A Word From Your Senior Editor

Dear authors and readers,

At the beginning of the 5th year of life of EurJIC there is a shared feeling of satisfaction for the high ISI ranking obtained by the Journal (2.222 is the first Impact Factor). It represents the success of the whole community of Inorganic Chemistry. Also the opinion that the chemistry of metal ions is growing in relative importance together with the growth of metal-based catalysis, material sciences, life sciences and environmental chemistry can be heard in Inorganic Chemistry circles. Together with this expansion of inorganic chemistry, the comprehension of the mechanisms of reactions and transformations increases, thanks to the new power of analytical and theoretical tools.

First Impact Factor 2.222

It is with pleasure that we note that the Nobel Committee awarded the Nobel Prize in Chemistry for 2001 to William S. Knowles and Ryoji Noyori for their work on chirally catalysed hydrogenation reactions, and K. Barry Sharpless for his work on chirally catalysed oxidation reactions. They can be defined as organometallic/metallorganic chemists! This must give impetus to this branch of Inorganic Chemistry.

Impetus to Organometallic Chemistry

The number of chemical societies that own the journal has also increased. We welcome the Hungarian Chemical Society and its members, and in particular the Hungarian Academy of Sciences, who merged one of their chemical journals with EurJIC to make this cooperation possible. Once again, one more journal has disappeared through this amalgamation.

Tenth participating society

I would also like to express my gratitude to the Editors and Advisory Board members for their dedication to the Journal. In particular I would like to mention Robert Schoonheydt, Sergio Cenini, and Jacques Livage, who have enthusiastically served until now, and to welcome Guy Bertrand, Pablo Espinet, Anton W. Gal, Tamás Kiss, Maurizio Peruzzini, Rinaldo Poli, Eduardo Ruiz-Hitzky, and Dieter Vogt, the newly appointed members – a dynamic organization thrives on the new ideas that a continuous rotation of the members brings.

New board members

In wishing you a successful new year, I also solicit you to sustain the journal in all the ways that you can: the success of the journal is due to contributors and referees and, of course, to readers.

Finally, the present standard of the journal could not be reached without the excellent performances of the managing editor and of the editorial team.

Thanks to all of them. Our aim for next year is to publish, fast, the best papers in the field.

Ivano Bertini
Senior Editor

 Eur. J. Inorg. Chem. **2002**, 4–5 © WILEY-VCH Verlag GmbH, 69451 Weinheim, Germany, 2002 1434–1948/02/0101–0004 $ 17.50+.50/0

A Word From Your Editorial Office:

Many people from authors, referees, and editors to compositors, bookbinders, freelance copy-editors and language-polishers put their best work into producing a high-quality journal. My thanks go to all of them. It has been an exciting year for the European Journal of Inorganic Chemistry, commonly called EurJIC by the ten European Chemical Societies, who own the journals. The nickname, pronounced "Your"JIC, caught on and has now been anchored in the new design of the cover. This innovation was prompted by the long-awaited ISI Impact Factor, which was announced to be 2.222, a good start. A high impact can only come from excellent papers from our authors − now each month authors will have the opportunity to present their chemistry on the front cover. We invite our authors to submit suggestions for this coveted position.

Authors invited to submit cover picture

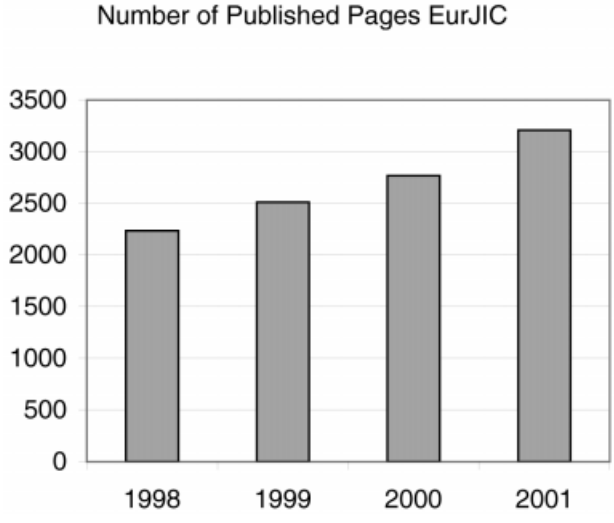

Last year EurJIC provided you with about 400 more pages of high-quality chemistry than in 2000. Publication times have been reduced (t_{50} now 4.6 months from received date to Web publication for the last quarter of 2001), although we are generous with the time we allow authors to include the improvements suggested by the referees, in order to achieve optimum quality. We do not automatically consider a paper that required over six weeks for revision as a new submission. Precedence is an important aspect for EurJIC, so we request the resubmission of a manuscript only if additional experimental work constitutes a significant part of the revision. We also like to provide referees with enough time to assess a manuscript critically and provide the author with stimulating comments. To reduce postal delays, we send PDF files to request a referee report. Nevertheless, you ALWAYS have the option of asking for a hard copy. I appeal to referees not to click away such e-mails. If your workload does not allow a timely assessment of the manuscript, let the office know promptly. Only if all steps in peer review are efficient, can we give authors the fast response that they expect.

Publication Times shortened

New technologies have also shortened publication times. The EarlyView feature of Wiley Inter Science gives you fully citable papers from EurJIC up to five weeks in advance of print. In particular Short Communications form the focus of this service. Thus the accelerated procedure that starts with the submission of an urgent article ends only with particularly rapid electronic publication.

And finally I would like to thank all Advisory Board Members and all authors who contacted us with suggestions in 2001. Only such open channels of communication can make EurJIC "Your Journal" for top papers in inorganic, bioinorganic, solid-state, physical inorganic and organometallic chemistry.

Coordinating Managing Editor European Journals:
Karen Hindson

and your Editorial Team:
Udo Eberhardt, Andrew Frankland, and Robert Temme

EurJIC
European Journal of Inorganic Chemistry

January 2002
Issue 1
Pages 1–264

COVER PICTURE

The cover picture shows a schematic view of silene plastocyanin (PDB ID: 1BYO, ref.[2] of the text) interacting with *tetra*-lysine. Details are discussed in the Microreview by S. Hirota and O. Yamauchi on page 17 ff.

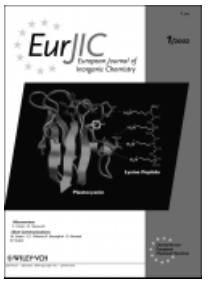

MICROREVIEW

Contents

17 **S. Hirota,* O. Yamauchi***

Interactions in Plastocyanin–Lysine Peptide and Related Systems

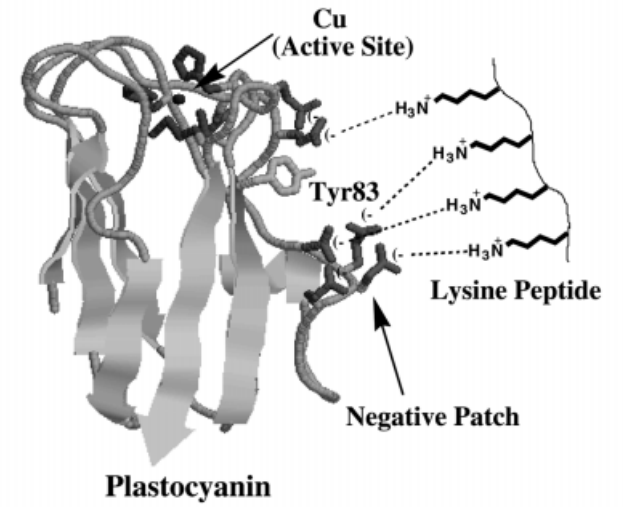

Keywords: Electron transfer / Proteins / Peptides / Structure–activity relationships

 © WILEY-VCH Verlag GmbH, 69451 Weinheim, Germany, 2002 1434–1948/02/0101–0007 $ 17.50+.50/0

Interactions in Plastocyanin−Lysine Peptide and Related Systems

Shun Hirota*[a] and Osamu Yamauchi*[b]

Keywords: Electron transfer / Proteins / Peptides / Structural change / Structure−activity relationships

The structure–function relationship of proteins is one of the major topics of protein studies. In spite of the importance of intermolecular interactions between proteins, which could control their functions, there are only a limited number of detailed studies on the protein structural changes induced by interaction with a protein or a peptide, because the associated changes in properties are small. Charged peptides, however, may be useful for studying the molecular recognition character of proteins and their interaction-induced structural changes, since they do not have any visible absorption. The active site Cu of plastocyanin (PC) exhibited a longer Cu–S(Cys) bond length and a higher redox potential on binding of a lysine peptide, suggesting that lysine peptides induce a structural change in PC to adapt the copper site for facile electron transfer. Structural changes were also observed for cytochrome (cyt) *f*, cyt *c*, and cytochrome *c* peroxidase on interaction with charged peptides.

1. Introduction

Structure−function relationship is one of the major topics in protein studies. In cells, each protein has to recognize its partner effectively, and thus the molecular recognition of proteins has been studied extensively. Intermolecular interactions between proteins and the induced structural changes, which may control their functions, are also important to understand the structure−function relationship of proteins. However, there are only a limited number of detailed studies on the structural changes induced by molecular interactions, because of the lack of a useful method.

[a] Department of Chemistry, Graduate School of Science, Nagoya University,
Chikusa-ku, Nagoya 464-8602, Japan
Fax: (internat.) + 81-52/789-2953
E-mail: k46230a@nucc.cc.nagoya-u.ac.jp
[b] Unit of Chemistry, Faculty of Engineering, Kansai University,
Yamate-cho, Suita, Osaka 564-8680, Japan
Fax: (internat.) + 81-6/6330-3770
E-mail: osamuy@ipcku.kansai-u.ac.jp

Shun Hirota was born in Port Jefferson, New York, in 1965. He obtained his Master's degree from Kyoto University in 1992. He received his Ph.D. degree in 1995 from the Graduate University for Advanced Studies under the supervision of Professor Teizo Kitagawa at the Institute for Molecular Science, Okazaki, Japan. He was a JSPS Research Fellow from 1994 to 1996 and joined Professor Luigi G. Marzilli's research group in the Chemistry Department, Emory University, Atlanta, Georgia, USA in 1995. Since 1996, he has been an assistant professor in the Department of Chemistry, Graduate School of Science, Nagoya University. He has been working in the field of bioinorganic chemistry, and his research interests include structure−function relationship and reaction mechanisms of metalloproteins.

Osamu Yamauchi was born in Nagoya in 1936. He received his Master's degree from Kyoto University in 1961. After spending two years at a pharmaceutical company as research staff member, he resumed his graduate studies at Kyoto University, receiving his Doctor's degree in pharmaceutical sciences in 1967. He was appointed Associate Professor at Osaka University in 1967 and Professor at Kanazawa University in 1980. In 1987 he was appointed Professor at the Department of Chemistry, Nagoya University. He retired from Nagoya University in 2000 and is now Professor at Kansai University and Professor Emeritus of Nagoya University. His research interests include weak interactions involving metal-coordinated amino acids and metalloproteins, self-organization of complex molecules, reactivity of aromatic rings in the vicinity of the metal center, metal-pterin chemistry, and other areas of bioinorganic chemistry.

MICROREVIEWS: This feature introduces the readers to the authors' research through a concise overview of the selected topic. Reference to important work from others in the field is included.

 © WILEY-VCH Verlag GmbH, 69451 Weinheim, Germany, 2002 1434−1948/02/0101−0017 $ 17.50+.50/0

Electron-transfer proteins are indispensable for life. Many of them are charged on their surface and/or have a specific charged site for a specific protein−protein complex formation, and the electrostatic interaction is one of the main forces that guide them to form such a complex for electron transfer. For example, plastocyanin (PC), a mobile electron-transfer protein existing in the thylakoid lumen of photosynthetic organisms, is negatively charged at neutral pH for higher plant and green algae PCs, whereas PCs from cyanobacteria are characterized by high pI values. Higher plant and green algae PCs contain consecutive acidic residues (negative patch) located at the solvent-accessible site near the tyrosine residue remote from the Cu center.[1,2] PC receives an electron from cytochrome *f* (cyt *f*) of the cytochrome b_6f complex, which is an integral oligomeric membrane protein complex existing in the photosynthetic organism. By X-ray structural studies, a lysine (Lys) residue rich positively charged site (positive patch) has been revealed to exist at the solvent-exposed site of cyt *f*,[3] and the electrostatic interaction between the negative patch of PC and the positive patch of cyt *f* has been inferred to be the force for the formation of the cyt *f*·PC complex.

An NMR spectroscopic study on the Cd-substituted PC·cytochrome *c* (cyt *c*) complex indicated that the PC·cyt *c* complex consists of a highly dynamic ensemble of structures.[4] Theoretical docking models demonstrated three docked complexes between PC and cyt *f* and suggested that the negative patch of PC is not important in the active electron transfer complex, although it is important for the initial binding.[5,6] Kostić et al. proposed that PC and cyt *f* or cyt *c* bind and react with each other in different configurations resulting from the protein−protein interaction termed as the gating process for electron transfer,[7−9] showing possible configurations for the diprotein complex by computer simulation.[10,11] A paramagnetic NMR spectroscopy and restrained rigid-body molecular mechanics study also indicated that the electrostatic interactions guide PC and cyt *f* into a position that is optimal for electron transfer,[12] whereas electron transfer has been shown to occur via His87 to Cu in PC by mapping NMR chemical-shift changes.[13] However, kinetic evidence for multiple binary complexes has been obtained for the protein docking and gated electron-transfer reactions between zinc cyt *c* and a new PC from the fern *Dryopteris crassirhizoma*,[14] which has a very large acidic surface extending into the area that is hydrophobic in other PCs.[15]

Cyt *c* is a well-known electron-transfer heme protein which is positively charged at neutral pH,[16,17] whereas cytochrome *c* peroxidase (C*c*P), an electron-transfer partner of cyt *c*, is negatively charged at neutral pH.[18] The cyt *c*·C*c*P complex was therefore predicted to be formed by the electrostatic interaction, which has been verified by the X-ray crystal structure analysis of the cyt *c*·C*c*P complex.[19]

Redox-inactive inorganic compounds have been utilized to study the molecular recognition character of electron-transfer proteins. NMR spectroscopic investigations on the complex formation between proteins and Cr^{III} compounds were made,[20,21] and $[Cr(NH_3)_6]^{3+}$ was shown to interact with both the hydrophobic and negative patches of PC,[21] whereas it bound to several sites on the surface of cyt *c*.[20] Sykes et al. showed that small redox-inactive inorganic compounds inhibit electron transfer between PC and cyt *c*,[22] cyt *f*,[23] or inorganic redox partners,[24−26] which has been explained by competitive inhibition due to interaction between the positive charge of the redox-inactive inorganic compound and the negative charge of PC.

2. Plastocyanin−Lysine Peptide Interaction

2.1 Molecular Recognition

Since the electrostatic interaction is essential for complex formation between these electron transfer proteins, we came upon the idea of using charged peptides as models for the protein interacting sites (Figure 1). Positively charged peptides interact with the aspartyl (Asp) and glutamyl (Glu) residues of the negatively charged sites of proteins, whereas negatively charged peptides can interact with the Lys residues of the positively charged sites. Actually, positively charged lysine peptides interacted with the consecutive Asp and Glu residues of the negative patch of PC and competitively inhibited electron transfer from reduced cyt *f* or cyt *c* to oxidized PC (Figure 2).[27] The inhibitory effects of lysine peptides on electron transfer were explained as competitive inhibition due to neutralization of the PC negative patch by formation of PC·lysine peptide complexes (Figure 3). Upon decreasing the net charge of the PC negative patch by mutation, the electron transfer rates from reduced cyt *c* to oxidized PC and the inhibiting effect of lysine peptide decreased. These results strongly indicate that the negative patch of PC is the dominant cyt *c*/*f* recognition site.

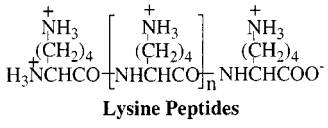

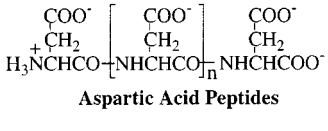

Figure 1. Chemical structures of lysine and aspartic acid peptides

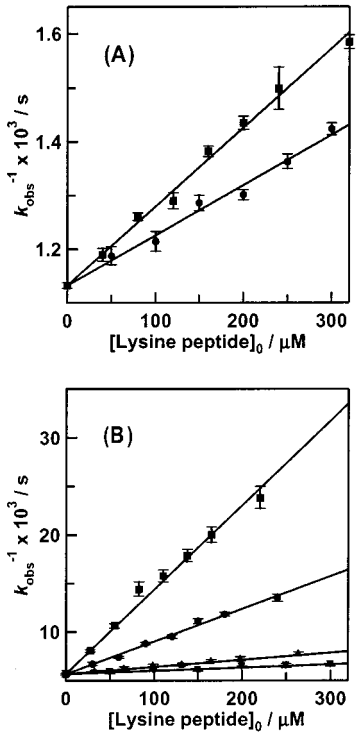

Figure 2. Plots of the reciprocal electron transfer rate constants ($1/k_{obs}$) from reduced cyt *f* or cyt *c* to oxidized PC vs. the initial concentrations of lysine peptides: *di*- (▼), *tri*- (▲), *tetra*- (•), and *penta*-Lys (■); (A) reduced cyt *f*-oxidized PC and (B) reduced cyt *c*-oxidized PC electron-transfer systems; protein concentrations: PC, 5 μM; cyt *f* and cyt *c*, 0.5 μM; Tris-HCl buffers (10 mM), pH = 7.3, containing 10 mM (A) and 60 mM NaCl (B), respectively, were used; modified from refs.[27,54]

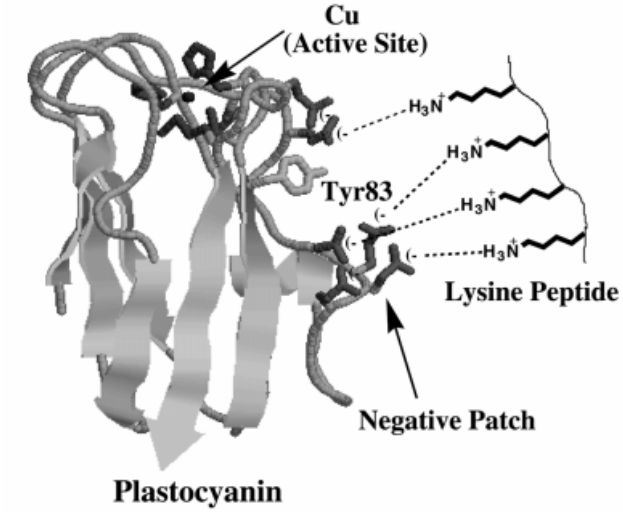

Figure 3. A schematic view of silene PC (PDB 1BYO, ref.[2]) interacting with *tetra*-Lys

The observed inhibition may be interpreted by considering formation of two complexes, a PC·cyt *c*/*f* complex where electron transfer subsequently occurs, and a PC·lysine peptide complex that competitively inhibits formation of the PC·cyt *c*/*f* complex and thus inhibits electron transfer. The complex formations are expressed by Equation (1) and Equation (2), where K_{OS} and K_i are the association constants for PC_{ox}·cyt c/f_{red} and PC_{ox}·lysine peptide complexes, respectively, and k_e represents the electron-transfer rate constant.

$$PC_{ox} + \text{cyt } f/c_{red} \underset{}{\overset{K_{OS}}{\rightleftharpoons}} (PC_{ox}\cdot \text{cyt } f/c_{red})_R \xrightarrow{k_e} (PC_{red}\cdot \text{cyt } f/c_{ox})_R \quad (1)$$

$$PC_{ox} + \text{lysine peptide} \overset{K_i}{\rightleftharpoons} (PC_{ox}\cdot\text{lysine peptide})_R \quad (2)$$

The suffixes ox and red refer to the oxidized and reduced states, and R denotes that the complex is formed at the Cu-remote negative patch of PC. If we write the observed rate constant as k_{obs}, $K_{OS} \times k_e$ as k, and the initial concentrations of PC and lysine peptide as $[PC]_0$ and $[\text{lysine peptide}]_0$, we obtain the relationship

$$\frac{1}{k_{obs}} = \frac{K_i}{k[PC]_0}[\text{lysine peptide}]_0 + \frac{1}{k[PC]_0} \quad (3)$$

Plots of $1/k_{obs}$ against $[\text{lysine peptide}]_0$ give straight lines, substantiating the validity of the assumptions leading to Equation (3). K_i values obtained from least-squares fitting of the data for the cyt *c*−PC electron-transfer system (Figure 2, B) with Equation (3) are listed in Table 1. The association constants for the PC·lysine peptide complexes increase as the length and thus the charge of the peptide increase, which shows that PC effectively recognizes the sites with four or more positive charges. The inhibitory effects demonstrate that these lysine peptides, especially *tetra*- and *penta*-Lys, function as models for the PC interacting site of proteins.

Table 1. Association constants (K_i) for PC−lysine peptide complexes obtained by least-squares fitting of the data in Figure 2 (B) with Equation (3)

Length of lysine peptide	K_i/M^{-1} [a]
di	550±130
tri	1400±200
tetra	5900±300
penta	15300±1000

[a] In 10 mM Tris-HCl buffer, pH = 7.3, containing 10 mM NaCl at 15 °C.

Interactions of lysine peptides with PC were also studied by measuring electron transfer between $[Fe(CN)_6]^{4-}$ and oxidized PC in the presence of the peptides.[28] Lysine peptides up to *penta*-Lys promoted electron transfer from $[Fe(CN)_6]^{4-}$ to PC.[28] The electron transfer promoting effects of lysine peptides may be due to formation of PC·lysine peptide or lysine peptide·$[Fe(CN)_6]^{4-}$ complexes, subsequently forming an electron transferring complex, PC·lysine peptide·$[Fe(CN)_6]^{4-}$, without repulsion of the negative charges.

Table 2. Absorption maximum wavelengths, average ν_{Cu-S} frequencies, EPR parameters, and midpoint redox potentials ($E_{midpoint}$) of wild-type and Tyr83 mutant PCs

Species	Wavelength[a] [nm]	ν_{Cu-S} [b] [cm^{-1}]	EPR parameters $g_{\|\|}$	$\|A_{\|\|}\|$	$E_{midpoint}$[c] [mV]
wild-type	597.5	418.4	2.242	6.2	344
Y83F	597.5	417.9	2.256	5.7	340
Y83S	595.5	420.6	2.239	6.5	325
Y83L	595.5	423.3	2.238	6.5	320
Y83H	598.0	417.0	2.246	6.2	382

[a] Error ±0.5 nm. – [b] Error ±1.0 cm^{-1} for the calculated values. – [c] Versus NHE; measured in 10 mM phosphate buffer, pH = 7.4; error ±5 mV.

2.2 Relationship Between the Spectroscopic and Electrochemical Properties of PC

PC is classified as a type 1 copper protein and contains one copper atom, which is coordinated to two histidine nitrogen atoms, one methionine sulfur atom, and one cysteine sulfur atom in a distorted tetrahedral geometry according to the crystal structures of its oxidized and reduced forms.[1,2,29,30] Oxidized type 1 copper proteins exhibit unique spectroscopic properties, such as a low energy ligand-to-metal charge transfer (LMCT) band near 600 nm in the absorption spectrum and a narrow hyperfine coupling constant ($|A_{||}| < 90{\cdot}10^{-4}$ cm^{-1}) in the electron paramagnetic resonance (EPR) spectrum.[31,32]

Studies on the relationship between the structural and spectroscopic properties of type 1 copper proteins have been reported.[32–42] The general relationship will be discussed along with the properties of wild-type and Tyr83 mutant PCs (Table 2, Figure 4).[43] The spectroscopic and electrochemical properties of the wild-type and Tyr83 mutant PCs were similar but slightly different. In the absorption spectra, an intense band around 600 nm has been assigned to the cysteine thiolate [S(Cys)]-to-Cu^{II} LMCT band (Figure 5).[31,32] Y83H mutant PC which has a longer wavelength peak for this 600-nm band, exhibits an increase and decrease in the intensities of the 460- and 700-nm bands, respectively, compared with the corresponding bands of other PCs.[43] The ratio of the intensity of the 460-nm absorption band to that of the 600-nm band has been found to correlate with the rhombicity of the EPR signal for type 1 copper proteins,[35] and the rhombic distortion has been suggested to be associated with a stronger binding of the axial ligand and a concomitant shift from a trigonal planar toward a tetrahedrally distorted Cu site geometry.[35–37] Actually, wild-type PC which showed a stronger 460-nm absorption band than that of the Y83S or Y83 L proteins, exhibited a more rhombic EPR spectrum with larger $g_{||}$ and smaller $|A_{||}|$ values (Table 2), suggesting a more tetrahedral geometry for the Cu^{II} site.

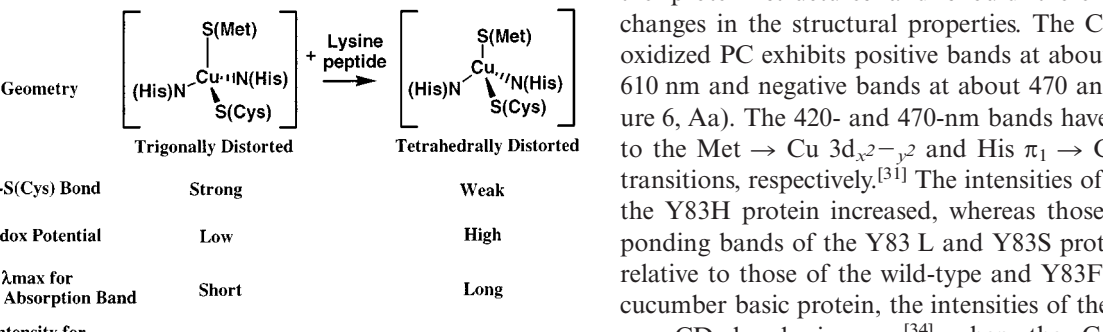

Figure 4. Relationship among the spectroscopic and electrochemical properties and the Cu active site geometry of oxidized PC

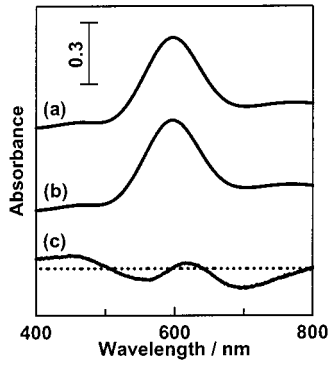

Figure 5. Absorption spectra of oxidized PC with (a) and without *penta*-Lys (b) and their difference spectrum (a – b) multiplied by 20 (c); the baseline of the difference spectrum is shown as a dotted line; concentrations of PC and *penta*-Lys were 100 and 330 μM, respectively; sodium phosphate buffer (10 mM), pH = 7.4, was used; modified from ref.[53]

The circular dichroism (CD) spectra are very sensitive to the protein structures and should therefore reflect the changes in the structural properties. The CD spectrum of oxidized PC exhibits positive bands at about 420, 560, and 610 nm and negative bands at about 470 and 760 nm (Figure 6, Aa). The 420- and 470-nm bands have been assigned to the Met → Cu $3d_{x^2-y^2}$ and His π_1 → Cu $3d_{x^2-y^2}$ CT transitions, respectively.[31] The intensities of these bands of the Y83H protein increased, whereas those of the corresponding bands of the Y83 L and Y83S proteins decreased, relative to those of the wild-type and Y83F proteins.[43] In cucumber basic protein, the intensities of the 420- and 470-nm CD bands increase[34] when the Cu–S(Cys) and Cu–S(Met) bond lengths are extended and shortened by 0.1 and 0.2 Å, respectively,[44] and the Cu–S(Cys) stretching (ν_{Cu-S}) frequency is lower [45] then that in PC.

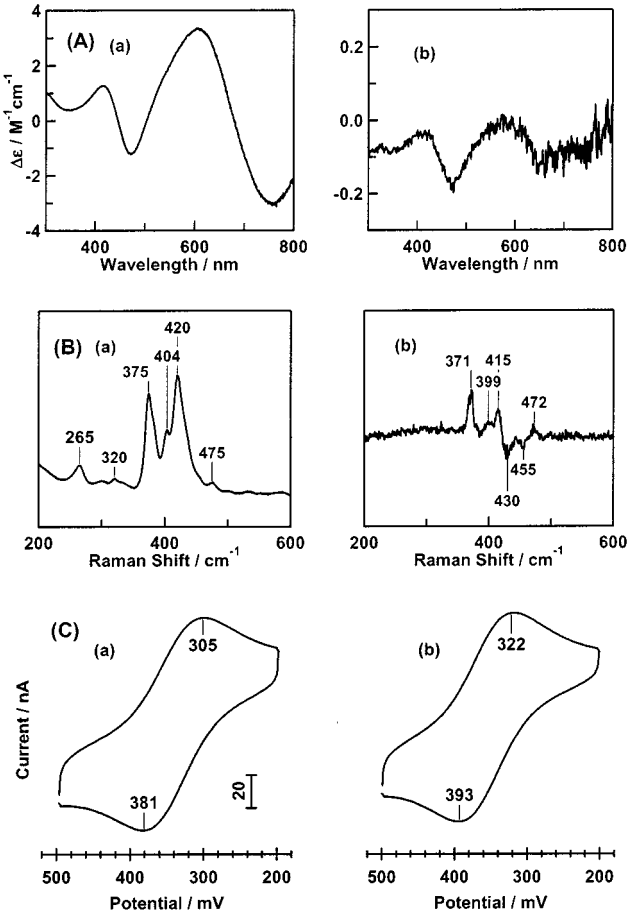

Figure 6. (A) CD spectra of oxidized PC without *tetra*-Lys (a) and the difference CD spectrum obtained by subtracting the CD spectrum from that with *tetra*-Lys (600 μM) (b); (B) RR spectra in the 200−600 cm^{-1} region for oxidized PC without *penta*-Lys (a) and the difference RR spectrum obtained by subtracting the RR spectrum from that with *penta*-Lys (660 μM) (b); (C) cyclic voltammograms of PC without (a) and with *penta*-Lys (260 μM) (b); concentration of PC was 70, 500, and 100 μM for A, B, and C, respectively; sodium phosphate buffer (10 mM), pH = 7.4, was used; modified from refs.[27,43]

Resonance Raman (RR) spectroscopy is a powerful method for investigating the character of the Cu−S(Cys) bond in type 1 copper proteins by exciting the Raman scattering near the S(Cys)-to-Cu^{II} CT band.[40,46−49] The ν_{Cu-S} frequency is shown to be a sensitive probe of the Cu−S(Cys) bond strength and copper coordination geometry for proteins with cysteine thiolate coordination.[39−42] It is closely related to the electron-transfer exothermicity for several type 1 copper proteins.[38] In practice, several bands are observed at 374−475 cm^{-1} for the RR spectrum of oxidized PC excited near its S(Cys)-to-Cu^{II} CT band (Figure 6, Ba), which is mainly due to the mixing of the Cu−S stretch with several angle bendings of the coordinated Cys side chain.[40,46−49] The weighted average frequency based on the S-isotope dependence was shown to correlate with the Cu−S(Cys) distance for azurin, another type 1 copper protein, and its mutants.[39] The average ν_{Cu-S} frequencies of wild-type and Tyr83 mutant PCs were therefore calculated from the intensities and frequencies of three major RR bands, which mainly contain contributions from the ν_{Cu-S} (Table 2).[50] The average ν_{Cu-S} frequency was in the order Y83 L > Y83S > Y83F ≈ wild-type > Y83H, suggesting a stronger Cu−S(Cys) bond in this order. Species exhibiting a more intense 460-nm absorption band exhibits a smaller average ν_{Cu-S}. A similar relationship has also been found by comparison of the properties of type 1 and type 2 cystein-coordinated copper proteins.[40]

As regards the redox potential, Y83F mutant PC exhibited a potential similar to that of wild-type PC, whereas the potentials of Y83S and Y83 L PCs shifted to lower values and the potential of Y83H PC shifted to a higher value relative to that of wild-type PC, where species with a higher ν_{Cu-S} frequency and a stronger Cu−S(Cys) bond exhibited a lower redox potential (Table 2).

The spectroscopic and electrochemical properties of PC may be summarized as follows. Species exhibiting a more intense 460-nm absorption band and a longer wavelength for the 600-nm absorption band show a more tetrahedral geometry for the Cu site, a smaller average ν_{Cu-S} frequency, and a higher redox potential. A weaker Cu−S(Cys) bond would create a weaker ligand field with the Cys ligand, and thus the energy of the S(Cys)-to-Cu^{II} CT band would decrease and the redox potential of Cu would shift to a higher value. In PC, the Cu−S(Met) bond is the longest metal−ligand bond,[1,2] and a stronger Cu−S(Met) axial bond has been suggested to cause a larger displacement of the Cu^{II} from the trigonal plane containing two histidine nitrogen atoms and one cysteine sulfur atom, shifting the active site coordination structure toward a tetrahedral geometry.[35] Comparison between several type 1 copper proteins showed that proteins with a higher energy ligand field associated with rotation of the Cu $d_{x^2-y^2}$ half-filled HOMO exhibit longer Cu−S(Cys) and shorter Cu−S(Met) bonds with a more tetrahedral geometry.[34,35] A weaker Cu−S(Cys) bond would therefore induce a structural change with a shorter Cu−S(Met) bond and a more tetrahedral Cu^{II} geometry, which has been detected by comparison of the Y83H protein with the Y83S and Y83 L proteins (Table 2).

2.3 Active Site Structural Change Induced by Interaction with Lysine Peptide

Redox-induced conformational changes in PC have been studied by infrared spectroscopy, and protonation of (an) Asp or Glu side chain(s) upon PC oxidation, at acidic pH, has been indicated.[51] Recently, Ag- and Cd-substituted PC were used as models for native Cu^{I} and Cu^{II} PCs, respectively, and the metal site structure depending on the charge of the metal ion has been indicated to influence the dissociation between PC and photosystem I.[52] Lysine peptides are very useful for investigating the molecular interaction-induced structural changes of metalloproteins having absorption bands in the visible region, since the peptides do not have any absorptions in the visible region. In this section, we focus on the active site structural changes of oxid-

ized PC by interaction with lysine peptide at its negative patch (Figure 3).

The interaction of PC with lysine peptides was investigated by absorption, CD, and RR spectroscopy, and electrochemical measurements, which revealed changes in the active site Cu coordination geometry upon binding of a lysine peptide at the negative patch.[27,43,53] In the difference absorption spectrum between the spectra with and without *penta*-Lys, peaks and troughs were detected at about 460 and 630 nm and at about 560 and 700 nm, respectively (Figure 5, c). These peaks revealed that the 600-nm absorption band shifts to a longer wavelength and the intensities of the 460- and 700-nm absorption bands increase and decrease, respectively, on interaction with a lysine peptide. As discussed in section 2.2, the intensity increase of the 460-nm absorption band and the shift of the 600-nm absorption band to a longer wavelength can be associated with the lengthening of the Cu−S(Cys) bond and the change from a trigonal planar toward a more tetrahedral Cu site geometry.[35−37] The Cu−S(Cys) bond should therefore be elongated and the Cu site should become more tetrahedral on interaction with the lysine peptide. These structural changes at the Cu site are caused by an electrostatic interaction of the PC negative patch with the lysine peptide, since the intensities of the peaks observed in the difference spectra decreased when NaCl was added to the solution. Moreover, the observed spectral changes decreased when the charges at the negative patch were decreased by site-directed mutagenesis.[27]

The intensities of the peaks and troughs in the difference spectra increased with the concentration of the lysine peptide and became saturated at a certain peptide concentration (Figure 7).[53] The observed intensity changes in the absorption spectra can be interpreted by considering the formation of a 1:1 PC·lysine peptide complex according to Equation (2). If we write the difference between the observed absorption changes at 630 and 560 nm upon lysine peptide binding as ΔΔAbs, the difference between the corresponding absorption coefficient changes as ΔΔε, the concentrations of PC and lysine peptide as [PC] and [lysine peptide], respectively, and the cell length used for the measurements as l, we obtain the relationship of Equation (4).

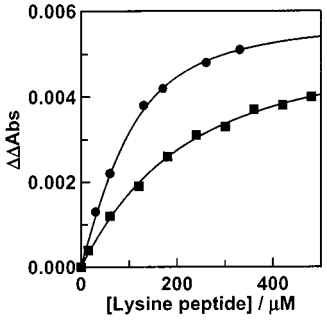

Figure 7. Plots of ΔΔAbs vs. [lysine peptide], together with least-squares fitted lines according to Equation (4); ■ = *tetra*- and • = *penta*-Lys; concentration of PC was 100 μM; modified from ref.[43]

$$\Delta\Delta Abs = \frac{\Delta\Delta\varepsilon \times l}{2}\left\{\left([PC] + [\text{lysine peptide}] + \frac{1}{K_i}\right) - \left[\left([PC] + [\text{lysine peptide}] + \frac{1}{K_i}\right)^2 - 4\,[PC]\,[\text{lysine peptide}]\right]^{1/2}\right\} \quad (4)$$

The K_i values (8000 ± 4000 and 24000 ± 5000 M^{-1} for *tetra*- and *penta*-Lys, respectively) were obtained by least-squares fitting of the experimental data with Equation (4) (Figure 7). Since the fitting was successful, it is reasonable to assume that only one lysine peptide is bound to the negative patch of PC, which is in agreement with the previous conclusion derived from the inhibitory character of lysine peptide on electron transfer from cyt *c* or cyt *f* to PC (see section 2.1).[27,54] The association constants between PC and lysine peptide obtained from the difference absorption spectra were larger than those obtained from electron transfer experiments,[27] which is probably due to NaCl added to the solution to make the electron transfer rate detectable. Absorption spectral studies with various lysine peptides showed that PC interacts effectively only with lysine peptides equal to or longer than *tetra*-Lys, due to the increase in the charges and stronger electrostatic interaction, where a similar conclusion was drawn from the inhibitory effect on electron transfer (see section 2.1). In connection with the absorption change by lysine peptide binding, the association constants between PC and cyt *f* or cyt *c* have been obtained by measuring the increase of the Soret band intensity of cyt *f* or cyt *c* on PC binding.[55−57]

The difference CD spectra of oxidized wild-type and Tyr83 mutant PCs in the presence and absence of *tetra*-Lys are shown in Figure 6, Ab. A positive peak at about 420 nm and a negative peak at about 470 nm were detected in the difference spectra, which demonstrate changes in their CD spectra and thus in the active site structure on interaction with *tetra*-Lys. Since the intensities of the 420- and 470-nm CD bands increase, the Cu−S(Cys) and Cu−S(Met) bond lengths should become longer and shorter, respectively, for PC by interaction with lysine peptides (see section 2.2). When *tetra*-Lys was added to PC, the Raman bands at 375−475 cm^{-1} shifted slightly to lower frequencies with a concomitant slight increase in the intensities of some lower frequency bands in this region, especially the ν_{Cu-S} related 375- and 422-cm^{-1} bands. These results indicate that the Cu−S(Cys) bond was weakened on addition of a lysine peptide. Interestingly, the RR spectral changes of PC were the same for PC−cyt *c* and PC−lysine peptide interactions, indicating that lysine peptides are excellent models for the PC recognition site of proteins. However, ESR spectroscopic measurements on oxidized PC gave no significant change on the Cu^{2+} signal upon addition of lysine peptides.[27,43] The lack of EPR spectroscopic detection of the structural change of PC on addition of lysine peptides could be due to the fact that EPR spectroscopy is more sensitive to the Cu−N bond geometry, while the 375−475-cm^{-1} RR bands are related to the Cu-coordinated Cys residue. In line with this, the 265-cm^{-1} RR band that is as-

signed to the Cu−His stretching mode did not show any change on interaction with lysine peptides.

Electrochemical measurements showed that the redox potential of PC shifted to a higher potential upon lysine peptide binding, which suggests that the structural change induced by binding of lysine peptides to PC adapts the copper site for facile electron transfer (Figure 6, C). This structural change might be related to the report by Kostić et al., who proposed that PC and cyt *c* or cyt *f* bind and react with each other in different configurations resulting from the protein−protein interaction termed as the gating process for electron transfer,[7−9,58] showing possible configurations for the diprotein complex by computer simulation.[10,11]

For the electron transfer from cyt *f* to PC, Tyr83 which is located near the negative patch of PC has been proposed to be involved in the electron transfer pathway, since the reaction rate decreased upon replacement of Tyr with other amino acid residues.[56,57] Ullmann et al. demonstrated by molecular dynamics the possible occurrence of a cation−π interaction at the Tyr83 site, which might be important for electron transfer from cyt *f* to PC.[11] On the other hand, Tyr83 mutants showed minor effects on the interaction between PC and PSI, and electron transfer from PC to $P700^+$ was proposed to occur at the hydrophobic patch.[59−61] Recently, electron transfer from cyt *f* to PC was inferred by NMR spectroscopic measurements to occur via His87 of the hydrophobic patch.[13] Since the structural changes observed for wild-type and Tyr83 mutant PCs by complex formation with lysine peptides were similar,[43] the structural change due to binding of lysine peptides to PC is concluded not to be transmitted through the path of Tyr83−Cys84−copper by a cation−π interaction.

In summary, when wild-type PC interacted with lysine peptide, the intensity of the 460-nm absorption band increased, the maximum wavelength for the 600-nm absorption band became longer, the average ν_{Cu-S} frequency became lower, and the redox potential shifted to a higher value. All these changes may be associated with a slightly more tetrahedral geometry for the Cu site, further supporting the proposal that PC suffers a structural change on interaction with its redox partner, cyt *f*, for facile electron transfer from it.

3. Other Protein−Charged Peptide Interactions

3.1 Interaction of Cyt *f* and Cyt *c* with Aspartic Acid Peptides

Positively charged aspartic acid peptides up to *penta*-Asp (Figure 1) served as competitive inhibitors of electron transfer from cyt *c* or cyt *f* to PC.[54] *Tetra*- and *penta*-Asp also served as competitive inhibitors of electron transfer from $[Fe(CN)_6]^{4-}$ to oxidized cyt *c*.[28] A cyt *c*/*f*·aspartic acid peptide complex is formed by the electrostatic interaction between the aspartic acid peptides and the Lys residues at the surface of cyt *c* or cyt *f*, and the electron-transfer inhibitory effects of aspartic acid peptides are ascribed to formation of the cyt *c*/*f*·aspartic acid peptide complex, similar to that of the PC·lysine peptide complex.

Changes in the absorption spectrum of cyt *c* in the Soret region were detected when aspartic acid peptides, up to *penta*-Asp, were added to the cyt *c* solution (Figure 8, A).[54] These changes were the same as those observed when cyt *c* interacted with PC, indicating that aspartic acid peptides interacted with cyt *c* in the same way as PC. Conformational changes of cyt *c* due to interaction with aspartic acid peptides observed by RR spectroscopy (Figure 8, B) were also similar to those reported for cyt *c* bound to its native partner, cytochrome *c* oxidase,[62] which indicates that aspartic acid peptides interact with cyt *c* in the same way as cytochrome *c* oxidase and serve as good models for the protein interacting sites. Electrochemical measurements showed that the redox potential of cyt *c* and cyt *f* shifts to lower potentials by 7−20 mV upon aspartic acid peptide binding, indicating the enhancement in the electron donor ability of both cyt *c* and cyt *f* upon complex formation with the aspartic acid peptide.[54] The changes in the absorption spectrum and redox potential increased with the length and concentration of the aspartic acid peptides used. The observed structural and redox changes of cyt *c* and cyt *f* are therefore attributed to adduct formations with aspartic acid peptides by electrostatic interactions.

The redox potential of silene PC and *Brassica komatsuna* cyt *f* are 343 and 364 mV, respectively, when no charged

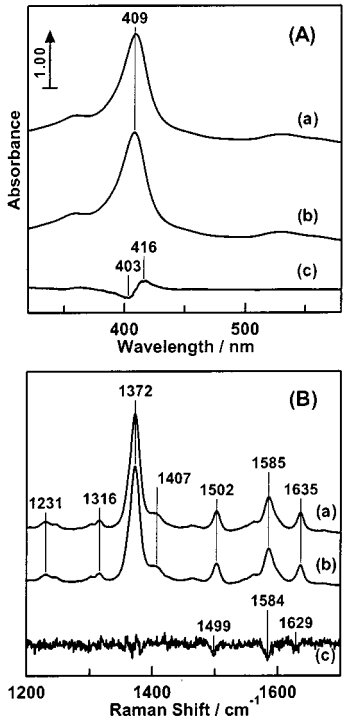

Figure 8. (A) Absorption spectra of oxidized cyt *c* with (a) and without *tetra*-Asp (b) and their difference spectrum (spectrum a − spectrum b) multiplied by 30 (c); (B) resonance Raman spectra in the 1200−1700 cm^{-1} region for cyt *c* with (a) and without *penta*-Asp (b) and their difference spectrum (spectrum a − spectrum b) multiplied by 15 (c); concentration of cyt *c* was 100 and 50 μM for A and B, respectively; Tris-HCl buffer (10 mM), pH = 7.4, was used; modified from ref.[54]

peptides are bound to them,[28,54] and considering their redox potentials, it appears unlikely that efficient electron transfer would occur between these proteins. Our observation that the redox potential of PC shifts to a higher potential and that of cyt *f* to a lower one, upon binding of charged peptides, suggests that redox potential shifts due to complex formation facilitate electron transfer between these proteins of non-physiological interaction and could also facilitate it between their physiological partners.

3.2 Cyt *c*−Cytochrome *c* Peroxidase System

The structural change of oxidized C*c*P due to interaction with lysine peptides was studied by measurements on electron transfer between reduced cyt *c* and C*c*P^{IV}=O (Trp191$^{\cdot+}$) and the absorption spectra in the presence of lysine peptides.[63] Lysine peptides competitively inhibited electron transfer from cyt *c* to C*c*P, which indicated that they interacted with C*c*P at the same site where cyt *c* binds and would be effective models for the C*c*P interacting site of cyt *c*.

Peaks were observed in the difference absorption spectrum of C*c*P between the spectra in the presence and absence of lysine peptides, demonstrating a structural perturbation of C*c*P, at least at its heme site, also occurs on interaction with the lysine peptides (Figure 9). This interaction was also proved to be electrostatic, since no significant peak was detected in the difference absorption spectrum measured in the presence of NaCl.

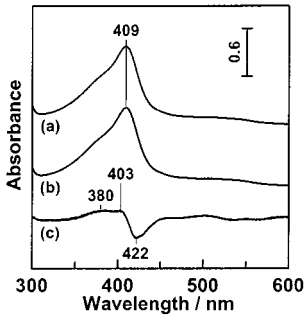

Figure 9. Absorption spectra of oxidized C*c*P with (a) and without *tetra*-Lys (b) and their difference spectrum multiplied by 20 (c); concentrations of C*c*P and *tetra*-Lys were 10 and 100 μM, respectively; Tris-HCl buffer (10 mM), pH = 7.8, was used; modified from ref.[63]

4. Conclusion

We propose that charged peptides are useful for studying the molecular recognition character of proteins and their structural changes induced by the molecular interaction. In particular, charged peptides which are good models of the protein interaction sites could be used for investigating the molecular interaction induced structural changes of metalloproteins which have absorption bands in the visible region, since the peptides have no visible absorption.

Positively charged lysine peptides inhibited electron transfer from reduced cyt *f* or cyt *c* to oxidized PC. Likewise, aspartic acid peptides served as competitive inhibitors of electron transfer from cyt *c* or cyt *f* to PC. They also served as inhibitors of electron transfer from $[Fe(CN)_6]^{4-}$ to oxidized cyt *c*. These inhibitory characters are ascribable to the formation of protein−peptide complexes which inhibit formation of the electron transfer complexes.

Changes in the absorption spectrum which were observed on addition of lysine peptides to the PC solution have been ascribed by RR spectroscopic studies to the change in the active site Cu−Cys geometry upon binding of lysine peptide to the PC negative patch. Similar absorption changes were observed for the PC−cyt *c* interaction, demonstrating that cyt *c* and lysine peptides interact with PC in a similar way. Electrochemical measurements showed that the redox potential of PC shifts to a higher potential upon lysine peptide binding, which suggested that lysine peptides induce a structural change in PC to adapt the copper site for facile electron transfer.

Changes in the absorption spectrum of cyt *c* in the Soret region were also detected when aspartic acid peptides were added to the cyt *c* solution. These changes were similar to those observed when cyt *c* interacted with PC, indicating that PC and aspartic acid peptides interact with cyt *c* in a similar way. Conformational changes of cyt *c* due to interaction with aspartic acid peptides observed in the RR spectra were also similar to those reported for cyt *c* when bound with its native partner, cytochrome *c* oxidase. Electrochemical measurements showed that the redox potential of cyt *c* and cyt *f* shifted to lower potentials upon aspartic acid peptide binding, showing the enhancement in the electron donor ability of both cyt *c* and cyt *f* upon complex formation with the aspartic acid peptide.

Acknowledgments

We are deeply indebted to the co-workers whose names are listed in the papers cited in the references for their contribution and enthusiasm. The support of the research by the Ministry of Education, Culture, Sports, Science and Technology of Japan is gratefully acknowledged.

[1] [1a] P. M. Colman, H. C. Freeman, J. M. Guss, M. Murata, V. A. Norris, J. A. M. Ramshaw, M. P. Venkatappa, *Nature* **1978**, *272*, 319−324. [1b] J. M. Guss, H. C. Freeman, *J. Mol. Biol.* **1983**, *169*, 521−563.
[2] H. Sugawara, T. Inoue, C. Li, M. Gotowda, T. Hibino, T. Takabe, Y. Kai, *J. Biochem.* **1999**, *125*, 899−903.
[3] S. E. Martinez, D. Huang, A. Szczepaniak, W. A. Cramer, J. L. Smith, *Structure* **1994**, *2*, 95−105.
[4] M. Ubbink, D. S. Bendall, *Biochemistry* **1997**, *36*, 6326−6335.
[5] D. C. Pearson, Jr., E. L. Gross, E. S. David, *Biophys. J.* **1996**, *71*, 64−76.
[6] D. C. Pearson, Jr., E. L. Gross, *Biophys. J.* **1998**, *75*, 2698−2711.
[7] M. M. Crnogorac, C. Shen, S. Young, Ö. Hansson, N. M. Kostić, *Biochemistry* **1996**, *35*, 16465−16474.
[8] M. M. Ivković-Jensen, N. M. Kostić, *Biochemistry* **1996**, *35*, 15095−15106.
[9] M. M. Ivković-Jensen, N. M. Kostić, *Biochemistry* **1997**, *36*, 8135−8144.
[10] G. M. Ullmann, N. M. Kostić, *J. Am. Chem. Soc.* **1995**, *117*, 4766−4774.

[11] G. M. Ullmann, E.-W. Knapp, N. M. Kostić, *J. Am. Chem. Soc.* **1997**, *119*, 42−52.
[12] M. Ubbink, M. Ejdebäck, B. G. Karsson, D. S. Bendall, *Structure* **1998**, *6*, 323−335.
[13] M. Ejdebäck, A. Bergkvist, B. G. Karlsson, M. Ubbink, *Biochemistry* **2000**, *39*, 5022−5027.
[14] E. V. Pletneva, D. B. Fulton, T. Kohzuma, N. M. Kostić, *J. Am. Chem. Soc.* **2000**, *122*, 1034−1046.
[15] T. Kohzuma, T. Inoue, F. Yoshizaki, Y. Sasakawa, K. Onodera, S. Nagatomo, T. Kitagawa, S. Uzawa, Y. Isobe, Y. Sugimura, M. Gotowda, Y. Kai, *J. Biol. Chem.* **1999**, *274*, 11817−11823.
[16] T. Takano, R. E. Dickerson, *J. Mol Biol.* **1981**, *153*, 79−94.
[17] G. W. Bushnell, G. V. Louie, G. D. Brayer, *J. Mol. Biol.* **1990**, *214*, 585−595.
[18] B. C. Finzel, T. L. Poulos, J. Kraut, *J. Biol. Chem.* **1984**, *259*, 13027−13036.
[19] H. Pelletier, J. Kraut, *Science* **1992**, *258*, 1748−1755.
[20] S. Bagby, P. C. Driscoll, K. G. Goodall, C. Redfield, H. A. O. Hill, *Eur. J. Biochem.* **1990**, *188*, 413−420.
[21] D. J. Cookson, M. T. Hayes, P. E. Wright, *Biochim. Biophys. Acta* **1980**, *591*, 162−176.
[22] S. K. Chapman, C. V. Knox, A. G. Sykes, *J. Chem. Soc., Dalton Trans.* **1984**, 2775−2780.
[23] D. Beoku-Betts, S. K. Chapman, C. V. Knox, A. G. Sykes, *Inorg. Chem.* **1985**, *24*, 1677−1681.
[24] S. K. Chapman, I. Sanemasa, A. G. Sykes, *J. Chem. Soc., Dalton Trans.* **1983**, 2549−2553.
[25] S. K. Chapman, A. D. Watson, A. G. Sykes, *J. Chem. Soc., Dalton Trans.* **1983**, 2543−2548.
[26] J. McGinnis, J. D. Sinclair-Day, A. G. Sykes, *J. Chem. Soc., Dalton Trans.* **1986**, 2007−2009.
[27] S. Hirota, K. Hayamizu, M. Endo, T. Hibino, T. Takabe, T. Kohzuma, O. Yamauchi, *J. Am. Chem. Soc.* **1998**, *120*, 8177−8183.
[28] S. Hirota, M. Endo, T. Tsukazaki, T. Takabe, O. Yamauchi, *J. Biol. Inorg. Chem.* **1998**, *3*, 563−569.
[29] J. M. Guss, P. R. Harrowell, M. Murata, V. A. Norris, H. C. Freeman, *J. Mol. Biol.* **1986**, *192*, 361−387.
[30] H. C. Freeman, in *Coordination Chemistry − 21* (Ed. J. L. Laurent), Pergamon Press, Oxford, U.K., **1981**, vol. 21, p. 29−51.
[31] A. A. Gewirth, E. I. Solomon, *J. Am. Chem. Soc.* **1988**, *110*, 3811−3819.
[32] E. I. Solomon, M. J. Baldwin, M. D. Lowery, *Chem. Rev.* **1992**, *92*, 521−542.
[33] K. Pierloot, J. O. A. De Kerpel, U. Ryde, M. H. M. Olsson, B. O. Roos, *J. Am. Chem. Soc.* **1998**, *120*, 13156−13166.
[34] L. B. LaCroix, D. W. Randall, A. M. Nersissian, C. W. G. Hoitink, G. W. Canters, J. S. Valentine, E. I. Solomon, *J. Am. Chem. Soc.* **1998**, *120*, 9621−9631.
[35] Y. Lu, L. B. LaCroix, M. D. Lowery, E. I. Solomon, C. J. Bender, J. Peisach, J. A. Roe, E. B. Gralla, J. S. Valentine, *J. Am. Chem. Soc.* **1993**, *115*, 5907−5918.
[36] A. A. Gewirth, S. L. Cohen, H. J. Schugar, E. I. Solomon, *Inorg. Chem.* **1987**, *26*, 1133−1146.
[37] J. Han, T. M. Loehr, Y. Lu, J. S. Valentine, B. A. Averill, J. Sanders-Loehr, *J. Am. Chem. Soc.* **1993**, *115*, 4256−4263.
[38] D. F. Blair, G. W. Campbell, J. R. Schoonover, S. I. Chan, H. B. Gray, B. G. Malmstrom, I. Pecht, B. I. Swanson, W. H. Woodruff, W. K. Cho, A. M. English, H. A. Fry, V. Lum, K. A. Norton, *J. Am. Chem. Soc.* **1985**, *107*, 5755−5766.
[39] B. C. Dave, J. P. Germanas, R. S. Czernuszewicz, *J. Am. Chem. Soc.* **1993**, *115*, 12175−12176.
[40] C. R. Andrew, H. Yeom, J. S. Valentine, B. G. Karlsson, N. Bonander, G. van Pouderoyen, G. W. Canters, T. M. Loehr, J. Sanders-Loehr, *J. Am. Chem. Soc.* **1994**, *116*, 11489−11498.
[41] C. R. Andrew, J. Sanders-Loehr, *Acc. Chem. Res.* **1996**, *29*, 365−372.
[42] C. R. Andrew, J. Han, T. den Blaauwen, G. van Pouderoyen, E. Vijgenboom, G. W. Canters, T. M. Loehr, J. Sanders-Loehr, *J. Biol. Inorg. Chem.* **1997**, *2*, 98−107.
[43] S. Hirota, K. Hayamizu, T. Okuno, M. Kishi, H. Iwasaki, T. Kondo, T. Hibino, T. Takabe, T. Kohzuma, O. Yamauchi, *Biochemistry* **2000**, *39*, 6357−6364.
[44] J. M. Guss, E. A. Merritt, R. P. Phizackerley, H. C. Freeman, *J. Mol. Biol.* **1996**, *262*, 686−705.
[45] T. Sakurai, S. Sawada, A. Nakahara, *Inorg. Chim. Acta* **1986**, *123*, L21−L22.
[46] J. Sanders-Loehr, in *Bioinorganic Chemistry of Copper* (Eds.: K. D. Karlin, Z. Tyeklár), Chapman & Hall, New York, **1993**, p. 51−63.
[47] W. H. Woodruff, R. B. Dyer, J. R. Schoonover, in *Biological Applications of Raman Spectroscopy* (Ed. T. G. Spiro), John Wiley, New York, **1988**, vol. 3, p. 413−438.
[48] D. Qiu, S. Dong, J. A. Ybe, M. H. Hecht, T. G. Spiro, *J. Am. Chem. Soc.* **1995**, *117*, 6443−6446.
[49] D. Qiu, S. Dasgupta, P. M. Kozlowski, W. A. Goddard, III, T. G. Spiro, *J. Am. Chem. Soc.* **1998**, *120*, 12791−12797.
[50] S. Dong, T. G. Spiro, *J. Am. Chem. Soc.* **1998**, *120*, 10434−10440.
[51] S. G. Taneva, U. Kaiser, A. A. Donchev, M. I. Dimitrov, W. Mäntele, A. Muga, *Biochemistry* **1999**, *38*, 9640−9647.
[52] E. Danielsen, H. V. Scheller, R. Bauer, L. Hemmingsen, M. J. Bjerrum, Ö. Hansson, *Biochemistry* **1999**, *38*, 11531−11540.
[53] S. Hirota, K. Hayamizu, T. Takabe, O. Yamauchi, *Inorg. React. Mech.* **2000**, *2*, 113−118.
[54] S. Hirota, M. Endo, K. Hayamizu, T. Tsukazaki, T. Takabe, T. Kohzuma, O. Yamauchi, *J. Am. Chem. Soc.* **1999**, *121*, 849−855.
[55] S. He, S. Modi, D. S. Bendall, J. C. Gray, *EMBO J.* **1991**, *10*, 4011−4016.
[56] S. Modi, M. Nordling, L. G. Lundberg, Ö. Hansson, D. S. Bendall, *Biochim. Biophys. Acta* **1992**, *1102*, 85−90.
[57] S. Modi, S. He, J. C. Gray, D. S. Bendall, *Biochim. Biophys. Acta* **1992**, *1101*, 64−68.
[58] L. Qin, N. M. Kostić, *Biochemistry* **1993**, *32*, 6073−6080.
[59] M. Nordling, K. Sigfridsson, S. Young, L. G. Lundberg, Ö. Hansson, *FEBS Lett.* **1991**, *291*, 327−330.
[60] K. Sigfridsson, S. Young, Ö. Hansson, *Biochemistry* **1996**, *35*, 1249−1257.
[61] W. Haehnel, T. Jansen, K. Gause, R. B. Klösgen, B. Stahl, D. Michl, B. Huvermann, M. Karas, R. G. Herrmann, *EMBO J.* **1994**, *13*, 1028−1038.
[62] P. Hildebrandt, F. Vanhecke, G. Buse, T. Soulimane, A. G. Mauk, *Biochemistry* **1993**, *32*, 10912−10922.
[63] S. Hirota, T. Tsukazaki, O. Yamauchi, *Biochem. Biophys. Res. Commun.* **2000**, *268*, 395−397.

Received April 12, 2001
[I01132]

Protonated Trithiocarbonic Acid − Synthesis, Spectroscopic Characterization and the Crystal Structure of $C(SH)_3^+AsF_6^-$

Rolf Minkwitz,*[a] Frank Neikes,[a] and Ulrike Lohmann[a][†]

Keywords: Carbocations / NMR spectroscopy / Raman spectroscopy / Protonation / Sulfur / Superacidic systems

Protonation of trithiocarbonic acid H_2CS_3 in the superacidic system HF/MF_5 (M = As, Sb) results in the generation and isolation of the extremely water-sensitive salts $C(SX)_3^+MF_6^-$ (M = As, Sb; X = H, D). The slightly yellow salts decompose above 233 K with the formation of $SX_3^+MF_6^-$ and CS_2. These new salts are characterized by vibrational and NMR spectroscopy and $C(SH)_3^+AsF_6^-$ by X-ray diffraction.

Introduction

The NMR spectroscopic evidence that protonated carbonic acid is stable in the superacidic system HSO_3F/SbF_5 below 273 K was found in 1968 by Olah. Based on his extensive ^{13}C NMR investigations he proposed a trihydroxycarbenium ion structure and explained the remarkable thermal stability by comparison with the high resonance stability of protonated guanidine.[1,2] The existence of a symmetrical structure protonated at the carbonyl oxygen atom is supported by theoretical studies.[3−5] The crystal structure of protonated carbonic acid was recently determined by Minkwitz and co-workers [Equation (1)]; the IR spectra of free and sublimable carbonic acid were also reported.[6,7]

$$(Me_3SiO)_2CO + HF/MF_5 \rightarrow 2\ Me_3SiF + C(OH)_3^+MF_6^- \ (M = As, Sb) \quad (1)$$

Formal replacement of the OH groups by SH groups leads to the mono-, di- and trithio-analogues compounds. The evidence for the existence of these species were given by ^1H-NMR studies in the super-acidic system HSO_3F/SbF_5 by Olah.[8] In contrast to the carbonic acid, trithiocarbonic acid can easily be synthesized and isolated from the reaction of barium trithiocarbonate with hydrochloric acid.[9] The physical and spectroscopic data as well as the crystal structures of the reaction products of trithiocarbonic acid with bromine, thiophosgene and chlorosulfane have been reported.[10−14]

In our investigations on protonated carbonic and thiocarbonic acids and their derivatives such as the $(MeO)_2COH^+$, $(MeO)(MeS)CSH^+$ and $(MeS)_2CSH^+$ cations, the determination of the crystal structure of trimercaptocarbenium hexafluoroarsenate was reported.[15−17]

[a] Anorganische Chemie, Fachbereich Chemie der Universität Dortmund,
44221 Dortmund, Germany
[†] Deceased.

Results and Discussion

Formation of $C(SX)_3^+$ Salts and NMR Spectra

Protonated trithiocarbonic acid is available by the reaction of trithiocarbonic acid with the superacid XF/MF_5 (X = H, D; M = As, Sb) [Equation (2)].

$$H_2CS_3 + HF/MF_5 \rightarrow H_3CS_3^+MF_6^- \quad (2)$$

To avoid the formation of arsenate and antimonate sulfide it is necessary to condense hydrofluoric acid and the Lewis acid alternately in layers. The yellowish, unpleasant smelling and extremely water-sensitive hexafluorometallates decompose, in the case of the arsenate salt, at 208 K and in the case of the antimonate salt at 218 K. The salts are clearly more unstable than the trihydroxycarbenium salts (273 K), and after one day storage under inert conditions at 203 K the decomposition products $SX_3^+MF_6^-$ (X = H, D; M = As, Sb) and CS_2 can be observed spectroscopically [Equation (3)].[1,6]

$$C(SX)_3^+MF_6^- \rightarrow SX_3^+MF_6^- + CS_2 \ (X = H, D; M = As, Sb) \quad (3)$$

This is similar to the decomposition of the trihydroxycarbenium cation as reported by Olah.[1]

The ^1H NMR spectra of freshly prepared $C(SH)_3^+AsF_6^-$ and $C(SH)_3^+SbF_6^-$ dissolved in SO_2 with TMS as external standard at −60 °C show one signal at δ = 8.3 and one at δ = 8.0 for the equivalent mercapto groups. These results are similar to the chemical shifts reported previously by Olah and Minkwitz.[8,15,16] The difference of 0.49 ppm from the reported chemical shift by Olah is explainable by different solvents and temperatures. The ^{13}C NMR signals could not be measured because of poor solubility in SO_2. In solution, the new salts are about 20 K more stable than in the solid state.

 © WILEY-VCH Verlag GmbH, 69451 Weinheim, Germany, 2002 1434−1948/02/0101−0027 $ 17.50+.50/0

Raman Spectra of $C(SX)_3^+MF_6^-$ (M = As, Sb; X = H, D)

The observed Raman frequencies of the $C(SX)_3^+MF_6^-$ (X = H, D; M = As, Sb) are summarized in Table 1. The assignments for the $C(SX)_3^+$ cations were made by comparison with the calculated frequencies of $(CH_3S)_2CS$ and several alkylxanthogenates.[15,16,18−20] The recorded Raman frequencies of protonated, deuterated and free trithiocarbonic acid are also shown in Table 1. The IR spectra could not be measured due to the high reactivity and spontaneous decomposition on the IR window material (Si or CsBr) at 193 K.

Table 1. Raman frequencies and possible assignments of H_2CS_3 and $C(SH)_3^+MF_6^-$ (X = H, D; M = As, Sb)

$(HS)_2CS$	$(XS)_3C^+AsF_6^-$		$(XS)_3C^+SbF_6^-$		Possible assignment
	X = H	X = D	X = H	X = D	
2530 sh	2526		2569 w	1873 sh	ν SX
2512	2514 m	1837 m	2509 sh	1832 sh	
2493 m			2464 s	1810 sh	
2395 sh			2396 br	1754 br	
1116 sh	1123 w			1093 s	
1095 s			1101 s	1072 s	ν C=S
1082 sh		1040 w		1055 s	
1002 m	972 w	960 w	1003 w	972 m	δ CSX
879 m	862 w		882 m	888 m	ν_{as} CS
813 w			823 w	837 w	ν_s CS
654 w				690 m	τ CSX
501 s	517 s	512 s	506 m	508 s	δ SC=S
	459 w	476 m			
		435 w			δ SCS
431 w	404 w	404 w			
291 m	279 m	270 m	277 sh	277 sh	γ SCS
266 m		221 m			γ SCS
	683 m	685 m	655 w	661 m	$\nu_{(1)}$ MF_6^-
	575 w	573 w	580 vw	582 vw	$\nu_{(2)}$ MF_6^-
	370 w	370 w	296 w	298 m	$\nu_{(5)}$ MF_6^-

There are significant differences in the frequency of the SH and CS stretching modes between the spectra of the hexafluroantimonate and hexafluoroarsenate salts. The spectrum of $C(SH)_3^+SbF_6^-$ shows a broad, slightly split line between 2569 and 2396 cm^{-1} similar to the spectra of trithiocarbonic acid, whereas the hexafluoroarsenate spectrum shows a sharp line shifted to higher frequencies by about 70 cm^{-1}. This means that there is a similar association of the molecules due to hydrogen bonds between the antimonate species and the free acid. The sulfur atoms function as both proton and electron donors. The existence of two maximums in the broad SH line can be explained by different SH bonds, similar to the previously reported IR spectra of dialkylphosphinicdithio acids.[21] The annealing of H_2CS_3 and $C(SH)_3^+SbF_6^-$ results in a decreasing width and a shift to higher frequencies of the SH valence mode, as described by Allen and co-workers. The result of these effects is that there are weaker hydrogen bonds in the arsenate species than in the hexafluoroantimonate salts. The observed H/D shift of about 700 cm^{-1} is similar to the expected shift reported by Teller and Redlich.[22]

The second significant difference between the hexafluoroarsenate and -antimonate salts is observed in the C=S valence mode region. The strongest line in the spectra of $X_3CS_3^+SbF_6^-$ (X = H, D) is observed at 1100 cm^{-1} and, analogous to H_2CS_3, is assigned to the C=S stretching mode. However, in the spectra of $X_3CS_3^+AsF_6^-$ (X = H, D) only a very weak line is observed. The measured frequencies and intensities in the region of the C−S stretching mode are similar and independent of the anion. It is doubtful if this difference can be explained by different interactions in the solid state or by different structures in the solid depending on the superacid used. For all substances the characteristic SC=S deformation mode is observed as a very sharp and intense line at 500 cm^{-1}. The vibrational modes of the anions are observed in their typical regions assuming O_h symmetry.

Crystal Structure of $C(SH)_3^+AsF_6^-$

Trimercaptocarbenium hexafluoroarsenate crystallises in the triclinic space group $P\bar{1}$ (no. 2) with six units per cell and the dimensions a = 800.8(2), b = 1154.6(2), c = 1499.7(3) pm, α = 107.74(3)°, β = 99.04(3)° and γ = 104.35(3)° (Table 2).[23] The bond lengths and angles are listed in Table 3. Figure 1 shows the salt with atom labels, and the arrangement of the $C(SH)_3^+AsF_6^-$ in the unit cell is depicted in Figure 2. The antimony and sulfur atoms

Table 2. Crystal data and structure refinement for $C(SH)_3^+AsF_6^-$

Formula	$CH_3AsF_6S_3$
Space group	$P\bar{1}$
Unit cell dimensions	a = 800.8(2) pm; α = 107.74(3)°
	b = 1154.6(2) pm; β = 99.04(3)°
	c = 1499.7(3) pm; γ = 104.35(3)°
Volume [Å^3]	1238.1(4)
Density (calculated) [g cm^{-3}]	2.415
Z	6
Molecular weight [g mol^{-1}]	300.13
Absorption coefficient [mm^{-1}]	4.913
Temperature [K]	173
λ (Mo-K_α) [Å]	0.71069
Crystal size [mm]	0.1 × 0.05 × 0.08
θ range for data collection [°]	1.95−26.3
Index ranges	$-9 \le h \le 9$; $-12 \le k \le 14$;
	$-16 \le l \le 17$
F(000)	864
Reflections collected	6182
Independent reflections	4373 [R(int) = 0.047]
R[a] [$I > 2\sigma(I)$]	$R1$ = 0.0328, $wR2$ = 0.0592
R[a] (all data)	$R1$ = 0.0636, $wR2$ = 0.0646
Largest diff. peak and hole [e Å^3]	0.461/−0.853
Free parameter	337
Goodness-of-fit on F^2	0.838
Programs used	SHELX,[29,30] SHELXTL Plus,[31] PARST,[32] MISSYM,[33] PLATON,[34] DENZO,[35] SCALEPACK[36,37]
Refinement method	Full-matrix least-squares on F^2

Table 3. Bond lengths [Å], angles [°] and contacts [Å] for $C(SH)_3^+AsF_6^-$[a]

As(1)F(11)	1.687(4)	F(11)−As(1)−F(12)	87.6(3)
As(1)−F(12)	1.699(4)	F(11)−As(1)−F(13)	178.0(2)
As(1)−F(13)	1.670(4)	F(11)−As(1)−F(14)	89.9(3)
As(1)−F(14)	1.689(4)	F(11)−As(1)−F(15)	90.6(2)
As(1)−F(15)	1.708(3)	F(11)−As(1)−F(16)	89.4(2)
As(1)−F(16)	1.720(3)	F(12)−As(1)−F(13)	91.0(3)
As(2)−F(21)	1.704(3)	F(12)−As(1)−F(15)	90.6(2)
As(2)−F(22)	1.727(4)	F(12)−As(1)−F(16)	89.1(2)
As(2)−F(23)	1.706(3)	F(13)−As(1)−F(14)	91.6(3)
As(2)−F(24)	1.716(3)	F(13)−As(1)−F(15)	90.7(2)
As(2)−F(25)	1.722(3)	F(13)−As(1)−F(16)	89.3(2)
As(2)−F(26)	1.713(3)	F(14)−As(1)−F(12)	177.2(2)
As(3)−F(31)	1.719(4)	F(14)−As(1)−F(15)	90.5(2)
As(3)−F(31a)	1.719(4)	F(14)−As(1)−F(16)	89.8(2)
As(3)−F(32)	1.727(3)	F(15)−As(1)−F(16)	179.7(2)
As(3)−F(32a)	1.727(3)		
As(3)−F(33)	1.711(3)	F(21)−As(2)−F(22)	89.9(2)
As(3)−F(33a)	1.711(3)	F(21)−As(2)−F(23)	90.4(2)
As(4)−F(41)	1.710(3)	F(21)−As(2)−F(24)	90.1(2)
As(4)−F(41b)	1.710(3)	F(21)−As(2)−F(25)	89.8(2)
As(4)−F(42)	1.727(3)	F(21)−As(2)−F(26)	179.4(2)
As(4)−F(42b)	1.727(3)	F(22)−As(2)−F(23)	179.7(2)
As(4)−F(43)	1.729(3)	F(22)−As(2)−F(24)	89.6(2)
As(4)−F(43b)	1.729(3)	F(22)−As(2)−F(25)	89.4(2)
S(11)−C(1)	1.683(5)	F(22)−As(2)−F(26)	90.0(2)
S(12)−C(1)	1.708(6)	F(23)−As(2)−F(24)	90.5(2)
S(13)−C(1)	1.701(6)	F(23)−As(2)−F(25)	90.5(2)
S(11)−H(11)	1.135(2)	F(23)−As(2)−F(26)	89.8(2)
S(12)−H(12)	1.358(2)	F(24)−As(2)−F(25)	179.0(2)
S(13)−H(13)	1.329(2)	F(24)−As(2)−F(26)	90.5(2)
S(21)−C(2)	1.702(6)	F(25)−As(2)−F(26)	89.6(2)
S(22)−C(2)	1.692(6)		
S(23)−C(2)	1.694(6)	F(31)−As(3)−F(31a)	180.0
S(21)−H(21)	1.039(2)	F(31)−As(3)−F(32)	89.6(2)
S(22)−H(22)	1.197(2)	F(31)−As(3)−F(32a)	90.4(2)
S(23)−H(23)	1.217(2)	F(31)−As(3)−F(33)	89.5(2)
S(31)−C(3)	1.712(6)	F(31)−As(3)−F(33a)	90.5(2)
S(32)−C(3)	1.684(6)	F(31a)−As(3)−F(32)	90.4(2)
S(33)−C(3)	1.686(6)	F(31a)−As(3)−F(32a)	89.6(2)
S(31)−H(31)	1.160(2)	F(31a)−As(3)−F(33)	90.5(2)
S(32)−H(32)	1.261(2)	F(31a)−As(3)−F(33a)	89.5(2)
S(33)−H(33)	1.276(2)	F(32)−As(3)−F(32a)	180.000(2)
		F(32)−As(3)−F(33)	90.5(2)
C(1)−S(11)−H(11)	104.5(2)	F(32)−As(3)−F(33a)	89.5(2)
C(1)−S(12)−H(12)	101.4(2)	F(32a)−As(3)−F(33)	89.5(2)
C(1)−S(13)−H(13)	91.8(2)	F(32a)−As(3)−F(33a)	90.5(2)
		F(33)−As(3)−F(33a)	180.000(3)
C(2)−S(21)−H(21)	89.7(2)		
C(2)−S(22)−H(22)	95.1(2)	F(41)−As(4)−F(41b)	180.000(3)
C(2)−S(23)−H(23)	100.7(2)	F(41)−As(4)−F(42)	89.6(2)
		F(41)−As(4)−F(42b)	90.4(2)
C(3)−S(31)−H(31)	92.4(2)	F(41)−As(4)−F(43)	90.1(2)
C(3)−S(32)−H(32)	107.5(2)	F(41)−As(4)−F(43b)	89.9(2)
C(3)−S(33)−H(33)	86.9(2)	F(41b)−As(4)−F(42)	90.4(2)
		F(41b)−As(4)−F(42b)	89.6(2)
S(11)−C(1)−S(12)	120.3(3)	F(41b)−As(4)−F(43)	89.9(2)
S(11)−C(1)−S(13)	120.5(3)	F(41b)−As(4)−F(43b)	90.1(2)
S(13)−C(1)−S(12)	119.2(3)	F(42)−As(4)−F(42b)	180.000(1)
		F(42)−As(4)−F(43)	89.6(2)
S(22)−C(2)−S(21)	119.1(4)	F(42)−As(4)−F(43b)	90.4(2)
S(22)−C(2)−S(23)	120.6(3)	F(42b)−As(4)−F(43)	90.4(2)
S(23)−C(2)−S(21)	120.3(3)	F(42b)−As(4)−F(43b)	89.6(2)
		F(43)−As(4)−F(43b)	180.000(3)
S(32)−C(3)−S(31)	119.0(3)		
S(32)−C(3)−S(33)	121.5(3)		
S(33)−C(3)−S(31)	119.5(3)		

Table 3 *Continued)*

S(11)···F(15c)	2.896(1)	S(11)···F(24d)	3.394(1)
S(12)···F(33e)	3.371(1)	S(12)···F(41f)	3.329(2)
S(13)···F(22)	3.397(1)	S(21)···F(16g)	3.317(1)
S(21)···F(14g)	3.737(1)	S(23)···F(23)	2.990(1)
S(21)···F(32h)	2.954(1)	S(33)···F(43)	3.506(1)
S(31)···F(13)	3.362(1)	S(33)···F(16g)	3.343(2)
S(33)···F(25)	3.052(1)		

[a] Symmetry operations: (a) $1 - x, -y + 2, -z + 2$; (b) $-x, -y + 3, -z + 2$; (c) $x + 1, +y - 1, +z$; (d) $-x + 1, -y + 2, -z + 1$; (e) $x, +y, +z - 1$; (f) $-x, -y + 2, -z + 1$; (g) $x + 1, +y, +z$; (h) $x, +y + 1, +z$.

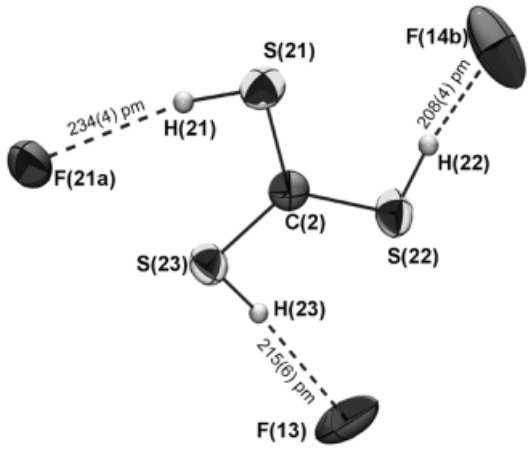

Figure 1. Projection of a selected $C(SH)_3^+$ cation with contacts; thermal ellipsoids are drawn at the 50% probability level

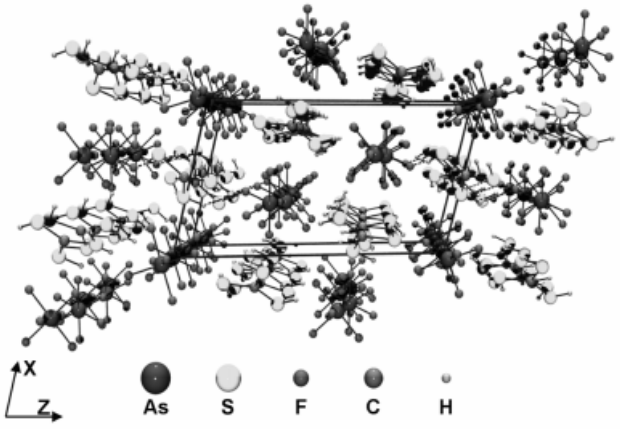

Figure 2. Projection of the $C(SH)_3^+AsF_6^-$ salt

were found by the Patterson method. All other atoms were determined by difference Fourier synthesis. A final refinement with anisotropic (except H atoms) thermal parameters gave a value of $R = 0.0328$.

The ideal octahedron structure of the anion is not distorted (O_h symmetry), with almost ideal angles of 90° and lengths of nearly 171 pm, similar to those in known structures.[6,24]

The CS_3 skeleton is surrounded by sulfur atoms in a trigonal planar geometry with angles of about 120° and average bond lengths of 169 pm. The still small differences in the length of the CS bonds imply a non-equal allocation of the positive charge over the sp^2-hybridised CS_3 group. The protons are not located in the CS_3 planes, therefore the symmetry is lowered to C_1 explaining the split SH valence mode in the Raman spectra. This geometry is similar to the structures of the $(CH_3S)_2CSH^+$ and $(CH_3O)(CH_3S)CSH^+$ cations where all cations posses a central sp^2 carbon atom, a delocalised positive charge and terminal groups which are not located in the CX (X = O,S) plane. The three symmetry-independent $C(SH)^+$ cations develop hydrogen bonds with S···F contacts, 10% below the sum of the Van der Waals radii, of about 289.6 pm, 295.4 pm, 305.2 pm and 299 pm.[25]

Experimental Section

All synthetic work and sample handling was performed by employing standard Schlenk techniques and a standard vacuum line (stainless steel or glass). SbF_5 (Merck) was fractionally distilled. Drying of HF and SO_2 were carried out by known literature methods.[26] Reactions in HF/DF were carried out in a KEL-F reactor with a KEL-F valve.[27] Infrared spectra were recorded with a Bruker IFS 113V spectrophotometer. The spectra of dry powders were obtained on a CsI plate in a cooled IR cell.[28] The Raman spectra were recorded with a T64000 (ISA) using a CCD detector (EEV CCD15-11) and an Ar^+ laser tube (514.5 nm) from Spectra Physics. The spectra were recorded in a glass cell cooled with liquid nitrogen. The NMR spectra were recorded with a Bruker DPX 300 spectrometer with TMS as external standard. Single crystals were placed in Lindemann capillaries in a cooled stream of dry nitrogen, and the X-ray diffraction study was carried out at −100 °C using an Enraff Nonius Kappa-CCD Mach3 automated diffractometer with an Oxford Cryosystem cooling unit.

Preparation of $C(SX)_3^+MF_6^-$ (X = H, D; M = As, Sb)

Caution! All contact with these compounds should be avoided as the hydrolysis of AsF_6^- and SbF_6^- salts forms HF, which burns the skin and causes irreparable damage. Safety precautions should be taken when using and handling these materials.

In a typical experiment H_2CS_3 (0.22 g) and anhydrous XF (X = H, D; 4 g) were combined at −196° C in a KEL-F reactor. AsF_5 (0.34 g) or SbF_5 (0.44 g) was then added to this mixture at −196 °C and the contents of the reactor were warmed up to −78 °C. After 10 minutes, the slow removal of all volatile material at −78 °C in vacuum resulted in a slightly yellow solid residue that was identified as $C(SX)_3^+MF_6^-$ (X= H, D; M= As, Sb). The remaining $C(SH)_3^+AsF_6^-$ contained crystals suitable for X-ray diffraction studies. The salts can be stored for one day under inert conditions at −70 °C.

Acknowledgments

This works was supported by the Deutsche Forschungsgemeinschaft and the Fonds der Chemischen Industrie.

[1] G. A. Olah, M. White, *J. Am. Chem. Soc.* **1968**, *90*, 1884−1889.
[2] G. A. Olah, M. White, *J. Am. Chem. Soc.* **1969**, *91*, 5801−5810.
[3] G. Rasul, V. P. Reddy, L. Z. Zdunk, G. K. S. Prakash, G. A. Olah, *J. Am. Chem. Soc.* **1993**, *115*, 2236−2238.
[4] H. Egsgaard, C. Carlsen, *J. Chem. Soc., Faraday Trans.* **1989**, *85*, 3403−3411.
[5] D. Ohlmann, C. M. Marchand, H. Grützmacher, G. S. Chen, D. Farmer, R. Glaser, A. Currao, R. P. H. Nesper, *Angew. Chem.* **1996**, *108*, 317−320; *Angew. Chem. Int. Ed. Engl.* **1996**, *35*, 300−303.
[6] R. Minkwitz, S. Schneider, *Angew. Chem.* **1999**, *111*, 749−751; *Angew. Chem. Int. Ed. Engl.* **1999**, *38*, 713−715.
[7] W. Hage, K. R. Liedl, A. Hallbrucker, E. Mayer, *Science* **1998**, *279*, 1332−1335.
[8] G. A. Olah, A. T. Ku, M. White, *J. Org. Chem.* **1969**, *34*, 1827−1832.
[9] G. Gattow, B. Krebs, *Z. Anorg. Allg. Chem.* **1963**, *321*, 143−160.
[10] B. Krebs, G. Gattow, *Naturwiss.* **1964**, *51*, 554.
[11] B. Krebs, G. Gattow, *Z. Anorg. Allg. Chem.* **1965**, *340*, 294−311.
[12] G. Gattow, *Angew. Chem.* **1964**, *76*, 581−582.
[13] J. Wortmann, G. Kiel, G. Gattow, *Z. Anorg. Allg. Chem.* **1970**, *376*, 64−72.
[14] M. Schmidt, *Angew. Chem.* **1961**, *73*, 394−398.
[15] R. Minkwitz, F. Neikes, *Inorg. Chem.* **1999**, *38*, 5960−5963.
[16] R. Minkwitz, F. Neikes, *Eur. J. Inorg. Chem.* **2000**, 2283−2287.
[17] R. Minkwitz, F. Neikes, *Eur. J. Inorg. Chem.* **2000**, 1261−1265.
[18] K. Herzog, J. Fabian, *Z. Phys. Chem.* **1995**, *191*, 159−177.
[19] R. Mattes, G. Pauleickhoff, *Spectrochimica Acta* **1973**, *29A*, 1339−1344.
[20] K. Klaesser, G. Gattow, *Z. Anorg. Allg. Chem.* **1981**, *481*, 135−142.
[21] G. Allen, R. O. Coclough, *J. Chem. Soc.* **1957**, 3912−3915.
[22] J. Weidlein, U. Müller, K. Dehnicke, G. Thieme, Stuttgart **1982**.
[23] Crystallographic data (excluding structure factors) for the structure of $(HS)_3C^+AsF_6^-$ reported in this paper have been deposited with the Cambridge Crystallographic Data Centre as supplementary publication no. CCDC-411938. Copies of the data can be obtained free of charge onapplication to The Director, CCDC, 12 Union Road, Cambridge CB2 1EZ, UK [Fax: (internat.) +44-1223/336-033; E-mail: deposit@chemcrys.cam.ac.uk].
[24] R. Minkwitz, S. Schneider, M. Seifert, *Z. Anorg. Allg. Chem.* **1996**, *622*, 1404−1410.
[25] A. Bondi, *J. Phys. Chem.* **1964**, *68 (3)*, 441.
[26] G. Brauer, *Handbuch der präparativen anorganischen Chemie*, 2 Aufl., F. Enke, Stuttgart **1975**.
[27] A. Werner, *Dissertation*, Universität Dortmund, **1988**.
[28] L. Bayerdorfer, R. Minkwitz, J. Jander, *Z. Anorg. Allg. Chem.* **1972**, *392*, 137−142.
[29] G. M. Sheldrick, *SHELXL 93*, Universität Göttingen, **1993**.
[30] G. M. Sheldrick, *SHELXS 86*, Universität Göttingen, **1986**.
[31] G. M. Sheldrick, *SHELXTL Plus Ver. 3.4*, An integrated System for Solving, Refining and Displaying Crystal Structures from Diffraction Data., Universität Göttingen.
[32] M. Nardelli, *Comput. Chem.* **1993**, *7*, 95−98.
[33] Y. Le Page, *J. Appl. Crystallogr.* **1987**, *20*, 264−269.
[34] A. L. Spek, *The EUCLID Package*, Computational Crystallography, (Hrsg. D. Sayre), Claredon Press, Oxford, **1982**.
[35] *KappaCCD package*, NONIUS BV, Roentgenweg 1, Delft Netherlands.
[36] Z. Otwinowsky, W. Minor, *Methods in Enzymology* **1997**, *276*, 307−326.
[37] *International Tables for X-ray Crystallography*, Vol. IV, Kynoch Press, Birmingham 1974.

Received March 14, 2001
[I01099]

1-Aminoboratabenzene Complexes of Scandium Group Metals[‡]

Bing Wang,[a] Xiaolai Zheng,[a] and Gerhard E. Herberich*[a]

Keywords: Boron / Group 3 metals / Metallocenes / Boratabenzene / Lithium

The syntheses of the new lithium boratabenzenes Li(3,5-$Me_2C_5H_3BNiPr_2$), Li(**3**), and Li_2[(3,5-$Me_2C_5H_3BNMe)_2$-$(CH_2)_2$], Li_2(**5**), via the dicarbanion route are described. Lithium 1-aminoboratabenzenes react with metal trihalides in toluene (110 °C, 3 d) to give the stepped ladder dimers [(3,5-$Me_2C_5H_3BNMe_2)_2Y(\mu$-Cl)$_2$Li]$_2$, (**12**), [(3,5-$Me_2C_5H_3BNMe_2)_2$-$Lu(\mu$-Cl)$_2$Li]$_2$ (**13**), and the mononuclear complexes YCl[3,5-$Me_2C_5H_3BN(SiMe_3)_2]_2$ (**18**), LuCl[3,5-$Me_2C_5H_3BN(SiMe_3)_2]_2$ (**19**), and ScCl(3,5-$Me_2C_5H_3BNiPr_2)_2$ (**20**). When donor solvents such as THF or THP are used, analogous reactions take place at ambient temperature, giving solvates such as (3,5-$Me_2C_5H_3BNMe_2)_2Sm(\mu$-Cl)$_2$Li(THF) (**15**), (3,5-$Me_2C_5H_3BNMe_2)_2Y(\mu$-Cl)$_2$Li(THP) (**16**), (3,5-$Me_2C_5H_3BNi$-$Pr_2)_2Y(\mu$-Cl)$_2$Li(THF)$_2$ (**21**), (3,5-$Me_2C_5H_3BNiPr_2)_2Sm(\mu$-Cl)$_2$Li(THF)$_2$ (**22**), and the ansa complexes [(3,5-$Me_2C_5H_3BNMeCH_2)_2$]Lu(μ-Cl)$_2$Li(THF)$_2$ (**23**) and [(3,5-$Me_2C_5H_3BNMeCH_2)_2$]Lu(μ-Cl)$_2$Li(THP)$_2$ (**24**). The bridge cleavage product Y(acac)(3,5-$Me_2C_5H_3BNMe_2)_2$ (**14**) is obtained from **12** and Na(acac) in toluene at ambient temperature. The complexes **12**, **14**, **16**, **18**·PhMe, **19**·PhMe, **20** (as two polymorphs **α-20** and **β-20**), **21**, and **24** (as the *rac*-stereomer) are characterized by single-crystal structure determinations. In all structures except those of the mononuclear complexes **18** and **19**, the ring-ring rotational positions are close to 180°, cf. e.g. **14**, or to 60°, cf. e.g. **20**; these conformations minimize transannular ligand-ligand repulsions. The internal coordination of a *B*-NMe_2 sidearm, which is unprecedented, is found in the structures of the stepped ladder dimers **12** and **13**, and in the mononuclear complexes **15** and **16**. According to solution NMR spectroscopy, all complexes are dynamic with respect to ring-ring rotation and, in the cases with internal coordination, they are dynamic with respect to the interchange between free and coordinated *B*-NMe_2 sidearms.

Introduction

Boratabenzenes are close relatives of the more familiar cyclopentadienides; this is particularly true of the systematic aspects of their salts and complexes.[2] The boratabenzene chemistry of the scandium group metals is still relatively unexplored, despite an early communication in this field.[2b] We have described the first bis(boratabenzene)scandium chlorides, which were synthesized from $ScCl_3$ and lithium boratabenzenes.[2b,3] Bazan et al. demonstrated that Fu's borabenzene trimethylphosphane adduct $C_5H_5BPMe_3$ [4] reacts with $Sc(THF)_2Ph_3$ to give (1-phenylboratabenzene)scandium complexes.[5] More recently we reported on the synthesis and structural chemistry of the dinuclear (1-methylboratabenzene)yttrium complex [Y(μ-Cl)(3,5-$Me_2C_5H_3BMe)_2]_2$.[6]

Closely related works involve compounds of magnesium in group 2,[7] and a very large variety of complexes of group 4 metals, mainly of zirconium.[4a,5,8] It was decided to study these compounds as they are novel, and because they are thought to mimic catalyst systems of modern Ziegler−Natta olefin polymerization processes that are derived from CpZr and CpTi complexes. Some of the catalyst systems so obtained are rather similar to those derived from $ZrCl_2Cp_2$,[8m] and others display considerably modified properties,[5,8f−8l] thus widening the range of the potential applications of these complexes. A similar parallel between cyclopentadienyl and boratabenzene complexes may be expected for catalysts of the scandium group metals,[9] providing a further incentive to explore the chemistry of boratabenzene complexes of the Sc group metals.

The goal of the present paper is to report on the syntheses and structures of Sc, Y, Sm, and Lu bis(boratabenzene) complexes that bear a *B*-amino group. It will be seen that the presence of a *B*-amino group provides a remarkably rich structural chemistry to this class of complexes.

Results and Discussion

Lithium Boratabenzenes

Lithium boratabenzenes are the most common source of boratabenzene ligands. Their properties are greatly influenced by the *B*-bonded substituents. *B*-(dialkylamino)boratabenzenes differ from boratabenzenes with innocent substituents at boron such as Li(C_5H_5BPh),[10] Li(C_5H_5BMe),[11a] Li(C_5H_5BtBu),[11a] and Li(C_5H_5BH).[4a]

[‡] Borabenzene Derivatives, 37. − Part 36: Ref.[1a]

[a] Institut für Anorganische Chemie, Technische Hochschule Aachen
52056 Aachen, Germany
Fax: (internat.) + 49-(0)241/809-2288
E-mail: gerhard.herberich@ac.rwth-aachen.de

 © WILEY-VCH Verlag GmbH, 69451 Weinheim, Germany, 2002 1434−1948/02/0101−0031 $ 17.50+.50/0

The dialkylamino group strongly perturbs the aromatic π-electron system of the boratabenzene ring. This was first demonstrated for the parent compound $Li(C_5H_5BNMe_2)$, Li(**1**),[11] and was later brought into a wider perspective.[12] Furthermore, and as will be detailed below, the amino functionality may also act as a Lewis base towards the Li^+ ions.

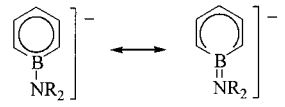

1$^-$

We prefer the more easily accessible 3,5-dimethyl derivatives and use $Li(3,5\text{-}Me_2C_5H_3BNMe_2)$, Li(**2**),[3] the diisopropylamino compound $Li(3,5\text{-}Me_2C_5H_3BN\textit{i}Pr_2)$, Li(**3**), the bis(trimethylsilyl)amino compound $Li[3,5\text{-}Me_2C_5H_3BN(SiMe_3)_2]$,[3] Li(**4**), and the bifunctional boratabenzene $Li_2[(3,5\text{-}Me_2C_5H_3BNMeCH_2)_2]$, Li_2(**5**).

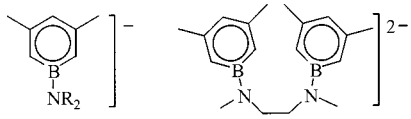

2$^-$: R = Me

3$^-$: R = *i* Pr

4$^-$: R = $SiMe_3$

5^{2-}

The syntheses of these ligand systems were based on what we call the dicarbanion route.[13] Double potassiation of 2,4-dimethylpenta-1,3-diene (and double bond isomers) gave the dipotassio derivative $K_2[CH_2CMeCHC(CH_2)_2]$ (**6**), which on treatment with BCl_2NMe_2 afforded the 1,2,3,6-tetrahydroborinine (**7a**). After distillation, **7a** is partially isomerized to the dihydroborinine isomers (**8a**) and (**9a**). Treatment with strong bases such as LDA or $LiN(SiMe_3)_2$ resulted in double bond migration and deprotonation to give the boratabenzene as the TMEDA solvate Li(TMEDA)(**2**),[13] or as the donor-free salt Li(**2**).[3] This synthesis is readily reproduced with much better yields than originally published. The new salt Li(**3**) and its TMEDA solvate were obtained analogously. Attempted preparation of Li(**4**) by this method resulted in a low yield (22%) of the ring closure product **7c**, and the subsequent deprotonation by $LiN(SiMe_3)_2$ failed altogether.[14]

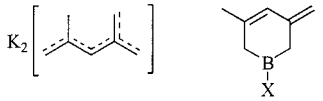

6

7

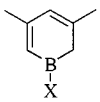

8

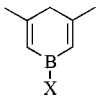

9

a: X = NMe_2, **b**: X = NPr^i_2, **c**: $N(SiMe_3)_2$, **d**: X = Cl

As an alternative, the substituent at boron may be modified. This has previously been described for the compounds of the series **a**,[3] and for our pinene-fused boratabenzenes.[15] Three steps are required: i) isomerization of **7a** with HCl to give the less sensitive isomers **8a/9a**; ii) treatment of the mixture **8a/9a** with BCl_3 to produce the chloro compounds **8d/9d**; iii) introduction of the desired new substituent, i.e. in the present case the $N(SiMe_3)_2$ group was introduced by the reaction of the chloro compounds **8d/9d** with a mixture of the secondary amine $NH(SiMe_3)_2$ and NEt_3, to give **8c/9c**, which was then metalated in the usual way.[3]

In a straightforward adaptation of this procedure the chloro compounds **8d/9d** were treated with $(CH_2NHMe)_2$/NEt_3 (1:1) to produce a mixture of ethylene-linked bis(aminodihydroborinines) **10**. Subsequent metalation with $LiN(SiMe_3)_2$ gave the new salt Li_2(**5**) in a high yield. The closely related bis(boratabenzene) $Li_2[(C_5H_5BNMeCH_2)_2]$ has recently been synthesized in a similar manner.[8a]

Complexes: General Comments

The most common cyclopentadienyl complexes of the scandium group metals are the bis(cyclopentadienyl)metal halides.[9] The smaller central metals usually form dinuclear complexes, such as $[Sc(\mu\text{-}Cl)Cp_2]_2$,[16a] and $Yb[(\mu\text{-}Cl)(C_5H_4Me)_2]_2$,[16b] and the larger central metals have a tendency to form higher aggregates. If the Cp ligand is sterically demanding as in the case of the pentamethylcyclopentadienyl ligand Cp*, mononuclear complexes such as $ScClCp^*_2$[17] are favored, despite their coordinative unsaturation. Larger central metals allow the formation of oligomers. For example, $(YClCp^*)_2$ displays a half-bridged dimeric structure $Cp^*_2YCl(\mu\text{-}Cl)YCp^*_2$,[18a] and the corresponding Sm complex is a cyclotrimer $[Sm(\mu\text{-}Cl)Cp^*_2]_3$.[18b] Thus, a subtle interplay of electronic requirements, steric hindrance, and presumably of the (often ignored) lattice energy of the crystal (cf. ref.[6]) determines the structural type observed for a particular compound.

At the outset of this work we decided to study simple metathetical reactions of scandium group metal trihalides with lithium boratabenzenes in a 1:2 ratio. In the related cyclopentadienyl chemistry, refluxing benzene has occasionally been used as the reaction medium[19] to prevent the formation of solvates that is common when the reactions are carried out in THF. In NMR spectroscopic tube experiments we found that higher reaction temperatures were required; heating the suspension of the reactants in toluene at 110 °C for 3 days gave satisfactory results in most cases. In the case of $SmCl_3$/Li(**2**), ill-defined reactions took place above 40 °C; thus THF was used. Other reactions were also carried out in ethereal solvents. Table 1 gives an overview of all products, isolated and characterized; of these, the complexes **11** and **17** have been described in previous work.[3]

Table 1. 1-Aminoboratabenzene complexes

11	$[Sc(\mu\text{-}Cl)(3,5\text{-}Me_2C_5H_3BNMe_2)_2]_2$[3]
12	$[(3,5\text{-}Me_2C_5H_3BNMe_2)_2Y(\mu\text{-}Cl)_2Li]_2$
13	$[(3,5\text{-}Me_2C_5H_3BNMe_2)_2Lu(\mu\text{-}Cl)_2Li]_2$
14	$Y(acac)(3,5\text{-}Me_2C_5H_3BNMe_2)_2$
15	$(3,5\text{-}Me_2C_5H_3BNMe_2)_2Sm(\mu\text{-}Cl)_2Li(THF)$
16	$(3,5\text{-}Me_2C_5H_3BNMe_2)_2Y(\mu\text{-}Cl)_2Li(THP)$
17	$ScCl[3,5\text{-}Me_2C_5H_3BN(SiMe_3)_2]_2$[3]
18	$YCl[3,5\text{-}Me_2C_5H_3BN(SiMe_3)_2]_2$
19	$LuCl[3,5\text{-}Me_2C_5H_3BN(SiMe_3)_2]_2$
20	$ScCl(3,5\text{-}Me_2C_5H_3BN\textit{i}Pr_2)_2$
21	$(3,5\text{-}Me_2C_5H_3BN\textit{i}Pr_2)_2Y(\mu\text{-}Cl)_2Li(THF)_2$
22	$(3,5\text{-}Me_2C_5H_3BN\textit{i}Pr_2)_2Sm(\mu\text{-}Cl)_2Li(THF)_2$
23	$[(3,5\text{-}Me_2C_5H_3BNMeCH_2)_2]Lu(\mu\text{-}Cl)_2Li(THF)_2$
24	$[(3,5\text{-}Me_2C_5H_3BNMeCH_2)_2]Lu(\mu\text{-}Cl)_2Li(THP)_2$

Metallocenoids with 1-(Dimethylamino)-3,5-dimethylboratabenzene Ligands

In our earlier work, we obtained the Sc complex **11** from the reaction of $ScCl_3$ with Li(**2**) (ratio 1:2) in toluene. The crystal of complex **11** displays a unique N−B−C η^3-coordination of one boratabenzene ring and a normal, facially bonded second boratabenzene ligand. In solution, the structure is dynamic with effective D_{2h} symmetry.[3] The analogous reactions of the trihalides YCl_3 and $LuCl_3$ with Li(**2**) in toluene produced the dinuclear bis(boratabenzene) complexes **12** and **13** as pale yellow platelets, which, surprisingly, contained two equivalents of loosely bound LiCl. The attempted recrystallization from hot toluene resulted in the very slow separation of solid LiCl. Treatment of complex **12** with sodium acetylacetonate [≡ Na(acac)] gave the bridge cleavage product **14**, which crystallized from toluene as large yellow blocks.

The structure of this mononuclear complex **14** (Figure 1) is discussed in some detail. The overall structure is that of a bent sandwich with a bending angle of 136.1°, and with the acac ligand in the pseudoequatorial plane. The two boratabenzene rings are roughly planar with the boron atom bending away from the metal by 6.3° in the first ring [C11..C15,B1], and by 12.2° in the second ring [C21..C25,B2]. The Y−(C_5B) distance is 2.319 Å for the first ring and 2.355 Å for the second ring. The Y atom is shifted towards the γ ring carbon atoms, the slip distortions[21] are 0.078 Å for the first ring and 0.129 Å for the second ring.

Several details of the structure reflect the importance of intramolecular repulsive ligand-ligand interactions. The two ligands adopt an antiperiplanar conformation. Thus, the rings are eclipsed and the three ring substituents of one ring are staggered with respect to those of the other ring. This motif is found in all structures of this paper, except those of the mononuclear complexes **18** and **19** (see below). The larger folding angle, metal-to-ligand distance, and slip distortion for the second ring relative to the first ring is caused by the transannular repulsion exerted by C13 and the 3,5-methyl groups with C16 and C17. The acac ligand is almost perfectly planar, but bent along the line O1,O2 away from the nearby NMe_2 group of the first ligand; the distance of the Y atom from the acac plane is 0.33 Å. The average B−N distance of 1.403 Å is close to that of typical aminoboranes [1.41 Å].[22] This observation indicates considerable B−N π-interactions which increase with the increasing charge of the central metal and increasing transfer of electron density from the boratabenzene rings to the metal.[7] In benzene, the structure of **14** possesses an effective C_{2v} symmetry, according to NMR spectroscopy, indicating a low barrier to the ring-ring rotation and also to an inversion of the Y(acac) ring in solution.

The nature of the LiCl coordination in **12** and **13** could be clarified by a structure determination of complex **12.** This compound is an approximately centrosymmetric stepped ladder dimer (Figure 2). The new motif of this structure is the internal coordination of a *B*-NMe_2 sidearm of a bent sandwich unit, to a Li^+ of a second bent sandwich, resulting in a central $[YCl_2Li]_2$ unit with a distorted tetrahedral coordination sphere around the Li^+ ions.

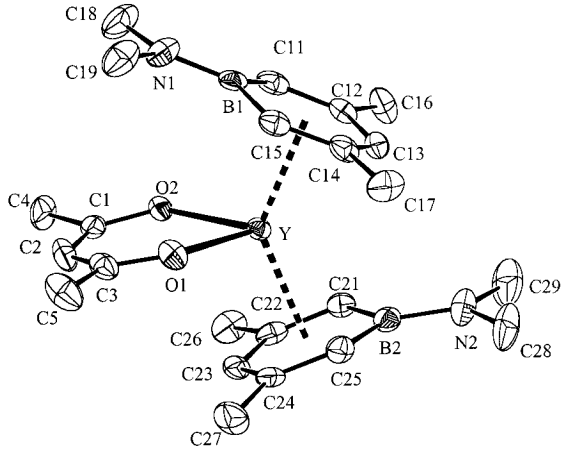

Figure 1. Molecular structure (PLATON plot, see ref.[20], at the 30% probability level) of **14** in the crystal. Selected bond lengths [Å] and bond angles [°]:Y−O1 2.205(5), Y−C1n 2.667(7) for C13 to 2.731(7) for C11, Y−B1 2.847(8), B1−N1 1.394(10), Y−O2 2.200(5), Y−C2n 2.694(7) for C23 to 2.755(7) for C21, Y−B2 2.941(8), B2−N2 1.411(10), O1−Y−O2 79.25(18).

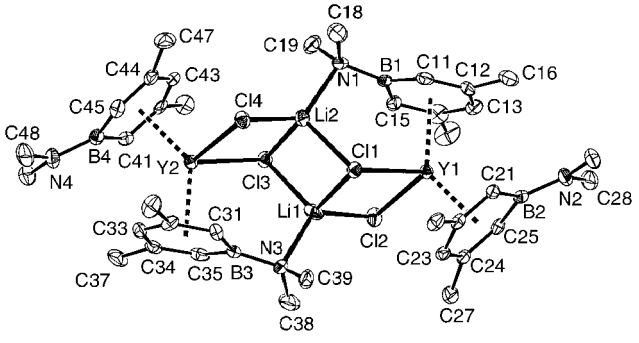

Figure 2. Molecular structure (PLATON plot, see ref.[20], at the 30% probability level) of **12** in the crystal. Selected bond lengths [A]:Y1−Cl1 2.645(2), Y1−Cl2 2.627(2), Y2−Cl3 2.667(2), Y2−Cl4 2.622(2), Li1−Cl1 2.451(13), Li1−Cl2 2.326(12), Li1−Cl3 2.300(15), Li1−N3 2.093(13), Li2−Cl1 2.345(14), Li2−Cl3 2.400(14), Li2−Cl4 2.336(14), Li2−N1 2.081(14), B1−N1 1.472(10), B2−N2 1.449(9), B3−N3 1.475(10), B4−N4 1.447(9).

The coordination of the *B*-dialkylamino group to a metal center has previously been observed in the chiral (*S*)-2-(methoxymethyl)pyrrolidine derivative Li(3,5-$Mo_2C_5H_3B$-SMP),[1b] in the Mg compound $Mg(THF)_2(3,5\text{-}Me_2C_5H_3BNMe_2)_2$,[7] and in the Sc complex **11**.[3] In all these complexes, the relevant B−N bonds are lengthened because of the polarization exerted by the positive metal center. The same is true for **14**, where the distances B1−N1 and B3−N3 [1.474 Å (av.)] with coordinated N centers are longer than the distances B2−N2 and B4−N4 [1.448 Å (av.)] with free N centers. The Li−N bond lengths [2.087 Å (av.)] and may be compared with those in $[LiCH_2CH_2CH_2NMe_2]_4$ [2.068 Å (av.)].[23] It may be speculated that complex **11** has a different structural type because of the smaller ionic radius of Sc^{3+},[24] suggesting that increased ligand-ligand repulsions disfavor structures with two facially bonded boratabenzene ligands.

The attempted preparation of an analogous, solvent-free Sm complex gave an intractable brown material. The alternative use of THF as the solvent readily gave the Sm complex **15** as large purple crystals that still contained coordinated LiCl and one equivalent of THF. Unfortunately, the quality of these crystals was not satisfactory for single crystal structure analysis. In the related cyclopentadienyl chemistry, complexes of the type $Cp''_2Ln(\mu\text{-}Cl)_2Li(OR_2)_2$ with tetrahedrally coordinated lithium, e.g. $(Me_3SiC_5H_4)_2Y(\mu\text{-}Cl)_2Li(THF)_2$ [25a] and $Cp^*_2Yb(\mu\text{-}Cl)_2Li(OEt_2)_2$,[25b] are common. Therefore, we guessed that the structure of **15** was similar, but with an extra solvate molecule due to the compensating internal coordination of the NMe_2 group. We then prepared the analogous Y complex **16** with a coordinated THP, in the same way as complex **15** using THP as the solvent. Complex **16** can also be prepared by simply dissolving the stepped ladder complex **12** in THP and subsequent crystallization. The pale yellow crystals of complex **16** displays the expected mononuclear structure, with an internally coordinated NMe_2 sidearm to yttrium (Figure 3). The coordination of the two ring ligands to the metal shows marked differences. The first ring [C11..C15,B1] with the coordinated sidearm is planar [largest deviation 0.029 Å at C11], with a small slip distortion of 0.066 Å and a long B1−N1 bond length [1.466(8) Å], while the second ring [C21..C25,B2] shows the usual folding along the line C21,C25 with a folding angle of 13(1)°, a large slip distortion of 0.163 Å and a short B2−N2 bond length [1.429(8) Å]. The central YCl_2Li ring is folded by 51.7(3)° bringing the Li^+ center into the vicinity of N1, however, the resulting bond Li−N1 [2.189(11) Å] remains relatively long.

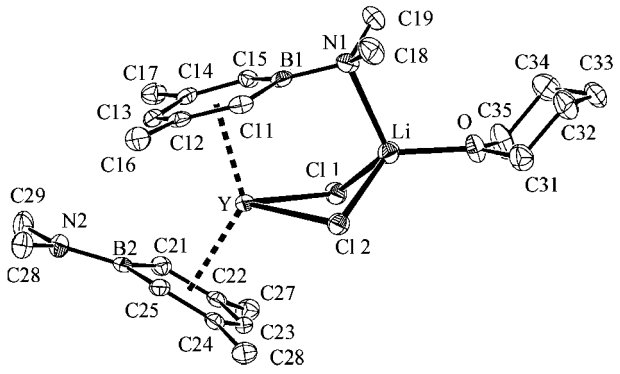

Figure 3. Molecular structure (PLATON plot, see ref.[20], at the 30% probability level) of **16** in the crystal. Selected bond lengths [Å] and bond angles [°]:Y−Cl1 2.6337(17), Y−Cl2 2.6338(17), Y−C1n 2.680(5) for C13 to 2.754(5) for C15, Y−B1 2.832(7), B1−N1 1.466(8), Y−C2n 2.664(5) for C23 to 2.739(5) for C21, Y−B2 2.939(6), B2−N2 1.429(8), Li−Cl1 2.400(10), Li−Cl2 2.371(10), Li−O 1.883(10), Li−N1 2.189(11), Cl1−Y−Cl2 82.00(5), Li−Cl1−Y 80.9(2), Li−Cl2−Y 81.5(2), Cl1−Li−Cl2 92.8(4), angle sum for $BNMe_2$ at N1 344.9° and at N2 360.0°.

Metallocenoids with Bulky *B*-(Amino) Substituents

Sterically demanding *N*-substituents were introduced with the aim to prevent the *B*-NMe_2 sidearm from coordinating to the metal centers. Reactions of the bis(trimethylsilyl)amino derivative Li(**4**) in toluene provided the Sc complex **17**,[3] and the Y and Lu complexes **18** and **19** as mononuclear complexes. The new complexes **18** and **19** crystallize from toluene as yellow rods which contain one equivalent of toluene. The molecular structure of **18** (Figure 4) (in the toluene/containing cocrystal) is essentially the same as that of **17**,[3] a two bladed propeller with crystallographic C_2 symmetry and a relatively short Y−Cl bond coinciding with the two fold symmetry axis. The toluene/containing cocrystal of the Lu complex **19** is isomorphous to that of **18**; for selected data see legend of Figure 4. The bending angles are 138.6° for **18** and 140.5° for **19**, and are close to the value of 140.8° observed for the Sc compound

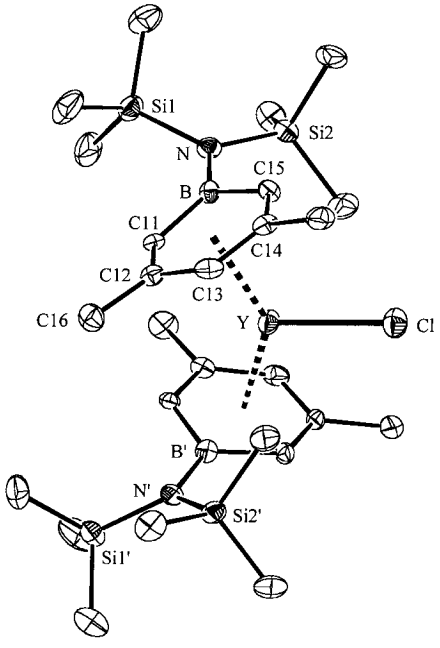

Figure 4. Molecular structure (PLATON plot, see ref.[20], at the 30% probability level) of **18** in the toluene/containing cocrystal and data for **18** and **19**. Selected bond lengths [Å] for **18**: Y−Cl 2.522(2), Y−C1n 2.667(7) for C12 to 2.738(6) for C11, Y−B 2.882(7), B−N 1.493(8), C11−B 1.497(8). C15−B 1.522(9). Selected bond lengths [Å] for **19**: Lu−Cl 2.475(3), Lu−C1n 2.605(9) for C13 to 2.683(8) for C11, Lu−B 2.853(9), B−N 1.464(11), C11−B 1.525(12). C15−B 1.531(11).

17.[3] As discussed recently, the B−N bond length in 1-(dimethylamino)boratabenzene complexes strongly depends on the polarizing influence of the central metal (i.e. primarily on the formal charge of the central metal).[7] The B−N bond lengths in ligand **4** are always relatively long [1.493(8) for **18**, 1.46(1) for **19**, and 1.471(3) Å for **17**]. This indicates weakened B−N π-interactions due to the polarizing influence of the positive Si centers, and presumably also because of the steric repulsion between the borabenzene ring and the close *Si*−Me groups. The large interplanar angles between the C_5B and NSi_2 planes [41.3° for **18**, and 42.2° for **19**] also suggest a rather soft torsional mode around the B−N bond. The fact that even the Y complex **18** is a monomer suggests that ligand **4** provides a more efficient steric protection than the Cp* ligand.

In the following experiments we reduced the size of the substituent at boron and treated $ScCl_3$ with Li(**3**) in a toluene suspension. Thus, we obtained the Sc complex **20** as red crystals. The crystal structure determination of **20** was complicated due to the existence of two modifications. The data of the high-temperature modification **α-20** (Figure 5a and 5b) were collected at −40 °C. The space group of **α-20** was found to be *C*2/*c*; the molecule of **20** possesses crystallographic C_2 symmetry (as in **17**−**19**), but an unusual anisotropic displacement parameter for the Cl atom (perpendicular to the Sc−Cl vector and mainly in the pseudoequatorial plane). This indicates some disorder. This disorder could be due to a large-amplitude vibration for the Sc−Cl bending, or could be a positional disorder of the chlorine atom.

As the temperature is reduced, a reversible phase transition and the formation of twinned crystals of the low-temperature modification **β-20** are observed. The data were collected at −73 °C. The crystal symmetry is now $P\bar{1}$, and the molecular symmetry is reduced to C_1 (Figure 6). The solved structure is less accurate for the low-temperature modification because of the twinning problem. The resulting molecular structure is closely related to those of **18** and **19**.

Attempts to prepare a Y complex analogous to **20** using toluene as the solvent were unsuccessful, only oily materials were obtained. When THF was used as the solvent, complex **21** was readily isolated as yellow crystals, and analogous Sm complex **22** was obtained as purple crystals. The crystals of **21** were of suitable quality to allow a structure determination. The molecular structure of **21** (Figure 7) is related to that of **16**. Since internal coordination of the B−N*i*Pr$_2$ group is now unfavorable because of the larger size of the dialkylamino group, a second donor molecule is added to the coordination sphere of Li instead, and the central Y(μ-Cl)$_2$Li core is planar.

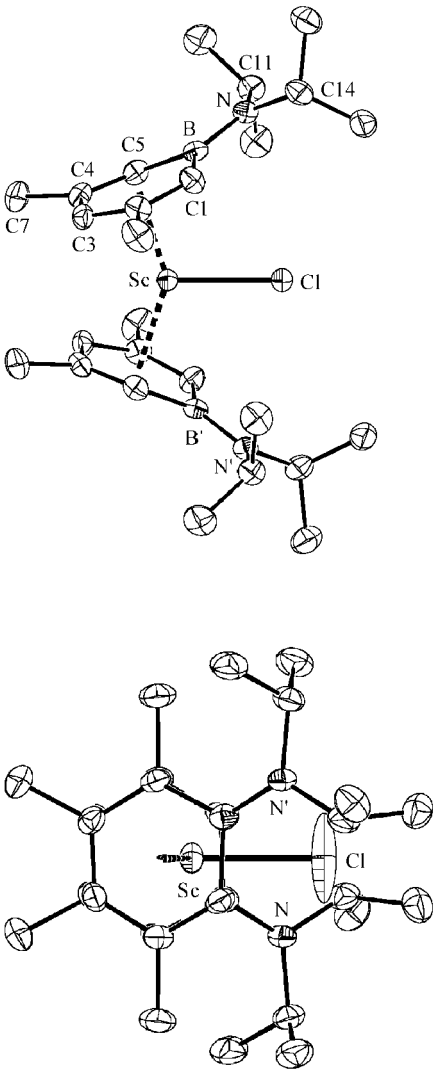

Figure 5. Left: Side-view of the molecular structure (PLATON plot, see ref.[20], at the 30% probability level) of **α-20** in the crystal. Right: Top-view showing the unusual displacement ellipsoid of the Cl atom in the high temperature α-modification. Selected bond lengths [Å] for **α-20**: Sc−Cl 2.377(2), Sc−Cn 2.463(3) for C3 to 2.571(3) for C1, Sc−B 2.756(3), B−N 1.412(4), C1−B 1.542(4). C5−B 1.539(4).

A *B*,*B*′-Bridged ansa Complex

Finally, we treated $LuCl_3$ with the bis(boratabenzene) salt Li_2(**5**) in THF and obtained the complex (**5**)Lu(μ-Cl)$_2$Li(THF)$_2$ (**23**). Crystallization from toluene gave large yellow rods, which according to NMR spectroscopy contained half an equivalent of toluene. The crystals readily lost toluene on standing, thus precluding the characterization by elemental analysis and also the determination of the crystal structure. A completely analogous preparation in THP as the solvent gave the solvate (**5**)Lu(μ-Cl)$_2$Li(THP)$_2$ (**24**), this time without the incorporation of toluene. The crystal structure determination proves the presence of an ansa-bridge that contains two nitrogen stereocenters in an approximate C_2-symmetry (Figure 8). In other words, we find the exclusive formation of the racemic form. We also note that the steric constraints of the ansa-bridge do not permit a perfectly eclipsed arrangement of the two boratabenzene rings. The compounds **23** and **24** are the first examples of group 3 ansa complexes with boratabenzene ligands. In group 4 a number of ansa complexes have been synthesized,[8a,8f,8g] and Ashe III et al. have

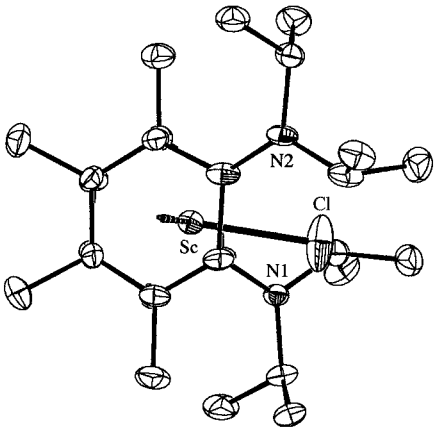

Figure 6. Top-view of the molecule (PLATON plot, see ref.[20], at the 30% probability level) of **β-20** in the crystal. Sc−Cl 2.385(3) Å.

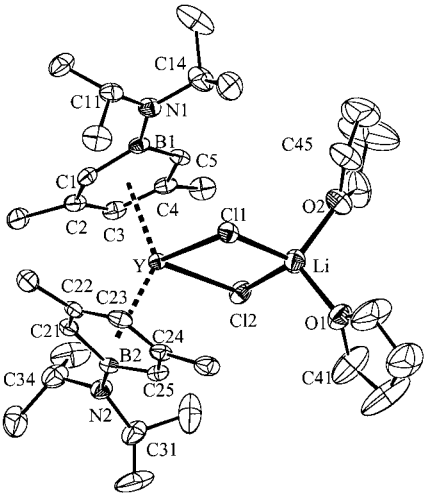

Figure 7. Molecular structure (PLATON plot, see ref.[20], at the 30% probability level) of **21** in the crystal. Selected bond lengths [Å] and bond angles [°]:Y−Cl1 2.628(2), Y−Cl2 2.624(2), Y−Cn 2.683(5) for C3 to 2.782(5) for C5, Y−B1 2.938(5), B1−N1 1.437(6), Y−C2n 2.686(5) for C23 to 2.794(5) for C25, Y−B2 2.912(5), B2−N2 1.445(7), Li−Cl1 2.346(10), Li−Cl2 2.333(11), Li−O1 1.901(11), Li−O2 1.913(11), Cl1−Y−Cl2 84.65(5), Cl1−Li−Cl2 98.2(4), Y−Cl1−Li 88.4(3), Y−Cl2−Li 88.7(3), O1−Li−O2 108.0(5), Cl1−Li−O1 116.5(5), Cl1−Li−O2 110.6(5), Cl2−Li−O1 110.7(5), Cl2−Li−O2 112.9(5).

shown that the exclusive formation of a related *rac*-stereomer is the result of thermodynamic control.[8a]

Conclusions

In this paper we have extended our earlier work on bis(boratabenzene)scandium complexes and have developed a chapter on the systematic synthetic and structural chemistry of 1-aminoboratabenzene complexes of scandium group metals. The ability of the *B*-dimethylamino group to coordinate to Li^+ centers gives rise to unusual structures such as the stepped ladder structures of **12** and **13**, and to the mononuclear complexes **15** and **16**. With larger substituents at boron this ability is suppressed. Both the 1-di-

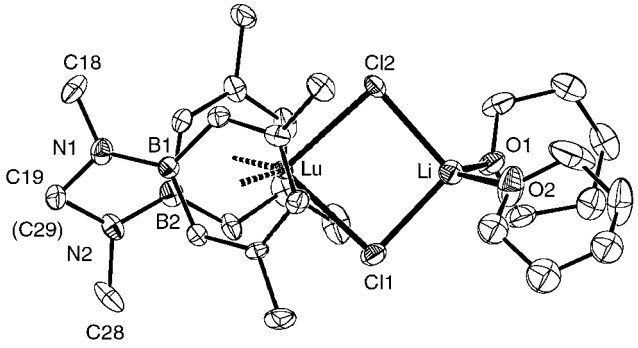

Figure 8. Top-view of the molecular structure (PLATON plot, see ref.[20], at the 30% probability level) of **24** in the crystal. Selected bond lengths [Å] and bond angles [°]:Lu−Cl1 2.579(3), Lu−Cl2 2.583(3), Lu−C1n 2.673(8) for C12 to 2.709(11) for C14, Lu−B1 2.873(12), B1−N1 1.440(15), Lu−C2n 2.671(9) for C23 to 2.702(11) for C21 and C25, Lu−B2 2.857(12), B2−N2 1.424(15), Li−Cl1 2.34(2), Li−Cl2 2.41(2), Li−O1 1.91(2), Li−O2 1.88(3), Cl1−Y−Cl2 85.4(1), Cl1−Li−Cl2 95.0(7), Lu−Cl1−Li 90.6(5), Lu−Cl2−Li 88.7(5), O1−Li−O2 112.5(11), Cl1−Li−O1 111.9(11), Cl1−Li−O2 110.1(9), Cl2−Li−O1 111.9(9), Cl2−Li−O2 114.2(11). The dihedral angle N1−C19−C29−N2 is 73.0(9)°.

isopropylamino ligand **3** and the 1-bis(trimethylsilyl)amino ligand **4** stabilize the coordinatively highly unsaturated mononuclear complexes **17**−**20**, and both these ligands seem to be more effective in this respect than the pentamethylcyclopentadienyl ligand Cp^*. We have also prepared the first group 3 ansa-bridged complexes **23** and **24**.

In most structures a strong preference for the eclipsed ring-ring conformations with 60° and 180° torsional angles is seen, which is enforced by transannular repulsions between the ring substituents in the 1,3,5-positions. In solution, all molecules are dynamic and display the highest possible effective symmetries in their NMR spectra.

Finally, we note that we still do not have boratabenzene complexes of the larger central metals, such as the early lanthanides, the divalent lanthanides, as well as of Th and U. Furthermore, the reaction chemistry of the bonds in the mouth of the bent sandwich molecules remains essentially untouched. We hope that this paper will stimulate other chemists to pursue these open aspects in the future.

Experimental Section

General: All manipulations were carried out under an inert atmosphere of nitrogen by means of standard Schlenk techniques. Hexane was distilled from Na/K alloy and toluene from sodium; Et_2O, THF, and THP were distilled from sodium benzophenone ketyl. Anhydrous lanthanide trichlorides were purchased from commercial sources and used as received. Elemental analyses were performed by Analytische Laboratorien, D-51779 Lindlar, Germany.

NMR spectra were recorded on a Varian Unity 500 (^{1}H, 499.6 MHz. ^{13}C, 125.6 MHz; ^{11}B, 160.3 MHz; ^{7}Li, 194.2 MHz) at ambient temperature. Chemical shifts are given in ppm; they are relative to internal TMS for ^{1}H and ^{13}C, to external $BF{\cdot}OEt_2$ for ^{11}B, and to external $LiBr/D_2O$ for ^{7}Li. Electron-impact mass spectra were recorded on a Finnigan MAT-95 at a nominal electron energy of 70 eV.

1-(Diisopropylamino)-5-methyl-3-methylene-1,2,3,6-tetrahydroborinine (7b): A solution of LiBu in hexane (1.6 M, 281 mL, 0.45 mol) was added to a suspension of KOBu*t* (50.5 g, 0.45 mol) in hexane at 0 °C. After the mixture was stirred at room temperature for 3 h, 2,4-dimethylpenta-1,3-diene[26] (21.6 g, 0.225 mol) in hexane (100 mL) was added and the reaction system was heated under reflux for 20 h. A precipitate of the dipotassio- compound was filtered off and washed thoroughly with hot hexane (3 × 500 mL). The solid was then suspended in hexane (250 mL) and was slowly added to a solution of BCl_2NiPr_2 [27] (40.3 g, 0.222 mol) in hexane/THF (4:1, 560 mL) at 0 °C. The mixture was stirred overnight and a white precipitate of KCl was removed by filtration. After removal of all volatiles, **7b** was collected by condensation (80 °C, 10^{-2} mbar) as a colorless liquid (30.3 g, containing 90% **7b**, 0.133 mol, 60%). On standing at room temperature overnight, **7b** solidified to form large needles, which afforded a spectroscopically pure sample of **7b**.

Data for 7b: ^{1}H NMR (500 MHz, $CDCl_3$): δ = 1.55 (br. s, 2 H, 6-H), 1.81 (s, 5-Me), 2.07 (br. s, 2 H, 2-H), 4.63 (m, 1 H, CH_2=), 4.66 (m, 1 H, CH_2=), 6.01 (m, 4-H), N*i*Pr$_2$: 1.12 (d, *J* = 7.0 Hz, 2 Me), 1.23 (d, *J* = 7.0 Hz, 2 Me), 3.54 (m, NCH), 3.73 (m, NCH). $^{13}C\{^1H\}$ NMR (126 MHz, $CDCl_3$): δ = 24.0 and 27.3 (C-2,6), 26.6 (5-Me), 107.9 (CH_2=), 126.6 (C-4), 139.9 (C-5), 146.8 (C-3), N*i*Pr$_2$: 22.5 (Me), 24.0 (Me), 45.7 (NCH), 48.0 (NCH). ^{11}B NMR (160 MHz, $CDCl_3$): δ = 44.6. MS (70 eV): *m*/*z* (%) = 206 (87) [M^+ + H], 190 (100) [M^+ − Me], 105 (10) [M^+ − N*i*Pr$_2$], 100 (12) [N*i*Pr$_2^+$]. $C_{13}H_{24}BN$ (205.2): calcd. C 76.11, H 11.79, N 6.83; found C 76.28, H 11.99, N 7.56.

1-[Bis(trimethylsilyl)amino]-5-methyl-3-methylene-1,2,3,6-tetrahydroborinine (7c): A crop of the dipotassio- compound, prepared from KOBu*t* (42.1 g, 0.37 mol), LiBu (1.6 M in hexane, 238 mL, 0.38 mol), and 2,4-dimethylpenta-1,3-diene (17.3 g, 0.18 mol), was suspended in hexane (250 mL). The suspension was added to a solution of $BCl_2N(SiMe_3)_2$ [28] (42.1 g, 0.17 mol) in hexane/THF (4:1, 450 mL) at 0 °C. Workup as described for **7b** gave, after condensation (140 °C, 10^{-2} mbar), a colorless liquid of **7c** together with some impurities (12.1 g, containing ca. 82% **7c**, 0.037 mol, 22%).

Data for 7c: ^{1}H NMR (500 MHz, $CDCl_3$): δ = 0.25 (s, 2 $SiMe_3$), 1.82 (s, 5-Me), 1.65 (br. s, 2 H, 6-H), 2.06 (br. s, 2 H, 2-H), 4.60 (m, 1 H, CH_2=), 4.70 (m, 1 H, CH_2=), 6.00 (m, 4-H) − $^{13}C\{^1H\}$ NMR (126 MHz, $CDCl_3$): δ = 4.4 ($SiMe_3$), 26.6 (5-Me), 30.7 and 33.8 (C-2,6), 108.7 (CH_2=), 126.9 (C-4), 138.7 (C-5), 146.2 (C-3). ^{11}B NMR (160 MHz, $CDCl_3$): δ = 57.9. MS (70 eV): *m*/*z* (%) = 265 (47) [M^+], 250 (100) [M^+ − Me], 146 (40) [$Si_2Me_6^+$], 73 (79) [$SiMe_3^+$].

Lithium 1-(Diisopropylamino)-3,5-dimethylboratabenzene [Li(3)]: A solution of $LiN(SiMe_3)_2$ in hexane (1.0 M, 20 mL, 20 mmol) was added dropwise to a solution of 1-(diisopropylamino)-5-methyl-3-methylene-1,2,3,6-tetrahydroborinine (**7b**) (4.10 g, 20 mmol) in ether (35 mL) at −78 °C. The mixture was kept at this temperature for 2 h, and was then allowed to warm to ambient temperature. A fine white precipitate gradually formed in the reaction system. After the suspension was stirred for 7 days, the solid was collected by filtration through a frit, washed with hexane (3 ′ 20 mL), and dried overnight under high vacuum to give Li(**3**) as an air- and moisture-sensitive, white powder (3.21 g, 76%).

Data for Li(3): ^{1}H NMR (500 MHz, [D_8]THF): δ = 2.03 (s, 6 H, 3-/5-Me), 5.15 (s, 4-H), 5.30 (s, 2-/6-H), N*i*Pr$_2$: 1.15 (d, *J* = 7.0 Hz, 4 Me), 3.66 (sept, *J* = 7.0 Hz, 2 NCH). $^{13}C\{^1H\}$ NMR (126 MHz, [D_8]THF): δ = 26.0 (3-/5-Me), 100.2 (C-4), 110.9 (br, C-2,6), 142.3 (C-3,5), N*i*Pr$_2$: 23.2 (Me), 46.1 (NCH). ^{11}B NMR (160 MHz, [D_8]THF): δ = 30.5.

TMEDA Solvate Li(TMEDA)(3): The lithium salt Li(**3**) (0.59 g, 2.80 mmol) was added to a solution of TMEDA (0.32 g, 2.80 mmol) in hexane (30 mL). The solution was filtered through a frit to remove some insoluble material and kept at −30 °C overnight to give Li(TMEDA)(**3**) (0.80 g, 87%) as moisture- and air-sensitive colorless rods.

Data for Li(TMEDA)(3): ^{1}H NMR (500 MHz, C_6D_6): δ = 2.34 (s, 3-/5-Me), 5.53 (s, 4-H), 5.81 (s, 2-/6-H), N*i*Pr$_2$: 1.46 (d, *J* = 6.7 Hz, 4 Me), 3.93 (sept, *J* = 6.7 Hz, 2 NCH), TMEDA: 1.45 (s, 2 NCH_2), 1.73 (s, 2 NMe_2). $^{13}C\{^1H\}$ NMR (126 MHz, C_6D_6): δ = 26.5 (3-/5-Me), 100.4 (C-4), 110.9 (br, C-2,6), 142.4 (C-3,5), N*i*Pr$_2$: 23.4 (Me), 46.2 (NCH), TMEDA: 45.1 (NMe_2), 55.8 (NCH_2). ^{11}B NMR (160 MHz, C_6D_6): δ = 31.4. $C_{19}H_{39}BLiN_3$ (327.3): calcd. C 69.73, H 12.01, N 12.84; found C 69.73, H 11.86, N 13.03.

1,1′-(*N*,*N*′-Dimethylethylenediamino)bis(3,5-dimethyldihydroborinines) 10: A mixture of *N*,*N*′-dimethylethylenediamine (0.99 g, 11.2 mmol) and triethylamine (2.28 g, 22.5 mmol) was added dropwise to a solution of 1-chloro-3,5-dimethyldihydroborinines[3] (3.15 g, 22.4 mmol) in hexane (25 mL) at 0 °C. The reaction mixture was stirred at ambient temperature for 6 h. A white precipitate, presumed to be $NHEt_3Cl$, was removed by filtration and washed with hexane (3 × 20 mL). The combined filtrate was evaporated to dryness under vacuum to give a pale yellow solid of **10** (2.19 g, 66%) as a mixture of isomers.

Lithium 1,1′-(*N*,*N*′-Dimethylethylenediamino)bis(3,5-dimethylboratabenzene) [Li_2(5)]: A solution of $LiN(SiMe_3)_2$ in hexane (1.0 M, 14.2 mL, 14.2 mmol) was added dropwise to a solution of the dihydroborinines **10** (2.10 g, 7.09 mmol) in ether (10 mL) at −78 °C. The mixture was allowed to warm to ambient temperature and a white precipitate formed. After the suspension was stirred for 1 day, the solid was collected by filtration through a frit, washed with hexane (3 ′ 10 mL), and dried overnight under high vacuum to give Li_2(**5**) as an extremely air- and moisture- sensitive white powder (1.90 g, 87%).

Data for Li_2(5): ^{1}H NMR (500 MHz, [D_6]DMSO): δ = 1.93 (s, 3-/3′-/5-/5′-Me), 2.66 (s, 2 NMe), 2.90 (s, 2 NCH_2), 4.89 (s, 4-/4′-H), 4.94 (s, 2-/2′-/6-/6′-H). $^{13}C\{^1H\}$ NMR (126 MHz, [D_6]DMSO): δ = 26.5 (3-/3′-/5-/5′-Me), 37.9 (NMe), 50.7 (NCH_2), 102.7 (C-4,4′), 108.7 (br, C-2,2′,6,6′), 139.4 (C-3,3′,5,5′). ^{11}B NMR (160 MHz, [D_6]DMSO): δ = 32.4.

Complex [(3,5-$Me_2C_5H_3BNMe_2$)$_2$Y(μ-Cl)$_2$Li]$_2$ (12): A suspension of YCl_3 (2.52 g, 12.9 mmol) and Li(3,5-$Me_2C_5H_3BNMe_2$) [Li(**2**)] (4.13 g, 26.6 mmol) in toluene (60 mL) was stirred at 110 °C for 3 days. An insoluble material, presumed to be LiCl, was filtered off and washed with toluene (20 mL). The combined yellow filtrate was concentrated to ca. 10 mL and kept at room temperature overnight to give **12** as air- and moisture-sensitive, pale yellow platelets. Crystallization of the concentrated mother liquor afforded a second crop of **12** (total: 3.44 g, 64%).

Data for 12: ^{1}H NMR (500 MHz, C_6D_6): δ = 2.24 (s, 3-/5-Me), 2.79 (s, NMe_2), 5.76 (s, 2-/6-H), 5.85 (s, 4-H). $^{13}C\{^1H\}$ NMR (126 MHz, C_6D_6): δ = 26.9 (3-/5-Me), 40.1 (NMe_2), 107.9 (C-4), 115.5 (br, C-2,6), 153.7 (C-3,5). ^{11}B NMR (160 MHz, C_6D_6): δ = 37.3. ^{7}Li NMR (194 MHz, C_6D_6): δ = 0.22. $C_{36}H_{60}B_4Cl_4Li_2N_4Y_2$ (925.7): calcd. C 46.71, H 6.53, N 6.05; found C 47.41, H 6.61, N 6.27.

Complex [(3,5-$Me_2C_5H_3BNMe_2$)$_2$Lu(μ-Cl)$_2$Li]$_2$ (13): Treatment of $LuCl_3$ (465 mg, 1.65 mmol) with Li(3,5-$Me_2C_5H_3BNMe_2$) [Li(**2**)] (531 mg, 3.42 mmol), as described for **12,** produced **13**. After crystallization from toluene (ca. 5 mL) at ambient temperature, air- and

moisture-sensitive, pale yellow platelets were obtained (770 mg, 85%).

Data for 13: ^{1}H NMR (500 MHz, C_6D_6): δ = 2.29 (s, 3-/5-Me), 2.77 (s, NMe_2), 5.67 (s, 2-/6-H), 5.85 (s, 4-H). $^{13}C\{^1H\}$ NMR (126 MHz, C_6D_6): δ = 27.0 (3-/5-Me), 40.0 (NMe_2), 107.2 (C-4), 113.8 (br, C-2,6), 153.6 (C-3,5). ^{11}B NMR (160 MHz, C_6D_6): δ = 37.0. ^{7}Li NMR (194 MHz, C_6D_6): δ = 0.19. $C_{36}H_{60}B_4Cl_4Li_2Lu_2N_4$ (1097.8): calcd. C 39.39, H 5.51, N 5.10; found C 39.62, H 5.55, N 5.28.

Complex Y(acac)(3,5-$Me_2C_5H_3BNMe_2$)$_2$ (14): Sodium acetylacetonate[29] (114 mg, 0.94 mmol) was added to a yellow solution of [(3,5-$Me_2C_5H_3BNMe_2$)$_2$YCl(LiCl)]$_2$ (**12**) (423 mg, 0.46 mmol) in toluene (15 mL). The reaction mixture was stirred at ambient temperature overnight. An insoluble material, presumed to be a mixture of LiCl and NaCl, was removed by filtration and washed with toluene (5 mL). The combined filtrate was concentrated to ca. 5 mL under vacuum. Large yellow crystals of **14** formed after the liquid was stored at −30 °C for 2 days. Crystallization of the concentrated mother liquor afforded a second crop of **14** (total: 282 mg, 64%), as air- and water-sensitive crystals.

Data for 14: ^{1}H NMR (500 MHz, C_6D_6): δ = 2.05 (s, 2 3-/5-Me), 2.92 (s, 2 NMe_2), 5.52 (t, *J* = 1.8 Hz, 2 4-H), 5.67 (d, *J* = 1.8 Hz, 2 2-/6-H), acac: 1.67 (s, 2 Me), 5.15 (s, CH). $^{13}C\{^1H\}$ NMR (126 MHz, C_6D_6): δ = 25.8 (3-/5-Me), 39.1 (NMe_2), 105.1 (C-4), 112.3 (br, C-2,6), 152.0 (C-3,5), acac: 27.2 (C-1,5), 102.2 (C-3), 191.1 (C-2,4). ^{11}B NMR (160 MHz, C_6D_6): δ = 33.4. MS (70 eV): *m*/*z* (%) = 484 (8) [M^+], 385 (<1) [M^+ − acac], 336 (37) [M^+ − $Me_2C_5H_3BNMe_2$], 149 (100) [$Me_2C_5H_3BNMe_2^+$], 134 (28) [149$^+$ − Me]. $C_{23}H_{37}B_2N_2O_2Y$ (485.1): calcd. C 57.07, H 7.70, N 5.79; found C 56.69, H 8.08, N 5.78.

Complex (3,5-$Me_2C_5H_3BNMe_2$)$_2$Sm(μ-Cl)$_2$Li(THF) (15): $SmCl_3$ (277 mg, 1.08 mmol) was added, with stirring, to a solution of Li(3,5-$Me_2C_5H_3BNMe_2$) [Li(**2**)] (343 mg, 2.21 mmol) in THF (20 mL). The reaction mixture was stirred at ambient temperature for 8 h to give a purple solution. The THF was evaporated under reduced pressure, and toluene (10 mL) was then added to the residue. The resulting mixture was stirred vigorously for 1 h. An insoluble material was removed by filtration and washed with toluene (5 mL). The combined filtrate was concentrated to ca. 5 mL and stored at 4 °C to give **15** as moisture-sensitive, purple crystals (397 mg, 62%).

Data for 15: ^{1}H NMR (500 MHz, C_6D_6): δ = 0.61 (br. s, 12 H, 3-/5-Me), 3.68 (br. s, 2 NMe_2), 6.50 (br. s, 2 2-/6-H), 15.84 (br. s, 2 4-H), THF: 1.64 (br, CH_2CH_2), 4.28 (br, 2 OCH_2). $^{13}C\{^1H\}$ NMR (126 MHz, C_6D_6): δ = 27.1 (3-/5-Me), 41.0 (NMe_2), 99.3 (br, C-4), 103.8 (br, C-2,6), 159.2 (C-3,5), THF: 25.6 (CH_2CH_2), 69.4 (OCH_2). ^{11}B NMR (160 MHz): δ = 46.2. ^{7}Li NMR (194 MHz, C_6D_6): δ = 6.51. $C_{22}H_{38}B_2Cl_2LiN_2OSm$ (596.4): calcd. C 44.30, H 6.42; found C 44.20, H 6.05.

Complex (3,5-$Me_2C_5H_3BNMe_2$)$_2$Y(μ-Cl)$_2$Li(THP) (16). − Method 1: Treatment of YCl_3 (239 mg, 1.23 mmol) with Li(3,5-$Me_2C_5H_3BNMe_2$) [Li(**2**)] (384 mg, 2.48 mmol) in THP (20 mL), as described for **15**, gave **16**. After crystallization from toluene (ca. 5 mL) at ambient temperature, air- and moisture-sensitive, pale yellow crystals were obtained (371 mg, 55%). **Method 2:** Crystallization of [(3,5-$Me_2C_5H_3BNMe_2$)$_2$YCl(LiCl)]$_2$ (**12**) (565 mg, 0.61 mmol) from THP (8 mL) at ambient temperature gave **16** as pale yellow crystals (556 mg, 83%).

Data for 16: ^{1}H NMR (500 MHz, C_6D_6): δ = 2.31 (s, 2 3-/5-Me), 2.81 (s, 2 NMe_2), 5.86 (s, 2 2-/6-H), 6.06 (s, 2 4-H), THP: 1.08 (br, 2 H, $OCH_2CH_2CH_2$), 1.18 (br, 4 H, OCH_2CH_2), 3.42 (t, 4 H, OCH_2). $^{13}C\{^1H\}$ NMR (126 MHz, C_6D_6): δ = 26.7 (3-/5-Me), 39.5 (NMe_2), 108.5 (C-4), 117.1 (br, C-2,6), 151.6 (C-3,5), THP: 22.8 ($OCH_2CH_2CH_2$), 26.0 (OCH_2CH_2), 69.5 (OCH_2). ^{11}B NMR (160 MHz, C_6D_6): δ = 34.9. ^{7}Li NMR (194 MHz, C_6D_6): δ = −0.20. $C_{18}H_{30}B_2Cl_2LiN_2Y(C_5H_{10}O)_{0.8}$ (531.7): calcd. C 49.69, H 7.20, N 5.27; found C 49.73, H 7.15, N 5.31.

Complex YCl[3,5-$Me_2C_5H_3BN(SiMe_3)_2$]$_2$ (18): Treatment of YCl_3 (218 mg, 1.12 mmol) with Li[3,5-$Me_2C_5H_3BN(SiMe_3)_2$] [Li(**4**)] (613 mg, 2.26 mmol) in toluene (15 mL), as described for **12**, gave **18**·(PhMe). After crystallization at −30 °C, air- and moisture-sensitive, yellow crystals were obtained (571 mg, 78%), which seem to easily lose part of the cocrystallized toluene.

Data for 18: ^{1}H NMR (500 MHz, CD_2Cl_2): δ = 0.19 [s, $N(SiMe_3)_2$], 2.36 (s, 3-/5-Me), 5.82 (br, 4-H), 6.06 (d, *J* = 1.2 Hz, 2-/6-H). $^{13}C\{^1H\}$ NMR (126 MHz, CD_2Cl_2): δ = 4.4 ($SiMe_3$), 27.1 (3-/5-Me), 112.1 (C-4), 129.3 (br, C-2,6), 154.1 (C-3,5). $^{11}B\{^1H\}$ NMR (160 MHz, CD_2Cl_2): δ = 39.2. $C_{26}H_{54}B_2ClN_2Si_4Y(C_7H_8)_{0.5}$ (699.1): calcd. C 50.68, H 8.36, N 4.01; found C 50.30, H 8.11, N 3.81.

Complex LuCl[3,5-$Me_2C_5H_3BN(SiMe_3)_2$]$_2$ (19): Treatment of $LuCl_3$ (364 mg, 1.29 mmol) with Li[3,5-$Me_2C_5H_3BN(SiMe_3)_2$] [Li(**4**)] (729 mg, 2.69 mmol) in toluene (20 mL), as described for **12**, afforded **19**·(PhMe). After crystallization at −30 °C, air- and moisture-sensitive, yellow rods were obtained (686 mg, 72%), which seem to easily lose part of the cocrystallized toluene.

Data for 19: ^{1}H NMR (500 MHz, C_6D_6): δ = 0.37 [s, $N(SiMe_3)_2$], 2.33 (s, 3-/5-Me), 5.52 (br, 4-H), 6.19 (br, 2-/6-H). $^{13}C\{^1H\}$ NMR (126 MHz, C_6D_6): δ = 4.6 ($SiMe_3$), 27.1 (3-/5-Me), 108.6 (C-4), 110.4 (br, C-2,6), 157.0 (C-3,5). ^{11}B NMR (160 MHz, C_6D_6): δ = 38.9. $C_{26}H_{54}B_2ClLuN_2Si_4$ $(C_7H_8)_{0.5}$ (785.2): calcd. C 45.13, H 7.45, N 3.57; found C 44.87, H 7.30, N 3.76.

Complex ScCl(3,5-$Me_2C_5H_3BNiPr_2$)$_2$ (20): Treatment of $ScCl_3$ (192 mg, 1.27 mmol) with Li(3,5-$Me_2C_5H_3BNiPr_2$) [Li(**3**)] (543 mg, 2.57 mmol) in toluene (20 mL), as described for **12,** afforded **20**. After crystallization at −30 °C, air- and moisture-sensitive, red crystals were obtained (391 mg, 63%).

Data for 20: ^{1}H NMR (500 MHz, $C_6D_5CD_3$): δ = 1.95 (s, 3-/5-Me), 5.56 (br. s, 2-/6-H), 5.61 (t, *J* = 1.7 Hz, 4-H), N*i*Pr_2: 1.26 (br, 4 Me), 3.78 (br, 2 NCH). $^{13}C\{^1H\}$ NMR (126 MHz, $C_6D_5CD_3$): δ = 26.5 (3-/5-Me), 109.1 (C-4), 117.7 (br, C-2,6), 152.4 (C-3,5), N*i*Pr_2: 23.2 (Me), 46.5 (NCH). ^{11}B NMR (160 MHz, $C_6D_5CD_3$): δ = 34.7. MS (70 eV): *m*/*z* (%) = 488 (3) [M^+], 473 (4) [M^+ − Me], 453 (<1) [M^+ − Cl], 284 (3) [M^+ − $Me_2C_5H_3BNiPr_2$], 205 (25) [$C_{13}H_{24}BN^+$], 190 (100) [$C_{13}H_{24}BN^+$ − Me]. $C_{26}H_{46}B_2ClN_2Sc$ (488.7): calcd. C 63.90, H 9.49, N 5.73; found C 63.65, H 9.66, N 5.66.

Complex (3,5-$Me_2C_5H_3BNiPr_2$)$_2$Y(μ-Cl)$_2$Li(THF)$_2$ (21): Treatment of YCl_3 (206 mg, 1.05 mmol) with Li(3,5-$Me_2C_5H_3BNiPr_2$) [Li(**3**)] (452 mg, 2.14 mmol) in THF (20 mL), as described for **15**, afforded **21**. After crystallization at −30 °C, air- and moisture-sensitive, yellow rods were obtained (399 mg, 64%).

Data for 21: ^{1}H NMR (500 MHz, C_6D_6): δ = 2.40 (s, 2 3-/5-Me), 5.74 (s, 2 4-H), 5.92 (s, 2 2-/6-H), N*i*Pr_2: 1.43 (d, 8 Me), 3.94 (br, 4 NCH), THF: 1.34 (br, 2 CH_2CH_2), 3.58 (br, 4 OCH_2). $^{13}C\{^1H\}$ NMR (126 MHz, C_6D_6): δ = 27.4 (3-/5-Me), 104.5 (C-4), 117.5 (br, C-2,6), 151.7 (C-3,5), N*i*Pr_2: 23.4 (*i*Pr-Me), 46.4 (NCH), THF: 25.4 (CH_2CH_2), 68.4 (OCH_2). ^{11}B NMR (160 MHz, C_6D_6): δ = 34.0. ^{7}Li NMR (194 MHz, C_6D_6): δ = −0.33. $C_{34}H_{62}B_2Cl_2Li$-

N_2O_2Y (719.3): calcd. C 56.78, H 8.69, N 3.90; found C 57.14, H 8.91, N 3.95.

Complex $(3,5\text{-}Me_2C_5H_3BNiPr_2)_2Sm(\mu\text{-}Cl)_2Li(THF)_2$ (22): Treatment of $SmCl_3$ (286 mg, 1.11 mmol) with $Li(3,5\text{-}Me_2C_5H_3BNiPr_2)$ [Li(**3**)] (490 mg, 2.32 mmol) in THF (20 mL), as described for **15**, afforded **22**. After crystallization at 4 °C, air- and moisture-sensitive, purple rods were obtained (428 mg, 65%).

Data for 22: ^{1}H NMR (500 MHz, C_6D_6): δ = 2.35 (br. s, 2 3-/5-Me), 7.06 (br. s, 2 2-/6-H), 12.09 (br. s, 2 4-H), N*i*Pr$_2$: 1.0(br, 8 Me), 3.71 (br. s, 4 NCH), THF: 1.57 (br, 2 CH_2CH_2), 3.89 (br, 4 OCH_2). $^{13}C\{^1H\}$ NMR (126 MHz, C_6D_6): δ = 29.1 (3-/5-Me), 96.0 (C-4), 106.6 (br, C-2,6), 159.1 (C-3,5), N*i*Pr$_2$: 22.8 (Me), 46.5 (NCH), THF: 25.6 (CH_2CH_2), 68.72 (OCH_2). ^{11}B NMR (160 MHz, C_6D_6): δ = 37.8. ^{7}Li NMR (194 MHz, C_6D_6): δ = 1.59. $C_{26}H_{46}B_2Cl_2LiN_2Sm(C_4H_8O)_{1.5}$ (744.7): calcd. C 51.61, H 7.85, N 3.76; found C 51.70, H 7.66, N 4.60.

Complex $[(3,5\text{-}Me_2C_5H_3BNMeCH_2)_2]Lu(\mu\text{-}Cl)_2Li(THF)_2$ (23): Treatment of $LuCl_3$ (437 mg, 1.54 mmol) with $Li_2[(3,5\text{-}Me_2C_5H_3BNMeCH_2)_2]$ [Li_2(**5**)] (510 mg, 1.66 mmol) in THF (20 mL), as described for **15**, afforded **23**. After crystallization at ambient temperature, air- and moisture-sensitive, large yellow rods were obtained (689 mg, 65%).

Data for 23: ^{1}H NMR (500 MHz, C_6D_6): δ = 2.45 and 2.48 (s, 2 3-/5-Me), 5.19, 5.78, 6.02 (s, 2H each, 2-/4-/6-H), ansa-bridge: 2.76 and 4.18 (m, 2H each, NCH_2CH_2N), 3.08 (s, 2 NMe), THF: 1.32 (br, 2 CH_2CH_2), 3.52 (br, 4 OCH_2). $^{13}C\{^1H\}$ NMR (126 MHz, C_6D_6): δ = 27.3 and 27.8 (3-/5-Me), 107.9 (C-4), 104.8 and 112.6 (br, C-2,6), 150.8 and 155.7 (C-3,5), ansa-bridge: 37.7 (NMe), 50.7 (NCH_2), THF: 25.4 (CH_2CH_2), 68.4 (OCH_2). ^{11}B NMR (160 MHz, C_6D_6): δ = 34.8. ^{7}Li NMR (194 MHz, C_6D_6): δ = −0.43.

Complex $[(3,5\text{-}Me_2C_5H_3BNMeCH_2)_2]Lu(\mu\text{-}Cl)_2Li(THP)_2$ (24): Treatment of $LuCl_3$ (266 mg, 0.95 mmol) with $Li_2[(3,5\text{-}Me_2C_5H_3BNMeCH_2)_2]$ [Li_2(**5**)] (307 mg, 1.00 mmol) in THP (15 mL) afforded large yellow rods of **24** (478 mg, 70%).

Data for 24: ^{1}H NMR (500 MHz, C_6D_6): δ = 2.45 and 2.52 (s, 2 3-/5-Me), 5.20, 5.84, 6.02 (s, 2H each, 2-/4-/6-H), ansa-bridge: 2.75 and 4.18 (m, 2 H each, NCH_2CH_2N), 3.09 (s, 2 NMe), THP: 1.23 (br, 2 $OCH_2CH_2CH_2$), 1.24 (br, 4 OCH_2CH_2), 3.47 (br, 4 OCH_2). $^{13}C\{^1H\}$ NMR (126 MHz, C_6D_6): δ = 27.3 and 27.9 (3-/5-Me), 107.9 (C-4), 104.8 and 112.5 (br, C-2,6), 150.8 and 155.9 (C-3,5), ansa-bridge: 37.7 (NMe), 50.7 (NCH_2), THP: 23.1 ($OCH_2CH_2CH_2$), 26.3 (OCH_2CH_2), 69.0 (OCH_2). ^{11}B NMR (160 MHz, C_6D_6): δ = 34.8. ^{7}Li NMR (194 MHz, C_6D_6): δ = −0.62. $C_{28}H_{48}B_2Cl_2LiLuN_2O_2$ (719.1): calcd. C 46.77, H 6.73, N 3.90; found C 46.73, H 6.84, N 4.05.

X-ray Crystal Structure Determinations: Diffraction intensity data were collected on ENRAF-Nonius CAD4 diffractometers equipped with graphite monochromators. Crystal data, data collec-

Table 2. Crystal data, data collection parameters, and convergence results for **12**, **14**, **16**, **18**·(PhMe) and **19**·(PhMe)

	12	**14**	**16**	**18**·PhMe	**19**·PhMe
Empirical formula	$C_{36}H_{60}B_4Cl_4Li_2N_4Y_2$	$C_{23}H_{37}B_2N_2O_2Y$	$C_{23}H_{40}B_2Cl_2LiN_2OY$	$C_{33}H_{62}B_2ClN_2Si_4Y$	$C_{33}H_{62}B_2ClLuN_2Si_4$
Molecular mass	925.65	484.09	548.96	745.20	831.25
Crystal system	Triclinic	triclinic	triclinic	orthorhombic	orthorhombic
Space group	$P\bar{1}$	$P\bar{1}$	$P\bar{1}$	$P2_12_12$	$P2_12_12$
Radiation (λ [Å])	Mo-K_α (0.71073)	Mo-K_α (0.71073)	Mo-K_α (0.71073)	Mo-K_α (0.71073)	Mo-K_α (0.71073)
a [Å]	12.149(2)	8.6551(5)	8.139(2)	13.042(2)	12.999(5)
b [Å]	13.526(2)	10.603(4)	11.013(3)	18.451(6)	18.468(7)
c [Å]	14.736(8)	14.21(1)	15.890(5)	8.548(3)	8.550(4)
α [deg]	101.56(2)	84.93(6)	77.80(2)		
β [deg]	90.44(2)	81.08(6)	83.70(3)		
γ [deg]	107.82(1)	78.45(4)	80.97(2)		
V [Å^3]	2252(2)	1260(2)	1370.5(8)	2057(2)	2052.5(15)
Z	2	2	2	2.00	2.00
$d_{calcd.}$ [g/cm^3]	1.36	1.28	1.33	1.20	1.35
F(000)	952	508	572	792	856
μ [cm^{-1}]	28.47	23.47	23.53	16.28	26.15
Absorption correction	Numerical	empirical	empirical	numerical	numerical
Max./min. transmission	0.609/0.409	0.999/0.749	0.999/0.599	0.556/0.410	0.565/0.413
θ range [deg]	3.2−27.0	3.0−26.0	3.0−27.0	3.1−27.0	3.1−25.5
Temperature [K]	213	223	213	213	223
Scan mode	ω−2θ	ω	ω−2θ	ω−2θ	ω
Crystal size [mm]	0.34 × 0.30 × 0.18	0.30 × 0.25 × 0.20	0.64 × 0.47 × 0.45	0.56 × 0.24 × 0.22	0.61 × 0.49 × 0.29
Reflections collected	18652	5390	9507	6957	4843
Reflections unique	9811	4929	5957	4482	3803
Reflections observed	3695	2551	3720	2007	2640
Criterion for observation	$I > 2\,\sigma(I)$	$I > 2\,\sigma(I)$	$I > 2\,\sigma(I)$	$I > 2\,\sigma(I)$	$I > 2\,\sigma(I)$
Variables	485	281	297	206	206
R_1 [a], observed (all data)	0.064 (0.190)	0.079 (0.179)	0.067(0.118)	0.070 (0.182)	0.046 (0.079)
wR_2[b], observed (all data)	0.093 (0.115)	0.129 (0.152)	0.136(0.148)	0.082 (0.102)	0.090 (0.100)
GOF[c]	0.771	0.914	0.967	0.844	0.987
Max. resd. density [e/Å^3]	0.73	0.52	1.16	0.33	0.97

[a] $R_1 = \|F_o| - |F_c\|/|F_o|$. − [b] $wR_2 = [w(F_o^2 - F_c^2)^2/w(F_o^2)^2]^{1/2}$, where $w = 1/[\sigma^2(F_o^2) + (aP)^2]$ and $P = [\max(F_o^2,0) + 2F_c^2]/3$. − [c] GOF = $[w(F_o^2 - F_c^2)^2/(n - p)]^{1/2}$.

Table 3. Crystal data, data collection parameters, and convergence results for **α-20**, **β-20**, **21**, and **24**

	α-20	**β-20**	**21**	**24**
Empirical formula	$C_{26}H_{46}B_2ClN_2Sc$	$C_{26}H_{46}B_2ClN_2Sc$	$C_{34}H_{62}B_2Cl_2LiN_2O_2Y$	$C_{28}H_{48}B_2Cl_2LiLuN_2O_2$
Molecular mass	488.70	488.70	719.26	719.11
Crystal system	Monoclinic	triclinic	triclinic	orthorhombic
Space group	*C*2/*c*	$P\bar{1}$	$P\bar{1}$	$P2_12_12_1$
Radiation (λ [Å])	Mo-K_α (0.71073)	Cu-K_α (1.54056)	Mo-K_α (0.71073)	Mo-K_α (0.71073)
a [Å]	10.247(1)	8.264(2)	11.784(5)	9.353(3)
b [Å]	13.083(3)	8.308(2)	13.481(2)	12.582(7)
c [Å]	21.883(5)	21.83(1)	15.312(3)	27.855(6)
α [deg]		96.78(4)	64.34(2)	
β [deg]	102.91(1)	98.83(5)	88.79(2)	
γ [deg]		103.62(2)	68.13(2)	
V [Å^3]	2859(2)	1421(1)	2006.0(10)	3278(2)
Z	4	2	2	4.00
$d_{calcd.}$ [g/cm^3]	1.13	1.14	1.19	1.46
F(000)	1056	528	764	1456
μ [cm^{-1}]	3.65	32.30	16.24	32.01
Absorption correction	not applied	empirical	empirical	numerical
Max./min. transmission		0.998/0.919	0.999/0.739	0.379/0.282
θ range [deg]	3.1−27.0	4.1−74.8	3.1−26.0	3.1−27.0
Temperature [K]	233	200	213	223
Scan mode	ω−2θ	ω	ω−2θ	ω−2θ
Crystal size [mm]	0.50 × 0.45 × 0.40	0.35 × 0.30 × 0.20	0.62 × 0.30 × 0.23	0.49 × 0.42 × 0.41
Reflections collected	10680	10125	11051	10006
Reflections unique	3123	5854	7851	6896
Reflections observed	1293	2126	4729	5590
Criterion for observation	$I > 2\,\sigma(I)$	$I > 2\,\sigma(I)$	$I > 2\,\sigma(I)$	$I > 2\,\sigma(I)$
Variables	238	299	409	342
R_1 [a], observed (all data)	0.051 (0.137)	0.140 (0.226)	0.067 (0.128)	0.051 (0.075)
wR_2 [b], observed (all data)	0.092 (0.105)	0.312 (0.354)	0.137 (0.154)	0.120 (0.131)
GOF[c]	0.746	0.907	0.926	1.056
Max. resd. density [e/Å^3]	0.60	1.89	0.61	1.62

[a] $R_1 = \|F_o| - |F_c\|/|F_o|$. − [b] $wR_2 = [w(F_o^2 - F_c^2)^2/w(F_o^2)^2]^{1/2}$, where $w = 1/[\sigma^2(F_o^2) + (aP)^2]$ and $P = [\max(F_o^2,0) + 2F_c^2]/3$. − [c] GOF = $[w(F_o^2 - F_c^2)^2/(n - p)]^{1/2}$.

tion parameters, and convergence results are listed in Tables 2 and 3. Before averaging over symmetry-related reflections, numerical[30] or empirical absorption[31] corrections were applied to the data sets with absorption coefficients (μ) larger than 10 cm^{-1}. Structures were solved by direct methods with the help of the SHELXS-97 program[32] and refined on reflection intensities (F^2) using the SHELXL-97 program.[33] In the final least-squares refinements, all non-hydrogen atoms were assigned anisotropic displacement parameters. In the case of **α-20**, the hydrogen atoms were refined isotropically. For all other structures, hydrogen atoms were included as riding with fixed displacement parameters [C−H = 0.98 Å, $U_{iso}(H) = 1.3\ U_{eq}(C)$].

Crystallographic data (excluding structure factors) for the structures reported in this paper have been deposited with the Cambridge Crystallographic Data Centre as supplementary publications nos. CCDC-166215 (**12**), CCDC-166216 (**14**), CCDC-166217 (**16**), CCDC-166218 (**18**·PhMe), CCDC-166219 (**19**·PhMe), CCDC-166220 (**α-20**), CCDC-166221 (**β-20**), CCDC-166222 (**21**), and CCDC-166223 (**24**). Copies of the data can be obtained free of charge on application to the CCDC, 12 Union Road, Cambridge CB2 1EZ, UK [Fax: (internat.) + 44 (0)1223/336−033; E-mail: deposit@ccdc.cam.ac.uk].

Acknowledgments

We thank Dr. A. Fischer and Dr. J. Ni for helpful advice regarding the synthesis of Li_2(**5**) and Dr. U. Englert concerning the X-ray structure determinations. This work was generously supported by the Deutsche Forschungsgemeinschaft and the Fonds der Chemischen Industrie.

[1] [1a] X. Zheng, G. E. Herberich, *Eur. J. Inorg. Chem.* **2001**, 3013−3019; [1b] X. Zheng, G. E. Herberich, *Organometallics*, **2001**, *20*, 3097−3100.

[2] [2a] G. C. Fu, *Adv. Organomet. Chem.* **2001**, *47*, 101−119; [2b] A. J. Ashe III, S. Al-Ahmad, X. Fang, *J. Organomet. Chem.* **1999**, *581*, 92−97; [2c] G. E. Herberich, *Boratabenzene Chemistry Revisited*, in *Advances in Boron Chemistry* (Ed.: W. Siebert), The Royal Society of Chemistry: Cambridge, U. K., **1997**; Special Publication No. 201, p. 211−223; [2d] G. E. Herberich in *Comprehensive Organometallic Chemistry II* (Eds.: E. W. Abel, F. G. A. Stone, G. Wilkinson), Pergamon Press, Oxford, **1995**, Vol. 1 (Volume ed.: C. E. Housecraft), p. 197−216; [2e] G. E. Herberich, H. Ohst, *Adv. Organomet. Chem.* **1986**, *25*, 199−236.

[3] G. E. Herberich, U. Englert, A. Fischer, J. Ni, A. Schmitz, *Organometallics* **1999**, *18*, 5496−5501.

[4] [4a] S. Qiao, D. A. Hoic, G. C. Fu, *J. Am. Chem. Soc.* **1996**,

118, 6329−6330; [4b] D. A. Hoic, J. R. Wolf, W. M. Davis, G. C. Fu, *Organometallics* **1996**, *15*, 1315−1318.
[5] M. A. Putzer, J. S. Rogers, G. C. Bazan, *J. Am. Chem. Soc.* **1999**, *121*, 8112−8113.
[6] X. Zheng, B. Wang, U. Englert, G. E. Herberich, *Inorg. Chem.* **2001**, *40*, 3117−3123.
[7] X. Zheng, U. Englert, G. E. Herberich, J. Rosenplänter, *Inorg. Chem.* **2000**, *39*, 5579−5585.
[8] [8a] A. J. Ashe III, S. Al-Ahmad, X. Fang, J. W. Kampf, *Organometallics* **2001**, *20*, 468−473; [8b] G. E. Herberich, U. Englert, B. Ganter, M. Pons, *Eur. J. Inorg. Chem.* **2000**, 979−986; [8c] G. C. Bazan, W. D. Cotter, Z. J. A. Komon, R. A. Lee, R. J. Lachicotte, *J. Am. Chem. Soc.* **2000**, *122*, 1371−1380; [8d] A. J. Ashe, III, S. Al-Ahmad, J. W. Kampf, *Organometallics* **1999**, *18*, 4234−4236; [8e] A. J. Ashe III, X. Fang, J. W. Kampf, *Organometallics* **1999**, *18*, 1363−1365; [8f] J. S. Rogers, R. J. Lachicotte, G. C. Bazan, *J. Am. Chem. Soc.* **1999**, *121*, 1288−1298; [8g] A. J. Ashe III, S. Al-Ahmad, X. Fang, J. W. Kampf, *Organometallics* **1998**, *17*, 3883−3888; [8h] R. W. Barnhart, G. C. Bazan, T. Mourey, *J. Am. Chem. Soc.* **1998**, *120*, 1082−1083; [8i] J. S. Rogers, G. C. Bazan, C. K. Sperry, *J. Am. Chem. Soc.* **1997**, *119*, 9305−9306; [8j] A. J. Ashe III, S. Al-Ahmad, J. W. Kampf, V. G. Young, Jr., *Angew. Chem.* **1997**, *109*, 2104−2106; *Angew. Chem. Int. Ed. Engl.* **1997**, *36*, 2014−2016; [8k] G. E. Herberich, U. Englert, A. Schmitz, *Organometallics* **1997**, *16*, 3751−3757; [8l] G. C. Bazan, G. Rodriguez, A. J. Ashe III, S. Al-Ahmad, J. W. Kampf, *Organometallics* **1997**, *16*, 2492−2494; [8m] G. C. Bazan, G. Rodriguez, A. J. Ashe III, S. Al-Ahmad, C. Müller, *J. Am. Chem. Soc.* **1996**, *118*, 2291−2292.
[9] [9a] F. T. Edelmann in *Metallocenes* (Eds.: A. Togni, R. L. Halterman), Wiley-VCH, Weinheim, Germany, **1998**, Vol. 1, p. 55−110; [9b] P. J. Chirik, J. E. Bercaw, in *Metallocenes* (Eds.: A. Togni, R. L. Halterman), Wiley-VCH, Weinheim, Germany, **1998**, Vol. 1, p. 111−152; [9c] G. Bombieri, G. Paolucci, *Organometallic p Complexes of f-elements*, in *Handbook on the Physics and Chemistry of Rare Earths* (Eds.: K. A. Gschneidner, Jr., L. Eyring), Elsevier Science, Amsterdam, The Netherlands, **1998**, Vol. 25, p. 265−413; [9d] H. Schumann, J. A. Meese-Marktscheffel, L. Esser, *Chem. Rev.* **1995**, *95*, 865−986.
[10] A. J. Ashe III, P. Shu, *J. Am. Chem. Soc.* **1971**, *93*, 1804−1805.
[11] [11a] G. E. Herberich, B. Schmidt, U. Englert, *Organometallics* **1995**, *14*, 471−480; [11b] G. E. Herberich, B. Schmidt, U. Englert, T. Wagner, *Organometallics* **1993**, *12*, 2891−2893.
[12] D. A. Hoic, M. DiMare, G. C. Fu, *J. Am. Chem. Soc.* **1997**, *119*, 7155−7156.
[13] G. E. Herberich, U. Englert, M. U. Schmidt, R. Standt, *Organometallics* **1996**, *15*, 2707−2712.
[14] B. Wang, Dissertation, Technische Hochschule Aachen, Aachen, Germany, **2001**.
[15] G. E. Herberich, U. Englert, B. Ganter, M. Pons, R. Wang, *Organometallics* **1999**, *18*, 3406−3413.
[16] [16a] J. L. Atwood, K. D. Smith, *J. Chem. Soc., Dalton Trans.* **1973**, 2487−2490; [16b] E. C. Baker, L. D. Brown, K. N. Raymond, *Inorg. Chem.* **1975**, *14*, 1376−1379.
[17] M. E. Thompson, S. M. Baxter, A. R. Bulls, B. J. Burger, M. C. Nolan, B. D. Santarsiero, W. P. Schaefer, J. E. Bercaw, *J. Am. Chem. Soc.* **1987**, *109*, 203−219.
[18] [18a] W. J. Evans, T. T. Peterson, M. D. Rausch, W. E. Hunter, H. Zhang, J. L. Atwood, *Organometallics* **1985**, *4*, 554−559; [18b] W. J. Evans, D. K. Drummond, J. W. Grate, H. Zhang, J. L. Atwood, *J. Am. Chem. Soc.* **1987**, *109*, 3928−3936.
[19] [19a] F. Bottomley, D. E. Paez, P. S. White, *J. Organomet. Chem.* **1985**, *291*, 35−41; [19b] W. Lamberts, H. Lueken, *Inorg. Chim. Acta* **1987**, *132*, 119−122; [19c] W. Lamberts, B. Hessner, H. Lueken, *Inorg. Chim. Acta* **1987**, *139*, 215−217; [19d] W. J. Evans, D. K. Drummond, *Organometallics* **1988**, *7*, 797−802.
[20] A. L. Spek, *Acta Crystallogr., Sect. C* **1990**, *46*, 34.
[21] The slip distortion is defined as the distance between the geometric mean of the C5B plane and the projection of the central metal onto this plane.
[22] P. Paetzold, *Adv. Inorg. Chem.* **1987**, *31*, 123−170.
[23] G. W. Klumpp, M. Vos, F. J. J. de Kanter, C. Slob, H. Krabbendam, A. L. Spek, *J. Am. Chem. Soc.* **1985**, *107*, 8292−8294.
[24] [24a] R. D. Shannon, *Acta Crystallogr., Sect. A* **1976**, *32*, 751−767; [24b] Y. Q. Jia, *J. Solid State Chem.* **1991**, *95*, 184−187.
[25] [25a] J. L. Atwood, W. E. Hunter, R. D. Rogers, J. Holton, J. McMeeking, R. Pearce, M. F. Lappert, *J. Chem. Soc., Chem. Commun.* **1978**, 140−142; [25b] P. L. Watson, J. F. Whitney, R. L. Harlow, *Inorg. Chem.* **1981**, *20*, 3271−3278.
[26] The isomer mixture of 2,4-dimethylpentadienes was prepared from a MeMgI Grignard reagent and mesityloxide, followed by dehydration at the distillation temperature: [26a] O. N. Jitkow, M. T. Bogert, *J. Am. Chem. Soc.* **1941**, *63*, 1979−1984; [26b] R. G. Kelso, K. W. Greenlee, J. M. Derfer, C. E. Boord, *J. Am. Chem. Soc.* **1955**, *77*, 1751−1755.
[27] W. Gerrard, H. R. Hudson, E. F. Mooney, *J. Chem. Soc.* **1960**, 5168−5172.
[28] P. Geymayer, E. G. Rochow, U. Wannagat, *Angew. Chem.* **1964**, *74*, 499−500; *Angew. Chem. Int. Ed. Engl.* **1964**, *3*, 633−634.
[29] R. S. P. Coutts, P. C. Wailes, *J. Organomet. Chem.* **1970**, *25*, 117−122.
[30] P. Coppens, L. Leiserowitz, D. Rabinovich, *Acta Crystallogr.* **1965**, *18*, 1035−1038.
[31] A. C. T. North, D. C. Phillips, F. S. Mathews, *Acta Crystallogr., Sect. A* **1968**, *24*, 351−359.
[32] G. M. Sheldrick, *SHELXS-97*, *Program for Structure Solution*, University of Göttingen, Göttingen, Germany, **1997**.
[33] G. M. Sheldrick, *SHELXL-97*, *Program for Structure Refinement*, University of Göttingen, Göttingen, Germany, **1997**.

Received June 29, 2001
[I01240]

Complexes of the (Tetramethylcyclobutadiene)cobalt Fragment with Boratabenzene Ligands and an Unprecedented Formation of a Borabenzene Complex − Structures of $(C_4Me_4)Co(3,5\text{-}Me_2C_5H_3BSnMe_3)$ with an Sn−B Bond and of the Dinuclear Complex $[(C_4Me_4)Co(3,5\text{-}Me_2C_5H_3B)]_2O$[‡]

Gerhard E. Herberich,*[a] Tushar S. Basu Baul,[a,b] and Ulli Englert[a]

Keywords: Boron / Cobalt / Tin / Borabenzene / Boratabenzene / Cyclobutadiene

The yellow-orange boratabenzene complex Cb*Co(3,5-$Me_2C_5H_3BNMe_2$) (**1**) (Cb* = C_4Me_4) was readily obtained from $[Cb^*Co(NCMe)_3]PF_6$ and Li(TMEDA)(3,5-$Me_2C_5H_3BNMe_2$). Methanolysis of **1** afforded Cb*Co(3,5-$Me_2C_5H_3BOMe$) (**2**). Complex **2** reacted with MeLi and with BCl_3 to give the *B*-methyl analogue **3** and the *B*-chloro compound **4**, respectively. The chloro compound **4** reacted with *i*Bu_2AlH, TlF, and $LiSnMe_3$ to afford the *B*-hydrido derivative **5**, the *B*-fluoro complex **6**, and the *B*-(trimethylstannyl) compound **7**, respectively. A single-crystal structure determination of **7** gave an Sn–B bond length of 2.236(5) Å. The B–O–B-linked dinuclear complex $[(C_4Me_4)Co(3,5\text{-}Me_2C_5H_3B)]_2O$ (**8**) was also characterized structurally. The amino compound **1** underwent an unprecedented quaternization with iodomethane to produce [Cb*Co(3,5-$Me_2C_5H_3BNMe_3$)]I (**10**) which possesses a borabenzene–trimethylamine ligand. Compound **10** is the first borabenzene complex of a metal outside the chromium group. When treated with Bu_4NCN in CH_2Cl_2 nucleophilic substitution of the NMe_3 group took place to give the *B*–CN derivative **11** which is the first *B*-cyanoboratabenzene complex.

Introduction

In the chemistry of borabenzene derivatives[2] it has become customary to distinguish between boratabenzene ions **A** and neutral borabenzene adducts **B**. The area of boratabenzene salts and complexes, especially those of the low-valent d-metals, is well developed. In the most recent years, the first compounds of Mg,[3] of group-3 metals,[1,4] and complexes of the group-4 metals[4b,5] were described. There are also a few studies of p-element compounds.[6] On the other hand, the scope and number of borabenzene adducts is still rather limited,[7] and very few complexes of these have been prepared. Those that have been synthesised are in all cases tricarbonyl compounds of group-6 metals,[7c,8] such as e.g. $Cr(CO)_3(C_5H_5BNC_5H_5)$ and its homologues of Mo and W.[8c]

This paper deals with (boratabenzene)(tetramethylcyclobutadiene)cobalt complexes Cb*Co(C_5H_5BX) (Cb = C_4H_4, cyclobutadiene; Cb* = C_4Me_4). In two previous papers,

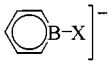

A

X = e.g. Me, Ph, NMe_2

B

X = e.g. py, PMe_3, CN*t*Bu

neutral sandwich complexes CbCo(C_5H_5BR) (R = Me,Ph)[9] and Cb*Co(C_5H_5BR) (R = Me, Ph) together with derivatives[10] have been described. In this paper we show that the new metallo-electrophile $[Cb^*Co(NCMe)_3]^+$[11] provides an efficient entry into this class of complexes (with the compounds **1**−**8**) and we present an unprecedented formation of a novel borabenzene complex $\mathbf{9}^+$ in the form of its iodide **10** [≡ (**9**)I] and its transformation into a *B*-cyano compound **11**.

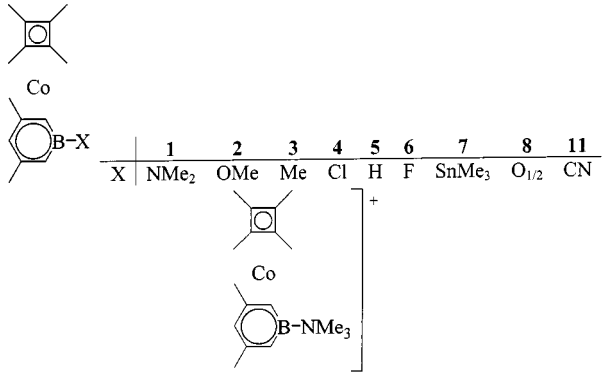

9a$^+$

[‡] Borabenzene Derivatives, 38. − Part 37: Ref.[1]

[a] Institut für Anorganische Chemie, Technische Hochschule Aachen
52056 Aachen, Germany
Fax: (internat.) + 49-(0)241/8888-288
E-mail: gerhard.herberich@ac.rwth-aachen.de
[b] Chemical Laboratory, Regional Sophisticated Instrumentation Centre, North-Eastern Hill University,
Bijni Complex, Shillong 793003, India

 © WILEY-VCH Verlag GmbH, 69451 Weinheim, Germany, 2002 1434−1948/02/0101−0043 $ 17.50+.50/0

Table 1. Overview of reactions

Substrate	Reagent	Product
Cb*Co(3,5-$Me_2C_5H_3BNMe_2$) (**1**)	MeOH (neat)	Cb*Co(3,5-$Me_2C_5H_3BOMe$) (**2**)
Cb*Co(3,5-$Me_2C_5H_3BOMe$) (**2**)	MeLi in Et_2O	Cb*Co(3,5-$Me_2C_5H_3BMe$) (**3**)
Cb*Co(3,5-$Me_2C_5H_3BOMe$) (**2**)	BCl_3 in CH_2Cl_2	Cb*Co(3,5-$Me_2C_5H_3BCl$) (**4**)
Cb*Co(3,5-$Me_2C_5H_3BCl$) (**4**)	$AlHiBu_2$ in toluene	Cb*Co(3,5-$Me_2C_5H_3BH$) (**5**)
Cb*Co(3,5-$Me_2C_5H_3BCl$) (**4**)	TlF, suspension in CH_2Cl_2	Cb*Co(3,5-$Me_2C_5H_3BF$) (**6**)
Cb*Co(3,5-$Me_2C_5H_3BCl$) (**4**)	$LiSnMe_3$ in THF	Cb*Co(3,5-$Me_2C_5H_3BSnMe_3$) (**7**)
Cb*Co(3,5-$Me_2C_5H_3BSnMe_3$) (**7**)	O_2, trace	[Cb*Co(3,5-$Me_2C_5H_3B]_2O$ (**8**)
Cb*Co(3,5-$Me_2C_5H_3BNMe_2$) (**1**)	MeI in THF	[Cb*Co(3,5-$Me_2C_5H_3BNMe_3$)]I (**10**)
[Cb*Co(3,5-$Me_2C_5H_3BNMe_3$)]I (**10**)	Bu_4NCN in CH_2Cl_2	Cb*Co(3,5-$Me_2C_5H_3BCN$) (**11**)

Results and Discussion

Synthesis of Cb*Co(3,5-$Me_2C_5H_3BNMe_2$) (1)

Reaction of the metallo-electrophile [Cb*Co(NCMe)$_3$]PF_6 [11] with the lithium boratabenzene Li(TMEDA)(3,5-$Me_2C_5H_3BNMe_2$)[12] in acetonitrile at ambient temperature resulted in the smooth formation of the sandwich complex **1**, which could be isolated as a yellow-orange crystalline solid in high yield (78%). The complex is highly soluble in most common organic solvents and is markedly sensitive to air and humidity. Because of its ready availability complex **1** has become the starting point for the syntheses described below; Table 1 gives an overview of the reactions involved.

Nucleophilic Substitution at the Boron Atom

Complex **1** can readily be modified by nucleophilic substitution at the boron atom. This is a well-known type of reaction that was observed for the first time in 1971[13] and was later established as a versatile and general synthetic method, e.g. in work with boratabenzene ligands,[14] with 2,5-dihydro-1,2,5-thiadiboroles,[15] with 1,4-diboracyclohexadienes,[16] and with 1*H*-borole ligands.[17]

Methanolysis of **1** takes place in refluxing methanol to give the methoxy compound **2** which is more reactive than **1** and a useful synthetic intermediate. Complex **2** readily reacts with MeLi in ether to afford the 1,3,5-trimethyl compound **3**, and with BCl_3 in dichloromethane solution to produce the *B*-chloro derivative **4**, which, to the best of our knowledge, is the first *B*-chloroboratabenzene complex. Complex **4** can be treated with diisobutylaluminium hydride to give a *B*-hydrido complex **5**. We note in this context, that the first *B*-hydrido complex Fe($C_5H_5BH)_2$ to be described was prepared by a similar nucleophilic substitution reaction.[14] Reaction of **4** with TlF produced the *B*-fluoro complex **6**; the B−F bond in this molecule is seen as a doublet in the $^{11}B\{^1H\}$ NMR spectrum with $^1J(^{19}F-^{11}B) = 55$ Hz. The only previous example of a *B*-fluoroboratabenzene complex is [Ir($PEt_3)_3$(3,5-$Me_2C_5H_3BF$)]($BF_4)_2$ which was obtained from an iridabenzene precursor and BF_3.[18] The nucleophiles used up to this point are of largely different character and the yields obtained are generally quite satisfactory (70−86%).

Treatment of the *B*-chloro complex **4** with $LiSnMe_3$ [19] afforded the anticipated *B*-(trimethylstannyl) derivative **7**, again as yellow-orange crystals. The presence of an Sn−B bond is readily seen in the $^{11}B\{^1H\}$ NMR spectrum of **7**, in the form of tin satellites, and in the $^{119}Sn\{^1H\}$ NMR spectrum, which displays a quadruplet with $^1J(^{119}Sn-^{11}B) = 869$ Hz. This may be compared with the 2,3-dihydro-1*H*-1,3,2-azadiborole **12a** that has an Me_3Sn−B single bond with a trigonal boron atom, and displays $^1J(^{119}Sn-^{11}B) = 1031$ Hz.[20] Alternatively, this may be compared to Li[H_3BSnMe_3] with a tetrahedral boron atom showing $^1J(^{119}Sn-^{11}B) = 554$ Hz.[21] Direct coupling constants qualitatively reflect the amounts of s-orbital contribution to the bonding between the two atoms involved. Thus, the data show that the s-orbital contribution of the boron atom in the Sn−B bond of **7** is only moderately reduced as compared to situations with truly trigonal boron atoms and, on the other hand, confirm that the boron orbital involved in the Co−B bonding largely retains its p-orbital character.

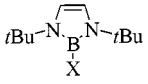

12a: X = $SnMe_3$, **b:** X = CN

Compound **7** is sensitive to air, but not more so than the more sensitive examples **1**, **4**, and **5**. When compound **7** was recrystallized, crystals appeared in the mother liquor that were identified by single-crystal structure determination as the *B*,*B*′-oxo linked dinuclear complex **8**.

Quaternization at the *B*-Amino Group

The *B*-amino group of **1** constitutes a Lewis basic reaction center. Treatment of **1** in THF with iodomethane at ambient temperature resulted in a slow quaternization and formation of the iodide (**9**)I ≡ **10**. This unusual reaction transforms a boratabenzene ligand into a borabenzene−trimethylamine ligand, or in more general terms, a ligand of type **A** into a ligand of type **B**. It also provides access to the first borabenzene complex outside the chromium triad. It is likely that other 1-aminoboratabenzene complexes will display an analogous reactivity, pro-

vided the nucleophilicity of the *B*-amino group is not reduced by strong π-interactions with the boron center or by the presence of sterically hindering *N*-alkyl groups.

A broad range of nucleophilic substitution reactions has been reported for the borabenzene adduct $C_5H_5BPMe_3$;[8b] the corresponding tricarbonylchromium complex $Cr(CO)_3(C_5H_5BPMe_3)$ is much more reactive, at least when treated with $LiC{\equiv}CSiMe_3$.[8b] We found that the NMe_3 group of **10** could readily be substituted on treatment with tetrabutylammonium cyanide in dichloromethane at ambient temperature. The reaction afforded the *B*-cyanoboratabenzene complex **11**, which is the first *B*-cyanoboratabenzene complex to be described.

We are not aware of other sandwich or half-sandwich complexes with a *B*-cyano group as part of a boron ring ligand. The ^{11}B chemical shift of **11** is at remarkably high field, as often observed for compounds with triple-bond systems (CO, CN, and CCR) attached to a boron atom.[22] A comparison of compounds **12a** and **12b** provides a pertinent example with $\delta(^{11}B) = 25.8$ for **12a** and $\delta(^{11}B) = 11.9$ for **12b**.[20] Note that the value for **12a** is in the typical range for this class of compounds,[22] while the value for **12b** is again at unusually high field.

Structure of Cb*Co(3,5-$Me_2C_5H_3BSnMe_3$) (7)

Crystals of **7** that were suitable for single-crystal X-ray work were obtained by slow crystallization from hexane (Figure 1, Table 2). The main aim of this study was the determination of the Sn−B bond length. The structure is described in some detail because of the high quality of the data obtained.

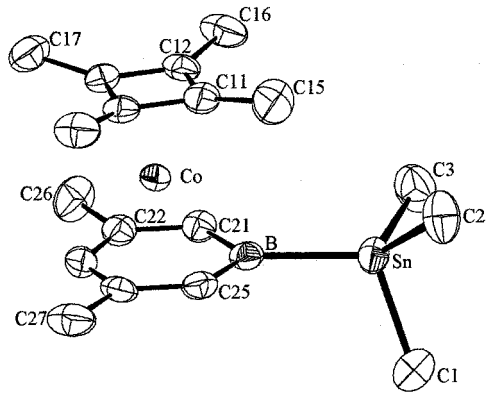

Figure 1. Molecular structure (PLATON plot, see ref.[23] at the 50% probability level) of **7** in the crystal

The molecular structure of **7** is that of a typical sandwich complex, and in its details it is typical of an electron-rich 18e complex. The cyclobutadiene ring is planar and the boratabenzene ring is nearly so [maximum deviation from the best plane 0.023(5) Å at B]. The metal atom is shifted away from the boron atom toward the opposite carbon atom [slip distortion: 0.043 Å] and the boron atom is bent away from the metal atom [folding angle of the boratabenzene ring: 3.5(7)°]. On the other hand, the bonding around the boron atom is strictly trigonal planar (angle sum at boron: 360.0°). Both the slip distortion and the folding angle are comparatively small. The two rings are almost perfectly coplanar [interplanar angle: 1.4(3)°], and the distances of the metal atom to the ring planes amount to 1.7026(6) Å for the Cb* ring and to 1.5622(6) Å for the borabenzene ring.

Table 2. Selected bond lengths [Å] and bond angles [°] of **7**

Co−C11	1.984(5)	Sn−C1	2.158(6)
Co−C12	1.985(4)	Sn−C2	2.150(6)
Co−C13	1.990(4)	Sn−C3	2.148(6)
Co−C14	1.983(4)	Sn−B	2.236(5)
Co−C21	2.122(4)	C21−C22	1.407(6)
Co−C22	2.100(5)	C22−C23	1.415(7)
Co−C23	2.078(5)	C23−C24	1.400(7)
Co−C24	2.122(4)	C24−C25	1.417(7)
Co−C25	2.126(4)	C21−B	1.506(7)
Co−B	2.214(5)	C25−B	1.519(7)
C1−Sn−C2	102.6(3)	C1−Sn−B	109.5(2)
C1−Sn−C3	106.9(3)	C2−Sn−B	121.5(2)
C2−Sn−C3	103.2(3)	C3−Sn−B	111.9(2)
Sn−B−C21	121.4(4)	Sn−B−C25	124.9(3)
C21−B−C25	113.7(4)		

A particularly interesting aspect of the structure is the presence of a $B{-}SnMe_3$ group. The Sn−B distance amounts to 2.236(5) Å and the torsional position of the $SnMe_3$ group is such that one *Sn*−Me substituent adopts a *transoid* position relative to the metal atom. This reduces the transannular repulsion between the remaining two *Sn*−Me substituents and the Cb* counter-ligand. Structurally documented and comparable Sn−B bonds are still rare. The closely related complex Cp*Fe($C_5H_5BSnMe_3$) shows the same Sn−B distance of 2.237(5) Å[24] and the observed Sn−B distance is, for instance, 2.274(5) Å for **12a**,[20] and 2.286 and 2.277(17) Å for (*E*)-$Me_3Sn(iPr_2N)$-BCHCHB($NiPr_2$)$SnMe_3$.[25]

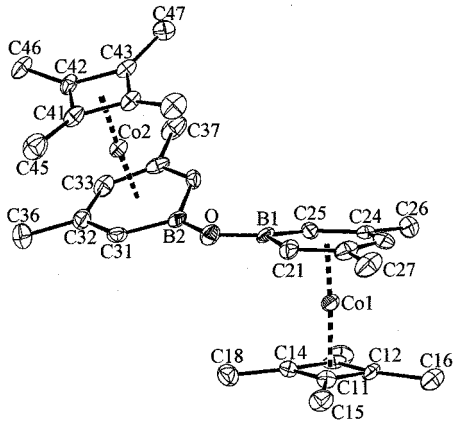

Figure 2. Molecular structure (PLATON plot, see ref.[23] at the 30% probability level) of **8** in the crystal; selected bond lengths [Å] and bond angles [°]: Co−C(Cb*) 1.969 (av.), Co−$C_{1,5}$(C_5B) 2.119 (av.), Co−$C_{2,4}$(C_5B) 2.082 (av.), Co−C_3(C_5B) 2.055 (av.), Co1−B1 2.283(9), Co2−B2 2.267(10), O−B1 1.367(10), O−B2 1.404(11); B1−O−B2 131.1(7), O−B1−C21 118.7(8), O−B1−C25 128.8(8), O−B2−C31 120.5(8), O−B2−C35 126.2(8), C21−B−C25 112.0(8), C31−B−C35 112.5(8)

Structure of [Cb*Co(3,5-$Me_2C_5H_3B$)]$_2$O (8)

Crystals of **8** deposited from the mother liquor of the crystallization of **7** after prolonged standing. Compound **8** had presumably formed from **7** and traces of oxygen. The molecules of **8** (Figure 2) consist of two sandwich units with structural features close to those of **7** and a B−O−B bridge linking the two. The B−O bond lengths and the B−O−B angle are in the expected ranges.[26] The bridging ligand is not planar; the observed twisting of the chain C25,B1,O,B2,C35 reduces the repulsive 1,5-interaction between the carbon atoms C25 and C35.

Conclusion

The recently discovered metallo-electrophile [Cb*Co(NCMe)$_3$]PF_6 could readily be combined with boratabenzene salts such as Li(TMEDA)(3,5-$Me_2C_5H_3BNMe_2$) to produce the *B*−NMe_2 complex **1**. This complex may be used as a starting point for the development of bora- and boratabenzene derivatives with the Cb*Co complex fragment. It readily underwent a quaternization with iodomethane to afford complex **11**, which is the first representative of a new type of borabenzene complexes. Nucleophilic substitution at the boron atom has not often been used previously with complex borabenzene derivatives. In this paper we have made use of this type of reaction to synthesize several compounds with uncommon substituents at the boron atom.

Experimental Section

General: Reactions were carried out under dinitrogen by employing conventional Schlenk techniques. Hexane was distilled from potassium, toluene from sodium, THF and Et_2O from sodium benzophenone ketyl, and CH_2Cl_2 from CaH_2. Alumina was heated under high vacuum at 300 °C prior to use and was deactivated (5% H_2O, deoxygenated) after cooling. Melting points were determined in sealed capillaries with a Büchi 510 melting point apparatus and are uncorrected. Elemental analyses were performed by the Analytische Laboratorien, Prof. Dr. H. Malissa and G. Reuter GmbH, 51789 Lindlar. NMR spectra were recorded with a Varian Unity 500 (^{1}H: 499.6 MHz. ^{13}C{^{1}H}: 125.6 MHz; ^{11}B{^{1}H}: 160.3 MHz. ^{19}F: 470.1 MHz; ^{119}Sn: 186.3 MHz) and a Varian VXR 300 (^{1}H: 300 MHz. ^{13}C{^{1}H}: 75.4 MHz). Chemical shifts are given in ppm; they were measured at ambient temperature and are quoted relative to internal TMS for ^{1}H and ^{13}C, relative to external BF_3·OEt_2 for ^{11}B, to external $CFCl_3$ for ^{19}F, and relative to external $SnMe_4$ for ^{119}Sn. Deuterated solvents for NMR spectroscopy were degassed, dried and stored over molecular sieves (4 Å; Merck). Assignments are based on APT and DEPT spectra. IR spectra were measured with a Nicolet Avatar 360 FT IR instrument.

Cb*Co(3,5-$Me_2C_5H_3BNMe_2$) (1): A freshly prepared solution of [Cb*Co(NCMe)$_3$]PF_6 [11] (1.66 g, 4.25 mmol) in acetonitrile (40 mL) was added with stirring to Li(TMEDA)(3,5-$Me_2C_5H_3BNMe_2$)[12] (1.22 g, 4.49 mmol), and stirring was continued at ambient temperature for 5 h. The volatiles were then removed under vacuum and the resulting residue was triturated with hexane. The extract was filtered through a frit covered with alumina (deactivated with 5% H_2O, 5-cm layer) at −80 °C, and the elution was completed with 60 mL of hexane. The volatiles were removed from the hexane solution. The product was crystallized from pentane at −30 °C as yellow-orange crystalline solid. Concentrating the mother liquor and cooling afforded a second crop of **1** (combined yield: 1.05 g, 78%); m.p. 66−67 °C, soluble in all common organic solvents. $C_{17}H_{27}BCoN$ (315.2): calcd. C 64.79, H 8.64, N 4.44; found C 64.71, H 8.77, N 4.90. ^{1}H NMR (CD_2Cl_2): δ = 1.36 (s, Cb*), 2.18 (s, 3-/5-Me), 3.76 (d, 2-/6-H), 4.77 (t, 4-H, $^4J_{24}$ = 1.2 Hz), 2.76 (s, NMe_2). ^{13}C{^{1}H} NMR (CD_2Cl_2): δ = 9.7 (C_4*Me*$_4$), 22.6 (3-/5-Me), 39.2 (NMe_2), 77.5 (br, C-2,6), 77.8 (*C*$_4$Me$_4$), 85.2 (C-4), 112.4 (C-3,5); reliable spectra could be obtained more easily from toluene solutions of **1** because of the higher solubility of **1** in this solvent. ^{11}B{^{1}H} NMR (CD_2Cl_2): δ = 22.0.

Cb*Co(3,5-$Me_2C_5H_3BOMe$) (2): A solution of **1** (0.53 g, 1.68 mmol) in methanol (15 mL, 0.37 mol) was heated under reflux at 65 °C for 24 h. After careful removal of the volatiles, the resulting residue was crystallized from hexane to give **2** (0.43 g, 86%) as an orange crystalline solid; m.p. 46−47 °C. $C_{16}H_{24}BCoO$ (302.1): calcd. C 63.61, H 8.01; found C 63.59, H 8.18. ^{1}H NMR (CD_2Cl_2): δ = 1.38 (s, Cb*), 2.04 (s, 3-/5-Me), 3.59 (s, OMe), 3.96 (d, 2-/6-H), 4.86 (t, 4-H, $^4J_{24}$ = 1.0 Hz). ^{13}C{^{1}H} NMR (CD_2Cl_2): δ = 9.5 (C_4*Me*$_4$), 22.8 (3-/5-Me), 53.4 (OMe), 78.2 (*C*$_4$Me$_4$), 80.6 (br, C-2,6), 87.0 (C-4), 113.4 (C-3,5). ^{11}B{^{1}H} NMR (CD_2Cl_2): δ = 25.4.

Cb*Co(3,5-$Me_2C_5H_3BMe$) (3): A solution of MeLi (1.52 mL, 1.6 M in diethyl ether, 2.43 mmol) was added dropwise to a stirred solution of **2** (0.38 g, 1.25 mmol) in diethyl ether (20 mL) at −80 °C. The reaction mixture was stirred for additional 30 min under cold conditions, then allowed to warm to room temperature and stirring was continued for 24 h. After removal of the volatiles in a vacuum, the resulting residue was dissolved in hexane. Filtration and concentration gave **3** (0.31 g, 86%) as an orange-yellow crystalline solid; m.p. 127−128 °C. $C_{16}H_{24}BCo$ (286.1): calcd. C 67.17, H 8.45; found C 66.77, H 8.66. ^{1}H NMR (CD_2Cl_2): δ = 0.49 (s, BMe), 1.38 (s, Cb*), 2.04 (s, 3-/5-Me), 4.34 (d, 2-/6-H), 5.01 (t, 4-H), $^4J_{24}$ = 1.0 Hz. ^{13}C{^{1}H} NMR (CD_2Cl_2): δ = 0.6 (br, BMe), 9.5 (C_4*Me*$_4$), 22.6 (3-/5-Me), 77.9 (*C*$_4$Me$_4$), 88.9 (C-4), 95.0 (br, C-2,6), 112.7 (C-3,5). ^{11}B{^{1}H} NMR (CD_2Cl_2): δ = 22.4.

Cb*Co(3,5-$Me_2C_5H_3BCl$) (4): A solution of BCl_3 in dichloromethane (2.97 mL, 1.56 M, 4.63 mmol) was added dropwise to a stirred solution of **2** (0.47 g, 1.55 mmol) in hexane (20 mL) at 0 °C. Rapid formation of a precipitate was seen. Stirring was continued for 1 h; then the reaction mixture was allowed slowly to warm to room temperature (12 h). After removal of the volatiles, the resulting residue was dissolved in dichloromethane and filtered through alumina (deactivated with 5% H_2O, 3 cm layer) using the same solvent as eluent. Removal of the solvent left **4** (0.33 g, 70%) as a fine microcrystalline, deep yellow solid; m.p. 159−160 °C. $C_{15}H_{21}BClCo$ (306.5): calcd. C 58.78, H 6.91; found C 58.81, H 6.97. ^{1}H NMR (CD_2Cl_2): δ = 1.39 (s, Cb*), 2.08 (s, 3-/5-Me), 4.50 (d, 2-/6-H), 5.09 (t, 4-H), $^4J_{24}$ = 1.0 Hz. ^{13}C{^{1}H} NMR (CD_2Cl_2): δ = 9.4 (C_4*Me*$_4$), 22.3 (3-/5-Me), 80.3 (*C*$_4$Me$_4$), 89.8 (C-4), 91.8 (br, C-2,6), 113.1 (C-3,5). ^{11}B{^{1}H} NMR (CD_2Cl_2): δ = 23.7.

Cb*Co(3,5-$Me_2C_5H_3BH$) (5): To a stirred solution of **4** (0.24 g, 0.78 mmol) in hexane (40 mL) was added diisobutylaluminium hydride in toluene (2.24 mL, 1 M, 2.24 mmol) at −80 °C. The reaction mixture was stirred for 30 min, then it was allowed slowly to warm to room temperature (12 h). The solvents were evaporated under vacuum, and the residue was dissolved in hexane (10 mL) and cooled to −80 °C. Anhydrous methanol (ca. 6 drops) and pyridine (ca. 4 drops) were added. The mixture was stirred for 30 min and

then was allowed to warm to room temperature. Filtration through a cold frit (−80 °C) containing alumina (deactivated with 5% H_2O, 5 cm layer) with diethyl ether as eluent and subsequent concentration of the filtrate gave **5** (0.18 g, 86%) as an orange colored solid; m.p. 138−139 °C. $C_{15}H_{22}BCo$ (272.1): calcd. C 66.22, H 8.15; found C 66.97, H 8.36. ^1H NMR (CD_2Cl_2): δ = 1.39 (s, Cb*), 2.08 (s, 3-/5-Me), 4.65 (dd, $^3J_{12}$ = 4.1, $^4J_{24}$ = 1.1 Hz, 2-/6-H), 5.11 (t, $^4J_{24}$ = 1.1 Hz, 4-H). $^{13}C\{^1H\}$ NMR (CD_2Cl_2): δ = 9.9 (C_4Me_4), 22.7 (3-/5-Me), 79.3 (C_4Me_4), 90.1 (C-4), 96.6 (br, C-2,6), 112.5 (C-3,5). ^{11}B NMR (CD_2Cl_2): δ = 16.8 [d, $^1J(^{11}B-^1H)$ = 110.0 Hz].

Cb*Co(3,5-Me$_2$C$_5$H$_3$BF) (6): A solution of **4** (0.18 g, 0.58 mmol) in dichloromethane (20 mL) was treated with excess TlF (0.26 g, 1.16 mmol) and stirred at room temperature for 3 d. The reaction mixture was filtered and normal workup gave **6** (0.13 g, 76%) as a yellow crystalline solid; m.p. 151−152 °C. $C_{15}H_{21}BCoF$ (290.1): calcd. C 62.11, H 7.30; found C 62.20, H 7.40. ^1H NMR (CD_2Cl_2): δ = 1.40 (s, Cb*), 2.06 (s, 3-/5-Me), 4.12 (d, 2-/6-H), 4.95 (t, 4-H, $^4J_{24}$ = 1.0 Hz). $^{13}C\{^1H\}$ NMR (CD_2Cl_2): δ = 9.5 (C_4Me_4), 22.5 (3-/5-Me), 79.4 (C_4Me_4), 83.3 (br, C-2,6), 88.1 (C-4), 114.1 (C-3,5). $^{11}B\{^1H\}$ NMR (CD_2Cl_2): δ = 27.0 [d, $^1J(^{19}F-^{11}B)$ = 55 Hz]. ^{19}F NMR (CD_2Cl_2): δ = −174 (br, with 90 Hz splitting).

Cb*Co(3,5-Me$_2$C$_5$H$_3$BSnMe$_3$) (7): A solution of **4** (0.22 g, 0.71 mmol) in THF (10 mL) was added dropwise to an ice-cooled solution of $LiSnMe_3$ [prepared from Sn_2Me_6 (0.23 g, 0.70 mmol) in THF (5 mL) and MeLi in diethyl ether (0.43 mL, 1.65 M, 0.70 mmol) at −80 °C].[19] Stirring was continued for 1 h; then the reaction mixture was allowed to warm to room temperature (12 h). After removal of the volatiles under vacuum, the resulting residue was dissolved in hexane and filtered through a cold frit (−80 °C) containing alumina (deactivated with 5% H_2O, 1-cm layer) with hexane as eluent. Concentration of the eluate yielded **7** (0.25 g, 81%) as yellow-orange crystals; m.p. 110−111 °C. $C_{18}H_{30}BCoSn$ (434.9): calcd. C 49.72, H 6.95; found C 49.57, H 7.35. ^1H NMR (CD_2Cl_2): δ = 0.02 [s, $^2J(^{119}Sn-^1H)$ = 41.4 Hz, $SnMe_3$], 1.37 (s, Cb*), 2.08 (s, 3-/5-Me), 4.83 (d, 2-/6-H), 5.17 (t, 4-H), $^4J_{24}$ = 1.5 Hz. $^{13}C\{^1H\}$ NMR (CD_2Cl_2): δ = −10.4 [s, $^1J(^{119}Sn-^{13}C)$ = 201.6 Hz, $SnMe_3$], 10.1 (C_4Me_4), 22.5 (3-/5-Me), 80.0 (C_4Me_4), 90.8 (C-4), 101.1 (br, C-2,6), 112.1 (C-3,5). $^{11}B\{^1H\}$ NMR (CD_2Cl_2): δ = 20.9 [s, $^1J(^{119}Sn-^{11}B)$ = 0.86 kHz]. $^{119}Sn\{^1H\}$ NMR (CD_2Cl_2): δ = −105.3 [q, $^1J(^{119}Sn-^{11}B)$ = 869 Hz].

Byproduct 8: On standing, the mother liquor of the above preparation of **7** deposited orange-colored crystals of **8**; m.p. 189−190 °C. The compound was identified and characterized by an X-ray structure determination.

[Cb*Co(3,5-Me$_2$C$_5$H$_3$BNMe$_3$)]I (10): MeI (0.16 g, 1.12 mmol) in THF (10 mL) was added dropwise to a solution of **1** (0.35 g, 1.11 mmol) in the same solvent (20 mL) with stirring. A yellow precipitate appeared after ca. 40 min and stirring was continued at ambient temperature for 10 h. The crude product was collected on a frit, washed with THF (2 × 5 mL), then with diethyl ether (2 × 10 mL), and dried under vacuum. The product was dissolved in hot chloroform; subsequent slow cooling to −30 °C yielded **10** (0.43 g, 86%) as yellow microcrystals; m.p. 198−199 °C, soluble in chloroform, dichloromethane, acetone, and methanol. $C_{18}H_{30}BCoIN$ (457.1): calcd. C 47.03, H 6.62; found C 46.78, H 6.62. ^1H NMR (CD_2Cl_2): δ = 1.42 (s, Cb*), 2.18 (s, 3-/5-Me), 3.29 (s, NMe_3), 4.71 (d, 2-/6-H), 5.30 (t, 4-H, $^4J_{24}$ = 1.0 Hz). $^{13}C\{^1H\}$ NMR (CD_2Cl_2): δ = 10.3 (C_4Me_4), 22.4 (3-/5-Me), 54.0 (NMe_3), 82.5 (C_4Me_4), 83.4 (br, C-2,6), 93.2 (C-4), 114.4 (C-3,5). $^{11}B\{^1H\}$ NMR (CD_2Cl_2): δ = 25.3.

Cb*Co(3,5-Me$_2$C$_5$H$_3$BCN) (11): A solution of tetrabutylammonium cyanide (0.20 g, 0.74 mmol) in dichloromethane (10 mL) was added dropwise to a solution of **10** (0.30 g, 0.66 mmol) in the same solvent (10 mL). The reaction mixture was stirred for 24 h. After removal of the volatiles, the residue was extracted in toluene (40 mL). Filtration through alumina (deactivated with 5% H_2O, 3-cm layer) using toluene/diethyl ether (95:5, v/v) as eluent, subsequent removal of the volatiles under vacuum, and recrystallisation from dichloromethane/diethyl ether (1:1) yielded **11** (0.15 g, 79%) as a yellow-orange solid; m.p. 155−156 °C. $C_{16}H_{21}BCoN$ (297.1): calcd. C 64.69, H 7.12, N 4.71; found C 65.12, H 7.24, N 5.08. ^1H NMR (CD_2Cl_2): δ = 1.42 (s, Cb*), 2.11 (s, 3-/5-Me), 4.87 (d, 2-/6-H), 5.27 (t, 4-H, $^4J_{24}$ = 1.5 Hz). $^{13}C\{^1H\}$ NMR (CD_2Cl_2, −50 °C): δ = 9.4 (C_4Me_4), 22.0 (3-/5-Me), 81.4 (C_4Me_4), 91.4 (C-4), 96.7 (br, C-2,6), 112.2 (C-3,5), 131.4 (br, CN). $^{11}B\{^1H\}$ NMR (CD_2Cl_2): δ = 7.4. IR (CD_2Cl_2): ν(CN) = 2198 cm^{-1}.

X-ray Crystal Structure Determinations: Diffraction intensity data were collected with ENRAF-Nonius CAD4 diffractometers equipped with graphite monochromators. Crystal data, data collection parameters, and convergence results are listed in Table 3. Before averaging over symmetry-related reflections, numerical[27] or empirical absorption[28] corrections were applied to the data sets. Structures were solved by direct methods with the help of the SHELXS-97 program[29] and refined on reflection intensities (F^2) using the SHELXL-97 program.[30] In the final least-squares refinements, all non-hydrogen atoms were assigned anisotropic displacement parameters. Hydrogen atoms were included as riding with

Table 3. Crystal data, data collection parameters, and convergence results for **7** and **8**

	7	**8**
Empirical formula	$C_{18}H_{30}BCoSn$	$C_{30}H_{42}B_2Co_2O$
Molecular weight	434.87	558.16
Crystal system	triclinic	monoclinic
Space group	$P\bar{1}$	$P2_1/c$
Radiation (λ [Å])	Mo-K_α (0.71073)	Mo-K_α (0.71073)
a [Å]	7.321(1)	15.907(2)
b [Å]	10.285(1)	13.664(3)
c [Å]	13.6514(8)	14.581(1)
α [°]	77.861(7)	90
β [°]	82.530(7)	115.750(6)
γ [°]	82.98(1)	90
V [Å^3]	991.6(2)	2854.5(8)
Z	2	4
$d_{calcd.}$ [g/cm^3]	1.46	1.30
$F(000)$	440	1176
μ [mm^{-1}]	20.99	11.79
Absorption correction	numerical	empirical
Max./min. transmission	0.622/0.523	1.000/0.886
θ range [°]	3.1−28.0	3.1−26.0
Temperature [K]	223	233
Scan mode	ω−2θ	ω−2θ
Crystal size [mm]	0.50 × 0.31 × 0.20	0.50 × 0.45 × 0.40
Reflections collected	9522	9361
Reflections unique	4766	5031
Reflections observed	3531	2205
Criterion for observation	$I > 2\,\sigma(I)$	$I > 2\,\sigma(I)$
Variables	199	328
R_1 [a], observed (all data)	0.049 (0.069)	0.079 (0.187)
wR_2[b], observed (all data)	0.118 (0.124)	0.131 (0.152)
GOF[c]	1.01	0.89
Max. resd. density [e/Å^3]	1.85	0.54

[a] $R_1 = \Sigma||F_o| - |F_c||/\Sigma|F_o|$. [b] $wR_2 = [\Sigma w(F_o^2 - F_c^2)^2/\Sigma w(F_o^2)^2]^{1/2}$, where $w = 1/[\sigma^2(F_o^2) + (aP)^2]$ and $P = [\max(F_o^2,0) + 2F_c^2]/3$. [c] GOF = $[\Sigma w(F_o^2 - F_c^2)^2/\Sigma(n - p)]^{1/2}$.

fixed displacement parameters [C−H = 0.98 Å, U_{iso}(H) = 1.3 U_{eq}(C)]. Crystallographic data (excluding structure factors) for the structures reported in this paper have been deposited with the Cambridge Crystallographic Data Centre as supplementary publications nos. CCDC-167066 (**7**) and -167065 (**8**). Copies of the data can be obtained free of charge on application to the CCDC, 12 Union Road, Cambridge CB2 1EZ, U. K. [Fax: (internat.) + 44-1223/336-033; E-mail: deposit@ccdc.cam.ac.uk].

Acknowledgments

We thank Mikhail V. Butovskii (Diploma Chemist; M. V. Lomonosov Moscow State University), for providing us with the salt [Cb*Co(NCMe)$_3$]PF$_6$ and for help with NMR measurements. This work was generously supported by the Deutsche Forschungsgemeinschaft and the Fonds der Chemischen Industrie. T. S. B. B. thanks North-Eastern Hill University, Shillong (India), for the grant of study leave.

[1] B. Wang, X. Zheng, G. E. Herberich, *Eur. J. Inorg. Chem.*, in press.
[2] [2a] G. C. Fu, *Adv. Organomet. Chem.* **2001**, *47*, 101−119. [2b] A. J. Ashe III, S. Al-Ahmad, X. Fang, *J. Organomet. Chem.* **1999**, *581*, 92−97. [2c] G. E. Herberich, "Boratabenzene Chemistry Revisited", in *Advances in Boron Chemistry* (Ed.: W. Siebert), The Royal Society of Chemistry, Cambridge, U. K., **1997**, special publication no. 201, p. 211−223. [2d] G. E. Herberich, in *Comprehensive Organometallic Chemistry II* (Eds.: E. W. Abel, F. G. A. Stone, G. Wilkinson), Pergamon Press, Oxford, **1995**, vol. 1 (Ed.: C. E. Housecroft), p. 197−216. [2e] G. E. Herberich, H. Ohst, *Adv. Organomet. Chem.* **1986**, *25*, 199−216.
[3] X. Zheng, U. Englert, G. E. Herberich, J. Rosenplänter, *Inorg. Chem.* **2000**, *39*, 5579−5585.
[4] [4a] G. E. Herberich, U. Englert, A. Fischer, J. Ni, A. Schmitz, *Organometallics* **1999**, *18*, 5496−5501. [4b] M. A. Putzer, J. S. Rogers, G. C. Bazan, *J. Am. Chem. Soc.* **1999**, *121*, 8112−8113.
[5] For leading references see: [5a] A. J. Ashe III, S. Al-Ahmad, X. Fang, J. W. Kampf, *Organometallics* **2001**, *20*, 468−473. [5b] G. C. Bazan, W. D. Cotter, Z. J. A. Komon, R. A. Lee, R. J. Lachicotte, *J. Am. Chem. Soc.* **2000**, *122*, 1371−1380. [5c] J. S. Rogers, R. J. Lachicotte, G. C. Bazan, *J. Am. Chem. Soc.* **1999**, *121*, 1288−1298. [5d] G. E. Herberich, U. Englert, A. Schmitz, *Organometallics* **1997**, *16*, 3751−3757. [5e] G. C. Bazan, G. Rodriguez, A. J. Ashe III, S. Al-Ahmad, C. Müller, *J. Am. Chem. Soc.* **1996**, *118*, 2291−2292.
[6] [6a] X. Zheng, G. E. Herberich, *Eur. J. Inorg. Chem.*, submitted. [6b] G. E. Herberich, X. Zheng, J. Rosenplänter, U. Englert, *Organometallics* **1999**, *18*, 4747−4752. [6c] G. E. Herberich, J. Rosenplänter, B. Schmidt, U. Englert, *Organometallics* **1997**, *16*, 926−931. [6d] U. Englert, G. E. Herberich, J. Rosenplänter, *Z. Anorg. Allg. Chem.* **1997**, *623*, 1098−1102. [6e] G. E. Herberich, H. J. Becker, C. Engelke, *J. Organomet. Chem.* **1978**, *153*, 265−270.
[7] [7a] X. Zheng, G. E. Herberich, *Organometallics* **2000**, *19*, 3751−3757. [7b] G. E. Herberich, U. Englert, B. Ganter, M. Pons, R. Wang, *Organometallics* **1999**, *18*, 3406−3413. [7c] J. Tweddell, D. A. Hoic, W. M. Davis, G. C. Fu, *J. Org. Chem.* **1997**, *62*, 8286−8287. [7d] S. Qiao, D. A. Hoic, G. C. Fu, *Organometallics* **1997**, *16*, 1501−1502. [7e] D. A. Hoic, J. R. Wolf, W. M. Davis, G. C. Fu, *Organometallics* **1996**, *15*, 1315−1318. [7f] G. Maier, H. P. Reisenauer, J. Henkelmann, C. Kliche, *Angew. Chem.* **1988**, *100*, 303; *Angew. Chem. Int. Ed. Engl.* **1988**, *27*, 295−296. [7g] R. Boese, N. Finke, J. Henkelmann, G. Maier, P. Paetzold, H. P. Reisenauer, G. Schmid, *Chem. Ber.* **1985**, *118*, 1644−1654.
[8] [8a] M. C. Amendola, K. E. Stockman, D. A. Hoic, W. M. Davis, G. C. Fu, *Angew. Chem.* **1997**, *109*, 278−281; *Angew. Chem. Int. Ed. Engl.* **1997**, *36*, 267−269. [8b] S. Qiao, D. A. Hoic, G. C. Fu, *J. Am. Chem. Soc.* **1996**, *118*, 6329−6330. [8c] R. Boese, N. Finke, T. Keil, P. Paetzold, G. Schmid, *Z. Naturforsch., Teil B* **1985**, *40*, 1327−1332.
[9] G. E. Herberich, H. J. Becker, B. Hessner, L. Zelenka, *J. Organomet. Chem.* **1985**, *280*, 147−151.
[10] G. E. Herberich, A. K. Naithani, *J. Organomet. Chem.* **1983**, *241*, 1−14.
[11] [11a] M. V. Butovskii, U. Englert, A. A. Fil'chikov, G. E. Herberich, A. R. Kudinov, *Eur. J. Inorg. Chem.*, in preparation. [11b] A. R. Kudinov, V. I. Meshcheryakov, P. V. Petrovskii, M. I. Rybinskaya, *Izv. Akad. Nauk, Ser. Khim.* **1999**, 177−179; *Russ. Chem. Bull.* **1999**, *48*, 176−178.
[12] G. E. Herberich, U. Englert, M. U. Schmidt, R. Standt, *Organometallics* **1996**, *15*, 2707−2712.
[13] G. E. Herberich, G. Greiss, H. F. Heil, J. Müller, *J. Chem. Soc., Chem. Commun.* **1971**, 1328−1329.
[14] A. J. Ashe III, W. Butler, H. F. Sandford, *J. Am. Chem. Soc.* **1979**, *101*, 7066−7067.
[15] W. Siebert, R. Full, J. Edwin, K. Kinberger, *J. Organomet. Chem.* **1977**, *131*, 1−22.
[16] G. E. Herberich, B. Hessner, *Chem. Ber.* **1982**, *115*, 3115−3127.
[17] G. E. Herberich, U. Englert, M. Hostalek, R. Laven, *Chem. Ber.* **1991**, *124*, 17−24.
[18] J. R. Bleeke, R. Behm, Y.-F. Xie, M. Y. Chiang, K. D. Robinson, A. M. Beatty, *Organometallics* **1997**, *16*, 606−623.
[19] S. Sharma, A. C. Oehlschlager, *J. Org. Chem.* **1989**, *54*, 5064−5073.
[20] L. Weber, E. Dobbert, H.-G. Stemmler, B. Neumann, R. Boese, D. Bläser, *Eur. J. Inorg. Chem.* **1999**, 491−497.
[21] W. Biffar, H. Nöth, H. Pommerening, R. Schwerthöffer, W. Storch, B. Wrackmeyer, *Chem. Ber.* **1981**, *114*, 49−60.
[22] For reference data see: [22a] H. Nöth, B. Wrackmeyer, in *NMR Basic Principles and Progress*, vol. 14 (Eds.: P. Diehl, E. Fluck, R. Kosfeld), Springer Verlag, Berlin, **1978**. [22b] B. Wrackmeyer, *Annu. Rep. NMR Spectrosc.* **1988**, *20*, 61−203. [22c] A. R. Siedle, *Annu. Rep. NMR Spectrosc.* **1988**, *20*, 205−314.
[23] A. L. Spek, *Acta Crystallogr. Sect.* **1990**, *A46*, C34.
[24] G. E. Herberich, U. Englert, M. König, unpublished work.
[25] P. Frankhauser, H. Pritzkow, W. Siebert, *Z. Naturforsch., Teil B* **1994**, *49*, 250−254.
[26] A. F. Wells, *Structural Inorganic Chemistry*, 4th ed., Clarendon Press, Oxford, **1974**, p. 861−862.
[27] P. Coppens, L. Leiserowitz, D. Rabinovich, *Acta Crystallogr.* **1965**, *18*, 1035−1038.
[28] A. C. T. North, D. C. Phillips, F. S. Mathews, *Acta Crystallogr., Sect. A* **1968**, *24*, 351−359.
[29] G. M. Sheldrick, *SHELXS-97*, *Program for Structure Solution*, University of Göttingen, Göttingen, Germany, **1997**.
[30] G. M. Sheldrick, *SHELXL-97*, *Program for Structure Refinement*, University of Göttingen, Göttingen, Germany, **1997**.

Received July 19, 2001
[I01269]

DNA as a Catalyst and Catalytic Template for the Racemisation of Metal Tris-Phenanthroline Complexes

Alison Rodger,*[a] Bengt Nordén,[b] P. Mark Rodger,[a] and Paula J. Bates[c]

Keywords: Circular dichroism / Bioinorganic chemistry / Coordination chemistry / Racemisation

[Fe(1,10-phenanthroline)$_3$]$^{2+}$ is known to racemise in solution and DNA is known to shift the equilibrium point of the Δ/Λ-[Fe(1,10-phenanthroline)$_3$]$^{2+}$ mixture from 50:50 to a position favouring a slight excess of the Δ enantiomer. In this paper it is shown that DNA catalyses the racemisation reaction, presumably by providing vibrational energy to species that bind in a less favoured mode for that enantiomer. The racemisation of [Co(1,10-phenanthroline)$_3$]$^{3+}$, however, is not enhanced by DNA unless [Co(1,10-phenanthroline)$_3$]$^{2+}$ is also added to the solution. In this case, the DNA acts as a template to facilitate the $Co^{II} \rightleftarrows Co^{III}$ electron transfer. Racemisation occurs while the [Co(1,10-phenanthroline)$_3$]$^{n+}$ is in the labile Co^{II} form.

Introduction

The presence of DNA has long been known to shift the position of the Δ/Λ equilibrium of [Fe(1,10-phenanthroline)$_3$]$^{2+}$ in favour of the Δ enantiomer on a timescale of minutes to hours.[1,2] There is also a suggestion in the literature that [Co(1,10-phenanthroline)$_3$]$^{3+}$ rapidly racemises over a period of minutes,[3] despite the well accepted stability of Co^{III} d^6 amine systems, and there is some suggestion that DNA affects this rate. We therefore chose to investigate both these racemisation reactions in the presence and absence of DNA in order to determine what if any role DNA plays in the kinetics.

Results and Discussion

[Fe(1,10-phenanthroline)$_3$]$^{2+}$: DNA Catalyses a Reaction

The results of the kinetic experiments with a range of DNA:Δ and DNA:Λ ratios for [Fe(1,10-phenanthroline)$_3$]$^{2+}$ are given in Table 1. All CD traces (not shown) fitted to a single exponential decay; the rate of change in the CD signal that is given in the final column is the constant in the exponent. For the simple case of free solution racemisation, the rate constant for the, for example, Δ→ Λ reaction is half the exponent constant, as shown below. The error range quoted shows the scatter between repeat runs. The rate of racemisation in the DNA-free systems at 20 °C and 25 °C, assuming a simple Arrhenius behaviour, gives an activation energy of about 40 kJ mol^{-1}. Mudasir et al. recently reported a rate constant for the racemisation of the Λ enantiomer at room temperature (stated to be approximately 25 °C) to be (0.72 ± 0.05)×10^{-3} s^{-1}.[4] Their value was estimated from two runs where points were measured at intervals (rather than the

Table 1. Rate of change of CD signals for both enantiomers of [Fe(1,10-phenanthroline)$_3$]$^{2+}$ in aqueous solution with and without calf thymus DNA; the columns give the following data: (1) DNA concentration (in base), (2) Δ- or (3) Λ-[Fe(1,10-phenanthroline)$_3$]$^{2+}$ concentrations, (4) DNA:ligand ratio, (5) final CD reading in millidegrees, and (6) the single exponential decay constant for the CD signal as a function of time; all data were collected at 20 °C except for the final row; the value in brackets indicates the variation between identical runs

[DNA]/μM	[Δ]/μM	[Λ]/μM	Ratio	Final CD/mdeg	k×1000/s^{-1}
0	121		0:∞	0	0.43 (±0.005)
301	121		2.5:1	6	0.53 (±0.01)
608	121		5:1	11	0.78 (±0.01)
1210	121		10:1	22	0.95 (±0.01)
2540	121		21:1	31	1.44 (±0.005)
0		112	0:∞	0	0.43 (±0.005)
280		112	2.5:1	4	0.63 (±0.01)
560		112	5:1	10	0.76 (±0.01)
1120		112	10:1	21	0.83 (±0.005)
2352		112	21:1	29	1.05 (±0.01)
0 (25 °C)		112		0	0.56 (±0.01)

[a] Department of Chemistry, University of Warwick Coventry CV4 7AL, UK
Fax: (internat.) + 44-24/7652-4112
E-mail: a.rodger@warwick.ac.uk
[b] Department of Physical Chemistry, Chalmers University of Technology
Gothenburg, Sweden, 41296, Sweden
Fax: (internat.) + 46-31/772-3858
[c] James Graham Brown Cancer Center, Department of Medicine, University of Louisville, 204B Baxter Building,
570 S. Preston Street, Louisville, KY 40202, USA
Fax: (internat.) + 1-502/852-2356

 © WILEY-VCH Verlag GmbH, 69451 Weinheim, Germany, 2002 1434−1948/02/0101−0049 $ 17.50+.50/0

trace monitored continuously as in our experiments). Assuming their data has been correctly analyzed, in order to be consistent with our data, the room temperature in their experiments must have been above 25 °C (≈28 °C) or their error has been underestimated.

The first observations to be made from our data are that the end point of the kinetics is the same for given concentrations of metal complex and DNA independent of which enantiomer is added initially; however, the value of the end point CD signal varies as a function of the DNA concentration. This variation is due to the DNA shifting the position of the Δ/Λ equilibrium (the end point is when the equilibrium is established) as previously observed by Härd and Nordén[1,2] and also the perturbation of the CD of the cations on binding to DNA. The final observed CD signal at 545 nm is always positive. As the unbound metal complex will be a 50:50 mixture of the two enantiomers at the conclusion of the kinetics, and so have no net CD, this means that the bound metal complexes must always have a net positive CD. Two factors might contribute to this: a Pfeiffer-effect shift in the equilibrium between the two enantiomers to give an excess of one enantiomer[1,2] and/or a positive CD signal being induced into the transition metal complex transitions due to their interaction with the DNA.[5]

To try to understand this behaviour at a molecular level it is helpful to consider the binding modes that have been established[5−7] for $[Ru(1,10\text{-phenanthroline})_3]^{2+}$ (which does not racemise in solution) since previous experience suggests that any information on binding modes determined for ruthenium complexes can be transferred to the iron(II) complex with the same ligands since the charge and steric effects are almost identical. At low ligand loadings, the Δ enantiomer is predominantly a minor groove binder with either one or two chelates pointing into the groove, whereas the Λ enantiomer is 90% in a major groove mode with a chelate partially inserted between two base pairs and with a lower equilibrium binding constant than the Δ enantiomer. When its preferred DNA binding modes have been fully occupied, each enantiomer then occupies less favoured modes and the Λ enantiomer on average binds more strongly.[5,7] Whether the site preference is perturbed by the presence of the other enantiomer is not clear, although the racemate-induced CD spectra[5] suggest the binding modes are not changed when the other enantiomer is present. However, the two enantiomers must reduce each other's binding constants since the racemate binds more weakly to DNA than either enantiomer.[5] For $[Ru(1,10\text{-phenanthroline})_3]^{2+}$ above ≈5:1 DNA:Δ or DNA:Λ ratios the most favoured sites are occupied. Thus in our experiments with $[Fe(1,10\text{-phenanthroline})_3]^{2+}$, except at the beginning of the 2.5:1 runs, it is reasonable to conclude that each enantiomer occupies its preferred site at all times. This means that we therefore have conditions where the Δ enantiomer binds more strongly than the Λ enantiomer, so the positive final CD could simply be due to the Pfeiffer effect causing an excess of Δ.

The other observation to be taken from Table 1 is that the racemisation rates of both enantiomers speed up when DNA is present, although to differing extents. At high DNA concentrations, where the Δ enantiomer has a stronger DNA binding constant,[5] the rate of racemisation of this enantiomer is the faster, whereas at lower DNA concentrations, where the Λ enantiomer binds more strongly to DNA this enantiomer's rate is more enhanced.

The rate enhancements observed in the presence of DNA might be due to the shift of the equilibrium position of the reaction or might be due to the DNA facilitating the reaction and providing a slightly lower energy pathway for racemisation. In order to determine which of these is occurring, let us assume that the latter is not the case, in other words, the DNA-bound molecules do not rearrange (or do so at the free solution rate), and deduce the consequences. We are therefore assuming that the presence of the DNA affects only the concentration of free molecules in solution that can rearrange and plays no direct role in the racemisation reaction, acting only to change the end point of the reaction due to the differing percentages of the two bound enantiomers.

Racemisation reactions probed using CD spectroscopy measure the rate of change of the CD signal (rather than the actual disappearance of one reactant or appearance of one product). To determine the rate of change of the metal complex concentration in the presence of DNA we need to determine the concentrations of each species present as a function of time and multiply by the appropriate Δε values and path lengths (Beer−Lambert analogue). In addition to assuming that the DNA-bound metal complexes cannot racemise, let us also assume that the bound and free forms are in fast equilibrium relative to the rate of racemisation (a reasonable assumption even if the on-rate is diffusion controlled, as the off-rate will be at worst in the microsecond domain given the binding constants of refs.[5,7]). This is schematically illustrated as in Equation (1)

$$\begin{array}{ccc} x + S_f & \xleftrightarrow{K_x} & X \\ k_1 \downarrow\uparrow k_1 & & \\ y + S_f & \xleftrightarrow{K_y} & Y \end{array} \quad (1)$$

where S_f is the concentration of free sites on DNA, x is the free concentration of the enantiomer that begins in excess, X is its bound concentration, k_1 is the rate constant for the conversion of one enantiomer to the other in free solution, K_x is the equilibrium binding association constant for species x with DNA, and the y symbols relate to the other enantiomer.

Because the DNA binding is in fast equilibrium, the rate of change of x and y may be written as in Equation (2):

$$\begin{aligned} \frac{dx}{dt} &= k_1(-x + y) \\ \frac{dy}{dt} &= k_1(x - y) \end{aligned} \quad (2)$$

or in matrix notation as Equation (3):

$$\frac{d\mathbf{c}}{dt} = \Lambda\,\mathbf{c}$$
$$\text{where } \mathbf{c} = \begin{pmatrix} x \\ y \end{pmatrix} \text{ and } \Lambda = k_1 \begin{pmatrix} -1 & 1 \\ 1 & -1 \end{pmatrix} \quad (3)$$

Solving Equation (3) gives Equation (4):

$$x(t) = \frac{x_o}{2}(1 + e^{-2k_1 t})$$
$$y(t) = \frac{x_o}{2}(1 - e^{-2k_1 t}) \quad (4)$$

where x_o is the starting concentration of x.

The CD signal as a function of time may be written according to Equation (5):

$$CD(t) = \Delta\varepsilon_x(x(t) - y(t)) + \Delta\varepsilon_X X(t) + \Delta\varepsilon_Y Y(t) K_y \quad (5)$$

where $\Delta\varepsilon_x$ is the CD extinction coefficient for the unbound enantiomer that is in excess at the beginning of the reaction, $\Delta\varepsilon_X$ is the CD extinction coefficient for X when it is bound to DNA etc. Since

$$K_x = \frac{X(t)}{x(t) S_f(t)} \quad (6)$$

from Equations (4) and (5) we may deduce Equation (7):

$$CD(t) = \Delta\varepsilon_x(x_o e^{-2k_1 t}) + \Delta\varepsilon_X K_x\left(\frac{x_o}{2} + \frac{x_o}{2} e^{-2k_1 t}\right) S_f(t) \ldots$$
$$\ldots + \Delta\varepsilon_Y K_y\left(\frac{x_o}{2} - \frac{x_o}{2} e^{-2k_1 t}\right) S_f(t) \quad (7)$$

which is the CD signal as a function of time *if the enantiomers may only racemise in free solution*.

The two sources of time dependence in Equation (7) are the single exponential decay terms with constant $-2k_1$ and $S_f(t)$. The latter can be deemed approximately time independent since the binding constants of the two enantiomers are similar. (At high DNA:metal complex ratios, by analogy with [Ru(1,10-phenanthroline)$_3$]$^{2+}$, 99% of the metal complex will be bound and 1% free for both enantiomers so the amount of free DNA is large and does not vary much during the reaction. At low DNA:metal complex ratios very little of the DNA is unoccupied throughout the reaction. So in both cases, $S_f(t)$ is approximately constant in any one run.) Thus, if racemisation occurs only for free metal complexes [as required for Equation (7)], then the rate of decay of the CD signal is $-2k_1$ for all DNA concentrations. Table 1 summarizes how the rate of decay of the CD signal *changes* with DNA concentration; we therefore must conclude that both enantiomers also rearrange when bound to the DNA and Equation (7) is not valid. In other words *the DNA acts as a catalyst for this reaction, slightly lowering the activation energy relative to the free solution value.*

One can speculate as to how the DNA achieves its catalytic effect. The most likely possibility is that the metal complexes will be moving on and off the DNA and if one enantiomer hits the DNA in one of its less favoured binding positions (e.g. the wrong groove) then during its time on the DNA it is encouraged to bind more strongly by changing its handedness. The natural breathing motions of the DNA would help provide the energy required to break the metal−ligand bond (as required for metal tris-chelate racemisation reactions, with a few exceptions such as dithiocarbamate complexes[8,9]) and the DNA will encourage the formation and net accumulation of the desired product for that DNA binding mode.

[Co(1,10-phenanthroline)$_3$]$^{3+}$: DNA as a Catalytic Template

Following literature claims of racemisation of [Co(1,10-phenanthroline)$_3$]$^{3+}$ [3] in the presence of DNA on a timescale too fast for NMR experiments, we attempted to characterize the kinetics of this process. However, we found no evidence of racemisation for the Co^{III} complex prepared as described in the Exp. Sect. either with or without DNA in the solution. We concluded that the previously observed effect must have been due to trace amounts of the labile Co^{II} complex remaining in solution — our oxidation conditions involved chlorine gas. Electron transfer occurs readily between the Co^{II} and Co^{III} tris-phenanthroline complexes and the Co^{II} form is labile and racemises readily. The net effect of this is the racemisation of the Co^{III} complex. We therefore probed the kinetics of the racemisation of [Co(1,10-phenanthroline)$_3$]$^{3+}$ in the presence of [Co(1,10-phenanthroline)$_3$]$^{2+}$ and DNA.

The racemisation of the Co^{III} complex proceeds slowly in the presence of the Co^{II} complex with a half life of the order of hours (depending on reagent concentrations) rather than minutes or seconds. In a series of experiments at widely varying concentrations of the two metal complexes and DNA, we observed that the DNA causes a significant increase in the rate of racemisation of the Co^{III} complex in the presence of the Co^{II} complex. In other words the DNA enhances the catalytic activity of the Co^{II} complex taking it to half lives of a few seconds (at high enough concentrations, see Table 2). As with [Fe(1,10-phenanthroline)$_3$]$^{3+}$, the rate of change of CD as a function of time in an individual run follows a simple exponential decay; however, the dependence of the rate on the concentration of each reagent is not straightforward as illustrated by a data set for the Λ-enantiomer in Table 2. These observations can be understood when it is realised that the DNA is forming a template to facilitate the electron transfer reaction between two cobalt tris-phenanthroline complexes of different oxidation states. The DNA may also be playing a more active role in the electron transfer. Increased concentrations of the cobalt complexes make such encounters on the DNA more likely. If, for example, Co^{III} is in excess, however, it will inhibit Co^{II} binding and decrease the effect. Similarly, decreasing

Table 2. Rate of change of CD signals for Λ-[Co(1,10-phenanthroline)$_3$]$^{3+}$ in aqueous solution in the presence of (±)-[Co(1,10-phenanthroline)$_3$]$^{2+}$ and calf thymus DNA; the columns give the following data: (1) DNA concentration, (2) Λ-[Co(1,10-phenanthroline)$_3$]$^{2+}$ concentration, (3) (±)-[Co(1,10-phenanthroline)$_3$]$^{2+}$ concentration, (4) DNA:Co^{III} ligand ratio, (5) the single exponential decay constant for the CD signal as a function of time; all data were collected at 20 °C. The +3 charged Co^{III} complex binds much more strongly to DNA than does the Co^{II} complex, hence its smaller concentrations

[DNA]/μM	[Λ-Co^{III}]/μM	[±-Co^{II}]/μM	DNA:Co^{III}	$k\times100$/s^{-1}
790	69	500	11.4:1	18
790	69	1000	11.4:1	23
790	69	1500	11.4:1	20
790	56	250	14:1	22
790	111	250	7.1:1	21
790	166	250	4.8:1	17
790	222	250	3.6:1	11
790	277	250	2.9:1	12
160	56	450	2.9:1	14
160	111	450	1.4:1	9
160	166	450	0.96:1	7
160	222	450	0.72:1	6.5
160	277	450	0.58:1	5
160	56	250	2.9:1	10
160	111	250	1.4:1	8
160	166	250	0.96:1	6
160	222	250	0.72:1	5
160	277	250	0.58:1	3.5

the DNA concentration increases the likelihood of an encounter between the reacting species until the same saturation occurs.

In conclusion, we have shown that DNA catalyses the racemisation reaction of both Δ- and Λ-[Fe(1,10-phenanthroline)$_3$]$^{2+}$ but has no effect on the stability of Δ- and Λ-[Co(1,10-phenanthroline)$_3$]$^{3+}$. However, in the presence of (±)-[Co(1,10-phenanthroline)$_3$]$^{2+}$ DNA increases the effectiveness of the Co^{II} complex catalysis of the racemisation of both Δ- and Λ-[Co(1,10-phenanthroline)$_3$]$^{3+}$ by acting as a template to enhance the rate of electron transfer between the labile Co^{II} and stable Co^{III} species. The concentration dependence of this process is complicated and maximized for DNA concentrations that encourage Co^{II} and Co^{III} to be bound together on the DNA. Too high a concentration of DNA reduces the nearest-neighbour interaction of the cobalt complexes and too high a concentration of one complex relative to the other means that complexes of different oxidation state are less likely to meet. The Co^{II}, with its intrinsically weaker binding constant, is particularly likely to be displaced. Thus we have an example of a DNA-catalyzed reaction where the DNA does not chemically take part but does provide some energy (about 40 kJ mol^{-1}) to help the rearrangement, and another reaction where DNA is a catalytic template.

Experimental Section

The Δ- and Λ-enantiomers of [Fe(1,10-phenanthroline)$_3$]$^{2+}$ were produced from cold (just above 0 °C) 0.025 M ferroin solution (Aldrich) by adding potassium antimonyl tartrate (also at 0 °C) in a 2:1 molar ratio. $NaClO_4$ (Aldrich) was added to the filtrate and the resulting crystals were collected. The L-enantiomer of antimonyl tartrate (Aldrich) was used to produce the Λ-enantiomer of [Fe(1,10-phenanthroline)$_3$]$^{2+}$. The D-enantiomer of antimonyl tartrate, used to produce the Δ-enantiomer of [Fe(1,10-phenanthroline)$_3$]$^{2+}$, was made by mixing D-tartaric acid and KOH and then adding Sb_2O_3, all in equimolar ratios. The solution was either boiled until all the Sb_2O_3 appeared to have dissolved or, for better yield, heated under reflux for 2 days. The solution was filtered and the filtrate left to evaporate to dryness producing D-potassium antimonyl tartrate. [Fe(1,10-phenanthroline)$_3$]$^{2+}$ enantiomeric purity was determined using the literature values of $\varepsilon_{510\ nm}$ = 11200 mol^{-1} dm^3 cm^{-1} and $\Delta\varepsilon_{545\ nm}$ = 20.0 mol^{-1} dm^3 cm^{-1} for the Δ enantiomer.[10] The Δ enantiomer proved to be 90% enantiomerically pure and the Λ enantiomer 103% (suggesting the literature value for Δε is an underestimate).

The racemisation kinetics of [Fe(1,10-phenanthroline)$_3$]$^{2+}$ were monitored at 20 °C at 545 nm in the presence and absence of calf thymus DNA (Sigma, highly lyophilised sodium salt) using a Jasco J-720 spectropolarimeter. Concentrations in DNA base were determined using $\varepsilon_{258\ nm}$ = 6600 mol^{-1} dm^3 cm^{-1}.[11] All runs could be fitted with a simple single exponential decay (using Kaleidagraph) and the results are reported in Table 1 in terms of the decay constants of the CD signal. All runs were repeated at least once. To ensure that the solutions did not racemise during preparation the [Fe(1,10-phenanthroline)$_3$]$^{2+}$ was kept cold until mixed with the DNA solutions. In fact, the apparent first-order nature of the kinetics [even under stopped flow conditions where data collection started after tens of ms (data not shown)] meant this precaution proved to be unnecessary.

Λ-[Co(1,10-phenanthroline)$_3$]$^{2+}$ was synthesized according to ref.[12] analogously to the [Fe(1,10-phenanthroline)$_3$]$^{2+}$ case. To produce the Co^{III} complexes, the least soluble antimonyl tartrate salt was isolated and then oxidized with chlorine gas to give yellow crystals of resolved [Co(1,10-phenanthroline)$_3$]$^{3+}$. As discussed above it proved crucial to fully oxidize the Co^{II} at this stage. The Δ-enantiomer was prepared analogously to the Λ-enantiomer using the potassium antimonyl D-tartrate as for the Fe complexes. This method gave a >90% yield and higher enantiomeric purity than the Lee method (17% yield).[12] Alternative literature methods for producing enantiomerically pure Co^{III} tris-chelates are more complicated and require expensive reagents.[13] [Co(1,10-phenanthroline)$_3$]$^{3+}$ enantiomeric purity was determined using the literature values of $\varepsilon_{273\ nm}$ = 68000 mol^{-1} dm^3 cm^{-1} and $\Delta\varepsilon_{281\ nm}$ = 222.0 mol^{-1} dm^3 cm^{-1} for the Δ enantiomer.[14] The Δ-enantiomer was 90% enantiomerically pure and the Λ-enantiomer 94%.

The racemisation kinetics of [Co(1,10-phenanthroline)$_3$]$^{3+}$ was monitored using a Jasco J-720 at 379 nm in a 1 cm cuvette or at 307 nm in a 0.8 mm cuvette with a Biologique SFM-3 stopped-flow system attached between the sample compartment and the photomultiplier tube. In the stopped flow system: the light beam was focused with a single lens;[15] data were collected with a band width of 2 nm, response time of 1 s; and the samples were loaded as follows: syringe 1: Co^{III} sample; syringe 2: premixed Co^{II} sample and DNA; syringe 3: water.

[1] T. Härd, B. Nordén, *Biopolymers* **1986**, *25*, 1209−1228.
[2] T. Härd, C. Hiort, B. Nordén, *J. Biomol. Struct. Dyn.* **1987**, *5*, 89−96.
[3] J. P. Rehmann, J. K. Barton, *Biochem.* **1990**, *29*, 1701−1709.
[4] Mudasir, N. Yoshioka, H. Inoue, *J. Inorg. Biochem.* **1999**, *77*, 239−247.
[5] C. Hiort, B. Nordén, A. Rodger, *J. Am. Chem. Soc.* **1990**, *112*, 1971−1982.
[6] I. S. Haworth, A. H. Elcock, J. Freeman, A. Rodger, W. G. Richards, *J. Biomol. Struct. Dyn.* **1991**, *9*, 23−44.
[7] D. Z. Coggan, I. S. Haworth, P. J. Bates, A. Robinson, A. Rodger, *Inorg. Chem.* **1999**, *38*, 4486−4497.
[8] A. F. Williams, *A Theoretical Approach to Inorganic Chemistry*, Springer-Verlag, Heidelberg, FRG, New York, **1979**.
[9] B. F. G. Johnson, A. Rodger, *Inorg. Chem.* **1989**, *28*, 1003−1006.
[10] S. F. Mason, B. J. Peart, *J. Chem. Soc., Dalton Trans.* **1973**, 949−955.
[11] H. R. Mahler, B. Kline, B. D. Mehrota, *J. Mol. Biol.* **1964**, *9*, 801−810.
[12] C. S. Lee, *Inorg. Chem.* **1966**, *5*, 1397−1399.
[13] L. S. Dollimore, R. D. Gillard, *J. Chem. Soc., Dalton Trans.* **1973**, 933−940.
[14] J. Ferguson, C. J. Hawkins, A. P. Kane-Maguire, H. Lip, *Inorg. Chem.* **1969**, *8*, 771−779.
[15] A. Rodger, M. Carey, "Stopped-flow circular dichroism" in *Spectrometry and spectrofluorimetry: A practical approach* (Ed.: M. Gore), **2000**.

Received May 7, 2001
[I01156]

The First Assembly of a Nest-Shaped Heterothiometallic Cluster and a Polyoxometalate Anion − Synthesis, Characterization, and Strong Third-Order Nonlinear Optical Response

Chi Zhang,*[a,b,c] Yinglin Song,[a] Fritz E. Kühn,*[b] Yan Xu,[d] Xinquan Xin,[d] Hoongkun Fun,[a,b,c] and Wolfgang A. Herrmann*[b]

Keywords: Polyoxometalates / Transition metals / Cluster compounds / Nonlinear optics

Two heterothiometallic cluster compounds $[MOS_3Cu_3(4\text{-pic})_6]\cdot 0.5[M_2O_7]$ (M = Mo **1**, W **2**) having a cationic cluster skeleton and a polyoxometalate cluster anion, as well as two other clusters $[MOS_3Cu_3(4\text{-pic})_6]\cdot[BF_4]$ (M = Mo **3**, W **4**) have been synthesized for nonlinear optics studies. Single-crystal X-ray diffraction data show that cluster **1** adopts a very interesting arrangement with a cationic nest-shaped cluster skeleton and a polyoxomolybdenum cluster anion. This is the first time that such a skeleton has been found for an Mo/S/Cu heterothiometallic cluster compound and it represents a distinct structural type as compared to the analogous nest-shaped clusters seen with a neutral or an anionic skeleton. The nonlinear optical properties of these four clusters have been investigated with an 8 ns pulsed laser at 532 nm, and optical self-focusing effects have been observed. Clusters **1** and **2** with the polyoxometalate cluster anion exhibit stronger third-order nonlinear optical absorption than clusters **3** and **4** having only a pseudo-halogen group as the anion, which can be attributed to skeletal differences. Clusters **1** and **2** also exhibit very large optical limiting effects toward the ns incident pulsed laser as compared with clusters **3** and **4** and other shaped clusters with the same skeleton factors studied previously. This demonstrates the influence of the cluster skeleton on the nonlinear optical performance.

Introduction

The chemistry of transition metal sulfur clusters has attracted considerable attention[1] and represents an important and active area of research concerning advanced materials, biological processes, and catalytic reactions.[2−4] This is because these clusters possess interesting electronic, biological, optical, structural, and catalytic properties and show promising potential as biological models of some nitrogenases or various other metalloenzymes,[4a,5] as active centers relevant to some industrial catalytic processes,[1a] and as precursor molecules of optically functional materials for optical limiting applications and optical signal detection techniques.[2] Currently, the tremendous interest in these clusters is mainly focused on the search for better materials with third-order nonlinear optical (NLO) properties and superior optical limiting (OL) effects, not only for applications in protecting optical sensors and human eyes from high-intensity laser hazards, but also for their utilization in optical communication, optical signal processing and transmission, optical data acquisition and storage, optical computing, and optic-electronic modulation.

The ongoing research and development in this promising field shows that, in contrast to the other most frequently mentioned NLO materials, such as phthalocyanine or fullerene C_{60} and derivatives thereof,[6,7] these clusters possess the combined advantages of both organic molecules and inorganic compounds: large modifiable structures and structures containing many heavy metal atoms. One of the most important and promising features of these heterothiometallic clusters is the possibility of modifying and eventually optimizing the building blocks through subtle modifications at the molecular level. Thus, all of the structural units, terminal ligands, skeletal elements, and constituent components can be altered just like organic molecules so that the NLO properties can be adjusted through structural manipulation. On the other hand, the incorporation of heavy metal atoms may introduce more sublevels into the energy hierarchy as compared to organic molecules with the

[a] Department of Applied Physics,
Harbin Institute of Technology,
Harbin 150001, P. R. China
[b] Anorganisch-Chemisches Institut der Technischen Universität München,
Lichtenbergstrasse 4, 85747 Garching bei München, Germany
[c] Department of Chemistry, University of Kansas,
Lawrence, Kansas 66045, USA
[d] State Key Laboratory of Coordination Chemistry,
Department of Chemistry, Nanjing University,
Nanjing 210093, P. R. China
[e] X-ray Crystallography Unit, School of Physics,
Universiti Sains Malaysia 11800, USM,
Penang, Malaysia

 © WILEY-VCH Verlag GmbH, 69451 Weinheim, Germany, 2002 1434−1948/02/0101−0055 $ 17.50+.50/0

same number of skeleton atoms. This permits more allowed electron transitions, thereby leading to larger NLO effects, especially those beneficial to NLO applications. Our studies on these clusters have demonstrated that, unlike some traditional NLO materials, their skeletons and constituent elements have a considerable influence on their NLO performances, which results in the Mo(W)/S/Cu(Ag) clusters exhibiting rather diverse combinations of NLO effects. Clusters having a cubane-like shape,[2a,8] a half-open cubane-like shape,[2b,9] and a hexagonal prism-shape[10] show strong nonlinear absorption. Strong nonlinear refraction effects are exhibited by some nest-shaped,[11] twin-nest-shaped,[12] and butterfly-shaped clusters.[13] The previously described twenty-nuclear supra-cage-shaped cluster[2d] possesses very large nonlinear susceptibility, while hexagonal prism-shaped clusters,[10] pentanuclear planar "open" clusters,[14] and cluster polymers[15] exhibit large optical limiting properties. Nevertheless, there remains a challenge to develop optically functional materials with strong third-order NLO properties and superior OL effects, and to establish the general relationships between the cluster molecular structures and their NLO performances.

In our systematic efforts to investigate the possibilities of controlling the size and composition of the cluster skeletons and their third-order NLO properties, including the OL effects, as well as the coordination chemistry of thiometalates with Lewis-base adducts through modification of their backbone, we describe herein the synthesis of a series of nest-shaped clusters **1**−**4** by ligand-redistribution reactions, and report the characterization of their structures by X-ray crystallography. To our surprise, the unexpected products, clusters **1** and **2**, adopt a very interesting arrangement with a cationic nest-shaped cluster skeleton and a polyoxometalate cluster anion. This is the first time that such a skeleton has been found for an Mo/S/Cu(Ag) heterothiometallic cluster compound. The results of *Z*-scan experiments show that these clusters possess strong NLO absorptive abilities and effective optical self-focusing behavior, which are simulated by excited-state absorption theory. Large optical limiting effects of this series of clusters are observed in the OL measurements. The third-order nonlinear optical susceptibilities $\chi^{(3)}$ and the third-order nonlinear hyperpolarizabilities γ of these clusters are also reported.

Results and Discussion

Synthetic Reactions

The cationic cluster skeleton $[MOS_3Cu_3(4\text{-pic})_6]^+$ (M = Mo, W; 4-pic = 4-picoline) present in clusters **1**−**4** was straightforwardly prepared in two steps by a ligand-redistribution reaction. In the first step, the copper complex bearing mixed ligands was pre-synthesized as an intermediate, which did not have to be isolated from the reaction system. In the present case, the starting material CuX [X = Cl^-, $(CH_3CN)_4BF_4^-$] was treated with 4-picoline, which served as both the reaction solvent and the σ-donor ligand. Since 4-pic exhibits a strong super-conjugation effect from the methyl group to the pyridine ring, it can be expected to show a high tendency to coordinate to Cu atoms. The gradual dissolution of CuX with the formation of a light-yellow solution were consistent with the formation of the intermediate product, i.e. the Lewis-base adduct $CuX(4\text{-pic})_3$.[16] Then the synthon thiometalate $[MOS_3]^{2-}$ was added to the reaction system as a bidentate ligand. The solution immediately turned from light-yellow to black-red (or orange-red) in color, which suggested that the target cluster compounds had been formed. Since the sequence of some Cu^I-philic ligands of Mo(W)/S/Cu(Ag) compounds can be regarded as $S^{2-} >$ (py, PPh_3) $> X^-$ (X = Cl, Br, I, CN), the former ligands can substitute part or all of the latter ligands, while the required coordination number of copper is not more than four. Two bonds of $CuX(4\text{-pic})_3$ were broken by the attack of the S^{2-} of the $[MOS_3]^{2-}$ moiety and in forming the final cationic cluster skeleton.

At the stage of forming the final cluster molecules, the BF_4^- anion in the reaction systems of clusters **3** and **4** can help to achieve a charge balance with the cationic cluster skeleton $[MOS_3Cu_3(4\text{-pic})_6]^+$ leading to formation and precipitation of the clusters $[MOS_3Cu_3(4\text{-pic})_6]\cdot[BF_4]$ (M = Mo **3**, W **4**) as expected (Scheme 1). To our surprise, the same does not take place in the reactions leading to the formation of clusters **1** and **2**. This is due to the fact that the expected target clusters $[MOS_3Cu_3(4\text{-pic})_6]\cdot Cl$ were not formed in the same way. These target clusters were to have been prepared to explore the relationship between the constituent components of the clusters and their NLO properties through comparing the isomorphous clusters with the same cationic cluster skeleton and different anions. Previous work has shown that large cations of appropriate size may combine with the anionic cluster skeletons through either charge-transfer or other non-bonding interactions.[17] In such a reaction system, the oxophilic Ca^{2+}, La^{3+}, and Nd^{3+} cations may be coordinated by the oxygen atoms of DMSO or DMF to form the larger bivalent and trivalent complex cations $[M(DMSO)_x]^{n+}$ or $[M(DMF)_x]^{n+}$ (M = Ca, La, Nd; x = 6, 8; n = 2, 3). These complex cations can induce the cluster anions in the solution to assemble into some special structural types of heterothiometallic clusters. In the present reaction systems involving clusters **1** and **2**, we assume that the crystallizing procedure, not being performed in an oxygen- and moisture-free environment, results in the transformation of excess $[MOS_3]^{2-}$ into $[M_2O_7]^{2-}$ (M = Mo, W) due to exposure to oxygen and atmospheric moisture. The polyoxometalate anion $[M_2O_7]^{2-}$, being larger than the Cl^- anion, is much more effective in precipitating the cationic cluster skeletons. Even

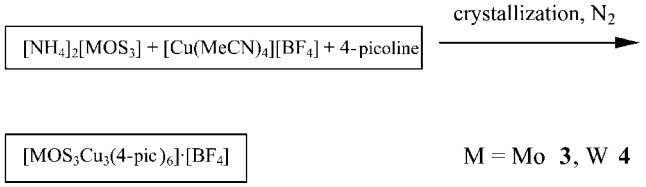

Scheme 1

if the clusters $[MOS_3Cu_3(4\text{-pic})_6]\cdot Cl$ have already formed, the small Cl^- anion can still be easily displaced by $[M_2O_7]^{2-}$. Since the polyoxometalate anion $[M_2O_7]^{2-}$ with the larger, more suitable size can stabilize an appropriately sized cation, the original cluster cations $[MOS_3Cu_3(4\text{-pic})_6]^+$ tend to combine with this large polyoxometalate anion $[M_2O_7]^{2-}$ by the assembly reaction in solution, finally crystallizing from the solution in the form of the interesting cluster skeleton with a cationic nest-shaped cluster skeleton and a polyoxometalate cluster anion (Scheme 2).

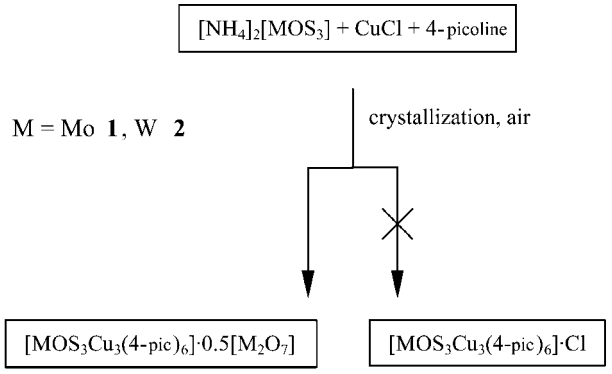

Scheme 2

Structural Description

The crystal structures of these clusters $[MOS_3Cu_3(4\text{-pic})_6]\cdot L$ (M = Mo, W; L = 0.5 M_2O_7, BF_4) reveal a nest-shaped cluster cation and a polyoxometalate cluster anion in the case of **1**, or a pseudo halogen group BF_4^- anion in the case of **4**. To the best of our knowledge, the nest-shaped clusters always adopt the configuration of a neutral skeleton, e.g. $[MOS_3Cu_3I(py)_5]$,[11b] or an anionic skeleton, e.g. $[Bu_4N]_2[MOS_3Cu_3BrCl_2]$[11a] or $[PPh_4]_2[MOS_3(CuCl)_3]$[18] (M = Mo, W). This is the first time that clusters such as **1**, with a cationic nest-shaped cluster skeleton and a polyoxometalate cluster anion, have been found for Mo/S/Cu(Ag) systems and they show a surprising difference in comparison with their nest-shaped cluster analogues. ORTEP plots of clusters **1** and **4** are shown in Figures 1 and 2. Selected

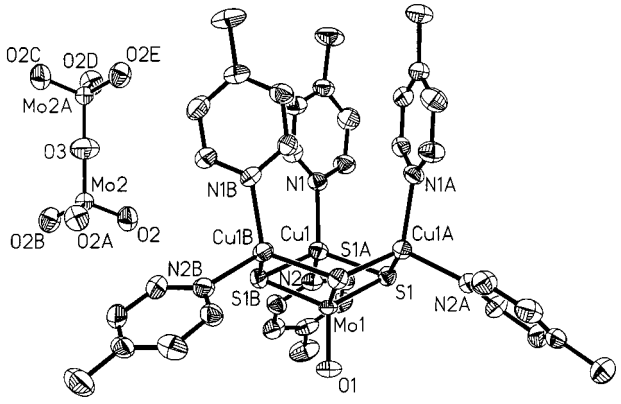

Figure 1. A perspective view of the structure of cluster $[MoOS_3Cu_3(4\text{-pic})_6]\cdot 0.5[Mo_2O_7]$ (**1**)

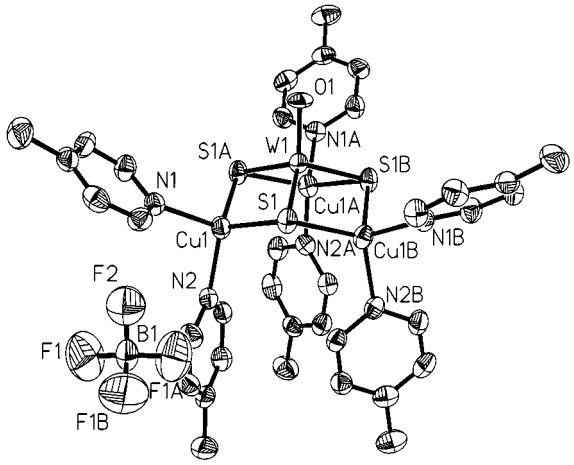

Figure 2. A perspective view of the structure of cluster $[WOS_3Cu_3(4\text{-pic})_6]\cdot[BF_4]$ (**4**)

bond lengths and angles are listed in Tables 1 and 2. Since the structures of the $[MOS_3Cu_3(4\text{-pic})_6]^+$ cation in clusters **1** and **4** are isomorphous, only the structure of cluster **1** is described in detail.

The cationic skeleton of **1**, with an $MoOS_3Cu_3$ aggregate, displays a nest-shaped structure. The central Mo atom is tetrahedrally coordinated by three S atoms and one O atom. The Mo(1)−O(1) bond length of 1.699(8) Å is characteristic of a double bond, while the three equivalent Mo−S bond lengths of 2.2692(17) Å are in the typical range for single bonds. Compared to the free $[MoOS_3]^{2-}$ ion, the $MoOS_3$ fragment adopts an ideal crystallographic C_3 symmetry at 0.3333, 0.3333, z axis through the Mo(1) atom and the O(1) atom, with three equal S−Mo−S bond angles [107.78(5)°]. In addition, weak interactions exist between the Mo atom and the three Cu atoms, while the Mo−Cu distances [2.6879(9) Å] in cluster **1** are slightly shorter than those in $[MoCu_3OS_3(PPh_3)_3\{S_2P(OBu)_2\}]$ [2.739(3) Å][19] and $[MoCu_3OS_3(PPh_3)_3(CH_3COO)]$ [2.710(1) Å].[20] The three Cu atoms exhibit the same coordination mode. Each adopts a distorted tetrahedral geometry and is coordinated by two μ_3-S atoms and two 4-pic ligands, forming three almost equivalent $CuS_2(4\text{-pic})_2$ units. These three $CuS_2(4\text{-pic})_2$ units are joined by a central Mo atom through three pairs of S−S edges, thereby forming the skeleton of the cation $[MOS_3Cu_3(4\text{-pic})_6]^+$. Since they have similar coordination environments, there is no obvious difference between Cu(1), Cu(1A), and Cu(1B). The Cu(1)−S(1) bond length [2.2777(19) Å] is almost identical to the Cu(1)−S(1)($-x + y + 1, -x + 3, z$) [2.2789(18) Å] and S(1)−Cu(1)($-y + 3, x - y + 2, z$) bond lengths [2.2789(18) Å], but the Cu(1)−N(1) distance [2.059(6) Å] is a little shorter than the Cu(1)−N(2) distance [2.107(6) Å]. On the other hand, the average Cu−S bond length [2.2785(18) Å] in cluster **1** is greater than that in its anionic analogue $[Bu_4N]_2[MoOS_3Cu_3BrCl_2]$ [2.238(3) Å] and is akin to that in its neutral analogue $[MoOS_3Cu_3I(py)_5]$ [2.288(5) Å]. This may be attributed to the fact that in cluster **1** and $[MoOS_3Cu_3I(py)_5]$ there is a strong super-conjugation effect in the pyridine

Table 1. Selected bond lengths [Å] and angles [°] for the cluster $[MoOS_3Cu_3(4\text{-pic})_6]\cdot 0.5[Mo_2O_7]$ (1). − Symmetry transformations used to generate equivalent atoms: #1: $-x + y + 1, -x + 3, z$; #2: $-y + 3, x - y + 2, z$; #3: $-y + 1, x - y + 2, z$; #4: $-x + y - 1, -x + 1, z$; #5: $-x, -y + 2, -z$

Mo(1)−O(1)	1.699(8)	Mo(2)−O(2)	1.705(7)
Mo(1)−S(1)	2.2692(17)	Mo(2)−O(2)#3	1.705(7)
Mo(1)−S(1)#1	2.2692(17)	Mo(2)−O(2)#4	1.705(7)
Mo(1)−S(1)#2	2.2692(17)	Mo(2)−O(3)	1.8557(13)
Mo(1)−Cu(1)	2.6879(9)	O(3)−Mo(2)#5	1.8557(13)
Mo(1)−Cu(1)#1	2.6879(9)	Cu(1)−S(1)	2.2777(19)
Mo(1)−Cu(1)#2	2.6879(9)	Cu(1)−S(1)#1	2.2789(18)
Cu(1)−N(1)	2.059(6)	S(1)−Cu(1)#2	2.2789(18)
Cu(1)−N(2)	2.107(6)		
O(1)−Mo(1)−S(1)	111.12(5)	O(2)#3−Mo(2)−O(3)	110.8(3)
O(1)−Mo(1)−S(1)#1	111.12(5)	O(2)−Mo(2)−O(3)	110.8(3)
O(1)−Mo(1)−S(1)#2	111.12(5)	O(2)#4−Mo(2)−O(3)	110.8(3)
S(1)#1−Mo(1)−S(1)	107.78(5)	Mo(2)−O(3)−Mo(2)#5	180.0
S(1)#1−Mo(1)−S(1)#2	107.78(5)	Cu(1)−S(1)−Cu(1)#2	112.93(8)
S(1)#2−Mo(1)−S(1)	107.78(5)	Mo(1)−S(1)−Cu(1)	72.48(5)
O(2)#3−Mo(2)−O(2)	108.1(3)	Mo(1)−S(1)−Cu(1)#2	72.45(5)
O(2)#3−Mo(2)−O(2)#4	108.1(3)	S(1)−Cu(1)−S(1)#1	107.15(8)
O(2)−Mo(2)−O(2)#4	108.1(3)	N(1)−Cu(1)−N(2)	105.3(2)

Table 2. Selected bond lengths [Å] and angles [°] for the cluster $[WOS_3Cu_3(4\text{-pic})_6]\cdot[BF_4]$ (**4**). − Symmetry transformations used to generate equivalent atoms: #1: $-x + y, -x + 1, z$; #2: $-y + 1, x - y + 1, z$; #3: $-x + y, -x, z$; #4: $-y, x - y, z$

W(1)−O(1)	1.772(8)	Cu(1)−S(1)	2.303(2)
W(1)−S(1)	2.2568(19)	S(1)−Cu(1)#1	2.287(2)
W(1)−S(1)#1	2.2568(19)	Cu(1)−S(1)#2	2.287(2)
W(1)−S(1)#2	2.2568(19)	Cu(1)−N(1)	2.098(7)
W(1)−Cu(1)	2.7037(10)	Cu(1)−N(2)	2.029(7)
W(1)−Cu(1)#1	2.7037(10)	F(1)−B(1)	1.308(6)
W(1)−Cu(1)#2	2.7037(11)	F(2)−B(1)	1.316(7)
O(1)−W(1)−S(1)	110.56(5)	N(2)−Cu(1)−N(1)	106.2(3)
O(1)−W(1)−S(1)#1	110.56(5)	S(1)#2−Cu(1)−S(1)	105.77(10)
O(1)−W(1)−S(1)#2	110.56(5)	N(2)−Cu(1)−S(1)	112.62(19)
S(1)−W(1)−S(1)#2	108.36(6)	N(1)−Cu(1)−S(1)#2	108.33(18)
S(1)#1−W(1)−S(1)	108.36(6)	N(1)−Cu(1)−S(1)	106.62(19)
S(1)#1−W(1)−S(1)#2	108.36(6)	N(2)−Cu(1)−S(1)#2	116.81(19)
W(1)−S(1)−Cu(1)	72.72(6)	F(1)−B(1)−F(2)	106.2(7)
W(1)−S(1)−Cu(1)#1	73.03(6)	F(1)#3−B(1)−F(1)#4	112.5(6)
Cu(1)#1−S(1)−Cu(1)	113.99(9)	F(1)#4−B(1)−F(2)	106.2(7)

ring that may result in 4-pic or py showing a high tendency to coordinate to a Cu atom, while the coordination between the Cu atom and the S atoms is weakened accordingly.

The unexpected polyoxometalate dianion $[Mo_2O_7]^{2-}$ formed in the present case originated from the adventitious introduction of air during the crystallization period. The dianion possesses a strict crystallographic C_2 symmetry, in which two MoO_4 tetrahedra share a vertex. The two equivalent MoO_3 moieties in the $[Mo_2O_7]^{2-}$ anion are oriented essentially perpendicularly to their respective Mo(2)−O(3) bonds in an almost eclipsed arrangement. All three independent Mo(2)−O(2) bond lengths are equal [1.705(7) Å] and are slightly longer than the Mo(1)−O(1) bond lengths, this being characteristic of a double bond, while the Mo(2)−O(3) bond lengths [1.8557(13) Å] are in the typical range for single bonds. All six independent O(2)−Mo(2)−O(2)($-x + y - 1, -x + 1, z$) bond angles are the same [108.1(3)°] and are clearly smaller than the O(1)−Mo(1)−S(1) and O(2)−Mo(2)−O(3) bond angles. It is interesting and noteworthy that the O(1)−Mo(1)−S(1) [111.12(5)°] and O(2)−Mo(2)−O(3) [110.8(3)°] bond angles are in the same range, which may be attributed to the Mo(2)−O(3) bond length being typical of a single bond, like the Mo(1)−S single bond. It is also noteworthy that the $[Mo_2O_7]^{2-}$ anion shows a perfectly straight Mo−O−Mo axis in the present case with the Mo(2)−O(3)−Mo(2)($-x, -y + 2, -z$) bond angle being equal to 180.0°, which is clearly different from that described previously [Mo−O−Mo angle 153.6(5)°].[21]

Spectral Characterization

The IR spectra of the $[MOS_3Cu_3(4\text{-pic})_6]\cdot L$ clusters (M = Mo, W; L = 0.5 M_2O_7, BF_4) exhibit strong characteristic bands at 436 cm^{-1} (**1**), 428 cm^{-1} (**2**), 437 cm^{-1} (**3**), and 428 cm^{-1} (**4**) attributable to the μ_3-S stretching vibration, while very strong absorptions at 908 cm^{-1} (**1**), 925 cm^{-1} (**2**), 910 cm^{-1} (**3**), and 924 cm^{-1} (**4**) can be attributed to the characteristic $\nu(M-O_t)$ vibration of the bridging MOS_3 group. In addition, due to the presence of $[M_2O_7]^{2-}$ anions, the absorption at 885 cm^{-1} (**1**) and 865 cm^{-1} (**2**) in the IR region may correspond to the stretching vibration of M−O double bonds in $[M_2O_7]^{2-}$ anions (M = Mo, W).

The similarity in the structures of these clusters leads to similar electronic spectra, as shown in Figure 3. The red shifts in the spectra of clusters **1** and **3** are expected, since these species contain one Mo atom instead of one W atom. The first absorption peaks of these four clusters located at 424 nm ($3.8\cdot10^3$ $cm^{-1}\cdot mol^{-1}\cdot dm^3$) (**1**), 392 nm ($6.1\cdot10^3$ $cm^{-1}\cdot mol^{-1}\cdot dm^3$) (**2**) and 407 nm ($3.1\cdot10^3$ $cm^{-1}\cdot mol^{-1}\cdot dm^3$) (**3**), 376 nm ($3.9\cdot10^3$ $cm^{-1}\cdot mol^{-1}\cdot dm^3$) (**4**) can be assigned to charge-transfer bands of the type $(\pi)S\rightarrow(d)M$ (M = Mo, W) arising from the MOS_3 moiety. The charge-transfer bands of **1** and **3** are blue-shifted, while those of **2** and **4** are red-shifted compared to those of the free $[MOS_3]^{2-}$ anion (459 nm for Mo and 375 nm for W,

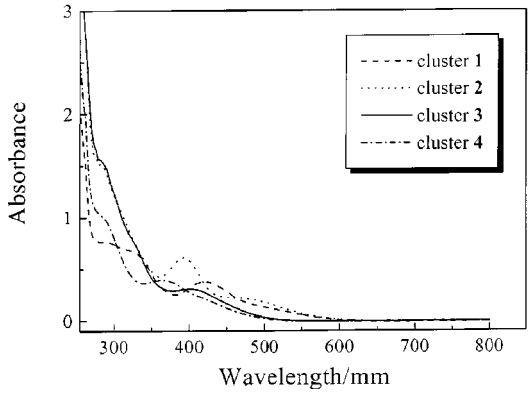

Figure 3. Electronic spectra of $1.0\cdot10^{-4}$ mol·dm^{-3} MeCN solutions of clusters **1**−**4** with an optical pathlength of 1 cm

respectively).[22] The electronic spectra of these four clusters show relatively low linear absorption in the visible and near-infrared regions, promising low intensity loss, and little temperature change caused by photon absorption when pulsed light propagates in the materials, showing that the clusters have potential as optical limiters.

Nonlinear Optical Properties

The third-order nonlinear optical (NLO) properties and the optical limiting (OL) performances of clusters **1**−**4** in MeCN solution were investigated with an 8-ns duration incident pulsed laser at 532 nm. The nonlinear absorption components of clusters **1**−**4** were evaluated by *Z*-scan experiments with an open-aperture configuration (Figure 4). The NLO absorption data obtained under the conditions used in this study can be adequately described by Equations (1) and (2),[23] which describe a third-order NLO absorptive process:

$$T(Z)=\frac{1}{\sqrt{\pi}\,q(Z)}\int_{-\infty}^{+\infty}\ln[1+q(Z)e^{-\tau^2}]\,d\tau \qquad (1)$$

$$q(Z)=\int_{0}^{+\infty}\int_{0}^{+\infty}\alpha_2\frac{I_0}{1+(Z/Z_0)^2}e^{[-2(r/\varpi_0)^2-(t/t_0)^2]}\;\frac{1-e^{-\alpha_0 L}}{\alpha_0}r\,dr\,dt \qquad (2)$$

Here, α_0 and α_2 are linear and effective third-order NLO absorptive coefficients, light transmittance T is a function of the sample's Z-position (with respect to focal point Z = 0), Z is the distance of the sample from the focal point, L is the sample thickness, I_0 is the peak irradiation intensity at focus, $Z_0 = \pi\omega_0^2/\lambda$, where ω_0 is the spot radius of the laser pulse at focus and λ is the laser wavelength, r is the radial coordinate, t is the time, and t_0 is the pulse width.

The nonlinear refractive properties of clusters **1**−**4** were assessed by dividing the normalized Z-scan data obtained under the closed-aperture configuration by the normalized Z-scan data obtained under the open-aperture configuration (Figure 5). An effective third-order nonlinear refractive index n_2 can be derived from the difference between normalized transmittance values at valley and peak positions ($\Delta T_{v\text{-}p}$) using Equation (3), where I is the incident pulsed light intensity.[24]

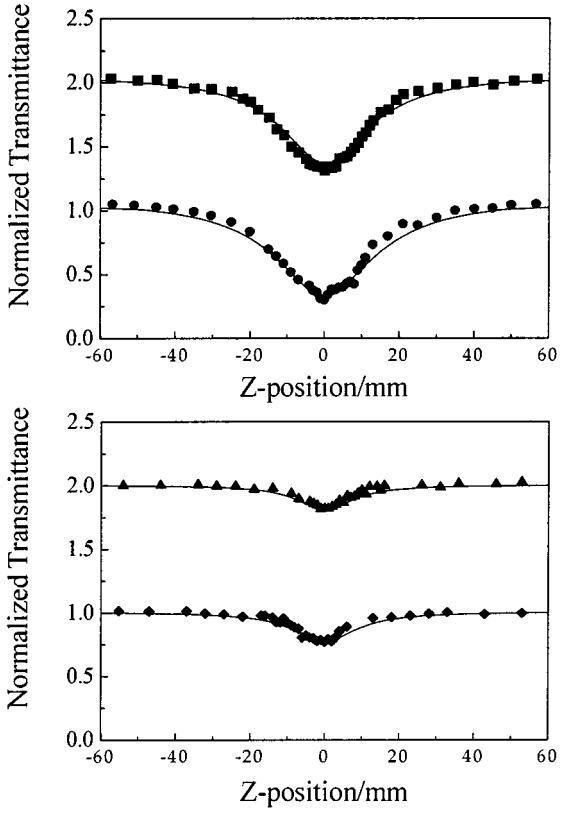

Figure 4. Open-aperture *Z*-scan data of clusters **1** (filled squares), **2** (filled circles), **3** (filled triangles), and **4** (filled diamonds) in MeCN solution at 532 nm with 8 ns wide laser pulses; the solid curves are the theoretical fits based on *Z*-scan theoretical calculations; the *Z*-scan data of both **1** and **3** have been shifted vertically by 1 unit for presentation purposes

$$n_2=\frac{\lambda\alpha_0}{0.812\,\pi I(1-e^{-\alpha_0 L})}\Delta T_{V-P} \qquad (3)$$

Based on our previous time-resolved nonlinear transmission studies[14a] and the NLO experimental results reported here, we can reasonably conclude that the physical origin of the observed reverse saturable absorption (RSA) in clusters **1**−**4** can be attributed to excited-state absorptive nonlinearities. Figures 4 and 5 show the typical NLO absorptive and refractive effects, respectively, of clusters **1**−**4**, in which the filled squares **1**, circles **2**, triangles **3**, and diamonds **4** represent the experimental data from the *Z*-scan measurements, while the solid lines represent the theoretical fitting on the basis of Equations (1)−(3) to the experimental data. A reasonably good fit between the experimental data and theoretical curves was obtained, which suggests that the experimentally obtained NLO effects are effectively third-order in nature. The effective α_2 values of $1.1\cdot10^{-9}$ m·W^{-1} (**1**), $1.2\cdot10^{-9}$ m·W^{-1} (**2**), $5.8\cdot10^{-10}$ m·W^{-1} (**3**), $6.3\cdot10^{-10}$ m·W^{-1} (**4**), and n_2 values of $1.22\cdot10^{-8}$ esu (esu = $7.162\cdot10^{13}$ m^5·v^{-2}) (**1**), $7.18\cdot10^{-9}$ esu (**2**), $6.52\cdot10^{-9}$ esu (**3**), and $5.93\cdot10^{-10}$ esu (**4**), were derived for the samples from

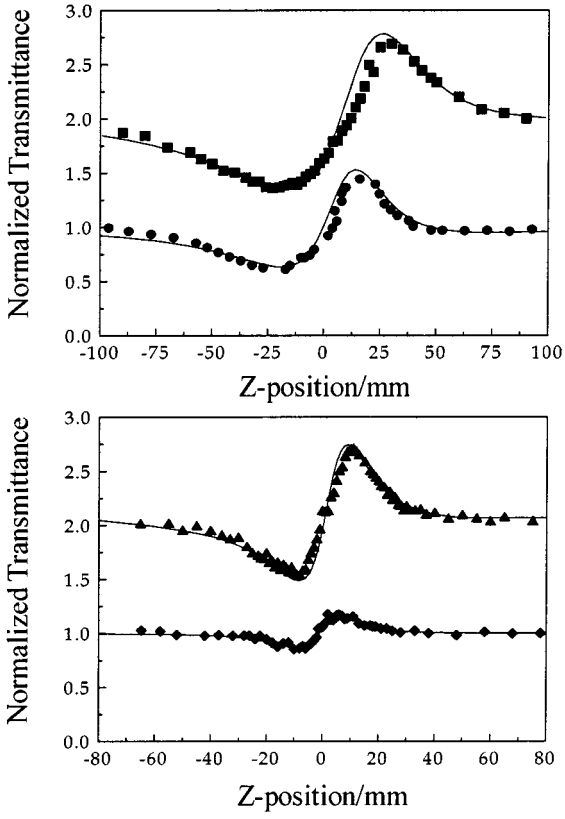

Figure 5. Closed-aperture *Z*-scan data of clusters **1** (filled squares), **2** (filled circles), **3** (filled triangles), and **4** (filled diamonds) in MeCN solution at 532 nm with 8 ns wide laser pulses; the solid curves are the theoretical fits based on *Z*-scan theoretical calculations; the *Z*-scan data of both **1** and **3** have been shifted vertically by 1 unit for presentation purposes

their respective theoretical curves. In accordance with the observed α_2 and n_2 values, the modulus of the effective third-order susceptibility $\chi^{(3)}$ can be calculated by Equation (4).[23a]

$$|\chi^{(3)}| = \sqrt{\left(\left|\frac{9\times10^{8}\varepsilon_0 n_0^2 c^2}{2\nu}\alpha_2\right|^2 + \left|\frac{cn_0^2}{80\pi}n_2\right|^2\right)} \quad (4)$$

Here, ν is frequency of the laser light, n_0 is the linear refractive index of the sample, and ε_0 and c are the permittivity and the speed of light in a vacuum, respectively. For $3.52\cdot10^{-4}$ (**1**), $2.67\cdot10^{-4}$ (**2**), $4.82\cdot10^{-4}$ (**3**), and $3.75\cdot10^{-4}$ mol·dm^{-3} (**4**) MeCN solutions, the $\chi^{(3)}$ values were calculated to be $8.7\cdot10^{-10}$ (**1**), $9.3\cdot10^{-10}$ (**2**), $2.6\cdot10^{-10}$ (**3**), and $3.1\cdot10^{-10}$ esu (**4**). The corresponding moduli of the hyperpolarizabilities γ of $1.32\cdot10^{-30}$ esu (**1**) and $1.87\cdot10^{-30}$ esu (**2**), $2.89\cdot10^{-31}$ esu (**3**) and $4.43\cdot10^{-31}$ esu (**4**), were separately obtained from $\chi^{(3)} = \gamma\cdot NF^4$, where N is the number density (concentration) of the clusters in the samples and $F^4 = 3.1$ is the local field correction factor.

From the above discussions, we can reasonably state that clusters **1**−**4** exhibit similar NLO properties. All exhibit strong RSA and effective self-focusing performances, as depicted in Figures 4 and 5. In the light of the aforementioned nonlinear absorptive and refractive experimental data, an obvious skeleton atom effect on the nonlinear optical properties was observed. For clusters **1**, **2** and **3**, **4**, a significant improvement in the NLO absorptive effects was observed on going from Mo-containing cluster **1** to W-containing cluster **2**, and from cluster **3** to cluster **4**, respectively, i.e. with increasing size of metal atom; this is indicative of a heavy atom effect. On the other hand, although the clusters **1**−**4** possess the same cationic cluster skeleton, their different anions, especially the polyoxometalate anions in clusters **1** and **2**, result in stronger nonlinear absorptive performances and larger $\chi^{(3)}$ values being observed for clusters **1** and **2** as compared to those of clusters **3** and **4**, which demonstrates the evident skeleton influence on the NLO properties of clusters **1**−**4**.

The presence of the combined effects of strong RSA and self-focusing in clusters **1**−**4** may significantly enhance the overall optical limiting (OL) performance of these four clusters. The optical limiting effects of clusters **1**−**4** are depicted in Figure 6. The linear and nonlinear transmission data (open triangles for **1**, filled squares for **2**, open circles for **3**, and filled diamonds for **4**) were measured with 532 nm laser pulses of 8-ns duration at cluster concentrations of $3.52\cdot10^{-4}$ (**1**), $2.67\cdot10^{-4}$ (**2**), $4.82\cdot10^{-4}$ (**3**), and $3.75\cdot10^{-4}$ mol·dm^{-3} (**4**) in MeCN solution. Figure 6 shows how the transmittances of the cluster sample solutions decrease as the laser fluence increases, and how the solution becomes increasingly less transparent as the incident fluence rises, characterizing the typical optical limiting effects. Experiments using neat MeCN solvent gave no detectable OL effect. This indicates that solvent contributions are negligible. The values of the limiting threshold, which is defined as the incident fluence at which the actual transmittance falls to 50% of the corresponding linear transmittance, were measured as 0.26 J·cm^{-2} (**1**), 0.20 J·cm^{-2} (**2**), 0.45 J·cm^{-2} (**3**), and 0.34 J·cm^{-2} (**4**), with the same linear transmittance of 72% in each case.

Table 3 lists the heterothiometallic clusters presented here and investigated previously, together with their limiting thresholds, along with data for some other frequently mentioned OL materials. From the perspective of the OL application, the present four clusters having a nest-shaped skeleton are clearly better than the known good optical limiting materials fullerene C_{60}[6b] and cubane-like shaped clusters,[2a,8] while their limiting thresholds are greater than those of phthalocyanine derivatives,[7b] the hexagonal prism-shaped cluster $[Mo_2Ag_4S_8(PPh_3)_4]$,[10b] and some pentanuclear planar "open" shaped clusters $[MS_4Cu_4L_2(py)_6]$,[14] which are among the best optical limiting materials reported to date. Comparison of clusters **1**, **2** and clusters **3**, **4** allows a comparison of Mo- and W-containing systems. The W-containing clusters always seem able to outperform their corresponding Mo-containing counterparts in OL performance at a given wavelength and with similar linear transmittance, just as in this report where the OL effect of **2** is superior to that of **1**, while **4** is better than **3**. This is consistent with the fact that the OL effects of Ag-containing clusters are better than those of their Cu-containing homologues, which may be due to the

Table 3. The limiting thresholds of some OL materials measured at 532 nm with ns laser pulses

Compound	Structure	Solvent	Linear transmission (%)	Limiting Threshold [J cm^{-2}]	ref.
C_{60}	–	toluene	62	1.6	[6b]
$[Bu_4N]_3[WS_4Cu_3Br_4]$	Cubane-like shaped	MeCN	70	1.1	[8a,8b]
$[Bu_4N]_3[WS_4Ag_3Br_4]$	Cubane-like shaped	MeCN	70	0.6	[8a,8b]
$[Bu_4N]_3[MoS_4Ag_3BrI_3]$	Cubane-like shaped	MeCN	70	0.5	[2a]
$[Bu_4N]_3[MoS_4Ag_3Br_4]$	Cubane-like shaped	MeCN	72	0.7	[8b]
$[Bu_4N]_3[MoS_4Ag_3BrCl_3]$	Cubane-like shaped	MeCN	70	0.6	[2a]
$[Et_4N]_4[Mo_2O_2S_6Cu_6Br_2I_4]$	Twin-nest shaped	MeCN	70	2	[12b]
$[MoOS_3Cu_3(PPh_3)_3\{S_2P(OBu)_2\}]$	Open cubane-like shaped	CH_2Cl_2	90	5	[19]
$[MoS_4Ag_3(PPh_3)_3\{S_2P(OBu)_2\}]$	Open cubane-like shaped	CH_2Cl_2	90	0.8	[19]
$[MoOS_3Cu_3(4\text{-pic})_6]\cdot 0.5[Mo_2O_7]$	Nest shaped	MeCN	72	0.26	this work
$[WOS_3Cu_3(4\text{-pic})_6]\cdot 0.5[W_2O_7]$	Nest shaped	MeCN	72	0.20	this work
$[MoOS_3Cu_3(4\text{-pic})_6]\cdot[BF_4]$	Nest shaped	MeCN	72	0.45	this work
$[WOS_3Cu_3(4\text{-pic})_6]\cdot[BF_4]$	Nest shaped	MeCN	72	0.34	this work
$[MoS_4Cu_6I_4(py)_4]_n$	Two-dimensional network polymer	DMSO	–	0.6	[15b]
$\{[Et_4N]_2[MoS_4Cu_4(CN)_4]\}_n$	Three-dimensional framework polymer	DMF	70	0.28	[15a]
$\{[Et_4N]_2[WS_4Cu_4(CN)_4]\}_n$	Three-dimensional framework polymer	DMF	70	0.15	[15a]
Phthalocyanine derivatives	–	toluene	85	0.1	[7b]
$[Mo_2Ag_4S_8(PPh_3)_4]$	Hexagonal-prism shaped	MeCN	92	0.1	[10b]
$[Et_4N]_2[MoS_4Cu_4(SCN)_4(2\text{-pic})_4]$	Planar "open" shaped	DMF	84	0.5	[14a,14b]
$[Et_4N]_2[WS_4Cu_4(SCN)_4(2\text{-pic})_4]$	Planar "open" shaped	DMF	86	0.3	[14a,14b]
$[MoS_4Cu_4Cl_2(py)_6]$	planar "open" shaped	DMF	78	0.15	[14a]
$[WS_4Cu_4Cl_2(py)_6]$	planar "open" shaped	DMF	64	0.10	[14a]
$[MoS_4Cu_4Br_2(py)_6]$	Planar "open" shaped	DMF	72	0.10	[14a]
$[WS_4Cu_4Br_2(py)_6]$	Planar "open" shaped	DMF	72	0.08	[14a]
$[MoS_4Cu_4I_2(py)_6]$	Planar "open" shaped	DMF	72	0.08	[14a]
$[WS_4Cu_4I_2(py)_6]$	Planar "open" shaped	DMF	72	0.07	[14a]

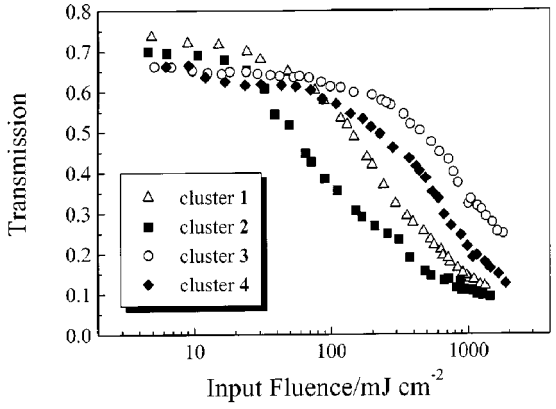

Figure 6. The 8 ns optical limiting effects of clusters **1**–**4** in MeCN solution; the energy transmission is plotted *vs.* the input fluence

heavy-atom effect. The importance of the heavy atom effect with regard to the efficiency of nonlinear absorption and the OL capabilities has already been noted in the case of the metallophthalocyanine system.[7b,25] Moreover, the OL behavior of cluster **1** is greater than that of cluster **3** and the limiting threshold of **2** is superior to that of **4**, which suggests a cluster skeleton effect on their NLO and OL properties. It has been proven that both the cluster skeletons and the heavy atoms are responsible for the NLO effects of the heterothiometallic clusters,[14a] although which one plays a more active and important role in their NLO performances is still not very clear. It currently represents a great challenge and considerable efforts still need to be made to further explore this promising field of research.

Experimental Section

General: All reactions and manipulations were conducted using standard Schlenk techniques under an atmosphere of nitrogen unless specifically mentioned. The compounds $(NH_4)_2[MOS_3]$ (M = Mo, W) were prepared according to the literature.[22] Likewise, the complex $[Cu(MeCN)_4]\cdot[BF_4]$ was synthesized based on a literature procedure.[26] The solvents were carefully dried and distilled prior to use; other chemicals were generally used as received from commercial sources. – Elemental analyses for carbon, hydrogen, and nitrogen were performed on a Perkin–Elmer 240C elemental analyzer. – Infrared spectra were recorded with a Nicolet FT-170SX Fourier transform spectrometer (KBr pellets). – Electronic spectra were measured on a Shimadzu UV-3100 spectrophotometer.

$[MoOS_3Cu_3(4\text{-pic})_6]\cdot 0.5[Mo_2O_7]$ (1): CuCl (0.297 g, 3 mmol) was added to 4-picoline (20 mL) and the solution was stirred for ca. 5 min at room temperature. Then, $(NH_4)_2MoOS_3$ (0.293 g, 1.2 mmol) was added. The reaction mixture immediately turned black-red. After stirring for a further 10 min, the solution was filtered to afford a black-red filtrate. Black-red crystals (0.132 g, 19.8%) were obtained after several days by layering the filtrate with *i*PrOH in air. – $C_{36}H_{42}Cu_3Mo_2N_6O_{4.5}S_3$ (1109.5): calcd. C 39.0, H 3.8, N 7.6; found C 38.7, H 3.9, N 7.8. – UV/vis (MeCN, λ_{max}/nm, 10^3 ε/cm$^{-1}\cdot$mol$^{-1}\cdot$dm^3): 424 (3.8), 326 (6.8), 290 (7.7). – IR (KBr pellets): $\tilde{\nu}$ = 1615 (vs), 1421 (s), 908 (vs), 885 (s), 813 (vs), 492 (vs), 436 (vs).

Table 4. Crystal data for $[MoOS_3Cu_3(4\text{-pic})_6]\cdot 0.5[Mo_2O_7]$ (**1**) and $[WOS_3Cu_3(4\text{-pic})_6]\cdot[BF_4]$ (**4**)

Compound	**1**	**4**
Empirical formula	$C_{36}H_{42}N_6Cu_3Mo_2O_{4.5}S_3$	$C_{36}H_{42}N_6BCu_3F_4OS_3W$
Molecular mass	1109.44	1132.22
Temperature [K]	293(2)	293(2)
Radiation	Mo-K_α (λ = 0.71073 Å)	Mo-K_α (λ = 0.71073 Å)
Crystal color and habit	black-red block	orange-red block
Crystal size [mm]	0.26 × 0.24 × 0.10	0.54 × 0.44 × 0.32
Crystal system	Trigonal	Trigonal
Space group	*P*-3	*P*-3
a [Å]	12.95640(10)	12.6610(18)
b [Å]	12.95640(10)	12.6610(18)
c [Å]	15.26030(10)	15.684(3)
V [Å^3]	2218.51(3)	2177.3(6)
Z	2	2
$D_{calcd.}$ [g·cm^{-3}]	1.661	1.727
F (000)	1110	1116
μ [mm^{-1}]	2.149	4.275
Collection range [°]	$1.33 < \theta < 28.33$	$1.30 < \theta < 25.01$
Scan method	ω scan	ψ scan
Index ranges	$-15 \le h \le 16$ $-17 \le k \le 9$ $-20 \le l \le 18$	$0 \le h \le 15$ $-15 \le k \le 0$ $0 \le l \le 18$
Reflections collected/unique	15712/3640 [R_{int} = 0.0876]	2839/2550 [R_{int} = 0.0847]
Absorption correction	empirical	empirical
Data/restraints/parameters	3640/6/165	2550/8/167
Goodness-of-fit on F^2	1.033	1.073
Final *R* indices [$I > 2\sigma(I)$]	R_1 = 0.0682, wR_2 = 0.2113	R_1 = 0.0563, wR_2 = 0.1542
R indices (all data)	R_1 = 0.1070, wR_2 = 0.2398	R_1 = 0.0769, wR_2 = 0.1640
Largest diff. peak and hole [e·Å^{-3}]	1.340 and −2.776	2.485 and − 2.142

$[WOS_3Cu_3(4\text{-pic})_6]\cdot 0.5[W_2O_7]$ (2): Cluster **2** was synthesized following the same procedure as used in the preparation of cluster **1**, except that $(NH_4)_2WOS_3$ (0.398 g, 1.2 mmol) was used instead of $(NH_4)_2MoOS_3$ (1.2 mmol). Orange-red crystals (0.143 g, 18.5%) were obtained. − $C_{36}H_{42}Cu_3N_6O_{4.5}S_3W_2$ (1285.3): calcd. C 33.6, H 3.3, N 6.5; found C 34.0, H 3.5, N 6.8. − UV/vis (MeCN, λ_{max}/nm, 10^3 ε/cm^{-1}·mol^{-1}·dm^3): 392 (6.1), 283 (15.2). − IR (KBr pellets): $\tilde{\nu}$ = 1615 (vs), 1423 (s), 925 (vs), 865 (s), 813 (vs), 492 (vs), 428 (vs).

$[MoOS_3Cu_3(4\text{-pic})_6]\cdot[BF_4]$ (3): $Cu(MeCN)_4BF_4$ (0.944 g, 3 mmol) was added to 4-picoline (20 mL) and the solution was stirred for ca. 5 min at room temperature. Then, $(NH_4)_2MoOS_3$ (0.244 g, 1 mmol) was added. The reaction mixture immediately turned deep-red. After stirring for a further 10 min, the solution was filtered to afford a deep-red filtrate. Deep-red crystals (0.818 g, 78.3%) were obtained after several days by layering the filtrate with *i*PrOH. − $C_{36}H_{42}BCu_3F_4MoN_6OS_3$ (1044.3): calcd. C 41.4, H 4.1, N 8.1; found C 41.6, H 4.3, N 8.2. − UV/vis (MeCN, λ_{max}/nm, 10^3 ε/cm^{-1}·mol^{-1}·dm^3): 407 (3.1), 281 (15.8). − IR (KBr pellets): $\tilde{\nu}$ = 1614 (vs), 1420 (s), 910 (vs), 813 (vs), 492 (vs), 437 (vs).

$[WOS_3Cu_3(4\text{-pic})_6]\cdot[BF_4]$ (4): Cluster **4** was synthesized following the same procedure as used in the preparation of cluster **3**, except that $(NH_4)_2WOS_3$ (0.332 g, 1 mmol) was used instead of $(NH_4)_2MoOS_3$ (1 mmol). Orange-red crystals (0.965 g, 85.2%) were obtained. − $C_{36}H_{42}BCu_3F_4N_6OS_3W$ (1132.2): calcd. C 38.2, H 3.8, N 7.4; found C 38.3, H 3.9, N 7.5. − UV/vis (MeCN, λ_{max}/nm, 10^3 ε/cm^{-1}·mol^{-1}·dm^3): 376 (3.9), 284 (10.7). − IR (KBr pellets): $\tilde{\nu}$ = 1614 (vs), 1420 (s), 924 (vs), 813 (vs), 492 (vs), 428 (vs).

Crystal Structure Determinations: Well-shaped single crystals of clusters **1** and **4** of suitable dimensions were selected and mounted on glass fibers. The diffraction data for **1** were collected on a Siemens Smart CCD area-detector diffractometer using the ω-scan technique. The data reductions for **1** were performed on a Silicon Graphics Indy workstation using Smart-CCD software. The diffraction data for **4** were collected on an Enraf−Nonius CAD4 four-circle diffractometer with unit-cell parameters determined from the automatic centering of 25 reflections by the least-squares method. Intensities were corrected for Lorentz polarization effects and an absorption correction was applied using the ψ-scan technique. The structures of both **1** and **4** were solved by direct methods and refined by full-matrix least-squares against F^2 using the SHELXL-97 programs.[27] All non-hydrogen atoms were refined anisotropically by the full-matrix least-squares method. The hydrogen atoms were placed in their calculated positions, assigned fixed isotropic thermal parameters, and allowed to ride on their respective parent atoms. The data processing and structure refinement parameters are listed in Table 4.

Crystallographic data (excluding structure factors) for the cluster structures reported in this paper have been deposited with the Cambridge Crystallographic Data Centre as supplementary publications nos. CCDC-164299 (cluster **1**) and CCDC-164300 (cluster **4**). Copies of the data can be obtained free of charge on application to the CCDC, 12 Union Road, Cambridge CB2 1EZ, U.K. [Fax: (internat.) +44 (0)1223/336033; E-mail: deposit@ccdc.cam.ac.uk].

Optical Measurements: A solution of the respective cluster **1**−**4** in MeCN was placed in a 5-mm quartz cuvette for optical limiting

property measurements, which were performed with linearly polarized 8-ns pulses at $\lambda = 532$ nm generated from a Q-switched frequency-doubled Nd:YAG laser. The clusters **1**−**4** proved to be stable towards air and laser light under the experimental conditions. The spatial profiles of the optical pulses were of near-Gaussian transverse mode. The pulsed laser was focused onto the sample cell using a mirror of focal length 30 cm. The spot radius of the laser beam was measured as 55 μm (half-width at $1/e^2$ maximum). The energy of the input and output pulses was measured simultaneously by precision laser detectors (Rjp-735 energy probes), which were linked to a computer through an IEEE interface,[28] while the incident pulse energy was varied by a Newport Com. attenuator. The interval between the laser pulses was chosen as 1 s to avoid the influence of thermal and long-term effects.

The third-order NLO absorptive and refractive properties of clusters **1**−**4** were determined by performing *Z*-scan measurements.[23a] The samples were mounted on a translation stage that was controlled by computer to move along the axis of the incident laser beam (*Z*-direction) with respect to the focal point rather than being positioned at its focal point. To determine both the sign and magnitude of the nonlinear refraction, a 0.2 mm diameter aperture was placed in front of the transmission detector and the transmittance was recorded as a function of the sample position on the *Z* axis (closed-aperture *Z*-scan). To determine the nonlinear absorption, the *Z*-dependent sample transmittance was measured without the aperture (open-aperture *Z*-scan).

Acknowledgments

Dr. C. Zhang greatly appreciates the Alexander von Humboldt Foundation for awarding a Humboldt Research Fellowship. Financial support from the National Science Foundations of China and the USA, the Foundations of the Harbin Institute of Technology and the Universiti Sains Malaysia is acknowledged. C. Z. thanks Scott E. Boesch, Dr. Douglas R. Powell, and Dr. Masood Khan for their helpful discussions.

[1] [1a] E. I. Stiefel, K. Matsumoto, *Transition Metal Sulfur Chemistry: Biological and Industrial Significance*, American Chemical Society, Washington DC, **1996**. – [1b] I. Dance, K. Fisher, *Prog. Inorg. Chem.* **1994**, *41*, 637−803. – [1c] S. C. Lee, R. H. Holm, *Angew. Chem. Int. Ed. Engl.* **1990**, *29*, 840−856.

[2] [2a] S. Shi, W. Ji, S. H Tang, J. P. Lang, X. Q. Xin, *J. Am. Chem. Soc.* **1994**, *116*, 3615−3616. – [2b] S. Shi, Z. R. Chen, H. W. Hou, X. Q. Xin, K. B. Yu, *Chem. Mater.* **1995**, *7*, 1519−1524. – [2c] P. E. Hoggard, H. W. Hou, X. Q. Xin, S. Shi, *Chem. Mater.* **1996**, *8*, 2218−2222. – [2d] S. Shi, W. Ji, X. Q. Xin, *J. Phys. Chem.* **1995**, *99*, 894−898.

[3] [3a] J. B. Howard, D. J. Low, *Chem. Rev.* **1996**, *96*, 2965−2982. – [3b] R. H. Holm, *Adv. Inorg. Chem.* **1992**, *38*, 1−71. – [3c] D. Coucouvanis, *Acc. Chem. Res.* **1991**, *24*, 1−8. – [3d] T. Shibahara, *Coord. Chem. Rev.* **1993**, *123*, 73−147. – [3e] B. C. Wiegand, C. M. Friend, *Chem. Rev.* **1992**, *92*, 491−504.

[4] [4a] A. Muller, E. Diemann, H. Bogge, *Angew. Chem. Int. Ed. Engl.* **1981**, *20*, 934−955. – [4b] C. Zhang, G. C. Jin, J. X. Chen, X. Q. Xin, K. P. Qian, *Coord. Chem. Rev.* **2001**, *213*, 51−77. – [4c] H. W. Hou, X. Q. Xin, S. Shi, *Coord. Chem. Rev.* **1996**, *153*, 25−56. – [4d] S. Sarkar, S. B. S. Mishra, *Coord. Chem. Rev.* **1984**, *59*, 239−264.

[5] [5a] J. Kim, D. C. Rees, *Science* **1992**, *257*, 1677−1682. – [5b] M. K. Chan, J. Kim, D. C. Rees, *Science* **1993**, *260*, 792−794. – [5c] J. T. Bolin, N. Campobasso, S. W. Muchmore, *Molybdenum Enzymes, Cofactors and Model Systems*, American Chemical Society, Washington DC, **1993**.

[6] [6a] L. W. Tutt, A. Kost, *Nature* **1992**, *356*, 225−226. – [6b] D. G. McLean, R. L. Sutherland, M. C. Brant, D. M. Brandelik, P. A. Fleitz, T. Pottenger, *Opt. Lett.* **1993**, *18*, 858−860. – [6c] Y. L. Song, G. Y. Fang, Y. X. Wang, S. T. Liu, C. F. Li, L. C. Song, Y. H. Zhu, Q. M. Hu, *Appl. Phys. Lett.* **1999**, *74*, 332−334. – [6d] Y. P. Sun, J. E. Riggs, *Int. Rev. Phys. Chem.* **1999**, *18*, 43−90.

[7] [7a] J. W. Perry, K. Mansour, I. Y. S. Lee, X. L. Wu, P. V. Bedworth, C. T. Chen, D. Ng, S. R. Mardar, P. Miles, T. Wada, M. Tian, H. Sasabe, *Science* **1996**, *273*, 1533−1536. – [7b] J. W. Perry, K. Mansour, S. R. Marder, K. J. Perry, D. Alvarez Jr., L. Choong, *Opt. Lett.* **1994**, *19*, 625−627. – [7c] C. F. Li, L. Zhang, M. Yang, H. Wang, Y. X. Wang, *Phys. Rev. A* **1994**, *49*, 1149−1157.

[8] [8a] S. Shi, W. Ji, J. P. Lang, X. Q. Xin, *J. Phys. Chem.* **1994**, *98*, 3570−3572. – [8b] W. Ji, H. J. Du, S. H. Tang, S. Shi, *J. Opt. Soc. Am. B* **1995**, *12*, 876−881.

[9] [9a] Z. R. Chen, H. W. Hou, X. Q. Xin, K. B. Yu, S. Shi, *J. Phys. Chem.* **1995**, *99*, 8717−8721. – [9b] H. W. Hou, B. Liang, X. Q. Xin, K. B. Yu, P. Ge, W. Ji, S. Shi, *J. Chem. Soc., Faraday Trans.* **1996**, *92*, 2343−2346.

[10] [10a] G. Salane, T. Shibahara, H. W. Hou, X. Q. Xin, S. Shi, *Inorg. Chem.* **1995**, *34*, 4785−4789. – [10b] W. Ji, S. Shi, H. J. Du, P. Ge, S. H. Tang, X. Q. Xin, *J. Phys. Chem.* **1995**, *99*, 17297−17301. – [10c] T. Xia, A. Dogariu, K. Mansour, D. J. Hagan, A. A. Said, E. W. Van Stryland, S. Shi, *J. Opt. Soc. Am. B* **1998**, *15*, 1497−1501.

[11] [11a] H. W. Hou, X. R. Ye, X. Q. Xin, J. Liu, M. Q. Chen, S. Shi, *Chem. Mater.* **1995**, *7*, 472−476. – [11b] P. Ge, S. H. Tang, W. Ji, S. Shi, H. W. Hou, D. L. Long, X. Q. Xin, S. F. Lu, Q. J. Wu, *J. Phys. Chem. B* **1997**, *101*, 27−31.

[12] [12a] H. W. Hou, D. L. Long, X. Q. Xin, X. Y. Huang, B. S. Kang, P. Ge, W. Ji, S. Shi, *Inorg. Chem.* **1996**, *35*, 5363−5367. – [12b] H. W. Hou, X. Q. Xin, J. Liu, M. Q. Chen, S. Shi, *J. Chem. Soc., Dalton Trans.* **1994**, 3211−3214.

[13] S. Shi, H. W. Hou, X. Q. Xin, *J. Phys. Chem.* **1995**, *99*, 4050−4053.

[14] [14a] C. Zhang, Y. L. Song, B. M. Fung, Z. L. Xue, X. Q. Xin, *Chem. Commun.* **2001**, 843−844. – [14b] C. Zhang, Y. L. Song, G. C. Jin, G. Y. Fang, Y. X. Wang, S. S. S. Raj, H. K. Fun, X. Q. Xin, *J. Chem. Soc., Dalton Trans.* **2000**, 1317−1323.

[15] [15a] C. Zhang, Y. L. Song, Y. Xu, H. K. Fun, G. Y. Fang, Y. X. Wang, X. Q. Xin, *J. Chem. Soc., Dalton Trans.* **2000**, 2823−2829. – [15b] H. W. Hou, Y. T. Fan, C. X. Du, Y. Zhu, W. L. Wang, X. Q. Xin, M. K. M. Low, W. Ji, H. G. Ang, *Chem. Commun.* **1999**, 647−648.

[16] [16a] J. C. Dyason, L. M. Englehardt, P. C. Healy, C. Pakawatchai, A. H. White, *Inorg. Chem.* **1985**, *24*, 1950−1957. – [16b] J. C. Dyason, P. C. Healy, C. Pakawatchai, V. A. Patrick, A. H. White, *Inorg. Chem.* **1985**, *24*, 1957−1960. – [16c] E. W. Ainscough, A. G. Bingham, A. M. Brodie, K. L. Brown, *J. Chem. Soc., Dalton Trans.* **1984**, 989−991.

[17] [17a] H. Yu, W. J. Zhang, X. T. Wu, T. L. Sheng, Q. M. Wang, P. Lin, *Angew. Chem. Int. Ed.* **1998**, *37*, 2520−2521. – [17b] Q. Huang, X. T. Wu, J. X. Lu, *Chem. Commun.* **1997**, 703−704. – [17c] Q. Huang, X. T. Wu, Q. M. Wang, T. L. Sheng, J. X. Lu, *Angew. Chem. Int. Ed. Engl.* **1996**, *35*, 868−870. – [17d] Q. Huang, X. T. Wu, J. X. Lu, *Inorg. Chem.* **1996**, *35*, 7445−7447.

[18] A. Muller, U. Schimanski, J. Schimanski, *Inorg. Chim. Acta* **1983**, *76*, L245−L246.

[19] D. L. Long, S. Shi, X. Q. Xin, B. S. Luo, L. R. Chen, X. Y. Huang, B. S. Kang, *J. Chem. Soc., Dalton Trans.* **1996**, 2617−2622.

[20] D. X. Zeng, W. Ji, W. T. Wong, W. Y. Wong, X. Q. Xin, *Inorg. Chim. Acta* **1998**, *279*, 172−177.

[21] V. W. Day, M. F. Fredrich, W. G. Klemperer, W. Shum, *J. Am. Chem. Soc.* **1977**, *99*, 6146−6148.

[22] J. W. McDonald, G. D. Friesen, L. D. Rosenhein, W. E. Newton, *Inorg. Chim. Acta* **1983**, *72*, 205−210.
[23] [23a] M. Sherk-Bahae, A. A. Said, T. H. Wei, D. J. Hagan, E. W. Van Stryland, *IEEE J. Quantum Electron.* **1990**, *26*, 760−769. – [23b] A. A. Said, M. Sherk-Bahae, D. J. Hagan, T. H. Wei, J. Wang, J. Young, E. W. Van Stryland, *J. Opt. Soc. Am. B* **1992**, *9*, 405−414.
[24] M. Sherk-Bahae, A. A. Said, E. W. Van Stryland, *Opt. Lett.* **1989**, *14*, 955−957.
[25] T. H. Wei, D. J. Hagan, M. J. Sence, E. W. Van Stryland, J. W. Perry, D. R. Coulter, *Appl. Phys. B* **1992**, *54*, 46−51.
[26] E. Heckel, German Patent, 1,230,025, *Chem. Abstr.* **1967**, *66*, 46487e.
[27] G. M. Sheldrick, *SHELXL-97*, *Program for Crystal Structure Determination*, University of Göttingen, Germany, **1997**.
[28] M. Sheik-Bahae, D. C. Hutchings, D. J. Hagan, E. W. Van Stryland, *IEEE J. Quantum Electron.* **1991**, *27*, 1296−1309.

Received May 31, 2001
[I01200]

Reactions of Secondary Dithioxamides with $[(\eta^6\text{-}p\text{-cymene})RuCl(\mu\text{-}Cl)]_2$: The Role of Steric Hindrance on Amidic Nitrogen in Determining the Reaction Products

Santo Lanza,*[a] Giuseppe Bruno,[a] Francesco Nicolò,[a] Archimede Rotondo,[a] and Giuseppe Tresoldi[a]

Keywords: N ligands / Bimetallic complexes / Ruthenium / Ion pairs / Chiral auxiliaries

The reactions of secondary dithioxamides H_2R_2DTO **1**–**11** [R = methyl **1**, ethyl **2**, *n*-propyl **3**, *n*-butyl **4**, isoamyl **5**, benzyl **6**, *p*-tolyl **7**, (*R*)-1-phenylethyl **8**, (*R*,*S*)-1-phenylethyl **9**, isopropyl **10**, cyclohexyl **11**] with the chloride-bridge dimer $[(\eta^6\text{-}p\text{-cymene})RuCl(\mu\text{-}Cl)]_2$ complex readily afforded either bimetallic ruthenium complexes of formula $[(\eta^6\text{-}p\text{-cymene})RuCl_2](\mu\text{-}R_2DTO)$ (R = methyl **12a**, R = ethyl, **12b**, R = *n*-propyl **12c**; R = *n*-butyl **12d**; R = isoamyl **12e**; R = benzyl **12f**; R = *p*-tolyl **12g**) or mononuclear "piano stool" geometry ion pairs $\{(\eta^6\text{-}p\text{-cymene})RuCl(H_2R_2DTO)^+,(Cl^-)$ κ-*S*,*S*′ Ru} [R = (*R*)-1-phenylethyl, **13a**; R = (*R*,*S*)-1-phenylethyl, **13b**; R = isopropyl, **13c**; R = cyclohexyl, **13d**]. The driving force of the reactions was the bulkiness of the R groups attached to dithioxamides, leading respectively from primary and aromatic *N*-bonded carbons to neutral bimetallic species **12a**–**g**, or from secondary *N*-bonded carbons to monometallic **13a**–**d** species. These latter compounds could be easily dehydrohalogenated to give neutral "piano stool" complexes $[(\eta^6\text{-}p\text{-cymene})RuCl(HR_2DTO)$ κ-*S*,*S*′ Ru] [R = (*R*)-1-phenylethyl **14a**; R = (*R*,*S*)-1-phenylethyl **14b**; R = isopropyl **14c**; R = cyclohexyl **14d**]. All complexes were characterised in solution by ^1H and $^{13}C\{^1H\}$ NMR spectroscopy. Complex **12f** was also characterised by mass spectrometry, and **12g** by solid state X-ray crystallography.

Introduction

Dimeric $[(\eta^6\text{-arene})RuCl(\mu\text{-}Cl)]_2$ species provide an ideal way of entering the synthesis of η^6-monoarene "three legged piano stool" ruthenium complexes, where the η^6-coordinated arene are the "bench", and the other ligands "the legs" of the stool.[1] However, when the $[(\eta^6\text{-arene})RuCl(\mu\text{-}Cl)]_2$ chloride-bridge dimers are reacted under particular experimental conditions with binucleating chelate ligands, binuclear complexes of the type $[(\mu\text{-L-L})\{RuCl_2(\eta^6\text{-arene})\}_2]$ can be also obtained.[2] Mononuclear η^6-arene ruthenium complexes revealed themselves as effective enantioselective catalysts in a number of asymmetric organic transformations when ruthenium is itself presented as a stereogenic centre or ligands are chiral species such as BINAP[3] or aminophosphanyl-phosphinite.[4]

We have previously reported that the platinum complexes [Pt(PN)Cl(HR_2DTO) κ-*S*,*S*′ Pt] (PN = 2-diphenylphosphanyl-pyridine. HR_2DTO^- = alkyl-substituted dithioxamidato) react with the ruthenium dimer $[(\eta^6\text{-}p\text{-cymene})RuCl(\mu\text{-}Cl)]_2$ giving rise to heterobimetallic "piano stool" ruthenium complexes:[5]

In complex **I** (Figure 1), the ruthenium is a stereogenic centre since the three legs of the stool are different. The stereochemistry of **I** remains ambiguous if one considers only the configuration of the ruthenium centre; thus, we have proposed that the best way to describe the asymmetry of **I** is to consider the Ru−Pt axis as an unprecedented element of chirality. As a matter of fact, the reactivity of [Pt(PN)Cl(HR_2DTO) κ-*S*,*S*′ Pt] type compounds opens the way to a new class of organometallic complexes. When these square planar complexes containing *S*,*S*′-coordinated

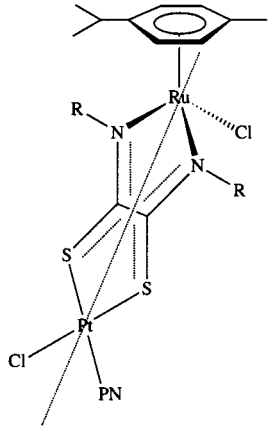

Figure 1. [Pt(PN)Cl(μ-R_2DTO)Ru(*p*-cymene)Cl, κ-*S*,*S*′ Pt, κ-*N*,*N*′ Ru] **I**

[a] Dipartimento di Chimica Inorganica, Chimica Analitica e Chimica Fisica, Università di Messina,
Salita Sperone, 31 (Vill. S. Agata), 98166 Messina, Italy
Fax: (internat.) + 39-090393756
E-mail: Lanza@chem.unime.it

 © WILEY-VCH Verlag GmbH, 69451 Weinheim, Germany, 2002 1434−1948/02/0101−0065 $ 17.50+.50/0

dithioxamides are forced to chelate by the unusual *N,N′*-coordination mode with a second prochiral metal fragment such as $[Ru(\eta^6\text{-}p\text{-cymene})Cl]^+$, new binuclear species exhibiting very interesting stereochemical features are formed. Starting from this point, we found it interesting to see how un-coordinated secondary dithioxamides react with the ruthenium dimer $[(\eta^6\text{-}p\text{-cymene})RuCl(\mu\text{-}Cl)]_2$. The coordination chemistry of secondary dithioxamides ligands is very rich; the multi-site donor nature of the two nitrogen and two sulfur atoms, their respective hard and soft character, the possibility of modulating electronic and geometrical properties by loss of one or two protons, and finally, the dicompartmental rigid structure of the dianionic rubeanate ligand have been largely exploited to form complexes of different coordination type, geometries, and nuclearity.[6] The organometallic chemistry of these ligands, on the contrary, has hitherto been rather unexplored: only one report has appeared in the last few years,[7] even though the alkyl groups of secondary dithioxamides could be usefully exploited as molecular probes or as electronic, steric, and enantioselective tools for modelling peculiar properties of the molecules.

The present paper stems from a systematic study devoted to the synthesis of η^6-arene-ruthenium(II) complexes containing dithioxamides: the aim of the research is to investigate the stereochemical effect of R groups in [RHNSC−CSNHR] or [RHNSC−CSNHR′] molecules in determining the possible stereoselective synthesis of half-sandwich molecules like **I**. In the following we report results concerning the reactions $[(\eta^6\text{-}p\text{-cymene})RuCl(\mu\text{-}Cl)]_2$ with a series of disubstituted dithioxamides bearing alkyl substituents of varying molecular complexity.

Results and Discussion

Structurally, the ligands [RHNSC−CSNHR] used in the present study can be divided into three families, according to the nature of the carbon bonded to the amidic nitrogens: i) primary [R = methyl (**1**), ethyl (**2**), *n*-propyl (**3**), *n*-butyl (**4**), isoamyl (**5**), and benzyl (**6**); ii) aromatic [*p*-tolyl (**7**)]; and iii) secondary [(*R*)-1-phenylethyl (**8**), (*R*,*S*)-1-phenylethyl (**9**), isopropyl (**10**), and cyclohexyl (**11**)].

The reactions of ligands **1**−**7** with $[(\eta^6\text{-}p\text{-cymene})RuCl(\mu\text{-}Cl)]_2$ in chloroform lead to the bimetallic complexes **12a**−**g** in high yields (Scheme 1).

In these compounds the two ruthenium atoms are connected by a dianionic rubeanate frame in an NS−NS binucleating mode, which is the usual coordination mode observed in many other inorganic bi- and polymetallic complexes.[8]

^{1}H NMR spectra of compounds **12a**−**g** show cymene ring protons as four doublets and methyl groups of the isopropyl moiety of cymene as two doublets. $^{13}C\{^1H\}$ NMR spectra, in turn, show four resonances corresponding to CH carbons of cymene ring, and two featuring cymene isopropyl CH_3 carbons (see Exp. Sect.). These spectral patterns are observed since ruthenium atoms are stereogenic, hence

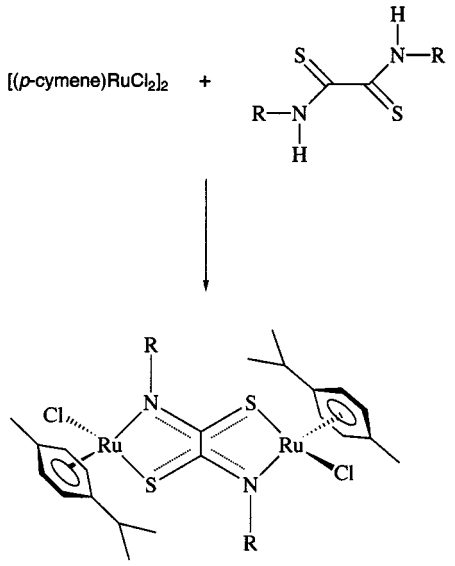

Scheme 1. Reactions of $[(\eta^6\text{-}p\text{-cymene})RuCl(\mu\text{-}Cl)]_2$ with the ligands **1**−**7**

the plane perpendicular to the *p*-cymene and passing through the quaternary phenyl carbons C^1 and C^4 is not a symmetry plane. Consequently, the methyl protons of the isopropyl group and the aromatic protons (H^2 and H^6) in the *ortho* position with respect to the same group, as well as H^3 and H^5, are diastereotopic. At the same time NCH_2−R protons in **12a**−**g** are diastereotopic, and appear in the ^{1}H NMR spectra as an ABC_n (n = 0, 1, 2, 3) spin systems. As explained previously, pseudo-octahedral ruthenium atoms are both stereogenic since they are surrounded by four different ligands, hence two diastereomers could have been formed in which the two ruthenium atoms could have equal or opposite configurations. However, we have observed that the reaction is totally diastereoselective and an X ray analysis of **12f** (Figure 2 and Table 1) revealed that only the compound with ruthenium atoms in the opposite configuration is formed.

Compounds **12a**−**g** are highly symmetric *meso* molecules, due to the presence of a centre of inversion in the middle of the central C−C bond of the rubeanate frame. We attempted to destroy this centre of inversion by three distinct strategies: i) metathesis of one of the two chlorides on ruthenium atoms; ii) use of a dithioxamide bearing an optically pure substituent on nitrogens; iii) use of an unsymmetrically disubstituted dithioxamide. This latter procedure is under investigation, since some additional problems concerning stereoselectivity arose that are not yet fully understood. As far as the metathesis of the chloride ligand, our attempt to change only one chloride with iodide failed. Consequently, we have used the enantiopure homochiral dithioxamide **8** to get into asymmetric ruthenium dimers of the type **12a**−**g** by depletion of the inversion centre. This ligand however, as well as **9**−**11**, undergoes a different reaction leading to the monomeric "piano stool" type complexes **13a**−**d** (Scheme 2).

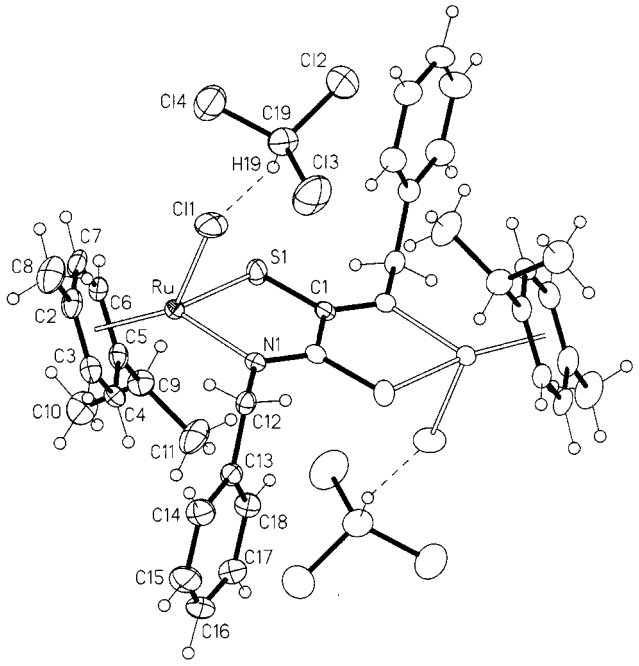

Figure 2. View of the whole molecule of **12f·2CHCl₃** at a crystallographic inversion centre, showing the labelling scheme of its half independent moiety. Thermal ellipsoids are drown at 30% probability, while hydrogen size is arbitrary

Table 1. Crystallographic data for **12f·2CHCl₃**

empirical formula	$C_{36}H_{42}Cl_2N_2Ru_2S_2 \cdot 2\ CHCl_3$
formula mass	1078.66
crystal dimensions	0.30 × 0.25 × 0.18 mm
crystal colour and form	yellow, prismatic
crystal system	triclinic
space group	$P\bar{1}$ (no. 2)
Unit cell dimensions	a = 9.515(1) Å
	b = 10.195(1) Å
	c = 12.391(2) Å
	α = 77.88(1)°
	β = 78.13(1)°
	γ = 71.64(1)°
V	1102.7(2) Å^3
Z	1
F(000)	542
$\rho_{calcd.}$	1.624 g/cm^3
μ	1.294 mm^{-1}
λ (graphite-monochromated)	0.71073 Å (Mo-K_α)
2θ range	3−50°
number of data collected (2θ − ω)	4597
number of data independent	3572 ($R_{int.}$ = 0.0232)
number of data refined	2222 [$F \geq 4\ \sigma(F)$]
number of variables	238
R[a]	0.0418/0.0725
(refined/all data)	
Rw[b] (refined/all data)	0.0493/0.1100
GOF[c] (refined/all data)	0.69/0.69
Max. diff. peak and hole	0.49/−0.48 eÅ^{-3}
Max. and mean shift/esd	0.002/0.001

[a] $R = [\Sigma||F_o| - |F_c||]/\Sigma|F_o|$. [b] $R_w\ [\Sigma w(|F_o| - |F_c|)^2/\Sigma w|F_o|^2]^{1/2}$. [c] $GOF = [\Sigma w(|F_o| - |F_c|)^2/(N_{observns} - N_{var})]^{1/2}$.

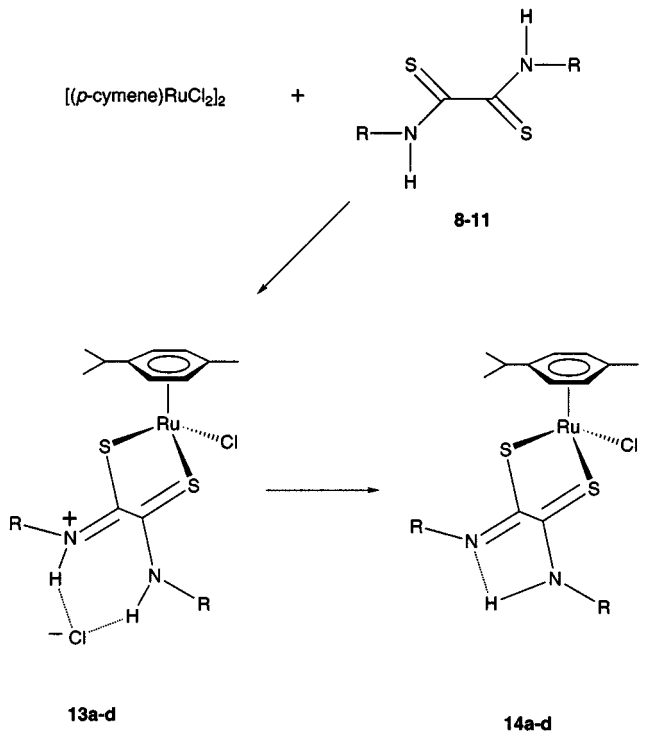

Scheme 2. Reactions of [(η⁶-*p*-cymene)RuCl(μ-Cl)]₂ with the ligands **8−11**

The N−H proton resonances at δ ≈ 13 in **13a−d** suggest that amidic nitrogens are engaged in an =N−H···Cl⁻···H−N= interaction.[6] This proves that the dithioxamide molecules are linked to ruthenium through sulfur atoms. Considering this and the absence of structural data, the geometry of **13a−d** compounds seems to be defined. Mass spectrum of **13a** shows a low intensity but significant peak at M^+ = 634, characterised by the usual ruthenium isotopomers pattern. More intense peaks observed in the spectrum are attributable to HCl, *p*-cymene, and 1-phenylethyldithioxamide. Compounds **13a−d** are tight contact ion pairs, extensively associated (Beer's law holds in the range 5 × 10^{-5} to 6 × 10^{-6} M), in which the steric repulsion between amidic hydrogens requires a torsion angle between the two NCS moieties in the neutral dithioxamide ligand. In fact, the co-planarity of the thioamide groups in an *S*,*S*′-coordinated neutral disubstituted dithioxamide would require a nonbonded H···H distance of ca. 1.4 Å between the amide protons. It may be emphasised that extremely short nonbonded H···H distances have been reported in the range 1.71−1.74 Å.[9]

A series of crystal structures performed on different metal complexes (copper, zinc, bismuth, and tin) containing neutral dithioxamides coordinated in the *S*,*S*′-mode, and having different geometrical environments (square-planar, tetrahedral, octahedral, bipyramidal) have appeared in the literature.[10] In all of them, in the solid state, a torsion angle between the two NCS fragments of about 40° was measured, which, being independent from both the metal and its geometrical environment, can be taken as a characteristic of any neutral *S*,*S*′-coordinated dithioxamides. In spite of

their chemical unequivalence, only one set of NMR signals for the dithioxamide alkyl groups of **13a−d** has been observed; as previously suggested, in the NMR time scale, fast HCl-mediated exchange should be responsible for the alkyl averaging.[11] Compounds **13a−d** can be easily dehydrohalogenated to give neutral rubeanate complexes **14a−d** in a pure form, by means of double phase reaction on a chromatographic column (see Exp. Sect.). HCl can also be removed from **13a−d** ion pairs by means of classical Brønsted bases such as alkylamines, and can be easily added to **14a−d** neutral complexes to restore the ion pairs **13a−d**. This easy and reversible protonation further supports *S*,*S*′ coordination in **14a−d**, as well as in **13a−d**. Complexes **13a** and **14a** are optically pure chiral molecules of C_1 symmetry; therefore in these species, RNCS fragments are diastereotopic, and accordingly two sets of signals appear in the NMR spectra. These complexes present optically pure chiral chelate ligands bonded to the metal by sulfur atoms. It is worth mentioning that in recent years new chiral auxiliaries appearing in the literature have attracted increasing interest and have found applications in synthetic organic chemistry.[12] Several different chiral chelates including diphosphane,[13] diamine,[14] diimine,[15] dithiol ligands,[16] and "mixed" chelates, e.g., S−N[17,18] and P−N[18] combinations, have been incorporated into the catalyst precursors and successfully employed in enantioselective synthesis (up to 90% enantiomeric excess often reported).

Compounds **13b** and **14b** were obtained from a dithioxamide, prepared by racemic phenylethylamine; the diastereoisomeric mixture was not separated, but characterised in solution by NMR spectra subtraction procedure. The reaction of $[(\eta^6\text{-arene})RuCl(\mu\text{-}Cl)]_2$ with **9** produces a mixture containing 50% of the racemate (*R*,*R*) and (*S*,*S*) and 50% of the two (*R*,*S*) and (*S*,*R*) *meso* forms. The NMR spectra of the (*R*,*R*) and (*S*,*S*) racemate is of course equal to that of the optical pure (*R*,*R*) enantiomer **13a**; thus by subtraction of the **13a** spectrum from that of the mixture, the spectrum of the two **13b** *meso* forms of C_s symmetry can be obtained. The diastereoisomers **13b** give rise to perfectly superimposable ^1H and ^{13}C NMR spectra which, owing to the internal reflection plane, show a single set of NMR signals; the two *meso* forms depict an interesting example of stereogenic achirotopic ruthenium centre.[19]

The different reactivity towards ruthenium(*p*-cymene)dichloro dimer of benzyl dithioxamide with respect to 1-phenylethyldithioxamide is rather surprising: a striking change in the reaction products and in the coordination mode of the ligands follows a small change in the molecular complexity of R substituents on nitrogen. This probably means that the *N*,S binucleation is a more favourable coordination mode of dithioxamide ligands towards the organoruthenium fragment $[(arene)RuCl]^+$: a better 'hard/soft' interaction and less steric hindrance should be achieved when only one alkyl substituent interacts with *p*-cymene ring. Vice versa is true when the ligands have sterically hindered amidic nitrogens, the *S*,*S*′ *cis*-chelation should be easier and mononuclear "piano stool" complexes formed preferentially. Actually, dithioxamide ligands other than **6**, **8**, and **9** were designed to verify if the steric hindrance on nitrogen could be responsible for the different reaction paths. Thus, we prepared **1**, **2**, **3**, **4**, and **5** where R = $-CH_2-R'$ (R′ = H, methyl, ethyl, propyl, isobutyl) at the scope of varying the molecular complexity of R′ while leaving the structure of the carbon attached to nitrogen unchanged. Alternatively, **10** and **11** were prepared to increase steric hindrance on the carbon directly attached to nitrogen, and **7** was prepared because the aromatic carbon on nitrogen is part of a flat structure, which does not have three-dimensional hindrance. The analysis of the reaction products confirms that the bulk on the nitrogen-bonded carbon is the structural property of secondary dithioxamides that leads to the synthesis of piano stool complexes **13a−d** rather than to the binuclear compounds **12a−g**.

Conclusions

Secondary dithioxamides *N*-substituted with substituents of various complexity were reacted with ruthenium(*p*-cymene)dichloro dimer. Binuclear $[(p\text{-cymene})ClRu]_2$ (μ-$R_2N_2S_2H_2$ κ-*N*,*S* Ru κ-*N*′,*S*′ Ru′) were synthesized when R = methyl, ethyl, *n*-propyl, *n*-butyl, isoamyl, *p*-tolyl. Mononuclear "piano stool" complexes $\{Ru(p\text{-cymene})Cl(H_2R_2N_2S_2C_2)^+, Cl^-\}$ and $[Ru(p\text{-cymene})Cl(H_2R_2N_2S_2C_2)]$ were obtained when R = cyclohexyl, isopropyl, 1-phenylethyl.

These results suggest that the bulk on the nitrogen-bonded carbon is the structural property of secondary dithioxamides that leads to the synthesis of piano stool complexes rather than to the binuclear compounds. This observation opens interesting perspectives; in fact, unsymmetrically disubstituted dithioxamides [RHNSC−CSNHR′] properly designed could provide binuclear as well as "piano stool" mononuclear chiral diastereomers. Furthermore, the tuning of steric effects, both on nitrogen substituents and on η^6-arene "stools", could promote stereoselective synthesis of "piano stool" type $[(\eta^6\text{-arene})Ru(HDTO)Cl]$ complexes.

Molecular Structure of $[(\eta^6\text{-}p\text{-Cymene})RuCl]_2$(μ-*N*,*N*′-dibenzyl-dithioxamidato κ-*N*,*S* Ru κ-*N*′,*S*′ Ru′)·2$CHCl_3$ (12f·2$CHCl_3$)

The complex consists of two $[(\eta^6\text{-}p\text{-cymene})RuCl]^+$ units *N*,*S*-bis-chelated by a planar bridge [(*N*,*N*′-dibenzyl-dithioxamidato)]$^{2-}$. The compound co-crystallises with solvent molecules (ratio 1:2) interacting with the chloride of the ruthenium moieties: H(19)···Cl(1) 2.407(9) Å, C(19)···Cl(1) 3.327(9) Å, C(19)−H(19)···Cl(1) 160.5(9)°. The observed decay of the diffraction data is due to the crystal packing deterioration due to loss of co-crystallised $CHCl_3$. In the solid state the middle point of the NSC−CSN is both a crystallographic and molecular inversion centre; thus the asymmetric unit contains only half complex moiety H-bonded to a chloroform molecule, as shown in Figure 2.

By considering the (η⁶-*p*-cymene) ligand as a unique coordination site represented by the centre of the benzene ring (Xcym in Table 2), the ruthenium geometry might be described as a significantly distorted tetrahedron. This deformation as evidenced by the space-filling model is mainly due to the metal d orbitals orientation (that is octahedral); these develop bonds toward ligands: the "three legs of the stool" are nearly 90° mutually oriented. The Ru−Ccym bond lengths shift from 2.170(7) for C(4) to 2.256(6) Å for C(2) with the average value 2.198(8) Å; the metal distance from the benzene centre is 1.685(6) Å. The ruthenium coordination geometry is the same as that of [(η⁶-*p*-cymene)RuCl(μ-bis(2-hydroxypropyl)-DTO)Pt(2-diphenylphosphanyl-pyridine)Cl] reported in our previous work[5] on DTO chirality, where ruthenium and platinum are *N*,*N*′- and *S*,*S*′-chelated, respectively. The difference arises from the *N*,*N*′-ditolyl-dithioxamidato, which undergoes *S*,*N*-chelation in order to better distribute the steric hindrance between tolyl substituents and *p*-cymene on two ruthenium centres. This arrangement, similar to an already reported *SN* coordination,[20] causes the C_i symmetry of the binuclear complex (if the tetrahedral ruthenium atom is a chiral centre, then the whole molecule is a *meso* form) and the formation of the observed centrosymmetric crystal packing in the solid state. The coordination through the bigger sulfur atom causes a slight elongation of the Ru−N bond with respect to the mean 2.06(1) Å value reported for the *N*,*N*-chelation.[21]

Table 2. Selected interatomic distances (Å) and angles (deg) for **12f·2CHCl₃**

Ru−Cl(1)	2.418(2)	Ru−S(1)	2.357(2)
Ru−N(1)	2.105(6)	Ru−Xcym	1.685(6)
Ru−C(2)	2.256(6)	Ru−C(3)	2.222(8)
Ru−C(4)	2.170(7)	Ru−C(5)	2.175(7)
Ru−C(6)	2.174(7)	Ru−C(7)	2.188(6)
C(2)−C(3)	1.39(1)	C(2)−C(7)	1.40(1)
C(2)−C(8)	1.52(1)	C(3)−C(4)	1.425(9)
C(4)−C(5)	1.41(1)	C(5)−C(6)	1.42(1)
C(5)−C(9)	1.52(1)	C(6)−C(7)	1.409(9)
C(9)−C(10)	1.52(1)	C(9)−C(11)	1.53(1)
S(1)−C(1)	1.724(7)	C(1)−C(1′)	1.46(1)
N(1)−C(1′)	1.314(7)	N(1)−C(12)	1.46(1)
C(12)−C(13)	1.49(1)		
N(1)−Ru−Xcym	133.7(3)	S(1)−Ru−Xcym	127.9(3)
Cl(1)−Ru−Xcym	126.3(3)	S(1)−Ru−N(1)	81.2(2)
Cl(1)−Ru−N(1)	83.3(2)	Cl(1)−Ru−S(1)	88.23(8)
C(7)−C(2)−C(8)	121.0(7)	C(3)−C(2)−C(8)	120.7(7)
C(3)−C(2)−C(7)	118.2(7)	C(2)−C(3)−C(4)	121.2(7)
C(3)−C(4)−C(5)	120.9(7)	C(4)−C(5)−C(9)	122.7(7)
C(4)−C(5)−C(6)	117.2(7)	C(6)−C(5)−C(9)	120.0(6)
C(5)−C(6)−C(7)	121.0(6)	C(2)−C(7)−C(6)	121.4(7)
C(5)−C(9)−C(11)	113.4(7)	C(5)−C(9)−C(10)	111.0(7)
C(10)−C(9)−C(11)	110.8(7)	Ru−N(1)−C(1′)	122.1(5)
Ru−S(1)−C(1)	100.3(2)	S(1)−C(1)−N(1′)	123.9(5)
S(1)−C(1)−C(1′)	118.2(5)	C(1)−C(1′)−N(1)	117.9(6)
C(12)−N(1)−C(1′)	118.5(6)	Ru−N(1)−C(12)	118.9(4)
N(1)−C(12)−C(13)	114.2(6)		

The DTO bridge exhibits a flat arrangement, observed in all the known complexes of the bis-chelating dithioxamide derivatives. The Ru atom is 0.116(1) Å out of the mean plane of the perfectly planar NSC−CSN fragment, in whose respect the tolyl substituent is disposed orthogonally [dihedral angle 81.5(2)°, torsion angle C(1′)−NCH₂−C_{phen} −92.7(8)°] to minimise the hindrance with the ruthenium bonded *p*-cymene. The C(1)−C(1′) distance of 1.46(1) Å is evidence of the large conjugation on the whole NSC−CSN system, as compared with the tilted conformation of the mono-chelate neutral *S*,*S*′-coordinated complexes with the C−C distance over 1.5 Å.[21]

Experimental Section

General Remarks: ^{1}H and ^{13}C{^{1}H} NMR spectra were recorded, at 298 K, on a Bruker ARX-300 spectrometer equipped with a broad-band probe operating at 300.13 and 75.46 MHz, respectively [δ (ppm) relative to Me_4Si, *J*(Hz)]. Electronic impact (EI) mass spectra were recorded with a Finnigan MAT 90 reverse-geometry double-focusing mass spectrometer. Sample was introduced into the EI source by a heated direct inlet probe. Ion source conditions: ionisation energy 70 eV; acceleration voltage 5 kV; temperature 220 °C.

The reagents are commercially available products used as purchased. Solvents were freshly distilled from sodium wire under a nitrogen atmosphere.

The dithioxamides **1**, **5**, **6**, **8**, **9**, **10**, **11**,[26] **7**,[27] and the starting complex [(η⁶-*p*-cymene)$RuCl_2$]$_2$ [28] were prepared according to known procedures. Compounds **2**, **3**, and **4**, already known,[26] were prepared with the following improved procedure: $H_4N_2C_2S_2$ (1 g, 8.32 mmol) was suspended in 50 mL of water and six fold excess (49.9 mmol) of the corresponding amine was added to the mixture. On stirring, yellow micro crystals of the product separated in a highly pure form.

[Ru(*p*-Cy)Cl]₂(μ-Me₂DTO) (12a): To a solution of [(η⁶-*p*-cymene)$RuCl_2$]$_2$ (612.4 mg, 1 mmol) in chloroform (100 mL), was added ligand **1** (148.2 mg, 1 mmol) and the mixture allowed to stand for 0.5 h at room temperature. After this time, the solution was concentrated to 10 mL and petroleum ether 40−60 (about 100 mL) added. A red brown solid precipitated, which was dissolved in the minimum amount of chloroform and purified by chromatography on silica with chloroform as eluent. The pure product was finally obtained by precipitation adding petroleum ether 40−60 (about 100 mL) to concentrated portions (about 10 mL) of eluates. Yield: 516 mg, 75%. ^{1}H NMR ($CDCl_3$): δ = 1.16, 1.23 [2 d, $^3J_{H,H}$ = 6.7 Hz, 6 H each, $CH(CH_3)_2$, cymene], 2.18 (s, 6 H, CH_3, cymene), 2.81 [seven lines, 2 H, $^3J_{H,H}$ = 6.7 Hz, $CH(CH_3)_2$, cymene], 3.88 (s, 6 H, NCH_3), 5.06, 5.18, 5.26, 5.42, (4 d, 2 H each, $^3J_{H,H}$ = 5.9 Hz, $H^{2,3,5,6}$, cymene). ^{13}C{^{1}H} NMR ($CDCl_3$): δ = 18.8 (s, CH_3, cymene), 22.0, 22.7 [2 s, $CH(CH_3)_2$, cymene], 30.9 [s, $CH(CH_3)_2$, cymene], 50.6 (s, NCH_3), 81.3, 81.8, 85.6, 85.8, (4 s, $C^{2,3,5,6}$, cymene), 99.9, 104.2, (2 s, $C^{1,4}$, cymene), 188.7 (s, CS). $C_{24}H_{34}Cl_2N_2Ru_2S_2$ (687.72): calcd. C 41.92, H 4.98, N 4.07, S 9.32, Cl 10.31; found C 41.40, H 4.92, N 4.00, S 9.40, Cl 10.24.

[Ru(*p*-Cy)Cl]₂(μ-Et₂DTO) (12b): This reddish compound was obtained as described for **12a** by using **2** (176.3 mg, 1 mmol) in place of **1**. Yield: 501 mg, 70%. ^{1}H NMR ($CDCl_3$): δ = 1.14, 1.23 [2 d, 6 H each, $^3J_{H,H}$ = 6.6 Hz, $CH(CH_3)_2$, cymene], 1.47 (t, 6 H, $^3J_{H,H}$ = 6.6 Hz, NCH_2CH_3), 2.20 (s, 6 H, CH_3, cymene), 2.81 [seven lines, 2 H, $^3J_{H,H}$ = 6.6 Hz, $CH(CH_3)_2$, cymene], 4.08, 4.57 (2 dq, 2 H each, $^2J_{H,H}$ = 13.6 Hz, $^3J_{H,H}$ = 7.0 Hz, NCH_2CH_3),

4.99, 5.14, 5.31, 5.40, (4 d, 2 H each, $^3J_{H,H}$ = 6.6 Hz, $H^{2,3,5,6}$, cymene). $^{13}C\{^1H\}$ NMR ($CDCl_3$): δ = 11.9 (s, NCH_2CH_3), 18.5 (s, CH_3, cymene), 21.8, 22.8 [2 s, $CH(CH_3)_2$, cymene], 30.7 [s, $CHCH_3)_2$, cymene], 58.3 (s, NCH_2CH_3), 80.4, 81.7, 85.1, 86.5, (4 s, $C^{2,3,5,6}$, cymene), 100.0, 104.5 (2 s, $C^{1,4}$, cymene), 188.3 (s, CS). $C_{26}H_{38}Cl_2N_2Ru_2S_2$ (715.77): calcd. C 43.63, H 5.35, N 3.91, S 8.96, Cl 9.91; found C 43.41, H 5.38, N 3.82, S 8.98, Cl 9.70.

[Ru(*p*-Cy)Cl]$_2$(μ-*n*Pr$_2$DTO) (12c): This compound was obtained as a reddish powder from [(η^6-*p*, cymene)$RuCl_2]_2$ (612.4 mg, 1 mmol) and **3** (204.3 mg, 1 mmol) following the procedure reported for **12a**. Yield: 521 mg, 70%. ^1H NMR ($CDCl_3$): δ = 1.14, 1.23 [2 d, 6 H each, $^3J_{H,H}$ = 6.6 Hz, $CH(CH_3)_2$, cymene], 1.22 (t, 6 H, $^3J_{H,H}$ = 7.3 Hz, $NCH_2CH_2CH_3$), 1.52÷1.96 (m, 4 H, $NCH_2CH_2CH_3$), 2.19 (s, 6 H, CH_3, cymene), 2.81 [seven lines, 2 H, $^3J_{H,H}$ = 6.8 Hz, $CH(CH_3)_2$, cymene], 3.91, 4.46, (2 m, 2 H each, $^2J_{H,H}$ = 13.0 Hz, $^3J_{H,H}$ = 6.0 Hz, $NCH_2CH_2CH_3$), 4.97, 5.13, 5.28, 5.38 (4 d, 2 H each, $^3J_{H,H}$ = 6.8 Hz, $H^{2,3,5,6}$, cymene). $^{13}C\{^1H\}$ NMR ($CDCl_3$): δ = 12.0 (s, $NCH_2CH_2CH_3$), 18.6 (s, CH_3, cymene), 22.7, 22.8 [2 s, $CH(CH_3)_2$, cymene], 20.1 (s, $NCH_2CH_2CH_3$), 30.7 [s, $CH(CH_3)_2$, cymene], 65.7 (s, $NCH_2CH_2CH_3$), 80.5, 81.5, 85.5, 86.5 (4 s, $C^{2,3,5,6}$, cymene), 100.0, 105.0 (2 s, $C^{1,4}$, cymene), 189.0 (s, CS). $C_{28}H_{42}Cl_2N_2Ru_2S_2$ (743.82): calcd. C 45.21, H 5.69, N 3.77, S 8.62, Cl 9.53; found C 45.35, H 5.71, N 3.65, S 8.53, Cl 9.38.

[Ru$_2$(*p*-Cy)$_2$Cl$_2$](μ-*n*Bu$_2$DTO) (12d): This reddish compound was prepared as described for **12a** by using **4** (232.4 mg, 1 mmol) in place of **1**. Yield: 540 mg, 70%. ^1H NMR ($CDCl_3$): δ = 1.04 (t, 6 H, $^3J_{H,H}$ = 7.1 Hz, $NCH_2CH_2CH_2CH_3$), 1.14, 1.24 [2 d, 6 H each, $^3J_{H,H}$ = 6.9 Hz, $CH(CH_3)_2$, cymene], 1.42÷2.19 (m, 8 H, $NCH_2CH_2CH_2CH_3$), 2.20 (s, 6 H, CH_3, cymene), 2.81 [seven lines, 2 H, $^3J_{H,H}$ = 6.9 Hz, $CH(CH_3)_2$, cymene], 3.98, 4.52 (2 dt, 2 H each, $^2J_{H,H}$ = 13.5 Hz, $^3J_{H,H}$ = 6.9 Hz, $NCH_2CH_2CH_2CH_3$), 4.98, 5.13, 5.30, 5.39, (4 d, 2 H each, $^3J_{H,H}$ = 5.5 Hz, $H^{2,3,5,6}$, cymene). $^{13}C\{^1H\}$ NMR ($CDCl_3$): δ = 14.0 (s, $NCH_2CH_2CH_2CH_3$), 18.7 (s, CH_3, cymene), 21.0 (s, $NCH_2CH_2CH_2CH_3$), 22.7, 21.9 [2 s, $CH(CH_3)_2$, cymene], 28.5 (s, $NCH_2CH_2CH_2CH_3$), 30.7 [s, $CH(CH_3)_2$, cymene], 69.9 (s, $NCH_2CH_2CH_2CH_3$), 80.4, 81.6, 84.9, 86.7, (4 s, $C^{2,3,5,6}$, cymene), 99.9, 104.6 (2 s, $C^{1,4}$, cymene), 189.9 (CS). $C_{30}H_{46}Cl_2N_2Ru_2S_2$ (771.8): calcd. C 46.68, H 6.01, N 3.63, S 8.31, Cl 9.19; found C 46.69, H 6.11, N 3.48, S 8.24, Cl 9.10.

[Ru(*p*-Cy)Cl]$_2$(μ-Isoamyl$_2$DTO) (12e): This reddish compound was prepared as described for **12a** by using **5** (260.5 mg, 1 mmol) in place of **1**. Yield: 600 mg, 70%. ^1H NMR ($CDCl_3$): δ = 1.03 [d, 6 H, $^3J_{H,H}$ = 7.3 Hz, $NCH_2CH_2CH(CH_3)_2$], 1.15, 1.25 [2 d, 6 H each,, $^3J_{H,H}$ = 6.9 Hz, $CH(CH_3)_2$, cymene], 1.62−2.19 [m, 6 H, $NCH_2CH_2CH(CH_3)_2$], 2.19 (s, 6 H, CH_3, cymene), 2.82 [seven lines, $^3J_{H,H}$ = 6.9, 2 H, $CH(CH_3)_2$, cymene], 4.03, 4.50 [2 dt, 2 H each, $^2J_{H,H}$ = 13.2 Hz, $^3J_{H,H}$ = 5.9 Hz, $NCH_2CH_2CH(CH_3)_2$], 4.99, 5.21, 5.31, 5.40 (4 d, 2 H each, $^3J_{H,H}$ = 5.6 Hz, $H^{2,3,5,6}$, cymene). $^{13}C\{^1H\}$ NMR ($CDCl_3$): δ = 18.7 (s, CH_3, cymene), 22.0, 22.7 [2 s, $CH(CH_3)_2$, cymene], 22.7 [s, $NCH_2CH_2CH(CH_3)_2$], 27.2 [s, $NCH_2CH_2CH(CH_3)_2$], 34.7 [s, $CH(CH_3)_2$, cymene], 34.8 [s, $NCH_2CH_2CH(CH_3)_2$], 62.8 [s, $NCH_2CH_2CH(CH_3)_2$], 80.2, 81.2, 84.7, 86.9, (4 s, $C^{2,3,5,6}$, cymene), 99.7, 104.5 (2 s, $C^{1,4}$, cymene), 188.0 (CS). $C_{32}H_{50}Cl_2N_2Ru_2S_2$ (799.93): calcd. C 48.05, H 6.30, N 3.50, S 8.02, Cl 8.86; found C 48.10, H 6.40, N 3.40, S 8.00, Cl 8.81.

[Ru(*p*-Cy)Cl]$_2$(μ-Benzyl$_2$DTO) (12f): This reddish compound was prepared as described for **12a** by using **6** (324.5 mg, 1 mmol) in place of **1**. Yield: 588 mg, 70%. ^1H NMR ($CDCl_3$): δ = 1.14, 1.33 [2d, 3 H each, $^3J_{H,H}$ = 6.8 Hz, $CH(CH_3)_2$, cymene], 2.10 (s, 3 H, CH_3, cymene), 2.68 [seven lines, 1 H, $^3J_{H,H}$ = 6.8 Hz, $CH(CH_3)_2$, cymene], 4.20, 4.50 (2 d, 2 H each, $^2J_{H,H}$ = 14.7 Hz $NCH_2C_6H_5$), 4.65, 4.71, 5.17, 5.21, (4d, 1 H each, $^3J_{H,H}$ = 5.5 Hz, $H^{2,3,5,6}$, cymene), 7.37 (m, 3 H, $H^{m,p}$ of $NCH_2C_6H_5$), 7.51 (d, 2 H, $^3J_{H,H}$ = 7.6 Hz, $H_o$of $NCH_2C_6H_5$). $^{13}C\{^1H\}$ NMR ($CDCl_3$): δ = 18.4 (s, CH_3, cymene), 21.6, 22.3 [2 s, $CH(CH_3)_2$, cymene], 30.7 [s, $CH(CH_3)_2$, cymene], 66.3 (s, $NCH_2C_6H_5$), 79.7, 82.0, 83.3, 83.8, (4 s, $C^{2,3,5,6}$, cymene), 99.4, 105.0 (2 s, $C^{1,4}$, cymene), 128.1−129.1 (CH^{Ph} of $NCH_2C_6H_5$), 133.9 (s, C_{quat} of $NCH_2C_6H_5$), 187.2 (s, CS). $C_{36}H_{42}Cl_2N_2Ru_2S_2$ (839.91): calcd. C 51.48, H 5.04, N 3.34, S 7.63, Cl 8.44; found C 51.43, H 5.10, N 3.32, S 7.60, Cl 8.20.

[Ru(*p*-Cy)Cl]$_2$(μ-*p*-Tolyl$_2$DTO) (12g): This reddish compound was prepared as described for **12a** by using **7** (324.5 mg, 1 mmol) in place of **1**. Yield: 588 mg, 70%. ^1H NMR ($CDCl_3$): δ = 1.07, 1.10 [2 d, 6 H each, $^3J_{H,H}$ = 6.9 Hz, $CH(CH_3)_2$, cymene], 2.05 (s, 6 H, CH_3, cymene), 2.42 (s, 6 H, $NC_6H_5CH_3$), 2.61 [seven lines, 2 H, $^3J_{H,H}$ = 6.9 Hz, $CH(CH_3)_2$, cymene], 4.60, 4.76, 4.79, 5.01 (4 d, 2 H each, $^3J_{H,H}$ = 5.7 Hz, $H^{2,3,5,6}$, cymene), 7.25 (2 d, 4 H, $^3J_{H,H}$ = 8.4 Hz, H_m of $NC_6H_4CH_3$), 7.44 (m, 4 H, H_o of $NC_6H_4CH_3$). $^{13}C\{^1H\}$ NMR ($CDCl_3$): δ = 18.7 (s, CH_3, cymene), 21.3 (s, $NC_6H_5CH_3$), 21.6, 22.9 (2 s, $CH(CH_3)_2$, cymene), 30.7 [s, $CH(CH_3)_2$, cymene], 81.4, 81.5, 84.4, 87.5 (4 s, $C^{2,3,5,6}$, cymene), 100.9, 103.7 (2 s, $C^{1,4}$, cymene), 123.4, 129.5 (2 s, CH_{Ph} of $NC_6H_5CH_3$), 135.7, 152.9 (2 s, C_{quat} of $NC_6H_5CH_3$), 192.4 (s, CS). $C_{36}H_{42}Cl_2N_2Ru_2S_2$ (839.91): calcd. C 51.48, H 5.04, N 3.34, S 7.63, Cl 8.44; found C 51.35, H 5.09, N 3.28, S 7.65, Cl 8.32.

Complex {[Ru(*p*-Cy)Cl(H$_2$-(R)-1-phenylethyl$_2$DTO)]$^+$, (Cl^-)} (13a): To a solution of $[(\eta^6$-*p*-cymene)$RuCl_2]_2$ (612.4 mg, 1 mmol) dissolved in chloroform (100 mL), was added **8** (657.0 mg, 2 mmol), and the mixture allowed to stand for 0.5 h at room temperature. After this time the solution was concentrated to a small volume (about 10 mL), and petroleum ether 40−60 (100 mL) was added. Complex **13a** precipitated as a brown powder. Yield: 622 mg, 98% − ^1H NMR ($CDCl_3$): δ = 1.13, 1.16 [2 d, 3 H each, $^3J_{H,H}$ = 7.0 Hz, $CH(CH_3)_2$, cymene], 1.89, 1.93 [2 d, 3 H each, $^3J_{H,H}$ = 7.0 Hz, $NHCH(CH_3)Ph$], 2.19 (s, 3 H, CH_3, cymene), 2.62 [seven lines, 1 H, $^3J_{H,H}$ = 7.0 Hz, $CH(CH_3)_2$, cymene], 5.26, 5.41 [2 q, 1 H each, $^3J_{H,H}$ = 7.0 Hz, $NHCH(CH_3)Ph$], 5.39, 5.45, 5.51, 5.56, (4 d, 1 H each, $^3J_{H,H}$ = 5.9 Hz, $H^{2,3,5,6}$, cymene), 7.34 [m, 6 H, $H_{m,p}$ of $NHCH(CH_3)Ph$], 7.56, 7.61 [2 d, 4 H, $^3J_{H,H}$ = 7.0 Hz, H_o of $NHCH(CH_3)Ph$], 13.3 [br. s, 2 H, $NHCH(CH_3)Ph$]. $^{13}C\{^1H\}$ NMR (298 K, $CDCl_3$): δ = 18.7 (s, CH_3, cymene), 21.5, 22.4 [2 s, $NHCH(CH_3)Ph$], 22.2, 22.5 [2 s, $CH(CH_3)_2$, cymene], 31.2 [s, $CH(CH_3)_2$, cymene], 60.5, 61.0 [2 s, $NHCH(CH_3)Ph$], 86.5, 86.7, 87.4, 87.8 (4 s, $C^{2,3,5,6}$, cymene), 104.3, 107.7 (2 s, $C^{1,4}$, cymene), 127.4−128.8 [CH_{Ph} of $NHCH(CH_3)Ph$], 139.8, 140.4 [2 s, C_{quat} $NHCH(CH_3)Ph$], 186.9, 187.1 (2 s, CS). $C_{28}H_{34}Cl_2N_2RuS_2$ (634.69): calcd. C 52.99, H 5.40, N 4.41, S 10.10, Cl 11.17; found C 52.88, H 5.52, N 4.45, S 10.05, Cl 11.12.

{Ru(*p*-Cy)Cl(H$_2$-(*R*,S)-1-phenylethyl$_2$DTO)$^+$, (Cl^-)} (13b): This brown compound was prepared as described for **13a** by using **9** (657.0 mg, 2 mmol) in place of **8**. Yield: 609 mg, 96%. ^1H NMR ($CDCl_3$): δ = 1.08 [d, 6 H, $^3J_{H,H}$ = 7.0 Hz, $CH(CH_3)_2$, cymene], 1.93 [d, 6 H, $^3J_{H,H}$ = 7.0 Hz, $NHCH(CH_3)Ph$], 2.13 (s, 3 H, CH_3, cymene), 2.52 [seven lines, 1 H, $^3J_{H,H}$ = 7.0 Hz, $CH(CH_3)_2$, cymene], 5.37, 5.49 (2 d, 2 H each, $^3J_{H,H}$ = 5.9 Hz, $H^{2,3,5,6}$, cymene), $NHCH(CH_3)Ph$ obscured by *p*-cymene ring signals, 7.33 [m, 6 H, $H_{m,p}$ of $NHCH(CH_3)Ph$], 7.58 [d, 4 H, $^3J_{H,H}$ = 7.0 Hz, H_o $NHCH(CH_3)Ph$], 13.4 [br. s, 2 H, $NHCH(CH_3)Ph$]. $^{13}C\{^1H\}$ NMR ($CDCl_3$): δ = 18.4 (s, CH_3, cymene), 21.6 and 22.3 [2 s, $CH(CH_3)_2$, cymene], 22.4 (s, $NHCH(CH_3)Ph$], 30.7 [s, $CH(CH_3)_2$, cymene], 60.6 [s, $NHCH(CH_3)Ph$], 79.7, 83.3 (2s, $C^{2,3,5,6}$, cymene), 99.4, 105.0 (2 s, $C^{1,4}$, cymene), 128.58 −140.19 (aromatic carbons of $NHCH(CH_3)Ph$), 185.8 (s, CS). − $RuC_{28}H_{34}N_2S_2Cl_2$ (634.69):

calcd. C 52.99, H 5.40, N 4.41, S 10.10, Cl 11.17; found C 52.87, H 5.53, N 4.44, S 10.07, Cl 11.15.

{Ru(*p*-Cy)Cl(H_2-*i*Pr_2DTO)$^+$, (Cl^-)} (13c): This brown compound was prepared as described for **13a** by using **10** (408.6 mg, 2 mmol) in place of **8**. The reaction product was a diastereoisomer mixture analysed without purification. Yield: 490 mg, 96%. ^{1}H NMR ($CDCl_3$): δ = 1.24 [d, 6 H, $^3J_{H,H}$ = 6.9 Hz, CH(CH_3)$_2$, cymene], 1.24 [d, 12 H, $^3J_{H,H}$ = 6.9 Hz, NHCH(CH_3)$_2$], 5.64, 5.49 (2 d, 2 H each, $^3J_{H,H}$ = 6.0 Hz, $H^{2,3,5,6}$, cymene), 2.26 (s, 3 H, CH_3, cymene), 2.81 [seven lines, 1 H, $^3J_{H,H}$ = 6.9 Hz, C*H*(CH$_3$)$_2$, cymene], 12.6 [br. s, 2 H, N*H*CH(CH$_3$)$_2$], 4.17 [seven lines, $^3J_{H,H}$ = 6.9 Hz, 2 H, NHC*H*(CH$_3$)$_2$], − ^{13}C{^{1}H} NMR ($CDCl_3$): δ = 18.6 (s, CH_3, cymene), 22.2 [s, CH(*C*H$_3$)$_2$, cymene], 24.6, 24.8 [2 s, NHCH(*C*H$_3$)$_2$], 31.0 [s, *C*H(CH$_3$)$_2$, cymene], 59.9 [s, NH*C*H(CH$_3$)$_2$], 86.1, 87.0 (2 s, $C^{2,3,5,6}$, cymene), 103.9, 107.1 (2 s, $C^{1,4}$, cymene), 184.4 (s, *C*S). − $RuC_{18}H_{30}N_2S_2Cl_2$ (510.55): calcd. C 42.35, H 5.92, N 5.49, S 12.56, Cl 13.89; found C 42.27, H 5.98, N 5.45, S 12.55, Cl 13.90.

{Ru(*p*-Cy)Cl[H_2-(cyclohexyl)$_2$DTO]$^+$ (Cl^-)} (13d): This brown compound was prepared as described for **13a** by using **11** (569.0 mg, 2 mmol) in place of **8**. Yield: 567 mg, 95%. ^{1}H NMR ($CDCl_3$): δ = 1.28 [d, 6 H, $^3J_{H,H}$ = 6.7 Hz, CH(CH_3)$_2$, cymene], 1.86 (m, 20 H, CH_2 of NHC_6H_{11}), 2.29 (s, 3 H, CH_3, cymene), 2.84 [seven lines, 1 H, $^3J_{H,H}$ = 6.7 Hz, C*H*(CH$_3$)$_2$, cymene], 4.21 (m, 2 H, CH of NHC_6H_{11}), 5.50, 5.66 (2d, 2 H each, $^3J_{H,H}$ = 5.9 Hz, $H^{2,3,5,6}$, cymene), 12.6 (br. s, 2 H, N*H*C_6H_{11}). ^{13}C{^{1}H} NMR ($CDCl_3$): δ = 18.9 (s, CH_3, cymene), 22.5 [s, CH(*C*H$_3$)$_2$, cymene], 24.8, 25.0, 25.1, 30.0, 30.1 (5 s, CH_2 of NHC_6H_{11}), 31.3 [s, *C*H(CH$_3$)$_2$, cymene], 60.3 (s, CH of NHC_6H_{11}), 86.3, 87.3 (2 s, $C^{2,3,5,6}$, cymene), 104.1, 107.5, (2 s, $C^{1,4}$, cymene), 184.8 (s, *C*S). − $RuC_{24}H_{38}N_2S_2Cl_2$ (590.68): calcd. C 48.80, H 6.48, N 4.74, S 10.86, Cl 12.00; found C 48.84, H 6.55, N 4.71, S 10.80, Cl 12.04.

Ru(*p*-Cy)Cl[H-(*R*)-1-(phenylethyl)$_2$DTO] (14a): A solution of **13a** (634.7 mg, 1 mmol) dissolved in about 15 mL of chloroform was purified by column chromatography. During chromatography, owing to HCl loss, the brown solution turned yellow. The yellow eluate was concentrated to a small volume (about 10 mL), and then petroleum ether/diethyl ether (boiling range 40−60 °C) was added (about 100 mL). The complex precipitated as yellow powder. Yields: 425 mg, 71%. ^{1}H NMR ($CDCl_3$): δ = 1.21, 1.22 [2 d, 3 H each, $^3J_{H,H}$ = 7.0 Hz, CH(CH_3)$_2$, cymene], 1.56 and 1.58 [2 d, 3 H each, $^3J_{H,H}$ = 7.0 Hz, NHCH(CH_3)Ph], 2.25 (s, 3 H, CH_3, cymene), 2.79 [seven lines, 1 H, $^3J_{H,H}$ = 7.0 Hz, C*H*(CH$_3$)$_2$, cymene], 5.2 [NHC*H*(CH$_3$)Ph partially obscured by *p*-cymene ring signals], 5.36 (m, 4 H, $H^{2,3,5,6}$, cymene), 7.35 [m, 10 H, $H_{o,m,p}$ of NHCH(CH$_3$)Ph], − ^{13}C{^{1}H} NMR ($CDCl_3$): δ = 18.6 (s, CH_3, cymene), 21.0, 22.4 [2s, NHCH(*C*H$_3$)Ph], 22.4 and 22.5 [2 s, (CH*C*H$_3$)$_2$, cymene], 30.9 [s, *C*H(CH$_3$)$_2$, cymene], 55.8, 58.0 [2 s, NH*C*H(CH$_3$)Ph], 84.5, 84.6, 85.7, 85.8 (4 s, $C^{2,3,5,6}$, cymene), 101.6, 104.7 (2 s, $C^{1,4}$, cymene), 126.61−143.08 [C_{Ph} of NHCH(CH$_3$)Ph], 177.9, 181.0 (2 s, *C*S). − $RuC_{28}H_{33}N_2S_2Cl$ (598.23): calcd. C 56.22, H 5.56, N 4.68, S 10.72, Cl 5.93; found C 56.25, H 5.55, N 4.72, S 10.80, Cl 5.85.

Ru(*p*-Cy)Cl[H-(*R*,S)-1-(phenylethyl)$_2$DTO] (14b): This compound was obtained by following the procedure reported for **14a**, starting from complex **13b** (634.7 mg, 1 mmol). Yields: 425 mg, 71%. ^{1}H NMR ($CDCl_3$): δ = 1.12 [d, 6 H, $^3J_{H,H}$ = 7.0 Hz, CH(CH_3)$_2$, cymene], 1.59 [d, 6 H, $^3J_{H,H}$ = 7.0 Hz, NHCH(CH_3)Ph], 2.21 (s, 3 H, CH_3, cymene), 2.66 [seven lines, 1 H, $^3J_{H,H}$ = 7.0 Hz, C*H*(CH$_3$)$_2$, cymene], ≈ 5.3 [m, NHC*H*(CH$_3$)Ph partially obscured by *p*-cymene ring signals], 5.36 (m, 4 H, $H^{2,3,5,6}$, cymene), 7.3 [m, 10 H, $H_{o,m,p}$ of NHCH(CH$_3$)Ph]. ^{13}C{^{1}H} NMR ($CDCl_3$): δ = 18.5 (s, CH_3, cymene), 20.9, 22.4 [2 s, NHCH(*C*H$_3$)Ph], 22.4 [s, CH(*C*H$_3$)$_2$], 30.8 [s, *C*H(CH$_3$)$_2$, cymene], 57.9 [s, NH*C*H(CH$_3$)Ph], 84.6, 85.5, (2 s, $C^{2,3,5,6}$, cymene), 101.6, 104.7 (2 s, $C^{1,4}$, cymene), 128.4−143.3 [aromatic carbons of NHCH(CH$_3$)Ph], 179.6 (1s, *C*S). − $RuC_{28}H_{33}N_2S_2Cl$ (598.23): calcd. C 56.22, H 5.56, N 4.68, S 10.72, Cl 5.93; found C 56.23, H 5.57, N 4.70, S 10.82, Cl 5.83.

[Ru(*p*-Cy)Cl(H−*i*Pr_2DTO)] (14c): This compound was obtained following the procedure reported for **14a**, starting from **13c** (510.5 mg, 1 mmol). Yields: 379 mg, 80%. ^{1}H NMR ($CDCl_3$): δ = 1.24 [d, 6 H, $^3J_{H,H}$ = 6.8 Hz, CH(CH_3)$_2$, cymene], 1.25 [d, 12 H, $^3J_{H,H}$ = 5.8 Hz, NCH(CH_3)$_2$], 2.24 (s, 3 H, CH_3, cymene), 2.85 [seven lines, 1 H, $^3J_{H,H}$ = 6.8 Hz, C*H*(CH$_3$)$_2$, cymene], 4.36 [seven lines, 2 H, $^3J_{H,H}$ = 5.8 Hz, NC*H*(CH$_3$)$_2$], 5.30, 5.47 (2 d, 2 H each, $^3J_{H,H}$ = 5.8 Hz, $H^{2,3,5,6}$, cymene). − $RuC_{18}H_{29}N_2S_2Cl$ (474.09): calcd. C 45.60, H 6.17, N 5.91, S 13.52, Cl 7.48; found C 45.52, H 6.27, N 5.90, S 13.48, Cl 7.55.

{Ru(*p*-Cy)Cl[H−(cyclohexyl)$_2$DTO]} (14d): This compound was obtained following the procedure reported for **14a**, starting from complex **13d** (590.7 mg, 1 mmol). Yields: 432 mg, 78%. ^{1}H NMR ($CDCl_3$): δ = 1.25 [d, 6 H, $^3J_{H,H}$ = 6.9 Hz, CH(CH_3)$_2$, cymene], 1.25−2.02 (m, 20 H, CH_2 of $NHCC_6H_{11}$), 2.23 (s, 3 H, CH_3, cymene), 2.84 [seven lines, 1 H, $^3J_{H,H}$ = 6.90 Hz, C*H*(CH$_3$)$_2$, cymene], 4.04 (m, 2 H, CH of $NHCC_6H_{11}$), 5.30, 5.45 (2 d, 2 H each, $^3J_{H,H}$ = 6.3 Hz, $H^{2,3,5,6}$, cymene). ^{13}C {^{1}H} NMR ($CDCl_3$): δ = 18.4 (s, CH_3, cymene), 22.2 [s, CH(*C*H$_3$)$_2$, cymene], 24.2, 24.4, 25.3, 31.2, 31.5, (5 s, CH_2 of $NHCC_6H_{11}$), 30.6 [s, *C*H(CH$_3$)$_2$, cymene], 57.2 (s, CH of $NHCC_6H_{11}$), 85.2, 84.0 (2 s, $C^{2,3,5,6}$, cymene), 104.1, 101.1 (2 s, $C^{1,4}$, cymene), 177.4 (s, *C*S). − $RuC_{24}H_{37}N_2S_2Cl$ (554.22): calcd. C 52.01, H 6.73, N 5.05, S 11.57, Cl 6.40; found C 52.07, H 6.75, N 5.01, S 11.51, Cl 6.47.

Single-Crystal X-ray Diffraction Studies of 12f: Suitable crystals of the complex **12f** (with R = R′ = benzyl) were obtained by slow evaporation of solvent from a chloroform/MeOH (1:1) solution. Diffraction data were collected on a Siemens R3m/V automatic four-circle diffractometer. Lattice parameters were obtained from least-squares refinement of the setting angles of 30 reflections within 15 ≤ 2θ ≤ 30° range. A summary of the crystallographic data and the structure refinement is reported in Table 1. A significant crystal deterioration was evidenced by the measurement of three standard reflections, monitored every 97 measurements. When the standard intensities decreased below 40% of the starting values, a new crystal was mounted to complete data collection (one third of the whole data). The reflection intensities were evaluated by a learnt-profile procedure[22] among 2θ shells, and then corrected for Lorentz-polarization effects. The data of each set were scaled on the standard intensities separately, while an inter-scaling factor was included and refined in the last least-square model recycling. No account was taken for absorption and extinction effects.

The structure was resolved by standard methods with the SHELXTL-PLUS system[23] and subsequently completed by a combination of least-squares technique and Fourier Syntheses. All non-hydrogen atoms were refined anisotropically. Whilst the final difference Fourier maps showed several hydrogen positions, the H atoms were placed in calculated positions (d_{X-H} = 0.960 Å) and included in the refinement among the "riding model" method with a unique common refined thermal isotropic displacement parameter [U_{iso} = 0.064(6) Å^2]. The refinement was carried out by the full-matrix least-squares technique, minimising the function $\Sigma w(|F_o| - |F_c|)^2$. In the last difference Fourier map, obtained with

the final weighting scheme $w^{-1} = [\sigma^2(F) + 0.0023*(F)^2]$, the minimum and maximum density residuals were −0.48 and 0.49 eÅ^{-3}, respectively. Neutral-atom scattering factors and anomalous dispersion corrections come from ref.[24]

All calculations were performed using the SHELXTL-PLUS system. The final geometrical calculations and drawings were carried out with the PARST program[25] and the XP utility of the Siemens package, respectively. Selected bond lengths and bond angles are reported in Table 2. By considering that the complex **12f** is placed at a crystallographic inversion centre, Figure 2 shows the atom-labelling scheme of the asymmetric moiety, which represents half a molecule.

Crystallographic data for the structure reported in this paper have been deposited with the Cambridge Crystallographic Data Centre as supplementary publication no. CCDC 164512. Copies of the data can be obtained free of charge on applicaton to The Director, CCDC, 12 Union Road,m Cambridge CB2 1EZ, UK [Fax: (internat.) + 44 (1223) 336-033; E-mail: deposit@ccdc.cam.ac.uk

[1] For a review see: M. A. Bennett, C. Kahn, E. Wenger, in "*Comprehensive Organometallic Chemistry*" vol. VII p. 473, (Eds.: Abel, Stone, Wilkinson), Pergamon Press, **1995**.

[2] [2a] H. Werner, R. Werner, *Chem. Ber.* **1982**, *115*, 3766. [2b] S. K. Mandal, A. R. Chakravarty, *Polyhedron* **1992**, *11*, 823. [2c] F. Faraone, G. A. Loprete, G. Tresoldi, *Inorg. Chim. Acta* **1979**, *34*, L251. [2d] F. Estevan, P. Lahuerta, J. LaTorre, A. Sanchez, C. Sieiro, *Polyhedron* **1987**, *6*, 437.

[3] [3a] R. Noyori, H. Takaya, *Acc. Chem. Res.* **1990**, *23*, 345. [3b] K. T. Wan, M. E. Davis, *Tetrahedron: Asymmetry* **1993**, *4*, 2461. [3c] P. Krasik, H. Alper, *Tetrahedron: Asymmetry* **1992**, *3*, 1283.

[4] F. Hapiot, F. Agbossou, A. Mortreux, *Tetrahedron: Asymmetry* **1994**, *5*, 515.

[5] S. Lanza, G. Bruno, F. Nicolò, R. Scopelliti, *Tetrahedron: Asymmetry* **1996**, *12*, 3347.

[6] G. Rosace, G. Bruno, L. Monsù Scolaro, F. Nicolò, S. Sergi, S. Lanza, *Inorg. Chim. Acta* **1993**, *208*, 59 and references therein.

[7] S. Lanza, L. Monsù Scolaro, G. Rosace, *Inorg. Chim. Acta* **1994**, *227*, 63.

[8] [8a] J. J. Girerd, S. Jeannin, Y. Jeannin, O. Kahn, *Inorg. Chem.* **1978**, *17*, 3034. [8b] C. Chauvel, J. J. Girerd, Y. Jeannin, O. Kahn, G. Lavigne, *Inorg. Chem.* **1979**, *18*, 3015.

[9] O. Ermer, S. A. Mason, *J. Chem. Soc., Chem. Commun.* **1983**, 53.

[10] [10a] O. L. Antolini, A. C. Fabretti, G. Franchini, L. Menabue, G. C. Pellacani, H. O. Desseyn, R. Dommisse, H. C. Hofmans, *J. Chem. Soc., Dalton Trans.* **1987**, 1921. [10b] M. G. B. Drew, J. M. Kisenyi, G. R. Willey, *J. Chem. Soc., Dalton Trans.* **1984**, 1723.

[11] G. Rosace, G. Giuffrida, M. Saitta, G. Guglielmo, S. Campagna, S. Lanza, *Inorg. Chem.* **1996**, *35*, 6816.

[12] R. Noyori, "*Asymmetric Catalyst in Organic Synthesis*", John Wiley & Sons, New York, **1994**.

[13] [13a] P. B. Mackenzie, J. Whelan, B. Bosnich, *J. Am. Chem. Soc.* **1985**, *107*, 2046. [13b] P. R. Auburn, P. B. Mackenzie, B. Bosnich, *J. Am. Chem. Soc.* **1985**, *107*, 2033. [13c] T. Hayashy, A. Yamamoto, *Tetrahedron Lett.* **1988**, *29*, 669. [13d] T. Hayashy, A. Yamamoto, Y. Yto, E. Nishioka, H. Miura, K. Yanagy, *J. Am. Chem. Soc.* **1989**, *111*, 6031. [13e] M. Savamura, H. Nagata, H. Sakamoto, Y. Yto, *J. Am. Chem. Soc.* **1992**, *114*, 2586.

[14] [14a] A. Togni, *Tetrahedron: Asymmetry* **1991**, *2*, 683. [14b] D. Tanner, *Angew. Chem. Int. Ed. Engl.* **1994**, *33*, 599.

[15] [15a] A. Pfaltz, *Acc. Chem. Res.* **1993**, *26*, 339. [15b] P. von Matt, A. Pfaltz, *Angew. Chem. Int. Ed. Engl.* **1993**, *32*, 556. [15c] K. Ohkita, H. Kurosawa, T. Hasegawa, T. Hirao, I. Ikeda, *Organometallics* **1993**, *12*, 3211.

[16] C. Claver, S. Castillon, N. Ruitz, G. Delogu, S. Fabbri, S. Gladiali, *J. Chem. Soc., Chem. Commun.* **1993**, 1883.

[17] J. Sprinz, M. Kiefer, G. Helmchen, M. Reggelein, G. Huttner, J. M. J. Williams, *Tetrahedron Lett.* **1993**, *34*, 2015.

[18] G. C. Frost, J. M. J. Williams, *Tetrahedron: Asymmetry* **1993**, *4*, 1785.

[19] K. Mislow, J. Siegel, *J. Am. Chem. Soc.* **1984**, *106*, 3319.

[20] G. Garcia, I. Solano, G. Sanchez, M. D. Santana, G. Lopez, J. Casabo, E. Molins, C. Miravitlles, *J. Organomet. Chem.* **1994**, *467*, 119.

[21] Search results on analogous DTO fragments through CSDS release 5.18 (october 1999): F. H. Allen, J. E. Davies, J. J. Galloy, O. Johnson, O. Kennard, C. F. Macrae, E. M. Mitchell, G. F. Mitchell, J. M. Smith, D. G. Watson, *J. Chem. Info. Comp. Sci.* 31, 187, **1991**.

[22] R. Diamond, *Acta Crystallogr., Sect. A* **1969**, *25*, 43.

[23] SHELXTL-PLUS, version 4.2, Siemens Analytical X-ray Instruments Inc., Madison Wisconsin, **1991**.

[24] *'International Tables for X-ray Crystallography'*, vol. IV, Kynoch Press, Birmingham, **1974**.

[25] M. Nardelli, *Comput. Chem.* **1983**, *7*, 95 − locally modified version).

[26] R. N. Hurd, G. De La Mater, G. C. McElheny, R. J. Tuner, V. H. Wallingford, *J. Org. Chem.* **1961**, *26*, 3980.

[27] M. C. Aversa, P. Bonaccorsi, D. W. Bruce, F. Caruso, P. Giannetto, S. Lanza, S. Morrone, *Inorg. Chim. Acta* **1997**, *256*, 235.

[28] [28a] M. A. Bennett, A. K. Smith, *J. Chem. Soc., Dalton Trans.* **1974**, 233. [28b] R. A. Zelonka, M. C. Baird, *Can. J. Chem.* **1972**, *50*, 3063.

Received June 4, 2001
[I01202]

Tetra(pyrrolidino)diborane(4), $[(C_4H_8N)_2B]_2$, as a New Improved Alternative Synthetic Route to Bis(pinacolato)diborane(4) − Crystal Structures of the Intermediates

Hijazi Abu Ali,[a] Israel Goldberg,[b] and Morris Srebnik*[a]

Keywords: Boranes / Tris(pyrrolidino)borane / Tetra(pyrrolidino)diborane(4) / Solvolysis / Bis(pinacolato)diborane(4)

The compound tetra(pyrrolidino)diborane(4) (**3**) is an important new and alternative precursor for the preparation and synthesis of bis(pinacolato)diborane(4). The latter is the major intermediate among the diborane derivatives used for many addition and insertion reactions into multiple bonds. The crystal structure of **3** and its precursor, tris(pyrrolidino)-borane, **1**, were determined. In addition the solvolysis reactions and solution behavior of **3** with alcohols were examined.

Introduction

Derivatives of diboranes,[1] in particular tetraalkoxydiboranes, have become increasingly important as a result of the accelerating use of the Suzuki coupling reaction in the synthesis of complex molecular species.[2] The preparation of arylboronates from tetraalkoxydiboranes,[3] and the addition of tetraalkoxydiboranes across alkenes,[4] alkynes,[5] diynes,[4e,5c] enynes,[4e] allenes,[4e,10a,10b] 1,3-butadienes,[4e,6] methylenecyclopropanes,[7] allylic acetates,[8] α,β-unsaturated compounds[4d,9] and various other substrates[10] have contributed to the development of the chemistry of diboranes.[11] Tetraalkoxydiboranes are generally prepared from tetradialkylaminodiboranes, by Wurtz coupling of the corresponding bis(dialkylamino)haloboranes,[12] or by reaction of bis(dialkylamino)dichlorodiboranes with lithium amides.[13] The tetraalkoxydiboranes are then obtained by solvolysis of the tetradialkylaminodiboranes with alcohols.[14]

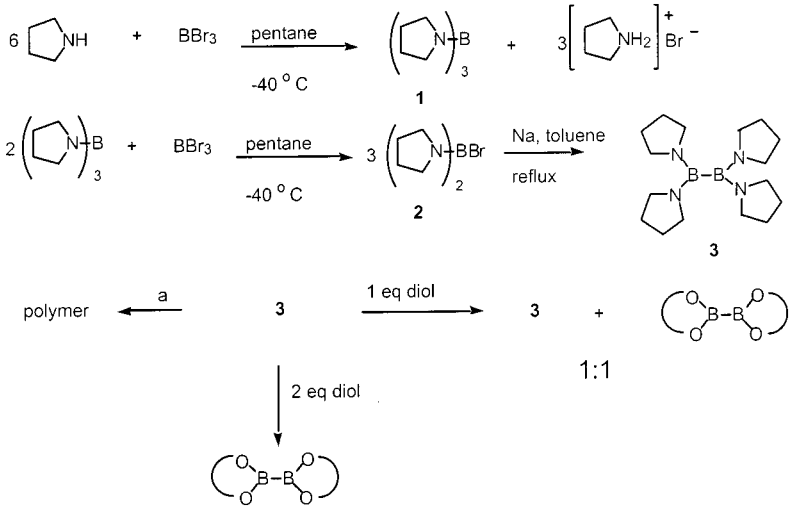

a. $CDCl_3$ or acetone, 1 day; or CO/toluene 4h. Diol=pinacol or 2-ethoxy-1,3-propoanediol

Scheme 1. Synthesis and reactions of **3**

While many tetradialkylaminodiboranes have been prepared by the above methods, few structures have been reported. In this paper we describe an improved synthesis of

[a] Department of Medicinal Chemistry and Natural products, School of Pharmacy, Hebrew University in Jerusalem, Jerusalem, 91120 Israel
Fax: (internat.) +972−2/675−8201
E-mail: msrebni@md2.huji.ac.il
[b] School of Chemistry, Tel-Aviv University, Ramat-Aviv 69987, Tel-Aviv, Israel

 © WILEY-VCH Verlag GmbH, 69451 Weinheim, Germany, 2002 1434−1948/02/0101−0073 $ 17.50+.50/0

3,[12b] its crystal structure, solution structure and solvolysis reactions, which have not been reported on previously. Compound **3**, we believe, is an important new and alternative precursor for the preparation of bis(pinacolato)diborane(4) which is the major intermediate among the diborane derivatives used for many addition and insertion reactions (see the extended reference list in the manuscript). This crucial compound can be obtained from tetra(dimethylamino)diborane(4), as described by Nöth.[15] This is the only synthetic route for this compound reported in the literature. There are several distinct disadvantages with this route. The preparation of bis(pinacolato)diborane(4) by the published route requires the use of dimethylamine, a dangerous gas above 7° C that is not easy to handle. In addition, dimethylamine is on the list of restricted chemicals, and thus is not available in many parts of the world. Alternatively, pyrrolidine is a stable liquid (87−88° C), easy to handle and is not on any restricted list of chemicals. Further, we have determined that **3**, which is a solid, is more stable to air and hydrolysis than tetra(dimethylamino)diborane(4), which is a very sensitive liquid [Various $(R_2N)_2BX$ compounds, where R = Et, *i*Pr, etc and X = Cl, Br, failed to give B−B compounds in the dehalogenation step]. However, dipyrrolidino behaved like dimethylamine, in that bis(pyrrolidino)bromoborane, **2**, was debrominated by sodium to give **3**. The precursor, tris(pyrrolidino)borane,**1**, is readily prepared from one equiv. of BBr_3 in pentane at − 40° C and six equiv. of pyrrolidine. After filtering the bromide salt, distillation afforded **1**. Bis(pyrrolidino)bromoborane was prepared from one equiv. of BBr_3 in pentane at − 40° C and two equiv. of **1** (Scheme 1). We have determined the stability of **3** in various solvents and found that the compound, while readily converted into tetraalkoxydiboranes by alcohols, polymerizes in the presence of acetone, chloroform, THF and CO/toluene. It is very stable to inert solvents like benzene, toluene and hydrocarbons.

Results and Discussion

Compound **1** crystallizes with four molecules in the asymmetric unit cell, two of which are shown in (Figure 1). The molecular entities have a planar BN_3 core, but they differ slightly in the conformation of the peripheral ring fragments. The latter are bent above and below the BN_3 plane, and are affected by severe disorder problems (in two of the four species). This is consistent with the low crystal density and loose intermolecular organization which facilitate the assumedly dynamic conformational behavior of the saturated rings at 110 K (Even at this low temperature the observed disorder of these rings could not be accounted for by a suitable combination of several static structures with partial occupancies and acceptable geometries. However, this order may still be static with several closely related positions, as this might also give rise to overlapped atoms that are not easy to resolve into separate positions). The bond lengths and angles involving B and N are similar to those previously observed in related triazaborane structures.[16]

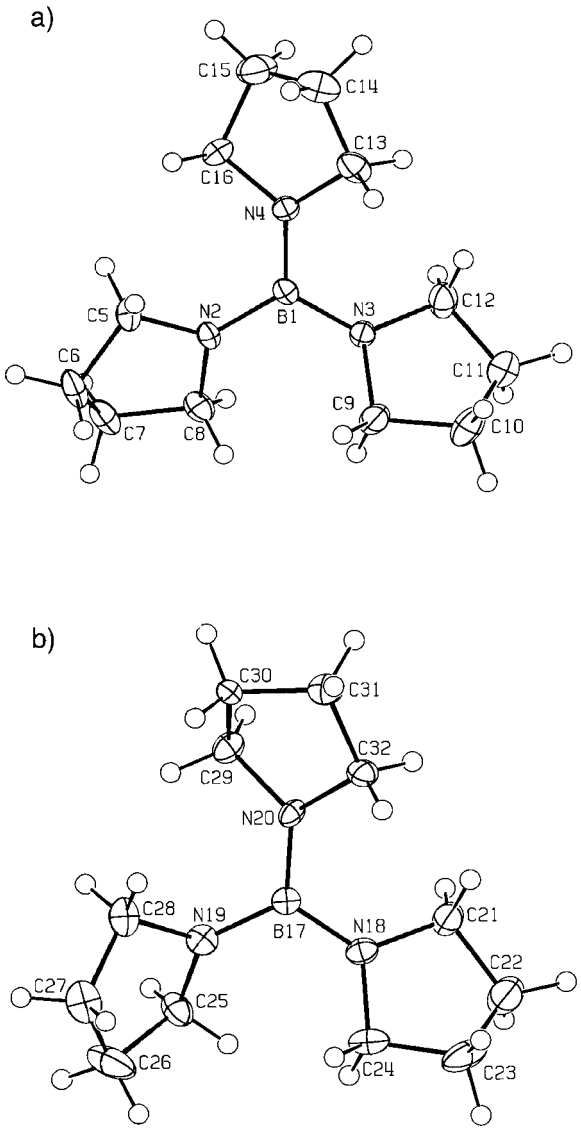

Figure 1. View of the molecular structure of **1** showing the atom numbering scheme (only the two ordered species of the asymmetric unit are shown). Ellipsoids represent thermal displacement parameters at the 50% probability level. The conformational lability of these species is reflected in the larger volume and higher anisotropy of the peripheral C-atoms. Selected bond lengths (Å) and angles (°) include: B1−N2 1.457(5), B1−N3 1.434(5), B1−N4 1.429(5), B17−N18 1.430(5), B17−N19 1.449(5), B17−N20 1.430(5), mean C−N 1.465, mean C−C 1.529; sum of angles at B1 360.0; sum of angles at B17 359.9.

The crystal structure is illustrated in (Figure 2). It shows a layered arrangement of the roughly flat molecules parallel to the *ab* plane of the unit-cell, that is stabilized by weak van der Waals forces between the lipophilic surfaces of adjacent species.

The molecular structure of **3** is shown in (Figure 3). It has a crystallographic twofold rotational axis which coincides with the B−B bond. As in related compounds, it maintains the trigonal planar geometry around the boron atoms. However, the observed B−B distance of 1.739(4) Å is slightly longer than in previously reported analogues. [12b,13,17] This may be due to the bulky pyrrolidino

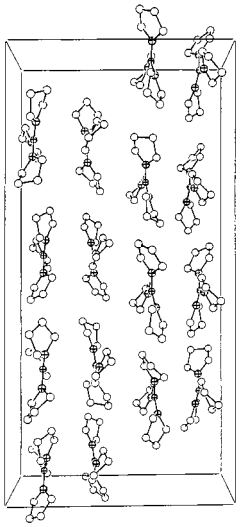

Figure 2. Crystal structure of **1** viewed approximately down the *a* axis (*b* is vertical) which shows the contents of a single unit-cell and the hypercentric layered molecular organization.

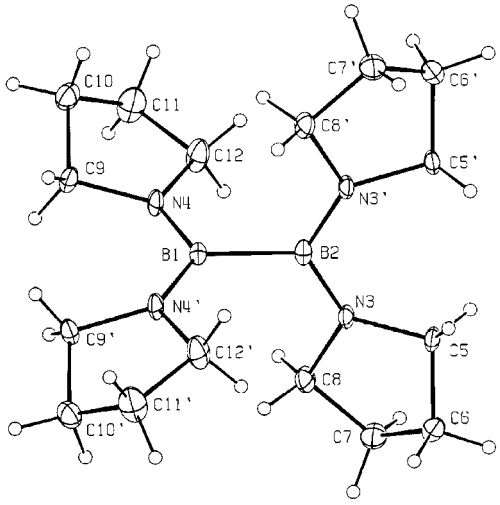

Figure 3. View of the molecular structure of **3**, showing the atom numbering scheme. Ellipsoids represent thermal displacement parameters at the 50% probability level. The molecules are located in the crystal on twofold symmetry axes; primed atoms are related to nonprimed atoms by symmetry transformation: $1 - x, y, 11/2 - z$. Selected bond lengths (Å) and angles (°) include: B1−B2 1.739(4), B1−N3 1.424(2), B1−N4 1.427(2), mean C−N 1.472, mean C−C 1.523, N4−B1−N4′ 121.7(2), N3−B2−N3′ 120.8(2), N4−B1−B2 119.1(1), N3−B2−B1 119.6(1), N4−B1−B2−N3 −103.6(1), N4−B1−B2−N3′ 76.4(1).

groups around the boron atoms. The molecule adopts a staggered conformation around the B−B bond (Figure 4) in order to avoid collision between the inner hydrogen atoms. The N−B−B−N torsion angles are 76.4 and 103.6°.[12b] The crystal structure is stabilized by weak van der Waals forces between the lipophilic surfaces of adjacent molecules, and readily cleaves along the interfaces between the molecular layers (Figure 4).

Compound **3** is monomeric in solvents like benzene or in hydrocarbons. It is more stable in air than tetra(dimethylamino)diborane(4). In terms of chemical reactivity

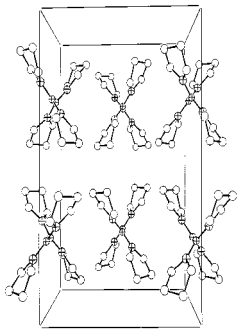

Figure 4. View of the crystal structure of **3** down the *b* axis of the unit cell (contents of 11/2 unit cells are shown). Note the staggered disposition of the five-membered rings with respect to the B−B bond, and the layered organization of the molecular entities in the crystals of this material.

and solvolysis, the pyrrolidino compound behaves in a similar manner to the tetradimethylamino analogue, but is more reactive than other tetradialkylamine derivatives. It reacts with one equiv. of pinacol to give a 1:1 mixture of bis(pinacolato)diborane(4),[15] and starting material. However, with two equiv. of pinacol, pure bis(pinacolato)diborane(4) is obtained in an 83% yield (Scheme 1). With two equiv. of 2-ethoxy-1,3-propanediol, the corresponding 2,2′-bis(5-ethoxy-1,3-dioxa-2-boracyclohexane), $[(C_5H_{10}O_3)B]_2$, is produced. Allowing a solution of freshly prepared **3** in $CDCl_3$, acetone or in CO in toluene, for 4 h results in the disappearance of starting material and the precipitation of a new compound, as indicated by ^1H, ^{13}C, ^{11}B NMR, GCMS and GPC analysis (Scheme 1). GPC analysis of the new compound indicates that it is a polymer (M_w = 19,458; M_n = 19,139; M_w/M_n = 1.02).[18] The small signals in the variable-temperature NMR spectra (Figure 5) at around δ = 1.75 and 2.95 are not impurities, but rather arise from the formation of a polymer, the structure of which has not yet been determined. However, a variable-temperature

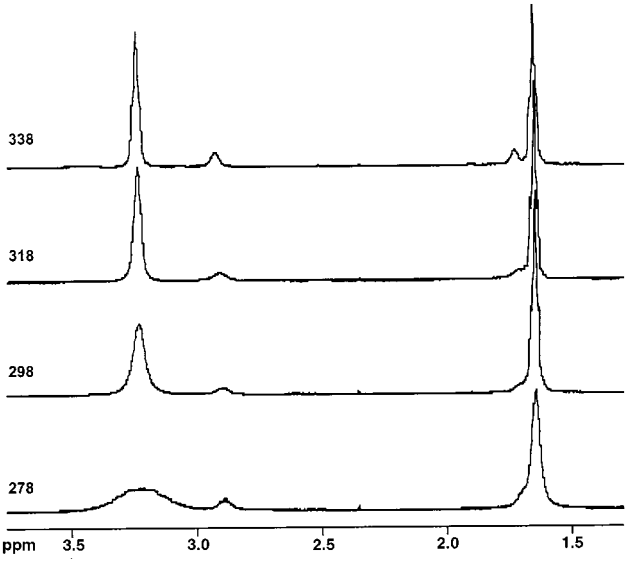

Figure 5. Variable-temperature (K) ^1H NMR spectra of **3** in $CDCl_3$.

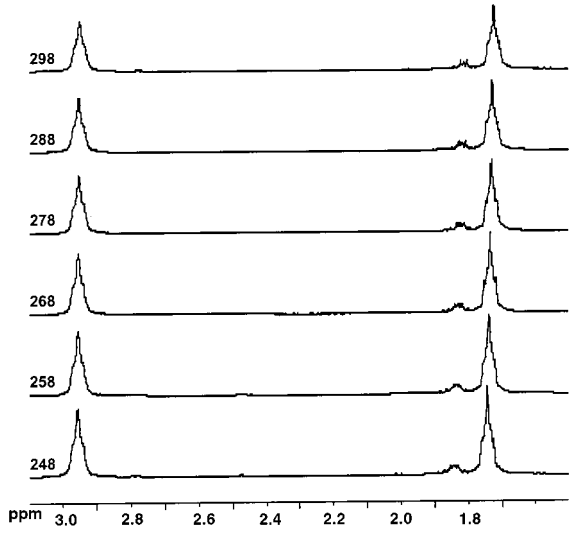

Figure 6. Variable-temperature (K) ^{1}H NMR spectra of the polymer in $CDCl_3$.

NMR spectroscopic study of the polymer in $CDCl_3$ has been performed (Figure 6). The signal of the monomer at $\delta = 1.64$ is shifted downfield in the polymer, while the signal at $\delta = 3.23$ is shifted upfield.

The ^{1}H NMR spectrum of **3** at 25 °C initially shows two broad singlets at $\delta = 1.64$ and 3.23. In the ^{13}C NMR spectrum, the C1 carbon atom of the pyrrolidino ring cannot be seen at room temperature. These phenomena may be due to the proximity of C1 to the boron atom, as well as the tumbling effect that takes place for large molecules in solution. Such spectra could also result from the restricted rotation around the B−B or B−N bond, or from both. However, when a $CDCl_3$ solution of **3** is heated from 278 to 338 K, the broad signals in the ^{1}H NMR spectrum are resolved into triplets ($^3J = 6.5$ Hz) (Figure 5), whereas C1 in the ^{13}C NMR spectrum is resolved into a singlet at $\delta = 49.43$. For the monomer, temperatures lower than 278 K result in the broadening of both signals in the ^{1}H NMR spectrum, and all splitting is lost, while for the polymer, lower temperatures give enhanced signals.

Conclusion

We have discovered that tetra(pyrrolidino)diborane(4) (**3**) is an excellent new precursor for the preparation of bis(pinacolato)diborane(4). Its crystal structure has been determined, as well as that of tris(pyrrolidino)borane. We have shown that **3** is stable in benzene, toluene and hydrocarbons, but tends to polymerize in acetone, chloroform, THF, and CO/toluene. We found that most bis(dialkylamino)-haloboranes are not suitable for the coupling reaction and give primarily the tris(dialkylamino)boranes and very low yields of the B−B product. Thus, tetra(pyrrolidino)diborane(4) is a valuable precursor for the preparation of bis(pinacolato)diborane(4) (obtained in an 83% yield), and is an alternative to $B_2(NMe_2)_4$.

Experimental Section

General Remarks: All reactions were carried under a nitrogen atmosphere using vacuum line and glove box techniques. Solvents were purified by distillation from appropriate drying agents under a nitrogen atmosphere. Starting materials were purchased from commercial suppliers and used without further purification. − ^{1}H and ^{13}C NMR spectra were recorded in $CDCl_3$ solution using a Varian Unity (300 or 75 MHz) spectrometer with Me_4Si as an internal standard. ^{11}B NMR spectra were recorded with a Bruker MSL-400 (128 MHz) spectrometer using $BF_3{\cdot}OEt_2$ as an external standard. − GC/MS spectra were obtained on a HP GCD PLUS instrument in EI mode on a 30 m methylsilicone column.

$(C_4H_8N)_3B$ (1): Pyrrolidine (86 g, 1.21 mol) and pentane (150 mL) was put into a dry 500 mL flask, closed with a rubber septum, under a nitrogen atmosphere. The flask was placed in a dry ice bath (− 78° C). Tribromoborane (51.25 g, 0.20 mol) was added slowly under nitrogen into a flask containing pentane (50 mL) which had been cooled to about − 40° C. This solution was added dropwise, with stirring, to the cooled amine-pentane solution. After an additional 3 h, the solution was allowed to warm to room temperature. The mixture was filtered under a nitrogen atmosphere, and pentane was added to transfer the solid to the filter funnel. The pentane was removed from the clear solution under vacuum, and the residue was distilled under vacuum to give colorless crystals (35.80 g, 81%). M.p. 40° C, b.p. 105° C/1.5Torr. − ^{1}H NMR ($CDCl_3$): $\delta = 1.66$ (t, 12 H, CH_2, $^3J_{H\text{-}H} = 6.6$ Hz), 3.04 (t, 12 H, CH_2N, $^3J_{H\text{-}H} = 6.6$ Hz). − ^{13}C{^{1}H} NMR ($CDCl_3$): $\delta = 24.61$ (CH_2), 46.84 (CH_2N). − ^{11}B NMR ($CDCl_3$): $\delta = 23.75$. − MS (EI), *m/z* (%) = 221 (20.4) [M^+], 192 (10.14), 178 (12.19), 151 (100), 123 (12.00), 109 (10.36), 82 (32.06), 70 (15.39), 40 (21.65). − $C_{12}H_{24}N_3B$: calcd. C 65.17, H 10.94, N 19.00; found C 64.96, H 10.81, N 18.81.

$(C_4H_8N)_2BBr$ (2): A solution of tribromoborane (16.29 g, 0.065 mol) in pentane (50 mL) was added to a vigorously-stirred solution of tris(pyrrolidino)borane (30 g, 0.13 mol) in pentane (150 mL) at − 50 to − 40° C, over a period of 20 min.. After an additional 3 h, the solution was allowed to warm to room temperature. The pentane was removed by rapid distillation at 1.5 Torr and the residue was distilled at 0.5 Torr giving the product as a pure liquid (39.51 g, 84%). B.p. 90° C \0.5Torr. − ^{1}H NMR ($CDCl_3$): $\delta = 1.71$ (t, 8 H, CH_2, $^3J_{H\text{-}H} = 6.75$ Hz), 3.31 (t, 8 H, CH_2N, $^3J_{H\text{-}H} = 6.75$ Hz). − ^{13}C{^{1}H} NMR ($CDCl_3$): $\delta = 26.56$ (CH_2), 50.01 (CH_2N). ^{11}B NMR ($CDCl_3$): $\delta = 24.51$ − $C_8H_{16}N_2BBr$: calcd. C 41.60, H 6.98, N 12.13; Br, 34.60; found C 41.31, H 7.21, N 11.46; Br, 34.93.

$[(C_4H_8N)_2B]_2$ (3): A solution of bis(pyrrolidino)bromoborane (21.8 g, 0.094 mol) in dry toluene (6 mL) was added slowly to highly-dispersed molten sodium (2.6 g, 0.11 mol) in dry toluene (20 mL) at 110 ° C. After 4 h, the resulting solids were filtered under a nitrogen atmosphere. The toluene was removed from the filtrate by vacuum distillation and the residue distilled at 160 ° C\0.5 Torr to give the product as a clear liquid, which on cooling gave colorless crystals (7.1 g, 50%). M.p. 75 °C, b.p. 160 °C\0.5 Torr. − ^{1}H NMR ($CDCl_3$) at 338 K: $\delta = 1.64$ (broad t, 16 H, CH_2, $^3J = 6.5$ Hz), 3.23 (broad t, 16 H, CH_2N). − ^{13}C{^{1}H} NMR ($CDCl_3$) at 338 K: $\delta = 26.53$ (CH_2), 49.43 (CH_2N). ^{11}B NMR ($CDCl_3$): $\delta = 33.96$. − MS (EI): *m/z* (%) = 302 (23.4) [M^+], 230 (100), 203 (46.6), 202 (39.2), 163 (64), 151(100), 133 (24.5), 107 (29.7), 82 (100), 70 (93.4). − $C_{16}H_{32}N_4B_2$: calcd. C 63.61, H 10.67, N 18.54; found C 63.53, H 10.69, N 18.27.

$[(C_5H_{10}O_3)B]_2$: A solution of tetra(pyrrolidino)diborane(4) (3.0 g, 0.01 mol) in benzene (20 mL) was added to a vigorously stirred

Table 1. Crystal data and structure refinement for **1** and **3**

Compound	**1**	**3**
Empirical formula	$C_{12}H_{24}BN_3$	$C_{16}H_{32}B_2N_4$
Molecular mass	221.15	302.08
Color	Colorless	Colorless
Temperature (K)	110(2)	110(2)
Wavelength (Å)	0.71070	0.71070
Crystal dimension (mm)	0.55 × 0.45 × 0.15	0.35 × 0.25 × 0.20
Crystal system	Monoclinic	Orthorhombic
Space group	$P2_1/n$	*Pbcn*
a (Å)	9.3780 (1)	10.6990 (4)
b (Å)	33.3540 (1)	9.3420 (5)
c (Å)	16.3120 (1)	17.6500 (8)
α (deg)	90	90
β (deg)	91.34	90
γ (deg)	90	90
V (Å^3)	5100.90 (2)	1764.12 (14)
Z	16	4
$D_{calcd.}$ (g cm^{-3})	1.152	1.137
*F*000	1952	664
μ (mm^{-1})	0.069	0.067
θ limits (deg)	2.22/25.34	3.80/25.36
Reflns unique	9151	1602
No. of data measured	15872	1873
Restraints	0	0
hkl limits	0,11/0,40/ −19,19	0,12/0,11/0,21
No. of variables	578	101
No. of data with $[I > 2\sigma(I)]$[a]	4774	1234
Final[b] *R* indices $[I > 2\sigma(I)]$[a]		
R1wR2	0.0824	0.0754
	0.2320	0.1948
Largest diff peak and hole (e/ Å^3)	0.692 and − 0.725	0.727 and − 0.313
GOF	1.05	1.06

[a] $[I > 3\sigma(I)]$ for **1**. − [b] $R_1 = \|\|F_o\| - \|F_c\|\| / |F_o|$ $wR2 = \{[w(F_0^2 - F_c^2)^2] / [w(F_o^2)^2]\}^{1\backslash 2}$.

solution of 2-ethoxy-1,3-propanediol (2.4 g, 0.02 mol) in benzene (10 mL) at 25 ° C. A solution of 3 M HCl /ether (15 mL) was added to the resulting mixture. After 6 h, the mixture was filtered and the benzene was removed under vacuum to give the product as an oily material, which was purified by silica gel chromatography eluting with 10% ether/petroleum ether (2.0 g, 78%). − ^{1}H NMR ($CDCl_3$): δ = 1.13 (t, 6 H, CH_3, ^3J = 7.0 Hz), 3.50 (q, 4 H, CH_2, ^3J = 7.0 Hz), 3.53 (m, 2 H, CH, ^3J = 5.0 Hz), 3.87 (dd, 8 H, CH_2, ^3J = 5.0 Hz). − ^{13}C{^{1}H} NMR ($CDCl_3$): δ = 15.31 (CH_3), 64.36 (O*CH*$_2$CH$_3$), 63.19 (CH_2), 71.50 (CH). − ^{11}B NMR ($CDCl_3$); δ = 27.49. − MS (EI): *m/z* (%) = 213 [M$^+$ − 45] (1.11), 171 (6.6), 143 (9.7), 129 (10.3), 115 (14.7), 101 (21.1), 72 (100), 45 (20.6), 29 (61.6). − $C_{10}H_{20}O_6B_2$: calcd. C 46.55, H 7.76; found C 46.13, H 7.55.

X-ray Crystallographic Study: Single crystals of **1** and **3** suitable for X-ray diffraction analysis were obtained from a saturated pentane solution at ≈ −20 °C. The crystal data and structure refinement for both are summarized in Table 1. **$(C_4H_8N)_3B$ (1)**. Crystals of this low-melting compound are extremely sensitive to air and moisture, and were coated with a layer of hydrocarbon oil in order to minimize deterioration. The X-ray diffraction measurements were carried out at ca. 110 K on a Nonius−Kappa CCD diffractometer, using Mo-K_α (λ = 0.7107 Å) radiation and 0.9° φ and Ω scans. The structure was solved by direct methods (SIR-92)[19] and refined by full-matrix least-squares based on F^2 for all reflections (SHELXL-97).[20] All non-hydrogen atoms were refined with anisotropic displacement parameters. The hydrogen atoms were located in calculated positions to correspond to standard bond lengths and angles, and were included in the refinement with isotropic displacement parameters using a riding model. Even at 110 K, the molecular structure of this compound is affected by severe conformational disorder of the five-membered rings. The asymmetric unit of the observed structure consists of four molecular entities that exhibit somewhat different conformations and varied degrees of disorder. The latter is reflected in the large-amplitude thermal displacement parameters of the C atoms, and could not be modeled; it is particularly evident in two out of the four crystallographically independent species. The dynamic nature of the structure gives rise to a large percentage of weak reflections in the diffraction pattern (revealing the appearance of several superlattice peaks as well), and affects the precision of this determination.

$[(C_4H_8N)_2B]_2$ (3): The analyzed crystal of **3** was coated with a layer of hydrocarbon oil in order to minimize deterioration and mounted on a glass fiber. The X-ray diffraction measurements were carried out as for **1**, using 1.0° Phi and Omega scans; solution and refinement were as for **1**.

Crystallographic data (excluding structure factors) for the structures reported in this paper have been deposited with the Cambridge Crystallographic Data Centre as supplementary publication no. CCDC-165578 (**1**) and CCDC-165579 (**3**). Copies of the data can be obtained free of charge on application to CCDC, 12 Union Road, Cambridge CB2 1EZ, UK [Fax: (internat.) + 44−1223/336−033; E-mail: deposit@ccdc.cam.ac.uk].

Acknowledgments

The authors thank the Israeli Science Foundation, MECC and the Horowitz Fund for support of this work.

[1] [1a] G. Lesley, T. B. Marder, N. C. Norman, C. R. Rice, *Main Group Chem. News* **1997**, *5*, 4. – [1b] T. B. Marder, N. C. Norman, *Top. Catal.* **1998**, *5*, 63. – [1c] T. Ishiyama, N. Miyaura, *J. Organomet. Chem.* **2000**, *611*, 392.

[2] A. Suzuki, *J. Organomet. Chem.* **1999**, *576*, 147. – [2b] N. Miyaura, A. Suzuki, *Chem. Rev.* **1995**, *95*, 2457.

[3] T. Ishiyama, M. Murata, N. Miyaura, *J. Org. Chem.* **1995**, *60*, 7508.

[4] [4a] T. B. Marder, N. C. Norman, C. R. Rice, *Tetrahedron Lett.* **1998**, 155. – [4b] C. N. Iverson, M. R. Smith, III, *Organometallics* **1997**, *16*, 2757. – [4c] T. Ishiyama, M. Yamamoto, N. Miyaura, *Chem. Commun.* **1997**, 689. – [4d] K. Takahashi, T. Ishiyama, N. Miyaura, *Chem. Lett.* **2000**, 982. – [4e] L. B. Han, M. Tanaka, *Chem. Commun.* **1999**, 395. – [4f] C. Y. Dai, E. G. Robins, A. J. Scott, W. Clegg, D. S. Yufit, J. A. K. Howard, T. B. Marder, *Chem. Commun.* **1998**, 1983. – [4g] R. T. Baker, P. Nguyen, T. B. Marder, S. A. Wescott, *Angew. Chem. Int. Ed. Engl.* **1995**, *34*, 1336.

[5] [5a] T. Ishiyama,N. Matsuda, M. Murata, F. Ozawa, A. Suzuki, N. Miyaura, *Organometallics* **1996**, *15*, 713. – [5b] T. Hiyama, M. Yamamoto, N. Miyaura, *Chem. Lett.* **1996**, 1117. – [5c] G. Lesley, P. Nguyen, N. J. Taylor, T. B. Marder, A. J. Scott, W. Clegg, N. C. Norman, *Organometallics* **1996**, *15*, 5137. – [5d] T. Ishiyama, N. Matsuda, N. Miyaura, A. Suzuki, *J. Am. Chem. Soc.* **1993**, *115*, 11018. – [5e] C. N. Iverson, M. R. Smith, III, *Organometallics* **1996**, *15*, 5155. – [5f] K. M. Anderson, M. J. G. Lesley, N. C. Norman, A. G. Orpen, J. Starbuck, *New J. Chem.* **1999**, *23*, 1053. – [5g] M. Suiginome, T. Matsuda, Y. Ito, *Organometallics* **1998**, *17*, 5233. Boryl alkynes: – [5h] M. Bluhm, A. Maderna, H. Pritzkow, S. Bethke, R. Gleiter, W. Siebert, *Eur. J. Inorg. Chem.* **1999**, 1693.

[6] [6a] T. Ishiyama, M. Yamamoto, N. Miyaura, *Chem. Commun.* **1996**, 2073. – [6b] W. Clegg, T. R. F. Johann, T. B. Marder, N. C. Norman, A. G. Orpen, T. M. Peakman, M. J. Quayle, C. R. Rice, A. J. Scott, *J. Chem. Soc., Dalton Trans.* **1998**, 1431.

[7] T. Ishiyama, S. Momota, N. Miyaura, *Synlett* **1999**, *11*, 1790.

[8] T. Ishiyama, T.-a. Ahiko, N. Miyaura, *Tetrahedron Lett.* **1996**, *37*, 6889.

[9] [9a] Y. G. Lawson, M. J. G. Lesley, T. B. Marder, N. C. Norman, C. R. Rice, *Chem. Commun.* **1997**, 2051. – [9b] H. Ito, H. Yamanaka, J. Tateiwa, A. Hosomi, *Tetrahedron Lett.* **2000**, *41*, 6821.

[10] [10a] T. Ishiyama, T. Kitano, N. Miyaura, *Tetrahedron Lett.* **1998**, *39*, 2357. – [10b] F. Y. Yang, C. H. Cheng, *J. Am. Chem. Soc.* **2001**, *123*, 761. Aryl halides see: – [10c] T. Ishiyama, Y. Itoh, T. Kitano, N. Miyaura, *Tetrahedron Lett.* **1997**, *38*, 3447. Imines, see; – [10d] G. Mann, K. D. John, R. T. Baker, *Org. Lett.* **2000**, *2*, 2105. – [10e] T. M. Cameron, R. T. Baker, S. A. Wescott, *Chem. Commun.* **1998**, 2395. Hydrazines, see: – [10f] H. Hommer, H. Nöth, H. Sachdev, M. Schmidt, H. Schwenk, *Chem. Ber.* **1995**, *128*, 1187. Carbenoids, see: – [10g] T. Hata, H. Kitagawa, H. Masai, T. Kurahashi, M. Shimuzu, T. Hiyama, *Angew. Chem. Int. Ed.* **2001**, *40*, 790.

[11] Mechanism: [11a] G. R. Clark, G. J. Irvine, W. R. Roper, L. J. Wright, *Organometallics* **1997**, *16*, 5499. – [11b] C. Dai, G. Stringer, T. B. Marder, A. J. Scott, W. Clegg, N. C. Norman, *Inorg. Chem.* **1997**, *36*, 272. – [11c] T. B. Marder, N. C. Norman, C. R. Rice, E. G. Robins, *Chem. Commun.* **1997**, 53. – [11d] G. J. Irvine, M. J. G. Lesley, T. B. Marder, N. C. Norman, C. R. Rice, E. G. Robins, W. R. Roper, G. R. Whittell, L. J. Wright, *Chem. Rev.* **1998**, *98*, 2685. – [11e] W. Clegg, F. J. Lawlor, T. B. Marder, P. Nguyen, N. C. Norman, A. G. Orpen, M. J. Quayle, C. R. Rice, A. J. Scott, F. E. S. Souza, G. Stringer, G. R. Whittell, *J. Chem. Soc., Dalton Trans.* **1998**, 301. Theoretical studies on alkenes and alkynes: – [11f] Q. Cui, D. G. Musaev, K. Morokuma, *Organometallics* **1997**, *16*, 1355. – [11g] R. Chadha, N. K. Ray, *J. Phys. Chem.* **1982**, *86*, 3293. – [11i] L. Ahmed, J. Castillo, D. A. Saulys, J. A. Morrison, *Inorg. Chem.* **1992**, *31*, 706. – [11j] R. Chadha, N. K. Ray, *Theo. Chim. Acta* **1982**, *60*, 573. – [11k] Q. Cui, D. G. Musaev, K. Morokuma, *Organometallics* **1998**, *17*, 1383. – [11l] Q. Cui, D. G. Musaev, K. Morokuma, *Organometallics* **1998**, *17*, 742.

[12] [12a] R. J. Brotherton, A. L. McCloskey, L. L. Petterson, H. Steinberg, *J. Am. Chem. Soc.* **1960**, *82*, 6242. – [12b] H. Nöth, H. Pommerening, W. Rattay, H. Schick, *Chem. Ber.* **1994**, *127*, 1605.

[13] H. Nöth, J. Knizek, W. Pinikwar, *Eur. J. Inorg. Chem.* **1999**, 1931.

[14] R. J. Brotherton, A. L. McCloskey, J. L. Boone, H. M. Manasevit, *J. Am. Chem. Soc.* **1960**, *82*, 6245.

[15] [15a] H. Nöth, *Z. Naturforsch., Teil B* **1984**, *39*, 1463. – [15b] T. Ishiyama, M. Murata, Ahiko,A. T-N. Miyaura, *Org. Synth.* **1999**, *77*, 176.

[16] [16a] B. Wrackmeyer, B. Schwarze, W. Milius, *Inorg. Chim. Acta* **1996**, *241*, 87–93. – [16b] G. J. Bullen, *J. Chem. Soc., Dalton Trans.* **1981**, 511–514. – [16c] G. Schmid, R. Boese, D. Blaser, *Z. Naturforsch., Teil B* **1982**, *37*, 1230. – [16d] H. Nöth, *Z. Naturforsch., Teil B* **1983**, *38*, 692.

[17] [17a] G. Ferguson, M. Parvez, R. P. Brint, D. C. M. Power, T. R. Spalding, D. R.d. Loy, *J. Chem. Soc., Dalton Trans.* **1986**, 2283. – [17b] W. Clegg, M. R. J. Elsegood, F. J. Lawlor, N. C. Norman, N. L. Pickett, E. G. Robins, A. J. Scott, P. Nguyen, N. J. Taylor, T. B. Marder, *Inorg. Chem.* **1998**, *37*, 5289.

[18] The structure of the polymer is being investigated and will be published seperately.

[19] A. Altomare, M. C. Burla, M. Camalli, M. Cascarano, C. Giacovazzo, A. Guagliardi, G. Polidori, *J. Appl. Cryst.* **1994**, *27*, 435.

[20] Sheldrick, G. M. SHELXL-97. Program for the Refinement of Crystal Structures from Diffraction Data, University of Goettingen, Germany, **1997**.

Received June 17, 2001
[I01216]

Synthesis and Characterization of Dirhodium(II,II)−Porphyrin-Based Multiredox Systems

Sandra Lo Schiavo,*[a] Scolastica Serroni,[a] Fausto Puntoriero,[a] Giuseppe Tresoldi,[a] and Pasquale Piraino[a]

Keywords: Rhodium / Porphyrins / Electrochemistry / Luminescence

Dirhodium(II,II)–porphyrin-based multiredox systems were easily prepared by combining the versatile reactivity, both axial and equatorial, of the $[Rh_2(form)_2(O_2CCF_3)_2(H_2O)_2]$ (form = *N*,*N*′-di-*p*-tolylformamidinate) complex and the well-known coordination capability of *meso*-substituted phenylporphyrins. In this way, redox systems featured by porphyrins axially or equatorially coordinated to the dirhodium subunits were obtained. Electrochemical and luminescence properties of the new assemblies were also investigated. Porphyrin–dirhodium(II,II) multiredox assemblies were synthesized by exploiting both the classical axial and the peculiar equatorial reactivity of the complex $[Rh_2(form)_2(O_2CCF_3)_2(H_2O)_2]$ (**1**) (form = *N*,*N*′-di-*p*-tolylformamidinate). The species $[Rh_2(form)_2(PCOO)_2]$ (**2**), featuring two bridged (carboxyphenyl)porphyrins in the equatorial positions, was prepared by metathetical reaction of **1** with the sodium salt of *meso*-5-(4-carboxyphenyl)-5,10,15-triphenylporphyrin (PCOO). Conversely, redox systems in which porphyrins are axially ligated to dirhodium were obtained by treating **1** with a variety of functionalized *meso*-pyridylporphyrins. Depending on the number and position of the peripheral pyridyl substituents, assemblies with different nuclearity, both in terms of metal and porphyrin subunits, were isolated. The 1:2 dirhodium/porphyrin adduct, $[Rh_2(form)_2(O_2CCF_3)_2(PyP)_2]$ (**3**) was obtained by treatment of **1** with triphenyl(pyridyl)porphyrin (PyP). By combination of **1** with the *cis*-5,10-diphenyl-15,20-dipyridylporphyrin (*cis*-DPyP) the molecular square box, $[Rh_2(form)_2(CF_3CO_2)_2(cis\text{-DPyP})]_4$ (**4**) was isolated in good yield. The reaction of **1** with 5,10,15,20-tetrakis(4-pyridyl)porphyrin (TPyP) is dependent on the experimental conditions and led to two different products: the grid polymer $[\{Rh_2(form)_2(CF_3CO_2)_2\}_2(TPyP)]_n$ (**5**) and the symmetric tetramer $[\{Rh_2(form)_2(CF_3CO_2)_2\}_4(TPyP)]$ (**6**), respectively. All the products were characterized by conventional spectroscopic methods. Proton NMR spectroscopy resulted particularly useful for the characterization of dirhodium–phenyl(pyridyl)porphyrin aggregates. The 2,6-pyridyl proton resonances are highly affected by coordination and experience significantly upfield shifts with respect to the corresponding unbound porphyrin. Systems **2**, **3**, **4**, and **6** underwent many redox processes in the potential window under investigation (+2; −1.4 V), each one of them can be assigned to the specific subunits of the molecular arrays. The emission studies performed on the same aggregates revealed that the porphyrin-based emission was significantly quenched by, most likely, reductive electron transfer from dirhodium subunits to the excited porphyrin chromophores. Such a process appears to be larger in the pyridylporphyrin–dirhodium systems with respect to the (carboxyphenyl)porphyrin ones.

Introduction

Redox multicomponent systems continue to be a topic of current interest owing to their diverse potential of application in the field of the molecular materials. Apart from their molecular properties (magnetism, electrical conductivity) these systems, depending on their structural features, may also display interesting specific functions (catalytic, host−guest interactions, electron reservoir, etc.) or act as models for electron or energy transport.[1] The choice of the redox components represents a crucial point in the synthetic approach to redox systems. The inclusion of transition metals constitutes one of the most promising means of introducing redox activity in a multicomponent system. These, besides acting as redox-active moieties, may play an important role from a synthetic point of view.[2] In fact, the self-assembly by metal complexation has provided a widely used route to supramolecular arrays.

Our experience in the chemistry of redox-active dirhodium(II,II) complexes, with lantern structures, led us to explore the possibility to build dirhodium multiredox based systems. By exploiting the metal-mediated self-assembly process, we recently succeeded in preparing a series of multiredox molecular square boxes incorporating two or four dirhodium(II,II) units, as redox metal centres, and dicarboxylate dianions as connectors.[3] The electrochemical

[a] Dipartimento di Chimica Inorganica, Chimica Analitica e Chimica Fisica, Università di Messina,
Salita Sperone n. 31, 98166 Vil. S. Agata, Messina, Italy
E-mail: loschiavo@chem.unime.it

 © WILEY-VCH Verlag GmbH, 69451 Weinheim, Germany, 2002 1434−1948/02/0101−0079 $ 17.50+.50/0

investigations performed on these square boxes $[Rh_2(form)_2(dicarboxylate)]_4$ [form = *N*,*N*′-di-*p*-tolylformamidinate, dicarboxylate = oxalate (ox) or terephthalate (tp)] featuring the *cis*-$Rh_2(form)_2$ moieties as angular components and *trans*-dicarboxylates as ligand connectors, provided evidence that no significant electronic interaction was operating among the dirhodium centres. The same electrochemical behaviour was also observed by introducing the redox active connector, *meso*-carboxyphenyl-functionalized porphyrin, 5,10-bis(4-carboxyphenyl)-15,20-diphenylporphyrin [$P(COO)_2$] into the cyclic structure. In fact, the porphyrin−dirhodium(II,II) macrocycle $[Rh_2(form)_2\{P(COO)_2\}]_2$ exhibits a CV pattern consistent with four independent redox centres releasing electrons at potential values that are mostly unchanged with respect to those of the parent species.[3]

Porphyrins are particularly attractive as building blocks for molecular materials as they couple a rich photochemistry to some interesting redox properties. They are among the most popular emitters, and indeed porphyrin-based molecules play the role of photo-active subunits in most natural photosynthetic systems,[4a] as well as in many artificial systems for solar energy conversion processes.[4b] The emission studies performed on the $[Rh_2(form)_2\{P(COO)_2\}]_2$ metallacycle revealed a luminescence decrease with respect to the free porphyrin, attributed to a reductive electron-transfer quenching of the porphyrin excited state by the dirhodium subunits.[3]

As a continuation of this study we planned the synthesis of new redox- and photo-active porphyrin−dirhodium(II,II) assemblies. The construction of such new assemblies was achieved by combining the versatile reactivity of the $[Rh_2(form)_2(O_2CCF_3)_2(H2O)_2]$ (**1**) complex[5,6] with the coordination capability of *meso*-substituted phenylporphyrins.[7]

Complex **1**, besides the well-known axial reactivity of dirhodium(II,II), allows the introduction at the equatorial position of bridging, neutral or charged, ligands.[6] Such a synthetic approach, successfully applied to the building of the above-mentioned square molecular boxes,[3] allows us to bridge carboxyphenylporphyrins at the equatorial positions of the dirhodium(II,II) species.

On the other hand, the classical axial reactivity of dirhodium(II,II) may be exploited to synthesise dirhodium(II,II)−pyridylporphyrin arrays with different shape or topology, depending on the number and geometry of the peripheral pyridyl substituents. Furthermore, dirhodium(II,II) may be used as *exo*-bidentate connectors, providing the right linear component to form square molecular boxes or grid polymers when combined with the appropriate angular component.1

In the present paper we report on the synthesis and characterization of a number of redox dirhodium(II,II)−porphyrin assemblies, with *meso*-substituted phenylporphyrins axially or equatorially ligated to dirhodium moieties. The electrochemical as well as the luminescence properties of the new multiredox systems have been also investigated.

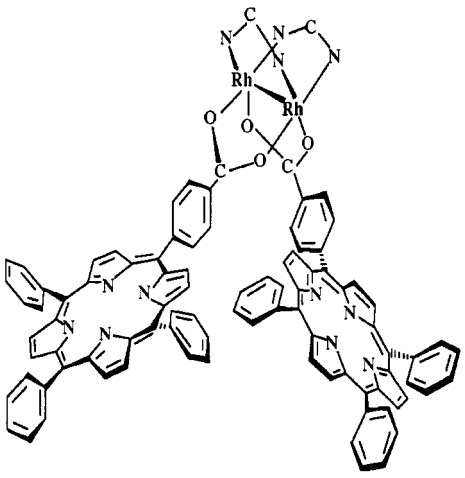

Figure 1. Structure proposed for $[Rh_2(form)_2(PCOO)_2]$ (**2**)

Results and Discussion

Synthesis and Characterization

$[Rh_2(form)_2(PCOO)_2]$ (2)

Dirhodium(II,II) systems bearing porphyrins in their equatorial positions have been synthesized by metathetical reaction of **1** with the sodium salt of *meso*-5-(4-carboxyphenyl)-10,15,20-triphenylporphyrin (PCOO). The addition of $[Rh_2(form)_2(CF_3COO)_2(H_2O)_2]$ (**1**) to a methanol/water solution of PCOONa (prepared in situ by treatment of the (carboxyphenyl)porphyrin with NaOH, see Exp. Sect.) affords $[Rh_2(form)_2(PCOO)_2]$ (**2**) in good yield. Compound **2** is a dark red-violet solid dissolving well in benzene and chlorinated solvents, sparingly in coordinating solvents such as acetone, acetonitrile, and alcohols. Elemental analysis, IR and NMR spectroscopic data are in agreement with the proposed structure (Figure 1), which retains the lantern structure of the parent complex **1**, i.e. with the two formamidinate and porphyrincarboxylate groups symmetrically bridged in a *cisoid* arrangement around the Rh_2^{4+} core.

The proton NMR spectrum of **2** does not differ significantly from those of the precursor subunits, with the exception of the pyrrole proton pattern, which consists of a rather broad singlet at $\delta = 8.88$, while in uncoordinated carboxyphenylporphyrin it appears as two doublets and one singlet. As already observed for the dirhodium−porphyrin molecular square box $[Rh_2(form)_2\{P(COO)_2\}]_2$ also bearing carboxyphenylporphyrins in the equatorial position, the electronic absorption spectrum of **2** appears as the sum of those of their constituents, suggesting that no significant electronic interaction is operating among the redox centres.

Reations of $Rh_2(form)_2(CF_3COO)_2(H_2O)_2$ (1) with Mixed meso-(4-Pyridyl)phenylporphyrins

Dirhodium(II,II)−porphyrin-based systems were also obtained by exploitation the classical axial reactivity of the

dirhodium(II,II) complexes towards Lewis bases. To this aim, the reactions of **1** with a series of functionalized *meso*-pyridylporphyrins were investigated.

$[Rh_2(form)_2(CF_3CO_2)_2(PyP)_2]$ (3)

The reaction of **1** with 5,10,15-triphenyl-20-(4-pyridyl)-porphyrin (PyP) led to the $[Rh_2(C_{15}H_{15}N_2)_2(CF_3CO_2)_2(PyP)_2]$ (**3**) adduct containing, as expected, two PyP axially coordinated to the dirhodium system via the peripheral pyridyl groups (Figure 2). The NMR spectra and the presence in the IR spectra of $\nu_{asym}(CO_2)$ and $\nu(N-C-N)$ bands at 1626 and 1594 (s) cm^{-1}, respectively, very similar to those of the parent complex **1**, confirm that the Rh_2^{4+} core remains unchanged upon the reaction.

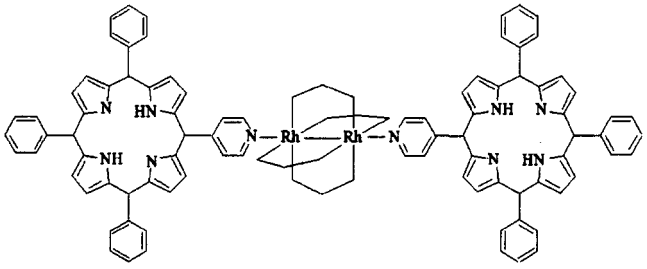

Figure 2. Structure proposed for $[Rh_2(form)_2(O_2CCF_3)_2(PyP)_2]$ (**3**)

Table 1. 300 MHz ^1H NMR chemical ($CDCl_3$, room temp.) shift for the (2,6- and 3,5-pyridyl)porphyrin protons; 2D ^1H NOESY spectra were performed to determine the correct assignment

Free porphyrins	2,6	3,5	Complexes	2,6	3,5
PyP	9.01	8.16	**3**	8.31	7.90
cis-DPyP	9.02	8.15	**4**	8.42	7.93
TPyP	9.06	8.16	**6**	7.78	7.97

Proton NMR spectroscopy is very diagnostic of the pyridylporphyrin coordination.[7] In the NMR spectra of pyridylporphyrins axially ligated to dirhodium(II,II) (present work), we found an upfield shift of the 2,6-pyridyl proton resonances (Table 1), which may be attributed to the π-back-donation from dp orbitals of the metal centre to π-anti-bonding orbitals of the porphyrin system. Consistently, the proton spectrum of **3** displays, for the 2,6-pyridyl protons, a doublet centred at δ = 8.31, with a $J_{H,H}$ coupling constant of 5.4 Hz, significantly upfield shifted as compared to free porphyrin (δ = 9.01), while the 3,5-pyridyl proton resonances are translated only by 0.26 upfield from the free one (δ = 7.90 vs. 8.16, respectively) (2D ^1H NOESY spectra were performed to determine the correct assignment). On the contrary, no shift is observed for the phenyl as well as for pyrrole proton resonances upon coordination.

$[Rh_2(form)_2(CF_3CO_2)_2(cis\text{-}DPyP)]_4$ (4)

Dirhodium(II,II) species, besides providing angular building blocks for the construction of molecular boxes, as we and others recently demonstrated,[3,8] exhibit the right properties (rigidity, geometry, and axial coordination capability) to act as *exo*-bidentate connectors of angular species leading to square molecular boxes. With this aim we explored the reactions of **1** with the 5,10-diphenyl-15,20-dipyridylporphyrin (*cis*-DPyP), which has in the past was been used successfully as an angular connector of transition metal complexes leading to square molecular boxes.[7a,7b,7f−7h]

Reaction of **1** with 1 mol-equiv. of *cis*-DPyP, in $CHCl_3$, at room temperature led to the formation of a 1:1 stoichiometry adduct, as indicated by elemental analysis and proton NMR integration data. Such a stoichiometry, in principle, may be indicative of the desired square box as well as of a polymeric species. The proper mass spectroscopic studies (MALDI, FAB- and ESI-MS), which in the lack of X-ray diffractometry data constitute the most powerful tool for establishing the nuclearity of such macrocycles, did not give unambiguous results, but, in any case showed no peaks due to long chain order oligomers.[9] No evidence of polymeric materials both as a precipitate and soluble by-products was observed, even by monitoring the reaction by NMR spectroscopy. These observations, along with the chemical and redox properties and the NMR investigations, suggest for **4** the cyclic structure showed in Figure 3.

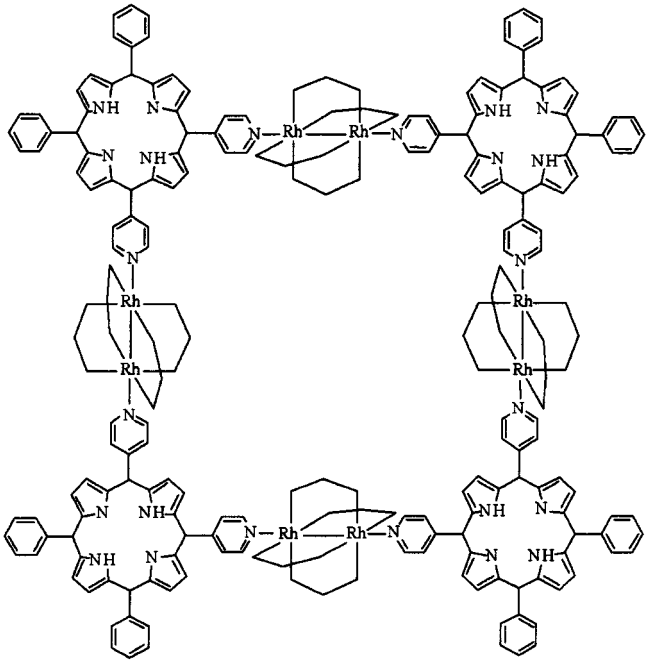

Figure 3. Structure proposed for $[Rh_2(form)_2(O_2CCF_3)_2(cis\text{-}DPyP)_2]_4$ (**4**)

This compound is, in fact, soluble in benzene and chlorinated solvents (interestingly, it is more soluble than the precursor *cis*-DPyP), but not in alcohols or acetonitrile or other coordinating solvents. Secondly, the proton spectra appear very simple and with well-resolved signals in agreement with a species at high symmetry, and finally, the redox properties are consistent with the proposed molecular structure (see below).

The inspection of the proton spectra reveals that the proton pattern resonances related to the dirhodium unit differ slightly from those of the starting building-block, while some differences are observed for the porphyrin proton resonances with respect to the free one. Consistent with the proposed structure, two equally intense doublets are observed for the (2,6- and 3,5-pyridine)porphyrin protons at $\delta = 8.42$ and 7.93, respectively, significantly shifted from free *cis*-DPyP ($\delta = 9.02$ and 8.15, respectively). Also, the phenyl as well as the pyrrole proton patterns are in agreement with a *cis* coordination for the bound *cis*-diphenyldipyridylporphyrin.[7a,7b,7f−7h] The two magnetically equivalent phenyl rings afford, in fact, two distinct proton sets for the two pairs of *ortho*- and (*meta* + *para*)-H, not shifted from free *cis*-DPyP. A slight overlapping is observed in the pyrrole proton patterns, which consist of two doublets and one singlet, accounting for four and eight protons each, respectively [three doublets are observed for free *cis*-DPyP, with a 2:4:2 proton ratio]. This is very likely caused by the pyrrole protons located inside the macrocycle that experience a downfield shift of $\delta = 0.03$ as compared to the unbound porphyrin.

$[\{Rh_2(form)_2(CF_3CO_2)_2\}_2(TPyP)]_n$ (5) and $[\{Rh_2(form)_2(CF_3CO_2)_2\}_4(TPyP)]$ (6)

The reaction of **1** with 5,10,15,20-tetrakis(4-pyridyl)porphyrin (TPyP) yielded different products depending on the molar ratio, as well as on the order of addition, of the reactants. The addition of **1** to a chloroform solution of TPyP led to a rust-coloured precipitate having a 1:2 stoichiometry between the dirhodium species and the TPyP porphyrin. Its insolubility in the most common solvents prevented its spectroscopic characterization and argues for the formation of a grid polymeric material of formula $[\{Rh_2(C_{15}H_{15}N_2)_2(CF_3CO_2)_2\}_2(TPyP)]_n$ (**5**).

When the reaction was performed in the presence of an excess of **1** (see Exp. Sect.), the species $[\{Rh_2(C_{15}H_{15}N_2)_2(CF_3CO_2)_2\}_4(TPyP)]$ (**6**), bearing four dirhodium subunits symmetrically coordinated to TpyP, was obtained in high yield. Elemental analyses and proton NMR integration agree with the requirements of the tetramer formulation as shown in Figure 4.

Consistently the aromatic region of ^1H NMR spectrum (Figure 5) shows only two doublets for the 2,6- and 3,5-pyridine protons at $\delta = 7.78$ and 7.97 ($J = 6.4$ Hz), respectively, significantly shifted with respect to those of free TPyP ($\delta = 9.06$ and 8.16, respectively), while, as expected for such a highly symmetric species, only one singlet at $\delta = 8.97$ is observed for the eight pyrrole protons, upfield shifted by 0.13 with respect to those of the free TPyP.[6d,6g] No changes are observed in the proton patterns related to the dirhodium subunits with respect to the parent complex **1**.

Complex **6** was very soluble in noncoordinating solvents (Et_2O, chlorinated solvents, etc.), remarkably more soluble than TPyP, and was stable as solid for a long time. In solution it slowly decomposed (3−4 d) releasing the parent complex **1** and an insoluble rust-coloured precipitate that was identified as **5** by IR and elemental analyses.

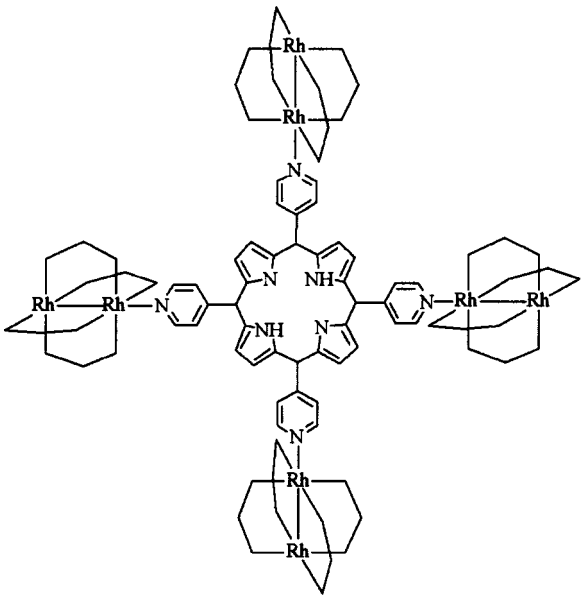

Figure 4. Structure proposed for $[\{Rh_2(form)_2(O_2CCF_3)_2\}_4(TPyP)]$ (**6**)

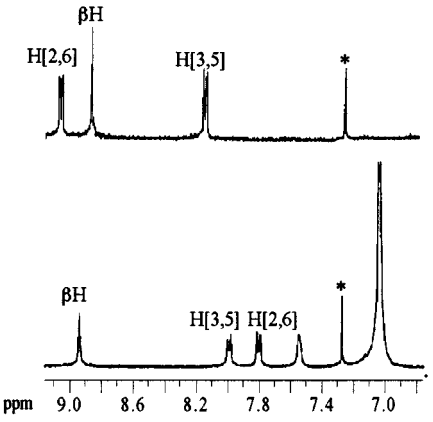

Figure 5. Aromatic region of the ^1H NMR spectra [$CDCl_3$ (*) room temp.] of TPyP (top) and (**6**) (bottom)

Electronic Spectra of 3, 4, and 6

The electronic absorption spectra of **3**, **4**, and **6** do not reveal significant modifications in the Soret and Q bands as compared to those of the unbound pyridylporphyrins, suggesting, once again, the absence of significant electronic interactions among porphyrin and the dirhodium subunits, as already observed for $[Rh_2(form)_2\{P(COO)_2\}]$ (**2**) and the square box $[Rh_2(form)_2\{P(COO)_2\}]_2$.

Electrochemistry

The new multicomponent redox systems exhibit several oxidation processes and one reduction process in the poten-

Table 2. Redox data of the new compounds; experiments were performed in argon-purged 1,2-dichloroethane solutions; all the processes are reversible except where otherwise noted; <#>: numbers of exchanged electrons

Complexes	Oxidation, *U* [V] vs. SCE[a]	Reduction, *U* [V] vs. SCE[a]
2	+0.37 <1>; +1.17 <2>[b]; +1.38 <1>[b]	−1.19 <2>[c]
3	+0.59 <1>; +1.17 <2<; 1.54[b] <1>	−1.11 <2>
4	+0.53 <4>; +1.24 <4>[c]; +1.60 <4>[b]	−1.10 <4>[c]
6	+0.60 <4>; +1.50 <4>[c]	−1.02 <1>[b]
1[d]	+0.59 <1>; +1.40 <1>	

[a] $E_{1/2}$ values are reported for reversible processes and E_{peak} values are reported for irreversible processes. [b] Irreversible process. [c] Quasi-reversible process. [d] Data obtained in dichloromethane solution.[10]

tial window examined (+ 2, −1.4 V vs. SCE), as evidenced by the redox data gathered in Table 2.

The first oxidation (+0.37 V vs. SCE) of complex **2** (Figure 6a) is attributed to the oxidation of the Rh_2^{4+} subunit, on the basis of: i) the reversibility of the process, ii) the number of electrons exchanged, iii) comparison with the potential of the oxidation process of the same subunit in the square species $[Rh_2(form)_2\{P(COO)_2\}]_2$ (+0.38 V vs. SCE).[3] Comparison with the molecular square $[Rh_2(form)_2\{P(COO)_2\}]_2$ also allowed us to attribute the second oxidation of **3** to the simultaneous one-electron oxidation of the two porphyrin subunits and the third one to the Rh_2^{5+}/Rh_2^{6+} process.

As far as compound **3** is concerned, it is interesting to note that its structure is similar to that of **2**, in particular, one "central" Rh_2^{4+} subunit is connected to two "peripheral" porphyrin fragments. However, significant differences in the properties of **2** and **3** may arise from the different nature of the linkages between subunits and from the presence, in compound **3**, of strong electron-withdrawing CF_3COO^- groups on the Rh_2^{4+} subunit (see Figures 1 and 2, respectively). Compound **3** indeed shows a redox pattern (Figure 6b) similar to that of **2**, and the attribution of the various processes to specific subunits is the same (see above). The relevant differences are the potentials of the oxidation processes centred in the Rh_2^{4+} subunit, that are substantially shifted to more positive values (ca. 200 mV; see Table 2). This is also in agreement with the oxidation reported for $[Rh_2(form)_2(CF_3COO)_2(H_2O)_2]$.[5,10]

Compound **4** exhibits three oxidation processes, each one involving four electrons. Comparison with the data of the parent compounds allows us to assign the observed processes as follows: the first process is due to four simultaneous one-electron Rh_2^{4+}/Rh_2^{5+} processes, the second one to the porphyrin subunits, and the third one to four simultaneous one-electron Rh_2^{5+}/Rh_2^{6+} processes. According to redox data shown in Table 2, the oxidation of the porphyrin fragments in **4** is more difficult than the analogous processes in **2** and **3**. This can be rationalised by considering

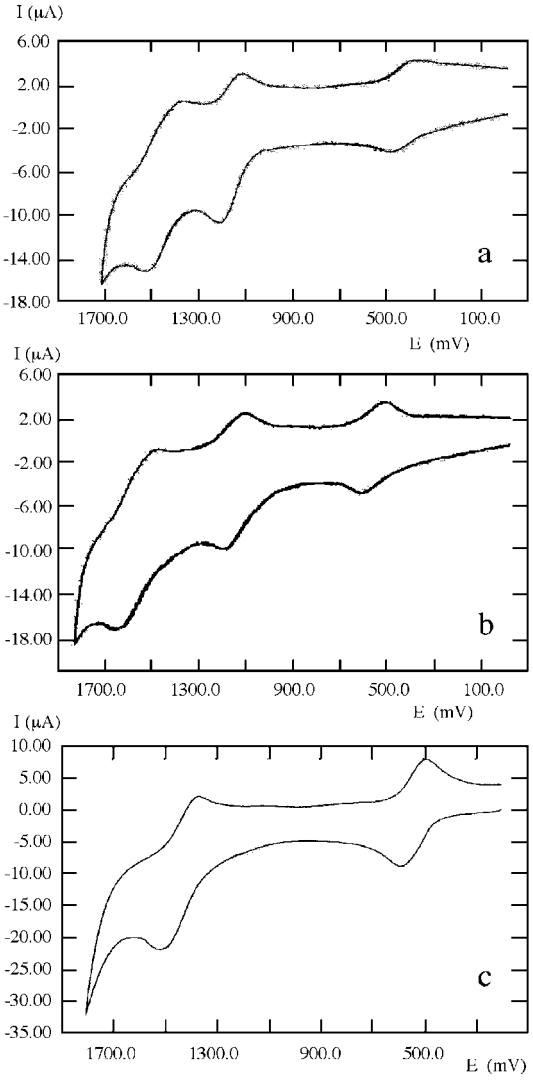

Figure 6. Cyclic voltammograms of compounds of **2** (a), **3** (b), and **6** (c); only the oxidation portion is shown

that: i) in **4** each porphyrin is connected to *two* already oxidized Rh_2^{5+} subunits when their oxidation occurs, ii) the presence of two pyridine groups most likely stabilises porphyrin orbitals.

The oxidation pattern of compound **6** is slightly different from those of the other new species reported here, in that it consists of only two processes in the potential window investigated (Figure 6c). Based on the number of exchanged electrons and of the potential values, it is possible to assign the observed processes to the successive one-electron oxidations of the four dirhodium subunits, i.e. Rh_2^{4+}/Rh_2^{5+} and Rh_2^{5+}/Rh_2^{6+} processes. The lack of the porphyrin-centred oxidation between the two dirhodium-based processes, opposed to the behaviour of the other new compounds, is probably due to the presence of the four already oxidized Rh_2^{5+} subunits, which displaces porphyrin oxidation to more positive potentials (after the second dirhodium-based oxidation). Moreover, the presence of four pyridine groups on the porphyrin fragment may also concur with this displacement.

On reduction, all the new species show a single process that is easily assigned to a porphyrin-centred reduction.[3] The number of exchanged electrons in each process is equal to the number of identical porphyrin subunits present in the examined compound. It is interesting to note that on increasing the number of pyridines the reduction process moves to less negative potentials (Table 2).

Luminescence

On the basis of the redox properties of the multicomponent systems **2**, **3**, **4**, and **6**, it was expected that the dirhodium(II,II) subunits could play the role of efficient quenchers of porphyrin-based luminescence by electron transfer. This was confirmed by the observed emission data, which are reported in Table 3 along with those related to the unbound chromophores PCOO, PyP, *cis*-DPyP, and TPyP.

Table 3. Luminescence data for the multicomponent systems **2**, **3**, **4**, and **6**, together with the related free porphyrins in air-equilibrated dichloromethane at room temperature

Compounds	Emission maxima [nm][a]	τ [ns]	ΔG [eV][b]
P(COO)	648	8.6	
2	648	1.5	−0.35
PyP	650	8.5	
3	no emission	−	−0.21
cis-DPyP	655	8.5	
4	no emission	−	−0.20
TPyP	655	8.5	
6	no emission	−	−0.27

[a] Only the highest-energy feature of the emission spectrum, taken as the E_{00} energy, is reported. [b] Driving force for the reductive electron transfer quenching, calculated as in Equation (1) (see text).

As expected, the uncoordinated porphyrins are strong emitters under the experimental conditions used. However, such an emission is significantly reduced in **2**, whereas **3**, **4**, and **6** do not exhibit any emission at all. This finding clearly indicates that a quenching of the porphyrin-based emission occurs in the studied multicomponent complexes due to the presence of the dirhodium subunits. A possible mechanism for the quenching is reductive electron transfer. Actually, the driving force ΔG for reductive electron transfer quenching of the porphyrin-based excited state by the dirhodium(II,II) subunits can be approximated by Equations (1) and (2), where entropy contributions and work terms are neglected.[11]

$$\Delta G = e[E_{ox} - {}^*E_{red}] \quad (1)$$

$${}^*E_{red} = E_{red} + E_{00} \quad (2)$$

In these Equations, E_{ox} is the oxidation potential of the dirhodium(II,II) subunit(s), E_{red} is the reduction potential of the porphyrin subunit(s), and E_{00} is the energy of the luminescent excited state of the corresponding model compounds, approximate to the highest-energy feature of the emission spectra. The ΔG values obtained are also shown in Table 2 and indicate that electron transfer from the dirhodium subunits to the excited porphyrin chromophores is moderately exergonic in all the cases. Electron transfer rate constants for moderately exergonic processes depend on the electronic interactions between the partners, in turn governed by several factors such as donor−acceptor distance, nature of spacers, and reorganization energy.[11] Compound **2** is luminescent, although with a reduced lifetime compared to PCOO. So the rate of the process k_{et} for this system can be easily obtained by Equation (3), in which τ_0 is the luminescence lifetime of the free porphyrin, PCOO, and τ is the luminescence lifetime of the species in the presence of the quencher, **2**.

$$k_{et} = 1/\tau - 1/\tau_0 \quad (1)$$

From the data in Table 3, k_{et} is 5.2×10^8 s^{-1} in **2**. It could be noted that this value is smaller than that estimated by a different method (luminescence quantum yield comparison between the free chromophore and chromophore-quencher systems) for a molecular square basically containing the same components.[3] However, in complex **2** each chromophore is connected to a single dirhodium(II,II) quencher, while in the molecular square compound reported in literature the chromophore was connected to two potentially quencher subunits, which both could contribute to the quenching process.

Complexes **3**, **4**, and **6** do not exhibit any emission, so the electron transfer rate constants cannot be evaluated by Equation (3). However, the complete quenching of the porphyrin emission in these complexes suggests that the electron transfer rate constants in **3**, **4**, and **6** are probably at least one order of magnitude larger than the value obtained for **3**. Differences in the driving force cannot be responsible for the difference in the electron-transfer rate, in that they are in the opposite direction (Table 3). The reason probably lies in the nature of the linkage between the chromophore(s) and the quencher subunits. Apparently, the pyridine linkage which is present in **3**, **4**, and **6** allows a better electronic coupling between donor and acceptor partners than the bridged carboxylate one, operating in **2** and in the molecular square $[Rh_2(form)_2\{P(COO)_2\}]_2$.

It should be noted that the occurrence of electron transfer between porphyrin and dirhodium subunits, which indicates that electronic coupling between the subunits takes place, is not in contradiction with the negligible interactions inferred by absorption spectra and redox properties. It is well known that electronic coupling as small as tens of cm^{-1}, which hardly cause changes in absorption spectra and redox properties of the individual subunits of the multicomponent arrays, are sufficient to promote fast intercomponent energy and/or electron-transfer processes.[12]

Conclusions

In the present paper, we have reported the results of our studies aimed at the synthesis and characterization of dirhodium−porphyrin assemblies as models of photoactive multiredox systems. The synthesis of such new assemblies

was achieved by combining the versatile reactivity, both axial and equatorial, of the $[Rh_2(form)_2(O_2CCF_3)_4(H_2O)_2]$ (**1**) complex with the coordination capability of *meso*-substituted phenylporphyrins. In this way, systems, featuring pyridylporphyrins axially coordinated or (carboxyphenyl)porphyrins equatorially bridged to the dirhodium subunits, were readily obtained. We have also explored the possibility of building dirhodium−porphyrin-based molecular square boxes. The capability of **1** to act as a precursor for new mixed dirhodium complexes, via the *cis*-$Rh_2(form)_2$ moieties, has already been exploited to synthesize the molecular square box $[Rh_2(form)_2\{P(COO)_2\}]_2$.[3] The square molecular box $[Rh_2(form)_2(CF_3CO_2)_2(cis\text{-DPyP})]_4$ (**4**), in which the dirhodium subunit acts as an *exo*-bidentate ligand, was obtained by assembling **1** with the *cis*-5,10-diphenyl-15,20-dipyridylporphyrin (*cis*-DPyP), which in turn constitutes the angular building block. It should also be remarked that the synthesis of the tetramer species $[\{Rh_2(form)_2(CF_3CO_2)_2\}_4(TPyP)]$ was achieved by reaction of **1** with 5,10,15,20-tetrakis(4-pyridyl)porphyrin (TPyP).

All the new systems undergo many redox processes in the potential window under investigation. It is important to stress that the redox patterns, especially in the oxidation part, are strictly related to the structure of the compounds.

In the multicomponent porphyrin−dirhodium assemblies studied here, the porphyrin-based emission is significantly quenched, most likely by reductive electron transfer from the dirhodium subunits to the excited porphyrin chromophores, a process which is moderately exergonic in all the cases. The rate constants of the processes appear to be larger in the compounds in which a pyridine linkage between dirhodium and porphyrin subunits is present compared with the compound in which the linkage is realized through bridging carboxylates, suggesting that the donor−acceptor electronic coupling is larger in the former cases.

Experimental Section

Materials: The starting complex $[Rh_2(form)_2(CF_3COO)_2(H_2O)_2]$ was prepared according to literature data.[5] The *meso*-5-(4-carboxyphenyl)-10,15,20-triphenylporphyrin was purchased from Mid-Century Company, Illinois. All other chemicals are commercially available and used as supplied. None of the compounds here reported were air-sensitive, but all reactions were carried out under dry nitrogen. Elemental analyses were performed by REDOX snc Laboratorio di Microanalisi, Monza, Italy.

Apparatus: Infrared spectra were recorded on KBr pellets with a Perkin−Elmer FT 1720X spectrometer. Electronic absorption spectra were recorded with a Perkin−Elmer Lambda 5 UV/Visible spectrophotometer. The NMR measurements were performed with a Bruker AMX 300 spectrometer using standard pulse sequences. Electrochemical measurements were carried out in argon-purged 1,2-dichloroethane at room temperature with a PAR 273 multipurpose equipment interfaced to a PC. The working electrode was a glassy carbon (8 mm^2, Amel) electrode. The counter electrode was a Pt wire, and the quasi-reference electrode was an Ag wire (ferrocene was used as internal standard). The concentration of the complexes was about 5×10^{-4} M. Tetrabutylammonium hexafluorophosphate was used as supporting electrolyte and its concentration was 0.05 M. Cyclic voltammograms were obtained at scan rates of 20, 50, 200, and 500 mV/s. For reversible processes, half-wave potentials (vs. SCE) were calculated as the average of the cathodic and anodic peaks. The criteria for reversibility were the separation between cathodic and anodic peaks, the close to unity ratio of the intensities of the cathodic and anodic currents, and the constancy of the peak potential on changing the scan rate. For irreversible processes, the values reported in Table 2 are the peaks estimated by differential pulse voltammetry (DPV). The number of exchanged electrons was measured with differential-pulse voltammetry (DPV) experiments performed with a scan rate of 20 mV/s, a pulse height of 75 mV, and a duration of 40 ms. Experimental error on the redox potentials was ± 10 mV. For the irreversible or quasi-reversible processes, an estimation of the number of the electrons involved can be inferred by current intensity of the anodic (for oxidation processes) or cathodic (for reduction processes) peaks. The luminescence experiments were performed in air-equilibrated dichloromethane solution at 298 K. Luminescence spectra were obtained with a Jobin Yvon-Spex Fluoromax 2 fluorimeter (experimental error on luminescence maxima was ± 4 nm). The spectra were corrected for detector response. The luminescence lifetimes were measured by an Edinburgh FL 900 Single-Photon-Counting Spectrometer (experimental error on lifetimes was ± 10%).

Preparations

$Rh_2(form)_2(PCOO)_2$ (2): To a mixture of methanol (50 mL) and 5-(4-carboxyphenyl)-10,15,20-triphenylporphyrin (0.150 g, 0.228 mmol) was added an aqueous solution (5 mL) of NaOH (0.010 g, 0.250 mmol). The resulting solution was stirred for ca. 1 h and then filtered. A chloroform solution (10 mL) of **1** (0.139 g, 0.152 mmol) was added dropwise to the filtrate, and the resulting mixture stirred for 36 h. After this time, the resulting brown red solid was collected by filtration, dissolved in 30 mL of benzene and the resulting mixture filtered. By addition of *n*-heptane (30 mL) to the filtrate, **2** was obtained as a red-brown microcrystalline precipitate. Yield: 0.185 g (62%). $C_{120}H_{88}N_{12}O_4Rh_2$ (1967.92): calcd. C 73.24, H 4.51, N 8.54; found C 73.34, H 4.58, N 8.60. IR (KBr pellet, nujol mulls): $\tilde{\nu}$ = 1619 [m, $\nu_{asym}(CO_2)$], 1593 cm^{-1} [s, ν(N−C−N)]. UV/Vis (C_6H_6): λ_{max} = 423.8, 514.4, 549.0, 591.2, 649.2 nm. ^{1}H NMR (CD_2Cl_2): δ = −2.66 (s, 4 H), 2.32 (s, 12 H), 7.16 (m, 16 H), 7.75 (m, 22 H), 8.20 (m, 14 H), 8.50 (d, 4 H, J = 8 Hz), 8.83 (br. s, 16 H).

$[Rh_2(form)_2(CF_3CO_2)_2(PyP)_2]$ (3): A chloroform solution (20 mL) of **1** (0.100 g, 0.110 mmol) was added to a solution of PyP (0.135 g, 0.220 mmol) in the same solvent (50 mL), and the resulting red-violet solution stirred for ca. 24 h. After this time, the solution was filtered and the solvents were evaporated to dryness using a rotary evaporator. The residue was washed with *n*-hexane and recrystallized from chloroform/*n*-heptane. Compound **3** was obtained as a dark-violet precipitate. Yield: 0.208 g (90%). $C_{120}H_{88}F_6N_{14}O_4Rh_2$ (2109.93): calcd. C 68.31, H 4.20, F 5.40, N 9.29; found C 68.12, H 4.30, F 5.35, N 9.22. IR (KBr pellet, nujol mulls): $\tilde{\nu}$ = 1626 [m, $\nu_{asym}(CO_2)$], 1594 cm^{-1}[s, ν(N−C−N)]. UV/Vis ($CHCl_3$): λ_{max} = 419, 515, 549, 589, 644 nm. ^{1}H NMR ($CDCl_3$): δ = −2.79 (s, 2 H), 2.22 (s, 12 H), 7.02 (m, 16 H), 7.54 (t, br, 2 H), 7.77 (m, 20 H), 7.90 (d, J = 5.4 Hz, 4 H), 8.24 (m, 10 H), 8.31 (d, J = 5.4 Hz, 4 H), 8.82 (d, 4 H, J = 4.83 Hz), 8.86 (s, 8 H), 8.95 (d, 4 H, J = 4.83 Hz).

$[Rh_2(form)_2(CF_3CO_2)_2(cis\text{-DPyP})]_4$ (4): A chloroform solution (75 mL) of *cis* -DPyP (0.087 g, 0.142 mmol) was added to a solution of **1** (0.130 g, 0.142 mmol) in the same solvent (30 mL). The resulting red-violet solution was stirred for 24 h, then filtered and

dried using a rotary evaporator. The residue was washed with *n*-hexane, and then dissolved in benzene (50 mL) and the resulting solution filtered. The addition of *n*-heptane to the filtrate afforded **5** as a dark-violet solid. Yield: 0.138 g (65%). $C_{76}H_{58}F_6N_{10}O_4Rh_2$ (5980.70): calcd. C 61.05, H 3.91, F 7.62, N 9.37; found C 60.95, H 3.96, F 7.49, N 9.29. IR (KBr pellet, nujol mulls): $\tilde{\nu}$ = 1622 [m, $\nu_{asym}(CO_2)$], 1592 cm^{-1} [s, ν(N−C−N)]. UV/Vis ($CHCl_3$): λ_{max} = 419, 515, 549, 589, 644 nm. ^1H NMR ($CDCl_3$): δ = −2.76 (s, 2 H), 2.13 (s, 12 H), 7.00 (m, 16 H), 7.51 (t, br, 2 H), 7.77 (m, 6 H, *m*-,*p*-H Ph), 7.93 (d, br, 4 H), 8.2 (m, 4 H, *o*-H Ph), 8.42 (d, br, 4 H), 8.78 (d, 2 H, J = 4.62 Hz), 8.87 (s, 4 H), 8.93 (d, 2 H, J = 4.62 Hz).

$[\{Rh_2(form)_2(CF_3CO_2)_2\}_2(TPyP)]_n$ (5): A chloroform solution (70 mL) of TPyP (0.040 g, 0.066 mmol) was added to a solution of **1** (0.120 g, 0.132 mmol) in the same solvent (30 mL). Immediately, **6** was formed as a red-brown precipitate. The resulting mixture was stirred overnight, and then the precipitate was collected by filtration, washed several times with $CHCl_3$, and dried in vacuo. Yield: 0.141 g (90%). $C_{108}H_{86}F_{12}N_{16}O_8Rh_4$ (2375.59): calcd. C 54.61, H 3.65, F 9.60, N 9.43; found C 54.43, H 3.64, F 9.43, N 9.44. IR (KBr pellet, nujol mulls): $\tilde{\nu}$ = 1626 [m, $\nu_{asym}(CO_2)$], 1594 cm^{-1} [s, ν(N−C−N)]. The low solubility of **5** prevented a full spectroscopic characterization.

$[\{Rh_2(form)_2(CF_3CO_2)_2\}_4(TPyP)]$ (6): A chloroform solution (70 mL) of TpyP (0.033 g,053 mmol) was added to a solution of **1** (0.120 g, 0.218 mmol) in the same solvent (30 mL). The resulting solution was stirred for 24 h and then left to stand for ca. 2 d. Then the solution was dried using a rotary evaporator, and the residue washed with *n*-hexane. Crystallization of the residue by diethyl ether/*n*-hexane (0 °C) afforded **6** as a dark-red microcrystalline solid. Yield: 0.135 g (60%). $C_{176}H_{146}F_{24}N_{24}O_{16}Rh_8$ (4132.48): calcd. C 51.15, H 3.56, F 11.03, N 8.13; found C 51.30, H 3.62, F 11.00, N 8.21. IR (KBr pellet, nujol mulls): $\tilde{\nu}$ = 1626 [m, $\nu_{asym}(CO_2)$], 1594 cm^{-1} [s, ν(N−C−N)]. UV/Vis ($CHCl_3$): λ_{max} = 419, 515, 549, 589, 644 nm. ^1H NMR ($CDCl_3$): δ = −2.90 (s, 2 H), 2.26 (s, 48 H), 7.0 (m, 64 H), 7.52 (t, br, 8 H), 7.78 (d, J = 6.4 Hz, 8 H), 7.97 (d, J = 6.4 Hz, 8 H), 8.97 (s, 8 H).

Acknowledgments

We thank the Italian CNR and the MURST for financial support.

[1] [1a] M. R. Wasielewski, *Chem. Rev.* **1992**, 435−461. [1b] H. Kurreck, M. Huber, *Angew. Chem. Int. Ed. Engl.* **1995**, *34*, 849−866. [1c] J.-M. Lehn, *Supramolecular Chemistry*, VCH Publishers, New York, **1995**. [1d] P. L. Boulas, M. Gòmez-Kaifer, L. Echegoyen, *Angew. Chem. Int. Ed.* **1998**, *37*, 216−247.

[2] [2a] S. Leninger, B. Olenyuk, P. J. Stang, *Chem. Soc. Rev.* **2000**, 853−908. [2b] B. Olenyuk, A. Fechtenkotter, P. J. Stang, *J. Chem. Soc., Dalton Trans.* **1998**, 1707−1729. [2c] M. Fujita, *Chem. Soc. Rev.* **1998**, 417−425. [2d] B. J. Hollyday, C. A. Mirkin, *Angew. Chem. Int. Ed.* **2001**, *40*, 2022−2043. [2e] P. N. W. Baxter, R. G. Khoury, J.-M. Lehn, G. Baum, D. Fenske, *Chem. Eur. J.* **2000**, 4140−4148 and refs. therein.

[3] S. Lo Schiavo, G. Pocsfalvi, S. Serroni, P. Cardiano, P. Piraino, *Eur. J. Inorg. Chem.* **2000**, 1371−1375.

[4] [4a] J. Deinsenhofer, H. Michel, *Angew. Chem. Int. Ed. Engl.* **1989**, *28*, 829−847. [4b] D. Gust, T. A. Moore, A. L. Moore, *Acc. Chem. Res.* **2001**, *34*, 40−48, and refs. therein. [4c] S. Anderson, H. Anderson, A. Bashall, M. McPartlin, J. K. M. Sanders, *Angew. Chem. Int. Ed. Engl.* **1995**, *34*, 1096−1099. [4d] A. Harriman, J. Sauvage, *Chem. Soc. Rev.* **1996**, 41−48. [4e] R. V. Slone, D. I. Yoon, R. M. Calhoun, J. T. Hupp, *J. Am. Chem. Soc.* **1995**, *117*, 11813−11814. [4f] A. Prodi, M. T. Indelli, C. J. Kleverlaan, F. Scandola, E. Alessio, T. Gianferrara, L. G. Marzilli, *Chem. Eur. J.* **1999**, 2668−2679. [4g] K. Sugiura, Y. Fujimoto, Y. Sakata, *Chem. Commun.* **2000**, 1105−1106.

[5] P. Piraino, G. Bruno, S. Lo Schiavo, F. Laschi, P. Zanello, *Inorg. Chem.* **1987**, *26*, 91−96.

[6] [6a] P. Piraino, G. Bruno, S. Lo Schiavo, F. Laschi, P. Zanello, *Inorg. Chem.* **1987**, *26*, 2205−2211. [6b] G. A. Rizzi, M. Casarin, E. Tondello, P. Piraino, G. Granozzi, *Inorg. Chem.* **1987**, *26*, 3406−3409. [6c] E. Rotondo, B. E. Mann, P. Piraino, G. Tresoldi, *Inorg. Chem.* **1989**, *28*, 3070−3073. [6d] E. Rotondo, G. Bruno, F. Nicolò, S. Lo Schiavo, P. Piraino, *Inorg. Chem.* **1991**, *30*, 1195−1200. [6e] P. Piraino, G. Tresoldi, S. Lo Schiavo, *Inorg. Chim. Acta* **1993**, *203*, 101−105. [6f] G. Bruno, G. De Munno, G. Tresoldi, S. Lo Schiavo, P. Piraino, *Inorg. Chem.* **1992**, *31*, 1538−1540. [6g] S. Lo Schiavo, M. S. Sinicropi, G. Tresoldi, C. G. Arena, P. Piraino, *J. Chem. Soc., Dalton Trans.* **1994**, 1517−1522. [6h] G. Tresoldi, G. De Munno, F. Nicolò, S. Lo Schiavo, P. Piraino, *Inorg. Chem.* **1996**, *35*, 1377−1381.

[7] [7a] C. M. Drain, J.-M. Lehn, *Chem. Commun.* **1994**, 2313−2315. [7b] J. Fan, J. A. Whiteford, B. Olenyuk, M. D. Levin, P. J. Stang, E. B. Fleisher, *J. Am. Chem. Soc.* **1999**, *121*, 2741−2752. [7c] P. J. Stang, J. Fan, B. Olenyuk, *Chem. Commun.* **1997**, 1453−1454. [7d] R. V. Slone, J. T. Hupp, *Inorg. Chem.* **1997**, *36*, 5422−5423. [7e] L. Pan, B. C. Noll, X. Wang, *Chem. Commun.* **1999**, 157−158. [7f] E. Iengo, B. Milani, E. Zangrando, S. Geremia, E. Alessio, *Angew. Chem. Int. Ed.* **2000**, *39*, 1096−1099. [7g] E. Alessio, M. Macchi, S. Heath, L. G. Marzilli, *Chem. Commun.* **1996**, 1411−1412. [7h] E. Alessio, E. Ciani, E. Iengo, V. Y. Kukushkin, L. G. Marzilli, *Inorg. Chem.* **2000**, *39*, 1434−1443. [7i] E. Alessio, S. Geremia, S. Mestroni, E. Iengo, B. Milani, E. Zangrando, *Inorg. Chem.* **1999**, *38*, 869−875 and refs. therein.

[8] [8a] F. A. Cotton, L. M. Daniels, C. Lin, C. A. Murrillo, *J. Am. Chem. Soc.* **1999**, *121*, 4538−4539. [8b] R.-P. Bonar-Law, T. D. McGrath, N. Singh, J. F. Bickley, A. Steiner, *Chem. Commun.* **1999**, 2457−2458.

[9] It is very likely that thermal and collision dissociation of the assembly occurs under the applied ESI conditions, as no pyridylporphyrin−dirhodium aggregate studied here gave significant ES mass spectra.

[10] S. Lo Schiavo, G. Bruno, P. Zanello, F. Laschi, P. Piraino, *Inorg. Chem.* **1997**, *36*, 1004−1012.

[11] *Electron Transfer in Chemistry*, vols. 1−5 (Ed.: V. Balzani), Wiley-VCH, Weinheim, **2001**.

[12] [12a] F. Scandola, M. T. Indelli, C. Chiorboli, C. A. Bignozzi, *Top Curr. Chem.* **1990**, *158*, 73−95. [12b] V. Balzani, A. Juris, M. Venturi, S. Campagna, S. Serroni, *Chem. Rev.* **1996**, *96*, 759−778.

Received June 27, 2001
[I01236]

Kinetics and Reaction Mechanisms of Complexes with Cobalt−Carbon σ Bonds of the Type $\{(NH_3)_5Co-R\}^{n+}$ in Aqueous Solutions, a Pulse Radiolysis Study

Nurit Shaham,[a] Alexandra Masarwa,[a] Yoseph Matana,[b] Haim Cohen,[a,b] and Dan Meyerstein*[a,c]

Keywords: Cobalt / Kinetics / N ligands / Reaction mechanisms / Radiolysis

The kinetics of formation of complexes with cobalt–carbon σ bonds in the reaction between $\{Co^{II}(NH_3)_5H_2O\}^{2+}$ or $\{Co^{II}(NH_3)_6\}^{2+}$ with different aliphatic radicals was studied in aqueous solutions using the pulse radiolysis technique. The formation of the complexes $\{(NH_3)_5Co^{III}–R\}^{n+}$ obey pseudo first order rate laws and the rate constants for R = CH_3 and $CH_2CO_2^-$ are $(3.0\pm0.3)\times10^7$ and $(2.1\pm0.3)\times10^7$ $M^{-1}s^{-1}$, respectively. The UV/Vis spectra of the complexes are reported and found to be in agreement with previous results for analogous complexes. The results point out that the reactions $(NH_3)_5Co^{III}–R + R^{\cdot} + NH_3 \rightarrow Co(NH_3)_6^{2+} + R_2$ are fast thus limiting the radical route as a synthetic tool for the $(NH_3)_5Co^{III}–R$ complexes.

Introduction

The properties of complexes with cobalt−carbon σ bonds were widely studied for two main reasons:

1. The importance of the coenzyme vitamin B_{12}.

2. The kinetic stability of the cobalt−carbon σ bond, which provides the ability to synthesize a variety of complexes of this type.

The discovery that coenzyme B_{12} is a cobalt(III) complex containing a cobalt−carbon σ bond initiated many studies concerning the mechanisms of formation and decomposition of these bonds. It was argued that a prerequisite for the formation of a stable alkylcobalt(III) compound is an unsaturated equatorial ligand system. Thus, the complexes studied so far mainly contained ligands, which are considered coenzyme vitamin B_{12} analogues, i.e. unsaturated ligands bound to the cobalt ion in a planar configuration as analogous to the corrins,[1] e.g. unsaturated tetraazamacrocylic ligands.[2−4] These ligands stabilize the cobalt ion in three oxidation states; +1, +2 and +3. Alkylcobalt(III) compounds containing solely saturated ligands have been reported for relatively few cases,[4−6] the ligands were mainly saturated tetraazamacrocyclic ones, these complexes have been prepared employing various synthetic methods. Meyerstein et al.[7] studied the formation and decomposition of $(nta)Co^{III}-R$ complexes formed in the reactions of (nta)cobalt(II) complexes with various aliphatic radicals $^{\cdot}R$ [where nta is nitriloacetate, $N(CH_2CO_2^-)_3$], to elucidate the factors affecting the rates of cobalt−carbon bond formation. It was found that the stability of the cobalt−carbon bond towards homolytic cleavage is in the order $CH_3 > CH_2OH > CH(CH_3)OH > C(CH_3)_2OH$. The results also pointed out, that nta indeed stabilizes transient complexes of the type $\{(nta)Co^{III}-R(H_2O)\}^-$. The formation and decomposition mechanisms were further studied using the high-pressure technique.[8] It was concluded that metal−carbon bond formation is very similar to ligand-exchange processes in terms of volume changes, and follows an I_d mechanism in the case of cobalt(II). Homolysis of the cobalt−carbon bond is presumably accompanied by an additional contribution due to the volume difference between the low spin $LCo^{III}-R$ complexes and the high-spin $LCo^{II}(H_2O)$ complexes.[9] Recently, Kofod et al.[10,11] prepared several alkylcobalt(III) complexes with ammonia ligands such as $\{(NH_3)_5Co^{III}-CH_3\}^{2+}$, *trans*-$\{Co(en)_2(NH_3)(CH_3)\}^{2+}$ and $\{Co(NH_3)_6\}$-*mer*,*trans*-$\{Co(NO_2)_3(NH_3)_2(CH_3)\}_2$-*trans*-$\{Co(NO_2)_4(NH_3)_2\}$. Kofod[10] synthesized and spectroscopically characterized the complex $\{(NH_3)_5Co^{III}-CH_3\}^{2+}$ by alkylation of $Co(NH_3)_6^{2+}$ using methylhydrazine with dioxygen as the oxidizing agent, a route that had originally been developed for the preparation of organocobalt(III) compounds with unsaturated ligands.

Basically the strength of the cobalt−carbon σ bond depends on several factors:

1. The equatorial ligands, which influence the redox potential of the central cobalt ion. Changes in the structure and identity of the ligands cause changes in the properties of the complexes. The redox potential of the central cobalt ion is affected by the σ donor character of the ligands.

[a] Department of Chemistry, Ben-Gurion University of the Negev, Beer-Sheva, Israel
[b] Nuclear Research Centre Negev, Beer-Sheva, Israel
[c] The College of Judea and Samaria, Ariel, Israel

 © WILEY-VCH Verlag GmbH, 69451 Weinheim, Germany, 2002 1434−1948/02/0101−0087 $ 17.50+.50/0

2. The character of the ligand in the *trans* position to the R group. It was shown that for a series of cobalt−methyl compounds ligands in the *trans* position [e.g.: CN^-, NO_2^-, H_2O, NH_3 and en (1,2-ethanediamine)], considerably affect the cobalt−carbon bond length and the UV/Vis absorption spectra (in agreement with the spectroscopic series $H_2O < NH_3 < CN^- \approx NO_2^-$).[12]

3. The character of the substituents on the aliphatic residue, R.

4. Steric hindrance which stems from the equatorial ligand structure and from the substituents on R.

It was decided to check whether the complexes $\{(NH_3)_5Co^{III}-R\}^{n+}$ can be synthesized according to Equation (1). This would open up the possibility of synthesizing a large variety of these complexes using radiation chemistry techniques. The results indicate that this technique might indeed be used, though it has its limitations. The new complexes were characterized spectrophotometrically, and their kinetics of formation and decomposition were studied.

$$\{(NH_3)_5Co(H_2O)\}^{2+} + {}^{\cdot}R \longrightarrow \{(NH_3)_5Co^{III}\text{-}R\}^{n+} \quad (1)$$

Results

N_2O-saturated aqueous solutions containing $(0.2-4.0)\times10^{-3}$ M $CoSO_4$, 20% NH_3 and in addition 1 M of one of the following substances, CH_3OH, CH_3COONa or $(CH_3)_2SO$, were irradiated by a short electron pulse from the linear accelerator. The experimental results, see below, point out, that under these conditions the primary radicals are transformed into the desired aliphatic radicals during the pulse. As the reaction of the $^{\cdot}OH$ radicals with NH_3 under our experimental conditions (ca. 11 M NH_3), competes with the reaction of $^{\cdot}OH$ radicals with $CH_3CO_2^-$ and CH_3OH,[13] see Table 1, the results (vide infra) indicate that the produced $^{\cdot}NH_2$ radicals react with the organic substrates to produce the desired aliphatic radicals by analogous reactions to those of the $^{\cdot}OH$ radical. This result is not surprising as the dissociation energy of the H_2N-H bond is considerably larger than that of the C−H bonds in $CH_3CO_2^-$ and CH_3OH.[14]

Table 1. Rate constants relevant to this study

Reaction	k [$M^{-1}s^{-1}$]
$(CH_3)_2SO + {}^{\cdot}OH \rightarrow (CH_3)_2S^{\cdot}(O)OH$	6.6×10^9 [21]
followed by:	
$(CH_3)_2S^{\cdot}(O)OH \rightarrow {}^{\cdot}CH_3 + (CH_3)S(O)OH$	1.5×10^7 [s^{-1}] [21]
$(CH_3)_2SO + {}^{\cdot}H \rightarrow (CH_3)_2S(OH)^{\cdot}$	2.7×10^6 [22]
$(CH_3)_2SO + e^-_{aq} \rightarrow$ products	1.6×10^6 [23]
$CH_3COO^- + {}^{\cdot}OH \rightarrow {}^{\cdot}CH_2COO^- + H_2O$	8.5×10^7 [24]
$CH_3COO^- + {}^{\cdot}H \rightarrow {}^{\cdot}CH_2COO^- + H_2$	3.5×10^5 [25]
$CH_3COO^- + e^-_{aq} \rightarrow$ products	$< 1.0\times10^6$ [26]
$CH_3OH + {}^{\cdot}OH \rightarrow {}^{\cdot}CH_2OH + H_2O$	9.7×10^8 [13]
$CH_3OH + {}^{\cdot}H \rightarrow {}^{\cdot}CH_2OH + H_2$	2.6×10^6 [13]
$CH_3OH + e^-_{aq} \rightarrow$ products	$< 1.0\times10^4$ [13]
$NH_3 + {}^{\cdot}OH \rightarrow {}^{\cdot}NH_2 + H_2O$	1.0×10^8 [13]

In all the systems studied a formation reaction was observed after the formation of the aliphatic radicals (Figure 1). The formation of the intermediates (for methyl and acetate) obey pseudo-first-order rate laws (Figure 1). The observed rates are proportional to the initial concentration of $[(NH_3)_5Co(H_2O)]^{2+}$ or $[Co(NH_3)_6]^{2+}$ (Figure 2). The rates are independent of the concentration of all other components of the solution, pulse intensity and the wavelength at which the reaction is observed. The products are unstable, vide infra, i.e. they are not $(NH_3)_5Co(H_2O)^{2+}$ or $Co(NH_3)_6^{3+}$. Therefore it is reasonable to propose that the intermediates formed in this process are of the type $\{(NH_3)_5Co^{III}-R\}^{2+}$, i.e. complexes with cobalt−carbon σ bonds, and that the reactions observed are as described in Equation (1). The results are summed up in Table 2. Though the straight lines in Figure 2 have no positive intercept, i.e. the reactions $R^{\cdot} + R^{\cdot} \rightarrow R_2$ do not compete with Equation (1) under the experimental conditions, the yield of the intermediates $(NH_3)_5Co^{III}-R$, as measured by its absorption, increases with an increase in $[(NH_3)_5Co(H_2O)^{2+}]$ (Figure 3). The spectra of the intermediates formed, Table 3, are similar to those of other complexes of this type,[10] a typical spectrum is shown in Figure 4.

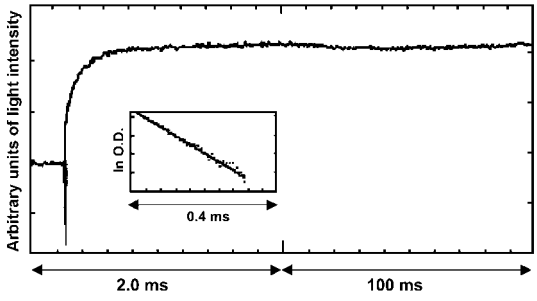

Figure 1. Formation kinetics of $[(NH_3)_5Co^{III}-CH_2CO_2^-]^+$; computer output of light intensity vs. time; N_2O-saturated solution with 1 M CH_3CO_2Na, 1×10^{-3} M $CoSO_4$, ca. 20% NH_3, the solution was irradiated with a maximum pulse and the kinetics were followed at 300 nm

Table 2. Measured rates of reaction of aliphatic radicals with $\{(NH_3)_5Co(H_2O)\}^{2+}$

Reaction	k_{1meas} [$M^{-1}s^{-1}$][a]
$\{(NH_3)_5Co(H_2O)\}^{2+} + {}^{\cdot}CH_3 \rightarrow \{(NH_3)_5Co-CH_3\}^{2+}$	3.4×10^7
$\{(NH_3)_5Co(H_2O)\}^{2+} + {}^{\cdot}CH_2COO^- \rightarrow \{(NH_3)_5Co-CH_2COO^-\}^+$	2.1×10^7
$\{(NH_3)_5Co(H_2O)\}^{2+} + {}^{\cdot}CH_2OH \rightarrow \{(NH_3)_5Co-CH_2OH\}^{2+}$	[b]

[a] The measured values are somewhat higher than k_1, see discussion. [b] The results imply that this process is an equilibrium process with a very small equilibrium constant, therefore it is difficult to establish this rate constant.

Mechanism of Decomposition of the Complexes $\{(NH_3)_5Co^{III}-R\}^{n+}$

The decomposition processes for all the intermediates in this study obey first-order rate laws. The measured decom-

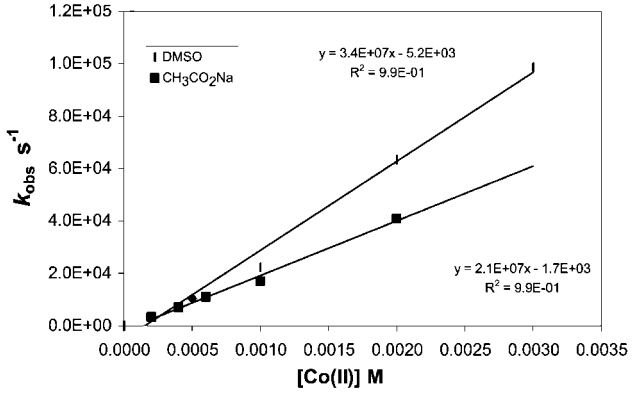

Figure 2. Dependence of the rate of formation of $\{(NH_3)_5Co-CH_3\}^{2+}$ and of $\{(NH_3)_5Co-CH_2CO_2^-\}^+$ on $\{(NH_3)_5Co(H_2O)\}^{2+}$; solution composition: N_2O saturated, $(0.2-4.0)\times10^{-3}$ M $CoSO_4$, ca. 20% NH_3 and 1.0 M DMSO or CH_3CO_2Na

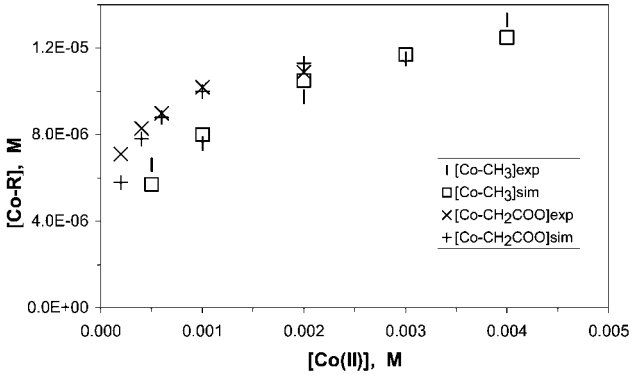

Figure 3. Dependence of $[\{(NH_3)_5Co-CH_3\}^{2+}]$ and $[(NH_3)_5Co-CH_2COO\}^+]$ on $[\{(NH_3)_5Co(H_2O)\}^{2+}]$; experimental and simulated data; solution composition: N_2O saturated, $(0.5-4.0)\times10^{-3}$ M $CoSO_4$, ca. 20% NH_3 and 1.0 M DMSO or 1 M CH_3CO_2Na; measured at 350 and 300 nm, respectively, and simulated with 1.6×10^{-5} and 1.3×10^{-5} M/pulse dose rates

Table 3. UV/Vis absorption maxima of the intermediates of the type $\{(NH_3)_5Co-R\}^{n+}$

Intermediate	λ_{max} [nm]	ε_{max} [$M^{-1}cm^{-1}$]
$\{(NH_3)_5Co-CH_3\}^{2+}$	362, 494	183, 50
$\{(NH_3)_5Co-CH_2COO^-\}^+$	370, 505	82, 50
$\{(NH_3)_5Co-CH_2OH\}^{2+}$	330	175[a]

[a] Assuming that all the radicals react to yield the intermediate.

position rate constants (samples irradiated in a ^{60}Co γ-source) are summed up in Table 4 [as the equilibrium constant for the formation of $\{(NH_3)_5Co^{III}-CH_2OH\}^{2+}$ is small, the observed decomposition is due to the reaction between two CH_2OH radicals ($k = 1.5\times10^9$ $M^{-1}s^{-1}$)[15]]. The final products of the decomposition reaction of the intermediate $\{(NH_3)_5Co-CH_3\}^{2+}$ were analyzed using GC and were found to be mainly ethane and methane. The ratios between ethane and methane formed were measured

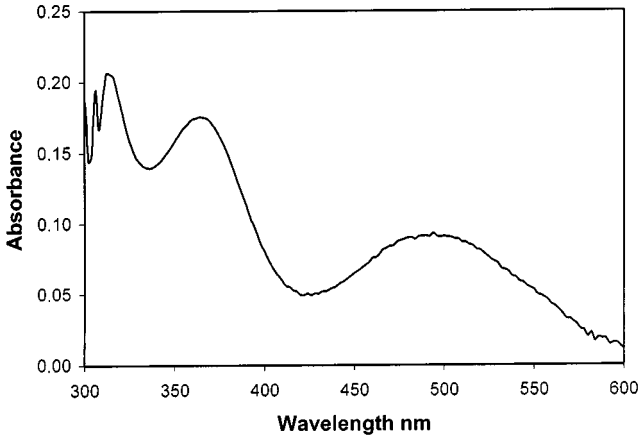

Figure 4. Spectrum of the intermediate $\{(NH_3)_5Co-CH_3\}^{2+}$; experimental conditions: N_2O saturated, 1×10^{-3} M $CoSO_4$, ca. 20% NH_3 and 1.00 M DMSO, the solution was irradiated for 15 min in the ^{60}Co source

Table 4. Measured decomposition rate constants of the complexes $\{(NH_3)_5Co-R\}^{n+}$

Complex	k [s^{-1}]
$\{(NH_3)_5Co-CH_3\}^{2+}$	2.2×10^{-4}
$\{(NH_3)_5Co-CH_2COO^-\}^+$	5.3×10^{-4}

and were found to decrease with the increase of the initial $[(NH_3)_5Co(H_2O)]^{2+}$ concentration, and increase with the number of pulses delivered to the sample, Table 5.

Table 5. Relative yields of C_2H_6 and CH_4 formed in the $(CH_3)_2SO$ system; solution composition: N_2O saturated, ca. 20% NH_3 and 1.00 M DMSO; samples were irradiated by consecutive pulses in the linear accelerator

$[Co^{2+}]$ [M]	No. of pulses	Ethane/methane[a] (experimental)	Ethane/methane (simulation)
4.0×10^{-4}	10	3.6	4.7
6.0×10^{-4}	10	3.0	3.2
1.0×10^{-3}	10	2.3	2.0
2.0×10^{-3}	10	1.5	1.05
1.0×10^{-3}	6	1.54	1.35
1.0×10^{-3}	4	1.50	1.05

[a] The pulses were given before the decomposition reaction occurs.

Discussion

Formation and Decomposition of the Complex $\{(NH_3)_5Co-CH_3\}^{2+}$

The experimental results indicate:

1) The reaction of the $^{\cdot}CH_3$ radical with the cobalt complex is relatively fast and the kinetics follows a pseudo-first-order rate law. The intercept of the line in Figure 2 is close to zero, i.e. K_1 is large and k_{-1} is small.

$$\{(NH_3)_5Co(H_2O)\}^{2+} + {}^{\cdot}CH_3 \underset{k_{-1}}{\overset{k_1}{\rightleftharpoons}} \{(NH_3)_5Co^{III}\text{-}CH_3\}^{2+} \quad (2)$$

2) However, surprisingly the yield of the intermediate formed also depends on the initial cobalt complex concentration, Figure 3.

3) The decomposition reaction of the complex $\{(NH_3)_5Co^{III}-CH_3\}^{2+}$ obeys a first-order rate law, with a rate that does not depend on the concentrations of the solution components, i.e. the decomposition reaction does not proceed by homolysis.

4) The major final product is ethane, which is surprising for a first-order decomposition of the intermediate. The ratio of [ethane]/[methane] formed depends on the initial $[Co(NH_3)_6^{2+}]$ and the total number of pulses delivered to the sample, Table 5.

These results seemed to suggest that the ethane is not a product of the decomposition of the intermediate complex, $\{(NH_3)_5Co^{III}-CH_3\}^{2+}$, which decomposes heterolytically according to Equation (3). The ethane might alternatively be formed by Equation (4), however the small intercept in Figure 2 rules out that this is the major source of ethane, and suggests that Equation (5) also occurs. Reactions analogous to Equation (5) were observed for a variety of complexes, Table 6. If the rate constant of Equation (5) is high enough it will compete with Equation (2), thus explaining qualitatively the dependence of the $[C_2H_6]/[CH_4]$ ratio on the $[Co(NH_3)_6^{2+}]_0$ concentration and on the number of pulses delivered to the solution, Table 5.

Table 6. Rates of reaction of methyl radicals with $\{LM-CH_3\}^{n+}$

Reaction	$2k$ [$M^{-1}s^{-1}$]	Ref.
$\{(NH_3)_5Co-CH_3\}^{2+} + {}^{\cdot}CH_3$	$(6\pm3)\times10^8$	this work
$\{(nta)(H_2O)Co-CH_3\}^{-} + {}^{\cdot}CH_3$	$(7.5\pm2.0)\times10^7$	[27]
$\{(nta)(H_2O)Fe-CH_3\}^{-} + {}^{\cdot}CH_3$	$(1.1\pm0.3)\times10^9$	[28]
$\{(nta)(H_2O)Mn-CH_3\}^{-} + {}^{\cdot}CH_3$	$(3.2\pm0.6)\times10^9$	[28]
$\{(cyclam)(H_2O)Ni-CH_3\}^{2+} + {}^{\cdot}CH_3$	8×10^7	[27]
$\{(hedta)Fe-CH_3\}^{2+} + {}^{\cdot}CH_3$	$(2.7\pm0.2)\times10^7$	[9]

$$\{(NH_3)_5Co^{III}-CH_3\}^{2+} \xrightarrow{H_2O} \{(NH_3)_5Co(H_2O)\}^{3+} + CH_4 \quad (3)$$

$k = 2.2\times10^{-4}\ s^{-1}$

$$2\,{}^{\cdot}CH_3 \longrightarrow C_2H_6 \quad (4)$$

$k = 1.6\times10^9\ M^{-1}s^{-1}$ [16]

$$\{(NH_3)_5Co^{III}-CH_3\}^{2+} + {}^{\cdot}CH_3 \longrightarrow \{(NH_3)_5Co(H_2O)\}^{2+} + C_2H_6 \quad (5)$$

To check whether the addition of Equation (5) to the reaction scheme indeed explains the experimental results and in order to estimate the rate constant of this reaction, the dependence of the ratio $[C_2H_6]/[CH_4]$ was simulated. The simulation experiment was done using the pro-K global analysis/simulation software (Applied Photophysics). The simulation was run assuming that only Equations (2), (4) and (5) have to be included, since Equation (3) is relatively very slow, and assuming that the concentration of methane formed equals the final concentration of the intermediate complex $\{(NH_3)_5Co-CH_3\}^{2+}$. The simulation had to account for the dependence of the $[C_2H_6]/[CH_4]$ ratio in the products on the $[Co(NH_3)_6^{2+}]_0$ concentration and on the number of consecutive pulses delivered to the sample, Table 5. The results clearly indicate that methane is mainly formed during the first pulses, while Equation (5) dominates during later pulses and ethane is primarily formed, Table 5. Initially the measured $k_1 = 3.4\times10^7\ M^{-1}s^{-1}$ was used to obtain a first estimate for k_5. Subsequently, the effect of the thus calculated k_5 on k_1 was examined, by simulating the rates of intermediate formation and both rates were iteratively adjusted. The following values best fit the experimental data: $k_1 = (3.0\pm0.3)\times10^7\ M^{-1}s^{-1}$ and $k_5 = (6\pm3)\times10^8\ M^{-1}s^{-1}$. Using these rate constants the concentrations of $\{(NH_3)_5Co-CH_3\}^{2+}$ by one pulse were calculated and the thus simulated data compared with those experimentally obtained from the optical density (O.D.) due to the transient complex, Figure 3. Obviously these rate constants simulate well with this data. The simulation points out that the yield of ethane according to Equation (4)[16] is negligible under most experimental conditions; k_5 can be compared to other reported values for analogous reactions, see Table 6. The rate constant for Equation (5) is at the higher end of the published data for these types of reactions.

It is of interest to compare the properties of $\{(nta)(H_2O)Co^{III}-CH_3\}^{-}$ [7] and $\{(NH_3)_5Co\text{-}CH_3\}^{2+}$. The former decomposes homolytically considerably faster than the heterolytic decomposition of the latter one. This is probably due to the fact that $\{Co(NH_3)_6\}^{2+}$ is a considerably stronger reducing agent than $\{Co(nta)(H_2O)_2\}^{-}$ [17] and therefore the electrons of the metal−carbon σ bond are nearer to the cobalt center in the $\{(nta)(H_2O)Co^{III}-CH_3\}^{-}$ complex. In other words the cobalt−carbon bond in $\{(NH_3)_5Co\text{-}CH_3\}^{2+}$ has a more ionic nature than that in $\{(nta)(H_2O)Co^{III}-CH_3\}^{-}$ which is more covalent and therefore tends more towards homolysis.

Formation and Decomposition of the Complex $\{(NH_3)_5Co-CH_2CO_2^{-}\}^{+}$

The acetate system behaves analogously to the methyl system. Formation and decomposition rates were measured (Tables 2 and 4) and corresponding dependencies of the formation rate constant and the intermediate concentration on initial cobalt(II) concentration were found (Figures 2 and 3). Therefore it is reasonable to conclude that the same reaction mechanism [analogous to Equations (2)−(5)] applies. The final products in this system were not measured as one of the possible products − acetate − is identical to the starting material. The rate for the reaction of the acetate radical with the intermediate (k_5 analogue) for this system was derived from a simulation of the dependency of the intermediate concentration versus the initial Co^{II} concentration (Figure 3) using the measured formation constant and a radical reaction constant (k_4 analogue) of $5.0\times10^8\ M^{-1}s^{-1}$.[15] The derived rate constant for the reaction of the intermediate with the acetate radical, $k_{5'} = (1\pm0.5)\times10^7$

$M^{-1}s^{-1}$, is considerably lower than that for the methyl system. This observation is tentatively attributed to higher steric hindrance in this system.

Formation and Decomposition of the Complex $\{(NH_3)_5Co-CH_2OH\}^{2+}$

The formation constant of the intermediate $\{(NH_3)_5Co-CH_2OH\}^{2+}$ could not be measured as in this case the back reaction of Equation (6), the homolysis, is apparently fast.

$$\{(NH_3)_5Co(H_2O)\}^{2+} + {}^{\cdot}CH_2OH \rightleftharpoons \{(NH_3)_5Co^{III}-CH_2OH\}^{2+} \quad (6)$$

The experimental results point out that the equilibrium constant of Equation (6) is much smaller than that measured for the analogous intermediate with nta as ligand. In the nta analog it was suggested[7] that the intermediate formed is $\{(nta)(Co^{III}-CH_2O^-\}$, this intermediate does not decompose readily according to the homolytic reaction since it is stabilized by partial bonding of the oxygen atom to the cobalt center due to electrostatic interactions;[7] i.e. the intermediate formed is:

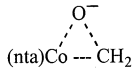

As in the NH_3 system the intermediate formed is $\{(NH_3)_5Co\text{-}CH_2OH\}^{2+}$ and no *cis* ammonia release is expected[18] as no such stabilization is possible and it decomposes very fast according to the homolytic pathway.

Spectra of the Complexes $\{(NH_3)_5Co^{III}-R\}^{n+}$

The general spectra of the $\{(NH_3)_5Co^{III}-R\}^{n+}$ complexes resemble the spectrum of the complex $\{(NH_3)_5Co^{III}-CH_3\}^{2+}$,[10] and the spectra of the complexes $\{(H_2O)(nta)Co^{III}-R\}^{2+}$.[7] This confirms the identity of the nature of the transient complexes formed, as complexes of cobalt(III) with cobalt−carbon σ bonds, $\{(NH_3)_5Co^{III}-R\}^{n+}$.

Concluding Remarks

The rate constants measured in this study, for the formation of the cobalt complexes with the cobalt−carbon σ bonds, with the different radicals, are similar to the known rate constants for ligand exchange of the complex $\{Co(H_2O)_6\}^{2+}$ in aqueous solutions, $k = 5\times10^6\ s^{-1}$. Reactions leading to the formation of the metal−carbon bonds clearly proceed according to the inner-sphere mechanism. The results are thus in agreement with a mechanism where the rate-determining step is the ligand-exchange step. Similar conclusions were reported previously for a variety of reactions in which metal−carbon σ bonds are formed by radical reactions.[2,7,19]

A comparison of the rates of reaction of ${}^{\cdot}CH_3$ radicals with a variety of complexes of the type $L_mM^{n+1}-CH_3$, Table 6, is of interest. Though all the other reactions measured are for $L_mM^{n+1}-CH_3$ complexes which decompose homolytically, the rate constant for $\{(NH_3)_5Co^{III}-CH_3\}^{2+}$, which decomposes heterolytically, falls well into the observed range for the other reactions, i.e. the rate constants of these reactions do not depend strongly on the "ionicity" or "covalency" of the metal−carbon σ bond. Contrary to the previously published systems, which decompose homolytically (with the exception of the copper systems, which decompose in a bimolecular reaction), $\{(NH_3)_5Co-CH_3\}^{2+}$ decomposes heterolytically, implying that the $Co-CH_3$ bond is considerably more ionic.

In principle two possible mechanisms might be envisioned for the radical complex reaction:

a) a second CH_3 radical coordinates at the *cis* position to the first one, followed by reductive elimination of ethane:

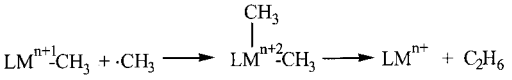

b) the second CH_3 radical attacks, and binds to, the carbon atom bound to the central metal cation:

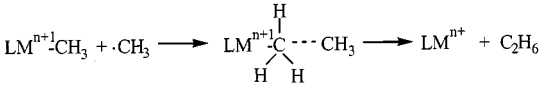

Reaction a) can be disqualified, based on the velocity of the reaction, as the derived reaction rate for the process is significantly faster than typical ligand exchange reactions for such a system. Recently, van Eldik et. al.[18] measured the ligand exchange rate for the *trans*-labilized NH_3 ligand of the $\{(NH_3)_5Co-CH_3\}^{2+}$ system as $k_{sat} = 1.8\ s^{-1}$ (a *cis* ligand should be more difficult to exchange). This mechanism is also in agreement with the observation that $k_{(NH_3)_5Co^{III}-CH_3 + {}^{\cdot}CH_3} >> k_{(NH_3)_5Co^{III}-CH_2CO_2^- + {}^{\cdot}CH_2CO_2^-}$ as the latter reaction is sterically hindered.

Complexes with cobalt−carbon σ bonds can be synthesized by a radical process. Nevertheless, this technique has a disadvantage, the results imply that the reaction according to Equation (5) is very fast, especially for systems without steric hindrance, in comparison to Equation (2). Therefore, the attainable yields of the desired intermediates are expected to be relatively low.

Experimental Section

Materials: All solutions were prepared from AR grade chemicals and from distilled water which was further purified by passing through a Milli Q Millipore setup, final resistivity > 10 MΩ/cm.

pH: The pH was measured with a Corning 22 pH meter and adjusted by addition of $HClO_4$ and/or NaOH.

Radiolytic Technique: Pulse radiolysis experiments were carried out using the Varian 7715 linear electron accelerator at the Hebrew

University of Jerusalem. The pulse duration was 0.1−1.5 μs with a 200-mA current of 5-MeV electrons. The dose per pulse was 3−30 Gray. Irradiations were carried out in a 4-cm spectrosil optical cell, the analyzing light was passed three times through the cell. A 150-W xenon arc produced the analyzing light. The experimental setup was identical with that described earlier in detail.[20] For dosimetry, an N_2O-saturated solution containing 1×10^{-3} M $Fe(CN)_6^{4-}$ was used. The yield was measured by using $\varepsilon_{420} = 1000\ M^{-1}cm^{-1}$. The values of the molar extinction coefficient calculated from the dosimetry measurements have an error limit of ±15% due to the scatter in the pulse intensity and due to uncertainties in G values. A ^{60}Co source, Noratom, with a dose rate of ca. 6 Gray/min was used for low-dose rate experiments and product analysis.

Product Analysis: GC analysis: 30-mL samples in closed glass vials under N_2O were irradiated by the linear accelerator and/or by the ^{60}Co source. The gaseous products were analyzed using a Varian Model 3700 gas chromatograph.

Production of Radicals: The radiolysis of water in dilute aqueous solutions can be summarized as follows:

$$H_2O \xrightarrow{e^-,\gamma} {}^{\cdot}OH\,(2.65);\ {}^{\cdot}H\,(0.60);\ e^-_{aq}\,(2.65);\ H_2\,(0.45);\ H_2O_2\,(0.75) \qquad (7)$$

(G values in parentheses, are defined as the number of molecules of each product/100 eV radiation absorbed by the solution).[20] In concentrated solutions the yields of the radicals are somewhat higher and those of H_2O_2 and H_2 are somewhat lower. In N_2O-saturated solutions the hydrated electron is converted into the hydroxyl radical via:[13]

$$e^-_{aq} + N_2O \longrightarrow N_2 + {}^{\cdot}OH + OH^- \qquad (8)$$
$$k = 9.1\times10^9\ M^{-1}s^{-1}$$

at pH > 3 the contribution of ·H atoms to the total free radical yield is less than 10%. Methyl radicals were produced by reactions summarized in Table 1. The other alkyl radicals used in this study were prepared by hydrogen abstraction reactions of the primary radicals with the appropriate aliphatic solutes, these reactions are also summarized in Table 1.

Acknowledgments

This study was supported in part by a grant from the Budgeting and Planning Committee of The Council of Higher Education and the Israel Atomic Energy Commission. D. M. wishes to thank the Alexander von Humboldt Foundation for support and Mrs. Irene Evens for her ongoing interest and support.

[1] J. Halpern, *Acc. Chem. Res.* **1982**, *15*, 238.
[2] H. Elroi, D. Meyerstein, *J. Am. Chem. Soc.* **1978**, *100*, 5540.
[3] J. F. Endicott, K. P. Balakrishnan, C. L. Wong, *J. Am. Chem. Soc.* **1980**, *102*, 551.
[4] C. Y. Mok, J. F. Endicott, *J. Am. Chem. Soc.* **1978**, *100*, 123.
[5] T. S. Roche, J. F. Endicott, *J. Am. Chem. Soc.* **1972**, *94*, 8622.
[6] T. S. Roche, J. F. Endicott, *J. Am. Chem. Soc.* **1974**, *13*, 1575.
[7] D. Meyerstein, H. A. Schwarz, *J. Chem. Soc., Faraday Trans. 1* **1988**, *84*, 2933−2949.
[8] R. van Eldik, H. Cohen, D. Meyerstein, *Angew. Chem. Int. Ed. Engl.* **1991**, *30*, 1158.
[9] S. Goldstein, G. Czapski, R. van Eldik, N. Shaham, H. Cohen, D. Meyerstein, *Inorg. Chem.*, in press.
[10] P. Kofod, *Inorg. Chem.* **1995**, *34*, 2768.
[11] P. Kofod, P. Harris, S. Larsen, *Inorg. Chem.* **1997**, *36*.
[12] Y. Abe, H. Ogino, *Bull. Chem. Soc. Jpn.* **1989**, *62*, 56.
[13] G. V. Buxton, C. L. Greenstock, W. P. Helman, A. B. Ross, *J. Phys. Chem. Ref. Data* **1988**, *17*, 513−886.
[14] T. L. Cottrell, *The Strengths of Chemical Bonds*, 2nd ed., Butterworths, London, **1958**.
[15] M. Simic, P. Neta, E. Hayon, *J. Phys. Chem.* **1969**, *73*, 3794.
[16] P. Neta, J. Grodkowsk, A. B. Ross, *J. Phys. Chem. Ref. Data* **1996**, *25*, 709−1050.
[17] IUPAC Stability Constants Database, Academic Software, **1993**.
[18] C. Ducker-Benfer, M. S. A. Hamza, C. Eckhardt, R. van Eldik, *Eur. J. Inorg. Chem.* **2000**, 1563.
[19] R. van Eldik, H. Cohen, D. Meyerstein, *Inorg. Chem.* **1994**, *33*, 1566.
[20] M. S. Matheson, L. M. Dorfman, *Pulse Rdiolysis*; MIT press, Cambridge, **1969**.
[21] D. Veitwisch, E. Janata, K. D. Asmus, *J. Chem. Soc., Perkin Trans. 2* **1980**, 146.
[22] S. A. Chandhri, M. Goebl, T. Freyholdt, K. D. Asmus, *J. Am. Chem. Soc.* **1984**, *106*, 5988.
[23] A. M. Koulkes-pujo, B. D. Michael, E. J. Hart, *J. Radiat. Phys. Chem.* **1971**, *3*, 33.
[24] H. Cohen, D. Meyerstein, *Inorg. Chem.* **1986**, *25*, 1506.
[25] P. Neta, G. R. Holdern, R. H. Schuler, *J. Phys. Chem.* **1971**, *75*, 449.
[26] S. Gordon, E. J. Hart, M. S. Matheson, J. Rabani, J. K. Thomas, *Discuss. Faraday Soc.* **1963**, *36*, 193.
[27] A. Sauer, H. Cohen, D. Meyerstein, *Inorg. Chem.* **1989**, *28*, 2511−2512.
[28] H. Cohen, D. Meyerstein, *Inorg. Chem.* **1988**, *27*, 3429.

Received July 3, 2001
[O01247]

Electronic Properties of the Axial Co−C and Co−S Bonds in B_{12} Systems − A Density Functional Study

Lucio Randaccio,*[a] Silvano Geremia,[a] Mauro Stener,[a] Daniele Toffoli,[a] and Ennio Zangrando*[a]

Keywords: Cobalamines / Coenzymes / Density functional calculations / X-ray diffraction

The numerous accurate structural data of cobalamins now available allows us to optimize the geometry of these systems, based on a simplified model by using density functional theory (DFT) calculations. This approach, which reproduces the trend of the experimental distances derived from EXAFS and X-ray crystal structures in the corrin macrocycle, permit us to interpret the electronic properties in the NB3–Co–X axial system. In particular, the results are analyzed for cobalamins containing a sulfur ligand which exhibits a "regular" *trans* influence, i.e., when the Co–S bond shortens, the *trans* Co–NB3 bond lengthens. This feature appears in contrast with an anomalous effect ("inverse" *trans* influence) postulated a few years ago by analyzing the structural data of several alkylcobaloximes, $LCo(DH)_2R$, a simple B_{12} model, and attributed principally to the electronic properties of the alkyl group R. The present study on the NB3–Co–S fragment does not indicate that the "inverse" *trans* influence is a general rule in cobalamins. The accurate crystal structures of the $[(SO_3)Cbl](NH_4)$ and [(thiourea)Cbl](PF_6) cobalamins based on synchrotron diffraction data at 100 K are also reported for comparison with the theoretical study. The former crystal structure, including one co-crystallized glycerol molecule, presents "for the first time" an ordered hydrogen-bonding pattern for the solvent molecules.

Introduction

Methionine synthase, whose cofactor is methylcobalamin (MeCbl; R = Me; Scheme 1) catalyzes the conversion of homocysteine to methionine.[1] The MeCbl-based enzymes (methyltransferases) catalyze the transfer of methyl groups from a nitrogen atom of methyltetrahydrofolate to cob(I)alamin (to form MeCbl) for onward transmission to an S atom of homocysteine. The enzymatic scheme proposed for the methionine synthase requires a reversible heterolytic cleavage of the Co−Me bond in the methyl carbocation and the strongly nucleophilic cob(I)alamin species.[2] In order to interpret the MeCbl function, several reactions of thiolates with organocobalt B_{12} model complexes have been carried out. However, the reports of these reactions were controversial.[3] Alkylthiolate cobalamin complexes, RS−Cbl, are also of interest as analogues of the RS and Co^{II}Cbl radical pair involved[4] in the mechanism of the coenzyme B_{12} (AdoCbl) dependent ribonucleotide reductase.[5]

Hence, knowledge of the properties and the behavior of thiolate−cobalamins is of significant interest. However, few thiolates have been isolated and characterized so far, and these have been principally by EXAFS[6] and NMR spectroscopy,[7,8] the former study also including (HSO_3)Cbl.

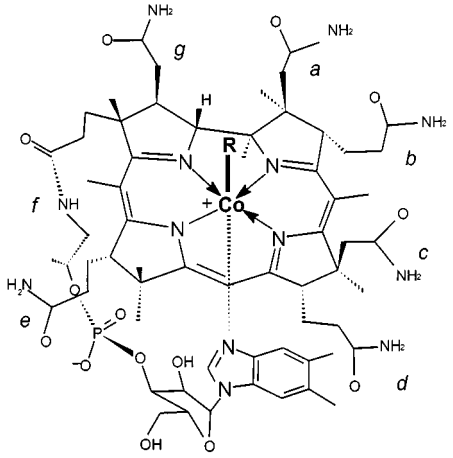

Scheme 1. Cobalamin

Only recently has the structural characterization of the NB3−Co−S fragment in $[(SO_3)Cbl](NH_4)$ (**1**) and $[(NH_2)_2CSCbl]Cl$ (**2**) been reported.[9]

Combining EXAFS and crystallographic results, it was concluded[6] that the S-containing ligands, such as thiolates and HSO_3^- have a weak *trans*-influencing ability, similar to that of H_2O[10] or CN.[11] Inversely, SO_3^{2-} exerts a strong *trans* influence similar to that of the methyl group.[9]

[a] Dipartimento di Scienze Chimiche, Università di Trieste
Via Giorgieri 1, 34127 Trieste, Italy
Fax: (internat.) + 39-040/676-3903
E-mail: zangrando@univ.trieste.it

 © WILEY-VCH Verlag GmbH, 69451 Weinheim, Germany, 2002 1434−1948/02/0101−0093 $ 17.50+.50/0

In order to verify the *trans* influence of HSO_3^-, we tried to prepare (HSO_3)Cbl according to a previous report.[6] The successive crystallographic analysis, described here, revealed that the compound is better formulated as $[(SO_3)Cbl](NH_4)$·glycerol solvate (**3**). Furthermore, in order to provide a more widespread comparison, the structural determination of $[(NH_2)_2CSCbl](PF_6)$ (**4**), more accurate than that of **3**, is also reported.

It is clear that the understanding of the chemical behavior of cobalamins requires an in-depth study of their electronic properties. However, despite the numerous experimental results, only a few attempts to understand their behavior on theoretical grounds have been carried out so far, principally on simple models[12] and in a few instances on R(Co−corrin)base (Scheme 2).[13] These studies, sometimes reaching conflicting conclusions, have been based on semiempirical approaches.[14] More recently, density functional theory (DFT) has been applied to calculate the geometry of some alkyl(Co−corrin)bases [15,16] and Co−corrin.[17] Furthermore, up to a few years ago, structural data on cobalamins were too low in accuracy for meaningful comparisons to be made.[18] Here, we report a theoretical approach, based on application of the density functional theory to the simplified model X(R)(Co−corrin)Bzm (Bzm = 5,6-dimethylbenzimidazole, X = R if alkyl group; Scheme 2), since the accurate structural data of several cobalamins is now available.[9−11,19,20] To complement this theoretical approach, which compares, for the first time, the electronic properties of the Co−S and Co−C bonds in the corrin model of cobalamins, some relationships with accurate structural data are reported.

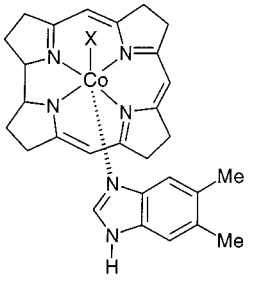

Scheme 2. Model corrin system used for calculations

Crystallographic Results

Crystal Packing

The cobalamin molecules are packed in their crystals in such a way as to form large cavities, in which solvent molecules are located (or ionic species when present, as in ClCbl·2LiCl[20]). These cavities may be described as being made by a central channel, running along a crystallographic 2_1 axis, and connected to side pockets at intervals defined by this axis.[19] The channel content is characterized by a disordered pattern of water molecules, while an ordered scheme of full-occupancy water molecules characterizes the pockets.[19]

Moreover, the crystal packing of isomorphous cobalamins can be divided into four clusters (I−IV),[9,18] according to the *c*/*a* and *b*/*a* ratios of the unit cell parameters. Isostructural cobalamins, which belong to the same cluster, display very similar amide side chain conformations,[9] and hence a closely related arrangement of solvent molecules within the pocket. Cobalamin **3** has unit cell parameters very similar to those of **1**, in spite of the presence of one glycerol molecule per Co atom and, hence, it still belongs to cluster I, which is characterized by an intramolecular H bond between the amide chain *c* and the axial sulfite ligand. Analogously, cobalamin **4** belongs to cluster II, as does $[(NH_2)_2CSCbl]Cl$ (**2**), and it does not exhibit any intramolecular H bond, the chain *c* points away from the axial thio-

Table 1. Hydrogen-bond scheme of water molecules (Ow), glycerol oxygen atoms (Og) and NH_4^+ within the pocket of compound **3**

	Occupancy	H bonds	H donors	H acceptors
Og1			Ow11	O3
Og2			N40	O44
Og3			N29, Ow9, Ow14	O1
NH_4^+		4		O4P, O62, O8R, O39
Ow1		3	N52	Ow2, O58
Ow2		3	Ow1	Ow3, O5P
Ow3		4	Ow2, O7R	O4P, Ow4
Ow4		4	Ow3, N59	O62, Ow12
Ow6		4	Ow7, Ow12 [Ow13]	Ow9, O33
Ow7		4	O8R, Ow8 [Ow15]	Ow6, Ow15 [Ow8]
Ow8		2 (3)	[Ow7]	O44, Ow7 [O6R]
Ow9		3	Ow6	O3, Og3 [Ow14]
Ow10	0.5	4	Ow11, Ow15 [Ow12]	O51, Ow12 [Ow15]
Ow11		4	N29, N45	Ow10, Og1
Ow12	0.59(2)	3	Ow4, Ow10	Ow6
Ow13	0.41(2)	2	Ow14 (?)	Ow6
Ow14	0.5	3 (?)	Ow9	Ow13 (?), Og3
Ow15		3	Ow7 [Ow10]	O39, Ow10 [Ow7]

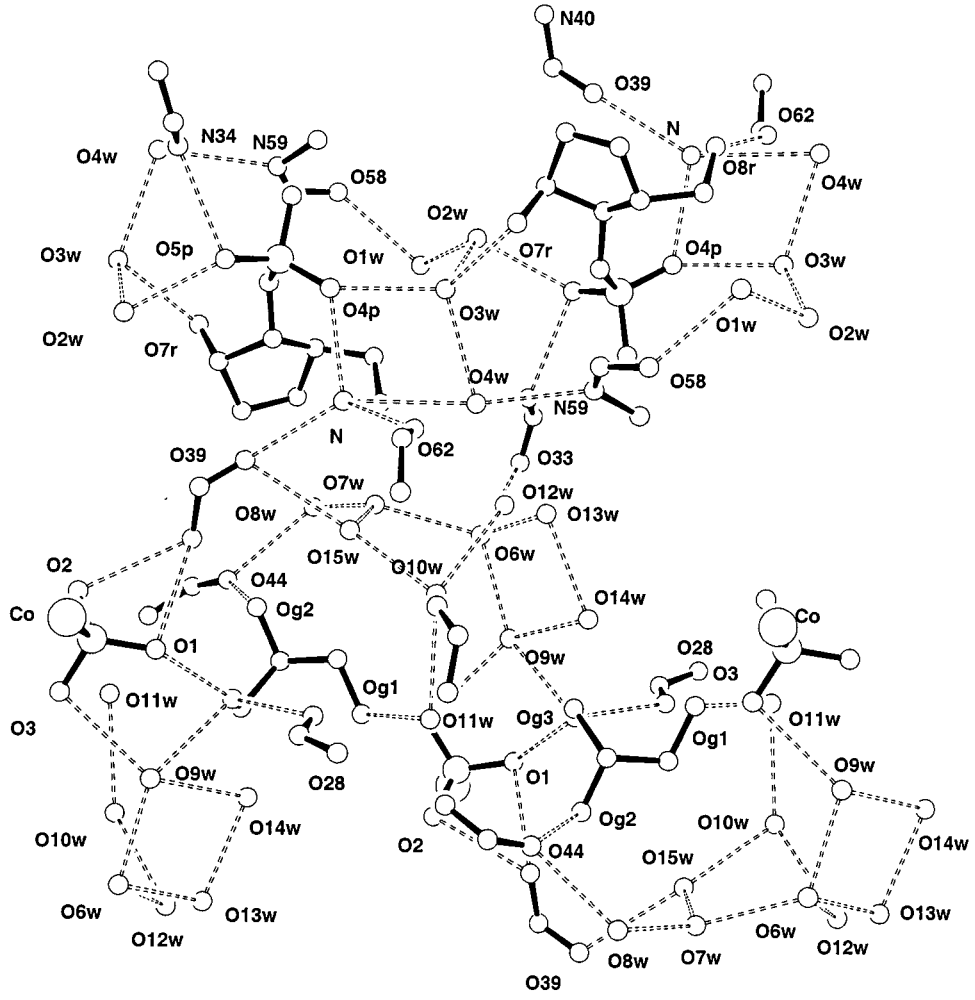

Figure 1. Hydrogen-bonding scheme (dashed lines) within the pocket for **3**; the content of a portion of the channel, running approximately along the horizontal direction of the figure, is also shown

urea ligand. The proposed H-bond scheme for **3** is given in Table 1 and the scheme within the cavity is shown in Figure 1. The structure within the pocket essentially corresponds to that found in **1** (see Figure 2 of ref.[9]), with only slight modifications (involving Ow3, Ow4, and OR7), as might be expected from the H-bond donor/acceptor scheme found in the crystal structure of vitamin B_{12r}, determined by neutron diffraction.[21] The glycerol molecules and the SO_3^{2-} groups are located within the channel, *where for the first time in a cobalamin crystal structure, the solvent molecules exhibit an ordered H-bond pattern*.

The H-bonding scheme within the cavity of **4** is significantly more detailed than that found in **2**, showing an ordered arrangement of the water molecules with full occupancy in the pocket and a disordered one in the channel, as has usually been the case in cobalamin crystal structures reported thus far. Of the disordered PF_6^- anion, the species with the highest occupancy (0.65) is located in the interface region, whereas the lower one (0.35) is in the channel.

Molecular Structure

The ORTEP drawings of **3** and **4** are shown in Figure 2 and Figure 3, respectively, and coordination distances are given in Table 2, where they are compared with those detected in the crystal structures of **1** and **2**. The folding angles, φ, defined as the dihedral angle between the two best-fit planes through N21/C4/C5/C6/N22/C9/C10 and C10/C11/N23/C14/C15/C16/N24, are also given in Table 2.

The axial distances in **1** and **3** are similar, whereas the Co−NB3 and Co−S distances are longer in **4** with respect to those of **2**. While the low accuracy of the latter structure[9] justifies the difference in the Co−NB3 distances, the discrepancy is more evident in the Co−S bond lengths. Actually, a re-examination of the difference Fourier map of **2** revealed a peak, along the Co−S bond, which could be assigned to a partially occupied (0.27) oxygen atom of a water ligand. This affected the previous refinement, which resulted in an artificial shortening of the Co−S distance.

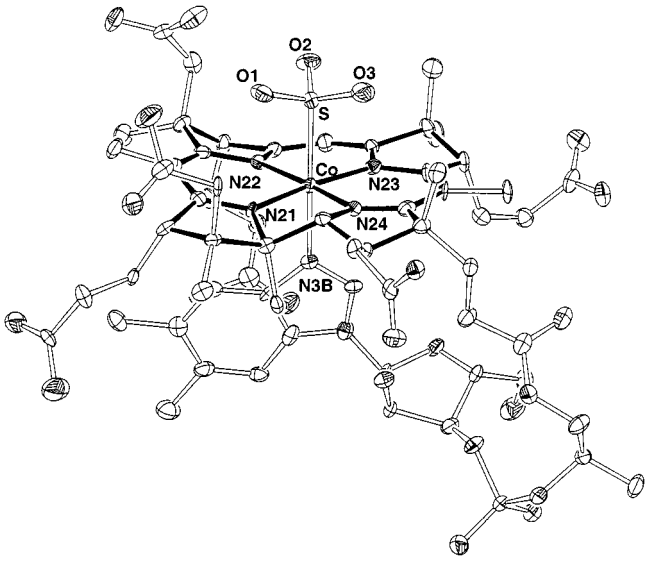

Figure 2. ORTEP drawings of **3** (thermal ellipsoids drawn at 50% probability level); solid bonds indicate the corrin ring

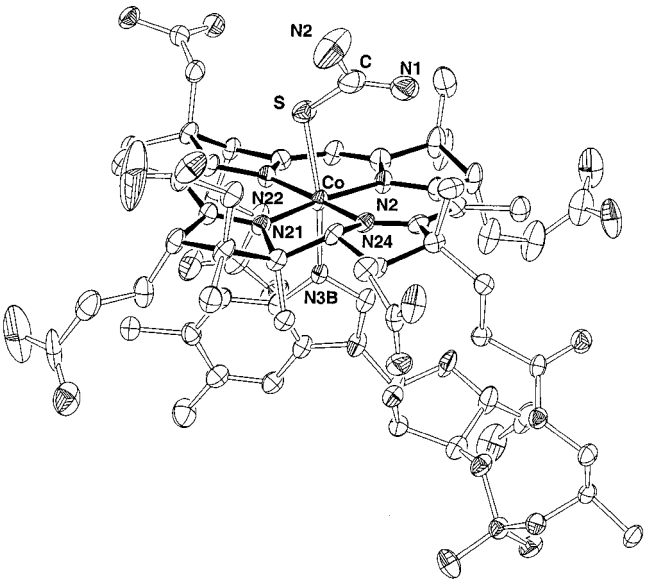

Figure 3. ORTEP drawings of **4** (thermal ellipsoids drawn at 30% probability level); solid bonds indicate the corrin ring

Table 2. Coordination distances [Å] and folding angle φ [°] in (SO_3)Cbl (**1**, **3**) and $(NH_2)_2$CSCbl (**2**, **4**)

	1	3	2	4
Co−S	2.231(1)	2.241(2)	2.216(7)	2.300(2)
Co−NB3	2.134(4)	2.156(5)	2.01(1)	2.032(5)
Co−N21	1.870(3)	1.883(5)	1.853(9)	1.884(5)
Co−N22	1.913(2)	1.911(5)	1.894(9)	1.916(4)
Co−N23	1.890(3)	1.904(5)	1.91(1)	1.926(5)
Co−N24	1.886(4)	1.901(5)	1.881(9)	1.895(4)
φ	16.3(1)	16.5(2)	14.9(3)	14.5(1)

Comparison of data confirms the previous finding that the Co−NB3 distance in the sulfite derivative is significantly longer than that in the thiourea analogue. On the other hand, the Co−S distance in the latter is about 0.06 Å longer than the corresponding values in **1** and **3**. Therefore, our previous conclusion,[9] that the Co−SO_3 and Co−$SC(NH_2)_2$ bond lengths were very similar, must be revised.

The sulfite geometry in **3** is characterized by S−O distances in the range 1.459(5)−1.490(5) Å and by approximately tetrahedral angles around S, which do not differ significantly from those found in **1** (Table 3). The orientation of SO_3 with respect to the equatorial plane appears to be determined by the intramolecular H bond [3.001(8) Å] between O2S and the NH_2 group of the amide chain *c*. In **4**, the Co−S−C angle is 118.9(3)° and the approximately planar S−$C(NH_2)_2$ group is oriented with respect to the equatorial moiety in such a way that the N21−Co−S−C and Co−S−C−N2 torsion angles are 107.1(4) and −143.7(8)°, respectively. The thiourea N1 atom is involved in a H bond with a water molecule [N1···Ow9 [2.99(1) Å].

The value of 10^7 of the equilibrium constant for the substitution of water by sulfite in aquocobalamin,[22] and the close similarities of the Co−SO_3 fragment geometry in **1** and **3**, strongly suggest the [(SO_3)Cbl](NH_4) formulation for **3**. Furthermore, the site assigned to the NH_4^+ ion corresponds to that occupied by K^+ in the isostructural CNCbl·KCl,[11] which belongs to the same cluster I. In addition, it has been claimed that (HSO_3)Cbl may be prepared from aquocobalamin,[6] by dissolving it in sodium acetate buffer (pH = 5) and adding sodium sulfite.[23] Thus, these results appear to favor the (HSO_3)Cbl formulation for **3**, assuming that the ammonium cation position is occupied by a water molecule (as found in **4**). However, this appears unlikely because of the four H-bond short contacts around this site (2.886, 2.734, 2.800, and 2.796 Å with O39, OP4, O62, and OR8, respectively, Table 1) should require a water molecule to be involved in bifurcate (probably long) H bonds. An early report[24] indicated that in acetate buffer at pH = 5.0, the complex exists as sulfitocobalamin, as evidenced by both IR spectroscopy (which showed no significant change over a pH range of 4−14) and electrophoresis (which indicates an overall charge of −1). Finally, the calculated geometry for the HSO_3^- group does not reproduce the experimental data as it does for the thiourea derivative (see below).

Discussion

Comparison of X-ray (XRD) and EXAFS Results

Several accurate X-ray structural determinations of the axial distances in cobalamins are now available.[9−11,19,20] Comparison with those previously determined by EXAFS may be useful in order to establish the reliability of bond lengths determined solely by using the first-shell Fourier filter analysis of EXAFS data.[6,25] In particular, such a comparison is important in view of the recent controversial EX-

Table 3. Calculated and experimental bond lengths [Å] and angles [°] of the Co−SO_3 fragment in **1** and **3** and of the Co−$SC(NH_2)_2$ in **4**; the calculated geometry for the HSO_3^- derivative is also reported

	1	**3**	calcd.	HSO_3 calcd.		**4**	calcd.
S−O1	1.466(4)	1.487(5)	1.469	1.625	S−C	1.724(8)	1.705
S−O2	1.452(4)	1.459(5)	1.461	1.440	C−N1	1.32(1)	1.321
S−O3	1.472(4)	1.490(5)	1.465	1.445	C−N2	1.31(1)	1.330
Co−S−O1	108.5(1)	108.6(2)	104.5	105.6	Co−S−C	118.9(3)	116.5
Co−S−O2	108.6(2)	108.5(2)	101.9	111.5	S−C−N1	122.3(7)	124.7
Co−S−O3	109.0(2)	108.4(2)	104.0	108.2	S−C−N2	116.6(7)	115.8
O1−S−O2	109.5(2)	110.2(3)	115.0	102.8	N1−C−N2	121.1(8)	119.4
O1−S−O3	109.4(3)	109.8(3)	115.4	107.1			
O2−S−O3	111.9(3)	111.4(3)	113.8	120.5			

AFS results concerning the considerable lengthening of the Co−N axial bond (by about 0.3 Å) in the protein-bound B_{12} coenzyme with respect to the free coenzyme.[26,27] In molecular biology, EXAFS is an ideal complement to biocrystallography in establishing the coordination distances in metalloenzyme and, under favorable circumstances, it can give coordination distances with an accuracy of 0.01 Å.[28] However, the analysis generally furnishes several solutions,[26] often difficult to interpret without comparison with accurate X-ray structural data, which often cannot be obtained for metalloproteins. Thus, such a dramatic impasse may be overcome if a model with precisely determined structure is available. Comparison of data for cobalamins, reported in Table 4, shows that the equatorial Co−Neq distances obtained by EXAFS and XRD are very similar. In fact, those determined by EXAFS range from 1.88(1) to 1.91(1) Å,[6] very close to the mean value of 1.895 Å based on 14 accurate X-ray structural determinations of R(X)−Cbl.[11] On the other hand, differences between axial distances, determined by means of EXAFS and XRD, range from −0.14 to +0.22 Å (Table 4). Thus, for example, the trend of the *trans* influence of the R(X) group, derived from EXAFS spectroscopy, is completely different. Such a large discrepancy has been ascribed to the presence of the four equatorial nitrogen atoms, which limits the accuracy of the axial distances because their contribution to the EXAFS spectrum interferes with that of the axial ligands.[27,29] The treatment of EXAFS data with the global mapping technique[26] has solved such a discrepancy in the case of $(H_2O)Cbl^+$, although it has been pointed out that multiple solutions are generally possible.[27,29] Thus, for $(H_2O)Cbl^+$, an alternative solution gave Co−N and Co−O distances in agreement with the crystallographic results (Table 4). More recently, an improvement of the global mapping technique, which reduces the parameters/observables ratio, has been proposed for the interpretation of EXAFS spectra of simple cobaloximes, a B_{12} model.[29] However, the lack of any structural information may sometimes render the choice among different solutions difficult.

Table 4. Cobalamins Co−X and Co−NB3 axial distances [Å] determined by X-ray diffraction (XRD) and EXAFS with relative differences Δ; the references in the footnotes correspond to XRD and EXAFS data, respectively

X	Co−X XRD	Co−X EXAFS	Δ	Co−NB3 XRD	Co−NB3 EXAFS	Δ
H_2O[a][b]	1.952(2)	1.90(2)	−0.05	1.925(2)	2.14(3)	0.22
H_2O[c]		1.97(2)	0.02		1.89(2)	−0.03
CN[d][b]	1.886(4)	1.90(3)	0.01	2.041(3)	2.15(3)	0.11
SO_3[e][f]	2.236(2)	2.35(2)	0.11	2.145(5)	2.16(4)	0.02
Me[b][d]	1.979(4)	2.00(3)	0.02	2.162(4)	2.20(3)	0.04
Ado[g][c]	2.033(4)	2.03(2)	0.00	2.237(3)	2.19(1)	−0.05
Cob(II)-alamin[h][i]	–	–	–	2.13(2)	1.99(3)	−0.14

[a] Ref.[10] – [b] Ref.[25]; EXAFS study based on a first shell Fourier filter analysis. – [c] Ref.[26]; EXAFS analysis based on a global mapping technique. – [d] Ref.[11] – [e] Mean value from structural data of **1** and **3**. – [f] Ref.[6]; the EXAFS study, based on a first shell Fourier filter analysis, refers to $(HSO_3)Cbl$. – [g] Ref.[32] – [h] B. Kräutler, W. Keller, C. Kratky, *J. Am. Chem. Soc.* **1989**, *111*, 8936−8938. – [i] I. Sagi, M. D. Wirt, E. Chen, S. Frisbie, M. R. Chance, *J. Am. Chem. Soc.* **1990**, *112*, 8639−8644.

DFT-Optimized Geometry

Calculated and experimental coordination distances for several cobalamins are reported in Table 5. As expected,[30] calculated distances are shorter than the experimental ones, with the exception of the axial distances of the sulfite derivative and, to a lesser extent, of the Co−OH_2 and Co−CF_3 distances. The relatively enormous lengthening of the calculated axial distances in the SO_3^{2-} derivative corresponds to large deviations from the tetrahedral value for the angles about the sulfur atom (Table 3). In fact, calculated Co−S−O (in the range 101.9−104.5°) and O−S−O angles (in the range 113.8−115.4°) are larger and smaller, respectively, than the experimental ones. This inconsistency in the geometry can be attributed to the repulsion of the negatively charged oxygen atoms of SO_3^{2-}. Analogous comparison for the thiourea derivative does not show any discrepancy (Table 3). Calculations carried out for the HSO_3^- derivative also indicate that "addition" of a proton to SO_3^{2-} decreases the O···O repulsion, reducing the angular distortion in the $CoSO_3$ fragment. If the calculated values for the latter are considered, instead of those of sulfite, the experimental trend of the axial distances, when X is varied, is very

Table 5. Experimental (at 100 K) and calculated coordination distances [Å] for several cobalamin derivatives; experimental data from ref.[11], if not otherwise stated

X	Co−NB3		Co−X		Co−N21		Co−N24		Co−N22		Co−N23	
	exp.	calcd.	exp.	calcd.	exp.	calcd.	exp.	calcd.	exp.	calcd.	exp.	calcd.
H_2O	1.925(2)	*1.881*	1.952(2)	*1.964*	1.881(2)	*1.858*	1.879(2)	*1.844*	1.897(2)	*1.886*	1.904(2)	*1.895*
Cl	1.981(3)	*1.972*	2.252(1)	*2.193*	1.873(3)	*1.847*	1.880(3)	*1.829*	1.902(3)	*1.892*	1.914(3)	*1.898*
CN[a]	2.041(3)	*2.002*	1.886(4)	*1.823*	1.881(3)	*1.840*	1.883(3)	*1.848*	1.911(3)	*1.882*	1.920(3)	*1.903*
CF_3[d]	2.05(1)	*2.051*	1.88(1)	*1.929*	1.870(9)	*1.842*	1.917(9)	*1.836*	1.95(1)	*1.888*	1.89(1)	*1.898*
Me	2.162(4)	*2.100*	1.979(4)	*1.942*	1.877(4)	*1.835*	1.874(4)	*1.829*	1.922(4)	*1.885*	1.918(4)	*1.890*
CMe_3	–	*2.174*	–	*2.082*	–	*1.833*		*1.822*		*1.895*		*1.898*
$SC(NH_2)_2$, **4**	2.032(5)	*1.974*	2.300(2)	*2.241*	1.884(5)	*1.853*	1.895(4)	*1.833*	1.916(4)	*1.901*	1.926(5)	*1.898*
SMe	2.04[b]	*2.028*	2.26[b]	*2.228*	–	*1.842*	–	*1.827*	–	*1.895*	–	*1.898*
HSO_3	–	*2.071*	–	*2.171*	–	*1.850*	–	*1.833*	–	*1.894*	–	*1.891*
SO_3[c]	2.145(5)	*2.170*	2.236(2)	*2.293*	1.877(4)	*1.840*	1.888(4)	*1.823*	1.912(4)	*1.875*	1.897(4)	*1.887*
Mean					1.878	*1.844*	1.888	*1.832*	1.916	*1.889*	1.910	*1.896*
Δ					0.014	*0.025*	0.043	*0.026*	0.053	*0.026*	0.036	*0.016*

[a] The calculated and experimental C−N bond lengths and Co−C−N angles are 1.166, 1.161(5) Å, and 175.4, 178.2(3)°, respectively. – [b] Estimated values (see text). – [c] Experimental mean values from structural data of **1** and **3**. – [d] X. Zou, K. L. Brown, *Inorg. Chim. Acta* **1998**, *267*, 305−308.

well reproduced. Thus it seems likely that the longer values of the calculated axial distances in $(SO_3)Cbl^-$ are due to a calculation artifact, ascribable to the high negative charge localized on the sulfite O atoms. This excess of charge should be caused by the lack, in the model molecule employed in calculations, of the interactions with the solvent (via H bonds), which delocalize the partial negative charge in the real system. This artifact gives rise to a strong apparent repulsion between the O atoms, indicated in the calculated structure by the flattening of the S tetrahedron towards the equatorial moiety (Table 3), which, in turn, enhances the steric repulsion with the macrocycle and provokes a lengthening of the Co−S bond, as well as a flattening of the corrin ligand (steric *cis* influence). In fact, the calculated folding angle φ of 10.26° [14.12° for $(HSO_3)Cbl$], is significantly smaller than the experimental one of 16.4° in the sulfite derivative. Consequently, the benzimidazole group is repelled away from the corrin with a concurrent lengthening of the Co−NB3 distance (steric *trans* influence).

The plots of calculated Co−NB3 and Co−X distances against the corresponding experimental values show fairly linear trends, excluding the calculated values for SO_3^{2-} (Figure 4). It should be stressed that in the simplified model of the corrin ligand used in the present calculations, H atoms have replaced the side groups. This does not allow consideration of the intramolecular interactions of the axial ligands with the corrin side chains. These interactions, such as the intramolecular H bonds between X and the corrin side chain *c* (when present), could affect the axial distances to some extent. It is of interest to compare the calculated axial distances for CN and Me derivatives of Table 5 with those obtained by Jensen et al.[16] by DFT calculations using the B3LYP method. These authors have found Co−C distances only marginally longer (ca. 0.03 Å), but Co−NB3 distances about 0.2 Å longer, than those calculated by our method.

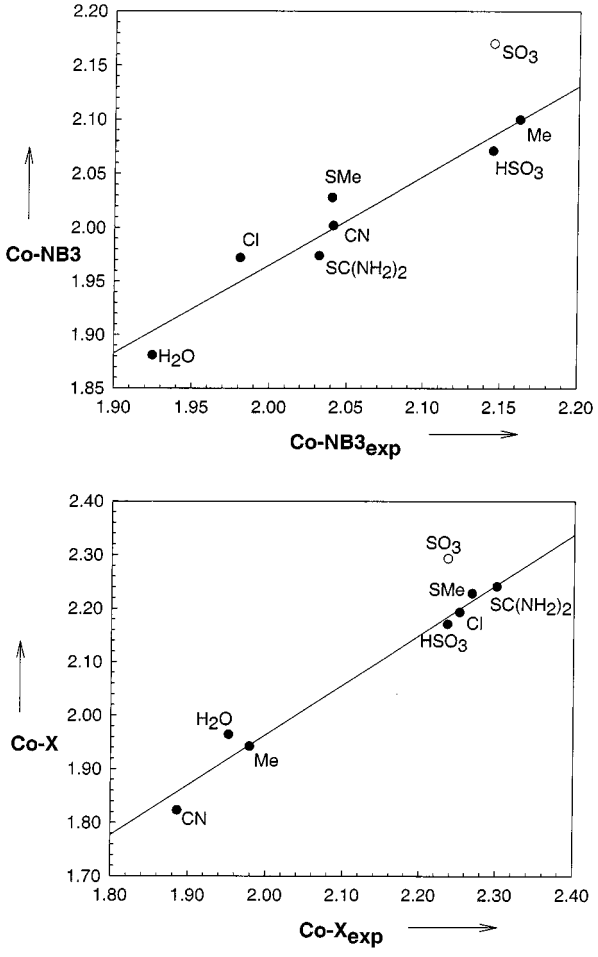

Figure 4. Plot of calculated Co−NB3 and Co−X distances [Å] in cobalamins vs. the corresponding experimental values; only experimental distances with e.s.d. values < 0.005 Å have been included (the experimental value of SO_3 is used also for HSO_3, see text)

Table 6. Calculated corrin distances [Å] in the XCo(corrin)Bzm system (X = H_2O and Me_3C) and in the Co^{II}(corrin), in comparison with experimental mean values from highly accurate structural data for several cobalamins

	H_2O[a]	Me_3C[a]	Co^{II}(corrin)[b]	Cbl(exp)[c]
Co−N21, Co−N24	1.858, 1.844	1.833, 1.822	1.85	1.878(3), 1.889(2)
Co−N22, Co−N23	1.886, 1.895	1.895, 1.898	1.90	1.907(3), 1.907(4)
N21−C1, N24−C19	1.457, 1.462	1.458, 1.454	1.49	1.500(6), 1.486(2)
C1−C2, C18−C19	1.516, 1.510	1.513, 1.513	−[d]	1.580(4), 1.530(4)
C2−C3, C17−C18	1.526, 1.529	1.527, 1.527	1.54	1.567(4), 1.560(5)
C3−C4, C16−C17	1.490, 1.491	1.493, 1.493	1.51	1.517(2), 1.535(4)
N21−C4, N24−C16	1.296, 1.298	1.295, 1.297	1.32	1.294(3), 1.300(2)
C1−C19	1.502	1.502	1.52	1.543(3)
C4−C5, C15−C16	1.412, 1.407	1.408, 1.407	1.41	1.444(4), 1.442(4)
C5−C6, C14−C15	1.360, 1.369	1.364, 1.364	1.37	1.363(3), 1.368(2)
N22−C6, N23−C14	1.373, 1.369	1.369, 1.368	1.39	1.401(3), 1.397(2)
N22−C9, N23−C11	1.336, 1.342	1.337, 1.338	1.37	1.340(3), 1.345(4)
C6−C7, C13−C14	1.488, 1.490	1.492, 1.495	1.51	1.545(3), 1.520(3)
C7−C8, C12−C13	1.520, 1.518	1.520, 1.517	1.53	1.550(2), 1.550(4)
C8−C9, C11−C12	1.482, 1.484	1.487, 1.487	−[d]	1.508(3), 1.512(4)
C9−C10, C10−C11	1.377, 1.374	1.374, 1.374	1.38	1.372(4), 1.386(3)

[a] Present work. − [b] Ref.[17]; a C_2 symmetry has been assumed in these calculations. − [c] Ref.[11] − [d] Missing data in ref.[17]

The experimental trend of the equatorial distances is well reproduced, with the Co−N21 and Co−N24 distances shorter than the Co−N22 and Co−N23 (Table 5). The calculated distances within the equatorial Co−corrin moiety are essentially unaffected by the axial ligands. In Table 6 a comparison for X = CMe_3 (the strongest σ-donating and bulkiest group) and for X = H_2O (the weakest σ-donating and the less bulky one) is reported. The C_2 symmetry of the corrin unit is quite well preserved, with differences in the symmetry equivalent to distances not exceeding 0.008 Å for X = H_2O, and 0.004 Å for X = CMe_3. The comparison of corrin distances shows no significant influence of the X axial ligand, since the differences between analogous distances also do not exceed 0.008 Å. However, the deviation from planarity, signified by φ values of 16.91 and 6.82° for the H_2O and CMe_3 derivatives, respectively, reflects the bulk of the axial ligand.

The trend of the experimental distances in the delocalized moiety of the corrin (Scheme 2) is fairly well reproduced (Table 6). The calculated values of the C−C single bonds of the pyrrole rings are shorter, by 0.02−0.06 Å, than those determined experimentally, the larger differences involve the more "crowded" bonds, such as C_q-C_q, where C_q represents a quaternary C atom. These discrepancies should be ascribed to the simplified equatorial ligand used in the calculations. This cannot reproduce the *steric pressure exerted by the side chains which lengthen in cobalamins the corrin C−C single bonds.*[10] On the contrary, the expected trend (short−long−short distances) in the pyrrole fragment $C(sp^2)-C(sp^3)-C(sp^3)-C(sp^2)$ is well reproduced.

It is interesting to compare the present results with those of Rovira et al.[17] derived by means of density functional molecular dynamics within the Car−Parrinello scheme for the square-planar Co(corrin), assumed to have C_2 symmetry. It was found that the corrin distances were not influenced at all by the oxidation state +1 ($S = 0$), or +2 ($S = 1$) of the metal center. The calculated distances reproduced the experimental trend in the delocalized moiety of the corrin (Table 6). As expected, the pyrrole C−C single bonds were shorter, to a greater or lesser extent, than the experimental ones, but longer than our calculated values, by about 0.02 Å. On the contrary, the calculated Co−N equatorial distances of the present work compare well with those of Rovira. Therefore, the axial ligands do not appear to influence the equatorial distances, as suggested by those authors.[17]

Electronic Properties of the Co−C and Co−S Bonds

Mullikan populations (MP) on the NB3−Co−X fragment are given in Table 7. As it is well known, Mulliken population analysis allows a partial charge to be attributed to a particular atom in a molecule. This procedure is not rigorous, since there is not a physical definition of the atomic charge within a molecule; however, it can be very helpful for interpretative purposes.[31]

Table 7. Mullikan population on the NB3−Co−X fragment for several cobalamins X-Cbl

X	NB3	Co	X
H_2O	−.4673	.7290	.2842
Cl	−.4757	.4524	−.2269
CN	−.4874	.5280	−.3270
CF_3	−.4924	.4311	−.0416
Me	−.5000	.5449	.0726
CMe_3	−.4966	.6481	.1029
$SC(NH_2)_2$	−.4781	.3813	.7247
SMe	−.4844	.3745	.0792
HSO_3	−.4862	.3205	.1737
SO_3	−.4952	.3308	−.4111

The only linear relationship is found between MP of NB3 and the calculated Co−NB3 distances, as shown in Figure 5 for several X groups. The trend of the Mulliken charge on the NB3 group, reported in Table 7 is surprising to some

extent, especially if the observed random fluctuation of the charge on Co and X group is considered. This behavior may be rationalized if we consider the nature of the chemical bonds in which the metal atom is involved. In fact, while the NB3 group is always connected to the Co atom, preserving the nature of the atom pair, the nature of the atom of the X group connected to Co varies and it is therefore more difficult to compare the Mulliken charges on Co and X groups along the series. Apart from the stability of the Mulliken charge on NB3, it is interesting to observe that the negative charge increases when the *trans* influence of the X group becomes higher. This finding is consistent with a model of the NB3−Co chemical bond in terms of electronic charge donation from the nitrogen atom to the metal ion. In fact, the NB3−Co distance increases with the increase of the *trans* influence of X, and consequently the weakening of the latter bond leaves an excess of negative charge on the NB3 atom.

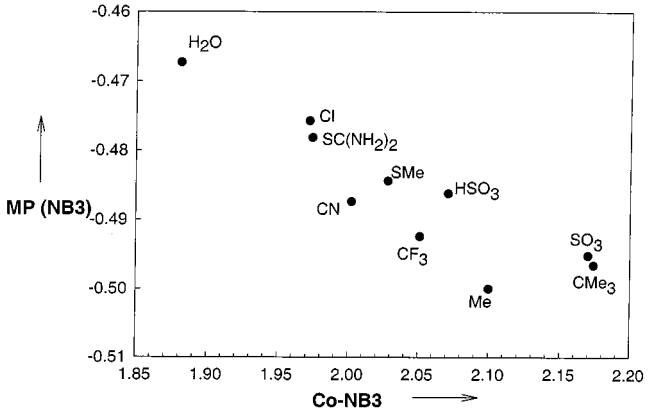

Figure 5. Plot of Mullikan population (MP) on NB3 vs. the calculated Co−NB3 distances [Å] for several X groups

Some peculiarities of the Mulliken charges on Co and X are worth noting. First, the positive charge of the metal ion is lower (< 0.4 au) when the Co is bound to a sulfur atom of the X group, irrespective of the position of the system along the series of increasing *trans* influence. This behavior can be explained by the "soft" character of the sulfur atom, which may be seen as an "electron reservoir" and is therefore able to screen more effectively the positive metal charge than the other ligands. The second interesting point is the very high positive charge of the thiourea. This finding clearly indicates that a strong conjugation is present in this ligand between the lone pairs of N and the C−S double bond. The latter is further polarized by the presence of the positive metal ion, which should enhance the conjugation via a Co−S π donation to the metal ion. Finally, the third observation regards the very high negative charge (−0.41 au) present on the SO_3 group. It has already been pointed out that the theory does not compare favorably with experimental data for this system, as previously described.

The NB3−Co−SR Fragment

Recently, we have found a good linear relationships between the Co−N and Co−X axial distances in cobalamins in comparison with the corresponding variables in cobaloximes, $LCo(DH)_2R$ (where DH = monoanion of dimethylglyoxime, L = neutral Lewis base, R = alkyl group).[11] This allowed an evaluation of the Co−NB3 and Co−SMe distances in cobalamins.[9] On the basis of these linear equations, slightly modified by including the recent data of the more accurate structures of MeCbl, CNCbl,[11] and AdoCbl,[32] ($r^2 = 0.980$, $n = 6$ for the Co−S bond and $r^2 = 0.966$, $n = 7$ for the Co−NB3 bond) the Co−SMe and Co−NB3 distances are found to be 2.26 and 2.04 Å, respectively. During the preparation of the present manuscript, we became aware of an accurate structural determination of (γ-glutamylcysteinyl)cobalamin (GCS-Cbl),[33] where the Co−S and Co−NB3 bond lengths were found to be 2.267(2) and 2.049(6) Å, respectively. These values are very close to those predicted above.

When X = HSO_3^-, SMe, and $SC(NH_2)_2$, the trend for the calculated Co−NB3 distances (Table 5) is as follows:
$SC(NH_2)_2$ (1.974) < SMe (2.028) < HSO_3^- (2.071 Å)
Inversely, the Co−S distances increase in the opposite order:
$SC(NH_2)_2$ (2.241) > SMe (2.228) > HSO_3^- (2.171 Å)

The above trends give an example of a "regular" *trans* influence, which is when the Co−S bond shortens and the Co−NB3 bond lengthens. A plot of the Co−NB3 vs. Co−S distances is reported in Figure 6. Correspondingly, the positive charge on Co (MP) decreases with the lengthening of the Co−NB3 distance, but it increases with the Co−S bond, shortening from $SC(NH_2)_2$ to HSO_3^- (Figure 7, bottom).

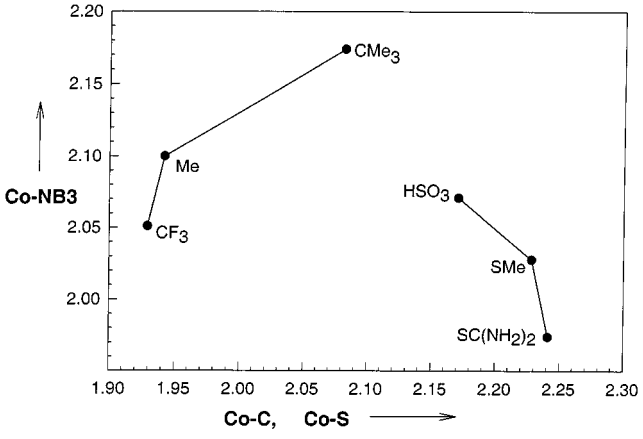

Figure 6. Plot of calculated Co−NB3 distances vs. the corresponding Co−X distances [Å] in cobalamins with alkyl and sulfur ligands

On the other hand, an "inverse" *trans* influence (i.e. both the Co−NB3 and Co−R distances increase) has been found[15] when the σ-donating ability of the R group increases from CN to Et. This finding was obtained by DFT calculations applied to the same simplified model corrin we have used in the present calculation.

Although the present Co−NB3 distances are approximately 0.15 Å shorter (and even more) than those calculated

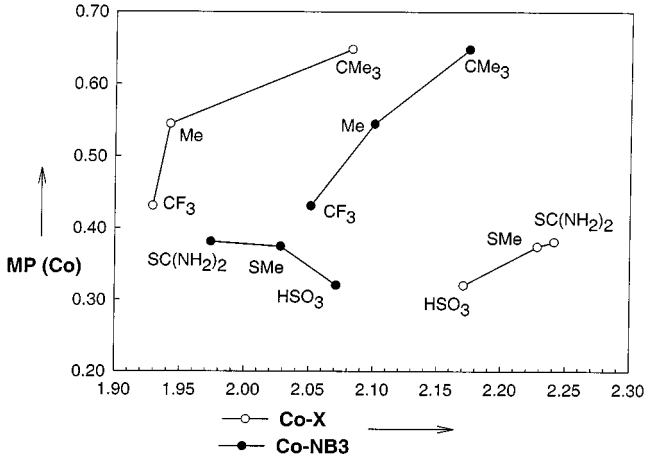

Figure 7. Plot of the Mullikan population (MP) on cobalt vs. the calculated axial bond lengths in cobalamins with alkyl (upper) and sulfur ligands (bottom)

by Andruniow et al.,[15] we have found this "inverse" *trans* influence for R = CF_3, Me and CMe_3 (Figure 6 and Table 5). Consistently, the positive charge on Co significantly increases with the lengthening of both the Co−NB3 and Co−C bonds (Figure 7, top). These findings appear to suggest that the different trend of the charge on Co with axial distances, in the two series containing S and C ligands, may be related to the "regular" or "inverse" *trans* influence of Figure 6. In fact, in the "regular" *trans* influence, the increase of the σ donation of the L group is reflected by the decrease of the Co positive charge. Therefore, the effect appears to be electronic in nature. On the other hand, in the "inverse" *trans* influence the positive metal charge increases with the σ-donating power of the R group. Thus, it cannot be an electronic, but rather a steric effect, due to the larger dimension of the σ-donor group (CMe_3). The steric repulsion, caused by the bulk of R, lengthens both the Co−R (steric *cis* influence) and Co−Nax (steric *trans* influence) distances and consequently the σ donation from ligands to the metal decreases, leading to a more positively charged metal.

The "inverse" *trans* influence, derived through an analysis of structural data in several alkylcobaloximes, $LCo(DH)_2R$, a simple B_{12} model,[34] was attributed principally to the electronic properties of R. However, it has been shown that in these complexes the bulk of R (independently of its electronic properties) also contributes significantly in determining the Co−R distance, because of its interaction with the equatorial ligand.[35] In fact, compared to the Me analogue, alkylcobaloximes with strong electronic withdrawing and bulky R groups, such as $CH(CN)CH_2CN$,[36] and $CF(CF_3)_2$,[37] show a significant lengthening of the Co−C bond (up to 0.08 Å) and a shortening of the Co−L bond (up to 0.03 Å). The present analysis of the NB3−Co−S fragment geometry does not support the idea that the "inverse" *trans* influence is a general rule also in cobalamins.

Experimental Section

Materials: Commercial samples of $(H_2OCbl)Cl$, stated purity by manufacturer about 96%, were purchased from Fluka. The other reactants were reagent grade and used without further purification. The complexes $[C_{62}H_{88}CoN_{13}O_{17}PS](NH_4)\cdot 12(H_2O)$ $(C_3H_8O_3)$ (**3**) and $[C_{63}H_{92}CoN_{15}O_{14}PS](PF_6)\cdot 13.3(H_2O)$ (**4**) were prepared in situ, growing the single crystals by the hanging drop method of vapor diffusion.

Preparation of 3: 2 μL of an aqueous $(H_2OCbl)Cl$ solution at 25 mg/mL was mixed with 2 μL of the precipitant solution containing $(NH_4)_2SO_4$, 20% glycerol, and 0.06 M $NaHSO_3$. Typical concentration range for precipitants were 20−45% in $(NH_4)_2SO_4$. Suitable single crystals were obtained only with 45% $(NH_4)_2SO_4$. Addition of LiCl did not result in formation of crystals. Attempts with PEG (with or without LiCl) were unsuccessful. The formation of the sulfite derivative, starting from $NaHSO_3$, is due to the high formation constant ($pK = -7$, with respect to the aquocobalamin) of $(SO_3)Cbl^-$, which allows its formation even in acid conditions (pH close to 4), where the concentration ratio $[HSO_3^-]/[SO_3^{2-}]$ is about 1000.

Preparation of 4: Several attempts to grow high quality single crystals were carried out, exploiting the procedure previously described,[10] slightly modified by addition of $(NH_4)PF_6$ in the ranges 0.10−0.50 M (by 0.05 M steps) and 0.05−0.16 M (by 0.01 M steps) and by substituting $(NH_4)_2SO_4$ with 20% glycerol as precipitant agent. Single crystals were obtained when 2 μL of an aqueous $(H_2OCbl)Cl$ solution at 25 mg/mL was mixed with 2 μL of the precipitant solution $(NH_4)PF_6$ (0.13 M), 20% glycerol and 0.30 M thiourea.

X-ray Structural Determinations: Diffraction experiments were carried out at the X-ray diffraction beamline of the Elettra Synchrotron, Trieste (Italy), using the rotating crystal method. Data were collected on a 345 mm MAR image plate with crystals mounted in loops and frozen to 100 K using a nitrogen-stream cryo-cooler. Crystallographic data for **3** and **4** are given in Table 8. The diffraction data were integrated using the DENZO program [38] and reflections subsequently were scaled and merged using the SCALEPACK program.[38] Friedel equivalent reflections were not merged and no absorption correction was applied. The phase problem was solved using the coordinates of an isomorphous structure as a starting model. The structural parameters were refined by full-matrix least squares on F^2 for all data using SHELXL-97.[39] The Fourier and Fourier difference maps clearly indicated that in **3** the PF_6^- anion is disordered over two different sites with occupancy factors of 0.65 and 0.35. Final *R* factors and details of refinements are reported in Table 8. Crystallographic data (excluding structure factors) for the structures reported in this paper have been deposited with the Cambridge Crystallographic Data Centre as supplementary publication, CCDC-161809 (**3**) and -161810 (**4**). Copies of the data can be obtained free of charge on application to CCDC, 12 Union Road, Cambridge CB2 1EZ, UK [Fax: (internat.) + 44-1223/336-033; E-mail: deposit@ccdc.cam.ac.uk].

Computational Method: The electronic structures of the systems under study were determined by solving the Kohn−Sham equations,[40] in the framework of Density Functional Theory (DFT), employing the ADF suite of quantum chemistry packages.[41,42] The simplified model for the corrin ligand, shown in Scheme 2, was used as in previous calculations.[13,15] During the SCF procedure, the Local Density Approximation (LDA) to the exchange correlation energy functional was applied, accordingly to the Vosko, Wilk

Table 8. Crystal data and structure refinement parameters of compounds **3** and **4**

	3	**4**
Empirical formula	$C_{65}H_{124}CoN_{14}O_{32}PS$	$C_{63}H_{118.60}CoF_6N_{15}O_{27.30}P_2S$
Formula mass	1735.74	1790.06
Crystal system	orthorhombic	orthorhombic
Space group	$P2_12_12_1$	$P2_12_12_1$
a [Å]	16.125(5)	15.758(4)
b [Å]	20.827(8)	22.698(4)
c [Å]	24.515(4)	24.765(7)
V [Å^3]	8233(4)	8858(4)
Z	4	4
$\rho_{calcd.}$ [g cm^{-3}]	1.400	1.342
μ [mm^{-1}]	0.345	0.345
Radiation, λ [Å]	synchrotron, 0.8558	synchrotron, 0.8558
$F(000)$	3704	3788
$2\theta_{max}$ [°]	54	56
No. reflns. total, unique	9932, 9267	12657, 12139
R(int.)	0.0523	0.0576
No. reflns $I > 2\sigma$ (I)	9139	11295
No. of parameters	1055	1103
Goodness-of-fit	1.045	1.054
$R1$[a]	0.0603	0.0778
$wR2$[a]	0.1763	0.2169

[a] $R1 = \Sigma||F_o| - |F_c||/\Sigma|F_o|$; $wR2 = [\Sigma w\,(|F_o|^2 - |F_c|^2)^2/\Sigma w(F_o^2)^2]^{1/2}$.

and Nusair VWN parameterization.[43] The basis set consisted of Slater Type Orbitals (STO) taken from the database of ADF: For all the atoms a Double Zeta plus Polarization (DZP) frozen core set was chosen, with the exception of the cobalt atom where, as suggested by a previous study,[30] the more extended Triple Zeta (TZ) frozen core was utilized. The geometry of the systems was optimized employing a quasi-Newton procedure with analytical energy gradients and default convergence criteria. Since we are mainly interested in the geometry of the systems, the VWN exchange-correlation potential was employed, which performs better and is more accurate for structural analysis than the more demanding GGA potentials, as has been already pointed out in a previous computational study on transition metal compounds.[30] A larger basis set (TZP) has been tested for the SO_3 group with the aim of improving the capability of the method in order to describe negative fragments with a diffuse electron density. However, we did not observe any improvement. It can therefore be concluded that the method employed gives reliable results, and that the cause of the disagreement with the experiment must be found elsewhere.

Acknowledgments

This work was supported by Ministero dell'Università e della Ricerca Scientifica e Tecnologica (Rome) (PRIN 9803184222).

[1] C. L. Drennan, M. M. Dixon, D. M. Hoover, J. T. Jarret, C. W. Goulding, R. G. Mattews, M. L. Ludwig, in Vitamin B_{12} and B_{12}-Proteins (Eds.: B. Kräutler, D. Arigoni, B. T. Golding), Wiley-VCH, Weinheim, **1998**, pp. 133−155.
[2] [2a] R. G. Matthews, J. T. Drummond, *Chem. Rev.* **1990**, *90*, 1275−1290. − [2b] R. G. Matthews, in Chemistry and Biochemistry of B_{12} (Ed.: R. Banerjee), J. Wiley & Sons Inc., New York, **1999**, pp. 681−706.
[3] S. M. Polson, L. Hansen, L. G. Marzilli, *Inorg. Chem.* **1997**, *36*, 307−313.
[4] N. E. Brasch, T.-L. C. Hsu, K. M. Doll, R. G. Finke, *J. Inorg. Biochem.* **1999**, *76*, 197−209.
[5] [5a] S. S. Licht, S. Booker, J. Stubbe, *Biochemistry* **1999**, *38*, 1221−1233. − [5b] S. Licht, G. J. Gerfen, J. Stubbe, *Science* **1996**, *271*, 477−481.
[6] E. M. Scheuring, I. Sagi, M. R. Chance, *Biochemistry* **1994**, *33*, 6310−6315.
[7] K. L. Brown, X. Zou, S. R. Savon, D. W. Jacobsen, *Biochemistry* **1993**, *32*, 8421.
[8] T.-L. C. Hsu, N. E. Brasch, R. G. Finke, *Inorg. Chem.* **1998**, *37*, 5109−5116. A preliminary structural analysis of the C_5F_5S−Cbl from this laboratory gave Co−S and Co−NB3 distances of 2.295(9) and 1.95(3) Å, respectively.
[9] L. Randaccio, S. Geremia, G. Nardin, M. Slouf, I. Srnova, *Inorg. Chem.* **1999**, *38*, 4087−4092.
[10] C. Kratky, G. Färber, K. Gruber, K. Wilson, Z. Dauter, H.-F. Nolting, R. Konrat, B. Kräutler, *J. Am. Chem. Soc.* **1995**, *117*, 4654−4670.
[11] L. Randaccio, M. Furlan, S. Geremia, M. Slouf, I. Srnova, D. Toffoli, *Inorg. Chem.* **2000**, *39*, 3403−3413.
[12] [12a] G. N. Schrauzer, L. P. Lee, J. W. Sibert, *J. Am. Chem. Soc.* **1970**, *92*, 2997−3005. − [12b] L. Salem, O. Eisenstein, N. T. Anh, H.-B. Burgi, A. Devaquet, G. Segal, A. Veillard, *Nouv. J. Chem.* **1977**, *1*, 335−348. − [12c] C. Mealli, M. Sabat, L. G. Marzilli, *J. Am. Chem. Soc.* **1987**, *109*, 1593−1594. − [12d] D. W. Christianson, W. N. Lipscomb, *J. Am. Chem. Soc.* **1985**, *107*, 2682−2686. − [12e] L. M. Hansen, P. N. V. Pavan Kumar, D. S. Marynick, *Inorg. Chem.* **1994**, *33*, 728−735.
[13] [13a] L. Zhou, N. M. Kostic, *Inorg. Chem.* **1987**, *26*, 4194−4197. − [13b] L. M. Hansen, A. Derecskei-Kovacs, D. S. Marynick, *J. Mol. Struct.* **1998**, *431*, 53−57.
[14] L. Randaccio, *Comments Inorg. Chem.* **1999**, *21*, 327−376.
[15] [15a] T. Andruniow, M. Z. Zgierski, P. M. Kozlowski, *Chem. Phys. Lett.* **2000**, *331*, 502−508; *Chem. Phys. Lett.* **2000**, *331*, 509−512. − [15b] T. Andruniow, M. Z. Zgierski, P. M. Kozlowski, *Chem. Phys. Lett.* **2000**, *331*, 509−512. − [15c] T. Andruniow, M. Z. Zgierski, P. M. Kozlowski, *J. Phys. Chem. B* **2000**, *104*, 10921−10927.
[16] K. P. Jensen, S. P. A. Sauer, T. Liljefors, P.-O. Norrby, *Organometallics* **2001**, *20*, 550−556
[17] C. Rovira, K. Kunc, J. Hutter, M. Parrinello, *Inorg. Chem.* **2001**, *40*, 11−17.
[18] K. Gruber, G. Jogl, G. Klintschar, C. Kratky, in *Vitamin B_{12}*

and B_{12}-Proteins (Eds.: B. Kräutler, D. Arigoni, B. T. Golding), Wiley-VCH, Weinheim, **1998**, pp. 335−347.
[19] [19a] J. P. Bouquiere, J. L. Finney, H. F. J. Savage, *Acta Crystallogr., Sect. B* **1994**, *50*, 566−578. − [19b] J. P. Bouquiere, J. L. Finney, M. S. Lehmann, P. F. Lindley, H. F. J. Savage, *Acta Crystallogr., Sect. B* **1993**, *49*, 79−89. − [19c] H. F. J Savage, *Biophysics* **1986**, *50*, 947−965. − [19d] H. F. J Savage, *Biophysics* **1986**, *50*, 967−980. − [19e] H. F. J. Savage, J. L. Finney, *Nature (London)* **1986**, *322*, 717−720.
[20] L. Randaccio, M. Furlan, S. Geremia, M. Slouf, *Inorg. Chem.* **1998**, *37*, 5390−5393.
[21] P. Langan, M. Lehmann, C. Wilkinson, G. Jogl, C. Kratky, *Acta Crystallogr., Sect. D* **1999**, *55*, 51−59.
[22] J. M. Pratt, in *B_{12} (Ed.: D. Dolphin), Wiley and Sons, New York, **1982**, vol. 1, p. 325−392.*
[23] E. Pezacka, R. Green, D. W. Jacobsen, *Biochem. Biophys. Res. Commun.* **1990**, *169*, 443−450.
[24] R. A. Firth, H. A. O. Hill, J. M. Pratt, R. G. Thorp, R. J. P. Williams, *J. Chem. Soc. A* **1969**, 381−386.
[25] I. Sagi, M. R. Chance, *J. Am. Chem. Soc.* **1992**, *114*, 8061−8066.
[26] E. M. Scheuring, R. Padmakumar, R. Banerjee, M. R. Chance, *J. Am. Chem. Soc.* **1997**, *119*, 12192−12200.
[27] F. Champloy, G. Jogl, R. Reitzer, W. Buckel, H. Boethe, B. Beatrix, G. Broeker, A. Michalowicz, W. Meyer-Klaucke, C. Kratky, *J. Am. Chem. Soc.* **1999**, *121*, 11780−11789.
[28] H. Bertagnolli, T. S. Ertel, *Angew. Chem.* ***1994***, *106*, 15−37; *Angew. Chem. Int. Ed. Engl.* **1994**, *39*, 45−66.
[29] E. Fonda, A. Michalowicz, L. Randaccio, G. Tauzher, G. Vlaic, *Eur. J. Inorg. Chem.*, **2001**, 1269−1278.
[30] M. Stener, M. Calligaris, *J. Mol. Struct. (Theochem)* **2000**, *497*, 91−104.
[31] A. Szabo and N. Ostlund, *Modern Quantum Chemistry*, Macmillan Publishing Co., New York, **1982**.
[32] L. Randaccio, et al., data from this laboratory, in preparation.
[33] R.G. Finke, private communication.
[34] D. J. A. De Ridder, E. Zangrando, H. B. Burgi, *J. Mol. Struct.* **1996**, *374*, 63−83.
[35] L. Randaccio, S. Geremia, E. Zangrando, C. Ebert, *Inorg. Chem.* **1994**, *33*, 4641−4650.
[36] J. P. Charland, W. M. Attia, L. Randaccio, L. G. Marzilli, *Organometallics* **1990**, *29*, 1367−1375.
[37] P. J. Toscano, H. Brand, S. Liu, J. Zubieta, *Inorg. Chem.* **1990**, *29*, 2101−2105
[38] Z. Otwinowski, W. Minor, *Methods Enzymol.* **1996**, *276*, 307−326.
[39] G. M. Sheldrick, *SHELXL-97, Program for Structure Refinement*, Universität Göttingen, Germany, ***1997***.
[40] R. G. Parr, W. Yang, in *Density Functional Theory of Atoms and Molecules* (Eds.: R. Breslow, J. B. Goodenough, J. Halpern, J. S. Rowllinson), Oxford University Press, New York, ***1989***.
[41] E. J. Baerends, D. E. Ellis, P. Ros, *Chem. Phys.* **1973**, *2*, 41.
[42] C. Guerra Fonseca, J. G. Snijders, G. te Velde, E. J. Baerends, *Theor. Chem. Acc.* **1998**, *99*, 391−403.
[43] S. H. Vosko, L. Wilk, M. Nusair, *Can. J. Phys.* **1980**, *58*, 1200.
Received July 6, 2001
[I01253]

Ion Conducting Behavior in $(Lu_{1-x}M_x)_2(WO_4)_3$ Solid Solutions (M = Sm, Ho, Er) with the $Sc_2(WO_4)_3$ Type Structure

Nobuhito Imanaka,*[a] Joachim Köhler,[b] Shinji Tamura,[a] and Gin-ya Adachi[a]

Keywords: Conducting materials / Ceramics / Electrochemistry / Tungsten / Solid-phase synthesis

Solid solutions in the trivalent cationic conducting system $(Lu_{1-x}M_x)_2(WO_4)_3$ (M = Er, Ho, Sm) that crystallize in the $Sc_2(WO_4)_3$ type structure were prepared and their conducting behaviors were characterized electrochemically. The partial replacement of the Lu^{3+} cation site in $(Lu_{1-x}M_x)_2(WO_4)_3$ by larger M^{3+} cations caused a crystal lattice expansion. Due to the opened ion-migration pathways, the solid solutions generally exhibited an increased cationic conductivity relative to pure $Lu_2(WO_4)_3$. The ion conductivity can be optimized by substituting the appropriate amount of M^{3+} into $(Lu_{1-x}M_x)_2(WO_4)_3$ in order to adjust the expansion of the migration pathways for the Lu^{3+} cations. Furthermore, a relationship between the average ionic radius of the trivalent cations involved and the ionic conductivity was characterized which makes it possible to predict the composition of the optimum ion-conducting compound in each solid solution system with the $Sc_2(WO_4)_3$ type structure.

Introduction

Compounds that crystallize in the scandium tungstate $Sc_2(WO_4)_3$ type structure and behave as trivalent cationic solid electrolytes have been intensively studied in recent years.[1−9] This research has focused mainly on the synthesis of various isostructural compounds with $Sc_2(WO_4)_3$-type structures and their characterization with respect to the trivalent cationic conduction properties. The $Sc_2(WO_4)_3$-type structure, in general $M_2(XO_4)_3$, is adopted by a huge number of tungstates (X = W) and molybdates (X = Mo). Considering $M_2(WO_4)_3$, M can be represented by trivalent cations of the heavier rare earth metals Er−Lu, Sc or by trivalent cations of the main group elements In and Al;[10] the corresponding molybdates, $M_2(MoO_4)_3$, are formed by Ho−Lu, Sc, In and Al.[10] In addition, it is possible to synthesize solid solutions by the partial replacement of a given M^{3+} cation with another trivalent cation B^{3+} $[(M_{1-x}B_x)_2(XO_4)_3]$[11] or by replacing the anionic part of the structure to give $M_2(W_{1-y}Mo_yO_4)_3$.[12] Furthermore, simultaneous substitutions in both the cationic as well as anionic part can be performed resulting in solid solutions such as $[M_2(WO_4)_3]_{1-x}[B_2(MoO_4)_3]_x$.[13] The number of possible compounds further increases when trivalent cations that are not usually able to form tungstates with the $Sc_2(WO_4)_3$ structure type are substituted into the host lattice. For example, $Gd_2(WO_4)_3$ crystallizes with the insulating $Eu_2(WO_4)_3$-type structure. However, a certain amount of Gd^{3+} (up to 60% of the trivalent cations) can be incorporated into $Sc_2(WO_4)_3$ maintaining the $Sc_2(WO_4)_3$-type structure and exhibiting ionic conduction characteristics.[14]

The ion conducting properties of a remarkable number of compounds with the $Sc_2(WO_4)_3$ type structure have been determined. It has been shown that the ion-conducting behaviors are strongly dependent on the nature of the trivalent cations. However, ordering principles are needed to manage and to oversee the huge amount of different conduction data.

Recently, the existence of such a principle was indicated during systematic investigations in the solid solution systems $(Sc_{1-x}M_x)_2(WO_4)_3$ (M = Lu, Dy, Gd) and $[Sc_2(WO_4)_3]_{1-x}[M_2(MoO_4)_3]_x$ (M = Lu, Gd, Sm, Nd). In these compounds, the Sc^{3+} conductivity was shown to be dependent on the crystal lattice expansion.[13,15]

It is the aim of this paper to determine whether this relationship can be generalized and extended to other solid solution systems with another trivalent-cation conducting tungstate series, such as trivalent ion species with ionic radii appreciably larger than that of Sc^{3+}. For this purpose, solid solutions in the system $(Lu_{1-x}M_x)_2(WO_4)_3$ (M = Er, Ho, Sm), which behave as Lu^{3+} ion conductors, have been prepared and characterized for the first time. The Lu^{3+} ion conducting system has been chosen for two reasons: i) the cationic radius of Lu^{3+} ($r_{Lu}{}^{3+}$ = 0.1001 nm)[16] is considerably larger than that of Sc^{3+} ($r_{Sc}{}^{3+}$ = 0.0885 nm),[16] and ii) because of the fast ion-conduction properties of $Lu_2(WO_4)_3$ {among compounds with the $Sc_2(WO_4)_3$-type structure,

[a] Department of Applied Chemistry, Faculty of Engineering, Osaka University,
2-1 Yamadaoka, Suita, Osaka 565-0871, Japan
Fax: (internat.) + 81-6/6879-7354
E-mail: imanaka@chem.eng.osaka-u.ac.jp
[b] Degussa Metals Catalysts Cerdec AG, Fuel Cell Division, Rodenbacher Chaussee 4, P. O. Box 1351, 63403 Hanau, Germany

 © WILEY-VCH Verlag GmbH, 69451 Weinheim, Germany, 2002 1434−1948/02/0101−0105 $ 17.50+.50/0

Table 1. Ionic radii of some selected trivalent cations corresponding to the coordination number of six[16]

Cation	Sc	In	Lu	Er	Ho	Dy	Gd	Sm	Nd
Radius / nm	0.0885	0.0940	0.1001	0.1030	0.1041	0.1052	0.1078	0.1098	0.1123

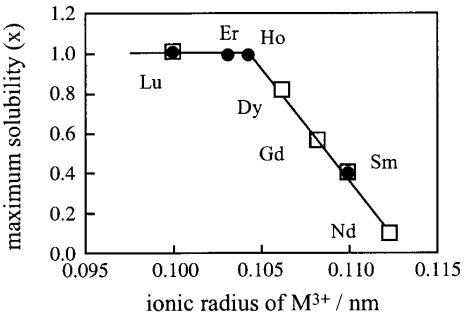

Figure 1. A plot of the maximum substitution rate in $(Lu_{1-x}M_x)_2(WO_4)_3$ (M = Sm, Ho, Er) (•) and in $(Sc_{1-x}M_x)_2(WO_4)_3$ (M = Lu, Dy, Gd) and $[Sc_2(WO_4)_3]_{1-x}[M_2(MoO_4)_3]_x$ (M = Lu, Gd, Sm, Nd) (□) solid solutions versus the ionic radius of the substituting cation M

$Lu_2(WO_4)_3$ exhibits the second highest conductivity [the optimum conducting compound is $Sc_2(WO_4)_3$ itself][1,5].

Results and Discussion

The ionic radii of several trivalent cations are summarized in Table 1 according to the coordination number of six in an octahedral environment.[16] Solid solutions between $Lu_2(WO_4)_3$ and $M_2(WO_4)_3$, with the $Sc_2(WO_4)_3$-type structure, are formed. Changing the size of the trivalent cation M^{3+} leads to drastically altered conditions for the formation of solid solutions. This relationship is displayed in Figure 1, where the solubility of $M_2(WO_4)_3$ in $Lu_2(WO_4)_3$ is given as a function of the ionic radius of M. For better illustration, the corresponding data of the previously described solid solutions in the systems $(Sc_{1-x}M_x)_2(WO_4)_3$ (M = Lu, Dy, Gd)[15] and $[Sc_2(WO_4)_3]_{1-x}[M_2(MoO_4)_3]_x$ (M = Lu, Gd, Sm, Nd)[13] are also shown. The ionic radii of W^{6+} (0.056 nm)[16] and Mo^{6+} (0.055 nm)[16] are almost identical and a corresponding influence on the mutual solubility can be neglected. For example, both $Gd_2(WO_4)_3$ and $Gd_2(MoO_4)_3$ can be dissolved into $Sc_2(WO_4)_3$ to about 60 mol %.[13,15] Thus, a direct comparison of the tungstate and molybdate systems, as shown in Figure 1, is possible. It can be seen that solid solutions between different tungstates/molybdates can be formed over the entire composition range ($0 < x < 1$) only for dopant cations M^{3+} with an ionic radius smaller than 0.105 nm. This value seems to be a stability limit for the $Sc_2(WO_4)_3$-type structure. The incorporation of larger cations causes a gradual decrease of the solid solution limit with increasing ionic radius of M^{3+}; for example, $x = 0.6$ for M = Gd ($r_{Gd}^{3+} = 0.1078$ nm[16]) and $x = 0.4$ for M = Sm ($r_{Sm}^{3+} = 0.1098$ nm[16]). Cations larger than Nd^{3+} cannot be dissolved into the $Sc_2(WO_4)_3$-type structure. The large cations cause strong local distortions in the crystal lattice which in turn collapses at a certain dopant level in order to release the strain and to form a new type of crystal structure. For example, pure $Gd_2(WO_4)_3$ and $Sm_2(WO_4)_3$ do not form the $Sc_2(WO_4)_3$-type structure but rather crystallize in the $Eu_2(WO_4)_3$-type structure.[10] Higher concentrations of M ($x > 0.6$ for M = Gd or $x > 0.4$ for M = Sm) in $(Lu_{1-x}M_x)_2(WO_4)_3$ destabilize the $Sc_2(WO_4)_3$ structure and favor the formation of either solid solutions in the corresponding $Eu_2(WO_4)_3$-type structure or mixtures of $Lu_2(WO_4)_3$ and $M_2(WO_4)_3$. On the other hand, $Er_2(WO_4)_3$ and $Ho_2(WO_4)_3$ crystallize in the $Sc_2(WO_4)_3$ type, and complete solid solution formation with $Lu_2(WO_4)_3$ becomes possible.

$Sc_2(WO_4)_3$, $Lu_2(WO_4)_3$ as well as the corresponding solid solutions $(Lu_{1-x}M_x)_2(WO_4)_3$ (M = Er, Ho, Sm) behave as trivalent cation conductors[13] and the ion-conduction properties vary with changing size and concentration of the different M^{3+} cations. The main effect of the incorporated larger M^{3+} cations in the $(Lu_{1-x}M_x)_2(WO_4)_3$ solid solutions is to increase the lattice parameters *a*, *b*, and *c*, as indicated by the corresponding shifted d-spacings of individual peaks in the X-ray diffraction pattern.[13] The size of the unit cell increases isotropically and linearly with increasing substitution ratio, as shown in Figure 2 for solid solutions in the $(Lu_{1-x}Er_x)_2(WO_4)_3$ system. The substitution ratio is directly related to the average radius of the trivalent cations r_m [$r_m = (1-x)\cdot r_{Lu}^{3+} + x\cdot r_M^{3+}$]. The linear dependence between the average cationic radius and the cell volume, as shown in Figure 2, will be of importance for the subsequent discussion.

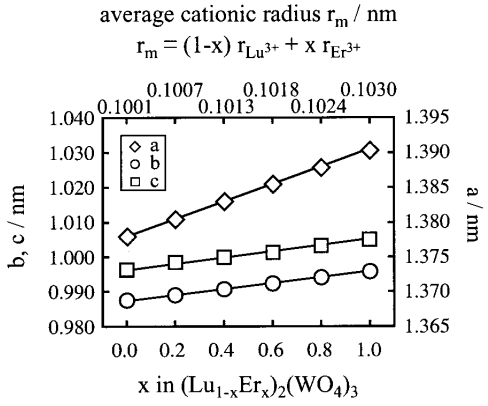

Figure 2. A plot of the lattice cell parameter of $(Lu_{1-x}Er_x)_2(WO_4)_3$ solid solutions versus the composition and the average trivalent cationic radius, r_m

Table 2. The trivalent-cation conducting properties of pure $Lu_2(WO_4)_3$ and $(Lu_{1-x}M_x)_2(WO_4)_3$ solid solutions (M = Er, Ho, Sm) for different degrees of doping x; upper row: conductivity at 600 °C (log $\sigma_{600\,°C}$); middle row: activation energy E_a in kJ/mol; bottom row: average trivalent-cation radius r_m in nm [$r_m = (1 - x)\cdot r_{Lu}^{3+} + x \cdot r_M^{3+}$]; the compounds showing an optimum performance are marked in bold

M	x							
	0.1	0.2	0.3	0.4	0.5	0.6	0.8	1.0
	−4.413	−4.413	−4.413	−4.413	−4.413	−4.413	−4.413	−4.413
Lu	50.6	50.6	50.6	50.6	50.6	50.6	50.6	50.6
	0.1001	0.1001	0.1001	0.1001	0.1001	0.1001	0.1001	0.1001
		−4.350		−4.262	**−4.260**	−4.306	−4.384	−4.490
Er		48.7		45.7	**45.6**	48.5	52.5	55.9
	0.1007		0.1013	**0.1016**	0.1019	0.1024	0.1030	
		−4.307	−4.248	**−4.222**		−4.256	−4.286	−4.638
Ho		52.6	58.0	**44.1**		50.3	52.9	58.3
	0.1009	0.1013	**0.1017**		0.1025	0.1033	0.1041	
	−4.224	−4.435						
Sm	**47.5**	48.0						
	0.1011	0.1020						

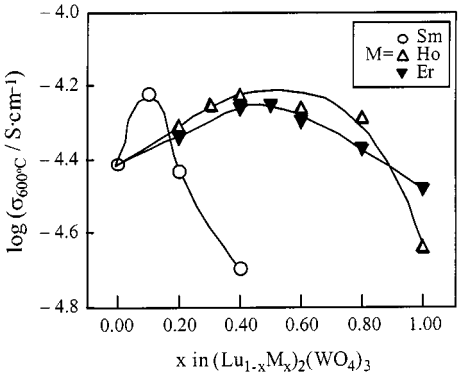

Figure 3. A plot of the trivalent cation conductivity at 600 °C (log $\sigma_{600\,°C}$) versus the compositional parameter, x, for the $(Lu_{1-x}M_x)_2(WO_4)_3$ solid solutions with M = Sm (○), Ho (□), Er (▼)

The conductivities of several $(Lu_{1-x}M_x)_2(WO_4)_3$ solid solutions differing in the compositional parameter x have been determined. The corresponding conductivity data at 600 °C (log $\sigma_{600\,°C}$) are tabulated in Table 2 in addition to the corresponding activation energies (E_a) as well as the average ionic radii of the involved trivalent cations. The activation energies are calculated from the log σT vs. 1/T relationship in the temperature range of 400−700 °C by using the common Arrhenius equation. A plot of the trivalent ion conductivities (log σ) of $(Lu_{1-x}M_x)_2(WO_4)_3$ at 600 °C versus the $M_2(WO_4)_3$ content (x) in $(Lu_{1-x}M_x)_2(WO_4)_3$ (M = Er, Ho, Sm) is shown in Figure 3. As a result, by expanding the crystal lattice due to the incorporation of larger cations M^{3+} into $(Lu_{1-x}M_x)_2(WO_4)_3$, the migration pathways within the crystal structure become more opened, which leads to a reduction in the electrostatic interaction between the mobile trivalent cations and the anionic host lattice. Thus, the migration of the trivalent Lu^{3+} cations is improved and increased conductivities are obtained in comparison to pure lutetium tungstate.

However, although the unit cell expands continuously over the whole composition region ($0 < x < 1$) and a corresponding continuous enhancement of the conductivity would be expected, a more complex behavior of log σ is found depending on the concentration and the size of the substituting cation, M^{3+}. Starting from the viewpoint of pure $Lu_2(WO_4)_3$, the conductivity increases continuously with increasing x because of the opening of the migration pathways due to the incorporation of the larger cation M^{3+}. However, at a certain composition, log σ reaches a maximum and the addition of further $M_2(WO_4)_3$ only reduces the ion-conduction properties. In our previous studies, trivalent cations with an ionic radius larger than Lu^{3+} are shown to be less mobile due to steric reasons.[5] Thus, although the crystal lattice is continuously expanding with increasing substitution ratio, the ionic conductivity decreases after reaching a maximum due to the exchange of mobile Lu^{3+} cations by M^{3+} cations that show a less-mobile behavior in $(Lu_{1-x}M_x)_2(WO_4)_3$ solid solutions. The corresponding activation energies seem to confirm the aforementioned assumption by exhibiting the same dependency on the composition in each single system as the conductivity. The lowest and highest activation energies were observed (see Table 2) in solid solutions with the best and worst conductivities, respectively. This behavior is fully consistent with the corresponding results in the solid solution systems $(Sc_{1-x}M_x)_2(WO_4)_3$ (M = Lu, Dy, Gd) and $[Sc_2(WO_4)_3]_{1-x}[M_2(MoO_4)_3]_x$ (M = Lu, Gd, Sm, Nd), where the Sc^{3+} cations have been unambiguously identified as the main charge-carrying species in the high ion-conducting compounds.[13,15]

Although the optimum conductivity in each single system (different systems refer to different M^{3+} cations) is observed for different compositions [different x in $(Lu_{1-x}M_x)_2(WO_4)_3$] in Table 2, the maximum appears at almost the same average ionic radius, r_m, of the concerned trivalent cations. A similar behavior was also observed during systematic investigations in the solid solution systems $(Sc_{1-x}M_x)_2(WO_4)_3$ (M = Lu, Dy, Gd) and $[Sc_2(WO_4)_3]_{1-x}[M_2(MoO_4)_3]_x$ (M = Lu, Gd, Sm, Nd).[13,15] The corresponding relationship between the conductivity

(log σ) and the average ionic radius, r_m, is shown in Figure 4, with the Sc^{3+}-conducting systems included for comparison (Figures 4b and 4c). The maximum ion conductivity in each solid solution system, corresponding to the main conducting species (Sc^{3+} or Lu^{3+} cations), appears at a similar average trivalent cationic radius within the Sc^{3+}- and Lu^{3+}-conducting compounds, respectively. It amounts to approximately 0.0938−0.0943 nm in $(Sc_{1-x}M_x)_2(WO_4)_3$ and $[Sc_2(WO_4)_3]_{1-x}[M_2(MoO_4)_3]_x$ and to about 0.1011−0.1017 nm in the $(Lu_{1-x}M_x)_2(WO_4)_3$ solid solutions. The size of the trivalent cations is directly related to the expansion of the crystal lattice (cf Figure 2), i.e. to the extension of the migration pathways. According to the different ionic size of Sc^{3+} and Lu^{3+}, the optimum conductivities in $(Lu_{1-x}M_x)_2(WO_4)_3$ appear for compounds with a larger lattice cell volume ($V_{opt-cell}$ = 1.41−1.42 nm^3) than the $(Sc_{1-x}M_x)_2(WO_4)_3$ and $[Sc_2(WO_4)_3]_{1-x}[M_2(MoO_4)_3]_x$ solid solutions ($V_{opt-cell}$ = 1.29−1.31 nm^3). Comparing these optimum cell volume to the ionic size of the charge-carrying Lu^{3+} ($Vr_{Lu}{}^{3+}$ = 0.0042 nm^3) and Sc^{3+} ($Vr_{Sc}{}^{3+}$ = 0.0029 nm^3) cations by forming the corresponding quotients $V_{opt-cell}/Vr_M{}^{3+}$ leads to values of 0.00297 (Lu^{3+}) and 0.00223 (Sc^{3+}). The similarity of these values might indicate the existence of a certain cell volume/cation size relation of approximately 0.002−0.003, which is most appropriate for the transport of trivalent cations within the $Sc_2(WO_4)_3$-type structure series. While this simple model is based only on steric considerations and neglects a more complex situation including polarizabilities, electrostatic interactions, and local ordering of the different cation types, which might also influence the migration behavior of the cations within the conduction layers to some extent, it provides information which makes it possible to roughly predict the composition of the optimum conducting compound of mixed solid solutions crystallizing with $Sc_2(WO_4)_3$-type structures, despite its simplicity.

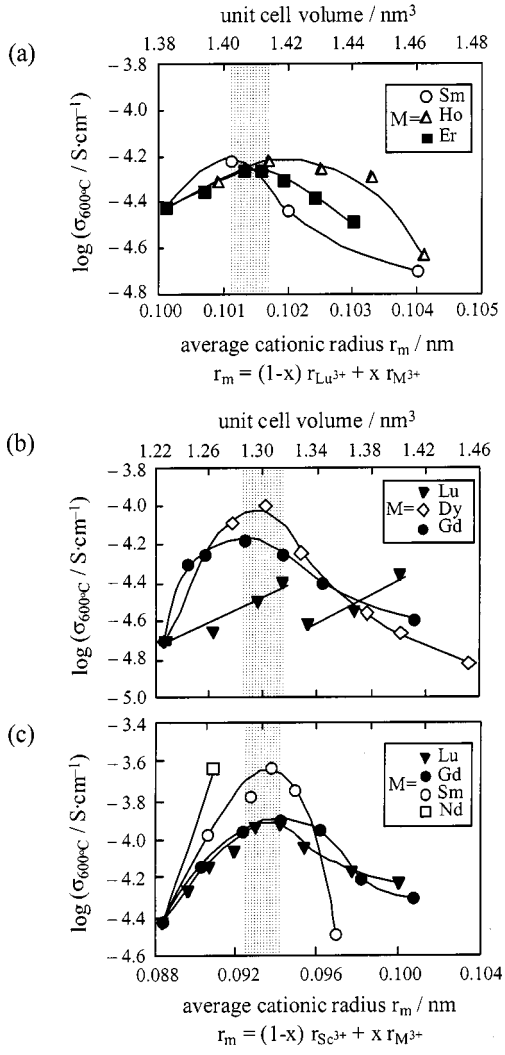

Figure 4. A plot of the trivalent cation conductivity at 600 °C (log $\sigma_{600\ °C}$) versus the average trivalent cationic radius, r_m, for: (a) $(Lu_{1-x}M_x)_2(WO_4)_3$ solid solutions [M = Sm (○), Ho (□), Er (■)]; (b) $(Sc_{1-x}M_x)_2(WO_4)_3$ solid solutions[12] [M = Lu (▼), Dy (◇), Gd (•)]; (c) $[Sc_2(WO_4)_3]_{1-x}[M_2(MoO_4)_3]_x$ solid solutions[13] [M = Lu (▼), Gd (•), Sm (○), Nd (□)]; the shaded region corresponds to the optimal cationic radius where the highest conductivity data can be observed

Conclusions

The trivalent-cation conducting solid solution system of $(Lu_{1-x}M_x)_2(WO_4)_3$ (M = Er, Ho, Sm) shows a monotonous expansion of crystal lattice by substituting Lu^{3+} cation site for larger M^{3+} cations. Due to the linear relationship between the average cationic radius and the unit cell volume of the solid solutions, the optimum ion-conducting compound in a certain solid solution system with a given M^{3+} cation can be easily elucidated only by calculating the $V_{opt-cell}/Vr_M{}^{3+}$ quotient (0.002−0.003) to adjust the expansion of the crystal lattice in an optimum surroundings for the mobile cations. Ideally, only the compound with the composition which corresponds to that optimum unit cell volume need be prepared. This provides a helpful tool for the understanding of the trivalent cationic conduction characteristics in the various tungstate and molybdate compounds with the $Sc_2(WO_4)_3$-type crystal structure.

Experimental Section

Polycrystalline $(Lu_{1-x}M_x)_2(WO_4)_3$ solid solutions (M = Er, Ho, Sm) were prepared in conventional solid-state reactions by heating a thoroughly ground mixture of reagent grade Lu_2O_3, WO_3, and the lanthanide oxides M_2O_3 (purity of all reagents 99.9% or higher) in the corresponding stoichiometric ratio at a temperature of 1200 °C for 24 h in an oxygen atmosphere. After regrinding, the procedure was repeated with the same experimental conditions. The colors of the obtained powders are white (Lu/Gd compounds), pink (Lu/Er), slight yellow (Lu/Ho), and salmon-pink (Lu/Sm). The resulting materials were characterized by X-ray powder diffraction analysis (XRD) using Cu-K_α radiation (Mac Science M18XHF diffractometer).

For the electrical conductivity measurements, pelletized samples of $(Lu_{1-x}M_x)_2(WO_4)_3$ were sintered in an oxygen atmosphere for 12 h at 1200 °C, and sputtered on opposite faces with ionically blocking platinum. Electrical conductivity measurements such as impedance analysis and time-dependent dc-polarization measurements of all

samples were performed following the usual procedures as reported elsewhere.[1−9] In dc electrolysis experiments, the $(Lu_{1-x}M_x)_2(WO_4)_3$ samples were exposed to a direct voltage of 6V for about 4−6 weeks at 800−850 °C in air, using ion-blocking Pt electrodes. After the electrolysis procedure, the cathodic and anodic surfaces as well as the bulk of the samples were characterized by electron-probe microanalysis(EPMA).

Acknowledgments

This work was partially supported by a Grant-in-Aid for Scientific Research No. 09215223 on Priority Areas (No. 260), Nos. 06241106, 06241107, and 093065 from The Ministry of Education, Science, Sports and Culture. It was also supported by the "Research for the Future, Preparation and Application of Newly Designed Solid Electrolytes (JSPS RFTF96P00102)" program from the Japan Society for the Promotion of Science (JSPS). J. Köhler gratefully acknowledges his postdoctoral fellowship for foreign researchers in Japan from the JSPS.

[1] J. Köhler, N. Imanaka, G. Adachi, *Chem. Mater.* **1998**, *10*, 3790−3812.
[2] N. Imanaka, Y. Kobayashi, G. Adachi, *Chem. Lett.* **1995**, 433−434.
[3] Y. Kobayashi, T. Egawa, S. Tamura, N. Imanaka, G. Adachi, *Chem. Mater.* **1997**, *9*, 1649−1654.
[4] N. Imanaka, G. Adachi, *J. Alloys and Comp.* **1997**, *250*, 492−500.
[5] N. Imanaka, Y. Kobayashi, K. Fujiwara, T. Asano, Y. Okazaki, G. Adachi, *Chem. Mater.* **1998**, *10*, 2006−2012.
[6] N. Imanaka, M. Hiraiwa, S. Tamura, G. Adachi, H. Dabkowska, A. Dabkowski, J. E. Greedan, *Chem. Mater.* **1998**, *10*, 2542−2545.
[7] Y. Kobayashi, S. Tamura, N. Imanaka, G. Adachi, *Solid State Ionics* **1998**, *113−115*, 545−552.
[8] N. Imanaka, S. Tamura, Y. Kobayashi, Y. Okazaki, M. Hiraiwa, T. Ueda, G. Adachi, *J. Alloys and Comp.* **2000**, *303−304*, 303−306.
[9] N. Imanaka, T. Ueda, Y. Okazaki, S. Tamura, G. Adachi, *Chem. Mater.* **2000**, *12*, 1910−1913.
[10] K. Nassau, H. J. Levinstein, G. M. Loiacono, *J. Phys. Chem. Solids* **1965**, *26*, 1805−1816.
[11] Y. Kobayashi, T. Egawa, S. Tamura, N. Imanaka, G. Adachi, *Solid State Ionics* **1999**, *118*, 325−330.
[12] Y. Kobayashi, PhD Thesis of Osaka University **1998**.
[13] J. Köhler, N. Imanaka, G. Adachi, *J. Mater. Chem.* **1999**, *9*, 1357−1362.
[14] Y. Kobayashi, T. Egawa, S. Tamura, N. Imanaka, G. Adachi, *Solid State Ionics* **1998**, *111*, 59−65.
[15] G. Adachi, J. Köhler, N. Imanaka, *Electrochemistry* **1999**, *67*, 744−751.
[16] R. D. Shannon, *Acta Crystallogr., Sect. A* **1976**, *32*, 751−767.
[17] As in previous reports on trivalent cation compounds with the $Sc_2(WO_4)_3$-type structure,[1−9] the conducting properties of the $(Lu_{1-x}M_x)_2(WO_4)_3$ solid solutions (M = Er, Ho, Sm) have been characterized by several electrochemical methods, including time-dependent polarization measurements (under various atmospheres) and dc electrolysis experiments. As a main result, the electrical conductivity in the $(Lu_{1-x}M_x)_2(WO_4)_3$ solid solutions is found to be purely cationic with an ion-transference number higher than $t_i^+ = 0.99$. No electronic or anionic O^{2-} conduction has been observed. The migrating cations have been directly identified by EPMA for the samples after the dc electrolysis using the same experimental setup as reported elsewhere.[1−9] Thus, the data presented are discussed in terms of trivalent cationic conduction.

Received July 9, 2001
[I01254]

Syntheses and Characterization of Copper(II) Complexes of the New Ligands *N*-[(2-Pyridyl)methyl]-2,2′-dipyridylamine and *N*-[Bis(2-pyridyl)methyl]-2-pyridylamine

Simon P. Foxon,[a] Olaf Walter,[b] and Siegfried Schindler*[a]

Keywords: Copper / Oxygen / Coordination chemistry / Ligand effects / Tripodal ligands

The two new ligands *N*-[(2-pyridyl)methyl]-2,2′-dipyridylamine (**L1**) and *N*-[bis(2-pyridyl)methyl]-2-pyridylamine (**L2**) have been synthesized and the copper(II) complexes $[Cu(\mathbf{L1})_2(CH_3OH)_2](ClO_4)_2$, $[Cu(\mathbf{L1})_2(H_2O)_2](ClO_4)_2$, $[Cu_3(\mathbf{L1})_2(DMF)_2Cl_6]$, $[Cu(\mathbf{L1})Cl_2]_n$, $[Cu(\mathbf{L2})(Cl)(ClO_4)]$, and $[Cu(\mathbf{L2})Cl_2]$ have been structurally characterised. The reactions of dioxygen with the copper(I) complexes with ligands **L1** and **L2** were investigated, but no copper–dioxygen intermediates could be detected spectrophotometrically.

Introduction

A large number of biologically important metalloproteins utilise copper ions in their active sites for the redox-processing of molecular dioxygen.[1−6] Examples include hemocyanin (O_2 carrier in the blood of arthropods and molluscs), tyrosinase (*o*-phenol monooxygenase), and other oxidases, which couple oxidation of the substrate with copper-mediated reduction of dioxygen to hydrogen peroxide or water.[7−11]

The function of the metalloprotein is closely related to the structure of its active site, i.e. the geometrical arrangement of amino acid residues around the copper ions. There has been considerable interest in the design of ligands and the characterisation of copper complexes that may constitute models of the active site structure in such metalloproteins.[1,4−6,12−16] In particular, copper complexes of tris(2-pyridylmethyl)amine (tmpa) and closely related ligands have been widely employed in order to explore and understand the thermodynamic and kinetic aspects of the reaction of copper(I) compounds with dioxygen.[1,17−22]

We recently carried out a detailed study on a family of three ligands closely related to tmpa, in which each "arm" of the tripodal parent ligand tmpa was systematically lengthened by the insertion of a methylene spacer group.[23] This systematic approach allowed an evaluation of the effect of the chelate ring size on the following properties: copper(I)-oxygen reactivity, the coordination geometry around the copper ion, the Cu^{II}/Cu^{I} redox couple, and spectroscopic features (UV/Vis, EPR).

The properties of these complexes were found to be strongly affected by changing the chelate ring size and, therefore, we also became interested in performing a similar investigation in which the tripodal ligand, tmpa, had each "arm" systematically shortened (Scheme 1). The tripodal amine, tris(2-pyridyl)amine (tpa; unfortunately tmpa has also been abbreviated as tpa in the literature) has been known for a long time,[24] but the two ligands *N*-[(2-pyridyl)-methyl]-2,2′-dipyridylamine (**L1**) and *N*-[bis(2-pyridyl)methyl]-2-pyridylamine (**L2**), intermediate between tmpa and tpa, are as yet unknown in the literature.

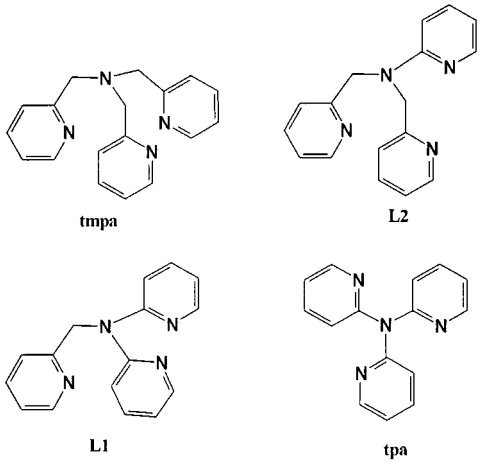

Scheme 1. The ligands tpa, **L1**, **L2**, and tmpa

Herein, we report the synthesis of these two new ligands and the characterisation of their copper(II) complexes, as

[a] Institute of Inorganic Chemistry, University of Erlangen-Nürnberg,
Egerlandstraße 1, 91058 Erlangen, Germany
Fax: (internat.) + 49-(0)9131−85 27 387
E-mail: schindls@anorganik.uni-erlangen.de
[b] ITC-CPV, Forschungszentrum Karlsruhe GmbH, ITC-CPV, Postfach 3640, 76021 Karlsruhe, Germany

 © WILEY-VCH Verlag GmbH, 69451 Weinheim, Germany, 2002 1434−1948/02/0101−0111 $ 17.50+.50/0

well as some preliminary studies of the reactivity of the copper(I) complexes with dioxygen.

Results and Discussion

The ligands *N*-[(2-pyridyl)methyl]-2,2′-dipyridylamine (**L1**) and *N*-[bis(2-pyridyl)methyl]-2-pyridylamine (**L2**) were synthesized by nucleophilic substitution reactions of the precursor amines with 2-picolyl chloride (Scheme 2). The resulting ligands were isolated in multigram quantities in modest yields. The two ligands are crystalline solids and were obtained in a highly pure state by recrystallisation from an appropriate solvent (see Exp. Sect.).

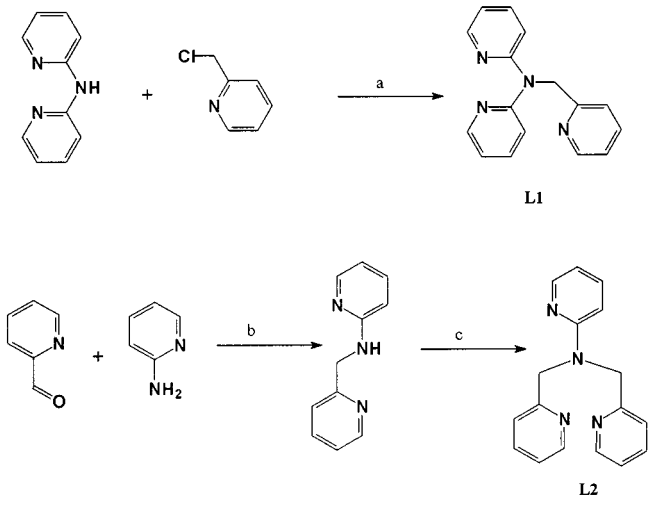

Scheme 2. Synthesis of the ligands **L1** and **L2**; reagents and conditions: **a**: KOH/DMSO, room temp., 2 h. **b**: i. benzene, reflux, 18 h, ii. $NaBH_4$, 18 h. **c**: i. NaH, DMF, room temp., 1 h, ii. picolyl chloride, DMF, room temp., 18 h

The copper(II) complexes used in this study were prepared by adding a copper(II) salt to the appropriate ligand. Crystals suitable for single-crystal X-ray diffraction studies were obtained either by slow evaporation of the solvent(s) from solutions in methanol, water, acetonitrile, or mixtures thereof, or by slow diffusion of diethyl ether into solutions of the complexes in DMF or acetonitrile.

L1 is a versatile ligand. It incorporates rigidity in the form of the dipyridyl moiety, while "flexibility" is provided by the pendant pyridyl "arm". The dipyridyl moiety of **L1** acts as a rigid bidentate donor to the copper(II) centres and it is observed that in the structures presented herein, the third pyridyl nitrogen atom does not coordinate to the same copper(II) centre. We demonstrate in this work that by changing the solvent and counteranions a variety of unique and different structures incorporating the common motif of ligand **L1** can readily be prepared.

Ligand **L2** is closely related to bis(2-pyridylmethyl)amine (dipica), but has been derivatised by the incorporation of an extra pyridine moiety. This introduces the possibility of additional coordination and hence the formation of new coordination compounds.

It should be noted that the proposed formulae obtained on the basis of elemental analyses of the copper(II) complexes differ from the structures obtained by single-crystal X-ray diffraction studies. This is due to the removal of solvent molecules from the crystal lattices in preparing samples for elemental analysis.

X-ray Structures

A summary of the crystallographic data and refinement parameters for the structures reported in this study can be found in Table 1. Selected bond lengths and angles for the copper(II) complexes are reported in Table 2.

Ligand L1

Crystals of **L1** were obtained by slow evaporation of the solvent from a solution of the ligand in acetonitrile at room temperature. An ORTEP representation of the crystal structure of ligand **L1** is shown in Figure 1. The crystal structure of **L1** shows no extraordinary features and is comparable to the reported structures of tpa and its derivatives.[25,26]

$[Cu(L1)_2(CH_3OH)_2](ClO_4)_2$ (1a)

Blue block-shaped crystals of **1a** were grown by slow diffusion of diethyl ether into a solution of the complex in DMF/methanol. The structure of the cation of **1a** is shown in Figure 2, while the coordination parameters around the copper(II) centre are listed in Table 2.

The structure of **1a** (Figure 2) reveals that two molecules of **L1** coordinate to the central copper(II) ion. Each **L1** molecule coordinates to the copper(II) centre through the two pyridine nitrogen atoms, N(2) and N(3), of the dipyridyl moiety. Due to the copper ion occupying a crystallographic inversion centre, the coordinated pyridyl nitrogen atoms and the copper(II) ion are rigorously coplanar. The equatorial ligands form a rectangular rather than a square basal plane around the copper(II) ion, as is evident from the N−N distances [$N(2)-N(3)^i$ = 2.9627(13) Å, N(2)−N(3) = 2.7365(13) Å]. Two methanol molecules are coordinated to the copper(II) ion in the axial positions. The resulting geometry around the copper(II) coordination sphere in **1a** can be described as elongated tetragonal [Cu(1)−N(2) = 2.0181(13) Å, Cu(1)−N(3) = 2.0150(13) Å, Cu(1)−O(1) = 2.4187(13) Å], which is characteristic of d^9 hexacoordinate copper(II) complexes. Furthermore, the methanol molecules are not perpendicular to the equatorial plane, which is evident from the angles [N(3)−Cu(1)−O(1) = 94.41(5)°, $N(3)^i$−Cu(1)−O(1) = 85.59(5)°], with each methanol molecule being *slightly* tilted towards the uncoordinated pyridyl moiety. This is perhaps unsurprising, considering the interesting and unexpected observation of a strong *intramolecular* hydrogen bonding interaction between the "pendant" pyridyl nitrogen N(4) and O(1) of the methanol molecule in the structure of **1a** [O(1)···N(4) = 2.7472(13) Å].

Although methanol is not a particularly good ligand, especially when bound at the axial coordination positions of the Jahn−Teller sensitive copper(II) ion, metal-bound methanol molecules have been observed in transition metal

Table 1. Crystallographic data from the X-ray diffraction studies of **L1**, **1a**−**1d**, **2a**, and **2b**

	L1	1a	1b	1c	1d	2a	2b
Empirical formula	$C_{16}H_{14}N_4$	$C_{34}H_{36}Cl_2CuN_8O_{10}$	$C_{38}H_{46}Cl_2CuN_{10}O_{12}$	$C_{44}H_{56}Cl_6Cu_3N_{12}O_4$	$C_{16}H_{14}Cl_2CuN_4$	$C_{17}H_{16}Cl_2CuN_4O_4$	$C_{17}H_{18}Cl_2CuN_4O$
M_r	262.31	851.14	969.28	1220.32	396.75	474.78	428.79
Temperature [K]	200(2)	200(2)	200(2)	200(2)	200(2)	200(2)	200(2)
Radiation used (λ [Å])	Mo-K_α (0.71073)	Mo-K_α (0.71073)	Mo-K_α (0.71073)	Mo-K_α (0.71073)	Mo-K_α (0.71073)	Mo-K_α (0.71073)	Mo-K_α (0.71073)
Crystal description	colourless block	blue block	blue block	blue block	green plates	green block	green plates
Crystal size [mm]	0.6 × 0.6 × 0.3	0.6 × 0.6 × 0.4	0.8 × 0.8 × 0.5	0.3 × 0.2 × 0.2	0.4 × 0.1 × 0.1	0.2 × 0.2 × 0.2	0.3 × 0.3 × 0.2
Crystal system	monoclinic	triclinic	monoclinic	triclinic	monoclinic	monoclinic	monoclinic
Space group	$P2_1/n$ (No. 14)	$P\bar{1}$ (No. 2)	$C2/c$ (No. 15)	$P\bar{1}$ (No. 2)	$P2(1)$ (No. 4)	$P2_1/n$ (No. 14)	$P2_1/n$ (No. 14)
a [Å]	8.976(3)	9.1818(5)	23.377(2)	8.9545(19)	7.6273(12)	8.2210(5)	8.6690(8)
b [Å]	15.083(6)	9.9260(6)	13.6502(13)	12.024(2)	13.947(2)	14.6760(9)	11.8603(11)
c [Å]	10.354(2)	11.2268(6)	14.4648(14)	13.303(3)	7.9549(13)	15.4302(9)	17.1999(16)
α [°]	90	71.3840(10)	90	82.53(2)	90	90	90
β [°]	111.61(2)	78.2960(10)	108.3600(10)	81.60(2)	111.556(2)	102.1950(10)	91.7060(13)
γ [°]	90	69.0490(10)	90	69.17(2)	90	90	90
V [Å^3]	1303.3(7)	900.99(9)	4380.7(7)	1319.6(5)	787.1(2)	1819.67(19)	1767.7(3)
Z	4	1	4	1	2	4	4
F(000)	552	439	2012	625	402	964	876
$\rho_{calcd.}$ [g·cm^{-3}]	1.337	1.569	1.470	1.536	1.674	1.733	1.611
μ [mm^{-1}]	0.083	0.825	0.693	1.555	1.730	1.528	1.551
Total reflections	13336	9534	22317	14042	8461	19367	18264
Unique reflections	3128	4231	5315	6240	3740	4444	4314
R(int)	0.0275	0.0105	0.0166	0.0260	0.0477	0.0512	0.0370
Scan range θ [°]	2.51 to 28.32	1.92 to 28.24	1.75 to 28.32	1.82 to 28.29	2.75 to 28.30	1.94 to 28.28	2.09 to 28.29
Completeness to $\theta_{max.}$ [%]	93.0	94.9	93.4	95.3	98.5	94.8	93.9
Index ranges	$-11 \le h \le 11$	$-12 \le h \le 12$	$-30 \le h \le 30$	$-11 \le h \le 11$	$-9 \le h \le 10$	$-10 \le h \le 10$	$-11 \le h \le 11$
	$-19 \le k \le 19$	$-12 \le k \le 12$	$-18 \le k \le 18$	$-16 \le k \le 16$	$-18 \le k \le 18$	$-19 \le k \le 19$	$-14 \le k \le 15$
	$-13 \le l \le 13$	$-14 \le l \le 14$	$-19 \le l \le 19$	$-17 \le l \le 17$	$-10 \le l \le 10$	$-19 \le l \le 20$	$-22 \le l \le 22$
Data/restraints/parameters	3128/0/185	4231/0/260	5315/0/295	6240/0/325	3740/1/213	4444/0/258	4314/0/233
$R1$,[a][b] $wR2$ [$I > 4\sigma(I)$][c]	0.0477, 0.1314	0.0318, 0.0883	0.0298, 0.0827	0.0361, 0.0783	0.0930, 0.2637	0.0367, 0.0758	0.0333, 0.0826
$R1$,[a][d] $wR2$ (all data) [c][d]	0.0540, 0.1377	0.0340, 0.0902	0.0323, 0.0852	0.0545, 0.0835	0.1191, 0.2836	0.0618, 0.0846	0.0412, 0.0875
Goodness-of-fit on F^2 [e]	1.039	1.051	1.076	1.042	1.083	1.018	1.079
Max./min. el. dens. [e.Å^{-3}]	0.360, −0.425	0.749, −0.429	0.354, −0.495	0.382, −0.484	3.918, −0.665	0.553, −0.456	0.496, −0.694

[a] $R1 = \Sigma||F_o| - |F_c||/\Sigma|F_o|$. [b] Denotes the value of the residual considering only the reflections with $I > 4\sigma(I)$. [c] $wR2 = \{\Sigma[w(F_o^2 - F_c^2)^2]/\Sigma[w(F_o^2)^2]\}^{1/2}$; $w = 1/[\sigma^2(F_o^2) + (aP)^2 + bP]$, $P = [\max(F_o^2 \text{ or } 0) + 2(F_c^2)]/3$. [d] Denotes the value of the residual considering all the reflections. [e] $S = [\Sigma w(F_o^2 - F_c^2)^2]/[(n - p)^{1/2}]$, n: number of data, p: parameters used.

complexes, particularly when stabilized by hydrogen bonding within solvated "cavities".[27] A similar observation of an *intramolecular* hydrogen bond between copper(II)-bound solvent molecules and pendant pyridyl moieties has been demonstrated by Mascharak et al. in the case of a ligand system incorporating an amide functionality.[28]

$[Cu(L1)_2(H_2O)_2](ClO_4)_2 \cdot 2DMF$ (1b)

The crystal structure of **1b** (Figure 3) displays similarities to that of **1a**. The geometry around the copper(II) coordination sphere in **1b** can also be described as elongated tetragonal [Cu(1)−(N2) = 2.0156(11) Å, Cu(1)−N(3) = 2.0175(11) Å, Cu(1)−O(1) = 2.3847(11) Å]. In this structure, there is a dihedral angle of 55.22° between the coordinated pyridyl rings of the two **L1** ligands. Furthermore, two water molecules occupy the axial sites of the copper(II) centre. They each form two strong hydrogen bonds; one *intramolecular* hydrogen bond to the pendant pyridyl "arm" [O(1)−N(4) = 2.8396(11) Å] and an *intermolecular* hydrogen bond to a DMF solvent molecule [O(1)−O(2)DMF = 2.7969(11) Å]. The copper(II) centre does not lie on an inversion centre and therefore the basal plane of the four equatorial nitrogen atoms does not form a perfect square basal plane.

In contrast to the well-known ligand tmpa (Scheme 1), there have been surprisingly few structurally characterised copper(II) complexes of tris(2-pyridyl)amine (tpa) reported in the literature; a search of the Cambridge Structural Data Base[29] reveals there to be only four.[30−33] In three of these four examples, two tpa ligands are found to be ligated to the copper(II) centre, while the other example is a larger tetrameric array.[33] In all the characterised structures, only two of the three pyridine nitrogen atoms are found to coordinate to the copper(II) centre. The single-crystal X-ray structures of the cations of **1a** and **1b** display similar features to those reported for the copper(II) complex $[Cu(tpa)_2(MeCN)_2](SO_3CF_3)_2$.[32] In this structure, the copper(II) ion is also found to occupy a crystallographic inversion centre. The tpa moiety coordinates to the copper(II) centre in an identical manner as observed for **L1**, and the two axial sites are occupied by acetonitrile solvent molecules. The third pyridine moiety of tpa remains uncoordinated. However, the crystal structures of **1a** and **1b** show one notable and interesting difference from that of $[Cu(tpa)_2(MeCN)_2](SO_3CF_3)_2$. The coordination of methanol molecules to the copper(II) centre of **1a** and of water molecules to the copper(II) centre in **1b** is stabilised by *intramolecular* hydrogen bonds formed between the coordinated solvent

Table 2. Selected bond lengths (Å) and angles (deg.) for compounds **1a−1d**, **2a**, and **2b**

1a

Cu(1)−N(2)	2.0181(13)	Cu(1)−N(3)^{i}	2.0150(13)	Cu(1)−O(1)	2.4187(13)
Cu(1)−N(2)^{i}	2.0182(13)	Cu(1)−N(3)	2.0150(13)	Cu(1)−O(1)^{i}	2.4187(13)
N(3)−Cu(1)−N(3)^{i}	180.0	O(1)−Cu(1)−O(1)^{i}	180.0	N(3)−Cu(1)−N(2)	85.45(5)
N(2)−Cu(1)−O(1)^{i}	89.29(5)	N(2)−Cu(1)−O(1)	90.71(5)	N(3)−Cu(1)−N(2)^{i}	94.55(5)
N(3)−Cu(1)−O(1)	94.41(5)	N(3)−Cu(1)−O(1)^{i}	85.59(5)	N(2)^{i}−Cu(1)−O(1)^{i}	90.71(5)

Symmetry transformations used to generate equivalent atoms: $-x, y, -z$

1b

Cu(1)−N(2)	2.0156(11)	Cu(1)−N(3)^{i}	2.0174(11)	Cu(1)−O(1)^{i}	2.3847(11)
Cu(1)−N(2)^{i}	2.0156(11)	Cu(1)−N(3)	2.0175(11)	Cu(1)−O(1)	2.3847(11)
N(2)^{i}−Cu(1)−N(2)	92.10(6)	N(3)^{i}−Cu(1)−N(3)	96.86(6)	O(1)^{i}−Cu(1)−O(1)	176.12(6)
N(2)−Cu(1)−N(3)^{i}	175.56(4)	N(2)−Cu(1)−N(3)	85.64(5)	N(2)−Cu(1)−O(1)^{i}	86.06(4)
N(3)−Cu(1)−O(1)^{i}	87.03(4)	N(2)−Cu(1)−O(1)	96.64(4)	N(3)^{i}−Cu(1)−O(1)	87.03(4)
N(3)−Cu(1)−O(1)	90.40(4)				

Symmetry transformations used to generate equivalent atoms: $-x, y, -z + 1/2$

1c

Cu(1)−N(1)	2.0307(19)	Cu(1)−Cl(1)	2.2769(8)	Cu(1)−N(2)	2.0161(19)
Cu(1)−Cl(2)	2.2687(9)	Cu(1)−O(1)	2.2870(18)	Cu(2)−N(4)^{i}	1.988(2)
Cu(2)−N(4)	1.988(2)	Cu(2)−Cl(3)	2.2396(9)		
N(2)−Cu(1)−N(1)	84.31(8)	N(2)−Cu(1)−Cl(2)	90.05(6)	N(1)−Cu(1)−Cl(2)	168.79(5)
N(2)−Cu(1)−Cl(1)	170.07(6)	Cl(2)−Cu(1)−Cl(1)	93.20(3)	N(2)−Cu(1)−O(1)	93.57(8)
Cl(2)−Cu(1)−O(1)	100.93(6)	N(4)−Cu(2)−N(4)^{i}	180.0	N(4)−Cu(2)−Cl(3)	89.78(6)
N(4)−Cu(2)−Cl(3)^{i}	90.22(6)				

Symmetry transformations used to generate equivalent atoms: $-x, -y, -z$

1d

Cu(1)−N(1)	2.421(7)	Cu(1)−N(3)	2.027(5)	Cu(1)−N(3)^{i}	2.027(5)
Cu(1)−Cl(1)	2.2762(17)	Cu(1)−Cl(1)^{i}	2.2762(17)	N(3)−Cu(1)−N(3)^{i}	84.5(3)
N(3)−Cu(1)−N(1)	84.64(19)	N(3)−Cu(1)−Cl(1)^{i}	168.04(16)	N(3)−Cu(1)−Cl(1)	91.03(15)
Cl(1)^{i}−Cu(1)−Cl(1)	91.20(10)	Cl(1)−Cu(1)−N(1)	106.01(12)		

Symmetry transformations used to generate equivalent atoms: $x, -y + 1/2, z$

2a

Cu(1)−N(2)	1.982(2)	Cu(1)−N(3)	1.991(2)	Cu(1)−N(1)	2.073(2)
Cu(1)−Cl(1)	2.2265(7)	Cu(1)−O(1)	2.4837(7)	N(2)−Cu(1)−N(3)	161.15(9)
N(2)−Cu(1)−N(1)	83.89(8)	N(3)−Cu(1)−N(1)	81.39(8)	N(2)−Cu(1)−Cl(1)	98.87(7)
N(3)−Cu(1)−Cl(1)	99.47(6)	N(1)−Cu(1)−Cl(1)	154.73(6)	O(1)−Cu(1)−N(1)	104.39(6)
O(1)−Cu(1)−N(2)	82.88(7)	O(1)−Cu(1)−N(3)	89.43(7)	O(1)−Cu(1)−Cl(1)	100.87(7)

2b

Cu(1)−N(2)	1.9798(17)	Cu(1)−N(3)	1.9836(17)	Cu(1)−Cl(1)	2.2619(6)
Cu(1)−Cl(2)	2.3271(6)	Cu(1)−N(1)	2.3399(17)		
N(2)−Cu(1)−N(3)	160.70(7)	N(2)−Cu(1)−Cl(1)	95.39(5)	N(3)−Cu(1)−Cl(1)	96.61(6)
N(2)−Cu(1)−Cl(2)	91.12(5)	N(3)−Cu(1)−Cl(2)	89.76(5)	Cl(1)−Cu(1)−Cl(2)	138.82(2)
N(2)−Cu(1)−N(1)	80.89(6)	N(3)−Cu(1)−N(1)	79.94(6)	Cl(1)−Cu(1)−N(1)	121.83(4)
Cl(2)−Cu(1)−N(1)	99.35(4)				

molecules and each pendant pyridyl "arm" as discussed above.

$[Cu_3(L1)_2(DMF)_2Cl_6]\cdot 2DMF$ (1c)

Crystals of **1c** suitable for single-crystal X-ray diffraction analysis were grown over a period of a few days by slow diffusion of diethyl ether into a solution of the complex in DMF at room temperature. Single-crystal X-ray diffraction analysis revealed that **1c** crystallises in the triclinic space group $P\bar{1}$. The structure is shown in Figure 4, while the coordination parameters around the copper(II) centres are listed in Table 2.

The first striking observation is that the coordination complex contains more than one copper ion. The crystal structure reveals a ratio of three copper(II) ions to two **L1** molecules (Figure 4). The coordination geometry around

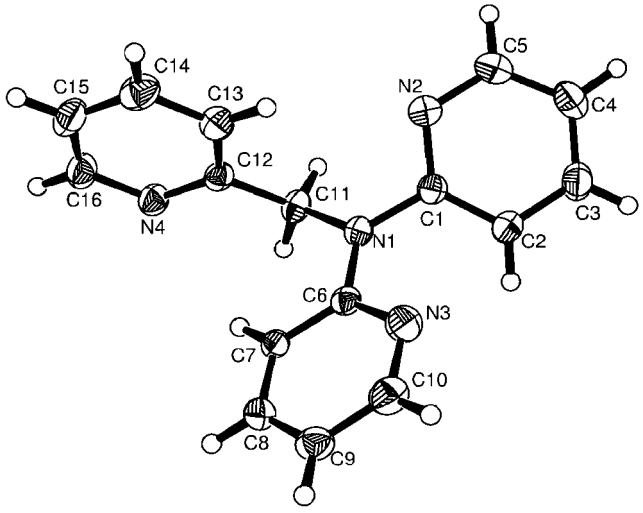

Figure 1. ORTEP representation (50% thermal probability ellipsoids) of the crystal structure of **L1**

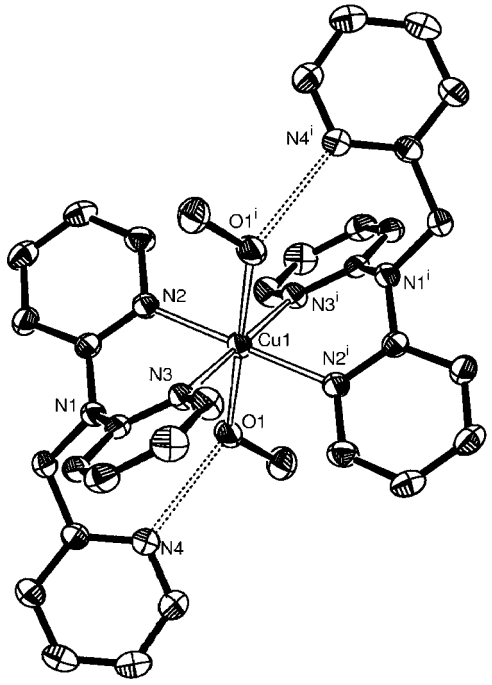

Figure 2. ORTEP representation (50% thermal probability ellipsoids) of the crystal structure of the cation of **1a**; perchlorate anions have been omitted for clarity

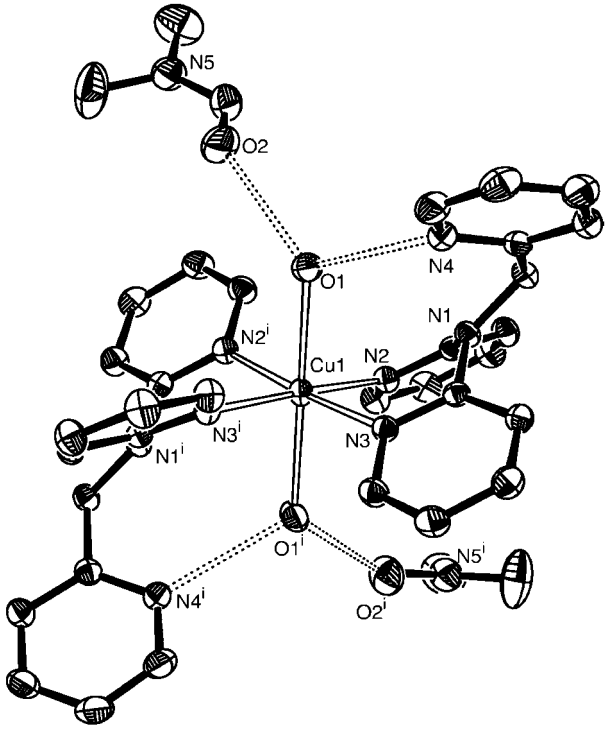

Figure 3. ORTEP representation (50% thermal probability ellipsoids) of the crystal structure of the cation of **1b**; perchlorate anions have been omitted for clarity

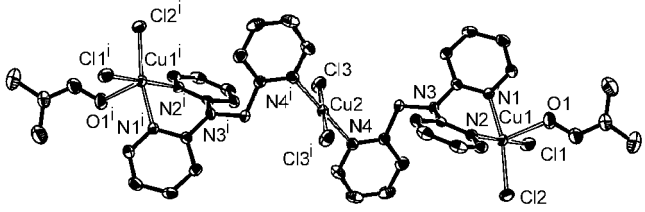

Figure 4. ORTEP representation (50% thermal probability ellipsoids) of the crystal structure of **1c**; two DMF solvent molecules have been omitted for clarity

Cu(1) can be described as being close to square pyramidal, with N(1) and N(2) of the dipyridyl moiety of **L1** and two chloride anions, Cl(1) and Cl(2), forming the square basal plane [Cu(1)−N(2) = 2.0161(19) Å, Cu(1)−N(1) = 2.0307(19) Å, Cu(1)−Cl(2) = 2.2687(9) Å, Cu(1)−Cl(1) = 2.2769(8) Å]. The oxygen atom O(1) of a DMF solvent molecule occupies the axial position [Cu(1)−O(1) = 2.2870(18) Å]. The Cu(1) ion is found to be displaced from the basal plane by 0.179 Å. In common with the two previously described structures incorporating **L1**, N(4) of the third pyridyl arm is found not to coordinate to the Cu(1) centre. In contrast to the two previous structures, however, N(4) is unable to take part in *intramolecular* hydrogen bonding interactions with the coordinated anions and solvent molecule. Instead, N(4) coordinates to a second copper(II) ion in the structure, Cu(2) [Cu(2)−N(4) = 1.988(2) Å]. Cu(2) is found to occupy the crystallographic inversion centre of the unit cell. Another ligand of **L1** is coordinated through $N(4)^i$ [related to N(4) by the operation of inversion at Cu(2)] to Cu(2). A chloride ion Cl(3) and its symmetry-equivalent $Cl(3)^i$ complete the coordination sphere around Cu(2) [Cu(2)−Cl(3) = 2.2396(9) Å]. No other anions or DMF solvent molecules are found to occupy the vacant axial coordination sites of the Cu(2) centre. Due to the crystallographic restraint imposed on Cu(2), the coordination geometry around the Cu(2) ion can be rigor-

ously defined as square planar. Two DMF solvent molecules (not shown) complete the structure.

$[Cu(L1)Cl_2]_n$ (1d)

Thin plate-like crystals of **1d** were grown by slow evaporation of the solvents from a solution of the complex in aqueous acetonitrile. The crystal structure is shown in Figure 5, while the coordination parameters around the copper(II) centre are listed in Table 2. During the refinement procedure, high residual electron densities were observed in the Fourier difference map. This is a direct result of the low crystal quality (possibly due to extremely thin plates being stuck together) resulting in high residual electron densities along the crystallographic twofold screw axis.

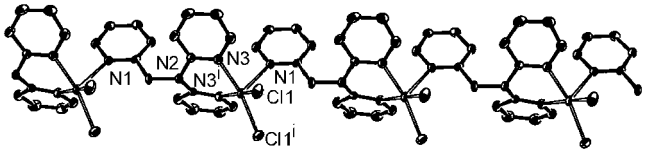

Figure 5. ORTEP representation (50% thermal probability ellipsoids) of the crystal structure of **1d**

The most striking feature is that **1d** has an infinite polymeric structure in the solid state. The ORTEP plot in Figure 5 shows three of the repeating units. The asymmetric unit cell consists of one half of a molecule of the formula "[Cu(**L1**)Cl_2]". The other symmetry-equivalent "half" of the structure is generated by reflecting the asymmetric unit contents through a mirror-plane consisting of the atoms Cu(1), N(1), N(2), and C(1)−C(6). The basal plane around each copper(II) centre in this structure is identical and is comprised of two pyridine nitrogen atoms of the dipyridyl moiety, N(1) and N(2), and two chloride anions, Cl(1) and Cl(2) [Cu(1)−N(1) = 2.033(14) Å, Cu(1)−N(2) = 2.014(14) Å, Cu(1)−Cl(2) = 2.275(5) Å, Cu(1)−Cl(1) = 2.276(5) Å]. The third pyridyl "arm" of **L1**, containing N(4), is not found to coordinate to the same copper(II) centre, as was seen in the structure of **1c**, but rather to a neighbouring copper(II) centre occupying the vacant axial position [N(4)−Cu(2) = 2.427(6) Å] and thus completing the distorted square-pyramidal coordination geometry around the copper(II) centre. No solvent molecules were found within the crystal lattice.

The two copper(II) chloride complexes of **L1** included in our study, **1c** and **1d**, show the effect of solvent coordination upon the nature of the final copper(II) complex obtained. Crystals of **1c**, the structure presented in Figure 4, were grown from a DMF-containing solution. In the crystal structure, DMF was found to occupy the axial site of the distorted square-pyramidal coordination environment of Cu(1) and consequently of its symmetry-equivalent $Cu(1)^i$ as well.

On moving to a medium containing predominantly acetonitrile, crystals of **1d** were obtained, the structure of which is shown in Figure 5. Here, the crystal structure revealed that no solvent molecules are coordinated to the copper(II) centres. The structure of **1d** shows similarities to that of **1c** in that N(4) of the pendant pyridyl "arm" coordinates to a neighbouring copper(II) centre. However, in contrast to the structure of **1c**, the N(4) atom in **1d** is found to occupy the axial coordination position around the square-pyramidal copper(II) centres, previously occupied by a DMF molecule in **1c**. It is interesting to note that no bridging by the chloride ion takes place, a common occurrence in copper halide polymeric structures.

$[Cu(L2)(Cl)(ClO_4)]$ (2a)

Blue block-shaped crystals of **2a** suitable for single-crystal X-ray analysis were grown by slow diffusion of diethyl ether into a solution in acetonitrile. An ORTEP plot of the crystal structure is presented in Figure 6. Selected crystallographic data and bond angles and distances are listed in Table 1 and 2, respectively.

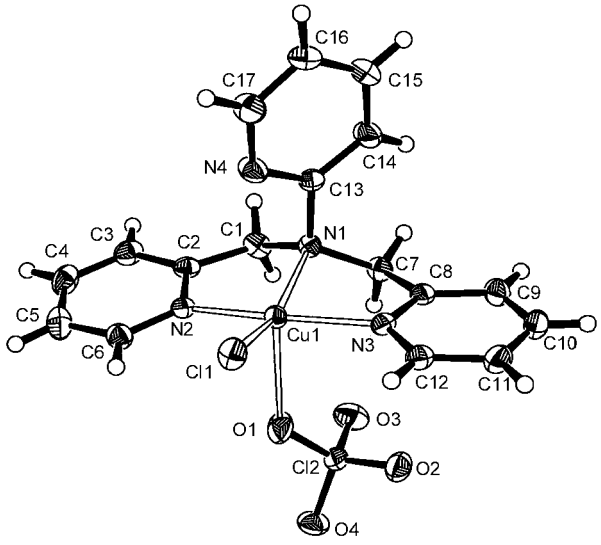

Figure 6. ORTEP representation (50% thermal probability ellipsoids) of the crystal structure of **2a**

As shown in Figure 6, two of the pyridyl rings of **L2** coordinate to the copper(II) centre in **2a**. The copper(II) centre is pentacoordinate, being coordinated by the pyridyl nitrogen atoms N(2) and N(3), the tertiary amine nitrogen N(1), chloride ion Cl(1), and O(1) of the perchlorate anion. The coordination environment around the copper(II) centre is best described as distorted square-pyramidal, with N(1), N(2), N(3), and Cl(1) forming the basal plane [Cu(1)−N(2) = 1.982(2) Å, Cu(1)−N(3) = 1.991(2) Å, Cu(1)−N(1) = 2.073(2) Å, Cu(1)−Cl(1) = 2.2265(7) Å] and O(1) of the perchlorate anion occupying the axial position [Cu(1)−O(1) = 2.4837(7) Å]. The coordination of the perchlorate anion in **2a** is also evident from the IR spectrum recorded from a Nujol mull. The strong band at

1089 cm^{-1} can be assigned as the coordinated perchlorate anion.

$[Cu(L2)Cl_2]\cdot H_2O$ (2b)

Green crystals suitable for single-crystal X-ray analysis were grown by slow evaporation of the solvents from a solution in aqueous methanol. An ORTEP plot of the crystal structure is displayed in Figure 7. Selected crystallographic data and bond lengths and angles are listed in Table 1 and 2, respectively.

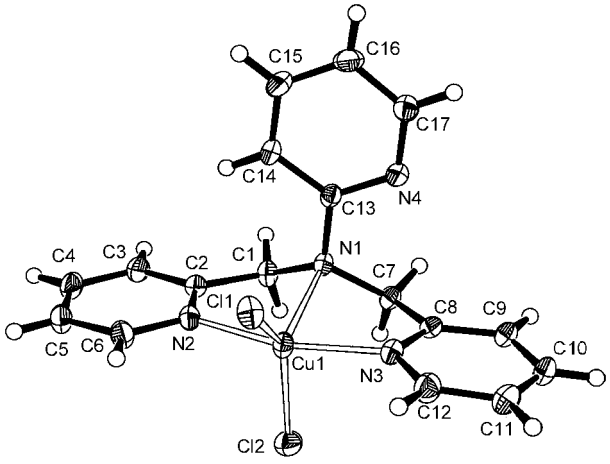

Figure 7. ORTEP representation (50% thermal probability ellipsoids) of the crystal structure of **2b**; a solvating water molecule has been omitted for clarity

As shown in Figure 7, and as was observed for **2a**, only two of the pyridyl rings of **L2** coordinate to the copper(II) centre in **2b**. The copper(II) centre is five-coordinate, being ligated by the pyridyl nitrogen atoms N(2) and N(3), the tertiary amine nitrogen N(1), and two chloride ions [Cu(1)−N(2) = 1.9798(17) Å, Cu(1)−N(3) = 1.9836(17) Å, Cu(1)−Cl(1) = 2.2619(6) Å, Cu(1)−Cl(2) = 2.3271(6) Å, Cu(1)−N(1) = 2.3399(17) Å]. At first sight, the geometry around the copper(II) centre might appear to be distorted trigonal bipyramidal, with the pyridyl nitrogen atoms N(2) and N(3) occupying the axial positions and the two chloride ions and N(1) occupying the equatorial plane. However, closer inspection reveals that the coordination environment around the Cu(1) centre is nearer to that found in square-pyramidal coordination complexes, with N(2), N(3), Cl(1), and Cl(2) forming the basal plane and the apical position being occupied by N(1). This is substantiated by examining the bond angles around the Cu(1) centre involving the atoms Cl(1), Cl(2), and N(1) [122°, 99°, 139° (sum = 360°)], which deviate from the value of 120° expected for a regular trigonal-bipyramidal geometry. Furthermore, the bond angle N(2)−Cu(1)−N(3) = 160.70(7)° is clearly less than 180°. This bond angle is a result of the small bite angles in each of the two five-membered chelate rings involving Cu(1), N(1), N(2), or N(3). These distortions and the value of the trigonality index τ of 0.36 (the index τ is zero for a square pyramid and unity for a trigonal bipyramid)[34] suggest that the coordination environment around Cu(1) is best described as trigonal-bipyramidal distorted square-based pyramidal (TBDSBP).

Ligand **L2** is a derivative of the parent amine (dipica) [dipica = bis(2-pyridylmethyl)amine] and shows a similar mode of coordination to copper(II) ions.[35−37] **L2** differs in that it possesses an additional pyridyl ring on the secondary aliphatic amine nitrogen atom, increasing the potential for additional coordination. There are numerous examples of derivatives of dipica, and the resulting ligands and metal complexes show interesting and novel properties.[38,39]

The structure of **2b** is similar to that reported for a copper complex of a derivatised dipica ligand.[38] This ligand was prepared by converting the secondary amine functional group of the precursor amine dipica into a tertiary amide group. The coordination parameters around the copper(II) centre are close to those seen in **2b**. In the structure, the tertiary amido nitrogen atom occupies the apical position at the copper(II) centre, with the other four ligating atoms (two pyridyl nitrogen atoms and two chloride ions) forming a distorted square plane in a similar manner to that shown in Figure 7. The coordination environment around the copper(II) centre is best described as trigonal-bipyramidal distorted square-based pyramidal (TBDSBP), having a trigonality index τ of 0.30.

UV/Vis Spectroscopy

The copper(II) complexes of **L2** are characterised by a rather broad d−d absorption band (ca. 650−1000 nm) in their solution (acetonitrile) electronic spectra; a low- or high-energy shoulder is often present as well, or occasionally two distinct absorption maxima are observed. In many cases, it has been demonstrated that the presence of a single d−d band with a low-energy shoulder is typical of a trigonal-bipyramidal geometry at copper, whereas an absorption with a high-energy shoulder indicates a square-pyramidal geometry. Examination of the electronic spectroscopic data of the copper(II) complexes of **L2** (see Exp. Sect.) indicates that, on the basis of this criterion, **2a** adopts a square-pyramidal geometry, whereas **2b** can best be described as having a geometry around the copper(II) centre close to trigonal bipyramidal. Complexes of **L1** are characterised by a rather broad absorption band at around 650 nm, indicating a square-pyramidal geometry in solution.

Electrochemistry

The half-wave potentials of complexes **1a**, **1d**, **2a**, and **2b** were determined by cyclic voltammetry in acetonitrile; the results are summarised in Table 3. All compounds displayed a reversible cyclic voltammogram, demonstrating that stable copper(I) complexes of the two ligands can be formed. Figure 8 shows the cyclic voltammogram of **2b**. Complexes with **L1** as a ligand are more easily reduced than those with **L2** as a ligand.

Table 3. Cyclic voltammetry of **1a**, **1d**, **2a**, and **2b** in acetonitrile

Compound[a]	E_p^{red} (V)	E_p^{ox} (V)	$E_{1/2}$ (V)	ΔE (mV)
1a	+0.31	+0.57	+0.44	260
1d	+0.31	+0.58	+0.45	270
2a	+0.11	+0.24	+0.18	130
2b	+0.07	+0.23	+0.15	160

[a] All potentials measured with a glassy carbon electrode vs. Ag/AgCl using $[NBu_4]PF_6$ (0.1 M) as electrolyte; scan rate: 100 mV s^{-1} in MeCN [$E_{1/2} = (E_p^{red} + E_p^{ox})/2$; $\Delta E = E_p^{ox} - E_p^{red}$].

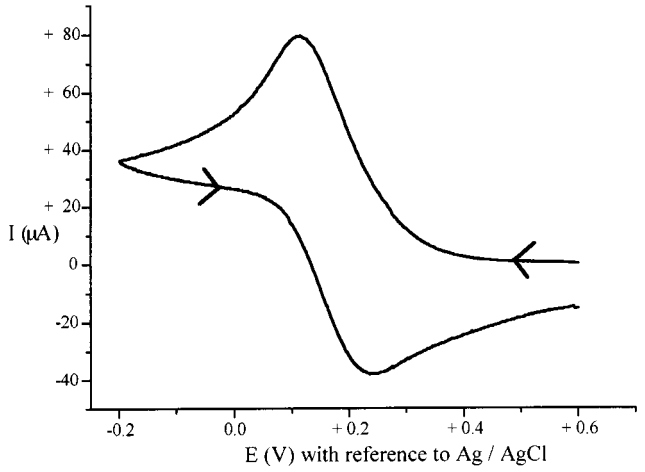

Figure 8. Cyclic voltammogram of **2b** in acetonitrile at 298 K; scan rate = 100 mV s^{-1}; concentration of complex = 1 mM; concentration of the supporting electrolyte $[NBu_4]PF_6$ = 0.1 M

Reactions of Dioxygen with Copper(I) Complexes of L1 and L2

As yet, we have been unable to isolate solid copper(I) complexes of **L1** or **L2**; only yellow-orange oils have been obtained. Therefore, to gain information on the reactions of dioxygen with the copper(I) complexes of **L1** or **L2**, these compounds were prepared in situ by mixing stoichiometric amounts of copper(I) salts with the ligands in acetone or propionitrile. Reactions of these solutions with dioxygen were investigated under the same conditions as employed for $[Cu(tmpa)(CH_3CN)]^+$ and its derivatives, using low-temperature stopped-flow techniques.[23] We observed that the copper complexes of both ligands were slowly oxidised, but in contrast to $[Cu(tmpa)(CH_3CN)]^+$ no "dioxygen adducts" were observed as intermediates.

Our earlier findings clearly demonstrated the influence of chelate ring size on the stability (or inertness) of copper "dioxygen" complexes.[23] $[Cu(tmpa)(CH_3CN)]^+$ reacts very rapidly with dioxygen to first form a superoxo complex, which reacts further to form a peroxo complex that is stable at low temperatures. Only one chelate ring is enlarged in $[Cu(pmea)]^+$, but we found that no superoxo complex could be detected in the course of its reaction with dioxygen; the initially formed peroxo complex rapidly underwent further reactions. In contrast to the findings for $[Cu(pmea)]^+$, a stopped-flow kinetic investigation showed that neither a superoxo nor a peroxo intermediate was observable during the reaction of $[Cu(pmap)]^+$ with dioxygen. $[Cu(tepa)]^+$ was found not to react with dioxygen. It was thus concluded that increasing the chelate ring size suppresses the formation of stable dioxygen adduct complexes in this series.

Unfortunately, reducing the chelate ring size by using **L1** or **L2** as described herein did not lead to a more stable copper superoxo or peroxo complex because intramolecular coordination of one of the pyridine donors was suppressed. The reaction of the copper(I) complex of tpa with dioxygen has been investigated previously and a cubane-like cluster was obtained as a product.[33] The authors did not report any dioxygen adduct complex as an intermediate during the course of this reaction.

Conclusions

We have reported the synthesis and characterisation of two new ligands, **L1** and **L2**, together with a series of copper(II) complexes derived from these ligands. The crystal structures of the complexes of **L1** demonstrate that in each case one of the three pyridyl donors remains uncoordinated, as observed in the copper complexes of tpa. However, the crystal structures of **1a** and **1b** show an important difference to copper tpa complexes: the coordination of methanol molecules to the copper(II) centre of **1a** and of water molecules in **1b** is stabilised by *intramolecular* hydrogen bonding between the coordinated solvent molecules and each pendant pyridyl "arm". Furthermore, using chloride as an anion in the syntheses of the copper(II) complexes of **L1** demonstrated an interesting solvent effect. In DMF, the trinuclear complex **1c**, incorporating coordinated DMF molecules is obtained, thus preventing the formation of a polymeric material. In contrast, in acetonitrile, no solvent molecules are coordinated and a polymeric complex **1d** is formed instead.

Ligand **L2** can be regarded as a derivative of bis(2-pyridylmethyl)amine (dipica) and the two complexes **2a** and **2b** are related to the complexes with dipica as ligand. **L2** differs from dipica in that it possesses a third pyridyl ring (not coordinated in **2a** and **2b**), increasing the potential for additional coordination.

As yet, it has not been possible to obtain copper(I) complexes of ligands **L1** or **L2** in a solid form, but reactions of dioxygen with these compounds formed in situ from a copper(I) salt and the ligand have been investigated. In contrast to the reaction of dioxygen with the copper(I) complex of tmpa, no dioxygen adducts could be observed as intermediates. Instead, complexes of both ligands were slowly oxidized to the copper(II) complexes, in line with their rather positive redox potentials.

Experimental Section

General Remarks: Reagents and solvents used were of commercially available reagent quality. Acetonitrile, propionitrile, diethyl ether,

and acetone were dried by standard methods. $[Cu(CH_3CN)_4]ClO_4$ and $[Cu(CH_3CN)_4]PF_6$ were synthesized according to literature procedures.[40] The purities of the ligands were assessed by TLC, elemental analysis, and ^1H and ^{13}C NMR. UV/Vis spectra were measured on a Hewlett−Packard 8452 A spectrophotometer using standard 1 cm quartz cuvettes. ^1H and ^{13}C NMR spectra were recorded on a Bruker DXP 300 AVANCE spectrometer. Infrared spectra were recorded from samples in either Nujol mulls or KBr pellets on an ATJ Mattson Infinity 60 AR FT-IR instrument. Cyclic voltammetry was performed using an EG&G Model 263 potentiostat at 25 °C at a scan rate of 100 mV s^{-1}. The solutions under investigation contained 1 mM copper complex and 0.1 M $[NBu_4]PF_6$ in acetonitrile that had been deoxygenated by bubbling nitrogen through it. A conventional H-type cell was used, with glassy carbon, Pt, and Ag/AgCl as working, counter, and reference electrodes, respectively.

Variable-Temperature Stopped-Flow Measurements: Solutions of the complexes for the collection of time-resolved UV/Vis spectra were prepared in a glovebox and transferred to the low-temperature stopped-flow instrument by means of syringes. Dioxygen-saturated solutions were prepared by bubbling dioxygen through propionitrile or acetone in syringes (solubility of dioxygen in propionitrile at 25 °C is 0.0088 M,[20] while in acetone it is 0.0102 M[41]). The reactions were studied under pseudo-first-order conditions ([complex] $<$ $[O_2]$), and time-resolved UV/Vis spectra of the reactions of dioxygen with copper(I) complexes were recorded with a modified Hi-Tech SF-3 L low-temperature stopped-flow unit (Salisbury, U.K.) equipped with a J&M TIDAS 16−500 photodiode-array spectrophotometer (J&M, Aalen, Germany).

Syntheses of Ligands and Complexes

Caution! Perchlorate salts are potentially explosive and should be handled with great care.

***N*-[(2-Pyridyl)methyl]-2,2′-dipyridylamine (L1):** Powdered potassium hydroxide (5.2 g, 93 mmol) was added to DMSO (40 mL). 2,2′-Dipyridylamine (3.42 g, 20 mmol) was added to this mixture. The resulting deep-orange coloured solution was stirred at room temperature for 45 min. 2-Picolyl chloride hydrochloride (3.28 g, 20 mmol) was then added and the orange solution was stirred at room temperature for 1 h. It was then diluted with water (50 mL), which led to the immediate deposition of a fine yellow precipitate. This precipitate was collected by filtration, washed with water (3 × 30 mL), and the yellow solid was recrystallised from hexane (75 mL) containing the minimum volume of dichloromethane. On cooling to 0 °C, fine yellow crystals formed. These were collected by filtration, washed with a little cold hexane, and dried to yield **L1** as a pale-yellow solid (2.9 g, 55%, 11 mmol). $C_{16}H_{14}N_4$: calcd. C 73.26, H 5.38, N 21.36; found C 73.31, H 5.50, N 21.23. M.p. 106−108 °C. FDI-MS: m/z = 262 [M^+]. ^1H NMR ($CDCl_3$, 300 MHz): δ = 5.60 (s, 2 H, $-CH_2-$), 6.82−6.86 (m, 2 H, ArH), 7.05−7.09 (m, 1 H, ArH), 7.24−7.32 (m, 3 H, ArH), 7.48−7.55 (m, 3 H, ArH), 8.28−8.30 (m, 2 H, ArH), 8.52 (d, 1 H, ArH). ^{13}C NMR ($CDCl_3$, 75 MHz): δ = 53.6, 114.4, 117.3, 121.2, 121.6, 136.5, 137.3, 148.2, 149.0, 156.8, 159.5. IR (KBr): $\tilde{\nu}$ = 3059 (w), 3004 (w), 2961 (w), 2925 (w), 2362 (w), 2337 (w), 1967 (w), 1943 (w), 1915 (w), 1893 (w), 1874 (w), 1845 (w), 1829 (w), 1796 (w), 1778 (w), 1737 (w), 1717 (w), 1701 (w), 1651 (w), 1585 (s), 1564 (m), 1470 (s), 1427 (s), 1379 (m), 1349 (m), 1325 (m), 1281 (m), 1260 (m), 1245 (m), 1225 (m), 1209 (m), 1173 (w), 1149 (m), 1130 (w), 1088 (m), 1044 (w), 983 (w), 901 (w), 873 (w), 772 (m), 753 (m), 737 (m), 661 (w), 612 (w), 585 cm^{-1} (w).

***N,N*-(2-Pyridyl)(2-pyridylmethyl)amine:** A solution of 2-pyridinecarboxaldehyde (9.2 mL, 96 mmol) and 2-aminopyridine (7.5 g, 80 mmol) in benzene (150 mL) was refluxed for 18 h with the continuous removal of water by means of a Dean−Stark trap. The solvent was subsequently removed in vacuo and the residue was taken up in absolute ethanol (200 mL). To this yellow solution, $NaBH_4$ (4.0 g, 105.8 mmol) was added and the solution was stirred at room temperature for 18 h. The excess $NaBH_4$ was then cautiously quenched by adding first water (100 mL) and then saturated aqueous NH_4Cl solution (100 mL) at 70 °C. Thereafter, the volatiles were removed in vacuo and the residue was redissolved in water (200 mL). The resulting aqueous solution was extracted with ethyl acetate (3 × 150 mL) and the combined organic fractions were dried over anhydrous magnesium sulfate. Upon removal of the solvent, a viscous yellow oil was obtained. The product was purified by vacuum distillation to yield a pale-yellow viscous liquid (6.0 g, 41%, 32.4 mmol). FDI-MS: m/z = 185 [M^+]. ^1H NMR ($CDCl_3$, 300 MHz): δ = 4.65 (d, 2 H, $-CH_2-$, $^3J_{H,H}$ = 5.3 Hz), 5.86 (br, 1 H, NH), 6.43−6.45 (m, 1 H, ArH), 6.53−6.58 (m, 1 H, ArH), 7.13−7.17 (m, 1 H, ArH), 7.30−7.40 (m, 2 H, ArH), 7.58−7.63 (m, 1 H, ArH), 8.09−8.11 (m, 1 H, ArH), 8.54−8.55 (m, 1 H, ArH). ^{13}C NMR ($CDCl_3$, 75 MHz): δ = 47.2, 107.7, 112.9, 121.6, 122.0, 136.6, 137.3, 147.9, 149.0, 158.3, 158.5. IR (KBr): $\tilde{\nu}$ = 3278 (br, m), 3084 (m), 3056 (m), 3018 (m), 2927 (w), 2865 (w), 1603 (s), 1571 (s), 1506 (s), 1490 (s), 1438 (m), 1332 (m), 1293 (m), 1254 (w), 1151 (m), 1120 (w), 1084 (w), 1049 (w), 983 (m), 771 (m), 686 (m), 611 (m), 527 cm^{-1} (m).

***N*-[Bis(2-pyridyl)methyl]-2-pyridylamine (L2):** Sodium hydride (60% dispersion in mineral oil; 1.3 g, 32.5 mmol) was added to anhydrous DMF (100 mL) under nitrogen. The resulting grey slurry was stirred at room temperature until hydrogen evolution had ceased (ca. 0.5 h). A solution of *N,N*-(2-pyridyl)(2-pyridylmethyl)amine (5.0 g, 27 mmol) in anhydrous DMF (60 mL) was then added dropwise to the sodium hydride slurry. The resulting orange solution was stirred until hydrogen evolution had ceased (ca. 1 h). To the amine carbanion, a solution of 2-picolyl chloride (free base) (3.79 g, 30 mmol) in anhydrous DMF (50 mL) was added dropwise and the brown solution was stirred overnight at room temperature. The light-orange solution obtained was then cautiously quenched by the addition of water (200 mL), and brine (50 mL) was also added. The aqueous solution was exhaustively extracted with dichloromethane (4 × 150 mL). The combined organic phases were washed with brine (200 mL) and dried over anhydrous magnesium sulfate. Removal of the solvent in vacuo yielded the crude product as a light-tan coloured solid. It was taken up in warm diethyl ether (100 mL), which led to the separation of a brown oil. The ethereal solution was decanted and the solvent was removed in vacuo. The crude cream-coloured product was recrystallised once from diethyl ether. On cooling to 0 °C, a fine white precipitate appeared, which was collected by filtration and dried in vacuo (5.3 g, 70%, 19.2 mmol). $C_{17}H_{16}N_4$: calcd. C 73.89, H 5.84, N 20.27; found C 73.94, H 5.97, N 20.03. M.p. 92−94 °C. FDI-MS: m/z = 276 [M^+]. ^1H NMR ($CDCl_3$, 300 MHz): δ = 4.99 (s, 4 H, $-CH_2-$), 6.47−6.61 (m, 2 H, ArH), 7.11−7.15 (m, 2 H, ArH), 7.22−7.25 (m, 2 H, ArH), 7.34−7.40 (m, 1 H, ArH), 7.55−7.60 (m, 2 H, ArH), 8.18 (d, 1 H, ArH), 8.54 (d, 2 H, ArH). ^{13}C NMR ($CDCl_3$, 75 MHz): δ = 54.1, 106.1, 112.7, 121.1, 122.0, 136.6, 137.5, 148.0, 149.4, 158.1, 158.7. IR (KBr): $\tilde{\nu}$ = 3046 (w), 3006 (w), 2964 (w), 2924 (w), 2924 (w), 2362 (w), 2338 (w), 1965 (w), 1916 (w), 1867 (w), 1843 (w), 1831 (w), 1768 (w), 1736 (w), 1719 (w), 1701 (w), 1596 (m), 1564 (m), 1492 (m), 1434 (m), 1391 (w), 1351 (m), 1283 (w), 1241 (w), 1180 (w), 1152 (w), 1094 (w), 1069 (w), 1047 (w),

976 (w), 938 (w), 884 (w), 848 (w), 779 (w), 753 (m), 664 (w), 635 (w), 615 (w), 589 (w), 568 (w), 545 cm^{-1} (w).

$[Cu(L1)_2(CH_3OH)_2](ClO_4)_2$ (1a): To a solution of **L1** (0.1 g, 0.38 mmol) in methanol (3 mL) was added a solution of $Cu(ClO_4)_2 \cdot 6H_2O$ (0.071 g, 0.19 mmol) in methanol (3 mL). Diethyl ether (100 mL) was then added, which led to the deposition of a fine blue precipitate. The mixture was stirred for a few minutes and then filtered. Dark-blue block-shaped crystals suitable for X-ray analysis were grown by slow evaporation of the solvents from a solution in aqueous methanol.

$[Cu(L1)_2(H_2O)_2](ClO_4)_2 \cdot 2DMF$ (1b): To a solution of **L1** (0.1 g, 0.38 mmol) in methanol (3 mL) was added a solution of $Cu(ClO_4)_2 \cdot 6H_2O$ (0.071 g, 0.19 mmol) in methanol (3 mL). Diethyl ether (100 mL) was then added, which led to the deposition of a fine blue precipitate. The mixture was stirred for a few minutes and then filtered. The precipitate was collected by filtration to give the crude product as a light-blue solid (0.135 g, 86%). Dark-blue block-shaped crystals suitable for X-ray analysis were grown by vapour diffusion of diethyl ether into a solution in DMF. $C_{32}H_{32}N_8Cu Cl_2O_{10}$: calcd. C 46.70, H 3.92, N 13.61; found C 46.49, H 3.83, N 13.36. UV/Vis [CH_3CN; λ_{max}, nm (ε, M^{-1} cm^{-1})]: 210 (8970), 250 (8847), 294 (8048), 410 (109), 656 (79).

$[Cu_3(L1)_2(DMF)_2Cl_6]$ (1c): Ligand **L1** (0.10 g, 0.38 mmol) in DMF and $CuCl_2 \cdot 2H_2O$ (0.065 g, 0.38 mmol) in DMF (2 mL) were combined. Diethyl ether was then slowly allowed to diffuse into the resulting solution of **1c**. After a few days, blue/green block-shaped crystals of **1c** were formed.

$[Cu(L1)Cl_2]_n$ (1d): To a solution of **L1** (0.1 g, 0.38 mmol) in acetonitrile (3 mL) was added a solution of $CuCl_2 \cdot 2H_2O$ (0.066 g, 0.38 mmol) in methanol (5 mL). The mixture was stirred for a few minutes and then filtered. Crystals suitable for X-ray analysis formed soon thereafter (0.65 g, 50%).

$[Cu(L2)Cl]ClO_4$ (2a): To a solution of **L2** (0.1 g, 0.36 mmol) in methanol (10 mL) was added a solution of $Cu(ClO_4)_2 \cdot 6H_2O$ (0.067 g, 0.18 mmol) and $CuCl_2 \cdot 2H_2O$ (0.036 g, 0.18 mmol) in methanol (5 mL). The mixture was stirred for a few minutes and then filtered. Diethyl ether (100 mL) was quickly added to the filtrate, which led to the deposition of a sky-blue precipitate. This precipitate was collected by filtration and dried in vacuo to yield a light-green solid (0.16 g, 90%, 0.33 mmol). Crystals suitable for X-ray analysis were grown by vapour diffusion of diethyl ether into a solution in DMF. $C_{17}H_{16}N_4CuCl_2O_4$: calcd. C 43.01, H 3.82, N 11.80; found C 43.04, H 3.43, N 11.64. UV/Vis [CH_3CN, (ε, M^{-1} cm^{-1})]: λ_{max} = 214 (14372), 260 (20809), 366 (417), 708 nm (125).

$[Cu(L2)Cl_2]$ (2b): To a solution of **L2** (0.1 g, 0.36 mmol) in methanol (10 mL) was added a solution of $CuCl_2 \cdot 2H_2O$ (0.062 g, 0.36 mmol) in methanol (5 mL). The mixture was stirred for a few minutes and then filtered. Diethyl ether (100 mL) was quickly added to the filtrate, which led to the deposition of a green precipitate. This precipitate was collected by filtration and dried in vacuo to yield a light-green solid (0.13 g, 86%, 0.31 mmol). Crystals suitable for X-ray analysis were grown from methanol/water (2:1; 10 mL). $C_{17}H_{16}N_4CuCl_2$: calcd. C 49.71, H 4.42, N 13.64; found C 49.87, H 4.15, N 13.50. UV/Vis [CH_3CN (ε, M^{-1} cm^{-1})]: λ_{max} = 212 (12735), 228 (11593), 260 (12801), 800 nm (320).

X-ray Crystallographic Study: Crystal data and experimental conditions are listed in Table 1. Selected bond lengths and bond angles with standard deviations in parentheses are presented in Table 2. Intensity data were collected on a Siemens SMART 1000 CCD diffractometer using graphite-monochromated Mo-K_α radiation (λ = 0.71073 Å). Exposure times were 10 s per frame for **L1**, **1a**, **1b**, and **1c** and 20 s per frame for **1d**, **2a**, and **2b**, collected using the ω-scan technique (Δω = 0.45° for **L1**, **1a**, **1b**, and **1c** and 0.4° for **1d**, **2a**, and **2b**). The collected reflections were corrected for Lorentz, polarization, and absorption effects. The structures were solved by direct methods and refined by full-matrix least-squares methods on F^2.[42–44]

Crystallographic data (excluding structure factors) for the structures reported in this paper have been deposited with the Cambridge Crystallographic Data Centre as supplementary publication nos. CCDC-167124–167130. Copies of the data can be obtained free of charge on application to the CCDC, 12 Union Road, Cambridge CB2 1EZ, U.K. [Fax: (internat.) +44 (0)1223 336033; E-mail: deposit@ccdc.cam.ac.uk].

Acknowledgments

The authors gratefully acknowledge financial support from the DFG (S. Schindler) and the DAAD (S. P. Foxon), and Prof. Rudi van Eldik (University of Erlangen-Nürnberg) for his support of this work.

[1] K. D. Karlin, A. D. Zuberbühler, in *Bioinorganic Catalysis*, 2nd Edition (Eds.: J. Reedijk, E. Bouwman), Marcel Dekker, New York, **1999**, pp. 469–534.
[2] S. Fox, K. D. Karlin, in *Active Oxygen in Biochemistry* (Eds.: J. S. Valentine, C. S. Foote, A. Greenberg, J. F. Liebman), Blackie Academic and Professional, Chapman & Hall, Glasgow, **1995**, pp. 188–231.
[3] W. Kaim, J. Rall, *Angew. Chem.* **1996**, *108*, 47–64; *Angew. Chem. Int. Ed. Engl.* **1996**, *35*, 43–60.
[4] N. Kitajima, *Adv. Inorg. Chem.* **1992**, *39*, 1–77.
[5] N. Kitajima, Y. Moro-oka, *Chem. Rev.* **1994**, *94*, 737–757.
[6] K. D. Karlin, Z. Tyeklár (Eds.), *Bioinorganic Chemistry of Copper*, Chapman & Hall, New York, **1993**.
[7] E. I. Solomon, U. M. Sundaram, T. E. Machonkin, *Chem. Rev.* **1996**, *96*, 2563–2605.
[8] K. A. Magnus, H. Ton-That, J. E. Carpenter, *Chem. Rev.* **1994**, *94*, 727–735.
[9] M. E. Cuff, K. I. Miller, K. E. van Holde, W. A. Hendrickson, *J. Mol. Biol.* **1998**, *278*, 855–870.
[10] H. Decker, R. Dillinger, F. Tuczek, *Angew. Chem. Int. Ed.* **2000**, *39*, 1591–1595.
[11] J. P. Klinman, *Chem. Rev.* **1996**, *96*, 2541–2561.
[12] E. Spodine, J. Manzur, *Coord. Chem. Rev.* **1992**, *119*, 171–198.
[13] H.-C. Liang, M. Dahan, K. D. Karlin, *Curr. Opin. Chem. Biol.* **1999**, *3(2)*, 168–175.
[14] K. D. Karlin, *Science* **1993**, *261*, 701–708.
[15] A. G. Blackman, W. B. Tolman, in *Structure & Bonding: Metal-Oxo and Metal-Peroxo Species in Catalytic Oxidations* (Ed.: B. Meunier), Springer, Berlin, **2000**, vol. 97, pp. 179–211.
[16] S. Schindler, *Eur. J. Inorg. Chem.* **2000**, 2311–2326.
[17] R. R. Jacobson, Z. Tyeklár, A. Farooq, K. D. Karlin, S. Liu, J. Zubieta, *J. Am. Chem. Soc.* **1988**, *110*, 3690–3692.
[18] Z. Tyeklár, R. R. Jakobson, N. Wei, N. N. Murthy, J. Zubieta, K. D. Karlin, *J. Am. Chem. Soc.* **1993**, *115*, 2677–2689.
[19] M. J. Baldwin, P. K. Ross, J. E. Pate, Z. Tyeklár, K. D. Karlin, E. I. Solomon, *J. Am. Chem. Soc.* **1991**, *113*, 8671–8679.
[20] K. D. Karlin, N. Wei, B. Jung, S. Kaderli, P. Niklaus, A. D. Zuberbühler, *J. Am. Chem. Soc.* **1993**, *115*, 9506–9514.
[21] K. D. Karlin, S. Kaderli, A. D. Zuberbühler, *Acc. Chem. Res.* **1997**, *30*, 139–147.
[22] K. D. Karlin, D.-H. Lee, S. Kaderli, A. D. Zuberbühler, *Chem. Commun.* **1997**, 475–476.
[23] M. Schatz, M. Becker, F. Thaler, F. Hampel, S. Schindler, R.

R. Jacobsen, Z. Tyeklár, N. N. Murthy, P. Ghosh, Q. Chen, J. Zubieta, K. D. Karlin, *Inorg. Chem.* **2001**, *40*, 2312−2322.
[24] J. P. Wibaut, G. L. La Bastide, *Recl. Trav. Chim. Pays-Bas* **1933**, *52*, 493−498.
[25] W. Yang, L. Chen, S. Wang, *Inorg. Chem.* **2001**, *40*, 507−515.
[26] W. Yang, H. Schmider, Q. Wu, Y. Zhang, S. Wang, *Inorg. Chem.* **2000**, *39*, 2397−2404.
[27] C. J. Boxwell, P. H. Walton, *Chem. Commun.* **1999**, 1647−1648.
[28] J. M. Rowland, M. M. Olmstead, P. K. Mascharak, *Inorg. Chem.* **2000**, *39*, 5326−5332.
[29] F. H. Allen, J. E. Davies, J. J. Galloy, O. Johnson, O. Kennard, C. F. Macrae, E. M. Mitchell, G. F. Mitchell, D. G. Watson, *J. Chem. Inf. Comput. Sci.* **1991**, *31*, 187−204.
[30] P. A. Anderson, F. R. Keene, J. M. Gulbis, E. R. T. Tiekink, *Z. Kristall.* **1993**, *206*, 275−278.
[31] D. Boys, C. Escobar, W. Zamudio, *Acta Crystallogr., Sect. C* **1992**, *48*, 1118−1120.
[32] P. L. Dedert, J. S. Thompson, J. A. Ibers, T. M. Marks, *Inorg. Chem.* **1982**, *21*, 969−977.
[33] P. L. Dedert, T. Sorrell, J. A. Ibers, T. M. Marks, *Inorg. Chem.* **1982**, *21*, 3506−3517.
[34] A. W. Addison, T. N. Rao, J. Reedijk, J. van Rijn, G. C. Verschoor, *J. Chem. Soc., Dalton Trans.* **1984**, 1349−1356.
[35] H. J. Hoorn, P. de Joode, W. L. Driessen, J. Reedijk, *Recl. Trav. Chim. Pays-Bas* **1996**, *115*, 191−197.
[36] M. Palaniandavar, R. J. Butcher, A. W. Addison, *Inorg. Chem.* **1996**, *35*, 467−471.
[37] M. Palaniandavar, S. Mahadevan, M. Köckerling, G. Henkel, *J. Chem. Soc., Dalton Trans.* **2000**, 1151−1154.
[38] C. Cox, D. Ferraris, N. N. Murthy, T. Lectka, *J. Am. Chem. Soc.* **1996**, *118*, 5332−5333.
[39] N. Niklas, O. Walter, R. Alsfasser, *Eur. J. Inorg. Chem.* **2000**, 1723−1731.
[40] G. J. Kubas, B. Monzyk, A. L. Crumbliss, *Inorg. Synth.* **1979**, *19*, 90−92.
[41] P. Lühring, A. Schumpe, *J. Chem. Eng. Data* **1989**, *34*, 250−252.
[42] *Siemens Area Detector Absorption Correction, Siemens.*
[43] G. M. Sheldrick, *SHELX-97*, Universität Göttingen, **1997**.
[44] L. Zsolnai, *XPMA, ZORTEP*, Universität Heidelberg, **1997**.

Received July 24, 2001
[I01276]

Novel Chiral Metallocenophanes Derived from [2.2]Paracyclophane and Their Use in Olefin Polymerization[‡]

Henning Hopf,*[a] Sethuraman Sankararaman,[b] Ina Dix,[a] Peter G. Jones,[c] Helmut G. Alt,*[d] and Andrea Licht[d]

Keywords: Metallocenophanes / Planar chirality / Fulvenes / Metallacycles / Olefin polymerization

The 4-fulvenyl[2.2]paracyclophane (**1**) was transformed, by treatment with lithium aluminium hydride and methyllithium in tetrahydrofuran, to the corresponding cyclopentadienyl anions **6** and **8**, respectively. The iron complex **7** was prepared from **6**, while **8** was converted into the metal complexes **9** (Fe complex), **10** (Ti), **11** (Zr), **12** (Ti), and **13** (Zr). All new metallocene complexes were characterized by their spectroscopic data. In addition, a single crystal X-ray crystallographic analysis was performed for complex **11**. The metallacyclic zirconocene complex **15** was synthesized by the reaction of the dichloride derivative **13** with two equivalents of *n*-butyllithium. After activation of complexes **10**–**13** and **15** with methylalumoxane (MAO) they were used for the catalytic polymerization of ethene and propene.

Introduction

Chiral metallocene complexes are important reagents and catalysts in stereoselective synthesis of organic fine chemicals and polymers.[2] In principle, chirality may be generated in a metallocene moiety by the introduction of both achiral and chiral substituents. Whereas in the latter case the resulting metallocene unit necessarily has to be chiral, the former case is more complex. Chirality, and especially the resolution of the enantiomers of the substituted metallocene complexes, now depends on various factors, including the height of the rotational barrier and the substitution pattern. For example, a metallocene complex carrying two achiral, non-identical substituents in one cyclopentadienyl ring will always be chiral and in principle resolvable, regardless of the barrier of rotation of the five-membered rings. Placing one substituent in either ring, however, does not necessarily induce chirality. Provided the rotational barrier of this derivative is sufficiently low, one conformation having a plane of symmetry is always accessible and the metallocene complex is hence unresolvable. One of the most widely used ways of reducing conformational mobility in metallocene complexes consists of the introduction of a molecular bridge between the two "decks" of the metal organic compound.[3,4] As far as chiral substituents are concerned, we are interested in combining molecules with a chiral plane, in particular monosubstituted [2.2]paracyclophanes, with a metallocene. Because of the rigidity of the molecular framework, these cyclophanes are always chiral, regardless of the type of the substituent and its position in these bridged aromatic compounds. By condensing 1,3-cyclopentadiene and indene with 4-formyl-[2.2]paracyclophane, i.e. applying the Thiele fulvene synthesis to this aldehyde, we have recently been able to prepare a number of fulvenyl paracyclophanes.[5] In the present paper we describe the preparation of ferrocene, zirconocene, and titanocene complexes of these new chiral ligands, and we report on first polymerization experiments in which these metal complexes (in racemic form) were used as catalysts for the polymerization of olefins (ethene, propene).

Results and Discussion

Stereochemistry of Addition of Methyllithium to 4-(6-Fulvenyl)[2.2]paracyclophane (1)

The formation of cyclopentadienyl anions by addition of organolithium reagents to the 6-position of fulvenes is a

[‡] Metallocenophanes, XI. – Part X: Ref.[1]
[a] Institut für Organische Chemie, Technische Universität Braunschweig,
Hagenring 30, 38106 Braunschweig, Germany
Fax: (internat.) + 49-(0)531/391-5388
E-mail: h.hopf@tu-bs.de
[b] Department of Chemistry, Indian Institute of Technology, Madras 600036, India
Fax: (internat.) + 91-44/235-0509
E-Mail: sanka@acer.iitm.ernet.in
[c] Institut für Anorganische und Analytische Chemie, Technische Universität Braunschweig,
Postfach 3329, 38023 Braunschweig, Germany
Fax: (internat.) + 49-(0)531/391-5387
E-mail: jones@xray36.anchem.nat.tu-bs.de
[d] Laboratorium für Anorganische Chemie, Universität Bayreuth
Universitätsstrasse 30, NW I, 95440 Bayreuth, Germany
Fax: (internat.) + 49-(0)921/55-2157
E-mail: helmut.alt@uni-bayreuth.de

 © WILEY-VCH Verlag GmbH, 69451 Weinheim, Germany, 2002 1434–1948/02/0101–0123 $ 17.50+.50/0

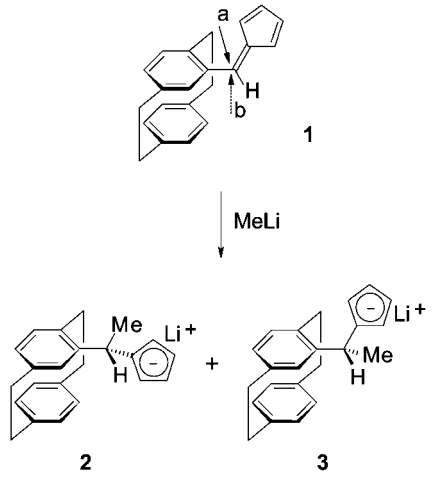

Scheme 1. Stereochemistry of addition of methyllithium to the fulvene **1**

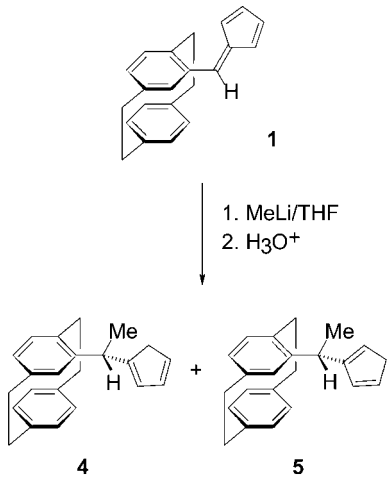

Scheme 2. Addition of methyllithium to the fulvene **1**

well-known process for generating these species, which are necessary for subsequent metallocene formation.[6,7] To investigate the stereochemistry of this process we selected the fulvene derivative **1** (Scheme 1), which is easily available in gram quantities.[5]

Unlike in the 4-formyl and 4-acetyl derivatives of [2.2]paracyclophane,[8] the conformation of the substituent in 4-fulvenyl[2.2]paracyclophane (**1**) is rigid. In our earlier studies we had shown by NMR spectroscopy and X-ray crystal structure analysis[5] that the most stable conformation of **1** in solution and in the solid state is the one in which the proton at C-6 of the fulvene ring is located in the intraannular space of the cyclophane part of the hydrocarbon, the bulky cyclopentadienyl unit pointing towards the exterior. The barrier for rotation around the C−C bond connecting the cyclophane residue and the fulvene unit is high (26 kcal·mol^{-1}). Addition of methyllithium to **1** at C-6 to provide the corresponding cyclopentadienyl anion led to the generation of a new chiral centre, and in principle a pair of diastereomeric cyclopentadienides (**2** and **3**) could be obtained, depending on the approach of the nucleophile as shown by pathways **a** and **b** in Scheme 1. However, in the former pathway the methyllithium approaches from the exterior of the cyclophane unit and it is sterically less hindered compared to pathway **b**. In this latter trajectory the approach of the metal organic reagent is sterically demanding because of hindrance by the bridge hydrogen atoms and also the unsubstituted aromatic ring of the phane unit. Both these effects essentially block one face of the C-6 position of the fulvene substituent. The approach of methyllithium via pathway **a** should hence be preferred, leading to the formation of a single diastereomer of the cyclopentadienide.

In order to verify this hypothesis, we added methyllithium to the racemic mixture of **1** and subsequently quenched the reaction mixture with acid. Careful analysis of the high-resolution ^{1}H and ^{13}C NMR spectra clearly indicated the formation of two isomeric products **4** and **5** in a nearly 2:1 ratio (Scheme 2), each one as a single diastereomer. In the ^{1}H NMR spectrum of the mixture of **4** and **5** the methine proton (C*H*−CH_3) appeared as overlapping quadruplets at δ_H = 3.90 and 3.87 (J = 7.1 Hz) and the methyl protons as a single doublet at δ = 1.23 (J = 7.1 Hz). In the corresponding ^{13}C NMR spectrum the methine carbon atom was registered at δ_C = 38.0 and 37.43 and the methyl carbon atom at δ_C = 23.59 and 22.92. The methylene carbon atom of the cyclopentadiene ring appeared at δ_C = 42.77 and 41.12.

Thus, we conclude that the addition of methyllithium to fulvene **1** is highly stereoselective in that the methyl group approaches from the less hindered face of the fulvene (pathway **a** in Scheme 1), leading to the formation of a single diastereomer of the cyclopentadienyl anion. This diastereomer is a crucial intermediate en route to the metallocenes. This argument is further substantiated by the X-ray crystal structure of the zirconocene dichloride **11** (to be discussed below) that clearly reveals the stereochemistry of the newly generated chiral center upon addition of methyllithium. It should be mentioned that the diastereoselectivity of the addition of organometallic reagents to the 4-formyl- and 4-acetyl derivatives of [2.2]paracyclophane is poor because of the high conformational mobility of these functional groups in comparison to the fulvenyl substituent.[7]

Synthesis of Metallocenes

The ferrocene derivatives **7** and **9** were prepared by reaction of the corresponding lithium cyclopentadienides **6** and **8**, respectively, with $FeCl_2$ in anhydrous tetrahydrofuran (Scheme 3). In both complexes the proton resonance signals corresponding to the cyclopentadienyl ring appeared between δ = 4.0−4.5 in the ^{1}H NMR spectra (Cp_2Fe: δ_H = 4.0−4.2). In the ^{13}C NMR spectra the corresponding carbon atoms were registered in the range δ_C = 65−70 (Cp_2Fe: δ_C = 65−67). Further, it is also evident from the NMR spectra that both **7** and **9** were produced as a 1:1 mixture of diastereomers. In the ^{1}H NMR spectrum of **9** the methyl

groups produced two overlapping doublets (δ_H = 1.52 and 1.50). In the ^{13}C NMR spectrum of both compounds two sets of signals for each carbon atom were present indicating the formation of two isomers. Finally, in the mass spectra of these ferrocene derivatives the molecular ion peak appeared as the base peak, corresponding to the generation of the respective ferrocenium ions of **7** and **9**.

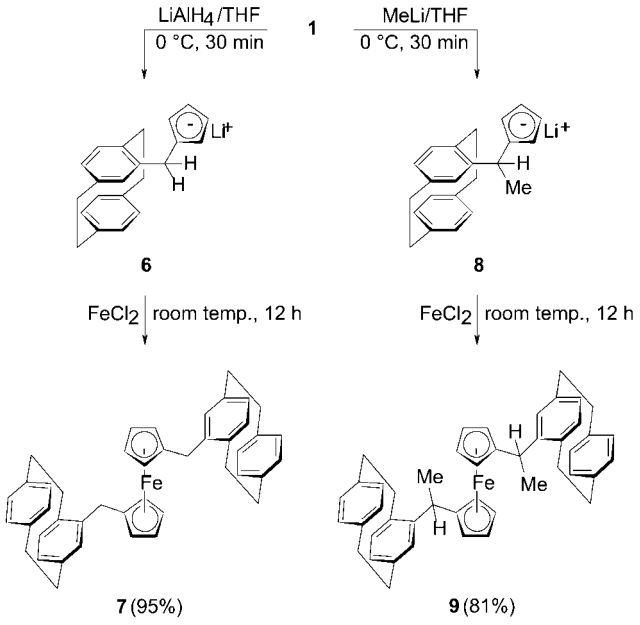

Scheme 3. Synthesis of the ferrocenes **7** and **9** from the fulvene **1**

The metallocene dichloride derivatives **10** and **11** were synthesized by reaction of the lithium cyclopentadienide **8** with $TiCl_4$ and $ZrCl_4$, respectively, as shown in Scheme 4. Both **10** and **11** were obtained as a 1:1 mixture of two diastereomers, as evident from the ^1H and ^{13}C NMR spectra. In the case of **10** the methine proton (C*H*−CH_3) appeared as overlapping quadruplets for the two diastereoisomers at δ = 4.52 and 4.56, and the methyl protons at δ_H = 1.35 and 1.31, each as a well-resolved doublet (J = 6.9 Hz).

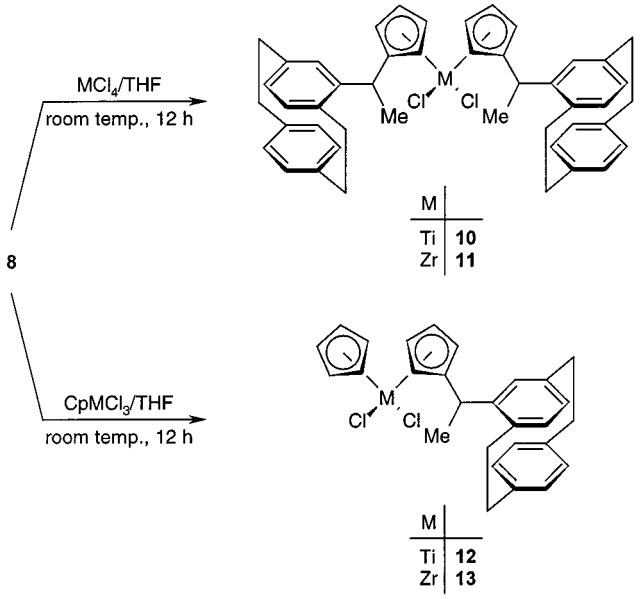

Scheme 4. Synthesis of metallocene dichlorides from the fulvene **1**

The cyclopentadienyl protons were registered in the same region as the aromatic protons of the cyclophane unit between δ = 6.0 and 7.0. (Cp_2TiCl_2, δ_H = 6.59). However, in the ^{13}C NMR spectrum of **10** the carbon signals corresponding to the cyclopentadienyl unit appeared at lower δ_C values in the region of 110 to 120, in contrast to the aromatic carbon atoms, which absorbed above δ = 130. Similarly, in the case of **11** the methine proton (C*H*−CH_3) appeared as overlapping quadruplets at δ_H = 4.48 and 4.46 and the methyl protons at δ_H = 1.44 and 1.42 as two overlapping doublets (J = 6.8 Hz). In the mass spectra of **10** and **11** the molecular ions generate a cluster of peaks due to the isotopes of chlorine and the metal atom. The intensities of these peaks matched with the calculated values based on the natural isotopic abundances of chlorine and the metal atom. Finally, the structure of the zirconocene dichloride **11** was confirmed by single crystal X-ray crystallographic analysis as shown in Figure 1.

Compound **11** crystallizes with two independent half molecules and two molecules of deuteriochloroform in the asymmetric unit. The two half molecules are completed by the operation of a twofold axis. The centrosymmetric space group *Pbcn* only allows the determination of the relative configuration of the two diastereomeric molecules; both showing the same relative configuration (4*R*,17*S*). The angles between the cyclopentadiene units in the molecules amount to 54.42(11)° (C19 to C23) and 56.69(10)° (C19′ to C23′). To minimize the electronic repulsion of the π-systems, the angles between the four coplanar carbon atoms in the [2.2]paracyclophane units and the cyclopentadiene units are 78.29(10)° (C4/C5/C7/C8 to C19−C23) and 70.75(10)° (C4′/C5′/C7′/C8′ to C19′−C23′), corresponding to an approximately perpendicular arrangement. The zirconium atoms show a distorted tetrahedral coordination involving the two chlorine atoms and the centroids of the π-cyclopentadienyl units. The Zr−C bonding to the cyclopentadienyl moieties can be described as pentahapto coordinated, since the distances between the metal atoms and the coordinated carbons atoms deviate from each other negligibly: 2.483(3) to 2.561(3) Å (C19 to C23) and 2.477(3) to 2.578(3) Å (C19′ to C23′). The average Zr−C distance amounts to 2.515 Å for Zr and 2.518 Å for Zr′ and is in good agreement with the vapor-phase electron-diffraction study of the (π-$C_5H_5)_2ZrCl_2$ molecule:[9] 2.522(5) Å. The centroids of the cyclopentadienyl rings are separated from the heavy atoms by 2.209 Å (Zr) and 2.214 Å (Zr′). The Zr−Cl bond lengths of 2.442(1) (Zr−Cl) and 2.444(8) Å (Zr′−Cl′) are very close to the sum of Pauling radii (2.44 Å)[10] and correspond to the values found in other zirconium complexes with coordinated cyclopentadienyl groups.[11,12] The Cl−Zr−Cl angles of 95.9(4) (Zr) and 95.8(4)° (Zr′) are somewhat less than the 97.1° for (π-$C_5H_5)_2ZrCl_2$.[11]

The ordered deuteriochloroform molecule C99−Cl99 is stabilized by Cl···Cl interactions in the range of the double

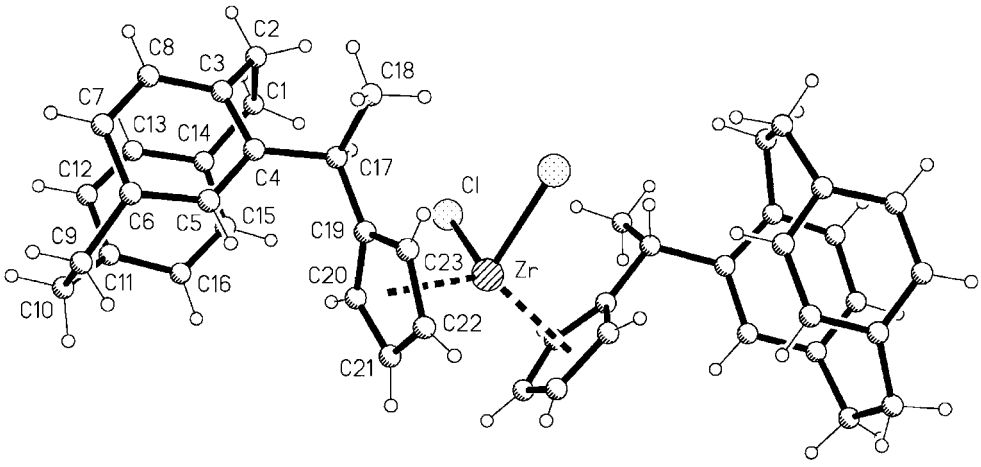

Figure 1. The structure of one independent molecule of **11** in the crystal; radii are arbitrary

van-der-Waals radius. This molecule connects the two independent zirconocenes to another via two chlorine atoms and interacts via the third chlorine atom with the other solvent molecule: Cl′···Cl99 3.633(1) Å, Cl···Cl98 3.518(1) Å, Cl97···Cl94 3.654(7) Å.

The mixed ligand metallocene dichloride derivatives **12** and **13** were prepared by metathetic reaction of **8** with $CpTiCl_3$ and $CpZrCl_3$, respectively, in anhydrous tetrahydrofuran (Scheme 4). Both **12** and **13** formed as single diastereomers, as evident from the ^1H and ^{13}C NMR spectroscopic data. For example, the methine proton of **12** appeared as a quadruplet at $\delta_H = 4.54$ and the methyl protons absorbed as a doublet at $\delta_H = 1.30$ ($J = 7.0$ Hz). Analogously, in the case of **13** the methine proton was registered as a quadruplet $\delta_H = 4.40$ and the methyl protons appeared as a doublet at $\delta_H = 1.35$ ($J = 7.0$ Hz). In both complexes **12** and **13** the unsubstituted cyclopentadienyl ligand protons are represented by a sharp singlet at $\delta = 6.61$ and 6.52, respectively (for five proton integration) in the ^1H NMR spectra. In the ^{13}C NMR spectra the corresponding carbon atoms appear as a single resonance line at $\delta = 119.9$ and 115.8, respectively, indicating free rotation of the cyclopentadienyl ligand in these complexes.

Synthesis of a Metallacyclic Zirconocene Complex by Using a CH Bond Activation Reaction

The metallocene dichloride complex **13** is well suited as a starting material for the synthesis of metallacyclic complexes. Only a single reaction product was obtained when **13** was treated with two equivalents of *n*-butyllithium in toluene. The key reaction step in this transformation is a CH bond activation that led to cyclometallation as shown in Scheme 5.

During this reaction a zirconocene dibutyl complex **14**,[13] which was stable in solution at low temperatures (−40 °C) for several minutes, was formed as an intermediate. The unsubstituted parent compound of this complex was characterized using NMR spectroscopy.[14]

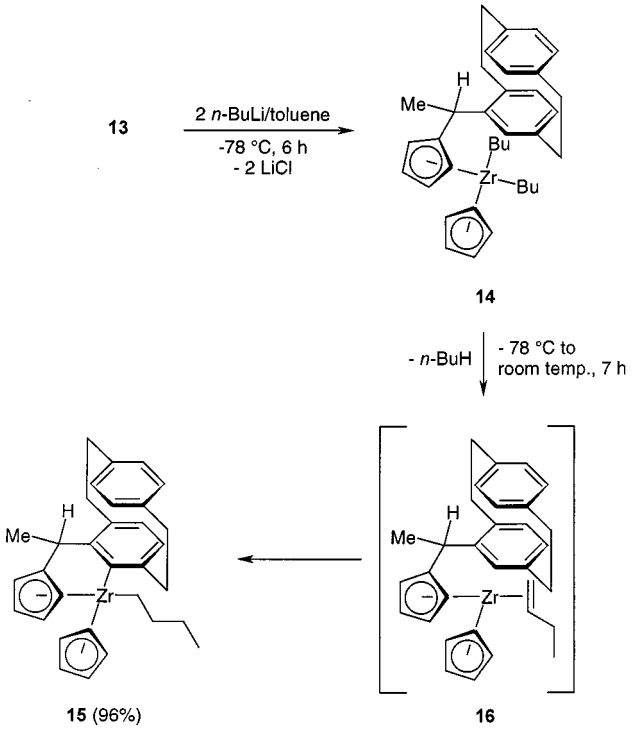

Scheme 5. Synthesis of the metallacyclic complex **15** from the metallocene dichloride complex **13**

Subsequently, **14** is proposed to lose *n*-butane[15,16] in a β-H transfer reaction, resulting in the formation of a reactive (η^2-butene) complex, **16**. "$Cp_2Zr(\eta^2$-butene)", generated as an intermediate during the reaction of Cp_2ZrCl_2 with two equivalents of *n*-butyllithium, has been stabilized with trimethylphosphane and characterized.[17−19] One phenyl moiety of the [2.2]paracyclophane group of **16** shown in Scheme 5 then reacted further to yield the corresponding metallacycle **15** by a CH bond activation and hydrogen transfer reaction.[20] The proposed structure of metallacycle **15** is based on comparison with similar

phenylalkyl-substituted zirconocene complexes[21] and the steric situation at the cyclophane moiety. Within the reaction pathway only one isomer is formed (see NMR spectroscopic data) that can have either (*R*) or (*S*) configuration at the 1,1-ethylidene bridge.

Polymerization Experiments

The resultant metallocene complexes are precursors for homogeneous ethylene and propylene polymerization. The complexes are activated by adding a 3000-fold molar excess of MAO. The formation of an active catalyst system is indicated by a colour change.

a) Ethylene Polymerization

The polymerization activities of the activated metallocene complexes, the number average of the molecular weight M_n, the weight average M_w, the centrifuge average M_z, the viscosity average M_η, and the polydispersity D of the resulting polyethylenes are listed in Table 1.

Table 1. Overview of the ethylene polymerization experiments and polymer analytical results. High temperature gel permeation chromatography (HT-GPC): M_n = number average of the molecular weight (kg/mol), M_w = weight average of the molecular weight (kg/mol), M_z = centrifuge average of the molecular weight (kg/mol), M_η = viscosity average of the molecular weight (kg/mol), D = polydispersity ($D = M_w/M_n$)

Metallocene complex	Activity [g PE / g M / h] M = Ti, Zr	Fouling	HT-GPC M_n M_w M_z M_η D
10 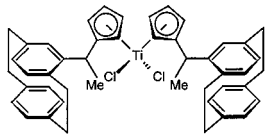	96000	middle	1350 17590 395510 9770 13.0
11 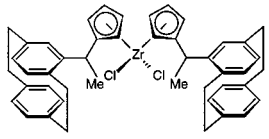	562400	middle	370 4580 230360 2480 12.2
12 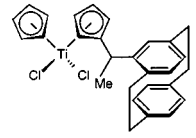	36200	low	280 2570 39530 1630 9.1
13 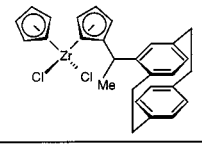	1442000	low	290 1490 8590 1220 5.2
15 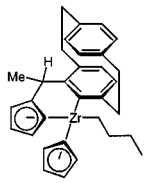	310000	low	370 3240 292010 3240 8.8

The central metal has a strong influence on the polymerization behaviour of the metallocene complexes;[21] in both bis[(paracyclophanyl)ethylcyclopentadienyl]metallocene and [(paracyclophanyl)ethylcyclopentadienyl]-(cyclopentadienyl)metallocene complexes, the zirconium complexes $(Cp')_2ZrCl_2$ (**11**) and $Cp'CpZrCl_2$ (**13**) are much more active than the corresponding titanium complexes $(Cp')_2TiCl_2$ (**10**) and $Cp'CpTiCl_2$ (**12**). The reason for this effect is the lower thermal stability of the titanium analogues.[22]

The bulky paracyclophanyl moiety exerts two different influences on the active metal centre. On the one hand, steric crowding can have a stabilizing effect on sensitive metal centres, as in the case of the titanium complexes.[23] Therefore, the productivity of $(Cp')_2TiCl_2$ (**10**) containing two bulky moieties is higher than that of $Cp'CpTiCl_2$ (**12**) containing only one bulky group, despite the stronger blockage of the active metal centre.

On the other hand, steric crowding lowers the productivity, as in the case of the zirconium complexes. The productivity of $(Cp')_2ZrCl_2$ (**11**) is much lower than that of $Cp'CpZrCl_2$ (**13**). Similarly, steric overloading is responsible for the lower productivity of the metallacyclic zirconium complex **15** compared to the corresponding precursor **13**. After activation of the metallacycle with MAO, the ring could be expanded during the polymerization process by repeated ethylene insertion into the metal−carbon σ bond of the metallacycle.[24,25] Finally, an insoluble polymer was formed that was directly attached to one π-ligand of the active catalyst cation. The polyethylene fixed to the paracyclophanyl moiety increased the steric overloading and lowered the productivity of complex **15** significantly (Scheme 6).

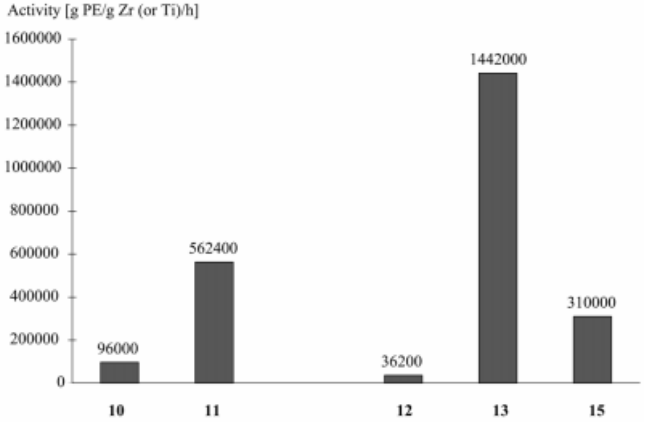

Scheme 6. Comparison of the catalytic activities of the metallocene complexes **10**−**13** and **15** for the polymerization of ethylene

This incorporation of the zirconium complex into the polymer backbone is an elegant and inexpensive way to inherently increase heterogeneity and form a supported and self-immobilizing catalyst for ethylene polymerization. As a result of the conversion, the polyolefins formed with the

heterogeneous catalysts precipitate onto the catalyst's surface and not onto internal wall surfaces, causing reactor fouling. The conversion of a homogeneous metallocene/MAO catalyst into a heterogeneous catalyst is absolutely necessary for the "slurry loop" process.

b) Propylene Polymerization

The polymerization activities of the activated metallocene complexes, the molecular weights, and the isotacticities of the resulting polypropylenes are listed in Table 2.

Table 2. Overview of the propylene polymerization experiments and polymer analytical results.

Metallocene complex	Activity [g PP / g Zr / h]	Molecular mass[a] M^+ [*m*/*z*]	Tacticity (only isotactic contribution mmmm)[b] [%]
13 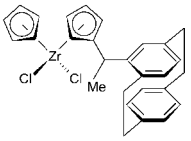	49370	Low-molecular weighted oil 952[c]	4.6
15 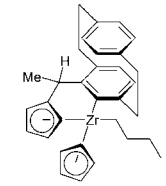	39350	Low-molecular weighted oil 953[c]	4.8

[a] Determined by mass spectrometry due to the low molecular weight. – [b] Determined by ^{13}C NMR spectroscopy (solvent 1,2,4-trichlorobenzene/1,1,2,2-tetrachlorodeuterioethane; 60° C). – [c] Highest peak in mass spectrum.

The synthesized metallocene complexes were activated with MAO; only the monosubstituted Cp′CpZrCl_2 (**13**) and the corresponding metallacycle **15** were active in the propylene polymerization with a productivity of 49370 g PP/g Zr/h (**13**) and 39350 g PP/g Zr/h (**15**). The produced polypropylenes were atactic, low-molecular weight oils with an isotactic share of only 4.6% (**13**) and 4.8% (**15**).

The comparatively low activity in propylene polymerization can be explained by the steric crowding of the active centre. The bulky paracyclophanyl group not only blocks the access of the monomer to the metal but also the growth and orientation of the polymer chain. The atactic character of the polymer is the result of random coordination of the prochiral monomer to the metal. This random coordination is probably due to the lack of a favoured configuration of the catalyst. The low-molecular weight is an indication of early termination reactions.

Experimental Section

The instrumentation used in this study has been described in the previous publications of this series.[1]

Addition of Methyllithium to Fulvene 1: Formation of 4-[1-(1-Cyclopenta-1,3-dienyl)ethyl][2.2]paracyclophane (4) and 4-[1-(2-Cyclopenta-1,3-dienyl)ethyl][2.2]paracyclophane (5): To an ice-cold solution of fulvene **1** (0.28 g, 1 mmol) in 5 mL of anhydrous THF, was added dropwise an ethereal solution of MeLi (0.65 mL of 1.6 M solution, 1.1 mmol) under N_2. The initially dark-red solution turned yellow. After 30 min of stirring, 10 mL of 1 N HCl was added and the mixture was extracted with dichloromethane. The organic layer was separated and washed with saturated brine solution and dried with anhydrous magnesium sulfate. Evaporation of the solvent yielded a yellow viscous oil (0.3 g, 100%) consisting of a mixture of compounds **4** and **5** in a 2:1 ratio (NMR analysis). – ^1H NMR ($CDCl_3$, 400 MHz): δ = 1.23 (d, *J* = 7.1 Hz, 3 H), 2.65–3.10 (m, 9 H), 3.40 (m, 1 H), 3.87 and 3.90 (overlapping quadruplets, *J* = 7.1 Hz, 1 H), 5.85 and 6.00 (broad s, 2 × 1 H), 6.10–6.30 (m, 4 H), 6.35–6.55 (m, 4 H), 6.65 (m, 1 H). – ^{13}C NMR ($CDCl_3$, 100 MHz): δ = 22.8 (q), 23.5 (q), 33.2 (t), 33.3 (t), 34.7 (t), 35.1 (t), 35.2 (t), 35.3 (t), 35.3 (t), 37.3 (d), 37.9 (d), 41.0 (t), 42.7 (t), 127.4 (d), 128.5 (d), 130.1 (d), 130.3 (d), 130.5 (d), 130.9 (d), 130.9 (d), 131.3 (d), 132.1 (s), 132.3 (d), 132.5 (d), 132.6 (d), 132.6 (d), 132.9 (d), 133.0 (d), 133.7 (d), 134.4 (d), 135.4 (d), 135.4 (d), 136.9 (s), 137.0 (s), 139.3 (s), 139.4 (s), 139.4 (s), 139.5 (s), 139.7 (s), 139.7 (s), 144.5 (s), 145.3 (s), 149.6 (s), 151.8 (s). – MS (EI, 70 eV): *m*/*z* (%) = 301 (10), 300 [M^+] (44), 196 (30), 195 (76), 181 (42), 165 (34), 155 (12), 153 (12), 142 (11), 141 (12), 128 (16), 119 (18), 104 (14), 91 (14), 86 (18), 84 (28).

Bis[(4-[2.2]paracyclophanyl)methylcyclopentadienyl]iron(II) (7): To an ice-cold, stirred solution of fulvene **1** (0.57 g, 2 mmol) in 20 mL of anhydrous THF, was added $LiAlH_4$ (76 mg, 2 mmol) under N_2. The initially dark-red solution turned yellow. After stirring for 30 min at 0 °C the solution was added dropwise with a syringe to a stirred, ice-cold slurry of $FeCl_2$ (130 mg, 1 mmol) in 20 mL of anhydrous THF. After the addition was complete the solution was warmed to room temp. and stirred overnight. The reaction was quenched by dropwise addition of 20 mL of 1 N HCl. The organic layer was separated and the aqueous layer was extracted with dichloromethane (2 × 20 mL). The combined organic layers were washed with water (20 mL) and dried ($MgSO_4$). Removal of the solvent yielded a brownish yellow solid (0.6 g, 95%) that was purified for analytical purposes by column chromatography on silica gel with pentane and dichloromethane (1:1, v/v) to yield ferrocene **7** as a bright yellow solid, m.p. 196–200 °C- IR (KBr): $\tilde{\nu}$ = 2924 cm^{-1}, 2851, 1593, 1412, 716, 502. – UV/Vis ($CHCl_3$): λ_{max} (log ε) = 266 nm (3.87), 300 (3.27), 314 (3.12). – ^1H NMR ($CDCl_3$, 400 MHz): δ = 2.80 (m, 2 H), 2.93 (m, 2 H), 2.98–3.25 (m, 12 H), 3.34 (m, 2 H), 3.51 (m, 2 H), 3.89 (broad s, 4 H), 3.95 (broad s, 4 H), 6.00 (s, 2 H), 6.36 (m, 2 H), 6.40 (m, 4 H), 6.46 (m, 2 H), 6.52 (m, 2 H), 6.68 (m, 2 H). – ^{13}C NMR ($CDCl_3$, 100 MHz): δ = 33.5 (t), 33.9 (t), 34.0 (t), 34.2 (t), 35.0 (t), 35.3 (t), 67.9 (d), 68.1 (d), 69.1 (d), 69.6 (d), 69.8 (d), 87.5 (s), 128.5 (d), 128.6 (d), 130.5 (d), 132.2 (d), 132.2 (d), 133.1 (d), 133.2 (d), 134.5 (d), 134.7 (d), 134.7 (d), 137.3 (s), 137.3 (s), 139.3 (s), 139.5 (s), 139.6 (s), 140.4 (s), 140.5 (s). – MS (EI, 70 eV): *m*/*z* (%) = 627 (50), 626 [M^+] (100), 522 (16), 521 (10), 405 (12), 342 (16), 341 (16), 340 (26), 300 (14), 237 (12), 181 (20), 180 (22), 179 (56), 164 (20), 104 (18). – HMRS: *m*/*z* calcd. for $C_{44}H_{42}Fe$: 626.2636; found 626.2627. – $C_{44}H_{42}Fe$ (626.3): calcd. C 84.31, H 6.76; found C 84.34, H 6.69.

Bis[1-(4-[2.2]paracyclophanyl)ethylcyclopentadienyl]iron (II) (9): To an ice-cold, stirred solution of fulvene **1** (0.57 g, 2 mmol) in 20 mL of anhydrous THF, was added dropwise an ethereal solution of MeLi (1.25 mL of 1.6 M solution, 2 mmol) under N_2. The initially dark-red solution turned yellow. After 30 min the solution was ad-

ded dropwise with a syringe to a stirred, ice-cold slurry of $FeCl_2$ (130 mg, 1 mmol) in 20 mL of anhydrous THF. After the addition the solution was stirred at room temp. overnight and worked up as described for **7** to yield a dark-red solid (0.52 g, 81%). The crude product was purified by column chromatography on silica gel with pentane and dichloromethane (1:1, v/v) to yield ferrocene **9** as a bright yellow solid, m.p. 200−202 °C; 1:1 mixture of diastereomers as inferred from the NMR spectra. − IR (KBr): $\tilde{\nu}$ = 2926 cm^{-1}, 2851, 1591, 1411, 901, 716. − UV/Vis ($CHCl_3$): λ_{max} (log ε) = 262 nm (4.05), 296 (3.42), 310 (3.36). − ^1H NMR ($CDCl_3$, 400 MHz): δ = 1.50 and 1.52 (overlapping doublets, *J* = 7.4 Hz, 6 H), 2.75 (m, 2 H), 2.90−3.30 (m, 12 H), 3.50 (m, 2 H), 3.90 (m, 2 H), 4.18 (s, 2 H), 4.32 (d, *J* = 10.8 Hz, 2 H), 4.41 (s, 2 H), 4.50 (d, *J* = 11.4 Hz, 2 H), 5.74 (s, 1 H), 5.76 (s, 1 H), 6.25 (m, 4 H), 6.35 (m, 2 H), 6.55 (m, 4 H), 6.64 (d, *J* = 7.5 Hz, 1 H), 6.68 (d, *J* = 7.4 Hz, 1 H). − ^{13}C NMR ($CDCl_3$, 100 MHz): δ = 23.4 (q), 23.5 (q), 33.0 (t), 33.0 (t), 34.8 (t), 34.9 (t), 35.1 (t), 35.2 (t), 36.4 (d), 36.6 (d), 67.9 (d), 68.3 (d), 68.5 (d), 68.6 (d), 69.0 (d), 69.5 (d), 69.8 (d), 92.9 (s), 93.2 (s), 130.2 (d), 130.2 (d), 130.3 (d), 130.8 (d), 130.9 (d), 132.4 (d), 132.4 (d), 132.6 (d), 132.7 (d), 132.9 (d), 132.9 (d), 135.1 (d), 135.1 (d), 136.3 (s), 136.3 (s), 139.2 (s), 139.3 (s), 139.5 (s), 139.5 (s), 139.6 (s), 139.6 (s), 146.2 (s), 146.2 (s). − MS (EI, 70 eV): *m*/*z* (%) = 655 (50), 654 [M^+] (100), 640 (8), 639 (10), 535 (10), 420 (12), 419 (38), 355 (20), 354 (26), 315 (20), 251 (20), 193 (52), 179 (32), 165 (22), 104 (45). − $C_{46}H_{46}Fe$ (654.7): calcd. C 84.37, H 7.09; found C 84.32, H 7.09.

Bis{[1-(4-[2.2]paracyclophanyl)]ethylcyclopentadienyl}titanium Dichloride (10): A solution of the lithium cyclopentadienide (**8**) (2 mmol in 20 mL of anhydrous THF, prepared by the method described above for the synthesis of **9**) was added dropwise with a syringe to a stirred, ice-cold solution of $TiCl_4$ (190 mg, 1 mmol) in 20 mL of anhydrous THF. During the addition the yellowish solution turned dark red. The reaction mixture was stirred at room temp. for 12 h and worked up as described for **7** to yield a red solid (0.57 g, 83%). This solid was further purified by recrystallization by dissolving it in a minimum amount of dichloromethane and adding pentane until a slight turbidity appeared. Upon cooling the solution in the freezer (−25 °C), the titanocene dichloride **10** was obtained as a bright red solid, m.p. > 250 °C (dec.). − IR(KBr): $\tilde{\nu}$ = 2925 cm^{-1}, 2852, 1592, 1486, 824, 717. − UV/Vis ($CHCl_3$): λ_{max} (log ε) = 260 nm (4.49), 396 (3.44). − ^1H NMR ($CDCl_3$, 400 MHz): δ = 1.31 (d, *J* = 6.9 Hz, 3 H), 1.35 (d, *J* = 7.0 Hz, 3 H), 2.65 (m, 2 H), 2.85−3.15 (m, 10 H), 3.20 (m, 2 H), 3.45 (m, 2 H), 4.52 and 4.56 (two overlapping quadruplets, 2 H, *J* = 6.9 and 7.0 Hz), 5.49 (m, 1 H), 5.53 (m, 1 H), 6.20 (m, 2 H), 6.25−6.40 (m, 6 H), 6.45−6.60 (m, 8 H), 6.58 (m, 1 H), 6.69 (m, 1 H), 6.71 (m, 1 H), 6.75 (m, 1 H), 6.86 (m, 1 H). − ^{13}C NMR ($CDCl_3$, 100 MHz): δ = 22.2 (q), 22.3 (q), 33.3 (t), 33.3 (t), 34.9 (t), 35.0 (t), 35.2 (t), 35.3 (t), 38.5 (d), 38.6 (d), 109.8 (d), 110.8 (d), 119.9 (d), 119.9 (d), 120.8 (d), 121.0 (d), 122.2 (d), 122.2 (d), 129.6 (d), 129.7 (d), 130.6 (d), 130.7 (d). 131.5 (d), 131.5 (d), 132.1 (d), 132.6 (d), 132.6 (d), 133.1 (d), 135.9 (d), 136.0 (d), 137.0 (s), 137.1 (s), 139.3 (s), 139.3 (s), 139.7 (s), 139.8 (s), 139.8 (s), 142.3 (s), 143.0 (s), 144.9 (s), 145.0 (s). − MS (EI, 70 eV): *m*/*z* (%) = 716 [M^+] (3), 598 (12), 419 (8), 384 (34), 383 (22), 382 (30), 300 (16), 299 (10), 298 (22), 278 (12), 196 (20), 195 (78), 194 (18), 193 (100), 192 (12), 181 (20), 180 (18), 179 (32), 178 (34), 165 (50), 119 (42), 105 (54), 104 (30), 78 (230), 77 (12).

Bis{[1-(4-[2.2]paracyclophanyl)]ethylcyclopentadienyl}zirconium Dichloride (11): Compound **11** was prepared by the procedure described for the synthesis of **10**, using $ZrCl_4$ (230 mg, 1 mmol). The crude product was obtained as a grey solid (0.70 g, 92%). The solid was triturated with diethyl ether (20 mL) and filtered to obtain pure zirconocene dichloride **11** as a tan-coloured solid (0.37 g). Further recrystallization from dichloromethane in the freezer (−25 °C) yielded colourless crystals of **11**, m.p. 280−285 °C (dec.). The ether soluble portion was evaporated to dryness and the ^1H NMR spectrum of this solid (0.31 g) indicated mainly **11**, along with small amounts of **4** and **5**. − IR (KBr): $\tilde{\nu}$ = 2926 cm^{-1}, 1592, 833, 821. − UV/Vis ($CHCl_3$): λ_{max} (log ε) = 296 nm (3.52), 340 (3.27), 372 (2.85). − ^1H NMR ($CDCl_3$, 400 MHz): δ = 1.42 and 1.44 (two overlapping doublets, 3 H each, *J* = 6.8 Hz), 2.72 (m, 2 H), 2.90−3.10 (m, 8 H), 3.15 (m, 2 H), 3.25 (m, 2 H), 3.53 (m, 2 H), 4.46 and 4.48 (two overlapping quadruplets, 1 H each, *J* = 6.8 Hz), 5.52 (d, *J* = 1.1 Hz, 1 H), 5.54 (d, *J* = 1.2 Hz, 1 H), 6.25−6.45 (m, 8 H), 6.45−6.65 (m, 8 H), 6.75 (m, 2 H), 6.82 (m, 2 H). − ^{13}C NMR ($CDCl_3$, 100 MHz): δ = 22.6 (q), 33.3 (t), 33.3 (t), 34.9 (t), 34.9 (t), 35.2 (t), 35.3 (t), 37.6 (d), 37.7 (d), 106.5 (d), 107.1 (d), 115.1 (d), 115.2 (d), 116.9 (d), 117.4 (d), 118.0 (d), 118.4 (d), 129.5 (d), 129.6 (d), 130.3 (d), 130.4 (d), 131.4 (d), 131.4 (d), 132.1 (d), 132.6 (d), 133.1 (d), 135.8 (d), 136.9 (s), 136.9 (s), 137.9 (s), 138.3 (s), 139.3 (s), 139.3 (s), 139.7 (s), 139.8 (s), 145.2 (s), 145.2 (s). − MS (EI, 70 eV): *m*/*z* (%) = 763 (0.8), 761 (0.8), 760 (1.8), 759 (1.4), 758 (1.4) [molecular ions], 668 (46), 465 (10), 463 (16), 462 (10), 459 (22), 359 (28), 357 (38), 355 (44), 300 (62), 196 (30), 195 (100), 194 (36), 181 (56), 164 (52), 155 (16), 119 (30), 104 (28). − $C_{46}H_{46}ZrCl_2$ (761.0): calcd. C 72.4, H 6.04, Cl 9.33; found C 71.57, H 6.04, Cl 9.59.

Cyclopentadienyl[1-(4-[2.2]paracyclophanyl)ethylcyclopentadienyl]-titanium Dichloride (12): A solution of the lithium cyclopentadienide (**8**) (2.0 mmol in 20 mL of anhydrous THF) was added dropwise to a stirred, ice-cold solution of $CpTiCl_3$ (0.44 g, 2.0 mmol) in 20 mL of anhydrous THF. During the addition, the colour of the solution turned from yellow to dark red. After stirring at room temp. for 12 h, the reaction was worked up as described above to yield a dark red solid (0.9 g, 94%). Recrystallization from a mixture of dichloromethane and ether in the freezer (−25 °C) yielded the product as dark red needles (0.52 g), m.p. 208 °C (dec.). − IR (KBr): $\tilde{\nu}$ = 3106 cm^{-1}, 2926, 2852, 1590, 856, 822. − UV/Vis ($CHCl_3$): λ_{max} (log ε) = 258 nm (4.42), 392 (3.32). − ^1H NMR ($CDCl_3$, 400 MHz): δ = 1.30 (d, *J* = 7.0 Hz, 3 H), 2.71 (m, 1 H), 2.90−3.05 (m, 4 H), 3.14 (m, 1 H), 3.26 (m, 1 H), 3.48 (m, 1 H), 4.54 (q, *J* = 7.0 Hz, 1 H), 5.50 (d, *J* = 1.1 Hz, 1 H), 6.22 (m, 1 H), 6.30−6.45 (m, 3 H), 6.54 (m, 4 H), 6.61 (s, 5 H), 6.73 (m, 1 H), 6.90 (m, 1 H). − ^{13}C NMR ($CDCl_3$, 100 MHz): δ = 22.3 (q), 33.2 (t), 34.9 (t), 35.1 (t), 35.3 (t), 38.4 (d), 110.2 (d), 119.9 (d), 120.3 (d), 120.4 (d), 123.7 (d), 129.6 (d), 130.5 (d), 131.5 (d), 132.1 (d), 132.6 (d), 133.1 (d), 135.9 (d), 137.0 (s), 139.3 (s), 139.7 (s), 139.7 (s), 143.3 (s), 144.8 (s). − MS (EI, 70 eV): *m*/*z* (%) = 486 (5), 485 (7), 484 (22), 483 (14), 482 (30) [molecular ions], 450 (12), 448 (16), 447 (30), 446 (18), 411 (26), 410 (60), 409 (18), 408 (22), 345 (32), 344 (26), 343 (74), 315 (28), 313 (42), 305 (32), 300 (32), 299 (100), 278 (22), 277 (26), 275 (33), 262 (28), 207 (30), 195 (90), 180 (36), 179 (50), 165 (50), 119 (100), 104 (28), 78 (10).

Cyclopentadienyl[1-(4-[2.2]paracyclophanyl)ethylcyclopentadienyl]-zirconium Dichloride (13): The complex was prepared by employing the procedure described for **12** using $CpZrCl_3$ (0.52 g, 2 mmol). The crude product was obtained as a tan-coloured solid (0.66 g, 64%) that was purified by recrystallization from a mixture of dichloromethane and diethyl ether in the freezer (−25 °C) to yield pure **13** as a colourless solid, m.p. 142−145 °C (dec.). − IR (KBr): $\tilde{\nu}$ = 2927 cm^{-1}, 1591, 835, 821, 813. − UV/Vis ($CHCl_3$): λ_{max} (log ε) = 296 nm (3.51), 330 (sh, 3.25), 378 (2.60). − ^1H NMR ($CDCl_3$, 400 MHz): δ = 1.35 (d, *J* = 7.0 Hz, 3 H), 2.72 (m, 1 H), 2.90−3.30

(m, 6 H), 3.49 (m, 1 H), 4.40 (q, J = 7.0 Hz, 1 H), 5.46 (s, 1 H), 6.20 (m, 1 H), 6.28−6.35 (m, 2 H), 6.38 (m, 1 H), 6.45 (m, 2 H), 6.52 (s, 5 H), 6.55 (m, 2 H), 6.69 (m, 1 H), 6.80 (m, 1 H). − ^{13}C NMR ($CDCl_3$, 100 MHz): δ = 22.6 (q), 33.2 (t), 34.9 (t), 35.1 (t), 35.3 (t), 37.6 (d), 103.4 (s), 106.7 (d), 115.5 (d), 115.8 (d), 117.0 (d), 119.0 (d), 129.6 (d), 130.3 (d), 131.4 (d), 132.1 (d), 132.6 (d), 133.1 (d), 135.8 (d), 136.8 (s), 138.4 (d), 139.3 (s), 139.7 (s), 139.8 (s), 145.1 (s). − MS (EI, 70 eV): *m/z* (%) = 530 (5), 529 (5), 528 (10), 527 (6), 526 (16), 525 (10), 524 (12) [molecular ions], 494 (20), 493 (18), 492 (54), 491 (30), 490 (76), 489 (50), 488 (100), 475 (12), 473 (12), 459 (12), 452 (16), 388 (20), 387 (20), 386 (36), 385 (36), 384 (52), 369 (14), 359 (14), 357 (28), 355 (26), 300 (24), 299 (26), 231 (40), 229 (26), 227 (38), 225 (36), 195 (72), 193 (38), 179 (76), 165 (76), 152 (12), 128 (12), 119 (40), 104 (42), 91 (12), 78 (14). − $C_{28}H_{28}ZrCl_2$ (526.7): calcd. C 63.87, H 5.38, Cl 13.35; found C 63.15, H 5.38, Cl 12.13.

X-ray Crystallography: A summary of the crystal data, data collection, and refinement parameters for the crystal structure of **11** is given in Table 3.

Table 3. X-ray structure refinement of **11**

Compound	**11**
Empirical formula	$C_{48}H_{46}Cl_8D_2Zr$
M_r	1001.69
Crystal habit	colourless tablet
Crystal size [mm]	0.35×0.31×0.13
Crystal system	Orthorhombic
Space group	*Pbcn*
Cell constants:	
a [Å]	30.6365(10)
b [Å]	14.0545(5)
c [Å]	20.9986(7)
V [Å^3]	9041.6
Z	8
D_x [Mg·m^{-3}]	1.472
μ [mm^{-1}]	0.750
Transmissions	0.73−0.93
F(000)	4032
T [°C]	−130
$2\theta_{max}$	56
No. of reflections:	
measured	127800
unique	11476
R_{int}	0.062
Parameters	554
Restraints	48
$wR(F^2$, all refl.)	0.127
$R(F, >4\sigma(F))$	0.044
S	1.01
max. Δρ [e·Å^{-3}]	1.20

Structure Determination of 11: A cut tablet was mounted on a glass fibre in inert oil and transferred to the cold gas stream of a Bruker SMART 1000 CCD diffractometer fitted with a Siemens LT-2 low-temperature attachment. Data were collected with ω- and φ-scans using graphite-monochromated Mo-K_α radiation (λ = 0.71073 Å). An absorption correction was performed using the multi-scan method (program SADABS). All unique data were used for calculations (program SHELXL-97, G. M. Sheldrick, University of Göttingen). The structure was solved by direct methods and refined anisotropically by full-matrix least-squares on F^2. The deuteriochloroform molecule containing C96 is severely disordered. Two alternative positions were refined with occupancies of 0.600(3) for C96/Cl94/Cl95/Cl96 and 0.400(3) for C96′/Cl91/Cl92/Cl93, but the high residual electron density in the solvent region indicates further disorder. The hydrogen atoms were refined with a riding model or as rigid methyl groups.

Crystallographic data (excluding structure factors) for the structure(s) included in this paper have been deposited with the Cambridge Crystallographic Data Centre as supplementary publication no. CCDC-171642. Copies of the data can be obtained free of charge on application to CCDC, 12 Union Road, Cambridge CB2 1EZ, UK [Fax: (internat.) + 44-1223/336-033; E-mail: deposit@ccdc.cam.ac.uk].

Butyl(η^5-cyclopentadienyl)[η^5:η^1-1-(4-[2.2]paracyclophanyl)ethylcyclopentadienyl]zirconium (15): *n*-Butyllithium (1.1 mL, 1.75 mmol) was added to a suspension of metallocene dichloride complex **13** (0.46 g, 0.88 mmol) in 50 mL of toluene at −78 °C under argon. After warming the reaction mixture to room temp. and stirring it for 11 h, the initially light brown suspension had turned into an orange solution. The reaction mixture was filtered through sodium sulfate. Removal of the solvent yielded a red oil (0.43 g, 96%). − ^{1}H NMR (C_6D_6, 250 MHz): δ = 0.59 (m, 1 H), 0.82 (m, 1 H), 1.05 (t, J = 14.3 Hz, 3 H), 1.12 (d, J = 7.0 Hz, 3 H), 1.39 (m, 2 H), 1.57 (m, 4 H), 2.64 (m, 2 H), 2.92 (m, 4 H), 2.97 (d, J = 7.0 Hz, 1 H), 4.97 (m, 1 H), 5.19 (m, 1 H), 5.68 (s, 5 H), 5.96 (s, 2 H), 6.35 (m, 1 H), 6.36 (m, 1 H), 6.40 (m, 1 H), 6.48 (m, 1 H), 6.83 (m, 2 H). − ^{13}C NMR (C_6D_6, 62.9 MHz): δ = 14.2 (CH_3), 21.7 (CH_3), 30.1 (CH_2), 34.3 (CH_2), 35.3 (CH_2), 35.9 (CH_2), 39.0 (CH_2), 39.6 (CH), 58.5 (CH_2), 101.3 (CH), 105.5 (CH), 110.2 (CH), 113.7 (CH), 117.8 (CH), 128.7 (CH), 130.3 (CH), 132.3 (CH), 133.3 (CH), 133.3 (CH), 133.6 (C_q), 135.5 (CH), 139.6 (C_q), 139.8 (C_q), 143.2 (C_q), 147.3 (C_q), 181.8 (C_q). − MS (EI, 70 eV): *m/z* (%) = 512 (10), 511 [M$^+$] (8), 457 (58), 455 (75), 453 (100), 451 (10), 352 (5), 348 (10), 347 (50), 345 (10), 321 (7), 181 (2), 165 (2), 92 (5), 91 (4).

Activation of the Metallocene Complexes with MAO: The respective metallocene complex, 10−15 mg, was activated with MAO (30% in toluene) (Zr/Al = 1:3000). A portion of the catalyst solution containing 0.5−1.5 mg metallocene complex was used within 1 h for the homo-polymerization of the olefin.

Homo-Polymerization of Ethylene: *n*-Pentane (500 mL) and the catalyst solution were placed in a 1-L Büchi laboratory autoclave. The autoclave was thermostated at 60 °C. An ethylene pressure of 10 bar (99.98% ethylene) was applied after an internal temperature of 50 °C had been reached. The mixture was stirred for 1 h at 60 (±2) °C. The reaction was terminated by releasing the pressure from the reactor. The obtained polymer was dried in vacuo.

Homo-Polymerization of Propylene in Bulk: The catalyst solution was placed in a 1-L Büchi laboratory autoclave followed by the condensation of 500 mL of propylene (polymerization grade). The autoclave was thermostated at 60 °C and the mixture was stirred for 1 h at 60 (±2) °C. The reaction was terminated by releasing the pressure from the reactor.

Acknowledgments

S. S. thanks the Alexander von Humboldt Foundation for a fellowship, and the Indian Institute of Technology, Madras, India, for leave. We also gratefully acknowledge the continuous support of our studies by the Fonds der Chemischen Industrie.

[1] H. Hopf, P. G. Jones, P. Bubenitschek, F. R. Heirtzler, *Z. Kristallogr.* **1996**, *211*, 357−358.
[2] For a recent review on frontiers in metal-catalyzed polymerizations see issue number 4 of *Chem. Rev.* **2000**, *100*, 1169−1681.
[3] F. R. W. P. Wild, L. Zsolnai, G. Huttner, H.-H. Brintzinger, *J. Organomet. Chem.* **1982**, *232*, 233−247.
[4] For a recent summary on single-site metal catalysts see: G. W. Coats, *Chem. Rev.* **2000**, *100*, 1223−1252.
[5] S. Sankararaman, H. Hopf, I. Dix, P. G. Jones, *Eur. J. Org. Chem.* **2000**, 2703−2709.
[6] J. C. Leblanc, C. Moise, *J. Organomet. Chem.* **1976**, *120*, 65−71.
[7] G. R. Knox, P. L. Pauson, *J. Chem. Soc.* **1961**, 4615−4618 and refs. cited therein.
[8] For a detailed discussion of the addition of metal organic reagents to carbonyl groups in [2.2]paracyclophanes, i.e. a study of the effects of Cram's rule in a planar chiral system, see: Th. Laue, PhD dissertation, Braunschweig, **1991**.
[9] I. A. Ronova, N. V. Alekseev, N. I. Gapotchenko, Yu. T. Struchkov, *J. Organomet. Chem.* **1970**, *25*, 149−151.
[10] L. Pauling, *The Nature of the Chemical Bond*, Cornell University Press, Ithaca, N. Y., **1960**, pp. 221−264.
[11] K. Prout, T. S. Cameron, R. A. Forder, S. R. Critchley, B. Denton, G. V. Rees, *Acta Crystallogr., Sect. B* **1974**, *30*, 2290−2304.
[12] C. H. Saldarragia-Molina, A. Clearfield, I. Bernal, *Inorg. Chem.* **1974**, *13*, 2880−2885.
[13] E. Negishi, F. E. Cederbaum, T. Takahashi, *Tetrahedron Lett.* **1986**, *27*, 2829−2832.
[14] E. Negishi, T. Takahashi, *Acc. Chem. Res.* **1994**, *27*, 124−130.
[15] D. P. Lewis, R. J. Whitby, R. V. H. Jones, *Tetrahedron* **1995**, *51*, 4541−4550.
[16] M. R. Kesti, R. M. Waymouth, *Organometallics* **1992**, *11*, 1095−1103.
[17] E. Negishi, S. J. Holmes, J. M. Tour, J. A. Miller, F. E. Cederbaum, D. R. Swanson, T. Takahashi, *J. Am. Chem. Soc.* **1989**, *111*, 3336−3346.
[18] P. Binger, P. Müller, R. Benn, A. Rufinska, B. Gabor, C. Krüger, P. Betz, *Chem. Ber.* **1989**, *122*, 1035−1042.
[19] R. Goddard, P. Binger, S. R. Hall, P. Müller, *Acta Crystallogr., Sect. C* **1990**, *46*, 998 −1001.
[20] E. H. Licht, H. G. Alt, M. M. Karim, *J. Organomet. Chem.* **2000**, *599*, 261−274.
[21] H. G. Alt, A. Köppl, *Chem. Rev.* **2000**, *100*, 1205−1221.
[22] H.-H. Brintzinger, D. Fischer, R. Mülhaupt, B. Rieger, R. Waymouth, *Angew. Chem.* **1995**, *107*, 1255−1283; *Angew. Chem. Int. Ed. Engl.* **1995**, *34*, 1143−1171.
[23] W. Kaminsky, M. Arndt, *Adv. Polym. Sci.* **1997**, *127*, 143−187.
[24] B. Peifer, W. Milius, H. G. Alt, *J. Organomet. Chem.* **1998**, *553*, 205−220.
[25] H. G. Alt, *J. Chem. Soc., Dalton Trans.* **1999**, 1703−1709.

Received May 10, 2001
[I01166]

The Tricarbonylchromium Complex of a Trimethyltin-Substituted *N*-(Triisopropylsilyl)indole − A Dynamic NMR Study of Multiple Independent Rotation Processes in the Solid State with an X-ray Diffraction Structure and Molecular Mechanics Calculations

Abil E. Aliev,[a] J. Edgar Anderson,*[a] David Butler,[a] Jorge Gonzalez-Outeiriño,[a] Lodovico Lunazzi,*[b] Andrea Mazzanti,[b] Jonathan W. Steed,[c] and René Wilhelm[d]

Keywords: NMR spectroscopy / Solid-state structures / Tin / Chromium / Molecular modeling / X-ray diffraction

The title compound was studied by dynamic NMR spectroscopy in solution and in the solid state, and by MM3 molecular mechanics calculations of model compounds. Barriers to rotation of the trimethyltin group, the tricarbonylchromium group, the triisopropylsilyl group, and the isopropyl groups were all too small to measure by NMR in solution i.e. less than about 5 kcal/mol. All of these barriers could be measured, however, in the solid state, are of different sizes, and are surprisingly large, up to 12.9 kcal/mol. A crystal structure determination shows close intermolecular interactions of these triple rotors that explain these high rotation barriers.

Introduction

Dynamic NMR studies of intramolecular motions in the solid state promise to provide particularly interesting insights when energy barriers found are markedly different from those in solution. Rotational barriers in the solid state are expected to be higher than in solution, since the lattice will usually further hinder any intramolecular process.[1,2] A crystal structure provides direct information on intermolecular interactions that may explain these differences. We now report an investigation of the title compound **1** with a variety of triple rotors.[3] Rotations involve the trimethylstannyl group, the tricarbonylchromium group, and all four bonds to the silicon atom in the *N*-(triisopropylsilyl) (*N*-TIPS) group, so six different bonds in all were investigated. Each rotation has a substantial barrier in the solid state, yet all the corresponding processes in solution were fast on the NMR timescale at all accessible temperatures.

An X-ray diffraction study shows that these groups are strongly hindered by groups in neighbouring molecules, but since barrier sizes are different, the rotations do not appear to be correlated. The parent *N*-(triisopropylsilyl)indole (**2**) was also studied by dynamic NMR in order to assist in elucidating the conformational process in the *N*-TIPS group. Furthermore, MM3 molecular mechanics calculations[4] were carried out on **2** and on 4-(trimethylstannyl)indole (**3**).

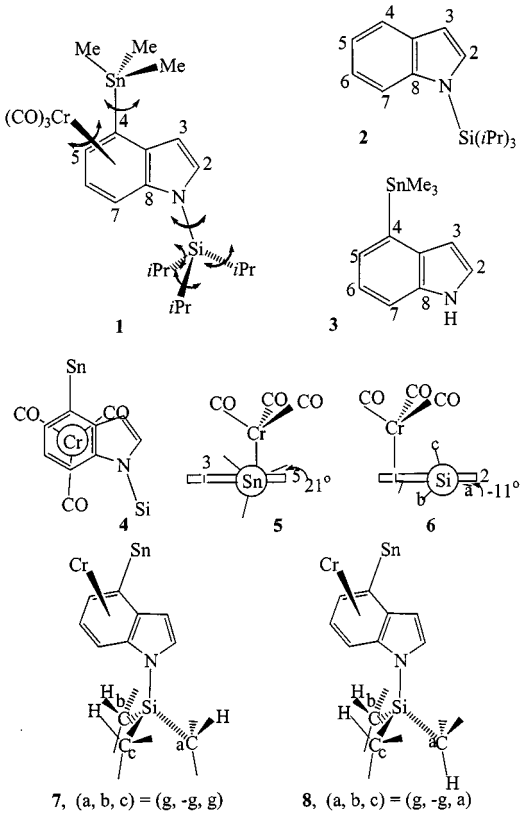

[a] Chemistry Department, University College, Gower Street, London, WC1E 6BT, United Kingdom
E-mail: j.e.anderson@ucl.ac.uk
[b] Dipartimento di Chimica Organica, "A. Mangini", Universita di Bologna, Viale Risorgimento 4, 40136 Bologna, Italy
E-mail: lunazzi@ms.fci.unibo.it
[c] Chemistry Department, King's College, Strand, London, WC2R 2LS, United Kingdom
[d] Chemistry Department, Imperial College, London, SW7 2AZ, United Kingdom

Results

Structure

The NMR results are best interpreted in terms of the molecular structure found in the crystal, with some assistance from MM3 calculations for an isolated molecule of the parent *N*-(triisopropylsilyl)indole (**2**), so these structural studies will be reported first. It should be noted that the solution or gas-phase conformations might be different from that of the crystal, particularly for the *N*-TIPS group. The structure of **1** in the crystal is shown in Figure 1 along with two different representations of parts of the unit cell to indicate intermolecular interactions.

The compound is chiral and there are four molecules of each enantiomer in the unit cell. Figure 1 (a and b), show a molecule in the crystal with the (*S*) configuration, based on C(11) as the chiral centre in that diagram, with Sn, Cr, C(6), and C(10) as substituents.[5] Equally, diagrams **1**, and **4**−**7** show the (*S*) configuration, and the discussion below refers to this. As many molecules exist in the (*R*) configuration in the crystal and in solution, with torsion angles of opposite sign,[6] so the discussion could be extended mutatis mutandis to cover them. Greater detail of the crystal structure is given in the Exp. Sect.

The tricarbonylchromium conformation is as in formula **4**. Both the trimethyltin and TIPS groups are in *peri* positions on the indole ring, and have a conformation with two substituents R towards the other *peri* position on either side of the plane and the third substituent close to the plane away from the *peri* interaction, as shown diagrammatically[6] in **5** and **6**. Within the *N*-TIPS group, the isopropyl group conformations can be defined by the N−Si−C−H^n torsion angles, and in the crystal these are (g, $-g$, g) for the groups a−c in the order shown in **6**. Thus reasonably, the two out-of-plane isopropyl groups that flank the *peri* position have their methine proton nearest to that position (see **7**). Molecular mechanics calculations for *N*-(triisopropylsilyl)indole (**2**) located a range of minima, each of which, like **6**, has one Si−*i*Pr bond near to the plane close to the C-2 position of the indole ring. These con-

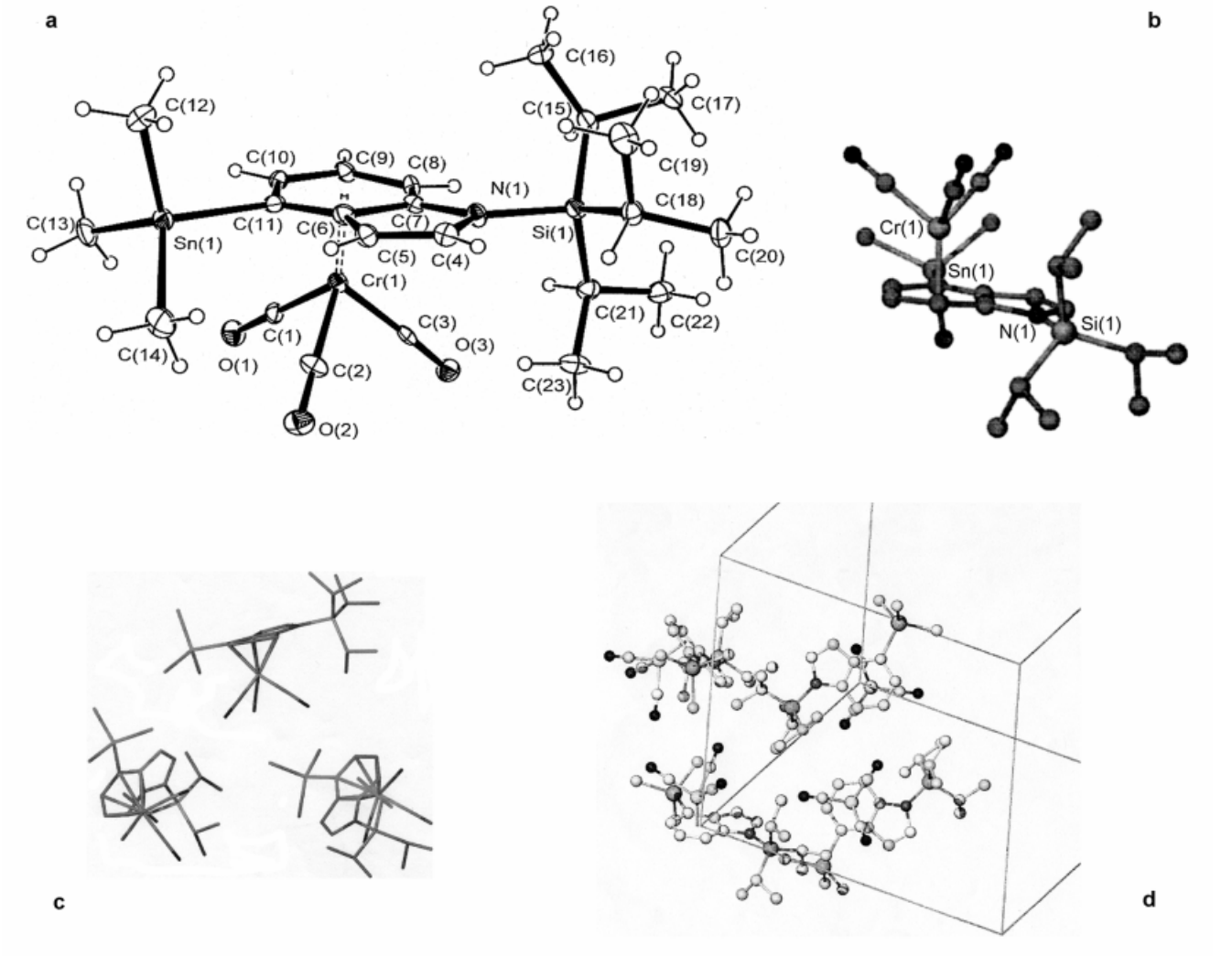

Figure 1. Crystal structure of compound **1**; a, b: ORTEP view and a view (≡ **6**) of the (*S*) configuration, respectively; c, d: parts of the unit cell

formational minima, listed in Table 1 along with the experimentally determined conformation for **1**, differ in the rotational arrangement of the three isopropyl groups as defined by the three N−Si−C−H torsion angles.[7−11] The most stable conformation, as shown in diagram **8**, is (*g*, −*g*, *a*) rather than (*g*, −*g*, *g*) (diagram **7**), which is calculated to be 1.19 kcal/mol less stable, but is the conformation found in the crystal. The structural difference between **7** and **8** is quite small, involving little more than 120° of rotation of the isopropyl group nearest to the tricarbonylchromium group. The calculated and measured torsion angles for the conformation **7**, found in the crystal, agree well.

Table 1. MM3 calculations of steric energies of conformations of *N*-(triisopropylsilyl)indole (**2**); conformations are described by the angle α, the torsion angle φ_a made with the indole plane by the isopropyl group, and the H−C−Si−N torsion angles φ_n, quoted in the alphabetical order shown; the experimental values for the (*g*, −*g*, *g*) conformation are included beneath the calculated values for that conformation

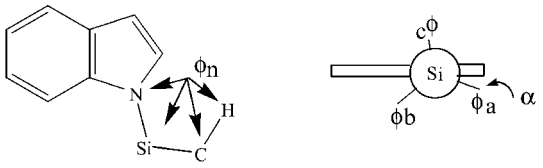

Conformation		Relative steric energy [kcal/mol]	α	φ_a	φ_b	φ_c
(*g*, −*g*, *a*)	**8**	0.00	−14	50	−71	−177
(*a*, *g*, −*g*)		1.14	0	180	79	−78
(*g*, −*g*, *g*)	**7**	1.19	−4	48	−79	48
(*g*, −*g*, *g*)	[a]	–	−11	46	−81	56
(*a*, −*g*, −*g*)		1.44	−14	171	−81	−63
(*a*, −*g*, *a*)		1.66	−12	−173	−55	−151
(*g*, −*g*, −*g*)		2.08	−14	49	−78	−82
(−*g*, −*g*, −*g*)		3.16	−12	−40	−55	−55
(*a*, *a*, *a*)		6.53	−8	−174	135	153

[a] Crystal values for compound **1**.

NMR Spectra

In the ^{13}C NMR spectrum of compound **1** in solution at room temperature, a set of signals corresponding to rapid rotation of all groups is seen, and at 133 K the singlets from the trimethyltin and isopropylsilyl groups are essentially unchanged with no sign of incipient dynamic broadening. While the carbonyl carbon signal is so broad as to be undetectable at this low temperature, this appears to be an effect of relaxation rather than a dynamic process. We conclude that all rotations are still fast on the NMR timescale for compound **1** *in solution* at that low temperature, so the associated barriers would be less than about 5 kcal/mol.

Several regions of ^{13}C CPMAS NMR spectra of crystalline compound **1** under various conditions are shown in Figures 2, 3, and 4, and described fully in the Exp. Sect. While the signals of the isopropyl methyl carbon atoms and aromatic carbon atoms are quite sharp at room temperature (line width at half-height $\Delta\nu_{1/2} \approx 50-60$ Hz), the isopropyl methine ($\Delta\nu_{1/2} \approx 90$ Hz), the trimethyltin ($\Delta\nu_{1/2} \approx 120$ Hz), and carbonyl ($\Delta\nu_{1/2} \approx 250$ Hz) signals are very broad. In contrast to the solution behaviour, all of the signals, except those for aromatic carbon atoms, show dynamic behaviour as the temperature is lowered, eventually showing decoalescence over different temperature ranges, suggesting three different conformational processes. We will discuss these in turn.

As the temperature was lowered from ambient, the broad trimethyltin carbon signal in the CPMAS spectrum sharpened and became more intense initially, then broadened in a conventional dynamic sense, and eventually split below about 233 K to give three singlets, see Figure 4 (spectra at 213 K and 173 K). A complete line-shape treatment yields rate constants at a series of temperatures (see Table 2), and a barrier to rotation in the solid state of 11.1 kcal/mol.

The room-temperature singlet due to the isopropyl methine carbon atoms in the CPMAS spectrum of **1** broadened rather more noticeably than the methyl singlet and split below about 273 K into what eventually became three equal signals. That methyl carbon singlet split below about 253 K into six signals, two of which overlapped. The variable-temperature spectra are shown in Figure 4, and chemical shifts are listed in Table 4 in the Exp. Sect. A complete line-shape fit of spectra at several temperatures led to rate constants shown in Table 2 and a barrier to rotation of about 12.9 kcal/mol for conformational interconversion of the TIPS group in the solid state. As the temperature was raised from room temperature, both signals of the isopropyl carbon atoms broadened compared with others in the spectrum.

The broad signal for the carbonyl carbon atoms in the CPMAS spectrum at room temperature disappeared completely at about 253 K as the temperature was lowered, and reappeared as a very broad singlet at about 213 K. This signal increased in intensity and split at about 193 K to appear at 173 K as a 1:1:1 triplet, see Figure 3. A complete line-shape fit of spectra towards the low-temperature limit could not be achieved, suggesting that the broadening e.g. at 193 K was not due to conformational exchange. Thus, with such an exchange, the peak at $\delta \approx 233$ should have been broader than the two peaks at $\delta \approx 240$ at 193 K, but it was not. The appearance as a singlet above room temperature but as a triplet at 173 K nonetheless indicates that rotation of the tricarbonylchromium group had become slow. This together with a consideration of the temperature range suggests the barrier is between 8 and 12 kcal/mol.

Each of these signals we have discussed showed additional changes at temperatures above the conventional dynamic-NMR range involving broadening and more or less disappearance of singlet signals as the temperature was further raised. In two cases and putatively in the third this was followed by a resharpening of the singlet signals at even higher temperatures. These not unprecedented

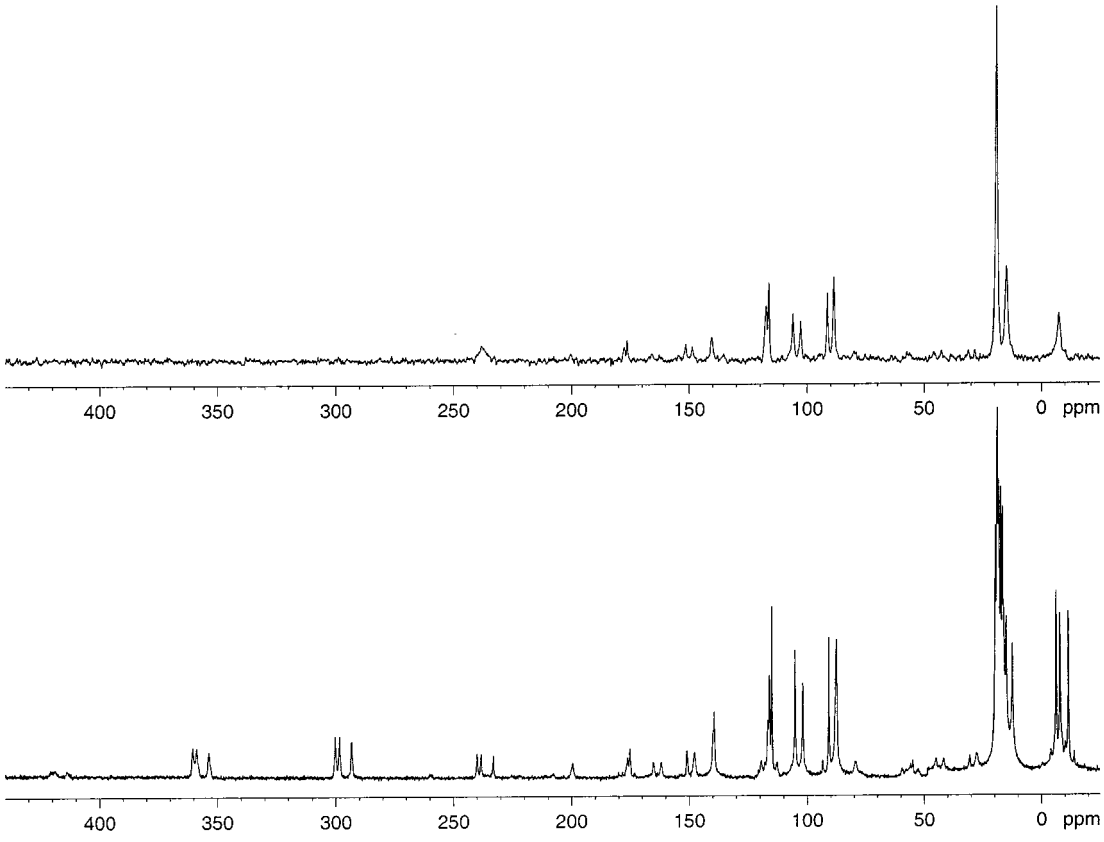

Figure 2. CPMAS ^{13}C NMR spectra of compound **1** at 173 K (bottom) and 297 K (top) − the more intense peaks are between $\delta = -12$ and +22, between $\delta = +85$ and +120, and between $\delta = +232$ and +242; other peaks are side-bands

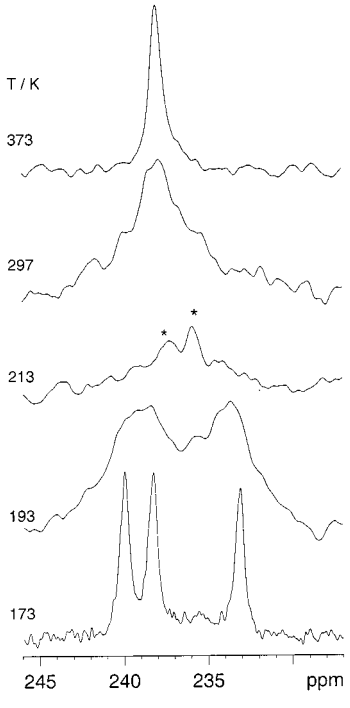

Figure 3. CPMAS ^{13}C NMR spectra of the carbonyl region of compound **1** at various temperatures; * indicates side-bands

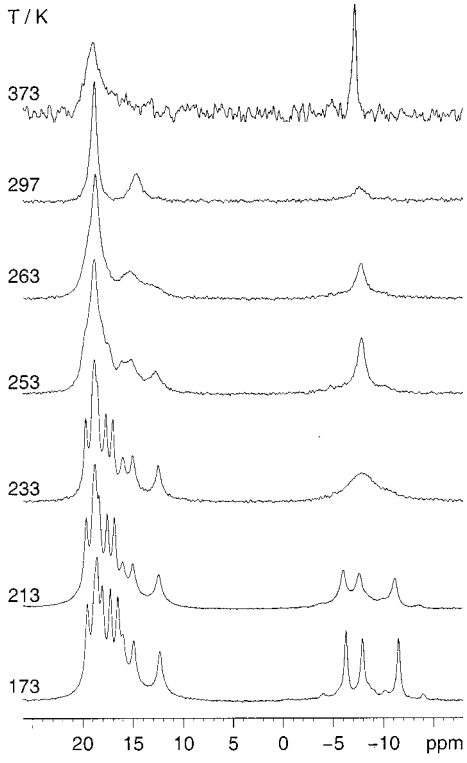

Figure 4. CPMAS ^{13}C NMR spectra of the upfield region of compound **1** at various temperatures

Table 2. Rate constants [s^{-2}] for rotation in compound **1** from complete line-shape analysis in NMR spectra

Temperature	*N*-TIPS rotation	$SnMe_3$ rotation
275 K	400	
268 K	180	
260 K	70	2500
245 K		600
238 K		400
230 K		120

observations[12−14] are a feature of dynamic NMR spectroscopy in the solid state and will be discussed below.

The striking result, therefore, for compound **1** is the NMR observation of three different dynamic processes with barriers up to 12.9 kcal/mol in the solid state. These processes are taking place at a much greater rate in solution, meaning that all barriers must be less than 5 kcal/mol.

Discussion

The barrier of 11.1 kcal/mol for rotation of the trimethyltin group in the solid state is remarkable. Such a symmetrical threefold rotation process of an MR_3 group attached to an aromatic ring should have a low barrier. Thus, the barrier to rotation of a *tert*-butyl group on a benzene-type ring is less (perhaps much less) than 5 kcal/mol, since such barriers have been determined by dynamic NMR in solution only when there was an adjacent *ortho* or *peri* substituent.

Trimethyltin group rotation barriers should certainly be markedly smaller than this, since the four longer Sn−C bonds (211−215 pm) reduce steric hindrance compared with C−C bonds (153−155 pm) in a *tert*-butyl group. There is both experimental and computational evidence confirming that the trimethyltin rotation barriers are very small in the fluid state. Thus, in 1,8-bis(trimethylstannyl)naphthalene (**9**), the barrier is 4.7 kcal/mol,[15] whereas in 1,8-di-*tert*-butylnaphthalene (**10**), the *tert*-butyl group rotational barrier is about 6.5 kcal/mol.[16] The presence of two rotors may of course mean that these are not simple rotation processes.

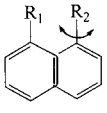

9 $R_1 = R_2 = SnMe_3$
10 $R_1 = R_2 = CMe_3$
11 $R_1 = H$, $R_2 = CH_2CMe_3$
12 $R_1 = H$, $R_2 = N(i\text{Pr})_2$
13 $R_1 = H$, $R_2 = Si(i\text{Pr})_3$

Table 3 shows molecular mechanics calculations (MM3) of rotational barriers in an isolated molecule in a series of trimethylstannyl- and *tert*-butyl-substituted aromatic compounds. The calculated values for trimethylstannyl group rotation barriers are very much smaller than those for *tert*-butyl groups, and clearly fall well below the range that might be measured by dynamic NMR studies even under the most favourable circumstances.

Table 3. MM3 calculated rotational barriers [kcal/mol] for *tert*-butyl and trimethyltin aromatic compounds

	Rotational barrier X = C	Rotational barrier X = Sn
Me_3X−benzene	0.46	0.03
1-Me_3X−naphthalene	3.67	1.97
4-Me_3X−indole	2.18	1.05

The fact that barriers are threefold, involving 120° of rotation, is one reason for their small size. Interestingly, higher, NMR-accessible rotational barriers have been found for less symmetrical $MR^1R^2R^3$ substituents when the rotation is twofold or even more so, onefold. Thus for 1-substituted naphthalenes, a barrier of 5.3 kcal/mol has been measured for 1-neopentylnaphthalene (**11**) (twofold)[17] and of 15.3 kcal/mol for 1-(diisopropylamino)naphthalene (**12**) (onefold).[18] These various points combine to suggest that the trimethylstannyl group rotation barriers should be very low for **1** in solution. The 11.1 kcal/mol barrier observed for the trimethylstannyl group rotation in **1** in the solid state is thus surprisingly high and is presumably due almost completely to interactions beyond the molecule itself.

There has already been some exploration,[7−11] of the conformational possibilities for three isopropyl or similar groups attached to a tetrahedral atom, including triisopropylsilyl groups.[10,11] The most recent report[11] includes results both in solution and the solid state for compound **13** with a TIPS group attached to the 1-position in naphthalene. All the more stable conformations calculated have the same arrangement about the C(ring)−Si bond analogous to **6**, with one isopropyl group close to the plane of the ring towards the 2-position. This, unsurprisingly, is the same conformation we now report for the N−Si bond of compound **1** both in the crystal and by calculation.

The conformation about the three Si−diisopropyl bonds has to be considered next, since each C−Si−C−H torsion angle in **13** and each N−Si−C−H torsion angle in **1** can be either +*gauche* or −*gauche* or *anti*, see **7** and **8**. The crystal structure of **1** shows the (*g*, −*g*, *g*) conformation, but information beyond this depends on NMR observations and calculations.

The solution NMR of compound **13** is much more interesting than that of compound **1**, since processes become slow on the NMR time scale at low temperatures and two different more or less equally populated conformations interconvert slowly at about 128 K. At even lower temperatures interconversion of isopropyl groups within these conformations became slow, the barriers to these processes being between 5.7 and 6.25 kcal/mol. In contrast, the solution spectra of compound **1** and of *N*-(triisopropyl)indole (**2**) are temperature-independent, so barriers are significantly lower.

In the solid state, NMR shows that compound **13** persists in adopting two conformations that show distinct spectra below about 223 K. Distinct barriers to rotation about the

different C−Si bonds could not be determined from the spectra, but rotation in the lattice has a barrier about 5 kcal/mol greater than in solution.

The ^{13}C NMR results for the TIPS group of compound **1** in the solid state can readily be interpreted in terms of the bond conformations found in the crystal structure. The changes in the isopropyl group signals lead to a barrier of 12.9 kcal/mol, compared with less than 5 kcal/mol in solution, but they cannot be used to distinguish the N−Si and the three C−Si bond rotations.

MM3 calculations suggest (see Table 1), that the (*g*, −*g*, *g*) conformation for **1** has torsion angles gratifyingly similar to those found in the crystal, but that this conformation is about 1.19 kcal/mol less stable than the (*g*, −*g*, *a*) conformation and 0.04 kcal/mol less stable than the (*a*, −*g*, *g*) conformation. This last conformation is too symmetrical to explain the low-temperature NMR spectra, except by invoking an unsymmetrical lattice. The fact that the most stable calculated conformation (*g*, −*g*, *a*) is not the one found in the crystal (*g*, −*g*, *g*), need not reflect shortcomings of the calculations, for it may be evidence of a conformational change induced by crystal lattice forces.

In view of the results in Table 3 for calculated barriers to trimethylstannyl group rotation, it is of interest to know the difference in *N*-TIPS rotation barriers to be expected when the 1-naphthyl group of **13** is replaced by the *N*-indolyl group of **1**. Calculation of TiPSi rotational barriers is complicated, however, as one torsion usually entrains another.[10] We therefore calculated the barrier to a simplified 120° rotation about the *peri* bond for **13** and for *N*-TIPS-indole (**2**) in the conformation with isopropyl groups (*g*, *g*, *g*). This is not a very stable conformation, but the calculation is straightforward since the three *gauche* isopropyl group conformations need not rearrange dramatically during the overall rotation. The barrier to rotation about the *peri* bond in these circumstances is calculated to be 5.6 kcal/mol for **13**, and only 3.2 kcal/mol for the indole **2**. Since the experimental solution barrier in **13** is about 6 kcal/mol this suggests that the barrier for reorientation in the TIPS group of **1** in solution be very much less than 5 kcal/mol. In this light, the 11.9 kcal/mol barrier found for **1** in the solid state is uncommonly high.

There have already been extensive NMR[14,19−22] and other studies[14] of the tricarbonylchromium η^6 complexes of aromatic compounds in the solid state. In crystals of the simple highly symmetrical benzene complex,[19] two distinct processes are taking place: Firstly there is an in-plane rotation of the benzene ligand in 60° jumps, with a barrier of 3.7−4.7 kcal/mol. This was studied using solid-state wideline ^2H wideline NMR techniques.[21] Additionally, there is a dynamic process in which tricarbonylchromium fragments rotate by 120° steps with respect to the crystal lattice (a crystallographic mirror plane bisects the molecule) with a barrier of about 17 kcal/mol.

Even more relevant to our work is what is known from NMR studies of tricarbonylchromium complexes of a set of polymethylbenzenes in the solid state.[14] A range of behaviour has been observed, but there are some general features. At low temperatures the carbonyl carbon signal appears either as a 1:1:1 triplet or a 2:1 doublet indicating that reorientation involving the carbonyl group is slow. On raising the temperature, signals broaden and coalesce, then continue to broaden until they disappear. At temperatures between 20 and 40°C and higher, the broad signal reappears and becomes sharper as the temperature rises.

The carbonyl spectrum of compound **1** in the solid state fits with this pattern, but it is interesting to note that for nine of the ten compounds studied,[14] the changes took place over a higher temperature range than for **1**, implying a higher reorientation barrier. The main difference between **1** and the polymethylbenzenes is that close π-stacking of the aromatic rings is absent in the crystal due to the presence of the bulky trimethylstannyl and TiPSi groups. Lattice effects on rotation in **1** are thus less critical.

Only the pentamethylbenzene complex shows the tricarbonylchromium group rotating with a lower barrier, about 7.5 kcal/mol, but in this case the aromatic ring is not reorienting even at room temperature. The barrier is 17 kcal/mol in benzenetricarbonylchromium,[18] and is even higher in the more symmetrical mesitylene and hexamethylbenzene complexes. Since the barriers reflect intermolecular interactions in different crystal environments, too much time should not be spent on comparisons.

The apparent disappearance of the carbonyl signal over a temperature range above coalescence is most likely associated with the very high chemical shift anisotropy of the CO carbon atoms ($\Delta\sigma \approx 430$ ppm). In the intermediate exchange region (relative to the chemical shift anisotropy), the CO line width $\Delta\nu_{1/2}$ will be of the order of $\Delta\sigma$ (ca. 33 kHz), which means that the spin-spin relaxation time (T_2) will be of the order of 10 μs. This is comparable to the dead-time delay used (15 μs in our experiments), hence complete loss of signal intensity for the CO carbon atoms is observed as a result of T_2 relaxation during the dead-time. For aliphatic carbon atoms, on the other hand, $\Delta\sigma$ is near 0 ppm and corresponding T_2 effects can be safely ignored.

The broadening of the $SnMe_3$ signals in the solid-state NMR spectrum as the temperature is raised from 273 K to room temperature, reaches a maximum breadth at about room temperature (Figure 4). This indicates that the bond rotation frequency at this temperature is comparable to the proton decoupling frequency used, and line broadening results.[12−14] Since the decoupling power used corresponds to a frequency of ca. 50 kHz, we can conclude that the frequency of rotation for the ring−Sn bond is of the same order at 297 K, the temperature of maximum signal broadening, whence the rotational barrier is calculated to be 10.9 kcal/mol at this temperature. This barrier value agrees well with that derived independently from the classical dynamic NMR changes at much lower temperatures shown in Figure 4.

In the same way, the two isopropyl carbon peaks at room temperature begin to broaden as the temperature is raised beyond about 353 K, this being more marked with the methine carbon signal. This is attributed to the onset of the same decoupling frequency effect.

A feature that emerges from the crystal structure of **1** is the interaction of adjacent molecules, and this is of course related to the high rotational barriers reported. The crystal is racemic with eight molecules in the unit cell, four of each enantiomer. Figure 1 (c) shows how three molecules of the same configuration are grouped round a central area with each one of the three molecules turning a different feature towards this centre, either a trimethyltin group, a tricarbonylchromium group, or a triisopropylsilyl group. Figure 1 (d) shows other interactions of adjacent molecules. At the top are two molecules whose contact is through the TIPS groups of each; at the bottom, contact is through a TIPS and a trimethyltin group. These and other views of groups of molecules all indicate that the principal interaction of neighbouring molecules is between TIPS and trimethyltin groups, and it is not surprising that these groups have particularly high rotation barriers in the solid state.

We failed to observe any of these exchange processes for **1** by solution NMR even at 133 K. All six rotation barriers clearly become much lower when derivative **1** passes from the solid to fluid solution state, as reported in a number of other cases.

Experimental Section

The synthesis of complex **1** has been described previously.[3]

High-resolution solid-state ^{13}C NMR spectra were recorded at 75.5 MHz with a Bruker MSL300 spectrometer (7.05 T) using a standard Bruker double-resonance magic angle sample spinning (MAS) probe. The samples were fitted into the cylindrical zirconia rotor (7 mm external diameter) and then spun at MAS frequency in the range 3−7 kHz (with stability better than ca. ±5 Hz). High-resolution solid-state ^{13}C NMR spectra were recorded using cross-polarisation (CP), MAS, and high-power ^{1}H decoupling applied during acquisition. Typical operating conditions for ^{13}C CPMAS experiments were: ^{1}H 90° pulse duration = 5 μs; contact time = 1 ms; recycle delay = 2 s. The stability and accuracy of the temperature controller used (Bruker B-VT1000) were ca. ±1 K. The ^{13}C chemical shifts are given relative to tetramethylsilane (Table 4). Fitting of the dynamic NMR changes in the trimethyltin and isopropylmethine signals with temperature was on the basis of a three-site mutual exchange. Fitting of the isopropylmethyl signal was on the basis of a six-site mutual exchange, which may not be strictly appropriate, but in view of the small chemical shift range of the six signals is likely to yield a reasonable approximation for that signal. Details of the crystal structure determination are shown in Table 5. Crystals were mounted on a thin glass fibre using silicon grease and cooled on the diffractometer to 100 K using an Oxford Cryostream low-temperature attachment. Approximate unit cell dimensions were determined by the Nonius Collect program[23] from 5 index frames of width 2° in using a Nonius Kappa CCD diffractometer, with a detector-to-crystal distance of 30 mm. The Collect program was then used to calculate a data collection strategy to 99.5% completeness for 2θ = 27.5° using a combination of 2° and ω scans of 10 s·deg^{-1} exposure time. Crystals were indexed using the DENZO-SMN package[24] and positional data were refined along with diffractometer constants to give the final unit cell parameters. Integration and scaling (DENZO-SMN, Scalepack[24]) resulted in unique data sets corrected for Lorentz and polarisation effects and for the effects of crystal decay and absorption by a combination of averaging of equivalent reflections and an overall volume and scaling correction. Structures were solved using SHELXS-97[25] and developed by alternating least-squares cycles

Table 4. NMR spectroscopic data for compound **1**

	^{13}C, solution Ambient temp.	^{13}C, solid state Ambient temp.	183 K	^{1}H, solution Ambient temp.
C=O	236.2	238	233.1 238.2 239.9	
aromatic	84.0, 89.1 97.9, 106.8 138.5	88.5, 91.3 102.7, 105.9 116.2, 117.5 140.3	87.5, 90.7 101.8, 105.0 115.0, 116.0 139.3	5.10 (1 H) 6.35 (1 H) 7.1−7.5
*i*Pr CH_3	18.1	18.9	19.5, 18.6, 18.1 17.3, 16.5	1.20
*i*Pr CH	12.8	14.7	12.4, 15.0, 16.5	1.70
Sn CH_3	−8.2	−7.5	−6.3, −7.9, −11.5	0.5

Table 5. Crystal data and structure refinement for $[Cr(CO)_3SnMe_3C_8H_5NSi(iPr)_3]$

Identification code	sntipsa
Empirical formula	$C_{23}H_{35}CrNO_3SiSn$
Molecular mass	572.30
Temperature	100(2) K
Wavelength	0.71073 Å
Crystal system	orthorhombic
Space group	*Pbcn*
Unit cell dimensions	a = 17.1962(19) Å b = 18.1537(19) Å c = 16.717(2) Å
Volume	5218.6(10) Å
Z	8
Density (calculated)	1.457 Mg/m^3
Absorption coefficient	1.442 mm^{-1}
F(000)	2336
Crystal size	0.20 × 0.20 × 0.15 mm
θ range for data collection	2.04 to 27.50°.
Index ranges	$-22 \le h \le 19$ $-23 \le k \le 22$ $-21 \le l \le 19$
Reflections collected	21815
Independent reflections	5909 [R(int) = 0.1597]
Completeness to θ = 27.50°	98.6%
Max./min. transmission	0.8128/0.7614
Refinement method	Full-matrix least squares on F^2
Data/restraints/parameters	5909/0/281
Goodness-of-fit on F^2	0.942
Final R indices [$I > 2\sigma(I)$]	$R1$ = 0.0549, $wR2$ = 0.0974
R indices (all data)	$R1$ = 0.1414, $wR2$ = 0.1222
Extinction coefficient	0.00014(8)
Largest diff. peak and hole	1.109 and −0.910 e·Å^{-3}

and difference Fourier synthesis (SHELXL-97[3]) with the aid of the program XSeed.[26] All non-hydrogen atoms were modelled anisotropically, while hydrogen atoms were assigned an isotropic thermal parameter 1.2 times that of the parent atom (1.5 for terminal atoms) and allowed to ride. All calculations were carried out with either a Silicon Graphics Indy workstation or an IBM-compatible PC. Crystal data for **1**: $C_{23}H_{35}CrNO_3SiSn$, M = 572.30 g·mol^{-1}, orthorhombic, space group *Pbcn*, a = 17.1962(19), b = 18.1537(19), c = 16.717(2) Å, V = 5218.6(10) Å^3, D_c = 1.457 Mg·m^{-3}, Z = 8, μ= 14.42 cm^{-1}, T = 100(2) K, Reflections measured: 21 815, unique data: 5909, parameters: 281, $R1$ [$F^2 > 2\sigma(F^2)$] 0.0549, $wR2$ (all data) 0.1222. Crystallographic data (excluding structure factors) for the structure reported in this paper have been deposited with the Cambridge Crystallographic Data Centre as supplementary publication no. CCDC-167381. Copies of the data can be obtained free of charge on application to CCDC, 12 Union Road, Cambridge CB2 1EZ, UK [Fax: int. code + 44-1223/336-033; E-mail: deposit@ccdc.cam.ac.uk].

Acknowledgments

We thank the EPSRC and King's College London for the provision of the X-ray diffractometer and the Nuffield Foundation for the provision of computing equipment.

[1] [1a] F. G. Riddell, S. Arumugam, K. D. M. Harris, *J. Am. Chem. Soc.* **1993**, *115*, 1881; – [1b] F. G. Riddell, G. Bernath, F. Fulop, *J. Am. Chem. Soc.* **1995**, *117*, 2327.

[2] D. Braga, *Chem. Rev.* **1992**, *92*, 633.

[3] P. J. Beswick, C. S. Greenwood, T. J. Mowlem, G. Nechvatal, D. A. Widdowson, *Tetrahedron* **1988**, *44*, 7325.

[4] N. L. Allinger, Y. H. Yu, J.-H. Lii, *J. Am. Chem. Soc.* **1989**, *111*, 8551.

[5] R. S. Cahn, C. K. Ingold, V. Prelog, *Angew. Chem.* **1966**, *78*, 413; *Angew. Chem. Int. Ed. Engl.* **1966**, *5*, 385.

[6] The torsion angles in **5**, **6** are taken from the crystal, but numbering is in terms of diagram **1**. The torsion angle C2−N−Si−C_a is negative in the chiral crystal, so for achiral **2**, calculated conformations for the *N*-TIPS groups will be normalised to the conformation in which this torsion angle is likewise negative.

[7] J. E. Anderson, K. H. Koon, J. E. Parkin, *Tetrahedron* **1985**, *41*, 561.

[8] J. E. Anderson, B. R. Bettels, *Tetrahedron* **1990**, *46*, 5353.

[9] I. Columbus, S. E. Biali, *J. Org. Chem.* **1993**, *58*, 7020.

[10] J. E. Anderson, D. Casarini, L. Lunazzi, A. Mazzanti, *Eur. J. Org. Chem.* **2000**, *65*, 479.

[11] J. E. Anderson, D. Casarini, L. Lunazzi, A. Mazzanti, *J. Org. Chem.* **2000**, *65*, 1729. The conformations for the TIPS group adopted by compound **13** are firstly (*g*, −*g*, *a*) and secondly a rapid equilibration between (*g*, −*g*, *g*) and (*a*, −*g*, *g*).

[12] W. P. Rothwell, J. S. Waugh, *J. Chem. Phys.* **1981**, *74*, 2721.

[13] P. J. Barrie, J. E. Anderson, *J. Chem. Soc., Perkin Trans. 2* **1992**, 2031, and earlier results cited therein.

[14] P. J. Barrie, C. A. Mitsopoulou, M. Motevalli, E. W. Randall, *J. Chem. Soc., Dalton Trans.* **1997**, 353.

[15] F. A. L. Anet, D. Donovan, U. Sjostrand, F. Cozzi, K. Mislow, *J. Am. Chem. Soc.* **1980**, *102*, 5941

[16] J. E. Anderson, R. W. Franck, W. L. Mandella, *J. Am. Chem. Soc.* **1972**, *94*, 4608.

[17] J. E. Anderson, D. J. D. Barkel, *J. Chem. Soc., Perkin Trans. 2* **1984**, 1053.

[18] [18a] D. Casarini, E. Foresti, L. Lunazzi, D. Macciantelli, *J. Am. Chem. Soc.* **1988**, *110*, 4527. – [18b] D. Casarini, S. Davalli, L. Lunazzi, D. Macciantelli, *J. Org. Chem.* **1989**, *54*, 4616.

[19] A. E. Aliev, K. D. M. Harris, F. Guillaume, P. J. Barrie, *J. Chem. Soc., Dalton Trans.* **1994**, 3193, and earlier work cited therein.

[20] P. Delise, G. Allegra, E. R. Mognaschi, A. Chierico, *J. Chem. Soc., Faraday Trans. 2* **1975**, *71*, 207.

[21] A. E. Aliev, K. D. M. Harris, F. Guillaume, *J. Phys. Chem.* **1995**, *99*, 1156.

[22] P. J. Barrie, C. A. Mitsopoulou, E. W. Randall, *J. Chem. Soc., Dalton Trans.* **1995**, 2125.

[23] R. Hooft, *Collect*, Nonius B. V., Delft, **1998**.

[24] Z. Otwinowski, W. Minor, in *Methods in Enzymology* (Eds.: C. W. Carter, R. M. Sweet), Academic Press, New York, **1996**, vol. 276, pp. 307−326.

[25] G. M. Sheldrick, *SHELXL-97*, University of Göttingen, **1997**.

[26] L. J. Barbour, *XSeed, A Program of the Manipulation and Display of Crystallographic Models*, University of Missouri, Columbia, **1999**.

Received June 5, 2001
[I01204]

Semi-Rigid Bis-Phosphane Ligands for Metallamacrocycle Formation

Susan K. Armstrong,*[a] Ronald J. Cross,[b] Louis J. Farrugia,[b] David A. Nichols,[b] and Alexis Perry[b]

Keywords: Phosphanes / Metallacycles / Platinum / Ditopic ligands / X-ray structures

Efficient syntheses are described for the new bridging bis-phosphanes DPPN (**4**) and DPEN (**5**) built around the restricted rigidity of a 2,7-dialkoxynaphthalene backbone. These show marked preference for bridging pairs of metal atoms (Pt^{II}, Mo^0) to form metallamacrocycles or oligomers. Single-crystal X-ray structure determinations of four dimeric complexes with Pt^{II} and Mo^0 are reported. The dimeric platinum complexes can be obtained as the kinetically favoured *trans*,*trans* products, which isomerise to the *cis*,*cis* forms in the presence of free ligand. *cis*,*cis*-$[Pt_2Cl_4(DPEN)_2]$ (**12**) shows marked hydroformylation catalytic activity.

Introduction

Wide bite-angle and bridging phosphane ligands and their metal complexes have recently undergone a marked resurgence of interest. Some bis-phosphanes, like van Leeuwen's "xantphos" **1** (Scheme 1) and related ligands with calculated bite angles around 110−115°, are well suited to *cis* chelation in a trigonal bipyramidal complex.[1,2] The xanthene skeleton imposes a well-defined bite angle on such ligands, which has been linked to the high activity of hydroformylation catalysts derived from them, particularly rhodium and platinum derivatives.[3,4] *trans*-Spanning bis-phosphane ligands and their metal complexes have recently been reviewed.[5] *trans*-Spanning has been reliably achieved by, among others, Venanzi and co-workers, who used the rigid benzo[c]phenanthrene skeleton in ligands **2** (Scheme 1).[6] More flexible long-chain bis-phosphanes occasionally coordinate *trans*, though these are often in equilibria with other geometries[7] unless constrained by other ligands. An alternative strategy has been to synthesise some *trans*-spanning ligands in situ.[8,9] Ditopic bis-phosphanes are designed for coordination to two metal centres, with[10] or without (e.g. Faraone's ligand **3**[11]) metal−metal bonding. A further class of ligands involves monophosphanes on solid supports, whose coordination geometry is subject to different controls.[12,13]

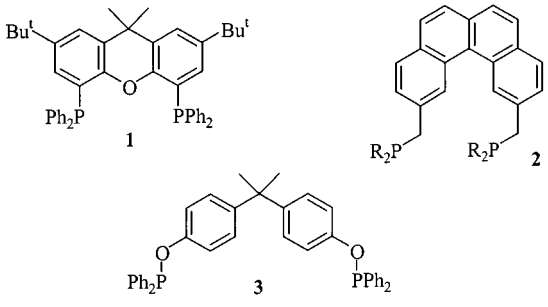

Scheme 1

We were interested to study the complexation behaviour of novel phosphanes, designed to be wide-angle chelators or bridging, and the catalytic activity of their transition metal complexes. For a ligand to be widely used, it must be readily available, with a short and high-yielding synthesis. We report here the efficient syntheses and complexing properties of two new semi-rigid, ditopic bis-phosphane ligands which further explore the relationship between ligand geometry and the structures of their transition metal complexes. The work extends recent reports on the formation of metallamacrocycles using related ligand types.[11]

Results and Discussion

Two new bis-phosphane ligands, 2,7-bis(3-diphenylphosphanylpropoxy)naphthalene (DPPN) **4** and 2,7-bis(2-diphenylphosphanylethoxy)naphthalene (DPEN) **5** (Scheme 2), were designed to allow similar separation be-

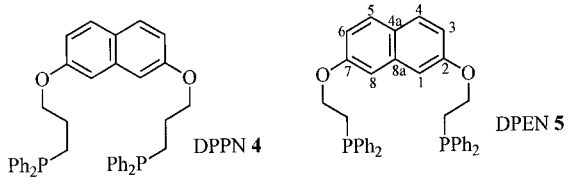

Scheme 2

[a] Department of Chemistry, University of Glasgow, Glasgow G12 8QQ, UK
Fax: (internat.) + 44-141/330-4888
E-mail: s.armstrong@chem.gla.ac.uk
[b] Department of Chemistry, University of Glasgow, Glasgow G12 8QQ, UK
Fax: (internat.) + 44-141/330-4888

 © WILEY-VCH Verlag GmbH, 69451 Weinheim, Germany, 2002 1434−1948/02/0101−0141 $ 17.50+.50/0

tween the P atoms to that found in the Venanzi ligands of type **2**, but with a more flexible ligand backbone. Bisphosphanes **2** suffer from lengthy and low-yielding synthetic approaches. By contrast, we sought ligands which could be synthesised by short, straightforward routes.

Ligand Synthesis

For the synthesis of DPPN **4** (Scheme 3), 2,7-dihydroxynaphthalene was alkylated with allyl bromide to give bisallyl ether **6** by a modification of the literature procedure. Addition of 18-crown-6 to the reaction mixture, and improved purification methods, enabled us to improve the published yield of 45% crude[14] or 27% pure[15] to a relatively good 59% of recrystallised product. Ultraviolet irradiation of bis-ether **6** and diphenylphosphane in the absence of solvent gave the bis-phosphane DPPN (**4**) in an overall yield for this two-step synthesis of 41%. DPPN is a very viscous colourless oil which oxidises slowly in air (more rapidly in solution). In the synthesis of DPEN (**5**), the same starting material was alkylated with ethyl bromoacetate to give bis-ester **7**, which was reduced to the corresponding diol **8**[16] and then converted into bis-mesylate **9**. Treatment of **9** with lithium diphenylphosphide gave the bis-phosphane DPEN (**5**) in an overall yield of 49%. DPEN is a white, crystalline air-stable solid which oxidises slowly in solution.

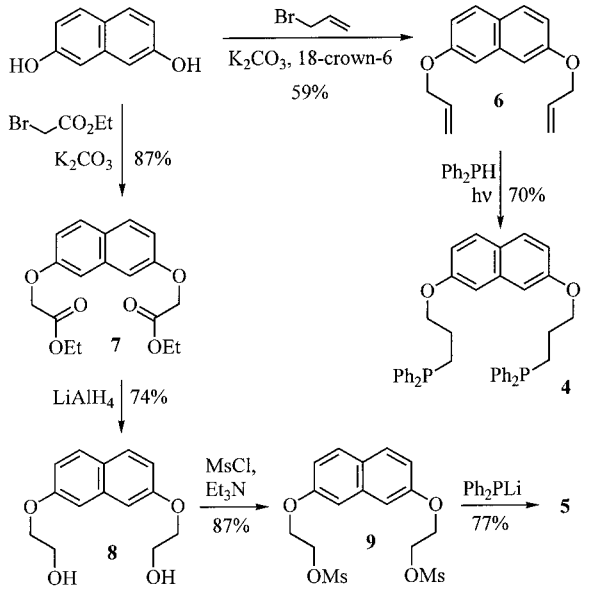

Scheme 3

Platinum(II) Complexes

The formation of square-planar platinum(II) complexes is known to be dependent on a number of factors, both kinetic and thermodynamic, including solvent polarity,[17] the *trans* effect of resident ligands, and the order of adding the reagents.[18,19] In addition, when polydentate ligands are involved, solution concentration exerts an effect, with high dilution favouring monomers whilst higher concentrations can promote dimer or oligomer formation. With suitable magnetic nuclei, the geometry of the products can often be determined from the magnitude of the coupling constants to ^{195}Pt. These are greatly dependent on the *trans* influence of the ligands opposite. For example, a phosphane *trans* to chloride has $^{1}J_{P\text{-}Pt}$ about 3500 Hz whereas a phosphane *trans* to another phosphane has $^{1}J_{P\text{-}Pt}$ near 2500 Hz.[20]

The geometry of the platinum complexes formed from DPEN (**5**) was dependent on the reaction conditions. Addition of up to one equivalent of **5** in dichloromethane to a solution of $[PtCl_2(SMe_2)_2]$ (**10**; *cis*/*trans* mixture) in the same solvent produced a complex mixture of products (Scheme 4). The $^{31}P\{^{1}H\}$ NMR spectrum of this mixture consisted of about ten signals, of varying intensities, with their associated ^{195}Pt satellites. Analysis of the ^{31}P-^{195}Pt coupling constants showed that it contained signals due to both *cis*- and *trans*-coordinated phosphanes. Only one compound, significantly less polar than the rest, could be isolated from the mixture by column chromatography. The $^{31}P\{^{1}H\}$ NMR spectrum of this complex gave $J_{Pt\text{-}P}$ = 2562 Hz indicating *trans* coordination of the ligand. A FAB mass spectrum indicated that the complex was dimeric. Slow diffusion of diethyl ether into a concentrated dichloromethane solution of the complex produced yellow prisms, and a single crystal X-ray analysis (Figure 1) showed the complex to be the metallamacrocycle *trans*,*trans*-$[Pt_2Cl_4(DPEN)_2]$ (**11**). The yield of **11** was only 10%, however, and the remainder of the products in the mixture could not be separated; their behaviour on chromatography and on attempted crystallisation suggested facile interconversion.

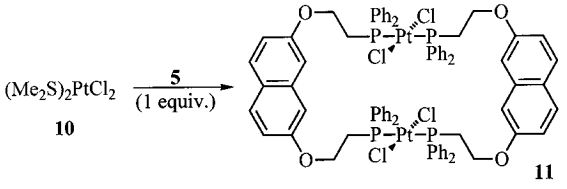

Scheme 4

Figure 1 shows that complex **11** forms a centrosymmetric dimer with the DPEN ligand bridging between Pt centres in a mutually *trans*,*trans* arrangement, as expected from the colour and the NMR evidence. The four ligating P and Cl atoms form a slightly distorted square planar arrangement (these four atoms deviate from their least-squares plane by ±0.03 Å). The nearly linear $PtCl_2$ unit is displaced towards the centre of the metallamacrocyclic ring and towards the other centrosymmetrically related Pt atom [Pt(1)···Pt(1)^{ii} = 10.691(1) Å]. The space-filling diagram of **11** (Figure 2) shows the hetero-ring system to have a central hydrophobic cavity of radius ≈5 Å.

When this experiment was repeated using **4**, an intractable mixture of complexes was again produced. The $^{31}P\{^{1}H\}$ NMR spectrum of the crude product again showed a mixture of signals, of varying intensities, with their associated ^{195}Pt satellites. Analysis of the ^{31}P-^{195}Pt coupling constants showed that it contained signals due to both *cis*- and

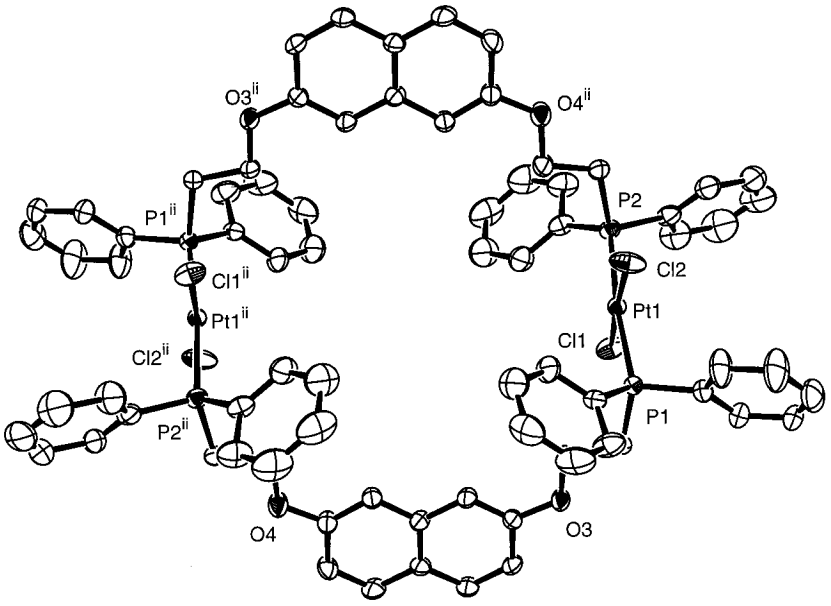

Figure 1. Ortep plot of compound **11** with thermal ellipsoids shown at the 30% probability level; atoms with primed labels are related to unprimed atoms by the symmetry operation ($1 - x$, $2 - y$, $1 - z$); selected bond lengths (Å) and angles (°): Pt−Cl(1) 2.2982(15), Pt−Cl(2) 2.2879(16), Pt−P(1) 2.3113(14), Pt−P(2) 2.3057(15), Pt···Pt^{ii} 10.692(1) ; Cl(1)−Pt−P(1) 92.02(5); Cl(1)−Pt−P(2), 88.70(6); Cl(2)−Pt−P(1) 87.75(6), Cl(2)−Pt−P(2) 91.27(6), Cl(1)−Pt−Cl(2) 177.29(8), P(1)−Pt−P(2) 174.32(5)

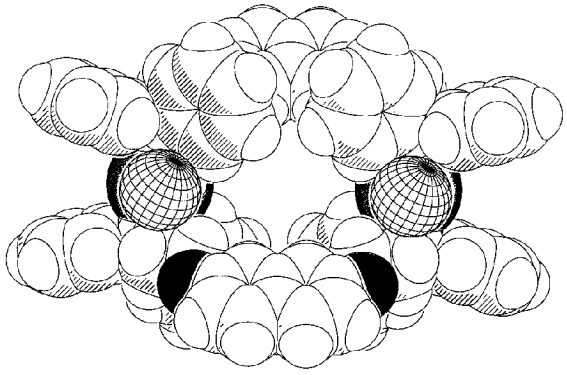

Figure 2. Space-filling plot of compound **11** showing the central cavity of the metallamacrocycle

trans-coordinated phosphanes, but in this case no single complex could be isolated by either chromatography or crystallisation.

Other methods of treating either **4** or **5** with Pt^{II} complex **10** produced a quite different outcome. The major products in almost all cases were the *cis,cis* complexes **12** (of DPEN) and **13** (of DPPN) (Scheme 5). These complexes show $J_{Pt\text{-}P}$ of 3627 Hz and 3646 Hz respectively, indicating exclusively *cis* coordination of the phosphanes. They were shown to be dimeric by FAB-MS, and to be *cis,cis*-dimers by single crystal X-ray analysis (Figures 3 and 4). Complex geometry was independent of precursor concentration over a range of 1.5−39 mmol l^{-1}, and apparently independent of solvent polarity (20% CH_2Cl_2 in toluene gave identical results to chloroform). Use of an excess of the bis-phosphane invariably resulted in formation of *cis,cis* complexes **12** or **13** as the sole or overwhelmingly major product. Similarly on inverse addition, i.e. addition of **10** to the bis-phosphane, the *cis,cis* complexes were the only products visible by ^{31}P NMR spectroscopy. These results led us to conclude that *cis,cis* complexes **12** and **13** were the thermodynamic products, and equilibration to them was catalysed by an excess of the phosphane, either by adding an excess of the ligand, or by having the excess present during the (inverse) addition of the platinum precursor. The mixture formed on "normal" addition of one equivalent of phosphane appeared to be a mixture of kinetic and thermodynamic products, of which the *trans,trans*-dimer **11** was the only one isolated. We tested this hypothesis by treating such mixtures with an excess of the bis-phosphane ligand **4** or **5** and in both cases the *cis,cis* complexes **12** and **13** became the only products observed by ^{31}P NMR spectroscopy.

Figure 3 shows that complex **12** forms a centrosymmetric dimer, this time with the DPEN ligand bridging between Pt centres in a mutually *cis,cis* arrangement. The geometry about the Pt centre shows a slight tetrahedral distortion away from a regular square planar environment. The "twist" angle between the $PtCl_2$ plane and the PtP_2 plane is 12.7°. The Pt−P bonds are shorter and Pt−Cl bonds longer than observed for **11**, consistent with the differing *trans* influences. The $PtCl_2$ groups lie exterior to the metallamacrocycle and the 2,7-dialkoxynaphthalene rings of the DPEN ligands are approximately parallel to each other and nearly in van der Waals contact, as shown in Figure 5. Figure 4 shows that complex **13** forms another centrosymmetric dimer, with the DPPN ligand bridging between Pt centres again in a mutually *cis,cis* arrangement. The geometry about the Pt centre is a more regular square-planar

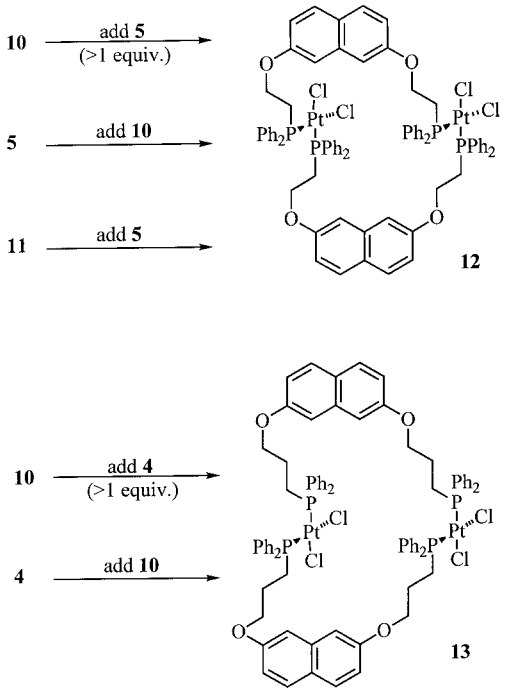

Scheme 5

environment than found in **12** – the "twist" angle between the $PtCl_2$ plane and the PtP_2 plane is only 3.3°. The Pt−P and Pt−Cl bond lengths are very similar to those observed for **12**. The longer "reach" of the DPPN ligands allows the two $PtCl_2$ groups to lie interior to the metallamacrocycle so that the Cl(1)···Cl(1)^{ii} non-bonded distance is 3.942 Å, about 0.4 Å longer than the sum of van der Waals radii. This is shown in Figure 6.

It was observed by $^{31}P\{^1H\}$ NMR spectroscopy that treatment of a solution of pure *trans,trans*-dimer **11** with a small amount of **5** at room temperature rapidly converted it to the *cis,cis*-dimer **12** in the few minutes taken to obtain a spectrum. At lower temperatures, however, it was possible to observe the isomerisation process (Figure 7). A $^{31}P\{^1H\}$ NMR spectrum (Figure 7, trace a) was obtained from a solution of *trans,trans*-dimer **11** before cooling to 203 K. A few crystals of **5** were then added to the sample tube which was briefly shaken before being immediately frozen in liquid nitrogen and returned to the NMR probe. Over two hours at 203 K (traces b and c), little change was observed to the signal with J = 2530 Hz (δ = 6.4) representing *trans,trans*-dimer **11**, although a few signals for intermediates did appear at δ = 10.7 and δ = 5.7. On warming to 223 K, the signal with J = 2530 Hz rapidly broadened and eventually vanished (trace d). On warming to 243 K, it was replaced by a signal with J = 3624 Hz (δ = 6.1) representing the *cis,cis*-dimer **12**. After 40 minutes at this temperature, the broad signals representing intermediates had disappeared, and the only significant species present were the *cis,cis*-dimer **12** and free phosphane at δ = −24 (trace e). No further change was observed after 19 h at room temperature (trace f). The broadness of the signals (traces b−d) did not allow identification of the intermediate fluxional five-coordinate platinum complexes.

Other Metal Complexes

In view of the interesting metallamacrocycles **11**−**13** formed by DPEN (**5**) and DPPN (**4**) with Pt^{II}, and their isomerisation behaviour, a brief investigation was made of the complexation of these new ligands with a wider range of transition metals. The results were, however, harder to obtain and interpret than with platinum.

Stirring an equimolar mixture of **5** and $[PdCl_2(MeCN)_2]$ overnight in dichloromethane produced a yellow solid, the $^{31}P\{^1H\}$ NMR spectrum of which consisted of several singlets. All attempts to isolate a pure complex from the mixture were unsuccessful, although a FAB mass spectrum suggested that the main species present was again dimeric and corresponded to $[Pd_2Cl_4(DPEN)_2]$. Attempts to prepare rhodium complexes of DPEN were unsuccessful. Reactions with (acetylacetonato)Rh(norbornadiene), (1,5-cyclooctadiene)$_2Rh_2Cl_2$, $[RhCl(CO)(PPh_3)_2]$ and $[RhCl(PPh_3)_3]$ all produced intractable mixtures from which no complexes could be isolated.

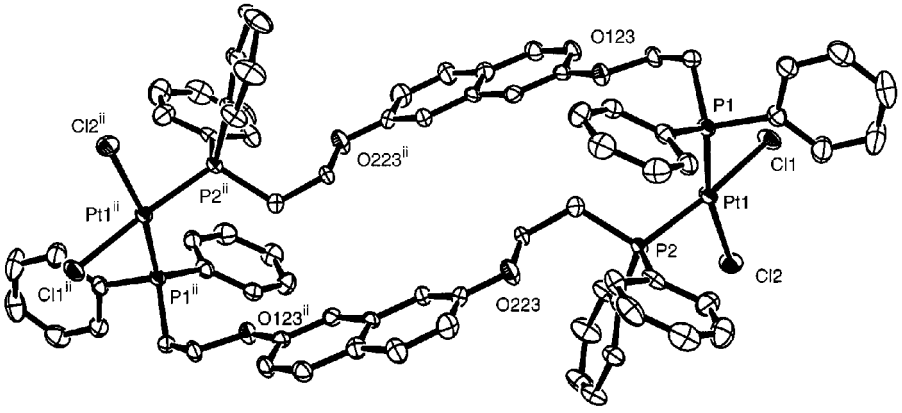

Figure 3. Ortep plot of compound **12** with thermal ellipsoids shown at the 50% probability level; atoms with primed labels are related to unprimed atoms by the symmetry operation (1 − x, 1 − y, −z); selected bond lengths (Å) and angles (°): Pt−Cl(1) 2.3495(19), Pt−Cl(2) 2.3566(18), Pt−P(1) 2.2567(18), Pt−P(2) 2.2479(19), Pt···Pt^{ii} 14.174(1); Cl(1)−Pt−Cl(2) 87.56(7), P(1)−Pt−P(2) 97.54(7)

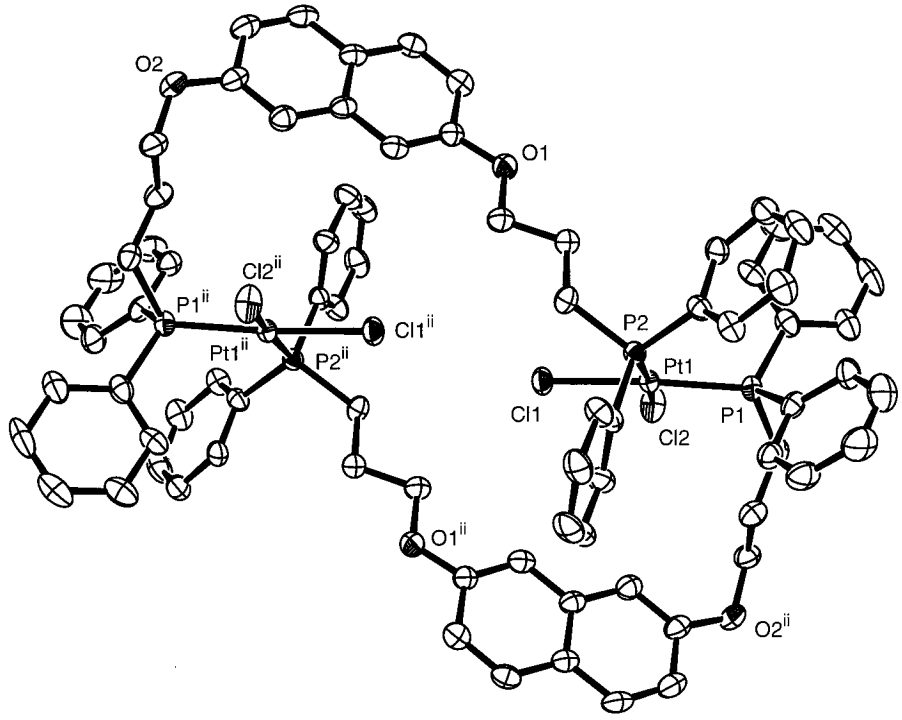

Figure 4. Ortep plot of compound **13** with thermal ellipsoids shown at the 50% probability level; atoms with primed labels are related to unprimed atoms by the symmetry operation ($-x$, $-y$, $1-z$); selected bond lengths (Å) and angles (°): Pt−Cl(1) 2.3500(9), Pt−Cl(2) 2.3467(10), Pt−P(1) 2.2544(9), Pt−P(2) 2.2510(9), Pt···Pt^{ii} 8.369(1); Cl(1)−Pt−Cl(2) 86.20(7), P(1)−Pt−P(2) 98.41(7)

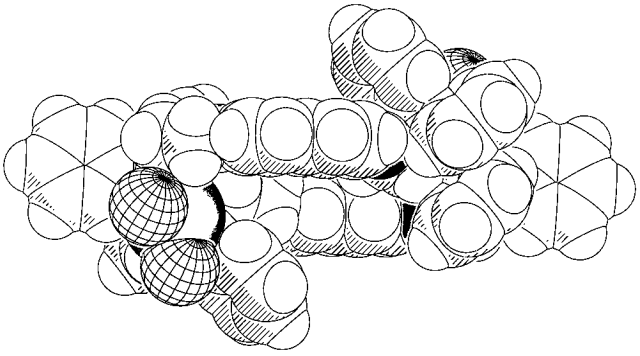

Figure 5. Space-filling plot of compound **12** showing the parallel close packing of the 2,7-dialkoxynaphthalene rings

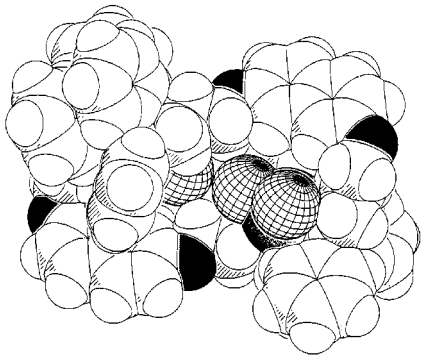

Figure 6. Space-filling plot of compound **13** showing the close Cl···Cl contact

Refluxing a suspension of **5**, molybdenum hexacarbonyl and sodium borohydride in ethanol[21] produced a pale-yellow solid, shown by single crystal X-ray analysis to be the *cis,cis*-dimer $[Mo_2(CO)_8(DPEN)_2]$ (**14**) (Scheme 6 and Figure 8). The DPEN ligand adopts a similar conformation to that observed in **12**. The phosphane ligands coordinate in a *cis* fashion to the Mo centres and the two $Mo(CO)_4$ moieties lie exterior to the metallacyclic ring. The 2,7-dialkoxynaphthalene rings of the DPEN are approximately parallel to each other, as seen in **12**.

Catalytic Application

Recent work by van Leeuwen and co-workers on the catalytic hydroformylation of alkenes has highlighted an important application of phosphanes with wide bite angles.[1] They have reported excellent linear/branched product selectivity in the hydroformylation of terminal alkenes when the wide-angle bis-phosphane "xantphos" (**1**) or the corresponding bis-arsane is used in a Pt/Sn catalyst system. With this in mind, we set out to investigate whether our bridging bis-phosphanes would give similar catalytic activity. We note that the dimeric complex *cis,cis*-$[Pt_2Cl_4(DPEN)_2]$ (**12**) has a P−Pt−P angle (97.5°) in the normal range for a complex having two *cis*-coordinated monophosphane ligands.[22−24] The ditopic ligands in a dimeric complex cannot, however, be expected to behave exactly as independent monodentate phosphanes, nor yet as the two phosphanes of a chelating ligand such as **1**. We applied van Leeuwen's procedure to the hydroformylation of 1-octene with *cis,cis*-$[Pt_2Cl_4(DPEN)_2]$ (**12**) as the catalyst.

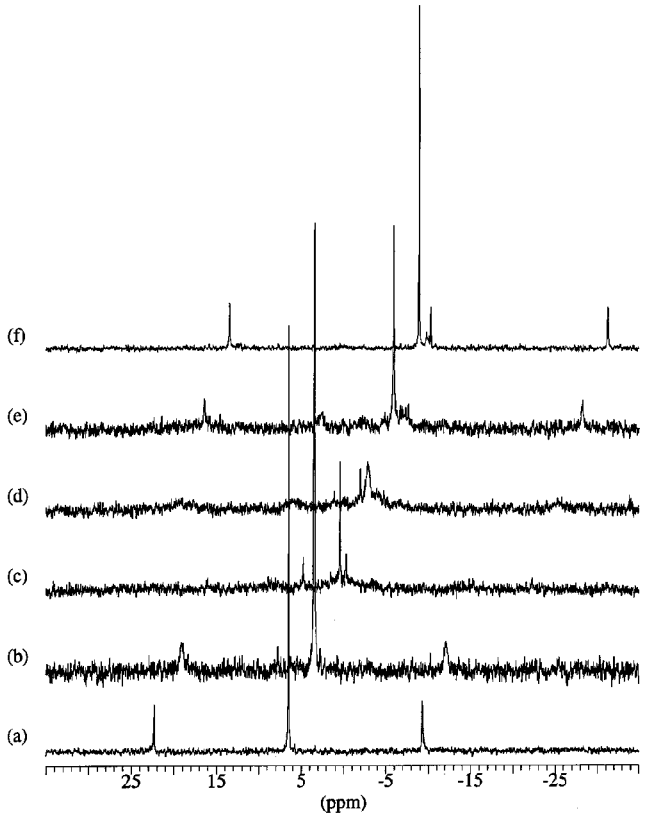

Figure 7. Stacked ^{31}P NMR spectra showing the changing Pt−P coupling constant on warming the mixture of complex **11** and DPEN **5** from 203 K; the spectra have been normalised to take account of the number of scans, but were run unlocked. They are plotted with an increment of 3 ppm between traces, and with traces (a) and (f) plotted at half the vertical intensity of the intervening spectra. Traces: (a) 298 K before commencing experiment; (b) 203 K after 35 min; (c) 203 K after 160 min; (d) 223 K after 210 min; (e) 243 K after 290 min; (f) 298 K after 24 h

The substrate was heated to 60 °C under an atmosphere of CO (20 bar) and H_2 (20 bar) in the presence of **12** (0.4 mol %) and $SnCl_2$ (0.8 mol %). After 18 hours, GCMS and ^1H NMR analysis of the mixture showed complete conversion of 1-octene to nonanal (87%) and 2-methyloctanal (11%) (both of which tended to trimerise in solution) with 2% of an unidentified by-product (Scheme 7). This activity and selectivity compares reasonably well with previously reported, monomeric, hydroformylation catalysts.

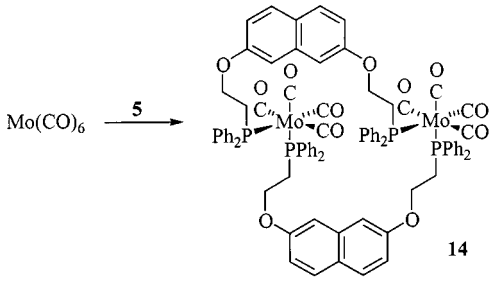

Scheme 6

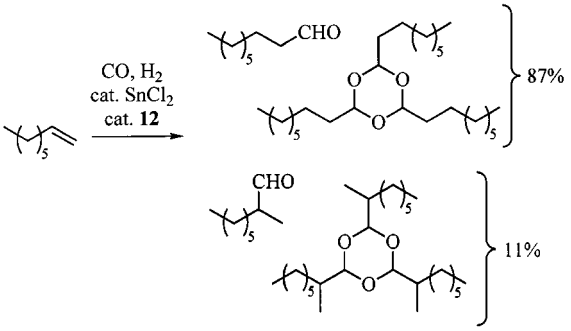

Scheme 7

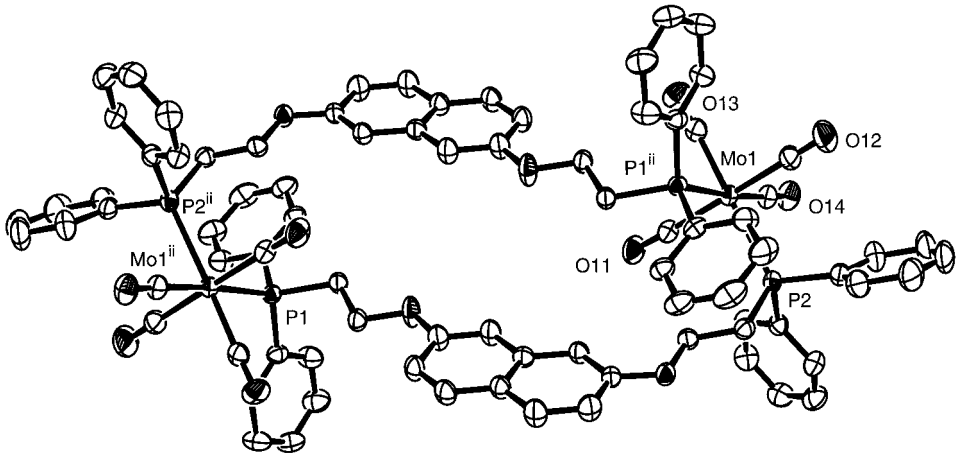

Figure 8. Ortep plot of compound **14** with thermal ellipsoids shown at the 50% probability level; atoms with primed labels are related to unprimed atoms by the symmetry operation (−*x*, −*y*, 1 − *z*); selected bond lengths (Å) and angles (°): Mo−P(1) 2.5434(9), Mo−P(2) 2.5536(9), Mo···Mo^{ii} 13.720(1); P(1)−Mo−P(2) 98.75(3)

Conclusion

Short, straightforward and efficient syntheses of two new bis-phosphane ligands, DPPN (**4**) and DPEN (**5**), have been developed. Both ligands are ditopic: in transition metal complexation, dimeric or oligomeric complexes are greatly favoured. No monomeric complexes have been observed using Pt^{II}, Pd^{II} or Mo^0.

In the case of platinum, although kinetic conditions lead to a mixture of products, employing an excess of ligand to catalyse isomerisation allows clean formation of the 28-membered metallamacrocycle **12** from DPEN (**5**) and the 32-membered metallamacrocycle **13** from DPPN (**4**). These complexes feature *cis* coordination at both square-planar metal centres. The synthesis of a 28-membered molybdenum macrocycle **14** also revealed a preference for *cis* coordination, in this case as part of an octahedral geometry. The very strong preferences of these ligands for forming metallamacrocyclic complexes is interesting, particularly when contrasted with the strong preference for *trans*-chelation shown by Venanzi's related ligands **2**: clearly, formation of monomers with *trans*-coordinated phosphanes is not favoured by ligands of this general shape and size unless rigid steric constraints prevent bridging.

The potential importance of ditopic bis-phosphanes and their macrocyclic transition metal complexes is demonstrated by the activity and linear selectivity of platinum complex **12** as a hydroformylation catalyst.

Experimental Section

General Remarks: All reactions were carried out using oven-dried glassware under a nitrogen atmosphere using standard Schlenk techniques unless stated otherwise. THF and CH_2Cl_2 were freshly distilled from sodium/benzophenone and calcium hydride respectively. Pet. ether refers to petroleum ether boiling between 40 and 60 °C. $PtCl_2(SMe_2)_2$ was prepared by the literature method.[18] Other reagents and starting materials were used as supplied without further purification. Column chromatography was carried out using silica gel (finer than 230 mesh ASTM) and reagent grade solvents which were not purified further before use.

All NMR spectra were obtained from $CDCl_3$ solutions unless stated otherwise. ^1H and ^{13}C NMR spectra were recorded using a Bruker DPX 400 spectrometer operating at 400 and 100 MHz, respectively. ^{31}P NMR spectra were recorded using a Bruker WP 200 SY spectrometer operating at 81 MHz. Chemical shifts (δ) are given in ppm relative to residual $CHCl_3$ (δ = 7.27) for ^1H, $CDCl_3$ (δ = 77.0) for ^{13}C, and 85% H_3PO_4 (δ = 0.0, external) for ^{31}P. Coupling constants (*J*) are given in Hz. Infra-red spectral analysis was performed on a Jasco 410 spectrometer, using KBr discs; absorbances are quoted in wavenumbers (cm^{-1}). Mass spectra were obtained using a JMS 700 spectrometer operating, unless stated otherwise, in FAB mode for coordination complexes, whose isotope patterns matched calculated patterns in all cases,[25] and in EI mode for their organic precursors. GC-MS was carried out using a Hewlett Packard 5890 Series II model GC, with a mass selective detector type 5971.

2,7-Bisallyloxynaphthalene (6): Potassium carbonate (3.80 g, 27.5 mmol) and 18-crown-6 (496 mg, 1.88 mmol) were added to a solution of 2,7-dihydroxynaphthalene (2.00 g, 12.5 mmol) in acetone (30 mL) under air. The mixture was refluxed for 1 h and then allyl bromide (2.7 mL, 31 mmol) was added and the mixture refluxed for a further 15 h. The reaction mixture was allowed to cool, filtered and then concentrated. The crude product was purified by column chromatography (silica, 5% EtOAc/hexane) and recrystallised from hexane to give bis-ether **6** as colourless plates (1.76 g, 59%): m.p. 60−62 °C [ref.[15] 62.5−63 °C (MeOH)]. ^1H NMR: δ = 4.65 (dt, *J* = 5.3, 1.4 Hz, 4 H, CH_2O), 5.33 (dq, *J* = 10.5, 1.4 Hz, 2 H, CH_AH_B=CH), 5.48 (dq, *J* = 17.3, 1.5 Hz, 2 H, CH_AH_B=CH), 6.13 (ddt, *J* = 17.2, 10.5, 5.3 Hz, 2 H, CH_2=C*H*), 7.02−7.05 (m, 4 H, $C_{3,6}$ H, $C_{1,8}$ H), 7.66 (d, *J* = 8.6 Hz, 2 H, $C_{4,5}$ H). ^{13}C NMR: δ = 68.8 (CH_2O), 106.5 (C_3, C_6), 116.4 (C_1, C_8), 117.7 (CH_2=CH), 124.4 (C_{4a}), 129.1 (C_4, C_5), 133.2 (CH_2=*C*H), 135.8 (C_{8a}), 157.1 (C_2, C_7). IR: $\tilde{\nu}$ = 3084 w, 2921 w, 2866 w, 1631 m, 1514 m, 1425 m, 1387 m, 1250 m, 1209 s, 1017 m, 936 m, 823 m. MS: *m*/*z* (%) = 240 (100) [M^+], 212 (13) [M^+ − CO], 199 (24) [M^+ − allyl], 185 (39), 171 (94) [M^+ − allyl − CO], 143 (25), 128 (35), 102 (26).

DPPN (4): Bisallyloxynaphthalene **6** (500 mg, 2.08 mmol) was dissolved in diphenylphosphane (0.90 mL, 5.2 mmol) and the resulting solution was irradiated with ultraviolet light from a medium-pressure mercury lamp for 18 h. The gelatinous mass was then washed with pentane, dissolved in ethyl acetate and concentrated. The crude product was purified by column chromatography (silica, 5% EtOAc/pet. ether) to give DPPN **4** as a very viscous colourless oil (891 mg, 70%). ^1H NMR: δ = 1.99−2.05 (m, 4 H, CH_2CH_2P), 2.27−2.31 (m, 4 H, CH_2P), 4.13 (t, *J* = 6.3 Hz, 4 H, CH_2O), 6.97−7.00 (m, 4 H, $C_{1,8}$ H, $C_{3,6}$ H), 7.32−7.38 (m, 12 H, Ph), 7.44−7.50 (m, 8 H, Ph), 7.64 (d, *J* = 9.6 Hz, 2 H, $C_{4,5}$ H). ^{13}C NMR: δ = 24.5 (d, *J* = 12 Hz, CH_2CH_2P), 25.8 (d, *J* = 17 Hz, CH_2P), 68.2 (d, *J* = 14 Hz, CH_2O), 106.1 (s, C_3, C_6), 116.2 (s, C_1, C_8), 124.2 (s, C_{4a}), 128.4−128.6 (m, Ph *p*-C and Ph *m*-C), 129.0 (s, C_4, C_5), 132.7 (d, *J* = 18 Hz, Ph *o*-C), 135.9 (s, C_{8a}), 138.4 (d, *J* = 13 Hz, Ph *i*-C), 157.4 (s, C_2, C_7). $^{31}P\{^1H\}$ NMR: δ = −16.4 (s, PPh_2). IR (neat): $\tilde{\nu}$ = 3069 m, 2944 m, 1627 s, 1514 s, 1434 s, 1387 s, 1253 m, 1210 s, 1159 m, 1026 m, 832 m, 751 s, 699 s. MS: *m*/*z* (%) = 612 (11) [M^+], 582 (13) [M^+ − CH_2O], 496 (64) [M^+ − $C_6H_{12}O_2$], 227 (29) [$Ph_2P(CH_2)_3^+$], 199 (100) [$CH_2PPh_2^+$], 183 (50). HRMS: calculated for $C_{40}H_{38}O_2P_2$: 612.2347; found 612.2347.

2,7-Bis(ethoxycarbonylmethoxy)naphthalene (7): Potassium carbonate (34.5 g, 250 mmol) and ethyl bromoacetate (6.1 mL, 55 mmol) were added to a solution of 2,7-dihydroxynaphthalene (4.00 g, 25.0 mmol) in acetone (100 mL) under air and the mixture was refluxed for 21 h. The reaction mixture was allowed to cool, filtered and then concentrated to give diester **7** (7.19 g, 87%). A portion was recrystallised from ethanol to give diester **7** as a white microcrystalline solid: m.p. 124−125 °C [ref.[26] 126 °C (EtOH)]. ^1H NMR: δ = 1.31 (t, *J* = 7.1 Hz, 6 H, CH_3CH_2O), 4.30 (q, *J* = 7.1 Hz, 4 H, CH_3CH_2O), 4.72 (s, 4 H, CH_2C=O), 6.98 (d, *J* = 2.5 Hz, 2 H, $C_{1,8}$ H), 7.10 (dd, *J* = 8.9, 2.5 Hz, 2 H, $C_{3,6}$ H), 7.69 (d, *J* = 8.9 Hz, 2 H, $C_{4,5}$ H). ^{13}C NMR: δ = 14.1 (CH_3CH_2O), 61.4 (CH_3CH_2O), 65.4 (CH_2C=O), 106.7 (C_3, C_6), 116.4 (C_1, C_8), 125.2 (C_{4a}), 129.4 (C_4, C_5), 135.3 (C_{8a}), 156.5 (C_2, C_7), 168.8 (C=O). IR: $\tilde{\nu}$ = 2993 w, 2916 w, 1760 s, 1629 m, 1203 s, 1076 m, 847 w, 834 w. MS: *m*/*z* (%) = 332 (100) [M^+].

2,7-Bis(2′-hydroxyethoxy)naphthalene (8): A solution of lithium aluminium hydride (0.85 g, 22 mmol) in THF (50 mL) was cooled to 0 °C and a solution of diester **7** (6.84 g, 20.6 mmol) in THF (85 mL) was added. The resulting mixture was stirred for 60 min and then allowed to warm to room temperature and stirred overnight. Further portions of $LiAlH_4$ (1.3 g in total) were added until

the reaction had gone to completion as indicated by TLC. The reaction mixture was quenched with EtOAc and then satd. aq. potassium sodium tartrate solution was added. The mixture was filtered, extracted with EtOAc, dried (Na_2SO_4) and concentrated to give diol **8** (3.79 g, 74%). A portion was recrystallised from methanol to give diol **8** as a white microcrystalline solid: m.p. 151−152 °C [ref.[16] 152−153 °C]. ^{1}H NMR: δ = 2.04 (t, *J* = 6.1 Hz, 2 H, OH), 4.03 (td, *J* = 4.2, 5.3 Hz, 4 H, C*H*$_2$OH), 4.20 (t, *J* = 4.5 Hz, 4 H, C*H*$_2$CH$_2$OH), 7.03 (dd, *J* = 8.8, 2.5 Hz, 2 H, $C_{3,6}$ H), 7.07 (d, *J* = 2.4 Hz, 2 H, $C_{1,8}$ H), 7.68 (d, *J* = 8.9 Hz, 2 H, $C_{4,5}$ H). ^{13}C NMR: δ = 61.5 (CH_2OH), 69.2 (*C*H$_2$CH$_2$OH), 106.3 (C_3, C_6), 116.3 (C_1, C_8), 125.2 (C_{4a}), 129.3 (C_4, C_5), 135.4 (C_{8a}), 157.2 (C_2, C_7). IR: ṽ = 3334 br, 2931 w, 2882 w, 1631 s, 1387 m, 1213 s, 1081 m, 838 m. MS: *m*/*z* (%) = 248 (77) [M$^+$], 204 (35), 160 (100).

2,7-Bis(2′-hydroxyethoxy)naphthalene bis(methanesulfonate)ester (9): Methanesulfonyl chloride (1.6 mL, 21 mmol) and triethylamine (2.9 mL, 21 mmol) were added to a solution of diol **8** (2.17 g, 8.75 mmol) in THF (100 mL) and the mixture was stirred for 30 min at room temperature. The reaction mixture was then filtered and the solvent removed. The residue was dissolved in EtOAc, washed with water, dried (Na_2SO_4) and concentrated. The crude product was recrystallised from dichloromethane and methanol to give dimesylate **9** as colourless plates (3.09 g, 87%): m.p. 134−135 °C. ^{1}H NMR: δ = 3.12 (s, 6 H, CH_3S), 4.36−4.38 (m, 4 H, C*H*$_2$CH$_2$OS), 4.64−4.66 (m, 4 H, CH_2OS), 7.01−7.05 (m, 4 H, $C_{3,6}$ H, $C_{1,8}$ H), 7.70 (d, *J* = 8.7 Hz, 2 H, $C_{4,5}$ H). ^{13}C NMR: δ = 37.8 (CH_3SO_2), 65.8 (CH_2), 67.9 (CH_2), 106.5 (C_3, C_6), 116.3 (C_1, C_8), 125.0 (C_{4a}), 129.5 (C_4, C_5), 135.5 (C_{8a}), 156.7 (C_2, C_7). IR: ṽ = 3025 w, 2941 w, 1629 s, 1517 m, 1353 s, 1256 m, 1216 s, 1171 s, 1069 m, 1024 m, 981 s, 930 s, 822 s. MS: *m*/*z* (%) = 404 (57) [M$^+$], 123 (100) [$C_2H_4OMs^+$], 79 (28) [$SO_2CH_3^+$]. $C_{16}H_{20}O_8S_2$ (404.45): calcd. C 47.51, H 4.98; found C 47.49, H 4.88.

DPEN (5): *n*-Butyllithium (2.5 M solution in hexanes, 2.3 mL, 5.75 mmol) was added to a solution of diphenylphosphane (1.0 mL, 5.75 mmol) in THF (6 mL). After stirring at room temperature for 15 minutes, a solution of dimesylate **9** (1.04 g, 2.57 mmol) in THF (60 mL) was added and the mixture stirred overnight. The solvent was removed and the residue dissolved in dichloromethane, washed with water, dried ($MgSO_4$) and concentrated. The crude product was recrystallised from ethyl acetate and pet. ether and washed with pentane to give DPEN (**5**) as white needles (1.15 g, 77%): m.p. 137−138 °C. ^{1}H NMR: δ = 2.65 (t, *J* = 7.7 Hz, 4 H, CH_2P), 4.22 (q, *J* = 7.5 Hz, 4 H, CH_2O), 6.80 (d, *J* = 2.2 Hz, 2 H, $C_{1,8}$ H), 6.90 (dd, *J* = 8.9, 2.3 Hz, 2 H, $C_{3,6}$ H), 7.35−7.42 (m, 12 H, Ph), 7.51−7.55 (m, 8 H, Ph), 7.60 (d, *J* = 8.9 Hz, 2 H, $C_{4,5}$ H). ^{13}C NMR: δ = 28.3 (d, *J* = 13 Hz, CH_2P), 65.2 (d, *J* = 27 Hz, CH_2O), 106.0 (s, C_3, C_6), 116.3 (s, C_1, C_8), 124.3 (s, C_{4a}), 128.6 (d, *J* = 7 Hz, Ph *m*-C), 128.8 (s, Ph *p*-C), 129.0 (s, C_4, C_5), 132.7 (d, *J* = 19 Hz, Ph *o*-C), 135.7 (s, C_{8a}), 137.9 (d, *J* = 12 Hz, Ph *i*-C), 156.9 (s, C_2, C_7). ^{31}P{^{1}H} NMR: δ = −22.8 (s, PPh_2). IR: ṽ = 3066 w, 2914 w, 1630 s, 1514 m, 1433 s, 1211 s, 1168 m, 1018 m, 834 m, 741 s, 697 s. MS: *m*/*z* (%) = 584 (4) [M$^+$], 553 (5) [M$^+$ − CH_3O], 371 (23) [M$^+$ − $C_2H_4PPh_2$], 341 (42) [M$^+$ − $C_2H_4PPh_2$], 328 (21), 212 (83) [$C_2H_3PPh_2^+$], 183 (100) [$C_{13}H_{11}O^+$]. HRMS: calculated for $C_{38}H_{34}O_2P_2$: 584.2034; found 584.2037.

***trans,trans*-[Pt$_2$Cl$_4$(DPEN)$_2$] (11):** A solution of DPEN (**5**; 250 mg, 0.43 mmol) in dichloromethane (8 mL) was added dropwise over 5 minutes to a solution of [$PtCl_2(SMe_2)_2$] (**10**; 167 mg, 0.43 mmol) in dichloromethane (5 mL). The mixture was stirred at room temperature for 5 min and then the solvent was removed. Column chromatography (silica, CH_2Cl_2) of the crude product mixture gave **11** as a yellow solid (37 mg, 10%). Slow diffusion of Et_2O into a CH_2Cl_2 solution of **11** produced yellow prisms suitable for X-ray analysis. ^{1}H NMR: δ = 3.08−3.15 (m, 8 H, CH_2P), 4.00−4.05 (m, 8 H, CH_2O), 6.70 (d, *J* = 2.3 Hz, 4 H, $C_{1,8}$ H), 6.85 (dd, *J* = 8.8, 2.4 Hz, 4 H, $C_{3,6}$ H), 7.42 (t, *J* = 7.6 Hz, 16 H, Ph *o*-H), 7.50 (t, *J* = 7.4 Hz, 8 H, Ph *p*-H), 7.54 (d, *J* = 8.9 Hz, 4 H, $C_{4,5}$ H), 7.81 (dt, *J* = 7.0, 5.6 Hz, 16 H, Ph *m*-H). ^{13}C NMR: δ = 28.9 (CH_2P), 62.4 (t, *J* = 4 Hz, CH_2O), 105.0 ($C_{3,6}$), 115.8 ($C_{1,8}$), 123.6 (C_{4a}), 127.6 (t, *J* = 5 Hz, Ph *m*-C), 128.3 ($C_{4,5}$) 128.8 (Ph *ipso*-C), 130.1 (Ph *p*-C), 133.0 (t, *J* = 6 Hz, Ph *o*-C), 134.9 (C_{8a}), 156.1 ($C_{2,7}$). ^{31}P{^{1}H} NMR: δ = 9.00 (*J* = 2563 Hz). IR: ṽ = 3053 w, 2919 w, 1631 s, 1513 m, 1435 s, 1253 m, 1209 s, 1158 m, 1101 m, 740 m, 691 s. MS: *m*/*z* (%) = 1701 (1.8) [$Pt_2Cl_4(DPEN)_2^+$], 1665 (1.3) [M$^+$ − Cl], 1628 (0.8) [M$^+$ − 2Cl]. HRMS: calculated for $C_{76}H_{69}Cl_4O_4P_4Pt_2$: 1701.2200; found 1701.2217.

***cis,cis*-[Pt$_2$Cl$_4$(DPEN)$_2$] (12). By Addition of an Excess of Phosphane:** A solution of DPEN (**5**; 150 mg, 0.26 mmol) in dichloromethane (8 mL) was added dropwise to a solution of [$PtCl_2(SMe_2)_2$] (**10**; 67 mg, 0.17 mmol) in toluene (90 mL) and dichloromethane (15 mL) and the mixture was stirred for 18 h at room temperature. The white precipitate formed was collected by filtration to obtain *cis,cis*-[$Pt_2Cl_4(DPEN)_2$] (**12**; 104 mg, 72%). Recrystallisation from a concentrated chloroform solution of **12** gave colourless prisms. ^{1}H NMR: δ = 2.88−2.94 (m, 8 H, CH_2P), 4.56 (quintet, *J* = 6.4 Hz, 8 H, CH_2O), 6.76 (d, *J* = 2.2 Hz, 4 H, $C_{1,8}$ H), 6.83 (dd, *J* = 8.8, 2.3 Hz, 4 H, $C_{3,6}$ H), 7.22 (br t, *J* = 6.9 Hz, 16 H, Ph *o*-H), 7.37 (t, *J* = 7.3 Hz, 8 H, Ph *p*-H), 7.48 (d, *J* = 8.9 Hz, 4 H, $C_{4,5}$ H), 7.57, (dd, *J* = 8.1, 10.7 Hz, 16 H, Ph *m*-H). ^{13}C NMR: δ = 30.3 (5-line m,[27] J_{P-C} = 22 Hz, CH_2P), 64.8 (CH_2O), 107.2 ($C_{3,6}$), 116.3 ($C_{1,8}$), 124.9 (C_{4a}), 128.8 (t, *J* = 5 Hz, Ph *m*-C), 129.4 ($C_{4,5}$), 130.1 (4 line m,[27] J_{P-C} = 32 Hz, Ph *i*-C), 131.5 (br. s, *p*-C), 133.7 (t, *J* = 5 Hz, *o*-C), 135.9 (C_{8a}), 156.6 (C_2). ^{31}P{^{1}H} NMR: δ = 6.49 (PPh_2, J_{Pt-P} = 3627 Hz). IR: ṽ = 1631 s, 1436 m, 1209 m, 694 m. MS: *m*/*z* (%) = 1701 (2.5) [$Pt_2Cl_4(DPEN)_2^+$], 1665 (13) [M$^+$ − Cl], 1629 (2) [M$^+$ − 2Cl]. HRMS: calculated for $C_{76}H_{68}Cl_3O_4P_4Pt_2$: 1665.2433; found 1665.2432. $C_{76}H_{68}Cl_4O_4P_4Pt_2$ (1701.3): calcd. C 53.7, H 4.03; found C 52.9, H 3.97.

***cis,cis*-[Pt$_2$Cl$_4$(DPEN)$_2$] (12). By Inverse Addition:** A solution of [$PtCl_2(SMe_2)_2$] (**10**; 167 mg, 0.43 mmol) in dichloromethane (5 mL) was added dropwise over 5 minutes to a stirred solution of DPEN (**5**; 250 mg, 0.43 mmol) in dichloromethane (8 mL). After 7 minutes, the solvent was removed to give a white solid (414 mg) consisting largely of *cis,cis*-[$Pt_2Cl_4(DPEN)_2$] (**12**; identified by ^{1}H and ^{31}P NMR spectroscopy and by MS) together with small quantities of higher oligomers.

***cis,cis*-[Pt$_2$Cl$_4$(DPPN)$_2$] (13):** A solution of [$PtCl_2(SMe_2)_2$] (**10**; 128 mg, 0.33 mmol) in dichloromethane (4 mL) was added dropwise over 5 minutes to a solution of DPPN (**4**; 200 mg, 0.33 mmol) in dichloromethane (4.5 mL). After 7 minutes the solvent was removed to give *cis,cis*-[$Pt_2Cl_4(DPPN)_2$] (**13**) as a white solid (281 mg, 97%) which contained small quantities of a closely similar compound, presumed from NMR and MS evidence to be a *cis,cis,cis*-trimer. Recrystallisation from dichloromethane produced **13** as colourless prisms suitable for X-ray analysis. ^{1}H NMR (CD_2Cl_2): δ = 2.20−2.30 (m, 8 H, C*H*$_2$CH$_2$P), 2.45−2.55 (m, 8 H, CH_2P), 4.15 (t, *J* = 6.1 Hz, 8 H, CH_2O), 6.91 (dd, *J* = 2.4, 8.8 Hz, 4 H, $C_{3,6}$ H), 7.10−7.14 (m, 16 H, Hs *meta* to P), 7.21 (s, 4 H, $C_{1,8}$-H), 7.29 (t, *J* = 7.0 Hz, 8 H, Hs *para* to P), 7.41 (dd, *J* = 8.2, 10.0 Hz, 16 H, Hs *ortho* to P), 7.62 (d, *J* = 8.9 Hz, 4 H, $C_{4,5}$ H). ^{31}P{^{1}H} NMR: δ = 7.18 (*J* = 3646 Hz). MS: *m*/*z* (%) = 1757 (1.3) [$Pt_2Cl_4(DPPN)_2^+$], 1721 (9.5) [$Pt_2Cl_3(DPPN)_2^+$], 1685 (2.5) [$Pt_2Cl_2(DPPN)_2^+$].

NMR Study of the Isomerisation of *trans,trans*-[$Pt_2Cl_4(DPEN)_2$] (11) to *cis,cis*-[$Pt_2Cl_4(DPEN)_2$] (12): A solution of *trans,trans*-[$Pt_2Cl_4(DPEN)_2$] (**11**; approx. 10 mg) in $CDCl_3/CH_2Cl_2$ was placed in an NMR tube and cooled to 203 K within the NMR machine. A ^{31}P NMR spectrum was taken. A microspatula was then used to add the minimum quantity of DPEN (**5**; approx. 0.5 mg) to the sample, which was briefly shaken then immediately frozen in liquid nitrogen and returned to the NMR machine. The sample was warmed to 298 K over 27 hours, during which time the sample was converted into *cis,cis*-[$Pt_2Cl_4(DPEN)_2$] (**12**). $^{31}P\{^1H\}$ NMR: initial: $\delta = 6.94$ ($J = 2530$ Hz); final: $\delta = 6.12$ ($J = 3624$ Hz). See Figure 7 for details.

[$Mo_2(CO)_8(DPEN)_2$] (14): $Mo(CO)_6$ (50 mg, 0.19 mmol) and $NaBH_4$ (13 mg, 0.35 mmol) were added to a suspension of DPEN (**5**; 100 mg, 0.17 mmol) in ethanol (5 mL). The mixture was refluxed for 15 h then allowed to cool to room temperature, by which time the initial white precipitate had become yellow. Water (10 mL) was added, the mixture filtered and the product washed from the resulting solid with dichloromethane. The solvent was then removed to give a pale-yellow solid (71 mg). Colourless prisms of complex **14** grown from a CH_2Cl_2 solution were suitable for X-ray analysis. ^1H NMR: $\delta = 2.50-2.55$ (m, 8 H, CH_2P), 4.08−4.13 (m, 8 H, CH_2O), 6.85−6.95 (m, 8 H, $C_{3,6}$ H and $C_{1,8}$ H) 7.27−7.45 (m, 40 H, PPh_2), 7.62 (d, $J = 9$ Hz, 4 H, $C_{4,5}$ H). $^{31}P\{^1H\}$ NMR: $\delta = 19.39$. MS: *m/z* (%) = 1586 (0.28) [$Mo_2(CO)_8(DPEN)_2^+$], 1530 (0.18) [$Mo_2(CO)_6(DPEN)_2^+$], 1474 (0.21) [$Mo_2(CO)_4(DPEN)_2^+$], 1446 (0.23) [$Mo_2(CO)_3(DPEN)_2^+$], 1411 (0.57).

Hydroformylation of 1-Octene using *cis,cis*-[$Pt_2Cl_4(DPEN)_2$] (12): A solution of *cis,cis*-[$Pt_2Cl_4(DPEN)_2$] (**12**; 54 mg, 0.03 mmol), $SnCl_2$ (12 mg, 0.06 mmol) and 1-octene (1.38 mL, 8.1 mmol) in dichloromethane (25 mL) in a reaction vessel was placed in a stainless steel autoclave. The reaction mixture was placed under 20 bar of CO and 20 bar of H_2 at 60 °C for 18 h. GCMS showed 100% conversion of 1-octene; this was confirmed by ^1H NMR spectoscopy. GC: t_R = 7.07 minutes (11.1%, 2-methyloctanal), 8.73 minutes (87.3%, nonanal), 50.11 minutes (1.6%, unidentified). Due to aldehyde trimerisation the ^1H NMR spectrum showed two sets of signals associated with nonanal, and two associated with 2-methyloctanal. Nonanal monomeric form: ^1H NMR: $\delta = 0.89$ (m, 3 H, CH_3), 1.29 [m, 12 H, $CH_3(CH_2)_6$], 2.43 (td, $J = 1.8$, 7.3 Hz, 2 H, CH_2CHO), 9.67 (s, 1 H, CHO). Nonanal cyclic trimer form: ^1H NMR: $\delta = 0.89$ (m, 9 H, 3 × CH_3), 1.29 [m, 36 H, $CH_3(CH_2)_6$], 1.57 (m, 6 H, 3 × $OCHCH_2$), 4.84 (t, $J = 5.3$ Hz, 3 H, 3 × OCH). 2-Methyloctanal monomeric form: ^1H NMR: $\delta = 0.89$ (m, 3 H, CH_3CH_2), 1.01 (d, $J = 7.0$ Hz, 3 H, CH_3CH), 1.29 [m, 10 H, $CH_3(CH_2)_5$], 2.25 (m, 1 H, $CHCH_3$), 9.51 (d, 1 H, CHO). 2-Methyloctanal cyclic trimer form: ^1H NMR: $\delta = 0.86$ (m, 9 H, 3 × CH_3CH_2), 0.89 (d, J =

Table 1. Experimental details of the crystallographic study

	11	**12**	**13**	**14**
Formula	$C_{76}H_{68}Cl_4O_4P_4Pt_2$	$C_{76}H_{68}Cl_4O_4P_4Pt_2$ ·6$CHCl_3$	$C_{80}H_{76}Cl_4O_4P_4Pt_2$ ·7CH_2Cl_2	$C_{84}H_{68}Cl_4Mo_2O_{12}P_4$ ·4CH_2Cl_2
Colour	pale yellow	colourless	colourless	colourless
M_r	1701.2	2417.4	2351.8	1924.9
Space group	*P*1bar	*P*1bar	$P2_1/n$	*P*1bar
Crystal system	triclinic	triclinic	monoclinic	triclinic
a (Å)	9.9438(9)	10.8061(4)	14.5506(1)	10.6251(2)
b (Å)	14.7383(13)	11.1389(5)	23.0337(2)	12.0645(3)
c (Å)	15.132(2)	20.6078(8)	15.0485(1)	21.4369(6)
α (°)	71.990(11)	81.450(2)		87.325(1)
β (°)	89.553(9)	77.570(2)	98.0901(6)	87.773(1)
γ (°)	83.186(7)	76.863(2)		65.051(1)
V (Å^3)	2093.1(4)	2345.97(16)	4993.37(6)	2488.2(1)
Z	1	1	2	1
$D_{calcd.}$ (g·cm^{-3})	1.35	1.71	1.564	1.285
F(000)	840	1188	2332	980
μ(Mo-K_α)	3.583	3.720	3.390	0.583
Crystal size	0.35 × 0.25 × 0.10	0.5 × 0.15 × 0.10	0.5 × 0.45 × 0.4	0.4 × 0.3 × 0.25
Transmission coefficients (range)	0.584–0.261	0.717–0.461	0.160–0.119	0.868–0.800
T (K)	298	173	150	150
θ angle (°)	2.7–26.0	3.4–26.0	2.1–30.0	2.9–27.6
No. of data collected	9714	24638	62058	19519
No. of unique data	8220	9021	14472	11202
h, *k*, *l* range	−1 → 12	−12 → 13	−20 → 20	−13 → 13
	−18 → 18	−13 → 13	−32 → 32	−15 → 15
	−18 → 18	−25 → 25	−15 → 21	−25 → 27
R_{int}	0.0312	0.0567	0.0442	0.0348
No. of data in refinement	8220	9021	14472	11202
No. of refined parameters	358	515	515	514
Final *R* [$I \geq 2\sigma(I)$] (all data)	0.0385 (0.0681)	0.0575 (0.0840)	0.0351 (0.0508)	0.0541 (0.0758)
*wR*2 [$I \geq 2\sigma(I)$] (all data)	0.0862 (0.0929)	0.117 (0.1277)	0.0933 (0.0980)	0.1353 (0.1455)
Goodness of fit *S*	0.949	1.062	1.032	1.019
Largest remaining feature in electron density map, max./min. e·Å^{-3}	0.72/–1.16	2.75/–1.98	1.50/–1.37	0.80/–0.57
Max shift/esd in last cycle	0.002	0.002	0.001	0.005

8.0 Hz, 9 H, 3 × CH_3CH), 1.29 [m, 30 H, 3 × $CH_3(CH_2)_5$], 1.57 (m, 3 H, 3 × OCHCH), 4.82 (m, 3 H, 3 × OCH).

Crystallographic Structure Determinations: Details of data collection procedures and structure refinements are given in Table 1. Single crystals of suitable size were attached to glass fibres using acrylic resin, and mounted on a goniometer head in a general position. All samples suffered solvent loss, this being particularly severe for compounds **12** and **13**, which required that these crystals were glued to the glass fibre under solvent and transferred as rapidly as possible to the cold stream of the Oxford Instruments Cryostream. For compounds **12**, **13** and **14**, low temperature data were collected on a Bruker-Nonius KappaCCD diffractometer, running under the Collect software, while data for compound **11** were collected on a Enraf−Nonius Turbo-CAD4 diffractometer at ambient temperature. Graphite monochromated X-radiation (λ = 0.71073 Å) was used for all studies. Precise unit cell dimensions for the CAD4 dataset were determined from 25 high-angle reflections which were flagged during data collection. Precise unit cell dimensions for the KappaCCD data-sets were determined by post-refinement using the Scalepack[28] program. Frame images were integrated using Denzo-SMN[28] and the resultant raw intensity files processed using a locally modified version of DENZOX[29] and then sorted and merged using SORTAV.[30] Empirical absorption corrections by the method of Blessing[31] for compounds **12**, **13** and **14** and Stuart and Walker[32] for **11** were applied to the data. No significant crystal decay was noted for any sample. The structures were solved by DIRDIF-99,[33] SIR-92[34] or SHELXS-97.[35] All non-H atoms were allowed anisotropic thermal motion. Aliphatic and aromatic C−H hydrogen atoms were included at calculated positions, with C−H = 0.96 Å, and were refined with a riding model and with U_{iso} set to 1.2 times that of the attached C atom. Refinement was with SHELXL97−2[35] using full-matrix least-squares on F^2 and all the unique data. All samples showed the presence of disordered solvent molecules, and the SQUEEZE procedure of Spek and van der Sluis[36] was used to model this extra electron density where appropriate. For compound **11** an extra 47 e/cell were indicated, this being potentially due to CH_2Cl_2, H_2O or Et_2O. For compound **12** three independent ordered molecules of $CHCl_3$ per asymmetric unit were found, and only a small residual solvent accessible void totalling ≈40 Å^3 was left. The SQUEEZE was not considered necessary in this case. For compound **13**, two ordered and one disordered CH_2Cl_2 molecules per asymmetric unit were found, along with indications of a further 1/2 molecule. An extra 83 e/cell were recovered by the SQUEEZE procedure, consistent with a 1/2 molecule of CH_2Cl_2. This was thus included in the cell contents. For compound **14** two ordered molecules of CH_2Cl_2 were observed as well as large voids containing further disordered solvent. The SQUEEZE procedure recovered 38 e/cell, consistent with a further 1/2 molecule of CH_2Cl_2. Neutral atom scattering factors, coefficients of anomalous dispersion and absorption coefficients were obtained from reference.[37] Thermal ellipsoid plots were obtained using the program ORTEP-3 for Windows.[38] All calculations were carried out using the WinGX package[39] of crystallographic programs.

Crystallographic data (excluding structure factors) for the structures reported in this paper have been deposited with the Cambridge Crystallographic Data Centre as supplementary publication nos. CCDC-165290 (**11**), CCDC-165291 (**12**), CCDC-165292 (**13**) and CCDC-165293 (**14**). Copies of the data can be obtained free of charge on application to CCDC, 12 Union Road, Cambridge CB2 1EZ, UK [Fax: (internat.) +44−1223/336−033; E-mail: deposit@ccdc.cam.ac.uk].

Acknowledgments

We are grateful to Mr James Gall for assistance with NMR spectroscopy, to Dr David Rycroft for assistance with Figure 7, and to Glasgow University Chemistry Department for financial support of this work. We thank EPSRC for a grant (GR/M91433) towards the purchase of a Kappa CCD diffractometer.

[1] L. A. van der Veen, P. K. Keeven, P. C. J. Kamer, P. W. N. M. van Leeuwen, *Chem. Commun.* **2000**, 333−334, and references therein.
[2] P. Wasserscheid, H. Waffenschmidt, P. Machnitzki, K. W. Kottsieper, O. Stelzer, *Chem. Commun.* **2001**, 451−452.
[3] M. Kranenburg, Y. E. M. van der Burgt, P. C. J. Kamer, P. W. N. M. van Leeuwen, K. Goubitz, J. Fraanje, *Organometallics* **1995**, *14*, 3081−3089.
[4] L. A. van der Veen, P. H. Keever, G. C. Schoemaker, J. N. H. Reek, P. C. J. Kamer, P. W. N. M. van Leeuwen, M. Lutz, A. L. Spek, *Organometallics* **2000**, *19*, 872−883.
[5] C. A. Bessel, P. Aggarwal, A. C. Marschilok, K. J. Takendi, *Chem. Rev.* **2001**, *101*, 1031−1066.
[6] H.-B. Bürgi, J. Murray-Rust, M. Camalli, F. Caruso, L. M. Venanzi, *Helv. Chim. Acta* **1989**, *72*, 1293−1300, and references therein.
[7] D. C. Smith, G. M. Gray, *Inorg. Chem.* **1998**, *37*, 1791−1797.
[8] W. J. Perez, C. H. Lake, R. F. See, L. M. Toomey, M. R. Churchill, K. J. Takeuchi, C. P. Radano, W. J. Boyko, C. A. Bessel, *J. Chem. Soc., Dalton Trans.* **1999**, 2281−2292.
[9] E. B. Bauer, J. Ruwwe, J. M. Martín-Alvarez, T. B. Peters, J. C. Bohling, F. A. Hampel, S. Szafert, T. Liz, J. A. Gladysz, *Chem. Commun.* **2000**, 2261−2262.
[10] P. Braunstein, J. Durand, M. Knorr, C. Strohmann, *Chem. Commun.* **2001**, 211−212.
[11] C. G. Arena, D. Drommi, F. Faraone, C. Graiff, A. Tiripicchio, *Eur. J. Inorg. Chem.* **2001**, 247−255.
[12] A. C. Comely, S. E. Gibson, N. J. Hales, *Chem. Commun.* **2000**, 305−306.
[13] R. J. P. Corriu, C. Hoarau, A. Mehdi, C. Reyé, *Chem. Commun.* **2000**, 71−72.
[14] L. Prajer-Janczewska, J. Wroblewski, *Pol. J. Chem.* **1980**, *54*, 1431−1437. This paper does not give full characterisation of bis-ether **6**.
[15] N. P. Buu-Hoi, D. Lavit, *J. Chem. Soc.* **1956**, 1743−1748. This paper does not give full characterisation of bis-ether **6**.
[16] cf G. T. Crisp, Y.-L. Jiang, P. J. Pullman, C. De Savi, *Tetrahedron* **1997**, *53*, 17489−17500. This paper does not give full characterisation of diol **8**.
[17] W. E. Hill, J. G. Taylor, C. P. Falshaw, T. J. King, B. Beagley, D. M. Tonge, R. G. Pritchard, C. A. McAuliffe, *J. Chem. Soc., Dalton Trans.* **1986**, 2289−2295.
[18] F. R. Hartley, *The Chemistry of Platinum, Palladium*, Applied Science Publishers, London, **1973**.
[19] U. Belluco, *Organometallic Coordination Chemistry of Platinum*, Academic Press, London, **1974**.
[20] S. O. Grim, R. L. Keiter, W. McFarlane, *Inorg. Chem.* **1967**, *6*, 1133−1137.
[21] See: K. Burgess, M. J. Ohlmeyer, K. H. Whitmire, *Organometallics* **1992**, *11*, 3588−3600.
[22] G. G. Messmer, E. L. Amma, J. A. Ibers, *Inorg. Chem.* **1967**, *6*, 725−730.
[23] L. Manojlovic-Muir, K. W. Muir, T. Solomun, D. W. Meek, J. L. Peterson, *J. Organomet. Chem.* **1978**, *146*, C26−C28.
[24] A. N. Caldwell, L. Manojlovic-Muir, K. W. Muir, *J. Chem. Soc., Dalton Trans.* **1977**, 2265−2269.
[25] Sheffield ChemPuter Isotope Pattern Calculation, M. Winter, **1998**, http://www.chem.shef.ac.uk/chemistry/chemputer/isotopes. html

[26] M. Janczewski, B. Dabrowska, B. Florkiewicz, *Przemysl. Chem.* **1958**, *37*, 784−787; *Chem. Abs.* **1959**, 17983. This paper does not give full characterisation of bis-ester **7**.
[27] D. A. Redfield, J. H. Nelson, L. W. Cary, *Inorg. Nucl. Chem. Lett.* **1974**, *10*, 727−733.
[28] Z. Otwinowski, W. Minor, *Processing of X-ray Diffraction Data Collected in Oscillation Mode*, *Methods in Enzymology*, Volume 276: Macromolecular Crystallography, part A (Eds.: C. W. Carter, R. M. Sweet), Academic Press, **1997**, p.307−326.
[29] DENZOX − Program for processing Denzo x files R. H. Blessing, **1997**. Modified for KappaCCD data, L. J. Farrugia, K. W. Muir, **2001**.
[30] R. H. Blessing, *J. Appl. Cryst.* **1997**, *30*, 421−426.
[31] R. H. Blessing, *Acta Crystallogr., Sect. A* **1995**, *51*, 33−38.
[32] N. Walker, D. Stuart, *Acta Crystallogr., Sect. A* **1983**, *39*, 158−166.
[33] DIRDIF-99 program system. P. T. Beurskens, G. Beurskens, R. de Gelder, S. Garcia-Granda, R. O. Gould, R. Israel, J. M. M. Smits, Crystallography Laboratory, University of Nijmegen, The Netherlands, **1999**.
[34] A. Altomare, G. Cascarano, C. Giacovazzo, A. Guagliardi, *J. Appl. Cryst.* **1993**, *26*, 343−350.
[35] SHELX-97 programs for crystal structure analysis; G. M. Sheldrick, University of Göttingen, Germany, **1997**, Release 97−2.
[36] P. van der Sluis, A. L. Spek, *Acta Crystallogr., Sect. A* **1990**, *46*, 194−201.
[37] Table 4.2.4.2, 4.2.6.8 & 6.1.1.4 from *International Tables for Crystallography, Volume C Mathematical, Physical and Chemical Tables*, Kluwer, Dordrecht, **1995**.
[38] L. J. Farrugia, *J. Appl. Cryst.* **1997**, *30*, 565.
[39] L. J. Farrugia, *J. Appl. Cryst.* **1999**, *32*, 837−838.

Received June 29, 2001
[I01242]

The Insertion of Heterocumulenes into Zn−H and Zn−OH Bonds of Pyrazolylborate−Zinc Complexes

Michael Rombach,[a] Horst Brombacher,[a] and Heinrich Vahrenkamp*[a]

Dedicated to Professor Ernst Anders on the occasion of his 60th birthday

Keywords: Zinc / Pyrazolylborate ligands / Heterocumulenes / Insertion / Hydroxide ligands / Enzyme models

The pyrazolylborate–zinc complexes $Tp^{Ph,Me}$Zn–H and $Tp^{Ph,Me}$Zn–OH undergo insertion reactions with heterocumulenes. CO_2, CS_2 and RNCS insert into the Zn–H function to yield the corresponding Zn–OCH(O), Zn–SCH(S) and Zn–SCH(NR) complexes. The primary products resulting from the insertion of CS_2, COS and RNCS into the Zn–OH function undergo rearrangements and subsequent reactions. $Tp^{Ph,Me}$Zn–OH and CS_2 or COS yield $Tp^{Ph,Me}$Zn–SH and COS or CO_2, whereas with RNCS the complexes $Tp^{Ph,Me}$Zn–SC(O)NHR are formed. In the presence of alcohols these are incorporated in the Zn–OH insertion products: CS_2/methanol yields $Tp^{Ph,Me}$Zn–SC(S)OMe and RNCS/ethanol yields $Tp^{Ph,Me}$Zn–SC(NR)OEt. All product types were characterized by X-ray crystallography. The reactions and structures support the four-centre reaction mechanism proposed for hydrolytic zinc enzymes.

Introduction

Hydrolytic zinc enzymes normally contain a zinc-aqua unit L_nZn-OH_2 in the resting state which becomes active by conversion into the powerful nucleophile L_nZn-OH.[1,2] In one of the simplest zinc-enzyme-catalyzed processes, the hydration of CO_2 by carbonic anhydrase,[3] the primary step consists formally of the insertion of CO_2 into this Zn−OH function producing an intermediate zinc-bicarbonate complex. Numerous research groups,[4,5] including ourselves,[6−9] have tried to model the function of carbonic anhydrase using $Zn-OH_2$ or Zn−OH complexes. Until now, however, zinc-bicarbonate complexes, which seem to be the most labile intermediates, have been elusive. Their existence as intermediates and the mechanistic details of the $Zn-OH/CO_2$ reaction have been elucidated in great detail by mechanistic and theoretical investigations.[3,10]

Our activities in this field are centred on the easily accessible pyrazolylborate-zinc hydroxide complexes Tp*Zn−OH, which we have called the Freiburg enzyme model.[11] We have described some reactions of these complexes with CO_2,[6−8] and related heterocumulenes such as CS_2 and RNCS,[7,12] and we have developed mechanistic proposals for the hydrolytic function of the Zn−OH unit based on preparative and kinetic work[13] as well as on theoretical considerations[12] and a structure correlation analysis.[13]

A characteristic feature of the Tp*Zn−OH/heterocumulene reactions is that their primary reaction products undergo subsequent reactions, either by proton migration or solvent incorporation.[6−8,12] In order to learn more about the possible primary products we therefore looked for a Tp*Zn complex as a starting material which bears a nucleophilic yet nonprotic ligand X capable of allowing insertion of the heterocumulene into the Zn−X function. We found that Zn−SH or Zn−SR complexes are not suitable for this purpose due to reluctance of the sulfur ligands to undergo Zn−S bond cleavage.[14,15] It turned out, however, that the Zn−H function in Tp*Zn−H complexes has all of the desired characteristics. This paper describes the heterocumulene reactions of $Tp^{Ph,Me}$Zn−H (**1**). The related reactions of $Tp^{Ph,Me}$Zn−OH (**2**), which have also yielded new insights, are included. The independent chemistry of $Tp^{Ph,Me}$Zn−OR complexes which bear the highly nucleophilic and extremely labile alkoxide ligands will be described in a separate paper.[16]

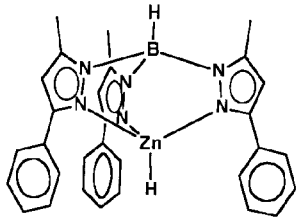

$Tp^{Ph,Me}$Zn-H

1

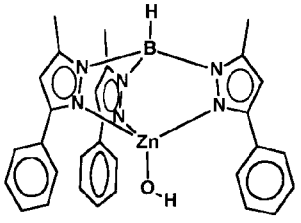

$Tp^{Ph,Me}$Zn-OH

2

[a] Institut für Anorganische und Analytische Chemie der Universität Freiburg,
Albertstraße 21, 79104 Freiburg, Germany
Fax: (internat.) + 49-761/203-6001
E-mail: vahrenka@uni-freiburg.de

 © WILEY-VCH Verlag GmbH, 69451 Weinheim, Germany, 2002 1434−1948/02/0101−0153 $ 17.50+.50/0

Results and Discussion

Reactions of $Tp^{Ph,Me}Zn-H$

$Tp^{tBu}Zn-H$ was prepared previously by Parkin from ZnH_2 and the ligand,[17] and $Tp^{p\text{-}Tol,Me}Zn-H$ by Kläui from the corresponding fluoride and triethylsilane.[18] The reactivity of the former towards protic reagents and alkyl halides had already been studied, as had its reaction with CO_2 to form $Tp^{tBu}Zn$-formate, which was characterized spectroscopically.[17]

We chose the Kläui method to prepare **1**. Both the formation of $Tp^{Ph,Me}Zn-F$ from $KTp^{Ph,Me}$, $Zn(ClO_4)_2$ and KF and its conversion into **1** with triethylsilane are high yield processes. The hydride complex **1** is remarkably stable. It melts without decomposition above 200 °C, and can be handled for short periods in the open atmosphere. Its ^1H NMR spectrum in $CDCl_3$ shows the hydride resonance at $\delta = 4.06$, which is in the range observed for the other two Tp*Zn−H complexes.

The structure of the hydride complex **1** is displayed in Figure 1. Although an electron density which roughly corresponds to that of a hydrogen atom could be localized at the position given in the figure, it is unrealistic to assign it to the zinc-bound hydride due to the observed distance of 1.9 Å, which is well above the accepted Zn−H distance of ca. 1.60 Å.[19] Compound **1** shares this feature with $Tp^{tBu}Zn-H$,[17] for which the hydride position was also not located but whose ZnN_3H arrangement is practically identical to that in **1**. Thus the main purpose of Figure 1 is to show the encapsulation of the Zn−H function by the phenyl groups on the pyrazole rings and to give one representative drawing of the complete pyrazolylborate ligand $Tp^{Ph,Me}$ which is omitted for clarity in all subsequent figures.

$Tp^{Ph,Me}Zn-H$ reacts readily with CO_2 or CS_2 in excess at ambient temperature to yield the corresponding formate or dithioformate complexes **3** and **4**. The transfer of the hydridic H atom from zinc to carbon, i.e. the insertion of the heterocumulene into the Zn−H function, is obvious from the NMR spectroscopic data and was confirmed by the structure determinations (see below). Likewise the isothiocyanates RNCS (R = methyl, phenyl and *p*-nitrophenyl) are inserted with formation of the corresponding iminothioformates **5a−c**. All three are crystalline solids with high thermal stabilities, whose formate nature is again evident from the formate proton resonances in the ^1H NMR spectrum.

$Tp^{Ph,Me}Zn$-OCHO **3** $Tp^{Ph,Me}Zn$-SCHS **4**

$Tp^{Ph,Me}Zn$-SCH(NR)

5a: R = CH_3, **5b**: R = C_6H_5, **5c**: R = C_6H_4-*p*-NO_2

The structure determinations of **3**, **4** and **5c** revealed the common features and characteristic differences of the species. In all drawings the attachment of the pyrazolylborate ligand to zinc is reduced to the attachment of its nitrogen donors for the purpose of an unobscured view of the heterocumulene-derived ligand. The latter is displayed such that its bond to zinc is vertical and the least-squares plane including its bond to zinc is in the plane of the drawing.

The formate complex **3** (Figure 2) is the first structurally authenticated formate complex in the group of TpZn-carboxylate complexes. The attachment of the formate ligand to zinc with a somewhat elongated Zn−O1 bond and a rather weak, but non-negligible, Zn···O2 interaction must be classified as semibidentate. In comparison, the acetate in $Tp^{tBu}Zn-OC(O)Me$ is clearly monodentate with Zn−O1 = 1.86 Å and Zn−O2 = 2.95 Å.[17] The extensive discussion of bidentate bonding of ligands to TpZn units[5,13] has identified another indicator for the strength of the interaction of the zinc ion with the second donor of the bidentate ligand. This is the position of the pyrazolylborate nitrogen *trans* to this second donor. In the case of **3** this is N2. N2 is not precisely *trans* to O2 (N2−Zn−O2 = 169.0°), it is not part of the planar ZnOOCH array (displacement 0.20 Å), and its bond to zinc is not longer than the other two Zn−N bonds. Thus the formate attachment is actually weakly semibidentate, resembling the nitrate attachment in $Tp^{tBu}Zn-ONO_2$.[20]

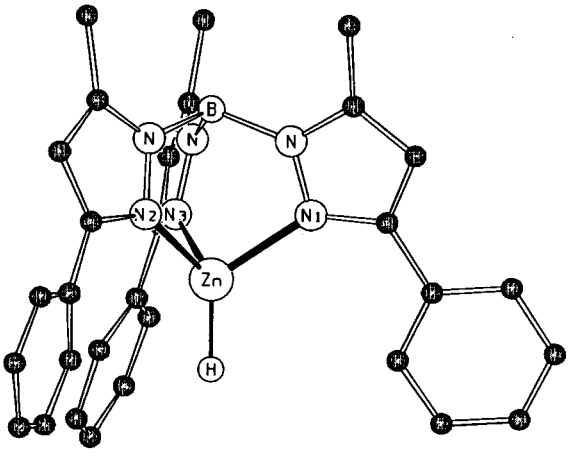

Figure 1. Molecular structure of $Tp^{Ph,Me}Zn-H$ (**1**); bond lengths: Zn−N1 2.079(5), Zn−N2 2.081(4), Zn−N3 2.054(5) Å

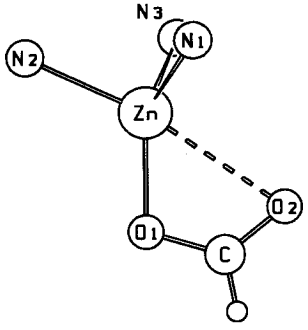

Figure 2. Zinc coordination in $Tp^{Ph,Me}Zn-OCHO$ (**3**); bond lengths: Zn−O1 1.918(3), Zn···O2 2.642(3), Zn−N1 2.034(5), Zn−N2 2.058(4), Zn−N3 2.068(4), O1−C 1.277(7), O2−C 1.208(7) Å; bond angles: Zn−O1−C 106.6(4), O1−C−O2 124.2(5)°

The dithioformate complex **4** (Figure 3) is, to the best of our knowledge, the first structurally authenticated classical coordination compound with a dithioformate ligand. In contrast, dithioformate complexes are not uncommon in organometallic chemistry where, as a rule, the dithioformate ligand bridges two metal atoms.[21] In **4** the attachment and orientation of the HCS_2 unit is quite similar to that of the HCO_2 unit in **3**. Again, the Zn−S2 interaction is not only obvious from the Zn−S2 distance of 3.02 Å but also from the strict planarity of the Zn−SCHS array and the *trans* arrangement of N3 and S2 with a bond angle of 176.3°. The N3 nitrogen is 0.13 Å above the Zn−SCHS plane, and its Zn−N bond is 0.07 Å longer than the average of the other two Zn−N bonds. The dithioformate ligand itself shows no unusual features, displaying an sp^2 carbon, a short C−S1 single bond and a long C−S2 double bond, in agreement with the semibidentate attachment. Thus the protection in the ligand pocket around zinc allows the labile dithioformate to exist as a stable dithiocarboxylic acid derivative with completely normal bonding parameters.

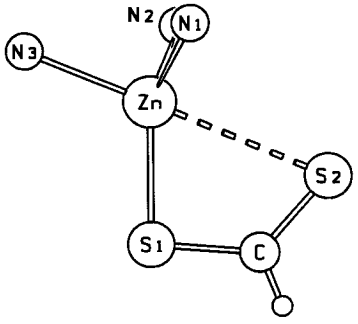

Figure 3. Zinc coordination in $Tp^{Ph,Me}Zn-SCHS$ (**4**); bond lengths: Zn−S1 2.291(1), Zn···S2 3.019(1), Zn−N1 2.019(2), Zn−N2 2.065(2), Zn−N3 2.111(2), S1−C 1.694(3), S2−C 1.623(3) Å; bond angles: Zn−S1−C 96.64(12), S1−C−S2 126.8(2)°

The iminothioformate ligand in **5c** (Figure 4) shows the closest approximation to a bidentate attachment. The Zn−S bond is longer than that in **4** and the Zn−N7 distance is close to that of a single bond. The array of Zn, S, N1, N7 and C is planar within ± 0.03 Å, and the N1−Zn−N7 angle is 177.1°. We see no obvious reason why the weakly bound N7 nitrogen in **5c** should be a better donor for zinc than the weakly bound O2 oxygen in **3** or the S2 sulfur in **4**. But while the whole range of attachments between monodentate and symmetrically bidentate is observed for zinc carboxylates[5,13] or zinc dithiocarboxylates and related species,[22,23] the unsymmetrical four-membered Zn−S−C−N chelate ring as in **5c** seems to be typical for zinc complexes of such ligands, specifically those derived from 2-mercaptopyridine-like heterocycles.[24−26] The basic form of the ligand in **5c**, iminothioformic acid HC(SH)(NH), exists only as thioformamide $HC(S)NH_2$. Its *N*-substituted derivatives, HC(SH)(NR), represented by the iminothioformate ligand in **5c**, can, however, exist as such under very favourable conditions.[27] We are not aware, however, that an anionic ligand of the type HC(S)(NR) has been used in a coordination compound before.

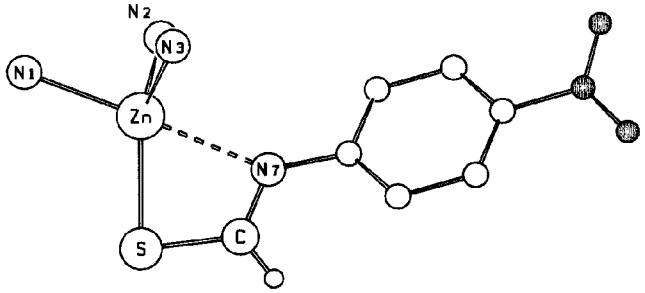

Figure 4. Zinc coordination in $Tp^{Ph,Me}Zn-SCH(NC_6H_4$-*p*-$NO_2)$ (**5c**); bond lengths: Zn−S 2.341(1), Zn···N7 2.373(3), Zn−N1 2.127(3), Zn−N2 2.048(3), Zn−N3 2.074(3), S−C 1.704(4), N7−C 1.277(5) Å; bond angles: Zn−S−C 83.24(14), Zn−N7−C 91.8(3), S−C−N7 118.7(3)°

Reactions of $Tp^{Ph,Me}Zn-OH$

We have previously described reactions of Tp*Zn−OH complexes with CO_2 in alcohols,[7,8] with CS_2 in alcohols[7] and in nonprotic solvents,[12] and with phenylisothiocyanate.[7] We had two reasons to repeat such reactions with $Tp^{Ph,Me}Zn-OH$ (**2**). Firstly, it was hoped that they would proceed like the reaction of $Tp^{Ph,Me}Zn-H$ (**1**) without subsequent reactions, thereby giving access to carbonic acid derivatives analogous to the formic acid derivatives **3**−**5**. Secondly, the favourable crystallization tendency of all $Tp^{Ph,Me}Zn-X$ complexes should allow for structural comparisons between the formic acid and carbonic acid derived complexes. The first expectation was not fulfilled: all heterocumulene insertions were accompanied by subsequent reactions. The structural comparisons, however, proved to be valuable.

The investigation of the reaction of **2** with CS_2 under nonprotic conditions was initiated by the theoretical prediction that it would lead to $Tp^{Ph,Me}Zn-SH$ and COS.[12] To our surprise this was actually the case and has resulted in a fruitful collaboration with the theoretical group of Anders.[12] In water-free dichloromethane, **2** and a stoichiometric amount of CS_2 were converted quantitatively to $Tp^{Ph,Me}Zn-SH$[14] and COS within 12 hours at room temperature. The COS resulting from this reaction in toluene was identified by mass spectrometry. Thereby it was found that under these conditions it was contaminated with CO_2, leading to the assumption that COS itself undergoes the same reaction. This was verified subsequently by the isolation of $Tp^{Ph,Me}Zn-SH$, again in a high yield, from the reaction of **2** with COS. The theoretical analysis of these interconversions,[12] whose insertion mechanism and proton migrations are of relevance for the functionality of the zinc enzyme carbonic anhydrase, will be published separately.[28] In the context of the present work these findings confirm the observation that insertions into the Zn−OH function of Tp*Zn−OH complexes will be accompanied by molecular rearrangements.

The simplest of these rearrangements, an OH/NH tautomerization, was now observed when reacting **2** with isothiocyanates in water-free dichloromethane. Methyl and

phenyl isothiocyanate yielded the thiocarbamate complexes **6a** and **6b**, respectively. Insertion alone would result in the iminothiocarbonate complexes $Tp^{Ph,Me}Zn-SC(NR)OH$. The migration of the OH proton to the more basic nitrogen should be a facile process.

$Tp^{Ph,Me}Zn\text{-}S\text{-}CO\text{-}NHR$

6a: R = CH_3, **6b**: R = C_6H_5

Esterification rather than proton migration was the subsequent reaction when performing such insertions in the presence of alcohols. As observed before for a related system,[7] CS_2 was inserted in the presence of one equivalent of methanol to yield the xanthogenate complex **7**. The insertion of *p*-nitrophenyl isothiocyanate in ethanol-stabilized chloroform produced the iminothiocarbonate complex **8**. Both results can be interpreted as an esterification of the primary insertion products $Tp^{Ph,Me}Zn-S-CS-OH$ and $Tp^{Ph,Me}Zn-S-C(NR)-OH$. However, initial replacement of OH by OR to form $Tp^{Ph,Me}Zn-OR$ as the species which is then subjected to insertion, cannot be ruled out with complete certainty. Although the alkoxides Tp*Zn−OR exist only in extremely low concentrations as equilibrium species of Tp*Zn−OH in alcohol solvents,[29] they might be the precursors of the product complexes **7** and **8**.

$Tp^{Ph,Me}Zn\text{-}S\text{-}CS\text{-}OMe$ **7** $\qquad$ $Tp^{Ph,Me}Zn\text{-}S\text{-}C(NC_6H_4NO_2)\text{-}OEt$ **8**

The molecular structure of the thiocarbamate complex **6a** (Figure 5) corresponds to that of the related thiocarboxylate complexes Tp*Zn−S−CO−R,[30] and the ligand attachment, orientation and bond lengths are quite similar to the only other structurally characterized zinc complex of this type, a bis(thiocarbamato)-bis(amine) zinc complex.[31] The long C···O distance indicates a very weak C···O interaction, as does the uniformity of the Zn−N distances. The fact that the carbamate oxygen rather than the carbamate nitrogen is in the vicinity of the zinc ion points to steric rather than electronic reasons for the arrangement of the thiocarbamate ligand. The Zn−S−C−O array is only roughly planar (± 0.08 Å) and N2 is displaced 0.4 Å from this plane. The bond lengths and angles within the thiocarbamate ligand are normal, therefore the attachment of the thiocarbamate ligand to zinc causes no unusual bonding features for the metal ion or for the ligand.

The structure of the xanthogenate complex **7** (Figure 6) complements that of $Tp^{Cum,Me}Zn-S-CS-OEt$.[7] Unlike in **6a** the sterically more demanding OR unit of the xanthogenate ligand is oriented towards zinc rather than the second sulfur atom. This points to a Zn···O interaction, as does the Zn···O distance which corresponds to that in the formate complex **3**. Likewise, the strict planarity of all five atoms of the Zn−S−CS−O unit and the displacement of N1 by 0.25 Å from this plane correspond to the situation in **3**, grouping the xanthogenate ligand in the weakly semibidentate class. The bonding details of the $MeOCS_2$ ligand

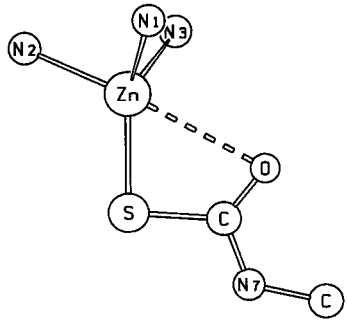

Figure 5. Zinc coordination in $Tp^{Ph,Me}Zn-S-CO-NHMe$ (**6a**); bond lengths: Zn−S 2.244(1), Zn···O 2.869(4), Zn−N1 2.085(3), Zn−N2 2.091(3), Zn−N3 2.044(3), S−C 1.734(5), C−O 1.223(5), C−N7 1.348(6) Å; bond angles: Zn−S−C 94.15(17), S−C−O 124.1(4)°

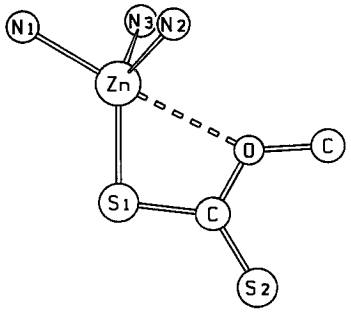

Figure 6. Zinc coordination in $Tp^{Ph,Me}Zn-S-CS-OMe$ (**7**); bond lengths: Zn−S1 2.244(3), Zn···O 2.685(3), Zn−N1 2.051(7), Zn−N2 2.036(8), Zn−N3 2.031(7), S1−C 1.72(1), C−S2 1.62(1), C−O 1.37(1) Å; bond angles: Zn−S1−C 97.5(4), S1−C−O 111.2(7)°

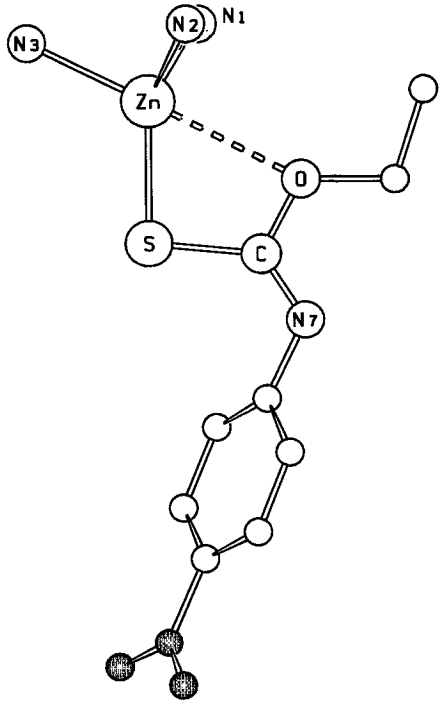

Figure 7. Zinc coordination in $Tp^{Ph,Me}Zn-S-C(NR)-OEt$ (**8**); bond lengths: Zn−S 2.254(2), Zn···O 2.680(5),Zn−N1 2.038(7), Zn−N2 2.034(6), Zn−N3 2.087(7), S−C 1.75(1), C−N7 1.27(1), C−O 1.35(1) Å; bond angles: Zn−S−C 95.8(3), S−C−O 112.1(6)°

in **7** are in full agreement with those of the $EtOCS_2$ ligand, as discussed in comparison with reference compounds for $Tp^{Cum,Me}Zn-S-CS-OEt$.[7]

The iminothiocarbonate ligand in **8** (Figure 7) seems to represent a type of ligand that has been unknown in coordination chemistry so far. Its attachment to zinc is quite similar to that of the xanthogenate ligand in **7**, however. This extends to the molecular details of the ligand as well as to its zinc−ligand interactions. Although the Zn···O contact shows the same interatomic distance as that in **7**, it seems to be somewhat stronger, as evidenced by the extension of the Zn−N3 bond *trans* to the Zn···O interaction, the O−Zn−N3 angle of 178.3° and the position of N3 in the plane defined by the Zn−S−C−O unit. It is noteworthy to compare the orientations of the *p*-nitrophenyl groups in **5c** (Figure 4) and **8**, which again point to the fact that electronic rather than steric influences determine the preferred donor for the weak interaction with the zinc ion.

Mechanistic Implications

The theoretical and mechanistic analysis of the key reaction of hydrolytic zinc enzymes − the nucleophilic attack of the Zn−OH function at the electrophilic centre of the substrate, specifically CO_2 − has led to the proposal that a four-centre mechanism prevails.[3,11,12] In this process, as displayed below for the hydration of CO_2, the zinc-bound OH is a leaving group, and the transformation of CO_2 to bicarbonate proceeds via the bidentate to the monodentate attachment of the latter.

The insertions of the heterocumulenes described here result in bonding situations which model transient bonding situations along the reaction coordinate of the enzymatic process. Three stages can be identified: Situation **A** is represented by the structures of **7** and **8** which contain the weakly bound oxygen donor as an alkoxide function which models the OH function of the enzyme. The substrate (CO_2 being modelled by CS_2 or RNCS) is attached in a four-centre fashion, and the Zn−OR bond is noticeably weakened. Situation **B** results from **A** either by proton transfer (Lipscomb mechanism[3]) or by internal rotation (Lindskog mechanism[3]). It is best represented by the structure of **5c** with a rather strong Zn−N interaction. The transition from situation **B** to **C** with a progressive weakening of the Zn···O interaction is represented by the structures of **3**, **6a** and **4**, in that order. While the formate ligand in **3** is an example of semibidentate coordination, the thiocarbamate ligand in **6a** is close to being monodentate. The six structures described here do not represent situation **C** (strictly monodentate). The latter is, however, approximated in our complexes $Tp^{Ph}Zn-SC(O)CH_3$ [30] and $Tp^{tBu,Me}Zn-OC(O)OCH_3$.[6]

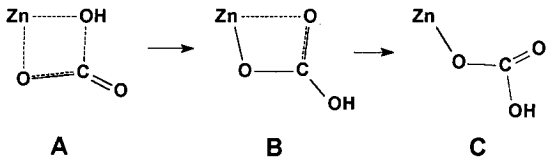

We have discussed in detail the changes in the coordination sphere of zinc upon the transition from **A** to **B**, as modelled by Tp*Zn(X)(Y) complexes.[11] The six structures in this paper provide further examples for this discussion which describes the path from the substrate attachment to the OH elimination as a transition along the Berry coordinate of the Berry pseudorotation of AB_5 molecules. They represent various stages of the interconversion between square-pyramidal and trigonal-bipyramidal coordination of zinc, as can be seen from their trans N−Zn−X angles (see Figure 2−7) ranging from 169−178°. Likewise their "percentage of trigonal-bipyramidal" values, as calculated by the dihedral angle method[13] range from 62% (**6a**) to 72% (**4**). A detailed discussion of these features, however, is not appropriate, as the distortions in the coordination sphere of zinc are spread over a range which is too narrow.

In summary, the chemical interconversions described in this paper have shown that the strong Zn−X nucleophiles Zn−H and Zn−OH can attack and incorporate all classical heterocumulenes and thereby model the biological Zn−OH/CO_2 chemistry. The structures of the resulting complexes have provided valuable insights into the molecular transformations occurring during the hydration of CO_2 as catalyzed by the zinc enzyme carbonic anhydrase.

Experimental Section

General: For general working and measuring procedures, see ref.[32] All reactions were performed in air- and water-free solvents under an inert atmosphere. $Tp^{Ph,Me}Zn-OH$[33] and COS[34] were prepared by the published procedures.

$Tp^{Ph,Me}Zn-F$: A solution of $Zn(ClO_4)_2 \cdot 6H_2O$ (1.43 g, 3.83 mmol) in 20 mL of methanol was added with stirring to a solution of $KTp^{Ph,Me}$ [33] (2.00 g, 3.83 mmol) in 100 mL of dichloromethane. A colourless precipitate was formed. After 2 h of stirring a solution of KF (222 mg, 3.83 mmol) in 10 mL of methanol was added. After stirring for 20 h and filtration the solution was reduced to 50 mL in vacuo and kept at −20 °C. $Tp^{Ph,Me}Zn-F$ (1.83 g, 84%) precipitated as colourless crystals, m.p. 244 °C. $C_{30}H_{28}BFN_6Zn$ (567.8): calcd: C 63.46, H 4.97, N 14.80, Zn 11.50; found C 62.44, H 4.92, N 14.51, Zn 11.69. ^1H NMR ($CDCl_3$): δ = 2.53 [s, 9 H, Me(pz)], 6.22 [s, 3 H, H(pz)], 7.33−7.49 (m, 9 H, Ph), 7.91 (d, *J* = 7.4 Hz, 6 H, Ph). ^{19}F NMR ($CDCl_3$): δ = 219.6.

1: A solution of $Tp^{Ph,Me}Zn-F$ (1.50 g, 2.64 mmol) and Et_3SiH (4.2 mL, 3.07 g, 26.0 mmol) in 25 mL of toluene was heated to reflux for 2 days. Upon cooling to room temp. the product was precipitated. All volatiles were removed in vacuo, and the residue was recrystallized from hot toluene, yielding 1.31 g (90%) of **1** as colourless crystals, m.p. 239 °C. $C_{30}H_{29}BN_6Zn$ (549.8): calcd: C 65.54, H 5.38, N 15.29, Zn 11.89; found C 64.72, H 5.37, N 14.75, Zn 11.79. ^1H NMR ($CDCl_3$): δ = 2.47 [s, 9 H, Me(pz)], 4.06 (s, 1 H, ZnH), 6.17 [s, 3 H, H(pz)], 7.19−7.36 (m, 9 H, Ph), 7.72 (d, *J* = 8.0 Hz, 6 H, Ph).

3: CO_2 gas, which was dried by passing through a suspension of P_2O_5 in toluene, was bubbled through a solution of **1** (200 mg, 0.36 mmol) in 30 mL of toluene for 1 h. Evaporation to dryness and recrystallization from hot acetonitrile yielded 164 mg (76%) of **3** as colourless crystals, m.p. 252 °C. $C_{31}H_{29}BN_6O_2Zn$ (593.8):

calcd: C 62.70, H 4.92, N 14.15; found C 62.44, H 4.92, Zn 14.18. ^{1}H NMR ($CDCl_3$): δ = 2.53 [s, 9 H, Me(pz)], 6.21 [s, 3 H, H(pz)], 7.34 (m, 9 H, Ph), 7.58 (m, 7 H, Ph and HCO_2).

4: A solution of **1** (100 mg, 0.18 mmol) and CS_2 (138 mg, 1.82 mmol) in 15 mL of toluene was stirred at 40 °C for 16 h. Evaporation to dryness and recrystallization from hot acetonitrile yielded 97 mg (85%) of **4** as pale yellow crystals, m.p. 204 °C. $C_{31}H_{29}BN_6S_2Zn$ (625.9): calcd: C 59.48, H 4.67, N 13.43, S 10.25; found C 59.67, H 4.71, N 13.70, S 9.98. ^{1}H NMR ($CDCl_3$): δ = 2.56 [s, 9 H, Me(pz)], 6.17 [s, 3 H, H(pz)], 7.32 (m, 9 H, Ph), 7.53 (m, 6 H, Ph), 10.24 (s, 1 H, HCS_2).

5a: Like **4**, from **1** (200 mg, 0.36 mmol) and CH_3NCS (27 mg, 0.36 mmol). Yield 118 mg (52%) of **5a** as colourless crystals, m.p. 214 °C. $C_{32}H_{32}BN_7SZn$ (622.9): calcd: C 61.70, H 5.18, N 15.74, S 5.15; found C 62.10, H 5.26, N 16.09, S 4.76. ^{1}H NMR ($CDCl_3$): δ = 1.60 (s, 3 H, NMe), 2.55 [s, 9 H, Me(pz)], 6.17 [s, 3 H, H(pz)], 7.30 (m, 9 H, Ph), 7.63 (m, 7 H, Ph and HC).

5b: A solution of **1** (200 mg, 0.36 mmol) and C_6H_5NCS (49 mg, 0.36 mmol) in 30 mL of toluene was heated to reflux for 15 h. Evaporation to dryness and recrystallization from hot acetonitrile yielded 164 mg (66%) of **5b** as colourless crystals, m.p. 181 °C. $C_{37}H_{34}BN_7SZn$ (685.0): calcd: C 64.88, H 5.00, N 14.31, S 4.68; found C 64.34, H 4.99, N 14.23, S 4.33. ^{1}H NMR ($CDCl_3$): δ = 2.56 [s, 9 H, Me(pz)], 5.59 (m, 3 H, Ph-NCS), 6.14 [s, 3 H, H(pz)], 6.72 (m, 2 H, Ph-NCS), 7.24 (m, 9 H, Ph), 7.54 (m, 6 H, Ph), 7.72 (s, 1 H, HC).

5c: A solution of **1** (200 mg, 0.36 mmol) and *p*-NO_2-C_6H_4NCS (66 mg, 0.36 mmol) in 30 mL of acetonitrile was stirred for 15 h. Evaporation to 15 mL in vacuo and cooling to −20 °C resulted in the crystallization of 173 mg (65%) of yellow **5c**, m.p. 239 °C. $C_{37}H_{33}BN_8O_2SZn$ (730.0): calcd: C 60.88, H 4.56, N 15.35, S 4.39; found C 60.92, H 4.59, N 15.57, S 4.21. ^{1}H NMR ($CDCl_3$): 2.57 [s, 9 H, Me(pz)], 5.64 (d, *J* = 8.2 Hz, 2 H, C_6H_4), 6.15 [s, 3 H, H(pz)], 7.24 (m, 9 H, Ph), 7.50 (m, 6 H, Ph), 7.64 (d, *J* = 8.2 Hz, 2 H, C_6H_4), 7.81 (s, 1 H, HC).

Reaction of 2 with CS_2: A mixture of **2** (25.0 mg, 44 μmol) and CS_2 (336 mg, 4.42 mmol) in 5 mL of toluene under an atmosphere of argon in a sealed 10 mL flask was stirred for 40 h. GC-MS analysis of samples taken from the gas phase with a syringe showed them to contain CO_2 and COS in about a 1:2 ratio.

$Tp^{Ph,Me}Zn-SH$ from 2 and CS_2: A solution of **2** (250 mg, 0.44 mmol) and CS_2 (37.0 mg, 0.49 mmol) in 20 mL of dichloromethane was stirred for 16 h. Evaporation to dryness and recrystallization from acetonitrile yielded 157 mg (61%) of $Tp^{Ph,Me}Zn-SH$.[14]

$Tp^{Ph,Me}Zn-SH$ from 2 and COS: COS gas was passed for 15 min through a solution of **2** (250 mg, 0.44 mmol) in 20 mL of dichloromethane/toluene (4:1). After stirring for 15 h, evaporation to dryness and recrystallization from acetonitrile yielded 183 mg (71%) of $Tp^{Ph,Me}Zn-SH$.[14]

6a: A solution of **2** (250 mg, 0.44 mmol) and CH_3NCS (32.3 mg, 0.44 mmol) in 20 mL of dichloromethane was heated to reflux for 40 h. Evaporation to dryness and recrystallization from benzene yielded 266 mg (84%) of **6a** as colourless crystals, m.p. 184 °C. $C_{32}H_{32}BN_7OSZn{\cdot}C_6H_6$ (638.9 + 78.1): calcd: C 63.65, H 5.34, N 13.67, S 4.47; found C 63.43, H 5.33, N 13.77, S 4.62. ^{1}H NMR ($CDCl_3$): δ = 1.91 (s, 3 H, NCH_3), 2.52 [s, 9 H, Me(pz)], 4.90 (s, 1 H, NH), 6.13 [s, 3 H, H(pz)], 7.30 (m, 15 H, Ph + C_6H_6), 7.67 (m, 6 H, Ph).

6b: Like **6a** from **2** (250 mg, 0.44 mmol) and C_6H_5NCS (59.7 mg, 0.44 mmol). Yield 290 mg (77%) of **6b** as colourless crystals, m.p.

Table 1. Crystallographic data

	1	**3**	**4**	**5c**	**6a**	**7**	**8**
Molecular mass	$C_{30}H_{29}BN_6Zn$	$C_{31}H_{29}BN_6O_2Zn$	$C_{31}H_{29}BN_6S_2Zn$	$C_{37}H_{33}BN_8O_2SZn$	$C_{32}H_{32}BN_7OSZn{\cdot}C_6H_6$	$C_{32}H_{31}BN_6OS_2Zn$	$C_{39}H_{37}BN_8O_3SZn{\cdot}CH_2Cl_2$
Crystal size [mm]	549.8	593.8	625.9	730.0	717.0	656.0	858.9
Space group	$P\bar{1}$	$P\bar{1}$	$P2_1/n$	$P\bar{1}$	*P*-1	$P2_1/c$	$P2_1/c$
Z	2	2	4	2	2	4	4
a [Å]	11.685(2)	11.840(6)	10.016(1)	9.540(2)	11.551(2)	12.575(1)	12.076(3)
b [Å]	12.194(2)	12.108(6)	15.644(2)	13.367(3)	12.234(2)	23.533(2)	23.142(6)
c [Å]	15.451(2)	12.448(5)	18.912(2)	14.981(4)	15.261(2)	11.416(1)	14.448(4)
α [°]	83.83(3)	115.772(9)	90	67.735(4)	69.137(3)	90	90
β [°]	84.99(3)	108.802(9)	95.781(2)	77.237(5)	84.569(3)	111.952(2)	92.611(6)
γ [°]	64.99(3)	98.909(7)	90	87.478(5)	63.035(3)	90	90
V [Å^3]	1981.4(7)	1427.3(11)	2948.4(5)	1722.6(7)	1790.4(5)	3133.4(6)	4034(2)
d(calcd.) [g·cm^{-3}]	0.95	1.38	1.41	1.41	1.33	1.39	1.41
μ(Mo-K_α) [mm^{-1}]	0.64	0.90	1.01	0.82	0.79	0.95	0.84
hkl range	*h*: −13 to 14 *k*: 0 to 15 *l*: 0 to 15	*h*: −15 to 15 *k*: −15 to 4 *l*: −13 to 13	*h*: −13 to 13 *k*: −20 to 20 *l*: −24 to 17	*h*: −12 to 12 *k*: −17 to 17 *l*: −19 to 19	*h*: −15 to 15 *k*: −16 to 15 *l*: −20 to 20	*h*: −16 to 16 *k*: −30 to 31 *l*: −14 to 15	*h*: −16 to 15 *k*: −30 to 30 *l*: −19 to 19
Measured reflections	8119	4289	18352	15817	16506	28597	36370
Independent reflections	7737	4279	7019	7891	8447	7647	9789
Observed refl. [$I > 2\sigma(I)$]	4548	3070	3890	3649	3911	2066	2595
Parameters	469	370	370	451	442	389	505
Refined reflections	7737	4279	7019	7891	8447	7647	9789
R_1(obs.refl.)	0.075	0.074	0.041	0.056	0.054	0.086	0.089
wR_2(all refl.)	0.228	0.196	0.096	0.146	0.154	0.342	0.288
Residual electron density [e/Å^3]	+1.0/-0.6	+1.5/-1.5	+0.4/-0.4	+0.7/-0.6	+0.5/-0.6	+0.7/-0.7	+0.7/-1.1

188 °C. $C_{37}H_{34}BN_7OSZn·2C_6H_6$ (701.0 + 156.2): calcd: C 68.66, H 5.41, N 11.44, S 3.74; found C 68.60, H 5.53, N 11.15, S 3.93. ^{1}H NMR ($CDCl_3$): δ = 2.53 [s, 9 H, Me(pz)], 6.17 [s, 3 H, H(pz)], 6.66 (d, *J* = 8.1 Hz, 2 H, NPh), 6.86 (m, 1 H, NPh), 7.04 (m, 2 H, NPh), 7.22 (m, 9 H, Ph), 7.35 (s, 12 H, C_6H_6), 7.61 (m, 6 H, Ph).

7: A solution of **2** (250 mg, 0.44 mmol), CS_2 (37.0 mg, 0.49 mmol) and CH_3OH (15.6 mg, 0.49 mmol) in 20 mL of dichloromethane was stirred for 16 h. Evaporation to dryness and recrystallization from acetonitrile yielded 228 mg (79%) of **7** as colourless crystals, m.p. 222 °C. $C_{32}H_{31}BN_6OS_2Zn$ (656.0): calcd: C 58.59, H 4.76, N 12.81, S 9.78; found C 58.67, H 4.84, N 12.81, S 9.98. ^{1}H NMR ($CDCl_3$): δ = 2.55 [s, 9 H, Me(pz)], 2.64 (s, 3 H, OMe), 6.16 [s, 3 H, H(pz)], 7.31 (m, 9 H, Ph), 7.53 (m, 6 H, Ph).

8: A solution of **2** (250 mg, 0.44 mmol) and *p*-NO_2-C_6H_4NCS (79.6 mg, 0.44 mmol) in 40 mL of chloroform containing ca. 1% of ethanol as a stabilizer was heated to reflux for 40 h. All volatiles were removed in vacuo, and the residue was dissolved in 10 mL of *n*-heptane/dichloromethane (4:1). Slow evaporation of the dichloromethane resulted in the precipitation of 145 mg (42%) of **8** as yellow crystals which lost the solvent of crystallization upon drying in vacuo, m.p. 234 °C. $C_{39}H_{37}BN_8O_3SZn$ (774.0): calcd: C 60.52, H 4.82, N 14.48, S 4.14; found C 60.39, H 4.66, N 14.70, S 4.38. ^{1}H NMR ($CDCl_3$): δ = 0.17 [t, *J* = 6.9 Hz, 3 H, CH_3(Et)], 2.57 [s, 9 H, Me(pz)]; 2.72 [q, *J* = 6.9 Hz, 2 H, CH_2(Et)], 6.19 [s, 3 H, H(pz)], 6.78 (m, 2 H, C_6H_4), 7.37 (m, 9 H, Ph), 7.65 (m, 6 H, Ph), 8.12 (m, 2 H, C_6H_4).

Structure Determinations:[35] All crystals were obtained as described above from the reaction solutions. Diffraction data were recorded at 180 K (**1** at room temp.) on a Bruker Smart CCD diffractometer and subjected to an empirical absorption correction (program SADABS). The structures were solved with direct methods and refined anisotropically with the SHELX program suite.[36] Hydrogen atoms were included with fixed distances and isotropic temperature factors 1.5 times those of their attached atoms. Parameters were refined against F^2. The *R* values are defined as $R_1 = \Sigma|F_o - F_c|/\Sigma F_o$ and $wR_2 = \{\Sigma[w(F_o^2 - F_c^2)^2]\Sigma[w(F_o^2)^2]\}^{1/2}$. Drawings were produced with SCHAKAL.[37] Table 1 lists the crystallographic data.

Acknowledgments

This work was supported by the Deutsche Forschungsgemeinschaft and the Fonds der Chemischen Industrie. We are indebted to Mrs. Petra Klose for technical assistance and to Drs. Werner Deck and Alexander Trösch for help with the crystallography.

[1] *Bioinorganic Chemistry* (Eds.: I. Bertini, H. B. Gray, S. J. Lippard, J. S. Valentine), University Science Books, Mill Valley, California, **1994**.
[2] W. Kaim, B. Schwederski, *Bioanorganische Chemie*, Teubner Studienbücher, Stuttgart, **1995**.
[3] *Carbonic Anhydrase* (Eds.: F. Botrè, G. Gros, B. T. Storey), VCH Publishers, Weinheim, **1991**.
[4] For the literature up to 1982, see: R. S. Brown, J. Huguet, N. J. Curtis, in *Metal Ions in Biological Systems* (Ed.: H. Sigel), Vol. 15, Marcel Dekker, New York, **1983**.
[5] For more recent references, see G. Parkin, *Adv. Inorg. Chem.* **1995**, *42*, 291−393.
[6] R. Alsfasser, M. Ruf, S. Trofimenko, H. Vahrenkamp, *Chem. Ber.* **1993**, *126*, 703−710.
[7] M. Ruf, H. Vahrenkamp, *Inorg. Chem.* **1996**, *35*, 6571−6578.
[8] M. Ruf, F. A. Schell, R. Walz, H. Vahrenkamp, *Chem. Ber./Recueil* **1997**, *130*, 101−104.
[9] A. Trösch, H. Vahrenkamp, *Inorg. Chem.* **2001**, *40*, 2305−2311.
[10] For a summary of references, see S. Sinnecker, M. Bräuer, W. Koch, E. Anders, *Inorg. Chem.* **2001**, *40*, 1006−1013.
[11] H. Vahrenkamp, *Acc. Chem. Res.* **1999**, *32*, 589−596.
[12] M. Bräuer, E. Anders, S. Sinnecker, W. Koch, M. Rombach, H. Brombacher, H. Vahrenkamp, *Chem. Commun.* **2000**, 647−648.
[13] M. Rombach, C. Maurer, K. Weis, E. Keller, H. Vahrenkamp, *Chem. Eur. J.* **1999**, *5*, 1013−1027.
[14] M. Rombach, H. Vahrenkamp, *Inorg. Chem.* in print.
[15] U. Brand, M. Rombach, J. Seebacher, H. Vahrenkamp, *Inorg. Chem.* in print.
[16] H. Brombacher, H. Vahrenkamp, work in progress.
[17] A. G. Looney, R. Han, I. B. Gorell, M. Cornebise, K. Yoon, G. Parkin, A. L. Rheingold, *Organometallics* **1995**, *14*, 274−284.
[18] W. Kläui, U. Schilde, M. Schmidt, *Inorg. Chem.* **1997**, *36*, 1598−1601.
[19] N. A. Bell, P. T. Moseley, H. M. M. Shearer, C. B. Spencer, *Acta Crystallogr., Sect. B* **1980**, *36*, 2950−2954.
[20] R. Han, G. Parkin, *J. Am. Chem. Soc.* **1991**, *113*, 9707−9708.
[21] H. C. Böttcher, M. Graf, K. Merzweiler, C. Wagner, *Z. Anorg. Allg. Chem.* **2000**, *626*, 597−603.
[22] M. Bonamico, G. Dessy, V. Fares, L. Scaramuzza, *J. Chem. Soc., Dalton Trans.* **1972**, 2515−2517.
[23] J. A. McCleverty, N. J. Morrison, N. Spencer, C. C. Ashworth, N. A. Bailey, M. R. Johnson, J. M. A. Smith, B. A. Tabbiner, C. R. Taylor, *J. Chem. Soc., Dalton Trans.* **1980**, 1945−1957.
[24] M. Ruf, K. Weis, H. Vahrenkamp, *Inorg. Chem.* **1997**, *36*, 2130−2137.
[25] M. A. Romero, M. P. Sanchez, M. Quiros, F. Sanchez, J. M. Salas, M. N. Moreno, R. Faure, *Can. J. Chem.* **1993**, *71*, 29−33.
[26] M. L. Godino-Salido, M. D. Gutierrez-Valero, R. Lopez-Garzon, J. M. Moreno-Sanchez, *Inorg. Chim. Acta* **1994**, *221*, 177−181.
[27] R. S. Hosmane, B. B. Lim, *Tetrahedron Lett.* **1985**, *26*, 1915−1918. W. Walter, K. J. Reubke, *Chem. Ber.* **1969**, *102*, 2117−2128.
[28] E. Anders et al. and H. Vahrenkamp et al., work in progress.
[29] C. Bergquist, H. Storrie, H. Koutcher, B. M. Bridgewater, R. A. Friesner, G. Parkin, *J. Am. Chem. Soc.* **2000**, *122*, 12651−12658.
[30] R. Alsfasser, A. K. Powell, S. Trofimenko, H. Vahrenkamp, *Chem. Ber.* **1993**, *126*, 685−694.
[31] D. L. Greene, B. J. McCormick, C. G. Pierpont, *Inorg. Chem.* **1973**, *12*, 2148−2152.
[32] M. Förster, R. Burth, A. K. Powell, T. Eiche, H. Vahrenkamp, *Chem. Ber.* **1993**, *126*, 2643−2648.
[33] M. Ruf, R. Burth, K. Weis, H. Vahrenkamp, *Chem. Ber.* **1996**, *129*, 1251−1257.
[34] E. Fluck, F. Horn, *Synth. Inorg. Met. Org. Chem.* **1972**, *2*, 341−343.
[35] The crystallographic data of the structures described in this paper were deposited with the Cambridge Crystallographic Data Centre as supplementary publication no. CCDC − 166856 for **1**, 166855 for **3**, 166954 for **4**, 166857 for **5c**, 166859 for **6a**, 166860 for **7** and 166858 for **8**. Copies of these data are available free of charge from the following address: The Director, CCDC, 12 Union Road, Cambridge, CB2 1EZ, UK [Fax: (internat.) +49−1223/336−033; E-mail: deposit@ccdc.cam.ac.uk].
[36] G. M. Sheldrick, *SHELX-86* and *SHELXL-93*, *Programs for Crystal Structure Determination*, Universität Göttingen, **1986** and **1993**.
[37] E. Keller, *SCHAKAL for Windows*, Universität Freiburg, **1998**.

Received July 10, 2001
[I01257]

The First Structurally Characterized 4-Halo-2,5-Cyclohexadienone Transition Metal Complex

Udo Radius*[a] and Juri Attner[a]

Keywords: Coordination chemistry / Macrocyclic ligands / Calixarenes / Molybdenum / Tungsten

The calix[4]arene molybdenum imido complex [CaxO_4Mo(N*t*Bu)] (**1**) reacts with HCl to give, in a reversible reaction, the 1,2-addition product [Cax(OH)O_3Mo(N*t*Bu)Cl] (**4**). Reaction with $PhICl_2$ does not lead to scission of the imido group either, but results in an unprecedented 1,6-addition of chlorine to the metallocalixarene to give a molybdenum 4-chloro-2,5-cyclohexadienone complex [Cax$^{Cl}O_4$Mo(N*t*Bu)Cl] (**5**), which has been structurally characterized. This compound is the first example of a structurally characterized 4-halo-2,5-cyclohexadienone transition metal complex.

Introduction

Macrocyclic ligands have played an important role in the development of modern coordination chemistry and continue to do so.[1] Macrocyclic complexes are usually associated with high thermodynamic and kinetic stability and are therefore used as templates in supramolecular chemistry, in multi-component assembly processes, and as molecular receptors for guest molecules. Such ligands can act as spectator ligands for organometallic transformations at the metal atom.[2] However, in many cases, the ligands are also involved in the reaction processes. In metalloporphyrin chemistry, for example, reactions at the porphyrin periphery are quite common and these ligands are susceptible to redox processes and electrophilic as well as nucleophilic attack.[3]

Calix[4]arenes or calix[4]arene ethers,[4] with a pre-organized set of oxygen donor atoms in a quasi-planar arrangement, may be regarded as oxygen analogues of porphyrins and related nitrogen-containing macrocyclic ligands. These molecules have received considerable attention because of their host−guest chemistry and their ability to bind metals.[4,5] In the last few years, the potential of these types of ligands in organometallic and coordination chemistry has been clearly demonstrated. The simplest of the calixarenes, the calix[4]arene system, usually binds in a tetradentate fashion and retains its *cone*-like appearance.[5] In contrast to transition metal chemistry involving porphyrins, tetraazaannulenes, calixpyrroles, and related nitrogen donor ligands,[6] the calix[4]arene backbone is usually not involved in organometallic transformations.[7] Calix[4]arenes are therefore ideal co-ligands in transition metal chemistry, they tolerate acidic, basic, reductive, and oxidative conditions.

We report herein on a selective halogenation of the macrocyclic ligand in a metallocalix[4]arene through an unprecedented 1,6-chlorination. The resulting product represents the first isolated and structurally characterized 4-halo-2,5-cyclohexadienone complex.

Results and Discussion

As part of our program on molybdenum calix[4]arene complexes,[8] we have synthesized molybdenum imido complexes previously.[8b] The ultimate aim of this work was the synthesis of compounds of the general type [CaxO_4MoX_2] or [CaxO_4MoXX′] (Cax = hydrocarbon backbone of the *p-tert*-butylcalix[4]arene, $C_{44}H_{52}$; X = monoanionic ligand), which represent important starting materials for molybdenocalix[4]arene chemistry. Since the direct reaction of [$MoCl_5$] with *p-tert*-butylcalix[4]arene does not afford calix[4]arene molybdenum halides,[8a] we were led to investigate the reaction of [CaxO_4Mo(N*t*Bu)] (**1**) with HCl and Cl_2. Preliminary experiments revealed that a solution of [CaxO_4W(N*t*Bu)] (**2**) in dichloromethane reacts spontaneously with gaseous HCl at −20 °C to give the known calix[4]arene tungsten dichloro complex [CaxO_4WCl_2] (**3**).[7d]

Whereas the imido ligand $[NR]^{2-}$ in **2** can be selectively replaced by two chloride ligands $[Cl]^-$, the reactivity of the analogous molybdenum compound **1** with respect to hydrochlorination is totally different (see Scheme 1). The reaction of **1** with one equivalent of HCl affords a dark-violet solution, which contains, according to NMR spectroscopy, a compound with local C_s symmetry of the calix[4]arene ligand, presumably [Cax(OH)O_3Mo(N*t*Bu)Cl] (**4**). The ^{1}H NMR spectrum of **4** features three signals due to the *t*Bu protons and three signals due to the protons of the methylene bridges, with relative integrals of 1:1:2. The signal of the OH proton can be detected at δ = 15.5. This low field

[a] Institut für Anorganische Chemie, Universität Karlsruhe (TH), Engesserstraße, Geb. 30.45, 76128 Karlsruhe, Germany
E-mail: uradius@achibm6.chemie.uni-karlsruhe.de

 © WILEY-VCH Verlag GmbH, 69451 Weinheim, Germany, 2002 1434−1948/02/0101−0161 $ 17.50+.50/0

resonance is indicative of protonation at the basic oxygen atoms of the calix[4]arene ligand. Similarly downfield shifted signals have been detected previously, for example in [{Cax(OH)$_2$O$_2$Mo$_2$(OAc)$_2$}(THF)], as reported by Lippard and co-workers.[9] However, the exact stereochemistry at the molybdenum center in **4** has not been established and protonation at the imido nitrogen atom cannot be totally excluded at present. We were not able to substitute the imido group, even by using a slight excess of HCl. The use of a larger amount of HCl in the reaction does not lead to scission of the imido group through proton transfer, but rather to decomposition of **4**. The protonated ligand Cax(OH)$_4$ was unequivocally detected in these reaction mixtures.

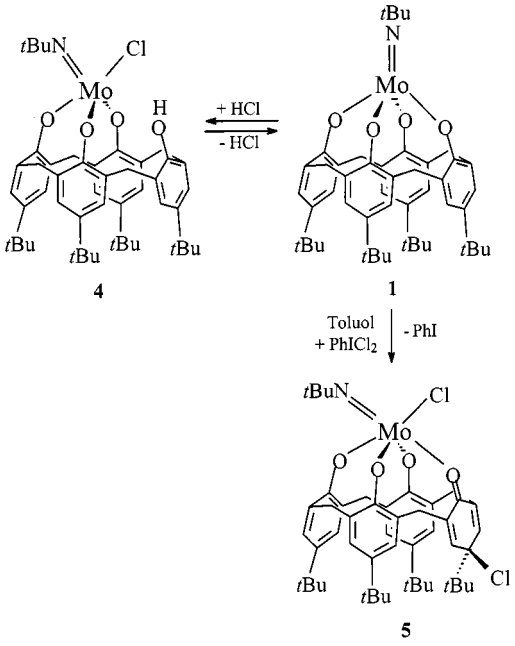

Scheme 1

Complex **4** decomposes to starting material **1** when solutions of this compound are concentrated in vacuo. The addition of HCl to **1** is totally reversible over several cycles. Reducing the pressure leads to elimination of HCl from **4**, and all attempts to remove **4** from equilibrium or to crystallize the complex have so far proved unsuccessful. Complex **4** could only be detected in solution and, as shown in Scheme 1, is the net result of a reversible 1,2-addition of HCl to the metal−oxygen bond of **1**.

The molybdenum imido function of **1** is similarly unreactive with respect to chlorine-transfer reagents. The addition of an equimolar amount of PhICl$_2$ to a solution of **1** in toluene causes a spontaneous color change of the reaction mixture to dark violet. After workup, the molybdenum complex [Cax^{Cl}O$_4$Mo(N*t*Bu)Cl] (**5**) could be isolated in good yield (see Scheme 1). Calix[4]arene Cax(OH)$_4$ does not react with PhICl$_2$ under comparable reaction conditions.

Spectroscopic data of the reaction product are in good agreement with an addition of Cl$_2$ to the imido compound **1**. The FD mass spectrum features a molecular peak at *m*/*z* = 885 (78%), which is the sum of the molar masses of **1** and Cl$_2$. The ^{1}H NMR spectrum of **5** shows a typical pattern for a pseudo-C_s-symmetric structure of the calix[4]arene ligand in solution. The resonance of the imido *t*Bu protons is detectable at δ = 1.44, ca. 0.4 ppm further upfield than in the case of the starting compound **1**. The ^{13}C NMR spectrum features signals for quaternary carbon atoms with unusual shifts for calix[4]arene complexes, a resonance at δ = 42.5, and a signal at δ = 191.2. These signals can be attributed to a carbon atom of a *C*(*t*Bu)Cl group and to a carbonyl carbon atom, respectively. Furthermore, the infrared spectrum of **5** shows a strong band at 1668 cm^{-1} in the typical absorption region of carbonyl groups of α,β-unsaturated ketones.[10] These ^{13}C NMR and IR spectroscopic results suggest a 1,6-addition of chlorine to the molybdenum imido complex **1**, one chlorine atom being located at the metal atom and the other at the *para* position of one of the phenoxide units of the calix[4]arene ligand (see Scheme 1).

The result of an X-ray crystallographic study of crystals of **5** is shown in Figure 1 and confirms the structure proposed above. Complex **5** crystallizes in the monoclinic space group $P2_1/c$ with four formula units and four additional hexane molecules in the unit cell. The molybdenum atom is sixfold coordinated by four oxygen atoms O(1) to O(4), a nitrogen atom, and the chlorine atom Cl(1). Whereas the N−Mo−O(1) arrangement is almost linear with an angle of 176.2(15)°, the O(2)−Mo−O(4) and O(3)−Mo−Cl(1) angles of 159.6(12)° and 164.1(9)° demonstrate the distortion from an idealized octahedron. The molybdenum−oxygen distances to the oxygen atoms of the phenolate groups O(2), O(3), and O(4) are within the typ-

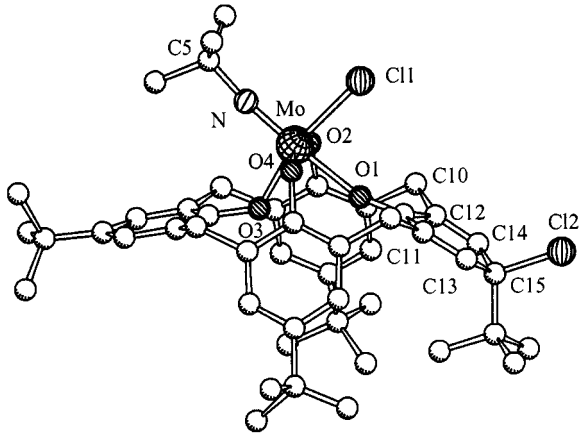

Figure 1. SCHAKAL plot of the molecular structure of [Cax^{Cl}O$_4$-Mo(N*t*Bu)Cl] **5**; hydrogen atoms are omitted for clarity and disorders of the *t*Bu groups are not resolved in the drawing; selected bond lengths [pm] and angles [°]: Mo−Cl(1): 241.0(1), Mo−N: 170.3(4), Mo−O(1): 216.0(3), Mo−O(2): 193.7(3), Mo−O(3): 191.9(3), Mo−O(4): 194.2(3), O(1)−C(10): 122.1(5), C(10)−C(11): 144.7(5), C(10)−C(12): 145.7(5), C(11)−C(13): 133.1(6), C(12)−C(14): 132.5(6), C(13)−C(15): 150.9(6), C(14)−C(15): 149.9(6), C(15)−Cl(2): 183.3(5), O(2)−C(20): 136.6(5), O(3)−C(30): 135.1(5), O(4)−C(40): 136.8(5); Mo−N−C(5): 173.0(4), Mo−O(1)−C(10): 163.1(3), Mo−O(2)−C(20): 125.3(2), Mo−O(3)−C(30): 119.6(3), Mo−O(4)−C(40): 124.6(2), N−Mo−O(1): 176.2(2), Cl(1)−Mo−O(3): 164.1(9), O(1)−Mo−O(3): 81.6(1), O(2)−Mo−O(4): 159.6(2)

ical range for molybdenum(VI) calix[4]arene complexes,[8] being between 191.9(3) pm and 194.2(3) pm; the Mo−Cl(1) distance of 241.0(1) pm is also unexceptional.[11] Interestingly, the molybdenum−nitrogen bond length to the imido ligand N atom of 170.3(4) pm is approximately 1.5 pm shorter than the Mo−N distance in the starting compound **1**, and the Mo−N−C(5) group is close to linear. These structural parameters are, as was likewise shown for **1**, in accordance with the triple bond character of the molybdenum−nitrogen bond.[12]

Significantly elongated with respect to the other molybdenum−oxygen bond lengths is the Mo−O(1) distance of 216.0(3) pm. This correlates with a short O(1)−C(10) contact of 122.1(5) pm, which is in the range for C=O double bonds.[13] The carbon atoms C(10) to C(15) of the carbon ring system connected to O(1) show alternating C−C bond lengths of 145.2(5) pm on average for $C_{ipso}-C_{ortho,}$ 132.8(6) pm for $C_{ortho}-C_{meta}$, and 150.4(6) pm for $C_{meta}-C_{para}$. This is in accordance with a description of the previously aromatic unit of the calix[4]arene as an α,β-unsaturated ring system. The C(15)−Cl(2) distance of 183.3(5) pm corresponds to a carbon−chlorine bond length involving an sp^3-hybridized carbon atom. As a net result, the structure of complex **5** in solution and in the solid state is best described as the 1,6-addition product of chlorine to **1**. To the best of our knowledge, no such selective 1,6-addition of chlorine to an organic or inorganic substrate has ever been observed previously.

Conclusion

The occurrence of electrophilic halogen attack in electrophilic aromatic substitution reactions,[14] especially on phenols,[15] is well-known. Such attack occurs in reactions in which a halogen atom replaces a substituent on the aromatic ring and the resulting kinetically unstable 4-halo-2,5-cyclohexadienone usually decomposes after the initial attack. If the starting phenol has a hydrogen atom in the *para* position, the dienone enolizes to the 4-halo product. With *p*-alkylphenols, the initial halogen attack leads to an "*ipso*-dienone". This can be used for further reactions, e.g. Diels−Alder reactions, or it can revert to the starting material through dehalogenation. 4-Alkyl-4-chloro-2,5-cyclohexadienones have previously been isolated by Fischer and Henderson.[16] Steroidal derivatives have been structurally characterized, as have related polyhalogenated compounds.[17] Calix[4]arene $Cax(OH)_4$ itself does not react with $PhICl_2$ under the reaction conditions that lead to **5**, giving an indication of the importance of the metal complex fragment coordinated at the calix[4]arene ligand in determining the outcome of the reaction.

The cyclohexadienone part of the macrocyclic ligand in **5** is the first example of a structurally characterized 4-halo-4-alkyl-2,5-cyclohexadienone in the coordination sphere of a transition metal complex. This moiety is stabilized by the highly Lewis acidic molybdenum(VI) complex fragment. After initial chlorine attack at the negatively charged and therefore activated ring system of the calix[4]arene ligand, the molecule does not regain its aromaticity but remains with an intact cyclohexadienone system, this being stabilized by attack of chlorine at the (positively charged) metal atom.

Experimental Section

General details were as given in our earlier reports.[8] Compounds **1** and **2** were prepared as described previously;[8b] $PhICl_2$ was prepared according to a published procedure.[18]

[$CaxO_4WCl_2$] (3) from [$CaxO_4W(N$*t*Bu)] (2): Gaseous HCl was for a short time passed into a solution of [$CaxO_4W(N$*t*Bu)] (**2**; 200 mg) in CH_2Cl_2 (20 mL), during which the color of the solution changed from yellow to dark red. After stirring for 5 min, all volatile materials were removed in vacuo. The main component of the remaining solid was identified as the known calix[4]arene tungsten complex [$CaxO_4WCl_2$] (**3**).[7d]

[Cax(OH)O_3Mo(N*t*Bu)Cl] (4): [$CaxO_4Mo(N$*t*Bu)] (**1**; 100 mg, 0.123 mmol) and pyHCl (14.0 mg, 0.123 mmol) were taken up in C_6D_6 (1.00 mL) in an NMR tube. The main species present in the resulting violet reaction mixture was identified by ^{1}H NMR spectroscopy as the addition product [Cax(OH)O_3Mo(N*t*Bu)Cl] (**4**). ^{1}H NMR (C_6D_6): δ = 0.69 [s, 18 H, $C(CH_3)_3$], 1.33 [s, 9 H, $C(CH_3)_3$], 1.35 [s, 9 H, $C(CH_3)_3$], 1.40 [s, 9 H, $NC(CH_3)_3$], 3.28 (d, $^2J_{H,H}$ = 13.9 Hz, 2 H, CH_2), 3.52 (d, $^2J_{H,H}$ = 14.7 Hz, 2 H, CH_2), 5.05 (d, $^2J_{H,H}$ = 14.5 Hz, 4 H, CH_2), 6.71 (d, $^4J_{H,H}$ = 2.4 Hz, 2 H, Aryl-H_m), 6.91 (d, $^4J_{H,H}$ = 2.4 Hz, 2 H, Aryl-H_m), 7.24 (s, 2 H, Aryl-H_m), 7.28 (s, 2 H, Aryl-H_m), 15.47 (br. s, 1 H, OH).

Evaporation of the volatiles from the solution led only to the starting material **1**. Compound **4** could also be obtained by the reaction of **1** with a stoichiometric amount of HCl in toluene or benzene.

[$Cax^{Cl}O_4$Mo(N*t*Bu)Cl] (5): A solution of [$CaxO_4Mo(N$*t*Bu)] (**1**; 800 mg, 0.99 mmol) in toluene (40 mL) was treated with $PhICl_2$ (271 mg, 0.99 mmol) and the resulting dark-violet solution was stirred for 8 h at room temperature. All volatile material was then removed in vacuo and the solid residue was extracted into hexane (60 mL). Removal of the solvent and drying in vacuo afforded **5** as a dark-violet solid; yield: 594 mg (68%). Crystals of **5** suitable for X-ray crystallography were obtained from saturated solutions of the compound in hexane. ^{1}H NMR ($CDCl_3$): δ = 1.02 [s, 9 H, $C(CH_3)_3$], 1.12 [s, 18 H, $C(CH_3)_3$], 1.33 [s, 9 H, $C(CH_3)_3$], 1.44 [s, 9 H, $NC(CH_3)_3$], 3.09 (d, $^2J_{H,H}$ = 13.2 Hz, 2 H, CH_2), 3.35 (d, $^2J_{H,H}$ = 14.6 Hz, 2 H, CH_2), 4.04 (d, $^2J_{H,H}$ = 13.2 Hz, 2 H, CH_2), 4.57 (d, $^2J_{H,H}$ = 14.6 Hz, 2 H, CH_2), 6.80 (d, $^4J_{H,H}$ = 2.4 Hz, 2 H, Aryl-H_m), 7.02 (d, $^4J_{H,H}$ = 2.4 Hz, 2 H, Aryl-H_m), 7.04 (s, 2 H, Aryl-H_m), 7.07 (s, 2 H, Aryl-H_m). $^{13}C\{^1H\}$ NMR ($CDCl_3$): δ = 25.87 [$C(CH_3)_3$], 26.24, 28.62, 31.63 [$C(CH_3)_3$], 31.73 [$C(CH_3)_3$], 31.95 [$C(CH_3)_3$], 33.06 (CH_2), 34.06, 34.36 [$C(CH_3)_3$], 35.73 (CH_2), 42.52 [C(*t*Bu)Cl], 73.25 [$NC(CH_3)_3$], 124.42, 125.16, 126.46 (Aryl-C_m), 127.46, 127.56, 127.84, 139.89 (Aryl-C_o), 144.53, 144.88, 145.34 (Aryl-C_p), 148.08 (Aryl-C_m), 167.62, 168.33 (Aryl-C_i), 191.17 (Aryl-C=O). IR (KBr): $\tilde{\nu}$ = 1668 cm^{-1} [vs br, ν(C=O)]. FD-MS (10 kV): *m*/*z* (%) = 885 (78) $[M + 2H]^+$, 815 (31) $[M + H - NC_4H_9]^+$, 792 (100) $[M - C_4H_9 - Cl]^+$. EI-MS: *m*/*z* (%) = 847 (1) $[M - Cl - H]^+$, 813 (4) $[M - 2Cl]^+$, 791 (62) $[M - Cl - C_4H_9]^+$, 735 (27) $[M - Cl - 2(C_4H_9)]^+$. $C_{48}H_{61}Cl_2NO_4Mo$ (882.9): calcd. C 65.30, H 6.96, N 1.59; found C 64.93, H 7.05, N 1.84.

X-ray Crystallographic Study: Data were collected on a Stoe-IPDS diffractometer (Ag-K_α radiation, λ = 0.56087 Å), *T* = 205(2) K;

data collection and refinement: SHELXS-97[19] and SHELXL-97,[20] monoclinic, space group $P2_1/c$; lattice constants a = 17.453(4), b = 13.199(3), c = 23.524(5) Å, β = 96.02(2)°; V = 5389.0(19) Å^3, Z = 4, μ(Ag-K_α) = 0.944 mm^{-1}, $2\Theta_{max}$ = 39°; 9292 independent reflections measured, of which 6564 were considered observed with $I > 2\sigma(I)$; max./min. residual electron density 0.70 and −0.65 e/Å^3. 561 parameters (Mo, O, and N anisotropic; C anisotropic except disordered *t*Bu groups and solvent molecule; the positions of the H atoms were calculated for idealized positions); R_1 = 0.056; wR_2 = 0.1378.

Crystallographic data (excluding structure factors) for the structures reported in this paper have been deposited with the Cambridge Crystallographic Data Centre as supplementary publication no. CCDC-163977. Copies of the data can be obtained free of charge on application to the CCDC, 12 Union Road, Cambridge, CB2 1EZ, U.K. [Fax: (internat.) +44 (0)1223/336033; E-mail: deposit@ccdc.cam.ac.uk].

Acknowledgments

This work was supported by the Deutsche Forschungsgemeinschaft and the Fonds der Chemischen Industrie. We kindly thank Professor D. Fenske for his continuing support and interest in our work. A gift of metal chlorides from Fa. H. C. Starck GmbH, Goslar, is gratefully acknowledged.

[1] L. H. Gade, *Koordinationschemie*, Wiley-VCH, Weinheim, **1998**, chapters 1−3, 21.

[2] [2a] F. Vögtle, *Supramolekulare Chemie*, Wiley, Chichester, **1993**. [2b] J. M. Lehn, *Supramolekulare Chemie*, VCH Verlagsgesellschaft, Weinheim, **1995**. [2c] W. Kaim, B. Schwerdinski, *Bioanorganische Chemie*, Teubner, Stuttgart, **1995**. [2d] E. C. Constable, *Metal and Ligand Reactivity − An Introduction to the Organic Chemistry of Metal Complexes*, VCH Verlagsgesellschaft, Weinheim, **1996**.

[3] [3a] L. R. Milgram, *The Colours of Life − An Introduction to the Chemistry of Porphyrins and Related Compounds*, Oxford University Press, Oxford, **1997**. [3b] K. M. Smith, *Porphyrins and Metalloporphyrins*, Elsevier, Amsterdam, **1975**. [3c] D. Dolphin, *The Porphyrins*, Academic Press, New York, **1978**. [3d] T. Mashiko, D. Dolphin, in *Comprehensive Coordination Chemistry* (Eds.: G. Wilkinson, R. D. Gillard, J. A. McCleverty), Pergamon, Oxford, **1987**, vol. 2, chapter 21.1.

[4] [4a] C. D. Gutsche, *Calixarenes*, Royal Society of Chemistry, Cambridge, **1989**. [4b] J. Vincens, V. Böhmer (Eds.), *Calixarenes*: *A Versatile Class of Macrocyclic Compounds*, Kluwer Academic Publishers, Dordrecht, **1991**. [4c] J. Vincens, Z. Asfari, J. M. Horrowfield (Eds.), *Calixarenes 50th Anniversary: Commemorative Issue*, Kluwer Academic Publishers, Dordrecht, **1994**. [4d] C. D. Gutsche, *Calixarenes Revisited*, Royal Society of Chemistry, Cambridge, **1998**. [4e] M. Lucinat, R. Ungaro (Eds.), *Calixarenes in Action*, Imperial College Press, London, **2000**. [4f] G. J. Lumetta, R. D. Rogers, A. S. Gopalan, *Calixarenes for Separations*, American Chemical Society, Washington D.C., **2000**.

[5] [5a] C. Floriani, *Chem. Eur. J.* **1999**, *5*, 19−23. [5b] C. Wieser, C. B. Dieleman, D. Matt, *Coord. Chem. Rev.* **1997**, *165*, 93−161. [5c] D. M. Roundhill, *Prog. Inorg. Chem.* **1995**, *43*, 533−565.

[6] [6a] D. Mansuy, M. Lange, J. C. Chottard, J. F. Bartoli, B. Chevrier, R. Weiss, *Angew. Chem.* **1978**, *90*, 828−829; *Angew. Chem. Int. Ed. Engl.* **1978**, *17*, 817−818. [6b] P. J. Brothers, J. P. Collman, *Acc. Chem. Res.* **1986**, *19*, 209−215. [6c] D. Mansuy, *Pure Appl. Chem.* **1987**, *59*, 759−770. [6d] F. Montanari, L. Casella, *Metalloporphyrin Catalyzed Oxidations*, Kluwer, Dordrecht, **1994**. [6e] H. Brand, J. Arnold, *Coord. Chem. Rev.* **1995**, *140*, 137. [6f] T. Aida, S. Inoue, *Acc. Chem. Res.* **1996**, *29*, 39−48. [6g] P. M. Jordan (Ed.), *Biosynthesis of Tetrapyrroles*, Elsevier, New York, **1991**. [6h] C. Floriani, *Chem. Commun.* **1996**, 1257−1263. [6i] P. A. Gale, J. L. Sessler, V. Kral, *Chem. Commun.* **1998**, 1−8. [6j] F. A. Cotton, J. Czuchajowska, *Polyhedron* **1990**, *9*, 2553−2566. [6k] P. Mountford, *Chem. Soc. Rev.* **1998**, *27*, 105−115.

[7] The scission of the *t*Bu groups or *ipso*-nitration reactions in *p-tert*-butylcalixarenes using Lewis acids under acidic conditions are well-known; see, for example: [7a] H. Kämmerer, G. Happel, V. Böhmer, D. Rathay, *Monatsh. Chem.* **1978**, *109*, 767−773. [7b] C. D. Gutsche, J. J. Levine, *J. Am. Chem. Soc.* **1982**, *104*, 2652−2653. [7c] O. Mogck, V. Böhmer, G. Ferguson, W. Vogt, *J. Chem. Soc., Perkin Trans. 1* **1996**, 1711−1715. A similar type of reaction has also been observed for a metallocalix[4]arene: [7d] F. Corazza, C. Floriani, A. Chiesi-Villa, C. Rizzoli, *Inorg. Chem.* **1991**, *30*, 4465−4468.

[8] [8a] U. Radius, J. Attner, *Eur. J. Inorg. Chem.* **1998**, 299−303. [8b] U. Radius, J. Attner, *Eur. J. Inorg. Chem.* **1999**, 2221−2231. [8c] J. Attner, U. Radius, *Chem. Eur. J.* **2001**, *7*, 783−790.

[9] [9a] J. Acho, S. J. Lippard, *Inorg. Chim. Acta* **1995**, *229*, 5−8. [9b] J. Acho, T. Ren, J. W. Yun, S. J. Lippard, *Inorg. Chem.* **1995**, *34*, 5226−5233.

[10] M. Hesse, H. Meier, B. Zeeh, *Spektroskopische Methoden in der organischen Chemie*, 3rd Edition, Thieme, Stuttgart, **1987**, 27−67.

[11] G. Orpen, L. Brammer, F. H. Allen, O. Kennard, D. G. Watson, *J. Chem. Soc., Dalton Trans.* **1989**, S1−S89.

[12] [12a] W. A. Nugent, B. L. Haymore, *Coord. Chem. Rev.* **1980**, *31*, 123−175. [12b] D. E. Wigley, *Prog. Inorg. Chem.* **1994**, *42*, 239−482. [12c] W. A. Nugent, J. M. Mayer, *Metal−Ligand Multiple Bonds − The Chemistry of Transition Metal Complexes Containing Oxo, Nitrido, Imido, Alkylidene, or Alkylidyne Ligands*, Wiley, New York, **1988**.

[13] J. March, *Advanced Organic Chemistry*, 4th Edition, Wiley, NewYork, **1992**, p. 21.

[14] [14a] F. A. Carey, R. J. Sundberg, *Advanced Organic Chemistry, Part A: Structure and Mechanism*, 2nd edition, Plenum Press, New York, **1984**, chapter 9. [14b] F. A. Carey, R. J. Sundberg, *Advanced Organic Chemistry, Part B: Reactions and Synthesis*, 2nd edition, Plenum Press, New York, **1984**, chapter 8.1. [14c] H. R. Christen, F. Vögtle, *Grundlagen der Organischen Chemie*, 2nd edition, Otto Salle Verlag, Frankfurt/Main, **1989**, chapter 15. [14d] A. Streitwieser, C. H. Heathcock, E. M. Kosower, *Organische Chemie*, 2nd edition, VCH, Weinheim, **1994**, chapter 23. [14e] H. Beyer, W. Walter, W. Francke, *Lehrbuch der Organischen Chemie*, 23rd edition, S. Hirzel Verlag, Stuttgart, **1998**, chapter 5, especially 5.5. [14f] M. Sainsbury, *Aromatenchemie*, VCH, Weinheim, **1995**.

[15] [15a] J. H. P. Tyman, *Synthetic and Natural Phenols*, Elsevier, Amsterdam, **1996**. [15b] P. B. D. de la Mare, *Electrophilic Halogenation*, Cambridge University Press, Cambridge, **1976**. [15c] P. B. D. de la Mare, *Acc. Chem. Res.* **1974**, *7*, 361−368.

[16] [16a] A. Fischer, G. N. Henderson, *Can. J. Chem.* **1979**, *57*, 552−557. [16b] A. Fischer, G. N. Henderson, *Can. J. Chem.* **1983**, *61*, 1045−1052.

[17] [17a] F. Mukawa, *J. Chem. Soc., Perkin Trans. 1* **1988**, 457−460. [17b] A. M. Soerensen, B. Jerslev, *Acta Chem. Scand.* **1968**, *22*, 319−327.

[18] H. J. Lucas, E. R. Kennedy, *Org. Synth.*, Wiley, New York, **1955**, *3*, 482−483.

[19] G. M. Sheldrick, *SHELXS-97: Program for Crystal Structure Solution*, Universität Göttingen, **1997**.

[20] G. M. Sheldrick, *SHELXL-97: Program for Crystal Structure Refinement*, Universität Göttingen, **1997**.

Received August 3, 2001
[I01287]

Electron Transfer in Mn-Tripod Complexes

Ulrich Kölle*[a] and Ulli Englert[a]

Keywords: Electrochemistry / Electron transfer / Tripodal ligands / Manganese

A heterogeneous electron-transfer rate constant $k_0 \approx 7–8 \times 10^{-7}$ cm s^{-1} for the reduction/oxidation of the bis-tripod complex $[CpCo^{III}\{P(OEt)_2O\}_3]_2Mn^{III/II}$ redox couple was measured by cyclic voltammetry. The homogeneous self-exchange rate was calculated as $k_2 = 4.25 \cdot 10^{-3}$ M^{-1}s^{-1} from the cross reaction of the Mn^{II} tripod complex with ferrocenium salt. X-ray structure determinations for both complexes showed a near regular octahedral oxygen coordination for the Mn^{II} complex and a sizeable Jahn–Teller distortion for the Mn^{III} complex. Applying current ET theory for the comparison of heterogeneous and homogeneous rates and estimates of reorganization energies leads to the conclusion that the major part of the latter is due to inner reorganization of the Mn tripod.

Introduction

The Kläui Tripod ligand $[CpCo^{III}\{P(OR)_2O\}_3]^-$ (see bold face part in Scheme 1) is unique as a tripodal oxygen ligand as it combines high complex stability constants with a relatively weak ligand field.[1] Thus, nearly all of the main group metals as well as the major part of the d- and f-block elements have been complexed by this ligand in the form of either (Trpd)ML or $(Trpd)_2M$ complexes, where M is fixed in a regular octahedral six oxygen environment. The 3d transition metal complexes are generally high spin with the exception of Co^{III}, which gives rise to a temperature-dependent spin equilibrium,[2–4] which is low spin at low temperatures and partly high spin at higher temperatures.

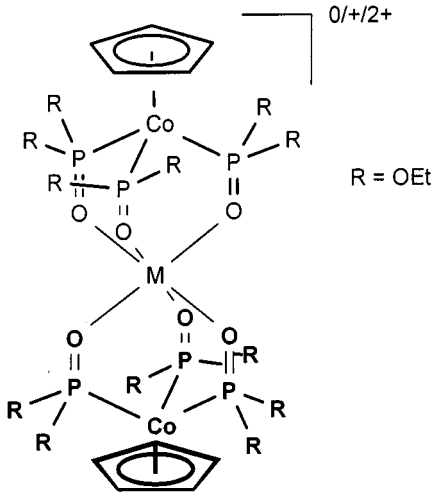

Scheme 1

These complexes are particularly well suited for redox studies,[5,6] since the ligand $[CpCo^{III}\{P(OR)_2O\}_3]^-$ itself offers a relatively broad potential window where the carrier metal Co^{III} is redox inert. This feature is explored by recording decomposition potentials for $(Trpd)_2M$ complexes featuring a redox-inert central metal. Reduction and oxidation limits depend somewhat on the charge of this central metal and have been determined as −1 and +0.76 V for the reduction and oxidation of the ligand anion $[CpCo\{P(OEt)_2O\}_3]^-$ (as the Na^+ salt), −1 V for $[CpCo\{P(OEt)_2O\}_3]_2Mg$ (reduction only) and −1.75 and +1.75 V for $[(CpCo\{P(OEt)_2O\}_3)_2Al]^+$. Reversible redox transitions for the central metal have been found to occur about 1 V more negative than those of the respective aqua ions $M(H_2O)_6^{3+/2+}$ for a variety of complexes of 3d metals.[5] Since for the latter the $M^{3+/2+}$ potentials become increasingly positive along the d block, tripod complexes allow us to determine redox transitions such as $Mn^{II/III/IV}$ and $Ni^{II/III}$ which are inaccessible for the aqua ions by direct electrochemical measurement. Table 1 lists observed redox transitions in $[CpCo\{P(OEt)_2O\}_3]_2M$ for 3d metals M. As can be clearly seen, a wide potential range is covered

Table 1. Redox transitions in $(Trpd)M^{n+}$ complexes

Electronic configuration	Transition $M^{n+}(L_{OEt})_2/M^{(n\pm1)+}(L_{OEt})_2$	$E_{1/2}$ [a]
d^0/d^1	Ti^{IV}/Ti^{III}	−0.30
d^1/d^2	V^{IV}/V^{III}	0.933
d^2/d^3	V^{III}/V^{II}	−1.54
d^3/d^4	Cr^{III}/Cr^{II}	−1.57
	Mn^{IV}/Mn^{III}	1.53
d^4/d^5	Mn^{III}/Mn^{II}	0.12
d^5/d^6	Fe^{III}/Fe^{II}	−0.72
d^6/d^7	Co^{III}/Co^{II}	0.745
d^7/d^8	Ni^{III}/Ni^{II}	1.255

[a] V vs. SCE in acetonitrile.

[a] Institute for Inorganic Chemistry, Aachen Technical University, 52056 Aachen, Germany

 © WILEY-VCH Verlag GmbH, 69451 Weinheim, Germany, 2002 1434–1948/02/0101–0165 $ 17.50+.50/0

by the accessible redox transitions and each electron configuration change d^{n+1}/d^n from $n = 0$ to 8 is represented by at least one redox pair. A second remarkable feature of the tripod complexes is their ready solubility in relatively nonpolar solvents. Thus neutral $(Trpd)_2M$ complexes (with a central metal M^{II}) are soluble in ether, dichloromethane and slightly soluble even in hydrocarbon solvents. Cationic $[(Trpd)_2M]PF_6$ (with a central metal M^{III}) complexes are readily dissolved in acetonitrile.

Due to the fixed geometry of the ligand sphere and the strictly outer-sphere character of the electron transfer, geometrical factors are identical for each of the above listed redox changes. Moreover, since the molecular dimensions of the complexes [about 27 × 23 Å for $P(OEt)_2$ tripod ligands] are rather large and the periphery of the molecule is strongly hydrophobic, solvation terms in the electron transfer process should play a minor role and are strictly identical in all cases. Therefore the differences in rate constants for transitions between different electron configurations reflect the geometrical change as well as an intrinsic barrier for an electron entering or leaving either a dσ or a dπ orbital, as well as electron repulsion and exchange terms.

The work presented here concentrates on the Mn^{II}/Mn^{III} couple as the most noteworthy and unusual redox couple within the bis tripod series.

Results

Heterogeneous Electron Transfer

Among all the redox couples studied the high spin $Mn^{III/II}$ pair is a highly remarkable case. Figure 1 depicts cyclic voltammograms at different scan rates starting either from the Mn^{II} or the Mn^{III} complex as the species in solution. As can be seen there is an extraordinarily large separation between the anodic and cathodic peak: $\Delta E_p = 1.03$ V at v = 50 mV/s to $\Delta E_p = 1.36$ V at v = 1000 mV/s. The much smaller peak height in the return sweep is not due to a chemical follow up reaction but rather to the diffusional broadening of the concentration gradient at the electrode

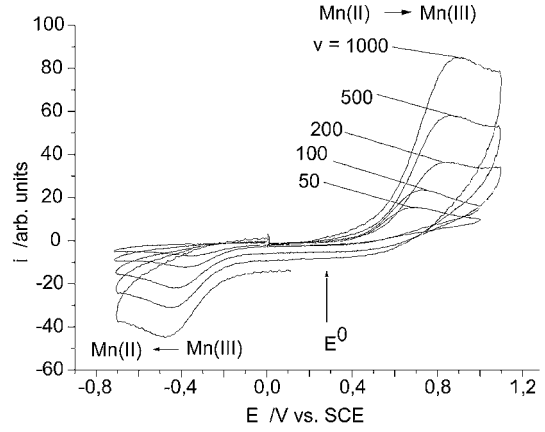

Figure 1. Cyclic voltammogram of $[CpCo\{P(OEt)_2O\}_3]_2Mn^{II}$ in CH_2Cl_2 at different sweep rates, 0.05 to 1.0 V/s

due to the prolonged time elapsed between the forward and the return sweep. The picture is symmetrical in that Mn^{II} oxidation or Mn^{III} reduction is the higher peak depending on the starting complex. This couple is an extreme case of chemically fully reversible non-Nernstian behavior with a very small heterogeneous electron-transfer constant.

The parameters were evaluated by digital simulation using the Gosser program adapted for Windows.[8] The heterogeneous transfer constant k_0 was adjusted mainly so as to match the experimental peak separation, whereas the transfer coefficient α was adjusted to the ratio of the cathodic to the anodic peak current as well as to the width of the peaks. Diffusion coefficients for the tripod couples had been determined previously as $\approx 3 \cdot 10^{-6}$ cm^2 s^{-1}.[8] The cyclic voltammograms recorded at sweep rates above 0.5 V/s require increasingly smaller k_0 values for simulation. This effect is traced back to the influence of uncompensated solution resistance at higher scan rates. Therefore values at $v = 0.05-0.5$ V s^{-1} giving $k_0 = 7-8 \cdot 10^{-7}$ cm s^{-1} are considered most reliable for this Mn^{II}/Mn^{III} couple.

In such cases the mean of the oxidation and reduction peak of the couple cannot simply be taken as the formal redox potential since this assumption is valid only under Nernstian or near Nernstian behavior. This problem was addressed by scrutinizing the oxidation of Mn^{II} with different ferrocenium salts of known reversible redox potential. Thus Mn^{II} is readily oxidized by the ferrocenium ion ($E_{1/2} = 0.400$ V vs. SCE) but not by the decamethylferrocenium ion ($E_{1/2} = -0.168$ V), whereas Mn^{III} does not oxidize ferrocene but does oxidize decamethylferrocene. The redox potential must thus be located between decamethylferrocene and ferrocene. The value for $E_{1/2}$ determined from simulation of the experimental cyclic voltammogram was 0.280 ± 0.008 V vs. SCE referred to $Fc^{+/0}$ vs. SCE as 0.4000 V.

Homogeneous Cross Reaction with Ferrocenium Ion

Direct determination of the self-exchange rate for the Mn tripod couple was not possible due to the lack of suitable signals in the NMR spectrum. Moreover, it was observed with a variety of other tripod couples that self exchange between tripod complexes is rather slow on the NMR time scale and exchange line broadening is small compared to the paramagnetic linewidth. A cross reaction with a transfer agent of known self-exchange rate was therefore sought in order to arrive at an estimate for the Mn self exchange reaction. The ferrocenium ion was found to be best suited for this purpose since its reversible potential is close to the $(Trpd)_2Mn^{III/II}$ potential. Self-exchange rates for the ferrocene/ferrocenium couple are known in a variety of solvents[9] and have been shown to be not very solvent dependent. Moreover, given the redox potential evaluated above, the driving force of the cross reactions is only about $\Delta E^0 = 0.12$ V. This low driving force places the reaction of Mn^{II}-tripod with the ferrocenium ion in a time domain suitable for stopped flow kinetics despite the rather high self-exchange rate of the latter of $\approx 10^7$ M^{-1} s^{-1}. A dichlorome-

Table 2. Crystal data and structure refinement for $(Trpd)_2Mn^{III}PF_6 \cdot CH_2Cl_2$ and $(Trpd)_2Mn^{II}$

Empirical formula	$C_{35}H_{72}Cl_2Co_2F_6MnO_{18}P_7$	$C_{34}H_{70}Co_2MnO_{18}P_6$
Molecular weight	1355.47	1125.57
Temperature	258 K	258 K
Wavelength	0.71073 Å	0.71073 Å
Crystal system	Monoclinic	Triclinic
Space group	*C*2/*c*	$P\bar{1}$
Unit cell dimensions	a = 21.596(8) Å	a = 12.406(6) Å; α= 92.43(3)°
	b = 12.197(2) Å; β = 107.58(3)°	b = 20.310(8) Å; β = 118.26(5)°
	c = 23.228(4) Å	c = 12.103(6) Å; γ = 75.90(4)°
Volume	5832(3) Å^3	2596(4) Å^3
Z	4	2
Density (calculated)	1.54 Mg/m^3	1.44 Mg/m^3
Absorption coefficient	1.123 mm^{-1}	1.103 mm^{-1}
Crystal size	0.6 × 0.6 × 0.4 mm	0.5 × 0.3 × 0.2 mm
Θ range for data collection	3.1 to 22.0 deg	3.1 to 25.0 deg.
Reflections collected	3676	8094
Independent reflections	3002 [R(int) = 0.039]	5748 [R(int) = 0.040]
Data/restraints/parameters	2479/155/323	3812/6/583
Final R indices	R = 0.103	R = 0.079
[$I > 0.5\sigma(I)$]	R_w = 0.077	R_w = 0.077
Largest diff. peak and hole	1.3931 and 0.8420 e.A^{-3}	0.6799 and −0.4675 e. Å^{-3}

thane solution of $(Trpd)_2Mn^{II}$ ($1.0 \cdot 10^{-2}$ M) and ferrocenium chloride ($1.3 \cdot 10^{-2}$ M) was mixed in a stopped flow cell at ambient temperature (22 °C) and the decay of the ferrocenium absorption [Equation (1)] was followed at 618 nm. Evaluation of the kinetic trace according to 2nd order kinetics gave a rate constant k_2 = 1400 s^{-1} M^{-1}.

$$(Trpd)_2Mn^{II} + Fc^+ \rightarrow (Trpd)_2Mn^{III\,+} + Fc \quad (1)$$

Structural Rearrangement Concomitant with Electron Transfer

A high spin d^4 electronic configuration is usually subject to substantial Jahn−Teller distortion. Since this distortion was originally anticipated as one of the principal factors for the exceptionally slow electron transfer in the $(Trpd)_2Mn$ case a quantization of the effect seemed highly desirable. We have thus undertaken single crystal X-ray structure determinations of both Mn complexes. Though bis-tripod complexes have been prepared throughout the transition series,[1] apart from the structure of a tripod-Na salt,[5] structural details of bis-tripod complexes have not been evaluated. The structures determined in this work are therefore the first X-ray structure determinations on bis-tripod complexes. $[CpCo\{P(OEt)_2O\}_3]_2Mn$ readily crystallizes from ether, whereas $[(CpCo^{III}\{P(OEt)_2O\}_3)_2Mn][PF_6] \cdot CH_2Cl_2$ crystallized by diffusion of ether into a dichloromethane solution. The structures were solved by direct methods[10] and refined on F^2.[11] Empirical absorption corrections[12] were applied to both data sets. Parameters for the structure determinations of the Mn^{II} and the Mn^{III} complex are given in Table 2.

$(Trpd)_2Mn^{II}$ crystallizes in the triclinic space group $P\bar{1}$ with two independent molecules in the unit cell. Since the most relevant structural features are expected to occur in the Mn−O bond lengths and angles we concentrate on these. Mn−O bond lengths in the two independent molecules are (three unrelated by symmetry in each molecule) 2.137(7), 2.146(7), 2.160(6) and 2.160(6), 2.155(7), 2.161(7) Å for Mn^{II}. They are nearly equal within the limits of error. The coordination environment of the Mn^{II} ion is a slightly distorted octahedron, with bond angles of 87.6(3) and 92.4(3)°.

The Mn^{III} complex crystallizes in the monoclinic space group *C*2/*c* with the complex molecule on a crystallographic inversion center. As far as Mn−O bond lengths are concerned, three distinctly different distances [1.981(5),

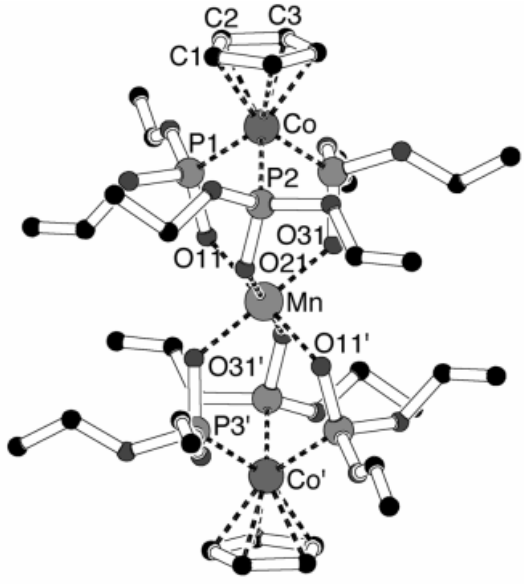

Figure 2. Perspective view of the $[(CpCo\{P(OEt)_2O\}_3)_2Mn]^+$ cation; see text for bond lengths and angles

2.053(4) and 1.923(4) Å] are found. The O−Mn−O bond angles differ only by about 2 °, ranging from 89 to 91°. There is thus a distinct deviation from the octahedral geometry, with each ligand giving rise to three different O−Mn bond lengths. The molecular symmetry of the MO_6 core in $[(Trpd)_2Mn^{III}]^+$ is thus C_i. Figure 2 shows a view of the molecule showing the overall atom connectivity.

Discussion

Comparison of Heterogeneous and Homogeneous Rate Constants

In view of the similarity of homogeneous electron transfer with electron transfer through an interface the rate constants k_{ex} and k_0 for either process of a given redox couple are related, as shown in Equation (2):

$$\frac{k_0}{A_{electrode}} = \left(\frac{k_{ex}}{A_{solution}}\right)^{1/2} \tag{2}$$

The applicability of Equation (2) to practical cases is, however, hampered by the inaccessibility of the frequency factors A.

Weaver[13] has suggested an expression [Equation (3)] that allows a direct comparison of the heterogeneous transfer rate of a redox couple with the rate of a cross reaction between this couple and a second oxidant/reductant:

$Red_1 + Ox_2 \rightarrow Ox_1 + Red_2$

where in our case index 1 refers to the Mn tripod and index 2 to ferrocene. The basic idea is to convert the heterogeneous constant to a pseudo-homogeneous one by treating the electrode as a surface with the dimensions of the coreactant in the bimolecular reaction [first term of the l.h.s. of Equation (3)].

$$\log\left(4\pi N_A r_h^2 k_{0,cor}\right) - \log(k_{ex}) = \log\left(\frac{\kappa_e \delta r_e}{\kappa_h \delta r_h}\right) + \ldots$$
$$\ldots \left[\Delta G^{\#}_{i,2} + \frac{N_A e^2}{4\pi\varepsilon_0}\left(\frac{1}{2r_2} - \frac{1}{(r_1 + r_2)} + \frac{1}{4r_{1-e}}\right)\left(\frac{1}{\varepsilon_{opt}} - \frac{1}{\varepsilon_s}\right)\right] / 2RT \tag{3}$$

In this equation $k_{0,cor}$ is the heterogeneous rate constant corrected for the driving force in the homogeneous reaction (0.12 V), κ a transmission coefficient, δr a reaction zone thickness and r_1, r_2, r_{1-e} are reactant radii and reactant electrode distances, respectively. The second term of the r.h.s. is the inner-shell reorganization of the coreactant (ferrocene) and the difference in outer-shell reorganization of self exchange and cross reaction. In general, κ and δr will be similar for both reactions, and for a fast reacting coreactant $\Delta G^{\#}_{i,2}$ will be small as well as $\Delta G^{\#}_{out}$ ($2r_2 \approx r_1 + r_2 < 4r_{1-e}$), which means that the first term of the r.h.s. vanishes and also that the bracketed term will be small, leading to Equation (4):

$$4\pi N_A r_h^2 k_{0,cor} = k_{ex} \tag{4}$$

Correcting k_0 for the driving force (0.12 V) gives $k_{0,cor} = 7.5 \cdot 10^{-6}$ cm s^{-1} and taking r_h as 27 Å, the radius of the tripod ligand, gives a value of $4.5 \cdot 10^3$ M^{-1} s^{-1} for the r.h.s. of Equation (4) compared to $1.4 \cdot 10^3$ M^{-1} s^{-1} for the measured rate of the cross reaction. Application of Equation (3) gives 3.5 for the r.h.s. as compared to 2.2 for the l.h.s., i.e. one order of magnitude difference. In view of the inherent assumptions, the similarity of the two values demonstrates that the same physical factors are responsible for homogeneous and heterogeneous electron transfer. Thus the very slow heterogeneous rate for the Mn couple is not an "electrochemical" effect

Estimate of the Self-Exchange Rate for the $(Trpd)_2Mn^{+/0}$ Couple

Self-exchange rates from cross reactions can be obtained using Marcus' cross relation [Equation (5)]:[14]

$$k_{12} = (\sqrt{k_{11}} k_{22} K_{12} f_{12}) W_{12} \tag{5}$$

which in the case of a small driving force and largely canceling work terms w_{ij} simplifies to Equation (6):

$$k_{12} \cong (\sqrt{k_{11}} k_{22} K_{12}) \tag{6}$$

Inserting the stopped flow determined value of k_{12} (1400 s^{-1} M^{-1} see above), the value 4.3 10^6 $M^{-1}s^{-1}$ as given for k_{ii}(ferrocene) in dichloromethane,[15] and the driving force of 0.12 V into Equation (6) gives a self exchange rate of $4.25 \cdot 10^{-3}$ $M^{-1}s^{-1}$ for the $(Trpd)_2Mn^{+/0}$ couple. This value signifies a rather slow exchange, surpassed among simple transition metal complexes only by a number of $Co^{II/III}$ couples with amine and pyridine ligands.[16]

Activation and Reorganization Energies

Using transition state theory[17] we may calculate activation and reorganization energies from Equation (7):

$$\frac{k_{obs}}{K_{os}} = k_{ex} = \nu_n \kappa \exp\left(-\frac{\Delta G^{\#}}{RT}\right) \tag{7}$$

Equation (7) is appropriate for homogeneous self exchange where k_{obs} in the domain far from the diffusion limit is directly related to k_{ex} only through the outer sphere complex formation constant K_{os}. In the case of one neutral reactant there will be no coulombic barrier to outer sphere complex formation, so K_{os} reduces to Equation (8):

$$K_{os} = \frac{4\pi N_A r^2 \delta r}{1000} \quad (8)$$

For the Mn tripod couple we set $\kappa = 1$ (adiabatic limit) and the frequency factor $\nu_n = 17.4 \cdot 10^{12}$ s^{-1} from a tentative assignment of a band at 580 cm^{-1} in the IR spectrum of M(tripod)$_2$ complexes to the M−O stretching vibration (a deviation from this value will have little influence on the final result).[18] Taking r = 27 Å and δr = 0.6 Å[19] gives K_{os} = 3.2 M^{-1} and, from Equation (7), $\Delta G^{\#}_{MnMn}$ = 92 kJ/mol.

Alternatively we may set $r^2 = r_{Fc} \cdot r_{Mn} = 3.8 \cdot 27$ Å^2 in Equation (8) for the cross reaction Equation (1) and 0.6 Å for δr, giving K_{os} = 0.46 M^{-1}. Similarly, the introduction of a frequency factor of 10^{13} s^{-1}, as a mean of the values derived for the Mn tripod and ferrocene,[9] and $k_{obs} = 1.4 \cdot 10^3$ M^{-1} s^{-1} in Equation (7) leads to $\Delta G^{\#}_{FcMn}$ = 54 kJ/mol.

For the cross reaction $\Delta G^{\#}$ can be divided into the driving force and reorganization free energy λ according to Equation (9):

$$\Delta G^{\#} = \frac{\lambda}{4}\left(1 + \frac{\Delta G^0}{\lambda}\right)^2 \quad (9)$$

leading to λ = 238 kJ/mol. (for $\Delta G° < \Delta G^{\#}$ and $\lambda \approx \Delta G^{\#}$) which must be compared to the value of approx. 370 kJ/mol for the self exchange reaction. To obtain the inner reorganization energy for the cross reaction from Equation (10):

$$\lambda = \lambda_{in} + \lambda_{out} \quad (10)$$

we estimate the outer (solvent) reorganization part through the familiar expression of Equation (11):

$$\lambda_{out} = \frac{e^2 N_A}{4\pi\varepsilon_0}\left(\frac{1}{2r_{Fc}} + \frac{1}{2r_{Mn}} - \frac{1}{R}\right)\left(\frac{1}{\varepsilon_{opt}} - \frac{1}{\varepsilon_s}\right) \quad (11)$$

where r_{Fe}, r_{Mn} and R are the radii of ferrocene, Mn tripod and intercomplex distance in the transition state, and ε_{opt} and ε_s are the optical (n^2) and static dielectric constants of the solvent (dichloromethane). Inserting the radii as above and taking R as the sum of the reactant radii one obtains λ_{out} = 62.4 kJ/mol (i.e. $\Delta G^{\#}_{out}$ = 15.6 kJ/mol) which is about one quarter of the total reorganization energy of the cross reaction. Since the inner reorganization energy for ferrocene as extracted from ferrocene/ferrocenium self exchange is small ($\Delta G^{\#}_{in}$ = 3.8 kJ/mol[20]) the major part, i.e. about 40 kJ/mol is left as the internal reorganization for the Mn part in the cross reaction. Doubling this value and adding the solvent reorganization energy evaluated through the appropriate version of Equation (11), ($\Delta G^{\#}_{out}$ = 6.4 kJ/mol) one arrives at 86.5 kJ/mol for the self exchange, in fair agreement with the value obtained from the rate calculated for Mn self exchange (92 kJ/mol, see above).

The most relevant species to compare with the tripod complexes are the aqua ions $M(H_2O)_6^{n+}$. In the case of the $Mn(H_2O)_6^{3+/2+}$ couple no direct measurement of the self-exchange rate constant exists. Whereas Diebler and Sutin[21] in earlier work proposed $k_{11} \approx 10^{-4}$ M^{-1}s^{-1} from cross reactions in different acid media, Macartney and Sutin in later work[22] extracted a range of self-exchange constants ranging from 10^{-9} to about 10^{-3} M^{-1}s^{-1} dependent on the partner in the cross reaction. These electron transfer reactions involving the strongly acidic $Mn(H_2O)_6^{3+}$ ion show branched kinetics in the rate law comprising acid dependent and acid independent paths. The nature of the actual transition state therefore cannot be deduced with certainty from the experiments, and neither is the outer sphere character of the redox transitions granted in each case. In spite of these uncertainties $Mn(H_2O)_6^{III/II}$ electron transfer appears to be among the slowest observed for first row transition metal aqua ions.

In view of a value of k_{ex} of $4 \cdot 10^{-3}$ M^{-1} s^{-1} found for the outer sphere tripod-$Mn^{III/II}$ self-exchange rate constant, the greater value of Macartney and Sutin appears as the more probable one since an outer-sphere reaction of the aqua ions should not be slower than that of the much larger tripod complexes.

It may be tempting to trace the rather slow $Mn^{III/II}$ self exchange back to the Jahn−Teller distortion of Mn^{III} and the mean value (0.167 Å) geometric rearrangement accompanying the redox change. However, the X-ray structure determination of a Mn^{III} alum did not reveal such an effect, not even an indication for a dynamic Jahn−Teller distortion.[23] Thus, $Mn^{III/II}$ electron exchange seems to be slow with and without Jahn−Teller distortion. Moreover, ET in other M^{II}/M^{III} tripod couples which can be expected to show similar differences in M−O distances in the two oxidation states is found to be orders of magnitude faster [$\log(k_{het}) \approx 10^{-2}$ cm s^{-1}]. There appears thus to be no simple relationship between the geometry difference of the two oxidation states and the electron transfer rate.

The particular kinetic inertness of the $Mn^{III/II}$ couple in electron transfer is obviously related to the high thermodynamic stability of the Mn^{II} state towards oxidation as well as reduction. This feature dominates the coordination chemistry of Mn^{II} and is even evident in organometallic complexes such as high spin manganocenes.[24] The origin of slow electron transfer kinetics is thus traced back to the destruction of the half-filled d shell, i.e. the loss of exchange energy, when going from Mn^{II} to Mn^{III}, a fact that hitherto has not been considered as a parameter in electron transfer theory.

Experimental Section

Tripod complexes were prepared from $[CpCo\{P(OEt)_2O\}_3]Na$ and the respective metal salt in water or dichloromethane according to ref.[5] Samples of neutral tripod complexes were recrystallized from toluene or diethyl ether and for cationic complexes from dichloromethane/ether. Crystals of $[(CpCo\{P(OEt)_2O\}_3)_2Mn][PF_6]\cdot CH_2Cl_2$ were grown by diffusion of ether into a dichloromethane solution.

Electrochemical measurements were performed using EG&G equipment as previously described.[7] The kinetics of the homogeneous cross reaction was performed with a home-made stopped flow apparatus built around a High-Tech Scientific optical mixing cell and recorded with a J&M Tidas Diode array spectrophotometer taking spectra at 12 ms intervals. At 22 °C a 10^{-2} M solution of $[CpCo\{P(OEt)_2O\}_3]_2Mn$ in CH_2Cl_2 was mixed with an equal volume of a 1.3 10^{-2} M solution of ferrocenium chloride in CH_2Cl_2 giving a final concentration of $5{\cdot}10^{-3}$ and $6.5{\cdot}10^{-3}$ M, respectively. The decay of the ferrocenium absorption at 618 nm was monitored. Under these conditions the reaction had a half-life of 0.84 s. The absorption decay was fitted to second order kinetics leaving k and the initial absorption as adjustable parameters.

Crystallographic data (excluding structure factors) for the structure(s) included in this paper have been deposited with the Cambridge Crystallographic Data Centre as supplementary publication nos. CCDC-162976 for $[CpCo^{III}\{P(OEt)_2O\}_3]_2Mn$ and -162977 for $[(CpCo^{III}\{P(OEt)_2O\}_3)_2Mn][PF_6]{\cdot}CH_2Cl_2$. Copies of the data can be obtained free of charge on application to CCDC, 12 Union Road, Cambridge CB2 1EZ, UK [Fax: (internat.) + 44-1223/336-033; E-mail: deposit@ccdc.cam.ac.uk].

Acknowledgments

This work was supported by the Stiftung Volkswagenwerk as part of the special program "Electron Transfer Reactions".

[1] W. Kläui, *Angew. Chem.* **1990**, *102*, 661−670; *Angew. Chem. Int. Ed. Engl.* **1990**, *29*, 627.
[2] W. Eberspach, N. El Murr, W. Kläui, *Angew. Chem.* **1982**, *94*, 919−920; *Angew. Chem. Int. Ed. Engl.* **1982**, *21*, 915.
[3] P. Gütlich, B. R. McGarvey, W. Kläui, *Inorg. Chem.* **1980**, *19*, 3704−3706.
[4] W. Kläui, W. Eberspach, P. Gütlich, *Inorg. Chem.* **1987**, *26*, 3977−3982.
[5] W. Kläui, A. Müller, W. Eberspach, R. Boese, I. Goldberg, *J. Am. Chem. Soc.* **1987**, *109*, 164−169.
[6] U. Kölle, W. Kläui, *Z. Naturforsch., Teil B* **1991**, *46*, 75−83.
[7] U. Kölle, A. Laguna, *Inorg. Chim. Acta* **1999**, *290*, 44−50.
[8] Version from K. Neuer-Edscheidt, cf. K. Neuer-Edscheidt, Diplom Thesis, Aachen, **1997**.
[9] R. M. Nielson, G. E. McManis, M. N. Golovin, M. J. Weaver, *J. Phys. Chem.* **1988**, *92*, 3441−3450.
[10] SHELX-97, Program for Structure Solution, G. M. Sheldrick, Univ. of Göttingen, **1997**.
[11] SHELX-97, Program for Structure Refinement, G. M. Sheldrick, Univ. of Göttingen, **1997**.
[12] A. C. T. North, D. C. Phillips, F. S. Mathews, *Acta Crystallogr., Sect. A* **1968**, *24*, 351−359.
[13] M. J. Weaver, *J. Phys. Chem.* **1990**, *94*, 8608−8613.
[14] For symbols and applicability of the simplified version see, for example, ref.[13] p. 42.
[15] E. S. Yang, M.-S. Chan, A. C. Wahl, *J. Phys. Chem.* **1980**, *84*, 3094−3099.
[16] C. Creutz, N. Sutin, in *Inorganic Reactions and Methods* (Ed.: J. J. Zuckerman), VCH, Weinheim 1986, p. 54.
[17] The treatment follows in part the presentation given by: N. Sutin, *Acc. Chem. Res.* **1982**, *15*, 275−282.
[18] W. Kläui, K. Dehnike, *Chem. Ber.* **1978**, *111*, 451−468.
[19] T. Gennett, D. F. Milner, M. J. Weaver, *J. Phys. Chem.* **1985**, *89*, 2787−2794.
[20] Calculated from values given in refs.[9,19] Note that the total measured reorganization energy is divided up for individual reaction partners, thus half the value determined for the self exchange reaction is taken as the reorganization energy for one molecule.
[21] H. Diebler, N. Sutin, *J. Phys. Chem.* **1964**, *68*, 174−180.
[22] D. H. Macartney, N. Sutin, *Inorg. Chem.* **1985**, *24*, 3403−3409.
[23] J. K. Beattie, S. P. Best, B. W. Skelton, A. H. White, *J. Chem. Soc., Dalton Trans.* **1981**, 2105−2111.
[24] We have found high spin Cp_2Mn to be neither reducible nor oxidizable electrochemically in THF between the limits −2.6 and 1.2 V vs. SCE (U. Koelle, unpublished results). In contrast, the low-spin complex Cp^*_2Mn is reported to lead to a stable anion in cyclic voltammetry in spite of the fact that Cp* (η^5-C_5Me_5) ligands shift reduction potentials to more negative values.

Received May 7, 2001
[I01155]

Mercury(II) Complexes with Heterocyclic Thiones − Preparation and Characterization of the 1:1 and 1:2 Mercury(II) Complexes with Benzo-1,3-imidazole-2-thione

Zora Popović,*[a] Željka Soldin,[a] Dubravka Matković-Čalogović,[a] Gordana Pavlović,[b] Maša Rajić,[c] and Gerald Giester[d]

Keywords: Mercury / Sulphur heterocycles / Crystal structure / TGA-DTA analysis

A series of complexes $HgX_2(bzimtH_2)$ and $HgX_2(bzimtH_2)_2$ (X = Cl^-, Br^-, I^-, SCN^-; $bzimtH_2$ = benzo-1,3-imidazole-2-thione) was obtained by reaction of the mercury(II) salts with benzo-1,3-imidazole-2-thione in the appropriate molar ratio (1:1 or 1:2). $Hg(bzimtH)_2$ was obtained by the deprotonation of $bzimtH_2$ with mercury(II) acetate (irrespective of the molar ratio of the reactants). The complexes were characterised by chemical and thermal analysis, IR, ^1H, and ^{13}C NMR spectroscopy, and some [$HgX_2(bzimtH_2)$, X = I^- and $HgX_2(bzimtH_2)_2$, X = I^- and SCN^-] by X-ray single crystal diffractometry. ^1H and ^{13}C NMR spectroscopic measurements in dimethyl sulphoxide revealed that the sulphur atom is coordinated to the mercury centre. The greatest complexation effects on the chemical shifts were observed for the thione carbon atom and thioamide proton. The crystal structures of $HgI_2(bzimtH_2)_2$ and $Hg(SCN)_2(bzimtH_2)_2{\cdot}C_2H_5OH$ consist of discrete monomeric molecules with halide or pseudohalide donor atoms and thione sulphur atoms tetrahedrally coordinated to the mercury atom. The structure of $HgI_2(bzimtH_2)$ is polymeric with a trigonal bipyramidal 3 + 2 coordination geometry around the mercury atom. Polymerisation occurs through Hg···I interactions with neighbouring molecules. The distribution of the π-electron density in $bzimtH_2$ corresponds to the thioketo tautomeric form in the solid state, and also in the DMSO solution of the complexes. Intermolecular hydrogen bonds of the type N–H···N, N–H···S and N–H···I are observed.

Introduction

The coordination chemistry of mercury(II) with sulphur-donor ligands is a topic of current research, largely because of the importance of such complexes as structural models in biological systems,[1] and also as solid-state materials.[2] The ability of mercury(II) halides and pseudohalides to form 1:1 and 1:2 complexes with neutral ligands has been known for years.[3,4] The most common neutral donors are phosphane and amine derivatives, and recently heterocyclic thiones.[5−7] Beside such complexes, heterocyclic thiones also give sulphide-like compounds of the type HgL_2 (L = deprotonated thione ligand), by deprotonation.[8,9]

The crystal structures of mercury(II) complexes with heterocyclic thiones revealed the monodentate thione sulphur-donating character of the ligand, although chelation was observed in a few cases.[8,10] The great structural variety of the aforementioned complexes reflects the flexibility of the coordination geometry of mercury. All structures can be regarded as being composed of an inner HgX_2 or HgX_3 unit. In these units the mercury behaves as a Lewis acid and becomes less strongly coordinated to an outer group. This leads to more highly coordinated species, HgX_2L_n or HgX_3L_m, where n is 2, 3 or 4, but m is most commonly 2. It is not fully clear what factors determine the coordination of mercury in such an environment. It is well known that mercury(II) halides form 1:1 or 1:2 complexes with neutral ligands, depending on the molar ratio of the reactants. The crystal structures of the 1:2 complexes usually consist of discrete monomeric molecules with a tetrahedrally coordinated mercury atom (more or less distorted). In contrast, the crystal structures of the 1:1 complexes often involve discrete dimeric molecules, with the mercury atom in a distorted tetrahedral environment.[8,12−16] We have examined a series of such complexes so as to gain an insight into the steric and electronic effects of halide or pseudohalide and heterocyclic thione ligands on the mercury coordination sphere, and into the donor potential towards the mercury atom.[8,11−16]

Continuing with our previous work, we now examine the structural characteristics of the 1:1 and 1:2 mercury(II) halide and mercury(II) thiocyanate complexes with benzo-1,3-

[a] Laboratory of General and Inorganic Chemistry, Faculty of Science, Chemistry Department, University of Zagreb,
Ul. kralja Zvonimira 8, 10000 Zagreb, Croatia
Fax: (internat.) + 385-1/4611191
E-mail: zpopovic@chem.pmf.hr
[b] Polytechnic of Karlovac,
I. Meštrovića 10, 47000 Karlovac, Croatia
[c] Laboratory for Thermal Analysis, Brodarski Institute, Marine Research and Special Technology,
Av. V. Holjevca 20, 10000 Zagreb, Croatia
[d] Institut für Mineralogie und Kristallographie, Geozentrum, Universität Wien,
Althanstrasse 14, 1090 Wien, Austria

 © WILEY-VCH Verlag GmbH, 69451 Weinheim, Germany, 2002 1434−1948/02/0101−0171 $ 17.50+.50/0

imidazole-2-thione in the solid state and in dimethyl sulphoxide.

Results and Discussion

Mercury(II) complexes $HgX_2(bzimtH_2)$ (**1**−**4**) and $HgX_2(bzimtH_2)_2$ (**5**−**8**) were prepared according to the following general procedure (Scheme 1). A methanol solution of $bzimtH_2$ was added dropwise to a methanol solution of the mercury(II) halide in the appropriate molar ratio. In the preparation of the thiocyanato complexes an ethanol solution was used instead of a methanol solution. Furthermore, due to the photosensitivity of the complexes, the reaction was performed in the dark. The reaction mixtures were left for a few days (with the exception of the thiocyanato complexes which were left for a few weeks), after which crystalline products formed and were filtered off, washed with cold methanol and dried. Complexes **1**−**8** are generally insoluble in common organic solvents, but fairly soluble in solvents with pronounced donor properties such as dimethyl sulphoxide (DMSO), dimethylformamide (DMF), pyridine etc. $Hg(bzimtH)_2$ (**9**) was obtained by treating mercury(II) acetate with $bzimtH_2$ in a 1:2 molar ratio in ethanol. Complex **9** is insoluble in common organic solvents and also insoluble in DMSO, DMF, pyridine, or similar solvents.

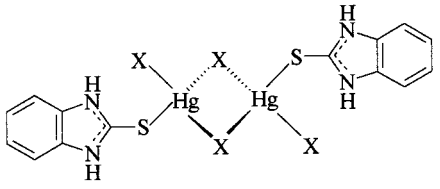

X = Cl⁻ (**1**), Br⁻ (**2**), SCN⁻ (**4**)

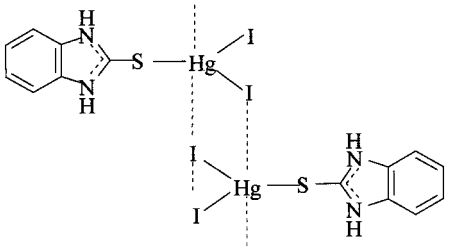

3

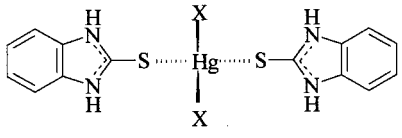

X = Cl⁻ (**5**), Br⁻ (**6**), I⁻ (**7**), SCN⁻ (**8**)

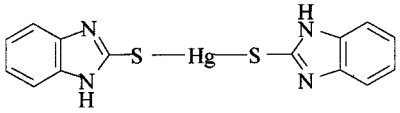

9

Scheme 1. Mercury(II) complexes of benzo-1,3-imidazole-2-thione

Infrared and NMR Spectra

The absence of the ν(S−H) absorption band at 2500 cm^{-1} in the spectrum of free $bzimtH_2$, as well as the presence of the ν(N−H) band confirm that the thione tautomer is the dominant form of the ligand in the solid state (Scheme 2, a). The spectra of **1**−**8** (Table 1) show strong absorption bands in the range 3180−3100 cm^{-1}, corresponding to the ν(N−H) stretching band. A small shift from the bands seen in the spectrum of free $bzimtH_2$ is observed, indicating that the nitrogen atom does not take part in the coordination to the mercury centre. This shift probably results from the variation in the hydrogen-bonding interactions and electronic changes within the ligand on coordination to the mercury ion. Absorption bands which are associated with the C−N vibration mode also show insignificant shifts, suggesting that $bzimtH_2$ is not bonded through the nitrogen atom. Coordination of the metal ion by the nitrogen atom in the thioamide ligands is accompanied by a negative shift of these bands. Such a shift, as well as the negative shift of the ν(N−H) absorption bands, is observed only in the spectrum of **9**, suggesting the existence of mercury and nitrogen interactions. Substitution of sulphur with selenium in $bzimtH_2$ was used to determine the vibrations related to the C−S modes.[17] In the IR spectrum of $bzimtH_2$, the region below 700 cm^{-1} undergoes substantial modification on selenation. Thus, the authors suggested the contribution of the C−S modes to these bands. In the spectra of **1**−**8**, a significant change in intensities and frequencies of these bands was observed, supporting the fact that $bzimtH_2$ is coordinated through the sulphur atom.

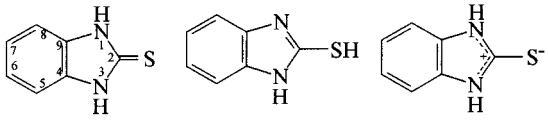

(a) (b) (c)

Scheme 2. (a) thione tautomer; (b) thiol tautomer; (c) zwitterionic resonance form of the thione tautomer

^1H and ^{13}C NMR spectroscopic data for **1**−**8** in their DMSO solutions are consistent with the finding that the sulphur atom is coordinated to the mercury atom, as previously found for similar mercury(II) complexes with imidazole-2-thione and some of its derivatives.[8,18−20] In the ^1H NMR spectra of $bzimtH_2$ and of complexes **1**−**8** (Table 2), the signals for the thioamide N−H protons (1-,3-H) are observed in the range δ = 12.50−13.90 (numbering of the carbon atoms is displayed in Scheme 2). The absence of the signal for the thiol proton (−SH, δ ≈ 3.5) in the ^1H NMR

Table 1. Major infrared bands [cm^{-1}] of $bzimtH_2$ and complexes **1−9**

Compound	ν(N−H)	C−N modes	C−S modes
$bzimtH_2$	3154 vs	1514 s, 1468 vs, 1357 s	661 s, 602 s, 482 m
$HgCl_2(bzimtH_2)$ (**1**)	3157 s, 3112 s	1508 vs, 1457 vs, 1347 m	663 m, 596 m, 478 w
$HgBr_2(bzimtH_2)$ (**2**)	3176 s, 3120 m, 3006 m	1510 s, 1460 vs, 1365 s, 1348 m	652 m, 598 s, 480 m
$HgI_2(bzimtH_2)$ (**3**)	3053 m	1498 vs, 1460 vs, 1360 m, 1344 m	642 m, 598 s, 478 m
$Hg(SCN)_2(bzimtH_2)$ (**4**)	3155 s, 3103 s	1507 s, 1458 vs, 1364 m, 1348 m	647 m, 598 m, 468 m
$HgCl_2(bzimtH_2)_2$ (**5**)	3147 s	1503 vs, 1457 vs, 1365 s, 1348 s	656 m, 598 s, 478 m
$HgBr_2(bzimtH_2)_2$ (**6**)	3175 s, 3118 s	1500 s, 1458 vs, 1336 m, 1347 s	656 m, 598 s, 477 m
$HgI_2(bzimtH_2)_2$ (**7**)	3156 s, 3117 s	1514 m, 1460 vs, 1360 s, 1344 s	642 m, 598 s, 480 m
$Hg(SCN)_2(bzimtH_2)_2$ (**8**)	3147 vs, 3104 s	1509 s, 1457 s, 1361 s, 1347 m	658 m, 600 s, 472 m
$Hg(bzimtH)_2$ (**9**)	3138 s, 3087 s	1498 m, 1441 vs, 1458 m, 1375 vs, 1348 s	646 m, 601 m

spectrum of free $bzimtH_2$ confirms that the thione tautomer is the dominant form in the DMSO solution and also in the solid state.[17,21] The ^1H NMR spectra also show that the 1- and 3-H protons are more deshielded in the complexes by δ = 1.40−1.81, than in the free thione molecule. The deshielding occurs as a result of the positive charge in the imidazole ring and the stronger hydrogen bonding in the complexes than in the free $bzimtH_2$. Broadening of the N−H signal in the complexes also supports hydrogen bonding. For all other protons, small complexation effects are detected, due to their greater distance from the binding site. For the thiocyanato complexes, the N−H resonance is not discernible due to strong hydrogen bonding. Additional evidence with regard to the coordination site in complexes **1−8** is provided by the ^{13}C NMR spectra (Table 3). The greatest change in the chemical shift was found for the thione carbon (C-2) signal, which shifts from δ = 7.10 to δ = 12.70. These upfield shifts are consistent with the reduction of the π-electron density in the exocyclic carbon−sulphur bond, which occurs as a result of the *S*-bonded $bzimtH_2$.

Table 2. ^{1} H NMR chemical shifts (δ in ppm) and complexation shifts[a] (Δδ in ppm) of $bzimtH_2$ and complexes **1−8**

Compound	[a]	1-,3-H	5-,8-H	6-,7-H
$bzimtH_2$	δ	12.50	7.12	7.12
$HgCl_2(bzimtH_2)$ (**1**)	δ	13.90	7.48	7.36
	Δδ	1.40	0.36	0.23
$HgBr_2(bzimtH_2)$ (**2**)	δ	13.68	7.45	7.33
	Δδ	1.18	0.33	0.21
$HgI_2(bzimtH_2)$ (**3**)	δ	13.61	7.45	7.33
	Δδ	1.11	0.33	0.21
$Hg(SCN)_2(bzimtH_2)$ (**4**)	δ	−	7.48	7.32
	Δδ	−	0.36	0.20
$HgCl_2(bzimtH_2)_2$ (**5**)	δ	13.57	7.27	7.27
	Δδ	1.07	0.15	0.15
$HgBr_2(bzimtH_2)_2$ (**6**)	δ	13.50	7.35	7.26
	Δδ	1.00	0.23	0.14
$HgI_2(bzimtH_2)_2$ (**7**)	δ	13.31	7.36	7.27
	Δδ	0.81	0.24	0.15
$Hg(SCN)_2(bzimtH_2)_2$ (**8**)	δ	−	7.38	7.31
	Δδ	−	0.26	0.19

[a] Complexation shift is defined as the ^1H chemical shift difference of corresponding nuclei in the complex and in the free thione molecule.

Table 3. ^{13} C NMR chemical shifts (δ in ppm) and complexation shifts[a] (Δδ in ppm) of $bzimtH_2$ and complexes **1−8**

Compound	[a]	C-2	C-4,-9	C-5,-8	C-6,-7
$bzimtH_2$	δ	168.5	132.5	109.8	122.6
$HgCl_2(bzimtH_2)$ (**1**)	δ	156.71	131.70	112.1	124.70
	Δδ	−11.79	−0.80	2.30	2.10
$HgBr_2(bzimtH_2)$ (**2**)	δ	156.72	131.72	112.0	124.68
	Δδ	−11.78	−0.78	2.20	2.08
$HgI_2(bzimtH_2)$ (**3**)	δ	158.1	131.8	111.9	124.5
	Δδ	−10.4	−0.70	2.10	1.90
$Hg(SCN)_2(bzimtH_2)$ (**4**)	δ	155.8	133.5	112.5	124.3
	Δδ	−12.7	1.00	2.70	1.70
$HgCl_2(bzimtH_2)_2$ (**5**)	δ	159.0	131.5	111.5	124.2
	Δδ	−9.50	−1.00	1.70	1.60
$HgBr_2(bzimtH_2)_2$ (**6**)	δ	160.2	131.8	111.3	124.0
	Δδ	−8.30	−0.70	1.50	1.40
$HgI_2(bzimtH_2)_2$ (**7**)	δ	161.4	132.21	111.4	124.1
	Δδ	−7.10	−0.29	1.60	1.50
$Hg(SCN)_2(bzimtH_2)_2$ (**8**)	δ	158.7	132.17	111.9	124.6
	Δδ	−9.80	−0.33	2.10	2.00

[a] Complexation shift is defined as the ^{13}C chemical shift difference of corresponding nuclei in the complex and in the free thione molecule.

Crystal Structures of 3, 7, and 8

Crystal Structure of $HgI_2(bzimtH_2)$ (3)

In the structure of **3**, the mercury atom is coordinated by two iodine atoms [Hg−I1 2.676(1) and Hg−I2 2.816(1) Å] and one sulphur atom from $bzimtH_2$ [Hg−S1 2.467(2) Å]. It has a distorted trigonal geometry (Figure 1, Table 4). The Hg−I1 bond is shorter than the sum of the covalent radii for the trigonal mercury and iodine atoms (1.39 + 1.33 Å),[22,23] while Hg−I2 is longer, since I2 acts as the bridging atom. Further, in the structure of $HgI_2(imtH_2)$[8] ($imtH_2$ = 1,3-imidazole-2-thione), the Hg−I(terminal) distance is shorter [2.6518(7) Å] and closer to the value for linear mercury coordination (2.63 Å), while the Hg−I(bridging) distance is very similar [2.8187(7) Å] (Table 5). A similar trigonal coordination pattern is found in the structure of $HgI_2(H_4pymtH)$[16] (H_4pymtH = 3,4,5,6-tetrahydropyrimidine-2-thione), where the thione ligand contains a saturated heterocyclic ring. The analogous Hg−I bond lengths are 2.6872(7) and 2.7044(6) Å, respectively. The Hg−S bond in

3 is slightly longer than the sum of the covalent radii for trigonal Hg and S atoms (2.43 Å).[22,23] It is longer, but not significantly, than the corresponding bond in $HgI_2(imtH_2)$ [2.460(2) Å].

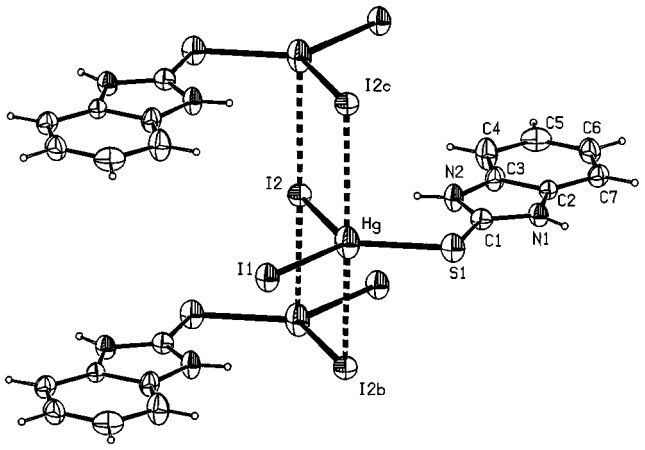

Figure 1. ORTEP drawing of di-μ-iodobis[iodo(benzo-1,3-imidazolium-2-thiolato-*S*)mercury(II)] (**3**), with the atom numbering scheme; the Hg···I contacts are drawn by dashed lines indicating trigonal pyramidal coordination around the mercury centre; symmetry transformation used to generate equivalent atoms: (b) = 1/2 − *x*, *y* − 1/2, 1 − *z* and (c) = 1/2 − *x*, *y* + 1/2, 1 − *z*; the thermal ellipsoids are at the 50% probability level at 200 K

Distortion of the trigonal geometry is determined by the bond angles, which are in the range from 112.94(4) to 127.34(6)°. The largest angle is that of S1−Hg−I1, and is accompanied by the short Hg−I1 bond length. In HgI_2(-$imtH_2$), where the Hg−I bond is shorter than that in **3**, the S−Hg−I angle is greater [134.63(5)°].

The number of atoms coordinated to mercury increases to five through Hg···I interactions with two neighbouring molecules which are related by mirror plane symmetry, thus effectively forming a trigonal-bipyramidal coordination sphere around the mercury centre, elongated in the axial direction [Hg···$I2^i$ 3.3774(6) Å; *i* = 1/2 − *x*, −1/2 + *y*, 1 − *z*]. By these interactions polymeric chains parallel to the *b* axis are formed. In $HgI_2(imtH_2)$ and $HgI_2(H_4pymtH)$, the mercury atom is disordered and is forced out of the mirror plane in order to form Hg···I contacts with distances of 3.486(1) and 3.517(3) Å, respectively. The distance to the other neighbouring I is very long (> 3.9 Å). While describing these two structures, we commented that if the mercury atom was in the mirror plane the distance to the neighbouring iodine atoms would be close to 3.7 Å which, in our opinion, would not be shorter than the sum of the van der Waals radii for Hg (1.55 to 1.65 Å)[24,25] and I (1.98 Å).[25] Therefore, only the 3 + 1 coordination was possible. The short Hg···I contacts and the 3 + 2 coordination in **3** are in support of our values.

In complex **3**, the larger $bzimtH_2$ allows shorter Hg···I contacts as a result of the hydrogen-bonding pattern. In the structure of $HgI_2(imtH_2)$,[8] only N−H···S intermolecular hydrogen bonds are formed (Table 5), while in **3** hydrogen bonds of the type N−H···I are observed, with values of 3.586(7) Å for the intramolecular, and 3.807(9) Å for the intermolecular hydrogen bonds (Table 6). We believe that the strength of Hg···I contacts in **3** is also influenced by the

Table 4. Selected interatomic distances [Å] and angles [°] for the compounds **3**, **7**, and **8**

	$HgI_2(bzimtH_2)$ (**3**)	$HgI_2(bzimtH_2)_2$ (**7**)	$Hg(SCN)_2(bzimtH_2)_2$·EtOH (**8**)
Interatomic distances			
Hg−X1[a]	2.676(1)	2.7204(8)	2.500(6)
Hg−X2[a]	2.816(1)	2.6970(9)	2.679(6)
Hg−X2[i]	3.3774(6)	–	–
Hg−S1	2.467(2)	2.612(2)	2.500(6)
Hg−S2	–	2.640(3)	2.508(6)
S1−C11 (S1−C1in **3**)	1.714(9)	1.709(9)	1.75(2)
S2−C21	–	1.715(9)	1.68(2)
C11−N11(C1−N1 in **3**)	1.35(1)	1.36(1)	1.32(3)
C11−N12 (C1−N2 in **3**)	1.33(1)	1.34 (1)	1.30(2)
C21−N21	–	1.33(1)	1.34(2)
C21−N22	–	1.35(1)	1.37(3)
C12−N11 (N1−C2 in **3**)	1.39(1)	1.39(1)	1.39(2)
C22−N21		1.39(1)	1.38(3)
C13−N12 (N2−C3 in **3**)	1.42(1)	1.37(1)	1.41(2)
C23−N22	–	1.39(1)	1.42(2)
Bond angles			
S1−Hg−X1	127.34(6)	109.41(6)	119.3(2)
S1−Hg−X2	119.72(6)	110.80(6)	99.8(2)
X1−Hg−X2	112.94(4)	124.43(3)	97.1(2)
S1−Hg−S2	–	88.36(8)	115.61(18)
S2−Hg−X1	–	102.94(6)	113.2(2)
S2−Hg−X2	–	114.86(6)	108.1(2)
I1−Hg−I2[i]	94.14(3)	–	–
S1−Hg−I2[i]	91.24(3)	–	–
I2−Hg−I2[i]	84.02(3)	–	–

[a] X1 = S3 in **8**; X2 = S4 in **8**; *i* = 1/2 − *x*, −1/2 + *y*, 1 − *z*.

Table 5. Selected structural parameters [Å] of mercury(II) iodide complexes with thione ligands

Compound	Coordination sphere	Hg−S	Hg−I and Hg···I	Hydrogen bonds	Ref.
HgI_2L_2					
$HgI_2(meimtH_2)_2$[a]	def. tetrahedron	2.526(3)	2.7866(11)	3.586 (N−H···I) inter	[20]
		2.571(3)	2.8047(9)	3.601 (N−H···I) intra	
$HgI_2(meimtH_2)_2$[b]	def. tetrahedron	2.520(3)	2.7809(9)	3.596(8) (N−H···I) intra	[14]
		2.576(3)	2.7999(8)	3.611(9) (N−H···I) inter	
$HgI_2(H_4pymtH)_2$	def. tetrahedron	2.612(2)	2.7123(5)	3.599(6) (N−H···S) inter	[13]
				3.725(5) (N−H···I) inter	
$HgI_2(bzimtH_2)_2$[c]	def. tetrahedron	2.612(2)	2.7204(8)	3.339(8) (N−H···S) inter	present
				3.553(8) (N−H···S) intra	work
		2.640(3)	2.6970(9)	3.657(7) (N−H···I) intra	
3.733(8) (N−H···I) inter					
HgI_2L					
$HgI_2(imtH_2)$	3+1 dimer	2.460(2)	2.8187(7)	2.692(2) (N−H···S) inter	[8]
			2.6518(7)		
			3.486(1) for Hg···I		
$HgI_2(H_4pymtH)$[c]	3+1 dimer	2.456(2)	2.6872(7)	3.696(4) (N−H···I) inter	[16]
			2.7044(6)		
			3.517(3) for Hg···I		
$HgI_2(bzimtH_2)$	3+2 polymer	2.467(2)	2.676(1)	3.586(7) (N−H···I) intra	present work
			2.816(1)		
			3.3774(6) for Hg···I	3.807(9) (N−H···I) inter	

[a] 160 K data. [b] 293 K data. [c] 200 K data.

extended π-delocalized ring system in $bzimtH_2$, which in comparison with the five-membered aromatic ring in $imtH_2$ and also with the saturated ring in H_4pymtH, enables a better π-stacking assembly of the ligand molecules. The stacking occurs along the *b* axis. Centrosymmetrical dimers parallel to the *ac* plane are formed through intermolecular hydrogen bonds. The intermolecular hydrogen bonds and Hg···I contacts interconnect molecules of **3** into a 2D network parallel to the *ab* plane (Figure 2).

Crystal Structure of $HgI_2(bzimtH_2)_2$ (7)

The molecular structure of **7** reveals a tetrahedrally coordinated mercury atom, with two thione sulphur atoms [Hg−S1 2.612(2) and Hg−S2 2.640(3) Å] and two covalently linked iodine atoms [Hg−I1 2.7204(8) and Hg−I2 2.6970(9) Å] (Figure 3). The Hg−S bond lengths are longer than the sum of covalent radii for tetrahedral Hg and S atoms (2.52 Å), but the Hg−I bond lengths are significantly shorter than 2.81 Å (1.48 + 1.33 Å).[22,24]

The tetrahedral environment is distorted since the bond angles are in the range from 88.36(8) to 124.43(3)° for S1−Hg−S2 and I1−Hg−I2, respectively. The largest bond angle is seen for the strong bonds formed with the iodine atoms.[14,16,20] In the structure of an analogous iodo derivative, $HgI_2(meimtH_2)_2$, the Hg−S distances are shorter and the Hg−I distances are longer than in **7** (Table 5).[14,20] This

Table 6. Hydrogen-bond geometry [Å, °] in **3**, **7**, and **8**

D−H···A	*d*(D−H)	*d*(H···A)	∠ (DHA)	*d*(D···A)	Symmetry code
$HgI_2(bzimtH_2)$ (**3**)					
N1−H1···I1^{i}	0.86	2.99	159	3.807(9)	*i* = 1 − *x*, *y*, 1 − *z*
N1−H1···I1^{ii}	0.86	2.99	159	3.807(9)	*ii* = 1 − *x*, −*y*, 1 − *z*
N2−H2···I2	0.86	2.73	174	3.586(7)	
$HgI_2(bzimtH_2)_2$ (**7**)					
N11−H11···I1^{iii}	0.86	2.98	147	3.733(8)	*iii* = 1 − *x*, 1 − *y*, 2 − *z*
N12−H12···I2	0.86	2.83	163	3.657(7)	
N21−H21···S2^{iv}	0.86	2.49	169	3.339(8)	*iv* = 1 − *x*, 1 − *y*, 1 − *z*
N22−H22···S1	0.86	2.81	146	3.553(8)	
$Hg(SCN)_2(bzimtH_2)_2$·EtOH (**8**)					
N11−H11...O1^{v}	0.86	1.95	172	2.81(3)	*v* = *x*, *y*, −1 + *z*
N12−H12...N4^{vi}	0.86	2.06	165	2.90(3)	*vi* = 1 − *x*, 1 − *y*, 1 − *z*
N21−H21...N3^{vii}	0.86	1.97	175	2.82(4)	*vii* = 1 − *x*, 1 − *y*, −*z*
N22−H22...N4	0.86	2.17	169	3.02(2)	

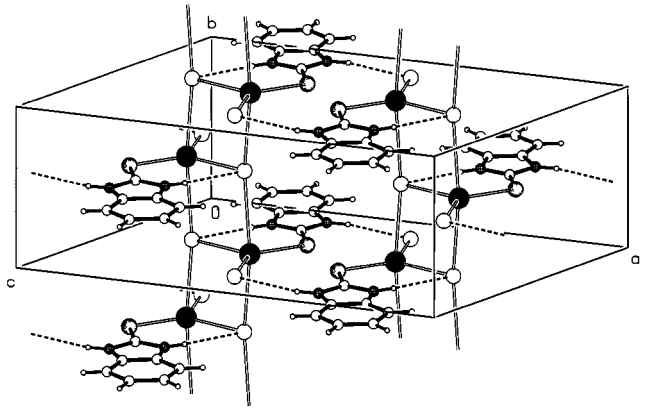

Figure 2. The crystal packing of **3** showing endless polymeric chains along the *b* axis and the centrosymmetrical dimer formed by hydrogen bonding in the *ac* plane; the N−H···I intra- and intermolecular hydrogen bonds are indicated by dashed lines

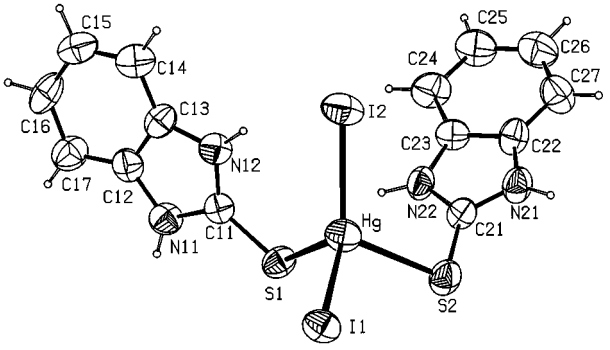

Figure 3. ORTEP drawing of bis[iodo(benzo-1,3-imidazolium-2-thiolato-*S*)]mercury(II) (**7**), with the atom numbering scheme; the thermal ellipsoids are at the 50% probability level at 293 K

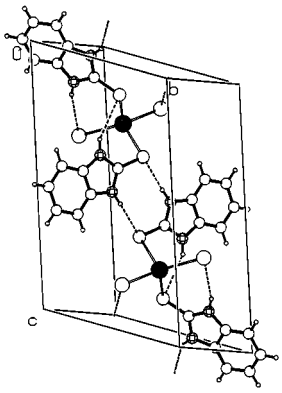

Figure 4. The crystal packing of **7**; dashed lines indicate N−H···S and N−H···I hydrogen-bonds

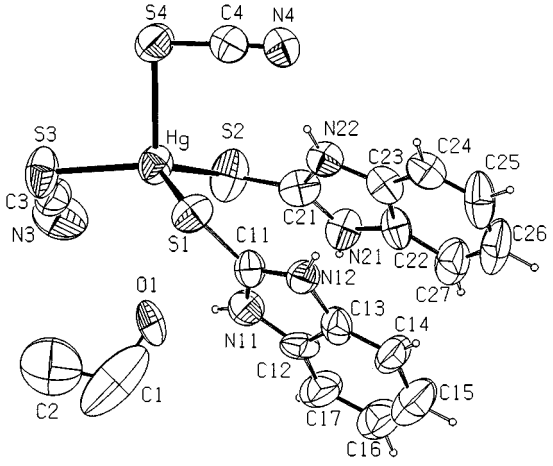

Figure 5. ORTEP drawing of the 1:1 ethanol solvate of bis[thiocyanato(benzo-1,3-imidazolium-2-thiolato-*S*)]mercury(II) (**8**), with the atom numbering scheme; the thermal ellipsoids are at the 50% probability level at 293 K

is caused by different intermolecular interactions. In both structures (obtained at 293[14] and at 160 K[20]), the NH groups of the imidazole ring take part in the intra- and intermolecular hydrogen bonds of the type N−H···I, and are in the range 3.586−3.611(9) Å. In **7**, the N−H···I hydrogen bonds are slightly longer (Table 6). Furthermore, in **7** there is an intermolecular bond of the type N−H···S with a length of 3.339(8) Å, and a longer intramolecular bond with a length of 3.553(8) Å (Table 6, Figure 4), while in $HgI_2(meimtH_2)_2$ such hydrogen bonds do not exist at all.

Crystal Structure of $Hg(SCN)_2(bzimtH_2)_2$·EtOH (8)

The less accurate geometrical parameters of **8** are associated with the significant intensity decay due to crystal decomposition under X-rays (see Exp. Sect.). The mercury atom is coordinated by two sulphur atoms of $bzimtH_2$ [Hg−S1 2.499(6) and Hg−S2 2.508(6) Å] and two sulphur atoms of SCN^- [Hg−S3 2.500(5) and Hg−S4 2.680(6) Å], thereby having a deformed tetrahedral geometry (Figure 5). The bond angles around the mercury centre range from 97.1(2)° for S3−Hg−S4, to 119.3(2)° for S1−Hg−S3. The Hg−S(thione) bond lengths are comparable with those observed in the structures of $Hg(SCN)_2(H_4pymtH)_2$[13] and the two polymorphs of $Hg(SCN)_2(pySH)_2$ (pySH = pyridine-2-thione)[11] [the bond ranges are 2.458(1)−2.526(2) Å for Hg−S(thione) bonds, and 2.556(2)−2.685(2) Å for Hg−S(SCN) bonds in these three structures].

The Hg−S1, Hg−S2, as well as the Hg−S3 bond in **8** are shorter than the sum of covalent radii for tetrahedral Hg and S atoms. This is an unexpected result for the Hg−S3 bond. In contrast, the Hg−S4 bond is among the longest ones found so far, but still in the range of the Hg−S(SCN) bonds. This could be due to the involvement of the N4 atom as a proton acceptor in both intra- and intermolecular N−H···N hydrogen bonds with the NH groups from $bzimtH_2$, while N3 participates only in one intermolecular hydrogen bond (Table 6).

Besides intra- and intermolecular N−H···N hydrogen bonds, an intermolecular N−H···O hydrogen bond, with a length of 2.82(3) Å (Table 6), forms between the complex and the ethanol molecules (Figure 6).

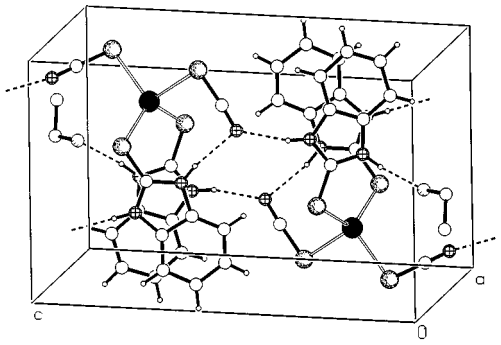

Figure 6. The crystal packing of **8**; dashed lines indicate intermolecular N−H···N and N−H···O hydrogen bonds between complex molecules and complex molecule and ethanol, respectively

Geometry of bzimtH$_2$ in 3, 7, and 8

The crystal structure of bzimtH$_2$ reveals a thioketo C=S bond length of 1.684(3) Å.[21] Such a bond possesses approx. 58% of the π-bond character. On complexation, the C=S bond exhibits a decrease in the π-bond character, to approx. 40%.[26]

The C−N bond lengths in all three complexes are similar to those in the free ligand,[21] with shorter C−N bonds involving the thioketo C atom and longer C−N bonds involving the C atoms common to the five- and six-membered ring. All C−N bonds are shorter than the theoretical C−N single bond length of 1.47 Å, and longer than the C=N double bond length of 1.27 Å (Table 4).[27]

The internal bond lengths, as well as the planarity of the bzimtH$_2$ molecule, strongly confirm that the aromatic character of the imidazole ring is preserved in the mercury(II) complexes, and suggest that the zwitterionic resonance form participates in the structure of the ligand (Scheme 2, c).

Thermal Analysis (TGA-DTA)

The samples of bzimtH$_2$ and **1**−**9** were heated from room temperature to 700 °C. Thermal data are summarised in Table 7. The DTA curve of free bzimtH$_2$ shows a single and broad endothermic peak at 300 °C that corresponds to its degradation.

The DTA and TGA curves for **1**−**8** essentially show two degradation processes. The TGA profile for these compounds suggests that bzimtH$_2$ is lost first (two endothermic overlapping peaks), and degradation of the mercury(II) halide or pseudohalide follows (determined by the third endothermic peak). Some of the complexes undergo melting as presented in Table 7. The relatively high melting points of these compounds suggest the presence of strong intermolecular bonding. The observed mass losses for the aforementioned processes are in good agreement with the calculated ones. The DTA curve for **9** shows three processes. Both endothermic minima at 240 °C and 290 °C, with a corresponding mass loss of 46.58%, represent degradation of the ligand due to the breaking of the C−S bond. Decomposition of the residue starts at 390 °C.

Experimental Section

Materials and Physical Measurements: Mercury(II) halides and benzo-1,3-imidazole-2-thione were used as received from Aldrich

Table 7. Thermoanalytical data for benzo-1,3-imidazole-2-thione and its mercury(II) complexes

Compound	Process	Temperature [°C]	Accumulated weight loss (%) Found	Calculated
bzimtH$_2$	degradation (*endo*)	292.87	100	100
HgCl$_2$(bzimtH$_2$) (**1**)	bzimtH$_2$ degradation (*endo*)	247.94, 303.98	70.05	71.14
	elimination of HgCl$_2$ (*endo*)	408.63	29.95	28.86
HgBr$_2$(bzimtH$_2$) (**2**)	melting (*endo*)	234.71	–	–
	bzimtH$_2$ degradation (*endo*)	overlap with melting	57.89	58.75
	elimination of HgBr$_2$ (*endo*)	322.33	42.11	41.25
HgI$_2$(bzimtH$_2$) (**3**)	melting (*endo*)	215.92	–	–
	bzimtH$_2$ degradation (*endo*)	226.50, 239.04	48.58	49.62
	elimination of HgI$_2$ (*endo*)	276.92	51.24	50.38
Hg(SCN)$_2$(bzimtH$_2$) (**4**)	melting (*endo*)	174.28	–	–
	bzimtH$_2$ degradation (*endo*)	209.63, 252.38	61.86	62.25
	elimination of Hg(SCN)$_2$ (*endo*)	363.20	38.14	38.14
HgCl$_2$(bzimtH$_2$)$_2$ (**5**)	bzimtH$_2$ degradation (*endo*)	255.11, 291.43	50.25	52.46
	elimination of HgCl$_2$ (*endo*)	381.74	49.75	47.54
HgBr$_2$(bzimtH$_2$)$_2$ (**6**)	melting (*endo*)	226.35	–	–
	bzimtH$_2$ degradation (*endo*)	overlap with melting	50.65	51.68
	elimination of HgBr$_2$ (*endo*)	335.33	49.35	48.32
HgI$_2$(bzimtH$_2$)$_2$ (**7**)	melting (*endo*)	213.82	–	–
	bzimtH$_2$ degradation (*endo*)	231.63, 240.21	40.12	39.75
	elimination of HgI$_2$ (*endo*)	275.31	59.88	60.25
Hg(SCN)$_2$(bzimtH$_2$)$_2$ (**8a**)	melting (*endo*)	174.26	–	–
	bzimtH$_2$ degradation (*endo*)	214.34, 268.33	47.59	48.61
	elimination of Hg(SCN)$_2$ (*endo*)	415.36	52.41	51.39
Hg(bzimtH)$_2$ (**9**)	bzimtH$^-$ degradation (*endo*)	243.14, 296.58	46.58	47.30
	elimination of HgS	350−400	53.42	52.70

without further purification. Mercury(II) thiocyanate was prepared by the reaction of mercury(II) nitrate monohydrate and ammonium thiocyanate. The mercury content in the complexes was determined by complexometric titration, with sodium diethyl dithiocarbamate, of the solution obtained after decomposition of the specimen in aqua regia.[28] CHNS analyses were performed in the Analytical Services Laboratories of the Institute Ruder Boškovic. The IR spectra were obtained from KBr pellets in the range 4000−450 cm^{-1} with a Perkin−Elmer FTIR 1600 spectrometer. The ^1H and ^{13}C NMR spectra were measured with a Varian Gemini 300 spectrometer, operating at 75.46 MHz for the ^{13}C nucleus. The samples were dissolved in [D_6]DMSO in 5-mm NMR tubes. The concentration was 0.05 M for ^1H NMR measurements and 0.25 M for the ^{13}C NMR measurements. Spectra were recorded at 20 °C. Chemical shifts (ppm) were referred to TMS. Digital resolution was 0.32 Hz per point in ^1H and 0.70 Hz per point in the ^{13}C one-dimensional spectra. The thermal measurements were performed using a simultaneous TGA-DTA analyser (TA Instruments, SDT Model 2960 coupled with MS). The samples were placed in small alumina sample pans. The TGA and DTA curves were obtained by placing the samples (approximately 2 mg in mass) in open sample pans, with a heating rate of 10 °C/min and nitrogen (purity > 99.996%) flowing at a rate of 50 mL/min. The SDT was calibrated with indium.

$HgCl_2(bzimtH_2)$ (1): A solution of benzo-1,3-imidazole-2-thione (0.25 g, 1.66 mmol) in 20 mL of methanol was added dropwise to a solution of mercuric chloride (0.4 g, 1.47 mmol) in 10 mL of methanol. A pale pink crystalline product was obtained the following day, which was filtered off, washed with cold methanol and dried in air. Yield: 0.50 g (81%). $C_7H_6Cl_2HgN_2S$ (421.7): calcd. C 19.92, H 1.42, Hg 47.57, N 6.64, S 7.59; found C 20.25, H 1.61, Hg 47.82, N 6.64, S 7.50.

$HgBr_2(bzimtH_2)$ (2): A solution of benzo-1,3-imidazole-2-thione (0.19 g, 1.26 mmol) in 20 mL of methanol was added dropwise to a solution of mercuric bromide (0.4 g, 1.11 mmol) in 10 mL of methanol. A pale yellow crystalline product was obtained the following day, which was filtered off, washed with cold methanol and dried in air. Yield: 0.45 g (79%). $C_7H_6Br_2HgN_2S$ (510.6): calcd. C 16.45, H 1.18, Hg 39.29, N 5.48, S 6.27; found C 17.07, H 1.06, Hg 39.58, N 5.41, S 6.35.

$HgI_2(bzimtH_2)$ (3): A solution of benzo-1,3-imidazole-2-thione (0.15 g, 0.99 mmol) in 10 mL of methanol was added dropwise to a solution of mercuric iodide (0.4 g, 0.88 mmol) in 20 mL of methanol. After a few days, the yellow crystals were filtered off, washed with cold methanol and dried in air. Yield: 0.50 (94%). $C_7H_6I_2HgN_2S$ (604.6): calcd. C 13.89, H 0.99, Hg 33.18, N 4.63; found C 14.38, H 1.54, Hg 33.32, N 5.22.

$Hg(SCN)_2(bzimtH_2)$ (4): A solution of benzo-1,3-imidazole-2-thione (0.21 g, 1.40 mmol) in 20 mL of 96% ethanol was added dropwise to a solution of mercuric thiocyanate (0.4 g, 1.26 mmol) in 120 mL of 96% ethanol. The reaction mixture was left in the dark due to the photosensitivity of the complex. After a few weeks, the yellow crystalline product was filtered off, washed with cold ethanol and dried in air. Yield: 0.36 g (61%). $C_9H_6HgN_4S_3$ (466.9): calcd. C 23.13, H 1.28, Hg 42.96, N 11.99, S 20.56; found C 23.08, H 1.49, Hg 43.27, N 11.88, S 20.58.

$HgCl_2(bzimtH_2)_2$ (5): A solution of benzo-1,3-imidazole-2-thione (0.49 g, 3.26 mmol) in 40 mL of methanol was added dropwise to a solution of mercuric chloride (0.4 g, 1.47 mmol) in 10 mL of methanol. A pale pink crystalline product was obtained the following day, which was filtered off, washed with cold methanol and dried in air. Yield: 0.62 g (74%). $C_{14}H_{12}Cl_2HgN_4S_2$ (571.9): calcd. C 29.38, H 2.10, Hg 35.08, N 9.79, S 11.19; found C 29.72, H 2.48, Hg 35.27, N 9.65, S 11.24.

$HgBr_2(bzimtH_2)_2$ (6): A solution of benzo-1,3-imidazole-2-thione (0.37 g, 2.46 mmol) in 30 mL of methanol was added dropwise to a solution of mercuric bromide (0.4 g, 1.11 mmol) in 10 mL of methanol. After a few days, the pale pink crystalline product was filtered off, washed with cold methanol and dried in air. Yield: 0.61 g (84%). $C_{14}H_{12}Br_2HgN_4S_2$ (660.8): calcd. C 25.42, H 1.82, Hg 30.36, N 8.47, S 9.69; found C 25.57, H 2.23, Hg 30.81, N 8.25, S 9.56.

$HgI_2(bzimtH_2)_2$ (7): A solution of benzo-1,3-imidazole-2-thione (0.29 g, 1.93 mmol) in 20 mL of methanol was added dropwise to a solution of mercuric iodide (0.4 g, 0.88 mmol) in 20 mL of methanol. After a few days, the yellow crystals were filtered off, washed with cold methanol and dried in air. Yield: 0.28 g (42%). $C_{14}H_{12}I_2HgN_4S_2$ (754.8): calcd. C 22.26, H 1.59, Hg 33.20, N 7.45; found C 22.00, H 1.79, N 8.60, Hg 33.70.

$Hg(SCN)_2(bzimtH_2)_2$·EtOH (8): A solution of benzo-1,3-imidazole-2-thione (0.42 g, 2.80 mmol) in 20 mL of 96% ethanol was added dropwise to a solution of mercuric thiocyanate (0.4 g, 1.26 mmol) in 120 mL of 96% ethanol. The reaction mixture was left in the dark due to the photosensitivity of the complex. After a few weeks, the pale yellow crystals were filtered off, washed with cold ethanol and dried in air. Yield: 0.55 g (71%). Since the crystals lose ethanol on standing, especially on grinding, analysis of the non-solvated sample has been carried out. $C_{16}H_{12}HgN_6S_4$ (617.1): calcd. C 31.11, H 1.94, Hg 32.50, N 13.61, S 20.74; found C 31.25, H 2.57, Hg 32.75, N 13.51, S 20.80.

$Hg(bzimtH)_2$ (9): A solution of benzo-1,3-imidazole-2-thione (0.41 g, 2.73 mmol) in 30 mL of methanol was added dropwise to a solution of mercuric acetate (0.4 g, 1.26 mmol) in 30 mL of methanol. The colourless crystalline product was filtered off, washed with cold methanol and dried in air. Yield: 0.51 g (81%). $C_{14}H_{10}HgN_4S_2$ (499.0): calcd. C 33.67, H 2.00, Hg 40.20, N 11.27, S 12.88; found C 33.02, H 2.52, Hg 40.25, N 11.00, S 12.80.

X-ray Crystallographic Structure Determination of 3, 7, and 8: Single-crystal X-ray diffraction data were collected for **3**, **7**, and **8** using Mo-K_α radiation (graphite monochromator). Data for the small crystals of **3** were collected with a Nonius Kappa CCD diffractometer (capillary optics) at 200 K, while those of **7** and **8** were collected at room temperature with the Philips PW1100 diffractometer. Crystal data and details of the data collection and refinement procedure are given in Table 8. The unit-cell parameters were obtained by the least-squares refinement procedure of the setting angles of well-centred reflections: 35 in the range $10.0° \leq \theta \leq 15.1°$ for **7**, 42 reflections in the range $10.0° \leq \theta \leq 16.5°$ for **8**, and of all reliable data in the structure of **3**. Data reduction was done by the Denzo-SMN program[29] for **3** and by the STADI4 program[30] for **7** and **8**. Due to the significant crystal decay of **8** under X-ray exposure (approx. 30% in 2 d), a reliable data set for the structure refinement was obtained from 3 crystals. Data were corrected for the Lorentz polarisation and absorption effects and then scaled. The numerical Gaussian method for absorption correction based on crystal dimensions was applied for **7** and **8** by the X-RED program,[31] while for **3**, a semi-empirical method was applied by XEMP.[32] The non-H atoms of the ethanol molecule in **8** exhibit large thermal displacement parameters due to crystal decay. The freshly prepared crystals could be described as a 1:1 ethanol solvate, but after the data collection procedure only half of the ethanol molecule is found within the asymmetric unit. The geometry of the

Table 8. General and crystal data and summary of intensity data collection and structure refinement for compounds **3**, **7**, and **8**; data in common: diffractometers used for data collection: PW1100 (Stoe upgraded) with λ(Mo-K_α) = 0.71073 Å at 293 K for **7** and **8** and Kappa CCD for **3** at 200 K

Compound	$HgI_2(bzimtH_2)$ (**3**)	$HgI_2(bzimtH_2)_2$ (**7**)	$Hg(SCN)_2(bzimtH_2)_2$·EtOH (**8**)
Empirical formula	$C_7H_6HgI_2N_2S$	$C_{14}H_{12}HgI_2N_4S_2$	$C_{18}H_{18}HgN_6OS_4$
M_r	604.59	754.79	663.21
Crystal system and habit	monoclinic, prism	triclinic, plate	triclinic, plates
Space group	$C2/m$	$P\bar{1}$	$P\bar{1}$
Crystal dimensions [mm]	0.065 × 0.049 × 0.048	0.285 × 0.142 × 0.045	0.547 × 0.490 × 0.042 0.731 × 0.419 × 0.042 0.600 × 0.400 × 0.051
Unit cell parameters:			
a [Å]	17.417(3)	8.1711(7)	7.8037(14)
b [Å]	6.7140(10)	8.6217(10)	10.285(3)
c [Å]	11.080(2)	14.7494(10)	15.202(3)
α [°]		76.246(9)	90.02(2)
β [°]	114.60(3)	81.199(9)	98.18(2)
γ [°]		86.001(11)	96.96(2)
V [Å^3]	1178.1(3)	996.80(16)	1198.6(5)
Z	4	2	2
D_c [gcm^{-3}]	3.409	2.515	1.838
μ [mm^{-1}]	18.442	11.030	6.786
F(000)	1056	684	614
2θ range for data collection [°]	3−29	3−27	3−27
h,k,l range	−22 to 20, −7 to 8, 13 to 14	−10 to 10, −10 to 10, 0 to 18	−9 to 9, −13 to 13, 0 to 19
Scan type	ω	ω	ω
No. measured reflections	7086	4430	5460
No. independent reflections (R_{int})	1488 (0.11)	4261 (0.032)	4850 (0.060)
No. refined parameters	80	208	271 (3 restraints)
No. observed reflections, $I \geq 2\sigma(I)$	1376	2654	3192
Transmission factors, min, max.[a]	0.352, 0.413	0.166, 0.609	0.034−0.752 for 1st crystal 0.167−0.3511 for 2nd crystal 0.0872 −0.7264 for 3rd crystal
Face indices, distances from centroid [mm]	−	(1 0 1, −1 0 −1) 0.0710 (−1 0 1; 1 0 −1) 0.0225 (0 1 1, 0 −1 −1) 0.1425	(1 0 0, −1 0 0) 0.2734; 0.3657; 0.300 (0 1 0, 0 −1 0) 0.1633; 0.2095;0.2000 (0 0 1; 0 0 −1) 0.0210; 0.0210; 0.0256
g_1, g_2 in w[b]	0.0821, 0	0.0632, 0	0.2000, 0
R[c], wR[d] [$I \geq 2\sigma(I)$]	0.0489, 0.1224	0.0461, 0.0964	0.1235, 0.3006
R, wR [all data]	0.0516, 0.1252	0.0961, 0.1137	0.1717, 0.3431
Goodness of fit on F^2, S[e]	1.041	0.986	1.323
Max., min. electron density [e·Å^{-3}][f]	2.18, −3.39	1.68, −1.79	−5.23, 4.24
Extinction coefficients, x[g]	0.0011(3)	−	−
Maximum Δ/σ	0.001	0.001	0.001

[a] Absorption correction type: semiempirical for **3** and numerical Gaussian for **7** and **8**. [b] $w = 1/[\sigma^2(F_o^2) + [g_1P + g_2P]$ where $P = (F_o^2 + 2F_c^2)/3$. [c] $R = \Sigma||F_o| - |F_c||/\Sigma|F_o|$. [d] $wR = [\Sigma(F_o^2 - F_c^2)^2/\Sigma w(F_o^2)^2]^{1/2}$. [e] $S = \Sigma[w(F_o^2 - F_c^2)^2/(N_{obs} - N_{param})]^{1/2}$. [f] In all structures the max. electron density in the last difference Fourier map is near Hg. [g] $F_c^2 = kF_c[1 + 0.001 \times F_c^2\lambda^3/\sin(2\theta)]^{-1/4}$, $k = 0.10926$.

EtOH molecule (C−C and C−O bonds and C−C−O angle) has been modelled with restraints. All structures were solved by direct methods in SHELXS,[33] and refined by the least-squares procedure with anisotropic thermal parameters for non-H atoms by the SHELXL97 program.[34] The hydrogen atoms were placed at calculated positions and refined by the riding model [Csp^2−H 0.93 Å; Nsp^2−H 0.86 Å; with U_{iso}(H) = 1.2 U_{eq}]. The molecular geometry calculations and drawings were performed by PLATON.[35] Crystallographic data (excluding structure factors) for the structure(s) reported in this paper have been deposited with the Cambridge Crystallographic Data Centre as supplementary publication no. CCDC-162383−162385 for complexes **3**, **7**, and **8**, respectively. Copies of the data can be obtained free of charge on application to CCDC, 12 Union Road, Cambridge CB2 1EZ, UK [Fax: (internat.) + 44-1223/336-033; E-mail: deposit@ccdc.cam.ac.uk].

Acknowledgments

This research was supported by the Ministry of Science and Technology of the Republic of Croatia (Grant nos. 119408 and 01920202).

[1] J. G. Wright, M. J. Natan, F. M. MacDonnell, D. M. Ralston, T. V. O'Halloran, *Prog. Inorg. Chem.* **1990**, *38*, 323−412 (and refs. therein).
[2] M. Bochmann, K. J. Webb, *J. Chem. Soc., Dalton Trans.* **1991**, 2325−2329.
[3] P. A. Dean, *Prog. Inorg. Chem.* **1978**, *24*, 109−178.
[4] D. P. Graddon, *Rev. Inorg. Chem.* **1982**, *4*, 211−282.
[5] E. S. Raper, *Coord. Chem. Rev.* **1985**, *61*, 115−184.
[6] E. S. Raper, *Coord. Chem. Rev.* **1996**, *153*, 199−255.
[7] E. S. Raper, *Coord. Chem. Rev.* **1997**, *165*, 475−567.

[8] Z. Popović, D. Matković-Čalogović, Ž. Soldin, G. Pavlović, N. Davidović, D. Vikić-Topić, *Inorg. Chim. Acta* **1999**, *294*, 35−46.
[9] Ž. Žugaj, Z. Popović, D. Mrvoš-Sermek, *Bull. Czech and Slovak Crystallogr. Association* **1998**, *5 (special i*ssue B, Abstracts) p. 322.
[10] A. K. Das, S. Seth, *J. Inorg. Biochem.* **1997**, *65*, 207−218.
[11] Z. Popović, D. Matković-Čalogović, J. Hasić, D. Vikić-Topić, *Inorg. Chim. Acta* **1999**, *285*, 208−216.
[12] G. Pavlović, Z. Popović, Ž. Soldin, D. Matković-Čalogović, *Acta Crystallogr., Sect. C* **2000**, *56*, 61−63.
[13] Z. Popović, G. Pavlović, D. Matković-Čalogović, Ž. Soldin, M. Rajić, D. Vikić-Topić, D. Kovaček, *Inorg. Chim. Acta* **2000**, *306*, 142−152.
[14] G. Pavlović, Z. Popović, Ž. Soldin, D. Matković-Čalogović, *Acta Crystallogr., Sect. C* **2000**, *56*, 801−803.
[15] Z. Popović, D. Matković-Čalogović, G. Pavlović, Ž. Soldin, G. Giester, M. Rajić, D. Vikić-Topić, *Croat. Chem. Acta* **2001**, *74*, 359−380.
[16] D. Matković-Čalogović, Z. Popović, G. Pavlović, Ž. Soldin, G. Giester, *Acta Crystallogr., Sect. C* **2001**, *57*, 409−411.
[17] F. A. Devillanova, G. Verani, *Aust. J. Chem.* **1980**, *33*, 279−286.
[18] R. Shunmugam, D. N. Sathyanarayana, *J. Coord. Chem.* **1983**, *12*, 151−156.
[19] E. S. Raper, J. R. Creighton, N. A. Bell, W. Clegg, L. Cucurull-Sánchez, *Inorg. Chim. Acta* **1998**, *277*, 14−20.
[20] N. A. Bell, T. N. Branston, W. Clegg, J. R. Creighton, L. Cucurull-Sánchez, M. R. J. Elsegood, E. S. Raper, *Inorg. Chim. Acta* **2000**, *303*, 220−227.
[21] K. Ravikumar, K. Ch. Mohan, M. Bidyasagar, G. Y. S. K. Swamy, *J. Chem. Crystallogr.* **1995**, *25*, 325−329.
[22] D. Grdenić, *Quat. Rev.* **1965**, *19*, 303−328.
[23] D. Matković-Čalogović, PhD Thesis (in Croatian; Abstract in English), University of Zagreb, **1994.**
[24] L. Pauling, The Nature of the Chemical Bond, Ithaca, New York, Cornell University Press, **1960.**
[25] A. Bondi, *J. Phys. Chem.* **1964**, *68*, 441−451.
[26] N. Trinajstić, *Tetrahedron Lett.* **1968**, 1529−1532.
[27] F. H. Allen, O. Kennard, D. G. Watson, L. Brammer, A. G. Orpen, R. Taylor, *J. Chem. Soc., Perkin Trans. 2* **1987**, S1.
[28] P. Gouverneur, W. Hoedeman, *Anal. Chim. Acta* **1964**, *30*, 519−523.
[29] Z. Otwinowski, W. Minor, *Processing of X-ray Diffraction Data Collected in Oscillation Mode*, in: *Methods in Enzymology*, vol. 276 (Eds.: C. W. Carter, Jr., R. M. Sweet), Macromolecular Crystallography, part A, Academic Press, London, **1997**, p.307.
[30] Stoe & Cie, *STADI4, Diffractometer Control Program for Windows*, Darmstadt, Germany, **1995**.
[31] Stoe & Cie, *X-RED, Data Reduction Program for Windows*, Darmstadt, Germany, **1995**.
[32] G. M. Sheldrick, *XEMP, Program for Semimpirical Absorption Correction*, University of Göttingen, Germany, **1988**.
[33] G. M. Sheldrick, *Acta Crystallogr., Sect. A* **1990**, *46*, 467.
[34] G. M. Sheldrick, *SHELXL97, Program for the Refinement of Crystal Structures*, University of Göttingen, Germany, **1997**.
[35] A. L. Spek, *Acta Crystallogr., Sect. A* **1990**, *46*, C34.

Received May 7, 2001
[I01159]

A Congested $Ru(dps)_2$ or $Ru(dprs)_2$ Core (dps = di-2-pyridyl sulfide; dprs = di-2-pyrimidinyl sulfide) Promotes Sulfur Inversion of *N*,*S*-Chelate Thioethers Containing CH_2R and 2-Pyridyl or 2-Pyrimidinyl Groups

Giuseppe Tresoldi,*[a] Sandra Lo Schiavo,[a] Santo Lanza,[a] and Paola Cardiano[a]

Keywords: Ruthenium / N ligands / S ligands / Sulfur inversion / Activation barriers

The thioethers L [L = 4-methylbenzyl 2-pyridyl sulfide (**L_1**), 4-chlorobenzyl 2-pyridyl sulfide (**L_2**), 3-chlorobenzyl 2-pyridyl sulfide (**L_3**), 1,4-bis(2-pyridylthiomethyl)benzene (**L_4**), 4-methylbenzyl 2-pyrimidinyl sulfide (**L_5**), and 4-chlorobenzyl 2-pyrimidinyl sulfide (**L_6**)], containing a CH_2R group bonded to the sulfur atom, were prepared and characterized. Compounds **L_1**, **L_2**, **L_3**, and **L_4** reacted with *cis*-Ru(*N*,*N*-dprs)$_2$Cl$_2$ or *cis*-Ru(*N*,*N*-dps)$_2$Cl$_2$ (dprs = di-2-pyrimidinyl sulfide, dps = di-2-pyridyl sulfide) leading to the complexes [Ru(*N*,*N*-dprs)$_2$(*N*,*S*-L)][PF$_6$]$_2$ and [Ru(*N*,*N*-dps)$_2$(*N*,*S*-L)][PF$_6$]$_2$. Similar products were obtained from [Ru(*N*,*N*-dps)$_2$(NO$_2$)(NO)][PF$_6$]$_2$ and **L_5** or **L_6**. As a consequence of the L ligand *N*,*S*-chelation, all the complexes contain the four-membered ring RuSCN(*Ru*–*N*). Since the ruthenium and sulfur atoms are stereogenic centres, with Δ and Λ, and *R* and *S* configurations, respectively, they led to four isomers, including the enantiomers. NMR investigations show that the sulfur inversion produces an exchange between the diastereoisomers Δ*R* and Δ*S*, as well as Λ*S* and Λ*R*. The one-dimensional band-shape analysis of the exchanging methylene proton signals showed that the inversion barriers ($\Delta G^{\ddagger}_{298\,K}$) for the dprs complexes are in the 54.9–53.8 kJ mol^{-1} range, with the two invertomers exhibiting similar abundance. Substitution of dprs with dps affects the relative invertomer population leaving the magnitude of $\Delta G^{\ddagger}_{298\,K}$ (52.0–50.6 kJ mol^{-1}) practically unchanged. Conversely, the substitution of the pyridine thioethers (**L_1**, **L_2**) with pyrimidine thioethers (**L_5**, **L_6**) influences the inversion barriers, and $\Delta G^{\ddagger}_{298\,K}$ values of 47.5 and 47.0 kJ mol^{-1} were found for [Ru(*N*,*N*-dps)$_2$(*N*,*S*-**L_5**)][PF$_6$]$_2$ and [Ru(*N*,*N*-dps)$_2$(*N*,*S*-**L_6**)][PF$_6$]$_2$, respectively. An intramolecular mechanism without any bond rupture is suggested on the basis of the $\Delta S^{\ddagger}$ values (negative or close to zero) and the NMR spectra, temperature-reversible and concentration-independent. The contemporary presence of the congested Ru(*N*,*N*-dps)$_2$ or Ru(*N*,*N*-dprs)$_2$ core and sterically demanding *N*,*S*-coordinated thioether ligands is invoked to explain the low energy barrier of the process. This hypothesis is also corroborated by the different behaviour observed for the complex [Ru(bipy)$_2$(*N*,*S*-**L_1**)][PF$_6$]$_2$.

Introduction

The chemistry of the ruthenium compounds containing 2,2′-bipyridine (bipy), polypyridine and similar ligands has been thoroughly explored over many years. This interest has stemmed mainly for the relevance of this chemistry to photophysical, photochemical, and redox phenomena.

Recently we have focused our attention on the bipy or bipy-like ruthenium(II) complexes in which one or more ligands are replaced by di-2-pyridyl sulfide (dps) or other bipy-like nonplanar ligands,[1−3] with the aim of modifying the chemical and physical properties of the complexes.

The dps ligand can in principle exhibit a variety of bonding modes to metal ions: *N*- or *S*-monodentate, *N*,*N*- or *N*,*S*-chelate and *N*,*N*- or *N*,*S*-bridging. However, normally it functions as an *N*,*N*-chelate ligand, adopting a twisted *N*,*N*-inside conformation.[1−11] The control of the coordination mode of this and similar ligands may be achieved by opportune choice of the starting complex. The complexes Ru(diimmine)$_2$Cl$_2$ (diimmine = bipy or 1,10-phenanthroline or similar ligands) are expected to favour the *N*,*N*-chelation,[12−14] whereas Ru(dps)$_2$Cl$_2$ or other sterically hindering diimmines are expected to give species in which dps exhibits a different bonding mode.[15,16]

As proof of this, the *cis*-Ru(bipy)$_2$ fragment favours the *N*,*N*-chelation of dps,[1] whereas the congested *cis*-Ru(*N*,*N*-dps)$_2$ fragment prevents the *N*,*N*-chelation and leads to *N*,*S*-coordinated dps complexes.[17] The crystal structure of [Ru(*N*,*N*-dps)$_2$(*N*,*S*-dps)][PF$_6$]$_2$·H$_2$O[17] clearly shows the distortion of the RuSCN(*Ru*−*N*) ring as well as the steric hindrance effect on the *N*,*S*-coordinate ligand. [The four-membered ring and the coordinated pyridine ring are almost coplanar whereas the pendant pyridine is rotated by 113.9(2)°.] The above complex and the similar species [Ru(*N*,*N*-dps)$_2$(*N*,*S*-phpys)][PF$_6$]$_2$ and [Ru(*N*,*N*-dprs)$_2$(*N*,*S*-phpys)][PF$_6$]$_2$ (phpys = phenyl pyridyl sulfide; dprs = di-2-pyrimidinyl sulfide), as a consequence of the *N*,*S*-coordination, exhibit a sulfur stereogenic centre (*R* and *S* configura-

[a] Dipartimento di Chimica Inorganica, Chimica Analitica e Chimica Fisica, Università di Messina,
98166 Messina, Italy
Fax: (internat.) + 39-090/393756
E-Mail: Tresoldi@chem.unime.it

Supporting information for this article is available on the WWW under http://www.eurjic.com or from the author.

 © WILEY-VCH Verlag GmbH, 69451 Weinheim, Germany, 2002 1434−1948/02/0101−0181 $ 17.50+.50/0

tions) and a pendant ring. The ^1H and ^{13}C NMR spectra were temperature-dependent and the fluxionality of the complexes was interpreted in terms of restricted rotation of the pendant rings and inversion at the sulfur atom. However, only an estimation of the activation energy data for the restricted rotation was possible due to the complex splitting patterns of the proton signals of the coordinated and pendant rings and the numerous partial overlaps of these signals.

In order to elucidate the mechanism of the sulfur inversion, in this paper we report on the synthesis of a series of the novel thioethers [4-methylbenzyl 2-pyridyl sulfide (**L$_1$**), 4-chlorobenzyl 2-pyridyl sulfide (**L$_2$**), 3-chlorobenzyl 2-pyridyl sulfide (**L$_3$**), 1,4-bis(2-pyridylthiomethyl)benzene (**L$_4$**), 4-methylbenzyl 2-pyrimidinyl sulfide (**L$_5$**), and 4-chlorobenzyl 2-pyrimidinyl sulfide (**L$_6$**)] containing sulfur-bonded CH_2R groups. We also report on their coordination chemistry that leads to the formation of the complexes [Ru(*N*,*N*-dprs)$_2$(*N*,*S*-L)][PF_6]$_2$, and [Ru(*N*,*N*-dps)$_2$(*N*,*S*-L)][PF_6]$_2$.

These tris(chelated) ruthenium complexes containing the *N*,*S*-coordinated thioethers exist as the enantiomers Δ and Λ, and in presence of the stereogenic sulfur atom (configuration *S* and *R*) four isomers can exist (Δ*S*, Δ*R*, Λ*S* and Λ*R*). When the thioether is *N*,*S*-chelated, the two methylene protons of the CH_2R group bonded to the sulfur atom are anisochronous. Their ^1H NMR signals are well separated by other signals and very sensitive to the inversion and racemisation processes.

By NMR studies in acetone two exchanging diastereoisomers were identified and the inversion at the sulfur atom examined. The complex [Ru(bipy)$_2$(*N*,*S*-**L$_1$**)][PF_6]$_2$ was also prepared and, in contrast to the other complexes, its NMR spectra, in the range 200−330 K are temperature-independent and show the presence of two non-exchanging isomers.

Results

Synthesis and Characterization of the 4-Methylbenzyl 2-Pyridyl Sulfide (L$_1$), 4-Chlorobenzyl 2-Pyridyl Sulfide (L$_2$), 3-Chlorobenzyl 2-Pyridyl Sulfide (L$_3$), 1,6-Bis(2-pyridylthiomethyl)benzene (L$_4$), 4-Methylbenzyl 2-Pyrimidinyl Sulfide (L$_5$), and 4-Chlorobenzyl 2-Pyrimidinyl Sulfide (L$_6$)

The novel thioether ligands were prepared by heating equimolar amounts of the appropriate mercapto and bromide derivative [2-sulfanylpyridine and 4-methylbenzyl bromide (**L$_1$**) or 4-chlorobenzyl bromide (**L$_2$**) or 3-chlorobenzyl bromide (**L$_3$**), 2-sulfanylpyrimidine and 4-methylbenzyl bromide (**L$_5$**), or 4-chlorobenzyl bromide (**L$_6$**)] in the presence of K_2CO_3 under reflux in DMF under N_2. Compound **L$_4$** was prepared from 2-sulfanylpyridine and α,α′-dichloro-*p*-xylene (or 2-bromopyridine and α,α′-disulfanyl-*p*-xylene) in a molar ratio of 2:1. The DMF was removed by distillation at 100 Torr. The thioethers were obtained as oils by extraction in CH_2Cl_2. Crystallization from CH_2Cl_2/heptane at room temperature (**L$_1$** and **L$_4$**) or at −18 °C (**L$_2$**, **L$_3$**, **L$_5$**, and **L$_6$**) gave white solids. The structures of these compounds were determined by a combination of elemental analysis and usual spectroscopic techniques. The ^1H and ^{13}C NMR spectroscopic data of the ligands in $(CD_3)_2CO$ are collected in Table 1 with the numbering scheme for proton and carbon assignments.

The pyridine proton signals of **L$_1$**, **L$_2$**, **L$_3$**, and **L$_4$** appear as four multiplets in the δ = 7.04−8.46 range, whereas the pyrimidine signals of **L$_5$** and **L$_6$** appear as a triplet and a doublet at δ = 7.15 and 8.59, respectively. The signals of methylene protons were found as singlets in the range δ = 4.37−4.46.

The ^{13}C signals were easily assigned. The pyridine quaternary carbon signals of **L$_1$**, **L$_2$**, **L$_3$**, and **L$_4$** are observed at δ ≈ 159.0, and other pyridine signals in the range δ = 120.2−150.1. The pyrimidine quaternary carbon signals of **L$_5$** and **L$_6$** are observed at δ ≈ 172.0, and other pyrimidine signals at δ ≈ 117.7 (C^5) and 158.1 (C^6 and C^4).

Synthesis of the Compounds

The air-stable compounds [Ru(*N*,*N*-dprs)$_2$(*N*,*S*-L)][PF_6]$_2$ (L = **L$_1$**, **L$_2$** and **L$_4$**), [Ru(*N*,*N*-dps)$_2$(*N*,*S*-L)][PF_6]$_2$ (L = **L$_1$**, **L$_2$** and **L$_3$**) and [Ru(*N*,*N*-bipy)$_2$(*N*,*S*-**L$_1$**)][PF_6]$_2$ were obtained by the reaction of the appropriate dichlorobis(diimmine) complex with an excess of L in boiling ethanol/water (1:1), followed by addition of aqueous NH_4PF_6. The complexes [Ru(*N*,*N*-dps)$_2$(*N*,*S*-**L$_5$**)][PF_6]$_2$ and [Ru(*N*,*N*-dps)$_2$(*N*,*S*-**L$_6$**)][PF_6]$_2$ were prepared from the nitrosyl compound [Ru(*N*,*N*-dps)$_2$(NO_2)(NO)][PF_6]$_2$.[1] All the complexes were soluble in acetone or acetonitrile and slightly soluble in methanol, ethanol, and water.

Conductivity measurements in acetonitrile solution indicate that these compounds are 1−2 electrolytes. Analytical and selected IR data are given in the Exp. Sect.

Dynamic NMR Studies

Variable-temperature ^1H NMR spectra of the compounds were obtained in $(CD_3)_2CO$ in the range 190−330 K. Selected data are listed in Table 2.

Solution Behaviour of the Complexes [Ru(*N*,*N*-dprs)$_2$(*N*,*S*-L$_1$)][PF_6]$_2$, [Ru(*N*,*N*-dprs)$_2$(*N*,*S*-L$_2$)][PF_6]$_2$ and [Ru(*N*,*N*-dprs)$_2$(*N*,*S*-L$_4$)][PF_6]$_2$

At 205 K the NMR spectra of these complexes show the presence of two slow-exchanging isomers in similar abundance. The spectrum of [Ru(*N*,*N*-dprs)$_2$(*N*,*S*-**L$_1$**)][PF_6]$_2$ is shown in Figure 1 and selected data are listed in Table 2. According to the presence of two isomers (population ratio 53:47) two signals are observed in the methyl region (Figure 1a) at δ = 2.28 and 2.27 (the first signal due to the major isomer). Furthermore, four doublets are observed in the methylene region: two doublets of minor intensity at δ = 5.20 and 4.13 (labelled A and B, respectively) and two doublets of major intensity at δ = 4.64 and 4.00 (labelled C and D, respectively). The H^3 pyridine signals appear (Figure 1b) at an abnormally low frequency (δ = 6.23 and 6.13, the first signal of major intensity) due to the strong shielding effect of the phenyl ring. Some signals partially over-

Table 1. ^1H and ^{13}C NMR spectroscopic data[a] of the new ligands

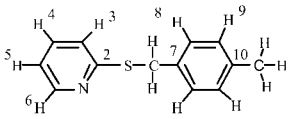

L_1

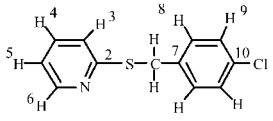

L_2

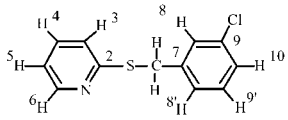

L_3

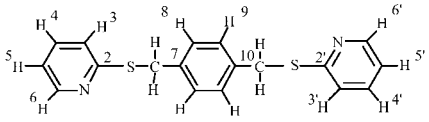

L_4

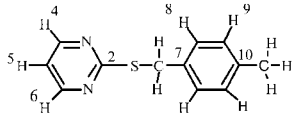

L_5

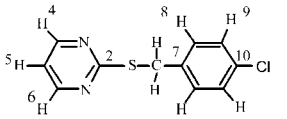

L_6

Ligand	Heterocyclic ring positions						Other positions					
	2	3	4	5	6	7	8	8'	9	10	CH_2	CH_3
L_1		7.21	7.55	7.04	8.45		7.09[b]		7.32[b]		4.44	2.27
	J_{H6H5} = 4.9		J_{H6H4} = 1.9		J_{H6H3} = 1.0							
	J_{H5H4} = 7.4		J_{H5H3} = 1.1		J_{H4H3} = 8.1							
	159.50	122.35	136.80	120.25	150.00	137.10	129.70		129.60	136.00	34.20	22.10
L_2		7.22	7.58	7.07	8.45		7.29[b]		7.44[b]		4.41	
	J_{H6H5} = 5.0		J_{H6H4} = 1.9		J_{H6H3} = 1.0							
	J_{H5H4} = 7.4		J_{H5H3} = 1.1		J_{H4H3} = 8.0							
	158.85	122.55	137.10	120.55	150.10	132.95	131.35		129.05	138.60	34.20	
L_3		7.23	7.60	7.09	8.46		7.39	7.48	7.29	7.23	4.46	
	J_{H6H5} = 5.0		J_{H6H4} = 1.9		J_{H6H3} = 1.0	$J_{H8H8'}$ = 2.0	J_{H8H9} = 6.8		J_{H8H10} = 1.5	J_{H8HCH_2} = 0.6	J_{H9HCH_2} = -0.3	
	J_{H5H4} = 7.4		J_{H5H3} = 1.1		J_{H4H3} = 8.0	$J_{H8'H9}$ = 0.6	$J_{H8'H10}$ = 2.6		J_{H9H10} = 8.0	$J_{H8'HCH_2}$ = 0.6	J_{H10HCH_2} = 0.2	
	158.65	122.55	137.10	120.60	150.10	134.25	129.55	130.65	127.65	128.20	33.35	142.20[c]
L_4		7.22	7.58	7.07	8.44		7.36		7.36		4.42	
	J_{H6H5} = 4.9		J_{H6H4} = 1.9		J_{H6H3} = 1.0							
	J_{H5H4} = 7.4		J_{H5H3} = 1.1		J_{H4H3} = 8.0							
	159.25	122.40	136.95	120.35	150.05	138.00	129.70		129.70	138.00	33.90	
L_5			8.59	7.15	8.59		7.11[b]		7.31[b]		4.37	2.27
			J_{H6H5} = 4.9									
	172.45		158.10	117.65	158.10	137.25	129.70		129.60	135.50	35.10	21.00
L_6			8.59	7.15	8.59		7.30[b]		7.47[b]		4.40	
			J_{H6H5} = 4.9									
	171.85		158.10	117.70	158.10	137.95	131.25		128.90	132.90	35.90	

[a] ^1HNMR spectra recorded at 300.13 MHz and ^{13}C NMR data at 75.56 MHz, T = 298 K in $(CD_3)_2CO$; δ values with respect to internal $SiMe_4$, J_{HH} in Hz. – [b] Unresolved AA'BB' system. – [c] Assigned to $C^{9'}$.

lapped are present in the range δ = 7.20−9.00 whereas in the range δ = 9.00−9.54 the H^6 pyridine and some pyrimidine signals are easily identified.

The almost complete assignment of the signals was based on low-temperature 2D COSY and phase-sensitive 2D NOESY (Figure 2a) experiments. In this way, 24 signals as doublet doublets were assigned to the protons of eight pyrimidine rings with coupling constant J_{45} = 4.60 Hz, J_{46} = 2.15 Hz, and J_{56} = 5.95. In particular, the H^6 pyrimidine protons of the major isomer are observed at δ = 8.79, 8.85, 8.88, and 9.36, while those of the minor isomer at δ = 8.88, 8.81, 9.22, and 9.54.

The 2D NOESY (Figure 2a) was performed at 230 K. At this temperature the significant signals are split and the interchange process is slow. The cross-peaks, due to chemical exchange of magnetization (Figure 2b), are detected between the methylene protons A−D as well as the B−C protons and, in the aromatic region, between the H^3 pyridine protons, between the $H^{6'}$ pyrimidine protons at δ = 9.54 and 9.36 as well as those at δ = 9.22 and 8.88. Figure 2a also shows the negative cross-peaks. The strong NOEs include intra-ring *ortho* interactions (e.g. 6−5, 5−4, and 4−3 in the *N,S*-coordinated pyridine ring and 6−5 in the pyrimidine rings), adjacent-group interactions (e.g. methyl/phenyl protons, not shown in figure, methylene/phenyl protons), and most significantly the following interactions: protons of phenyl ring/H^3 pyridine protons, H^6 pyridine protons and $H^{6'}$ pyrimidine protons at δ = 9.22 and 8.88, methylene proton of the major isomer at δ = 4.64/$H^{6'}$ pyrimidine protons at δ = 9.36. If we assume that there is no restricted rotation, e.g. methylene and phenyl groups freely rotate, since the ruthenium and sulfur atoms are stereogenic

Table 2. Selected ^{1}H NMR spectroscopic data

Complex	T [K][a]	*N,S*-ligand Heterocyclic ring				Other signals[b]				*N,N*-ligands
		H^3	H^4	H^5	H^6	CH_2	CH_2	J [Hz]	CH_3	Selected $H^{6'}$ protons
$[Ru(dprs)_2\mathbf{L_1}][PF_6]_2$	328	6.34	7.89	7.73	9.36	4.53	4.09	12.40	2.32	9.33 8.89
	205	6.23[c]	7.92[c]	7.76[c]	9.43[c]	4.64[c]	4.00[c]	12.45	2.28[c]	9.36[c] 8.88[c]
		6.13	7.87	7.74	9.41	5.20	4.13	12.80	2.27	9.54 9.22
$[Ru(dps)_2\mathbf{L_1}][PF_6]_2$	328	6.27	7.81	7.62	9.24	4.47	3.89	13.00	2.31	9.04 8.72
	205	6.05[c]	7.81[c]	7.64[c]	9.37[c]	5.05[c]	3.73[c]	13.00	2.26[c]	9.24[c] 8.98[c]
		6.17	7.84	7.66	9.34	4.74	3.91	12.55	2.27	9.06 8.57
$[Ru(dprs)_2\mathbf{L_2}][PF_6]_2$	328	6.45	7.92	7.75	9.37	4.58	4.19	12.90		9.32 8.89
	205	6.35	7.93	7.79	9.45	4.67	4.04	12.40		9.34 8.85
		6.28	7.90	7.77	9.41	5.27	4.25	13.10		9.52 9.23
$[Ru(dps)_2\mathbf{L_2}][PF_6]_2$	320	6.40	7.87	7.65	9.28	4.54	4.01	13.45		9.07 8.75
	205	6.23[c]	7.87[c]	7.70[c]	9.39[c]	5.11[c]	3.89[c]	13.10		9.22[c] 9.00[c]
		6.31	7.89	7.72	9.36	4.76	3.98	12.80		9.02 8.57
$[Ru(dps)_2\mathbf{L_3}][PF_6]_2$	328	6.38	7.85	7.64	9.26	4.51	3.99	13.25		9.03 8.72
	210	6.24[c]	7.85[c]	7.68[c]	9.38[c]	5.12[c]	3.86[c]	13.15		9.21[c] 9.00[c]
		6.29	7.87	7.70	9.36	4.77	3.93	12.65		9.03 8.55
$[Ru(dprs)_2\mathbf{L_4}][PF_6]_2$	318	6.28	7.86	7.47	9.39	4.53	4.16	13.00		9.37 8.99
		7.23[e]	7.60[e]	7.08[e]	8.43[e]	4.45[e]				
	210	6.23[c]	7.90[c]	7.77[d]	9.43[c]	4.63[c]	4.02[c]	12.50		9.36[c] 8.81[c]
		6.14	7.85		9.41	5.20	4.17	12.80		9.54 9.20
		7.30[e]	7.62[e]	7.14[e]	8.46[e]	4.41[e]				
$[Ru(dps)_2\mathbf{L_5}][PF_6]_2$	298		8.81	7.74	9.69	4.64	4.35	13.50	2.29	9.08 8.71
	195		8.86[c]	7.80[d]	9.78[c]	5.04[c]	4.34[c]	12.60	2.23[d]	9.29[c] 9.05[c]
			8.90		9.80	4.78	4.39	13.25		[f] [f]
$[Ru(dps)_2\mathbf{L_6}][PF_6]_2$	298		8.78	7.74	9.69	4.71	4.39	13.40		9.09 8.71
	195		8.84[c]	7.80[d]	9.77[c]	5.08[c]	4.40[c]	13.25		9.26[c] 9.03[c]
			8.88		9.80	4.80	4.42	13.25		[f] [f]
$[Ru(bipy)_2\mathbf{L_1}][PF_6]_2$	298	7.43[c]	8.12[c]	7.55[c]	7.88[c]	4.29[c]	3.81[c]	12.55	2.22[c]	9.66[c] 8.76[c]
		7.36	8.13	7.50	7.89	4.71	4.26	13.30	2.18	9.89 8.84

[a] Recorded in $(CD_3)_2CO$ at 300.13 MHz, δ in ppm with respect to internal $SiMe_4$. Coupling constants (Hz) in the pyridine rings: J_{43} = 7.7−8.1, J_{45} = 7.4−7.8, J_{65} = 4.8−5.5, J_{64} = 1.1−1.9, J_{53} = 0.7−1.3, and J_{63} = 0.7−0.8; in the pyrimidine rings: J_{65} = 5.5−6.0, J_{45} = 4.6−5.0, and J_{64} = 2.0−2.1. − [b] The phenyl signals are observed as unresolved AA′BB′ systems in the range δ = 7.2−7.8. − [c] Assigned to the major isomer. − [d] Overlapped signals of the two isomers. − [e] Uncoordinated side. − [f] Not assigned.

centres (configurations Δ and Λ, *R* and *S*, respectively), the complex has a total of four isomers including the enantiomers. Thus, the above-mentioned positive and negative cross-peaks found in the 2D NOESY imply that in the two isomers (Figure 3) the phenyl protons, in *ortho* positions with respect to the methylene group, are in close proximity to the H^3 pyridine protons (in Figure 3 only a phenyl *ortho*-proton is shown). Furthermore, the H^6 pyridine proton is in close proximity to the H^6 pyrimidine proton at δ = 8.88 (major isomer) or that at δ = 9.22 (minor isomer). Moreover, in the major isomer the methylene protons are in close proximity to the $H^{6'}$ pyrimidine proton at δ = 9.36. These results are indicative of a sulfur inversion, which exchanges the two diasteroisomers $\Delta R \rightleftarrows \Delta S$ (or $\Lambda S \rightleftarrows \Lambda R$), as depicted in Figure 3.

On warming the NMR solutions, all the spectral lines broaden. In particular the coalescence for the exchange $A \rightleftarrows D$ and $B \rightleftarrows C$ occurred around 280 K.

At 330 K, the highest temperature reached, two averaged methylene doublets and a single methyl signal were observed (Table 2). It is pertinent to note at this point that the splitting patterns of methylene protons, at high temperature, definitely eliminate the possibility of racemisation ($\Delta \rightleftarrows \Lambda$). In fact, in presence of a fast inversion and racemisation the averaged environments of the methylene protons should become equivalents. Furthermore, EXSY experiments in the range 300−330 K exclude a slow racemisation process. The complete assignment of the signals was performed with the help of the COSY spectrum. In the aromatic region, at this temperature, twelve pyrimidine proton signals due to four rings of the *N,N*-coordinated ligands are observed. In particular, the signals at δ = 9.33, 8.89 and 8.70 (two overlapped signals) were assigned to the H^6 pyrimidine protons, while four pyridine proton signals of the *N,S*-coordinated ligand are detected (Table 2).

The rates of the processes were deduced by band-shape analysis of the methylene signals, which are well separated by other signals and very sensitive to the process by virtue of the methylene closeness to the site of inversion. Some experimental and computer-simulated spectra are shown in Figure 4. As evident from the figure, the shifts are found to be strongly temperature-dependent. In order to correct for this temperature dependence a linear interpolation was used.[18] The resulting rate data were checked on the H^3 pyridine signals. Activation energy data were calculated from 16 independent fittings in the temperature range 205−330 K. Activation energy data for the other dprs com-

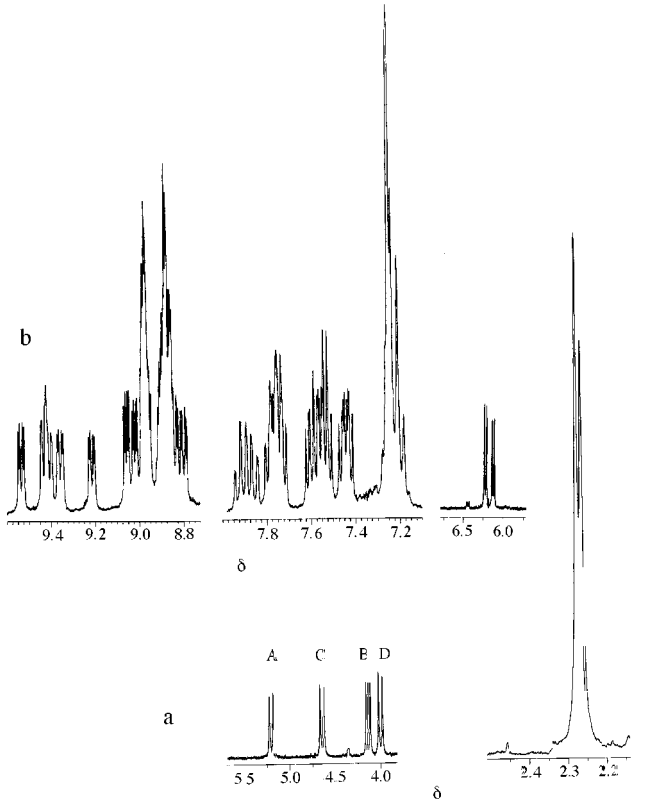

Figure 1. ^{1}H NMR spectrum of [Ru(*N,N*-dprs)$_2$(*N,S*-L$_1$)][PF$_6$]$_2$ at 205 K in (CD$_3$)$_2$CO; a) methylene and methyl region, b) aromatic region

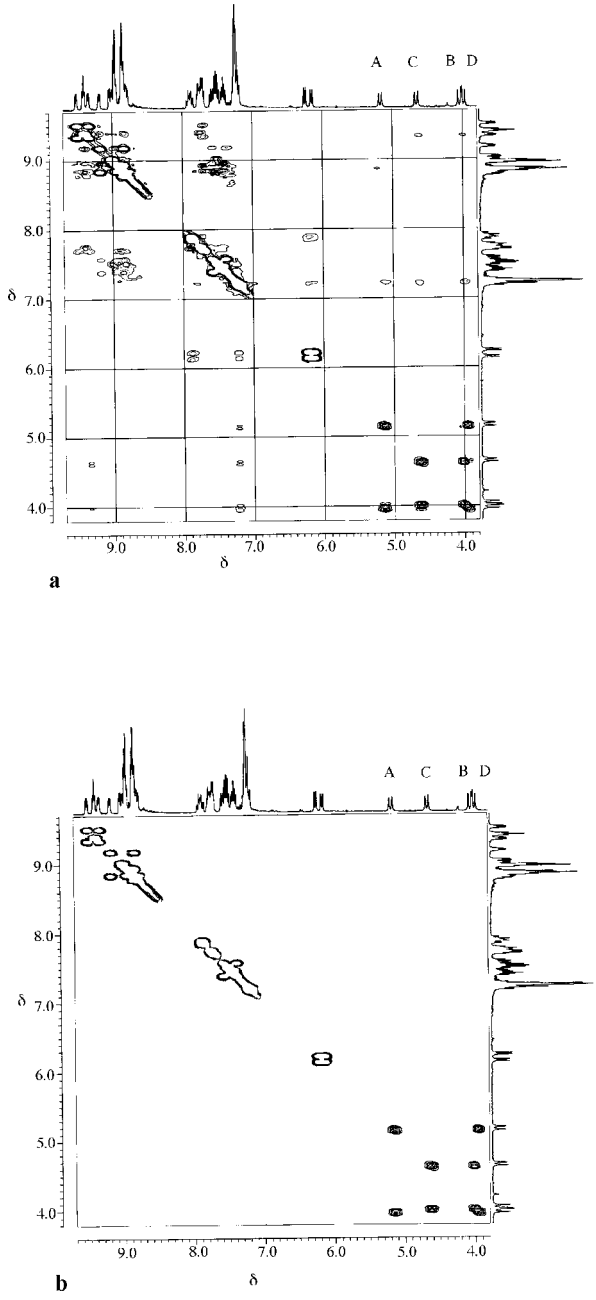

Figure 2. Phase-sensitive 2D NOESY of [Ru(*N,N*-dprs)$_2$(*N,S*-**L$_1$**)][PF$_6$]$_2$ at 230 K in (CD$_3$)$_2$CO; a) positive and negative cross-peaks, b) only positive cross-peaks

plexes were obtained by similar method and collected in Table 3.

The ^{13}C NMR spectra were easily interpreted, at least for the carbon signals of the *N,S*-ligand, by comparison of the spectra of the present complexes with those of the free ligands and other complexes containing *N,S*-chelated ligands,[17] with the help of CH-correlation experiments and jmod pulse sequences. ^{13}C NMR spectra of all three dprs complexes were similar (Table 4) and the results for [Ru(dprs)$_2$(*N,S*-**L$_1$**)][PF$_6$]$_2$ will serve to illustrate the analysis of the problem.

The ^{13}C NMR spectrum at 228 K comprised three regions of interest for the *N,S*-chelate ligand: (i) the methyl region that displayed the methyl resonances of the two isomers as overlapped signals at δ = 19.95; (ii) the methylene region with two signals at δ = 38.70 and 40.20 (the latter of the major isomer); (iii) the phenyl and pyridyl region (δ = 165−126) in which the C^7 quaternary carbon atoms of the two isomers are observed as overlapped signals. The C^3 pyridine carbon atom of the minor isomer and C^5 pyridine carbon atom of the major isomer led to superimposed signals whereas other resonances are well separated.

On warming the NMR solutions above 245 K some signals broaden, and in the range 265−285 K some signals vanish (in particular the methylene signals). In the fast exchange regime (328 K) averaged signals of the two isomers were observed (Table 4).

In the ^{13}C NMR spectrum of [Ru(dprs)$_2$(*N,S*-**L$_4$**)][PF$_6$]$_2$ the **L$_4$** carbon signals of the uncoordinated pyridyl ring and of the methylene group in the uncoordinated side are also observed. These signals and the corresponding signals of the free ligand show, at the same temperature, nearly the same chemical shift.

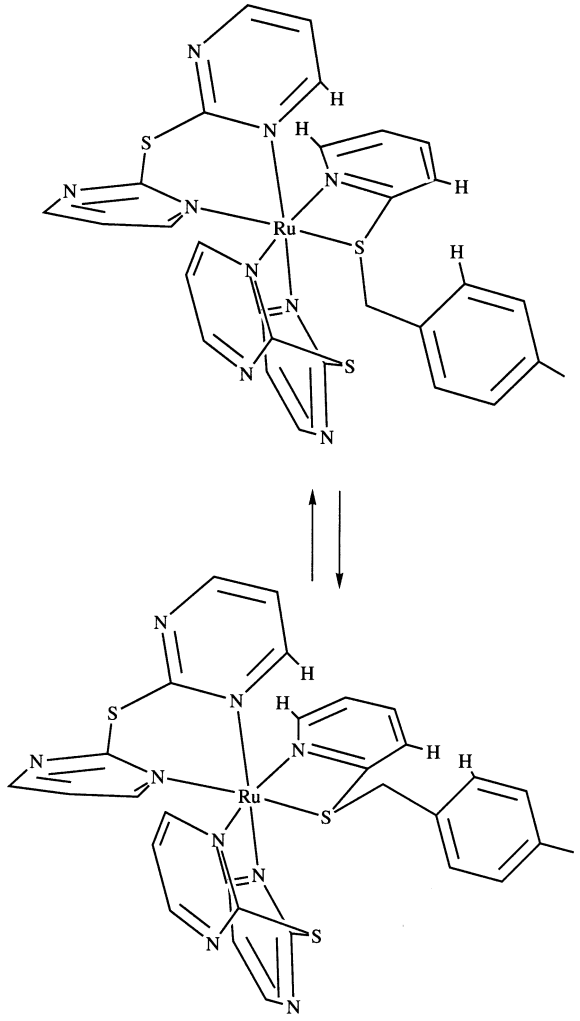

Figure 3. Schematic representation of the proposed structure for the diastereoisomers of $[Ru(N,N\text{-dprs})_2(N,S\text{-}\mathbf{L_1})][PF_6]_2$ and of the close proximity between the phenyl *ortho*-protons (only one is shown) and H^3 pyridine protons and that between the H^6 pyridine protons and H^6 pyrimidine proton at $\delta = 8.88$ (major isomer) or at $\delta = 9.22$ (minor isomer)

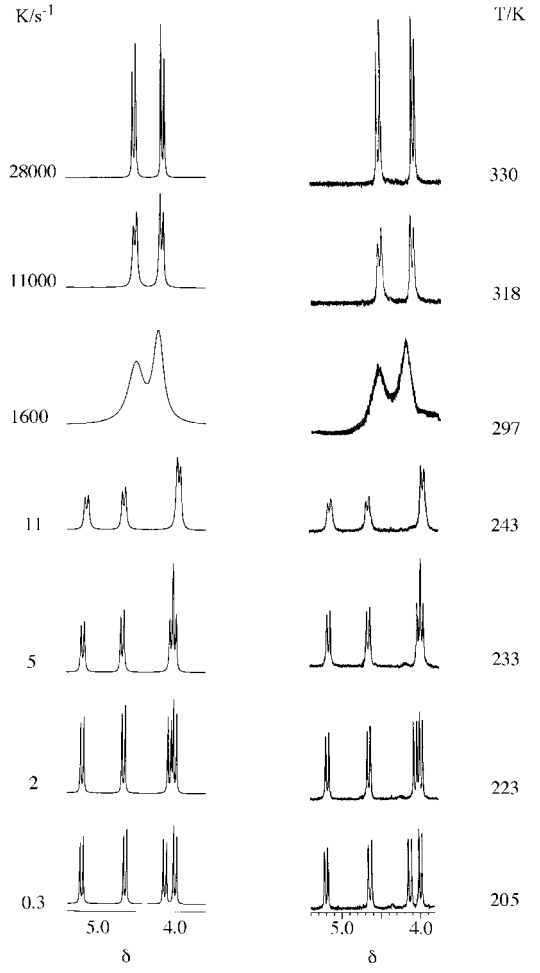

Figure 4. Selected variable-temperature ^1H NMR spectra of $[Ru(N,N\text{-dprs})_2(N,S\text{-}\mathbf{L_1})][PF_6]_2$ at 205 K in $(CD_3)_2CO$ (methylene region); computer-synthesised spectra of the same region are shown on the left

Solution Behaviour of the Complexes $[Ru(dps)_2(N,S\text{-}\mathbf{L_1})][PF_6]_2$, $[Ru(dps)_2(N,S\text{-}\mathbf{L_2})][PF_6]_2$ and $[Ru(dps)_2(N,S\text{-}\mathbf{L_3})][PF_6]_2$

Also for these complexes, two slow-exchanging isomers are present at 205 K, but the population ratio between the isomers is ca. 2:1 (Table 3). Furthermore, the methylene proton signals appear different with respect to those of the $[Ru(dprs)_2(N,S\text{-L})][PF_6]_2$ complexes in that now the methylene signals (Figure 5) of the minor isomer (C and D) are framed by those of the major isomer (A and B).

The 2D ^1H NOESY experiment on $[Ru(dps)_2(N,S\text{-}\mathbf{L_2})][PF_6]_2$ is shown in Figure 5. The positive cross-peaks show the chemical exchange between the methylene protons (A−D and B−C), between the H^6 pyrimidine protons at $\delta = 9.00$ and 8.57 (the first signal of major intensity), and between the H^6 pyrimidine protons at $\delta = 9.22$ and 9.02 (the first signal of major intensity). The most significant negative cross-peaks show strong NOEs due to the close proximity of phenyl protons and H^3 pyridine protons of *N*,*S*-chelated ligand and between the H^6 pyridine protons of *N*,*S*-chelated ligand and the H^6 pyridine protons of *N*,*N*-chelated ligands at $\delta = 9.00$ and 8.57, respectively. Thus, also in this case there are two exchanging diastereoisomers. In the major isomer the phenyl protons are in close proximity to the H^3 proton at $\delta = 6.23$ and in the minor isomer of the H^3 proton at $\delta = 6.31$. Rates of the process were deduced by band-shape analysis of the methylene signals. Also in this case a linear interpolation was necessary due to the strong temperature dependence of the signals. Activation energy data were collected in Table 3.

Solution Behaviour of the Complexes Containing Pyrimidine Thioethers as N,S-Ligands: $[Ru(dps)_2(N,S\text{-}\mathbf{L_5})][PF_6]_2$ and $[Ru(dps)_2(N,S\text{-}\mathbf{L_6})][PF_6]_2$

In contrast to the complexes containing pyridine thioethers as *N*,*S*-ligands, which showed some broad signals at room temperature (in particular broad methylene signals, see Figure 4), the ^1H NMR spectra of these complexes showed well-resolved signals in agreement with the presence

Table 3. Activation energy data

	Population (%)	$\Delta G^{\#}_{298\,K}$ [kJ mol^{-1}]	$\Delta H^{\#}$ [kJ mol^{-1}]	$\Delta S^{\#}$ [J K^{-1}mol^{-1}]
$[Ru(dprs)_2\mathbf{L_1}](PF_6)_2$	53:47	54.1 ± 0.2	48.9 ± 1.9	−17.4 ± 7.0
$[Ru(dprs)_2\mathbf{L_2}](PF_6)_2$	50:50	53.8 ± 0.1	44.9 ± 3.0	−30.0 ± 8.0
$[Ru(dprs)_2\mathbf{L_4}](PF_6)_2$	53:47	54.9 ± 0.2	49.2 ± 2.5	−19.2 ± 9.0
$[Ru(dps)_2\mathbf{L_1}](PF_6)_2$	60:40	51.8 ± 0.2	49.3 ± 1.6	−8.2 ± 5.9
$[Ru(dps)_2\mathbf{L_2}](PF_6)_2$	66:34	52.0 ± 0.6	53.1 ± 1.6	+3.4 ± 4.0
$[Ru(dps)_2\mathbf{L_3}](PF_6)_2$	67:33	50.6 ± 0.3	52.2 ± 1.8	+5.3 ± 7.0
$[Ru(dps)_2\mathbf{L_5}](PF_6)_2$	65:35	47.5 ± 0.5	40.0 ± 2.0	−25.0 ± 5.0
$[Ru(dps)_2\mathbf{L_6}](PF_6)_2$	65:35	47.0 ± 0.5	39.5 ± 2.0	−24.0 ± 5.0

Table 4. Selected ^{13}C NMR spectroscopic data

Complex	T [K][a]	*N,S*-coordinated ligand										
		Heterocyclic ring					Phenyl ring[b]				CH_2	CH_3
		C^2	C^3	C^4	C^5	C^6	C^7	C^8	C^9	C^{10}		
$[Ru(dprs)_2\mathbf{L_1}][PF_6]_2$	328	165.05	128.45	140.55	127.80	157.35	140.05	130.90	130.75	131.55	42.05	21.20
	228	163.25[c]	127.20[c]	138.65[c]	126.00[c]	155.60[c]	138.10[d]	129.40[c]	129.35[c]	130.55[c]	40.20[c]	19.95[d]
		164.40	126.10	138.95	126.20	155.40		129.50	129.25	131.10	38.70	
$[Ru(dps)_2\mathbf{L_1}][PF_6]_2$	328	164.95	127.70	139.75	126.85	157.90	139.75	130.85	130.60	131.80	42.40	21.15
	218	163.70[c]	127.30[c]	138.65[d]	125.95[c]	156.10[c]	137.65[d]	129.25[d]	128.90[c]	131.25[c]	40.60[c]	19.75[d]
		162.85	127.10		126.05	156.05			129.00	130.60	38.20	
$[Ru(dprs)_2\mathbf{L_2}][PF_6]_2$	320	164.60	128.30	140.60	127.75	157.20	135.20	132.45	130.00	133.65	41.00	
	228	164.15	127.35	139.20	126.35	155.70	133.40[d]	131.32	128.80	132.80[d]	39.45	
		162.90	126.35	138.90	126.15	155.45		131.20	128.70		38.10	
$[Ru(dps)_2\mathbf{L_3}][PF_6]_2$	320	164.55	127.65	139.85	127.10	158.00	137.55	130.35	135.20	129.30	41.50	
								130.15	129.35			
	218	163.50[c]	127.40[c]	138.75[d]	126.00[c]	156.15[c]	137.10[c]	128.35[c]	133.20[d]	127.90[d]	39.85[c]	
		162.35	127.15		126.40	156.25	136.40	128.20	127.90[d]		37.70	
$[Ru(dprs)_2\mathbf{L_4}][PF_6]_2$	318	165.10	128.50	140.60	127.90	157.45	141.10	131.10	130.80	136.30	42.00	
		159.20[e]	122.65[e]	137.40[e]	120.90[e]	150.40[e]					34.05[e]	
	228	163.30[c]	127.05[c]	138.65[d]	126.00[c]	155.60[c]	139.00[d]	129.50[c]	129.40[c]	132.50[c]	40.05[c]	
		164.45	126.20		126.05	155.35		129.60	129.25	133.00	38.50	
		157.35[e]	121.15[e]	136.15[e]	119.45[e]	148.90[e]					32.05[e]	
$[Ru(dps)_2\mathbf{L_5}][PF_6]_2$	298	174.00		159.35	122.85	165.35	138.65	130.35	129.95	132.15	40.10	20.75
	195	173.45[c]		159.35[c]	121.40[d]	163.80[c]	137.50[c]	129.20[c]	128.30[d]	131.85[d]	40.00[c]	19.45[c]
		172.80		158.45		163.85	137.70	129.30			38.00	19.35
$[Ru(dps)_2\mathbf{L_6}][PF_6]_2$	298	174.10		159.50	123.10	165.50	138.80	132.45	130.10	133.00	39.65	
	195	173.45[c]		159.35[c]	121.70[d]	163.85[c]	137.80[c]	130.35[c]	129.10[c]	132.00[d]	39.65[c]	
		172.45		158.45		163.75		130.45	129.00		37.00	
$[Ru(bipy)_2\mathbf{L_1}][PF_6]_2$	298	162.25[c]	128.55[c]	140.00[c]	125.20[c]	154.00[c]	138.85[c]	129.95[d]	128.85[c]	130.10[d]	38.25[c]	20.60[c]
		162.20	127.50	137.60	125.80	153.75	138.75		128.90		35.75	20.50

[a] Recorded in $(CD_3)_2CO$ at 75.56 MHz. – [b] Assignments of the quaternary phenyl carbon atoms C^7 and C^{10} possibly reversed. – [c] Assigned to the major isomer. – [d] Overlapped signals of the two isomers. – [e] Uncoordinated side.

of two fast-exchanging isomers (Figure 6). Unluckily, experimental difficulties ruled out the possibility of performing one- and two-dimensional experiments below 190 K. At this temperature the signal broadening, due to the inversion process, was not negligible and prevented the assignment of most signals. However, the band-shape analysis of the methylene signals above 190 K allows the evaluation of the activation energies. According to the fast inversion observed at room temperature, the mean values of the activation barriers, $\Delta G^{\ddagger}$ and $\Delta H^{\ddagger}$, for these complexes were 47.2 and 39.7 kJ mol^{-1}, respectively, whereas for the corresponding complexes containing thioarylpyridine as *N,S*-ligands (e.g. $[Ru(dps)_2(N,S\text{-}\mathbf{L_1})][PF_6]_2$ and $[Ru(dps)_2(N,S\text{-}\mathbf{L_2})][PF_6]_2$) the mean values were 52.9 and 49.6 kJ mol^{-1}, respectively.

Although some carbon signals (in particular of the minor isomer) were not observed in the slow exchange regime, the ^{13}C NMR spectra (Table 4) of $[Ru(dps)_2\,L][PF_6]_2$ complexes (L = $\mathbf{L_1}$, $\mathbf{L_2}$, $\mathbf{L_3}$, $\mathbf{L_5}$, and $\mathbf{L_6}$) confirm the presence of the two exchanging isomers.

Discussion

Our previous studies[17] on the dynamic behaviour of $[Ru(N,N\text{-dprs})_2(N,S\text{-phpys})][PF_6]_2$ and $[Ru(N,N\text{-dps})_2(N,S$-

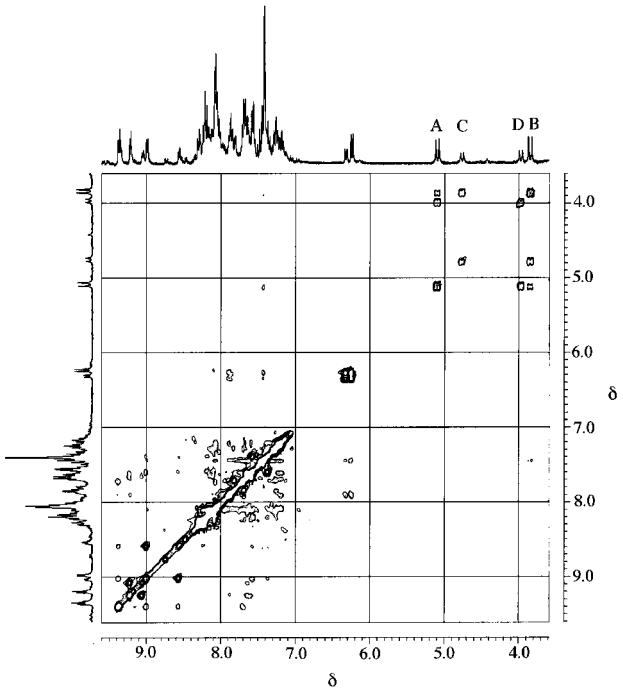

Figure 5. Phase-sensitive 2D NOESY of [Ru(*N*,*N*-dps)$_2$(*N*,*S*-**L$_2$**)][PF$_6$]$_2$ at 218 K in (CD$_3$)$_2$CO; positive and negative cross-peaks are shown

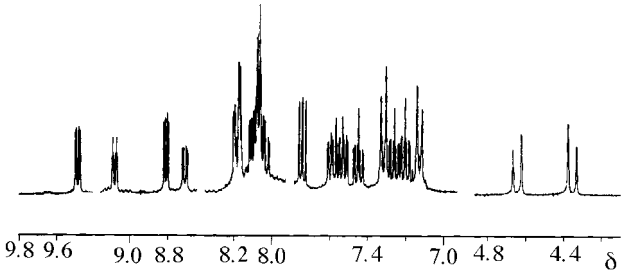

Figure 6. ^{1}H NMR spectrum of [Ru(*N*,*N*-dps)$_2$(*N*,*S*-L$_5$)][PF$_6$]$_2$ at 298 K in (CD$_3$)$_2$CO

phpys)][PF$_6$]$_2$ (phpys = phenyl pyridyl sulfide) show, in the range 180−240 K, that a restricted rotation of the pendant phenyl ring was operative, affecting only the phenyl proton signals. Above 240 K extensive internal arrangements, involving sulfur inversion were invoked to explain the higher temperature changes in the aromatic region of ^{1}H NMR spectra.

In contrast, the NMR spectra of the present complexes, at the lower temperatures reached (190 K), clearly show the presence of two slow-exchanging invertomers and the absence of any restricted rotation. Very likely, restricted rotation of the methylene or phenyl group occurs below the above temperature, but experimental difficulties ruled out the possibility of supporting this suggestion. Thus, the present tris(chelated) ruthenium complexes containing the ruthenium chiral atom (configurations Δ and Λ) and the sulfur chiral atom (configurations *S* and *R*) can exist only as four isomers. The process consistent with the NMR behaviour is the inversion at the sulfur atom ($R \rightleftarrows S$), whereas the possibility of racemisation ($\Delta \rightleftarrows \Lambda$) can be discarded.

The inversion at the sulfur atom may occur through one of three processes: a) a dissociative mechanism; b) a mechanism involving association of solvent or anion or free ligand; or c) intramolecular mechanism without any bond rupture. A dissociative mechanism with sulfur or nitrogen decoordination is unlikely on the basis of the $\Delta S^{\ddagger}$ values and ^{1}H NMR spectra, which are temperature-reversible and concentration-independent.

In particular, for the complexes containing pyrimidine thioether ligands, the dissociative mechanism may involve exchange of the coordinated and uncoordinated N-atoms through dissociation of the ruthenium−N bond, rotation around the pyrimidine−S bond, inversion at the sulfur atom and reformation of the pyrimidine−ruthenium bond. This mechanism can be definitively rejected in that it should make the H^6 and H^4 pyrimidine protons equivalent, whereas the latter protons are nonequivalent even when the process becomes fast at the NMR time scale. A dissociative mechanism involving nitrogen decoordination in the pyridine thioethers complexes can also be discarded on the basis of the pyridine basicity (pK_a = 5.25) being much larger than that of the pyrimidine (pK_a = 1.23), which suggests better σ-donor capability of the pyridine.

Even though the determination of $\Delta S^{\ddagger}$ values is based on extrapolation to $1/T = 0$ in the Eyring diagrams and, owing to the long distance over which this extrapolation has to be taken, is subject to considerable uncertainty, the data collected show that the activation entropies for [Ru(*N*,*N*-dprs)$_2$(*N*,*S*-L)][PF$_6$]$_2$ (L = **L$_1$**, **L$_2$**, and **L$_4$**) and [Ru(*N*,*N*-dps)$_2$(*N*,*S*-L)][PF$_6$]$_2$ (L = **L$_5$** and **L$_6$**) are, without doubt, negative (Table 3). Thus, the transition state conformations should be sterically even more congested than the ground state conformations, suggesting that a dissociative mechanism can be discarded. For [Ru(*N*,*N*-dps)$_2$(*N*,*S*-L)][PF$_6$]$_2$ (L = **L$_1$**, **L$_2$**, and **L$_3$**), the activation entropies are -8.2 ± 5.9 J K^{-1} mol^{-1}, $+3.4 \pm 4.0$ J K^{-1} mol^{-1}, and $+5.3 \pm 7.0$ J K^{-1} mol^{-1}, respectively. Although these values, different to those of other complexes, are close to zero, it is pertinent to note that the $\Delta G^{\ddagger}_{298\,K}$ values for the process in the corresponding dprs and dps complexes (Table 3) are of comparable magnitude, strongly suggesting that a similar mechanism is operative.

On the other hand, a mechanism involving association of solvent or anion or free ligand can be discarded on the basis of the following NMR findings: (i) the ^{1}H NMR spectra are temperature-reversible and concentration-independent; (ii) when free ligand is added separate signals are observed and the exchange rates are not affected; (iii) for the complex [Ru(dprs)$_2$(*N*,*S*-**L$_4$**)][PF$_6$]$_2$ the presence of the uncoordinated side in the thioether ligand does not affect the process; and (iv) addition of chloride or hexafluorophosphate anion does not affect the exchange rate.

The only mechanism, therefore, consistent with all the experimental results appears to be the pyramidal inversion without any bond rupture. However, the inversion barriers for the present complexes are low with respect to those

found in iron or ruthenium complexes containing bridging[19] or chelating[20] ligands, and other complexes containing *N,S*-coordinated ligands that form five-membered chelate rings.[21,22] Furthermore, decreasing the size of the ring containing the sulfur atom ought to make the access to the planar transition state more difficult, with a consequent increase in the pyramidal inversion energy barrier.[20]

The low $\Delta G^{\ddagger}$ values of the present complexes, which reflect differences between the ground- and transition-state energy, are mainly due to relatively high-energy ground states rather than low-energy transition states. This may be explained in terms of the contemporary presence of the congested Ru(*N,N*-dps)$_2$ or Ru(*N,N*-dprs)$_2$ fragments and steric demanding thioether ligands *N,S*-coordinated. This hypothesis is supported by the NMR spectra of the [Ru(bipy)$_2$(*N,S*-**L$_1$**)][PF$_6$]$_2$ that show the presence of two non-exchanging isomers, even at the highest temperatures achievable in acetone. The planar disposition of the bipy ligands in the last complex very likely reduces the steric hindrance of the [Ru(*N,N*-diimmine)$_2$ fragment and the ground-state energy with consequent increase of the $\Delta G^{\ddagger}$ value.

Conclusion

The synthesis of a series of novel thioethers bearing CH_2R groups allowed us to extend the chemistry of polypyridine ruthenium(II) compounds containing *N,S*-coordinated ligands with a four-membered chelate ring, and to elucidate the sulfur inversion mechanism. The pyramidal inversion, without bond rupture, is likely to be the only mechanism consistent with the dynamic behaviour of the present complexes. The steric hindrance of the ruthenium substrates and the steric demand of the thioether ligand *N,S*-coordinated appear to play a determinant role for the inversion process.

The process occurs at distinctly lower rates in the complexes containing pyridine thioethers (**L$_1$**, **L$_2$**, **L$_3$**, **L$_4$**) than in those containing pyrimidine derivatives (**L$_5$**, **L$_6$**), the differences in the averaged $\Delta G^{\ddagger}$ values being 8 kJ mol^{-1}. Steric and electronic effects may be invoked to explain this difference. In fact, the pyridine H^3 proton, in close proximity to the phenyl ring in the *N,S*-coordinated ligand, should increase the energy barrier of the dynamic process. On the other hand, the substitution in the thioether ligand of the pyridine with pyrimidine should weaken the ruthenium−sulfur bond (pyrimidine is a better electron-withdrawing group than pyridine) and decrease the energy barrier. Further attempts are in progress with the aim to study the effect of more or less congested Ru(*N,N*-diimine)$_2$ cores on the structure of the isomers and the exchange process.

Experimental Section

Di-2-pyridyl sulfide,[24] [Ru(dps)$_2$Cl$_2$]·2H$_2$O,[1] [Ru(dprs)$_2$Cl$_2$]·2H$_2$O,[17] and [Ru(dps)$_2$(NO)(NO$_2$)][PF$_6$]$_2$·H$_2$O[1] were prepared by published methods. Other reagents and solvents were used as received. − Elemental analyses were carried by Redox Microanalytical Laboratory of Cologno Monzese (Milano). − Conductivity measurements were done with a Radiometer CDM 3 conductivity meter. − Infrared spectra were recorded with an FT-IR 1720X spectrophotometer with samples as Nujol mulls placed between KBr plates. − The ^{1}H and ^{13}C NMR spectra were recorded with a Bruker AMX 300 spectrometer. The following Bruker programs were used: zg, homodecnew, zgpg, jmod, cosy, noesy.pt, hxco, invb. Simulations of static and dynamic spectra were performed using the G NMR program.

4-Methylbenzyl 2-Pyridyl Sulfide (L$_1$): The compounds 2-sulfanylpyridine (11.1 g, 0.1 mol), 4-methylbenzyl bromide (18.5 g, 0.1 mol), and potassium carbonate (11.0 g, 0.08 mol) were vigorously stirred in dimethylformamide (40 cm^3), and heated under reflux for 5 h, under N_2. The dimethylformamide was then distilled under reduced pressure (100 Torr) and the residue extracted with CH_2Cl_2 (ca. 250 cm^3). To the solution was added aluminium oxide (activated neutral, STD grade, 10 g). The mixture was allowed to stand until the solution was almost colourless (ca. 1 d). By evaporation of the filtered solution, a pale yellow oil was obtained that was dissolved in 150 cm^3 of CH_2Cl_2/heptane (1:2). A white solid was formed by slow concentration. Yield 11.0 g (51%). − Selected IR data (KBr): $\tilde{\nu}$ = 1578 vs, 1557 s, 1515 s, 1454 vs, 1415 vs, 1124 vs, 841 br, 758 vs, 740 ms, 726 s cm^{-1}. − $C_{13}H_{13}NS$ (215.31): calcd. C 72.50, H 6.10, N 6.50, S 14.90; found C 72.60, H 6.15, N 6.55, S 14.90.

4-Chlorobenzyl 2-Pyridyl Sulfide (L$_2$): This compound was obtained starting from 2-sulfanylpyridine (11.1 g, 0.1 mol), 4-chlorobenzyl chloride (16.1 g, 0.1 mol), and potassium carbonate (11.0 g, 0.08 mol) in dimethylformamide (40 cm^3) under reflux for 7 h, under N_2. After removal of the DMF, extraction with CH_2Cl_2 (ca 250 cm^3), and addition of aluminium oxide (10 g), the mixture was allowed to stand until the solution was colourless. The filtered solution was concentrated to give an oil that was kept at −24 °C. Colourless needles were formed. Yield 10.0 g (42%). − Selected IR data (KBr): $\tilde{\nu}$ = 1578 vs, 1556 vs, 1490 vs, 1453 vs, 1414 vs, 1122 vs, 1091 vs, 1015 vs, 853 br, 756 vs, 730 s, 725 s cm^{-1}. − $C_{12}H_{10}ClNS$ (235.73) calcd: C 61.15, H 4.30, N 5.95, S 13.60; found C 61.10, H 4.35, N 6.00, S 13.60.

3-Chlorobenzyl 2-Pyridyl Sulfide (L$_3$): This white compound was obtained in the same manner as above, starting from 2-sulfanylpyridine (11.1 g, 0.1 mol), 3-chlorobenzyl bromide (20.5 g, 0.1 mol), and potassium carbonate (11.0 g, 0.08 mol). Reaction time: 3 h. Yield 8.0 g (34%). − Selected IR data (KBr): $\tilde{\nu}$ = 1597s, 1579 vs, 1556 vs, 1453 vs, 1414 vs, 1123 vs, 876 br, 787 br, 757 vs, 725 vs cm^{-1}. − $C_{12}H_{10}ClNS$ (235.73): calcd. C 61.15, H 4.30, N 5.95, S 13.60; found C 61.20, H 4.35, N 6.00, S 13.70.

1,4-Bis[(phenylsulfanyl)methyl]benzene (L$_4$): The compounds 2-bromopyridine (15.8 g, 0.1 mol), 1,4-benzenedimethanethiol (8.52 g, 0.05 mol), and potassium carbonate (11 g, 0.08 mol) were vigorously stirred in dimethylformamide (40 cm^3) and heated under reflux for 5 h. The solvent was then removed ant the resulting brown solid extracted with a mixture (210 cm^3) of CH_2Cl_2 and heptane (1:2). The first crop of solid separated by slow evaporation (ca. 2 h) as a white pure product. To the solution was added the residue, CH_2Cl_2 (100 cm^3), and aluminium oxide (activated neutral, STD grade, 10 g). The mixture was allowed to stand until the solution was almost colourless (ca. 1 d). By slow concentration of the filtered solution the second crop of product was obtained. Total yield 19.5 g (60%). − Selected IR data (KBr): $\tilde{\nu}$ = 1576 vs, 1550 s, 1514 s, 1121 vs, 894 s, 823 s, 757 vs, 732 s, 724 vs, 504s cm^{-1}. −

$C_{18}H_{16}N_2S_2$ (324.46): calcd. C 66.65, H 4.95, N 8.65, S 19.75; found C 66.60, H 5.00, N 8.55, S 19.70. − Compound **L_4** was also obtained in the same way starting from 2-sulfanylpyridine (11.3 g, 0.1 mol) and α,α′-dichloro-*p*-xylene (8.75 g, 0.05 mol). Yield ca. 50%.

4-Methylbenzyl 2-Pyrimidinyl Sulfide (L_5): This white compound was obtained as like **L_2** from 2-sulfanylpyrimidine (11.2 g, 0.1 mol), 4-methylbenzyl bromide (18.5 g, 0.1 mol), and potassium carbonate (11.0 g, 0.08 mol). Yield 10.6 g (49%). − Selected IR data (KBr): $\tilde{\nu}$ = 1565 vs, 1546 vs, 1516 s, 1205 s, 1181 s, 1170 s, 803 s, 771 vs, 757 ms, 744 s. 727s cm^{-1}. − $C_{12}H_{12}N_2S$ (216.30): calcd: C 66.65, H 5.60, N 12.95, S 14.80; found C 66.60, H 5.65, N 12.85, S 14.90.

4-Chlorobenzyl 2-Pyrimidinyl Sulfide (L_6): This white compound was obtained like **L_2** from 2-sulfanylpyrimidine (11.2 g, 0.1 mol), 4-chlorobenzyl chloride (16.1 g, 0.1 mol), and potassium carbonate (11.0 g, 0.08 mol). Yield 10.6 g (45%). − (KBr): $\tilde{\nu}$ = 1566 vs, 1548 vs, 1490 s, 1206 s, 1184 s, 1159 s, 1093 vs, 1015 s, 812 s, 769 s, 750 vs, 722 s cm^{-1}. − $C_{11}H_9ClN_2S$ (236.72): calcd. C 55.80, H 3.85, N 11.85, S 13.55; found C 55.80, H 3.95, N 11.80, S 13.60.

$[Ru(dprs)_2(L_1)][PF_6]_2$: $[Ru(dprs)_2Cl_2]\cdot 2H_2O$ (0.196 g, 0.33 mmol) and **L_1** (0.190 g, 0.882 mmol) were heated under reflux in 60 cm^3 of ethanol/water (1:1). After 1 h, the red complex was dissolved and the yellow solution was filtered hot. By addition of 30 cm^3 of water containing 0.49 g (3 mmol) of NH_4PF_6 a yellow precipitate was obtained. It was filtered, washed with 50 cm^3 of cold water, and dried overnight. The solid was washed copiously with diethyl ether and dried again. It was then dissolved in acetone (20 cm^3), and diethyl ether (ca. 40 cm^3) was added slowly until a yellow solid was obtained. The compound was washed with diethyl ether and dried over P_4O_{10} under vacuum. Yield 0.165 g (50%). − Selected IR data (KBr): $\tilde{\nu}$ = 1619 br, 1577 s, 1549 s, 1167 s, 1127 s, 847 br, 768 s, 754 vs, 723 s, 558 vs cm^{-1}. − $C_{29}H_2F_{12}N_9P_2RuS_3$ (986.76): calcd. C 35.30, H 2.55, N 12.80, S, 9.75; found C 35.30, H 2.60, N 12.75, S 9.80. − Conductivity: Λ_M(MeCN, 2 × 10^{-4} mol dm^{-3}, 20 °C) = 270 S cm^2 mol^{-1}.

$[Ru(dprs)_2(L_2)][PF_6]_2$: The compound was obtained in the same way as the previous complex, starting from $[Ru(dprs)_2Cl_2]\cdot 2H_2O$ (0.196 g, 0.33 mmol) and **L_2** (0.208 g, 0.882 mmol). Yield 0.160 g (48%). − Selected IR data (KBr): $\tilde{\nu}$ = 1579 vs 1549 vs, 1492 s, 1396 vs, 1167 vs, 847 br, 768s, 754 vs, 558 vs cm^{-1}. − $C_{28}H_{22}ClF_{12}N_9P_2RuS_3$ (1007.18): calcd. C 33.40, H 2.20, N 12.50, S 9.55; found C 33.40, H 2.25, N 12.40, S 9.60. − Conductivity: Λ_M(MeCN, 2 × 10^{-4} mol dm^{-3}, 20 °C) = 290 S cm^2 mol^{-1}.

$[Ru(dprs)_2(L_4)][PF_6]_2$: The crude product was prepared in the same way as above, starting from $[Ru(dprs)_2Cl_2]\cdot 2H_2O$ (0.196 g, 0.333 mmol) and **L_4** (0.216 g, 0.666 mmol). The solid was dissolved in acetone (10 cm^3) and added to the top of a chromatography column (diameter 2 cm) packed with aluminium oxide [60 g; Aldrich, neutral, STD grade, 150 mesh, deactivated with water (2.4 g)]. The first orange band was eluted with acetone/CH_2Cl_2 (3:2) (60 cm^3) and acetone (ca 300 cm^3). The orange solid obtained by removal of the solvent was collected and washed with diethyl ether. Further elution with acetone (ca. 400 cm^3) gave a yellow band, which was concentrated (10 cm^3) and precipitated with diethyl ether (90 cm^3). The yellow solid obtained was washed copiously with diethyl ether and dried over P_4O_{10} under vacuum. Yield 0.140 g (30%). − Selected IR data (KBr): $\tilde{\nu}$ = 1617 br, 1577 vs, 1549 vs, 1511 ms, 1167 vs, 846 vs, 766 s, 754 vs, 723 ms, 558 vs cm^{-1}. − $C_{34}H_{28}F_{12}N_{10}P_2RuS_4$ (1095.91): calcd. C 37.25, H 2.60, N 12.80, S 11.70; found C 37.20, H 2.65, N 12.65, S 11.65. − Conductivity: Λ_M(MeCN, 2 × 10^{-4} mol dm^{-3}, 20 °C) = 295 S cm^2 mol^{-1}.

$[Ru(dps)_2(L_1)][PF_6]_2$: The compound was obtained in the same way as above, starting from $[Ru(dps)_2Cl_2]\cdot 2H_2O$ (0.195 g, 0.33 mmol) and **L_1** (0.190 g, 0.882 mmol). Yield 0.163 g (50%). − Selected IR data (KBr): $\tilde{\nu}$ = 1641 br, 1586 s, 1556 s, 1284 s, 1162 s, 1127 s, 845 br, 766 vs, 741 ms, 725 s, 558 vs cm^{-1}. − $C_{33}H_{29}F_{12}N_5P_2RuS_3$ (982.81): calcd. C 40.35, H 2.95, N 7.15, S 9.80; found C 40.40, H 3.00, N 7.05, S 9.85. − Conductivity: Λ_M(MeCN, 2 × 10^{-4} mol dm^{-3}, 20 °C) = 304 S cm^2 mol^{-1}.

$[Ru(dps)_2(L_2)][PF_6]_2$: The compound was obtained in the same way as above, starting from $[Ru(dps)_2Cl_2]\cdot 2H_2O$ (0.195 g, 0.33 mmol) and **L_2** (0.208 g, 0.882 mmol). Yield 0.134 g (40%). − Selected IR data (KBr): $\tilde{\nu}$ = 1588 vs, 1555 s, 1421 vs, 1284 s, 1163 s, 1129 s, 1087 s, 1063 s, 843 br, 768 vs, 740 ms, 727 s, 558 vs cm^{-1}. − $C_{32}H_{26}ClF_{12}N_5P_2RuS_3$ (1003.23): calcd. C 38.30, H 2.60, N 7.00, S 9.60; found C 38.40, H 2.70, N 7.00, S 9.65. − Conductivity: Λ_M(MeCN, 2 × 10^{-4} mol dm^{-3}, 20 °C) = 295 S cm^2 mol^{-1}.

$[Ru(dps)_2(L_3)][PF_6]_2$: The compound was obtained in the same way as above, starting from $[Ru(dps)_2Cl_2]\cdot 2H_2O$ (0.195 g, 0.33 mmol) and **L_3** (0.208 g, 0.882 mmol). Yield 0.167 g (50%). − Selected IR data (KBr): $\tilde{\nu}$ = 1588 vs, 1555 ms, 1422 vs, 1284 s, 1164 s, 1129 s, 1087 s, 1064 s, 845 br, 768 vs, 740 ms, 727 s, 558 vs cm^{-1}. − $C_{32}H_{26}ClF_{12}N_5P_2RuS_3$ (1003.23): calcd. C 38.30, H 2.60, N 7.00, S 9.60; found C 38.40, H 2.70, N 6.95, S 9.55. − Conductivity: Λ_M(MeCN, 2 × 10^{-4} mol dm^{-3}, 20 °C) = 290 S cm^2 mol^{-1}.

$[Ru(dps)_2(L_5)][PF_6]_2$: NaN_3 (0.0325 g, 0.5 mmol) was dissolved in warm methanol (8 cm^3) and added dropwise to a stirred solution of $[Ru(dps)_2(NO)(NO_2)][PF_6]_2\cdot H_2O$ (0.431 g, 0.5 mmol) in acetone (30 cm^3). The solution colour changed from yellow to dark-red. To the solution, protected from light, was added, after 3 min **L_5** (0.324 g, 1.5 mmol), after 2 min a 70% aqueous solution of HPF_6 (3 cm^3), and again a methanol (8 cm^3) solution of NaN_3 (0.0325 g, 0.5 mmol), dropwise. The mixture was stirred for 2 h, filtered, concentrated (20 cm^3), and the product precipitated with diethyl ether (100 cm^3). The yellow solid obtained was dried over P_4O_{10}, under vacuum, crystallised from acetone (10 cm^3) and diethyl ether (90 cm^3), washed with diethyl ether, and dried again. Yield 0.16 g (33%). − Selected IR data (KBr): $\tilde{\nu}$ = 1590 s, 1455 vs, 1423 s, 1286 s, 1165 s, 1064 s, 846 br, 770 s, 726 ms, 558 vs cm^{-1}. − $C_{32}H_{28}F_{12}N_6P_2RuS_3$ (983.80): calcd. C 39.05, H 2.85, N 8.55, S 9.80; found C 39.00, H 2.90, N 8.55, S 9.70. − Conductivity: Λ_M(MeCN, 2 × 10^{-4} mol dm^{-3}, 20 °C) = 305 S cm^2 mol^{-1}.

$[Ru(dps)_2(L_6)][PF_6]_2$: The complex was obtained in the same way as $[Ru(dps)_2(L_5)][PF6]_2$ using **L_6** (0.355 g, 1.5 mmol) instead of **L_5**. Yield 0.15 g (30%). − Selected IR data (KBr): $\tilde{\nu}$ = 1590 s, 1455 vs, 1422 s, 1286 s, 1164 s, 1064 s, 845 br, 770 s, 726 ms, 558 vs cm^{-1}. − $C_{31}H_{25}ClF_{12}N_6P_2RuS_3$ (1004.22): calcd. C 37.10, H 2.50, N 8.35, S 9.60; found C 37.10, H 2.60, N 8.25, S 9.70. − Conductivity: Λ_M(MeCN, 2 × 10^{-4} mol dm^{-3}, 20 °C) = 305 S cm^2 mol^{-1}.

$[Ru(bipy)_2(L_1)][PF_6]_2$: The compound was obtained in the same way as $[Ru(dps)_2(\mathbf{L_1})][PF_6]_2$, starting from $[Ru(bipy)_2Cl_2]\cdot 2H_2O$ (0.174 g, 0.33 mmol) and **L_1** (0.190 g, 0.882 mmol). Yield 0.153 g (50%). − Selected IR data (KBr): $\tilde{\nu}$ = 1605 vs, 1585 s, 1515 s, 1243 s, 1162 s, 1125 s, 1070 ms, 1046 ms, 850 br, 764 vs, 740 ms, 730 s, 558 vs cm^{-1}. − $C_{33}H_{29}ClF_{12}N_5P_2RuS$ (918.69): calcd. C 43.15, H 3.20, N 7.60, S 3.50; found C 43.10, H 3.30, N 7.50, S 3.55. − Conductivity: Λ_M(MeCN, 2 × 10^{-4} mol dm^{-3}, 20 °C) = 296 S cm^2 mol^{-1}.

Acknowledgments

This work was supported by the Ministero dell'Università e della Ricerca Scientifica e Tecnologica (Murst) of Italy.

[1] G. Bruno, F. Nicolò, S. Lo Schiavo, M. S. Sinicropi, G. Tresoldi, *J. Chem. Soc., Dalton Trans.* **1995**, 17−24.
[2] G. Bruno, F. Nicolò, G. Tresoldi, *Acta Crystallogr., Sect. C* **2000**, *56*, 282−283.
[3] G. Tresoldi, S. Lo Schiavo, P. Piraino, P. Zanello, *J. Chem. Soc., Dalton Trans.* **1996**, 885−892.
[4] D. C. Black, *Aust. J. Chem.* **1967**, *20*, 2101−2107.
[5] G. C. Pappalardo, A. Seminara, *J. Inorganic. Nucl. Chem.* **1976**, *38*, 1993−1995.
[6] A. Forchioni, V. Librando, G. C. Pappalardo, *J. Chem. Soc., Dalton Trans.* **1977**, 638−641.
[7] G. Tresoldi, P. Piraino, E. Rotondo, F. Faraone, *J. Chem. Soc., Dalton Trans.* **1991**, 425−430.
[8] G. Tresoldi, E. Rotondo, P. Piraino, M. Lanfranchi, A. Tiripicchio, *Inorg. Chim. Acta* **1992**, *194*, 233−241.
[9] G. De Munno, G. Bruno, E. Rotondo, G. Giordano, S. Lo Schiavo, P. Piraino, G. Tresoldi, *Inorg. Chim. Acta* **1993**, *208*, 67−75.
[10] F. Nicolò, G. Bruno, G. Tresoldi, *Acta Crystallogr., Sect. C* **1996**, *52*, 2188−2191.
[11] G. Tresoldi, S. Lo Schiavo, P. Piraino, *Inorg. Chim. Acta* **1997**, *254*, 381−385.
[12] R. Chotalia, E. C. Constable, M. J. Hannon, D. A. Thocher, *J. Chem. Soc., Dalton Trans.* **1995**, 3571−3580.
[13] M. Kakoti, A. K. Deb, S. Goswami, *Inorg. Chem.* **1992**, *31*, 1302−1304.
[14] A. Juris, V. Balzani, F. Barigelletti, S. Campagna, P. Belser, A. Von Zelewsky, *Coord. Chem. Rev.* **1988**, *84*, 85−277.
[15] A. Basu, T. G. Kasar, N. J. Sapre, *Inorg. Chem.* **1988**, *27*, 4539−4542.
[16] J. P. Collins, J. P. Sauvage, *Inorg. Chem.* **1986**, *25*, 135−141.
[17] R. Scopelliti, G. Bruno, C. Donato, G. Tresoldi, *Inorg. Chim. Acta* **2001**, *313*, 43−55.
[18] G. Binsch, H. Kessler, *Angew. Chem. Int. Ed. Engl.* **1980**, *6*, 411−428.
[19] S. D. Killops, S. A. R. Knox, *J. Chem. Soc., Dalton Trans.* **1978**, 1260 −1269.
[20] S. D. Killops, S. A. R. Knox, G. H. Riding, *J. Chem. Soc., Chem. Commun.* **1978**, 486−488
[21] E. W. Abel, D. Ellis, K. G. Orrell, *J. Chem. Soc., Dalton Trans.* **1992**, 2243−2249.
[22] E. W. Abel, P. J. Heard, K. G. Orrell, M. B. Hursthouse, M. A. Mazid, *J. Chem. Soc., Dalton Trans.* **1993**, 3795−3801.
[23] E. W. Abel, S. K. Bhargava, K. G. Orrell, *Prog. Inorg. Chem.* **1984**, *32*, 1−118.
[24] C. Chachaty, C. Pappalardo, C. G. Scarlata, *J. Chem. Soc., PerkinTrans. 2* **1976**, 1234−1238.

Received May 15, 2001
[I01170]

A Simple Example of the Fluxional Behaviour of Ruthenium-Coordinated C_2-Symmetric Monodentate Ligands − Synthesis, ^{1}H NMR Spectroscopic Study, and Crystal Structure of *cis*-[Ru(bpy)$_2$(4Pic)$_2$](PF$_6$)$_2$

Aldrik H. Velders,[a] Chiara Massera,[b] Franco Ugozzoli,[b] Marina Biagini-Cingi,[b] Anna M. Manotti-Lanfredi,[b] Jaap G. Haasnoot,[a] and Jan Reedijk*[a]

Keywords: Ruthenium / NMR spectroscopy / Nitrogen heterocycles / Fluxionality

In complexes of the type *cis*-[Ru(bpy)$_2$(L)$_2$](PF$_6$)$_2$ the fluxional behaviour (dynamics of rotation) of the monodentate heterocyclic ligands (L) in solution can be well investigated with ^{1}H NMR spectroscopy. As both the *cis*-[Ru(bpy)$_2$] moiety and the coordinated 4-picoline have a C_2 symmetry, no atropisomers of *cis*-[Ru(bpy)$_2$(4Pic)$_2$](PF$_6$)$_2$ are possible, and as a result a relatively easily understandable ^{1}H NMR spectrum is observed. The fast and slow rotation of the 4-picoline ligands have been monitored using variable-temperature 1D and 2D ^{1}H NMR spectroscopy. In addition the room temperature, solid state, X-ray structure is presented.

Introduction

The investigation of the coordinative and fluxional behaviour (dynamics of rotation) of metal-coordinated heterocyclic ligands is important for the understanding of the biological functions and activity of transition metal ions in living systems.[1,2] The solid-state and solution studies on platinum compounds with *cis* bifunctionally coordinated DNA (model) bases, have provided an enormous insight into the activity of these kinds of antitumour complexes on a molecular level.[3,4] Ruthenium complexes which are currently under investigation for their potential use as antitumour agents [2,5] are mostly octahedral six-coordinated complexes; the *cis* bifunctional coordination of heterocyclic ligands is therefore different from square-planar platinum complexes and is as yet not well understood. The ruthenium(II) antitumour complex *cis*-[Ru(dmso)$_4$Cl$_2$] was the first suitable system to study the coordinative and fluxional behaviour of *cis bis*-adducts of the type *cis*-[Ru(dmso)$_2$Cl$_2$(L)(L′)] with L and L′ being heterocyclic N-donor ligands.[6−12] The recent finding that structurally similar *cis*-dichlororuthenium(II) complexes of the type *cis*-[Ru(LL′)$_2$Cl$_2$] {in which LL′ is a chelating N-donor ligand like 2,2′-bipyridine[13] or 2-(phenyl)azopyridine[14]} show very different biological activity, inspired us to investigate in detail the coordination and the fluxional behaviour of monodentate heterocycles in the complexes of the type *cis*-[Ru(LL′)$_2$(L)$_2$](PF$_6$)$_2$.

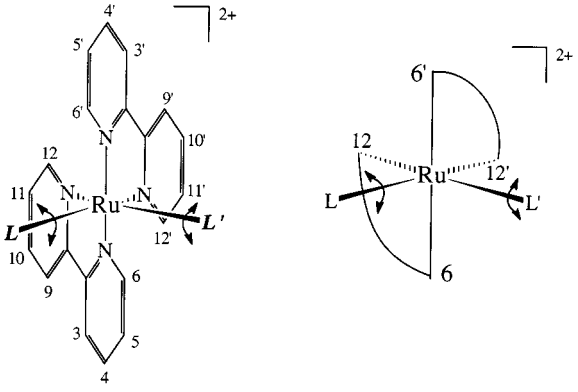

Scheme 1. Structural (left) and schematic (right) representation of the A enantiomer of the *cis*-[Ru(bpy)$_2$(L)$_2$]$^{2+}$ system and proton numbering scheme of the bpy

In the complexes *cis*-[Ru(bpy)$_2$(L)$_2$](PF$_6$)$_2$ (Scheme 1), in which the L's are imidazole-type ligands, the ligands can flip around their Ru−N axis, either fast or slowly on the NMR timescale, depending on the size of the substituents on the imidazole ring and on the temperature.[15,16] With the relatively small 1-methylimidazole (MeIm), the ^{1}H NMR spectrum of the complex shows fast rotation of the monodentate ligands at all the measured temperatures. The sterically more demanding 1,2-dimethylimidazole (Me2Im) and 1-methylbenzimidazole (MeBim) are fast rotating on the ^{1}H NMR timescale, at temperatures above room temp.,

[a] Leiden Institute of Chemistry, Gorlaeus Laboratories, Leiden University,
P. O. Box 9502, 2300 RA Leiden, The Netherlands
Fax: (internat.) + 31-71/527-4451
E-mail: reedijk@chem.leidenuniv.ni
[b] Dipartimento di Chimica Generale ed Inorganica, Chimica Analitica, Chimica Fisica, Università di Parma and Centro di Studio per la Strutturistica Diffrattometrica del C.N.R., Viale delle Scienze 78, 43100 Parma, Italy

Supporting information for this article is available on the WWW under http://www. eurjic.com or from the author.

 © WILEY-VCH Verlag GmbH, 69451 Weinheim, Germany, 2002 1434−1948/02/0101−0193 $ 17.50+.50/0

but are relatively slow rotating at temperatures below 0 °C.[15,16]

1-Methylimidazole, 1,2-dimethylimidazole, and 1-methylbenzimidazole are so-called lopsided ligands of which one site can be defined as the head (H) and the other as the tail (T). In octahedral sites, lopsided ligands can theoretically orient in 4 staggered positions, but in practice usually only one orientation is preferential. In *cis*-$[Ru(bpy)_2(L)_2](PF_6)_2$ (L = imidazole ligand) two staggered orientations are not accessible because of the steric bulk of the bidentate bpy; however, the imidazole ligands do occur in the other two orientations on the ruthenium. All the resulting four possible atropisomers have been observed and identified for the Me_2Im and MeBim complexes: two head-to-head (HH) isomers (which have the corresponding atoms of the imidazole at the same site of the N−Ru−N plane) and two head-to-tail (HT) isomers (in which the corresponding atoms of the imidazole ligands are at opposite sites of the N−Ru−N plane) (Scheme 2).[15,16] The two HT isomers, A and C, both have a twofold symmetry axis which causes the two bpy ligands and the two imidazole ligands to be identical and indistinguishable with ^{1}H NMR spectroscopy. Due to the twofold symmetry in the *cis*-$[Ru(bpy)_2]$ moiety, the hypothetical HH atropisomers, B and B′, are identical to each other; the HH orientation of the lopsided monodentate ligands causes the two bpy ligands in these atropisomers to be inequivalent, as can be observed with ^{1}H NMR spectroscopy. In general, the presence of atropisomers causes complex, but interesting spectra; therefore the use of a relatively simple system with high symmetry is important for a detailed understanding of the data.

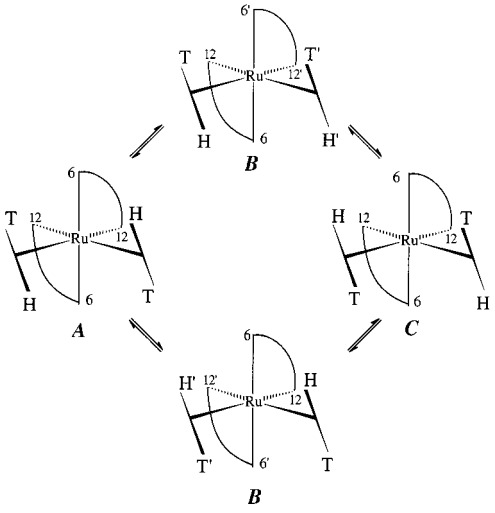

Scheme 2. Schematic representation of the 4 possible atropisomers of the A enantiomer of the *cis*-$[Ru(bpy)_2(L)_2]_2$, system. For L = 4-picoline these atropisomers all become identical

In the present study the synthesis and room temperature, solid state, X-ray structure of the high-symmetry molecule *cis*-$[Ru(bpy)_2(4Pic)_2](PF_6)_2$ (**1**) is described and the fluxional behaviour of the 4-picoline (4Pic) ligands in solution

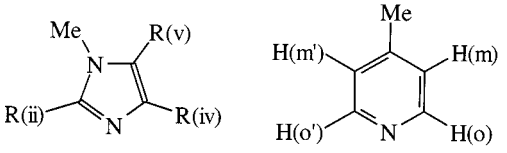

Scheme 3. Structural representation and proton numbering scheme of 1-Methylimidazoles (left) and 4-picoline (right)

is discussed. The rod-like 4Pic ligand coordinates via the N-atom, and therefore is not a lopsided ligand like the methylimidazole ligands (Scheme 3). The CH_3 groups of the 4Pic ligand rotate rapidly making the ligand rod like. Due to the three twofold symmetry axes present in complex **1** {one for the *cis*-$[Ru(bpy)_2]$ moiety and one for each Ru-picoline moiety}, no atropisomers of *cis*-$[Ru(bpy)_2(4Pic)_2](PF_6)_2$ are possible, resulting in fully interpretable ^{1}H NMR spectroscopic data.

Results and Discussion

Solid-State Structure

The *cis*-$[Ru(bpy)_2]$ moiety is chiral, and in the crystal structure of I both the A and A enantiomers have been found in the unit cell (complex A and B). In Figure 1 the molecular structure of one of the two symmetry-independent enantiomers is reported together with the atom numbering. The most significant geometrical parameters are summarized in Table 1. The structure of each enantiomer shows a six-coordinated pseudo-octahedral ruthenium ion with all ligands in a *cis* configuration. The Ru−N bond lengths for the bpy ligands in the two *cis*-$[Ru(bpy)_2(4Pic)_2]^{2+}$ moieties range from 2.042(4) to 2.084(4) Å and are significantly shorter than those involving the 4Pic ligands [2.103(4) to 2.122(4) Å]. These values are quite similar to those in *cis*$[Ru(bpy)_2(L)_2](BF_4)_2$, where

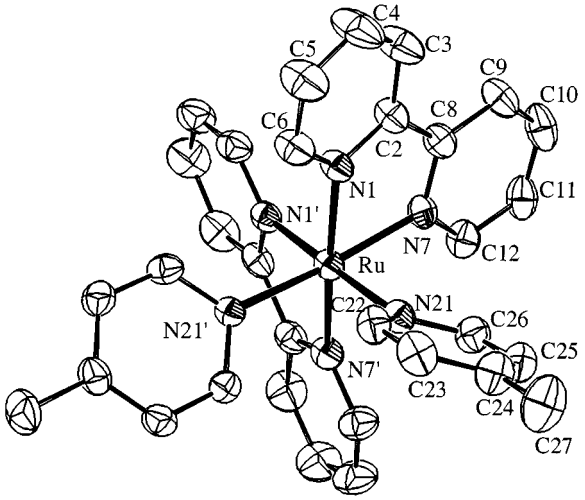

Figure 1. Thermal ellipsoid plot of one of the A enantiomers of 1. The PF_6^- anions, co-crystallised solvent molecules and protons are omitted for clarity. The view is approximately the same as in Schemes 1 and 2. Relevant data are given in Tables 1 and 2

Table 1. Selected bond lengths [Å] and bond angles [°] for the two independent complex units A and B of *cis*-$[Ru(bpy)_2(4Pic)_2](PF_6)_2$

	Complex A	Complex B
Rul−N7	2.060(4)	2.042(4)
Rul−Nl	2.084(4)	2.061(4)
Rul−Nl′	2.070(4)	2.073(4)
Rul−N7′	2.056(5)	2.053(5)
Rul−N21	2.103(4)	2.122(4)
Rul−N21′	2.104(5)	2.108(4)
N7−Rul−N1	78.7(2)	78.9(2)
Nl−Rul−N21	97.6(2)	99.1(2)
Nl′−Rul−N21	87.6(2)	85.6(2)
N7−Rul−Nl′	96.0(2)	96.2(2)
N7−Rul−N21′	90.4(2)	90.1(2)
Nl−Rul−N21′	84.9(2)	88.0(2)
Nl′−Rul−N21′	99.0(2)	98.3(2)
N21−Rul−N21′	90.6(2)	91.7(2)
N7−Ru I−N7′86.4(2)	87.1(2)	
N1−Rul−N7′	96.7(2)	94.3(2)
Nl′−Rul−N7′	79.1(2)	79.1(2)
N21−Rul−N7′	92.8(2)	91.2(2)
N7−Rul−N21	176.2(2)	177.2(2)
N1−Rul−Nl′	173.5(2)	172.1(2)
N7′−Rul−N21′	176.0(2)	175.9(2)

the Ru−N bond lengths range from 2.04 to 2.05 Å for the bpy ligands and from 2.09 to 2.10 Å for the Im ligands.[17] Labelling the bpy involving the N1 and N7 as bpy#1, that involving the Nl′ and N7′ as bpy#2, the 4-picoline involving N21 as 4Pic#1 and the 4-picoline involving the N21′ as 4Pic#2, the mean values of the dihedral angles between the least-squares plane through the ligands in the two *cis*-$[Ru(bpy)_2(4Pic)_2]^{2+}$ complexes are: 58.9(2)° (bpy#1−4Pic#1), 85.6(1)° (bpy#1−4Pic#2), 84.3(2)° (bpy#2−4Pic#1), 46.8(1)° (bpy#2−4Pic#2), 79.3(1)° (bpy#l-bpy#2) and 59.5(1)° (4Pic#1−4Pic#2).

In conclusion, in both *cis*-$[Ru(bpy)_2(4Pic)_2]^{2+}$ cations the 4Pic ligands, gauche to each other, are orthogonal only to one bpy, whereas they are tilted with respect to the other bpy on angles which range from 47 to 59°. The bond lengths and angles in the PF_6^- anions and in the acetone solvate molecule are as expected. The *cis*-$[Ru(bpy)_2(4Pic)_2]^{2+}$ cations interact with the PF_6^- anions through an array of CH···F hydrogen interactions.

Solution Structure

The ^{1}H NMR spectrum of **1** in [D_6]acetone at room temp. (Figure 2) shows a total of ten multiplet signals in the aromatic region, four doublets and four triplets of equal intensity and two doublets with an integral value twice as high as that of the other eight multiplets. All resonances could be assigned as shown in Figure 2 on the basis of COSY and NOESY spectra (see Supplementary Material), in a similar way as has been described for the analogous imidazole complexes.[15,16] The fact that the two H(*ortho*) protons [and the two H(*meta*) protons] resonate at the same frequency, indicates that the picolines rotate fast on the NMR timescale around their Ru−N axes. Upon lowering the temperature, the eight bpy signals show a small down-field shift, but remain sharp multiplets over the whole temperature range measured. In contrast, the two 4Pic doublets H(*ortho*) and H(*meta*), at δ = 8.4 and 7.3, respectively, first start broadening on lowering the temperature and finally, both, split up in two doublets at −90 °C separated by 56 and 27 Hz, respectively (Figure 2).

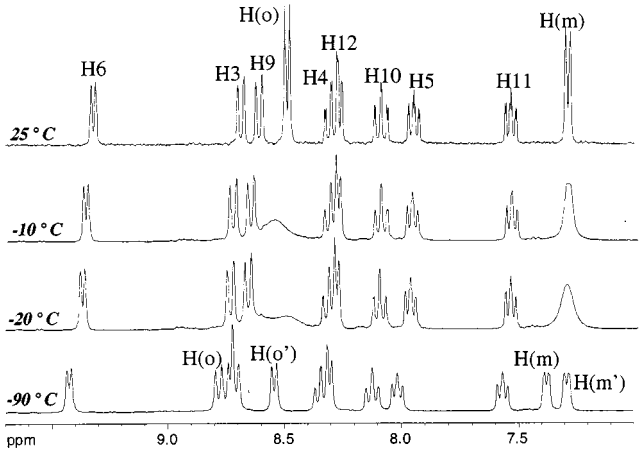

Figure 2. Aromatic region of the ^{1}H NMR spectra of I in [D_6]acetone at room temp., −10, −20, and −90 °C

The fact that the four aromatic 4-picoline protons have become inequivalent at low temperatures, whilst the two bpy ligands and the two picoline ligands remain indistinguishable, indicates that the 4Pic ligands slowly flip by 180° between two orientations, on the NMR timescale, and all four atropisomers depicted in Scheme 2 are present. Due to the symmetries present in the system (which makes the four atropisomers identical and thus indistinguishable) only a total of 12 resonances are found in the aromatic region of the spectrum.

2D NMR techniques like NOESY and **ROESY** are powerful methods for accurately determining the orientation of monodentate ligands in atropisomers and their rotational behaviour (via interligand NOE cross-peaks and exchange cross-peaks). In Figure 3 the aromatic region of a **ROESY** spectrum of I is shown and the most characteristic interligand cross-peaks are indicated. The most down-field shifted H(*ortho*) doublet shows a NOE cross-peak with the bpy H6, as well as the H12 (of the other bpy!) indicating this resonance belonging to the H(o) proton, which is wedged in between the two bpy ligands. The NOE cross-peak of the other H(*ortho*) doublet, H(o′), with only the H6 resonance confirms the assignment of this peak to the 4Pic H(o′) proton which is oriented in between a bpy and the other picoline. The relative down-field shift of the H(o) with respect to the H(o′) signal is nicely explained by the stronger deshielding the former protons experience with respect to the latter. In Figure 4, a space-filling model of I clearly shows the H(o) proton to be wedged in between the two bpy ligands, but not above the (shielding) aromatic pyridine rings. The H(o′) proton is situated close to one bpy on the opposite site with respect to where the H(o) of the other 4Pic is positioned, but in addition, this proton is oriented just above the aromatic ring of the neighbouring pico-

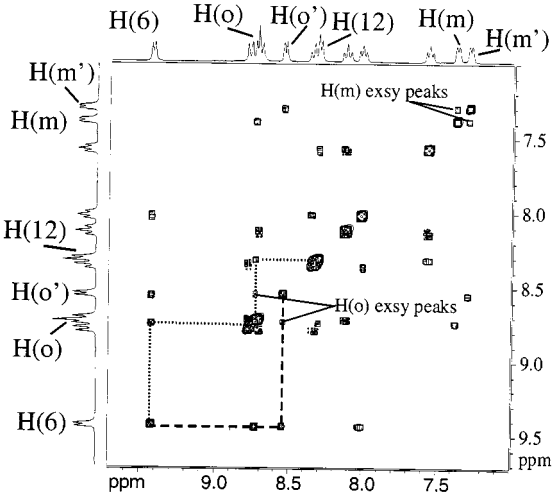

Figure 3. Positive (EXSY) and negative (NOE) level of the aromatic region of the **ROESY** spectrum of I in [D_6]acetone at −100 °C, recorded with a mix time of 500 ms. The H(o)−H6 and H(o)−H12, and the H(o′)−H12 NOE cross-peaks are indicated with a dotted and dashed line, respectively. The observed exchange peaks are between the H(o) and H(o′), and the H(m) and H(m)′ resonances

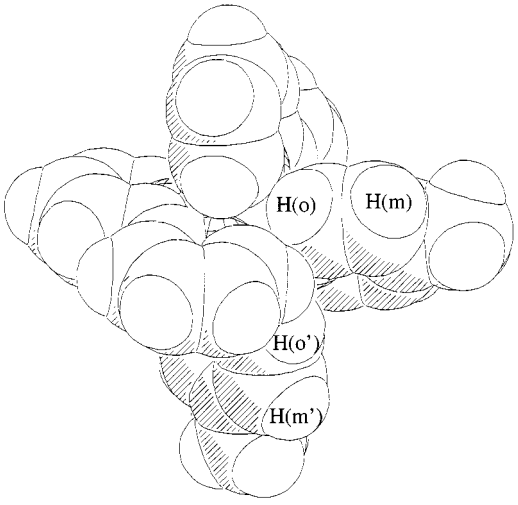

Figure 4. Space-filling representation of the solid state molecular structure of the A enantiomer of the cation of 1. The H(o) proton is clearly wedged in between the H6 site of one bpy and the H12 site of the other bpy, whilst the H(o′) proton is close to the pyridine rings of a bpy as well as the neighbouring 4-picoline

line ligand, which nicely supports the explanation of the relative upfield shift of 0.2 ppm of this proton. However, the solution and solid state orientations of the ligands should, by no means, be considered to be the same by default.

Although the VT ^{1}H NMR spectroscopic data indicate the slowing down of the rotation of the picolines around their Ru−N axes at lower temperatures, the ligands do not stand still on the NMR timescale at the lowest temperature investigated (−100 °C). In Figure 3 the exchange level of the ROESY spectrum is shown in which clear cross peaks are present between the two H(*ortho*) proton signals, H(o) and H(o′), of the picoline and also between the two H(*meta*) proton resonances, H(m) and H(m′). The picoline thus exhibits a greater fluxionality than the bulky MeBim and Me2Im ligands in the analogous complexes, that only show exchange cross-peaks at higher temperatures.[15,16] In practice this means that the four atropisomers of I can interchange even at temperatures as low as −90 to −100 °C, albeit slow on the NMR timescale. Picoline is obviously less hindered in its rotation around its Ru−N axis than are the bicyclic MeBim or the Me2Im in the $[Ru(bpy)_2(L)_2]^{2+}$ complexes. On the other hand, the VT NMR spectroscopic data of the 4Pic complex clearly show a slow rotation of the monodentate ligands at lower temperatures, whereas the MeIm complex does not reach the stage of slow rotation under the same conditions. Assuming the ruthenium(II)−nitrogen bonds to be similar in picoline and imidazole complexes, the six-membered ring ligand has its protons *ortho* to the coordinating nitrogen lying closer to the coordination plane than the analogous protons, H(ii) and H(iv), in the heterocyclic five-membered ring. As there are no electrostatic effects expected to influence the orientational and fluxional behaviour of the monodentate ligands in the complex *cis*-$[Ru(bpy)_2(L)_2](PF_6)_2$, the differences observed for complexes with different ligands can be attributed mainly to steric differences. For the above mentioned monodentate ligands the order of steric hindrance in these complexes is found to be:

$$\text{MeIm} < \text{4Pic} < \text{Me2Im} = \text{MeBim}$$

From the atropisomerisation study on the imidazole complexes,[15,16] it is reasonable to assume that the interconversion of the 4 rotamers of I occurs by the flipping of one picoline at a time, by 180°. As all the 4 rotamers are identical, the rate of the back and forward flipping of one picoline between two rotamers is the same. This facilitates the determination of the thermodynamic parameters, because the atropisomerisation process of **1** can now be regarded as a simple dynamic system with 2-site mutual exchange, i.e. two identical compounds interconverting into each other by the flipping of one picoline ligand. Using the temperatures (T_c and the rate constants (k_c) determined at the coalescence points of the H(*ortho*) signals (235 K, 124 s^{-1}) and the H(*meta*) signals (225 K, 60 s^{-1}), from the Eyring equation,[18] the consecutively determined free energy of activation $\Delta G^{\#}$ for the picoline rotation in I is 48 kJ·mol^{-1}, the free enthalpy of activation, $\Delta H^{\#}$, is 30 kJ·mol^{-1}, and the free entropy of activation, $\Delta S^{\#}$, is −75 J·K^{-1}·mol^{-1}. The Arrhenius activation energy E_A is found to be 32 kJ mol^{-1}.

Conclusion

The *cis*-$[Ru(bpy)_2Cl_2]$ complex has been investigated for its binding properties to DNA[13,19] and DNA model bases[20] and appears to be a borderline complex with respect to monofunctional or bifunctional coordination to DNA purines. The restricted rotational behaviour of lopsided methylimidazole ligands in *cis*-$[Ru(bpy)_2(L)_2](PF_6)_2$ has confirmed the steric hindrance of the bidentate ligands with

incoming N-heterocycles.[15,16] In the present study the *cis*-$[Ru(bpy)_2(4Pic)_2](PF_6)_2$ complex is shown to be a relatively simple, but very interesting system in the investigation of the fluxional behaviour of heterocyclic monodentate ligands on octahedral complexes. The differences in fluxional behaviour between the heterocyclic six-membered ring 4Pic and the five-membered ring MeIm ligands as observed with VT NMR spectroscopy in the complexes *cis*-$[Ru(bpy)_2(L)_2](PF_6)_2$ emphasise that the coordinative behaviour of heterocyclic ligands, on six-coordinated complexes like ruthenium is influenced by small differences in steric properties. In addition, the high symmetry complex **1** has allowed for relatively easy determination of the thermodynamic parameters of the fluxional behaviour of such complexes.

Experimental Section

General Remarks: NMR: Bruker DPX 300 MHz spectrometer. For [D_6]acetone as solvent, δH = 2.06, between −90 °C and +50 °C. NOESY[21] and ROESY[22,23] spectra with mixing times of 1.0 s and 0.5 s, respectively, were obtained using the Bruker pulse programs. Hydrated $RuCl_3$ was used as received from Johnson Matthey Inc. 2,2-Bipyridine (Fluka), 4-picoline (Merck) were used without further purification. *cis*-$[Ru(bpy)_2Cl_2]\cdot 2H_2O$ was prepared according to a literature procedure.[24]

***cis*-$[Ru(bpy)_2(4Pic)_2](PF_6)_2$ (1):** Preparation was performed by a method slightly different from that reported by Henderson et al.[25] *cis*-$[Ru(bpy)_2Cl_2]\cdot 2H_2O$ (0.26 g, 0.5 mmol) and 4-picoline (0.5 g, ca 5 mmol) in 50 mL of water were refluxed for 3 hours. At room temperature the reaction mixture was filtered and to the clear red solution a concentrated aqueous solution of NH_4PF_6 (1.6 g, 10 mmol) was added. The formed precipitate was isolated by filtration and washed with water. After recrystallisation from acetone/water, complex I was obtained as an orange red microcrystalline powder that was isolated by filtration and washed with diethyl ether. Yield: 0.30 g (75%), characterisation by NMR spectroscopy and elemental analyses. Recrystallisation from acetone/water yielded red crystals suitable for X-ray diffraction study. Because of the photolability of complex I the NMR samples were stored in the dark.

X-ray Crystallographic Study: Data were collected on a Bruker SMART diffractometer equipped with graphite monochromated Mo-K_α radiation source (λ = 0.71073 Å) and a CCD detector. The frames data were processed to give structure factors using the program SAINT.[26] The crystal data and the most relevant experimental parameters used in the X-ray measurements and in the crystal structure analyses are reported in Table 2. The phase problem was solved by Direct Methods by using SIR92[27] that revealed two independent complex molecules of formula $C_{32}H_{30}F_{12}N_6P_2Ru$ and one acetone solvent molecule in the asymmetric unit. Atomic coordinates and anisotropic thermal parameters were refined by blocked full-matrix least-squares methods on F^2 using the SHELXL-97 program.[28] The hydrogen atoms were placed at their calculated positions with the geometrical constraint C−H 0.96 A and refined "riding" on their corresponding carbon atoms. The final molecular geometry was analysed with the program PARST97.[29] All calculations were carried out on the DEC Alpha 250 workstation at the Centro di Studio per la Strutturistica Diffrattometrica of C.N.R., Parma. Crystallographic data (excluding structure factors) for the structure reported in this paper have been deposited with the Cambridge Crystallographic Data Centre as supplementary publication no. CCDC-143552. Copies of the data can be obtained free of charge on application to CCDC, 12 Union Road, Cambridge CB2 1EZ, UK [Fax: (internat.) +44−1223/336-033; E-mail: deposit@ccdc.cam.ac.uk].

Table 2. Crystallographic data and experimental details for the complex *cis*-$[Ru(bpy)_2(4Pic)_2](PF_6)_2$

Crystal data	
Empirical formula	$C_{67}H_{66}F_{24}N_{12}OP_4Ru_2$
Molecular mass	1837.335
Crystal size [mm]	0.4 × 0.3 × 0.4
Crystal system	triclinic
Space group	$P\bar{1}$
a [Å]	11.013(5)
b [Å]	14.020(5)
c [Å]	27.143(5)
α [°]	92.39(2)
β [°]	100.63(2)
γ [°]	110.10(2)
V [Å^3]	3843(2)
Z	2
d (calcd.) [gcm^{-3}]	1.588
F(000)	1848
Data collection	
T [K]	295
Index ranges	$-12 \le h \le 12$, $-15 \le k \le 15$, $-30 \le l \le 30$
Reflections collected	18829
Independent refections	10639 (R_{int} = 0.021)
Observed reflections	7910 [$F_o \ge 4\sigma(F_o)$]
Structure refinement	
Data/restraints/parameters	10639/0/1000
Weighting scheme	$w = [(\sigma^2(F_o^2) + (0.2P)^2]^{-1}$ where $P = (F_o^2 + 2F_c^2)/3$
Goodness-of-fit on F^2 [a]	0.664
Final R indices (obs. data)	$R1$ = 0.0496, $wR2$ = 0.150
R indices (all data)	$R1$ = 0.0662, $wR2$ = 0.168
Largest diff. Peak and hole [e/Å^3]	0.75, −0.70

[a] $R1 = \Sigma||F_o| - |F_c||/\Sigma|F_o|$, $wR2 = [\Sigma w(F_o^2 - F_c^2)^2/\Sigma wF_o^4\ ]^{1/2}$. Goodness-of-fit = $[\Sigma w(F_o^2 - F_c^2)^2/(n-p)]^{1/2}$, where n is the number of reflections and p the number of parameters.

Acknowledgments

The authors thank Johnson & Matthey (UK) for their generous loan of $RuCl_3\cdot 3H_2O$. This research is sponsored by the Council of Chemical Sciences of the Netherlands Organization for Scientific Research (NWO), and also support by COST Action D8/0017/97 (Metals in medicine) is kindly acknowledged. The authors wish to thank the Italian MURST and the Italian C. N. R. (Roma) for the financial support to this work.

[1] S. J. Lippard, J. M. Berg, *Principles of Bioinorganic Chemistry*, University Science Books, Mill Valley, California, **1994**.
[2] Z. Guo, P. J. Sadler, *Angew. Chem. Int. Ed.* **1999**, *38*, 1512.

[3] B. Lippert, *Cisplatin, Chemistry and Biochemistry of a Leading Anticancer Drug* Verlag Helvetica Chimica Acta, Zurich, Wiley-VCH, Weinheim, **1999**.
[4] J. Reedijk, *Chem. Commun.* **1996**, 801.
[5] M. J. Clarke, F. Zhu, D. R. Frasca, *Chem. Rev.* **1999**, *99*, 2511.
[6] E. Alessio, Y. H. Xu, S. Cauci, G. Mestroni, F. Quadrifoglio, P. Viglino, L. G. Marzilli, *J. Am. Chem. Soc.* **1989**, *111*, 7068.
[7] E. Alessio, L. Hansen, M. Iwamoto, L. G. Marzilli, *J. Am. Chem. Soc.* **1996**, *118*, 7593.
[8] E. Alessio, M. Calligaris, M. Iwamoto, L. G. Marzilli, *Inorg. Chem.* **1996**, *35*, 2538.
[9] E. Alessio, E. Zangrando, R. Roppa, L. G. Marzilli, *Inorg. Chem.* **1998**, *37*, 2458.
[10] L. G. Marzilli, M. Iwamoto, E. Alessio, L. Hansen, M. Calligaris, *J. Am. Chem. Soc.* **1994**, *116*, 815.
[11] L. G. Marzilli, P. A. Marzilli, E. Alessio, *Pure & Appl. Chem.* **1998**, *70*, 961.
[12] M. Iwamoto, E. Alessio, L. G. Marzilli, *Inorg. Chem.* **1996**, *35*, 2384.
[13] O. Nováková, J. Kaspárková, O. Vrána, P. M. van Vliet, J. Reedijk, V. Brabec, *Biochemistry* **1995**, *34*, 12369.
[14] A. H. Velders, H. Kooijman, A. L. Spek, J. G. Haasnoot, D. de Vos, J. Reedijk, *Inorg. Chem.* **2000**, *39*, 2966.
[15] A. H. Velders, A. C. G. Hotze, J. G. Haasnoot, J. Reedijk, *Inorg. Chem.* **1999**, *38*, 2762.
[16] A. H. Velders, A. C. G. Hotze, G. A. van Albada, J. G. Haasnoot, J. Reedijk, *Inorg. Chem.* **2000**, *39*, 4073.
[17] K. B. Reddy, M.-O. P. Cho, J. F. Wishart, T. J. Emge, S. S. Isied, *Inorg. Chem.* **1996**, *35*, 7241.
[18] H. Friebolin, *Basic One- and Two-dimensional NMR Spectroscopy*, VCH-Verlagsgesellschaft, Weinheim, **1991**.
[19] N. Grover, N. Gupta, H. H. Thorp, *J. Am. Chem. Soc.* **1992**, *114*, 3390.
[20] P. M. Van Vliet, J. G. Haasnoot, J. Reedijk, *Inorg. Chem.* **1994**, *33*, 1934.
[21] S. Macura, R. R. Ernst, *J. Mol. Phys.* **1980**, *41*, 95.
[22] T. L. Hwang, *J. Am. Chem. Soc.* **1992**, *114*, 3157.
[23] T. L. Hwang, *Magn. Reson. Chem.* **1992**, *30*, S24.
[24] B. P. Sullivan, D. J. Salmon, T. J. Meyer, *Inorg. Chem.* **1978**, *17*, 3334.
[25] L. J. Henderson Jr., M. Ollino, V. K. Gupta, G. R. Newkome, W. R. Cherry, *J. of Photochemistry* **1985**, *31*, 199.
[26] Siemens: *Area Detector Control Integration Software,* version 4.0 in SMART and SAINT, Siemens Analytical X-ray Instruments Inc., Madison, Winsconsin, **1996**.
[27] A. Altomare, M. C. Burla, M. Camalli, G. Cascarano, C. Giacovazzo, A. Guagliardi, G. Polidori, *J. App. Crystallogr.* **1994**, *27*, 435.
[28] G. M. Sheldrick, SHELXL-97, *Program for Crystal Structure Refinement*, University of Göttingen, **1997**; http://shelx.uni-ac.gwdg.de/she1x/index.html.
[29] M. Nardelli, *J. Appl. Crystallogr.* **1995**, *28*, 659.

Received June 26, 2001
[I01230]

Novel Monodentate Phosphoramidites By Chiral Pool Synthesis Starting from D-Mannitol, and Their Pd^{II} and Rh^{I} Complexes

Alexander Bayer,[a] Ulf Thewalt,[b] and Bernhard Rieger*[a]

Keywords: Asymmetric synthesis / Chiral pool / Rhodium / P ligands / Palladium

The new monodentate phosphoramidites **6a**–**e** were prepared in an ex-chiral-pool synthesis from readily available D-mannitol in high yields. A ring opening of 1,2;5,6-dianhydro-3,4-*O*-isopropylidene-D-mannitol (**4**) with nucleophiles provides the chiral diols **5a**–**e** with different steric demand as key intermediates. The ligands **6a**–**e** are synthesized by refluxing **5a**–**e** with hexamethyltriaminophosphane (HMTAP) and lead, after treatment with $[PdCl_2(COD)]$ or $[Rh(COD)_2][SO_3CF_3]$, to the corresponding Pd complex **8a** and rhodium(I) complexes **7a**–**e**, respectively. The *cis*-arrangement of the ligands and the C_2-symmetry of the complexes in the solid state is demonstrated by an X-ray structure investigation performed on **8a**. In addition, variable temperature NMR experiments show that **8a** keeps its C_2-symmetric coordination geometry even at temperatures up to 90 °C (decomposition).

Introduction

Worldwide activity in the development of C_2-symmetric, bridged bisphosphane complexes for asymmetric catalyzed reactions began in the late 1970's and continued strongly until the end of the 1980's. Then, major emphasis was spent on the development of biocatalysts for catalytic organic transformations. It is well known that both enzymes and organometallic complexes occupy their own specific catalytic field. In organometallic chemistry bidentate ligands were supposed to be superior to the monodentate ones as the resulting rigidity of the catalysts favors effective chiral induction.[1] Consequently, monodentate ligands were neglected in asymmetric hydrogenations until Pringle et al. questioned the superiority of bidentate structures. These authors found higher enantioselectivities (92% *ee*) using an asymmetric monophosphonite rather then the corresponding C_2-symmetric diphosphonite in the hydrogenation of methyl-2-acetamido acrylate.[2] Excellent enantioselectivities (>99% *ee*) have also been reported with monodentate phosphites[3] and phosphoramidites,[4,5] inducing a renaissance in the investigation of monodentate ligands of the above type. However, a disadvantage of these species is their limitation to the binaphthol backbone, which does not allow a rational catalyst design.

We report here on a straightforward and highly variable synthetic protocol based on an ex-chiral-pool synthesis starting from D-mannitol[6] to generate monodentate phosphoramidites bearing four stereogenic centers. This approach allows us to introduce a variety of substituents with different steric demand at key positions at the stereogenic centers by using selected nucleophiles in epoxide ring-opening reactions. The structure and dynamic behavior of the corresponding Pd^{II} and Rh^{I} complexes was investigated by a combination of X-ray diffraction in the solid state and variable temperature NMR spectroscopy in solution.

Results and Discussion

The starting material for our synthetic strategy is the commercially available and cheap D-mannitol (**1**), which was converted into the 1,2;3,4;5,6-tri-*O*-isopropylidene derivative (**2**). Subsequent acidic cleavage of two protecting groups yielded the 3,4-*O*-isopropylidene-D-mannitol (**3**) selectively.[7,8] 1,2;5,6-Dianhydro-3,4-*O*-isopropylidene-D-mannitol (**4**) was prepared from **3** in a simple one pot synthesis according to a literature procedure.[9] The stereoisomer 1,2;5,6-dianhydro-3,4-*O*-isopropylidene-L-iditol,[7] with a different configuration at carbon atoms C2 and C5, is also available and provides access to additional chiral diols. Ring-opening reactions using organolithium or Grignard compounds afford the chiral key-diols **5a**−**e**. Nucleophilic attack of $LiAlH_4$ opens the epoxide ring to form (2*R*,3*R*,4*R*,5*R*)-3,4-*O*-isopropylidene-2,3,4,5-hexanetetraol (**5a**).[10] Compounds **5b**−**e** were prepared by treatment with organocuprates − generated from the copper(I) bromide−dimethyl sulfide complex − and the correspond-

[a] Department of Inorganic Chemistry II, Materials and Catalysis, University of Ulm
Albert-Einstein-Allee 11, 89069 Ulm, Germany
Fax: (internat.) + 49-731/502-3039
E-mail: bernhard.rieger@chemie.uni-ulm.de
[b] Section for X-ray- and electron diffraction, University of Ulm
Albert-Einstein-Allee 11, 89069 Ulm, Germany

 © WILEY-VCH Verlag GmbH, 69451 Weinheim, Germany, 2002 1434−1948/02/0101−0199 $ 17.50+.50/0

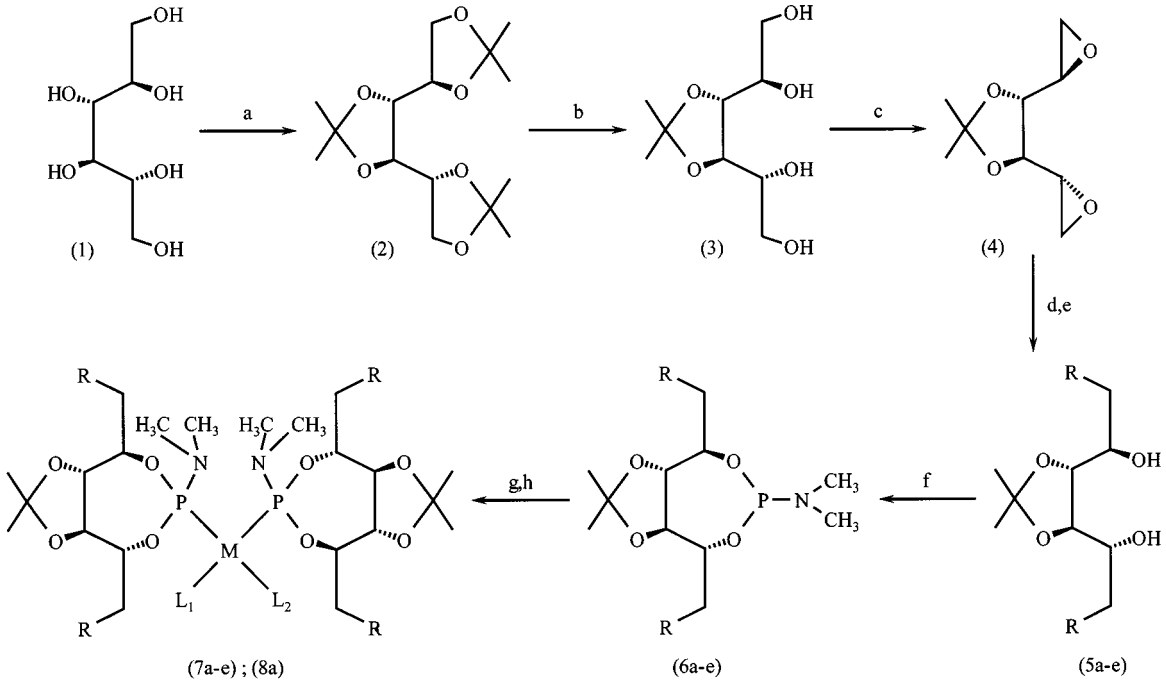

Figure 1. a) acetone, H_2SO_4; b) AcOH, H_2O, 40 °C; c) (i) trimethyl orthoacetate, PPTS, (ii) NEt_3, AcBr, (iii) K_2CO_3, MeOH; d) $LiAlH_4$, Et_2O, R = H; e) CuBr·SMe_2, RMgBr, THF/Et_2O, −40 °C, R = CH_3, C_2H_5, i-C_4H_9, C_6H_5; f) HMTAP, toluene, reflux; g) $Rh^I(COD)_2(SO_3CF_3)$, CH_2Cl_2, **7a**−**e**: M = Rh, L_1-L_2 = COD; h) $Pd^{II}(COD)Cl_2$, CH_2Cl_2, **8a**: M = Pd; L_1,L_2 = Cl

ing alkyl- or phenylmagnesium bromides in diethyl ether.[11] The monodentate phosphoramidites (**6a**−**e**) were formed in high yields by refluxing **5a**−**e** and HMTAP in toluene (Figure 1).

The corresponding yellow-orange Rh^I complexes **7a**−**e** and the pale yellow Pd^{II} complex **8a** were prepared by stirring two equivalents of monodentate ligand **6a**−**e** with $[Rh(COD)_2][SO_3CF_3]$ or $[PdCl_2(COD)]$ in dichloromethane.

We were not able to obtain suitable crystals of one of the rhodium(I) complexes for X-ray diffraction, but we succeeded in crystallizing the isoelectronic Pd^{II} species **8a** from methanol. Its X-ray structure clearly shows the *cis*-coordination of the two monodentate phosphoramidite ligands **6a** and the expected square-planar coordination environment of Pd^{II} (Figure 2a, Table 1) with a chiral, C_2-symmetric arrangement of both P ligands (Figure 2b).

No sign of other diastereomers (rotamers) could be found, indicating a stable chiral conformation, at least in the solid state. The side-view (Figure 2b) furthermore shows that the tunable substituents (Figure 1, CH_2−R) of the monodentate phosphoramidites (Figure 2, R = H; C1, C10) occupy the top-left and bottom-right quadrants, thus defining a chiral cage around the metal center, the size of which is determined by the nucleophile used for the epoxide ring-opening. Quadrant diagrams have often been used to explain the achieved enantioselectivity with several known asymmetric diphosphane-rhodium catalysts in hydrogenations. Knowles suggested to use X-ray structures to predict the absolute configuration of hydrogenation products from the chiral cage of the catalyst.[12] We are looking forward to check these predictions in applying **7a**−**e** in the asymmetric hydrogenation of prochiral olefins. The rigidity of the C_2-symmetric ligand arrangement in solution is further supported by variable temperature ^{31}P NMR spectroscopy. The spectra of **8a** show a sharp singlet at δ = 102.49, which remains unaltered between −30 °C and +90 °C (decomposition). The Rh^I complexes **7a**−**e** have ^{31}P NMR spectra with a single sharp doublet. Variable temperature NMR experiments performed on **7a** show an unaltered signal at δ = 118.92 between −30 °C and +60 °C, which again indicates the presence of a single isomer. At higher temperatures a second doublet grows at δ = 86.67, which could be due to a further complex species. This second species undergoes decomposition, as we noticed from a NMR measurement the next day, while the initial Rh^I complex is still present.

Conclusion

We have introduced an efficient, ex-chiral-pool synthetic route to a new family of chiral, monodentate phosphorus ligands with different steric demand. Their corresponding C_2-symmetric Rh^I and Pd^{II} complexes bear two *cis*-arranged ligands both in the solid state and in solution. In addition, the complexes are thermally stable up to 60 and 90 °C, respectively. Due to the variability of the ligand synthesis, changes of the configuration of the stereogenic cen-

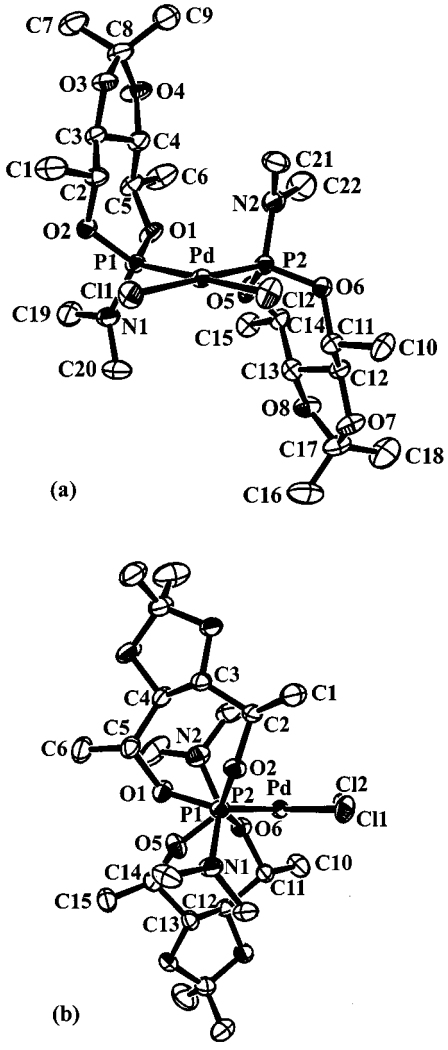

Figure 2. Molecular structure of **8a**; (a) front view: square-planar environment of Pd^{II}; (b) side view: C_2-symmetric arrangement; hydrogen atoms have been omitted for clarity

ters (Figure 2, C2, C5 and C11, C14) and modifications of their substitution can easily be introduced. This is a prerequisite for adopting the catalysts to new substrates in asymmetric transformations. Investigations on this topic are underway.

Experimental Section

General Remarks: All reactions and manipulations were performed using standard Schlenk techniques. The reagents were obtained from Aldrich, Fluka, Merck and Strem and used without purification. Diethyl ether, tetrahydrofuran, toluene and pentane were distilled from $LiAlH_4$, dichloromethane was distilled from CaH_2 under nitrogen.

Melting points were determined on a Büchi Melting Point B-540 and are uncorrected. Optical rotation was obtained on a POLARmonitor from IBZ Messtechnik. Elemental analyses were carried out on a Elementar Vario EL. Mass spectrometry was performed on a Finnigan MAT, TSQ 7000 (FAB, matrix: 2-nitrophenyloctyl ether) and a Finnigan MAT, SSQ 7000 (CI: CH_4. EI: 70 eV). ^1H, ^{13}C, and ^{31}P NMR spectra were recorded on Bruker DRX 400 spectrometer. Chemical shifts are reported in ppm downfield from tetramethylsilane with the solvent as the internal standard or 85% H_3PO_4 as the external standard.

Table 1. Selected bond lengths [Å] and angles [°] in **8a**

Bond lengths			
Pd−Cl1	2.3461(9)	C1−C2	1.500(4)
Pd−Cl2	2.3416(10)	C2−C3	1.510(4)
Pd−P1	2.2462(9)	C3−C4	1.507(4)
Pd−P2	2.2360(9)	C4−C5	1.519(4)
P1−O1	1.592(2)	C5−C6	1.503(5)
P1−O2	1.6082(18)	C7−C8	1.495(5)
P1−N1	1.620(3)	C8−C9	1.513(5)
N1−C19	1.474(4)	O3−C3	1.419(3)
N1−C20	1.461(4)	O3−C8	1.438(4)
O1−C5	1.459(3)	O4−C4	1.422(4)
O2−C2	1.462(3)	O4−C8	1.447(4)
Bond angles			
Cl1−Pd−Cl2	88.90(3)	C1−C2−C3	113.4(2)
P1−Pd−Cl1	86.92(3)	C2−C3−C4	115.7(2)
P1−Pd−P2	93.05(3)	C2−C3−O3	111.3(2)
P2−Pd−Cl2	91.16(3)	C3−O3−C8	105.7(2)
P1−Pd−Cl2	175.49(3)	O3−C3−C4	101.7(2)
P2−Pd−Cl1	179.10(3)	O3−C8−C7	107.7(3)
Pd−P1−O1	117.44(8)	O3−C8−C9	110.1(3)
Pd−P1−O2	112.22(7)	O3−C8−O4	105.8(2)
Pd−P1−N1	113.58(9)	C7−C8−C9	114.3(3)
O1−P1−O2	103.26(11)	C7−C8−O4	110.4(3)
O1−P1−N1	103.78(13)	C9−C8−O4	108.2(3)
O2−P1−N1	105.27(13)	C8−O4−C4	107.1(2)
P1−N1−C19	120.8(2)	O4−C4−C5	111.3(2)
P1−N1−C20	122.9(2)	O4−C4−C3	101.1(2)
C19−N1−C20	116.2(3)	C3−C4−C5	116.4(3)
P1−O1−C5	129.59(18)	C4−C5−C6	113.8(3)
P1−O2−C2	121.45(18)	C4−C5−O1	108.4(2)
C1−C2−O2	108.6(3)	O1−C5−C6	105.8(2)
C3−C2−O2	104.1(2)		

Synthesis of Chiral Diols 5a−e: The diols **5a** and **5b** were prepared according to known procedures.[10,11]

General Procedure for the Synthesis of 5c−e: $CuBr{\cdot}SMe_2$ (3 mmol) was added to a stirred suspension of the appropriate alkyl- or phenylmagnesium bromide (120 mmol) in diethyl ether (100 mL) at −40 °C. After stirring at −40 °C for 2 h, **4** (30 mmol) in 30 mL tetrahydrofuran was added. After 1 h stirring at room temperature the mixture was poured into a saturated aqueous NH_4Cl solution. The organic layer was extracted, washed with water, dried over Na_2SO_4 and the solvents evaporated to dryness to give the pure products **(5c−e)** after flash chromatography (eluting with hexane/EtOAc; 7:3).

(4*R*,5*R*,6*R*,7*R*)-5,6-*O*-isopropylidene-4,5,6,7-decanetetraol (5c): Oil. Yield: 6.78 g, 91.8%. $[\alpha]_D^{23} = +25.8$ ($c = 1.0$, $CHCl_3$). ^1H NMR (400 MHz, $CDCl_3$): δ = 3.61−3.59 (m, 2 H, CH), 3.55−3.49 (m, 2 H, CH), 1.74−1.66 (m, 2 H, CH_2), 1.58−1.45 (m, 2 H, CH_2), 1.45−1.33 (m, 4 H, CH_2), 1.32 (s, 6 H, CH_3), 0.91 (t, 6 H, CH_3). ^{13}C NMR: δ = 108.67, 83.24, 72.88, 36.34, 26.85, 18.26, 14.00. MS (CI): $MH^+ = 391$ (+MSTFA). $C_{13}H_{26}O_4$ (246.3): calcd. C 63.39, H 10.64; found C 62.68, H 10.60.

(5*R*,6*R*,7*R*,8*R*)-6,7-*O*-isopropylidene-2,11-dimethyl-5,6,7,8-dodecanetetraol (5d): Oil. Yield: 8.63 g, 95.1%. $[\alpha]_D^{24}$ = +29.2 (*c* = 1.0, $CHCl_3$). ^1H NMR (400 MHz, $CDCl_3$): δ = 3.65−3.63 (m, 2 H, CH), 3.55−3.48 (m, 2 H, CH), 1.80−1.71 (m, 2 H, CH_2), 1.60−1.50 (m, 2 H, CH_2), 1.44−1.35 (m, 4 H, CH_2), 1.34 (s, 6 H, CH_3), 1.28−1.18 (m, 2 H, CH), 0.89−0.86 (m, 12 H, CH_3). ^{13}C NMR: δ = 108.72, 83.16, 73.48, 34.20, 32.06, 28.11, 26.90, 22.81, 22.38. MS (CI): MH^+ = 447 (+MSTFA). $C_{17}H_{34}O_4$ (302.5): calcd. C 67.51, H 11.33; found C 66.37, H 10.97.

(2*R*,3*R*,4*R*,5*R*)-3,4-*O*-Isopropylidene-1,6-diphenyl-2,3,4,5-hexanetetraol (5e): Oil. Yield: 9.20 g, 89.6%. $[\alpha]_D^{23}$ = +43.2 (*c* = 1.0, $CHCl_3$). ^1H NMR (400 MHz, $CDCl_3$): δ = 7.33−7.20 (m, 10 H, $CH_{arom.}$), 3.82−3.72 (m, 4 H, CH), 3.18−3.13 (m, 2 H, CH_2), 2.74−2.68 (m, 2 H, CH_2), 1.48 (s, 6 H, CH_3). ^{13}C NMR: δ = 137.66, 129.68, 128.39, 126.42, 109.02, 82.34, 73.54, 40.26, 26.93. MS (CI): MH^+ = 343 (+MSTFA). $C_{21}H_{26}O_4$ (342.4): calcd. C 73.66, H 7.65; found C 72.56, H 7.63.

General Procedure for the Synthesis of 6a−e: Chiral diols **5a−e** (6.5 mmol), HMTAP (8.23 mmol) and 10 mg NH_4Cl were refluxed in toluene for 7 h. The mixture was concentrated under reduced pressure affording an oil. The oil was stirred in a small amount of diethyl ether, after which crystals formed.

(4*R*,5*S*,6*S*,7*R*)-5,6-*O*-Isopropylidene-2-dimethylamino-4,7-dimethyl-1,3,2-dioxaphosphepane-5,6-diol (6a): Yield: 1.66 g, 97.2%; m.p. 70 °C. $[\alpha]_D^{23}$= +10.2 (*c* = 1.0, $CHCl_3$). ^1H NMR (400 MHz, $CDCl_3$): δ = 3.95−3.85 (m, 3 H, CH), 3.53−3.48 (m, 1 H, CH), 2.58 (s, 3 H, N−CH_3), 2.56 (s, 3 H, N−CH_3), 1.38 (d, 3 H, CH_3), 1.34 (s, 6 H, CH_3), 1.33 (d, 3 H, CH_3). ^{13}C NMR: δ = 109.30, 83.72, 83.59, 72.39, 71.16, 35.00, 34.81, 26.95, 21.25, 19.98. ^{31}P NMR: δ = 142.71 (s). MS (CI): MH^+ = 264. $C_{11}H_{22}NO_4P$ (263.3): calcd. C 50.18, H 8.42, N 5.32; found C 49.16, H 8.35, N 5.40.

(4*R*,5*S*,6*S*,7*R*)-5,6-*O*-isopropylidene-2-dimethylamino-4,7-diethyl-1,3,2-dioxaphosphepane-5,6-diol (6b): Yield: 1.77 g, 93.7%; m.p. 44 °C. $[\alpha]_D^{23}$= +31.3 (*c* = 1.0, $CHCl_3$). ^1H NMR (400 MHz, $CDCl_3$): δ = 3.86−3.70 (m, 3 H, CH), 3.60−3.55 (m, 1 H, CH), 2.60 (s, 3 H, N−CH_3), 2.57 (s, 3 H, N−CH_3), 1.88−1.73 (m, 2 H, CH_2), 1.66−1.51 (m, 2 H, CH_2), 1.34 (s, 3 H, CH_3), 1.33 (s, 3 H, CH_3), 0.97 (t, 3 H, CH_3), 0.95 (t, 3 H, CH_3). ^{13}C NMR: δ = 109.29, 82.34, 82.10, 76.68, 75.17, 35.09, 34.89, 27.48, 26.91, 26.31, 9.26, 8.83. ^{31}P NMR: δ = 141.72 (s). MS (CI): MH^+ = 292. $C_{13}H_{26}NO_4P$ (291.3): calcd. C 53.60, H 9.00, N 4.81; found C 51.59, H 9.02, N 5.04.

(4*R*,5*S*,6*S*,7*R*)-5,6-*O*-Isopropylidene-2-dimethylamino-4,7-dipropyl-1,3,2-dioxaphosphe-pane-5,6-diol (6c): yield: 1.94 g, 93.6%; m.p. 87 °C. $[\alpha]_D^{23}$= +36.8 (*c* = 1.0, $CHCl_3$). ^1H NMR (400 MHz, $CDCl_3$): δ = 3.88−3.76 (m, 3 H, CH), 3.58−3.54 (m, 1 H, CH), 2.59 (s, 3 H, N−CH_3), 2.57 (s, 3 H, N−CH_3), 1.79−1.65 (m, 2 H, CH_2), 1.64−1.46 (m, 4 H, CH_2), 1.44−1.35 (m, 2 H, CH_2), 1.35 (s, 3 H, CH_3), 1.34 (s, 3 H, CH_3), 0.91 (t, 3 H, CH_3), 0.90 (t, 3 H, CH_3). ^{13}C NMR: δ = 109.32, 82.80, 82.62, 75.35, 74.04, 36.70, 35.46, 35.15, 34.95, 26.94, 26.87, 18.29, 17.89, 13.97. ^{31}P NMR: δ = 141.10 (s). MS (CI): MH^+ = 320. $C_{15}H_{30}NO_4P$ (319.4): calcd. C 56.41, H 9.47, N 4.39; found C 54.43, H 9.30, N 4.73.

(4*R*,5*S*,6*S*,7*R*)-5,6-*O*-Isopropylidene-2-dimethylamino-4,7-di-*iso*-pentyl-1,3,2-dioxaphosphe-pane-5,6-diol (6d): Yield: 2.33 g, 95.3%; mp: 67 °C. $[\alpha]_D^{23}$= +37.5 (*c* = 1.0, $CHCl_3$). ^1H NMR (400 MHz, $CDCl_3$): δ = 3.83−3.72 (m, 3 H, CH), 3.58−3.53 (m, 1 H, CH), 2.59 (s, 3 H, N−CH_3), 2.56 (s, 3 H, N−CH_3), 1.83−1.70 (m, 2 H, CH), 1.61−1.46 (m, 4 H, CH_2), 1.45−1.35 (m, 2 H, CH_2), 1.35 (s, 3 H, CH_3), 1.34 (s, 3 H, CH_3), 1.27−1.18 (m, 2 H, CH_2), 0.88−0.85 (m, 12 H, CH_3). ^{13}C NMR: δ = 109.30, 82.88, 82.61, 75.79, 74.60, 34.16, 33.97, 33.17, 32.97, 31.44, 31.41, 30.26, 30.19, 27.00, 25.97, 25.89, 21.82, 21.45. ^{31}P NMR: δ = 140.83 (s). MS (CI): MH^+ = 376. $C_{19}H_{38}NO_4P$ (375.5): calcd. C 60.78, H 10.20, N 3.73; found C 58.54, H 10.10, N 4.28.

(4*R*,5*S*,6*S*,7*R*)-5,6-*O*-isopropylidene-2-dimethylamino-4,7-dibenzyl-1,3,2-dioxaphosphepane-5,6-diol (6e): Yield: 2.61 g, 96.7%; mp: 64 °C. $[\alpha]_D^{23}$= +29.5 (*c* = 1.0, $CHCl_3$). ^1H NMR (400 MHz, $CDCl_3$): δ = 7.24−7.12 (m, 10 H, $CH_{arom.}$), 4.02−3.96 (m, 1 H, CH), 3.93−3.88 (m, 2 H, CH), 3.51−3.47 (m, 1 H, CH), 3.09−3.00 (m, 2 H, CH_2), 2.90−2.82 (m, 2 H, CH_2), 2.40 (s, 3 H, N−CH_3), 2.38 (s, 3 H, N−CH_3), 1.41 (s, 3 H, CH_3), 1.39 (s, 3 H, CH_3). ^{13}C NMR: δ = 137.78, 137.31, 130.24, 129.99, 127.88, 127.70, 126.16, 126.11, 109.58, 81.46, 81.16, 75.83, 74.05, 40.27, 39.18, 35.01, 34.88, 27.01, 26.89. ^{31}P NMR: δ = 141.30 (s). MS (CI): MH^+ = 416. $C_{23}H_{30}NO_4P$ (415.5): calcd. C 66.49, H 7.28, N 3.37; found C 64.02, H 7.33, N 4.22.

Synthesis of Rhodium(I) Complexes. General Procedure for the Synthesis of 7a−e: A solution of 2 equivalents of the corresponding monodentate phosphoramidite **6a−e** in 20 mL dichloromethane was added to a stirred solution of $[Rh(COD)_2][SO_3CF_3]$ (300 mg, 0.64 mmol) in 30 mL of dichloromethane at 0 °C. After stirring for 2 h at room temperature, the solvent was removed under reduced pressure. The resulting orange solid was washed twice with 50 mL pentane and dried in vacuo.

{Bis[(4*R*,5*S*,6*S*,7*R*)-5,6-*O*-isopropylidene-2-dimethylamino-4,7-dimethyl-1,3,2-dioxaphosphepane]Rh(COD)} Trifluoromethanesulfonate (7a): Yield: 557 mg, 98.2%. ^1H NMR (400 MHz, $CDCl_3$): δ = 5.53−5.45 (m, 2 H, CH_{COD}), 5.19−5.11 (m, 2 H, CH_{COD}), 4.33−4.23 (m, 2 H, CH), 4.09−3.99 (m, 2 H, CH), 3.42−3.36 (m, 2 H, CH), 3.30−3.24 (m, 2 H, CH), 3.03−2.98 (m, 12 H, N−CH_3), 2.77−2.31 (m, 8 H, CH_2 $_{COD}$), 1.39 (s, 6 H, CH_3), 1.36 (s, 6 H, CH_3), 1.33 (d, 6 H, CH_3), 1.29 (d, 6 H, CH_3). ^{31}P NMR: δ = 118.92 (d). MS (FAB): $[M - SO_3CF_3^-]^+$ = 737. $C_{31}H_{56}F_3N_2O_{11}P_2RhS$ (886.7): calcd. C 41.99, H 6.37, N 3.16; found C 41.42, H 5.97, N 3.18.

{Bis[(4*R*,5*S*,6*S*,7*R*)-5,6-*O*-isopropylidene-2-dimethylamino-4,7-diethyl-1,3,2-dioxaphosphepane]Rh(COD)} Trifluoromethanesulfonate (7b): Yield: 477 mg, 79.1%. ^1H NMR (400 MHz, $CDCl_3$): δ = 5.60−5.53 (m, 2 H, CH_{COD}), 5.32−5.25 (m, 2 H, CH_{COD}), 4.09−3.98 (m, 4 H, CH), 3.59−3.52 (m, 2 H, CH), 3.39−3.32 (m, 2 H, CH), 3.06−3.01 (m, 12 H, N−CH_3), 2.76−2.33 (m, 8 H, CH_2 $_{COD}$), 1.86−1.77 (m, 4 H, CH_2), 1.77−1.66 (m, 2 H, CH_2), 1.55−1.43 (m, 2 H, CH_2), 1.40 (s, 6 H, CH_3), 1.37 (s, 6 H, CH_3), 0.99−0.91 (m, 12 H, CH_3). ^{31}P NMR: δ = 118.06 (d). MS (FAB): $[M - SO_3CF_3^-]^+$ = 793. $C_{35}H_{64}F_3N_2O_{11}P_2RhS$ (942.8): calcd. C 44.59, H 6.84, N 2.97; found C 45.12, H 6.97, N 2.97.

{Bis[(4*R*,5*S*,6*S*,7*R*)-5,6-*O*-isopropylidene-2-dimethylamino-4,7-dipropyl-1,3,2-dioxaphosphepane]Rh(COD)} Trifluoromethanesulfonate (7c): Yield: 558 mg, 87.2%. ^1H NMR (400 MHz, $CDCl_3$): δ = 5.55−5.46 (m, 2 H, CH_{COD}), 5.29−5.21 (m, 2 H, CH_{COD}), 4.10−3.98 (m, 4 H, CH), 3.55−3.47 (m, 2 H, CH), 3.32−3.27 (m, 2 H, CH), 3.03−2.97 (m, 12 H, N−CH_3), 2.74−2.32 (m, 8 H, CH_2 $_{COD}$), 1.79−1.63 (m, 4 H, CH_2), 1.61−1.50 (m, 2 H, CH_2), 1.49−1.39 (m, 6 H, CH_2), 1.38 (s, 6 H, CH_3), 1.35 (s, 6 H, CH_3), 1.33−1.20 (m, 4 H, CH_2),0.94−0.87 (m, 12 H, CH_3). ^{31}P NMR: δ = 117.93 (d). MS (FAB): $[M - SO_3CF_3^-]^+$ = 849. $C_{39}H_{72}F_3N_2O_{11}P_2RhS$ (998.9): calcd. C 46.89, H 7.26, N 2.80; found C 46.38, H 7.11, N 2.87.

{Bis[(4*R*,5*S*,6*S*,7*R*)-5,6-*O*-isopropylidene-2-dimethylamino-4,7-di-*iso*-pentyl-1,3,2-dioxaphosphepane]Rh(COD)} Trifluoromethanesul-

fonate (7d): Yield: 692 mg, 97.3%. ^{1}H NMR (400 MHz, $CDCl_3$): δ = 5.55−5.48 (m, 2 H, CH_{COD}), 5.32−5.25 (m, 2 H, CH_{COD}), 4.11−3.96 (m, 4 H, CH), 3.54−3.48 (m, 2 H, CH), 3.36−3.30 (m, 2 H, CH), 3.03−2.97 (m, 12 H, N−CH_3), 2.75−2.32 (m, 8 H, CH_2 $_{COD}$), 1.81−1.69 (m, 4 H, CH_2), 1.68−1.58 (m, 2 H, CH), 1.57−1.46 (m, 4 H, CH_2), 1.45−1.40 (m, 2 H, CH), 1.39 (s, 6 H, CH_3), 1.36 (s, 6 H, CH_3), 1.32−1.11 (m, 8 H, CH_2), 0.91−0.82 (m, 24 H, CH_3). ^{31}P NMR: δ = 118.01 (d). MS (FAB): [M − $SO_3CF_3^-$]$^+$ = 961. $C_{47}H_{88}F_3N_2O_{11}P_2RhS$ (1111.1): calcd. C 50.81, H 7.98, N 2.52; found C 50.35, H 7.91, N 2.68.

{Bis[(4*R*,5*S*,6*S*,7*R*)-5,6-*O*-ispropylidene-2-dimethylamino-4,7-dibenzyl-1,3,2-dioxaphosphe-pane]Rh(COD)} Trifluoromethanesulfonate (7e): Yield: 743 mg, 97.5%. ^{1}H NMR (400 MHz, $CDCl_3$): δ = 7.37−7.08 (m, 20 H, $CH_{arom.}$), 5.47−5.39 (m, 2 H, CH_{COD}), 5.22−5.16 (m, 2 H, CH_{COD}), 4.44−4.38 (m, 2 H, CH), 4.13−4.05 (m, 2 H, CH), 3.53−3.48 (m, 2 H, CH), 3.17−3.10 (m, 2 H, CH), 2.75−2.33 (m, 8 H, CH_2 $_{COD}$), 2.52−2.47 (m, 12 H, N−CH_3), 1.50−1.45 (m, 2 H, CH_2), 1.44 (s, 6 H, CH_3), 1.43−1.36 (m, 2 H, CH_2), 1.32−1.24 (m, 2 H, CH_2), 1.24 (s, 6 H, CH_3), 1.23−1.15 (m, 2 H, CH_2). ^{31}P NMR: δ = 118.35 (d). MS (FAB): [M − $SO_3CF_{33}^-$]$^+$ = 1041. $C_{55}H_{72}F_3N_2O_{11}P_2RhS$ (1191.1): calcd. C 55.46, H 6.09, N 2.35; found C 54.25, H 6.19, N 2.67.

{Bis((4*R*,5*S*,6*S*,7*R*)-5,6-*O*-isopropylidene-2-dimethylamino-4,7-dimethyl-1,3,2-dioxaphosphepane]}$PdCl_2$ (8a): A solution of 2 equivalents of monodentate ligand **6a** in 50 mL dichloromethane was added to a stirred solution of [$PdCl_2$(COD)] (500 mg, 1.75 mmol) in 70 mL of dichloromethane at 0 °C. After stirring at room temperature for 2 h, the solvent was removed under reduced pressure. Washing the residue twice with 50 mL of diethyl ether and drying in vacuo resulted in a pale yellow powder. Yield: 749 mg, 60.8%. ^{1}H NMR (400 MHz, $CDCl_3$): δ = 4.82−4.73 (m, 2 H, CH), 4.38−4.31 (m, 2 H, CH), 3.64−3.60 (m, 2 H, CH), 3.49−3.45 (m, 2 H, CH), 2.92−2.89 (m, 12 H, N−CH_3), 1.47 (d, 6 H, CH_3), 1.37 (s, 12 H, CH_3), 1.36 (d, 6 H, CH_3). ^{13}C NMR: δ = 110.05, 83.61, 82.38, 74.13, 37.08, 26.75, 26.55, 18.89, 18.82. ^{31}P NMR: δ = 102.49 (s). MS (FAB): [M − $SO_3CF_3^-$]$^+$ = 669. $C_{22}H_{44}Cl_2N_2O_8P_2Pd$ (703.9): calcd. C 37.54, H 6.30, N 3.98; found C 36.80, H 6.34, N 4.09.

Table 2. Crystal data and refinement details for **8a**

	8a
Formula	$C_{22}H_{44}Cl_2N_2O_8P_2Pd$
M_r	703.83
Crystal system	Monoclinic
Space group	$P2_1$
a (Å)	8.098(2)
b (Å)	14.460(2)
c (Å)	13.910(3)
β (°)	96.06(3)
V (Å^3)	1619.6(6)
Z	2
$D_{calcd.}$ (g·cm^{-3})	1.443
μ (mm^{-1})	0.88
Crystal size (mm^3)	0.40 × 0.30 × 0.10
θ range (°)	2.04−25.98
Measured reflections	14673
Unique reflections	5968
R_{int}	0.039
Reflections with $I > 2\sigma(I)$	5543
Goodness-of-fit	1.01
R_1 [F, $I > 2\sigma(I)$]	0.025
R_1 (F, all data)	0.029
wR_2 (F^2, all data)	0.053
Min./max. in ΔF (e·Å^{-3})	−0.46/0.37
Absolute struct. parameter	−0.03

X-ray Crystallography of 8a: The crystal used in this study was mounted onto the end of an glass fiber. X-ray data were collected at −100 °C on a STOE IPDS unit (Imaging Plate Diffraction System). Graphite monochromated Mo-K_α radiation (λ = 0.71073 Å) was used. Crystal data are listed in Table 2 together with refinement details. Absorption corrections were not applied. The structure was solved by the Patterson method with the SHELXS-86 program.[13] The atomic coordinates and anisotropic thermal parameters of the non-hydrogen atoms were refined using the SHELXL-97 program;[14] full-matrix method, F^2 data. Hydrogen atoms were included in the final refinement cycles in a riding mode.
Crystallographic data (excluding structure factors) for the structure(s) included in this paper have been deposited with the Cambridge Crystallographic Data Centre as supplementary publication no. CCDC-165693. Copies of the data can be obtained free of charge on application to CCDC, 12 Union Road, Cambridge CB2 1EZ, UK [Fax: (internat.) + 44-1223/336-033; Email: deposit@ccdc.cam.ac.uk].

Acknowledgments

We thank the Deutsche Forschungsgemeinschaft for financial support of this work (Ri613/5−1). Alexander Bayer was further supported by a scholarship of the state of Baden-Württemberg.

[1] X. Zhang, *Enantiomer* **1999**, *4*, 541.
[2] C. Claver, E. Fernandez, A. Gillon, K. Heslop, D. J. Hyett, A. Martorell, A. G. Orpen, P. G. Pringle, *Chem. Commun.* **2000**, 961−962.
[3] M. T. Reetz, G. Mehler, *Angew. Chem.* **2000**, *112*, 4047−4049; *Angew. Chem. Int. Ed.* **2000**, *39*, 3889−3891.
[4] M. van den Berg, A. J. Minnaard, E. P. Schudde, J. van Esch, A. H. M. de Vries, J. G. de Vries, B. L. Feringa, *J. Am. Chem. Soc.* **2000**, *122*, 11539−11540.
[5] Phosphoramidites are also frequently used in the enantioselective copper-catalyzed conjugate addition of dialkylzinc reagents to enones, see: A. Alexakis, G. P. Trevitt, G. Bernardinelli, *J. Am. Chem. Soc.* **2001**, *123*, 4358−4359.
[6] D-Mannitol is also the starting material for the synthesis of bidentate ligands: A. Börner, J. Holz, G. Voss, R. Stürmer, DE 48 084 (18.06.1997); J. Holz, M. Quirmbach, U. Schmidt, D. Heller, R. Stürmer, A. Börner, *J. Org. Chem.* **1998**, *63*, 8031−8034.
[7] Y. Merrer, A. Dureault, C. Greck, D. Micas-Languin, C. Gravier, J. Depezay, *Heterocycles* **1987**, *25*, 541−548.
[8] L. F. Wiggins, *J. Chem. Soc.* **1946**, *13*, 13−14.
[9] B. B. Lohray, M. Chatterjee, Y. Jayamma, *Synth. Commun.* **1997**, *27*, 1711−1724.
[10] L. F. Wiggins, D. J. C. Wood, *J. Am. Chem. Soc.* **1950**, 1566−1575.
[11] P. Allevi, M. Anastasia, P. Ciuffreda, A. M. Sanvito, *Tetrahedron: Asymmetry* **1994**, *5*, 927−934.
[12] W. S. Knowles, *Acc. Chem. Res.* **1983**, *16*, 106−112.
[13] G. M. Sheldrick, *SHELXS-86*, Program for the Solution of Crystal Structures, Göttingen, **1986**.
[14] G. M. Sheldrick, *SHELXL-97*, Program for the Refinement of Crystal Structures, Göttingen, **1997**.

Received June 27, 2001
[I01233]

Pyrazolylborate Nickel(II) Complexes as Catalysts for the Formation of Polyketones from Ethene and Carbon Monoxide − Partial Hydrolysis of the Bis(pyrazolyl)borate Yields a Pyrazolyl(hydroxo)borate Ligand

Wolfgang Kläui,*[a] Barbara Turkowski,[a] Gerd Rheinwald,[b] and Heinrich Lang[b]

Keywords: Nickel / N ligands / Homogeneous catalysis / Copolymerization / Polyketones / Solvolysis

The new nickel(II) complex [Ni{BBN(pz)$_2$}(*o*-tol)(PPh$_3$)] (**1**) of the bis(pyrazolyl)borate ligand [BBN(pz)$_2$]$^-$ (BBN = 1,5 borabicyclo[3.3.1]nonane) has been prepared by reaction of [NiBr(*o*-tol)(PPh$_3$)$_2$] with K[BBN(pz)$_2$]. In the presence of moisture this reaction yields the nickel(II) complex [Ni{BBN(pz)(OH)}(*o*-tol)(PPh$_3$)] (**2**). The hydroxoborate ligand [BBN(pz)(OH)]$^-$ acts as an *N*,*O*-chelate ligand in **2**. Compound **1** and the analogous nickel complex [Ni{HB(3-Phpz)$_3$}(*o*-tol)(PPh$_3$] show very similar activity in the catalytic copolymerization of carbon monoxide and ethene. This suggests that the borane hydrogen and the noncoordinated pyrazolyl ring in the latter are not essential for the catalysis. Compound **2** is inactive. Both **1** and **2** were characterised by X-ray crystallography.

Introduction

Recently we have found that the nickel(II) complex [Ni{HB(3-Phpz)$_3$}(*o*-tol)(PPh$_3$)] catalyses the copolymerization of carbon monoxide and ethene under mild reaction conditions.[1] The coordination around nickel is planar with the tripodal tris(pyrazolyl)borate moiety acting as a bidentate ligand. In the solid state the third, noncoordinated pyrazolyl ring faces away from the coordination plane. This has the effect that borane hydrogen lies in the vicinity of nickel (Figure 1).

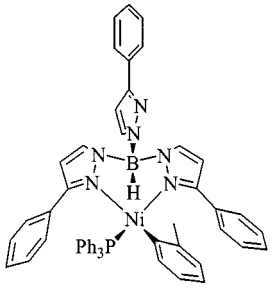

Figure 1. The structure of [Ni{HB(3-Phpz)$_3$}(*o*-tol)(PPh$_3$)]

It was not clear at all why this nickel(II) complex is catalytically active. Does the tridenticity of the ligand play a role? Is the borane hydrogen important for the catalysis?

[a] Institut für Anorganische Chemie und Strukturchemie der Universität Düsseldorf,
Universitätstraße 1, 40225 Düsseldorf, Germany,
Fax: (internat.) + 49-211/81-12287
E-mail: klaeui@uni-duesseldorf.de
[b] Lehrstuhl für Anorganische Chemie, Technische Universität Chemnitz,
Straße der Nationen 62, 09107 Chemnitz, Germany

To answer these questions, we have now synthesised an analogous nickel(II) complex with the dipodal bis(pyrazolyl)borate ligand [BBN(pz)$_2$]$^-$. The potassium salt of this ligand is accessible from BBN, potassium pyrazolide and pyrazole [Equation (1)].[2,3]

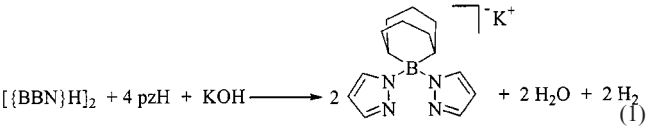

Herein we report the synthesis, crystal structure, and catalytic activity of the novel organonickel(II) complex [Ni{BBN(pz)$_2$}(*o*-tol)(PPh$_3$)] (**1**) (Figure 2).

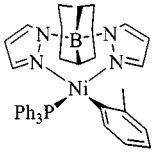

Figure 2. The structure of [Ni{BBN(pz)$_2$}(*o*-tol)(PPh$_3$)] (**1**)

Results and Discussion

Synthesis of the Nickel(II) Complexes

[Ni{BBN(pz)$_2$}(*o*-tol)(PPh$_3$)] (**1**) was prepared by reacting [NiBr(*o*-tol)(PPh$_3$)$_2$] with K[BBN(pz)$_2$] in THF (Scheme 1). In the presence of moisture the ligand [BBN(pz)$_2$]$^-$ partly hydrolyses to form a hydroxoborate. This in turn acts as an *N*,*O*-chelate ligand to give the unusual complex [Ni{BBN(pz)(OH)}(*o*-tol)(PPh$_3$)] (**2**).

 © WILEY-VCH Verlag GmbH, 69451 Weinheim, Germany, 2002 1434−1948/02/0101−0205 $ 17.50+.50/0

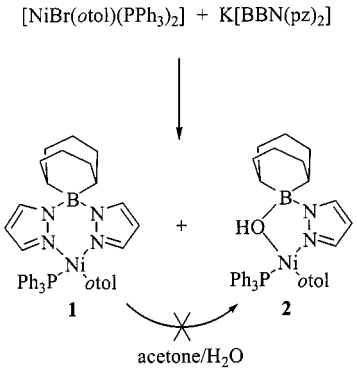

Scheme 1. Synthesis of the nickel complexes [Ni{BBN(pz)$_2$}-(*o*-tol)(PPh$_3$)] (**1**) and [Ni{BBN(pz)(OH)}(*o*-tol)(PPh$_3$)] (**2**)

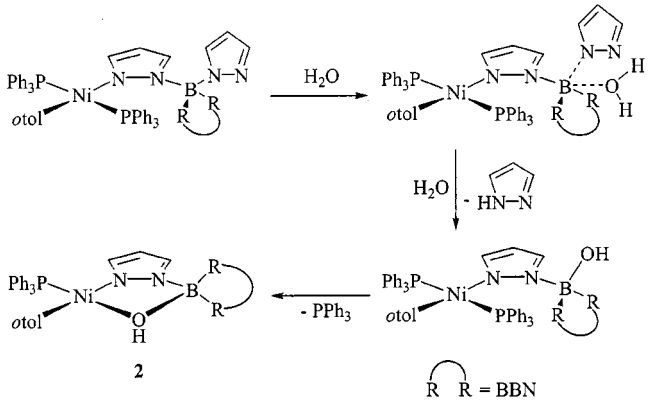

Scheme 2. Hydrolysis of the [BBN(pz)$_2$]$^-$ ligand during the synthesis of **2**

The ^{1}H NMR spectra of **1** and **2** are similar and show the expected signals. The signals of the pyrazolyl ring and of the methyl group of the *o*-tolyl ligand in **2** experience a low-field shift in comparison with the ones of **1**. The BBN signals of both nickel complexes in the range $\delta = 0.5-2.3$ are broad and unresolved. The signal shifted downfield to $\delta = 4.4$ is assigned to the C7 proton, which is oriented towards the nickel atom (see Figure 3). A similar effect has been observed in the nickel complex [Ni{Et$_2$B(pz)$_2$}$_2$].[4] The signal of the hydroxyl proton in **2** appears as a doublet at $\delta = -0.5$. A ^{1}H{^{31}P} NMR decoupling experiment shows that the doublet structure is due to a $^3J_{PH}$ coupling.

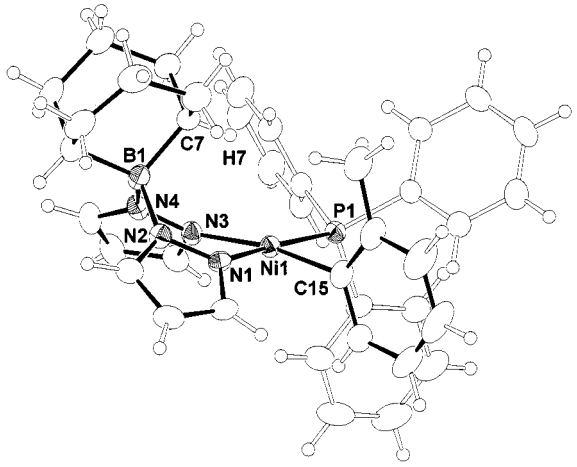

Figure 3. ZORTEP plot of [Ni{BBN(pz)$_2$}(*o*-tol)(PPh$_3$)] (**1**)

We have tried to pin down the conditions under which the hydroxoborate complex **2** is formed. From separate experiments we know that: (i) complex **1** does not hydrolyse to yield complex **2**, and (ii) the hydrolysis of the ligand [BBN(pz)]$^-$ in the absence of the nickel complex [NiBr(*o*-tol)(PPh$_3$)$_2$] is much slower than the formation of **2**. In Scheme 2 we have postulated how the formation of **2** could occur.[5]

Crystal Structures of the Nickel(II) Complexes

[Ni{BBN(pz)$_2$}(*o*-tol)(PPh$_3$)] (1)

The nickel complex **1** crystallises from acetone as dark yellow plates [monoclinic space group *Pn* with $a = 12.1313(8)$, $b = 13.0085(8)$, $c = 12.6192(8)$ Å, and $\beta = 107.492(2)°$]. The compound co-crystallizes with one molecule of acetone per formula unit. Figure 3 shows the structure of **1** in the crystal.

The four-coordinate nickel atom is in a planar arrangement. The bis(pyrazolyl)borate ligand coordinates in a bidentate fashion with a bite angle N1−Ni1−N3 of 89.80(13)°, and forms a six-membered chelate ring in a boat conformation. The *o*-tolyl ring is orientated nearly perpendicular to the coordination plane [torsion angle P1−Ni1−C15−C16: 99.2(4)°] in order to minimise the interaction with the neighbouring ligands.

The incorporated acetone molecule shows a weak non-classical hydrogen bond between H25 and the symmetry generated O1a (values are given in Table 1). The bond lengths and bond angles are in the expected[1] range (see Table 1).

[Ni{BBN(pz)(OH)}(*o*-tol)(PPh$_3$)] (2)

The nickel complex **2** crystallises from acetone as dark-yellow triclinic blocks [triclinic space group $P\bar{1}$ with $a = 12.1983(10)$, $b = 12.3689(10)$, $c = 13.7388(11)$ Å, $\alpha = 112.086(2)$, $\beta = 112.360(2)$ and $\gamma = 90.462(2)°$]. The compound co-crystallizes with one molecule of acetone per formula unit. Figure 4 shows the structure of **2** in the crystal.

The nickel atom is in a planar environment. The hydroxoborate ligand coordinates in a bidentate fashion with the nitrogen of the pyrazolyl ring and the oxygen of the hydroxyl group. The five-membered chelate ring shows an envelope conformation with a bite angle N1−Ni1−O1 of 81.5°.

The deviations from the least-squares plane including the atoms N1, N2, B1, O1, and Ni1 are: 0.0472(0.0008), 0.0488(0.0010), −0.1612(0.0010), 0.1836(0.0009) and −0.1184(0.0007) Å, respectively.

Table 1. Selected distances (Å) and angles (°) of **1**

Ni1−C15	1.898(4)	C15−Ni1−N1	88.45(17)
Ni1−N1	1.967(3)	C15−Ni1−N3	170.27(18)
Ni1−N3	1.988(3)	N1−Ni1−N3	89.80(13)
Ni1−P1	2.1603(11)	C15−Ni1−P1	84.64(15)
N2−B1	1.575(7)	N1−Ni1−P1	172.99(9)
N4−B1	1.590(6)	N3−Ni1−P1	97.21(11)
H7···Ni1	2.569	N2−N1−Ni1	122.3(3)
		N1−N2−B1	120.4(3)
		N2−B1−N4	100.8(3)
		N3−N4−B1	118.8(3)
		N4−N3−Ni1	124.5(2)
C25−H25	0.95	C25−H25−O1a[a]	142.6
H25−O1a[a]	2.552		
C25−O1a[a]	3.356		

[a] Symmetry operation: $a = -1/2 + x, 1 - y, -1/2 + z$.

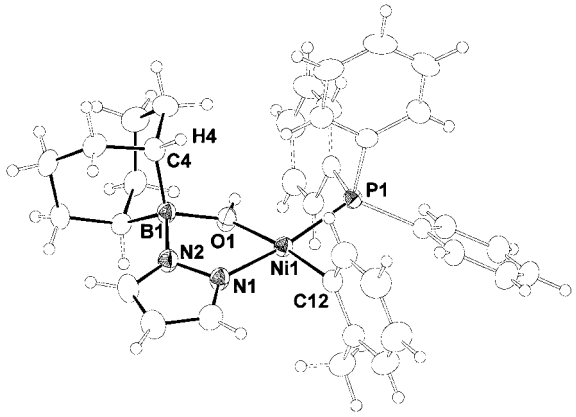

Figure 4. ZORTEP plot of [Ni{BBN(pz)(OH)}(*o*-tol)(PPh_3)] (**2**)

As in **1**, the incorporated acetone shows a weak nonclassical hydrogen bond between H1 and O2a as well as between H22 and O2b.

The bond lengths and bond angles are in the expected range.[1,6,7] Selected distances and angles of **2** are presented in Table 2.

Copolymerization Reactions with [Ni{$BBN(pz)_2$}(*o*-tol)(PPh_3)] (1)

The copolymerization of carbon monoxide and ethene was performed according to the reaction conditions reported for [Ni{$HB(3\text{-}Phpz)_3$}(*o*-tol)(PPh_3)] as catalyst.[1]

Table 2. Selected distances (Å) and angles (°) of **2**

Ni1−C12	1.8839(16)	C12−Ni1−O1	172.72(6)
Ni1−N1	1.8986(13)	N1−Ni1−O1	81.54(6)
Ni1−O1	1.9195(12)	C12−Ni1−P1	89.63(5)
Ni1−P1	2.1520(5)	C12−Ni1−N1	91.76(6)
O1−B1	1.590(6)	N1−Ni1−P1	171.27(4)
N2−B1	1.528(2)	O1−Ni1−P1	97.43(4)
H4···Ni	3.559	N2−N1−Ni1	116.56(10)
		N1−N2−B1	118.04(12)
		N2−B1−O1	97.83(12)
		B1−O1−Ni1	119.14(10)
C1−H1	0.916(19)	C1−H1−O2a[a]	153.48
H1−O2a[a]	2.4642		
C1−O2a[a]	3.3089		
C22−H22	0.98(2)	C22−H22−O2b[b]	162.98
H22−O2b[b]	2.4144		
C22−O2b[b]	3.3655		

[a] Symmetry operation: $a = 2 - x, 1 - y, 1 - z$. − [b] Symmetry operation: $b = 1 - x, 1 - y, 1 - z$.

The formation of polyketone is dependent on the carbon monoxide pressure (see Table 3)

The highest efficiency for the copolymerization of ethene and carbon monoxide with [Ni{$HB(3\text{-}Phpz)_3$}(*o*-tol)(PPh_3)] is observed with 3.5 bar of carbon monoxide.[1] Under the same reaction conditions complex **1** appears somewhat less efficient although the catalytic activity of [Ni{$HB(3\text{-}Phpz)_3$}(*o*-tol)(PPh_3)] and **1** is essentially the same.

The reaction of [$NiBr$(*o*-tol)(PPh_3)$_2$] with K[$BBN(pz)_2$] in the presence of moisture leads to the formation of [Ni{BBN(pz)(OH)}(*o*-tol)(PPh_3)] (**2**). However, **2** displays no activity in the formation of polyketone under the same reaction conditions as used with **1**. This is an interesting result as our group has recently found nickel complexes with *N*,*O*-chelate ligands that show a very high efficiency in the copolymerization of carbon monoxide and ethene.[6] It is still not clear which factors are essential for the catalytic activity of the nickel complexes. However, from the results described here we can conclude: (i) that the noncoordinated pyrazolyl ring of the tripodal nitrogen ligand in [Ni{$HB(3\text{-}Phpz)_3$}(*o*-tol)(PPh_3)] plays no important role in the copolymerization reaction, and (ii) that the borane hydrogen atom is not important for the catalytic activity via, for example, the formation of a nickel hydride species.

Table 3. Copolymerization of carbon monoxide and ethene at 60 °C in toluene; comparison of the nickel catalysts **1** and [Ni{$HB(3\text{-}Phpz)_3$}(*o*-tol)(PPh_3)][1]

Catalyst	Ethene pressure (bar)	CO pressure (bar)	Polyketone (g)	Efficiency (gPK/gNi)
1	40	20	0.47	60
1	40	10	0.70	90
1	40	3.5	0.38	50
[Ni{$HB(3\text{-}Phpz)_3$}(*o*-tol)(PPh_3)]	40	2.0	0.23	34
[Ni{$HB(3\text{-}Phpz)_3$}(*o*-tol)(PPh_3)]	40	3.5	1.15	167
[Ni{$HB(3\text{-}Phpz)_3$}(*o*-tol)(PPh_3)]	40	5.0	0.31	45

Experimental Section

General Remarks: All reactions were carried out under nitrogen using standard Schlenk techniques unless stated otherwise. All solvents were purified and degassed by standard procedures. THF for the synthesis of **2** was not dried. The compounds $K[BBN(pz)_2]$[3] and $[NiBr(o\text{-tol})(PPh_3)_2]$[8] were synthesized according to literature procedures. Filtration was done with 1 μm membrane filters (regenerated cellulose, Schleicher & Schuell). One dimensional ^1H and ^{31}P NMR spectra were recorded on a Bruker DRX 200 spectrometer at 296 K. The proton chemical shifts (δ) are given in ppm and referenced to the signal of partially deuterated $CDCl_3$ at δ = 7.3. The phosphorus chemical shifts are referenced to the signal of external H_3PO_4. Infrared spectra were recorded on a FT-IR Bruker IFS 66 spectrometer. EIMS data were recorded on a Varian MAT 311 A instrument, ionisation energy 70 eV. FAB mass spectra were recorded on a Finnigan MAT 8200 spectrometer using an NBA matrix. Elemental analyses were performed on a Perkin−Elmer CHN-2400/II elemental analyser.

Preparation of the Nickel(II) Complexes 1 and 2: A solution of $[NiBr(o\text{-tol})(PPh_3)_2]$ (1.0 g, 1.3 mmol) and $K[BBN(pz)_2]$ (0.39 g, 1.3 mmol) in 25 mL of dry THF for **1** or in 25 mL of wet THF for **2** was stirred overnight. The solvent was evaporated, the residue was taken up in dichloromethane and filtered through a membrane filter. After evaporation of the solvent the residue was washed with about 10 mL of hexane. Crystallisation from diethyl ether (**1**) or acetone (**1** and **2**) yielded **1** and **2** as yellow crystals suitable for X-ray analysis.

$[Ni\{BBN(pz)_2\}(o\text{-tol})(PPh_3)]$ (1): Yield: 0.51 g (57%). ^1H NMR ($CDCl_3$): δ = 1.3−2.3 (broad, 13 H, BBN), 2.3 (s, 3 H, *o*-tol C*H*$_3$), 4.4 (s, 1 H, BBN), 5.7 (t, 1 H, pyrazolyl C^4 *H*), 5.9 (dt, $^3J_{H,H}$ = 2, $^5J_{P,H}$ = 1 Hz, 1 H, pyrazolyl C^4 *H*), 6.4 (dd, $^3J_{H,H}$ = 7, *J* = 2 Hz, 1 H, *o*-tol), 6.6−6.7 (m, 2 H, *o*-tol), 6.8 (dd, $^3J_{H,H}$ = 2, $^5J_{P,H}$ = 1 Hz, 1 H, pyrazolyl C$^{3/5}$ *H*), 6.9 (d, $^3J_{H,H}$ = 2 Hz, 1 H, pyrazolyl C$^{3/5}$ *H*), 7.2−7.7 (m, 19 H, PPh_3, *o*-tol, pyrazolyl C$^{3/5}$ *H*). $^{31}P\{^1H\}$ NMR ($CDCl_3$): δ = 29.5. IR (KBr): $\tilde{\nu}$ = 2939 cm^{-1}, 2924, 2881, 2838 (m, C−H), 1499 (w, C=C), 1434, 1409 (m, P−C). MS

Table 4. Crystallographic data for $[Ni\{BBN(pz)_2\}(o\text{-tol})(PPh_3)]$ (**1**) and $[Ni\{BBN(pz)(OH)\}(o\text{-tol})(PPh_3)]$ (**2**)

	1	**2**
Crystal shape	plate	triclinic block
Crystal colour	yellow	yellow
Crystal size (mm^3)	0.5 × 0.4 × 0.08	0.46 × 0.36 × 0.18
Chemical formula	$C_{36}H_{42}BN_4NiP{\cdot}C_3H_6O$	$C_{36}H_{40}BN_2NiOP{\cdot}C_3H_6O$
Molecular weight	725.33	675.27
Crystal system	Monoclinic	Triclinic
Space group	*Pn*	$P\bar{1}$
a (Å)	12.1313(8)	12.1986(10)
b (Å)	13.0085(8)	12.3689(10)
c (Å)	12.6192(8)	13.7388(11)
α (°)	90	112.086(2)
β (°)	107.492(2)	112.360(2)
γ (°)	90	90.462(2)
Volume (Å^3)	1889.3(2)	1748.5(2)
Z	2	2
ρ (calcd., g/cm^3)	1.268	1.283
Radiation used (λ, Å)	Mo-K_α (0.7173)	Mo-K_α (0.7173)
Temperature (K)	173(2)	173(2)
Scan method	ω scans	ω scans
Linear absorption coefficient (mm^{-1})	0.591	0.637
Total reflections	8147	14631
Independent reflections	4348	9753
Unique reflections	3748	6793
Used reflections	4348	9753
R(int)	0.0944	0.0246
θ-Scan range (°)	1.57 to 29.24	1.76 to 30.88
Index ranges	$-16 \le h \le 4$ $-17 \le k \le 17$ $-10 \le l \le 16$	$-17 \le h \le 13$ $-17 \le k \le 17$ $-18 \le l \le 19$
Completeness to $\theta_{max.}$ (%)	75.2	88.5
F(000)	768	716
R,[a] wR^2 [$I > 2\sigma(I)$][b]	0.0423, 0.0931	0.0360, 0.0768
R indices (all data), wR^2	0.0551, 0.0963	0.0635, 0.0840
Maximum δ/σ	0.449	0.145
Max./min. e-density (e.Å^{-3})	0.715/−0.740	0.411/ −0.309
Used reflections	4348	9753
L. S. restraints	2	0
Refined parameters	454	599
Goodness-of-fit on F^2 [c]	1.014	0.933
Weighting scheme parameters *a*/*b* [d]	0.0635/0	0.0414/0

[a] $R_1 = \Sigma(||F_0| - |F_c||)/\Sigma|F_0|$. − [b] $wR^2 = [\Sigma[w(F_0^2 - F_c^2)^2]/\Sigma(wF_0^4)]^{1/2}$. − [c] $S = [\Sigma\, w(F_0^2 - F_c^2)^2]/(n - p)^{1/2}$, *n* = number of reflections, *p* = parameters used. − [d] Definition of *w* calculation: $w = 1/[\sigma^2(F_0^2) + (aP)^2 + bP]$ where $P = (F_0^2 + 2F_c^2)/3$.

(FAB$^+$): *m/z* (%) = 665 (6) [M$^+$ − H], 589 (1) [M$^+$ − pzH], 574 (72) [M$^+$ − *o*-tol], 556 (8) [M$^+$ − BBN], 507 (9) [M$^+$ − (*o*-tol, pzH)], 353 (100) [PPh$_3$(*o*-tol)]$^+$. $C_{39}H_{42}BN_4NiP{\cdot}C_3H_6O$ (725.34): calcd. C 69.55, H 6.67, N 7.72; found C 69.60, H 6.70, N 7.95.

[Ni{BBN(pz)(OH)}(*o*-tol)(PPh$_3$)] (2): Yield: 0.31 g (38%). ^{1}H NMR ($CDCl_3$): δ = −0.5 (d, $^3J_{P,H}$ = 1 Hz, 1 H, O*H*), 0.5 (s (broad), 1 H, BBN), 0.6 (s (broad), 1 H, BBN), 0.8−2.2 (broad, 12 H, BBN), 2.7 (s, 3 H, *o*-tol CH_3), 6.1 (dt, $^3J_{H,H}$ = 2, $^5J_{P,H}$ = 1 Hz, 1 H, pyrazolyl C^4 *H*), 6.2 (d, $^3J_{H,H}$ = 2 Hz, 1 H, pyrazolyl C$^{3/5}$ *H*), 6.5−6.8 (m, 3 H, *o*-tol), 7.3 (dt, $^3J_{H,H}$ = 8, *J* = 1 Hz, 1 H, *o*-tol), 7.3−7.6 (m, 15 H, PPh$_3$), 7.7−7.8 (m, 1 H, pyrazolyl C$^{3/5}$ *H*). $^{31}P\{^1H\}$ NMR ($CDCl_3$): δ = 30.6. IR (KBr): $\tilde{\nu}$ = 3630 cm^{-1} (s, sharp, O−H), 3043, 2978, 2936 (m, C−H), 2914 (s, C−H), 2863 (vs, C−H), 1497 (w, C=C), 1434 (s, P−C), 1404 (m, P−C). MS (EI, 220 °C): *m/z* (%) = 616 (3) [M$^+$], 550 (<1) [M$^+$ − pz], 524 (3) [M$^+$ − *o*-tol], 354 (20) [PPh$_3$(*o*-tol)]$^+$, 262 (100) [PPh$_3$]$^+$. $C_{36}H_{40}BN_2NiOP{\cdot}C_3H_6O$ (675.28): calcd. C 69.37, H 6.87, N 4.15; found C 69.31, H 6.85, N 4.27.

General Preparation for the Synthesis of Polyketone: Compound **1** (0.12 mmol, 0.086 g) in 10 mL of toluene was transferred into a 100 mL autoclave. The solution was pressurised with carbon monoxide and then with ethene and stirred with a magnetic stirrer at 60 °C for 16 h. The white solid was filtered off, washed with hexane, and dried (see Table 3).

Crystal Structure Analysis: For compounds **1** and **2** data collection was carried out using a CCD area detector SMART 1 K by Bruker AXS GmbH with graphite monochromated Mo-K_α radiation (λ = 0.71073 Å). Data collection was done at 173 K. For protection against oxygen or moisture, the preparation of single crystals was done in a perfluoroalkyl ether from ABCR GmbH & Co KG (viscosity 1600 cSt). The unit cell was determined with the program SMART.[9] For data integration and refinement of the unit cell the program SAINT[9] was used. The space group was determined using the programs XPREP[9] (**1**) and ABSEN[10] (**2**) and the empirical absorption correction was done with SADABS.[9] The structures were solved by direct methods using the programs SHELX-97[11] for (**1**) and SIR97[12] for (**2**), the structure refinement was based on least-squares methods based on F^2 with SHELX-97.[11] The plots of the molecular structures were visualised using the program ZORTEP.[13]

All non-hydrogen atoms were fully refined in the calculated positions. For **2** the hydrogen atoms were taken from the electron density difference map and refined freely. For **1** the hydrogen atoms were positioned as riding on their neighbouring atoms and refined depending on its position. The figure in parenthesis after each calculated value represents the standard deviation in units of the last significant digit. Crystal data and refinement parameters are summarized in Table 4.

Crystallographic data (excluding structure factors) for the structures reported in this paper have been deposited with the Cambridge Crystallographic Data Centre as supplementary publication no. CCDC-165852 (**1**) and 165853 (**2**). Copies of the data can be obtained free of charge on application to CCDC, 12 Union Road, Cambridge CB2 1EZ, UK [Fax: (internat.) + 44(1223)336−033; E-mail: deposit@ccdc.cam.ac.uk].

[1] B. Domhöver, W. Kläui, R. Bell, D. Motz, *Angew. Chem.* **1998**, *110*, 3218−3220; *Angew. Chem. Int. Ed.* **1998**, *37*, 3050−3052.
[2] S. Trofimenko, J. C. Calabrese, J. S. Thompson, *Angew. Chem.* **1989**, *101*, 207−208; *Angew. Chem. Int. Ed.* **1989**, *28*, 205−206.
[3] M. Bortolini, U. E. Bucher, H. Rüegger, L. M. Venanzi, *Organometallics* **1992**, *11*, 2514−2521.
[4] S. Trofimenko, *J. Am. Chem. Soc.* **1967**, *89*, 6288−6294.
[5] This reaction has been formulated in analogy to a similar reaction which has been observed by Macchioni et al.: G. Bellachioma, G. Cardaci, V. Gramlich, A. Macchioni, F. Pieroni, L. M. Venanzi, *J. Chem. Soc., Dalton Trans.* **1998**, 947−951.
[6] W. Kläui, J. Bongards, G. J. Reiß, *Angew. Chem.* **2000**, *112*, 4077−4079; *Angew. Chem. Int. Ed.* **2000**, *39*, 3894−3896.
[7] A. Y. Desjardins, K. J. Cavell, J. L. Hoare, B. W. Skelton, A. N. Sobolev, A. H. White, W. Keim, *J. Organomet. Chem.* **1997**, *544*, 163−174.
[8] M. Hidai, T. Kashiwagi, T. Ikeuchi, Y. Uchida, *J. Organomet. Chem.* **1971**, *30*, 279−284.
[9] Bruker AXS Inc., Madison, WI, USA, **1998**.
[10] P. McArdle, *J. Appl. Cryst.* **1996**, *29*, 306.
[11] G. M. Sheldrick, SHELX-97, Programs for Crystal Structure Analysis (Release 97-2), University of Göttingen, Germany **1997**.
[12] A. Altomare, M. C. Burla, M. Camalli, G. L. Cascarano, C. Giacovazzo, A. Guagliardi, A. G. G. Moliterni, G. Polidori, R. Spagna, *J. Appl. Cryst.* **1999**, *32*, 115−119.
[13] L. Zsolnai, G. Huttner, University of Heidelberg, Germany, **1994.**

Received June 27, 2001
[I01237]

Synthesis, Structure, and Catalytic Activity of Some New Chiral 2-Menthylindenyl and 2-Menthyl-4,7-dimethylindenyl Rhodium Complexes

Herbert Schumann,*[a] Oleg Stenzel,[a] Sebastian Dechert,[a] Frank Girgsdies,[a] Jochanan Blum,[b] Dmitri Gelman,[b] and Ronald L. Halterman[c]

Dedicated to Prof. Dr. Rudolf Taube on the occasion of his 70th birthday

Keywords: Homogeneous catalysis / Hydroformylation / Hydrogenation / Indenyl ligands / Rhodium

Optically active rhodium complexes containing the chiral, menthyl-substituted indenyl ligands (–)-2-menthyl-4,7-dimethylindene and (–)-2-menthylindene are described. Metathesis reactions of the chiral lithium salts of these indenyl systems with the appropriate starting materials yielded the complexes (–)-(2-menthyl-4,7-dimethylindenyl)$Rh(CO)_2$ (**2**), (–)-(2-menthyl-4,7-dimethylindenyl)Rh(dppe) (**3**), (+)-(2-menthylindenyl)Rh(dppe) (**5**), (–)-(2-menthylindenyl)$Rh(PMe_3)_2$ (**6**), and (–)-(2-menthylindenyl)Rh(nbd) (**8**). All compounds obtained were diastereomerically pure. The structures of **2**, **3**, and **6** were determined by single crystal X-ray diffractometry. Complexes **3** as well as (–)-bis(η^2-ethylene)(η^5-2-menthyl-4,7-dimethylindenyl)rhodium(I) (**9**), (–)-(cycloocta-1,5-diene)(η^5-1-menthyl-4,7-dimethylindenyl)rhodium(I) (**10**), (–)-(cycloocta-1,5-diene)(η^5-2-menthyl-4,7-dimethylindenyl)rhodium(I) (**11**), and (–)-(cycloocta-1,5-diene)(η^5-2-menthylindenyl)rhodium(I) (**12**) were found to be active as double bond hydrogenation catalysts. Two of them proved to induce asymmetry up to 18% *ee*. These complexes also promote the hydroformylation of olefins yielding both linear and branched aldehydes in varying ratios but hardly transfer chirality.

Introduction

Rhodium catalysts are widely used in organic synthesis and some are currently used in large-scale industrial processes.[1] Combining the high reactivity of rhodium with chiral phosphane, sulfide, or cyclopentadienyl ligands containing chiral substituents led to their wide application as asymmetric catalysts.[2,3] Over the last few years we have exploited the use of the inexpensive commercially available chiral compound menthol in combination with dinuclear rhodium complexes to prepare chiral catalysts. Using a menthyl-substituted phosphane as a chiral ligand in the complex $[(R^*Ph_2P)(CO)Rh(\mu\text{-}Cl)(\mu\text{-}SR)Rh(CO)(PPh_2R^*)]$ [R* = (+)-neomenthyl; R = *t*Bu, $CH_2CH_2Si(OEt)_3$] asymmetric hydrogenation of methyl (*Z*)-α-acetamidocinnamate could be performed. An optical purity of up to 97% *ee* at low conversions was achieved, but it dropped gradually when the reduction advanced.[4] Using a menthyl-substituted thiolato group as a chiral bridging ligand in (+)-*cis*-$[tBu_3P(CO)Rh(\mu\text{-}Cl)(\mu\text{-}SR^*)Rh(CO)PtBu_3]$ [R* = (+)-neomenthyl], an optical purity of up to 50% *ee* was obtained in moderate yields.[5] Our newly developed synthesis of conformationally well-defined, enantiomerically pure 3-menthylindenyl[6] and 2-menthylindenyl ligands[7] and their transition metal complexes,[8,9] enable us to describe in this paper a third example for exploiting the menthyl-derived chirality in catalysis.

[a] Institut für Chemie der Technischen Universität,
Straße des 17. Juni 135, 10623 Berlin, Germany,
Fax: (internat.) + 49-(0)30/3142-2168
E-mail: schumann@chem.tu-berlin.de
[b] Department of Organic Chemistry, Hebrew University,
Jerusalem 91904, Israel
Fax: (internat.) + 972-2/651-3832
E-mail: jblum@chem.ch.huji.ac.il
[c] Department of Chemistry and Biochemistry, University of Oklahoma,
620 Parrington Oval, Norman, OK 73019, USA
Fax: (internat.) + 1-405/325-6111
E-mail: rHalterman@ou.edu

Results and Discussion

Rhodium Complexes

The metathesis reaction of two equivalents of the lithium salt **1** with the binuclear rhodium complex $[(CO)_2Rh(\mu\text{-}Cl)_2Rh(CO)_2]$, in diethyl ether at 0 °C, followed by warming to room temperature, gave the corresponding indenyl complex **2** in 74% yield (Scheme 1). Although the indenyl ligand is chiral, owing to the menthyl substituent, it possesses homotopic π-faces and can form only one chiral indenyl metal complex after metalation. The crude product was obtained by removing the solvent, and purified by chromatography under an inert atmosphere on dried alumina with *n*-

 © WILEY-VCH Verlag GmbH, 69451 Weinheim, Germany, 2002 1434–1948/02/0101–0211 $ 17.50+.50/0

hexane as eluent, followed by crystallization from *n*-pentane. Contact with even traces of oxygen during chromatography led to the immediate decomposition of the complex and dimerization of the indenyl ligand to give 1,1′-bis(2-menthyl-4,7-dimethylindene) and 1,1′-bis(2-menthylindene), respectively.[10] Upon addition of bis(diphenylphosphanyl)ethane to **2**, followed by prolonged heating, **3** was obtained in 73% yield (Scheme 1).

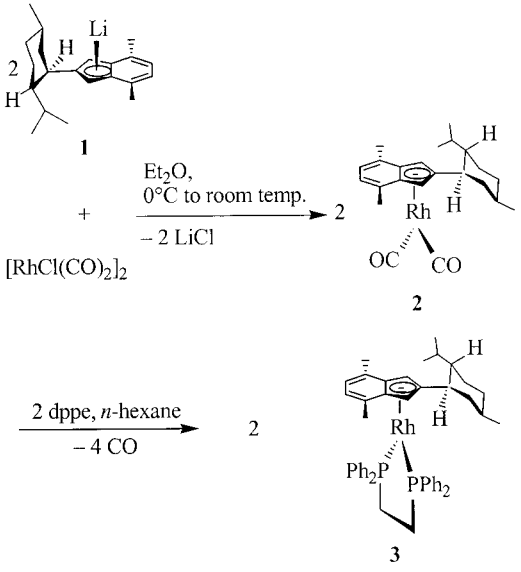

Scheme 1

The same substitution procedure could be used to obtain **5** and **6** by adding bis(diphenylphosphanyl)ethane or trimethylphosphane, respectively, to (−)-bis(η²-ethylene)(η⁵-2-menthylindenyl)rhodium(I) (**4**) (Scheme 2).

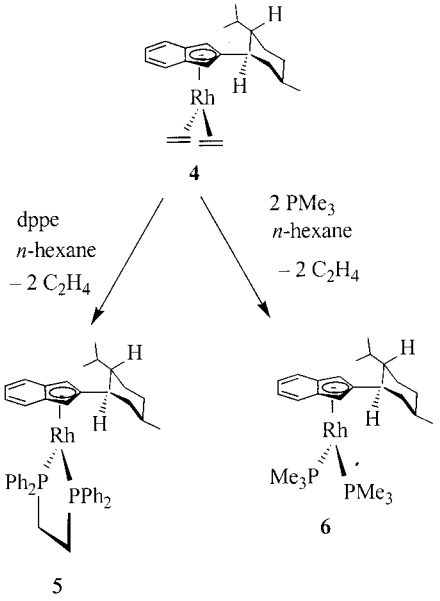

Scheme 2

The rhodium complex **8** was synthesized and isolated in 87% yield by the metathesis reaction of two equivalents of the lithium salt **7** with the binuclear rhodium complex [(nbd)Rh(μ-Cl)$_2$Rh(nbd)] (Scheme 3).

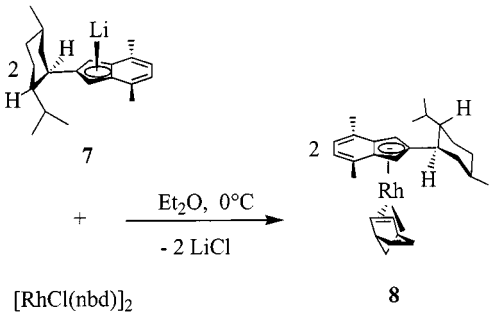

Scheme 3

In contrast to their solutions, pure crystalline **2**, **3**, **5**, and **8** are stable to air and moisture, while **6** readily decomposes. The complexes are soluble in polar solvents such as THF, pyridine, and diethyl ether as well as in aromatic solvents such as toluene, and in nonpolar solvents such as *n*-hexane.

Compounds **2**, **3**, and **6** gave suitable single crystals for X-ray diffraction analysis upon recrystallization from *n*-pentane. They crystallized in the same orthorhombic space group $P2_12_12_1$ with one or three crystallographically independent molecules in the asymmetric unit. The solid state structures of these molecules are shown in Figure 1, Figure 2, and Figure 3, respectively. The trimethylphosphane groups in **6** are disordered about two positions, with occupancy factors of 0.504(4) and 0.496(4), as shown in Figure 4.

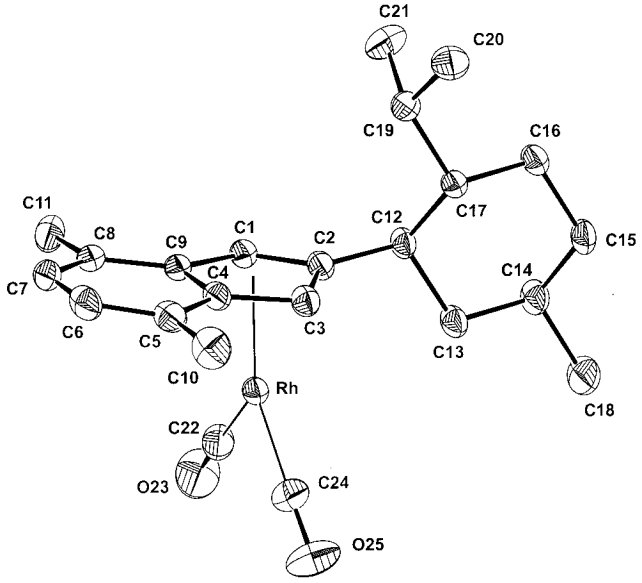

Figure 1. ORTEP drawing[11] of the molecular structure and numbering scheme of **2**, with 50% probability thermal ellipsoids; all hydrogens have been removed for clarity; selected bond lengths [Å] and bond angles [°] with estimated standard deviations:[12] Rh−Cg 1.9557(8), Rh−C(22) 1.861(2), Rh−C(24) 1.865(3), C(1)−C(2) 1.412(3), C(2)−C(3) 1.423(3), C(3)−C(4) 1.464(3), C(4)−C(9) 1.416(3), C(1)−C(9) 1.476(3), C(22)−O(23) 1.132(3), C(24)−O(25) 1.141(3); Cg−Rh−C(22) 135.24(8), Cg−Rh−C(24) 134.45(8), C(22)−Rh−C(24) 90.19(11), Rh−C(22)−O(23) 178.0(3), Rh−C(24)−O(25) 177.8(3)

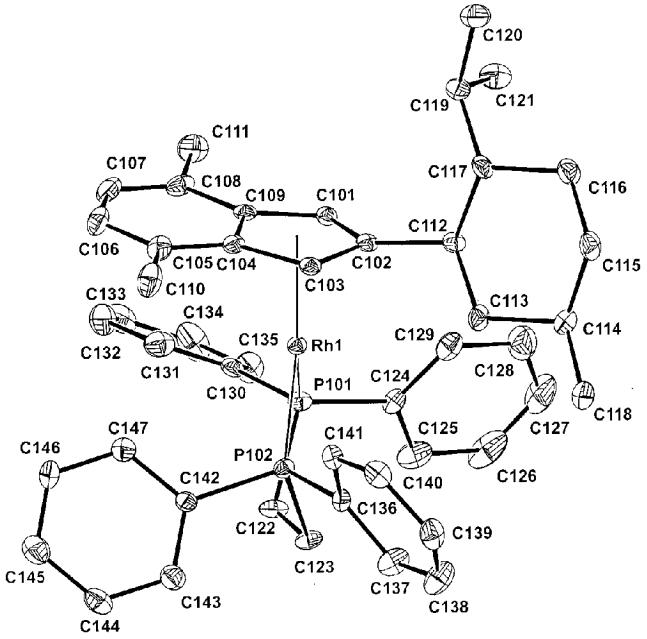

Figure 2. ORTEP drawing[11] of the molecular structure and numbering scheme of **3** (only one of the three crystallographically independent molecules is shown), with 30% probability thermal ellipsoids; all hydrogens have been removed for clarity; selected bond lengths [Å] and bond angles [°] with estimated standard deviations:[13] Rh(1)−Cg(1) 1.9782(19), Rh(2)−Cg(2) 1.9617(19), Rh(3)−Cg(3) 1.9880(19), Rh(1)−P(101) 2.2036(12), Rh(1)−P(102) 2.2063(13), Rh(2)−P(201) 2.1775(13), Rh(2)−P(202) 2.2094(14), Rh(3)−P(301) 2.1763(14), Rh(3)−P(302) 2.2322(13), C(101)−C(102) 1.435(6), C(102)−C(103) 1.418(6), C(103)−C(104) 1.461(6), C(104)−C(109) 1.436(7), C(101)−C(109) 1.440(6), C(201)−C(202) 1.443(6), C(202)−C(203) 1.421(6), C(203)−C(204) 1.442(7), C(204)−C(209) 1.432(7), C(201)−C(209) 1.437(7), C(301)−C(302) 1.437(6), C(302)−C(303) 1.407(6), C(303)−C(304) 1.456(6), C(304)−C(309) 1.428(7), C(301)−C(309) 1.450(6); Cg(1)−Rh(1)−P(101) 137.02(7), Cg(1)−Rh(1)−P(102) 138.57(7), Cg(2)−Rh(2)−P(201) 133.42(8), Cg(2)−Rh(2)−P(202) 141.36(8), Cg(3)−Rh(3)−P(301) 130.88(7), Cg(3)−Rh(3)−P(302) 143.98(7), P(101)−Rh(1)−P(102) 84.22(5), P(201)−Rh(2)−P(202) 85.20(5), P(301)−Rh(3)−P(302) 84.76(5), C(122)−P(101)−Rh(1) 111.28(16), C(123)−P(102)−Rh(1) 110.76(16), C(222)−P(201)−Rh(2) 110.59(16), C(223)−P(202)−Rh(2) 109.95(16), C(322)−P(301)−Rh(3) 109.36(18), C(323)−P(302)−Rh(3) 109.56(16)

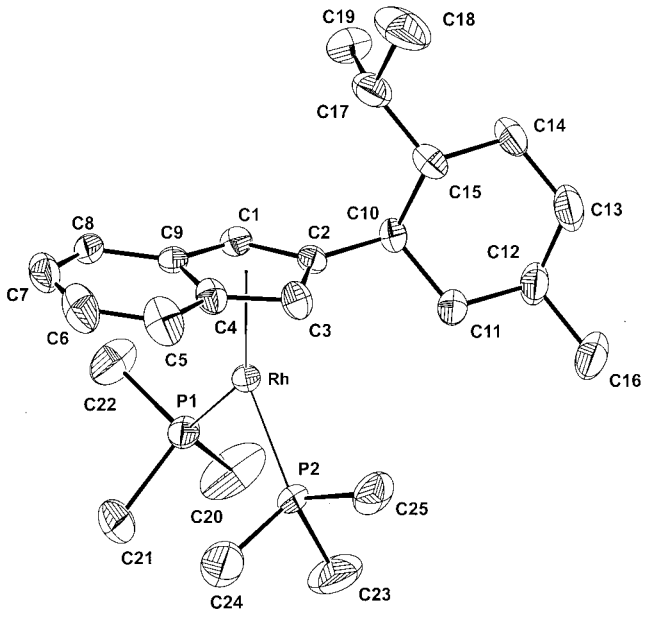

Figure 3. ORTEP drawing[11] of the molecular structure and numbering scheme of **6**, with 50% probability thermal ellipsoids; all hydrogens have been removed for clarity, and the disorder of the PMe_3 groups is omitted; selected bond lengths [Å] and bond angles [°] with estimated standard deviations:[14] Rh−Cg 1.9583(13), Rh−P(1a) 2.138(3), Rh−P(2a) 2.285(3), Rh−P(1b) 2.312(2), Rh−P(2b) 2.154(3), C(1)−C(2) 1.417(4), C(2)−C(3) 1.430(4), C(3)−C(4) 1.451(4), C(4)−C(9) 1.422(4), C(1)−C(9) 1.447(4), P(1a)−C(20a) 1.841(9), P(1a)−C(21a) 1.838(8), P(1a)−C(22a) 1.798(8), P(2a)−C(23a) 1.804(19), P(2a)−C(24a) 1.846(8), P(2a)−C(25a) 1.828(4), P(1b)−C(20b) 1.7758(13), P(1b)−C(21b) 1.836(8), P(1b)−C(22b) 1.823(7), P(2b)−C(23b) 1.828(16), P(2b)−C(24b) 1.817(8), P(2b)−C(25b) 1.810(8); Cg−Rh−P(1a) 136.14(9), Cg−Rh−P(2a) 125.68(10), Cg−Rh−P(1b) 123.64(8), Cg−Rh−P(2b) 141.07(9), P(1a)−Rh−P(2a) 96.19(10), P(1b)−Rh−P(2b) 94.64(9)

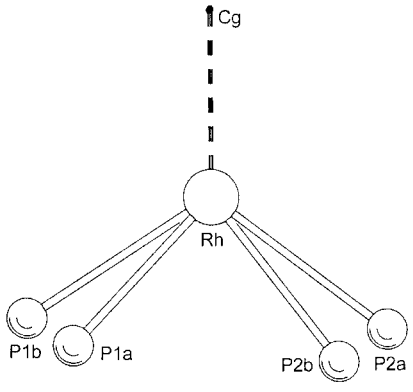

Figure 4. Disorder of **6** in the crystal[14]

All four complexes are monomeric, free of solvent, diastereomerically pure and clearly show the characteristic three stereocenters of the menthyl moiety. In all cases the transition metals of the formal oxidation state +1 are coordinated in a trigonal planar arrangement by the centroids of the cyclopentadienyl systems and the neutral ligands. It is particularly noteworthy that the terpene moiety adopts similar conformations, with the menthyl moiety being nearly perpendicular to the indenyl plane and the bulky isopropyl group pointing away from the metal. The corresponding dihedral angles[15] are: **2**: −8°; **3**: 24°, 29°, 17°; **6**: 14°. The average bonding distances of rhodium to the five-membered indenyl rings are 2.30 Å (**2**, **6**) and 2.32 Å (**3**); the average bond lengths for rhodium to the neutral ligands are 1.86 Å for complex **2**, 2.20 Å for complex **3**, and 2.22 Å for complex **6**. These distances are in close agreement with the bond lengths given for dicarbonyl(η^5-indenyl)rhodium (2.29 Å and 1.86 Å),[16] dicarbonyl(η^5-4,5,6,7-tetramethylindenyl)rhodium (2.29 Å and 1.86 Å),[17] (η^5-indenyl)bis(trimethylphosphane)rhodium(I) (2.32 Å and 2.21 Å),[18] and (η^5-indenyl)(methyl)[1,2-bis(diphenylphosphanyl)propane]-rhodium(III) (2.28 Å and 2.27 Å).[19] The CO−Rh−CO angle of 90.2° in **2** (91.7°[16] and 92.5°[17]) and the P(1)−Rh−P(2) angles of 84.2°, 85.2°, and 84.8° for **3** as well as 96.2° and 94.6° for **6** (96.7°[18] and 85.2°[19]) correlate with the corresponding angles in related complexes. The carbonyl ligands are almost linearly coordinated (177.9°). The average methyl−P−methyl angle of 99.9° is smaller

than the expected tetrahedral angle of 109.5°. It correlates with 101.5° in the compound $[Al_2Cl_2Me_4][(\eta^5$-cyclopentadienyl)bis(trimethylphosphane)rhodium(I)].[20]

The five-membered rings of the indenyl systems are not equally bound to Rh but resemble a distorted η^5-coordination. The bond lengths of the carbon atoms C(X01), C(X02), and C(X03) to the metal are 0.08−0.27 Å shorter than the bond lengths of the bridging atoms C(X04) and C(X09). In general, slip distortions Δ[21] and ring slippages RS[21] toward the C(X02) atoms are found. The values for Δ and RS are 0.186 Å and 0.189 Å in **2**, 0.157 Å, 0.152 Å, 0.177 Å and 0.175 Å, 0.180 Å, 0.243 Å in **3**, and 0.178 Å and 0.205 Å in **6**. The tendency towards a slight η^3-coordination accounts for the non-planar cyclopentadienyl ring and thus for the hinge angles HA[22] and fold angles FA.[22] The values for HA and FA are 10.6° and 10.5° in **2**, 7.7°, 6.8°, 8.0° and 8.3°, 5.4°, 8.1° in **3**, and 8.1° and 8.0° in **6**. The values are in the range expected for distorted η^5-coordination, as found in (COD)(η^5-indenyl)rhodium[23] (Δ = 0.152 Å, HA = 8.9°, FA = 7.4°), $(C_2H_4)_2$(η^5-indenyl)rhodium(I)[24] (Δ = 0.161 Å, HA = 8.1°, FA = 7.4°), bis(trimethylphosphane)(η^5-indenyl)rhodium(I)[25] (Δ = 0.201 Å, HA = 8.4°, FA = 7.9°) and fail to show the characteristics of η^3-coordination found in tris(dimethylphenylphosphane)(η^3-indenyl)rhodium(I)[26] (Δ = 0.79 Å, HA = 25°, FA = 28°). Such distortions are also detectable by the differences in the C−C bond lengths in the five-membered indenyl rings. The maximum variations of 0.06 Å (**2**), 0.05 Å (**3**), and 0.03 Å (**6**) are higher than can be accounted for by the influence of the condensed six-membered ring alone. In general the trend towards η^3-coordination is not strong; although the distortions are much higher than they are for the asymmetrical substituted (1-menthylindenyl)metal complexes, where the substitution patterns favor not only a distortion toward C(X02) but toward C(X03) as well.[8]

As the HOMO of the indenyl unit in rhodium complexes can best be stabilized at a rotation angle RA of 0°[16,18,24] the neutral ligands are aligned parallel to the longitudinal axis of indene. In these cases, values for RA of 0.1° (**2**), 1.8°, 11.4°, and 11.9° (**3**) as well as 6.3° and 3.5° (**6**) are observed.

NMR Spectra

The assignment of the ^{1}H and ^{13}C signals was based on ^{1}H,^{1}H COSY and ^{1}H,^{13}C correlated spectra as well as on two-dimensional NOE experiments. All described transition metal complexes exhibit C_1 symmetry in their solution NMR spectra. The neutral ligands dppe in **5** and PMe_3 in **6** exhibit two ^{31}P NMR signals and thus do not seem to rotate around the indenyl−rhodium axis on the NMR time scale as has been found for similar complexes.[27] For the two CO ligands in **2**, for example, only one signal occurs and for the four coordinating carbon atoms of the nbd ligand only two signals occur. This gives rise to an empirical low induction of the chiral indenyl ligand on the remote neutral ligands or to rotating ligands on the ^{13}C NMR time scale.

Characteristic $^1J_{CRh}$ coupling constants varying between 1.0 and 7.9 Hz for the five-membered indenyl rings and from 10.3 to 85.4 Hz for the neutral ligands could be determined. Higher coupling constants correlate to higher electron density, therefore the bridging atoms C^8 and C^9 are more weakly bonded in comparison to the atoms C^1 to C^3, which show higher values. This is consistent with the $\eta^2+\eta^3$-coordination found in the solid state structures. The higher $^1J_{XRh}$ values of the neutral ligands are due to the shorter bond lengths in comparison to the indenyl−rhodium bond.

Decoupled ^{103}Rh NMR spectra of **3** and **8** in Et_2O/D_2O (3:1) were recorded and chemical shifts between δ = −143.4 and −834.1 relative to hexachlororhodate in D_2O were observed. The intensity of the high-field shift increases along with the stronger σ-donor bonded to the metal[28] and higher alkylation of the indenyl ligand.[8]

Catalysis

Catalytical Hydrogenation

The applicability of the rhodium complex **3** and of the related compounds (−)-bis(η^2-ethylene)(η^5-2-menthyl-4,7-dimethylindenyl)rhodium(I) (**9**),[29] (−)-(cycloocta-1,5-diene)(η^5-1-menthyl-4,7-dimethylindenyl)rhodium(I) (**10**),[8] (−)-(cycloocta-1,5-diene)(η^5-2-menthyl-4,7-dimethylindenyl)rhodium(I) (**11**),[29] and (−)-(cycloocta-1,5-diene)(η^5-2-menthylindenyl)rhodium(I) (**12**)[29] (Scheme 4), described by us earlier, as hydrogenation catalysts was studied. The prochiral itaconic acid was chosen as the substrate.

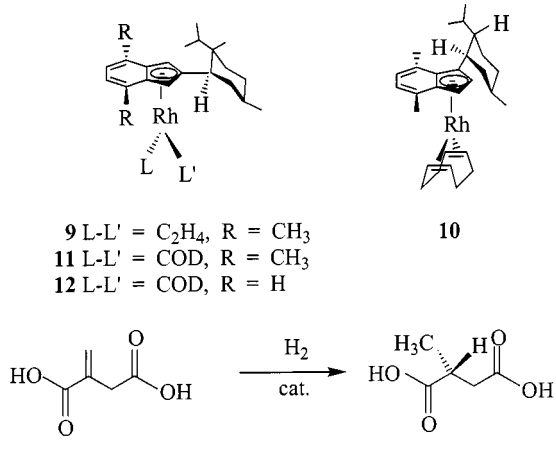

Scheme 4

All tested catalysts proved highly active. Usually a quantitative yield of the methylsuccinic acid was obtained within 4 h at 60−70 °C. However, only the two COD-containing rhodium-menthylindenyl complexes **10** and **11** were found to induce chirality, and lead to the formation of (*S*)-(−)-methylsuccinic acid in 18 and 16% *ee*, respectively. Complex **11** only has the chiral influence of the menthyl substituent, and the observed low stereoselectivity is similar to that seen with menthylcyclopentadienyl metal complexes.[30] Complex **10**, however, contains an additional facial chirality element, and gave an unexpectedly lower selectivity than other bis(1-menthylindenyl)metal catalyzed reactions.[31] It is rather

surprising that catalyst **12**, which has also a COD moiety but differs from **11** by having no indenyl-bound methyl groups, does not promote enantioselective hydrogenation of the itaconic acid.

Catalytic Hydroformylation

The observation that cyclohexene is hydroformylated in the presence of catalyst **2** at 120 °C and 40 bar CO/H_2, giving a quantitative yield of cyclohexanecarboxaldehyde within 3 h, led us to investigate the transformation of an olefin which can yield isomeric products. Using styrene as a prochiral substrate our rhodium complexes afforded 2- and 3-phenylpropanal (branched and linear products) in 23−100% yield. The results of some representative experiments are summarized in Table 1.

Table 1. Hydroformylation of styrene in the presence of some rhodium catalysts

Entry	Catalyst[a]	Total yield after 22 h	Linear/branched ratio
1	**2**	25	1:7.8[b]
2	**2**[c]	26	1:9.0
3	**3**	30	1:14.0
4	**4**	61	1:3.4
5	**10**	89[d]	1:6.2[e]
6	**11**	23	1:3.9
7	**12**	83	1:1.6

[a] Reaction conditions: 0.1 mol of styrene, 1 mmol of catalyst, 10 mL of toluene, 20 bar H_2, 20 bar CO, 60 °C, 22 h. [b] At 100−120 °C (2−4 h) the ratio became 1:0.8. [c] The complex was entrapped in a silica sol-gel matrix according to ref.[32]. [d] After 36.5 h. [e] At 100 °C the ratio became 1:1.1.

Due to the stereogenic centers in the catalyst precursors one would expect the chirality to be transferred to the branched aldehyde. However, styrene was found to undergo quantitative hydroformylation at 100 °C in the presence of **10** to give nearly identical amounts of the linear and the racemic branched aldehyde. As no chirality could be detected in the branched product, we lowered the temperature to 60 °C. At this temperature catalysts **2**, **3**, **4**, **11**, and **12** led to 23−83% aldehydes after 22 h, and even under these conditions no appreciable chirality transfer was observed: the highest *ee* value of 3% was obtained with catalyst **3** (entry 3).

Although we did not visually detect the separation of any metallic rhodium during the hydroformylation that could have been responsible for the achiral processes, we performed an experiment with sol-gel entrapped complex **2** to prevent any possible decomposition of the original chiral catalyst (entry 2). We found, however, that the homogeneous and the immobilized catalysts gave almost identical results and no significant enantioselectivity could be detected. Another reason for the atactic activity might have been the formation of achiral complexes of the type $RhH(CO)_2(L)(L')$ by substitution of the indenyl moiety. However, these complexes could still not explain the different linear/branched ratios, as they vary with changes of the indenyl (entry 6 vs. 7) and the neutral ligands. Values between 1:0.78 (catalyst **2** at 120 °C) and 1:14 (catalyst **3** at 60 °C) were found. The highest selectivity is obtained using the bulky dppe ligand, and the selectivity decreases with increasing temperature. Typically, linear/branched ratios of 1:1 and 1:3 are mentioned in the literature.[33]

In addition to styrene, *n*-dodecene was also reacted in the presence of catalyst **2** at different temperatures and pressures. Samples of the reaction mixture were withdrawn every hour and analyzed by GC and ^1H NMR spectroscopy. After 6 h (80 bar total pressure) conversions of 97% were obtained at 80 °C. If the temperature was lowered to 60 °C only 38% yield was obtained.

When using 1-dodecene as a substrate partial isomerization of the double bond occurred prior to the hydroformylation. In addition to 1-tridecanal and 2-methyldodecanal in the ratio 1:0.7, 3-ethylundecanal and 4-propyldecanal were formed in 8 and 7% yield (80 °C and 80 bar). This isomerization of 1-dodecene to 2- and 3-dodecene does not occur at 60 °C.[34]

Conclusions

Metathesis reactions of $[RhCl(L)(L')]_2$, with chiral, menthyl-functionalized indenyl salts and ligand substitution reactions provide a convenient entry into chiral rhodium complexes. X-ray diffraction analyses of the monomeric, stereomerically pure complexes **2**, **3**, and **6** confirm the enantiomeric purity of the stereogenic centers in the ligands and that the indenyl moiety is $\eta^2+\eta^3$-coordinated. Complex **3** and the analogeous rhodium complexes **9**, **10**, **11**, and **12** show a high activity in the catalytic hydrogenation of itaconic acid. Both catalysts **10** and **11** induced chirality in the product. Complexes **2**−**4** and **10**−**12** show considerable activity in the hydroformylation of olefins with highly varying linear/branched ratios between 1:0.78 and 1:14 but promote very little chirality transfer.

Experimental Section

All operations involving organometallic compounds were carried out under an inert atmosphere of nitrogen or argon using standard Schlenk techniques in dry, oxygen-free solvents. Melting points were measured in sealed capillaries with a Büchi 510 melting point apparatus and are uncorrected. Optical rotations were determined on a Schmidt+Haensch Polartronic-D and a Perkin−Elmer model 141 polarimeter. The NMR spectra were recorded on a Bruker ARX 200 (^1H: 200 MHz; ^{13}C: 50.32 MHz; ^{31}P: 80.94 MHz) or ARX 400 (^1H: 400 MHz; ^{13}C: 100.64 MHz; ^{103}Rh: 12.60 MHz) spectrometer at ambient temperature. Chemical shifts are reported in ppm relative to the ^1H or the ^{13}C signal of the deuterated solvents. Chemical shifts of ^{31}P and ^{103}Rh are given relative to 85% phosphoric acid in D_2O and hexachlororhodate in D_2O. The IR spectra were recorded on a Nicolet Magna System 750 spectrometer. Mass spectra (EI, 70 eV) were obtained using a Varian MAT 311 A/AMD instrument. Only significant fragments containing the isotopes of the highest abundance are listed. Relative intensities in % are given in parentheses. Elemental analyses were performed on a Perkin−Elmer Series II CHNS/O Analyzer 2400. (−)-(2-Men-

thyl-4,7-dimethylindenyl)lithium (**1**),[7] (−)-(2-menthylindenyl)lithium (**7**),[7] tetracarbonyldi-μ-chlorodirhodium(I),[35] (−)-bis(η²-ethylene)(η⁵-2-menthyl-4,7-dimethylindenyl)rhodium(I) (**9**),[29] (−)-bis(η²-ethylene)(η⁵-2-menthylindenyl)rhodium(I) (**4**),[29] (−)-(cycloocta-1,5-diene)(η⁵-1-menthyl-4,7-dimethylindenyl)rhodium(I) (**10**),[8] (−)-(cycloocta-1,5-diene)(η⁵-2-menthyl-4,7-dimethylindenyl)rhodium(I) (**11**),[29] and (−)-(cycloocta-1,5-diene)(η⁵-2-menthylindenyl)rhodium(I) (**12**)[29] were prepared according to published procedures. 1,2-Bis(diphenylphosphanyl)ethane and di-μ-chlorobis(η⁴-norbornadiene)dirhodium(I) were used as purchased without further purification.

(−)-Dicarbonyl(η⁵-2-menthyl-4,7-dimethylindenyl)rhodium(I) (2): (−)-(η⁵-2-menthyl-4,7-dimethylindenyl)lithium (**1**) (0.62 g, 2.15 mmol) was added to a solution of tetracarbonyldi-μ-chlorodirhodium(I) (0.42 g, 1.08 mmol) in diethyl ether (15 mL) at 0 °C. The suspension was stirred for 3 h, heated to 25 °C and stirred for further 10 h. The solvent was removed under vacuum (10^{-2} mbar), leaving a solid which was subsequently suspended in *n*-hexane (2 mL) and fractionally chromatographed under nitrogen on alumina. Elution with *n*-hexane initially gave colorless and finally yellow solutions. The solvents of the yellow fractions were removed under vacuum (10^{-2} mbar) yielding an orange solid. Recrystallization from warm *n*-pentane (5 mL) gave 0.70 g (74%) of **2** as orange crystals, m.p. 125 °C dec. $[\alpha]_D^{25} = -31.8$ (*c* = 7.6, *n*-hexane). ^{1}H NMR ([D$_6$]benzene, 400 MHz): δ = 0.67 (d, ^3J = 7.0 Hz, 3 H, H$^{7'/9'/10'}$), 0.68 (d, ^3J = 6.9 Hz, 3 H, H$^{7'/9'/10'}$), 0.93 (d, ^3J = 6.5 Hz, 3 H, H$^{7'/9'/10'}$), 0.80−2.05 (m, 10 H, H$^{1',2',3',4',5',6',8'}$), 2.14 (s, 3 H, H$^{10/11}$), 2.15 (s, 3 H, H$^{10/11}$), 4.48 (d, ^4J = 2.0 Hz, 1 H, H$^{1/3}$), 5.50 (d, ^4J = 2.0 Hz, 1 H, H$^{1/3}$), 6.67 (m, 2 H, H^{5,6}). ^{13}C{^{1}H} NMR ([D]chloroform, 50.32 MHz): δ = 15.6, 18.07, 18.11, 21.6, 22.8 (C$^{7',9',10,10',11}$), 25.0, 35.4, 47.8 (C$^{2',5',6'}$), 28.2, 33.6, 40.2, 50.5 (C$^{1',3',4',8'}$), 72.1 (d, $^1J_{CRh}$ = 3.2 Hz, C$^{1/3}$), 75.9 (d, $^1J_{CRh}$ = 3.1 Hz, C$^{1/3}$), 114.3 (d, $^1J_{CRh}$ = 2.1 Hz, C$^{8/9}$), 115.8 (d, $^1J_{CRh}$ = 2.0 Hz, C$^{8/9}$), 128.1 (d, $^1J_{CRh}$ = 1.6 Hz, C^2), 125.07, 125.08 (C^{4,7}), 125.5, 125.6 (C^{5,6}), 191.3 (d, $^1J_{CRh}$ = 85.4 Hz, CO). IR (CsI): $\tilde{\nu}$ = 3043 cm^{-1} (w), 3025 (w), 2953 (s), 2929 (s), 2919 (s), 2877 (m), 2868 (m), 2859 (m), 2847 (m), 2031 (s), 2016 (m), 1971 (s), 1942 (m), 1835 (w), 1819 (m), 1699 (w), 1634 (w), 1589 (w), 1502 (m), 1445 (m), 1377 (m), 1367 (m), 1362 (m), 1348 (m), 1307 (m), 1288 (m), 1274 (m), 1261 (m), 1247 (w), 1182 (m), 1165 (w), 1139 (w), 1127 (m), 1084 (m), 1036 (m), 1004 (m), 922 (m), 860 (m), 818 (m), 684 (w), 574 (w), 569 (w), 563 (w), 552 (m), 543 (w), 510 (m), 502 (m), 491 (m), 279 (m). MS (68 °C): *m*/*z* (%) = 440 (5) [M]$^+$, 412 (11) [(CO)(C$_{21}$H$_{29}$)Rh]$^+$, 384 (4) [(C$_{21}$H$_{29}$)Rh]$^+$, 382 (100) [C$_{21}$H$_{27}$Rh]$^+$, 245 (1) [C$_{11}$H$_{10}$Rh]$^+$. C$_{23}$H$_{29}$O$_2$Rh (440.39): calcd. C 62.73, H 6.64; found C 62.30, H 6.23.

(−)-(η⁵-2-Menthyl-4,7-dimethylindenyl){η²-1,2-bis(diphenylphosphanyl)ethane}rhodium(I) (3): 1,2-Bis(diphenylphosphanyl)ethane (0.32 g, 0.80 mmol) was added to a solution of **2** (0.35 g, 0.79 mmol) in *n*-hexane (40 mL) at 0 °C. The orange solution (gas evolution!) was stirred for 2 h at room temperature and heated for 10 h to 60 °C. The solvent was removed under vacuum (10^{-2} mbar), leaving a solid which was suspended in *n*-hexane (10 mL), filtered with a d4 frit and washed three times with *n*-hexane (10 mL). The filtrate was cooled to −78 °C, decanted and the solvent was removed under vacuum (10^{-2} mbar). Fractional chromatography under nitrogen on alumina using *n*-hexane and *n*-hexane/ethyl acetate (10:1) as eluent gave yellow solutions. The solvent was removed under vacuum (10^{-2} mbar) yielding an orange solid. Recrystallization from warm *n*-pentane (5 mL) gave 0.45 g (73%) of **3** as orange crystals, m.p. > 240 °C. $[\alpha]_D^{25} = -76.0$ (*c* = 0.5, diethyl ether). ^{1}H NMR ([D$_6$]benzene, 200 MHz): δ = 0.67 (d, ^3J = 6.9 Hz, 3 H, H$^{9'/10'}$), 0.77 (d, ^3J = 6.9 Hz, 3 H, H$^{9'/10'}$), 0.81 (d, ^3J = 6.5 Hz, 3 H, H$^{7'}$), 0.81−1.95 (m, 14 H, H$^{1',2',3',4',5',6',8'}$, PCH_2), 2.03 (s, 3 H, H$^{10/11}$), 2.19 (s, 3 H, H$^{10/11}$), 5.23 (m, 1 H, H$^{1/3}$), 5.37 (m, 1 H, H$^{1/3}$), 6.93 (m, 2 H, H^{5,6}), 7.04−7.55 [m, 20 H, C*H*(Phenyl)]. ^{13}C{^{1}H} NMR ([D$_6$]benzene, 50.32 MHz): δ = 15.6, 18.8, 19.5, 21.7, 23.3 (C$^{7',9',10,10',11}$), 30.1 (d, $^1J_{CP}$ = 24.8 Hz, P*C*H$_2$), 30.6 (d, $^1J_{CP}$ = 24.7 Hz, P*C*H$_2$), 25.3, 35.8, 46.3 (C$^{2',5',6'}$), 28.0, 34.1, 41.2, 51.0 (C$^{1',3',4',8'}$), 71.6 (m, C$^{1/3}$), 74.4 (m, C$^{1/3}$), 114.3 (d, $^1J_{CRh}$ = 1.6 Hz, C$^{8/9}$), 115.7 (d, $^1J_{CRh}$ = 1.6 Hz, C$^{8/9}$), 120.6, 121.8 (C^{5,6}), 123.3 (C$^{4/7}$), 123.4 (d, $^1J_{CRh}$ = 7.9 Hz, C^2), 124.2 (C$^{4/7}$), 127.5−133.6 [m, *C*H(Phenyl)], 140.3 [d, $^1J_{CP}$ = 35.4 Hz, *C*^{q}(Phenyl)]. ^{31}P NMR ([D$_6$]benzene, 80.94 MHz): δ = 75.01 (m). ^{103}Rh NMR ([D]chloroform/diethyl ether (1:3), 12.60 MHz): δ = −834.10. IR (CsI): $\tilde{\nu}$ = 3070 cm^{-1} (m), 3052 (m), 3002 (w), 2954 (s), 2915 (s), 2870 (m), 2852 (m), 1586 (w), 1571 (w), 1482 (m), 1433 (s), 1385 (w), 1374 (m), 1367 (m), 1337 (w), 1095 (s), 921 (m), 824 (m), 815 (m), 792 (w), 743 (m), 699 (s), 694 (s), 683 (m), 527 (s), 489 (m), 446 (w), 203 (m). MS (209 °C): *m*/*z* (%) = 782 (33) [M]$^+$, 739 (3) [C$_{44}$H$_{46}$P$_2$Rh]$^+$, 501 (21) [(C$_{26}$H$_{24}$P$_2$)Rh]$^+$. C$_{47}$H$_{53}$P$_2$Rh (782.79): calcd. C 72.12, H 6.82; found C 71.76, H 6.48.

(+)-(η⁵-2-Menthylindenyl){η²-1,2-bis(diphenylphosphanyl)ethane}rhodium(I) (5): In analogy to the preparation of **3**, (−)-bis(η²-ethylene)(η⁵-2-menthylindenyl)rhodium(I) (**4**) (0.42 g, 1.02 mmol) was reacted at room temperature with 1,2-bis(diphenylphosphanyl)ethane (0.40 g, 1.00 mmol) in *n*-hexane (20 mL) at 0 °C. After 3 days, workup, chromatography and recrystallization from *n*-pentane at −28 °C, red crystals of **5** (0.52 g, 69%) were obtained, m.p. 119 °C dec. $[\alpha]_D^{25} = 63.7$ (*c* = 1.4, benzene). ^{1}H NMR ([D$_6$]benzene, 400 MHz): δ = 0.65 (m, 1 H, H$^{2'}$), 0.66 (d, ^3J = 6.8 Hz, 3 H, H$^{9'/10'}$), 0.73 (d, ^3J = 6.8 Hz, 3 H, H$^{9'/10'}$), 0.80 (d, ^3J = 6.8 Hz, 3 H, H$^{7'}$), 0.82 (m, 1 H, H$^{6'}$), 0.95 (m, 1 H, H$^{5'}$), 1.04 (m, 1 H, H$^{4'}$), 1.24 (m, 1 H, H$^{1'}$), 1.29 (m, 4 H, PCH_2), 1.60 (m, 1 H, H$^{5'}$), 1.70 (m, 1 H, H$^{6'}$), 1.82 (m, 1 H, H$^{2'}$), 1.86 (m, 1 H, H$^{8'}$), 1.89 (m, 1 H, H$^{3'}$), 5.16 (m, 1 H, H$^{1/3}$), 5.36 (m, 1 H, H$^{1/3}$), 7.01, 7.02, 7.04, 7.05 (m, 4 H, H^{4,5,6,7}), 7.08−7.54 [m, 20 H, C*H*(Phenyl)]. ^{13}C{^{1}H} NMR ([D$_6$]benzene, 100.64 MHz): δ = 15.6, 21.7 (C$^{9'/10'}$), 23.1 (C$^{7'}$), 25.2 (C$^{5'}$), 27.9 (C$^{8'}$), 29.5 (m, P*C*H$_2$), 33.9 (C$^{1'}$), 35.6 (C$^{6'}$), 40.9 (C$^{3'}$), 46.2 (C$^{2'}$), 50.8 (C$^{4'}$), 74.0 (m, C$^{1/3}$), 74.3 (m, C$^{1/3}$), 114.6 (d, $^1J_{CRh}$ = 1.0 Hz, C$^{8/9}$), 116.7 (d, $^1J_{CRh}$ = 1.2 Hz, C$^{8/9}$), 117.1, 117.4, 119.5, 120.9 (C^{4,5,6,7}), 124.7 (d, $^1J_{CRh}$ = 6.5 Hz, C^2), 126.7−134.5 [m, *C*H(Phenyl)], 139.5−141.0 [m, *C*^{q}(Phenyl)]. ^{31}P NMR ([D$_6$]benzene, 80.94 MHz): δ = 73.76 (m, $^1J_{PRh}$ = 213.4 Hz), 78.11 (m, $^1J_{PRh}$ = 225.1 Hz). IR (CsI): $\tilde{\nu}$ = 3096 cm^{-1} (m), 3049 (m), 2958 (s), 2927 (s), 2912 (s), 2868 (m), 2847 (m), 1585 (w), 1484 (m), 1459 (m), 1434 (s), 1431 (s), 1248 (s), 1095 (m), 922 (m), 747 (m), 735 (s), 696 (s), 681 (m), 527 (s), 491 (m), 449 (w). MS (83 °C): *m*/*z* (%) = 754 (100) [M]$^+$, 711 (2) [C$_{42}$H$_{42}$P$_2$Rh]$^+$, 501 (51) [C$_{26}$H$_{24}$P$_2$Rh]$^+$, 424 (9) [C$_{20}$H$_{19}$P$_2$Rh]$^+$, 356 (1) [(C$_{19}$H$_{25}$)Rh]$^+$. C$_{45}$H$_{49}$P$_2$Rh (754.74): calcd. C 71.61, H 6.54; found C 72.05, H 6.51. Mol wt. cryosc in benzene: 783.

(−)-(2-Menthylindenyl)bis(trimethylphosphane)rhodium(I) (6): In analogy to the preparation of **5**, a mixture of **4** (0.49 g, 1.19 mmol) and trimethylphosphane (0.30 g, 3.94 mmol) in *n*-hexane (20 mL) was reacted at 0 °C. After 10 h at room temperature, workup, chromatography and recrystallization from warm *n*-pentane, red crystals of **6** (0.47 g, 77%) were obtained, m.p. 157 °C. $[\alpha]_D^{25} = -47.7$ (*c* = 0.5, diethyl ether). ^{1}H NMR ([D$_6$]benzene, 400 MHz): δ = 0.81 (d, ^3J = 7.0 Hz, 3 H, H$^{9'/10'}$), 0.88 (d, ^3J = 6.8 Hz, 3 H, H$^{9'/10'}$), 0.94 (m, 1 H, H$^{6'}$), 0.99 (d, ^3J = 6.4 Hz, 3 H, H$^{7'}$), 1.04 [m, 9 H, P^2(CH_3)$_3$], 1.06 (m, 1 H, H$^{2'}$), 1.07 (m, 1 H, H$^{5'}$), 1.08 [m, 9 H, P^1(CH_3)$_3$], 1.27 (m, 1 H, H$^{4'}$), 1.39 (m, 1 H, H$^{1'}$), 1.70 (m, 1

H, H$^{5'}$), 1.76 (m, 1 H, H$^{6'}$), 2.17 (m, 1 H, H$^{8'}$), 2.22 (m, 1 H, H$^{3'}$), 2.41 (m, 1 H, H$^{2'}$), 4.80 (m, 1 H, H$^{1/3}$), 4.96 (m, 1 H, H$^{1/3}$), 6.91 (m, 1 H, H^{5,6}), 7.06 (m, 2 H, H^{4,7}). $^{13}C\{^1H\}$ NMR ([D$_6$]benzene, 100.64 MHz): δ = 15.9, 21.9 (C$^{9',10'}$), 23.1 (C$^{7'}$), 23.5 [dvt, $^1J_{CP}$ = 8.6, $^2J_{CRh}$ = 2.2 Hz, P(*C*H$_3$)$_3$], 23.8 [dvt, $^1J_{CP}$ = 8.6, $^2J_{CRh}$ = 2.2 Hz, P(*C*H$_3$)$_3$], 25.3 (C$^{5'}$), 27.9 (C$^{8'}$), 33.8 (C$^{1'}$), 35.7 (C$^{6'}$), 41.5 (C$^{3'}$), 48.9 (C$^{2'}$), 50.7 (C$^{4'}$), 69.1 (dd, $^2J_{CP}$ = 14.5, $^1J_{CRh}$ = 3.2 Hz, C$^{1/3}$), 73.0 (dd, $^2J_{CP}$ = 14.5, $^1J_{CRh}$ = 3.2 Hz, C$^{1/3}$), 113.67, 113.69 (C^{4,7}), 116.9, 118.4 (C^{8,9}), 119.5, 119.6 (C^{5,6}), 125.6 (d, $^1J_{CRh}$ = 7.5 Hz, C^2). $^{31}P\{^1H\}$ NMR spectroscopy ([D$_6$]benzene, 80.94 MHz): δ = −6.60 (d, $^1J_{P(2)Rh}$ = 120.4, $^2J_{P(1)P(2)}$ = 50.4 Hz, P^2), −3.95 (dd, $^1J_{P(1)Rh}$ = 119.2, $^2J_{P(1)P(2)}$ = 50.4 Hz, P^1). MS (114 °C): *m*/*z* (%) = 508 (100) [M]$^+$, 493 (1) [$C_{24}H_{40}P_2Rh$]$^+$, 465 (1) [$C_{22}H_{36}P_2Rh$]$^+$, 432 (3) [$C_{22}H_{34}PRh$]$^+$, 356 (1) [($C_{19}H_{25}$)Rh]$^+$, 255 (4) [$C_6H_{18}P_2Rh$]$^+$. $C_{25}H_{43}P_2Rh$ (wt 508.47): calcd. C 59.05, H 8.52; found C 59.54, H 8.52.

(−)-(η^5-2-Menthylindenyl)(η^4-norbornadiene)rhodium(I) (8): In a similar manner to the synthesis of **2**, di-μ-chlorobis(η^4-norbornadiene)dirhodium(I) (0.96 g, 2.08 mmol) was reacted with **7** (1.21 g, 4.65 mmol) in diethyl ether (20 mL) at 0 °C. A yellow powder of **7** (1.63 g, 87%) was obtained after workup, chromatography, and recrystallization from warm *n*-pentane, m.p. 104 °C. $[\alpha]_D^{25}$ = −64.0 (*c* = 2.3, diethyl ether). ^1H NMR ([D$_6$]benzene, 400 MHz): δ = 0.72 (d, ^3J = 7.0 Hz, 3 H, H$^{9'/10'}$), 0.75 (d, ^3J = 6.9 Hz, 3 H, H$^{9'/10'}$), 0.82 [m, 2 H, C*H*$_2$(nbd)], 0.98 (m, 1 H, H$^{6'}$), 1.05 (m, 1 H, H$^{5'}$), 1.11 (d, ^3J = 6.5 Hz, 3 H, H$^{7'}$), 1.13 (m, 1 H, H$^{4'}$), 1.33 (m, 1 H, H$^{2'}$), 1.52 (m, 1 H, H$^{1'}$), 1.67 (m, 1 H, H$^{5'}$), 1.75 (m, 1 H, H$^{8'}$), 1.80 (m, 1 H, H$^{6'}$), 2.30 (m, 1 H, H$^{3'}$), 2.71 (m, 1 H, H$^{2'}$), 3.05 [m, 2 H, C*H*CH$_2$(nbd)], 3.30 [m, 4 H, C*H*(nbd)], 4.88 (s. br., 1 H, H$^{1/3}$), 4.94 (s. br., 1 H, H$^{1/3}$), 7.05 (m, 2 H, H^{5,6}), 7.23 (m, 2 H, H^{4,7}). $^{13}C\{^1H\}$ NMR ([D$_6$]benzene, 50.32 MHz): δ = 15.7, 21.7 (C$^{9',10'}$), 23.2 (C$^{7'}$), 25.2 (C$^{5'}$), 27.9 (C$^{8'}$), 33.9 (C$^{1'}$), 35.6 (C$^{6'}$), 37.8 [d, $^1J_{CRh}$ = 15.4 Hz, *C*H(nbd)], 38.1 [d, $^1J_{CRh}$ = 10.3 Hz, *C*H(nbd)], 41.1 (C$^{3'}$), 47.9 [d, $^2J_{CRh}$ = 2.7 Hz, *C*HCH$_2$(nbd)], 48.2 (C$^{2'}$), 50.6 (C$^{4'}$), 58.3 [d, $^3J_{CRh}$ = 6.7 Hz, *C*H$_2$(nbd)], 72.0 (d, $^1J_{CRh}$ = 4.6 Hz, C$^{1/3}$), 75.5 (d, $^1J_{CRh}$ = 4.6 Hz, C$^{1/3}$), 108.8 (d, $^1J_{CRh}$ = 3.2 Hz, C$^{8/9}$), 110.4 (d, $^1J_{CRh}$ = 3.1 Hz, C$^{8/9}$), 119.3, 119.5 (C^{4,7}), 121.6 (d, $^1J_{CRh}$ = 6.1 Hz, C^2), 122.0 (C$^{5/6}$), 122.3 (C$^{5/6}$). ^{103}Rh NMR ([D]chloroform/diethyl ether (1:3), 12.60 MHz): δ = −143.40. IR (CsI): $\tilde{\nu}$ = 3053 cm^{-1} (m), 2981 (m), 2954 (s), 2919 (s), 2868 (m), 2850 (m), 1713 (m), 1605 (w), 1454 (m), 1383 (m), 1347 (m), 1299 (m), 1260 (w), 1171 (m), 1063 (m), 748 (s), 735 (s), 567 (m), 493 (m), 459 (w), 358 (m), 309 (w). MS (103 °C): *m*/*z* (%) = 448 (100) [M]$^+$, 405 (16) [$C_{23}H_{26}Rh$]$^+$, 356 (3) [($C_{19}H_{25}$)Rh]$^+$, 309 (22) [$C_{16}H_{14}Rh$]$^+$, 217 (1) [C_9H_6Rh]$^+$, 195 (3) [C_7H_8Rh]$^+$. $C_{26}H_{33}Rh$ (448.46): calcd. C 69.64, H 7.42; found C 69.73, H 7.62.

Hydrogenation of Itaconic Acid: Typically, a mini-autoclave was charged under nitrogen in a glove box with the chiral rhodium catalyst (1 mmol) and a solution of itaconic acid (2.6 g, 20 mmol) in methanol (7 mL). The autoclave was sealed, purged three times with H_2 and pressurized to 14 bar. The reaction vessel was placed in a preheated oil bath thermostated at the desired temperature (accuracy ±0.5 °C). After 4 h the autoclave was cooled, opened and its contents were treated with 10% aqueous NaOH (5 mL). The rhodium catalyst was extracted with diethyl ether (3 × 5 mL). Addition of excess 3 M HCl to the aqueous solution, threefold extraction with diethyl ether (20 mL), drying with Na_2SO_4 and removal of the solvent under vacuum (10^{-2} mbar) afforded methylsuccinic acid as a colorless powder in quantitative yield. When catalyst **10** was employed at 60 °C or catalyst **11** at 70 °C, the *ee* values of the resulting (−)-methylsuccinic acid were 18 and 16%, respec-

Table 2. Crystal data and structure refinement for **2**, **3**, and **6**

Compound	**2**	**3**	**6**
Empirical formula	$C_{23}H_{29}O_2Rh$	$C_{47}H_{53}P_2Rh$	$C_{25}H_{43}P_2Rh$
M_r [g·mol^{-1}]	440.39	728.79	508.47
Crystal system	orthorhombic	orthorhombic	orthorhombic
Space group	$P2_12_12_1$ (No. 19)	$P2_12_12_1$ (No. 19)	$P2_12_12_1$ (No. 19)
a [Å], α [°]	11.0197(2), 90	19.5844(1), 90	8.7390(16), 90
b [Å], β [°]	13.0781(2), 90	22.8322(1), 90	8.838(2), 90
c [Å], γ [°]	14.9456(3), 90	27.4046(4), 90	34.919(10), 90
V [Å^3]	2153.91(7)	12254.1(2)	2697.1(11)
Z	4	12	4
ρ $_{calcd.}$ [g/cm^3]	1.358	1.273	1.252
μ (Mo-K_α) [mm^{-1}]	0.806	0.527	0.760
F(000)	912	4920	1072
Cystal size [mm^3]	0.63 × 0.52 × 0.32	0.40 × 0.32 × 0.28	0.58 × 0.23 × 0.22
θ $_{min}$, θ $_{max}$ [°]	2.07, 27.49	1.28, 27.50	1.17, 27.50
Index ranges	$-11 \le h \le 14$	$-25 \le h \le 25$	$-7 \le h \le 11$
	$-13 \le k \le 16$	$-15 \le k \le 29$	$-11 \le k \le 10$
	$-18 \le l \le 19$	$-35 \le l \le 34$	$-45 \le l \le 42$
Reflections collected	16446	95295	20726
Independent reflections	4946 [R_{int} = 0.0361]	28116 [R_{int} = 0.1051]	6183 [R_{int} = 0.0482]
Max., min. transmission	0.7477, 0.5332	0.8955, 0.7370	0.8832, 0.7132
Data, restraints, parameters	4946/0/240	28116/0/1366	6183/0/334
GOF on F^2	1.038	1.030	1.000
R indices [$I > 2\sigma(I)$]	R_1 = 0.0214	R_1 = 0.0567	R_1 = 0.0335
	wR_2 = 0.0498	wR_2 = 0.0797	wR_2 = 0.0687
R indices (all data)	R_1 = 0.0231	R_1 = 0.0988	R_1 = 0.0437
	wR_2 = 0.0506	wR_2 = 0.0916	wR_2 = 0.0737
Abs. structure param.	−0.03(2)	−0.043(17)	0.01(3)
Residual el. density	max. 0.236	max. 0.468	max. 0.342
[e/Å^3]	min. −0.534	min. −0.535	min. −0.859

tively. Complexes **3**, **9** and **12** proved equally active as hydrogenating catalysts but did not induce asymmetry in the product.

Hydroformylation Reactions: In a typical experiment a mini-autoclave was charged under nitrogen in a glove box with a mixture of styrene (10.4 g, 0.1 mol), the appropriate rhodium complex (1 mmol) and toluene (10 mL). The reaction vessel was purged three times with nitrogen and loaded with 20 bar each of H_2 and CO. The autoclave was placed in a thermostated oil bath and heated at 60 °C for 22 h. After cooling, the autoclave was opened, the toluene was distilled off, and the catalyst was removed by filtration through a silica 60 column, using hexane as eluent. The hexane also eluted the linear aldehyde, $C_6H_5CH_2CH_2CHO$. The branched product $C_6H_5CH(CHO)CH_3$, was eluted with a 8:2 ratio of hexane/diethyl ether. The ratio of the two products was determined by NMR spectroscopy. Polarimetric measurements indicated that the enantiomeric excess of (−)-$C_6H_5CH(CHO)CH_3$ was low in all experiments and did not exceed 3%. The hydroformylation experiments with the various catalysts are summarized in Table 1.

Crystal Structure Determination: Data were collected on a Siemens SMART CCD diffractometer (graphite monochromated Mo-K_α radiation, $\lambda = 0.71073$ Å) with an area detector by use of ω scans at room temperature for **2** and at 173 K for **3** and **6**. The structures were solved by direct methods using SHELXS-97[36] and refined on F^2 using all reflections with SHELXL-97.[37] All non-hydrogen atoms were refined anisotropically. The hydrogen atoms were placed in calculated positions and assigned to an isotropic displacement parameter of 0.08 Å^2. The idealized methyl groups were allowed to rotate about their X−C bond. Absolute structure parameters were determined according to Flack[38] with SHELX-97. SADABS[39] was used to perform area-detector scaling and absorption corrections. The maximum and minimum transmission factors and the resulting crystallographic data are given in Table 2. The geometrical aspects of the structures were analyzed by using the PLATON program.[40]

Crystallographic Data (excluding structure factors) for the structures reported in this paper have been deposited with the Cambridge Crystallographic Data Centre as supplementary publication nos. CCDC-165792 (**2**), CCDC-165793 (**3**), and CCDC-165794 (**6**). Copies of the data can be obtained free of charge on application to CCDC, 12 Union Road, Cambridge CB2 1EZ, UK [Fax: (internat.) +44-1223/336-033; E-mail: deposit@ccdc.cam.ac.uk].

Acknowledgments

This work was supported by the Fonds der Chemischen Industrie, the Deutsche Forschungsgemeinschaft (Graduiertenkolleg "Synthetische, mechanistische und reaktionstechnische Aspekte von Metallkatalysatoren"), and the Partnerships between the Technische Universität Berlin and The Hebrew University of Jerusalem and the University of Oklahoma. We thank Marco Haumann for performing the hydroformylation experiments of 1-dodecene.

[1] K. Weissermel, H.-J. Arpe, *Industrielle Organische Chemie*, Wiley-VCH, Weinheim, Germany, **1998**.
[2] *Applied Homogeneous Catalysis with Organometallic Compounds* (Eds.: B. Cornils, W. A. Herrmann), Wiley-VCH: Weinheim, Germany, **1996**.
[3] *Metallocenes* (Eds.: A. Togni, R. L. Halterman), Wiley-VCH: Weinheim, Germany, **1998**.
[4] M. Eisen, J. Blum, H. Schumann, B. Gorella, *J. Mol. Catal.* **1989**, *56*, 329−33.
[5] M. Eisen, P. Weitz, S. Shtelzer, J. Blum, H. Schumann, B. Gorella, F. H. Görlitz, *Inorg. Chim. Acta* **1991**, *188*, 167−176.
[6] H. Schumann, O. Stenzel, F. Girgsdies, R. L. Halterman, *Organometallics* **2001**, *20*, 1743−1751.
[7] R. L. Halterman, D. R. Fahey, E. F. Bailly, D. W. Dockter, O. Stenzel, J. L. Shipman, M. A. Khan, S. Dechert, H. Schumann, *Organometallics* **2000**, *19*, 5464−5470.
[8] H. Schumann, O. Stenzel, S. Dechert, F. Girgsdies, R. L. Halterman, *Organometallics* **2001**, *20*, 2215−2225.
[9] H. Schumann, O. Stenzel, S. Dechert, R. L. Halterman, *Organometallics* **2001**, *20*, 1983−1991.
[10] Compare the X-ray structure of *rac*-1,1′-bis(2,4,7-trimethylindene): O. Stenzel, H. G. Raubenheimer, M. Esterhuysen, *Acta Crystallogr. Sect. C*, accepted for publication.
[11] L. Zsolnai, H. Pritzkow, *ZORTEP ORTEP Program for PC*, Universität Heidelberg, **1994**.
[12] Cg defines the centroid of the ring atoms C(1), C(2), C(3), C(4), C(9).
[13] Cg(X) defines the centroid of the ring atoms C(X01), C(X02), C(X03), C(X04), C(X09).
[14] Cg defines the centroid of the ring atoms C(1), C(2), C(3), C(4), C(9); P(1), C(20), C(21), C(22) and P(2), C(23), C(24), C(25) are disordered about positions a and b, with occupancy factors of 0.504(4) and 0.496(4).
[15] Dihedral angle = angle between H(1) and H(10) or H(X01) and H(X12), respectively. Negative values correspond to H(10) or H(X12) pointing away from the metal.
[16] A. K. Kakkar, N. J. Taylor, J. C. Calabrese, W. A. Nugent, D. C. Roe, E. A. Connaway, T. B. Marder, *J. Chem. Soc., Chem. Commun.* **1989**, 990−992.
[17] A. K. Kakkar, N. J. Taylor, T. B. Marder, J. K. Shen, N. Hallinan, F. Basolo, *Inorg. Chim. Acta* **1992**, *198*, 219−231.
[18] T. B. Marder, J. C. Calabrese, D. C. Roe, T. H. Tulip, *Organometallics* **1987**, *6*, 2012−2014.
[19] F. Morandini, G. Pilloni, G. Consiglio, A. Sironi, M. Moret, *Organometallics* **1993**, *12*, 3495−3503.
[20] J. M. Mayer, J. C. Calabrese, *Organometallics* **1984**, *3*, 1292−1298.
[21] Slip distortion Δ = difference in the average metal to carbon distances: 0.5·[M − C(X04) + M − C(X09)] − 0.5·[M − C(X01) + M − C(X03)]; ring slippage RS = distance of the normal of the least-squares ring plane defined by C(X01), C(X02), C(X03), C(X08), C(X09) to the metal atom and the centroid of the five-membered ring.[17]
[22] Hinge angle = angle between normals to the least-squares planes defined by C(X01), C(X02), C(X03) and C(X01), C(X09), C(X04), C(X03); fold angle = angle between normals to the least-squares planes defined by C(X01), C(X02), C(X03) and C(X04), C(X05), C(X06), C(X07), C(X08), C(X09).[17]
[23] R. T. Baker, T. H. Tulip, *Organometallics* **1986**, *5*, 839−845.
[24] M. Mlekuz, P. Bougeard, B. G. Sayer, M. J. McGlinchey, C. A. Rodger, M. R. Churchill, J. W. Ziller, S. K. Kang, T. A. Albright, *Organometallics* **1986**, *5*, 1656−1663.
[25] L. Salvatella, A. Mokrane, A. Cartier, M. F. Ruiz-López, *J. Org. Chem.* **1998**, *63*, 4664−4670.
[26] J. S. Merola, R. T. Kacmarcik, D. van Engen, *J. Am. Chem. Soc.* **1986**, *108*, 329−331.
[27] [27a] A. Salzer, C. Täschler, *J. Organomet. Chem.* **1985**, *294*, 261−266. [27b] J. Müller, H. O. Stühler, W. Goll, *Chem. Ber.* **1975**, *108*, 1074−1086.
[28] E. Maurer, S. Rieker, M. Schollbach, A. Schwenk, T. Egolf, W. von Philipsborn, *Helv. Chim. Acta* **1982**, *65*, 26−45.
[29] H. Schumann, O. Stenzel, S. Dechert, F. Girgsdies, R. L. Halterman, *Organometallics* accepted for publication.
[30] [30a] E. Cesarotti, R. Ugo, R. J. Vitiello, *J. Mol. Catal.* **1981**, *12*, 63−69. [30b] E. Cesarotti, R. Ugo, H. B. Kagan, *Angew. Chem.* **1979**, *91*, 842−843; *Angew. Chem. Int., Ed. Engl.* **1979**, *18*, 779−780.
[31] [31a] G. Erker, M. Aulbach, M. Knickmeier, D. Wingbermühle, C. Krüger, M. Nolte, S. Werner, *J. Am. Chem. Soc.* **1993**, *115*,

4590−4601. [31b] D. Y. Kondakov, E. Negishi, *J. Am. Chem. Soc.* **1995**, *117*, 10771−10772. [31c] E. Negishi, D. Y. Kondakov, *Chem. Soc. Rev.* **1996**, 417−430.

[32] H. Sertchook, D. Avnir, J. Blum, F. Joó, Á. Kathó, H. Schumann, R. Weimann, S. Wernick, *J. Mol. Catal. A: Chem.* **1996**, *108*, 153−160.

[33] [33a] R. Paciello, L. Siggel, M. Röper, *Angew. Chem.* **1999**, *111*, 2045−2048; *Angew. Chem. Int. Ed.* **1999**, *38*, 1920−1923. [33b] L. A. van der Veen, P. C. J. Kamer, P. W. N. M. van Leeuwen, *Angew. Chem.* **1999**, *111*, 349−351; *Angew. Chem. Int. Ed.* **1999**, *38*, 336−338. [33c] G. Chelucci, M. Marchetti, B. Sechi, *J. Mol. Catal. A: Chem.* **1997**, *122*, 111−114. [33d] G. J. H. Buisman, L. A. van der Veen, A. Klootwijk, W. G. J. de Lange, P. C. J. Kamer, P. W. N. M. van Leeuwen, D. Vogt, *Organometallics* **1997**, *16*, 2929−2939. [33e] B. Breit, R. Winde, K. Harms, *J. Chem. Soc., Perkin Trans. 1* **1997**, 2681−2682. [33f] C. G. Arene, F. Nicolo, D. Drommi, G. Bruno, F. Faraone, *J. Chem. Soc., Dalton Trans.* **1996**, 4357−4363.

[34] [34a] V. S. Nair, S. P. Mathew, R. V. Chaudhari, *J. Mol. Catal. A: Chem.* **1999**, *143*, 99− 110. [34b] I. Ojima, K. Kato, M. Okabe, T. Fuchikami, *J. Am. Chem. Soc.* **1987**, *109*, 7714−7720.

[35] J. A. McCleverty, G. Wilkinson, *Inorg. Synth.* **1966**, *8*, 211−214.

[36] G. M. Sheldrick, *SHELXS-97 Program for the Solution of Crystal Structures*; Universität Göttingen, **1997**.

[37] G. M. Sheldrick, *SHELXL-97 Program for the Refinement of Crystal Structures*; Universität Göttingen, **1997**.

[38] H. D. Flack, *Acta Crystallogr., Sect. A* **1983**, *39*, 876−881.

[39] G. M. Sheldrick, *SADABS Program for Empirical Absorption Correction of Area Detector Data*; Universität Göttingen, **1996**.

[40] A. L. Spek, *PLATON A Multipurpose Crystallographic Tool*, Utrech University, **2000**.

Received July 1, 2001
[I01243]

Metal-Ion Extraction by Immobilised Aza Crown Ethers

Leon G. A. van de Water,[a] Willem L. Driessen,*[a] Jan Reedijk,[a] and David C. Sherrington[b]

Keywords: Aza crown ethers / Functional polymers / Cadmium / Silver

The immobilisation of [15]aneNO$_4$, [15]aneN$_2$O$_3$, and [18]aneN$_2$O$_4$ onto the oxirane and thiirane containing copolymers *p*(GMA-O) and *p*(GMA-S) resulted in six aza crown ether containing polymers with interesting metal-ion affinities. The pendent hydroxy or thiol groups, originating from the polymeric backbones, appeared to play an important role in the observed metal-ion affinities. The metal-ion affinity of *p*(GMA-O)-[15]aneN$_2$O$_3$ for a range of cations was found to decrease with decreasing ionic radius: $Ag^+ > Pb^{2+} > Cd^{2+} > Cu^{2+}$. The thiol-containing analogue of this polymer, *p*(GMA-S)-[15]aneN$_2$O$_3$, showed a reversed Cd^{2+}/Cu^{2+} selectivity. This illustrates the capability of pendent hydroxy groups to seriously reduce the stability of complexes of small cations compared to those of large cations. All the modified oxirane resins tested were found to be Ag^+-selective in the presence of a range of divalent (heavy) transition-metal ions. The difference in ring size between [15]aneN$_2$O$_3$ and [18]aneN$_2$O$_4$ was found to have a significant effect on the uptake values of Cu^{2+} and Zn^{2+}, as these ions are too small to fit into the ligand cavity of [18]aneN$_2$O$_4$. The uptake values for the larger Ag^+ and Pb^{2+} were found to be similar for both resins. Loaded resins were successfully regenerated (with an efficiency of 99%) by treatment with 2.0 m acid solutions (Pb^{2+} and Cd^{2+}) or with a 3.35 m NH_3 + 2.0 m NH_4NO_3 solution (Ag^+).

Introduction

Heavy-metal ions, like Cd^{2+}, Pb^{2+}, Hg^{2+}, and Cr^{3+}, exhibit toxic effects in biological systems, even at low concentration levels, as organic tissues exhibit affinity for many heavy-metal ions. Accumulation often occurs in particular organs and this results in undesired health effects.[1] Although the removal of these toxic metal ions from the environment has attracted much attention over the past decades, the pollution of surface and ground water remains a serious problem.[2] Purification systems for the removal of these toxic metal ions from aqueous solutions should possess a high degree of selectivity for heavy- and transition-metal ions due to the presence of relatively large amounts of alkali and alkaline earth metal ions in surface and ground water. Apart from toxic metal ions, those with a high commercial value also need to be recovered. Examples of these are Rh, Ir, Pd (applied in catalysis), Pt (catalysis, medicine), Ag (^{111}Ag-based immunotherapy, photographic technology), and Au (jewellery, medicine).[3]

Crown ethers are a class of ligands with metal-ion affinities that are a function of the nature, number, and spatial arrangement of the donor atoms, substitutions of the ligand backbone, the flexibility, and the hole size of the macrocycle. For instance, all-oxygen crown ethers have been found to be selective for alkali and alkaline earth metal ions, and there appears to be a correlation between ionic radius and macrocyclic cavity size.[4] The affinity of crown ethers that contain nitrogen and/or sulfur donor atoms is directed more towards (heavy) transition metal ions, and the size selectivity of this type of crown ether is much lower.[5]

Selective extraction of heavy-metal ions from aqueous solutions may be accomplished by functionalising non-hydrophobic[6] supporting materials with (multidentate) ligands, which contain donor atoms with affinity for the target metal ion(s).[7,8] In the present study, copolymers of ethylene glycol dimethacrylate (EDMA) (as the crosslinker) and glycidyl methacrylate [*p*(GMA-O)[9]], or its sulfur analogue [*p*(GMA-S)[10]] have been used as supporting materials (see Scheme 1). These polar copolymers can be functionalised easily by a ring-opening of the oxirane and thiirane moieties with nucleophiles, thereby generating additional hydroxy or thiol groups on the polymer.

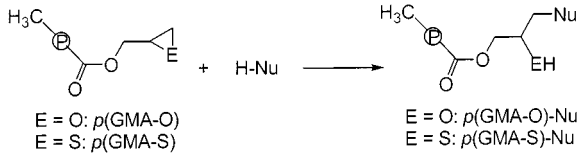

Scheme 1. Functionalisation of *p*(GMA-O) and *p*(GMA-S) with a nucleophile (H-Nu)

[a] Leiden Institute of Chemistry, Gorlaeus Laboratories, Leiden University,
P. O. Box 9502, 2300 RA Leiden, The Netherlands
Fax: (internat.) + 31-71/527-4671
E-mail: Driessen@chem.leidenuniv.nl
[b] Department of Pure and Applied Chemistry, University of Strathclyde, Thomas Graham Building,
295 Cathedral Street, Glasgow G1 1XL, United Kingdom

 © WILEY-VCH Verlag GmbH, 69451 Weinheim, Germany, 2002 1434–1948/02/0101–0221 $ 17.50+.50/0

When a crown ether is used as the nucleophile, a so-called lariat ether is formed on the polymer, whereby both the crown ether and the pendent hydroxy or thiol groups may be involved in metal-ion binding. Lariat ethers are known to be very suitable for selectively binding metal ions.[11] The results of the immobilisation of the tetrathia-monoaza crown ligand [16]aneNS$_4$ onto both *p*(GMA-O) and *p*(GMA-S), and the metal-ion binding studies of the resulting functionalised polymers, have been reported previously.[12] Both functionalised polymers were found to have a high capacity and selectivity towards Ag^+ ions, due to the high affinity of soft sulfur atoms for soft Ag^+ ions. The affinity for Pb^{2+} and Cd^{2+}, however, was found to be much lower, as the thioether ligands on the polymers form only moderately stable complexes with these latter metal ions. To improve the extraction of these metal-ion species, the immobilisation of three macrocyclic ligands without sulfur-donor atoms, 1,4,7,10-tetraoxa-13-azacyclopentadecane ([15]aneNO$_4$), 1,4,10-trioxa-7,13-diazacyclopentadecane ([15]aneN$_2$O$_3$), and 1,4,10,13-tetraoxa-7,16-diazacyclooctadecane ([18]aneN$_2$O$_4$) is reported here. In Scheme 2, the immobilisation reactions onto *p*(GMA-O) and *p*(GMA-S) are illustrated for [18]aneN$_2$O$_4$. The metal-ion uptake results, both under competitive and non-competitive conditions, the regeneration characteristics of the metal-loaded polymers, and distribution-coefficient determinations of these six functionalised polymers (**1**−**6**) are presented here.

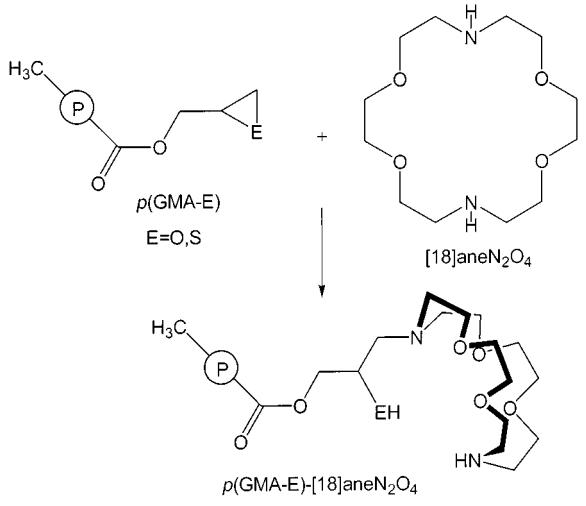

Scheme 2. Immobilisation of [18]aneN$_2$O$_4$ onto *p*(GMA-O) and *p*(GMA-S)

Results and Discussion

Crown Ether Modified Polymers

The microanalytical data of the functionalised resins **1**−**6** are presented in Table 1. Three different batches have been synthesised for each of the resins **3** and **5**. Oxirane and thiirane conversions are relative values with respect to the oxirane and thiirane concentrations on the starting polymers. Conversions and ligand concentrations are based on the nitrogen contents of the functionalised resins. The ligand concentrations of modified thiirane resins are less accurate than those of modified oxirane resins, due to the presence of a small amount of nitrogen in the starting polymer *p*(GMA-S).

The reactivity of [15]aneNO$_4$ is considerably higher than that of the other two macrocyclic ligands, the ligand concentration on **1** being 1.58 mmol/g and the ligand concentrations on **3** and **5** being approximately 0.80 mmol/g and 0.60 mmol/g, respectively. The presence of unchanged oxirane and thiirane groups on the modified resins is unlikely as either methanol, that was used in the immobilisation reactions, or traces of water may have reacted with these groups. This is confirmed by the IR spectra of the resins: characteristic peaks originating from both the epoxy group {850, 910 cm^{-1} (epoxy-ring vibration) and 1340, 1480 cm^{-1} [δ(CH)epoxy]}, or the thiirane group {615, 910 cm^{-1} (thiirane-ring vibration) and 1330, 1440 cm^{-1} [δ(CH)thiirane]}, have disappeared, indicating complete conversion of the epoxy and thiirane groups.

The solid-state CP MAS ^{13}C NMR spectra of the starting polymers *p*(GMA-O) and *p*(GMA-S) and of the modified resins indicate that peaks originating from the ligands, occurring at δ = 70.1 (*C*H$_2$-O), have appeared in the spectra of the modified polymers. This is in accordance with the ^{13}C NMR spectroscopic data of the free macrocycles in solution. The *C*H$_2$-N peak, found at δ ≈ 49 in solution, is obscured by the intense backbone peak at δ = 45.2. The CH$_2$ (epoxy) peak at δ = 48.0 and the CH$_2$ (thiirane) peaks

Table 1. Microanalytical data, oxirane/thiirane-group conversions, and ligand concentrations of the resins, based on the weight-% nitrogen; conversions and ligand concentrations of the modified thiirane resins are less accurate and are given in parentheses

	Resin	% C	% H	% N	% S	Conversion [%]	Ligand conc. [mmol/g]
1	*p*(GMA-O)-[15]aneNO$_4$	55.58	7.72	2.22		62	1.58
2	*p*(GMA-S)-[15]aneNO$_4$	51.84	7.01	1.32		(28)	(0.66)
3a	*p*(GMA-O)-[15]aneN$_2$O$_3$	57.30	7.47	2.29		25	0.82
3b	*p*(GMA-O)-[15]aneN$_2$O$_3$	57.05	7.46	2.48		27	0.88
3c	*p*(GMA-O)-[15]aneN$_2$O$_3$	57.38	7.47	2.03		21	0.73
4	*p*(GMA-S)-[15]aneN$_2$O$_3$	54.39	6.94	1.49	6.54	(21)	(0.44)
5a	*p*(GMA-O)-[18]aneN$_2$O$_4$	56.31	7.42	1.85		20	0.66
5b	*p*(GMA-O)-[18]aneN$_2$O$_4$	56.25	7.32	1.48		15	0.52
5c	*p*(GMA-O)-[18]aneN$_2$O$_4$	56.13	7.35	1.96		22	0.70
6	*p*(GMA-S)-[18]aneN$_2$O$_4$	51.01	6.79	1.57	7.44	(15)	(0.39)

at δ = 30.5 and 38.3 are no longer present in the spectra of the modified oxirane and thiirane resins.

Metal-Uptake Experiments

All metal-uptake experiments were performed as a function of the pH. Buffered metal chloride solutions were used for the experiments involving Cu^{2+}, Cd^{2+}, Zn^{2+}, Co^{2+}, Ni^{2+}, and Ca^{2+}, whilst for the experiments involving Ag^{+} and Pb^{2+} (competitive as well as non-competitive) nitrate salts were used. In these latter experiments, the pH was adjusted with dilute HNO_3 or with dilute NH_3. No Ag^{+}-uptake experiments were performed with modified thiirane resins, as the thiol groups on these resins are known to irreversibly bind large amounts of Ag^{+} ions.[12]

Because resins **1**−**6** have different ligand concentrations, it would not be correct to compare the capacity values (*C* in mmol/g resin) of the different resins. Therefore, the ligand occupation (*L* in %) was calculated in order to have a more appropriate basis for comparison of the resins, where *L* (in %) = [uptake capacity (*C*) for M^{n+} (in mmol/g resin)]/[ligand concentration (in mmol/g resin)].

[15]aneNO_4

The metal-ion uptake results with **1** {*p*(GMA-O)-[15]aneNO_4} under non-competitive conditions are presented in Figure 1 (a). The maximum uptake of Ag^{+} is 0.74 mmol/g at pH = 6.6 (47% ligand occupation), and is clearly a function of the pH. Cd^{2+} is the only other metal ion that is extracted significantly, although the maximum uptake is only 0.22 mmol/g at pH = 1.2. The Cd^{2+} uptake is probably due to the binding of polychlorocadmates to the resin.[12−14] The Ca^{2+} and Na^{+} uptakes have also been determined, since oxa crown ethers are known to form stable complexes with alkali and alkaline earth metal ions, but no uptake was observed.

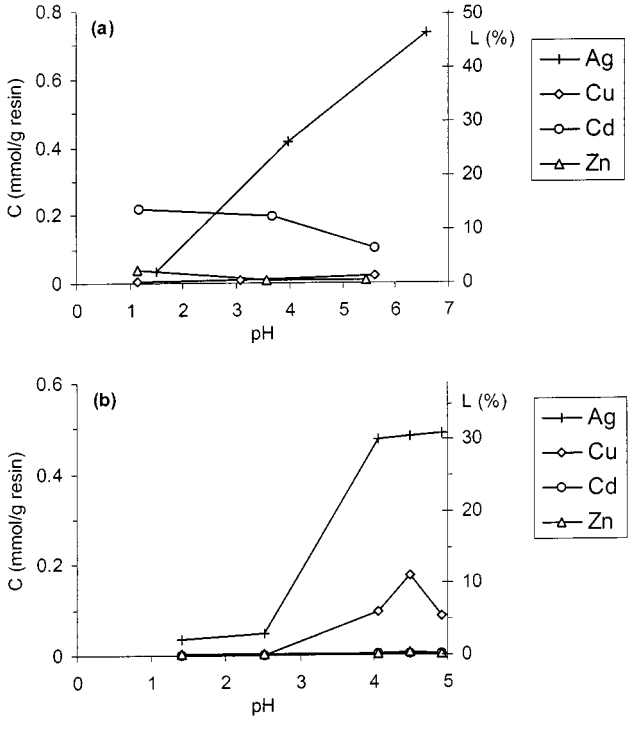

Figure 1. Metal-ion uptake behaviour of **1** {*p*(GMA-O)-[15]aneNO_4}: a) under non-competitive conditions; b) under competitive conditions, using metal nitrates

The experiment under competitive conditions (using metal nitrates) shows that Ag^{+} is the predominantly adsorbed species, although some Cu^{2+} is also extracted, see Figure 1 (b). This Cu^{2+} uptake is not in agreement with the non-competitive experiment, where no Cu^{2+} uptake was observed. The most likely explanation for this phenomenon is that the high acetate concentration in the non-competitive experiment (originating from the buffer) prevents the binding of Cu^{2+} to the ligands on the resin, as these acetate ions themselves are relatively strong ligands for Cu^{2+}. The absence of an acetate buffer in the competitive experiment thus allows Cu^{2+} ions to bind to the resin. The competitive experiment also shows that, at low pH, no Cd^{2+} is taken up. This behaviour is in agreement with the hypothesis that the Cd^{2+} uptake in the non-competitive experiment is due to the formation of polychloro species, as chloride ions were present in the non-competitive experiment and absent in the competitive experiment.

The capacity of modified thiirane resin **2** was determined for Cu^{2+}, Cd^{2+}, Zn^{2+}, and Ca^{2+}. The maximum uptake values of these metal ions were found to be 0.19 mmol/g, 0.18 mmol/g, 0.12 mmol/g, and 0.03 mmol/g, respectively. A significant part of this uptake, however, can be ascribed to the thiol groups on the resin. This is suggested by blank experiments with a resin containing only thiol and hydroxy groups, which showed an uptake of 0.14 mmol/g Cu^{2+} and 0.09 mmol/g Cd^{2+}. The competitive experiment with **2** shows that the resin is moderately Cu^{2+} selective, the maximum uptake being 0.15 mmol/g at pH 6.0.

[15]aneN_2O_3

The uptake results with **3b** {*p*(GMA-O)-[15]aneN_2O_3} under non-competitive conditions are presented in Figure 2 (a). The highest uptake is observed for Ag^{+}, 0.52 mmol/g at pH = 6.4 (ligand occupation of 59%). The metal uptake of all tested species shows a pronounced pH dependence, which is probably due to protonation of the nitrogen atom(s) of [15]aneN_2O_3 at low pH. In fact, Cd^{2+} is the only species that is adsorbed at low pH. The Cd^{2+} uptake at high pH is slightly lower than the Pb^{2+} uptake, but it clearly exceeds the uptake of Cu^{2+}. The observed order in the metal-uptake values, $Ag^{+} > Pb^{2+} > Cd^{2+} > Cu^{2+} > Co^{2+} > Zn^{2+} \approx Ni^{2+}$, is different from the order found for the formation constants of complexes of the free macrocycle [15]aneN_2O_3 with these metal ions in aqueous solution: $Cu^{2+} > Cd^{2+} > Pb^{2+} \approx Ag^{+} > Zn^{2+} > Co^{2+} > Ni^{2+}$.[15] In contrast, the order of stability constants of these cations with two structurally related cryptands (see Figure 3) in aqueous solution was found to be $Ag^{+} > Pb^{2+} > Cu^{2+} > Cd^{2+}$, Zn^{2+}, Co^{2+}, Ni^{2+} for cryptand-211, and $Pb^{2+} > Ag^{+} > Cd^{2+} > Cu^{2+} > Zn^{2+} > Co^{2+} > Ni^{2+}$ for cryptand-221.[15] The difference between the order of the stability constants of crown ether [15]aneN_2O_3 on one hand, and resin **3b** and cryptands-211 and -221 on the other hand, must be due to the presence of additional oxygen-

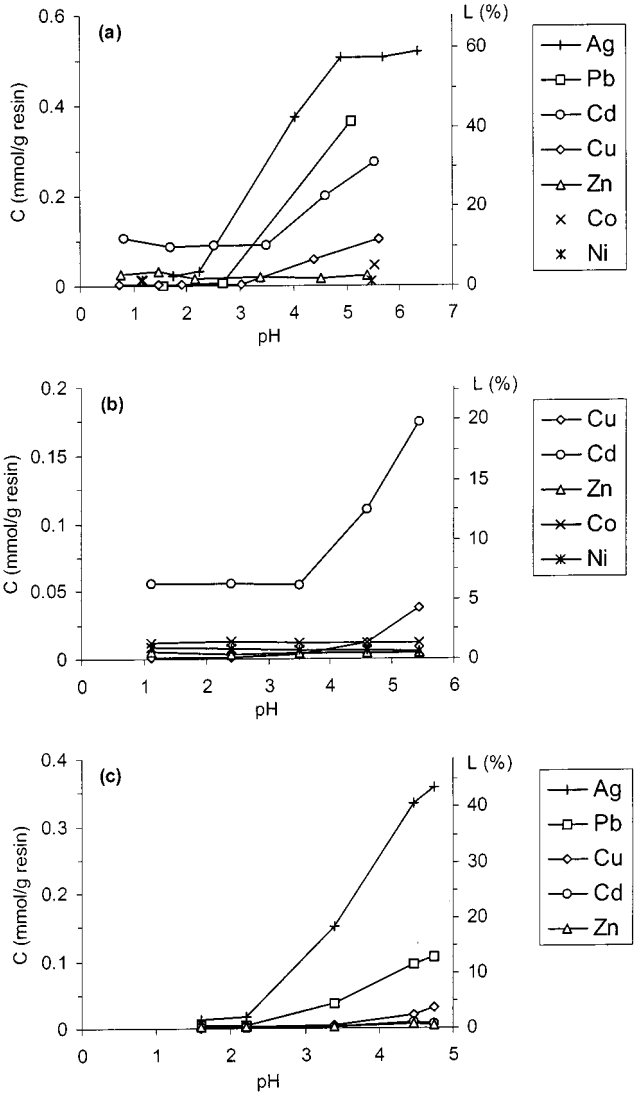

Figure 2. Metal-ion uptake behaviour of **3b** {*p*(GMA-O)-[15]aneN$_2$O$_3$}: a) under non-competitive conditions; b) under competitive conditions using metal chlorides; c) under competitive conditions using metal nitrates

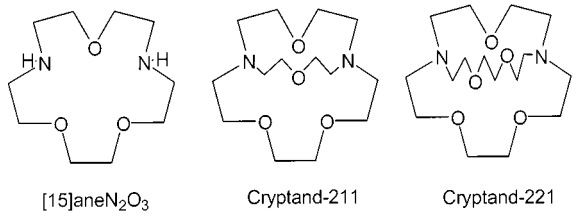

Figure 3. Structural formulae of [15]aneN$_2$O$_3$, cryptand-211 and cryptand-221

donor atoms on resin **3b** (the hydroxy groups originating from the backbone) and on the cryptands. These additional oxygen donors may change the stability of the different metal complexes.

The metal uptake by **3b** seems to be related to the ionic radii of the metal-ion species, as the metal uptake decreases with decreasing ionic radius, see Table 2. Exceptions to this trend are Ag^+ and Cu^{2+}. The relatively high value for Ag^+ can be explained by the different valencies of the tested metal ions. Ag^+ is the only monovalent species, and a higher uptake may be explained by the fact that only one negative charge has to be compensated for upon coordination, either by deprotonation of the immobilised ligand, or by the coordination of an accompanying anion. The somewhat high uptake of Cu^{2+}, compared to Co^{2+}, Zn^{2+}, and Ni^{2+}, can be ascribed to the high affinity of Cu^{2+} for nitrogen ligands.

Table 2. Ionic radii and uptake values for **3b** {*p*(GMA-O)-[15]aneN$_2$O$_3$}; ionic radii are all appropriate for coordination number 6

	Ionic radius [Å]	Uptake by **3b** [mmol/gram]
Pb^{2+}	1.19	0.36
Ag^+	1.15	0.52
Cd^{2+}	0.95	0.27
Co^{2+}	0.75	0.05
Zn^{2+}	0.74	0.02
Cu^{2+}	0.73	0.10
Ni^{2+}	0.69	0.01

The size-selective uptake by **3b** {*p*(GMA-O)-[15]aneN$_2$O$_3$} may be explained by the presence of the pendent hydroxyethyl groups, originating from the backbone. This additional coordinating oxygen donor imposes extra steric crowding on a metal ion that is already coordinated by the crown ether, and this steric crowding is best accommodated by the largest metal ions, whereas the stability of the complexes of small ions, such as Cu^{2+} and Zn^{2+}, is seriously reduced.[16,17] This results in the observed selectivity for Cd^{2+} over Cu^{2+}, Cd^{2+} over Zn^{2+}, and Pb^{2+} over Zn^{2+}. This effect is similar to the observed higher stability of large cations with the cryptands-211 and -221 in comparison with the parent macrocycle [15]aneN$_2$O$_3$.[15] The effect of the addition of hydroxyalkyl groups to oxa-aza ethers on the stability of the corresponding metal-ion complexes has been described in several papers.[16–18]

The selectivity for Cd^{2+} over Cu^{2+} is illustrated by the results of the competitive experiment, using metal chlorides [see Figure 2 (b)]. Hardly any Cu^{2+} is adsorbed between pH = 1 and 4.6, and only at pH = 5.4 some Cu^{2+} was found to be co-extracted with Cd^{2+}. The selectivity for Cd^{2+} over Cu^{2+} at pH = 4.6 is 10:1.

The selectivity for Cd^{2+} over Cu^{2+} and for Cd^{2+} over Zn^{2+} has been further investigated. In the presence of a tenfold excess of Cu^{2+}, the Cd^{2+} selectivity at pH = 4.9 is reduced to only 1.8:1, and at pH = 5.9 this is only 0.8:1, which suggests that an excess of Cu^{2+} causes a severe decrease in the Cd^{2+} selectivity. The selectivity for Cd^{2+} over Zn^{2+} is of interest as these species belong to the same group of the periodic table and hence often occur together in nature. The Cd^{2+}/Zn^{2+} selectivity in the competitive experiment, with equal amounts of Cd^{2+} and Zn^{2+} ions, is as high as 37:1 at pH = 5.4 [see Figure 2 (b)]. In an experiment at pH = 5.8, with Zn^{2+} present in a tenfold excess, the

Cd^{2+}/Zn^{2+} selectivity appears to still be 8.8:1. *p*(GMA-O)-[15]aneN_2O_3 thus exhibits a very reasonable selectivity for Cd^{2+} over Zn^{2+}, which can be ascribed to the difference in octahedral ionic radii (0.95 Å versus 0.74 Å). Similarly, cryptand-221 was reported to form complexes with Cd^{2+} and Zn^{2+} which significantly differ in stability, log*K* being 10.04 in the case of Cd^{2+} and 5.41 in the case of Zn^{2+}.[15] For [15]aneN_2O_3, the difference in log*K* values was found to be much smaller: 6.46 for Cd^{2+} versus 5.19 for Zn^{2+}.

The result of the competitive experiment, using metal nitrates, is depicted in Figure 2 (c). The same trend as under non-competitive conditions is observed: **3b** {*p*(GMA-O)-[15]aneN_2O_3} predominantly adsorbs Ag^+, although some Pb^{2+} is co-extracted at higher pH. The Ag^+ uptake at pH = 4.7 is 0.36 mmol/g.

The results of the non-competitive experiment with **4** {*p*(GMA-S)-[15]aneN_2O_3} are presented in Figure 4 (a), and show that the Cu^{2+} uptake exceeds the Cd^{2+} uptake. No correlation between the uptake and the ionic radii of the metal ions is observed, indicating that the role of the pendent thiol groups is entirely different from the role that pendent hydroxy groups play. The coordination of these thiol groups enhances the stability of the Cu^{2+} complex on the resin more than that of the Cd^{2+} complex. The maximum uptake of Cu^{2+} is 0.24 mmol/g (at pH = 5.7), for Cd^{2+} this is 0.18 mmol/g (at pH = 5.6). The experiment, under competitive conditions [Figure 4 (b)], shows that *p*(GMA-S)-[15]aneN_2O_3 is Cu^{2+}-selective in the presence of other divalent metal chlorides. Upon changing the polymeric backbone from *p*(GMA-O) to *p*(GMA-S), a reversed Cu^{2+}/Cd^{2+} selectivity is obtained, which can only be ascribed to the different effect that the pendent hydroxy and thiol groups have on the stability of the complexes formed on the resins. The donor strength of thiol groups towards (heavy) transition metal ions is higher than that of hydroxy groups, and this bond strength effect predominates any destabilising steric effect of the additional donor groups. In other words, the Cu^{2+} complex on *p*(GMA-S)-[15]aneN_2O_3 is stabilised by the pendent thiol group, where, in the case of *p*(GMA-O)-[15]aneN_2O_3, the steric effect of the pendent hydroxyethyl group predominates the bond strength effect of this group.

[18]aneN_2O_4

A range of metal ions has been tested under non-competitive conditions with **5a** {*p*(GMA-O)-[18]aneN_2O_4}, see Figure 5. The metal-ion uptake values are in the order $Ag^+ > Pb^{2+} > Cd^{2+} > Cu^{2+}, Zn^{2+}$. The solution data[15] are somewhat different as in this case the Cu^{2+} complex was found to be more stable than the Cd^{2+} complex, which again may be due to the presence of the additional hydroxyethyl groups on the polymer, which destabilises the Cu^{2+} complex. The uptake of Ag^+ and Pb^{2+} is very similar to that of **3b**. The uptake curves again show a pH dependence, and the maximum uptake of Ag^+ is again higher than that of Pb^{2+}, 0.61 mmol/g for Ag^+ at pH = 6.4 (ligand occupation of 92%) vs. 0.37 mmol/g for Pb^{2+} at pH = 5.1 (ligand occupation of 56%). The ligand occupations of Ag^+ and Pb^{2+} are (slightly) higher than those found with **3b**, suggesting that the larger macrocyclic cavity slightly enhances the stability of the Ag^+ and Pb^{2+} complexes. This effect was also observed for [18]aneN_2O_4 in solution.[15] The Cd^{2+} capacity of **5a** is lower than that of **3b** and is not a function of the pH. The uptake at low pH (pH = 1 and 2), which may be due to polychlorocadmate complexes (such as $[CdCl_4]^{2-}$), is higher than for resin **3b**, suggesting that this complex anion fits better into the larger binding cavity of **5a**. At increasing pH, no increased Cd^{2+} uptake is observed, which suggests that the Cd^{2+} ion cannot effectively be accommodated in the ligand cavity of *p*(GMA-O)-[18]aneN_2O_4. Cu^{2+} and Zn^{2+} are not extracted at all by **5a**, which is an illustration of the fact that they are too small for the macrocyclic cavity of [18]aneN_2O_4.

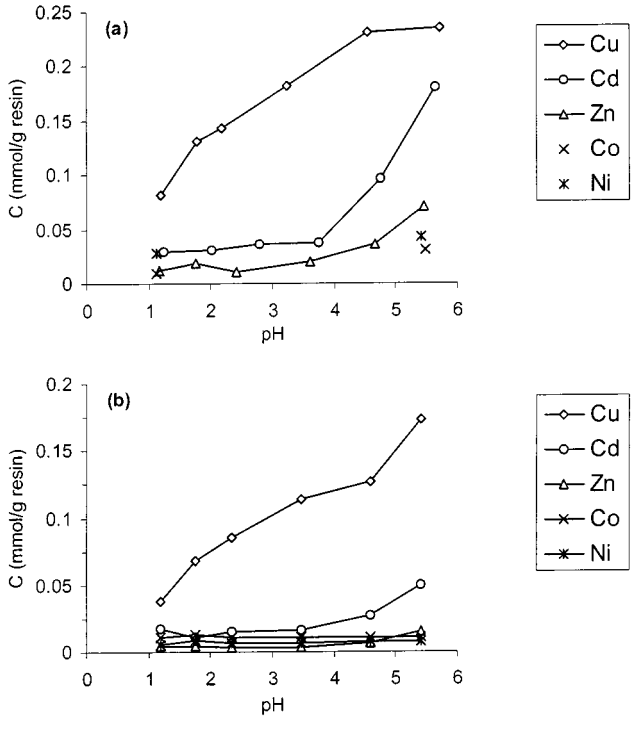

Figure 4. Metal-ion uptake behaviour of **4** {*p*(GMA-S)-[15]aneN_2O_3}: a) under non-competitive conditions; b) under competitive conditions using metal chlorides

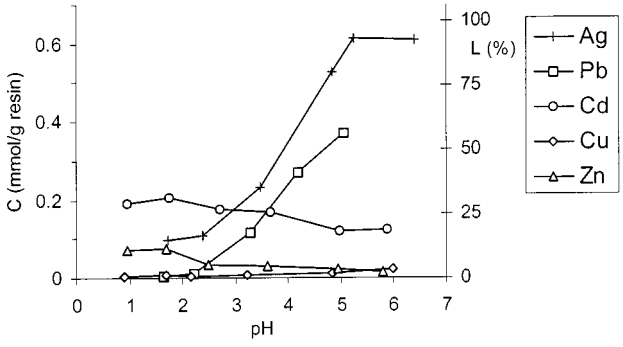

Figure 5. Metal-ion uptake behaviour of **5a** {*p*(GMA-O)-[18]aneN_2O_4} under non-competitive conditions

[18]aneO$_6$ is known to have a high affinity for K^+ and, to a lesser extent, for Na^+. The uptake of these two species by *p*(GMA-O)-[18]aneN$_2$O$_4$ was therefore investigated and appeared to be remarkably low, the maximum value for K^+ being 0.03 mmol/g at pH = 6.2.

The competitive experiment with **5a**, using the chlorides of Cu^{2+}, Cd^{2+}, Zn^{2+}, Co^{2+}, and Ni^{2+}, shows hardly any metal uptake at all. Only some Cd^{2+} is extracted over the whole pH range, the maximum uptake being only 0.09 mmol/g at pH = 1.7. This illustrates that these metal-ion species are too small to be accommodated in the macrocyclic cavity of [18]aneN$_2$O$_4$, and thus form very weak complexes with the resin. The competitive experiment using metal nitrates shows that both Ag^+ and Pb^{2+} are extracted, albeit to a small extent. The maximum values for these ions at pH = 4.8 are 0.17 mmol/g and 0.15 mmol/g, respectively.

The capacity of the modified thiirane resin **6** has been determined under non-competitive conditions, using buffered metal chloride solutions of Cu^{2+}, Cd^{2+}, Zn^{2+}, Co^{2+}, and Ni^{2+}. The maximum uptake values for all these metal-ion species has been observed at pH = 5.5, the values being 0.29 mmol/g, 0.23 mmol/g, 0.10 mmol/g, 0.04 mmol/g and 0.04 mmol/g, respectively. A solution of Pb(NO$_3$)$_2$, of which the pH was adjusted to 4.9, has been used to determine the Pb^{2+} uptake, which appeared to be 0.45 mmol/g.

The competitive experiment, using metal chlorides, reveals that **6** extracts both Cu^{2+} and Cd^{2+}, the maximum uptake of these metals being 0.21 mmol/g and 0.10 mmol/g, respectively.

Regeneration Experiments

The small quantity of **1** {*p*(GMA-O)-[15]aneNO$_4$} available, allowed only one regeneration experiment. The Ag^+-loaded resin was successfully regenerated with a 1.0 M HNO_3 solution, which left only 3.0% of the initial amount of Ag^+ on the resin.

Modified oxirane resin **3c** {*p*(GMA-O)-[15]aneN$_2$O$_3$} was loaded with Ag^+, Pb^{2+}, and Cd^{2+} at pH values where maximum uptake was observed in the non-competitive experiments. Aqueous solutions of acid (2.0 M HNO_3 in the case of Ag^+ and Pb^{2+}, and 2.0 M H_2SO_4 for Cd^{2+}), 3.35 M NH_3 in combination with 2.0 M NH_4NO_3, and 1.0 M $(NH_2)_2CS$ were used as potential stripping agents. The results are presented in Table 3.

Table 3. Relative amounts of residual Ag^+, Pb^{2+}, and Cd^{2+} on **3c** {*p*(GMA-O)-[15]aneN$_2$O$_3$} (in %) after stripping with 2.0 M HNO_3/H_2SO_4, 3.35 M NH_3 + 2.0 M NH_4NO_3 and 1.0 M $(NH_2)_2CS$

Stripping agent	Ag^+	Pb^{2+}	Cd^{2+}
HNO_3/H_2SO_4	5.74	0.55	1.12
NH_3 + NH_4NO_3	1.47	50.6	1.52
$(NH_2)_2CS$	16.4	37.5	14.5

The binding of metal ions by **3c** is due to the coordination of amines, oxygen ethers and hydroxyethyl moieties. Dilute acid is therefore likely to be an effective stripping agent, as the metal-binding sites can easily be protonated, and may subsequently release metal ions. This appears to be the case, as the residual amounts of Ag^+, Pb^{2+}, and Cd^{2+} on the resin after treatment with acid are only 5.7%, 0.6% and 1.1%, respectively. The stripping of Ag^+, however, appears to be more successful with NH_3 + NH_4NO_3, leaving only 1.5% of the initial amount of Ag^+ on the resin. Apparently, NH_3 is able to compete with the amines of the ligands on the resin in the case of Ag^+. This is probably due to the high stability of the formed $[Ag(NH_3)_2]^+$ complexes in solution. Cd^{2+} is also successfully stripped in this way, but when stripping with NH_3 + NH_4NO_3 is attempted for the Pb^{2+}-loaded resin, 51% of the initial amount of Pb^{2+} remains on the resin.

$(NH_2)_2CS$, which appeared to be the most successful stripping agent for the removal of metal ions from resins containing [16]aneNS$_4$,[12] appears to be the least effective agent for the removal of Ag^+, Pb^{2+}, or Cd^{2+} from *p*(GMA-O)-[15]aneN$_2$O$_3$. Unlike *p*(GMA-O)-[15]aneN$_2$O$_3$, however, *p*(GMA-O)-[16]aneNS$_4$ binds metal ions through its sulfur atoms, and $(NH_2)_2CS$ appears to be particularly useful for the disruption of these metal ion−sulfur bonds. On the other hand, *p*(GMA-O)-[15]aneN$_2$O$_3$ only contains oxygen- and nitrogen-donor atoms, and therefore other stripping agents are required, such as acid or NH_3 + NH_4NO_3.

Distribution-Coefficient Measurements

Distribution coefficients were determined for Ag^+, Pb^{2+}, Cu^{2+}, and Cd^{2+} with resins **3c** {*p*(GMA-O)-[15]aneN$_2$O$_3$} and **5c** {*p*(GMA-O)-[18]aneN$_2$O$_4$}. The results are presented in Table 4 and Figure 6. The experiments were performed at pH values where maximum uptake in the non-

Table 4. log*D* values for modified oxirane resins **3c** {*p*(GMA-O)-[15]aneN$_2$O$_3$} and **5c** {*p*(GMA-O)-[18]aneN$_2$O$_4$} with Ag^+, Pb^{2+}, Cu^{2+}, and Cd^{2+}; the pH of the experiment is indicated in parentheses

Resin	Ag^+	Pb^{2+}	Cu^{2+}	Cd^{2+}
p(GMA-O)-[15]aneN$_2$O$_3$	4.65 (6.8)	3.01 (5.1)	1.57 (5.9)	2.1 (5.9)
p(GMA-O)-[18]aneN$_2$O$_4$	3.69 (5.7)	2.66 (5.4)	0.42 (5.9)	1.60 (2.1)

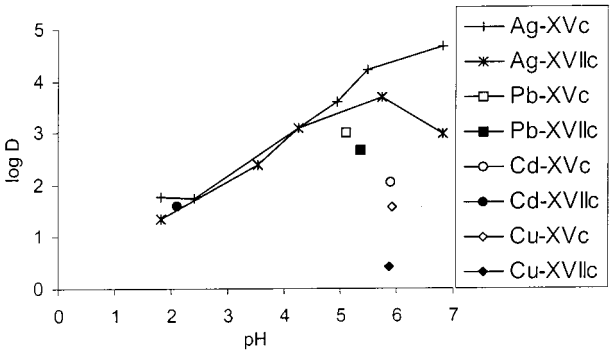

Figure 6. Distribution coefficients (log*D*) for Ag^+, Pb^{2+}, Cu^{2+}, and Cd^{2+} with **3c** {*p*(GMA-O)-[15]aneN$_2$O$_3$} and **5c** {*p*(GMA-O)-[18]aneN$_2$O$_4$}

competitive experiments was observed. In the case of Ag^+, log*D* values were determined as a function of the pH.

The results show the same trend as has been observed in the batch metal-uptake experiments: Both resins form their most stable complexes with Ag^+, and the stability is clearly a function of the pH. The stability of the Ag^+-p(GMA-O)-[18]aneN_2O_4 complex at pH = 6.8 is lower than at pH = 5.7, in contrast to the non-competitive uptake experiment and also in contrast to the log*D* curve of the Ag^+-p(GMA-O)-[15]aneN_2O_3 complex. A possible explanation for this may be that only a very small amount of Ag^+ was present in the log*D* experiments. At pH = 6.8, the small amount of NH_3 that was used to adjust the pH may have been enough to keep a significant part of the Ag^+ in solution. In the capacity measurements under non-competitive conditions, a larger excess of Ag^+ ions with respect to NH_3 was used, and the effect of the NH_3 is therefore likely to be smaller in that case.

The influence of the ring size on the log*D* values is not the same for each metal-ion species. Although the log*D* values of all metal ions are higher with *p*(GMA-O)-[15]aneN_2O_3, the difference is rather small in the case of Ag^+ and Pb^{2+}. This indicates that both the 18-membered and the 15-membered macrocycle form stable complexes with these metal-ion species. In the case of Cu^{2+}, however, the difference in the log*D* values is significant: 1.57 with *p*(GMA-O)-[15]aneN_2O_3 and only 0.42 with *p*(GMA-O)-[18]aneN_2O_4 at pH = 5.9. This illustrates once more that the cavity size of [18]aneN_2O_4 is too large for Cu^{2+}, whereas the [15]aneN_2O_3-containing resin yields somewhat more stable Cu^{2+} complexes. The log*D* value found for Cu^{2+} with *p*(GMA-O)-[16]aneNS_4 was found to be somewhat higher[12] (2.1), suggesting that the absence of thioethers in the immobilised macrocyclic ligands decreases the stability of the corresponding Cu^{2+} complexes. The log*D* values obtained for Cd^{2+} are similar to those found for *p*(GMA-O)-[16]aneNS_4.[12] These results are in accordance with chromatography experiments involving mixed-donor crown ethers, immobilised onto thin layer plates.[19] A range of macrocycles were impregnated on silica plates and mixtures of metal ions were separated on the basis of their different R_f values. The observed stability trends were $Cu^{2+} > Cd^{2+} > Ba^{2+}$ for macrocycles containing N and S donor atoms and $Ba^{2+} > Cd^{2+} > Cu^{2+}$ for those containing N and O donors.[19]

Conclusion

The immobilisation of [15]aneN_2O_3 onto *p*(GMA-O) resulted in a resin with a high capacity for Ag^+, and a somewhat lower capacity for Pb^{2+} and Cd^{2+}. A correlation between the ionic radii and the uptake values was observed for a range of metal ions. With decreasing ionic radius, a decrease in metal-ion uptake was observed. This effect was not observed for *p*(GMA-S)-[15]aneN_2O_3. The size selectivity is most probably due to the presence of pendent hydroxy groups on the modified oxirane resin. These additional neutral oxygen-donor atoms are known to destabilise complexes of small metal ions more than those of larger metal ions do. This effect only becomes apparent when crown ethers without sulfur atoms are applied, since no size selectivity due to the pendent hydroxy groups was observed for *p*(GMA-O)-[16]aneNS_4 and other thia crown ether containing modified oxirane resins.[12,20] With *p*(GMA-O)-[15]aneN_2O_3, Cd^{2+} over Cu^{2+} and Zn^{2+}, and Pb^{2+} over Cu^{2+} and Zn^{2+} selectivities have been obtained.

p(GMA-S)-[15]aneN_2O_3 shows a reversed Cd^{2+}/Cu^{2+} selectivity, which is due to the presence of pendent thiol rather than pendent hydroxy groups on the resin. Thiol groups have a higher donor strength, and their stabilising effect is larger on Cu^{2+} complexes than on Cd^{2+} complexes, and loss of the Cd^{2+} over Cu^{2+} selectivity, observed for *p*(GMA-O)-[15]aneN_2O_3, is the result.

The distribution-coefficient measurements show that Cu^{2+} forms less stable complexes with *p*(GMA-O)-[15]aneN_2O_3 than with resins containing thia crown ethers.[12] This suggests that the presence of thioethers, in the macrocyclic ligands, increases the stability of the Cu^{2+}. *p*(GMA-O)-[18]aneN_2O_4 extracts amounts of Ag^+ and Pb^{2+} that are similar to *p*(GMA-O)-[15]aneN_2O_3, but the uptake of Cd^{2+}, Cu^{2+}, and Zn^{2+} appeared to be drastically reduced. The cavity size of [18]aneN_2O_4 is apparently too large to accommodate these latter metal ions. As with *p*(GMA-O)-[15]aneN_2O_3, the ionic radius of the metal ions is an important factor in the interpretation of the uptake results obtained. The increase in the cavity size of the macrocycle has its largest effect on the smallest metal ions, as the difference in the log*D* value of the small Cu^{2+} ion with *p*(GMA-O)-[15]aneN_2O_3 and *p*(GMA-O)-[18]aneN_2O_4 illustrates. For large metal-ion species, such as Ag^+ and Pb^{2+}, comparable log*D* values have been obtained for the two resins.

Regeneration experiments, performed with Ag^+-, Pb^{2+}-, and Cd^{2+}-loaded *p*(GMA-O)-[15]aneN_2O_3, showed that stripping with 2.0 M acid is successful for Pb^{2+} and Cd^{2+}. The combination of NH_3 + NH_4NO_3 appeared to be the most successful method for Ag^+. It was not possible to remove the metal ions with $(NH_2)_2CS$ from the loaded resins, in contrast to the loaded resins that contain thia crown ethers. Apparently, the type of donor atoms that bind a metal ion determines the type of stripping agent that is best applicable.

The absence of sulfur atoms in the crown ethers that have been described in the present study has resulted in selectivity patterns that are governed by several factors. The ring size of the macrocycle, the effect of the pendent hydroxy groups and the relative positions of the metal ions and the donor atoms on the HSAB scale all become important when oxygen donor atoms, which are relatively weak donor atoms for (heavy) transition-metal ions, are used in crown ether containing metal-ion extractants. This has resulted in functionalised polymers with an enhanced affinity for large heavy-metal ions such as Cd^{2+} and Pb^{2+}, compared to resins containing thia-aza crown ethers.

Experimental Section

Starting Materials: [15]aneNO$_4$ and [15]aneN$_2$O$_3$ were purchased from Aldrich, and [18]aneN$_2$O$_4$ was obtained from Fluka. All other reagents and solvents were purchased from commercial sources and were used as received, unless stated otherwise. DMF was stored under dinitrogen over molecular sieves (4 Å). Toluene was distilled from sodium metal and stored under dinitrogen over molecular sieves (4 Å). Methanol was distilled from magnesium and stored under dinitrogen over molecular sieves (4 Å).

Physical and Chemical Measurements: The metal contents of the digested samples (vide infra) of loaded resins were measured by atomic absorption spectroscopy (AAS) with a Perkin−Elmer 3100 AAS and flame emission spectrometer, using a linear calibration method. − Elemental analyses (C,H,N,S) were carried out by the Microanalytical Department of the University College of Dublin (Republic of Ireland). − Solid-state CP MAS ^{13}C NMR spectra (cross polarisation and magic-angle spinning) were recorded with a Bruker MSL-400 spectrometer, operating at 100.6 MHz for ^{13}C. The sample spinning rate was 7000 Hz. The cross-polarisation contact time was 1.0 ms, with 3−5 s recycle delays between successive scans. − ^{1}H NMR and ^{13}C NMR spectra were recorded with a 200 MHz JEOL JNM FT NMR spectrometer. Chemical shifts are quoted with respect to TMS as an internal reference.

Synthesis of the Ion Exchangers: Oxa-aza crown ethers were immobilised onto *p*(GMA-O) and *p*(GMA-S), according to the same general procedure.[12,21] The synthetic details for resins **1**−**6** are presented in Table 5. The epoxide concentration on *p*(GMA-O) was 4.21 mmol/g in all cases. The *p*(GMA-S) batch that was used for the synthesis of *p*(GMA-S)-[15]aneNO$_4$ contained 2.76 mmol thiirane groups per g, the thiirane contents of the batches used for *p*(GMA-S)-[15]aneN$_2$O$_3$ and *p*(GMA-S)-[18]aneN$_2$O$_4$ were 2.35 mmol/g and 3.00 mmol/g, respectively. The reaction temperature was 80 °C in all cases. After each immobilisation, unchanged ligand was collected, analysed by NMR spectroscopy, and re-used in some cases.

To a solution of the ligand in toluene or in a mixture of toluene and methanol (1:1, v/v), *p*(GMA-O) or *p*(GMA-S) was added (molar ratio ligand/epoxide/thiirane groups, 1.5:1) and the mixture was heated at 75−100 °C under dinitrogen for 5 d. The resulting resins were filtered off and purified by Soxhlet extraction with toluene (6 h) and ethanol (6 h), respectively. The resins were dried in vacuo at 50 °C for 16 h. Finally, the resins were conditioned with 0.5 M H_2SO_4 (30 min) and 0.5 M NaOH (30 min), washed with water and dried in vacuo at 50 °C for 48 h. The ligand concentrations of the functionalised polymers were calculated on the basis of the weight-% of nitrogen (microanalysis), whereby allowances were made for the nitrogen content of the thiirane-containing *p*(GMA-S) backbone, as traces of (thio)urea were left after the conversion of oxirane to thiirane.[10,12]

Metal-Uptake Experiments: The metal-uptake experiments, with the exception of those involving Ag^+ and Pb^{2+}, were performed using standard metal chloride solutions of 0.16 M and 0.6 M buffer solutions of NaCl/HCl (pH = 0.9−2.3) and NaOAc/HOAc (pH = 2.5−6.0). All experiments were performed in polyethylene bottles mounted on a shaker at room temperature. The capacities for Cu^{2+}, Cd^{2+}, Zn^{2+}, Ni^{2+}, Co^{2+}, and Ca^{2+} under non-competitive conditions were determined as a function of the pH. Batches of 70−100 mg of resin were used, together with a mixture of 25 mL of metal-ion solution and 25 mL of buffer. For the determination of the Cu^{2+} capacities at pH > 5, a lower Cu^{2+} concentration (10 mL of the standard Cu^{2+} solution and 40 mL of buffer) was used to prevent precipitation of Cu^{II} hydroxides. After a shaking time of 48 h, the samples were filtered, washed with water, ethanol and diethyl ether, and dried in vacuo at 50 °C.

Batch metal-uptake experiments under competitive conditions were performed with standard metal chloride solutions of Cu^{2+}, Cd^{2+}, Zn^{2+}, Ni^{2+}, and Co^{2+} in a pH range of 0.9 to 6. Batches of 70−100 mg of resin were used, together with a mixture of 5 mL of each metal ion solution and 25 mL of buffer. After a shaking time of 48 h, the samples were further handled as described for the non-competitive experiments.

Table 5. Synthetic details of immobilisation reactions of N,O-mixed donor crown ethers (Tol = toluene; IPA = 2-propanol; reaction time = 5 d)

Ligand	Support epoxide/thiirane	Solvent	Product (yield)
[15]aneNO$_4$	*p*(GMA-O)	Tol (20 mL)	*p*(GMA-O)-[15]NO$_4$
1.85 g, 8.44 mmol	1.34 g, 5.62 mmol		**1** (2.04 g)
[15]aneNO$_4$	*p*(GMA-S)	Tol (15 mL)	*p*(GMA-S)-[15]NO$_4$
1.09 g, 4.97 mmol	1.20 g, 3.31 mmol		**2** (1.26 g)
[15]aneN$_2$O$_3$	*p*(GMA-O)	Tol (20 mL)	*p*(GMA-O)-[15]N$_2$O$_3$
1.00 g, 4.58 mmol	0.73 g, 3.05 mmol		**3a** (0.88 g)
[15]aneN$_2$O$_3$	*p*(GMA-O)	Tol (50 mL)	*p*(GMA-O)-[15]N$_2$O$_3$
3.00 g, 13.7 mmol	2.18 g, 9.16 mmol		**3b** (2.67 g)
[15]aneN$_2$O$_3$	*p*(GMA-O)	Tol (40 mL)/	*p*(GMA-O)-[15]N$_2$O$_3$
4.48 g, 20.5 mmol	3.25 g, 13.7 mmol	MeOH (40 mL)	**3c** (3.80 g)
[15]aneN$_2$O$_3$	*p*(GMA-S)	Tol (15 mL)/	*p*(GMA-S)-[15]N$_2$O$_3$
2.25 g, 10.3 mmol	2.94 g, 6.87 mmol	MeOH (15 mL)	**4** (3.17 g)
[18]aneN$_2$O$_4$	*p*(GMA-O)	Tol (30 mL)/	*p*(GMA-O)-[18]N$_2$O$_4$
3.00 g, 11.4 mmol	1.81 g, 7.62 mmol	MeOH (30 mL)	**5a** (2.20 g)
[18]aneN$_2$O$_4$	*p*(GMA-O)	Tol (30 mL)/	*p*(GMA-O)-[18]N$_2$O$_4$
2.60 g, 9.91 mmol	1.40 g, 5.89 mmol	MeOH (30 mL)	**5b** (1.65 g)
[18]aneN$_2$O$_4$	*p*(GMA-O),	Tol (20 mL)/	*p*(GMA-O)-[18]N$_2$O$_4$
2.35 g, 8.96 mmol	1.42 g, 5.97 mmol	IPA (20 mL)	**5c** (1.79 g)
[18]aneN$_2$O$_4$	*p*(GMA-S)	Tol (25 mL)/	*p*(GMA-S)-[18]N$_2$O$_4$
1.76 g, 6.71 mmol	1.49 g, 4.47 mmol	IPA (25 mL)	**6** (1.57 g)

Batch metal-uptake experiments involving Ag^+ and Pb^{2+} were performed using standard metal nitrate solutions of 0.10 M. The capacities for Ag^+ and Pb^{2+} were determined with batches of 70−100 mg of resin over a pH range of 1 to 6. The pH of the metal solutions was adjusted with dilute HNO_3 and dilute NH_3, respectively. In the case of Pb^{2+}, pH values higher than 5.3 were not attainable due to precipitation of $Pb(OH)_2$. The experiments involving Ag^+ were performed under exclusion of light.

Batch metal-uptake experiments involving Ag^+ and Pb^{2+} under competitive conditions were performed using standard metal nitrate solutions (0.10 M) of Ag^+, Pb^{2+}, Cu^{2+}, Cd^{2+}, and Zn^{2+}. Batches of 70−100 mg of resin were used, together with a mixture of 10 mL of each of the metal solutions, and the pH was adjusted in the same way as in the non-competitive experiments with Ag^+ and Pb^{2+}. The samples were shaken for 48 h and further handled as described for the metal chloride experiments.

In the regeneration experiments, a range of potential stripping agents were tested for their ability to remove metal ions from loaded resins. A sufficient amount of ion exchanger was loaded with the appropriate metal ion solution and subsequently contacted with aqueous solutions of a range of acids or competing ligands, using parts of the same batch of loaded resin.

Distribution coefficients [D = (mg M^{n+}/g of dry resin)/(mg M^{n+}/mL of solution)] were determined as a function of pH according to Roozemond et al.[22] In each case, 0.2 g of resin, 25 mL of buffer solution and 25 mL of an appropriate metal ion solution, containing such an amount of metal ions that the polymer-bound ligands were present in about eightfold excess, were shaken for 48 h. In the case of Ag^+ and Pb^{2+}, no buffer solutions were used, instead the pH was adjusted with dilute HNO_3 or NH_3.

Samples for metal analysis were prepared by heating the loaded samples overnight with concentrated H_2SO_4 (reflux) and subsequently with concentrated HNO_3 until clear solutions were obtained.

Acknowledgments

Mr. J. G. Hollander is gratefully acknowledged for the collection of the solid-state CP MAS ^{13}C NMR spectra presented in this paper. Dr. W. Buijs (DSM Research) is thanked for his suggestions and fruitful discussions and Ing. F. ten Hoonte is acknowledged for technical assistance.

[1] O. Andersen, *Chem. Rev.* **1999**, *99*, 2683.
[2] A. T. Yordanov, D. M. Roundhill, *Coord. Chem. Rev.* **1998**, *170*, 93.
[3] R. A. Beauvais, S. D. Alexandratos, *React. Funct. Polym.* **1998**, *36*, 113.
[4] J. D. Lamb, R. M. Izatt, J. J. Christensen, D. J. Eatough, *Coordination Chemistry of Macrocyclic Compounds* (Ed.: G. A. Melson), Plenum, New York, **1979**, pp. 145−217.
[5] J. S. Bradshaw, R. M. Izatt, *Acc. Chem. Res.* **1996**, *30*, 338.
[6] P. M. van Berkel, W. L. Driessen, G. J. A. A. Koolhaas, J. Reedijk, D. C. Sherrington, *J. Chem. Soc., Chem. Commun.* **1995**, 147.
[7] P. M. van Berkel, M. Punt, G. J. A. A. Koolhaas, W. L. Driessen, J. Reedijk, D. C. Sherrington, *React. Funct. Polym.* **1997**, *32*, 139.
[8] H. J. Hoorn, P. de Joode, W. L. Driessen, J. Reedijk, *React. Funct. Polym.* **1997**, *32*, 169.
[9] F. Svec, J. Hadril, J. Coupek, J. Kalal, *Angew. Makromol. Chem.* **1975**, *48*, 135.
[10] B. D. Moore, D. C. Sherrington, A. Zitsmanis, *J. Mater. Chem.* **1992**, *2*, 1231.
[11] T. Nabeshima, N. Tsukada, K. Nishijima, H. Ohshiro, Y. Yano, *J. Org. Chem.* **1996**, *61*, 4342.
[12] L. G. A. van de Water, F. ten Hoonte, W. L. Driessen, J. Reedijk, D. C. Sherrington, *Inorg. Chim. Acta* **2000**, *303*, 77.
[13] P. M. van Berkel, D. C. Sherrington, *Polymer* **1996**, *37*, 1431.
[14] C. Knakkergaard Möller, *Acta Chem. Scand., Ser. A* **1979**, *33*, 11.
[15] F. Arnaud-Neu, B. Spiess, M.-J. Schwing-Weill, *Helv. Chim. Acta* **1977**, *60*, 2633.
[16] R. D. Hancock, A. E. Martell, *Chem. Rev.* **1989**, *89*, 1875.
[17] R. D. Hancock, R. Bhavan, P. W. Wade, J. C. A. Boeyens, S. M. Dobson, *Inorg. Chem.* **1989**, *28*, 187
[18] R. D. Hancock, H. Maumela, A. S. de Sousa, *Coord. Chem. Rev.* **1996**, *148*, 315.
[19] E. I. Morosanova, I. M. Maksimova, Yu. A. Zolotov, *Zh. Anal. Khim.* **1992**, *47*, 1854.
[20] L. G. A. van de Water, W. L. Driessen, J. Reedijk, manuscript in preparation.
[21] P. M. van Berkel, M. Punt, G. J. A. A. Koolhaas, W. L. Driessen, J. Reedijk, D. C. Sherrington, *React. Funct. Polym.* **1997**, *32*, 139.
[22] D. A. Roozemond, F. den Hond, J. B. J. Veldhuis, H. Strasdeit, W. L. Driessen, *Eur. Polym. J.* **1988**, *24*, 868.

Received February 28, 2001
[I01072]

Synthesis, Chemistry, and Catalytic Activity of Ruthenium Diaminodiphosphane Complexes − Crystal Structures of *trans*-[$RuCl_2\{\kappa^3$-$Ph_2PC_6H_4CH{=}NC_6H_{10}N(H)CH_2C_6H_4PPh_2\}(PPh_3)$] and *cis*-[$RuCl_2\{\kappa^4$-$Ph_2PC_6H_4CH{=}NC_6H_{10}N(H)CH_2C_6H_4PPh_2\}$]

Wai-Kwok Wong,*[a] Xiao-Ping Chen,[a] Wei-Xiong Pan,[b] Jian-Ping Guo,[a] and Wai-Yeung Wong[a]

Keywords: Ruthenium / N,P ligands / Catalysis / Oxidations

The interaction of $[RuCl_2(PPh_3)_3]$ with one equivalent of *N*,*N*′-bis[2-(diphenylphosphanyl)benzyl]-1*R*,2*R*-cyclohexanediamine [1*R*,2*R*-P(NH)(NH)P] in dichloromethane at room temperature gave *trans*-[$RuCl_2\{\kappa^3$-1*R*,2*R*-P(NH)(NH)P$\}(PPh_3)$] (**1**). When heated under reflux in toluene under a nitrogen atmosphere, **1** was converted into *trans*-[$RuCl_2\{\kappa^4$-1*R*,2*R*-P(NH)(NH)P$\}$] (**2**). However, when **1** was stirred at room temperature in air, it was oxidized to *trans*-[$RuCl_2\{\kappa^3$-1*R*,2*R*-PN(NH)P$\}(PPh_3)$] (**3**). Depending on the reaction conditions, **3** was converted into *trans*-[$RuCl_2\{\kappa^3$-1*R*,2*R*-P(NH)(NH)P=O$\}(PPh_3)$] (**4**) when heated to 80 °C in toluene in air, to *cis*-[$RuCl_2\{\kappa^4$-1*R*,2*R*-PN(NH)P$\}$] (**5**) when stirred at room temperature in acetone in air, or to *trans*-[$RuCl_2\{\kappa^4$-1*R*,2*R*-PN(NH)P$\}$] (**6**) when heated under reflux in acetone under a nitrogen atmosphere. When heated under reflux in toluene under a nitrogen atmosphere, **5** isomerized to **6** quantitatively. When heated under reflux in mesitylene under a nitrogen atmosphere, **6** was slowly reduced to **2**. The solid state structures of **3** and **5** were ascertained by X-ray crystallography. Catalytic studies showed that **1** could catalyze the oxidation of alkanes and alkenes with molecular oxygen.

Introduction

Transition-metal complexes with chiral diamino-, diimino-, and diamidodiphosphane ligands have been shown to be effective catalysts for asymmetric hydrogen-transfer reactions,[1] epoxidations,[2] and allylic alkylations,[3−4] respectively. Thus, the synthesis of chiral diamino-, diimino-, and diamidodiphosphane ligands and their application as auxiliaries for the preparation of chiral catalysts have aroused considerable recent interest. We have investigated the preparation and chemistry of diamino-, diimino-, and diamidodiphosphane ligands,[5−10] and reported the synthesis of *N*,*N*′-bis[2-(diphenylphosphanyl)benzyl]-1*R*,2*R*-cyclohexanediamine [1*R*,2*R*-P(NH)(NH)P] and its Ru^{II},[7] Cu^{I}, and Ag^{I} complexes.[8] In this report, we describe the synthesis, reactivity, and catalytic activity of *trans*-[$RuCl_2\{\kappa^3$-1*R*,2*R*-P(NH)(NH)P$\}(PPh_3)$] (**1**).

Results and Discussion

Unlike the reaction with $[RuCl_2(DMSO)_4]$ in refluxing toluene, which gave the complex *trans*-[$RuCl_2\{\kappa^4$-1*R*,2*R*-P(NH)(NH)P$\}$] (**2**),[7] 1*R*,2*R*-P(NH)(NH)P reacted with $[RuCl_2(PPh_3)_3]$ in dichloromethane at room temperature to give *trans*-[$RuCl_2\{\kappa^3$-1*R*,2*R*-P(NH)(NH)P$\}(PPh_3)$] (**1**), which was fully characterized by elemental analysis, NMR spectroscopy, and mass spectrometry. The ^{31}P NMR spectrum of **1** exhibited two doublets at δ = 48.6 (d, $^2J_{PP}$ = 28.9 Hz) and 38.9 (d, $^2J_{PP}$ = 28.9 Hz) for the coordinated P atom of the P(NH)(NH)P ligand and PPh_3, respectively, and a singlet at δ = −13.3 (s) for the dangling P atom of the P(NH)(NH)P ligand. The positive FAB mass spectrum of **1** showed a peak corresponding to its molecular ion $[M]^+$ at *m*/*z* = 1096 for ^{102}Ru and ^{35}Cl. The tridentate nature of the P(NH)(NH)P ligand was also confirmed by X-ray crystallography. While this work was in progress, the synthesis and structure of **1** appeared in the literature.[11] Our structural and spectroscopic data of **1** agree with the literature data.

When heated to reflux in toluene under a nitrogen atmosphere, **1** was converted quantitatively to *trans*-[$RuCl_2\{\kappa^4$-1*R*,2*R*-P(NH)(NH)P$\}$] (**2**), which was confirmed by comparing the spectroscopic data with the literature values.[1,7] However, when stirred in dichloromethane in air at room temperature, **1** was converted into *trans*-[$RuCl_2\{\kappa^3$-1*R*,2*R*-PN(NH)P$\}(PPh_3)$] (**3**) (Scheme 1). The structure of **3** was established by X-ray crystallography (Figure 1). Selected bond lengths and bond angles are given in Table 1.

Structural analysis revealed that the κ^3-1*R*,2*R*-P(NH)(NH)P ligand had been oxidized to a κ^3-1*R*,2*R*-

[a] Department of Chemistry, Hong Kong Baptist University, Waterloo Road, Kowloon Tong, Hong Kong, P. R. China
[b] Department of Chemistry, Tsinghua University, Beijing, 100084, P. R. China

 © WILEY-VCH Verlag GmbH, 69451 Weinheim, Germany, 2002 1434−1948/02/0101−0231 $ 17.50+.50/0

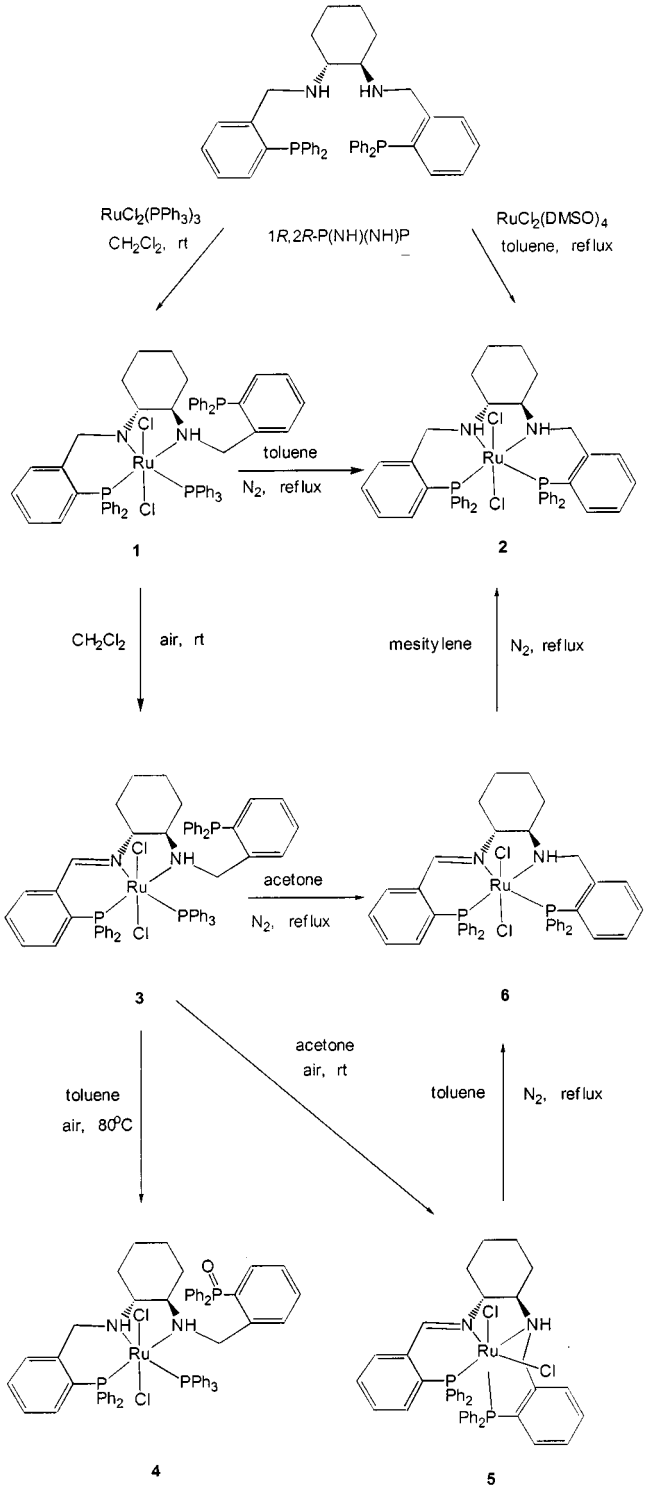

Scheme 1

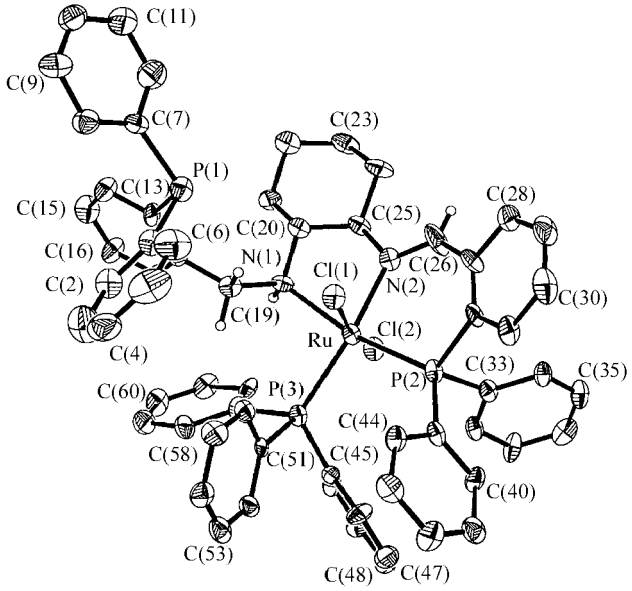

Figure 1. A perspective drawing of compound **3**. All the phenyl and cyclohexyl protons are omitted for clarity

Table 1. Selected bond lengths (Å) and bond angles (°) for compounds **3** and **5**

Compound **3**			
Ru−P(2)	2.261(2)	Ru−P(3)	2.355(2)
Ru−Cl(1)	2.452(2)	Ru−Cl(2)	2.405(2)
Ru−N(1)	2.192(6)	Ru−N(2)	2.059(7)
N(1)−C(19)	1.505(8)	N(1)−C(20)	1.488(8)
N(2)−C(25)	1.527(9)	N(2)−C(26)	1.28(1)
N(1)−Ru−N(2)	79.4(3)	N(1)−Ru−P(2)	168.2(2)
N(1)−Ru−P(3)	92.4(2)	N(1)−Ru−Cl(1)	86.4(2)
N(1)−Ru−Cl(2)	90.0(2)	N(2)−Ru−P(2)	89.6(2)
N(2)−Ru−P(3)	170.0(2)	N(2)−Ru−Cl(1)	81.7(2)
N(2)−Ru−Cl(2)	86.4(2)	P(2)−Ru−P(3)	98.9(1)
P(2)−Ru−Cl(1)	87.8(1)	P(2)−Ru−Cl(2)	93.6(1)
P(3)−Ru−Cl(1)	103.7(1)	P(3)−Ru−Cl(2)	87.9(1)
Cl(1)−Ru−Cl(2)	168.0(1)	N(1)−C(19)−C(18)	118.2(7)
N(2)−C(26)−C(27)	123(1)		
Compound 5			
Ru−P(1)	2.299(2)	Ru−P(2)	2.270(2)
Ru−Cl(1)	2.453(1)	Ru−Cl(2)	2.442(1)
Ru−N(1)	2.026(5)	Ru−N(2)	2.142(4)
N(1)−C(1)	1.295(6)	N(1)−C(2)	1.521(7)
N(2)−C(8)	1.497(5)	N(2)−C(7)	1.500(6)
N(1)−Ru−N(2)	82.5(2)	N(1)−Ru−P(1)	94.9(1)
N(1)−Ru−P(2)	94.1(1)	N(1)−Ru−Cl(1)	85.1(1)
N(1)−Ru−Cl(2)	168.8(1)	N(2)−Ru−P(1)	90.3(1)
N(2)−Ru−P(2)	169.3(1)	N(2)−Ru−Cl(1)	80.8(1)
N(2)−Ru−Cl(2)	88.3(1)	P(1)−Ru−P(2)	100.2(1)
P(1)−Ru−Cl(1)	171.0(1)	P(1)−Ru−Cl(2)	91.5(1)
P(2)−Ru−Cl(1)	88.8(1)	P(2)−Ru−Cl(2)	93.8(1)
Cl(1)−Ru−Cl(2)	87.2(1)	N(1)−C(1)−C(27)	127.4(6)
N(2)−C(8)−C(9)	114.0(4)		

PN(NH)P ligand with the amino group *trans* to the PPh_3 group oxidized to an imino group. The N(1)−C(19) and N(2)−C(26) distances of 1.505(8) and 1.28(1) Å are consistent with a carbon−nitrogen single and double bond, respectively. The Ru atom adopts a slightly distorted octahedral geometry with a *trans*-$RuCl_2$ arrangement. The [1*R*,2*R*-PN(NH)P] ligand acts as a tridentate ligand with one of the two phosphanyl groups being uncoordinated. The sixth site is occupied by a PPh_3 ligand. The Ru−P, Ru−Cl, and Ru−N distances are in the range expected for similar com-

plexes of general formula [$RuCl_2${P(NH)(NH)P}].[1,7,11] The Ru−N distances [Ru−N(1) 2.192(6), Ru−N(2) 2.059(7) Å] reflect that the imino nitrogen, N(2), is more tightly bound to the Ru centre than the amino nitrogen, N(1). The Ru−P distance of the PPh_2 group [Ru−P(2) 2.261(2) Å] is shorter than that of the PPh_3 group [Ru−P(3) 2.355(2) Å]. This may be a reflection of the chelate effect as well as the *trans* influence. The closing of the Cl(1)−Ru−Cl(2) angle [168.0°(1)] reflects the steric crowding and chelate ring strain in the complex, as the chloro ligands are pushed away from the bulky PPh_3 toward the imino moiety *trans* to it. The solid-state structure is supported by ^1H, ^{13}C and ^{31}P NMR, IR, and MS data. The $^{31}P\{^1H\}$ NMR spectrum of **3** exhibits two doublets and a singlet at δ = 55.5 (d, $^2J_{PP}$ = 27.2 Hz), 31.1 (d, $^2J_{PP}$ = 27.2 Hz), and −14.9 (s), which can be assigned to P(2), P(3), and P(1) (see Figure 1 for atom numbering), respectively. The presence of the imino group is further supported by the ^1H NMR spectrum and ^{13}C NMR spectrum, which shows a doublet at δ = 8.55 (d, $^4J_{P-CH}$ = 8.8 Hz, 1 H) for the proton and a singlet at δ = 164.9 for the carbon of the -CH=N- group. Furthermore, the IR spectrum shows the $\nu_{C=N}$ absorption at 1621 cm^{-1}. The positive FAB mass spectrum exhibits the molecular ion peak $[M]^+$ at *m*/*z* = 1094.

When heated to 80 °C in air in toluene, **3** was converted quantitatively to a purple red species, **4**, within 4 h. The $^{31}P\{^1H\}$ NMR spectrum of **4** exhibited two doublets and a singlet at δ = 47.1 (d, $^2J_{PP}$ = 28.8 Hz), 39.1 (d, $^2J_{PP}$ = 28.8 Hz), and 30.6 (s). The chemical shifts of the two doublets are very similar to those of **1**. Thus, the doublets at δ = 47.1 and 39.1 can be assigned to the phosphorus atoms of the tridentate ligand and PPh_3, respectively. The $^{31}P\{^1H\}$ NMR spectroscopic data suggest that the imino group in **3** has been reduced to an amino group. This is supported by the absence of the imino proton, imino carbon, and the $\nu_{C=N}$ band in the ^1H NMR, ^{13}C NMR, and IR spectra, respectively. The chemical shift of the singlet corresponds to that of a phosphane oxide, suggesting that the pendant phosphane had been oxidised to a phosphane oxide. This is further supported by the IR data, which shows the $\nu_{P=O}$ absorption at 1191 cm^{-1}, and the mass spectroscopic data (FAB, positive), which displays the molecular ion peak $[M]^+$ at *m*/*z* = 1112. Based on the spectroscopic data, compound **4** was formulated as *trans*-[$RuCl_2${κ^3-1*R*,2*R*-P(NH)(NH)P=O}(PPh_3)] with the structure shown in Scheme 1.

When stirred at room temperature in acetone in air, however, **3** was converted into a mixture of compounds. The ^{31}P NMR spectrum of the reaction mixture showed that in addition to **4** (approximately 5%), a new species **5** was also observed, which exhibited a pair of doublets at δ = 51.5 (d, $^2J_{PP}$ = 30.3 Hz) and 46.3 (d, $^2J_{PP}$ = 30.3 Hz). Compounds **4** and **5** could be easily separated by column chromatography. The structure of **5** was ascertained by X-ray crystallography (Figure 2). Crystals of **5**·H_2O suitable for X-ray diffraction study were grown by slow evaporation of **5** in an acetone/hexane mixture. The water molecule probably came from acetone, which had not been dried prior to use. Selected bond lengths and bond angles are given in Table 1. Structural analysis revealed that the tridentate κ^3-1*R*,2*R*-PN(NH)P ligand had become a tetradentate κ^4-1*R*,2*R*-PN(NH)P ligand with the imino nitrogen N(1) and the phosphorus atom P(1) of the aminophosphanyl group *trans* to the Cl atoms. The Ru atom had adopted a slightly distorted octahedral geometry with a *cis*-$RuCl_2$ arrangement. The Cl(1)−Ru−Cl(2) bond angle is 87.2(1)°. The Ru−P, Ru−Cl, and Ru−N distances are similar to those of **3**. The differences in Ru−P [Ru−P(1) 2.299(2), Ru−P(2) 2.270(2) Å], Ru−Cl [Ru−Cl(1) 2.453(1), Ru−Cl(2) 2.442(1) Å], and Ru−N [Ru−N(1) 2.026(5), Ru−N(2) 2.142(4) Å] distances are a reflection of the *trans* influence. The N(2)−C(8) and N(1)−C(1) distances of 1.497(5) and 1.295(6) Å are consistent with a carbon−nitrogen single and double bond, respectively.

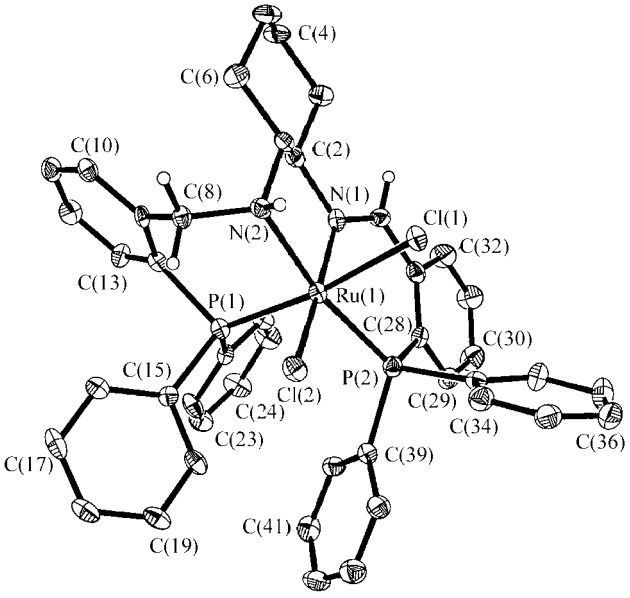

Figure 2. A perspective drawing of compound **5**; all the phenyl and cyclohexyl protons are omitted for clarity

When heated under reflux in toluene under a nitrogen atmosphere for 12 h, **5** was converted quantitatively (by ^{31}P NMR) to a red species **6**. In its ^{31}P NMR spectrum, **6** exhibited two doublets at δ = 54.3 (d, $^2J_{PP}$ = 26.7 Hz) and 36.1 (d, $^2J_{PP}$ = 26.7 Hz), which could be assigned to the PPh_2 groups attached to the imino and amino group, respectively. In its mass spectrum (FAB, positive), **6** exhibited the $[M]^+$ peak at *m*/*z* = 832 for ^{102}Ru and ^{35}Cl. Thus, compound **6** can be formulated as *trans*-[$RuCl_2${κ^4-1*R*,2*R*-PN(NH)P}]. Compound **6** could also be obtained quantitatively (by ^{31}P NMR) when an acetone solution of **3** was heated to reflux under a nitrogen atmosphere for 12 h. A ^{31}P NMR study showed that the imino group of **6** could be slowly reduced to an amino group upon prolong heating in a high boiling hydrocarbon solvent under a nitrogen atmosphere. When **6** was heated under reflux in mesitylene under a nitrogen atmosphere, the $^{31}P\{^1H\}$ NMR spectrum of the

solution showed that as well as the resonances of **6**, a singlet at δ = 46.5 corresponding to a resonance of **2** emerged. After heating for 48 h under reflux the reaction proceeded cleanly with about 50% of **6** being converted into **2**, based on ^{31}P NMR spectroscopic data. No other phosphorus-containing species could be observed. The mechanism of this reduction is not clear, but it is very likely that the hydrogen source for the reduction is the solvent.

Catalytic Oxidation

Preliminary results showed that under oxygen, **1** catalysed the oxidation of octane primarily to 2-, 3-, and 4-octanone, hexene to 1,2-hexanediol, and styrene to benzoic acid (Table 2). For the octane oxidation, the effect of temperature was more critical than pressure. For example, when the catalytic reaction was carried out at 130 °C and an oxygen pressure of 5 MPa, the turnover frequency (TOF) was 67. A drop in oxygen pressure to 2.4 MPa did not affect the TOF significantly. The TOF was about 62. However, when the temperature was decreased to 110 °C, the TOF dropped to about 0.4. The activity of $[RuCl_2(PPh_3)_3]$ as a catalyst for the oxidation of styrene and octane with oxygen were also examined. The results (the last two entries of Table 2) showed that under the same conditions $[RuCl_2(PPh_3)_3]$ catalysed the oxidation of styrene with oxygen to benzaldehyde and styrene oxide with a very low conversion (0.4%), and was inactive toward the oxidation of octane with oxygen. Thus, **1** is a better catalyst than $[RuCl_2(PPh_3)_3]$ for the oxidation of styrene and octane with oxygen.

Ruthenium-catalysed oxidation of alkane with peroxo species has drawn considerable interest recently. However, most of the studies were concentrated on the use of peroxo species as oxidants in the catalytic reaction;[12−14] there were very few studies using molecular oxygen as oxidant.[15] The present study provides an additional example of a catalytic system where molecular oxygen can be used to oxidise a saturated hydrocarbon. The mechanism of the catalytic oxidation is not clear. However, based on the reactivity of **1** with air, compounds **3** and **4** may be involved as intermediates in the catalytic cycle. The transformation of **3** to **4** is rather unusual. Rather than just oxidising the pendant phosphane to a phosphane oxide, the oxidation was accompanied by the reduction of an imino group to an amino group.

Experimental Section

General Procedures: Unless otherwise stated, all reactions were carried out under an atmosphere of dry nitrogen using standard Schlenk and vacuum-line techniques. Solvents were dried by standard procedures, distilled, and deaerated prior to use. All chemicals

Table 2. Catalytic oxidation of 1-hexene, styrene and octane with O_2 using **1** as catalyst

Substrate	Temp (°C)	O_2 Pressure (MPa)	Conversion (%)[a]	TOF (h^{-1})[a]	Product[b]	Selectivity (%)[c]
1-Hexene[d]	130	5.0	39	4633	1,2-hexanediol	55
Styrene[e]	130	3.9	93	3038	benzaldehyde	1
					benzoic acid	85
Octane[f]	130	5.0	70	67	butanoic acid	12
					4-octanone	11
					3-octanone	12
					2-octanone	25
					4-octanol	0.2
					3-octanol	0.2
					2-octanol	0.4
	130	2.4	57	62	butanoic acid	9
					4-octanone	12
					3-octanone	16
					2-octanone	23
					4-octanol	0.7
					3-octanol	1
					2-octanol	1.3
	110	4.4	0.4	0.4	butanoic acid	10
					4-octanone	43
					3-octanone	25
					2-octanone	22
Styrene[g]	130	3.9	0.4	11	benzaldehyde	75
					styrene oxide	21
Octane[h]	130	2.4	0	0	−	0

[a] Determined by GLC analysis based on the starting substrate using acetophenone as an internal standard. [b] Identified by GC-MS. [c] Determined by GLC analysis based on the converted substrate using acetophenone as an internal standard. [d] Substrate (2.0 g): catalyst (1 mg) = 26100 (mole ratio), reaction time = 2 h. [e] Substrate (2.7 g): catalyst (2 mg) = 14200 (mole ratio), reaction time = 4 h. [f] Substrate (1.4 g): catalyst (2 mg) = 6700 (mole ratio), reaction time = 64 h. [g] Catalyst: $RuCl_2(PPh_3)_3$, substrate (2.7 g): catalyst (2 mg) = 12500 (mole ratio), reaction time = 4 h. [h] Catalyst: $RuCl_2(PPh_3)_3$, substrate (1.4 g): catalyst (2 mg) = 5900 (mole ratio), reaction time = 17 h.

used were of reagent grade, obtained from the Aldrich Chemical Company, and, where appropriate, were degassed before use. The compounds 1*R*,2*R*-P(NH)(NH)P[8] and $[RuCl_2(PPh_3)_3]$[16] were prepared according to literature methods. Microanalyses were performed at the Shanghai Institute of Organic Chemistry, Chinese Academy of Sciences. The IR spectra (KBr pellets) were recorded on a Nicolet Nagna-IR 550 spectrometer, and NMR spectra on a JEOL EX270 spectrometer. Chemical shifts of ^1H NMR spectra were referenced to internal deuterated solvents and then recalculated to TMS (δ = 0.00), those of $^{31}P\{^1H\}$ NMR spectra were referenced to external 85% H_3PO_4. Low-resolution mass spectra were obtained on a Finnigan MAT SSQ-710 or MAT 95 spectrometer in positive FAB mode and reported as *m*/*z*. Gas chromatograms were obtained on a HP 5890 GC system or a HP 6890−5972 GC-MSD system. The progress of all the reactions was monitored by $^{31}P\{^1H\}$ NMR spectroscopy.

Preparation of *trans*-[RuCl$_2${κ^3-1*R*,2*R*-P(NH)(NH)P}(PPh$_3$)] (1): A solution of 1*R*,2*R*-P(NH)(NH)P (0.212 g, 0.320 mmol) and $[RuCl_2(PPh_3)_3]$ (0.305 g, 0.318 mmol) in CH_2Cl_2 (20 cm^3) was stirred under a nitrogen atmosphere at room temperature for 4 h. The solution was filtered and the solvent of the filtrate was removed in vacuo to give a dark red residue. The residue was dissolved in a minimum amount of chloroform and purified by chromatography on a silica gel column using chloroform as eluent to give an orange band. Removal of the solvent from the orange band gave an orange solid, which was recrystallized from dichloromethane/hexane to give orange crystals. Yield: 0.264 g, 64%; m.p. 186−187 °C (decomp). IR (KBr): $\tilde{\nu}$ = 3257 cm^{-1} w, 3186 w, 3047 m, 2930 w, 1490 m, 1434 s, 1189 w, 1086 m, 1035 w, 994 m, 958 w, 753 s, 702 vs, 574 w, 552 s and 467 w. ^1H NMR: ($CDCl_3$): δ = 6.41−7.82 (m, 43 H), 3.98 (m, 2 H), 3.79 (m, 2 H), 3.53 (m, 2 H), 3.04 (m, 1 H), 2.57 (m, 1 H), 0.98−1.48 (m, 8 H). $^{31}P\{^1H\}$ NMR ($CDCl_3$): δ = 47.0 (d, $^2J_{PP}$ = 28.2 Hz), 39.3 (d, $^2J_{PP}$ = 28.2 Hz), −13.1 (s). $C_{62}H_{59}Cl_2N_2P_3Ru{\cdot}CH_2Cl_2{\cdot}CHCl_3$ (1301.37): calcd. C 59.07, H 4.80, N 2.15; found C 59.09, H 4.81 , N 2.14. LRMS (FAB+): *m*/*z* = 1096 [M]$^+$ for ^{102}Ru and ^{35}Cl. $[\alpha]_D^{20}$ = 55.83 (*c* = 0.5, CH_2Cl_2).

Preparation of *trans*-[RuCl$_2${κ^4-1*R*,2*R*-P(NH)(NH)P}] (2): A solution of **1** (0.081 g, 0.074 mmol) in toluene (10 cm^3) was heated to reflux under a nitrogen atmosphere for 12 h. After cooling to room temperature, the solution was filtered, and the solvents evaporated to dryness in vacuo to give an orange residue. The residue was washed with diethyl ether (2 × 5 cm^3) and recrystallized from a CH_2Cl_2/hexane mixture to give orange crystals of **2**. Yield: 0.060 g, 97% (0.072 mmol). The identity of **2** was confirmed by comparing the IR, NMR [^1H and $^{31}P\{^1H\}$], and MS (FAB+) data of **2** with those of an authentic sample of *trans*-[RuCl$_2${κ^4-1*R*,2*R*-P(NH)(NH)P}].

Preparation of *trans*-[RuCl$_2${κ^3-1*R*,2*R*-PN(NH)P}(PPh$_3$)] (3): A solution of **1** (0.020 g, 0.018 mmol) in dichloromethane (5 cm^3) was allowed to stir at room temperature in air. The progress of the reaction was monitored by $^{31}P\{^1H\}$ NMR spectroscopy. After 2 days, the ^{31}P NMR spectrum showed that **1** had completely reacted. The solution was then filtered and the filtrate was evaporated to dryness. The residue was dissolved in a minimum amount of chloroform and purified by chromatography on a silica gel column using chloroform as eluent to give a red band, which upon work-up and crystallisation from a $CHCl_3$/THF/hexane mixture gave red crystals of **3**. Yield: 0.018 g, 91%; m.p. 148−149 °C (decomp). IR (cm^{-1}, in KBr): $\tilde{\nu}$ = 3258 w, 3058 m, 2929 m, 2865 w, 1621 m, 1584 w, 1481 m, 1430 s, 1093 m, 751 s, 705 vs and 524 s. ^1H NMR ($CDCl_3$): δ = 8.55 (d, $^4J_{P-H}$ = 8.8 Hz, 1 H), 5.94−8.02 (m, 43 H), 4.55 (m, 1 H), 3.86−4.21 (m, 4 H), 3.03 (m, 1 H), 2.26 (m, 1 H), 0.96−1.35 (m, 6 H). $^{13}C\{^1H\}$ NMR ($CDCl_3$): δ = 164.9 (s), 126.8−136.1 (m), 64.5 (s), 53.7 (s), 43.6 (s), 40.4 (s), 29.2(s). $^{31}P\{^1H\}$ NMR ($CDCl_3$): δ = 55.5 (d, $^2J_{PP}$ = 27.2 Hz), 31.1 (d, $^2J_{PP}$ = 27.2 Hz), −14.9 (s). $C_{62}H_{57}Cl_2N_2P_3Ru{\cdot}CH_2Cl_2{\cdot}C_6H_{14}$ (1266.15): calcd. C 65.46, H 5.81, N 2.21; found C 65.09, H 5.86, N 2.19. LRMS (FAB+): *m*/*z* = 1094 [M]$^+$ for ^{102}Ru and ^{35}Cl. $[\alpha]_D^{20}$ = 60.90 (*c* = 0.5, CH_2Cl_2).

Preparation of *trans*-[RuCl$_2${κ^3-1*R*,2*R*-P(NH)(NH)P=O}(PPh$_3$)] (4): A solution of **3** (0.050 g, 0.046 mmol) in toluene (10 cm^3) was heated to 80 °C in air. After heating at 80 °C in air for 4 h, the solution turned purple red and the ^{31}P NMR signals due to **3** had completely disappeared. The solvent was subsequently removed in vacuo to give a purple red residue, which upon crystallization from a $CHCl_3$/THF/hexane mixture gave purple red crystals. Yield: (quantitative by $^{31}P\{^1H\}$ NMR), 0.050 g, 98%; m.p. 198−199 °C (decomp). IR (KBr): $\tilde{\nu}$ = 3263 cm^{-1} w, 3048 m, 2929 w, 2852 w, 1584 w, 1486 m, 1429 s, 1305 w, 1264 m, 1191 s, 1124 s, 1088 s, 1026 m, 995 m, 803 m, 747 s, 721 s, 695 vs, 550 vs and 534 s. ^1H NMR ($CDCl_3$): δ = 6.20−8.10 (m, 43 H), 3.91 (m, 4 H), 3.57 (m, 2 H), 3.05 (m, 1 H), 2.65 (m, 1 H), 0.80−1.60 (m, 8 H). $^{13}C\{^1H\}$ NMR ($CDCl_3$): δ = 126.8−136.6 (m), 60.8 (s), 49.0 (s), 48.7 (s), 31.1 (s), 24.8 (s). $^{31}P\{^1H\}$ NMR ($CDCl_3$): δ = 47.1 (d, $^2J_{PP}$ = 28.8 Hz), 39.1 (d, $^2J_{PP}$ = 28.8 Hz), 30.6 (s). $C_{62}H_{59}Cl_2N_2OP_3Ru{\cdot}C_4H_{10}O{\cdot}CHCl_3$ (1304.54): calcd. C 61.69, H 5.25, N 2.15; found C 61.51, H 5.75, N 2.01. LRMS (FAB+): *m*/*z* = 1112 [M]$^+$ for ^{102}Ru and ^{35}Cl. $[\alpha]_D^{20}$ = 34.95 (*c* = 0.5, CH_2Cl_2).

Preparation of *cis*-[RuCl$_2${κ^4-1*R*,2*R*-PN(NH)P}] (5): A solution of **3** (0.050 g, 0.046 mmol) in acetone (10 cm^3) was stirred in air at room temperature for 4 days. The solution was filtered and the solvent from the filtrate was removed in vacuo to give a dark red residue. The residue was dissolved in a minimum amount of chloroform and purified by chromatography on a silica gel column using chloroform as eluent to give a red band. This was followed by eluting with acetone to afford another red band. The red band from chloroform, after work up, was identified as the starting material **3** (0.028 g, 56% recovery).

Removal of the solvent from the second red band led to a red solid, which upon crystallisation from a $CHCl_3$/THF/hexane mixture gave red crystals of **5**. Yield: 0.016 g, 42%; m.p. 102−104 °C (decomp). IR (KBr): $\tilde{\nu}$ = 3253 cm^{-1} w, 3058 m, 2924 m, 1623 m, 1486 m, 1439 s, 1113 m, 761 s, 710 vs and 539 s. ^1H NMR ($CDCl_3$): δ = 8.69 (s, 1 H), 6.00−7.89 (m, 28 H), 4.85 (m, 1 H), 4.10−4.28 (m, 2 H), 3.61 (m, 1 H), 2.99 (m, 1 H), 1.93−2.38 (m, 3 H), 0.88−1.40 (m, 5 H). $^{31}P\{^1H\}$ NMR ($CDCl_3$): δ = 51.5 (d, $^2J_{PP}$ = 30.3 Hz), 46.3 (d, $^2J_{PP}$ = 30.3 Hz). $C_{44}H_{42}Cl_2N_2P_2Ru{\cdot}3H_2O$ (886.80): calcd. C 59.59, H 5.46, N 3.16; found C 59.05, H 5.75, N 3.25. LRMS (FAB+): *m*/*z* = 832 [M]$^+$ for ^{102}Ru and ^{35}Cl. $[\alpha]_D^{20}$ = 60.18 (*c* = 0.5, CH_2Cl_2).

Preparation of *trans*-[RuCl$_2${κ^4-1*R*,2*R*-PN(NH)P}] (6). Method (a): A solution of **5** (0.030 g, 0.036 mmol) in toluene (10 cm^3) was heated under reflux overnight under a nitrogen atmosphere. The solution was filtered and the solvent from the filtrate was removed in vacuo to give a dark red residue. The dark residue was washed with Et_2O (2 × 5 cm^3) and recrystallized from a dichloromethane/hexane mixture to give red crystals of **6**. Yield: 0.029 g, 97%; m.p. 198−200 °C. IR (KBr): $\tilde{\nu}$ = 3258 cm^{-1} w, 3054 m, 2924 m, 1629 m, 1481 m, 1430 s, 1114 m, 747 s, 700 vs and 524 s. ^1H NMR ($CDCl_3$): δ = 9.41 (s, 1 H), 6.21−7.83 (m, 28 H), 4.55 (m, 2 H), 3.68 (m, 1 H), 2.21−2.80 (m, 4 H), 1.01−1.56 (m, 6 H). $^{31}P\{^1H\}$ NMR ($CDCl_3$): δ = 54.3 (d, J_{PP} = 26.7 Hz), 36.1 (d, J_{PP} =

Table 3. Crystallographic data for compounds **3** and **5**

Compound	**3**	**5**
Empirical formula	$C_{62}H_{57}Cl_2N_2P_3Ru{\cdot}C_4H_8O$	$C_{44}H_{42}Cl_2N_2P_2Ru{\cdot}H_2O$
Formula mass	1167.08	850.71
Colour and habit	Red block	Red block
Crystal size/mm	0.10 × 0.10 × 0.15	0.10 × 0.12 × 0.15
Crystal system	Orthorhombic	Orthorhombic
Space group	$P2_12_12_1$	$P2_12_12_1$
a/Å	10.349(1)	12.705(1)
b/Å	17.752(2)	13.393(1)
c/Å	31.719(3)	22.432(2)
V/Å^3	5827(1)	3817.0(6)
Z	4	4
$D_{calcd.}$/g·cm^{-3}	1.330	1.477
Absorption coefficient/mm^{-1}	0.487	0.673
F(000)	2424	1744
Θ range/°	1.72 to 27.53	1.77 to 27.54
Reflections collected	34944	22625
Independent reflections	13174 (R_{int} = 0.1841)	8598 (R_{int} = 0.0957)
Goodness-of-fit on F^2	0.712	0.744
Final *R* indices [$I > 2\sigma(I)$]	$R1$ = 0.0546 $wR2$ = 0.0853	$R1$ = 0.0458 $wR2$ = 0.0607

26.7 Hz). $C_{44}H_{42}Cl_2N_2P_2Ru{\cdot}CH_2Cl_2{\cdot}C_6H_{14}$ (1003.86): calcd. C 61.02, H 5.82, N 2.79; found C 60.33, H 5.31, N 2.36. LRMS (FAB+): *m*/*z* = 832 $[M]^+$ for ^{102}Ru and ^{35}Cl. $[\alpha]_D^{20}$ = 56.07 (*c* = 0.5, CH_2Cl_2).

Method (b): A solution of **3** (0.050 g, 0.046 mmol) in acetone (10 cm^3) was heated to reflux under a nitrogen atmosphere for 12 h. The solution was filtered and the solvent was removed in vacuo from the filtrate to give a dark red residue. The dark residue was washed with Et_2O (2 × 5 cm^3) and recrystallized from a chloroform/hexane mixture to give red crystals of **6**. Yield: 0.037 g, 97%.

Thermolysis of 6: A solution of **6** (0.020 g, 0.024 mmol) in mesitylene (10 cm^3) was heated under reflux under a nitrogen atmosphere for 48 h. The $^{31}P\{^1H\}$ NMR spectrum of the solution showed that as well as the resonances due to **6**, a new singlet at δ = 46.5 had appeared. The solution was filtered and the solvent removed from the filtrate in vacuo, to give a dark red residue. The residue was dissolved in a minimum amount of chloroform and purified by chromatography on a silica gel column using chloroform as eluent to give two red bands. Work up of the first band gave orange crystals of **2** (0.010 g, 50% yield) and second band red crystals of **6** (0.009 g, 45% recovery). Their identities were confirmed by comparing their IR, NMR (^{1}H and ^{31}P), and MS (FAB+) data with those of authentic samples of **2** and **6**.

Catalytic Studies: Catalytic experiments were carried out in a 50-cm^3 stainless steel autoclave (model FW-005) equipped with a temperature control unit. ***Caution:*** *The catalytic reactions must be carried out with safety protection as the reactions may become very violent and explode.* All the catalytic reactions, unless otherwise stated, were carried out in the absence of any solvent. Upon transferring the catalyst, the substrate and a magnetic stirring bar to the autoclave, the autoclave was flushed with oxygen three times by pressurising the autoclave to the desired pressure for 30 s before releasing the pressure. After the autoclave had been thoroughly flushed with oxygen, it was pressurised to the desired oxygen pressure, stirred and quickly raised to the desired temperature. The reaction mixture was allowed to react at the desired temperature for the desired period before it was cooled to room temperature. Then the pressure of the autoclave was released slowly and the reaction mixture was analysed by GC. The identities of the products were verified by GC-MS. Control experiments without the catalysts were performed under identical conditions. The results of the catalytic studies are listed in Table 2.

X-ray Crystallography: Pertinent crystallographic data and other experimental details are summarized in Table 3. Crystals of **3**·C_4H_8O and **5**·H_2O suitable for X-ray diffraction study were grown by slow evaporation of **3** in a THF/hexane mixture and **5** in an acetone/hexane mixture, respectively. The crystals were wrapped in epoxy glue to prevent them from losing solvent, and mounted on a thin glass fibre. No decay in intensity was encountered during the data collection. Intensity data were collected at 293 K on a Bruker Axs SMART 1000 CCD area-detector diffractometer using graphite-monochromated Mo-K_α radiation (λ = 0.71073 Å). The collected frames were processed with the software SAINT[17] and an absorption correction was applied (SADABS)[18] to the collected reflections. The space groups of each crystal were determined from the systematic absences and Laue symmetry check and confirmed by successful refinement of the structure. The structures of all compounds were solved by direct methods (SHELXTL)[19] and refined against F^2 by full-matrix least-squares analysis. All non-hydrogen atoms were refined anisotropically. Hydrogen atoms were generated in their idealized positions and allowed to ride on their respective parent carbon atoms. The Flack parameter for compounds **3** and **5** is 0.07(4) and −0.04(3), respectively.

Crystallographic data (excluding structure factors) for the structures reported in this paper have been deposited with the Cambridge Crystallographic Data Centre as supplementary publication nos. CCDC-161383 (**3**) and CCDC-164794 (**5**). Copies of the data can be obtained free of charge on application to CCDC, 12 Union Road, Cambridge CB2 1EZ, UK [Fax: (internat.) + 44-1223/336-033; E-mail: deposit@ccdc.cam.ac.uk].

Acknowledgments

W.-K. Wong thanks the Hong Kong Baptist University and the Hong Kong Research Grants Council (HKBU 2053/97P) for financial support.

[1] J. X. Gao, T. Ikariya, R. Noyori, *Organometallics* **1996**, *15*, 1087−1089.
[2] R. M. Stoop, A. Mezzetti, *Green Chemistry* **1999**, 39−41.
[3] B. M. Trost, *Acc. Chem. Res.* **1996**, *29*, 355−364.
[4] C. P. Butts, J. Crosby, G. C. Lloyd-Jones, S. C. Stephen, *Chem. Commun.* **1999**, 1707−1708 and refs. therein.
[5] W. K. Wong, J. X. Gao, Z. Y. Zhou, T. C. W. Mak, *Polyhedron* **1993**, *12*, 1415−1417.
[6] J. X. Gao, H. L. Wan, W. K. Wong, M. C. Tse, W. T. Wong, *Polyhedron* **1996**, *15*, 1241−1251.
[7] W. K. Wong, T. W. Chik, X. Feng, T. C. W. Mak, *Polyhedron* **1996**, *15*, 3905−3907.
[8] W. K. Wong, T. W. Chik, K. N. Hui, I. Williams, X. Feng, T. C. W. Mak, C. M. Che, *Polyhedron* **1996**, *15*, 4447−4460.
[9] W. K. Wong, J. X. Gao, W. T. Wong, C. M. Che, *Polyhedron* **1993**, *12*, 2063−2066.
[10] W. K. Wong, J. X. Gao, W. T. Wong, W. C. Cheng, C. M. Che, *J. Organomet. Chem.* **1994**, *471*, 277−282.
[11] R. M. Stoop, S. Bachmann, M. Valentini, A. Mezzetti, *Organometallics* **2000**, *19*, 4117−4126.
[12] C. M. Che, K. W. Cheng, M. C. W. Chan, T. C. Lau, C. K. Mak, *J. Org. Chem.* **2000**, *65*, 7996−8000.
[13] S. I. Murahashi, N. Komiya, Y. Oda, T. Kuwabara, T. Naota, *J. Org. Chem.* **2000**, *65*, 9186−9193.
[14] N. Komiya, S. Noji, S. I. Murahashi, *Chem. Commun.* **2001**, 65−66.
[15] A. S. Goldstein, R. H. Beer, R. S. Drago, *J. Am. Chem. Soc.* **1994**, *116*, 2424−2429.
[16] S. J. La Placa, J. A. Ibers, *Inorg. Chem.* **1965**, *4*, 778−783.
[17] *SAINT, Reference Manual*, Siemens Energy and Automation, Madison, WI, **1994−1996**.
[18] G. M. Sheldrick, SADABS, Empirical Absorption Correction Program, University of Göttingen, **1997**.
[19] G. M. Sheldrick, *SHELXTL Reference Manual, ver.5.1*, Siemens, Madison, WI, **1997**.

Received June 11, 2001
[I01212]

Donor−Acceptor Interaction in Cationic Archetype Mono- and Dinuclear Sesquifulvalene Complexes $[(\eta^5\text{-}C_5H_5)Fe\{\mu\text{-}(\eta^5\text{-}C_5H_4)(\eta^7\text{-}C_7H_6)\}M'L']^{n+}$ (n = 1, 2)

Timo Meyer-Friedrichsen,[a] Christoph Mecker,[a] Marc H. Prosenc,[a] and Jürgen Heck*[a]

Dedicated to Prof. Dr. Thiem on the occasion of his 60th birthday

Keywords: Nonlinear optics / Sesquifulvalene complexes / Structure determination / Cyclic voltammetry / Iron / Ruthenium

In order to gain a deeper insight into structure-property relationships of the donor (D)–acceptor (A) interactions in cationic sesquifulvalene complexes the mono- and dicationic complexes $[(\eta^5\text{-}C_5H_5)Fe\{\mu\text{-}(\eta^5\text{-}C_5H_4)(\eta^7\text{-}C_7H_6)\}M'L']^+$ were synthesized as BF_4 and PF_6 salts: M′L′ = $Cr(CO)_3$ (**3**PF_6); M′L′ = none (**4**BF_4); M′L′ = $Ru(\eta^5\text{-}C_5H_5)^+$ [**5**$(PF_6)_2$]; M′L′ = $Ru(\eta^5\text{-}C_5Me_5)^+$ [**6**$(PF_6)_2$]. The ferrocenyl substituent works as the electron donor and the tropylium moiety as the electron acceptor. For the electronic ground state the NMR spectroscopic results demonstrate an increasing charge delocalization in the order M′L′ = $Cr(CO)_3$ < $Ru(\eta^5\text{-}C_5Me_5)^+$ < $Ru(\eta^5\text{-}C_5H_5)$ < none. The same order of the acceptor moieties is observed for the difference between the oxidation and reduction potentials, which are related to an electrochemically reversible and a complete irreversible one-electron transfer, respectively. A comparison of the structural data of **3**–**6** reveals a small but distinct contribution of the cross-conjugated mesomeric form to the bis(aromatic) mesomeric form in the ground state of the sesquifulvalene complexes, which increases, when the electron-withdrawing ability of the acceptor becomes stronger. The UV/Vis spectra are dominated by two intense absorption bands in the visible and near-UV region, which are assigned to a low-energy donor-(metal)–acceptor charge-transfer (D–A CT) transition and to a high-energy donor(ligand)–acceptor charge-transfer (L–A CT) transition. For these archetype sesquifulvalene complexes the first hyperpolarizability β was determined by means of hyper-Rayleigh scattering (HRS). Whereas for **3** no second harmonic signal could be detected and **4** shows fluorescence due to two-photon absorptions, **5** and **6** possess appreciable β values.

Introduction

Structure-property relationships in nonlinear optical (NLO) chromophores have proven to be very useful, in particular for organic polyene-bridged donor−acceptor (D−A) molecules, as it has been demonstrated for the bond-length alternation (BLA) in relation to second harmonic generation (SHG).[1,2] As in D−A substituted polyenes, a description of the bonding situation in mono- and dinuclear sesquifulvalene complexes which demonstrates weak to strong NLO effects, is achieved by different mesomeric forms. The ground state is mainly represented by the polar bisaromatic form **A** as deduced by means of several structure determinations, whereas the excited CT state is supposed to have more contributions from the cross-conjugated form **B** (Figure 1).[3,4]

It would be worthwhile to know, whether a contribution of the cross-conjugated form **B** to the ground state would affect the SHG according to the BLA in acyclic α,ω-donor−acceptor substituted conjugated polyenes.

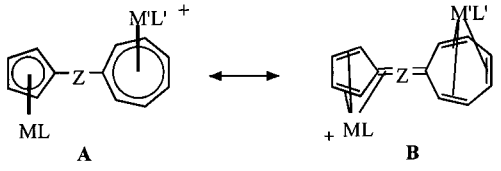

Figure 1. The bis(aromatic) (**A**) and cross-conjugated (**B**) form of mono- and dinuclear sesquifulvalene complexes [e.g. ML = $Fe(\eta^5\text{-}C_5H_5)$; M′L′ = none, $Cr(CO)_3$; Z denotes a conjugated π-bridge]

The crystal structure determinations of the hitherto structurally characterized mono- and dinuclear sesquifulvalene-type complexes do not indicate any significant contribution of the cross-conjugated form **B** to the ground state. This is partly due to the poor quality of the crystals, resulting in a low accuracy of the crystal structure analyses, and partly due to the fact that there are no structural changes, which point to the lack of any remarkable delocalization of charge.[3−7] However, we were now able to determine the structures of some sesquifulvalene complexes, wherein the five- and seven-membered rings are directly connected, in sufficiently high quality to discuss some structure−property relationships. In this paper we additionally present syntheses, spectroscopic and redox properties of the mono- and dinuclear archetype

[a] Institut für Anorganische und Angewandte Chemie
Martin-Luther-King-Platz 6, 20146 Hamburg, Germany
Fax: (internat.) + 49-(0)40/42838-6945
E-mail: heck@chemie.uni-hamburg.de

 © WILEY-VCH Verlag GmbH, 69451 Weinheim, Germany, 2002 1434−1948/02/0101−0239 $ 17.50+.50/0

sesquifulvalene complexes depicted in Figure 2, as well as results of NLO studies concerning the SHG. The spectroscopic and redox data are discussed in comparison to the corresponding properties of the tropylium cation and its complexes shown in Figure 2.

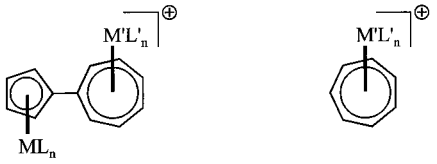

Figure 2. Archetype sesquifulvalene complexes of the general composition $[MLFe\{\mu\text{-}(\eta^5\text{-}C_5H_4)(\eta^7\text{-}C_7H_6)\}M'L']^+$ [ML = $(\eta^5\text{-}C_5H_5)Fe$; M′L′ = $Cr(CO)_3$ (**3**), none (**4**), $Ru(\eta^5\text{-}C_5H_5)^+$ (**5**), $Ru(\eta^5\text{-}C_5Me_5)^+$ (**6**)], and the tropylium cation **7** and its M′L′ complexes [M′L′ = none (**7**), $Cr(CO)_3$ (**8**), $Ru(\eta^5\text{-}C_5H_5)^+$ (**9**), $Ru(\eta^5\text{-}C_5Me_5)^+$ (**10**)]

Results and Discussion

Synthesis

For the cationic target complexes the starting compound is the monohydro-sesquifulvalene complex **1**, which is readily prepared by the nucleophilic addition of monolithiated ferrocene[8] to the tropylium cation (Scheme 1a).[3,4] The subsequent preparation of the cationic dipolar sesquifulvalene complexes is determined by the nature of the electron-accepting function. The reaction of the cycloheptatriene complex **1** with $Cr(CO)_3(EtCN)_3$ [9] yields the dimetallic monohydro-sesquifulvalene complex **2** (Scheme 1b) which is converted into the dipolar monocationic, dinuclear product **3** after the hydride elimination by the trityl cation (Scheme 1c).

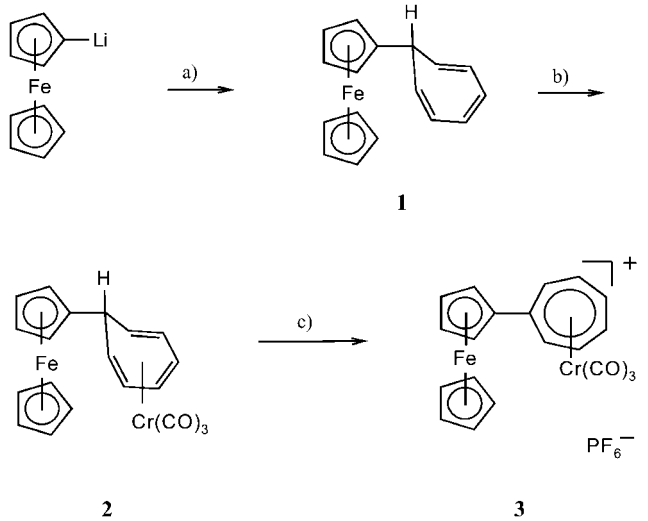

Scheme 1. Synthesis of the dimetallic monohydro-sesquifulvalene complexes **2** and the formation of the monocationic dinuclear sesquifulvalene complex **3:** a) $[C_7H_7]PF_6$, Et_2O; b) $Cr(CO)_3(EtCN)_3$, THF; c) $[Ph_3C]PF_6$, CH_2Cl_2

The preparation of the dicationic congeners **5** and **6** occurs by a hydride abstraction from **1**, revealing the cationic ferrocenyl-substituted tropylium compound **4**,[10] and is accomplished by the coordination of the proper metal−ligand fragment $Ru(\eta^5\text{-}C_5R_5)^+$ [11a,11b] to the tropylium moiety (Scheme 2).

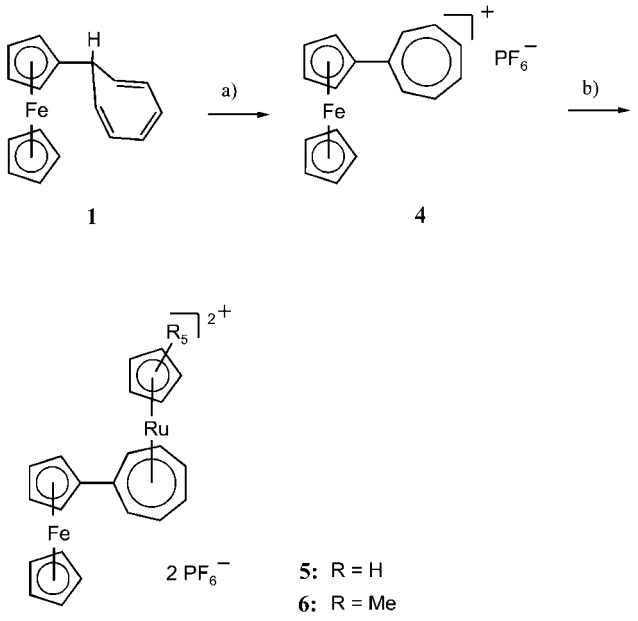

Scheme 2. Synthesis of the monometallic monocationic and dinuclear dicationic sesquifulvalene complexes **4**, **5**, and **6**, respectively: a) $[Ph_3C]PF_6$, CH_2Cl_2; b) $[(\eta^5\text{-}C_5R_5)Ru(MeCN)_3]PF_6$ (R = H, Me), CH_2Cl_2

Most remarkable in the course of the synthesis of the cationic sesquifulvalene complexes is a dramatic color change upon hydride abstraction. The dichloromethane solutions of the ferrocenyl derivatives change color from orange or brick-red to deep green-blue on going from the neutral monohydro-sesquifulvalene complexes to the cationic sesquifulvalene species.

NMR Spectroscopy

The assignment of the ^1H and ^{13}C NMR signals was performed using the splitting pattern in the ^1H NMR spectra, and by means of $^1H^1H$ and $^1H^{13}C$ correlation spectroscopy. From the NMR spectroscopic data in Table 1, which also includes the data of the unsubstituted tropylium cation and its M′L′ complexes [M′L′ = $Cr(CO)_3$ (**8**), $Ru(\eta^5\text{-}C_5H_5)^+$ (**9**), $Ru(\eta^5\text{-}C_5Me_5)^+$ (**10**)], it becomes evident that the shift ranges of the acceptor of the sesquifulvalene complexes correspond to the shifts of the signals of the unsubstituted tropylium cation **7** and its complexes **8**−**10**. In general a high-field shift of the signals of the tropylium moiety is also observed when the ferrocenyl donor is bound to the seven-membered ring. This effect of the donor substituent is also recognized for the distal ligands L′ whose signals are slightly high-field shifted when **5** and **6** are compared with **9** and **10**. Additionally, the small low-field shift of the resonance signal of the carbonyl ligands in **3** compared to **8** is in agreement with a slight increase in electron density on the metal center Cr, upon donor substitution on the tropylium ring. The high-field shift of the resonance signals of

Table 1. ^{1}H and ^{13}C NMR shifts of the cationic sesquifulvalene complexes $[(\eta^5\text{-}C_5H_5)Fe\{\mu\text{-}(\eta^5\text{-}C_5H_4)(\eta^7\text{-}C_7H_6)\}M'L']^+$ [M′L′ = $Cr(CO)_3$ (**3**), none (**4**), $Ru(\eta^5\text{-}C_5H_5)^+$ (**5**), $Ru(\eta^5\text{-}C_5Me_5)^+$ (**6**)], and, for comparison, the ^{1}H and ^{13}C NMR spectroscopic data of the tropylium cation $[C_7H_7]^+$ (**7**) and its complexes $[(\eta^7\text{-}C_7H_7)M'L']^+$ [M′L′ = $Cr(CO)_3$ (**8**), $Ru(\eta^5\text{-}C_5H_5)^+$ (**9**), $Ru(\eta^5\text{-}C_5Me_5)^+$ (**10**)]

	^{1}H NMR[a]						^{13}C NMR[a]						
M′L′	C_5H_4	CpFe	1-,6-H	2-,5-H	3-,4-H	L′	C_5H_4	CpFe	C-7	C-1,-6	C-2,-5	C-3,-4	L′
$Cr(CO)_3$ (**3**)	4.97, 5.12	4.28	6.45	6.75	6.55	–	81.3, 70.8, 76.0	72.9	133.1	99.8	105.6	104.7	223.9 (CO_3)
none (**4**)	5.45, 5.51	4.41		8.26−8.49		–	84.5, 73.4, 81.8	75.7	175.8	147.9	148.1	148.8	–
$Ru(\eta^5\text{-}C_5H_5)^+$ (**5**)	5.33, 5.47	4.37	7.27	7.34	7.60	6.11 ($\eta^5\text{-}C_5H_5$)	81.4, 72.2, 81.5	75.4	138.7	92.9	102.0	104.1	91.3 ($\eta^5\text{-}C_5H_5$)
$Ru(\eta^5\text{-}C_5Me_5)^+$ (**6**)	5.27, 5.34	4.36	7.09	7.10	7.35	1.98 ($\eta^5\text{-}C_5Me_5$)	77.6, 71.6, 79.6	74.1	133.8	97.8	104.2	105.3	109.9 ($\eta^5\text{-}C_5Me_5$) 10.4 ($\eta^5\text{-}C_5Me_5$)
none (**7**)	–	–		9.38 (C_7H_7)		–	–	–		156.6 (C_7H_7)			
$Cr(CO)_3$ (**8**)	–	–		6.67 ($\eta^7\text{-}C_7H_7$)		–	–	–		106.5 ($\eta^7\text{-}C_7H_7$)			221.7 (CO_3)
$Ru(\eta^5\text{-}C_5H_5)^+$ (**9**)	–	–		7.8 ($\eta^7\text{-}C_7H_7$)		6.37 ($\eta^5\text{-}C_5H_5$)	–	–		107.5 ($\eta^7\text{-}C_7H_7$)			93.1 ($\eta^5\text{-}C_5H_5$)
$Ru(\eta^5\text{-}C_5Me_5)^+$ (**10**)	–	–		7.48 ($\eta^7\text{-}C_7H_7$)		2.23 ($\eta^5\text{-}C_5Me_5$)	–	–		107.6 ($\eta^7\text{-}C_7H_7$)			112.6 ($\eta^5\text{-}C_5Me_5$) 10.9 ($\eta^5\text{-}C_5Me_5$)

[a] Solvent: CD_3NO_2 rel. TMS, numbering scheme see Figure 4.

the tropylium moiety goes along with a general low-field shift of the ferrocene signals, which increases in the order M′L′ = $Cr(CO)_3$ < $Ru(\eta^5\text{-}C_5Me_5)^+$ < $Ru(\eta^5\text{-}C_5H_5)^+$ < none. This behavior of the dipolar sesquifulvalene complexes **3**−**6** clearly elucidates a strong donor (metallocene)−acceptor (tropylium moiety) interaction in the ground state and, moreover, points to a growing charge delocalization in the same order.

Redox Properties

Cyclic voltammetry studies were conducted on all of the sesquifulvalene complexes as well as for the unsubstituted tropylium cation (**7**) and the corresponding mononuclear complexes $[(\eta^7\text{-}C_7H_7)M'L']^+$ [M′L′ = $Cr(CO)_3$ (**8**), $Ru(\eta^5\text{-}C_5H_5)^+$ (**9**), $Ru(\eta^5\text{-}C_5Me_5)^+$ (**10**)]. Electrochemical studies on **7**,[12] **8**,[13] and **9**[11a] have already been described. However, since the published data were obtained under different conditions, the reduction potentials of **7**−**9** were revised under conditions comparable to those applied for the sesquifulvalene complexes. As is known from the literature, the tropylium cation **7** and its complex congeners **8** and **9** undergo irreversible one-electron reduction steps, which is in agreement with the results obtained for the sesquifulvalene complexes (vide infra). The reduction potentials (Table 2) obtained for the tropylium derivatives **7**−**10** change in the order of M′L′ = $Cr(CO)_3$ < $Ru(\eta^5\text{-}C_5Me_5)^+$ < none < $Ru(\eta^5\text{-}C_5H_5)^+$, and illustrate an increase in the electron-withdrawing ability roughly in accordance with the NMR spectroscopic data.

Table 2. Cyclic voltammetry data of the cationic sesquifulvalene complexes $[(\eta^5\text{-}C_5H_5)Fe\{\mu\text{-}(\eta^5\text{-}C_5H_4)(\eta^7\text{-}C_7H_6)\}M'L']^+$ (**3**−**6**) and the mononuclear tropylium species $[(\eta^7\text{-}C_7H_7)M'L']^+$ (**7**−**10**)

M′L′		$E_{1/2}$ [a][b]	ΔE_p [c]	E_{pc} [a][b][d]	ΔE[e]
$Cr(CO)_3$	**3**	0.32	72	−1.14	1.46
none	**4**	0.42	74	−0.59	1.01
$Ru(\eta^5\text{-}C_5H_5)^+$	**5**	0.44	84	−0.61	1.05
$Ru(\eta^5\text{-}C_5Me_5)^+$	**6**	0.44	69	−0.84	1.28
none	**7**			−0.63[f][g]	
$Cr(CO)_3$	**8**			−1.20[h]	
$Ru(\eta^5\text{-}C_5H_5)^+$	**9**			−0.52[g]	
$Ru(\eta^5\text{-}C_5Me_5)^+$	**10**			−0.78	

[a] Obtained from $MeNO_2$ solutions, 0.4 M $[nBu_4N]PF_6$, room temperature, reference electrode Ag/AgCl. − [b] In V vs. $Fe(C_5H_5)_2/[Fe(C_5H_5)_2]^+$. − [c] $\Delta E_p = |E_{pa} - E_{pc}|$ in mV, ΔE_p(ferrocene) = 73 mV, scan rate: 100 mV/s. − [d] Peak potential of the irreversible one-electron reduction, scan rate: 100 mV/s. − [e] $\Delta E = E_{1/2} - E_{pc}$ in mV. − [f] See also ref.[12] − [g] See also ref.[11a] − [g] See also ref.[13]

The cyclic voltammograms of the corresponding cationic sesquifulvalene complexes **3**−**6** also reveal an irreversible one-electron reduction process in the potential domain of the unsubstituted tropylium species (Figure 3) in addition to an oxidation step in the range of free ferrocene. The potentials of the electrochemically irreversible reduction of the sesquifulvalene complexes are slightly cathodically shifted with respect to the unsubstituted tropylium cations **7**−**10** (Table 2) as expected, due to the electron-donating property of the ferrocenyl substituent.

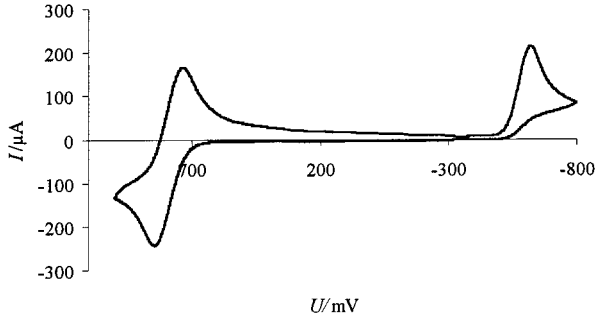

Figure 3. Representative cyclic voltammogram of the cationic sesquifulvalene complexes $[(\eta^5\text{-}C_5H_5)Fe\{\mu\text{-}(\eta^5\text{-}C_5H_4)(\eta^7\text{-}C_7H_6)\}M'L']^+$ [here M′L′ = none (**4**); for more details see Table 2]

The oxidation step involves an electrochemically reversible one-electron transfer, which is 320−440 mV anodically shifted with respect to free ferrocene (Table 2) caused by the electron-withdrawing ability of the tropylium moiety. The anodic shift of the oxidation potentials changes in the order M′L′ = $Cr(CO)_3$ < none < $Ru(\eta^5\text{-}C_5Me_5)^+$ = $Ru(\eta^5\text{-}C_5H_5)^+$. This order differs somewhat from the outcome of

the NMR spectroscopic study. This may be due to the fact, that in the NMR spectroscopic studies only the donor−acceptor interaction of the ground state is measured, whereas in cyclic voltammetry experiments the donor−acceptor interactions of the starting complex as well as of the oxidized (or reduced) product, including reorganization energies, will contribute to the oxidation (or reduction) potential.

Assuming that the oxidation potentials roughly correlate with the energy of the HOMO and the reduction potentials to the energy of the LUMO, the differences of the redox potentials E (Table 2) allow the tentative conclusion that the HOMO−LUMO gap for the sesquifulvalene complexes **3**−**6** should roughly decrease in the order M′L′ = $Cr(CO)_3$ > $Ru(\eta^5\text{-}C_5Me_5)^+$ > $Ru(\eta^5\text{-}C_5H_5)^+$ > none.

Crystal Structure Analyses

Crystal structure analyses were obtained for all of the sesquifulvalene complexes studied, and selected structural data are listed in Table 3. The crystal structure of complex **3** [M′L′ = $Cr(CO)_3$] has already been published,[3] as well as the molecular structure of **4** as a hexafluorophosphate salt.[14] However, **4** was synthesized as a tetrafluoroborate salt and the molecular structure data were obtained with higher accuracy.[4]

Solving the molecular structure of complex **6** [M′L′ = $Ru(\eta^5\text{-}C_5Me_5)^+$] proved to be more difficult because of the presence of three different independent molecules, and the intercalation of four independent solvent molecules of $MeNO_2$ as evidenced by means of NMR spectroscopy and elemental analysis. The structural data of all three independent molecules of **6** are in agreement within the margin of error. In Table 3 the selected structural data of only one independent molecule of the unit cell of **6** are presented. The molecular structures of the sesquifulvalene complexes **5** and **6** are depicted in Figure 4.

The molecular structures of the sesquifulvalene complexes **3**−**6** have an almost coplanar alignment of the sesquifulvalene rings. The twisting angle between the best planes of the five- and seven-membered rings varies between 0 and 17° for **4** and **6**, respectively. The dinuclear complexes exhibit a *transoid* conformation of the complex moieties due to the nonbonding repulsions between the metal fragments in a *cisoid* conformation. A *cisoid* conformation is observed only for complexes with increased length of the π-bridge between the five- and seven-membered ring.[3−7]

Since mutual electronic influence of the donor and acceptor group is expected to affect the molecular structure, the discussion concerning the structural details is focussed on geometric parameters directly related to the sesquifulvalene entity (Figure 5). As for sesquifulvalenes themselves the bonding situation in their complexes can in principle be described in terms of two mesomeric forms, the bis(aromatic) form **A** and the cross-conjugated form **B** (Figure 1), which is composed of an η^6-fulvene complex and a free or coordinated cycloheptatriene moiety. For both types of complexes characteristic structural features are expected

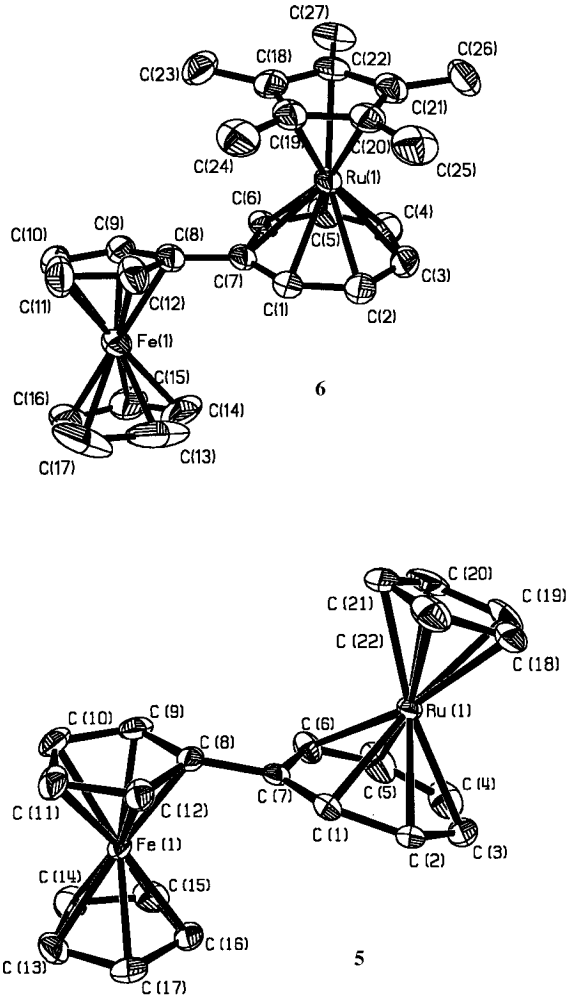

Figure 4. Molecular structures of the cationic sesquifulvalene complexes $[(\eta^5\text{-}C_5H_5)Fe\{\mu\text{-}(\eta^5\text{-}C_5H_4)(\eta^7\text{-}C_7H_6)\}M'L']^+$ [M′L′ = $Ru(\eta^5\text{-}C_5H_5)^+$ (**5**), $Ru(\eta^5\text{-}C_5Me_5)^+$ (**6**); 50% ellipsoids, the hydrogen atoms, solvent molecules and counter ions are omitted for clarity, for **6** only one independent molecule is shown]

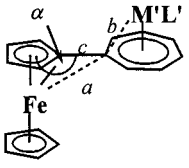

Figure 5. Schematic presentation of the molecular structure of the sesquifulvalene complexes including the notations of special geometric parameters found in Table 3

which are known from corresponding mononuclear complexes and their uncoordinated monocyclic organic species.[15−17]

In fact, a comparison of the structural data listed in Table 3, on average, reveals a characteristic long-short pattern of the endocyclic C−C bonds for the coordinated or free tropylium moiety, which is less significant in the dinuclear species. In accordance to it, the C−C distances between the bridge-head carbon atom C8 and the proximal carbon atoms C9 and C12 of the five-membered ring are distinctly longer than the C−C distances within the endocyclic buta-

Table 3. Selected interatomic distances [pm] and angles [°] (compare Figure 5) of the cationic sesquifulvalene complexes $[(\eta^5\text{-}C_5H_5)Fe\{\mu\text{-}(\eta^5\text{-}C_5H_4)(\eta^7\text{-}C_7H_6)\}M'L']^+$ [M′L′ = $Cr(CO)_3$ (**3**), none (**4**), $Ru(\eta^5\text{-}C_5H_5)^+$ (**5**), $Ru(\eta^5\text{-}C_5Me_5)^+$ (**6**)] and the corresponding structural parameters of the fulvene complex $[(\eta^5\text{-}C_5H_5)Fe\{\eta^6\text{-}C_5H_4C(C_6H_5)_2\}]BF_4$ (**11**) (see ref.[17a])

M′L′ =	$Cr(CO)_3$ [a] **3**	none[b] **4**	$Ru(\eta^5\text{-}C_5H_5)^+$ **5**	$Ru(\eta^5\text{-}C_5Me_5)^+$ **6**	**11**[c]
C1−C7	141.1(10)	141.5(3)	142.7(4)	143.1(7)	
C1−C2	137.7(12)	137.7(4)	140.4(4)	141.3(8)	
C2−C3	140.3(12)	140.0(4)	141.0(5)	142.7(9)	
C3−C4	138.5(14)	136.1(7)	137.7(6)	141.4(9)	
C4−C5	139.7(13)		141.8(6)	142.0(9)	
C5−C6	138.9(11)		140.8(4)	140.8(8)	
C6−C7	141.4(10)		142.7(4)	144.3(7)	
C7−C8[d]	145.1(10)	145.0(5)	145.2(4)	145.3(7)	141.6(10)
C8−C9	144.1(10)	144.6(3)	144.9(4)	144.7(7)	144.5(10)
C8−C12	143.7(10)		144.1(4)	144.6(8)	143.8(10)
C9−C10	141.2(12)	142.7(4)	141.4(5)	141.7(9)	140.2(11)
C10−C11	138.6(12)	141.2(6)	141.0(5)	142.1(10)	142.5(11)
C11−C12	138.4(12)		141.7(4)	142.3(9)	141.3(9)
Fe···C7[e]	305.0(7)	305.1(3)	290.4(4)	303.9(6)	271.5(6)
Fe−C8	202.0(6)	203.5(3)	201.3(3)	202.5(5)	200.9(7)
Fe−C9	202.0(7)	204.8(3)	202.7(3)	203.7(5)	201.8(8)
Fe−C10	203.1(9)	206.8(3)	206.3(3)	203.7(6)	208.5(8)
Fe−C11	206.0(8)		206.6(3)	205.0(7)	209.5(6)
Fe−C12	204.4(7)		203.9(3)	202.3(6)	206.0(8)
M′−Cn[f]	221.4(7)− 224.1(7)		226.0(6)− 228.2(5)	222.5(3)− 227.4(3)	
M′−C7[g]	232.0(6)		244.7(3)	234.2(5)	
α[h] [°]	176.5	175.5	167.5	174.7	159.3
γ[i] [°]	10.0(4)	0.0	10.5(4)	17.0(3)	

[a] Ref.[3] − [b] Ref.[4] − [c] Ref.[17a] − [d] Bridging carbon−carbon bond *c*. − [e] Nonbonding Fe−C7 distance *a*. − [f] Cn denotes C1−C6 of the tropylium moiety, only the upper and lower values are given. − [g] Metal−carbon bond *b*. − [h] Bending angle between the vector which bisects the substituted five-membered ring and includes the bridge-head carbon atom C8, and the vector of the carbon−carbon bond C7−C8. − [i] γ denotes the twisting angle between the five- and seven-membered ring.

diene unit C9...C12. A similar bond length variation is found in η^6-fulvene complexes, although to a larger extent.[17] This characteristic bond length pattern goes along with a decrease of the bending angle α and the distance *a* between the Fe atom of the ferrocenyl unit and the bridge-head carbon atom C7 of the seven-membered ring, which are the most important structural features indicating the contribution of the cross-conjugated mesomeric form **B** to the electronic ground state (see Figure 1). The bending angle α and the distance Fe···C7 decrease in the order M′L′ = $Cr(CO)_3$ > $Ru(\eta^5\text{-}C_5Me_5)^+$ > none > $Ru(\eta^5\text{-}C_5H_5)^+$. Similarly, a considerable increase of the bond length *b* between M′ (Cr or Ru) and C7 is observed with respect to the remaining metal−carbon bond lengths of the tropylium complexes (M′−Cn, see Table 3), which amounts to about 10 pm for **3** and **6**, but about 20 pm for **5**. Apparently, the gradual change from an aromatic to a fulvene-like coordination mode is a result of an increased D−A interaction due to the growing electron-withdrawing ability of the acceptor.[18]

Electronic Excitation

UV/Vis spectroscopic studies were performed with solutions of different solvent polarity such as dichloromethane and nitromethane, to elucidate solvatochromism which gives an indication of the dipole change Δμ between the ground and the excited state,[19] and is thus relevant for the first hyperpolarizability β according to the two-level approximation.[20,21] The UV/Vis spectra of the complexes under study contain two strong absorption bands in the visible and near-UV region (Figure 6, Table 4), which undergo considerable negative solvatochromism, i.e. hypsochromic shift with increasing solvent polarity. These two bands are characteristic for dipolar ferrocene bearing NLO chromophores. Recently, it was shown by means of DF calculations that for (*E*)-1-ferrocenyl-2-(*p*-nitrophenyl)ethene the high-energy absorption band must be assigned to a cyclo-

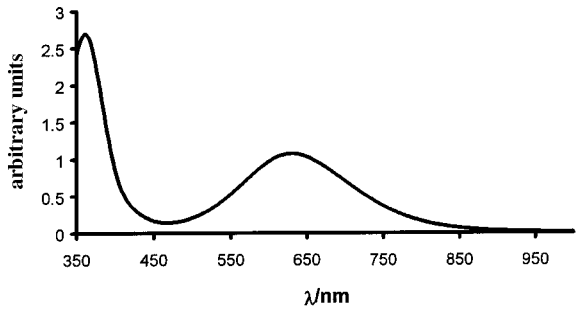

Figure 6. Representative UV/Vis spectrum of the dinuclear sesquifulvalene complexes $[(\eta^5\text{-}C_5H_5)Fe\{\mu\text{-}(\eta^5\text{-}C_5H_4)(\eta^7\text{-}C_7H_6)\}M'L'](PF_6)_2$ [here: M′L′ = $Ru(\eta^5\text{-}C_5H_5)$ (**5**)] obtained from CH_2Cl_2 solution

Table 4. UV/Vis data of the cationic sesquifulvalene complexes $[(\eta^5\text{-}C_5H_5)Fe\{\mu\text{-}(\eta^5\text{-}C_5H_4)(\eta^7\text{-}C_7H_6)\}M'L']^+$ [$M'L' = Cr(CO)_3$ (**3**), none (**4**), $Ru(\eta^5\text{-}C_5H_5)^+$ (**5**), $Ru(\eta^5\text{-}C_5Me_5)^+$ (**6**)], and the experimental first hyperpolarizability β obtained by means of hyper-Raleigh scattering measurements (see ref.[24])

	λ_{max}(LA−CT)[a][b] (ε)[c]			λ_{max}(DA−CT)[a][b] (ε)[c]				
M′L′	CH_2Cl_2	$MeNO_2$	$\Delta\tilde{\nu}$[d]	CH_2Cl_2	$MeNO_2$	$\Delta\tilde{\nu}$[d]	β[HRS][e] [f]	β_0[g] [f]
$Cr(CO)_3$ (**3**)	408 (2600)	395	−807	590 (3100)	574 (4880)	−473	n.d.[h]	
none (**4**)	400 (14710)	395 (13355)	−317	725 (3565)	700 (3335)	−493	f[i]	
$Ru(\eta^5\text{-}C_5H_5)^+$ (**5**)	374	–		637	614 (5270)	−588	125	28
$Ru(\eta^5\text{-}C_5Me_5)^+$ (**6**)	360	–		628	605 (4510)	−605	115	23

[a] Obtained from ca. 10^{-5} M solutions. – [b] λ_{max} in nm. – [c] Extinction coefficient in $M^{-1}cm^{-1}$. – [d] $\Delta\tilde{\nu} = \tilde{\nu}(CH_2Cl_2) - \tilde{\nu}(MeNO_2)$ in cm^{-1}. – [e] Referenced against *p*-nitroaniline (*p*-NA): $\beta(MeNO_2) = 34.6 \cdot 10^{-30}$ esu[37]. – [f] Given as units of 10^{-30} esu. – [g] Calculated from $\beta_0 = \beta(HRS)\,[(1-4\lambda^2_{max}/\lambda^2)(1-\lambda^2_{max}/\lambda^2)]$.[21] – [h] n.d.: HRS signal not detectable. – [i] f: fluorescent.

pentadienyl ligand−acceptor charge-transfer (L−A CT) transition whereas the low-energy absorption band is caused by a donor (metal)−acceptor charge-transfer (D−A CT) transition.[22] The CT transitions both provide a delocalization or even transfer of the positive charge from the tropylium moiety to the donor upon excitation, which is experimentally proven by the negative solvatochromism.[23]

This assignment is also supported by the fact that both of the CT transitions are strongly influenced by the nature of the acceptor, which is in accordance with recently published results about sesquifulvalene complexes with more extended π-bridges between the metallocene donor and the tropylium moiety acceptor.[3−5] However, the electronic influence of the acceptor on the L−A and D−A CT transitions is different. The D−A CT transitions decrease in energy in the order $M'L' = Cr(CO)_3 > Ru(\eta^5\text{-}C_5Me_5)^+ > Ru(\eta^5\text{-}C_5H_5)^+ >$ none. This order correlates with that of the HOMO−LUMO splitting assumed from the cyclic voltammetry results. The order varies for the L−A CT transition: $M'L' = Ru(\eta^5\text{-}C_5Me_5) > Ru(\eta^5\text{-}C_5H_5)^+ >$ none $> Cr(CO)_3$. The extraordinary low-energy shift of the D−A CT band of the mononuclear complex **4** compared to the dinuclear species may be explained by the formation of additional molecular orbitals (MO) upon coordination of a metal−ligand fragment, thus forming occupied bonding MOs which would be lower in energy, and empty antibonding MOs which would be higher in energy compared to the orbitals of the initial uncoordinated tropylium moiety.

As mentioned before the electronic excitations are governed by a distinct blue-shift on increasing the solvent polarity. The extent of the solvatochromism for both of the absorption bands can only be determined for **3** and **4**, since the maximum of the high-energy L−A CT absorption band of **5** and **6** in CH_3NO_2 is too far blue-shifted into the absorption region of the solvent to be determined. Nevertheless, from the obtained data it turns out that the change in polarity is similar for both of the CT transitions, and hence both should contribute to the first hyperpolarizability.[20,21]

NLO Measurements

The low-lying excited states of the sesquifulvalene complexes under study along with their facile polarizability, indicated by their pronounced solvatochromism, makes these types of complexes very promising for the second harmonic generation. Due to the cationic nature of the sesquifulvalene complexes the hyper-Rayleigh scattering (HRS)[24] is the only method for determining the first hyperpolarizability β which represents the molecular capability of transforming incoming light with frequency ω to frequency 2ω. However, a draw-back of the HRS method may be fluorescence due to two-photon absorption.[25−27] After realizing the problem of multiphoton absorption induced fluorescence concerning the determination of the first hyperpolarizability, several techniques have been investigated to overcome this problem. These include long-wavelength measurements,[28,29] time-resolved HRS[28] measurements of the two-photon fluorescence spectrum to abstract the fluorescence contribution to the HRS signal,[30] and a high-frequency demodulating technique to suppress the multiphoton fluorescence contribution to the HRS signal.[25]

A ''low-cost'' check for the two-photon fluorescence was recently described,[4,5] and uses bandpass filters with peak transmittance at different wavelengths introduced in front of the photomultiplier of the HRS set-up. The broad fluorescence signal, which yields the emission maximum at λ/2 of the fundamental wavelength, is easily discerned from the narrow second harmonic signal at λ/2.

In the course of this study the mononuclear complex **4** indicates two-photon fluorescence (Figure 7) whereas for **3** no intensity for the second harmonic signal was detected (Table 4). For the remaining complexes **5** and **6** the first hyperpolarizability β has been determined. The static first hyperpolarizability β_0 has been calculated by means of the two-level model,[21] taking into account the low-energy D−A CT transition. Nevertheless, it has to be emphasized that the high-energy L−A CT transition will also contrib-

ute to the first hyperpolarizability as indicated by the solvatochromism. The experimentally obtained first hyperpolarizability β and the calculated static hyperpolarizability β_0 for **5** and **6** (Table 4) are comparable although slightly larger for **5** with M′L′ = Ru(η^5-C_5H_5)$^+$ which has been shown to be the stronger electron-accepting moiety by means of NMR spectroscopy and cyclic voltammetry studies. However, the β and β_o values are not large and are comparable with the ferrocenyl-substituted (borabenzene)cobalt complex cation [CpFe{μ-(η^5-C_5H_4)(η^6-B(C_5H_5)}CoCp]$^+$.[18] Their values are difficult to discuss with respect to increasing D−A interaction due to (i) the margin of error in the determination of the first hyperpolarizability by HRS, (ii) the fact that the SHG signal occurs in the region of considerable D−A CT absorption, and (iii) the contribution of both the L−A CT and D−A CT transition to the SHG.

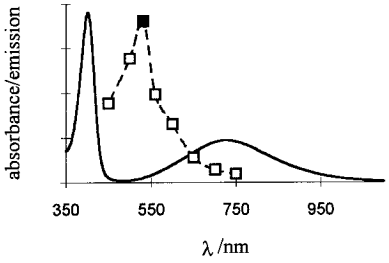

Figure 7. Absorption and emission spectrum of **4**

Conclusions

A series of cationic ferrocenyl-containing mono- and dimetallic dipolar sesquifulvalene complexes [CpFe{μ-(η^5-C_5H_4)(η^7-C_7H_6)M′L′]$^+$ [M′L′ = $Cr(CO)_3$, none, Ru(η^5-C_5H_5)$^+$, Ru(η^5-C_5Me_5)$^+$] were synthesized and both spectroscopically and structurally characterized. In these complexes the metallocenyl unit acts as an electron donor and the positively charged tropylium moiety as an electron acceptor. From the NMR spectroscopic data an increased delocalization of the positive charge is concluded for the ground state in the series M′L′ = $Cr(CO)_3$ < Ru(η^5-C_5Me_5)$^+$ < Ru(η^5-C_5H_5)$^+$ < none. The increased delocalization of the positive charge goes along with a growing contribution of the cross conjugated mesomeric form **B** to the bis(aromatic) mesomeric form **A** in the electronic ground state (Figure 1) as confirmed by gradual structural changes: i) the increasing bond length alternation in the five-membered ring, ii) the decreasing bending angle α between the C_5H_4 plane and the bonding vector of the bond C7−C8 linking the five- and seven-membered ring, and iii) the decreasing distance between the Fe atom of the ferrocene and the bridge-head carbon atom C7 of the seven-membered ring. The electronic excitation reveals two absorption bands in the visible and near-UV region that are assigned to an energetically low-lying D−A CT transition and an energetically higher lying L−A CT transition. Both CT transitions will contribute to the efficiency of the second harmonic generation. However, the first hyperpolarizability β, which is determined by HRS, is only obtained for the dinuclear species **5** [M′L′ = Ru(η^5-C_5H_5)$^+$] and **6** [M′L′ = Ru(η^5-C_5Me_5)$^+$]. For complex **4** fluorescence was observed whereas for **3** no SHG could be observed.

Experimental Section

Manipulations were carried out under dry nitrogen using standard Schlenk techniques. Solvents were saturated with nitrogen. Diethyl ether (Et_2O), tetrahydrofuran (THF), *n*-hexane and toluene were freshly distilled from the appropriate alkali metal or metal alloy. Dichloromethane (CH_2Cl_2) and nitromethane ($MeNO_2$) were dried with calcium hydride. NMR: Varian Gemini 200 BB; Bruker AM 360; measured at 295 K rel. TMS. UV/Vis: Perkin−Elmer Model 554. IR: nujol mull, KBr cells, FT-IR, Perkin−Elmer Model 325. MS: Finnigan MAT 311 A (EI-MS). Elemental analyses: CHN-O-Rapid, Fa. Heraeus. Tropylium hexafluorophosphate (**7**),[31] monolithioferrocene,[8] triphenylcarbenium hexafluorophosphate/tetrafluoroborate,[32] tricarbonyltris(propionitrile)chromium(0),[9,33] tris(acetonitrile)(η^5-cyclopentadienyl)ruthenium(II) hexafluorophosphate,[34] tris(acetonitrile)(η^5-pentamethylcyclopentadienyl)ruthenium(II) hexafluorophosphate,[11b] tricarbonyl(η^7-cycloheptatrienylium)chromium(0) hexafluorophosphate (**8**),[35] (2,4,6-cycloheptatrien-1-yl)ferrocene (**1**), tricarbonyl[η^6-1-(ferrocenyl)cycloheptatriene]chromium(0) (**2**)[3,4] and tricarbonyl[(η^7-1-(ferrocenyl)cycloheptatrienylium]chromium(0) hexafluorophosphate (**3**)[3] were synthesized according to literature procedures.

1-(Ferrocenyl)cycloheptatrienylium Tetrafluoroborate ($4BF_4$): A solution of $[Ph_3C]BF_4$ (610 mg, 1.85 mmol) in CH_2Cl_2 (20 mL) was added to a solution of **1** (510 mg, 1.85 mmol) in CH_2Cl_2 (20 mL) and stirred for 30 min at room temperature. The color of the solution turned from brick-red to deep green-blue. The product precipitates on addition of Et_2O. The crystalline material was filtered off and recrystallized by gas-phase diffusion of Et_2O into a concentrated solution of $\mathbf{4}BF_4$ in CH_2Cl_2. Yield: 410 mg (61%) of black-blue cubes. ^{1}H NMR (CD_3NO_2): δ = 8.49−8.26 (m, 6 H, C_7H_6), 5.51 (pt, *J* = 2.0 Hz, 2 H, C_5H_4), 5.45 (pt, *J* = 2.0 Hz, 2 H, C_5H_4), 4.41 (s, 5 H, C_5H_5). ^{13}C NMR (CD_3NO_2): δ = 175.8 (C-7), 148.8 (C-3,-4), 148.1 (C-2,-5), 147.9 (C-1,-6), 84.5 [$C_q(C_5H_4)$], 81.8 (C_5H_4), 75.7 (C_5H_5), 73.4 (C_5H_4). IR (KBr): $\tilde{\nu}$ = 3100, 3060, 1498, 1443, 1383, 1272, 1084 (ν_{B-F}), 1059, 1035 cm^{-1}. $C_{17}H_{15}BF_4Fe$ (362.0): calcd. C 56.41, H 4.18; found C 56.14, H 4.16.

{(Tricarbonyl)(η^7-cycloheptatrienylium-1-yl)chromium(0)}ferrocene Hexafluorophosphate ($3PF_6$): The synthesis performed was slightly modified according to the literature procedure.[3] Instead of $[Ph_3C]BF_4$ the PF_6 salt was used. The reaction was conducted at 0 °C. Quantities used: [η^5-C_5H_5)Fe{μ-(η^5-C_5H_4)(η^6-C_7H_7)}Cr(CO)$_3$] (**2**) (150 mg, 0.36 mmol) in CH_2Cl_2 (20 mL), $[Ph_3C]PF_6$ (140 mg, 0.36 mmol) in CH_2Cl_2 (10 mL). Yield: 120 mg (61%) of blue-black needles. ^{1}H NMR (CD_3NO_2): δ = 6.75 (m, 2 H, 2-,5-H), 6.55 (dd, *J* = 6.1, 2.9 Hz, 2 H, 3-,4-H), 6.45 (d, *J* = 9.5 Hz, 2 H, 1-,6-H), 5.12 (pt, *J* = 2.0 Hz, 2 H, C_5H_4), 4.97 (pt, *J* = 2.0 Hz, 2 H, C_5H_4), 4.28 (s, 5 H, C_5H_5). ^{13}C NMR (CD_3NO_2): δ = 223.87 (CO), 133.13 (C-7), 105.59 (C-2,5), 104.71 (C-3,-4), 99.76 (C-1,-6), 81.32 [$C_q(C_5H_4)$], 75.97 (C_5H_4), 72.88 (C_5H_5), 70.82 (C_5H_4). IR (KBr): $\tilde{\nu}$ = 3100, 2038 (ν_{CO}), 1996 (ν_{CO}), 1549, 1487, 1384, 1291, 838 (ν_{P-F}) cm^{-1}; (CH_3NO_2): $\tilde{\nu}$ = 2054 (ν_{CO}), 2014 (ν_{CO}) cm^{-1}. UV/Vis (CH_3NO_2): λ_{max} (ε) = 395 (5280), 574 (4880) nm (M^{-1}·cm^{-1}). $C_{20}H_{15}CrF_6FeO_3P$ (556.2): calcd.: C 43.19, H 2.72; found C 42.68, H 2.97.

Generel Procedure for the Preparation of the Dicationic Dinuclear Sesquifulvalene Complexes: A solution of the monocationic tropylium compound **4** in CH_2Cl_2 was treated with an equimolar amount of the appropriate (cyclopentadienyl)ruthenium salt and stirred overnight. The precipitated product was filtered off, washed with CH_2Cl_2, and recrystallized from $MeNO_2/Et_2O$.

(η^5-Cyclopentadienyl)[η^7-1-(ferrocenyl)cycloheptatrienylium]-ruthenium(II) Bis(hexafluorophosphate) [5(PF_6)$_2$]: Quantities used: [(η^5-C_5H_5)Fe(η^5-C_5H_4−C_7H_6)]PF_6 (**4**PF_6) (280 mg, 0.67 mmol), [(η^5-C_5H_5)Ru(CH_3CN)$_3$]PF_6 (290 mg, 0.67 mmol), CH_2Cl_2 (30 mL). Yield: 402 mg (82%) of deep blue, rhombic plates. ^{1}H NMR (CD_3NO_2): δ = 7.60 (dd, *J* = 5.4, 2.0 Hz, 2 H, 3-,4-H), 7.34 (m, 2 H, 2-,5-H), 7.27 (d, *J* = 9.8 Hz, 2 H, 1-,6-H), 6.11 (s, 5 H, C_5H_5'), 5.47 (pt, 2 H, C_5H_4), 5.33 (pt, 2 H, C_5H_4), 4.37 (s, 5 H, C_5H_5). ^{13}C NMR (CD_3NO_2): δ = 138.7 (C-7), 104.1 (C-3,-4), 102.0 (C-2,-5), 92.9 (C-1,-6), 91.3 (C_5H_5'), 81.5 (C_5H_4), 81.4 [$C_q(C_5H_4)$], 75.4 (C_5H_5), 72.2 (C_5H_4). IR (KBr): $\tilde{\nu}$ = 3126, 1548, 1498, 1474, 1420, 1301, 1266, 834 (ν_{P-F}) cm^{-1}. UV/Vis (CH_3NO_2): λ_{max} (ε) = 614 (5270) nm ($M^{-1}\cdot cm^{-1}$). $C_{22}H_{20}F_{12}FeP_2Ru$ (731.3): calcd. C 36.14, H 2.76; found C 35.80, H 2.76.

[η^7-1-(Ferrocenyl)cycloheptatrienylium](η^5-pentamethylcyclopentadienyl)ruthenium(II) Bis(hexafluorophosphate) [6(PF_6)$_2$]: Quantities used: [(η^5-C_5H_5)Fe(η^5-C_5H_4−C_7H_6)]PF_6 (**4**PF_6) (160 mg, 0.38 mmol), [(η^5-C_5Me_5)Ru(CH_3CN)$_3$]PF_6 (192 mg, 0.38 mmol), CH_2Cl_2 (20 mL). Yield: 213 mg (70%) of violet-blue rhombic plates. ^{1}H NMR (CD_3NO_2): δ = 7.35 (m, 2 H, 3-,4-H), 7.10 (m, 2 H, 2-,5-H), 7.09 (d, *J* = 7.3 Hz, 2 H, 1-,6-H), 5.34 (pt, 2 H, C_5H_4), 5.27 (pt, 2 H, C_5H_4), 4.36 (s, 5 H, C_5H_5), 1.98 (s, 15 H, C_5Me_5). ^{13}C NMR (CD_3NO_2): δ = 133.8 (C-7), 109.9 (C_5Me_5), 105.3 (C-3,-4), 104.2 (C-2,-5), 97.8 (C-1,-6), 79.6 (C_5H_4), 77.6 [$C_q(C_5H_4)$], 74.1 (C_5H_5), 71.6 (C_5H_4), 10.4 (C_5Me_5). IR (KBr): $\tilde{\nu}$= 3086, 2978, 1628, 1546, 1474, 1383, 1292, 1027, 837 (ν_{P-F}) cm^{-1}. UV/Vis (CH_3NO_2): λ_{max} (ε) = 605 (4510) nm ($M^{-1}\cdot cm^{-1}$). $C_{27}H_{30}F_{12}FeP_2Ru \times 4/3(CH_3NO_2) \times 1/3\ H_2O$ (888.77): calcd. C 38.24, H 3.93, N 2.10; found C 37.01, H 3.89, N 2.13.

Tricarbonyl(η^7-cycloheptatrienylium)chromium(0) Hexafluorophosphate (8PF_6): The synthesis was performed with a slight modification from the literature procedure.[35] To a solution of [(η^6-C_7H_8)Cr(CO)$_3$] (190 mg, 0.8 mmol) in CH_2Cl_2 (10 mL), a solution of [Ph_3C]PF_6 (320 mg, 0.8 mmol) in CH_2Cl_2 (10 mL), was added. The reaction mixture was stirred for 30 min at room temperature. The product was precipitated upon addition of Et_2O. The crystalline material was filtered off and recrystallized by gas-phase diffusion of Et_2O into a concentrated solution of **8**PF_6 in $MeNO_2$. Yield: 210 mg (70%) of red cubes. ^{1}H NMR (CD_3NO_2): δ = 6.67 (s, C_7H_7). ^{13}C NMR (CD_3NO_2): δ = 221.69 (CO), 106.51 (C_7H_7). IR (KBr): $\tilde{\nu}$ = 3092, 2067 (ν_{CO}), 2026 (ν_{CO}), 1455, 839 (ν_{P-F}) cm^{-1}; ($MeNO_2$): $\tilde{\nu}$ = 2069 (ν_{CO}), 2029 (ν_{CO}) cm^{-1}. UV/Vis (CH_3NO_2): λ_{max} (ε) = 400 (sh) (160) nm ($M^{-1}\cdot cm^{-1}$). $C_{10}H_7CrF_6O_3P$ (372.1): calcd. C 32.28, H 1.90; found C 32.06, H 2.12.

Table 5. Crystallographic data of [(η^5-C_5H_5)Fe(η^5-C_5H_4)(C_7H_6)]BF_4 (**4**BF_4), [(η^5-C_5H_5)Fe{μ-(η^5-C_5H_4)(η^7-C_7H_6)}Ru(η^5-C_5H_5)](PF_6)$_2$ [**5**(PF_6)$_2$], [(η^5-C_5H_5)Fe{μ-(η^5-C_5H_4)(η^7-C_7H_6)}Ru(η^5-C_5Me_5)](PF_6)$_2$ [**6**(PF_6)$_2$]

	4	5	6
Empirical formula	$C_{17}H_{15}BF_4Fe$	$C_{22}H_{20}F_{12}FeP_2Ru$	$C_{28.33}H_{34}F_{12}FeN_{1.33}O_{2.83}P_2Ru$
Formula mass	361.95	731.24	888.77
T [K]	173(2)	173(2)	173(2)
λ [pm]	71.073	71.073	71.073
Crystal system	orthorhombic	triclinic	triclinic
Space group	*Pnma*	$P\bar{1}$	$P\bar{1}$
a [pm]	2175(2)	942.6(2)	1749.2(4)
b [pm]	990.0(2)	1059.2(1)	1756.9(4)
c [pm]	688.1(3)	1235.2(2)	1767.0(4)
α [°]	90	75.908(1)	90.94(3)
β [°]	90	89.32	90.99(3)
γ [°]	90	82.381(1)	91.23(3)
V [10^6 pm^3]	1482.0(15)	1185.59(3)	5427.8(19)
Z	4	2	6
$\rho_{calcd.}$ [mg/m^3]	1.622	2.048	1.625
μ [mm^{-1}]	1.055	1.490	0.999
F (000)	736	720	2664
Crystal size [mm^3]	0.6 × 0.4 × 0.1	0.6 × 0.3 × 0.05	0.8 × 0.5 × 0.3
Scan range [°]	2.78−30.10	1.70−29.13	2.31−27.56
Index range	$-1 \le h \le 30$	$-12 \le h \le 12$	$0 \le h \le 22$
	$-13 \le k \le 1$	$-14 \le k \le 14$	$-22 \le k \le 22$
	$-1 \le l \le 9$	$-16 \le l \le 7$	$-23 \le l \le 23$
Reflections measured	2293	8200	26691
Reflections unique	1773	5834	25070
R_{int}	0.0175	0.0358	0.0740
Parameters	131	343	1353
Reflections $I > 4\ \sigma(I)$	2293	5834	20345
GoF[a]	1.061	0.971	1.058
$R1/wR^2$ [$I > 2(I)$][b]	0.0496/0.1280	0.0371/0.0854	0.0792/0.2199
$R1/wR^2$ (all data)[b]	0.0690/0.1172	0.0452/0.0884	0.0923/0.2350
Resd. min/max. [e/Å^3]	−0.647/0.549	−1.59/1.02	−1.952/1.858

[a] GoF (goodness of fit) = $[\Sigma w(F_o^2 - F_c^2)^2/(n-p)]^{1/2}$ (*n* = numbers of reflections, *p* = numbers of parameters). − [b] $R1 = \Sigma||F_o| - |F_c||/\Sigma|F_o|$; $wR2 = [\Sigma w(F_o^2 - F_c^2)^2/\{\Sigma w(F_o^2)^2\}]^{1/2}$.

(η^7-Cycloheptatrienylium)(η^5-cyclopentadienyl)ruthenium(II) Bis-(hexafluorophosphate) [9(PF_6)$_2$]: The synthesis was performed with a slight modification from the literature[11a] (see also the preparations of **5**PF_6 and **6**PF_6). Quantities used: [C_7H_7]PF_6 (**7**) (120 mg, 0.5 mmol), CH_2Cl_2 (20 mL), [(η^5-C_5H_5)Ru(CH_3CN)$_3$]PF_6 (220 mg, 0.5 mmol). Yield: 160 mg (80%) of a pale yellow solid. ^{1}H NMR (CD_3NO_2): δ = 7.80 (s, 7 H, C_7H_7), 6.37 (s, 5 H, C_5H_5). ^{13}C NMR (CD_3NO_2): δ = 107.51 (C_7H_7), 93.07 (C_5H_5). IR (KBr): $\tilde{\nu}$ = 3127, 3085, 2971, 1458, 1421, 832 (ν_{P-F}) cm^{-1}. $C_{12}H_{12}F_{12}P_2Ru$ (547.2): calcd. C 26.34, H 2.21; found C 26.30, H 2.55.

(η^7-Cycloheptatrienylium)(η^5-pentamethylcyclopentadienyl)-ruthenium(II) Bis(hexafluorophosphate) [10(PF_6)$_2$]: The synthesis was performed under identical conditions as for **9**(PF_6)$_2$. Quantities used: [C_7H_7]PF_6 (**7**) (100 mg, 0.4 mmol), CH_2Cl_2 (20 mL), [(η^5-C_5Me_5)Ru(CH_3CN)$_3$]PF_6 (200 mg, 0.4 mmol). Yield: 150 mg (80%) of pale yellow prisms. ^{1}H NMR (CD_3NO_2): δ = 7.48 (s, 7 H, C_7H_7), 2.23 (s, 15 H, C_5Me_5). ^{13}C NMR (CD_3NO_2): δ = 112.58 (C_5Me$_5$), 107.60 (C_7H_7), 10.91 (C_5Me_5). IR (KBr): $\tilde{\nu}$ = 3084, 2972, 1475, 1456, 1420, 1391, 1082, 1028, 832 (ν_{P-F}) cm^{-1}. $C_{17}H_{22}F_{12}P_2Ru$ (617.4): calcd. C 33.07, H 3.49; found C 32.82, H 3.55.

X-ray Structure Determination: Crystals of **4**BF_4, **5**(PF_6)$_2$, and **6**(PF_6)$_2$ suitable for an X-ray structure determination, were obtained by gas-phase diffusion of Et_2O into an $MeNO_2$ solution of the complex. The data were collected with four-circle diffractometers [**4**BF_4, and **6**(PF_6)$_2$: Hilger and Watts, Mo-K_α, λ = 0.71073 Å; **5**(PF_6)$_2$: Siemens aix, Mo-K_α, λ = 0.71073 Å]. The structures were solved by direct methods (SHELXS-86) and the refinements on F^2 were carried out by full-matrix least-squares techniques (SHELXL-93).[36] All non hydrogen atoms were refined with anisotropic thermal parameters. The hydrogen atoms were refined with a fixed isotropic thermal parameter related by a factor of 1.2 to the value of the equivalent isotropic parameter of their carrier atom. Weights were optimized in the final refinement cycles. In the structure of **6**, four independent molecules of CH_3NO_2 are present within the asymmetric unit. The position of an additional water molecule could be detected and was refined. An extinction coefficient correction of 0.0011 was applied. For more information see Table 5. Crystallographic data for the structures reported in this paper have been deposited at the Cambridge Crystallographic Data Centre as supplementary publication no. CCDC-142001 [**5**(PF_6)$_2$], and -42000 [**6**(PF_6)$_2$]. Copies of the data can be obtained free of charge on application to CCDC, 12 Union Road, Cambridge CB2 1EZ, UK [Fax: (internat.) + 44−1223/336−033; E-mail: deposit@ccdc.cam.ac.uk].

Cyclic Voltammetry: Measurements were performed in $MeNO_2$ with 0.4 M [N(nBu)$_4$]PF_6 as supporting electrolyte. An Amel 5000 system was used with a Pt wire as the working electrode and a Pt plate (0.6 cm^2) as the auxiliary electrode. The potentials were measured against Ag/Ag$^+$ and are referenced against $E_{1/2}$([Fe(C_5H_5)$_2$]/[Fe(C_5H_5)$_2$]$^+$) = 0 V.

Hyper-Rayleigh Scattering: Hyper-Rayleigh scattering measurements were performed with a pulsed Nd:YAG laser at a wavelength of λ = 1064 nm. For the experimental setup see ref.[24] Solutions of the complexes in $MeNO_2$ with concentrations in the range of 10^{-4} to 10^{-6} M were used with *p*-nitroaniline as a reference [β($MeNO_2$) = 34.6·10^{-30} esu].[37] Fluorescence checks were made by replacing the interference filter in front of the photomultiplier tube with filters that have transmittances at 400, 450, 500, 532, 560, 600, 650, and 700 nm.[4]

Acknowledgments

This work was supported by the Deutsche Forschungsgemeinschaft (DFG, HE 1309/3), by the European Community (COST D4/003/94, TMR FMRX-CT98−0166), and by the Fonds der Chemischen Industrie. We thank the DEGUSSA AG for a donation of $RuCl_3$ and Sartorius GmbH for a donation of microfilters.

[1] [1a] S. R. Marder, D. N. Beratan, L.-T. Cheng, *Science* **1991**, *252*, 103. [1b] S. R. Marder, G. B. Gorman, F. Meyers, J. W. Perry, G. Bourhill, J.-L. Brédas, B. M. Pierce, *Science* **1994**, *265*, 632. [1c] F. Meyers, S. R. Marder, B. M. Pierce, J.-L. Brédas, *J. Am. Chem. Soc.* **1994**, *116*, 10703. [1d] S. R. Marder, B. Kippelen, A. K.-Y. Jen, N. Peyghambarian, *Nature* **1997**, *388*, 845.

[2] J.-L. Brédas, *Adv. Mater.* **1995**, *7*, 263.

[3] U. Behrens, H. Brussaard, U. Hagenau, J. Heck, E. Hendrickx, J. Körnich, J. G. M. van der Linden, A. Persoons, A. L. Spek, N. Veldmann, B. Voss, H. Wong, *Chem. Eur. J.* **1996**, *2*, 98.

[4] H. Wong, T. Meyer-Friedrichsen, T. Farrell, C. Mecker, J. Heck, *Eur. J. Inorg. Chem.* **2000**, 631.

[5] J. Heck, S. Dabek. T. Meyer-Friedrichsen, H. Wong, *Coord. Chem. Rev.* **1999**, *190−192*, 1217.

[6] [6a] M. Tamm, T. Jentzsch, W. Werncke, *Organometallics* **1997**, *16*, 1418. [6b] M. Tamm, A. Gregorzewski, T. Steiner, T. Jentzsch, W. Werncke, *Organometallics* **1996**, *15*, 4984. [6c] M. Tamm, A. Grzegorzewski, T. Steiner, *Chem. Ber./Recueil* **1997**, *130*, 225.

[7] M. Tamm, T. Bannenberg, K. Baum, R. Fröhlich, T. Steiner, T. Meyer-Friedrichsen, J. Heck, *Eur. J. Inorg. Chem.* **2000**, 1161.

[8] F. Rebiere, O. Samuel, H. B. Kagan, *Tetrahedron Lett.* **1990**, *31*, 3121; U. T. Müller-Westerhoff, Z. Yuan, G. Ingram, *J. Organomet. Chem.* **1993**, *463*, 163; D. Guillaneux, H. B. Kagan, *J. Org. Chem.* **1995**, *60*, 2502.

[9] G. J. Kubas, *Inorg. Chem.* **1983**, *22*, 692.

[10] M. Cais, A. Eisenstadt, *J. Am. Chem. Soc.* **1967**, *89*, 5468.

[11] [11a] R = H: A. M. NcNair, D. C. Boyd, D. A. Bohling, T. P. Gill, K. R. Mann, *Inorg. Chem.* **1987**, *26*, 1182. [11b] R = Me: B. Steinmetz, W. A. Schenk, *Organometallics* **1999**, *18*, 943; P. J. Fagan, M. D. Ward, J. C. Calabrese, *J. Am. Chem. Soc.* **1989**, *111*, 1698.

[12] A. M. Romanin, A. Venzo, A. Ceccon, *J. Electroanal. Chem.* **1980**, *112*, 147.

[13] A. M. Romanin, A. Ceccon, A. Venzo, *J. Electroanal. Chem.* **1981**, *130*, 245.

[14] S. K. Brownstein, E. J. Gabe, R. C. Hynes, *Can. J. Chem.* **1992**, *70*, 1011.

[15] M. J. Barrow, O. S. Mills, *J. Chem. Soc., Chem. Commun.* **1971**, 119.

[16] J. D. Dunitz, P. Pauling, *Helv. Chim. Acta* **1960**, *43*, 2188.

[17] [17a] U. Behrens, *J. Organomet. Chem.* **1979**, *182*, 89. [17b] M. Watanabe; I. Motoyama, T. Takayama, *J. Organomet. Chem.* **1996**, *524*, 9. [17c] S. Barlow, L. M. Henling, M. W. Day, S. R. Marder, *Chem. Commun.* **1999**, 1567. [17d] A. I. Yanovsky, Y. T. Struchkov, A. Z. Kreindlin, M. I. Rybinskaya, *J. Organomet. Chem.* **1989**, *369*, 125.

[18] U. Hagenau, J. Heck, E. Hendrickx, A. Persoons, T. Schuld, H. Wong, *Inorg. Chem.* **1996**, *35*, 7863.

[19] P. Suppan, N. Ghoneim, in: *Solvatochromism*, Paston Press, Ltd., Norfolk, **1997**; N. Mataga, T. Kubota, *Molecular Interactions and Electronic Spectra*; Marcel Dekker; New York, **1970**, chapter 8.

[20] L. Oudar, D. S. Chemla, *Chem. Phys.* **1977**, *66*, 2664.

[21] E. Hendrickx, K. Clays, A. Persoons, C. Dehu, J. L. Brédas, *J. Am. Chem. Soc.* **1995**, *117*, 3547.

[22] [22a] S. Barlow, H. E. Bunting, C. Ringham, J. C. Green, G. U. Bublitz, S. G. Boxer, J. W. Perry, S. R. Marder, *J. Am. Chem. Soc.* **1999**, *121*, 3715. [22b] S. Barlow, S. R. Marder, *Chem. Commun.* **2000**, 1555.

[23] C. Reichard, *Solvents and Solvent Effects in Organometallic Chemistry*, 2nd ed., VCH, Weinheim, **1988**.
[24] K. Clays, A. Persoons, *Rev. Sci. Instrum.* **1992**, *63*, 3285.
[25] K. Clays, E. Hendrickx, T. Verbiest, A. Persoons, *Adv. Mater.* **1998**, *10*, 643; G. Olbrechts, T. Munters, K. Clays, A. Persoons, O.-K. Kim, L.-S. Choi, *Opt. Mater.* **1999**, *12*, 221.
[26] J. J. Wolff, R. Wortmann, *Adv. Phys. Org. Chem.* **1999**, *32*.121.
[27] S. Stadler, G. Bourhill, C. Bräuchle, *J. Phys. Chem.* **1996**, *100*, 6927.
[28] S. Stadler, R. Dietrich, G. Bourhill, C. Bräuchle, *Opt. Lett.* **1996**, *21*, 251−253
[29] M. A. Pauley, C. H. Wang, *Rev. Sci. Instrum.* **1999**, *70*, 1277.
[30] N. W. Song, T.-I. Kang, S. C. Jeung, S.-J. Joan, B. R. Cho, D. Kim, *Chem. Phys. Lett.* **1996**, *261*, 307; O. K. Song, J. N. Woodford, C. H. Wang, *J. Phys. Chem. A* **1997**, *101*, 3222
[31] K. Conrow, *Org. Synth., Coll. Vol.* **1973**, vol. V, p. 1138.
[32] G. A. Olah, J. J. Svoboda, J. A. Olah, *Synthesis* **1972**, 544.
[33] J. A. S. Howell, B. F. G. Johnson, J. Lewis, *J. Chem. Soc., Dalton Trans.* **1974**, 293.
[34] T. P. Gill, K. R. Mann, *Organometallics* **1982**, *1*, 485.
[35] E. W. Abel, M. A. Bennett, R. Burton, G. Wilkonson, *J. Chem. Soc.* **1958**, 4559.
[36] G. M. Sheldrick, *SHELXS-86 − program for crystal structure determination*, University of Göttingen, Germany, **1986**; G. M. Sheldrick, *SHELXL-93 − program for crystal structure refinement*, University of Göttingen, Germany, **1993**.
[37] T. Verbiest, K. Clays, S. Samyn, J. Wolff, D. Reinhoudt, A. Persoons, *J. Am. Chem. Soc.* **1994**, *116*, 9320.

Received June 21, 2001
[I01222]

Bis(keto-phosphane) and Bis(enolato-phosphane) Ruthenium Complexes − Synthesis and X-ray Structure Determination of RuCl(NO)[η^2-*(P,O)*-$Ph_2PCH{=}C(tBu)O]_2$

Bernard Demerseman*[a] and Loïc Toupet[b]

Keywords: Ruthenium / O,P ligands / Carbonyl ligands / Nitrosyl ligands / Isomerizations

A slow reaction consisting of a cleavage of one Ru–Cl bond occurred when a mixture of $RuCl_2[Ph_2PCH_2C(tBu){=}O]_2$ (**1**) and $[NH_4][PF_6]$ was dissolved in methanol as shown by a subsequent reaction with carbon monoxide affording the stable cationic derivative $\{RuCl(CO)[Ph_2PCH_2C(tBu){=}O]_2\}[PF_6]$ (**2**). By contrast, the straightforward reaction of **1** with carbon monoxide yielded $RuCl_2(CO)[Ph_2PCH_2C(tBu){=}O][Ph_2PCH_2C(=O)tBu]$ (**3**) which contains unreactive Ru–Cl bonds. The isomerization of **2,** which is induced under sun light exposure, is the preliminary step to the selective formation of the *all-cis* bis(enolato-phosphane) derivative *(ccc)*-$Ru(CO)_2[\eta^2$-*(P,O)*-$Ph_2PCH{=}C(tBu)O]_2$ (**9**). The isomeric bis(enolato-phosphane) derivative *(cct)*-$Ru(CO)_2[\eta^2$-*(P,O)*-$Ph_2PCH{=}C(tBu)O]_2$ (**10**), with *trans* phosphorus and *cis* carbonyl ligands, respectively, was selectively obtained under mild basic conditions, starting from *(cct)*-$RuCl_2(CO)_2[Ph_2PCH_2C(=O)tBu]_2$ (**4**), which results from the reaction of **3** with carbon monoxide under thermal activation. Through an oxidative addition process, the reaction of **1** with $[NO][BF_4]$ yielded $\{RuCl_2(NO)[Ph_2PCH_2C(tBu){=}O][Ph_2PCH_2C(=O)tBu]\}[BF_4]$ (**13**) with *trans* phosphorus and *trans* chloride ligands, respectively. Simple deprotonation of **13** generated the enolato-phosphane Ru^{IV} complex $RuCl_2(NO)[Ph_2PCH{=}C(tBu)O][Ph_2PCH_2C(=O)tBu]$ (**14**) which retains the same geometry. Under basic conditions, the bis(enolato-phosphane) derivative $RuCl(NO)[\eta^2$-*(P,O)*-$Ph_2PCH{=}C(tBu)O]_2$ (**15**) was obtained. The formation of **15** surprisingly showed a *trans* to *cis* rearrangement of the two phosphorus coordinating atoms, as further confirmed by an X-ray structure determination.

Introduction

Several pathways are available to the coordinatively saturated keto-phosphane complex $RuCl_2[\eta^2$-*(P,O)*-keto-phosphane$]_2$ for the incorporation of a donor ligand L (Scheme 1). These include: (i) a transformation of the coordination mode of the functional phosphane involving opening of the Ru-oxygen bond, (ii) the abstraction of one chloride generating a cationic derivative, or (iii) the formal (and nonreductive) elimination of HCl under basic conditions, facilitated by concomitant enolisation of the keto-phosphane ligand. To date, the first of these mechanistic possibilities, namely the change in coordination mode from η^2-*(P,O)* to η^1-*(P)* is well documented.[1−13] In order to emphasise the interest of an alternative preliminary cleavage of one Ru−Cl bond, the synthesis of a coordinatively unsaturated and highly reactive $\{RuCl[\eta^2$-*(P,N)*-functional phosphane$]_2\}^+$ species has been achieved starting from $RuCl_2[\eta^2$-*(P,N)*-functional phosphane$]_2$ complexes.[14] We report herein further comparison between these distinct reactivities, starting from a $RuCl_2[\eta^2$-*(P,O)*-keto-phosphane$]_2$ complex, namely $RuCl_2[Ph_2PCH_2C(tBu){=}O]_2$ (**1**)[11] and using carbon monoxide as an entering substrate L. The generation, under mild basic conditions, of rigid and strongly bound η^2-*(P,O)*-enolato-phosphane ligands leading to

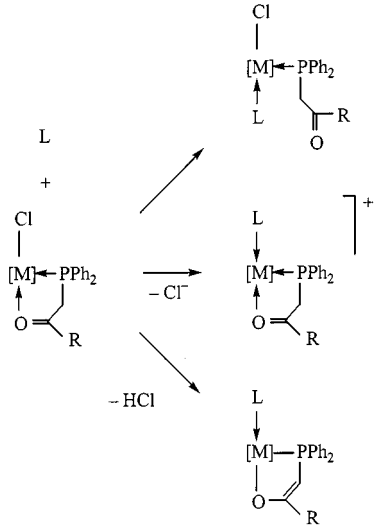

Scheme 1

[a] Laboratoire de Chimie de Coordination et Catalyse, UMR-CNRS 6509, Campus de Beaulieu, Université de Rennes I, 35042 Rennes Cédex, France
E-mail: Bernard.Demerseman@univ-rennes1.fr
[b] Groupe Matière Condensée et Matériaux, UMR-CNRS 6626, Campus de Beaulieu, Université de Rennes I, 35042 Rennes Cédex, France

stability in stereoisomeric $Ru(CO)_2[\eta^2$-*(P,O)*-$Ph_2PCH{=}C(t\mathrm{Bu})O]_2$ derivatives is of interest. The reaction of $[NO][BF_4]$ with **1** afforded a new family of ruthenium(IV) derivatives. The bis(enolato-phosphane) complex $RuCl(NO)[\eta^2$-*(P,O)*-$Ph_2PCH{=}C(t\mathrm{Bu})O]_2$ has been characterised by an X-ray structure determination.

Results and Discussion

1. Cationic (Keto-phosphane) Complexes Involving Carbon Monoxide

A cleavage of one Ru−Cl bond is likely to have occurred when $RuCl_2[Ph_2PCH_2C(t\mathrm{Bu}){=}O]_2$ (**1**) (which behaves in solution as a mixture of two isomers with *cis* phosphorus and *trans* or alternatively *cis* chlorine coordinating atoms)[11] was reacted with a solution of $[NH_4][PF_6]$ in methanol. The examination of the resulting orange solution by $^{31}P\{^1H\}$ NMR spectroscopy showed a new set of resonances consisting of an AB spin system as expected for two inequivalent phosphorus *nuclei* and the observation of a low coupling constant value (^2J = 40.0 Hz) which indicated a retention of their mutual *cis* arrangement.[15] A subsequent admittance of a carbon monoxide atmosphere resulted in the formation of the cationic complex $\{RuCl(CO)[\eta^2$-*(P,O)*-$Ph_2PCH_2C(t\mathrm{Bu}){=}O]_2\}[PF_6]$, **2**, which was isolated as orange-yellow crystals in 65% yield (Scheme 2). The structure of **2** was determined from a combination of elemental analysis, IR spectroscopy and ^1H, $^{31}P\{^1H\}$, $^{13}C\{^1H\}$, and ^{13}C NMR spectroscopy. Elemental analysis indicated a retention of one chlorine atom *per* Ru. The $^{31}P\{^1H\}$ NMR spectrum consisted of an AB spin system and a high coupling constant value (^2J = 328 Hz) indicated a relative *trans* arrangement of the two phosphorus *nuclei*. The IR spectrum of **2** indicated that the two keto-phosphane ligands [ν(C=O): 1621 and 1596 cm^{-1}] are η^2-*(P,O)*-coordinated,[11] and produced a very strong absorption attributed to the carbon monoxide ligand [ν(C≡O): 1991, 1977 cm^{-1} (the absorption is slightly split at its summit, most likely due to a solid state effect)]. The examination of **2** by ^1H and $^{13}C\{^1H\}$ NMR spectroscopy provided further evidence for one carbon monoxide ligand and two inequivalent keto-phosphane ligands, thus again indicating that the two coordinated oxygen atoms are located in a relative *cis* arrangement. The neutral complex $RuCl_2(CO)[\eta^2$-*(P,O)*-$Ph_2PCH_2C(t\mathrm{Bu}){=}O][\eta^1$-*(P)*-$Ph_2PCH_2C(=O)t\mathrm{Bu}]$ (**3**)[11] was obtained when a solution of **1** and $[NH_4][PF_6]$ in methanol was stirred under a carbon monoxide atmosphere. Attempts to obtain **2** by reacting **3** with $[NH_4][PF_6]$ or $Ag[BF_4]$ failed.

A preliminary cleavage of one Ru−Cl bond from **1** may account for the formation of **2** and not surprisingly, the reaction of $Ag[BF_4]$ with a solution of **1** in dichloromethane similarly generated a new species as shown by $^{31}P\{^1H\}$ NMR spectroscopy (see Exp. Sect.). Removal of the solvent resulted in the fast decomposition and further characterisation of the likely unsaturated species was not attempted. The distinct chemical pathways leading to **2** and **3** involve a *cis* to *trans* rearrangement of the phosphorus coordinating atoms. Requirement of an entrance of carbon monoxide *trans* relative to a coordinated oxygen atom may be responsible for the rearrangement achieving *trans* O−Ru−CO arrangements in **2** and **3**. Since complex **3** reversibly adds carbon monoxide to generate the fragile derivative *all-trans* $RuCl_2(CO)_2[\eta^1$-*(P)*-$Ph_2PCH_2C(=O)t\mathrm{Bu}]_2$ (**3′**)[11] (Scheme 2), we looked for a comparison between the hemilabile properties of the keto-phosphane ligands in complexes **2** and **3**.

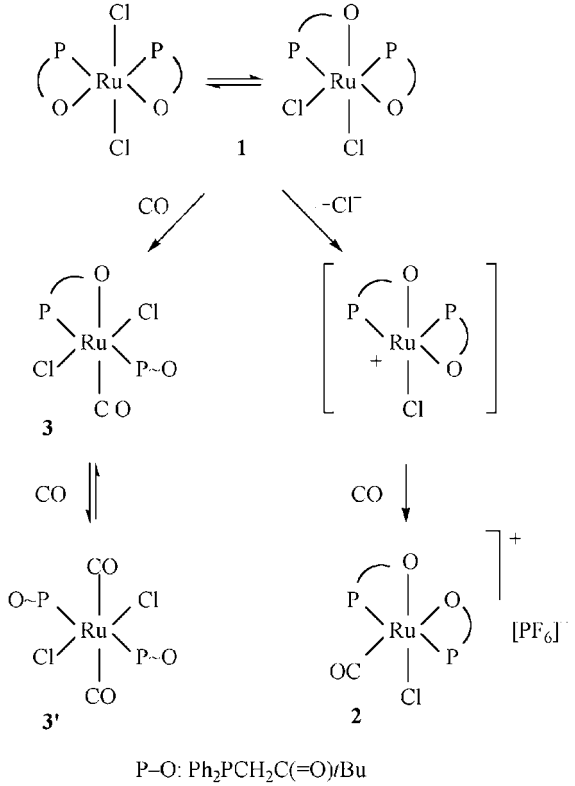

Scheme 2

Under a moderate thermal activation, as previously reported, when starting from $RuCl_2$[ether-phosphane]$_2$ complexes,[10] complex **3** irreversibly added carbon monoxide to yield $RuCl_2(CO)_2[Ph_2PCH_2C(=O)t\mathrm{Bu}]_2$ the *cis,cis,trans* stereoisomer, **4** (Scheme 3) as it is thermodynamically favoured and stable. Thus, complex **4** was isolated as colourless crystals in 92% yield after a solution of **3** in hot toluene (85 °C) was stirred under a carbon monoxide atmosphere. The IR spectrum of **4** showed the two carbonyl ligands [ν(C≡O): 2056, 1992 cm^{-1}] to be in a relative *cis* arrangement besides a single absorption [ν(C=O): 1705 cm^{-1}] as expected for two equivalent η^1-*(P)*-coordinated keto-phosphanes. The $^{31}P\{^1H\}$ NMR spectrum consisted of a single resonance and the ^1H NMR spectrum showed the resonance attributed to the four equivalent PCH_2 protons as a virtual triplet. A clean reaction occurred when a stoichiometric amount of $Ag[BF_4]$ was added to a solution of **4** in dichloromethane and afforded the expected cationic derivative **5** which was also isolated as colourless crystals in 80% yield (Scheme 3). The formation of **5** merely consists of the removal of one chloride ligand from **4** allowing an η^2-*(P,O)*-coordination of one keto-phosphane ligand. As ex-

pected, the two keto-phosphane ligands in **5** were found inequivalent by $^{31}P\{^1H\}$ NMR spectroscopy and the observation of a high coupling constant value (^2J = 305 Hz) indicated a relative *trans* arrangement of the phosphorus *nuclei*. The IR spectrum of **5** showed that the two carbonyl ligands [ν(C≡O): 2072, 2015 cm^{-1}] are in a relative *cis* arrangement but that the distinct absorptions [ν(C=O): 1707, 1614 cm^{-1}] are attributable to the two keto-phosphane ligands, which are η^1-*(P)*- and η^2-*(P,O)*-coordinated, respectively.

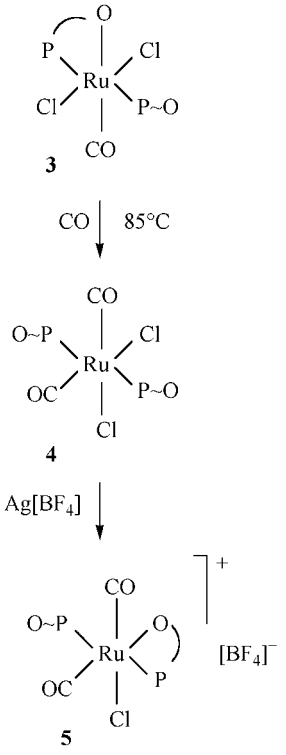

Scheme 3

Complexes **2** and **5** are both stable and inert under a carbon monoxide atmosphere. Thus, a straightforward comparison of their structures is enough to emphasise an unusual strength of the O→Ru bonds in cationic complex **2**: an easy cleavage would allow carbon monoxide fixation by **2** resulting in formation of **5**.

Emphasising the easiness of photochemical activation, sun light exposure of a dichloromethane solution of **2** cleanly produced a pale precipitate of **6** which was collected in 82% yield (Scheme 4). In contrast, complex **2** decomposed under thermal activation (ethanol at reflux). The $^{31}P\{^1H\}$ NMR spectrum of **6** disclosed besides a single resonance, an AB spin system with a low coupling constant value (^2J = 24.0 Hz), thus suggesting a mixture of two species. At least one of them involves two phosphorus coordinating atoms in a relative *cis* arrangement. The ^1H NMR spectrum only allowed the determination of the relative abundance of the major unsymmetrical species in solution, and owing to a very low solubility, we failed to obtain a tractable $^{13}C\{^1H\}$ NMR analysis. Therefore, we sought for chemical evidence providing further information concerning the structure of **6**.

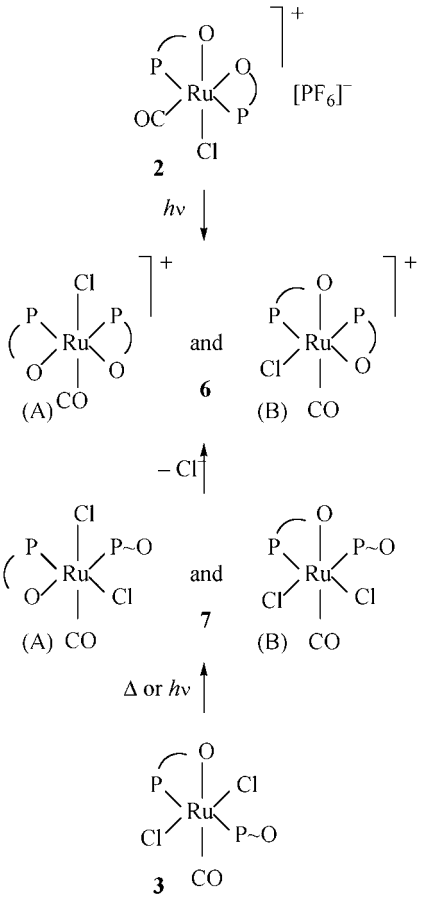

Scheme 4

A rearrangement of complex **3** similarly occurred under sun light exposure but also under thermal activation, to afford **7** as a mixture of two isomers both disclosing a relative *cis* arrangement of the phosphorus atoms by $^{31}P\{^1H\}$ NMR spectroscopy (Scheme 4). As expected for a mixture of two isomers, the $^{13}C\{^1H\}$ NMR spectrum disclosed two C≡O resonances and the observation of low $^2J_{PC}$ coupling constant values (^2J = 23 and 27 Hz, respectively) indicated that carbon monoxide was located in a *cis* position relative to the two phosphorus atoms. Only two structures, namely (A) and (B) in Scheme 4, remained conceivable on the basis of a *facial* arrangement of a carbon monoxide ligand and two phosphorus coordinating atoms. When compared to ether-phosphane complexes,[11] the relative abundance of the two isomers was also found to be solvent dependent by ^1H NMR spectroscopy (see Exp. Sect.), but no fluxional process between the coordinating modes of the two keto-phosphane ligands was observed at ambient temperature. Of further interest with respect to this study is the addition of $[NH_4][PF_6]$ to a solution of **7** in methanol which immediately resulted in the formation of a precipitate of **6.** Abstraction of one chloride ligand located *trans* relative to a phosphorus atom in **7**, affords the mixture of isomers which is assumed for **6** (Scheme 4).

2. Neutral Bis(enolato-phosphane) Complexes Involving Carbon Monoxide

Owing to the very low solubility of **6** and the presence of two isomers for both **6** and **7**, some doubt remained concerning their structures. Complex **6** reacted with acetonitrile and K_2CO_3 resulting in a nearly quantitative formation of the neutral bis(enolato-phosphane) complex Ru(CO)(MeCN)[η^2-*(P,O)*-$Ph_2PCH{=}C(t\text{Bu})O]_2$ (**8**) and further reaction of **8** with carbon monoxide selectively led to the bis(enolato-phosphane) derivative *all-cis* $Ru(CO)_2[\eta^2$-*(P,O)*-$Ph_2PCH{=}C(t\text{Bu})O]_2$ (**9**) the structure of which was unambiguously determined (Scheme 5). $^{31}P\{^1H\}$ NMR spectroscopic studies were enough to specify the structure of **9** and indicated two inequivalent enolato-phosphane ligands and also showed that the phosphorus atoms are in a relative *cis* arrangement (^2J = 24.0 Hz). The ^1H NMR spectrum of **9** showed two distinct PCH= protons whereas a relative *cis* arrangement of the two carbonyl ligands was inferred from both IR and $^{13}C\{^1H\}$ NMR spectroscopy.

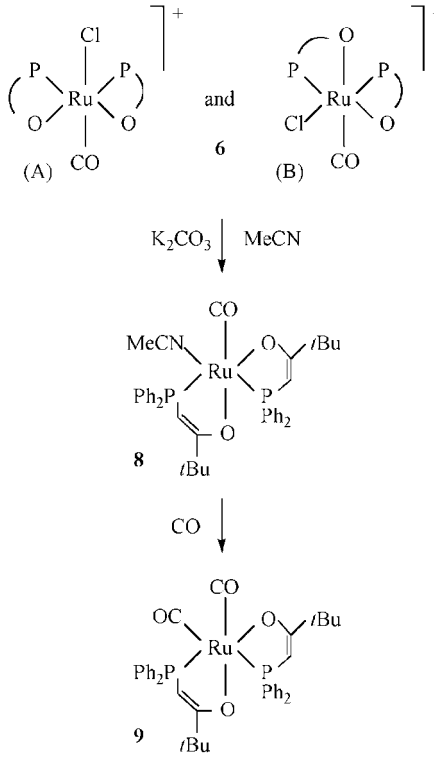

Scheme 5

The reaction of **4** or **5** with carbon monoxide under basic conditions (K_2CO_3 in methanol) was found to be very selective and afforded the bis(enolato-phosphane) derivative $Ru(CO)_2[\eta^2$-*(P,O)*-$Ph_2PCH{=}C(t\text{Bu})O]_2$ (**10**) with *cis* carbonyl ligands, *cis* oxygen and *trans* phosphorus coordinating atoms (Scheme 6). Complex **10** is a stereoisomer of **9**. Its IR spectrum indicated the relative *cis* arrangement of the two C≡O ligands and the conversion of both keto-phosphanes from **4** (or **5**), into enolato-phosphane ligands that were found to be equivalent by $^{31}P\{^1H\}$ NMR spectroscopy. The ^1H NMR spectrum of **10** showed the resonance, attributed to the two equivalent PCH= protons, as a virtual triplet, as expected from a mutual *trans* arrangement of the two phosphorus coordinating atoms.

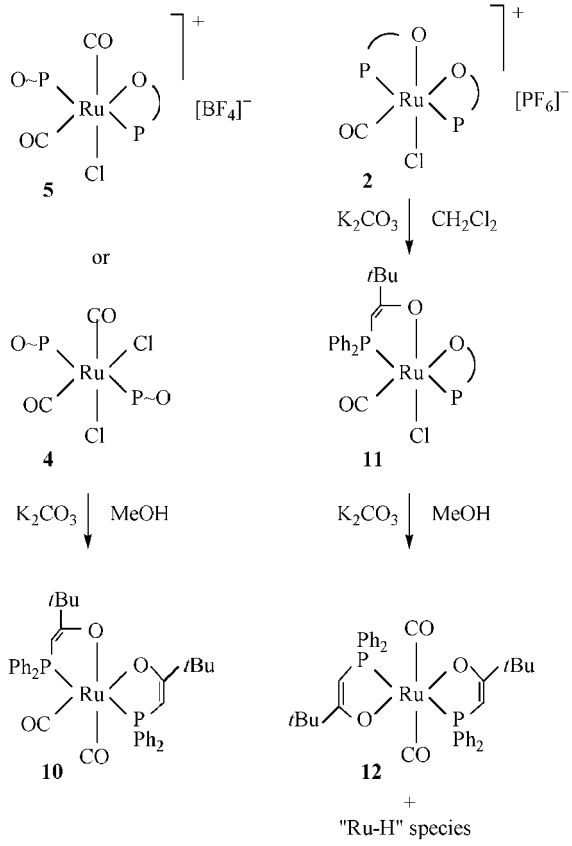

Scheme 6

Owing to its structure with *trans* phosphorus and *cis* oxygen coordinating atoms, the cationic complex **2** may appear as a precursor for the access to **10**. However, the reaction of **2** and K_2CO_3 in dichloromethane selectively afforded the *all-trans* derivative **11** (Scheme 6). We had previously reported the synthesis of **11** starting from **3** and allowing the access of a third stereoisomer of **9** and **10**, namely *all-trans* $Ru(CO)_2[\eta^2$-*(P,O)*-$Ph_2PCH{=}C(t\text{Bu})O]_2$ (**12**).[11] When compared to the nearly quantitative synthesis of **9** and **10**, complex **12** was previously obtained in a markedly lower yield (24%). Therefore, the formation of **12** was re-investigated. Complex **11** was reacted with K_2CO_3 in methanol under a carbon monoxide atmosphere and the resulting crude material was examined by $^{31}P\{^1H\}$NMR spectroscopy that disclosed a mixture of **12** and of a second unidentified species but neither **9** nor **10** were detected. Fractional crystallization allows pure **12** to be obtained but we failed to isolate the second species which is likely a Ru−H complex as suggested by ^1H NMR spectroscopy (see Exp. Sect.).

3. Neutral Bis(enolato-phosphane) Complexes Involving Nitrogen Monoxide

The nitrosonium cation $[NO]^+$ is isoelectronic with carbon monoxide but also a strong oxidising reagent and the reaction of $[NO][BF_4]$ with a $RuCl_2$(ether-phosphane)$_2$ complex had proved to result in a Ru^{II} to Ru^{III} oxidation.[1] By contrast, the reaction of **1** with $[NO][BF_4]$ in dichloromethane afforded an orange solid that may be assumed to mainly contain *all-trans* (on the basis of two *trans* phosphorus and two *trans* chlorine coordinating atoms) $\{RuCl_2(NO)[Ph_2PCH_2C(t\text{Bu})=O][Ph_2PCH_2C(=O)t\text{Bu}]\}$-$[BF_4]$ (**13**). The structure of **13** was suggested by spectroscopic studies. The IR spectrum of **13** showed besides the characteristic absorption attributed to the $[BF_4]^-$ counter anion, a very strong absorption attributed to a nitrosyl ligand [ν(NO): 1884 cm^{-1}] and two absorptions [ν(C=O): 1701 cm^{-1} and 1595 cm^{-1}] emphasising two distinct keto-phosphane ligands, that are η^1-*(P)*- and η^2-*(P,O)*-coordinated, respectively. $^{31}P\{^1H\}$ NMR spectroscopy indicated a relative *trans* arrangement of the two inequivalent phosphorus *nuclei*, but ^1H NMR spectroscopy indicated two equivalent PCH_2 protons for each keto-phosphane, as may be expected when two chloride ligands are in a relative *trans* arrangement. Unfortunately, attempts of purification of **13** failed, instead affording the stable enolato-phosphane derivative *all-trans* $RuCl_2(NO)[Ph_2PCH=C(t\text{Bu})O]$-$[Ph_2PCH_2C(=O)t\text{Bu}]$ (**14**) (Scheme 7). The structure of **14** was similarly determined by spectroscopic studies but also elemental analysis and a peculiarly easy deprotonation of the η^2-*(P,O)*-coordinated keto-phosphane ligand in **13** straightforwardly accounts for the formation of **14**. A formal removal of HCl from **14** was achieved under basic conditions (KOH or K_2CO_3 in methanol) and afforded the bis(enolato-phosphane) complex $RuCl(NO)[Ph_2PCH=C(t\text{Bu})O]_2$ (**15**) which surprisingly showed a relative *cis* arrangement of the phosphorus coordinating atoms (Scheme 7). The spectroscopic data collected for **15** only allowed us to further specify a structure involving two distinct enolato-phosphane ligands but did not provide any information on the symmetry.

A complete determination of the structure of **15** was achieved by an X-ray analysis that revealed a distorted octahedron (Figure 1). Examination of bond angles clearly indicated that the nitrosyl ligand behaves as a 3e-donor [O(1)−N(1)−Ru: 172.88(16)°] and is located *trans* relative to an oxygen atom [N(1)−Ru−O(3): 174.40(7)°].[16] The two phosphorus atoms are in a relative *cis* arrangement [P(1)−Ru−P(2): 101.685(18)°] and located *trans* relative to the oxygen [O(2)−Ru−P(1): 167.43(4)°] and chlorine [Cl(1)−Ru−P(2): 166.697(19)°] atoms. The two Ru−O bond lengths [Ru−O(3): 1.9930(13), Ru−O(2): 2.0820(13) Å] account for distinct *trans* influences from nitrosyl and phosphorus, whereas the two Ru−P bonds lengths [Ru−P(1): 2.3409(5), Ru−P(2): 2.3646(5) Å] remain close. The lengths of the C=C bonds involved in the two cycles [C(1)−C(2): 1.350(3), C(19)−C(20): 1.365(3) Å] are normal as expected for enolato-phosphane ligands.

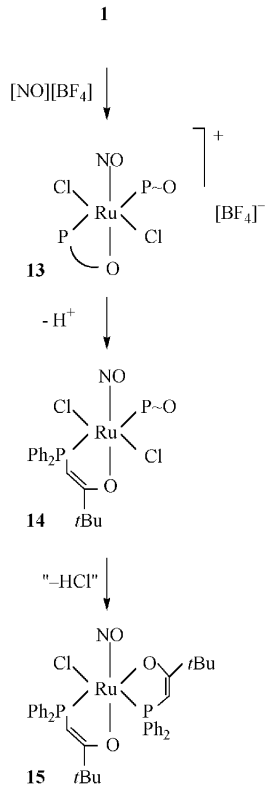

Scheme 7

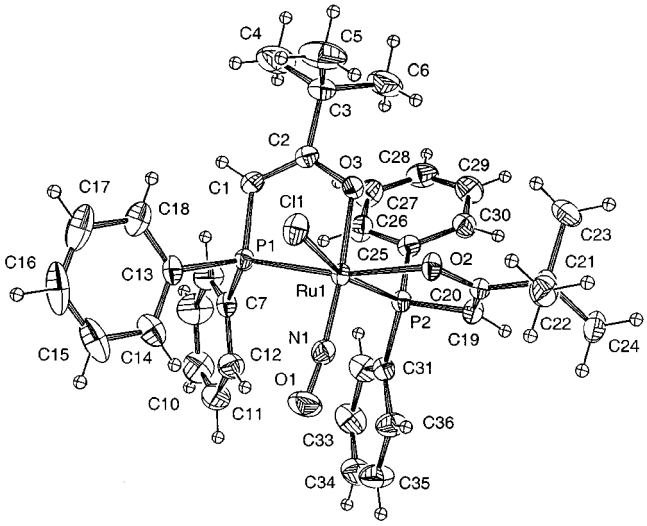

Figure 1. ORTEP drawing of $RuCl(NO)[Ph_2PCH=C(t\text{Bu})O]_2$ **(15)** showing 50% thermal ellipsoids; selected bond lengths (Å) and angles (°): Ru(1)−N(1) 1.7355(17), Ru(1)−O(3) 1.9930(13), Ru(1)−O(2) 2.0820(13), Ru(1)−P(1) 2.3409(5), Ru(1)−P(2) 2.3646(5), Ru(1)−Cl(1) 2.4193(5), O(1)−N(1) 1.162(2), C(1)−C(2) 1.350(3), C(19)−C(20) 1.365(3), N(1)−Ru(1)−O(3) 174.40(7), N(1)−Ru(1)−O(2) 99.30(7), O(3)−Ru(1)−O(2) 86.30(6), N(1)−Ru(1)−P(1) 92.74(5), O(3)−Ru(1)−P(1) 81.67(4), O(2)−Ru(1)−P(1) 167.43(4), N(1)−Ru(1)−P(2) 94.15(6), O(3)−Ru(1)−P(2) 86.65(4), O(2)−Ru(1)−P(2) 81.16(4), P(1)−Ru(1)−P(2) 101.685(18), N(1)−Ru(1)−Cl(1) 94.42(6), O(3)−Ru(1)−Cl(1) 85.82(4), O(2)−Ru(1)−Cl(1) 87.42(4), P(1)−Ru(1)−Cl(1) 88.051(18), P(2)−Ru(1)−Cl(1) 166.697(19), O(1)−N(1)−Ru(1) 172.88(16)

The *trans* to *cis* rearrangement of the two phosphorus coordinating atoms which is involved in the **14** to **15** transformation is intriguing because no pentacoordinated intermediate that still contains a strongly bonded enolato-phosphane ligand is expected from **14**. A possible pathway leading to **15** will consist of a preliminary deprotonation of the η^1-*(P)*-coordinated keto-phosphane in **14**. The coordination of the anionic oxygen atom may occur as a result of the ability of nitrosyl ligands to behave as either a 3e or 1e donor and this will generate an heptacoordinated intermediate transiently scrambling the octahedral structure.[17] Subsequent elimination of one chloride anion achieves the formation of **15**. From a steric point of view, complex **15** seems very close when compared to the bis(enolato-phosphane) complexes **9**, **10** and **12**, which seem equally stable, providing evidence for a lack of steric constraints.

Conclusion

The coordination of the oxygen atoms from the two keto-phosphane ligands leads to an unusually strong stabilization in the cationic complex $\{RuCl(CO)[Ph_2PCH_2C(tBu)=O]_2\}[PF_6]$ (**2**). The stereoisomeric *all-cis*, *cct,* and *all-trans* $Ru(CO)_2[\eta^2$-*(P,O)*-$Ph_2PCH=C(tBu)O]_2$ complexes, were selectively obtained under mild conditions and such a result indicates high energetic barriers between the three corresponding families of compounds. Thus, the behaviour of complex **2** under mild basic conditions clearly shows **2** to be an *all-trans* derivative. However, the families are strongly related to the number x of carbon monoxide ligands: the observation of the *cct* family requires $x = 2$ whereas only *all-trans* and *all-cis* derivatives are observed when $x = 1$, and a distinct geometry was observed when $x = 0$. As new evidence for synthetic usefulness, the precursor $RuCl_2[Ph_2PCH_2C(tBu)=O]_2$ (**1**) is able to coordinate not only carbon monoxide but also the isolelectronic nitrosonium cation. The coordination of $[NO]^+$ thus provides an entry to a family of octahedral ruthenium (IV) complexes such as $RuCl(NO)[\eta^2$-*(P,O)*-$Ph_2PCH=C(tBu)O]_2$, (**15**), the reactivity of which is under investigation.

Experimental Section

General: The reactions were performed according to Schlenk type techniques. Solvents were distilled under an inert atmosphere after drying according to conventional methods. Elemental analyses were performed by the "Service de Microanalyse du CNRS" Vernaison, France. Infrared spectra were recorded on a Nicolet 205 FT-infrared spectrometer as Nujol mulls. NMR spectra were recorded at 297 K on AC 300 FT Bruker instrument (^{1}H: 300.13, ^{13}C: 75.47, ^{31}P: 121.50 MHz; absolute values of coupling constants in Hz) and referenced internally to the solvent peak. The following abbreviations are used: s, singlet; d, doublet; t, triplet; vt, virtual triplet; m, unresolved multiplet. The precursor complex $RuCl_2[Ph_2PCH_2C(tBu)=O]_2$ (**1**) was synthesised as reported previously.[11]

Generation of the $\{RuCl[Ph_2PCH_2C(tBu)=O]_2\}^+$ Species: An aliquot of the solution resulting from the reaction of **1** with NH_4PF_6 in methanol (see synthesis of **2**) was examined by $^{31}P\{^1H\}$ NMR spectroscopy (MeOH/$CDCl_3$): δ = 62.8 (d), 70.7 (d), ^2J = 38 Hz. However, a second and minority species was detected: δ = 67.1 (d), 68.4 (d), ^2J = 37 Hz. In another experiment, an equivalent amount of $Ag[BF_4]$ was added to a solution of **1** in CH_2Cl_2. The mixture was stirred for 1 h and decanted. The supernatant solution was examined by $^{31}P\{^1H\}$ NMR spectroscopy (CH_2Cl_2/CD_2Cl_2): δ = 63.7 (d), 73.2 (d), ^2J = 39 Hz. Only one species was observed in CH_2Cl_2 suggesting that the observation of a second set of resonances in methanol indicated a solvated species.

***trans-(P,P)*-$\{RuCl(CO)[Ph_2PCH_2C(tBu)=O]_2\}[PF_6]$ (2):** A mixture consisting of sample **1** (5.20 g, 7.02 mmol) and NH_4PF_6 (1.20 g, 7.36 mmol) in methanol (80 mL), under an inert atmosphere, was stirred overnight to obtain an orange solution that was then stirred for 2 h under a carbon monoxide atmosphere. The resulting yellow precipitate was collected by filtration and then extracted with dichloromethane (40 mL). The solution was filtered and the filtrate was covered with methanol (20 mL) and diethyl ether (130 mL) to afford orange-yellow crystals. Yield: 4.00 g, 65%. IR: ν(C≡O) = 1991, 1977 cm^{-1}; ν(C=O) = 1621, 1596 cm^{-1}. $^{31}P\{^1H\}$ NMR (CD_2Cl_2): δ = 35.0 (d), 48.4 (d, ^2J = 328 Hz). ^{1}H NMR (CD_2Cl_2): δ = 0.93 (s, 9 H, *t*Bu), 1.06 (s, 9 H, *t*Bu), 3.72 (dd, 1 H, $^2J_{H,H}$ = 18.7, $^2J_{PH}$ = 11.2 Hz, PCH_2, H_a), 3.97 (dd, 1 H, $^2J_{H,H}$ = 17.9, $^2J_{PH}$ = 11.1 Hz, P′CH_2, H_a), 4.74 (ddd, 1 H, $^2J_{H,H}$ = 17.9, $^2J_{PH}$ = 11.4, $^4J_{PH}$ = 3.1 Hz, P′CH_2, H_b), 4.83 (ddd, 1 H, $^2J_{H,H}$ = 18.7, $^2J_{PH}$ = 10.4 Hz, $^4J_{PH}$ = 1.5 Hz, PCH_2, H_b), 7.45−7.99 (m, 20 H, Ph). $^{13}C\{^1H\}$ NMR (CD_2Cl_2): δ = 26.7 (s, C*Me*$_3$), 26.8 (s, C*Me*$_3$), 42.9 (d, $^1J_{PC}$ = 26.2 Hz, PCH_2), 43.4 (d, $^1J_{PC}$ = 26.9 Hz, PCH_2), 47.1 (d, $^3J_{PC}$ = 2.9 Hz, *C*Me$_3$), 47.7 (d, $^3J_{PC}$ = 3.4 Hz, *C*Me$_3$), 127.4−134.3 (m, 2 Ph_2P groups), 202.3 (dd, $^2J_{PC}$ = 13.6 and 11.4 Hz, C≡O), 235.9 (dd, $^2J_{PC}$ = 6.2, $^3J_{PC}$ = 4.9 Hz, C=O), 239.6 (dd, $^2J_{PC}$ = 5.5, $^3J_{PC}$ = 3.8 Hz, C=O). $C_{37}H_{42}ClF_6O_3P_3Ru$ (878.2): calcd. C 50.61, H 4.82, Cl 4.04, P 10.58; found C 50.82, H 4.89, Cl 4.03, P 10.23.

***ttt*-$RuCl_2(CO)[Ph_2PCH_2C(=O)tBu][Ph_2PCH_2C(tBu)=O]\cdot 2/3CH_2Cl_2$ (3):** The synthesis of **3** starting from **1** was reported previously.[11] A more straightforward synthesis starting from $[RuCl_2(p\text{-cymene})]_2$ is described herein. A mixture consisting of a sample of $[RuCl_2(p\text{-cymene})]_2$ (3.91 g, 6.38 mmol) and keto-phosphane $Ph_2PCH_2C(tBu)=O$ (7.26 g, 25.5 mmol) was dissolved in dichloromethane (60 mL) and methanol (140 mL) was then added. This mixture was stirred for 3 days under a carbon monoxide atmosphere and the resulting orange-yellow slurry was concentrated under vacuum. Diethyl ether was first added to collect the yellow precipitate. The solid was washed with diethyl ether then dried under vacuum and identified as *all-trans* $RuCl_2(CO)_2[Ph_2PCH_2C(=O)tBu]$, **3′**, by IR spectroscopy.[11] (Yield: 8.30 g, 82%). The crude product was dissolved in dichloromethane (50 mL) and the orange solution was stirred overnight in an open Erlenmeyer flask allowing the evolution of one mol of carbon monoxide. The solution was then covered with ethanol (250 mL) and the natural preferential evaporation of dichloromethane resulted in the formation of yellow crystals of **3**. Yield: 7.75 g, 74%. IR and NMR spectroscopic data as reported previously.[11]

***cct*-$RuCl_2(CO)_2[Ph_2PCH_2C(=O)tBu]_2$ (4):** A mixture consisting of a sample of **1** (4.06 g, 4.92 mmol) (or corresponding amounts of **3** or **3′**) and hot toluene (50 mL, 85 °C) was stirred for 2 days under a carbon monoxide atmosphere. The resulting colourless solution was evaporated under vacuum to leave a solid that was dissolved in dichloromethane (20 mL). Methanol (35 mL) was added and slow

evaporation of the solution afforded colourless crystals of **4**. Yield: 3.59 g, 92%. IR: ν(C≡O) = 2056, 1992 cm^{-1}; ν(C=O) = 1705 cm^{-1}. $^{31}P\{^1H\}$ NMR (CD_2Cl_2): δ = 19.2 (s). ^1H NMR (CD_2Cl_2): δ = 0.82 (s, 18 H, 2 *t*Bu), 4.43 (vt, 4 H, $|^2J_{PH} + {}^4J_{PH}|$ = 7.7 Hz, 2 PCH_2), 7.38−7.84 (m, 20 H, Ph). $C_{38}H_{42}Cl_2O_4P_2Ru$ (796.7): calcd. C 57.29, H 5.31, Cl 8.90, P 7.78; found C 57.40, H 5.29, Cl 8.85, P 7.76.

{RuCl(CO)$_2$[Ph$_2$PCH$_2$C(=O)*t*Bu][Ph$_2$PCH$_2$C(*t*Bu)=O]}[BF$_4$] (5): A mixture consisting of a sample of **4** (1.00 g, 1.26 mmol) and $Ag[BF_4]$ (0.25 g, 1.28 mmol) in dichloromethane (30 mL) was stirred overnight. The resulting solution was decanted, then filtered and covered with diethyl ether (80 mL) to afford colourless crystals of **5**. Yield: 0.86 g, 80%. IR: ν(C≡O) = 2072, 2015 cm^{-1}; ν(C=O) = 1707, 1614 cm^{-1}. $^{31}P\{^1H\}$ NMR (CD_2Cl_2): δ = 19.3 (d), 44.8 (d, ^2J = 305 Hz). ^1H NMR (CD_2Cl_2): δ = 1.02 (s, 9 H, *t*Bu), 1.05 (s, 9 H, *t*Bu), 4.04 (dd, 1 H, $^2J_{H,H}$ = 17.0, $^2J_{PH}$ = 10.2 Hz, P′CH_2, H_a), 4.15 (dd, 1 H, $^2J_{H,H}$ = 18.5, $^2J_{PH}$ = 11.8 Hz, PCH_2, H_a), 4.51 (dd, 1 H, $^2J_{H,H}$ = 16.8, $^2J_{PH}$ = 9.1 Hz, P′CH_2, H_b), 4.79 (dd, broad, 1 H, $^2J_{H,H}$ ≈ 18.5 Hz, $^2J_{PH}$ ≈ 12.0 Hz, PCH_2, H_b), 7.35−7.90 (m, 20 H, Ph). $C_{38}H_{42}BClF_4O_4P_2Ru$ (848.0): calcd. C 53.82, H 4.99, Cl 4.18, P 7.30; found C 53.66, H 5.11, Cl 5.02, P 7.06, retention of some dichloromethane is likely to be responsible for the high chlorine value.

***cis*-*(P,P)*-{RuCl(CO)[Ph$_2$PCH$_2$C(*t*Bu)=O]$_2$}[PF$_6$] (6):** A Schlenk flask was filled with a solution consisting of a sample of **2** (4.11 g, 4.68 mmol) in dichloromethane (60 mL). The flask was then exposed to sunlight. After three weeks (corresponding to ≈ 70 h of exposure according to our feasibility) the resulting cream-coloured precipitate was collected by filtration, then washed with diethyl ether (50 mL). Yield: 3.39 g, 82%. IR: ν(C≡O) = 1995 cm^{-1}; ν(C=O) = 1613 cm^{-1}. $^{31}P\{^1H\}$ NMR (CD_2Cl_2), asterisk marked values for the unsymmetrical isomer: δ = 55.3* (d), 56.2 (s), 62.5* (d), ^2J = 24 Hz*. ^1H NMR (CD_2Cl_2), asterisk marked values for the unsymmetrical and major (3:1) isomer: δ = 1.15* (s, *t*Bu), 1.41 (s, *t*Bu), 1.45* (s, *t*Bu), 3.63* (dd, $^2J_{H,H}$ = 18.6 Hz, $^2J_{PH}$ = 9.9 Hz, 1 H from a PCH_2 group), 4.21−4.30 (m, 2 H from PCH_2* groups, and 4 H from the two equivalent PCH_2 that showed close chemical shifts of the inequivalent protons), 4.56* (dd, $^2J_{H,H}$ = 18.7 Hz, $^2J_{PH}$ = 10.2 Hz, 1 H from a PCH_2 group), 6.56−7.87 (m, 20 H, Ph, both isomers). $C_{37}H_{42}ClF_6O_3P_3Ru$ (878.2): calcd. C 50.61, H 4.82, Cl 4.04, P 10.58; found C 50.71, H 4.92, Cl 4.18, P 10.69.

***ccc*-RuCl$_2$(CO)[Ph$_2$PCH$_2$C(=O)*t*Bu][Ph$_2$PCH$_2$C(*t*Bu)=O] (7):** A mixture consisting of a sample of **3** (7.53 g, 9.12 mmol) and toluene (80 mL), was heated to reflux for 20 h to afford a pale-yellow precipitate that was collected by filtration then washed with hexane and dried under vacuum. Yield: 5.63 g, 80%. Exposure of a solution of **3** in dichloromethane (as detailed for synthesis of **6**) to sunlight afforded a mixture of **6** and remaining **3**. Despite the fact that pale-yellow crystals were obtained upon addition of diethyl ether to a concentrated solution of the crude solid in dichloromethane, we failed to obtain **7** in a high state of purity as shown by elemental analyses. IR: ν(C≡O) = 1968 cm^{-1}; ν(C=O) = 1703, 1629 cm^{-1}. $^{31}P\{^1H\}$ NMR ($CDCl_3$), asterisk marked values for the major isomer: δ = 41.7 (broad), 47.4* (d), 47.8* (d), 59.7 (d, ^2J = 23 and 27 Hz*). $C_{37}H_{42}Cl_2O_3P_2Ru$ (768.7): calcd. C 57.82, H 5.51, Cl 9.22, P 8.06; found C 56.96, H 5.56, Cl 10.62, P 7.90. Attempts at recrystallization from hot acetonitrile yielded yellow crystals that retain acetonitrile (≈ 1.3 MeCN/Ru) but no significant change was observed from $^{31}P\{^1H\}$ NMR and IR spectroscopy. A concomitant crystallization of the two isomeric forms with only one retaining some solvent may account for the failure in obtaining a satisfactory elemental analysis. $^{31}P\{^1H\}$ NMR (CD_2Cl_2), asterisk marked values for the major isomer: δ = 39.9 (broad), 45.8* (d), 47.8* (d), 58.8 (d, ^2J = 23 and 27 Hz*). ^1H NMR (CD_2Cl_2), asterisk marked values for the major isomer: δ = 0.59 (s, *t*Bu), 0.70* (s, *t*Bu), 1.05 (s, *t*Bu), 1.28* (s, *t*Bu), 1.94 (s, MeCN), 2.62 (m, broad, 1 H from a PCH_2 group), 3.14 (m, broad, 1 H from a PCH_2 group), 4.02−4.30 (m, 5 H from PCH_2 groups), 4.67* (dd, $^2J_{H,H}$ = 17.2 Hz, $^2J_{PH}$ = 7.4 Hz, 1 H from a PCH_2 group), 6.75−7.86 (m, Ph). $^{13}C\{^1H\}$ NMR (CD_2Cl_2): δ = 2.2 (s, *Me*CN), 25.8 (s, C*Me*$_3$), 25.8 (s, C*Me*$_3$), 27.0 (s, C*Me*$_3$), 27.0 (s, C*Me*$_3$), 36.9 (d, $^1J_{PC}$ = 28.0 Hz, PCH_2), 37.4 (d, $^1J_{PC}$ = 33.4 Hz, PCH_2), 45.4 (d, $^3J_{PC}$ = 1.5 Hz, *C*Me$_3$), 45.9 (m, 2 *C*Me$_3$), 46.0 (d, $^3J_{PC}$ = 3.9 Hz, *C*Me$_3$), 47.2 (d, broad, $^1J_{PC}$ = 35.3 Hz, PCH_2), 49.0 (d, $^1J_{PC}$ = 31.5 Hz, PCH_2), 117.1 (s, Me*C*N), 127.7−137.5 (phenyl-groups resonances), 197.9 (dd, $^2J_{PC}$ = 17.7 and 13.0 Hz, C≡O), 204.3 (dd, $^2J_{PC}$ = 17.5 and 14.3 Hz, C≡O), 209.6 (d, $^2J_{PC}$ = 6.4 Hz, C=O), 209.7 (d, $^2J_{PC}$ = 10.7 Hz, C=O), 227.9 (d, $^2J_{PC}$ = 3.3 Hz, C=O), 228.4 (broad, C=O). Isomeric ratio as determined by ^1H NMR spectroscopy: 3:1 in $CDCl_3$, < 5:4 in CD_2Cl_2.

***ccc*-Ru(CO)(MeCN)[Ph$_2$PCH=C(*t*Bu)O]$_2$ (8):** A mixture consisting of a sample of **6** (3.39 g, 3.86 mmol), K_2CO_3 (1.20 g, 8.68 mmol) and acetonitrile (50 mL), was stirred overnight and then evaporated to dryness. The remaining solid was extracted with dichloromethane (50 mL). The solution was filtered and the clear filtrate was evaporated under vacuum to leave a cream-coloured powder that was found by NMR spectroscopy and elemental analysis to be pure. Yield: 2.62 g, 92%. IR: ν(C≡N) = 2325 cm^{-1}; ν(C≡O) = 1924 cm^{-1}; ν(C=CO) = 1506, 1493 cm^{-1}. $^{31}P\{^1H\}$ NMR (CD_2Cl_2): δ = 45.3 (d), 48.8 (d), ^2J = 27. ^1H NMR (CD_2Cl_2): δ = 0.92 (s, 9 H, *t*Bu), 1.22 (s, 9 H, *t*Bu), 1.54 (s, 3 H, MeCN), 4.09 (d, 1 H, $^2J_{PH}$ = 3.5 Hz, PCH=), 4.46 (d, 1 H, $^2J_{PH}$ = 2.0 Hz, P′CH=), 6.83−7.66 (m, 20 H, Ph). $^{13}C\{^1H\}$ NMR (CD_2Cl_2): δ = 3.1 (s, *Me*CN), 29.6 (s, C*Me*$_3$), 30.1 (s, C*Me*$_3$), 39.1 (dd, $^3J_{PC}$ = 12.6 Hz, $^4J_{PC}$ = 3.6 Hz, *C*Me$_3$), 39.2 (d, $^3J_{PC}$ = 12.6 Hz, *C*Me$_3$), 69.7 (d, $^1J_{PC}$ = 61.1 Hz, PCH=), 73.5 (d, $^1J_{PC}$ = 62.9 Hz, PCH=), 120.0 (d, $^3J_{PC}$ = 14.3 Hz, Me*C*N), 127.4−133.6 (m, phenyl-groups resonances), 134.2 (d, $^1J_{PC}$ = 51.5 Hz, PhP, *ipso*), 137.4 (d, $^1J_{PC}$ = 56.5 Hz, PhP, *ipso*), 138.9 (d, $^1J_{PC}$ = 53.1 Hz, PhP, *ipso*), 140.0 (d, $^1J_{PC}$ = 49.7 Hz, PhP, *ipso*), 198.9 (d, $^2J_{PC}$ = 17.1 Hz, =CO), 198.9 (d, $^2J_{PC}$ = 10.8 Hz, =CO), 202.7 (dd, $^2J_{PC}$ = 17.5 and 13.0 Hz, C≡O). $C_{39}H_{43}NO_3P_2Ru$ (736.8): calcd. C 63.58, H 5.88, N 1.90, P 8.41; found C 63.28, H 6.12, N 1.96, P 8.72.

***ccc*-Ru(CO)$_2$[Ph$_2$PCH=C(*t*Bu)O]$_2$·1/6CH$_2$Cl$_2$ (9):** A solution consisting of a sample of **8** (2.50 g, 3.39 mmol) and dichloromethane (35 mL), was stirred under carbon monoxide for 20 h, and then evaporated under vacuum to dryness to leave a white solid. Yield: 2.38 g, 95%. IR: ν(C≡O) = 2051, 1972 cm^{-1}; ν(C=CO) = 1507, 1500 cm^{-1}. $^{31}P\{^1H\}$ NMR (C_6D_6): δ = 34.3 (d), 44.0 (d, ^2J = 24 Hz). ^1H NMR (C_6D_6): δ = 1.22 (s, 9 H, *t*Bu), 1.52 (s, 9 H, *t*Bu), 4.41 (dd, 1 H, $^2J_{PH}$ = 3.1 Hz, $^4J_{PH}$ = 0.7 Hz, PCH=), 4.65 (d, 1 H, $^2J_{PH}$ = 4.0 Hz, P′CH=), 6.84−7.63 (m, 20 H, Ph). $^{13}C\{^1H\}$ NMR (C_6D_6): δ = 30.0 (s, C*Me*$_3$), 30.5 (s, C*Me*$_3$), 39.8 (dd, $^3J_{PC}$ = 12.6, $^4J_{PC}$ = 2.7, *C*Me$_3$), 39.8 (d, $^3J_{PC}$ = 12.6 Hz, *C*Me$_3$), 70.8 (dd, $^1J_{PC}$ = 60.6 Hz, $^3J_{PC}$ = 3.1 Hz, PCH=), 71.8 (d, $^1J_{PC}$ = 64.6 Hz, PCH=), 128.1−140.8 (m, phenyl-groups resonances), 191.2 (dd, $^2J_{PC}$ = 102.3 and 11.7 Hz, C≡O), 199.7 (dd, $^2J_{PC}$ = 15.3 and 10.8 Hz, C≡O), 200.4 (dd, $^2J_{PC}$ = 15.3, $^3J_{PC}$ = 1.8 Hz, =CO), 200.8 (d, $^2J_{PC}$ = 14.4 Hz, =CO). $C_{38}H_{40}O_4P_2Ru$·1/6CH_2Cl_2 (737.9): calcd. C 62.12, H 5.51, Cl 1.60, P 8.40; found C 62.14, H 5.66, Cl 1.27, P 8.03.

***cct*-Ru(CO)$_2$[Ph$_2$PCH=C(*t*Bu)O]$_2$ (10):** A sample of **1** (4.60 g, 5.57 mmol) was converted into crude **4** (as detailed above) before

adding K_2CO_3 (1.00 g, 7.24 mmol) and methanol (50 mL). This mixture was stirred for 7 days at room temperature. The solvent was then removed under vacuum to leave a white solid that was extracted with dichloromethane (30 mL). The solution was filtered and methanol (40 mL) was added to the colourless filtrate. Through slow evaporation, the mixture afforded colourless crystals of **10**. Yield: 3.04 g, 75%. IR: ν(C≡O) = 2029, 1963 cm^{-1}; ν(C=CO) = 1494 cm^{-1}. $^{31}P\{^1H\}$ NMR (CD_2Cl_2): δ = 44.4 (s). ^1H NMR (CD_2Cl_2): δ = 0.97 (s, 18 H, 2 *t*Bu), 4.48 (vt, 2 H, $|^2J_{PH} + {}^4J_{PH}|$ = 5.8 Hz, 2 PCH=), 7.36−7.80 (m, 20 H, Ph). $C_{38}H_{40}O_4P_2Ru$ (723.8): calcd. C 63.06, H 5.57, P 8.56; found C 63.22, H 5.77, P 8.47.

Formation of *ttt*-RuCl(CO)[$Ph_2PCH{=}C(tBu)O$][$Ph_2PCH_2C(tBu){=}O$] (11): The synthesis of **11** by reacting **3** with K_2CO_3 in dichloromethane has been reported previously.[11] Starting from **2**, complex **11** was selectively obtained also.

Formation of *ttt*-Ru(CO)$_2$[$Ph_2PCH{=}C(tBu)O$]$_2$ (12): A mixture consisting of a sample of **1** (0.77 g, 1.04 mmol) and K_2CO_3 (0.31 g, 2.24 mmol) in methanol (30 mL), was stirred for 4 days under a carbon monoxide atmosphere. The solvent was then removed under vacuum and the residue was extracted with dichloromethane (30 mL). A white powder was obtained after filtration of the solution and subsequent evaporation. The examination of the solid by NMR spectroscopy disclosed a mixture of two complexes when very weak additional resonances are omitted. $^{31}P\{^1H\}$ NMR ($CDCl_3$): δ = 27.1 (s, complex **12**)[11] and 29.9 (d), 51.5 (d) ^2J = 242 Hz (unidentified compound). ^1H NMR ($CDCl_3$), selected values attributed to the unidentified compound: δ = − 5.07 (dd, 1 H, $^2J_{PH}$ = 20.4 and 19.5 Hz, RuH), 3.92 (dd, 1 H, $^2J_{H,H}$ = 17.0 Hz, $^2J_{PH}$ = 6.8 Hz, PCH_2, H_a), 4.13 (dd, $^2J_{H,H}$ = 17.0 Hz, 1 H, $^2J_{PH}$ = 7.6 Hz, PCH_2, H_b), 4.62 (dd, 1 H, $^2J_{PH}$ = 3.5 Hz, $^4J_{PH}$ = 3.0 Hz, PCH=).

***ttt*-RuCl$_2$(NO)[$Ph_2PCH_2C(=O)tBu$][$Ph_2PCH_2C(tBu){=}O$][BF_4] (13):** A sample of **1** (5.00 g, 6.75 mmol) and [NO][BF_4] (0.85 g, 7.28 mmol) were successively added to cold dichloromethane (60 mL, −80 °C). The mixture was allowed to reach ambient temperature and stirred overnight. The resulting solution was evaporated under vacuum to obtain an orange solid (5.52 g). The NMR spectroscopic analysis of this crude material indicated a mixture of several products and we failed to isolate a pure compound after recrystallization from a dichloromethane/diethyl ether mixture. When additional weak IR absorptions and NMR resonances are omitted, the collected spectroscopic data suggested the assumed structure. IR: ν(NO) = 1884 cm^{-1}; ν(C=O) = 1701 cm^{-1}, 1595 cm^{-1}. $^{31}P\{^1H\}$ NMR (CD_2Cl_2): δ = 20.3 (d), 49.8 (d, ^2J = 371 Hz). ^1H NMR (CD_2Cl_2): δ = 0.84 (s, 9 H, *t*Bu), 1.05 (s, 9 H, *t*Bu), 4.39 (dd, 2 H, $^2J_{PH}$ = 9.1 Hz, $^4J_{PH}$ = 2.4 Hz, PCH_2), 4.70 (d, broad, 2 H, $^2J_{PH}$ = 10.0 Hz, P′CH_2), 7.00−7.70 (m, 20 H, Ph). Attempts at recrystallization of the compound from slow evaporation of its solution in a dichloromethane/ethanol mixture afforded orange crystals of the enolato-phosphane derivative **14** instead of **13**.

***ttt*-RuCl$_2$(NO)[$Ph_2PCH{=}C(tBu)O$][$Ph_2PCH_2C(=O)tBu$] (14):** Complex **14** was obtained in 65% yield relative to **1** after recrystallization of **13** in a dichloromethane/ethanol mixture (see synthesis of **13**) or alternatively by reacting **13** with K_2CO_3 in dichloromethane. Further recrystallization from a dichloromethane/methanol mixture afforded orange needles. IR: ν(NO) = 1858 cm^{-1}; ν(C=O) = 1702 cm^{-1}; ν(C=CO): 1520 cm^{-1}. $^{31}P\{^1H\}$ NMR (CD_2Cl_2): δ = 14.9 (d, PCH_2), 53.1 (d, PCH=, ^2J = 385 Hz). ^1H NMR (CD_2Cl_2): δ = 0.87 (s, 9 H, *t*Bu), 0.98 (s, 9 H, *t*Bu), 4.29 (dd, 2 H, $^2J_{PH}$ = 9.9 Hz, $^4J_{PH}$ = 1.8 Hz, PCH_2), 4.63 (dd, 1 H, $^2J_{PH} \approx {}^4J_{PH} \approx$ 4.1 Hz, PCH=), 7.37−7.78 (m, 20 H, Ph). $^{13}C\{^1H\}$ NMR (CD_2Cl_2): δ = 26.4 (s, C*Me*$_3$), 28.9 (s, C*Me*$_3$), 33.4 (d, $^1J_{PC}$ = 30.4 Hz, PCH_2), 38.6 (d, $^3J_{PC}$ = 12.3 Hz, *C*Me$_3$), 45.6 (d, $^3J_{PC}$ = 1.8 Hz, *C*Me$_3$), 72.1 (dd, $^1J_{PC}$ = 63.8 Hz, $^3J_{PC}$ = 1.8 Hz, PCH=), 128.5 (d, $^2J_{PC}$ = 10.9 Hz, Ph_2P, *ortho*), 128.6 (d, $^2J_{PC}$ = 10.0 Hz, Ph_2P, *ortho*), 129.8 (dd, $^1J_{PC}$ = 43.8 Hz, $^3J_{PC}$ = 2.4 Hz, Ph_2P, *ipso*), 130.9 (d, $^4J_{PC}$ = 2.7 Hz, Ph_2P, *para*), 131.1 (d, $^4J_{PC}$ = 2.3 Hz, Ph_2P, *para*), 132.0 (dd, $^1J_{PC}$ = 57.2 Hz, $^3J_{PC}$ = 2.3 Hz, Ph_2P, *ipso*), 133.1 (dd, $^3J_{PC}$ = 9.1 Hz, $^5J_{PC}$ = 1.7 Hz, Ph_2P, *meta*), 134.3 (d, $^3J_{PC}$ = 8.8 Hz, Ph_2P, *meta*), 198.6 (dd, $^2J_{PC}$ = 16.9 Hz, $^3J_{PC}$ = 8.9 Hz, =CO), 209.8 (d, $^2J_{PC}$ = 5.4 Hz, C=O). ^{13}C NMR (CD_2Cl_2), selected values: δ = 33.4 (td, $^1J_{HC}$ = 130 Hz, PCH_2), 72.1 (ddd, $^1J_{HC}$ = 169 Hz, PCH=). $C_{36}H_{41}Cl_2NO_3P_2Ru$ (769.7): calcd. C 56.18, H 5.37, Cl 9.21, N 1.82, P 8.05; found C 55.84, H 5.43, Cl 9.85, N 1.84, P 7.79.

***ccc*-RuCl(NO)[$Ph_2PCH{=}C(tBu)O$]$_2$ (15):** **1** (5.30 g, 7.16 mmol) and [NO][BF_4] (0.93 g, 7.96 mmol) produced crude complex **13** and this was added to ethanol (80 mL) and then KOH (0.80 g, 14.3 mmol) and the mixture was stirred at ambient temperature for 2 days. The resulting orange slurry was evaporated under vacuum to leave a solid that was extracted with dichloromethane (60 mL). The solution was filtered and the filtrate was covered with methanol (150 mL) to afford well-formed orange-red crystals. Yield: 3.02 g, 58%. Complex **15** may be similarly obtained starting from **14**. IR: ν(NO) = 1805 cm^{-1}; ν(C=CO) = 1507, 1497 cm^{-1}. $^{31}P\{^1H\}$ NMR (CD_2Cl_2): δ = 40.7 (d), 46.5 (d), ^2J = 20. ^1H NMR (CD_2Cl_2): δ = 0.95 (s, 9 H, *t*Bu), 1.35 (s, 9 H, *t*Bu), 4.22 (dd, $^2J_{PH}$ = 6.3 Hz, 1 H, $^4J_{PH}$ = 1.4 Hz, PCH=), 4.63 (d, 1 H, $^2J_{PH}$ = 5.6 Hz, P′CH=), 7.00−7.64 (m, 20 H, Ph). $^{13}C\{^1H\}$ NMR (CD_2Cl_2): δ = 29.0 (s, C*Me*$_3$), 29.7 (s, C*Me*$_3$), 39.1 (d, $^3J_{PC}$ = 12.6 Hz, *C*Me$_3$), 39.7 (dd, $^3J_{PC}$ = 12.6 Hz, $^4J_{PC}$ = 4.5 Hz, *C*Me$_3$), 71.1 (dd, $^1J_{PC}$ = 65.5 Hz, $^3J_{PC}$ = 1.8 Hz, PCH=), 73.5 (d, $^1J_{PC}$ = 66.4 Hz, PCH=), 128.2−137.0 (m, phenyl-groups resonances), 198.0 (d, $^2J_{PC}$ = 13.5 Hz, =CO), 201.3 (dd, $^2J_{PC}$ = 10.3 Hz, $^3J_{PC}$ = 3.1 Hz, =CO). $C_{36}H_{40}ClNO_3P_2Ru$ (733.2): calcd. C 58.97, H 5.50, Cl 4.84, N 1.91, P 8.45; found C 58.80, H 5.54, Cl 4.79, N 1.95, P 8.66.

Crystal Data for 15: $C_{36}H_{40}ClNO_3P_2Ru$, M = 733.15, crystal size 0.40 × 0.38 × 0.32, monoclinic, space group $P2_1/c$, Z = 4, a = 18.2203(2) Å, b = 10.9932(1) Å, c = 18.3698(3) Å, β = 109.1277(6)°, U = 3476.42(8) Å^3, $\delta_{calcd.}$ = 1.401 g cm^{-3}, T = 293(2) K, $F(000)$ = 1512, Mo-K_α radiation (λ = 0.71069 Å), μ = 0.655 mm^{-1}, 7952 reflections measured in the range 2.28° ≤ θ ≤ 27.50°, 7952 unique (R_{int} = 0.03%) which were used in all calculations. The structure was refined using full-matrix least-squares on F^2 to R_1 = 0.0296, wR_2 = 0.0745, S = 1.071, for 6891 reflections (>2σ) and 398 refined parameters, R_1(all data) = 0.0371, wR_2(all data) = 0.0805, goodness-of-fit on F^2 = 1.071. The sample was studied with a NONIUS Kappa CCD diffractometer with graphite monochromator. The cell parameters were obtained with Denzo and Scalepack.[18] The data collection ($2\theta_{max}$ = 60°, 148 frames via 1.9° ω rotation and 13 s per frame, index ranges 0 ≤ h ≤ 23, 0≤ k ≤ 14, −23 ≤ l ≤ 22) gave 19547 reflections.[19] The data reduction led to 7952 independent reflections from which 6891 had $I > 2\sigma(I)$. The structure was solved with SIR-97 which revealed the non hydrogen atoms.[20] After anisotropic refinement, many hydrogen atoms may be found with Fourier difference calculations. The whole structure was refined with SHELXL97 by full-matrix least-squares methods on F^2 [x, y, z, β_{ij} for Ru, P, Cl, O, C and N atoms; x, y, z in riding mode for H atoms; $w = 1/[\sigma^2(F_0^2) + (0.038P)^2 + 1.72P]$ where $P = (F_0^2 + 2F_c^2)/3$ with the resulting R = 0.029, wR = 0.075 and S = 1.071 (residual around solvent molecules); minimum and maximum final electron density: −0.619 and 0.695 eÅ^{-3}].[21] ORTEP views were prepared with PLATON98.[22]

Crystallographic data (excluding structure factors) for the structure reported in this paper have been deposited with the Cambridge Crystallographic Data Centre as supplementary publication no. CCDC-165881. Copies of the data can be obtained free of charge on application to the CCDC, 12 Union Road, Cambridge CB2 1EZ, U.K. [Fax: (internat.) + 44−1223/336−033; E-mail: deposit@ccdc.cam.ac.uk].

Acknowledgments

This work was supported by the "Centre National de la Recherche Scientifique". The authors are grateful to J.-P. Guégan for NMR technical assistance.

[1] J. C. Jeffrey, T. B. Rauchfuss, *Inorg. Chem.* **1979**, *18*, 2658−2666.
[2] P. Braunstein, D. Matt, Y. Dusausoy, *Inorg. Chem.* **1983**, *22*, 2043−2047.
[3] P. Braunstein, D. Matt, D. Nobel, S.-E. Bouaoud, B. Carluer, D. Grandjean, P. Lemoine, *J. Chem. Soc., Dalton Trans.* **1986**, 415−419.
[4] E. Lindner, U. Schober, R. Fawzi, W. Hiller, U. Englert, P. Wegner, *Chem. Ber.* **1987**, *120*, 1621−1628.
[5] E. Lindner, B. Karle, *Chem. Ber.* **1990**, *123*, 1469−1473.
[6] A. Bader, E. Lindner, *Coord. Chem. Rev.* **1991**, *108*, 27−110.
[7] E. Lindner, A. Möckel, H. A. Mayer, R. Fawzi, *Chem. Ber.* **1992**, *125*, 1363−1367.
[8] E. Lindner, A. Möckel, *Z. Naturforsch., Teil B* **1992**, *47*, 693−696.
[9] H. Werner, A. Stark, M. Schulz, J. Wolf, *Organometallics* **1992**, *11*, 1126−1130.
[10] E. Lindner, A. Möckel, H. A. Mayer, H. Kühbauch, R. Fawzi, M. Steimann, *Inorg. Chem.* **1993**, *32*, 1266−1271.
[11] B. Demerseman, R. Le Lagadec, B. Guilbert, C. Renouard, P. Crochet, P. H. Dixneuf, *Organometallics* **1994**, *13*, 2269−2283.
[12] P. Braunstein, Y. Chauvin, J. Nähring, Y. Dusausoy, D. Bayeul, A. Tiripicchio, F. Ugozzoli, *J. Chem. Soc., Dalton Trans.* **1995**, 851−862.
[13] E. Lindner, S. Pautz, M. Haustein, *Coord. Chem. Rev.* **1996**, *155*, 145−162.
[14] J.-Y. Shen, C. Slugovc, P. Wiede, K. Mereiter, R. Schmid, K. Kirchner, *Inorg. Chim. Acta.* **1998**, *268*, 69−76.
[15] D. W. Krassowski, J. H. Nelson, K. R. Brower, D. Hauenstein, R. A. Jacobson, *Inorg. Chem.* **1988**, *27*, 4294−4307.
[16] R. Eisenberg, C. D. Meyer, *Accounts. Chem. Res.* **1975**, *8*, 26−34
[17] E. Hauptman, M. Brookhart, P. J. Fagan, J. C. Calabrese, *Organometallics* **1994**, *13*, 774−780.
[18] Z. Otwinowski, W. Minor, Processing of X-ray Diffraction Data Collected in Oscillation Mode, *Macromol. Crystallogr. A* **1997**, *276*, 307−326.
[19] *NONIUS KappaCCD Software*, Nonius BV, Delft, The Netherlands, **1999**.
[20] *SIR-97 − A New Tool for Crystal Structure Determination and Refinement*: A. Altomare, M. C. Burla, M. Camalli, G. Cascarano, C. Giacovazzo, A. Guagliardi, A. G. G. Moliterni, G. Polidori, R. Spagna, *J. Appl. Crystallogr.* **1998**, *31*, 74−77.
[21] G. M. Sheldrick, *SHELXL97 − Program for the Refinement of Crystal Structures*, University of Göttingen, Germany, **1997**.
[22] A. L. Spek, *PLATON − A Multipurpose Crystallographic Tool*, University of Utrecht, The Netherlands, **1998**.

Received June 29, 2001
[I01241]

Preparation and Properties of Rh^I and Ir^I Ethylene Complexes Containing the Chiral *P,N*-Chelate Ligand (4*S*)-2-[2-(Diphenylphosphanyl)phenyl]-4-isopropyl-1,3-oxazoline

Daniel Carmona,*[a] Joaquina Ferrer,[a] Elena Lalaguna,[a] Mónica Lorenzo,[a] Fernando J. Lahoz,[a] Sergio Elipe,[a] and Luis A. Oro[a]

Keywords: N,P ligands / Chirality / NMR spectroscopy / Alkene ligands / Iridium / Rhodium

The synthesis and characterization of the chiral complexes [MCl(η^2-C_2H_4)(PN)] [M = Rh (**1**), Ir (**2**)] and [IrCl(η^2-C_2H_4)$_2$(PN)] (**3**) {PN = (4*S*)-2-[2-(diphenylphosphanyl)-phenyl]-4-isopropyl-1,3-oxazoline}, including the X-ray crystal structure of **2**, are reported. The solution behavior has been studied by NMR spectroscopy. For the rhodium complex **1** it is shown that a rotation of the olefin about the Rh-midpoint of the ethylene axis must be operating in solution at ambient temperature. The iridium analogue **2** is, however, stereochemically rigid and interconverts in solution, in the presence of ethylene, with the bis-ethylene derivative **3**.

Introduction

Many important enantioselective catalytic reactions employ transition metal complexes with chiral ligands as catalysts.[1] In this context, chiral chelate phosphino−oxazoline ligands have recently proven to be useful in the control of the enantioselectivity of various metal-catalyzed asymmetric reactions.[2] The pronounced difference in electronic as well as steric properties between the two chelating atoms (hard N and soft P) has been shown to be the key to these reactions. Most of the published work in this field focuses on the catalytic aspects of the reactions and, in some instances, the involved metallic species have not been fully characterized. For example, although mixtures of chiral phosphino−oxazoline ligands and different diolefin rhodium(I) complexes have been successfully applied as catalysts in the hydrosilylation of ketones, the potentially active complexes formed have not been characterized.[2a−2c] Analogously, asymmetric allylic alkylations have been carried out using catalysts prepared in situ from [Ir(μ-Cl)(cod)]$_2$ and phosphino−oxazoline ligands.[2d] However, the crystal structure of a cationic iridium complex [Ir(cod)(PN)]$^+$ {PN = (4*S*)-2-[2-(diphenylphosphanyl)phenyl]-4-isopropyl-1,3-oxazoline, Figure 1} − an efficient catalyst for the enantioselective hydrogenation of prochiral imines − has been determined by X-ray diffraction.[2e] In the present paper, we report the preparation, characterization, and NMR spectroscopic properties of the new rhodium(I) and iridium(I) ethylene complexes [RhCl(η^2-C_2H_4)(PN)] (**1**) and [IrCl(η^2-C_2H_4)$_n$(PN)] [*n* = 1 (**2**), 2 (**3**)] containing the chelating enantiopure ligand PN. In the rhodium complex **1** the ethylene is fluxional. Three motions can be envisaged for coordinated ethylene: i) rotation about the metal−alkene bond, ii) rotation about the carbon−carbon bond, and iii) alkene dissociation.[3] The spectroscopic data indicated that, whereas the olefin rotation takes place at an intermediate rate at room temperature, the intermolecular exchange of ethylene is very slow.

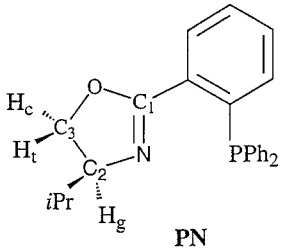

PN

Figure 1. (4*S*)-2-[2-(diphenylphosphanyl)phenyl]-4-isopropyl-1,3-oxazoline (PN)

Results and Discussion

The reaction of the dimers [M(μ-Cl)(η^2-C_2H_4)$_2$]$_2$ (M = Rh,[4] Ir[5]) with PN, in a 1:2 molar ratio, led to an orange precipitate which was analyzed as [MCl(η^2-C_2H_4)(PN)] [M = Rh (**1**), Ir (**2**)]. However, when the mononuclear tetrakis(ethylene)iridium(I) complex [IrCl(η^2-C_2H_4)$_4$][5] was reacted in diethyl ether with PN (1:1 molar ratio, 20 °C), a

[a] Departamento de Química Inorgánica, Instituto de Ciencia de Materiales de Aragón, Universidad de Zaragoza-Consejo Superior de Investigaciones Científicas,
50009 Zaragoza, Spain
Fax: (internat.) + 34-76/761-187
E-mail: dcarmona@posta.unizar.es

Supporting information for this article is available on the WWW under http://www.eurjic.com or from the author.

 © WILEY-VCH Verlag GmbH, 69451 Weinheim, Germany, 2002 1434−1948/02/0101−0259 $ 17.50+.50/0

mixture of the mono- (**2**) and the bis(ethylene) complex [IrCl(η^2-C_2H_4)$_2$(PN)] (**3**) was obtained instead (Scheme 1). Complexes **1** and **2** decomposed slowly as solids, even under an atmosphere of ethylene, over a period of a few days and did so more rapidly in solution (several hours). In solution, at temperatures higher than −10 °C, the pentacoordinate adduct **3** is also unstable to the loss of ethylene.

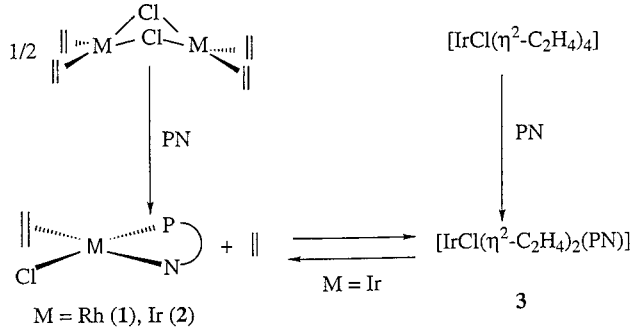

Scheme 1

Only one set of signals was observed in the NMR spectra of compounds **1** and **2**, indicating that, in both cases, one single geometrical isomer exists in solution. The $^{13}C\{^1H\}$ NMR spectrum of the rhodium complex **1**, measured in $CDCl_3$ at −40 °C, showed two doublets at δ = 58.81 and 53.48 for the ethylene carbons, with $^1J_{RhC}$ coupling constants of 14.7 and 11.5 Hz, respectively.[6] Because no $^{13}C-^{31}P$ coupling was observed, we assume that the olefin and the phosphorus atom of the phosphino−oxazoline ligand occupy positions mutually *cis*. NOE measurements at −80 °C in CD_2Cl_2 showed interactions between the ethylene protons at ca. δ = 3.32 and some of the phenyls protons of the phosphino−oxazoline ligand. However, no NOE enhancement of the ethylene protons was observed when the CH_3 protons of the isopropyl oxazoline group were irradiated. These NOE data support the above-mentioned *cis* disposition. In the case of the iridium complex **2**, two sharp singlets at δ = 44.90 and 38.11 were observed, at ambient temperature, for the C_2H_4 carbons. Furthermore, the ^{13}C and ^1H NMR spectra of complex **1** showed a temperature dependence for the signals of the ethylene ligand, clearly indicating fluxionality: in the ^{13}C NMR spectrum, at room temperature, only one broad signal centered at ca. δ = 55.9 (line-width at half-height of 150 Hz) appeared for the C_2H_4 carbons, while the other peaks remained sharp. Upon heating to 45 °C (the rate of ethylene loss precluded measurements at higher temperatures) this signal becomes sharper indicating the equivalence of the two carbons.

The ^1H NMR spectra provided additional information about the behavior of the molecules in solution. Thus, at room temperature, the four ethylene protons of the rhodium complex **1** gave rise, in deuterated chloroform, to a broad resonance centered at ca. δ = 3.0 (line-width at half-height of 150 Hz), which progressively sharpened upon heating (line-width at half-height of 75 Hz at 45 °C). Unfortunately, a sharp time-averaged spectrum was not obtained. On cooling to −40 °C, the broad signal resolved into three broad humps centered at ca. δ = 3.32, 2.25 and 2.08, with respective integrals of 2, 1, and 1 protons. On the other hand, at room temperature, the signal of added ethylene,[7] at ca. δ = 5.4, showed only a slight broadening (line-width at half-height of 24 Hz), indicating that the exchange equilibrium between **1** and free ethylene is slow. An estimate of the barrier for the fluxional process in **1** gives a value of about 54 kJ·mol^{-1}, obtained as the resonances begin to broaden above the limiting low-temperature spectrum.[8] This value is similar to those found for other 16-electron square-planar rhodium(I) or platinum(II) ethylene derivatives such as [Rh(acac)(η^2-C_2H_4)$_2$] (51.3 kJ·mol^{-1})[9] or [Pt(acac)X(η^2-C_2H_4)] [X = Cl (52.3 kJ·mol^{-1}),[10] Br (53.1 kJ·mol^{-1}),[11] in which the fluxional mechanism has been proposed to be the rotation of the olefin about the metal-centroid of the olefin axis. The encountered value for the activation energy definitively ruled out the possibility of intermolecular exchange of the ethene molecule as the main fluxional process because the rhodium−ethylene bond dissociation energy has been measured as ca. 130 kJ·mol^{-1}.[12] On the other hand, a rotation about the carbon−carbon double bond axis would disrupt the coordination bond and the expected energy requirements would be therefore greater than the 54 kJ·mol^{-1} observed.[13] Consequently, to account for the equilibration of the protons and the carbons of the olefin in the rhodium complex, an intramolecular restricted rotation about the rhodium−alkene bond must be operating. The unequivocal detection of this mode of rotation (through the ^{13}C NMR measurements) was facilitated by the chirality of the PN ligand. It should be noted that in symmetrical, nonrigid, square-planar ethylene complexes it is not possible to distinguish between the two intramolecular motions because it is invisible to conventional spectroscopic probes, whereas experiments using complexes with chiral centers allow the distinction between rotation about the metal−alkene or the carbon−carbon axes.

For the iridium complex [IrCl(η^2-C_2H_4)(PN)] (**2**), ^1H NMR measurements revealed that the fluxional movement of the ethylene ligand was slowed down since its proton resonances appeared invariantly as three broad peaks at δ = 2.80, 2.02 and 1.67 (2,1,1 protons, respectively) from ambient temperature to 45 °C. At room temperature, its ^{31}P NMR spectrum consisted of a narrow singlet at δ = 9.42. Ethylene rotation barriers are usually higher in Ir^I compounds than in their Rh^I analogues. Thus, for example, the reported ethylene rotation barrier for [(η^5-C_5H_5)Rh(η^2-C_2H_4)$_2$][14] is 65.6 kcal mol^{-1}, while it is 80.7 kJ·mol^{-1} for the analogous iridium complex;[15] as in our case, no rotation has been observed for related penta- or tetracoordinated complexes of Ir^I.[16] Although it is not clear how the metal and alkene characteristics may affect the relative importance of the σ and the π back-donation,[17] the more basic iridium atom will most probably give rise to a stronger metal−ligand π-interaction. The stronger back-donation to the empty π* orbitals of the ethylene will additionally weaken the C=C bond, and this may be a plausible explanation for the higher barrier for the rotation of the olefin observed in the iridium complexes.

As stated above, the bis(ethylene)iridium complex **3** loses ethylene above −10 °C to form complex **2**. The ^{31}P NMR spectrum of CD_2Cl_2 solutions of **3**, at ambient temperature, displayed a broad signal centered at δ = 8.9 (linewidth at half-height of 73 Hz). This signal sharpened progressively as the temperature increased and became sharp at 45 °C. Below −20 °C, the singlet splits into two broad signals of approximately the same intensity centered at δ = 9.4 and 0.4. The relative intensity of these signals changes with temperature, the amount of the resonance at higher field increasing as the temperature decreases. Thus, at −40 °C the ratio (signal at ca. δ = 9.4 to signal at ca. δ = 0.4) was 2:8 and at −90 °C, 1:9. When ethylene was bubbled through the mixture at −40 °C (2 min) the resonance centered at ca. δ = 9.4 disappeared, whereas the signal at ca. δ = 0.4 remained. Removal of the ethylene atmosphere, by passing a stream of argon, regenerated the signal at δ = 9.4. A reversible equilibrium [Equation (1)] between species **2** (δ = 9.43, −40 °C) and **3** (δ = 0.35, −40 °C) can explain all these observations. As expected, bubbling ethylene or lowering the temperature displaces equilibrium 1 to the right and vice versa.

$$\underset{\mathbf{2}}{[IrCl(\eta^2\text{-}C_2H_4)(PN)]} + C_2H_4 \rightleftharpoons \underset{\mathbf{3}}{[IrCl(\eta^2\text{-}C_2H_4)_2(PN)]} \quad (1)$$

Recently, Milstein et al.[16b] reported that in the related $[IrCl(\eta^2\text{-}C_2H_4)_2L_2]/[IrCl(\eta^2\text{-}C_2H_4)L_2]$ (L = PEt_3) system, the bis(ethylene) adduct is more stable than the mono(ethylene) one. As the authors stated, the strong electron-donating character of the PEt_3 ligands could stabilize the pentacoordinated species. In good agreement with this proposal is the fact that, in the analogous PPh_3 system, the bis(ethylene) adduct is unstable to the loss of ethylene at temperatures higher than −50 °C.[18] Therefore, our results are in agreement with the expected intermediate electron-donating properties of the PN ligand.

We have carried out a crystal X-ray diffraction study of complex **2** in order to establish unambiguously the proposed structure. A molecular representation of the molecule is shown in Figure 2. Selected bond lengths and angles are given in Table 1.

The principal structural feature of **2** is the square-planar geometry about the iridium atom with the coordinated ethylene molecule nearly perpendicular to the best PN−Ir−Cl plane and *cis* to the phosphorus atom of the phosphino−oxazoline, as indicated by the spectroscopic data. As is usually observed in square-planar olefin complexes, the structure shows some deviation from ideal symmetry[19] [max. dev. 0.125(1) Å out of coordination plane for Cl atom]. The ethylene C−C bond is inclined at 84.7(3)° to the coordination plane and its center is 0.044(6) Å out of this plane. The C=C bond length is 1.392(8) Å, quite similar to the bond length found in the closely related square-planar Ir^I−ethylene complex *trans*-$[IrCl(\eta^2\text{-}C_2H_4)(PPh_3)_2]$ [1.376(10) Å][19] and compares well with the range of other reported Ir^I−ethylene complexes [1.35−1.47 Å, mean value 1.411(3) Å].[20] The PN ligand and the iridium atom form a six-membered chelate ring, puckered towards a screw-boat conformation[21] [Q = 0.604(3), F = 19.0(5)°, q = 61.8(5)°], with all three carbon atoms situated above the plane of the complex.

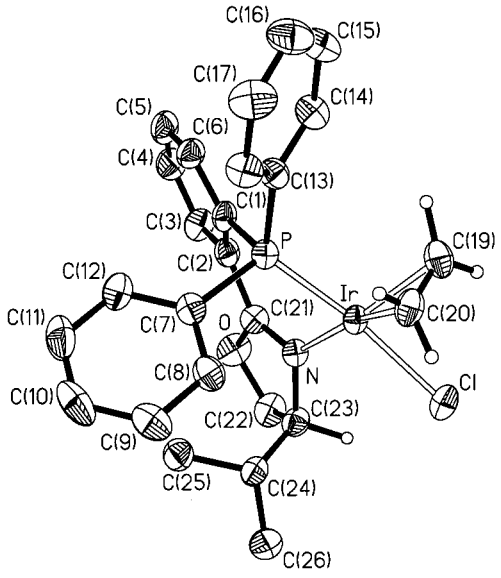

Figure 2. A molecular representation of complex **2** showing the atomic labelling scheme used; hydrogens are shown for the ethylene ligand and the asymmetric carbon of the oxazoline ligand

Table 1. Selected bond lengths (Å) and angles (°) for complex **2**

Bond lengths (Å)		Bond angles (°)	
Ir−N	2.084(4)	N−Ir−P	86.70(12)
Ir−P	2.1741(14)	N−Ir−Cl	90.20(13)
Ir−Cl	2.4170(13)	N−Ir−G[a]	176.3(2)
Ir−C(19)	2.123(6)	P−Ir−Cl	172.90(5)
Ir−C(20)	2.137(5)	P−Ir−G[a]	95.73(17)
Ir−G[a]	2.013(6)	Cl−Ir−G[a]	87.69(17)
C(19)−C(20)	1.392(8)	C(19)−Ir−C(20)	38.2(2)

[a] G represents the midpoint of the olefinic C(19)−C(20) bond.

Experimental Section

General Comments: The compounds described herein were handled with exclusion of air by using standard Schlenk techniques. All solvents were dried by known procedures and distilled under argon prior to use. NMR spectra were recorded on a Varian UNITY, a Varian Gemini 2000, or a Bruker ARX 300 MHz spectrometers. Chemical shifts (δ values) are given relative to TMS (^1H and ^{13}C) or to 85% H_3PO_4 aqueous solution (^{31}P). Coupling constants (J) are given in Hertz. For proton and carbon labelling, see Figure 1. Infrared spectra were recorded as Nujol mulls on polyethylene sheets using a Nicolet 550 spectrometer. The C, H and N analyses were performed on a Perkin−Elmer 2400 CHNS/O analyzer. The precursors $[Ir(\mu\text{-}Cl)(\eta^2\text{-}C_8H_{14})_2]_2$,[22] $[M(\mu\text{-}Cl)(\eta^2\text{-}C_2H_4)_2]_2$ (M = Rh, Ir)[4,5] and $[IrCl(\eta^2\text{-}C_2H_4)_4]$[5] and the ligand (4*S*)-2-[2-(di-

phenylphosphanyl)phenyl]-4-isopropyl-1,3-oxazoline (PN)[23] were prepared according to published procedures.

Synthesis of [RhCl(η²-C_2H_4)(PN)] (1): A solution of PN (237 mg, 0.634 mmol) in dichloromethane (2 mL) was added to a suspension of [Rh(μ-Cl)(η²-C_2H_4)$_2$]$_2$ (124 mg, 0.319 mmol) in diethyl ether (10 mL) at ambient temperature under argon. After 1 h, the resulting solution was concentrated to ca. 5 mL and a solid precipitated. The solvent was removed with a syringe and the solid residue washed with cold Et_2O and dried in vacuo to give **1** as an orange powder. Yield 285 mg (83%). Solid **1** must be stored under ethylene at 4 °C. $C_{26}H_{28}ClNOPRh$ (539.57): calcd. C 57.87, H 5.23, N 2.59; found C 57.85, H 5.37, N 2.44. ^{1}H NMR ($CDCl_3$, room temp.): δ = 8.00−6.98 (m, 14 H, Ph's of PN), 5.46 (ddd, *J* = 2.7, 5.5, 8.7, 1 H, H_g of PN), 4.26 (m, 2 H, H_c and H_t of PN), 2.45 (dsept, *J* = 2.7, 7.0, 1 H, C*H*Me$_2$ of PN), 3.01 (br. s, 4 H, C_2H_4), 0.79 (d, *J* = 7.0, 3 H, Me of PN), 0.05 (d, *J* = 7.0, 3 H, Me of PN). ^{13}C NMR ($CDCl_3$, −40 °C): δ = 161.79 (d, J_{PC} = 7.8, C_1 of PN), 135.2−126.9 (m, Ph's of PN), 70.43 (s, C_2/C_3 of PN), 67.79 (s, C_3/C_2 of PN), 58.81 (d, $^1J_{RhC}$ = 14.71, C_2H_4), 53.48 (d, $^1J_{RhC}$ = 11.54, C_2H_4), 30.83 (s, *C*HMe$_2$ of PN), 18.86 (s, Me of PN), 12.83 (s, Me of PN). ^{31}P NMR ($CDCl_3$, room temp.): δ = 52.5 (d, $^1J_{RhP}$ = 177). IR: ν(CN) 1616 cm^{-1}; ν(CO) 1242 cm^{-1}.

Synthesis of [IrCl(η²-C_2H_4)(PN)] (2): Under argon, a red suspension of the bis(ethylene)iridium(I) dimer [Ir(μ-Cl)(η²-C_2H_4)$_2$]$_2$ [5b] (75 mg, 0.132 mmol) in diethyl ether (15 mL) was cooled to −20 °C and PN was added (98 mg, 0.262 mmol). A deep red solution was immediately formed and after a short time a red powder precipitated. After stirring the solution for one hour, solid **2** was filtered off, washed with diethyl ether and dried in vacuo. Yield 116 mg (70%). Complex **2** must be stored under ethylene at 4 °C. $C_{26}H_{28}ClIrNOP$ (629.11): calcd. C 49.64, H 4.48, N 2.23; found C 50.24, H 4.74, N 2.02. ^{1}H NMR ($CDCl_3$, room temp.): δ = 8.07−7.01 (m, 14 H, Ph's of PN), 5.72 (m, *J* = 2.7, 1 H, H_g of PN), 4.32 (m, 2 H, H_c and H_t of PN), 2.49 (dsept, *J* = 2.7, 7.0, 1 H, C*H*CMe$_2$ of PN), 2.80 (br. s, 2 H, C_2H_4), 2.02 (br. s, 1 H, C_2H_4), 1.67 (br. s, 1 H, C_2H_4), 0.81 (d, *J* = 7.0, 3 H, Me of PN), 0.16 (d, *J* = 7.0, 3 H, Me of PN). ^{13}C NMR ($CDCl_3$, room temp.): δ = 162.10 (d, J_{PC} = 5.96, C_1 of PN), 137.0−127.0 (m, Ph′s of PN), 70.58 (s, C_2/C_3 of PN), 68.35 (s, C_3/C_2 of PN), 44. 90 (s, C_2H_4), 38.11 (s, C_2H_4), 31.09 (s, *C*HMe$_2$ of PN), 18.66 (s, Me of PN), 13.32 (s, Me of PN). ^{31}P NMR ($CDCl_3$, room temp.): δ = 9.42 (s). IR (Nujol): ν(CN) 1616 cm^{-1}; ν(CO) 1245 cm^{-1}.

Preparation of a Mixture of [IrCl(η²-C_2H_4)(PN)] (2) and [IrCl(η²-C_2H_4)$_2$(PN)] (3): Ethylene was bubbled through a pale orange suspension of [Ir(μ-Cl)(η²-C_8H_{14})$_2$]$_2$ (100 mg, 0.112 mmol) in diethyl ether (5 mL) at −20 °C. After stirring for 15 min, PN (83 mg, 0.222 mmol) was added to the resulting colorless solution containing the tetrakis(ethylene)iridium(I) [IrCl(η²-C_2H_4)$_4$]. After 20 min stirring, an orange solid precipitated which was filtered off under an argon atmosphere and dried in vacuo. The solid obtained was characterized as a mixture of **2** and **3**.

3: ^{1}H NMR (CD_2Cl_2, −90 °C): δ = 8.40−6.90 (m, 14 H, Ph's of PN), 5.56 (m, 1 H, H_g of PN), 4.55 (m, 2 H, H_c and H_t of PN), 2.72 (br. s, 1 H, C_2H_4), 2.63 (br. s, 1 H, C_2H_4), 2.44 (m, 2 H, C*H*CMe$_2$ of PN and 1 H of C_2H_4), 2.22 (br. s, 1 H, C_2H_4), 2.04 (br. s, 2 H, C_2H_4), 1.74 (br. s, 2 H, C_2H_4), 0.90 (br. s, 3 H, Me of PN), 0.83 (br. s, 3 H, Me of PN). ^{31}P NMR (CD_2Cl_2, −90 °C): δ = 0.40 (s).

Crystallographic Data Collection and Refinement of the Structure: Crystals suitable for X-ray diffraction were grown by slow diffusion of pentane into a solution of **2** in dichloromethane under an ethylene atmosphere; a red irregular block (0.36 × 0.38 × 0.42 mm) was glued to the end of a glass fiber and mounted on a four-circle diffractometer (Siemens P4) working with graphite-monochromated Mo-K_α radiation (λ = 0.71073 Å) and operating at 173 K. A summary of crystal data, intensity collection procedure, and refinement parameters for the structural analysis is reported in Table 2. Precise lattice parameters were determined by a least-squares fit from 64 centered reflections in the region 25 ≤ 2θ ≤ 38°. Three standard reflections were monitored every 97 measured reflections to check crystal and instrument stability throughout data collection; no significant variations of the intensities were observed. All data were corrected for Lorentz and polarization effects, and a semiempirical (ψ-scan method) absorption correction was also applied.[24] The structure was solved by Patterson and conventional Fourier techniques, and refined by full-matrix least-squares methods on F^2 (SHELXL-97)[25] with initial isotropic thermal parameters. Anisotropic thermal parameters were used in the last cycles of refinement for all non-hydrogen atoms. The hydrogen atoms of the methyl groups were included in calculated positions (C−H = 0.98 Å), and the remaining hydrogens were located in difference Fourier maps; all were included in the refinement riding on their respective carbon atom with four different common isotropic thermal parameters for the distinct types of H atoms. The absolute structure was estimated by the refinement of the Flack parameter, *x* = −0.006(7).[26] Atomic scattering factors, corrected for anomalous dispersion for heavy atoms, were taken from ref.[27] Crystallographic data for the structure reported in this paper have been deposited at the Cambridge Crystallographic Data Centre as supplementary publication no. CCDC-167640. Copies of the data can be obtained free of charge on application to CCDC, 12 Union Road, Cambridge CB2 1EZ, UK [Fax: (internat.) + 44−1223/336−033; Email: deposit@ccdc.cam.ac.uk].

Table 2. Crystal data and data collection and refinement for complex **2**

Formula	$C_{26}H_{28}ClIrNOP$
Mol. wt.	629.11
Space group	orthorhombic, $P2_12_12_1$ (no. 19)
a, Å	10.7695(9)
b, Å	12.9389(11)
c, Å	17.5393(15)
V, Å^3	2444.0(3)
Z	4
D_{calcd}, g cm^{-3}	1.710
m, mm^{-1}	5.66
No. of data collected	6042 (4 ≤ 2θ ≤ 54°)
No. of unique data	5304 (R_{int} = 0.0234)
Min, max transm fact	0.056, 0.081
No. data/params/restraints	5304/286/0
*R*1 (*F*) [$F^2 \geq 4\sigma(F^2)$][a]	0.0262
wR (all data)[b]	0.0622
S[c]	1.027

[a] $R_1(F) = \Sigma||F_o| - |F_c||/\Sigma|F_o|$ for 5036 observed reflections. [b] $wR(F^2) = \{\Sigma[w(F_o^2 - F_c^2)^2]/\Sigma[w(F_o^2)^2]\}^{1/2}$; $w^{-1} = [\sigma^2(F_o^2) + (0.0330P)^2 + 3.98P]$, where $P = [\max(F_o^2, 0) + 2F_c^2)]/3$. [c] $S = \{\Sigma[w(F_o^2 - F_c^2)^2]/(n - p)\}^{1/2}$, where *n* is the number of reflections and *p* the number of parameters.

Acknowledgments

We thank the Dirección General de Investigación Científica y Técnica for financial support (Projects PB96/0845 and BQU2000-0907). S. E. thanks the DGICYT for a fellowship.

[1] [1a] *Catalytic Asymmetric Synthesis* (Ed.: I. Ojima), VCH, Weinheim, **1993**. [1b] R. Noyori, *Asymmetric Catalysis in Organic Synthesis*, John Wiley and Sons, New York, **1994**. [1c] H. Brunner, *Handbook of Enantioselective Catalysis*, VCH, Weinheim, **1993**. [1d] *Comprehensive Asymmetric Catalysis*, (Eds.: E. N. Jacobsen, A. Pfaltz, H. Yamamoto), Springer, **1999**.

[2] [2a] L. M. Newman, J. M. J. Williams, R. McCague, G. A. Potter, *Tetrahedron: Asymmetry* **1996**, *6*, 1597−1598. [2b] T. Langer, J. Janssen, G. Helmchen, *Tetrahedron: Asymmetry* **1996**, *7*, 1599−1602. [2c] A. Sudo, H. Yoshida, K. Saigo, *Tetrahedron: Asymmetry* **1997**, *8*, 3205−3208. [2d] J. Janssen, G. Helmchen, *Tetrahedron Lett.* **1997**, *38*, 8025−8026. [2e] P. Schnider, G. Koch, R. Prétot, G. Wang, F. M. Bohnen, C. Krüger, A. Pfaltz, *Chem. Eur. J.* **1997**, *3*, 887−892. [2f] D. Carmona, C. Cativiela, S. Elipe, F. J. Lahoz, M. P. Lamata, M. P. López-Ram de Víu, L. A. Oro, C. Vega, F. Viguri, *Chem. Commun.* **1997**, 2351−2352. [2g] G. Helmchen, S. Kudis, P. Sennhenn, H. Steinhagen, *Pure Appl. Chem.* **1997**, *69*, 513−518. [2h] G. C. Lloyd-Jones, C. P. Butts, *Tetrahedron* **1998**, *54*, 901−914. [2i] R. Prétot, G. C. Lloyd-Jones, A. Pfaltz, *Pure Appl. Chem.* **1998**, *70*, 1035−1040. [2j] O. Loiseleur, M. Hayashi, M. Keenan, N. Schmees, A. Pfaltz, *J. Organomet. Chem.* **1999**, *576*, 16−22. [2k] G. Helmchen, *J. Organomet. Chem.* **1999**, *576*, 203−214.

[3] B. E. Mann, in *Comprehensive Organometallic Chemistry* (Eds.: G. Wilkinson, F. G. A. Stone, E. W. Abel), Pergamon Press, Oxford, **1982**, vol.3, pp. 103−109.

[4] R. Cramer, in *Inorg. Synth.* (Ed.: G. W. Parshall), McGraw-Hill, New York, **1974**, *15*, pp.14−16.

[5] [5a] A. L. Onderdelinden, A. Van der Ent, *Inorg. Chim. Acta* **1972**, *6*, 420−426. [5b] M. A. Arthurs, J. Bickerton, S. R. Stobart, J. Wang, *Organometallics* **1998**, *17*, 2743−2750.

[6] [6a] A. C. Jesse, M. A. M. Meester, D. J. Stufkens, K. Vrieze, *Inorg. Chim. Acta* **1978**, *26*, 129−136. [6b] M. C. Nicasio, M. Paneque, P. L. Pérez, A. Pizzano, M. L. Poveda, L. Rey, S. Sirol, S. Taboada, M. Trujillo, A. Monge, C. Ruiz, E. Carmona, *Inorg. Chem.* **2000**, *39*, 180−188.

[7] W. J. Oldham, Jr., D. M. Heinekey, *Organometallics* **1997**, *16*, 467−474.

[8] J. V. Faller, in *Encyclopedia of Inorganic Chemistry* (Ed.: R. B. King), Wiley, New York, **1994**, vol. 7, pp. 3914−3933.

[9] M. Herberhold, C. G. Kreiter, G. O. Wiedersatz, *J. Organomet. Chem.* **1976**, *120*, 103−130.

[10] C. E. Holloway, G. Hulley, B. F. G. Johnson, J. Lewis, *J. Chem. Soc. (A)* **1969**, 53−57.

[11] C. E. Holloway, G. Hulley, B. F. G. Johnson, J. Lewis, *J. Chem. Soc. (A)* **1970**, 1653−1658.

[12] R. C. Mehrotra, A. Singh, *Organometallic Chemistry: A Unified Approach*, Wiley, New York, **1992**.

[13] J. V. Faller, B. V. Johnson, *J. Organomet. Chem.* **1975**, *88*, 101−113.

[14] R. Cramer, J. B. Kline, J. D. Roberts, *J. Am. Chem. Soc.* **1969**, *91*, 2519−2524.

[15] L. P. Szajek, R. J. Lawson, J. R. Shapley, *Organometallics* **1991**, *10*, 357−361.

[16] [16a] P. P. Deutsch, R. Eisenberg, *J. Am. Chem. Soc.* **1990**, *112*, 714−721. [16b] M. Aizenberg, D. Milstein, T. H. Tulip, *Organometallics* **1996**, *15*, 4093−4095. [16c] E. G. Lundquist, J. C. Huffman, K. Folting, K. G. Caulton, *Angew. Chem. Int. Ed. Engl.* **1988**, *27*, 1165−1167. [16d] E. G. Lundquist, K. Folting, W. E. Streib, J. C. Huffman, O. Eisenstein, K. G. Caulton, *J. Am. Chem. Soc.* **1990**, *112*, 855−863.

[17] [17a] M. J. S. Dewar, *Bull. Soc. Chim. Fr.* **1951**, *18*, C17. [17b] J. Chatt, L. A. Duncanson, *J. Chem. Soc.* **1953**, 2939−2947. [17c] B. Akermark, S. Glaser, L. Öhrström, K. Zetterberg, *Organometallics* **1991**, *10*, 733−736.

[18] A. Van der Ent, A. L. Onderdelinden, *Inorg. Chim. Acta* **1973**, *7*, 203−208.

[19] R. J. Restivo, G. Ferguson, T. L. Kelly, C. V. Senoff, *J. Organomet. Chem.* **1975**, *90*, 101−109.

[20] F. H. Allen, J. E. Davies, J. J. Galloy, O. Johnson, O. Kennard, C. F. Macrae, E. M. Mitchell, G. F. Mitchell, J. M. Smith, D. G. Watson, *J. Chem. Inf. Comput. Sci.* **1991**, *31*, 187.

[21] D. Cremer, J. A. Pople, *J. Am. Chem. Soc.* **1975**, *97*, 1354−1358.

[22] A. Van der Ent, A. L. Onderdelinden, in *Inorg. Synth.* (Eds.: A. Wold, J. K. Ruff), McGraw-Hill, New York, **1973**, *14*, pp. 94−95.

[23] J. V. Allen, G. J. Dawson, C. G. Frost, J. M. J. Williams, *Tetrahedron* **1994**, *50*, 799−808.

[24] A. C. T. North, D. C. Phillips, F. S. Mathews, *Acta Crystallogr., Sect. A* **1968**, *24*, 351−359.

[25] G. M. Sheldrick, *SHELXL-97 Program for Crystal Structure Solution and Refinement*; University of Göttingen, **1997**.

[26] H. D. Flack, *Acta Crystallogr., Sect. A* **1983**, *39*, 876.

[27] *International Tables For Crystallography*; Kynoch Press, Birmingham, **1974**, vol. IV.

Received July 20, 2001
[I01272]

EurJIC
European Journal of Inorganic Chemistry

February 2002
Issue 2
Pages 265–496

COVER PICTURE

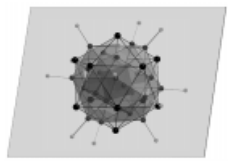

The cover picture shows the penetrating polyhedra of copper and tellurium atoms that are found in the molecular structure of the mixed-valence copper telluride cluster $[Cu_{26}Te_{12}(PEt_2Ph)_{12}]$ (copper atoms: blue; tellurium atoms: black; phosphorus atoms: green; organic groups omitted). Polyhedral substructures are very often found in the cluster frameworks of small or middle-sized, phosphane-ligated copper chalcogenide clusters, since highly symmetric atomic arrangements play a key role in the formation of the most stable isomers. Another approach tomeet the symmetry requirements is realized by large $[Cu_{2n}E_n(PR_3)_m]$ clusters (E = S, Se, Te) that adopt layer-type molecular structures when $2n$ is 70 or more. Hence, they denote the transition to the structural features of binary copper chalcogenide phases. The structural properties of copper sulfide, copper selenide and copper telluride clusters that were developed from single-crystal X-ray analyses, as well as the results of further physico-chemical or quantum-chemical investigations on these substances, are comprehensively discussed in the microreview by D. Fenske et al.

MICROREVIEW

Contents

279 **S. Dehnen, A. Eichhöfer, D. Fenske***

Chalcogen-Bridged Copper Clusters

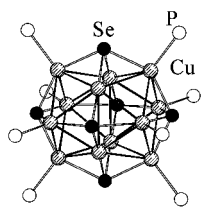

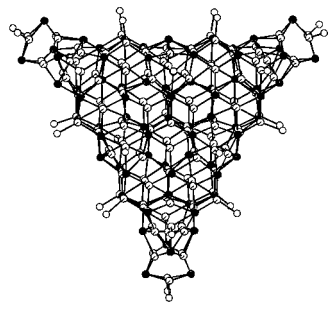

Keywords: Copper / Sulfur / Selenium / Tellurium / Clusters

 © WILEY-VCH Verlag GmbH, 69451 Weinheim, Germany, 2002 1434–1948/02/0202–0269 $ 17.50+.50/0

SHORT COMMUNICATIONS

319 **B. Ronig, I. Pantenburg, L. Wesemann***

Meltable Stannaborate Salts

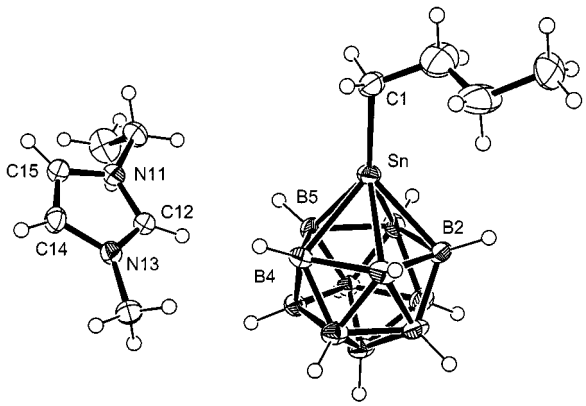

Keywords: Boranes / Ionic liquids / Tin / Cations

323 **K. E. Berg, Y. Pellegrin, G. Blondin, X. Ottenwaelder, Y. Journaux, M. M. Canovas, T. Mallah, S. Parsons, A. Aukauloo***

A Unique Heterotopic Ligand for Sequential Synthesis of Polymetallic Complexes

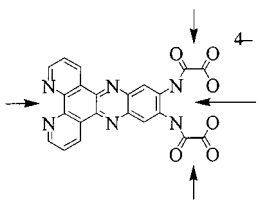

Keywords: Copper / Heterotopic ligands / Iron / Metalations / Oxamate

327 **I.-P. Lorenz,* M. Maier, K. Polborn**

New Organometalated Phosphinato-*O,O′* Ligands in the Planar Eight-Membered Ring $[\{Cp(CO)_2Fe\}t BuPO_2FeCl_2]_2$

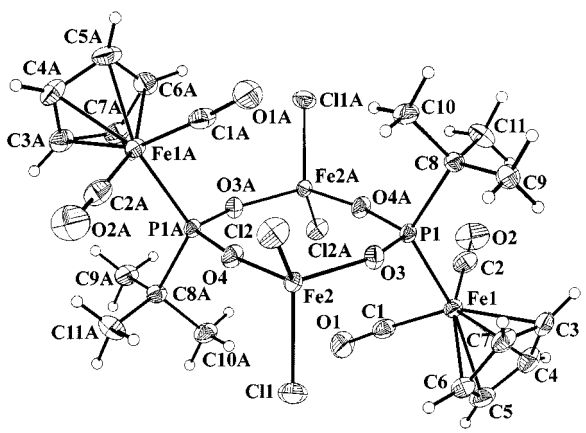

Keywords: Iron / Heterocycles / O ligands / Oxidations / Self-assembly

331 **E. Schulz Lang,* R. A. Zan, C. C. Gatto, R. A. Burrow, E. M. Vázquez-López**

Syntheses and Structures of New Tellurium–Mercury Clusters with Twelve- and Six-Membered Rings

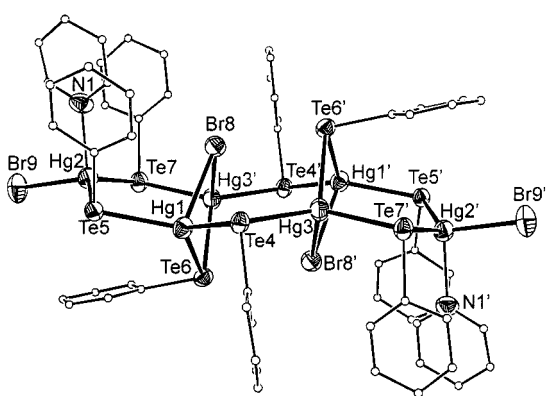

Keywords: Tellurium / Mercury / Cluster compounds / Metallacycles

335 **M. Staffilani, P. Belser,* L. De Cola, F. Hartl***

Redox Control of Conformation and Luminescence of a Dinuclear Ruthenium(II) Complex with a Bis-dipyridophenazine Bridging Ligand

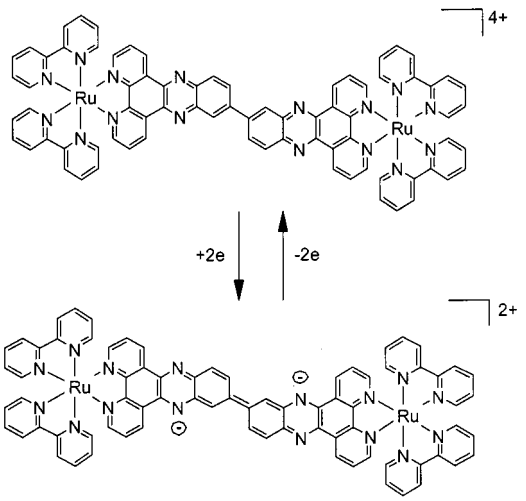

Keywords: Ruthenium / Spectroelectrochemistry / Redox control / Cyclic voltammetry / Electron transfer / Bridging ligands

FULL PAPERS

341 **N. Wiberg,* T. Blank, K. Amelunxen, H. Nöth, H. Schnöckel, E. Baum, A. Purath, D. Fenske**

Ditrielanes $(R_3Si)_2E-E(SiR_3)_2$ and Heterocubanes $(R_3Si)_4E_4Y_4$ (R_3Si = tBu$_3$Si, tBu$_2$PhSi; E = Al, Ga, In, Tl; Y = O, Se)

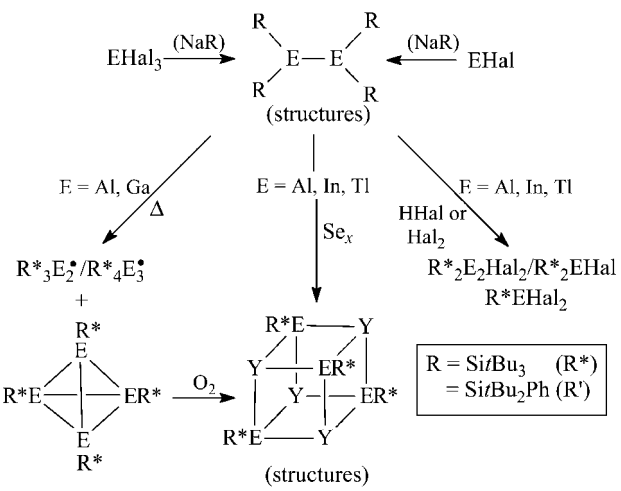

Keywords: Aluminium / Ditrielanes / Gallium / Heterocubanes / Indium / Silicon / Thallium

351 **N. Wiberg,* T. Blank, M. Westerhausen, S. Schneiderbauer, H. Schnöckel, I. Krossing, A. Schnepf**

Disodium Tetrasupersilyltetragallanediide $Na_2Ga_4R^*_4\cdot 2THF$ (R^* = SitBu$_3$) – Preparation of a Novel Gallium Cluster Compound via Dichlorodisupersilyldigallane $R^*_2Ga_2Cl_2$

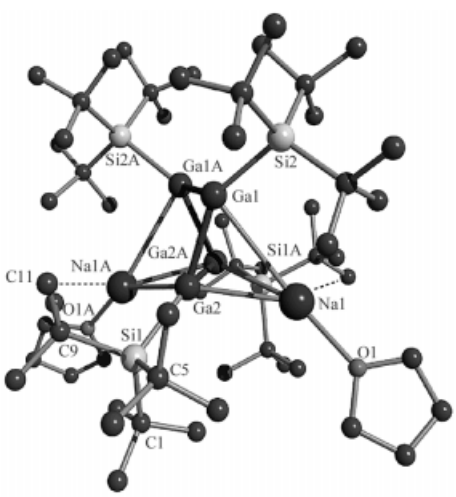

Keywords: Clusters / Gallium / Oligogallanes / Silicon / Sodium

357 **K. Chichak, U. Jacquemard, N. R. Branda***

The Construction of (Salophen)ruthenium(II) Assemblies Using Axial Coordination

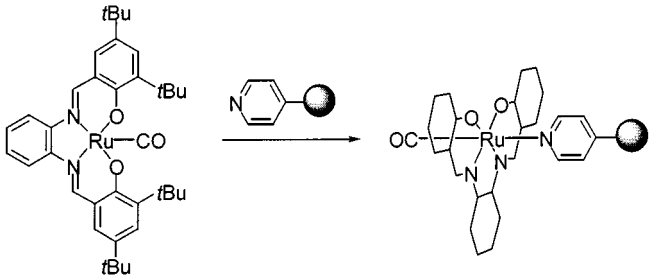

Keywords: Axial coordination / N,O ligands / Ruthenium / Schiff bases / Supramolecular chemistry

369 **A. C. G. Hotze, M. E. T. Broekhuisen, A. H. Velders, K. van der Schilden, J. G. Haasnoot, J. Reedijk***

Unusual Coordination of the Rare Neutral Imine Tautomer of 9-Methyladenine Chelating in the *N*6,*N*7-Mode to Ruthenium(II) Complexes

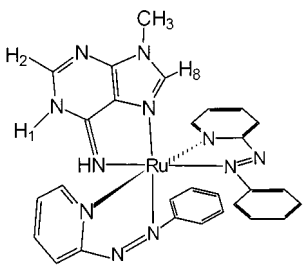

Keywords: Ruthenium / Cytotoxicity / NMR spectroscopy / DNA model bases

377 **M. Hoogenraad, K. Ramkisoensing, S. Gorter, W. L. Driessen, E. Bouwman, J. G. Haasnoot, J. Reedijk,* T. Mahabiersing, F. Hartl**

Electrochemical and Catalytic Properties of Novel Manganese(III) Complexes with Substituted 2-(2′-Hydroxyphenyl)oxazoline Ligands − X-ray Structures of Tris[5-methyl-2-(2′-oxazolinyl)-phenolato]manganese(III) and Tris[5-chloro-2-(2′-oxazolinyl)phenolato]manganese(III)

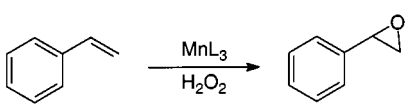

Keywords: Manganese / Spectroelectrochemistry / Cyclic voltammetry / Homogeneous catalysis / Oxidations

389 **M. Westerhausen,* T. Bollwein, N. Makropoulos, S. Schneiderbauer, M. Suter, H. Nöth, P. Mayer, H. Piotrowski, K. Polborn, A. Pfitzner**

Zinc- and Tin-Mediated C−C Coupling Reactions of Metalated (2-Pyridylmethyl)(trialkylsilyl)amines − Mechanistic, NMR Spectroscopic, and Structural Studies

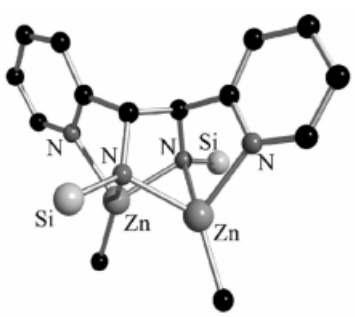

Keywords: Amides / C−C coupling / Magnesium / Metalations / Metallacycles / Pyridyl ligands / Tin / Zinc

405 **E. Polo,* A. Barbieri, S. Sostero, M. L. H. Green**

Zirconocenes as Photoinitiators for Free-Radical Polymerisation of Acrylates

Keywords: Metallocenes / Zirconium / Photolysis / Homogeneous catalysis / Polymerizations

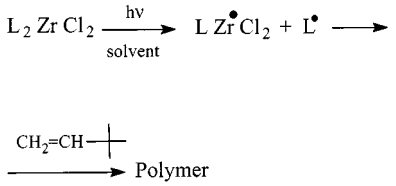

411 **R. Blom,* O. Swang**

Dynamic Behaviour of Tris(2-methylallyl)-chromium − NMR and DFT Results

Keywords: Chromium / Allyl complexes / Paramagnetism / NMR spectroscopy / Density-functional calculations

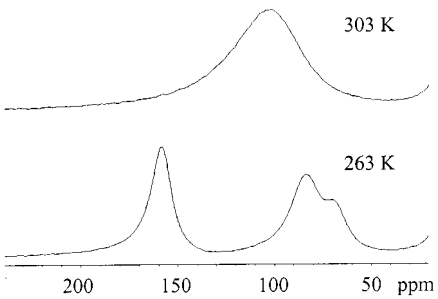

417 **M. Galanski,* W. Zimmermann, M. Berger, C. Baumgartner, G. Giester, B. K. Keppler***

Carboxylation of 2-Hydroxyethyl-Substituted Tetrachloro(ethane-1,2-diamine)platinum(IV) Complexes − A New Synthetic Approach to Anticancer Platinum Compounds

Keywords: Platinum / Structure elucidation / Carboxylation / Antitumor agents

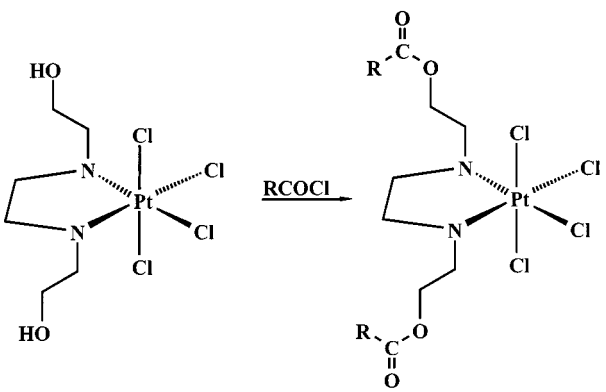

423 **N. Navon,* A. Burg, H. Cohen, R. van Eldik, D. Meyerstein**

Ligand Effects on the Reactivity of $Cu^{I}L$ Complexes Towards $Cl_3CCO_2^-$

Keywords: Copper / Ligands / Redox chemistry / Kinetics / Reaction mechanisms

$$Cu(I)L^i/Cu^-_{aq} + Cl_3CCOO^- \longrightarrow (L^iCu^{II}Cl)/(CuCl)^+ + {}^{\cdot}CCl_2COO^-$$

$$Cu(I)L^i/Cu^-_{aq} + {}^{\cdot}CCl_2COO^- \longrightarrow (L^iCu^{II}\text{-}CCl_2CO_2^-)/(Cu^{II}\text{-}CCl_2CO_2^-)$$

$$(L^iCu^{II}\text{-}CCl_2CO_2^-)/(Cu^{II}\text{-}CCl_2CO_2^-) + H_3O^+ \longrightarrow Cu^{2+}_{aq} + HCCl_2COO^- + L^i$$

$$(Cu(II)L^i)^+/Cu^{2+}_{aq} + {}^{\cdot}CCl_2COO^- \longrightarrow (L^iCu^{III}\text{-}CCl_2CO_2^-)/(Cu^{III}\text{-}CCl_2CO_2^-)^+$$

$$(L^iCu^{III}\text{-}CCl_2CO_2^-)/(Cu^{III}\text{-}CCl_2CO_2^-)^+ + Cu(I)L^j/Cu^+_{aq} \longrightarrow (L^iCu^{II}\text{-}CCl_2CO_2^-)/(Cu^{II}\text{-}CCl_2CO_2^-) + Cu(II)L^{i+}/Cu^{2+}_{aq}$$

431 **G. Minghetti,* A. Doppiu, S. Stoccoro, A. Zucca, M. A. Cinellu, M. Manassero,* M. Sansoni**

Reactivity of $Ph_2P(O)py$-2 with Platinum(II) Alkyl Derivatives − Building-up of a Chiral Phosphorus Atom through C,N-Cyclometallation

Keywords: Platinum / N ligands / Cyclometallation / Alkyl derivatives / Crystal structure

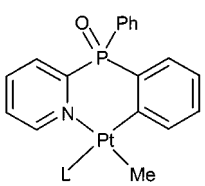

439 **P. Pelagatti,* A. Bacchi, M. Carcelli, M. Costa, H.-W. Frühauf, K. Goubitz, C. Pelizzi, M. Triclistri, K. Vrieze**

Methyl- and Acetylpalladium(II) Complexes Containing a P,N,O Tridentate Hydrazone Ligand

Keywords: Hydrazones / Insertions / Palladium / Tridentate ligands

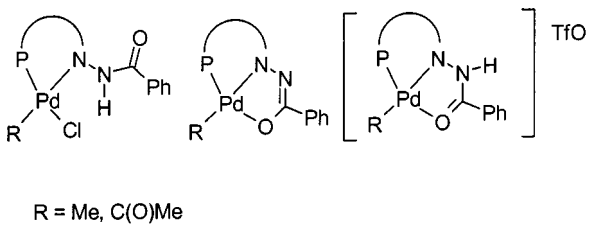

447 **T. Moriuchi, M. Nishiyama, T. Hirao***

A Zinc(II) Complex Composed of a Tridentate Ligand Bearing Podand Pyrenyl Moieties

Keywords: Coordination modes / N ligands / Crystal engineering / Zinc / Receptors

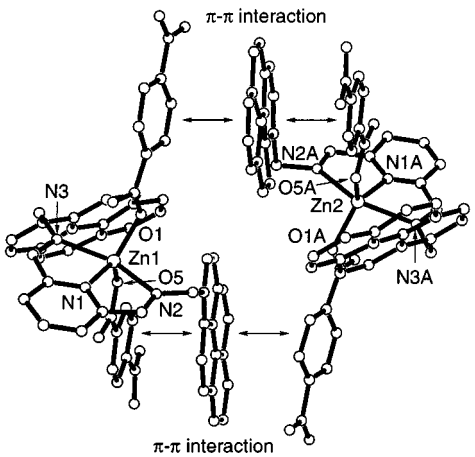

453 **W. J. Evans,* D. G. Giarikos, M. A. Greci, J. W. Ziller**

Direct Synthesis of Heterometallic Europium/Barium Complexes: $H_2[Eu_2Ba_6O_2(OiPr)_{16}(THF)_4]$ and $EuBa_2(OC_6H_4Me\text{-}4)_7(diglyme)_2(DME)$

Keywords: Europium / Barium / Heterometallic complexes / Isopropoxide complexes

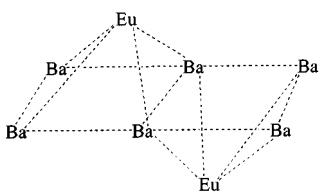

457 **T. Sciarone, J. Hoogboom, P. P. J. Schlebos, P. H. M. Budzelaar, R. de Gelder, J. M. M. Smits, A. W. Gal***

(Diene)rhodium and -iridium Complexes of Pyridinophane Ligands

Keywords: Diene ligands / Fluxionality / Iridium / Oxidations / Rhodium

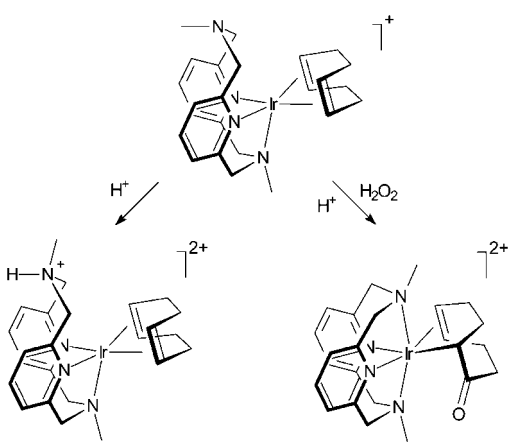

465 **M. Vázquez, M. R. Bermejo,* M. Fondo, A. García-Deibe, A. M. González, R. Pedrido**

New Helical Complexes with a Bis(bidentate) Schiff Base Ligand Containing a Flexible Spacer

Keywords: Supramolecular chemistry / Helical structures / Schiff bases / Electrochemistry

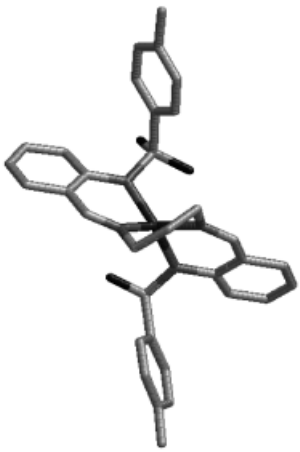

473 **B. Keita, I. M. Mbomekalle, L. Nadjo,* R. Contant**

Compared Behaviours of Dawson-Type Tungstodiarsenates and -diphosphates

Keywords: Polyanions / Tungsten / Arsenic / Phosphorus / Electrochemistry

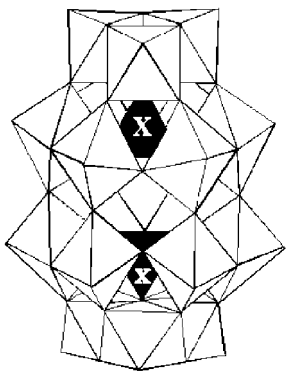

481 **M. Bakir**

Synthesis, Characterization and Structural Studies on the First Rhenium Complex with Di(2-pyridyl) Ketone 2,4-Dinitrophenylhydrazone (dpkdnph), *fac*-[$Re(CO)_3$(dpkdnph)Cl]

Keywords: Rhenium / Carbonyl ligands / Hydrazones

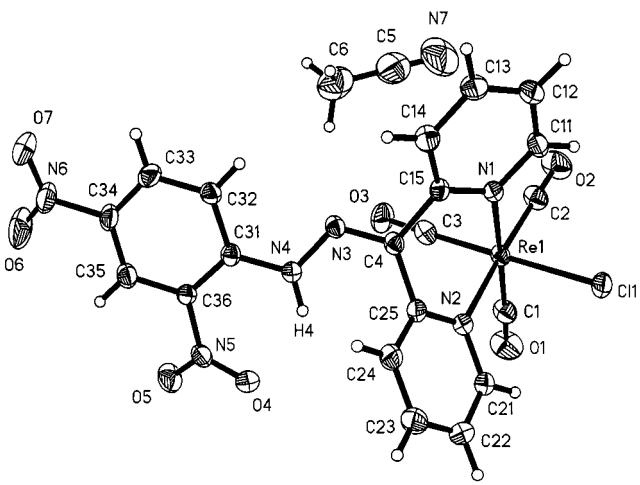

487 **S. Striegler,* E. Tewes**

Investigation of Sugar-binding Sites in Ternary Ligand−Copper(II)−Carbohydrate Complexes

Keywords: Carbohydrates / Copper / Molecular imprinting / N ligands / UV/Vis spectroscopy

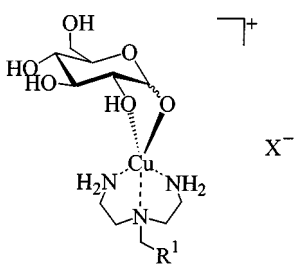

R^1 =

X^- = OH^- or $HCOO^-$

Chalcogen-Bridged Copper Clusters

Stefanie Dehnen,[a] Andreas Eichhöfer,[b] and Dieter Fenske*[a]

Dedicated to Professor Günter Schmid on the occasion of his 65th birthday

Keywords: Copper / Sulfur / Selenium / Tellurium / Clusters

The investigation of coinage metal molecular clusters bridged by chalcogen atoms represents an area of ever increasing activity in recent chemical and material science research. This is largely due to the relatively high ionic and even higher electric conductivity of binary coinage metal chalcogenides, which leads to properties intermediate between those of semiconducting and metallic phases. In addition, the size-dependency of the chemical, physical, and structural properties of substances on going from small molecules to bulk materials is of general interest. Approaches towards the synthesis and investigation of such clusters have included the study of colloidal nanoparticles with a narrow size distribution, as well as the formation and isolation of crystalline cluster compounds amenable to structural determination by single-crystal X-ray diffraction analysis. Irrespective of the chosen synthesis route, the molecules have to be kinetically protected from decomposition to the thermodynamically favored binary phases by a suitable ligand sphere, often consisting of tertiary phosphane molecules, or a combination of phosphanes and organic groups. In this report, we concentrate on the syntheses and structural as well as physical properties of ligand-stabilized, chalcogen-bridged copper clusters, which have been comprehensively studied by means of experimental and quantum chemical investigations.

[a] Institut für Anorganische Chemie der Universität Karlsruhe (TH),
Engesserstraße, Geb. 30.45, 76128 Karlsruhe, Germany
Fax: (internat.) +49 (0)721/608-7021
E-mail: Dieter.Fenske@chemie.uni-karlsruhe.de
[b] Institut für Nanotechnologie, Forschungszentrum Karlsruhe GmbH,
Postfach 3640, 76021 Karlsruhe, Germany
Fax: (internat.) +49 (0)7247/82-6368

1. Introduction

The synthesis of chalcogen-bridged molecular clusters of the coinage metal elements represents an area of ever increasing activity in recent chemical and material science research. This can be mainly ascribed to two aspects. Firstly, binary coinage metal chalcogenides exhibit relatively high

Andreas Eichhöfer (left) was born in Hünfeld, Germany, in 1964. He received his diploma in 1991, and subsequently graduated in 1993 in the group of Prof. D. Fenske at the university of Karlsruhe with a doctoral degree on metal-phosphorous cluster complexes. He then moved to the group of Prof. G. Fritz at the same institute to work on carbosilanes as precursor compounds for the fabrication of SiC fibers. After that he returned to his previous group and became a research scientist at the Institute of Nanotechnology at the Forschungszentrum Karlsruhe in 1999, where he is currently investigating the syntheses and properties of semiconductor cluster compounds.

Stefanie Dehnen (center) was born in Gelnhausen, Germany, in 1969. She obtained her diploma from the University of Karlsruhe in 1993 and her doctoral degree in 1996 under the supervision of Prof. D. Fenske on experimental and theoretical investigations of copper sulfide and copper selenide clusters. After a postdoctoral stay with Prof. R. Ahlrichs (1997) she returned to the inorganic chemistry department at the University of Karlsruhe where she is presently preparing her Habilitation. In 1997, she was awarded a Feodor-Lynen-Stipendium of the Alexander-von-Humboldt-Stiftung, and in 1998, she received a Margarete-von-Wrangell-Habilitations-Stipendium of the state of Baden-Württemberg. Her current research interests comprise the synthesis, structural elucidation and chemical reactivity of binary or ternary polyanions of main group elements.

Dieter Fenske (right) was born in Dortmund, Germany, in 1942. He studied chemistry at the University of Münster where he also received his doctoral degree in 1973 with Prof. H. J. Becher. After the completion of his Habilitation at the University of Münster in 1978, he became Professor of Inorganic Chemistry at the University of Karlsruhe in 1981. Five years later, he was offered a Chair of Inorganic Chemistry at the University of Frankfurt, from where he returned to the University of Karlsruhe in 1988 to become Chair of Inorganic Chemistry. He received offers for the same position from the Universities of Marburg and Münster and is a laureate of the Leibniz Award and the Wilhelm Klemm Award. In 1998 he became Director of the Institute of Nanotechnology at the Forschungszentrum Karlsruhe. His research field concerns the synthesis, structures, and properties of main group element-bridged clusters of transition metals, especially group 8–10 elements.

MICROREVIEWS: This feature introduces the readers to the authors' research through a concise overview of the selected topic. Reference to important work from others in the field is included.

 © WILEY-VCH Verlag GmbH, 69451 Weinheim, Germany, 2002 1434–1948/02/0202–0279 $ 17.50+.50/0

ionic[1] and even higher electric[2] conductivity in the solid state, leading to properties intermediate between those of semiconducting and metallic phases. Secondly, the size-dependence of the chemical, physical, and structural properties of substances on going from small molecules to bulk materials is of general interest.[3] Several research groups have concentrated on the synthesis and properties of colloid nanoparticles with narrow cluster size distributions.[4] Another approach is the formation and isolation of crystalline cluster compounds suitable for single-crystal X-ray diffraction analysis. In both cases, the molecules have to be kinetically protected from further reaction to the thermodynamically favored binary phases. Therefore, a ligand sphere coordinating to the outer metal or chalcogen atoms is necessary; in most cases this consists of tertiary phosphane molecules or a combination of phosphanes and organic groups.

In this paper, we focus on ligand-stabilized, chalcogen-bridged copper clusters, which have hitherto been the most frequently studied. Experimental[5−33] and quantum chemical[34−37] investigations have been undertaken during the last decade in order to study the transition from the definitely non-metallic Cu_2E monomer (E = S, Se, Te) to the bulk Cu_2E.[38−40] From a synthetic point of view, the most important result was the elucidation of the close relationship between the chosen reaction conditions and the formation of the desired products, together with the use of this knowledge in the synthesis of different cluster types.[9−31] Furthermore, the great number of isolated and structurally characterized cluster compounds and the comprehensive computational work[34−37] in this area has allowed the delineation and rationalization of size-dependent structure principles for these molecules. Last but not least, various calculations and measurements have been carried out to obtain insights into the physical properties of the cluster materials.[32,33]

2. General Synthetic Routes

The compounds are − with some exceptions − highly air- and moisture-sensitive. Therefore, all reaction steps have to be carried out under strict exclusion of air and moisture in a high purity dried nitrogen atmosphere by employing standard Schlenk-line techniques on a double-manifold vacuum line. All solvents must be dried and freshly distilled prior to use.

Most chalcogen-bridged copper compounds have been synthesized according to the following general reaction pathway and possess one of the given formulae (Scheme 1).

The CuX-to-phosphane ratio, the counterion X of the copper salt, and especially the nature of the phosphane used, are very important. In the first step, the phosphane complexes the copper salt to generate a reactive species, the reactivity of which can be subtly regulated by the choice of X and PR_2R'. Furthermore, the driving force of the reactions is the formation of thermodynamically stable $SiMe_3X$ and can thus be controlled by the choice of X according to

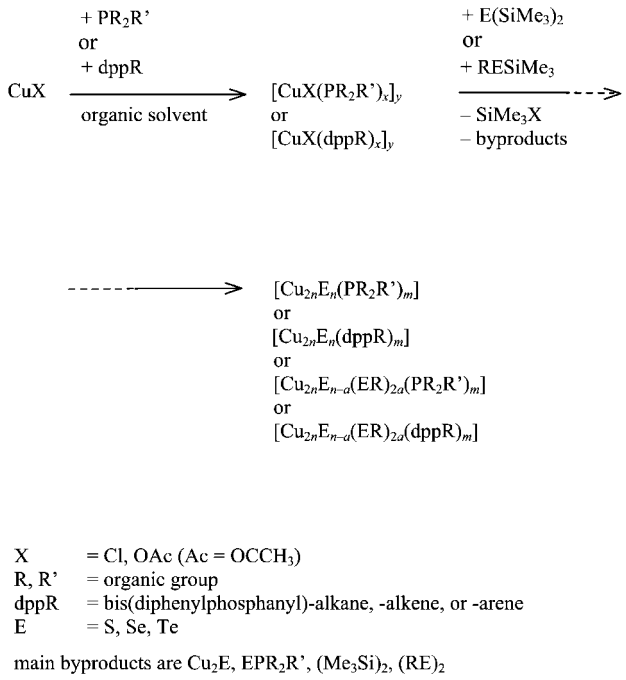

Scheme 1. General synthetic route for the formation of phosphane-ligated chalcogen-bridged copper clusters

the bond strength of the Si−X bond.[41] Finally, the steric demand of the PR_2R' molecules on the cluster surface − as measured by Tolman's cone angle θ[42] (see Table 1) − is related, although not linearly, to the final size and shape of the copper chalcogenide core.

Table 1. Values of Tolman's cone angle θ for phosphanes PR_2R' used in the syntheses of copper chalcogenide clusters (ref.[42])

PR_2R'	θ [°]
PMe_2Ph	127
PEt_3	132
$PnPr_3$	132
PEt_2Ph	136
$PPhnPr_2$	136
$PEtPh_2$	141
PPh_2nPr	141
PPh_3	145
$PMeiPr_2$	146
$PCyPh_2$	153
$PiPr_3$	160
$PtBu_2Me$	161
$PnButBu_2$	165
PCy_3	170
$PtBu_3$	182

In addition, other reaction conditions such as the chosen solvent, the reaction temperature, or the temperature program strongly influence the course of the synthesis. It has been shown that, under similar reaction conditions, the use of derivatives $RE(SiMe_3)$ (R = organic group) leads to the formation of completely different structures to those reactions employing $Se(SiMe_3)_2$. The reason for this is the different reactivity of the reactants as well as partly incomplete Se−C bond cleavage. Thus, some RE^- fragments are bound

at the periphery of the cluster framework, acting as terminal ligands in addition to the phosphane groups.

Regarding the given general formula of the products, the copper atoms can be assigned a formal charge of 1+ while the chalcogen ligands are formally viewed as E^{2-} or RE^{-} groups. However, some of the selenium-bridged species and many copper telluride clusters form non-stoichiometric compounds that display mixed-valence metal centers, leading either to an overall electron deficiency or an electron excess. This corresponds to observations made for the binary phases Cu_2S, $Cu_{2-x}Se$, and $Cu_{2-x}Te$.[38−40]

Even though most ligated copper chalcogenide clusters have been prepared as described herein, it should be mentioned that other synthetic routes to ligated or "naked" $[Cu_{2n}E_n]$ cluster compounds have been studied. Besides syntheses in solvent environments[5−31] that led to the formation of, for example, $[PhMe_3As]_4[Cu_8\{S_2C_2(CN)_2\}_6]$,[5] $(Me_4N)_2[Cu_5(SPh)_7]$,[6] $(Ph_4P)_4[Cu_{12}S_8]$,[7] or $[Cu_6\{Se(2,4,6\text{-}iPr_3C_6H_2)\}_6]$,[8] ligand-free particles have been obtained and characterized by means of laser ablation techniques in combination with mass spectrometry.[32]

3. Synthesis Details, Molecular Structures, and Stabilities

3.1. Sulfur-Bridged Copper Clusters

3.1.1. Syntheses

The reactions yielding the phosphane-ligated, sulfur-bridged copper clusters that have been isolated and structurally characterized to date are summarized in Scheme 2, in order of increasing cluster size.

Sulfur-bridged clusters could not be obtained by reactions starting from copper halides. The reason for this is the lower reactivity of primary copper acetate-phosphane complexes compared to the analogous halide complexes, as a result of the chelating acetate ligands that can be displaced in a double-step substitution of selenium ligands for oxygen.[43] Reactants of higher reactivity lead directly to the formation and precipitation of Cu_2S, even at low temperatures. The kinetic restrictions at the beginning of the synthesis are in addition to those at the end of the cluster growth. The phosphane molecules have to provide a certain minimum steric demand and it has not yet proved possible to generate sulfur-bridged copper clusters with PMe_3 ligands.

3.1.2. Structures and Stabilities

Half of the total number of known copper sulfide clusters have the general formula $[Cu_{12}S_6(PR_2R')_8]$, which represents the smallest known copper chalcogenide $[Cu_{2n}E_n]$ cluster core (**1**−**5**).[13,15,18] The respective molecular structures correspond to one of two possible isomers that can both be derived from a highly symmetric polyhedron of metal and chalcogen atoms. The highly symmetrical conformation is the reason for the strong preference for "Cu_{12}" species. An

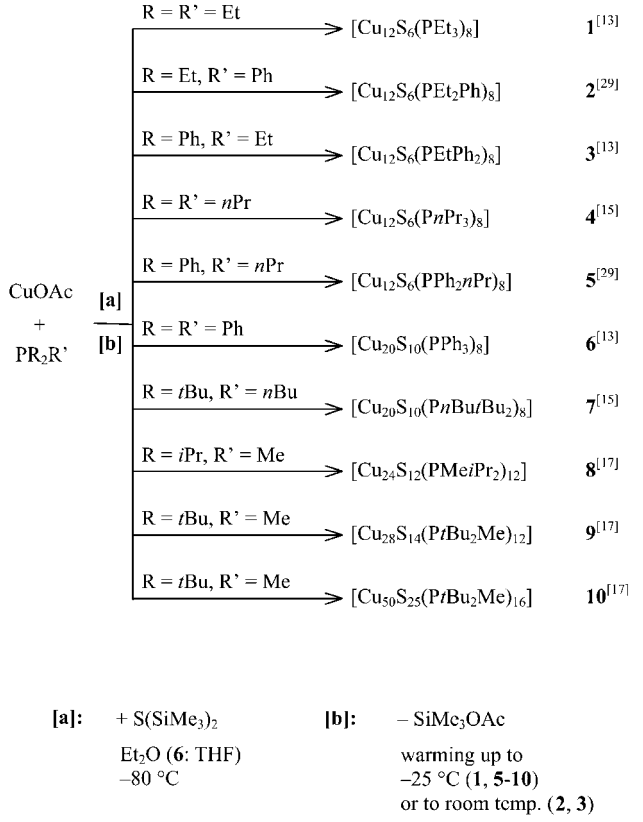

Scheme 2. Survey of the synthesis of sulfur-bridged copper clusters protected by terminal phosphane ligands

S_6 octahedron is penetrated by a Cu_{12} cubooctahedron. However, the latter is distorted as a result of the coordination of the phosphane ligands, as there is only enough space for eight rather than twelve phosphane molecules at the cluster surface within a reasonable Cu−P bond length. Different distributions of the terminal ligands with respect to the cubooctahedron atoms lead to the formation of isomers I or II, respectively. Both cluster structures, as well as a computed hypothetical "naked", undistorted $[Cu_{12}S_6]$ core,[35] are shown in Figure 1.

In the "Cu_{12}" clusters, two coordination modes of the copper atoms can be observed. The four copper atoms that are not bound by phosphane ligands are almost linearly coordinated by sulfur atoms and are positioned either in the equatorial Cu_4 ring of the cubooctahedron (I) or two each reside in the top and bottom Cu_4 planes (II). The eight remaining copper atoms bound by the PR_2R' groups are surrounded in an almost trigonal-planar manner by two sulfur neighbors and one phosphorus atom. The phosphane molecules can be thought of as "pulling" their respective metal atoms out of the basic Cu_{12} polyhedron, whereas the "naked" copper atoms are slightly displaced towards the cluster center. All the sulfur ligands act as μ_4-bridges between copper atoms. In molecules of type I, the eight phosphorus atoms are arranged around the cluster surface so as to form an approximate cube, whereas in the other isomer, if the phosphorus atoms are formally linked, a P_8 Δ-dodecahedron is obtained. Both arrangements are among the most stable polyhedra of eight points on the surface of a sphere.

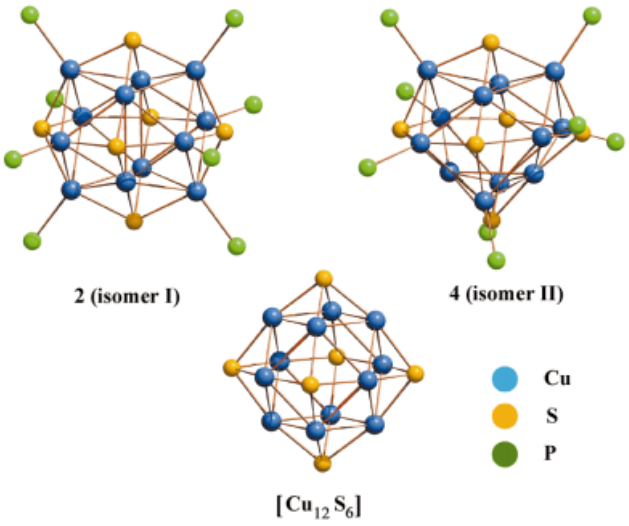

Figure 1. Molecular structures of $[Cu_{12}S_6(PEt_2Ph)_8]$ (**2**) and $[Cu_{12}S_6(PnPr_3)_8]$ (**4**) (without organic groups) and of a calculated "naked" $[Cu_{12}S_6]$ core

Quantum chemical investigations with the program system TURBOMOLE,[44,45] employing MP2[46] and DFT[47] methods, were carried out assigning the highest possible symmetry in order to explain the obvious experimental preference for type I clusters over those of type II.[36] For model ligands PH_3 (MP2 and DFT; highest possible symmetry: D_{4h} for type I or S_4 for type II), both structures representing local minima on the energy hypersurface were found to be isoenergetic within the limits of the methods used. On calculating clusters $[Cu_{12}S_6(PR_3)_8]$ with R = Et or R = Pr according to both structural isomers (DFT; highest possible symmetry: C_{4h} or S_4), i.e. one real (**1**, **4**) and one hypothetical species each, one does not find a direct correlation between the substituents on the phosphorus atoms and the thermodynamic stabilization. Thus, further kinetic effects such as solubility and mobility of the organic groups at the experimental temperatures (>> 0 K) probably play key roles in the choice of isomers. The fact that the same cone angle values are found for PEt_3 and $PnPr_3$ underlines this conclusion (see Table 1).

Another pair of isomers is formed in the presence of the sterically more demanding phosphanes PPh_3 or $PnButBu_2$, where there are 20 copper atoms in the cluster framework.[13,15] The respective molecular structures of **6** (type I) and **7** (type II) are shown in Figure 2.

Again, the positions of the eight Cu−P groups determine the shapes of the clusters, the cores of which can be regarded as distortions of the formal condensation product of two of the $Cu_{12}S_6$ units shown in Figure 1. This relationship is particularly clear when "Cu_{12}" and "Cu_{20}" clusters of type I are compared. After the loss of one apical sulfur ligand and four phosphane molecules from each, as well as one Cu_4 ring, a $[Cu_8S_5(PR_3)_4]$ and a $[Cu_{12}S_5(PR_3)_4]$ fragment are fused in such a way that two face-sharing fragments of the "Cu_{12}" cubooctahedra of cluster type I (idealized symmetry of the Cu−S−P core: D_{4h}) are obtained in

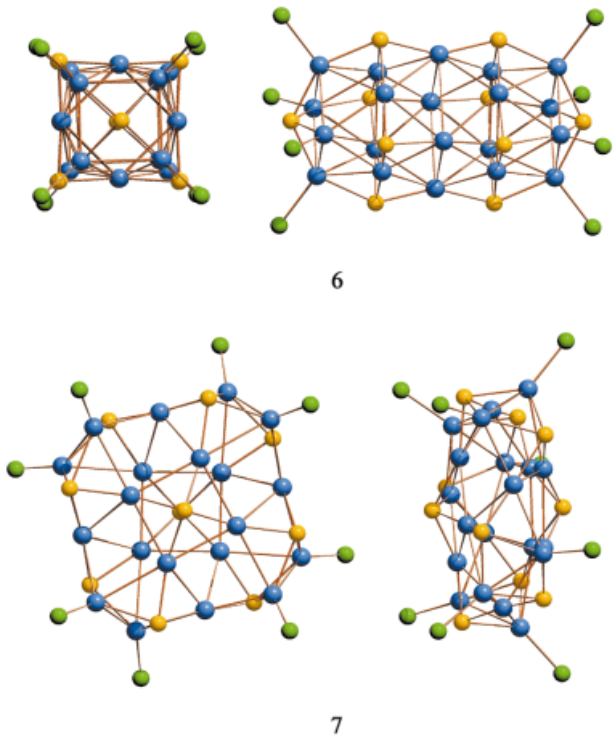

Figure 2. Molecular structures of $[Cu_{20}S_{10}(PPh_3)_8]$ (**6**) (top) and $[Cu_{20}S_{10}(PnButBu_2)_8]$ (**7**) (bottom) (without organic groups), each shown both along and perpendicular to the $S_{apical}-S_{apical}$ axis

the case of **6**. In **7** (type II, idealized symmetry of the Cu−S−P core: D_4), the ligands do not occupy coordination sites at the two outer Cu_4 rings but bind to the second and fourth rings resulting in the oblate and slightly twisted isomer. The respective S_{10} polyhedra are a bicapped tetragonal prism (**6**) and a highly compressed, bicapped tetragonal anti-prism (**7**). A tetragonal prismatic P_8 arrangement is found in **6**, while a P_8 tetragonal anti-prism is found in **7**. Coordination numbers and geometries are similar to the situation in the "Cu_{12}" species.

The structural differences between pairs of isomeric copper sulfide clusters can clearly be ascribed to the coordination sites of the phosphane groups, which are directed towards the respective copper atoms by their own steric demand to give the best protecting ligand shell around the Cu−S core. If different phosphanes display the same cone angle, isoenergetic structural isomers result, so that further kinetic aspects will dominate, as shown for the "Cu_{12}" species. If the PR_2R' groups are so small that even variation of the ligand positions does not result in a complete ligand sphere, or if the phosphane molecules are so bulky that one would have to have one fewer ligand, resulting in a non-ideal P_n polyhedron and an incomplete ligand sphere, the cluster growth continues until the optimum ratio of $[Cu_{2n}S_n]$ core and PR_2R' number and arrangement is achieved.

A continuation of the cluster growth also takes place in the presence of $PMeiPr_2$. Being too bulky for an arrangement of eight molecules around a $[Cu_{12}S_6]$ core and not generating a suitable ligand sphere with six terminal li-

gands, the phosphane groups enforce a formal dimerization of "Cu_{12}" clusters to the $[Cu_{24}S_{12}]$ core in **8**.[17] Figure 3 shows the formal dimerization of two "$[Cu_{12}S_6(PR_2R')_8]$" clusters of type II, which results in the molecular structure of **8** after the loss of four phosphane groups.

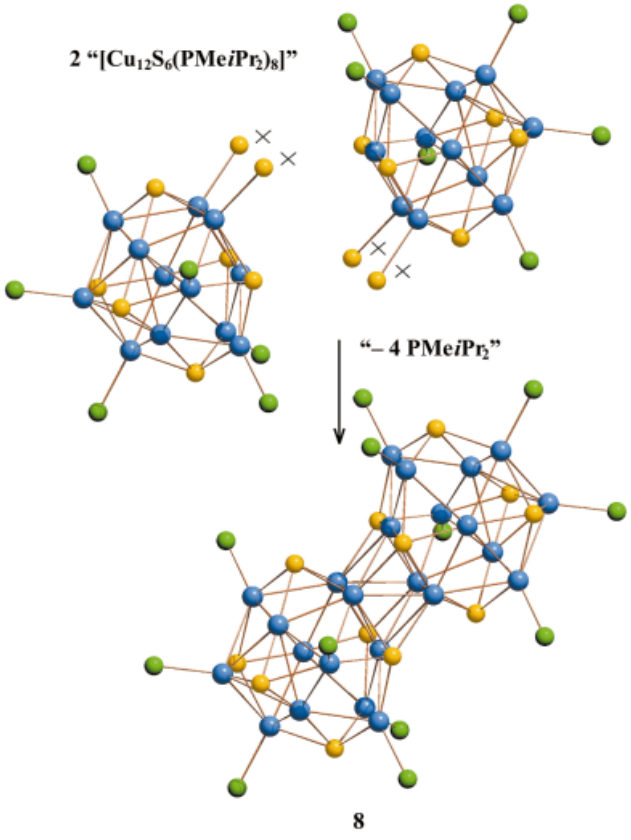

Figure 3. Formal dimerization/condensation reaction of two hypothetical clusters "$[Cu_{12}S_6(MeiPr_2)_8]$", resulting in the molecular structure of $[Cu_{24}S_{12}(PMeiPr_2)_{12}]$ (**8**) (without organic groups); phosphane ligands that are formally lost during the dimerization/condensation are drawn yellow and are marked by a cross

In contrast to the formal condensation (2 × "Cu_{12}") − 4 Cu → "Cu_{20}", which leads to the sharing of a Cu_4 rectangular face in **6**, in this case one observes a fusion of two Cu_3 triangular faces of the two basic cubooctahedra, forming a Cu_6 octahedron around the inversion center of the cluster. These six copper atoms show a novel coordination pattern. They are surrounded exclusively by sulfur neighbors in a trigonal-planar geometry. Conversely, the four sulfur atoms in the cluster center are found to act as μ_5-bridges, whereas all sulfur ligands in the clusters discussed so far and all the other ones in **8** are μ_4-bridging. The μ_5-bridges exhibit longer average Cu−S bond lengths than the μ_4-bridging sulfur ligands, as they bind to four copper neighbors with normal distances [2.159(3)−2.378(3) Å] and form one significantly longer Cu−S bond to a copper atom of the opposite asymmetric unit [2.485(3), 2.509(3) Å].

In the molecular structure of **8**, one observes the beginning of a transition from the so-called "small" copper sulfide clusters to the "middle-sized" species. Both cluster sizes possess spherical Cu−S−P frameworks with copper centers near the S_n polyhedron edges, but the "middle-sized" examples show some new structural features besides those already found for the "small" clusters: coordination numbers other than four for sulfur atoms, and copper centers that bind to more than two sulfur neighbors.

This same observation can be made for clusters **9** and **10**, particularly for the latter.[17] Unlike the species already discussed, these two clusters are topologically unrelated to the smaller examples. However, they are structurally related between themselves, and are actually formed in the same reaction. The molecular structures of **9** and **10** are shown in Figure 4, emphasizing their structural relationship by respective orientation. The basic S_{14} and S_{25} polyhedra are compared in Figure 5.

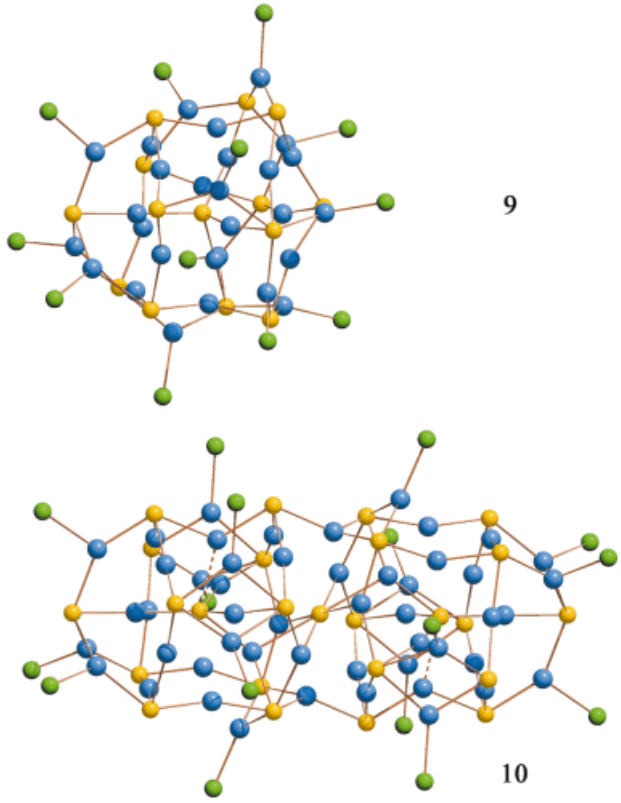

Figure 4. Molecular structures of $[Cu_{28}S_{14}(PtBu_2Me)_{12}]$ (**9**) and $[Cu_{50}S_{25}(PtBu_2Me)_{16}]$ (**10**) (without organic groups)

Besides various bridging modes of the sulfur atoms (μ_3 to μ_5 in **9**; μ_4 to μ_6 in **10**) and the greater numbers of three sulfur ligands around several of the copper atoms in **10**, both systems show another new structural feature characterizing "middle-sized" Cu−S clusters: Only for these two largest examples of copper sulfide cluster compounds does one find sulfur atoms inside an outer Cu−S shell, generating inner Cu−S units. In **9**, one sulfur ligand lies at the center of a distorted S_{13} deltahedron. Four copper atoms then bond around the central sulfur atom to yield an inner $[SCu_4]$ unit. The remaining copper centers are positioned either slightly below the surface of the S_{13} polyhedron if they show no Cu−P bonds, or slightly above if they are

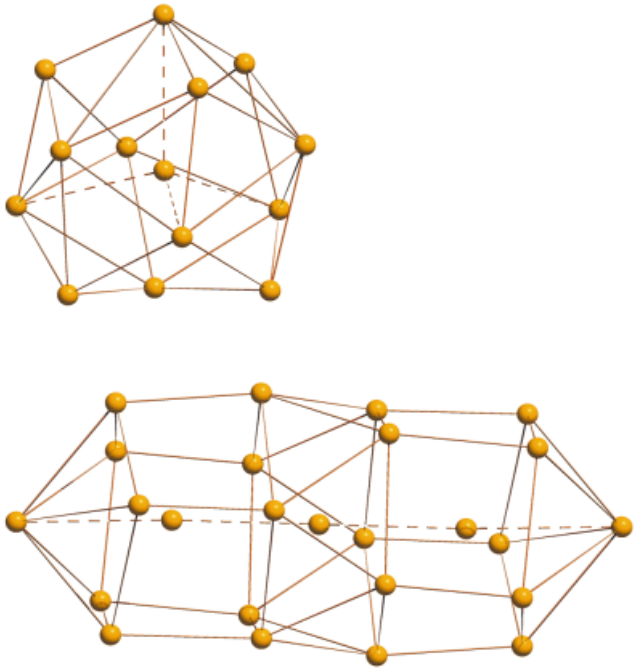

Figure 5. S_{14} (top) and S_{25} (bottom) polyhedra in **9** and **10**, respectively; the straight lines between the S atoms do not represent bonding interactions, but merely help to visualize the geometries of the polyhedra

bound by phosphane groups. A near C_3 symmetry of the Cu−S core is lost because of the "irregular" position of a single copper atom, which is also responsible for the μ_3- or μ_5-bridging mode of two sulfur ligands. The spherical cluster core is enclosed by a distorted icosahedron made up of the twelve phosphorus atoms. The sulfur substructure of **10** constitutes a cylinder-shaped polyhedron of near D_{5d} symmetry with a length of 17.14 Å. Underlining the supposition that **10** is formed through a form of dimerization−condensation from **9**, three inner sulfur atoms are present. Two of them − formally equivalent to the central sulfur atom in **9** − are also μ_4-bridging, resulting in an [SCu_4] fragment. However, one of the respective copper centers belongs to the cluster surface rather than being an inner metal atom, as a result of the structural differences between **9** and **10** when considering the center in **10**. Here, one observes the most unusual aspect of any of the copper sulfide clusters yet reported. The central sulfur ligand binds to six nearest copper atoms in a slightly corrugated chair-type manner. This arrangement, which is not found in any of the known copper sulfide compounds, displays very long Cu−S distances in the range of 2.633(4)−2.673(5) Å, which are about 0.3−0.5 Å longer than standard Cu−S bonds. Considering the ten next nearest copper atoms, 2.896(5)−3.814(5) Å out from the sulfur center, a near-spherical [SCu_{16}] arrangement is found for the cluster center. These structural observations are evidence for an interstitial S^{2-} anion rather than a covalently-bonded sulfur ligand. A summary of interatomic distances found in known copper sulfide systems for the different coordination numbers around copper is given in Table 2.

Considering the Cu−S distances listed in Table 2, one can recognize a first step in the direction of solid-state Cu−S phases in the structure of **10**.

By a comprehensive ab initio study of clusters [$Cu_{2n}S_n(PH_3)_m$] (n = 1−4, 6, 10; m = 0, 2, 4, 6, 8) at the MP2 level (program system TURBOMOLE), stabilization energies for the attachment of successive Cu_2S units to a given "naked" cluster (n = 1−4, 6, 10; m = 0; Figure 6), as well as the variation in the phosphane binding energies for clusters containing up to twelve copper atoms (n = 1−4, 6; m > 0; Figure 7), were calculated.[35]

For "naked" clusters, the stabilization energies increase continuously with the cluster size, which shows that the investigated molecules are thermodynamically unstable species in vacuo and that they have to be stabilized by ligands. Moreover, the increment in the stabilization energy per monomer unit decreases with increasing cluster size in the expected way, since it should theoretically converge at infinite cluster size, i.e. solid Cu_2S. Finally, the calculated Cu−P binding energy per Cu−P bond decreases rapidly from a value of ca. 140 kJ·mol^{-1} for [$Cu_2S(PH_3)_2$] − with a short relaxation when the Cu/P ratio is decreased (1 for n = 1−3, >1 for n = 4, 6) − to a value of ca. 56 kJ·mol^{-1} for the "Cu_{12}" species. Even if one assigns a higher Cu−P binding energy to the "real" tertiary phosphanes that bind to organic groups, it is evident that the phosphane ligands are bonded only very weakly to the copper sulfide core. Therefore, an additional stabilization by solvents or a crystal lattice is required.

3.2. Selenium-Bridged Copper Clusters

3.2.1. Syntheses

Scheme 3 summarizes the reactions yielding all PR_2R'-ligated, selenium-bridged copper clusters that have been isolated and structurally characterized to date, in order of increasing cluster size.

Unlike the sulfur-bridged compounds, the synthesis of selenium-bridged clusters can start from either copper acetate or copper chloride. This can be attributed to the lower standard formation enthalpy of Cu_2Se ($\Delta H_f° = -65.2$ kJ·mol^{-1})[49] when compared to its sulfur analogue Cu_2S ($\Delta H_f° = -81.2$ kJ·mol^{-1}).[50] Thus, the formation of Cu_2Se does not occur as rapidly as that of Cu_2S, although $Se(SiMe_3)_2$ is, in principle, more reactive than $S(SiMe_3)$. The cluster growth and protection of selenium-bridged clusters can therefore often be observed even at room temperature. However, with copper acetate as the starting material and by choosing low temperatures, one can obtain smaller clusters that could be considered as intermediates in the formation of the larger molecules. In addition to a great number of "stoichiometric" compounds that formally contain Cu^+ and Se^{2-}, some clusters have been characterized as having a Cu:Se ratio of less than two, indicating mixed-valence metal centers. All selenium ligands have a formal charge of −2 as one does not find any Se−Se binding inter-

Table 2. Interatomic distances of selected $Cu^{I}-S$ systems and metallic copper

System	Cu−Cu [Å]	Cu−S distances for the different coordination numbers (*CN*) [Å]			ref.
		CN = 2	*CN* = 3	*CN* = 4	
Cu−S clusters	2.511−2.985	2.111−2.291	2.103−2.673	–	[13−15,17,29]
$[Cu_{12}S_8]^{2-}$	2.774−2.950	2.156−2.179	–	–	[7]
ternary M−Cu^{I}−S phases	2.60−2.96	2.13−2.17	2.17−2.53	2.37−2.55	[48]
binary $Cu_{2-x}S$ phases	2.59−2.97	2.06	2.28−2.33	2.15−2.59	[38]
copper metal	2.56	–	–	–	[38a]

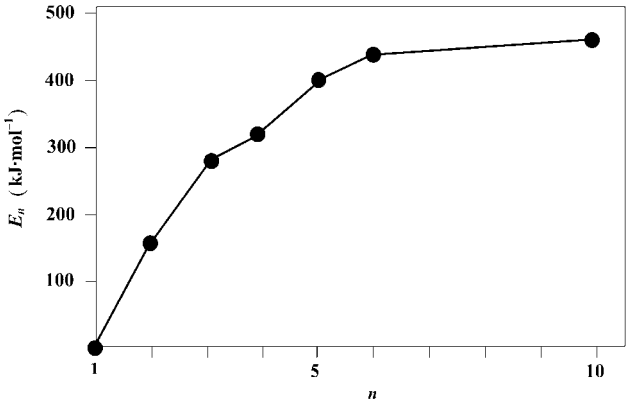

Figure 6. Variation in the stabilization energies per monomer unit in "naked" clusters $[Cu_{2n}S_n]$ (n = 1−4, 6, 10) with the given values taking into account the total energies of the most stable structural isomers computed at the MP2 level

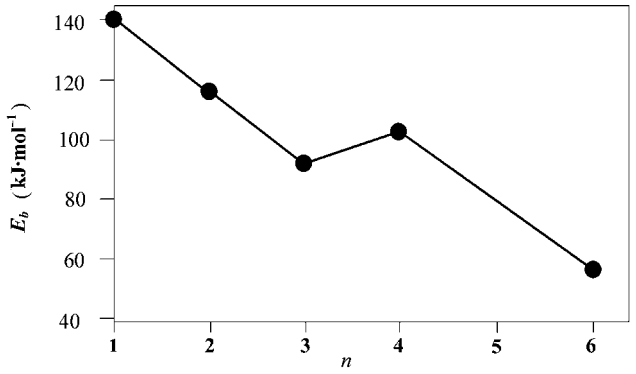

Figure 7. Variation in the Cu−P binding energies per Cu−P bond in phosphane-ligated clusters $[Cu_{2n}S_n(PH_3)_m]$ (n = 1−4, 6; m = 2, 4, 6, 8) with the given values taking into account the total energies of the most stable structural isomers computed at the MP2 level with respect to the total energy of PH_3 calculated by the same method

actions; therefore, one can assign Cu^{I} and Cu^{II} centers within the same cluster core in **14**, **17**, **27**, and **33**. The phosphane ligands again play a key role in determining the observed cluster sizes and shapes. The number of observed compositions is approximately four times that of the number of copper sulfide species, and the cluster growth proceeds to much higher nuclearity. Again, the lower tendency for precipitation of the binary phase can be invoked to account for this observation.

Another route to selenium-bridged copper clusters is by synthesis using $RSeSiMe_3$ (R = organic group) in the presence of either tertiary phosphanes or chelating ligands such as 1,2-bipyridyl, diphenylphosphanyl acid, or bidentate phosphanes dppR (R = organic spacer). The compounds prepared in this way are listed in Scheme 4 in order of increasing size.

Again, one finds clusters containing exclusively Cu^{I} centers, as well as compounds with mixed-valence metal centers. In contrast to the compounds presented in Schemes 2 and 3, one of the selenido/selenolato-bridged clusters (**52**; see below) apparently contains Cu^{0} as well as Cu^{I}. Apart from this peculiarity, the cluster size and conformation of the Se^{2-}/SeR^{-}-bridged compounds is not only influenced by the nature and steric demand of the phosphane used, but is also dependent on the spatial properties of the organic substituent on the selenium reactant. This determines both the Se^{2-}/SeR^{-} ratio as well as the arrangements of the Se^{2-} ligands positioned inside the cluster core and of the SeR^{-} ligands on the periphery of the molecules.

3.2.2. Structures and Stabilities

3.2.2.1. Se^{2-}-Bridged Copper Clusters

The subtle, nonlinear structural influence of the phosphane ligands allows the formation of different clusters of sometimes significantly different size and shape in the presence of the same phosphane. The isolation of a particular cluster compound is then determined by the choice of reaction conditions. Conversely, the use of different PR_2R' ligands can lead to clusters of the same $[Cu_{2n}Se_n]$ cores that may display differing numbers of terminal ligands and/or structural isomerism. These observations have already been illustrated and explained for the sulfur-bridged copper clusters, but they are more important for the Cu−Se species and a much greater structural variety is found. As with the copper sulfide compounds, one can distinguish between "small" and "middle-sized" clusters with regard to their shape and the coordination properties of the atoms involved. However, a third group, the "large" clusters, exists for the Cu−Se system. Whereas the transition from the first to the second type of molecular size is rather smooth, a clear break occurs when the number of copper atoms exceeds 59.

The only composition and structure that is equivalent for both copper sulfide and selenide clusters is $[Cu_{12}E_6(PR_2R')_8]$ (E = S, Se; PR_2R' = $PEtPh_2$, $PnPr_3$; respective cone angles: 141°, 132°). Compounds **11**[13] and **12**[29] are topologically identical to their sulfur analogues **3**

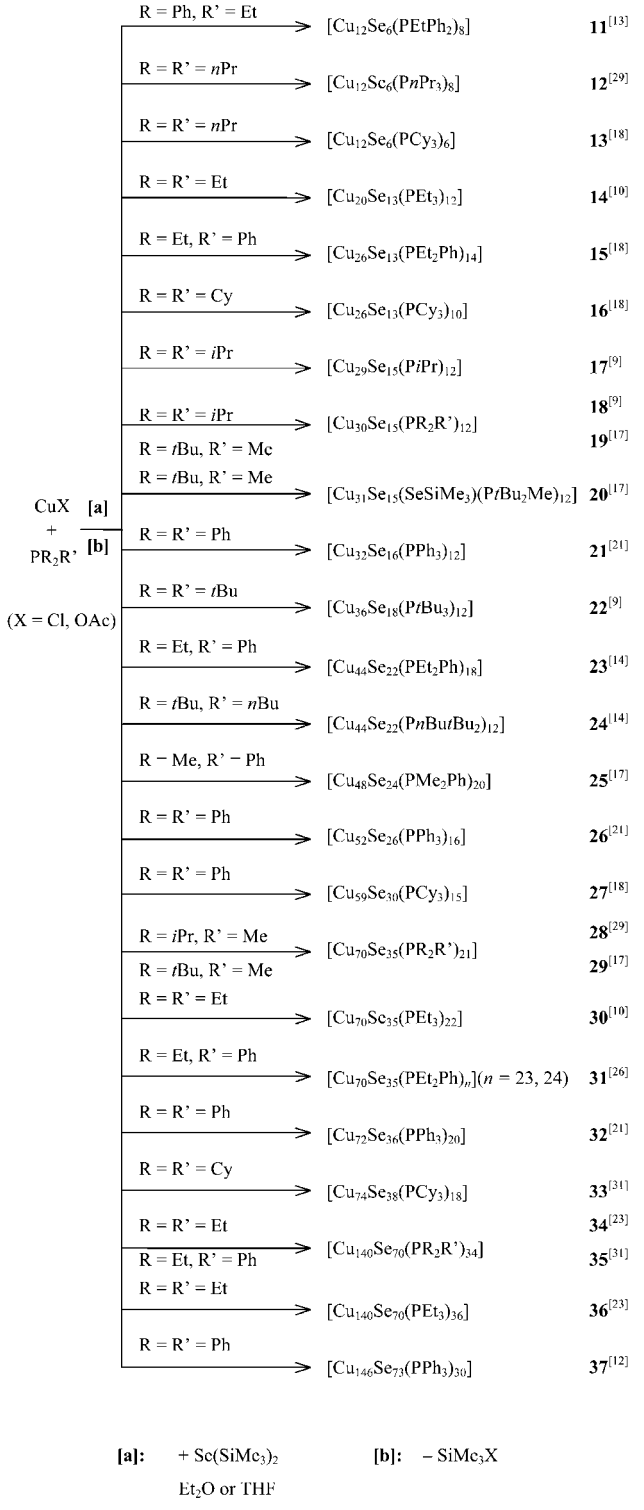

Scheme 3. Survey of the synthesis of selenium-bridged copper clusters protected by terminal phosphane ligands

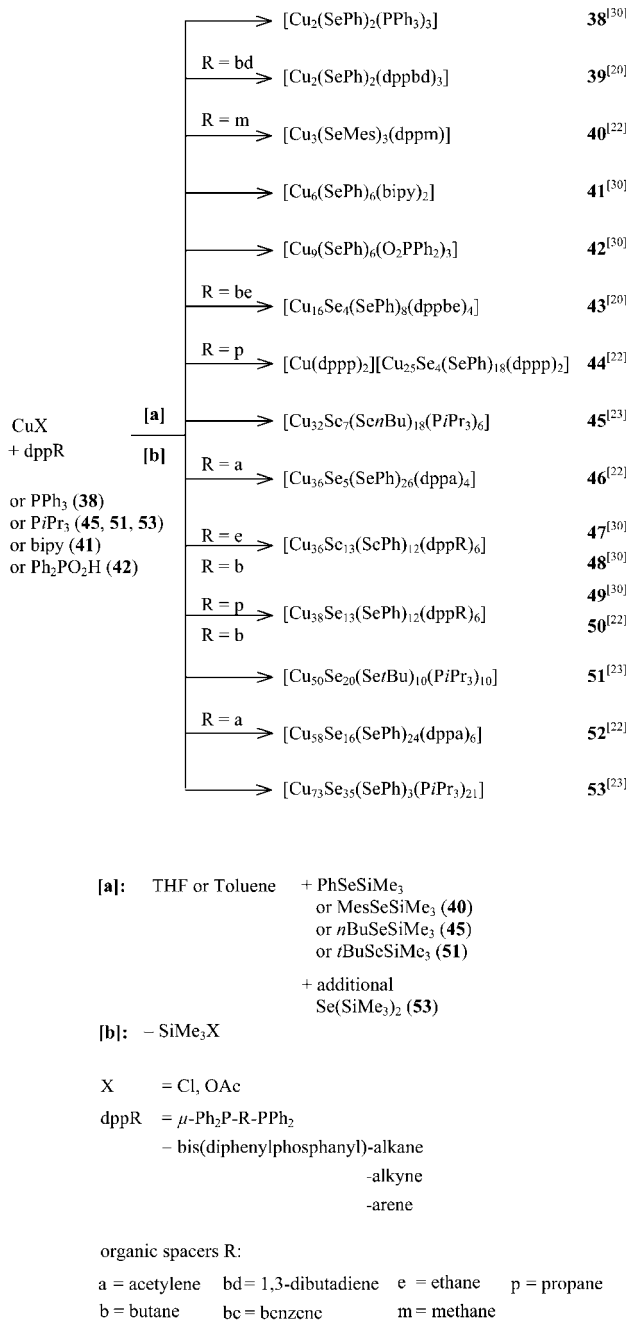

Scheme 4. Survey of the synthesis of selenido/selenolato-bridged copper clusters protected by monodentate or chelating bidentate ligands

and **4**. The use of a much bulkier phosphane ligand, PCy_3, does not lead to a condensation or dimerization of cluster cores as observed for **6**−**8**, which contain PR_2R' groups of medium or large steric bulk. In contrast to the copper sulfide clusters in the presence of PPh_3, $PnButBu_2$, or $PMeiPr_2$, a reduction to six terminal ligands is acceptable in the case of **13**[18] (Figure 8) and the resulting ligand shell can encapsulate the $Cu_{12}Se_6$ cluster core. The clearly larger cone angle of PCy_3 compared to PPh_3, $PnButBu_2$, or $PMeiPr_2$ (170° *vs.* 145°, 146°, or 165°) is sufficient to allow a distorted P_6 octahedron to protect the copper selenide framework. However, as might be expected, a third version of the distortion of the $[Cu_{12}E_6]$ core is observed in this case.

Considering the clusters presented thus far, there seems to be a strong preference for highly symmetrical substructures of all the components involved in the heavy atom framework. Capped or uncapped, sometimes condensed,

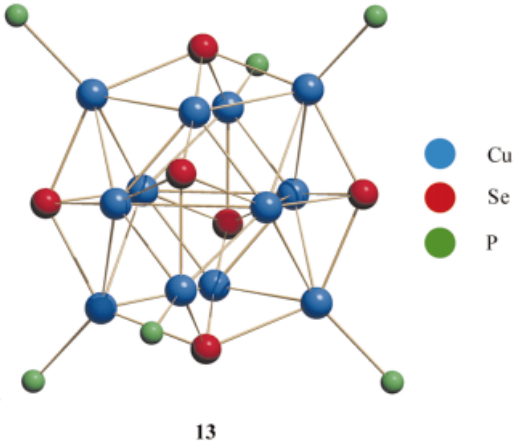

Figure 8. Molecular structure of $[Cu_{12}Se_6(PCy_3)_6]$ (**13**) (without organic groups)

octahedral, prismatic, cubic, dodecahedral, cubooctahedral, or icosahedral arrangements of either metal, chalcogen, or phosphorus atoms penetrate or enclose each other in all the structures. Among the compounds discussed, the "Cu_{12}" molecules possess the most symmetrical substructures. However, selenium ligands evidently prefer higher bridging modes. Therefore, the formation of "small" clusters with mostly μ_4-bridging selenium ligands is disfavored and these are consequently less common than larger ones. For the Cu−Se clusters, three further "middle-sized" compounds can be considered with regard to their symmetry properties as well as for a further illustration of the structural influence of the phosphanes. The cluster frameworks of **14**[10] and the $[Cu_{26}Se_{13}]$ isomers **15**[18] and **16**[18] can again be described as alternate packings of copper, selenium, and phosphorus polyhedra, respectively. However, regular polyhedra are only observed in the structures of **14** and **15**, whereas the $[Cu_{26}Se_{13}]$ core of **16**, being surrounded by only ten PCy_3 ligands instead of 14 PEt_2Ph groups, does not conform to a known polyhedral pattern. The molecular structures of **14**−**16** are shown in Figure 9.

To some extent, **14** and **15** are topologically related as both contain a centered icosahedron of selenium atoms. However, the penetrating polyhedra of copper atoms have different shapes according to the differing numbers of copper atoms and Cu−PR_2R' fragments (**14**: R = R′ = Et, **15**: R = Et, R′ = Ph) in the two clusters (Figure 10).

In **14**, a Cu_8 cube surrounds the inner selenium atom below Se_3 faces of the Se_{12} icosahedron. An outer Cu_{12} icosahedron follows, which is positioned above and rotated by 90° with respect to the Se_{12} shell. The eight copper centers inside the cluster thus form tetrahedral $[CuSe_4]$ groups and the twelve outer ones display an $[Se_3CuP]$ environment by binding to the similarly orientated P_{12} icosahedron formed by the PEt_3 ligands. In **15**, the inner selenium atom has twelve nearest copper neighbors that form an icosahedron, each edge being positioned below an Se−Se edge of the enclosing Se_{12} polyhedron and lying perpendicular to it, resulting in a coordinative occupation of one copper atom per Se_3 face. Slightly above the Se_{12} icosahedral surface, an

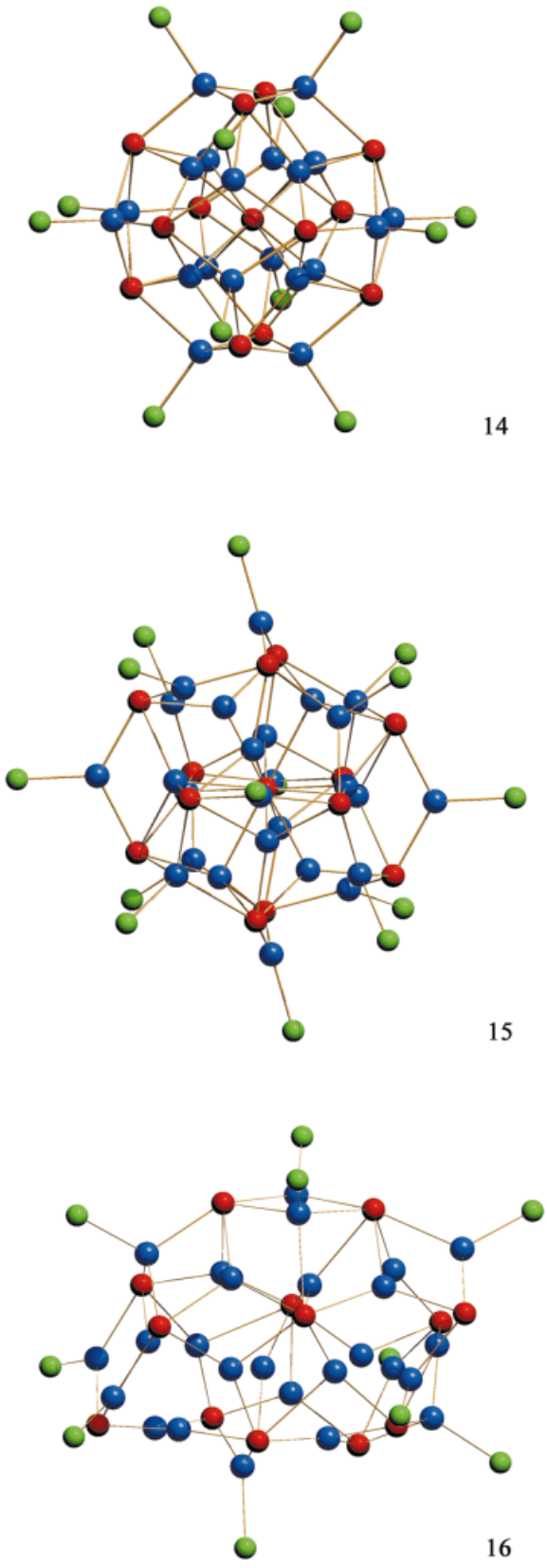

Figure 9. Molecular structures of $[Cu_{20}Se_{13}(PEt_3)_{12}]$ (**14**), $[Cu_{26}Se_{13}(PEt_2Ph)_{14}]$ (**15**), and $[Cu_{26}Se_{13}(PCy_3)_{10}]$ (**16**) (without organic groups)

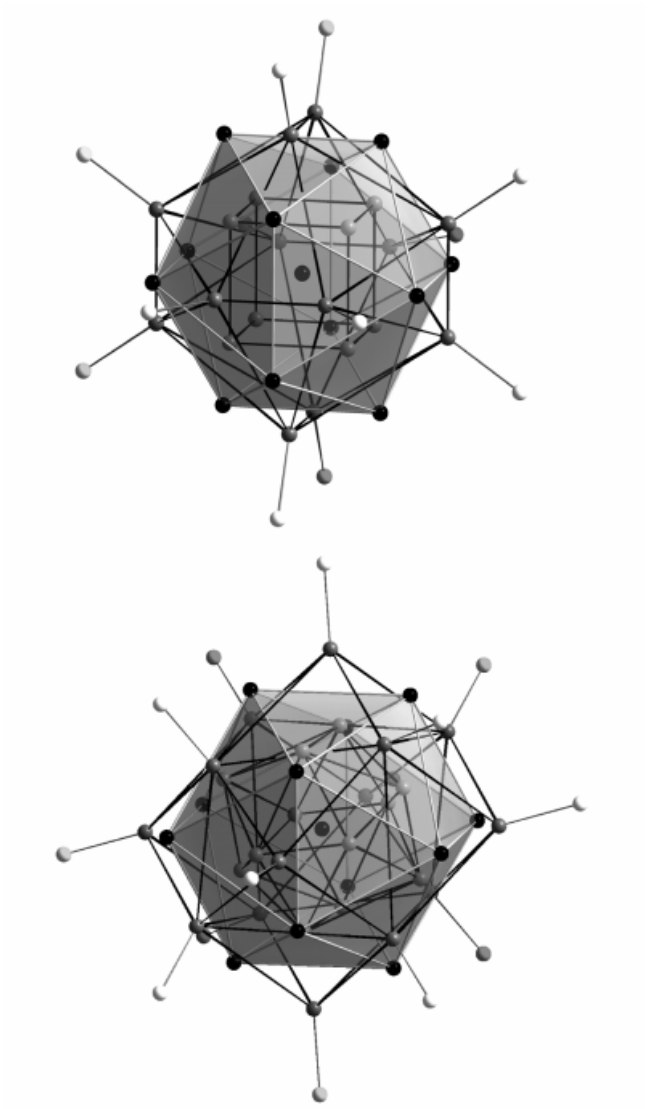

Figure 10. A comparison of the interpenetrating polyhedra in **14** (top) and **15** (bottom) that form the heavy atom cluster cores; the lines merely represent polyhedral edges and do not imply bonding interactions

arrangement of 14 $Cu-PEt_2Ph$ units can be described as a sixfold capped cube. The twelve inner copper atoms and the eight metal centers of the capped cube, which all reside near Se_3 faces, are approximately tetrahedrally coordinated by either four selenium ligands or three selenium ligands and one phosphorus ligand. This is characteristic of those clusters larger than those classified as "small". The six remaining $Cu-PEt_2Ph$ fragments are situated above six Se−Se edges and therefore represent tricoordinated $[Se_2CuP]$ units, as found in both "small" and "middle-sized" clusters. On comparing the Cu/Se ratios for **14** and **15**, the fundamental difference that can be invoked to account for the structural differences becomes apparent. Cluster **14** represents a mixed-valence compound formally incorporating six Cu^{II} and 14 Cu^{I} centers to neutralize the 26− charge of the Se_{13} substructure. However, the intermetallic distances in **14** [Cu(1)−Cu(1): 2.821(4), Cu(1)−Cu(2): 2.678(4) Å] do not indicate significant interatomic interactions despite the partial depletion of electrons. The only structural indication of different valence situations in **14** or **15** is that, apart from equal average Cu−P bond lengths (2.247 Å in **14** and **15**) and similar average intermetallic distances Cu−Cu (2.707 Å in **14**, 2.682 Å in **15**), one finds significantly shorter average Cu−Se bonds in the mixed-valence compound **14** (2.365 Å) than in **15** (2.457 Å). The molecular structure of **16** differs from those of **14** and **15** in that the selenium substructure consists of a very irregular Se_{13} deltahedron. Twelve of the copper centers and ten $Cu-PCy_3$ fragments bind to the Se_{13} polyhedron in such a way that they are again three- or four-coordinated. Unlike the situation in **14** or **15**, one additionally observes four copper atoms that are almost linearly coordinated by two selenium neighbors. This pattern is typical for "small" Cu−E clusters and again underlines the partial maintenance of these properties in the "middle-sized" compounds. The structure of **16** acutally resembles more the molecular structures of the next larger clusters **17**−**19** (Figure 11), being reduced by three or four copper atoms, two selenium, and two phosphane ligands.

Like the "Cu_{12}"−"Cu_{20}", the "Cu_{12}"−"Cu_{24}", or the "Cu_{28}"−"Cu_{50}" relationship discussed for copper sulfide clusters, the molecular structures of **14** and **15** can be seen to be closely related, at least in principle, even though the numbers and ratios of heavy atoms are very different. In contrast, a similar number of copper and selenium atoms *can* but does not always lead to a topological relationship (cf. **15/16**). Compounds **17**−**21**[9,17,21] contain 29, 30, 31, or 32 copper atoms and either 15 or 16 selenium ligands. Nevertheless, three completely different molecular frameworks are observed. The first structure type is adopted by **17**,[9] **18**,[9] and **19**.[17] As an example, the molecular structure of **17** is shown in Figure 11.

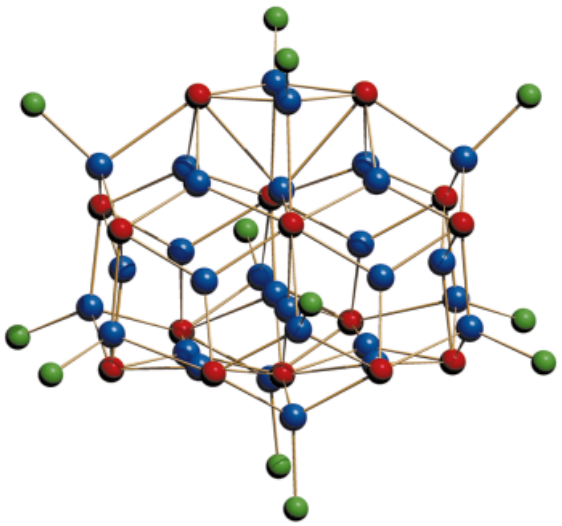

17

Figure 11. Molecular structure of $[Cu_{29}Se_{15}(PiPr)_{12}]$ (**17**) (without organic groups)

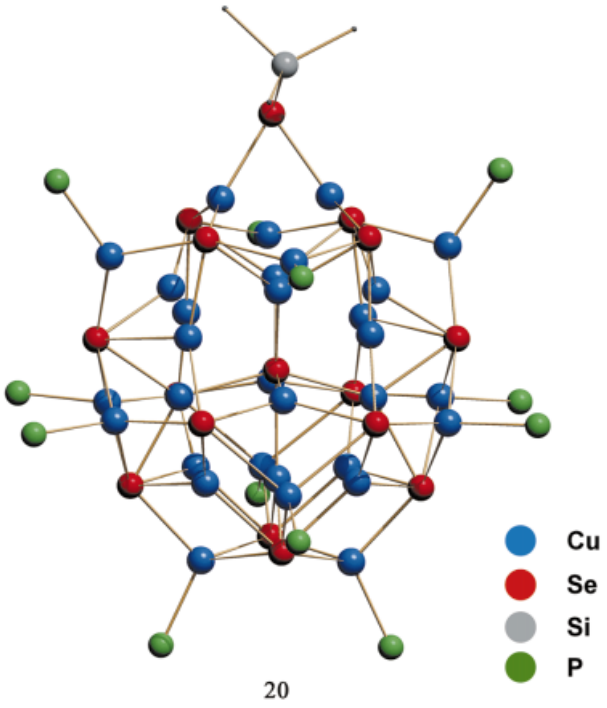

Figure 12. Molecular structure of $[Cu_{31}Se_{15}(SeSiMe_3)(PtBu_2Me)_{12}]$ (**20**) (without organic groups)

Although the number of copper atoms in **17** is one less than in **18** or **19**, indicating a mixed-valence situation in this system, all the clusters show equivalent Cu−Se−P cores. The additional copper atom in **18** or **19** is positioned in the cluster center. A reaction employing the same reactants and temperatures as for the synthesis of **19**, but using a 40% higher $PtBu_2Me$:CuOAc ratio, yields compound **20**[17] (see also Scheme 8). Although the cluster core of **20** (Figure 12) can also be described in terms of five parallel planes of copper and selenium atoms that are then surrounded by twelve phosphane ligands, analogous atomic arrangements or corresponding polyhedra in **19** or **20** are not found.

The $SeSiMe_3$ group, which is unique in the copper chalcogenide clusters, not only influences the molecular structure of **20**, but also indicates the obvious reason for the structural differences. Compound **20** can be viewed as a "frozen" intermediate en route to the formation of a larger cluster such as the "Cu_{70}" cluster **29**[17] (see below), since it still bears a leaving group. The latter uniquely acts as a protecting unit in addition to the phosphane ligands and consequently further cluster growth is slowed down to such an extent that compound **20** crystallizes instead. Thus, its formation is naturally independent of the cluster growth yielding **19**. A third structure type for this size of cluster is found for **21**,[21] as shown in Figure 13. The selenium atoms form a flattened polyhedron consisting of non-bonded Se_3 triangles. One observes four distinct copper environments: 24 of the copper atoms cap the selenium triangles, and of these 16 are bonded only to selenium ligands producing a distorted trigonal-planar coordination geometry slightly below the Se_3 faces. The other eight of these copper centers

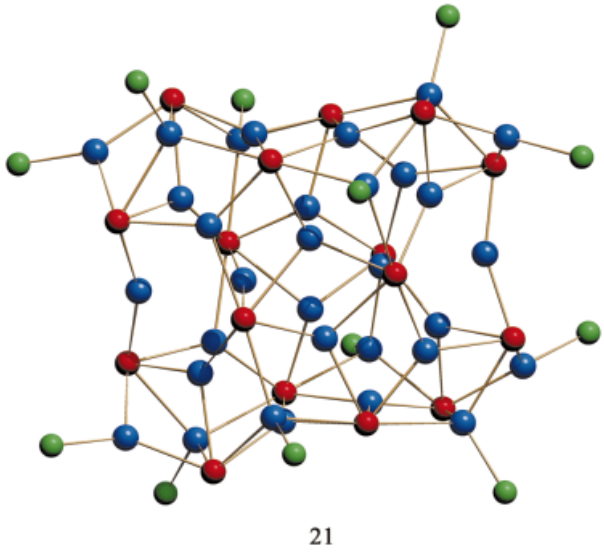

Figure 13. Molecular structure of $[Cu_{32}Se_{16}(PPh_3)_{12}]$ (**21**) (without organic groups)

are also coordinated by a phosphane ligand, giving a tetrahedral environment with the copper atoms situated on the exterior of the selenium substructure. Of the remaining copper atoms, four are coordinated in a quasi-linear fashion to two selenium ligands, and four are bonded in a distorted trigonal-planar manner to two selenium neighbors and one phosphorus atom from PPh_3. These coordination patterns, as well as bridging modes of μ_5 and μ_6 for the selenium ligands, are common for "middle-sized" Cu−E clusters. Compounds **16**, **17**, and **21** also represent exceptions for their cluster size in that they do not contain copper or selenium atoms inside an approximately spherical Cu−Se shell. All other "middle-sized" clusters containing 20 or more copper atoms (beginning with compound **14**) feature central copper atoms (**18**, **19**) or central selenium ligands (**14**, **15**, **20**).

The larger molecules **22**−**27**[9,14,17,18,21] all feature selenium atoms enclosed within an Se_n polyhedron (n = 18, 22, 24, 26, or 30). The number of inner selenium ligands increases with increasing cluster size from one central atom (**22**),[9] through two inner atoms (**23**−**25**),[14,17] to three selenium centers inside the cluster core (**26**, **27**).[18,21] The respective underlying selenium substructures are summarized and compared in Figure 14.

Even though these six compounds can be considered as spherical, "middle-sized" clusters, and all possess central units within a Cu−Se surface, two distinct basic shapes can be discerned. Compounds **22** and **26** (Figure 15) are based on a triangular structure, whereas **23**−**25** and **27** form ellipsoid-type cluster surfaces (Figures 16 and 17).

The molecular structure of **22** displays idealized D_3 symmetry, while the Cu−Se core of **26** shows near C_3 symmetry, although in neither case is this realized in the crystal (**22**: C_2 symmetry; **26**: C_1 symmetry). Along the idealized threefold axes, one finds one selenium ligand at the top and one at the bottom of the approximate flattened trigonal prism

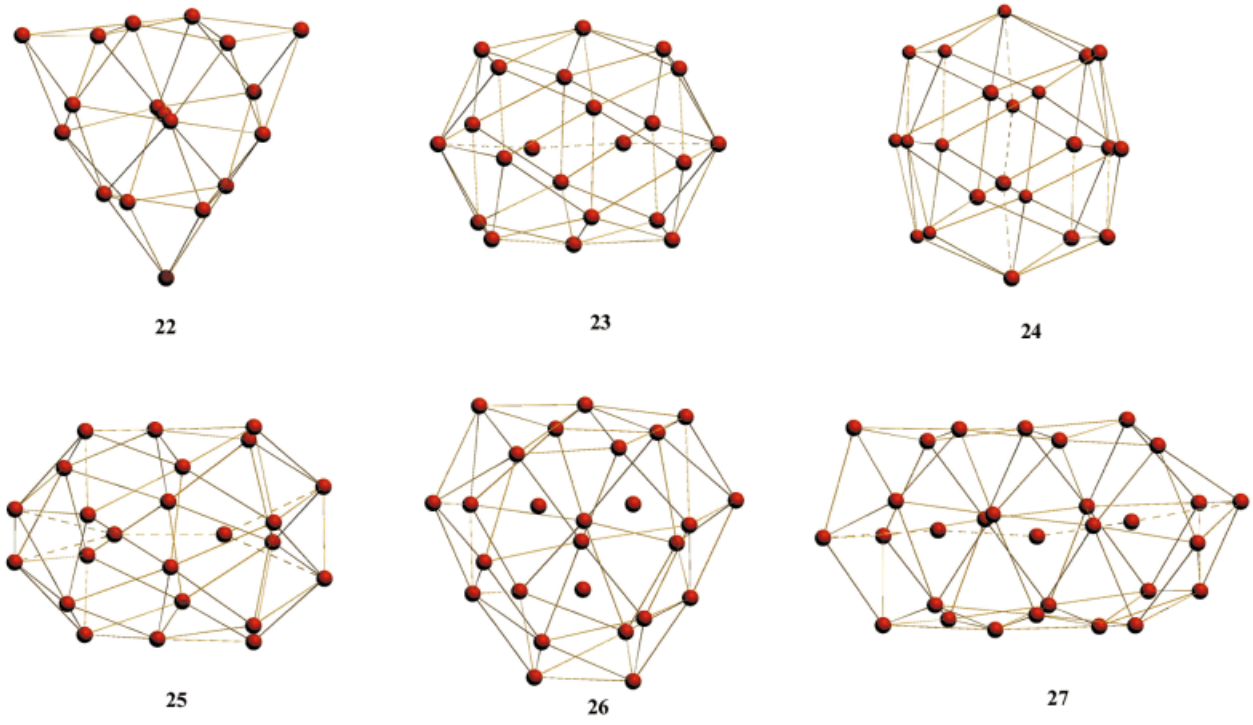

Figure 14. Selenium substructures in **22**−**27** (from top left to bottom right); the Se−Se lines do not represent bonding interactions, but merely help to visualize the geometries of the polyhedra

formed by the cluster atoms. In **22**, a third selenium ligand is positioned between these two at the cluster center. Conversely, in **26** a triangle of three inner selenium atoms lies at the center of the Cu−Se core, and two copper atoms are arranged along the near C_3 axis, between this Se_3 triangle and the two aforementioned selenium ligands. Considering first the central cores, the clusters are formed in the usual way by alternating bonds from copper to selenium atoms. For **22**, this leads to [Se_2Cu], [Se_3Cu], or [Se_2CuP] coordination environments around the copper centers and μ_3- to μ_6-bridging selenium ligands with Cu−Se distances of 2.347(4)−2.875(5) Å. The larger cluster core of **26** consequently features higher coordination numbers, including almost tetrahedral [Se_3CuP] arrangements besides di- or tricoordinated copper atoms as found in **22**, and the selenium atoms act as μ_4- to μ_8-bridges with a wide Cu−Se distance range of 2.19−2.91 Å. Twelve P*t*Bu_3 ligands enclose the copper selenide core of **22** in the following way. Six are bonded over rectangular faces when the cluster is viewed in a simplified manner as a trigonal prism. Six further P*t*Bu_3 units are situated over the respective triangular faces. In addition to nine PPh_3 ligands that are bonded over the rectangular faces of the "prismatic" Cu−Se core in **26**, seven phosphane groups surround the cluster core in a different manner on the two triangular faces in such a way that three are positioned on one side and four on the other.

By using different phosphane ligands and changing the CuOAc/PR_2R' molar ratios and final reaction temperatures, the structural isomers **23** and **24** can be obtained. The spatial demands of the phosphane ligands enabled ligand shells composed of either 18 PEt_2Ph or 12 P*n*Bu*t*Bu_2 groups to adequately protect a [$Cu_{44}Se_{22}$] core. In **23**, the phosphorus atoms form a quite regular polyhedron of alternating, eclipsed P_3, P_6, P_6, and P_3 rings perpendicular to the long axis of the cluster. The twelve phosphorus atoms at the periphery of the cluster core in **24** constitute a highly distorted icosahedron. As a result of the different numbers and arrangements of PR_2R' ligands, which modify the core geometry in the usual way by "pulling" the ligated copper atoms out of the Cu−Se core to some extent, some differences are observed when the copper selenide frameworks are considered in detail. This is clearly apparent when the respective Se_{22} substructures are compared (Figure 14). Both can be described as a staggered arrangement of three Se_6 rings, the middle one being larger than the outer rings. One additional selenium ligand caps each of the two terminal Se_6 faces of the face-sharing hexagonal anti-prisms. Apart from different distortions of these peripheral Se_{20} polyhedra (total lengths or widths of the Se_{22} substructures according to the orientations in Figure 14: 11.43 or 8.64 Å in **23**; 8.34 or 10.60 Å in **24**), the relative positions of the inner Se_2 units are perpendicular to each other. One can therefore consider units of twelve copper and two selenium atoms in each cluster core that have completely different orientations, a consequence of the significantly different situations on the cluster surface mentioned above. The isomerism observed with the "Cu_{44}" clusters again shows that certain [$Cu_{2n}E_n$] compositions represent "islands of stability" − within given limits of structural isomers − that are obtained experimentally whenever a suitable ligand shell

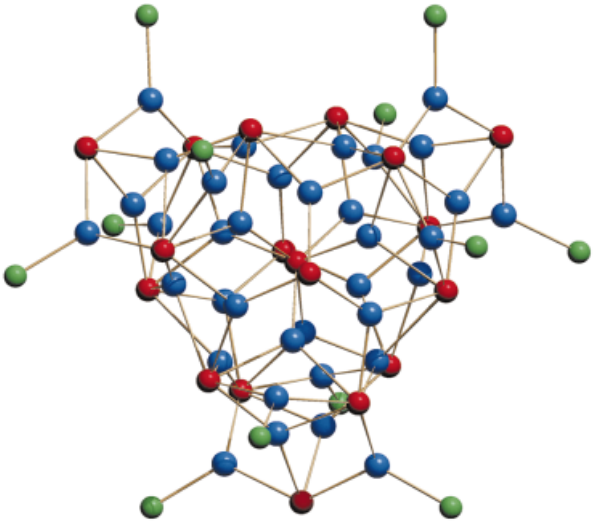

22

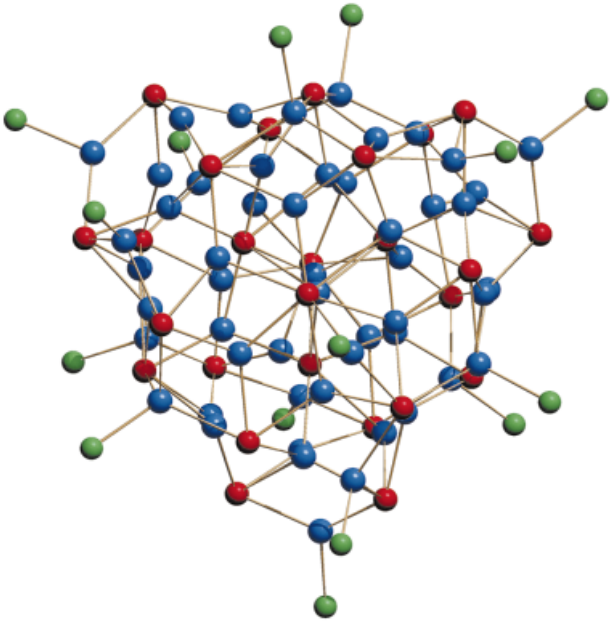

26

Figure 15. Molecular structures of $[Cu_{36}Se_{18}(PtBu_3)_{12}]$ (**22**) and $[Cu_{52}Se_{26}(PPh_3)_{16}]$ (**26**) (without organic groups)

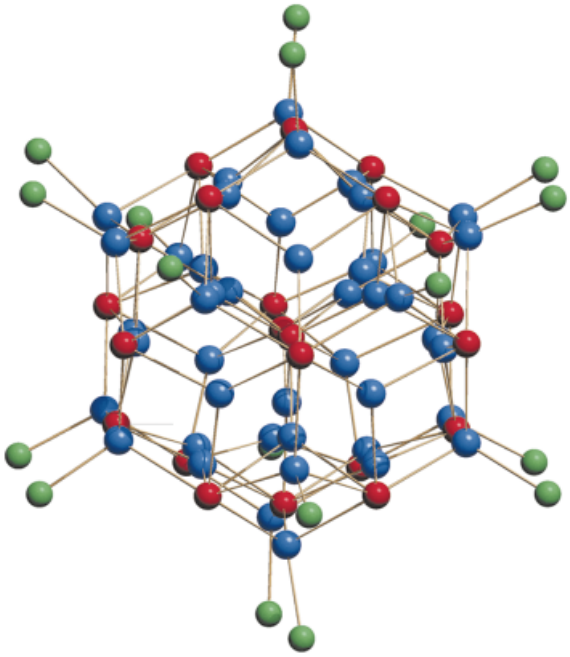

23

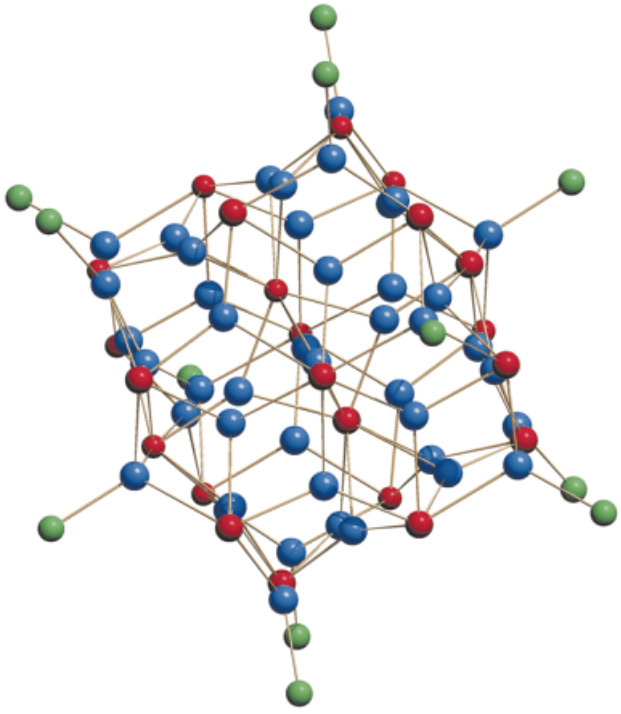

24

Figure 16. Molecular structures of $[Cu_{44}Se_{22}(PEt_2Ph)_{18}]$ (**23**) and $[Cu_{44}Se_{22}(PnButBu_2)_{12}]$ (**24**) (without organic groups)

can be realized by means of the available phosphane molecules.

Two further ellipsoid-like arrangements are found for clusters **25** and **27**, respectively. Apparently, it is not possible for a phosphane shell composed of PMe_2Ph ligands (cone angle: 127°) to surround a $[Cu_{44}Se_{22}]$ cluster. Instead, the smallest compound to be sufficiently stable and insoluble to allow its isolation is the slightly larger cluster **25**, although this is structurally related to the smaller species **23**. The ellipsoid-like Se_{24} substructure of **25** (Figure 14) can be derived from the Se_{22} arrangement in **23** by simple substitution of each of the single Se caps in the smaller

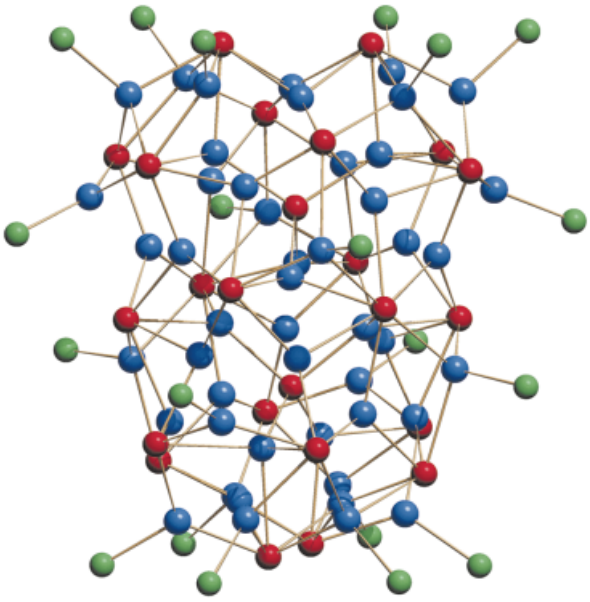

25

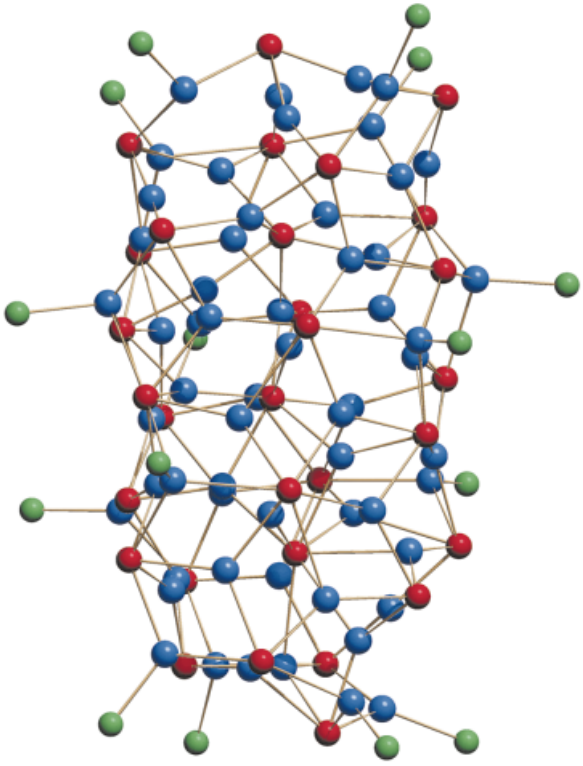

27

Figure 17. Molecular structures of $[Cu_{48}Se_{24}(PMe_2Ph)_{20}]$ (**25**) and $[Cu_{59}Se_{30}(PCy_3)_{15}]$ (**27**) (without organic groups)

polyhedron by two selenium ligands capping the outer Se_6 rings. Again, one finds all the coordination features typical for "middle-sized" Cu−Se clusters, even four copper atoms showing an almost tetrahedral environment of four selenium ligands. However, unlike all the smaller clusters that contain selenium atoms inside the cluster core, **25** features two tetrahedral $[SeCu_4]$ units − these being linked by a *trans*-edge junction through a compressed Cu_4 tetrahedron − with a uniquely low bridging mode (μ_4) for the two inner selenium ligands (cf. the bridging modes of the inner selenium ligands in **14**, **15**, **20**, **22**−**24**: μ_5 to μ_8, μ_{12}). Besides **14** and **17**, **27** is the third copper selenide cluster that has too few metal centers for an overall +1 oxidation state for the copper atoms. However, no single Cu^{2+} center can be assigned and the lack of one electron is likely to be delocalized over the whole cluster framework. As with **23**−**25**, the molecule is oblong in shape. It represents the largest spherical copper selenide cluster yet known, and thus it concludes the series of "middle-sized" Cu−Se clusters. The selenium atoms form a highly irregular Se_{27} polyhedron around three inner chalcogen centers (Figure 14), which can alternatively be viewed as an approximate arrangement of the selenium ligands into three layers. The molecular structure of **27** includes all possible coordination environments around copper atoms, i.e. $[Se_2Cu]$, $[Se_3Cu]$, $[Se_4Cu]$, $[Se_2CuP]$, and $[Se_3CuP]$. Selenium ligands are observed to act as μ_4-, μ_5-, μ_6-, or μ_7-bridges.

Summarizing the structural properties of the "small" Cu−Se clusters **11**−**13**, and the "middle-sized" ones **14**−**27**, the spherical shape and the absence of any topological relationship with the bulk material Cu_2Se are a central feature. Only the tendency towards higher coordination numbers at the copper centers, i.e. three and four, with increasing cluster size approaches the situation in the binary phase. However, the main difference between "small" and "middle-sized" clusters is the occurrence of inner atoms that first appear within a copper selenide core of 33 atoms (**14**). The coordination patterns in the "middle-sized" molecules typically show a mixture of higher and lower coordination numbers or bridging modes, whereas only lower coordination numbers are observed in "small" clusters.

Although only eleven more copper atoms are observed in compounds **28**−**31**[10,17,26,29] than in **27**, these represent the smallest examples of a new type of copper selenide clusters. The so-called "large" Cu−Se clusters are characterized by significantly different cluster shapes, structural principles, and relationships to the bulk material than the smaller species. Clusters **28**−**37** display *A*-*B*-*A*-type packed layers of selenium atoms that form large triangles. At first sight, this might appear to be reminiscent of the "triangular" structures of **22** or **26**. However, a closer look clearly reveals the differences between these two clusters and the layer-type structures of the "large" clusters. Compounds **28**−**37** are all based on three *hcp* selenium layers, of which the middle one is the largest. Figure 18 shows the selenium networks of the "large" clusters **28**[29] (as an example of a $Cu_{70}Se_{35}$ core), **32**[21] ($Cu_{72}Se_{36}$ core), **33**[31] ($Cu_{74}Se_{38}$ core), **34**[23] ($Cu_{140}Se_{70}$ core), and **37**[12] ($Cu_{146}Se_{73}$ core). It is worth

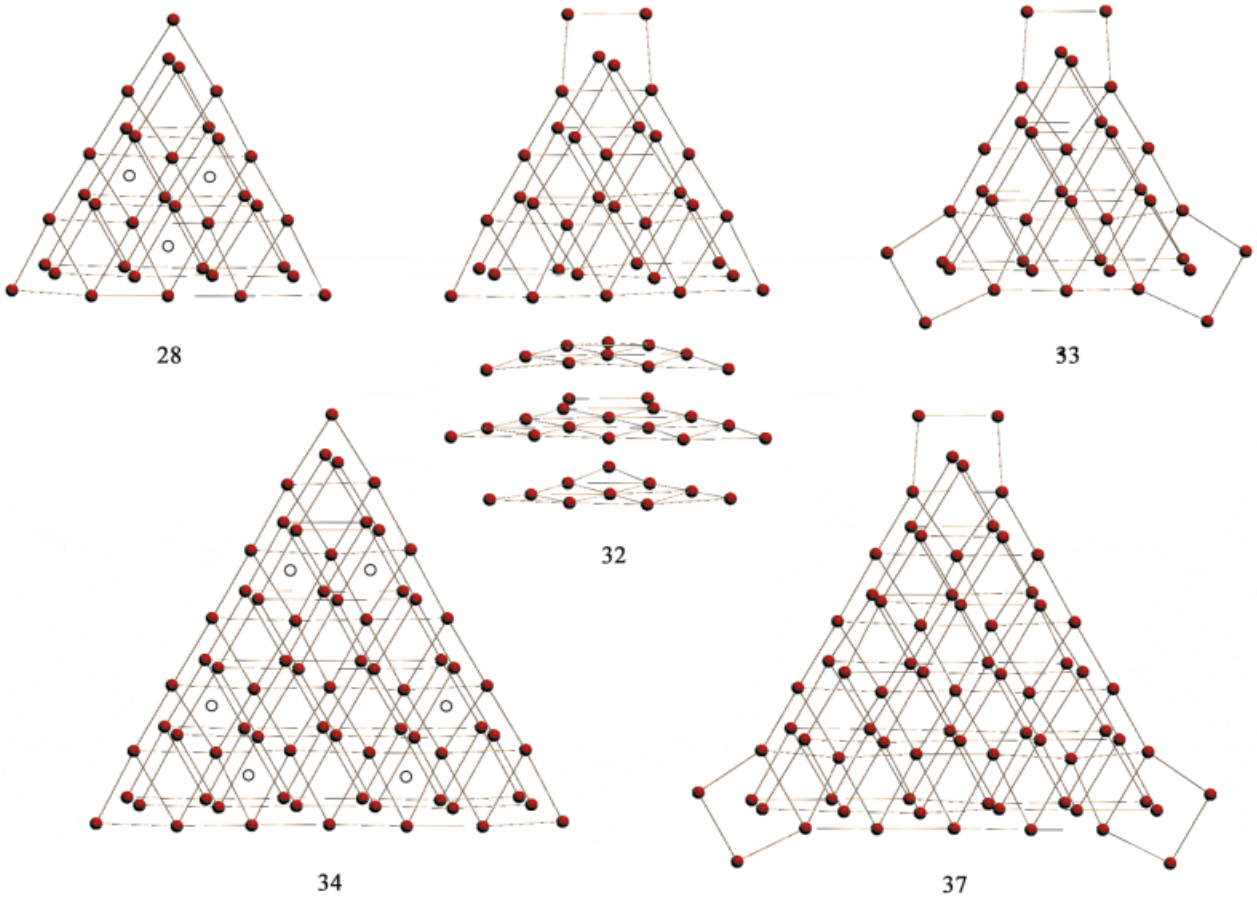

Figure 18. Selenium substructures in **28**, **32**, **33**, **34**, and **37** (from top left to bottom right) that contain 35, 36, 38, 70, or 73 selenium atoms; the drawn Se−Se contacts do not represent binding interactions, but merely serve to visualize the *A-B-A* packing of selenium atoms in three layers; this is additionally demonstrated by the supplementary view of the Se_{36} substructure of **32** (top middle); open circles mark disorder positions of copper atoms (see text)

mentioning that this structural pattern seems to be exceptionally favored for huge copper selenide clusters since it is observed over a size range from "Cu_{70}" to "Cu_{146}", i.e. over a more than twofold increase in the nuclearity.

Clusters **28**−**31** contain Se_{10}, Se_{15}, and Se_{10} layers that form perfect triangles. Thus, the next largest selenium substructure should be formed by an arrangement of triangular Se_{15}, Se_{21}, and Se_{15} layers incorporating one more row of selenium atoms each. However, the corresponding "[$Cu_{102}Se_{51}$]" cluster core is not yet known. Instead, one observes the formation of intermediate clusters incorporating selenium layers similar to those in **28**−**31**, but with the middle one deviating from a perfectly triangular shape. In **32**, one corner of the middle layer is modified with respect to the corresponding layer of the "Cu_{70}" clusters in that two selenium atoms replace one former corner atom. Similarly, all three corners are modified in this way to result in the $Se_{10}-Se_{18}-Se_{10}$ selenium framework of **33**; this compound is another "Cu-deficient" cluster featuring fewer copper centers than Cu_{2n} with respect to Se_n. The third "ideal" cluster composition has been observed in compounds **34**−**36**. The underlying selenium layers contain 21, 28, and 21 atoms, respectively. By replacing all corner selenium centers of the middle triangle by two chalcogen atoms, one obtains the Se_{73} substructure that is observed in **37**. For this third possible size, successive modification of one or two triangle corners of the middle layer has not yet been observed, whereas for the first size (35 selenium atoms), a modification of one or three corners has been found.

The reason for the missing "Cu_{102}" cluster might be related to the primary steps of the cluster growing mechanism. Selenium networks consisting of three triangular *hcp* layers based on $0.5\cdot[n\cdot(n+1)]$ selenium atoms (n = number of straight rows in the triangular network) in *A-B-A* order permit three possible orientations of the central threefold axis of the network {layers with a central Se atom are those containing $0.5\cdot[n\cdot(n+1)]$ atoms, where $n = (3m+1)$, i.e. Se_1, Se_{10}, Se_{28}, etc.; layers where $n = 3m$ or $n = (3m+2)$ have a central hole: Se_3, Se_6, Se_{15}, Se_{21}, Se_{36}, Se_{45}, etc.}: one either finds a hole (representing the unoccupied *C* position), one selenium atom in the middle layer (located in a *B* position), or two selenium atoms belonging to the two outer layers (located in *A* positions). Since all the "large" Cu−Se clusters characterized to date have only been consistent with the last two possibilities, the presence of a central Cu_xSe_y axis ($Se_A-Cu-Cu-Se_A$ in **28**−**33**; $Cu-Se_B-Cu$ in **34**−**37**) would seem to be necessary for the formation of a stable cluster core. Assuming that the cluster growth starts

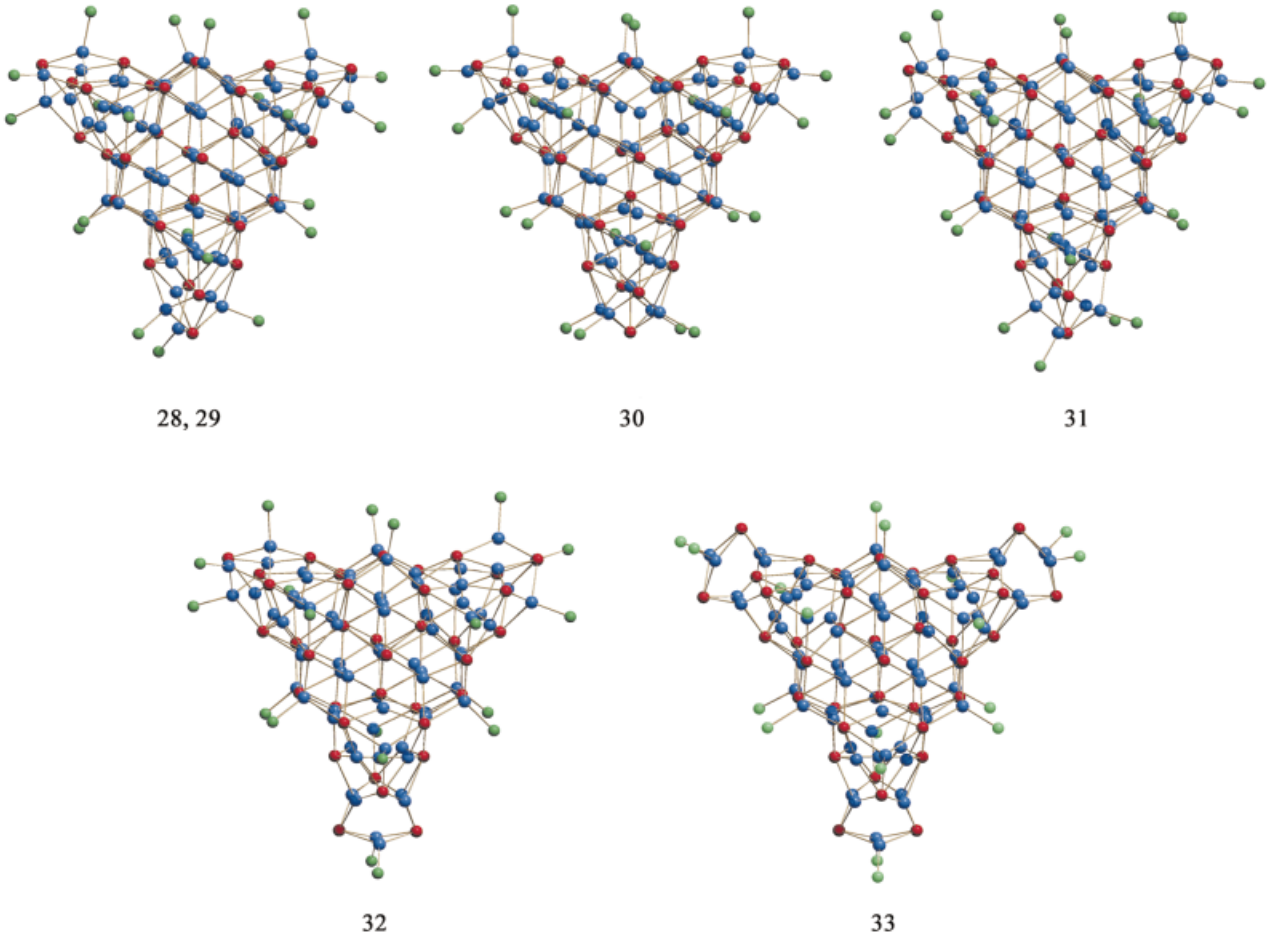

Figure 19. Molecular structures of $[Cu_{70}Se_{35}(PR_2R'_{21}]$ (R = *i*Pr, *t*Bu; R′ = Me) (**28**, **29**), $[Cu_{70}Se_{35}(PEt_3)_{22}]$ (**30**), $[Cu_{70}Se_{35}(PEt_2Ph)_n]$ (n = 23, 24) (**31**), $[Cu_{72}Se_{36}(PPh_3)_{20}]$ (**32**), and $[Cu_{74}Se_{38}(PCy_3)_{18}]$ (**33**) (without organic groups); two copper atoms that are positioned around the central Se−Cu−Cu−Se axis are statistically distributed with occupancies of 0.67 over three positions in **28**, **29**, and **31**

from the center of the molecule, the need for such a $[Cu_2Se]$ or a $[Cu_2Se_2]$ fragment situated along the C_3 axis appears understandable for a non-spherical cluster. Therefore, only those molecules that contain either one (middle; cf. **34**−**37**) or two (outer; cf. **28**−**33**) selenium layers with a central selenium atom instead of a central triangular hole are formed and observed experimentally. Both the Se_{15} and the Se_{21} layers that would conceivably form a "Cu_{102}" molecule do not contain central selenium atoms, thus suggesting why the $[Cu_{102}Se_{51}]$ core has not been observed.

In Figure 19, the cluster cores of the clusters containing 70 (**28**−**31**), 72 (**32**), and 74 (**33**) copper atoms are compared.

The "Cu_{70}" core is quite tolerant with regard to its ligand shell. An increase in the spatial demand of the PR_2R' molecules is not strictly coupled with a decreasing number of terminal ligands. However, one still finds a rough correlation, since 21 of the bulkier phosphane ligands PMe*i*Pr$_2$ (cone angle: 146°) and P*t*Bu$_2$Me (cone angle: 161°) are arranged around the Cu−Se core in **28** and **29**, whereas 22, and 23 or 24, terminal ligands are observed for the smaller phosphanes PEt_3 (cone angle: 132°; **30**) or PEt_2Ph (cone angle: 136°; **31**), respectively. Clusters **28**, **29**,[17] and **31**[26] differ marginally in their molecular structures. The only observable difference between **28** and **29** is a slightly less complete ligand shell achieved by the less sterically demanding PMe*i*Pr$_2$ groups. Cluster **31** displays a disorder problem with the PEt_2Ph groups, such that it cannot be determined with complete certainty whether the total number of phosphane ligands amounts to 23 or 24. Accordingly, for the formation of the cluster, another two (or three) additional phosphane molecules − compared to **28** or **29** − are situated at the triangle corners in such a way that two (or three) corners possess four instead of three Cu−PEt_2Ph groups, while one (or no) corner still bears three groups. The intermediate number of phosphane ligands, 22, is accompanied by a more distinct structural modification in **30**. Again, this affects the corner region. In contrast to all the corner arrangements of copper and selenium atoms in the other "Cu_{70}" clusters, none of which can be described in terms of regular patterns, in **30**[10] only two corners have an irregular structure. The third one shows a highly symmetrical $[Cu_9Se_3(PEt_3)_4]$ configuration featuring a centered cube of copper atoms that is capped on three faces by μ_4-selenium ligands and bears a square of four phosphane groups on the four outer atoms. This peculiarity of one cluster corner in

30 is one of two reasons for the absence of pseudo-threefold molecular symmetry. A C_3 symmetry of the $[Cu_{70}Se_{35}]$ core of **28**, **29**, or **31** is additionally approached − apart from one "wrong" Cu−PR_2R' position in **28** and **29** − by the statistical disorder of two copper atoms. The latter are distributed over three positions − each with site occupancies of 0.67 − forming a triangle around and perpendicular to the Se−Cu−Cu−Se pseudo-threefold axis running through the center of the molecule. In Figure 18, the three disorder sites are marked with open circles. The disorder of the PEt_2Ph ligands in **31** also leads to a pseudo-C_3 axis if 24 phosphane groups are assigned to the ligand shell. In contrast, close inspection of the cluster center in **30** reveals an unoccupied copper atom position. The two other metal atom sites are fully occupied, leading to a lower − yet crystallographically realized − C_2 symmetry.

The molecular structure of **32** can be derived from that of **28** or **29** in a simple manner if one first fully occupies all the copper atom positions around the Se−Cu−Cu−Se axis as mentioned above, and then formally substitutes one corner selenium atom by an $[Se_2(CuPPh_3)_2]$ unit after removal of three PPh_3 ligands at that corner. This leads to a modification of the middle selenium layer, as discussed earlier. Additionally, the number of phosphane groups that enclose the respective corner is reduced to two, since two of the three copper atoms that are coordinated by PR_2R' ligands in the analogous corner in **28** or **29** remain "naked" in **32**. Modification of all three cluster corners in this way, again together with full occupation of the Cu_3 group around the cluster center, generates the structure of the mixed-valence cluster framework in **33**. With idealized C_{3h} symmetry for the cluster framework, the symmetry of the molecule does not exceed C_2 in the crystal due to slight distortions and the positions of the organic groups bonded to the phosphorus atoms.

The largest copper selenide clusters yet known contain 140 or 146 copper atoms and 70 or 73 selenium ligands, respectively. The molecular structures of **34**, **36**,[23] and **37** are shown in Figure 20.

The different number of PR_2R' groups observed in **34** or **35**,[31] on the one hand, and in **36** on the other, affects the molecular structures in a different manner as seen for the "Cu_{70}" species **30** and **31**. Considering the corners again, **34**, with 34 terminal PEt_3 ligands, resembles an enlarged analogue of **30**. As in the smaller compound, two corners are arranged irregularly, whereas the third shows the regular, centered-cubic pattern. On increasing the number of PEt_3 groups to 36, as in **36**, all three corners now show this ordered arrangement of copper, selenium, and phosphorus atoms. This corner unit, which is only found for the PEt_3-ligated "large" Cu−Se clusters, underlines the structural relationship between **30**, **34**, and **36**, and again highlights the steric influence of a particular PR_2R' ligand. All other phosphane ligands that surround "large" copper selenide clusters feature larger cone angles, which could be the reason for the adoption of a more staggered arrangement if four Cu−PR_2R' units are present at a corner. Consequently, in **35**, all three corners show arrangements like that in the smaller analogue **31**. Disorder of copper atoms that increases the apparent idealized molecular symmetry is again present in the "Cu_{140}" clusters. A twofold disorder of one copper atom, between positions on the pseudo-C_3 axis (above and below the central selenium atom), results in an apparent "$Cu_{0.5}$"−Se−"$Cu_{0.5}$" central axis. In addition, four copper atoms are disordered over six equivalent sites, each with occupancies of 0.67. As for the "Cu_{70}" clusters, these sites lie within the plane of the middle selenium layer. However, in contrast to the smaller clusters **28**, **29**, and **31**, where the disorder sites form part of the $[Cu_3Se_3]$ hexagon at the center of the clusters, the six disorder sites in **34**−**36** are more distant from the cluster centers, as marked with open circles in Figure 18.

The formal replacement of each of the three corner selenium atoms and twelve PR_2R' molecules in **36** by three $[Se_2Cu(PR_2R')_2]$ units, as well as full occupation of all the copper sites present in the "Cu_{140}" clusters, exactly yields the composition and D_{3d} symmetric molecular structure of **37**. Thus, the structural relationship between **36** and **37** is analogous to that between the "Cu_{70}" and the "Cu_{72}" and "Cu_{74}" clusters.

All the "large" Cu−Se clusters show an *A-B-A* packing of hexagonal layers of selenium atoms. The metal centers occupy either trigonal or tetrahedral holes, or are situated outside the selenium layers in trigonal or tetrahedral coordination environments. Thus, the layer-type clusters clearly show a closer relationship to solid-state structures than do the spherical ones. However, for the $Cu_{2-x}Se$ phases, hexagonal structures are unknown and only cubic modifications are found. Interestingly, for the Cu_2S (chalcosine) high-temperature phase,[38] a hexagonal lattice with mainly trigonally-surrounded copper atoms, with some tetrahedrally and linearly coordinated ones, does exist. In contrast, the cubic $Cu_{2-x}Se$ crystal structures[39] can be derived from an antifluorite lattice[51] by positioning the selenium atoms at defined lattice sites, and positioning six to eight copper atoms per unit cell − according to the phase composition − in trigonal, tetrahedral, or octahedral holes. In α-Cu_2Se, the metal centers are positioned in an ordered manner within the selenium lattice, whereas in β-Cu_2Se they are statistically disordered over the observed sites. Even though the reported structural properties of copper selenide binary phases are not uniform, there is a clear agreement regarding the dominant coordination number of four for the copper atoms and the absence of any linearly-coordinated metal centers. Due to the hexagonal modification and the preferred coordination number of three for the copper atoms, the layer-type Cu−Se clusters approach the bulk material situation only in principle. Table 3 summarizes the interatomic distances in several copper(I) selenide compounds with respect to different coordination numbers around the metal atoms (cf. Table 2 for Cu−S systems).

Regarding the copper selenide clusters reviewed here, it is clear that a given phosphane ligand does not just generate clusters within a given size range, with another PR_2R' ligand resulting in the next largest clusters, and so on. Instead, it is evident that even very different types of phos-

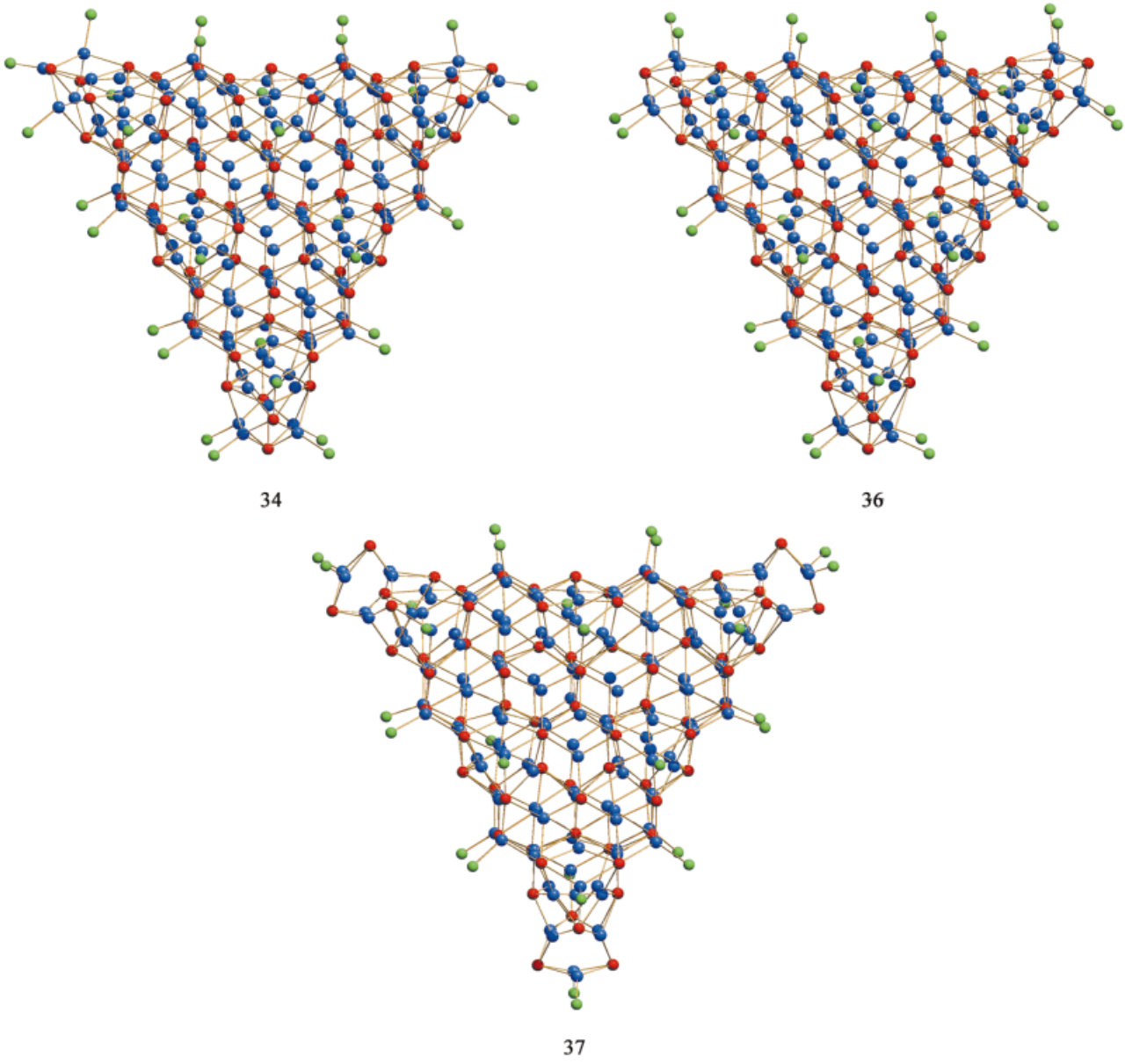

Figure 20. Molecular structures of $[Cu_{140}Se_{70}(PEt_3)_{34}]$ (**34**), $[Cu_{140}Se_{70}(PEt_3)_{36}]$ (**36**), and $[Cu_{146}Se_{73}(PPh_3)_{30}]$ (**37**) (without organic groups); in **34** and **36**, the two central copper atoms each have occupancies of 0.5, to result in one atom overall, which is statistically distributed over two sites; six further copper atoms are assigned occupancies of 0.67, resulting in four instead of six metal atoms in the overall formula

Table 3. Interatomic distances of selected Cu^I−Se systems

System	Cu−Cu [Å]	Cu−S distances for the different coordination numbers (*CN*) [Å]			Ref.
		CN = 2	*CN* = 3	*CN* = 4	
Cu−Se clusters	2.427−3.047	2.169−2.295	2.317−2.897	2.291−2.986	[9,10,12−14,17,18,21]
Cu^I−(Se_n) complexes	2.77 (av.)	−	2.37 (av.)	−	[52]
α-$KCuSe_4$	2.64−3.00	−	2.35−2.50		[53]
Binary $Cu_{2-x}Se$ phases	2.35−2.92	2.06	2.28−2.33	2.15−2.59	[39]

phanes, of different steric bulk, can lead to the formation and crystallization of similar, isomeric, or even identical Cu−Se cores if the ligand shells comply with certain requirements of regular geometry and thus protective properties. Inspection of Scheme 3 reveals that several clusters, varying significantly in size, may be formed in the presence of the same phosphane, although under different reaction conditions, so long as various suitable ligand shells can be

realized. In order to illustrate the size dependence of the cluster core on the use of different copper salts, reaction stoichiometries, solvents, and reaction temperatures, selected cluster formation reactions are shown in Schemes 5, 6, 7, and 8 with precise specifications of the respective conditions. Each scheme deals with one phosphane type.

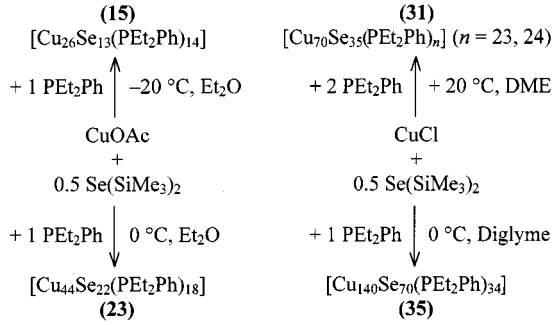

Scheme 5. Synthesis of various copper selenide clusters in the presence of PEt_2Ph under different reaction conditions

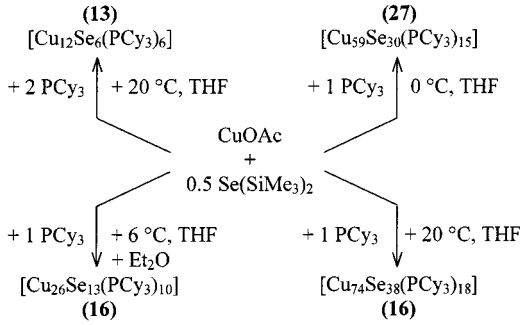

Scheme 6. Synthesis of various copper selenide clusters in the presence of PCy_3 under different reaction conditions

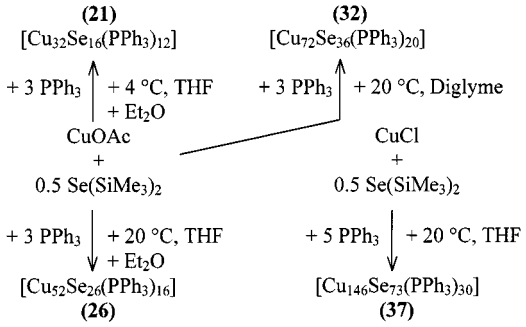

Scheme 7. Synthesis of various copper selenide clusters in the presence of PPh_3 under different reaction conditions

As for the copper sulfide clusters, comprehensive theoretical investigations within the MP2 approximation (program system TURBOMOLE) were carried out for the $[Cu_{2n}Se_n]$ clusters.[34] Again, stabilization energies per monomeric unit for a "naked" cluster growth from $n = 1$ through $n = 2-4$, 6 to $n = 10$ were calculated, along with phosphane binding energies for mono-, di-, tri-, tetra-, and hexameric species. The results are presented in Figures 21 and 22, respectively. The corresponding graphs for the Cu−S clusters, shown in Figures 6 and 7, respectively, are given once more for comparison purposes.

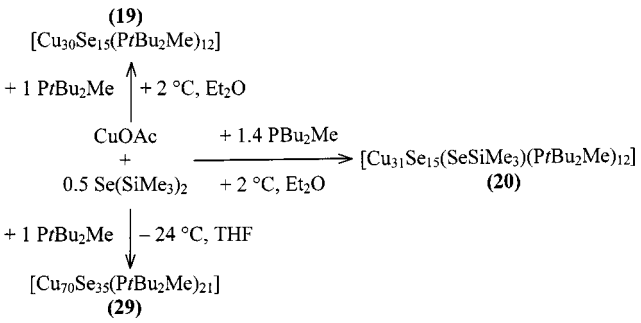

Scheme 8. Synthesis of various copper selenide clusters in the presence of $PtBu_2Me$ under different reaction conditions

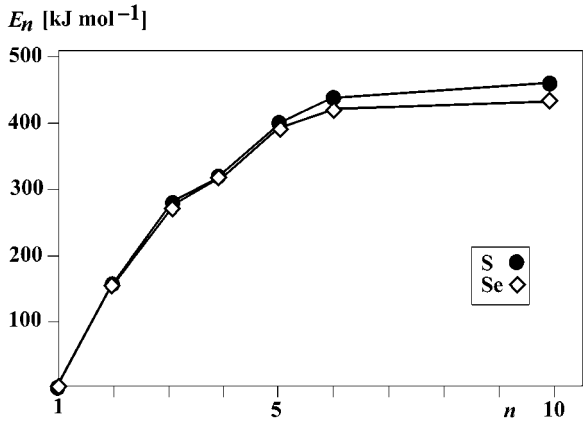

Figure 21. Variation of the stabilization energies per monomer unit in "naked" clusters $[Cu_{2n}E_n]$ (E = S, Se; $n = 1-4$, 6, 10) with the given values taking into account the total energies of the most stable structural isomers computed at the MP2 level

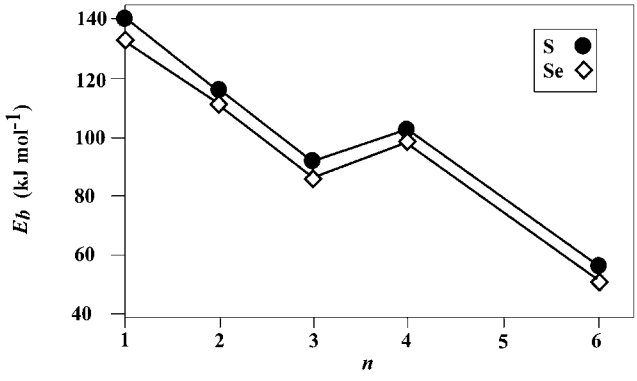

Figure 22. Variation of the Cu−P binding energies per Cu−P bond in phosphane-ligated clusters $[Cu_{2n}E_n(PH_3)_m]$ (E = S, Se; $n = 1-4$, 6; $m = 2$, 4, 6, 8); the given values taking into account the total energies of the most stable structural isomers computed at the MP2 level with respect to the total energy of PH_3 calculated by the same method

The variations in both energies are similar for the quantum chemically investigated sulfur- and selenium-bridged copper clusters. Thus, the kinetic rather than the thermodynamic stabilities of the species, and the very low

Cu−P binding energy, are the same as for the Cu−S compounds. Additionally, a comparison of the energetic properties of sulfur- vs. selenium-bridged copper clusters leads to two results. First, after nearly identical stabilization energies (maximum differences: ±5 kJ·mol^{-1}, < 2%) up to $n = 4$, a slightly higher stabilization for the Cu−S species is seen from $n = 6$ onwards. This correlates with a larger absolute value for the formation enthalpy of solid Cu_2S ($\Delta H_f° = -81.2$ kJ·mol^{-1}) than for solid Cu_2Se ($\Delta H_f° = -65.2$ kJ·mol^{-1}). However, the differences between the stabilization energies per monomeric unit for the calculated, rather small clusters do not exceed 5%. Thus, it is understandable why laser ablation spectra of copper chalcogenides do not vary much for the different chalcogens. Secondly, the Cu−P bond energies are generally 4−7 kJ·mol^{-1} (4−9%) higher for the sulfur-bridged compounds. This correlates with the discrepancy between the experiments reported by Dance et al.,[32] which show similar behavior for different chalcogens − in agreement with the calculations on "naked" species − and the experimental observations of significant differences in the syntheses and structures of phosphane-coordinated sulfur- and selenium-bridged copper clusters. The larger Cu−P binding energies computed for Cu−S clusters, relative to those computed for their Cu−Se analogues, help to explain the different ranges of observed products in the following way. Assuming that on going from the Cu−Se to the Cu−S systems the activation energy E_a for the Cu−P bond cleavage increases by a similar value as the Cu−P binding energy itself, a decrease in the respective reaction rate constant k can be calculated by means of the Arrhenius equation[54] [Equation (1)].

$$k = A \cdot e^{-E_a/RT} \quad (1)$$

At a typical cluster formation temperature of $T = 250$ K, an increase in the activation energy E_a of about 5 kJ·mol^{-1} causes a reduction in the rate constant k by one order of magnitude. Thus, the cluster growth that is initiated by the loss of a primary terminal phosphane ligand shell will occur at a lower rate for sulfur-bridged clusters. Consequently, unlike the selenium-bridged copper clusters, the Cu−S species show a much lower tendency to aggregate beyond "Cu_{12}".

3.2.2.2. Se^{2-}/SeR^--Bridged Copper Clusters

The use of alkylated or arylated derivatives $RSeSiMe_3$ (R = organic group) results in aggregation according to another mechanism, and leads to the formation of selenido/selenolato-bridged copper clusters. The given synthetic route using $RSeSiMe_3$ (Schemes 1 and 4) has not produced any selenolato-free species. This observation is at variance with those made for similar reactions with tellurolato reactants $RTeSiMe_3$ (see below). The experimentally isolated and characterized compounds listed in Scheme 4 display significantly different structures with respect to the purely E^{2-}-bridged molecules (E = S, Se). This applies even for reactions in the presence of tertiary phosphanes PPh_3 or P*i*Pr$_3$ used for the syntheses of the copper selenide clusters. The expanded ligand properties of SeR^-, which can act as both a bridging and a terminal ligand, lead to the crystallization of low nuclearity complexes with two, three, six, or nine metal centers (**38**−**42**),[20,22,30] if Se−C bond cleavage is suppressed. Larger cluster compounds can be isolated whenever Se^{2-} particles are produced during the reaction to facilitate the formation of inner selenium bridges. However, those molecules containing both selenide and selenolato ligands show structural patterns that are also common for Cu−Se clusters as far as the inner core is concerned. Figure 23 depicts compounds **38**−**42**, which only contain selenolato ligands and not selenide.

The binuclear complexes **38**[30] and **39**[20] formally show analogous molecular formulae but differ structurally according to the requirements of the different ligating components that are present. These requirements are of structural relevance for all Se^{2-}/SeR^--bridged copper clusters, as outlined in the following. Firstly, bidentate phosphanes dppR (R = organic spacer) bridge two copper centers at the periphery of the polynuclear complex or cluster molecule and therefore act simultaneously as both protecting groups and linking molecules. Secondly, selenolato ligands SeR^- have the capability to bridge between two *or* three metal centers. Additionally, they *can* be terminally bonded, as in **39**, when the Cu−Cu distance (9.01 Å) is too large for a monoatomic μ_2-bridge. Thirdly, tertiary phosphanes PR_2R' act exclusively as terminal ligands. Therefore, the copper atoms in **38** are bridged by $SePh^-$ fragments at a Cu−Cu distance of 2.846(1) Å. The molecular structure of **40**[22] also conforms to these constraints, again with the ubiquitous key factor of optimal protection of the heavy atom framework by organic groups. Compounds **41**[30] and **42**[30] are the only examples that could be isolated employing the bidentate amine ligand bipyridyl (**41**) or diphenylphosphanyl acid Ph_2PO_2H (**42**). Compound **41** seems to represent a "snapshot" molecule during cluster growth, since two $[Cu(bipy)]^+$ fragments are unsymmetrically attached to a regular cluster center. The latter is formed by a distorted Cu_4 tetrahedron [Cu−Cu: 2.650(4)−2.824(4) Å], the six edges of which are each μ_2-bridged by $SePh^-$ ligands. However, four of the phenyl selenolato groups act as μ_3-bridges in the molecule, since two bind to each of the additional $Cu(bipy)^+$ units. Having achieved charge neutrality, the sufficiently protected compound precipitated in this low nuclearity state. Much higher molecular symmetry − even crystallographic symmetry − is found for **42**. Two six-membered $Cu_3(SePh)_3$ rings are linked by three "naked" copper centers leading to a μ_3-bridging function of the $SePh^-$ groups. Additionally, the rings are clamped by three $Ph_2PO_2^-$ ligands, which bind to the six copper atoms in the two six-membered rings. Twelve phenyl groups perfectly wrap the uncharged cluster and therefore allow the termination of atomic aggregation and crystallization in THF.

As was found for the copper chalcogenide clusters **1**−**37**, the nature of the phosphane ligands plays a key role in determining the size and structures of the observed product molecules, even though they are no longer the sole protective groups at the cluster peripheries. Great success in the synthesis of copper selenide/selenolate clusters was achieved by the use of bidentate phosphanes. The variation of or-

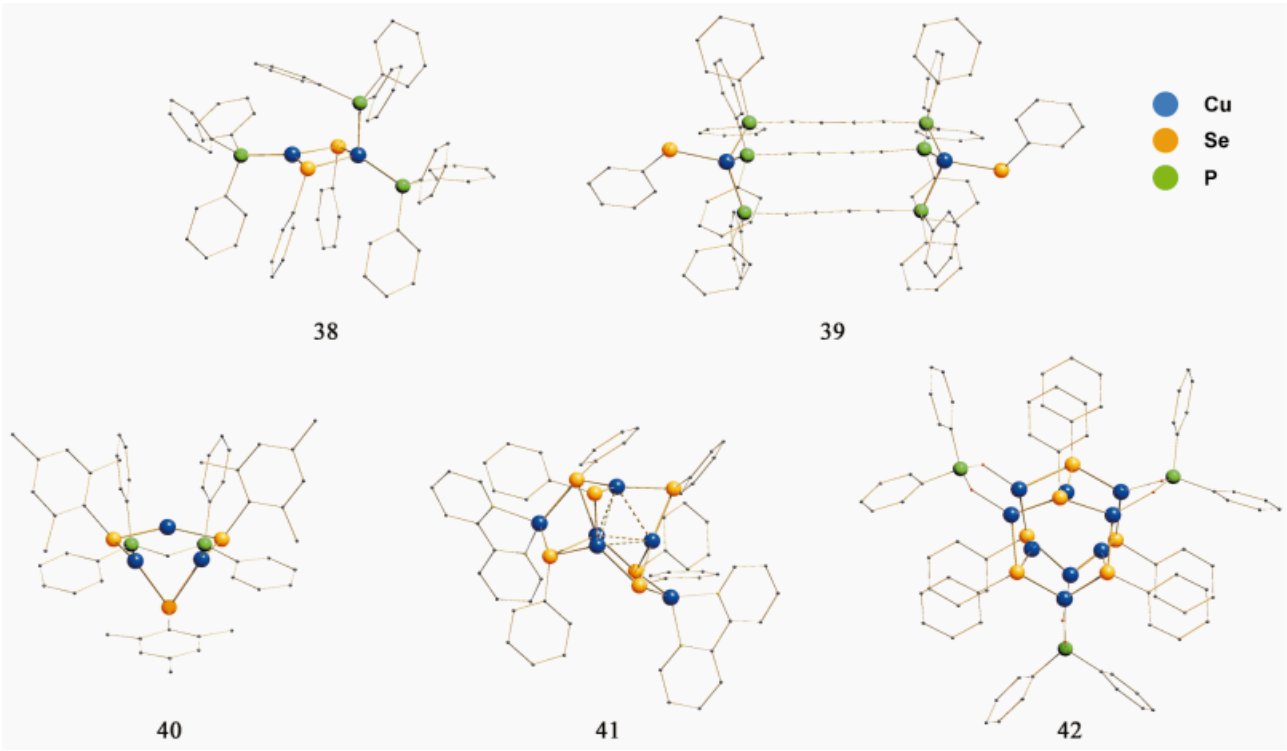

Figure 23. Molecular structures of $[Cu_2(SePh)_2(PPh_3)_3]$ (**38**), $[Cu_2(SePh)_2(dppbd)_3]$ (**39**), $[Cu_3(SeMes)_3(dppm)]$ (**40**), $[Cu_6(SePh)_6(bipy)_2]$ (**41**), and $[Cu_9(SePh)_6(O_2PPh_2)_3]$ (**42**) (without hydrogen atoms)

ganic spacers between the two ligating $[Ph_2P]$ fragments replaces the former variation of organic substituents R of PR_2R' in the selenolate-free clusters. Again, a given dppR ligand does not inflexibly restrict the synthesis to the formation of one single cluster product. Other reaction conditions discriminate between several potential compounds that can all be conveniently protected by the phosphane employed. Thus, with ethane, propane, butane, acetylene, or benzene spacers, one obtains clusters with 16, 25, 36, 38, or 58 copper centers (**43**,[20] **44**,[22] **46**−**50**,[22,30] **52**[22]), respectively. The only tertiary phosphane PR_3 to have been successfully used for the formation of higher nuclearity $Se^{2-}/SePh^-$-bridged copper clusters is P*i*Pr$_3$. With this ligand, the synthesis of molecules featuring 32, 50, or even 73 metal centers (**45**, **51**, and **53**)[23] was observed, depending on the reaction conditions. Figure 24 shows the molecular structures of **43** and the anion in **44**, which represents the only ionic copper selenide cluster compound isolated to date.

Both clusters are oblong in shape. The selenium substructure of **43** can, however, be viewed as an incipient hexagonal packing of selenium atoms. The middle "layer" consists of six atoms arranged in a zigzag fashion, while the two enclosing "layers" each contain three selenium centers occupying the quasi *A* position with respect to the quasi *B* position of the atoms in between. Four of the chalcogen bridges do not bind to phenyl groups and act as μ_4- or μ_6-bridging ligands. The $SePh^-$ ligands bind to two or three copper neighbors each, and at the same time contribute to the protection of the Cu−Se core by means of their organic substituents. Six copper atoms are linearly coordinated by two

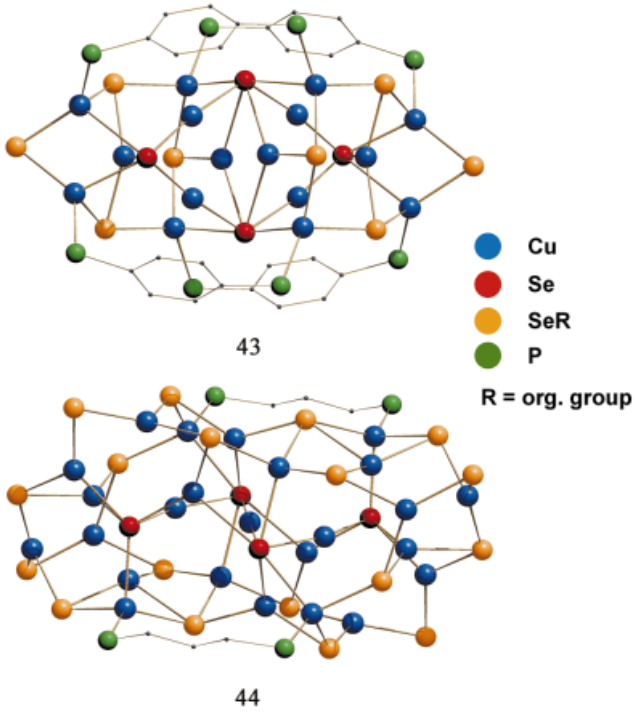

Figure 24. Molecular structures of $[Cu_{16}Se_4(SePh)_8(dppbe)_4]$ (**43**) and the anion in $[Cu(dppp)_2][Cu_{25}Se_4(SePh)_{18}(dppp)_2]$ (**44**) (without terminal phenyl groups)

selenium ligands, two show an almost trigonal-planar $[Se_3Cu]$ coordination, whereas the remaining eight metal centers occupy the centers of slightly distorted $[Se_3P]$ tetra-

hedra. Unlike in **43**, the chalcogen framework of **44** is composed of an ellipsoid-type deltahedron of four Se^{2-} ligands and 18 selenium atoms of the $SePh^-$ groups. Again, the bridging mode of the chalcogen centers is higher for the "naked" ligands (μ_5 or μ_7) than for the $SePh^-$ fragments (μ_2 to μ_4 with regard to the Cu−Se bonds). Eighteen copper atoms are positioned at the cluster periphery and belong to almost planar [Se_3Cu] or distorted tetrahedral [Se_3CuP] units. The observation that less linear [Se_2Cu] arrangements are present (four in **43**, three in **44**) underlines the trend to higher coordination numbers at the metal center with increasing molecular size, as reported for the copper selenide clusters without selenolato ligands. The cluster core is large enough to accommodate seven inner copper atoms that are either two-, three-, or four-coordinated by selenium neighbors. Comparing the compositions of **43** and the anion in **44**, one perceives an increasing preference for ligation by $SePh^-$ ligands rather than by phosphane donors. This may be explained by the dual character of the $SePh^-$ groups, which primarily form fairly stable Cu−Se cluster bonds, but also bear protective organic substituents. Thus, the ratio of selenolato selenium atoms to phosphorus atoms increases from 1:1 in **43** to 4.5:1 in **44**.

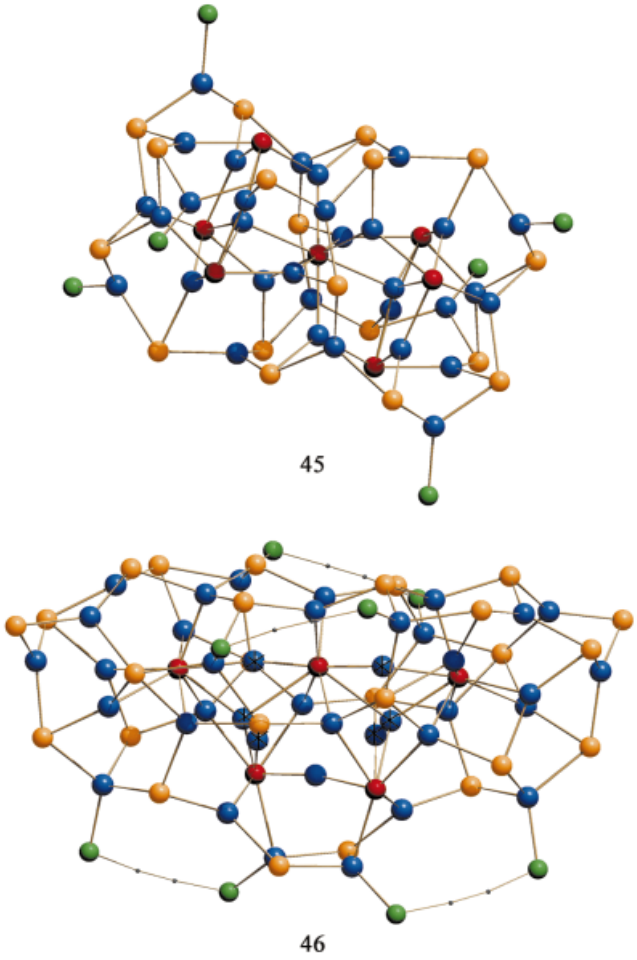

Figure 25. Molecular structures of $[Cu_{32}Se_7(SenBu)_{18}(PiPr_3)_6]$ (**45**) and $[Cu_{36}Se_5(SePh)_{26}(dppa)_4]$ (**46**) (without *n*-butyl, isopropyl, or phenyl groups); three copper atoms (marked with an asterisk) in the cluster center of **46** are distributed over six sites with occupancies of 0.5

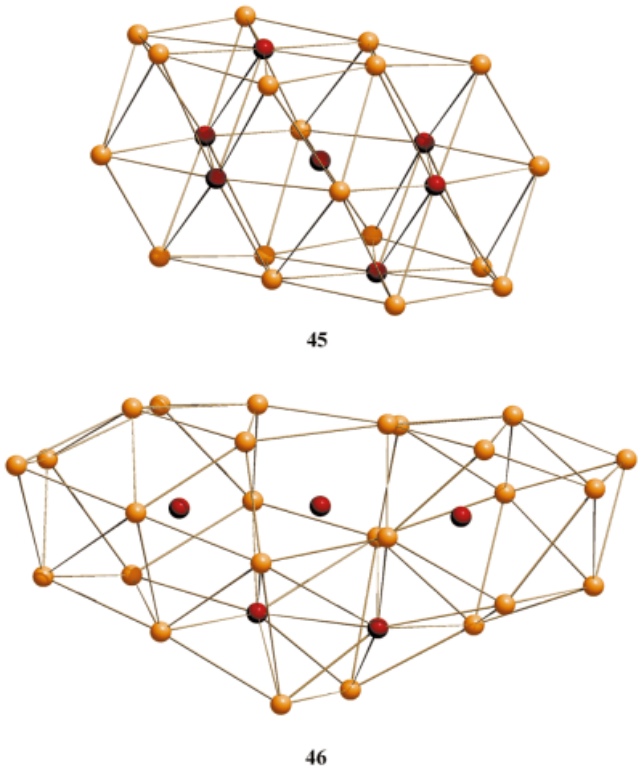

Figure 26. Selenium substructures in **45** (top) and **46** (bottom); the Se−Se lines do not represent bonding interactions, but merely help to visualize the *A-B-C* packing of selenium atoms in three layers in **45** or explain the geometry of the polyhedron in **46**

The molecular structures of the cluster compounds **45** and **46** are shown in Figure 25, while Figure 26 compares the selenium substructures in these two clusters.

As in the comparison between **43** and **44**, we again have a smaller cluster for which the structure is based on a regular packing of selenium atoms in hexagonal layers (**45**) and a larger, rather spherically shaped compound that features a polyhedral selenium framework (**46**). However, the selenium layers in the $SenBu^-$-bridged species **45** are packed in an *A-B-C* fashion similar to the Cu_2Se solid-state structure, which is unparalleled for all copper chalcogenide clusters characterized to date. This similarity between the atomic arrangement of a cluster molecule and the non-molecular Cu_2Se suggests that a nanosized fragment of a bulk structure may indeed be stabilized by coating the surface with suitable groups. This tendency has also been observed in three silver selenide/selenolate clusters, $[Ag_{112}Se_{32}(SenBu)_{48}(PtBu_3)_{12}]$, $[Ag_{114}Se_{34}(SenBu)_{46}(PtBu_3)_{14}]$, and $[Ag_{172}Se_{40}(SenBu)_{92}(dppp)_4]$.[55] Compound **45** is the only copper selenide/selenolate compound that contains $SenBu^-$ groups like those found in these silver clusters. It is not yet proven, but is nevertheless conceivable, that the packing of the selenium atoms is influenced by the nature of the organic group attached to the selenolato ligand. The chalcogen layers in **45** are centered by a large planar rhombus of nine selenium atoms. Five of them are "naked" Se^{2-} ligands in

the cluster network, while the four vertex atoms belong to Se*n*Bu$^-$ groups. Above and below this middle layer, one finds two similar but truncated rhombuses consisting of only eight selenium atoms, the "central" ones not being bonded to organic substituents. However, the size dependency of the structural properties seems to be different from that of the selenolato-free copper clusters. Thus, layer-type structures are observed even for smaller molecules like **43** or **45**, as well as for larger spherical ones. Additionally, a return to lower average coordination numbers in larger clusters may arise, as observed in **45**. The location of the copper atoms in **45** can be described with reference to the selenium grid. The six phosphane-bound copper centers bind to two selenium atoms of Se*n*Bu$^-$ ligands and are situated on the cluster periphery. Six copper atoms are located approximately within the selenium layers and have trigonal-planar coordination geometries with normal Cu−Se bond lengths of 2.406(2)−2.483(2) Å. The other 20 metal centers are positioned between the layers of selenium atoms. Two of these show ideal tetrahedral environments, while the others are shifted away from the centers of tetrahedral holes. As a result, each of these displays only three normal Cu−Se bonds, with the fourth Cu−Se distance being relatively long (3.18−3.35 Å). The tendency to occupy tetrahedral holes − even unsymmetrically − is again consistent with the structural properties of bulk Cu_2Se. In **46**, five inner Se^{2-} ligands are enclosed by a shell of 26 $SePh^-$ fragments. The bridging modes of the Se^{2-} ligands amount to μ_7 or μ_8, whereas the selenium atoms of the $SePh^-$ groups act only as μ_2- to μ_4-bridges between adjacent copper atoms. The copper centers show coordination numbers of two, three, or four, within $[Se_2Cu]$, $[Se_3Cu]$, and $[Se_4Cu]$ or $[Se_3CuP]$ units, respectively. Depending on their position inside the cluster or at the surface, the selenium neighbors of the metal atoms are exclusively Se^{2-}, or both Se^{2-} and $SePh^-$ ligands. As for compounds **43** or **44**, the number of terminal selenolato groups is greater than the number of ligating phosphorus atoms (SeR/P ratios: 3:1 in **45**, 3.25:1 in **46**).

Four very similar Cu/Se/SePh clusters are formed in the presence of either dppe, dppp, or dppb (**47**−**50**). The syntheses of the isomeric, mixed-valence compounds **47** and **48**, containing 36 copper centers, were carried out in THF. The isomeric "Cu_{38}" clusters **49** and **50**, which formally contain exclusively Cu^+, were crystallized from toluene. Besides the different solvents, the reactions producing the dppb-ligated compounds **48** and **50** differed in the CuCl:dppb ratios (3.1:1 for **48**, 5:1 for **50**). In Figure 27, the molecular structures of **47** and **49** are given as examples.

Cluster **47** crystallizes in the trigonal space group $R\bar{3}$, whereas **48**−**50** crystallize in triclinic $P\bar{1}$. Despite the different crystallographic symmetries, all four compounds display very similar structural properties. A closer look at the atomic arrangements may explain the preference for this prototypical cluster framework in terms of the highly symmetrical substructures. A central selenium atom positioned at the inversion centers of the clusters is surrounded by a distorted icosahedron of twelve copper atoms. The latter is itself enclosed by another distorted Se_{12} icosahedron. An

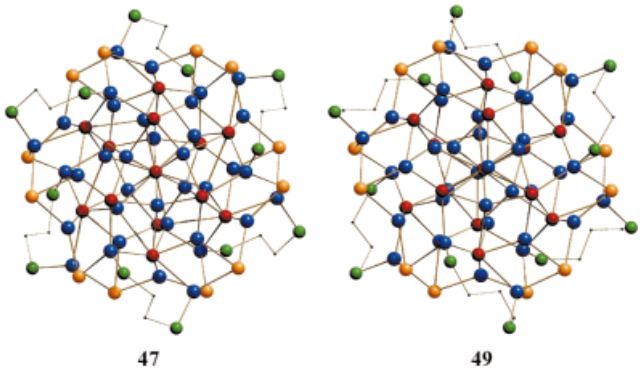

Figure 27. Molecular structures of $[Cu_{36}Se_{13}(SePh)_{12}(dppe)_6]$ (**47**) and $[Cu_{38}Se_{13}(SePh)_{12}(dppp)_6]$ (**49**) (without phenyl groups)

alternate packing of Cu_{12} and Se_{12} icosahedra has already been discussed for the Cu−Se clusters **14** and **15** (Figures 9 and 10). In these compounds, one polyhedron is positioned with its edges perpendicular to the edges of the polyhedron beneath. Unlike that pattern, the Se_{12} and Cu_{12} icosahedra in **47**−**50** are arranged such that one of the idealized fivefold axes of one polyhedron is parallel to one of the idealized threefold axes of the other and vice versa. The central $[Se_{13}Cu_{12}]$ unit of **47** is shown as an example in Figure 28.

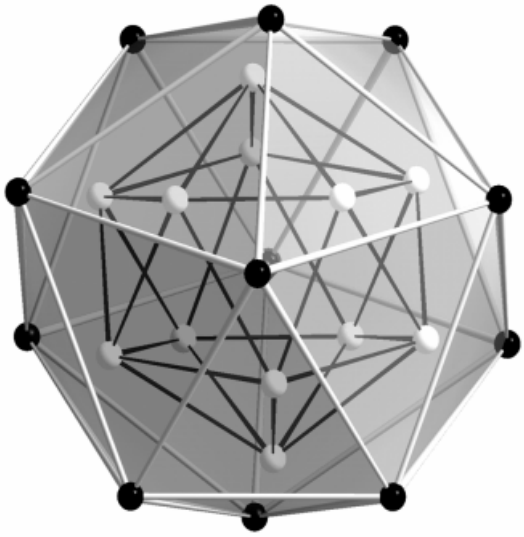

Figure 28. The central $[Se_{13}Cu_{12}]$ unit in **47**; the drawn lines only represent polyhedral edges and do not imply bonding interactions

In this way, six edges and six faces of the Cu_{12} icosahedron are bridged by the selenide ligands that form the Se_{12} polyhedron. The cluster core is then extended to the periphery by coordination of the Se_{12} substructure by another 24 copper atoms, twelve of which are ligated by the six dppR ligands. All 24 of these copper atoms are also bridged by twelve μ_3-$SePh^-$ groups, which are positioned at the cluster surface between the phosphane molecules. Except for the μ_{12}-bridging central selenium atom, the selenide ligands act as μ_6-bridges (six in both **47** and **48**, all twelve in **49** and **50**) or μ_5-bridges (six in both **47** and **48**) between copper centers. The different numbers of copper neighbors

per selenium atom in **47** or **48** on the one hand, and in **49** or **50** on the other, is caused by two copper atoms being formally absent in the molecular structures of **47** or **48**, resulting in the mixed-valence situation, but present in **49** and **50**. The respective copper atoms each coordinate to one of the Se_{12} icosahedral faces and form a straight Cu−Se−Cu axis, with the central selenium atom in the middle. At the same time, this $[Cu_2Se]$ arrangement represents an idealized threefold axis that is not realized crystallographically in **49** or **50**. The metal centers are surrounded in a distorted trigonal-planar or tetrahedral fashion. All Cu−Se distances in the mixed-valence clusters lie within the range of the Cu−Se bond lengths in all four clusters [2.301(4)−2.888(3) Å] and thus give no evidence for any localization of the Cu^{2+} centers. However, the range of the Cu−Cu contacts in **47** or **48** [2.511(3)−2.943(4) Å] is rather narrower than that found for **49** or **50** [2.305(4)−3.040(3) Å]. The spherical, somewhat oblate molecules show a maximum total diameter of 23.9−25.7 Å.

The use of different selenolato sources and different optimized reaction conditions leads to three different copper selenide/selenolate clusters with terminal $PiPr_3$ ligands, i.e. **45** (Figures 25 and 26), **51**, and **53**. The latter is synthesized in an unusual manner by the use of both $PhSeSiMe_3$ and $Se(SiMe_3)_2$ in the same reaction and is discussed below. Scheme 9 summarizes the syntheses of the $PiPr_3$-ligated clusters, specifying the reaction conditions in detail. Figure 29 shows the molecular structure of compound **51**.

Looking at Figure 29, one gets the impression that "normal" cluster growth occurred in the presence of a tertiary phosphane, and with Se−C bond cleavage, to result in the formation of a copper selenide cluster represented by the $[Cu_{40}Se_{20}]$ central unit of **51**. Only the lateral attachment of two symmetry-equivalent $[Cu_5(SetBu)_5(PiPr_3)_2]$ fragments reminds us of the presence of the selenolato reactant. This is in contrast to the equally $PiPr_3$-ligated structure of **45**, which shows only seven Se^{2-} ligands along with 18 $SetBu^-$ groups. No definite correlation between the clearly different courses of cluster formation and the respective reaction conditions can be delineated based on such a limited sample size, but it is very likely that the Cu:P ratio of the reactants and the temperature play important roles. The copper atoms in **51** bind to Se^{2-}, $SePh^-$, and $PiPr_3$ ligands in different ratios to achieve coordination numbers of two (albeit with a bent coordination geometry indicating a weak third interaction), three, or four. The selenium atoms bearing *tert*-butyl groups act as μ_3-bridges between copper atoms, whereas the Se^{2-} ligands bridge between five, six, or seven copper neighbors. The molecules are protected in the usual way by the $PiPr_3$ ligands and the organic substituents of the $SetBu^-$ groups.

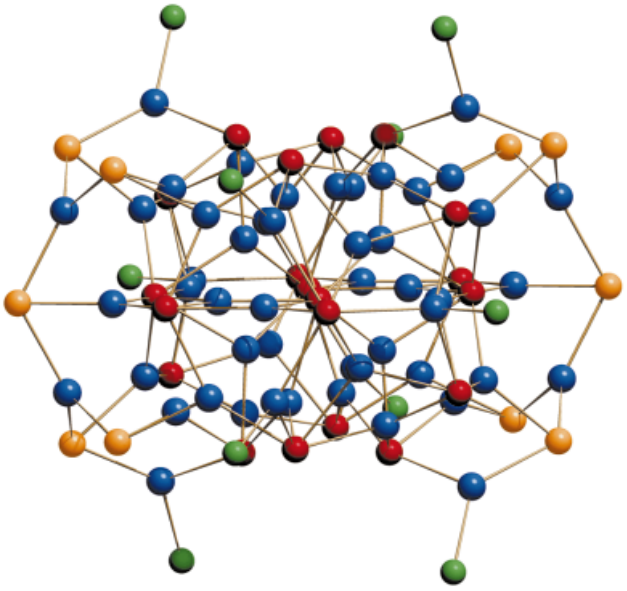

Figure 29. Molecular structure of $[Cu_{50}Se_{20}(SetBu)_{10}(PiPr_3)_{10}]$ (**51**) (without organic groups)

The molecular structure of another dppR-ligated copper cluster (R = a = acetylene) with both selenido and selenolato ligands, **52**, again possesses a high symmetry. This time, the molecular symmetry is underlined by a very high crystallographic symmetry. The compound crystallizes in the cubic space group $F\bar{4}3c$ and thus represents the second known copper chalcogenide cluster besides **14** (space group $Fm\bar{3}$) with a cubic crystal lattice. The molecular structure of **52** is illustrated in Figure 30.

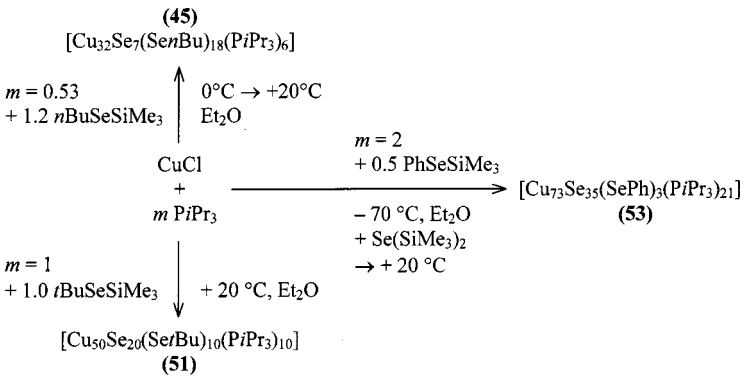

Scheme 9. Synthesis of various selenido/selenolato-bridged copper clusters in the presence of $PiPr_3$ under different reaction conditions

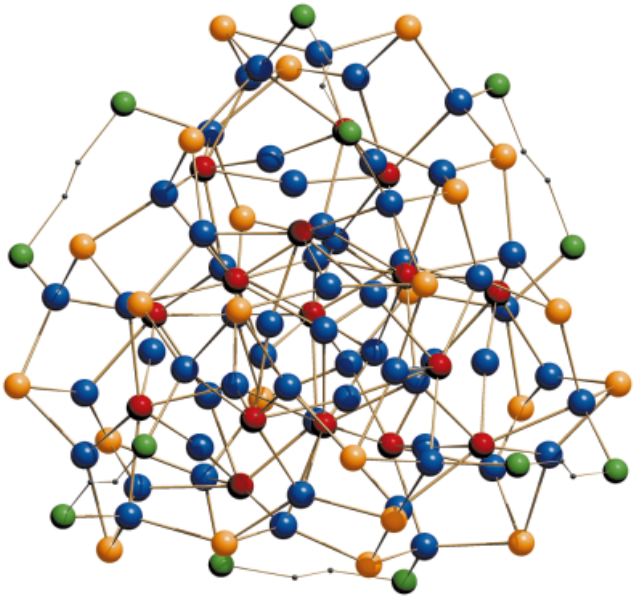

52

Figure 30. Molecular structure of $[Cu_{58}Se_{16}(SePh)_{24}(dppa)_6]$ (**52**) (without phenyl groups)

As observed for compounds **47**−**50**, the cluster core is oblate in shape, but in contrast to **47**−**50** it is not based on icosahedral fragments. Instead, a central Cu_4 tetrahedron shares its corners with four further Cu_4 units, which, in turn, share their *trans* faces with a Cu_6 octahedron. The remaining 30 copper atoms are situated between these polyhedra or are connected at the exterior of the polyhedral arrangement. The copper substructure of **52** is shown in Figure 31.

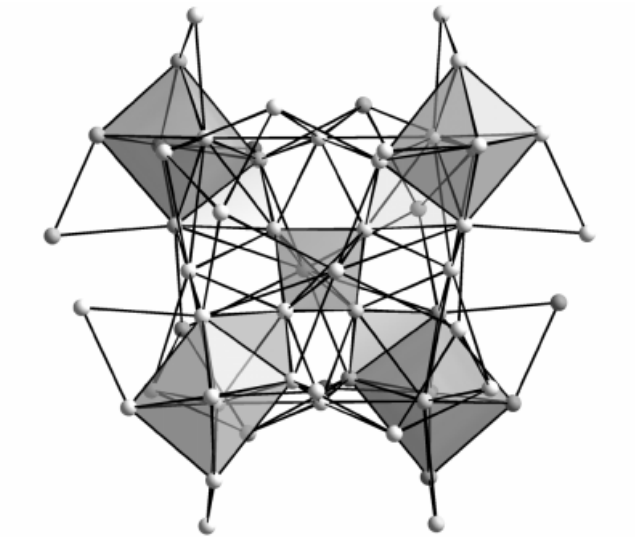

Figure 31. The copper substructure in **52**; the connected Cu_4 tetrahedra and Cu_6 octahedra are highlighted by gray shading; Cu−Cu distances are drawn up to 3.012(4) Å

Even though the Cu_{58} substructure has to be assigned a formal charge 56+ (assuming Se^{2-} and $SePh^-$ ligands as well as electroneutrality in the sum), which implies an extraordinary mixed-valence Cu^+/Cu^0 compound, one does not find any indication of exceptional Cu−Cu binding interactions. The Cu−Cu distances lie within the usual range of 2.540(3)−3.012(4) Å. Thus, the cluster core is held together by bridging selenido or selenolato ligands in the usual way. The former act as μ_5- or μ_6-bridges, while the latter form μ_3-bridges between adjacent copper atoms. Despite the large cluster size, metal centers with near-linear, trigonal-planar, and tetrahedral coordination are observed. Therefore, it is again apparent that the size-dependencies of the structural principles discussed for chalcogenolato-free copper sulfide or copper selenide clusters are generally invalid in the Cu/Se/SeR cluster systems. Six dppa ligands and 24 phenyl groups of the $SePh^-$ fragments protect the cluster molecule. Hence, **52** continues the series of compounds that show a significant preference for protection by the SeR^- groups rather than by the phosphane ligands. The clusters **43** and **47**−**51** represent exceptions from this series as their SeR/P ratios all amount to 1:1.

The largest cluster that displays both Se^{2-} as well as SeR^- ligands in the cluster framework is **53**. Its molecular structure is shown in Figure 32.

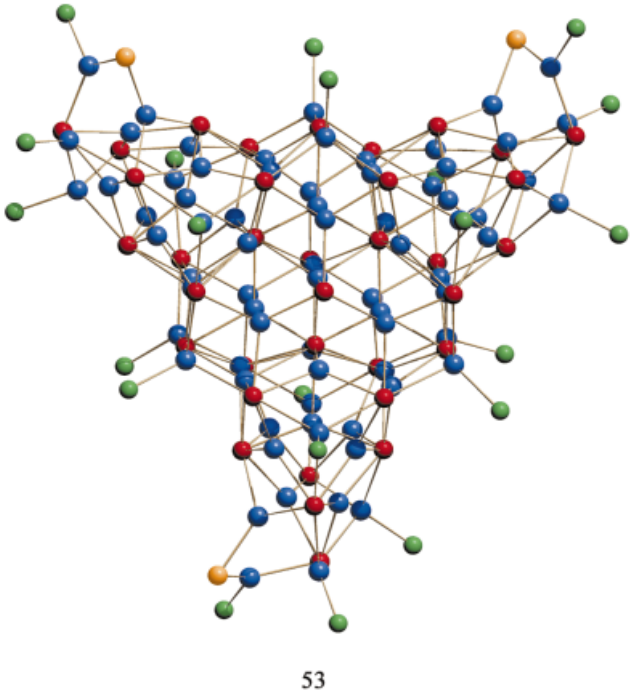

53

Figure 32. Molecular structure of $[Cu_{73}Se_{35}(SePh)_3(PiPr_3)_{21}]$ (**53**) (without organic groups)

This cluster displays a $[Cu_{70}Se_{35}]$ core, which is identical to that observed in **28** and **29** (Figures 18 and 19). Only three additional Cu−SePh fragments positioned at the corners of the triangular molecule distinguish **53** from the slightly smaller "Cu_{70}" clusters. The fact that one observes a typical copper selenide cluster structure with only a few

selenolato groups present is surprising, since $PhSeSiMe_3$ was the first selenium source to be added during the synthesis. This again illustrates the distinct preference for the "Cu_{70}" molecular structure, which is formed whenever the reaction conditions (Scheme 9) and the solubility situation enable the cluster growth to proceed until this large cluster compound crystallizes.

3.2.3. Optical Spectra and Thermal Behavior

The discrete molecular cluster species reviewed thus far are ideal subjects for studying the molecular quantum size effect,[3] which is one of the most absorbing questions connected with research in the field of cluster chemistry. In this regard, one must investigate the electronic properties of the cluster species, and first of all the relationship between cluster size and the HOMO−LUMO gap. Theoretical investigations have provided preliminary answers to this question.[34,37] The first dipole- and spin-allowed singlet or triplet excitations of selected "naked" copper selenide clusters $[Cu_{2n}Se_n]$ (up to $n = 15$) were calculated at the CIS level[56] (CIS = configuration interaction considering single excitations) for structures previously optimized for the same symmetry employing the CCSD(T) method[57] [CCSD(T) = coupled cluster approximation up to single and double excitation with additional consideration of third excitations by means of perturbation theory] ($n = 1, 2$) or the MP2 method ($n > 2$). Triplet excitations were investigated in order to take into account the fact that relativistic effects (spin-orbit coupling)[58] are significant in Cu−Se compounds. The results are presented in Figure 33.

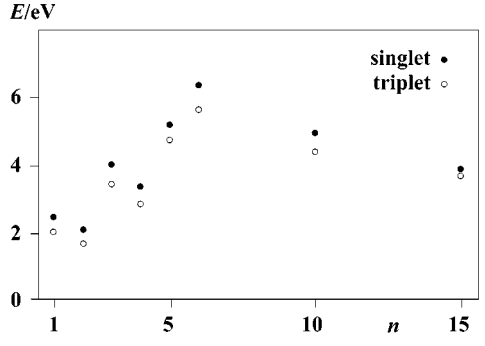

Figure 33. First dipole- and spin-allowed singlet or triplet excitations of selected "naked" copper selenide clusters $[Cu_{2n}Se_n]$ (up to $n = 15$), calculated at the CIS level (CIS = configuration interaction with single excitations) for structures previously optimized for the same symmetry employing the CCSD(T) method [CCSD(T) = coupled cluster up to single and double excitation with additional consideration of third excitations by means of perturbation theory] ($n = 1, 2$) or the MP2 method ($n > 2$)

The changes in the energy values for singlet or triplet excitations with increasing cluster size show similar trends, with the triplet excitation energies being 0.2−0.7 eV lower than the singlet ones. The excitation energies increase with a slight oscillation to a value of around 6 eV for the hexamer ($n = 3$), decreasing thereafter down to a value of ca. 3.8 eV for the $[Cu_{30}Se_{15}]$ species. The initial increase in the excitation energy values can be explained firstly by a stabilization of selenium *p*-orbitals by admixture of *s*-, *p*-, or *d*-contributions from the copper atoms, and secondly by an increasing degree of completion of the selenium shell around the copper substructure. The latter reduces the space for electrons in excited states with *s*-character. Thus, for $[Cu_{12}Se_6]$, significant *p*-type contributions are observed for the calculated transitions. The two exceptions ($n = 2, 4$) to this trend feature less compact molecular structures, which lead to lower excitation energies. Once the covering of selenium atoms on the copper framework has been completed, the overall size of the cluster molecules becomes more important. This confirms the assumption of separating the Se-*p* and Cu-*s* states to form valence and conducting bands. For clusters of ever increasing size, and ultimately bulk Cu_2Se, the first excitation energy should approach a value of ca. 1 eV.[59,60] According to the quantum chemical investigations, "naked" "middle-sized" copper selenide clusters should be colorless insulators that gradually adopt semiconductor properties with increasing cluster size. Calculations on small PH_3- or PMe_3-ligated copper selenide clusters indicate an increase in the first excitation energies compared to the corresponding "naked" clusters. Estimating a degree of error of about 1.5 eV, the respective transitions could indeed lead to the absorption of violet light, in agreement with the observed red color of the small copper selenide clusters.

The crystals obtained in the cluster formation reactions are colored. The intensity of the color increases on going from sulfur- to selenium- to tellurium-bridged compounds (see below), as expected for an increase in covalent or (semi)metallic binding properties. Small copper sulfide or selenide clusters form light-red, orange, or purple crystals. With increasing cluster size, the color becomes dark-red, reddish-black, and finally black with a metallic sheen. The optical spectra of some copper selenide cluster compounds were studied by means of solid-state UV/Vis spectroscopy. The single-crystalline samples were powdered and sus-

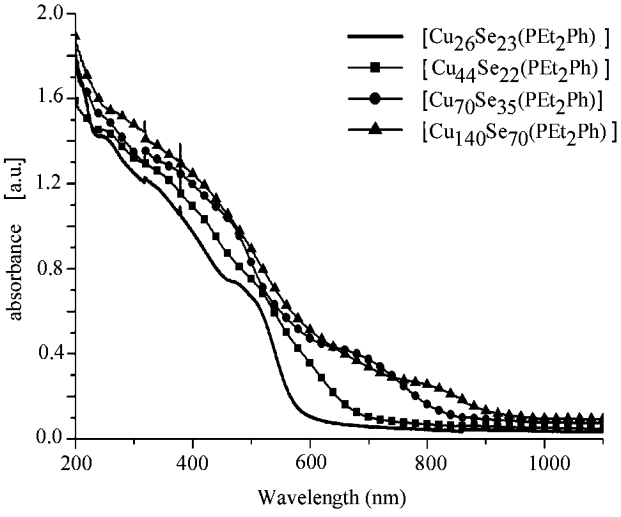

Figure 34. Solid-state UV/Vis absorption spectra of PEt_2Ph-ligated compounds **15**, **23**, **31**, and **35** that contain 26, 44, 70, and 140 copper atoms; for the measurements, powdered single-crystalline samples in mineral oil were placed between two quartz plates

pended in mineral oil between two quartz plates. Figure 34 shows the absorption spectra of the PEt_2Ph-ligated compounds **15**, **23**, **31**, and **35**, which contain 26, 44, 70, and 140 copper atoms, respectively. The influence of the phosphane ligands should be broadly the same for all four clusters, hence the increments in the position of the absorption band can be attributed solely to the increasing size and structural changes of the Cu−Se framework.

A shift of the absorption band to higher wavelengths with increasing cluster size is observed. In principle, this is consistent with a decrease in the HOMO−LUMO gap in the same direction. Although the experimental value for the band gap in Cu_2Se (1.1 eV, i.e. 1127 nm, from optical measurements;[59] 0.37 eV, i.e. 3350 nm, from electrochemical measurements[61]) is not reached, the trend can be explained in terms of the quantum size effect. An approximation of the HOMOs and LUMOs with increasing nuclearity is clearly observed. The broadness of the bands in the cluster spectra may be a result of the measurements being made at room temperature and/or a charge-transfer contribution to the observed transitions.

It has been known for several years that Cu−P bond cleavage occurs upon heating the copper selenide clusters, forming Cu_2Se as a black powder. In addition, XPS experiments (XPS = X-ray photoelectron spectroscopy) have shown that partial removal of the terminal ligands under the experimental conditions (room temperature, high vacuum) leads to an aggregation of the remaining clusters to larger, still ligated particles with a very narrow size distribution.[33] This agrees with the results of the quantum chemical investigations, which indicated the clusters to be metastable species with respect to the binary chalcogenide Cu_2E, and pointed to very low calculated Cu−P binding energies (see above). Thermogravimetric analysis of **31** (Figure 35) showed that all the phosphane ligands are removed in a single-step process within 20 minutes. The temperature required for this process is dependent on the experimental pressure.

Carrying out the experiment at normal pressure in a nitrogen flow, the ligands are all lost at 226 °C. On reducing the pressure down to $2\cdot10^{-6}$ mbar, this temperature decreases to 145 °C. However, on calculating the mass difference, one observes a loss of 33.6% rather than the 35.6% that should have been lost theoretically. This observation, as well as a residue of 1.2% carbon in the resulting copper selenide powders, indicates a slight amount of decomposition of the PR_2R' ligands. Following the process by means of powder diffraction, the intense reflections of the crystalline cluster in the range $2\Theta = 2-10°$ disappear during the thermogravimetric experiments, and are replaced by lower intensity reflections in the 2Θ range 10−55°. Sharp reflections from crystalline α-Cu_2Se are finally observed after annealing the powder at 600 °C. The Scherrer equation[62] [Equation (2)] gives a relationship between the medial peak width β and the particle size *D*.

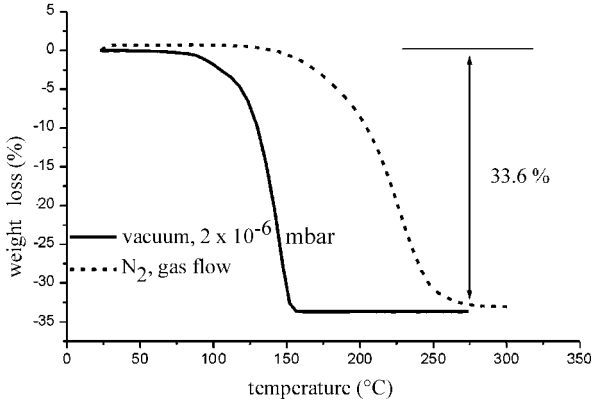

Figure 35. Results of a thermogravimetric analysis of **31** under different pressures

$$D = (K\cdot\lambda\cdot57.3)/(\beta\cdot\cos\theta) \quad (2)$$

where *D* is the average particle size perpendicular to the reflecting plane, *K* is the atomic form factor (here 1.0), λ is the wavelength of the X-ray radiation (here Cu-K_α: λ = 1.5418 Å), β is the peak width measured at half maximum intensity, and θ is the diffraction angle.

After calibration of the peak width at half maximum intensity for the diffractometer using LaB_6, an average particle size of $D = 117$ Å could be calculated for Cu_2Se powders generated by heating **31** to 150 °C at $2\cdot10^{-6}$ mbar for 20 min. This value for *D* is 7.8 times the size of the $[Cu_{70}Se_{31}]$ core of **31** (15 Å). The results give a further indication of a partial, controlled collapse of the cluster particle lattice.

3.3. Tellurium-Bridged Copper Clusters

In this section we focus on the description of the syntheses and structures of ligand-stabilized copper telluride cluster molecules. Solid-state copper tellurides as well as ternary alkali metal copper telluride compounds, which consist of *n*-dimensionally linked copper telluride clusters, are beyond the scope of this review. Their syntheses have become more frequent, although there are still only a limited number of examples, e.g. KCuTe,[63] NaCuTe,[48a] KCu_3Te_2,[64] $NaCu_3Te_2$,[65] $K_2Cu_5Te_5$,[66] and $K_4Cu_8Te_{11}$,[67] all of which have been prepared by means of melt reactions. The recently synthesized compound $K_3Cu_{11}Te_{16}$ [68] is the first example of a ternary alkali metal copper telluride crystallized from supercritical 1,2-diaminoethane.

3.3.1. Synthesis

According to the reaction pathways shown in Scheme 10, the syntheses of ligand-stabilized copper telluride clusters have mainly been achieved in one of three different ways.[11,16,19,20,24,25,31,69]

The reaction of copper(I) acetate with $Te(SiMe_3)_2$ at low temperatures (−50 to −20 °C) yields small cluster compounds with stoichiometric compositions. At higher reaction temperatures, up to 25 °C, larger clusters can be isolated that are mostly of the mixed-valence type. Similar mixed-valence compounds have also been isolated from reactions of copper(I) chloride with $Te(SiMe_3)_2$ at lower tem-

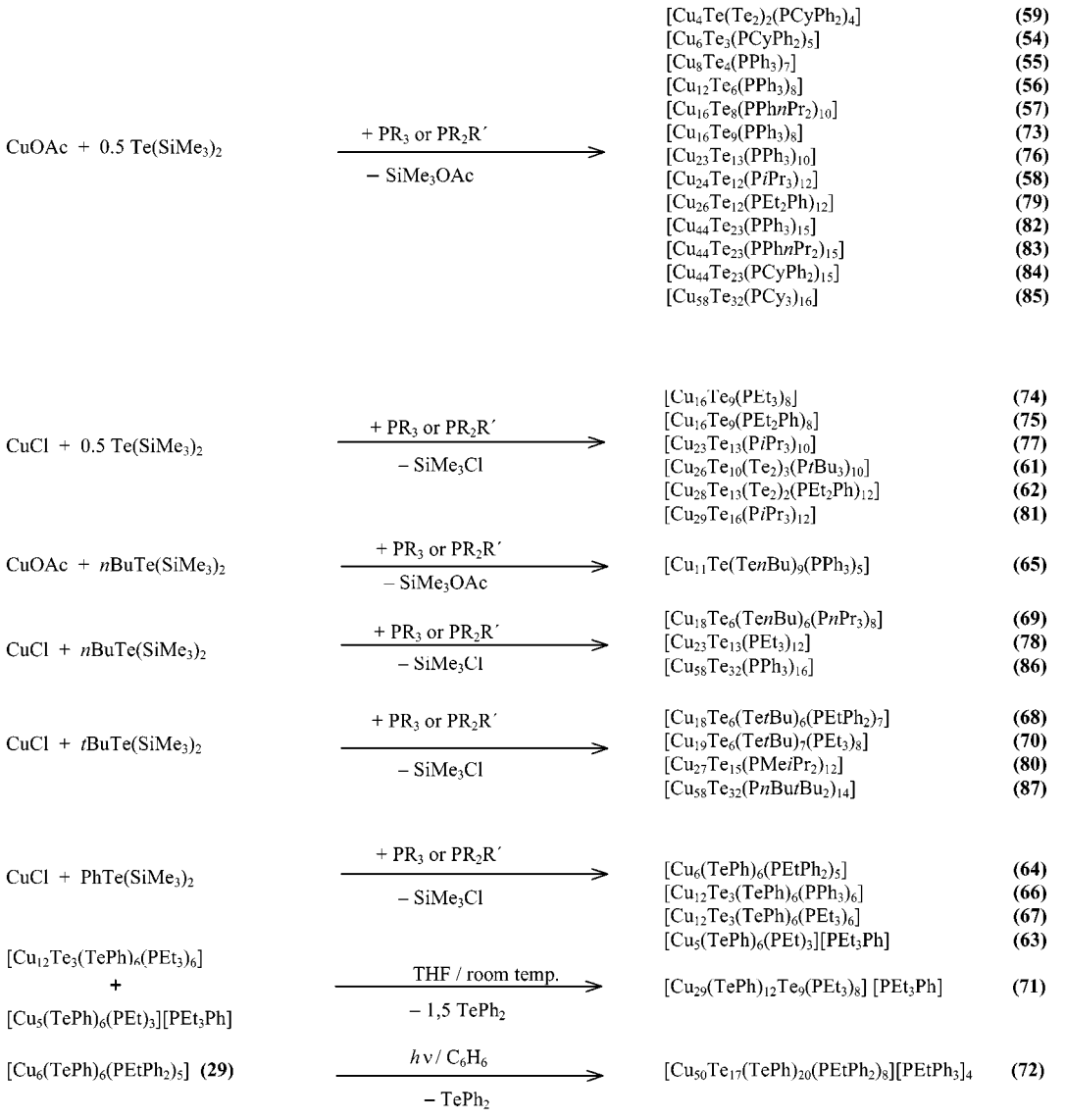

Scheme 10. Survey of the reaction pathways for the synthesis of ligand-stabilized tellurido or tellurido/tellurolato-bridged copper clusters

peratures (down to −70 °C). By treating copper(I) chloride or copper(I) acetate with tellurolate compounds $RTeSiMe_3$ (R = *t*Bu, *n*Bu, Ph), one obtains clusters containing both RTe^- and Te^{2-} ligands as a result of the facile cleavage of the Te−C bond. In some cases, we isolated clusters featuring Te−Te bridges. Examples of syntheses of larger copper telluride clusters starting from cluster precursors are the light-induced formation of $[Cu_{50}Te_{17}(TePh)_{20}(PEtPh_2)_8][PEtPh_3]_4$ (**72**) from $[Cu_6(TePh)_6(PEtPh_2)_5]$ (**64**) in benzene,[19] and the co-condensation of $[Cu_{12}Te_3(TePh)_6(PEt_3)_6]$ (**67**) with $[Cu_5(TePh)_6(PEt)_3][PEt_3Ph]$ (**63**) to form $[Cu_{29}(TePh)_{12}Te_9(PEt_3)_8]$ $[PEt_3Ph]$ (**71**).[69]

Table 4 summarizes all the Cu−Te cluster compounds that have been synthesized and structurally characterized by single-crystal X-ray diffraction analysis to date. The species can be subdivided into four main groups, three of which consist of compounds of stoichiometric compositions $[Cu_{2n}Te_{n-x}(TeR)_{2x}(PR_2R')_m]$ that differ in the nature of their tellurium ligands, while the fourth represents the group of mixed-valence clusters.

3.3.2. Structures

The structures of the tellurium-bridged copper clusters (Figures 39−42; see below) differ from those of the copper sulfide or selenide clusters, with the exception of some smaller ones. This can be understood against the background of the larger atomic and ionic radii of the tellurium atoms compared to the lighter chalcogen atoms, allowing higher coordination numbers and therefore new binding geometries, which lead to different structures. In addition, one finds a greater tendency to form mixed-valence clusters. This is in line with the existence of many stable binary compounds with compositions $Cu_{2-x}Te$[40] and with the situ-

Table 4. Classification of copper telluride clusters into stoichiometric or mixed-valence systems according to the types of tellurium ligands

Stoichiometric						Mixed-valence	
with only Te^{2-} ligands		with additional Te−Te bridges		with additional TeR^- ligands			
$[Cu_6Te_3(PCyPh_2)_5]$	**(54)**[31]	$[Cu_4Te(Te_2)_2(PCyPh_2)_4]$	**(59)**[31]	$[Cu_5(TePh)_6(PEt)_3][PEt_3Ph]$	**(63)**[69]	$[Cu_{16}Te_9(PPh_3)_8]$	**(73)**[24]
						$[Cu_{16}Te_9(PEt_3)_8]$	**(74)**[11]
						$[Cu_{16}Te_9(PEt_2Ph)_8]$	**(75)**[11]
$[Cu_8Te_4(PPh_3)_7]$	**(55)**[24]	$[Cu_4(Te_2)_2(PiPr_3)_4]$	**(60)**[11]	$[Cu_6(TePh)_6(PEtPh_2)_5]$	**(64)**[19]	$[Cu_{23}Te_{13}(PPh_3)_{10}]$	**(76)**[24]
						$[Cu_{23}Te_{13}(PiPr_3)_{10}]$	**(77)**[11]
						$[Cu_{23}Te_{13}(PEt_3)_{12}]$	**(78)**[16]
$[Cu_{12}Te_6(PPh_3)_8]$	**(56)**[24]	$[Cu_{26}Te_{10}(Te_2)_3(PtBu_3)_{10}]$	**(61)**[11]	$[Cu_{11}Te(TenBu)_9(PPh_3)_5]$	**(65)**[16]	$[Cu_{26}Te_{12}(PEt_2Ph)_{12}]$	**(79)**[24]
$[Cu_{16}Te_8(PPhnPr_2)_{10}]$	**(57)**[24]	$[Cu_{28}Te_{13}(Te_2)_2(PEt_2Ph)_{12}]$	**(62)**[11]	$[Cu_{12}Te_3(TePh)_6(PPh_3)_6]$	**(66)**[19]	$[Cu_{27}Te_{15}(PMeiPr_2)_{12}]$	**(80)**[25]
				$[Cu_{12}Te_3(TePh)_6(PEt_3)_6]$	**(67)**[69]		
$[Cu_{24}Te_{12}(PiPr_3)_{12}]$	**(58)**[24]			$[Cu_{18}Te_6(TetBu)_6(PEtPh_2)_7]$	**(68)**[25]	$[Cu_{29}Te_{16}(PiPr_3)_{12}]$	**(81)**[11]
				$[Cu_{18}Te_6(TenBu)_6(PnPr_3)_8]$	**(69)**[16]		
				$[Cu_{19}Te_6(TetBu)_7(PEt_3)_8]$	**(70)**[25]	$[Cu_{44}Te_{23}(PPh_3)_{15}]$	**(82)**[24]
						$[Cu_{44}Te_{23}(PPhnPr_2)_{15}]$	**(83)**[24]
						$[Cu_{44}Te_{23}(PCyPh_2)_{15}]$	**(84)**[24]
				$[Cu_{29}(TePh)_{12}Te_9(PEt_3)_8]$-$[PEt_3Ph]$	**(71)**[69]	$[Cu_{58}Te_{32}(PCy_3)_{16}]$	**(85)**[31]
						$[Cu_{58}Te_{32}(PPh_3)_{16}]$	**(86)**[16]
						$[Cu_{58}Te_{32}(PnButBu_2)_{14}]$	**(87)**[25]
				$[Cu_{50}Te_{17}(TePh)_{20}(PEtPh_2)_8]$-$[PEtPh_3]_4$	**(72)**[19]		

ation found in the ternary alkali copper telluride compound $K_2Cu_5Te_5$.[66]

In the case of copper telluride clusters, we have not yet reached the turning point in size where the whole core structures display bulk structure characteristics, as seen for the copper selenide species. Nevertheless, the tellurium frameworks in the largest cluster compounds, **85**−**87**, display hexagonal structure properties. Powder diffraction patterns of Cu_2Te could also be indexed on the basis of a hexagonal cell of tellurium atoms, although the structural details for bulk Cu_2Te have not yet been completely established.[40b]

In all the copper tellurium cluster molecules, the tellurium atoms form polyhedra with triangular faces. In the larger ones, some of the tellurium atoms are located inside the polyhedra. For smaller cluster molecules, the tellurium polyhedra can usually be derived from classical polyhedra (Figure 36). Those of the larger ones often show unusual cage structures. The distances between the tellurium atoms are usually nonbonding, except for the Te−Te units in **59**−**62** (Table 5).

The copper atoms reside in the holes and on the surface of the polyhedra and are coordinated by either two, three, or four tellurium atoms, with some being additionally coordinated by one further phosphane ligand (Figure 37).

The Cu−Te distance ranges that are regarded as bonding contacts are listed in Table 6 for all the clusters under discussion. Even though coordination numbers (*CN*) for Te^{2-} ligands range from 4 to 12 and those for TeR^- are usually smaller (*CN* = 2, 3, 4), there is no significant difference in the average Cu−Te distances for the Te^{2-} and TeR^- ligands.

Those tellurium atoms that are located in the center of the cluster molecules tend to bond to a large number of copper atoms. In some compounds, the copper atoms themselves form polyhedra, which can be described as Frank−Kasper polyhedra.[70] In these cases, the clusters consist of interpenetrating Frank−Kasper polyhedra, which are well-known from a number of intermetallic phases (e.g. Laves phases) (Figure 38).

However, the observed Cu−Cu distances (Table 7) give no indication of strong metal−metal, i.e. d^{10}−d^{10} interactions. Theoretical investigations pointed to the same conclusion.[34b,71] The shortest Cu−Cu contacts were observed in the molecular structures of **62** (2.383 Å) and **78** (2.382 Å), but these involve copper atoms exhibiting elongated thermal ellipsoids.

In the following section, all cluster structures will be briefly described and discussed according to the division into four groups indicated in Table 4.

3.3.2.1. Stoichiometric Clusters Containing Only Te^{2-} Ligands

The molecular structures of the stoichiometric copper telluride clusters **54**−**58** are shown in Figure 39.

In **54**, three tellurium atoms form a triangle, in the center of which a copper atom is coordinated in a slightly distorted triangular fashion. Four $[CuPPh_2Cy]$ units are doubly-bridging two of the edges. The third edge is bridged by a copper atom, which is coordinated by two phosphane ligands.

The tellurium atoms in **55** form a tetrahedron, the six edges of which are bridged by $[CuPPh_3]$ groups. An additional μ_3-$[CuPPh_3]$ fragment is bonded to a Te_3 face, and one naked copper atom is located in the center of the Te_4 tetrahedron.

Cluster **56** features a Te_6 octahedron. Six $[CuPPh_3]$ groups act as μ_2-bridges above six of the octahedral edges. Two further $[CuPPh_3]$ groups are coordinated by three tellurium atoms, giving a tetrahedral environment about the

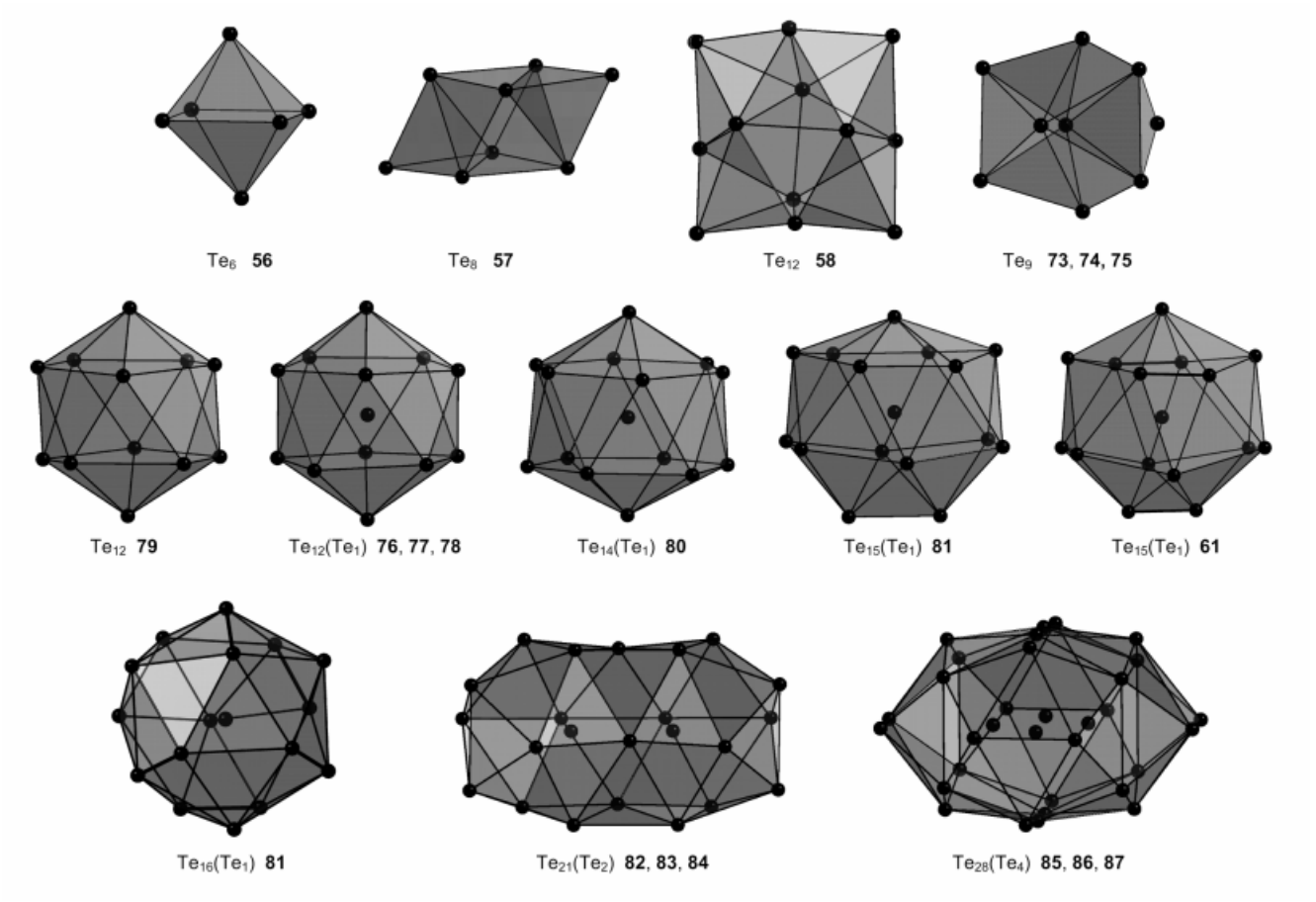

Figure 36. Tellurium polyhedra in copper telluride clusters (values for Te−Te distances in Table 5); connections to the central tellurium atoms are omitted for clarity; direct Te−Te bonds in **61** are drawn in bold

Table 5. Te−Te distances [Å] in copper telluride cluster molecules

with only Te^{2-} ligands		Stoichiometric with additional Te−Te bridges			Mixed-valence with additional TeR^- ligands			
	nonbonding		within Te−Te bridges	nonbonding		nonbonding		nonbonding
54	4.323−4.645	**59**	2.811; 2.799	4.375−4.382	**63**	3.831−4.807	**73**	4.165−4.687
							74	4.134−4.677
							75	4.140−4.652
55	4.556−4.662	**60**	2.791	4.234	**64**	4.022−4.713	**76**	4.083−4.663
							77	3.937−4.722
							78	4.246−4.577
56	4.486−4.764	**61**	2.878; 2.891; 2.895	4.180−4.883	**65**	4.009−4818	**79**	4.302−4.599
57	4.210−4.796	**62**	2.893; 2.897; 3.150; 3.183; 3.360; 3.531;	4.260−4.649	**66**	3.892−4.596	**80**	4.019−4.787
					67	4.053−4.653		
58	4.126−4.697				**68**	3.947−4.737	**81**	3.922−4.801
					69	3.822−4.795		
					70	3.907−4.765	**82**	3.967−4.752
							83	3.967−4.746
							84	3.924−4.768
					71	3.634−4.927	**85**	3.658−4.939
							86	3.733−4.944
							87	3.825−4.800
					72	3.583−4.868		

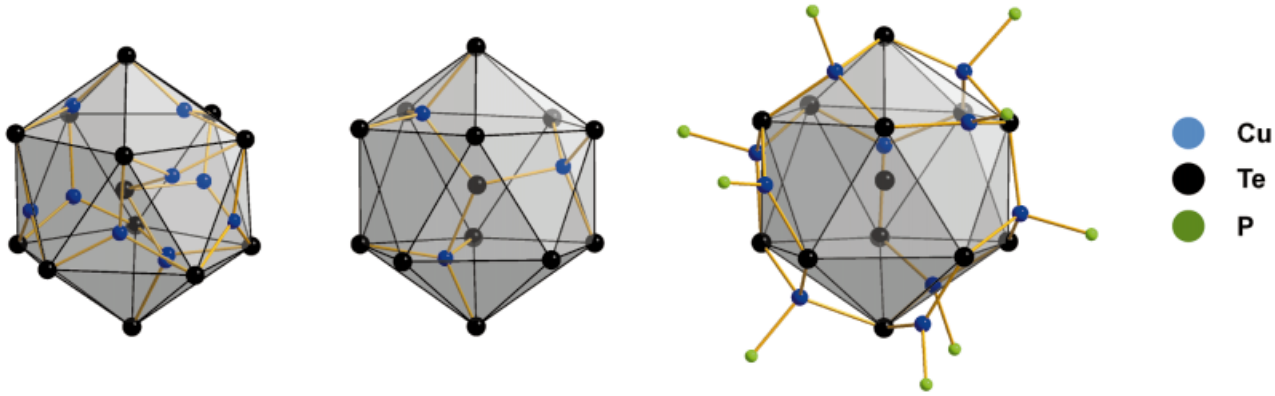

Figure 37. Different coordination modes of copper atoms in copper telluride clusters shown using the structure of **76** as an example; left-hand picture: μ_3-copper atoms only coordinated by tellurium atoms situated within the tellurium polyhedron; middle picture: μ_4-copper atoms only coordinated by tellurium atoms; right-hand picture: μ_3- and μ_4-copper atoms located at the surface of the tellurium polyhedra coordinated by tellurium atoms and one phosphane ligand

Table 6. Cu−Te contacts [Å] in copper telluride cluster molecules

with only Te^{2-} ligands		Stoichiometric with additional Te−Te bridges		with additional TeR^- ligands			Mixed-valence	
					Cu−TeR	$Cu-Te(-Cu)_n$		
54	2.518−2.782	**59**	2.525−2.769	**63**		2.490−2.660	**73**	2.511−2.790
							74	2.526−2.856
							75	2.540−2.791
55	2.532−2.925	**60**	2.574−2.856	**64**		2.511−2.854	**76**	2.530−3.128
							77	2.533−3.327
							78	2.468−2.961
56	2.552−3.187	**61**	2.521−3.337	**65**	2.600−2.897	2.553−3.104	**79**	2.585−2.818
57	2.549−2.794	**62**	2.420−3.310	**66**	2.623−2.743	2.607−2.665	**80**	2.538−3.183
				67	2.606−2.769	2.627−2.666		
58	2.525−2.904			**68**	2.578−2.924	2.519−2.767	**81**	2.567−2.757
				69	2.565−2.889	2.468−2.742		
				70	2.569−3.066	2.504−2.758	**82**	2.589−2.979
							83	2.588−3.033
							84	2.576−3.007
				71	2.576−3.140	2.552−2.855	**85**	2.403−3.115
							86	2.514−3.100
							87	2.515−3.078
				72	2.522−2.926	2.537−2.922		

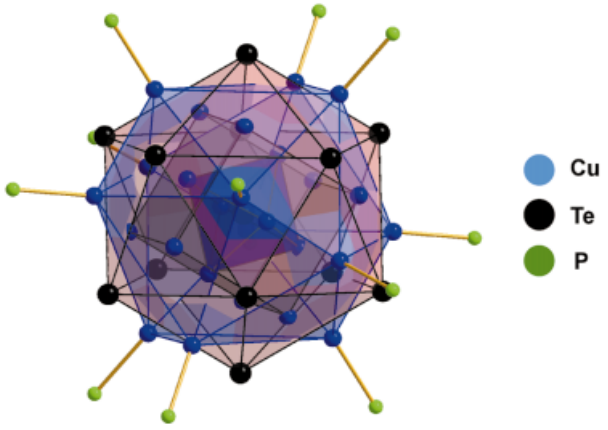

Figure 38. Interpenetrating copper and tellurium polyhedra in **79**

copper atoms. The other four copper atoms are each coordinated by three tellurium atoms. Thus, **56** represents a novel isomer of the $[Cu_{12}E_6(PR_3)_8]$ clusters (see above), which was not observed for E = S, Se.

An octahedron of tellurium atoms is also found in **57**. However, two further tellurium atoms additionally cap two opposite triangular faces. Eight [CuPPh*n*Pr$_2$] groups are bonded along the edges of this polyhedron. Of the other eight copper centers, two are tetrahedrally coordinated by one phosphane and a Te_3 face. The six remaining metal atoms are bonded in a distorted trigonal-planar mode by three tellurium atoms, and are located inside the cluster cavity.

The Te_{12} substructure of **58** cannot be described as a classical deltahedron, but rather shows an arrangement of two highly distorted face-sharing tetragonal antiprisms. Four [CuP*i*Pr$_3$] groups bridge one Te−Te non-bonding edge

Table 7. Cu−Cu contacts [Å] in copper telluride cluster molecules

with Te^{2-} ligands		Stoichiometric with Te−Te bridges		with RTe^- ligands		Mixed-valence	
54	2.510−2.625	**59**	2.797	**63**	2.587−2.613	**73**	2.478−2.730
						74	2.481−2.729
						75	2.475−2.742
55	2.510−2.625	**60**	2.609−2.641	**64**	2.568−2.747	**76**	2.490−2.714
						77	2.507−2.775
						78	2.382−2.725
56	2.479−2.724	**61**	2.581−2.793	**65**	2.469−2.800	**79**	2.566−2.747
57	2.529−2.795	**62**	2.383−2.797	**66**	2.552−2.727	**80**	2.539−2.721
				67	2.563−2.698		
58	2.523−2.764			**68**	2.459−2.774	**81**	2.563−2.763
				69	2.483−2.946		
				70	2.466−2.764	**82**	2.466−2.734
						83	2.476−2.788
						84	2.453−2.789
				71	2.479−2.786	**85**	2.426−2.800
						86	2.448−2.801
						87	2.433−2.796
				72	2.462−2.799		

each, and eight [CuP*i*Pr$_3$] units act as μ_3-bridges above Te_3 faces. The other twelve copper atoms are each surrounded by three tellurium atoms and are slightly shifted away from the Te_3 planes towards the center of the molecule.

3.3.2.2. Stoichiometric Clusters Containing Te−Te Bridges

Some reactions of copper(I) chloride or copper(I) acetate lead to the formation of copper telluride clusters that contain Te−Te bridges (**59**−**62**; Figure 40).

In **59**, three tellurium atoms form an approximate isosceles triangle with a Te−Te bond along the short edge (Te−Te: 2.791 Å). The two longer edges of the triangle are bridged by one [CuPPh$_2$Cy] unit each. The two other copper atoms are located above and below the triangular face and are additionally coordinated by phosphane ligands.

The four copper atoms in **60** form a "butterfly" structure bridged by two ditelluride ligands (Te−Te: 2.800−2.812 Å). Each copper atom is additionally coordinated by a phosphane ligand.

Clusters **61** and **62** are spherical molecules based on tellurium polyhedra, parts of which are strongly distorted due to the presence of Te−Te bonds. Both compounds display Frank−Kasper polyhedra containing 15 (**61**) or 16 (**62**) tellurium atoms centered by one additional tellurium ligand. The tellurium polyhedron of **61** is similar to that observed in **20**, although it differs in the presence of three Te−Te bonds (2.936−3.011 Å). The copper atoms are bonded to the tellurium atoms in a different arrangement to that in **20**. Eight [CuP*t*Bu$_3$] units are situated above Te_3 faces of the polyhedron, while two such units are edge-bridging. Eleven further copper atoms are coordinated by three tellurium atoms, eight of which are localized below Te_3 faces, while the other three bind between the central tellurium atom and the tellurium atoms of the polyhedron. The remaining copper atoms are localized in the center of the molecule and are each tetrahedrally surrounded by four tellurium atoms.

In **62**, two of the copper centers display relatively high thermal parameters, from which it can be concluded that their positions are only partly occupied. A deficiency of electrons at the tellurium atoms resulting from the partial occupation of copper sites could either be formally delocalized in the valence band or localized as a ditelluride group following a structural deformation similar to a Peierls deformation.[72] Considering the tellurium polyhedra, the molecular structure of **62** shows two short Te−Te bonds (2.848 and 2.876 Å) and four Te−Te distances in the range 3.150−3.351 Å. The latter tellurium atoms have thermal ellipsoids that are elongated in the direction of the formal Te−Te bond. As the Te−Te bonds and copper centers seem to be disordered to a certain extent in **62**, the given formula represents the idealized composition of a stoichiometric cluster compound with three Te−Te bonds. The situation in **62** can therefore be viewed as being somewhat similar to that in CuS, a well-known mixed-valence compound that can be described as $(Cu^+)_2Cu^{2+}(S_2)^{2-}S^{2-}$ or as $(Cu^+)_3(S_2)^{2-}S^-$.[73]

3.3.2.3. Stoichiometric Clusters Containing Tellurido and Tellurolato Ligands

In a different approach towards the synthesis of copper telluride cluster compounds, we used alkyl- and aryl(trimethylsilyl)tellurium compounds RTeSiMe$_3$ (R = organic group). Due to the facile cleavage of the carbon−tellurium bond, one obtains clusters featuring either exclusively TeR^- ligands, a mixture of TeR^- and Te^{2-} ligands, or solely Te^{2-} ligands. The tellurium atoms of the tellurolato ligands bridge at most two or three copper atoms, whereas "naked" Te^{2-} ligands can coordinate to up to seven copper atoms. The polyhedra of tellurium atoms usually possess unusual structures, even in the smaller clusters. In the larger clusters, one already observes the characteristics of layer-type ar-

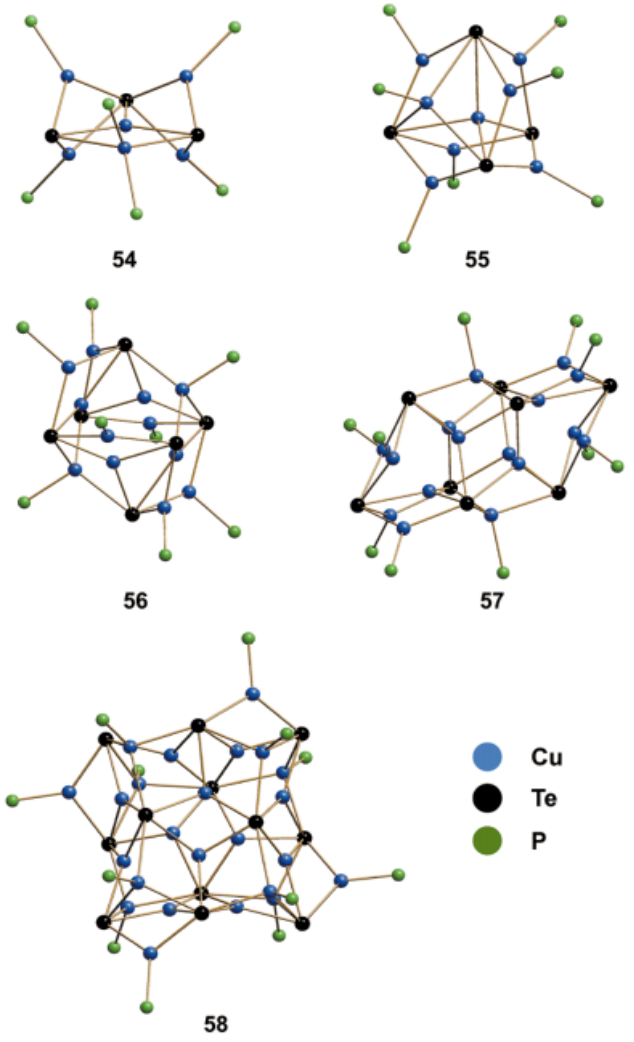

Figure 39. Molecular structures of stoichiometric copper telluride clusters $[Cu_6Te_3(PCyPh_2)_5]$ (**54**), $[Cu_8Te_4(PPh_3)_7]$ (**55**), $[Cu_{12}Te_6(PPh_3)_8]$ (**56**), $[Cu_{16}Te_8(PPhnPr_2)_{10}]$ (**57**), and $[Cu_{24}Te_{12}(PiPr_3)_{12}]$ (**58**); C and H atoms are omitted for clarity

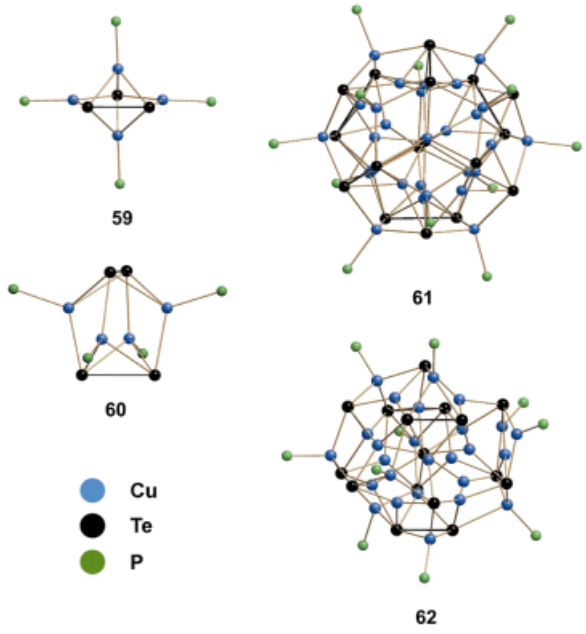

Figure 40. Molecular structures of stoichiometric copper telluride clusters $[Cu_4Te(Te_2)_2(PCyPh_2)_4]$ (**59**), $[Cu_4(Te_2)_2(PiPr)_4]$ (**60**), $[Cu_{26}Te_{10}(Te_2)_3(PtBu_3)_{10}]$ (**61**), and $[Cu_{28}Te_{13}(Te_2)_2(PEt_2Ph)_{12}]$ (**62**) containing Te−Te bridges; C and H atoms are omitted for clarity

rangements of tellurium atoms. As in the cluster compounds discussed earlier, the copper atoms are coordinated in linear, trigonal, or tetrahedral geometries by tellurium atoms. Metal centers coordinated by two or three chalcogens may also be ligated by a phosphane ligand. The molecular structures of the copper telluride/tellurolate clusters **63**−**66** and **68**−**72** are shown in Figure 41.

The ionic cluster compound **63** contains six $TePh^-$ ligands, the tellurium atoms of which define an octahedron. In contrast to **64** (see below), all the tellurolato ligands act as μ_2-bridges. There are two distinct coordination geometries around the copper centers. Two of the metal centers are located inside the cluster below Te_3 faces. The others are coordinated by three tellurium atoms above Te_3 faces, and are also ligated by one phosphane ligand each.

The structure of **64** is also based on a non-bonded octahedral array of tellurolato ligands. With the exception of one tellurium atom, which forms two Cu−Te bonds, all of these are bridging three copper sites. Four of the copper atoms adopt tetrahedral geometries, either with three tellurium atoms and one phosphorus ligand or through two Cu−Te and two Cu−P bonds. The other two copper atoms lie in opposite deltahedral Te_3 faces of the Te_6 octahedron. Compound **64** is therefore related to the recently published homoleptic hexanuclear copper selenolate complex $[Cu_6\{Se(2,4,6\text{-}iPr_3C_6H_2)\}_6]$.[8]

In **65**, the nine tellurium atoms of the tellurolato ligands form three-quarters of a cubooctahedron, which is capped on the hexagonal face by the Te^{2-} ligand. Seven $TenBu^-$ groups act as μ_3-bridges between copper atoms, while the other two bind to four copper atoms. The "naked" tellurium atom at the base of the cluster coordinates to seven copper atoms. Five of the eleven metal atoms are ligated by triphenylphosphane ligands, four of which are tetrahedrally coordinated due to three additional Cu−Te bonds. One $[CuPPh_3]$ unit bridges only two tellurium atoms, resulting in an almost trigonal-planar coordination environment. Three of the six interstitial copper atoms exhibit tetrahedral coordination geometries, while the other three show three bonding contacts to tellurium atoms and have nearly trigonal-planar coordination geometries.

Clusters **66** and **67** are identical except for the organic groups R of the PR_3 ligands. Both contain two tellurolato layers of three $TePh^-$ groups each and one central tellurido layer of three Te^{2-} ligands. The resulting Te_9 polyhedron can alternatively be viewed as two face-sharing Te_6 octahedra. Six of the twelve copper atoms are coordinated in a distorted trigonal fashion by three tellurium atoms, resulting in shorter contacts to the Te^{2-} ligands than to the $TePh^-$. The other six copper atoms are tetrahedrally surrounded by three tellurium atoms and one phosphane li-

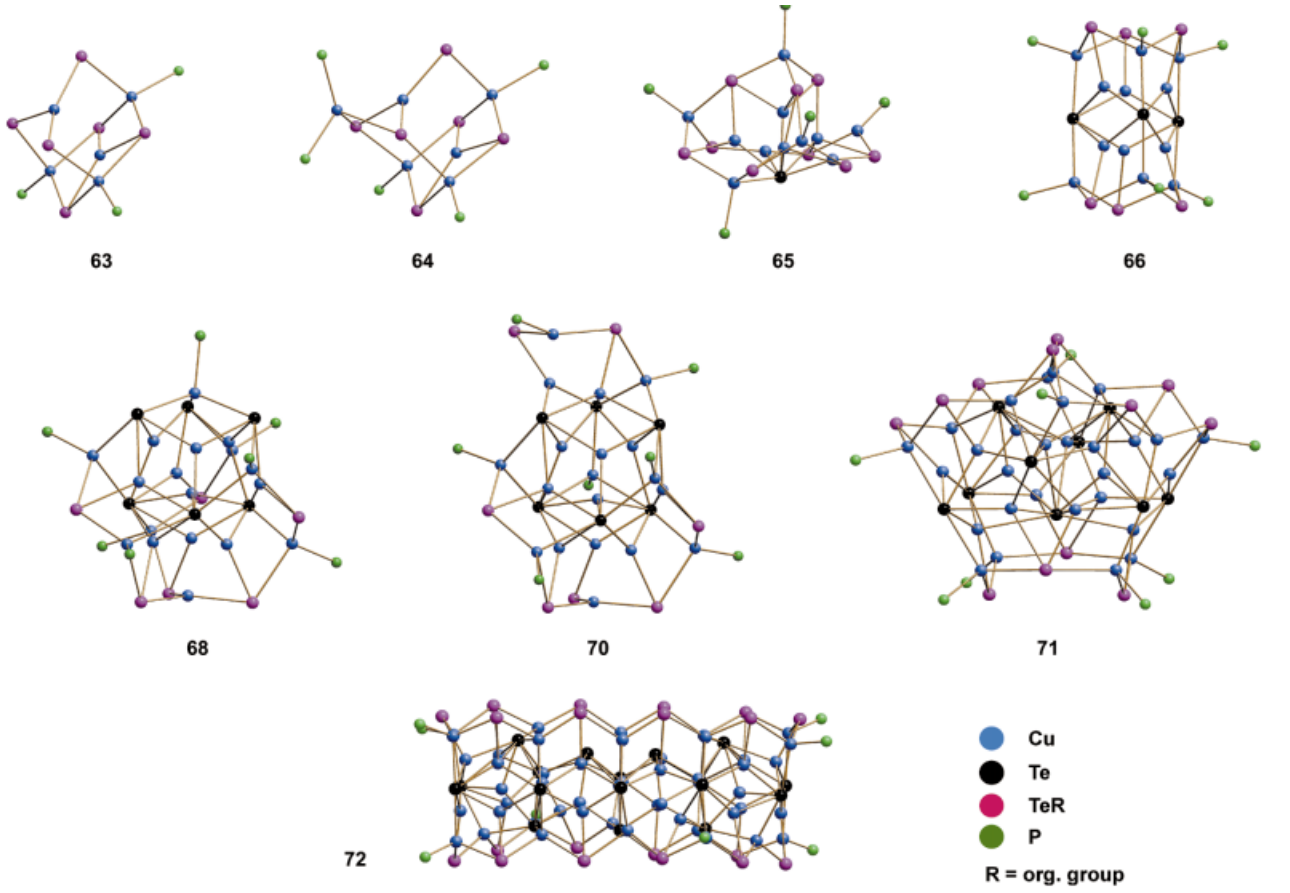

Figure 41. Molecular structures of stoichiometric copper telluride/tellurolate clusters $[Cu_5(TePh)_6(PEt)_3][PEt_3Ph]$ (**63**), $[Cu_6(TePh)_6(PEtPh_2)_5]$ (**64**), $[Cu_{11}Te(Te\mathit{n}Bu)_9(PPh_3)_5]$ (**65**), $[Cu_{12}Te_3(TePh)_6(PPh_3)_6]$ (**66**), $[Cu_{18}Te_6(Te\mathit{t}Bu)_6(PEtPh_2)_7]$ (**68**), $[Cu_{19}Te_6(Te\mathit{t}Bu)_7(PEt_3)_8]$ (**70**), $[Cu_{29}(TePh)_{12}Te_9(PEt_3)_8][PEt_3Ph]$ (**71**), and $[Cu_{50}Te_{17}(TePh)_{20}(PEtPh_2)_8][PEtPh_3]_4$ (**72**) containing TeR^- ligands; C and H atoms are omitted for clarity

gand. Compounds **66** and **67** might be viewed as condensation products of two $(TePh)_6$ frameworks like those found in **64**.

The molecular structures of **68** and **69** differ only by an extra phosphane ligand bonded to the former, in line with the smaller cone angle of $P\mathit{n}Pr_3$ relative to that of $PEtPh_2$. The layering of the tellurium atoms is clearly evident, and the twelve atoms adopt a distorted hexagonal packing. The three layers consist of a "top" layer of three "naked" Te^{2-} ligands, a second layer of three $Te\mathit{n}Bu^-$ and three Te^{2-} ligands, with the former lying at the corners of the triangular array, and a third basal triangle consisting of another three $Te\mathit{n}Bu^-$ groups. Eight of the copper atoms cap open Te_3 triangular faces, with a fourth bonding interaction to a phosphane ligand. Of the interstitial copper atoms, seven display only three bonding contacts to the neighboring tellurium atoms, while three metal atoms are tetrahedrally surrounded by tellurium atoms.

Compared to **68** and **69**, **70** contains one additional [Cu-Te*t*Bu] group. However, the structures are partly comparable. Again, a layering of the tellurium atoms can be observed, which is related to that in **68** and **69** as follows. There are now four formal layers of tellurium atoms, with one $Te\mathit{t}Bu^-$ group less in the former middle layer, and two additional $Te\mathit{t}Bu^-$ groups at the "top" of the molecule forming the fourth layer. One of the seven $Te\mathit{t}Bu^-$ ligands acts only as a doubly-bridging ligand, whereas the other six form μ_3-bridges between copper atoms. The six Te^{2-} ligands and 16 of the copper centers are situated in similar positions as in **68** or **69**. Three further copper atoms are located between the "top" Te−Te unit and the adjacent "naked" Te_3 layer. The similarities and differences between the structures of **68**, **69**, and **70** demonstrate the complicated influence of the phosphane ligands, which have different cone angles, and of the tellurolate ligands, which have different degrees of flexibility in their organic substituents. These systems may stem from a common intermediate, but due to the different steric demands of the ligands they develop in different ways.

The synthesis of the ionic cluster compound, **71**, is the only example to date of a co-condensation reaction of two smaller clusters to form a larger one. However, the structure of **71** cannot be considered as being built-up from recognizable structural fragments of the precursor compound. The tellurium atoms form an unusual polyhedron consisting of twelve $TePh^-$ ligands and nine Te^{2-} ligands. Two of the tellurolato ligands act as μ_4-bridges, while the other ten act as μ_3-bridging atoms between the copper centers. The tel-

luride ligands each coordinate six, seven, eight, or ten copper atoms with Cu−Te distances between 2.58 and 3.14 Å. Eight of the copper atoms coordinated by phosphane ligands cap Te_3 faces at the cluster surface, while four further copper atoms without phosphane ligands coordinate to Te_3 faces from the inside of the cluster core. The remaining 17 copper atoms are surrounded in a tetrahedral manner in the center of the molecule. Interestingly, a structurally related silver tellurium compound, $[Ag_{30}(TePh)_{12}Te_9(PEt_3)_{12}]$,[69] can be prepared by the direct reaction of AgCl with $Te(SiMe_3)_2$/$PhTeSiMe_3$, which is in contrast to the synthesis of **71**. This cluster represents the only known example of a copper-telluride-tellurolate cluster that shows a distinct structural relationship with its silver analogue.

Upon standing in daylight, solutions of **64** in benzene gradually darken to a brown color. Over the course of several days, brown platelets of the ionic, mixed tellurido/tellurolato cluster **72** crystallize from these solutions. In contrast, when solutions of **64** in benzene are protected from light, they show no sign of darkening, even after several weeks at room temperature. The detection of a $^{125}Te\{^1H\}$ NMR signal at $\delta = 688$ reveals the formation of $TePh_2$ in the solution, giving good evidence for the mechanism of formation of the "naked" tellurido ligands. The most striking feature of the cluster core is the manner in which the tellurium ligands are arranged: the molecule consists of "top" and "bottom" layers of μ_3-$TePh^-$ ligands with a central tellurido (Te^{2-}) layer. Sandwiched between these are the 50 copper atoms along with the remaining seven tellurido ligands. The 20 phenyltellurolato ligands are each bonded to three copper atoms and, in conjunction with the eight coordinated PEt_2Ph ligands, serve to effectively stabilize the inner copper telluride core. The telluride ligands of the middle Te_{10} layer act as μ_6- and μ_7-bridges between the copper sites. The seven remaining Te^{2-} centers function as μ_6-, μ_7-, or μ_8-ligands. Eight of the copper atoms are bonded to Te_3 faces at the surface of the cluster molecule and to one phosphane ligand. The 42 copper atoms in the center of the molecule are either trigonally (18) or tetrahedrally (24) coordinated by their tellurium neighbors.

3.3.2.4. Mixed-Valence Clusters

Counting the electrons for **73**−**85** on the assumption of Te^{2-} and Cu^+ leads to an overall electron excess for **79** and to electron deficiencies for the other compounds. These compounds can therefore be thought of as being of mixed-valence type. The molecular structures of **73**, **76**, **79**−**82**, and **85** are depicted in Figure 42.

The smallest mixed-valence cluster molecules, **73**−**75**, feature 16 copper atoms arranged around a Te_9 polyhedron. However, the tellurium substructure cannot be derived from the skeleton of **57** by simply adding one tellurium atom, as one might have assumed. Two of the copper atoms that are coordinated by a phosphane ligand bridge Te−Te nonbonding edges. The other six $[CuPR_2R']$ units bridge three tellurium atoms, the copper atoms thus being tetrahedrally coordinated. The remaining eight copper atoms are coordinated by three tellurium atoms in a distorted trigonal-planar manner. Assuming that the tellurium atoms have a formal charge of 2−, one can formally assign 14 Cu^+ centers and two Cu^{2+} centers. However, the co-existence of Cu^{2+} and Te^{2-} is unlikely for thermodynamic reasons because of an electron-transfer process from the reducing Te^{2-} ligand to the oxidizing Cu^{2+} center. An assignment of

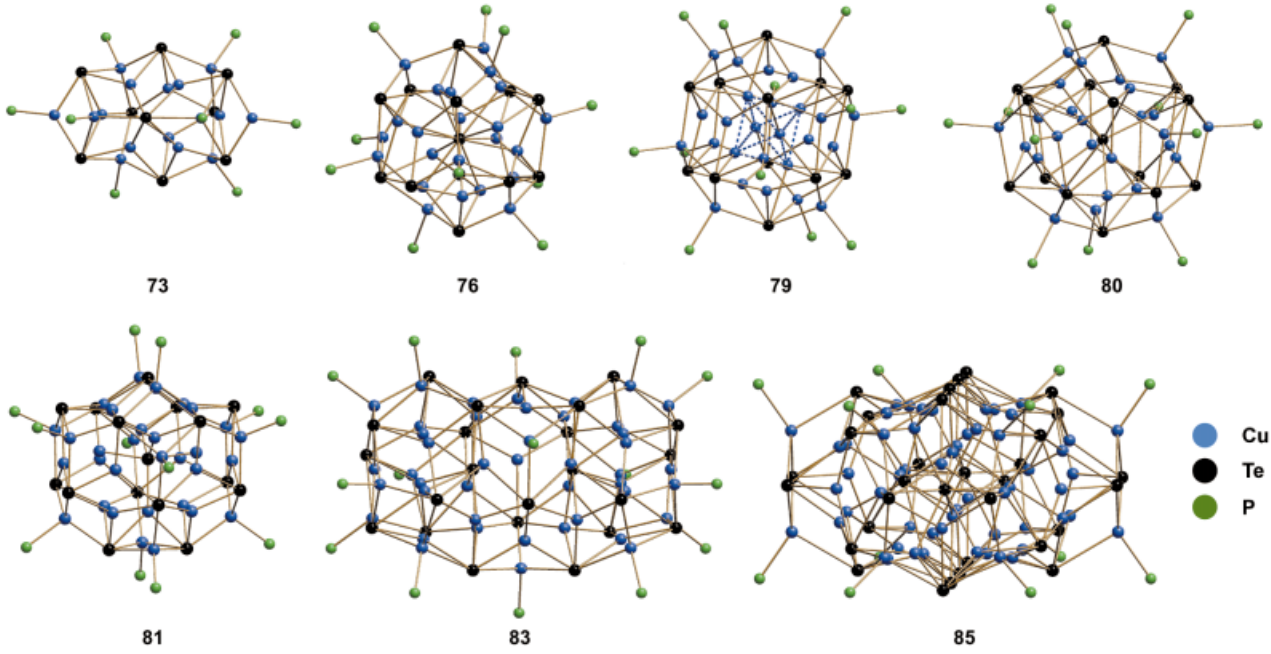

Figure 42. Molecular structures of mixed-valence copper telluride clusters $[Cu_{16}Te_9(PPh_3)_8]$ (**73**), $[Cu_{23}Te_{13}(PPh_3)_{10}]$ (**76**), $[Cu_{26}Te_{12}(PEt_2Ph)_{12}]$ (**79**), $[Cu_{27}Te_{15}(PMe\textit{i}Pr_2)_{12}]$ (**80**), $[Cu_{29}Te_{16}(P\textit{i}Pr_3)_{12}]$ (**81**), $[Cu_{44}Te_{23}(PPh_3)_{15}]$ (**82**), and $[Cu_{58}Te_{32}(PCy_3)_{16}]$ (**85**); C and H atoms are omitted for clarity

16 Cu^+, seven Te^{2-}, and two Te^- is not supported by structural means. The compounds should therefore rather be described in terms of a "pure" Cu^+ substructure ligated by tellurium centers with an average charge of −1.78. This electron deficiency can be delocalized in the valence band of the compound, as has recently been shown by calculations on the electron-rich compound **79** (see below).[74]

Thirteen tellurium atoms form a distorted, centered icosahedron in the closely-related compounds **76**−**78**. In **76** and **77**, ten of the 20 Te_3 faces are bridged by copper-phosphane units, whereas ten more copper atoms are situated below the remaining faces, either trigonally coordinated or tetrahedrally surrounded due to an additional Cu−Te bond to the central tellurium atom. Compound **78** needs twelve phosphane ligands for a sufficient shielding of the cluster core. This can be ascribed to the smaller steric demand of the phosphane PEt_3 (Table 1) compared to PPh_3. As a result, in **78**, twelve of the copper atoms are coordinated above Te_3 faces and eight below. The three remaining copper atoms in all three compounds are positioned inside the respective icosahedra. They each have three tellurium neighbors, two of which belong to the Te_{12} shell, while the third is the central tellurium ligand. Formal counting of charges leads to an electron excess of three and, assigning a charge of 1+ to every copper atom as discussed above, an average charge of −1.77 is obtained for the 13 tellurium ligands.

An icosahedron of tellurium atoms is also found in **79** but, in contrast to those observed in **76**−**78**, it does not contain a central atom. The arrangement of the copper atoms above the Te_3 faces is similar to that found in **78**. This might have been anticipated, given the Tolman angle for both phosphanes. Twelve $[CuPEt_2Ph]$ units are bonded above Te_3 faces and eight copper atoms cap the other Te_3 faces from the interior. In contrast to the situation in **76**−**78**, in **79** six rather than three copper atoms are located in the center of the cluster molecule, forming an octahedron with intermetallic distances between 2.592 and 2.607 Å. These distances lie within the range of Cu−Cu distances measured in the other copper telluride clusters under investigation. Therefore, it cannot be concluded from these distances whether d^{10}−d^{10} interactions are present within the Cu_6 octahedron. However, it is remarkable that two of the copper atoms must be formally uncharged Cu^0 atoms, alongside 24 Cu^+ centers, if one assigns a formal charge of 2− to all the tellurium ligands. Calculations of the electronic band structure reveal that a localization of the oxidation states does not occur and that the excess electron density cannot be assigned to d^{10}−d^{10} interactions.[74] The "additional" electron pair, which arises if one assigns exclusively Cu^+ and Te^{2-} centers, is better described as an MO embedded in the valence band of tellurium 5p orbitals and copper 4s orbitals.

The cluster molecules **80** and **81** are constructed in an analogous way. Both compounds consist of tellurium polyhedra which, however, form Frank−Kasper polyhedra: **80** contains a Te_{14} polyhedron, while **81** is based on a Te_{15} polyhedron. Both chalcogen substructures enclose an additional tellurium ligand at the center. Similar to the situations in **76**−**79**, all Te_3 faces are μ_3-capped by copper atoms. The Te_{14} polyhedron displays 24 such faces and the Te_{15} substructure forms 26 Te_3 triangles. Copper atoms that are additionally coordinated by a phosphane ligand are situated above the Te_3 faces, while the other copper atoms lie below, as observed previously. In both **80** and **81**, twelve copper atoms that are coordinated by a phosphane ligand are tetrahedrally coordinated above the cluster surface. One then finds 17 (**81**) or 15 (**80**) copper atoms below the Te_3 faces in the two cluster structures. Similarly to the situation in **76**−**78**, three metal centers are situated inside the polyhedral cages. Assuming that only Cu^+ centers and Te^{2-} ligands are present, three electrons are formally missing in each compound. Therefore, **80** and **81** are also compounds of mixed-valence type, each featuring three formal Cu^{2+} centers. However, from the structural data it is again impossible to divide the atomic positions into those that are occupied by Cu^{2+} and those that are Cu^+ sites.

The largest copper telluride cluster molecules synthesized to date are also mixed-valence compounds. Compounds **82**−**87** display ellipsoidal tellurium deltahedra with an increasing number of inner tellurium atoms, ranging from two inner tellurium atoms in **82**−**84**, to four such tellurium atoms in the centers of the molecular structures of **85**−**87**. As usual, the copper atoms that are coordinated by phosphane ligands are coordinated above the Te_3 triangles on the cluster surface. The other copper atoms are either coordinated by three or, especially in the cluster center, by four tellurium ligands. The structures of **85**−**87** already suggest the formation of distorted layers of tellurium atoms showing incipient characteristics of bulk Cu_2Te.[40] However, the turning point has not yet been reached for copper telluride cluster compounds. If one continues the reported tendency for ever bigger molecules being required for the observation of bulk structure properties on going from Cu−S to Cu−Se clusters, the cluster size that might begin to show Cu_2Te structural characteristics should in fact be considerably larger than a "Cu_{58}" species, and probably even larger than a "Cu_{70}" analogue of the turning point to "large" clusters found for the copper selenide system.

3.3.3. Optical Spectra in the Solid State

The colors of the microcrystalline powders of the various copper telluride clusters already reveal differences in the electronic properties of the compounds. Larger clusters are significantly darker in color than the smaller ones. For a more detailed investigation, UV/Vis spectra of the stoichiometric clusters **55** and **57**, as well as of the mixed-valence compounds **73**, **76**, **79**, and **83** were measured in the solid state.[24] Absorption spectra of the crystalline samples were measured in transmission mode from suspensions in Nujol between two quartz plates. As representative examples, the spectra of **57**, **73**, and **83** are shown in Figure 43.

In line with its red color, **57** exhibits charge-transfer bands between 600 and 200 nm, together with bands that can be assigned to transitions related to the ligands. The UV/Vis spectrum of **73** also shows similar bands between

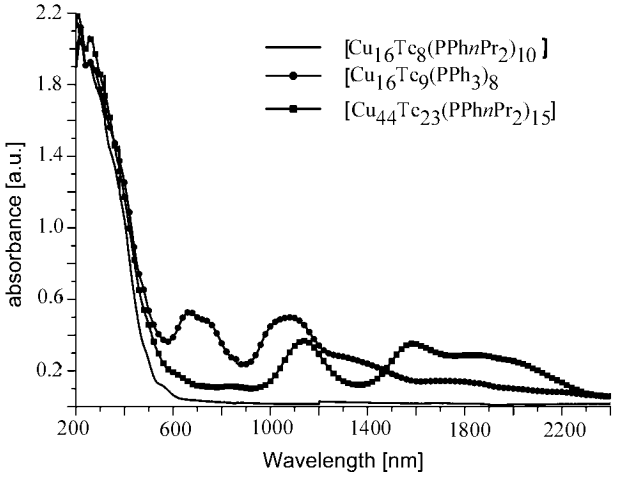

Figure 43. The UV/Vis solid-state absorption spectra (Nujol mulls) of copper telluride clusters $[Cu_{16}Te_8(PPh_nPr_2)_{10}]$ (**57**), $[Cu_{16}Te_9(PPh_3)_8]$ (**73**), and $[Cu_{44}Te_{23}(PPh_nPr_2)_{15}]$ (**83**)

600 and 200 nm, but additionally displays broad and weaker peaks at higher wavelengths, specifically at 670, 750, 1050, and 1350 nm. As outlined above, **73** can be described as a mixed-valence compound with an overall electron deficiency that is delocalized in the valence band. In general, compounds containing metal atoms in formally different oxidation states exhibit interesting spectroscopic behavior. Depending on the degree of delocalization of the charges over the molecular framework, one may detect additional bands in the near-infrared region. According to the classification of Robin and Day,[75] which describes the different degrees of electron delocalization between the metal atoms, the copper telluride clusters under investigation should belong to class IIIa (metal clusters). In this class, metal centers with different valencies cannot be distinguished and total delocalization of the charge is achieved. The larger cluster **83** also formally contains an electron deficiency of two and thus shows broad peaks that are shifted even further to longer wavelengths than in the case of **73**. Since the energy of the mixed-valence transition is strongly correlated with the degree of delocalization, an even better charge delocalization − i.e. a smaller transition energy − is observed for **83**, as might have been expected for such a large cluster. In **79**, the assignment of formal charges results in two Cu^0 atoms and 24 Cu^+ centers, which implies a formal electron excess of two. In principle, this should also cause mixed-valence bands. However, the absorption spectrum of **79** only shows a red shift of the onset of the charge-transfer bands with respect to **57** from 600 to 800 nm. It cannot yet be established whether this is a general behavior of the two different types of mixed-valence copper telluride clusters possessing either an electron deficiency or an electron excess.

4. Conclusion and Outlook

Reactions of copper salts such as copper(I) acetate and copper(I) chloride with silylated chalcogen compounds $E(SiMe_3)_2$ or $RE(SiMe_3)$ (E = S, Se, Te; R = organic group) in the presence of tertiary phosphane ligands lead to the formation of ligand-stabilized copper chalcogenide or copper chalcogenide/chalcogenolate cluster molecules of different sizes. The synthesis of the cluster molecules is influenced in a complex manner by the reactants, ligands, and solvents used, and by the reaction temperature.

All copper sulfide clusters characterized to date show spherical molecular structures that give an insight into the structural principles of $[Cu_2E]_n$ aggregates. Rules that lead to maximum stability have been delineated by comparing the observed structures, and by quantum-chemically investigating a series with up to 20 copper atoms. They are strictly adhered to by small clusters, and remain widely valid for the larger Cu−S cluster compounds.

In the case of the copper selenide clusters, the molecular structures of smaller or middle-sized clusters of up to 59 copper atoms exhibit spherical cluster shapes and also follow the structural principles elucidated for the copper sulfide species. These cluster structures differ significantly from those of the larger molecules that possess hexagonal lattices of selenium atoms. Hence, the cluster formation of the smaller copper chalcogenide clusters seems to follow spontaneous aggregation processes leading to molecular species, whereas the crystallization of the larger ones represents instead the incipient formation of ordered solid-state structures. Although the final structure determination of the low-temperature α-Cu_2Se phase is still a point of discussion, the best refinement of the data is achieved by assuming a cubic lattice of selenium atoms with copper atoms occupying the tetrahedral and trigonal holes.[76] Therefore, it is possible that the cluster molecules display fragments of a new structure type of an as yet unknown Cu_2Se polymorph.

In contrast to the clusters containing sulfur or selenium ligands, copper telluride systems show a significant tendency to form non-stoichiometric clusters, with either an electron deficiency or an electron excess. This is not only evident from the overall charge, but is also shown by the occurrence of intervalence bands in the optical spectra of these compounds. Structural considerations as well as calculations on the electronic band structure reveal that a localization of the different formal oxidation states is not possible. Even though compound **79** contains a central Cu_6 octahedron with sufficiently short Cu−Cu distances, the charge excess cannot be assigned to $d^{10}-d^{10}$ interactions. The "additional" electron pair that arises from the formal assignment of charges Cu^+ and Te^{2-} is instead delocalized in an MO embedded in the tellurium(5*d*)−copper(4*s*) valence band. The distinct differences from the Cu_2S or Cu_2Se mixed-valence cluster systems can generally be attributed to the small differences between the ionization potentials (IP), electron affinities (EA), and electronegativities (EN) of copper and tellurium, which do not allow a discrete separation into Cu^+ and Te^{2-} centers [IP(Cu): 745.4, IP(Te): 869.2; EA(Cu): 118.5, EA(Te):190.2; EN(Cu, Pauling): 1.9, EN(Te): 2.1].

In the future, we aim to further investigate the thermal properties of these materials and to use them as precursor

compounds for the synthesis of nanostructured Cu_2E (E = S, Se, Te) phases. This will include the preparation of thin films of these materials, which may have applications in solar cell technology, as well as the synthesis of $Cu_{2-x}E$ compounds of precise, known compositions that may show interesting magnetic and electrical properties.

Acknowledgments

This work has been supported by the Deutsche Forschungsgemeinschaft (SFB 195), the State of Baden-Württemberg, the Fonds der Chemischen Industrie, and the Forschungszentrum Karlsruhe GmbH. We wish to acknowledge the financial support throughout this long period of time. The authors also gratefully acknowledge the help of Dr. Chris Anson in correcting the English.

[1] V. A. Fedorin, *Semiconductors* **1993**, *27*, 354−357.
[2] [2a] B. A. Mansour, S. E. Demian, H. A. Zayed, *J. Mater. Sci.* **1992**, *3*, 249−252; [2b] Z. Vučić, O. Milat, V. Horvatić, Z. Ogorelek, *Phys. Rev.* **1981**, *B24*, 5398−5401.
[3] [3a] G. Nimtz, P. Marquard, H. Gleiter, *J. Cryst. Growth* **1988**, *86*, 66−79; [3b] J. Koutecky, P. Fantucci, *Chem. Rev.* **1986**, *86*, 539−587; [3c] M. D. Morse, *Chem. Rev.* **1986**, *86*, 1049−1071; [3d] M. M. Kappes, *Chem. Rev.* **1988**, *88*, 369−389; [3e] H. Weller, *Angew. Chem.* **1993**, *105*, 43−50; *Angew. Chem. Int. Ed. Engl.* **1993**, *32*, 88−95.
[4] [4a] H. Weller, *Angew. Chem.* **1998**, *110*, 1748−1749; *Angew. Chem. Int. Ed.* **1998**, *37*, 1658−1659; [4b] A. P. Alivisatos, *Science* **1996**, *271*, 933−937; [4c] H. Weller, *Angew. Chem.* **1996**, *108*, 1159−1161; *Angew. Chem. Int. Ed. Engl.* **1996**, *35*, 1079−1081; [4d] *Clusters and Colloids* (Ed.: G. Schmid), VCH, Weinheim, **1995**.
[5] [5a] J. P. Fackler, Jr., D. Coucouvanis, *J. Am. Chem. Soc.* **1966**, *88*, 3913−3920; [5b] L. E. McCandlish, E. C. Bissell, D. Coucouvanis, J. P. Fackler, K. Knox, *J. Am. Chem. Soc.* **1968**, *90*, 7357−7359.
[6] I. G. Dance, *Aust. J. Chem.* **1978**, *31*, 2195−2206.
[7] P. Betz, B. Krebs, G. Henkel, *Angew. Chem.* **1984**, *96*, 293−294; *Angew. Chem. Int. Ed. Engl.* **1984**, *23*, 311−312.
[8] D. Ohlmann, H. Pritzkow, H. Grützmacher, M. Anthamatten, P. Glaser, *J. Chem. Soc., Chem. Commun.* **1995**, 1011−1012.
[9] D. Fenske, H. Krautscheid, S. Balter, *Angew. Chem.* **1990**, *102*, 799−801; *Angew. Chem. Int. Ed. Engl.* **1990**, *29*, 796−798.
[10] D. Fenske, H. Krautscheid, *Angew. Chem.* **1990**, *102*, 1513−1516; *Angew. Chem. Int. Ed. Engl.* **1990**, *29*, 1452−1454.
[11] D. Fenske, J. C. Steck, *Angew. Chem.* **1993**, *105*, 254−257; *Angew. Chem. Int. Ed. Engl.* **1993**, *32*, 238−242.
[12] H. Krautscheid, D. Fenske, G. Baum, M. Semmelmann, *Angew. Chem.* **1993**, *105*, 1364−1367; *Angew. Chem. Int. Ed. Engl.* **1993**, *32*, 1303−1305.
[13] S. Dehnen, A. Schäfer, D. Fenske, R. Ahlrichs, *Angew. Chem.* **1994**, *106*, 786−790; *Angew. Chem. Int. Ed. Engl.* **1994**, *33*, 764−768.
[14] S. Dehnen, D. Fenske, *Angew. Chem.* **1994**, *106*, 2369−2372; *Angew. Chem. Int. Ed. Engl.* **1994**, *33*, 2287−2289.
[15] S. Dehnen, D. Fenske, A. C. Deveson, *J. Clust. Sci.* **1996**, *7(3)*, 351−369.
[16] J. F. Corrigan, S. Balter, D. Fenske, *J. Chem. Soc., Dalton Trans.* **1996**, 729−738.
[17] S. Dehnen, D. Fenske, *Chem. Eur. J.* **1996**, *2*, 1407−1416.
[18] A. Deveson, S. Dehnen, D. Fenske, *J. Chem. Soc., Dalton Trans.* **1997**, 4491−4498.
[19] J. F. Corrigan, D. Fenske, *Angew. Chem.* **1997**, *109*, 2070−2071; *Angew. Chem. Int. Ed. Engl.* **1997**, *36*, 1981−1983.
[20] M. Semmelmann, D. Fenske, J. F. Corrigan, *J. Chem. Soc., Dalton Trans.* **1998**, 2541−2546.
[21] A. Eichhöfer, D. Fenske, *J. Chem. Soc., Dalton Trans.* **1998**, 2969−2972.
[22] M. Bettenhausen, A. Eichhöfer, D. Fenske, M. Semmelmann, *Z. Anorg. Allg. Chem.* **1999**, *625*, 593−601.
[23] N. Zhu, D. Fenske, *J. Chem. Soc., Dalton Trans.* **1999**, 1067−1075.
[24] A. Eichhöfer, J. F. Corrigan, D. Fenske, E. Tröster, *Z. Anorg. Allg. Chem.* **2000**, *626*, 338−348.
[25] N. Zhu, D. Fenske, *J. Clust. Sci.* **2000**, *11*, 135−151.
[26] H. Krautscheid, Ph. D. Thesis, University of Karlsruhe, **1991**.
[27] J. C. Steck, Ph. D. Thesis, University of Karlsruhe, **1992**.
[28] S. Balter, Ph. D. Thesis, University of Karlsruhe, **1994**.
[29] S. Dehnen, Ph. D. Thesis, University of Karlsruhe, **1996**.
[30] M. Semmelmann, Ph. D. Thesis, University of Karlsruhe, **1997**.
[31] A. Eichhöfer, D. Fenske, unpublished results.
[32] J. H. El Nakat, I. G. Dance, K. J. Fisher, G. D. Willet, *Inorg. Chem.* **1991**, *30*, 2957−2958.
[33] [33a] D. van der Putten, D. Olevano, R. Zanoni, H. Krautscheid, D. Fenske, *J. Electron. Spectrosc. Relat. Phenom.* **1995**, *76*, 207−211; [33b] A. Enderle, Diploma Thesis, University of Karlsruhe, **1993**; [33c] U. Stöhr, Diploma Thesis, University of Karlsruhe, **1993**.
[34] [34a] A. Schäfer, C. Huber, J. Gauss, R. Ahlrichs, *Theor. Chim. Acta* **1993**, *87*, 29−40; [34b] A. Schäfer, R. Ahlrichs, *J. Am. Chem. Soc.* **1994**, *116*, 10686−10692.
[35] S. Dehnen, A. Schäfer, R. Ahlrichs, D. Fenske, *Chem. Eur. J.* **1996**, *2*, 429−435.
[36] K. Eichkorn, S. Dehnen, R. Ahlrichs, *Chem. Phys. Lett.* **1998**, *284*, 287−292.
[37] A. Schäfer, Ph. D. Thesis, University of Karlsruhe, **1994**.
[38] [38a] *Structural Inorganic Chemistry* (Ed.: A. F. Wells), 5th ed., Clarendon Press, Oxford, **1984**; [38b] H. T. Evans, *Z. Kristallogr.* **1979**, *150*, 299−301.
[39] [39a] R. D. Heyding, R. M. Murray, *Can. J. Chem.* **1976**, *54*, 841−848; [39b] P. Rahlfs, *Z. Phys. Chem.* **1936**, *B31*, 157−159; [39c] W. Borchert, *Z. Kristallogr.* **1945**, *106*, 5−24; [39d] A. L. N. Stevels, *Philips Res. Rep. Suppl.* **1969**, *9*, 124; [39e] A. L. N. Stevels, F. Jellinek, *Recl. Trav. Chim.* **1971**, *90*, 273−283; [39f] A. Tonjec, Z. Ogorelec, B. Mestnik, *J. Appl. Crystallogr.* **1975**, *8*, 375−379.
[40] [40a] R. Blachnik, M. Lasocka, U. Walbrecht, *J. Sol. State Chem.* **1983**, *48*, 431−438; [40b] Y. G. Asadov, L. V. Rustamova, G. B. Gasimov, K. M. Jafarov, A. G. Babajev, *Phase Transitions* **1992**, *38*, 247−259.
[41] G. H. Aylward, T. J. V. Findlay, *Datensammlung Chemie*, VCH, Weinheim, **1986**, p. 125.
[42] C. A. Tolman, *Chem. Rev.* **1977**, *77*, 313−348.
[43] [43a] *Comprehensive Coordination Chemistry* (Ed.: G. Wilkinson), Vol. 5, Pergamon Press, Oxford, **1987**, p. 583f; [43b] M. G. B. Drew, A. H. B. Othman, D. A. Edwards, R. Richards, *Acta Crystallogr., Sect. B* **1975**, *31*, 2695−2697.
[44] [44a] R. Ahlrichs, M. Bär, M. Häser, H. Horn, C. Kölmel, *Chem. Phys. Lett.* **1995**, *242*, 652−660; [44b] O. Treutler, R. Ahlrichs, *J. Chem. Phys.* **1995**, *102*, 346−354; [44c] A. Schäfer, H. Horn, R. Ahlrichs, *J. Chem. Phys.* **1992**, *97*, 2571−2577.
[45] [45a] K. Eichkorn, O. Treutler, H. Öhm, M. Häser, R. Ahlrichs, *Chem. Phys. Lett.* **1995**, *242*, 652−660. [45b] K. Eichkorn, F. Weigend, O. Treutler, R. Ahlrichs, *Theor. Chim. Acta* **1997**, *97*, 119−124.
[46] C. Møller, M. S. Plesset, *Phys. Rev.* **1934**, *46*, 618.
[47] [47a] R. G. Parr, W. Yang, *Density Functional Theory of Atoms and Molecules*, Oxford University Press, New York, **1988**; [47b] T. Ziegler, *Chem. Rev.* **1991**, *91*, 651−667.
[48] [48a] G. Savelsberg, H. Schäfer, *Z. Naturforsch., Teil B* **1978**, *33*, 711−713; [48b] V. C. Burschka, *Z. Anorg. Allg. Chem.* **1980**, *463*, 65−71; [48c] R. S. Hall, J. M. Stewart, *Acta Crystallogr., Sect. B* **1973**, *29*, 579−581; [48d] J. E. Iglesias, K. E. Pachali, H. Steinfink, *J. Solid State Chem.* **1974**, *9*, 6−14.
[49] D'Ans, Lax, *Taschenbuch für Chemiker und Physiker*, Vol. 3 (Ed.: R. Blachnik), Springer, Berlin, Heidelberg, **1998**, p. 440.

[50] D'Ans, Lax, *Taschenbuch für Chemiker und Physiker*, Vol. 3 (Ed.: R. Blachnik), Springer, Berlin, Heidelberg, **1998**, p. 436.
[51] A. F. Hollemann, E. Wiberg, *Lehrbuch der Anorganischen Chemie*, W. de Gruyter, Berlin, **1985**, p.148.
[52] [52a] U. Müller, M.-L. Ha-Eierdanz, G. Kräuter, K. Dehnicke, *Z. Naturforsch., Teil B* **1990**, *45*, 1128−1132; [52b] J. Cusick, M. L. Scudder, D. C. Craig, I. G. Dance, *Polyhedron* **1989**, *8*, 1139−1141.
[53] [53a] M. G. Kanatzidis, Y. Park, *J. Am. Chem. Soc.* **1989**, *111*, 3767−3769; [53b] A. C. Sutorik, M. G. Kanatzidis, *J. Am. Chem. Soc.* **1991**, *113*, 7754−7755.
[54] G. Wedler, *Lehrbuch der Physikalischen Chemie*, VCH, Weinheim, **1987**, p. 168.
[55] D. Fenske, N. Zhu, T. Langetepe, *Angew. Chem.* **1998**, *110*, 2784−2788; *Angew. Chem. Int. Ed.* **1998**, *37*, 2640−2644.
[56] [56a] J. B. Foresman, M. Head-Gordon, J. A. Pople, M. J. Frisch, *J. Phys. Chem.* **1992**, *96*, 135−149; [56b] R. McWheeny, *Methods of Molecular Quantum Mechanics*, 2nd ed., Academic Press, London, **1992**.
[57] K. Raghavachari, G. W. Trucks, J. A. Pople, M. Head-Gordon, *Chem. Phys. Lett.* **1989**, *157*, 479−483.
[58] F. Schwabl, *Quantenmechanik*, Springer, Heidelberg, **1990**, p. 189f.
[59] A. A. Voskanyan, P. N. Inglizyan, S. P. Lalykin, I. A. Plyutto, Y. M. Shevchenko, *Fiz. Tekh. Poluprovodn.* **1978**, *12*, 2096−2099.
[60] E. J. D. Garba, R. L. Jacobs, *Physica B+C* **1986**, *138*, 253−260.
[61] S. N. Mostafa, S. A. Schiman, *Ber. Bunsenges. Phys. Chem.* **1983**, *87*, 113−119.
[62] P. Scherrer, *Göttinger Nachrichten* **1918**, *2*, 98f.
[63] Y. Park, Ph. D. Thesis, Michigan State University, **1992**.
[64] K. O. Klepp, *J. Less Common Met.* **1987**, *128*, 79−89.
[65] G. Savelsberg, H. Schäfer, *Mater. Res. Bull.* **1981**, *16*, 1291−1297.
[66] Y. Park, D. C. Degroot, J. Schindler, C. R. Kannewurf, M. G. Kanatzidis, *Angew. Chem.* **1991**, *103*, 1404−1407; *Angew. Chem. Int. Ed. Engl.* **1991**, *30*, 1325−1328.
[67] [67a] Y. Park, M. G. Kanatzidis, *J. Chem. Mater.* **1991**, *3*, 781−783; [67b] X. Zhang, Y. Park, T. Hogan, J. L. Schindler, C. R. Kannewurf, S. Seong, T. Albright, M. G. Kanatzidis, *J. Am. Chem. Soc.* **1995**, *117*, 10300−10310.
[68] M. Emirdag, G. L. Schimek, J. W. Kolis, *J. Chem. Soc., Dalton Trans.* **1999**, 1531−1532.
[69] D. Fenske, J. F. Corrigan, in *Metal Clusters in Chemistry* (Eds.: P. Braunstein, L. A. Oro, P. R. Raithby), Wiley-VCH, Weinheim, **1999**, Vol. 3, p. 1302.
[70] [70a] F. C. Frank, J. S. Kasper, *Acta Crystallogr.* **1958**, *11*, 184−190; [70b] F. C. Frank, J. S. Kasper, *Acta Crystallogr.* **1959**, *12*, 483−499.
[71] [71a] C. Kölmel, R. Ahlrichs, *J. Phys. Chem.* **1990**, *94*, 5536−5542; [71b] F. A. Cotton, X. Feng, M. Matusz, R. Poli, *J. Am. Chem. Soc.* **1988**, *110*, 7077−7083; [71c] K. M. Merz, R. Hoffmann, *Inorg. Chem.* **1988**, *27*, 2120−2127.
[72] U. Müller, *Anorganische Strukturchemie*, 2nd Ed., B. G. Teubner, Stuttgart, **1991**, p. 101f.
[73] [73a] F. Jellinek, in *MTP International Review of Science, Inorganic Chemistry Series One*, *Vol. 5* (Ed.: D. W. Sharp), Butterworths, London, **1972**, p. 339; [73b] C. W. Folmer, F. Jellinek, *J. Less Common Met.* **1980**, *76*, 153−162.
[74] R. Ahlrichs, J. Besinger, A. Eichhöfer, D. Fenske, A. Gbureck, *Angew. Chem.* **2000**, *112*, 4089−4099; *Angew. Chem. Int. Ed.* **2000**, *39*, 3923−3933.
[75] M. B. Robin, P. Day, *Adv. Inorg. Radiochem.* **1967**, *10*, 247−422.
[76] S. Kashida, J. Akai, *J. Phys. C: Solid State Phys.* **1988**, *21*, 5329−5336.

Received March 28, 2001
[I01112]

Meltable Stannaborate Salts

Benno Ronig,[a] Ingo Pantenburg,[a] and Lars Wesemann*[a]

Keywords: Boranes / Ionic liquids / Tin / Cations

In a one-pot procedure, four imidazolium salts of alkylated stanna-*closo*-dodecaborate anions were synthesized. Alkyl substituents at the stannaborate anion and imidazolium cation were varied between ethyl and butyl, resulting in a range of melting points from 55 to 105 °C. The structures in the solids were determined in the case of [EMIM][Et–$SnB_{11}H_{11}$] (**1**) and [EMIM][Bu–$SnB_{11}H_{11}$] (**2**).

Introduction

Salts with a melting point under 100 °C are named ionic liquids, and are currently of growing interest.[1,2] This might be due to the expected high potential of these salts as an alternative reaction media in processes of technical relevance. The almost undetectable volatility of these compounds is one reason they might substitute conventional solvents. Obviously, the cation in these salts plays an important role for the low melting point and so far work is concentrated on *N*,*N*′-dialkylimidazolium and *N*-alkylpyridinium ions. A variety of classical, weak coordinating anions ($AlCl_4^-$, BF_4^-, PF_6^-, $CF_3SO_3^-$, NO_3^-, etc.) with these imidazolium or pyridinium cations exhibit the interesting properties of ionic liquids. Recently, C. A. Reed has presented the first studies on ionic liquids based on carborate salts of imidazolium and pyridinium cations.[3] Melting points down to 45 °C were determined for [*N*-ethyl-*N*′-methylimidazolium][propylcarba-*closo*-dodecaborate(12)]. Since the heteroborate anions are prominent for their very weak coordinating abilities, and they show resistance towards moisture and air, it is worthwhile to study these salts. We are currently investigating the chemistry of the easily accessible *closo*-heteroborate $[SnB_{11}H_{11}]^{2-}$. In this publication, we present imidazolium salts of the alkylated stanna-*closo*-dodecaborate with low melting points.

Results and Discussion

The synthesis of the nearly icosahedral stannaborate cluster was discovered by Todd in 1992,[4] and recently we have shown that this dianion can be used as a ligand in transition metal chemistry.[5] The air-stable stanna-*closo*-dodecaborate salt can be synthesized with a variety of counter-cations, offering the possibility of further modifying the solubility of the cluster salt. A key compound in this context is the tributylammonium salt $[Bu_3NH]_2[SnB_{11}H_{11}]$, since it drops out of water and the cations can be easily replaced by interaction with a base like KH. The ionic liquids of the alkylstannaborate anion are straightforwardly synthesized in to a two-step procedure. Starting from $[Me_3NH][B_{11}H_{14}]$ the stannaborate $[Bu_3NH]_2[SnB_{11}H_{11}]$ was synthesized in amounts of five grams and a yield of ca. 85% (Scheme 1).

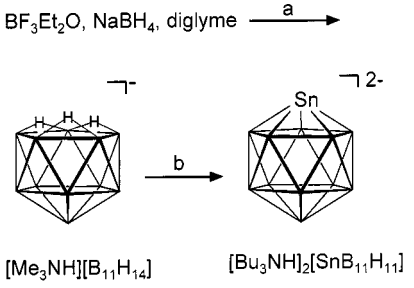

Scheme 1. a) 1. 106 °C, 2. H_2O, $[Me_3NH]Cl$; b) 1. 4 equiv. BuLi, 2. $SnCl_2$, 3. H_2O, $[Bu_3NH]Cl$

The air-stable stannaborate was treated with 1 equiv. of the respective alkyl iodide. After this quantitative alkylation, 2 equiv. of super-hydride $KHBEt_3$ were added in order to substitute the ammonium against the potassium cation. The solvent was changed to water and the ionic liquid was precipitated in high yield after addition of the respective imidazolium iodide (Scheme 2).

The new salts **1**–**4** were characterized by elemental analysis, DSC, NMR, and IR spectroscopy, and in the case of **1** and **2** also by single-crystal X-ray structure analysis. In contrast to the ionic liquids based on the classical anions like $[AlCl_4]^-$ or $[BF_4]^-$, the synthesized stannaborate salts were not hygroscopic, and showed no tendency to react with water and air even at higher temperatures. After melt-

[a] Institut für Anorganische Chemie, Universität zu Köln,
Greinstraße 6, 50939 Köln, Germany
Fax: (internat.) + 49-(0)221/470-4899
E-mail: lars.wesemann@uni-koeln.de

 © WILEY-VCH Verlag GmbH, 69451 Weinheim, Germany, 2002 1434–1948/02/0202–0319 $ 17.50+.50/0

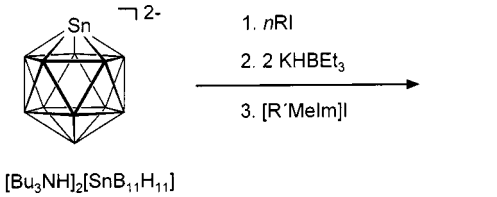

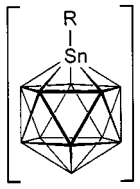

[R´MeIm]

	1	2	3	4
R	Et	Bu	Et	Bu
R´	Et	Et	Bu	Bu
yield (%)	73	62	61	60
MP(°C)	106	80	64	55

Scheme 2

ing the borates **1**−**4** at 200 °C for several hours, repeated elemental analyses confirmed the correct composition. In the series of the imidazolium salts **1**−**4**, the lowest melting point of 55 °C was achieved for the derivative with the butyl substituents at the imidazolium cation and the tin atom in the cluster. According to this concept, we tried to synthesize the octyl-substituted salt, but were not able to purify this waxy solid for satisfactory elemental analysis.

The imidazolium salts **1** and **2** crystallized in the monoclinic space group $P2_1/c$ and showed no disorder in the solid state. For both compounds, we did not find any indications for cation−anion contacts. In Figures 1 and 2, an ORTEP plot of the salts is shown. The interatomic distances in **1** and **2** are not unusual, and selected values and angles are listed in the captions of Figures 1 and 2.

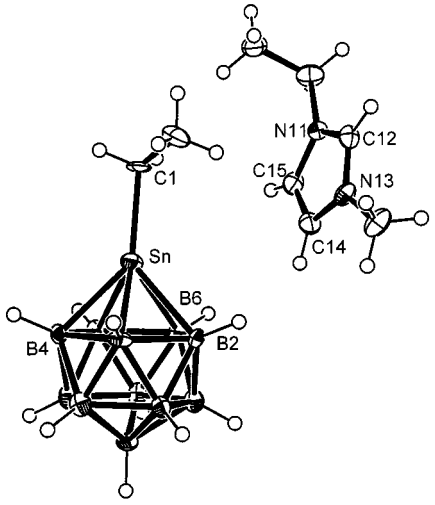

Figure 1. ORTEP drawing of the salt **1**; thermal ellipsoids are drawn at the 50% probability level; selected interatomic distances [Å]: Sn−C1 2.148(4), Sn−B2 2.308(5), Sn−B3 2.323(5), Sn−B4 2.311(6), Sn−B5 2.299(5), Sn−B6 2.298(6), N11−C12 1.332(7), C12−N13 1.332(7), N13−C14 1.380(7), C14−C15 1.353(8), C15−N11 1.380(8)

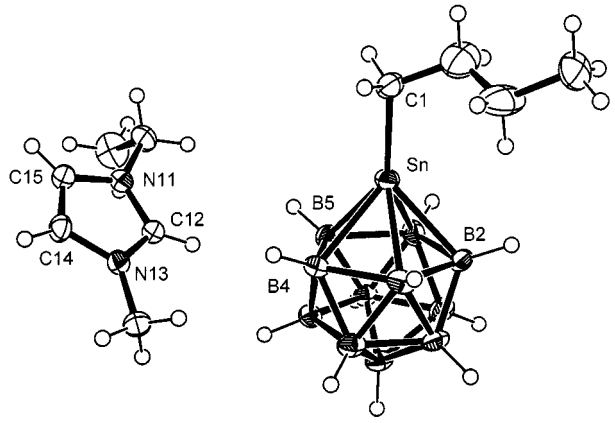

Figure 2. ORTEP drawing of the salt **2**; thermal ellipsoids are drawn at the 50% probability level; selected interatomic distances [Å]: Sn−C1 2.122(5), Sn−B2 2.307(6), Sn−B3 2.314(5), Sn−B4 2.312(5), Sn−B5 2.303(6), Sn−B6 2.312(5), N11−C12 1.335(6), C12−N13 1.329(6), N13−C14 1.386(6), C14−C15 1.355(7), C15−N11 1.376(6)

Conclusion

The quantitative alkylation of the stannaborate dianion offers the possibility of introducing this heteroborate into imidazolium salts exhibiting a low melting point. Positional disorder in the solid state is not an indicator for the relative low melting point of **1** and **2**.

Experimental Section

General: All experiments were carried out under dry nitrogen using standard Schlenk techniques. Solvents were freshly distilled under an inert gas from appropriate drying agents. All imidazolium iodides were prepared according to procedures known from the literature.[6] NMR spectroscopy was performed with a Bruker AC 200 spectrometer (^{1}H: 200 MHz, int. TMS; ^{13}C{^{1}H}: 50 MHz, int. TMS; ^{11}B and ^{11}B{^{1}H}: 64 MHz, ext. $BF_3{\cdot}OEt_2$). IR spectrometer: IFS66v/s Bruker. Elemental analyses were carried out in the Institut für Anorganische Chemie der Universität zu Köln with a Heraeus C,H,N,O-Rapid analyser. DSC measurements were performed with a Netzsch STA 409-Skimmer thermal analyser.

[EMIM][1-Et−SnB$_{11}$H$_{11}$] (1): 1-Iodoethane (0.08 mL, 0.99 mmol) was added to a solution of $[Bu_3NH]_2[SnB_{11}H_{11}]$ (510 mg, 0.82 mmol) in 40 mL of THF at room temperature. The mixture was heated under reflux for 3 h. Afterwards, the solvent was evaporated in vacuum and the residue dried for another 24 h. This was then dissolved in 20 mL of THF and treated with $LiHBEt_3$ (1.95 mL, 1 M solution in THF, 1.95 mmol). The solution was stirred for another 2 h and volatiles were removed in vacuum. The remaining white solid was dissolved in 50 mL of H_2O and [EMIM]I (0.40 g, 1.68 mmol) was added. The white precipitate was filtered off and dried in vacuum. Single crystals were obtained by slow evaporation of methanol from the product. Yield: 234 mg, 0.60 mmol, 73.3%. ^{1}H NMR (CD_2Cl_2): δ = 1.58 (t, ^3J = 7.3 Hz, 3 H, $SnCH_2CH_3$), 1.69 (t, ^3J = 7.8 Hz, 3 H, NCH_2CH_3), 2.62 (q, ^3J = 7.8 Hz, 2

H, SnCH_2CH$_3$), 3.97 (s, 3 H, NCH_3), 4.27 (q, ^3J = 7.3 Hz, 2 H, NCH_2CH$_3$), 0.99 (t, ^3J = 7.1 Hz, 3 H, CH$_2$CH$_2$CH_3), 7.30 (s, 2 H, NC*H*C*H*N), 8.69 (s, 1 H, NC*H*N). ^{11}B{^{1}H} NMR (CD$_2$Cl$_2$): δ = −12.5 (s, B12), −17.0 (s, B2−6 and B7−11). ^{13}C{^{1}H} NMR (CD$_2$Cl$_2$): δ = 9.0 (SnCH$_2$*C*H$_3$), 13.7 (Sn*C*H$_2$CH$_3$), 15.5 (NCH$_2$*C*H$_3$), 37.1 (N*C*H$_3$), 46.0 (N*C*H$_2$CH$_3$), 122.3 (N*C*H$_2$CH$_2$N), 124.1 (NCH$_2$*C*H$_2$N), 135.8 (N*C*H$_2$N). $C_8H_{27}B_{11}N_2Sn$ (388.9): calcd. C 24.71, H 7.00, N 7.20; found C 25.41, H 7.02, N 7.43. DSC: M.p. 105.7 °C. IR (KBr): ṽ = 2490 (vs), 2866 (vw), 2926 (w), 2958 (w), 3095 (s), 3097 (s), 3109 (s), 3140 (s), 3159 cm^{-1} (w).

X-ray Crystallographic Analysis of 1: $C_8H_{27}B_{11}N_2Sn$, formula mass 388.92 g/mol; monoclinic, space group $P2_1/c$ (no.14); a = 7.451(1), b = 17.564(2), c = 14.081(2) Å, β = 99.09(2)°, V = 1819.7(4) Å^3, Z = 4, $d_{calcd.}$ = 1.420 g·cm^{-3}, μ(Mo-K_α) = 1.392 mm^{-1}. Image Plate STOE (IPDS) diffractometer; Mo-K_α radiation (λ = 0.71073 Å); graphite monochromator. Data collection at 170 K on a crystal of dimensions 0.2 × 0.2 × 0.1 mm, using ω scans in the range 2.3° ≤ θ ≤ 27.0°, yielded 15956 reflections. The data were corrected for Lorentz and polarization effects. Numerical absorption corrections with programs X-RED (Stoe, Darmstadt, **2001**) and X-SHAPE (Stoe, Darmstadt, **1999**): T_{min}/T_{max} = 0.7474/0.8849. 3925 unique reflections with $I > 2\,\sigma(I)$ remained for structure solution by direct methods.[7] The structure model was completed by Fourier difference synthesis, F^2 refinement;[8−10] anisotropic parameters for non-hydrogen atoms and hydrogen atoms placed in calculated positions (C−H = 0.98 Å; B−H = 1.1 Å). Convergence obtained for 200 variables, 3925 data, and R_1(all) = 0.094, wR_2(all) = 0.087, GooF = 0.826. A final difference Fourier map showed the highest peak with 0.56 e·Å^{-3} 1.22 Å from B2 and the deepest hole with −1.40 e·Å^{-3} 0.02 Å from the Sn.

[EMIM][1-Bu−SnB$_{11}$H$_{11}$] (2): 1-Iodobutane (0.05 mL, 0.44 mmol) was added to a solution of [Bu$_3$NH]$_2$[SnB$_{11}$H$_{11}$] (235 mg, 0.38 mmol) in 40 mL of THF at room temperature. The mixture was heated under reflux for 3 h. Afterwards, the solvent was evaporated in vacuum and the residue dried for another 24 h. This was then dissolved in 20 mL of THF and treated with LiHBEt$_3$ (0.83 mL, 1 M solution in THF, 0.83 mmol). The solution was stirred for another 2 h and volatiles were removed in vacuum. The remaining white solid was dissolved in 50 mL of H$_2$O and [EMIM]I (0.18 g, 0.76 mmol) was added. The white precipitate was filtered off and dried in vacuum. Single crystals were obtained by slow evaporation of methanol from the product. Yield: 113 mg, 0.27 mmol, 62%. ^{1}H NMR (CD$_2$Cl$_2$): δ = 0.99 (t, ^3J = 7.1 Hz, 3 H, CH$_2$CH$_2$CH_3), 1.57 (m, 5 H, CH$_2$CH_2CH$_3$ and NCH$_2$CH_3), 1.99 (m, 2 H, SnCH$_2$CH_2CH$_2$), 2.70 (t, ^3J = 7.1 Hz, 2 H, SnCH_2), 3.97 (s, 3 H, NCH_3), 4.27 (q, ^3J = 7.3 Hz, 2 H, NCH_2CH$_3$), 7.30 (s, 2 H, NC*H*C*H*N), 8.69 (s, 1 H, NC*H*N). ^{11}B{^{1}H} NMR (CD$_2$Cl$_2$): δ = −12.3 (s, B12), −16.9 (s, B2−6 and B7−11). ^{13}C{^{1}H} NMR (CD$_2$Cl$_2$): δ = 13.5 (CH$_2$CH$_2$*C*H$_3$), 15.5 (NCH$_2$*C*H$_3$), 16.9 (SnCH$_2$*C*H$_2$), 26.8 (SnCH$_2$*C*H$_2$), 30.3 (Sn*C*H$_2$), 37.1 (N*C*H$_3$), 46.1 (N*C*H$_2$CH$_3$), 122.3 (N*C*H$_2$CH$_2$N), 124.1 (NCH$_2$*C*H$_2$N), 136.0 (N*C*H$_2$N). $C_{10}H_{31}B_{11}N_2Sn$ (417.0): calcd. C 28.80, H 7.42, N 6.72; found C 29.02, H 7.21, N 6.76. DSC: M.p. 80.3 °C. IR (KBr): ṽ = 2496 (vs), 2849 (vw), 2866 (vw), 2922 (w), 2957 (w), 3093 (s), 3113 (s), 3146 cm^{-1} (s)

X-ray Crystallographic Analysis of 2: $C_{10}H_{31}B_{11}N_2Sn$: formula mass 416.97 g/mol; monoclinic, space group $P2_1/c$ (no.14); a = 11.378 (1), b = 11.030 (1), c = 16.911 (2) Å, β = 100.81(2)°, V = 2084.6 (4) Å^3, Z = 4, $d_{calcd.}$ = 1.329 g·cm^{-3}, μ(Mo-K_α) = 1.220 mm^{-1}. Image Plate STOE (IPDS) diffractometer; Mo-K_α radiation (λ = 0.71073 Å); graphite monochromator. Data collection at 170 K on a crystal of dimensions 0.3 × 0.25 × 0.1 mm using ω scans in the range 1.8° ≤ θ ≤ 24.1° yielded 12909 reflections. The data were corrected for Lorentz and polarization effects. Numerical absorption corrections with programs X-RED (Stoe, Darmstadt, **2001**) and X-SHAPE (Stoe, Darmstadt, **1999**): $T_{min.}/T_{max}$ = 0.7218/0.8928. 3287 unique reflections with $I > 2\,\sigma(I)$ remained for structure solution by direct methods.[7] The structure model was completed by Fourier difference synthesis, F^2 refinement;[8−10] anisotropic parameters for non-hydrogen atoms, and hydrogen atoms placed in calculated positions (C−H = 0.98 Å; B−H = 1.1 Å). Convergence obtained for 219 variables, 3287 data, and R_1(all) = 0.072, wR_2(all) = 0.069, GooF = 0.878. A final difference Fourier map showed the highest peak with 0.92 e·Å^{-3} 1.03 Å from C3 and the deepest hole with −0.50 e·Å^{-3} 0.38 Å from H2a.

Crystallographic data (excluding structure factors) for the structures reported in this paper have been deposited with the Cambridge Crystallographic Data Centre as supplementary publications no. CCDC-169179 (**1**) and -169180 (**2**). Copies of the data can be obtained free of charge on application to CCDC, 12 Union Road, Cambridge CB2 1EZ, UK [Fax: (internat.) + 44-1223/336-033; E-mail: deposit@ccdc.cam.ac.uk].

[BMIM][1-Et−SnB$_{11}$H$_{11}$] (3): Salt **3** was synthesised according to the procedure outlined for the synthesis of **1**, starting from [Bu$_3$NH]$_2$[SnB$_{11}$H$_{11}$] (413 mg, 0.67 mmol) with 1-iodoethane (0.06 mL, 0.74 mmol) and LiHBEt$_3$ (1.44 mL, 1 M solution in THF, 1.44 mmol). The salt was precipitated by adding [BMIM]I (0.36 g, 1.35 mmol). The white solid was dried in vacuum. Yield: 170 mg, 0.41 mmol, 61.2%. ^{1}H NMR (CD$_2$Cl$_2$): δ = 0.97 (t, ^3J = 7.3 Hz, 3 H, CH$_2$CH$_2$CH_3), 1.39 (m, 2 H, CH$_2$CH_2CH$_3$), 1.69 (t, ^3J = 7.8 Hz, 3 H, SnCH$_2$CH_3),), 1.89 (m, 2 H, NCH$_2$CH_2CH$_2$),), 2.62 (q, ^3J = 7.8 Hz, 2 H, SnCH_2), 3.98 (s, 3 H, NCH_3), 4.21 (q, ^3J = 7.3 Hz, 2 H, NCH_2CH$_3$), 7.30 (s, 2 H, NC*H*C*H*N), 8.70 (s, 1 H, NC*H*N). ^{11}B{^{1}H} NMR (CD$_2$Cl$_2$): δ = −11.9 (s, B12), −17.1 (s, B2−6 and B7−11). ^{13}C{^{1}H} NMR (CD$_2$Cl$_2$): δ = 9.0 (CH$_2$CH$_2$*C*H$_3$), 13.6 (SnCH$_2$*C*H$_3$), 13.7 (CH$_2$*C*H$_2$CH$_3$), 19.7 (NCH$_2$CH$_2$*C*H$_2$), 32.3 (Sn*C*H$_2$), 37.2 (N*C*H$_3$), 50.7 (N*C*H$_2$CH$_3$), 122.6 (N*C*H$_2$CH$_2$N), 124.0 (NCH$_2$*C*H$_2$N), 136.2 (N*C*H$_2$N). $C_{10}H_{31}B_{11}N_2Sn$ (417.0): calcd. C 28.80, H 7.42, N 6.72; found C 29.25, H 7.48, N 6.87. DSC: M.p. 64.0 °C. IR (KBr): ṽ = 2501 (vs), 2868 (w), 2930 (w), 2958 (s), 3093 (s), 3115 (s), 3109 (s), 3142 (w), 3157 cm^{-1} (w).

[BMIM][1-Bu−SnB$_{11}$H$_{11}$] (4): Salt **4** was synthesised according to the procedure outlined for the synthesis of **1**, starting from [Bu$_3$NH]$_2$[SnB$_{11}$H$_{11}$] (302 mg, 0.49 mmol) with 1-iodobutane (0.07 mL, 0.61 mmol) and LiHBEt$_3$ (1.00 mL, 1 M solution in THF, 1.00 mmol). The salt was precipitated by adding [BMIM]I (0.275 g, 1.16 mmol). The light yellow-brown solid was dried in vacuum. The residue was dissolved in 5 mL of acetone, and precipitated by adding 20 mL of water. The light brown salt was filtered and dried in vacuum. Yield: 130 mg, 0.29 mmol, 60%. ^{1}H NMR (CD$_2$Cl$_2$): δ = 0.97 (m, 6 H, CH$_2$CH_3 and CH$_2$CH_3), 1.37 (m, 4 H, SnCH$_2$CH$_2$CH_2 and NCH$_2$CH$_2$CH_2), 1.63 (m, 4 H, SnCH$_2$CH_2CH$_2$ and NCH$_2$CH$_2$CH_2), 1.88 (m, 2 H, NCH$_2$CH_2), 2.66 (m, 2 H, SnCH_2CH$_2$), 3.98 (s, 3 H, NCH_3), 4.20 (t, ^3J = 7.3 Hz, 2 H, NCH_2CH$_3$), 7.28 (s, 2 H, NC*H*C*H*N), 8.70 (s, 1 H, NC*H*N). ^{11}B{^{1}H} NMR (CD$_2$Cl$_2$): δ = −12.1 (s, B12), −16.9 (s, B2−6 and B7−11). ^{13}C{^{1}H} NMR (CD$_2$Cl$_2$): δ = 13.5 (CH$_2$CH$_2$*C*H$_3$), 15.5 (NCH$_2$*C*H$_3$) 16.9 (SnCH$_2$*C*H$_2$), 26.8 (SnCH$_2$*C*H$_2$), 30.3 (Sn*C*H$_2$), 37.1 (N*C*H$_3$), 46.1 (N*C*H$_2$CH$_3$), 122.3 (N*C*H$_2$CH$_2$N), 124.1 (NCH$_2$*C*H$_2$N), 136.0 (N*C*H$_2$N).

$C_{12}H_{35}B_{11}N_2Sn$ (445.1): calcd. C 32.39, H 7.93, N 6.29; found C 32.22, H 7.33, N 7.07. DSC: M.p. 54.9 °C. IR (KBr): $\tilde{\nu}$ = 2505 (vs), 2856 (w), 2870 (w), 2926 (s), 2957 (s), 3097 (s), 3111 (w), 3140 (s), 3159 cm^{-1} (w).

[1] K. R. Seddon, *J. Chem. Tech. Biotechnol.* **1997**, *68*, 351−356.
[2] P. Wasserscheid, W. Keim, *Angew. Chem.* **2000**, *112*, 3926−3945; *Angew. Chem. Int. Ed.* **2000**, *39*, 3772−3789.
[3] A. S. Larsen, J. D. Holbrey, F. S. Tham, C. A. Reed, *J. Am. Chem. Soc.* **2000**, *122*, 7264−7272.
[4] R. W. Chapman, J. G. Kester, K. Folting, W. E. Streib, L. J. Todd, *Inorg. Chem.* **1992**, *31*, 979−983.
[5] T. Marx, L. Wesemann, S. Dehnen, I. Pantenburg, *Chem. Eur. J.* **2001**, *7*, 3025−3032, and references therein.
[6] J. D. Holbrey, K. R. Seddon, *J. Chem. Soc., Dalton Trans.* **1999**, 2133−2139.
[7] [7a] *X-RED 1.22, Data Reduction for STAD4 and IPDS*, Fa. Stoe & Cie, Darmstadt, **2001**.[7b] *X-SHAPE 1.06, Crystal Optimization for Numerical Absorption Correction*, Fa. Stoe & Cie, Darmstadt, **1999**.
[8] *WINGX 1.63*: L. J. Farrugia, *J. Appl. Crystallogr.* **1999**, *32*, 837−838.
[9] *SIR 92 − A program for crystal structure solution*: A. Altomare, G. Cascarano, C. Giacovazzo, A. Guagliardi, *J. Appl. Crystallogr.* **1993**, *26*, 343−350.
[10] G. M. Sheldrick, *SHELXL 93, Program for the Refinement of Crystal Structures*, Göttingen, **1993**.

Received August 27, 2001
[I01331]

A Unique Heterotopic Ligand for Sequential Synthesis of Polymetallic Complexes

Katja E. Berg,[a][‡] Yann Pellegrin,[a] Geneviève Blondin,[a] Xavier Ottenwaelder,[a] Yves Journaux,[a] María Moragues Canovas,[a] Talal Mallah,[a] Simon Parsons,[b] and Ally Aukauloo*[a]

Keywords: Copper / Heterotopic ligands / Iron / Metalations / Oxamate

A new organic ligand bearing four coordination sites that may be metallated in a stepwise manner is described, together with its Cu^{II} and Fe^{II} derivatives. This may be considered as the first ligand precursor for trimetallic systems.

Introduction

The design of new coordination complexes that play the role of ligands in the elaboration of polymetallic complexes is one of the challenging issues in the domain of modern inorganic chemistry.[1] The preparation of such complexes using a "step-by-step" approach is a prerequisite to building molecular extended systems with new architectures or even discrete molecules containing an increasing number of metallic centres with predetermined physical properties.[2−13]

Oxamato ligands have been extensively used to generate families of polymetallic compounds according to a sequential strategy.[2−7] However, the pitfall of this generation of oxamato complexes was the isolation of only heterobimetallic complexes. In order to overcome this drawback, it seems evident that the ligand must embody predetermined instructions that will, under the supervision of the chemist, lead toward the desired edifice. Recently, Chaudhuri et al. described a well-founded route leading to the formation of discrete heterotrimetallic complexes in a stepwise fashion.[14] Thus, in comparison to the chemistry described for instance with $[Cu(opba)]^{2-}$ [opba = *o*-phenylenebis(oxamato)],[2,3] an additional chelating anchor in the initial building block should consequently allow us to synthesize molecules of higher nuclearity and dimensional arrays.

In this communication, we describe the synthesis of an organic ligand that contains three different types of coordination sites. The chemical difference in the binding nature of the three coordination sites of the ligand renders the metalation process selective, allowing stepwise reactions that may lead to novel higher nuclearity trimetallic systems, be it discrete or extended in nature. Herein we report the preparation and the crystal structure of the first coordination complex $[\mathbf{L}Cu]^{2-}$ where $H_4\mathbf{L}$ stands for *N*,*N*′-(dipyrido[3,2-*a*:2′,3′-*c*]phenazine-11,12-diyl)bis(oxamic acid). The versatility of this ligand **L** towards selective metalation is also shown with the characterisation of the $[Fe(\mathbf{L_1})_3]^{2+}$ complex together with the tetranuclear $[Fe(\mathbf{L}Cu)_3]^{4-}$ adduct.

The synthesis of the heterotopic ligand follows the condensation of *o*-diones with aromatic *o*-diamines as shown in Scheme 1.[15] The ethyl ester derivative, noted $\mathbf{L_1}$, was isolated quantitatively as a yellow powder by condensation of equimolar amounts of **1**[16] and 1,10-phenanthroline-5,6-dione[17] in refluxing methanol.

Selective metalation of the bis(oxamato) cavity with a copper(II) ion was carried out in basic medium by slow addition of a copper(II) salt in solution, and the corresponding phosphonium salt was obtained by metathesis. Insertion of a copper ion in the bis(oxamato) cavity was evidenced by a red shift of about 50 cm^{-1} for the C=O stretching. Crystallisation in a mixture of acetonitrile and water gave red tablets that were analysed by X-ray diffraction. The structure of $[\mathbf{L}Cu](PPh_4)_2{\cdot}0.5CH_3CN$ consists of the dianionic copper(II) complex, tetraphenylphosphonium cations, and acetonitrile molecules of crystallisation. As shown in Figure 1, a perspective side view of the dianion complex $\mathbf{L}Cu^{2-}$ indicates an almost planar structure of the ligand skeleton with maximum deviation from the mean molecular plane of 0.317(3) Å for atom O(17).

The copper atom sits in a planar-trapezoidal N_2O_2 coordination environment. The average bond lengths between

[‡] Present address: Department of Chemistry, Stanford University, Stanford, CA 94305-5080, USA
[a] Laboratoire de Chimie Inorganique, UMR 8613, Université Paris-Sud,
91405 Orsay, France
Fax: (internat.) + 33-1/69154754
E-mail: aukauloo@icmo.u-psud.fr
[b] Department of Chemistry, The University of Edinburgh, West Mains Road, Edinburgh, EH9 3JJ, United Kingdom

 © WILEY-VCH Verlag GmbH, 69451 Weinheim, Germany, 2002 1434−1948/02/0202−0323 $ 17.50+.50/0

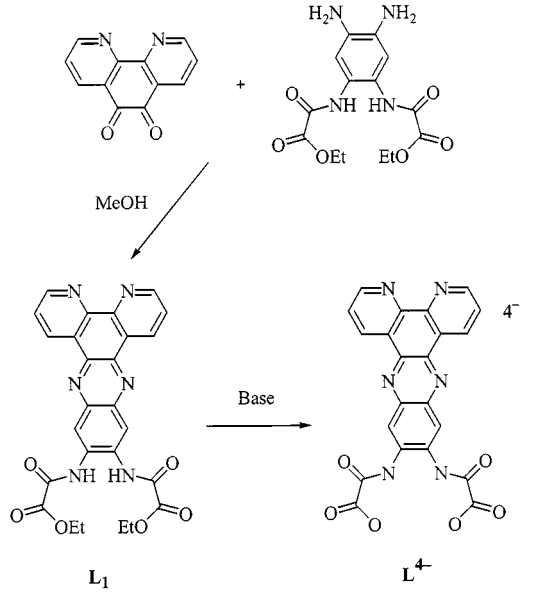

Scheme 1

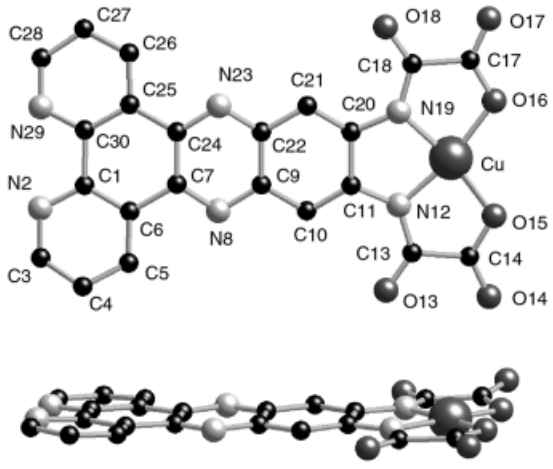

Figure 1. Different views of $[\mathbf{L}Cu]^{2-}$ with the atom numbering scheme (H atoms have been omitted)

the copper and the two deprotonated nitrogen atoms of the amide functions and the two oxygen atoms from the carboxylate groups are 1.898 and 1.936 Å, respectively. Comparatively, these bond lengths are in agreement with those found for similar environments of copper(II).[18] To the best of our knowledge, this is the first X-ray structure whereby a phenanthroline-carrying ligand is not involved in the coordination sphere of the metal ion. The solid-state EPR spectrum (100 K) of this copper complex, shown in Figure 2, is characteristic of a copper(II) ion in a square-planar geometry. The best agreement between the experimental solid-state spectrum and the simulated one was obtained for the following parameters: $A_{\perp} = 33.275$ G, $A_{\parallel} = 214.587$ G, $g_{\perp} = 2.040$, and $g_{\parallel} = 2.191$.

Benefiting from the high affinity constant of the iron(II) ion for phenanthroline to form the tris(phenanthroline) complex ($K_c = 10^{21}$),[19] we set out to metallate the phen-

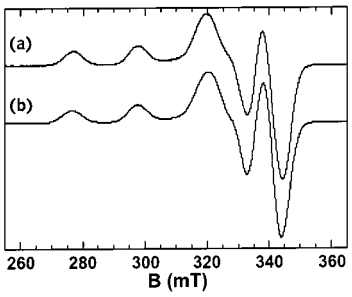

Figure 2. Solid-state EPR spectra (100 K) of [**L**Cu]-$(PPh_4)_2 \cdot 0.5CH_3CN$: (a) experimental; (b) simulated

anthroline end of the $\mathbf{L_1}$ ligand. The ^{1}H NMR spectrum of the $[Fe(\mathbf{L}_1)_3]^{2+}$ clearly indicates that the compound is diamagnetic and all signals of the ligand are present. The less resolved signals and the chemical shifts for the protons carried by the phenanthroline skeleton are attributable to the presence of the iron(II) ion. No apparent shift was observed for the proton signals of the ethyl groups indicating that no metal ion was coordinated to this cavity. This was also confirmed by infrared spectroscopy where no shift in the vibration frequencies of the carbonyl groups was observed.

Finally, treatment of $[Fe(\mathbf{L}_1)_3]^{2+}$ with an adequate amount of tetramethylammonium hydroxide in an aqueous solution, followed by addition of a copper(II) salt, gave, after conventional work up, a deep red solid. The infrared spectrum of $(NMe_4)_4[Fe(\mathbf{L}Cu)_3] \cdot 10H_2O$ indicates the presence of a tetramethylammonium cation and metalation of the oxamato cavity. The pattern of the signals is similar to that of the mononuclear counterpart, bringing thus a solid evidence that all the oxamate groups are coordinated in the same fashion. The more convincing piece of evidence of the content of copper ions for complex $(NMe_4)_4$-$[Fe(\mathbf{L}Cu)_3] \cdot 10H_2O$ comes from the magnetic susceptibility measurement where the χT value for a wide range of temperatures equals to the sum of three spins $S = 1/2$ for each corresponding copper(II) ion.

We have shown in this report the versatility of this new heterotopic ligand in the design of multinuclear compounds in a rationale way. We are currently using the tetranuclear complex as ligand to bind a third generation of metal ions through the external oxygen atoms of the oxamato groups to give discrete molecules or an extended network of heteropolymetallic compounds.

Experimental Section

Diethyl *N*,*N*′-(Dipyrido[3,2-*a*:2′,3′*c*]phenazine-11,12-diyl)bis(oxamate) ($\mathbf{L_1}$): To a stirred solution of 1,10-phenanthroline-5,6-dione[17] (0.42 g, 2 mmol) in methanol (100 mL) under reflux was added dropwise a slurry of the diamine **1**[16] (0.68 g, 2 mmol) in methanol (50 mL). After the addition was completed, the mixture was kept under constant stirring for 30 min. The deep yellow precipitate was filtered off, washed with ether and dried under vacuum (0.92 g, 90%). ^{1}H NMR ([D$_6$]DMSO): δ = 1.38 (t, 3 H), 4.40 (q, 4 H), 7.95 (dd, 2 H), 8.64 (s, 2 H), 9.26 (dd, 2 H), 9.55 (dd, 2 H), 10.9 (s, 2

H). IR (KBr): $\tilde{\nu}$ = 3285 cm^{-1} (NH), 1755 and 1695 cm^{-1} (C=O).

$(PPh_4)_2$[CuL]: To a suspension of **L_1** (513 mg, 1 mmol) in water (25 mL) was added a methanolic solution of Me_4NOH (25%) (1.7 mL, 4 mmol). After complete dissolution, an aqueous solution of $Cu(NO_3)_2 \cdot 3H_2O$ (246 mg, 1 mmol) was added dropwise with stirring. The dark brown solution was filtered to remove any insoluble material and concentrated under reduced pressure. To the solution was added an excess of Ph_4PCl and the complex extracted twice with dichloromethane. The organic phase was dried with $MgSO_4$, filtered and the solvents were evaporated to dryness yielding a red solid. Crystallisation in a mixture of acetonitrile and water (90:10) afforded well-shaped crystals of the copper complex suitable for X-ray analysis. IR (KBr): $\tilde{\nu}$ = 1675 and 1645 cm^{-1} (C=O).

$[Fe(L_1)_3](BF_4)_2 \cdot 2H_2O$: In methanol (30 mL), **L_1** (154 mg, 0.3 mmol) was suspended and a methanolic solution (10 mL) of $Fe(BF_4)_2 \cdot 6H_2O$ (33 mg, 0.1 mmol) was added dropwise, giving a deep red solution. A red solid was isolated after concentration of the reaction mixture and precipitation with diethyl ether (90%). ^1H NMR ([D_6]DMSO): δ = 1.38 (t, 3 H), 4.46 (q, 4 H), 7.82 (dd, 2 H), 7.95 (dd, 2 H), 8.74 (s, 2 H), 9.62 (dd, 2 H), 11.2 (s, 2 H). IR (KBr): $\tilde{\nu}$ = 3415 cm^{-1} (NH), 1745 and 1710 cm^{-1} (C=O). $C_{78}H_{64}N_{18}O_{20}B_2F_8Fe$ (1802.9): calcd. C 51.96, H 3.58, N 13.98; found C 50.99, H 3.49, N 14.14.

$(NMe_4)_4[Fe(CuL)_3] \cdot 10H_2O$: The synthesis of $[Fe(LCu)_3]^{6-}$ was similar to that of $[LCu]^{2-}$, starting with $[Fe(L_1)_3]^{2+}$ in methanol and adding 12 equiv. of base and 3 equiv. of the copper(II) salt. It was isolated as a red solid by concentration of the filtered solution and precipitation with diethyl ether. IR (KBr): $\tilde{\nu}$ = 1670 and 1635 cm^{-1} (C=O). $C_{72}H_{60}Cu_3FeN_{22}O_{28}$ (2080.3): calcd. C 47.35, H 4.46, Cu 9.16, Fe 2.68, N 14.81; found C 47.18, H 4.86, Cu 9.22, Fe 2.56, N 14.86.

Crystal Data for $(PPh_4)_2$[CuL]·0.5CH_3CN: $C_{71}H_{49.5}CuN_{6.5}O_6P_2$, M = 1433.11, $P\bar{1}$, a = 11.141(3), b = 14.724(5), c = 19. 586(6) Å, α = 75.617(2), β = 75.43(2), γ = 84.592(2) °, V = 3010.3(16) $Å^3$, T = 220 K, Z = 2, 14106 reflections measured, of which 10676 were unique (R_{int} = 0.0190). Data collection, solution, and refinement: ω-θ, standard Patterson methods with subsequent full-matrix least-squares refinement. Shelxl-97.[20] The final $wR(F^2)$ was 0.1893 (all data). The crystal drawings were carried out with the Crystal Maker program.[21] Crystallographic data (excluding structure factors) reported in this paper have been deposited at the Cambridge Crystallographic Data Centre and allocated the deposition number CCDC-164965. Copies of the data can be obtained free of charge on application to CCDC, 12 Union Road, Cambridge CB2 11Z, UK [Fax: (internat.) + 44-1223/336-033; E-mail: deposit@ccdc.cam.ac.uk].

Acknowledgments

We thank STINT (The Swedish Foundation for International Cooperation in Research and Higher Education), the CNRS (Centre National de Recherche Scientifique) and the European community for financial support (TMR programs "Ru−Mn Artificial Photosynthesis" Contract FMRX-CT96−0031 and "MolNanoMag" Contract HPRN-CT-1999−00012).

[1] O. Kahn, *Adv. Inorg. Chem.* **1995**, *43*, 179−259.
[2] Y. Pei, Y. Journaux, O. Kahn, *Inorg. Chem.* **1988**, *27*, 399−404.
[3] Y. Pei, Y. Journaux, O. Kahn, *Inorg. Chem.* **1989**, *28*, 100−103.
[4] M. Mitsumi, H. Okawa, H. Sakiyama, M. Ohba, N. Matsumoto, T. Kurisaki, H. Wakita, *J. Chem. Soc., Dalton Trans.* **1993**, 2991−2994.
[5] R. Ruiz, J. Faus, F. Lloret, M. Julve, Y. Journaux, *Coord. Chem. Rev.* **1999**, *193−195*, 1069−1117 and references therein.
[6] Y. Pei, Y. Journaux, O. Kahn, A. Dei, D. Gatteschi, *J. Chem. Soc., Chem. Commun.* **1986**, 1300−1301.
[7] J. Ribas, C. Diaz, R. Costa, Y. Journaux, C. Mathonière, O. Kahn, A. Gleizes, *Inorg. Chem.* **1990**, *29*, 2042−2047.
[8] A. Aukauloo, X. Ottenwaelder, R. Ruiz, Y. Journaux, Y. Pei, E. Rivière, M. C. Muñoz, *Eur. J. Inorg. Chem.* **2000**, *5*, 951−957.
[9] V. Gadet, T. Mallah, I. Castro, M. Verdaguer, *J. Am. Chem. Soc.* **1992**, *114*, 9213−9214.
[10] T. Mallah, S. Thiébaut, M. Verdaguer, P. Veillet, *Science* **1993**, *262*, 1554−1557.
[11] W. R. Entley, G. S. Girolami, *Science* **1995**, *268*, 397−400.
[12] S. Ferlay, T. Mallah, R. Ouahès, P. Veillet, M. Verdaguer, *Nature* **1995**, *378*, 701−703.
[13] A. Scuiller, T. Mallah, A. Nivorozkhin, J.-L. Tholence, M. Verdaguer, P. Veillet, *New J. Chem.* **1996**, *20*, 1−3.
[14] V. C. Verani, T. Weyhermuller, E. Rentschler, E. Bill, P. Chaudhuri, *Chem. Commun.* **1998**, *22*, 2475−2476.
[15] M. J. Crossley, P. L. Burn, S. J. Langford, J. K. Prashar, *J. Chem. Soc., Chem. Commun.* **1995**, 1921−1923.
[16] A. Aukauloo, X. Ottenwaelder, unpublished results.
[17] M. Yamada, Y. Tanaka, Y. Yoshimoto, S. Kuroda, I. Shimao, *Bull. Chem. Soc. Jpn.* **1992**, *65*, 1006−1011.
[18] B. Cervera, J. L. Sanz, M. J. Ibanez, G. Vila, F. Lloret, M. Julve, R. Ruiz, X. Ottenwaelder, A. Aukauloo, S. Poussereau, Y. Journaux, M. C. Muñoz, *J. Chem. Soc., Dalton. Trans.* **1998**, 781−790.
[19] A. Ringbom, in *Complexation in Analytical Chemistry*, John Wiley & Sons, **1963**, p.284.
[20] G. M. Sheldrick, Institut für Anorganische Chemie der Universität, Tammanstrasse 4, 3400 Göttingen, Germany, **1998**.
[21] D. Palmer, *CrystalMaker*, Bicester, **1993**.

Received September 5, 2001
[I01344]

New Organometalated Phosphinato-*O*,*O*′ Ligands in the Planar Eight-Membered Ring [{Cp(CO)$_2$Fe}*t*BuPO$_2$FeCl$_2$]$_2$

Ingo-Peter Lorenz,*[a] Markus Maier,[a] and Kurt Polborn[a]

Keywords: Iron / Heterocycles / O ligands / Oxidations / Self-assembly

By simple oxidation of the diferriophosphonium salt [Fp$_2$P(H)*t*Bu]$_2$FeCl$_4$ (**1′d**) with air the planar eight-membered heterocycle {Fp*t*BuPO$_2$FeCl$_2$}$_2$ (**2**) was generated. Compound **2** contains two organometalated phosphinato-*O*,*O*′ ligands bridging two tetrahedrally configured iron(III) centres [Fp = CpFe(CO)$_2$ = ferrio]. The new ferrio phosphinato ligand Fp*t*BuPO$_2^-$ was synthesized in a controlled manner for the first time. Compound **1′d** was obtained by the so-called insertion reaction of Fp$_2$ and *t*BuPCl$_2$, or by the silyl method using CpFe(CO)$_2$Cl and *t*BuP(SiMe$_3$)$_2$, both in toluene with traces of water present.

Introduction

The phosphinato ligand R$_2$PO$_2^-$ has a significant position among the classical ligands. Their syntheses, stability, and complex chemical behaviour towards the main group and transition elements (mono-, bidentate and bridging ligands), as well as their applications, especially as coordination polymers, has been the subject of numerous publications.[1] Within the scope of our investigations on organometalated phosphorus compounds,[2] which follow the isolobal theory, we succeeded in the synthesis and structural characterisation of the cage-like molecule [{CpFe(CO)$_2$(Mes)PO$_2$}$_4${MesPO$_3$Fe$_2$(OH)Cl}$_2$].[3] Besides the phosphonato ligand RPO$_3^{2-}$, it contains for the first time the organometalated phosphinato ligand FpRPO$_2^-$ (Fp = CpFe(CO)$_2$; R = Mes). The very complex framework of 4 iron(III) and 6 phosphorus centres connected by oxygen atoms, was formed unexpectedly by simple oxidation of the ferriophosphonium salt [Fp$_2$P(H)Mes]Cl with air.[3] Our attempts to separate the novel ferriophosphinato ligand from this cage compound have not been hitherto successful.

Mono-, di- and triferriophosphanes Fp$_n$PR$_{3-n}$ (n = 1−3) can be easily oxidised to the corresponding organometallated (chalcogeno)phosphoranes Fp$_n$PR$_{3-n}$(E) (E = O, S, Se), as well as the organic derivatives PR$_3$.[4] While the organic phosphonium salts [PR$_4$]X are normally air-stable, the diferriophosphonium salts [Fp$_2$P(H)R]X (X = any anion) turned out to be very reactive towards oxidising reagents, especially air oxygen.[3]

In the following, we report on the simple and selective transformation of a dimetalated phosphonium salt into an eight-membered planar ring molecule containing two Fe^{III} centres as well as two bidentate bridging ferriophosphinato-*O*,*O*′ ligands.

[a] Department Chemie, Universität München
Butenandtstr. 5−13, 81377 München, Germany
Fax: (internat.) + 49-(0)89/2180-7867
E-Mail: ipl@cup.uni-muenchen.de

Results and Discussion

Our aim was to prove the surprising result of the oxidation of the PH-functionalized diferrio(mesityl)phosphonium salt [Fp$_2$P(H)Mes]Cl with air, leading to the cage molecule.[3] Therefore, we first synthesized a series of PH- and PCl-functionalized diferrio(organyl)phosphonium salts of the type [Fp$_2$P(X)R]$_2$FeCl$_4$ (X = H, Cl; R = Me, Et, *i*Pr, *t*Bu, Ph, *p*Tol, Xyl, Mes), which could then be oxidized. We used the so-called insertion method, which is the reaction of RPCl$_2$ with the dimer {CpFe(CO)$_2$}$_2$ (Scheme 1).

Depending on the substituent R and the solvent, we were able to obtain both the corresponding PCl- and PH-functionalized diferriophosphonium salts. In toluene at 80 °C both derivatives were obtained concurrently, whereby traces of H$_2$O played a role. Whereas in the case of R = Me, Et, Ph, and Tol, only the PCl phosphonium salts [Fp$_2$P(Cl)R]$_2$FeCl$_4$ (**1a**, **b**, **e**, and **f**) were formed, for R = *i*Pr, *t*Bu, Xyl, and Mes; however, the PH derivatives [Fp$_2$P(H)R]$_2$FeCl$_4$ (**1′c**, **d**, **g**, and **h**) were also obtained in considerable amounts, besides the PCl compounds. The best yields for **1a**−**h** and **1′a**−**h** were achieved when the starting materials Fp$_2$ and RPCl$_2$ were used in a 3:2 ratio. When dichloromethane was used as the solvent, only the PCl derivatives **1b**−**d** were formed at room temp. As NMR experiments with the combinations H$_2$O/toluene, D$_2$O/toluene, and H$_2$O/C$_6$D$_6$ and absolutely dry toluene as the solvent have shown, the hydrogen atom is derived from traces of water in the toluene. It is surprising that the P−Cl moiety, once formed could not be transformed into the PH entity. Further experiments showed that P−Cl could be changed into P−OH or P−OR by reaction with H$_2$O or ROH, respectively.[5]

 © WILEY-VCH Verlag GmbH, 69451 Weinheim, Germany, 2002 1434−1948/02/0202−0327 $ 17.50+.50/0

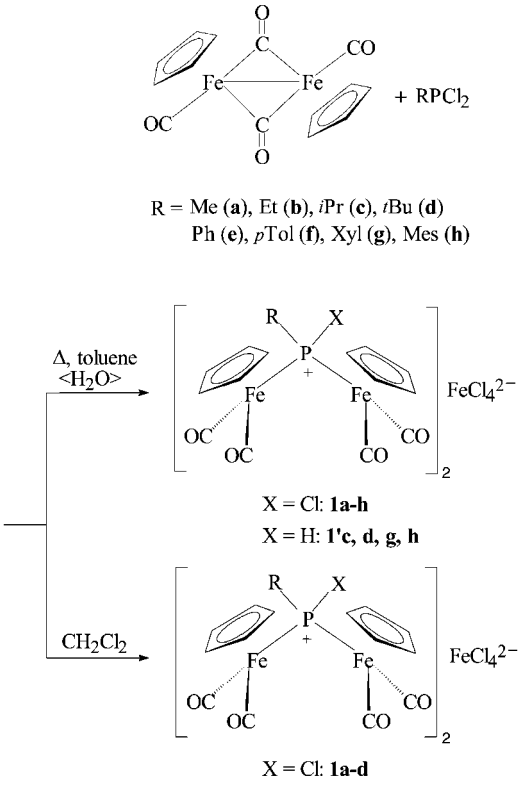

Scheme 1

We were not able to successfully obtain single crystals of any PH derivative, $[Fp_2P(H)R]_2FeCl_4$, but we succeeded in obtaining single crystals of the PCl compounds, $[Fp_2P(Cl)R]_2FeCl_4$ (R = Me, Et, *i*Pr, *t*Bu) **1a**−**d**. In this context, however, we only report on the molecular structure of the *tert*-butyl derivative **1d**, instead of the analogous **1′d**, which is the starting material for the formation of the novel ring molecule **2**. Compound **1′d** was obtained by using the silyl method, where $CpFe(CO)_2Cl$ was treated with *t*BuP-$(SiMe_3)_2$ in toluene at room temperature in the presence of traces of water (Scheme 2).

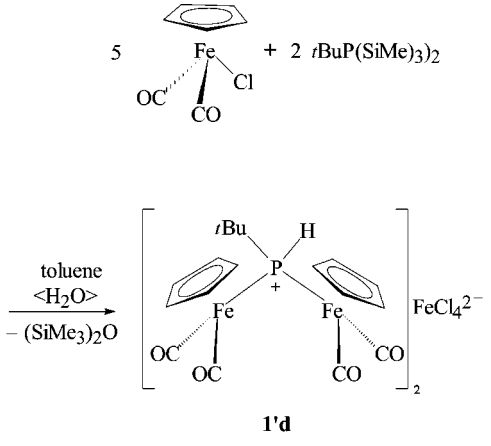

Scheme 2

The phosphonium salts **1a**−**h** and **1′c**, **d**, **e**, **g**, and **h** were treated with air oxygen for periods ranging from a few days to weeks. Only the mixed PH/Cl-functionalized salt with R = *t*Bu (**1d/1′d**) yielded a homogeneous product with **2**, besides the by-product ferrocene. Related experiments showed that the pure, rather stable PCl derivative **1d** could not be oxidized to give **2**. On the other hand, the oxidation of the pure PH compound **1′d** gave a greater yield of **2** than using the mixed salt **1d/1′d**. A plausible reaction mechanism is shown in Scheme 3, in which the balance of electrons and stoichiometry is correct. In the first step, the phosphonium cation is oxidised by oxygen under elimination of one ferrio group. In the next step, the resulting unstable monoferriophosphinic acid reacts with the $FeCl_4^-$ counter anion, which is derived by oxidation from the $FeCl_4^{2-}$ present in the starting material **1′d**. The resulting eight-membered ring of **2** seems to be the consequence of self assembling under thermodynamic control.

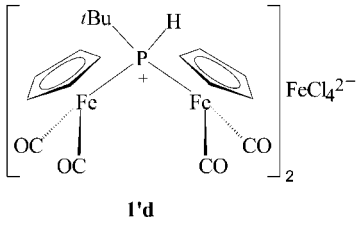

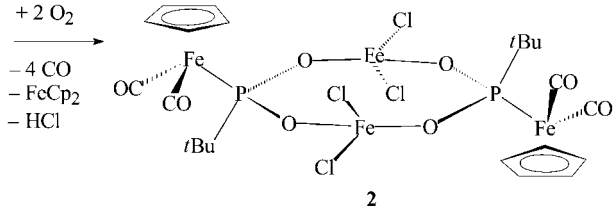

Scheme 3

The IR spectra (solid, KBr) of the mixed compound **1d/1′d** and the pure **1d** and **1′d** show the characteristic vibrations $\nu(CO_t)$ at 2055, 2031, and 1989 cm^{-1}. The ^{31}P NMR spectrum of **1d** shows a singlet at $\delta = 289$ and that of **1′d** shows a doublet at $\delta = 31$ ($^1J_{PH} = 303$ Hz), which are in the expected regions. The ^1H NMR spectra of both compounds **1d** and **1′d** show two signals at $\delta = 5.36$ (s, Cp) and 1.29 (s, Me), **1′d** additionally a doublet at $\delta = 3.40$ ($^1J_{PH} = 303$ Hz). In the FAB$^+$ (*m*NBA) mass spectra the parent signals are found at *m*/*z* = 477 [M(*PCl*)]$^+$ (**1d**) and 443 [M(*PH*)]$^+$ (**1′d**), respectively. In the case of the mixed salt **1d/1′d**, both signals appear in a 1:1 ratio. The elemental analysis does not indicate any exact product distribution in the mixed salt, the Cl value, however, points to an excess of the PCl-functionalised derivative **1d** in the mixed salt.

All attempts to obtain single crystals of **1′d** failed. The PCl-functionalised derivative **1d**, however, could be obtained as single crystals suitable for an X-ray structure analysis. In **1d**[6] both the Fe atoms and the central P atom are

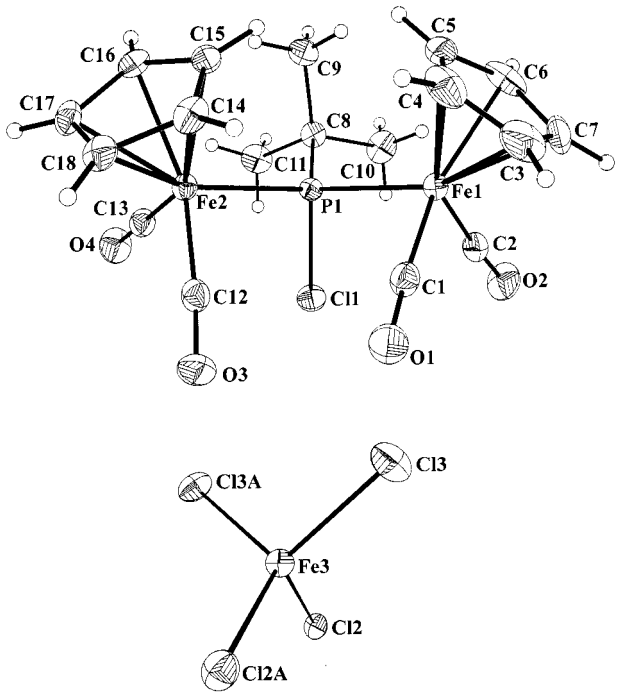

Figure 1. Molecular structure of **1d** (only 1 cation and the anion) in the crystal; selected bond lengths [Å] and angles [°]: Fe1−P1 2.3070(9), Fe2−P1 2.2930(10), P1−Cl1 2.0989(11), P1−C8 1.900(3), Fe3−Cl*n* 2.3159(11), 2.3231(10); Fe1−P1−Fe2 119.78(4), Fe1−P1−Cl1 102.46(4), Fe1−P1−C8 114.47(11), Fe2−P1−Cl1 102.46(4), Fe2−P1−C8 114.66(11), Cl1−P1−C8 98.57(11), Cl*x*−Fe3−Cl*y* 103.67(6), 115.52(4), 107.96(4), 106.52(6)

pseudo-tetrahedrally coordinated (Figure 1). The two Fe−P distances have the same size and fit very well within the range of symmetric diferriophosphonium salts.[2] There is no bonding interaction between the two Fe centres (Fe−Fe 3.979 Å). Because of the steric effect of the two ferrio groups, the tetrahedron of the P atom is strongly distorted [Fe1−P1−Fe2 119.78(4)°; Cl1−P−C8 98.57(11)°].

Compound **2** is slightly soluble and paramagnetic (μ_B = 6.04 B.M.).[7] Therefore, NMR measurements were not possible, and the spectroscopic characterization was restricted. The IR spectrum of **2** shows, besides the absorptions of the Cp and *t*Bu groups, those of the corresponding ν(CO) at 2044 and 1999 cm^{-1} and ν(PO_2) at 1070 and 971 cm^{-1}. In the EI (*m*NBA) mass spectrum the signal of highest mass appears at *m*/*z* = 791 as the fragment $[M - 2\ CO]^+$; the further fragmentation includes Cl and CO eliminations with signals at *m*/*z* = 719, 692, and 664 $[M - 2\ CO - 2Cl - nCO]^+$ (*n* = 0−2).

The solution of the composition and the structure of **2** could only be achieved by a single-crystal X-ray diffraction analysis[6] (Figure 2). Accordingly, **2** consists of a nearly planar centrosymmetric eight-membered ring with alternating O−P−O−Fe positions and C_i symmetry. The four tetrahedra at both P and Fe centres are linked by four common O atoms. The maximum deviation of the least-squares plane over all atoms is 0.067 Å. The heterocycle of **2** has a diameter of about 4.7 Å (Fe2−Fe2A 4.576 Å, P1−P1A 4.792 Å). The tetrahedra are completed at the Fe atoms by

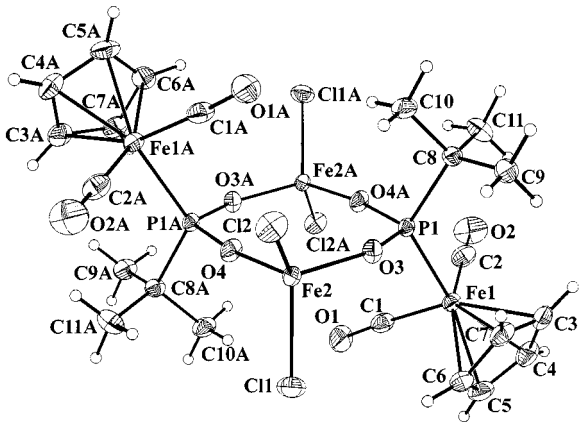

Figure 2. Molecular structure of **2** (only 1 cation and the anion) in the crystal; selected bond lengths [Å] and angles [°]: P1−Fe1 2.2190(11), P1−C8 1.860(4), P1−O3 1.552(3), P1−O4A 1.555(2), Fe2−O3 1.845(3), Fe2−O4 1.825(3), Fe2−Cl1 2.2029(12), Fe2−Cl2 2.1910(12); O3−P1−O4A 108.6(2), Fe2−O3−P1 146.5(2), P1−O4A−Fe2A 171.5(2), O3−P1−C8 103.7(2), O3−P1−Fe1 109.82(11), O3−Fe2−O4 110.80(12), O3−Fe2−Cl1 107.04(9), O3−Fe2−Cl2 109.43(9), Cl1−Fe2−Cl2 110.60(5)

two Cl atoms, and at the P atoms by a ferrio and a *t*Bu group. The P−O and Fe−O distances are in pairs nearly in the same range [P1−O3 1.552(3), P1−O4A 1.555(2) Å, Fe2−O3 1.845(3), Fe2−O4 1.825(2) Å]. The exocyclic distances P1−Fe1, P1−C8 and Fe2−Cl1 are 2.219(0), 1.860(4) and 2.203(0) Å. The corresponding ring angles of the Fe and P atoms are quite similar [O3−Fe2−O4A 110.80(12), O3−P1−O4A 108.6(2)°], the angles including the substituents, however, differ more noticeably [Cl1−Fe2−Cl2 110.60(5), Fe1−P1−C8 120.44(13)°]. The angles at the ring O atoms are surprisingly different [P1−O3−Fe2 146.5(2)° and P1A−O4−Fe2 171.5(2)°].

The structural constitution of **2** is very similar to that of cyclic tetrametaphosphates[7] and dimeric diorganophosphinato complexes of transition metals,[1] which in contrast are not planar. Formally, **2** can be regarded as the dimeric compound of a (*tert*-butyl)(ferrio)phosphinato-*O*,*O*′ complex of tetrahedrally configured Fe^{III}, where the phosphinato ligand is not behaving as a chelating ligand towards *one* Fe^{III} atom, but as a bridging ligand between *two* Fe^{III} centres. Theoretical calculations (B3LYP, hybrid density functional theory) indicate a planar ring skeleton with island-like π-electron delocalisation.[9]

Our experimental results are a first step towards the synthesis of novel organometalated phosphinato ligands, for which a similar manifold coordination chemistry and field of application is expected as for the organic phosphinato ligands. Because of the simultaneous coupling to two metal centres − perhaps two different ones − they seem to be more interesting.

Experimental Section

1d/1′d: A solution of $\{CpFe(CO)_2\}_2$ (2.0 g, 5.64 mmol) and *t*$BuPCl_2$ (0.3 mL, 3.7 mmol) in 80 mL of toluene was stirred at 80 °C for 12 h. A yellow solid precipitated that was filtered off, washed

with 50 mL of dry toluene, and dried in vacuo. Yield: 1.4 g (75%) of **1d/′d** as a bright yellow powder, no correct elemental analysis was obtained because of the existence of a mixture of PCl- and PH-functionalised product.

1d: A solution of $\{CpFe(CO)_2\}_2$ (2 g, 5.64 mmol) and tBuPCl$_2$ (0.3 mL, 3.7 mmol) in 20 mL of dichloromethane was kept at room temperature for up to 1 week. The product **1d** separated as very thin plates at the surface of the glass. Yield: 0.2 g (10%). FAB$^+$ MS (*m*NBA): *m*/*z* = 477 [M]$^+$. IR (KBr): ν(CO) = 1987, 2003, 2030, 2050 cm^{-1}. ^{31}P NMR (CD_3CN, 109.4 MHz): δ = 289. ^{13}C NMR (CD_3CN, 67.9 MHz): δ = 211 (CO), 90 (Cp), 50 [$C(CH_3)_3$], 30 (CH_3). ^{1}H NMR (CD_3CN, 270.2 MHz): δ = 5.55 (Cp), 1.45 (CH_3). $C_{36}H_{38}Cl_6Fe_5O_8P_2$ (1152.6): calcd. C 37.5, H 3.3, Cl 18.4; found C 36.7, H 3.1, Cl 18.4.

1′d: A solution of $CpFe(CO)_2Cl$ (5.0 g, 23.54 mmol) and 1 mL (4.70 mmol) of tBuP(SiMe$_3$)$_2$ in 100 mL of toluene was stirred at 25 °C for 12 h. A yellow solid precipitated, which was filtered off, washed with 80 mL of dry toluene, and dried in vacuo. Yield: 4.2 g (82%). FAB$^+$ MS (*m*-NBA): *m*/*z* = 443 [M]$^+$. IR (KBr): ν(CO) = 1987, 2024, 2034 cm^{-1}. ^{31}P NMR (CD_3CN, 109.4 MHz): δ = 27 (d, $^1J_{PH}$ = 303 Hz). ^{13}C NMR (CD_3CN, 67.9 MHz): δ = 91 (Cp), 50 [$C(CH_3)_3$], 30 (CH_3). ^{1}H NMR (CD_3CN, 270.2 MHz): δ = 5.41 (Cp), 3.4 (d, $^1J_{PH}$ = 303 Hz, PH), 1.27 (d, $^3J_{PH}$ = 18 Hz, CH_3). $C_{36}H_{40}Cl_4Fe_5O_8P_2$ (1083.7): calcd. C 39.9, H 3.7, Cl 13.1; found C 38.7, H 3.5, Cl 16.2.

2: A solution of **1′d** (140 mg, 0.12 mmol) in 12 mL of acetonitrile was kept for about 2 weeks in an air atmosphere. After this time, small prismatic, deep purple-red single crystals of **2** separated at the bottom of the vessel. They were isolated by decantation of the solution. In the mother liquor some of product **2** still remained, which could not, however, be separated as a pure product. Yield: 33 mg (33%). EI MS (*m*NBA): *m*/*z* = 791 [M − 2 CO]$^+$, 692, 664 [M − 2 CO − 2 Cl − *n*CO (*n* = 0, 2)]$^+$. IR (KBr): ν(PO_2) = 971, 1070 cm^{-1}, ν(CO) = 1999, 2044 cm^{-1}. $C_{22}H_{28}Cl_4Fe_4O_8P_2{\cdot}2CH_3CN$ (929.7): calcd. C 33.6, H 3.7, Cl 15.1; found C 33.1, H 3.9, Cl 14.3.

Acknowledgments

We thank the Fonds der Chemischen Industrie for financial support. The doctoral scholarship for M. M. of the Freistaat Bayern is appreciated.

[1] Selected examples: [1a] E. Lindner, S. Trad, S. Hoehne, H.-H. Oetjen, *Z. Naturforsch., Teil B* **1979**, *34*, 1203−1212 (and cit. ref.). [1b] W. V. Cicha, J. S. Haynes, K. W. Oliver, S. J. Rettig, R. C. Thompson, J. Trotter, *Can. J. Chem.* **1985**, *63*, 1055−1062. [1c] A. Bino, L. Sissman, *Inorg. Chim. Acta* **1987**, *128*, L21−L22. [1d] P. Betz, A. Bino, *Inorg. Chim. Acta* **1988**, *147*, 109−113. [1e] D. S. Bohle, H. Vahrenkamp, *Inorg. Chem.* **1990**, *29*, 1097−1099. [1f] S.-J. Liu, R. J. Staples, J. P. Fackler, Jr., *Polyhedron* **1992**, *11*, 2427−2430. [1g] M. McCann, E. Murphy, C. Cardin, M. Covery, *Polyhedron* **1993**, *12*, 1725−1731. [1h] C. M. Barnes, D. S. Bohle, S. K. Madsen, *Inorg. Chem.* **1994**, *33*, 6411−6414. [1i] N. S. Dean, L. M. Mokry, M. R. Bond, C. J. O'Connor, C. J. Carrano, *Inorg. Chem.* **1996**, *35*, 2818−2825. [1j] N. S. Dean, M. R. Bond, C. J. O'Connor, C. J. Carrano, *Inorg. Chem.* **1996**, *35*, 7643−7648.

[2] [2a] G. Effinger, W. Hiller, I.-P. Lorenz, *Z. Naturforsch., Teil B* **1987**, *42*, 1315−1327. [2b] I.-P. Lorenz, C. Klasen, S. Schmid, G. Beuter, *J. Organomet. Chem.* **1992**, *428*, 363−378. [2c] I.-P. Lorenz, C. Klasen, S. Schmid, *Z. Naturforsch., Teil B* **1993**, *48*, 705−712. [2d] I.-P. Lorenz, W. Pohl, H. Nöth, M. Schmid, *J. Organomet. Chem.* **1994**, *475*, 211−221. [2e] I.-P. Lorenz, W. Pohl, H. Nöth, M. Schmid, *Z. Naturforsch., Teil B* **1995**, *50*, 1485−1493. [2f] I.-P. Lorenz, W. Pohl, K. Polborn, *Chem. Ber.* **1996**, *129*, 11−13.

[3] I.-P. Lorenz, W. Pohl, H. Nöth, *Angew. Chem.* **1997**, *109*, 55−56; *Angew. Chem. Int. Ed. Engl.* **1997**, *36*, 55−56.

[4] I.-P. Lorenz, P. Mürschel, W. Pohl, K. Polborn, *Chem. Ber.* **1995**, *128*, 413−416.

[5] M. Maier, PhD Thesis, University of Munich, **2001**.

[6] X-ray structure analyses: **1d:** $C_{38}H_{41}Cl_6Fe_5NO_8P_2$, M_r = 1193.6, purple crystals, 0.43 × 0.37 × 0.13 mm, monoclinic, space group *P*2/*c*, *a* = 14.501(2) Å, *b* = 8.938(2) Å, *c* = 18.017(3) Å, β = 92.999(14)°, *Z* = 2, *V* = 2332.0(7) Å^3, $\rho_{calcd.}$ = 1.700 Mg/m^3, μ = 1.979 mm^{-1}, *F*(000) = 1204, diffractometer: Enraf−Nonius CAD4, Mo-K_α (λ = 0.71073 Å), *T* = 293(2) K, θ = 2.26−23.96°, reflections collected 3804, independent reflections 3645 [*R*(int) = 0.0174], 2995 observed reflections [$I > 2\sigma(I)$], final *R* indices [$I > 2\sigma(I)$]: *R*1 = 0.0294, *wR*2 = 0.0640, *R* indices (all data): *R*1 = 0.0426, *wR*2 = 0.0724, goodness-of-fit on F^2: 1.086, largest diff. peak and hole: 0.336 and −0.247 e·A^{-3}, absorption correction: semi-empirical from ψ-scans, max./min. transmission: 0.9991/0.8336, refinement method: full-matrix least squares on F^2, data/restraints/parameters: 3645/0/276. **2:** $C_{26}H_{34}Cl_4Fe_4N_2O_8P_2$, M_r = 929.69, deep purple crystals, 0.53 × 0.4 × 0.13 mm, triclinic, space group *P*$\bar{1}$, *a* = 9.592(2) Å, *b* = 9.622(2) Å, *c* = 11.944(3) Å, α = 82.29(2), β = 72.50(2), γ = 64.06(2)°, *Z* = 1, *V* = 945.4(4) Å^3, $\rho_{calcd.}$ = 1.633 Mg/cm^{-3}, μ = 1.916 mm^{-1}, *F*(000) = 470, diffractometer: Enraf−Nonius CAD4, Mo-K_α (λ = 0.71073 Å), *T* = 293(2) K, θ = 2.59−23.97°, reflections collected: 3150, independent reflections 2952 [*R*(int) = 0.0146], 2517 observed reflections [$I > 2\sigma(I)$], final *R* indices [$I > 2\sigma(I)$] *R*1 = 0.0343, *wR*2 = 0.0864, *R* indices (all data): *R*1 = 0.0439, *wR*2 = 0.0937, goodness-of-fit on F^2: 1.091, largest diff. peak and hole: 0.269 and −0.296 e·A^{-3}, absorption correction: semi-empirical from ψ-scans, max./min. transmission: 0.9995/0.7440, refinement method: full-matrix least squares on F^2, data/restraints/parameters: 2952/0/211. Crystallographic data for the structures reported in this paper have been deposited with the Cambridge Crystallographic Data Centre as supplementary publication no. CCDC-112648 (**1d**) and -112647 (**2**). Copies of the data can be obtained free of charge on applicaton to CCDC, 12 Union Road, Cambridge CB2 1EZ, UK [Fax: (internat.) + 44-1223/336-033; E-mail: deposit@ccdc.cam.ac.uk].

[7] Magnetic measurement of **2:** $C_{26}H_{34}Cl_4Fe_4N_2O_8P_2$: μ_B = 6.04; Θ = −58.44 K; we thank Dr. R. Hoffmann for the measurement.

[8] A. Durif in *The Chemistry of Inorganic Homo- and Heterocycles*, vol 2 (Eds.: I. Haiduc, D. B. Sowerby), Academic Press, London, **1987**, p. 659−679.

[9] I.-P. Lorenz, M. Maier, A. Schulz, paper in preparation.

Received July 26, 2001
[I01279]

Syntheses and Structures of New Tellurium−Mercury Clusters with Twelve- and Six-Membered Rings

Ernesto Schulz Lang,*[a] Renato A. Zan,[a] Claudia C. Gatto,[a] Robert A. Burrow,[a] and Ezequiel M. Vázquez-López[b]

Keywords: Tellurium / Mercury / Cluster compounds / Metallacycles

Clusters with polycyclic twelve-membered rings were formed exclusively from the reaction of $[Hg(TePh)_2]$ with HgX_2 in pyridine. Clusters with just six members were formed from the same reaction in DMSO. In both cases, the solvent was coordinated to the clusters. The clusters, $[Hg_6(\mu\text{-}Br)_2Br_2(\mu\text{-}TePh)_8(py)_2]$ and $[Hg_3X_3(\mu\text{-}TePh)_3]\cdot 2DMSO$ (X = Cl, Br, I), were characterized by single-crystal X-ray crystallography.

Mercury chalcogenide compounds have found considerable use in industry, especially as low band gap semiconductors, in photovoltaic applications, and IR detection devices.[1] The synthesis and structural characterization of metal chalcogenide molecules with a defined size and structure provide an interesting approach to this class of materials.[2] Coordination compounds can be adequate precursors because the structure and properties of the resulting material can be modified by the synthesis conditions or the nature and properties of the ligands. Diorganochalcogenide compounds, RE−ER (E = S, Se, Te), could be optimal ligands, because they react with mercury under mild conditions to yield $[Hg(ER)_2]$ complexes. Although they eventually form polymeric structures by weak intermolecular Hg···E interactions,[3,4] the sulfide and selenide derivatives react with equimolar amounts of $HgCl_2$ in pyridine to yield metallacyclic compounds $[Hg_4Cl_4(\mu\text{-}ER)_4(py)_n]$ (E = S, R = *t*Bu, *n* = 2;[5] E = Se, R = Et, *n* = 4; E = Se, R = *t*Bu, *n* = 4.[3]) The different stoichiometry of the compounds appears to depend on the steric hindrance between pyridine and organic substituent R. Surprisingly, analogous tellurium derivatives have not been reported until now. As part of our interest in organotelluride chemistry,[6] we have investigated the reaction of $[Hg(TePh)_2]$[7] with $HgBr_2$ in coordinating solvents, in which only the first is soluble.

The solid isolated from the reaction mixture could be fully characterized as the cluster $[Hg_6(\mu\text{-}Br_2)Br_2(\mu\text{-}TePh)_8(py)_2]$ (**1**) by single-crystal X-ray diffraction[8] (Figure 1). The structure of **1** exemplifies a rare multinuclear compound. The molecule can be considered as being formed from two six-membered $Hg_3(\mu\text{−}TePh)_3$ rings that are bridged by two (μ-TePh) ligands. Additionally, a bromine atom asymmetrically bridges the two mercury atoms in each ring [Hg(1)−Br(8) 2.941(2), Hg(3)−Br(8) 2.845(2) Å]. A terminal bromine atom coordinates to the third mercury atom at a shorter distance [Hg(2)−Br(9) 2.641(2) Å].

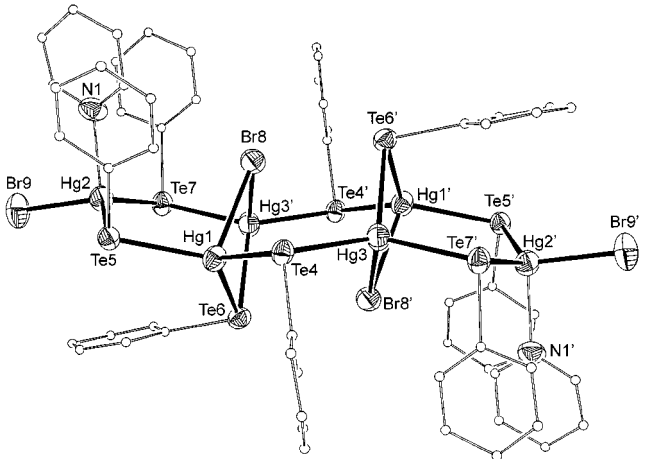

Figure 1. Structure of **1** (with H atoms omitted and each carbon atom represented by a conventional radius for clarity); selected bond lengths [Å]: Hg(1)−Te(4) 2.7489(13), Hg(1)−Te(6) 2.7552(15), Hg(1)−Te(5) 2.7796(13), Hg(1)−Br(8) 2.941(2), Hg(2)−N(1) 2.421(19), Hg(2)−Br(9) 2.641(2), Hg(2)−Te(5) 2.7432(13), Hg(2)−Te(7) 2.7568(15), Hg(3)−Te(7)′ 2.7511(13), Hg(3)−Te(4) 2.7564(13), Hg(3)−Br(8)′ 2.845(2), Hg(3)−Te(6)′ 2.8500(15), Te(6)−Hg(3)′ 2.8501(15), Te(7)−Hg(3)′ 2.7511(13); ′ = $-x+1, -y, -z+1$

The structure of **1** resembles those found of $[Et_4N]_4[Hg_7(\mu\text{-}Se)_6(\mu\text{-}Se_2)(\mu_3\text{-}Se)_2]$[9a] (Figure 2A) and $[nBu_4N]_4[Hg_4(\mu\text{-}Te)_2(\mu\text{-}Te_2)_2(\mu\text{-}Te_3)_2]$[9b] (Figure 2B), both of which contain only two coordinated chalcogen atoms. In these anionic clusters, two Hg_3Se_3 or $Hg_2(Te_3)Te$ rings are

[a] Laboratório de Materiais Inorgânicos, Universidade Federal de Santa María,
97119-900 Santa Maria, RS, Brazil
Fax: (internat.) + 55-55/220-8031
E-mail: eslang@base.ufsm.br
[b] Departamento de Química Inorgánica, Facultade de Ciencias-Química, Universidade de Vigo,
36200 Vigo, Galicia, Spain

 © WILEY-VCH Verlag GmbH, 69451 Weinheim, Germany, 2002 1434−1948/02/0202−0331 $ 17.50+.50/0

bridged by Se^{2-}, Se_2^{2-}, and $HgSe_2^{2-}$, or Te_2^{2-} and Te^{2-} units. The Hg−Hg distances in **1** [Hg(1)−Hg(3) = 3.6249(11) Å is the shortest] preclude a metal−metal interaction.

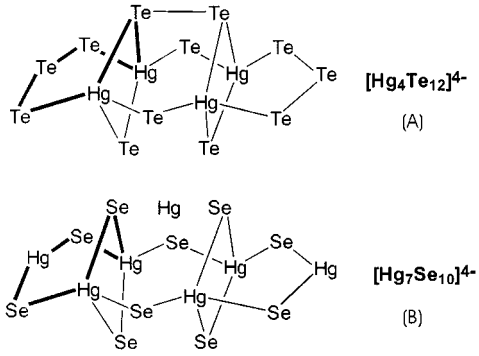

Figure 2. Structures of the clusters $[Hg_7(\mu\text{-}Se)_6(\mu\text{-}Se_2)(\mu_3\text{-}Se)_2]^{4-}$ [9a] (A) and $[Hg_4(\mu\text{-}Te)_2(\mu\text{-}Te_2)_2(\mu\text{-}Te_3)_2]^{4-}$ [9b] (B)

Although the coordination geometry around all the mercury atoms in **1** is a distorted tetrahedron, two different environments coexist about the atoms: $HgBrTe_3$ [for Hg(1) and Hg(3)] and $HgBrTe_2N$ [for Hg(2)]. No compounds with the same environment around the three-coordinate Te atom (two Hg atoms and an alkyl or aryl group) have been reported in the Cambridge Crystallographic Database.[10] However, the Hg−Te bond lengths [2.7423(13)−2.8500(15) Å] are similar to those found in other mercury(II) tellurides containing two-coordinate Te atoms (two Hg atoms)[9b,13] or three-coordinate with two Hg atoms and one P atom.[12] The only other reported Hg−Te distances for three-coordinate Te (two Hg atoms and a Te atom) are much longer.[9a,9b] The Hg−Br and Hg−N distances are normal.[13] All the Te atoms are trigonal-pyramidal with each bonding to two Hg atoms and a carbon atom of the phenyl group [bond angles ranging between Hg(1)−Te(6)−Hg(3) 80.57(4)° and C(71)−Te(7)−Hg(3)′ 104.6(5)°; ′ = $-x + 1$, $-y$, $-z + 1$].

Compound **1** is sparingly soluble in most organic solvents except pyridine, DMSO, and DMF. Furthermore, **1** is a very stable compound and was the main product formed when mixtures of $[Hg(TePh)_2]$ and $HgBr_2$ and an excess of other ligand (for instance PPh_3) in pyridine were allowed to crystallize. On the other hand, all attempts to substitute pyridine for another ligand were unsuccessful.

The reaction of $[Hg(TePh)_2]$ and $HgBr_2$ in DMSO yielded a crystalline light yellow solid (**2a**), whose composition was determined by single-crystal X-ray diffraction as $[Hg_3Br_3(TePh)_3]\cdot 2DMSO$.[13] The molecular structure of **2a** (Figure 3) consists of a six-membered ring with alternating Hg and Te atoms in a chair conformation. Although a similar conformation is observed as for **1**, in this case the orientation of all phenyl groups of the TePh ligands are on the same side of the ring (in **1**, two groups occupy one side and one group occupies the other). A terminal bromine atom coordinates to each mercury atom. The Hg−Te and Hg−Br distances are similar to the corresponding distances observed in **1**. If we consider only the interactions noted above, the coordination geometry around the mercury atom would be trigonal-planar. However, two DMSO molecules (one of them crystallographically disordered about two positions) occupy positions on either side of the Hg_3Te_3 ring with the oxygen atoms directed to the center of the ring. The distance of O(21) to the mercury atoms is shorter than that of O(11) [Hg(1)−O(21) 3.176(11), Hg(2)−O(21) 2.832(9), Hg(3)−O(21) 2.908(9), Hg(1)−O(11) 3.2380(15), Hg(2)−O(11) 3.344(9) and Hg(3)−O(11) 3.346(8) Å]. Atom O(21) seems to establish a weak interaction with the tellurium atoms; the Te···O(21) distances range between 3.161(8) and 3.252(9) Å. Each mercury atom also interacts weakly with the bromine atoms of the neighboring molecules [Hg(1)···Br(1)′ = 3.2380(15), Hg(2)···Br(2)′′ = 3.4881(15) and Hg(3)···Br(3)′′′ = 3.4640(16) Å; ′ = $x + 1$, $-y + 1$, $-z$; ′′ = $-x + 1$, $-y + 1$, $-z + 1$; ′′′ = $-x + 1$, $-y$, $-z + 1$]. If all weak interactions are considered, the resulting coordination polyhedron around the mercury atom can be described as a strongly distorted octahedron, while the co-

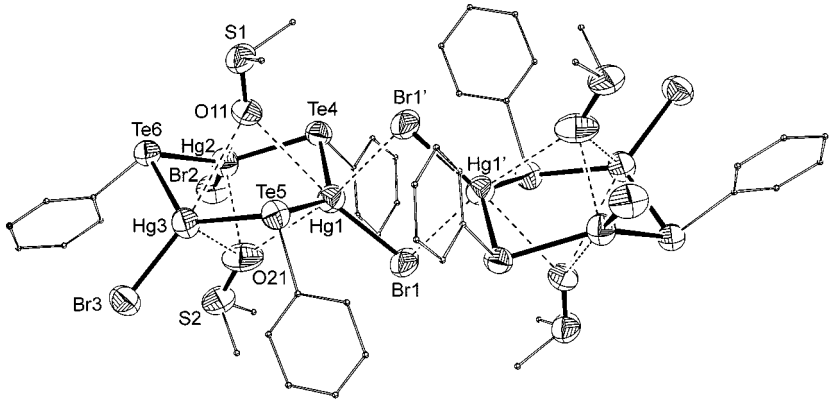

Figure 3. Two molecules of **2a**, showing intermolecular interactions (H atoms are omitted and each carbon atom represented by a conventional radius for clarity); selected bond lengths [Å]: Hg(1)−Br(1) 2.6134(13), Hg(1)−Te(4) 2.6884(9), Hg(1)−Te(5) 2.6974(9), Hg(2)−Br(2) 2.5859(15), Hg(2)−Te(6) 2.6855(9), Hg(2)−Te(4) 2.7139(9), Hg(3)−Br(3) 2.5824(13), Hg(3)−Te(5) 2.6929(9), Hg(3)−Te(6) 2.7062(9), Hg(1)−Br(1)′ 3.2380(15); ′ = $-x + 1, -y + 1, -z$

ordination geometry about the tellurium atoms is trigonal-pyramidal with the Hg−Te−Hg angles approximately 90°.

As compound **1** comprises $Hg_3(\mu\text{-}TePh)_3$ units, **2a** therefore could be considered to be its structural precursor. An interesting aspect is that changing the reaction solvent affects the stoichiometry as well as the structure of the resulting compound. Furthermore, the DMSO molecules in **2a** seem to shield the mercury atoms, but they are not strongly bonded to them. The compounds $[Hg_3Cl_3(\mu\text{-}TePh)_3]\cdot 2DMSO$ (**2b**) and $[Hg_3I_3(\mu\text{-}TePh)_3]\cdot 2DMSO$ (**2c**), which are isostructural with analogs **2a**, were also characterized. Studies to evaluate the stoichiometry and structure of the products from the reaction of **2** with other ligands in different solvents are underway in our laboratory.

Experimental Section

$(PhTe)_2Hg$ (0.61 g, 1.0 mmol) was dissolved in 10 mL of dry pyridine for **1** or DMSO for **2a**, and subsequently $HgBr_2$ (0.36 g, 1 mmol) was added under dry N_2. After stirring for 4 h at room temperature, the yellow solution was filtered. The addition of ethanol (2 mL) produced yellow crystals after a week (**1**: 0.497 g, 60% yield based on $HgBr_2$, m.p. 104 °C; **2a**: 0.172 g, 32% yield based on $HgBr_2$, m.p. 118 °C; **2b**: 0.223 g, 45% yield based on $HgCl_2$, m.p. 106−107 °C; **2c**: 0.263 g, 45% yield based on HgI_2, m.p. 125−126 °C).

Acknowledgments

This work was supported with funds from CNPq and FAPERGS (Brazil). E. S. L. thanks the AECI (Ministerio de Asuntos Exteriores, Spain) for a travel grant.

[1] C. J. Warren, R. C. Haushalter, A. B. Bocarsly, *J. Alloys Comp.* **1995**, *229*, 175−205.
[2] I. Dance, K. Fisher, *Prog. Inorg. Chem.* **1994**, *41*, 637−803.
[3] A. P. Arnold, A. J. Canty, B. W. Skelton, A. H. White, *J. Chem. Soc., Dalton Trans.* **1982**, 607−613.
[4] E. S. Lang, E. M. Vázquez-López, M. M. Dias, U. Abram, *Z. Anorg. Allg. Chem.* **2000**, *626*, 784−788.
[5] A. J. Canty, C. L. Raston, A. H. White, *Aust. J. Chem.* **1978**, *31*, 677−684. See also for 4-methylpyridine derivative: A. J. Canty, C. L. Raston, A. H. White, *Aust. J. Chem.* **1979**, *32*, 311−320.
[6] E. S. Lang, R. M. Fernandes, Jr., E. T. Silveira, U. Abram, E. M. Vázquez-López, *Z. Anorg. Allg. Chem.* **1999**, *625*, 1401−1404.
[7] Y. Okamoto, T. Yano, *J. Organomet. Chem.* **1971**, *29*, 99−103.
[8] Crystal data for **1**: $C_{58}H_{50}Br_4Hg_6N_2Te_8$, triclinic, $P\bar{1}$ (no. 2), a = 12.1079(7), b = 12.2316(7), c = 15.6690(9) Å, α = 69.6370(10), β = 67.5350(10), γ = 63.1920(10)°, V = 1870.09(19) Å^3, Z = 2, Mo-K_α (λ = 0.71073 Å), 8655 unique reflections (R_{int} = 0.1305). Final residuals R_1 = 0.0760 and wR_2 = 0.1937 [$I > 2\sigma(I)$], 287 parameters, as supplementary publication no. CCDC-164994.
[9] [9a] K.-W. Kim, M. G. Kanatzidis, *Inorg. Chem.* **1991**, *30*, 1966−1969. [9b] R. C. Haushalter, *Angew. Chem.* **1985**, *97*, 433; *Angew. Chem. Int. Ed. Eng.* **1985**, *24*, 433−435. [9c] R. C. Burns, J. D. Corbett, *Inorg. Chem.* **1981**, *20*, 4433−4434.
[10] F. H. Allen, O. Kennard, *Chem. Des. Autom. News* **1993**, *8*, 31−37.
[11] C. E. Holloway, M. Melnik, *Main Group Met. Chem.* **1994**, *17*, 799−885.
[12] L. Huang, R. A. Zingaro, E. A. Meyers, J. H. Reibenspies, *Heteroatom Chem.* **1996**, *7*, 57.
[13] Crystal data for **2a**: $C_{22}H_{27}Br_3Hg_3O_2S_2Te_3$, triclinic, $P\bar{1}$ (no. 2), a = 10.2766(11), b = 14.1892(15), c = 14.5784(15) Å, α = 62.235(2), β = 72.606(2), γ = 89.866(2)°, V = 1771.3(3) Å^3, Z = 2, Mo-K_α (λ = 0.71073 Å), 10380 unique reflections (R_{int} = 0.0468). Final residuals R_1 = 0.0419 and wR_2 = 0.0833 [$I > 2\sigma(I)$], 326 parameters, supplementary publication no. CCDC-164992. Crystal data for **2b**: $C_{22}H_{27}Cl_3Hg_3O_2S_2Te_3$, triclinic, $P\bar{1}$ (no. 2), a = 11.1468(9), b = 12.2189(10), c = 14.1336(11) Å, α = 107.2810(10), β = 107.752(2), γ = 100.832(2)°, V = 1666.5(2) Å^3, Z = 2, Mo-K_α (λ = 0.71073 Å), 10206 unique reflections (R_{int} = 0.0403). Final residuals R_1 = 0.0518 and wR_2 = 0.1260 [$I > 2\sigma(I)$], 316 parameters, supplementary publication no. CCDC-164991. Crystal data for **2c**: $C_{22}H_{27}Hg_3I_3O_2S_2Te_3$, triclinic, $P\bar{1}$ (no. 2), a = 11.1372(9), b = 12.4649(10), c = 15.4378(12) Å, α = 111.868(2), β = 102.381(2), γ = 102.1630(10)°, V = 1840.2(3) Å^3, Z = 2, Mo-K_α (λ = 0.71073 Å), 10874 unique reflections (R_{int} = 0.1094). Final residuals R_1 = 0.0676 and wR_2 = 0.1602 [$I > 2\sigma(I)$], 304 parameters, supplementary publication no. CCDC-164993. Crystallographic data (excluding structure factors) for the structures have been deposited with the Cambridge Crystallographic Data Center. Copies of the data can be obtained free of charge on application to the CCDC, 12 Union Road, Cambridge CB2 1EZ, UK [Fax: (internat.) + 44-1223/336-033; E-mail: deposit@ccdc.cam.ac.uk], citing the supplementary publication numbers above.

Received September 27, 2001
[I01365]

Redox Control of Conformation and Luminescence of a Dinuclear Ruthenium(II) Complex with a Bis-dipyridophenazine Bridging Ligand

Mara Staffilani,[a] Peter Belser,*[b] Luisa De Cola,[a] and František Hartl*[a]

Keywords: Ruthenium / Spectroelectrochemistry / Redox control / Cyclic voltammetry / Electron transfer / Bridging ligands

This spectroelectrochemical study deals with an interesting luminescent dinuclear complex $[\{Ru(bpy)_2\}_2(\mu\text{-bdppz})]^{4+}$ ($\mathbf{1}^{4+}$), where bpy stands for 2,2′-bipyridine and bdppz for 1,1′-dipyrido[3,2-*a*:2′,3′-*c*]phenazin-1,1′-yldipyrido[3,2-*a*:2′,3′-*c*]phenazine. The electronic coupling between the phenazine moieties through the central C–C bond can be easily modified as a function of the ligand oxidation state. Upon stepwise one-electron reduction in acetonitrile, complex $\mathbf{1}^{4+}$ is reversibly transformed into $\mathbf{1}^{3+}$ and $\mathbf{1}^{2+}$, with consequent major structural and electronic changes of the bridging ligand and with quenched MLCT emission of the excited $Ru(bpy)_2$ moieties.

Introduction

The control of the electronic interaction between different molecular components opens new strategies for the construction of nanometre-sized molecular devices, for example in the field of information and data storage.[1] The possibility to modulate the physical response of chromophoric units by an external stimulus such as redox- or light-driven reaction is a fascinating and booming research topic.[2] An important issue for experimental and theoretical investigations in coordination chemistry in this area is tuneable electronic communication between remote redox-active metal centres with attached chromophoric units or other functionalities (e.g. sensors). The key position of the connecting wire in such an assembly of molecular components can be occupied by a well-defined di- or oligonucleating ligand with tuneable energies of its frontier orbitals and molecular structure as a function of its oxidation state.[3] In this work we focus on an interesting dinucleating α-diimine ligand 1,1′-dipyrido[3,2-*a*:2′,3′-*c*]phenazin-1,1′-yldipyrido[3,2-*a*:2′,3′-*c*]-phenazine (bdppz) and its homodinuclear complex $[\{Ru(bpy)_2\}_2(\mu\text{-bdppz})]^{4+}$ ($\mathbf{1}^{4+}$; bpy = 2,2′-bipyridine).[4,5] The bridging ligand consists of two well-known 1,1′-dipyrido[3,2-*a*:2′,3′-*c*]phenazine (dppz)[4c,6] moieties linked by a C−C bond (see Scheme 1). It is noteworthy that the central part of the bdppz ligand, reaching up to the phenazine nitrogens, formally corresponds to the bridging 3,3′,4,4′-tetraimino-3,3′,4,4′-tetrahydrobiphenyl (tib) ligand with interesting conformation, electronic and redox properties studied in its homodinuclear complex $[\{Ru(bpy)_2\}_2(\mu\text{-tib})]^{4+}$.[7] Comparison between the bdppz and tib ligands will follow.

[a] Institute of Molecular Chemistry, Universiteit van Amsterdam, Nieuwe Achtergracht 166, 1018 WV Amsterdam, The Netherlands
E-mail: hartl@anorg.chem.uva.nl
[b] Institute of Inorganic and Analytical Chemistry, University of Fribourg, Pérolles, 1700 Fribourg, Switzerland
E-mail: peter.belser@unifr.ch

Results and Discussion

The cyclic and differential pulse voltammograms of $\mathbf{1}^{4+}$ in butyronitrile (Figure 1) reveal a two-electron anodic process (Table 1) that corresponds to unresolved one-electron oxidations of both Ru^{II} centres to Ru^{III} in $\mathbf{1}^{6+}$. The inefficient electronic communication between the two remote Ru centres through the bridging ligand in $\mathbf{1}^{4+}$ is caused to some extent by a large twist at the central C−C bond, in analogy with the related but less extended tib quinonediimine system, that better conjugates the chromophores;[7] the poor overlap between the $d_\pi(Ru)$ orbitals and the central phenazine π-system is also important in this regard.[8,9] The initial reduction of $\mathbf{1}^{4+}$ is indeed largely localised on the phenazine nitrogens of the C−C-linked dppz moieties and occurs as two separate reversible one-electron steps (Table 1). The 2,2′-bipyridine ligands remain insensitive to the reduction of the bridge and reduce reversibly pair-wise in unresolved two-electron processes (Table 1). These assignments have received unambiguous support from the redox properties of the reference[8b] mononuclear complex $[Ru(bpy)_2(dppz)]^{2+}$ ($\mathbf{2}^{2+}$) (Scheme 1 and Table 1) and related diruthenium systems.[9] The pairwise response of the 2,2′-bipyridine ligands to the reduction indicates the persistent inefficient electronic interaction between the ruthenium centres across the presumably planar two-electron reduced bdppz bridge, in contrast to the tib ligand.[7]

The absorption properties of the dinuclear complex $\mathbf{1}^{4+}$ undergo major changes upon stepwise reduction to $\mathbf{1}^{2+}$ in

 © WILEY-VCH Verlag GmbH, 69451 Weinheim, Germany, 2002 1434−1948/02/0202−0335 $ 17.50+.50/0

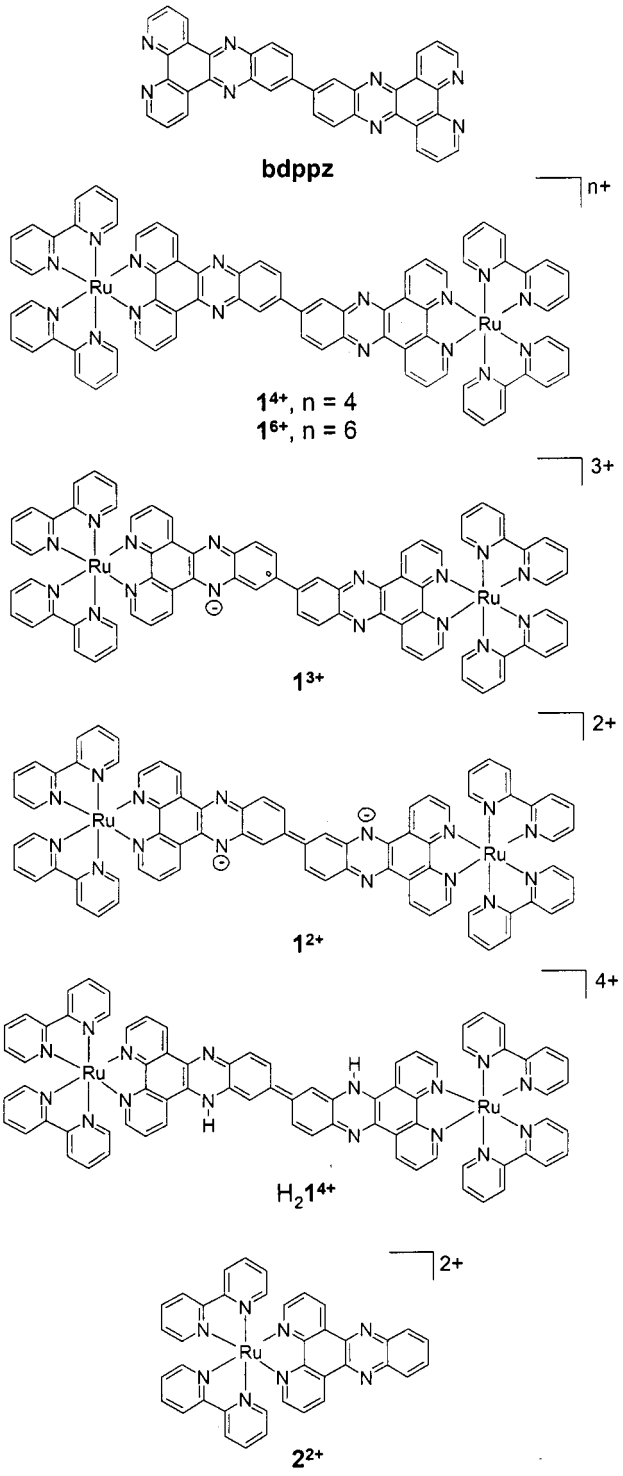

Scheme 1

a UV/Vis spectroelectrochemical cell[10] (Figure 2). The absorption band of $\mathbf{1}^{4+}$ at 407 nm belongs to an intraligand (IL) π-π* transition localised on the phenazine moieties of the bdppz ligand. This band is indeed present in the absorption spectrum of the bdppz ligand, at 413 nm in dichloromethane (insert to Figure 2); it disappears from the absorption spectrum of $\mathbf{1}^{4+}$ upon reduction to $\mathbf{1}^{3+}$ (Figure 2). The pronounced shoulder at 454 nm in the absorption spectrum

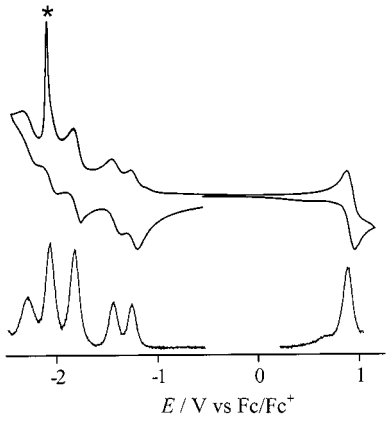

Figure 1. Cyclic voltammogram (top; v = 100 mV s^{-1}) and differential pulse voltammogram (bottom) of $5 \cdot 10^{-4}$ M $\mathbf{1}^{4+}$ recorded at a Pt disk electrode in butyronitrile/10^{-1} M Bu_4NPF_6 at 293 K; the asterisk indicates an overlapping adsorption peak

Table 1. Electrochemical data[a] for dinuclear $\mathbf{1}^{4+}$ and mononuclear $\mathbf{2}^{2+}$

Complex	bpy$^{-1/0}$	bdppz$^{-2/-1}$	bdppz$^{-1/0}$	dppz$^{-1/0}$	Ru$^{II/III}$
1^{4+}	−1.80 (2)	−1.42 (1)	−1.23 (1)		+0.91 (2)
	−2.04 (2)				
2^{2+}	−1.80 (1)			−1.39 (1)	+0.94(1)
	−2.06 (1)				
2^{2+} [b]	−1.73 (1)			−1.23 (1)[c]	+0.95(1)
	−1.93 (1)				

[a] Electrode potentials ($E_{1/2}$, V vs. Fc/Fc$^+$), with the number of transferred electrons in brackets. Experimental conditions: Pt disk working electrode, scan rate 100 mV/s, butyronitrile/10^{-1} M Bu_4NPF_6, 293 K. [b] Experiment in the presence of 1 equivalent of CF_3SO_3H. [c] Cathodic process followed by protonation; reverse oxidation of $H\mathbf{2}^{2+}$ occurs at $E_{p,a}$ = −0.29 V.

of $\mathbf{1}^{4+}$ is assigned to a set of metal-to-ligand [d_π(Ru)-to-π* (bpy)] charge transfer (MLCT) transitions, consistent with the assignments reported for $\mathbf{2}^{2+}$ [4c] and related diruthenium complexes.[9] The shoulder indeed disappears upon the 2e-oxidation of the ruthenium ions to Ru^{III} in $\mathbf{1}^{6+}$ (Scheme 1)[11] but remains almost unchanged upon reduc-

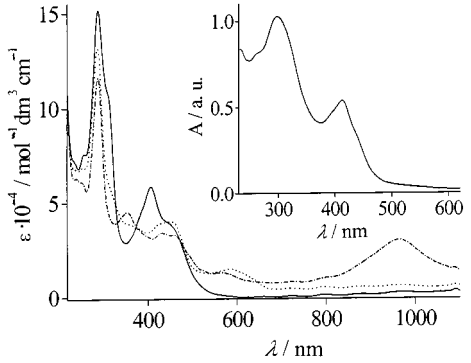

Figure 2. UV/Vis spectra of $5 \cdot 10^{-4}$ M $\mathbf{1}^{4+}$ (——), $\mathbf{1}^{3+}$ (− − −) and $\mathbf{1}^{2+}$ (−·−·−) in butyronitrile/$3 \cdot 10^{-1}$ M Bu_4NPF_6, recorded in an OTTLE cell;[10] inset: UV/Vis spectrum of the noncoordinated bdppz ligand (saturated solution in dichloromethane)

tion of $\mathbf{1}^{4+}$ to $\mathbf{1}^{3+}$ (Figure 2). A new structured absorption band of 1e-reduced $\mathbf{1}^{3+}$ at ca 580 nm belongs to IL transitions due to the radical $[bdppz]^{\cdot-}$ ligand (Figure 2), similarly to that reported for $\mathbf{2}^{2+}$.[8b] Importantly, when proceeding further with the reduction to $\mathbf{1}^{2+}$, a new broad and intense low-lying absorption band arises at 965 nm (Figure 2). It corresponds to an IL π-π* transition within the new π-system of the planar C=C-linked phenazine moieties of $[bdppz]^{2-}$. This absorption band shifts to 650 nm in the UV/Vis spectrum of the complex $H_2\mathbf{1}^{4+}$ (Figure 3 and Scheme 1) formed by protonation of the negatively charged phenazine nitrogens in $\mathbf{1}^{2+}$ (see Exp. Sect.). It is noteworthy that $H_2\mathbf{1}^{4+}$ deprotonates smoothly back to orange $\mathbf{1}^{4+}$ upon addition of H_2O_2.

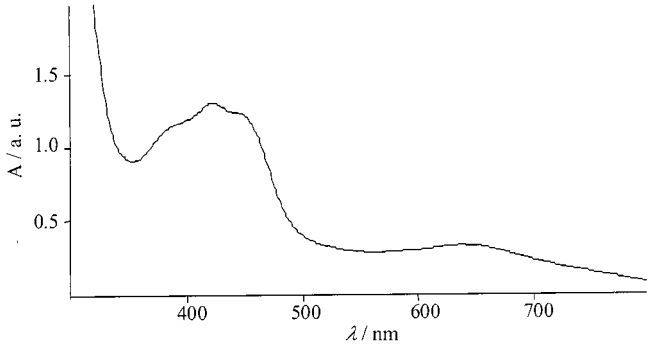

Figure 3. UV/Vis spectrum of $H_2\mathbf{1}^{4+}$ produced by chemical reduction of $\mathbf{1}^{4+}$ with Zn in deaerated acidified acetonitrile

The chemical reversibility of the coupled reduction/protonation processes and their localisation on the phenazine moieties was also revealed by cyclic voltammetry. For reference $\mathbf{2}^{2+}$, the phenazine-centred reduction at the dppz ligand in acetonitrile becomes electrochemically irreversible in the presence of exactly one equivalent of trifluoromethanesulfonic acid. The cyclic voltammogram indeed exhibits a large separation between the reduction of $\mathbf{2}^{2+}$, at $E_{p,c} = -1.23$ V, and the reverse anodic process, at $E_{p,a} = -0.29$ V, assigned to the oxidation of $H\mathbf{2}^{2+}$. In contrast, the bpy-centred cathodic steps are much less affected by the protonation, only being shifted by ca. 100 mV to more positive potentials, while the ruthenium-centred oxidation remains unchanged (Table 1). The product $H\mathbf{2}^{2+}$ does not decompose during the complete cyclic voltammetric scan (v = 100 mV/s), as testified by identical $i_{p,c}$ (reduction of $\mathbf{2}^{2+}$) and $i_{p,a}$ (oxidation of $H\mathbf{2}^{2+}$) peak current values. An analogous voltammetric response was also observed for dinuclear $\mathbf{1}^{4+}$ in acidified acetonitrile; however, the voltammetric peaks associated with the electrochemical reduction and coupled protonation of the phenazine nitrogen sites become very broad and determination of the cathodic and anodic peak potentials lacks precision.

The emission of complex $\mathbf{1}^{4+}$ at 650 nm with lifetime τ = 130 ns in acetonitrile (Figure 4) becomes completely quenched upon the stepwise electrochemical reduction to $\mathbf{1}^{3+}$ and $\mathbf{1}^{2+}$. The same result was obtained for reference $\mathbf{2}^{2+}$ and 1e-reduced $\mathbf{2}^{+}$. The corresponding experiments were conveniently run in situ within the thin-layer spectroelectrochemical cell, as described in the Exp. Sect. The luminescence can be switched OFF and ON repeatedly between $\mathbf{1}^{3+}$ and $\mathbf{1}^{4+}$, respectively. For $\mathbf{1}^{3+}$ (and $\mathbf{2}^{+}$) the quenching is attributed to efficient electron transfer from the electrochemically reduced phenazine moiety of bdppz (or dppz, in the case of $\mathbf{2}^{+}$) to the excited $*\{Ru^{III}(bpy^{\cdot-})\}$ unit. The value of the Gibbs energy change associated with the electron transfer process can be estimated through the zero-zero excitation energy E_{00} and the electrochemical potentials of the ground-state redox couples [Equation (1), for $\mathbf{1}^{3+}$], where $E°(bpy^{-1/0})$ denotes the 1e-reduction of the $Ru(bpy)_2$ moiety.

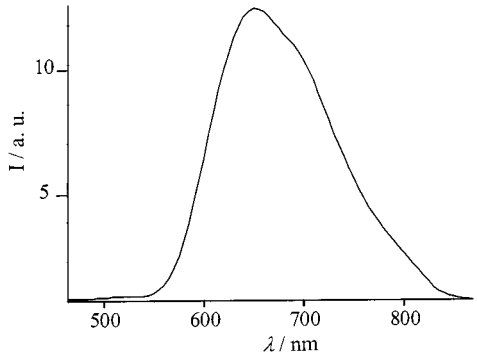

Figure 4. Emission of $\mathbf{1}^{4+}$ in acetonitrile, recorded upon excitation with 450 nm light

$$\Delta G° = E°(bdppz^{-1/0}) - E°(bpy^{-1/0}) - E_{00} = -1.23 - (-1.80) - 2.14\ eV < 0 \quad (1)$$

No luminescence was observed for 2e-reduced $\mathbf{1}^{2+}$ or its protonated form $H_2\mathbf{1}^{4+}$ (see Exp. Sect.), probably due to its low-lying non-luminescent bdppz-centred π-π* excited state (see above).

In conclusion, we present the redox behaviour of a diruthenium complex where the phenazine portion of the bridging bdppz ligand can be reversibly reduced in two separate one-electron steps. Interestingly, in the two-electron reduced state the bdppz ligand becomes planar. Its central C−C-linked bis(phenazine) portion responds to the reductions similarly to the less extended bis(*o*-quinonediimine) tib ligand.[7] In the planar conformation the bridging $[bdppz]^{2-}$ ligand is characterized by a new low-lying excited state, localised on the planar C=C-linked bis(phenazine) portion, that acts as an energy trap for the higher-lying (MLCT) excited states. Importantly, the energy of the lowest excited state can be increased upon reversible protonation. These properties of the binucleating bdppz ligand classify it as a redox- and pH-controllable molecular switch of long-distance electron/energy transfer in appropriately selected donor-acceptor dyads. In this regard, detailed photophysical and spectroelectrochemical investigations of bdppz-bridged homo- and heterodinuclear complexes are in progress.

Experimental Section

General: All solvents and reagents used in the preparations were reagent grade, purchased from Fluka or Aldrich, and used as supplied. Silica gel preparative plates and aluminium oxide chromatographic columns were used for purification of the metal complexes. The preparative SiO_2 plates were made of silica gel purchased from Merck (60, particle size 0.040−0.063 mm) and prepared according to the procedure indicated by Merck. Aluminium oxide for chromatography was purchased from Fluka (type 507 C neutral, Brockmann grade I, particle size 0.05−0.15 mm, pH 7.0 ± 0.5). For electrochemistry, butyronitrile (Acros) was dried over CaH_2 and freshly distilled under nitrogen prior to use; acetonitrile (Fluka, spectroscopic grade) was used as received. The supporting electrolyte Bu_4NPF_6 (Aldrich) was recrystallized twice from ethanol and dried overnight under reduced pressure at 60 °C.

^{1}H NMR spectra were recorded on a Varian Gemini 300 (300.075 MHz) spectrometer; chemical shifts are given in ppm, using the solvent itself as internal standard. Assignment of the signals was performed using the COSY technique. The numbering of the protons is shown in Scheme 2. ESI (Electron Spray Ionisation) mass spectra were obtained with a Bruker FTMS 4.7 T Bio APEXII spectrometer. UV/Vis absorption spectra were recorded on a Hewlett Packard 8453 diode-array spectrophotometer, and the reported emission spectrum (corrected for the photomultiplier response) on a Spex 1681 spectrophotometer (λ_{exc} = 450 nm).

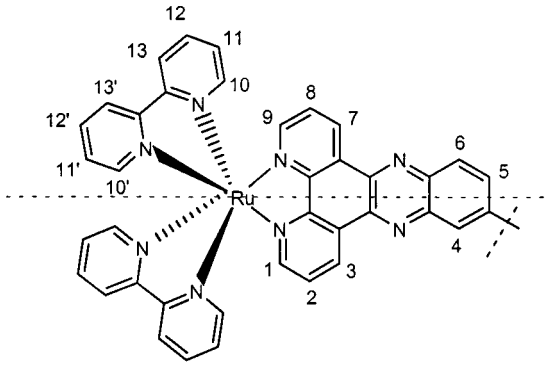

Scheme 2

Cyclic voltammetric and differential pulse voltammetric scans were performed with a gas-tight single-compartment cell under an atmosphere of dry nitrogen or argon. The cell was equipped with a Pt disk working (apparent surface area of 0.42 mm^2), Pt wire auxiliary, and Ag wire pseudoreference electrodes. The working electrode was carefully polished with a 0.25 μm-grain diamond paste between scans. All redox potentials are reported against the ferrocene-ferrocenium (Fc/Fc^+) redox couple used as an internal standard[12] ($E_{1/2}$ = 0.42 V vs. SCE in acetonitrile). The potential control was achieved with a PAR Model 283 potentiostat. UV/Vis spectroelectrochemical experiments were performed with an optically transparent thin-layer electrochemical (OTTLE) cell,[10] equipped with a Pt minigrid working electrode and quartz optical windows. The controlled-potential electrolyses were carried out with a PA4 potentiostat (EKOM, Czech Republic). All electrochemical samples were $5\cdot10^{-4}$ M in the studied complex and contained $3\cdot10^{-1}$ M Bu_4NPF_6. The spectroelectrochemical cell was also conveniently employed for recording emission spectra during the electrochemical quenching experiments and determination of emission lifetime. In this case the emission spectra were recorded using an optical fibre connected to a nitrogen laser and a streak camera (Hamamatsu C5680−21), equipped with a M 5677 sweep unit. Excitation at 337 nm was achieved by a pulsed (fwhm 600 ps) nitrogen laser (LTB, MGS 405 TD) operating at a repetition rate of 20 Hz.

1,1′-Dipyrido[3,2-*a*:2′,3′-*c*]phenazin-1,1′-yldipyrido[3,2-*a*:2′,3′-*c*]-phenazine (bdppz): 1,10-phenanthroline-5,6-dione[4] (0.420 g, 2.0 mmol) and 3,3′,4.4′-biphenyltetramine (0.214 g, 1.0 mmol) were suspended in 10 mL acetic acid (100%) and heated at 120 °C for 1 h. After cooling to room temperature, 100 mL of water was added to the reaction mixture. The olive-green precipitate was filtered off, washed with water, aqueous sodium hydrogen carbonate (10%) and again with water. The solid was dried under vacuum at 50 °C (0.484 g, yield 86%). The bdppz ligand is practically insoluble in all common solvents, therefore a direct analytical proof has not been possible.

[{Ru(bpy)$_2$}$_2$(μ-bdppz)](PF$_6$)$_4$ (1^{4+}): [$Ru(bpy)_2Cl_2$]·$2H_2O$ (0.104 g, 0.2 mmol),[5] bdppz (0.056 g, 0.1 mmol) and 2 drops of HPF_6 (60% solution in water) were suspended in ethylene glycol (6 mL) and heated in a microwave oven (3 times for 2 min). The solvent was removed under reduced pressure. Water (20 mL) and NH_4PF_6 (1 g) were then added to produce a red precipitate that was separated by suction filtration. The crude product was purified on a column of neutral aluminium oxide (10 × 2 cm) with acetone/water (98:2) as eluent. The orange-red band (TLC: R_f = 0.22, support SiO_2, eluent $MeCN/H_2O/MeOH/KNO_3$ 4:1:1:0.1) was collected, the solvents were removed under reduced pressure and the residual solid was further purified on SiO_2 plates ($MeCN/H_2O$/*tert*-butyl alcohol/KNO_3 4:1:1:0.1). Isolation (with acetone/NH_4PF_6 as eluent) of the orange-red band gave the pure product (0.055 g, 28% yield). ^{1}H NMR (CD_3CN): bdppz signals δ = 7.92 (dd, 4 H, H2 and H8), 8.20 (d, 4 H, H1 and H9), 8.69 (d, 2 H, H6), 8.76 (d, 2 H, H5), 9.04 (s, 2 H, H4), 9.71 (d, 4 H, H3 and H7); bpy signals δ = 7.28 (dd, 2 H, H11), 7.47 (dd, 4 H, H11′), 7.75 (d, 4 H, H10), 7.86 (d, 4 H, H10′), 8.03 (dd, 4 H, H12), 8.12 (dd, 4 H, H12′), 8.53 (d, 4 H, H13), 8.56 (d, 4 H, H13′). See Scheme 2 for proton numbering. ESI-MS: *m*/*z* = 839.59 [$M^+ - 2PF_6^-$], 551.74 [$M^+ - 3PF_6^-$], 347.56 [$M^+ - 4PF_6^-$]. HRMS for $C_{76}H_{50}N_{16}Ru_2$ (1389.5): calcd. 347.5617; found 347.5618.

Reversible Protonation of 2e-Reduced 1^{2+}: The doubly protonated complex H_2**1**$^{4+}$ was prepared in situ by reducing **1**$^{4+}$ with metallic zinc in acidified acetonitrile or acetone. The parent complex (4.6 mg, $2.3\cdot10^{-3}$ mmol) was dissolved in 50 mL of the solvent. This solution (8 mL) was acidified with HCl (2 mL) and stirred with added Zn granules (1 g, about 1 mm size) for 15 min. The UV/Vis spectrum of the product (see Figure 3) was identical with that of H_2**1**$^{4+}$ generated in situ by reducing **1**$^{4+}$ in acetonitrile in the UV/Vis spectroelectrochemical cell in the presence of exactly two equivalents of trifluoromethanesulfonic acid. Addition of hydrogen peroxide to the green solution of H_2**1**$^{4+}$ resulted in a rapid and complete recovery of orange **1**$^{4+}$, as confirmed by UV/Vis spectroscopy.

[1] *Molecular Electronics* (Eds.: J. Jortner, M. Ratner), Blackwell, London, **1997.**
[2] [2a] V. Balzani, F. Scandola, *Supramolecular Photochemistry*, Ellis Horwood, Chichester. **1991**. [2b] V. Balzani, F. Scandola, *Comprehensive Supramolecular Chemistry* (Ed.: D. N. Reinhoudt), Pergamon Press, Oxford, **1996**, Vol.10. [2c] A. P. de

Silva, H. Q. N. Gunaratne, T. Gunnlaugsson, A. J. M. Huxley, C. P. McCoy, J. T. Rademacher, T. E. Rice, *Chem. Rev.* **1997**, *97*, 1515−1566.
[3] [3a] T. E. Keyes, R. J. Foster, P. M. Jayaweera, C. G. Coates, J. J. McGarvey, J. G. Vos, *Inorg. Chem.* **1998**, *37*, 5925−5932, and reference 2 therein. [3b] L. De Cola, P. Belser, *Coord. Chem. Rev.* **1998**, *177*, 301−346.
[4] [4a] P. Lincoln, B. Nordén, *Chem. Commun.* **1996**, 2145−2146. [4b] S. Bernhard, P. Belser, *Synthesis* **1996**, 192−194. [4c] E. Amouyal, A. Homsi, J.-C. Chambron, J.-P. Sauvage, *J. Chem. Soc., Dalton Trans.* **1990**, 1841−1845.
[5] B. P. Sullivan, D. J. Salmon, T. J. Meyer, *Inorg. Chem.* **1978**, *17*, 3334−3341.
[6] J. C. Chambron, J. P. Sauvage, *Chem. Phys. Lett.* **1991**, *182*, 603−607.
[7] [7a] P. R. Auburn, A. B. P. Lever, *Inorg. Chem.* **1990**, *29*, 2551−2553. [7b] F. Hartl, T. L. Snoeck, D. J. Stufkens, A. B. P. Lever, *Inorg. Chem.* **1995**, *34*, 3887−3894.
[8] [8a] G. Albano, P. Belser, C. Daul, *Inorg. Chem.* **2001**, *40*, 1408−1413. [8b] J. Fees, W. Kaim, M. Moscherosch, W. Matheis, J. Klíma, M. Krejčík, S. Záliš, *Inorg. Chem.* **1993**, *32*, 166−174. [8c] M. R. Waterland, K. C. Gordon, J. J. McGarvey, P. M. Jayaweera, *Dalton Trans.* **1998**, 609−616.
[9] [9a] J. Bolger, A. Gourdon, E. Ishow, J.-P. Launay, *Inorg. Chem.* **1996**, *35*, 2937−2944. [9b] E. Ishow, A. Gourdon, J.-P. Launay, C. Chiorboli, F. Scandola, *Inorg. Chem.* **1999**, *38*, 1504−1510.
[10] M. Krejčík, M. Daněk, F. Hartl, *J. Electroanal. Chem.* **1991**, *317*, 179−187.
[11] M. Staffilani, F. Hartl, unpublished results.
[12] G. Gritzner, J. Kůta, *Pure Appl. Chem.* **1984**, *56*, 461−466.

Received August 15, 2001
[I01312]

Ditrielanes $(R_3Si)_2E-E(SiR_3)_2$ and Heterocubanes $(R_3Si)_4E_4Y_4$ (R_3Si = tBu_3Si, tBu_2PhSi; E = Al, Ga, In, Tl; Y = O, Se)[‡]

Nils Wiberg,*[a] Thomas Blank,[a] Kerstin Amelunxen,[a] Heinrich Nöth,[a][‡‡] Hansgeorg Schnöckel,[b][‡‡] Elke Baum,[b][‡‡] Andreas Purath,[b][‡‡] and Dieter Fenske[b][‡‡]

Keywords: Aluminium / Ditrielanes / Gallium / Heterocubanes / Indium / Silicon / Thallium

Ditrielanes $R^*_2E-ER^*_2$ (R^* = Si*t*Bu$_3$; E = Al, In, Tl), $R'_2E-ER'_2$ (R' = Si*t*Bu$_2$Ph; E = In, Tl) and $R^*_2Ga-GaR^*(SiMe_3)$ are prepared in alkanes (i) from ECl_3 (E = Al, In, Tl) and NaR^* via isolable R^*_2ECl (reaction of $GaCl_3$ and NaR^* leads to $R^*_2Ga{\cdot}GaR^*$ instead of $R^*_2Ga-GaR^*_2$), (ii) from EBr (E = In, Tl) and NaR^* or NaR' (reaction of AlBr or GaBr and NaR^* leads to $R^*_4Al_4$ or $R^*_8Ga_{18}$ and $R^*_8Ga_{22}$), (iii) from $NaGa_2R^*_3$ and Me_3SiCl. According to X-ray structure analyses, the ditrielanes contain two planar groups R_2EE which are orthogonal to each other (R = R^*; angle REER ca. 90°) or nearly orthogonal (R = R'; angle REER ca. 80°). All compounds are deeply colored. The λ_{max} value of the visible absorption shifts with increasing atomic number of E and with the increasing angle between the R_2EE planes to longer wavelengths (ruby $R^*_4Al_2$, deep-violet $R^*_4In_2$, dark-green $R^*_4Tl_2$; red-violet R'_4In_2, dark-blue R'_4Tl_2). Thermolysis of $R^*_4E_2$ in alkanes at about 100 °C leads to $R^*_3Al_2^{\cdot}$/$R^*_4Al_3^{\cdot}$/$R^*_4Al_4$, to $R^*_3Ga_2^{\cdot}$/$R^*_4Ga_4$, to $(R^*_4In_6)$/$R^*_8In_{12}$ and to Tl, respectively. R'_4E_2 thermolizes under formation of an In or Tl mirror. The ditrielanes $R^*_4E_2$ are stable against MeOH at normal conditions, but react with HBr under Si–E and E–E bond cleavage with the formation of R^*EBr_2 (e.g. R^*InBr_2) besides R^*H and H_2. Air transforms the ditrielanes into R^*OH or $R'OH$. On the other hand, halogens oxidize $R^*_4E_2$ under formation of R^*_2EHal (e.g. R^*_2AlI), R^*EHal_2 (e.g. R^*InBr_2) or thermolysis products of the dihalides (e.g. R^*Br/TlBr). Selenium gives with $R^*_4E_2$ heterocubanes $R^*_4E_4Se_4$ (E = Al, In, Tl). Analogous heterocubanes $R^*_4E_4O_4$ (E = Al, Ga) are synthesized from tetrahedranes $R^*_4E_4$ and oxygen. X-ray structure analyses for $R^*_4In_4Se_4$, $R^*_4Al_4O_4$ – besides the mentioned ditrielanes – are presented.

Introduction

Silyltrielanes $REHal_2$ and R_2EHal with R = R*= Si*t*Bu$_3$ (supersilyl) or R = R' = Si*t*Bu$_2$Ph and E = triel = B, Al, Ga, In, Tl, introduced in preceding publications,[1−3] are synthesized with the purpose of dehalogenation to form silylated triel cluster compounds. Indeed, silylditrielanes R_2E-ER_2 (R = R*, R'; E = Al, Ga, In, Tl) represent examples with the smallest triel clusters. Its syntheses, characterization, reactions and X-ray structure analyses are presented afterwards together with some heterocubanes $R^*_4E_4Y_4$, which represent reaction products of $R^*_4E_2$ and selenium as well as $R^*_4E_4$ and oxygen (for preliminary communications, relevant to this subject, see refs.[4,5]; for syntheses of some larger silylated triel clusters from R^*EHal_2 and R^*_2EHal see refs.[6−8]).

In fact, except for the compounds dealt with in this publication, only three other examples of *silyl-ditrielanes*, namely $[(Me_3Si)_3Si]_4E_2$ with E = Ga,[9] In,[10] Tl[11] have been published to date. On the other hand, some *organyl-* and *aminyl-ditrielanes* R_4E_2 are known with R = $CH(SiMe_3)_2$/E = Al,[12] Ga,[13] In;[14] R = 2,4,6-*i*Pr$_3$C$_6$H$_2$/E = Al,[15] Ga,[16] In;[17] R = 2,4,6-$(CF_3)_3C_6H_2$/E = Ga,[18] In;[18] R = 2,2,6,6-$Me_4NC_5H_6$/E = Ga;[19] and R_2 = −*t*BuN−MeSi(N*t*Bu)$_2$SiMe−N*t*Bu−/E = Ga,[20] In[20] amongst others (for aminylditrielanes cf. in addition ref.[21]).

Results and Discussion

Syntheses of $R^*_4E_2$ and R'_4E_2 (R* = Si*t*Bu$_3$, R' = Si*t*Bu$_2$Ph)

According to Scheme 1, the reactions of NaR* with *triel(III) compounds* $\mathbf{EX_3}$ (E = Al, Ga, In, Tl; X = Cl, Br) in alkanes at room temperature lead to tetrasupersilylditrielanes $R^*_2E-ER^*_2$ [**1**−**4**; due steric and/or electronic reasons, instead of $R^*_4Ga_2$ (**2**) only the radical $R^*_3Ga_2^{\cdot}$ (**2a**) is isolated[5]]. Isolable intermediates are R^*EHal_2 [1,2] and R^*_2EHal.[1,2] As already discussed elsewhere,[5] NaR* reacts with R^*_2EHal under NaHal elimination to radicals $R^{*\cdot}$ and

[‡] Compounds of Silicon and Homologues, 150; Supersilyl Compounds of Boron and Homologues, 17. − Part 149 and 16: N. Wiberg, T. Blank, H.-W. Lerner, H. Nöth, T. Habereder, D. Fenske, Z. Naturforsch., Teil B **2001**, *56*, 652−658.

[a] Department Chemie der Universität München, Butenandtstraße 5−13 (Haus D), 81377 München, Germany
[b] Institut für Anorganische Chemie der Universität, Engesserstraße, Geb. 30.45, 76128 Karlsruhe, Germany

[‡‡] X-ray structure analyses.

 © WILEY-VCH Verlag GmbH, 69451 Weinheim, Germany, 2002 1434−1948/02/0202−0341 $ 17.50+.50/0

$R^*_2E^{\cdot}$. For steric reasons only the dimerization of the radicals under formation of R^*_2 and $(R^*_2E)_2$ is possible and no recombination of both radicals to form R^*_3E occurs (the cone angle for R* amounts to 130°;[15] even $R^*_2Tl^+$ and NaR* give $R^*_4Tl_2$ and not R^*_3Tl[7]). Obviously, the same is valid for the reaction of the triel(III) compound BX_3 (X = Cl, Br) and NaR*, with the difference that dimerization of the radicals $R^*_2B^{\cdot}$ obtained from R^*BHal_2 [2] and R^*_2BHal[2] is also not possible for steric reasons. Therefore, in the place of $R^*_4B_2$ other products are formed possibly from the anion $R^*_2B^-$, obtained according to the reaction $R^*_2B^{\cdot} + NaR^* \rightarrow NaBR^*_2 + R^{*\cdot}$.[2]

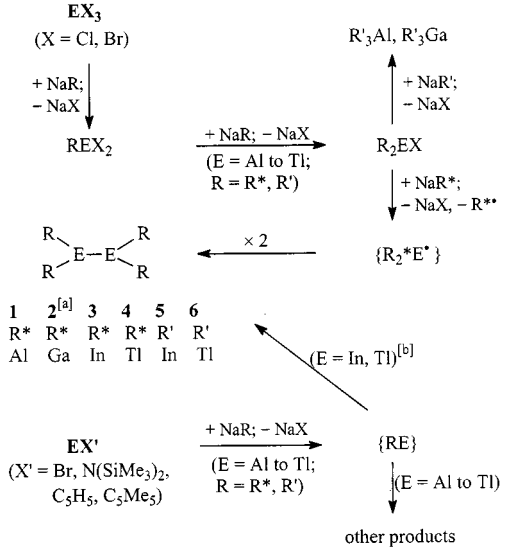

Scheme 1. Syntheses of ditrielanes R_4E_2 with E = Al, Ga, In, Tl and R = R* = Si*t*Bu$_3$ and R = R′ = Si*t*Bu$_2$Ph: [a] instead of $R^*_4Ga_2$ the radical $R^*_3Ga_2^{\cdot}$ (**2a**) is formed (cf. Scheme 2); [b] in the presence of NaR

The reactions of NaR′ instead of NaR* with $\mathbf{EX_3}$ (E = Al, Ga, In; X = Cl, Br) in alkanes (Scheme 1) lead to isolable monotrielanes R'_3E and not to ditrielanes $R'_2E{-}ER'_2$, via $R'EHal_2$ (isolated)[3] and R'_2EHal (not isolated).[3] Certainly, this time the exchange of halogen in R'_2EHal for R′ is possible for steric reasons {the reaction of $GaCl_3$ with $LiSi(SiMe_3)_2$ leads analogously to $[(Me_3Si)_3Si]_3Ga$,[22] whereas $InCl_3$ and $LiSi(SiMe_3)_3$ gives $[(Me_3Si)_3Si]_4In_2$ [10]}.

For the reactions of NaR* or NaR′ with *triel(I) compounds* **EX**, those of InBr or TlBr produce the ditrielanes $R^*_4In_2$, R'_4In_2, or $R^*_4Tl_2$, R'_4Tl_2 (**3**−**6**) besides disilanes R^*_2 and R'_2 as well as indium or thallium, respectively (Scheme 1). In fact, the ditrielane formation is fully unclear to date. Nevertheless, silyltrielylenes RE may probably be the first products of the **EX**/NaR reactions. On the other hand, the action of NaR* on GaBr gives the gallium cluster compounds $R^*_8Ga_{18}$ and $R^*_8Ga_{22}$,[23] the formation of which indicates another possible way of stabilization of gallylene R*Ga. The reaction of AlBr with NaR* leads to $R^*_4Al_4$ (**12**).[24]

The diindanes **3** and **5** are also produced in alkanes from InX [X = $N(SiMe_3)_2$, C_5H_5, C_5Me_5] and NaR* as well as NaR′, and the dithallane **6** forms from $TlN(SiMe_3)_2$ and NaR*. By analogy $[(Me_3Si)_3Si]_4Tl_2$ is prepared from $TlN(SiMe_3)_2$ and $RbSi(SiMe_3)_3$.[11] On the other hand, the reaction of C_5Me_5In with NaR* gives − besides **3** − the octaindane $R^*_6In_8$,[6] whereas the reaction of $TlN(SiMe_3)_2$ with NaR′ leads to an insoluble black substance, not identified to date. Obviously, the indylene R*In or thallylene R′Tl, possibly formed as intermediates in the latter cases, may polymerize with or without elimination of R. In accordance with this, the action of $LiC(SiMe_3)_3$ on InBr leads − possibly by way of $(Me_3Si)_3CIn$ − to $[(Me_3Si)_3C]_4In_4$.[25] In addition, it is worth mentioning that the diindane **3** also forms by reaction of $R^*_6In_8$ (see above) with NaR* in heptane at 25 °C or with Na in benzene at 95 °C.

In concluding this part, we again point to the difficulty of preparing $R^*_4Ga_2$ (**2**), due to its instability against decomposition into $R^*_3Ga_2^{\cdot}$ (**2a**) and $R^{*\cdot}$ (cf. Scheme 2). To date, only one supersilyldigallane, namely $R^*_3Ga_2(SiMe_3)$ (**2b**), has been prepared by reaction of Me_3SiCl with the THF adduct of $NaGa_2R^*_3$, obtained by reduction of **2a** with Na in THF:[5] **2a** + Na and then $Me_3SiCl \rightarrow$ **2b** + NaCl (cf. Scheme 2). Preparation methods for R'_4Al_2 and R'_4Ga_2 are still lacking. Here amongst others, the reactions of *triel(II) compounds* $\mathbf{EX_2}$ like $Ga_2X_4{\cdot}2D$ (D = donor) with NaR′ must be studied, as it is known that the reactions of $Ga_2Br_4{\cdot}2$dioxane or $In_2Br_4{\cdot}2$TMEDA with $LiCH(SiMe_3)_2$ lead to $[(Me_3Si)_2CH]_4Ga_2$ or $[(Me_3Si)_2CH]_4In_2$,[13,14] and the reaction of $Ga_2Cl_4 \equiv Ga^+[GaCl_4]^-$ with $LiSi(SiMe_3)_3{\cdot}$THF to $[(Me_3Si)_3Si]_4Ga_2$.[9]

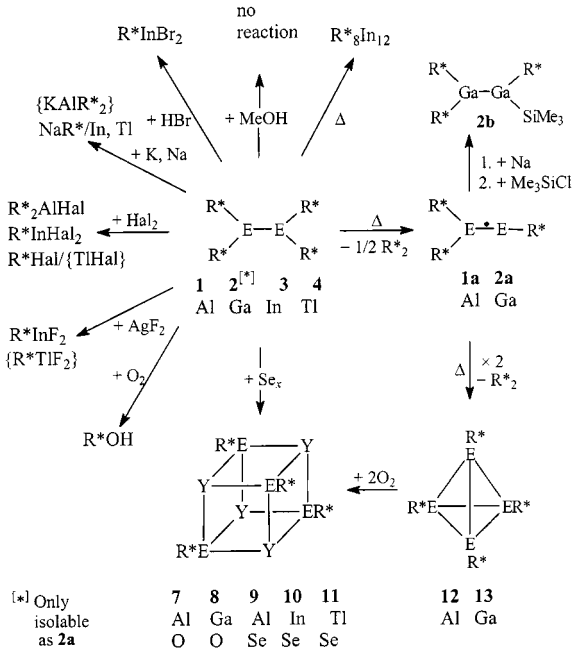

Scheme 2. Reactions and thermolyses of ditrielanes $R^*_4E_2$ (E = Al, Ga*), In, Tl; R* = Si*t*Bu$_3$) as well as formation of heterocubanes $R^*_4E_4Y_4$ (E = Al, Ga, In, Tl; Y = O, Se); compounds in brackets are unstable and/or not fully characterized

Table 1. Characterization of ditrielanes R_4E_2 and heterocubanes $R^*_4E_4Y_4$ with R = Si*t*Bu$_3$ (R*), Si*t*Bu$_2$Ph (R′), SiMe$_3$, E = triel and Y = chalcogen

	M.p. [°C][a]	Color	λ_{max} [nm][b]	NMR (C_6D_6): δ(Si*t*Bu$_3$/Si*t*Bu$_2$) ^{1}H	^{13}C[c]	^{29}Si/^{79}Se	E−E [Å][d]	Si−E [Å]	E−Y [Å]	Si−E−Si [°]	Y−E−Y/E−Y−E [°]	τ [°][d]
1: $R^*_4Al_2$	63/dec.	ruby	525	1.36	25.6/35.6	44.7	2.751	2.717	−	128.3	−/−	90.0
2a: $R^*_3Ga_2$	55/dec.	dark-blue		−[e]	−/−[e]	−[e]	2.420	2.50[f]		140.7	−/−	83.5
2b: $R^*_3Ga_2SiMe_3$		red		1.26[g]	25.4/32.4[g]	48.4[g]		−			−/−	
				1.28[g]	25.6/33.9[g]	44.8[g]						
3: $R^*_4In_2$		deep-violet	560	1.35	26.8/34.0	76.8	2.928	2.786[f]	−	130.1	−/−	87.0
4: $R^*_4Tl_2$	56/dec.	dark-green	628	1.32	28.6/33.1	99.5	2.961	2.779[f]	−	130.5[f]	−/−	89.6
5: R'_4In_2		red-violet	530	1.24	23.6/31.9	54.4	2.938	2.737[f]	−	121.4[f]	−/−	79.9
6: R'_4Tl_2	125/dec.	dark-blue	591	1.29	27.0/32.5	103.7	2.881	2.682[f]	−	122.8[f]	−/−	82.2
7: $R^*_4Al_4O_4$		colorless		1.31	24.1/32.2		2.61			−		−
8: $R^*_4Ga_4O_4$	367/dec.	colorless		1.34	24.1/31.9	26.5	2.71	2.49	1.84	−	89.2/90.8	−
9: $R^*_4Al_4Se_4$		light-red		1.34	25.2/32.9	−178		2.42	1.92	−	89.9/90.1	−
10: $R^*_4In_4Se_4$		yellow		1.33	25.5/32.2	44.6/−322	3.55	2.57	2.68	−	96.8/82.9	−
11: $R^*_4Tl_4Se_4$						88.6/−498				−		−

[a] dec. = decomposition. [b] In heptane. [c] First/second shift CMe_3/CMe_3. [d] τ = Si−E−E−Si angle; *d* (E−E)/τ for R_4E_2 with R = Dsi = CH(SiMe$_3$)$_2$, Tip = 2,4,6-*i*Pr$_3$C$_6$H$_2$, Pip = 2,2,6,6-Me$_4$NC$_5$H$_6$, Mes′ = 2,4,6-(F$_3$C)$_3$C$_6$H$_2$, Hsi = Si(SiMe$_3$)$_3$, R′′ = 1/2 −*t*BuN−MeSi(N*t*Bu)$_2$SiMe−N*t*Bu−. E = Al: Dsi$_4$Al$_2$ 2.660/8; Tip$_4$Al$_2$ 2.647/44.8; E = Ga: Dsi$_4$Ga$_2$ 2.541/4.9, Pip$_4$Ga$_2$ 2.525/31, Tip$_4$Ga$_2$ 2.515/43.8, Mes′$_4$Ga$_2$ 2.479/?, Hsi$_4$Ga$_2$ 2.599/80; E = In: R′′$_4$In$_2$ 2.768/0, Dsi$_4$In$_2$ 2.828/6.8, Tip$_4$In$_2$ 2.775/48, Mes′$_4$In$_2$ 2.744/86, Hsi$_4$In$_2$ 2.868/78.6; E = Tl: Hsi$_4$Tl$_2$ 2.914/78.1.[9−19] [e] Not seen in the NMR spectrum. [f] Mean value. [g] First/second shift R^*_2Ga/R*Ga; Me$_3$Si: δ(^{1}H/^{13}C/^{29}Si) = 0.173/1.29/19.4.

Characterization of $R^*_4E_2$ and R'_4E_2 (R* = Si*t*Bu$_3$, R′ = Si*t*Bu$_2$Ph)

Table 1 summarizes the ditrielanes **1**−**6** prepared by us, together with some characteristic properties. The compounds are remarkable colored and more or less soluble in organic media. They melt with decomposition (see below) and are air-sensitive. In addition, the ditrielanes **1**, **4** and **6** are highly unstable in the presence of light [$R^*_4Al_2$/daylight → *tetrahedro*-$R^*_4Al_4$/R^*_2 (in weeks); $R^*_4Tl_2$/R'_4Tl_2/daylight → Tl/R^*_2/R'_2 (in hours)].

The ^{1}*H NMR* and ^{13}*C NMR* shifts of the *t*Bu groups of $R^*_4E_2$ and R'_4E_2 appear − according to its peripheral position − in small regions [δ(^{1}H) = 1.24−1.36; δ(^{13}C) = 31.9−35.6/23.6−28.8]. On the other hand, the ^{29}*Si NMR* shifts show E-specific areas at δ ≈ 45−50 for E = Al, Ga, δ ≈ 55−75 for E = In, and δ ≈ 95−105 for E = Tl.

The color of ditrielanes R_4E_2, that is λ_{max} of its *UV/Vis spectra*, depends on the nature of the triel E and on the geometry of the central framework (planar, gauche, orthogonal) which itself is essentially determined by the steric behavior of R. (Certainly, the electronic behavior of R is essential too.) Figure 1 shows the UV/Vis spectra of the ditrielanes R_4E_2 with fixed substituent R = R* and fixed REER torsion angles τ (90°). Evidently, with increasing atomic number of the triel, λ_{max} of $R^*_4E_2$, shifts to longer wavelengths (525/560/628 nm for **1**/**3**/**4**), corresponding to a bathochromic colorshift from ruby (**1**) to deep-violet (**3**) to dark-green (**4**; accordingly, λ_{max} of **2**, not isolated to date, should have an absorption maximum of about 540 nm). Obviously, according to Table 1, the same is valid for **5** and **6** (τ about 80°; red-violet and dark-blue).

On the other hand, the color of ditrielanes R_4E_2 with fixed triel E shows a bathochromic shift with increasing REER torsion angle τ. Accordingly, the dialanes

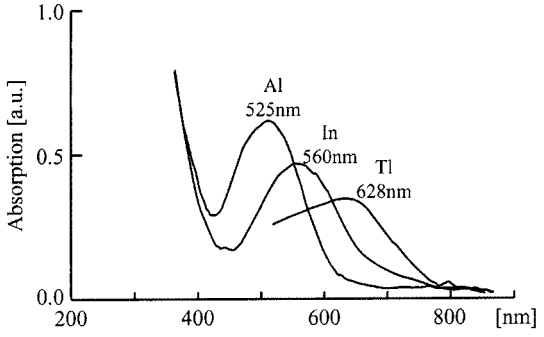

Figure 1. UV/Vis spectra of ditrielanes $R^*_2E-ER^*_2$ (E = Al, In, Tl; ε ≈ 50000 for λ_{max})

[(Me$_3$Si)$_2$CH]$_4$Al$_2$ [12]/[2,4,6-*i*Pr$_3$C$_6$H$_2$]$_4$Al$_2$ [15]/$R^*_4Al_2$ with τ = 8/45/90° are colorless/yellow-green/ruby (λ_{max} = 370/420/525 nm), the diindanes [(Me$_3$Si)$_2$CH]$_4$In$_2$ [14]/R'_4In_2/$R^*_4In_2$ with τ = 6/80/90° are orange-red/red-violet/deep-violet (λ_{max} = 380/530/560 nm), or the dithallanes R'_4Tl_2/$R^*_4Tl_2$ with τ = 82/90° are dark-blue/dark-green (λ_{max} = 591/628 nm). [For electronic effects of R cf. yellow [(Me$_3$Si)$_2$CH]$_4$Ga$_2$ (planar)[13] and more electronegatively substituted colorless R′′$_4$Ga$_2$ (evidently planar as R′′$_4$In$_2$) with R′′ = 1/2 −*t*BuN−MeSi(N*t*Bu)$_2$SiMe−N*t*Bu−.[20]]

Reactions of $R^*_4E_2$ and R'_4E_2 (R* = Si*t*Bu$_3$, R′ = Si*t*Bu$_2$Ph)

In the following, the behavior of R_4E_2 (R = R*, R′) against acids/bases, redox agents and heat is discussed. The first step of the mentioned reactions may involve addition of a donor or cleavage of the E−E bond as well as cleavage of the Si−E bonds leading to compounds which themselves

may give secondary products. Selected reactions that we studied are shown in Scheme 2.

We have never observed − probably for steric reasons − a formation of adducts $R_4E_2{\cdot}D$ of the mentioned ditrielanes **1** and **3**−**6** with Donors D (e.g. halogenides, ethers). This is unlike other − less overcrowded − ditrielanes which may work as *Lewis acids* [cf. for example the adducts $Dis_4Al_2{\cdot}D$ with Dis = $CH(SiMe_3)_2$ and D = Br^-, H^-, Me^- [26]]. In addition, the ditrielanes **1** and **3** are methanol-stable (certainly, MeOH would act first as a donor against $R^*_4E_2$ in the course of methanolyses). Also, our ditrielanes do not work as *Brönsted acids* (e.g. against NaR*, NaR′) unlike Dis_4Al_2 with Dis = $CH(SiMe_3)_2$.[26]

On the other hand, $R^*_4In_2$ (**3**) transforms, with excess hydrogen bromide, in benzene at 25 °C into R^*InBr_2 and R*H (molar ratio 1:1) and also H_2 (Scheme 2). Obviously, **3** behaves here as a *Lewis base* against HBr. The reaction may proceed either by $R^*_4In_2 + 4\ HBr \rightarrow R^*_2In_2Br_2 + 2\ R^*H + 2\ HBr \rightarrow 2\ R^*InBr_2 + 2\ R^*H + H_2$ (cf. reaction of Dis_4Ga_2 with RCOOH[26]) or − less likely − by $R^*_4In_2 + 4\ HBr \rightarrow 2\ R^*_2InBr + H_2 + 2\ HBr \rightarrow 2\ R^*InBr_2 + 2\ R^*H + H_2$ (cf. reaction of Dis_4Al_2 with LiOR;[26] certainly, an In−In bond cleavage with HBr would require the ditrielane to be a Lewis base, which is not true for **3** but might be observed for $R^*_2In_2Br_2$). In this connection, it is worth mentioning that $R^*_4Tl_2$ (**4**) reacts with HBr in a molar ratio of 1:2 (THF, −30 °C) with the formation of R*H and a red substance. The latter compound may be the dithallane $R^*_2Tl_2Br_2$ according to NMR spectroscopy. It slowly decomposes already at −30 °C into R*Br and a black residue which has not yet been characterized (for some reactions of halosupersilylthallanes cf. ref.[7]). We could synthesize the orange digallane $R^*_2Ga_2Cl_2$ by reaction of $R^*GaCl_2{\cdot}THF$ and potassium in heptane, which − according to X-ray structure analysis − exists as a dimer with the As_4S_4 structure (exchange of As/S against Ga/Cl).[27]

Other examples for acid/base reactions of R_4E_2 may be that of $R^*_4Tl_2$ (**4**) and R'_4Tl_2 (**6**) with Ph_3CCl in benzene or cyclohexane at 0 °C which lead exclusively to R^*_2/R'_2 and a colorless residue (TlCl?). Certainly, the course of the mechanism is completely unclear at this time. The acid/base reactions of ditrielanes R_4E_2 (R = R*, R′) with $EHal_3$, which may lead to haloditrielanes $R_nE_2Hal_{4-n}$ (cf. R_nEHal_{3-n} [1,2]), have to be studied.

According to Scheme 2, the ditrielanes $R^*_4E_2$ can be both *oxidized* (e.g. with halogens, chalcogenes) and *reduced* (e.g. with alkali metals). The dialane $R^*_4Al_2$ (**1**) reacts cleanly in alkanes at 50 °C with iodine or hydrogen − according to Scheme 2 − under formation of the monotrielanes R^*_2AlX (X = I, H), as published elsewhere.[5] Obviously, the products are probably formed from the sterically overcrowded dialane as follows: $\mathbf{1} \leftrightarrows 2\ R^*_2Al^{\cdot}$; $2\ R^*_2Al^{\cdot} + X_2 \rightarrow 2\ R^*_2AlX$. Bromine transforms $R^*_4In_2$ (**3**) into R^*InBr_2 and R*Br (Scheme 2). The reaction may proceed either by In−In or by In−Si bond cleavage via R^*_2InBr or $R^*_2In_2Br_2$. Bromination of $R^*_4Tl_2$ (**4**) results − possibly by way of R^*TlBr_2 finally to TlBr ($R^*TlBr_2 \rightarrow R^*Br + TlBr$). Fluorination of $R^*_4In_2$ (**3**) with AgF_2 produces − according to Scheme 2 − the dihalide R^*InF_2 ($\mathbf{3} + 4\ AgF_2 \rightarrow 2\ R^*InF_2 + 2\ R^*F + 4\ AgF$). R^*TlF_2 possibly plays the role of an intermediate in the reaction of $R^*_4Tl_2$ (**4**) with AgF_2, finally leading to TlF ($R^*TlF_2 \rightarrow R^*F + TlF$).

The main products of the reactions of ditrielanes **1**, **3**−**6** with air are the silanols $t\mathrm{Bu}_3\mathrm{SiOH}$ (Scheme 2) and $\mathrm{Ph}t\mathrm{Bu}_2\mathrm{SiOH}$. Selenium transforms $R^*_4E_2$ (**1**, **3** and **4**) − according to Scheme 2 − into the heterocubanes $R^*_4E_4Se_4$ (**9**, **10**, **11**) and also R^*_2 (no R^*_2Se is formed). This is unlike the reactions of Dis_4E_2 [Dis = $CH(SiMe_3)_2$; E = Al, Ga, In] with transfer agents for chalcogens Y like Me_3NO, Me_2SO, and Et_3PY among others, which lead to compounds $Dis_2E-Y-EDis_2$.[26] The mechanism for the formation of **9**−**11** is still unclear. Perhaps, the ditrielanes $R^*_4E_2$ react with Se_x − for steric reasons − not to selanes $R^*_2E-Se-ER^*_2$ but to diselanes $R^*_2E-SeSe-ER^*_2$ which − via R^*_2 and $R^*E(Se)_2ER^*$ (central four-membered ESeESe ring) − transform into the heterocubanes.

On the other hand, heterocubanes $R^*_4E_4O_4$ (**7** and **8**) are produced − according to Scheme 2 − by reaction of the tetrahedranes $R^*_4Al_4$ (**12**)[24] and $R^*_4Ga_4$ (**13**)[28] with oxygen instead of selenium (cf. Scheme 2). In fact, **12** and **13** are − like other known silyl-substituted tetrahedranes (e.g. $[(Me_3Si)_3Si]_4Ga_4$ [29]) and unlike organyl-substituted tetrahedranes (e.g. $[(Me_3C)_3Si]_4Ga_4$ [30] and $[(Me_3Si)_3C]_4In_4$ [31]) − extremely oxygen-sensitive ($[(Me_3Si)_3C]_4In_4$ may be oxidized with *o*-nitrosotoluene[31]). Certainly, **12** and **13** also react with the oxygen homologues that − as is known − even attack organyl-substituted tetrahedranes like $[(Me_3Si)_3C]_4Ga_4$ [30] and $[(Me_3Si)_3C]_4In_4$ [21]. In this connection the question arises whether the latter reactions can be reversed. In fact, deselenation of **10** should give the tetrahedrane $R^*_4In_4$ which has not be prepared to date.[6] For characteristic properties of the mentioned heterocubanes cf. Table 1.

The reactions of ditrielanes with alkali metals have not been studied in detail, thus far. Obviously, potassium transforms the dialane $R^*_4Al_2$ (**1**) in pentane at room temperature into an insoluble compound which is also obtained from R^*_2AlHal (Hal = Cl, Br) and K and reacts with Ph_3CH under formation of R^*_2AlH (for details cf. ref.[2]). On the other hand, $R^*_4In_2$ (**3**) or $R^*_4Tl_2$ (**4**) give with sodium in benzene or cyclohexane at 40 °C − according to Scheme 2 − supersilylsodium NaR* and In or Tl along with R^*_2/R*H. Radical anions $R_4E_2^{\cdot -}$, which form by reaction of alkali metals with organylditrielanes,[26] are not observed in the case of the ditrielanes **1**, **3** and **4** (certainly, electron intake leads to a planarisation of the ditrielanes,[24] which is sterically impossible for $R^*_4E_2$).

Regarding the redox reactions of R_4E_2 (R = R*, R′) so far discussed, there is some reason from mass spectrometric studies (see below) to believe that they start with the formation of radicals $R_2E^{\cdot}$. As stated elsewhere,[5] *thermolysis in solution* leads in the case of $R^*_4Al_2$ (**1**), probably by a fast and reversible Al−Al bond dissociation, to radicals $R^*_2Al^{\cdot}$ in low equilibrium concentration, but at the same time by a slow and irreversible Si−Al bond dissociation to radicals $R^{*\cdot}$ and $R^*_3Al_2^{\cdot}$ (**1a**). The latter are stable at room

temperature and transform at 80−100 °C − according to Scheme 2 − possibly via $R^*_2Al_2$ into isolable trialanyl radicals $R^*_4Al_3^{\cdot}$ and *tetrahedro*-tetraalane $R^*_4Al_4$ (**12**),[5] whereas the radicals $R^{*\cdot}$ dimerize under formation of the disilane R^*_2 (the radical $R^*_4Al_3^{\cdot}$ may be formed by addition of $R^*_2Al_2$ and $R^*_2Al^{\cdot}$, and the tetrahedrane **12** by dimerization of $R^*_2Al_2$).[5] On the other hand, $R^*_4Ga_2$ (**2**) very easily thermolizes in solution into $R^{*\cdot}$ and the isolable digallanyl radical $R^*_3Ga_2^{\cdot}$ (**2a**) making the isolation of the digallane **2** unsuccessful to date[5] (the formation of $R^*_2Ga^{\cdot}$, the precursor of **2**, from R^*_2GaHal and NaR*, only occurs at temperatures where **2** already decomposes into **2a**). The radicals **2a** themselves decompose in alkanes at 100 °C − according to Scheme 2 − possibly via $R^*_2Ga_2$ into the *tetrahedro*-tetragallane $R^*_4Ga_4$ (**13**) along with R^*_2 and R*H.[28]

According to ESR spectroscopic studies, alkane solutions of $R^*_4In_2$ (**3**) and $R^*_4Tl_2$ (**4**) always contain radicals, the nature of which, however, is unclear. Interestingly, heating of equimolar amounts of **1** and **3** in alkanes at 90 °C do not lead to any cross-over product $R^*_2Al-InR^*_2$, but only to the thermolysis products of **1** (see above), leaving **3** intact. At 100 °C the diindane **3** thermolizes very slowly in alkanes with the formation of the dodecaindane $R^*_8In_{12}$ along with R^*_2 and R*H (cf. Scheme 2).[6] Thus, an intermediate is formed which may be $R^*_4In_6$ (in fact, it reacts like $R^*_6In_8$ with NaR* under formation of **3**, see preparation of the diindane). By the way, $R^*_8In_{12}$ also forms by thermolysis of $R^*_6In_8$ in benzene at 100 °C. The dithallane **4** slowly (in hours) decomposes in alkanes at 40 °C into R^*_2 and a dark brown residue (Tl?). The ditrielanes R'_4E_2 (**5**, **6**) are more stable than $R^*_4E_2$ (**3**, **4**) and thermolize in C_6D_6 at 140 °C (**5**) or 106 °C (**6**) under formation of R′D and In or Tl mirrors, respectively.

In high vacuum, the mentioned ditrielanes R_4E_2 (R = R*, R′) are comparably volatile. From the mass spectrum (chemical ionization with NH_3^+) of $R^*_4Al_2$ (**1**), $R^*_4In_2$ (**3**), R'_4In_2 (**5**) and R'_4Tl_2 (**6**) the $M/2^+$ peak is seen instead of an M^+ peak, which is an indication that the ditrielanes vaporize under cleavage of the E−E bonds. Accordingly its *thermolysis* in the *gas phase* takes place under formation of radicals $R_2E^{\cdot}$. In addition, the mass spectra (CI) of **1** (but not of **3**, **5** and **6**) shows peaks for fragments with an intact E−E framework, namely $R^*_2Al_2^+ + H$ and $R^*_2Al_2^+ - t$Bu. Obviously, the steric overcrowding of **1** facilitates not only Al−Al, but also Si−Al bond cleavage (in fact, the digallane **2** exists as radical **2a**; see above).

Structures of $R^*_4E_2$, R'_4E_2 and $R^*_4E_4Y_4$ (R* = Si*t*Bu$_3$, R′ = Si*t*Bu$_2$Ph; Y = O, Se)

The structures of $R^*_4In_2$ (**3**; revisited),[4] $R^*_4Tl_2$ (**4**), R'_4In_2 (**5**), R'_4Tl_2 (**6**), $R^*_4Al_4O_4$ (**7**) and $R^*_4In_4Se_4$ (**10**) are shown in Figures 2−4, together with selected bond lengths and angles. For comparison, bond lengths and angles of $R^*_4Al_2$ (**1**)[5] and $R^*_4Ga_4O_4$ (**8**) [28] are also quoted. In addition, Table 1 presents bond lengths and angles of the ditrielanes and heterocubanes under discussion as well as E−E bond lengths and R−E−E−R torsion angles of other ditrielanes R_4E_2.

According to X-ray structure analyses and Figure 2, in **1**, **3** and **4** the Al, In and Tl atoms are planar coordinated with two Si atoms and one triel atom E, whereby the $EESi_2$ planes are orthogonal or nearly orthogonal to each other (cf. Table 1). Interestingly, in ditrielanes R_4E_2 with sterically less overcrowded silyl substituents the angles between the EER_2 planes decrease with decreasing bulkiness of R and are 79.9° for **5** and 82.2° for **6**, according to Figure 3 and Table 1 {for comparison $[(Me_3Si)_3Si]_4E_2$: 80° (Ga)[9]/78.6° (In)[10]/78.1° (Tl)}.[11] Significant smaller angles between the EER_2 planes show the organylditrielanes Tip_4E_2 and − above all − Dsi_4E_2 [for E = Al/Ga/In in Tip_4E_2 with Tip = 2,4,6-*i*Pr$_3$C$_6$H$_2$ 45/44/48° and in Dsi_4E_2 with Dsi = $(Me_3Si)_2CH$ 8/5/7°; cf. Table 1].

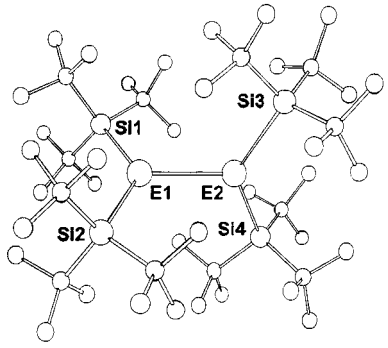

Figure 2. Crystal structures of **1**, **3** and **4** with atom numbering (SCHAKAL; H atoms omitted for clarity); selected distances [Å] and angles [°] with standard deviations: **$R^*_4Al_2$** (local symmetry D_{2d}; E1/E2 = Al1/Al1A; Si1/Si2/Si3/Si4 = Si1/Si1A/Si1B/Si1C; see ref.[5]): Al1−Al1A 2.751(2), Al1−Si1 2.717(5), Si−C (mean value) 1.97; Si1−Al1−Si1A 128.26(5), Si1−Al1−Al1A 115.87(2), C−Si−C (mean value) 109.1; Si−Al−Al−Si 90.0; **$R^*_4In_2$** (local symmetry ca. D_{2d}; E1/E2 = In1/In1A; Si1/Si2/Si3/Si4 = Si1/Si2/Si1A/Si2A): In1−In1A 2.928(3), In1−Si1 2.7835(6), In1−Si2 2.7886(6), Si−C (mean value) 1.96; Si1−In1−Si2 130.13(2), Si1−In1−In1A 115.4(1), Si2−In1−In1A 114.42(1), C−Si−C (mean value) 109.6; Si−In−In−Si 87.0; **$R^*_4Tl_2$** (local symmetry ca. D_{2d}; E1/E2 = Tl1/Tl2): Tl1−Tl2 2.961(1), Tl1−Si1 2.768(3), Tl1−Si2 2.779(4), Tl2−Si3 2.788(3), Tl2−Si4 2.781, Si−C (mean value) 1.95; Si1−Tl1−Si2 130.4(1), Si3−Tl2−Si4 130.5(1), Si1−Tl1−Tl2 114.7(2), Si2−Tl1−Tl2 114.9(2), Si3−Tl2−Tl1 114.4(1), Si4−Tl2−Tl1 115.1(1), C−Si−C (mean value) 110.1; Si−Tl−Tl−Si 89.6

The space-filling properties of the groups R* and R′ lead to unusually long E−E distances in **1** (2.75 Å), **3** (2.93 Å), **5** (2.94 Å), **4** (2.96 Å) and **6** (2.88 Å). Those in $R^*_4E_2$ are longer than those found in any dialane, diindane or dithallane with a covalent E−E bond (cf. Table 1, footnote[d]). As expected, the E−E distances in R_4E_2 increase with increasing bulkiness of R [CH(SiMe$_3$) (Dsi) < 2,4,6-*i*Pr$_3$C$_6$H$_2$ (Tip) < Si(SiMe$_3$)$_3$ (Hsi) < Si*t*Bu$_3$ (R*)], but naturally are also dependent on τ; they amount to 2.65/2.66/2.75 Å for $Dsi_4Al_2/Ti_4Al_2/R^*_4Al_2$; 2.54/2.52/2.60 Å for $Dsi_4Ga_2/Tip_4Ga_2/Hsi_4Ga_2$; 2.83/2.78/2.87/2.93 Å for $Dsi_4In_2/Tip_4In_2/Hsi_4In_2/R^*_4In_2$; and 2.91/2.96 Å for $Hsi_4Tl_2/R^*_4Tl_2$ (cf. Table 1). Interestingly, the E−E distance decreases on going from R_4Al_2 to analogously substituted R_4Ga_2 by ca. 0.1 Å. This may be due to a decrease of the triel atomic

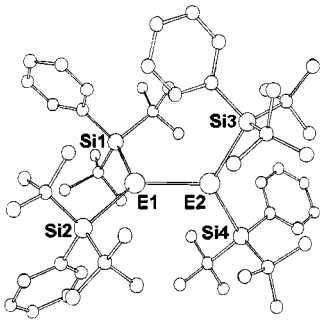

Figure 3. Crystal structures of **5**, **6** with atom numbering (SCHAKAL; H atoms omitted for clarity); selected distances [A] and angles [°] with standard deviations: **R′$_4$In$_2$** (E1/E2 = In1/In2): In1−In2 2.938(1), In1−Si1 2.655(2), In1−Si2 2.795(1), In2−Si3 2.826(2), In2−Si4 2.671(1), Si−C (mean value) 1.96; Si1−In1−Si2 122.74(5), Si3−In2−Si4 120.10(5), Si1−In1−In2 117.73(4), Si2−In1−In2 119.43(4), Si3−In2−In1 113.50(4), Si4−In2−In1 126.39(3), C−Si−C (mean value) 110.4; Si−In−In−Si 79.9; **R′$_4$Tl$_2$** (E1/E2 = Tl1/Tl2): Tl1−Tl2 2.881(2), Tl1−Si1 2.674(2), Tl1−Si2 2.685(2), Tl2−Si3 2.685(2), Tl2−Si4 2.687(2), C−Si (mean value) 1.93; Si1−Tl1−Si2 120.69(6), Si3−Tl2−Si4 124.96(6), Si1−Tl1−Tl2 123.37(5), Si2−Tl1−Tl2 115.93(5), Si3−Tl2−Tl1 119.20(5), Si4−Tl2−Tl1 115.76(5), C−Si−C (mean value) 110.5; Si−Tl−Tl−Si 82.19

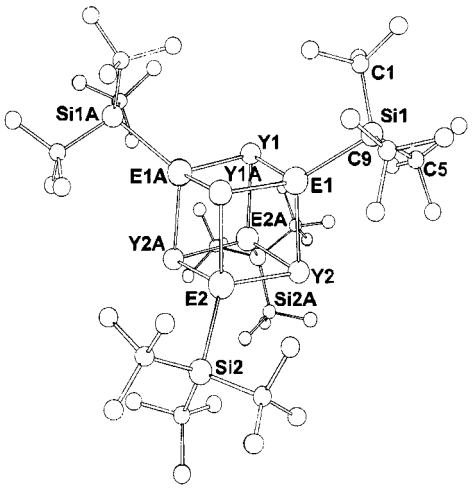

Figure 4. Crystal structures of **7**, **8**, **9** with atom numbering (SCHAKAL; H atoms omitted for clarity); selected distances [A] and angles [°] with standard deviations [R*$_4$Al$_4$O$_4$ together with R*$_4$Al$_4$ (molar ratio 1:2) in the crystal]: **R*$_4$Al$_4$O$_4$** (local symmetry C_2; E =Al, Y = O): Al1−O2 1.826(7), Al1−O1A 1.831(6), Al1−O1 1.838(6), Al1A−O1 1.831(6), Al2−O2A 1.836(6), Al2−O2 1.837(6), Al2−O1A 1.840(6), Al2A−O1 1.840(6), Al2A−O2 1.836(6), Al−Al (mean value) 2.612, Si1−Al1 2.486(1), Si2−Al2 2.486(1), Si−C (mean value) 1.94; Al1A−O1−Al1 90.7(3), Al1A−O1−Al2A 90.7(3), Al1−O1−Al2A 90.4(3), Al1−O2−Al2A 90.9(3), Al1−O2−Al2 91.0(3), Al2A−O2−Al2 90.8(3), O2−Al1−O1A 89.4(3), O2−Al1−O1 89.5(3), O1A−Al1−O1 89.3(3), O2A−Al2−O2 89.2(3), O2A−Al2−O1A 89.1(3), O2−Al2−O1A 88.8(3), Al−Al−Al (mean value) 60.0, Si−Al−Al (mean value) 144.7, Si−Al−O (mean value) 126.0, C−Si−C (mean value) 111.8; **R*$_4$Ga$_4$O$_4$** (local symmetry C_2; E = Ga, Y = O; see ref.[23]): Ga1−O1A 1.923(4), Ga1−O1 1.912(4), Ga1−O2 1.909(4), Ga2−O1A 1.915(3), Ga2−O2 1.902(4), Ga2−O2A 1.928(4), Ga−Ga (mean value) 2.712, Ga1−Si1 2.425(1), Ga2−Si2 2.423(1), Si−C (mean value) 1.93; O2−Ga1−O1 90.2(2), O1−Ga1−O1A 89.7(2), O2−Ga1−O1A 89.96(2), O2−Ga2−O2A 90.1(2), O2−Ga2−O1A 90.2(2), O1A−Ga2−O2A 89.5(1), Ga1A−O1A−Ga2 90.3(2), Ga2−O1A−Ga1 89.7(2), Ga1A−O1A−Ga1 90.3(2), Ga2−O2−Ga1 90.5(2), Ga2−O2−Ga2A 89.9 (2), Ga1−O2−Ga2A 90.0(2), Si−Ga−Ga (mean value) 144.5, Si−Ga−O (mean value) 123.7, C−Si−C (mean value) 112.3; **R*$_4$In$_4$Se$_4$** (local symmetry C_2; E = In, Y = Se): In1−Se1A 2.681(1), In1−Se1 2.682(1), In1−Se2 2.681(1), In2−Se1A 2.680(2), In2−Se2 2.675(1), In2−Se2A 2.677, In−In (mean value) 3.553, In1−Si1 2.577(2) In2−Si2 2.565(3), Si−C (mean value) 1.95; Se2−In1−Se1 96.27(2), Se1−In1−Se1A 95.93(2), Se2−In1−Se1A 97.01(3), Se2−In2−Se2A 97.16(2), Se2−In2−Se1A 97.19(3), Se1A−In2−Se2A 96.97(2), In1A−Se1A−In2 82.76(2), In2−Se1A−In1 82.44(2), In1A−Se1A−In1 83.57(2), In2−Se2−In1 82.54(2), In2−Se2−In2A 82.45(2), In1−Se2−In2A 83.39, In−In−In (mean value) 60.0, Si−In−In (mean value) 144.9, Se−In−Se (mean value) 96.5, In−Se−In (mean value) 82.9, Si−In−Se (mean value) 120.3, C−Si−C (mean value) 112.2

radius in the direction Al → Ga because of a d-orbital contraction which only effects r_{Ga}, but not r_{Al}. Cf. remarks in ref.[41] It is possible that the atomic radii r_{Al}/r_{Ga} = 1.25/1.26 Å normally used[32] are incorrect and may be exchanged by calculated mean values 1.30/1.24 Å (accordingly r_{In}/r_{Tl} amounts to 1.43/1.53 Å).[10] This means that the steric hindrance increases on going from **1** to **2** with the consequence that **2** is much more unstable with respect to elimination of R* than the dialane. Indeed, **2a** is isolated instead of **2**.

Another consequence of the steric hindrance of the R* or R′ groups to each other in the R_2E and REER parts of the ditrielanes R_4E_2 are unusually long Si−E distances {found in R*$_4$Al$_2$/R*$_4$In$_2$/R*$_4$Tl$_2$/R′$_4$In$_2$/R′$_4$Tl$_2$ 2.72/2.79/2.78/2.74/2.68 Å and in [(Me$_3$Si)$_3$Si]$_4$E$_2$ 2.41 (Ga)[9]/2.66 (In)[10]/2.67 Å (Tl)[11]}. For the same reason the Si−E−Si bond angles are certainly somewhat larger than 120° but much smaller than occurs in the less crowded halogenides R*$_2$EHal (R*$_4$Al$_2$/R*$_4$In$_2$/R*$_4$Tl$_2$/R′$_4$In$_2$/R′$_4$Tl$_2$: 128/130/130/121/123°; R*$_2$EHal about 150°, see ref.[2]).

The central frameworks of the heterocubanes R*$_4$E$_4$O$_4$ (**7**, **8**[28]), shown in Figure 4, form nearly nondistorted cubes, the corners of which are alternatively occupied by E and O atoms (mean angles AlOAl/OAlO = 90.8/89.2°; GaOGa/OGaO = 90.1/89.9°; cf. also Table 1). Obviously, the oxidation of the tetrahedranes R*$_4$Al$_4$ (**12**) or R*$_4$Ga$_4$ (**13**) to **7** or **8** which are also described as E_4 tetrahedranes each with a face capped by a chalcogen atom (cf. Scheme 2), leads to an expansion of the Al$_4$/Ga$_4$ cores as seen by the E−E distances in **13** (2.57 Å) and **8** (2.71 Å). Indeed, the X-ray structure analysis of **7** refers to crystals that contain **7** and **12** in a molar ratio of 1:2. As is known from crystals containing **8** and **13**, bond lengths and angles lie between those of **8** and **13**. Therefore, the E−E distances in pure **7** are certainly somewhat longer than the 2.61 Å obtained (found for **12** 2.60 Å).

According to Figure 4, the heterocubane R*$_4$In$_4$Se$_4$ (**10**) is analogously structured to **7** or **8**. Certainly, the In$_4$Se$_4$ cube deviates somewhat from being regular (mean angles InSeIn/SeInSe = 82.9/96.8°; cf. also Table 1), and the expansion of the In$_4$ tetrahedrane by going from R*$_4$In$_4$ [not synthesized to date; In−In distance must be even shorter than in **3** (2.93 Å)] to **10** (In−In distance 3.55 Å) is very pronounced. Altogether, the heterocubane **10** is analogously structured to the many other heterocubanes $R_4E_4Y_4$ (E = Al, Ga, In; Y = S, Se, Te) which have been prepared to date (e.g. cf. refs.[30,31]).

Experimental Section

General Remarks: All experiments were carried out in flame-dried glass apparatus with standard Schlenk techniques under dry argon or nitrogen. During all manipulations, air and moisture were strictly excluded. The solvents (pentane, heptane, benzene, cyclohexane, toluene, tetrahydrofuran) were distilled from sodium/lead or sodium/benzophenone. Available for use were: H_2, HBr, Cl_2, Br_2, I_2, Se, Ph_3CH, Ph_3CCl, Bu_3SnH, $AlBr_3$, $GaCl_3$, $InBr_3$, InBr, $TlCl_3$, TlBr and AgF_2. The following compounds were synthesized according to literature procedures: NaR*,[33] NaR*·2THF,[33] NaR′,[3] R*$_2$AlHal,[2] C_5H_5In,[34] C_5Me_5In,[35] $TlN(SiMe_3)_2$,[36] C_5H_5Tl,[37] R*$_4$Al$_4$,[24] and R*$_4$Ga$_4$.[28] Synthesis of $InN(SiMe_3)_2$ resulted from the addition of $LiN(SiMe_3)_2$ (0.897 g, 5.36 mmol)[40] in 10 mL of THF to InCl (0.806 g, 5.36 mmol) in 20 mL of THF (−78 °C). After warming to 25 °C, the light-yellow solution contained $InN(SiMe_3)_2$ exclusively according to the NMR spectra. Filtration of the insoluble residue (LiCl) and removal of all volatile compounds with an oil-pump vacuum led to colorless $InN(SiMe_3)_2$ in quantitative yield. ^{1}H NMR (C_6D_6, int. TMS): δ = 0.324. ^{13}C{^{1}H} NMR (C_6D_6, int. TMS): δ = 5.96. ^{29}Si{^{1}H} NMR (C_6D_6, ext. TMS): δ = 2.69. The products R*$_2$,[33] R*H,[33] R*Hal,[33] R*OH,[38] R*C_6H_5,[33] NaR′,[3] R′$_2$,[39] R′H,[39] R′OH[39] were identified by comparison with authentic samples [tBu$_3$Si in R*OH: δ(^{1}H) = 1.090; δ(^{13}C) = 22.67/29.69; δ(^{29}Si) = 10.30; tBu$_2$Si in R′$_2$: δ(^{1}H) = 1.244, δ(^{13}C) = 28.00/33.05, δ(^{29}Si) = 139.5; tBu$_2$Si in R′H: δ(^{1}H) = 1.063, δ(^{13}C) = 19.1/29.2, δ(^{29}Si) = 13.4; tBu$_2$Si in R′OH: δ(^{1}H) = 1.073; δ(^{13}C) = 21.5/28.5; δ(^{29}Si) = 1.01]. For NMR spectra a Jeol GX-270 (^{1}H/^{13}C/^{29}Si: 270.17/67.94/53.67 MHz) and Jeol EX-400 (^{1}H/^{13}C/^{29}Si: 399.78/100.54/79.43 MHz) were used. The ^{29}Si NMR spectra were recorded with the INEPT or DEPT pulse sequence using empirically optimized parameters for the mentioned groups. For mass spectra a Varian CH7 and a MStation JMS 700 of Jeol were used, for UV/Vis spectra a 555-UV/Vis spectrometer from Perkin−Elmer.

Syntheses, Thermolysis and Reactions of R*$_4$Al$_2$ (1). − (i): $AlBr_3$ (0.537 g, 2.01 mmol) and NaR* (1.35 g, 6.07 mmol) in 60 mL of heptane (−78 °C) gave, after heating at room temperature for 24 h, **1** and R*$_2$ in a molar ratio of 1:1 (according to NMR spectra) along with NaBr. After filtration of the insoluble residue (NaBr) and concentration of the filtrate to 20 mL, tetrasupersilyldialane **1** (0.762 g, 0.896 mmol; 89%) was obtained in 1 week at −23 °C as air-sensitive, methanol-stable, benzene-labile, photo- and thermolabile, ruby crystals which decomposed at 63 °C (the oxidation with *air* leads to R*OH as the only R*-containing compound). **1** also forms from equimolar amounts of R*$_2$AlHal (Hal = Cl, Br) and NaR* in pentane (see ref.[5]). $C_{48}H_{108}Al_2Si_4$ (851.7): calcd. C 67.34, H 12.73; found C 67.69, H 12.78. NMR: see Table 1. UV/Vis (heptane): λ_{max} = 525 nm (ε ≈ 50000). MS (EI; 70 eV): m/z = 452 (1) [R*$_2$Al$_2^+$], 395 (11) [R*$_2$Al$_2^+$ − tBu], 425 (4) [R*$_2$Al$^+$], 368 (8) [R*$_2$Al$^+$ − C_4H_8], 226 (13) [R*Al$^+$]. CI (NH_3; 25−50 °C): m/z = 453 (95) [R*$_2$Al$_2^+$ + H], 395 (15) [R*$_2$Al$_2^+$ − tBu], 442 (20) [R*$_2$Al$^+$ + NH_3], 425 (40) [R*$_2$Al$^+$], 216 (100) [SitBu$_3^+$ + NH_3], 199 (5) [SitBu$_3^+$]. X-ray structure analysis: see Figure 2 and ref.[5] − **(ii):** For thermolysis of **1** see ref.[5] − **(iii):** Irradiation of **1** (0.016 mmol) in C_6D_{12} (0.6 mL) slowly leds (in weeks) to **12**,[24] R*$_2$ and R*H in a molar ratio of ca. 1:1:3. − **(iv):** For reaction of hydrogen and iodine with **1** see ref.[5]; for reaction with oxygen see above; for reaction with selenium see below. − **(v):** In the presence of 0.8 mmol of potassium (K), a red solution of R*$_4$Al$_2$ (0.042 g, 0.05 mmol) in 10 mL of pentane transforms over 24 h to a gray residue (intermediate colors: violet, green, colorless). The solution then contains R*$_2$ and R*H according to NMR specroscopy. The residue reacts with Ph_3CH to form R*$_2$AlH.[5]

Synthesis, Thermolysis and Reactions of R*$_3$Ga$_2$˙ (2a); Formation of R*$_3$Ga$_2$(SiMe$_3$) (2b). − (i): $GaCl_3$ (0.184 g, 1.045 mmol) and NaR*·2THF (1.35 mmol) in 20 mL of pentane (−30 °C) gave, after warming to room temperature over 24 h, black-blue **2a** (detected by ESR spectroscopy) and R*$_2$ (detected by NMR spectroscopy) along with NaCl. After filtration of the insoluble residue (NaCl), concentration of the filtrate to 7 mL and cooling to −23 °C, superdisilane R*$_2$ formed as colorless crystals and then trisupersilyldigallanyl (**2a**) (0.110 g, 0.15 mmol, 14.4%) over 5 d as oxygen- and moisture-sensitive black-blue crystals, which decomposed at ca. 55 °C. **2a** was also formed from equimolar amounts of R*$_2$GaHal (Hal = Cl, Br) and NaR* in heptane.[5] For characterization and for thermolysis (formation of **13**) and reduction of **2a** (formation of $NaGa_2R^*_3$·3THF) see ref.[5] − **(ii):** Reaction of 0.1 mL of tributylstannane with **2a** in 10 mL of pentane immediately leds to a deep-red solution with − according to NMR spectroscopy (C_6D_6) − an unidentified substance with R* groups [δ(^{1}H) = 1.107, 1.214, 1.322] along with R*H and R*$_2$. The latter decomposed under decolorization of the C_6D_6 solution. − **(iii):** Reaction of chlorine (0.038 mmol) in 0.1 mL of CCl_4 with **2a** (0.04 mmol) in 10 mL of pentane (−78 °C) immediately led to a deep-red solution which contained − according to NMR spectroscopy (C_6D_6) − unidentified substances with R* groups [δ(^{1}H) = 1.092, 1.205, 1.238, 1.260; δ(^{29}Si) = 6.27, 17.56, 39.91, 51.22] along with R*H, R*$_2$, R*Cl and R*$_2$GaCl. One compound was identical to the substance found from R*$_4$Tl$_2$ with Na in C_6D_6 [δ(^{1}H/^{29}Si) = 1.092/6.27] and obviously contains no Ga and Tl, respectively. The other compounds may be the digallane R*$_3$Ga$_2$Cl or products formed from it. − **(iv):** For synthesis of trisupersilyltrimethylsilyldigallane R*$_3$Ga$_2$(SiMe$_3$) (**2b**) from $NaGa_2R^*_3$·3THF and Me_3SiCl and for characterization of this digallane see ref.[8]

Syntheses, Thermolysis and Reactions of R*$_4$In$_2$ (3). − (i): $InCl_3$ (0.778 g, 3.50 mmol) and NaR*·2THF (10.5 mmol) in 40 mL of THF (−78 °C) gave **3** and R*$_2$ in a molar ratio of 1:1 (according to NMR spectra) along with NaCl after warming to room temperature over 5 h. After exchange of THF with 80 mL of toluene, filtration of the insoluble residue (NaCl) and concentration of the filtrate to 20 mL, 0.112 g (1.09 mmol; 63%) of tetrasupersilyldiindane **3** was obtained over some days at −23 °C as air-sensitive, methanol-stable, deep-violet crystals which decomposed at 125 °C (the oxidation with air led to R*OH as the only R*-containing compound). **3** and In (or Na_xIn_y) is also formed from InBr (2.91 mmol) and NaR* (2.91 mmol) in 25 mL of THF (warming from −78 °C to 25 °C[4]) or from C_5H_5In (3.24 mmol) and NaR* (2.50 mmol) in 40 mL of pentane (warming from −78 °C to 25 °C, 12 h), or from $InN(SiMe_3)_2$ (0.49 mmol) and NaR* (0.49 mmol) in 15 mL of pentane (warming from −78 °C to 25 °C, 14 d). $C_{48}H_{108}In_2Si_4$ (1027.4): calcd. C 56.12, H 10.60; found C 55.75, H. 10.53. NMR: see Table 1. UV/Vis (heptane): λ_{max} = 560 nm (ε ≈ 50000). MS (EI; 70 eV): m/z = 513 (19) [R*$_2$In$^+$], 457 (3) [R*$_2$In$^+$ − C_4H_8], 314 (100) [R*In$^+$]. CI (NH_3; 25−50 °C): m/z = 513 [R*$_2$In$^+$]. X-ray structure analysis: see Figure 2 and ref.[4] Remarks: Reaction of equimolar amounts of C_5Me_5In and NaR* in pentane (warming from −120 °C to −78 °C/48 h, then to 25 °C) led to **3** and R*$_6$In$_8$ in a molar ratio of 1:1.[6] R*$_6$In$_8$ itself thermolized in C_6D_6 at 100 °C/20 d into R*$_8$In$_{12}$ besides R*D/In and reacted with NaR* in heptane (warming from −78 °C to 25 °C) or with Na in C_6D_6 at 95 °C with the formation of **3** and R*$_2$/In (or Na_xIn_y). − **(ii):** Thermolysis of **3** in alkanes at 100 °C took place via an unidentified intermediate (R*$_4$In$_6$?) with the formation of R*$_8$In$_{12}$;[6] the

intermediate transformed, in the presence of NaR*·2THF in heptane, into **3** and an unidentified residue (In or Na_xIn_y). Thermolysis of **3** (0.191 mmol) in the presence of **1** (0.101 mmol) in 20 mL of heptane (5 h, 90 °C) led to the thermolysis products of **1**[5]; **3** remained unchanged. − **(iii):** Irradiation of **3** has not been studied thus far. − **(iv):** The reaction of silver difluoride (AgF_2) with **3** led to R^*InF_2, see ref.[1]; for the reaction with oxygen see above; for the reaction with selenium see below. − **(v):** Reaction of sodium (0.9 mmol) and **3** (0.01 mmol) in 0.7 mL of C_6D_6 led at 40 °C and 3 d to R^*_2, R*D, $R^*C_6D_5$ and NaR* in a molar ratio of ca. 1:2:2:7 with a color change from deep-violet to red and formation of a residue (In or Na_xIn_y), according to NMR spectra. − **(vi):** After warming hydrogen bromide (HBr) (0.41 mmol) and **3** (0.071 mmol) in 0.6 mL of C_6D_6 from −78 °C to room temperature (decolorization, formation of H_2), the solution contained R^*InBr_2 [2] and R*H in a molar ratio of ca. 1:1, according to NMR spectroscopy. − **(vii):** After warming bromine (Br_2) (0.07 mmol) and **3** (0.061 mmol) in 4 mL of pentane from −78 °C to room temperature (decolorization), the solution contained R^*InBr_2 [2] and R*Br in a molar ratio of ca. 1:1 along with a grayish residue, according to NMR spectroscopy.

Syntheses, Thermolysis and Reactions of $R^*_4Tl_2$ (4). − (i): A solution of $TlCl_3$ (0.584 g, 1.88 mmol) and NaR*·2THF (5.64 mmol) in 30 mL of THF was kept at −78 °C for 20 h and then warmed to room temperature. The dark green solution − over a black residue − then contained an unidentified compound [multiplet at $\delta(^{29}Si)$ = 166.2 which points at a substance with two or more Tl atoms]. After filtration of the insoluble residue (NaCl) and concentration of the filtrate to 10 mL, tetrasupersilyldithallane **4** (0.035 g, 0.030 mmol; 24%) was obtained over 14 d at −23 °C as air-sensitive, methanol-stable, deep green crystals which decomposed at 56 °C (the oxidation with air led to R*OH as the only R*-containing compound). The reaction of $TlN(SiMe_3)_2$ (0.272 g, 0.746 mmol) and NaR* (0.166 g, 0.746 mmol) in 30 mL of pentane led to $NaN(SiMe_3)_2$ [40] and R^*_2 after 72 h at −90 °C and warming to −30 °C, according to NMR spectroscopy [$\delta(^{29}Si)$ = 166.2]. Then, after concentration of the solution to 10 mL, crystals of deep-green **4** were obtained at −23 °C in 14 d. Crystalline **4** and Tl (or Na_xTl_y) also formed from TlBr and NaR* in THF (warming from −78 °C to 25 °C)[4] or from C_5H_5Tl (1.785 mmol) and NaR* (1.785 mmol) in 40 mL of pentane at −80 °C. ^1H NMR (C_6D_6, int. TMS): δ = 1.318 (d, $^4J_{HTl}$ = 8.4 Hz, 108 H, Si*t*Bu$_3$). $^{13}C\{^1H\}$ NMR (C_6D_6, int. TMS): δ = 28.6/33.1 (d/d, $^2J_{CTl}/^3J_{CTl}$ = 155.8/49.9 Hz, (12 C/36 C, *C*Me$_3$/C*Me*$_3$). $^{29}Si\{^1H\}$ NMR (C_6D_6, ext. TMS): δ = 99.5 (two doublets with $^1J_{Si}{}^{205/203}{}_{Tl}$ = 1628/1610 Hz; the absence of $^2J_{Si}{}^{205/203}{}_{Tl}$ is unclear, 4 Si, Si*t*Bu$_3$). UV/Vis (heptane): λ_{max} = 628 nm (ε ≈ 50000). X-ray structure analysis: see Figure 2. − **(ii):** Thermolysis of **4** in alkanes at 40 °C led to R^*_2 and a dark-brown residue (Tl?). − **(iii):** Irradiation of **4** in C_6D_{12} with daylight led to R^*_2 and Tl over a few hours. − **(iv):** Reaction of silver difluoride (AgF_2) with **4** led to R*F and R^*_2, see ref.[2]; for the reaction with oxygen see above; for the reaction with selenium see below. − **(v):** By dropwise addition of bromine (Br_2) in 10 mL of pentane to **4** (0.1 mmol) in 15 mL of pentane (−78 °C), the solution decolorized with the formation of a residue (TlBr?) and contained only R*Br according to NMR spectroscopy − **(vi):** After warming hydrogen bromide (HBr) (0.358 mmol) and **4** (0.166 mmol) in 0.6 mL of [D_8]THF at temperature of liquid nitrogen to −30 °C, the solution changed its color from deep green to red. It then contained a thallium compound which − according to NMR spectroscopy at −30 °C in C_6D_8O − may have the composition R*BrTl−TlBrR* [$\delta(^1H)$ = 1.322 (d, $^4J_{HTl}$ = 8.4 Hz, Si*t*Bu$_3$); $\delta(^{29}Si)$ = 98.9 (two d, $^1J_{Si}{}^{205/203}{}_{Tl}$ = 1451/1438 Hz, Si*t*Bu$_3$]. The solution decolorized after warming to room temperature and then contained R*Br. At the same time a residue [colorless TlBr, black $(R^*Tl)_n$?][7] was formed. The decomposition partly took place at −30 °C. − **(vii):** After warming a mixture of triphenylmethyl chloride (Ph_3CCl) (0.083 mmol) and **4** (0.082 mmol) in 0.6 mL of pentane from −196 °C to 25 °C (decolorization; formation of TlCl?), the solution then contained R^*_2 according to NMR spectroscopy. − **(viii):** Reaction of sodium (Na) (0.9 mmol) and **4** (0.01 mmol) in 0.7 mL of C_6D_6 led at 40 °C in 1 d, under change of color from deep-green to brown and formation of a residue (Tl or Na_xTl_y) to R^*_2, R*D and NaR* (molar ratio ca. 1:1:1), according to NMR spectroscopy, along with an unidentified substance [$\delta(^1H)$ = 1.104; $\delta(^{29}Si)$ = 6.3].

Syntheses and Thermolysis of R'_4In_2 (5). − (i): A mixture of InBr (0.207 g, 1.06 mmol) and NaR′ (0.254 g, 1.05 mmol) in 30 mL of pentane/18 mL of THF was kept for 12 h at −78 °C. After warming to 25 °C, the color of the solution changed from yellow to green to deep-violet and it then contained − according to NMR spectroscopy − **5** and R'_2 in a molar ratio of 1:1. After filtration of the insoluble residue (NaBr, In) and concentration of the filtrate to 10 mL, tetrakis(di-*tert*-butylphenylsilyl)diindane (**5**) (0.168 g, 0.152 mmol; 85%) was obtained as red-violet, air-sensitive crystals. **5** was also formed from C_5Me_5In (0.155 g, 0.620 mmol) and NaR′ (0.151 g, 0.622 mmol) in 20 mL of pentane (12 h at −78 °C or 6 h at −120 °C). After warming to 25 °C, the solution exclusively contained − according to NMR spectroscopy − **5** and R'_2 in a molar ratio of 1:1. The concentrated filtrate led to crystalline R'_4In_2 (0.090 g, 0.080 mmol; 75%) at −23 °C. ^1H NMR (C_6D_6, int. TMS): δ = 1.242 (s, 72 H, Si*t*Bu$_2$), 7.840/7.179 (m/m, 8 H/12 H, *m*-/*o*-,*p*-CH of Ph). $^{13}C\{^1H\}$ NMR (C_6D_6, int. TMS): δ = 23.6/31.9 (s/s, 8 C/24 C, *C*Me$_3$/C*Me*$_3$), 127.8/128.1/128.3/136.9 (s/s/s/s, 8 C/4 C/8 C/4 C, *m*-/*p*-/*o*-/*i*-CH of Ph). $^{29}Si\{^1H\}$ NMR (C_6D_6, ext. TMS): δ = 54.4 (s, 4 Si, Si*t*Bu$_2$). UV/Vis (heptane): λ_{max} = 530 nm (ε ≈ 50000). MS (CI: NH_3; 25−50 °C): *m*/*z* = 553 [R'_2In^+]. X-ray structure analysis: see Figure 3. − **(ii):** Thermolysis of 0.127 mmol of **5** in 0.6 mL of C_6D_{12} at 140 °C/12 h led to R′D and an In mirror; some **5** remained unchanged. − **(iii):** The oxidation of **5** with air led to R′OH as the only R′-containing compound.

Syntheses, Thermolysis and Reactions of R'_4Tl_2 (6). − (i): A mixture of TlBr (0.225 g, 0.790 mmol) and NaR′ (0.192 g, 0.790 mmol) in 20 mL of THF was kept for 12 h at −90 °C. After warming to 25 °C, the color of the solution changed from yellow to dark-blue, and it then contained − according to NMR spectroscopy − **6** and R'_2 in a molar ratio of 1:1. After filtration of the insoluble residue (NaBr, Tl) and concentration of the filtrate to 5 mL, tetrakis(di-*tert*-butylphenylsilyl)dithallane (**6**) (0.151 g, 0.117 mmol; 94%) was obtained as air-sensitive, photo-labile, black-blue crystals which decomposed at 125 °C. ^1H NMR (C_6D_6, int. TMS): δ = 1.290 (broad, 72 H, Si*t*Bu$_2$), 7.814/7.528 (m/m, 8 H/12 H, *m*-/*o*-/*p*-CH of Ph). $^{13}C\{^1H\}$ NMR (C_6D_6, int. TMS): δ = 27.0/32.5 (broad/broad, 8 C/24 C, *C*Me$_3$/C*Me*$_3$), 128.6/135.9/137.0/137.7 (s/s/s/s, 8 C/4 C/8 C/4 C, *m*-/*p*-/*o*-/*i*-CH of Ph). $^{29}Si\{^1H\}$ NMR (C_6D_6, ext. TMS): δ = 103.7 (2 doublets with $^1J_{Si}{}^{205/203}{}_{Tl}$ = 982/973 Hz; the absence of $^1J_{Si}{}^{205/203}{}_{Tl}$ is unclear; 4 Si, Si*t*Bu$_2$). UV/Vis (heptane): λ_{max} = 591 nm (ε ≈ 50000). MS (CI; NH_3; 25−50 °C): *m*/*z* = 643 (R'_2Tl^+). X-ray structure analysis: see Figure 3. Remarks: Reaction of equimolar amounts of $TlN(SiMe_3)_2$ and NaR′ in alkanes did not lead to **6**, but to a black residue [$(R'Tl)_x$?].[5] − **(ii):** Thermolysis of 0.113 mmol of **6** in 0.6 mL of C_6D_{12} at 106 °C/48 h completely led to R′D and a Tl mirror. − **(iii):** Irradiation of **6** in C_6D_{12} with daylight led to R'_2 and Tl over a few hours. − **(iv):** After warming a mixture of 0.036 mmol of triphenylmethyl chloride (Ph_3CCl) and **6** (0.020 mmol) in 0.6 mL of C_6D_{12} from −78 °C to 25 °C, it turned

from black-blue to colorless within 10 min (formation of TlCl?), and then contained only R′$_2$, according to NMR spectroscopy. − **(v):** The oxidation of **6** with air led to R′OH as the only R′-containing compound.

Syntheses of R*$_4$E$_4$Y$_4$ (E = triel, Y = O, Se). − (i): Reaction of gray selenium (Se$_x$) (0.022 g, 0.273 mmol) in 0.8 mL of C_6D_{12} with **1** (0.122 g, 0.144 mmol) led to R*$_4$Al$_4$Se$_4$ (**9**) and R*$_2$ and R*H at 60 °C over 12 h. From the reaction mixture at 5 °C **9** was obtained as air- and moisture-sensitive light-red crystals which were not suitable for X-ray analysis but certainly contained molecules structured like **10** (see below). $C_{48}H_{108}Al_4Se_4Si_4$ (1221.5): calcd. C 29.53, H 5.57; found C 29.85, H 5.64. ^{1}H NMR (C_6D_6, int. TMS): δ = 1.337 (s, 108 H, Si*t*Bu$_3$). ^{13}C{^{1}H} NMR (C_6D_6, int. TMS): δ = 25.2/32.9 (s/s, 12 C/36 C, *C*Me$_3$/*C*Me$_3$). ^{29}Si NMR: Not observed. ^{79}Se NMR (C_6D_6, ext. SeMe$_2$ in C_6D_6): δ = −178.4 (s, 4 Se). − **(ii):** Reaction of gray selenium (Se$_x$) (0.054 g, 0.681 mmol) in 30 mL of heptane with R*$_4$In$_2$ (0.350 g, 0.341 mmol) led at 90 °C in 7 h to R*$_4$In$_4$Se$_4$ (**10**), R*$_2$ and R*H. All the volatile compounds were removed in an oil-pump vacuum, the residue was taken up in heptane (30 mL), the precipitate (Se) was then filtered off from the solution and the latter concentrated to 10 mL. From the solution at −23 °C **10** (0.123 g, 0.089 mmol; 46%) was obtained as air- and moisture-sensitive yellow crystals. $C_{48}H_{108}In_4Se_4Si_4$ (1572.9): calcd. C 36.66, H 6.92; found C 36.32, H 6.87. ^{1}H NMR (C_6D_6, int. TMS): δ = 1.328 (s, 108 H, Si*t*Bu$_3$). ^{13}C{^{1}H} NMR (C_6D_6, int. TMS): δ = 25.5/32.2 (s/s, 12 C/36 C, *C*Me$_3$/C*Me*$_3$). ^{29}Si{^{1}H} NMR (C_6D_6, ext. TMS): δ = 44.6 (s, 4 Si, Si*t*Bu$_3$). ^{79}Se NMR (C_6D_6, ext SeMe$_2$ in C_6D_6): δ = −322.4 (s, 4 Se). X-ray structure analysis: see Figure 4. − **(iii):** Reaction of gray selenium (Se$_x$) (0.014 g, 0.178 mmol) in 5 mL of pentane with **4** (0.107 g, 0.090 mmol) led to R*$_2$, R*H and a new substance at −30 °C in 8 h [δ(^{29}Si) = 88.56; δ(^{79}Se) = −498.3] which then decomposed at −25 °C in hours. It possibly contained molecules R*$_4$Tl$_4$Se$_4$ (**11**) structured like **9** [δ(^{79}Se) = −178.4] or **10** [δ(^{79}Se) = −322.4]. − **(iv):** From a solution of **12** (0.05 mmol) in 2 mL of heptane in the presence of traces of dry oxygen (O_2) a mixture of **7**/**12** was formed in 2 weeks as air- and moisture-sensitive violet crystals (for **12** see ref.[25]). Further oxidation of **7**/**12** leads to colorless **7**. ^{1}H NMR (C_6D_6, int. TMS): δ = 1.31 (s, 108 H, Si*t*Bu$_3$ of **7**), 1.36 (s, 108 H, Si*t*Bu$_3$ of **12**). ^{13}C{^{1}H} NMR (C_6D_6, int. TMS): δ = 24.1/32.2 (s/s, 12 C/36 C, *C*Me$_3$/C*Me*$_3$ of **7**), 25.5/32.8 (s/s, 12 C/36 C, *C*Me$_3$/C*Me*$_3$ of **12**). ^{29}Si{^{1}H} NMR (C_6D_6, ext. TMS): δ = 16.2 (s, 4 Si, Si*t*Bu$_3$ of **12**), not observed (Si*t*Bu$_3$ of **7**). X-ray structure analysis: see Figure 4. − **(v):** For synthesis of colorless R*$_4$Ga$_4$O$_4$ (**8**), see ref.[28]; X-ray analysis: see Figure 4.

X-ray Structure Determinations: Siemens P4 with an area detector for R*$_4$Al$_2$, R*$_4$Al$_4$O$_4$, R*$_4$Ga$_4$O$_4$, STOE IPDS with an area detector for R*$_4$In$_2$, R*$_4$Tl$_2$, R*$_4$In$_4$Se$_4$, R′$_4$In$_2$, R′$_4$Tl$_2$. Crystals were mounted in perfluorpolyether oil. The structures were solved by direct methods [SHELXS-97/SHELXL-97: R*$_4$Al$_2$; XS (SHELXS, version 5)/SHELXL-93: R*$_4$Al$_4$O$_4$, R*$_4$Ga$_4$O$_4$; SHELXS/SHELXL-93: R*$_4$In$_2$, R*$_4$Tl$_2$, R*$_4$In$_4$Se$_4$, R′$_4$In$_2$, R′$_4$Tl$_2$] and full matrix against F^2. All non-hydrogen atoms were refined anisotropically and H atoms were included in the refinement at calculated positions with a riding model and fixed isotropic U_i values. All *t*Bu groups of **4** were rotationally disordered; this could explain the high *R* values of the dithallane structure. The structures of the compounds that are shown in Figures 2−4, crystallographic details are summarized in Table 2. Crystallographic data (excluding structure factors) for the structures reported in this paper have been deposited with the Cambridge Crystallographic Data Centre as supplementary publications no. CCDC-163234 (R*$_4$In$_2$), -163352 (R*$_4$Tl$_2$), -163236 (R′$_4$In$_2$), -163353 (R′$_4$Tl$_2$), -163233 (R*$_4$Al$_4$O$_4$/2R*$_4$Al$_4$), -163235 (R*$_4$In$_4$Se$_4$) (for R*$_4$Al$_2$ see ref.[5], for R*$_4$Ga$_4$O$_4$ see ref.[28]). Copies can be obtained free of charge on application

Table 2. Selected parameters of the X-ray structure analyses of the compounds shown in the first line

	R*$_2$Al−AlR*$_2$ [5]	R*$_2$In−InR*$_2$	R*$_2$Tl−TlR*$_2$	R′$_2$In−InR′$_2$	R′$_2$Tl−TlR′$_2$	R*$_4$Al$_4$O$_4$ [a]	R*$_4$Ga$_4$O$_4$ [22]	R*$_4$In$_4$Se$_4$
Formula	$C_{48}H_{108}Al_2Si_4$	$C_{48}H_{108}In_2Si_4$	$C_{48}H_{108}Tl_2Si_4$	$C_{56}H_{92}In_2Si_4$	$C_{56}H_{92}Si_4Tl_2$	$C_{48}H_{108}Al_4Si_4O_4$	$C_{48}H_{108}Ga_4Si_4O_4$	$C_{48}H_{108}In_4Si_4Se_4$
M_r	851.69	1027.37	1206.49	1107.33	1286.46	969.65	1140.65	1572.85
T [K]	173	200	193	193	293	203	173	190
Mo-K_α [Å]	0.71073	0.71073	0.71073	0.71073	0.71073	0.71073	0.71073	0.71073
System	orthorhombic	monoclinic	monoclinic	triclinic	triclinic	monoclinic	trigonal	cubic
Space group	$I\bar{4}$	*C*2/*c*	*C*2/*c*	$P\bar{1}$	$P\bar{1}$	*C*2/*c*	$R3\bar{c}$	$Pa\bar{3}$
a [Å]	15.4599(1)	21.2994(9)	20.396(4)	13.108(3)	13.188(4)	23.692(1)	19.807(3)	23.701(4)
b [Å]	15.4599(1)	14.905(1)	15.437(3)	14.394(3)	13.386(5)	12.716(2)	19.807(3)	23.728(8)
c [Å]	13.204	21.539(1)	41.621(8)	19.708(4)	19.815(6)	25.109(2)	61.772(11)	23.747(6)
α [°]	90	90	90	83.52(3)	84.31(4)	90	90	89.94(4)
β [°]	90	103.189(5)	99.97(3)	80.50(3)	80.59(3)	115.901(3)	90	89.85(3)
γ [°]	90	90	90	63.23(3)	63.45	90	120	89.89(3)
V [Å^3]	3155.82(3)	6657.6(7)	12906(45)	3271.2(11)	3085.8(17)	6804.8(10)	20987.3	13355(6)
Z	2	8	8	1	2	4	12	8
ρ [Mg/m^3]	0.896	1.181	1.242	1.124	1.394	0.985	1.172	1.565
μ [mm^{-1}]	0.147	0.797	5.086	0.807	5.325	0.171	1.626	3.643
F(000)	956	2536	4912	1164	1302	2244	7922	6272
2θ [°]	3.72−58.14	5.46−54.04	4.70−54.24	3.88−51.8	5.78−55.92	3.60−55.18	2.72−58.98	4.86−48.24
Ranges	$-19 \le h \le 20$; $-20 \le k \le 20$; $-16 \le l \le 16$	$-27 \le h \le 26$; $-18 \le k \le 19$; $-27 \le l \le 27$	$-21 \le h \le 25$; $-19 \le k \le 11$; $-53 \le l \le 53$	$-12 \le h \le 16$; $-13 \le k \le 16$; $-24 \le l \le 24$	$-16 \le h \le 16$; $-16 \le k \le 17$; $-26 \le l \le 26$	$-29 \le h \le 29$; $-6 \le k \le 15$; $-32 \le l \le 32$	$-25 \le h \le 25$; $-25 \le k \le 25$; $-76 \le l \le 74$	$-24 \le h \le 27$; $-27 \le k \le 27$; $-27 \le l \le 19$
All reflections	9338	6763	25125	13569	18424	13628	39018	41507
Observed (> 4σ)	3403	6763	12448	9606	12799	6841	5157	3531
R_{int}	0.0197	0.00	0.0912	0.0545	0.0539	0.0552	0.0279	0.123
x/*y* [b]	0.9573/0.9436	0.8548/0.6605	1/1	1/1	1/1	0.1292/18.7670	0.0272/37.5392	1/1
*R*1 [c]	0.0461	0.0264	0.1044	0.0498	0.0505	0.0696	0.0284	0.0496
*wR*2 [c]	0.1519	0.0780	0.2784	0.1463	0.1154	0.2063	0.0650	0.1226
GOOF	1.304	0.968	0.976	1.063	−	1.082	1.131	0.954
Electron density [eÅ^3]: max./min.	1.513/−0.288	0.429/−0.803	4.588/−3.002	0.804/−0.738	3.172/−2.083	1.317/−0.660	0.340/−0.414	3.172/−2.083

[a] R*$_4$Al$_4$O$_4$ and R*$_4$Al$_4$ in mol ratio 1:2. [b] $w^{-1} = \sigma^2F_o^2 + (xP)^2 + yP$ with $P = (F_o^2 + 2F_c^2)/3$. [c] $F > 4\sigma(F)$.

to CCDC, 12 Union Road, Cambridge CB2 1 EZ, UK [Fax. (internat.) + 44-1223/336-033); E-mail: deposit@ccdc.cam.ac.uk].

Acknowledgments

We are grateful to the Deutsche Forschungsgemeinschaft and the Fonds of Chemische Industrie for their financial support.

[1] N. Wiberg, K. Amelunxen, H.-W. Lerner, H. Nöth, J. Knizek, I. Krossing, *Z. Naturforsch., Teil B* **1997**, *53*, 333−348.
[2] N. Wiberg, K. Amelunxen, T. Blank, H.-W. Lerner, K. Polborn, H. Nöth, R. Littger, M. Rackl, M. Schmidt-Amelunxen, H. Schwenk-Kircher, M. Warchold, *Z. Naturforsch., Teil B* **2001**, *56*, 634−651.
[3] N. Wiberg, T. Blank, H.-W. Lerner, H. Nöth, T. Habereder, D. Fenske, *Z. Naturforsch., Teil B* **2001**, *56*, 652−658.
[4] N. Wiberg, K. Amelunxen, H. Nöth, M. Schmidt, H. Schwenk, *Angew. Chem.* **1996**, *108*, 110−112; *Angew. Chem. Int. Ed. Engl.* **1996**, *35*, 65−67.
[5] N. Wiberg, K. Amelunxen, T. Blank, H. Nöth, J. Knizek, *Organometallics* **1998**, *17*, 5431−5433; N. Wiberg, T. Blank, W. Kaim, B. Schwerderski, G. Linti, *Eur. J. Inorg. Chem.* **2000**, 1475−1481; N. Wiberg, T. Blank, K. Amelunxen, H. Nöth, T. Habereder, W. Kaim, M. Wanner, *Eur. J. Inorg. Chem.* **2001**, 1719−1727 and refs. cited.
[6] N. Wiberg, T. Blank, H. Nöth, W. Ponikwar, *Angew. Chem.* **1999**, *111*, 887−890; *Angew. Chem. Int. Ed.* **1999**, *38*, 839−841; N. Wiberg, T. Blank, A. Purath, G. Stößer, H. Schnöckel, *Angew. Chem.* **1999**, *111*, 2745−2748; *Angew. Chem. Int. Ed.* **1999**, *38*, 2563−2565.
[7] N. Wiberg, T. Blank, H.-W. Lerner, D. Fenske, G. Linti, *Angew. Chem.* **2001**, *113*, 1275−1278; *Angew. Chem. Int. Ed.* **2001**, *40*, 1232−1235.
[8] M. Kehrwald, W. Köstler, A. Rodig, G. Linti, T. Blank, N. Wiberg, *Organometallics* **2001**, *20*, 860−868; N. Wiberg, T. Blank, H. Nöth, M. Suter, M. Warchhold, *Eur J. Inorg. Chem.* **2002**, in preparation; cf. also refs.[23,27]
[9] G. Linti, W. Köstler, *Angew. Chem.* **1996**, *108*, 593−595; *Angew. Chem. Int. Ed. Engl.* **1996**, *35*, 550−552.
[10] R. Wochele, W. Schwarz, K. W. Klinkhammer, K. Locke, J. Weidlein, *Z. Anorg. Allg. Chem.* **2000**, *626*, 1963−1973.
[11] S. Henkel, K. W. Klinkhammer, W. Schwarz, *Angew. Chem.* **1994**, *106*, 721−722; *Angew. Chem. Int. Ed. Engl.* **1994**, *33*, 681−683.
[12] W. Uhl, *Z. Naturforsch., Teil B* **1988**, *43*, 1113−1118.
[13] W. Uhl, M. Layh, T. Hildenbrand, *J. Organomet. Chem.* **1989**, *364*, 289−300.
[14] W. Uhl, M. Layh, W. Hiller, *J. Organomet. Chem.* **1989**, *368*, 139−153.
[15] R. J. Wehmschulte, K. Ruhlandt-Senge, M. M. Olmstead, H. Hope, B. E. Sturgeon, P. P. Power, *Inorg. Chem.* **1993**, *32*, 2983−2984.
[16] X. He, R. A. Bartlett, M. M. Olmstead, K. Ruhlandt-Senge, B. E. Sturgeon, P. P. Power, *Angew. Chem.* **1993**, *105*, 761−762; *Angew. Chem. Int. Ed. Engl.* **1993**, *32*, 717−718.
[17] P. J. Brothers, K. Hübler, B. C. Noll, M. M. Olmstead, P. P. Power, *Angew. Chem.* **1996**, *108*, 2528−2530; *Angew. Chem. Int. Ed. Engl.* **1996**, *35*, 2355−2357.
[18] R. D. Schluter, A. H. Cowley, D. A. Atwood, R. A. Jones, M. R. Bond, C. J. Carrano, *J. Am. Chem. Soc.* **1993**, *115*, 2070−2071.
[19] G. Linti, R. Frey, M. Schmidt, *Z. Naturforsch., Teil B* **1994**, *49*, 958−962.
[20] M. Veith, F. Goffing, S. Becker, V. Huch, *J. Organomet. Chem.* **1991**, *406*, 105−107.
[21] M. Veith, A. Spaniol, J. Pöhlmann, F. Gross, V. Huch, *Chem. Ber.* **1993**, *126*, 2625−2635; C. H. Galka, L. H. Gade, *Inorg. Chem.* **1999**, *38*, 1038−1039 and refs. cited; K. W. Klinkhammer, S. Henkel, *J. Organomet. Chem.* **1994**, *480*, 167−171 and refs. cited.
[22] R. Wochele, W. Schwarz, K. W. Klinkhammer, J. Weidlein, *Z. Anorg. Allg. Chem.* **2000**, *626*, 833−835.
[23] A. Donchev, A. Schnepf, G. Stößer, E. Baum, H. Schnöckel, T. Blank, N. Wiberg, *Chem. Eur. J.* **2001**, 3348−3353.
[24] A. Purath, C. Dohmeier, A. Ecker, H. Schnöckel, K. Amelunxen, T. Passler, N. Wiberg, *Organometallics* **1998**, *17*, 1894−1896.
[25] W. Uhl, R. Graupner, M. Layh, U. Schütz, *J. Organomet. Chem.* **1995**, *493*, C1−C5; W. Uhl, A. Janatschak, W. Saak, M. Kaupp, R. Wartchow, *Organometallics* **1998**, *17*, 5009−5017.
[26] W. Uhl, *Angew. Chem.* **1993**, *105*, 1449−1461; *Angew. Chem. Int. Ed. Engl.* **1993**, *32*, 1386−1398 and refs. cited; W. Uhl, *Coord. Chem. Rev.* **1997**, *163*, 1−32 and refs. cited.
[27] N. Wiberg, T. Blank, M. Westerhausen, S. Schneiderbauer, H. Schnöckel, I. Krossing, A. Schnepf, *Eur. J. Inorg. Chem.* **2002**, 351−356. In addition to $R^*_2Ga_2Cl_2$ the silyldigallanes $[(Me_3Si)_3Si]_2Ga_2Hal_2$ (Hal = Cl, Br) are known: G. Linti, W. Köstler, *Angew. Chem.* **1996**, *108*, 593−595; *Angew. Chem. Int. Ed.* **1996**, *35*, 550−552; M. Kehrwald, W. Köstler, A. Rodig, G. Linti, T. Blank, N. Wiberg, *Organometallics* **2001**, *20*, 860−868.
[28] N. Wiberg, K. Amelunxen, H.-W. Lerner, H. Nöth, W. Ponikwar, H. Schwenk, *J. Organomet. Chem.* **1999**, *574*, 246−251.
[29] G. Linti, *J. Organomet. Chem.* **1996**, *520*, 107−113.
[30] W. Uhl, M. Benter, W. Saak, *Z. Anorg. Allg. Chem.* **1998**, *624*, 1622−1628 and refs. cited.
[31] W. Uhl, R. Graupner, M. Pohlmann, S. Pohl, W. Saak, *Chem. Ber.* **1996**, *129*, 143−146 and refs. cited; W. Uhl, M. Pohlmann, *Chem. Commun.* **1998**, 451−452.
[32] Holleman-Wiberg, *Lehrbuch der Anorganischen Chemie*, 101st ed., deGruyter, Berlin, **1995**; 1st engl. ed., Academic Press, London, **2001**.
[33] N. Wiberg, K. Amelunxen, H.-W. Lerner, H. Schuster, H. Nöth, I. Krossing, M. Schmidt-Amelunxen, T. Seifert, *J. Organomet. Chem.* **1997**, *542*, 1−18.
[34] O. T. Beachley, J. C. Pazik, T. E. Glassmann, M. R. Churchill, J. C. Fettinger, R. Blom, *Organometallics* **1988**, *7*, 1051−1059.
[35] O. T. Beachley, B. Blom, M. R. Churchill, K. Faegri Jr., J. C. Fellinger, J. C. Pazik, L. Victoriano, *Organometallics* **1989**, *8*, 346−356.
[36] K. W. Klinkhammer, S. Henkel, *J. Organomet. Chem.* **1994**, *480*, 167−171.
[37] E. O. Fischer, *Angew. Chem.* **1957**, *69*, 201−205; F. A. Cotton, L. T. Reynolds, *J. Am. Chem. Soc.* **1958**, *80*, 269−274.
[38] M. Weidenbruch, H. Pesel, *Z. Naturforsch., Teil B* **1978**, *33*, 1465−1467.
[39] H.-W. Lerner, S. Scholz, M. Bolte, *Z. Anorg. Allg. Chem.* **2001**, *627*, 1638−1642.
[40] U. Wannagat, H. Niederprüm, *Chem. Ber.* **1961**, *94*, 1540−1543.
[41] Electrostatic repulsions of the E atoms in organyl- and silyldi-trielanes R_2E-ER_2 which are stronger for dialanes than for digallanes due to higher similar charges on E in the first case may result in a bond length shortening in direction Al−Al → Ga−Ga (electronegativities: C/Si/Al/Ga = 2.50/1.74/1.47/1.82[32]). On the other hand, the Si−Al/Si−Ga distances in $(tBu_2PhSi)_3E$ (2.59/2.58 Å)[3] or in R^*_2ECl (2.53/2.49 Å)[2] shorten in direction Si−Al → Si−Ga, though the electrostatic attractions of Si−E are stronger in the first case. The latter facts confirm the stated decrease of the atomic radius by going from Al (1.30 Å) to Ga (1.24 Å). The bond lengths shortening in direction X−Al → X−Ga (the same non-metal X) may be decreased, or even reversed as a consequence of decreasing electrostatic attractions of X and Al/Ga atoms in direction X−Al → X−Ga (for more electronegative partners X like halogens X−Al bonds are always shorter than X−Ga bonds; e.g. 2.16/2.25 Å in R^*_2Al-Cl R^*_2Ga-Cl[2]).

Received June 5, 2001
[I01208]

Disodium Tetrasupersilyltetragallanediide $Na_2Ga_4R^*_4$·2THF ($R^* = Si\mathit{t}Bu_3$) – Preparation of a Novel Gallium Cluster Compound via Dichlorodisupersilyldigallane $R^*_2Ga_2Cl_2$[‡]

Nils Wiberg,*[a] Thomas Blank,[a] Matthias Westerhausen,[a][‡‡] Stefan Schneiderbauer,[a][‡‡] Hansgeorg Schnöckel,[b] Ingo Krossing,[b][‡‡] and Andreas Schnepf[b][‡‡]

Keywords: Clusters / Gallium / Oligogallanes / Silicon / Sodium

Red tetragallanediide $Na_2Ga_4R^*_4$·2THF was prepared by reduction of the monogallane R^*GaCl_2·THF in heptane or the *tetrahedro*-tetragallane $R^*_4Ga_4$ in benzene/tetrahydrofuran (THF) with sodium at 100 °C. Potassium worked analogously as a reduction agent. As an intermediate of the dehalogenation of R^*GaCl_2·THF, the orange digallane $R^*_2Ga_2Cl_2$ and the dark violet tetrahedrane $R^*_4Ga_4$ were formed. The extreme air- and moisture-sensitive $Na_2Ga_4R^*_4$·2THF was stable against Me_3SiCl, but reacted with oxygen under formation of $R^*_4Ga_4$, and with GaBr under formation of several products (isolation and X-ray structure analysis of R^*GaBr_2·THF). According to X-ray structure analyses, (i) the tetragallanediide contains a nonplanar Ga_4 ring with short Ga–Ga bonds, whereby three Ga atoms on opposite sides of the ring are each connected with one of the two Na(THF) groups, (ii) the digallane is dimeric, whereby it takes the structure of As_4S_4 (exchange of As/S against Ga/Cl). The possible ways of R^*GaCl_2·THF reduction are discussed, an explanation of the structure of $Na_2Ga_4R^*_4$·2THF is given, and halides $R_nE_nHal_2$ (E = Al–Tl) are presented.

Introduction

Uncharged or negatively charged cluster compounds R_mE_n of the heavier main group III elements Al, Ga, In, Tl have – unlike such compounds with clusters of boron B[1] – only been known quite recently. In fact, the former clusters tend to disproportionate into R_3E and E (or R_2 and E). However, this process can be hindered by employing bulky substituents R.

A particularly great number of sterically overloaded, non- or negatively charged clusters R_mGa_n of gallium, the element that forms the focus of this publication, have been synthesized to date (cf. ref.[2] and references for over 30 gallium cluster compounds cited therein). For example, with supersilyl ($Si\mathit{t}Bu_3$ = R*) which we use as a bulky substituent R, the following gallium cluster compounds have hitherto been prepared: $R^*_3Ga_2^{\cdot}$,[3] $R^*_3Ga_2^-$,[3] $R^*_4Ga_3^{\cdot}$,[3] $R^*_4Ga_3^-$,[3] $R^*_4Ga_4$,[4] $R^*_6Ga_8$,[5] $R^*_6Ga_8^{2-}$,[5] $R^*_6Ga_{10}^-$,[6] $R^*_6Ga_{13}^-$,[6] $R^*_8Ga_{18}$,[2] and $R^*_8Ga_{22}$.[2] Herein, we report on the reduction of R^*GaCl_2·THF with alkali metals M. This led, via the dimeric digallane $R^*_2Ga_2Cl_2$ (**1**) and the already known[4] tetrahedrane $R^*_4Ga_4$ (**3**), to the cluster compound $Na_2Ga_4R^*_4$·2THF (**2**). This cluster **2** contains the dianion $R^*_4Ga_4^{2-}$, which, after dark-red $Tip_6Ga_4^{2-}$ (Tip = 2,4,6-*i*$Pr_3C_6H_2$)[7] and dark-red $Dis_2Ga_4^{2-}$ [Dis = 2,6-(Tip)$_2C_6H_3$],[8] represents a third tetragallanediide thus far prepared with a novel butterfly-shaped Ga_4 framework [$Tip_6Ga_4^{2-}$ contains a star-shaped Ga_4 framework, similar to the neutral, light orange Tip_6Ga_4,[7] and $Dis_2Ga_4^{2-}$ (neutral species unknown) contains a square-shaped Ga_4 framework[8]]. Dimeric $R^*_2Ga_2Cl_2$, on the other hand, is analogously structured as the already published dimeric $R_2E_2X_2$ with E/R = Ga/Si(SiMe$_3$)$_3$ [9] and In/C(SiMe$_3$)$_3$ [10] (X in each case is Cl or Br). Indeed, there have also been indications of the existence of $R^*_2E_2Hal_2$ with other main group III elements E ($R^*_2B_2Cl_2$, $R^*_2In_2Br_2$, $R^*_2Tl_2Br_2$ among others),[11] but to date no X-ray structure analyses exist from the latter compounds.

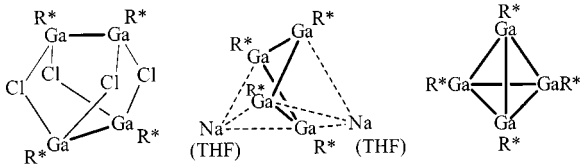

[‡] Compounds of Silicon and Homologues, 151; Compounds of Boron and Homologues, 19. – Part 150 and 17: Ref.[11]

[a] Department Chemie der Universität München, Butenandtstraße 5–13 (Haus D) 81377 München, Germany
[b] Institut für Anorganische Chemie der Universität Karlsruhe, Engesserstraße, Geb. 30.45, 76128 Karlsruhe, Germany

[‡‡] X-ray structure analyses

 © WILEY-VCH Verlag GmbH, 69451 Weinheim, Germany, 2002 1434–1948/02/0202–0351 $ 17.50+.50/0

Results and Discussion

Syntheses and Reactions of 1 and 2

As was stated in a preceding publication,[12] the reduction of R*$GaCl_2$·THF (THF = tetrahydrofuran) with sodium in heptane at 100 °C gave, according to equation (a) in Scheme 1, the violet tetrasupersilyl-*tetrahedro*-tetragallane R*$_4Ga_4$ (**3**) and an unidentified water- and oxygen-sensitive red gallium cluster compound. We have since been able to identify the red compound as $Na_2Ga_4R^*_4$·2THF (**2**) (see Scheme 1; interestingly, the reaction of homologous R*$AlCl_2$·THF with Na does not proceed in this way; see ref.[12]). As with sodium, potassium reduced R*$GaCl_2$·THF under formation of a THF adduct of $K_2Ga_4R^*_4$. After filtration of the insoluble material and exchange of heptane for benzene, the tetragallanediide slowly crystallized (in weeks) at 5 °C as red prisms that were extremely water- and oxygen-sensitive. Indeed, in the presence of traces of air the tetragallanediide was oxidized to **3** according to $R^*_4Ga_2^{2-} \leftrightarrows R^*_4Ga_4 + 2e^-$ [reverse of equation (d) in Scheme 1]. Thereby, the tetrahedrane was formed as an intermediate that itself rapidly reacted with oxygen under formation of the heterocubane $R^*_4Ga_4O_4$ [the latter hydrolyzed to R*Ga(OH)$_2$].[4] Certainly, oxidation of **2** with R*Br should quantitatively lead to **3** (ref.[3]).

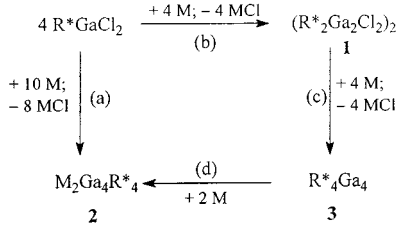

Scheme 1. Reaction of R*$GaCl_2$·THF with alkali metals M = Na, K (THF excluded for clarity; R* = Si*t*Bu_3)

Besides **3**, as a further intermediate of the reduction of R*$GaCl_2$·THF with alkali metals, the water- and oxygen-sensitive digallane $(R^*_2Ga_2Cl_2)_2$ (**1**) could be isolated as orange crystals [equation (b) in Scheme 1]. The reduction of **1** then led, by way of the tetrahedrane **3**, to the tetragallanediide **2** [equation (c) and (d) in Scheme 1]. In fact, **3** could be reduced according to equation (d) in Scheme 1 with Na in a mixture of benzene and THF at 100 °C. In this respect, the latter reaction offered another possibility for producing **2**.

Certainly, the first reaction of R*$GaCl_2$·THF with M = Na or K – leading via **1** and **3** to **2** – consists of an exchange of chlorine by M [equation (a) in Scheme 2]. Possibly, R*GaClM forms from R*$GaCl_2$·THF/Na via the radical R*GaCl$^{\cdot}$, which would then be rapidly reduced by Na. Therefore, the radical concentration would remain low, forestalling a radical dimerization. In fact, the formed gallanide R*GaClM could obviously then react with the starting material R*$GaCl_2$ under formation of **1** [equation (b) in Scheme 2] or might – more probably for steric reasons – eliminate MCl with formation of the gallylene R*Ga, which after insertion into a Ga–Cl bond of R*$GaCl_2$ would give the isolated product **1** [equations (c), (d) in Scheme 2; cf. dehalogenation of R*$SiHal_3$ (ref.[13])].

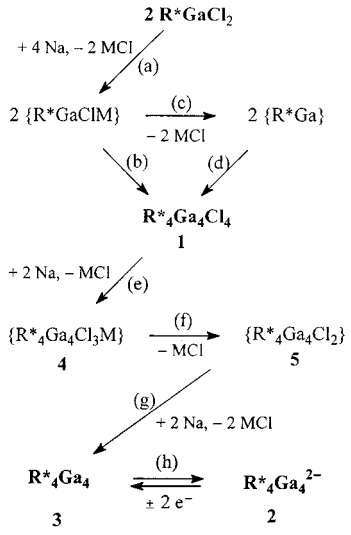

Scheme 2. Possible ways from R*$GaCl_2$·THF/Na in heptane at 100 °C, via **1** (and perhaps **4** and **5**) to **3** and its reduction product **2** (M = Na or K; R* = Si*t*Bu_3; THF excluded for clarity); bold-face formulae refer to isolated products

Further intermediates on the way from R*$GaCl_2$·THF to **3** were definitively not seen. Obviously, all these formed much more slowly from reactants than they transformed into following products. Certainly, many ways are imaginable that lead to the tetragallanediide. To our mind, the reaction of **1** with M transforms via $R^*_4Ga_4Cl_3M$ (**4**) and $R^*_4Ga_4Cl_2$ (**5**) into **3** [equations (e), (f), and (g) in Scheme 2]. A fast reduction of **3** finally gives **2** [equation (h) in Scheme 2]. In fact, compounds related to **4** and **5**, namely $R_4Ga_4I_3^-$ [R = $Si(SiMe_3)_3$][6] and $R_4In_4Br_2$ [R = $C(SiMe_3)_3$][10] could be isolated (cf. Figure 4; compound **5** might be prepared by mild chlorination of **3**).

Structures of 1, 2, and R*$GaBr_2$·THF

Figure 1 shows the structure of the molecule $Na_2Ga_4R^*_4$·2THF (**2**) in the crystal (red prisms, monoclinic, *C*2/*c*) together with selected bond lengths and angles. The central structural element of **2** is a nonplanar, butterfly-shaped Ga_4 ring with nearly equal Ga–Ga bond lengths (2.43 Å; distances of opposite Ga atoms 3.21 Å), and nearly equal Ga–Ga–Ga bond angles (82.6°) as well as Ga–Ga–Ga–Ga torsion angles (39.4°; the angle between the Ga–Ga–Ga planes amounts to 122.9°). In the course of the two-electron reduction of the tetrahedrane $R^*_4Ga_4$ (Ga–Ga distances 2.57 Å[4]) the Ga–Ga bonds shorten (by 0.14 Å on average) and the Ga_4 cluster opens. In fact, the Ga–Ga distances in **2** are comparable to the Ga–Ga bond length in R^*_2Ga–GaR* (2.43 Å), which itself relates to a bond order of 1.5 (see ref.[3]; the mean Ga–Ga distances in

Tip_6Ga_4,[7] $Tip_6Ga_4^{2-}$,[7] and $Dis_2Ga_4^{2-}$ [8] amount to 2.47, 2.39 and 2.46 Å).

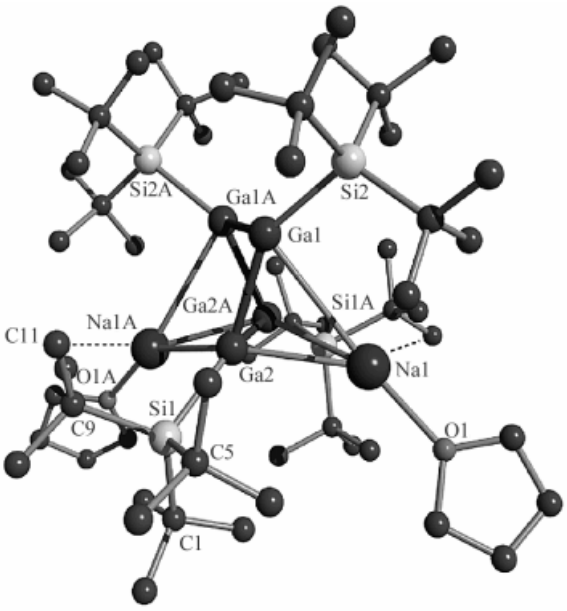

Figure 1. A view of molecule **2** (local symmetry C_2) in the crystal (H atoms excluded for clarity); the dotted line represents the (electrostatic) contacts of Na^+ with a CH_3 group of Si*t*Bu$_3$; selected bond lengths [Å] and angles [°]: Ga1−Ga1A 2.416(1), Ga1−Ga2 2.4238(6), Ga1−Si2 2.4488(9), Ga1−Na1 3.470(1), Ga1−Ga2A 3.206(1) Ga2−Si1 2.4401(8), Ga2−Ga2A 2.4530(8), Ga2−Na1 2.934(1), Ga2−Na1A 3.303, Si−C (mean value) 1.96, C11−Na1A 2.988(4), Na1−O1 2.252(3); Ga1A−Ga1−Ga2 82.98(1), Ga1A−Ga1−Si2 132.11(3), Ga2−Ga1−Si2 140.49(2), Ga1A−Ga1−Na1 106.74(3), Ga2−Ga1−Na1 56.41(3), Si2−Ga1−Na1 91.32(3), Ga1−Ga2−Si1 133.30(2), Ga1−Ga2−Ga2A 82.20(2), Si1−Ga2−Ga2A 142.99(2), Ga1−Ga2−Na1 80.11(3), Si1−Ga2−Na1 115.52(4), Ga2A−Ga2−Na1 75.03(4), Ga1−Ga2−Na1A 111.70(3), Si1−Ga2−Na1A 92.33(4), Ga2A−Ga2−Na1A 59.12(4), Na1−Ga2−Na1A 129.14(3), C−Si−C (mean value) 110.1; Ga1−Ga2−Ga2A−Ga1A 39.32, Ga2−Ga2A−Ga1A−Ga1 39.39

To explain the structure of **2**, one can assume that each Na atom transfers its s electron *entirely* to the Ga_4 cluster, which then works as a 2π-aromatic system with shortened and nearly equal Ga−Ga bonds (see Figure 2a). Obviously, the nonplanarity of the Ga_4 ring in **2** is, in this case, a consequence of steric hindrance of the four supersilyl groups with respect to each other (as a consequence of the overcrowding, **2** does not react with Me_3SiCl). Incidentally, 1,2-dihydro-1,3-diborets $R_4B_2C_2$ (R = organyl, silyl) also show a nonplanar 2π-aromatic B_2C_2 ring.[14]

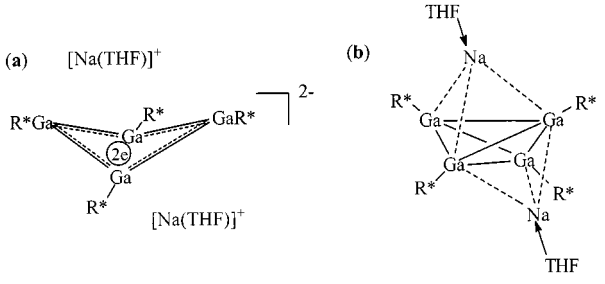

Figure 2. Illustration of the central framework of **2** (a) as a 2π-aromatic system, (b) as a twofold-capped tetrahedron

If on the other hand, each Na atom transfers its s electron only *partly* to Ga_4 in **2**, the Na_2Ga_4 framework of the molecule must be viewed as a whole. The Wade-Mingos rules (cf. ref.[1]) − which associate the number of cluster electrons with the cluster structure − predict a bicapped tetrahedron (see Figure 2b) for the Na_2Ga_4 part of **2**, according to the present $10 = 2n - 2$ cluster electrons [n = number of cluster atoms that deliver 1 electron (Na·THF) or 2 electrons (GaR*) each]. An argument for the latter description is the stability of the tetragallanediide even in pure THF [no indication of formation of independent cations $Na(THF)_n^+$]. Therefore, it might be imaginable that the reaction of **2** with GaBr results in an exchange of $Na(THF)^+$ against the "isoelectronic" Ga^+ under production of the novel gallium cluster compound $R^*_4Ga_6$ which is in great demand. In fact, **2** and GaBr transform in pentane/toluene/THF into the gallane R^*GaBr_2·THF (see below) and other products (not identified to date).

According to Figure 1, the Na atoms in **2** are each coordinated with three Ga atoms (Na−Ga distances 2.93/3.30/3.45 Å) on opposite sides of the Ga_4 ring, and in addition with the O atom of one THF molecule (Na−O distance 2.52 Å), as well as one CH_3 group of the substituents Si*t*Bu$_3$ (Na−C distance 2.99 Å). The mean values of the Si−Ga bond lengths (2.44 Å), C−Si bond lengths (1.96 Å), and C−Si−C bond angles (110.1°) are normal for supersilylated gallium cluster compounds.[2−6]

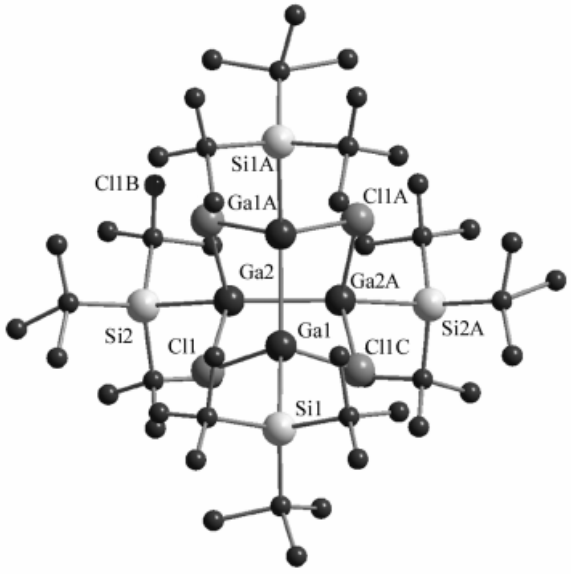

Figure 3. A view of the molecule **1** (local symmetry approx. S_4) in the crystal (H atoms excluded for clarity); selected bond lengths [Å] and angles [°]: Ga1−Ga1A/Ga2−Ga2A 2.546(3)/2.548(3), Ga1−Cl1/Ga2−Cl1 2.415(3)/2.403(3), Ga1−Si1/Ga2−Si2 2.473(4)/2.469(4), Si−C (mean value) 1.95; Cl1−Ga1−Cl1C/Cl1−Ga2−Cl1B 90.6(2)/90.6(2), Cl1−Ga1−Ga1A/Cl1−Ga2−Ga2A 100.38(9)/100.58(9), Ga1−Cl1−Ga2 101.72(10), Cl1−Ga1−Si1/Cl1−Ga2−Si2 104.96(9)/104.46(9), Si1−Ga1−Ga1A/Si2−Ga2−Ga2A 143.64(9)/144.07(9), C−Si−C (mean value) 112.0, C−Si−Ga (mean value) 106.8

Figure 3 shows the structure of the molecule $R^*_4Ga_4Cl_4$ (**1**) together with selected bond lengths and angles. Hereafter, dichlorodisupersilyldigallane $R^*_2Ga_2Cl_2$ represents a dimer, whereby the central Ga_4Cl_4 framework is structured analogously to As_4S_4 [1] [exchange of As/S by Ga/Cl; $(HGa)_4Cl_4$ is isoelectronic with As_4S_4]. The Ga atoms are distorted-tetrahedrally coordinated by Si, Ga, and 2Cl (angles Si−Ga−Cl/Si−Ga−Ga/Cl−Ga−Ga/Cl−Ga−Cl ca. 105/144/100/90°). The Cl atoms are two-coordinated by 2Ga (angle Ga−Cl−Ga ca. 102°). The two $R^*Cl_2Ga-GaCl_2R^*$ moieties show eclipsed conformations.

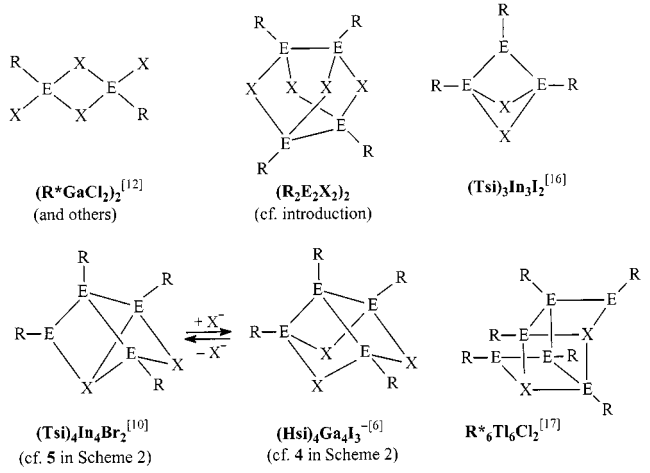

Figure 4. Examples of dihalides with the formulae $R_nE_nX_2$ [R = Si*t*Bu$_3$ (R*), Si(SiMe$_3$)$_3$ (Hsi), C(SiMe$_3$)$_3$ (Tsi); E = Al−Tl; X = halogen] and their adducts with halides [e.g. REX_3^-,[8] $R_2E_2X_4^{2-}$,[8] and $R_4E_4X_3^-$ (see above)[8]]; for monohalides $R_{n-1}E_nX$ with n = 1, 2, 3 see refs.[11,12,17]

The Ga−Ga distances in **1** (2.55 Å) are longer than those in the hitherto studied digallanes R_4Ga_2, $R_2Ga_2Hal_2$ (monomer or dimer), $R_2Ga_2Hal_4^{2-}$, $R_2Ga_2Hal_2$·2D (D = ethers, amines, phosphanes), and $Ga_2Hal_6^{2-}$ (2.39 to 2.54 Å).[3] Thereby, the Ga−Ga bond lengths shorten by going from $R^*_4Ga_4Cl_4$ [2.55 Å; R* = supersilyl Si(CMe$_3$)$_3$] to the analogously structured $R_4Ga_4Cl_4$ [2.50 Å; R = hypersilyl Si(SiMe$_3$)$_3$][9] due to steric effects. Certainly, the size of the supersilyl groups is not sufficient to prevent a dimerization of $R^*_2Ga_2Cl_2$, as is true for $Mes^*_2Ga_2Cl_2$ (Mes* = supermesityl = 2,4,6-*t*Bu$_3$C$_6$H$_2$),[15] but obviously it hinders the transformation of **1** into an adduct $R^*_2Ga_2Cl_2$·2THF in the presence of THF. The Ga−Cl distances in **1** (2.42 Å) are significantly longer than those in dimeric R^*GaCl_2 (2.18 to 2.39 Å) or monomeric R^*_2GaCl (2.25 Å).[12]

Indeed, dimeric **1** represents one member of compounds of formulae $R^*_nGa_2Cl_{4-n}$ or more generally, $R_nGa_2Hal_{4-n}$ with n = 2. Among the other members, $R^*_3Ga_2Cl$ (n = 3) is possibly obtained as the product of chlorination of the radical $R^*_3Ga_2^{\cdot}$,[3] whereas $R^*_4Ga_2$ (n = 4) loses R* and exists only as radical $R^*_3Ga_2^{\cdot}$.[11] The digallanes $R^*Ga_2Cl_3$ (n = 1) and Ga_2Cl_4 (n = 0) are unknown to date. Certainly, Ga_2Cl_4, with a structure like **1** (exchange of R* with Cl, e.g. by reaction of **1** with HCl in alkanes at low temperatures) is isomeric to the long-known $Ga^+GaCl_4^-$.[1]

On the other hand, $R^*_2Ga_2Cl_2$ represents one homologue of compounds of formulae $R^*_nGa_nCl_2$, or more generally, $R_nE_nHal_2$ (E = triel = element of the third main group), that are themselves halogen derivatives, $R^*_{n+2-m}E_nHal_m$, of compounds with the general formulae $R^*_{n+2}E_n$ (m = 0). Figure 4 shows some examples of $R_nE_nHal_2$ and their ad-

Table 1. Selected parameters from the X-ray structure analyses of $Na_2Ga_4R^*_4$·2THF (**2**), $(R^*_2Ga_2Cl_2)_2$ (**1**), and R^*GaBr_2·THF

	$Na_2Ga_4R^*_4$·2THF (**2**)	$(R^*_2Ga_2Cl_2)_2$ (**1**)	R^*GaBr_2·THF
Empirical formula	$C_{56}H_{124}Ga_4Na_2O_2Si_4$	$C_{48}H_{108}Cl_4Ga_4Si_4$	$C_{16}H_{35}Br_2OSi$
M_r	1266.84	1218.43	501.07
Crystal size [mm]	0.1 × 0.2 × 0.2	0.25 × 0.2 × 0.2	0.3 × 0.5 × 0.5
System	monoclinic	orthorhombic	orthorhombic
Space group	*C*2/*c*	*Cmcm*	*Pbca*
a [Å]	24.274(5)	23.855(7)	13.784(3)
b [Å]	12.863(3)	13.654(3)	13.301(3)
c [Å]	24.683(5)	23.814(5)	24.049(5)
β [°]	116.62(3)	90.00	90.00
V [Å^3]	6890(3)	7757(3)	4409(2)
Z	4	4	8
D [mg m^{-3}]	1.217	1.074	1.510
F(000)	2696	2660	2032
μ [mm^{-1}]	1.664	1.599	4.926
2θ [°]	4.48−52.00	8.58−52.04	4.58−51.88
Refl. collected	15373	20584	28425
indep. (R_{int})	6453 (0.0312)	3938 (0.0936)	4289 (0.0000)
obsd. [F>4σ(F)]	4957	2489	2347
GOOF	0.917	1.075	0.745
h,*k*,*l* ranges	$-29 \le h \le 26$	$-29 \le h \le 29$	$0 \le h \le 16$
	$0 \le k \le 15$	$-16 \le k \le 16$	$0 \le k \le 16$
	$0 \le l \le 30$	$-29 \le l \le 29$	$-29 \le l \le 0$
*R*1 [F>4σ(F)]	0.0326	0.0994	0.0393
*wR*2 (all data)	0.0778	0.2777	0.0931
max./min. diff peak [e·Å^{-3}]	0.524/−0.429	1.306/−0.824	1.020/−0.869

ducts with halogenides, the structures of which are known (obviously, the Ga atoms in $R_nE_nHal_2$ try to obtain the coordination number 4 by forming inter- or intramolecular halogen bridges).

The molecule R*$GaBr_2$·THF, which was obtained as one of the products of the reaction of **2** with GaBr (see above), but has already been synthesized by reaction of $GaBr_3$ with NaR* in THF[12] is analogously structured as the other donor adducts R*$EHal_2$·D (E = B to Tl),[12] and shows a distorted tetrahedral coordination of Ga with one Si atom (from R*), two Cl atoms, and one O atom (from THF). For bond lengths and angles of dibromosupersilylgallane−tetrahydrofuran(1:1), the structure of which is not discussed in detail, see ref.[18]. Further data can be found in Table 1.

Experimental Section

General: All experiments were performed under purified nitrogen or in vacuo, using Schlenk techniques. Available for use were: Na, K, C_6D_6, C_4D_8O, Me_3SiCl, and the solvents heptane, benzene, and tetrahydrofuran. The following compounds were synthesized according to literature procedures: R*$GaCl_2$·THF,[12] and R*$_4Ga_4$ (**3**).[4] For NMR spectra a Jeol GSX-270 and Jeol EX-400 were available. The ^{29}Si NMR spectra were recorded with the INEPT or DEPT pulse sequence using empirically optimized parameters for the mentioned groups.

Synthesis of the THF Adducts of $M_2Ga_4R^*_4$ (M = Na, K). − (i): 0.402 g (0.975 mmol) of R*$GaCl_2$·THF and 1.00 g (43.5 mmol) of Na were heated for 7 h in 20 mL of heptane at 100 °C. According to NMR (C_6D_6), the reaction mixture (now red) then contained compound **2**. After filtration of the heptane-insoluble materials, evaporation of volatile products under an oil-pump vacuum, and dissolution of the residue in 5 mL of benzene, 0.080 g (0.06 mmol; 26%) of disodium tetrasupersilyltetragallanediide−tetrahydrofuran(1:2) (**2**) was obtained in 8 weeks at 5 °C as water- and oxygen-sensitive, red prisms. ^{1}H NMR (C_6D_6, int. TMS): δ = 1.47 (broad, 4 Si, Si*t*Bu_3), 1.32/3.40 (m/m, 8 H/8 H, CH_2/CH_2O). ^{13}C{^{1}H} NMR (C_6D_6, int. TMS): δ = 23.1/25.2 (s/s, 6 C/6 C, *C*Me_3/*C*Me_3), 30.2/34.4 (s/s, 18 C/18 C, C*Me*$_3$/C*Me*$_3$), 25.5/67.9 (s/s, 8 H/8 H, CH_2/CH_2O). ^{29}Si{^{1}H} NMR (C_6D_6, ext. TMS): δ = 40.7/48.6 (s/s, 2 Si/2 Si, Si*t*Bu_3/Si*t*Bu_3). X-ray structure analysis: see Figure 1. Remarks: a) The insoluble material of the reaction mixture consists of **3**, among others; identification by comparison with an authentic sample[4]. It was separable from insoluble Na and NaCl by dissolving it in 10 mL of THF (see ref.[12]). b) After dissolving 0.015 g (0.01 mmol) of **2** in 0.5 mL of [D_8]THF, no changes in color or NMR spectra were observed. − **(ii):** Heating of **3** (0.095 g, 0.88 mmol) and 0.005 g (0.218 mmol) of Na in 0.4 mL of C_6D_6/0.1 mL of THF for 2 h at 100 °C led − according to NMR − exclusively to the formation of **2**. For characterization see above. − **(iii):** The reaction of R*$GaCl_2$·THF with K in heptane at 100 °C (cf. reaction with Na, above) led to a solution, in 7 h, containing a substance that was probably a THF adduct of dipotassium tetrasupersilyltetragallanediide $K_2Ga_4R^*_4$. The ^{1}H, ^{13}C, and ^{29}Si NMR shifts of this substance were identical with those for **2** (see above).

Reactions of the THF Adducts of $M_2Ga_4R^*_4$ (M = Na, K). − (i): Red **2** (0.015 g, 0.01 mmol) in 0.5 mL of C_6D_6 reacted with traces of oxygen, in the first instance under formation of the violet tetrahedrane **3**, which then transformed into the colorless heterocubane R*$_4Ga_4O_4$ (identification of the products by comparison with authentic samples[4]). Obviously, the same is valid for the THF adduct of $K_2Ga_4R^*_4$. − **(ii):** Chlorotrimethylsilane (Me_3SiCl) did not react with **2** in benzene even at 100 °C. − **(iii):** Gallium monobromide (GaBr)[19] (0.9 mmol) in 3 mL of toluene/1 mL of THF was added to 0.4 mmol of **2** in 20 mL of heptane at −78 °C. After warming the solution to room temperature, and evaporation of volatile products under an oil-pump vacuum, a dark brown residue was obtained. Extraction of the latter with pentane gave a metallic residue (Ga) and a violet solution that contained several compounds, according to NMR. Colorless crystals of dibromosupersilylgallane−tetrahydrofuran(1:1) R*$GaBr_2$·THF (identified by comparison with an authentic sample[12] and by X-ray structure analysis) were obtained from the pentane extract. Obviously, the solution contains in addition, violet tetrasupersilyl-*tetrahedro*-tetragallane (**3**) among others.

Synthesis of Dimeric $R^*_2Ga_2Cl_2$ (1): R*$GaCl_2$·THF (0.514 g, 1.247 mmol) and 1.50 g (38.4 mmol) of K were heated for 2 h in 40 mL of heptane at 100 °C. According to NMR, the solution then contained **1** (besides small amounts of R*$GaCl_2$·THF and the THF adduct of $K_2Ga_4R^*_4$). After filtration of the insoluble materials (K and KCl), evaporation of the volatile products under an oil-pump vacuum, and dissolution of the residue in 8 mL of heptane, 0.09 g (0.07 mol; 28%) of the dimeric dichlorotetrasupersilyldigallane $R^*_2Ga_2Cl_2$ (**1**) was obtained in 6 weeks at −25 °C as water- and oxygen-sensitive orange crystals. ^{1}H NMR (C_6D_6, int. TMS): δ = 1.346 (s, 108 H, Si*t*Bu_3). ^{13}C{^{1}H} NMR (C_6D_6, int. TMS): δ = 25.2/32.6 (s/s, 12 C/36 C, *C*Me_3/C*Me*$_3$). ^{29}Si{^{1}H} NMR (C_6D_6, ext. TMS): δ = 30.9 (s, 4 Si, Si*t*Bu_3). X-ray structure analysis: see Figure 3. Remarks: The ^{29}Si NMR signal at δ = 30.9 was also observed, besides signals for R*$GaCl_2$·THF and for **2** by way of the reaction of R*$GaCl_2$·THF with Na in heptane at 100 °C after 30 min. Consequently, **1** was also intermediately formed during the reduction of R^*_2GaCl·THF with Na.

X-ray Structure Determinations: Data collections were performed using Mo-K_α radiation with a STOE IPDS diffractometer at T = 200 K (**2**, R*$GaBr_2$·THF) or with a Siemens SMART diffractometer at 193 K (**1**). Structures were solved with direct methods. Refinement was with full matrix on F^2. All non-hydrogen atoms were included as riding models with fixed isotropic U values in the final refinement. Due to high thermal motion and disordering within the Si*t*Bu_3 substituents only a rather poor-quality X-ray structure determination of **1** was achieved. For further data, see Table 1. Crystallographic data (excluding structure factors) for the structures reported have been deposited with the Cambridge Crystallographic Data Centre as supplementary publication no. CCDC-165315 (**2**), -167434 (**1**), and -167745 (R*$GaBr_2$·THF). Copies of the data can be obtained free of charge on application to CCDC, 12 Union Road, Cambridge, CB2 1EZ, UK [Fax: (internat.) + 44-1223/336-033; E-mail: deposit@ccdc.cam.ac.uk].

Acknowledgments

We are grateful to the Deutsche Forschungsgemeinschaft and the Fonds der Chemischen Industrie for generous financial support.

[1] See textbooks of Inorganic Chemistry.
[2] A. Donchev, A. Schnepf, G. Stößer, E. Baum, H. Schnöckel, T. Blank, N. Wiberg, *Chem. Eur. J.* **2001**, 3348−3353.
[3] N. Wiberg, T. Blank, K. Amelunxen, H. Nöth, J. Knizek, T. Habereder, W. Kaim, M. Wanner, *Eur. J. Inorg. Chem.* **2001**, 1719−1727.

[4] N. Wiberg, K. Amelunxen, H.-W. Lerner, H. Nöth, W. Ponikwar, H. Schwenk, *J. Organomet. Chem.* **1999**, *574*, 246−251.
[5] N. Wiberg, T. Blank, H. Nöth, M. Suter, M. Warchhold, *Eur. J. Inorg. Chem.*, in press.
[6] M. Kehrwald, W. Köstler, A. Rodig, G. Linti, T. Blank, N. Wiberg, *Organometallics* **2001**, *20*, 860−867.
[7] R. J. Wehmschulte, P. P. Power, *Angew. Chem.* **1998**, *110*, 3344−3346; *Angew. Chem. Int. Ed.* **1998**, *37*, 3152−3154.
[8] B. Twamley, P. P. Power, *Angew. Chem.* **2000**, *112*, 3643−3646; *Angew. Chem. Int. Ed.* **2000**, *39*, 3500−3503.
[9] A. Schnepf, E. Weckert, G. Linti, H. Schnöckel, *Angew. Chem.* **1999**, *111*, 3578−3581; *Angew. Chem. Int. Ed.* **1999**, *38*, 3381−3383; G. Linti, W. Köstler, *Angew. Chem.* **1996**, *108*, 593−595; *Angew. Chem. Int. Ed. Engl.* **1996**, *35*, 550−552.
[10] W. Uhl, S. Melle, *Chem. Eur. J.* **2001**, *7*, 4216−4221.
[11] N. Wiberg, T. Blank, K. Amelunxen, H. Nöth, H. Schnöckel, E. Baum, A. Purath, D. Fenske, *Eur. J. Inorg. Chem.* **2001**, 341−350.
[12] N. Wiberg, K. Amelunxen, H.-W. Lerner, H. Nöth, J. Knizek, I. Krossing, *Z. Naturforsch., Teil B* **1998**, *53*, 333−348; N. Wiberg, K. Amelunxen, T. Blank, H.-W. Lerner, K. Polborn, H. Nöth, R. Littger, M. Rackl, M. Schmidt-Amelunxen, H. Schwenk-Kircher, M. Warchhold, *Z. Naturforsch., Teil B*, **2001**, *56*, 634−651.
[13] N. Wiberg, W. Niedermayer, *J. Organomet. Chem.* **2001**, *628*, 57−64.
[14] M. Hildenbrand, H. Pritzkow, W. Siebert, *Angew. Chem.* **1985**, *97*, 769−770; *Angew. Chem. Int. Ed. Engl.* **1985**, *24*, 759−760.
[15] A. H. Cowley, A. Decken, C. A. Olazabal, *J. Organomet. Chem.* **1996**, *524*, 271−273.
[16] W. Uhl, S. Melle, G. Geiseler, K. Harms, *Organometallics* **2001**, *20*, 3355−3357.
[17] N. Wiberg, T. Blank, H.-W. Lerner, D. Fenske, G. Linti, *Angew. Chem.* **2001**, *113*, 1275−1278; *Angew. Chem. Int. Ed.* **2001**, *40*, 1232−1235.
[18] Bond lengths [Å] and angles [°] of R*GaBr$_2$·THF: Ga−O 2.027(3), Ga−Br 2.360(1), Ga−Si 2.426(1), Si−C (mean value) 1.93; O−Ga−Br 98.10(10)/98.32(9), Br−Ga−Br 105.55(3), O−Ga−Si 114.32(9), Br−Ga−Si 118.88(4)/118.08(4), C−Si−C (mean value) 112.1.
[19] C. Dohmeier, D. Loos, H. Schnöckel, *Angew. Chem.* **1996**, *108*, 141−161; *Angew. Chem. Int. Ed. Engl.* **1996**, *35*, 129−149.

Received August 8, 2001
[I01302]

The Construction of (Salophen)ruthenium(II) Assemblies Using Axial Coordination

Kelly Chichak,[a] Ulrich Jacquemard,[a] and Neil R. Branda*[a,b]

Keywords: Axial coordination / N,O ligands / Ruthenium / Schiff bases / Supramolecular chemistry

Mononuclear and binuclear carbonylruthenium(II) complexes with N_2O_2 Schiff base ligands based on 3,5-di-*tert*-butylsalicylaldehyde and three different *ortho*-diamines have been prepared. The mononuclear Ru(BSP)(CO) [BSP = *N*,*N*′-bis(3,5-di-*tert*-butylsalicylidene)-1,2-phenylenediamine] complex **4** acts as a versatile supramolecular synthon, as illustrated by the fact that it spontaneously forms linear and three-dimensional assemblies through axial coordination with pyridyl Lewis bases. Using this motif, neutral and charged assemblies **6**, **9**, and **12** were prepared. The versatility of the salophen ligand was highlighted by the preparation of bimetallic carbonylruthenium(II) compounds **14**–**17** from 1,2,4,5-tetraaminobenzene and 2,3,7,8-tetraaminodibenzo-[1,4]dioxin. The bimetallic complexes were isolated as a mixture of *cis* and *trans* diastereomers with respect to the spatial relationship between the two axially bound carbon monoxide ligands. The electronic spectral and electrochemical properties of the pyridyl adducts **5**, **15**, and **17** were compared. The properties of **17** closely resembled **5** due to the insulating effect of the extended central tetraamino fragment, while **15** behaved as a single, novel chromophore. The electrochemical studies revealed that the central tetraamino linker regulates the communication between the two metal centers of **15** and **17**. It was found that the two metal atoms of **15** sense each other to a larger extent than those of **17**.

Introduction

The use of vacant axial coordination sites on metalloporphyrins in conjunction with substituted pyridines in order to create supramolecular assemblies with well-defined architectures and novel properties has been well exploited and extensively documented.[1] The construction of more elaborate porphyrin-based assemblies would provide access to new materials with tunable optical and electrochemical properties, suitable for modeling photosynthetic functions such as energy capture and transfer reactions, as well as new photonic devices such as solar cells and gated molecular circuitry.[2] However, there are significant shortcomings when substituted porphyrins are used. The syntheses tend to give low yields and it is tedious to isolate and purify the macrocycles, making the "design-to-realization" period for the highly functionalized porphyrin building blocks lengthy. Alternative molecular platforms that provide free binding sites suitable for axial coordination, which are more conducive to convenient synthesis, modification and isolation need to be explored.

Metallosalens **1** [salen = *N*,*N*′-bis(salicylidene)ethylenediamine] and metallosalophens **2** [salenophen = *N*,*N*′-bis(salicylidene)-1,2-phenylenediamine] have received little attention as sources of planar supramolecular building blocks. These tetravalent ligands are particularly attractive for several reasons: 1) they are conveniently prepared in a single synthetic step by condensing substituted *ortho*-diamines with salicylaldehyde, and as a result, can be readily tailored by modifying the substituents on the diamine synthon; 2) they form stable coordination compounds with a wide variety of metal ions, which can be easily isolated; 3) if the appropriate metal ion is inserted into the ligands, the resulting complexes display accessible axial Lewis-acidic sites. Despite this appeal, we are aware of only one report describing the use of metallosalens or metallosalophens in the construction of multicomponent supramolecular assemblies through axial coordination. In this report, the authors describe how 4,4′-bipyridine axially coordinates to two methyl(salen)cobalt(III) complexes to produce a linear three-component assembly.[3]

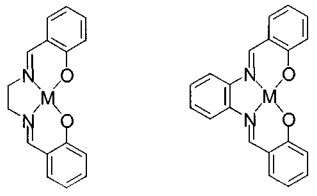

1 **2**

Our recent success in constructing multicomponent assemblies using axial coordination to (porphyrin)ruthenium-

[a] Department of Chemistry, University of Alberta, Edmonton, Alberta, T6G 2G2, Canada
[b] Current address: Department of Chemistry, Simon Fraser University
8888 University Drive, Burnaby, B. C., V5A 1S6, Canada
Fax: (internat.) + 1-604/291-3765
E-mail: nbranda@sfu.ca

 © WILEY-VCH Verlag GmbH, 69451 Weinheim, Germany, 2002 1434–1948/02/0202–0357 $ 17.50+.50/0

(II) synthons[4] prompted us to evaluate the versatility of the (salophen)ruthenium(II) analogues in supramolecular chemistry. The reported examples of axial coordination to carbonyl(salen)ruthenium(II) and carbonyl(salophen)ruthenium(II) complexes are limited in their scope and have certainly not been given the same degree of attention as their porphyrin counterparts. Here, we describe the application of the Ru(BSP)(CO) building block **4** [BSP = *N*,*N*′-bis(3,5-di-*tert*-butylsalicylidene)-1,2-phenylenediamine] in the generation of supramolecular linear and three-dimensional assemblies **6**, **9**, and **12**. The syntheses and characterization of bis(metallosalophen) complexes **14**−**17** are also reported.

Results and Discussion

Synthesis of the (Salophen)ruthenium(II) Building Block

In an early report involving metal−carbonyl insertion into salens, Calderazzo and co-workers describe the reaction of the unsubstituted ligand **1** (M = 2 H) with $Ru_3(CO)_{12}$ to produce a metallosalen dimer in high yield.[5] Owing to the insolubility of this dimeric product, it was characterized primarily using elemental analysis techniques, which gave the correct 1:1 metal-to-ligand stoichiometry for the coordination compound but not its three-dimensional structure. The authors postulated that the dimer is held together through axial coordination to the ruthenium center of each monomer by one of the Lewis basic oxygen atoms of the other. This claim was based on the fact that analogous iron(III) coordination compounds have been characterized in the solid state. In a later report, Farrell and co-workers described how the [Ru(**1**)(CO)]$_2$ dimer can be broken into its monomeric fragments only when heated in pyridine, where it dissociates to yield the pyridine-coordinated metallosalen monomer Ru(CO)(py)(salen).[6] Khan and co-workers described an alternative, milder approach to metal−carbonyl insertion, whereby a variety of chloro- and methoxy-substituted salens and salophens were treated with $Cs_2[RuCl_4(CO)(H_2O)]$.[7] To the best of our knowledge, the axial coordinating behavior of these chloro- and methoxy-substituted ruthenium(II) Schiff base complexes has not been reported.

In light of the dimerization product described by Calderazzo and Farrell, and the less than satisfactory structural and binding information on the reported metallo-Schiff base complexes, we sought a more soluble salophen ligand that is amenable to facile characterization in self-assembly processes. We chose *N*,*N*′-bis(3,5-di-*tert*-butylsalicylidene)-1,2-phenylenediamine (**3**) which precipitates as a yellow solid when 3,5-di-*tert*-butylsalicylaldehyde and 1,2-diaminobenzene are condensed in hot ethanol.[8] Metal insertion was accomplished by heating ligand **3** with an excess of $Ru_3(CO)_{12}$ in toluene (Scheme 1). Ru(BSP)(CO) (**4**) was isolated as a burgundy air-stable solid by a combination of column chromatography through activated alumina and recrystallization from aqueous ethanol. The isolation of **4** as a monomer was first suggested by the absence of signals in the positive ion ES mass spectrum, corresponding to higher aggregates or multiply charged species, and then by the ease of forming axially coordinated supramolecular assemblies (see later). In addition to peaks corresponding to the parent ion (*m*/*z* = 668) and the loss of carbon monoxide (*m*/*z* = 640), the ES mass spectrum of a nitromethane solution of **4** contains peaks corresponding to the hydrated (*m*/*z* = 686) and solvated (*m*/*z* = 729 for $[M + CH_3NO_2]^+$) coordination compounds. We are assuming that the molecule of the solvent (CH_3NO_2 or H_2O) most likely occupies the axial site on the metal center. Clearly, the presence of the bulky *tert*-butyl substituents on the salophen ligand inhibits the dimerization of Ru(BSP)(CO) (**4**). Similar results have been reported for the zinc analogues of these types of coordination compounds.[9] Computer-assisted molecular modeling of **4** reveals that the sterically demanding *tert*-butyl substituents prevent the metallosalophens from approaching each other, thus inhibiting the formation of an analogous dimer to that originally reported by Calderazzo.

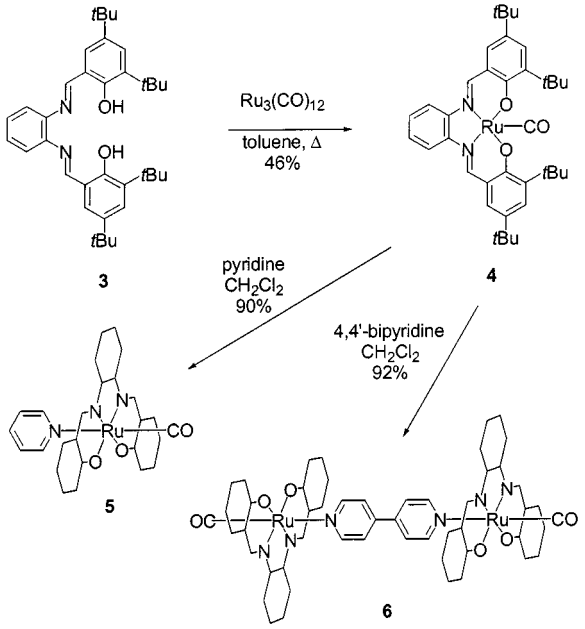

Scheme 1

The pyridine adduct Ru(BSP)(CO)(py) (**5**) was constructed when **4** was treated with an excess of pyridine in dichloromethane at room temperature. Compound **5** was isolated as a purple solid, by filtering the solution through silica gel which effectively removed any unchanged **4** as the pyridyl adduct is the only compound that elutes with CH_2Cl_2. The formation of **5** is confirmed by the upfield shifts ($\Delta\delta$ = −0.6 to −0.1) of the signals for the protons on the coordinated pyridine because these protons lie within the shielding regions of the aromatic rings of the salophen (Table 1). The generation of **5** using such mild conditions clearly indicates that, although the bulkiness of the *tert*-butyl substituents inhibits the dimerization of **4**, they do not impede the approach of Lewis bases such as pyridine towards the metal center. The ES mass spectrum

Table 1. Selected ^{1}H NMR spectroscopic data of the pyridyl-coordinated metallosalophen assemblies prepared in this study

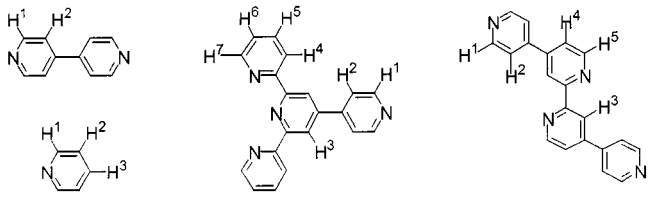

Compound	δ (Δδ)[a]						
	H^1	H^2	H^3	H^4	H^5	H^6	H^7
5[b]	8.12 (−0.46)	7.09 (−0.18)	7.59 (−0.10)				
6[b]	8.19 (−0.52)	7.16 (−0.40)					
9a[c]	8.48 (−0.48)	8.16 (−0.13)	9.39 (−0.17)	7.63 (−0.20)	8.00 (−0.13)	7.21 (−0.15)	8.91 (−0.17)
9b[c]	8.53 (−0.47)	8.27 (−0.12)	9.55 (−0.20)	7.38 (−0.21)	7.95 (−0.13)	7.11 (−0.15)	8.27 (−0.12)
12a[c]	8.23 (−0.79)	7.58 (−0.66)	9.04 (−0.49)	7.45 (−0.62)	7.88 (−0.58)		
12b[c]	8.24 (−0.56)	7.59 (−0.33)	9.03 (−0.52)	7.56 (−0.47)	7.54 (−0.58)		
15[b] [d]	8.20 (−0.38)	7.16 (−0.11)	7.64 (−0.05)				
17[b] [d]	8.16 (−0.42)	7.14 (−0.13)	7.63 (−0.06)				

[a] Upfield shifts of the signals for the protons in the assemblies relative to those in free pyridine for assemblies **5**, **15 (*cis*)** and **15 (*trans*)**, and **17 (*cis*)** and **17 (*trans*)**, 4,4′-bipyridine for assembly **6**, complex **7** for assembly **9a**, tetrapyridine **8** for assembly **9b**, complex **10** for assembly **12a**, and tetrapyridine **11** for assembly **12b**. [b] In CH_2Cl_2. [c] In [D_6]acetone. [d] As a mixture of both *cis*- and *trans*-isomers.

of **5** shows a peak for the parent ion (m/z = 747), as well as peaks corresponding to the exchange of pyridine with a nitromethane solvent molecule (m/z = 729), to the loss of pyridine (m/z = 668) and to the loss of both axial ligands (m/z = 640). The intense band for $\tilde{\nu}$(CO) in the IR spectrum of **5** is shifted to a higher frequency (1944 cm^{-1}) than that for **4** (1931 cm^{-1}), as is expected for the strengthening of the CO bond on addition of a π-acid.[10] The magnitude of this shift is comparable with that reported for the $\tilde{\nu}$(CO) of the metallosalen **1** [M = Ru(CO)], as the [Ru(**1**)(CO)]$_2$ dimer is converted into its pyridine adduct.[6]

Construction of Neutral Assemblies

The use of the novel metallosalophen **4** as a supramolecular synthon was studied using ^{1}H NMR spectroscopy and then by the isolation of several air-stable multicomponent assemblies. A linear trimeric assembly [Ru(BSP)(CO)]$_2$(4,4′-bpy) (**6**) was prepared by treating a dichloromethane solution of 4,4′-bipyridine with 2.2 equiv. of Ru(BSP)(CO) (**4**) in the same solvent (Scheme 1). The ^{1}H NMR spectrum of **6**, whether generated in situ or isolated as described for **5**, shows the expected upfield shifts for the signals assigned to the protons of the coordinated 4,4′-bipyridine fragment (Figure 1 and Table 1). Our studies reveal that ligand exchange is slow on the NMR timescale and sharp peaks, that do not change, of the statistical mixture of mono- and di-addition products are visible when 1.0 mol-equiv. of **4** is added (Figure 1). The ES mass spectrum of **6** exhibits a parent ion peak (m/z = 1492), as well as a peak (m/z = 824) corresponding to the loss of one metallosalophen. The spectrum also contains peaks that correspond to the fragmentation of the metallosalophen as previously seen for **4** and **5**. The IR spectrum of toluene solutions of **6** exhibits an intense band for $\tilde{\nu}$(CO) at 1947 cm^{-1}.

Construction of Charged Assemblies

Metallosalophen assemblies incorporating coordination compounds as the central fragments were also prepared (Scheme 2). Addition of 2.0 mol-equiv. of Ru(BSP)(CO) (**4**) to the bis[4′-(4′′′-pyridyl)-2,2′:6′,2′′-terpyridine]ruthenium complex **7**[11] in acetone afforded the triad **9a**, which was isolated as a purple solid by precipitation with pentane. The iron analogue **9b** was readily synthesized from its simplest building blocks in a single self-assembly process, when equal parts of 4′-(4′′′-pyridyl)-2,2′:6′,2′′-terpyridine (**8**)[12] and Ru(BSP)(CO) (**4**) were added to an acetone solution containing 0.5 mol-equiv. of Fe(BF$_4$)$_2$(H$_2$O)$_6$. The ES mass spectra of both **9a** and **9b** each show parent ion peaks (m/z = 1028 for [M − 2 PF$_6$]$^{2+}$ and 1006 for [M − 2 BF$_4$]$^{2+}$), as well as peaks corresponding to the loss of one metallosalophen (m/z = 695 for [M − **4** − 2 PF$_6$]$^{2+}$ and 672 for [M − **4** − 2 BF$_4$]$^{2+}$). The IR spectrum for **9a** and

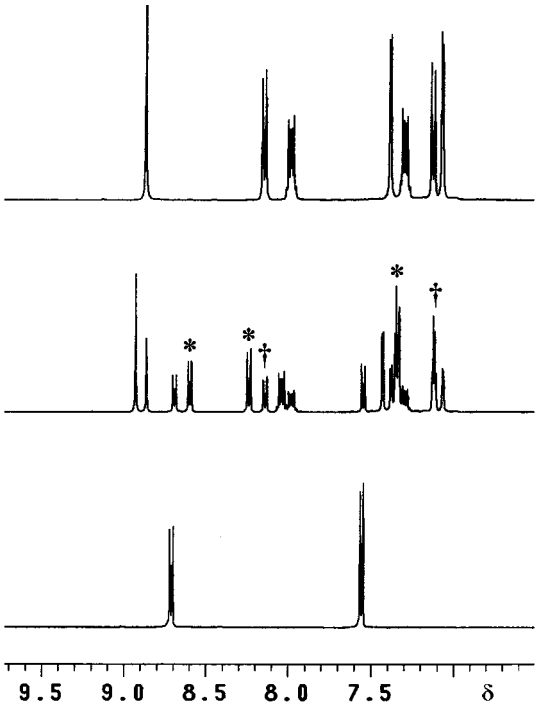

Figure 1. ^{1}H NMR (300 MHz) spectra of 4,4′-bipyridine (bottom trace), **4** + 1.0 equiv. of 4,4′-bipyridine (center trace), and **4** + 0.5 equiv. of 4,4′-bipyridine (top trace); signals corresponding to the protons of 4,4′-bipyridine for both the mono- (*) and the di-coordination (†) assemblies are highlighted; all spectra were run in CD_2Cl_2

9b obtained in the solid state exhibits intense bands for $\tilde{\nu}$(CO) at 1933 and 1934 cm^{-1}, respectively.

The syntheses of the octahedral ruthenium(II) and iron(II) assemblies **12a** and **12b** were accomplished according to our recently reported metal-directed synthesis employed to prepare the corresponding metalloporphyrin analogues (Scheme 2).[4a] The addition of [D_6]acetone to a 3:6:1 molar mixture of solid 4,4′-di(4′′-pyridyl)-2,2′-bipyridine (**11**),[13] Ru(BSP)(CO) (**4**), and $Fe(BF_4)_2(H_2O)_6$, followed by 5 min of heating, cleanly afforded assembly **12b**. The octahedral assembly **12a** was prepared by treating the pre-assembled ruthenium(II) core fragment **10** with a slight excess of **4**. The ES mass spectra of both **12a** and **12b** each show a peak corresponding to the dications (*m*/*z* = 2519 for [M − 2 PF_6]$^{2+}$ and 2496 for [M − 2 BF_4]$^{2+}$, respectively), as well as peaks for the loss of subsequent metallosalophens. The IR spectra for **12a** and **12b** obtained in the solid state exhibit intense bands for $\tilde{\nu}$(CO) at 1947 and 1946 cm^{-1}, respectively.

Synthesis of Bis(salophens)

Illustrative examples that highlight the versatility of the salophen ligand are bis(metallosalophen) complexes **14**−**17**. These metallosalophens offer two accessible axial metal binding sites, separated by different intermetal distances based on the size of the tetraamine synthon (7.62 Å for **14** and **15**, and 12.32 Å for **16** and **17**). The corresponding salophen ligands used to prepare these complexes were synthesized by condensing the 1,2,4,5-tetraaminobenzene hydrochloride salt for **14**, and the 2,3,7,8-tetraaminodibenzo-[1,4]dioxin hydrochloride salt **13**[14] for **16**, with 3,5-di-*tert*-butylsalicylaldehyde in ethanol under reflux (Scheme 3). Metal insertion was accomplished by heating the resulting salophens with $Ru_3(CO)_{12}$ in either toluene or diglyme, followed by purification using column chromatography through alumina. Complexes **14** and **16** were isolated as deep-red air-stable solids.

The ES mass spectrum of **14** shows the parent ion peak (*m*/*z* = 1258), as well as peaks corresponding to the solvated complex (*m*/*z* = 1336 for [M + H_2O + CH_3NO_2]$^+$, 1318 for [M + CH_3NO_2]$^+$ and 1370 for [M − CO + H_2O + 2 CH_3NO_2]$^+$). The ES mass spectrum of **16** shows a similar trend. The IR spectra for these bis(metallosalophens) obtained in the solid state exhibit intense bands for $\tilde{\nu}$(CO) at 1950 cm^{-1} for **14**, and at 1943 cm^{-1} for **16**.

The ^{1}H NMR spectrum of **14** in acetone reveals that the isolated product is a mixture of *cis* and *trans* diastereomers based on how the two carbonyl ligands project in space with respect to each other.[15] This is manifested as the appearance of two singlets of equal intensity assigned to the C−H protons on the central tetraaminobenzene ring fragment of **14**. The production of these stereoisomers is not unexpected, since the chelation sites are far away from each other so that they can act independently during the metal-insertion reactions. The diastereomeric mixture is even more apparent in the case of the pyridine adduct **15**, which was formed by treating complex **14** with pyridine, followed by the filtering of the solution through a plug of silica gel to remove trace amounts of unchanged **14**. The ^{1}H NMR spectrum of **15** shows an analogous pair of singlets assigned to the C−H hydrogen atoms on the central tetraaminobenzene fragment. The signals corresponding to the protons of the imine and flanking *tert*-butyl substituents on the bis(salophen) ligand, as well as C−H protons on the coordinated pyridine also appear as duplicate signals. These environmental effects are not limited to ^{1}H NMR spectroscopy, but are also apparent in the ^{13}C NMR spectrum for **15**, which contains duplicate signals for the coordinated pyridine ligand. On the other hand, the symmetrical nickel(II) analogue of **13** (Figure 2), prepared as a burgundy precipitate by treating the metal-free salophen ligand with 5 equiv. of $Ni(OAc)_2(H_2O)_4$, shows an absence of signal splitting in both the ^{1}H and ^{13}C NMR spectra (see Exp. Sect.).

The ^{1}H NMR spectra of the coordination compounds using the larger bis(metallosalophens) **16** and **17** show an absence of signal splitting for all protons, due to the greater separation between the two coordination sites. The ^{13}C NMR spectrum of **16** also lacks any signal splitting, however, the ^{13}C NMR spectrum of **17** exhibits two sets of signals corresponding to the coordinated pyridine ligands. All of the carbon atoms on the salophen ligand remain unaffected and appear as one set of signals. Again, the symmetrical nickel(II) analogue of **16** (Figure 2) does not show any multiple peaks in its NMR spectra.

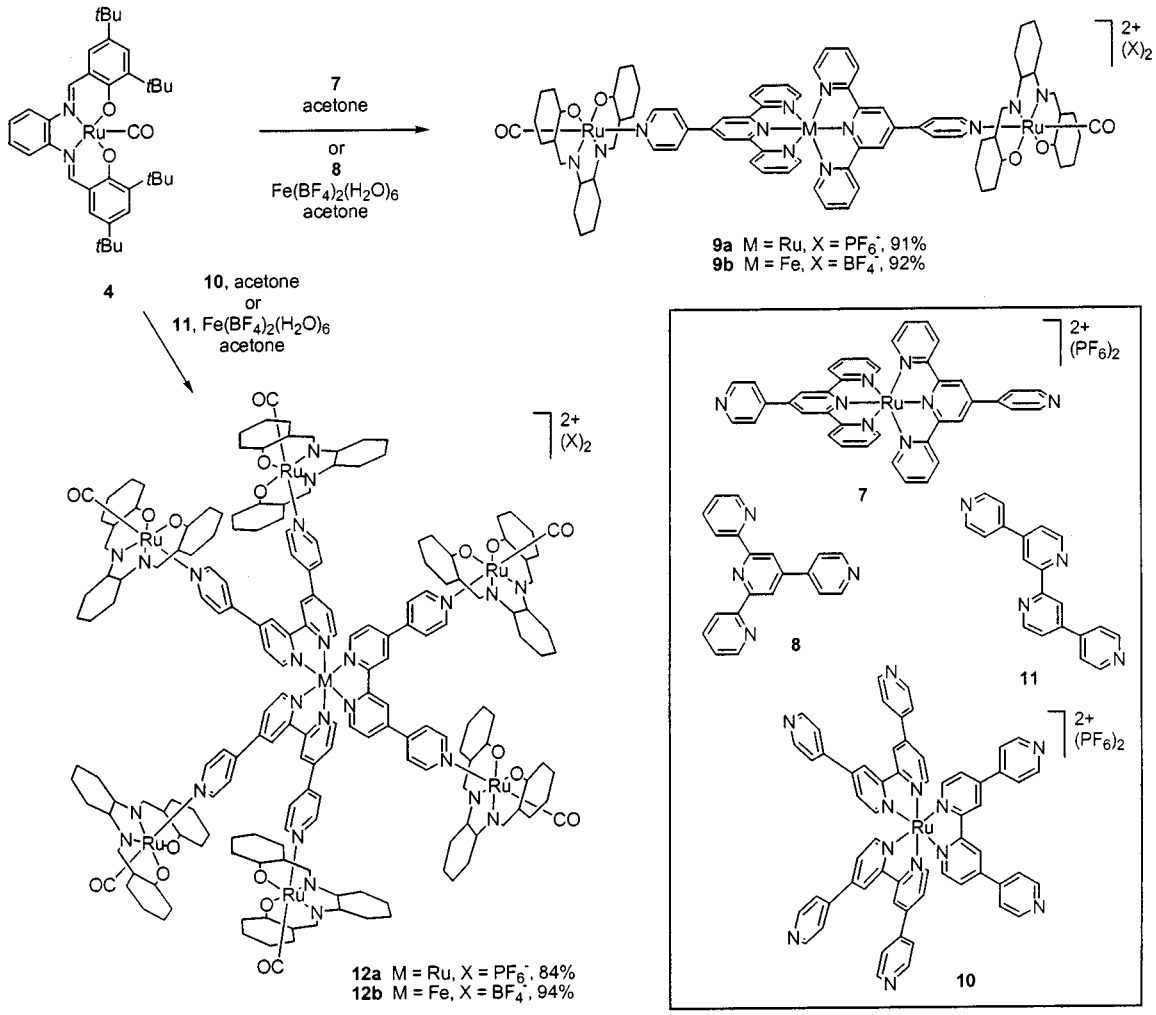

Scheme 2

The ES mass spectrum of **15** shows the parent ion peak (m/z = 1416) and peaks corresponding to the loss of pyridine (m/z = 1338 for $[M - py]^+$ and 1258 for $[M - 2\,py]^+$). The ES mass spectrum of **17** shows a similar pattern. The IR spectra of the pyridine complexes **15** and **17** in the solid state show two intense overlapping bands for the stretching vibrations of the axial carbon monoxide (1955 cm^{-1} and 1924 cm^{-1} for **15**, 1951 cm^{-1} and 1934 cm^{-1} for **17**). The IR spectra measured in toluene exhibit two completely resolved $\tilde{\nu}$(CO) at 1944 cm^{-1} and 1924 cm^{-1} for **15**, and at 1947 cm^{-1} and 1934 cm^{-1} for **17**. A solvent dependency was also observed for the $\tilde{\nu}$(CO) of both pyridine complexes, and the IR spectra of dichloromethane solutions show a single band at 1940 cm^{-1} and 1931 cm^{-1} for **15** and **17**, respectively.

The convenience of incorporating the bis(metallosalophens) into supramolecular chemistry becomes clear when their syntheses are compared with that of the analogous bis(metalloporphyrin) **18a**. Although the metal insertion into Crossley's bis(porphyrin)[16] proceeded uneventfully by heating the bis(porphyrin) with an excess of $Ru_3(CO)_{12}$ in phenol, the preparation of the free-based porphyrin was accomplished in 5 steps giving a 50% yield as reported by Burn and co-workers.[17] This is a significant drawback when compared with our single-step preparation of the bis(salophen) precursor to **14**, and the two-step procedure for the precursor of **16**. The bis(metalloporphyrin) **18a** was purified as a brown air-stable solid by a combination of column chromatography through water-activated alumina and recrystallization from aqueous ethanol. When an excess of pyridine was added to **18a** in dichloromethane, the more Lewis-basic amine immediately displaced the labile ethanol affording the pyridine adduct.

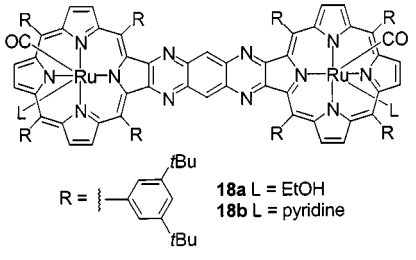

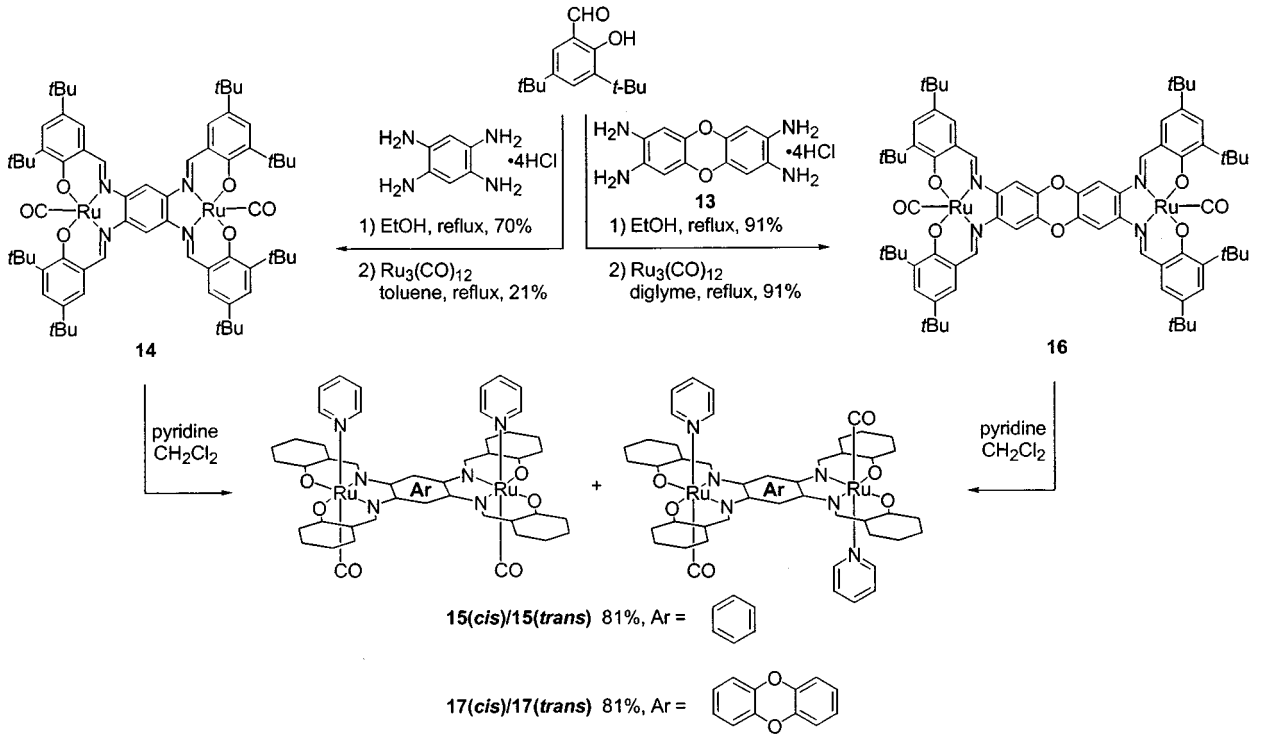

Scheme 3

UV/Vis Spectroscopic Analysis

Initial photophysical studies reveal that UV/Vis absorption spectra of metallosalophen assemblies **6**, **9**, and **12** are essentially the sum of the absorption spectra of the corresponding components, and electronic absorptions are limited to minor shifts ($\Delta\lambda = \pm 2$ nm) (Table 2), although the steady-state emission spectra vary significantly (not shown). A more detailed description of the supramolecular absorption and emission properties of the metallosalophen assemblies will be the subject of a separate report.

The absorption spectra of dichloromethane solutions of **5**, **15** (as the mixture of *cis* and *trans* isomers), and **17** (as the mixture of *cis* and *trans* isomers) are characterized by intense ligand-centered (LC) bands with maxima in the 250−400 nm region (Figure 3).[7,18] These bands have been designated as π−π* and n−π* transitions for the electrons localized on the azomethine group of the Schiff base ligand. The bands at longer wavelengths are most likely due to ligand(π)−metal(d*) charge transfer, as has been reported for similar complexes.[7,18a,18c] The similarity of the electronic spectra of complexes **5** and **17** suggests that the central dibenzodioxin fragment effectively separates the metal centers from each other, allowing them to act independently. However, this effect does not apply to complex **15**, which exhibits a unique pattern of red-shifted charge-transfer bands. This observation is indicative of the fact that **15** is behaving as one extended chromophore and not as two independent metallosalophens.

Electrochemistry of Bis(salophens)

The cyclic voltammograms of dichloromethane solutions of complexes **5**, **15** (as the mixture of *cis* and *trans* isomers), and **17** (as the mixture of *cis* and *trans* isomers) do not show any reduction waves at negative potentials, but do show two quasi-reversible ($\Delta E = 70-90$ mV) oxidation waves centered at 0.58 V (assigned as a Ru^{II}/Ru^{III} process) and 1.29 V (assigned as a Ru^{III}/Ru^{IV} process) vs. saturated Ag/AgCl (Figure 4).[18a] For the scan rates used, the cathodic-to-anodic peak current ratio (i_{pc}/i_{pa}) is constantly equal to unity for the first oxidation and slightly less than unity for the second oxidation; the quotient of the anodic peak current and the square root of the scan rate ($i_{pa}/v^{1/2}$) remains constant. Complex **5** is well behaved, showing two one-electron oxidations at 0.56(7) and 1.29(4) V. For the bimetallic species **15** and **17**, the first oxidation waves are two-electron processes [actually, two one-electron oxidations at each ruthenium(II) center] and are shifted to slightly more positive potentials [0.60(0) and 0.58(2) V for **15** and **17**, respectively]. This indicates that the metal centers do not communicate with each other for the Ru^{II}/Ru^{III} couple. The second oxidation wave of the bimetallic species are split into two one-electron oxidation waves at 1.27(7)/1.36(8) V for **15** and 1.28(4)/1.33(0) for **17**, indicative of weak interactions between the covalently linked metallosalophens. This metal-to-metal communication is amplified in the case of the smaller complex **15** ($\Delta V = 91$ mV), as compared with the larger complex **17** ($\Delta V = 50$ mV).

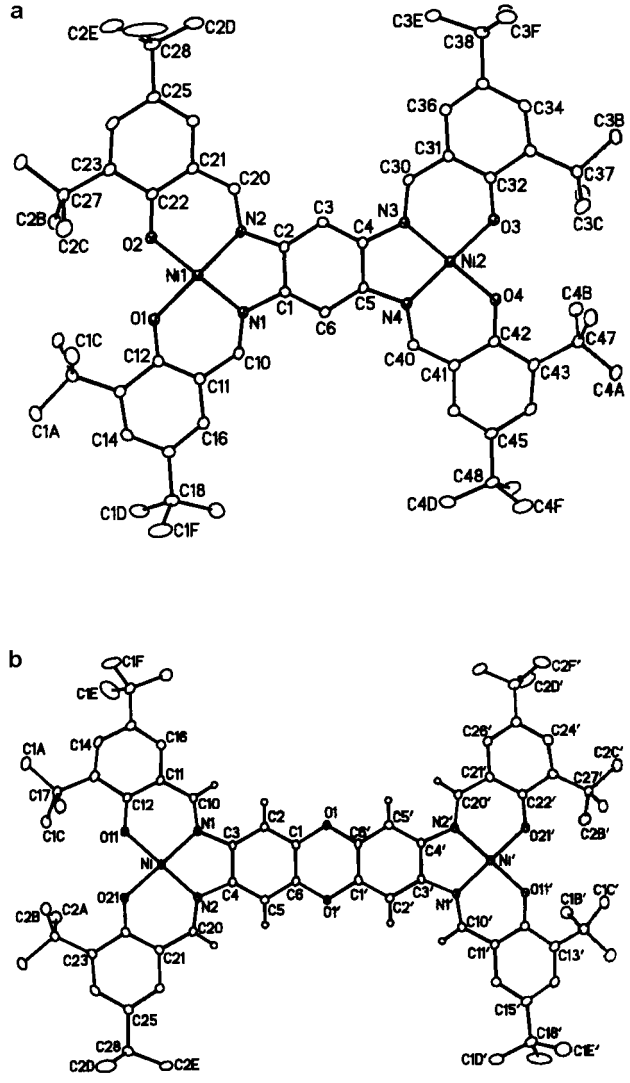

Figure 2. Molecular structures of the nickel(II) analogues of (a) **14** and (b) **16** in the crystal; solvent molecules (acetone/CH_2Cl_2 for **14** and THF for **16**) have been removed for clarity; the thermal ellipsoids are drawn at the 20% probability level

Table 2. Selected UV/Vis absorption data of the pyridyl-coordinated metallosalophen assemblies prepared in this study

Compound	λ_{max} [nm] (log ε [$M^{-1}cm^{-1}$])[a]					
4	258 (4.48)	306 (4.26)	382 (4.38)	491 (3.91)	541[b] (3.75)	
5	264 (4.68)	310 (4.38)	391 (4.60)	503 (4.02)	555[b] (3.09)	
6	264 (4.81)	310 (4.56)	391 (4.70)	501 (4.17)	555[b] (4.00)	
9a	276 (5.01)	312 (4.88)	330 (4.77)	390 (4.74)	493 (4.59)	555[b] (4.18)
9b	282 (5.02)	291 (5.02)	327 (4.82)	393 (4.75)	508 (4.35)	573[b] (4.52)
12a	255 (5.34)	311 (5.19)	388 (5.18)	490 (4.77)	555[b] (4.53)	
12b	285 (5.39)	311 (5.16)	391 (5.21)	506 (4.72)	555[b] (4.70)	
15[c]	313 (4.58)	325 (4.57)	407 (4.62)	492 (4.42)	551[b] (4.37)	614[b] (4.35)
17[c]	263 (4.75)	304 (4.70)	317 (4.70)	400 (4.80)	520 (4.29)	566[b] (4.22)

[a] Run in deoxygenated CH_2Cl_2 at 10^{-4} to 10^{-5} M. [b] Observed as a shoulder. [c] As a mixture of both *cis* and *trans* isomers.

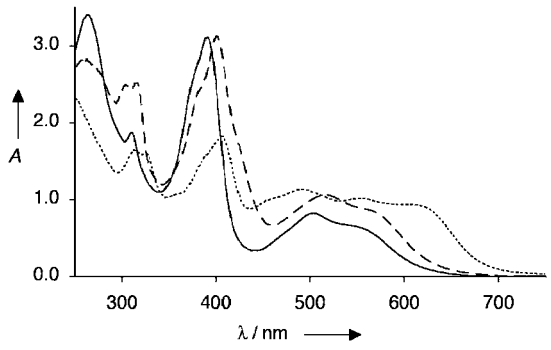

Figure 3. UV/Vis absorption spectra of Ru(BSP)(CO)(py) (**5**) (solid line), $Ru_2[(BS2P)(CO)_2(py)_2]$ (**15**, both isomers) (dotted line), and $Ru_2[(BS2DP)(CO)_2(py)_2]$ (**17**, both isomers) (dashed line) in CH_2Cl_2 at room temperature

Conclusion

In summary, this work highlights the fact that mononuclear and binuclear ruthenium(II) carbonyl Schiff base complexes can be prepared in a facile manner from *ortho*-diamines and 3,5-di-*tert*-butylsalicylaldehyde. We have also established that Ru(BSP)(CO) (**4**) has the same axial coordination properties as our previously reported Ru(CO)(TTP) supramolecular synthons. The ease with which salophens can be modified represents a significant synthetic advantage over its metalloporphyrin analogue, as was demonstrated by the formation of the carbonylbis(metallosalophens)ruthenium(II). The ease of synthetically tailoring the *ortho*-diamine synthon of the salophen ligands should spark efforts to further develop this class of supramolecular building blocks.

Experimental Section

General Remarks: All solvents (Caledon) were distilled prior to use. Solvents used for UV/Vis spectroscopy were deoxygenated by bubbling argon through the solvent. Solvents for NMR analysis (Cambridge Isotope Laboratories) were used as received. All reagents and starting materials were purchased from Aldrich. *N*,*N*′-Bis(3,5-di-*tert*-butylsalicylidene)-1,2-phenylenediamine (**3**),[8] $[Ru(pytpy)_2][PF_6]_2$ (**7**)[11] [pytpy = 4′-(4′′′-pyridyl)-2,2′:6′,2′′-terpyridine], 4′-(4′′′-pyridyl)-2,2′:6′,2′′-terpyridine (**8**),[12] $[Ru(dpybpy)_3][PF_6]_2$ (**10**)[4a] [dpybpy = 4,4′-di(4′′-pyridyl)-2,2′-bipyridine], and 4,4′-di(4′′-pyridyl)-2,2′-bipyridine (**11**)[13] were prepared as described in the literature. ^1H NMR characterizations were performed with a Varian Inova-500 instrument, working at 499.92 or with a Varian Inova-300 instrument, working at 299.96 MHz. Chemical shifts (δ) are reported in ppm relative to tetramethylsilane using the residual solvent peak as a reference standard. FT-IR measurements were performed using a Nicolet Magna-IR 750

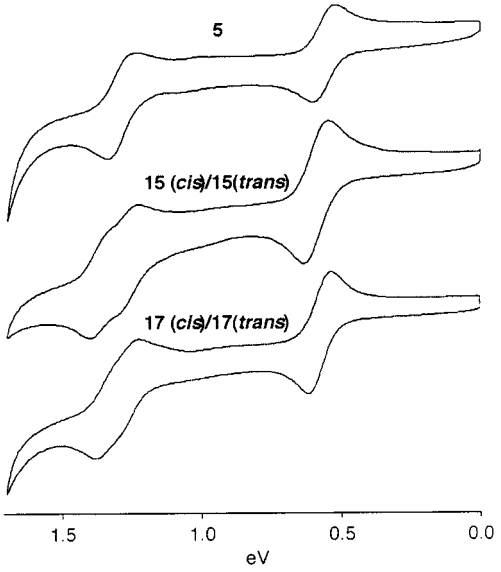

Figure 4. Cyclic voltammograms of (a) Ru(BSP)(CO)(py) (**5**), (b) $Ru_2[(BS2P)(CO)_2(py)_2]$ (**15**, both isomers), and (c) $Ru_2[(BS2DP)(CO)_2(py)_2]$ (**17**, both isomers) at identical scan rates of 50 mV/s in CH_2Cl_2 with 0.1 M TBAP at room temperature

microscope. UV/Vis measurements were performed using a Varian Cary 400 Scan spectrophotometer. Cyclic voltammetry measurements were performed in CH_2Cl_2 using a PINE bipotentiostat, a platinum working electrode, a platinum counter electrode and an Ag/AgCl reference electrode, and tetrabutylammonium hexafluorophosphate as the electrolyte. MALDI mass spectra were recorded with an Applied Biosystems Voyager Elite equipped with delayed extraction and an ion mirror (reflectron). Electrospray ionization mass spectra were recorded with a Micromass ZabSpec Hybrid Sector-TOF with positive mode electrospray ionization. All isotopic abundances match the calculated values.

Ru(BSP)(CO) (4): A solution of *N*,*N*′-bis(3,5-di-*tert*-butylsalicylidene)-1,2-phenylenediamine (**3**) (130 mg, 0.242 mmol) and $Ru_3(CO)_{12}$ (65.0 mg, 0.102 mmol) in toluene (5 mL) was heated under reflux for 15 h under argon. The reaction mixture was cooled to room temperature, filtered through Celite, and concentrated under reduced pressure. The resulting dark red residue was chromatographed on alumina (II−III) eluting first with toluene to remove an orange band, followed by CH_2Cl_2 to remove a yellow band, and then with a mixture of EtOH/CH_2Cl_2 (5:95) to remove a red-pink band. The red-pink band was concentrated to dryness under vacuum affording **4** as a glassy red solid that was recrystallized from aqueous EtOH. Yield: 73 mg (46%). ^{1}H NMR (300 MHz, [D$_6$]acetone, 22 °C): δ = 9.34 (s, 2 H), 8.29 (dd, *J* = 3.3, 9.6 Hz, 2 H), 7.48 (d, *J* = 2.7 Hz, 2 H), 7.40 (d, *J* = 2.7 Hz, 2 H), 7.33 (dd, *J* = 3.3, 9.6 Hz, 2 H), 1.55 (s, 18 H), 1.33 (s, 18 H). ^{13}C NMR APT (125.7 MHz, [D$_6$]acetone, 22 °C): δ = 170.6 (C), 157.2 (CH), 146.9 (C), 142.7 (C), 135.2 (C), 131.0 (CH), 130.1 (CH), 126.7 (CH), 121.7 (C), 116.1 (CH), 36.6 (C), 34.5 (C), 31.7 (CH_3), 30.4 (CH_3). HRMS (ES+): *m*/*z* = 668.2552 [M$^+$]. Selected IR: $\tilde{\nu}$ = 1931 (CO) cm^{-1}.

Ru(BSP)(CO)(py) (5): A solution of pyridine (0.25 mL) in CH_2Cl_2 (5 mL) was treated with Ru(BSP)(CO) (**4**) (38.0 mg, 0.055 mmol) and stirred at room temperature for 30 min. Silica gel (1 g) was added and the solvents were evaporated. The solid residue was applied to a small column of silica gel (1 × 2 cm) and eluted with CH_2Cl_2. The first band was collected and concentrated to dryness affording **5** as a purple solid. Yield: 37 mg (90%).^{1}H NMR (300 MHz, CD_2Cl_2, 22 °C): δ = 8.90 (s, 2 H), 8.12 (m, 2 H), 8.01 (dd, *J* = 3.3, 9.9 Hz, 2 H), 7.59 (m, 1 H), 7.42 (d, *J* = 2.7 Hz, 2 H), 7.32 (dd, *J* = 3.3, 9.6 Hz, 2 H), 7.09 (m, 4 H), 1.56 (s, 18 H), 1.28 (s, 18 H). ^{13}C NMR APT (125.7 MHz, CD_2Cl_2, 22 °C): δ = 170.0 (C), 155.0 (CH), 149.5 (CH), 145.9 (C), 143.0 (C), 138.0 (CH), 135.1 (C), 130.1 (CH), 130.0 (CH), 126.2 (CH), 124.6 (CH), 120.5 (C), 115.1 (CH), 36.3 (C), 34.1 (C), 31.4 (CH_3), 29.9 (CH_3). HRMS (ES+): *m*/*z* = 747.2974 [M$^+$]. Selected IR: $\tilde{\nu}$ = 1942 (CO) cm^{-1}.

[Ru(BSP)(CO)]$_2$[4,4′-bipy] (6): A solution of 4,4′-bipyridine (3.9 mg, 0.025 mmol) in CH_2Cl_2 (5 mL) was treated with Ru(BSP)(CO) (**4**) (35.0 mg, 0.051 mmol) and stirred at room temperature for 30 min. Silca gel (1 g) was added and the solvents were evaporated. The solid residue was applied to a small column of silica gel (1 × 2 cm) and eluted with CH_2Cl_2. The first band was collected and concentrated to dryness affording **6** as a purple solid. Yield: 34.0 mg (92%).^{1}H NMR (300 MHz, CD_2Cl_2, 22 °C): δ = 8.91 (s, 4 H), 8.19 (dd, *J* = 1.5, 6.6 Hz, 4 H), 8.02 (dd, *J* = 3.6, 9.9 Hz, 4 H), 7.43 (d, *J* = 2.4 Hz, 4 H), 7.34 (dd, *J* = 3.3, 9.6 Hz, 4 H), 7.16 (dd, *J* = 1.5, 6.6 Hz, 4 H), 7.11 (d, *J* = 2.4 Hz, 4 H), 1.50 (s, 36 H), 1.27 (s, 36 H). ^{13}C NMR APT (125.7 MHz, CD_2Cl_2, 22 °C): δ = 169.9 (C), 155.1 (CH), 150.3 (CH), 146.4 (C), 145.8 (C), 143.0 (C), 135.2 (C), 130.0 (CH), 126.1 (CH), 122.4 (CH), 120.5 (C), 115.1 (CH), 36.2 (C), 34.1 (C), 31.3 (CH_3), 29.9 (CH_3). MS (ES+): *m*/*z* = 1492 [M$^+$]. Selected IR: $\tilde{\nu}$ = 1938 (CO) cm^{-1}.

[Ru(BSP)(CO)]$_2$[Ru(pytpy)$_2$][PF$_6$]$_2$ (9a): A solution of [Ru(pytpy)$_2$][PF$_6$]$_2$ (**7**)[11] (2.2 mg, 2.2 μmol) in acetone (5 mL) was treated with Ru(BSP)(CO) (**4**) (3.4 mg, 5.0 μmol) and stirred at room temperature for 30 min. The solvents were evaporated and the resulting solid was triturated in a mixture of Et_2O/pentane (20:80) and dried under vacuum. Yield: 4.7 mg (91%). ^{1}H NMR (300 MHz, [D$_6$]acetone, 22 °C): δ = 9.40 (s, 4 H), 9.39 (s, 4 H), 8.91 (d, *J* = 8.1 Hz, 4 H), 8.48 (d, *J* = 6.6 Hz, 4 H), 8.39 (dd, *J* = 3.6, 9.9 Hz, 4 H), 8.17 (d, *J* = 6.6 Hz, 4 H), 8.00 (t, *J* = 7.8 Hz, 4 H), 7.63 (d, *J* = 4.8 Hz, 4 H), 7.50 (d, *J* = 2.4 Hz, 4 H), 7.40 (m, 8 H), 7.21 (t, *J* = 6.0 Hz, 4 H), 1.61 (s, 36 H), 1.32 (s, 36 H). MS (ES+): *m*/*z* = 1028 [M − 2 PF$_6$]$^{2+}$. Selected IR: $\tilde{\nu}$ = 1933 (CO) cm^{-1}.

[Ru(BSP)(CO)]$_2$[Fe(pytpy)$_2$][BF$_4$]$_2$ (9b): A solid mixture of 4′-(4′′′-pyridyl)-2,2′:6′,2′′-terpyridine (**8**)[12] (3.1 mg, 0.01 mmol), $Fe(BF_4)_2(H_2O)_6$ (1.7 mg, 5.0 μmol), and Ru(BSP)(CO) (**4**) (15.0 mg, 0.022 mmol) was dissolved in acetone (5 mL) and stirred at room temperature for 30 min. The solvents were evaporated and the resulting solid product was triturated in a mixture of Et_2O/pentane (20:80) and dried under vacuum. Yield: 20.1 mg (92%).^{1}H NMR (300 MHz, [D$_6$]acetone, 22 °C): δ = 9.56 (s, 4 H), 9.42 (s, 4 H), 8.86 (d, *J* = 7.8 Hz, 4 H), 8.53 (d, *J* = 6.6 Hz, 4 H), 8.40 (dd, *J* = 3.3, 9.6 Hz, 4 H), 8.27 (d, *J* = 6.6 Hz, 4 H), 7.95 (t, *J* = 7.8 Hz, 4 H), 7.50 (d, *J* = 2.4 Hz, 4 H), 7.40 (m, 12 H), 7.11 (t, *J* = 6.0 Hz, 4 H), 1.63 (s, 36 H), 1.32 (s, 36 H). MS (ES+): *m*/*z* = 1006 [M − 2 BF$_4$]$^{2+}$. Selected IR: $\tilde{\nu}$ = 1934 (CO) cm^{-1}.

[Ru(BSP)(CO)]$_6$[Ru(dpybpy)$_3$][PF$_6$]$_2$ (12a): A solution of [Ru(dpybpy)$_3$][PF$_6$]$_2$ (**10**)[4a] (2.0 mg, 1.5 mmol) in acetone (5 mL) was treated with Ru(BSP)(CO) (**4**) (6.4 mg, 9.6 mmol) and stirred under reflux for 30 min. The solvents were evaporated and the resulting solid product was triturated in a mixture of Et_2O/pentane (20:80) and dried under vacuum. Yield: 6.8 mg (84%).^{1}H NMR (500 MHz, [D$_6$]acetone, 22 °C): δ = 9.27 (s, 12 H), 9.04 (s, 6 H), 8.31 (m, 12

H), 8.23 (d, J = 6.5 Hz, 12 H), 7.88 (d, J = 6.0 Hz, 6 H), 7.58 (d, J = 6.5 Hz, 12 H), 7.45 (m, 18 H), 7.38 (dd, J = 3.5, 9.5 Hz, 12 H), 7.30 (s, 12 H), 1.55 (s, 108 H), 1.30 (s, 108 H). MS (ES+): m/z = 2519.5 $[M - 2\,PF_6]^{2+}$. Selected IR: $\tilde{\nu}$ = 1946 (CO) cm^{-1}.

$[Ru(BSP)(CO)]_2[Fe(dpybpy)_2][BF_4]_2$ (12b): A solid mixture of 4,4′-di(4′′-pyridyl)-2,2′-bipyridine (**11**)[13] (1.2 mg, 3.9 μmol), $Fe(BF_4)_2(H_2O)_6$ (0.5 mg, 1.5 μmol), and Ru(BSP)(CO) (**4**) (6.5 mg, 9.5 μmol) was dissolved in acetone (5 mL) and stirred under reflux for 30 min. The solvents were evaporated and the resulting solid product was triturated in a mixture of Et_2O/pentane (20:80) and dried under vacuum. Yield: 7.1 mg (94%). ^1H NMR (500 MHz, [D$_6$]acetone, 22 °C): δ = 9.28 (s, 12 H), 9.03 (s, 6 H), 8.32 (m, 12 H), 8.24 (d, J = 7.0 Hz, 12 H), 7.59 (d, J = 7.0 Hz, 12 H), 7.56 (dd, J = 1.5, 6.0 Hz, 6 H), 7.54 (d, J = 6.0 Hz, 6 H) 7.45 (m, 12 H), 7.38 (dd, J = 3.5, 10.0 Hz, 12 H), 7.31 (d, J = 2.5 Hz, 12 H), 1.57 (s, 108 H), 1.31 (s, 108 H). MS (ES+): m/z = 2496.5 $[M - 2\,BF_4]^{2+}$. Selected IR: $\tilde{\nu}$ = 1946 (CO) cm^{-1}.

***N*,*N*′′,*N*′′′,*N*′′′′-Tetra-(3,5-di-*tert*-butylsalicylidene)-1,2,4,5-phenylenetetraamine [Bis(salophen) Precursor to 14] (BS2P):** 3,5-Di-*tert*-butylsalicylaldehyde (1.00 g, 4.27 mmol) and 1,2,4,5-benzenetetramine tetrahydrochloride (250 mg, 0.880 mmol) were heated in EtOH (5 mL) under reflux for 15 h. The solution was cooled to −10 °C and stirred for 3 h. The yellow-orange precipitate was collected by filtration, washed with EtOH and dried under vacuum. Yield: 610 mg (70%). M.p. 285−286 °C. ^1H NMR (360 MHz, CD_2Cl_2, 27 °C): δ = 13.53 (s, 4 H), 8.83 (s, 4 H), 7.49 (d, J = 2.2 Hz, 4 H), 7.32 (d, J = 2.3 Hz, 4 H), 7.25 (s, 4 H), 1.52 (s, 36 H), 1.33 (s, 36 H). ^{13}C NMR APT (125.7 MHz, $CDCl_3$, 27 °C): δ = 164.7 (CH), 158.7 (C), 141.6 (C), 140.6 (C), 137.3 (C), 128.6 (CH), 127.0 (CH), 118.4 (C), 111.2 (CH), 35.2 (C), 34.1 (C), 31.5 (CH_3), 29.5 (CH_3). MS (ES+): m/z = 1004 $[M + H]^+$. IR: $\tilde{\nu}$ = 2962, 2908, 2870, 1653, 1615, 1607, 1580, 1492, 1463, 1440, 1392, 1362, 1316, 1273, 1250, 1168, 1027, 983, 963, 937, 909, 882, 874, 866, 837, 771, 749, 686, 642 cm^{-1}.

$Ru_2[(BS2P)(CO)_2]$ (14): A solution of BS2P (200 mg, 0.20 mmol), $Ru_3(CO)_{12}$ (102 mg, 0.16 mmol) in toluene (5 mL) was heated under reflux for 40 h, under argon. The reaction mixture was cooled to room temperature, filtered through Celite and concentrated under reduced pressure. The resulting dark red residue was chromatographed on alumina (II−III), eluting first with $CHCl_3$ to remove a red-orange band, followed by EtOH/$CHCl_3$ (5:95) to remove a purple band. The purple band was concentrated to dryness under vacuum affording the product as a glassy purple solid. Yield: 52.0 mg (21%). ^1H NMR (300 MHz, [D$_6$]acetone, 22 °C): δ = 9.41 (s, 4 H), 9.14 (s, 1 H), 9.13 (s, 1 H), 7.51 (d, J = 2.7 Hz, 4 H), 7.31 (d, J = 2.4 Hz, 4 H), 1.56 (s, 36 H), 1.36 (s, 36 H). ^{13}C NMR APT (125.7 MHz, [D$_6$]acetone, 22 °C): δ = 170.9 (C), 156.9 (CH), 144.7 (C), 142.9 (C), 135.5 (C), 130.6 (CH), 130.4 (CH), 121.8 (C), 101.3 (CH), 36.7 (C), 34.5 (C), 30.3 (CH_3), 31.7 (CH_3). MS (ES+): m/z = 1258 $[M^+]$. UV/Vis (CH_2Cl_2): λ_{max} [nm] (log ε [$M^{-1}cm^{-1}$]) = 320 (4.58), 395 (4.62), 486 (4.47), 539sh (3.75) 568sh (4.42), 579sh (4.41). Selected IR: $\tilde{\nu}$ = 1950 (CO) cm^{-1}.

$Ru_2[(BS2P)(CO)_2(py)_2]$ (15): A solution of pyridine (0.25 mL) in dichloromethane (5 mL) was treated with $Ru_2[(BS2P)(CO)_2]$ (**14**) (35.0 mg, 0.055 mmol) and stirred at room temperature for 30 min. The solvents were evaporated and the residue applied to a small column of silica gel (1 × 2 cm) and eluted with CH_2Cl_2. The first band was collected and concentrated to dryness affording a dark purple solid. Yield: 32.0 mg (81%). ^1H NMR (500 MHz, CD_2Cl_2, 22 °C): δ = 9.04 (s, 2 H), 8.52 (s, 1 H), 8.51 (s, 1 H), 8.20 (m, 4 H), 7.64 (m, 2 H), 7.47 (d, J = 2.5 Hz, 4 H), 7.28 (d, J = 2.5 Hz, 4 H), 7.16 (m, 4 H), 1.56 (s, 18 H), 1.55 (s, 18 H), 1.35 (2 s, 36 H). ^{13}C NMR APT (125.7 MHz, CD_2Cl_2, 22 °C): δ = 170.3 (C), 154.3 (CH), 149.6 (CH), 149.5 (CH), 143.5 (C), 143.2 (C), 143.2 (C), 138.2 (C), 135.6 (C), 130.6 (CH), 130.1 (CH), 130.0 (CH), 124.8 (CH), 124.6 (CH), 120.9 (C), 99.7 (CH), 99.6 (CH), 36.35 (C), 34.3 (C), 31.6 (CH_3), 29.9 (CH_3). MS (ES+): m/z = 1416 $[M^+]$. Selected IR: $\tilde{\nu}$ = 1954, 1924 (CO) cm^{-1}.

Ni_2(BS2P): A solution of BS2P (100 mg, 0.1 mmol), $Ni(OAc)_2(H_2O)_4$ (124 mg, 0.5 mmol) in absolute EtOH (5 mL) was heated under reflux for 2 h. The reaction mixture was cooled to room temperature and the red solid was collected by filtration, washed with cold EtOH and dried under vacuum. Yield: 100 mg (89%). ^1H NMR (300 MHz, CD_2Cl_2, 22 °C): δ = 8.33 (s, 4 H), 8.01 (s, 2 H), 7.46 (d, J = 2.7 Hz, 4 H), 7.28 (d, J = 2.4 Hz, 4 H), 1.45 (s, 36 H), 1.36 (s, 36 H). ^{13}C NMR APT (125.7 MHz, $CDCl_3$, 22 °C): δ = 165.4 (C), 153.5 (CH), 141.5 (C), 140.9 (C), 137.4 (C), 131.2 (CH), 126.5 (CH), 119.7 (C), 98.5 (CH), 35.9 (C), 34.0 (C), 31.2 (CH_3), 29.7 (CH_3). MS (MALDI, no matrix): m/z = 1116 $[M^+]$. UV/Vis (CH_2Cl_2): λ_{max} [nm] (log ε [$M^{-1}cm^{-1}$]) = 268 (4.78), 322 (4.45), 374sh (4.46), 394 (4.55), 494 (4.58), 541sh (4.50). IR: $\tilde{\nu}$ = 2957, 2907, 2869, 1703, 1616, 1589, 1546, 1522, 1495, 1462, 1423, 1385, 1359, 1322, 1258, 1177, 1130, 1026, 971, 933, 916, 868, 828, 788, 749, 654, 637 cm^{-1}.

2,3,7,8-Tetraaminodibenzo-[1,4]-dioxin Tetrahydrochloride (13):[14] Tin metal (7.0 g, 59 mmol) was added in small portions to a suspension of 2,3,7,8-tetranitrodibenzo-[1,4]-dioxin (1.70 g, 4.7 mmol) in concentrated hydrochloric acid (25 mL). The reaction became extremely exothermic after 30 min at which point the color of the suspension changed from yellow to creamy-white. The mixture was heated under reflux for 8 h to dissolve any residual solid tin metal. The mixture was filtered leaving a white solid. The product was washed with concentrated HCl, then with EtOH and finally with Et_2O, and dried under vacuum. Yield: 1.35 g (74%). ^1H NMR (300 MHz, D_2O/CF_3CO_2H, 22 °C): δ = 6.63 (s). ^{13}C NMR APT (125.7 MHz, D_2O/CF_3CO_2H, 22 °C): δ = 140.6 (C), 123.1 (C), 112.4 (CH). MS (ES+): m/z = 244 $[M - 4\,HCl]^+$.

***N*,*N*′′,*N*′′′,*N*′′′′-Tetra(3,5-di-*tert*-butylsalicylidene)dibenzo-[1,4]-dioxin-2,3,7,8-tetraamine [Bis(salophen) Precursor to 16] (BS2DP):** 3,5-Di-*tert*-butylsalicylaldehyde (750 mg, 3.20 mmol) and 2,3,7,8-tetraaminodibenzo-1,4-dioxin tetrahydrochloride (310 mg, 0.795 mmol) were heated in EtOH (18 mL) under reflux for 15 h. The solution was cooled to −10 °C and stirred at that temperature for 3 h. The yellow precipitate was collected by filtration, washed with cold EtOH and dried under vacuum. Yield: 802 mg (91%). M.p. > 350 °C. ^1H NMR (500 MHz, [D$_8$]THF, 22 °C): δ = 13.57 (br. s, 4 H), 8.85 (s, 4 H), 7.46 (d, J = 2.5 Hz, 4 H), 7.37 (d, J = 2.5 Hz, 4 H), 7.14 (s, 4 H), 1.45 (s, 36 H), 1.33 (s, 36 H). ^{13}C NMR APT (125.7 MHz, [D$_8$]THF, 22 °C): δ = 165.9 (CH), 159.5 (C), 141.6 (C), 141.0 (C), 140.3 (C), 137.6 (C), 128.7 (CH), 128.2 (CH), 119.7 (C), 108.2 (CH), 35.8 (C), 34.8 (C), 31.8 (CH_3), 30.0 (CH_3). MS (ES+): m/z = 1109 $[M + H]^+$. IR: $\tilde{\nu}$ = 2957, 2907, 2870, 1615, 1593, 1489, 1440, 1393, 1369, 1307, 1275, 1252, 1229, 1203, 1167, 937, 875, 861, 811, 774, 687 cm^{-1}.

$Ru_2[(BS2DP)(CO)_2]$ (16): A solution of BS2DP (250 mg, 0.225 mmol) and $Ru_3(CO)_{12}$ (220 mg, 0.470 mmol) in diglyme (15 mL) was heated at 135 °C for 12 h. The reaction mixture was cooled to room temperature, filtered and concentrated to dryness under reduced pressure. The resulting dark red residue was chromatographed on alumina (II−III) eluting first with $CHCl_3$ to remove a yellow and an orange band, followed by EtOH/$CHCl_3$ (5:95) to remove a red-pink band. The latter was concentrated to dryness

under vacuum affording a glassy purple solid. Yield: 277 mg (91%). ^{1}H NMR (300 MHz, [D$_6$]acetone, 22 °C): δ = 9.20 (s, 4 H), 7.96 (s, 4 H), 7.49 (d, *J* = 2.7 Hz, 4 H), 7.41 (d, *J* = 2.4 Hz, 4 H), 1.55 (s, 36 H), 1.35 (s, 36 H). ^{13}C NMR APT (125.7 MHz, [D$_6$]acetone, 22 °C): δ = 170.6 (C), 157.1 (CH), 143.2 (C), 142.7 (C), 140.4 (C), 135.4 (C), 130.9 (CH), 130.2 (CH), 121.8 (C), 103.5 (CH), 36.6 (C), 34.5 (C), 31.7 (CH$_3$), 30.4 (CH$_3$). MS (ES+): *m*/*z* = 1363 [M$^+$]. UV/Vis (CH$_2$Cl$_2$): λ$_{max}$ [nm] (log ε [M^{-1}cm^{-1}]) = 262 (4.67), 302 (4.59), 313 (4.61), 375sh (4.59), 393 (4.64), 420sh (4.44), 507 (4.30) 550sh (4.19). Selected IR: $\tilde{\nu}$ = 1943 (CO) cm^{-1}.

Ru$_2$[(BS2DP)(CO)$_2$(py)$_2$] (17): A solution of pyridine (0.25 mL) in CH$_2$Cl$_2$ (5 mL) was treated with **16** (50 mg, 0.055 mmol) and stirred at room temperature for 30 min. The solvents were evaporated to dryness and the residue was applied to a small column of silica gel (1 × 2 cm) and eluted with CH$_2$Cl$_2$. The first band was collected and concentrated to dryness under vacuum affording a dark purple solid. Yield: 51.4 mg (81%). ^{1}H NMR (300 MHz, CD$_2$Cl$_2$, 22 °C): δ = 8.72 (s, 4 H), 8.16 (m, 4 H), 7.63 (t, *J* = 2.4 Hz, 2 H), 7.60 (s, 4 H), 7.43 (d, *J* = 2.4 Hz, 4 H), 7.14 (m, 8 H), 1.54 (s, 36 H), 1.32 (s, 36 H). ^{13}C NMR APT (125.7 MHz, CD$_2$Cl$_2$, 22 °C): δ = 170.0 (C), 154.5 (CH), 149.5 (CH), 149.5 (CH), 143.1 (C), 142.1 (C), 139.9 (C), 138.1 (CH), 135.3 (C), 130.2 (CH), 130.0 (CH), 124.7 (CH), 124.6 (CH), 120.5 (C), 102.5 (CH), 36.3 (C), 34.2 (C), 31.4 (CH$_3$), 29.9 (CH$_3$). MS (ES+): *m*/*z* = 1522 [M$^+$]. Selected IR: $\tilde{\nu}$ = 1951, 1934 (CO) cm^{-1}.

Ni$_2$(BS2DP): A solution of **BS2DP** (150 mg, 0.135 mmol) and Ni(OAc)$_2$(H$_2$O)$_4$ (168 mg, 0.676 mmol) in diglyme (15 mL) was heated at 140 °C for 10 h under argon. The reaction mixture was cooled to room temperature and the red solution was concentrated to dryness. The residue was suspended in hot 95% EtOH (30 mL), filtered while hot and washed with EtOH. The product was then dried under vacuum. Yield: 140 mg (85%). ^{1}H NMR (300 MHz, [D$_8$]THF, 22 °C): δ = 8.40 (s, 4 H), 7.63 (s, 2 H), 7.41 (d, *J* = 2.7 Hz, 4 H), 7.26 (d, *J* = 2.4 Hz, 4 H), 1.47 (s, 36 H), 1.33 (s, 36 H). ^{13}C NMR APT (125.7 MHz, [D$_8$]THF, 22 °C): δ = 165.4 (C), 156.2 (CH), 141.0 (C), 141.0 (C), 140.1 (C), 137.2 (C), 130.9 (CH), 127.8 (CH), 120.9 (C), 103.2 (CH), 36.6 (C), 34.6 (C), 31.6 (CH$_3$), 30.3 (CH$_3$). MS (MALDI, no matrix): *m*/*z* = 1222 [M$^+$]. UV/Vis (CH$_2$Cl$_2$): λ$_{max}$ [nm] (log ε [M^{-1}cm^{-1}]) = 246sh (4.74), 270 (4.88), 304sh (4.61), 313 (4.63), 392 (4.65), 429 (4.63), 505 (4.40). IR: $\tilde{\nu}$ = 2956, 2908, 2869, 1617, 1590, 1526, 1494, 1480, 1464, 1429, 1386, 1358, 1322, 1298, 1258, 1238, 1207, 1175, 1130, 1024, 960, 934, 917, 867, 842, 787, 676, 638 cm^{-1}.

Porphyrin Complex 18a: A solution of Crossely's bis(porphyrin) (225 mg, 0.100 mmol) and Ru$_3$(CO)$_{12}$ (215 mg, 0.338 mmol) in phenol (2.0 g) was heated under reflux for 1 h, under argon. The reaction mixture was cooled to room temperature and diluted with EtOH (2 mL), and the crude product was precipitated by adding water. The crude product was collected by filtration and washed with H$_2$O/EtOH (50:50) to remove the phenol. The dark brown solid was dissolved in toluene and chromatographed on alumina (II−III) eluting first with toluene to remove an orange band, followed by CH$_2$Cl$_2$ to remove a yellow band, and then with a mixture of EtOH/CH$_2$CH$_2$ (5:95) to remove a dark brown band. The latter

Table 3. Crystallographic data for the nickel(II) analogues of **14** and **16**

	14	**16**
Empirical formula	$C_{66}H_{86}N_4Ni_2O_4{\cdot}1.4C_3H_6O{\cdot}0.3CH_2Cl_2$	$C_{72}H_{84}N_4Ni_2O_6{\cdot}2C_4H_8O$
Molecular mass	1226.83	1367.09
Crystal size [mm]	0.38 × 0.37 × 0.33	0.28 × 0.27 × 0.08
Crystal system	orthorhombic	monoclinic
Space group	*Pbcn* (no. 60)	$P2_1/c$ (no. 14)
a [Å]	27.4494(13)	10.6955(15)
b [Å]	21.7996(11)	14.073(2)
c [Å]	23.3535(12)	25.424(4)
β [°]		95.733
Z	8	2
V [Å^3]	13974.4(12)	3807.7(9)
Density [g cm^{-3}]	1.166	1.192
μ [mm^{-1}]	0.612	0.550
Data collection 2θ limit [°]	52.82	52.82
Total data collected	88377	16031
Independent reflections	14337	7685
Observed data with $I \geq 2\sigma(I)$	10691	4974
Absorption correction method	*SADABS*	*SADABS*
Range of transmission factors	0.8236−0.8007	0.9574−0.8613
Data/restraints/parameters	14337/15[a] /740	7685/0/424
Goodness-of-fit on F^2	1.054	0.972
Final *R* indices [$I \geq 2\sigma(I)$][b]		
$R_1 = [F_o^2 \geq 2\sigma(F_o^2)]$	0.0667	0.0519
$wR_2 = [F_o^2 \geq -3\sigma(F_o^2)]$	0.2130	0.1291
Largest difference peak/hole	2.350/−1.647 e·Å^{-3}	0.577/−0.273 e·Å^{-3}

[a] The following distance restraints were applied to the disordered solvent acetone and dichloromethane molecules: *d*(O2S−C5S) = *d*(O3S−C8S) = 1.22 Å; *d*(C4S−C5S) = *d*(C5S−C6S) = *d*(C8S−C9S) = 1.54 Å; *d*(O2S···C4S) = *d*(O2S···C6S) = *d*(O3S···C9S) = 2.40 Å; *d*(C4S···C6S) = *d*(C9S···C9S′) = 2.67 Å; *d*(Cl1S−C7S) = *d*(Cl2S−C7S) = *d*(Cl3S−C10S) = 1.80 Å; *d*(Cl1S···Cl2S) = *d*(Cl3S···Cl3S′) = 2.95 Å [primed atoms are related to unprimed ones by the crystallographic twofold rotational axis (0, *y*, $^1/_4$)]. [b] $R_1 = \Sigma||F_o| - |F_c||/\Sigma|F_o|$; $wR_2 = \{\Sigma[w(F_o^2 - F_o^2)^2]/\Sigma[w(F_o^4)]\}^{1/2}$.

was concentrated to dryness under vacuum and recrystallized from hydrous ethanol to give a brown solid. Yield 168 mg (65%). ^{1}H NMR (500 MHz, CD_2Cl_2, 22 °C): δ = 8.75 (s, 4 H), 8.72 (d, J = 5.0 Hz, 4 H), 8.63 (d, J = 5.0 Hz, 4 H), 8.53 (s, 2 H), 8.11 (m, 4 H), 8.06 (m, 4 H), 8.02 (m, 8 H), 7.99 (m, 4 H), 7.83 (m, 4 H), 1.56 (m, 144 H), 0.83 (broad, EtOH). ^{13}C NMR (125.7 MHz, CD_2Cl_2, 22 °C): δ = 153.1, 149.4, 149.3, 149.2, 147.0, 144.4, 143.0, 141.6, 141.5, 139.9, 137.1, 132.8, 131.0, 132.43, 129.5, 129.3, 129.2, 129.2, 128.9, 128.8, 125.9, 121.5, 120.3, 120.2, 35.4, 35.3, 32.3, 31.9. MS (ES+): m/z = 2508 [M − 2 EtOH]$^+$. Selected IR: $\tilde{\nu}$ = 1956 (CO) cm^{-1}.

Porphyrin(pyridine) Complex 18b: A solution of pyridine (0.25 mL) in dichloromethane (5 mL) was treated with porphyrin complex **18a** (30.0 mg, 0.012 mmol) and stirred at room temperature for 30 min. The solvents were evaporated and the residue applied to a small column of silica gel (1 × 2 cm) and eluted with CH_2Cl_2. The first band was collected and concentrated to dryness affording a dark brown solid. Yield: 20.0 mg (63%). ^{1}H NMR (300 MHz, CD_2Cl_2, 22 °C): δ = 8.69 (s, 4 H), 8.65 (d, J = 4.8, Hz 4 H), 8.57 (d, J = 4.8 Hz 4 H), 8.45 (s, 2 H), 8.05 (m, 4 H), 8.03 (m, 4 H), 7.96 (m, 8 H), 7.90 (m, 4 H), 7.81 (m, 4 H), 6.29 (t, J = 7.5 Hz, 2 H), 5.46 (t, J = 7.5 Hz, 4 H), 2.13 (d, J = 5.1 Hz, 4 H), 1.55 (s, 72 H), 1.53 (s, 36 H), 1.52 (s, 36 H). ^{13}C NMR (125.7 MHz, CD_2Cl_2, 22 °C): δ = 153.4, 149.4, 149.3, 149.3, 149.2, 149.0, 146.4, 144.8. 143.9, 142.6, 141.7, 141.7, 139.8, 136.5, 135.4, 135.4, 132.8, 132.1, 131.4, 130.0, 129.8, 129.5, 129.4, 129.0, 128.7, 128.6, 125.5, 122.6, 121.4, 120.2, 120.1, 35.4, 35.3, 32.3, 31.8. MS (ES+): m/z = 2508 [M − 2 py]$^+$. Selected IR: $\tilde{\nu}$ = 1966 (CO) cm^{-1}.

X-ray Crystallographic Study: The crystallographic data for the complexes Ni_2(BS2P), and Ni_2(BS2DP) are shown in Table 3. Crystals of Ni_2(BS2P) were grown from a mixture acetone/CH_2Cl_2 and crystals of Ni_2(BS2DP) were grown from THF. X-ray data were collected with a Bruker PLATFORM/SMART 1000 CCD at 193 K using a graphite-monochromated Mo-K_α radiation (λ = 0.71073 Å) by taking ω scans at 0.2° intervals. The structures were solved by direct methods/fragment search using the computer program DIRDIF-96 and refined by full-matrix least squares, with anisotropic displacement parameters for the non-hydrogen atoms, using the computer program SHELXL-93. Hydrogen atoms were introduced in their idealized positions as indicated by the sp^2 or sp^3 geometries of their attached carbon atoms. Crystallographic data (excluding structure factors) for the structures reported in this paper have been deposited with the Cambridge Crystallographic Data Centre as supplementary publication no. CCDC-162995 (**14**) and -162996 (**16**). Copies of the data can be obtained free of charge on application to CCDC, 12 Union Road, Cambridge CB2 1EZ, UK [Fax: (internat.) + 44-1223/336-033; E-mail: deposit@ccdc.cam.ac.uk].

Acknowledgments

This work was supported by the University of Alberta and the Natural Sciences and Engineering Research Council of Canada. We are grateful Dr. Robert McDonald for the X-ray crystallographic analysis.

[1] [1a] T. Imamura, K. Fukushima, *Coord. Chem. Rev.* **2000**, *198*, 133−156. [1b] M. J. Gunter, N. Bampos, K. D. Johnstone, J. K. M. Sanders, *New J. Chem.* **2001**, *25*, 166−173. [1c] J. E. Redman, N. Feeder, S. J. Teat, J. K. M. Sanders, *Inorg. Chem.*, in print, advance article. [1d] E. Iengo, E. Zangrando, S. Mestroni, G. Fronzoni, M. Stener, E. Alessio, *J. Chem. Soc., Dalton Trans.* **2001**, 1338−1346. [1e] U. Michelsen, C. A. Hunter, *Angew. Chem. Int. Ed.* **2000**, *39*, 764−767. [1f] R. A. Haycock, A. Yartsev, U. Michelsen, V. Sundström, C. A. Hunter, *Angew. Chem. Int. Ed.* **2000**, *39*, 3616−3619. [1g] Y. Diskin-Posner, S. Dahal, I. Goldberg, *Angew. Chem. Int. Ed.* **2000**, *39*, 1288−1292. [1h] A. Prodi, M. T. Indelli, C. J. Kleverlaan, F. Scandola, E. Alessio, T. Gianferrara, L. G. Mazilli, *Chem. Eur. J.* **1999**, *5*, 2668−2679.

[2] [2a] D. Gust, T. A. Moore, A. L. Moore, *Acc. Chem. Res.* **2001**, *34*, 40−48. [2b] M. Andersson, M. Linke, J.-C. Chambron, J. Davidsson, V. Heitz, J.-P. Sauvage, L. Hammarström, *J. Am. Chem. Soc.* **2000**, *122*, 3526−3527. [2c] L. Flamigni, I. M. Dixon, J.-P. Collin, J.-P. Sauvage, *Chem. Commun.* **2000**, 2479−2480. [2d] R. K. Lammi, A. Ambroise, T. Balasubramanian, R. W. Wagner, D. F. Bocian, D. Holten, J. S. Lindsey, *J. Am. Chem. Soc.* **2000**, *122*, 7579−7591. [2e] S. I. Yang, J. Li, H. S. Cho, D. Kim, D. F. Bocian, D. Holten, J. S. Lindsey, *J. Mater. Chem.* **2000**, *10*, 283−296. [2f] J. Brettar, J.-P. Gisselbrecht, M. Gross, N. Solladié, *Chem. Commun.*, in print, advanced article. [2g]S. Richeter, C. Jeandon, R. Ruppert, H. J. Callot, *Chem. Commun.* **2001**, 91−92. [2h] C. M. Drain, X. Shi, T. Milic, F. Nifiatis, *Chem. Commun.* **2001**, 287−288. [2i] S. Yagi, I. Yonekura, M. Awakura, M. Ezoe, T. Takagishi, *Chem. Commun.* **2001**, 557−558. [2j] A. Nakano, T. Yamazaki, Y. Nishimura, I. Yamazaki, A. Osuka, *Chem. Eur. J.* **2000**, *6*, 3254−3271. [2k] N. Aratani, A. Osuka, Y. H. Kim, D. H. Jeong, D. Kim, *Angew. Chem. Int. Ed.* **2000**, *39*, 1458−1462. [2l] K. KilsÅ, J. Kajanus, A. N. Macpherson, J. MÅrtensson, B. Albinsson, *J. Am. Chem. Soc.* **2001**, *123*, 3069−3080. [2m] H. Imahori, K. Tamaki, D. M. Guldi, C. Luo, M. Fujitsuka, O. Ito, Y. Sakata, S. Fukuzumi, *J. Am. Chem. Soc.* **2001**, *123*, 2607−2617. [2n] H. Imahori, H. Norieda, H. Yamada, Y. Nishimura, I. Yamazaki, Y. Sakata, S. Fukuzumi, *J. Am. Chem. Soc.* **2001**, *123*, 100−110. [2o] K. Ogawa, Y. Kobuke, *Angew. Chem. Int. Ed.* **2000**, *39*, 4070−4073. [2p] F. Fungo, L. A. Otero, L. Sereno, J. J. Silber, E. N. Durantini, *J. Mater. Chem.* **2000**, *10*, 645−650. [2q] Y. Sakakibara, S. Okutsu, T. Enokida, T. Tani, *Thin Solid Films* **2000**, *363*, 29−32.

[3] A. W. Herlinger, K. Ramakrishna, *Polyhedron* **1985**, *4*, 551−561.

[4] [4a] K. Chichak, N. R. Branda, *Chem. Commun.* **2000**, 1211−1212. [4b] K. Chichak, M. C. Walsh, N. R. Branda, *Chem. Commun.* **2000**, 847−848. [4c] K. Chichak, N. R. Branda, *Chem. Commun.* **1999**, 523−524.

[5] F. Calderazzo, C. Floriani, R. Henzi, F. L'Eplattenier, *J. Chem. Soc. A* **1969**, 1378−1386.

[6] N. Farrell, M. N. De Oliveira Bastos, A. A. Neves, *Polyhedron* **1983**, *2*, 1243−1246.

[7] M. M. Taqui Khan, Z. A. Shaikh, *Ind. J. Chem.* **1992**, *31A*, 191−194.

[8] J. Wöltinger, J.-E. Bäckvall, Á. Zsigmond, *Chem. Eur. J.* **1999**, *5*, 1460−1467.

[9] A. L. Singer, D. A. Atwood, *Inorg. Chim. Acta* **1998**, *277*, 157−162.

[10] For a good discussion of pyridine as a π-acid in ruthenium(II) carbonyl complexes, see: R.-J. Cheng, S.-H. Lin, H.-M. Mo, *Organometallics* **1997**, *16*, 2121−2126.

[11] E. C. Constable, A. M. W. Cargrill Thompson, *J. Chem. Soc., Dalton Trans.* **1994**, 1409−1418.

[12] E. C. Constable, A. M. W. Cargrill Thompson, *J. Chem. Soc., Dalton Trans.* **1992**, 2947−2950.

[13] R. J. Morgan, A. D. Baker, *J. Org. Chem.* **1990**, *55*, 1986−1993.

[14] For the synthesis of the dibenzodioxin fragment, see: [14a] R. C. Cambie, S. J. Janssen, P. S. Rutledge, P. D. Woodgate, *J. Organomet. Chem.* **1991**, *420*, 387−418. For the nitration of

the dibenzodioxin fragment, see: [14b] H. Gilman, J. J. Dietrich, *J. Am. Chem. Soc.* **1958**, *80*, 366−368. For the reduction of the nitrated compound, see: [14c] W. Knobloch, H. Niedrich, *Chem. Ber.* **1958**, *91*, 2562−2566.

[15] A pair of *cis* and *trans* diastereomers has also been reported for multimetallic porphyrin monomers: S. C. Darling, P. K. Y. Goh, N. Bampos, N. Feeder, M. Montalti, L. Prodi, B. F. G. Johnson, J. K. M. Sanders, *Chem. Commun.* **1998**, 2031−2032.

[16] M. J. Crossley, P. L. Burn, *J. Chem. Soc., Chem. Commun.* **1987**, 39−40.

[17] V. Promarak, P. L. Burn, *J. Chem. Soc., Perkin Trans. 1* **2001**, 14−20.

[18] [18a] A. M. El-Hendawy, A. H. Alkubaisi, A. El-Ghany El-Kourashy, M. M. Shanab, *Polyhedron* **1993**, *12*, 2343−2350. [18b] M. M. Taqui Khan, Z. A. Shaikh, R. I. Kureshy, A. B. Boricha, *Polyhedron* **1992**, *11*, 91−100. [18c] M. M. Taqui Khan, D. Srinivas, R. I. Kureshy, N. H. Khan, *Inorg. Chem.* **1990**, *29*, 2320−2326.

Received April 30, 2001
[I01149]

Unusual Coordination of the Rare Neutral Imine Tautomer of 9-Methyladenine Chelating in the *N*6,*N*7-Mode to Ruthenium(II) Complexes

Anna C. G. Hotze,[a] Marjolein E. T. Broekhuisen,[a] Aldrik H. Velders,[a][+] Karlijn van der Schilden,[a] Jaap G. Haasnoot,[a] and Jan Reedijk*[a]

Keywords: Ruthenium / Cytotoxicity / NMR spectroscopy / DNA model bases

The coordination of the DNA model base 9-methyladenine (9-MeAde) to both complexes *cis*-[Ru(bpy)$_2$Cl$_2$] and α-[Ru(azpy)$_2$(NO$_3$)$_2$] is reported. Structural characterisation using 2D NMR techniques and variable-temperature NMR studies between 25 and –55 °C show that in the compounds α-[Ru(azpy)$_2$(9-MeAde)](PF$_6$)$_2$ (**1**) and *cis*-[Ru(bpy)$_2$(9-MeAde)](PF$_6$)$_2$ (**2**), 9-MeAde is coordinated to the ruthenium ion in a chelating mode via its N7 and exocyclic N6 atoms. The NMR spectroscopic data unambiguously prove the occurrence of the rare imine tautomer of 9-MeAde in these complexes, which is clearly stabilised by the bidentate coordination of 9-MeAde in both complexes. Variable-temperature NMR spectra and 2D COSY data show that the H2 resonance of 9-MeAde in **1** and **2** appears as a doublet at low temperatures and shows a COSY cross peak to the NH1 resonance of 9-MeAde, which confirms the protonation at the N1 site. This protonated N1 site, together with an observed pK_a of ca. 6.5 of compound **1** is in agreement with the presence of the imine tautomeric form of 9-MeAde. As the binding mode of 9-MeAde to both *cis*-[Ru(bpy)$_2$] and α-[Ru(azpy)$_2$] moieties is the same, this binding mode does not explain the earlier observed difference in cytotoxicity between *cis*-[Ru(bpy)$_2$Cl$_2$] and α-[Ru(azpy)$_2$Cl$_2$].

Introduction

Currently, several ruthenium complexes are under investigation for their antitumour properties, and amongst them are polypyridyl−ruthenium complexes.[1−3] The in vitro cytotoxicity of three isomeric bis(2-phenylazopyridine)ruthenium(II) complexes, [Ru(azpy)$_2$Cl$_2$], has recently been reported.[4] The so-called α isomer, α-[Ru(azpy)$_2$Cl$_2$] (α corresponding with the isomer in which the coordinating pairs Cl, N(py), and N(azo) are *cis*, *trans*, and *cis*, respectively), shows remarkably high cytotoxicity against a series of tumour-cell lines.[4] This high cytotoxicity is in contrast to the low cytotoxicity of its isomeric complexes[4] β-[Ru(azpy)$_2$Cl$_2$] and γ-[Ru(azpy)$_2$Cl$_2$] and the structurally related complex[5] *cis*-[Ru(bpy)$_2$Cl$_2$] (where bpy is 2,2′-bipyridine). Therefore, in the search for a structure-activity relationship of antitumour-active ruthenium complexes, the investigation of complexes of the type *cis*-[Ru(LL)$_2$Cl$_2$] (with LL being a heterocyclic bidentate ligand like azpy or bpy) is very useful. Since it is generally accepted that DNA might be the target for antitumour-active ruthenium complexes,[1−3] as in the case for antitumour-active platinum complexes,[6−8] the interaction of the [Ru(azpy)$_2$Cl$_2$] complexes with DNA model bases has been studied.[3,9] The α-[Ru(azpy)$_2$Cl$_2$] compound is poorly soluble in aqueous solutions, and therefore the analogous water-soluble nitrate complex, α-[Ru(azpy)$_2$(NO$_3$)$_2$], has been synthesized and used for DNA model base binding studies.[9]

The reaction of the DNA model base 9-ethylguanine (9-EtGua) to α-[Ru(azpy)$_2$(NO$_3$)$_2$] and the structurally similar, but noncytotoxic *cis*-[Ru(bpy)$_2$Cl$_2$], results in monofunctional binding of 9-EtGua in both cases.[9,10] The 9-EtGua binding studies and rotational aspects of smaller model bases, like 1-methylbenzimidazole, show that the α-[Ru(azpy)$_2$] moiety[3] is more versatile in its coordination to heterocycles than the *cis*-[Ru(bpy)$_2$] moiety.[11,12] To obtain a better understanding of all factors influencing the biological properties of α-[Ru(azpy)$_2$Cl$_2$] and *cis*-[Ru(bpy)$_2$Cl$_2$] (Figure 1), the binding of other DNA model bases and oligonucleotides is under investigation. The interaction with the DNA model base 9-methyladenine is presented in this paper. Of all DNA nucleobases, the adenine base exhibits the most flexible binding-site behaviour with metal ions.[13] In 9-substituted adenine derivatives the ring nitrogen atoms N1 and N7 are the predominant binding sites.[13] In certain cases metal ions may also bind to the exocyclic amino group after deprotonation of the exocyclic N6 nitrogen atom.[14−18]

Bidentate coordination of adenine derivatives is shown in dinuclear complexes in which the adenine derivative acts as

[a] Leiden Institute of Chemistry, Gorlaeus Laboratories, Leiden University,
P. O. Box 9502, 2300 RA Leiden, The Netherlands
Fax: (internat.) + 31-71/527-4671
E-mail: reedijk@chem.leidenuniv.nl
[+] Magnetic Resonance Center (CERM), University of Florence, Via Luigi Sacconi, 6, 50019, Sesto Fiorentino (Florence), Italy
Supporting information for this article is available on the WWW under http://www.eurjic.com or from the author.

 © WILEY-VCH Verlag GmbH, 69451 Weinheim, Germany, 2002 1434−1948/02/0202−0369 $ 17.50+.50/0

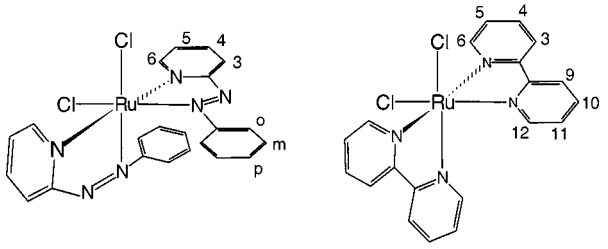

Figure 1. Comparison of the schematic structures of the Λ enantiomers of α-[Ru(azpy)$_2$Cl$_2$] (left) and *cis*-[Ru(bpy)$_2$Cl$_2$] (right)

a bridging ligand between the two metal sites. This bridging coordination occurs via the N6 and N7 atoms of the 9-ethyladenine (9-EtAde), like in the dinuclear Mo structure[19] [Mo$_2$(O$_2$CCHF$_2$)$_2$(9-EtAde)$_2$(MeCN)$_2$](BF$_4$)$_2$·2MeCN and a related dinuclear Rh structure.[20,21] In the tetrameric carbonylrhodium(I) complex [(CO)$_2$Rh(μ-3-MeAde$_{-H}$)]$_4$ the bridging *N*6,*N*7 coordination of deprotonated 3-methyladenine (3-MeAde) is also shown.[22] In a dirhenium carboxylate complex the bridging coordination of adenine occurs via its N1 and N6 atoms.[23] Bidentate coordination in which the N6 and N7 atoms of adenine (Ade) derivatives are coordinated to the same metal site have been reported for the tetrameric (cymene)Ru^{II} complex[24] [{Ru(Ade$_{-H}$)-(η^6-*p*-cymene)}$_4$](CF$_3$SO$_3$)$_4$, the trinuclear complex [{Ru(9-EtAde$_{-H}$)(η^6-*p*-cymene)}$_3$](CF$_3$SO$_3$)$_3$, and in related complexes[25] with adenosine bases. Also, in the case of other metal complexes like Mo, Ir, and Rh, an *N*6,*N*7 coordination of adenine derivatives to one metal site has been observed.[26−28]

In DNA, adenine is mainly present in its amine tautomeric form (Figure 2) in which form it can take part in Watson−Crick base pairing with thymine. It is estimated[29]

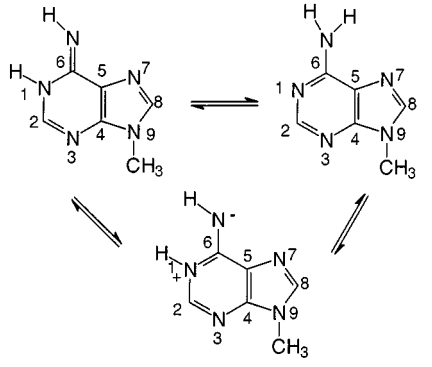

Figure 2. Tautomeric structures of 9-MeAde: the imine form (left) the amine form (right) and the zwitterionic form (bottom)

that the ratio of the amine to the imine tautomer (Figure2) in neutral adenine is approximately 10^4 to 10^5. This tautomeric equilibrium might be influenced by metal coordination.[29−31] To the best of our knowledge, only a few examples of metallated adenine derivatives are known in which it is explicitly proven by NMR spectroscopy and/or a crystal structure that the adenine derivative is in the neutral imine form.[14,17−21] The imine form of adenine in DNA might result in nucleobase mispairing, which eventually results in mutations if not repaired.[29,30] Regarding the potential antitumour activity of ruthenium complexes, it is of biological relevance to obtain a better insight in their binding to adenine derivatives. In this paper the binding of 9-methyladenine (9-MeAde) to α-[Ru(azpy)$_2$(NO$_3$)$_2$] and *cis*-[Ru(bpy)$_2$Cl$_2$] is presented. NMR spectroscopic data show that in these adducts, 9-MeAde is coordinated in its rare imine form, likely stabilised by the *N*6,*N*7 coordination.

Results and Discussion

Synthesis and Characterisation

On dissolving α-[Ru(azpy)$_2$(NO$_3$)$_2$] in H$_2$O, hydrolysis of the nitrate ions occurs, resulting in α-[Ru(azpy)$_2$(H$_2$O)$_2$]$^{2+}$,[3,9] which consecutively coordinates to 9-MeAde. Also upon reaction of *cis*-[Ru(bpy)$_2$Cl$_2$] and 9-MeAde it is the aqua complex, *cis*-[Ru(bpy)$_2$(H$_2$O)$_2$]$^{2+}$, that coordinates to 9-MeAde. The reaction of α-[Ru-(azpy)$_2$(NO$_3$)$_2$] with 9-methyladenine (9-MeAde) was carried out at 40 °C because we have observed[9] that isomerisation from the α to the β isomer in aqueous solution does not occur at or below 40 °C. Both in α-[Ru(azpy)$_2$(NO$_3$)$_2$] and in *cis*-[Ru(bpy)$_2$Cl$_2$], two coordination sites, which are identical due to the presence of a C_2 axis in the complexes, are in theory available for coordination to DNA model bases after hydrolysis of the anions. However, NMR spectroscopy clearly proves the coordination of only one 9-MeAde ligand to the α-[Ru(azpy)$_2$] and *cis*-[Ru(bpy)$_2$] moieties. Also, when the reaction of α-[Ru(azpy)$_2$(NO$_3$)$_2$] or *cis*-[Ru(bpy)$_2$Cl$_2$] with 9-MeAde was repeated in a ratio 1:2, no bifunctional adducts of the type α-[Ru(azpy)$_2$(9-MeAde)$_2$](PF$_6$)$_2$ or *cis*-[Ru(bpy)$_2$(9-MeAde)$_2$](PF$_6$)$_2$ were obtained. The starting materials α-[Ru(azpy)$_2$(NO$_3$)$_2$] and *cis*-[Ru(bpy)$_2$Cl$_2$] were racemic mixtures containing equal amounts of Λ and Δ isomers, but as 9-MeAde is not chiral, no diastereoisomers were formed and consequently only one set of signals was observed. Nucleosides do have a chiral centre and on reaction of α-[Ru(azpy)$_2$(NO$_3$)$_2$] with guanosine[9] and adenosine[32] two different sets of signals were observed for the diastereoisomeric complexes. The binding pattern of adenine derivatives to metal complexes

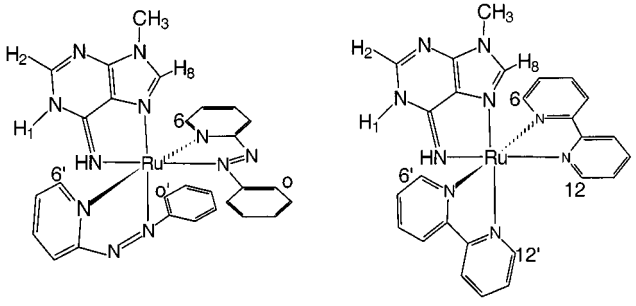

Figure 3. *N*6,*N*7-Bidentate coordination of 9-MeAde in the Λ enantiomers of α-[Ru(azpy)$_2$(9-MeAde)](PF$_6$)$_2$ (left) and *cis*-[Ru(bpy)$_2$(9-MeAde)](PF$_6$)$_2$ (right) (with proton numbering used for the NMR assignments)

is known to be very complex (vide supra), and the bidentate coordination of 9-MeAde to the α-[Ru(azpy)$_2$] and *cis*-[Ru(bpy)$_2$] moieties was not for certain beforehand. Moreover, NMR characterisation of bidentate coordination and confirmation of the imine tautomer of adenine derivatives in metal complexes is not very clear from literature, and especially the assignment of adenine resonances is sometimes confusing.[20,21] Therefore, in the presented work, a detailed NMR study was performed in order to investigate the binding mode of 9-MeAde in the bifunctional ruthenium(II) complexes.

Mass spectrometry data of α-[Ru(azpy)$_2$(9-MeAde)](PF$_6$)$_2$ show two molecule-ion peaks; apparently a part of the sample is protonated and a part of the sample is deprotonated, i.e. *m*/*z* = 616 {α-[Ru(azpy)$_2$(9-MeAde)]$^{2+}$ − H$^+$}$^+$ and *m*/*z* = 308 {α-[Ru(azpy)$_2$(9-MeAde)]$^{2+}$}. The same observation was made in *cis*-[Ru(bpy)$_2$(9-MeAde)](PF$_6$)$_2$, i.e. two signals appear in the mass spectra, belonging to *cis*-[Ru(bpy)$_2$(9-MeAde)]$^{2+}$ and {*cis*-[Ru(bpy)$_2$(9-MeAde)]$^{2+}$ − H$^+$}$^+$. The elemental analysis of *cis*-[Ru(bpy)$_2$(9-MeAde)](PF$_6$)$_2$ shows the presence of co-crystallised water and acetone. The pseudo-crystalline material did not allow single-crystal X-ray analysis.

NMR Structural Characterisation of α-[Ru(azpy)$_2$(9-MeAde)](PF$_6$)$_2$

The ^{1}H NMR spectrum of the reaction product of α-[Ru(azpy)$_2$(NO$_3$)$_2$] with 9-methyladenine (9-MeAde), i.e. α-[Ru(azpy)$_2$(9-MeAde)](PF$_6$)$_2$ (**1**), in [D$_6$]acetone at 25 °C (see Figure 4, Table 1) shows two sets of azpy signals, which are the first indication of the formation of a 1:1 adduct. The α-[Ru(azpy)$_2$] backbone is C_2-symmetric, so both coordination sites are equivalent. The coordination of a DNA model base to one of the two coordination sites results in a compound that no longer has a C_2 axis, resulting in non-equivalent azpy ligands. The integration of the signals of 9-MeAde relative to the azpy signals confirms the monofunctional coordination of 9-MeAde. The assignment of all signals was made from 2D NOESY and COSY NMR spectroscopic data at 25 °C and variable-temperature ^{1}H NMR measurements (vide infra). Characteristic signals of coordinated 9-MeAde are H8 at δ = 8.51, H2 at δ = 8.18, NH1 as a broad signal at δ = 12, and the NH6 signal overlapping with the *meta* signals at δ ≈ 7.4. These NMR spectroscopic data do not answer the question whether 9-MeAde is present in its neutral imine form or protonated amine form, since four resonances of 9-MeAde would be expected in both cases. This question will be addressed in the next section.

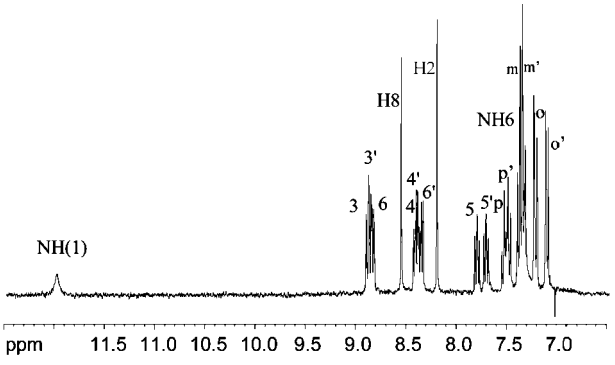

Figure 4. Low-field region of the ^{1}H NMR spectrum of α-[Ru(azpy)$_2$(9-MeAde)](PF$_6$)$_2$ in [D$_6$]acetone at 25 °C

No isomerisation of the α-[Ru(azpy)$_2$] moiety had taken place, since the interligand NOE cross-peak between the pyridine H6 protons and the phenyl ring *ortho* signals, H6-*o*′ and H6′-*o*, indicate presence of the α isomer.[3,9] The H8 resonance of the coordinated 9-MeAde was determined by its intraligand NOE cross peak with the CH$_3$ signal. The H8 signal of the coordinated 9-MeAde has an NOE cross peak to the *ortho* signal of one of the azpy ligands. This confirmed the *N*7 coordination of 9-MeAde and indicated the orientation of 9-MeAde in the complex with the H8 situated above the aza bond of the azpy ligand. In comparison to the resonance of H6, the signal of H6′ is shifted upfield by almost 0.5 ppm. This is easily explained by the orientation of 9-MeAde, which causes the H6′ of the azpy ligand to be shielded by the five-membered ring of 9-MeAde.

The experimental conditions used for the reaction of α-[Ru(azpy)$_2$(NO$_3$)$_2$] and 9-MeAde were the same as for the analogous reaction with 9-EtGua previously reported,[9] resulting in α-[Ru(azpy)$_2$(9-EtGua)(H$_2$O)](PF$_6$)$_2$ with a coordinated water molecule in the final adduct. Therefore, a coordinated water molecule was to be expected in the complex with 9-MeAde; however, the ^{1}H NMR spectrum shows no resonance to be assigned to this coordinated water ligand. This observation, in fact, is the first indication of a bidentate coordination of 9-MeAde to the α-[Ru(azpy)$_2$] moiety. Even though in theory, the absence of the proton

Table 1. Proton chemical shift values [ppm] for 9-methyladenine (9-MeAde) and α-[Ru(azpy)$_2$(9-MeAde)](PF$_6$)$_2$ (**1**) in D$_2$O (a) and [D$_6$]acetone (b) at 25 °C

	6/6′	3/3′	4/4′	5/5′	*p*/*p*′	*m*/*m*′	*o*/*o*′	H8	H2	NH(1)	NH(6)
9-MeAde (a)								8.20	7.93		
9-MeAde (b)								7.81	8.20		7.2
1 (a)	8.51	8.75	8.26/	7.59	7.51	7.33	7.06	8.07	8.02		
pH < 5	7.95	8.75	8.26	7.59	7.51	7.33	7.22				
1 (b)	8.83	8.91	8.38	7.80	7.50	7.39	7.24	8.53	8.20	11.9	7.4
	8.35	8.91	8.41	7.71	7.48	7.38	7.12				

resonance of coordinated water could also be caused by rapid exchange with residual water present in [D_6]acetone. To exclude the possibility of water exchange by traces of H_2O in [D_6]acetone (98%), [D_6]acetone (100%) was used, and again no proton resonance of a coordinated water molecule could be assigned.

The ^{1}H NMR spectrum of **1** in D_2O at 25 °C and pH ≈ 5, shows that the H8 resonance (δ = 8.10) is shifted downfield in comparison to the free ligand (δ = 7.93), whereas the H2 resonance is shifted upfield (from δ = 8.20 for the free ligand to δ = 8.03 in the complex). In [D_6]acetone the H8 (δ = 8.52) resonance of 9-MeAde in the complex is shifted significantly downfield corresponding to the free base (δ = 7.81) (Table 1). This downfield shift is most probably due to the deshielding effect of the phenyl ring of the azpy ligand. The phenyl ring rotates fast on the NMR time scale around the CN axis, but is likely to spend most of the time in an orientation with the phenyl ring not in-plane with the chelate, but more perpendicular to it. This would imply the H(*o*) atoms to be on average close to the H8, which is confirmed by the NOE cross peak between these two signals.

Variable-Temperature NMR Experiments of α-[Ru(azpy)$_2$-(9-MeAde)](PF$_6$)$_2$

The above-mentioned NMR spectroscopic data of **1** at room temperature show four aromatic 9-MeAde signals that suggest the 9-MeAde to be present in the imine tautomer. Therefore, the possible imine tautomer and coordination mode of 9-MeAde in the complex was further investigated by using variable-temperature NMR, as it is known that low-temperature measurements can shift signals apart and slow down rotational or exchange properties. In fact, upon lowering the temperature of **1** in [D_6]acetone from

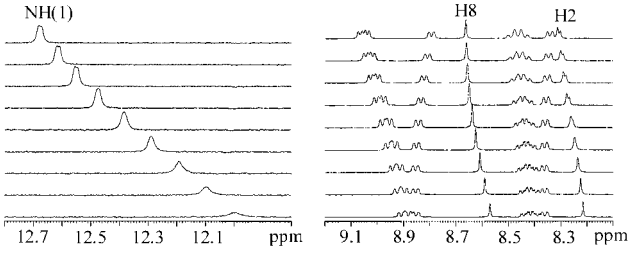

Figure 5. Variable-temperature ^{1}H NMR spectra of parts of the aromatic region of α-[Ru(azpy)$_2$(9MeAde)](PF$_6$)$_2$ in [D_6]acetone from 25 °C (bottom spectrum) to −55 °C (top spectrum); the shifting and sharpening of the NH1 signal (left) and the doubling of the H2 signal (right), prove the protonated N1 site

room temperature (25 °C) to −55 °C (Figure 5), the low-field broad signal (δ = 11.9) sharpened and shifted downfield (δ = 12.7). More importantly, the H2 signal of 9-MeAde also shifted downfield and became a doublet at −25 °C (see Figure 5). At temperatures below −55 °C, the H2 signal overlaps with the H6′ signal (not shown in Figure 5). 2D COSY experiments at −50 °C provide a cross peak between the singlet at δ = 12.8 and the doublet at δ = 8.3 (see Figure 6). This cross peak unambiguously confirms the signal at δ = 12.8 to be the NH1 (which means that this site is protonated) and the signal at δ = 8.3 to be the H2 proton. Although the NH1 resonance is not as clearly split into a doublet as the H2 resonance, probably due to line-broadening as the result of exchange with bulk water present in [D_6]acetone, the ^3J coupling of NH1 (which is hardly seen) is the same as the H2 resonance, i.e. 2.9 Hz. The exchange of the NH1 with bulk water is confirmed by the EXSY cross peak between residual water present in [D_6]acetone and the NH1 signal. In the 2D ROESY spectrum a weaker cross peak between the bulk water resonance and H2 was also observed, which is attributed to an exchange-COSY signal. The fact that the ^3J splitting of the H2 resonance is only observed at low temperatures is due to slower exchange of the NH1 proton with bulk water.

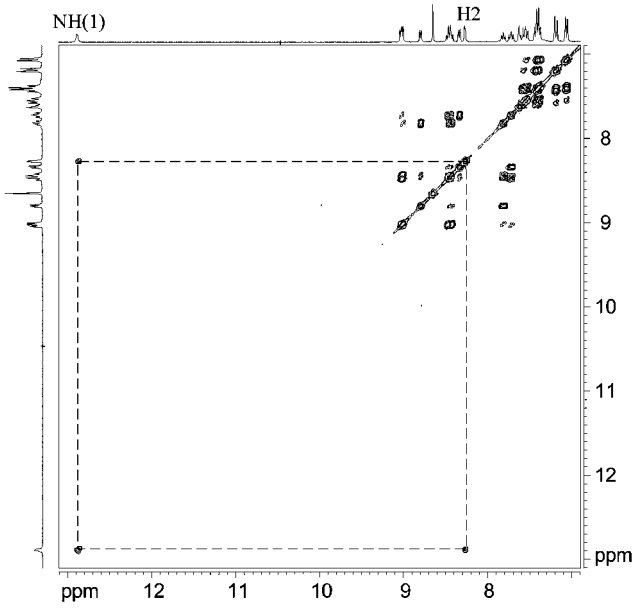

Figure 6. Low-field region of the COSY spectrum of α-[Ru(azpy)$_2$(9-MeAde)](PF$_6$)$_2$ in [D_6]acetone at −50 °C; the cross peak between the 9-MeAde NH(1) and H2 resonances is indicated with a dashed line

As the adduct **1** was isolated at pH ≈ 5, the protonation of N1 is not likely when 9-MeAde is in its amine form as the pK_a of an *N*7-metallated 9-MeAde is thought to be < 4, as in the case of Pt complexes.[33,34] Thus, in compound **1** the N1 protonation would only be possible if the 9-MeAde was present in its imine form. However, 9-MeAde being present in the zwitterionic form (Figure 2) could not a priori be excluded, as in that case the N1 and N6 atoms were also both protonated. For example, in the case of a (cymene)Ru^{II} complex [{Ru(Ade$_{-H}$)(η^6-*p*-cymene)}$_4$]-(CF$_3$SO$_3$)$_4$, Ade is probably present in the zwitterionic form, as shown by the relatively long N6−C6 distance in the crystal structure.[24] The combination of NMR spectroscopic and crystal structural data of the complex[19] [Mo$_2$(O$_2$CCHF$_2$)$_2$(9-EtAde)$_2$(MeCN)$_2$](BF$_4$)$_2$·2MeCN is in agreement with the results presented here. This crystal structure shows that the 9-EtAde molecules are bridging

ligands coordinated via the N7 and N6 nitrogen atoms and, importantly, are present in the neutral imine tautomer. The ^{1}H NMR spectrum of this Mo structure at −40 °C shows the NH1 signal at low field and the H2 resonance of 9-EtAde as a doublet, and so these resonances have a similar appearance as the 9-MeAde resonances of the present sample **1** at −55 °C. This confirms the presence of the imine form of 9-MeAde in sample **1**. In DNA, adenine in the imine form is very exceptional, but metal coordination might influence the equilibrium.[29−31] The imine form of 9-MeAde in **1** must apparently be stabilised by the bidentate coordination via the N7 and exocyclic N6 atoms. The presence of 9-MeAde coordinated in a bidentate fashion in **1** was also confirmed by the absence of an NMR signal of a coordinated water (vide supra), and by the pH experiments showing only one protonation step (vide infra).

As at low temperatures, 9-MeAde resonances no longer overlap with azpy resonances. 2D NOESY experiments were also performed at −50 °C. For example, at −50 °C the NH6 singlet was clearly seen at δ = 7.6, whereas at room temperature this signal showed overlap with the *meta* signals at δ ≈ 7.4. 2D NOESY and ROESY NMR spectroscopic data (600 MHz, Figure 7) at −50 °C show NOE signals between the H8 and H_o resonances, and between the NH6 and H6 resonances, confirming the orientation of 9-MeAde caused by the chelating mode of 9-MeAde via its N7 and N6 nitrogen atoms, i.e. the H8 positioned above the aza bond and the NH6 close to the H6 of the azpy ligand. In the NOE level of the 2D ROESY spectrum NH1 shows an NOE cross peak to NH6, which confirms the imine form. The NH1−NH6 distance (2.25 Å) of 9-EtAde, which is also present in the neutral imine form in the structure $[Rh_2(DTolF)_2(9\text{-}EtAde)_2(CH_3CN)][BF_4]_2$ (DTolF = *N*,*N*′-*para*-ditolylformamidinate), shows that an NOE cross-peak between NH1 and NH6 in compound **1** is likely.[20,21] However, the assignment[20] of the NH1 and NH6 signals of $[Rh_2(DTolF)_2(9\text{-}EtAde)_2(CH_3CN)][BF_4]_2$ is confusing as it was done by selective decoupling. By this method it is impossible to discriminate between both signals. On the other hand, it is also stated[21] that the NH1 and H2 resonances of $[Rh_2(DTolF)_2(9\text{-}EtAde)_2(CH_3CN)][BF_4]_2$ were determined by selective decoupling. In this presented work we have shown that 2D COSY NMR is a powerful technique for assigning the NH1 and H2 resonances of 9-MeAde in the imine form, and by using 2D NOESY NMR, the coupling between the NH1 and NH6 resonances proves the assignment of the NH6 resonance of 9-MeAde.

Protonation and Deprotonation of α-[Ru(azpy)$_2$(9-MeAde)](PF$_6$)$_2$

A pH titration of **1** in the pH range from 1 to 14, followed by ^{1}H NMR spectroscopy, shows only one protonation step, indicating a pK_a of 6.5 for NH1 (see Supporting Information, S1). The fact that only one protonation step was observed confirms the bidentate coordination of 9-MeAde. In the case of α-[Ru(azpy)$_2$(9-EtGua)(H$_2$O)](PF$_6$)$_2$, two protonation steps were observed;[9] one for N1 of 9-EtGua and one for coordinated

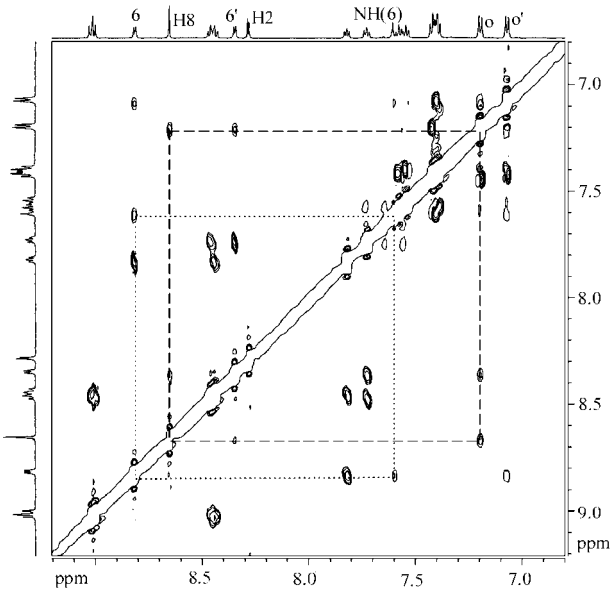

Figure 7. Aromatic region of the NOESY spectrum of α-[Ru(azpy)$_2$(9-MeAde)](PF$_6$)$_2$ in [D$_6$]acetone at −50 °C; the cross peaks between the 9-MeAde H8 and H_o resonances and the H6 and NH(6) signals are indicated with dashed and dotted lines, respectively

H_2O. The acidity of the free imine tautomer of 9-MeAde is estimated to have a pK_a for N1 of about 12.[15] In the case of adenine in the Hg complex [Hg(9-MeAde-*N*6)(1,3-dimeU-*C*5]NO_3·H_2O, in which 9-MeAde is present in its imine form and coordinated only via its exocyclic N6 nitrogen atom, the pK_a for deprotonation of NH1 is 4.5.[15] Therefore, in **1** the effect of ruthenium(II) is an increase in the acidity by about 5.5 log units in comparison to the acidity of the free imine tautomer of 9-MeAde; this shift seems to be reasonable in comparison to the Hg compound.[15]

The deprotonation behaviour of 9-MeAde of **1** in [D$_6$]-acetone was more complicated than in water. Depending on the pH at which the product of the reaction between α-[Ru(azpy)$_2$(NO$_3$)$_2$] and 9-MeAde was isolated, a mixture of **1** and the deprotonated form, α-[Ru(azpy)$_2$(9-MeAde$_{-H}$)](PF$_6$) (**1$_{-H}$**) could be obtained. In the ^{1}H NMR spectrum of either pure **1** or a mixture of **1** and **1$_{-H}$**, one set of signals was observed at room temperature. In the fully protonated sample, lowering the temperature of the sample only resulted in a shift of the signals and appearance of the NH1 and H2 resonances as doublets, as mentioned above and shown in Figure 5. However, in the case of a sample in which both **1** and **1$_{-H}$** were present, lowering the temperature resulted in ^{1}H NMR spectra showing signal broadening (from ca. 5 °C to −45 °C) and on further cooling, re-sharpening in two sets of signals at −75 °C (in a **1**/**1$_{-H}$** ratio of 1.5:1). This signal broadening and re-sharpening is likely due to **1** and **1$_{-H}$** being in fast exchange at the NMR time-scale at room temperature, intermediate exchange at temperatures from ca. 5 °C to −45 °C, and at slow exchange at −75 °C, resulting in the appearance of signals of both **1** and **1$_{-H}$**. After addition of some HNO_3

(1 M) to this sample of **1** and $\mathbf{1_{-H}}$, ^{1}H NMR spectroscopic data at −75 °C showed that the signals of $\mathbf{1_{-H}}$ were converted into one set of resonances (those of **1** only). Similarly, the addition of an excess of triethylamine in situ to **1** in [D_6]acetone at −75 °C resulted in one set of signals of α-[Ru(azpy)$_2$(9-MeAde$_{-H}$)](PF_6). In particular, the disappearance of the NH1 signal and the appearance of H2 as a singlet resonance instead of a doublet after addition of excess triethylamine in situ, indicated deprotonation of the NH1 site of 9-MeAde in the imine form. The significant upfield shift of the NH6 signal to δ = 5.7 can be seen as a characteristic after deprotonation of the NH1 site.

NMR Structural Characterisation of *cis*-[Ru(bpy)$_2$(9-MeAde)](PF_6)$_2$

The downfield region of the ^{1}H NMR spectrum of *cis*-[Ru(bpy)$_2$(9-MeAde)](PF_6)$_2$ (**2**) at 25 °C in [D_6]acetone (Table 2) shows two sets of bpy multiplet signals and the characteristic four singlet signals (H8, H2, NH1, and NH6) of the coordinated 9-MeAde ligand. The fact that the two bpy ligands were non-equivalent upon coordination of 9-MeAde, and the integration of the signals of 9-MeAde relative to the bpy signals, confirmed the presence of just one molecule of 9-MeAde. With the use of 2D NOESY and COSY experiments the bpy and 9-MeAde signals were assigned. The H8 resonance of 9-MeAde was assigned using the intraligand NOE coupling between the CH_3 and H8 signals. Interestingly, the H8 signal appears at higher field than the H2 resonance in contrast to the signals observed in the analogous ^{1}H NMR spectrum of **1** in which the H8 and H2 resonances appear in opposite order. The H8 signal at δ = 8.00 is shifted downfield with respect to the H8 of free 9-MeAde. The H2 resonance at δ = 8.11 is shifted upfield (δ = 0.3) relative to free 9-MeAde. Similar to the previously discussed NMR spectroscopic data of **1**, the absence of a coordinated water signal in the ^{1}H NMR spectrum of **2** suggests the bidentate coordination of 9-MeAde to the *cis*-[Ru(bpy)$_2$] moiety.

Variable-temperature ^{1}H NMR spectra show, similar to **1**, downfield shifting and sharpening of the NH1 signal of 9-MeAde and downfield shifting of the H2, H8, and NH6 signals of 9-MeAde upon decreasing the temperature. Remarkable again, is the splitting of the H2 signal into a doublet, most clearly seen at −50 °C (Figure 8). The NH1 and H2 signals were confirmed by a COSY cross peak between these two signals (see Supporting Information, Figure S2). A 2D ROESY NMR spectrum (600 MHz) (see Supporting Information, Figure S3) at −50 °C shows an NOE cross peak between NH1 and NH6 and together with the COSY cross peak NH1−H2, this confirms the imine tautomer of 9-MeAde. The H6 signal of bpy shows an NOE cross peak to NH6 and the H8 resonance shows an NOE cross peak to the H6′ signal. These NOE data are in agreement with the orientation of 9-MeAde caused by the bidentate coordination via its N7 and N6 nitrogen atoms. In summary, the 2D NMR spectroscopic data and variable-temperature ^{1}H NMR measurements indicate that in **2** 9-MeAde is in the neutral imine form and this tautomeric form is most likely stabilised by the chelating coordination via its N7 and N6 atoms. In this coordination mode the large difference in chemical shift of the H6 and H6′ resonances is explained because the H6′ atom is in the shielding cone of 9-MeAde.

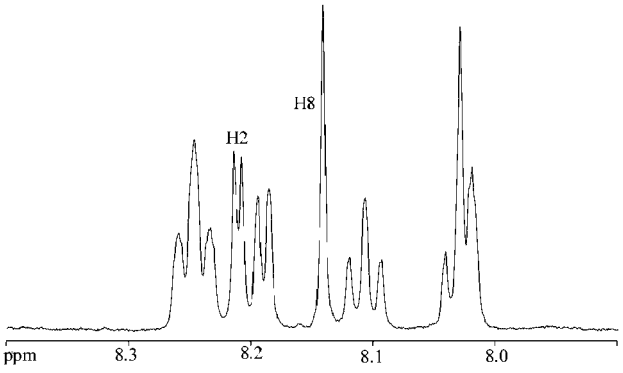

Figure 8. Enlargement of the aromatic region of the ^{1}H NMR spectrum in [D_6]acetone at −50 °C of *cis*-[Ru(bpy)$_2$(9-MeAde)](PF_6)$_2$ showing the 9-MeAde H2 signal as a doublet

Analogous to the results of **1**, after addition of triethylamine in situ at −50 °C, the ^{1}H NMR spectra of **2** show the disappearance of the NH1 signal, the appearance of the H2 signal, no longer as a doublet, and the NH6 resonance dramatically shifted upfield to δ = 5.3. These results are consistent with the formation of *cis*-[Ru(bpy)$_2$(9-MeAde$_{-H}$)](PF_6), in which 9-MeAde is still present in the imine form, now deprotonated at N1. Unfortunately, due to the poor solubility of **2** in water, the pK_a of this compound could not be determined.

Conclusions

The strong differences in biological activity between the structurally similar complexes *cis*-[Ru(bpy)$_2$Cl$_2$] and α-[Ru(azpy)$_2$Cl$_2$] encouraged us to investigate the binding of DNA model bases to the hydrolysis products of both com-

Table 2. Proton chemical shift values [ppm] for *cis*-[Ru(bpy)$_2$(9-MeAde)](PF_6)$_2$ (**2**) in [D_6]acetone at 25 °C

	6/6′	5/5′	4/4′	3/3′	12/12′	11/11′	10/10′	9/9′	H8	H2	NH(1)	NH(6)
2[a]	9.32 8.59	8.00 7.63	8.22/ 8.22	8.77 8.77	8.11 8.00	7.77 7.75	8.07 8.00	8.70 8.65	8.00	8.11	11.7	7.01

[a] The proton chemical shift values of **2** in D_2O could not be determined due to poor solubility of **2** in D_2O.

plexes. In this paper the coordination of 9-MeAde to both *cis*-$[Ru(bpy)_2(H_2O)_2]^{2+}$ and α-$[Ru(azpy)_2(H_2O)_2]^{2+}$ is presented. NMR spectroscopic data prove that, although the ruthenium ions in these two complexes have two available coordination sites, only one 9-MeAde coordinates to the metal ion. NMR structural characterisation using 2D NMR techniques and variable-temperature ^1H NMR spectra show that in both compounds α-$[Ru(azpy)_2$(9-MeAde)$](PF_6)_2$ (**1**) and in *cis*-$[Ru(bpy)_2$(9-MeAde)$](PF_6)_2$ (**2**), 9-MeAde is present in its rare neutral imine tautomeric form, apparently stabilised by the chelating coordination via its N7 and exocyclic N6 atoms. As the coordination mode of 9-MeAde is the same in both the azpy complex **1**, as in the bpy complex **2**, the difference in cytotoxicity of the parent chloride complexes cannot be explained by differences in the coordination of 9-MeAde around the ruthenium centre. At present, further investigation is focussed on the steric properties of the *cis*-$[Ru(LL)_2Cl_2]$ complexes (with LL being a heterocyclic bidentate ligand), to investigate the influence of steric hindrance of the LL ligand toward the free coordination sites in order to obtain a structure-activity relationship of antitumour-active ruthenium complexes. Nevertheless, the interesting imine tautomer of 9-MeAde, stabilised by the bidentate coordination to the ruthenium ion reported here, represents a structural model for any metal ion of interest with a nucleobase where coordination influences the tautomeric equilibrium. There might be biological consequences of the occurrence of the imine form of 9-MeAde upon coordination of 9-MeAde to ruthenium(II). It has already been questioned whether Pt coordination does shift the tautomer equilibrium towards the imine form, but Lippert et al. reported[35] that for the compound $[Cl_3Pt(9MeA)]^-$ the shift in favour for the imine tautomer is too small to explain the observed preferential Ademine−Thymine (AT) transversion. It is generally accepted that the mutation pathway of the AT transversion involves a pairing between one of the two adenines in the rare imine tautomer and the other adenine in the normal amine tautomer in a *syn* conformation.[35] Speculatively, the obvious shift towards the imine tautomer of 9-MeAde presented in this study might result in AT transversions when these ruthenium compounds coordinate to DNA.

In conclusion, a very interesting bidentate coordination of 9-MeAde in the complexes α-$[Ru(azpy)_2$(9-MeAde)$](PF_6)_2$ and *cis*-$[Ru(bpy)_2$(9-MeAde)$](PF_6)_2$ is observed in which 9-MeAde is present in its neutral imine tautomer.

Experimental Section

General Remarks: NMR experiments were performed at 300.13 MHz with a Bruker 300 DPX spectrometer and at 600.13 MHz with a Bruker 600 DPX spectrometer. Spectra were recorded in $[D_6]$acetone, calibrated on the residual solvent peak (δ_H = 2.06) using standard Bruker pulse programs. NOESY and ROESY spectra were recorded with mixing times of 1.0 and 0.5 s, respectively. The pH-dependent experiments were performed in D_2O and the pH was adjusted by HNO_3 (0.1 M) and NaOH (0.1 M). The direct pH-meter readings were used to estimate the pK_a values (no correction for the pD value was performed). Elemental analyses were carried out by the Chemical Services Unit of the University College, Dublin. Mass spectra were obtained by the chemical services of the Gorlaeus Laboratories with a Finnigan MAT 900 instrument equipped with an electrospray interface (ESI). Hydrated $RuCl_3$ was used as received from Johnson and Matthey, Inc. 2-(Phenylazopyridine) and α-$[Ru(azpy)_2Cl_2]$ were synthesised according to published methods.[36−38] α-$[Ru(azpy)_2(NO_3)_2]$ was prepared as described previously.[9] 9-Methyladenine was prepared by methylation of adenine with methyl iodide.[39] *cis*-$[Ru(bpy)_2Cl_2]$ $2H_2O$ was prepared according to a literature procedure.[40]

α-$[Ru(azpy)_2$(9-MeAde)$](PF_6)_2$ (1): 9-Methyladenine (0.027 g, 0.18 mmol) was added to solution of α-$[Ru(azpy)_2(NO_3)_2]$ (0.10 g, 0.17 mmol) in 32 mL of water. The purple reaction mixture was stirred at 40 °C for 7 d. After filtration, a concentrated aqueous solution of NH_4PF_6 was added and the precipitate was collected by filtration. The purple solid was purified by dissolution in acetone and addition of diethyl ether, and this purification step was repeated several times. Yield 0.12 g (77%). ESI MS: *m*/*z* = 616 (92) $\{\alpha\text{-}[Ru(azpy)_2(9\text{-}MeAde)]^{2+} - H^+\}^+$, 308 (100) $\{\alpha\text{-}[Ru(azpy)_2(9\text{-}MeAde)]^{2+}\}$. $C_{28}H_{25}F_{12}N_{11}P_2Ru$ (906.58): calcd. C 37.1, H 2.78, N 17.0; found C 37.1, H 2.76, N 16.1.

***cis*-$[Ru(bpy)_2$(9-MeAde)$](PF_6)_2$ (2):** A mixture of *cis*-$[Ru(bpy)_2Cl_2]$ (0.100 g, 0.19 mmol) and 9-MeAde (0.035 g, 0.23 mmol) in 70 mL of water and 30 mL of ethanol was heated under reflux for 16 h. The reaction mixture was concentrated by rotary evaporation and filtered at room temperature before a concentrated aqueous solution of NH_4PF_6 was added. The resulting orange precipitate was isolated by filtration and recrystallised from acetone/water. The orange crystalline material was washed with diethyl ether. Yield: 0.08 g (68%). ESI MS: *m*/*z* = 562 (68) $\{cis\text{-}[Ru(bpy)_2(9\text{-}MeAde)]^{2+} - H^+\}^+$,281 (100) $\{cis\text{-}[Ru(bpy)_2(9\text{-}MeAde)]^{2+}\}$. $C_{26}H_{23}F_{12}N_9P_2Ru{\cdot}C_3H_6O{\cdot}2.5H_2O$ (852.53 + 58 + 45): calcd. C 36.8, H 2.77, N 13.3; found C 36.8, H 3.05, N 13.3.

Note added in proof (November 9, 2001): The proposed structural details of **1** and **2** as discussed in this paper are confirmed by the recently elucidated crystal structure of α-$[Ru(azpy)_2$(3-MeAde)$](PF_6)$, which will be reported soon.

Acknowledgments

We thank C. Erkelens and A. W. M. Lefeber for assistance with the NMR pulse techniques and Johnson Matthey Chemicals for a generous loan of $RuCl_3{\cdot}3H_2O$. This research was sponsored by the Council for Chemical Sciences of The Netherlands Organisation for Scientific Research. Additional support from COST Action D8 (1997−2001) (Chemistry of Metals in Medicine) is gratefully acknowledged.

[1] M. J. Clarke, F. Zhu, D. R. Frasca, *Chem. Rev.* **1999**, *99*, 2511.
[2] B. K. Keppler, *Metal Complexes in Cancer Chemotherapy*, VCH Verlagsgesellschaft, Weinheim, Germany, **1993**.
[3] A. H. Velders, Leiden University, PhD thesis, **2000**.
[4] A. H. Velders, H. Kooijman, A. L. Spek, J. G. Haasnoot, D. de Vos, J. Reedijk, *Inorg. Chem.* **2000**, *39*, 2966.
[5] O. Nováková, J. Kaspárková, O. Vrána, P. M. van Vliet, J. Reedijk, V. Brabec, *Biochemistry* **1995**, *34*, 12369.

[6] B. Lippert, *Cisplatin. Chemistry and Biochemistry of a Leading Anticancer Drug*, Verlag Helvetica Chimica Acta and Wiley-VCH, Zürich and Weinheim, **1999**.
[7] J. Reedijk, *Chem. Commun.* **1996**, 801.
[8] E. R. Jamieson, S. J. Lippard, *Chem. Rev.* **1999**, *99*, 2467.
[9] A. C. G. Hotze, A. H. Velders, F. Ugozzoli, M. Biagini-Cingi, A. M. Manotti-Lanfredi, J. G. Haasnoot, J. Reedijk, *Inorg. Chem.* **2000**, *39*, 3838.
[10] P. M. Van Vliet, J. G. Haasnoot, J. Reedijk, *Inorg. Chem.* **1994**, *33*, 1934.
[11] A. H. Velders, A. C. G. Hotze, J. G. Haasnoot, J. Reedijk, *Inorg. Chem.* **1999**, *38*, 2762.
[12] A. H. Velders, A. C. G. Hotze, G. Van Albada, J. G. Haasnoot, J. R. Reedijk, *Inorg. Chem.* **2000**, *39*, 4073.
[13] J. Arpalahti, K. D. Klika, S. Molander, *Eur. J. Inorg. Chem.* **2000**, 1007.
[14] A. H. Velders, B. van der Geest, H. Kooijman, A. L. Spek, J. G. Haasnoot, J. Reedijk, *Eur. J. Inorg. Chem.* **2001**, 369.
[15] F. Zamora, M. Kunsman, M. Sabat, B. Lippert, *Inorg. Chem.* **1997**, *36*, 1583.
[16] M. J. Clarke, *J. Am. Chem. Soc.* **1978**, *100*, 5068.
[17] J. Arpahlahti, K. D. Klika, *Eur. J. Inorg. Chem.* **1999**, 1199.
[18] J. Viljanen, K. D. Klika, R. Sillanpää, J. Arpalahti, *Inorg. Chem.* **1999**, *38*, 4924.
[19] E. F. Day, C. A. Crawford, K. Folting, K. R. Dunbar, G. Christou, *J. Am. Chem. Soc.* **1994**, *116*, 9339.
[20] K. V. Catalan, D. J. Mindiola, D. L. Ward, K. R. Dunbar, *Inorg. Chem.* **1997**, *36*, 2458.
[21] K. V. Catalan, J. S. Hess, M. M. Maloney, D. J. Mindiola, D. L. Ward, K. R. Dunbar, *Inorg. Chem.* **1999**, *38*, 3904.
[22] W. S. Sheldrick, B. Gunther, *J. Organomet. Chem.* **1991**, *402*, 265.
[23] M. E. Prater, D. J. Mindiola, X. Ouyang, K. R. Dunbar, *Inorg. Chem. Commun.* **1998**, *1*, 475.
[24] S. Korn, W. S. Sheldrick, *Inorg. Chim. Acta* **1997**, *254*, 85.
[25] S. Korn, W. S. Sheldrick, *J. Chem. Soc., Dalton Trans.* **1997**, 2191.
[26] P. Annen, S. Schildberg, W. S. Sheldrick, *Inorg. Chim. Acta* **2000**, *307*, 115.
[27] R. H. Fish, *Coord. Chem. Rev.* **1999**, *185/186*, 569.
[28] L. Y. Kuo, M. G. Kanatzidis, M. Sabat, A. L. Tipton, T. J. Marks, *J. Am. Chem. Soc.* **1991**, *113*, 9027.
[29] B. Lippert, *J. Chem. Soc., Dalton Trans.* **1997**, 3971.
[30] B. Lippert, H. Schollhorn, U. Thewalt, *Inorg. Chim. Acta* **1992**, *200*, 723.
[31] J. V. Burda, J. Sponer, J. Leszczynski, *J. Biol. Inorg. Chem.* **2000**, *5*, 178.
[32] A. C. G. Hotze, unpublished results.
[33] B. Song, J. Zhao, R. Griesser, C. Meiser, H. Sigel, B. Lippert, *Chem. Eur. J.* **1999**, *5*, 2374.
[34] J. H. J. den Hartog, H. van den Elst, J. Reedijk, *J. Inorg. Biochem.* **1984**, 83.
[35] B. Lippert, H. Schoellhorn, U. Thewalt, *Inorg. Chim. Acta* **1992**, 198−200.
[36] R. A. Krause, K. Krause, *Inorg. Chem.* **1980**, *19*, 2600.
[37] T. Bao, K. Krause, R. A. Krause, *Inorg. Chem.* **1988**, *27*, 759.
[38] S. Goswami, A. R. Chakravarty, A. Chakravorty, *Inorg. Chem.* **1981**, *29*, 2246.
[39] E. G. Talman, W. Bruning, J. Reedijk, A. L. Spek, N. Veldman, *Inorg. Chem.* **1997**, *36*, 854.
[40] B. P. Sullivan, D. J. Salmon, T. J. Meyer, *Inorg. Chem.* **1978**, *17*, 3334.

Received May 17, 2001
[I01175]

Electrochemical and Catalytic Properties of Novel Manganese(III) Complexes with Substituted 2-(2′-Hydroxyphenyl)oxazoline Ligands − X-ray Structures of Tris[5-methyl-2-(2′-oxazolinyl)phenolato]manganese(III) and Tris[5-chloro-2-(2′-oxazolinyl)phenolato]manganese(III)

Marcel Hoogenraad,[a] Kevita Ramkisoensing,[a] Syb Gorter,[a] Willem L. Driessen,[a] Elisabeth Bouwman,[a] Jaap G. Haasnoot,[a] Jan Reedijk,*[a] Taasje Mahabiersing,[b] and František Hartl[b]

Keywords: Manganese / Spectroelectrochemistry / Cyclic voltammetry / Homogeneous catalysis / Oxidations

A series of manganese complexes of the type MnL_3 were synthesised and characterised, with HL being (substituted) 2-(2′-hydroxyphenyl)oxazoline ligands. The molecular structures of [Mn(5′-Mephox)$_3$] and [Mn(5′-Clphox)$_3$] reveal their meridional configuration with a significant Jahn–Teller distortion. The ligand substituents exert a significant influence on the redox and catalytic properties of the manganese complexes. Cyclic voltammetry experiments show that the electrochemically quasi-reversible Mn^{II}/Mn^{III} and reversible Mn^{III}/Mn^{IV} redox couples shift towards higher potentials with more electron-withdrawing substituents. The same trend applies for the oxidation of the manganese(IV) complexes. Electrolysis experiments monitored with UV/Vis and EPR spectroscopy revealed that the reduction of the manganese(III) complexes to manganese(II), and their oxidation to manganese(IV) are both chemically reversible, while subsequent oxidation of the manganese(IV) species was found to be irreversible. All complexes are active oxidation catalysts with dihydrogen peroxide as the oxidant. In the oxidation of styrene, up to 220 turnover numbers were obtained towards styrene oxide. The turnover numbers in the oxidation reactions as well as the selectivity in the oxidation of styrene and *cis*-stilbene are affected significantly by the substituents, but no clear correlation with the electrochemical properties was observed. The most striking substituent effect is the higher stability of [Mn(5′-NO_2phox)$_3$] compared to the other complexes during styrene oxidation with dihydrogen peroxide in methanol.

Introduction

The presence of manganese at the active site of a wide variety of enzymes involved in oxidation catalysis has inspired the synthesis and study of manganese complexes as structural or functional models for these enzymes.[1,2] Several of these complexes have successfully been used in bleaching reactions[2] or in (asymmetric) oxidation reactions of organic substrates.[3] In most oxidation reactions, oxidants such as *tert*-butyl hydroperoxide, sodium hypochlorite, or iodosylbenzene are used. These reagents are relatively expensive and environmentally unacceptable. There is a wide interest in the use of cleaner and cheaper oxidants like molecular oxygen or hydrogen peroxide. Coordination compounds known to use hydrogen peroxide as oxidant in oxidation are manganese complexes with 1,4,7-trimethyl-1,4,7-triazacyclononane (Me_3tacn) and derived ligands and Mn−porphyrin catalysts.[4]

The introduction of substituents on the ligands has been shown to affect various properties of the catalysts. For instance, in the Mn−Me_3tacn complexes, the presence of substituents at the nitrogen atoms at the 1-, 4-, and 7-positions in the triazacyclononane ring is essential for the catalytic activity.[2] Another example is the introduction of halogen or nitro groups on porphyrin catalysts, which resulted in a higher resistance towards oxidative degradation.[5] The higher stability probably arises from a combination of electronic effects, replacement of C−H bonds by less oxidisable carbon−halogen bonds and steric crowding to reduce intermolecular catalyst degradation. As for porphyrin complexes, the catalytic efficiency of Mn−salen complexes has been reported to improve by introduction of electron-withdrawing nitro substituents.[6] However, in Mn(salen)-catalysed asymmetric epoxidation reactions, the enantiomeric excess (*ee*) of the product was significantly lower if catalysts containing ligands with electron-withdrawing substituents were used.[3,7] In fact, the most commonly used Mn−salen catalysts contain only alkyl, or alkyl and aryl groups as substituents. The use of these complexes results in high enanti-

[a] Leiden Institute of Chemistry, Gorlaeus Laboratories, Leiden University,
P. O. Box 9502, 2300 RA Leiden, The Netherlands
Fax: (internat.) + 31-71/527-4671
E-mail: reedijk@chem.leidenuniv.nl
[b] Institute of Molecular Chemistry, University of Amsterdam, Nieuwe Achtergracht 166, 1018 WV Amsterdam, The Netherlands

 © WILEY-VCH Verlag GmbH, 69451 Weinheim, Germany, 2002 1434−1948/02/0202−0377 $ 17.50+.50/0

omeric excesses of the product, but the catalyst stability is rather low, usually resulting in turnover numbers below 40 for reactions with dihydrogen peroxide as the oxidant.[3]

The didentate ligand 2-(2′-hydroxyphenyl)oxazoline (Hphox) has, like the salen ligands, a mixed N,O donor set. It is readily accessible and more stable against hydrolysis than the salen ligands.[8] Complexes with Hphox ligands and various transition metal complexes,[9,10] including manganese(III),[1,11−13] have been shown to catalyse oxidation reactions. We now wish to report novel manganese complexes MnL_3 [with HL being substituted 2-(2′-hydroxyphenyl)oxazoline ligands, see Scheme 1], their electrochemical properties, and their use as catalysts for oxidation reactions with dihydrogen peroxide as the oxidant.

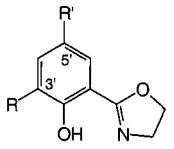

ligand	R	R′	ligand	R	R′
Hphox	H	H	H-5′-Mephox	H	CH_3
H-5′-NO_2phox	H	NO_2	H-3′-Mephox	CH_3	H
H-3′,5′-dClphox	Cl	Cl	H-5′-MeOphox	H	OCH_3
H-5′-Clphox	H	Cl			

Scheme 1. Structures of the ligands

Results and Discussion

Syntheses and Characterization of the [MnL_3] Complexes

Complexes of the type [MnL_3] were obtained by two different methods. The syntheses of [Mn(5′-Clphox)$_3$], [Mn(3′-Mephox)$_3$], [Mn(5′-Mephox)$_3$], and [Mn(5′-MeOphox)$_3$] from $Mn(OAc)_2$ and the appropriate ligand in methanol, are similar to the synthesis of [Mn(phox)$_3$].[12] The synthesis of [Mn(5′-NO_2phox)$_3$] and [Mn(3′,5′-dClphox)$_3$] was accomplished by applying the procedure used for the synthesis of [tris(8-oxyquinoline)−manganese(III)].[14] This latter method involves the addition of an ethanolic solution of the ligand to $Mn(OAc)_3$ in ethanol. In this manner, a dark brown precipitate could be isolated within a number of hours, which − after recrystallisation − afforded the desired compounds in good purity.

For all complexes, the parent peak observed in the electrospray mass spectra was the $[MnL_2]^+$ fragment. Further characterisation of the complexes was performed with IR and UV/Vis spectroscopy. The UV/Vis spectra of the complexes, except [Mn(5′-NO_2phox)$_3$], exhibit a ligand-to-metal charge transfer (LMCT) band around 370 nm and π→π* transitions of the ligand at around 310, 260, and 210 nm. No d-d transitions are observed due to the poor solubility of the complexes. The π→π* transitions are also present in the spectra of the free ligands. For [Mn(5′-NO_2phox)$_3$], two intense absorption bands at 340 and 222 nm are observed. These bands are also observed in the free ligand and can be ascribed to π→π* transitions (see the spectroelectrochemical section below). For all complexes, the manganese(III) oxidation state is confirmed by the absence of an EPR signal (at 77 K and 298 K) and by the magnetic moments at room temperature ranging from 4.10 μ_B ([Mn(3′,5′-dClphox)$_3$]) to 4.96 μ_B ([Mn(5′-MeOphox)$_3$]). These data are close to the spin-only value of 4.92 μ_B for high-spin manganese(III), the deviation being caused by orbital effects. ^{1}H NMR spectroscopy of the complexes have been used,[1,13] however, the paramagnetic ^{1}H NMR signals of these complexes could not be assigned; in order to assign the signals, systematic substitution of the hydrogen atoms is required.

Molecular Structure of [Mn(5′-Mephox)$_3$]

In the unit cell of [Mn(5′-Mephox)$_3$], with $Z = 4$, two similar, independent molecules are present. The crystallographic data are presented in Table 1.

Table 1. Crystallographic data for *mer*-[Mn(5′-Mephox)$_3$] and *mer*-[Mn(5′-Clphox)$_3$]

	[Mn(5′-Mephox)$_3$]	[Mn(5′-Clphox)$_3$]
Empirical formula	$C_{30}H_{30}MnN_3O_6$	$C_{27}H_{21}Cl_3MnN_3O_6$
Molecular mass	583.52	644.78
Crystal dimensions [mm]	0.55×0.3×0.2	0.45×0.35×0.1
Symmetry cell setting	triclinic	triclinic
Symmetry space group	P$\bar{1}$	P$\bar{1}$
a [Å]	12.725(7)	7.943(5)
b [Å]	14.299(6)	12.237(12)
c [Å]	16.16(2)	15.301(5)
α [°]	92.61(3)	68.40(3)
β [°]	107.52(3)	79.62(5)
γ [°]	105.15(3)	83.53(5)
Cell volume [Å^3]	2684(2)	1358.5(16)
Z	4	2
F(000)	1216	656
$D_{calcd.}$ [g cm^{-3}]	1.445(2)	1.576(2)
μ (Mo-K$_\alpha$) [mm^{-1}]	0.54	0.83
T [K]	77	293
R	0.058	0.039
wR	0.083	0.053
S	1.259	1.12
No residual density outside [e Å^{-3}]	−3.00, 1.45	−1.33, 0.95

A Platon[15] plot of one of the independent molecules of [Mn(5′-Mephox)$_3$] is shown in Figure 1. The molecular structure largely resembles that of [Mn(phox)$_3$],[12] having the MnN_3O_3 chromophore in a meridional configuration with a significant tetragonal distortion. The absence of

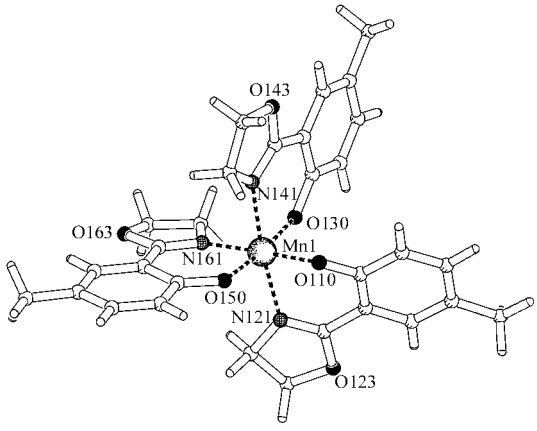

Figure 1. Platon[15] projection of one of the independent molecules of *mer*-[Mn(5′-Mephox)$_3$]

counter ions and the differences in the Mn−L bond lengths due the Jahn−Teller effect, characteristic for a d^4 configuration, confirm the manganese(III) oxidation state.

Selected bond lengths and bond angles for one [Mn(5′-Mephox)$_3$] molecule are given in Table 2. The differences in the ligand−metal bond lengths between the two independent molecules fall within 0.01 Å, while the bond angles deviate within a few degrees. The largest difference is found for the angle contained by the *trans*-O−Mn−O bonds, that expands from 173.15(18)° in one independent molecule to 177.7(2)° in the other. The structure of [Mn(5′-Mephox)$_3$] (Figure 1) has the elongated Jahn−Teller axis along the N(121)−Mn−N(141) bonds, as revealed by the long bond lengths Mn−N(121) and Mn−N(141) of 2.232(5) and 2.246(5) Å, respectively, compared to 2.033(6) Å for the Mn−N(161) bond. The Mn−O bond lengths are around 1.90 Å.

Table 2. Selected bond lengths [Å] and angles [°] of one molecule of *mer*-[Mn(5′-Mephox)$_3$] and of *mer*-[Mn(5′-Clphox)$_3$]

[a]	[Mn(5′-Mephox)$_3$]	[Mn(5′-Clphox)$_3$]
Mn1−O10	1.898(5)	1.894(4)
Mn1−O30	1.896(6)	1.927(5)
Mn1−O50	1.912(6)	1.889(4)
Mn1−N21	2.232(5)	2.238(6)
Mn1−N41	2.246(5)	2.244(5)
Mn1−N61	2.033(6)	2.033(5)
O10−Mn1−N21	84.4(2)	85.13(18)
O10−Mn1−O30	91.7(3)	91.92(18)
O10−Mn1−N41	90.4(2)	90.28(17)
O10−Mn1−O50	92.4(3)	177.57(18)
O10−Mn1−N61	177.6(2)	90.1(2)
N21−Mn1−O30	90.1(2)	90.5(2)
N21−Mn1−N41	173.8(2)	172.67(18)
N21−Mn1−O50	95.8(2)	94.19(18)
N21−Mn1−N61	93.3(2)	91.5(2)
O30−Mn1−N41	86.5(2)	84.0(2)
O30−Mn1−O50	173.15(18)	90.42(18)
O30−Mn1−N61	87.9(3)	177.57(19)
N41−Mn1−O50	87.9(2)	90.63(18)
N41−Mn1−N61	91.9(2)	94.2(2)
O50−Mn1−N61	88.3(3)	87.58(19)

[a] Due to the presence of two independent molecules in the asymmetric unit, the donor atoms for [Mn(5′-Mephox)$_3$] listed in this Table should be read as O1xx and N1xx.

Molecular Structure of [Mn(5′-Clphox)$_3$]

The crystallographic data are presented in Table 1. The unit cell, with $Z = 2$, contains the two meridional stereoisomers of the complex. Selected bond lengths and bond angles are given in Table 2. The structure of [Mn(5′-Clphox)$_3$] (Figure 2) has the elongated Jahn−Teller axis along the N21−Mn−N41 axis as shown by the long bond lengths Mn−N21 and Mn−N41 of 2.238(6) and 2.244(5) Å, respectively, compared to 2.033(5) Å for the Mn−N61 bond. The Mn−O bond lengths are around 1.90 Å. The ligand bite angle varies between 84.0(2)° and 87.58(19)° for the O30−Mn1−N41 and O10−Mn1−N21 angles, respectively.

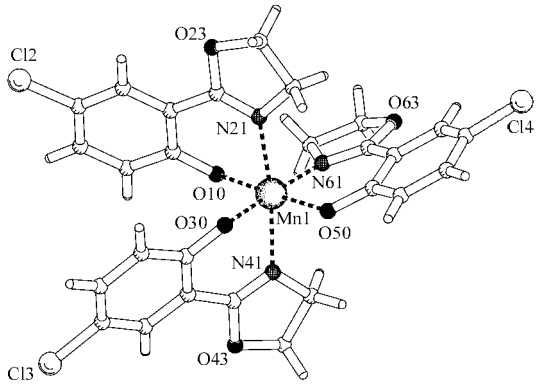

Figure 2. Platon[15] projection of *mer*-[Mn(5′-Clphox)$_3$]

As a matter of fact, all bond angles and distances for [Mn(5′-Mephox)$_3$] and [Mn(5′-Clphox)$_3$] are uneventful and very similar to those of [Mn(phox)$_3$].[12] The Mn−N bond lengths of these complexes of the type [MnL$_3$] vary from 2.033(5) to 2.060(2) Å for the equatorial Mn−N bonds and from 2.192(2) to 2.246(2) Å for the axial Mn−N bonds, while the Mn−O bond lengths are between 1.8823(17) and 1.958(2) Å.

Redox Properties of the [MnL$_3$] Complexes

Cyclic Voltammetry

The redox properties of the [MnL$_3$] complexes were investigated in acetonitrile. The potentials are given against Ag/AgCl. The investigated phox-type ligands were not redox-active between +2.00 and −2.00 V, except for H-5′-NO_2phox, which is reducible at −1.22 V (see below).

The [MnL$_3$] complexes show a (quasi)reversible one-electron cathodic wave ascribed to the reduction of manganese(III) to manganese(II), and a fully reversible one-electron anodic wave corresponding to the oxidation of manganese(III) to manganese(IV). The $E_{1/2}$ and ΔE_p values for these redox couples (Table 3) are strongly influenced by the ligand substituents.

The Mn^{III}/Mn^{IV} redox couples are fully reversible, as indicated by the peak-to-peak separations ranging from 65 to 90 mV and the i_{pc}/i_{pa} ratio of 1.[16] The linear relationship

Table 3. Electrochemical data for the oxidation and reduction of the manganese(III) centre of the [MnL$_3$] complexes

Complex[a]	Mn^{III}/Mn^{II} $E_{1/2}$	ΔE_p	Mn^{III}/Mn^{IV} $E_{1/2}$	ΔE_p
[Mn(5′-NO_2phox)$_3$]	+0.12	80	+0.87	65
[Mn(3′,5′-dClphox)$_3$]	−0.07	100	+0.75	65
[Mn(5′-Clphox)$_3$]	−0.26	120	+0.60	75
[Mn(phox)$_3$]	−0.42	260	+0.48	85
[Mn(5′-Mephox)$_3$]	−0.45	180	+0.42	60
[Mn(3′-Mephox)$_3$]	−0.52	230	+0.40	90
[Mn(5′-MeOphox)$_3$]	−0.49	220	+0.41	90

[a] In acetonitrile solutions containing 0.05 M Bu_4NPF_6 at a scan rate of 0.10 V/s; $E_{1/2}$ in V (vs. Ag/AgCl), ΔE_p in mV.

between the peak current i_{pa} and the square root of the scan rate (v) in the range of 0.2 to 2 V/s is indicative of a diffusion-controlled process.[16] The marked positive shift of both the reduction and oxidation potentials of the $[MnL_3]$ complexes with the electron-withdrawing substituents on the phox ligands closely resembles the redox properties of related mononuclear manganese(IV)[17] and manganese(III)[18,19] complexes with substituted phenolate ligands showing the same trend. For the Mn^{III}/Mn^{II} redox couples, large differences between the complexes are observed in the ΔE_p value. For the Mn−phox complexes with the electron-withdrawing substituents, the peak-to-peak separation lies between 80 and 120 mV, just slightly above the value expected for a electrochemically reversible process.[16] However, the complexes with more electron-donating ligands show much larger peak-to-peak separation, indicating quasi-reversible redox processes.

At higher potentials, yet another anodic process is observed for the formally manganese(IV) centre. The ligand substituents again exert a significant effect on the oxidation potentials (Table 4). No clear correlation exists in this case between the substituent's nature and the ΔE_p values.

Table 4. Electrochemical data for the Mn−phox complexes: electrochemically irreversible oxidations of the manganese(IV) species at higher potentials

Complex[a]	E_{pa}	E_{pc}	ΔE_p
$[Mn(5'\text{-}NO_2phox)_3]^+$	+1.59	+1.37	220
$[Mn(3',5'\text{-}dClphox)_3]^+$	+1.28	+1.14	140
$[Mn(5'\text{-}Clphox)_3]^+$	+1.31	+1.16	150
$[Mn(phox)_3]^+$	+1.30	+1.06	240
$[Mn(5'\text{-}Mephox)_3]^+$	+1.13	+0.95	180
$[Mn(3'\text{-}Mephox)_3]^+$	+1.17	+0.90	270
$[Mn(5'\text{-}MeOphox)_3]^+$	+0.98	−	−

[a] In acetonitrile solutions containing 0.05 M Bu_4NPF_6 at a scan rate of 0.10 V/s; E_{pa} and E_{pc} in V (vs. Ag/AgCl), ΔE_p in mV.

The oxidation of the manganese(IV) complexes is chemically irreversible, as evidenced by the peak-current ratios i_{pc}/i_{pa}, significantly smaller than 1 at moderate scan rates. The cyclic voltammogram of $[Mn(5'\text{-}MeOphox)_3]$ does not show any cathodic counter-peak on the reverse scan beyond the oxidation of the manganese(IV) compound.

Reduction of the formally manganese(II) species was observed, in the available potential window, only for the complexes with the most electron-withdrawing phox ligands, $[Mn(3',5'\text{-}dClphox)_3]$ and $[Mn(5'\text{-}NO_2phox)_3]$ (Figure 3). In both cases, the reduction of the manganese(II) species consumed more than one electron, as deduced from the comparison of the corresponding cathodic peak currents with those for the reversible Mn^{III}/Mn^{II} and Mn^{III}/Mn^{IV} couples. The reduction of $[Mn(5'\text{-}NO_2phox)_3]^-$ at $E_{pc} = -1.56$ V produced a species that could be further reduced at $E_{pc} = -1.81$ V. The latter cathodic step is chemically reversible, pointing to the reduction of the nitro groups on the phox ligands. The cyclic voltammogram of the uncoordinated H-5′-NO_2phox ligand shows an irreversible reduction step at $E_{pc} = -1.22$ V, followed by a quasi-reversible

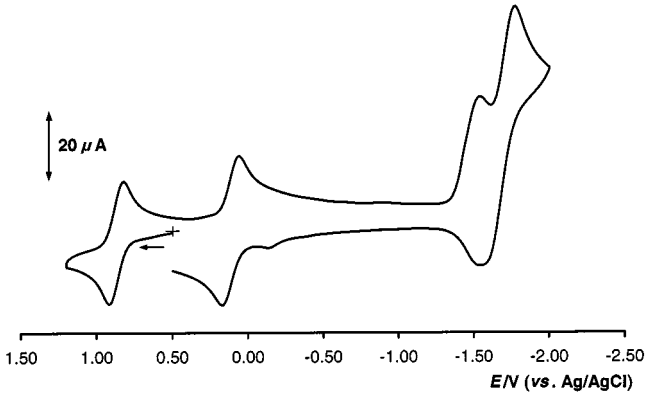

Figure 3. Cyclic voltammogram of $[Mn(5'\text{-}NO_2phox)_3]$ at a scan rate of 0.10 V/s in an acetonitrile solution containing 0.05 M Bu_4NPF_6

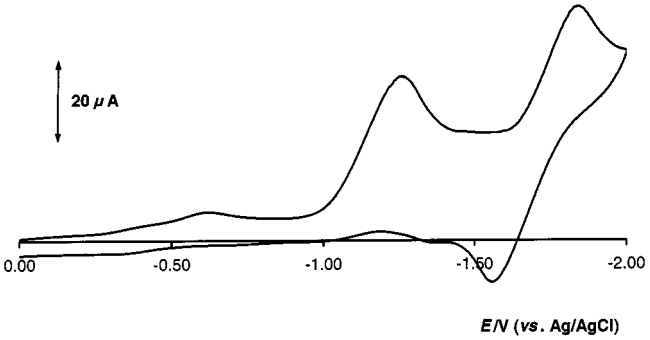

Figure 4. Cyclic voltammogram of H-5′-NO_2phox at a scan rate of 0.10 V/s in an acetonitrile solution containing 0.05 M Bu_4NPF_6

step at $E_{1/2} = -1.68$ V (Figure 4). The potential of this quasi-reversible step is nearly identical with that of the reversible cathodic process ($E_{1/2} = -1.66$ V), following the irreversible reduction of $[Mn(5'\text{-}NO_2phox)_3]^-$, suggesting that the irreversible process in the complex results in dissociation of at least one $[5'\text{-}NO_2phox]^-$ ligand. This anionic compound is obviously also produced during the irreversible reduction of H-5′-NO_2phox at $E_{pc} = -1.22$ V. Further evidence for this explanation was obtained from corresponding UV/Vis spectroelectrochemical experiments (vide infra). This behaviour is in agreement with that reported for the 4-nitro-thiophenolate anion ($[4\text{-}O_2NC_6H_4S]^-$), which can be reduced, reversibly, at the nitro group.[20] The latter cathodic process also occurred upon the reduction of the complex $[Pt^{II}(bpy^{\cdot-})(4\text{-}O_2NC_6H_4S)_2]^-$.[20] In view of these arguments, it is not surprising that the irreversible reduction of $[Mn(3',5'\text{-}dClphox)_3]^-$ at $E_{pc} = -1.86$ V is not followed by such a reversible cathodic step because further reduction of the liberated $[3',5'\text{-}dClphox]^-$ ligand is not facile. The reduction of the latter Mn^{II} complex was followed instead by a minor, irreversible wave at $E_{pc} = -2.10$ V, belonging to a secondary product that remains unassigned.

The strong dependence of the electrode potentials on the electron-withdrawing (NO_2, Cl) or electron-donating (Me, MeO) character of the phox substituents implies that the frontier molecular (redox) orbitals of the high-spin man-

ganese(III) complexes possess a significant contribution from the phox ligands. This qualitative presumption has been indeed confirmed by Extended Hückel calculations with the programme CACAO,[21] using the X-ray structure data of $[Mn(phox)_3]$. The calculated data show that the closely spaced HOMO and HOMO-1 ($\Delta E = 0.064$ eV) frontier orbitals of the complex are delocalised over the manganese(III) ion and the phox ligands. The one-electron containing HOMO possesses 69% Mn and 22% phenolate character. The singly occupied HOMO-1 has a similar character, with a slightly larger phenolate contribution (27%) and smaller Mn contribution (65%). The oxidation and reduction processes of the studied $[ML_3]$ complexes to the manganese(IV) and manganese (II) complexes, respectively, may therefore be assigned as predominantly metal-localized, although with a significant ligand influence.

UV/Vis Spectroelectrochemistry with $[Mn(phox)_3]$ and $[Mn(5'\text{-}NO_2phox)_3]$

A valuable approach in investigating the redox behaviour of the Mn−phox complexes of the type $[MnL_3]$ is to monitor the spectroscopic changes during electrolysis with methods such as UV/Vis and EPR spectroscopy. With these spectroelectrochemical methods, the chemical reversibility of the redox processes can be studied on the time scale of minutes. UV/Vis spectroelectrochemistry has been employed for mononuclear manganese complexes with nitrogen ligands[22] and mixed oxygen/nitrogen ligands.[23] To obtain more insight into the redox behaviour of $[Mn(phox)_3]$ and $[Mn(5'\text{-}NO_2phox)_3]$, the changes in their UV/Vis spectra were studied during electrolysis in acetonitrile at room temperature. The results are summarized in Table 5.

Table 5. UV/Vis absorption bands of the formally manganese(II), manganese(III), and manganese(IV) compounds, recorded in the course of the spectroelectrochemical experiments

Complex	λ_{max} (ε)[a]
$[Mn(phox)_3]^+$	216, 293 (1.2×10^4), 380 (sh), 430 (sh), 575 (4.0×10^3)
$[Mn(phox)_3]$	216, 319 (9.7×10^3), 360 (sh)
$[Mn(phox)_3]^-$	222, 349 (1.5×10^4)
$[Mn(5'\text{-}NO_2phox)_3]^+$	211, 230, 320 (4.0×10^4), 390 (sh), 582 (7.6×10^3)
$[Mn(5'\text{-}NO_2phox)_3]$	222, 358 (4.4×10^4)
$[Mn(5'\text{-}NO_2phox)_3]^-$	222, 340 (sh), 397 (6.2×10^4)

[a] In acetonitrile; λ_{max} in nm, ε in $M^{-1}\cdot cm^{-1}$; the ε values for the bands around 210−220 nm vary depending on the concentration of the complexes; sh = shoulder.

The reduction of $[Mn(phox)_3]$ at −0.55 V resulted in a colour change from green to light-brown. The most remarkable feature in the UV/Vis spectra of the manganese(II) product is the appearance of a peak at 349 nm, attributed to an LMCT transition. The π→π* transition of the ligand shifted slightly from 216 to 222 nm. Isosbestic points are observed at 381, 329, 242, and 214 nm. Reoxidation of the stable manganese(II) species at −0.29 V resulted in complete reappearance of the initial UV/Vis spectrum of $[Mn(phox)_3]$.

The reduction of $[Mn(5'\text{-}NO_2phox)_3]$ at +0.08 V resulted in a yellow solution. In the UV/Vis spectra, the shift of the absorption peak at 358 nm to 397 nm is attributed to changes in the intense π→π* transition of the nitro group (Figure 5).

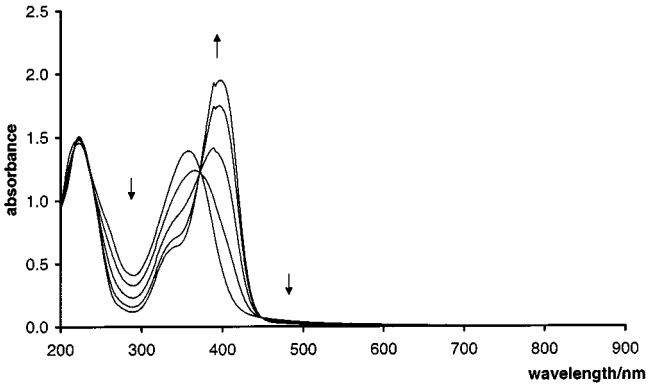

Figure 5. UV/Vis spectroscopic changes recorded during the electrochemical reduction of $[Mn(5'\text{-}NO_2phox)_3]$ from manganese(III) to manganese(II)

The peak at 222 nm, ascribed to the aromatic π→π* transition, hardly changes. Two isosbestic points occur at 372 and 449 nm. The presence of the π→π*(NO_2) absorption band makes it difficult to compare the spectra of the manganese(II) complexes $[Mn(5'\text{-}NO_2phox)_3]^-$ and $[Mn(phox)_3]^-$. However, the shoulder in the spectrum of the manganese(II) species at 340 nm has presumably the same origin as the peak at 349 nm in the UV/Vis spectrum of $[Mn(phox)_3]^-$. This observation is important, because it indicates that one-electron-reduced $[Mn(phox)_3]^-$ and $[Mn(5'\text{-}NO_2phox)_3]^-$ are electronically similar. Both anionic complexes are also inherently stable.

Cyclic voltammetry revealed that the anionic complexes $[Mn(3',5'\text{-}dClphox)_3]^-$ and $[Mn(5'\text{-}NO_2phox)_3]^-$ undergo irreversible reduction that may result in dissociation of one or more anionic phox ligands (see previous section). This assumption could be confirmed by UV/Vis spectroelectrochemistry. The UV/Vis spectra recorded during the reduction of $[Mn(5'\text{-}NO_2phox)_3]^-$ at −1.56 V exhibit isosbestic points at 483, 408, and 207 nm and a shift of the intense absorption band due to the π→π*(NO_2) transition from 397 nm to 426 nm (Figure 6).

Importantly, the UV/Vis spectrum of the product (absorption maxima at 426, 330 and 228 nm) is identical with that of $[5'\text{-}NO_2phox]^-$ recorded after the one-electron reduction of H-5′-NO_2phox (Figure 6, inset). This result implies that the irreversible reduction of $[Mn(5'\text{-}NO_2phox)_3]^-$ indeed affords the uncoordinated $[5'\text{-}NO_2phox]^-$ ligand, which dissociates due to the decreased positive charge on the manganese centre in the primarily $Mn^{II}\rightarrow Mn^{I}$ electron-transfer step. The liberated anion $[5'\text{-}NO_2phox]^-$ is further reversibly reduced at the NO_2 group at $E_{1/2} = -1.66$ V, resulting in the formation of $[5'\text{-}NO_2phox]^{2-}$. As expected, the latter reduction process increases the energy of the

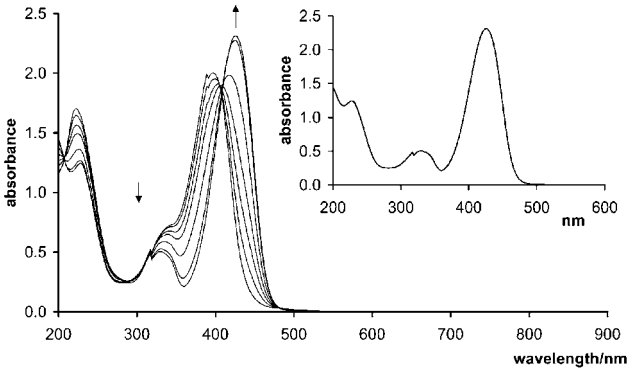

Figure 6. UV/Vis spectroscopic changes recorded during the in situ irreversible reduction of $[Mn(5'\text{-}NO_2phox)_3]^-$; inset: UV/Vis spectrum of $[5'\text{-}NO_2phox]^-$ formed during the irreversible reduction of $[H\text{-}5'\text{-}NO_2phox]^-$

$\pi\rightarrow\pi^*(NO_2)$ electronic transition[20] and the corresponding absorption band shifts from 426 nm for $[5'\text{-}NO_2phox]^-$ to 291 nm for $[5'\text{-}NO_2phox]^{2-}$.

The oxidation of the Mn−phox complexes to the manganese(IV) species is fully reversible according to cyclic voltammetry. The spectroelectrochemical experiments show that this also applies for the time scale of minutes. In the UV/Vis spectra recorded during the stepwise electrolytic oxidation of $[Mn(5'\text{-}NO_2phox)_3]$ at 0.90 V, two isosbestic points are observed at 331 and 408 nm (Figure 7).

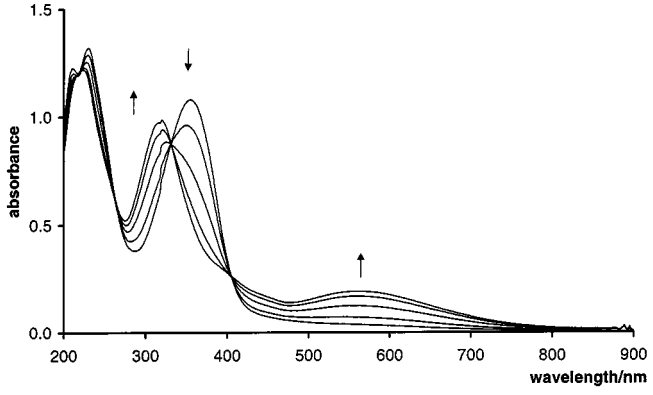

Figure 7. UV/Vis spectroscopic changes recorded during the electrochemical oxidation of $[Mn(5'\text{-}NO_2phox)_3]$ from manganese(III) to manganese(IV)

The most important feature in the UV/Vis spectrum of the manganese(IV) complex is the new broad absorption band at 582 nm; based on its intensity, it can be assigned to an LMCT transition. This visible absorption results in the dark blue colour of the complex, also known for some other manganese(IV) complexes.[24,25] The $\pi\rightarrow\pi^*(NO_2)$ transition shifts from 358 to 320 nm. Further oxidation of $[Mn(5'\text{-}NO_2phox)_3]^+$ at +1.59 V led to irreversible disappearance of the LMCT band and degradation of the complex.

UV/Vis spectra collected during the stepwise oxidation of $[Mn(phox)_3]$ at +0.52 V, show new absorption maxima at 575 and 293 nm. Isosbestic points are present at 371, 332 and 277 nm. The new broad peak at 575 nm corresponds to that at 582 nm in the UV/Vis spectrum of the dark blue $[Mn(5'\text{-}NO_2phox)_3]^+$ complex, indicating that similar complexes are formed. The $[Mn(phox)_3]^+$ compound shows a small oxidation wave at +1.30 V. The UV/Vis spectra taken during this anodic step reveal a new absorption band at 424 nm and isosbestic points at 470 and 371 nm, while all other UV/Vis bands are diminished. Continued anodic scan shows a large wave at +1.72 V, with a peak current of approximately three times the intensity compared to the reversible one-electron oxidation of manganese(III) to manganese(IV). Similar to the oxidation of $[Mn(5'\text{-}NO_2phox)_3]^+$, irreversible disappearance of all UV/Vis absorption bands indicate oxidative degradation of the phox derivative.

EPR Spectroelectrochemistry with $[Mn(phox)_3]$ and $[Mn(5'\text{-}NO_2phox)_3]$

The UV/Vis spectroelectrochemical experiments prove that the manganese(II) and manganese(IV) complexes were stable on a time scale of several minutes. For EPR spectroelectrochemistry butyronitrile was used due to fairly good solubility of the complexes in this solvent, particularly at low temperatures. As no EPR signals of the starting complexes or their reduced or oxidized forms were observed at 223 K, EPR spectroelectrochemical experiments were performed at 77 K in a solid matrix of the frozen solutions that had first been subjected to bulk electrolysis at the E_{pa} or E_{pc} values of the precursor manganese(III) compounds upon the UV/Vis spectroscopic control (see Figures 5 and 7). The EPR spectra of the stable manganese(II) complexes show a typical six-line hyperfine signal due to coupling of the electron spin with the nuclear spin of ^{55}Mn ($I = 5/2$).[26] The EPR signals of both $[Mn(5'\text{-}NO_2phox)_3]^-$ and $[Mn(phox)_3]^-$ occur at $g = 2.00$ with $a_{Mn} = 9.0$ mT.

At 77 K, no EPR signals were observed for the oxidized manganese(IV) products $[Mn(phox)_3]^+$ and $[Mn(5'\text{-}NO_2phox)_3]^+$, even though spectra are commonly observed for other manganese(IV) complexes.[26] Their absence in this case cannot be readily explained. The cyclovoltammetric and UV/Vis spectroelectrochemical data nevertheless reveal that oxidation of $[Mn(phox)_3]$ and $Mn(5'\text{-}NO_2phox)_3]$ results in the formation of stable isostructural manganese(IV) complexes, so relaxation phenomena are likely responsible for this observation.

Catalytic Studies with the $[ML_3]$ Complexes

Oxidation of Styrene

The effect of the ligand substituents on the catalytic activity of the studied complexes $[MnL_3]$ was investigated for the oxidation of styrene in methanol at room temperature, as well as in acetone at 0 °C. The successful use of acetone as a solvent at 0 °C has been reported for oxidations with dihydrogen peroxide catalysed by Mn−Me_3tacn complexes.[27] Such reaction conditions also proved to be very suitable for the Mn−phox-catalysed oxidations. The catalytic efficiency for the different $[MnL_3]$ complexes, ex-

Table 6. Turnover numbers in the oxidation of styrene with dihydrogen peroxide in methanol or acetone catalysed by Mn−phox complexes

Catalyst	Methanol[a] Styrene oxide	Benzaldehyde	Acetone[b] Styrene oxide	Benzaldehyde	Diol[c]
[Mn(5′-NO_2phox)$_3$]	34[d]	2	207	5	18
[Mn(3′,5′-dClphox)$_3$]	23	2	108	4	5
[Mn(5′-Clphox)$_3$]	27	2	192	4	12
[Mn(phox)$_3$]	34	2	220	5	11
[Mn(5′-Mephox)$_3$]	24	2	181	4	9
[Mn(3′-Mephox)$_3$]	27	2	80	3	3
[Mn(5′-MeOphox)$_3$]	5	2	76	2	5

[a] Reactions were carried out under standard conditions: 14 μmol of the indicated Mn−phox complex was dissolved, with stirring, in 20 mL of methanol at room temperature. Subsequently, 14 mmol of substrate, 2.0 mmol of 1-MeIm, and 21 mmol of dihydrogen peroxide were added (t = 0); turnover numbers are the total turnover numbers obtained at t = 15 min. [b] Reactions were carried out under standard conditions: 10 mL of acetone and 21 mmol of dihydrogen peroxide were stirred at 0 °C for 30 min. Subsequently, 14 mmol of substrate, 2.0 mmol of 1-MeIm, and 14 μmol of the indicated Mn−phox complex were added (t = 0); turnover numbers are the total turnover numbers obtained at t = 15 min. [c] 1-Phenyl-1,2-ethanediol. [d] 72, 3, and 2 turnover numbers towards styrene oxide, benzaldehyde, and 1-phenyl-1,2-ethanediol, respectively, as determined at t = 120 min (end of the reaction).

Table 7. Turnover numbers and *cis*/*trans* ratios of the products in the oxidation of *cis*-stilbene by Mn−phox complexes with dihydrogen peroxide

Complex[a]	*cis*-Oxide	*trans*-Oxide	Benzaldehyde	Ratio *cis*/*trans*
[Mn(5′-NO_2phox)$_3$]	32	64	2	1:2.0
[Mn(3′,5′-dClphox)$_3$]	22	37	2	1:1.7
[Mn(5′-Clphox)$_3$]	18	50	2	1:2.8
[Mn(phox)$_3$]	17	50	2	1:2.9
[Mn(5′-Mephox)$_3$]	13	46	1	1:3.5
[Mn(3′-Mephox)$_3$]	9	31	2	1:3.4
[Mn(5′-MeOphox)$_3$]	4	19	1	1:4.8

[a] Reactions were carried out by stirring 10 mL of acetone and 21 mmol of H_2O_2 at 0 °C: after 30 min, subsequently 5.0 mmol of the substrate, 2.0 mmol of 1-methylimidazole, and 14 μmol of the complex were added (t = 0); turnover numbers are the total turnover numbers obtained at t = 15 min.

pressed in turnover numbers, is listed in Table 6. All reactions were performed in the presence of 2.0 mmol of 1-methylimidazole (1-Meim). An alkaline additive is required for reactions with manganese catalysts and H_2O_2; it is thought that the additive might act as a base and as an axial ligand.[12]

Small amounts of the side product benzaldehyde were obtained in all reactions. For the reactions in acetone, 1-phenyl-1,2-ethanediol was also detected as a side product. The turnover numbers towards the main product, styrene oxide, are significantly influenced by the substituents on the ligands in the [MnL_3] complexes. For the reactions in methanol, all Mn−phox complexes gave turnover numbers towards styrene oxide between 23 and 34 after 15 min, which represents an efficiency of approximately 2% relative to dihydrogen peroxide. The results in acetone show a dramatic increase in turnover numbers compared to the reactions in methanol. The efficiency relative to the oxidant increased simultaneously, varying from 5 to 15%.

In both solvents, [Mn(phox)$_3$] and [Mn(5′-NO_2phox)$_3$] show the highest efficiency. The use of Mn−phox complexes with more electron-donating ligands resulted in a significant decrease in efficiency compared to [Mn(phox)$_3$], while the use of complexes with electron-withdrawing ligands only resulted in a slightly lower efficiency. The turnover numbers obtained with the least efficient Mn−phox catalyst, [Mn(5′-MeOphox)$_3$], are relatively more enhanced in acetone compared to methanol. For the reactions in acetone, the influence of the presence of a substituent at the 3′-position is more pronounced compared to the reactions in methanol. The complexes with such ligands, [Mn(3′,5′-dClphox)$_3$] and [Mn(3′-Mephox)$_3$], exhibited much lower efficiency compared to complexes with a substituent at the 5′-position only.

Oxidation of Stilbene

In oxidation reactions of *cis*-alkenes catalysed by manganese complexes, such as Mn−salen,[7] isomerisation can occur, resulting in both *cis*- and *trans*-epoxides. For the Mn−salen complexes, this effect has been studied in detail. It has been found that the *cis*/*trans* ratio is mainly influenced by the reaction conditions,[28] the oxidant,[28,29] and the substituents on the ligand.[6,30] The oxidation of *cis*-stilbene with Mn−phox complexes results in both *cis*- and *trans*-stilbene oxide. Oxidation of *cis*-stilbene was performed with all studied [MnL_3] complexes (Table 7).

In all described reactions more *trans*- than *cis*-stilbene oxide was formed, together with small amounts of the cleavage product benzaldehyde. The ligand substituents clearly

affected the *cis*/*trans* ratio of the stilbene oxides, the complexes with electron-withdrawing ligands produced a larger amount of *cis*-stilbene oxide, while the reaction with [Mn(5′-MeOphox)$_3$] resulted in the largest relative fraction of *trans*-stilbene oxide.

The catalytic activity of the unsubstituted precursor catalyst [Mn(phox)$_3$] under similar reaction conditions for the oxidation of *trans*-stilbene and cyclohexene was also studied. Oxidation of *trans*-stilbene resulted in a TON of 49 towards the *trans*-stilbene epoxide and a TON of 3 towards the by-product benzaldehyde. Oxidation of cyclohexene with [Mn(phox)$_3$] gave a TON of 98 towards the epoxide, and additionally the allylic oxidation products were formed with a TON of 28.

Catalyst Stability

In both methanol and acetone, the catalytic reactions with most of the Mn−phox complexes were very fast during the first few minutes, and no clear differences in the reaction rates were found. After 15 min, no catalytic activity could be observed. The only exception is the [Mn(5′-NO$_2$phox)$_3$] catalyst, which remained active for up to 1 h. For [Mn(phox)$_3$] and [Mn(5′-NO$_2$phox)$_3$], the total turnover numbers to styrene oxide in time is depicted in Figure 8.

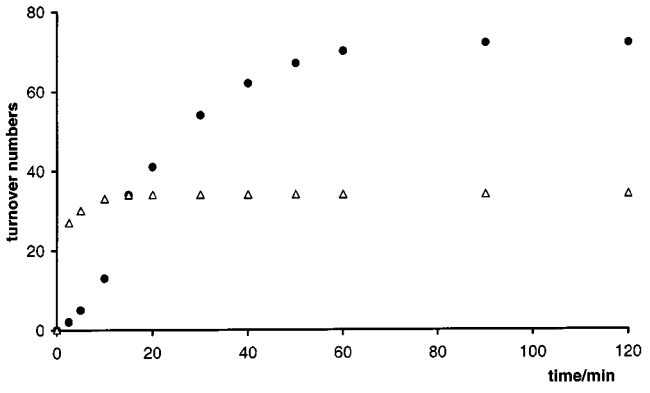

Figure 8. Oxidation of styrene with dihydrogen peroxide in methanol: cumulative turnover number in time towards styrene oxide; • = [Mn(5′-NO$_2$phox)$_3$] as catalyst; Δ = [Mn(phox)$_3$] as catalyst

The oxidation reaction with [Mn(phox)$_3$] was initially very fast, but the activity quickly diminished, with a concomitant loss of colour. In contrast, a significantly slower colour change was observed for the [Mn(5′-NO$_2$phox)$_3$]-catalysed reaction. The oxidation with this catalyst had a short induction period. Catalytic activity persisted for 1 h, resulting in a total turnover number of 72 towards styrene oxide. With both catalysts, benzaldehyde was formed in the first minutes of the reaction, while 1-phenyl-1,2-ethanediol was formed in a gradually increasing amount.

Concluding Remarks

A series of novel, readily available manganese complexes of the type [MnL$_3$] with phenol-substituted 2-(2′-hydroxyphenyl)oxazoline ligands have been synthesized. The complexes are nearly isostructural, as evidenced by the results from X-ray crystallographic studies of [Mn(phox)$_3$],[12] [Mn(5′-Mephox)$_3$] and [Mn(5′-Clphox)$_3$].

The substituents on the phenolate ring of the ligands influence the redox properties of the complexes. The electrochemically quasi-reversible Mn^{II}/Mn^{III} and reversible Mn^{III}/Mn^{IV} redox couples sensitively shifted towards higher potentials with more electron-withdrawing substituents. The same trend applies for the irreversible oxidation of the manganese(IV) complexes. (Spectro)electrochemical studies show that the manganese centre could coordinate all three anionic phox ligands in the formal oxidation states Mn^{II}, Mn^{III}, and Mn^{IV} without any pronounced change of the complex structure. The UV/Vis spectra document that reoxidation of the manganese(II) product and the back-reduction of the manganese(IV) species led to the recovery of the parent [MnL$_3$] species, proving that these redox processes are chemically reversible. In contrast to this stability, oxidation of manganese(IV) or reduction of manganese(II) resulted in decomposition, in the latter case involving the dissociation of at least one anionic [5′-NO$_2$phox]$^-$ ligand. The dissociation of the anionic phox ligand(s) probably also takes place during the reduction of [Mn(3′,5′-dClphox)$_3$]$^-$. The other formally manganese(II) anionic complexes were reduced at significantly more negative potentials and the corresponding cathodic waves were not observed within the available potential window. Ligand dissociation during the reduction of the manganese(II) complexes is not surprising, as the manganese(I) ion is hardly capable of coordinating exclusively strong σ- and π-donors, such as the anionic phox ligands.

The Mn−phox complexes are all active catalysts for the oxidation of styrene and *cis*- and *trans*-stilbene with dihydrogen peroxide as the oxidant. The substituents on the phenolate ring of the ligands significantly influenced the turnover numbers and selectivities in the oxidation reactions. The effect of the ligand substituents on the turnover numbers is roughly similar in acetone and methanol. However, considerably higher turnover numbers were obtained for styrene oxidation in acetone than in methanol, resulting in a turnover number of up to 220 towards styrene oxide with [Mn(phox)$_3$] as the catalyst, which also corresponds to increased efficiency towards dihydrogen peroxide from 2 to 15%. Although a clear general pattern can be noticed, exact correlation between the redox properties of the complexes and the turnover numbers and selectivities obtained in oxidation catalysis could not be found. This variation was probably caused by the effects that the ligands have on various reactions in solution, such as equilibria between different complexes in solution, dihydrogen peroxide decomposition and oxidation of the substrate.

The most remarkable substituent effect, the higher stability against oxidative degradation of the Mn−phox complex with the most electron-withdrawing substituents, [Mn(5′-NO$_2$phox)$_3$], was observed both in the electrochemical experiments and in oxidation catalysis. Further studies

on stability and decomposition will be published elsewhere.[31]

Experimental Section

General Remarks: The ligands were synthesised according to the synthesis for Hphox.[8] The synthesis of $[Mn(phox)_3]$ has been published before.[12] Solvents of technical grade, p.a. grade, or, for acetonitrile (Rathburn), HPLC grade quality were used as received. All p.a. grade solvents were purchased from Baker, except for acetone (Acros). Deuterated solvents for NMR measurements were obtained from Euriso-top ($CDCl_3$ and $[D_6]$DMSO) or Cambridge Isotope Laboratories, Inc. (CD_3OD). The following materials were supplied by Merck: Na_2SO_4, ferrocene, $Mn(OAc)_2{\cdot}4H_2O$, 2-aminoethanol, dihydrogen peroxide (35% in water), styrene, benzyl alcohol, and benzaldehyde. All other chemicals used were purchased from Acros.

Ligands

H-5′-NO_2phox: Starting from 15.35 g (78 mmol) of methyl 5-nitrosalicylate: Yield 7.21 g (35 mmol, 45%) of a yellow powder. ^{1}H NMR ($[D_6]$DMSO): δ = 4.17 (t, 2 H, NCH_2), 4.53 (t, 2 H, OCH_2), 7.07 (d, 1 H, H3′), 8.25 (dd, 1 H, H4′), 8.58 (d, 1 H, H6′), 13.1 (br, 1 H, OH). ^{13}C NMR ($[D_6]$DMSO): δ =52.0 (C4), 68.2 (C5), 109.4 (C1′), 118.5 (C3′), 124.3 (C5′), 128.9 (C6′), 138.1 (C4′), 164.9 (C2′), 165.9 (C2).

H-3′,5′-dClphox: Starting from 18.23 g (82 mmol) of methyl 3,5-dichlorosalicylate: Yield 16.35 g (70 mmol, 85%) of a pale yellow solid. ^{1}H NMR ($CDCl_3$): δ = 4.13 (t, 2 H, NCH_2), 4.47 (t, 2 H, OCH_2), 7.43 (d, 1 H, H6′), 7.52 (d, 1 H, H4′), 12.6 (br, 1 H, OH). ^{13}C NMR ($CDCl_3$): δ =53.3 (C4), 67.4 (C5), 112.3 (C1′), 122.4 (C3′), 122.9 (C5′), 126.0 (C6′), 132.9 (C4′), 154.6 (C2′), 165.1 (C2).

H-5′-Clphox: Starting from 10.69 g (58 mmol) of methyl 5-chlorosalicylate: Yield 7.40 (38 mmol, 66%) of a pale pink solid. ^{1}H NMR ($[D_6]$DMSO): δ = 4.07 (t, 2 H, NCH_2), 4.48 (t, 2 H, OCH_2), 7.02 (d, 1 H, H3′), 7.49 (m, 2 H, CH4′, H6′), 12.28 (s, 1 H, OH). ^{13}C NMR (D_6[DMSO]): δ =53.0 (C4), 67.3 (C5), 111.3 (C1′), 118.3 (C4′), 122.2 (C5′), 126.6 (C6′), 133.1 (C4′), 157.8 (C2′), 164.3 (C2).

H-5′-Mephox: Starting from 7.83 g (47 mmol) of methyl 5-methylsalicylate: Yield 6.18 g (35 mmol, 74%) of a pale pink solid. ^{1}H NMR ($CDCl_3$): δ = 2.23 (s, 3 H, CH_3), 4.02 (t, 2 H, NCH_2), 4.37 (t, 2 H, OCH_2), 6.79 (d, 1 H, H4′), 7.14 (d, 1 H, H3′), 7.39 (s, 1 H, H6′). ^{13}C NMR ($CDCl_3$): δ =20.3 (CH_3), 53.4 (C4), 66.6 (C5), 110.2 (C1′), 116.4 (C3′), 127.6 (C5′), 127.8 (C6′), 134.0 (C4′), 157.6 (C2′), 166.1 (C2).

H-3′-Mephox: Starting from 7.18 g (55 mmol) of ethyl 3-methylsalicylate: Yield 6.23 g (35 mmol, 88%) of a pale pink solid. ^{1}H NMR ($CDCl_3$): δ = 2.27 (s, 3 H, CH_3), 4.02 (t, 2 H, NCH_2), 4.35 (t, 2 H, OCH_2), 6.75 (t, 1 H, H5′), 7.20 (d, 1 H, H4′), 7.47 (d, 1 H, H6′). ^{13}C NMR ($CDCl_3$): δ =15.9 (CH_3), 53.4 (C4), 66.7 (C5), 110.0 (C1′), 118.0 (C5′), 125.5 (C6′), 125.7 (C3′), 134.1 (C4′), 158.1 (C2′), 166.5 (C2).

H-5′-MeOphox: Starting from 8.92 g (49 mmol) of methyl 5-methoxysalicylate: Yield 3.50 g (18 mmol, 37%) of a pale pink solid. ^{1}H NMR (CD_3OD): δ = 3.72 (s, 3 H, $ArOCH_3$), 4.05 (t, 2 H, NCH_2), 4.41 (t, 2 H, OCH_2), 6.84 (d, 1 H, H3′), 6.96 (dd, 1 H, H4′), 7.12 (d, 1 H, H6′). ^{13}C NMR (CD_3OD): δ =54.5 (C4), 56.4 ($ArOCH_3$), 68.2 (C5), 111.6 (C1′), 112.3 (C6′), 118.4 (C3′), 121.7 (C4′), 153.2 (C2′), 154.8 (C5′), 166.9 (C2).

General Synthetic Procedure for the Complexes $[Mn(5'\text{-}NO_2phox)_3]$ and $[Mn(3',5'\text{-}dClphox)_3]$: The appropriate ligand (3.0 mmol), dissolved in 10 mL of ethanol, was added to a solution of $Mn(OAc)_3{\cdot}2H_2O$ (0.27 g, 1.0 mmol) in 10 mL of ethanol. The product slowly precipitated as a black solid. Recrystallisation from ethanol afforded a black crystalline product.

$[Mn(5'\text{-}NO_2phox)_3]$: Yield 0.51 g (0.75 mmol, 75%). IR: $\tilde{\nu}$ = 1622 (s), 1312 (s), 1121 (m), 1058 (m), 871 (m), 838 (m), 714 cm^{-1} (m). $C_{27}H_{21}MnN_6O_{12}$: calcd. C 47.94, H 3.13, N 12.42; found C 47.68, H 3.37, N 12.12. ES-MS: *m*/*z*: 468 $[Mn(5'\text{-}NO_2phox)_2]^+$, 209 [H-5′-$NO_2$phox + H^+]. μ_{eff} = 4.87 μ_B (at 22.5 °C).

$[Mn(3',5'\text{-}dClphox)_3]$: Yield 0.51 g (0.68 mmol, 68%). IR: $\tilde{\nu}$ = 1617 (s), 1582 (m), 1437 (s), 1418 (s), 1370 (m), 1308 (m), 1234 (s), 1194 (m), 954 (m), 872 (m), 784 (s), 751 (m), 738 cm^{-1} (m). $C_{27}H_{18}Cl_6MnN_3O_6$: calcd. C 43.35, H 2.43, N 5.62; found C 43.08, H 2.45, N 5.31. ES-MS: *m*/*z*: 519, 517, 515 $[Mn(3',5'\text{-}dClphox)_2]^+$, 234, 232 [H-3′,5′-dClphox + H^+]. μ_{eff} = 4.10 μ_B (at 22.5 °C).

$[Mn(5'\text{-}Clphox)_3]$: To a solution of $Mn(OAc)_2{\cdot}4H_2O$ (0.25 g, 1.0 mmol) in 20 mL of MeOH was added 0.59 g (3.0 mmol) of H-5′-Clphox. After the addition of 10 mL of diethyl ether, the ligand dissolved and within several minutes the solution turned dark green. The dark green complex precipitated within 1 d. Recrystallisation from ethanol afforded X-ray quality crystals. Yield 0.52 g (0.81 mmol, 81%). IR: $\tilde{\nu}$ = 1622 (s), 1458 (s), 1405 (m), 1314 (s), 1237 (s), 1224 (s), 1100 (m), 1055 (m), 941 (m), 827 (m), 820 (m), 728 cm^{-1} (m). $C_{27}H_{21}Cl_3MnN_3O_6$: calcd. C 50.30, H 3.28, N 6.52; found C 50.41, H 3.30, N 6.33. ES-MS: *m*/*z*: 449, 447 $[Mn(5'\text{-}Clphox)_2]^+$, 200, 198, [H-5′-Clphox + H^+]. μ_{eff} = 4.74 μ_B (at 22.5 °C).

General Synthetic Procedure for $[Mn(3'\text{-}Mephox)_3]$, $[Mn(5'\text{-}Mephox)_3]$ and $[Mn(5'\text{-}MeOphox)_3]$: A solution of the ligand (3.0 mmol) and 0.30 g (3.0 mmol) of triethylamine in 10 mL of methanol was added to a solution of $Mn(OAc)_2{\cdot}4H_2O$ (0.25 g, 1.0 mmol) in 10 mL of methanol. The solution turned dark green immediately and within a number of days the complex precipitated. The complexes were recrystallised from methanol/water (2:1) ($[Mn(3'\text{-}Mephox)_3]$ and $[Mn(5'\text{-}MeOphox)_3]$) or ethanol ($[Mn(5'\text{-}Mephox)_3]$).

$[Mn(5'\text{-}Mephox)_3]$: Yield 0.43 g (0.72 mmol, 72%). X-ray quality crystals were obtained after recrystallisation from methanol. IR: $\tilde{\nu}$ = 1626 (s), 1601 (m), 1552 (m), 1485 (m), 1472 (s), 1323 (s), 1257 (m), 1242 (s), 1233 (s), 1201 (m), 1074 (m), 1057 (s), 866 (m), 826 (m), 792 cm^{-1} (m). $C_{30}H_{30}MnN_3O_6$: calcd. C 61.75, H 5.18, N 7.20; found C 61.53, H 5.32, N 7.30. ES-MS: *m*/*z*: 583 $[Mn(5'\text{-}Mephox)_3]^+$, 407 $[Mn(5'\text{-}Mephox)_2]^+$, 178 [H-5′-Mephox + H^+]. μ_{eff} = 4.47 μ_B (at 22.5 °C).

$[Mn(3'\text{-}Mephox)_3]$: Yield 0.45 g (0.77 mmol, 77%). IR: $\tilde{\nu}$ = 1622 (s), 1561 (m), 1424 (s), 1394 (m), 1382 (m), 1322 (m), 1252 (m), 1239 (s), 1136 (m), 1088 (m), 955 (m), 863 (m), 748 cm^{-1} (m). $C_{30}H_{30}MnN_3O_6$: calcd. C 61.75, H 5.18, N 7.20; found C 61.33, H 5.05, N 7.14. ES-MS: *m*/*z*: 407 $[Mn(3'\text{-}Mephox)_2]^+$, 17[H-3′-Mephox + H^+]. μ_{eff} = 4.82 μ_B (at 22.5 °C).

$[Mn(5'\text{-}MeOphox)_3]$: Yield 0.50 g (0.79 mmol, 79%). IR: $\tilde{\nu}$ = 1633 (m), 1601 (s), 1558 (m), 1471 (s), 1416 (m), 1273 (m), 1242 (m), 1206 (s), 1184 (m), 1040 (m), 815 (m), 794 cm^{-1} (m). $C_{30}H_{30}MnN_3O_9$: calcd. C 57.06, H 4.79, N 6.65; found C 57.10, H 4.73, N 6.65. ES-MS: *m*/*z*: 631 $[Mn(5'\text{-}MeOphox)_3]^+$, 439 $[Mn(5'\text{-}MeOphox)_2]^+$. μ_{eff} = 4.96 μ_B (at 22.5 °C).

X-ray Crystallographic Study: The data were collected with an Enraf−Nonius CAD-4 diffractometer with graphite-monochromated Mo-K_α radiation (λ = 0.71073 Å) and ω-2θ scan. The cell dimensions were determined by 24 independent reflections. The data were corrected for linear decay, but not for absorption effects. Atomic scattering factors and anomalous dispersion constants were taken from the International Tables for X-ray Crystallography.[32] For both compounds the positions of the heavy atoms were determined from Patterson maps (DIRDIF).[33] The remainder of the non-hydrogen atoms were found in subsequent ΔF syntheses (XTAL).[34] Hydrogen atoms were placed at calculated positions and were not included in refinement. Full-matrix least-squares refinement (XTAL)[34] on F of the positional and the anisotropic thermal parameters of the non-hydrogen atoms. The hydrogen atoms, with fixed isotropic thermal parameters, were included, riding on a fixed distance of their parent atoms. Crystallographic data (excluding structure factors) for the structures reported in this paper have been deposited with the Cambridge Crystallographic Data Centre as supplementary publications no. CCDC-144587 [Mn(5′-Mephox)$_3$] and -144588 [Mn(5′-Clphox)$_3$]. Copies of the data can be obtained free of charge on application to CCDC, 12 Union Road, Cambridge CB2 1EZ, UK [Fax: (internat.) + 44-1223/336-033; E-mail: deposit@ccdc.cam.ac.uk].

Equipment: IR spectra were recorded with a Perkin−Elmer FT-IR Paragon 1000 spectrometer. Samples were measured as KBr pellets. ^{1}H and ^{13}C NMR (^{1}H decoupled) spectra of the ligands were recorded with Jeol JNM-FX 200 or Bruker 300 DPX MHz spectrometers. ^{1}H NMR spectra of the complexes (up to 0.2 mM) were recorded with a Bruker 300 DPX MHz spectrometer. These spectra were collected using an inversion recovery pulse sequence π-τ-π/2. The value of τ (12 or 13 ms) was chosen such that the paramagnetic signals were relaxed, while the signals from the diamagnetic compounds in solution remained inverted. Other operating parameters were as follows: spectrometer frequency 300.13 Hz; data block size (SI) 32 K; acquisition time 200 ms; line broadening 5 Hz; window 30 kHz. Elemental analyses were carried out by the Microanalytical Laboratory, University College Dublin or at Leiden University with a Perkin−Elmer series II CHNS/O analyser 2400. A Johnson Matthey Alfa Products Mk1 magnetic susceptibility balance was used to determine the magnetic moments of the powdered complexes at room temperature. Standard electrospray mass spectra of the complexes were recorded with a Finnigan MAT TSQ-70 mass spectrometer, equipped with an electrospray interface (ESI). The spectra were collected by constant infusion of the analyte, dissolved in a methanol/water (80:20) mixture containing 1% acetic acid. A Varian Star 3400CX gas chromatograph with a J&W Scientific/Fisons DB-1701 (14% cyanopropylphenyl-methylpolysiloxane) column was used for analysis of the oxidation experiments. The turnover numbers given are the total turnover numbers per manganese ion after the indicated period of time. All reactions were performed at least in duplicate.

Cyclic Voltammetry: The cyclic voltammetry measurements were performed with an Autolab PGstat10 potentiostat controlled by the GPES4 software. A three-electrode system was used, consisting of a glassy carbon (GC) working electrode, a platinum (Pt) auxiliary electrode, and an Ag/AgCl reference electrode. All potentials are given versus Ag/AgCl. The experiments were carried out in acetonitrile at room temperature under argon with tetrabutylammonium hexafluorophosphate (Aldrich) as the supporting electrolyte. Under these conditions, the ferrocene/ferrocenium (Fc/Fc$^+$) couple was located at +0.44 V with a peak separation of 80 mV. Except for H-5′-NO_2phox that shows a reduction wave at −1.22 V (see above), the other ligands are not redox-active between +2.00 and −2.00 V.

Spectroelectrochemistry and Bulk Electrolysis: Butyronitrile (Acros Chimica, analytical grade) was dried with CaH_2 and freshly distilled under nitrogen. The samples were prepared under nitrogen using standard Schlenk techniques. The spectroelectrochemical experiments were conducted with saturated solutions of the complexes containing 0.3 M Bu_4NPF_6, recrystallised twice from absolute ethanol and dried in vacuo at 80 °C for 10 h. A PA4 potentiostat (EKOM, Czech Republic) was used to carry out the controlled-potential electrolyses. Bulk electrolyses were carried out in a gas-tight cell that consisted of three chambers separated at the bottom by S4 frits, with a Pt working electrode (120 mm^2 surface) in the middle, and Ag wire pseudo-reference and Pt gauze auxiliary electrodes in the lateral chambers. Chemical reduction was achieved with cobaltocene ($CoCp_2$; Aldrich), $E_{1/2}$ = −1.34 V vs. Fc/Fc$^+$. The UV/Vis spectroelectrochemical experiments at room temperature were performed with a previously described[35] Optically Transparent Thin-Layer Electrochemical (OTTLE) cell equipped with a Pt mini-grid working electrode (32 wires/cm) and quartz optical windows. The UV/Vis spectra were recorded with a software-updated Perkin−Elmer Lambda 5 spectrophotometer. X-band EPR spectra were obtained in an airtight tube cell at 77 K with a Varian Century E-104A spectrometer. EPR g values were determined relative to the 2,2′-diphenyl-1-picrylhydrazyl radical (DPPH; Aldrich) as an external "g mark" (g = 2.0037).

MO Calculations: Extended Hückel calculations were performed with the computer program CACAO (Computer Aided Composition of Molecular Orbitals).[36] The calculations were based on the X-ray diffraction data for [Mn(phox)$_3$].[12]

Catalytic Oxidation Reactions: Blank experiments were carried out in the absence of the catalyst or using manganese salts or ligands only. These experiments did not result in any epoxidation activity. Hydrogen peroxide decomposition (catalase activity) was observed with some of the reaction conditions, but systematic studies to this reaction have not been performed. − **In Methanol:** Upon stirring, 14 μmol of the catalyst was dissolved in 20 mL of MeOH at room temperature. To the resulting green solution, 14 mmol of styrene, 5.0 mmol of chlorobenzene, and 2.0 mmol of 1-methylimidazole (1-Meim) were added, followed (at t = 0 min) by 21 mmol of dihydrogen peroxide (35% in water). Except for the solution of [Mn(5′-NO_2phox)], which slowly started to turn pale yellow after t = 10 min, the colour of the solutions of the other complexes became yellowish to colourless within the first few minutes of the reactions. At t = 15 min, a sample was taken for analysis using gas chromatography with chlorobenzene as the internal standard. − **In Acetone:** Dihydrogen peroxide (21 mmol of a 35% solution in water) and 10 mL of acetone were stirred for 30 min at 0 °C. Thereafter, 14 mmol of styrene, 5.0 mmol of chlorobenzene, and 2.0 mmol of 1-Meim were added, followed by 14 μmol of the powdered catalyst (t = 0). The green solution changed to a slightly red-brown colour within the first few minutes of the reaction. After 10 min, the solution slowly turned to pale green-yellow. At t = 15 min, a sample was taken for analysis using gas chromatography with chlorobenzene as the internal standard. ***Caution!*** The mixture of acetone and dihydrogen peroxide is potentially explosive, especially under acidic conditions.[37,38] However, it can be handled safely by performing reactions on a small scale at 0 °C, using slightly alkaline conditions, as described above.

Acknowledgments

This work was carried out as part of the Innovation Oriented Research Programme on Catalysis (IOP Katalyse, no. IKA94056)

sponsored by the Netherlands Ministery of Economic Affairs. We would like to acknowledge Dr. J. G. de Vries (DSM, The Netherlands) and Dr. R. Hage (Unilever, The Netherlands) for useful discussions.

[1] M. Hoogenraad, *PhD thesis*, Leiden University, **2000**.
[2] R. Hage, *Recl. Trav. Chim. Pays-Bas.* **1996**, *115*, 385−395.
[3] T. Katsuki, in *Catalytic Asymmetric Synthesis* (Ed.: I. Ojima), Wiley-VCH, Weinheim, **2000**, p. 287.
[4] W. R. Sanderson, *Pure Appl. Chem.* **2000**, *72*, 1289.
[5] A. M. d′A. Rocha Gonsalves, M. M. Pereira, *J. Mol. Catal. A* **1996**, *113*, 209−221.
[6] K. Srinivasan, P. Michaud, J. K. Kochi, *J. Am. Chem. Soc.* **1986**, *108*, 2309−2320.
[7] M. Palucki, N. S. Finney, P. J. Pospisil, M. L. Güler, T. Ishida, E. N. Jacobsen, *J. Am. Chem. Soc.* **1998**, *120*, 948−954.
[8] H. R. Hoveyda, V. Karunaratne, S. J. Rettig, C. Orvig, *Inorg. Chem.* **1992**, *31*, 5408−5416.
[9] G. Mugesh, H. B. Singh, R. J. Butcher, *Eur. J. Inorg. Chem.* **2001**, 669−678.
[10] M. Gómez, S. Jansat, G. Muller, G. Noguera, H. Teruel, V. Moliner, E. Cerrada, M. Hursthouse, *Eur. J. Inorg. Chem.* **2001**, 1071−1076.
[11] M. Gómez-Simón, S. Jansat, G. Muller, D. Panyella, M. Font-Bardía, X.-J. Solans, *J. Chem. Soc., Dalton Trans.* **1997**, 3755−3764.
[12] M. Hoogenraad, K. Ramkisoensing, H. Kooijman, A. L. Spek, E. Bouwman, J. G. Haasnoot, J. Reedijk, *Inorg. Chim. Acta* **1998**, *279*, 217−220.
[13] M. Hoogenraad, K. Ramkisoensing, W. L. Driessen, H. Kooijman, A. L. Spek, E. Bouwman, J. G. Haasnoot, J. Reedijk, *Inorg. Chim. Acta* **2001**, *320*, 117−126.
[14] P. Basu, A. Chakravorty, *Inorg. Chem.* **1992**, *31*, 4980−4986.
[15] A. L. Spek, *PLATON, a multipurpose crystallographic tool*, Utrecht University, the Netherlands, **2000**; internet: http://www.cryst.chem.uu.nl/platon/
[16] D. H. Evans, K. M. O'Connell, R. A. Petersen, M. J. Kelly, *J. Chem. Educ.* **1983**, *60*, 290293.
[17] M. Koikawa, H. Okawa, S. Kida, *J. Chem. Soc., Dalton Trans.* **1988**, 641−645.
[18] M. R. Bermejo, A. Castiñeiras, J. C. Garcia-Monteagudo, M. Rey, A. Sousa, M. Watkinson, C. A. McAuliffe, R. G. Pritchard, R. L. Beddoes, *J. Chem. Soc., Dalton Trans.* **1996**, 2935−2945.
[19] R. I. Kureshy, N. H. Khan, S. H. R. Abdi, A. K. Bhatt, *J. Mol. Catal. A* **1996**, *110*, 33−40.
[20] J. A. Weinstein, N. N. Zheligovskaya, M. Y. Melnikov, F. Hartl, *J. Chem. Soc., Dalton Trans.* **1998**, 2459−2466.
[21] C. Mealli, D. M. Proserpio, *J. Chem. Educ.* **1990**, *67*, 399−402.
[22] M. M. Morrison, D. T. Sawyer, *Inorg. Chem.* **1978**, *17*, 333−337.
[23] K. Yamaguchi, D. T. Sawyer, *Inorg. Chem.* **1985**, *24*, 971−976.
[24] U. Auerbach, T. Weyhermüller, K. Wieghardt, B. Nuber, E. Bill, C. Butzlaff, A. X. Trautwein, *Inorg. Chem.* **1993**, *32*, 508−519.
[25] O. Schlager, K. Wieghardt, B. Nuber, *Inorg. Chem.* **1995**, *34*, 6456−6452.
[26] J. R. Pilbrow, *Transition Ion Electron Paramagnetic Resonance*, Oxford University Press, Oxford, **1990**.
[27] C. Zondervan, R. Hage, B. L. Feringa, *Chem. Commun.* **1997**, 419−420.
[28] T. Linker, *Angew. Chem. Int. Ed. Engl.* **1997**, *36*, 2060−2062.
[29] N. S. Finney, P. J. Pospisil, S. Chang, M. Palucki, R. G. Konsler, K. B. Hansen, E. N. Jacobsen, *Angew. Chem. Int. Ed. Engl.* **1997**, *36*, 1720−1723.
[30] R. I. Kureshy, N. H. Khan, S. H. R. Abdi, P. Iyer, A. K. Bhatt, *J. Mol. Catal. A* **1997**, *120*, 101−108.
[31] M. Hoogenraad, H. Kooijman, A. L. Spek, E. Bouwman, J. G. Haasnoot, J. Reedijk, manuscript in preparation.
[32] *International Tables for Crystallography*, vol. C (Ed.: A. J. C. Wilson), Kluwer Academic Publishers, Dordrecht, **1992**.
[33] P. T. Beurskens, G. Admiraal, G. Beurskens, W. P. Bosman, R. O. García-Granda, R. O. Gould, J. M. M. Smits, C. Smykalla, *The DIRDIF Program System*, Technical report of the Laboratory of Crystallography, University of Nijmegen, **1992**.
[34] S. R. Hall, G. S. D. King, J. M. Stewart, *XTAL3.4 User's manual*, Universities of Western Australia and Maryland, **1995**.
[35] M. Krejčík, M. Daněk, F. Hartl, *J. Electroanal. Chem.* **1991**, *317*, 179−187.
[36] C. Mealli, D. M. Proserpio, *CACAO version 3.3*, University of Florence, Italy, **1993**.
[37] L. Bretherick, *Handbook of Reactive Chemical Hazards*, Butterworths, London, **1975**.
[38] C. J. M. Stirling, *Chem. Br.* **1969**, *5*, 36.

Received June 21, 2001
[I01223]

Zinc- and Tin-Mediated C−C Coupling Reactions of Metalated (2-Pyridylmethyl)(trialkylsilyl)amines − Mechanistic, NMR Spectroscopic, and Structural Studies

Matthias Westerhausen,*[a] Tobias Bollwein,[a] Nikolaos Makropoulos,[a] Stefan Schneiderbauer,[a][‡] Max Suter,[a][‡] Heinrich Nöth,[a][‡] Peter Mayer,[a][‡] Holger Piotrowski,[a][‡] Kurt Polborn,[b][‡] and Arno Pfitzner[c][‡]

Keywords: Amides / C−C coupling / Magnesium / Metalations / Metallacycles / Pyridyl ligands / Tin / Zinc

The zincation of (2-pyridylmethyl)(triisopropylsilyl)amine (**1**) gives dimeric methylzinc (2-pyridylmethyl)(triisopropylsilyl)-amide (**2**). Further addition of dimethylzinc to a toluene solution of **2** at raised temperatures yields the C–C coupling product [1,2-dipyridyl-1,2-bis(triisopropylsilylamido)ethane]-bis(methylzinc) (**3**). Heating of molten **2**, or UV irradiation of **2**, results in the formation of **3** and zinc bis[(2-pyridylmethyl)-(triisopropylsilyl)amide] (**4**). The reaction between the zinc dihalide complexes of **1** [**5a** (X = Cl) and **5b** (X = Br)] and methyllithium yields the C–C coupling product **3** and the heteroleptic complex **2**, observed by NMR spectroscopy. During this reaction, zinc metal precipitates. The magnesiation of **1** with dibutylmagnesium gives magnesium bis[(2-pyridylmethyl)(triisopropylsilyl)amide] (**6**) in a quantitative yield. Subsequent addition of dimethylmagnesium results in a dismutation reaction and the formation of heteroleptic methylmagnesium (2-pyridylmethyl)(triisopropylsilyl)amide (**7**). Treatment of **1** with dimethylmagnesium also gives **7**. This complex slowly undergoes an intramolecular metalation during which dark red single crystals of (tetrahydrofuran)-magnesium 2-(triisopropylsilylamidomethylidene)-1-azacyclohexa-3,5-dien-1-ide (**8**) precipitate. In this compound the aromaticity of the pyridyl fragment is abolished. The magnesiation of (*tert*-butyldimethylsilyl)(2-pyridylmethyl)amine (**I**) proceeds quantitatively to give methylmagnesium (*tert*-butyldimethylsilyl)(2-pyridylmethyl)amide (**9**). This compound also undergoes an intramolecular metalation reaction, which results in the loss of the aromaticity of the pyridyl substituent and the formation of (tetrahydrofuran)magnesium 2-(*tert*-butyldimethylsilylamidomethylidene)-1-azacyclohexa-3,5-dien-1-ide (**10**). The metalation of **1** with tin(II) bis[bis(trimethylsilyl)amide] yields [bis(trimethylsilyl)amido]tin(II) (2-pyridylmethyl)(triisopropylsilyl)amide (**11**). The elimination of tin metal occurs even at room temperature, and the C–C coupling product [1,2-dipyridyl-1,2-bis(triisopropylsilylamido)ethane]tin(II) (**12**) is formed. The metalation of (*tert*-butyldimethylsilyl)(2-pyridylmethyl)amine with $Sn[N(SiMe_3)_2]_2$ gives [bis(trimethylsilyl)amido]tin(II) (*tert*-butyldimethylsilyl)(2-pyridylmethyl)amide (**13**). Within a few minutes, precipitation of tin metal takes place and the C–C coupled product [1,2-bis(*tert*-butyldimethylsilylamido)-1,2-dipyridylethane]tin(II) (**14**) is produced. In order to examine the importance of the pyridyl ligand for the C–C coupling reactions, zinc bis[*N*-(*tert*-butyldimethylsilyl)benzylamide] (**15**) was prepared by means of the metathesis reaction between lithium *N*-(*tert*-butyldimethylsilyl)benzylamide and zinc(II) halide. Treatment of **15** with dimethylzinc yields heteroleptic methylzinc *N*-(*tert*-butyldimethylsilyl)benzylamide (**16**). Refluxing of **16** with an excess of dimethylzinc in toluene does not give any C–C coupling reactions.

Introduction

A novel oxidative C−C coupling reaction subsequent to zincation of (*tert*-butyldimethylsilyl)(2-pyridylmethyl)amine (**I**) has been found.[1] The metalation of amine **I** with dimethylzinc yielded dimeric methylzinc (*tert*-butyldimethylsilyl)(2-pyridylmethyl)amide (**II**), according to Scheme 1. Either thermal decomposition or the addition of another equivalent of dimethylzinc at elevated temperatures then resulted in the oxidative C−C coupling reaction and hence in the formation of [1,2-bis(*tert*-butyldimethylsilylamido)-1,2-dipyridylethane]bis(methylzinc) (**III**) and the precipitation of zinc metal. The thermal decomposition of **II** also resulted in the formation of amine **I**, which was zincated by **II** still present to give zinc bis[(*tert*-butyldimethylsilyl)(2-pyridylmethyl)amide] (**IV**), according to Scheme 2.[1]

[a] Department Chemie, Ludwig-Maximilians-Universität München,
Butenandtstraße 9 (Haus D), 81377 München, Germany
Fax: (internat.) + 49-(0)89/2180-7867
E-mail: maw@cup.uni-muenchen.de
[b] Department Chemie, Ludwig-Maximilians-Universität München, Butenandtstraße 13 (Haus F), 81377 München, Germany
[c] Anorganische Chemie II, Universität Siegen,
57068 Siegen, Germany
Fax: (internat.) + 49-(0)271/7402555
[‡] Crystal structure determinations.

 © WILEY-VCH Verlag GmbH, 69451 Weinheim, Germany, 2002 1434−1948/02/0202−0389 $ 17.50+.50/0

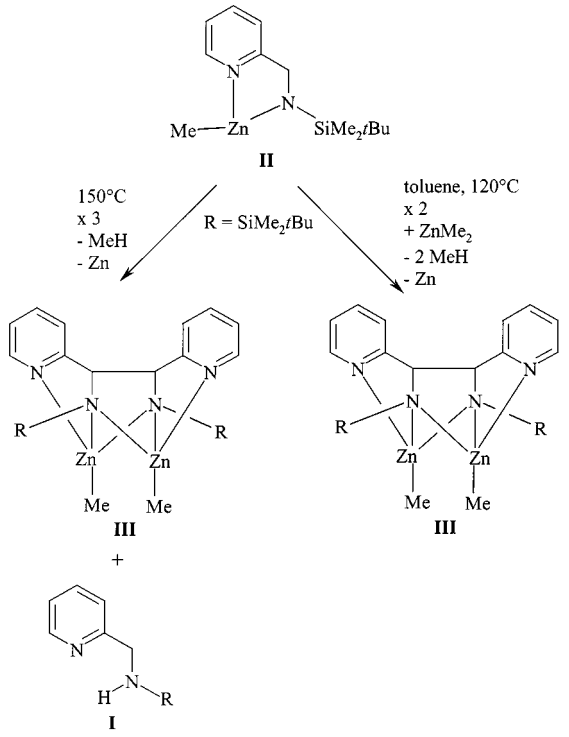

Scheme 1

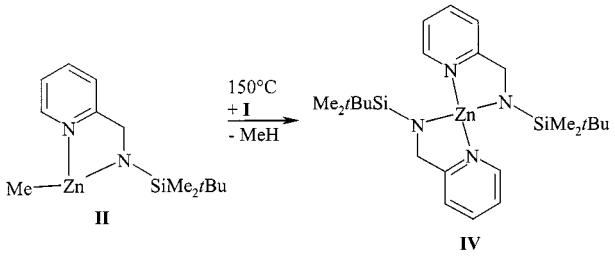

Scheme 2

The reaction between *N*,*N*′-di(*tert*-butyl)-1,4-diazabutadiene and dialkylzinc offered three different possible reaction pathways:[2,3] *C*-alkylation (**A**),[4,5] radical formation (**B**),[6,7] and *N*-alkylation (**C**)[4,5] after a homolytic Zn−C bond cleavage. An overview of these reactions is given in Scheme 3. The radicals **B** were in equilibrium with the dimeric species, as shown in this reaction diagram.[2,8,9] Mechanistically the formation of the C−C-coupled dimer can be explained by recombination of radicals.

This mechanism is not transferable to the oxidative C−C coupling reaction described here, for several reasons. During the zincation and subsequent C−C coupling, no radicals were detected by ESR spectroscopy and neither was a monomer−dimer equilibrium observed. In order to investigate the mechanism of the oxidative C−C coupling reaction shown in Scheme 1, it was necessary to address several questions: the influence of the steric hindrance of the *N*-bonded trialkylsilyl group, the standard potential E^0(M/M^{2+}) of the metalation reagent, and the role of the pyridyl substituent.

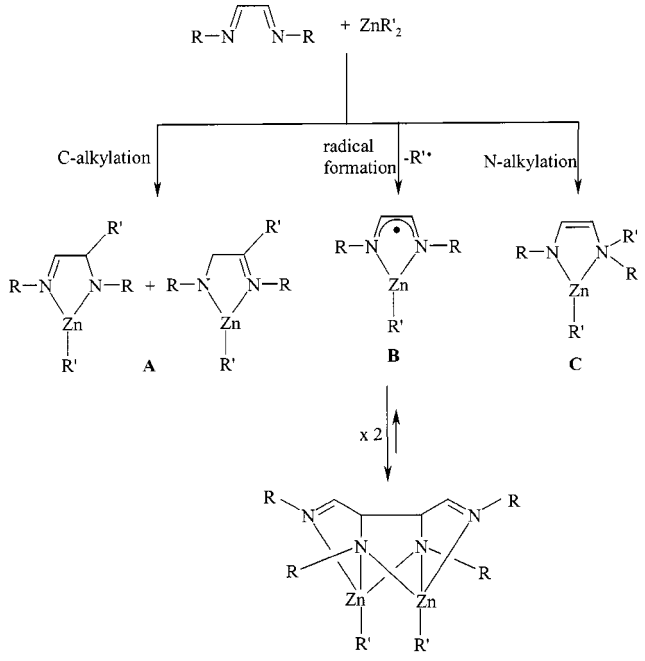

Scheme 3

Results and Discussion

Synthesis and Mechanistic Studies

It has already been shown that methylzinc (*tert*-butyl)(2-pyridylmethyl)amide undergoes a monomer/dimer equilibrium favoring the dimeric molecule **VI** (Scheme 4),[2,8] which has also been structurally characterized.[9] The substitution of the *tert*-butyl group for a trialkylsilyl substituent results in drastic changes in the chemical and physical behavior of these molecules. On one hand, the *N*-trialkylsilyl substitution prevents the monomerization process, while on the other a novel synthetic route to these tetradentate ligands in a quantitative yield is possible, by means of the C−C coupling reaction.

Influence of the Size of the Trialkylsilyl Substituents

The lithiation of 2-(aminomethyl)pyridine and the subsequent metathesis reaction with chlorotriisopropylsilane yields (2-pyridylmethyl)(triisopropylsilyl)amine (**1**). The zincation of **1** gives dimeric methylzinc (2-pyridylmethyl)-

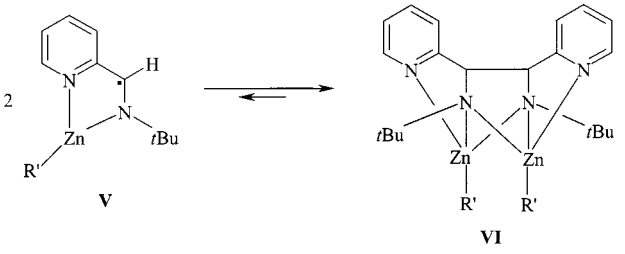

Scheme 4

(triisopropylsilyl)amide (**2**), with a central Zn_2N_2 ring. The addition of dialkylzinc to a solution of **2** in toluene at raised temperatures results in a C−C coupling reaction and the formation of [1,2-bis(triisopropylsilylamido)-1,2-dipyridylethane]bis(methylzinc) (**3**). Heating of molten **2**, or UV irradiation of **2**, yields **3** and zinc bis[(2-pyridylmethyl)(triisopropylsilyl)amide] (**4**) in an equimolar ratio, together with zinc and methane. Compound **4** represents a structure similar to **IV**, the only difference being the substituents at the silicon atom.

The quantitative synthesis of **3** is achieved by means of a reaction between **1** and at least 1.5 equiv. of dimethylzinc. The mechanistic picture is presented in Scheme 5. The first step is the complexation of dimethylzinc by **1**, as described below for the zinc dihalide complexes and similar to already published adducts.[6,10] Subsequently, the amine moiety is zincated. The methylene groups are then metalated by a methylzinc moiety. Whether this zincation step happens intramolecularly (monomolecular) or intermolecularly (bimolecular or even higher order) is uncertain, especially in view of the fact that the compounds described above are dimeric both in the solid state and in solution. The relaxation of the anionic charge produces a bis(amide). However, this intermediate forms only at higher temperatures and was not observable in the zinc-mediated C−C coupling reaction. At these temperatures, the zinc atom could be eliminated as Zn^0, with (pyridylmethylidene)(trialkylsilyl)amine being formed. In the presence of additional dimethylzinc and another equivalent of **2**, the C−C coupling occurs immediately with evolution of methane (mass spectrometric identification) and precipitation of zinc metal (proof by X-ray powder diffraction[1]). Because of the dimeric nature of **2**, only the (*R*,*R*) and the (*S*,*S*) isomers of **3** are formed, and no *meso* isomer is observed. The steric demand of the trialkylsilyl groups influences the conformation of the dimeric methylzinc (2-pyridylmethyl)(trialkylsilyl)amide as shown in Scheme 6 (structure types **D** and **E**), but not the reactivity towards dimethylzinc.

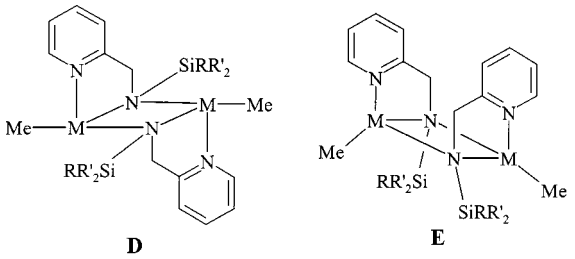

Scheme 6. Schematic drawing of the two possible conformations **D** and **E** for the dimeric derivatives of the type $[R-M-N(SiRR'_2)CH_2-py]_2$ with M as Zn (**2** and **II**) and Mg (**7** and **9**)

Mixing of compounds **III** and **3** in toluene does not afford the mixed compound with a triisopropylsilyl group at one nitrogen atom and a *tert*-butyldimethylsilyl substituent at the other, which we also interpret as support for the ionic mechanism. However, irradiation of this mixture does produce this mixed derivative, most probably through a C−C bond cleavage, as shown for the equilibrium in Scheme 4 for the *N*-*tert*-butyl derivative.

Another possibility for the synthesis of **3** is shown in Scheme 7. Treatment of **1** with zinc dihalides yields the corresponding adducts **5a** (X = Cl) and **5b** (X = Br), which are only partly soluble in common organic solvents. The addition of methyllithium to **5b** results in the formation of the C−C coupling product **3** and the heteroleptic complex **2**, as observed by NMR spectroscopy. During this reaction, zinc metal precipitates in accordance with the proposed mechanism.

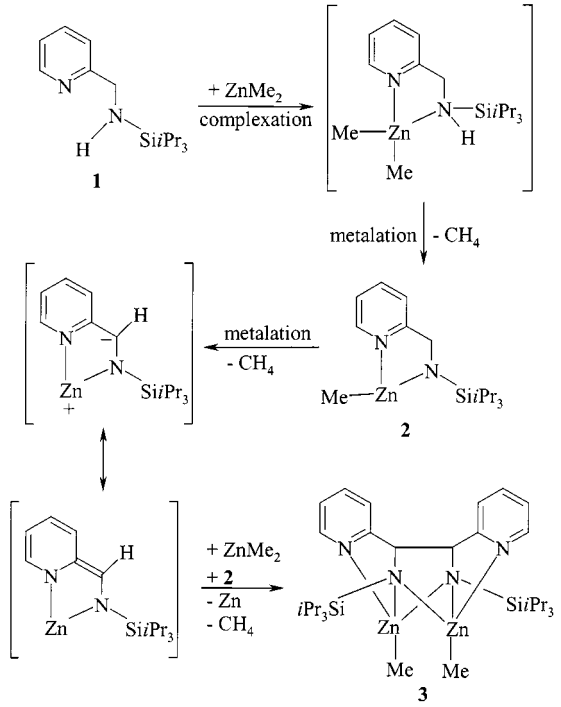

Scheme 5

Influence of the Standard Potential $E^0(M/M^{2+})$

If the reaction were to be performed with other metals, other pathways should be followed, depending on the potential $E^0(M/M^{2+})$, which for zinc is −0.7626 V.[11] In order to investigate the reaction mechanism, the less noble magnesium [$E^0(Mg/Mg^{2+}) = -2.356$ V[11]] and the nobler tin [$E^0(Sn/Sn^{2+}) = -0.137$ V[11]] were applied. The magnesiation of **1** with dibutylmagnesium gives magnesium bis[(2-pyridylmethyl)(triisopropylsilyl)amide] (**6**) in a quantitative yield. Subsequent addition of dimethylmagnesium results in a dismutation reaction and the formation of heteroleptic methylmagnesium (2-pyridylmethyl)(triisopropylsilyl)amide (**7**). Treatment of **1** with dimethylmagnesium in an equimolar ratio gives mainly **7**; the reaction solution turns dark, however. Reduction of the volume and cooling to approximately 5 °C results in the precipitation of dark red, single crystals of (tetrahydrofuran)magnesium 2-[(triisopropylsilyl)amidomethylidene]-1-azacyclohexa-3,5-dien-1-ide (**8**) in a rather low yield, embedded in a dark oil. The first reaction step is clearly the metalation of the amine **1**, followed

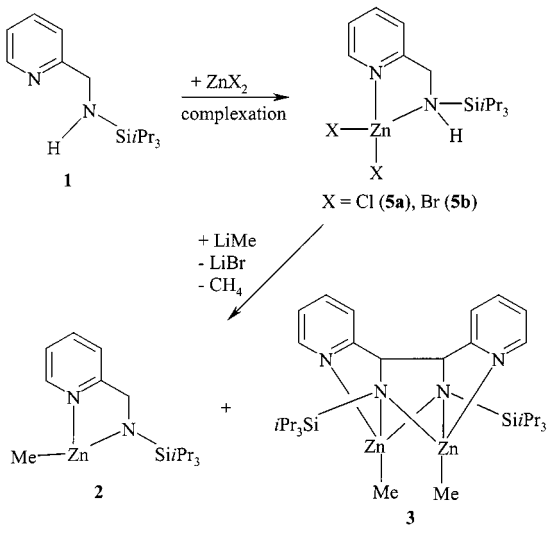

Scheme 7

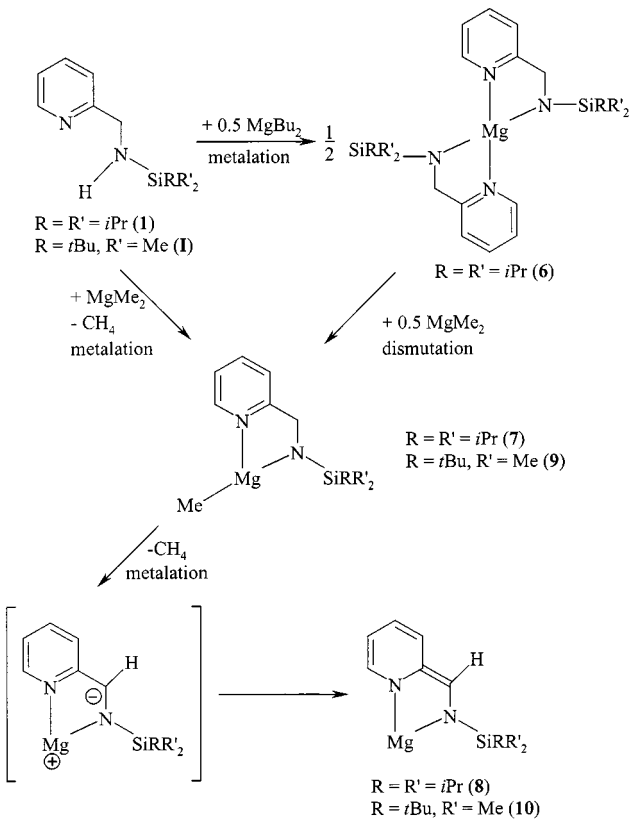

Scheme 8

by a further metalation of the methylene group. The anionic charge is then transferred to the pyridyl nitrogen atom, thus forming a bis(amide) as shown in Scheme 8. The stronger metalation power[12] of a magnesium-bonded methyl group allows intramolecular H abstraction and the breakdown of the aromaticity of the pyridyl moiety at lower temperatures. The reduced aromatic character of *C*-bonded pyridyl moieties is already well known in the case of [bis(2-pyridyl)methyl]lithium.[13–15] No precipitation of magnesium metal is observed in the course of this reaction. During the zincation of **1**, no similar zinc bis(amide) was detected, because on the one hand elevated temperatures are necessary for the metalation of the methylene fragment and on the other hand the reduction of the zinc dication is more easily accessible than that of the magnesium dication. Complex **8**, if dissolved in common organic solvents, decomposes into a variety of as yet unidentified products, which prevents spectroscopic characterization.

The magnesiation of (*tert*-butyldimethylsilyl)(2-pyridylmethyl)amine (**I**) proceeds quantitatively, to give methylmagnesium (*tert*-butyldimethylsilyl)(2-pyridylmethyl)amide (**9**). Even though this metalation is performed in THF, **9** crystallizes from a toluene solution isotypically to the corresponding zinc derivative,[1] as a dimer without coordination of further neutral coligands. This compound undergoes an intramolecular metalation reaction, which results in the loss of the aromaticity of the pyridyl substituent and the formation of (tetrahydrofuran)magnesium 2-[(*tert*-butyldimethylsilyl)amidomethylidene]-1-azacyclohexa-3,5-dien-1-ide (**10**). In a concentrated THF solution, dark red crystals, containing both the compounds **9** and **10** in an equimolar ratio, precipitate at 5 °C within 3 d. This magnesiation step occurs even in the dark and at low temperatures. Attempts to crystallize pure **10** were not successful. Thanks to this cocrystallization during the intramolecular magnesiation process, **9** and **10** were removed from the reaction solution environment, which allowed their molecular structures to be crystallographically determined, since the crystalline material constituting **10** decomposes very slowly in the solid state. In solution, however, as yet unknown decomposition reactions occur.

The metalation of **1** with tin(II) bis[bis(trimethylsilyl)amide][16–20] yields a green solution of [bis(trimethylsilyl)amido]tin(II) (2-pyridylmethyl)(triisopropylsilyl)amide (**11**). The elimination of tin metal occurs even at room temperature, as proven by X-ray powder diffraction analysis (Figure 1). In an equimolar quantity, the C–C coupling product tin(II) 1,2-dipyridyl-1,2-bis(triisopropylsilylamido)ethane (**12**) forms according to Scheme 9. Because of the size of the Sn^{2+} cation and the stereochemical activity of the lone pair, only one metal center is coordinated to this tetradentate ligand, through three nitrogen atoms. The magnetic equivalence of both pyridyl groups can be explained by a fast (on the NMR timescale) exchange reaction. NMR spectroscopic investigation of the crystals shows the presence of a small amount of the *meso* isomer **12′**, because the fixation of the geometry is less restrictive in regard to the reaction pathway due to the mononuclearity of these tin(II) complexes.

The smaller *tert*-butyldimethylsilyl group at the amide moiety gives products similar to those described above. The metalation of (*tert*-butyldimethylsilyl)(2-pyridylmethyl)amine **I** with $Sn[N(SiMe_3)_2]_2$ gives [bis(trimethylsilyl)amido]tin(II) (*tert*-butyldimethylsilyl)(2-pyridylmethyl)amide (**13**). Within a few minutes, the precipitation of tin

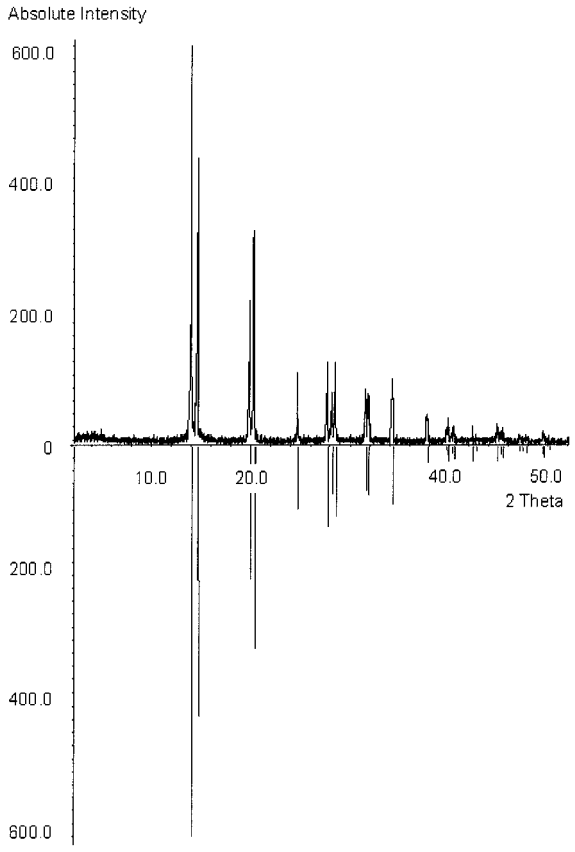

Figure 1. X-ray powder diffractogram of tin that precipitated during the C−C coupling reactions (top) and the reference line spectrum (bottom)

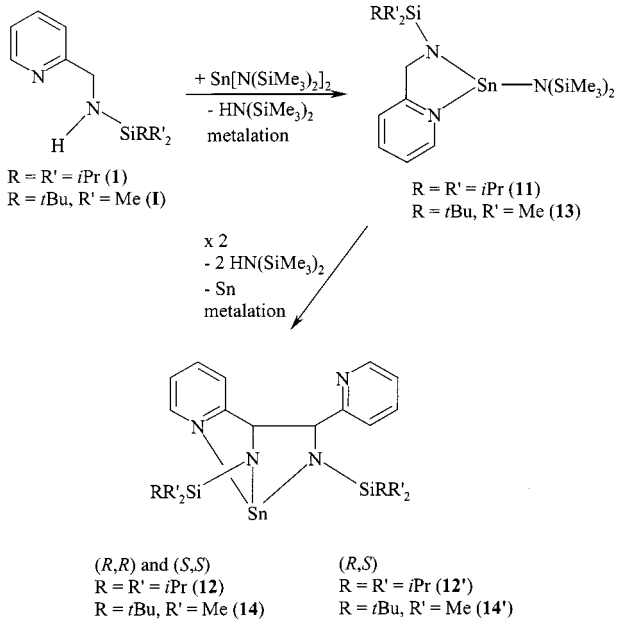

Scheme 9

metal and the C−C coupling reaction begin. Thanks to the less crowded trialkylsilyl substituent, the (*R*,*R*) and (*S*,*S*) isomers **14** are formed together with a small quantity of the *meso* form **14′**.

All these C−C coupling products are colorless and no equilibrium similar to the reaction described in Scheme 4 was observed. Solutions of these derivatives in toluene and heptane showed no EPR signal, and so there was no indication of a radical mechanism. We interpret all these findings in terms of the involvement of a polar reaction mechanism.

Importance of the Pyridyl Fragment

The pyridyl substituent could be important for this reaction in two ways. On the one hand, it might function as an anchor group to bind dimethylzinc and thus to enforce a close contact between the metalating reagent and the amine. On the other, the reaction mechanism involves a step in which the aromaticity of the pyridyl substituent is disturbed and a bis(amide) is formed. Therefore, the use of an *N*-silylated benzylamine (formal replacement of the pyridyl nitrogen atom by a CH fragment) was investigated. This change strongly decreased the reactivity of (benzyl)(*tert*-butyldimethylsilyl)amine towards dimethylzinc. The zincation did not offer access to the corresponding zinc amides.

In order to examine the importance of the pyridyl ligand for the C−C coupling reactions, zinc bis[(benzyl)(*tert*-butyldimethylsilyl)amide] (**15**) was prepared by lithiation of (benzyl)(*tert*-butyldimethylsilyl)amine (**V**)[21] and the subsequent metathesis reaction with zinc(II) halide according to Scheme 10. Treatment of **15** with dimethylzinc yielded heteroleptic methylzinc (benzyl)(*tert*-butyldimethylsilyl)amide (**16**).[22]

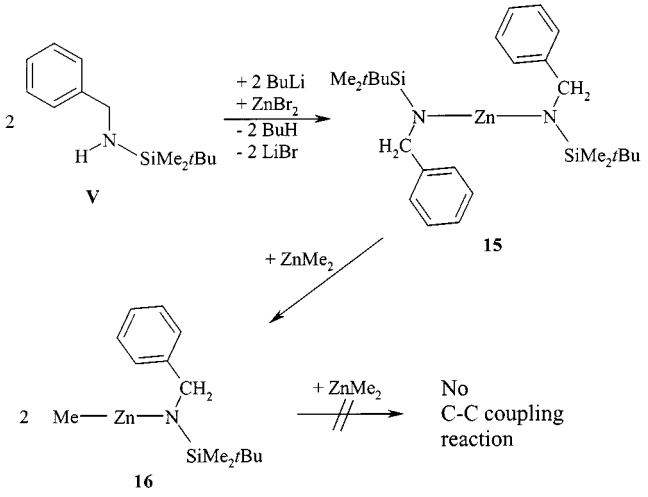

Scheme 10

Compound **16** behaves as a characteristic heteroleptic alkylzinc amide, as is well known for a wide variety of compounds of the general type R−Zn−NR′R′′ (see examples in the literature[23−26]). No C−C coupling reaction between **16** and excess dimethylzinc was observed, even in refluxing toluene.

From these observations, we conclude that a derivative with a disturbed aromatic character in the pyridyl fragment seems to play the key role in this mechanism. For the C−C coupling reaction, the presence of the methylpyridyl moiety

is essential, whereas the steric demand of the *N*-bonded trialkylsilyl substituent is only of secondary importance. The standard potential determines the reaction conditions for the C−C coupling. Whereas mild conditions are sufficient for the use of tin(II), the reaction solutions had to be heated to perform the coupling with zinc(II). Magnesium was not able to initiate the C−C bond formation but we were therefore able in this case to determine the crystal structures of molecules that most probably serve as intermediates in the metalation reactions with zinc(II) and tin(II) reagents.

Structural Investigations

Figure 2 shows the molecular structure and numbering scheme of **2**. The crystallographic C_2 axis generates the second half of the molecule; the symmetry-related atoms are marked with primes. Scheme 7 shows the possible conformations for dimeric methylzinc (2-pyridylmethyl)(trialkylsilyl)amides. Whereas type **D** is already known for the *N*-(*tert*-butyldimethylsilyl)-substituted derivative **II**,[1] compound **2** crystallizes in structure type **E**. However, the conformation of the dimer is without importance for the reactivity in the C−C coupling reaction. The central feature is the slightly folded Zn_2N_2 ring (folding angle 167.1°) with Zn−N bond lengths of approximately 211 pm (Table 1). The transannular Zn1···Zn1′ contact lies at 284.7 pm.

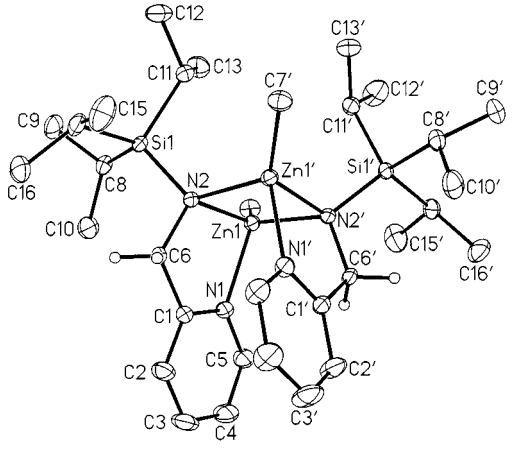

Figure 2. Molecular structure of **2**; the ellipsoids represent 40% probability; atoms generated by the crystallographic C_2 symmetry ($-x$, y, $-z + 1.5$) are marked with apostrophes; the hydrogen atoms are omitted for clarity, with the exception of those at C6/C6′

Figure 3 represents the molecular structure of **3**. The numbering scheme coincides with that of **2** and thus offers the possibility of direct comparison of the structural parameters (Table 1). The C−C coupling of the bidentate anions results in the formation of both the (*R*,*R*)- and the (*S*,*S*)-1,2-bis(pyridyl)-1,2-bis(triisopropylsilylamido)ethane dianions. Thanks to the crystallographically enforced inversion center, both of these isomers are included in the investigated single crystals, whereas no (*R*,*S*) isomer was observed either in the crystalline state or in solution.

The Zn−N bonds of the pyridine moiety are elongated in comparison to those in the sterically unhindered (bipyridine-*N*,*N*′)zinc dichloride, with values of 206 pm.[27] In the pyridine complex bis(1,4-dihydropyridyl)bis(pyridine-*N*)zinc,[28] on the other hand, Zn−N values of 198 and 213 pm have been observed for the anionic and the neutral ligands, respectively. Enhanced steric demand results in a further elongation of this bond, as shown for (bipyridine-*N*,*N*′)bis[bis(trimethylsilyl)methyl]zinc.[29]

The C6−C6′ bond formation increases the intramolecular steric strain, as is also demonstrated by the C6−C6′ bond length of 160 pm, a value in the same range as, for example, strongly strained [1.1.1]propellanes.[30] A slightly smaller value was previously found by van Koten and coworkers for compound **VI** [R = Et, 157.0(8) pm[2,9]]; the Zn−N bond lengths to the amido ligands show a mean value of 208.5 pm,[2,9] whereas values of 212.3 pm are observed in **3**. Furthermore, a strong folding of the Zn_2N_2 ring is imposed. Whereas the folding angle in **2** is 167.1°, the corresponding value after C−C bond formation lies at 109.9°. Because of this folding, the triisopropylsilyl substituents are pushed apart from each other and the *Zn*-bonded methyl groups move toward each other and consequently between the *i*Pr_3Si substituents. The Zn1−N2−Si1 angle is therefore enhanced. Furthermore, the short transannular Zn1···Zn1′ contact of 272.8 pm increases the electrostatic repulsion between the metal cations. In **VI**, a comparable metal−metal contact of 274.9(1) pm was found.[2] The rearrangement of the aliphatic substituents gives rise to a slight contraction of most of the bond lengths. The Zn1−C7 distance is approximately 3 pm smaller, whereas this trend is less dramatic for the Si1−N2 and Si1−C bonds.

Figure 4 shows the molecular structure and numbering scheme of **8**. The disordered THF molecule between these dimeric magnesium bis(amides) is neglected, due to the lack of short contacts between this solvent molecule and **8**. Derivative **8** represents the key compound in explaining the mechanism discussed above. The numbering scheme is similar to that shown for **2** and **3**; atoms generated by crystallographic inversion symmetry are marked with apostrophes. The central feature is the Mg_2N_2 ring with distorted tetrahedrally coordinated magnesium atoms. The N2−Mg1−N2′ angle in this centrosymmetric ring has a value of 95.2°. The Mg−O distances of 202.7 pm lie in the expected region.[31,32] Selected structural parameters are summarized in Table 1.

Special attention should be drawn to the amidomethylpyridyl fragment. The aromaticity of the pyridyl moiety is broken, and alternating long and short C−C bonds are observed. The negative charge is located on both the nitrogen atoms, thus giving a cyclic magnesium bis(amide). The N1−C5 distance of 135.9 pm represents a characteristic value for an N−C single bond to an sp^2-hybridized carbon atom, whereas the N1−C1 bond (140.7 pm) seems to be elongated. The N2−C6 distance of 145.6 pm is larger, due to the tetrahedral environment of N2 and the steric strain induced by the trialkylsilyl substituent. The C−C bonds of the pyridyl fragment show a slight degree of conjugation, as the C−C single bonds are shorter (mean value 142.6)

Table 1. Selected bond lengths [pm] and angles [°] of **2**, **3**, **8**, **9**, and **10**

Compound	**2**	**3**	**8**	**9**[a]	**9**[b]	**10**[b]
M1−N1	211.8(2)	210.9(3)	203.5(4)	211.8(4)	214.4(3)	203.1(3)
M1−N2	210.9(2)	212.2(3)	209.6(4)	215.7(4)	213.4(2)	206.4(3)
M1−N2′	209.9(2)	212.2(3)	208.6(3)	211.7(3)	211.7(3)	207.0(3)
M1−C7	198.4(2)	195.1(4)	202.7(3)[c]	213.2(5)	211.9(4)	199.3(3)[c]
M1···M1′	284.8(1)	272.78(9)	281.9(3)	293.4(3)	293.7(2)	281.0(2)
N1−C1	133.8(3)	133.5(5)	140.7(6)	134.3(5)	134.4(4)	140.1(4)
N1−C5	135.4(3)	133.7(5)	135.9(6)	135.6(6)	132.2(4)	136.7(4)
C1−C2	138.3(3)	137.6(6)	145.0(6)	140.3(6)	138.7(5)	144.2(5)
C1−C6	151.0(3)	151.0(5)	136.2(7)	151.7(6)	150.4(5)	137.0(5)
C2−C3	137.4(3)	138.3(7)	134.9(8)	136.6(7)	136.0(5)	135.8(6)
C3−C4	138.3(4)	135.9(8)	140.2(8)	137.6(8)	137.0(6)	139.9(6)
C4−C5	136.2(3)	137.1(7)	136.9(7)	135.6(7)	137.5(5)	135.4(6)
N2−C6	147.5(3)	146.8(4)	145.6(5)	148.0(4)	148.7(4)	146.1(4)
N2−Si1	174.6(2)	173.8(3)	174.4(3)	172.7(3)	173.0(2)	172.3(3)
C6−C6′	–	159.8(6)	–	–	–	–
M1−N2−M1′	85.18(7)	80.0(1)	84.8(1)	86.7(1)	87.39(9)	85.7(1)
N2−M1−N2′	94.14(7)	76.5(1)	95.2(1)	93.3(1)	92.61(9)	94.4(1)
M1−N2−C6	109.8(1)	94.1(2)	92.1(2)	109.4(3)	108.2(2)	99.9(2)
N2−C6−C1	115.7(2)	114.0(3)	123.6(5)	115.2(3)	114.9(3)	123.3(4)
C6−C1−N1	117.8(2)	114.7(3)	119.7(4)	119.3(4)	117.4(3)	118.9(3)
C1−N1−M1	113.4(1)	107.1(2)	104.9(3)	113.3(3)	112.7(2)	104.9(2)
N1−M1−N2	82.53(6)	83.0(1)	87.8(2)	82.2(2)	82.0(1)	88.2(1)
Si1−N2−C6	111.5(1)	117.8(2)	111.7(3)	114.2(2)	113.7(2)	117.4(2)
Si1−N2−M1	115.65(9)	128.1(2)	131.2(2)	111.6(2)	114.4(1)	128.3(2)
Si1−N2−M1′	120.48(9)	122.3(2)	128.4(2)	124.3(2)	122.5(1)	123.8(1)

[a] Data from the solid state structure of **9**. [b] Parameters from the crystal structure of **9·10**. [c] Mg1−O01.

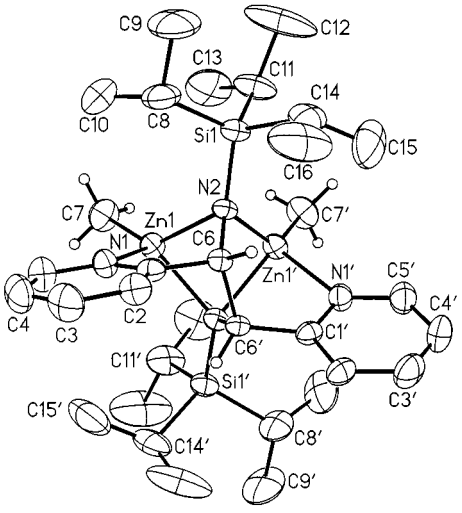

Figure 3. Molecular structure of **3**; the ellipsoids represent 40% probability; atoms generated by the crystallographic C_2 symmetry ($-x + 2$, y, $-z + 0.5$) are marked with apostrophes;the hydrogen atoms are omitted for clarity, with the exception of those at C6/C6′

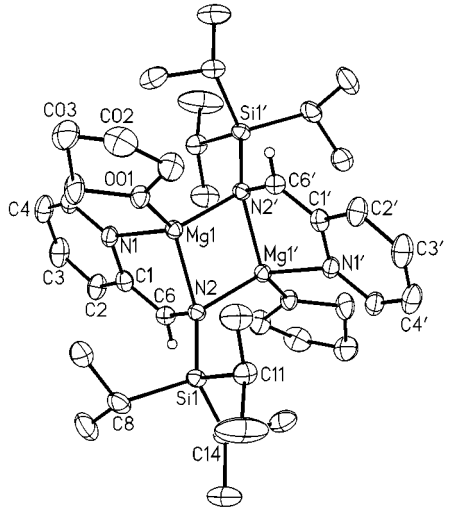

Figure 4. Molecular structure of **8**; the ellipsoids represent 40% probability; atoms generated by the crystallographic inversion symmetry ($-x$, $-y + 1$, $-z + 2$) are marked with apostrophes; the hydrogen atoms are omitted for clarity, with the exception of those at C6/C6′

than expected (reference value 1.48 pm[33]) whereas the C=C double bonds (mean value 136.0 pm) are widened (reference value 1.34 pm[33]).

The Mg1−N1 bond length of 203.5 pm is rather short, due to the low coordination number of N1 and the electrostatic attraction between the nitrogen atom and the metal center. The distorted tetrahedral surrounding and the steric shielding of N2 produce a longer N2−Mg1 bond length. The transannular Mg1···Mg1′ contact of 281.9 pm is rather short, however, this is a consequence of the small endocyclic Mg−N bonds lengths.

Figure 5 represents the molecular structure and numbering scheme of dimeric **9**. This molecule shows point symmetry and so structure type **D** is achieved. Atoms generated by the inversion symmetry are marked with apostrophes. In comparison with the isotypic zinc complex **II** and with **2**, the metal−carbon bonds of **9** are elongated by approxim-

ately 15 pm in accordance to the van der Waals radii difference (r_{Mg} = 170 pm; r_{Zn} = 140 pm[34]); however, the difference between the Mg−N and Zn−N bond lengths is far less distinct. Because of the slightly larger metal centers, the transannular M1···M1 contacts of **9** are larger than those in the similar zinc derivatives **II** and **2**. This is achieved by widening of the Mg1−N2−Mg1′ bond angle compared with the corresponding values in the zinc complexes.

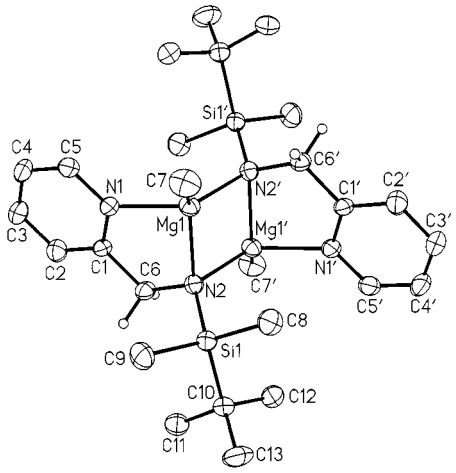

Figure 5. Molecular structure of **9**; the ellipsoids represent 40% probability; atoms generated by the crystallographic inversion symmetry ($-x + 1, -y + 1, -z$) are marked with apostrophes; the hydrogen atoms are omitted for clarity, with the exception of those at C6/C6′

Figure 6 represents the molecular structure and numbering scheme of **10**. This molecule cocrystallizes in an equimolar ratio with **9** as shown in Figure 7. The solid-state structure can be regarded as a layer structure, with the molecules of **9** in (*h*,*k*,0) and those of **10** in (*h*,*k*,0.5). Both these molecules show inversion symmetry and a nearly similar arrangement of their substituents. The magnesium atoms are in a distorted tetrahedral environment. The molecular structure of **9** is similar to the structure described above and no detailed discussion is necessary. However, **10** shows some remarkable structural features. The center of interest concerns the disturbed aromaticity of the pyridyl fragment, which is similar to that in **8**. Detailed discussion therefore seems unnecessary.

Mononuclear 1,2-dipyridyl-1,2-bis(trialkylsilylamido)-ethane complexes of tin(II) preferentially form as (*R*,*R*) and (*S*,*S*) isomers; however, a minor quantity of the *meso* form is also produced from this reaction. This situation allows these isomers to be compared in the crystalline state, and so the numbering schemes are alike for all these derivatives. Figures 8 to 10 show the molecular structures and numbering schemes of **12**, **12′**, and **14**, respectively; Table 2 contains selected structural data. The backbone consists of the stereogenic centers C1 and C2. The *Sn*-bonded pyridyl fragment is located at C1, whereas the uncoordinated pyridyl substituent is bonded to C2. The tin atoms are in a trigonal-pyramidal environment formed by the three nitrogen atoms N1, N2, and N21, whereas N22 shows no short contacts to any tin(II) centers. The Sn−N21 bond lengths are nearly 20

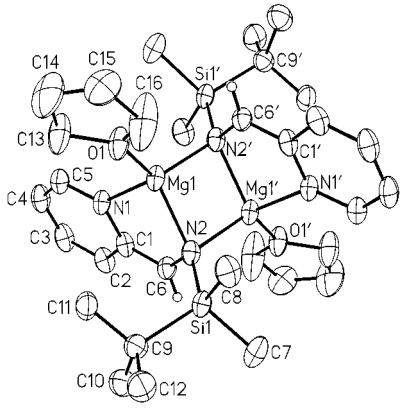

Figure 6. Molecular structure of **10**; the ellipsoids represent 30% probability; atoms generated by the crystallographic inversion symmetry ($-x + 2, -y + 2, -z + 1$) are marked with apostrophes; the hydrogen atoms are omitted for clarity, with the exception of those at C6/C6′

pm larger than the tin−nitrogen distances to the negatively charged atoms N1 and N2. The sterically less demanding *tert*-butyldimethylsilyl substituent allows shorter Sn−N bonds than the *N*-bonded triisopropylsilyl group. A remarkable difference concerns the newly formed C1−C2 bond. Whereas this bond is extremely long in compounds **12** and **12′**, a characteristic value of 153.5(6) is found in **14**. However, the ring strain in **14** gives rise to an elongated C1−C11 bond. A comparison of the structural parameters of **12** [(*R*,*R*) and (*S*,*S*) isomers] and **12′** (*meso* isomer) show two main differences, namely the smaller Sn−N21 bond length and the smaller Sn−N2−Si2 bond angle in **12′**. Both these observations can be attributed to reduced intramolecular steric strain in this isomer.

The stereochemically active lone pair at tin(II) gives rise to the pyramidal coordination sphere at the metal center. Similar observations are already well known for other tin(II) amides. The Sn−N1 and Sn−N2 bond lengths are comparable to those published for $Sn[N(SiMe_3)_2]_2$.[35−37] A higher coordination number of three[38] or four[39] at the tin(II) center results in longer Sn−N bonds.

In **14**, the nitrogen atoms N1 and N2 are in a planar environment (angle sums of N1 and N2: 359.3 and 359.7°). The larger trialkylsilyl substituents produce distortions and smaller angle sums at the amide moieties (**12**: N1 354.4°, N2 358.1°; **12′**: N1 357.8°, N2 350.2°).

NMR Spectroscopy

NMR spectroscopic data for the zinc- and magnesium-containing molecules are summarized in Table 3; the numbering scheme is given in Scheme 11. The influence of the trialkylsilyl substituents on the chemical shifts of the pyridylmethyl fragments is very small. The compound classes are therefore distinguishable by the δ values of the methylene moieties in the proton NMR experiments: the (2-pyridylmethyl)(trialkylsilyl)amines **1** (R = Si*i*Pr$_3$) and **I** (R = SiMe$_2$*t*Bu) show their resonances at δ = 4.1. Substitution of the H atom by a methylmetal fragment (**2** and **II**: Zn; **7** and **9**: Mg) produces a low-field shift of approximately 0.6 ppm,

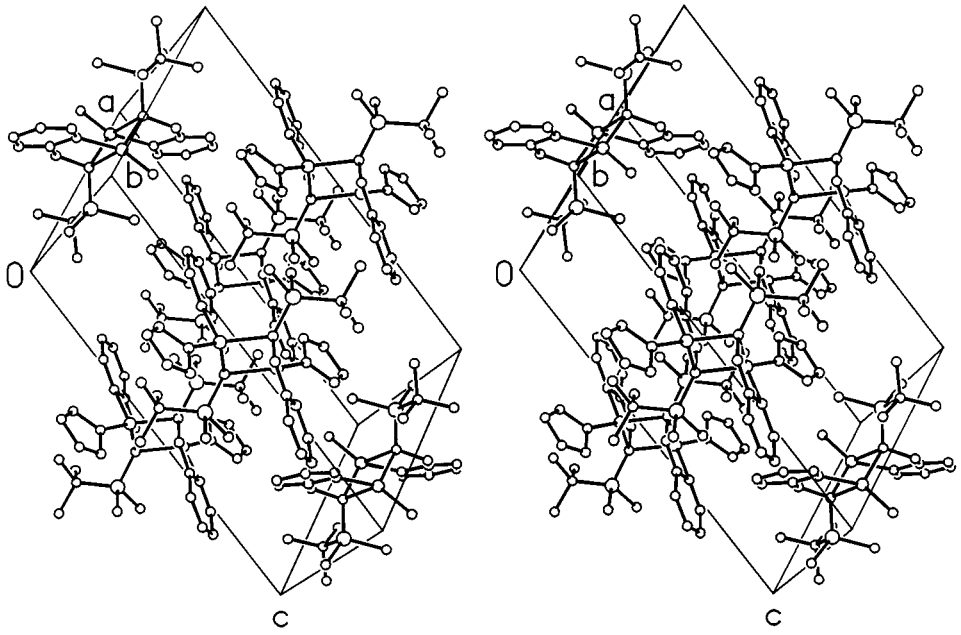

Figure 7. Representation of the arrangement of the molecules of **9·10** in the unit cell; the atoms are shown with arbitrary radii (see text)

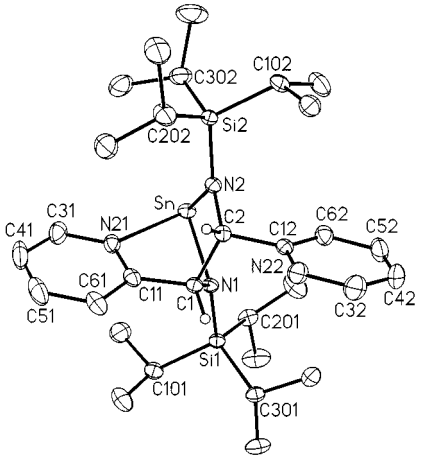

Figure 8. Molecular structure of **12**; the ellipsoids represent 40% probability; the hydrogen atoms are omitted for clarity, with the exception of those at C1 and C2

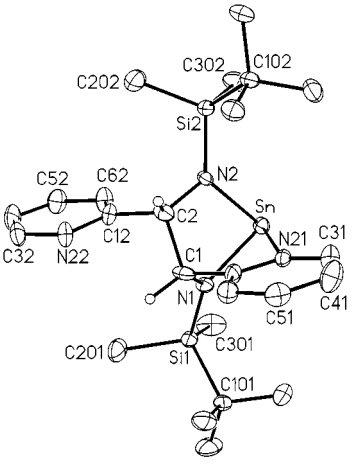

Figure 10. Molecular structure of **14**; the ellipsoids represent 40% probability; the hydrogen atoms are omitted for clarity, with the exception of those at C1 and C2

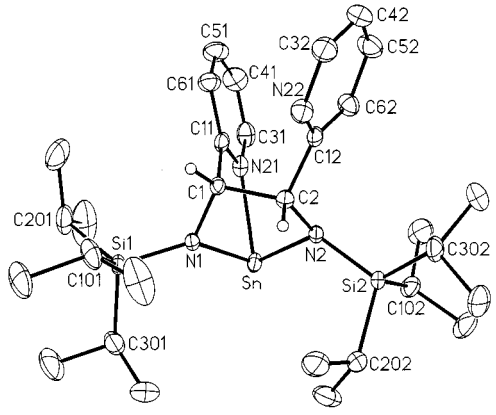

Figure 9. Molecular structure of **12′** (*meso* form); the ellipsoids represent 40% probability; the hydrogen atoms are omitted for clarity, with the exception of those at C1 and C2

whereas the C−C-coupled derivatives **3** and **III** give chemical shifts of $\delta = 4.0$. The resonances of these methylene moieties in metal bis[(2-pyridylmethyl)(trialkylsilyl)amide] (Zn: **4** and **IV**; Mg: **6**) appear at a rather low field at $\delta = 4.9$. Similar tendencies are deducible from the $^{13}C\{^1H\}$ NMR experiments; the amines **1** and **I** have values of $\delta = 48$, whereas the metalated amines show low-field shifts of approximately 6 ppm regardless of the metal (Zn or Mg). The C−C coupling gives chemical shifts of approximately $\delta = 67$ for these carbon atoms. In the NMR spectroscopic experiments, the influences both of the steric demand of the trialkylsilyl substituents and of the nature of the metal center (Zn or Mg) seem to play a minor role regarding the NMR spectroscopic data of the pyridylmethyl groups. The dependence on the solvent was elucidated for compound **9**; the influence of the solvent on the NMR spectroscopic data

Table 2. Selected bond lengths [pm] and angles [°] of **12**, **12′**, and **14**

Compound	**12**[a]	12′[b]	14[a]
Sn−N1	209.2(2)	209.9(3)	207.5(3)
Sn−N2	210.7(2)	213.1(3)	209.6(3)
Sn−N21	238.8(2)	231.8(3)	238.3(3)
N1−Si1	172.2(2)	172.4(3)	170.8(3)
N2−Si2	172.9(2)	173.3(3)	170.9(3)
C1−C2	157.1(3)	159.3(4)	153.5(6)
C1−N1	145.4(3)	145.7(4)	144.9(5)
C2−N2	146.2(3)	146.7(4)	145.1(5)
C1−C11	151.8(3)	150.6(5)	157.6(6)
C11−N21	134.1(3)	133.8(5)	133.4(5)
N21−C31	134.9(3)	133.9(5)	132.3(6)
C31−C41	136.8(5)	137.1(6)	137.8(7)
C41−C51	137.0(5)	138.5(6)	136.6(7)
C51−C61	138.8(4)	137.8(6)	135.9(6)
C11−C61	139.1(4)	138.5(5)	137.3(6)
C2−C12	151.7(3)	152.1(5)	154.0(6)
C12−N22	134.1(3)	133.1(4)	135.1(5)
N22−C32	134.4(4)	134.3(5)	131.3(5)
C32−C42	136.2(5)	137.3(6)	136.3(7)
C42−C52	137.3(5)	137.7(6)	137.7(7)
C52−C62	138.4(4)	137.3(6)	135.2(6)
C12−C62	137.7(4)	138.8(5)	138.5(6)
N1−Sn−N2	82.45(7)	82.2(1)	81.4(1)
N1−Sn−N21	74.35(7)	75.4(1)	75.3(1)
N2−Sn−N21	81.45(7)	82.5(1)	81.2(1)
C1−N1−Sn	101.8(1)	101.1(2)	102.6(2)
C1−N1−Si1	124.4(1)	123.4(2)	124.9(2)
Si1−N1−Sn	128.2(1)	133.3(2)	131.8(2)
C2−N2−Sn	109.8(1)	109.4(2)	110.9(2)
C2−N2−Si2	120.9(2)	123.6(2)	120.9(2)
Si2−N2−Sn	127.4(1)	117.2(1)	127.9(2)

[a] Data for the racemate composed of the (*R*,*R*) and (*S*,*S*) isomers. [b] Parameters for the (*R*,*S*) isomer (*meso* form).

is of the same magnitude as that of the substitution pattern.

The NMR parameters of the tin(II) complexes are summarized in Table 4. All these complexes are mononuclear, and variations in the NMR spectroscopic data are therefore to be expected. The solid-state structures of **12** and **14** show that only one pyridyl group bonds to the tin center, whereas the other one shows no short contacts to a metal atom. In solution, both pyridyl fragments are chemically and magnetically equivalent; the exchange process is fast on the NMR timescale even at low temperatures. In general, the δ values of the methylene fragments are shifted towards lower field, relative to the zinc and magnesium derivatives, in the proton and $^{13}C\{^1H\}$ NMR experiments. The $^{119}Sn\{^1H\}$ chemical shifts were found in the characteristic region for triply coordinated tin(II) compounds.[40−42]

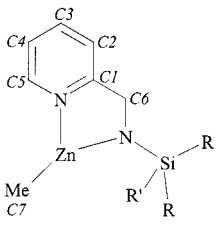

Scheme 11. Numbering scheme of the (2-pyridylmethyl)(trialkylsilyl)amide ligand for the assignment of the NMR spectroscopic data

The ^1H NMR spectroscopic data for **15** and **16**[22] are summarized in Table 5; the corresponding values for (benzyl)(trialkylsilyl)amine (**V**)[21] are also included for comparison. The low-field shift of the methylene moiety of **16** compared to **15** is contrary to the observations concerning the pyridyl compounds **2** and **4** as well as **II** and **IV**, respectively, where the ^1H NMR spectra show the CH_2 signals of the heteroleptic derivatives **2** and **II** at a higher field.

Conclusion

The zinc-mediated C−C coupling reaction is not dependent on the intramolecular steric strain introduced by the trialkylsilyl substituents. However, the use of the triisopropylsilyl ligand permitted the crystallographic characterization of the cyclic magnesium bis(amide) **8**, which is thought to be the intermediate in this reaction. The intermediate with the smaller *tert*-butyldimethylsilyl substituent cocrystallized with **9**, and its fast decomposition was prevented due to its removal from the reaction mixture. Furthermore, the solid-state structures of **2** and **II** vary with the steric demand of the trialkylsilyl group but the reactivity is all but retained. As one would expect, this coupling reaction is strongly dependent on the redox potential of the metal employed in this reaction. The pyridyl substituent is necessary to support the C−C coupling reaction. The key step of the mechanism is the metalation of the methylene group and a charge migration to the pyridyl nitrogen atom, thus forming a cyclic bis(amide). Because of the C−C coupling, the aromaticity of the pyridyl group is regained; this may be the driving force for this step. This also provides an explanation of why no similar molecule is observed in the zinc-mediated reaction: the elevated reaction temperature prevents the reaction from stopping at this step, since the reduction of the metal is too easy.

The zinc-mediated C−C coupling reaction results in the formation of the (*R*,*R*)- and (*S*,*S*)-isomeric 1,2-dipyridyl-1,2-bis(trialkylsilylamido)ethane ligand. The *meso* form is not observed in the course of this reaction. However, the tin-mediated C−C coupling yields a mixture of all possible isomers, although the demanding trialkylsilyl groups favor the (*R*,*R*) and (*S*,*S*) forms. Whereas the zinc- and magnesium-containing complexes crystallize as dimers, the mononuclear tin compounds are monomeric in the solid state and in solution.

This zinc-mediated C−C coupling reaction is novel in zinc chemistry. However, it allows the quantitative synthesis of a dinuclear zinc complex with the metal atoms in close contact with one another, due to the folding of the Zn_2N_2 ring. Further investigations will now concentrate on the influence of the trialkylsilyl substituents on the properties of these compounds and comparison with the *tert*-butyl-substituted derivatives described earlier by van Koten and coworkers.[2,9]

Table 3. NMR spectroscopic data of **1**−**7** and **9**; data for **I**−**IV** are also given for comparison

Compound Solvent	**1** C_6D_6	**2** C_6D_6	**3** C_6D_6	**4** C_6D_6	**5a** [D$_8$]THF	**5b** [D$_8$]THF	**6** C_6D_6
^{1}H							
δ(H2)	7.09	6.54	6.78	6.65	7.30	7.05	6.75
δ(H3)	7.15	6.79	6.95	6.83	7.68	7.52	6.96
δ(H4)	6.66	6.34	6.50	6.36	7.20	7.14	6.46
δ(H5)	8.48	7.75	8.06	7.91	8.44	8.41	7.91
δ(H6)	4.14[a]	4.67	4.06	4.94[b]	4.19	4.17	4.85[c]
δ(H7)	–	−0.13	0.21	–	–	–	–
δ(C*H*Me$_2$)	1.05	1.35	1.00	1.41	1.05	1.07	0.88
δ(CH*Me*$_2$)	1.06	1.33	0.91	1.36	1.05	1.07	0.88
δ(SiMe)	–	–	–	–	–	–	–
δ(SiMe)	–	–	–	–	–	–	–
δ(Si*t*Bu)	–	–	–	–	–	–	–
δ(NH)	1.28	–	–	–	n.o.[d]	n.o.[d]	–
^{13}C{^{1}H}							
δ(C1)	163.0	166.4	168.7	166.2	158.4	157.8	169.9
δ(C2)	120.4	121.1	119.8	121.1	122.4	122.3	120.6
δ(C3)	135.6	136.7	138.3	136.6	139.6	139.6	136.7
δ(C4)	121.0	121.6	122.3	121.7	123.8	123.8	122.1
δ(C5)	149.0	145.4	146.7	145.5	147.4	147.3	145.9
δ(C6)	48.4	54.4	67.0	54.2	47.2	47.3	53.6
δ(C7)	–	−14.7	−11.5	–	–	–	–
δ(SiCH)	11.9	13.6	14.3	14.2	11.9	12.0	13.7
δ(CH*Me*$_2$)	18.4	19.1	18.9	18.4	18.1	18.3	19.6
δ(SiMe)	–	–	–	–	–	–	–
δ(SiMe)	–	–	–	–	–	–	–
δ(Si*C*Me$_3$)	–	–	–	–	–	–	–
δ(SiC*Me*$_3$)	–	–	–	–	–	–	–
^{29}Si{^{1}H}							
δ(Si)	6.04	4.09	6.66	2.49	n.o.[d]	n.o.[d]	0.58

Compound Solvent	**7** C_6D_6	**I** C_6D_6	**II** C_6D_6	**III** C_6D_6	**IV** C_6D_6	**9** C_6D_6	**9** THF/C_6D_6
^{1}H							
δ(H2)	7.36	7.06	6.52	6.77	6.64	6.58	6.65
δ(H3)	7.77	7.17	6.85	6.97	6.84	6.92	6.83
δ(H4)	7.19	6.68	6.47	6.48	6.38	6.51	6.37
δ(H5)	8.14	8.47	8.25	7.98	7.95	8.28	7.91
δ(H6)	4.80	4.09	4.65	4.03	4.93[e]	4.70[f]	4.95
δ(H7)	−1.21	–	−0.25	−0.51	–	−0.72	n.o.
δ(C*H*Me$_2$)		–	–	–	–	–	–
δ(CH*Me*$_2$)		–	–	–	–	–	–
δ(SiMe)	–	0.01	−0.11	0.40	0.34	−0.12	0.29
δ(SiMe)	–	0.01	−0.11	0.15	0.28	−0.15	0.29
δ(Si*t*Bu)	–	0.87	1.10	0.82	1.27	1.07	1.27
δ(NH)	–	1.32	–	–	–	–	–
^{13}C{^{1}H}							
δ(C1)	169.6	163.2	165.5	168.5	166.4	167.0	170.1
δ(C2)	121.4	120.5	121.5	119.9	121.1	121.9	120.8
δ(C3)	137.7	135.7	137.5	138.4	136.2	138.3	136.8
δ(C4)	122.4	121.0	121.7	122.4	122.0	122.1	122.4
δ(C5)	146.2	148.9	145.4	146.7	145.6	146.9	146.1
δ(C6)	53.3	48.2	54.1	67.3	54.4	51.0	54.1
δ(C7)	−11.9	–	−12.6	−14.1	–	−15.2	−3.6
δ(SiCH)	13.5	–	–	–	–	–	–
δ(CH*Me*$_2$)	19.2	–	–	–	–	–	–
δ(SiMe)	–	−5.0	−3.6	−2.1	−3.0	−3.1	1.2
δ(SiMe)	–	−5.0	−3.6	−3.2	−3.3	−4.4	1.2
δ(Si*C*Me$_3$)	–	18.5	20.8	20.6	20.8	20.7	20.8
δ(SiC*Me*$_3$)	–	26.3	28.6	27.7	28.1	28.2	28.1
^{29}Si{^{1}H}							
δ(Si)	8.59	9.04	10.32	8.66	3.92	7.75	0.65
Ref.		[1]	[1]	[1]	[1]		

[a] Doublet due to coupling with NH group, $^3J_{H,H}$ = 7.6 Hz. [b] Mean value of an AB spin system, δ_A = 4.90, δ_B = 4.98, $^2J_{H,H}$ = 19.6 Hz. [c] Mean value of an AB spin system, δ_A = 4.81, δ_B = 4.89, $^2J_{H,H}$ = 21.0 Hz. [d] Not observed (n.o.). [e] Mean value of an AB spin system, δ_A = 4.91, δ_B = 4.95, $^2J_{H,H}$ = 19.9 Hz. [f] Mean value of an AB spin system, δ_A = 4.42, δ_B = 4.98, $^2J_{H,H}$ = 19.4 Hz.

Table 4. NMR parameters of **11**−**14**

Compound Solvent	**11** toluene/C_6D_6	**12** [D_8]THF	**13** toluene/C_6D_6	**14** [D_8]THF
^{1}H				
δ(H2)	6.61	7.77	6.53	7.69
δ(H3)	6.86	7.72	6.77	7.74
δ(H4)	6.42	7.17	6.32	7.17
δ(H5)	8.04	8.52	7.96	8.53
δ(H6)	4.99[a]	5.10	4.90[b]	5.06
δ(NSiMe_3)	0.23	−	0.26	−
δ(C*H*Me_2)	1.20	0.78/1.28	−	−
δ(CH*Me_2*)	1.27	0.69/1.12	−	−
δ(SiMe)	−	−	0.31	−0.47
δ(SiMe)	−	−	0.37	−0.33
δ(Si*t*Bu)	−	−	0.96	0.49
^{13}C{^{1}H}				
δ(C1)	167.0	167.0	166.8	166.5
δ(C2)	121.2	122.6	121.1	122.0
δ(C3)	138.4	137.0	138.3	137.0
δ(C4)	122.0	121.6	121.9	121.4
δ(C5)	144.8	146.5	145.1	146.5
δ(C6)	57.6	73.0	57.0	73.2
δ(NSiMe_3)	6.1	−	6.1	−
δ(C*H*Me_2)	13.9	13.5	−	−
δ(CH*Me_2*)	19.4	18.1/18.2	−	−
δ(SiMe)	−	−	−4.4	−4.5
δ(SiMe)	−	−	−2.0	−3.5
δ(Si*C*Me_3)	−	−	20.2	18.9
δ(SiC*Me_3*)	−	−	27.4	26.2
^{29}Si{^{1}H}				
δ(Si)	7.86	4.98	7.94	7.49
δ(NSiMe_3)	−2.49	−	−2.55	−
^{119}Sn{^{1}H}				
δ(Sn)	139.8	76.6	135.9	57.1

Mean value of an AB spin system, $\delta_A = 4.75$, $\delta_B = 5.05$, $^2J_{H,H} = 18.5$ Hz.

Table 5. NMR spectroscopic data of **15** and **16**; the parameters of **V** are included for comparison

Compound Solvent	**V**[18] CCl_4	**V** [D_8]THF	**15** [D_8]THF	**16** [D_8]THF
δ(SiMe_2)	0.03	0.02	0.02	−0.06
δ(*t*Bu)	0.86	0.92	0.96	0.85
δ(CH_2)	3.60	3.96	3.86	4.41
δ(Ph)	7.24	7.23	7.17	7.12
δ(ZnMe)	−	−	−	−0.81
δ(NH)	n.o.[a]	n.o.[a]	−	−

[a] Not observed (n.o.).

Experimental Section

General Remarks: All experiments and manipulations were carried out under argon. Reactions were performed with standard Schlenk techniques and dried, thoroughly deoxygenated solvents. (*tert*-Butyldimethylsilyl)(2-pyridylmethyl)amine (**I**),[1] tin(II) bis[bis(trimethylsilyl)amide],[16−20] (Benzyl)(*tert*-butyldimethylsilyl)amine,[21] and dimethylmagnesium[43] were prepared according to literature procedures. NMR spectra were recorded with Jeol GSX270 and EX400 spectrometers. A Nicolet 520 FT-IR spectrophotometer was used to record the IR spectra; solid substances were measured in nujol between KBr plates (vs very strong, s strong, m medium strong, w weak, vw very weak, sh shoulder). The low carbon and nitrogen values of the elemental analyses are the result of carbide, carbonate, and nitride formation during combustion of the compounds. The NMR parameters are listed in Tables 3−5.

2-(Triisopropylsilylaminomethyl)pyridine [(2-Pyridylmethyl)(triisopropylsilyl)amine] (1): 2-(Aminomethyl)pyridine (3.24 g, 30.0 mmol) was dissolved in THF (20 mL). At −78 °C, a hexane solution of *n*-butyllithium (2.5 M, 12.0 mL, 30.0 mmol) was added dropwise. After complete addition, chlorotriisopropylsilane (6.42 mL, 30.0 mmol), dissolved in THF (5 mL), was added to the still cooled solution. The solution was then slowly warmed to room temperature and all volatile materials were removed under vacuum. Pentane (15 mL) was added to the remaining pink suspension and all insoluble solids were removed by filtration. After that, all volatile materials were distilled again in vacuo at 120 °C. The remaining oily liquid consisted of analytically pure **1**, which turned brown immediately upon exposure to air; yield: 7.25 g (27.4 mmol, 91%). IR: $\tilde{\nu}$ = 3373 m, 3091 w, 3011 sh, 2942 vs, 2892 vs, 2863 vs, 2758 vw, 2722 w, 1700 vw, 1646 vw, 1592 s, 1571 s, 1464 vs, 1434 s, 1407 s, 1387 m, 1382 m, 1366 w, 1342 w, 1319 vw, 1294 vw, 1255 w, 1249 w, 1213 w, 1145 sh, 1125 s, 1094 m, 1084 m, 1070 m, 1047 m, 1013 m, 994 m, 952 vw, 918 w, 883 vs, 841 w, 799 m, 752 s, 728 w, 680 s, 639 m, 830 m, 602 w, 553 w, 502 w, 462 w, 404 vw cm^{-1}. MS (EI): *m*/*z* (%) = 265 (11), 264 (46) [M^+], 263 (100) [$M^+ - H$], 223 (5), 222 (19), 221 (70) [$M^+ - C_3H_7$], 220 (11), 219 (10), 136 (5), 135 (29), 134 (9), 87 (5), 73 (6), 59 (10). $C_{15}H_{28}N_2Si$ (264.48): calcd. C 68.11, H 10.67, N 10.59; found C 67.19, H 10.29, N 10.72.

Methylzinc (2-Pyridylmethyl)(triisopropylsilyl)amide (2): A toluene solution of dimethylzinc (2.0 M, 11.5 mL, 23.0 mmol) was added to **1** (6.03 g, 22.8 mmol) in 10 mL of toluene. After 10 h, the volume of the dark solution was reduced to a few milliliters. At 5 °C, colorless **2** (5.10 g, 7.41 mmol, 65% of the dimer) precipitated. M.p. 72−74 °C. IR: $\tilde{\nu}$ = 3393 vw, 3138 vw, 3081 vw, 2764 vw, 2726 vw, 2269 vw, 1987 vw, 1922 vw, 1868 vw, 1842 vw, 1635 vw, 1603 s, 1571 m, 1541 vw, 1507 vw, 1486 m, 1471 sh, 1463 m, 1431 s, 1406 w, 1389 w, 1383 w, 1357 w, 1320 vw, 1284 m, 1245 w, 1207 vw, 1151 m, 1123 w, 1100 w, 1054 m, 1063 vs, 1016 m, 1011 m, 1003 m, 995 m, 987 m, 972 sh, 917 m, 883 vs, 846 sh, 836 s, 823 m, 803 vs, 794 vs, 754 vs, 723 m, 647 vs, 625 s, 562 w, 508 s, 487 m, 471 m, 460 m, 445 m, 412 m cm^{-1}. MS (EI): *m*/*z* (%) = 341 (3) [M$^+$/2], 263 (7) [M$^+$/2 − ZnMe], 222 (21), 221 (100) [263 − C_3H_6], 219 (94), 135 (24), 134 (14). $[C_{16}H_{30}N_2SiZn]_2$ (687.78): calcd. C 55.88, H 8.79, N 8.15; found C 55.19, H 8.64, N 8.13.

[1,2-Dipyridyl-1,2-bis(triisopropylsilylamido)ethane]bis(methylzinc) (3): A toluene solution of dimethylzinc (2.0 M, 7.5 mL, 15.0 mmol) was added dropwise to a solution of **1** (1.63 g, 6.16 mmol) in toluene (5 mL). After 1 h, the green solution was heated under reflux for an additional 20 h. The volume of the solution was then reduced to half of its original amount. At 5 °C colorless crystals of **3** (1.18 g, 1.72 mmol, 56%) precipitated. M.p. 250 °C (dec.). IR: $\tilde{\nu}$ = 3099 m, 3077m, 2711 w, 1993 vw, 1956 vw, 1920 vw, 1601 vs, 1571 s, 1474 vs, 1439 vs, 1410 sh, 1388 s, 1382 sh, 1365 w, 1345 m, 1331 w, 1288 s, 1254 s, 1241 sh, 1233 sh, 1210 w, 1158 sh, 1148 vs, 1105 s, 1070 sh, 1050 sh, 1041 vs, 1019 vs, 994 s, 970 w, 918 vs, 884 vs, 847 m, 780 vs, 753 s, 721 vw, 686 sh, 671 vs, 654 vs, 644 vs, 631 sh, 607 s, 565 m, 529 vs, 512 vs, 477 s, 417 m, 392 vw, 331 w, 283 cm^{-1} w. MS (EI): *m*/*z* (%) = 265 (23), 264 (81) [$C_{15}H_{28}N_2Si$], 263 (100) [$C_{15}H_{27}N_2Si$], 221 (16) [263-C_3H_6], 220 (13), 219 (19), 135 (15). $C_{32}H_{58}N_4Si_2Zn_2$ (685.76): calcd. C 56.04, H 8.53, N 8.17; found C 55.52, H 8.40, N 7.63.

Zinc Bis[(2-pyridylmethyl)(triisopropylsilyl)amide] (4): An *n*-hexane solution of *n*-butyllithium (2.5 M, 2.8 mL, 7.0 mmol) was added dropwise to **1** (1.85 g, 7.0 mmol) in THF (10 mL) at −78 °C. The solution was then warmed to 0 °C and zinc(II) bromide (0.79 g, 3.5 mmol) was added. After this had been stirred for 10 h, all volatile materials were removed in vacuo at room temperature. From the remaining oil, 0.89 g of colorless waxy crystals of **4** (1.51 mmol, 43%) were isolated.

[(2-Pyridylmethyl)(triisopropylsilyl)amine-*N*,*N*′]zinc(II) Chloride (5a): A suspension of zinc(II) chloride (1.14 g, 8.37 mmol) in THF (7 mL) was added to a solution of **1** (2.22 g, 8.39 mmol) in THF. After 10 min of stirring, the solution was cooled to −20 °C and a colorless precipitate of **5a** (2.15 g, 5.38 g, 64%) formed. M.p. 203 °C. MS (EI): *m*/*z* (%) = 363 (77) [M$^+$ − Cl], 307 (16), 263 (13) [M$^+$ − $ZnCl_2$], 221 (64) [263 − C_3H_6], 207 (30), 155 (27) [Si*i*Pr$_3$ − H_2], 154 (100), 136 (72), 105 (33) [263 − HSi*i*Pr$_3$], 91 (43) [263 − HNSi*i*Pr$_3$], 43 (48) [C_3H_7]. $C_{15}H_{28}N_2SiZnCl_2$ (400.764): calcd. C 44.95, H 7.04, N 6.99; found C 41.84, H 6.45, N 7.32.

[(2-Pyridylmethyl)(triisopropylsilyl)amine-*N*,*N*′]zinc(II) Bromide (5b): Zinc(II) bromide (1.61 g, 7.15 mmol) was added at 0 °C to a solution of **1** (1.77 g, 7.15 mmol) in THF (10 mL). The brown suspension was stirred for 12 h. The precipitate was collected and washed with several portions of pentane. After drying in vacuo, colorless **5b** (3.12 g, 6.36 mmol, 89%) was isolated. M.p. 236 °C (dec.). IR: $\tilde{\nu}$ = 3216 m, 1608 s, 1572 m, 1473 m, 1444 m, 1433 m, 1397 w, 1383 m, 1366 vw, 1353 vw, 1284 w, 1253 w, 1227 vw, 1213 w, 1157 vw, 1105 w, 1069 w, 1054 w, 1029 s, 1007 m, 983 m, 964 w, 914 m, 883 s, 842 w, 826 vw, 802 vw, 768 s, 753 s, 723 s, 673 s, 653 w, 605 w, 552 vw, 488 w, 473 vw, 445 w, 414 w, 398 vw, 368 vw, 339 cm^{-1} vw. MS (EI): *m*/*z* (%) = 409 (2) [M$^+$ − Br], 263 (1) [M$^+$ − $ZnBr_2$], 222 (68), 221 (100) [263 − C_3H_6], 136 (49). $C_{15}H_{28}N_2SiZnBr_2$ (489.664): calcd. C 36.79, H 5.76, N 5.72, Br 32.63; found C 34.98, H 5.48, N 5.51, Br 33.5.

Magnesium Bis[(2-pyridylmethyl)(triisopropylsilyl)amide] (6): A solution of **1** (2.57 g, 9.7 mmol) in pentane (50 mL) was cooled to 0 °C. A hexane solution of dibutylmagnesium (1.0 M, 4.85 mL, 4.85 mmol) was added dropwise. After 24 h of stirring at room temperature, the volume of the solution was reduced to a few milliliters and toluene (30 mL) was added. Colorless needles of **6** (2.53 g, 4.61 mmol, 95%) precipitated within hours. Dec. 100 °C. IR: $\tilde{\nu}$ = 1661 w, 1630 w, 1592 s, 1570 m, 1464 vs, 1435 s, 1407 s, 1382 m, 1366 w, 1343 w, 1319 vw, 1292 vw, 1214 w, 1150 sh, 1124 s, 1094 s, 1072 s, 1047 s, 1013 s, 995 m, 918 w, 882 s, 841 w, 798 s, 753 m, 728 w, 673 s, 653 m, 639 m, 602 m, 553 m, 501 m, 404 cm^{-1} w. MS (70 eV, EI): *m*/*z* (%) = 503 (10), 429 (20), 355 (31), 281 (46), 221 (100) [py−CH_2−Si*i*Pr$_2$]. $C_{30}H_{54}MgN_4Si_2$ (551.26): calcd. C 65.36, H 9.87, N 10.16; found C 59.55, H 9.79, N 8.00.

Methylmagnesium (2-Pyridylmethyl)(triisopropylsilyl)amide (7). − Method A: Compound **1** (1.85 g, 7 mmol) was added dropwise at 0 °C to a THF/dioxane solution of dimethylmagnesium (7 mL, 1.0 M), dissolved in 25 mL of additional THF. After 3 d of stirring at room temperature, the volume of the solution was reduced and needles of **7** precipitated at 5 °C in a quantitative yield. − **Method B:** Compound **6** (2.7 mmol) was dissolved in THF (20 mL), and a THF/dioxane solution of dimethylmagnesium (2.7 mL, 1.0 M) was added at 0 °C. After stirring for 3 d, the same workup procedure as described for Method A was applied. This compound was characterized by NMR spectroscopy, due to its slow decomposition even at room temperature.

Methylmagnesium (*tert*-Butyldimethylsilyl)(2-pyridylmethyl)amide (9): Toluene (10 mL) was added to a THF/dioxane solution of dimethylmagnesium (1 M, 2.42 mL, 2.42 mmol) at 0 °C. (*tert*-Butyldimethylsilyl)(2-pyridylmethyl)amine (0.54 g, 2.42 mmol) was now added dropwise to this solution. After 72 h of stirring at room temperature, the volume was reduced to a few milliliters. Colorless crystals of **9** (0.53 g, 1.03 mmol, 85%) precipitated at 5 °C. Slow dec. at room temperature. IR: $\tilde{\nu}$ = 1654 w, 1601 s, 1592 sh, 1569 s, 1472 s, 1435 s, 1408 m, 1388 m, 1360 w, 1294 vw, 1284 vw, 1251 s, 1210 vw, 1150 sh, 1116 s, 1100 s, 1048 s, 1018 m, 1007 m, 941 m, 908 w, 830 vs, 806 sh, 775 s, 758 sh, 661 m, 643 sh, 629 w, 566 w, 534 m, 523 m, 497 m, 416 w, 405 w, 370 w, 334 cm^{-1} vw. MS (70 eV, EI): *m*/*z* (%) = 221 (100) [py−CH_2NSiMe$_2$*t*Bu], 207 (11) [py−CH_2NSiMe$_2$*t*Bu − Me], 191 (4) [py−CH_2NSiMe$_2$*t*Bu − 2 Me], 165 (83) [py−CH_2NSiMe$_2$], 134 (37) [py−CH_2NSi], 57 (21) [*t*Bu]. $C_{26}H_{48}Mg_2N_4Si_2$ (521.48): calcd. C 59.88, H 9.28, N 10.75; found C 58.31, H 9.26, N 10.01.6

Bis[(trimethylsilyl)amido]tin(II) (2-Pyridylmethyl)(triisopropylsilyl)-amide (11): Compound **1** (1.1 g, 4.1 mmol) was added at room temperature to a solution of of tin(II) bis[bis(trimethylsilyl)amide] (1.62 mL, 4.1 mmol) in 20 mL of toluene. After stirring for 6 d, the volume was reduced to a few milliliters and 5 mL of THF was added. Cooling to −20 °C afforded colorless crystals of **11**. This compound slowly underwent the C−C coupling reaction and so only the NMR spectroscopic data are presented in Table 4.

[1,2-Dipyridyl-1,2-bis(triisopropylsilylamido)ethane]tin(II) (12): Tin(II) bis[bis(trimethylsilyl)amide] (4.5 mL, 11.7 mmol) was added at room temperature to a solution of **1** (3.1 g, 11.7 mmol) in toluene (40 mL). During heating of this solution, the precipitation of tin metal was observed. After decantation, the volume of the solution

Table 6. Crystallographic data of **2**, **3**, **8**·0.5THF, **9**, **9·10**, **12**, **12′**, and **14** as well as details of the structure solution and refinement procedures

Compound	**2**	**3**	**8**·0.5THF	**9**
Empirical formula	$C_{16}H_{30}N_2SiZn$	$C_{32}H_{58}N_4Si_2Zn_2$	$C_{45}H_{76}Mg_2N_4O_2Si_2$	$C_{26}H_{48}Mg_2N_4Si_2$
Formula mass [g·mol^{-1}]	343.88	685.74	809.90	521.48
T [K]	173(2)	293(2)	193(2)	193(2)
Crystal system	monoclinic	monoclinic	triclinic	triclinic
Space group[46]	$C2/c$	$C2/c$	$P\bar{1}$	$P\bar{1}$
a [pm]	1619.3(2)	2179.2(5)	1014.8(3)	856.7(2)
b [pm]	1549.2(1)	945.2(1)	1023.8(3)	1013.2(3)
c [pm]	1523.5(2)	1855.7(2)	1168.9(3)	1056.1(3)
α [°]	90	90	79.262(4)	71.290(4)
β [°]	110.38(1)	104.40(1)	79.695(5)	83.638(4)
γ [°]	90	90	84.677(4)	68.268(4)
V [nm^3]	3.5828(7)	3.702(1)	1.1717(5)	0.8065(4)
Z	8	4	2	1
$d_{calcd.}$ [g·cm^3]	1.275	1.230	1.148	1.074
μ [mm^{-1}]	1.432	1.385	0.142	0.168
F(000)	1472	1464	442	284
Scan range [°]	$5.9 < 2\theta < 50.0$	$4.5 < 2\theta < 48.5$	$3.6 < 2\theta < 57.9$	$4.1 < 2\theta < 56.9$
Measured data	12279	5740	6683	4612
Unique data (R_{int})	3130 (0.1071)	2679 (0.0330)	3521 (0.0228)	2426 (0.0281)
Absorption. correction	none	semiempirical	SADABS	SADABS
Transmission, max./min.	−/−	1.000/0.806	0.986/0.972	1.000/0.538
Parameters	301	188	247	250
Restraints	0	0	0	0
wR_2[a] (all data, on F^2)	0.0813	0.1287	0.1950	0.2038
R_1 [a] (all data)	0.0367	0.0593	0.0839	0.0863
Data with $I > 2\sigma(I)$	2810	2187	2869	1666
R_1 [$I > 2\sigma(I)$]	0.0315	0.0457	0.0713	0.0700
Goof s[b] on F^2	1.057	1.070	1.116	1.009
Residual density [e·nm^{-3}]	765/−492	628/−683	395/−278	537/−0.436
CCDC-[47]	-138790	-138791	-155098	-155099

Compound	**9·10**	**12**	**12′**	**14**
Empirical formula	$C_{58}H_{104}Mg_4N_8O_2Si_4$	$C_{30}H_{52}N_4Si_2Sn$	$C_{30}H_{52}N_4Si_2Sn$	$C_{24}H_{40}N_4Si_2Sn$
Formula mass [g·mol^{-1}]	1155.09	643.64	643.64	559.47
T [K]	193(2)	200(3)	200(3)	200(2)
Crystal system	triclinic	triclinic	monoclinic	monoclinic
Space group[46]	$P\bar{1}$	$P\bar{1}$	$P2_1/n$	$P2_1/n$
a [pm]	969.42(9)	1116.7(1)	1660.0(4)	1050.15(7)
b [pm]	1083.2(1)	1156.5(1)	892.3(1)	2311.4(2)
c [pm]	1769.5(2)	1410.1(1)	2305.9(4)	1202.79(9)
α [°]	100.987(2)	89.31(1)	90	90
β [°]	105.153(2)	80.55(1)	101.84(3)	105.948(8)
γ [°]	97.908(2)	67.72(1)	90	90
V [nm^3]	1.7258(3)	1.6582(3)	3.343(1)	2.8072(4)
Z	1	2	4	4
$d_{calcd.}$ [g·cm^3]	1.111	1.289	1.279	1.324
μ [mm^{-1}]	0.165	0.867	0.860	1.013
F(000)	628	676	1352	1160
Scan range [°]	$2.4 < 2\theta < 58.2$	$3.8 < 2\theta < 51.8$	$4.9 < 2\theta < 52.0$	$5.0 < 2\theta < 51.8$
Measured data	10154	13104	15298	14494
Unique data (R_{int})	5340 (0.0320)	5998 (0.0250)	6166 (0.0837)	4314 (0.0650)
Absorption. correction	SADABS	numerical	numerical	numerical
Transmission, max./min.	1.000/0.810	0.907/0.878	0.893/0.640	0.942/0.862
Parameters	520	542	334	440
Restraints	0	0	0	0
wR_2 [a] (all data, on F^2)	0.1453	0.0642	0.1033	0.0731
R_1 [a] (all data)	0.0904	0.0291	0.0543	0.0507
Data with $I > 2\sigma(I)$	2900	5234	4832	3190
R_1 [$I > 2\sigma(I)$]	0.0503	0.0224	0.0406	0.0318
Goof s[b] on F^2	0.856	1.076	0.938	0.920
Residual density [e·nm^{-3}]	281/-272	517/-345	1028/-1778	682/-396
CCDC-[47]	-155100	-154568	-154569	-154570

[a] Definition of the R values: $R_1 = (\Sigma||F_o| - |F_c||)/\Sigma|F_o|$; $wR_2 = \{\Sigma[w(F_o^2 - F_c^2)^2]/\Sigma[w(F_o^2)^2]\}^{1/2}$ with $w^{-1} = \sigma^2(F_o^2) + (aP)^2$. [b] $s = \{\Sigma[w(F_o^2 - F_c^2)^2]/(N_o - N_p)\}^{1/2}$.

was reduced and 3.57 g of colorless crystals (5.56 mmol, 95%) precipitated at −20 °C. M.p. 102 °C. IR: $\tilde{\nu}$ = 1690 vw, 1663 vw, 1621 vw, 1599 vs, 1588 vs, 1565 vs, 1474 s, 1432 vs, 1387s, 1358 m, 1335 s, 1285 s, 1268 m, 1248 s, 1228 sh, 1207 vw, 1158 m, 1140 m, 1105 sh, 1086 vs, br, 1063 vs, br, 1045 vs, br, 1011 vs, 994 vs, 950 vs, 918 s, 896 sh, 883 vs, 861 vs, 820 s, 781 vs, 749 vs, 681 vs, 661 vs, 640 vs, 624 vs, 610 vs, 571 m, 538 m, 524 vs, 508 vs, 486 m, 476 m, 443 s, 421 m, 405 s, 315 w, 284 cm^{-1} m. MS (70 eV, EI): m/z (%) = 644

(0.2) [M^+], 601 (0.2) [$M^+ - i$Pr], 527 (0.2) [M^+ − Sn], 483 (1.1) [M^+ − Sn − iPr], 448 (0.2) [M^+ − Sn−py], 382 (32) [M^+ − py−CHNSi(iPr)$_3$], 263 (100) [py−CHNSi(iPr)$_3$], 219 (100) [py−CHNSi(iPr)$_2$], 134 (63). $C_{30}H_{52}N_4Si_2Sn$ (643.64): calcd. C 55.97, H 8.14, N 8.70; found C 55.97, H 8.33, N 8.54.

[Bis(trimethylsilyl)amido]tin(II) (*tert*-Butyldimethylsilyl)(2-pyridylmethyl)amide (13): Amine **I** (0.77 g, 3.46 mmol) was dissolved in toluene (20 mL). At room temperature, tin(II) bis[bis(trimethylsilyl-)amide] (1.35 mL 3.46 mmol) was added. After 6 d of stirring, the volume of the solution was reduced and **13** precipitated quantitatively at 5 °C as a polycrystalline material, which decomposed slowly even at room temperature. IR: $\tilde{\nu}$ = 2953 vs, 2894 vs, 2850 vs, 2799 w, 1993 vw, 1905 vw, 1854 vw, 1608 s, 1570 m, 1505 sh, 1485 m, 1470 s, 1440 s, 1420 m, 1387 m, 1358 w, 1281 s, 1251 vs, 1180 w, 1155 m, 1099 s, 1050 s, 1005 m, 993 m, 946 vs, 901 vs, 863 vs, 832 vs, 777 s, 757 s, 716 m, 700 m, 668 vs, 582 vw, 490 w, 463 vw, 416 vw, 361 w.

[1,2-Bis(*tert*-butyldimethylsilylamido)-1,2-dipyridylethane]tin(II) (14): Tin(II) bis[bis(trimethylsilyl)amide] (2 mL, 5.12 mmol) was added at room temperature to a solution of **I** (1.14 g, 5.12 mmol) in toluene (20 mL). Heating for 3 d at 80 °C resulted in the precipitation of tin metal. After removal of the metal, the volume of the solution was reduced. At −20 °C, 1.40 g of colorless crystals of **14** (2.55 mmol, 98%) precipitated. M.p. 143 °C. IR: $\tilde{\nu}$ = 1684 sh, 1656 w, 1601 s, 1587 s, 1567 s, 1470 vs, 1462 vs, 1440 s, 1432 s, 1416 m, 1410 m, 1356 m, 1338 w, 1319 m, 1285 m, 1252 vs, 1208 sh, 1154 m, 1141 m, 1102 s, 1090 vs, 1071 vs, 1046 s, 1014 s, 1005 s, 994 s, 969 vs, 958 s, 937 m, 922 s, 903 s, 886 vs, 829 vs, 807 vs, 776 vs, 767 vs, 748 vs, 673 m, 660 s, 641 s, 622 m, 606 s, 573 w, 545 m, 522 s, 490 m, 456 w, 415 m, 393 m, 371 w, 357 w, 335 vw, 323 vw, 300 vw, 283 cm^{-1} w. MS (70 eV, EI): *m*/*z* (%) = 441 (21) [M^+ − Sn], 383 (18) [M^+ − Sn-tBu], 356 (26) [M^+ − py], 252 (30), 221 (100) [$^1/_2M^+$ − Sn], 163 (68) [$^1/_2M^+$ − Sn -tBu], 149 (28) [$^1/_2M^+$ − Sn − tBu-Me], 107 (13), 75 (100), 59 (11) [tBu]. $C_{24}H_{40}N_4Si_2Sn$ (559.48): calcd. C 51.52, H 7.21, N 10.01, found C 51.29, H 7.45, N 9.72.

Zinc Bis[(benzyl)(*tert*-butyldimethylsilyl)amide] (15): A hexane solution of butyllithium (2.5 M, 3.95 mL, 9.88 mmol) was added dropwise at −78 °C to (*tert*-butyldimethylsilyl)(2-pyridylmethyl)amine (1.93 g, 8.99 mmol) in pentane (10 mL). During the warm-up, a colorless solid precipitated. This suspension was stirred at room temperature for an additional 8 h. At −18 °C the lithium salt crystallized and was isolated by decanting the mother liquor. This crystalline material was redissolved in pentane (25 mL) at 0 °C. Zinc(II) bromide (1.00 g, 4.44 mmol) was then added and the solution was stirred at room temperature for several days. A colorless precipitate formed and was separated. The volume of the solution was reduced to afford an oily residue. At −18 °C, 1.25 g of colorless crystals of **15** (2.47 mmol, 55%) grew in the oil. M.p. 65 °C. ^{1}H NMR ([D$_6$]benzene): δ = 7.17 (m, 5 H, Ph), 3.86 (s, 2 H, CH_2), 0.96 (s, 9 H, tBu), 0.02 (s, 6 H, $SiCH_3$). ^{13}C{^{1}H} NMR ([D$_6$]benzene): δ = 148.21 (C_q, Ph), 129.36 (Ph), 127.29 (Ph), 126.79 (Ph), 51.92 (CH_2), 27.31 (CCH_3), 19.76 (CCH_3), −3.63 ($SiCH_3$). ^{29}Si{^{1}H} NMR ([D$_6$]benzene): δ = 7.05. IR: $\tilde{\nu}$ = 3409 vw, 3087 vw, 3067 w, 3028 w, 2954 vs, 2926 vs, 2899 vs, 2883 vs, 2855 vs, 2806 sh, 2799 w, 2718 vw, 1680 sh, 1650 vs, 1619 sh, 1605 m, 1583 m, 1568 sh, 1537 vw, 1509 sh, 1494 m, 1471 vs, 1463 s, 1453 s, 1389 s, 1361 m, 1306 w, 1292 vw, 1252 vs, 1209 w, 1199 w, 1166 vw, 1115 s, 1102 s, 1070 m, 1028 m, 1007 m, 973 vw, 938 w, 912 vw, 898 w, 845 vs, 831 s, 814 s, 774 vs, 749 s, 728 m, 696 s, 663 m, 586 w, 561 w, 482 m, 420 w, 369 w, 334 cm^{-1} vw. MS (EI): *m*/*z* (%) = 504 (1) [M^+], 489 (1) [M^+ − Me], 447 (47) [M^+ − tBu], 367 (14), 353 (29), 165 (17) [$C_{13}H_{22}NSi$-C_4H_8], 164 (100) [$C_{13}H_{22}NSi$ − tBu], 162 (32), 148 (13), 135 (58), 91 (29) [Bzl], 73 (25) [$SiMe_2t$Bu − C_3H_6], 59 (41) [$SiMe_2t$Bu − C_4H_8], 57 (13) [tBu]. $C_{26}H_{44}N_2Si_2Zn$ (506.225): calcd. C 61.69, H 8.76, N 5.54, found C 61.95, H 9.17, N 5.42.

Crystal Structure Determinations: Data were collected with a STOE-IPDS diffractometer (compounds **2**, **12**, **12′**, and **14**) and a Siemens P4 diffractometer with a Siemens SMART-CCD area detector (compounds **8**·0.5THF, **9**, and **9·10**) using oil-coated, rapidly cooled single crystals.[44,45] The data for **3** were collected with a Nonius CAD4 diffractometer using a single crystal sealed in a glass capillary. In all cases, graphite-monochromated Mo-K_α radiation (λ = 71.073 pm) was used. Crystallographic parameters, details of data collection, and refinement procedures are summarized in Table 6.

The structures were solved by direct methods and refined with the software packages SHELXL-93 and SHELXL-97.[48] Neutral scattering factors were taken from Cromer and Mann[49] and those for the hydrogen atoms from Stewart et al.[50] The non-hydrogen atoms were refined anisotropically. The H atoms were considered with a riding model under restriction of ideal symmetry at the corresponding carbon atoms or refined isotropically. Crystallographic details can be obtained from the Cambridge Data Centre quoting the CCDC numbers given in Table 6.[47]

Acknowledgments

This work was financially supported by the Deutsche Forschungsgemeinschaft, Bonn, and the Fonds der Chemischen Industrie, Frankfurt/Main. We thank Mr. S. Correll for performing the X-ray powder diffraction experiments of precipitated zinc and tin metals and Dr. A. Lötz for the ESR experiments. Prof. G. van Koten (Utrecht University) provided helpful suggestions and contributions to the discussion of the mechanism. T. B. wishes to express his gratitude to the Fonds der Chemischen Industrie for a Ph.D. scholarship.

[1] M. Westerhausen, T. Bollwein, N. Makropoulos, T. M. Rotter, T. Habereder, M. Suter, H. Nöth, *Eur. J. Inorg. Chem.* **2001**, 851−857.
[2] G. van Koten, J. T. B. H. Jastrzebski, K. Vrieze, *J. Organomet. Chem.* **1983**, *250*, 49−61.
[3] M. Kaupp, H. Stoll, H. Preuss, W. Kaim, T. Stahl, G. van Koten, E. Wissing, W. J. J. Smeets, A. L. Spek, *J. Am. Chem. Soc.* **1991**, *113*, 5606−5618.
[4] E. Wissing, M. Kaupp, J. Boersma, A. L. Spek, G. van Koten, *Organometallics* **1994**, *13*, 2349−2356.
[5] E. Wissing, K. van Gorp, J. Boersma, G. van Koten, *Inorg. Chim. Acta* **1994**, *220*, 55−61.
[6] E. Wissing, S. van der Linden, E. Rijnberg, J. Boersma, W. J. J. Smeets, A. L. Spek, G. van Koten, *Organometallics* **1994**, *13*, 2602−2608.
[7] E. Wissing, E. Rijnberg, P. A. van der Schaaf, K. van Gorp, J. Boersma, G. van Koten, *Organometallics* **1994**, *13*, 2609−2615.
[8] J. T. B. H. Jastrzebski, J. M. Klerks, G. van Koten, K. Vrieze, *J. Organomet. Chem.* **1981**, *210*, C49−C53.
[9] A. L. Spek, J. T. B. H. Jastrzebski, G. van Koten, *Acta Crystallogr., Sect. C* **1987**, *43*, 2006−2007.
[10] M. Westerhausen, T. Bollwein, K. Polborn, *Z. Naturforsch., Teil B* **2000**, *55*, 51−59.
[11] J. Emsley, *The Elements*, W. de Gruyter, Berlin, **1994**.
[12] A. Boudier, L. A. Bromm, M. Lotz, P. Knochel, *Angew. Chem.* **2000**, *112*, 4584−4606; *Angew. Chem. Int. Ed.* **2000**, *39*, 4414−4435.
[13] H. Gornitzka, D. Stalke, *Angew. Chem.* **1994**, *106*, 695−698; *Angew. Chem. Int. Ed. Engl.* **1994**, *33*, 693−696.
[14] H. Gornitzka, D. Stalke, *Organometallics* **1994**, *13*, 4398−4405.

[15] T. Kottke, D. Stalke, *Chem. Ber./Recueil* **1997**, *130*, 1365−1374.
[16] D. H. Harris, M. F. Lappert, *J. Chem. Soc., Chem. Commun.* **1974**, 895−896.
[17] C. D. Schaeffer, J. J. Zuckerman, *J. Am. Chem. Soc.* **1974**, *96*, 7160−7162.
[18] M. J. S. Gynane, D. H. Harris, M. F. Lappert, P. P. Power, P. Rivière, M. Rivière-Baudet, *J. Chem. Soc., Dalton Trans.* **1977**, 2004−2009.
[19] P. J. Corvan, J. J. Zuckerman, *Inorg. Chim. Acta* **1979**, *34*, 255−258.
[20] N. Auner, U. Klingebiel, *Synthetic Methods of Organometallic and Inorganic Chemistry (Herrmann/Brauer)*, Thieme, New York, **1996**, vol. 2, p. 280, 288.
[21] J. R. Bowser, J. F. Bringley, *Synth. React. Inorg. Met. -Org. Chem.* **1985**, *15*, 897−905.
[22] T. Bollwein, Ph.D. Thesis, University of Munich (LMU), **2001**.
[23] I. B. Gorrell, A. Looney, G. Parkin, *J. Am. Chem. Soc.* **1990**, *112*, 4068−4069.
[24] M. G. Davidson, D. Elilio, S. L. Less, A. Martín, P. R. Raithby, R. Snaith, D. S. Wright, *Organometallics* **1993**, *12*, 1−3.
[25] M. M. Olmstead, W. J. Grigsby, D. R. Chacon, T. Hascall, P. P. Power, *Inorg. Chim. Acta* **1996**, *251*, 273−284.
[26] M. Westerhausen, T. Bollwein, A. Pfitzner, T. Nilges, H.-J. Deiseroth, *Inorg. Chim. Acta* **2001**, *312*, 239−244.
[27] M. A. Khan, D. G. Tuck, *Acta Crystallogr., Sect. C* **1984**, *40*, 60−62.
[28] A. L. Spek, *Cryst. Struct. Commun.* **1982**, *11*, 1621.
[29] M. Westerhausen, B. Rademacher, W. Schwarz, *J. Organomet. Chem.* **1992**, *427*, 275−287.
[30] M. D. Levin, P. Kaszynski, J. Michl, *Chem. Rev.* **2000**, *100*, 169−234.
[31] P. R. Markies, O. S. Akkerman, F. Bickelhaupt, W. J. J. Smeets, A. L. Spek, *Adv. Organomet. Chem.* **1991**, *32*, 147−226.
[32] C. E. Holloway, M. Melnik, *J. Organomet. Chem.* **1994**, *465*, 1−63.
[33] J. March, *Advanced Organic Chemistry*, 3rd ed., Wiley, New York, **1985**, p. 19.
[34] J. E. Huheey, *Anorganische Chemie: Prinzipen von Struktur und Reaktivität*, W. de Gruyter, Berlin, **1988**, p. 278−279.
[35] M. F. Lappert, P. P. Power, M. J. Slade, L. Hedberg, K. Hedberg, V. Schomaker, *J. Chem. Soc., Chem. Commun.* **1979**, 369−370.
[36] T. Fjeldberg, H. Hope, M. F. Lappert, P. P. Power, A. J. Thorne, *J. Chem. Soc., Chem. Commun.* **1983**, 639−641.
[37] T. Fjeldberg, A. Haaland, B. E. R. Schilling, M. F. Lappert, A. J. Thorne, *J. Chem. Soc., Dalton Trans.* **1986**, 1551−1556.
[38] B. S. Jolly, M. F. Lappert, L. M. Engelhardt, A. H. White, C. L. Raston, *J. Chem. Soc., Dalton Trans.* **1993**, 2653−2663.
[39] U. Kilimann, M. Noltemeyer, F. T. Edelmann, *J. Organomet. Chem.* **1993**, *443*, 35−42.
[40] M. F. Lappert, *Main Group Met. Chem.* **1994**, *17*, 183−207.
[41] B. Wrackmeyer, *J. Magn. Reson.* **1985**, *61*, 536−539.
[42] B. Wrackmeyer, K. Horchler, H. Zhou, *Spectrochim. Acta* **1990**, *46A*, 809−816.
[43] W. Strohmeier, F. Seifert, *Chem. Ber.* **1961**, *94*, 2356; see also: E. Weiss, *J. Organomet. Chem.* **1964**, *2*, 314−321.
[44] T. Kottke, D. Stalke, *J. Appl. Crystallogr.* **1993**, *26*, 615−619.
[45] D. Stalke, *Chem. Soc. Rev.* **1998**, *27*, 171−178.
[46] T. Hahn (Ed.), *International Tables for Crystallography*, vol. A ("Space Group Symmetry"), 2nd ed., D. Reidel, Dordrecht, **1984**.
[47] Crystallographic data (excluding structure factors) for the crystal structures have been deposited with the Cambridge Crystallographic Data Centre as supplementary publications as listed in Table 6. Copies of the data can be obtained on application to CCDC, 12 Union Road, Cambridge CB2 1EZ, UK [Fax: int. code + 44-1223/336-033; E-mail: deposit@ccdc.cam.ac.uk].
[48] G. M. Sheldrick, *SHELXL-93*, Universität Göttingen, **1993**; *SHELXL-97*, Universität Göttingen, **1997**.
[49] D. T. Cromer, J. B. Mann, *Acta Crystallogr.* **1968**, *24*, 321−324.
[50] R. F. Stewart, E. R. Davidson, W. T. Simpson, *J. Chem. Phys.* **1965**, *42*, 3175−3187.

Received January 10, 2001
[I01012]

Zirconocenes as Photoinitiators for Free-Radical Polymerisation of Acrylates

Eleonora Polo,*[a] Andrea Barbieri,[a] Silvana Sostero,[a] and Malcolm L. H. Green[b]

Keywords: Metallocenes / Zirconium / Photolysis / Homogeneous catalysis / Polymerizations

This paper reports the photochemical behaviour of unbridged (**1**–**6**) and bridged zirconocenes (**7r**, **7m**), whose substituents differ in both electron-donor and steric properties. The study of the electronic spectra and EPR spin-trapping experiments showed the photogeneration of ligand- and zirconium-centred radicals at wavelengths higher than 350 nm. This feature makes these complexes suitable as photoinitiators for radical polymerisation processes. *tert*-Butyl acrylate polymerisation has been studied in detail and the results are particularly encouraging as far as the reaction yields and the stereochemistry are concerned. In particular, the complexes **4**–**6**, due to the tuneability of their structure and their stability in solution, look the most promising reagents.

Introduction

Photochemical or photoinitiated polymerisations play a central role in several commercial technologies[1−3] and they are largely employed today in the areas of surface coatings, photoresists, adhesives, and holography. In particular, a growing area of interest is the design of new photoinitiators for use in pigmented coatings. Among those, initiators showing absorption peaks at wavelengths higher than 350 nm[4] are of particular interest since they can be used with the visible light produced by continuous wave lasers.

Photoinitiated reactions offer several potential advantages over conventional thermally activated processes since the absorption of a photon generates an electronic excited state whose chemical reactivity can differ substantially from that of the ground state. As a consequence, the involvement of an excited state can induce a reaction pathway that does not occur thermally or occurs only at very high temperatures.

Light is a clean, tuneable and versatile "reagent", since it allows the selective activation of a photoinitiator also in the presence of organic solvents and chemical contaminants. Regulation of light intensity affords a convenient means of controlling reaction kinetics and photoinitiation can also be spatially directed and turned on or off simply by switching the light source. Other potential advantages of the photochemical reactions include reduced energy requirements, increased shelf life of substrate formulations, and greater compatibility with heat-sensitive materials. Other commendable features are low toxicity and friendly environmental impact.

The desire to expand the application of photoinitiated chemistry beyond organic systems has led recently to the discovery of several classes of inorganic and organometallic photoinitiators.[5−9] Among them, metallocenes have attracted increasing interest because it is possible to tailor the polymer microstructure by systematic, rational variation of the cyclopentadienyl ligand substituents, whether they are connected by an interannular bridge or not. Moreover, they leave low-toxic residues and they photobleach with high efficiency, thus leaving clear or colourless coatings after exposure to argon lasers.[5]

Despite their importance in organometallic chemistry and catalysis, to now few studies have been performed on the photochemistry of metallocene complexes of Ti, Zr, and Hf.[10−17] Moreover, while the relationship between the catalytic activity of Group IV metallocenes and their structure has been thoroughly studied, very little is known about its correlation with their electronic properties.

In this paper we report the photochemical behaviour of zirconocenes, whose substituents differ in both electron-donor and steric properties. Several unbridged zirconium complexes have been studied: bis(η^5-cyclopentadienyl)zirconium dichloride (Cp_2ZrCl_2, **1**), bis(η^5-pentamethylcyclopentadienyl)zirconium dichloride ($Cp^*_2ZrCl_2$, **2**), bis(η^5-indenyl)zirconium dichloride (Ind_2ZrCl_2, **3**), bis(η^5-tetrahydroindenyl)zirconium dichloride (THI_2ZrCl_2, **4**), bis(η^5-hexahydroazulenyl)zirconium dichloride [$(C7)_2ZrCl_2$, **5**], and bis[η^5-(4,5,6,7,8,9-hexahydro-1*H*-cyclopentacyclooctenyl)]zirconium dichloride [$(C8)_2ZrCl_2$**6**].

They have been also compared with two bridged complexes, *rac*-[ethylenebis(4,7-dimethyl-η^5-1-indenyl)]zirconium dichloride (*rac*-$EBDMIZrCl_2$, **7r**), and its *meso* isomer *meso*-$EBDMIZrCl_2$ (**7m**), in order to check if some of the

[a] Dipartimento di Chimica, Centro di Studio su Fotoreattività e Catalisi del C. N. R.,
Via L. Borsari 46, 44100 Ferrara, Italy
Fax: (internat.) + 39-0532/240709
E-mail: tr3@unife.it
[b] Inorganic Chemistry Laboratory, University of Oxford
South Parks Road, Oxford OX1 3QR, United Kingdom
Fax: (internat.) + 44-1865/272690
E-mail: malcolm.green@chem.ox.ac.uk

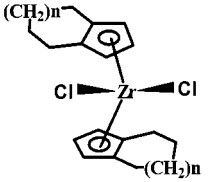

n = 1 **(4)**, 2 **(5)**, 3 **(6)**

original stereocontrol properties were retained after irradiation and could be applied in catalysis.

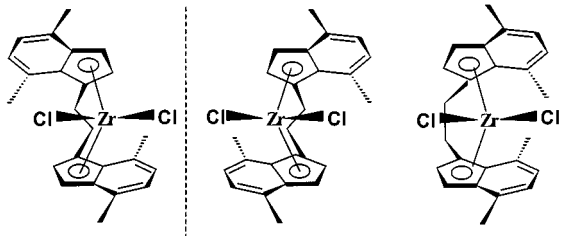

7r **7m**

Preliminary olefin photopolymerisation tests have also been carried out to verify their activity as photoinitiators for α-olefins.

Results and Discussion

Photochemistry

UV/Vis spectra of the zirconocenes under study were recorded in benzene, THF and CH_2Cl_2. No solvent effect was observed, neither on the λ_{max}, or on the ε_{max} values. The results are reported in Table 1. All complexes exhibit at least one electronic transition in the visible range of the spectrum (at $\lambda > 320$ nm) with ε values of the order of 10^3 $mol^{-1}\cdot L\cdot cm^{-1}$. The progressive red-shift of the bands as the electron-donor activity of the cyclopentadienyl substituents increases supports the hypothesis of LMCT character for the low-energy electronic transition.

Selective photolysis was carried out on the complexes at the wavelength corresponding to their LMCT transition, in order to ascertain if they can be employed as initiators in radical photopolymerisation and to optimise the reaction conditions. The primary quantum yield corresponding to the metal-ring cleavage is of the order of 0.28 for all the unbridged compounds, and of 0.11 for $EBDMIZrCl_2$ (**7r** and **7m**). Long-time photolysis led to the bleaching of the solutions due to evolution of the complexes, as determined by NMR analysis.

Table 1. Spectral band maxima of zirconocene complexes in solution (benzene, THF or CH_2Cl_2)

Zirconocene	λ_{max} [nm]	ε_{max} ($mol^{-1}\cdot L\cdot cm^{-1}$)
Cp_2ZrCl_2	290	2400
	340	620
$Cp^*_2ZrCl_2$	350	1580
	370	1990
Ind_2ZrCl_2	310	1475
	380	720
THI_2ZrCl_2	310	1600
	350	1100
$(C7)_2ZrCl_2$	310	2380
	345	1540
$(C8)_2ZrCl_2$	305	2920
	345	1720
meso-$EBDMIZrCl_2$	380	1130
rac-$EBDMIZrCl_2$	425	1350

The solvent nature strongly affects the stability of the complexes in solution, and it emphasises the differences among the metallocenes; in particular, in benzene and in toluene, (Figure 1) after 1 h of irradiation, only the 5−10% (by UV/Vis spectroscopy) of the complexes **4**−**6** were decomposed and the degradation rates were $Ind_2ZrCl_2 > Cp^*_2ZrCl_2 > Cp_2ZrCl_2 >> (THI)_2ZrCl_2 > (C7)_2ZrCl_2/(C8)_2ZrCl_2$.

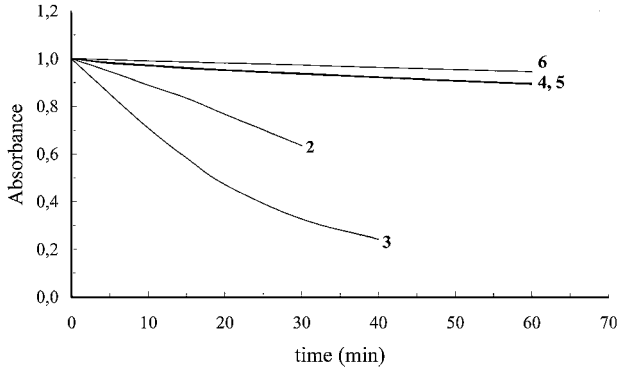

Figure 1. Absorption maxima decay of the zirconocenes **2**−**6** in benzene as a function of time

Pure solutions of **4**−**6** in benzene or in toluene were more stable and the photodecomposition was reversed after 24 h of storage in the dark. The initial spectral pattern and absorbance values were almost completely recovered.

Figure 2 shows that in THF the photodecomposition of the compounds **1**−**6** was faster (30−70%) and followed the same trend as in benzene solution. The increased rate of decomposition may be due to stronger coordinating properties of THF. We note that the UV/Vis spectra in THF have a different shape from those in toluene or benzene.

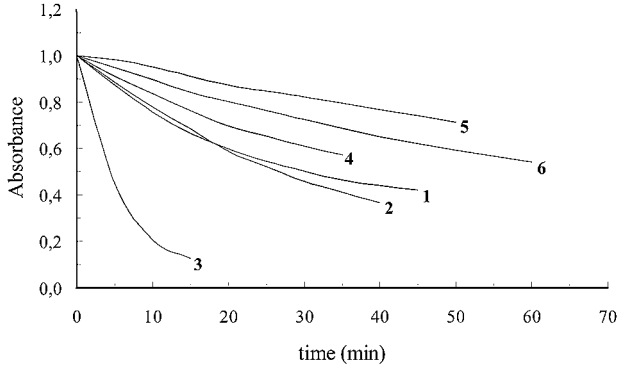

Figure 2. Absorption maxima decay of the zirconocenes **1**−**6** in THF as a function of time

EPR Spin Trapping Investigation

In order to assess the nature of the primary photochemical act, EPR/spin trapping experiments have been carried out by direct irradiation of benzene solutions of the zirconocenes inside the spectrometer cavity. Different spin traps, i.e. *N*-*tert*-butyl-α-phenylnitrone (PBN), nitrosodurene (ND), and 5,5-dimethyl-1-pyrroline *N*-oxide (DMPO), were used in order to identify unambiguously the nature of the radical species.[18−19] By comparison with NIEHS Spin Trap Database data,[20] the hyperfine coupling constants (*hfcc*) of the spin adducts detected and reported in Table 2, could be assigned to cyclopentadienyl-type radicals. Therefore, the primary photochemical act can be described by Scheme 1.

Table 2. Hyperfine coupling constants of cyclopentadienyl-type spin adducts (all values are expressed in Gauss)

Zirconocene	ND	PBN	DMPO
Cp_2ZrCl_2	a_N = 13.7	a_N = 14.6	a_N = 14.0
	a_H = 15.3	a_H = 2.9	a_H = 20.2
$Cp^*_2ZrCl_2$	a_N = 13.5	a_N = 14.6	a_N = 14.8
		a_H = 4.0	a_H = 20.3
Ind_2ZrCl_2	a_N = 13.8	a_N = 14.6	a_N = 14.0
	a_H = 15.4	a_H = 2.5	a_H = 20.0
THI_2ZrCl_2	a_N = 13.8	a_N = 14.6	a_N = 14.2
	a_H = 13.8	a_H = 3.2	a_H = 20.8
$(C7)_2ZrCl_2$	a_N = 13.8	a_N = 14.5	a_N = 14.2
	a_H = 15.9	a_H = 2.9	a_H = 20.4
$(C8)_2ZrCl_2$	a_N = 13.8	a_N = 14.7	a_N = 14.0
	a_H = 21.3	a_H = 3.0	a_H = 20.3
$EBDMIZrCl_2$	a_N = 14.0	a_N = 14.6	a_N = 14.3
	a_H = 9.8	a_H = 2.3	a_H = 20.4

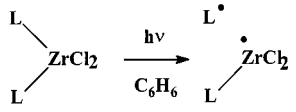

Scheme 1

The case of the bridged *rac*- and *meso*-metallocenes is rather complicated since the photodissociation of one of the two L−Zr bonds gives a biradical species as a consequence of the bridge and because the light causes also a partial interconversion between the two isomeric forms.[17] In this case, the primary photochemical act can be described by Scheme 2.

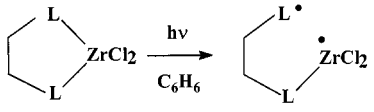

Scheme 2

The presence of radical intermediates in the zirconocenes' photochemical reactions suggests a possible use as photoinitiators for radical polymerisation processes. In order to test the effectiveness of these organometallic photoinitiators, similar EPR/spin trapping experiments were performed in the presence of different alkenes, i.e. 1-pentene, methyl methacrylate (MMA) and *tert*-butyl acrylate (*t*BA), and in different solvents, benzene and dichloromethane. During irradiation of the zirconocene/alkene mixtures the growth of a new EPR signal characteristic of a carbon-centred radical has been detected (a_N = 14.7−14.9 G; a_H = 3.0−3.6 G). The results are reported in Table 3.

Removal of the solvent left a polymeric film, while no polymer formation was observed even after prolonged irradiation in the absence of metallocenes. This observation supports the proposal that the radical species produced upon irradiation can add to the double bond of the monomers, thus initiating the radical polymerisation process. When the same experiments were carried in CH_2Cl_2, the $^{\cdot}CH_2Cl$ radical was also detected (a_N = 14.2 G; a_H = 3.1 G) (see Table 3, last column). This species can act as a second photoinitiator and this accounts for the higher monomer conversions obtained when the polymerisations were carried in halogenated solvents.[21−23]

The stability of the complexes in the presence of the monomers has been also determined. We found that in benzene and in toluene only 10% of the complexes was decomposed after 1 h of irradiation, whilst in THF the decomposition was more rapid and ca. 60% of the complexes **4−6** was decomposed, while the other metallocenes were completely decomposed in the same period.

Polymerisation Studies

On the basis of these findings, polymerisation tests were performed on *tert*-butyl acrylate, since the polymerisation of acrylates is of industrial interest and has been the subject of intensive experimental investigations and practical application. Recently, zirconocene complexes were introduced as catalysts or catalyst precursors for methyl methacrylate polymerisation.[24−27] We tested the most promising metallocenes in benzene and in CH_2Cl_2, and we can compare our data with what reported[28−34] for similar systems. We have also determined whether there is evidence for stereochemical control by the *ansa*-zirconocenes **7r** and **7m** (Table 4). The tacticity of the poly(*t*BA) formed has been estimated by deconvolution of the methine peaks which occurs at δ ≈ 42 in the ^{13}C NMR spectra (Figure 3).

The EPR data (vide supra) for the polymerisations in CH_2Cl_2 with the complexes **4−6** gave higher product yields than in benzene solutions due to the synergistic effect of the $^{\cdot}CH_2Cl$ radical. This effect was quite negligible with the *ansa*-bridged metallocenes **7r** and **7m**. The stereochemical outcome of the reaction was independent of the solvent and of stereochemistry of the compounds **7r** and **7m.**

The polymer yields shown in Table 4 compare favourably with the yields reported for polymerisations using chiral metallocenes with alumoxanes.[28] For example, after only 1 h, we have 22−36% polymer yield, when the literature values were only 13% after 17 h. The stereochemical properties of the polymers (Table 4) are comparable to those reported for other catalysts,[30−34] even though the latter had more complex and rigid stereochemical features.

Table 3. Hyperfine coupling constants of cyclopentadienyl-type spin adducts (all values are expressed in Gauss)

Zirconocene[a]	1-pentene in C_6H_6	MMA in C_6H_6	*t*BA in C_6H_6	*t*BA in CH_2Cl_2	
Cp_2ZrCl_2	a_N = 14.7	a_N = 14.7			
	a_H = 3.0	a_H = 3.6			
$Cp^*_2ZrCl_2$	a_N = 14.6	a_N = 14.7			
	a_H = 2.9	a_H = 3.7			
Ind_2ZrCl_2	a_N = 14.8				
	a_H = 2.9				
THI_2ZrCl_2	a_N = 14.8	a_N = 14.7	a_N = 14.9	a_N = 15.0	a_N = 14.0
	a_H = 3.0	a_H = 3.5	a_H = 3.4	a_H = 3.1	a_H = 3.1
$(C7)_2ZrCl_2$	a_N = 14.7	a_N = 14.6	a_N = 14.9	a_N = 15.2	a_N = 14.2
	a_H = 3.0	a_H = 3.5	a_H = 3.4	a_H = 3.4	a_H = 3.0
$(C8)_2ZrCl_2$	a_N = 14.7	a_N = 14.5	a_N = 14.9	a_N = 15.2	a_N = 14.3
	a_H = 3.0	a_H = 3.4	a_H = 3.4	a_H = 3.4	a_H = 3.2
EBDMIZrCl$_2$ *meso*			a_N = 15.0	a_N = 15.1	a_N = 14.2
			a_H = 3.5	a_H = 3.5	a_H = 3.0
EBDMIZrCl$_2$ *rac*			a_N = 15.2	a_N = 15.1	a_N = 14.2
			a_H = 3.6	a_H = 3.5	a_H = 3.0

[a] 8 mg of metallocene in 4 mL of a 20% solution of the monomer in benzene or dichloromethane.

Table 4. *tert*-Butyl acrylate polymerisation data

Zirconocene	20% *t*BA in C_6H_6				20% *t*BA in CH_2Cl_2			
	Yield[a]	Stereochemistry[b] (%)			Yield[a]	Stereochemistry[b] (%)		
		[rr]	[mr]	[mm]		[rr]	[mr]	[mm]
THI_2ZrCl_2	24	37	52	11	29	40	47	13
$(C7)_2ZrCl_2$	22	40	45	15	27	44	45	11
$(C8)_2ZrCl_2$	24	35	50	15	31	39	49	12
EBDMIZrCl$_2$ *meso*	36	41	47	12	38	41	48	10
EBDMIZrCl$_2$ *rac*	35	40	48	12	39	40	49	11

[a] Weight of polymer obtained/weight of monomer added. [b] Percent of syndiotactic [rr], isotactic [mm], and atactic [mr] triads in the isolated polymer, calculated from the deconvolution of the ^{13}C NMR peaks at $\delta = 41-43$.

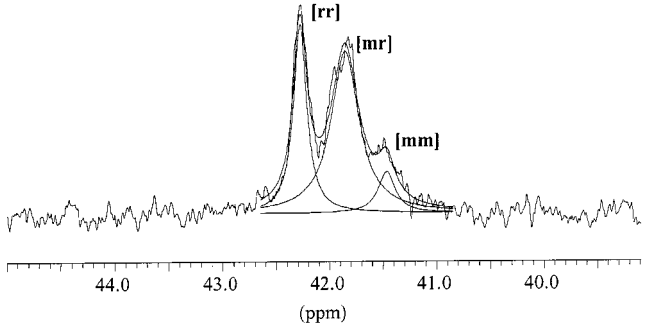

Figure 3. Methine region in the ^{13}C NMR spectrum of poly(*t*BA) obtained in CH_2Cl_2 (the single deconvoluted peaks are also represented)

Conclusion

Known and new zirconocene complexes are described here to be photoinitiators for radical polymerisation processes. *tert*-Butyl acrylate polymerisation has been studied in detail with both bridged (**7r** and **7m**) and unbridged complexes (**4**−**6**) and the results are particularly encouraging as far as the reaction yields and the stereochemistry are concerned. Also the use of non-halogenated solvents is environmentally desirable.

We propose to take advantage of the ability to modify the structure of the complexes **4**−**6**,[35] in order to tune the optical properties and radical stability.

Experimental Section

General Remarks: All manipulations of air- and/or moisture-sensitive materials were carried out under an inert gas using a dual vacuum/argon line and standard Schlenk techniques. All solvents were thoroughly dehydrated and deoxygenated under argon before use. They were dried and purified by refluxing under argon over a suitable drying agent (benzene, toluene and THF over Na/benzophenone ketyl; CH_2Cl_2 over CaH_2) followed by distillation, and stored under argon in Young's ampoules. Solvents and solutions were transferred, using a positive pressure of argon, through stainless-steel cannulae (diameter 0.5−2.0 mm) and mixtures were filtered in a similar way using modified cannulae which could be fitted with glass-fibre filter disks (Whatman GFC).

Preparation of the Complexes: Metallocenenes THI_2ZrCl_2 (**4**),[35] $(C7)_2ZrCl_2$ (**5**),[35] $(C8)_2ZrCl_2$ (**6**),[35] Ind_2ZrCl_2 (**3**),[36] and EBDMIZrCl$_2$ [37] were prepared as described previously; Cp_2ZrCl_2 (**1**), and $Cp^*_2ZrCl_2$ (**2**) were purchased from Sigma-Aldrich Chem. Co. and used without further purification.

NMR Spectra: ^1H (200.13 MHz) and ^{13}C (50.32 MHz) nuclear magnetic resonance spectra were recorded at room temperature

with a Bruker AC200 spectrometer. Spectra were referenced internally using the residual protio solvent resonance relative to tetramethylsilane ($\delta = 0$). Deuterated solvents were dried and distilled under argon over a suitable drying agent (CaH_2 for $CDCl_3$ and K for C_6D_6) and stored under argon in Young's ampoules.

EPR Studies: The spin traps PBN, ND and DMPO were purchased from Sigma-Aldrich Chem. Co. and used without further purification, except from DMPO, which was distilled under vacuum below 40 °C to remove paramagnetic impurities. The EPR/spin trapping experiments were performed with a Bruker EMX spectrometer, operating in the X-band (microwave frequency: 9.6 GHz; microwave power: 2 mW; modulation frequency: 100 kHz; modulation amplitude: 1 G; sweep rate: 50 G/min; time constant: 20 ms). Sample solutions were irradiated with a 350-W medium-pressure Hg lamp directly into the EPR spectrometer (Bruker ER-4104OR, TE102) cavity. Solid α,α′-diphenyl-β-picrylhydrazyl was used as external reference for *g* values. The *hfcc* values were calculated by best-fit simulation of experimental spectra using the NIEHS WinSim software.[38]

Photochemical Experiments: Irradiation was performed using an Oriel 500-W high-pressure Hg lamp using either a grating monochromator (Jasco CT-25A) or cut-off filters for wavelength selection. UV/Vis spectra were recorded with a Jasco UVIDEC-610 double-beam spectrophotometer.

Polymerisation Tests: 1-Pentene, methyl methacrylate and *tert*-butyl acrylate were dehydrated over molecular sieves (4Å) and freed from the stabilisers by filtration before use. In a typical experiment a 20% monomer solution in a 4-mL cuvette was irradiated for 1 h in the presence either of 7 mg of an unbridged metallocene at $\lambda = 350$ nm, or of 3 mg of an *ansa*-bridged metallocene at $\lambda = 410$ nm. After 1 h, the polymerisation was quenched with methanol and HCl, and the polymer was recovered after removal of the solvents under reduced pressure.

Acknowledgments

We thank the C. N. R. Short Term Fellowship Program (1996/97) for supporting the stay of E. P. in Oxford and Prof. O. Traverso of the University of Ferrara for helpful discussion.

[1] N. S. Allen (Ed.), *Photopolymerization and Photoimaging Science and Technology*, Elsevier, Amsterdam, **1989**.
[2] S. P. Pappas (Ed.), *Radiation Curing: Science and Technology*, Plenum Press, New York, **1992**.
[3] A. B. Scranton, C. N. Bowman, R. W. Peiffer (Eds.), *Photopolymerization: Fundamentals and Applications* (ACS Symp. Ser., no. 673), American Chemical Society, Washington, DC, **1997**.
[4] Ciba (Ed.), *Photoinitiators for UV curing. Key Products Selection Guide. Additives*, **1998** (brochure available at http://www.cibasc.com).
[5] B. M. Monroe, G. C. Weed, *Chem. Rev.* **1993**, *93*, 435−448.
[6] R. S. Davidson, *J. Photochem. Photobiol., A* **1993**, *69*, 263−275
[7] R. S. Davidson, *J. Photochem. Photobiol., A* **1993**, *73*, 81−96
[8] C. Kutal, *Coord. Chem. Rev.* **2001**, *211*, 353−368
[9] Y. Yamaguchi, B. J. Palmer, C. Kutal, *Macromolecules* **1998**, *31*, 5155−5157.
[10] W. Kaminsky, A. M. Schauwienold, F. Freidanck, *J. Mol. Catal. A: Chem.* **1996**, *112*, 37−42.
[11] A. L. Rheingold, N. P. Robinson, J. Whelan, B. Bosnich, *Organometallics* **1992**, *11*, 1869−1876.
[12] K. Schmidt, A. Reinmuth, U. Rief, J. Diebold, H. H. Brintzinger, *Organometallics* **1997**, *16*, 1724−1728.
[13] E. Vitz, C. H. Brubaker, Jr., *J. Organomet. Chem.* **1974**, *82*, C16.
[14] R. W. Harrigan, G. S. Hammond, M. B. Gray, *J. Organomet. Chem.* **1974**, *81*, 79−85.
[15] E. Vitz, P. J. Wagner, C. H. Brubaker Jr., *J. Organomet. Chem.* **1976**, *107*, 301−306.
[16] G. L. Lee, C. H. Brubaker, Jr., *Inorg. Chim. Acta* **1977**, *25*, 181−184.
[17] A. Barbieri, A. Droghetti, S. Sostero, O. Traverso, *J. Photochem. Photobiol., A* **1999**, *129*, 137−142.
[18] S. Sostero, D. Rehorek, O. Traverso, E. Polo, *Inorg. Chim. Acta* **1993**, *209*, 171−176.
[19] S. Di Martino, S. Sostero, O. Traverso, D. Rehorek, T. J. Kemp, *Inorg. Chim. Acta* **1990**, *176*, 107−112.
[20] A. S. W. Li, K. B. Cummings, H. P. RoethLing, G. R. Buetner, C. F. Chignell, *J. Magn. Reson.* **1988**, *79*, 140−142.
[21] H.-G. Woo, J.-Y. Park, L.-Y. Hong, S.-Y. Yang, H. You, H.-S. Ham, *Bull. Korean Chem. Soc.* **1996**, *17*, 582−585.
[22] H.-G. Woo, J.-Y. Park, H.-S. Ham, H.-R. Park, S.-D. Cho, Y.-H. Ko, W.-G. Kim, *Bull. Korean Chem. Soc.* **1997**, *18*, 444−447.
[23] H.-G. Woo, J. Y. Park, L.-Y. Hong, S.-Y. Yang, H. You, H.-S. Ham, *Bull. Korean Chem. Soc.* **1996**, *17*, 412−414.
[24] W. B. Farnham, W. R. Hertler, US Patent 4,728,706, **1988**.
[25] K.-H. Thiele, H.-J. Timpe, D. Schenke, B. Strehmel, DD Patent 297018, **1991**.
[26] C. Albrecht, W. Frass, R. Zertani, EP 573805, **1993**.
[27] R. Zertani, D. Mohr, K. Rode, EP 447930, **1991**.
[28] H. Deng, K. Soga, *Macromolecules* **1996**, *29*, 1847−1848.
[29] Y. Li, D. G. Ward, S. S. Reddy, S. Collins, *Macromolecules* **1997**, *30*, 1875−1883.
[30] P. A. Cameron, V. C. Gibson, A. J. Graham, *Macromolecules* **2000**, *33*, 4329−4335.
[31] M. H. Lee, J.-W. Hwang, Y. Kim, J. Kim, Y. Han, Y. Do, *Organometallics* **1999**, *18*, 5124−5129.
[32] C. Qian, W. Nie, J. Sun, *Organometallics* **2000**, *19*, 4134−4140.
[33] H. Frauenrath, H. Keul, H. Höcker, *Macromolecules* **2001**, *34*, 14−19.
[34] J. Q. Sun, Z. D. Pan, Y. Zhong, W. Q. Hu, S. L. Yang, *Eur. Polym. J.* **2000**, *36*, 2375−2380.
[35] E. Polo, R. M. Bellabarba, G. Prini, O. Traverso, M. L. H. Green, *J. Organomet. Chem.* **1999**, *577*, 211−218.
[36] E. Samuel, *Bull. Soc. Chim. Fr.* **1966**, *11*, 3548−3564.
[37] L. Resconi, F. Piemontesi, I. Camurati, D. Balboni, A. Sironi, M. Moret, H. Rychlicki, R. Ziegler, *Organometallics* **1996**, *15*, 5046−5059.
[38] D. R. Duling, *J. Magn. Reson. Ser. B* **1994**, *104*, 105−110.

Received August 3, 2001
[I01291]

Dynamic Behaviour of Tris(2-methylallyl)chromium − NMR and DFT Results

Richard Blom*[a] and Ole Swang[a]

Keywords: Chromium / Allyl complexes / Paramagnetism / NMR spectroscopy / Density-functional calculations

The variable-temperature ^{1}H NMR spectra of paramagnetic (2-Me-allyl)$_3$Cr in [D$_8$]toluene were recorded in the temperature range from 243 to 323 K. The changes observed in the spectra are interpreted in terms of intramolecular dynamic behaviour. Line-shape analyses gave an entropy of activation $\Delta H^{\ddagger}$ of 40(5) kJ/mol, and an entropy of activation $\Delta S^{\ddagger}$ of –31(4) J/mol·K for the observed transformation. This corresponds to a free energy of activation $\Delta G^{\ddagger}$ of 49(6) kJ/mol at 300 K. Different possible mechanisms were investigated by DFT. The presence of two different conformers, which were converted into each other by rotation of one allyl ligand around the allyl–chromium axis, may explain the observations.

Introduction

Homoleptic allyl complexes of the early transition elements (Groups 4−6) were prepared for the first time in the 1960s.[1] The complexes can act as one-component catalysts for polymerisation of 1-olefins and α,ω-dienes, both in homogeneous solutions and as deposits on oxide supports.[2] Despite their practical potential, the molecular structures of these complexes have not been determined experimentally, which is mostly due to their thermal instability. One property that has been widely studied for the Group 4 allyl complexes is the "rotation" of the allyl ligand that interchanges the *syn* and *anti* protons.[3] The activation energy for this transformation is typically found to be in the range 40 to 60 kJ/mol using variable-temperature NMR.

The Cr^{III} complex Cr(C$_3$H$_5$)$_3$ is paramagnetic, and has therefore not been analysed properly by NMR methods. An early crystal structure has been reported;[4] unfortunately, the quality of the data did not allow detailed structural information to be deduced, but the gross picture is a molecule with close to C_3 symmetry and close to trihapto-bonded allyl ligands. We recently reported the molecular structures of both Cr(allyl)$_3$ and Cr(2-Me-allyl)$_3$ from DFT calculations.[5] Both these molecules have C_{3h} symmetry. The dimeric Cr^{II} complex Cr$_2$(C$_3$H$_5$)$_4$, prepared by thermal decomposition of Cr(C$_3$H$_5$)$_3$, has been fully characterised by single-crystal X-ray diffraction;[6] it is diamagnetic and has thus also been characterised by ^{13}C NMR.[7]

In the present paper we report the observed high-power ^{1}H NMR spectra of (2-Me-allyl)$_3$Cr, dissolved in deuterated toluene, in the temperature range from −60 to +40 °C. From line-shape analysis, we have deduced the kinetic parameters for the transformation observed and we have used DFT calculations to test possible mechanisms that can explain the observed dynamics.

[a] SINTEF Applied Chemistry, Department of Hydrocarbon Process Chemistry,
P. O. Box 124 Blindern, 0314 Oslo, Norway
Fax: (internat.) + 47-2/206-7350
E-mail: Richard.Blom@chem.sintef.no

Results and Discussion

^{1}H NMR spectra recorded at different temperatures are shown in Figure 1. Except for a strong signal at $\delta \approx 0$ (not shown), no other signals, other than those shown in Figure 1, were observed in the range from $\delta = -5000$ to +5000. The signal at $\delta \approx 0$ results from the diamagnetic species present: the protons of the imperfectly deuterated solvent, residual pentane, and 2,5-dimethylhexa-1,5-diene, formed as a by-product during the synthesis. At low temperatures, there are three broad signals at $\delta \approx 70$, 85, and 160, with relative peak areas of roughly 1:2:3.

Normally, one would assign these three peaks to the three symmetrically independent protons present: the protons of the methyl groups, the *syn* protons and the *anti* protons. As the temperature increased, there seemed to be a coalescence of all peaks at approximately 295 K. The fact that all observed protons ended up being magnetically equivalent, indicates that either a facile proton exchange was taking place in the complex, or that our first interpretation is wrong. NMR signals from paramagnetic species are notoriously difficult to assign, and some peaks might not be observable due to extreme broadening by the paramagnetic centre present. If the latter were the case, the protons closest to the chromium atom would be most heavily influenced by the paramagnetic effect; hence, their resonances could be expected to be undetectable. An alternative assignment of the three peaks could then be that the three peaks stem from three individual methyl groups or from three different individual protons of the methyl groups. In either case, all protons of the methyl groups become equivalent at elevated

 © WILEY-VCH Verlag GmbH, 69451 Weinheim, Germany, 2002 1434−1948/02/0202−0411 $ 17.50+.50/0

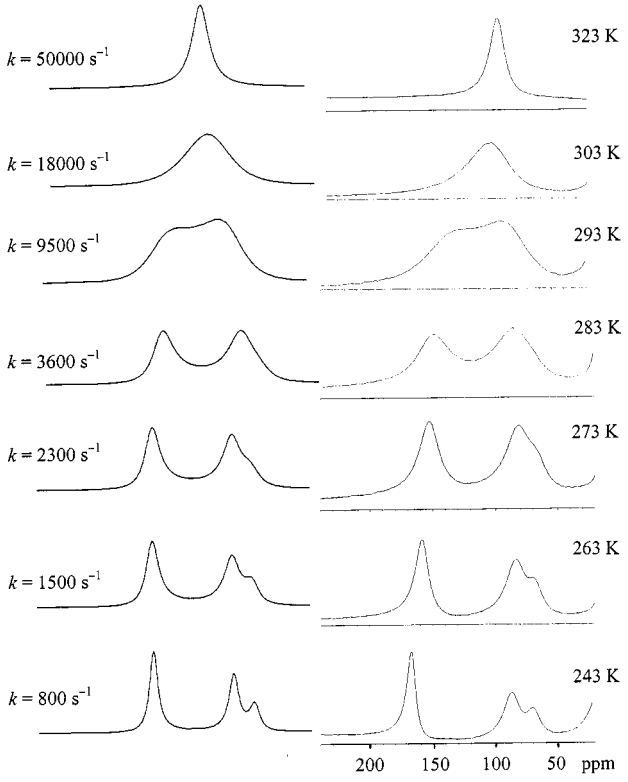

Figure 1. Experimental (right column) ^{1}H NMR spectra of (2-Me-allyl)$_3$Cr recorded in [D$_8$]toluene at the temperatures indicated; on the left are the modelled spectra shown with the corresponding rates

temperatures. Non-equivalent methyl groups can indicate that more than one conformation is present.

As noted above, NMR spectroscopy often gives little information on the structure of organometallic Cr^{III} complexes due to extreme line broadening.[8] The half-width of the peaks observed at low temperatures are large, the narrowest peak at $\delta = 160$ having a half-width of about 2400 Hz at 243 K, which is at the lower end of the estimated range suggested for Cr^{III} species (3000−25000 Hz at 500 MHz).[9] The enhancement of the nuclear longitudinal relaxation rate due to dipolar coupling to unpaired electrons is proportional to r^{-6}. The distance between the paramagnetic centre and the allylic protons is about 73% of the average distance to the methyl protons, meaning that the expected half-width of the allylic protons will be around 16000 Hz (80 ppm). Possible fluxional behaviour might increase the half-width further, and consequently the peaks would easily go into the background and thus remain unobserved. In addition, Cr(allyl)$_3$ does not give any peaks in the range from $\delta = -300$ to 300, which is a further indication that the allylic protons were not observed within this range for (2-Me-allyl)$_3$Cr.

The calculated structure of the tris(2-methylallyl)chromium molecule, structure **1** on the left in Figure 2, has been reported earlier.[5] It has C_{3h} symmetry and a ^{4}A′ electronic ground state, and in the following, its energy will be taken as the zero reference.

One might envisage three different interpretations of the observed NMR spectra:

A. Proton transfer from a methyl group to a terminal CH_2 group. The transfer may be either intra-allylic, or it may be a concerted mechanism involving all three allyl ligands.

B. Rotation of the allyl groups around the allyl−chromium axis. Actually, if we only observe the methyl groups, rotation around the allyl−metal axis cannot be separated, mechanistically, from the *syn*/*anti* exchange described in the introduction. Both routes were examined.

C. Rotation of the methyl groups.

Reaction path A may include an intermediate in which a hydrogen atom is removed from the methyl group of a 2-methylallyl ligand, giving an intermediate having both a hydrido and a trimethylenemethane ligand. For simplicity, the latter will be called corvyl[10] in the following discussion. This reaction path is shown as (i) in Figure 2. The intermediate, (corvyl)(hydrido)bis(2-methylallyl)chromium (**2**) was calculated to be as much as 105 kJ/mol higher in energy than its homoleptic allyl analogue. The distance between the hydrido ligand and one carbon atom of the corvyl ligand was chosen as a reaction coordinate for the reconstruction from (corvyl)(hydrido) to homoleptic triallyl. A transition state was found to be only 11 kJ/mol higher in energy than the (corvyl)(hydrido) intermediate, with a C−H distance of 1.66 Å. The complete exchange of a hydrogen atom requires the formation of (corvyl)(hydrido), then a 120° rotation of the corvyl ligand, followed by the reconnection of the corvyl and the hydrido ligands to a 2-methylallyl ligand. The exchange transforms a methyl group into a CH_2 group and at the same time transforms a CH_2 group into a methyl group. The activation energy of 116 kcal/mol is too high for reaction (i) to take place within the NMR timescale at the temperature in question, and hence other reaction paths must be investigated.

One could envisage a concerted transfer of hydrogen atoms between all three methylallyl groups. Structural optimisations were attempted in which all C−H distances for the transferring hydrogen atoms were constrained to be equal; the starting geometry is shown in Scheme 1. These attempts were fruitless, as they invariably converged to unphysical geometries of very high energies (> 250 kJ/mol). We therefore concluded that a proton transfer between the methyl group and the CH_2 group of the allyl ligand has too high a barrier, and thus cannot be used to explain the dynamics in the observed ^{1}H NMR spectra.

Our suggested mechanisms B and C are both based on the assumption that the allylic protons of the ligands are unobserved. Mechanism B concerns a rotation of one of the allyl ligands as shown as route (ii) in Figure 2. In the ground-state geometry all the methyl groups are connected by symmetry, and are thus expected to give only one peak in the ^{1}H NMR spectrum. However, by rotating one allyl group around the allyl−chromium axis by approximately 180°, a conformer is obtained in which all three methyl groups are, in principle, non-equivalent. This conformer **3** is expected to give three signals in the NMR spectrum, and

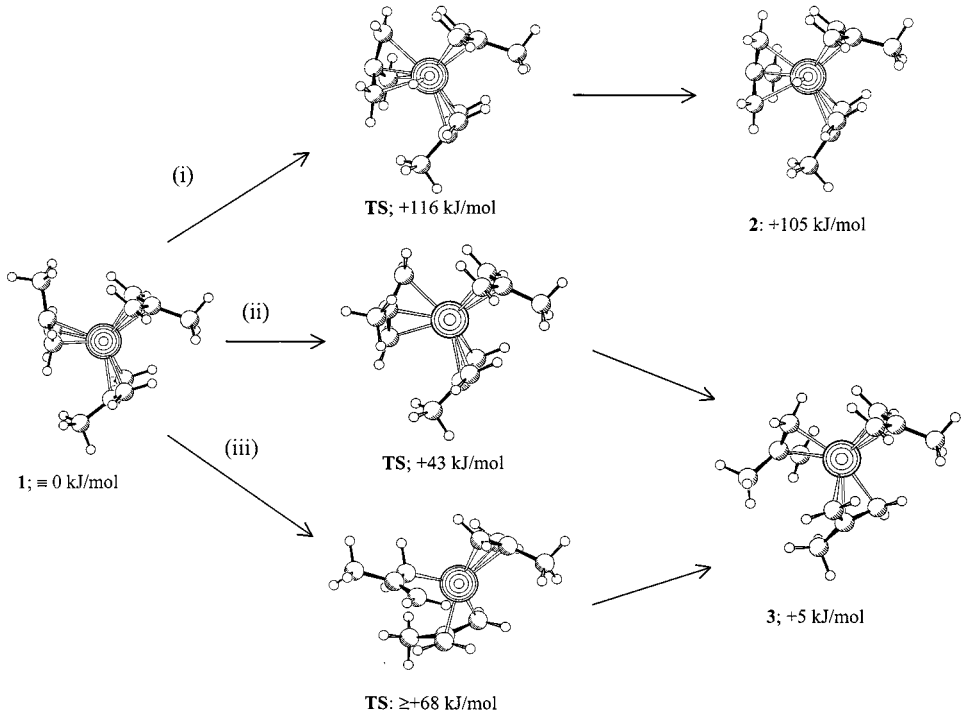

Figure 2. The structures and energies of central species and transition states (TS) obtained from DFT calculations: (i) transformation of one allyl ligand into a hydrido(trimethylenemethyl) complex; (ii) pure rotation of one allyl ligand around the allyl−chromium axis; (iii) $\eta^3 \rightarrow \eta^1 \rightarrow \eta^3$ transformation leading to the same conformer as route (ii); see text for more details

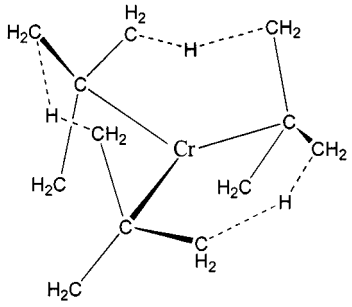

Scheme 1

the energy is only 5 kJ/mol higher than the ground-state geometry. The rotation goes through a transition state, the structure of which is shown in the centre of Figure 2, with a relative energy of 43 kJ/mol. Considering the accuracy of the DFT energies, it is reasonable to suggest that both conformers are present at low temperatures. A possible interpretation of the observed ^{1}H NMR spectra is then that the high-symmetry conformer **1** gives rise to the single peak at $\delta = 160$, while the two broad peaks at $\delta = 70$ and 87, of different intensities, are due to the three methyl peaks of conformer **3**. For the latter conformer there is an additional fluxionality due to the flipping of two methyl groups having van der Waals contacts from side to side. The barrier for this flipping was estimated from DFT modelling to be 8 kJ/mol. This is below the detection limit in the NMR experiment. At elevated temperatures, the rotation of the allyl groups becomes rapid, interchanging the two conformers rapidly at the NMR time scale, leaving only one single methyl peak at temperatures above 300 K. A rough lineshape analysis was carried out in order to estimate the activation energy for the rotation process assuming two different species, one species with nine magnetically equivalent protons, and a second species containing three magnetically inequivalent sets of protons. The modelled spectra are given on the left-hand side in Figure 1. From the analyses we obtained an enthalpy of activation $\Delta H^{\ddagger}$ of 40(5) kJ/mol and an entropy of activation $\Delta S^{\ddagger}$ of −31(4) J/mol·K, corresponding to a free energy of activation $\Delta G^{\ddagger}$ of 49(6) kJ/mol at 300 K. The equilibrium constant for the transformation **1** $\rightleftarrows$ **3** was estimated to be 1.2(1). The DFT activation barrier obtained is within the error of the experimental value.

Actually, another mechanism leading to **3** could include a pseudo-rotation that interchanges the (assumed unobserved) *syn* and *anti* protons of the allyl ligand. Such a "rotation" is believed to proceed first by transferring the η^3-allyl ligand into an η^1-bonding mode, followed by a rotation around the $C_\alpha-C_\beta$ bond, and finishing by re-transferring the allyl ligand into an η^3-bonded mode. Setting the $Cr-C_\alpha-C_\beta-C_{(methyl)}$ dihedral angle equal to 180°, and minimising all other degrees of freedom, we found a DFT energy of 69 kJ/mol. This energy, which may be regarded as

a lower limit for the reaction barrier, is significantly higher than the pure rotation around the allyl−metal axis. We infer that the latter mechanism will dominate over the former.

The last possibility that should be considered is mechanism C, rotation of the methyl groups. Methyl rotations are, in most cases, unobserved by dynamic NMR due to the low energy barrier. However, one might speculate if steric requirements and/or the paramagnetism and consequently large shift differences could lead to observable methyl rotations. DFT calculations give a barrier of 7 kJ/mol for the methyl rotation in the high-symmetry ground-state conformer, which is too low when compared to the experimental value.

Conclusions

The observed line widths in the ^{1}H NMR spectra of tris(2-methylallyl)chromium are in accordance with what one would expect from Cr^{III} complexes. The estimated free energy of activation deduced from line-shape analysis of the NMR spectra, 49(6) kJ/mol, is in accordance with a mechanism where two conformers are present, and the conformers can be transformed into one another by rotation of one allyl ligand around the allyl−chromium axis. The other mechanisms investigated by using DFT calculations all have energies that are discrepant with the experimental results. However, we can only explain our observations by assuming that the terminal allylic protons are not observed in the spectra. This assumption is reasonable in light of the close distances between these protons and the paramagnetic metal centre.

Experimental Section

Experimental Details: Tris-(2-methylallyl)chromium [(2-$CH_3C_3H_4)_3Cr$] was prepared according to known procedures.[11] The complex could be stored as a 0.050 M pentane solution (determined by ICP) at −40 °C for at least two weeks. All handling of the complex was carried out at temperatures below −20 °C under argon. NMR samples were prepared by transferring 0.5−1.0 mL of the pentane solution to an NMR tube connected to an argon/vacuum line. The pentane was removed at approximately −30 °C under reduced pressure. Then, 0.5 mL of [D_8]toluene was distilled into the NMR tube, which was kept in liquid nitrogen until it could be sealed. Before the tube was introduced into the NMR magnet, the solution was allowed to thaw at −78 °C in a dry-ice/ethanol bath. The NMR measurements were performed with a Bruker DMX 200 Avance spectrometer operating at 200 MHz. A high-power ^{1}H NMR probe was utilised to achieve a spectrum over a wide frequency range. The probe was capable of producing 90° radio frequency (rf) pulses as short as 1.5 ms. In the present experiments, a more moderate pulse power of approx. 3 ms 90° pulse was utilised. A pulse length of 1.2 ms was used, corresponding to approximately 40°. The sweep width was set to 1.3 MHz, the repetition time was 3.02 s, and 96 scans were acquired in every experiment. A 0.6 ms dead time was allowed between pulse and acquisition, and the acquisition time was 19.4 ms. Line-shape analysis was carried out using the program WINDNMR.[12] Due to a software limitation in the maximum possible natural half-width of the peaks, only spectra in the temperature range 263 to 303 K were used in the analysis.

Computational Details: The DFT calculations were carried out using the program system ADF, developed by Baerends et al.[13] The frozen-core approximation was used for all atoms except hydrogen, keeping the orbitals up to and including 2p for chromium and 1s for carbon frozen in their atomic shapes. The orbitals were described by Slater-type orbital (STO) basis sets. The number of unfrozen basis functions, in order of increasing angular momentum, was (5,3,3) for chromium, (2,2,1) for carbon, and (2,1) for hydrogen, yielding TZVP quality for Cr and DZVP for C and H (note that for Cr, the number of unfrozen orbitals is larger than the number of valence orbitals). Slater exchange and the VWN parameterisation of the LDA correlation energy,[14] with the gradient corrections of Becke[15] for exchange and of Perdew[16] for correlation, were used for the exchange-correlation energies; the gradient corrections were added self-consistently. The accuracy of the numerical integration was set to $10^{-6.0}$, which may be assumed to give a numerical noise level of less than 0.1 kcal/mol in the final energies.[17] The calculations were carried out while making no initial assumptions of molecular symmetry. The calculations were run without restrictions, with separate sets of Kohn−Sham orbitals for each spin. No vibrational spectra have been computed.

Acknowledgments

We would like to thank Per Olav Kvernberg at the University of Oslo for recording the NMR spectra. The work has been carried out with financial support from the Norwegian Research Council (Grant 110675/420), and a grant of computer time from the NOTUR program (http://www.notur.org).

[1] G. Wilke, B. Bogdanovic, P. Hardt, P. Heimbach, W. Keim, M. Kröner, W. Oberkirch, K. Tanaka, E. Steinrücke, D. Walter, H. Zimmermann, *Angew. Chem.* **1966**, *78*, 157; *Angew. Chem. Int. Ed. Engl.* **1966**, *5*, 151.

[2] D. G. H. Ballard, *Adv. Catal.* **1974**, *23*, 263; D. G. H. Ballard, W. H. Janes, T. Medinger, *J. Chem. Soc., Ser. B.* **1968**, 1168; D. G. H. Ballard, E. Jones, T. Meldinger, A. J. P. Pioli, *Die Makromol. Chemie*, **1971**, *148*, 175; V. A. Kormer, V. A. Vasilèv, N. A. Kalinicheva, O. I. Belgorodskaya, *J. Polym. Sci., Polym. Chem. Ed.* **1973**, *11*, 2557; E. A. Demin, V. A. Zakharov, Yu. I. Ermakov, S. S. Derbeneva, *Izv. Vyssh. Uchebn. Zaved. Khim. Khim. Tekhnol.* **1975**, *18*, 1283 (*Chem. Abstr.* **1975**, *83*, 206,624); V. K. Dudchenko, V. A. Zakharov, Z. K. Bukatova, Yu. I. Ermakov, *Kin. Katal.*, **1978**, *19*, 584; V. A. Zakharov, *Ind. J. Tech.* **1983**, *21*, 353; I. F. Gavrilenko, V. L. Sokolova, V. V. Sitnikova, E. I. Tinyakova, V. A. Dolgoplosk, *Kin. Katal.* **1991**, *32*, 1169; F. J. Karol, R. N. Johnsen, *J. Polym. Sci.* **1975**, *13*, 1607; R. N. Johnson, F. J. Karol (Union Carbide Corp.), US Patent 4,054,538, **1977**.

[3] J. K. Krieger, J. M. Deutch, G. M. Whitesides, *Inorg. Chem.* **1973**, *12*, 1535−1545; E. G. Hoffmann, R. Kallweit, G. Schroth, K. Seevogel, W. Stempfle, G. Wilke, *J. Organomet. Chem.* **1975**, *97*, 183−202.

[4] The crystal structure of $Cr(allyl)_3$ has been reported; see: H. Dietrich, *Acta Crystallogr., Sect. A* **1969**, *25*, 160. However, only the unit cell parameters are given; neither *R* factors nor individual interatomic distances or angles are reported.

[5] O. Swang, R. Blom, *J. Organomet. Chem.* **1998**, *561*, 29.

[6] T. Aoki, A. Furusaki, Y. Tomiie, K. Ono, K. Tanaka, *Bull. Chem. Soc. Jpn.* **1969**, *42*, 545.

[7] R. Benn, *Angew. Chem.* **1982**, *94*, 633.
[8] K. H. Theopold, *Acc. Chem. Res.* **1990**, *23*, 263.
[9] I. Bertini, C. Luchinat, *Coord. Chem. Rev.* **1996**, *150*, 77.
[10] From lat. *corvus* (crow). The ligand appears to grip the metal atom like a bird's claw.
[11] S. O'Brien, M. Fishwick, B. McDermott, M. G. H. Wallbridge, G. A. Wright, *Inorg. Synth.* **1972**, *13*, 73.
[12] *WINDNMR*, Version 1.50: H. J. Reich, *J. Chem. Educ.* **1997**, Software.
[13] *Amsterdam Density Functional (ADF)*, Release 2.3.0, Scientific Computing and Modelling, Dept. of Theoretical Chemistry, Vrije Universiteit, de Boelelaan 1083, 1081 HV Amsterdam. The method is described in the following publications: E. J. Baerends, *Chem. Phys.* **1973**, *2*, 41; Baerends, E. J., PhD Thesis, Vrije Universiteit Amsterdam, **1975**; W. Ravenek, *in Algorithms and Applications on Vector and Parallel Computers* (Eds.: H. J. J. te Riele, T. J. Dekker, H. A. van de Vorst), Elsevier, Amsterdam, **1987**; P. M. Boerrigter, G. te Velde, and E. J. Baerends, *Int. J. Quantum Chem.* **1988**, *33*, 87; G. te Velde, E. J. Baerends, *J. Comput. Phys.* **1992**, *99*, 84; C. Fonseca Guerra, O. Visser, J. G. Snijders, G. te Velde, E. J. Baerends, in *Methods and Techniques for Computational Chemistry* (Eds.: E. Clementi, G. Coronglu), METECC-95, STEF, Cagliari, **1995**.
[14] S. H. Vosko, L. Wilk, M. Nusair, *Can. J. Phys.* **1980**, *58*, 1200.
[15] A. D. Becke, *Phys. Rev.* **1988**, *A33*, 2786; *ACS Symp. Ser.* **1989**, *394*, 165; *Int. J. Quantum Chem.* **1989**, *S23*, 599; *Phys. Rev.* **1988**, *A38*, 2398.
[16] J. P. Perdew, *Phys. Rev.* **1986**, *B33*, 8822; Erratum: *Phys. Rev.* **1987**, *B34*, 7406.
[17] G. te Velde, E. J. Baerends, *J. Comp. Phys.* **1992**, *99*, 84.

Received August 27, 2001
[I01333]

Carboxylation of 2-Hydroxyethyl-Substituted Tetrachloro(ethane-1,2-diamine)-platinum(IV) Complexes — A New Synthetic Approach to Anticancer Platinum Compounds

Markus Galanski,*[a] Wolfgang Zimmermann,[a] Michael Berger,[a] Christian Baumgartner,[a] Gerald Giester,[b] and Bernhard Klaus Keppler*[a]

Keywords: Platinum / Structure elucidation / Carboxylation / Antitumor agents

The present study has focused on a general reaction procedure for the derivatization of hydroxyethyl-substituted tetrachloro(ethane-1,2-diamine)platinum(IV) compounds at peripheral hydroxyl groups using acyl chlorides. A new class of platinum(IV) complexes could be synthesized which now opens the possibility for the first time to couple the cytotoxic platinum(IV) moiety to carrier molecules like proteins and antibodies in a very selective way. Moreover, it is now possible to synthesize platinum(IV) complexes with ligands in the equatorial plane which are not very stable in the presence of oxidizing agents.

Introduction

Since its discovery as a very effective antitumour compound, cisplatin,[1,2] *cis*-diamminedichloroplatinum(II), has become the dominant anticancer drug in clinics worldwide. Numerous platinum complexes have been synthesized and tested with respect to their cancerostatic activity so far, but only the second and third generation complexes carboplatin, *cis*-diammine(1,1-cyclobutanedicarboxylato)-platinum(II), and oxaliplatin, (*trans*-*R,R*-cyclohexane-1,2-diamine)oxalatoplatinum(II), are in clinical use today.[3] Because of severe side-effects and limitations of the platinum based drugs in use, research has focused on four major goals: (i) reduction of toxicity; (ii) expansion of platinum chemotherapy to a broader range of cancers; (iii) circumvention of resistance to Pt drugs; and (iv) synthesis of platinum compounds for oral administration. At the moment, only a few Pt complexes are in clinical trials.[4,5] Besides ZD0473[6] a sterically hindered compound and BBR3464[7] a trinuclear complex, satraplatin[8] (JM216) an orally available platinum(IV) compound is under development in the clinic.

The synthesis of JM216 is not only an approach to a new class of Pt^{IV} antitumour agents, but it also constitutes a new synthetic pathway in platinum chemistry, which was previously limited to ligand substitution or oxidation of platinum(II) species with hydrogen peroxide or chlorine gas to the corresponding Pt^{IV} complexes. Kinetically inert hydroxoplatinum(IV) complexes were used and carboxylated with anhydrides, acyl chlorides, pyrocarbonates and isocyanates to form carboxylates, carbonates and carbamates.[9–13] Unfortunately, the reactions are limited to a few carboxylating agents. Moreover, carboxylates will be lost again after reduction of the platinum(IV) species in the body. This would be a problem when linking of antitumour platinum fragments to carrier molecules is planned using the method described before. Therefore, we have focused on derivatization of kinetically inert tetrachloroplatinum(IV) complexes not directly at the metal centre but at peripheral functional groups. For this purpose, hydroxyethyl-substituted tetrachloro(ethane-1,2-diamine)platinum(IV) complexes and acyl chlorides have been used to set up a general reaction procedure.

Results and Discussion

The synthesis of the hydroxyethyl-substituted tetrachloro(ethane-1,2-diamine)platinum(IV) complexes *N*-(2-hydroxyethyl)ethane-1,2-diamine and *N,N′*-bis(2-hydroxyethyl)ethane-1,2-diamine which were selected for the carboxylation reactions starts from K_2PtCl_4 (Scheme 1). In the free diamine ligands there is no chiral atom. After coordination of *N,N′*-bis(2-hydroxyethyl)ethane-1,2-diamine to the platinum(II) centre, two chiral nitrogen atoms are produced resulting in the *trans*-*R,R*-, *trans*-*S,S*-, and *cis*-*R,S*-isomers.[14,15] The coordination of *N*-(2-hydroxyethyl)-ethane-1,2-diamine to platinum generates two isomers (*R* and *S*). The oxidation to the corresponding Pt^{IV} species

[a] Institute of Inorganic Chemistry, Vienna University,
Waehringer Strasse 42, 1090 Vienna, Austria
Fax: (internat.) +43-1/4277-52680
E-mail: Keppler@ap.univie.ac.at
Galanski@ap.univie.ac.at
[b] Institute of Mineralogy and Crystallography, Vienna University,
Althanstrasse 14, 1090 Vienna, Austria

 © WILEY-VCH Verlag GmbH, 69451 Weinheim, Germany, 2002 1434–1948/02/0202–0417 $ 17.50+.50/0

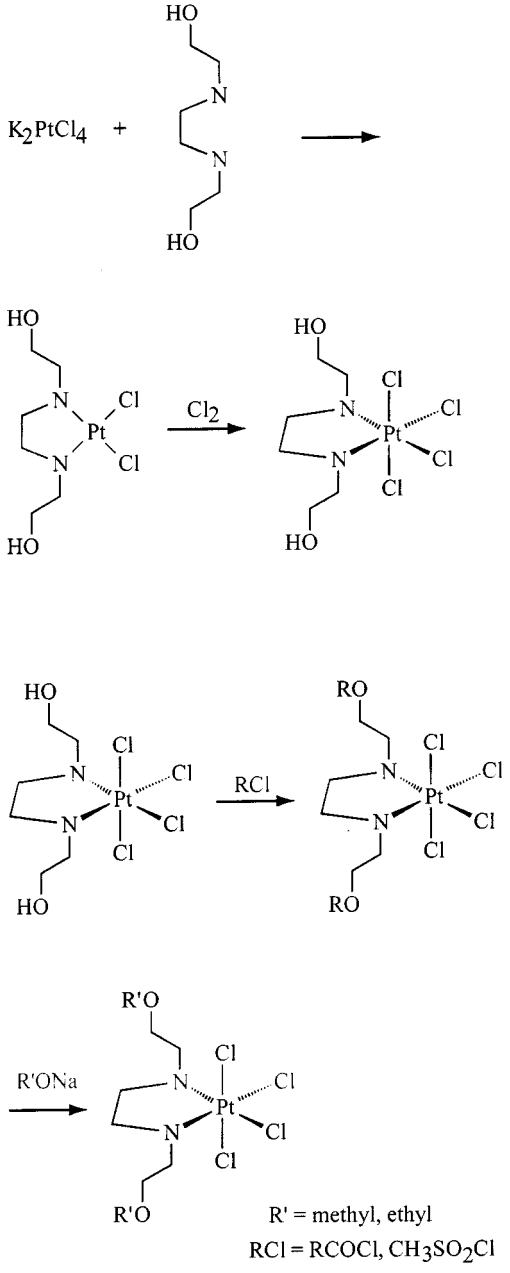

Scheme 1. Synthesis of the tetrachloro[*N,N'*-bis(2-hydroxyethyl)-ethane-1,2-diamine]platinum(IV) starting compound **2** and subsequent derivatization

was done in aqueous suspension with chlorine gas at room temperature.

For carboxylation of the peripheral OH groups, the tetrachloroplatinum(IV) compounds were suspended in dry acetone. After the addition of an excess of dry pyridine and acyl chloride, the mixture was stirred at room temperature and then under reflux. Water was added after cooling to room temperature. The precipitates were filtered off, dried, dissolved and precipitated with an appropriate organic solvent. The ether synthesis was carried out via sulfonation of the OH groups with mesyl chloride and subsequent reaction with sodium ethanolate or sodium methanolate without isolation of the intermediate ester.

The compounds were characterized by elemental analysis and, if soluble enough, by NMR spectroscopy. The theoretical values of the elemental analyses are in good agreement with those found experimentally. During the synthesis of the *N,N'*-bis(2-hydroxyethyl)-substituted (ethane-1,2-diamine)platinum(IV) complexes it was possible to isolate (*OC*-6-32)-*R,S*-tetrachloro[*N,N'*-bis(2-hydroxyethyl)ethane-1,2-diamine]platinum(IV) (**2**) and to resolve its structure by single crystal structure analysis (Figure 1).

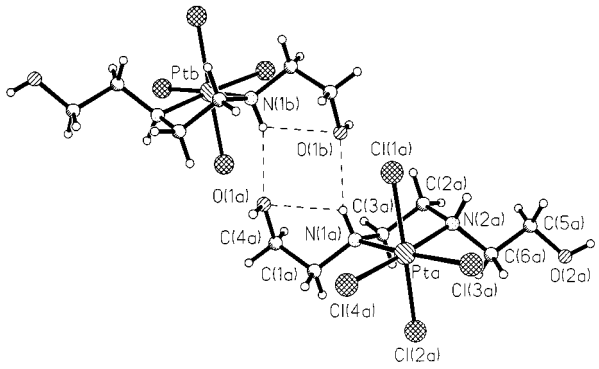

Figure 1. Structure of **2** in the crystal; selected distances (Å) and angles (°): Pt−N(1) 2.093(4), Pt−N(2) 2.086(4), Pt−Cl(1) 2.3094(13), Pt−Cl(2) 2.3202(13), Pt−Cl(3) 2.3227(13), Pt−Cl(4) 2.3259(12), C(2)−C(3) 1.499(7); N(1)−Pt−N(2) 84.57(17), N(1)−Pt−Cl(1) 87.68(12), N(2)−Pt−Cl(1) 86.47(13), N(1)−Pt−Cl(2) 90.54(12), N(2)−Pt−Cl(2) 93.56(13), Cl(1)−Pt−Cl(2) 178.20(5), N(1)−Pt−Cl(3) 174.31(12), N(2)−Pt−Cl(3) 89.87(12), Cl(1)−Pt−Cl(3) 90.81(5), Cl(2)−Pt−Cl(3) 90.99(5), N(1)−Pt−Cl(4) 94.75(12), N(2)−Pt−Cl(4) 176.98(13), Cl(1)−Pt−Cl(4) 90.56(5), Cl(2)−Pt−Cl(4) 89.38(5), Cl(3)−Pt−Cl(4) 90.75(5), C(3)−N(1)−Pt 105.5(3), C(2)−N(2)−Pt 106.9(3), N(2)−C(2)−C(3) 109.6(4), N(1)−C(3)−C(2) 109.2(4)

The O and N atoms are arranged in an octahedral manner around the platinum(IV) centre. The angular sum in the square planar plane (N1, N2, Cl3, Cl4) is 359.94°, with angles of 84.57(17)° (N2−Pt−N1), 90.75(5)° (Cl3−Pt−Cl4), 89.87(12)° (Cl3−Pt−N2) and 94.75(12)° (Cl4−Pt−N1). The Cl1−Pt−Cl2 axis is nearly linear with an angle of 178.20(5)°. The Pt−N and Pt−Cl distances [Pt−N1 2.093(4) Å, Pt−N2 2.086(4) Å, Pt−Cl1 2.3094(13) Å, Pt−Cl2 2.3202(13) Å, Pt−Cl3 2.3227(13), Å Pt−Cl4 2.3259(13) Å] are in the normal range for aminetetrachloroplatinum(IV) complexes. The bond lengths between the axial chloro ligands (Cl1 and Cl2) and Pt are significantly smaller than the corresponding Pt−Cl distances in the equatorial plane. The angular sum in the ethane-1,2-diamineplatinum(IV) chelate (five-membered ring) is 515.77°; the Pt−N1−C3−C2−N2 ring adopts a half-chair conformation with dihedral angles of 19.3, 44.7, 55.7, 35.9 and 8.9° at Pt−N1, N1−C3, C3−C2, C2−N2, and N2−Pt, respectively. The values found are in good agreement with those expected for cyclopentane in a half-chair conformation (13, 34, 42, 34 and 13°, respectively).

Furthermore, the structure of **2** is stabilized by intramolecular and intermolecular hydrogen bonds in the crystal. An intramolecular hydrogen bond is formed between N1 and O1, with a donor acceptor contact distance of 2.812 Å. O1

is also involved in the intermolecular hydrogen bond network with a very weak interaction to the proton at N1 (N1−H1···O1, N1−O1 3.186 Å). Moreover, intermolecular donor−acceptor contacts of 2.745 Å (O1−O2) and 3.254 Å (O2−Cl4), were found. A short intermolecular C−O contact of 3.195 Å (C2−O1, C2−H···O1) could be detected between O1 and C2 of the neighbouring ethane-1,2-diamine unit; this is in the typical range for C−H···O hydrogen bonds. It may indicate attractive interactions further stabilizing the structure of **2** in the crystal.

Besides the well-known procedures for the synthesis of platinum(IV) compounds, for example oxidation with H_2O_2 or Cl_2, or carboxylation of di- and tetrahydroxoplatinum(IV) complexes, a pathway to a new class of Pt^{IV} compounds is demonstrated.

In the present study simple acyl chlorides have been chosen for the carboxylation reaction, while hydroxyethyl-substituted tetrachloro(ethane-1,2-diamine)platinum(IV) complexes were used as the cytotoxic moiety. Tetrachloroplatinum(IV) compounds are kinetically inert so side products can be limited during the carboxylation. However, although it is known that tetrachloroplatinum(IV) complexes are easily reduced to their corresponding platinum(II) counterparts in vivo,[16] it occurs now without loss of the ester residue. Contrary to the limited possibilities of a carrier-mediated transport in platinum(IV) chemistry, a new synthetic approach to anticancer platinum(IV) compounds for drug targeting has been found. This new procedure is not only a completion of the synthesis of tumour inhibiting platinum-based drugs, but it also opens up the possibility for the first time of coupling the cytotoxic moiety to carrier molecules like proteins or antibodies in a very selective way. A platinum(IV) conjugate with albumine has recently been synthesized by us and will be published elsewhere. Moreover, it is now possible to synthesize platinum(IV) complexes with ligands (e.g. ethers, crown ethers) in the equatorial plane which are not very stable in the presence of oxidizing agents.

Conclusion

In conclusion it has been demonstrated that a new class of platinum(IV) complexes could be synthesized starting from tetrachloro[*N*-(2-hydroxyethyl)ethane-1,2-diamine]-platinum(IV) and tetrachloro[*N*,*N*′-bis(2-hydroxyethyl)-ethane-1,2-diamine]platinum(IV) by carboxylation of the peripheral hydroxyl groups with acyl chlorides.

Besides the synthesis of platinum(IV) compounds with ligands in the equatorial plane that are not very stable under oxidizing conditions, it is now possible for the first time to generate platinum(IV) conjugates with proteins or antibodies in a very selective way.

Experimental Section

General Remarks: All chemicals obtained from commercial suppliers were used as received and were of analytical grade. Water was doubly distilled. All synthetic procedures were carried out in the dark.

^1H and ^{13}C NMR experiments were performed at 200.13 MHz (^1H) and 50.32 MHz (^{13}C) on a Bruker Ac 200 MHz spectrometer at 24 °C with standard Bruker pulse programs.

Elemental analyses were performed by the microanalytical laboratory at the Universities of Heidelberg and Vienna.

Synthesis of Hydroxyethyl-Substituted (Ethane-1,2-diamine)platinum(II) and -(IV) Complexes. Dichloro[*N*,*N*′-bis(2-hydroxyethyl)-ethane-1,2-diamine]platinum(II) (1): A solution of *N*,*N*′-bis(2-hydroxyethyl)ethane-1,2-diamine (1.7916 g, 12.09 mmol) in 60 mL of ethanol was treated with K_2PtCl_4 (5.0176 g, 12.09 mmol). After addition of 115 mL of doubly distilled water the pH of the solution was adjusted to 7 using diluted hydrochloric acid and stirred at room temperature. The precipitate was collected over a period of 20 hours. During this time the pH was kept constant at 7 by addition of dilute NaOH. The yellow precipitate was washed with water and dried over P_4O_{10}. $C_6H_{16}Cl_2N_2O_2Pt$ (414.2): calcd. C 17.40, H 3.89, N 6.76, Cl 17.12, Pt 47.10; found C 17.45, H 3.63, N 6.62, Cl 17.45, Pt 47.23. Yield: 3.928 g, 78.5%.

Tetrachloro[*N*,*N*′-bis(2-hydroxyethyl)ethane-1,2-diamine]-platinum(IV) (2): Chlorine gas was bubbled through a suspension of dichloro[*N*,*N*′-bis(2-hydroxyethyl)ethane-1,2-diamine]platinum-(II) (2.000 g, 4.82 mmol) in 45 mL of water at room temperature. After 100 min the yellow precipitate was collected and washed with water (3 × 2 mL). The red filtrate thus obtained was then left to stand at room temperature for several days, after which time more product had precipitated. This precipitate was filtered off and washed with water. The precipitates were dried over P_4O_{10}. $C_6H_{16}Cl_4N_2O_2Pt$ (485.1): calcd. C 14.86, H 3.32, N 5.77, Cl 29.23, Pt 40.22; found C 14.74, H 3.35, N 5.75, Cl 28.94, Pt 40.16. Yield: 1.582 g, 68.0%.

Dichloro[*N*-(2-hydroxyethyl)ethane-1,2-diamine]platinum(II) (1a): A solution of *N*-(2-hydroxyethyl)ethane-1,2-diamine (2.514 g, 24.14 mmol) in 20 mL of water was treated with 150 mL of an aqueous solution of K_2PtCl_4 (10.006 g, 24.11 mmol). The pH was adjusted to 7 using diluted hydrochloric acid and stirred at room temperature. The precipitate was collected over a period of 20 hours. During this time the pH was kept constant at 7 by addition of dilute NaOH. The yellow precipitate was collected, washed with water and dried over P_4O_{10}. $C_4H_{12}Cl_2N_2O_2Pt$ (386.1): calcd. C 12.98, H 3.27, N 7.57, Cl 19.16, Pt 52.71; found C 12.94, H 3.24, N 7.54, Cl 19.28, Pt 52.75. Yield: 5.608 g, 63.0%.

Tetrachloro(*N*-(2-hydroxyethyl)ethane-1,2-diamine)platinum(IV) (2a): Synthesis and workup was performed as described for **2**. $C_4H_{12}Cl_4N_2O_2Pt$ (457.1): calcd. C 10.89, H 2.74, N 6.35, Cl 32.15, Pt 44.23; found C 10.87, H 2.77, N 6.31, Cl 32.09, Pt 44.15. Yield: 1.067 g, 45.0%.

Carboxylation Reactions and Ether Synthesis

Tetrachloro[*N*,*N*′-bis(2-octadecanoyloxyethyl)ethane-1,2-diamine]-platinum(IV) (3): Compound **2** (294.0 mg, 0.606 mmol) was suspended in dry acetone and mixed with dry pyridine (1.078 g, 13.63 mmol) and octadecanoic acid chloride (1.474 g, 4.87 mmol). The mixture was stirred at room temperature overnight and for 5 hours under reflux. After cooling to room temperature, 70 mL of water was added and the resulting mixture was stored overnight in the refrigerator. The precipitate was filtered off and washed thoroughly with water. After drying over P_4O_{10} the crude product was dissolved in 20 mL of chloroform and precipitated with diethyl

ether. The solid was washed several times with diethyl ether. After filtration the precipitate (light brownish) was dried over P_4O_{10}. $C_{42}H_{84}Cl_4N_2O_4Pt$ (1018.0): calcd. C 49.55, H 8.32, N 2.75, Pt 19.16; found C 49.18, H 8.06, N 2.83, Pt 19.52. Yield: 213 mg, 35%.

Tetrachloro[*N*,*N*′-*bis*(2-hexadecanoyloxyethyl)ethane-1,2-diamine]-platinum(IV) (4): The synthesis was carried out as described for **3**. $C_{38}H_{76}Cl_4N_2O_4Pt$ (961.9): calcd. C 47.45, H 7.96, N 2.91, Pt 20.28; found C 47.28, H 7.75, N 2.95, Pt 20.65. Yield: 181 mg, 47%.

{*N*,*N*′-Bis[2-(1-adamantanoyloxy)ethyl]ethane-1,2-diamine}-tetrachloroplatinum(IV) (5): The synthesis was carried out as described for **3**. ^{1}H NMR ($CDCl_3$): δ = 1.3−2.2 ($H_{adamantane}$), 2.7−4.6 (NC*H*$_2$, OC*H*$_2$), 6.3−8.9 (N*H*). ^{13}C NMR ($CDCl_3$): δ = 27.7 (C_{ad}), 36.3 (C_{ad}), 38.8 (C_{ad}), 40.9 (C_{ad}), 53.7 (N*C*H$_2$), 55.1 N*C*H$_2$), 60.7 (O*C*H$_2$), resonance for C=O was not found. $C_{28}H_{44}Cl_4N_2O_4Pt$ (809.6): calcd. C 41.54, H 5.48, N 3.46, Pt 24.10; found C 41.67, H 5.47, N 3.71, Pt 24.33. Yield: 302 mg, 60%.

{*N*,*N*′-Bis[2-(6,7,9,10,12,13,15,16-octahydrobenzo[*b*][1,4,7,10,13]-pentaoxacyclopentadecin-2-carbonyloxy)ethyl]ethane-1,2-diamine}-tetrachloroplatinum(IV) (6): The synthesis was carried out as described for **3**. The excess of free carboxylic acid is soluble in the water/acetone mixture; further workup is not necessary. $C_{36}H_{52}Cl_4N_2O_{14}Pt$ (1073.7): calcd. C 40.27, H 4.88, N 2.61, Pt 18.17; found C 39.96, H 4.84, N 2.71, Pt 18.37. Yield: 284 mg, 76%.

{*N*-[2-(1-Adamantanoyloxy)ethyl]ethane-1,2-diamine}tetrachloro-platinum(IV) (7): The synthesis was carried out as described for **3** with **2a** as starting compound. The precipitate was dried over P_4O_{10}. $C_{15}H_{26}Cl_4N_2O_2Pt$ (603.3): calcd. C 29.86, H 4.34, N 4.64, Pt 32.34; found C 30.28, H 4.39, N 4.39, Pt 32.23. Yield, 212 mg, 56%.

Tetrachloro[*N*,*N*′-*bis*(2-methoxyethyl)ethane-1,2-diamine]-platinum(IV) (8): Mesyl chloride (661 mg, 5.772 mmol) and dry pyridine (913 mg, 11.54 mmol) were added to a suspension of **2** (700 mg, 1.322 mmol) in dry chloroform. The mixture was stirred for 12 hours at room temperature and for 3 hours under reflux. After that, the suspension was evaporated to dryness and the resulting solid washed with ethanol and diethyl ether. The solid (yellow-brownish, 531 mg) was dried over P_4O_{10}. Some of the product (200 mg) was then reacted with an excess of $NaOCH_3$ (168 mg) in 10 mL of dry methanol. After stirring for eight hours at room temperature, the solution was reduced to 3 mL. Water (20 mL) was then added, and the precipitate was filtered off, washed with water and methanol and dried under reduced pressure. $C_8H_{20}Cl_4N_2O_2Pt$ (513.2): calcd. C 18.73, H 3.93, N 5.46, Pt 38.02; found C 18.26, H 4.02, N 5.53, Pt 37.96. Yield: 132 mg, 51%.

Tetrachloro[*N*-(2-ethoxyethyl)ethane-1,2-diamine]platinum(IV) (9): Mesyl chloride (727 mg, 6.348 mmol) and dry pyridine (1.004 g, 12.70 mmol) were added to a suspension of **2a** (700 mg, 1.587 mmol) in dry acetone. The mixture was stirred for 12 hours at room temperature and for 3 hours under reflux. After that, the suspension was filtered and reduced to 10 mL. Dry acetone (40 mL) and $NaOCH_2CH_3$ (2.159 g, 31.74 mmol) were then added. After stirring for eight hours at room temperature, the solution was reduced to 3 mL. Water (20 mL) was then added, and the precipitate was filtered off, washed with water and methanol and dried under reduced pressure. $C_6H_{16}Cl_4N_2O_1Pt$ (469.1): calcd. C 15.36, H 3.44, N 5.97, Pt 41.59; found C 14.79, H 3.40, N 5.72, Pt 41.67. Yield: 362 mg, 49%.

X-ray Crystallographic Study: X-ray diffraction measurements were performed on a Nonius Kappa instrument with a CCD detector at 293 K, using graphite-monochromated Mo-K_α radiation. Crystal data, data collection parameters and structure refinement details are given in Table 1. The structure was solved by direct methods and refined by full-matrix least-squares techniques. The non-H atoms were refined with anisotropic displacement parameters, while H atoms were calculated and allowed to ride. Details of the computer programs used are as follows: data reduction: DATAP;[17] structure solution: SHELXS-97;[18] structure refinement: SHELXL-97;[19] molecular diagram: ORTEP.[20] The scattering factors were obtained from a literature source.[21] Crystallographic data (excluding structure factors) for the structure reported in this paper have been deposited with the Cambridge Crystallographic Data Centre as supplementary publication no. CCDC-162129. Copies of the data can be obtained free of charge on application to CCDC, 12 Union Road, Cambridge CB2 1EZ, UK [Fax: (internat.) +44-1223/336-033; E-mail: deposit@ccdc.cam.ac.uk].

Table 1. Crystal data and details of data collection for **2**

	2
Chemical formula	$C_6H_{16}Cl_4N_2O_2Pt$
M (g mol^{-1})	485.10
Crystal system	Monoclinic
Space group	$P2_1/n$
a (Å)	6.990(1)
b (Å)	9.723(1)
c (Å)	19.099(3)
β (°)	92.12(1)
V (Å^3)	1297.2(3)
Z	4
D_c (g cm^{-3})	2.484
μ (cm^{-1})	116.2
F(000)	912
θ range for data collection (°)	2.35−28.99
h range	−8/8
k range	−10/11
l range	−24/24
No. uniq. measd. refls.	2866
No. refls. used in refinement	2866
No. parameters	139
R_{int}	0.0137
R_1 (obs.)	0.0272
wR_2 (all data)	0.0752
S	1.111
Largest diff. peak and hole (eÅ^3)	1.282 and −1.730

Acknowledgments

The support of the FWF (Fonds zur Foerderung der wissenschaftlichen Forschung) and COST (D8 program) is gratefully acknowledged. We thank Mrs. R. Strobl for administrative support in the preparation of the manuscript.

[1] B. Rosenberg, *Inderdiscip. Sci. Rev.* **1978**, *3*, 134−147.
[2] *Cisplatin: Chemistry and Biochemistry of a Leading Anticancer Drug* (Ed.: B. Lippert), Weinheim, Wiley-VCH, **1999**.
[3] P. J. O'Dwyer, P. Stevenson, S. W. Johnson, *Drugs* **2000**, *59*, 19−27.
[4] I. Judson, L. R. Kelland, *Drugs* **2000**, *59*, 29−36.

[5] E. Wong, C. M. Giandomenico, *Chem. Rev.* **1999**, *99*, 2451−2466.
[6] J. Holford, F. Raynaud, B. A. Murrer, K. Grimaldi, J. A. Hartley, M. Abrams, L. R. Kelland, *Anticancer Drug Des.* **1998**, *13*, 1−18.
[7] C. Sessa, G. Capri, L. Gianni, F. Peccatori, G. Grasselli, J. Bauer, M. Zucchetti, L. Vigano, A. Gatti, C. Minoia, P. Liati, S. Van den Bosch, A. Bernareggi, G. Gamboni, S. Marsoni, *Ann. Oncol.* **2000**, *11*, 977−983.
[8] M. J. McKeage, F. Raynaud, J. Ward, C. Berry, D. O'Dell, L. R. Kelland, B. Murrer, P. Santabarabara, K. R. Harrap, I. R. Judson, *J. Clin. Oncol.* **1997**, *15*, 2691−2700.
[9] C. M. Giandomenico, M. J. Abrams, B. A. Murrer, J. F. Vollano, M. I. Rheinheimer, S. B. Wyer, G. E. Bossard, J. D. Higgins III, *Inorg. Chem.* **1995**, *34*, 1015−1021.
[10] M. Galanski, B. K. Keppler, *Met-Based Drugs* **1995**, *2*, 57−63.
[11] M. Galanski, B. K. Keppler, *Inorg Chem.* **1996**, *35*, 1709−1711.
[12] M. Galanski, B. K. Keppler, *Inorg Chim. Acta* **1997**, *265*, 271−274.
[13] J. N. Jolley, A. I. Yanovsky, L- R. Kelland, K. B. Nolan, *J. Inorg. Biochem.* **2001**, *83*, 91−100.
[14] Q. Xu, A. R. Khokhar, J. L. Bear, *Inorg. Chim. Acta* **1999**, *292*, 107−111.
[15] M. Galanski, B. K. Keppler, *Met-Based Drugs* **2000**, *7*, 349−355.
[16] L. T. Ellis, H. M. Er, T. W. Hambley, *Aust. J. Chem.* **1995**, *48*, 793−806.
[17] P. Coppens, L. Leiserowitz, D. Rabinowich, *Acta Crystallogr.* **1965**, *18*, 1035−1038.
[18] G. M. Sheldrick, *SHELXS-97*, *Program for Crystal Structure Solution*, Universität Göttingen, **1997**.
[19] G. M. Sheldrick, *SHELXL-97*, *Program for Crystal Structure Refinement*, Universität Göttingen, **1997**.
[20] C.K. Johnson, *Rep. ORNL-5138*, OAK Ridge National Laboratory, OAK Ridge, TN, **1976**.
[21] *International Tables for X-ray Crystallography*, Kluwer Academic Press: Dodrecht, The Netherlands, **1992**, vol. C, Tables 4.2.6.8 and 6.1.1.4.

Received September 12, 2001
[I01356]

Ligand Effects on the Reactivity of $Cu^{I}L$ Complexes Towards $Cl_3CCO_2^-$

Nadav Navon,*[a] Ariela Burg,[a] Haim Cohen,[a,b] Rudi van Eldik,[c] and Dan Meyerstein[a,d]

Keywords: Copper / Ligands / Redox chemistry / Kinetics / Reaction mechanisms

The effect of the nature of the ligand L on the mechanism and kinetics of the reaction of $Cu^{I}L$ with $Cl_3CCO_2^-$ in aqueous solution is reported. The results demonstrate that the rate of the chlorine abstraction reaction, which is usually the rate-determining step in the process, is affected by: a) the redox potential of the $Cu^{II/I}L$ couple, b) the hybridization on Cu^{I} in the $Cu^{I}L$ complex, c) steric hindrance, d) electron density on the central Cu^{I} cation, at the binding site of the chlorine atom to be abstracted. Measurement of $\Delta V^{\neq}$ for the chlorine abstraction step indicates that this reaction proceeds by the inner-sphere mechanism, as expected. When the redox potential of the $Cu^{II/I}L$ couple is considerably cathodically shifted the transient complex $LCu^{II}–CCl_2CO_2^-$ is relatively long-lived.

Introduction

Copper(I) complexes catalyze a variety of organic reactions, which are of synthetic and of industrial importance.[1–3] Many of these processes are initiated by halide abstraction from aryl or alkyl halides. The halide abstraction reaction by the Cu^{I} catalyst is believed to be the rate-determining step of these processes. The addition of organic polyhalides to alkenes is a good example of such reactions.[3] The detailed mechanisms of these reactions have not been fully elucidated. Due to the low solubility of Cu^{I} halides and to the disproportionation of Cu^{+}_{aq} the concentration of Cu^{I} species in these systems is usually very low. In principle the addition of appropriate ligands for Cu^{I}, e.g. CH_3CN,[4] alkenes[5] and NH_3 [5] increases the concentration of the Cu^{I} species in the system and is therefore expected to increase the rate of the catalytic process. Tri- and tetradentate ligands, which stabilize Cu^{I}, were indeed shown to accelerate catalytic processes.[6–8] However, these ligands might also affect the reactivity of the Cu^{I} complexes due to one, or more, of the following reasons:

1. If the stability constant of the Cu^{I} complex with the ligand is larger than that of the corresponding Cu^{II} complex then the redox potential of the $Cu^{II/I}$ couple is shifted anodically, i.e. the Cu^{I} complex is a weaker reducing agent than Cu^{+}_{aq}, and vice versa.

2. Ligands can slow down the rate of Cu^{I} reactions due to steric effects.

3. Ligands might impose a coordination geometry, which affects the energy of the transition state thus affecting the rate of the reaction.

The effect of ligands that stabilize copper(I) on the rates and mechanisms of the catalytic processes was not studied in detail. The effect of fumarate on the reaction of Cu^{+}_{aq} with Cl_3CCOO^- (TCA) was recently[6] studied. The results demonstrate that the rate of reaction between Cu^{I}-($HOOCCH=CHCOO^-$) and Cl_3CCOO^- is very slow. Cl^- is a product of the reaction, its yield equals half the concentration of $Cu^{I}L$. The general reaction mechanism is:

$$Cu^{+}_{aq} + L \rightleftarrows Cu^{I}L \quad (1)$$

$$Cu^{I}L/Cu^{+}_{aq} + Cl_3CCOO^- \rightarrow (LCu^{II}Cl)/(CuCl)^+ + {}^{\cdot}CCl_2COO^- \quad (2)$$

$k_2 = 6.0 \pm 1.0\ M^{-1}s^{-1}$ for Cu^{+}_{aq} and $k_2 < 0.015\ M^{-1}s^{-1}$ for $Cu^{I}(HOOCCH=CHCOO^-)$

$$Cu^{I}L/Cu^{+}_{aq} + {}^{\cdot}CCl_2COO^- \rightarrow (LCu^{II}-CCl_2CO_2^-)^-/(Cu^{II}-CCl_2CO_2^-) \quad (3)$$

$$(LCu^{II}-CCl_2CO_2^-)^-/(Cu^{II}-CCl_2CO_2^-) + H_3O^+ \rightarrow Cu^{2+}_{aq} + HCCl_2COO^- + L \quad (4)$$

$$(Cu^{II}L)^+/Cu^{2+}_{aq} + {}^{\cdot}CCl_2COO^- \rightarrow (LCu^{III}-CCl_2CO_2^-)/(Cu^{III}-CCl_2CO_2^-)^+ \quad (5)$$

$$(LCu^{III}-CCl_2CO_2^-)/(Cu^{III}-CCl_2CO_2^-)^+ + Cu^{I}L/Cu^{+}_{aq} \rightarrow (LCu^{II}-CCl_2CO_2^-)^-/(Cu^{II}-CCl_2CO_2^-) + Cu^{II}L^+/Cu^{2+}_{aq} \quad (6)$$

These results indicate that carrying out catalytic processes in the absence of a large excess of alkenes is desired. It seemed of interest to extend this study to the effect of other ligands on this reaction. For this purpose the following ligands were chosen:

1. CH_3CN, which is often used as a solvent for the catalytic processes.

[a] Chemistry Department, Ben-Gurion University of the Negev, Beer-Sheva, Israel
[b] Nuclear Research Centre Negev, Beer-Sheva, Israel
[c] Institute for Inorganic Chemistry, University of Erlangen-Nürnberg, 91058 Erlangen, Germany
[d] The College of Judea and Samaria, Ariel, Israel

 © WILEY-VCH Verlag GmbH, 69451 Weinheim, Germany, 2002 1434–1948/02/0202–0423 $ 17.50+.50/0

2. NH_3, a σ-donor ligand that shifts the redox potential of the Cu^{II}/Cu^{I} couple somewhat cathodically.

3. L^1 [7] and L^2,[8] ligands that were recently designed with the aim to stabilize Cu^{I} while cathodically shifting the redox potential of the Cu^{II}/Cu^{I} couple. It was therefore hoped that they will accelerate catalytic processes in which the Cu^{I} acts as a reducing agent in the rate determining step.

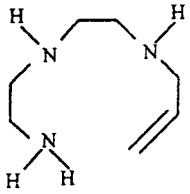

L^1

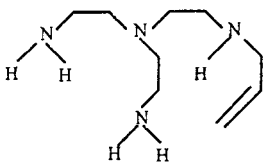

L^2

It was hoped that the choice of different types of ligands for this study might shed light on the factors affecting the rates of halide abstraction reactions by Cu^{I} complexes and thus enable the design of improved catalytic processes. In order to gain more insight on the detailed mechanism of the reaction of Cu^{+}_{aq} with $Cl_3CCO_2^-$ the volume of activation of this reaction was determined. The experimental conditions were identical to those used for the determination of the volume of activation for the reaction of Cu^{+}_{aq} with O_2,[9] i.e. He-saturated solutions containing 0.05 M $CuSO_4$, 1.0 M CH_3OH, 0.01 M Cl_3CCO_2Na, $1.0\cdot10^{-4}$ M HOOCCH=CHCOO$^-$ at pH = 3.0 were irradiated at different pressures.

Results and Discussion

In the following sections the effects of each ligand on the mechanism and kinetics of the reaction of Cu^{I} with CCl_3COO^- is described and discussed separately. Then the effects of the ligands are compared and general conclusions are derived.

CH_3CN

Acetonitrile forms the complexes $Cu(CH_3CN)_n^+$, n = 1−4, with Cu^{I} in aqueous solutions. In the concentration range of $(0.05-1.5)\cdot10^{-1}$ M CH_3CN the main complexes present in the solutions are $Cu^{I}(CH_3CN)^+$ and $Cu^{I}(CH_3CN)_2^+$.

$$Cu^{+}_{aq} + CH_3CN \rightleftarrows Cu(CH_3CN)^+ \quad \log\beta_1 = 3.27^{[4a]} \tag{7a}$$

$$Cu^{+}_{aq} + 2\,CH_3CN \rightleftarrows Cu(CH_3CN)_2^+ \quad \log\beta_2 = 4.32^{[4b]} \tag{7b}$$

Since these complexes have no absorption bands in the near UV/Vis region, the effect of acetonitrile on the rate of the reaction of $Cu^{I}L$ with $CCl_3CO_2^-$ was studied in the presence of low concentrations of fumaric acid. The Cu^{I}(fumaric acid) complex has a strong absorption band in the near UV region[10] and the ligand exchange reaction Cu^{+}_{aq} + HOOCCH=CHCOO$^-$ ⇄ $Cu^{I}(HO_2CCH=CHCO_2^-)$ is very fast.[11a] The addition of fumarate thus simplifies the use of spectrophotometry in order to follow the rate of reaction of Cu^{I}. The technique used was pulse radiolysis. When N_2O-saturated aqueous solutions at pH = 3.0 containing $5.0\cdot10^{-2}$ M $CuSO_4$, 1.0 M CH_3OH, $2.0\cdot10^{-4}$ M fumaric acid and $(0.05-1.5)\cdot10^{-1}$ M CH_3CN are irradiated, all the primary radicals are transformed according reactions (7)−(11) to a mixture of Cu^{+}_{aq}, Cu^{I}(fumaric acid) and $Cu^{I}(CH_3CN)_n^+$.[6,12]

$$^{\cdot}OH/^{\cdot}H + CH_3OH \rightarrow {}^{\cdot}CH_2OH + H_2O/H_2 \quad k_{OH} = 4.6\cdot10^8\ M^{-1}s^{-1},^{[13]}\ k_H = 1.6\cdot10^6\ M^{-1}s^{-1}\ ^{[13]} \tag{8}$$

$$^{\cdot}CH_2OH + Cu^{2+}_{aq} \rightarrow Cu^{+}_{aq} + CH_2O + H_3O^+ \quad k = 1.6\cdot10^8\ M^{-1}s^{-1}\ ^{[10]} \tag{9}$$

$$e^-_{aq} + Cu^{2+}_{aq} \rightarrow Cu^{+}_{aq} \quad k = 3.3\cdot10^{10}\ M^{-1}s^{-1}\ ^{[13]} \tag{10}$$

$$Cu^{+}_{aq} + HOOCCH=CHCOO^- \rightleftarrows Cu^{I}(HOOCCH=CHCOO^-) \tag{11}$$

at pH = 3.65, $k_{11} = 1.7\cdot10^9\ M^{-1}s^{-1}$;[11] at pH =3.65, $k_{-11} = 2.4\cdot10^5\ M^{-1}s^{-1}$ [11]

This mixture reacts with the H_2O_2 formed by the pulse and the excess Cu^{I} is long-lived.[6,11] The mixture of Cu^{+}_{aq}, Cu^{I}(HOOCCH=CHCOO$^-$) ($K = 8.7\cdot10^3\ M^{-1}$ at pH = 3.0 [11] and $Cu^{I}(CH_3CN)_n^+$ thus reaches equilibrium within less than 50 μs after the pulse.

The complex Cu^{I}(HOOCCH=CHCOO$^-$) has an absorption band at λ_{max} = 346 nm.[11] When $(0.5-4.0)\cdot10^{-2}$ M trichloroacetic acid is added to the solutions the disappearance of Cu^{I}(HOOCCH=CHCOO$^-$) is observed within several hundreds of seconds.

The kinetics of this process were followed spectrophotometrically, using the M→L charge transfer band of the complex Cu^{I}(HOOCCH=CHCOO$^-$). The kinetics obey a first-order rate law, i.e. the reaction exhibits a first-order dependence on the concentration of Cu^{I}. The observed rate of this process is proportional to the concentration of the trichloroacetate, Figure 1, and decreases with the increase in the acetonitrile concentration, Figure 2. In order to obtain an upper limit for the rate constant of the reaction between $Cu^{I}(CH_3CN)_2^+$ and Cl_3CCOO^-, the rate was measured in solutions containing high concentrations of acetonitrile [$(0.05-1.5)\cdot10^{-1}$ M] in the presence of three different concentrations of fumarate ($2.0\cdot10^{-4}$, $6\cdot10^{-4}$ and $2\cdot10^{-3}$ M) at a constant concentration of Cl_3CCOO^- ($2.0\cdot10^{-2}$ M). The results are presented in Figure 2. The results demonstrate that the rate decreases as the concentration of acetonitrile is increased and seems to approach a limiting value, at [CH_3CN] = 0.15 M the same k_{obs} ($3.0\cdot10^{-3}$ s^{-1}) is measured for the three systems. In these systems at [CH_3CN] = 0.15 M, between 96.5% (for [fumarate] = $2.0\cdot10^{-3}$ M) and 99.5% (for [fumarate] = $2.0\cdot10^{-4}$ M) of the Cu^{I} is present in the form of the $Cu^{I}(CH_3CN)_2^+$,

$Cu^{I}(CH_3CN)_3^+$ and less than 0.2% Cu^+_{aq} in the latter system. The calculated rate of the reaction between $Cu^{I}(CH_3CN)_2^+$ and Cl_3CCOO^- is $k_{11} = 0.15$ $M^{-1}s^{-1}$, which is considerably higher than that which can be attributed to Cu^+_{aq} present in these solutions.

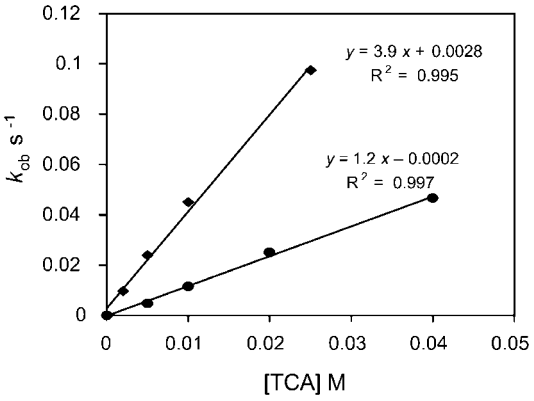

Figure 1. Dependence of the rate of the disappearance of Cu^{I}-(HOOCCH=CHCOO$^-$) on $[Cl_3CCO_2^-]$; ■ N_2O saturated solutions, containing $5\cdot10^{-2}$ M $CuSO_4$, $2\cdot10^{-4}$ M fumaric acid, 1 M CH_3OH and $0.1-2.5\cdot10^{-2}$ Cl_3CCO_2H at pH = 3.0; • same solution but with 0.02 M CH_3CN

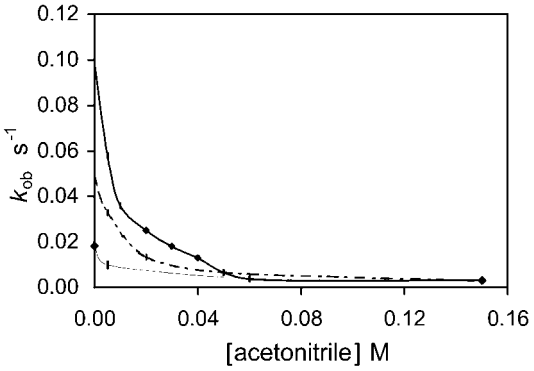

Figure 2. Dependence of the observed rate constant on $[CH_3CN]$; solution composition: N_2O saturated, containing $5\cdot10^{-2}$ M $CuSO_4$, $(0.2-2.0)\cdot10^{-4}$ M fumaric acid: ····· $2.0\cdot10^{-3}$ M, –·–·– $6.0\cdot10^{-4}$ M, —— $2.0\cdot10^{-4}$ M, 0–0.15 M CH_3CN, 1 M CH_3OH and $2.0\cdot10^{-2}$ Cl_3CCO_2H at pH = 3.0

$$Cu(CH_3CN)_n^+ + Cl_3CCOO^- \rightarrow {}^{\cdot}CCl_2CO_2^- + Cu(CH_3CN)_nCl^+ \quad (12)$$

As reaction (2) and/or (12) are the rate-determining steps the observed rate equals $2k_{12}$, therefore $k_{12} = 0.075 \pm 0.011$ $M^{-1}s^{-1}$ for $Cu(CH_3CN)_2^+$. The reaction mechanism is analogous to reactions (1)–(6). Reaction (2) occurs via Cu^+_{aq} and/or via the $Cu^{I}(CH_3CN)_n^+$ reaction (12). The rate of reaction is independent of the concentration of all other components of the solution (i.e. of $[CuSO_4]$, $[CH_3OH]$) and the pulse intensity. Analysis of the results presented in Figure 1, remembering that k [Cu^{I}(HOOCCH=CHCO$_2^-$) + $Cl_3CCO_2^-$] < 0.015 $M^{-1}s^{-1}$ and k[$Cu^{I}(CH_3CN)^+_2$ + $Cl_3CCO_2^-$] = 0.075 $M^{-1}s^{-1}$, indicates that the contribution of Cu^+_{aq} to the observed rate is 0.24 s^{-1}, therefore a rate of 0.96 s^{-1} has to the attributed to the reaction of $Cu^{I}(CH_3CN)^+$ with $Cl_3CCO_2^-$.

The kinetics are then described by the following equations:

$Cu^+_{aq} + L \rightleftarrows Cu^{I}L$
(L = fumarate)
$Cu^+_{aq} + n\ CH_3CN \rightleftarrows Cu^{I}(CH_3CN)^{n+}$

$$Cu^{I}(CH_3CN)^+ + TCA \xrightarrow{k_2} P$$

(TCA = trichloroacetate; P = products)
$d[P]/dt = k_2[Cu^{I}]_T[TCA]$
$K_1 = [Cu^{I}L]/[Cu^+_{aq}][L]$, $\beta_1 = [Cu^{I}(CH_3CN)^+]/[Cu^+_{aq}][CH_3CN]$, $\beta_2 = [Cu^{I}(CH_3CN)_2^+]/[Cu^+_{aq}][CH_3CN]^2$
$[Cu^{I}]_T = [Cu^+_{aq}] + [CuL] + [Cu^{I}(CH_3CN)^+] + [Cu^{I}(CH_3CN)_2^+]$

Inserting the known values of K_1, β_1, β_2, [L] and $[CH_3CN]$, one obtains $k_2 = 0.62 \pm 0.012$ $M^{-1}s^{-1}$ for $Cu^{I}(CH_3CN)^+$.

NH_3

In order to measure the rate of reaction between $Cu^{I}(NH_3)_2^+$ and Cl_3CCOO^-, Ar-saturated solutions containing $5.0\cdot10^{-4}$ M or $1.0\cdot10^{-3}$ M Cu^{I} and 1.0 M NH_3 were prepared. Under these conditions the Cu^{I} complex present in the solution is $Cu^{I}(NH_3)_2^+$ due to equilibrium (13).

$$Cu^+_{aq} + 2\ NH_3 \rightleftarrows Cu^{I}(NH_3)_2^+ \quad (13)$$
$$\log \beta_2 = 10.4^{[14]}$$

These solutions were mixed in a fast-mixing cell with Ar-saturated solutions containing $(0.1-1.0)\cdot10^{-2}$ M Cl_3CCOO^-. Soon after the mixing, the formation of an absorption band at $\lambda = 620$ nm, typical for $Cu^{II}(NH_3)_4^{2+}$,[5] was observed. The kinetics of this process obey a first-order rate law, i.e. the reaction exhibits a first-order dependence on the concentration of Cu^{I}. The observed rate is propor-

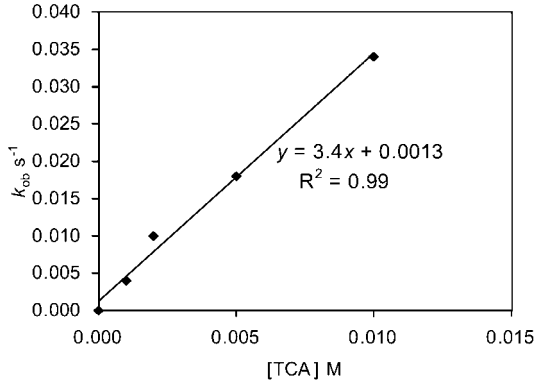

Figure 3. Dependence of the observed rate constant on $[Cl_3CCO_2^-]$; solution composition: Ar-saturated, containing $1.0\cdot10^{-3}$ M Cu^{I}, 1 M NH_3 and $(0.1-1.0)\cdot10^{-2}$ M $Cl_3CCO_2^-$ at pH = 11.0

tional to the concentration of the trichloroacetate, Figure 3. The kinetic equations that describe this system are as follows:

$$\begin{aligned} &Cu(NH_3)_2^+ + TCA \rightarrow P \\ &(P = \text{products}) \\ &d[P]/dt = k_{14}[Cu(NH_3)_2^+][TCA], [TCA] >> \\ &[Cu(NH_3)_2^+], k_{obs} = k_{14}[TCA] \end{aligned} \quad (14)$$

The rate constant is calculated from the slope of the line in Figure 3 as $k = 3.4 \pm 0.5$ M^{-1}s^{-1}. The yield of $Cu^{II}(NH_3)_4^{2+}$, measured in solutions containing an excess of Cu^I in comparison to Cl_3CCOO^-, is in agreement with the expected ratio $Cu^{II}(NH_3)_4^{2+}$/TCA = 2. These results are in agreement with the mechanism described in reactions (2)−(6). Equation (14a) is analogous to reaction (2).

$$Cu(NH_3)_2^+ + ClCCOO_2^- \rightarrow {}^{\cdot}CCl_2CO_2^- + Cu(NH_3)_2Cl^+ \quad (14a)$$

As reaction (14a) is the rate-determining step the observed rate equals $2k_{14}$, therefore $k_{14a} = 1.7 \pm 0.25$ M^{-1}s^{-1}.

L^1

L^1 forms a complex with Cu^I according to Equation (15).

$$\begin{aligned} &Cu^+_{aq} + L^1 \rightleftarrows (CuL^1)^+ \\ &\log K = 11.94^{[7]} \end{aligned} \quad (15)$$

In order to measure the rate of the reaction between $(CuL^1)^+$ and Cl_3CCOO^-, Ar-saturated solutions containing $1.0 \cdot 10^{-3}$ M $(CuL^1)^+$ at pH = 7.0 were prepared. These solutions were mixed in a fast-mixing cell with Ar-saturated solutions containing $(0.16-2.0) \cdot 10^{-1}$ M Cl_3CCOO^-. After mixing, the disappearance of the absorption band at $\lambda = 236$ nm, due to $[CuL^1]^+$,[7] is observed. The kinetics of this process obey a first-order rate law for the concentration of Cu^I. The observed rate is proportional to the concentration of trichloroacetate, Figure 4. The rate constant calculated from the slope of the line in Figure 4, $k = 0.27 \pm 0.04$ M^{-1}s^{-1}. The yield of $[CuL^1]^{2+}$, measured in solutions containing an excess of Cu^I, is in agreement with the expected ratio $[CuL^1]^{2+}$/TCA = 2. Thus, for each mol TCA two mol of $[CuL^1]^+$ are transformed into $[CuL^1]^{2+}$.

These results are in agreement with the mechanism described in reactions (2)−(6). Equation (16) is analogous to Equation (2).

$$(CuL^1)^+ + Cl_3CCOO^- \rightleftarrows {}^{\cdot}CCl_2CO_2^- + L^1Cu^{II}Cl^+ \quad (16)$$

As reaction (16) is the rate-determining step the observed rate equals $2k_{16}$, therefore $k_{16} = 0.14 \pm 0.02$ M^{-1}s^{-1}.

L^2

L^2 forms a complex with Cu^I according to Equation (17).[8]

$$\begin{aligned} &Cu^+_{aq} + L^2 \rightleftarrows [CuL^2]^+ \\ &\log K = 13.40 \end{aligned} \quad (17)$$

In order to measure the rate of the reaction between $(CuL^2)^+$ and Cl_3CCOO^-, the stopped-flow technique was used. Ar-saturated solutions containing $8.0 \cdot 10^{-4}$ M $(CuL^2)^+$ at pH = 6.5 were mixed with Ar-saturated solutions containing $(0.5-2.0) \cdot 10^{-1}$ M Cl_3CCOO^- and 0.5 M $NaClO_4$ at the same pH. After the mixing, two processes were observed (Figure 5). The first process, the formation of an absorption band at $\lambda = 350$ nm, occurs within a few seconds. The second process, the disappearance of the absorption band formed in the first process, occurs within several tens of seconds. The kinetics of the first process obey a first-order rate law in the concentration of Cu^I. The observed rate is proportional to the concentration of trichloroacetate (Table 1). The kinetics of the second process obey a first-order rate law and do not depend on the composition of the solutions, within the experimental error.

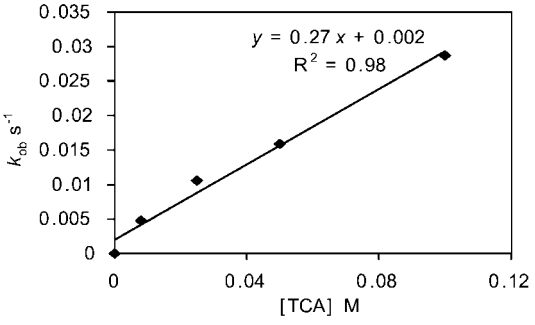

Figure 4. Dependence of the observed rate constant on $[Cl_3CCO_2^-]$; solution composition: Ar-saturated, containing $5.0 \cdot 10^{-4}$ M $(Cu^IL^1)^+$ and $(0.08-1.0) \cdot 10^{-1}$ M $Cl_3CCO_2^-$ at pH = 7.0

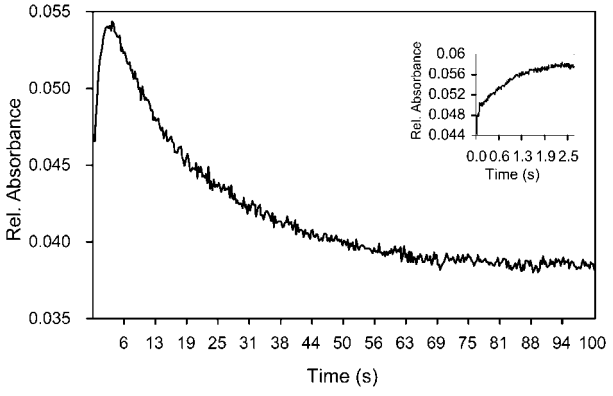

Figure 5. Computer output of the absorbance vs. time; experimental conditions: Ar-saturated solutions containing $8.0 \cdot 10^{-4}$ M $(CuL^2)^+$ at pH = 6.5 were mixed with Ar-saturated solutions containing 0.02 M $Cl_3CCO_2^-$ and 0.5 M $NaClO_4$ at the same pH measured at $\lambda = 350$ nm

Table 1. Observed rate constants in the L^2 system under different conditions; k_1: the observed rate constants of the first process (error limits ± 0.10); k_2: the observed rate constants of the second process (error limits ± 0.01)

	$[Cu^{I}L^2]^+$ $4.0\cdot10^{-4}$ M		$[Cu^{I}L^2]^+$ $4.0\cdot10^{-4}$ M $[Cu^{II}L^2]^{2+}$ $2.5\cdot10^{-4}$ M		$[Cu^{I}L^2]^+$ $4.0\cdot10^{-4}$ M $[Cu^{II}L^2]^{2+}$ $2.0\cdot10^{-3}$ M	
[TCA]	k_1 [s^{-1}]	k_2 [s^{-1}]	k_1 [s^{-1}]	k_2 [s^{-1}]	k_1 [s^{-1}]	k_2 [s^{-1}]
0.025	0.37	0.02	1.4	0.03	0.44	0.03
0.050	0.70	0.03	1.9	0.05	0.74	0.04
0.10	1.4	0.05	3.4	0.07	1.5	0.06

The effect of $[CuL^2]^{2+}$ on the rate of the processes was measured. Ar-saturated solutions containing $8.0\cdot10^{-4}$ M $[CuL^2]^+$ and $(0.5-4.0)\cdot10^{-3}$ M $[CuL^2]^{2+}$ at pH = 6.5 were mixed with Ar-saturated solutions containing $(0.5-2.0)\cdot10^{-1}$ M Cl_3CCOO^- and 0.5 M $NaClO_4$ at the same pH. The results are summed up in Table 1. The results show that the presence of $[CuL^2]^{2+}$ in similar concentrations as to those of $[CuL^2]^+$ accelerates the rate of the first process. However, in the presence of an excess of $[CuL^2]^{2+}$, in comparison to $[CuL^2]^+$, the rate of the first process is similar to that obtained in the absence of $[CuL^2]^{2+}$. The rate constant of the second process is independent of $[CuL^2]^{2+}$ within the experimental accuracy. The yield of Cl^- was determined and equals half the concentration of Cu^{I}. The yield of Cl^- is independent of the concentration of $[CuL^2]^{2+}$.

Based on these results and on the assumption that the absorption band at $\lambda = 350$ nm is due to the formation of the transient complex $L^2Cu^{II}-CCl_2CO_2^-$ (complexes with $Cu^{II}-C$ σ-bonds are known to absorb in this wavelength region[15]) it is reasonable to propose that the following reactions and kinetic equations describe the system:

$$Cu(I)L + RX \xrightarrow{k_I} Cu(II)L + {}^{\cdot}R + X^- \quad (I)$$

$(L - L^2, X - Cl^-, RX - ClC(Cl)_2CO_2^-)$

$$^{\cdot}R + Cu(I)L \xrightarrow{k_{II}} LCu(II)\text{-}R \quad (II)$$

$$^{\cdot}R + LCu(II)\text{-}R \xrightarrow{k_{III}} Cu(I)L + R_2 \quad (III)$$

$$^{\cdot}R + Cu(II)L \xrightarrow{k_{IV}} LCu(III)\text{-}R \quad (IV)$$

$$Cu(I)L + LCu(III)\text{-}R \xrightarrow{fast} LCu(II)\text{-}R + Cu(II)L \quad (V)$$

$$LCu(II)\text{-}R + H_3O^+ \xrightarrow[very\ slow]{k_{VI}} Cu(II)L + RH \quad (VI)$$

$k_{VI} = 0.04 \pm 0.02\ s^{-1}$

$$d[LCu(II)\text{-}R]/dt = k_{II}[^{\cdot}R][Cu(I)L] - k_{III}[^{\cdot}R][LCu(II)\text{-}R] + k_{IV}[^{\cdot}R][Cu(II)L]$$

Applying the steady-state assumption for $[^{\cdot}R]$:

$$d[^{\cdot}R]/dt = k_I[Cu^{I}L][RX] + (k_{II}[Cu^{I}L] + k_{III}[LCu^{II}-R] + k_{IV}[Cu^{II}L])[^{\cdot}R] = 0$$

$$[^{\cdot}R] = k_I[Cu^{I}L][RX]/(k_{II}[Cu^{I}L] + k_{III}[LCu^{II}-R] + k_{IV}[Cu^{II}L])$$

$$d[Cu^{II}-R]/dt = (k_{II}[Cu^{I}L] - k_{III}[Cu^{II}-R] + k_{IV}[Cu^{II}L])k_I[Cu^{I}L][RX]/(k_{II}[Cu^{I}L] + k_{III}[LCu^{II}-R] + k_{IV}[Cu^{II}L])$$

The latter rate law is in agreement with the experimental observations:

a) At low $[Cu^{II}L]$ the contribution of k_{IV} $[Cu^{II}L]$ to the nominator is larger than to the denominator as $(k_{II}[Cu^{I}L] + k_{III}[LCu^{II}-R]) > (k_{II}[Cu^{I}L] - k_{III}[LCu^{III}-R])$. It should be noted that $[Cu^{II}L]$ is always > 0 as it is formed in reaction (I).

b) At high $[Cu^{II}L]$, i.e. when $k_{IV}[Cu^{II}L] >> (k_{II}[Cu^{I}L] + k_{III}[LCu^{II}-R])$ the rate law is reduced to $d[Cu^{II}-R]/dt = k_I[Cu^{I}L][RX]$ and therefore it is concluded that the large error limit is due to the observation that $k_{IV}[Cu^{II}L]$ is still not large enough and that $[Cu^{II}L] > 0$ even when no $Cu^{II}L$ was added to the solutions.

$$(CuL^2)^+ + Cl_3CCOO^- \rightarrow {}^{\cdot}CCl_2CO_2^- + Cu(L^2)Cl^+ \quad (18)$$

$k_{18} = 7.0 \pm 2.0\ M^{-1}s^{-1}$

Volume of Activation

The volume of activation of reaction (2) for $Cu^+{}_{aq}$ was derived by measuring the pressure effect on the rate of this reaction in the presence of fumarate as the rate constant for the reaction of Cu^{I}(fumarate) with Cl_3CCOO^- is too slow to be measured.[6] The volume of activation was derived analogously to the method used for the reaction of $Cu^+{}_{aq}$ with O_2.[9] The observed volume of activation $\Delta V_2^{\neq}(Cu^+{}_{aq})_{obs} = -9.9 \pm 1.0$ mL/mol. However, as $\Delta V_1^0 = -4.5 \pm 1.0$ mL/mol one calculates $\Delta V_2^{\neq}(Cu^+{}_{aq}) = -14.4 \pm 2.0$ mL/mol. This result clearly demonstrates that reaction (2) proceeds via an associative transition state in agreement with expectations.

Ligand Effects on the Reactivity of $Cu^{I}L$

Before analyzing the ligand effect on the reaction mechanism and kinetics, the thermodynamics of the chlorine ab-

straction, the rate-determining step in most of the systems studied, should be considered.

The ΔH of the reactions between Cu^{I} and Cl_3CCOO^- in aqueous solution can be roughly estimated using the equation $\Delta H = \Delta H(Cl{-}CCl_2) - \Delta H^0_f(Cl_g) - \Delta H^0_f(Cl^-_{aq}) + [\Delta H^0_f(Cu^{2+}_{aq}) - \Delta H^0_f(Cu^+_{aq})]$. Thus $\Delta H = 3.5$ kcal mol^{-1} and $\Delta H = -2.7$ kcal mol^{-1} is obtained for Cu^+_{aq} and $[Cu^{I}L^2]^+$, respectively. [The calculation is based on data from ref.[16] assuming that the solvation energy of the radical $^{\cdot}CCl_2CO_2^-$ does not differ considerably from that of Cl_3CCOO^-. The ΔH calculation for $(Cu^{I}L^2)^+$ is based on the redox potential of the complex assuming a small ΔS value for this redox process.]

The small free energy gain, if any, in these reactions in combination with the low rates for the self exchange rate of Cu^{I} [$k(Cu^+_{aq}/Cu^{2+}_{aq}) = 5{\cdot}10^{-7}$ M^{-1}s^{-1}][17] and the probably low self exchange rate for the couple $Cl_3CCOO^-/{}^-Cl_3CCOO^-$ suggests that reaction (2) proceeds by the inner sphere mechanism and not by the outer sphere mechanism. The large negative volume of activation measured for reaction (2) verified this expectation.

Since the Cu^{I} complexes act as reducing agents in these reactions with Cl_3CCOO^- it seemed reasonable to expect that the rate constants of these reactions will be correlated to the redox potential of the $Cu^{II/I}L$ couples. The measured rate constants of these reactions for the different complexes and their redox potentials are summed up in Table 2. The results point out that there is no simple correlation between the redox potentials of the Cu^{I} complexes and the observed rate constants. The results thus demonstrate that the rate of this reaction also depends on other factors; in the following paragraphs these effects are discussed.

Table 2. A comparison between the rate constants of the reaction of the Cu^{I} complexes with that of $Cl_3CCO_2^-$ along with their redox potentials

Complex	k [M^{-1}s^{-1}][a]	$E^0_{Cu(II)L/Cu(I)L}$ [V]
Cu^+_{aq}	6.0	0.15
$(Cu^{I}L^2)^+$	7.0	−0.12[b]
$Cu^{I}(NH_3)_2^+$	1.2	0.032[c]
$Cu^{I}(CH_3CN)^+$	0.62	0.34[c]
$(Cu^{I}L^1)^+$	0.14	−0.035[d]
$Cu^{I}(CH_3CN)_2^+$	0.075	0.41[c]
Cu^{I}(fumarate)$^+$ [e]	< 0.015	0.38[c]

[a] The error limits for the rate constants are ± 15%. [b] Data taken from ref.[8] [c] The redox potentials were calculated using the stability constants of the complexes (error limits ± 10%). [d] Data taken from ref.[7] [e] Data taken from ref.[4]

$Cu^{I}(CH_3CN)^+$ and $Cu^{I}(CH_3CN)_2^+$ are weaker reducing agents than Cu^+_{aq} and indeed their rates of reaction with Cl_3CCOO^- are considerably smaller than that of Cu^+_{aq}, as expected. (However, other factors might contribute to the low reactivity of $Cu^{I}(CH_3CN)_2^+$, see below.)

Though $(Cu^{I}L^1)^+$ is a better reducing agent than $Cu^{I}(NH_3)_2^+$ its reactivity is lower. This observation is probably due to the steric hindrance imposed by the ligand. The reaction of $(Cu^{I}L^2)^+$ with Cl_3CCOO^- probably first requires a ligand exchange step, most likely a release of the alkene bonding. Still the rate of this reaction is similar to that of Cu^+_{aq} and 45 times faster than that of $(Cu^{I}L^1)^+$ despite the steric hindrance that the L^2 ligand imposes on the central copper cation. This is attributed to the redox potential of $(Cu^{I}L^2)^+$.

$Cu^{I}(NH_3)_2^+$ is a considerably stronger reducing agent than Cu^+_{aq}; however, $Cu^{I}(NH_3)_2^+$ is considerably less reactive towards Cl_3CCOO^- than Cu^+_{aq}. This observation is attributed to the fact that when the linear $Cu^{I}(NH_3)_2^+$ complex, which has an sp hybridization, reacts with Cl_3CCOO^- in an inner sphere process the hybridization has to be changed, probably to an sp^3 one, a process which costs energy and therefore slows down the reaction. A similar argument probably contributes to the low reactivity of $Cu^{I}(CH_3CN)_2^+$. On the other hand Cu^+_{aq} is $Cu(H_2O)_4^+$,[18] i.e. it has an sp^3 hybridization and the reaction probably proceeds by a ligand exchange step followed by the chlorine abstraction.

The complex $Cu^{I}(HOOCCH{=}CHCOO^-)$ is the least reactive complex towards Cl_3CCOO^- though it is a better reducing agent than $Cu^{I}(CH_3CN)_2^+$. The low reactivity of $Cu^{I}(HOOCCH{=}CHCOO^-)$ is attributed to the fact that the Cu^{I} forms a d-π* complex with the fumarate. This type of binding reduces the electron density in the position *trans* to the ligand and therefore decreases the complex reactivity. A similar phenomenon was found for the reaction between $Cu^{I}(HOOCCH{=}CHCOO^-)$ and dioxygen.[9]

Finally it should be pointed out that if $[Cu^{I}L^2]^+$ would be used under catalytic conditions the rate-determining step would not be the chlorine abstraction reaction but the decomposition of $L^2Cu^{II}{-}R$ which might complicate the reaction mechanism as reactions of $^{\cdot}R$ with $L^2Cu^{II}{-}R$ are plausible.[8] The stabilization of $L^2Cu^{II}{-}R$ is attributed to the redox potential of the $(CuL^2)^{2+/+}$ couple. Thus, the results point out that the cathodic shift of the redox potential of the $Cu^{II/I}$ couple might in some cases complicate catalytic processes. The transient $L^2Cu^{II}{-}CCl_2CO_2^-$ is the most stable LCu^{II}-alkyl complex in aqueous solution, observed to date.[15,19]

Conclusion

The implications of the results, presented in this study, on catalytic processes catalyzed by Cu^{I} complexes, in which the redox step is the rate-determining step, are:

1. Solvents such as acetonitrile, that form complexes with Cu^{I} and anodically shift its redox potential, decrease the reactivity. Therefore, in catalytic systems, the use of solvents that do not form Cu^{I} complexes will considerably improve the rate of the processes.

2. The observation that the $Cu^{I}(HOOCCH{=}CHCOO^-)$ complex reacts considerably slower than Cu^+_{aq} with Cl_3CCOO^- suggests that it would be advantageous to work in catalytic systems, which are all carried out in organic solvents, in the absence of a large excess of alkenes.

3. Ligands such as L^1 and L^2, which have substituents that bind to the central cation only in its uncommon oxida-

tion state, might be used to improve the properties of processes that are redox-catalyzed.

4. Even ligands that accelerate the rate of the redox step might slow down the catalytic processes if they stabilize one of the intermediates in the catalytic process.

Experimental Section

Materials: All solutions were prepared from A. R. grade chemicals and from distilled water further purified by passing through a Milli Q Millipore setup, final resistivity > 10 MΩ/cm. L^1 and L^2 were synthesized and analyzed by procedures described in refs.[7,8] Cl^- was analyzed by using a Dionex ion chromatograph. Solutions of $[Cu^{I}L^1]^+$ and $[Cu^{I}L^2]^+$ were prepared by the comproportionation process, reaction (19). Solid copper was added to deaerated solutions containing $CuSO_4$ and excess of L^1 or L^2 at pH = 6.5.

$$Cu^0_{(s)} + (Cu^{II}L)^{2+}_{aq} + L \rightleftarrows 2\,(Cu^{I}L)^+ \quad (19)$$

(L = L^1 or L^2)

Solutions of $Cu^{I}(NH_3)_2^+$ were prepared by comproportionation of $Cu(NH_3)_4^{2+}$ in 1 M NH_3.

Kinetic Measurements: Reactions with half lives longer than 2 s were carried out using a fast mixing cell (SFA-11 Rapid Kinetics Accessory Hi-Tech Scientific Ltd.), which was connected to a Hewlett Packard 8452A diode array spectrophotometer. Stopped flow experiments were carried out using an SX.18 Applied PhotoPhysics stopped flow that enables kinetic measurements of reactions with lifetimes of 2 ms. The detector was a 05−109 Spectra Kinetics Monochromator that enabled measurements in the range of 200−700 nm. The optical path was 10 nm.

Pulse-Radiolysis Experiments: These were carried out using the Varian 7715 linear electron accelerator of the Hebrew University of Jerusalem. The pulse duration was 0.1−1.5μs with a 200-mA current of 5-MeV electrons. The dose per pulse was 3−30 Gray. Irradiations were carried out in a 4-cm spectrosil optical cell, the analyzing light passed through the cell three times. A 150-W Xenon lamp produced the analyzing light. The experimental setup was identical to that described earlier in detail.[11] For dosimetry, an N_2O-saturated solution containing $1.0\cdot10^{-3}$ M KSCN was used. The yield of $(SCN)_2^{\cdot-}$ was measured by taking ε_{475} = 7600 $M^{-1}cm^{-1}$ and the dose per pulse was calculated assuming $G(SCN)_2^{\cdot-}$ = 6.0[20] and an optical path of 12.3 cm. High-pressure pulse-radiolysis experiments for the determination of volumes of activation were carried out using the technique recently described in detail.[21]

Acknowledgments

This study was supported in part by The Israel Science Foundation administered by The Israel Academy of Sciences and Humanities and by a grant from the Budgeting and Planning Committee of The Council of Higher Education and the Israel Atomic Energy Commission. D. M. wishes to express his thanks to Mrs. Irene Evens for her ongoing interest and support. R. v. E. is indebted to the Dozor Foundation that enabled his visit to Beer-Sheva, during which this study was performed.

[1] [1a] J. K. Kochi, *Organometallic Mechanisms and Catalysis*, Academic Press, New York, **1978**. [1b] L. Brandsma, S. F. Vasilevsky, H. D. Verkruijsse, *Application of Transition Metal Catalysis in Organic synthesis*, Springer, Berlin, **1998**. [1c] B. Cornils, W. A. Herrmann, *Applied Homogeneous Catalysis with Organometallic Compounds*, VCH, Weinheim, **1996**.
[2] M. A. Schwartz, J. D. Crowell, J. H. Musser, *J. Am. Chem. Soc.* **1972**, 4363−4364.
[3] D. Bellus, *Pure Appl. Chem.* **1985**, *57*, 1827−1838.
[4] [4a] A. Guenter, A. D. Zuberbuehler, *Chimia* **1970**, *24*, 340−342. [4b] A. D. Zuberbuhler, *Helv. Chim. Acta* **1970**, *53*, 278.
[5] F. A. Cotton, G. Wilkinson, *Advanced Inorganic Chemistry*, 4th ed., John Wiley & Sons, New York, **1980**.
[6] N. Navon, H. Cohen, D. Meyerstein, *Inorg. Chem.* **1997**, *36*, 3781−3783.
[7] N. Navon, G. Golub, H. Cohen, P. Paoletti, A. Bencini, B. Valtancoli, D. Meyerstein, *Inorg. Chem.* **1999**, *38*, 3484−3488.
[8] N. Navon, H. Cohen, P. Paoletti, A. Bencini, B. Valtancoli, D. Meyerstein, *Ind. Eng. Chem. Res.* **2000**, *39*, 3536−3540.
[9] N. Navon, H. Cohen, R. Van Eldik, D. Meyerstein, *J. Chem. Soc., Dalton Trans.* **1998**, 3663−3666.
[10] M. Freiberg, D. Meyerstein, *J. Chem. Soc., Faraday Trans. I* **1980**, *76*, 1825−1837.
[11] [11a] D. Meyerstein, *Inorg. Chem.* **1975**, *14*, 1716−1717. [11b] N. Navon, A. Masarwa, H. Cohen, D. Meyerstein, *Inorg. Chim. Acta* **1997**, *261*, 29−35.
[12] S. Goldstein, G. Czapski, R. Van Eldik, H. Cohen, D. Meyerstein, *J. Phys. Chem.* **1991**, *95*, 1282−1285.
[13] G. V. Buxton, C. V. Greenstock, W. P. Helman, A. B. Ross, *J. Phys. Chem. Ref. Data* **1988**, *17*, 513.
[14] J. F. Fisher, J. L. Hall, *Anal. Chem.* **1967**, 1550−1556.
[15] N. Navon, G. Golub, H. Cohen, D. Meyerstein, *Organometallics* **1995**, *261*, 29−35.
[16] *Handbook of Chemistry and Physics*, 60th ed. (Ed.: R. C. Weast), CRC Press, Boca Raton, FL, USA, **1979−1980**, p. D-70, F-234.
[17] M. J. Sisley, R. B. Jordan, *Inorg. Chem.* **1992**, *31*, 2880−2884.
[18] I. Persson, J. Penner-Hahn, K. O. Hodgson, *Inorg. Chem.* **1993**, *32*, 2497−2501.
[19] P. J. Chmielewski, L. Latos-Grazynski, I. Schmidt, *Inorg. Chem.* **2000**, *39*, 5475−5482.
[20] M. S. Matheson, M. L. Dorfman, *Pulse Radiolysis*, MIT Press Cambridge, MA, **1969**.
[21] R. van Eldik, D. Meyerstein, *Acc. Chem. Res.* **2000**, *33*, 207.

Received May 14, 2001
[I01177]

Reactivity of $Ph_2P(O)py$-2 with Platinum(II) Alkyl Derivatives − Building-up of a Chiral Phosphorus Atom through C,N-Cyclometallation

Giovanni Minghetti,*[a] Angelino Doppiu,[a] Sergio Stoccoro,[a] Antonio Zucca,[a] Maria Agostina Cinellu,[a] Mario Manassero,*[b] and Mirella Sansoni[b]

Keywords: Platinum / N ligands / Cyclometallation / Alkyl derivatives / Crystal structure

The reaction of $Ph_2P(O)py$-2 (HL) with methyl- and dimethylplatinum(II) derivatives afforded a series of six-membered *C,N*-cyclometallated species, [PtX(L′)(L)] (X=halide or Me; L′ = neutral ligand, e.g. SMe_2, $SOMe_2$, CO, PAr_3) arising from activation of one $C(sp^2)$–H bond of a phenyl substituent. The metallation entailed elimination of methane and caused the phosphorus atom to become chiral. The series includes the complex [Pt(Me)(CO)(L)] where the platinum atom is bonded to three different carbon atoms (C_{sp}^3, C_{sp}^2, C_{sp}). From the neutral species cationic derivatives $[Pt(L')(L'')(L)]^+$ (L′ = SMe_2, L′′ = CH_3CN; L′–L′′ = dppe; L′ = SMe_2 or $SOMe_2$, L′′ = H_2O) could be obtained. The new complexes were isolated and fully characterised by elemental analyses and spectroscopic techniques (IR, NMR, FAB-MS). The solid-state structures of [PtCl(SMe_2)(L)], [PtCl(CO)(L)], [Pt(Me)($SOMe_2$)(L)], and [Pt(SMe_2)(H_2O)(L)][BF_4] were determined by single-crystal X-ray diffraction.

Introduction

In recent years, coordination of pyridylphosphanes to typical soft acceptors such as Rh^I, Pd^{II}, or Pt^{II} has been extensively studied,[1] whereas much less investigated is the behaviour of the pyridylphosphane oxides.[2] In a previous paper we described the reactivity of palladium(II) and platinum(II) halides with the ligands $Ph_2P(O)CH(Me)py$-2 and $Ph_2P(O)CH_2py$-2.[3] We observed that they can act either as N-monodentate or N,O-*endo*-bidentate ligands to afford $[(HL)_2MX_2]$ or $[(HL)MX_2]$ adducts, respectively. In the case of $Ph_2P(O)py$-2, only a 1:1 species $[(HL)PdCl_2]$ was obtained; spectroscopic data are in agreement with a chelating behaviour to give a five-membered ring. In no case were the phenyl substituents involved; no C−H activation was observed to give cyclometallated species.

Now, following our interest in the reactivity of alkyl derivatives of platinum(II),[4] we report a study on the interaction of $Ph_2P(O)py$-2 with the methyl- and dimethylplatinum species *trans*-[PtCl(Me)(SMe_2)$_2$], $[Pt(Me)_2(\mu\text{-}SMe_2)]_2$, *trans*-[PtCl(Me)($SOMe_2$)$_2$], and *cis*-[Pt(Me)$_2$($SOMe_2$)$_2$] to afford a series of six-membered *N,C*-cyclometallated derivatives.

[a] Dipartimento di Chimica, Università di Sassari,
Via Vienna 2, 07100 Sassari, Italy
Fax: (internat.) + 39-079/212069
E-mail: mingh@ssmain.uniss.it
[b] Dipartimento di Chimica Strutturale e Stereochimica Inorganica, Università di Milano, Centro CNR,
Via Venezian 21, 20133 Milano, Italy
E-mail: m.manassero@csmtbo.mi.cnr.it

Results and Discussion

The N,O-ligand diphenyl(2-pyridyl)phosphane oxide (HL)[3] and the starting methyl- and dimethylplatinum complexes *trans*-[PtCl(Me)(SMe_2)$_2$],[5] *trans*-[PtCl(Me)-($SOMe_2$)$_2$],[6] $[Pt(Me)_2(\mu\text{-}SMe_2)]_2$,[5] and *cis*-[Pt(Me)$_2$-($SOMe_2$)$_2$][6] were obtained as previously described. The reaction of the chloro(methyl) complexes with the ligand affords compounds [PtCl(SMe_2)(L)] (**1**) and [PtCl(SO-Me_2)(L)] (**2**), respectively (see Scheme 1). Compounds **1** and **2** have been characterised by elemental analyses, conductivity measurements, FAB MS, IR, and ^1H-, and $^{31}P\{^1H\}$-NMR spectra. In the FAB MS spectra the molecular ions were observed at m/z = 570 and 586, respectively; in the IR spectra the absorption assigned to ν(P=O) is not significantly shifted with respect to the free ligand (1190 cm^{-1}), suggesting that the oxygen atom is not involved in the coordination to the platinum atom. In agreement, in the $^{31}P\{^1H\}$ NMR spectra, the resonances at δ = 31.15 (compound **1**) and 31.65 (compound **2**) are only slightly deshielded compared to that of the ligand (δ = 22.0). We have previously reported that in the adduct $[Pd(Cl)_2(HL)]$ (*N,O*-coordination) the ^{31}P resonance is strongly deshielded (δ = 60.5).

The ^1H NMR spectra allow a choice to be made between the two possible isomers having a Cl−Pt−C or a Cl−Pt−N *trans* arrangement; the H(6) proton of the pyridine ring is remarkably deshielded, as often observed for six-membered species with the chloride ligand *cis* to the nitrogen atom.[7] In addition, the very large value of $^3J_{Pt,H}$ relative to the methyl protons of SMe_2 in compound **1** supports the pres-

 © WILEY-VCH Verlag GmbH, 69451 Weinheim, Germany, 2002 1434−1948/02/0202−0431 $ 17.50+.50/0

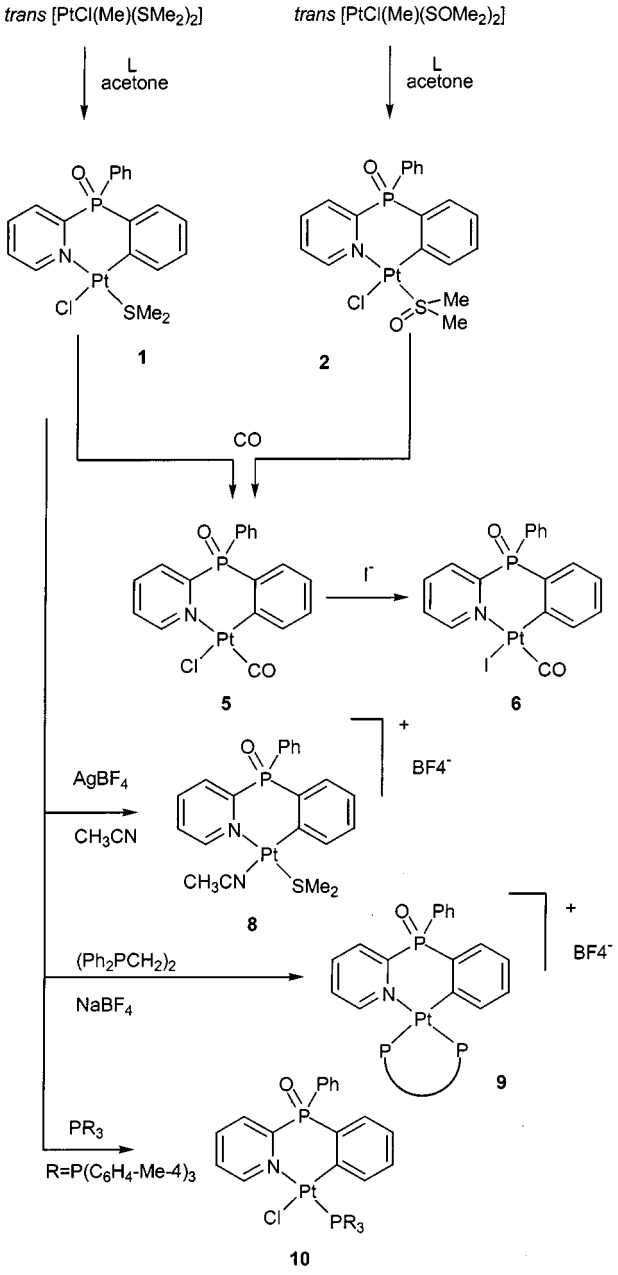

Scheme 1

ence of a ligand (in a *trans* configuration) with low *trans* influence.[8]

The methyl groups of the coordinated SMe_2 ligand are diastereotopic; one of them resonates at rather high field ($\delta = 1.63$) with respect to the other one ($\delta = 2.49$) ($\Delta\delta = 0.86$). The shift at higher field of one of the resonances is likely related to the shielding effect of the phenyl ring. In an attempt to obtain more information on the structure of compound **1** in solution, an NOE difference experiment was carried out, but failed owing to interconversion of the methyl groups, due to either dissociation/association or partially hindered rotation of the Pt−S bond.

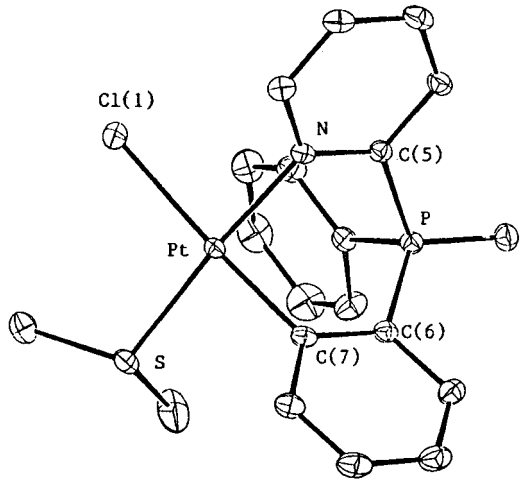

Figure 1. ORTEP view of compound **1**; thermal ellipsoids are drawn at the 30% probability level

Table 1. Selected bond lengths [Å] and angles [°] with e.s.d.s in parentheses

a) Compound **1**

Pt−Cl(1)	2.400(1)	Pt−S	2.268(1)
Pt−N	2.046(2)	Pt−C(7)	2.003(2)
Cl(1)−Pt−S	97.01(2)	Cl(1)−Pt−N	87.78(5)
Cl(1)−Pt−C(7)	176.81(7)	S−Pt−N	175.20(5)
S−Pt−C(7)	85.92(6)	N−Pt−C(7)	89.29(8)

b) Compound **5**

Pt−Cl	2.403(1)	Pt−N	2.069(3)
Pt−C(7)	2.028(3)	Pt−C(18)	1.897(4)
C(18)−O(2)	1.061(5)		
Cl−Pt−N	88.3(1)	Cl−Pt−C(7)	177.3(1)
Cl−Pt−C(18)	93.5(1)	N−Pt−C(7)	89.5(1)
N−Pt−C(18)	177.4(2)	C(7)−Pt−C(18)	88.8(2)

In the solid state, the nature of complex **1** was confirmed by X-ray diffraction. Suitable crystals were obtained by slow concentration of a $CHCl_3$ solution. The structure consists of the packing of $[PtCl(SMe_2)(L)]$ and $CHCl_3$ molecules in the molar ratio 1:1 with no unusual van der Waals contacts. An ORTEP view or the complex molecule is shown in Figure 1 and selected bond parameters are reported in Table 1.

The metal atom displays a square-planar coordination with a very slight square-pyramidal distortion, maximum distances from the best plane being −0.012(1) and +0.013(2) Å for Pt and C(7), respectively. The inner coordination sphere of the metal atom in the present compound is identical with that found in $[PtCl(SMe_2)(L^2)]$ (**13**) (HL^2= 6-*tert*-butyl-2,2′-bipyridine)[8] where the L^2 ligand is coordinated through a nitrogen atom and the C(3) atom of the substituted pyridine ring. Corresponding bond lengths involving the metal atom are all very similar in the two com-

pounds, thus, Pt−Cl = 2.400(1) (here) and 2.395(2) Å (**13**); similarly, Pt−S = 2.268(1) and 2.263(2) Å, Pt−N = 2.046(2) and 2.042(4) Å, and Pt−C = 2.003(2) and 1.990(5) Å, respectively, here and in **13**.

The Pt−N−C(5)−P−C(6)−C(7) six-membered ring is in a boat conformation, with atoms N, C(5), C(6), and C(7) strictly coplanar, and atoms Pt and P lying 1.008(1) and 0.752(2) Å above that plane, respectively. The best plane of atoms N, C(5), C(6), and C(7) forms dihedral angles of 44.4(1)° with the Pt−N−C(7) plane and of 41.2(1)° with the C(5)−P−C(6) plane.

Compound **2** is similar to **1**, having the $SOMe_2$ ligand in place of SMe_2; the ^1H NMR spectra provide evidence for the same isomer as **1** and an *S*-bonded dimethyl sulfoxide.

Both compounds **1** and **2** reacted under mild conditions with carbon monoxide to give **5**; the stretching vibration of the terminal CO is observed at a rather high value, 2122 cm^{-1} (Nujol) typical of platinum(II) species. The chloride ligand in complex **5** could be easily replaced by iodide through exchange with LiI. A lowering of ν(CO) in complex **6** [PtI(CO)L] ($\Delta\nu$ = 28 cm^{-1}) is consistent with substitution of iodide in exchange for the more electronegative chloride.

An ORTEP view of the molecular structure of **5** is shown in Figure 2, and selected bond parameters are listed in Table 1. Crystals of this compound contain molecules of **5** and water molecules in the molar ratio 1:0.667. In **5**, the Pt^{II} atom is in the usual square-planar coordination. Bond lengths and angles involving the Pt−Cl−(N,C) moiety are all very similar to those already discussed for compound **1**. The Pt−CO bond length [1.897(4) Å] is in good agreement with those found in $[Pt_2(Me)_2(CO)_2(N,C^{\wedge}C,N\text{-terpy-2H})]$[9] [1.890 Å (average of two)] and in [Pt(COPh)(Me)-(CO)(PPh_3)][10] [1.897(7) Å]. The C−O distance [1.061(5) Å] is rather short.

From compound **1**, the ligand SMe_2 could be substituted by other neutral ligands such as $P(C_6H_4\text{-Me-}4)_3$. In compound **10** the phosphane group is *trans* to the nitrogen atom as shown by the $^1J_{Pt,P}$ value of 4279 Hz.

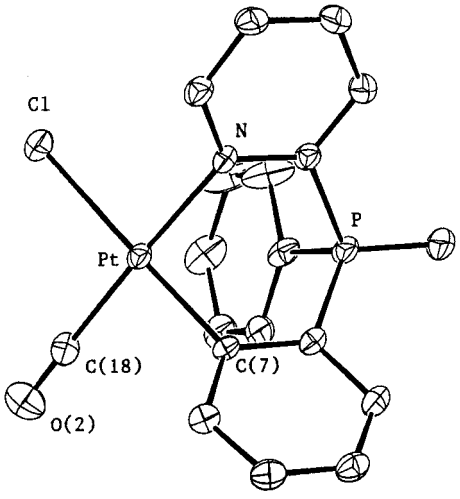

Figure 2. ORTEP view of compound **5**; thermal ellipsoids as in Figure 1

The chloride ion could be displaced by means of silver salts to give cationic species such as **8** {$[Pt(MeCN)(SMe_2)(L)][BF_4]$}, or by chelating ligands in the presence of a non-coordinating anion. Thus compound **9** {$[Pt(dppe)(L)][BF_4]$} could be easily isolated by reaction of **1** with dppe and $Na[BF_4]$ [dppe = 1,2-bis(diphenylphosphanyl)ethane]. In the cationic species **9**, in addition to the six-membered N,C-ring, a second five-membered ring was formed by chelation of dppe. The behaviour of the diphosphane is unambiguously shown by the $^{31}P\{^1H\}$ NMR spectrum. Noteworthy is the long-range coupling ($^4J_{P,P}$ = 9.2 Hz) between the ^{31}P nucleus in the C,N-cycle and the ^{31}P *trans* to the carbon atom. The molecular ion at *m/z* = 871 in the FAB mass spectrum confirms the nature of the cation.

The behaviour of the ligand HL towards the dimethyl derivatives $[Pt(Me)_2(\mu\text{-}SMe_2)]_2$ and *cis*-$[Pt(Me)_2(SOMe_2)_2]$ is similar to that observed in the case of the monoalkyl species. Indeed, metallation of a phenyl group occurs with loss of methane (Scheme 2) to give the six-membered *C*,*N*-metallated compounds **3** and **4**, respectively (Scheme 2).

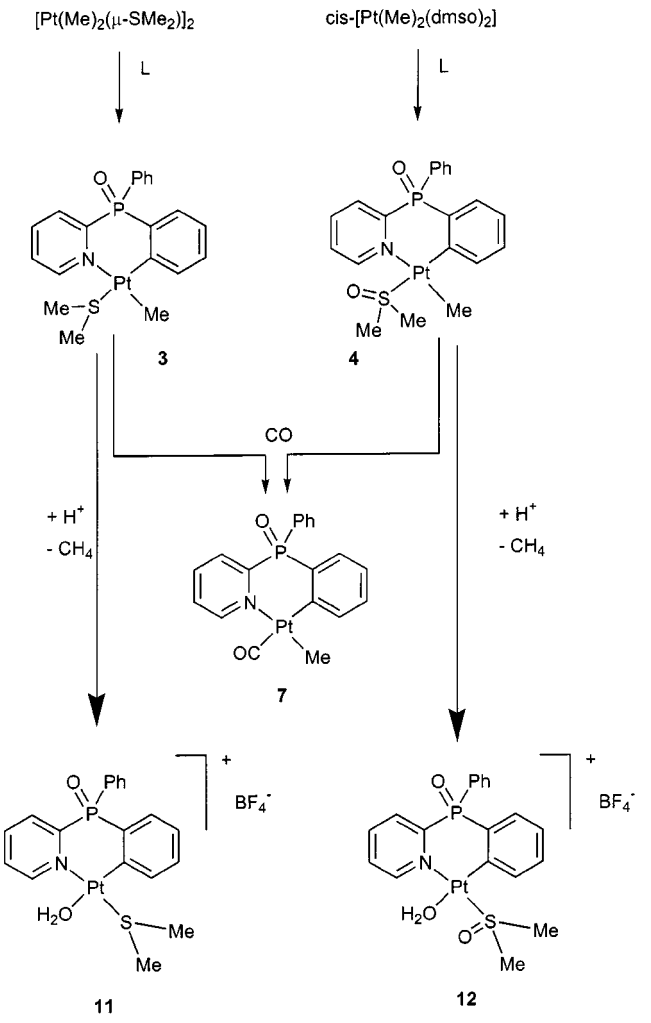

Scheme 2

One isomer only was formed having the methyl group *trans* to the nitrogen atom (as shown by ^{1}H NMR spectra). The structure in solution for **3** and **4** were ascertained by means of ^{1}H NMR NOE difference spectra, which unambiguously show that in $CDCl_3$ solution the methyl group is coordinated *trans* to the pyridine ring. For example, in the case of **3**, irradiation of the coordinated methyl group at $\delta = 0.59$ enhanced the doublet ($\delta = 7.52$) of the H *ortho* to the C(sp^2)−Pt bond. At variance, irradiation of the singlet at $\delta = 1.80$ (SMe_2) revealed contacts with the coordinated methyl group ($\delta = 0.59$) and the H(6) proton of the substituted pyridine ring ($\delta = 8.76$). Contacts among the C_6H_5 protons (two multiplets at $\delta = 7.30$ and 7.64) and the methyl group of the coordinated dimethyl sulfide suggest that in the boat conformation of the six-membered cyclometallated ring they are spatially close.

The structure consists of the packing of molecules of **4** and water molecules in the molar ratio 1:0.25. The asymmetric unity of **4**·0.25H_2O contains two crystallographically independent molecules of **4**. An ORTEP view of molecule A is shown in Figure 3. Selected bond parameters for both molecules are reported in Table 2. Corresponding bond lengths and angles in the two molecules are all very similar. Pt−N1 and Pt−S1 bond lengths (2.130 and 2.303 Å, respectively, average of two), are both elongated by the influence of the *trans*-carbon atoms. All other bond lengths and angles are normal.

Also, with these methyl species, carbon monoxide easily displaced the ligands SMe_2 or $SOMe_2$ from **3** and **4**, respectively, to afford the not trivial derivative **7** [Pt(Me)(CO)(L)] where three carbon ligands, C(sp^3), C(sp^2), C(sp) are assembled around the platinum center.

The CO ligand is coordinated *cis* to the pyridine ring as shown, inter alia, by ^{1}H NMR NOE difference spectra; irradiation of the singlet at $\delta = 0.76$ (CH_3−Pt) produced enhancement of the doublet at $\delta = 7.56$, assigned to the hydrogen atom *ortho* to the C(sp^2)−metal bond, proving that the coordinated methyl group is close in space to the metallated phenyl ring. In addition, the $^2J_{Pt,H}$ of the methyl protons (88.2 Hz) is consistent with a methyl group *trans* to a nitrogen atom.[4] Under mild conditions, no migration insertion to give an acyl group was observed.

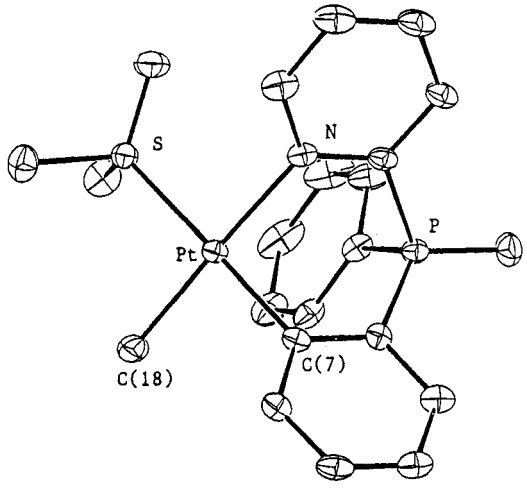

Figure 3. ORTEP view of compound **4**; thermal ellipsoids as in Figure 1

Table 2. Selected bond lengths [Å] and angles [°] with e.s.d.s in parentheses

a) Compound **4**

	Molecule A	Molecule B
Pt−S	2.305(2)	2.300(2)
Pt−N	2.139(5)	2.121(6)
Pt−C(7)	2.040(6)	2.032(6)
Pt−C(18)	2.074(8)	2.088(8)
S−Pt−N	90.8(1)	89.8(2)
S−Pt−C(7)	175.3(2)	176.9(2)
S−Pt−C(18)	91.4(2)	92.9(2)
N−Pt−C(7)	90.8(2)	88.7(2)
N−Pt−C(18)	177.7(2)	177.3(2)
C(7)−Pt−C(18)	87.0(3)	88.7(3)

b) Compound **11**

Pt−S	2.273(1)	Pt−O(2)	2.133(2)
Pt−N	2.036(3)	Pt−C(7)	1.986(3)
S−Pt−O(2)	91.2(1)	S−Pt−N	178.2(1)
S−Pt−C(7)	89.1(1)	O(2)−Pt−N	88.6(1)
O(2)−Pt−C(7)	177.9(1)	N−Pt−C(7)	91.2(1)

A remarkable result was obtained by reaction of compounds **3** and **4** with the complex acid [H_3O]-18-crown-6-[BF_4] (Scheme 2). We have preferred this acid because it is solid, easily obtainable, and can be weighted accurately so that an excess can be avoided. This excess could potentially also attack the Pt−C(sp^2) bond, destroying the cyclometallated ring. Indeed, the Pt−C(sp^3) bond is cleaved selectively with elimination of methane. In the resulting cationic derivatives, **11** and **12**, the fourth position in the coordination sphere of the platinum atom is filled by a molecule of water *trans* to the carbon atom. The isomerization observed is likely due to the remarkable difference of the lability production action (*trans* effect) between the C- and N-ligands.

Crystals of **11** suitable for X-ray diffraction were isolated from a dichloromethane solution. The structure of **11** consists of the packing of [Pt(OH_2)(SMe_2)(L)]$^+$ cations and [BF_4]$^-$ anions in the molar ratio 1:1. An ORTEP view of the cation in **11** is shown in Figure 4. Selected bond lengths and angles are listed in Table 2. The Pt−S, Pt−N, and Pt−C7 distances, 2.273(1), 2.036(3), and 1.986(3) Å, respectively, are very close to the corresponding distances already discussed for compound **1** [2.268(1), 2.046(2), and 2.003(2) Å, respectively]. The Pt−O2 bond length [2.133(2) Å] is significantly shorter than the Pt−OH_2 distance [2.186(2) Å] found in cation [Pt{C_6H_3(CH_2NMe_2)$_2$-2,6}(OH_2)]$^+$,[11] which to the best of our knowledge, is a rare example of a cyclometallated aqua complex of Pt^{II} for which a crystal structure determination has been reported.

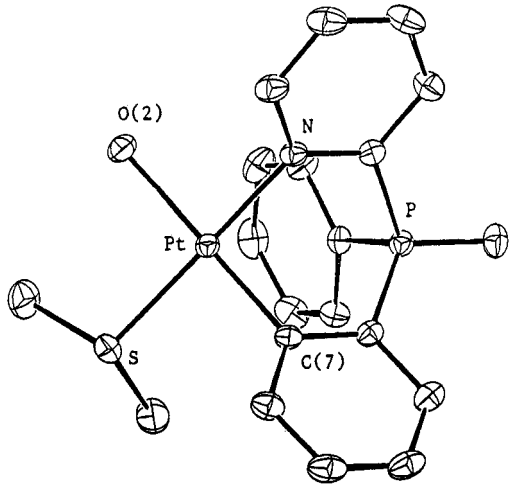

Figure 4. ORTEP view of the cation in compound **11**; thermal ellipsoids as in Figure 1

The hydrogen atoms of the coordinated water molecule are both involved in interionic hydrogen bonds, one towards the O1 phosphane oxide atom of a neighbouring cation [O2····O1 = 2.573(3) Å] and the other towards a fluorine atom of the $[BF_4]^-$ anion [O2····F1 = 2.719(4) Å], as shown in Figure 5.

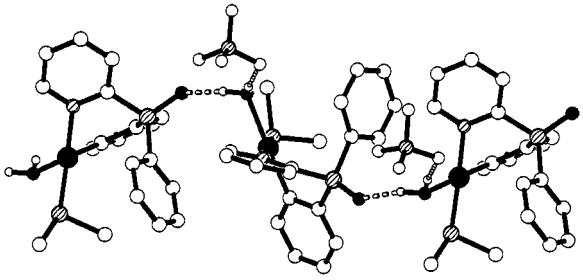

Figure 5. A view of the hydrogen-bonding network in the crystal packing of compound **11**

Conclusion

In a previous paper, we reported on the reactivity of some (2-pyridyl)phosphane oxides with platinum and palladium halides. At variance with the behaviour shown in the reaction with mono- and dimethyl derivatives, no involvement of the phenyl substituents was observed; only 1:1 or 1:2 (Pt/LH) adducts were obtained. It seems, therefore, that metallation is easier, at least in the case of platinum, when methane rather than hydrogen chloride elimination is involved. This points to methyl or methyl halide derivatives as suitable starting materials to achieve activation of $C(sp^2)-H$ bonds. It is worth underlining the fact that in this case, metallation entailed the building-up of a stereogenic centre, the phosphorus atom, inside the *C,N*-metallated ring. The behaviour of analogous intermediates of palladium(II) is currently under investigation.

Experimental Section

General: The ligand HL and the platinum complexes *trans*-$[PtCl(Me)(SMe_2)_2]$, $[Pt(Me)_2(\mu\text{-}SMe_2)]_2$, *trans*-$[PtCl(Me)(SOMe_2)_2]$, and *cis*-$[Pt(Me)_2(SOMe_2)_2]$, were obtained as previously described.[5−6] $[H_3O]$-18-Crown-6-$[BF_4]$ was synthesised as reported elsewhere.[12] All solvents were distilled and dried according to established methods. Elemental analyses were performed with a Perkin−Elmer Elemental Analyzer 240B by Mr. A. Canu (Dipartimento di Chimica, Università di Sassari). Infrared spectra were recorded with a Perkin−Elmer 983 spectrophotometer; the values are given in cm^{-1}. ^1H and $^{31}P\{^1H\}$ NMR spectra were recorded with a Varian VXR 300 spectrometer operating at 299.9 and 121.4 MHz, respectively. Chemical shifts are given in ppm relative to internal TMS (^1H) or external H_3PO_4 (^{31}P). Mass spectra were obtained with a VG 7070EQ instrument operating under FAB conditions with 3-nitrobenzyl alcohol as supporting matrix.

General Procedures: The compounds **1**−**4** were synthesised according to the following procedure. The relevant starting complex (ca. 0.1 g) and a stoichiometric amount of the ligand were dissolved in anhydrous acetone (ca. 30 mL). The solution was heated at reflux for 24 h under nitrogen, it was then concentrated to dryness. The solid was dissolved in dichloromethane (20 mL) and the resulting solution was filtered through Celite and concentrated to a small volume. Dropwise addition of *n*-hexane afforded a white crystalline solid, which was filtered off and collected. − Compound **5** was obtained in almost quantitative yield by carbonylation (p_{CO} = 1 bar) of a dichloromethane solution (5 mL) of either **1** or **2** (ca. 0.1 g) for 24 h at room temperature. Compound **7** was obtained from either **3** or **4** in quantitative yield, according to a similar procedure, but with shorter reaction time (6 h). − Compounds **11** and **12** were prepared in ca. 80% yield according to the following procedure. The relevant starting complex **1** or **2** (ca. 0.100 g), was dissolved in dichloromethane (5 mL) and a stoichiometric amount of the complex acid $[H_3O]$-18-crown-6-$[BF_4]$ was added. The solution was kept unstirred for 8 h. The white crystals that formed were washed with dichloromethane and collected.

[PtCl(SMe$_2$)(L)] (1): Yield 85%, m.p. 234−236 °C (dec.). $C_{19}H_{19}ClNOPSPt$ (570.9): calcd. C 39.96, H 3.36, N 2.45; found C 39.65, H 3.12, N 2.33. IR (Nujol): $\tilde{\nu}$ = 1583 m, 1559 m, 1196s, 692s, 545 vs, 502s, 306s, 279 s. ^1H NMR ($CDCl_3$): δ = 9.23 [dd, 1 H, $^3J_{Pt,H} \approx 49$, $^3J_{H,H}$ = 5.6, $^4J_{H,H} \approx 1$ Hz, H(6)], 8.57 (1 H, td, $^3J_{H,H}$ = 6.1 Hz), 8.1 (m, 2 H), 7.7−7.1 (m, 9 H), 2.49 (s, 3 H, $^3J_{Pt,H}$ = 53.7 Hz, SMe), 1.63 (s, 3 H, $^3J_{Pt,H}$ = 57.4 Hz, SMe). ^{31}P NMR ($CDCl_3$): δ = 31.15 (1 P, s, $^3J_{Pt,P}$ = 395.2 Hz). FAB^+: *m/z* = 570 [M^+], 535 [M − Cl], 508 [M − SMe_2], 473 [M − Cl − SMe_2].

[PtCl(SOMe$_2$)(L)] (2): Yield 89%, m.p. 242 °C (dec.). $C_{19}H_{19}ClNO_2PSPt$ (586.9): calcd. C 38.88, H 3.27, N 2.39; found C 39.06, H 3.42, N 2.35. IR (Nujol): $\tilde{\nu}$ = 1587 m, 1562 m, 1196s, 693s, 542 vs, 501s, 295 s. ^1H NMR ($CDCl_3$): δ = 9.11 [dd, 1 H, $^3J_{Pt,H} \approx 45$, $^3J_{H,H}$ = 5.6, $^4J_{H,H} \approx 1$ Hz, H(6)], 8.62 (1 H, td, $^3J_{H,H}$ = 6.1 Hz), 8.2−7.1 (m, 11 H), 3.40 (s, 3 H, $^3J_{Pt,H}$ = 23.4 Hz, OSMe), 2.55 (s, 3 H, $^3J_{Pt,H}$ = 26.0 Hz, OSMe). ^{31}P NMR ($CDCl_3$): δ = 31.65 (1 P, s, $^3J_{Pt,P}$ = 383.0 Hz). FAB^+: *m/z* = 586 [M^+], 551 [M − Cl], 508 [M − $SOMe_2$], 473 [M − Cl − $SOMe_2$].

[Pt(Me)(SMe$_2$)(L)] (3): Yield 87%, m.p. 155−160 °C. $C_{20}H_{22}NOPSPt$ (550.5): calcd. C, 43.63, H 4.04, N 2.54; found C 43.46, H 3.84, N 2.33. IR (Nujol): $\tilde{\nu}$ = 1582 m, 1562 m, 1164s, 691s, 544 vs, 494 m. ^1H NMR ($CDCl_3$): δ = 8.76 [dd, 1 H, $^3J_{Pt,H} \approx 20$, $^3J_{H,H}$ = 5.3, $^4J_{H,H}$ ca. 1 Hz, H(6)], 8.63 (1 H, td, $^3J_{H,H}$ = 6.3 Hz), 8.2−7.1 (m, 11 H), 1.80 [6 H, br. s, $S(Me)_2$], 0.59 (s, 3 H,

$^2J_{Pt,H}$ = 83.5 Hz, Pt-Me). ^{31}P NMR ($CDCl_3$): δ = 27.41 (1 P, s, $^3J_{Pt,P}$ = 351.7 Hz). FAB$^+$: *m*/*z* = 550 [M$^+$], 535 [M − Me], 488 [M − SMe_2], 473 [M − Me − SMe_2].

[Pt(Me)(SOMe$_2$)(L)] (4): Yield 90%, m.p. 183−185 °C. $C_{20}H_{22}NO_2PSPt$ (566.5): calcd. C, 42.40, H 3.92, N 2.47; found C 42.19, H 3.72, N 2.36. IR (Nujol): ṽ = 1584 m, 1562 m, 1191s, 689s, 540 vs, 504 m. ^{1}H NMR ($CDCl_3$): δ = 8.89 [d, 1 H, $^3J_{Pt,H}$ ≈ 18.1, $^3J_{H,H}$ = 5.3, $^4J_{H,H}$ ≈ 1 Hz, H(6)], 8.62 (t, 1 H, $^3J_{H,H}$ = 6.8 Hz), 8.2−7.2 (m, 11 H), 2.99 (s, 3 H, $^3J_{Pt,H}$ = 17.3 Hz, OSMe), 2.11 (s, 3 H, $^3J_{Pt,H}$ = 16.1 Hz, OSMe), 0.30 (s, 3 H, $^2J_{Pt,H}$ = 83.2 Hz, Pt-Me). ^{31}P NMR ($CDCl_3$): δ = 28.10 (1 P, s, $^3J_{Pt,P}$ = 346.4 Hz). FAB$^+$: *m*/*z* = 566 [M$^+$], 551 [M − Me], 488 [M − $SOMe_2$], 473 [M − Me − $SOMe_2$].

[PtCl(CO)(L)] (5): M.p. 221−223 °C. $C_{18}H_{13}ClNO_2PPt$ (536.8): calcd. C 40.27, H 2.44, N 2.61; found C 40.42, H 2.57, N 2.80. IR (Nujol): ṽ = 2122 vs, 1588 m, 1564 m, 1190 s, 689 s, 542 v s, 496 s, 303 s, 295 s. ^{1}H NMR ($CDCl_3$): δ = 9.09 [dd, 1 H, $^3J_{Pt,H}$ = 39.8, $^3J_{H,H}$ = 5.6, $^4J_{H,H}$ ≈ 1 Hz, H(6)], 8.69 (t, $^3J_{H,H}$ = 5.9 Hz, 1 H), 8.2 (m, 2 H), 7.8−7.2 (m, 9 H). ^{31}P NMR ($CDCl_3$): δ = 31.27 (1 P, s, $^3J_{Pt,P}$ = 322.7 Hz). FAB$^+$: *m*/*z* = 536 [M$^+$], 501 [M − Cl], 473 [M − Cl − CO].

[PtI(CO)(L)] (6): Compound **5** (0.034 g, 0.063 mmol) was dissolved in acetone (5 mL), LiI (0.025 g, 0.19 mmol) was added and the solution stirred for 1.5 h; then it was concentrated to dryness, the solid was dissolved with dichloromethane (10 mL) and the resulting solution was filtered, concentrated to small volume, and *n*-hexane (10 mL) added. The cream-yellow solid was filtered and collected. Yield 0.038 g (95%), m.p. 234−235 °C. $C_{18}H_{13}INO_2PPt$ (628.3): calcd. C 34.41, H 2.10, N 2.23; found C 34.21, H 1.91, N 2.37. IR (Nujol): ṽ = 2094 vs, 1588 m, 1562 m, 1210 s, 692 s, 542 vs, 501 s. ^{1}H NMR ($CDCl_3$): δ = 9.41 [d, 1 H, $^3J_{Pt,H}$ = 43.0, $^3J_{H,H}$ = 5.4 Hz, H(6)], 8.70 (t, $^3J_{H,H}$ = 6.3 Hz, 1 H), 8.25 (m, 1 H), 8.15 (t, $^3J_{H,H}$ = 7.8 Hz, 1 H), 7.8−7.2 (m, 9 H). ^{31}P NMR ($CDCl_3$): δ = 30.77 (1 P, s, $^3J_{Pt,P}$ = 319.7 Hz). FAB$^+$: *m*/*z* = 628 [M$^+$], 501 [M − I], 473 [M − I − CO].

[Pt(Me)(CO)(L)] (7): M.p. 195−197 °C (dec.). $C_{19}H_{16}NO_2PPt$ (516.4): calcd. C 44.19, H 3.13, N 2.71; found C 43.98, H 2.91, N 2.71. IR (Nujol): ṽ = 2051 vs, 1585 m, 1562 m, 1202 s, 693 s, 541 vs, 494 s. ^{1}H NMR ($CDCl_3$): δ = 8.86 [dd, 1 H, $^3J_{Pt,H}$ = 23.0, $^3J_{H,H}$ = 5.4, $^4J_{H,H}$ ≈ 1 Hz, H(6)], 8.73 (t, 1 H, $^3J_{H,H}$ = 6.3 Hz), 8.22−8.02 (m, 2 H), 7.7−7.2 (m, 9 H), 0.76 (s, 3 H, $^2J_{Pt,H}$ = 88.2 Hz, Me−Pt). ^{31}P NMR ($CDCl_3$): δ = 28.90 (1 P, s, $^3J_{Pt,P}$ = 292.2 Hz). FAB$^+$: *m*/*z* = 516 [M$^+$], 501 [M − Me], 473 [M − Me − CO].

[Pt(MeCN)(SMe$_2$)(L)][BF$_4$] (8): Compound **1** (0.100 g, 0.175 mmol) was dissolved in dichloromethane (10 mL), $AgBF_4$

Table 3. Crystallographic data

	1·$CHCl_3$	**5**·0·67H_2O
Empirical formula	$C_{20}H_{20}Cl_4NOPPtS$	$C_{18}H_{14.33}ClNO_{2.67}PPt$
M	690.33	548.84
Colour	colourless	pale yellow
Crystal system	monoclinic	trigonal
Space group	*C*2/*c* (no.15)	$R\bar{3}$ (no.148)
a [Å]	33.159(4)	33.736(5)
b [Å]	8.261(1)	33.736(5)
c [Å]	17.350(3)	8.645(1)
α [°]	90	90
β [°]	101.00(1)	90
γ [°]	90	120
V [Å^3]	4665.3(1.4)	8520.9(1.9)
Z	8	18
F(000)	2656	4692
D_c [g cm^{-3}]	1.966	1.925
T [K]	223	223
Crystal dimensions [mm]	0.31 × 0.39 × 0.48	0.11 × 0.14 × 0.45
μ(Mo-K_α) [cm^{-1}]	67.1	77.2
Min.−max. transmiss. factors	0.63−1.00	0.56−1.00
Scan mode	ω	ω
Frame width [°]	0.30	0.30
Time per frame [s]	20	25
No. of frames	2450	1321
Detector−sample distance [cm]	5.00	5.00
θ range [°]	3−26	3−26
Reciprocal space explored	full sphere	hemisphere
No. of reflections: total/independent	27531/5675	19256/4696
R_{int}	0.025	0.053
Final R_2, R_{2w} indices[a] (F^2, all reflections)	0.029, 0.043	0.043, 0.063
Conventional R_1 index [$I > 2\sigma(I)$]	0.016	0.028
Reflections with $I > 2\sigma(I)$	4809	3430
No. of variables	262	235
Goodness of fit[b]	0.94	0.97

[a] $R_2 = [\Sigma(|F_o^2 - kF_c^2|)/\Sigma F_o^2]$, $R_{2w}=[\Sigma w(F_o^2 - kF_c^2)^2/w(F_o^2)^2]^{1/2}$. [b] $[\Sigma w(F_o^2 - kF_c^2)^2/(N_o - N_v)]^{1/2}$, where $w = 4F_o^2/\sigma(F_o^2)^2$, $\sigma(F_o^2) = [\sigma^2(F_o^2) + (PF_o^2)^2]^{1/2}$, N_o is the number of observations, N_v the number of variables, and *P* the ignorance factor (= 0.03 for **1**·$CHCl_3$ and 0.04 for **5**·0.67H_2O).

(0.035 g, 0.180 mmol), dissolved in acetonitrile (5 mL) was added. The mixture was stirred in the absence of light for 0.5 h, then it was filtered through Celite and concentrated to about 3 mL; diethyl ether (20 mL) was added dropwise, the resulting crystalline solid was filtered off and washed with diethyl ether (3 × 5 mL). Yield 0.110 g (0.166 mmol, 95%), m.p. 198−201 °C. $C_{21}H_{22}BF_4N_2OPSPt$ (663.3): calcd. C 38.02, H 3.35, N 4.22; found C 38.02, H 3.11, N 4.09. IR (Nujol): $\tilde{\nu}$ = 2334 and 2303 m, 1588 m, 1562 m, 1205 s, 1055 vs, 696 s, 543 vs, 505 s. ^{1}H NMR ([D$_6$]acetone): δ = 9.24 [d, 1 H, $^3J_{Pt,H}$ = 47.8, $^3J_{H,H}$ = 5.9 Hz, H(6)], 8.60 (t, $^3J_{H,H}$ = 7.1 Hz, 1 H), 8.48 (t, $^3J_{H,H}$ = 7.8 Hz, 1 H), 8.04−7.10 (m, 10 H), 2.59 (s, 3 H, $^3J_{Pt,H}$ = 53.2 Hz, SMe), 2.55 (s, 3 H, MeCN), 1.76 (s, 3 H, $^3J_{Pt,H}$ = 61.0 Hz, SMe). ^{31}P NMR ($CDCl_3$): δ = 30.27 (1 P, s, $^3J_{Pt,P}$ = 384.5 Hz). FAB$^+$: *m*/*z* = 576 [M$^+$], 535 [M − MeCN], 473 [M − MeCN − SMe_2].

[Pt(dppe)(L)] [BF_4] (9): Compound **1** (0.051 g, 0.089 mmol) was dissolved in acetone (5 mL); $NaBF_4$ (0.011 g, 0.10 mmol) and dppe [1,2-bis(diphenylphosphanyl)ethane, 0.038 g, 0.095 mmol] were added. The solution was stirred for 6 h; it was then filtered and concentrated to a small volume; addition of *n*-hexane caused the precipitation of a white crystalline solid that was filtered off and collected. Yield 0.085 g (quantitative), m.p. 210 °C (dec.). $C_{43}H_{37}BF_4NOP_3Pt$ (958.6): calcd. C, 53.87, H 3.90, N 1.46; found C 53.73, H 3.67, N 1.28. IR (Nujol): $\tilde{\nu}$ = 1584 m, 1562 m, 1210 s, 1063 vs, 697 s, 534 vs, 491 s. ^{1}H NMR ([D$_6$]acetone): δ = 9.17 [1 H, br. s, $^3J_{Pt,H}$ = 37.6 Hz, H(6)], 8.70−6.70 (m, 32 H), 3.0−2.1 (m, 4 H, CH_2). ^{31}P NMR ([D$_6$]acetone): δ = 48.64 (1 P, d, $^4J_{P,P}$ = 9.2, $^1J_{Pt,P}$ = 1782 Hz), 33.12 (1 P, s, $^1J_{Pt,P}$ = 3737 Hz), 32.55 (1 P, d, $^4J_{P,P}$ = 9.2, $^3J_{Pt,P}$ = 277.0 Hz). FAB$^+$: *m*/*z* = 871 [M$^+$].

[PtCl[P(C_6H_4-Me-4)$_3$](L)] (10): Compound **1** (0.046 g, 0.081 mmol) was dissolved in dichloromethane (5 mL); P(C_6H_4-Me-4)$_3$ (0.025 g, 0.082 mmol) was added. The solution was stirred for 8 h, and then concentrated to a small volume. Addition of *n*-hexane caused the precipitation of a white crystalline solid that was filtered off and collected. Yield 0.065 g (quantitative), m.p. 195−196 °C. $C_{38}H_{34}ClNOP_2Pt$ (813.2): calcd. C 56.12, H 4.22, N 1.82; found C 55.95, H 3.99, N 1.97. IR (Nujol): $\tilde{\nu}$ = 1596 m, 1584 m, 1188 s, 694 s, 544 vs, 528 s, 512 m, 274m. ^{1}H NMR ($CDCl_3$): δ = 9.46 [1 H, br. s, $^3J_{Pt,H}$ = 31.7 Hz, H(6)], 8.56 (t, $^3J_{H,H}$ = 6.8 Hz, 1 H), 8.1−6.4 (m, 23 H), 2.33 (s, 9 H, Me). ^{31}P NMR ($CDCl_3$): δ = 31.00 (1 P, s, $^3J_{Pt,P}$ = 361.6 Hz), 10.10 (1 P, s, $^1J_{Pt,P}$ = 4279 Hz). FAB$^+$: *m*/*z* = 812 [M$^+$], 777 [M − Cl].

[Pt(H_2O)(SMe_2)(L)] [BF_4] (11): M.p. 204−206 °C (dec.). $C_{19}H_{21}BF_4NO_2PPtS$ (640.3): calcd. C 35.63, H 3.31, N 2.19; found C 34.43, H 3.11, N 2.11. IR (Nujol): $\tilde{\nu}$ = 3345 m, 1587 m, 1095

Table 4. Crystallographic data

	4·0·25H_2O	**11**
Empirical formula	$C_{20}H_{22.5}NO_{2.25}PPtS$	$C_{19}H_{21}BF_4NO_2PPtS$
M	571.04	640.32
Colour	colourless	colourless
Crystal system	monoclinic	monoclinic
Space group	*P*21/*c* (no.14)	*P*21/*n* (no.14)
a [Å]	17.326(2)	10.619(1)
b [Å]	14.451(1)	16.094(2)
c [Å]	16.925(2)	13.342(2)
α [°]	90	90
β [°]	99.45(1)	105.66(1)
γ [°]	90	90
V [Å^3]	4180.1(8)	2195.5(5)
Z	8	4
F(000)	2212	1232
D_c [g cm^{-3}]	1.815	1.937
T [K]	223	223
Crystal dimensions [mm]	0.11 × 0.17 × 0.23	0.17 × 0.17 × 0.28
μ(Mo-K_α) [cm^{-1}]	69.7	66.6
Min.−max. transmission factors	0.49−1.00	0.68−1.00
Scan mode	ω	ω
Frame width [°]	0.30	0.30
Time per frame [s]	30	25
No. of frames	1850	2450
Detector−sample distance [cm]	5.00	5.00
θ range [°]	3−26	3−26
Reciprocal space explored	full sphere	full sphere
No. of reflections: total/independent	39932/10552	27660/5624
R_{int}	0.071	0.035
Final R_2, R_{2w} indices[a] (F^2, all reflections)	0.090, 0.106	0.033, 0.054
Conventional R_1 index [$I > 2\sigma(I)$]	0.044	0.022
Reflections with $I > 2\sigma(I)$	6537	4656
No. of variables	478	271
Goodness of fit[b]	0.96	0.95

[a] $R_2=[\Sigma(|F_o^2 - kF_c^2|)/\Sigma F_o^2]$, $R_{2w} = [\Sigma w(F_o^2 - kF_c^2)^2/w(F_o^2)^2]^{1/2}$. [b] $[\Sigma w(F_o^2 - kF_c^2)^2/(N_o - N_v)]^{1/2}$, where $w = 4F_o^2/\sigma(F_o^2)^2$, $\sigma(F_o^2) = [\sigma^2(F_o^2) + (PF_o^2)^2]^{1/2}$, N_o is the number of observations, N_v the number of variables, and *P* the ignorance factor (= 0.06 for **4**·0.25H_2O and 0.04 for **11**).

vs, 696 s, 543 vs, 505 s. ^{1}H NMR ([D$_3$]acetonitrile): δ = 8.94 [d, 1 H, $^3J_{Pt,H}$ = 41.7, $^3J_{H,H}$ = 5.4 Hz, H(6)], 8.60−7.20 (m, 12 H), 2.41 (s, 3 H, $^3J_{Pt,H}$ = 55.2 Hz, SMe), 1.63 (s, 3 H, $^3J_{Pt,H}$ = 61.3 Hz, SMe). ^{31}P NMR ([D$_3$]acetonitrile): δ = 30.69 (1 P, s, $^3J_{Pt,P}$ = 388.3 Hz).

[Pt(H$_2$O)(SOMe$_2$)(L)] [BF$_4$] (12): M.p. 212−216 °C (dec.). $C_{19}H_{21}BF_4NO_3PPtS$ (656.3): calcd. C 34.76, H 3.23, N 2.13; found C 34.53, H 3.01, N 2.16. IR (Nujol): $\tilde{\nu}$ = 3345 m, 1588 m, 1562 m, 1176 s, 1090 vs, 695 s, 543 vs, 505 s. ^{1}H NMR ([D$_3$]acetonitrile): δ = 8.93 [d, 1 H, $^3J_{Pt,H}$ = 45.6, $^3J_{H,H}$ = 5.7 Hz, H(6)], 8.60−7.20 (m, 12 H), 3.09 (s, 3 H, $^3J_{Pt,H}$ = 24.5 Hz, OSMe), 2.47 (s, 3 H, $^3J_{Pt,H}$ = 32.0 Hz, OSMe). ^{31}P NMR ([D$_3$]acetonitrile): δ = 30.00 (1 P, s, $^3J_{Pt,P}$ = 384.5 Hz). FAB$^+$: *m*/*z* = 551 [M − H$_2$O], 473 [M − H$_2$O − SOMe$_2$].

X-ray Data Collection and Structure Determinations: Crystal data and other experimental details are summarized in Tables 3 and 4. The diffraction experiments were carried out with a Bruker SMART CCD area-detector diffractometer at 223 K using Mo-K_α radiation (λ = 0.71073 Å) with a graphite crystal monochromator in the incident beam. Cell parameters and orientation matrices were obtained from the least-squares refinement of 124 (for **1**·CHCl$_3$), 123 (for **5**·0.67H$_2$O), 59 (for **4**·0.25H$_2$O), and 112 (for **11**) reflections measured in three different sets of 15 frames each, in the range $3° < \theta < 23°$. At the end of data collections the first 50 frames, containing 417, 334, 335, and 267 reflections (for **1**·CHCl$_3$, **5**·0.67H$_2$O, **4**·0.25H$_2$O, and **11**, respectively) were recollected to have a monitoring of crystal decay, which was not observed, so no time-decay correction was needed. The collected frames were processed with the software SAINT,[13] and an empirical absorption correction was applied (SADABS)[14] to the collected reflections. Scattering factors and anomalous dispersion corrections were taken from ref.[15] The calculations were performed with a Pentium III PC using the Personal Structure Determination Package,[16] and the physical constants tabulated therein. The structures were solved by Patterson and Fourier methods and refined by full-matrix least squares, using all reflections and minimizing the function $\Sigma w(F_o^2 - k|F_c|^2)^2$ (refinement on F^2). Anisotropic thermal factors were refined for all the non-hydrogen atoms. The hydrogen atoms of the coordinated water molecule in **11** were detected in the final Fourier maps and not refined. The hydrogen atoms of the clathrate water molecules in **5**·0.67H$_2$O and **4**·0.25H$_2$O were neglected. All the other hydrogen atoms were placed in their ideal positions (C−H = 0.97 Å; *B* = 1.10 times that of the carbon atom to which they are attached) and not refined. The final Fourier maps show maximum residuals of 1.0(2) e/Å^3 at 0.76 Å from Pt for **1**·CHCl$_3$, 1.8(3) e/Å^3 at 0.91 Å from Pt for **5**·0.67H$_2$O, 3.0(7) e/Å^3 at 0.83 Å from Pt(A) for **4**·0.25H$_2$O, and 1.0(2) e/Å^3 at 0.89 Å from Pt for **11**. The atomic coordinates of the structure models have been deposited with the Cambridge Crystallographic Data Centre as supplementary publication no. CCDC-164381 (**1**·CHCl$_3$), -164382 (**5**·0.67 H$_2$O), -164383 (**4**·0.25 H$_2$O), -164384 **11**. Copies of the data can be obtained free of charge on application to CCDC, 12 Union Road, Cambridge CB2 1EZ, UK [Fax: (internat.) + 44-1223/336-033; E-mail: deposit@ccdc.cam.ac.uk].

Acknowledgments

Financial support from Università di Sassari and RAS (Regione Autonoma della Sardegna) is gratefully acknowledged.

[1] [1a] G. R. Newkome, *Chem. Rev.* **1993**, *93*, 2067−2089. [1b] Z. Z. Zhang, H. Cheng, *Coord. Chem. Rev.* **1996**, *147*, 1−39. [1c] P. Espinet, K. Soulantica, *Coord. Chem. Rev.* **1999**, *193*, 499−556 and references cited therein.

[2] [2a] F. E. Wood, M. M: Olmstead, J. P. Farr, A. J. Balch, *Inorg. Chim. Acta* **1985**, *97*, 77−83. [2b] J. A. Casares, P. Espinet, J. M. Martìnez-Illarduya, Y. S. Lin, *Organometallics* **1997**, *16*, 770−779. [2c] J. P. Damiano, V. Munyejabo, M. Postel, *Polyhedron* **1995**, *14*, 1229−1234. [2d] P. Guillame, M. Postel, *Inorg. Chim. Acta* **1995**, *233*, 109−112. [2e] Z. Zhang, X. Wsng, Z. Xi, R. Wanf, H. Wang, *Jiegou Huaxue* **1989**, *8*, 107. [2f] C. Abu-Gnim, I. Amer, *J. Organomet. Chem.* **1996**, *516*, 235−243. [2g] J. A. Casares, P. Espinet, J. M. Martìn-Alvarez, G. Espino, M. Pérez-Manrique, F. Vattier, *Eur. J. Inorg. Chem.* **2001**, 289−296.

[3] G. Minghetti, S. Stoccoro, M. A. Cinellu, A. Zucca, M. Manassero, M. Sansoni, *J. Chem. Soc., Dalton Trans.* **1998**, 4119−4126.

[4] A. Doppiu, M. A. Cinellu, G. Minghetti, S. Stoccoro, A. Zucca, M. Manassero, M. Sansoni, *Eur. J. Inorg. Chem.* **2000**, 2555−2563.

[5] J. D Scott, R. J. Puddephatt, *Organometallics* **1983**, *2*, 1643−1648.

[6] C. Eaborn, K. Kundu, A. J. Pidcock, *J. Chem. Soc., Dalton Trans.* **1981**, 933.

[7] e. g.: G. Minghetti, A. Zucca, S. Stoccoro, M. A. Cinellu, M. Manassero, M. Sansoni, *J. Organomet. Chem.* **1994**, *481*, 195−204.

[8] G. Minghetti, A. Doppiu, A. Zucca, S. Stoccoro, M. A. Cinellu, M. Manassero, M. Sansoni, *Chem. Heterocycl. Compd. (N. Y.)* **1999**, *35*, 992−1000.

[9] A. Doppiu, G. Minghetti, M. A. Cinellu, S. Stoccoro, A. Zucca, M. Manassero, *Organometallics* **2001**, *20*, 1148−1152.

[10] J. T. Chen, T. M. Huang, M. C. Cheng, Y. Wang, *Organometallics* **1990**, *9*, 539−541.

[11] M. Schmulling, D. M. Grove, G. van Koten, R. van Eldik, N. Veldman, A. L. Spek, *Organometallics* **1996**, *15*, 1384−1391

[12] R. Cheenevert, A. Rodrigue, M. Pigeon-Gosselin, R. Savoie, *Can. J. Chem.* **1982**, *60*, 853.

[13] *SAINT, Reference manual*, Siemens Energy and Automation, Madison, WI, **1994−1996**.

[14] G. M. Sheldrick, *SADABS, Empirical Absorption Correction Program*, University of Göttingen, **1997**.

[15] *International Tables for X-ray Crystallography*, Kynoch Press, Birmingham, **1974**, vol.4.

[16] [16a] B. A. Frenz, *Comput. Phys.* **1988**, *2*, 42. [16b] B. A. Frenz, *Crystallographic Computing 5*, Oxford University Press, Oxford, U. K., **1991**, chapter 11, p. 126.

Received June 4, 2001
[I01203]

Methyl- and Acetylpalladium(II) Complexes Containing a P,N,O Tridentate Hydrazone Ligand

Paolo Pelagatti,*[a] Alessia Bacchi,[a] Mauro Carcelli,[a] Mirco Costa,[b] Hans-Werner Frühauf,[c] Kees Goubitz,[d] Corrado Pelizzi,[a] Michele Triclistri,[b] and Kees Vrieze[c]

Keywords: Hydrazones / Insertions / Palladium / Tridentate ligands

The hydrazone ligand 2-(diphenylphosphanyl)benzaldehyde benzoylhydrazone (HPNO) forms the methyl Pd^{II} complex [Pd(HPN)(Me)Cl] (**1**) in high yield when treated with [(COD)Pd(Me)Cl] in dichloromethane or diethyl ether at room temperature. In complex **1**, the ligand remains neutral and is P,N bidentate. The deprotonation of the ligand by Et_3N affords [Pd(PNO)(Me)] (**2**), in which the anionic ligand is P,N,O tridentate. When **1** is treated with $AgCF_3SO_3$, the cationic complex $[Pd(HPNO)(Me)]^+[CF_3SO_3]^-$ (**3**) is formed; here the neutral ligand coordinates in a tridentate P,N,O fashion. All three methyl complexes were subjected to 30 atm of CO pressure, resulting in the isolation of the corresponding acetyl complexes [Pd(HPN)(MeCO)Cl] (**4**), [Pd(PNO)(MeCO)] (**5**) and $[Pd(HPNO)(MeCO)]^+[CF_3SO_3]^-$ (**6**). Complex **4** is completely stable in solution in the absence of CO, whereas **5** and **6** quickly decarbonylate to regenerate the starting methyl complexes **2** and **3**. Complexes **5** and **6** can also be obtained in high yields by treatment of **4** with Et_3N and $AgCF_3SO_3$, respectively. The X-ray crystal structures of the complexes **2**, **5** and **6** were determined.

Introduction

Recently, we have shown that ionisable tridentate hydrazone ligands of the type HNN′O, derived from the condensation of different hydrazides with 2-formyl- or 2-acetylpyridine, can give rise to two different kinds of methylpalladium(II) complexes: namely [Pd(HNN′)(Me)Cl] and [Pd(NN′O)(Me)], respectively.[1] In the first, the neutral ligands display an N,N′ bidentate behaviour, with the oxygen excluded from the coordination sphere, while in the second the anionic ligands bind palladium through all three donor atoms. Under a CO atmosphere, [Pd(HNN′)(Me)Cl] complexes convert quantitatively into the corresponding acetyl complexes [Pd(HNN′)(MeCO)Cl], and the ligands do not vary their coordination mode. Surprisingly, when the [Pd(NN′O)(Me)] complexes are subjected to a CO atmosphere they quickly decompose to Pd black, with isolation of a new organic molecule corresponding to the ligand acylated at the hydrazone nitrogen (Scheme 1).

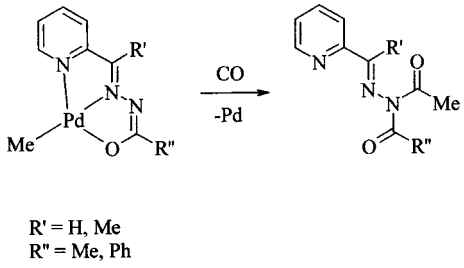

Scheme 1

With the aim of isolating acetyl palladium(II) complexes in which the metal is three-coordinated to an anionic ligand, we have introduced a P atom, with a higher affinity towards palladium, into the chelating system. The previously synthesised acylhydrazone ligand 2-(diphenylphosphanyl)benzaldehyde benzoylhydrazone (HPNO in Scheme 2),[2] was used in the synthesis of a series of methylpalladium(II) complexes, which were subsequently carbonylated in order to isolate the corresponding acetyl complexes. The HPNO ligand has already shown its versatility: depending on the experimental conditions it can be either

[a] Dipartimento di Chimica Generale ed Inorganica, Chimica Analitica, Chimica Fisica, Università degli Studi di Parma
Parco Area delle Scienze 17/A, 43100 Parma, Italy
Fax: (internat.) + 39-0521/905-557
E-mail: paolo.pelagatti@unipr.it
[b] Dipartimento di Chimica Organica ed Industriale, Università degli Studi di Parma
Parco Area delle Scienze 17/A, 43100 Parma, Italy
[c] Institute of Molecular Chemistry, Universiteit van Amsterdam
Nieuwe Achtergracht 166, 1018 WV Amsterdam, The Netherlands
[d] Institute of Molecular Chemistry, Laboratory of Crystallography, Universiteit van Amsterdam,
Nieuwe Achtergracht 166, 1018 WV Amsterdam, The Netherlands

 © WILEY-VCH Verlag GmbH, 69451 Weinheim, Germany, 2002 1434–1948/02/0202–0439 $ 17.50+.50/0

P,N bidentate or P,N,O tridentate when protonated, and P,N,O tridentate when deprotonated.[3]

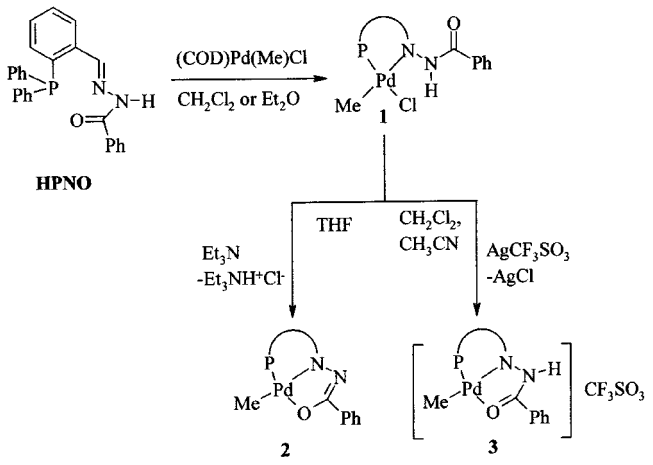

Scheme 2

We report in this paper on the synthesis and characterisation of a series of methylpalladium(II) complexes possessing HPNO as a ligand, as well as on their reactivity towards CO, with particular regard to the influence that the coordination mode of the ligand exerts on the carbonylation course.

Results and Discussion

The ligand HPNO reacts at room temperature with [(COD)Pd(Me)Cl], both in dichloromethane and diethyl ether, resulting in the formation of the complex [Pd(HPN)(Me)Cl] (**1**), in which the metal is coordinated by the neutral ligand in a P,N mode (Scheme 2). The large shifts to lower fields both of the signals of the phosphane moiety in the ^{31}P NMR spectrum (from $\delta = -12.5$ to 38.4) and of the HC=N proton in the ^{1}H NMR spectrum (from $\delta = 8.95$ to 9.53), relative to the free ligand, indicate the involvement of both the P and the N atom in the coordination. The exclusion of the oxygen from the coordination sphere is demonstrated by the strong IR stretching band at 1684 cm^{-1}, which is a value typical for an uncoordinated amide C=O group.[1][3a] The neutral character of the ligand is confirmed by a weak IR band at 3206 cm^{-1} and by a singlet at $\delta = 11.19$ in the ^{1}H NMR spectrum recorded in $CDCl_3$. The methyl group bonded to palladium resonates in the ^{1}H NMR spectrum as a doublet at $\delta = 0.73$, with a phosphorous coupling constant of 1.9 Hz; these are typical values for a phosphane and a methyl situated *cis* to one another in a square-planar arrangement around a palladium(II) ion.[4]

The addition of a slight excess of Et_3N to a THF solution of **1** causes the deprotonation of the ligand, affording the complex [Pd(PNO)(Me)] (**2**), in which the ligand is now P,N,O tridentate (Scheme 2). Both ν(N−H) and ν(C=O) are absent in the IR spectrum, while in the ^{31}P NMR spectrum there is a singlet at $\delta = 32.0$; the methyl group bonded to palladium is seen as a doublet centred at $\delta = 0.61$ in the ^{1}H NMR spectrum, with a phosphorous coupling constant equivalent to that found in **1**. The shielding of the signals observed in the NMR spectra of **2**, relative to those in **1**, is attributable to the higher electron density due to the anionic tridentate coordination on the metal. The HC=N proton resonates as a singlet at $\delta = 8.52$, a value very similar to those found for palladium(II) complexes of the type [Pd(PNO)X] (X = OAc, Cl, I, C≡C−R).[2,5] Yellow crystals suitable for X-ray analysis were collected after slow diffusion of *n*-hexane into a dichloromethane solution of **2** at −20 °C; the resulting structure confirmed the proposed nature of **2**.

The addition of a chloride scavenger, such as $AgCF_3SO_3$, to a dichloromethane solution of **1** resulted in the immediate precipitation of AgCl and isolation of the cationic methyl complex $[Pd(HPNO)(Me)]^+[CF_3SO_3]^-$ (**3**), in which the neutral ligand was P,N,O tridentate (Scheme 2). The ^{31}P NMR spectrum shows a singlet at $\delta = 36.2$, while the HC=N proton resonance is found as a singlet at $\delta = 9.36$. The involvement of the C=O in the coordination is proved by the lowering in frequency of the ν(C=O), which is now visible as a strong bifurcated band at 1560−1597 cm^{-1};[3,6] two strong signals always present at 1298 cm^{-1} and 1240 cm^{-1} in the IR spectrum testify to the presence of a triflate anion.[7] The neutral nature of the hydrazone is indicated both in the IR spectrum and in the ^{1}H NMR spectrum, by a weak band at 3189 cm^{-1} and by a broad singlet at $\delta = 13.49$; the strong deshielding of this last signal is due to the three-coordination of the ligand, which makes the hydrazone proton highly acidic. Finally, the methyl ligand gives rise to a doublet at $\delta = 0.87$, with a phosphorous coupling constant of 3 Hz, which is in agreement with the values found for cationic methylpalladium(II) complexes with phosphanyl-imine ligands.[4b]

All the isolated methyl complexes were treated with CO, with the aim of isolating the corresponding acetyl complexes. Complex **1** did not react either at 1 atm or at 10 atm of CO, but when 30 atm of CO were employed it converted completely into the acetyl [Pd(HPN)(MeCO)Cl] (**4**) within 22 h at room temperature (Scheme 3). The reaction was monitored by ^{1}H and ^{31}P NMR spectroscopy, in a single-crystal sapphire high pressure NMR tube. During the carbonylation the disappearance of the singlet of **1** and the simultaneous appearance of a new singlet at $\delta = 20.2$ was observed in the ^{31}P NMR spectrum, while in the ^{1}H NMR spectrum the doublet at $\delta = 0.73$ of **1** progressively disappeared in favour of a singlet at $\delta = 2.06$. These findings agreed with the formation of an acetylpalladium(II) complex,[4] but unfortunately it was not possible to detect any intermediate species. The IR spectrum of **4** in KBr showed a strong ν(C=O) vibration at 1696 cm^{-1}, which indicates the P,N bidentate coordination mode of the ligand; this band was distinguishable from the one due to the ν(MeCO), which was a sharp band at 1665 cm^{-1}. The ν(N−H) vibration was also visible as a weak band at 3204 cm^{-1}. Complex **4** was stable in $CDCl_3$ at room temperature, as demonstrated by the fact that no changes were observed in the ^{1}H

NMR spectrum over 24 h. Slow diffusion of diethyl ether into a $CDCl_3$ solution of **4** refrigerated at −20 °C provided pale yellow crystals suitable for X-ray analysis. Although it was not possible to complete the refinement of the structure, owing to the presence of a disordered solvent molecule, the diffractometric analysis did confirm the proposed structure, with the acetyl group *cis* to the phosphane.

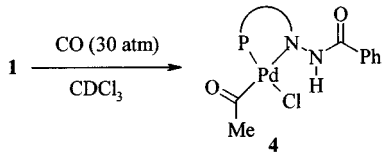

Scheme 3

On the basis of these results, all subsequent carbonylations were carried out at a CO pressure of 30 atm.

The carbonylation of **2** was carried out in a steel autoclave at 25 °C for 24 h, with dichloromethane or THF as solvent. After CO release and removal of the solvent, the ^1H NMR spectrum of the residue, recorded in $CDCl_3$, still showed the doublet due to the starting methyl complex **2** at $\delta = 0.61$, together with a new singlet at $\delta = 2.30$, indicative of the formation of the acetyl complex [Pd(PNO)(MeCO)] (**5**) (Scheme 4); the integrals of the two NMR lines were in a 1:2 ratio. However, when the solution was allowed to stand in the absence of CO, the singlet rapidly disappeared in favour of the more shielded doublet, and after a few hours only the signals belonging to **2** were present in the spectrum: in the absence of CO the rapid decarbonylation of **5** took place, without release of palladium black (Scheme 4). The same behaviour was observed in the ^{31}P NMR spectrum recorded in $CDCl_3$, in which there were two different singlets centred at $\delta = 25.0$ (**5**) and $\delta = 32.0$ (**2**). In the IR spectrum of the solid mixture, the ν(MeCO) of **5** was clearly visible at 1675 cm^{-1}; this did not vanish with time, showing that the decarbonylation occurs only in solution.

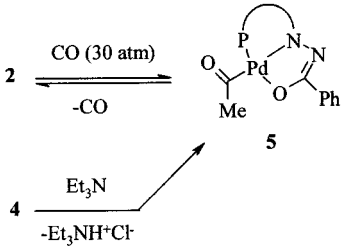

Scheme 4

The carbonylation of **3** was carried out in a steel autoclave for 24 h at 25 °C, with dichloromethane as solvent. The ^1H NMR spectrum of the residue in $CDCl_3$ again showed the doublet of the starting methyl at $\delta = 0.87$, but in addition there was a singlet centred at $\delta = 2.35$. The two lines were in a 4:1 ratio, indicating that only 20% of **3** had been converted into $[Pd(HPNO)(MeCO)]^+(CF_3SO_3)^-$ (**6** in Scheme 5). As already seen for **5**, but in an even faster process, complex **6** in solution lost CO to regenerate **3**; the decarbonylation process also took place in solution at −18 °C. The rapidity of the decarbonylation prevented the recording of the ^{31}P NMR spectra of **6**. The IR spectrum of the mixture showed a ν(MeCO) band at 1700 cm^{-1} and, as with **5**, decarbonylation in the solid state also did not take place in this case.

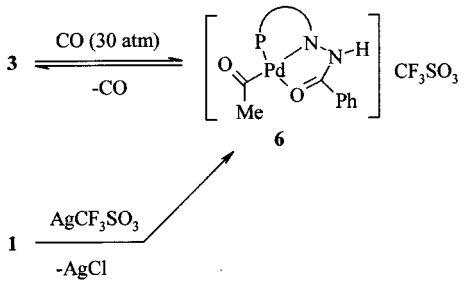

Scheme 5

With the aim of obtaining pure **5** and **6**, solutions of **4** in THF and in CH_2Cl_2 were treated with a slight excess of Et_3N and with a stoichiometric amount of $AgCF_3SO_3$, respectively (Schemes 4 and 5). In both cases, in order to prevent decarbonylation, the products were quickly precipitated with a large excess of diethyl ether. In this way **5** and **6** were obtained in good yields and purities. In solution, however, they rapidly lost CO, as already found during the NMR examination, but it was possible in both cases to collect crystals suitable for X-ray analysis from refrigerated THF/*n*-hexane mixtures, thus confirming the proposed structures.

The need to use high CO pressures for the conversion of the methyl complexes into the corresponding acetyl ones is not surprising with phosphane-containing ligands.[4a] Moreover, the decarbonylation undergone by **5** and **6** is a common process for three-coordinate acetylpalladium(II) complexes.[4b,8] However, is worth noting that the carbonylation of the three-coordinate methyl complex **2** did not result in the formation of palladium black and acylation of the ligand, contrary to what was seen with the related [Pd(NN′O)(Me)] complexes (Scheme 1).

The lack of acetyl transfer from palladium to the ligand in this system may be attributable to the presence of the soft phosphorus donor atom in the chelating ligand. The phosphorus coordinates more strongly than nitrogen, thus meaning that breaking of the Pd−P bond is now unlikely, and therefore our previous hypothesis[1] of a unidentate intermediate in the acylation of the N,N′,O ligands is corroborated.

Crystallographic Section

Complexes **2** and **5** are neutral, while complex **6** is cationic and was isolated as a triflate salt. Compound **5** crystallised with two independent, but not significantly different, molecules in the unit cell. The crystal structures and numbering schemes of compounds **2**, **5** (molecule A) and **6** are shown in Figure 1−3 respectively; selections of relevant

bond lengths and angles are given in Table 1, Table 2 and Table 3. The ligand behaves in all cases as a tridentate P,N,O donor, and the square planar geometry around palladium is completed by a methyl group in **2** and by an acetyl group in **5** and **6**. Two chelating rings are formed by coordination of the metal: the five-membered N−N−C−O−Pd ring is always strictly planar, while the six-membered N−C−C−C−P−Pd ring shows an envelope conformation with the phosphorus at the flap, a feature common in similar systems.[2,3,5] The distances between P and the mean plane containing the remaining five atoms varies from 0.38 Å in **2** to 0.52 Å in **6**. As commonly observed for analogous compounds,[1] the acyl groups in **5** and **6** are nearly perpendicular to the coordination planes, as indicated by the torsion angles: O1−Pd1−C27−O2 = 90(1)°, O3−Pd2−C55−O4 = 88(1)° (**5**, molecules A and B respectively) and O1−Pd−C27−O2 = −114.0(5)° (**6**). Minor differences due to subtle electronic effects are observed between some distances in the coordination systems among the three compounds: an apparent slight elongation of the Pd−N bond is observed on passing from the *trans* methyl [**2**, 2.058(1) Å] to the *trans* acyl group [**5**, 2.093(9) and 2.089(9) Å for molecules A and B] for the deprotonated form of the PNO ligand. These distances are longer than those observed in complexes with the same or a strictly related hydrazone ligand and containing as groups *trans* to N a chloride [2.001(2) Å],[3a] a *t*Bu-alkynyl [2.028(7) Å],[3a] an iodide [1.99(1), 2.03(1) Å],[5a] an acetate [1.974(4) Å][5b] or a phenylalkynyl [2.010(3) Å] moiety.[2] The major differences between the anionic (**2** and **5**) and the neutral forms (**6**) of the PNO ligand are confined mainly to the carbonyl bond of the N−C=O system. For the deprotonated ligand we observe a shift towards the enol form, as already shown by semiempirical calculations and crystal structures of the chloride and *t*Bu-alkynyl palladium complexes of the ligand.[3a] The contribution of the enol form causes the C−O bond length to be slightly longer in **2** and **5** [1.294(2) Å, **2**, 1.28(1) Å, **5**, both molecules] than in **6** [C−O = 1.246(6)

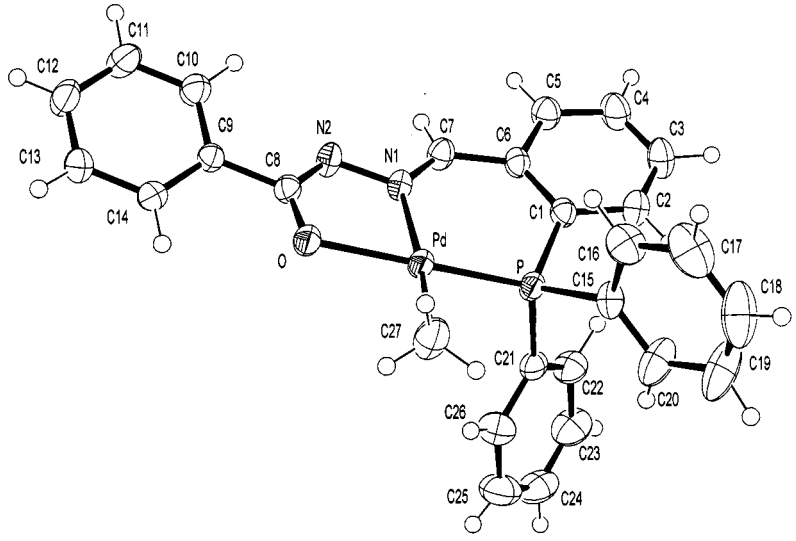

Figure 1. ORTEP diagram of compound **2**

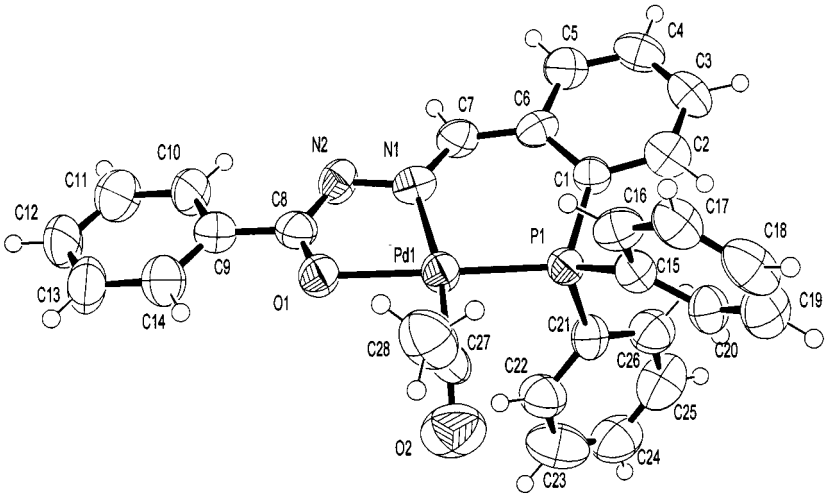

Figure 2. ORTEP diagram of compound **5** (molecule A)

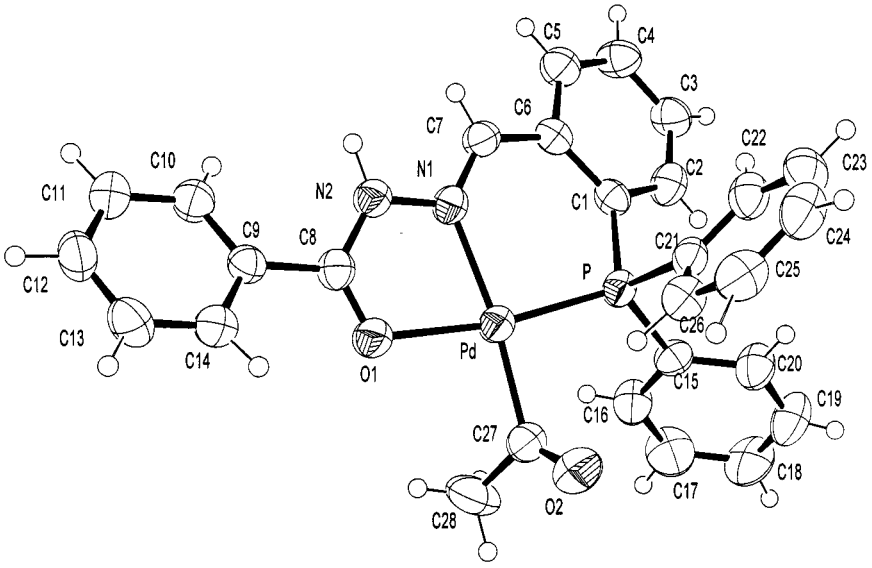

Figure 3. ORTEP diagram of compound **6**; the triflate ion has been omitted

Table 1. Selected bond lengths (Å) and angles (°) for **2**

Pd−C27	2.048(2)	C27−Pd−N1	171.37(8)
Pd−N1	2.058(1)	C27−Pd−O	94.73(7)
Pd−O	2.103(1)	N1−Pd−O	77.84(5)
Pd−P	2.1843(7)	C27−Pd−P	92.09(7)
O−C8	1.294(2)	N1−Pd−P	95.72(4)
N1−C7	1.291(2)	O−Pd−P	171.54(4)
N1−N2	1.398(2)	C1−P−Pd	111.01(5)
N2−C8	1.319(2)	C7−N1−Pd	131.4(1)
		N2−N1−Pd	114.7(1)
		C8−O−Pd	109.3(1)

Table 2. Selected bond lengths (Å) and angles (°) for **5**

Pd1−C27	2.01(1)	Pd2−C55	2.00(1)
Pd1−N1	2.093(9)	Pd2−N3	2.089(9)
Pd1−O1	2.100(8)	Pd2−O3	2.070(8)
Pd1−P1	2.204(3)	Pd2−P2	2.208(3)
O1−C8	1.28(1)	O3−C36	1.28(1)
O2−C27	1.20(2)	O4−C55	1.18(1)
N1−C7	1.29(1)	N3−C35	1.27(1)
N1−N2	1.40(1)	N3−N4	1.41(1)
N2−C8	1.33(1)	N4−C36	1.33(2)
C27−Pd1−N1	171.3(5)	C55−Pd2−N3	172.2(5)
C27−Pd1−O1	93.8(4)	C55−Pd2−O3	93.9(4)
N1−Pd1−O1	77.6(3)	N3−Pd2−O3	78.2(3)
C27−Pd1−P1	93.7(4)	C55−Pd2−P2	93.0(4)
N1−Pd1−P1	95.0(3)	N3−Pd2−P2	94.7(3)
O1−Pd1−P1	169.8(2)	O3−Pd2−P2	169.8(2)
C1−P1−Pd1	111.8(3)	C29−P2−Pd2	111.0(5)
C8−O1−Pd1	109.9(7)	C36−O3−Pd2	109.9(8)
C7−N1−Pd1	130.2(8)	C35−N3−Pd2	132.7(9)
N2−N1−Pd1	113.5(7)	N4−N3−Pd2	112.9(7)

Table 3. Selected bond lengths (Å) and angles (°) for **6**

Pd−C27	1.988(5)	C27−Pd−N1	172.6(2)
Pd−N1	2.100(4)	C27−Pd−O1	95.9(2)
Pd−O1	2.125(3)	N1−Pd−O1	76.8(1)
Pd−P	2.206(1)	C27−Pd−P	93.3(1)
O1−C8	1.246(6)	N1−Pd−P	94.0(1)
O2−C27	1.200(6)	O1−Pd−P	170.3(1)
N1−C7	1.291(6)	C1−P−Pd	109.7(1)
N1−N2	1.390(5)	C8−O1−Pd	113.0(3)
N2−C8	1.337(7)	C7−N1−Pd	132.2(3)
		N2−N1−Pd	110.5(3)

Å]; accordingly, the N−C(O) bond is shorter in the anionic form [1.319(2), 1.33(1), 1.33(2) Å for **2** and **5**, molecules A and B] than in the neutral one [1.337(7) Å for **6**]. Previous calculations[3a] have shown that the anionic charge is largely localized on the oxygen. The Pd−O bond is correspondingly stronger when the ligand has anionic character [2.103(1), 2.100(8), 2.070(8) Å in **2** and **5**] than in the neutral form [2.125(3) Å for **6**].

As observed in the similar compounds above, the terminal phenyl ring C9−C14 apparently has a certain degree of rotational freedom [N2−C8−C9−C10 ranging from −17.8(2) to 25.6(2)°] around the C8−C9 bond that, in all cases, does not appear to be involved in any double bond character delocalization with the hydrazone system [C8−C9 ranging from 1.47(2) to 1.492(2) Å].

The most relevant feature of the crystal packing of the three compounds is given by the charge-assisted hydrogen bond between the cationic complex and the triflate in **6**: N2−H···O5 (N2···O5 = 2.826Å; N2−H−O5 = 121.3°).

Conclusion

The tridentate P,N,O hydrazone ligand HPNO can form three different kinds of methylpalladium(II) complexes, in which it adopts different coordination modes: *i*) neutral P,N (**1**), *ii*) anionic P,N,O (**2**), and *iii*) neutral P,N,O (**3**). The isolation of one or the other depends on the experimental conditions. The methyl complexes **1**, **2** and **3** convert into the corresponding acetyl complexes **4**, **5** and **6** when subjected to high CO pressures; the carbonylations do not af-

fect the coordination modes of the ligand. The stability of the acetyl species in solution towards the loss of CO depends on the chelating behaviour of the ligand: only **4** is completely stable, whereas the three-coordinate acetyl derivatives **5** and **6** quickly decarbonylate to regenerate the starting methyl complexes. In contrast to the carbonylations with HNN′O ligands, no acetylation of HPNO was observed during the carbonylation of **2**. Pure **5** and **6** can be obtained by treating **4** with Et_3N and with $AgCF_3SO_3$, respectively.

Experimental Section

General Remarks: All reactions were performed under an atmosphere of nitrogen, by employing standard Schlenk techniques. Solvents were dried prior to use and stored under nitrogen. Elemental analysis (C, H, N and S) were performed with a Carlo Erba Mod. EA 1108 apparatus. Infrared spectra were recorded with a Nicolet 5PCFT-IR spectrophotometer in the 4000−400 cm^{-1} range as KBr disks. ^1H NMR spectra were obtained on a Bruker 300 FT instrument with $SiMe_4$ as internal standard, while $^{31}P\{^1H\}$NMR spectra were recorded on a Bruker CPX 200 FT with H_3PO_4 (85%) as external standard. MS spectra (C.I., methane) were recorded on a Finnigan SSQ 710 spectrometer. 2-(Diphenylphosphanyl)benzaldehyde benzoylhydrazone (HPNO) was synthesised as previously reported.[2] [(COD)Pd(Me)Cl] was prepared according to the literature,[8] while $AgCF_3SO_3$ was purchased from Aldrich.

[Pd(HPN)(Me)Cl] (1). Method a: HPNO (180 mg, 0.441 mmol) was dissolved in CH_2Cl_2 (30 mL), and [(COD)Pd(Me)Cl] (117 mg, 0.453 mmol) was added. The resulting yellow solution was stirred at room temperature for two hours and was then concentrated to a volume of about 5 ml; on addition of 40 mL of diethyl ether a yellow solid precipitated and was filtered off, washed with diethyl ether and dried in vacuum. Yield: 220 mg (88%).

Method b: [(COD)Pd(Me)Cl] (130 mg, 0.490 mmol) was suspended in diethyl ether (20 mL) and HPNO (200 mg, 0.490 mmol) was added; a yellow solid immediately precipitated. The mixture was stirred at room temperature for 2 hours and the solid was then removed by filtration, washed with diethyl ether and dried in vacuum. Yield: 263 mg (95%). $C_{27}H_{24}ClN_2OPPd$ (565.3): calcd. C 57.36, H 4.28, N 4.96; found C 56.98, H 4.22, N 4.84. ^1H NMR ($CDCl_3$): δ = 0.73 (d, $^3J_{P-H}$ = 1.9 Hz, 3 H, Pd-Me), 7.40−7.60 (m, 17 H, Ph), 8.25 [d, ^3J = 8.2 Hz, 2 H, Ph(C=O)], 9.53 (s, 1 H, CH=N), 11.19 (s, 1 H, N−H). ^{31}P NMR ($CDCl_3$): δ = 38.4 (s). IR (KBr): ṽ = 3206 w (N−H), 1684 s cm^{-1}(C=O). MS-CI: *m*/*z* = 527 $[M - HCl]^+$.

[Pd(PNO)(Me)] (2). Method a: HPNO (108 mg, 0.264 mmol) was dissolved in THF (20 mL) and Et_3N (40 mg, 0.395 mmol, 0.06 mL) was added. [(COD)Pd(Me)Cl] (70 mg, 0.264 mmol) was added to the pale yellow solution, whereupon triethylamine hydrochloride precipitated; after 3 hours of stirring at room temperature the mixture was filtered to afford a yellow solution, which was concentrated under vacuum to a volume of about 5 mL. Addition of 30 mL of diethyl ether and refrigeration at −20 °C overnight caused the precipitation of a yellow solid, which was filtered off, washed with diethyl ether and dried in vacuum. Yield: 67 mg (48%).

Method b: Compound **1** (70 mg, 0.124 mmol) was dissolved in THF (20 mL), and Et_3N (19 mg, 0.188 mmol, 0.03 mL) was added; the mixture was stirred at room temperature for 3 hours and then filtered, and the resulting yellow solution was worked up as reported in method *a*. Yield: 53 mg (82%). Crystals suitable for X-ray analysis were collected from a CH_2Cl_2/*n*-hexane mixture refrigerated at −20 °C. $C_{27}H_{23}N_2OPPd$ (528.9): calcd. C 61.32, H 4.38, N 5.30; found C 61.17, H 4.32, N 5.42. ^1H NMR ($CDCl_3$): δ = 0.61 (d, $^3J_{P-H}$ = 1.9 Hz, 3 H, Pd-Me), 7.39−7.60 (m, 17 H, Ph), 8.22 [dd, ^3J = 7.6, ^4J = 1.5 Hz, 2 H, Ph(C=O)], 8.52 (s, 1 H, CH=N). ^{31}P NMR ($CDCl_3$): δ = 32.0 (s). MS-CI: *m*/*z* = 528 $[M]^+$.

[Pd(HPNO)(Me)]$^+$[CF_3SO_3]$^-$ (3): Compound **1** (100 mg, 0.177 mmol) was placed in a Schlenk tube and dissolved in CH_2Cl_2 (15 mL). $AgCF_3SO_3$ (45 mg, 0.177 mmol) dissolved in CH_3CN (2 mL) was added, resulting in the immediate precipitation of AgCl. The resulting mixture was stirred at room temperature for 2 h, filtered and concentrated under vacuum; addition of Et_2O and refrigeration at −18 °C overnight afforded **3** as a microcrystalline yellow solid. Yield: 86 mg (72%). $C_{28}H_{24}F_3N_2O_4PPdS$ (678.9): calcd. C 49.53, H 3.56, N 4.13, S 4.72; found C 49.53, H 3.35, N 4.06, S 4.71. ^1H NMR ($CDCl_3$): δ = 0.87 (d, $^3J_{P-H}$ = 3 Hz, 3 H, Pd-Me), 7.40−8.03 (m, 17 H, Ph), 8.23 [d, ^3J = 7.9 Hz, 2 H, Ph(C=O)], 9.36 (s, 1 H, CH=N), 13.49 (s, 1 H, N−H). ^{31}P NMR ($CDCl_3$): δ = 36.2 (s). IR (KBr): ṽ = 3189 w (N−H), 1597 s − 1560 s (C=N + C=O), 1298 s − 1240 s cm^{-1} (S=O).

Synthesis of the Acetyl Complexes

Carbonylation Reactions: The carbonylation of complex **1** was carried out as described below. **Method a:** A magnetic stirring bar was placed in a 150 mL capacity steel autoclave, together with the complex (30 mg) dissolved in chloroform or dichloromethane (20 mL). The reactor was purged twice with CO and then pressurized to 30 atm. The mixture was stirred overnight at 25 °C, CO was then released, and the solution was filtered through celite in order to remove the traces of palladium black sometimes formed. The resulting yellow solution was treated with diethyl ether until precipitation of [Pd(HPN)(MeCO)Cl] (**4**). This was filtered and washed with diethyl ether. Yield: 37 mg (99%).

The same procedure applied to complexes **2** and **3** did not permit the isolation of pure acetyl complexes because of the decarbonylation that took place when the CO pressure was released.

Method b (Only for Complex 1): Complex **1** (20 mg, 0.035 mmol) was placed in a 5 mm o.d. single-crystal sapphire high-pressure NMR tube and dissolved in about 1 mL of deuterated chloroform. The tube was purged twice with CO and then pressurized at 30 atm. The reaction was followed by ^1H and ^{31}P NMR spectroscopy at 20 °C until the complete disappearance of the starting signals (20 h). The final solution was worked up as reported above.

SAFETY NOTE: Since high gas pressures are involved, safety precautions must be taken at all stages involving HP NMR tubes.[9]

[Pd(HPN)(MeCO)Cl] (4): $C_{28}H_{24}ClN_2O_2PPd{\cdot}CDCl_3$ (713.7): calcd. C 48.80, H 3.53, N 3.93; found C 49.00, H 3.71, N 3.90. ^1H NMR ($CDCl_3$): δ = 2.06 (s, 3 H, MeCO), 7.30−7.59 (m, 17 H, Ph), 8.02 [d, ^3J = 6.9 Hz, 2 H, Ph(C=O)], 9.63 (s, 1 H, CH=N), 11.84 (s, 1 H, N−H). ^{31}P NMR ($CDCl_3$): δ = 20.2 (s). IR (KBr): ṽ = 3204 w (N−H), 1696 s (C=O), 1665 s cm^{-1} (MeCO). Crystals suitable for X-ray diffraction were obtained by slow diffusion of diethyl ether into the deuterated chloroform solution of **4** at −20 °C.

[Pd(PNO)(COMe)] (5): Compound **4** (30 mg, 0.051 mmol) was dissolved in THF (20 mL) and treated with Et_3N (8 mg, 0.01 mL, 0.081 mmol). The mixture was stirred at room temperature for 2 h and then filtered; the resulting yellow solution was concentrated in

vacuum and **5** was precipitated with diethyl ether, filtered and dried in vacuum. Crystals suitable for X-ray analysis were obtained from a THF/*n*-hexane mixture, refrigerated to −18 °C. $C_{28}H_{23}N_2O_2PPd$ (556.9): calcd. C 60.39, H 4.16, N 5.03; found C 60.52, H 4.24, N 5.11. ^{1}H NMR ($CDCl_3$): δ = 2.30 (s, 3 H, MeCO), 8.18 [br. d, 2 H, Ph(C=O)], 8.51 (br, 1 H, CH=N). The other data are obscured by the signals of **2**. ^{31}P NMR ($CDCl_3$): δ = 25.0 (s). IR (KBr): $\tilde{\nu}$ = 1675 m cm^{-1} (MeCO).

[Pd(HPNO)(MeCO)]$^+$[CF_3SO_3]$^-$ (6): Compound **4** (30 mg, 0.044 mmol) was dissolved in CH_2Cl_2 (20 mL), and $AgCF_3SO_3$ (11.4 mg, 0.044 mmol) dissolved in acetonitrile (1 mL) was added. The mixture was stirred at room temperature for 2 h and then filtered, giving a yellow solution that was concentrated under reduced pressure. The product was precipitated by addition of diethyl ether, filtered and dried in vacuum. Crystals suitable for X-ray analysis were collected from a THF/*n*-hexane mixture refrigerated at −18 °C. $C_{29}H_{24}F_3N_2O_5PPdS$ (706.9): calcd. C 49.27, H 3.42, N 3.96, S 4.53; found C 49.38, H 3.38, N 4.02, S 4.30. ^{1}H NMR ($CDCl_3$): δ = 2.35 (s, 3 H, MeCO), 8.20 [br. d, 2 H, Ph(C=O)]. The other data were obscured by signals of **3**. IR (KBr): $\tilde{\nu}$ = 3183 w (N−H), 1700 s (MeCO), 1602 s (C=N), 1559 vs (C=O), 1296 vs − 1224 vs cm^{-1} (S=O).

X-ray Data Collection, Structure Determination and Refinement of Compounds 2, 5 and 6

Air-stable crystals suitable for structural determination by single-crystal X-ray diffraction were obtained for compounds **2**, **5** and **6**. Relevant details about X-ray experimental conditions, data collection and refinement are given in Table 4. Data for compounds **5** and **6** were collected on Siemens AED diffractometers, while for compound **2** a Philips PW1100 diffractometer was used and the ψ-scan empirical absorption correction was applied. For compounds **2** and **6**, graphite monochromated Mo-K_α radiation was used (λ = 0.71069Å). For the thick crystals of **5**, graphite monochromated Cu-K_α radiation (λ = 1.54184 Å) was chosen for data collection.

Data were corrected for Lorentz and polarisation effects. Crystal decay was observed for **5** and data were rescaled accordingly. The phase problem for all the compounds was solved by direct methods with SIR97.[10] Data refinement was performed by full-matrix, least-squares on $F2$ with SHELXL-97.[11] For compounds **5** and **6**, the Walker and Stewart[12] absorption correction was applied after the last isotropic refinement cycle. In all cases non-hydrogen atoms were refined anisotropically. While in compound **2** all hydrogen atoms were located in the Fourier maps and refined isotropically; in compound **6** some of them were placed in calculated positions. For compound **5**, all hydrogens were placed in calculated positions and constrained to ride on their carrying atoms. The geometry of the structures was inspected and analysed by PARST-97[13] and ORTEP-3[14] and compared with literature data with the aid of the Cambridge Structural Database software.[15]

Crystallographic data (excluding structure factors) for the structures reported in this paper have been deposited with the Cambridge Crystallographic Data Centre as supplementary publication nos. CCDC-155797 (**2**), -155798 (**5**) and -155799 (**6**). Copies of the data can be obtained free of charge on application to CCDC, 12 Union Road, Cambridge CB2 1EZ, UK [Fax: (internat.) + 44-1223/336-033; E-mail: deposit@ccdc.cam.ac.uk]

Acknowledgments

This work was partially supported by the MURST (Programmi di Ricerca Scientifica di interesse nazionale, cofin 1999). The CIM

Table 4. Crystal data and structure refinement

	2	**5**	**6**
Empirical formula	$C_{27}H_{23}N_2OPPd$	$C_{28}H_{23}N_2O_2PPd$	$C_{29}H_{24}F_3N_2O_5PPdS$
Formula mass	528.84	556.85	706.93
Wavelength	0.71069 Å	1.54184 Å	0.71069 Å
Crystal system	monoclinic	monoclinic	monoclinic
Space group	$C2/c$	$P2_1/c$	$P2_1/a$
Unit cell dimensions	a = 21.465(7) Å	a = 16.141(6) Å	a = 25.681(8) Å
	b = 12.612(4) Å	b = 15.259(6) Å	b = 10.919(4) Å
	c = 18.052(5) Å	c = 19.674(7) Å	c = 10.401(4) Å
	β = 106.31(2)°	β = 94.92(2)°	β = 99.19(2)°
Volume	4690(2) Å^3	4828(3) Å^3	2879(2) Å^3
Z	8	8	4
Calculated density	1.498 Mg/m^3	1.532 Mg/m^3	1.631 Mg/m^3
Absorption coefficient	0.881 mm^{-1}	7.054 mm^{-1}	0.835 mm^{-1}
F(000)	2144	2255	1424
Crystal size	0.4 × 0.4 × 0.3 mm	0.3 × 0.2 × 0.15 mm	0.5 × 0.3 × 0.3 mm
θ range	3.23 to 31.96°	3.67 to 65.12°	3.05 to 30.07°
Reflections collected/unique	13643/7070	8201/8201	8830/8427
Observed reflections [$I > 2\sigma(I)$]	5640	4359	3667
Refinement method	Full-matrix, least-squares on F^2	Full-matrix, least-squares on F^2	Full-matrix, least-squares on F^2
Data/restraints/parameters	7070/0/381	8201/0/615	8427/1/457
Goodness-of-fit on F^2	0.908	1.057	0.886
Final R indices [$I > 2\sigma(I)$]	$R1$[a] = 0.0258	$R1$[a] = 0.0752	$R1$[a] = 0.0598
	$wR2$[b] = 0.0668	$wR2$[b] = 0.2431	$wR2$[b] = 0.1603
R indices (all data)	$R1$[a] = 0.0383	$R1$[a] = 0.1185	$R1$[a] = 0.1203
	wR2[b] = 0.0717	$wR2$[b] = 0.2661	$wR2$[b] = 0.1829

[a] $R = \Sigma \, ||F_o| - |F_c|| / \Sigma \, |F_o|$. [b] $wR2 = \{\Sigma[w(F_0^2 - F_c^2)^2] / \Sigma \, [w(F_0^2)^2]\}^{1/2}$.

(Centro Interfacoltà di Misure G. Casnati) of the University of Parma is thanked for technical assistance. Particular thanks go to J. M. Ernsting (Institute of Molecular Chemistry, University of Amsterdam) for the recording of the HP NMR spectra.

[1] P. Pelagatti, M. Carcelli, F. Franchi, C. Pelizzi, A. Bacchi, A. Fochi, H.-W. Frühauf, K. Goubitz, K. Vrieze, *Eur. J. Inorg. Chem.* **2000**, 463−475.
[2] A. Bacchi, M. Carcelli, M. Costa, P. Pelagatti, C. Pelizzi, G. Pelizzi, *Gazz. Chim. Ital.* **1994**, *124*, 429−435.
[3] [3a] A. Bacchi, M. Carcelli, M. Costa, A. Fochi, C. Monici, P. Pelagatti, C. Pelizzi, G. Pelizzi, L. M. Sanjuan Roca, *J. Organomet. Chem.* **2000**, *593−594*, 180−191. [3b] P. Pelagatti, A. Bacchi, C. Bobbio, M. Carcelli, M. Costa, C. Pelizzi, C. Vivorio, *Organometallics* **2000**, *19*, 5440−5446.
[4] [4a] G. P. C. M. Dekker, A. Buijs, C. J. Elsevier, K. Vrieze, P. W. N. M. van Leeuwen, W. J. J. Smeets, A. L. Spek, Y. F. Wang, C. H. Stam, *Organometallics* **1992**, *11*, 1937−1948. [4b] R. E. Rülke, V. E. Kaasjager, P. Wehman, C. J. Elsevier, P. W. N. M. van Leeuwen, K. Vrieze, J. Fraanje, K. Goubitz, A. L. Spek, *Organometallics* **1996**, *15*, 3022−3031.
[5] [5a] A. Bacchi, M. Carcelli, M. Costa, A. Leporati, E. Leporati, P. Pelagatti, C. Pelizzi, G. Pelizzi, *J. Organomet. Chem.* **1997**, *535*, 107−120. [5b] P. Pelagatti, A. Bacchi, M. Carcelli, M. Costa, A. Fochi, P. Ghidini, E. Leporati, M. Masi, C. Pelizzi, G. Pelizzi, *J. Organomet. Chem.* **1999**, *583*, 94−105.
[6] [6a] P. Braunstein, Y. Chauvin, J. Nähring, A. DeCian, J. Fischer, A. Tiripicchio, F. Ugozzoli, *Organometallics* **1996**, *15*, 5551−5567. [6b] P. Braunstein, Y. Chauvin, J. Fischer, H. Olivier, C. Strohmann, D. V. Toronto, *New J. Chem.* **2000**, *24*, 437−445.
[7] [7a] G. A. Lawrence, *Chem. Rev.* **1986**, *86*, 17−33. [7b] P. J. Stang, Y.-H. Huang, A. M. Arif, *Organometallics* **1992**, *11*, 231−237. [7c] P. Burger, J. M. Baumeister, *J. Organomet. Chem.* **1999**, *575*, 214−222.
[8] [8a] H. A. Ankersmit, N. Veldman, A. L. Spek, K. Vrieze, G. van Koten, *Inorg. Chim. Acta* **1996**, *252*, 339−354. [8b] J. H. Groen, A. de Zwart, M. J. M. Vlaar, J. M. Ernsting, P. W. N. M. van Leeuwen, K. Vrieze, H. Kooijman, W. J. J. Smeets, A. L. Spek, P. H. M. Budzelaar, Q. Xiang, R. P. Thummel, *Eur. J. Inorg. Chem.* **1998**, 1129−1143.
[9] R. E. Rülke, J. M. Ernsting, A. L. Spek, C. J. Elsevier, P. W. N. M. van Leeuwen, K. Vrieze, *Inorg. Chem.* **1993**, *32*, 5769−5778.
[10] C. J. Elsevier, *J. Mol. Catal.* **1994**, *92*, 285−297.
[11] *SIR97: A New Program For Solving And Refining Crystal Structures*, A. Altomare, M. C. Burla, M. Camalli, G. Cascarano, C. Giacovazzo, A. Guagliardi, A. G. Moliterni, G. Polidori, R. Spagna, **1997**, Istituto di Ricerca per lo Sviluppo di Metodologie Cristallografiche C.N.R., Bari, Italy.
[12] G. Sheldrick, *SHELXL97*: *Program for Structure Refinement*, University of Göttingen, Germany, **1997**.
[13] N. Walzer, D. Stuart, *Acta Crystallogr., Sect. A* **1983**, *39*, 158−166.
[14] M. Nardelli, *PARST97*, *J. Appl. Crystallogr.* **1995**, *28*, 659.
[15] L. J. Ferrugia, *J. Appl. Crystallogr.* **1997**, *30*, 565.
[16] F. H. Allen, O. Kennard, R. Taylor, *Acc. Chem. Res.* **1983**, *16*, 146−153.

Received June 25, 2001
[I01229]

A Zinc(II) Complex Composed of a Tridentate Ligand Bearing Podand Pyrenyl Moieties

Toshiyuki Moriuchi,[a] Masahito Nishiyama,[a] and Toshikazu Hirao*[a]

Keywords: Coordination modes / N ligands / Crystal engineering / Zinc / Receptors

The structural characterization and function of Zn^{II} complexes composed of a tridentate ligand bearing podand pyrenyl moieties as a fluorophore [2,6-pyridinedicarboxaldehydebis(1-pyrenylmethylimine) (L^1)] are described. The tridentate podand ligand L^1 forms a 2:1 complex, $[Zn(L^1)_2(BF_4)_2]$, with $Zn(BF_4)_2$ although the 1:1 complex $[Zn(L^1)(OAc)_2]$ is obtained with $Zn(OAc)_2$. The X-ray crystal structure determination of $[Zn(L^1)_2(BF_4)_2]$ reveals that two tridentate podand ligands L^1 coordinate meridionally to Zn^{II} ion to give an orthogonally oriented molecular turn around the approximately octahedral Zn^{II} center. One pyridyl moiety of L^1 is sandwiched in between two podand pyrenyl moieties of another L^1 through π-π interactions, together with an extended π-stacking through π-π interactions between the pyrenyl moieties in the crystal packing. $[Zn(L^1)(OAc)_2]$ serves as a fluorophore metalloreceptor possessing a two-guest binding ability. $[Zn(L^1)(OAc)_2]$ affords the 1:2 complex $[Zn(L^1)(G^1)_2]$ (G = guest molecule) with 4-nitrobenzoate ion (G^1). The X-ray crystal structure of $[Zn(L^1)(G^1)_2]$ confirms that $Zn(L^1)^{2+}$ accommodates two 4-nitrobenzoate moieties and that the coordination geometry around Zn^{II} is a distorted square pyramid. Two independent molecules are present in the asymmetric unit to form the π-stacked dimer by face-to-face overlap. Fluorescence quenching of $[Zn(L^1)(G^1)_2]$ is observed by intramolecular electron transfer from the pyrenyl moieties to the Zn^{II}-bound 4-nitrobenzoates.

Introduction

The organization of host molecules by complexation with metal ions has attracted much attention.[1] Metalloreceptors, which possess metal binding sites and additional interaction sites of ligands, have been regarded as useful organized host molecules.[2] Such metalloreceptors can undergo the desired conformational change for binding of guest molecules. The utilization of the allosteric effect is also a convenient approach to organize component molecules.[3]

A change in the fluorescent properties is generally considered to be a signal that a guest binding process has occurred.[4] The pyrene unit is one of the most commonly used fluorophores due to its strong luminescence and chemical stability.[5] Another interesting feature of the pyrene unit is the π-π interaction between pyrene aromatic rings in the crystal packing, which can permit the formation of highly ordered molecular aggregates in the solid state by architecturally controlled self-assembly.[6]

The complexation of a tridentate ligand with a Zn^{II} ion is expected to provide two labile coordination sites. Another advantage in the use of Zn^{II} as a binding site is its photophysical innocuousness and its Lewis acidity towards binding anions.[7] Flexible podand ligands allow metal complexes to possess a varied geometry at the metal center due to their different modes of coordination.[8] On this basis, the introduction of pyrene units, which serve as a fluorophore and provide an additional site for π-π interaction, into the podand moieties of a tridentate ligand should provide an efficient Zn^{II} metalloreceptor possessing a two-guest binding ability through first- and second-sphere coordination. In this context, we describe herein the structural characterization and fluorescence properties of Zn^{II} complexes composed of a tridentate ligand bearing podand pyrenyl moieties.

Results and Discussion

The tridentate podand ligand, 2,6-pyridinedicarboxaldehydebis(1-pyrenemethylimine) (L^1), which was obtained by Schiff base condensation of 2,6-pyridinedicarboxaldehyde with 1-pyrenemethylamine in methanol, was used to serve as a tridentate ligand bearing podand pyrenyl moieties as the fluorophore and additional interaction sites. Treatment of the tridentate podand ligand L^1 with $Zn(BF_4)_2$ led to the formation of the 2:1 complex $[Zn(L^1)_2(BF_4)_2]$ (Scheme 1), although the 1:1 complex $[Zn(L^1)(OAc)_2]$ was produced with $Zn(OAc)_2$.

The structure of the 2:1 complex $[Zn(L^1)_2(BF_4)_2]$ was confirmed by X-ray crystallography (Table 1). The crystal structure of $[Zn(L^1)_2(BF_4)_2]$ revealed that two tridentate podand ligands L^1 coordinate meridionally to Zn^{II} ion to give an orthogonally oriented molecular turn around an approximately octahedral Zn^{II} center (Figure 1). Selected bond lengths and bond angles are listed in Table 2. Six of their

[a] Department of Applied Chemistry, Faculty of Engineering, Osaka University,
Yamada-oka, Suita, Osaka 565-0871, Japan
E-mail: hirao@ap.chem.eng.osaka-u.ac.jp

 © WILEY-VCH Verlag GmbH, 69451 Weinheim, Germany, 2002 1434−1948/02/0202−0447 $ 17.50+.50/0

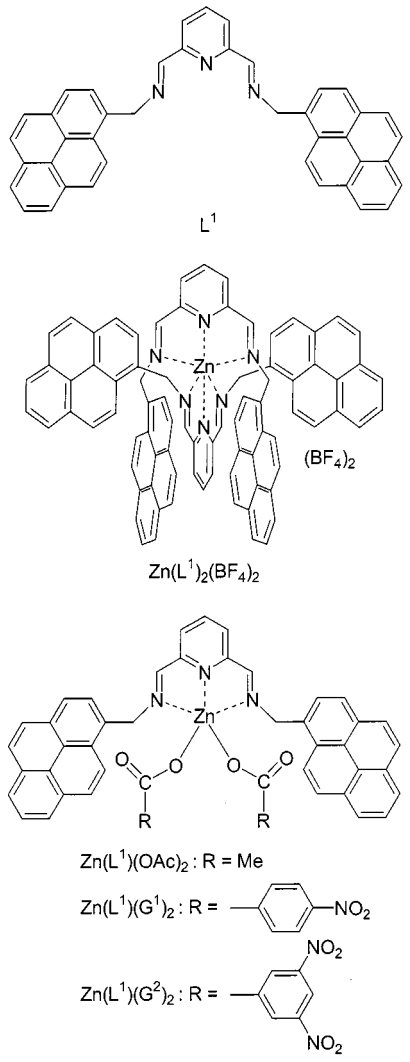

Scheme 1

Table 1. Crystallographic data for $[Zn(L^1)_2(BF_4)_2]$ and $[Zn(L^1)(G^1)_2]$

Empirical formula	$C_{82}H_{54}B_2F_8N_6Zn{\cdot}2CH_3OH$	$C_{55}H_{35}N_5O_8Zn$
Formula mass	1426.44	959.25
Crystal system	monoclinic	triclinic
Space group	$P2_1/n$ (No. 14)	$P\bar{1}$ (No. 1)
a [Å]	21.557(2)	12.4178(8)
b [Å]	17.783(2)	12.8828(8)
c [Å]	21.348(1)	15.7080(10)
α [°]		103.931(2)
β [°]	120.244(1)	110.1920(10)
γ [°]		100.0100(10)
V [Å^3]	7070.1(10)	2196.2(2)
Z	4	2
D_{calcd} [g cm^{-3}]	1.340	1.451
μ (Mo-K_α) [cm^{-1}]	4.23	6.26
T [°C]	23	25
λ(Mo-K_α) [Å]	0.71069	0.71073
$R1$[a] [$I > 2\sigma(I)$]	0.119	0.053
$wR2$[b] (all data)	0.371	0.084

[a] $R = \Sigma||F_o| - |F_c||/\Sigma|F_o|$. [b] $R_w = [\Sigma w(F_o^2 - F_c^2)^2/\Sigma w(F_o^2)^2]^{1/2}$.

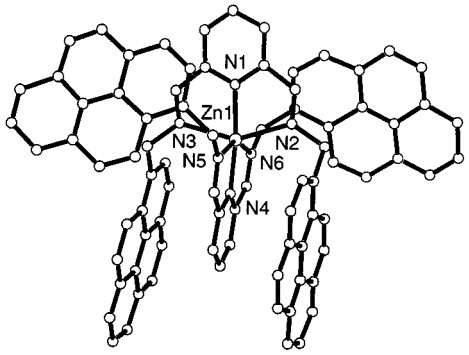

Figure 1. Molecular structure of $[Zn(L^1)_2(BF_4)_2]$ (hydrogen atoms and tetrafluoroborate ligands are omitted for clarity)

coordination sites are occupied by nitrogen donors of two pyridinedicarboxaldehydebisimine chelates. The N−Zn−N angles deviate from 90°, probably due to the formation of the five-membered chelate rings with extended conjugation. The most noteworthy structural feature is that one pyridyl moiety of L^1 is sandwiched between two podand pyrenyl moieties of another L^1 in a π-π interaction within which the distance between the pyridyl and pyrenyl moieties is ca. 3.5 Å. Furthermore, $[Zn(L^1)_2(BF_4)_2]$ shows extended π-stacking along a single axis in the crystal; the pyrenyl moieties are closely associated with the pyrenyl moieties of the neighboring molecules with ca. 3.5 Å separation and the remaining pyrenyl moieties surround the extended π-stacking through edge-to-face interaction with ca. 3.8 Å separation.

The coordinatively labile Zn^{II} center in $[Zn(L^1)(OAc)_2]$ bearing the tridentate podand ligand L^1 is able to provide two binding sites for two anions as guest molecules. The ancillary acetates were displaced by treatment of $[Zn(L^1)(OAc)_2]$ with the 4-nitrobenzoate ion (G^1), giving the 1:2 complex $[Zn(L^1)(G^1)_2]$ quantitatively. The 1:2 complex $[Zn(L^1)(G^2)_2]$ was obtained in a similar manner with the 3,5-dinitrobenzoate ion (G^2). The crystal structure of $[Zn(L^1)(G^1)_2]$ confirmed that $Zn(L^1)^{2+}$ accommodates two 4-nitrobenzoate ions and that two independent molecules are present in the asymmetric unit with almost the same conformation, as depicted in Figure 2. The structural parameter $\tau = (\beta - \alpha)/60$ for the coordination geometry of the five-coordinated complex proposed by Addison and Reedijik shows $\tau = 0.39$ and 0.33 for $[Zn(L^1)(G^1)_2]$, where α and β represent two basal angles ($\beta > \alpha$).[9] The parameters for an ideal square pyramidal and trigonal bipyramidal geometries are $\tau = 0$ ($\alpha = \beta = 180°$) and $\tau = 1$ ($\alpha = 120°$ and $\beta = 180°$), respectively. The τ values of $[Zn(L^1)(G^1)_2]$ indicate that the coordination geometry around Zn^{II} is a distorted square pyramid. Two imine nitrogens and two oxygens of the 4-nitrobenzoate moieties reside in the basal plane while one pyridyl nitrogen occupies the axial position. It is notable that two independent molecules overlap in a face-to-face manner to form a π-stacked dimer in which two 4-nitrobenzoate moieties lie in almost parallel planes and one pyrenyl moiety is sandwiched in-between. Furthermore, these π-stacked dimers are connected through

Table 2. Selected bond lengths [Å] and angles [°] for $[Zn(L^1)_2(BF_4)_2]$ and $[Zn(L^1)(G^1)_2]$

	$[Zn(L^1)_2(BF_4)_2]$	$Zn(L^1)(G^1)_2$ [a]	
Bond lengths			
Zn−N(1)	2.02(1)	2.043(11)	2.018(15)
Zn−N(2)	2.26(1)	2.254(14)	2.231(16)
Zn−N(3)	2.27(2)	2.211(15)	2.305(13)
Zn−N(4)	2.01(1)	−	−
Zn−N(5)	2.27(1)	−	−
Zn−N(6)	2.34(1)	−	−
Zn−O(1)	−	1.949(11)	1.976(10)
Zn−O(5)	−	1.871(10)	1.960(10)
Bond angles			
N(1)−Zn−N(2)	75.9(5)	73.5(5)	77.4(6)
N(1)−Zn−N(3)	73.3(6)	77.3(5)	71.9(5)
N(1)−Zn−N(4)	171.8(6)	−	−
N(1)−Zn−N(5)	107.2(4)	−	−
N(1)−Zn−N(6)	102.8(4)	−	−
N(2)−Zn−N(3)	149.2(5)	150.4(5)	149.1(5)
N(2)−Zn−N(4)	111.5(6)	−	−
N(2)−Zn−N(5)	94.9(4)	−	−
N(2)−Zn−N(6)	94.6(5)	−	−
N(3)−Zn−N(4)	99.3(7)	−	−
N(3)−Zn−N(5)	92.2(5)	−	−
N(3)−Zn−N(6)	94.1(4)	−	−
N(4)−Zn−N(5)	76.2(5)	−	−
N(4)−Zn−N(6)	73.8(5)	−	−
N(5)−Zn−N(6)	149.9(5)	−	−
N(1)−Zn−O(1)	−	127.2(4)	129.3(5)
N(1)−Zn−O(5)	−	121.6(5)	119.6(5)
N(2)−Zn−O(1)	−	95.0(5)	99.8(5)
N(2)−Zn−O(5)	−	102.0(5)	100.7(5)
N(3)−Zn−O(1)	−	99.0(5)	96.8(5)
N(3)−Zn−O(5)	−	97.0(5)	97.6(5)

[a] Two independent molecules exist in the asymmetric unit.

a π-π interaction with ca. 3.4 Å separation between the remaining pyrenyl moieties in the crystal.

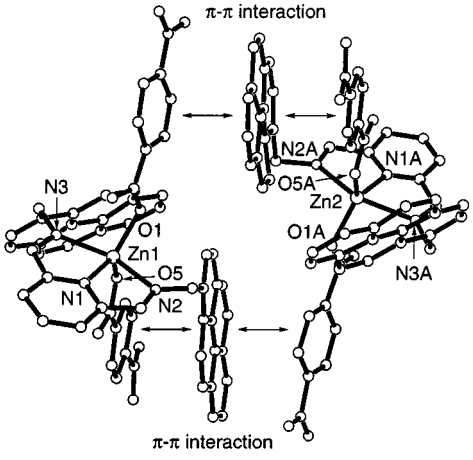

Figure 2. Molecular structure of $[Zn(L^1)(G^1)_2]$ (hydrogen atoms are omitted for clarity)

In the fluorescence spectra, the tridentate podand ligand L^1 shows both monomer and excimer emissions, as shown in Figure 3. $[Zn(L^1)(OAc)_2]$, on the other hand, only exhibits the monomer emission, due to a conformational change induced by complexation. Interestingly, fluorescence quenching was observed with $[Zn(L^1)(G^1)_2]$ by intramolecular electron transfer from the pyrenyl moieties to the Zn^{II}-bound 4-nitrobenzoates (Figure 4).[10] For the intramolecular electron-transfer process, the pyrenyl moieties and 4-nitrobenzoates should be close enough to each other for overlap of the orbitals. Both podand pyrenyl moieties are considered to interact with each Zn^{II}-bound 4-nitrobenzoate through π-π interactions by virtue of the flexibility of the podand pyrenylmethyl moieties in this system. The binding of two 3,5-dinitrobenzoates also resulted in fluorescence quenching in $[Zn(L^1)(G^2)_2]$.

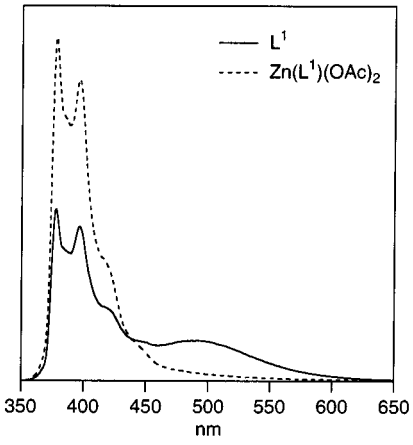

Figure 3. Fluorescence spectra of L^1 and $[Zn(L^1)(OAc)_2]$ in dichloromethane (1.0×10^{-5} M, $\lambda_{ex} = 344$ nm)

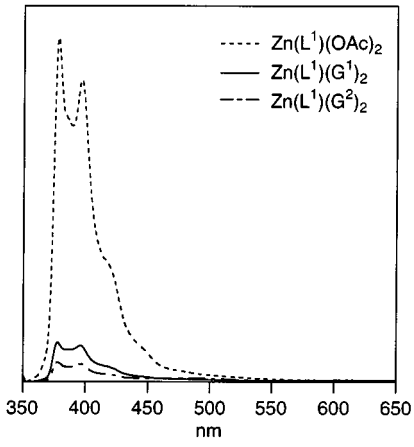

Figure 4. Fluorescence spectra of $[Zn(L^1)(OAc)_2]$, $[Zn(L^1)(G^1)_2]$, and $[Zn(L^1)(G^2)_2]$ in dichloromethane (1.0×10^{-5} M, $\lambda_{ex} = 344$ nm)

Conclusion

The synthesis, structural characterization, and fluorescence properties of Zn^{II} complexes composed of a tridentate ligand bearing podand pyrenyl moieties have been described. The tridentate podand ligand L^1 forms the 2:1 complex $[Zn(L^1)_2(BF_4)_2]$ with $Zn(BF_4)_2$ and the 1:1 complex $[Zn(L^1)(OAc)_2]$ with $Zn(OAc)_2$. The aggregation of py-

renyl moieties through π-π interaction resulted in extended π-stacking, which permits architecturally controlled self-assembly in the solid state.

The coordinatively labile Zn^{II} center in $[Zn(L^1)(OAc)_2]$ provided a metalloreceptor possessing a two-guest binding ability. Fluorescence quenching by intramolecular electron transfer from the pyrenyl moieties to the guest molecules within $[Zn(L^1)(G)_2]$ was attained due to the flexibility of the podand moieties. Investigations on the scope of the allosteric metalloreceptor are currently in progress.

Experimental Section

General Methods: All reagents and solvents were purchased from commercial sources and were further purified by standard methods if necessary. Melting points were determined on a Yanagimoto Micromelting Point Apparatus and are uncorrected. Infrared spectra were obtained with a Perkin−Elmer Model 1605 FT-IR. ^{1}H NMR spectra were recorded on a Varian Mercury 300 (300 MHz) spectrometer with tetramethylsilane as an internal standard. Mass spectra were run on a JEOL JMS-DX303HF mass spectrometer. Electronic spectra were obtained using a Shimazu MultiSpec-1500 photodiode array spectrophotometer. Fluorescence emission spectra were recorded using a Shimazu RF-5300PC spectrofluorophotometer and were not corrected for instrument response. Fluorescence emission measurements were carried out in degassed solvents at 25 °C.

Synthesis of 2,6-Pyridinedicarboxaldehydebis(1-pyrenemethylimine) (L^1): A mixture of 2,6-pyridinedicarboxaldehyde (0.27 g, 2.0 mmol), 1-pyrenemethylamine hydrochloride (1.07 g, 4.0 mmol), and triethylamine (1.4 mL, 10 mmol) in methanol (80 mL) was stirred under argon at room temperature for 3 h. The precipitate was collected by vacuum filtration and rinsed with methanol. The tridentate podand ligand L^1 was isolated in 96% yield by recrystallization from dichloromethane/ether. M.p. 196−198 °C (uncorrected). IR (KBr): $\tilde{\nu}$ = 1635, 1585 cm^{-1}. ^{1}H NMR (300 MHz, $CDCl_3$): δ = 5.61 (d, J = 1.5 Hz, 4 H), 7.75 (t, J = 7.8 Hz, 1 H), 8.20−7.99 (m, 18 H), 8.37 (d, J = 9.0 Hz, 2 H), 8.51 (t, J = 1.5 Hz, 2 H). $C_{41}H_{27}N_3 \cdot 0.5H_2O$ (570.7): calcd. C 86.29, H 4.95, N 7.36; found C 86.65, H 4.86, N 7.31.

Preparation of $[Zn(L^1)_2(BF_4)_2]$: A mixture of L^1 (112 mg, 0.20 mmol) and $Zn(BF_4)_2$ (24 mg, 0.10 mmol) in acetonitrile (10 mL) was stirred under argon at room temperature for 3 h. After evaporation of the solution, $Zn(L^1)_2(BF_4)_2$ was isolated in 84% yield by recrystallization from acetonitrile/methanol. M.p. 246−247 °C (decomp.). IR (KBr): $\tilde{\nu}$ = 1644, 1587 cm^{-1}. ^{1}H NMR (300 MHz, CD_3CN): δ = 4.88 (d, J = 1.5 Hz, 8 H), 6.09−5.99 (m, 6 H), 7.37 (d, J = 8.1 Hz, 4 H), 7.70 (t, J = 1.5 Hz, 4 H), 8.29−7.75 (m, 32 H). $C_{82}H_{54}B_2F_8N_6Zn \cdot 2CH_3OH$ (1426.5): calcd. C 70.73, H 4.38, N 5.89; found C 70.53, H 4.11, N 6.12.

Preparation of $[Zn(L^1)(OAc)_2]$: A mixture of L^1 (169 mg, 0.30 mmol) and $Zn(OAc)_2$ (55 mg, 0.30 mmol) in dichloromethane (20 mL) was stirred under argon at room temperature for 3 h. Most of the dichloromethane solvent was evaporated, and $[Zn(L^1)(OAc)_2]$ was precipitated with ether. The precipitate was collected by vacuum filtration and dried to give $[Zn(L^1)(OAc)_2]$ in 98% yield. M.p. 173−174 °C (decomp.). IR (KBr): $\tilde{\nu}$ = 1614, 1592 cm^{-1}. ^{1}H NMR (300 MHz, $CDCl_3$): δ = 2.17 (s, 6 H), 5.96 (d, J = 1.5 Hz, 4 H), 7.31 (d, J = 7.8 Hz, 2 H), 7.77 (t, J = 1.5 Hz, 2 H), 7.85 (t, J = 7.8 Hz, 1 H), 8.26−8.01 (m, 18 H). $C_{45}H_{33}N_3O_4Zn \cdot H_2O$ (763.2): calcd. C 70.82, H 4.62, N 5.51; found C 70.79, H 4.69, N 5.47.

Preparation of $[Zn(L^1)(G^1)_2]$: A mixture of $[Zn(L^1)(OAc)_2]$ (75 mg, 0.10 mmol) and potassium 4-nitrobenzoate (40 mg, 0.20 mmol) in methanol (15 mL) was stirred under argon at room temperature for 3 h, resulting in a yellow precipitate. The precipitate was collected by vacuum filtration and dried to give a quantitative yield of $[Zn(L^1)(G^1)_2]$. M.p. 237−238 °C (decomp.). IR (KBr): $\tilde{\nu}$ = 1632, 1590 cm^{-1}. ^{1}H NMR (300 MHz, $CDCl_3$): δ = 5.73 (d, J = 1.5 Hz, 4 H), 8.16−7.66 (m, 29 H), 8.30 (br. t, 2 H). $C_{55}H_{35}N_5O_8Zn$ (959.3): calcd. C 68.86, H 3.68, N 7.30; found C 68.51, H 3.89, N 7.24.

Preparation of $[Zn(L^1)(G^2)_2]$: A mixture of $[Zn(L^1)(OAc)_2]$ (75 mg, 0.10 mmol) and potassium 3,5-dinitrobenzoate (47 mg, 0.20 mmol) in methanol (15 mL) was stirred under argon at room temperature for 3 h, resulting in a yellow precipitate. The precipitate was collected by vacuum filtration and dried to give a quantitative yield of $[Zn(L^1)(G^2)_2]$. M.p. 256−257 °C (decomp.). IR (KBr): $\tilde{\nu}$ = 1626, 1591 cm^{-1}. ^{1}H NMR (300 MHz, $CDCl_3$): δ = 5.55 (d, J = 1.5 Hz, 4 H), 8.17−7.76 (m, 24 H), 8.36 (t, J = 2.1 Hz, 2 H), 8.38 (t, J = 7.8 Hz, 1 H), 8.75 (br. t, 2 H). $C_{55}H_{33}N_7O_{12}Zn \cdot 2H_2O$ (1085.33): calcd. C 60.87, H 3.44, N 9.03; found C 60.47, H 3.38, N 8.74.

X-ray Crystal Structure Determination: The measurement for $[Zn(L^1)_2(BF_4)_2]$ was made on a Rigaku RAXIS-RAPID Imaging Plate diffractometer with graphite-monochromated Mo-K_α radiation. A total of 56986 independent reflections was obtained of which 15981 were unique. The structure was solved by heavy-atom Patterson methods and expanded using Fourier techniques. The non-hydrogen atoms were refined anisotropically. $R1$ = 0.119, $wR2$ = 0.371. The measurement for $[Zn(L^1)(G^1)_2]$ was made on a Bruker SMART 1000 diffractometer with graphite-monochromated Mo-K_α radiation. A total of 12923 independent reflections were obtained of which 10897 were unique. The structure was solved by direct methods and expanded using Fourier techniques. The non-hydrogen atoms were refined anisotropically. $R1$ = 0.053, $wR2$ = 0.084. Crystallographic details are given in Table 1. Crystallographic data (excluding structure factors) for the structures reported in this paper have been deposited with the Cambridge Crystallographic Data Centre as supplementary publication nos. CCDC-169877 for $[Zn(L^1)_2(BF_4)_2]$ and CCDC-169878 for $[Zn(L^1)(G^1)_2]$. Copies of the data can be obtained free of charge on application to CCDC, 12 Union Road, Cambridge CB2 1EZ, UK [Fax: (internat.) +44-1223/336-033; E-mail: deposit@ccdc.cam.ac.uk].

Acknowledgments

Thanks are due to the Analytical Center, Faculty of Engineering, Osaka University.

[1] [1a] M. Kim, G. W. Gokel, *J. Chem. Soc., Chem. Commun.* **1987**, 1686−1688. [1b] H.-J. Schneider, D. Ruf, *Angew. Chem. Int. Ed. Engl.* **1990**, *29*, 1159−1160. [1c] C. A. Hunter, L. D. Sarson, *Angew. Chem. Int. Ed. Engl.* **1994**, *33*, 2313−2316. [1d] M. S. Goodman, J. Weiss, A. D. Hamilton, *Tetrahedron Lett.* **1994**, *35*, 8943−8946. [1e] M. S. Goodman, V. Jubian, B. Linton, A. D. Hamilton, *J. Am. Chem. Soc.* **1995**, *117*, 11610−11611. [1f] B. Linton, A. D. Hamilton, *Chem. Rev.* **1997**, *97*, 1669−1680.

[2] [2a] C. J. van Staveren, D. E. Fenton, D. N. Reinhoudt, J. van Eerden, S. Harkema, *J. Am. Chem. Soc.* **1987**, *109*, 3456−3458. [2b] P. Scrimin, P. Tecilla, U. Tonellato, N. Vignaga, *J. Chem. Soc., Chem. Commun.* **1991**, 449−451. [2c] J. E. Kickham, S. J. Loeb, S. L. Murphy, *J. Am. Chem. Soc.* **1993**, *115*, 7031−7032. [2d] T. Mizutani, T. Ema, T. Tomita, Y. Kuroda, H. Ogoshi, *J. Am. Chem. Soc.* **1994**, *116*, 4240−4250. [2e] M. J. Crossley, T. W. Hambley, L. G. Mackay, A. C. Try, R. Walton, *J. Chem. Soc., Chem. Commun.* **1995**, 1077−1079.

[3] [3a] T. Nabeshima, T. Inaba, N. Furukawa, T. Hosoya, Y. Yano, *Inorg. Chem.* **1993**, *32*, 1407−1416. [3b] M. Inouye, T. Konishi, K. Isagawa, *J. Am. Chem. Soc.* **1993**, *115*, 8091−8095. [3c] M. H. Al-Sayah, N. R. Branda, *Angew. Chem. Int. Ed.* **2000**, *39*, 945−947.

[4] A. P. de Silva, H. Q. N. Gunaratne, T. Gunnlaugsson, A. J. M. Huxley, C. P. McCoy, J. T. Rademacher, T. E. Rice, *Chem. Rev.* **1997**, *97*, 1515−1566.

[5] [5a] I. Aoki, H. Kawabata, K. Nakashima, S. Shinkai, *J. Chem. Soc., Chem. Commun.* **1991**, 1771−1773. [5b] S. Nishizawa, Y. Kato, N. Teramae, *J. Am. Chem. Soc.* **1999**, *121*, 9463−9464. [5c] N. J. van der Veen, S. Flink, M. A. Deij, R. J. M. Egberink, F. C. J. M. van Veggel, D. N. Reinhoudt, *J. Am. Chem. Soc.* **2000**, *122*, 6112−6113.

[6] [6a] G. R. Desiraju, A. Gavezzotti, *J. Chem. Soc., Chem. Commun.* **1989**, 621−623. [6b] M. Munakata, J. Dai, M. Maekawa, T. Kuroda-Sowa, J. Fukui, *J. Chem. Soc., Chem. Commun.* **1994**, 2331−2332.

[7] [7a] E. Kimura, T. Ikeda, M. Shionoya, M. Shiro, *Angew. Chem. Int. Ed. Engl.* **1995**, *34*, 663−664. [7b] G. De Santis, L. Fabbrizzi, M. Licchelli, A. Poggi, A. Taglietti, *Angew. Chem. Int. Ed. Engl.* **1996**, *35*, 202−204.

[8] [8a] T. Hirao, T. Moriuchi, T. Ishikawa, K. Nishimura, S. Mikami, Y. Ohshiro, I. Ikeda, *J. Mol. Catal. A: Chemical* **1996**, *113*, 117−130. [8b] F. A. Chavez, M. M. Olmstead, P. K. Mascharak, *Inorg. Chem.* **1997**, *36*, 6323−6327.

[9] A. W. Addison, T. N. Rao, J. Reedijk, J. van Rijn, G. C. Verschoor, *J. Chem. Soc., Dalton Trans.* **1984**, 1349−1356.

[10] An electron transfer process from the pyrenyl moiety to the 4-nitrobenzoate moiety is thermodynamically feasible, as indicated by the negative value of $\Delta G_{ET} = E(D^+/D) - E(A/A^-) - E^{0-0} = -0.6$ eV.

Received September 4, 2001
[I01361]

Direct Synthesis of Heterometallic Europium/Barium Complexes: $H_2[Eu_2Ba_6O_2(OiPr)_{16}(THF)_4]$ and $EuBa_2(OC_6H_4Me\text{-}4)_7(diglyme)_2(DME)$

William J. Evans,*[a] Dimitrios G. Giarikos,[a] Michael A. Greci,[a] and Joseph W. Ziller[a]

Keywords: Europium / Barium / Heterometallic complexes / Isopropoxide complexes

Convenient syntheses of mixed-metal Eu/Ba complexes starting from the elemental metals have been explored. A mixture of europium and barium ingots reacts in boiling 2-propanol to form a product which crystallizes from THF as the heterometallic complex formulated as $H_2[Eu_2Ba_6O_2(OiPr)_{16}(THF)_4]$ (**1**). An analogous reaction in the presence of *p*-cresol (HOC_6H_4Me-4) forms trimetallic $EuBa_2(OC_6H_4Me_4)_7(diglyme)_2(DME)$ (**2**), after recrystallization from THF/DME/diglyme (DME = 1,2-dimethoxyethane). Complex **1** exhibits an octametallic geometry comprised of two square pyramids with coplanar bases which share a basal edge and have apices on opposite sides. The six barium atoms occupy the basal positions and the two europium atoms are at the apices. Complex **2** exhibits a triangular arrangement of metal atoms with both terminal and bridging aryloxide ligands coordinated to the europium atom and bridging aryloxide and terminal ether ligands coordinated to the barium atoms.

Introduction

One approach to improve the performance of multi-metallic solid-state materials is to construct them from molecular precursors which have the metal components mixed with a predetermined stoichiometry at the molecular level.[1] To use this method to improve phosphors[2,3] that depend on the special fluorescent properties of europium,[4] convenient syntheses of heterometallic europium complexes are needed. Alkoxide or aryloxide complexes are desirable since they could be converted into oxide materials by sol-gel and thermal methods.[5] Preparation of such complexes directly from the metals is preferable, since it avoids the problems of drying and potential anion contamination which accompany the use of metal salts as precursors.

Although several routes to well-defined homometallic europium alkoxide complexes have been reported,[6−15] heterometallic species have remained elusive. For example, attempts to produce heterometallic Eu/alkaline earth species by direct reaction of the metal ingots with aryl alcohols in liquid ammonia were unsuccessful and produced only mixtures of homometallic species.[16]

We report here the direct synthesis of well-defined heterometallic europium alkoxide complexes by reaction of mixtures of europium and barium metal ingots with 2-propanol at reflux. Barium was chosen since it is a frequent heterocomponent in europium-based phosphors.[17−19] We also describe the variation in structure and metal stoichiometry induced in the isolated products by addition of *p*-cresol to the reaction mixture.

Results and Discussion

Synthesis

Mixtures of metallic europium and barium react with 2-propanol at reflux to form an ether-soluble product. Structural details could not be elucidated from the NMR spectra of the product due to the broadness and shifts in resonances caused by the paramagnetism of europium in this product. To unambiguously determine the nature of reaction products, crystallization was attempted from a variety of coordinating solvents and mixtures of solvents.

Single crystals of **1** could only be obtained from THF. Crystallization of the europium/barium/2-propanol reaction product from THF yielded single crystals which were found by X-ray diffraction to be $H_2[Eu_2Ba_6O_2(OiPr)_{16}(THF)_4]$ (**1**), see Figure 1. The magnetic moment of

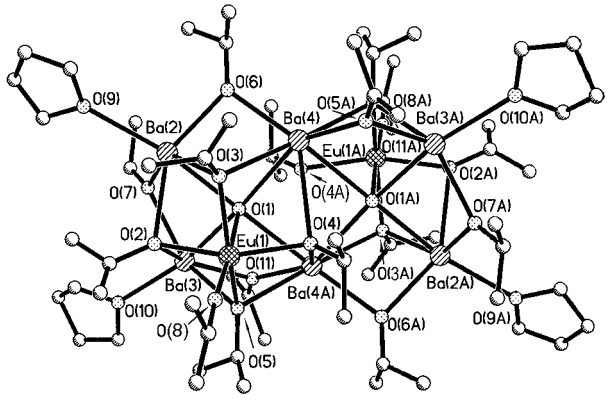

Figure 1. Ball-and-stick diagram of $H_2[Eu_2Ba_6O_2(OiPr)_{16}(THF)_4]$ (**1**); hydrogen atoms are omitted for the sake of clarity

[a] Department of Chemistry, University of California, Irvine, California 92697-2025, USA

this complex was consistent with the presence of trivalent, rather than divalent, europium.[20]

Reactions containing aryl alcohols were also examined, since they had previously been shown to be effective in generating crystalline polymetallic lanthanide complexes.[6,7,11−13,21] After heating a mixture of *p*-cresol and europium and barium metals in 2-propanol at reflux, removal of solvent resulted in a yellow solid. The solid failed to crystallize from THF, diglyme, diethyl ether, and DME, but formed crystals from a mixture of ethers (THF, DME, diglyme, 6:1:1). The fact that **2** crystallized only from a mixture of ethers, but not from any single ether suggested that there may be more than one type of ether in the product. IR data indicated that the product contained arlyoxide ligands. The effective magnetic moment of **2** was also consistent with the presence of Eu^{III}.[20] Elemental analysis was consistent with a 2:1 ratio of Ba/Eu. The structure was determined by X-ray diffraction to be $EuBa_2(OC_6H_4Me\text{-}4)_7(diglyme)_2(DME)$ (**2**), Figure 2.

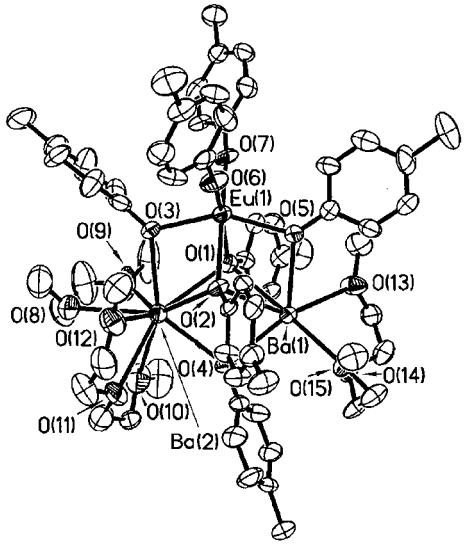

Figure 2. ORTEP diagram of the molecular structure of $EuBa_2(OC_6H_4Me\text{-}4)_7(diglyme)_2(DME)$ (**2**); thermal ellipsoids are drawn at the 30% probability level; hydrogen atoms are omitted for the sake of clarity

Structure of $H_2[Eu_2Ba_6O_2(OiPr)_{16}(THF)_4]$ (1)

Due to the limited quality of the data, only the atomic connectivity in this structure can be described. The metal atoms in **1** do not adopt a conventional eight-coordinate geometry, but rather form the vertices of two square pyramids which share an edge and have their apices on the opposite sides of the basal plane (Figure 3). This geometry

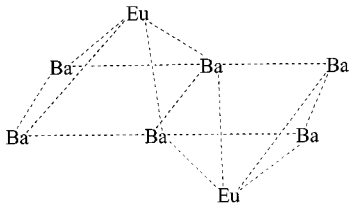

Figure 3. Metal framework in $H_2[Eu_2Ba_6O_2(OiPr)_{16}(THF)_4]$ (**1**)

is not unique to **1** and has been observed in $H_2[Ba_8O_2(OC_6H_5)_{14}(HMPA)_6]$ (**3**), and $H_2[Ba_2Sr_6O_2(OC_6H_5)_{14}(HMPA)_6]$ (**4**), both of which have the same general formula as **1**, namely $H_2[M_8O_2(ligand)_{20}]$.[22]

The two apical positions of the square pyramids in **1** are occupied by europium atoms and the six basal positions are occupied by barium atoms. Complex **4** also has a 3:1 ratio of metals (Sr/Ba) in the same geometry as **1**, but the set of two Ba atoms occupy the shared basal edge positions in **4** instead of the apical positions occupied by the set of two europium atoms in **1**. Both square-pyramidal units in **1** are symmetry-related due to a center of symmetry located between the two europium atoms. The metal···metal distances are given in Table 1.

Table 1. Metal−metal bond lengths [Å] in $H_2[Eu_2Ba_6O_2(OiPr)_{16}(THF)_4]$ (**1**)

Bond	**1**
Eu(1)···Ba(3)	3.737(1)
Eu(1)···Ba(2)	3.738(1)
Eu(1)···Ba(4A)	3.895(1)
Eu(1)···Ba(4)	3.896(1)
Ba(2)···Ba(3)	3.836(1)
Ba(2)···Ba(4)	3.892(1)
Ba(3)···Ba(4A)	3.886(1)
Ba(4)···Ba(3A)	3.886(1)
Ba(4)···Eu(1A)	3.895(1)

The five metal atoms of each square pyramid are connected by one μ_5-oxygen, four μ_3-O*i*Pr ligands bridging the triangular faces, and three μ-O*i*Pr ligands bridging the unshared basal edges of the square pyramid. In addition, there is one terminal isopropoxide ligand on each of the two europium atoms and there is one THF ligand attached to each of the four unshared basal corners of the square pyramids. This generates a six-coordinate europium atom and six- and eight-coordinate barium atoms. Two THF ligands also co-crystallize with each molecule of **1**, but do not interact with the metal centers. In addition to the components described so far, the presence of two protons is required to balance the charge between the observed cations and anions. Hydrogen atoms were not located in the X-ray study and there are no structural anomalies in **1** that would indicate their exact position, in contrast to the situation in **3** and **4**.[22]

Structure of $EuBa_2(OC_6H_4Me\text{-}4)_7(diglyme)_2(DME)$ (2)

The three metal atoms in **2** occupy a triangular arrangement with 4.1316(14) Å Ba(1)···Ba(2) nonbonding distances and 3.8440(13) and 3.8934(13) Å Eu(1)···Ba nonbonding distances. The metal atoms in **2** are connected by two μ_3-aryloxide ligands above and below the triangular plane and three μ_2-aryloxide ligands, each bridging one edge of the triangle. The europium atom has two additional terminal aryloxide ligands, which lead to a formal coordination number of six. The barium atoms have dissimilar coordination environments: each atom has one tridentate diglyme coordinated to it, but Ba(2) also has a bidentate DME. This

gives a formal coordination number of seven for Ba(1) and nine for Ba(2), with respect to the oxygen donor atoms, but further ligation is present, as described below. Bond lengths in **2** are shown in Table 2.

Table 2. Bond lengths [Å] in $EuBa_2(OC_6H_4Me\text{-}4)_7(diglyme)_2(DME)$ (**2**)

Eu(1)−O(1)	2.432(9)	Ba(1)−O(15)	2.815(10)
Eu(1)−O(2)	2.412(9)	Ba(2)−O(1)	2.822(9)
Eu(1)−O(3)	2.299(10)	Ba(2)−O(2)	2.829(9)
Eu(1)−O(5)	2.343(9)	Ba(2)−O(3)	2.751(9)
Eu(1)−O(6)	2.161(10)	Ba(2)−O(4)	2.675(9)
Eu(1)−O(7)	2.193(9)	Ba(2)−O(8)	2.918(11)
Ba(1)−O(1)	2.770(9)	Ba(2)−O(9)	2.909(11)
Ba(1)−O(2)	2.780(9)	Ba(2)−O(10)	2.893(12)
Ba(1)−O(4)	2.630(10)	Ba(2)−O(11)	2.943(11)
Ba(1)−O(5)	2.672(9)	Ba(2)−O(12)	2.815(11)
Ba(1)−O(13)	2.849(10)	Eu(1)···Ba(1)	3.844(1)
Ba(1)−O(14)	2.837(10)	Eu(1)···Ba(2)	3.893(1)

The 2.412(9) and 2.432(9) Å Eu−μ_3-O (OAr) (OAr = OC_6H_4Me-4) distances and the 2.161(10) and 2.193(9) Å Eu−O (terminal OAr) distances in **2** are in the range of those in the trivalent lanthanum 4-methylphenoxide complex $[Me_4N][La_2Na_2(\mu_4\text{-}OAr)(\mu_3\text{-}OAr)_2(\mu\text{-}OAr)_4(OAr)_2(THF)_5]$ [2.284(3) and 2.296(3) Å],[21] considering the differences in Shannon radii,[23] but they are shorter than the corresponding 2.350(5) Å distance in divalent $Eu_2(OC_6H_3Me_2\text{-}2,6)_4(DME)_3$.[6] The 2.299(10) and 2.343(9) Å Eu−μ-O (OAr) distances in **2** are also reasonable compared to those in trivalent $K_3Nd_2(\mu\text{-}OAr)_6(\mu_4\text{-}OAr)_3(THF)_7$ [24] and $\{[La_2Na_2(\mu_4\text{-}OAr)_3(\mu\text{-}OAr)_6(dioxane)_5](dioxane)\}_n$,[17] but they are shorter than the 2.479(3)−2.632(3), 2.447(5)−2.597(5), and 2.444(13)−2.581(12) Å Eu−O (μ-$OC_6H_3Me_2$-2,6) distances in the divalent complexes $Eu_2(OC_6H_3Me_2\text{-}2,6)_4$(*N*-methylimidazole)$_5$,[12] $Eu_2(OC_6H_3Me_2\text{-}2,6)_4(DME)_3$,[6] and $Eu_3(OC_6H_3Me_2\text{-}2,6)_6(THF)_6$,[14] respectively. In general, the differences in Eu−O bond lengths between **2** and divalent europium aryloxides in the literature correspond to the difference in Shannon radii between Eu^{III} and Eu^{II}.[23] This is in agreement with the magnetic data on **2** which indicate that the europium atom is trivalent.

The 2.630(10)−2.751(9) Å Ba−O (μ-OAr) and 2.770(9)−2.829(9) Å Ba−O (μ_3-OAr) distances in **2** are also similar to the corresponding average distances in $HBa_5(O)(OC_6H_5)_9(THF)_8$ [2.65(3) and 2.75(2) Å],[25] **3** [2.65(6) and 2.76(9) Å],[22] and those in $Ba_5(OH)(OC_6H_3Me_2\text{-}3,5)_9(THF)_5$ [26] [2.61(5) and 2.70(3) Å]. The 2.815(11)−2.943(11) Å Ba−O (ether) distances in **2** are in good agreement with the 2.814(6)−2.900(6) Å and 2.826(7)−2.919(8) Å distances in Ba(tetramethylheptanedionate)$_2$(triglyme)[27] and $KBa_2(OSiPh_3)_5(DME)_2$.[28]

In addition to coordination from oxygen atoms, Ba(1) exhibits close contacts with the *ipso*-carbon atoms, C(8) and C(1), from both μ_3-aryloxide ligands, with 3.229(13) and 3.254(14) Å Ba−C (*ipso*-Ar) distances, respectively. These distances are in the range of similar 2.981(6)−3.193(7) Å Ba−C (Ar) contacts in $[Ph_2P(4\text{-methylbenzylide})_2]_2Ba$.[29] The Ba−O−C (Ar) angles in **2** involving these two ligands also suggest that both phenyl rings are canted towards Ba(1): the angles involving Ba(1) [97.0(7) and 98.7(8)°] are more acute than those involving Ba(2) [127.5(8) and 128.3(8)]. Consideration of these two interactions increases the coordination number of Ba(1) to nine, the same as Ba(2).

Conclusion

Mixed metal complexes of europium and barium can be readily synthesized directly from the metals in 2-propanol at reflux. Varying Eu/Ba stoichiometries have been identified in crystalline systems depending on the crystallization conditions.

Experimental Section

General: All reactions were performed in a glovebox under nitrogen or by using standard Schlenk and vacuum line techniques under nitrogen. Europium and barium ingots were washed with hexanes, dried, and cut to appropriate size before use. 2-Propanol was dried by addition of 0.02 equiv. of sodium per equivalent of 2-propanol at 20° C, followed by vacuum transfer of the alcohol from this mixture into the reaction flasks. 4-Methylphenol (Aldrich) was dried and vacuum-distilled from molecular sieves (3 Å). Other solvents were dried and physical measurements were made as previously described.[15] Magnetic moments were measured by the method of Evans[30] with a General Electric QE300 NMR spectrometer. Elemental analyses were performed by Desert Analytics, Tucson, AZ with metal analyses done by atomic absorption spectroscopy.

$H_2[Eu_2Ba_6O_2(OiPr)_{16}(THF)_4]$ (1): Mixtures of europium (0.166 g, 1.1 mmol) and barium (0.408 g, 3 mmol) ingots, typically 0.5 mm in diameter, were combined in a round-bottom flask equipped with a stir bar and a Schlenk adapter. 2-Propanol (25 mL) was vacuum-transferred into the flask. The mixture was heated at reflux for 4 h and the solvent was removed under vacuum with slight heating to give an orange-brown solid (0.51 g, 50% yield based on Eu). A portion of this material (110 mg) was then dissolved in hot THF and centrifuged. Yellow crystals formed overnight at −31 °C (75 mg, 68%). $C_{64}H_{146}Ba_6Eu_2O_{22}$ (2395.74): calcd. C 32.08, H 6.14, Ba 34.39, Eu 12.69; found C 31.86, H 6.28, Ba 34.25, Eu 12.45. Magnetic susceptibility: $\chi_g^{298K} = 5.4 \times 10^{-6}$, $\mu_{eff}^{298K} = 4.2\ \mu_B$. IR (KBr): $\tilde{\nu}$ = 2948 s, 2858 m, 2770 m, 2670 w, 2581 m, 2353 w, 2104 w, 1933 w, 1731 w, 1457 m, 1368 m, 1348 m, 1239 w, 1150 s, 1040 w, 966 s, 902 w, 812 m, 763 w, 728 w, 510 m cm^{-1}. Space group: *C*2/*c*. Unit cell: *a* = 27.853(5), *b* = 24.263(3), *c* = 17.097(4) Å, β = 108.496(12)°, *V* = 10958(4) $Å^3$, *Z* = 4.

X-ray Data Collection and Solution and Refinement for $H_2[Eu_2Ba_6O_2(OiPr)_{16}(THF)_4]$ (1): A yellow crystal of approximate dimensions 0.30 × 0.23 × 0.23 mm was mounted on a glass fiber and transferred to the Siemens P4 diffractometer. The determination of symmetry, crystal class, unit cell parameters and the crystal's orientation matrix were carried out according to standard procedures.[31] Intensity data were collected at 163 K using the 2θ/ω scan technique with Mo-K_α radiation. The raw data were processed with a local version of CARESS[32] which employs a modified version of the Lehman−Larsen algorithm to obtain intensities and standard deviations from the measured 96-step peak profiles. All 7818 data were corrected for absorption and Lorentz and polarization effects and were placed on an approximately absolute scale. The diffrac-

tion symmetry was 2/*m* and the systematic absences were consistent with the centrosymmetric monoclinic space group *C*2/*c*. All calculations were carried out using the SHELXL program.[33] The analytical scattering factors for neutral atoms were used throughout the analysis.[34] The structure was solved by direct methods and refined on F^2 by full-matrix least-squares techniques. Hydrogen atoms were included using a riding model. Two molecules of THF were located per octametallic molecule of **1**. Only heteroatoms were refined anisotropically because of unacceptable thermal parameters for several carbon atoms after anisotropic refinement was attempted. Hence, only connectivity could be determined from these data.

$EuBa_2(OC_6H_4Me\text{-}4)_7(diglyme)_2(DME)$ (2): Europium (117 mg, 0.77 mmol) and barium (210 mg, 1.53 mmol) ingots and *p*-cresol (592 mg, 5.47 mmol) were combined in a round-bottom flask equipped with a stir bar and a Schlenk adapter. 2-Propanol (15 mL) was vacuum-transferred into the flask and the mixture was heated at reflux for 24 h. After the solvent was removed under vacuum with slight heating, 30 mL of THF, 5 mL of DME, and 5 mL of diglyme were added to the flask. After heating for 30 min, the entire product was soluble. Reduction of the solution volume to 5 mL by rotary evaporation led, over a period of 12 h, to the formation of crystals of **2** suitable for single-crystal X-ray diffraction (910 mg, 80%). $C_{65}H_{87}Ba_2EuO_{15}$ (1534.99): calcd. C 50.9, H 5.7, Eu 9.9; found C 50.8, H 5.9, Eu 10.4. Magnetic susceptibility: $\chi_g^{298K} = 3.5 \times 10^{-6}$, $\mu_{eff}^{298K} = 3.5\ \mu_B$. IR (KBr): $\tilde{\nu}$ = 3010 w, 2916 m, 2860 w, 1604 m, 1557 w, 1501 s, 1454 m, 1318 m, 1266 s, 1201 w, 1167 m, 1097 w, 1065 m, 1013 m, 933 w, 858 m, 824 s, 753 m, 580 w cm^{-1}. Temperature: 163 K. Crystal system: monoclinic. Space group: $P2_1/n$. Unit cell: a = 12.269(3), b = 24.750(5), c = 23.570(4) Å, β = 98.685(10)°, V = 7076(2) $Å^3$, Z = 4, $\rho_{calcd.}$ = 1.441 Mg/m^3, μ = 2.035 mm^{-1}.

X-ray Data Collection and Solution and Refinement for 2: A yellow crystal of approximate dimensions 0.20 × 0.10 × 0.10 mm was handled and raw data were processed as described above for **1**. All 9756 data were corrected for absorption and Lorentz and polarization effects and were placed on an approximately absolute scale. The diffraction symmetry was 2/*m* and the systematic absences were consistent with the centrosymmetric monoclinic space group $P2_1/n$. All calculations were as described for **1** above. The structure was solved by direct methods and refined on F^2 by full-matrix least-squares techniques. Minor disorder in the diglyme molecules was modeled by assigning partial occupancy to components of the disordered groups. Hydrogen atoms were included using a riding model. At convergence, $wR2$ = 0.1705 and GOF = 1.066 for 748 variables refined against all 9248 unique data [for refinement on F, $R1$ = 0.0631 for those 5757 data with $F > 4.0\sigma(F)$].

Crystallographic data (excluding structure factors) for the structures reported in this paper have been deposited with the Cambridge Crystallographic Data Centre as supplementary publication no. CCDC-171956 (**1**) and -171957 (**2**). Copies of the data can be obtained free of charge on application to CCDC, 12 Union Road, Cambridge CB2 1EZ, UK [Fax: (internat.) + 44-1223/336-033; E-mail: deposit@ccdc.cam.ac.uk].

Acknowledgments

For support of this research, we thank the Division of Chemical Sciences of the Office of Basic Energy Sciences of the Department of Energy.

[1] K. G. Caulton, L. Hubert-Pfalzgraf, *Chem. Rev.* **1990**, *90*, 969.
[2] R. C. Ropp, *Studies in Inorganic Chemistry 17*, *The Chemistry of Artificial Lighting Devices, Lamps, Phosphors and Cathode Ray Tubes*, Elsevier, New York, **1993**. S. Shionoya, W. M. Yen, *Phosphor Handbook*, CRC Press, Boca Raton, Florida, **1998**.
[3] G. Blasse, B. C. Grabmaier, *Luminescent Materials*, Springer-Verlag, New York, **1994**.
[4] J. R. McColl, F. C. Palilla, in *Industrial Applications of Rare Earth Elements* (Ed.: K. A. Gschneidner, Jr.), *ACS Symp. Ser.*, American Chemical Society, Washington, D. C., **1981**, vol. 164, chapter 10. W. A. Thorton, in *Industrial Applications of Rare Earth Elements* (Ed.: K. A. Gschneidner, Jr.), *ACS Symp. Ser.*, American Chemical Society, Washington, D. C., **1981**, vol. 164, chapter 11. R. C. Ropp, *Luminescence and the Solid State*, Elsevier Sci. Pub. Co., New York, **1991**.
[5] L. G. Hubert-Pfalzgraf, *New J. Chem.* **1987**, *11*, 663.
[6] L. Brown, M. K. S. Mazdiyasni, *Inorg. Chem.* **1970**, *9*, 2783.
[7] W. J. Evans, W. G. McClelland, M. A. Greci, J. W. Ziller, *Eur. J. Solid State Inorg. Chem.* **1996**, *33*, 145.
[8] W. J. Evans, M. A. Greci, J. W. Ziller, *J. Chem. Soc., Dalton Trans.* **1997**, *17*, 3035.
[9] W. J. Evans, M. A. Greci, M. A. Ansari, J. W. Ziller, *J. Chem. Soc., Dalton Trans.* **1997**, *23*, 4503.
[10] J. M. Carretas, J. Branco, J. Marçalo, J. C. Waerenborgh, N. Marques, A. Pires de Matos, *International Conference on f Elements*, 3, Paris, France, Sept. **1997**, P6/7−55.
[11] J. M. Carretas, J. Branco, J. Marçalo, J. C. Waerenborgh, N. Marques, A. Pires de Matos, *J. Alloys Compds.* **1998**, 275−277, 841.
[12] W. J. Evans, M. A. Greci, J. W. Ziller, *Inorg. Chem.* **1998**, *37*, 5221.
[13] W. J. Evans, M. A. Greci, J. W. Ziller, *Chem. Commun.* **1998**, 2367.
[14] W. J. Evans, M. A. Greci, J. W. Ziller, *Inorg. Chem. Commun.* **1999**, *2*, 530.
[15] W. J. Evans, M. A. Greci, J. W. Ziller, *Inorg. Chem.* **2000**, *39*, 3213.
[16] W. J. Evans, L. R. Chamberlain, T. A. Ulibarri, J. W. Ziller, *J. Am. Chem. Soc.* **1988**, *110*, 6423.
[17] T. L. Barry, *J. Electrochem. Soc.* **1968**, *115*, 1181.
[18] A. M. Pires, M. R. Davolos, O. L. Malta, *J. Luminesc.* **1997**, *72−74*, 244.
[19] A. M. Pires, M. R. Davolos, *Chem. Mater.* **2001**, *13* 21.
[20] W. J. Evans, M. A. Hozbor, *J. Organomet. Chem.* **1987**, *326*, 299.
[21] W. J. Evans, R. E. Golden, J. W. Ziller, *Inorg. Chem.* **1993**, *32*, 3041.
[22] K. G. Caulton, M. H. Chisholm, S. R. Drake, K. Folting, J. C. Huffman, *Inorg. Chem.* **1993**, *32*, 816.
[23] R. D. Shannon, *Acta Crystallogr., Sect. A* **1976**, *32*, 751.
[24] W. J. Evans, M. A. Ansari, J. W. Ziller, *Polyhedron* **1997**, *16*, 3429.
[25] K. G. Caulton, M. H. Chisholm, S. R. Drake, K. Folting, *J. Chem. Soc., Chem. Commun.* **1990**, 1349.
[26] P. Miele, J.-D. Foulon, N. Hovnanian, *Polyhedron* **1993**, *12*, 209.
[27] S. R. Drake, S. A. Miller, D. J. Williams, *Inorg. Chem.* **1993**, *32*, 3227.
[28] P. S. Coan, W. E. Streib, K. G. Caulton, *Inorg. Chem.* **1991**, *30*, 5019.
[29] S. Harder, M. Lutz, *Organometallics* **1997**, *16*, 225.
[30] D. F. Evans, *J. Chem. Soc.* **1959**, 2003.
[31] *XSCANS Software Users Guide*, Version 2.1, Siemens Industrial Automation, Inc., Madison, WI, **1994**.
[32] R. W. Broach, Argonne National Laboratory, Illinois, **1978**.
[33] G. M. Sheldrick, Siemens Analytical X-ray Instruments, Inc., Madison, WI, **1994**.
[34] *International Tables of X-ray Crystallography*, Kluwer Academic Publishers, Dordrecht, **1992**, vol. C.

Received May 2, 2001
[I01151]

(Diene)rhodium and -iridium Complexes of Pyridinophane Ligands

Timo Sciarone,[a,b] Johan Hoogboom,[a] Paul P. J. Schlebos,[a] Peter H. M. Budzelaar,[a] René de Gelder,[a] Jan M. M. Smits,[a] and Anton W. Gal*[a]

Keywords: Diene ligands / Fluxionality / Iridium / Oxidations / Rhodium

(Diene)rhodium(I) and -iridium(I) derivatives of the pyridinophane ligand L^4 and the analogous macrocycle L^6 have been prepared and characterized [diene = cyclooctadiene (COD) or norbornadiene (NBD)]. In all of the complexes, the ligand is coordinated in a κ^3-(amine)(pyridine)$_2$ fashion; a dynamic process, believed to be concerted, exchanges free and coordinated amine groups. $[L^4Ir(COD)]^+$ can be protonated at the amine nitrogen atom. It reacts with H_2O_2, but *only* in the presence of acid, to give an oxocyclooctenyl complex, formally a 4-e$^-$ oxidation product. X-ray structures of $[L^4Rh(COD)]PF_6$, $[L^6Rh(COD)]PF_6$, $[L^6Rh(NBD)]PF_6$, $[(L^4H)Ir(COD)](BF_4)_2$, and $[L^4Ir(C_8H_{11}O)](PF_6)_2$ are presented.

Introduction

Olefin oxidation at a transition metal center constitutes an important method for functionalizing hydrocarbons. Recent work by Klemperer,[1] Flood,[2] and ourselves[3–8] has shown that hard N- and O-donor ligands can be used to "trap" primary oxidation products such as metallaoxetanes and metalladioxolanes. The oxidation reactions have been found to be very sensitive to ligand variation. In order to explore these ligand effects further, we decided to investigate the (diene)rhodium and -iridium [diene = COD (cyclooctadiene), NBD (norbornadiene)] complexes of pyridinophane ligands L^4 and L^6.

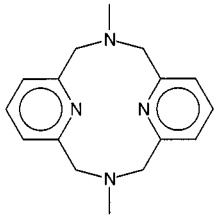

L^4

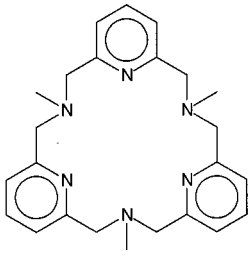

L^6

These ligands contain the same donor groups as the dipicolylamine (DPA) and tripicolylamine (TPA) ligands that we have studied previously,[5,6] but obviously have very different geometric constraints. Diene complexes are usually rather stable and thus provide a convenient starting point for further studies using more labile olefins. One Rh complex of L^4 has been reported,[9] but no Ir complexes. The coordination chemistry of L^6 appears to be relatively unexplored, and only complexes of two cryptand-like derivatives have been described.[10,11]

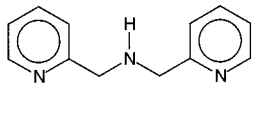

DPA

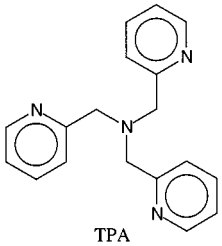

TPA

Results and Discussion

Synthesis

The syntheses of the ligands have been described by Bottino et al. (Scheme 1).[12] The ring-closure step in the syn-

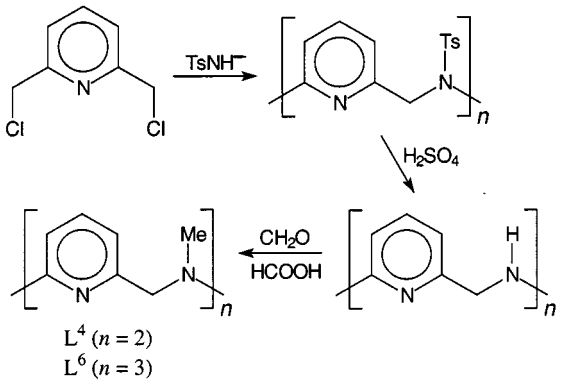

Scheme 1. Ligand synthesis

[a] Department of Inorganic Chemistry, University of Nijmegen, Toernooiveld 1, 6525 ED Nijmegen, The Netherlands
E-mail: gal@sci.kun.nl
[b] Present address: Stratingh Institute of Chemistry and Chemical Engineering, University of Groningen, Nijenborgh 4, 9747 AG Groningen, The Netherlands

Supporting information for this article is available on the WWW under http://www.eurjic.com or from the author.

 © WILEY-VCH Verlag GmbH, 69451 Weinheim, Germany, 2002 1434–1948/02/0202–0457 $ 17.50+.50/0

thesis always produces a mixture of bis- and tris(pyridine) ligands. The most convenient preparation of pure L^4 involves crystallization at the NH stage.[13] For the preparation of pure L^6, we separated the two components by chromatography at the *N*-tosyl stage; this was much less convenient and required large amounts of solvent.

Complexes of L^4 and L^6 were prepared by adding the ligand to a suspension of $[M(COD)Cl]_2$ (M = Rh, Ir) or $[Rh(NBD)Cl]_2$ in methanol. The products can be isolated as the PF_6, BF_4 or BPh_4 salts by precipitation, or as the chlorides by evaporation of the solvent.

Structure and Fluxionality

In all complexes the metal atom is coordinated to one amine nitrogen atom, two pyridine nitrogen atoms and the diene ligand. X-ray structures of $[L^4Rh(COD)]^+$, $[L^6Rh(COD)]^+$, and $[L^6Rh(NBD)]^+$ are shown in Figures 1, 2, and 3, respectively. The structures are all roughly square-pyramidal, with N_{amine} occupying the apical position. In $[L^4Rh(COD)]^+$, the methyl group at the noncoordinated amine group points away from the Rh atom. This is somewhat surprising, since in the only other complex of a κ^3-coordinated L^4 ligand reported to date $[L^4Mo(CO)_3]$[14] the methyl group points in the opposite direction.[15]

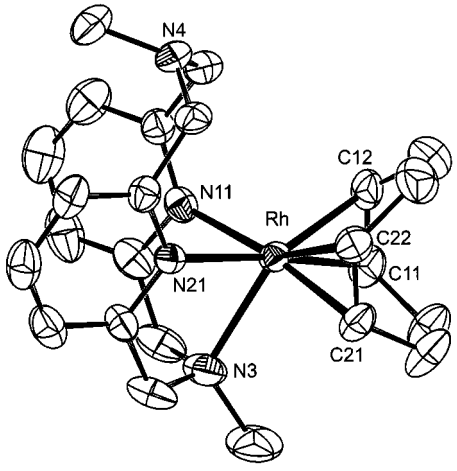

Figure 1. X-ray structure [40% TME (Thermal Motion Ellipsoids)] of $[L^4Rh(COD)]PF_6$; all hydrogen atoms and the counterion have been omitted; selected bond lengths [Å] and angles [°]: Rh−C11 2.105(7), Rh−C12 2.123(7), Rh−C21 2.119(8), Rh−C22 2.137(8), Rh−N11 2.183(6), Rh−N21 2.171(5), Rh−N3 2.336(7); N11−Rh−N21 75.9(2), N11−Rh−N3 77.0(2), N21−Rh−N3 77.0(2)

It is interesting to compare the structures of the L^4 and L^6 complexes with those of other tridentate N-donor ligands. We have recently reported the structures of several $Rh^I(COD)$ complexes of DPA-type ligands.[5] With one exception,[16] these all have $N_{py}-Rh-N_{py}$ angles of 87−92°. The $N_{py}-Rh-N_{py}$ angle in $[L^4Rh(COD)]^+$ is small (76°), undoubtedly because of steric constraints; in fact, it is close to the $N_{amine}-Rh-N_{py}$ angles (75−77° in our L^4 and L^6 complexes), and to the $N_{amine}-Rh-N_{amine}$ angles in $[Cn^*Rh(COD)]^+$ (77−80°) (Cn* = 1,4,7-trimethyl-1,4,7-triazacyclononane).[5] In contrast, the $N_{py}-Rh-N_{py}$ angles in the two L^6 complexes are normal (91° and 95°), showing that steric constraints are much less important there.

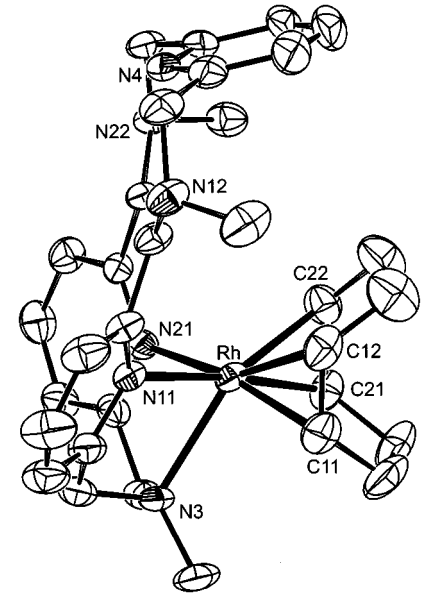

Figure 2. X-ray structure (40% TME) of $[L^6Rh(COD)]PF_6$; all hydrogen atoms and the counterion have been omitted; selected bond lengths [Å] and angles [°]: Rh−C11 2.124(5), Rh−C12 2.165(5), Rh−C21 2.101(5), Rh−C22 2.183(5), Rh−N11 2.311(4), Rh−N21 2.176(4), Rh−N3 2.343(4); N11−Rh−N21 91.48(14), N11−Rh−N3 75.86(14), N21−Rh−N3 75.15(15)

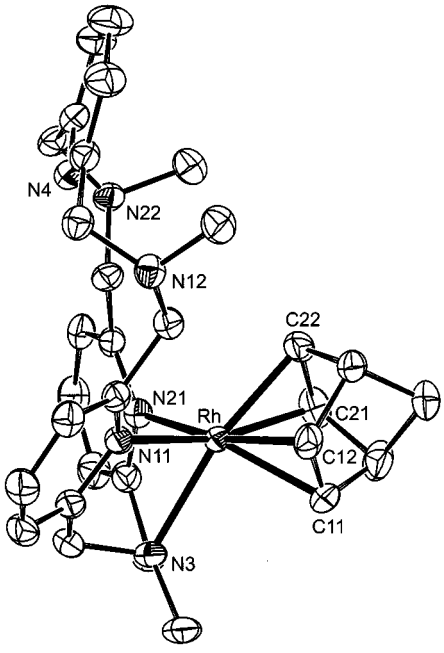

Figure 3. X-ray structure (40% TME) of $[L^6Rh(NBD)]PF_6$(acetone); all hydrogen atoms, the counterion and the acetone molecule of crystallization have been omitted; selected bond lengths [Å] and angles [°]: Rh−C11 2.152(4), Rh−C12 2.148(4), Rh−C21 2.054(4), Rh−C22 2.079(4), Rh−N11 2.310(3), Rh−N21 2.154(3), Rh−N3 2.278(3); N11−Rh−N21 94.71(12), N11−Rh−N3 75.95(12), N21−Rh−N3 74.84(12)

Ligand L^4 seems to be preorganized for κ^4 coordination. The κ^3-coordinated Mo complex mentioned above displays fluxional behaviour involving exchange of the two amine nitrogen atoms (Scheme 2) with activation parameters $\Delta H^{\ddagger} = 13.9$ kcal/mol, $\Delta S^{\ddagger} = -0.8$ cal/mol·K.

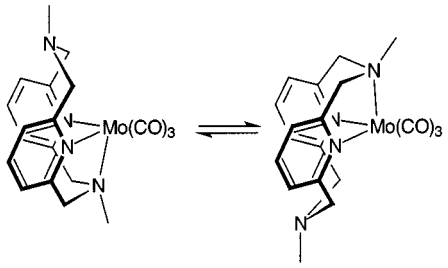

Scheme 2

The strongly broadened 1D ^{1}H NMR spectra and the negative cross-peaks in the NOESY spectra of our diene complexes indicate a similar fluxionality. The situation is complicated here by the occurrence of another fluxional process, namely diene rotation (Scheme 3). Diene rotation is common in five-coordinate complexes and would therefore be expected here; it exchanges the "top" and "bottom" halves of the diene ligand. Amine exchange would also exchange the diene halves; thus, the rate of diene rotation as determined by NMR includes a contribution from amine exchange. Variable-temperature NMR studies and full-spectrum NMR fits[17] were used to determine rate constants for $[L^4Rh(COD)]^+$, $[L^4Ir(COD)]^+$, and $[L^6Rh(COD)]^+$; the resulting activation parameters are shown in Table 1.

For the L^4 complexes, the total rate of COD rotation is significantly faster than the amine exchange in the temperature range of 0 to 100 °C, demonstrating that both processes indeed contribute. Interestingly, amine exchange has a lower activation *enthalpy*, but is still the slower process because of its more negative activation *entropy*. Since COD rotation is unlikely to be a dissociative process, these results

Table 1. Activation parameters for fluxionality of $LM(COD)^+$ complexes

Complex	Amine exchange[a] [b]		COD rotation[a] [b]	
	$\Delta H^{\ddagger}$	$\Delta S^{\ddagger}$	$\Delta H^{\ddagger}$	$\Delta S^{\ddagger}$
$[L^4Rh(COD)]PF_6$	12.0±0.3	−11.0±1.0	15.7±1.0	3.2±3.1
$[L^4Ir(COD)]PF_6$	14.0±0.2	−6.7±0.7	22.8±1.5	18.2±4.4
$[L^6Rh(COD)]PF_6$	11.8±0.3	−10.3±0.9		

[a] $\Delta H^{\ddagger}$ [kcal/mol], $\Delta S^{\ddagger}$ [cal/mol·K]. [b] Error margins are 1σ limits from Eyring fits.

suggest that metal−amine bond dissociation and formation occur simultaneously. Amine exchange is only slightly slower for Ir than for Rh, which agrees with this interpretation; for a dissociative process, the Ir analogue should have a much higher barrier.

For $[L^6Rh(COD)]^+$, COD rotation is always fast on the NMR timescale. The activation parameters for movement of the metal atom around the ring are similar to those found for amine exchange in $[L^4Rh(COD)]^+$, suggesting a similar mechanism involving repeated amine/pyridine exchange at Rh. The metal atom thus presumably moves between κ^3-(amine)(pyridine)$_2$ and κ^3-(amine)$_2$(pyridine) compartments of the macrocycle; the observed preference for the κ^3-(amine)(pyridine)$_2$ compartment suggests that this is the stronger donor site. Even at 100 °C, the two faces of the ring remain inequivalent, implying that the Rh(COD) fragment cannot move *through* the ring.

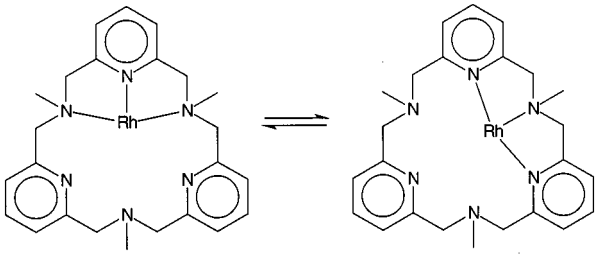

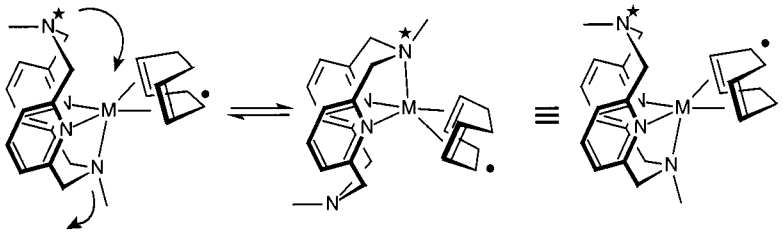

amine exchange

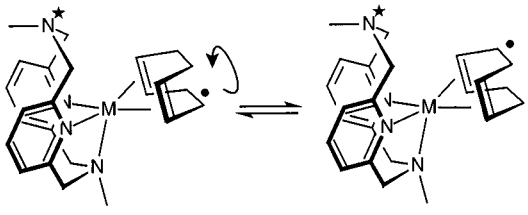

COD rotation

Scheme 3

Since L^6 has six N-donor atoms, one might wonder whether dinuclear complexes could be formed, in which one metal atom would occupy a κ^3-(amine)(pyridine)$_2$ compartment and the other a (less favourable) κ^3-(amine)$_2$(pyridine) compartment. However, treatment of L^6 with excess [Rh(diene)Cl]$_2$ produces the mononuclear complex as the only product. Possibly, there would be too much repulsion between the two diene fragments in a dinuclear complex. Also, the nitrogen lone pairs in the X-ray structures of [L^6Rh(COD)]$^+$ and [L^6Rh(NBD)]$^+$ are oriented in an unfavourable manner for coordination to the κ^3-(amine)$_2$(pyridine) compartment, as shown in Figures 2 and 3. We therefore conclude that formation of dinuclear complexes of L^6 is unlikely.

Protonation and Oxidation

Surprisingly, [L^4Ir(COD)]$^+$ reacts with H_2O_2 *only* in the presence of acid. Therefore, protonation was also investigated separately. Addition of a diethyl ether solution of HBF_4 to a solution of [L^4Ir(COD)]$^+PF_6$ in methanol produced a colourless solution. Evaporation of the solvent and dissolution of the product in methanol gave a yellow solution, from which red crystals precipitated overnight. The X-ray structure (Figure 4) shows these crystals to have the composition [(L^4H)Ir(COD)]$^+(BF_4)_2$; evidently, the lower solubility of the BF_4 salt resulted in selective precipitation of the complex with this counterion. Protonation has occurred on the dangling amine nitrogen atom. The hydrogen atom was located and refined; additional proof for protonation at the nitrogen atom comes from the C−N−C angles at the nitrogen atom (av. 110.2°), which are similar to those of the metal-coordinated nitrogen atoms in [(L^4H)Ir(COD)]$^+(BF_4)_2$ (av. 110.1°) and [L^4Rh(COD)]PF_6 (av. 109.9°) and definitely smaller than those around the dangling nitrogen atom in [L^4Rh(COD)]PF_6 (av. 115.6°). The methyl group on the ammonium nitrogen atom is now in the expected position, pointing towards the Ir atom; the ammonium proton forms a hydrogen bond with a fluorine atom of a BF_4 group. Apart from this, the structure of the dication is fairly similar to that of the unprotonated monocation [L^4Rh(COD)]$^+$.

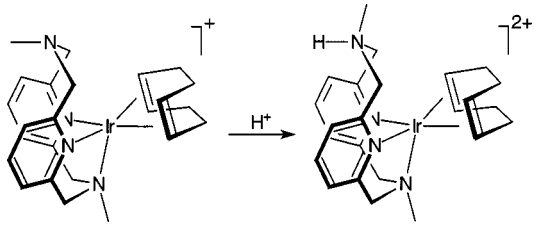

Addition of excess H_2O_2 to a solution of [L^4Ir(COD)]$^+$ and 1 equiv. of acid results in a fast reaction to give an oxocyclooctenyl complex [L^4Ir($C_8H_{11}O$)]$^{2+}$. This is a net 4-e$^-$ oxidation and we were unable to detect any intermediates by NMR; 1 equiv. of acid is consumed, but if only 0.5 equiv. of acid is used, half of the starting material is recovered unchanged. Crystals suitable for X-ray diffraction were obtained from acetone; they were found to contain

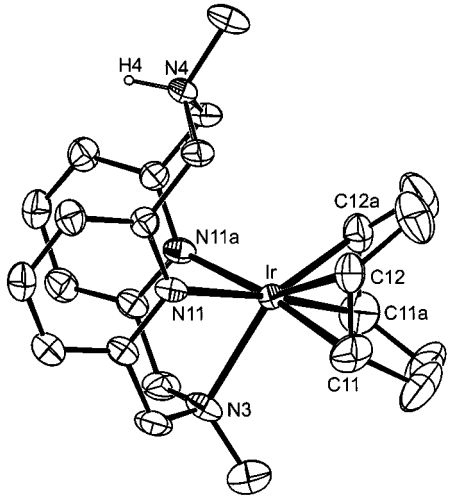

Figure 4. X-ray structure (50% TME) of [(L^4H)Ir(COD)]$(BF_4)_2$; all hydrogen atoms (except 4) and the counterion have been omitted; selected bond lengths [Å] and angles [°]: Ir−C11 2.091(7), Ir−C12 2.112(7), Ir−N11 2.169(5), Ir−N3 2.301(7); N11−Ir−N11a 74.6(3), N11−Ir−N3 77.9(2)

one molecule of diacetone alcohol of crystallization. The structure (Figure 5) shows that the ligand is now κ^4-coordinated. Compared with those in the Rh^I(COD) and Ir^I(COD) complexes described above, the Ir−N distances in this Ir^{III} derivative are shorter and the Ir−olefin distances longer, as expected. Perhaps somewhat surprisingly, all Ir−N distances are significantly shorter (by ca. 0.1 Å) than the corresponding Rh−N distances in [L^4RhCl_2]$^+$.[9]

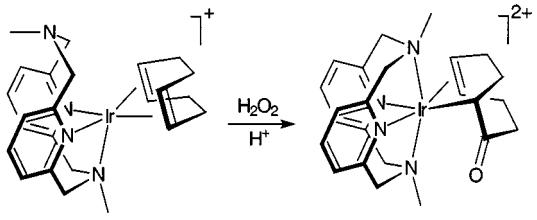

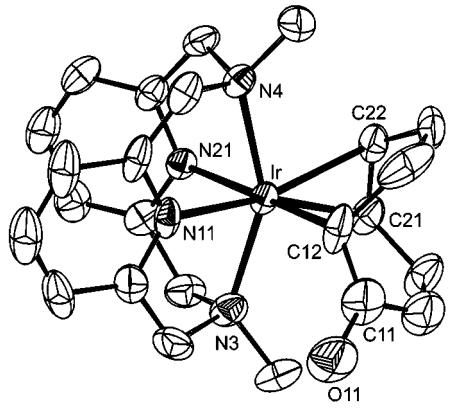

Figure 5. X-ray structure (30% TME) of [L^4Ir($C_8H_{11}O$)]$(PF_6)_2$(diacetone alcohol); all hydrogen atoms, the counterion and the molecule diacetone alcohol of crystallization have been omitted; selected bond lengths [Å] and angles [°]: Ir−C12 2.124(11), Ir−C21 2.242(10), Ir−C22 2.247(10), Ir−N11 2.031(8), Ir−N21 2.093(7), Ir−N3 2.213(10), Ir−N4 2.211(8), C11−O11 1.275(17); N11−Ir−N21 79.1(3), N11−Ir−N3 79.6(4), N21−Ir−N3 78.7(3), N11−Ir−N4 79.2(4), N21−Ir−N4 79.3(3), N3−Ir−N4 151.8(3)

Oxocyclooctadiene and oxoalkyl-allyl ligands somewhat similar to ours were obtained by Klemperer in the O_2 oxidation of Cp*Ir(COD).[18] He attributed their formation to a radical (autoxidation) mechanism; the reaction required rather drastic conditions. Since ligands, conditions and oxidants are different in our case, it is difficult to draw parallels between the two systems.

We have found that COD coordinated to Rh can be oxidized to an 9-oxabicyclo[4.2.1]nona-2,5-diyl fragment, presumably via a metallaoxetane intermediate.[3,5] (COD)Ir complexes can also be oxidized to oxetanes.[1,2,19] In both cases, the products rearrange to hydroxycyclooctenediyl complexes. In addition, we have observed that unsubstituted oxetanes can decompose to aldehydes, and can be oxidized to formylmethyl complexes.[8] On the basis of analogy, one possible mechanism for the formation of the oxocyclooctenyl complex could involve further oxidation of an initially formed metallaoxetane, represented schematically in Scheme 4.

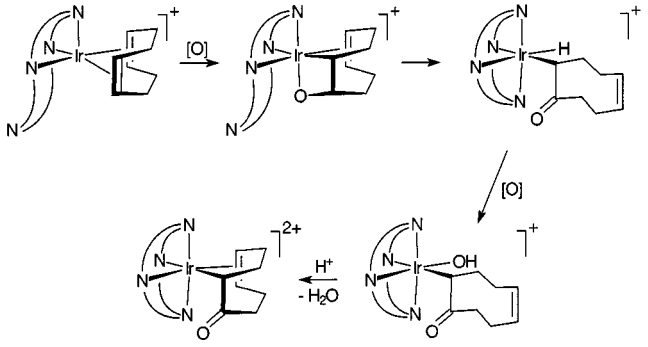

Scheme 4

The change in ligand coordination mode from κ^3 to κ^4 might be important here; it could result in displacement of the unchanged C=C bond from the metal atom, thus facilitating further reaction of the oxetane by relieving geometric constraints. Since we have not been able to observe any intermediates, we feel that further speculation on details of this reaction is not warranted.

The most interesting aspect of the H_2O_2 oxidation chemistry is probably the role of acid. Activation of H_2O_2 by acid is relatively common, but the H_2O_2 oxidation of $[(DPA)Rh(COD)]^+$ and $[(N\text{-Bu-DPA})Rh(COD)]^+$ does not require the addition of acid.[5] It might be that for the L^4 ligand, with substituents in the 6-positions of the pyridine rings, the increased steric hindrance prevents or slows down direct oxidation by H_2O_2. The isolation of the amine-protonated Ir complex makes it tempting to suggest that such a protonated species might also might also play a role in the oxidation by, for example, activating H_2O_2 near the metal centre, assisting in the first step of Scheme 4.

Conclusions

(Diene)rhodium and -iridium complexes of L^4 and L^6 pyridinophane ligands have five-coordinate structures in which the ligand is bound in a κ^3-(amine)(pyridine)$_2$ fashion. All Rh and Ir complexes are fluxional and show movement of the (diene)metal fragment over the ligand. Oxidation of $[L^4Ir(COD)]^+$ by H_2O_2 requires addition of acid, and then gives the oxocyclooctenyl complex in a net 4-e$^-$ oxidation reaction. In the absence of H_2O_2, acid protonates the dangling amine ligand; an amine-protonated species *might* also play a role in the oxidation reaction.

Experimental Section

General: All synthesis involving air-sensitive compounds were carried out by using standard Schlenk techniques. All solvents were distilled under nitrogen prior to use. Starting materials were prepared by literature methods: L^4/L^6,[12] $[Rh(COD)Cl]_2$,[20] $[Rh(NBD)Cl]_2$,[21] $[Ir(COD)Cl]_2$.[22] All other reagents were commercial products.

$[L^4Rh(COD)]PF_6$: $[Rh(COD)Cl]_2$ (13 mg, 0.026 mmol) was added to a solution of L^4 (14 mg, 0.052 mmol) in methanol (6 mL). The mixture turned yellow. After stirring for 1 h, the solution was filtered, and a solution of KPF_6 (40 mg, 0.22 mmol) in methanol (4 mL) was added. The mixture was concentrated to half its volume in vacuo, after which a yellow solid precipitated. The supernatant was removed with a Pasteur pipette. The resulting solid was washed with methanol (3 × 3 mL) and dried in vacuo. Yield: 0.35 g (75%). $[L^4Rh(COD)]PF_6$ is a yellow, air-stable solid. ^{1}H NMR (500 MHz, [D$_6$]acetone, 213 K): δ = 7.71 (t, J = 7.7 Hz, 2 H, py H_4), 7.36 (d, J = 7.7 Hz, 2 H, py H_3), 7.23 (d, J = 7.7 Hz, 2 H, py H_5), 6.22 (d, J = 14.0 Hz, 2 H, NCH_2), 4.97 (d, J = 17.0 Hz, 2 H, NCH_2), 4.49 (d, J = 14.0 Hz, 2 H, NCH_2), 4.30 (d, J = 17.0 Hz, 2 H, NCH_2), 3.79 (s, 3 H, CH_3), 2.89 (br, 2 H, C=CH), 2.59 (br, 2 H, C=CH), 2.44 (m, 2 H, =CCH_2), 2.27 (s, 3 H, CH_3), 1.94 (m, 2 H, =CCH_2), 1.76 (m, 2 H, =CCH_2), 1.61 (m, 2 H, =CCH_2). ^{1}H NOESY (200 MHz, [D$_6$]acetone, 298 K, exchange cross-peaks): δ = (7.23⇄7.36, Py-$H_{3,5}$), (4.97⇄6.22, NCH_2), (4.30⇄4.49, NCH_2), (3.5⇄4.1, C=CH), (2.27⇄3.79, CH_3). At this temperature all ligand signals except that of py-H_4 are severely broadened. ^{13}C{^{1}H} NMR (75 MHz, [D$_6$]acetone, 297 K): δ = 159 (2 C, py C_6), 158 (2 C, py C_2), 138 (2 C, py C_4), 126 (2 C, py C_5), 122 (2 C, py C_3), 80.7 (br, 2 C, =CH), 67.1 (2 C, NCH$_2$), 66.2 (br, 2 C, =CH), 65.0 (2 C, NCH_2), 51.8 (1 C, CH$_3$), 38.7 (1 C, CH$_3$), 32.6 (br, 2 C, = CHCH$_2$−), second =CHCH$_2$ obscured by acetone signal. FAB$^+$ MS (BPh$_4$ salt): m/z = 370 $[L^4Rh - H]^+$, 479 $[L^4Rh(COD)]^+$. IR (KBr): $\tilde{\nu}$ = 2976, 2943, 2906, 2895, 2852, 1603, 1463, 1450, 1105, 1035, 989, 874, 839, 771 cm^{-1}. $C_{24}H_{32}F_6N_4PRh$ (624.41): calcd. C 46.17, H 5.17, N 8.97; found C 46.42, H 4.91, N 8.61.

$[L^4Rh(NBD)]PF_6$: $[Rh(NBD)Cl]_2$ (107 mg, 0.23 mmol) was added to a solution of L^4 (125 mg, 0.47 mmol) in methanol (3 mL). The resulting yellow solution was stirred for 1 h. Upon addition of a solution of KPF_6 (343 mg, 1.86 mmol) in methanol (4 mL), a yellow solid precipitated. The solid was filtered off, washed with methanol (3 × 5 mL) and dried in vacuo. Yield: 215 mg (76%). ^{1}H NMR (500 MHz, [D$_6$]acetone, 273 K): δ = 7.60 (t, J = 7.8 Hz, 2 H, Py-H_4), 7.25 (d, J = 7.8 Hz, 2 H, Py-H_3), 7.15 (d, J = 7.8 Hz, 2 H, Py-H_5), 6.26 (d, J =14 Hz, 2 H, NCH_2), 4.96 (d, J = 16.0 Hz, 2 H, NCH_2), 4.47 (d, J = 14.0 Hz, 2 H, NCH_2), 4.34 (d, J = 16.0 Hz, 2 H, NCH_2), 4.11 (s, 3 H, CH_3), 3.99 (s, 2 H, NBD CH$_2$), 3.54 (m, 4 H, NBD =CH), 2.38 (s, 3 H, CH_3), 1.19 (s, 2 H, NBD =CCH). ^{1}H NOESY (200 MHz, [D$_6$]acetone, 298 K, exchange cross-peaks): δ = (7.15⇄7.19, Py-$H_{3,5}$), (5.02⇄6.23, NCH_2), (2.43⇄4.15, CH_3).

$^{13}C\{^1H\}$ NMR (75 MHz, [D$_6$]acetone, 297 K): δ = 159 (2 C, py C_2), 158 (2 C, py C_6), 137 (2 C, py C_4), 125 (2 C, py C_3), 121 (2 C, py C_5), 67.2 (2 C, NCH_2), 65.6 (2 C, NCH_2), 58.3 (4 C, NBD =C), 52.8 (1 C, NBD CH_2), 47.5 (1 C, CH_3), 39.4 (1 C, CH_3), 39.3 (2 C, NBD =CCH). FAB$^+$-MS: m/z = 370 [L^{4}Rh − H]$^+$, 463 [L^{4}Rh(NBD)]$^+$. IR (KBr): ṽ = 3004, 2941, 2892, 2861, 2813, 1601, 1573, 1464, 1449, 1430, 1305, 1168, 1101, 1034, 990, 968, 885, 839, 772, 557 cm^{-1}. We did not obtain a satisfactory elemental analysis for this complex: $C_{23}H_{28}F_6N_4PRh$ (608.37): calcd. C 45.41, H 4.64, N 9.21; found C 43.67, H 4.74, N 8.78.

[L^{6}Rh(COD)]PF$_6$: [Rh(COD)Cl]$_2$ (62 mg, 0.13 mmol) was added to a solution of L^6 (100 mg, 0.25 mmol) in methanol (10 mL). After the mixture had been stirred for 1 h, a solution of KPF_6 (184 mg, 1.0 mmol) in methanol (4 mL) was added. The reaction mixture was concentrated to half its volume in vacuo, after which a yellow solid precipitated. The product was filtered off, washed with methanol (3 × 2 mL) and dried in vacuo. Yield: 150 mg (79%). ^1H NMR (500 MHz, [D$_6$]acetone, 273 K): δ = 7.95 (t, J = 7.4 Hz, 1 H, py H_4), 7.92 (t, J = 7.4 Hz, 2 H, py H_4), 7.86 (d, J = 7.4 Hz, 2 H, py H_3), 7.50 (d, J = 7.4 Hz, 2 H, py H_5), 7.38 (d, J = 7.4 Hz, 2 H, py $H_{3,5}$), 5.07 (d, J = 17.0 Hz, 2 H, NCH_2), 4.96 (d, J = 17.0 Hz, 2 H, NCH_2), 4.57 (d, J = 15.0 Hz, 2 H, NCH_2), 4.24 (s, 4 H, NCH_2), 3.92 (d, J = 15.0 Hz, 2 H, NCH_2), 3.38 (s, 3 H, CH_3), 3.07 (br, 4 H, =CH), 2.49 (s, 6 H, CH_3), 2.35 (br, 4 H, =CCH_2), 1.55 (br, 4 H, =CCH_2). ^1H NMR (500 MHz, [D$_6$]acetone, 203 K): δ = 8.09 (t, J = 7.4 Hz, 1 H, py H_4), 7.97 (t, J = 7.4 Hz, 2 H, py H_4), 7.89 (d, J = 7.4 Hz, 2 H, py H_3), 7.63 (d, J = 7.4 Hz, 2 H, py H_5), 7.43 (d, J = 7.4 Hz, 2 H, py $H_{3,5}$), 4.78 (d, J = 17.0 Hz, 2 H, NCH_2), 4.72 (d, J = 17.0 Hz, 2 H, NCH_2), 4.52 (d, J = 15.0 Hz, 2 H, NCH_2), 4.26 (d, J = 13.0 Hz, 2 H, NCH_2), 4.19 (d, J = 13.0 Hz, 2 H, NCH_2), 3.88 (d, J = 15.0 Hz, 2 H, NCH_2), 3.42 (s, 3 H, CH_3), 3.15 (br, 2 H, =CH), 2.68 (br, 2 H, =CH), 2.59 (s, 6 H, CH_3), 2.30 (br, 2 H, =CCH_2), 1.97 (br, 2 H, =CCH_2), 1.51 (d, br, J = 8.1 Hz, 2 H, =CCH_2), 1.33 (d, br, J = 8.1 Hz, 2 H, =CCH_2). ^1H NOESY (chloride salt, 200 MHz, [D$_6$]acetone, 298 K, exchange cross-peaks): δ = (7.38⇄7.86, Py-$H_{3,5}$), (4.24⇄4.96, CH_2), (3.92⇄5.07), CH_2), (3.92⇄4.24, CH_2), (3.92⇄5.07, CH_2), (3.92⇄4.24, CH_2), (3.38⇄2.49, CH_3). $^{13}C\{^1H\}$ NMR (75 MHz, [D$_6$]acetone, 297 K): δ = 164 (2 C, py C_2), 160 (2 C, py C_6), 156 (2 C, py $C_{2,6}$), 139 (2 C, py C_4), 137 (1 C, py C_4), 124 (2 C, py C_3), 123 (2 C, py C_5), 122 (1 C, py $C_{3,5}$), 75.3 (br, 4 C, =CH), 64.5 (2 C, NCH_2), 63.7 (2 C, NCH_2), 63.0 (2 C, NCH_2), 47.7 (1 C, CH_3), 40.7 (2 C, NCH_3), 30.6 (4 C, =CCH_2), second =$CHCH_2$ signal obscured by acetone signal. FAB$^+$-MS (chloride salt): m/z = 403 [L^6 + H]$^+$, 425 [L^6 + Na]$^+$, 613 [L^{6}Rh(COD)]$^+$. IR (KBr): ṽ = 2931, 2884, 2866, 2844, 2796, 1602, 1584, 1572, 1455, 1427, 1159, 1116, 1094, 1040, 976, 877, 843, 800, 771, 558 cm^{-1}. $C_{32}H_{42}F_6N_6PRh$ (758.59): calcd. C 50.67, H 5.58, N 11.08; found C 49.84, H 6.05, N 10.38.

[L^{6}Rh(NBD)]PF$_6$: [Rh(NBD)Cl]$_2$ (57.2 mg, 0.12 mmol) was added to a solution of L^6 (100 mg, 0.25 mmol) and KPF_6 (184 mg, 1.0 mmol) in methanol (7.5 mL). The yellow reaction mixture was stirred for 1 h, after which the volume was concentrated to half its volume in vacuo. The product was precipitated by addition of water, filtered off, washed with diethyl ether (3 × 3 mL) and dried in vacuo. Yield: 140 mg (76%). ^1H NMR (500 MHz, [D$_6$]acetone, 273 K): δ = 7.94 (t, J = 7.6 Hz, 2 H, py H_4), 7.85 (t, J = 7.3 Hz, 1 H, py H_4), 7.79 (d, J = 7.6 Hz, 2 H, py H_3), 7.41 (d, J = 7.6 Hz, 2 H, py H_5), 7.38 (d, J = 7.3 Hz, 2 H, py $H_{3,5}$), 5.04 (d, J = 17.0 Hz, 2 H, NCH_2), 4.54 (d, J = 15.0 Hz, 2 H, NCH_2), 4.49 (d, J = 17.0 Hz, 2 H, NCH_2), 4.12 (s, 4 H, NCH_2), 3.95 (d, J = 15.0 Hz, 2 H, NCH_2), 3.58 (2 H, NBD CH_2), 3.08 (4 H, NBD = CH), 2.94 (s, 3 H, CH_3), 2.41 (s, 6 H, CH_3), 1.00 (2 H, NBD = CCH). ^1H NOESY (chloride salt, 200 MHz, [D$_6$]acetone, 298 K, exchange cross-peaks): δ = (7.52⇄7.70, py $H_{3,5}$), (7.36⇄7.81, py $H_{3,5}$ and py H_4), (4.48⇄5.08, NCH_2), (4.24⇄4.36, NCH_2), (4.14⇄5.08, NCH_2), (4.14⇄4.50, NCH_2), (2.46⇄2.95, CH_3). At this temperature all ligand signals are severely broadened. $^{13}C\{^1H\}$ NMR (75 MHz, [D$_6$]acetone, 297 K): δ = 168 (2 C, py $C_{2,6}$), 163 (2 C, py $C_{2,6}$), 162 (2 C, py $C_{2,6}$), 144 (2 C, py C_4), 142 (1 C, py C_4), 2 × 128 (4 C, py $C_{3,5}$), 126 (2 C, py $C_{3,5}$), 70 (2 C, NCH_2), 67 (2 C, NCH_2), 67 (2 C, NCH_2), 63 (2 C, NBD CH_2), 53 (2 C, NBD =CH), 52 (1 C, CH_3), 46 (4 C, NBD =CCH), 43 (2 C, CH_3). FAB$^+$-MS: m/z = 597 [L^{6}Rh(NBD)]$^+$. IR (KBr): ṽ = 2932, 2917, 2863, 2841, 1604, 1588, 1574, 1462, 1450, 1427, 1160, 1096, 1051, 875, 842, 793, 777, 558 cm^{-1}. We did not obtain a satisfactory elemental analysis for this complex: $C_{31}H_{38}F_6N_6PRh$ (742.55): calcd. C 50.14, H 5.16, N 11.32; found C 46.99, H 4.74, N 10.38.

[L^{4}Ir(COD)]PF$_6$: [Ir(COD)Cl]$_2$ (25 mg, 0.037 mmol) was added to a solution of L^4 (20 mg, 0.075 mmol) in methanol. After addition of KPF_6 (14 mg), a yellow precipitate was collected by filtration. This was dissolved in dichloromethane, KCl was filtered off, and the solvent was evaporated in vacuo. Yield: 46 mg (85%). ^1H NMR (400 MHz, [D$_6$]acetone, 298 K): δ = 7.73 (t, J = 7.7 Hz, 2 H, py H_4), 7.39 (d, J = 7.6 Hz, 2 H, py H_3), 7.33 (d, J = 7.8 Hz, 2 H, py H_5), 6.03 (d, J = 14.0 Hz, 2 H, NCH_2), 4.87 (d, J = 16.8 Hz, 2 H, NCH_2), 4.61 (d, J = 16.9 Hz, 2 H, NCH_2), 4.48 (d, J = 14.1 Hz, 2 H, NCH_2), 3.84 (s, 3 H, CH_3), 3.79 (br, 2 H, =CH), 2.98 (br, 2 H, =CH), 2.75, (br, 2 H, =CCH_2), 2.39 (br, 2 H, =CCH_2), 2.29 (s, 3 H, CH_3), 1.76 (d, J = 7.9 Hz, 2 H, =CCH_2), 1.30 (d, J = 8.9 Hz, 2 H, =CCH_2). ^1H NOESY (400 MHz, [D$_6$]acetone, 298 K, exchange peaks): δ = (3.84⇄2.29, CH_3). $^{13}C\{^1H\}$ NMR (75 MHz, [D$_6$]acetone, 298 K): δ = 162 (2 C, py C_2), 160 (2 C, py C_6), 139 (2 C, py C_3), 127 (2 C, py C_4), 122 (2 C, py C_5), 70 (2 C, NCH_2), 66 (2 C, NCH_2), 65 (2 C, =CH), 55 (1 C, CH_3), 46 (2 C, =CH), 39 (1 C, CH_3), 35 (2 C, =CCH_2), 30 (2 C, =CCH_2). FAB$^+$-MS: m/z = 569 [L^{4}Ir(COD)]$^+$, 192 [Ir]$^+$. $C_{24}H_{32}F_6IrN_4P$ (713.73): calcd. C 40.39, H 4.52, N 7.85; found C 39.99, H 4.18, N 7.64.

[(L^{4}H)Ir(COD)](BF$_4$)$_2$: A solution of HBF_4 in ether (54 wt%, 3.86 mL) was added at 0 °C to a suspension of [L^{4}Ir(COD)]PF$_6$ (20 mg, 0.028 mmol) in methanol. The solvents were removed in vacuo. Treatment of the residue with methanol gave a yellow solution, from which a yellow solid [(L^{4}H)Ir(COD)](BF$_4$)$_2$ could be isolated by addition of 5 mL of diethyl ether. Overnight, the solution deposited further red crystals, suitable for X-ray diffraction. The complex is only poorly soluble in most solvents, while solutions in acetonitrile and methanol slowly decompose. We could therefore only partially interpret the ^1H NMR spectrum and did not obtain useful ^{13}C NMR spectroscopic data. ^1H NMR (200 MHz, CD_3OD, 298 K): δ = 7.73 (t, J = 7.7 Hz, 2 H, py H_4), 7.60 (d, J = 7.3 Hz, 2 H, py H_3), 7.36 (d, J = 7.5 Hz, 2 H, py H_5), 6.39 (d, J = 12.9 Hz, 2 H, NCH_2), 5.16 (d, J = 13.1 Hz, 2 H, NCH_2), 4.71 (d, J = 16.7 Hz, 2 H, NCH_2), 4.48 (d, J = 16.9 Hz, 2 H, NCH_2), 3.70 (s, 3 H, CH_3), 2.70 (br, 2 H, =CH), 2.37 (br, 2 H, =CCH_2), 2.04 (br, 2 H, =CCH_2), 1.74 (br, 2 H, =CCH_2), 1.28 (br, 2 H, =CCH_2).

[L^{4}Ir(C$_8$H$_{11}$O)](PF$_6$)$_2$: H(OEt$_2$)$_2^+$B(Ar^F)$_4^-$ (28.4 mg, 0.028 mmol) was added to a solution of [L^{4}Ir(COD)]PF$_6$ (20 mg, 0.028 mmol) in acetonitrile. After 5 min, aqueous hydrogen peroxide (1%, 0.08 mL) was added, after which the mixture was stirred vigorously for 15 min. Removal of the solvent in vacuo gave a yellow solid, which could be dissolved in methanol. Addition of KPF_6 (14 mg) yielded a yellow solid, which could be "crystallised" as droplets from acetonitrile by slow diffusion of diethyl ether into the solution. Yield: 22 mg (90%). When the reaction was attempted with only 0.5 equiv. of H(OEt$_2$)$_2^+$B(Ar^F)$_4^-$, a 1:1 mixture of [L^{4}Ir(COD)]PF$_6$ and

$[L^4Ir(C_8H_{11}O)](PF_6)_2$ was isolated. $[L^4Ir(C_8H_{11}O)](PF_6)_2$ is an air-stable, yellow solid. ^1H NMR (600 MHz, [D$_6$]acetone, 298 K): δ = 8.15 (t, J = 8.16 Hz, 1 H, py H_4), 8.02 (t, J = 7.7 Hz, 1 H, py H_4), 7.70 (d, J = 8.1 Hz, 1 H, py H_3), 7.67 (d, J = 7.4 Hz, 1 H, py H_3), 7.65 (d, J = 7.8 Hz, 1 H, py H_5), 7.61 (d, J = 7.4 Hz, 1 H, py H_5), 6.94 (br, 1 H, =C*H*), 6.75 (br, 1 H, =C*H*), 5.47 (d, J = 16.7 Hz, 1 H, NCH_2), 5.31 (d, J = 16.3 Hz, 2 H, NCH_2), 4.79 (d, J = 16.8 Hz, 1 H, NCH_2), 4.75 (d, J = 16.7 Hz, 1 H, NCH_2), 4.64 (d, J = 16.3 Hz, 1 H, NCH_2), 4.62 (d, J = 15.9 Hz, 1 H, NCH_2), 4.31 (d, J = 16.3 Hz, 1 H, NCH_2), 3.76 (br, 1 H, COD CH_2), 3.51 (s, 3 H, CH_3), 3.22 (br, 1 H, COD CH_2), 3.14 (s, 3 H, CH_3), 3.12 (br, 1 H, COD CH_2), 2.99 (br, 1 H, COD CH_2), 2.67 (br, 1 H, COD CH_2), 2.53 (br, 1 H, COD CH_2), 2.38 (br, 1 H, COD CH_2), 1.83 (dd, J_1 = 9.7 Hz, J_2 = 15.9 Hz, 1 H, Ir-C*H*). One COD CH_2 proton signal is probably obscured by a solvent signal. $^{13}C\{^1H\}$ NMR (75 MHz, [D$_6$]acetone, 298 K): δ = 220.8 (1 C, *C*=O), 157.5 (1 C, py C_2), 157.0 (1 C, py C_2), 156.9 (1 C, py C_6), 156.5 (1 C, py C_6), 142.5 (1 C, py C_4), 142.2 (1 C, py C_4), 123.2 (1 C, py C_3), 123.1 (1 C, py C_3), 123.0 (1 C, py C_5), 122.7 (1 C, py C_5), 100.4 (1 C, =*C*H), 88.2 (1 C, =*C*H), 80.4 (1 C, N*C*H$_2$), 78.9 (1 C, N*C*H$_2$), 77.9 (1 C, N*C*H$_2$), 76.4 (1C, N*C*H$_2$), 57.1 (1 C, *C*H$_3$), 53.5 (1 C, *C*H$_3$), 38.1 (1 C, =C*C*H$_2$), 36.1 (1 C, O=C*C*H$_2$), 28.7 (1 C, =C*C*H$_2$), 28.6 (1 C, =C*C*H$_2$), 25.3 (1 C, Ir-*C*). ^1H NOESY (600 MHz, [D$_6$]acetone, 298 K, cross peaks): δ = (6.94/5.31, =C*H*/CH_2), (6.75/5.47, =C*H*/CH_2), (6.94/3.51, =C*H*/CH_3), (6.75/3.14 (=C*H*/CH_3). MALDI-TOF-MS: m/z = 583 $[L^4Ir(C_8H_{11}O)]^+$, 556 $[L^4Ir(C_8H_{11}O) - HCN]^+$, 493 [?]$^+$, 459 $[L^4Ir]^+$, 269 $[L^4H]^+$. $C_{24}H_{31}F_{12}IrN_4OP_2$ (873.68): calcd. C 32.99, H 3.58, N 6.41; found C 32.80, H 3.63, N 6.38. X-ray quality crystals were obtained by crystallization from acetone, and were found to contain one molecule of diacetone alcohol of crystallization (see below).

X-ray Structure Determinations: Single crystals were mounted in air on glass fibres. Intensity data were collected at room temperature with an Enraf−Nonius CAD4 single-crystal diffractometer. Unit-cell dimensions were determined from the angular setting of a limited number of reference reflections. Intensity data were corrected for Lorentz and polarization effects, and for absorption using a semiempirical ψ-scan correction.[23] Structures were solved by the DIRDIF[24] program system, using the PATTY[25] program to locate the heavy atom (Rh or Ir), and refined with standard methods (refinement against F^2 of all reflections) with SHELXL97.[26] All

Table 2. Details of X-ray structure determinations

Compound	$[L^4Rh(COD)]PF_6$	$[L^6Rh(COD)]PF_6$	$[L^6Rh(NBD)]PF_6 \cdot C_3H_6O$	$[(L^4H)Ir](BF_4)_2$	$[L^4Ir(C_8H_{11}O)](PF_6)_2 \cdot C_6H_{12}O_2$
Crystal colour	transparent yellow-brown	transparent brown-yellow	yellow, degraded, cracked	transparent dark red	transparent yellow
Crystal shape	fairly regular thick platelet	fairly regular platelet	regular fragment	rather irregular fragment	irregular fragment
Crystal size [mm]	0.31 × 0.26 × 0.11	0.42 × 0.39 × 0.08	0.44 × 0.40 × 0.23	0.39 × 0.33 × 0.21	0.39 × 0.36 × 0.31
Empirical formula	$C_{24}H_{32}F_6N_4PRh$	$C_{32}H_{42}F_6N_6PRh$	$C_{34}H_{44}F_6N_6OPRh$	$C_{24}H_{33}B_2F_8IrN_4$	$C_{30}H_{43}F_{12}IrN_4O_3P_2$
Molecular mass	624.42	758.60	800.63	743.36	989.82
Temperature [K]	293(2)	208(2)	208(2)	293(2)	293(2)
Radiation (graphite mon.)	Cu-K_α	Cu-K_α	Cu-K_α	Cu-K_α	Mo-K_α
Wavelength [Å]	1.54184	1.54184	1.54184	1.54184	0.71073
Crystal system, space group	monoclinic, *P*21/*c*	orthorhombic, *Pbca*	triclinic, *P*-1	orthorhombic, *Pnma*	monoclinic, *C*2/*c*
No. of unit-cell reflections,	12,	25,	25,	21,	25,
θ range [°]	22.435−45.250	40.367−46.985	34.259−39.151	40.232−46.897	18.474−20.669
a [Å]	8.828(11)	18.9991(9)	11.1345(5)	10.5427(11)	21.871(3)
b [Å]	15.163(3)	15.1936(7)	13.3241(10)	13.7308(7)	13.847(5)
c [Å]	18.949(2)	22.3517(8)	13.4933(7)	17.9889(5)	24.995(3)
α [°]	90	90	96.372(4)	90	90
β [°]	92.030(19)	90	109.201(5)	90	104.026(11)
γ [°]	90	90	103.779(10)	90	90
V [Å^3]	2535(3)	6452.2(5)	1796.51(18)	2604.1(3)	7344(3)
Z, calcd. density [Mg·m^{-3}]	4, 1.636	8, 1.562	2, 1.480	4, 1.896	8, 1.791
Abs. coefficient [mm^{-1}]	6.633	5.345	4.853	10.651	3.822
Scan	θ/2θ	θ/2θ	θ/2θ	θ/2θ	ω
F(000)	1272	3120	824	1456	3920
θ range for data collection [°]	3.73−70.22	3.96−69.99	3.49−64.97	4.05−69.89	3.06−26.31
Index ranges	$-10 \le h \le 0$ $0 \le k \le 18$ $-23 \le l \le 23$	$0 \le h \le 23$ $0 \le k \le 18$ $0 \le l \le 27$	$-12 \le h \le 13$ $-15 \le k \le 15$ $-15 \le l \le 0$	$-12 \le h \le 0$ $-15 \le k \le 0$ $0 \le l \le 21$	$-27 \le h \le 0$ $0 \le k \le 17$ $-30 \le l \le 31$
Refl. collected/unique (R_{int})	5137/4810 (0.0289)	6110/6110	6382/6091 (0.0138)	2573/2573	7608/7408 (0.0273)
Refl. observed [$I_o > 2\sigma(I_o)$]	3377	5225	5962	2200	5072
Abs. corr.	semiemp. ψ-scan	semiemp. ψ-scan	semiemp. ψ-scan	semiemp. ψ-scan + DIFABS	semiemp. ψ-scan
Range of rel. transm. factors	2.069 and 0.852	2.648 and 0.786	1.037 and 0.968	1.369 and 0.805	1.100 and 0.936
Data/restraints/parameters	4810/0/343	6110/0/418	6091/24/598	2573/2/189	7408/0/475
Goodness-of-fit on F^2	1.034	1.051	1.059	1.062	1.041
SHELXL-97 wt parameters	0.0912, 6.8763	0.1016, 16.9184	0.070, 4.396	0.0562, 9.6517	
Final $R1$, $wR2$ [$I > 2\sigma(I)$]	0.0601, 0.1472	0.0599, 0.1626	0.0447, 0.1207	0.0411, 0.0985	0.0588, 0.1406
$R1$, $wR2$ (all data)	0.0942, 0.1713	0.0683, 0.1713	0.0453, 0.1213	0.0515, 0.1036	0.0974, 0.1607
Diff. peak and hole [e·Å^{-3}]	1.813 and −0.981	1.422 and −1.418	1.690 and −0.970	1.294 and −1.229	2.600 and −1.155

non-hydrogen atoms were refined anisotropically; hydrogen atoms were refined isotropically in riding mode, unless otherwise noted. Geometrical calculations (PLATON[27]) revealed neither unusual geometric features, nor unusual short intermolecular contacts, no higher symmetry and no (further) solvent-accessible areas. Details of the data collection and structure determinations are collected in Table 2. − **[L^{4}Rh(COD)]PF$_6$:** Hydrogen atoms attached to C11, C12, C21, and C22 were freely refined. − **[L^{6}Rh(NBD)]PF$_6$·C$_3$H$_6$O:** The hydrogen atoms of the acetone methyl groups were refined as rigid rotors with idealized sp^3 hybridization and a C−H bond length of 0.97 Å to match maximum electron density in a difference Fourier map. All other hydrogen atoms were initially placed at calculated positions and were subsequently freely refined. − **[(L^{4}H)Ir(COD)](BF$_4$)$_2$:** The normal least-squares refinement procedure failed to give acceptable anisotropic displacement parameters for a number of atoms. Refinement in space group *Pna*21, although possible and resulting in an even lower *R* value (0.1118 vs. 0.1161 isotropic, 0.0607 vs. 0.0638 anisotropic), produced even worse displacement parameters. Because the irregular crystal shape prevented adequate analytic absorption correction, the DIFABS procedure[28] was applied after all atoms, including hydrogen atoms, had been refined isotropically in *Pnma*. After this correction, refinement in *Pnma* lowered the isotropic *R* value from 0.1161 to 0.0530, and the anisotropic *R* value from 0.0638 to 0.0410, with perfectly acceptable anisotropic displacement parameters. Further refinement in *Pna*21, however, again gave nonpositive definite values for most atoms. Besides this, there is no significant change/improvement in the geometry in those parts of the structure (esp. the COD moiety) that are possibly constrained most by the imposed symmetry. The statistical distribution of *E* values favours the centrosymmetric space group *Pnma*. However, all the structures containing cyclooctadiene that we have solved so far showed a twist in the COD moiety, through which an eclipsed conformation of the CH_2CH_2 groups is avoided. The mirror symmetry imposed on the COD moiety in space group *Pnma* does not conform with this convincing observation, and the refinement in *Pna*21 clearly shows the expected torsion in the COD moiety. Therefore, we believe that the average structure shows an overall centrosymmetric arrangement in which mainly the COD moiety is disordered to a certain extent, although there will also be some effect on the remainder of the structure. Unfortunately, if this is the case then the deviations from a centrosymmetric structure are not large enough to allow for a disorder refinement. The bond lengths in the COD fragment should be treated with caution. − **[L^{4}Ir(C$_8$H$_{11}$O)](PF$_6$)$_2$·C$_6$H$_{12}$O$_2$:** The diacetone alcohol molecule of crystallization shows large displacement parameters and is probably disordered. The assignments of O77 and O78 as oxygen atoms is based on bond lengths only, and that of O77 is not certain. The hydrogen bond involving H77 must therefore be regarded as tentative. − Crystallographic data (excluding structure factors) for the structures reported in this paper have been deposited with the Cambridge Crystallographic Data Centre as supplementary publication nos. CCDC-166291−166295. Copies of the data can be obtained free of charge on application to CCDC, 12 Union Road, Cambridge CB2 1EZ, UK [Fax: (internat.) + 44-1223/336-033; E-mail: deposit@ccdc.cam.ac.uk].

Supporting Information: Fitted rate constants for [L^{4}Rh(COD)]$^+$, [L^{6}Rh(COD)]$^+$, and [L^{4}Ir(COD)]$^+$ and the Arrhenius and Eyring plots used to derive activation parameters.

Acknowledgments

We are grateful to Prof. Dr. Hans-Jörg Krüger (Johannes Gutenberg-Universität Mainz, Germany) for communicating his modification of the synthesis of L^4 to us prior to publication.

[1] V. W. Day, W. G. Klemperer, S. P. Lockledge, D. J. Main, *J. Am. Chem. Soc.* **1990**, *112*, 2031.
[2] T. C. Flood, M. Iimura, J. M. Perotti, A. L. Rheingold, T. E. Concolino, *Chem. Commun.* **2000**, 1681.
[3] B. de Bruin, M. J. Boerakker, J. J. M. Donners, B. E. C. Christiaans, P. P. J. Schlebos, R. de Gelder, J. M. M. Smits, A. L. Spek, A. W. Gal, *Angew. Chem. Int. Ed. Engl.* **1997**, *36*, 2064.
[4] B. de Bruin, M. J. Boerakker, R. de Gelder, J. M. M. Smits, A. W. Gal, *Angew. Chem. Int. Ed.* **1999**, *111*, 118.
[5] B. de Bruin, J. A. Brands, J. J. J. M. Donners, M. P. J. Donners, R. de Gelder, J. M. M. Smits, A. W. Gal, A. L. Spek, *Chem. Eur. J.* **1999**, *5*, 2921.
[6] B. de Bruin, M. J. Boerakker, J. A. W. Verhagen, R. de Gelder, J. M. M. Smits, A. W. Gal, *Chem. Eur. J.* **2000**, *6*, 298.
[7] M. Krom, R. G. E. Coumans, J. M. M. Smits, A. W. Gal, *Angew. Chem. Int. Ed.* **2001**, *40*, 2106.
[8] B. de Bruin, J. A. W. Verhagen, C. H. J. Schouten, A. W. Gal, *Chem. Eur. J.* **2001**, *7*, 416.
[9] H. Sakaba, C. Kabuto, H. Horino, M. Arai, *Bull. Chem. Soc. Jpn.* **1990**, *63*, 1822.
[10] H. Takemura, N. Kon, K. Tani, K. Takehara, J. Kimoto, T. Shinmyozu, T. Inazu, *J. Chem. Soc., Perkin Trans. 1* **1997**, 239.
[11] J. Breitenbach, K. Rissanen, U. U. Wolf, F. Vögtle, *Chem. Ber.* **1991**, *124*, 2323.
[12] F. Bottino, M. de Grazia, P. Finocchario, F. R. Frinczek, A. Mamo, S. Pappalardo, *J. Org. Chem.* **1988**, *53*, 3521.
[13] H.-J. Krüger, personal communication.
[14] H. Kelm, H.-J. Krüger, *Eur. J. Inorg. Chem.* **1998**, 1381.
[15] Models indicate that the methyl orientation found in [L^{4}Rh(COD)]$^+$ should be the more hindered one, and PM3 calculations predict it to be 2.6 kcal/mol higher in energy than the alternative orientation. However, the X-ray structure of [L^{4}Rh(C$_2$H$_4$)$_2$]$^+$ shows the same methyl orientation as found here: M. Krom, T. Sciarone, J. Hoogboom, T. P. J. Peters, A. W. Gal, to be published.
[16] The parent complex [(DPA)Rh(COD)]$^+$ adopts a different conformation, in which the N_{amine} is *trans* to a C=C bond (see ref.[5]).
[17] gNMR development version V5.0 (P. H. M. Budzelaar). Temperature ranges used: [L^{4}Rh(COD)]$^+$ 300−373 K; [L^{4}Ir(COD)]$^+$ 323−373 K; [L^{6}Rh(COD)]$^+$ 298−363 K; data points spaced by ca. 10°.
[18] V. W. Day, T. A. Eberspacher, W. G. Klemperer, B. Zhong, *J. Am. Chem. Soc.* **1994**, *116*, 3119.
[19] R. J. N. A. M. Kicken, A. W. Gal, manuscript to be published.
[20] J. Chatt, J. Venanzi, *J. Chem. Soc.* **1957**, 4735.
[21] [21a] J. Chatt, J. Venanzi, *J. Chem. Soc.* **1957**, 4735. [21b] E. W. Abel, M. A. Bennett, G. Wilkinson, *J. Chem. Soc.* **1959**, 3178. [21c] R. R. Schrock, *J. Am. Chem. Soc.* **1971**, *93*, 2397.
[22] [22a] G. Winklaus, H. Singer, *Chem. Ber.* **1966**, *99*, 3610. [22b] A. van der Ent, A. L. Onderdelinden, *Inorg. Synth.* **1973**, *14*, 92.
[23] A. C. T. North, D. C. Philips, F. S. Mathews, *Acta Crystallogr., Sect. A* **1968**, *24*, 351.
[24] P. T. Beurskens, G. Beurskens, W. P. Bosman, R. de Gelder, S. Garcia-Granda, R. O. Gould, R. Israel, J. M. M. Smits, *DIRDIF-96. A computer program system for crystal structure determination by Patterson methods and direct methods applied to difference structure factors*, Crystallography Laboratory, University of Nijmegen, The Netherlands, **1996**.
[25] P. T. Beurskens, G. Beurskens, M. Strumpel, C. E. Nordman, in: *Patterson and Pattersons* (Eds.: J. P. Glusker, B. K. Patterson, M. Rossi), Clarendon Press, Oxford, **1987**, p. 356.
[26] G. M. Sheldrick, *SHELXL-97, Program for the refinement of crystal structures*, University of Göttingen, Germany, **1997**.
[27] A. L. Spek, *PLATON-93, Program for display and analysis of crystal and molecular structures*, University of Utrecht, The Netherlands, **1995**.
[28] N. Walker, D. Stuart, *Acta Crystallogr., Sect. A* **1983**, *39*, 158.

Received July 3, 2001
[I01246]

New Helical Complexes with a Bis(bidentate) Schiff Base Ligand Containing a Flexible Spacer

Miguel Vázquez,[a] Manuel R. Bermejo,*[a] Matilde Fondo,[a] Ana García-Deibe,[a] Ana M. González,[a] and Rosa Pedrido[a]

Keywords: Supramolecular chemistry / Helical structures / Schiff bases / Electrochemistry

Neutral complexes with the general empirical formula M(PTs) [M: Mn, Fe, Co, Cu, Zn, and Cd; H_2PTs: *N*,*N*′-bis(2-tosylaminobenzylidene)-1,3-diaminopropane] were obtained by means of an electrochemical procedure. All complexes were characterised by elemental analyses, mass spectrometry, IR and ^{1}H NMR spectroscopy, and magnetic measurements, where appropriate. Recrystallisation of the cobalt, copper, and zinc complexes yielded single crystals of [Co(PTs)] (**1**), [Cu(PTs)]·1.5CH_3CN (**2**) and [Zn(PTs)]$_2$·1.5H_2O·CH_3CN (**3**). Their X-ray characterisation shows that **1** and **2** are mononuclear tetrahedral single-stranded helical complexes in the solid state, while **3** is a double-helical compound containing a major and a minor groove, with the Schiff base acting as a bis(bidentate) N_4 donor.

Introduction

The study of supramolecular helical complexes has been the subject of considerable interest recently, in order to clarify the mechanisms of self-assembly processes.[1−5] From these studies, it was concluded that metal helicates are generated by the combination of appropriate ligands and metal ions with specific preferences for particular coordination geometries.

Interesting studies have been devoted to the development of synthetic procedures, in order to prepare new multidentate ligands with the potential ability of forming bridged polynuclear species.[6−11] A key parameter in the assembly of helicates is how a flexible polydentate ligand becomes partitioned into distinct metal binding sites. In many cases ligands have been constructed that contain several bidentate or terdentate domains separated by rigid or bulky groups. Thus, the domains are arranged such that each site will definitely bind to different metal ions rather than chelating to a single metal centre. Furthermore, the spacer groups usually contain aromatic moieties, which provoke π···π and/or CH···π non-covalent interactions that control the self-assembly process.

The supramolecular chemistry involving ligands containing flexible spacers has not been extensively investigated. In this case, the way in which the ligand is partitioned into binding sites mainly depends on the stereoelectronic preferences of the metal ion, and this type of ligand often leads to the isolation of mononuclear helical species.[12−14]

Our recent investigations on Schiff bases allowed us to isolate the bis(bidentate) N_4 ligand H_2PTs [IUPAC name: *N*,*N*′-bis(2-tosylaminobenzylidene)-1,3-diaminopropane] (Scheme 1), which contains a flexible spacer. Its X-ray structure[15] shows that it adopts an *anti*-opened conformation[16] in the solid state that should do it suitable to span two metal centres, generating double-helical complexes. This is the situation found in the related [Ni(PTs)]$_2$ complex.[17] In an attempt to know the role of the metal atom in the disposition of this type of ligand, we extended our investigations to the behaviour of H_2PTs. In order to check if the arrangement of the ligand is the same as that found for nickel,[17] its electrochemical interaction with manganese, iron, cobalt, copper, zinc and cadmium was studied and the results obtained are described here.

Results and Discussion

The Schiff base H_2PTs has been prepared as previously described and satisfactorily characterised by elemental analysis, FAB mass spectrometry, IR and ^{1}H NMR spectroscopy,[17] and X-ray diffraction studies.[15]

Synthesis of the Complexes

All the complexes were prepared by an electrochemical method previously described.[17,18] The electrochemical efficiency of the cell E_f was approximately 0.5 mol·F^{-1} in all cases, which is compatible with the reaction mechanism shown in Scheme 2.

Elemental analyses (Table 1) show that all metal ions react with the ligand in a 1:1 molar ratio affording complexes

[a] Departamento de Química Inorgánica, Facultade de Química, Universidade de Santiago de Compostela, 15706 Santiago de Compostela, Spain
Fax: (internat.) + 34-981/597-525
E-mail: qimb45@usc.es

 © WILEY-VCH Verlag GmbH, 69451 Weinheim, Germany, 2002 1434−1948/02/0202−0465 $ 17.50+.50/0

Table 1. Elemental analysis and some selected data for the complexes

Compound	Yield (%)	Colour	% C[a]	% H[a]	% N[a]	% S[a]	FAB[b]	μ[c]
Mn(PTs)	72	ochre	57.8 (58.0)	4.8 (4.7)	8.6 (8.7)	9.9 (10.0)	641	6.0
Fe(PTs)	65	red	57.9 (57.9)	4.6 (4.6)	8.6 (8.7)	9.7 (9.9)	642	5.1
Co(PTs)	70	garnet	57.8 (57.6)	4.4 (4.6)	8.7 (8.7)	9.6 (9.9)	646	4.3
Cu(PTs)	75	green	57.1 (57.2)	4.6 (4.6)	8.7 (8.6)	9.8 (9.8)	650	2.2
Zn(PTs)	81	yellow	56.9 (57.0)	4.8 (4.6)	8.4 (8.6)	9.9 (9.8)	651	
Cd(PTs)	77	yellow	53.4 (53.2)	4.1 (4.3)	7.7 (8.0)	9.0 (9.1)	701	

[a] Found (calculated). [b] amu; peaks corresponding to $[ML]^+$. [c] In BM.

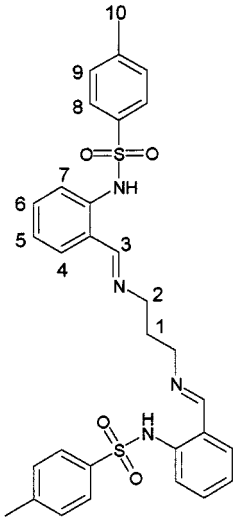

Scheme 1. H_2PTs

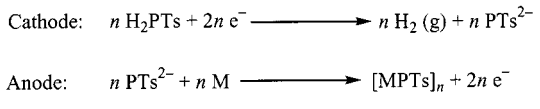

Scheme 2

of the bis(deprotonated) ligand $[PTs]^{2-}$ in high purity. These neutral metal complexes are obtained in high yields and appear to be stable in the solid state and in solution. Most of them are insoluble or sparingly soluble in water and common organic solvents, but soluble in polar coordinating organic solvents such as DMF, DMSO, and pyridine.

Crystal Structures

[Co(PTs)] (1) and [Cu(PTs)]·1.5CH$_3$CN (2)

The crystal structures of **1** and **2** are shown in Figures 1 and 2, respectively. Selected bond lengths and angles are displayed in Table 2.

Both compounds consist of discrete molecules of M(PTs) and show quite similar structures. In complex **2**, two acetonitrile solvates per complex molecule are present in the unit cell, one of them at 0.5 occupancy.

In both complexes, the ligand uses all its N-donor atoms to bind to the same metal centre. One oxygen atom of each

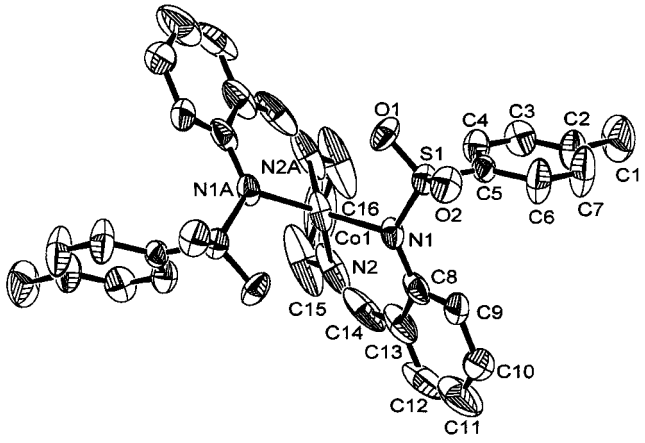

Figure 1. ORTEP view of complex **1** (thermal ellipsoids are drawn at 30% of probability level)

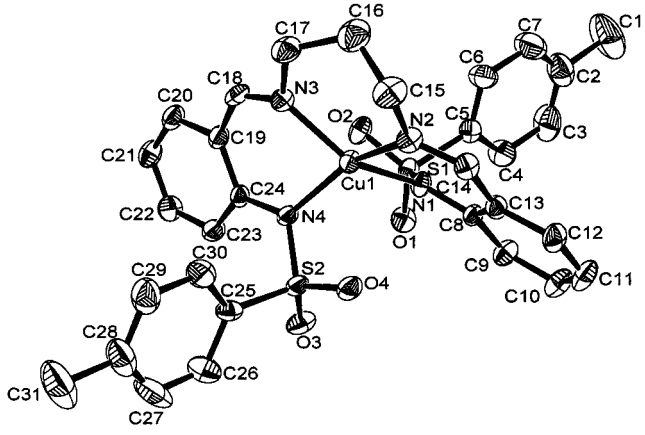

Figure 2. ORTEP view of complex **2** (thermal ellipsoids are drawn at 30% of probability level; hydrogen atoms and solvent molecules have been omitted for clarity)

tosyl group seems to weakly interact with the metal atom, the M···O distances (about 2.6 Å for **1** and 2.8 Å for **2**) are too long to be considered as true coordinated bonds, and therefore are best described as secondary intramolecular interactions. Thus, the metal centres are tetracoordinated, with the cobalt atom located in a twofold crystallographic axis in **1**. The geometry about the metal ions could be described as pseudo-tetrahedral, although the two terminal bidentate fragments are not mutually perpendicular. The dihedral angle θ between the two MNN terminal planes is 69.38° for **1** and 44.37° for **2**. This shows that the deviation

Table 2. Selected bond lengths [Å] and angles [°] for **1**−**3**

1		**2**		**3**			
Co(1)−N(1)	1.962(6)	Cu(1)−N(1)	1.985(5)	Zn(1)−N(1)	1.985(6)	N(5)−Zn(1)−N(2)	106.4(2)
Co(1)−N(1A)	1.962(6)	Cu(1)−N(2)	1.973(5)	Zn(1)−N(2)	2.027(6)	N(1)−Zn(1)−N(6)	111.5(2)
Co(1)−N(2)	2.020(11)	Cu(1)−N(4)	1.975(5)	Zn(2)−N(3)	2.026(6)	N(5)−Zn(1)−N(6)	92.9(2)
Co(1)−N(2A)	2.020(11)	Cu(1)−N(3)	1.981(5)	Zn(2)−N(4)	1.971(6)	N(2)−Zn(1)−N(6)	103.8(2)
N(1)−Co(1)−N(1A)	128.6(3)	N(2)−Cu(1)−N(4)	149.7(2)	Zn(1)−N(5)	1.987(6)	N(8)−Zn(2)−N(4)	139.7(2)
N(1)−Co(1)−N(2)	89.0(4)	N(2)−Cu(1)−N(3)	97.9(2)	Zn(1)−N(6)	2.039(6)	N(8)−Zn(2)−N(3)	110.7(2)
N(1)−Co(1)−N(2A)	128.1(3)	N(4)−Cu(1)−N(3)	89.2(2)	Zn(2)−N(7)	2.027(5)	N(4)−Zn(2)−N(3)	94.5(2)
N(1A)−Co(1)−N(2)	128.1(3)	N(2)−Cu(1)−N(1)	89.7(2)	Zn(2)−N(8)	1.964(6)	N(8)−Zn(2)−N(7)	93.8(2)
N(1A)−Co(1)−N(2A)	89.0(4)	N(4)−Cu(1)−N(1)	99.4(2)	N(1)−Zn(1)−N(5)	144.6(2)	N(4)−Zn(2)−N(7)	108.0(2)
N(2)−Co(1)−N(2A)	92.6(8)	N(3)−Cu(1)−N(1)	148.7(2)	N(1)−Zn(1)−N(2)	92.7(2)	N(3)−Zn(2)−N(7)	108.2(2)

from tetrahedral to square-planar geometry is higher for the copper complex ($\theta = 0$ for square-planar geometry and $\theta = 90$ for tetrahedral geometry). The wide range of angles observed around the metal centres [from 89.0(4) to 128.1(3)° for **1** and from 89.2(2) to 149.7(2)° for **2**] also shows the deviation from the ideal tetrahedral geometry. The M−N distances are typical of cobalt and copper complexes with this type of ligand,[19−20] although it should be noted that all the Cu−N bonds are very similar while the $Co-N_{amide}$ bonds are significantly shorter than the $Co-N_{imine}$ bonds (Table 2).

The tetradentate dianionic Schiff base PTs^{2-} wraps around the metal ions affording helical molecules in both cases. The screwed disposition of the ligand seems to be favoured by the presence of the two terminal bulky tosyl groups. The steric hindrance induced by these tosyl groups appears to provoke a twisting of the Schiff base, in order to minimise the steric interactions. Therefore, the torsion of the flexible spacer allows a remarkable shortening of the $N_{imine}\cdots N_{imine}$ distances relative to the free ligand (ca. 2.9 Å for **1** and **2**, and ca. 4.4 Å for free H_2PTs[15]). This permits the four nitrogen atoms to bind to the same metal centre, leading to the isolation of mononuclear, tetrahedral, single-stranded helical complexes. These compounds can be also classified as saturated,[4] as the Schiff base fulfil the stereochemical requirements of the cobalt and copper atoms. Both right- (*P*) and left-handed (*M*) helixes[4] can be simultaneously observed (in 50% yields) in the unit cell of **1** and **2**.

The PTs^{2-} ligand forms three six-membered chelate rings. The angles between adjacent calculated chelate planes show the screwing of the thread. The degree of twisting is much smaller for the copper complex than for the cobalt complex (the angles between adjacent chelates for **1** is 55.67° and for **2** are 29.78 and 12.68°). Besides, in the crystal structure it can be clearly seen that when the tosyl groups are excluded, the wrapping angle is smaller than 360°. This angle is significantly higher for the copper complex than for the cobalt complex (264° for **1** and 305° for **2**), and this trend correlates with the ionic radius, as expected.

Finally, no specific π-stacking interactions (face-face or face-edge π-π) can be identified, either between the benzylidene binding moieties or between terminal tosyl aromatic rings, which probably appear to be separated in order to minimise the steric hindrance.

[Zn(PTs)]$_2$·1.5H$_2$O·CH$_3$CN (3)

An ORTEP view of **3** is shown in Figure 3. Main bond lengths are shown in Table 2.

The unit cell of complex **3** consists of $[Zn(PTs)]_2$ discrete molecules, with lattice acetonitrile and disordered water. The complex is dinuclear and adopts an *anti*-opened conformation, with the Schiff bases acting as bis(bidentate) donors.[16] Its structure is quite similar to that of the related $[Ni(PTs)]_2$ complex.[17] Each Schiff base uses the amide and imine nitrogen atoms corresponding to one of its arms [N(1), N(2); N(5), N(6)] to bind to Zn(1), and the nitrogen donor atoms of the remaining arm [N(3), N(4); N(7), N(8)] to bind to the second zinc atom [Zn(2)]. One oxygen atom of each tosyl group weakly interacts with the metal centre [the Zn(1)···O(1), Zn(1)···O(6), Zn(2)···O(4) and Zn(2)···O(7) distances are ca. 2.6 Å]. These distances could be secondary intramolecular interactions, as seen in **1** and **2**, as well as in $[Ni(PTs)]_2$.[17] Therefore, each zinc centre has a four-coordinated pseudo-tetrahedral environment, bound to two imine and two amide nitrogen atoms.

The two ligands wrap around the metal−metal axis giving rise to a double-stranded dinuclear helical compound with a Zn···Zn separation of ca. 6.031 Å. This distance compares fairly well with that observed in its analogue nickel complex,[17] but is clearly shorter than that found for dizinc complexes with bis(bidentate) ligands containing a propylene spacer (11.29 Å).[21] The wrapping angle of both strands is ca. 240°, and shows less helical coiling of the ligand than for mononuclear complexes. Both (*P*,*P*) and (*M*,*M*) isomers are present in the unit cell in 50% yields.

The ligands form two six-membered chelate rings, one around each metal atom, which are nearly planar. The dihedral angles between the two ZnNN planes around the same zinc centre are 84.77° for Zn(1) and 82.51° for Zn(2), indicating the deviation of the coordination polyhedron from the ideal geometry. All the distances and angles are in the expected range for distorted tetrahedral zinc(II) complexes with Schiff bases.[22−23] The variety of angles [ranging from 92.7(2) to 144.6(2)° for Zn(1) and from 93.8(2)

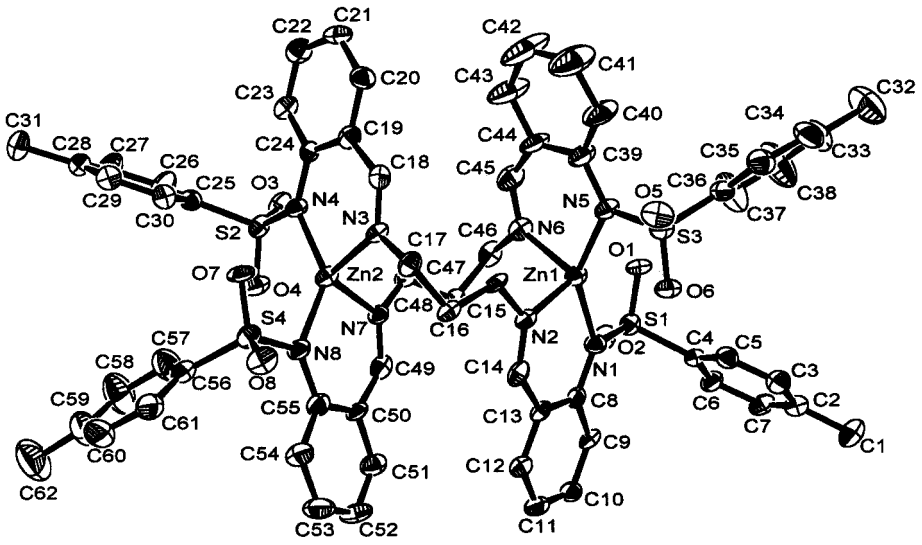

Figure 3. ORTEP view of complex **3** (thermal ellipsoids are drawn at 50% of probability level; hydrogen atoms and solvent molecules have been omitted for clarity)

to 139.7(2)° for Zn(2)] also show the distortion of the tetrahedral environment and that both metal atoms are not equivalent. All these features resemble those in the nickel analogue.[17] Besides, no symmetry elements relate the two ligands or the two halves of the same ligand. This leads to a certain degree of asymmetry in the complex, which gives rise to the formation of two different grooves (major and minor) (Figure 4), as seen in $[Ni(PTs)]_2$.[17] In addition, no π-interactions are observed between the aromatic rings.

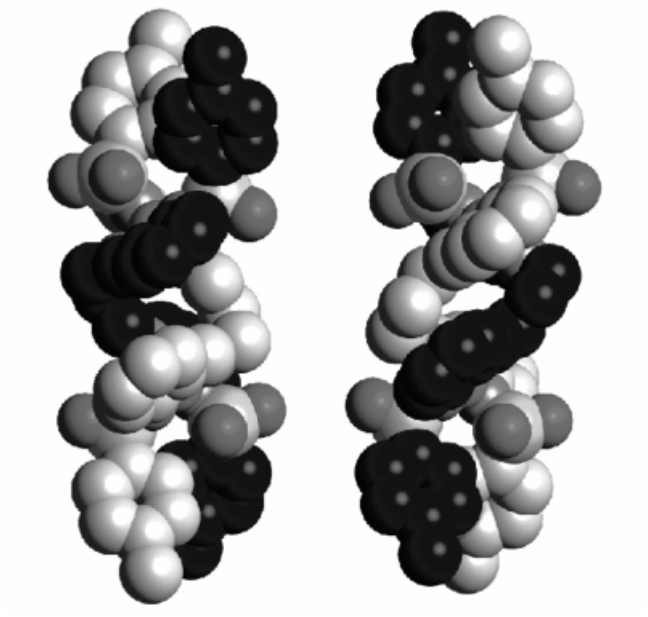

Figure 4. Space-filling representation of complex **1**, showing the minor (left) and major (right) grooves; both representations correspond to the same enantiomer, turned 180°

In spite of the detailed NMR spectroscopic studies of van Koten on dinuclear zinc complexes with diimine ligands,[24] not many complexes of this kind have been reported. There are some structurally characterised dizinc helical complexes described in the literature,[7,21,23–31] but only two helicates (one triple-stranded and one double-stranded) contain Schiff bases.[7,23] In these cases, the two bidentate domains are separated by a rigid spacer, which is the most general situation.[7,23,25–31] In fact, the structurally characterised zinc complexes derived from bis(bidentate) ligands containing flexible spacers are usually monohelical in the solid state,[13–14] and to the best of our knowledge, there are only two examples of bis(dipyrromethane)dizinc complexes with aliphatic spacers, where the extent of helicity is really small.[21] Therefore, the isolation of complex **3** further substantiates the NMR spectroscopic studies of van Koten and unequivocally demonstrates that Schiff bases with flexible spacers can generate zinc double-helical species.

IR Spectroscopy and FAB Mass Spectrometry

The IR spectra of all complexes show a strong band between 1641 and 1612 cm^{-1} due to the imine ν(C=N) group (Table 3). This is a negative shift of 4–23 cm^{-1} relative to the free ligand for all complexes except **3**. In the case of the zinc complex, the ν(C=N) band is shifted to higher wavenumbers (6 cm^{-1}), indicating a slight shift of charge towards the CN group on coordination. However, the ν(C–N) stretching frequency is shifted to lower wave-

Table 3. Selected IR data for the complexes (ṽ, cm^{-1})

Compound	ν(C=N)	ν(C–N)	$\nu_{as}(SO_2)$	$\nu_{s}(SO_2)$
H_2PTs	1635	1340	1287	1164
Mn(PTs)	1624	1304	1272	1158
Fe(PTs)	1612	1298	1260	1158
Co(PTs)	1630	1296	1264	1134
Cu(PTs)	1617	1297	1267	1137
Zn(PTs)	1641	1296	1264	1137
Cd(PTs)	1631	1294	1259	1128

Table 4. Selected ^{1}H NMR chemical shifts (δ values)

	H^1	H^2	H^3	H^5	H^4	H^7	H^6	H^9	H^{10}	H^8
H_2PTs	2.07 (q, 2 H)	3.80 (t, 4 H)	8.55 (s, 2 H)	7.08 (t, 2 H)	7.48 (m, 4 H)		7.37 (t, 2 H)	7.27 (d, 2 H)	2.25 (s, 6 H)	7.65 (d, 2 H)
Zn(PTs)	2.17 (st, 2 H)	4.20, 3.88 (m, 4 H)	8.67 (s, 2 H)	6.93 (t, 2 H)	7.34 (d, 2 H)	7.50 (d, 2 H)	7.27 (m, 4 H)		2.32 (s, 6 H)	7.77 (d, 2 H)
Cd(PTs)	2.03 (b, 2 H)	3.80 (b, 4 H)	8.48 (s, 2 H)	6.86 (t, 2 H)	7.20 (d, 2 H)	7.38 (d, 2 H)	7.15 (m, 4 H)		2.27 (s, 6 H)	7.84 (d, 2 H)

numbers (36−46 cm^{-1}) in all the complexes. This behaviour is compatible with the participation of both imine and amide nitrogen atoms in the coordination to the metal centres. In addition, two bands in the ranges 1259−1272 cm^{-1} and 1128−1158 cm^{-1} are assigned to the asymmetric and symmetric vibration modes of the SO_2 group.[32−33] Finally, no bands above 2500 cm^{-1} were detected for the complexes, indicating the deprotonation of the NH groups, and therefore the dianionic character of the ligand.

The FAB mass spectra show peaks assigned to the $[M(PTs)]^+$ fragments (Table 1) for all the complexes, indicating the coordination of the ligand to the metal centre. However, no other information about the nuclearity of the complexes can be drawn in this case study.

^{1}H NMR Spectroscopy

The ^{1}H NMR spectra of the zinc and cadmium complexes were recorded in [D_6]DMSO as the solvent at room temperature (Table 4), and in CD_3CN at low temperatures (273 and 233 K). The spectra do not change significantly with temperature. In fact, the spectra of the zinc complex recorded at the three different temperatures are identical. All spectra show a singlet set of proton resonances that could be fully assigned. This seems to indicate that there is a single species in solution. In all cases, the disappearance of the NH protons present in the free ligand is observed, which is in agreement with the bis(deprotonation) of the Schiff base. When the ^{1}H NMR spectra of the free ligand is compared with those of the complexes at room temperature, some clear differences are observed (Figure 5):

1. The imine hydrogen atom (3-H) shows a downfield shift for the zinc complex, whilst it is displaced upfield in the spectrum of the cadmium complex, indicating that the coordination of the imine group to the metal centre induces opposite shielding effects on this hydrogen atom. Only one signal is observed for the H-imine atom in **3** at different temperatures suggesting that only symmetric species exist in solution. The imine protons of the cadmium complex are flanked by satellites arising from spin-spin coupling to $^{111/113}$Cd, indicating that the complex is kinetically inert on the NMR timescale.

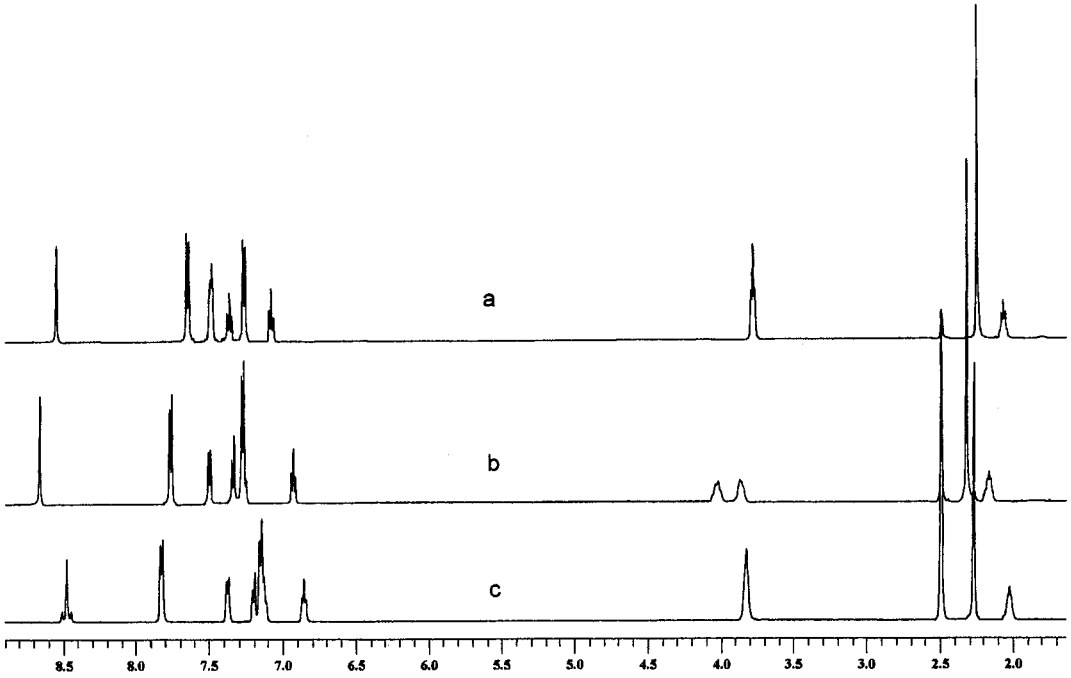

Figure 5. ^{1}H NMR spectra in [D_6]DMSO at room temperature for a) H_2PTS, b) Zn(PTs), and c) Cd(PTs)

2. The signals of the aromatic protons of the benzylidene ring are shifted upfield and the displacements are higher for the cadmium complex. The spectra show that complexation clearly affect the environments of 7-H and 4-H. In the spectra of the free ligand the signals are overlapped, while two sharp doublets are observed in the spectra of the complexes.

3. The signals of the aromatic protons of the tosyl groups also appear to be shifted on complexation, and the displacement is similar for the zinc and cadmium complexes.

4. Finally, the methylene protons of the cadmium and zinc complexes show different chiral behaviour in solution. The 2-H protons are equivalent in the free ligand and appear as a triplet at $\delta = 3.80$. However, for complex **3**, the 2-H protons appear as two multiplets at $\delta = 3.88$ and 4.20. This implies that the strong coordination of the hard imine nitrogen atom to the zinc atom removes the erstwhile enantiotopic nature of the protons making them diastereotopic, and the complex chiral. This is also supported by the central methylene 1-H protons, which in the free ligand appear as a quintuplet at $\delta = 2.07$, while in **3** they appear as a septuplet at $\delta = 2.17$ as a result of the coupling with two pairs of different protons. However, these central methylene hydrogen atoms seem to rotate freely as they are enantiotopic.

The spectrum of the cadmium complex is clearly different. Only one broad signal can be observed for the 2-H protons at room temperature, at $\delta = 3.80$. The 1-H protons also appear as a unique broad signal at $\delta = 2.03$. These signals get sharper on lowering the temperature, and a triplet (4 H) and a quintuplet (2 H) can clearly be observed for 2-H and 1-H, respectively. However, no splitting of the signal assigned to 2-H ($\delta = 3.80$) is observed. This indicates that all 2-H protons are equivalent, in contrast to that found in **3**, and therefore that the cadmium complex is not chiral in solution.

Magnetic Characterisation

Magnetic measurements at room temperature of all the paramagnetic compounds give similar values for the magnetic moments to those expected for magnetically diluted M^{II} ions. The magnetic moment of the manganese and copper complexes only allows for the confirmation of the +2 oxidation state for the central atom, indicating the deprotonation of the Schiff base ligand. The magnetic moments of Fe(PTs) and Co(PTs) are in agreement with high-spin M^{II} complexes. In both cases the magnetic moment is in the normal range for Fe^{II} (5.0−5.4 BM) and Co^{II} (4.3−4.8 BM) tetrahedral complexes. Thus, in view of the formulation of the complexes and their magnetic moments, it seems quite reasonable to propose a tetrahedral environment around the metal atom for all the paramagnetic complexes, as confirmed by the crystal structures of **1** and **2**.

Comparison of all the data obtained from the characterisation techniques employed herein with related complexes[17] leads us to conclude that zinc and nickel[17] form dinuclear double-stranded helicates, and Co and Cu yield mononuclear complexes with H_2PTs in the solid state. In addition, comparison of the ^{1}H NMR spectroscopic data of the Zn and Cd complexes seem to indicate that the tosyl groups behave in a similar way in both complexes and are not directly linked to the central atom, suggesting a tetrahedral environment for the metal centre in both cases. This tetrahedral environment can also be proposed for the other complexes on the basis of the magnetic measurements and X-ray results. Thus, the coordination preferences of the metal ion do not seem to have a profound effect on the disposition of the ligand and the nuclearity of the helix in this case study.

Experimental Section

General: Elemental analysis was performed with a Carlo Erba EA 1108 analyser. The NMR spectra were recorded with a Bruker AMX-500 spectrometer using [D_6]DMSO (296 K) and CD_3CN (273 and 233 K) as solvents. Infrared spectra were recorded as KBr pellets with a Bio-Rad FTS 135 spectrophotometer in the range 4000−600 cm^{-1}. Fast atom bombardment mass spectra (FAB) were obtained with a Kratos MS-50 mass spectrometer in *m*-nitrobenzyl alcohol as a matrix. Room-temperature magnetic measurements were performed using a Sherwood Scientific Magnetic Susceptibility Balance, calibrated using mercury tetrakis(isothiocyanato)cobaltate(II).

Syntheses: All the starting materials were purchased from Aldrich and used without further purification. 2-(Tosylamino)benzaldehyde was prepared according to literature methods[34] and was fully characterised.[35] *N*,*N*′-Bis(2-tosylaminobenzylidene)-1,3-diaminopropane (H_2PTs) was synthesised as previously reported by us and characterised by elemental analyses, melting point, IR, ^{1}H NMR spectroscopy and FAB mass spectroscopy and X-ray diffraction.[15,17]

Synthesis of the Metal Complexes: All complexes were prepared in a similar way, that can be exemplified by the isolation of [Co(PTs)] (**1**). A solution of H_2PTs (0.1 g, 0.15 mmol) in acetonitrile (80 mL), containing ca. 10 mg of tetramethylammonium perchlorate as the supporting electrolyte, was electrolysed for 1.8 h using a current of 5 mA. Concentration of the resultant solution to a third of its initial volume yielded a garnet solid that was washed with diethyl ether and dried in vacuo. Recrystallisation of the powder obtained in acetonitrile yielded single crystals of [Co(PTs)] (**1**), suitable for X-ray diffraction studies. The other complexes were obtained by the same method, using the appropriate metal anode. In the case of the manganese complex, the synthesis was performed in an inert gas under an argon stream. Recrystallisation of [Cu(PTs)] in acetonitrile and of [Zn(PTs)] by diffusion of ether into an acetonitrile solution, yielded crystals suitable for single X-ray analyses of [Cu(PTs)]·1.5CH_3CN (**2**) and [Zn(PTs)]$_2$·1.5H_2O·CH_3CN (**3**), respectively.

CAUTION: Perchlorate salts are potentially explosive and should therefore be handled with the appropriate care.

X-ray Crystallography: Crystals of **1** and **2**, suitable for X-ray diffraction studies, were grown as previously described. Data were collected at 298 K using a Siemens CCD diffractometer employing graphite-monochromated Mo-K_α ($\lambda = 0.71073$ Å) radiation, using the ω-scan mode. The structures were solved by direct methods[36] and refined by full-matrix least squares on F^2.[37] Absorption and incident beam corrections were applied (Sadabs). All non-hydrogen atoms were refined anisotropically. All hydrogen atoms were in-

Table 5. Crystal data and structure refinement

	1	**2**	**3**
Empirical formula	$C_{31}H_{30}CoN_4O_4S_2$	$C_{34}H_{34.5}CuN_{5.5}O_4S_2$	$C_{64}H_{66}N_9O_{9.5}S_4Zn_2$
Formula mass	654.64	711.83	1372.24
Crystal system	orthorhombic	monoclinic	monoclinic
Crystal size [mm]	0.40 × 0.20 × 0.15	0.50 × 0.4 × 0.25	0.30 × 0.25 × 0.25
a [Å]	9.292(3)	8.7453(4)	18.729(4)
b [Å]	26.518(13)	26.9760(12)	24.693(5)
c [Å]	12.458(3)	15.4879(6)	15.633(3)
α [°]	90	90	90
β [°]	90	101.1430(10)	107.097(10)
γ [°]	90	90	90
V [Å^3]	3069.8(20)	3584.9(3)	6910(2)
Space group	*Aba*2 (no. 41)	*P*21/*n* (no. 14)	*P*21/*c* (no. 14)
Z	4	4	4
Absorption coefficient [mm^{-1}]	0.737	0.769	0.875
Reflections collected	6232	14814	20423
Independent reflections	2689 [R_{int} = 0.0375]	6312 [R_{int} = 0.0719]	12646 [R_{int} = 0.0608]
Final *R* indices [$I > 2\sigma(I)$]	0.0504	0.0733	0.0713
R indices (all data)	0.0837	0.1239	0.1412

cluded in the model at geometrically calculated positions. Single crystals of **3** were grown as described above. Data were collected at 173 K using a Siemens CCD diffractometer employing graphite-monochromated Mo-K_α (λ = 0.71073 Å) radiation, using the φ- and ω-scan mode. The structure was solved by direct methods and refined by full-matrix least squares on F^2. Non-hydrogen atoms were refined anisotropically. All hydrogen atoms were included in calculated positions. Data processing and computation were carried out using the SHELX-97 program package.[38] Experimental details are shown in Table 5. Crystallographic data (excluding structure factors) for the structures reported in this paper have been deposited with the Cambridge Crystallographic Data Centre as supplementary publication nos. CCDC-166800 to -166802. Copies of the data can be obtained free of charge on application to CCDC, 12 Union Road, Cambridge CB2 1EZ, UK [Fax: (internat.) + 44-1223/336-033; E-mail: deposit@ccdc.cam.ac.uk].

Acknowledgments

The authors thank the Xunta de Galicia (PGIDT99PXI20903B) and the Ministerio de Educación y Ciencia (Spain) (PB98-0600) for financial support. M. V. thanks the Fundación Segundo Gil Dávila for a grant.

[1] J. M. Lehn, *Supramolecular Chemistry-Concepts and Perspectives*, VCH, Weinheim, **1995**.
[2] [2a] E. C. Constable, in: *Comprehensive Supramolecular Chemistry*, vol. 9 (Eds.: J. P. Sauvage, M. W. Hosseini), Pergamon Press, Oxford, **1996**, p. 213−252. [2b] E. C. Constable, C. E. Housecroft, M. Neuburger, D. Phillips, P. R. Raithby, E. Schofield, E. Sparr, D. A. Tocher, M. Zehnder, Y. Zimmermann, *J. Chem. Soc., Dalton Trans.* **2000**, 2219−2228.
[3] D. Philp, J. F. Stoddart, *Angew. Chem. Int. Ed. Engl.* **1996**, *35*, 1155−1196.
[4] C. Piguet, G. Bernarddinelli, G. Hopfgartner, *Chem. Rev.* **1997**, *97*, 2005−2062.
[5] G. F. Swiegers, T. J. Maleftse, *Chem. Rev.* **2000**, *100*, 3483−3537.
[6] [6a] M. J. Hannon, C. L. Painting, A. Jackson, J. Hamblin, W. Errington, *Chem. Commun.* **1997**, 1807−1808. [6b] N. W. Alcock, P. R. Barker, J. M. Haider, M. J. Hannon, C. L. Painting, Z. Pikramenou, E. A. Plummer, K. Rissanen, P. Saarenketo, *J. Chem. Soc., Dalton Trans.* **2000**, 1447−1461. [6c] L. J. Chields, N. W. Alcock, M. J. Hannon, *Angew. Chem. Int. Ed.* **2001**, *40*, 1079−1081.
[7] N. Yoshida, K. Ichikawa, *Chem. Commun.* **1997**, 1091−1092.
[8] C. R. Rice, S. Wörl, J. C. Jeffery, R. L. Paul, M. D. Ward, *J. Chem. Soc., Dalton Trans.* **2000**, 550−559.
[9] H-L. Zhu, Y-X. Tong, X-M. Cheng, *J. Chem. Soc., Dalton Trans.* **2000**, 4182−4186.
[10] [10a] J. Sanmartín, M. R. Bermejo, A. García-Deibe. O. Piro, E. E. Castellano, *Chem. Commun.* **1999**, 1953−1954. [10b] J. Sanmartín, M. R. Bermejo, A. M. García-Deibe, A. L. Llamas-Saiz, *Chem. Commun.* **2000**, 795−796. [10c] O. L Hoyos, M. R. Bermejo, M. Fondo, A. García-Deibe, A. M. González, M. Maneiro, R. Pedrido, *J. Chem. Soc., Dalton Trans.* **2000**, 3122−3127.
[11] L. Carbonaro, M. Isola, V. Liuzzo, F. Marchetti, F. Balzano, C. S. Pomelli, A. Raffaelli, *Eur. J. Inorg. Chem.* **2001**, 353−357.
[12] A. Jäntti, M. Wagner, R. Suontamo, E. Kolehmainen, K. Rissanen, *Eur. J. Inorg. Chem.* **1998**, 1555−1562.
[13] S. C. Shoner, A. M. Nienstedt, J. J. Ellison, I. Y. Kung, D. Barnhart, J. A. Kovaks, *Inorg. Chem.* **1998**, 5721−5726.
[14] M. H. W. Lam, D. Y. K. Lee, S. S. M. Chiu, K. W. Man, W. T. Wong, *Eur. J. Inorg. Chem.* **2000**, 1483−1488.
[15] J. Mahía, M. Maestro, M. Vázquez, M. R. Bermejo, J. Sanmartín, M. Maneiro, *Acta Crystallogr., Sect. C* **1999**, *55*, 1545−1546.
[16] N. Yoshida, H. Oshio, T. Ito, *J. Chem. Soc., Perkin Trans. 2* **1999**, 975−983.
[17] M. Vázquez, M. R. Bermejo, M. Fondo, A. M. González, J. Mahía, L. Sorace, D. Gatteschi, *Eur. J. Inorg. Chem.* **2001**, 1863−1868.
[18] C. Oldham, D. G. Tuck, *J. Chem. Educ.* **1982**, *59*, 420.
[19] A. Sousa, M. R. Bermejo, M. Fondo, A. García-Deibe, A. Sousa-Pedrares, O. Piro, *New J. Chem.* **2001**, *25*, 647−654.
[20] J. A. García-Vázquez, J. Romero, M. L. Durán, A. Sousa, A. D. Garnovskii, A. S. Burlov, D. A. Garnovskii, *Polyhedron* **1998**, *17*, 1547−1552.
[21] A. Thompson, D. Dolphin, *J. Org. Chem.* **2000**, *65*, 7870−7877.
[22] J. Romero, J. A. García-Vázquez, M. L. Durán, A. Castiñeiras,

A. Sousa, A. D. Garnovskii, D. A. Garnovskii, *Acta Chem. Scand.* **1997**, *51*, 672−675.
[23] N. Yoshida, K. Ichikawa, M. Shiro, *J. Chem. Soc., Perkin Trans. 2* **2000**, 17−26.
[24] C. G. van Stein, G. van Koten, H. Passenier, O. Steinebach, K. Vrieze, *Inorg. Chim. Acta.* **1984**, *89*, 79−87.
[25] G. Struckmeier, U. Thewalt, J. H. Furhop, *J. Am. Chem. Soc.* **1976**, *98*, 278−279.
[26] D. Wester, G. J. Palenik, *Inorg. Chem.* **1976**, *15*, 755−761.
[27] W. S. Sheldrick, J. Engel, *Acta Crystallogr., Sect. B* **1981**, *37*, 250−251.
[28] C. Lorenzini, C. Pelizzi, G. Pelizzi, G. Predieri, *J. Chem. Soc., Dalton Trans.* **1983**, 2155−2158.
[29] A. Bino, N. Cohen, *Inorg. Chim. Acta* **1993**, *210*, 11−16.
[30] R. Chotalia, E. C. Constable, M. Neuburger, D. R. Smith,, M. Zehnder, *J. Chem. Soc., Dalton Trans.* **1996**, 4207−4216.
[31] Y. Zhang, A. Thompson, S. J. Rettig, D. Dolphin, *J. Am. Chem. Soc.* **1998**, *120*, 13537−13538.
[32] M. Morioka, M. Kato, H. Yoshida, T. Ogata, *Heterocycles* **1997**, *45*, 1173−1181.
[33] K. Nakamoto, in: *Infrared and Raman Spectra of Inorganic and Coordination Compounds*, John Wiley & Sons, New York, **1997**.
[34] N. I. Chernova, Y. S. Ryabokobylky, V. G. Brudz, B. M. Bolotin, *Zh. Neorg. Khim.* **1971**, 1680−1687.
[35] J. Mahía, M. Maestro, M. Vázquez, M. R. Bermejo, A. M. Gonzalez, M. Maneiro, *Acta Crystallogr., Sect. C* **1999**, *55*, 2158−2160.
[36] G. M. Sheldrick, "SHELXS-86", in: *Crystallographic Computing* (Eds.: G. M. Sheldrick, C. Krueger, R. Goddard), Oxford University Press, **1985**.
[37] G. M. Sheldrick *SHELXL 93*, University of Göttingen, Germany, **1993**.
[38] G. M. Sheldrick, *SHELX-97 (SHELXS 97 and SHELXL 97), Programs for Crystal Structure Analyses*, University of Göttingen, Germany, **1998**.

Received July 12, 2001
[I01263]

Compared Behaviours of Dawson-Type Tungstodiarsenates and -diphosphates

Bineta Keita,[a] Israel Martyr Mbomekalle,[a] Louis Nadjo,*[a] and Roland Contant[b]

Keywords: Polyanions / Tungsten / Arsenic / Phosphorus / Electrochemistry

The lacunary α_2-$[As_2W_{17}O_{61}]^{10-}$ derived from the Dawson molecule α-$[As_2W_{18}O_{62}]^{6-}$ was used as a ligand for the following metal cations: Mn^{2+}, Fe^{3+}, Co^{2+}, Ni^{2+}, Cu^{2+} and Zn^{2+}. The cyclic voltammograms of this lacunary precursor species, as well as those of the substituted complexes were run in a medium at pH = 3. A systematic comparison was carried out with the electrochemical characteristics of the corresponding complexes derived from α-$[P_2W_{18}O_{62}]^{6-}$, with the aim of highlighting the differences in their behaviour, which could be ascribed to the identity of the central atoms. The study was also extended to the Fe^{3+} species of the α_1 series. The comparisons reveal that whatever the series, the first several voltammetric waves are driven in the positive potential direction by the presence of As as the central atom in the heteropolyanions. These results agree with those from crystallographic evaluations, and with the knowledge of the stability constants of the complexes, indirectly reveal a coherent picture of the behaviour of the vacant sites in the diarsenates and diphosphates. In particular, the influence of the central heteroatom on the redox and/or acid-base properties could be assessed and compared. Steric effects, expected on geometrical grounds, and already reflected in the values of the stability constants of the metal ion substituted compounds, also influence the cyclic voltammograms.

1. Introduction

Much work has been devoted to Dawson-type tungstodiphosphates. In particular, their ability to generate lacunary species, and hence metal cation substituted derivatives has received extensive attention.[1−10] The impetus was triggered by the pioneering remark that monosubstituted heteropolyanions can be considered as the analogues of metallated porphyrins, and can be used in catalytic processes with the advantage, over their organic counterparts, of their thermal stability, robustness and inertness toward oxidising environments.[11] In contrast, the corresponding diarsenates have been the subject of very few papers,[12−14] presumably owing to the assumption that a complete analogy should be expected between the two series of species. Actually, such an assumption would ignore the possibility that the change in the central heteroatom might bring about new physical, and correlatively, electronic, chemical and redox behaviours. Several papers[2,4] have shown the linear dependence of the first one-electron reduction potentials (under conditions of no protonation) on the overall negative charge of the heteropolyanions, in conjunction with the charge on the central heteroatom. Further, the influence of the central heteroatom (Si^{IV}, Ge^{IV}, P^{V}, As^{V}) on the stabilities of the metal(II) and alkaline ion complexes of selected heteropolytungstates[12,15] was published. However, most of these studies were performed in the Keggin series.

In our systematic study of the parameters which could modify the redox properties of heteropolyanions, and hence their electrocatalytic behaviour, several possibilities were identified. The pH of the solution is one obvious parameter. A rich series of possibilities is opened up by the substituent effect; the location of the heterometal in the framework, the nature, and the number of substituents may influence the interactions between the electroactive centres within the molecule.[6,9,16] Furthermore, a recent paper from our group[17] has stressed the change in symmetry of the charge distribution in lacunary species and in their first transition metal ion substituted derivatives, thus justifying the comparison between these two series of compounds, and not with the saturated precursors.[6,9,16,17]

Until now the influence of the central heteroatom in Dawson-type anions on their cyclic voltammograms was not explored. In this context, we are interested in comparing saturated and metal ion monosubstituted diarsenates with diphosphates. Particular attention will be paid to the location of the vacant site in the framework, to steric effects (in other words the ability of the vacant site to accommodate the substituent metal cation), and the physical and chemical behaviour.

2. Results

2.1. The Selection of Relevant Heteropolyanions

All the polyanions studied here can be considered as being primarily derived from α-$[P_2W_{18}O_{62}]^{6-}$ (abbreviated as

[a] Laboratoire de Chimie Physique, UMR 8000, CNRS, Electrochimie et Photoélectrochimie, Université Paris-Sud, Bâtiment 420,
91405 Orsay Cedex, France
Fax: (internat.) + 33-1/69154328
E-mail: louis.nadjo@lcp.u-psud.fr
[b] Laboratoire de Chimie des Métaux de Transition, UPRESA 7071, CNRS, Université Paris VI,
4, place Jussieu, 75252 Paris Cedex 05, France

 © WILEY-VCH Verlag GmbH, 69451 Weinheim, Germany, 2002 1434−1948/02/0202−0473 $ 17.50+.50/0

α-P_2W_{18} in the following) and α-$[As_2W_{18}O_{62}]^{6-}$ (abbreviated as α-As_2W_{18}). Although it has become classical, Figure 1 is shown for clarity. The tungsten atoms are numbered according to the IUPAC recommendations. The two P atoms are numbered 1 and 2 for the upper and the lower halves of the molecule, respectively. For example, considering the upper half of the molecule, and taking into account the numbering, the metal atoms in the "cap" occupy what will be termed the α_2 positions and those in the "belt" the α_1 positions. In the lacunary species, the vacancies (missing W atoms) are numbered in the same way and represented, when necessary, by □ in the formula of the anion. Any metal atom occupying the vacancy will keep the same index.

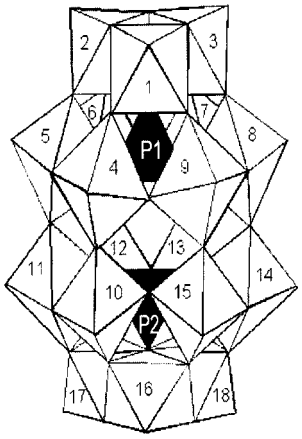

Figure 1. Idealised structure of α-$[P_2W_{18}O_{62}]^{6-}$ and its substitution derivatives

The following heteropolyanions were used: α-$[As_2W_{18}O_{62}]^{6-}$ (abbreviated as α-As_2W_{18}), α_1- and α_2-$[As_2W_{17}O_{61}]^{10-}$ (α_1- and α_2-As_2W_{17}), α_2-$[Mn(H_2O)(As_2W_{17}O_{61})]^{8-}$ (α_2-$As_2W_{17}Mn$), α_1- and α_2-$[Fe(H_2O)(As_2W_{17}O_{61})]^{7-}$ (α_1- and α_2-$As_2W_{17}Fe$), α_2-$[Co(H_2O)(As_2W_{17}O_{61})]^{8-}$ (α_2-$As_2W_{17}Co$), α_2-$[Ni(H_2O)(As_2W_{17}O_{61})]^{8-}$ (α_2-$As_2W_{17}Ni$), α_2-$[Cu(H_2O)(As_2W_{17}O_{61})]^{8-}$ (α_2-$As_2W_{17}Cu$), α_2-$[Zn(H_2O)(As_2W_{17}O_{61})]^{8-}$ (α_2-$As_2W_{17}Zn$), α-$[P_2W_{18}O_{62}]^{6-}$ (abbreviated as α-P_2W_{18}), α_1- and α_2-$[P_2W_{17}O_{61}]^{10-}$ (α_1- and α_2-P_2W_{17}), α_2-$[Mn(H_2O)(P_2W_{17}O_{61})]^{8-}$ (α_2-$P_2W_{17}Mn$), α_1- and α_2-$[Fe(H_2O)(P_2W_{17}O_{61})]^{7-}$ (α_1- and α_2-$P_2W_{17}Fe$), α_2-$[Co(H_2O)(P_2W_{17}O_{61})]^{8-}$ (α_2-$P_2W_{17}Co$), α_2-$[Ni(H_2O)(P_2W_{17}O_{61})]^{8-}$ (α_2-$P_2W_{17}Ni$), α_2-$[Cu(H_2O)(P_2W_{17}O_{61})]^{8-}$ (α_2-$P_2W_{17}Cu$), α_2-$[Zn(H_2O)(P_2W_{17}O_{61})]^{8-}$ (α_2-$P_2W_{17}Zn$). Their preparation and characterisation have already been described in detail.[6,8,9,12−15,18,19]

2.2. Electrochemistry

The main features of the electrochemical data are presented in Table 1, which allows a pertinent comparison of the reduction peak potentials pertaining to the first W wave for the As and P derivatives. The ΔE_p values can be considered as a self-consistent parameter, using the appropriate precursor lacunary species as a reference. Most of our study is devoted to derivatives that are substituted in the α_2 position. Strictly, the changes in acid-base properties from the lacunary precursor to the substituted species preclude the direct use of the ΔE_p values in obtaining reliable values for the stability constants of the complexes. As previously with tungstodiphosphates, the location of the vacant site, and subsequently of the substituent metal cation, is revealed by the characteristic fingerprint associated with the α_2 compounds in a medium with pH = 3,[10] where the first two two-electron W-centred processes are followed by two one-electron processes. From the two pH values studied (pH = 3 and 5), the first W wave is shifted roughly by 74 mV/pH, irrespective of the type of substituted tungstodiarsenate.

Table 1. Reduction peak potential vs. SCE for the first tungsten wave in α_2-$X_2W_{17}M$ complexes (X = As or P; M represents the substituent metal cation) and comparison with the appropriate lacunary species; supporting electrolyte: 0.2 M Na_2SO_4 + H_2SO_4 (pH = 3); scan rate 10 mV·s^{-1}; the results for the diphosphates were published previously in ref.[10], but here, for composite waves in this series, only the most negative peak potential was retained for clarity

Compound	$-E_p$ [mV] vs. SCE	$\delta\Delta E_p$ [mV][a]
α-As_2W_{18}	−18	−
α-P_2W_{18}	22	−
α_2-As_2W_{17} o	298	0
α_2-P_2W_{17} o	320	0
α_2-$As_2W_{17}Mn$	324	26
α_2-$P_2W_{17}Mn$	394	74
α_2-$As_2W_{17}Fe$	360	62
α_2-$P_2W_{17}Fe$	402	82
α_2-$As_2W_{17}Co$	346	48
α_2-$P_2W_{17}Co$	392	72
α_2-$As_2W_{17}Ni$	358	60
α_2-$P_2W_{17}Ni$	406	86
α_2-$As_2W_{17}Cu$	288	−10
α_2-$P_2W_{17}Cu$	306 (composite W/Cu wave)	−14
α_2-$As_2W_{17}Zn$	360	62
α_2-$P_2W_{17}Zn$	386	66

[a] $\Delta E_p = E_{p,lacunary} - E_{p,substituted}$.

At pH = 3, the first W wave for α-As_2W_{18} and α-P_2W_{18} features a one-electron process, as confirmed by controlled potential coulometry. Otherwise, throughout Table 1, the first redox process associated with the W centres involves two electrons. Examination of the values in this table underscores the previously demonstrated fact[9,10,16] that the appropriate comparison among the present compounds must be made between the precursor lacunary species and their metal ion substituted derivatives. In this series of "unsaturated" species, it can be seen that the first W wave is shifted in the positive potential direction in all the As compounds relative to the P derivatives. This trend appears even in the lacunary species and can be ascribed to the larger basicity of the reduced forms of the As derivatives. However, it is worth noting that these W peak potentials in the substituted As derivatives are rather close from one compound to

the next, except in the case of the Cu-substituted species. This observation would indicate, even in the case of the Fe derivative in which the reduction of the iron centre occurs prior to the W centres, that a roughly constant change in basicity exists between the precursor lacunary species and its metal ion complexes.

Several complementary results characteristic of the diarsenates are worth noting and are presented in Table 2. The influence of pH is obvious, except for the $Co^{2+/3+}$ redox couple. The pH dependence of the $Mn^{2+/3+}$ redox couple in α_2-$As_2W_{17}Mn$ is very apparent. The significance of this observation will be studied in conjunction with the electrocatalytic properties of this system. In the α_2 series it is found that the reduction peaks for the substituent cations, that are reduced in a potential domain close to that of the W centres, are observed at more positive potentials in the As than in the P derivatives; in the As compounds, the reduction peak potentials are located at −66 mV vs. SCE for Fe^{3+} and −212 mV vs. SCE for Cu^{2+}, compared with −130 mV and −306 mV, respectively for the P derivatives.

Table 2. Oxidation or reduction peak potentials for the electroactive substituent cations within the α_2-$As_2W_{17}M$ species (M represents the substituent metal cation) at pH = 3 and 5; scan rate 10 mV·s^{-1}

	$Mn^{2+/3+}$	$Mn^{3+/4+}$	$Fe^{3+/2+}$	$Co^{2+/3+}$	$Cu^{2+/0}$
E_p [mV] (pH = 3)	1040	1186	−66	1130	−212
E_p [mV] (pH = 5)	624	950	−134	1124	−270

A short comparison is made in Table 3, between some compounds of the α_1 series. The corresponding results of the α_2 series are added to facilitate further comments. The location of the vacant site has no influence (for As), or only a small influence (for P), on the reduction peak potential of the lacunary species, irrespective of the identity of the central atom. Even so, a small positive shift is observed for the diarsenates relative to the diphosphates. Substantially larger shifts in the same direction are seen for the first reduction process of W centres in the iron-substituted species. The same trend can be seen for the reduction of the Fe^{3+} centre within the heteropolyanions with regard to the comparison between the diarsenates and the diphosphates. It must be noted that the influence of the pH on the $Fe^{3+/2+}$ redox couple in the α_1 derivatives is rather small. In contrast, the maximum shift in the negative potential direction for the α_2 species is 68 mV for the As derivative and 46 mV for the P compound. It is also worth noting that the iron centre is less easily reduced in the α_1 than in the α_2 derivatives. Such an observation should be related to a more general problem; it has been proposed[20,21] that α-P_2W_{18} is first reduced at one of the twelve equivalent tungsten atoms in the "belt". Experimental evidence supports this fact.[22] This behaviour still holds for the α_1-substituted species, the first observed wave depends on the relative reducibility of the substituent cation and W. It is then conceivable that the reduction potential of this hetero-cation is influenced by the neighbouring W atoms.[6] This point is being elaborated and will be published in a forthcoming paper.[23]

Tables 1−3 are complemented by Figure 2, which displays cyclic voltammograms of selected representative heteropolyanions that show more specific descriptions of their behaviour. Figure 2A compares the cyclic voltammograms of the α_1- and α_2-$As_2W_{17}Fe$ derivatives at pH = 3, and Figure 2B compares those of the corresponding P derivatives. Provisionally, it must be pointed out that the characteristic fingerprint for the α_2-type derivatives is present, as expected. Although the assignment of the observed first wave might appear straightforward, the novelty of the compounds prompted us to carry out several complementary coulometric determinations. Controlled potential coulometric experiments at pH = 3, and at the relevant peak potential or just negative of this value, suggest that one electron per molecule of α_1- or α_2-$As_2W_{17}Fe$ is involved. The characteristic blue colour of the reduced W centres was not observed, thus confirming that only the Fe^{3+} centre was reduced. Complete reoxidation to the Fe^{3+} state was achieved, and this indicated the stability of the $Fe^{3+/2+}$ system within the heteropolyanions, at least on the coulometric

Table 3. Reduction peak potential vs. SCE for $Fe^{3+/2+}$ redox couple and first tungsten wave in complexes of the α_1 and α_2 series; electrolytes: pH = 3 and 5; scan rate 10 mV·s^{-1}; for further details, see text

Compound	pH	$-E_p$ [mV] (Fe^{3+}/Fe^{2+})wave	$-E_p$ [mV] (1st W wave)
α_1-$As_2W_{17}\square$	3	–	298
α_2-$As_2W_{17}\square$	3	–	298
α_1-$P_2W_{17}\square$	3	–	306
α_2-$P_2W_{17}\square$	3	–	320
α_1-$As_2W_{17}Fe$	3	114	350,[a] 468, 544
	5	128	498,[a] 558, 666
α_2-$As_2W_{17}Fe$	3	66	360
	5	134	510
α_1-$P_2W_{17}Fe$	3	198	500
	5	192	602
α_2-$P_2W_{17}Fe$	3	130	(340) 402[b]
	5	176	548

[a] The combined 1st and 2nd W waves are split into three components, the peaks of which are located at the potentials indicated in the table (see Figure 2A). [b] The number in parentheses corresponds to the first part of a composite wave.

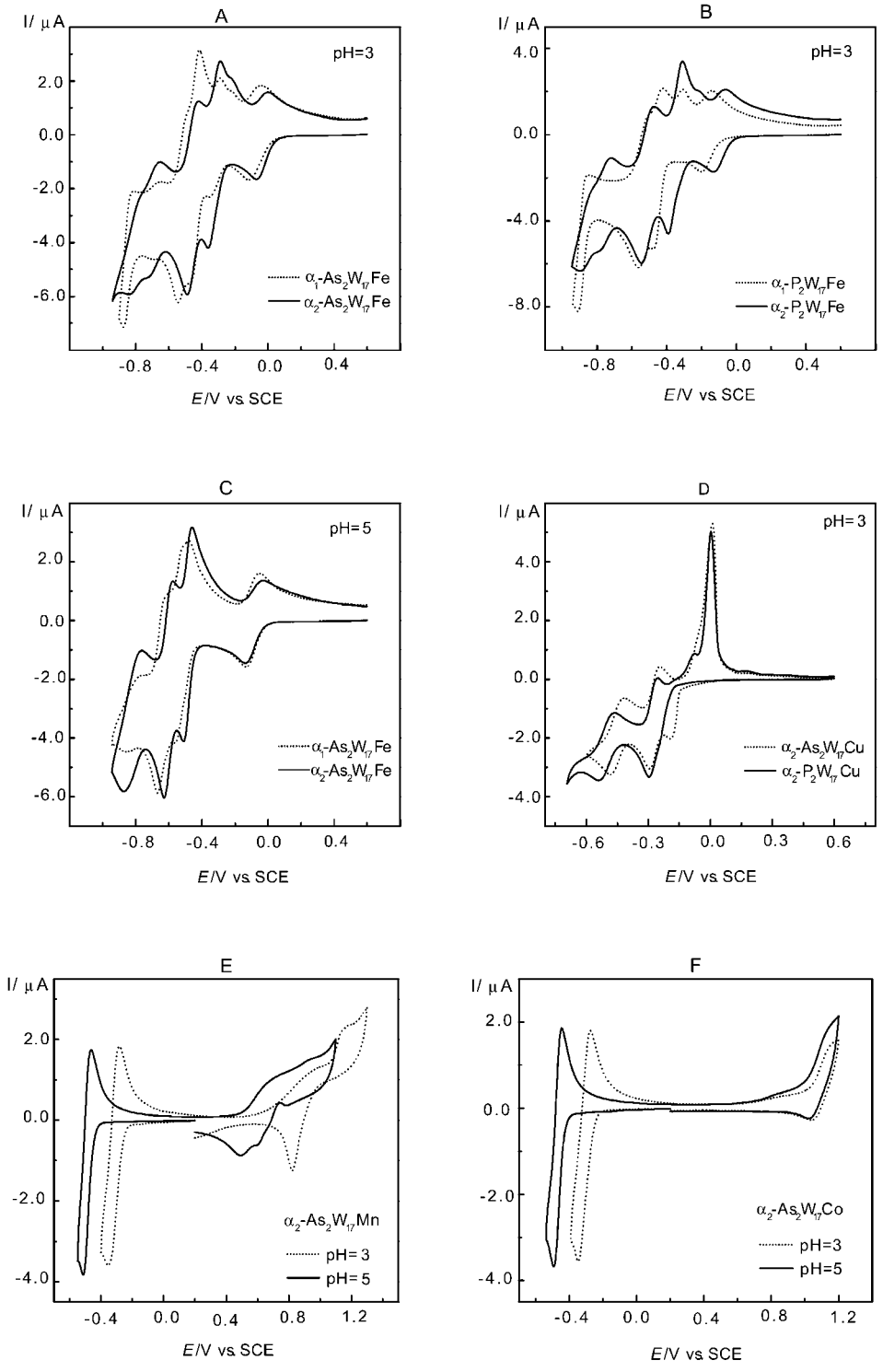

Figure 2. Cyclic voltammograms of a 5×10^{-4} M solution of the relevant heteropolyanion; working electrode glassy carbon; scan rate 10 $mV \cdot s^{-1}$, unless otherwise stated: A and B: 0.2 M Na_2SO_4 + H_2SO_4 (pH = 3); C: 0.4 M CH_3COONa + CH_3COOH (pH = 5); D: 0.2 M Na_2SO_4 + H_2SO_4 (pH = 3); scan rate 2 $mV \cdot s^{-1}$: E and F: 0.2 M Na_2SO_4 + H_2SO_4 (pH = 3) and 0.4 M CH_3COONa + CH_3COOH (pH = 5)

timescale. Under the same experimental conditions, a parallel behaviour was obtained for α_1- and α_2-$P_2W_{17}Fe$.[10,16] In Figure 2A, the Fe^{3+} reduction wave for α_2-$As_2W_{17}Fe$ is followed by two two-electron W waves. The same observation is seen for α_2-$P_2W_{17}Fe$ in Figure 2B, with a slight splitting of the first W wave in the P derivative. In contrast, for the α_1-$As_2W_{17}Fe$ derivative in Figure 2A, the expected two two-electron tungsten waves are separated into three components, with a remarkable reduction in the current of the first W wave and an enhancement of the intermediate part. A

different behaviour is displayed by α_1-$P_2W_{17}Fe$ in Figure 2B. An important negative shift of the first W wave, and a large enhancement of the first wave relative to the second wave is seen. Comparison of these two Figures indicates a sharp difference in the acid-base behaviour between the α_1 and α_2 derivatives in each series, and also between the α_1 derivatives of the two series. Such a difference between α_1-$As_2W_{17}Fe$ and α_2-$As_2W_{17}Fe$ is less striking at pH = 5, as can be seen in Figure 2C. The last example selected for comparison can be seen in Figure 2D, and involves α_2-$As_2W_{17}Cu$ and α_2-$P_2W_{17}Cu$. The cyclic voltammograms were run at pH = 3, and clearly show the good separation between the Cu^{2+}- and W^{6+}-centred processes in α_2-$As_2W_{17}Cu$, in contrast to the almost complete merging of the corresponding processes in α_2-$P_2W_{17}Cu$. Coulometry at the peak potential of the Cu^{2+} reduction wave in α_2-$As_2W_{17}Cu$ clearly showed the involvement of two electrons per molecule of heteropolyanion. No blue colour was observed, which would have indicated the concomitant reduction of the W centres. Using the same experimental conditions, it was necessary to use spectroelectrochemistry to appreciate the degree of separation of these two processes in α_2-$P_2W_{17}Cu$[24] Finally, Figure 2E,F illustrates the behaviour of the Mn^{2+} and Co^{2+} diarsenate derivatives at the two pH values studied. Two oxidation-reduction steps are easily observed for Mn^{2+} and one for Co^{2+}.

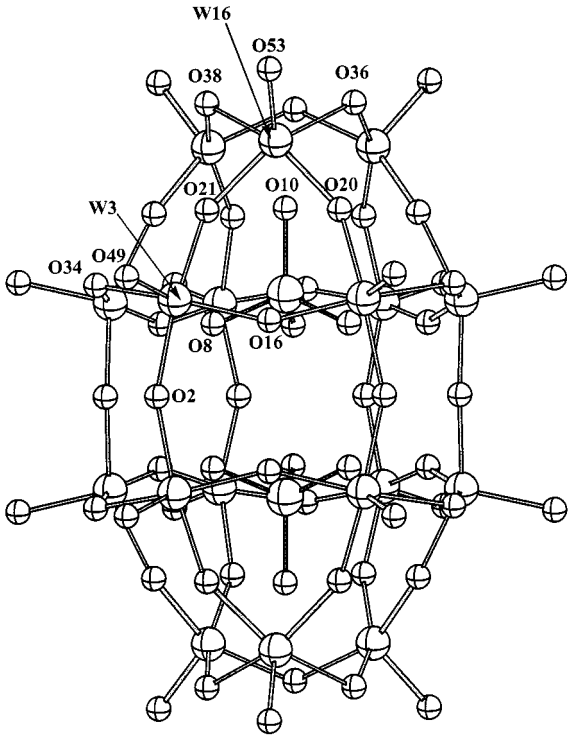

Figure 3. Numbering of atoms in the idealised structure of α-$[P_2W_{18}O_{62}]^{6-}$, used in the working out of crystallographic distances in Table 4

3. Discussion

We attempted to rationalise the experimental results by considering the interplay between several influences that ultimately determine the physical properties of the vacant site and hence, the behaviour of the substituted species. A crude evaluation of the size of the vacant site can be obtained by measuring the W−O distances around a selected W atom in the Dawson-type structure, with special attention being paid to the W−O terminal bond, which disappears when the vacancy is created. It is assumed during this process that the bond lengths or bond angles do not change on creating the vacant site. In this context, the numbering of atoms in the idealised structure in Figure 3 is based directly on the crystallographic results of D'Amour[25] and are used for the evaluation of the energies of molecular orbitals,[23] and more specifically here, for the determination of bond lengths. Table 4 shows the bond lengths recalculated from this idealised structure of P_2W_{18}. This evaluation of the sizes of vacant sites is primarily useful when comparing the behaviours of the derivatives of α_1- and α_2-P_2W_{18}.

Table 4. Mean W−O distances in Å in an idealised structure of $[P_2W_{18}O_{62}]^{6-}$

W3−O2	1.9220	W16−O10 (W−O−P)	2.3010
W3−O8 (W−O−P)	2.3196	W16−O20	1.9235
W3−O49	1.8986	W16−O21	1.9235
W3−O21	1.9401	W16−O36	1.9917
W3−O16	1.9575	W16−O38	1.9917
W3−O34 (W−O_t)	1.9147	W16−O53 (W−O_t)	1.8230

The two possible nonequivalent locations for a monovacant site are outlined by the W3−O and the W16−O distances; extraction of a W−O_t moiety from the appropriate position will create a vacant site in the so-called α_1 position for W3−O, or α_2 position for W16−O. Examination of the bond lengths would then suggest that the vacant site in the α_2 position is slightly larger than that in the α_1 position. However, this evaluation does not take into account the influence of the bond angles, which could minimise the difference in size between the two sites, whether the volume or the entrance surface is considered. In any case, a direct study of the size of the vacant site is severely plagued by the lack of precise crystallographic data on the lacunary species. As a matter of fact, it was pointed out that the vacancy in such species is statistically distributed over several or all of the equivalent positions.[26,27] Therefore, although the same kind of derivation as above could have been carried out using the crystallographic determinations on As_2W_{18} by Neubert and Fuchs,[28] we found that the following complementary qualitative observations might prove more useful. From a general point of view in the Dawson-type tungstodiphosphates and tungstodiarsenates, the physical behaviour of a vacancy depends on its location in the polyoxometalate frame. The greater rigidity of the α_1 sites compared with the relative fluidity of the α_2 sites might be explained as follows: a WO_6 octahedron in an α_1 position is once edge-shared and three times corner-shared, while in an α_2 position it is twice corner-shared and twice edge-

shared. Such an explanation clearly predicts the influence of the degree of matching between the size of the vacant site and the radius of the substituent cation on the stability constants of the complexes. Incidentally, it is worth noting that such a reasoning suggests a parallel behaviour for monolacunary Keggin species and α_2 Dawson-type lacunary compounds that possess the same kind of vacancy. Thus, the variations in the stability constants of the metal(II) and alkaline ion complexes of lacunary heteropolytungstates can be explained.[12,15] In contrast, it also justifies that the stability constants for the divalent metal ion complexes of α_1-P_2W_{17} □ and α_1-As_2W_{17} □ are not really affected by the nature of the central heteroatom.[12] Such an observation is important to propose a tentative explanation for some of the results in Table 3. The following suggestion can be made: the first W wave is driven in the positive potential direction in α_1-$As_2W_{17}Fe$ relative to the corresponding wave in α_1-$P_2W_{17}Fe$, due to the electronic effects of the central heteroatom, which ultimately is reflected in the relative basicity of the reduced species. The same influence holds for the compounds substituted in the α_2 position. Turning then to the general comparison between Dawson-type tungstodiphosphates and diarsenates, it can be assumed that, all things being equal, the size of the central atoms becomes the main relevant parameter. Considering the ionic radii of As^{5+} (0.46 Å) and P^{5+} (0.35 Å)[29] the larger space-filling ability of As should decrease the size of vacancies in the tungstodiarsenates relative to the -diphosphates. On this basis it is expected that the substituent cations would be attached less tightly in As than in the P derivatives. Stability constant values confirm this reasoning.[12] The only two examples of complexes in the present series in which the substituent cations are reduced in the vicinity of the W centres are the Fe^{III}- and Cu^{II}-substituted derivatives. The reduction potentials of these heterometal centres are substantially less negative in the As than in the P species, thus corroborating the expectations from the aforementioned reasoning.

4. Concluding Remarks

In the present work, Dawson-type tungstodiarsenates were synthesised, as well as their mono-lacunary species and several corresponding metal ion substituted derivatives. Attention was focused mainly on α_2-type derivatives, however, the Fe^{3+} derivatives of the α_1-, as well as the α_2-lacunary precursors were used. Systematic comparisons of the cyclic voltammograms of these compounds with those of tungstodiphosphates reveal that the first several voltammetric waves are driven in the positive potential direction by the presence of As as the central atom in the heteropolyanions. Precise crystallographic data are lacking for such compounds, in the diarsenate or in the diphosphate series. In spite of this situation, the present electrochemical results agree with the rough geometrical considerations, and with the knowledge of the stability constants of the metal ion substituted compounds indirectly reveal a coherent picture of the behaviour of the vacant sites in diarsenates and diphosphates. In particular, the influence of the central heteroatom on the redox and/or acid-base properties could be assessed and compared. Steric effects, expected on geometrical grounds, and already reflected in the values of the stability constants of the metal ion substituted compounds, also influence the cyclic voltammogram.

In conclusion, the identity of the central heteroatom substantially influences the redox behaviour of heteropolyanions, and must therefore be taken into account in our study of the parameters, which could modify electrocatalytic properties of this class of chemicals. It is rewarding to note that indirect methods can be used when evaluating the influence of changing the central atom in heteropolyanions. The study of multi-substitutions in the diarsenates and diphosphates is currently in progress.

5. Experimental Section

Pure water from a Milli-RO_4 unit, followed by a Millipore Q purification set was used throughout. All the chemicals were of high-purity grade and were used as received. H_2SO_4, Li_2SO_4, Na_2SO_4, CH_3COOH, CH_3COONa (Prolabo Normapur) were commercial products. In the present study, the medium of pH = 3 was made up with 0.2 M Na_2SO_4 + H_2SO_4 and that of pH = 5 with 0.4 M CH_3COONa + CH_3COOH. The heteropolyanions used in this work have been cited previously, along with appropriate abbreviations and preparations. Their stability was checked in a 0.2 M Na_2SO_4 + H_2SO_4 medium (pH = 3) using UV/Vis spectroscopy over a period of at least 24 h. The solutions were deaerated thoroughly for at least 30 min with pure argon and kept under argon during the electrochemical experiments**.** The source, mounting and polishing of the glassy carbon electrode (GC, Le Carbone Lorraine, France, 3 mm diameter) have been described.[5,6] The electrochemical setup was an EG & G 273 A driven by a PC with the 270 software. Potentials are quoted against the saturated calomel electrode (SCE), in a compartment separated from the test solution by a fine porosity glass frit. The counter electrode was platinum gauze with a large surface area in a separated compartment with a medium porosity glass frit. The UV/Vis spectra were recorded with a Perkin−Elmer Lambda 19 spectrophotometer. Experiments were performed at 23 ± 1 °C.

Acknowledgments

This work was supported by the CNRS (Laboratoire de Chimie Physique, UMR 8000, CNRS) and the University Paris XI. The help of Y. Jean, B. Levy and S. Blasco (Laboratoire de Chimie Physique) in the extraction of distances from crystallographic data and the numbering of the atoms in Figure 3 is gratefully acknowledged.

[1] C. L. Hill (Guest Ed.), *Chem. Rev.* **1998**, *98*, 1−389.
[2] M. T. Pope, *Heteropoly and Isopoly Oxometalates*, Springer-Verlag, Berlin, **1983**.
[3] M. T. Pope, A. Muller (Eds.), *Polyoxometalates: From Platonic Solids to Antiretroviral Activity*, Kluwer Academic Publications, Dordrecht, **1994**.
[4] M. Sadakane, E. Steckhan, *Chem. Rev.* **1998**, *98*, 219−237.
[5] A. Belhouari, B. Keita, L. Nadjo, R. Contant, *New J. Chem.* **1998**, 83−86.

[6] R. Contant, M. Abbessi, J. Canny, A. Belhouari, B. Keita, L. Nadjo, *Inorg. Chem.* **1997**, *36*, 4961−4967.
[7] B. Keita, L. Nadjo, R. Contant, *J. Electroanal. Chem.* **1998**, *443*, 168−174.
[8] R. Contant, M. Abbessi, J. Canny, B. Keita, A. Belhouari, L. Nadjo, *Eur. J. Inorg. Chem.* **2000**, 567−574.
[9] B. Keita, Y. W. Lu, L. Nadjo, R. Contant, M. Abbessi, J. Canny, M. Richet, *J. Electroanal. Chem.* **1999**, *477*, 146−157.
[10] B. Keita, F. Girard, L. Nadjo, R. Contant, J. Canny, M. Richet, *J. Electroanal. Chem.* **1999**, *478*, 76−82.
[11] L. C. Baker, Plenary Lecture. Proc. XV Int. Conf. Coord. Chem. 15th, Moscow, **1973**.
[12] R. Contant, *J. Chem. Res. (S)* **1984**, 120−121; (M) **1984**, 1063−1081.
[13] R. Contant, R. Thouvenot, *Can. J. Chem.* **1991**, *69*, 1498−1506.
[14] R. Contant, R. Thouvenot, *Inorg. Chim. Acta* **1993**, *212*, 41−50.
[15] R. Contant, J. P. Ciabrini, *J. Chem. Res. (S)* **1982**, 50−51; (M) **1982**, 641−660.
[16] B. Keita, A. Belhouari, L. Nadjo, R. Contant, *J. Electroanal. Chem.* **1998**, *442*, 49−57.
[17] B. Keita, Y. W. Lu, L. Nadjo, R. Contant, *Eur. J. Inorg. Chem.* **2000**, 2463−2471.
[18] R. Contant, *Inorg. Synth.* **1990**, *27*, 104−111.
[19] M. Abbessi, R. Contant, R. Thouvenot, G. Hervé, *Inorg. Chem.* **1991**, *30*, 1695−1702.
[20] G. M. Varga, E. Papaconstantinou, M. T. Pope, *Inorg. Chem.* **1970**, *9*, 662−667.
[21] R. Acerete, S. Harmalker, C. F. Hammer, M. T. Pope, L. C. W. Baker, *J. Chem. Soc., Chem. Commun.* **1979**, 777- 779.
[22] J. P. Ciabrini, R. Contant, J.-M. Fruchart, *Polyhedron* **1983**, *2*, 1229−1233.
[23] B. Keita, Y. Jean, B. Levy, R. Contant, Y. W. Lu, L. Nadjo, to be published.
[24] B. Keita, E. Abdeljalil, L. Nadjo, B. Avisse, R. Contant, J. Canny, M. Richet, *Electrochem. Commun.* **2000**, *2*, 145−149.
[25] H. D'Amour, *Acta Crystallogr., Sect. B* **1976**, *32*, 729−740.
[26] J. Fuchs, A. Thiele, R. Palm, *Z. Naturforsch., Teil B* **1981**, *36*, 544- 550.
[27] K. Y. Matsumoto, Y. Sasaki, *Bull. Chem. Soc. Jpn.* **1976**, *49*, 156- 158.
[28] H. Neubert, J. Fuchs, *Z. Naturforsch., Teil B* **1987**, *42*, 951−958.
[29] R. C. Weast (Ed.), *Handbook of Chemistry and Physics*, 66th ed., CRC Press, Inc., Boca Raton, Florida, USA, **1985**, p. F164.

Received August 6, 2001
[O01294]

Synthesis, Characterization and Structural Studies on the First Rhenium Complex with Di(2-pyridyl) Ketone 2,4-Dinitrophenylhydrazone (dpkdnph), *fac*-[Re(CO)$_3$(dpkdnph)Cl]

Mohammed Bakir[a]

Keywords: Rhenium / Carbonyl ligands / Hydrazones

When di(2-pyridyl) ketone 2,4-dinitrophenylhydrazone (dpkdnph) was allowed to react with [Re(CO)$_5$Cl] in refluxing toluene *fac*-[Re(CO)$_3$(dpkdnph)Cl] was formed in good yield. Spectroscopic measurements on *fac*-[Re(CO)$_3$(dpkdnph)Cl] revealed strong solvent dependence as manifested by the high sensitivity of its electronic absorption spectra to solvent variation. Electrochemical measurements on *fac*-[Re(CO)$_3$(dpkdnph)Cl] in DMF show electrochemical properties with quasi-reversible reductions following an irreversible one-electron transfer. Structural studies on a brown crystal of *fac*-[Re(CO)$_3$(dpkdnph)Cl]·CH$_3$CN grown from an acetonitrile solution of *fac*-[Re(CO)$_3$(dpkdnph)Cl] show well separated linear CH$_3$CN and pseudo-octahedral *fac*-[Re(CO)$_3$(dpkdnph)Cl], with the major distortion about rhenium being due to the bidentate binding of dpkdnph to form a six-membered Re–N–C–C–C–N metallacyclic ring in a boat conformation. The molecular packing shows a web of *fac*-[Re(CO)$_3$(dpkdnph)Cl]·CH$_3$CN units interlocked via a network of intra- and intermolecular non-covalent interactions that include donor/acceptor and hydrogen bonds.

Introduction

Hydrazones and their compounds have been extensively studied for their rich physicochemical properties, reactivity patterns and applications in many important chemical processes that include non-linear optics, medicine, molecular sensing and separations.[1−16] The synthesis and characterization of rhenium carbonyl compounds of di(2-pyridyl) ketone (dpk), di(2-pyridyl)amine (dpa), di(2-pyridyl) ketone oxime (dpk·oxime), and di(2-pyridyl) ketone *p*-nitrophenyl hydrazone (dpknph) were described by us previously.[17−20] Electrochemical measurements on *fac*-[Re(CO)$_3$(dpk)Cl] and *fac*-[Re(CO)$_3$(dpk.oxime)Cl] revealed strong solvent dependence and the possible use of *fac*-[Re(CO)$_3$(dpk)Cl] as an electrochemical sensor for electrophiles that include metal ions.[17−19] Optical and thermodynamic measurements in polar solvents on dpknph and *fac*-[Re(CO)$_3$(dpknph)Cl] show the presence of two charge-transfer bands for the free ligand and its metal compound; the electronic/charge transfer in *fac*-[Re(CO)$_3$(dpknph)Cl] is faster than that in dpknph, and therefore *fac*-[Re(CO)$_3$(dpknph)Cl] can be used as a spectrophotometric sensor for metal ions.[20,21] These results prompted us to explore how a variation in the ligand backbone affects the electrochemical and optical properties of the complex, and here I report the synthesis, characterization and solid-state structure of the first metal compound of di(2-pyridyl) ketone 2,4-dinitrophenyl hydrazone (dpkdnph). Although a variety of 2,4-dinitrophenylhydrazones have been reported, to the best of my knowledge there has been no report on the isolation of dpkdnph.[1]

[a] Department of Chemistry, The University of the West Indies-Mona Campus,
Kingston 7, Jamaica, W. I.

Results and Discussion

The reaction between [Re(CO)$_5$Cl] and dpkdnph in toluene under reflux gave *fac*-[Re(CO)$_3$(dpkdnph)Cl] in good yield. This reaction is similar to those reported for the synthesis of *fac*-[Re(CO)$_3$(L-L)Cl] (L-L = dpk, dpk.oxime, dpknph) from [Re(CO)$_5$Cl] and L-L in refluxing toluene.[17−20] The formulation of the isolated rhenium-carbonyl as *fac*-[Re(CO)$_3$(dpkdnph)Cl] is based on the results of a number of spectroscopic measurements and a comparison of these results with those reported for *fac*-[Re(CO)$_3$(L-L)Cl].[17−20] In the IR spectrum of *fac*-[Re(CO)$_3$(dpkdnph)Cl] three strong bands appeared in the ν(C=O) stretching region similar to those observed for *fac*-[Re(CO)$_3$(dpknph)Cl] and other tricarbonylhalorhenium(I) compounds with polypyridyl-like ligands, thus confirming the assigned *fac* geometry.[17−20] The ν(C=N) absorption of the hydrazone moiety and the combined ν(C=C) and ν(C=N) of the pyridine vibrations are normal and in the same region as in *fac*-[Re(CO)$_3$(dpknph)Cl].[20] A single absorption band was observed for the ν(NH) stretching mode signalling a free N−H in the solid state.[22] The ^{1}H NMR spectrum of *fac*-[Re(CO)$_3$(dpkdnph)Cl] (see Exp. Sect.) is solvent dependent, indicating a solvent-solute interaction. No evidence of paramagnetic line broadening or unusual shifts of resonances appeared in the spectra of this compound, thus confirming its diamagnetic character.

 © WILEY-VCH Verlag GmbH, 69451 Weinheim, Germany, 2002 1434−1948/02/0202−0481 $ 17.50+.50/0

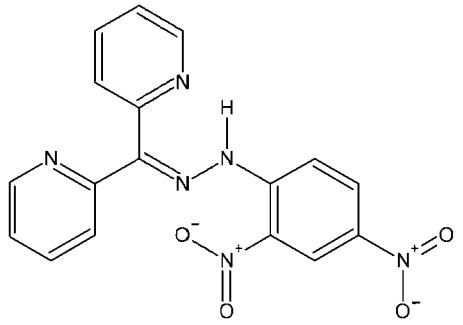

dpkdnph

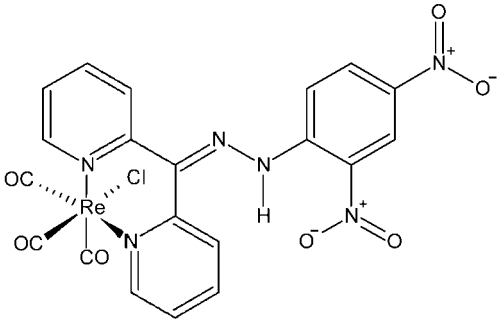

fac-Re(CO)$_3$(dpkdnph)Cl

The electronic absorption spectra of *fac*-[Re(CO)$_3$(dpkdnph)Cl] show spectral features similar to those reported for *fac*-[Re(CO)$_3$(dpknph)Cl], although subtle differences are apparent.[20,21] The charge-transfer bands in *fac*-[Re(CO)$_3$(dpkdnph)Cl] shift to high-energy relative to *fac*-[Re(CO)$_3$(dpknph)Cl] due to a decrease in the electron-withdrawing ability of dpkdnph compared to dpknph. In non-polar solvents such as CH_2Cl_2 a highly intense high-energy charge-transfer band appeared (Figure1a), in polar solvents such as CH_3CN two charge-transfer bands appeared (Figure 1b), and in highly polar solvents such as DMF a low-energy charge-transfer band appeared (Figure 1c). The intensity and location of these bands are solvent dependent. The gradual addition of a physical or chemical stimulus to a solution of *fac*-[Re(CO)$_3$(dpkdnph)Cl] causes an interconversion between the low- and high-energy intra-ligand charge-transfer bands of *fac*-[Re(CO)$_3$(dpkdnph)Cl]. For example, when a DMF solution of *fac*-[Re(CO)$_3$(dpkdnph)Cl] was exposed to sunlight, the intensity of the low-energy charge-transfer band decreased and the intensity of the high-energy band increased (Figure 2). The spectrophotometric response of *fac*-[Re(CO)$_3$(dpkdnph)Cl] towards physical and chemical stimuli is similar to that reported for *fac*-[Re(CO)$_3$(dpknph)Cl] and studies are in progress to explore the thermodynamics and kinetics of the interconversion between the high- and low-energy forms of *fac*-[Re(CO)$_3$(dpkdnph)Cl] and its use as a spectrophotometric sensor.

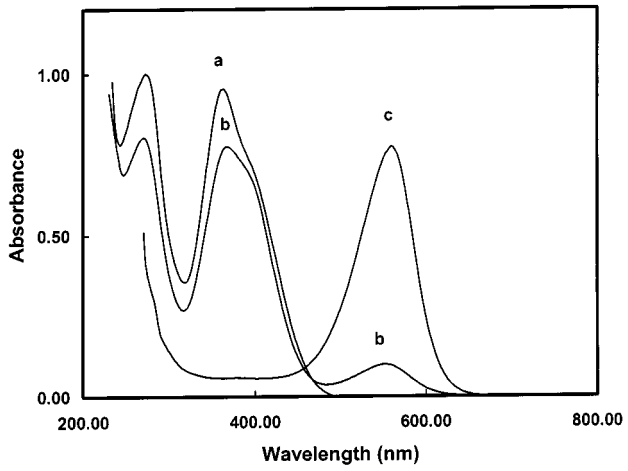

Figure 1. Electronic absorption spectrum of *fac*-[Re(CO)$_3$(dpkdnph)Cl] in: (a) CH_2Cl_2 (3.00×10^{-5} M); (b) CH_3CN (3.00×10^{-5} M); (c) DMF (1.00×10^{-5} M)

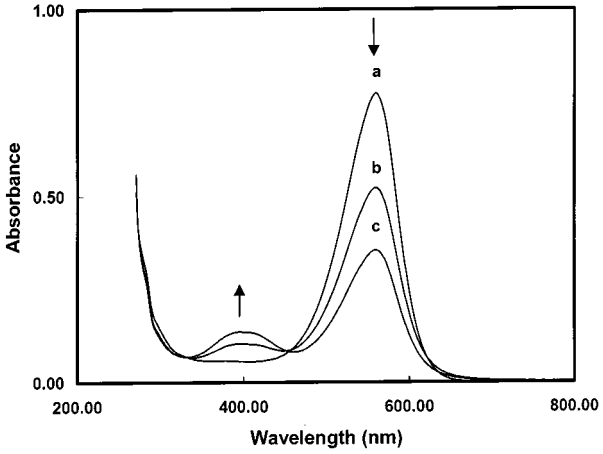

Figure 2. Electronic absorption spectrum of *fac*-[Re(CO)$_3$(dpkdnph)Cl] in DMF (1.00×10^{-5} M) (a) in the absence of sunlight, (b) after 3 h of sunlight exposure and (c) after 6 h of sunlight exposure

The electrochemical properties of *fac*-[Re(CO)$_3$(dpkdnph)Cl] in non-aqueous media were investigated using voltammetric techniques. Cyclic voltammograms of *fac*-Re(CO)$_3$(dpkdnph) in DMF are shown in Figure 3. In these voltammograms rich redox processes appeared. The first reduction wave at $E_{p,c} = -0.76$ V is one-electron and irreversible. Scan rate variations on this wave from 100−2000 mV/s revealed no sign of reversibility pointing to structural/chemical modification following the first electronic transfer. Two quasi-reversible reduction waves appeared at $E_p = -1.24$ V ($E_{p,c} = -1.29$ and $E_{p,a} = -1.18$ V) and -1.62 V ($E_{p,c} = -1.75$ and $E_{p,a} = -1.48$ V) pointing to the stability of the electrochemically generated species following the second and third electron transfer. The quasi-reversible reduction wave at -1.62 V is assigned to the $Re^{I/0}$ couple as it

falls in the potential range observed for such a couple in a variety of rhenium compounds of polypyridyl-like ligands of the type *fac*-[Re(CO)$_3$(L-L)Cl], where L-L = dpk, dpk.oxime, dpknph and others.[17−20] The irreversible oxidation wave at $E_{p,a}$ = +1.74 V carries a peak current larger than that observed for the first irreversible reduction wave and points to its multi-electron character. The peak potential of this wave and its multi-electron character is similar to that reported for *fac*-[Re(CO)$_3$(dpk.oxime)Cl] and suggests a metal-mediated oxidation of coordinated dpkdnph.[19] Electrochemically generated product waves appeared at $E_{p,a}$ = −1.62, +0.15, +0.55 and +0.98 V pointing to structural modifications following electron transfer(s). Their appearance, coupled with the reversibility of the reduction waves, points to the formation of electrochemically generated transient intermediates sensitive to their surroundings that can be used to explore the electrochemical behaviour of various substrates toward *fac*-[Re(CO)$_3$(dpkdnph)Cl] in a procedure similar to that reported for *fac*-[Re(CO)$_3$(dpk)Cl].[17,18]

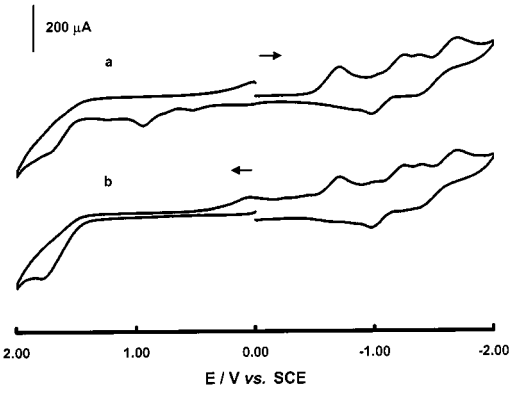

Figure 3. Cyclic voltammograms of *fac*-[Re(CO)$_3$(dpkdnph)Cl] in DMF solutions 0.1 M in [N(nBu)$_4$](PF$_6$)) at a glassy carbon working electrode at a scan rate of 400 mVs^{-1} vs. SCE

Single crystals of *fac*-[Re(CO)$_3$(dpkdnph)Cl]·CH$_3$CN were grown from an acetonitrile solution of *fac*-[Re(CO)$_3$-(dpkdnph)Cl] and the structure was determined using X-ray crystallography. An ORTEP drawing of *fac*-[Re(CO)$_3$(dpkdnph)Cl]·CH$_3$CN (Figure 4) shows well separated linear CH$_3$CN and pseudo-octahedral *fac*-[Re-(CO)$_3$(dpkdnph)Cl]. The distortion from an octahedral geometry about rhenium is due to the *N*,*N*-bidentate binding of dpkdnph and the formation of a six-membered metallacyclic ring (Re1−N1−C15−C00−C25−N5) in a boat conformation with the pyridine rings in a butterfly (Λ) formation. The N−N bite angle [N(1)−Re1−N(2)] of 83.03(11)° is of the same order as the 84.6° bite angles observed for the dpkO,OH in [ReOCl$_2$(dpkO,OH)],[23] and is larger than the 74.3° reported for bipy in *fac*-[Re(CO)$_3$-(bipy)(OPOF$_2$)].[24] These results reveal that the six-membered metallacyclic ring in rhenium compounds with polypyridyl-like ligands is less constrained than the five-membered metallacyclic ring in rhenium compounds with α-diimine ligands. The 2,4-dinitrophenylhydrazone moiety is planar with all nitrogen and carbon atoms sp^2 hybridized. The bond lengths and angles (Table 1) of the coordinated atoms are normal and similar to those reported for a variety of rhenium compounds of the type *fac*-[Re(CO)$_3$(N-N)X], where N-N = α-diimine ligand and X = anion.[24−26]

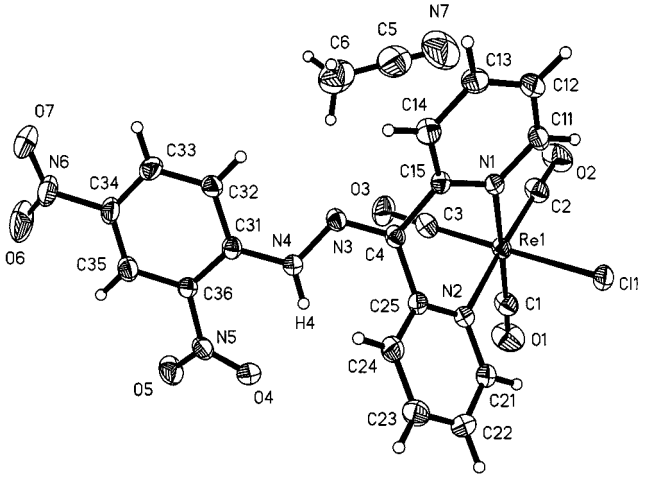

Figure 4. ORTEP drawings of the structure of *fac*-[Re(CO)$_3$(dpknph)Cl]·CH$_3$CN; thermal ellipsoids are drawn at the 30% probability level

Table 1. Bond lengths [Å] and angles [°] for *fac*-[Re(CO)$_3$(dpkdnph)Cl]·CH$_3$CN

Re(1)−C(3)	1.900(4)	C(3)−Re(1)−C(1)	89.73(18)
Re(1)−C(1)	1.909(4)	C(1)−Re(1)−C(2)	90.61(17)
Re(1)−C(2)	1.924(4)	C(3)−Re(1)−N(2)	94.66(14)
Re(1)−N(2)	2.187(3)	C(1)−Re(1)−N(2)	91.94(15)
Re(1)−N(1)	2.210(3)	C(2)−Re(1)−N(2)	175.43(15)
Re(1)−Cl(1)	2.4732(11)	C(1)−Re(1)−N(1)	174.87(15)
C(2)−O(2)	1.138(5)	N(2)−Re(1)−N(1)	83.10(11)
C(3)−O(3)	1.151(5)	N(1)−Re(1)−Cl(1)	85.09(8)
C(1)−O(1)	1.142(5)	O(2)−C(2)−Re(1)	179.0(4)
C(4)−N(3)	1.298(5)	O(3)−C(3)−Re(1)	178.4(4)
C(4)−C(25)	1.488(5)	O(1)−C(1)−Re(1)	176.4(4)
N(3)−N(4)	1.351(4)	N(3)−C(4)−C(15)	114.8(3)
N(4)−C(31)	1.368(4)	N(3)−C(4)−C(25)	124.9(3)
N(5)−O(5)	1.213(4)	C(4)−N(3)−N(4)	118.6(3)
N(5)−O(4)	1.228(4)	O(5)−N(5)−O(4)	123.1(3)
N(6)−O(6)	1.203(6)	O(6)−N(6)−O(7)	124.9(4)
N(6)−O(7)	1.240(6)	N(7)−C(5)−C(6)	177.2(10)

The packing of molecules (Figure 5) shows *anti*-parallel *fac*-[Re(CO)$_3$(dpkdnph)Cl]·CH$_3$CN units interlocked via a network of non-covalent interactions that include hydrogen bonding of the type X···H−C, where X = O, N or Cl and oxygen-nitrogen charge-transfer between the *ortho*-nitro groups of adjacent molecules. Selected views of the non-covalent interactions are shown in Figure 6 and their bond angles and distances are listed in Table 2. The amide (NH) proton of the hydrazone backbone forms an intramolecular classical hydrogen bond of the type N−H···O with the oxygen atom (O4) of the *ortho*-nitro group. The acetonitrile

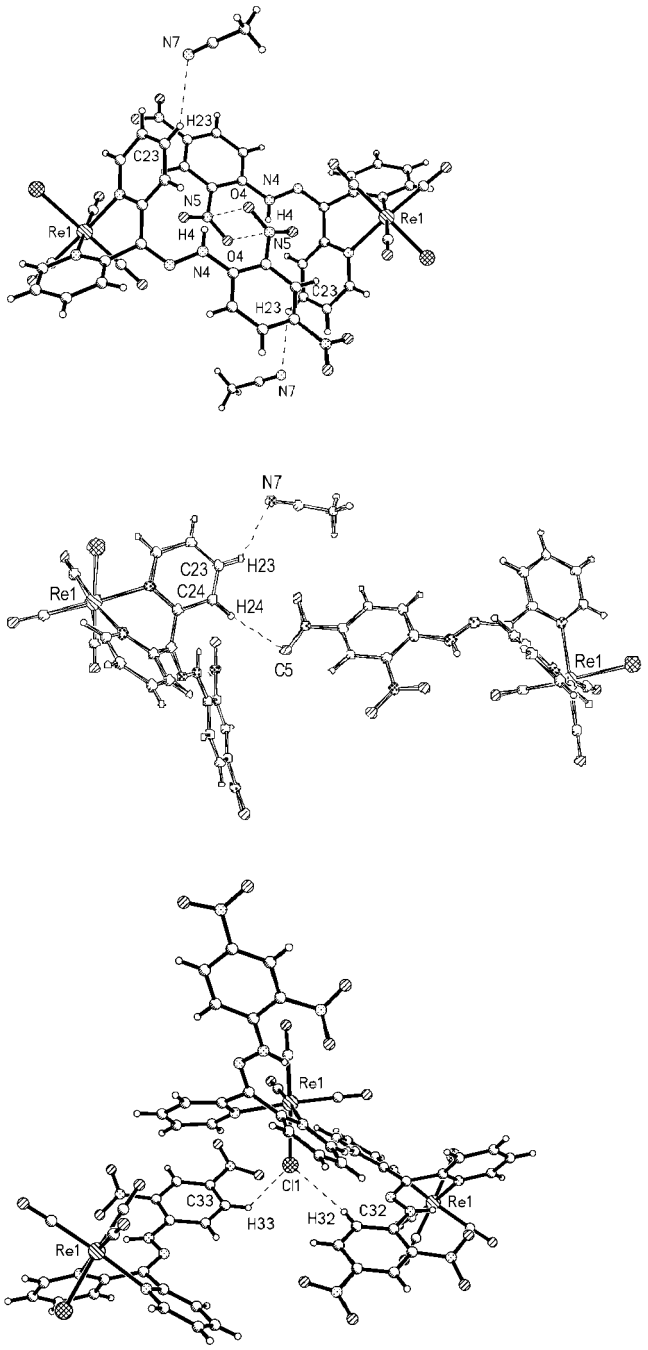

Figure 6. Selected views of the non-covalent bonding in the packed structure of *fac*-[$Re(CO)_3$(dpknph)Cl]·CH_3CN; non-covalent bonds are indicated by dashed lines

molecule binds to the adjacent proton (Figure 6b), whereas the *p*-nitro group binds to an adjacent *fac*-[$Re(CO)_3$-(dpkdnph)Cl] unit and the axial chloride doubly bridges two adjacent phenyl rings in a [C(32)−H(32)···Cl(1)···H(33)−C(33)] bonding form (Figure 6c). The bond lengths and angles of the non-covalent interactions are of the same order as those reported for a variety of compounds containing such bonds.[27−29] The difference in the oxygen−nitrogen bond length (Table 1) of the *para*-nitro group hints to an increase in electron density around the oxygen atom participating in the non-covalent C(24)−H(24)···O(6) interaction.

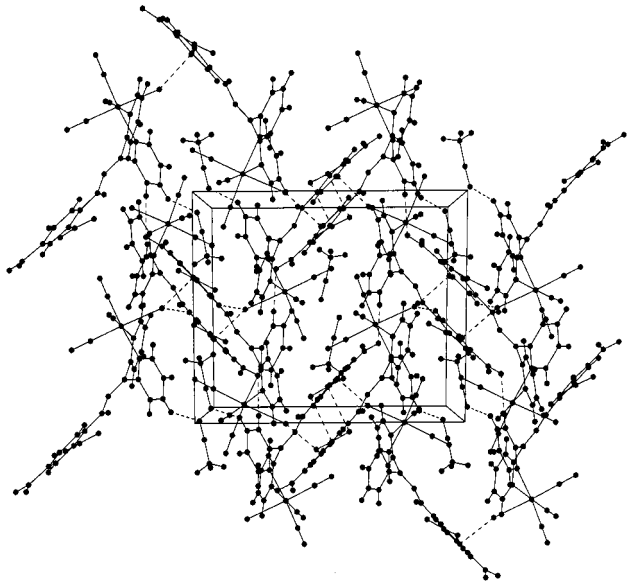

Figure 5. Packing of the molecules of *fac*-[$Re(CO)_3$-(dpkdnph)Cl]·CH_3CN in the unit cell; non-covalent bonds are indicated by dashed lines

Table 2. Bond lengths [Å] and angles [°] of the non-covalent interactions in the packed structure of *fac*-[$Re(CO)_3$-(dpkdnph)Cl]·CH_3CN

Bond[a]	Distance	Angle
O(4)···H(4)−N(4)	2.647	126.7
O(6)···H(24)−C(24)$^{(1)}$	2.450	166.3
N(7)···H(23)−C(23)$^{(2)}$	2.609	136.1
Cl(1)···H(32)−C(32)$^{(3)}$	2.790	146.7
Cl(1)···H(33)−C(33)$^{(4)}$	2.853	120.1
N(5)−O(4)···N(5)−O(4)$^{(5)}$	2.954	99.4, 80.6

[a] Symmetry transformations used to generate equivalent atoms: (1): $1/2 - x$, $1/2 + y$, $3/2 - z$; (2): $-1/2 + x$, $1/2 - y$, $1/2 + z$; (3): $-1/2 + x$, $1/2 - y$, $-1/2 + z$; (4): $3/2 - x$, $1/2 + y$, $3/2 - z$; (5): $1 - x$, $-y$, $2 - z$).

Owing to their convenient synthesis, rich physicochemical properties and potential use as molecular sensors, work is in progress to explore the electro-optical properties, solid state structures and solution conformations of a variety of di(2-pyridyl) ketone derivatives and their rhenium compounds.

Experimental Section

Reagents and Reaction Procedures: Solvents were reagent grade and thoroughly deoxygenated prior to use. All other reagents were obtained from commercial sources and used without further purification. All reactions were performed under a nitrogen atmosphere.

Physical Measurements: Electronic absorption spectra were recorded on a Perkin−Elmer Lambda 19 UV/Vis/NIR spectrometer. Solution ^{1}H NMR spectra were recorded on a Bruker ACE 200-MHz Fourier transform spectrometer and referenced to the residual protons in the deuterated solvent. Infrared spectra were recorded as KBr pellets on a Perkin−Elmer Spectrum 1000 FT-IR Spectrometer. Photochemical measurements were conducted on deoxygenated solutions before and after exposure to sunlight. Electrochemical measurements were performed with the use of a Princeton Applied Research (PAR) Model 173 potentiostat/galvanostat and Model 276 interface in conjunction with a 286 PC. Data were acquired with the EG&G PARC Headstart program and manipulated using Microsoft Excel Program. Measurements were performed in solutions that were 0.1 M in $[N(n\text{Bu})_4](PF_6)$.The $E_{p,a}$, $E_{p,c}$ and $E_p = (E_{p,a} + E_{p,c})/2$ values were referenced to the potassium chloride saturated calomel electrode, SCE, at room temperature and are uncorrected for junction potentials. The number of electrons in the redox waves was determined using the oxidative peak current of the reversible one electron $FeCp_2/FeCp_2^+$ couple as an internal standard. Electrochemical cells were of conventional design based on scintillation vials or H-cells. A glassy-carbon disc was used as the working electrode and Pt-wire as a counter electrode.

Analytical Procedures: Microanalyses were performed by MEDAC Ltd., Department of Chemistry, Brunel University, Uxbridge, United Kingdom.

Preparation of dpkdnph: A mixture of dpk (200 mg, 1.09 mmol), 2,4-dinitrophenylhydrazine (220 mg, 1.12 mmol), ethanol (100 mL) and conc. HCL (0.25 mL) was refluxed for 5 h. The resulting reaction mixture was allowed to stand at room temperature for 3 h. A yellow solid was filtered off, washed with diethyl ether, hexane and dried; yield 350 mg, 0.96 mmol (88%). $C_{17}H_{12}N_6O_4$ (364.3): calcd. C 56.04, H 3.33, N 23.06; found C 55.86, H 3.32, N 22.98. IR (KBr disk): ν(N−H) 3320 cm^{-1}. The low solubility of dpkdnph in polar and non-polar solvents prevented any solution measurements on this compound.

Preparation of *fac*-[Re(dpkdnph)(CO)$_3$Cl]: A mixture of $[Re(CO)_5Cl]$ (200 mg, 0.55 mmol), dpkdnph (250 mg, 0.67 mmol) and toluene (50 mL) was refluxed for 20 h. The resulting mixture was allowed to cool to room temperature and reduced in volume to ≈ 25 mL. A yellow solid was filtered off, washed with hexane and diethyl ether, and dried; yield 300 mg, 0.45 mmol (82%). $C_{20}H_{12}ClN_6O_7Re$ (670.0): calcd. C, 35.87, H 1.80, N 12.54; found C 35.91, H 1.91, N 12.48. IR (KBr disk): ν(C=O) 2020, 1900, 1890 cm^{-1}, ν(NO_2) 1340, ν(N−H) 3273. ^{1}H NMR ([D$_6$]DMSO): δ = 11.80 (s, 1 H, NH), 9.15 (d, 1 H, dnph), 8.95 (d, 1 H, dnph), 8.85 (s, 1H dnph), 8.50−8.00 (closely spaced overlapped triplets and doublets, 6 H, dpk), 7.8 (overlapped triplets, 2 H, dpk). In $CDCl_3$: δ = 11.98 (s, 1 H, NH), 9.40 (d, 1 H, dnph), 9.16 (s, 1 H, dnph), 9.14 (d, 1 H, dnph), 8.45 (d, 1 H, dpk), 8.25−8.10 {overlapped triplet (8.16) and doublet (8.15), 2 H, dpk}, 8.04 (t, 1 H, dpk), 7.85 (d, 2 H, dpk), 7.65 (t, 1 H, dpk), and 7.55 (t, 1 H, dpk). UV/Vis {CH_2Cl_2, nm(ε)}: 396 sh (28,700); 358 (37,600), 268 (39,400).

X-ray Crystallography: When *fac*-[Re(CO)$_3$(dpkdnph)Cl] was allowed to stand in acetonitrile solution for several days brown cubic crystals of *fac*-[Re(CO)$_3$(dpkdnph)Cl]·CH_3CN were obtained. A single crystal was selected and mounted on a glass fibre with epoxy cement. A Bruker diffractometer equipped with a Mo-K_α radiation source and a graphite monochromator was used for data collection, and the SHELXTL software package version 5.1 was used for structure solution. Cell parameters and other crystallographic information are given in Table 3 along with additional details concerning data collection.[30−32] The location of the rhenium atom was determined from a Patterson map, and the remaining non-hydrogen atoms were located in subsequent difference Fourier maps. All non-hydrogen atoms were refined with anisotropic thermal parameters. In the final least-squares cycle, 344 parameters were fitted to 4095 observations, for a data to parameters ratio of 11.90:1. The least-squares residuals and other relevant parameters are given in Table 3.

Table 3. Crystal data and structure refinement for *fac*-[Re(CO)$_3$(dpkdnph)Cl]·CH_3CN

Empirical formula	$C_{22}H_{15}ClN_7O_7Re$
Formula mass	711.06
Temperature	298(2) K
Wavelength	0.71073 Å
Crystal system	Monoclinic
Space group	$P2_1/n$
Unit cell dimensions	a = 12.1221(19) Å, α = 90°
	b = 14.226(2) Å, β = 98.691(13)°
	c = 14.6170(19) Å, γ = 90°
V	2491.7(7) Å^3
Z	4
Density (calculated)	1.895 mg/m^3
Absorption coefficient	5.042 mm^{-1}
F(000)	1376
Theta range for data collection	2.01 to 25.00 °
Reflections collected/unique	8326/4095 [R(int) = 0.0417]
Completeness to theta: 25.00	93.2%
Absorption correction	Empirical
Max. and min. transmission	0.3158 and 0.2749
Refinement method	Full-matrix least-squares on F^2
Data/restraints/parameters	4095/0/344
Final R indices [$I > 2\sigma(I)$]	$R1$ = 0.0227, $wR2$ = 0.0547
R indices (all data)	$R1$ = 0.0294, $wR2$ = 0.0568
Largest diff. peak and hole	0.646 and −0.695 e·A^{-3}

Acknowledgments

I acknowledge funding from the following: The University of the West Indies (UWI), Inter-America Development Bank (IDB) for funds to establish the X-ray laboratory at UWI-Mona.

[1] L. R. Sutton, A. J. Blake, W.-S. Li, M. Schröde, *J. Chem. Soc., Dalton Trans.* **1998**, 279−284.
[2] F. Pan, C. Bosshard, M. S. Wong, C. Serbutoviez, K. Schenk, V. Gramlich, P. Gunter, *Chem. Mater.* **1997**, *9*, 1328−1334.
[3] A. S. Batsanov, A. V. Churakov, M. A. M. Easson, L. J. Govenlock, J. A. K. Howard, J. M. Moloney, D. Parker, *J. Chem. Soc., Dalton Trans.* **1999**, 323−330.
[4] J. Frelek, J. Jagodziski, H. Meyer-Figge, W. S. Sheldrick, E. Wieteska, W. J. Szczepek, *Chirality* **2001**, *13*, 313−321.
[5] A. Bacchi, A. Bonini, M. Carcelli, F. Ferraro, E. Leporati, C. Pelizzi, G. Pelizzi, *J. Chem. Soc., Dalton Trans.* **1996**, 2699−2704.
[6] D. Armesto, A. Ramos, M. J. Ortiz, W. M. Horspool, M. J. Mancheno, O. Caballero, E. P. Mayoral, *J. Chem. Soc., Perkin Trans. 1* **1997**, 1535−1542.
[7] T. Odashima, M. Yamaguchi, H. Ishii, *Talanta* **1995**, *42*, 1229−1237.
[8] R. Hai-Ying He, X.-K. Jiang, *J. Phys. Org. Chem.* **1999**, *12*, 392−400.
[9] M. R. Maurya, S. Khurana, C. Schulzke, D. Rehder, *Eur. J. Inorg. Chem.* **2001**, 779−788.

[10] J. G. March, B. M. Simonet, F. Grases, *Analyst* **1999**, 897−900.
[11] D. Enders, R. Peters, R. Lochtman, G. Raabe, J. Runsink, J. W. Bats, *Eur. J. Org. Chem.* **2000**, 3399−3426.
[12] V. Atlan, H. Bienaymé, L. El Kaim, A. Majee, *Chem. Commun.* **2000**, 1585−1586.
[13] A. Carbayo, J. V. Cuevas, G. García-Herbosa, S. García-Granda, D. Miguel, *Eur. J. Inorg. Chem.* **2001**, 2361−2363.
[14] J. F. Hartwig, *Angew. Chem. Int. Ed.* **1998**, *37*, 2090−2093.
[15] C. Bosshard, K. Sutter, P. Pretre, J. Hullinger, M. Florsheimer, P. Kaatz, P. Gunter, *Organic Nonlinear Optical Materials*; Gordon and Breach Science Publishers, Amsterdam, **1995**.
[16] *Molecular Nonlinear Optics: Materials, Physics, Devices* (Ed.: J. Zyss), Academic Press, Boston, **1994**.
[17] M. Bakir, J. A. M. McKenzie, *Electroanal. Chem.* **1997**, *425*, 61−66.
[18] M. Bakir, J. A. M. McKenzie, *J. Chem. Soc., Dalton Trans.* **1997**, 3571−3578.
[19] M. Bakir, *J. Electroanal. Chem.* **1999**, *466*, 60−66.
[20] M. Bakir, K. Abdur-Rashid, *Transition Met. Chem.* **1999**, *24*, 384−388.
[21] M. Bakir, K. Abdur-Rashid, W. H. Mulder, *Talanta* **2000**, *51*, 735−741.
[22] *Tables of Spectral data for Structure Determination of Organic Compounds* (Eds.: F. L. Boschke, W. Fresenius, J. F. K. Huber, E. Pungor, G. A. Rechnitz, W. Simon, Th. S. West), Springer-Verlag, Berlin Heidelberg, **1983**.
[23] T. I. A. Gerber, H. J. Kemp, J. G. H. du Preez, G. Bandoli, *J. Coord. Chem.* **1993**, *28*, 329−336.
[24] E. Horn, M. R. Snow, *Aust. J. Chem.* **1980**, *33*, 2369−2376.
[25] W.-M. Xue, M. C.-W. Chan, Z.-M. Su, K.-K. Cheung, S.-T. Liu, C.-M. Che, *Organometallics* **1998**, *17*, 1622−1630.
[26] V. W.-W. Yam, K.-Z. Wang, C.-R. Wang, Y. Yang, K.-K. Cheung, *Organometallics* **1998**, *17*, 2440−2446.
[27] D. Braga, F. Grepioni, G. R. Desiraju, *Chem. Rev.* **1998**, *98*, 1375−1405.
[28] J. P. Glusker, M. Lewis, M. Rossi, *Crystal Structure Analysis for Chemists and Biologists*, Wiley-VCH, New York, **1994**.
[29] J. H. Williams, *Acc. Chem. Res.* **1993**, *26*, 593−598.
[30] Bruker-SHELXTL (**1997**). Software Version 5.1. Bruker AXS, Inc., Madison, Wisconsin, U.S.A.
[31] Bruker-XSCANS (**1996**). Software Version 2.2. Bruker AXS, Inc., Madison, Wisconsin, U.S.A.
[32] G. M. Sheldrick, SHELX-97 and SHELXL-97, University of Göttingen, Germany, **1997**.

Received September 10, 2001
[I01359]

Investigation of Sugar-Binding Sites in Ternary Ligand−Copper(II)−Carbohydrate Complexes

Susanne Striegler*[a] and Elfi Tewes[a]

Keywords: Carbohydrates / Copper / Molecular imprinting / N ligands / UV/Vis spectroscopy

Evaluation of the binding interactions between a template (such as a carbohydrate) and a functional monomer (such as a metal complex) is one of the key steps during the design of molecularly imprinted polymers. Since we are interested in the development of carbohydrate-imprinted polymers as functional enzyme mimics, we have evaluated the binding interactions of several carbohydrates with [(diethylenetriamine)copper(II)] dinitrate (**1**), [*N*-{(2-hydroxyethyl)ethylenediamine}copper(II)] dichloride (**8**), and [{4-(*N*-vinylbenzyl)-diethylenetriamine}copper(II)] diformate (**13**) in aqueous solution. The binding sites of epimeric carbohydrates in complex formation with different copper(II) complexes have been investigated for the first time. The ternary ligand–copper(II)–carbohydrate complexes produced have been characterized by determination of their stoichiometry and their binding strength, by UV/Vis spectroscopy at alkaline pH.

Introduction

The mimicking of carbohydrate recognition by synthetic receptors has attracted much attention, especially in supramolecular chemistry.[1−5] Several attempts to recognize carbohydrates selectively by means of synthetic receptors based on hydrogen bonding, charged interactions, or boronic acids have been made, and the progress achieved was recently reviewed in detail by Davis and Shinkai.[1,6] Hydrogen bonding interactions, which provide the major driving force for sugar binding in apolar organic media, become far less effective in aqueous media.[7] The binding interactions of synthetic receptors with carbohydrates in water should therefore rely on other forces, such as metal coordination.

Functional enzyme mimics can be engineered by the molecular imprinting technique, which is suitable for the development of robust, inexpensive, but highly selective polymers.[8−10] Molecular imprinting involves the preorganization of polymerizable functional monomers around a targeted template (such as a carbohydrate) in solution, forming a monomer−template assembly, followed by cross-linking polymerization to stabilize this arrangement in the three-dimensional polymeric material. The solvent serves as a porogen during the imprinting process and is responsible for the microporosity of the later polymer. During the imprinting process the functional monomers are placed complementarily to the functionality of the template (such as a carbohydrate) inside the polymer matrix. Functional cavities remain after removal of the template, and these enable the matrix to rebind its original template specifically. The preparation of these polymers can only be rationalised with precise knowledge of the binding interaction between the functional monomer and the targeted template (carbohydrate) prior to polymerization.[11,12]

Binding forces applied during the self-organization of functional monomers and carbohydrates as templates include covalent, noncovalent, and coordinative binding interactions. Wulff and co-workers introduced a covalent approach for the separation of racemates of glycosides and free carbohydrates.[13−15] The reversible formation of boronate esters between pairs of hydroxyl groups of the sugar molecule and *p*-vinylphenylboronic acid was used for preorganization of the functional monomer and the carbohydrate. The esters were characterized by common methods, such as ^{1}H and ^{13}C NMR spectroscopy, prior to polymerization. Mosbach and co-workers introduced a noncovalent approach for the investigation of sugar-imprinted polymers. Their study demonstrates the feasibility of noncovalent binding interactions for the preparation of sugar binding polymers, and the binding specificity of the resulting polymer sites.[16] Prior to polymerization, derivatized carbohydrates (templates) were prearranged through hydrogen bonding to methacrylic acid (functional monomer). The complex formation was assumed to be similar to that investigated for the previously reported self-organization of amino acids with methacrylic acid.[17] However, binding sites with high affinity and excellent anomeric and epimeric selectivity suitable for the separation of racemic mixtures were obtained. Arnold and co-workers have also developed a sensing device for glucose, based on an α-methyl-D-glucose-imprinted polymer.[18] Metal coordination was used as the

[a] Division of Inorganic Chemistry II, University of Ulm, Albert-Einstein-Allee 11, 89069 Ulm, Germany
Fax: (internat.) +49-(0)731/50-23039
E-mail: susanne.striegler@chemie.uni-ulm.de
Supporting information for this article is available on the WWW under http://www.eurjic.com or from the author.

 © WILEY-VCH Verlag GmbH, 69451 Weinheim, Germany, 2002 1434−1948/02/0202−0487 $ 17.50+.50/0

binding force between functional monomer and carbohydrate to generate a glucose-specific cavity inside the polymer. Isothermal titration calorimetry was applied in order to study the formation of a ternary triazacyclononane−Cu^{II}−glucose complex in solution at pH = 11.25 [K_{app} = 2.6 (±0.2) × 10^3 M^{-1}] and to study the binding interactions between the triazacyclononane−Cu^{2+} complex and *cis*-1,2- or *trans*-1,2-diols, such as 1,4-anhydroerythritol or 1,4-anhydro-L-threitol. Upon binding of *cis*-diols at high pH (> 9), the metal complex releases protons, which can be easily detected by a pH electrode. However, this sensing device is limited by its operation range, which is not suitable for sensing carbohydrates at physiological pH values.[19]

Taking advantage of the demonstrated recognition capability for *cis*-1,2-diols over *trans*-1,2-diols of metal-coordinated molecularly imprinted polymers, we are aiming to prepare molecularly imprinted polymers as enzyme mimics, that are operational at physiological pH. We have therefore investigated suitable binding interactions and binding sites prior to the imprinting of carbohydrates by metal coordination into polymeric materials. Accordingly, we now report for the first time on the evaluation of the binding sites of several closely related carbohydrates upon chelation to selected copper(II) complexes. We have also characterized the ternary ligand−Cu^{II}−carbohydrate complexes produced in terms of stoichiometry and binding strength.

Results and Discussion

Determination of the Stoichiometry of the Ternary Ligand−Copper(II)−Carbohydrate Complexes

Binding events in light-absorbing metal complexes can easily be observed by UV/Vis spectroscopy, while the application of NMR spectroscopy to the observation and characterization of binding events is widely used only for diamagnetic complexes. Therefore, a direct line of arguments relying on NMR spectroscopy does not appear to be applicable for systems containing paramagnetic copper(II) complexes. Accordingly, the following chain of indirect evidence is given.

The determination of the number of spectroscopic states in an equilibrium gives an insight into the number of complexes formed, and influences the choice of a suitable method to evaluate the binding constant, which strongly depends on the number of absorbing species. The association of a metal complex (M) with a carbohydrate (C) resulting in a ternary ligand−Cu^{II}−carbohydrate complex (MC) is described by Equation (1), its apparent binding constant $pK_{11} = -\log(K_{11}^{-1})$, whereas K_{11} is defined by Equation (2).[20] The number of spectroscopic states does not characterize intramolecular equilibria within ternary metal complexes.

$$M + C \leftrightharpoons MC \quad (1)$$

$$K_{11} = [MC]/([M] \times [C]) \quad (2)$$

When no complex formation between C and M takes place, M remains the only absorbing species in a one-state system, although the number of species (i.e., C and M) in this solution is two. Accordingly, a system containing two absorbing species (i.e., M and MC), refers to a two-state system and also to 1:1 complex formation if the carbohydrate C does not absorb within the selected wavelength range.[20]

If additivity of absorbances is assumed for two solutions k and n at any wavelength pair 1 and 2, Beer's law can be rewritten, resulting in Equations 3:

$$A_{1k} = \varepsilon_{1k}^{M}[M]_k + \varepsilon_{1k}^{MC}[MC]_k \quad (3a)$$

$$A_{1n} = \varepsilon_{1n}^{M}[M]_n + \varepsilon_{1n}^{MC}[MC]_n \quad (3b)$$

$$A_{2k} = \varepsilon_{2k}^{M}[M]_k + \varepsilon_{2k}^{MC}[MC]_k \quad (3c)$$

$$A_{2n} = \varepsilon_{2n}^{M}[M]_n + \varepsilon_{2n}^{MC}[MC]_n \quad (3d)$$

When $[M]_k + [MC]_k = [M]_n + [MC]_n = M_t$ (t = total; M_t is kept constant) and medium-independent spectra can be assumed, then $\varepsilon_{1k}^{M} = \varepsilon_{1n}^{M}$ and $\varepsilon_{1k}^{MC} = \varepsilon_{1n}^{MC}$. It also follows that the ratio of differences of the absorbances is a constant. Plots of $(A_{1k} - A_{1n})$ versus $(A_{2k} - A_{2n})$, $k \neq n$, give straight lines passing through the origin [Equation (4)]. The corresponding system has two spectroscopic states and refers to 1:1 complex formation.[20]

$$(A_{1k} - A_{1n}) = [(\varepsilon_{1k}^{MC} - \varepsilon_{1k}^{M}) \times (\varepsilon_{2k}^{MC} - \varepsilon_{2k}^{M})^{-1}] \times (A_{2k} - A_{2n}) \quad (4)$$

[(Diethylenetriamine)copper(II)] dinitrate — [CuDIEN]-$(NO_3)_2$ (**1**) — and glucose (**2**), galactose (**3**), mannose (**4**), or maltose (**5**) assemble at pH > 10.4 to give 1:1 complexes, resulting in two-state systems. This conclusion is based: (1) on the evaluation of the number of spectroscopic states, and (2) on the method of continuous variation (Job's method).[20] As a representative example for other calculations of numbers of spectroscopic states reported in this

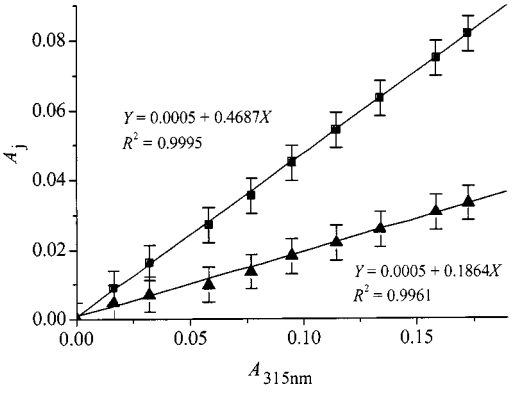

Figure 1. Plot of selected absorbances A_j [j = 325 nm (■) and 335 nm (▲)] over A_{315nm} from titration of [CuDIEN]$(NO_3)_2$ (**1**) with water at pH 12.4, 25 °C (calibration curve)

paper, the stoichiometry of the ternary complex formed from **1** and glucose (**2**) is determined by Equation (4) according to the plots shown in Figure 1 and Figure 2.

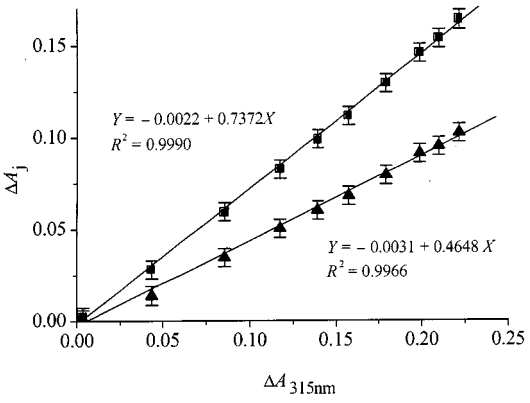

Figure 2. Plot of selected differences in absorbances $\Delta A_j = (A_{j,k} - A_{j,n})$ over $\Delta A_{315nm} = (A_{315nm,k} - A_{315nm,n})$ from titration of $[CuDIEN](NO_3)_2$ (**1**) with glucose (**2**) at j = 325 nm (■) and 335 nm (▲) for solution k containing **1** and **2** and solution n containing **1** at V_t = 2 mL, $[\mathbf{1}]_t$ = 2 mM, t = total, $A_{315nm,\mathbf{1}}$ = 0.0657, $A_{325nm,\mathbf{1}}$ = 0.0354, $A_{335nm,\mathbf{1}}$ = 0.0109, pH = 12.4, 25 °C

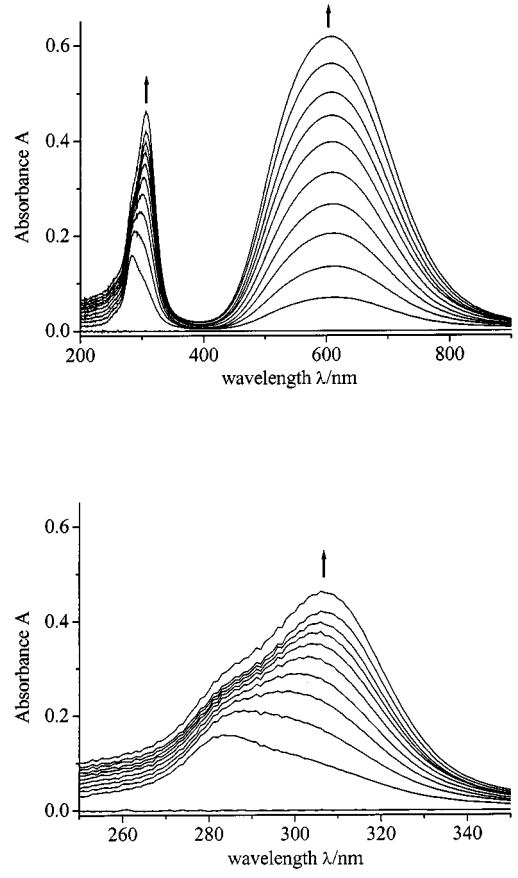

Figure 3. UV/Vis spectra observed during titration of $[CuDIEN](NO_3)_2$ (**1**) with glucose (**2**) at 25 °C in unbuffered, aqueous solution at pH = 12.4 according to Job's method; the concentrations of **1** and **2** were varied from 0−10 mM, while the sums of the total concentrations ($M_t + C_t$ = 10 mM) and the total volume of the solution (V_t = 2 mL) were kept constant

If the system contains only one absorbing species (i.e., M), no complex formation takes place and the slopes of the linearly fitted data for corresponding wavelength pairs in systems containing **1** or **1** and **2** would be identical. This is not observed here; therefore, association between **1** and **2** takes place and at least one ternary ligand−copper(II)−carbohydrate complex is formed (Figures 1 and 2). From the linear fit of the data, the current system can be described as a two-state system, based on 1:1 complex formation.[20]

The method of continuous variation (Job's method) was also applied to demonstrate association between **1** and **2**−**5**. Accordingly, the concentrations of **1** and the carbohydrates were varied, keeping the total concentration of the sugars and the metal complex constant. The titration data of **1** and **2** obtained by Job's method are shown as representative examples in Figures 3−5 and discussed below (for others, see Supporting Information).

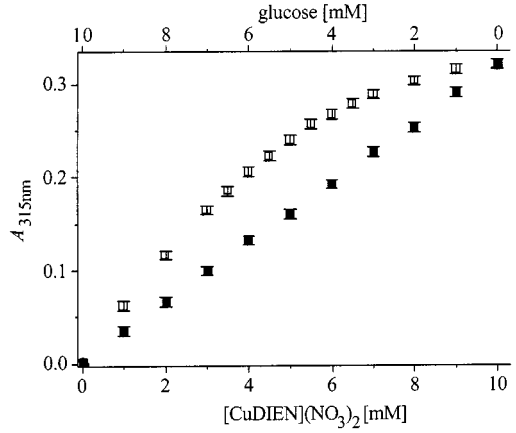

Figure 4. Plot of the absorbance A at 315 nm versus concentration of $[CuDIEN](NO_3)_2$ (**1**), observed during titration of **1** with glucose (**2**) (□) and during titration of **1** with water (■) according to Job's method at pH 12.4, 25 °C

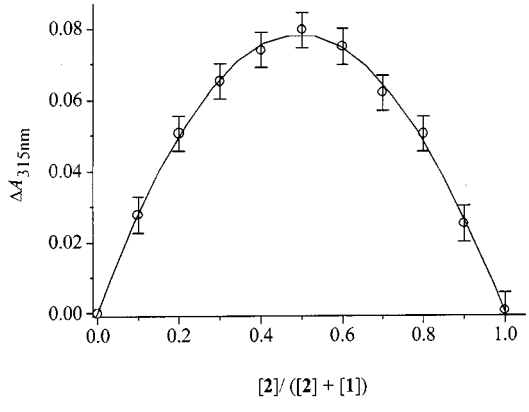

Figure 5. Plot of differences in absorbances ΔA at 315 nm between solutions containing $[CuDIEN](NO_3)_2$ (**1**) and glucose (**2**) and solutions containing pure **1** versus the molar ratio **2**/(**2** + **1**); the maximum is related to the molecular ratio of n and m in $n\mathbf{M} + m\mathbf{C} = \mathbf{M}_n\mathbf{C}_m$ and is defined by $n/(n + m)$; the ratio of $n/(n + m)$ = 0.5 corresponds to n = 1 and m = 1 and refers to 1:1 complex formation of **1** and **2** (Job plot)

There is no evidence for the occurrence of multiple equilibria or other complex formation if a 1:1 molar ratio of the compounds or an excess of ligand is applied. The complex formation is not observable by UV/Vis spectroscopy when the pH value is less than 10.4. In contrast, multiple equilibria are present for the association of glucuronic acid (**6**) with **1** (Figure 6).

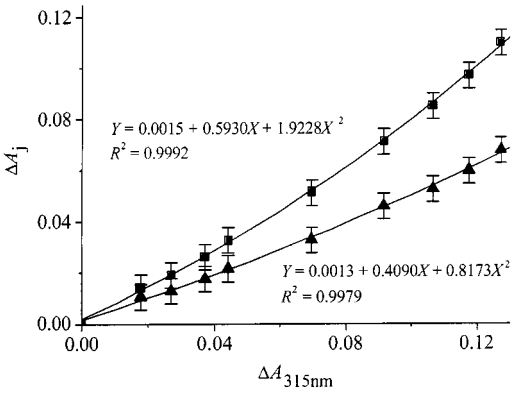

Figure 6. Plot of selected differences in absorbances $\Delta A_j = (A_{j,k} - A_{j,n})$ over $\Delta A_{315nm} = (A_{315nm,k} - A_{315nm,n})$ from titration of $[CuDIEN](NO_3)_2$ (**1**) with glucuronic acid (**6**) at j = 325 nm (■) and 335 nm (▲) for solutions k containing **1** and **6** and solution n containing **1**, V_t = 2 mL, $[\mathbf{1}]_t$ = 2 mM, t = total, $A_{315nm,\mathbf{1}} = 0.0657$, $A_{325nm,\mathbf{1}} = 0.0354$, $A_{335nm,\mathbf{1}} = 0.0109$, pH = 12.4, 25 °C

The nonlinear plot shows complex formation between **1** and **6** and accounts for the presence of more than two spectroscopic states due to multiple equilibria. The carboxylic group at the carbon C^6 of **6**, in contrast to **2**−**5**, offers an additional binding site to copper(II) complexes, which can be used for coordination or, in combination with the hydroxyl group at C^4, chelation to a copper(II) complex.

Evaluation of Suitable Ligand−Cu^{II} Complexes for Association with Carbohydrates

We also evaluated whether the reported binding constants of binary, nonpolymerizable Cu^{II}−ligand complexes can be used to interpret their association behavior with carbohydrates. Our idea behind this was: (1) to achieve fast accessibility and screening of potentially useful and structurally different Cu^{II}−ligand complexes, (2) to achieve increased stability of the Cu^{II} complex during the UV/Vis measurement, avoiding polymerization reactions, and (3) to demonstrate the similar association capabilities of structurally related Cu^{II} complexes with and without polymerizable ligands. Accordingly, we picked several tri- and bidentate Cu^{II} complexes with reported binding constants, in order to evaluate their complexation behavior with **2**−**5** (Figure 7).

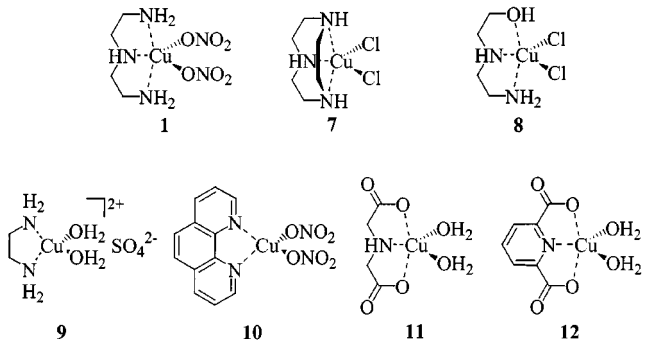

Figure 7. Structures of the copper(II) complexes **1**, **7**−**12**

The Cu^{II} complexes formed from tridentate N- and N,O-ligands **1**, [(triazacyclononane)copper(II)] dichloride $[Cu(TACN)]Cl_2$ (**7**),[18] and *N*-[{(2-hydroxyethyl)ethylenediamine}copper(II)] dichloride CuHEN (**8**), each associate with **2**−**5** with identical stoichiometries (see Supporting Information). In contrast, decomposition of [(ethylenediamine)copper(II)]sulfate (**9**), [(phenanthroline)copper(II)] dinitrate (**10**), copper(II)iminodiacetic acid (**11**), and copper(II)pyridinedicarboxylic acid (**12**) occurs in alkaline solution (pH > 10.4), which prevents the observation of complex formation with **2**−**5**. The formation of a precipitate, which was identified as copper(II) hydroxide, is due to the low chelating ability of the ligands ethylenediamine (EN), iminodiacetic acid (IDA), pyridinedicarboxylic acid (pdca), or phenanthroline (phen), to copper(II) in alkaline solution. Since strong binding of carbohydrates during molecular imprinting requires highly alkaline pHs, only copper(II) complexes stable under these conditions are useful. Surprisingly, *N*-(2-hydroxyethyl)ethylenediamine (HEN) is a suitable ligand for chelating copper(II) in alkaline solution according to our UV measurements, although the reported binding strength of HEN to copper(II) (pK^{Cu} = 10.09) is of the same order of magnitude as those reported for the tridentate IDA (pK^{Cu} = 10.56) or pdca (pK^{Cu} = 9.1), and the bidentate EN (pK^{Cu} = 10.49) or phen (pK^{Cu} = 9.12), while those for copper(II) complexes with tridentate N-ligands — TACN (pK^{Cu} = 15.5) or DIEN (pK^{Cu} = 15.9) — are much higher.[21] The advantage of the copper(II) complex **1** over **7** lies in the low cost of the diethylenetriamine ligand compared to triazacyclononane (1 g of TACN can be purchased from Aldrich for about US $350, whereas 1 g of DIEN costs only about US $0.02), while the binding strength to copper(II) is almost the same (pK^{Cu}_{TACN} = 15.5, pK^{Cu}_{DIEN} = 15.9).[21,22] Accordingly, we chose [{4-(*N*-vinylbenzyl)-diethylenetriamine}copper(II)] diformate $[Cu(styDIEN)](HCOO)_2$ (**13**) as a functional monomer for the preparation of molecularly imprinted polymers after characterization of the stoichiometry of the targeted ternary ligand−Cu^{II}−carbohydrate complexes from **13** and **2**−**5** (see Supporting Information).[23]

As demonstrated for CuHEN, the binding constants of known binary nonpolymerizable Cu^{II}−ligand complexes do not allow a generally valid interpretation of their association behavior with carbohydrates. In contrast, the complexation behavior of the polymerizable Cu^{II} complex **13** can be estimated from the known binding behavior of the corresponding nonpolymerizable Cu^{II} complex **1**.

Investigation of the Binding Sites of Selected Carbohydrates upon Interaction with Copper(II) Complexes

Carbohydrates exist in several equilibrium structures (i.e., α- and β-pyranoses, α- and β-furanoses, and an acyclic

form) and conformers. It is known that both *cis*- and *trans*-diols in six-membered rings can complex to metal ions, but that only *cis*-diols in five-membered rings do.[24] It is also generally accepted that the effectiveness of complexing sites can be listed in descending order: *cis*-diol on a five-membered ring > *cis*-diol on a six-membered ring > *trans*-diol on a six-membered ring.[25] The pyranoses of **2**−**4**, which are the main equilibrium structures in aqueous solution of the saccharides under investigation here,[30] are shown in Figure 8.

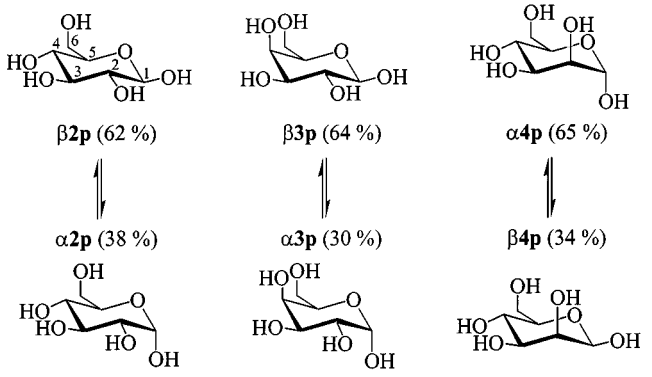

Figure 8. Percentage values of the main equilibria structures of glucose (**2**), galactose (**3**), and mannose (**4**) in aqueous solution at pH = 7 at 31 °C (**2**, **3**) and 44 °C (**4**);[30] missing percentage values refer to the furanose and the acyclic carbonyl forms; **p** = pyranose

Subsequently, we firstly determined whether multiple deprotonation of the carbohydrate occurs upon complexation with **1**, **7**, and **8** under the conditions applied, and secondly, which 1,2-diol groups of the carbohydrates **2**−**6** are involved in chelation to **1**, **7**, and **8**.

Multiple deprotonation of metal-bound carbohydrates is a well-known phenomenon in the solid state, particularly when pH values close to 14 are considered. Klüfers et al. reported on a crystal structure of fivefold deprotonated D-mannose as a ligand in homoleptic dinuclear metalates of trivalent iron, vanadium, chromium, aluminium, and gallium.[26] However, the systems under investigation here are clearly different in terms of concentration of the compounds, the kind and charge of the metal ion, and the identity of the metal atom-binding ligand. When the solutions both of the metal complex and of the sugar are adjusted to pH 12.4 prior to mixing, proton release during complex formation is directly related to the single or multiple deprotonation of the carbohydrate in a ternary ligand−copper(II)−carbohydrate complex and observable by a drop in the pH value of the solution.

Since ternary complexes formed both from singly deprotonated and from doubly deprotonated carbohydrate can coexist in equilibrium (Scheme 1), titration experiments were performed at 2, 5 and 10 mM concentrations of **1** with fortyfold, sixteenfold, and eightfold molar excesses of **2** to distinguish both possible binding modes (Figure 9).

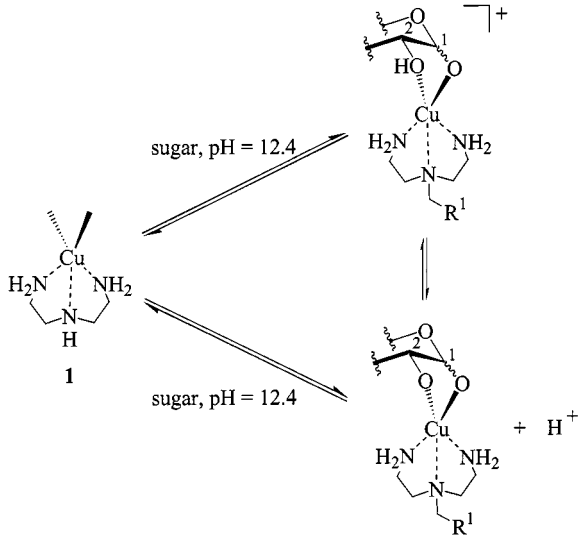

Scheme 1. Complex formation of $[Cu(DIEN)](NO_3)_2$ (**1**) with singly and doubly deprotonated carbohydrates at pH 12.4

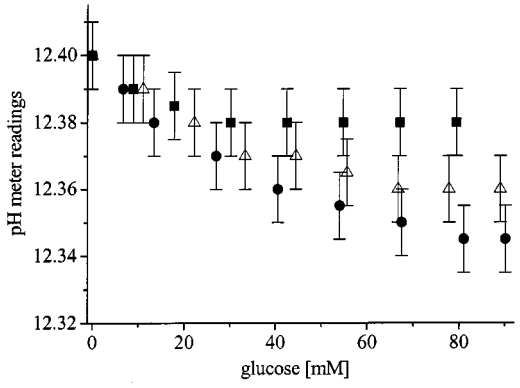

Figure 9. Plot of average pH meter readings from titration experiments of 2 mM (■), 5 mM (▲), and 10 mM (circle) $[CuDIEN](NO_3)_2$ (**1**) solution with up to fortyfold molar excesses of glucose (**2**) at 25 °C; each set of titration was performed three times and the error in the pH reading was within 0.01 units; total concentration of **1** and the total volume of the solution (V_t = 1 mL) were kept constant; nanopure water was sonicated and purged with argon prior to use; stock solutions were separately adjusted to pH 12.4 with $NaOH_{(aq)}$ and kept under argon prior to use

By using the Hendersson−Hasselbach equation and the reported first deprotonation constants of the carbohydrates,[21] we calculated the ratio of singly deprotonated and nondeprotonated sugars in the saccharide stock solution.[27] We further estimated the maximum amount of proton release during the formation of the ternary ligand−copper(II)−carbohydrate complexes for 2, 5, and 10 mM metal ion solution for complete dissociation of **2** into a singly deprotonated saccharide upon binding to the copper(II) complex. The pH value would be expected to drop from 12.40 to 12.38 for 2 mM, from 12.40 to 12.36 for 5 mM, and from 12.40 to 12.32 for 10 mM copper(II) ion solution. In contrast, the pH value of the solution for doubly deprotonated **2** should drop from 12.40 down to 12.34 for 2 mM, from 12.40 to 12.25 for 5 mM, and from 12.40 to 12.03 for 10 mM copper(II) solution. This larger drop is caused by

further dissociation of **2** and additional release of 1 mol proton/mol carbohydrate upon binding to the copper(II) ion. However, the observed changes in pH for the overall solutions of both 5 mM and 10 mM Cu^{II} concentrations correspond to singly deprotonated **2** as the main species in solution in the ternary ligand−copper(II)−carbohydrate complex (Figure 9). The drop in the pH value for the 2 mM solution is close to the experimental error and was not considered.

We therefore propose that complex formation between **1**, **7**, and **8** with **2** at pH = 12.40 takes place with singly deprotonated α-D-glucopyranose (pK_2^H = 12.28)[21] chelating the copper(II) complex through the hydroxyl groups at C^1 and C^2, this being the only equilibrium structure of glucose with a 1,2-*cis* arrangement of hydroxyl groups. The proposed complex formation between **13** and **2**−**5** for aqueous solution at alkaline pH is indicated in Scheme 2.

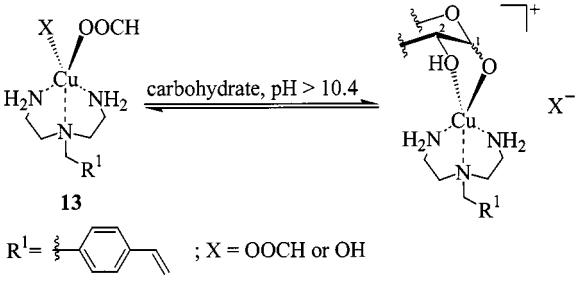

Scheme 2. Complex formation of [Cu(styDIEN)]$(HCOO)_2$ (**13**) with **2**−**5** at pH =12.40

If this assumption is valid, then the derivatizing carbon atoms C^1 and C^2 should have a strong influence on the binding behavior of glucose to **1**, **7**, and **8**. To obtain confirmation of this, we performed several experiments at pH = 12.40 with **1** as a model for the similar copper(II) complexes **7** and **8**. Firstly, blocking of the hydroxyl group of the anomeric carbon atom C^1 of **2** by using α-D-methylglucopyranoside or β-D-methylglucopyranoside resulted in no detectable binding interactions with **1**. Secondly, removal of the hydroxyl group at C^2 of **2** by using 2-desoxyglucose as ligand resulted in no ternary complex formation. Thirdly, blocking of the hydroxyl group at C^3 by using 3-*O*-methyl-D-glucose (**2a**) as ligand permitted the formation of a 1:1 complex with **1**. These experiments demonstrate that the free hydroxyl groups at carbon atoms C^1 and C^2 of **2** are essential for chelating the copper(II) complex **1** in alkaline solution, while the hydroxyl group at C^3 is not involved in complex formation of **1** and **2** under the provided conditions.

Galactose (**3**) differs from its epimer **2** in the configuration at carbon atom C^4, while the arrangement of the hydroxyl groups at C^1 and C^2 is identical. Complex formation with **3** and **1** can in principle occur through the hydroxyl groups at C^1 and C^2, at C^3 and C^4, or at C^4 and C^6. At pH = 12.40, deprotonation of the hydroxyl group at C^1 takes place (pK_3^H = 12.35)[21] in analogy to **2**, which would be expected to provide stronger and therefore preferable binding interactions with a copper(II) complex than those arising by chelation through the protonated hydroxyl groups at C^3 and C^4, or C^4 and C^6. Under the given conditions, the number of spectroscopic states corresponds to a two-state system and a 1:1 assembly of **3** with **1**. No evidence for multiple equilibria is given by the experimental data when a 1:1 molar ratio between **1** and **3**, or an excess of **3**, is provided during the experiments. Since no binding interactions between **1** and α-methyl-D-galactopyranoside or β-methyl-D-galactopyranoside are detectable, only the hydroxyl groups at the anomeric carbon C^1 and at C^2 of **3** are considered to chelate **1**, in agreement with the observations made for ternary complex formation of **1** with **2**.

Mannose (**4**) differs from its epimer **2** in the configuration at C^2. Chelation of **1** should preferentially be through the *cis*-diol groups at C^1, C^2, and C^3 of **4**. The binding interaction between **4** and **1** at pH = 12.40 was characterized as a two-state system corresponding to a 1:1 molar ratio during complex formation. A protonated hydroxyl group at C^2 of **4** is less likely to act as a donor group for two molecules of **1** at the same time, which is attributable to steric constraints during complexation. Since deprotonation of the hydroxyl group at C^1 of **4** occurs at pH = 12.40 (pK_4^H = 12.08),[21] analogously with **2** and **3**, participation of the deprotonated hydroxyl group at C^1 in chelation has the strongest influence on the complex formation between **1** and **4**. No binding interactions between α-methyl-D-mannopyranoside and **1** were observed even at pH = 12.40. This demonstrates that the deprotonated hydroxyl group at C^1 is necessary for strong binding, and suggests that the hydroxyl groups at C^2 and C^3 of **4** do not contribute significantly to the binding interactions with **1** under the given conditions.

Determination of the Binding Constant of Selected Copper(II) Complexes with Different Carbohydrates

The method of Rose and Drago was applied in order to determine the binding constants of the 1:1 complexes formed from **1**, **8**, and **13** with **2**−**5**.[20] This graphical tech-

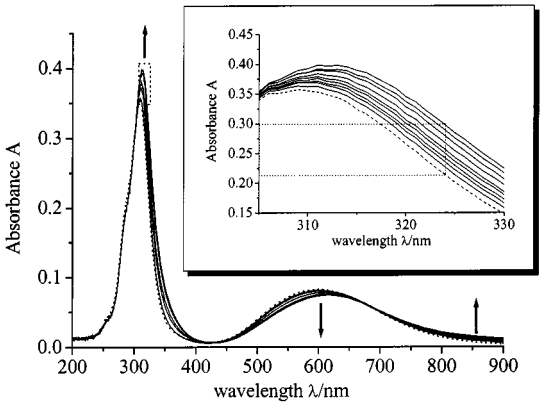

Figure 10. UV/Vis spectra obtained during titration of [Cu(styDIEN)]$(HCOO)_2$ (**13**) with glucose (**2**) at 25 °C in unbuffered, aqueous solution at pH = 12.40; ····· UV/Vis spectrum of **13** (1 mM); —— UV spectra of **13** after addition of **2** (2, 3, 4, 5, 6, 7, 8, 9, and 10 mol equivalents); the total concentration of **13** (M_t = 1 mM) and the total volume of the solution (V_t = 2 mL) were kept constant

nique does not require the assumption that $C = C_t$ made in the Scatchard plot analysis and is only applicable when the total concentration of the copper complex (C_t = 1 mM) and the total volume of the resulting solution (V_t = 2 mL) are kept constant.[28] As representative examples, the UV/Vis spectra obtained during titration of **13** with **2** at 25 °C in unbuffered, aqueous solution at pH 12.4 are depicted in Figure 10.

The binding strengths of the complexes formed from **1** and **6** were determined by nonlinear regression. The obtained apparent binding constants (pK_{11}) from the titration of **1**, **8**, and **13** with **2**−**6** are summarized in Table 1.

Table 1. Apparent binding constants (pK_{11}) for ternary complexes formed from [CuDIEN]$(NO_3)_2$ (**1**), CuHEN (**8**), and [Cu(styDIEN)]$(HCOO)_2$ (**13**) with the carbohydrates **2**−**6** at pH = 12.40

Compd.	pK_{11} [1]	pK_{11} [13]	pK_{11} [8]
2	3.73 ± 0.12	3.37 ± 0.31	3.61 ± 0.17
2a	3.71 ± 0.09	n.d.[a]	n.d.[a]
3	3.70 ± 0.09	3.41 ± 0.43	3.64 ± 0.12
4	3.68 ± 0.12	3.05 ± 0.41	3.38 ± 0.19
5	3.75 ± 0.12	3.41 ± 0.26	3.62 ± 0.09
6	3.48 ± 0.14	n.d.[a]	n.d.[a]
	1.36 ± 0.15	n.d.[a]	n.d.[a]

[a] n.d. = not determined.

The pK values for the complexes formed from **1**, **8**, and **13** with **2**−**5** are of the same order of magnitude. The ternary complexes formed from **2**, **3**, and **5** with **1**, **8**, or **13** show similar apparent binding constants, while those formed with **4** are smaller in each case. We attribute this to a rearrangement of the ligand−copper(II)−mannose complex when complex formation with the *cis*-1,2-diol at C^2 and C^3 occurs despite the preferential chelation through the hydroxyl groups at C^1 and C^2. Unfortunately, no binding interaction with α-methyl-D-mannopyranoside, which could have provided evidence for complex formation with the hydroxyl groups at C^2 and C^3, was observed by UV spectroscopy at alkaline pH values (see above and Supporting Information).

Since a carbohydrate is mostly deprotonated at a pH value larger than its pK (i.e., pK_2^H = 12.28), the binding strength of the coordinative bond to a metal complex increases with pH.[21] Therefore, the determined binding constants of the ternary complexes formed from **1** and **2** (pK_{11} = 3.73 ± 0.12 at pH = 12.40) or **13** and **2** (pK_{11} = 3.37 ± 0.31 at pH = 12.40) are of the same order of magnitude as those reported by Arnold for **7** and **2**, which were determined by isothermal titration calorimetry (pK_{11} = 2.6 ± 0.1 at pH = 11.25).[18]

In agreement with the number of spectroscopic states, two binding interactions are observed between **1** and **6**. The stronger (pK_{11} = 3.38 ± 0.14) is of the same order of magnitude as that observable between **1** and **2** (pK_{11} = 3.73 ± 0.12) and is due to chelation of **1** through the hydroxyl groups at C^1 and C^2 of **6**. The weaker binding interaction (pK_{11} = 1.36 ± 0.15) is caused by coordination of **1** by the carboxylic group of **6**, which is comparable to that observed for coordination of free copper(II) ions to **6** at neutral pH (pK_{11} = 1.44),[29] in which coordination of **6** is reported to be through the carboxylic group only. A detailed investigation of binding interactions between copper(II) complexes and disaccharides and other carbohydrates providing multiple points of interactions during complex formation is currently underway.

The binding strength of the ternary ligand−copper(II)−carbohydrate complex decreases to some extent when the secondary amino group in the DIEN ligand of **1** is alkylated with a styryl group to yield **13**, but it decreases only slightly when the HEN-based functional monomer **8** is used. Accordingly, the replacement of one amino group by a more weakly electron-donating hydroxyl group influences the stability of complexes formed with carbohydrates less than the alkylation of the secondary amino group in the DIEN-based functional monomer **1**. However, the determined binding strength for a ternary complex consisting of **13** and **2**−**5** [e.g., pK_{11} = 3.37 for complex formation of **13** with **2** (Table 1)] seems to be suitable for imprinting carbohydrates into a polymer matrix.

Determination of the Distribution of Species Participating in Complex Formation

Since different coordinating compounds (species) usually exist in equilibrium structures in aqueous solution, it is important, prior to a planned imprinting process, to examine the total amount of copper(II) bound in the formed ternary ligand−copper(II)−carbohydrate complex. We therefore evaluated the species distribution during complexation of **13** with **2**−**5** from their binding constants, with the SPE computer program.[22] The calculations suggested that only up to 80% of **13** (the overall concentration of which is kept at 2 mM) are bound in a 1:1 complex with **2**−**5** at pH = 12.4. This is not favorable for the planned imprinting process, since about 20% of the functional monomer would remain unbound and would therefore not be able to create specific cavities during polymerization, but would generate randomly distributed, nonspecific binding sites inside the polymer instead. Up to 100% complexation of the copper-containing functional monomer can be achieved by using an excess of carbohydrate, which does not interfere with the 1:1 ratio of complex formation as determined and described earlier.

Investigation of Carbohydrate Stability at Alkaline pH Values

It is known that a Lobry de Bruyn−van Ekenstein rearrangement as well as base-catalyzed fragmentation of aldoses and ketoses may occur under alkaline conditions.[30] Treatment of D-glucose with a 0.035% aqueous sodium hydroxide solution at 35 °C for 100 h results in a mixture containing D-fructose (28%), D-mannose (3%), and unchanged D-glucose (57%).[30] This behavior is not favorable either for carbohydrate chelation to copper(II) complexes, or for a planned imprinting process in which the original template has to be maintained during polymerization. Since we use

even more strongly alkaline conditions (pH = 12.40; i.e., about 0.1% aqueous sodium hydroxide) at 25 °C for strong carbohydrate binding to copper(II) complexes, we investigated the stability of **2**−**4** under these conditions by ^{1}H NMR spectroscopy. A set of ^{1}H NMR spectra recorded for **2** after its exposure to base is depicted in Figure 11 and Figure 12 (for others, see Supporting Information).

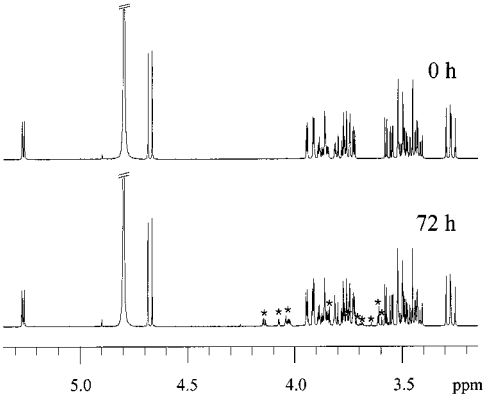

Figure 11. 400.1 MHz ^{1}H NMR spectra (303 K) of glucose (**2**) after exposure to pH = 12.40 at 25 °C for 0 and 72 h

The ^{1}H NMR spectra demonstrate the stability of **2**−**4** at pH = 12.40 for at least 1 h. Additional signals in the recorded ^{1}H NMR spectra occur for the first time only after 3 h. The original carbohydrates **2**, **3**, or **4** are maintained during the UV experiments, which are usually complete in under 20 minutes.

Polymerization methods commonly used during an imprinting process proceed for about 72 h at 60 °C and so, according to our results, are not applicable to the system described here, especially since even faster decomposition of the carbohydrate at the elevated temperature would be expected. A fast polymerization technique has been developed to prevent the carbohydrates from epimerization, isomerization, or fragmentation during the imprinting process under our conditions. The investigation of the obtained molecularly imprinted polymers is reported elsewhere.[23]

Conclusion

Careful characterization of the binding interactions between functional monomers (such as copper complexes) and targeted templates (such as carbohydrates) prior to polymerization is one of the key steps in the molecular imprinting technique. We therefore report here for the first time on the naturally accessible binding sites in several sugars — namely glucose (**2**), galactose (**3**), mannose (**4**), and maltose (**5**) — upon chelation to copper(II) complexes at alkaline pH values. Under these conditions, only the hydroxyl groups at C^1 and C^2 of the carbohydrates **2**−**5** are involved in formation of ternary ligand−copper(II)−carbohydrate complexes, which were characterized in terms of stoichiometry and binding strength at alkaline pH.

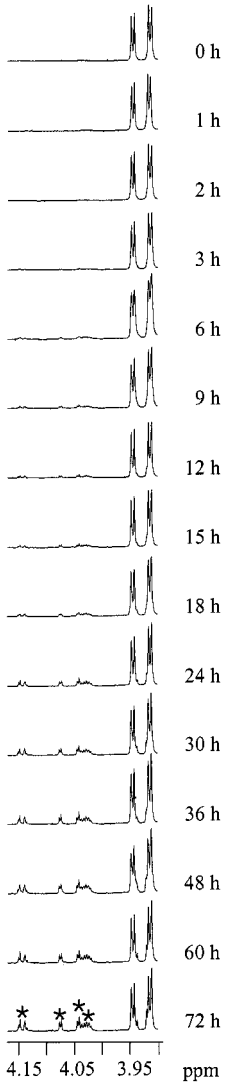

Figure 12. 400.1 MHz ^{1}H NMR signals (303 K) of protons 6a-H and 6b-H of **2** at 303 K after exposure of **2** to pH = 12.4 at 25 °C for 0, 1, 2, 3, 6, 9, 12, 15, 18, 24, 30, 36, 48, 60, and 72 h; the asterisks indicate the formation of new signals

Experimental Section

General Remarks: Methyl β-D-galactopyranoside, β-D-(+)-glucose (**2**), and maltose (**5**) were obtained from Sigma; sodium hydroxide, D-mannose (**4**), methyl α-D-galactopyranoside, methyl α-D-mannopyranoside, methyl β-D-glucopyranoside, and methyl α-D-glucopyranoside were obtained from Fluka; diethylenetriamine, 2-(2-aminoethylamino)ethanol, 3-*O*-methyl-D-glucose (**2a**), and 2-desoxy-D-glucose were obtained from Aldrich; nanopure water, cupric chloride dihydrate, cupric nitrate trihydrate, and D-(+)-galactose (**3**) were obtained from Merck Eurolab. Diethylenetriamine and 2-(2-aminoethylamino)ethanol were distilled prior to use. The nanopure water was sonicated and purged with argon prior to use. All other commercially available reagents were used as received from the supplier.

(Diethylenetriamine)copper(II) dinitrate (**1**),[31] [(1,4,7-triazacyclononane)copper(II)] dichloride (**7**),[32] [{4-(*N*-vinylbenzyl)-diethylenetriamine}copper(II)] diformate (**13**),[23] and [{*N*-(2-

hydroxyethyl)ethylenediamine}copper(II)] dichloride (**8**)[33] were prepared as described.

UV Experiments: All experiments described here were performed on a J & M TIDAS UV spectrophotometer (software SPECTRALYS Version 1.55) with Suprasil® standard cells (200−2000 nm) of 10 mm thickness and 700 μL volume at 25 °C. All experiments were done in unbuffered, degassed, nanopure water, the pH of which was freshly adjusted to pH 12.40 with NaOH for each set of titrations. Typically, 10 mM stock solutions of the appropriate copper complex and 25 mM stock solutions of the carbohydrates were prepared separately and kept at 25 °C. The total concentration of the absorbing copper complex (M_t = 1 mM in the case of **13**; M_t = 2 mM in the case of **1**, **7**, **8**) and the total volume of the resulting solutions (V_t = 2 mL) were kept constant during the titration experiments by addition of an appropriate amount of water. The UV/Vis absorbances of the resulting mixtures were measured immediately, over a range of 200−900 nm. The pH of the resulting solutions did not differ from the solutions prepared initially.

NMR Experiments: All NMR experiments were performed on a Bruker DRX 400 (^{1}H: 400.1 MHz; ^{13}C: 100.6 MHz), D_2O was used as solvent, and residual HDO was used as internal standard [δ = 4.80]. Chemical shifts (δ values) downfield from tetramethylsilane refer to the residual nondeuterated solvent signal.

Typically, **2**−**4** (1 g) was dissolved in H_2O (25 mL) at pH 12.4. The resulting solution was kept for 72 h at 25 °C. After 0, 1, 2, 3, 6, 9, 12, 15, 18, 24, 30, 36, 48, 60, and 72 h, 1 mL of the solution was removed and neutralized with HCl_{aq} (1 N, 30 μL), and the solvents were evaporated to dryness. The residue was taken up in 0.7 mL D_2O and the ^{1}H NMR spectra were recorded at 303 K.

Supporting Information (see footnote, page one) includes Job plots for the demonstration of association of the copper(II) complexes **1**, **13**, and **8** with the carbohydrates **2**−**5** at pH 12.4, 25 °C, and sets of time-dependent ^{1}H NMR spectra (400.1 MHz, D_2O, 303 K) of **3** and **4**.

Acknowledgments

A fellowship from the Margarete von Wrangell habilitation program from the state of Baden-Württemberg (S. S.) and financial support from the University of Ulm are gratefully acknowledged. The authors also thank Prof. Dr. G. Wulff, Düsseldorf, Germany and Prof. Dr. P. Klüfers, Munich, Germany for helpful discussions during the preparation of this manuscript.

[1] A. P. Davis, R. S. Wareham, *Angew. Chem.* **1999**, *111*, 3160−3179; A. P. Davis, R. S. Wareham, *Angew. Chem. Int. Ed.* **1999**, *38*, 2979−2996.
[2] S. David, *The Molecular and Supramolecular Chemistry of Carbohydrates*, Oxford University Press, Oxford **1997**.
[3] W. E. Stites, *Chem. Rev.* **1997**, *97*, 1232−1273.
[4] H. J. Schneider, A. Yatsimirski, *Principles and Methods in Supramolecular Chemistry*, John Wiley & Sons, Somerset, **2000**.
[5] J. W. Canary, B. C. Gibb, in *Prog. Inorg. Chem. Vol. 45* (Ed.: K. D. Karlin), John Wiley & Sons, New York, **1997**, pp 1−81.
[6] T. D. James, K. R. A. Samankumara Sandanayake, S. Shinkai, *Angew. Chem.* **1996**, *108*, 2038−2050; T. D. James, K. R. A. Samankumara Sandanayake, S. Shinkai, *Angew. Chem. Int. Ed. Engl.* **1996**, *35*, 1910−1922.
[7] Y. Nagai, K. Kobayashi, H. Toi, Y. Aoyama, *Bull. Chem. Soc. Jpn.* **1993**, *66*, 2965−2971.
[8] K. Haupt, K. Mosbach, *Chem. Rev.* **2000**, *100*, 2495−2504.
[9] M. E. Davis, *CATTECH* **1997**, *1*, 19−26.
[10] G. Wulff, *Angew. Chem.* **1995**, *107*, 1959−1979; G. Wulff, *Angew. Chem. Int. Ed. Engl.* **1995**, *34*, 1812−1832.
[11] F. H. Arnold, S. Striegler, V. Sundaresan, in *Molecular and Ionic Recognition with Imprinted Polymers* (Ed.: R. A. Bartsch, M. Maeda), American Chemical Society, Washington DC., **1998**, 109−118.
[12] K. Adbo, H. S. Andersson, J. Ankarloo, J. G. Karlsson, M. C. Norell, L. Olofsson, J. Svenson, U. Ortegren, A. Nicholls, *Bioorg. Chem.* **1999**, *27*, 363−371.
[13] G. Wulff, in *Frontiers in Biosensorics I − Fundamental Aspects* (Ed.: F. W. Scheller, F. Schubert, J. Fedrowitz), Birkhäuser Verlag, Basel, **1997**, 13−26.
[14] G. Wulff, S. Schauhoff, *J. Org. Chem.* **1991**, *56*, 395−400.
[15] G. Wulff, J. Haarer, *Makrom. Chem.* **1991**, *192*, 1329−1338.
[16] A. G. Mayes, L. I. Andersson, K. Mosbach, *Anal. Biochem.* **1994**, *222*, 483−488.
[17] B. Sellergren, M. Lepistoe, K. Mosbach, *J. Am. Chem. Soc.* **1988**, *110*, 5853−5860.
[18] G. H. Chen, Z. B. Guan, C. T. Chen, L. T. Fu, V. Sundaresan, F. H. Arnold, *Nat. Biotechnol.* **1997**, *15*, 354−357.
[19] F. H. Arnold, W. Zheng, A. S. Michaels, *J. Membr. Sci.* **2000**, *167*, 227−239.
[20] K. A. Connors, *Binding constants − The Measurement of Molecular Complex Stability*, John Wiley & Sons, New York, **1987**.
[21] NIST Critically Selected Stability Constants of Metal complexes, Reference database 46, Version 5.0, data collected and selected by A. E. Martell, R. M. Smith, U. S. Department of Commerce, National Institute of Standards and Technology, Gaithersburg, MD, USA, **1998**.
[22] A. E. Martell, R. I. Motekaitis, *Determination and Use of Stability Constants*, VCH Publishers, New York, **1988**.
[23] S. Striegler, *Tetrahedron* **2001**, *57*, 2349−2354.
[24] D. M. Whitfield, S. Stojkovski, B. Sarkar, *Coord. Chem. Rev.* **1993**, *122*, 171−225.
[25] S. J. Angyal, *Adv. Carbohydr. Chem. Biochem.* **1991**, *49*, 19−35.
[26] J. Burger, C. Gack, P. Klüfers, *Angew. Chem.* **1995**, *107*, 2950−2951; J. Burger, C. Gack, P. Klüfers, *Angew. Chem. -Int. Edit. Engl.* **1995**, *34*, 2647−2649.
[27] pH = pK_{sugar}^{H} + log([sugar-H]/[sugar]). The calculation suggests that 56.9% of **2**, 52.9% of **3**, and 69.6% of **4** are singly deprotonated in stock solutions at pH 12.4.
[28] This assumption is only appropriate if the total carbohydrate concentration C_t is much larger than the total concentration of the metal complex M_t.
[29] C. Makridou, M. Cromer-Morin, J. P. Scharff, *Bull. Soc. Chim. Fr.* **1977**, 59−63.
[30] P.M. Collins, R. J. Ferrier, *Monosaccharides − Their chemistry and their role in natural products*, John Wiley & Sons, Chichester, England, **1995**.
[31] R. Allmann, M. Krestl, C. Bolos, G. Manoussakis, G. St. Nikolov, *Inorg. Chim. Acta* **1990**, *175*, 255−260.
[32] W. F. Schwindinger, T. G. Fawcett, P. A. Lalancette, J. A. Potenza, H. J. Schugar, *Inorg. Chem.* **1980**, *19*, 1379−1381.
[33] J. G. Breckenridge, *Can J. Res., Sect. B* **1948**, *26*, 11−19.

Received April 25, 2001
[I01146]

EurJIC
European Journal of Inorganic Chemistry

March 2002
Issue 3
Pages 497–766

COVER PICTURE

The cover picture shows an electrospray mass spectrum obtained with a time of flight instrument of a mixture of Cu^{II} coordination polymers in solution. For these artificial nanostructures, electrospray mass spectrometry (ESMS) is the only analytical tool allowing an unambiguous characterisation. The largest polymer clearly identified consists of 47 units and has a molecular weight of 32901.4 D. Details are discussed in the article by E. Leize et al. on p. 573 ff.

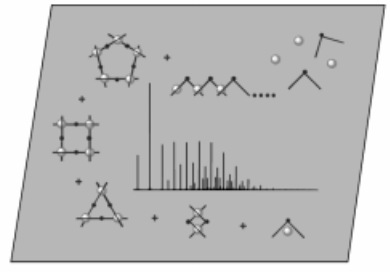

MICROREVIEW

Contents

515 **A. Delabie, K. Pierloot,* M. H. Groothaert, R. A. Schoonheydt, L. G. Vanquickenborne**

The Coordination of Cu^{II} in Zeolites – Structure and Spectroscopic Properties

Keywords: Zeolites / Copper / Ab initio calculations / Density functional calculations / ESR spectroscopy / UV/Vis spectroscopy / Heterogeneous catalysis

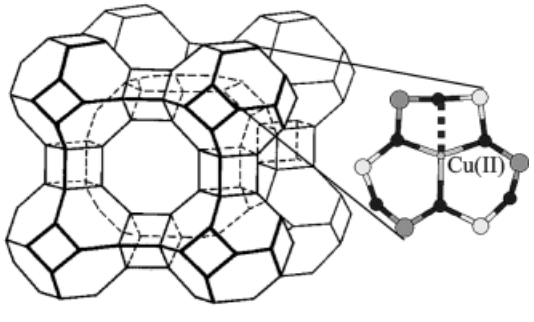

 © WILEY-VCH Verlag GmbH, 69451 Weinheim, Germany, 2002 1434–1948/02/0303–0501 $ 17.50+.50/0

SHORT COMMUNICATIONS

531 **M. Castriciano, A. Romeo, R. Romeo, L. Monsu′ Scolaro***

Mesoscopic Globular Self-assemblies of Platinum(II) Complexes Containing Porphyrins

Keywords: Platinum / Porphyrins / Nanostructures / Aggregation / Scanning probe microscopy

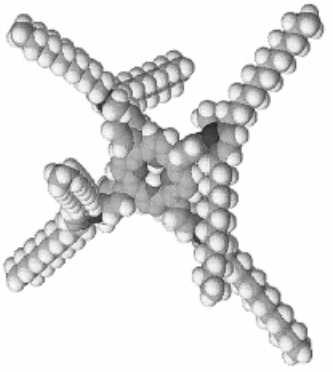

535 **H. Adams, D. Bradshaw, D. E. Fenton***

A Dinuclear Zinc(II) Complex of 2,6-bis{[(2-hydroxybenzyl)(2-pyridylmethyl)amino]methyl}-4-methylphenol Bearing an Exogenous Hydroxo Bridge

Keywords: N ligands / O ligands / Bridging ligands / Zinc

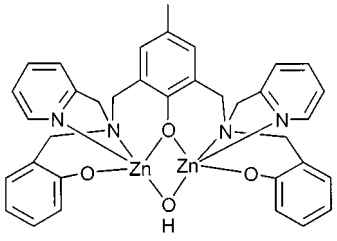

539 **M. Enders,* G. Ludwig, H. Pritzkow**

Olefin-Metal π-Interactions of Mercury and Zinc Ions in Complexes of Neutral Quinolylcyclopentadiene Derivatives

Keywords: Mercury / Zinc / N ligands / π interactions

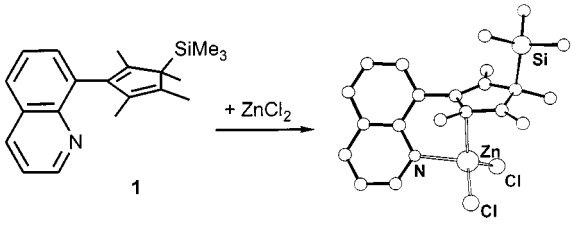

543 **D. L. Reger,* R. F. Semeniuc, M. D. Smith**

Self-Assembly of a Chiral Three Dimensional Architecture Composed of Two Different Silver(I) Helical Chains Connected by Bitopic Tris(pyrazolyl)methane Ligands

Keywords: Helical structures / Ligand design / Silver / Self-assembly

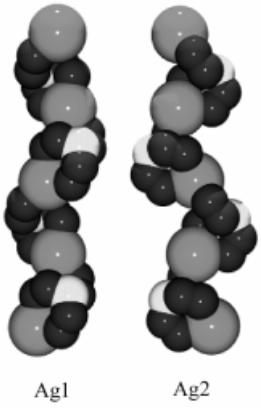

FULL PAPERS

547 **A. V. Olenev, A. I. Baranov, A. V. Shevelkov,* B. A. Popovkin**

A New Family of Supramolecular Complexes with 3D Cationic Hg/Z Frameworks, SnX_3^- Guest Anions (Z = P, As, Sb; X = Cl, Br, I): Crystal Structures and Host−Guest Interactions

Keywords: Host-guest systems / Tin / Supramolecular chemistry / Mercury / Ab initio calculations / Pnicogens

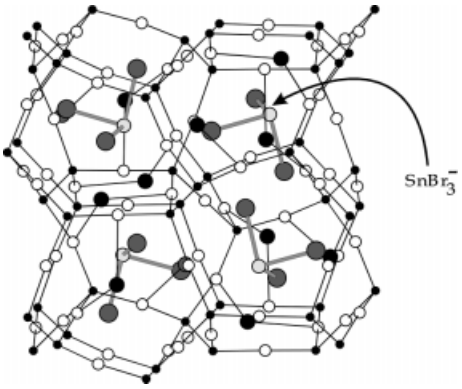

554 **K. C. Gordon,* A. K. Burrell, T. J. Simpson, S. E. Page, G. Kelso, M. I. J. Polson, A. Flood**

Probing the Nature of the Redox Products and Lowest Excited State of $[(bpy)_2Ru(\mu\text{-bptz})\text{-}Ru(bpy)_2]^{4+}$: A Resonance Raman Study

Keywords: Raman spectroscopy / Mixed-valent compounds / Ab initio calculations / Ruthenium(II) / Tetrazines

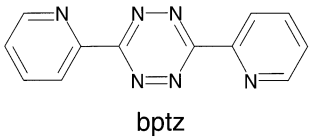

564 **R. Minkwitz,* M. Dzyk**

Trichlorohydroxyphosphonium Hexafluorometallate − Synthesis, Spectroscopic Characterization and Crystal Structure of $Cl_3POH^+AsF_6^-$

Keywords: Phosphonium salts / Superacidic systems / Structure elucidation / Vibrational spectroscopy

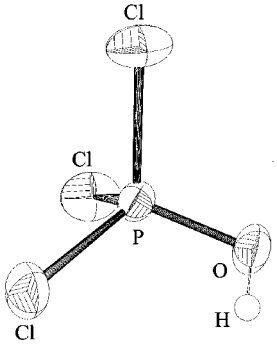

569 **R. Minkwitz,* M. Dzyk**

The Crystal Structures of the Trihalogenphosphonium Salts $X_3PH^+As_2F_{11}^-$ (X = Cl, Br)

Keywords: Phosphonium salts / Protonation / X-ray diffraction / Phosphorus / Main group elements

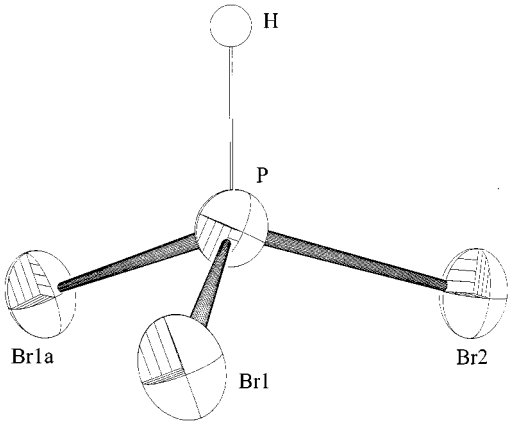

573 **H. Nierengarten, J. Rojo, E. Leize,* J.-M. Lehn, A. Van Dorsselaer**

High Molecular Weight Cu^{II} Coordination Polymers and Their Characterisation by Electrospray Mass Spectrometry (ESMS)

Keywords: Supramolecular chemistry / Copper / Polymers / Mass spectrometry / Self-assembly

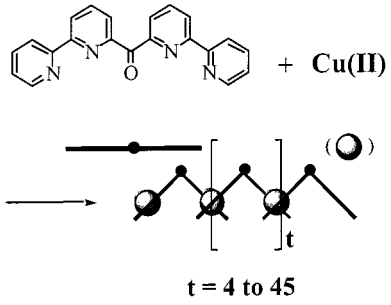

580 **M. S. A. Hamza, R. van Eldik,* P. L. S. Harper, J. M. Pratt,* E. A. Betterton**

Five-Coordination and Adduct Formation in Co^{III}−Corrinoids − Dissecting Ligand Substitution into Its Component Steps

Keywords: Adduct formation / Reaction mechanisms / Cobalt / Equilibrium / Ligand substitution / High-pressure chemistry / Kinetics

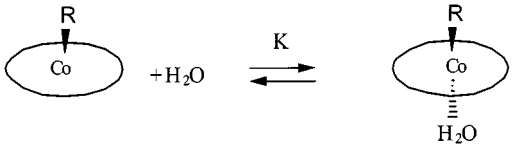

584 **E. Leiner, O. Hampe, M. Scheer***

Synthesis and Structure of Novel Complexes of Gallium

Keywords: Metathesis / Iron / Gallium / Cobalt / Cyclopentadienyl ligands

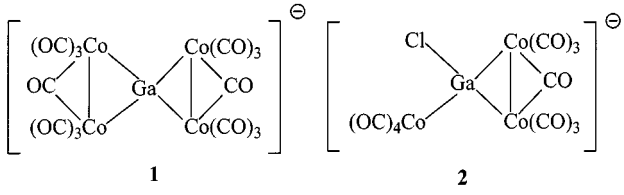

1 **2**

591 **C.-S. Lee, H. Kleinke***

Synthesis, Structure, and Thermoelectric Properties of the New Antimonide Sulfide $MoSb_2S$

Keywords: Antimony / Sulfur / Materials science / Chalcogens / Molybdenum

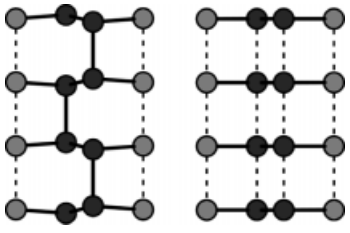

597 **K. Schmohl, D. Wandschneider, H. Reinke, A. Heintz, H. Oehme***

The Cationic Rearrangement of (3-Hydroxy-1-propenyl)tris(trimethylsilyl)silanes into (1-Trimethylsilyl-2-propenyl)bis(trimethylsilyl)silanols − Experimental and Theoretical Studies

Keywords: Alcohols / Rearrangements / Silanes / Silicon

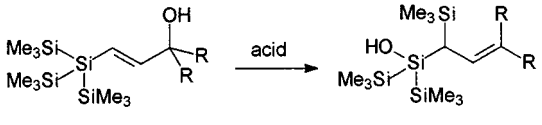

8b,c **13b,c**

R = Me, Ph

602 **H. Nöth,* T. Seifert**

Hydrazino Derivatives of Gallanes and Indanes − Synthesis and Structures

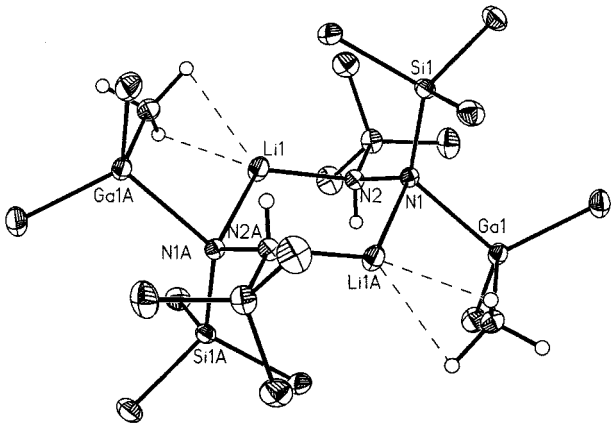

Keywords: Gallium / Indium / Cage compounds / Cleavage reactions / Hydrolysis

613 **A. Amoedo, M. Graña, J. Martínez, T. Pereira, M. López-Torres, A. Fernández, J. J. Fernández, J. M. Vila***

A Comparative Study of Cyclometallated Palladium(II) Compounds with Terdentate [C,N,S] Pincer Ligands − Crystal and Molecular Structure of [Pd{4-$MeC_6H_3C(Me)$=NNC(=S)-NHMe}(PPh_3)] and [Pd{4-$MeOC_6H_3C(H)$=N[2-$(SMe)C_6H_4$]}(Cl)]

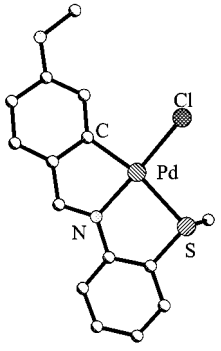

Keywords: C−H activation / Palladium / S ligands / Schiff bases

621 **D. Pappalardo,* C. Tedesco, C. Pellecchia**

New Neutral and Cationic Dialkylaluminium Complexes Bearing Imino-Amide or Imino-Phenoxide Ligands: Synthesis, Characterization and Reactivity With Olefins

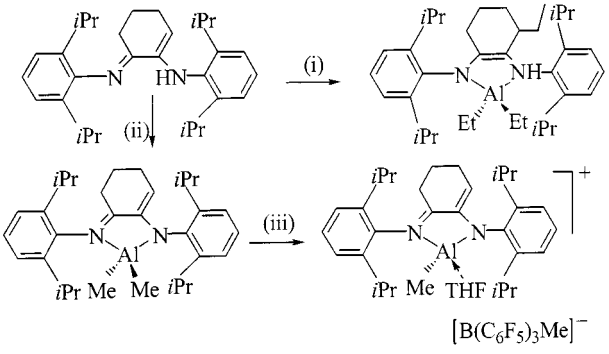

(i) heptane, $AlEt_3$; (ii) heptane, $AlMe_3$; (iii) $B(C_6F_5)_3$, THF

Keywords: Alkenes / N ligands / N,O ligands / Polymerization / Aluminum

629 **R. Romeo,* L. M. Scolaro, M. R. Plutino, A. Romeo, F. Nicolo, A. Del Zotto**

Ring Closure Kinetics of Bidentate Hemilabile P,N and P,S Ligands on a Platinum(II) Complex

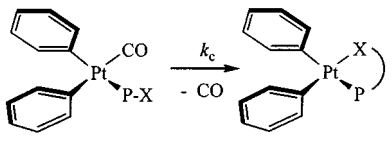

Keywords: N,P ligands / Kinetics / Platinum / Hydrogen bonds / Chelate effect

639

K. Guennou de Cadenet, R. Rumin, F. Y. Pétillon,* D. S. Yufit, K. W. Muir*

Activation and Functionalization of Vinylic C−F Bonds by Transition Metal Compounds: The Factors Determining Reactions between Nucleophiles and a (Perfluorovinyl)diiron(I) Complex; Syntheses of Diiron Derivatives Containing New C−N, C−S, C−H and C−O Bonds

Keywords: F activation / C−N, C−S coupling / Carbenes / Nucleophiles / Vinyl complexes

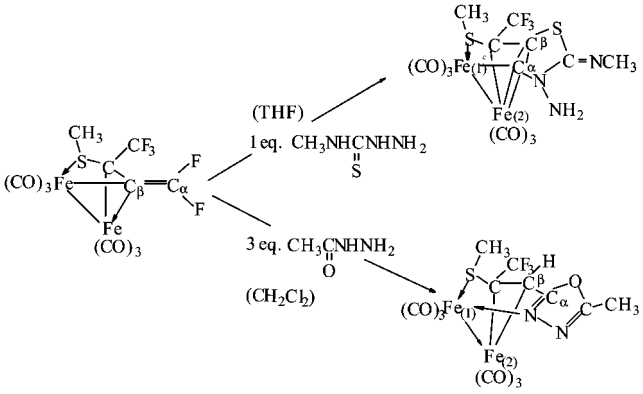

658

P. Schollhammer, B. Didier, N. Le Grand, F. Y. Pétillon,* J. Talarmin, K. W. Muir,* S. J. Teat

Transformations of Hydrazines $RNHNH_2$ (R = Me, Ph) at a Sulfur-Rich Bimetallic Site: Diazene−Diazenido−Isodiazene/Hydrazido-(2−) Interconversions

Keywords: N ligands / S ligands / X-ray diffraction / Metal-metal interactions / Molybdenum

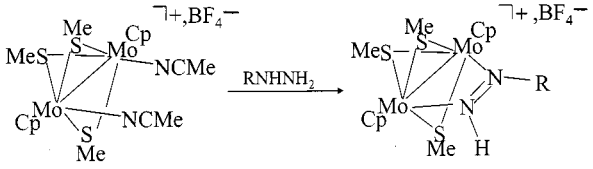

664

L.-J. Liang, Q.-H. Luo,* Q.-X. Li, M.-C. Shen, H.-W. Hu

New Fluorenyl-Substituted Dioxotetraamine Ligands and Their Copper(II) Complexes − Crystal Structure and Fluorescent Sensing Properties in Aqueous Solution

Keywords: Copper / Dioxotetraamines / Fluorescence / N ligands

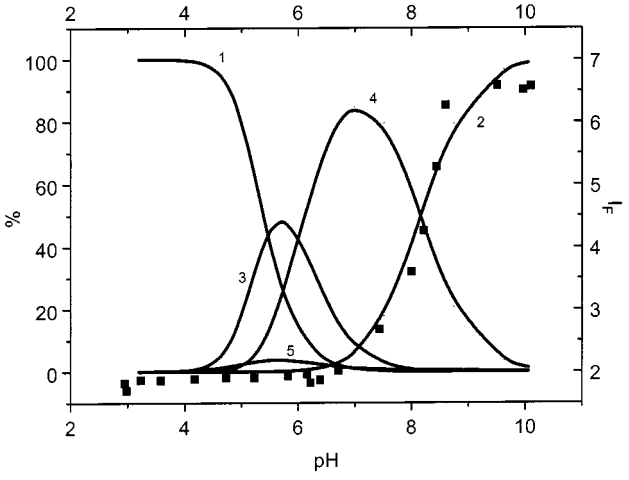

671

A. López-Hernández, R. Müller, H. Kopf, N. Burzlaff*

Bis(pyrazol-1-yl)acetato Ligands in Ruthenium Chemistry: Syntheses and Structures of Ruthenium(II) and Ruthenium(III) Complexes with bpza and bdmpza

Keywords: Ruthenium / N ligands / Scorpionates / Tripodal ligands / Structural chemistry

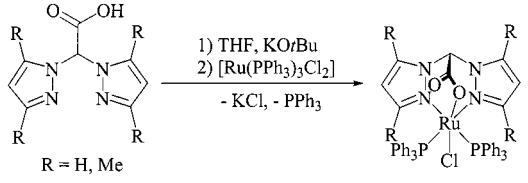

678 **V. V. Kotov,* E. V. Avtomonov,* J. Sundermeyer, K. Harms, D. A. Lemenovskii**

Alkyl(amino)- and Alkyl(chloro)phosphanyl-Substituted Cyclopentadienyl Complexes of Titanium and Zirconium

Keywords: Titanium / Zirconium / Cyclopentadienyl ligands / P ligands / Polymerisation

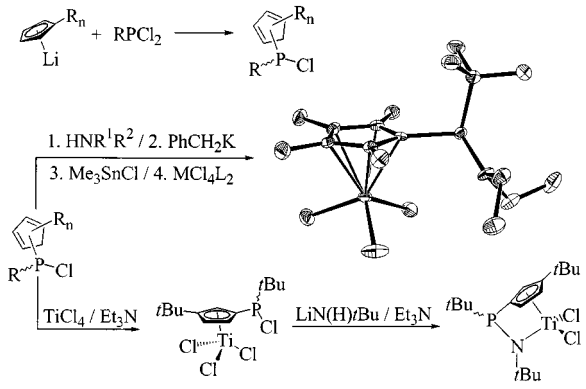

692 **J.-C. Moutet,* E. Saint-Aman, G. Royal, S. Tingry, R. Ziessel**

Electrochemical and Complexation Studies of Ferrocenyl Complexes Bearing Terpyridine or Phenanthroline Ligands

Keywords: N ligands / Sandwich complexes / Receptors / Cyclic voltammetry

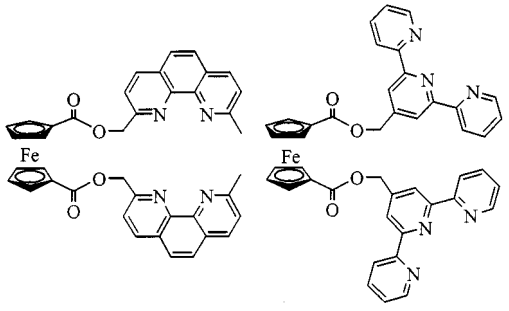

699 **H.-Z. Kou, S.-F. Si, S. Gao, D.-Z. Liao,* Z.-H. Jiang, S.-P. Yan, Y.-G. Fan, G.-L. Wang**

Two Ferromagnetic One-Dimensional Nickel(II) Complexes Containing the Diamagnetic $[Ni(CN)_4]^{2-}$ Group

Keywords: Cyanides / Bridging ligands / Nickel / Magnetic properties / Crystal structure

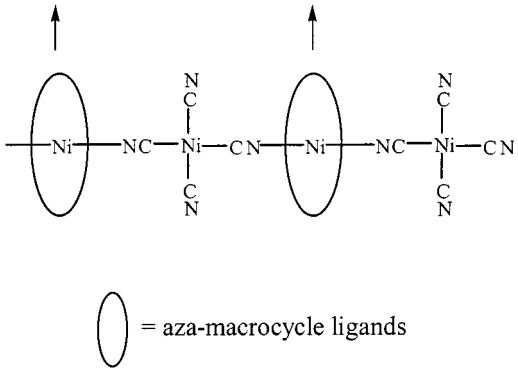

703 **M. Fondo, A. Sousa, M. R. Bermejo, A. García-Deibe, A. Sousa-Pedrares, O. L. Hoyos, M. Helliwell**

Electrochemical Synthesis and X-ray Characterisation of Cadmium Complexes Containing 2,6-Bis(1-salicyloylhydrazonoethyl)pyridine − the Influence of the Supporting Electrolyte on the Nature of the Isolated Compounds

Keywords: N ligands / Cadmium / Electrochemistry

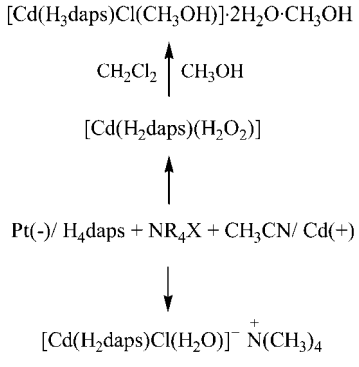

711 **C. G. Arena, F. Faraone,* C. Graiff, A. Tiripicchio**

Rhodium(I), Palladium(II), and Platinum(II) Complexes Containing New Mixed Phosphane−Phosphite Ligands − Effect of the Catalytic System Stability on the Enantioselective Hydroformylation of Styrene

Keywords: Rhodium / Palladium / Platinum / Chirality / P ligands / Hydroformylation

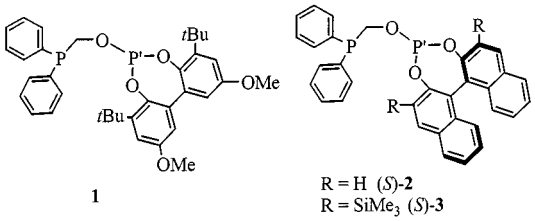

717 **U. Klingebiel,* P. Neugebauer, I. Müller, M. Noltemeyer, I. Usón**

2,5-Bis(di-*tert*-butylhydroxysilyl)furan as a Host Molecule for Potassium Fluoride, H_2O, NH_3 and $MeNH_2$

Keywords: Silicon / Furan / Host-guest complexes / Structure elucidation

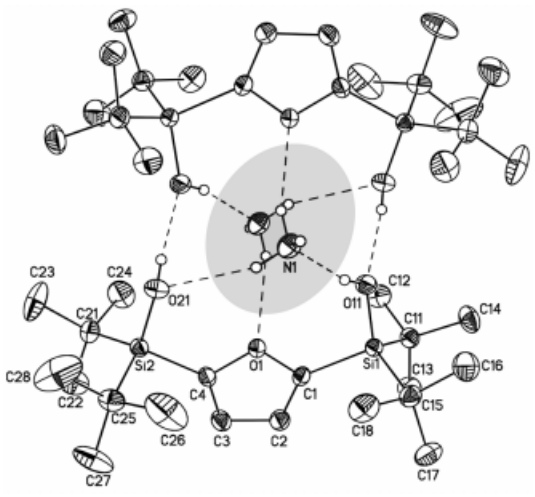

723 **G. R. Giesbrecht, J. C. Gordon,* J. T. Brady, D. L. Clark, D. W. Keogh, R. Michalczyk, B. L. Scott, J. G. Watkin**

Interactions of Remote Alkyl Groups with Lanthanide Metal Centers: Synthesis, Characterization and Ligand Redistribution Reactions of Heterobimetallic Species Containing Trialkylaluminum Fragments

Keywords: Lanthanides / Samarium / Aluminum / O ligands / Agostic interactions

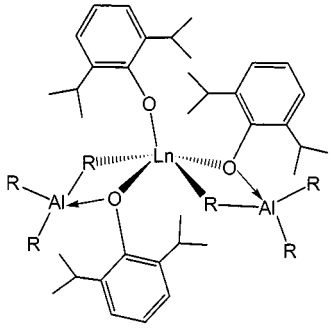

732 **F. Dahan, P. W. Dyer,* M. J. Hanton, M. Jones, D. M. P. Mingos, A. J. P. White, D. J. Williams, A.-M. Williamson**

Synthesis and Reactivity of Group 6 and 10 Complexes of the Bis(dialkylaminophosphanyl)-imine *i*PrN=C[$CH_2P(NiPr_2)_2$]$_2$

Keywords: P,N ligands / Chelates / Diaminophosphanes / Imines / Palladium

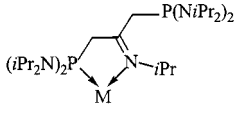

M= Pd(II), Pt (II), Cr(0), Mo(0)

743 **A. Selling,* I. Andersson, J. H. Grate, L. Pettersson**

Reduced Molybdovanadophosphates

Keywords: Polyoxometalates / NMR spectroscopy / Redox chemistry / Speciation / Formation constants

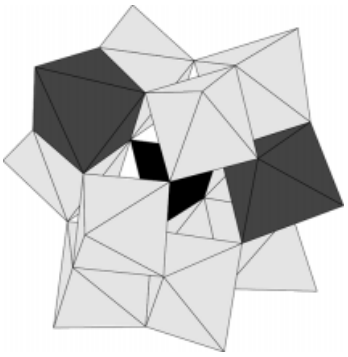

750 **E. J. Fernández, A. Laguna,* J. M. López-de-Luzuriaga, M. Monge, P. Pyykkö,* N. Runeberg**

A Study of the Interactions in an Extended Unsupported Gold-Silver Chain

Keywords: Gold / Silver / Ab initio calculations / N ligands

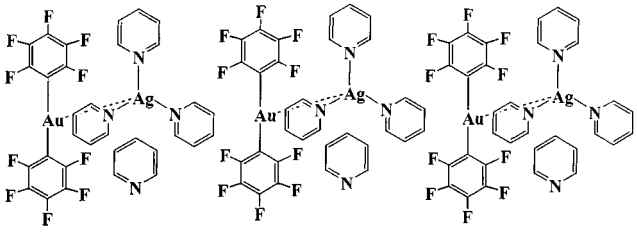

754 **T. Ruman, Z. Ciunik, J. Mazurek, S. Wolowiec***

Anionic Poly(pyrazolyl)borate Ligands Obtained from 3,5-Dimethylpyrazole and 3,5-Diphenylpyrazole and Their Cobalt(II) Complexes − X-ray Crystallographic and ^{1}H NMR Studies

Keywords: Cobalt / Borates / X-ray diffraction / NMR spectroscopy / N ligands

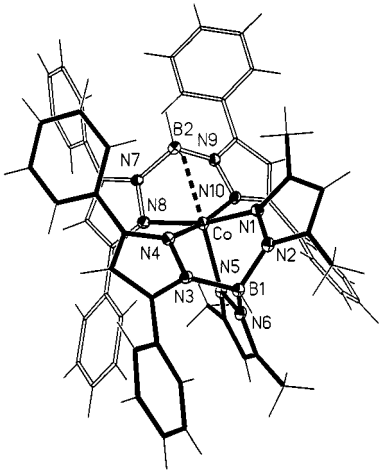

761 **R. Vogler, H. Vahrenkamp***

Dipeptides Made up Solely from Histidine: Solution Behaviour and Zinc Complexation

Keywords: Zinc / Peptides / Histidine / Complex stabilities

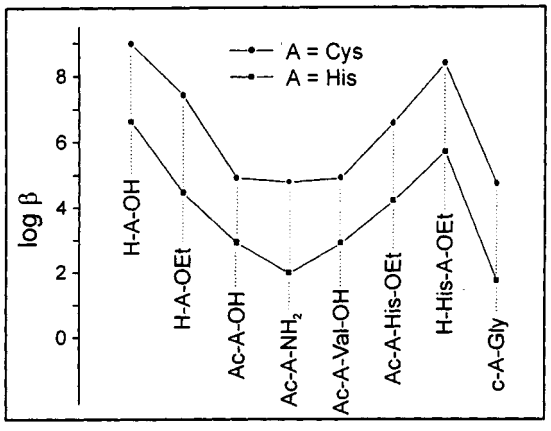

The Coordination of Cu^{II} in Zeolites − Structure and Spectroscopic Properties

Annelies Delabie,[a] Kristine Pierloot,*[a] Marijke H. Groothaert,[b] Robert A. Schoonheydt,[b] and Luc G. Vanquickenborne[a]

Keywords: Zeolites / Copper / Ab initio calculations / Density functional calculations / ESR spectroscopy / UV/Vis spectroscopy / Heterogeneous catalysis

Zeolites loaded with transition metal ions are promising heterogeneous catalysts. Knowledge about the location and structure of the metal centers is of paramount importance for the understanding of the catalytic potential of these materials. In this work, the spectroscopic studies of the coordination of Cu^{II} in zeolite A, ZK4, X, Y and mordenite are reviewed. Experimentally, diffuse reflectance spectroscopy (DRS) and electron spin resonance (ESR) spectroscopy have been applied to study the coordination of Cu^{II} in zeolites. Ab initio calculations on model clusters, representing the Cu^{II} sites in zeolites, are used for the interpretation of the experimental data. The combination of experimental spectroscopic information with theoretical results leads to a new and profound insight into the Cu^{II}–zeolite interaction.

1. Introduction

Zeolites are inorganic crystalline materials characterized by a regular structure of channels and cages of molecular dimensions. Their structure is built from tetrahedral units (TO_4), consisting of a central atom (T) − mostly Si^{IV} − coordinated to four oxygen atoms. Other atoms, especially

[a] Department of Chemistry, University of Leuven
Celestijnenlaan 200F, 3001 Heverlee-Leuven, Belgium
Fax: (internat.) + 32-16/327992
E-mail: Kristin.Pierloot@chem.kuleuven.ac.be
[b] Center for Surface Chemistry and Catalysis, University of Leuven
Kasteel Arenberg 23, 3001 Heverlee-Leuven, Belgium

Annelies Delabie (left top) completed her PhD study with the thesis "Computational study of transition metal ions in zeolites: structure, spectroscopy and reactivity" at the division of Quantum Chemistry, University of Leuven, Belgium, in May 2001 under the supervision of Professor Kristine Pierloot. Presently, she is a postdoctoral research fellow of the Flemish Fund of Scientific Research at the University of Leuven. She is the author of 12 scientific papers.

Kristine Pierloot (right top) is a Professor at the Department of Chemistry, University of Leuven. She received her PhD in Leuven in 1985 under the supervision of Professor Luc Vanquickenborne. She teaches general chemistry and computational chemistry. Her main research interest is the application of ab initio methods for the study of spectroscopic and magnetic properties of systems containing transition metals.

Marijke H. Groothaert (left center) was born in Neerpelt, Belgium in 1975. In 1998 she received her M. S. degree from the Faculty of Agricultural and Applied Biological Sciences, Catholic University of Leuven, Belgium. Since 1998 she is a PhD student at the Center for Surface Chemistry and Catalysis under the supervision of Professor Robert A. Schoonheydt. Her research is concentrated on the coordination of transition metal ions in zeolites and combines spectroscopic techniques with computational methods.

Robert A. Schoonheydt (left bottom) received his M. S. degree in 1966 and his PhD in 1970, both under the supervision of Professor Jan B. Uytterhoeven at the Catholic University of Leuven, Belgium. After one year as a postdoc with Professor Jack H. Lunsford in the Chemistry Department of Texas A&M University, USA, he returned to the Catholic University of Leuven as a National Fund of Scientific Research researcher. He became full professor in 1989. His teaching responsibilities include physical chemistry, analytical chemistry, and general thermodynamics for engineering students at the Faculty of Agricultural and Applied Biological Sciences. His research is concentrated in three areas: (1) spectroscopy and chemistry of surface transition metal ions, (2) molecular organization on clay surfaces, (3) theoretical modeling of molecule-surface interactions. He has authored more than 170 scientific papers, and is the editor of the book "Developments in the theory of chemical reactivity and heterogeneous catalysis". Presently, he is secretary-general of AIPEA and dean of the Faculty of Agricultural and Applied Biological Sciences. He also serves on the editorial board of Microporous and Mesoporous Materials, Applied Clay Science and European Journal of Inorganic Chemistry.

Luc G. Vanquickenborne (right bottom) is a Professor of theoretical chemistry at the Department of Chemistry, University of Leuven. He received his PhD and Dr. Hab. in Leuven, where he teaches quantum chemistry, computational chemistry, and inorganic chemistry. His main research interests are in the application of computational methods in different areas of chemistry.

MICROREVIEWS: This feature introduces the readers to the authors' research through a concise overview of the selected topic. Reference to important work from others in the field is included.

 © WILEY-VCH Verlag GmbH, 69451 Weinheim, Germany, 2002 1434−1948/02/0303−0515 $ 17.50+.50/0

Al^{III}, but also P^{V}, Ga^{III} and even transition metal ions can replace the central Si^{IV}. The tetrahedral units are linked by sharing all the oxygen atoms, leading to a wide variety of materials, differing in framework structure and chemical composition.[1] In the case of microporous solids (with aperture diameters from ca. 3 to 14 Å) the largest two subclasses are the aluminosilicates and aluminophosphates (the latter also known as ALPOs). This review will only deal with aluminosilicate zeolites. Other recent reviews focus on transition metal ions in aluminophosphate molecular sieves.[2,3]

As each Al^{III} incorporated in the silicate framework leads to one excess negative charge, an equivalent amount of extra-framework cations must be introduced to neutralize the structure. These cations, mostly Na^{I}, K^{I} and Ca^{II}, are present inside the cages and channels of the zeolite together with intrazeolitic water. They are not covalently bound to the zeolite framework and can therefore easily be replaced by transition metal ions by conventional aqueous ion exchange. After dehydration, these transition metal ions become localized. They are dispersed over the large internal surface of the zeolite, coordinating to the framework oxygen atoms. The obtained metal coordination environment is often not saturated, which means that these ions can act as coordination centers for adsorbed molecules or as catalytically active sites. The microporous character of the zeolite material puts limits on the size and shape of the interacting molecules, and hence enables shape selective reactions. Alternatively, transition metal ions can also be encountered at framework positions (the T atoms) in zeolites. In this case, the transition metal ions are already incorporated during the synthesis of the zeolite by so-called isomorphous substitution.

This review deals with studies of Cu^{II} in the zeolite channels, acting as a charge-compensating ion. These Cu−zeolites have been studied extensively because they display high activities for the catalytic and photocatalytic decomposition of NO and N_2O forming N_2 and O_2.[4−15] Also the selective reduction of NO by NH_3 or hydrocarbons is catalyzed by Cu−zeolites.[16−19]

A prerequisite for a fundamental understanding of the catalytic potential of Cu−zeolites is the knowledge of the location (and accessibility), coordination and electronic structure of the Cu ions. However, the location and coordination of transition metal ions inside zeolites are still a matter of debate. For aluminum-rich zeolites, one usually assigns the cations to well-defined rings or cages in the zeolite structure. The preference of the cation for occupation of these specific extra-framework sites can be thought of as arising from favorable interactions between the cation and the framework structure. The study of the distribution of the transition metal ions throughout the zeolite is usually referred to as cation siting.[20−21] On the other hand, it has also been suggested that the location of cations, especially divalent cations, is determined by the distribution of aluminum in the zeolite lattice.[22−25] Indeed, it can be expected, on the basis of simple electrostatic considerations, that divalent cations are preferentially located in the proximity of two framework aluminum atoms. The importance of charge compensation by aluminum must be emphasized in particular in the case of Si-rich zeolites. Unfortunately, the exact positions of aluminum ions in the zeolite lattice are unknown, and there is no general agreement on whether the distribution of aluminium is random or ordered.

We intend to give an overview of the studies on the siting and coordination of Cu^{II} in zeolites by means of spectroscopic and theoretical methods. Especially diffuse reflectance spectroscopy (DRS) and electron spin resonance (ESR) spectroscopy have been applied extensively in the study of the coordination of Cu^{II} in zeolites. We will focus on Cu^{II} in zeolite A, ZK4, X, Y and mordenite because of their well-documented literature. The spectroscopic fingerprints of the Cu^{II} species in these zeolites are now firmly established, as shown in a previous review[20] in 1993. However, there is still a good deal of disagreement on the interpretation of the spectroscopic data. At the time of the 1993 review, the spectroscopic fingerprints were mainly interpreted from XRD results or by means of semi-empirical calculations. Recently, however, it has become possible to study the coordination and spectroscopic features of Cu^{II} in zeolites by means of ab initio calculations.[26−32] Large model clusters were constructed, representing the possible Cu^{II} sites in the different zeolites. The structure of the Cu^{II} coordination environment was obtained from geometry optimizations based on density functional theory (DFT). Multiconfigurational perturbation theory (CASPT2) was used for the calculation of the spectroscopic features of these clusters. As will be shown in the present review, the combination of these ab initio results with the available experimental spectroscopic information is a powerful research tool, and leads to new and detailed information on the interaction of Cu^{II} with zeolites. We therefore present a summary of the new ab initio results and compare them with the older methods and interpretations.

We note that the present review will be limited to "model materials", i.e. with high Al contents (Si/Al ratio between 1 and 5) and with low Cu^{II} contents. Isolated and bare Cu^{II} sites are then present in the fully dehydrated state. Spectroscopic techniques clearly point to a limited number of well-defined Cu^{II} coordination modes in these zeolites, and the fingerprints can often be individually resolved, thereby facilitating the comparison with the ab initio results. On the other hand, several zeolites studied for catalytic processes contain Cu^{II} in larger than stoichiometric amounts. These so-called "overexchanged" zeolites do not only contain isolated Cu^{II} ions, but also Cu dimers or oxides. We have also incorporated some ab initio results for zeolite Y where the adsorption of one molecule (H_2O or NH_3) on the Cu^{II} site is studied.

The text is organized as follows: First, we recall the framework structures of zeolite A, faujasite and mordenite, together with a description of their most important cation sites. Next, we describe some of the major advantages and drawbacks of the spectroscopic techniques frequently used for the study of Cu^{II} in zeolites, mainly X-ray diffraction (XRD), diffuse reflectance spectroscopy and electron spin

resonance spectroscopy. We also discuss why theoretical calculations can be useful for the interpretation of the spectroscopic information. Finally, we present a critical overview of both experimental and theoretical spectroscopic studies of Cu^{II}−zeolites.

2. Overview of Zeolite Structures and Cation Sites

2.1 Zeolite A, ZK4, X and Y

The structure of zeolites with LTA (e.g. zeolite A, ZK4) or FAU topology (e.g. zeolite X, Y) can be visualized as a regular stacking of sodalite cages. The sodalite unit comprises 24 T atoms that make up a truncated octahedron, and 36 bridging oxygen atoms. Usually, the structure of a zeolite framework is represented in a schematic way. As shown in Figure 1, the vertices give the position of the T atoms, while the lines connecting the vertices represent the oxygen atoms.

One can see in Figure 1A that in zeolite A, the sodalite cages are connected through the oxygen four-membered rings. They enclose a larger volume, the supercage, with eight-membered ring apertures. The contours of this supercage are indicated in Figure 1A by dashed lines. The Si/Al ratio of zeolite A is 1, implying a strict alternation of Si and Al tetrahedra according to the Loewenstein rule.[33] ZK4 has the same topology as zeolite A, but a higher Si/Al ratio.

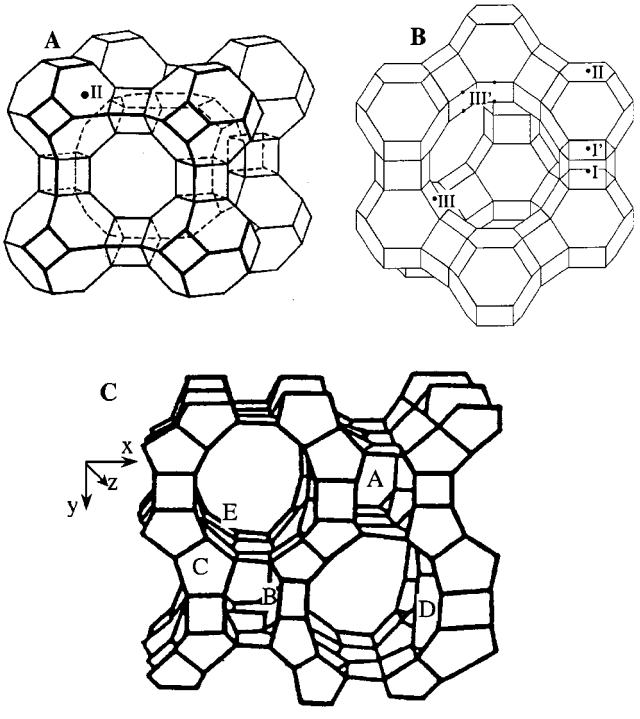

Figure 1. Schematic framework structure of zeolite A, ZK4 (A), zeolite X, Y (B) and mordenite (C); only the T atoms are shown on the vertices of the structure, the oxygen atoms are arranged in between; the location of the exchangeable cation sites is also indicated; the contours of the supercage in zeolite A are shown by dashed lines

For zeolite A and ZK4, only one site for Cu^{II} has been proposed: It is indicated as site II in Figure 1, at the oxygen six-membered ring between sodalite and supercage. The atomic structure of this six-membered ring is shown in Figure 2. This cation site has C_{3v} symmetry. One can see that there are six oxygen atoms available for coordination with the Cu^{II} ion. Three of them (indicated with O_A) are bent slightly inwards, and are therefore favorably located for coordination with a cation in the ring. The other three oxygen atoms (O_B) are bent outwards and therefore seem less accessible.

On the other hand, the sodalite cages can also be linked via the six-membered rings to form hexagonal prisms, as for the faujasite (FAU) topology (see Figure 1B). The interior supercage can be entered via twelve-membered rings, and is therefore much larger than the supercage of zeolite A. Zeolite X and Y are both members of the faujasite topology;

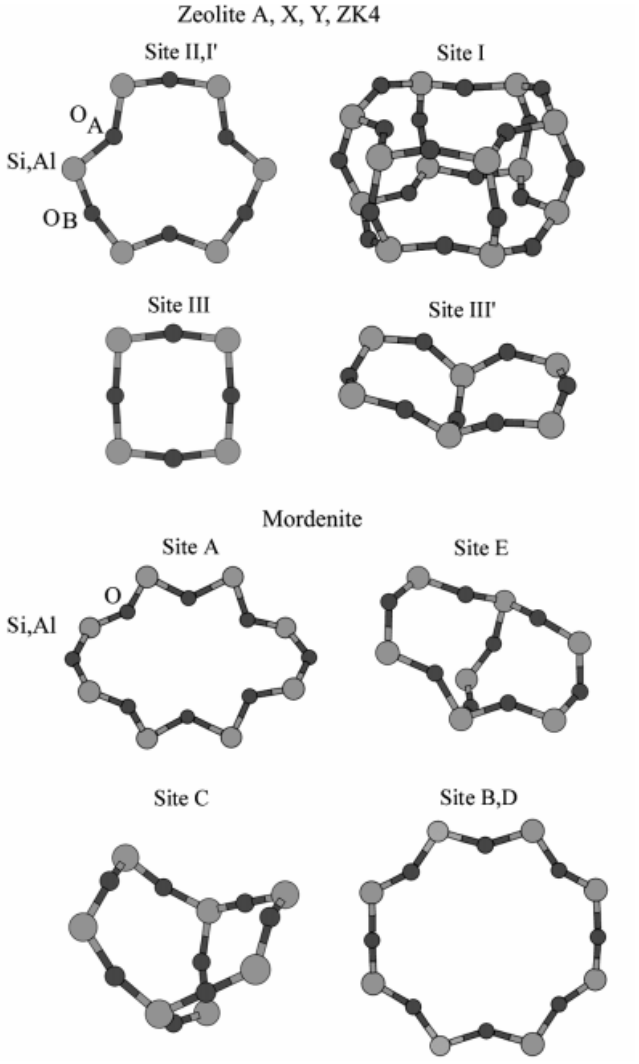

Figure 2. The common cation exchange sites of zeolite A and ZK4 (site II), X and Y (sites II, I′, I, III, III′) and mordenite (site A, E, C, B and D); the two types of oxygen atoms in sites II and I′ are labeled as O_A and O_B

they differ only by the aluminum content. Zeolite X has an Si/Al ratio between 1 and 1.25; faujasites with an Si/Al ratio higher than about 2 are generally referred to as zeolite Y.

As shown in Figures 1 and 2, many possible cation sites are present in the faujasite structure. Due to the tetragonal stacking of the sodalite cages, one can distinguish two distinct types of six-membered ring sites in faujasite. In Figure 2, these two types of six-membered rings are represented in the same picture, as they differ only by the zeolite surroundings extending beyond the atoms on display. One can, however, clearly see in Figure 1 that site II is the hexagonal window between the sodalite cage and the supercage, and it is therefore similar to site II in zeolite A. On the other hand, site I′ is one of the base planes of the hexagonal prism. A completely different cation site is the center of the hexagonal prism (site I), where the cations may obtain a sixfold coordination by binding with the three O_A oxygen atoms of the two six-membered ring base planes. Finally, cations may coordinate to oxygen atoms of the four-membered ring structures III and III′, located at the walls of the supercage.

2.2 Mordenite

Mordenite (MOR) is one of the pentasil zeolites. In these zeolites, five-membered ring building units (the pentasil units) are linked to form parallel columns. In the complex framework of mordenite (see Figure 1C), these columns are arranged along the *z* direction, so that they enclose a large, straight twelve-membered ring channel along the *z* direction, often referred to as the main channel, and eight-membered ring side-pockets. There is also an eight-membered ring zigzag channel, but as it runs in a direction perpendicular to the main channel, this channel is not visible in Figure 1C. The Si/Al ratio in the pentasil zeolites is usually considerably higher than in zeolite A and faujasite. The typical Si/Al ratio of mordenite is 5, but structures with higher Si/Al ratios can be synthesized.

The location of the cation sites in the mordenite structure is also indicated in Figure 1C, while the detailed structures of the sites can be seen in Figure 2. A first cation site in mordenite is site A, a twisted eight-membered ring located in the eight-membered ring side-pockets. The symmetry of this site is C_{2h}. The six most central oxygen atoms can coordinate with cations in this site. The E site is the planar six-membered ring in the twelve-membered ring channel. This six-membered ring is significantly different from the trigonal six-membered ring sites encountered in zeolite A and Y because it is formed by connecting two (bent) five-membered rings (see Figure 2). As a consequence, even an ideal E site in mordenite shows only C_s symmetry, whereas the highest possible symmetry of the six-membered ring sites in zeolite A and Y is C_{3v}. Cations in site E usually coordinate to the four central oxygen atoms of the six-membered ring. Other cation sites in mordenite are site D, the circular eight-membered rings situated at the walls of the large twelve-membered ring channel, and site B, a similar eight-membered ring in the side-pockets. There is also a boat-shaped site in the eight-membered ring channel of the zeolite; the latter site is composed of a non-planar six-membered ring (site C) in between two five-membered rings. As one can see from Figure 2, this six-membered ring also contains, like site E, an O−T−O bridge. The corresponding planar five-membered ring leads to the main channel of mordenite. It is not known which cation coordination environments can be achieved in site C. One can see from Figure 2 that site E and site C have the same topology, but a different shape.

3. Experimental and Theoretical Tools

3.1 Electron Spin Resonance

The first studies of the coordination of Cu^{II} in zeolites, starting from the year 1959, were based on ESR.[34,35] The ESR spectrum is very sensitive to the surroundings of the Cu^{II} ion, as manifested by the *g* tensor and the hyperfine splitting. The number of ESR signals present in the spectrum therefore indicates the number of different coordination environments of Cu^{II}. The initial goal of the ESR studies of Cu^{II}−zeolites was to draw conclusions concerning the coordination environment of Cu^{II} in unknown zeolite surroundings by comparing ESR spectroscopy data with that of Cu^{II} in crystals of known structure. However, since the ESR spectra turn out to be very sensitive to the degree of hydration, the temperature of the heat treatment during dehydration and the nature of other cations in the zeolite, the early reported ESR spectral parameters varied strongly from one report to another.[34−42] Over the years, a consensus emerged in the literature on the ESR parameters of the fully dehydrated Cu^{II}−zeolites, which are by now firmly established.[20] On the other hand, the interpretation of this spectroscopic information is not straightforward. One has attempted to obtain more information about the accessibility of the Cu^{II} species by studying the dependence of the ESR signal on the adsorption of small molecules on the Cu^{II} sites and on the degree of dehydration of the Cu^{II}−zeolite.

Additionally, the pulsed electron spin resonance technique called electron spin-echo (ESE) spectroscopy can measure the superhyperfine interaction between the Cu^{II} ion and nearby magnetic nuclei (for example ^{27}Al).[43] These very weak hyperfine interactions cannot be observed in a conventional ESR spectroscopy experiment, but they show up as a modulation of the decay of the time domain ESE spectrum. By proper analysis of this modulation one can determine the types, number and distances of magnetic nuclei surrounding the Cu^{II} ion.

In order to avoid magnetic dipole interactions between different Cu^{II} centers, the ESR spectra are recorded at low Cu^{II} exchange levels.[44]

3.2 Diffuse Reflectance Spectroscopy

Diffuse reflectance spectroscopy (DRS) allows the measurement of the electronic transitions in the UV/Vis/NIR region from a powdered zeolite sample. As the excitation en-

ergies of the transitions within the 3d shell depend on the ligand field surrounding of the transition metal ion, these spectra provide a "fingerprint" of the local Cu^{II} coordination environment in the considered zeolite. In many cases, however, not one but several different coordination environments are present inside the zeolite. Hence overlapping spectra are obtained, and the spectrum must be deconvoluted into its individual components.[45−48] DRS spectra are therefore often measured at low exchange levels, as it is assumed that under low load conditions only the preferential coordination sites are occupied.

ESR and DRS both have the advantage that, although their spectra may represent a superposition of several Cu^{II} coordinations, the local atomic environments of Cu^{II} can often be extracted from progressive loading and preferential site occupations.

3.3 X-ray Diffraction

X-ray diffraction (XRD) is the most direct method of obtaining the location of the exchangeable cations in the zeolite unit cell. However, a major limitation of XRD in the study of transition metal exchanged zeolites is that no distinction can be made between Si and Al in the lattice. The apparent symmetry of the coordination environment of cations obtained with XRD is therefore often too high. This means that the local effect of Al on the coordination environment of the cation cannot be investigated with XRD. Another disadvantage is that in the case of partial site occupancy XRD visualizes only an average structure for the given crystallographic site, whether it is occupied or empty. Hence, XRD as such provides only average information, pertaining to the overall structural integrity, as opposed to ESR and DRS, which reveal the local atomic environment of the transition metal ion.

Apart from these disadvantages, there are also limits in the preparation of suitable samples. With high-alumina zeolites (such as zeolite A, X and Y), it is usually possible to obtain concentrations of divalent cations in the zeolite matrix which are sufficiently high to allow determination of their location in the zeolite unit cell. However, with siliceous zeolites, levels of exchange are low. Since the unit cell of such zeolites is often large and has low symmetry, the limited number of available metal ions is distributed among several crystallographically different positions.

Ever since the first XRD study of Cu^{II} zeolite Y, the XRD structures of Cu^{II}−zeolites have been used to interpret the ESR signals and DRS spectra.[49] One should, however, be careful with such a comparison, not only because XRD reports only average Cu^{II} coordination environments, but also because the XRD results are reported for highly loaded Cu^{II} samples (close to complete exchange), while in ESR and DRS often zeolites with low Cu^{II} contents are studied.

3.4 Theoretical Calculations

Even the combination of complementary experimental techniques cannot always provide a conclusive picture of the siting of Cu^{II} ions in zeolites. As one will see from the literature overview in sections 4 and 5, different authors have proposed different sites for Cu^{II} in zeolites. In order to obtain a sound interpretation of the spectroscopic data, at the end of the 1970s Klier started to perform theoretical calculations.[50−52] He carried out semi-empirical calculations on a simple CuO_3 model to study the electronic structure of Cu^{II} in the trigonal six-membered ring site of zeolite Y, and proposed the first assignment of the ligand field bands measured by DRS. The group of Schoonheydt soon followed this example and studied the spectroscopic properties of Cu^{II} at several exchange sites (in zeolite Y, mordenite), with calculations based on the angular overlap model (AOM).[20,53−55] These theoretical results were used to provide an interpretation for the available ESR and DRS data. One disadvantage was that the only structural information available was obtained from XRD. These calculations were therefore performed at the average XRD structures.

Thanks to the rapid development of computer power, today it has become possible to perform ab initio calculations on model clusters large enough to represent the cation exchange sites in zeolites. Pierloot et al. have studied the coordination of Cu^{II} in various zeolites (zeolite A, Y, ZK4 and mordenite) with a cluster model approach.[26−32] The considered clusters include the Cu^{II} ion surrounded by a zeolite ring (or a combination of rings), terminated by either OH groups or hydrogen atoms. The structures of the cluster models were obtained from partial geometry optimizations, based on density functional theory (DFT). The spectroscopic features (ligand field excitation energies and ESR g factors) were calculated by means of the CASPT2 method, i.e. multiconfigurational perturbation theory. The calculated results were compared with the experimental DRS and ESR spectra. This comparison allowed detailed information about the Cu^{II} coordination in zeolites to be obtained. The present approach was also applied to study the coordination of Co^{II} in the six-membered ring sites in zeolites.[26,56] The main features of the electronic spectrum of Co^{II} in zeolite A and Y are successfully described.

We note that very recently Larsen et al. used DFT to calculate both ESR g values and A values of several vanadyl model complexes, in which H_2O molecules were used to represent the framework oxygen atoms.[57] Theory and experimental results were also combined here, but this time to interpret the ESR spectra of VO^{2+}-exchanged zeolites.

Another theoretical approach has been followed by Sauer and co-workers.[58−60] A combined quantum mechanics/interatomic potential function technique was developed, in which the cation exchange site is treated by quantum mechanical methods, while the periodic lattice is treated by an ion pair shell model potential. Using this method, the location, structure and coordination of isolated Cu^{I} ions in ZSM-5 were studied.[61,62] Photoluminescence energies of Cu^{I} sites were also calculated, and could help in assigning the observed bands of the Cu^{I} luminescence spectra.

We have also noted that during the last years, many other ab initio studies have concentrated on the catalytic potential of Cu-containing zeolites.[59,61−77] Various kinds of cluster

models have been constructed in order to represent the Cu^{II} coordination in the zeolite. There is, however, still no agreement about the active site and reaction mechanism of − for instance − the decomposition reactions of NO and N_2O.

3.5 Additional Observations

Although the previous techniques are most often used in order to probe the coordination environment of Cu^{II} in zeolites, other experimental techniques provide complementary information. Infrared spectroscopy of adsorption complexes in Cu−zeolites (mostly of NO and CO) is often used as a selective probe for Cu ions because there is a shift in the vibration frequencies depending on the copper oxidation state and its coordination environment. The technique can therefore be used to discriminate between different Cu sites.[23,78] Secondly, IR measurements have shown that cations induce local perturbations of the T−O−T bonds adjacent to the cation, reflected in a shift of the skeletal T−O−T vibrations.[79,80]

Determination of the Cu oxidation state, coordination number and Cu−O bond lengths can be achieved by X-ray absorption fine structure (XAFS) techniques.[81,82] However, for isolated Cu^{II} sites the EXAFS (extended X-ray absorption fine structure) spectrum only yields average Cu−O bond lengths and coordination numbers. Hence, this technique is not well suited to offer detailed information on the different Cu^{II} sites and is more often used to distinguish between isolated versus clustered Cu ions in over-exchanged zeolites.

The photoluminescence spectra of Cu^{I} ions are highly sensitive to their coordination environment. The $Cu^{I}(3d^{9}4s^{1})-Cu^{I}(3d^{10})$ transition energies have been measured by several groups for several zeolites. The group of Wichterlová started from the assumption that the Cu ions do not migrate upon reduction of Cu^{II} to Cu^{I}. Therefore they use the various bands in the luminescence spectra of Cu^{I} zeolites to distinguish between different types of Cu^{II}.[23−25]

Few NMR spectroscopic studies have been reported for studying the coordination of cations inside zeolites. They are based on ^{65}Cu NMR[83] or ^{129}Xe NMR spectra of Xenon adsorbed in various Cu−zeolite samples. Due to the large polarizability of the latter ion, its chemical shift is very sensitive to its environment.[84−86]

4. Cu^{II} in Zeolites A, ZK4, X and Y

Below, we present a literature overview of the spectroscopic and theoretical studies of Cu^{II} zeolites. Because of their related framework structures, zeolite A, ZK4, X and Y are treated together. The XRD results of Cu^{II}−zeolites will be discussed before the results of the spectroscopic studies (ESR and DRS), since they may give a first indication of the possible Cu^{II} sites in the zeolites. Next, the results of the ab initio calculations are summarized and compared with the earlier interpretations.

4.1 Diffraction Studies

The structure of fully exchanged Cu^{II} zeolite A was determined by single-crystal XRD in the cubic space group *Pm3m*.[87] All Cu^{II} ions are located in site II, on the threefold axes in the hexagonal six-membered rings. The coordination environment of Cu^{II} in this site is shown in Figure 3. The Cu^{II} ion is coordinated to three close-by oxygen atoms (O_A), at a distance of 2.14 Å. A second shell of three oxygen atoms is found at a distance of 2.85 Å from Cu^{II}. The Cu^{II} ion extends slightly into the large cavity, giving rise to an O_A-Cu-O_A angle of 119°.

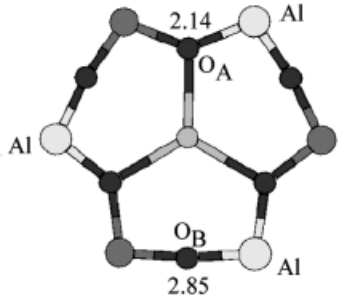

Figure 3. Trigonal coordination environment of Cu^{II} in the six-membered ring site II of zeolite A, as obtained from XRD;[87] Cu−O distances are given in Å; the labeling of the two types of oxygen atoms (O_A and O_B) is also indicated

On the other hand, XRD reveals several exchange sites for Cu^{II} in zeolite Y. Two XRD studies on $Cu^{II}-Y$ have indicated that the six-membered rings are the favored, although not the only possible cation sites for Cu^{II}. First, an X-ray powder diffraction study of a 50% exchanged $Cu^{II}-Y$,[49] reported that Cu^{II} ions are, for the most part, present in six-membered ring site I′. The large affinity of Cu^{II} for site I′ was ascribed to the opportunity to be firmly bound to three O_A atoms of the zeolite framework. The remaining Cu^{II} ions were located at the center of the hexagonal prism (site I) in an octahedral coordination environment.

Secondly, a single-crystal XRD experiment on a 90% exchanged $Cu^{II}-Y$ by Maxwell and de Boer[88] pointed to the presence of Cu^{II} ions in both six-membered rings I′ and II. The coordination environment is trigonal; the Cu−O distances are compared with the other XRD structures in Table 1. Only a very small fraction of the Cu^{II} ions were found in the hexagonal prism I, in a sixfold coordination environment. Finally, Cu^{II} ions were also found in the four-membered ring sites III and III′.

Table 1. Cu−O distances (given in Å) in the trigonal six-membered ring sites, obtained from X-ray diffraction studies on $Cu^{II}-A$ and $Cu^{II}-Y$

Zeolite	Site	$Cu-O_A$	$Cu-O_B$
$Cu^{II}-A$[87]	II	2.14	2.85
$Cu^{II}-Y$[49]	I′	2.00	2.91
$Cu^{II}-Y$[88]	II	2.22	2.92
	I′	2.12	2.95

Recently, a pulsed-neutron diffraction study of solid-state copper(II)-exchanged zeolite Y (with a Cu-exchange level of 87%) was also reported.[89] This study indicated that Cu^{II} occupies three sites. About half of the Cu^{II} ions were found in site III′, each coordinated in a near square-planar manner to four framework oxygen atoms. However, an undetected fifth ligand (H_2O, OH^- or Cl^-) may be present, coordinating axially to Cu^{II} so as to give a distorted square pyramid. 31% of Cu^{II} are placed at site I′ in a trigonal coordination with Cu−O distances of 2.17 Å. The remaining Cu^{II} ions are present in site I.

4.2 ESR Spectroscopic Results

Zeolite A and ZK4

In the first ESR studies of Cu^{II} in zeolite A no agreement was reached on the number of Cu^{II} species or the characteristic ESR parameters of these species.[90−92] Most of the later studies agree that only one axially symmetric signal is present in the ESR spectrum of fully dehydrated Cu^{II} zeolite A, described by $g_{//}$ = 2.37−2.41 (see Table 2).[20,28,53−55,93,94] The presence of one ESR signal is in good agreement with the XRD study, pointing to Cu^{II} at only one site, the trigonal six-membered ring II.[87] Kevan et al.[93−96] monitored the coordination of Cu^{II} in zeolite A during the process of dehydration by electron spin echo spectrometry. After complete dehydration, they described the Cu^{II} coordination as close to the plane of the six-membered ring site II, in a position displaced 0.2 Å into the supercage, where it is trigonally coordinated to three of the six lattice oxygen atoms. This coordination environment is very similar to that obtained by XRD (see Figure 3).

The coordination of Cu^{II} in ZK4 has also been studied. Two Cu^{II} species were detected by ESR spectroscopy, characterized by $g_{//}$ = 2.357 and 2.321.[97] The former signal was assigned to Cu^{II} in the six-membered ring site II, moved inside the sodalite cage, while the latter signal was attributed to Cu^{II} ions at the same site, but extended into the supercage. The presence of these two ESR signals in Cu^{II}−ZK4 was recently confirmed.[28] However, a totally different interpretation based on ab initio calculations was given, as will be detailed in section 4.4.

Table 2. An overview of the ESR parameters found in literature of Cu^{II} in various zeolites; for references, see text

Zeolite	$g_{//}$	$g_{\perp}$
Cu^{II}−zeolite A	2.37−2.41	2.06−2.07
Cu^{II}−ZK4	2.36	2.07
	2.32	2.07
Cu^{II}−zeolite Y	2.36−2.41	2.07−2.08
	2.30−2.34	2.05−2.07
Cu^{II}−zeolite X	2.37−2.38	2.06
	2.35	2.06
Cu^{II}−mordenite	2.32−2.34	2.05−2.06
	2.27−2.29	2.05−2.06

Zeolite Y and X

Most authors report at least two overlapping axial signals in Cu^{II}−zeolite Y.[20,28,36−42,53−55,86,92−94,98−103] Generally, there is agreement about the parameters describing these ESR spectra (see Table 2). One of the signals conforms to the one observed in zeolite A with $g_{//}^{(1)}$ = 2.36−2.41. The second signal is characterized by a much smaller $g_{//}$ value, $g_{//}^{(2)}$ = 2.30−2.34. It was suggested that these ESR signals are, within experimental accuracy, independent of the Si/Al ratio, the Si−Al ordering and the type of co-exchanged cation.[20,53] As such, they only reflect the type of coordination of Cu^{II} in the structure. However, the relative intensities of the two ESR signals vary with the Si/Al ratio, the type of co-cation and the Cu^{II} loading, and are indicative of the site preference of Cu^{II}.[20,53]

Interpretations of the two ESR signals of Cu^{II} in zeolite Y in terms of specific coordination environments at cation sites were published only after the first XRD study of Cu^{II}−Y became available. Almost all groups assign the two ESR signals to Cu^{II} at two different cation sites. However, different research groups have proposed different sites for Cu^{II}. Conesa and Soria[102,104−106] suggested that Cu^{II} remains mainly in the two types of trigonal six-membered rings in the final dehydrated state, at positions I′ and II. This interpretation is in agreement with subsequent studies by Herman[92] and Schoonheydt,[20] and was also confirmed by O_2 line-broadening experiments. The O_2 molecule can only enter the large supercage of zeolite Y, but it cannot access the smaller sodalite cages and hexagonal prisms (see also Figure 1B). One can therefore expect that the ESR signals of Cu^{II} in the supercage (site II, III, III′) will be broadened by the dipolar interaction between the O_2 molecule and Cu^{II} (the resolution and signal intensity decrease), while the ESR signals of Cu^{II} in the sodalite cage and hexagonal prism (site I, I′) are not affected. Since the ESR signal with $g_{//}^{(1)}$ = 2.38 disappears upon admission of oxygen, it was assigned to Cu^{II} in six-membered ring site II in the supercage, with Cu^{II} in a distorted trigonal coordination environment. This assignment also seems very reasonable, because of the similarity of the parameters of this signal with those of the Cu^{II} ions encountered in zeolite A, where the Cu^{II} ions are also present in site II. On the other hand, the signal with $g_{//}^{(2)}$ = 2.33 is insensitive to the presence of oxygen molecules and was assigned to Cu^{II} ions in site I′. As the latter ESR parameters are characteristic for a square-pyramidal coordination, Conesa and Soria suggested that the Cu^{II} ions in site I′ should remain coordinated to two water molecules in order to realize such a coordination.[106] On the other hand, Schoonheydt assigned this signal to naked Cu^{II} ions in site I′ in a trigonal coordination environment.[20] We will come back to this point in section 4.4.

In the Cu^{II}−zeolite X, two axial ESR signals are also observed.[20,36,42,107−110] A first signal conforms to the one observed in both zeolite A and Y, and is characterized by $g_{//}^{(1)}$ = 2.37−2.38. The second is described by a somewhat higher $g_{//}^{(2)}$ value than the second signal in zeolite Y, 2.35

instead of 2.30−2.34. Schoonheydt assigned the signal with $g_{//}^{(1)} = 2.37-2.38$ in zeolite X to Cu^{II} ions in site II, in line with the assignments of Cu^{II} zeolite A and Y. On the other hand, the second signal in Cu^{II}−X was assigned to a different site; since this ESR signal is also broadened by O_2, it was assigned to the Cu^{II} ions in the supercage at site III′.

A different site-dependent interpretation of the ESR signals in zeolite Y and X was provided by the group of Kevan, who used ESR spectroscopy in combination with electron spin echo (ESE) spectrometry.[21,97,103,109−113] These authors propose the same sites for Cu^{II} in zeolite X and Y. The ESR signal with $g_{//}^{(1)} = 2.39$ was attributed to an almost planar trigonal Cu^{II} coordination in the six-membered ring site I′ of zeolites X and Y. On the other hand, the signals with $g_{//}^{(2)} = 2.33$ and $g_{//}^{(2)} = 2.35$ in zeolite Y and X, respectively, were suggested to both correspond to Cu^{II} in the hexagonal prism I. This assignment is in agreement with the earliest XRD results[49] and with the findings of Iwamoto,[114] who studied the oxygen adsorption in Cu^{II}−zeolites Y by temperature-programmed desorption (TPD).

Matar and Goldfarb studied the interactions of the Cu^{II} cations with framework Al in zeolites A, X and Y in various stages of dehydration and after methanol adsorption by electron spin echo envelope modulation (ESEEM).[115−117] The spectra show contributions from two types of ^{27}Al nuclei. One type includes first-shell Al, bound to the oxygen atoms to which the Cu^{II} ion is coordinated; they are at about 3.1−3.4 Å from the Cu^{II} ion and exhibit relatively large isotropic hyperfine constants which indicate strong interaction with the framework oxygen atoms. The second type consists of distant Al nuclei, situated at distances larger than 5 Å. Orientation-selective ESEEM experiments provide additional structural information: The modulation of the first-shell Al in some cases showed strong orientation dependence. Based on these results, a link was proposed between the ESR $g_{//}$ values of the coordinated Cu^{II} and the position of this ion with respect to the aluminum atoms in the trigonal six-membered ring. The Cu^{II} ions situated close to a plane of Al nuclei are held responsible for the $g_{//}$ value of 2.33, whereas the larger $g_{//}$ value (2.38) is supposed to originate from Cu^{II} ions located away from the plane of Al nuclei. This interpretation is original in its suggestion that the different ESR signals might actually be due to Cu^{II} at one and the same site, but surrounded by different Al distributions. A somewhat similar idea will be backed by ab initio calculations (section 4.4), where it is shown that the ESR signals can indeed be explained by Cu^{II} in the six-membered ring site with different Al surroundings.

4.3 DRS and Ligand Field Theory

Klier was the first to interpret the diffuse reflectance spectrum of dehydrated Cu^{II}−zeolite Y.[50−52] This spectrum is composed of a narrow peak centered at 10900 cm^{-1} and two broader bands centered at 12700 and 14650 cm^{-1}. He studied the electronic structure of Cu^{II} positioned in the six-membered ring site, represented by a CuO_3 model. The presence of one hole in its 3d shell corresponds to the free $Cu^{II}(d^9)$ ion in a ^2D ground state. The C_{3v} symmetry of the oxygen environment imposes a splitting on the Cu^{II} ^2D ion term as shown in Figure 4A. The ground state is a degenerate ^2E, with the one hole in the 3d shell located in the e shell, consisting (to a first approximation) of the $3d_{x^2-y^2}$, $3d_{xy}$ orbitals. The Jahn−Teller effect was invoked, inducing an off-axial distortion to remove this degeneracy, as also shown in Figure 4A. Furthermore, the effect of spin-orbit coupling was considered. By fitting the energy of the three highest transitions to the experimental band positions, the Jahn−Teller coupling constant *b*, the spin-orbit coupling constant λ, and β, a structural parameter, were determined. As such, an O−Cu−O angle of 117° was determined, in (somewhat fortuitous) agreement with the angle found by XRD (of 115°). This means that the Cu^{II} ion would obtain an almost planar coordination in the six-membered ring. Klier's assignment of the ligand field transitions is presented in Table 3.

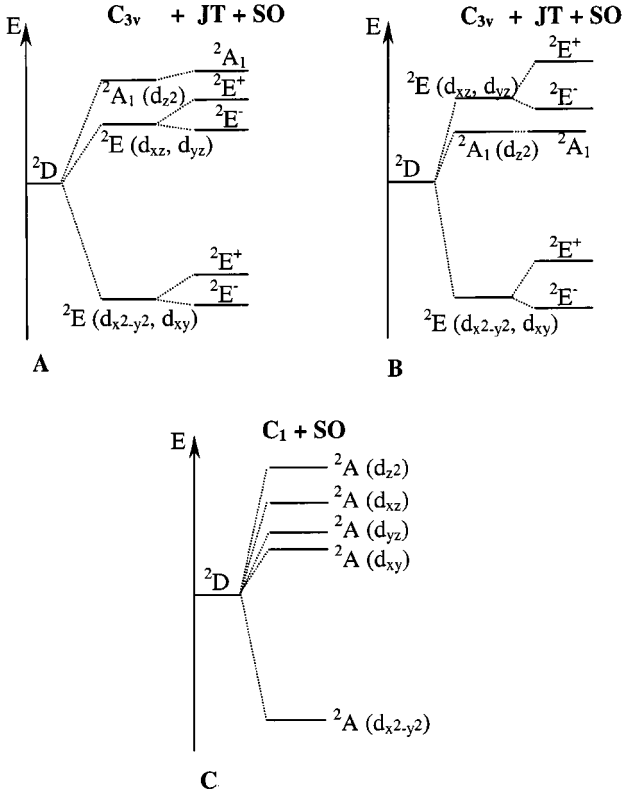

Figure 4. Energy term diagram for Cu^{II} in the trigonal six-membered ring site of zeolite A, ZK4, X, Y by Klier (A),[51] Schoonheydt (B)[53] and Pierloot (C)[28]

Table 3. Assignments of the ligand field bands of Cu^{II} in the trigonal six-membered ring site by various authors

Band maximum [cm^{-1}]	Assignments		
	Klier	Schoonheydt	Pierloot
10900	$^2E_1 \rightarrow {}^2E_2^-$	$^2E_1 \rightarrow {}^2A_1$	$X^2A \rightarrow b^2A$ $X^2A \rightarrow c^2A$
12700	$^2E_1 \rightarrow {}^2E_2^+$	$^2E_1 \rightarrow {}^2E_2^-$	$X^2A \rightarrow d^2A$
14650	$^2E_1 \rightarrow {}^2A_1$	$^2E_1 \rightarrow {}^2E_2^+$	$X^2A \rightarrow e^2A$

Packet and Schoonheydt[20,53−55] studied the coordination of Cu^{II} in various zeolites by combined DRS/ESR experiments. The ligand field band positions for Cu^{II} in zeolite A, X and Y are summarized in Table 4. As one can see, these spectra all show ligand field transitions at similar energies. In contrast to the ESR results, no pronounced difference is found between the DRS spectra of Cu^{II}−A on the one hand and Cu^{II}−X and −Y on the other hand. As already explained in section 4.2, the Cu^{II} ions were assigned to site II and I′ for zeolite Y, while sites II and III were proposed for Cu^{II} in zeolite X. These assignments were supported by calculations based on the angular overlap model (AOM).[20,53−55] Schoonheydt et al. further extended the work on the CuO_3 complex of Klier by also including the three more distant oxygen atoms of the six-membered ring. The two types of six-membered ring sites of zeolite Y, site I′ and II, were both considered. Not only were the three ligand field bands calculated but also the ESR parameters $g_{//}$, $A_{//}$ and $g_{\perp}$. In agreement with Klier, a distortion of the trigonal geometry of the six-membered rings was proposed, due to a Jahn−Teller effect. Spin-orbit coupling was taken into account. By the least-squares procedure, the values of six adjustable parameters were then optimized, the AOM spectroscopic parameters σ and π, a geometrical parameter, the Jahn−Teller parameter, the spin-orbit coupling constant and the Fermi contact parameter. The resulting assignment of the ligand field spectrum is compared to that of Klier in Figure 4 and Table 3. As one can see, the sequence of the $^2A_1$ and ^2E terms is reversed. The reason can be traced back to a different value for the π/σ ratio from both authors. The ligand field stabilization energy of Cu^{II} in site I′ and II was calculated. From these calculations, no site preference between type I′ and II six-membered rings could be predicted.

Both Klier and Packet obtained rather unusual values for the spectroscopic parameters from their ligand field calculations. The spectra of Klier were calculated at an extremely high π/σ ratio, while Packet reports a very large σ value. The origin of these unrealistic parameters may be because the semi-empirical calculations started from the average XRD structures of Cu^{II} sites and are therefore performed in fictitious high symmetry coordination environments. The possibility of symmetry reduction, for example by an asymmetric aluminum surrounding, was not considered. As was suggested by Goldfarb[115−117] and will also be shown in the following section, this factor does play a crucial role in the Cu^{II}−zeolite interaction.

Table 4. Overview of DRS band positions of Cu^{II} in various zeolites by Schoonheydt et al.[20]

Zeolite	Band I	Band II	Band III
Cu^{II}−zeolite A	10400	12200−12800	15000−15400
Cu^{II}−zeolite Y	10400−10800	12400−13000	14700−15100
Cu^{II}−zeolite X	10400−11100	12400−13000	14700−15100
Cu^{II}−mordenite	12500	13700	14800

4.4 Ab initio Studies of Cu^{II} in Trigonal Six-Membered Ring Sites

Recently, more advanced quantum chemical calculations have been performed in order to investigate the coordination and spectroscopic properties of Cu^{II} in the trigonal six-membered ring site.[27−29] The results point to a new interpretation of the ESR signals in zeolite A and Y. Ab initio calculations were performed on the cluster models shown in Figure 5. They consist of the Cu^{II} ion in the six-membered ring, with OH groups (Figure 5A, denoted as "large models") or hydrogen atoms (Figure 5B, denoted as "small models") inserted in order to saturate the dangling bonds of Si, Al. The cluster models are thus represented by the structural formula $CuO_6Si_{6-x}Al_x(OH)_{12}^{(2-x)+}$ and $CuO_6Si_{6-x}Al_xH_{12}^{(2-x)+}$. Different aluminum contents and distributions were studied in order to examine the local effect of aluminum on the coordination environment and the spectroscopic properties of Cu^{II} in the six-membered ring.

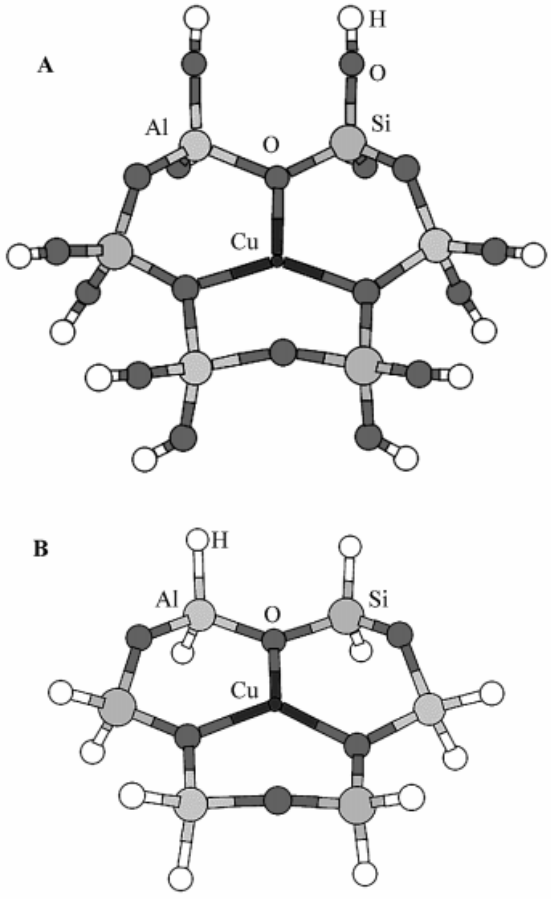

Figure 5. Cluster models for the ab initio calculations of Cu^{II} in the trigonal six-membered ring site in zeolites A, ZK4, X and Y: (A) the dangling bonds of the silicon or aluminum atoms are terminated by OH groups ("large models"); (B) the dangling bonds of the silicon or aluminum atoms are terminated by hydrogen atoms ("small models"); the clusters are depicted at the XRD starting geometry as obtained from the literature[77]

The coordination environment of Cu^{II} in the six-membered ring was obtained by partial geometry optimizations of the large clusters (Figure 5A). The starting geometry of

the cluster models is based on XRD data of Cu^{II}−zeolite A.[87] Partial geometry optimizations of these cluster compounds were performed; restrictions were applied to mimic the rigidity of the zeolite framework. The geometry optimizations were based on density functional theory (DFT) with the B3LYP functional in combination with basis sets from Schäfer et al.[118] The accuracy of the obtained B3LYP-DFT structures was checked by performing additional restricted CASPT2 geometry optimizations for a few clusters.[28] Significant corrections were only obtained for the negatively charged $CuO_6Si_3Al_3(OH)_{12}^-$ cluster model.

As for the calculation of the electronic spectra and the *g* factors, calculations based on multiconfigurational perturbation theory (CASPT2) were performed. Since these CASPT2 calculations demand a considerably larger computational effort than the DFT geometry optimizations, slightly smaller models were used, obtained by replacing the terminal OH groups in the optimized cluster models by hydrogen atoms. It was shown that this reduction of the cluster size does not affect the spectroscopic features of the central Cu^{II} ion to any significant extent.[26,28] In the CASPT2 calculations, the basis sets are atomic natural orbitals.[119] The reference active space consists of the Cu(3d) orbitals, an additional d-shell (to take into account the 3d-double shell effect) and one bonding oxygen valence orbital. The effect of spin-orbit coupling was taken into account by means of an effective one-electron operator.[120] Finally, the *g* tensors were calculated using second-order perturbation theory, introducing spin-orbit coupling and the magnetic field as simultaneous perturbations. More information about the details of the calculations can be found in the original papers.[27−29]

First, it was checked whether the ligand field spectrum of Cu^{II}−zeolite A can be explained by assuming Cu^{II} to be coordinated in the high-symmetric (C_{3v}) oxygen six-membered ring structure as reported on the basis of XRD (see Figure 3). However, the CASPT2 excitation energies of a six-membered ring cluster at the XRD geometry did not exceed 8500 cm^{-1} for the ligand field transitions. Even after invoking a Jahn−Teller distortion, the calculated excitation energies remained much too low to offer an explanation of the experimental DRS spectra of Cu^{II}−A, −Y.

In a next step, the DFT-optimized structures of model clusters with all possible aluminum distributions in the six-membered ring were considered. All structures were optimized without applying any symmetry restrictions. The optimized coordination environments are shown in Figure 6. Only one Al is present in ring A, while rings B and C contain two, and ring D three Al. As one can see, the calculated structures reveal strong local deformations of the six-membered rings; as a matter of fact, no symmetry whatsoever is retained. The distortions are due to the tendency of the Cu^{II} ion to obtain a fourfold coordination environment in the six-membered ring. One of the more distant O_B oxygen atoms (O_{B1}) is bent inwards in order to provide an additional short Cu−O bond. This fourfold coordination environment gives rise to a much higher ligand field as compared to the trigonal coordination; the CASPT2 excitation

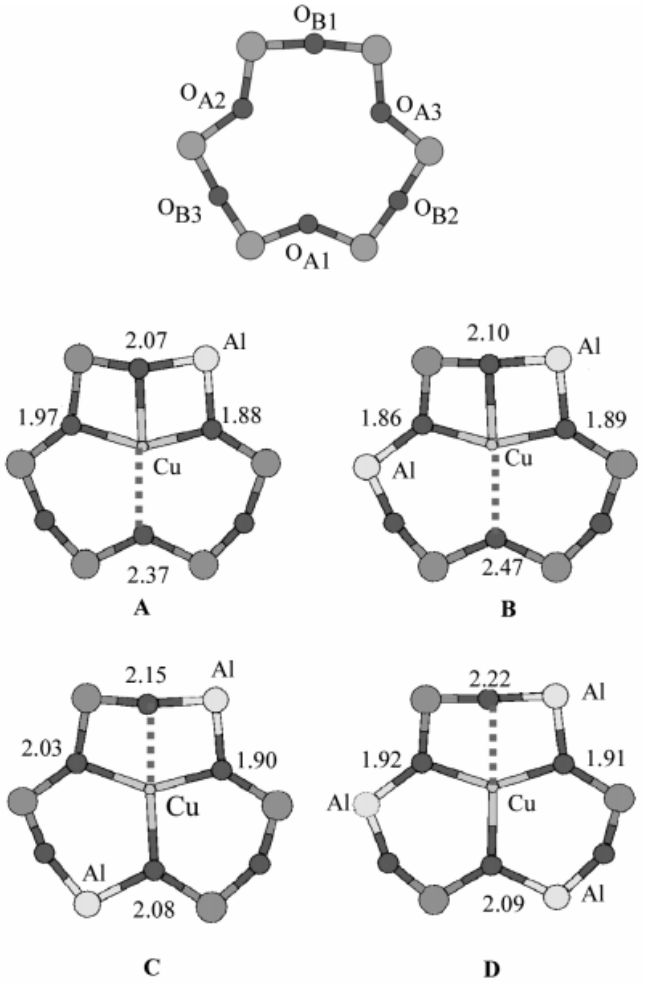

Figure 6. Calculated structures of Cu^{II} in the trigonal six-membered ring site; Cu−O distances are given in Å; cluster A contains only one Al, clusters B, C contain two Al, while three Al are present in cluster D; the coordination geometry of Cu^{II} is fourfold planar; one can clearly distinguish the two coordination modes in the six-membered ring: clusters A, B on the one hand and clusters C, D on the other hand; clusters A, B represent B3LYP-DFT structures, while cluster C, D contain a CASPT2-optimized Cu−O_{B1} bond

energies are calculated between 9500 and 15400 cm^{-1}, in good agreement with the experimental ligand field bands. The energy term diagram is shown in Figure 4C. A new assignment of the experimental ligand field bands is proposed, as shown in Table 3.

One can also see from Figure 6 that the cation shows a strong preference for coordination to oxygen atoms bound to Al rather than Si. This also means that the aluminum distribution may thoroughly influence the coordination environment of Cu^{II}. Two distinct fourfold coordination modes could be distinguished, depending on the number and relative positions of Al in the six-membered ring. In clusters A and B, the Cu−O_{B1} distance is much shorter than Cu−O_{A1}. On the other hand, Cu−O_{A1} is shorter than Cu−O_{B1} in rings C and D, due to the introduction of a second Al next to O_{A1}. The two coordination modes can also clearly be distinguished by looking at the calculated *g* factors. The $g_{//}$ value is systematically lower (2.31−2.33) for

the clusters A and B, than for the other group with clusters C and D (2.39−2.41). Based on the close correspondence between the calculated *g* factors and the experimental ESR signals of zeolite A and Y, a new interpretation of these signals is proposed. The occurrence of two ESR signals in zeolite Y as opposed to only one signal in zeolite A can be attributed to the higher Si/Al ratio in the former zeolite. In zeolite A, with an Si/Al ratio of 1, only the ring shown in Figure 6D can occur, explaining the single ESR signal with $g_{//} = 2.38$. On the other hand, rings with 1, 2 or 3 Al (all structures in Figure 6) can occur in zeolite Y, which leads to the two ESR signals. This new interpretation is corroborated by the experimental ESR signals obtained for Cu^{II}−ZK4 (with Si/Al > 1).[28,97] Also here, two ESR signals are observed, while only one six-membered ring site is present. On the other hand, the rather high $g_{//}^{(2)}$ value observed in the Cu^{II}−zeolite X remains puzzling.

Finally, we should remark that for clusters with more than 1 Al, there are different structural minima for Cu^{II} in the six-membered ring. The energy barriers for going from one minimum to another are low, which indicates that at room temperature Cu^{II} is likely to undergo a hopping process between the different minima. This also explains why the actual minima are not detected on the time-scale of an XRD measurement.

As a next step, the DFT/CASPT2 approach was applied to investigate how the coordination of Cu^{II} in the six-membered ring is influenced when an external ligand is adsorbed at the Cu^{II} ion.[29] The structures of the six-membered rings were reoptimized with B3LYP-DFT in the presence of one NH_3 or H_2O ligand. Adsorption on Cu^{II} in the two coordination modes in the six-membered ring may be compared by considering clusters B and D in Figure 6. For both clusters, it is found that the weakest of the four Cu−O bonds is partially given up upon adsorption of NH_3 or H_2O, and a new strong bond is formed with the extra-lattice ligand instead. This means that for cluster B, the $Cu-O_{A1}$ bond is partially relaxed, while in cluster D, the CuO_{B1} bond is relaxed. When the binding energies were calculated, it was found that adsorbed NH_3 systematically gives a stronger bond than H_2O.

The ligand field spectra of the clusters with external ligands were compared to those of the naked Cu^{II} clusters. The CASPT2 excitation energies of the adsorption complexes are calculated at a lower energy than that of the Cu^{II} clusters without adsorbent. This is in agreement with experimental observations; it is known that the partially hydrated or ammoniated Cu^{II}−Y samples are characterized by a ligand field band in the range 10500−12500 cm^{-1}, somewhat lower than the ligand field band for fully dehydrated Cu^{II}−Y.[29,121] It has indeed been proposed in the literature that the Cu^{II} species in these partially saturated samples are complexes with Cu^{II} coordinated to three lattice oxygen atoms of the six-membered ring site and one external ligand.[41,121] On the other hand, a trigonal bipyramidal complex with Cu^{II} coordinating to three oxygen atoms of the six-membered ring and two axial H_2O or NH_3 molecules has also been suggested.[101] So far, clusters with more than one external ligand have not been studied with the ab initio approach.

5. The Siting of Cu^{II} Ions in Mordenite

5.1 XRD

According to the best of our knowledge, XRD data on fully dehydrated Cu^{II}−mordenite are not available yet. Therefore, other XRD data are often consulted to obtain a first indication of possible coordination sites of Cu^{II}. In partially dehydrated Cu^{II}−mordenite,[122] three sites for Cu^{II} were determined. In site A (see Figure 1C) the Cu^{II} ions are not only coordinated to six lattice oxygen atoms of the eight-membered ring, but also to two water molecules. A second occupied site is the six-membered ring in the twelve-membered ring channel (site E), where the Cu^{II} ion is coordinated to four lattice oxygen atoms of the six-membered ring. The last and least occupied site is site D, where Cu^{II} is bound to three oxygen atoms of the circular eight-membered ring. It can, however, not be excluded that the Cu^{II} ion further migrates to other cation sites upon complete dehydration.

Most of the interpretations of the siting of Cu^{II} in mordenite are based on the much earlier XRD results of dehydrated Ca^{II} mordenite.[123] Four sites are occupied by Ca^{II}. Ca^{II} ions are first found in site A, where this ion is coordinated to six lattice oxygen atoms in C_{2h} symmetry. The second exchange site which is occupied by Ca^{II} is site E, where Ca^{II} is coordinated to four lattice oxygen atoms. A smaller portion of the Ca^{II} ions is located in the boat-shaped site in the eight-membered ring channel of the zeolite. This site is composed of a non-planar six-membered ring (site C) in between two bent five-membered rings. Finally, Ca^{II} ions were also found in site D. It should, however, be noted that the ion radius for Cu^{II} is much smaller than that of Ca^{II}, which can result in different preferential sites for dehydrated Cu^{II}− and Ca^{II}−mordenite. Moreover, it can also be expected that transition metal cations react differently with the zeolite than the closed shell alkaline-earth cations. Any interpretation of the spectroscopic signals in Cu^{II}−mordenite on the basis of these two available XRD studies is therefore speculative.

5.2 ESR and DRS Studies

In the first ESR studies of Cu^{II}-exchanged mordenite, two types of Cu^{II} cations, both in an axial environment, were detected, with $g_{//}^{(1)} = 2.32$ and $g_{//}^{(2)} = 2.27$ (as also reported in Table 2).[124,125] The two coordination environments were described as either four-coordinated square-planar (characterized by $g_{//}^{(2)} = 2.27$) or five-coordinated square-pyramidal (characterized by $g_{//}^{(1)} = 2.32$). An investigation of the Cu^{II} reducibility provided additional information on the coordination of these ions. The Cu^{II} ions in the close to square-planar coordination are readily reduced by CO at 400 °C, while the five-coordinated Cu^{II} ions are more stable to reduction by CO. It was therefore suggested that

the five-coordinated Cu^{II} ion compensates for the two elemental charges of the mordenite lattice and has no additional link to extra-lattice oxygen ligands. The reduction process for the latter species must involve the abstraction of an O^{2-} anion from the zeolitic framework and should prove difficult. Finally, the accessibility of the Cu^{II} species was examined. It was shown that both types of Cu^{II} ions interact with cation-radicals of large molecules such as benzene and *o*-xylene via a dipole−dipole interaction, implying that they must be located in sites that are accessible from the main channel.

Sass and Kevan[126] studied the coordination of Cu^{II} in mordenite in the presence of adsorbed molecules. Due to the very low Cu^{II} loadings (1 Cu^{II} per 30 unit cells), they observed only one ESR signal in CuNa−, CuK− and CuCa−mordenite, with $g_{//}^{(1)} = 2.32-2.33$. This Cu^{II} species was assigned to Cu^{II} in site A.

De Tavernier and Schoonheydt observed the same two Cu^{II} signals with ESR as Kucherov, and found that their relative intensities are dependent on the Cu^{II} loading, the Si/Al ratio and co-exchanged cations.[20,30,31,127] At small Cu^{II} loadings, only the ESR signal with $g_{//}^{(1)} = 2.33$ is detected. In the DRS spectrum of these samples, a ligand field band with maximum intensity at 13700 cm^{-1} is observed. In contrast with the DRS spectra of zeolite Y, the individual transitions of this band are not resolved. When the Cu^{II} loading is increased, the second signal ($g_{//}^{(2)} = 2.27$) also becomes apparent in the ESR spectrum. This goes along with a broadening of the DRS ligand field band. An interpretation of these combined DRS/ESR data of Cu^{II}−mordenite was provided on the basis of AOM calculations.[127] According to this interpretation only site A is occupied at low Cu^{II} exchange levels, in agreement with the assignment of Kevan. The weak coordination with six oxygen atoms at this site gives rise to the ESR signal with a $g_{//}^{(1)}$ value of 2.32. At higher copper loadings, a second exchange site, i.e. site E, becomes occupied. The fourfold Cu−oxygen coordination at this site was held responsible for the second ESR signal with $g_{//}^{(2)} = 2.27$.

Carl and Larsen[128,129] also decomposed the ESR spectrum of CuNa−mordenite into two axial signals, but with different parameters $g_{//} = 2.33$, $A_{//} = 164\ 10^{-4}\ cm^{-1}$ and $g_{//} = 2.34$, $A_{//} = 121\ 10^{-4}\ cm^{-1}$. While the first signal is in good correspondence with that found by de Tavernier, the second signal has an exceptionally low value of $A_{//}$ ($121\ 10^{-4}\ cm^{-1}$). A third ESR signal was also present, but its parameters could not be resolved.

The siting of Cu^{II} in various Si-rich zeolite matrices, including mordenite, has been studied extensively by Wichterlová et al.[23−25] They combined conventional ESR measurements with Cu^{I} luminescence and IR studies of adsorbed NO on Cu^{II} and also studied the reducibility of the Cu^{II} ions. It was assumed that the Cu^{I} siting and distribution reflect those of the Cu^{II} ion. As shown in Table 5, four main coordinations of the Cu ions, common in ZSM-5, mordenite, erionite, and zeolite beta, were distinguished. These authors concluded that the Cu^{II} siting in high silica zeolites is essentially controlled by the local Si−Al sequences in the framework, in agreement with the earlier suggestions of Kucherov.[124,125] Cu^{II} characterized by $g_{//}^{(1)} = 2.32$ is preferentially located in the close vicinity of two framework aluminum atoms. Here it obtains the square-pyramidal oxygen coordination. The Cu^{II} ions are strongly bound to the zeolite lattice and they are not easily reduced. A second type of Cu^{II}, characterized by a $g_{//}^{(2)}$ value of 2.27, has a square-planar oxygen coordination and is adjacent to a single aluminum atom. This site is easily reduced and was suggested to be responsible for the high and stable activity of Cu−zeolites in NO decomposition.[130,131] The possibility of an extra-framework oxygen ligand (O^- or OH^-) was, for the latter site, also considered.

From an FTIR study of the framework T−O−T vibrations, Wichterlová et al. also showed that the bonding of Cu^{II} (or other divalent cations) to the framework oxygen atoms causes local deformations in the zeolite framework.[79] Upon reduction of Cu^{II} to Cu^{I} or the adsorption of a ligand on the Cu^{II} ion, the band shifted to higher wavenumbers, indicating some relaxation of the framework.

5.3 Ab initio Studies of the Siting of Cu^{II} in Mordenite

Pierloot et al.[30,31] also performed ab initio calculations in order to interpret the two ESR signals of Cu^{II} in mordenite. Cluster models of several cation exchange sites in mordenite were constructed, based on the XRD structure of Ca^{II}−mordenite. These clusters consist of the ring systems in Figure 2 terminated by OH groups or hydrogen atoms. The considered sites were site A, as a representative of an oxygen eight-membered ring site, and sites E and C (see Figures 1C and 2).

The structure and spectroscopic features of Cu^{II} on these cation exchange sites were calculated with the DFT/CASPT2 approach, using a similar strategy as described in section 4.4. The effect of the aluminum distribution on the coordination environment, spectroscopic features and siting

Table 5. Spectroscopic signatures of Cu^{II} as established by Wichterlová et al.:[23−25] Cu^{+} emission wavelengths, IR frequencies of Cu^{2+}−NO, and ESR parameters of Cu^{2+}

Cu site	Cu^{+} emmision [nm]	Cu^{2+}−NO [cm^{-1}]	$g_{//}$	Al	Cu^{2+} coordination
Cu-I	450	1921 (1909)	2.31	Al pairs	square-pyramidal
Cu-II	480	1912	2.33	Al pairs	square-pyramidal
Cu-III	510	1906	−		
Cu-IV	540	1896	2.28	single Al	square-planar

of Cu^{II} was examined in detail. The calculated spectroscopic features were confronted with the experimental DRS and ESR data in order to understand the siting of Cu^{II} in mordenite.

The geometry optimizations of site-A clusters indicate that the Cu^{II} ion cannot acquire a fourfold coordination environment in this site. The distortions induced by Cu^{II} are insufficient to realize an optimal fourfold oxygen coordination. Eight-membered rings are simply too large to supply Cu^{II} with the desired planar oxygen four-coordination. This was also shown by a molecular modeling study of the coordination of Cu^{II} in mordenite.[132] As a consequence of the weak coordination, the obtained ligand field is not strong enough to explain the observed spectroscopic features of Cu^{II}−mordenite (the CASPT2 excitation energies remain below 10000 cm^{-1}). Therefore, the eight-membered ring sites in mordenite will be excluded from the following considerations.

As a next step, the coordination of Cu^{II} in the cluster models of site E and site C was studied. The geometry optimizations show that Cu^{II} can obtain a strong fourfold coordination environment in the planar rings of these sites, i.e. in the six-membered ring of site E and in the planar five-membered ring of site C. Let us first look at the results for site E. As for the trigonal six-membered ring site, two coordination modes can be distinguished in the six-membered ring of site E, depending on the relative positions of Al. A representative cluster of each of these two coordination modes is represented in Figure 7. Coordination mode I is realized if Al is present at the central positions in the six-membered ring. Then, an almost perfect square-planar coordination is obtained (see Figure 7), with four Cu−O distances of around 2 Å. This strong coordination gives rise to a ligand field spectrum at high energy (and is in agreement with experimental results), and axial g factors with a $g_{//}$ value around 2.27. On the other hand, more distorted coordination environments are present if Al is placed at less central positions, mode II in Figure 7. Cu^{II} forms a bond with one of the less central oxygen atoms due to the preference of Cu^{II} for coordination with oxygen atoms bound to Al. As can be seen from Figure 7, this results in a planar four-coordination with one rather large O−Cu−O angle. This distortion of the coordination environment slightly weakens the strength of the ligand field, resulting in higher characteristic $g_{//}$ values ($g_{//}$ = 2.30−2.32) for coordination mode II as compared with mode I.

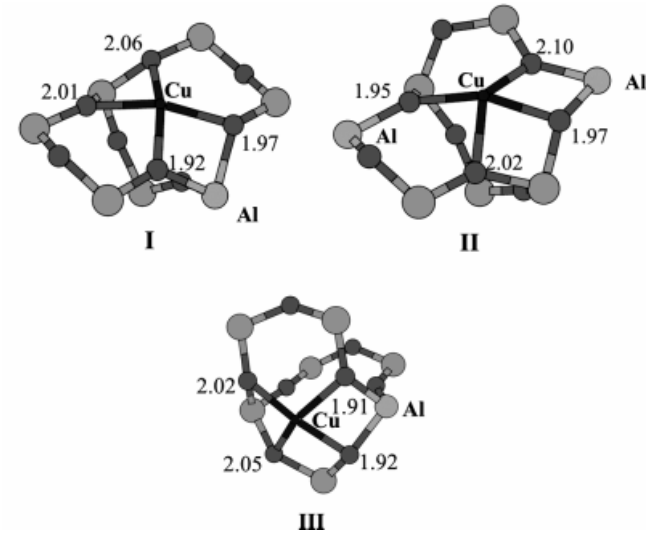

Figure 7. The representative coordination modes for Cu^{II} in mordenite; cluster I represents Cu^{II} in site E where one Al is present at a central position; the Cu^{II} ion obtains a planar fourfold coordination environment; cluster II represents Cu^{II} in site E with two Al at non-central positions; Cu^{II} is present in an irregular fourfold coordination environment; cluster III represents Cu^{II} in the planar five-membered ring in the main channel, where this ion obtains a fourfold pyramidal coordination; the Cu−O distances are given in Å

At site C, it was found that Cu^{II} acquires a pyramidal four-coordination in the planar five-membered rings, coordination mode III in Figure 7. Due to the small size of the five-membered ring, the Cu^{II} ion is located slightly above the plane of the oxygen atoms, in the main channel of mordenite. This pyramidal coordination is also characterized by $g_{//}$ = 2.27, and this third coordination mode can therefore not be distinguished from mode I in site E.

As one can see, the calculated g factors characterizing coordination mode I, II and III are in good agreement with the experimental ESR spectra. The ESR signal with $g_{//}^{(1)}$ = 2.33 is assigned to Cu^{II} in coordination mode II, while the second signal with $g_{//}^{(2)}$ = 2.27 can be assigned to Cu^{II} ions in coordination mode I and/or III. Additional considerations must be taken into account in order to explain the order in which the two ESR signals appear; first, it may be expected that the Cu^{II} ions prefer rings in which two Al are present above rings containing only one Al, due to electrostatic effects. Second, the rule of Takaishi for the ordered aluminum distribution in mordenite was invoked.[133][134] According to this rule, the five-membered rings in mordenite can never contain more than one Al. This also implies that not all six-membered rings with two Al in site E and C can occur (as linking five-membered rings forms them). Six-membered rings with 2 Al at central positions cannot be formed in mordenite; 2 Al must be placed at the non-central positions.

The following interpretation of the siting of Cu^{II} ions in mordenite is then proposed: at low Cu^{II} loadings, the Cu^{II} ions are found at the preferential sites, that is in rings with two aluminum atoms. Takaishi's rule excludes those aluminum distributions that might have provided Cu^{II} with a regular square-planar coordination in a ring containing 2 Al. As such, only coordination mode II (see Figure 7) is realized at the lowest Cu^{II} loadings, leading to only one ESR signal with $g_{//}$ = 2.33. The number of vacant six-membered rings decreases when the Cu^{II} loading increases. Therefore, rings with 1 Al also become occupied at higher Cu^{II} loadings, so that the more regular square-planar or square-pyramidal coordination modes in the planar five- and six-membered ring in the main channel are also formed. This gives rise to the second ESR signal, characterized by $g_{//}$ = 2.27. We remark that the Cu^{II} ions are located in the main channel of mordenite, and as such they are

well accessible for adsorbing molecules, in agreement with ESR results.[124]

Finally, the charge compensation of Cu^{II} in rings with only 1 Al was examined. In the literature, it is often suggested that Cu^{II} ions in the vicinity of only 1 Al are coordinated to an extra-lattice OH^- ligand in order to compensate for the local positive charge.[23,70,128,135] To test this hypothesis, additional calculations were performed for clusters with 1 Al, where Cu^{II} is also coordinated to OH^-. The optimized structures show that the Cu^{II} ion is in a planar threefold coordination environment. The Cu^{II} ion is moved outside the plane of the zeolite ring and remains coordinated to only two of the lattice oxygen atoms (the ones bound to Al) and the OH^- group. The latter bond has an unusually short Cu−O distance. This trigonal coordination is very unusual in the inorganic coordination chemistry of Cu^{II}. The $g_{//}$ factors characterizing this coordination (around 2.40) are much higher than the experimentally observed ESR signals. It is concluded that the $(Cu-OH)^+$ species are not present in the Cu^{II}−mordenite samples considered here. Charge compensation therefore only proceeds via Al in the lattice. In the case of Cu^{II} in rings with only 1 Al, this implies that charge compensation is also realized by Al in a next shell of the zeolite structure.

6. Concluding Remarks

The present work demonstrates that the structure and spectroscopic properties of transition metal ions in zeolites can successfully be explained by means of cluster model calculations using a combined DFT/CASPT2 treatment. Accurate structural information about the coordination of the transition metal ion and the distortions of the zeolite framework due to the metal adsorption is obtained from the partial geometry optimizations based on DFT. The spectroscopic features of the cluster models were calculated by means of the CASPT2 method. The ligand field excitation energies were predicted with an accuracy of less than 1000 cm^{-1}, while the ESR g factors were calculated with an accuracy of 0.03.

The DFT/CASPT2 approach allows a thorough investigation of the role of the Al distribution on the coordination environment and siting of the transition metal ion, which turns out, plays a crucial role in the cation−zeolite interaction. The main disadvantage of the cluster model approach could be the neglect of the effect of the rest of the zeolite crystal on the coordination environment of the transition metal ion. One may wonder whether restricted model clusters can correctly describe the cation exchange sites in the real zeolite matrix. However, the excitation energies and g factors crucially depend on the structure of the cluster model. The close correspondence between the experimental and calculated spectroscopic features therefore indirectly confirms the high quality of the DFT structures. The fact that the coordination environment and spectroscopic properties of transition metal ions in the considered zeolites can be described by the relatively small cluster models used in this work is an indication that they are essentially only dependent on the nearest neighbors of the cation. It would be interesting to examine the effect of the wider zeolite environment by using a QM/MM embedding procedure. In this method, the quantum mechanical (QM) description of the cluster is coupled with a classical description (with molecular modeling, MM) of the interactions between the cluster and its further environment.[58−60]

The study of the coordination of Cu^{II} in zeolite A, Y, ZK4 and mordenite has led to a new and profound insight in the Cu^{II}−zeolite interaction, which can be summarized by the following three rules:

(1) The presence of Cu^{II} in cation exchange sites in zeolites causes local distortions of the zeolite framework. The driving force for these structural deformations is the tendency of Cu^{II} to attain a four-coordinate square-planar coordination to the lattice oxygen atoms. This can be rationalized by means of molecular orbital theory; in a square-planar environment, Cu^{II} can maximize the σ interaction between the $Cu(3d_{x^2-y^2})$ orbital and the oxygen ligands. The Cu−O binding thus has a partially covalent character.

(2) Framework aluminum atoms strongly influence the coordination environment of Cu^{II}, since the cation preferentially coordinates to lattice oxygen atoms bound to Al. As there are different possible Al distributions in one site (for zeolites with Si/Al > 1), this can lead to different coordination modes for Cu^{II} in one site.

(3) Planar five- and six-membered rings are the ideal sites to accommodate the Cu^{II} ion, as the planar fourfold coordination is most easily achieved in these rings. Larger or twisted rings are avoided.

In the future, it will be interesting to examine and compare the reaction mechanism and reactivity of these transition metal ion centers for the N_2O and NO_x decomposition reactions.

Finally, the performance of the DFT/CASPT2 approach can also be compared to previous theoretical calculations of transition metal ions in zeolites, which were based on crystal or ligand field theory.[20,50−55] Whereas the crystal/ligand field calculations essentially had a rationalizing role, the current DFT/CASPT2 approach has proven to have a predictive value. As a first example, the DFT/CASPT2 calculations have revealed large local distortions of the zeolite structure due to the presence of the transition metal ion. These local deformations of the zeolite in the presence of divalent cations were already decided from IR spectroscopy experiments, where a shift of the framework T−O−T stretching vibrations is observed upon complexation with the cations,[79,80] and from ESEEM and ^{27}Al NMR spectroscopy experiments.[115] In this respect, the DFT structures offer detailed structural information about these distortions which has, so far, been inaccessible to experiment. Secondly, our new interpretation of the ESR signals of Cu^{II} in zeolite A and Y suggested the presence of two ESR signals in a related zeolite, namely Cu^{II}−ZK4. The subsequent ESR experiments on this zeolite indeed confirmed this prediction.

The new ab initio interpretations differ quite significantly from many previous ligand field results on the coordination

of Cu^{II} in zeolites. On the other hand, some of the main ideas of ligand field theory apparently survive. The predominant orbitals that constitute the complete basis of the whole ligand field framework are the metal d orbitals. And these very same orbitals play a crucial role in the construction of the complete active space of the ab initio work. The unique role of the $d_{x^2-y^2}$ orbital in the stabilization of the four-coordinate square-planar coordination is completely in line with simple ligand-field predictions.

Acknowledgments

This investigation has been supported by grants from the Flemish Science Foundation (FWO) and from the Concerted Research Action of the Flemish Government (GOA). M. G. thanks the Institute for the Promotion of Innovation by Science and Technology in Flanders (IWT) for a research grant.

[1] *Atlas of Zeolite Structure Types*, Structure Commission of the International Zeolite Association (IZA-SC), http://www.iza-structure.org/databases
[2] M. Hartmann, L. Kevan, *Chem. Rev.* **1999**, *99*, 635.
[3] B. M. Weckhuysen, R. R. Rao, J. A. Martens, R. A. Schoonheydt, *Eur. J. Inorg. Chem.* **1999**, 565.
[4] M. Iwamoto, H. Furukawa, Y. Mine, F. Uemura, S. Mikuriya, S. Kagawa, *J. Chem. Soc., Chem. Commun.* **1986**, 1273.
[5] M. Iwamoto, H. Yahiro, K. Tanda, N. Mizuno, Y. Mine, S. Kagawa, *J. Phys. Chem.* **1991**, *95*, 3727.
[6] Y. Li, W. K. Hall, *J. Phys. Chem.* **1990**, *94*, 6145.
[7] Y. Li, W. K. Hall, *J. Catal.* **1991**, *129*, 202.
[8] J. Valyon, W. K. Hall, *Catal. Lett.* **1993**, *19*, 109.
[9] M. Anpo, M. Matsuoka, K. Hanou, H. Mishima, H. Yamashita, H. H. Patterson, *Coord. Chem. Rev.* **1998**, *171*, 175.
[10] H. Esemann, H. Förster, *J. Mol. Struct.* **1999**, *482/483*, 7.
[11] Y. Li, J. N. Armor, *Appl. Catal. B: Environ.* **1992**, *1*, 21.
[12] F. Kapteijn, J. Rodriguez-Mirasol, J. A. Moulijn, *Appl. Catal. B: Environ.* **1996**, *9*, 25.
[13] F. Kapteijn, G. Marbán, J. Rodriguez-Mirasol, J. A. Moulijn, *J. Catal.* **1997**, *167*, 256.
[14] M. Shimokawabe, K. Hirano, N. Takezawa, *Catal. Today* **1998**, *45*, 117.
[15] A. Dandekar, M. A. Vannice, *Appl. Catal. B: Environ.* **1999**, *22*, 179.
[16] M. Shelef, *Chem. Rev.* **1995**, *95*, 209.
[17] H. Mishima, K. Hashmoto, O. Takehiko, M. Anpo, *Appl. Catal. B: Environ.* **1998**, *19*, 119.
[18] G. Centi, F. Razzini, A. Galli, *Res. Chem. Intermed.* **1998**, *24*, 541.
[19] E.-Y. Choi, I.-S. Nam, Y. G. Kim, *J. Catal.* **1996**, *161*, 597.
[20] R. A. Schoonheydt, *Catal. Rev. Sci. Eng.* **1993**, *35*, 129.
[21] L. Kevan, *Rev. Chem. Intermed.* **1987**, *8*, 53.
[22] C. J. J. den Ouden, R. A. Jackson, C. R. A. Catlow, M. F. M. Post, *J. Phys. Chem.* **1990**, *94*, 5286.
[23] J. Dědeček, Z. Sobalík, Z. Tvarůžková, D. Kaucký, B. Wichterlová, *J. Phys. Chem.* **1995**, *99*, 16327.
[24] B. Wichterlová, Z. Sobalík, A. Vondrová, *Catal. Today* **1996**, *29*, 149.
[25] B. Wichterlová, Z. Sobalík, J. Dědeček, *Catal. Today* **1997**, *38*, 199.
[26] K. Pierloot, A. Delabie, C. Ribbing, A. A. Verberckmoes, R. A. Schoonheydt, *J. Phys. Chem. B* **1998**, *102*, 10789.
[27] K. Pierloot, A. Delabie, A. A. Verberckmoes, R. A. Schoonheydt, in *Density Functional Theory, a Bridge between Chemistry and Physics* (Eds.: P. Geerlings, F. D. Proft, W. Langenaeker), VUB University Press, Brussels, **1999**, pp. 169−188.
[28] K. Pierloot, A. Delabie, M. H. Groothaert, R. A. Schoonheydt, *Phys. Chem. Chem. Phys.* **2001**, *3*, 2174.
[29] A. Delabie, K. Pierloot, M. H. Groothaert, B. M. Weckhuysen, R. A. Schoonheydt, *Micropor. Mesopor. Mat.* **2000**, *37*, 209.
[30] A. Delabie, K. Pierloot, M. H. Groothaert, B. M. Weckhuysen, R. A. Schoonheydt, *Phys. Chem. Chem. Phys.*, in press.
[31] A. Delabie, M. H. Groothaert, R. A. Schoonheydt, K. Pierloot, in *Proceedings of the 13th international zeolite conference* (Eds.: A. Galarneau, F. D. Renzo, F. Fajula, J. Vendrine), Elsevier Science, **2001**.
[32] M. H. Groothaert, R. A. Schoonheydt, A. Delabie, K. Pierloot, in *Unique metal Ion Structures in Solid Matrices. From Science to Application* (Eds.: B. Wichterlová, A. T. Bell), Kluwer Academic Publishers, Dordrecht, **2001**, pp. 205−219.
[33] W. Loewenstein, *Am. Miner.* **1942**, *39*, 92.
[34] R. J. Faber, M. T. Rogers, *J. Am. Chem. Soc.* **1959**, *81*, 1849.
[35] J. T. Richardson, *J. Catal.* **1967**, *9*, 172.
[36] U. Krüerke, P. Jung, *Z. Phys. Chem. (Frankfurt)* **1968**, *58*, 53.
[37] H. B. Slot, J. L. Verbeek, *J. Catal.* **1968**, *12*, 216.
[38] D. Mikheikin, V. A. Shvets, V. B. Kazanskii, *Kinet. Katal.* **1968**, *29*, 1395.
[39] C. Naccache, B. Taarit, *Chem. Phys. Lett.* **1971**, *11*, 11.
[40] J. Turkevich, Y. Ono, J. Soria, *J. Catal.* **1972**, *25*, 44.
[41] E. F. Vansant, J. H. Lunsford, *J. Phys. Chem.* **1972**, *76*, 2860.
[42] E. F. Vansant, *Recl. Trav. Chim.* **1973**, *11*, 1152.
[43] D. Goldfarb, in *Spectroscopy of transition metal ions on surfaces* (Eds.: B. M. Weckhuysen, P. Van Der Voort, G. Catana), Leuven University Press, **2000**, pp. 93−133.
[44] C. C. Chao, J. H. Lunsford, *J. Phys. Chem.* **1972**, *57*, 2890.
[45] A. A. Verberckmoes, B. M. Weckhuysen, J. Pelgrims, R. A. Schoonheydt, *J. Phys. Chem.* **1995**, *99*, 15222.
[46] A. A. Verberckmoes, B. M. Weckhuysen, R. A. Schoonheydt, K. Ooms, I. Langhans, *Anal. Chim. Acta* **1997**, *348*, 267.
[47] A. A. Verberckmoes, B. M. Weckhuysen, R. A. Schoonheydt, *Stud. Surf. Sci. Catal.* **1997**, *105*, 623.
[48] J. Dědeček, B. Wichterlová, *J. Phys. Chem. B* **1999**, *103*, 1462.
[49] P. Gallezot, Y. B. Taarit, B. Imelik, *J. Catal.* **1972**, *26*, 295.
[50] J. Texter, D. H. Storme, R. G. Herman, K. Klier, *J. Phys. Chem.* **1977**, *81*, 333.
[51] K. Klier, P. J. Hutta, R. Kellerman, *ACS Symp. Ser.* **1977**, *40*, 108.
[52] D. H. Storme, K. Klier, *ACS Symp. Ser.* **1980**, *135*, 155.
[53] D. Packet, R. A. Schoonheydt, *ACS Symp. Ser.* **1988**, *368*, 203.
[54] R. A. Schoonheydt, *Acad. Analecta* **1987**, *49*, 3.
[55] R. A. Schoonheydt, *J. Phys. Chem. Solids* **1989**, *50*, 523.
[56] A. A. Verberckmoes, R. A. Schoonheydt, A. Ceulemans, A. Delabie, K. Pierloot, *Mat. Res. Proc.* **1999**, 387.
[57] P. J. Carl, S. L. Isley, S. C. Larsen, *J. Phys. Chem. A* **2001**, *105*, 4563.
[58] M. Sierka, J. Sauer, *Faraday Discuss.* **1997**, *106*, 41.
[59] L. Rodriguez-Santiago, M. Sierka, V. Branchadell, M. Sodupe, J. Sauer, *J. Am. Chem. Soc.* **1998**, *120*, 1545.
[60] J. Sauer, *Chem. Rev.* **1989**, *89*, 199.
[61] P. Nachtigall, D. Nachtigallová, J. Sauer, *J. Phys. Chem. B* **2000**, *104*, 1738.
[62] D. Nachtigallová, P. Nachtigall, M. Sierka, J. Sauer, *Phys. Chem. Chem. Phys.* **1999**, *1*, 2019.
[63] W. F. Schneider, K. C. Hass, R. Ramprasad, J. B. Adams, *J. Phys. Chem. B* **1997**, *101*, 4353.
[64] W. F. Schneider, K. C. Hass, R. Ramprasad, J. B. Adams, *J. Phys. Chem. B* **1998**, *102*, 3692.
[65] W. F. Schneider, K. C. Hass, R. Ramprasad, J. B. Adams, *J. Phys. Chem.* **1996**, *100*, 6032.
[66] H. V. Brand, A. Redondo, P. J. Hay, *J. Phys. Chem. B* **1997**, *101*, 7691.
[67] Y. Yokomichi, H. Ohtsuka, T. Tabata, O. Okada, Y. Yokoi, H. Ishikawa, R. Yamaguchi, H. Matsui, A. Tachibana, T. Yamabe, *Catal. Today* **1995**, *23*, 431.
[68] Y. Yokomichi, T. Yamabe, H. Ohtsuka, T. Kakumoto, *J. Phys. Chem.* **1996**, *100*, 14424.
[69] N. U. Zhanpeisov, H. Nakatsuji, H. Hada, M. Anpo, *Catal. Lett.* **1996**, *42*, 173.

[70] B. L. Trout, A. K. Chakraborty, A. T. Bell, *J. Phys. Chem.* **1996**, *100*, 4173.
[71] B. L. Trout, A. K. Chakraborty, A. T. Bell, *J. Phys. Chem.* **1996**, *100*, 17582.
[72] R. J. Blint, *J. Phys. Chem.* **1996**, *100*, 19518.
[73] H. Oka, T. Okada, K. Hori, *J. Mol. Catal. A: Chem.* **1996**, *109*, 51.
[74] N. Tajima, M. Hashimoto, F. Toyama, A. M. El-Nahas, K. Hirao, *Phys. Chem. Chem. Phys.* **1999**, *1*, 3823.
[75] X. Solans-Monfort, V. Branchadell, M. Sodupe, *J. Phys. Chem. A* **2000**, *104*, 3225.
[76] M. J. Rice, A. K. Chakrabotry, A. T. Bell, *J. Catal.* **2000**, *194*, 278.
[77] M. J. Rice, A. K. Chakrabotry, A. T. Bell, *J. Phys. Chem. B* **2000**, *104*, 9987.
[78] J. M. Campos-Martin, A. Guerrero-Ruiz, J. L. G. Fierro, *Catal. Lett.* **1996**, *41*, 55.
[79] Z. Sobalík, Z.; J. Dedecek, I. Ikonnikov, B. Wichterlová, *Microporous Mesoporous Mater.* **1998**, *21*, 525.
[80] Z. Sobalík, Z. Tvarůžková, B. Wichterlová, *J. Phys. Chem. B* **1998**, *102*, 1077.
[81] H. Yamashita, M. Matsuoka, K. Tsuji, Y. Shioya, M. Anpo, M. Che, *J. Phys. Chem.* **1996**, *100*, 397.
[82] C. Lamberti, G. Spoto, D. Scarano, C. Pazé, M. Salvalaggio, S. Bordiga, A. Zecchina, G. T. Palomino, F. D'Acapito, *Chem. Phys. Lett.* **1997**, *269*, 500.
[83] S. Hu, A. Reimer, A. T. Bell, *J. Phys. Chem. B* **1997**, *101*, 1869.
[84] S.-B. Liu, B. M. Fung, T.-C. Yang, E.-C. Hong, C.-T. Chang, P.-C. Shih, F.-H. Tong, T.-L. Chen, *J. Phys. Chem.* **1994**, *98*, 4393.
[85] S.-B. Liu, T.-C. Yang, R.-Y. Lin, E.-C. Hong, T.-S. Lin, *Stud. Surf. Sci. Catal.* **1994**, *84*, 789.
[86] S.-B. Liu, T.-S. Lin, T.-C. Yang, T.-H. Chen, E.-C. Hong, R. Ryoo, *J. Phys. Chem.* **1995**, *99*, 8277v.
[87] H. S. Lee, K. Seff, *J. Phys. Chem.* **1981**, *85*, 397.
[88] I. E. Maxwell, J. J. de Boer, *J. Phys. Chem.* **1975**, *79*, 1874.
[89] R. M. Haniffa, K. Seff, *Microporous Mesoporous Mater.* **1998**, *25*, 137.
[90] N. N. Tikhomiroya, I. V. Nikolaeva, *Zh. Strukt. Khim.* **1969**, *10*, 547.
[91] R. A. Schoonheydt, P. Peigneur, J. B. Uytterhoeven, *J. Chem. Soc., Faraday Trans. 1* **1978**, *74*, 2550.
[92] R. G. Herman, D. R. Flentge, *J. Phys. Chem.* **1978**, *82*, 720.
[93] M. Narayana, L. Kevan, *J. Chem. Soc., Faraday Trans. 1* **1986**, *82*, 213.
[94] M. W. Anderson, L. Kevan, *J. Phys. Chem.* **1987**, *91*, 1850.
[95] T. Ichikawa, L. Kevan, *J. Chem. Soc., Faraday Trans. 1* **1981**, *77*, 2567.
[96] T. Ichikawa, L. Kevan, *J. Am. Chem. Soc.* **1981**, *103*, 5355.
[97] M. W. Anderson, L. Kevan, *J. Phys. Chem.* **1986**, *90*, 3206.
[98] D. R. Flentge, J. H. Lunsford, P. A. Jacobs, J. B. Uytterhoeven, *J. Phys. Chem.* **1975**, *79*, 354.
[99] R. G. Herman, J. H. Lunsford, H. K. Beyer, P. A. Jacobs, J. B. Uytterhoeven, *J. Phys. Chem.* **1975**, *79*, 2388.
[100] I. E. Maxwell, E. Drent, *J. Catal.* **1976**, *41*, 412.
[101] R. G. Herman, *Inorg. Chim. Acta* **1979**, *34*, 119.
[102] J. C. Conesa, J. Soria, *J. Chem. Soc., Faraday Trans. 1* **1979**, *75*, 406.
[103] J. S. Yu, L. Kevan, *J. Phys. Chem.* **1990**, *94*, 7612.
[104] J. C. Conesa, J. Soria, *J. Phys. Chem.* **1978**, *82*, 1847.
[105] J. C. Conesa, J. Soria, *J. Phys. Chem.* **1978**, *82*, 1575.
[106] J. C. Conesa, J. Soria, *J. Chem. Soc., Faraday Trans. 1* **1979**, *75*, 423.
[107] I. R. Leith, C. Kemball, H. F. Leach, *Chem. Commun.* **1971**, 407.
[108] I. R. Leith, H. F. Leach, *Proc. R. Soc. London, Ser A* **1972**, *330*, 247.
[109] J. S. Yu, L. Kevan, *J. Phys. Chem.* **1990**, *94*, 7620.
[110] J. S. Yu, L. Kevan, *J. Phys. Chem.* **1990**, *94*, 5595.
[111] T. Ichikawa, L. Kevan, *J. Am. Chem. Soc.* **1983**, *105*, 402.
[112] T. Ichikawa, L. Kevan, *J. Phys. Chem.* **1983**, *87*, 4433.
[113] J. S. Yu, L. Kevan, *J. Phys. Chem.* **1991**, *95*, 6648.
[114] M. Iwamoto, K. Maruyama, N. Yamazoe, T. Seiyama, *J. Phys. Chem.* **1977**, *81*, 622.
[115] D. Goldfarb, L. Kevan, *J. Magn. Reson.* **1989**, *82*, 270.
[116] D. Goldfarb, K. Zukerman, *Chem. Phys. Lett.* **1990**, *171*, 167.
[117] K. Matar, D. Goldfarb, *J. Phys. Chem.* **1992**, *96*, 3100.
[118] A. Schäfer, H. Horn, R. Ahlrichs, *J. Chem. Phys.* **1992**, *97*, 2571.
[119] K. Pierloot, B. Dumez, P.-O. Widmark, B. O. Roos, *Theor. Chim. Acta* **1995**, *90*, 87.
[120] C. Ribbing, C. Daniel, *J. Chem. Phys.* **1994**, *100*, 6591.
[121] W. De Wilde, R. A. Schoonheydt, J. B. Uytterhoeven, *ACS Symp. Ser.* **1977**, *40*, 132.
[122] M. P. Attfield, S. J. Weigel, A. K. Cheetham, *J. Catal.* **1997**, *170*, 227.
[123] W. J. Mortier, J. J. Pluth, V. J. Smith, *Mater. Res. Bull.* **1975**, *10*, 1037.
[124] A. V. Kucherov, A. A. Slinkin, D. A. Kondrat'ev, T. N. Bondarenko, A. M. Rubinstein, K. M. Minachev, *Zeolites* **1985**, *5*, 320.
[125] A. V. Kucherov, A. A. Slinkin, *Zeolites* **1986**, *6*, 175.
[126] C. E. Sass, L. Kevan, *J. Phys. Chem.* **1989**, *93*, 4669.
[127] S. de Tavernier, R. A. Schoonheydt, *Zeolites* **1991**, *11*, 155.
[128] P. J. Carl, S. C. Larsen, *J. Phys. Chem. B* **2000**, *104*, 6568.
[129] P. J. Carl, S. C. Larsen, *J. Catal.* **1999**, *182*, 208.
[130] B. Wichterlová, J. Dědeček, Z. Sobalík, A. Vondrová, K. Klier, *J. Catal.* **1997**, *169*, 194.
[131] B. Wichterlová, J. Dědeček, A. Vondrová, *J. Phys. Chem.* **1995**, *99*, 1065.
[132] V. Guliants, J. Mullhaupt, J. Newsam, A. Gorman, C. Freeman, *Catal. Today* **1999**, *50*, 661.
[133] T. Takaishi, M. Kato, K. Itabashi, *Zeolites* **1995**, *15*, 21.
[134] T. Takaishi, M. Kato, K. Itabashi, *J. Phys. Chem.* **1994**, *98*, 5742.
[135] M. L. Jacono, G. Fierro, R. Dragone, X. Feng, J. d'Itri, W. K. Hall, *J. Phys. Chem. B* **1997**, *101*, 1979.

Received July 13, 2001
[I01261]

Mesoscopic Globular Self-assemblies of Platinum(II) Complexes Containing Porphyrins

Mariangela Castriciano,[a] Andrea Romeo,[a] Raffaello Romeo,[a] and Luigi Monsu′ Scolaro*[a,b]

Keywords: Platinum / Porphyrins / Nanostructures / Aggregation / Scanning probe microscopy

Slow evaporation of an acetone or chloroform solution of the novel tetranuclear platinum(II) complex $[Pt(Lau_2dim)Me]_4$-$(TpyP)(CF_3SO_3)_4$ [Lau_2dim = didodecyldiimine; TpyP = 5,10,15,20-tetrakis(4-pyridyl)-21*H*,23*H*-porphyrin] on a glass surface affords globular micrometric sized aggregates.

Introduction

The formation of organized supramolecular structures of chromophores with well-defined shapes and sizes is a topic of relevant interest.[1] Their potential application in energy storage and conversion, supramolecular catalysis, optics and electronics can be easily recognized. In this respect, porphyrins and their metal derivatives are important compounds due to their favorable photophysical, electronic and catalytic properties. These features are strictly related to their aggregation state and strongly depend on the microstructural environment.[2] Specifically tailored porphyrins can be easily dissolved in micelles or liposomes[3] obtaining systems that assume the required stability, rigidity and orientation to perform specific functions, for example to mimic cytochrome P-450.[4] Amphiphilic porphyrins have been exploited in the preparation of simple micelles,[5] fibers[6] and vesicles,[7] while "octopus" porphyrins have shown their tendency to self-assemble in vesicles[8] or fibers[9] able to bind oxygen in an aqueous medium. The formation of porphyrin wheels or rings in the mesoscopic range has been achieved by simple solvent evaporation.[10]

Metal complexes can be conveniently exploited to synthesize properly modified porphyrins[11] or linked porphyrin arrays using the self-assembly idea.[12] We have recently reported on the application of platinum(II) organometallic complexes to the synthesis of tetrasubstituted porphyrins that are soluble in micellar phases.[13] We knew from a detailed kinetic investigation on cationic complexes of the type $[Pt(N\text{-}N)Me(Me_2SO)]^+$ (N-N = a series of diamines or diimines)[14] that the coordinated Me_2SO becomes very labile when N-N is a diimine. Therefore, we used the complex $[Pt(Cy_2dim)Me(Me_2SO)]^+$ (Cy_2dim = dicyclohexyldiimine) as a monofunctional building block for introducing the platinum molecular fragment and for accessing a specifically tailored porphyrin.[13]

This paper describes the formation of globular mesoscopic aggregates by simple evaporation of solutions containing a novel 5,10,15,20-tetrakis(4-pyridyl)-21*H*,23*H*-porphyrin (TpyP) derivative functionalized with a platinum(II) complex bearing long alkyl chains.

Results and Discussion

The synthetic route to the porphyrin platinum(II) complex $[Pt(Lau_2dim)Me]_4(TpyP)(CF_3SO_3)_4$ (**1**) (Lau_2dim = didodecyldiimine) can be summarized as follows (Scheme 1): (i) the diimine ligand Lau_2dim is readily prepared, according to a literature method,[15] by reacting dodecylamine and glyoxal in methanol; (ii) in analogy with a well-established procedure,[14] the diimine ligand is reacted with the complex *trans*-$[Pt(Me_2SO)_2MeCl]$ in methanol, in the presence of a stoichiometric amount of $AgCF_3SO_3$; separation of solid AgCl and cautious evaporation of the excess solvent affords the sulfoxide complex $[Pt(Lau_2dim)Me(Me_2SO)](CF_3SO_3)$; (iii) this latter compound is reacted with a stoichiometric amount of the TpyP porphyrin in chloroform leading almost quantitatively to the tetranuclear complex **1**. The gradual platination of the porphyrin can be monitored easily in situ by ^1H NMR spectroscopy, by titrating a solution of TpyP with the sulfoxide complex. The aromatic region of the spectrum shows a decrease of the signals for TpyP and a matching increase of the peaks due to intermediate mono-, di- and trisubstituted species, af-

[a] Dipartimento di Chimica Inorganica, Chimica Analitica e Chimica Fisica and ICTPN−CNR, Sezione di Messina - Università di Messina,
Salita Sperone, 31-Vill. S. Agata-98166 Messina, Italy
Fax: (internat.) +39-090/393-756
E-mail: monsu@chem.unime.it
[b] INFM, Unità di Messina
Salita Sperone, 31-Vill. S. Agata-98166 Messina, Italy
Supporting information for this article is available on the WWW under http://www.eurjic.com or from the author.

 © WILEY-VCH Verlag GmbH, 69451 Weinheim, Germany, 2002 1434−1948/02/0303−0531 $ 17.50+.50/0

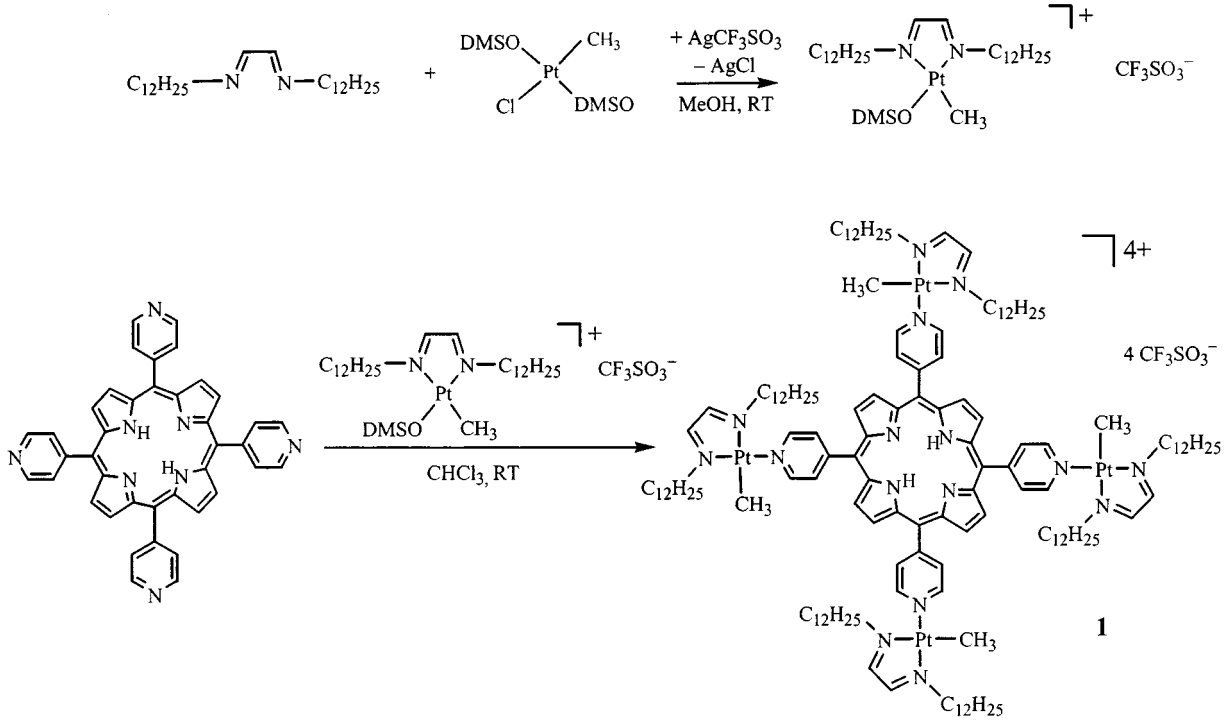

Scheme 1

fording eventually the required tetrasubstituted complex with a metal to porphyrin ratio of 4:1.

The UV/Vis electronic spectrum of **1** in acetone exhibits an intense Soret band at 422 nm ($\varepsilon = 2.76 \times 10^5$ м$^{-1}$cm^{-1}), which is bathochromically shifted with respect to the free TpyP porphyrin ($\Delta\lambda = +9$ nm, Figure 1). A series of four Q-bands are present at longer wavelengths. The resonance light-scattering[17] spectrum of the acetone solution of **1** exhibits a rather low intensity with respect to the neat solvent, and is strongly modulated by the absorbance of the sample, suggesting the monomeric nature of this complex in acetone. The platinated porphyrin is still emissive in acetone solutions. The fluorescence spectra display the typical two-band emission at 654 and 716 nm, very similar (even if partially quenched by the heavy atom effect) to those of the parent porphyrin and of other tetraaryl-substituted porphyrins (inset of Figure 1).[18] The excitation spectra match the absorption spectra.

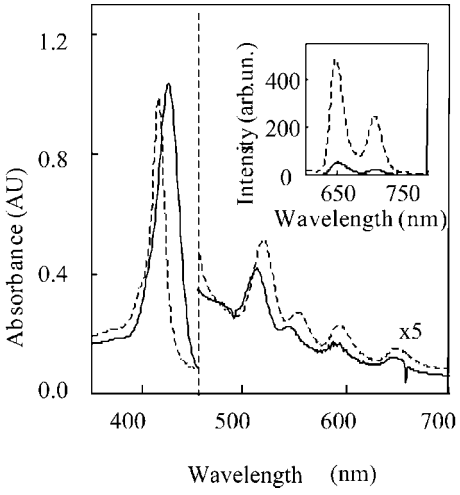

Figure 1. UV/Vis spectra of 5 μм solutions of TpyP (dashed line) and complex **1** (solid line) in acetone [the inset shows the fluorescence emission spectra of TpyP (dashed line) and complex **1** (solid line) in acetone ($\lambda_{exc} = 420$ nm; emissions are corrected for absorption)]

Chloroform or acetone solutions of complex **1** have been evaporated on glass cover slides. The resulting films exhibit an intense and sharp Soret band at 431 nm and the typical two-band emission fluorescence at 662 and 720 nm. Both the Soret and the emission features are bathochromically shifted with respect to the organic solution phase. These observations suggest a well-defined geometrical arrangement of porphyrins in the solid state, which could be accounted for by the occurrence of porphyrin−porphyrin interactions, in spite of the presence of the bulky alkyl side chains. These latter could be responsible for a further stabilization of the structure through hydrophobic interactions, which help to orientate the chromophore planes (Figure 2). Optical microscopy on these samples revealed a distribution of apparently globular objects, which are stable at 298 K for at least a week. After this period, the aggregates collapse in continuum unstructured layers. Scanning Electron Microscopy (SEM) has been exploited to investigate the morphology of this system. The SEM images (Figure 3) show a population of almost spherical aggregates with sizes spanning from 1000 up to 2000 nm. The presence of platinum in the aggregates is confirmed by Energy Dispersion Spectrometry (EDS), which shows the typical pattern of this element. The clear-cut evidence that compound **1** retains its identity in the globular aggregates has been proved by strip-

ping the compound from the glass with acetone and comparing the UV/Vis absorption and fluorescence emission of these solutions with those of **1** in the same solvent prior to deposition. Analogous experiments performed using solutions of [Pt(Lau$_2$dim)Me(Me$_2$SO)](CF$_3$SO$_3$) or of the platinated porphyrin compound [Pt(Cy$_2$dim)Me]$_4$(TpyP)(CF$_3$SO$_3$)$_4$ [13] resulted only in the formation of unstructured films, resembling a waxy layer.

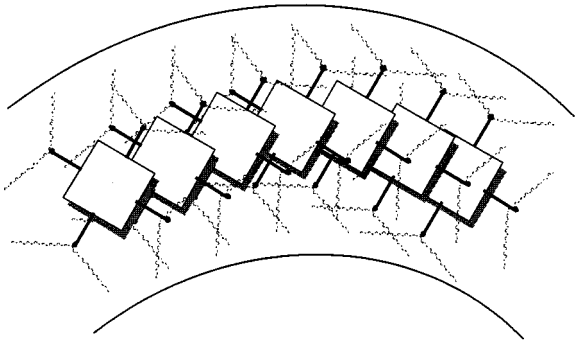

Figure 2. Schematic model for the arrangement of porphyrins in the aggregates

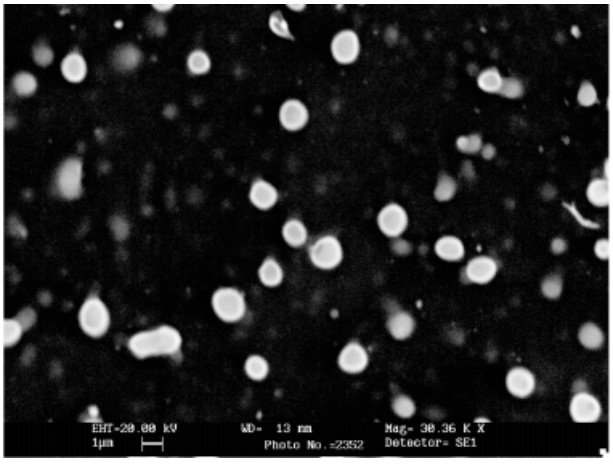

Figure 3. SEM image acquired on a sample of **1** deposited on glass from an acetone solution; the slide has been coated with graphite for EDS analysis

The growth of porphyrin wheels[10c] and of other well-defined patterns[19] of chromophores on different solid substrates has been explained on the basis of surface forces acting at the interface between the solid, the liquid and the gas phase. A similar mechanism could well apply to the growth of objects of spherical shape, even if a complete understanding deserves further investigations. The nature of the solvent does not allow a complete wettability of the glass substrate, leading to an increase of the contact angle. The droplets are pinned at the glass surface by the roughness of the surface or by defects present in the film. On evaporation the hydrophobic porphyrin concentrates in the droplet which tends to assume a spherical shape. The resulting structure should be stabilized by included solvent molecules. Further studies are in progress to test the catalytic ability of aggregated manganese(III) porphyrin derivatives in oxidative processes.

Experimental Section

General Procedures and Chemicals: All solvents were dried according to standard procedures by distillation under an oxygen-free nitrogen atmosphere from appropriate drying agents (i.e. dichloromethane from barium oxide and diethyl ether from sodium benzophenone ketyl). $CDCl_3$ was purchased from Cambridge Isotopes Laboratories (D, 99.8%). 5,10,15,20-tetrakis(4-pyridyl)-21*H*,23*H*-porphyrin (TpyP) was purchased from Aldrich. K_2PtCl_4 (Strem Chemical Co.) was purified from metallic Pt and K_2PtCl_6 by dissolving it in water and filtering. Tetramethyltin was received from Aldrich and its purity was checked by ^{1}H NMR spectroscopy. All the other reagents were of the highest commercial grade available and were used as received or were purified by distillation or recrystallization where necessary.

Instrumentation: ^{1}H and ^{13}C{^{1}H} NMR spectra were recorded at 298 K on a Bruker AMX R-300 spectrometer operating with a broad-band probe at 300.13 and 75.7 MHz for ^{1}H and ^{13}C nuclei, respectively. Chemical shifts (δ, ppm) are referred to $SiMe_4$. UV/Vis spectra were measured on a Hewlett Packard mod. HP 8453 diode array spectrophotometer. Fluorescence and resonance light scattering experiments were performed on a Jasco mod. FP-750 spectrofluorimeter equipped with a Hamamatsu R928 PMT using, in this latter case, a synchronous scan protocol with a right-angle geometry.[17] Microanalysis was performed by Redox Analytical Laboratories, Milan, Italy. SEM was performed on a LEO S420 Cambridge instrument operating with an accelerating potential of 20 kV. The samples were prepared by graphite coating for the EDS analysis.

Lau$_2$dim: Didodecyldiimine (Lau$_2$dim) was prepared following a literature method used for other dialkyl diimines.[15] The solid compound was crystallized from methanol. Yield 75%. $C_{26}H_{52}N_2$ (392.7): calcd. C 79.51, H 13.36, N 7.14; found C 79.3, H 13.5, N 7.10. ^{1}H NMR ($CDCl_3$): δ = 7.9 (s, 2 H), 3.55 (t, $^3J_{H-H}$ = 6.9 Hz, 4 H), 1.65 (m, 4 H), 1.24 (m, 36 H), 0.85 (t, $^3J_{H-H}$ = 6.6 Hz, 6 H). ^{13}C NMR ($CDCl_3$): δ = 162 (CH), 61 (C_1-N), 32 (C_2-N), 30 (C_3-N), 29 (2C), 27 (3C), 22 (3C), 15 (CH_3). MS-EI: *m*/*z* = 391 [M − H$^+$]. M.p. 63 °C.

[Pt(Lau$_2$dim)Me(Me$_2$SO)](CF$_3$SO$_3$): The precursor [Pt(Lau$_2$dim)-Me(Me$_2$SO)](CF$_3$SO$_3$) was prepared using a slightly modified literature method.[14] A weighed amount of *trans*-[Pt(Me$_2$SO)$_2$MeCl][16] (40.2 mg, 0.1 mmol) was reacted in methanol (70 mL) with an equimolar amount of $AgCF_3SO_3$ and the ligand Lau$_2$dim. After stirring for 30 min, AgCl was removed by centrifugation. The solvents were then evaporated under reduced pressure, and the resulting yellow-orange solid was dissolved in dichloromethane and filtered through a cellulose column to remove residual AgCl. The compound was precipitated by adding diethyl ether and cooling to −30 °C. 58 mg of the complex were recovered. Yield 70%. $C_{30}H_{61}F_3N_2O_4PtS_2$ (830.0): calcd. C 43.41, H 7.41, N 3.37; found C 43.2, H 7.2, N 3.5. ^{1}H NMR ($CDCl_3$): δ = 8.87 (s, $^3J_{Pt-H}$ = 46 Hz, 1 H), 8.84 (s, $^3J_{Pt-H}$ = 83 Hz, 1 H), 3.99 (t, 2 H), 3.77 (m, 2 H), 3.36 (s, $^3J_{Pt-H}$ = 32 Hz, 6 H), 1.67 (m, 4 H), 1.24 (m, 36 H), 0.87 (t, $^3J_{H-H}$ = 6 Hz, 6 H), 0.79 (s, $^2J_{Pt-H}$ = 70.2 Hz, 3 H). ^{13}C NMR ($CDCl_3$): δ = 173 (CH), 166 (CH′), 120.4 ($^2J_{F-C}$ = 320 Hz, CF_3), 62.3, 59.3 (C_2 + $C_{2'}$), 45.5 ($^2J_{Pt-C}$ = 84 Hz, Me_2SO), 41,

40.5 (C_3 + $C_{3'}$), 32−26.22 (18 C), 14 (C_{12} + $C_{12'}$), −9.6 ($^1J_{Pt-C}$ = 700 Hz, CH_3). MS-FAB: *m/z* = 680 [$M^+ - CF_3SO_3$].

[Pt(Lau$_2$dim)Me]$_4$(TpyP)(CF$_3$SO$_3$)$_4$ (1): [Pt(Lau$_2$dim)Me(Me$_2$SO)](CF$_3$SO$_3$) (54 mg, 0.064 mmol) was added to a stirred solution of TpyP (10 mg, 0.016 mmol) in 25 mL of freshly distilled chloroform. The solution was allowed to react for 2 hours, and the solvent was then removed under reduced pressure. The resulting deep purple compound was dissolved in acetone and precipitated by adding diethyl ether and cooling to −30 °C (46 mg). Yield 80%. $C_{152}H_{246}F_{12}N_{16}O_{12}Pt_4S_4$ (3626.3): calcd. C 50.35, H 6.84, N 6.18; found C 50.01, H 6.50, N5.98. ^{1}H NMR ($CDCl_3$): δ = 9.14 (m, $^3J_{H-H}$ = 5.5 Hz, 8 H), 8.97 (s, 8 H), 8.85 (s, 4 H), 8.71 (s, 4 H), 8.45 (m, $^3J_{H-H}$ = 5.5 Hz, 8 H), 3.99 (m, 8 H), 3.85 (m, 8 H), 1.85−1.05 (m, 160 H), 0.86 (m, $^3J_{H-H}$ = 6 Hz, 24 H), 0.60 (s, 12 H), −3.00 (s, 2 H). MS (MALDI-TOF): *m/z* = 1972 [M − 2Pt − $CF_3SO_3^+$], 1220.8 [M − 3Pt − $CF_3SO_3^+$]. UV/Vis (acetone): λ_{max} (ε) = 422 (276000), 514, 550, 592, 648 nm. UV/Vis (on glass): λ_{max} = 431, 521, 555, 598, 650 nm. Fluorescence emission (acetone): λ_{exc} = 420 nm; λ_{em} = 654, 716 nm. Fluorescence emission (on glass): λ_{exc} = 420 nm; λ_{em} = 662, 720 nm.

Deposition on Glass: Microscope slides, cleaned prior to use by immersion in a 1:1 mixture of concentrated NH_3 solution and 30+% H_2O_2, then rinsed with Milli-Q water and dried under a steam of N_2, were used as film substrates. A droplet of a 10^{-5}−10^{-4} M solution of **1** in acetone or chloroform (Aldrich, Spectral grade) was placed on the substrate and evaporation was achieved by gentle spinning at 298 K.

Supporting Information Available (see footnote on the first page of this article): ^{1}H NMR titration of TpyP with the precursor platinum(II) complex (Figure S1), UV/Vis and fluorescence emission of **1** in acetone solution and on glass surface (Figure S2 and S3), optical images (1000× magnification) of different porphyrin complexes (Figure S4) and Energy Dispersion Spectrometry (EDS) profile on samples of **1** deposited on glass (Figure S5).

Acknowledgments

The Authors wish to thank the Ministero dell'Università e della Ricerca Scientifica e Tecnologica (MURST), Programmi di Ricerca Scientifica di Rilevante Interesse Nazionale, Cofinanziamento 2000−2001 and CNR for financial support. We also thank Dr. Maurizio Triscari and Mr. Giuseppe Sabatino for SEM measurements, and Mr. Placido Mineo for technical support with MS spectra.

[1] [1a] J. M. Lehn, *Supramolecular Chemistry*, VCH, Weinheim, **1995**. [1b] J.-H. Fuhrhop, J. Koning, *Membranes and Molecular Assemblies: The Synkinetic Approach* (Ed.: J. F. Stoddart), RSC, **1994**.

[2] W. I. White, in *The Porphyrins* (Ed.: D. Dolphin), Academic Press, New York, **1978**, vol. 5, Chapter 7.

[3] [3a] K. M. Kadish, B. G. Maiya, C. Araullo-McAdams, *J. Phys. Chem.* **1991**, *95*, 427−431. [3b] K. M. Kadish, B. G. Maiya, C. Araullo-McAdams R. Guilard, *Inorg. Chem.* **1989**, *28*, 2725−2731. [3c] S. Mazumdar, *J. Phys. Chem.* **1990**, *94*, 5947−5949. [3d] M. J. Minch, G. La Mar, *J. Phys. Chem.* **1982**, *86*, 1400−1406.

[4] [4a] A. P. H. J. Schenning, J. H. Lutje Spelberg, D. H. W. Hubert, M. C. Feiters, R. J. M. Nolte, *Chem. Eur. J.* **1998**, *4*, 871−880. [4b] D. Mansuy, M. Fontecave, J.-F. Bartoli, *J. Chem. Soc., Chem. Commun.* **1983**, 253−254. [4c] A. M. d′ A. Rocha Gonsalves, R. A. W. Johnstone, M. M. Pereira, J. Shaw, A. J. F. do N. Sobral, *Tetrahedron Lett.* **1991**, *32*, 1355−1358. [4d] J. T. Groves, R. Neumann, *J. Am. Chem. Soc.* **1987**, *109*, 5045−5047.

[5] R. Guilard, N. Senglet, Y. H. Liu, D. Sazou, E. Findsen, D. Faure, T. Des Courieres, K. M. Kadish, *Inorg. Chem.* **1991**, *30*, 1898−1905.

[6] [6a] J.-H. Fuhrhop, C. Demoulin, C. Bottcher, J. Koning, U. Siggel, *J. Am. Chem. Soc.* **1992**, *114*, 4159−4165. [6b] J.-H. Fuhrhop, C. Demoulin, C. Bottcher, J. Koning, U. Siggel, *J. Am. Chem. Soc.* **1993**, *115*, 11036−11037. [6c] J.-H. Fuhrhop, U. Bindig, U. Siggel, *J. Chem. Soc., Chem. Commun.* **1994**, 1583−1584.

[7] T. Komatsu, E. Tsuchida, C. Bottcher, D. Donner, C. Messerschmidt, U. Siggel, W. Stocker, J. P. Rabe, J.-H. Fuhrhop, *J. Am. Chem. Soc.* **1997**, *119*, 11660−11665.

[8] T. Komatsu, K. Nakao, H. Nishide, E. Tsuchida, *J. Chem. Soc., Chem. Commun.* **1993**, 728−730.

[9] E. Tsuchida, T. Komatsu, K. Arai, H. Nishide, *J. Chem. Soc., Chem. Commun.* **1993**, 730−732.

[10] [10a] A. P. H. J. Schenning, F. B. G. Benneker, H. P. M. Geurts, X. Y. Liu, R. J. M. Nolte, *J. Am. Chem. Soc.* **1996**, *118*, 8549−8552. [10b] J. Hofkens, L. Latterini, P. Vanoppen, H. Faes, K. Jeuris, S. Defeyter, J. Kerimo, P. F. Barbara, F. C. Deschryver, A. E. Rowan, R. J. M. Nolte, *J. Phys. Chem. B* **1997**, *101*, 10588−10598. [10c] L. Latterini, R. Blossey, J. Hofkens, P. Vanoppen, F. C. Deschryver, A. E. Rowan, R. J. M. Nolte, *Langmuir* **1999**, *15*, 3582−3588.

[11] W. T. S. Huck, A. Rohrer, A. T. Anilkumar, R. H. Fokkens, N. M. M. Nibbering, F. C. J. M. van Veggel, D. N. Reinhoudt, *New J. Chem.* **1998**, *22*, 165−168.

[12] S. Leininger, B. Olenyuk, P. J. Stang, *Chem. Rev.* **2000**, *100*, 853−908.

[13] L. Monsù Scolaro, C. Donato, M. Castriciano, A. Romeo, R. Romeo, *Inorg. Chim. Acta* **2000**, *300−302*, 978−986.

[14] R. Romeo, L. Monsù Scolaro, N. Nastasi, G. Arena, *Inorg. Chem.* **1996**, *35*, 5087−5096.

[15] J. M. Kliegman, R. K. Barnes, *Tetrahedron* **1970**, *26*, 2555−2560.

[16] R. Romeo, L. Monsù Scolaro, *Inorg. Synth.* **1998**, *32*, 153−158.

[17] R. F. Pasternack, P. J. Collings, *Science* **1995**, *269*, 935−939.

[18] K. Kalyanasundaram, *Inorg. Chem.* **1984**, *32*, 2453−2459.

[19] C. J. Brinker, Y. F. Lu, A. Sellinger, H. Y. Fan, *Adv. Mater.* **1999**, *11*, 579−585.

Received August 3, 2001
[I01290]

A Dinuclear Zinc(II) Complex of 2,6-bis{[(2-hydroxybenzyl)(2-pyridylmethyl)amino]methyl}-4-methylphenol Bearing an Exogenous Hydroxo Bridge

Harry Adams,[a] Darren Bradshaw,[a] and David E. Fenton*[a]

Keywords: N ligands / O ligands / Bridging ligands / Zinc

Reaction of the symmetrical proligand H_3L with zinc(II) perchlorate gives a product from which the cationic complex $[Zn_2L(OH_2)_3]ClO_4$ and the neutral complex $[Zn_2L(OH)]$ co-crystallise in the triclinic space group $P\bar{1}$, with unit cell parameters a = 14.7647(13), b = 16.9376(14), c = 17.8089(15) Å, α = 68.634(2)°, β = 71.356(2)°, γ = 87.526(2)°. The dinuclear zinc centre in $[Zn_2L(OH_2)_3]^+$ is endogenously bridged by a cresolato-O atom; in $[Zn_2L(OH)]$ this bridging mode is enhanced by an exogenous hydroxo bridge.

Introduction

The symmetric "end-off" compartmental proligand 2,6-bis{[(2-hydroxybenzyl)(2-pyridylmethyl)amino]methyl}-4-methylphenol (H_3L) has been used to generate homodinuclear donor asymmetric nickel(II) ethanoato- and coordination number asymmetric zinc(II) ethanoato complexes.[1] The crystal structures revealed the presence of a (μ-cresolato)(μ-ethanoato)-bridged dinuclear core in each complex with the (μ-cresolato) bridge endogenous and the (μ-ethanoato) bridge exogenous in nature. Noncoordinated ethanoic acid molecules were tightly hydrogen-bonded to the pendant phenols of the ligand generating a double acid salt of the type $[CH_3COO\cdots H\cdots L\cdots H\cdots OOCCH_3]^{3-}$ in the dinickel complex and a single acid salt of the type $[CH_3COO\cdots H\cdots L]^{3-}$ in the dizinc complex. In both cases the ligand periphery has been extended to provide a supraligand in which the donor potential of the original ligand has been enhanced.

The presence of a noncoordinating anion, rather than ethanoate, should inhibit the formation of an anion-based exogenous bridge and encourage interaction of the dinuclear core with the solvent. The reaction of H_3L with zinc perchlorate was therefore investigated and herein we report the effect of a noncoordinating anion on product formation together with the crystal structure of the product.

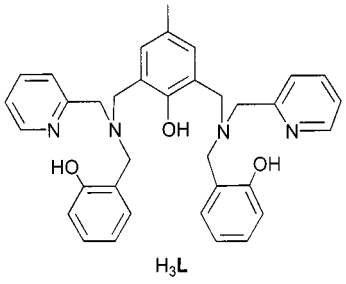

H_3L

Results and Discussion

H_3L was synthesized by modification of the method of Krebs et al.[2] and reacted with zinc(II) perchlorate in acetonitrile. Colourless crystals, suitable for X-ray structural determination, were obtained on standing. The crystal structure revealed that the cationic complex $[Zn_2L(OH_2)_3]ClO_4$ (**1**) and the neutral complex $[Zn_2L(OH)]$ (**2**) had co-crystallised. The molecular structures of the complexes are shown in Figures 1 and 2 with selected bond lengths and angles given in the captions to the figures. In addition to the complexes two disordered water molecules and a disordered acetonitrile molecule were present in the asymmetric unit.

The structure of complex **1** shows that the complex is coordination number asymmetric[3] with one zinc atom [Zn(1)] six-coordinate and the second [Zn(2)] five-coordinate. There is an endogenous cresolato bridge at the dinuclear centre but no exogenous bridge. Zn(1) is in a slightly distorted octahedral geometry with an N_2O_4 donor set derived from two ligand cresolato-O and pendant phenolato-O donor atoms [O(1) and O(2)], an articular tertiary aminic-N atom [N(1)], the pyridinyl-N atom [N(2)] and two *cis*-coordinated water molecules [O(4) and O(5)]. One water molecule is *trans* to the cresolato bridge and the other is *trans* to the articular tertiary amine as found at the six-coordinated metal atoms in the structure of the related dinickel(II) complex $[Ni_2L_A(OH_2)_4]\cdot CH_3COO^-\cdot C_3H_7NO\cdot 0.75H_2O$.[4] The three *trans*-axial angles at Zn(1) are 171.8

[a] Department of Chemistry, Dainton Building, The University of Sheffield, Sheffield S3 7HF, UK
Fax: (internat.) + 44-114/278-673
E-mail: d.fenton@sheffield.ac.uk

 © WILEY-VCH Verlag GmbH, 69451 Weinheim, Germany, 2002 1434–1948/02/0303–0535 $ 17.50+.50/0

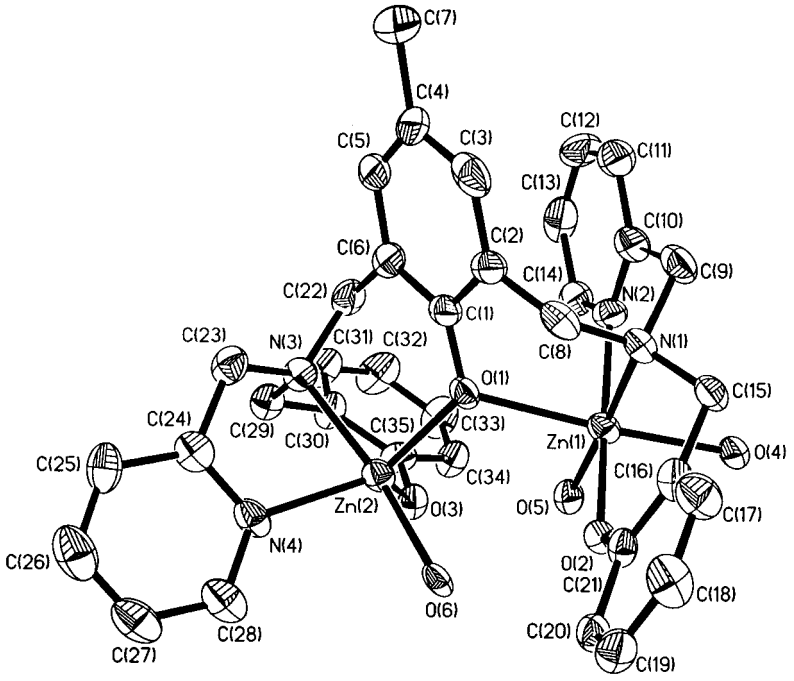

Figure 1. An ORTEP drawing of the molecular structure of the complex cation from (**1**), $[Zn_2L(OH_2)_3]^+$, showing the atom labelling; thermal ellipsoids for the non-hydrogen atoms are drawn at the 50% probability level; selected bond lengths (Å) and angles (°) at the zinc(II) atom: Zn(1)−O(1) 2.241(5), Zn(1)−O(2) 2.023(4), Zn(1)−N(1) 2.166(6), Zn(1)−N(2) 2.100(6), Zn(1)−O(4) 2.164(5), Zn(1)−O(5) 2.036(5), Zn(2)−O(1) 2.009(5), Zn(2)−O(3) 1.952(5), Zn(2)−O(6) 2.065(4), Zn(2)−N(3) 2.153(6), Zn(2)−N(4) 2.131(6), Zn(1)−Zn(2) 3.6162(12); O(2)−Zn(1)−N(2) 171.8(2), O(5)−Zn(1)−N(1) 177.9(2), O(1)−Zn(1)−O(4) 172.51(18), N(2)−Zn(1)−N(1) 82.1(2), N(1)−Zn(1)−O(2) 89.8(2), O(2)−Zn(1)−O(5) 91.26(19), O(5)−Zn(1)−N(2) 96.8(2), N(3)−Zn(2)−O(6) 167.9(2), O(1)−Zn(2)−O(3) 109.4(2), O(3)−Zn(2)−N(4) 117.7(2), N(4)−Zn(2)−O(1) 132.1(2), Zn(1)−O(1)−Zn(2) 116.5(2)

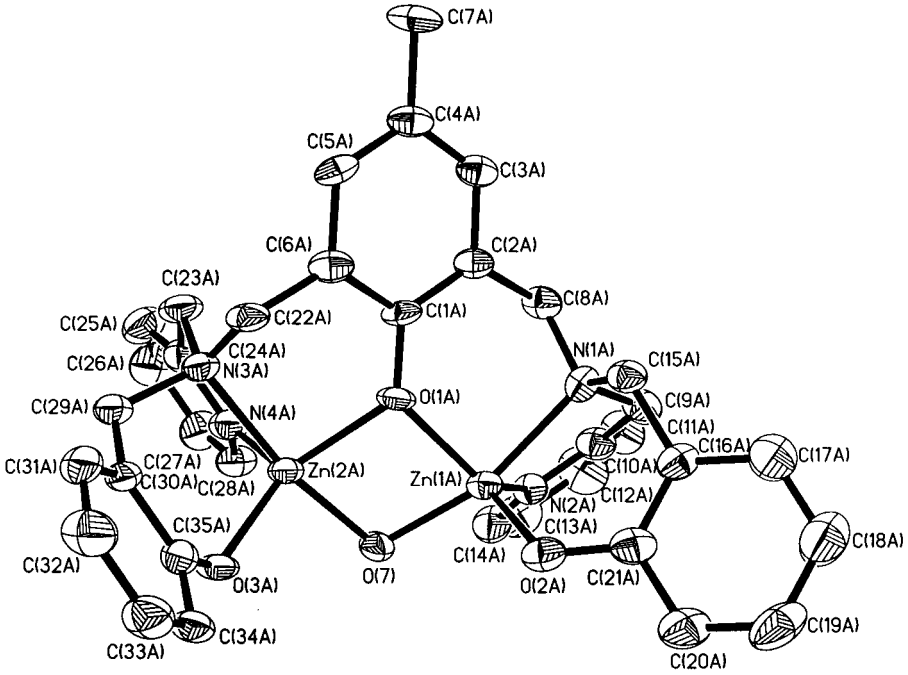

Figure 2. An ORTEP drawing of the molecular structure of $[Zn_2LOH]$ (**2**) showing the atom labelling; thermal ellipsoids for the non-hydrogen atoms are drawn at the 50% probability level; selected bond lengths (Å) and angles (°) at the zinc(II) atom: Zn(1A)−O(1A) 2.048(5), Zn(1A)−O(2A) 1.967(5), Zn(1A)−O(7) 1.990(5), Zn(1A)−N(1A) 2.179(6), Zn(1A)−N(2A) 2.107(6), Zn(2A)−O(1A) 2.066(5), Zn(2A)−O(3A) 1.989(5), Zn(2A)−O(7) 1.975(5), Zn(2A)−N(3A) 2.209(6), Zn(2A)−N(4A) 2.060(7), Zn(1A)−Zn(2A) 3.0696(13); O(7)−Zn(1A)−N(1A) 159.6(2), N(2A)−Zn(1A)−O(1A) 128.2(2), O(1A)−Zn(1A)−O(2A) 109.4(2), O(2A)−Zn(1A)−N(2A) 121.0(2), O(7)−Zn(2A)−N(3A) 169.3(2), O(1A)−Zn(2A)−O(3A) 130.4(2), O(3A)−Zn(2A)−N(4A) 115.8(2), N(4A)−Zn(2A)−O(1A) 112.8(2), Zn(1A)−O(1)−Zn(2A) 96.54(19), Zn(1A)−O(7)−Zn(2A) 101.5(2)

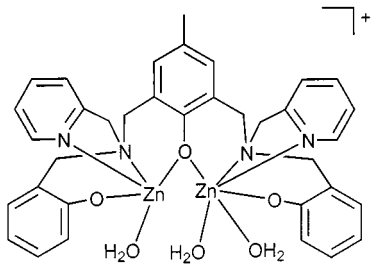

$[Zn_2L(OH_2)_3]^+$

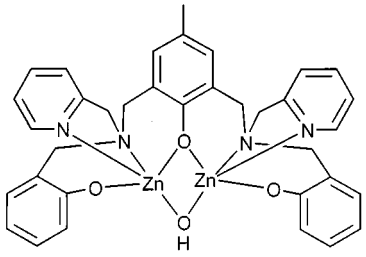

$[Zn_2L(OH)]$

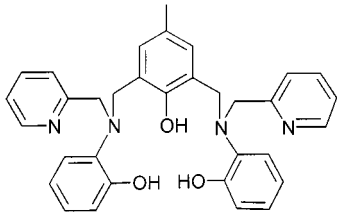

H_3L_A

[O(2)−Zn(1)−N(2)], 177.9 [O(5)−Zn(1)−N(1)] and 172.5° [O(4)−Zn(1)−O(1)].

The second zinc atom, Zn(2), is five-coordinate with an N_2O_3 donor set derived from the bridging cresolato-O and pendant phenolato-O donor atoms [O(1) and O(3)], an articular tertiary aminic-N atom [N(3)], the pendant pyridinyl-N atom [(N4)] and one coordinated water molecule [O(6)]. The degree of trigonality (τ) at Zn(2) is 0.60 signifying a distortion towards a trigonal bipyramidal geometry [a perfect trigonal bipyramidal geometry has τ = 1 and a perfect square pyramidal geometry has τ = 0.5].[5] The largest angle at Zn(2) is O(6)−Zn(2)−N(3) (167.9°) indicating that the water molecule and the articular aminic-N atom occupy the axial positions.

The second complex in the asymmetric unit, $[Zn_2L(OH)]$ (**2**), is a neutral dinuclear species with a (μ-cresolato)(μ-hydroxo) core. Both zinc atoms are five-coordinate with N_2O_3 donor sets made up of a bridging cresolato-O atom, a pendant phenolato-O atom, a pyridinyl-N atom, an articular tertiary aminic-N atom and a bridging hydroxo-O atom. The τ values of 0.52 [Zn(1A)] and 0.65 [Zn(2A)] show that the geometries at the metals are intermediate between trigonal bipyramidal and square pyramidal geometry. The largest angles at the metals are 159.6° [O(7)−Zn(1A)−N(1A)] and 169.3° [O(7)−Zn(2A)−N(3A)] showing that the O atom of the exogenous hydroxo bridge is *trans* to the articular tertiary aminic-N atom in each case.

The absence of an exogenous bridge in the complex cation from **1** promotes an intermetallic separation, Zn(1)−Zn(2), of 3.62 Å which is longer than that generally found in complexes bearing a (μ-cresolato)(μ-ethanoato)-bridged dinuclear core (≈3.41 Å)[1,6] and this is mirrored by the open Zn(1)−O(1)−Zn(2) angle of 116.5°. The separation Zn(1A)−Zn(2A) in complex **2** is 3.07 Å which is considerably shorter than those found in complexes with exogenously bridged bidentate bridges.[7] This is accompanied by a narrowing of the cresolato bridging angle [Zn(1A)−O(1A)−Zn(2A): 96.5°] *cf.* 116.5° in complex **1**. The Zn−OH−Zn bridge is slightly asymmetric with Zn−O distances of 1.975(5) and 1.990(5) Å. The bond lengths and angles at the dinuclear centre in complex **2** are similar to those found in the structure of $[Zn_2L_BOH(NO_3)_2]$ derived from the unsymmetrical compartmental ligand HL_B and used in the functional mimicking of metallo-β-lactams.[6] In this molecule the bridging bond angles at the phenolate- and hydroxo-O atoms are 98.2° and 105.7° respectively and the inter-zinc separation is 3.11 Å.

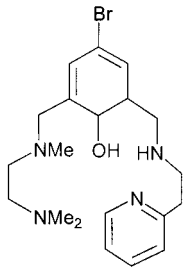

HL_B

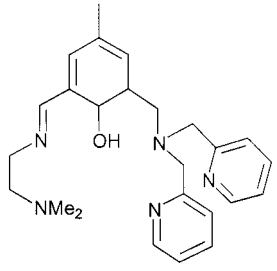

HL_C

In the crystal structures of dizinc(II)-containing metalloenzymes a water molecule or hydroxide anion shared by the zinc atoms frequently gives rise to a μ-hydroxo(*aqua*)-dizinc(II) motif[8,9] and the following metalloenzymes serve as representative examples: the metallo-β-lactamases from *Bacteriodes fragilis*[10,11] and *Stenotrophonomonas maltophilia*,[12] phospholipase C from *Bacillus cereus*,[13] P1 nuclease from *Penicillium citrium*[14] and bovine lens leucine aminopeptidase.[15,16] The first two examples have an unsupported water bridge and the Zn···Zn separation is approx. 3.5 Å, the next two examples are doubly bridged, by a water molecule and a bidentate carboxylato group, closing the Zn···Zn separation to approx. 3.3 Å. In the final example there is a triple bridge arising from a water molecule, a monodentate aspartate residue and a bidentate glutamate residue leading to a Zn···Zn separation of approx. 3.0 Å. Complex **2** has a double bridge constituted from two single oxygen atoms [(μ-cresolato)(μ-hydroxo)] and a Zn···Zn separation of 3.07 Å, and is thus similar to that found in bovine lens leucine aminopeptidase.

It is intriguing that the two complexes **1** and **2** co-crystallise and it is possible that conversion of **1** to **2** can occur if one of the polarisable water molecules on one Zn atom[17]

attacks the second Zn atom to displace bound water, thus forming the exogenous hydroxo bridge. Such an opportunity might also arise in the formation of μ-hydroxo bridges in dizinc(II)-containing metalloenzymes. A comparable co-crystallisation has been reported for the related complex $[Zn_2L_C(NCS)_3]$, derived from the phenol-based Schiff base compartmental ligand HL_C, in which one molecule has an exogenously bridging thiocyanate and two terminal thiocyanates, whereas the second molecule has no exogenous bridge and all three thiocyanates are terminal.[18]

Experimental Section

The Bulk Sample of $[ZnL]ClO_4 \cdot 3H_2O$: The proligand H_3L (133 mg, 0.24 mmol) was dissolved in warm CH_3CN (20cm^3) and $Zn(ClO_4)_2 \cdot 6H_2O$ (177 mg, 0. 48 mmol) added. The solution was refluxed gently for 1 h and then cooled to room temperature. Colourless crystals, suitable for X-ray structural analysis, were recovered on standing for one week. Yield: 154 mg (90%). MS (ES): *m*/*z* (%) = 687 (100) $[Zn_2L]^+$. IR (KBr disc): $\tilde{\nu}$ = 1609 cm^{-1} (C=N-pyr), 1572 (C=C-Ar), 1081 (ClO_4). $C_{35}H_{39}ClN_4O_{10}Zn_2$ (841.9): calcd. C 49.6, H 4.7, N 6.9, Cl 4.1; found C 49.9, H 4.7, N 6.7, Cl 4.1.

Caution! Although we have experienced no difficulties with the perchlorate salts they should nevertheless be regarded as hazardous and treated with care.

Crystal Data: $C_{72}H_{80}ClN_9O_{16}Zn_4$: M = 1624.38. Crystallises from CH_3CN as colourless blocks; crystal dimensions 0.28 × 0.15 × 0.06 mm^3. Triclinic, space group $P\bar{1}$, a = 14.7647(13), b = 16.9376(14), c = 17.8089(15) Å, α = 68.634(2)°, β = 71.356(2)°, γ = 87.526(2)°, U = 3916.3(6) Å^3, Z = 2, D_c = 1.377 Mg/m^3, Mo-K_α radiation (λ = 0.71073 Å), μ(Mo-K_α) = 1.312 mm^{-1}, F(000) = 1680. Data collected were measured on a Bruker Smart CCD area detector with an Oxford Cryosystems low temperature system at 150 K. Cell parameters were refined from the setting angles of 54 reflections (1.46 < θ < 28.32°). Reflections were measured from a hemisphere of data collected of frames each covering 0.3 degrees in omega. Of the 24262 reflections measured, all of which were corrected for Lorentz and polarisation effects and for absorption by semi-empirical methods based on symmetry-equivalent and repeated reflections (minimum and maximum transmission coefficients 0.7102 and 0.9254), 8804 independent reflections exceeded the significance level $|F|/\sigma(|F|) > 4.0$. The structure was solved by direct methods and refined by full-matrix least-squares methods on F^2. Hydrogen atoms were placed geometrically, except those on O1W, and refined with a riding model (including torsional freedom for methyl groups) and with U_{iso} constrained to be 1.2 (1.5 for methyl groups) times U_{eq} of the carrier atom. Refinement converged at a final R_1 = 0.0822 ($wR2$ = 0.2186, for all 17770 data, 913 parameters, mean and maximum δ/σ 0.004, 0.175) with allowance for the thermal anisotropy of all non-hydrogen atoms. The $[ClO_4]^-$ anion was disordered and refined to an occupancy of 41.0:59.0%; two disordered water molecules [O(2W) and O(3W)] were refined to occupancies of 52.0:48.0 and 51.0:49.0% respectively, and a disordered CH_3CN molecule was refined to an occupancy of 54.0:46.0%. Minimum and maximum final electron density: −1.176 and 2.371 e·Å^{-3}. A weighting scheme $w = 1/[\sigma^2(F_0^2) + (0.1212P)^2 + 0.00P]$ where $P = (F_0^2 + 2F_c^2)/3$ was used in the latter stages of refinement. Complex scattering factors were taken from the program package SHELXTL as implemented on a Viglen Pentium computer.[19]

Crystallographic data (excluding structure factors) for the structure reported in this paper have been deposited with the Cambridge Crystallographic Data centre as supplementary publication no. CCDC-171737. Copies of the data can be obtained free of charge on application to CCDC, 12 Union Road, Cambridge CB2 1EZ, UK [Fax: (internat.) +44-1223/336-033; E-mail: deposit@ccdc.cam.ac.uk].

Acknowledgments

We thank the BBSRC for a studentship (to D B) and the EPSRC for funds towards the purchase of the diffractometer.

[1] H. Adams, D. Bradshaw, D. E. Fenton, *Supramolecular Chem.* **2001**, *13*, 513−519.
[2] B. Krebs, K. Schepers, B. Bremer, G. Henkel, E. Althaus, W. Müller-Warmuth, K. Griesar, W. Haase, *Inorg Chem.* **1994**, *33*, 1907−1914.
[3] J. H. Satcher, Jr., M. W. Droege, T. J. R. Weakley, R. T. Taylor, *Inorg. Chem.* **1995**, *34*, 3317−3328.
[4] M. A. de Brito, A. J. Bortoluzzi, A. Greatti, A. S. Ceccato, A. C. Joussef, S. M. Drechsel, *Acta Crystallogr., Sect. C* **2000**, *56*, 1188−1190.
[5] A. W. Addison, T. N. Rao, J. Reedijk, J. van Rijn, G. C. Verschoor, *J. Chem. Soc., Dalton Trans.* **1984**, 1349−1356.
[6] N. V. Kaminskaia, B. Spingler, S. J. Lippard, *J. Am. Chem. Soc.* **2000**, *122*, 6411−6422.
[7] D. Bradshaw, PhD Thesis (University of Sheffield), **2001**.
[8] W. N. Lipscomb, N. Sträter, *Chem. Rev.* **1996**, *96*, 2375−2433.
[9] D. E. Wilcox, *Chem. Rev.* **1996**, *96*, 2435−2458.
[10] N. O. Concha, B. A. Rasmussen, K. Bush, O. Herzberg, *Structure* **1996**, *4*, 823−836.
[11] A. Carfi, E. Duée, R. Paul-Soto, N. Galleni, J.-M. Frére, O. Dideberg, *Acta Crystallogr., Sect. D* **1998**, *54*, 47−57.
[12] J. H. Ulla, T. R. Walsh, I. A. Taylor, D. C. Emery, C. S. Verma, S. J. Gamblin, J. Spencer, *J. Mol. Biol.* **1998**, *284*, 125−136.
[13] E. Hough, L. K. Hansen, B. Birknes, K. Jynge, S. Hansen, A. Hordvik, C. Little, E. J. Dodson, Z. Derewenda, *Nature(London)* **1989**, *338*, 357−360.
[14] A. Volbeda, A. Lahm, F. Sakijama, D. Suck, *EMBO J.* **1991**, *10*, 1607−1618.
[15] N. Strater, W. N. Lipscomb, *Biochemistry* **1995**, *34*, 14792−14800.
[16] Further examples of the μ-hydroxo(*aqua*)dizinc(II) motif may be found in the structures of phosphotriesterase from *Pseudomonas diminuta*[20] and dihydroorotase from *Escherichia coli*.[21] In both structures the dinuclear centre is doubly bridged, by a water molecule and a bidentate carbamate group from a carboxylated lysine residue.
[17] B. L. Vallee, D. S. Auld, *Proc. Natl. Acad. Sci. USA.* **1990**, *87*, 220−224.
[18] K. Abe, J. Izumi, M. Ohba, T. Yokoyama, H. Okawa, *Bull. Chem. Soc. Jpn.* **2001**, *74*, 85−95.
[19] SHELXTL version, An integrated system for solving and refining crystal structures from diffraction data (Revision 5.1), Bruker AXS Ltd., Madison., Wis., USA, **1997**.
[20] M. M. Benning, H. Shim, F. M. Raushel, H. M. Holden, *Biochemistry* **2001**, *40*, 2712−2722.
[21] J. B. Thoden, G. N. Phillips, Jr., T. M. Neal, F. M. Raushel, H. M. Holden, *Biochemistry* **2001**, *40*, 6989−6997.

Received October 5, 2001
[I01392]

Olefin-Metal π-Interactions of Mercury and Zinc Ions in Complexes of Neutral Quinolylcyclopentadiene Derivatives

Markus Enders,*[a] Gunter Ludwig,[a] and Hans Pritzkow[a]

Dedicated to Professor Walter Siebert on the occasion of his 65th birthday

Keywords: Mercury / Zinc / N ligands / π interactions

The donor-functionalised cyclopentadiene derivative **1** acts as a neutral chelate ligand and forms the zinc and mercury complexes **2** and **3** upon treatment with $HgCl_2$ or $ZnCl_2$. Due to the predefined geometry of **1**, the MCl_2 moieties are found in close proximity to the π-system of the cyclopentadiene. In the mercury compound **3** there is some evidence for a bond between the d^{10}-ion and the ring carbon atoms, although this is not conclusive. The zinc compound **2**, however, clearly shows an interaction between the metal atom and the cyclopentadiene fragment. At the same time the bond between the Cp ring and the Me_3Si group is weakened.

Introduction

Coordination compounds of d^{10}-metals with olefins are very common for Ni, Pd and Pt. The metal-olefin interaction is strengthened by back bonding of d-electrons into the anti-bonding olefin-π-orbitals. In d^{10}-metal ions with one or two positive charges, the d-orbitals are contracted and therefore the electrons in these orbitals are much less accessible for back bonding to π-acceptor ligands such as carbon monoxide or olefins. Therefore metal carbonyl or olefin complexes of group 11 cations or group 12 dications are much less common and are less stable than similar neutral group 10 compounds.[1] However, Hg^{2+} is known to interact with arenes and a few examples have been studied by X-ray diffraction.[2]

A metal ion can be fixed in proximity to an olefinic system by the judicious choice of rigid chelating ligands. With such ligands it is possible to study weak interactions between metal atoms and π-electrons. We report here the use of quinoline-functionalised cyclopentadiene derivatives for such investigations, as these ligands possess an adequate rigid geometry.

Results and Discussion

Previously we have found that quinoline-functionalised cyclopentadiene derivatives can bind transition metal atoms through the nitrogen donor and two carbon atoms of the cyclopentadiene ring.[3] Attempts to isolate similar compounds with d^{10}-metal cations have been unsuccessful. In order to increase the donor ability of the pentadiene system, the trimethylsilyl derivative **1** was used as a ligand. Compound **1** was described by us some time ago and it reacts with $TiCl_4$ or $ZrCl_4$ with elimination of Me_3SiCl and formation of η^5-cyclopentadienyl complexes.[4] The solid state structure of **1** has now been investigated and is shown in Figure 1. The Me_3Si group lies in the 3-position relative to the quinoline substituent. The bond C12−Si1 is relatively long [1.924(2) Å] compared to the same distance in other cyclopentadiene derivatives with a Me_3Si substituent [average value 1.88 Å].[5]

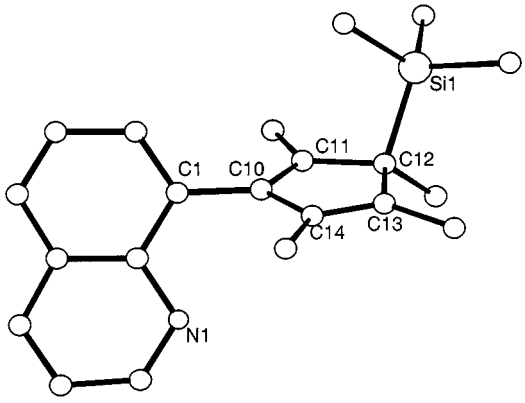

Figure 1. Solid-state structure of **1**; hydrogen atoms are omitted for clarity; selected bond lengths [Å]: C1−C10 1.482(2), C10−C11 1.357(2), C11−C12 1.504(2), C12−C13 1.508(2), C13−C14 1.352(2), C14−C10 1.464(2), C12−Si1 1.924(2), Si1−C_{Me} 1.863−1.869(2)

[a] Anorganisch-Chemisches Institut der Universität,
Im Neuenheimer Feld 270, 69120 Heidelberg, Germany
Fax: (internat.) + 49-(0)6221/545-609
E-mail: markus.enders@urz.uni-hd.de

Compound **1** was treated with zinc dichloride and with mercury dichloride (Scheme 1). In analogy to the synthesis of titanium or zirconium complexes, the elimination of trimethylsilyl chloride was expected with formation of cyclopentadienyl half-sandwich complexes. In fact anhydrous $ZnCl_2$, which is insoluble in toluene, slowly dissolves in the presence of a solution of **1** in toluene. After stirring for 16 h a yellow precipitate was obtained in 75% yield. Addition of hexane to a dichloromethane solution of this new compound led to the formation of yellow crystals suitable for X-ray diffraction. However, the structure analysis showed that an addition product of $ZnCl_2$ and **1** had been formed rather than the expected half-sandwich compound (Figure 2).

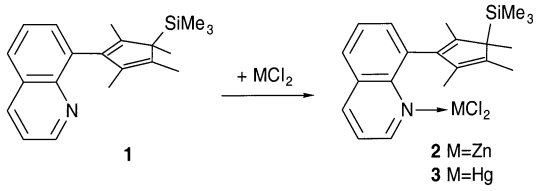

Scheme 1. Formation of **2** and **3**

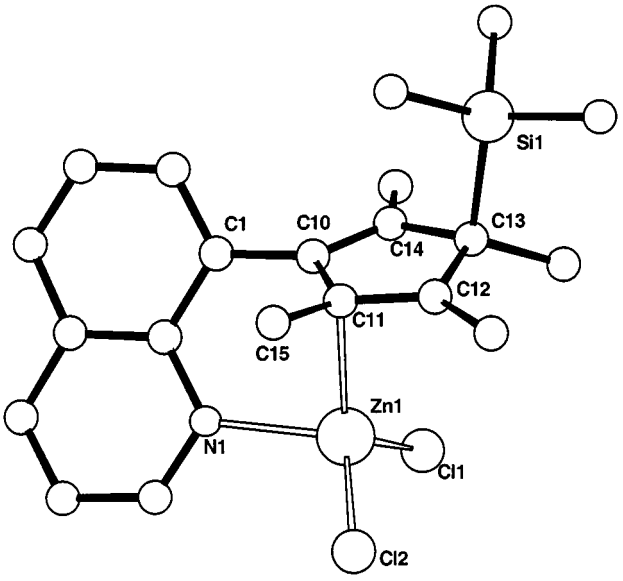

Figure 2. Solid-state structure of **2**; hydrogen atoms are omitted for clarity; selected bond lengths [Å] and angles [°]: C1−C10 1.475(3), C10−C11 1.467(3), C11−C12 1.376(3), C12−C13 1.486(3), C13−C14 1.486(3), C14−C10 1.358(3), C13−Si1 1.985(3), Si1−C_{Me} 1.856−1.867(3) Zn1−N1 2.080(2), Zn1−C11 2.316(2), Zn1−C12 2.735(2), Zn1−C10 2.639(2), Zn1−Cl1 2.216(1), Zn1−Cl2 2.219(1); C11−Zn1−Cl1 123.6(1), C11−Zn1−Cl2, 106.7(1), C11−Zn1−N1 89.4(1), Cl1−Zn1−Cl2 117.9(1), C10−C11−C15 123.8(2), C10−C11−C12 108.2(2), C12−C11−C15 126.3(2).

The zinc atom is coordinated in a distorted tetrahedral manner by two chlorine atoms, the nitrogen donor and one sp^2-carbon atom of the cyclopentadiene ring. The coordination of the neutral carbocyclic ring to the zinc atom is confirmed not only by a carbon-zinc distance of 2.316(2) Å but also by the strong pyramidalisation of the $ZnLCl_2$ fragment (L = nitrogen donor). The ligand framework in **2** shows some differences from the solid state structure of the free ligand **1**. Due to the interaction of the carbon atom C11 with the zinc atom, the bonding vector C11−C15 does not lie in the plane defined by the cyclopentadiene system but forms an angle of 15°. The Si1−C13 bonding vector approaches an orthogonal orientation (76°) to the best plane of the cyclopentadiene ring. In addition, the Si1−C13 bond length [1.985(3) Å] is considerably longer than the respective silicon-carbon bonds in **1**. To the best of our knowledge, the interaction of a zinc atom with a neutral olefinic π-system has not been observed previously in the solid state.[5] Many compounds are known where anionic $C_5R_5^-$ ligands bind to Zn^{2+} ions. In $[Zn(\eta^2\text{-}C_5H_5)_2]_n$ one zinc atom is coordinated by three cyclopentadienyl ligands in an η^2 binding mode with one short (2.04−2.19 Å) and one long (2.42−2.48 Å) metal-carbon bond.[6]

The NMR spectra of **2** show a higher symmetry than in the solid state. The four methyl substituents of the five-membered ring give only two signals in the ^1H and ^{13}C NMR spectrum. This can only be explained by a dynamic process where the zinc atom and the Me_3Si group are changing their positions at the five-membered ring. We were not able to freeze out this process by cooling to lower temperatures (down to 170 K in the ^1H NMR spectrum at 200 MHz). The ^1H NMR spectrum of the ligand **1** exhibits four broad resonances at room temperature for the four methyl groups of the ring. A fast exchange occurs at higher temperatures.[4] The higher fluxionality of **2** compared to that of **1** shows the influence of the zinc-carbon interaction, which weakens the bond between the $SiMe_3$ group and the five-remembered ring.

The reaction between **1** and $HgCl_2$ leads to an orange yellow solution, from which yellow needles of the new compound **3** were obtained by addition of hexane. The NMR spectra of redissolved crystals showed signals indicating the presence of several different species in solution. The elemental analysis proves that **3** is an adduct of **1** with one equivalent of $HgCl_2$. The X-ray analysis reveals that two isomers — a monomer and a dimer — are present in the solid state. The molecular structure of the monomeric complex is shown in Figure 3.

The mercury atom is surrounded by one nitrogen, two chlorine and two carbon atoms of the cyclopentadiene ring. The coordinated sp^2-carbon atoms are interconnected by a single bond [C31−C35: 1.479(6) Å]. The interaction between the metal and the two carbon atoms, with distances of 2.957(4) and 3.000(5) Å, seems to be weak. The N2−Hg2−Cl3−Cl4 unit remains nearly trigonal planar, in contrast to the geometry in the zinc compound **2**. In the dimeric isomer shown in Figure 4, the coordination number at mercury is higher. Three chlorine ligands, the nitrogen donor and two carbon atoms of the cyclopentadiene are connected to the metal atom. The two sp^2-carbon atoms are part of an olefinic C−C double bond [C10−C11: 1.359(5) Å]. This double bond is not lengthened by the interaction with the Hg^{2+} ions and is practically equal to the corresponding C−C double bond in **1** [1.357(2)]. The dis-

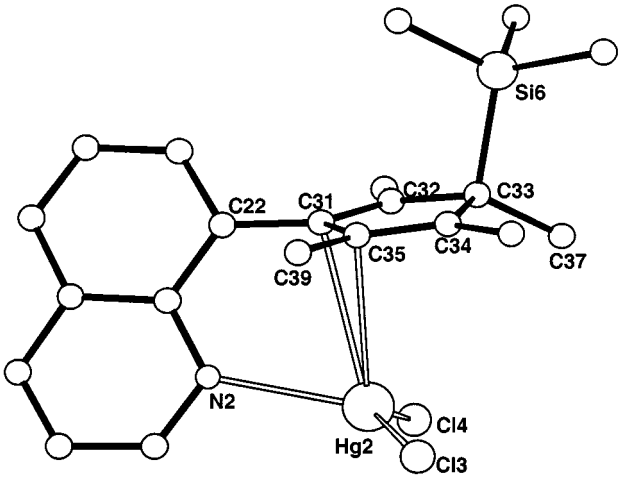

Figure 3. Part of the solid-state structure of **3** (monomeric Hg complex); hydrogen atoms are omitted for clarity; selected bond lengths[Å] and angles [°]: C22−C31 1.480(6), C31−C32 1.359(6), C32−C33 1.503(6), C33−C34 1.501(7), C34−C35 1.345(7), C35−C31 1.479(6), C33−Si6 1.956(5), Hg2−N2 2.391(4), Hg2−Cl3 2.356(1), Hg2−Cl4 2.358(1), Hg2−C31 2.957(4), Hg2−C35 3.000(5); N2−Hg2−Cl3 108.5(1), N2−Hg2−Cl4 110.5(1), Cl3−Hg2−Cl4 137.3(1)

tances between the mercury atoms and the linked carbon atoms are shorter in the dimeric compound (2.81 and 2.88 Å) than in the monomeric one (2.96 and 3.00 Å). In known Hg^{II}-arene complexes, the mercury-carbon distances vary considerably, from 2.56 Å[2a][2b] to 3.11 Å[2c][2d] and 3.33 Å.[2e]

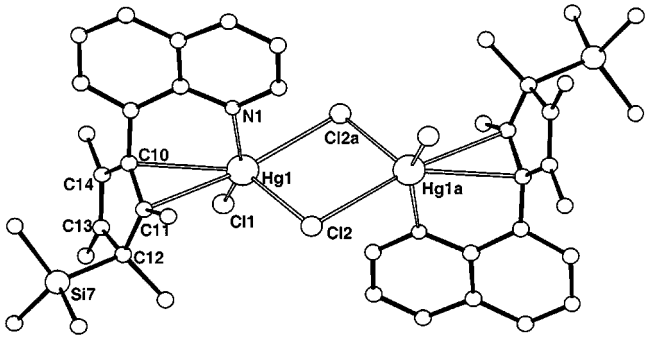

Figure 4. Part of the solid-state structure of **3** (dimeric Hg complex); hydrogen atoms are omitted for clarity; selected bond lengths[Å] and angles [°]: C10−C11 1.359(5), C11−C12 1.498(5), C12−C13 1.498(6), C13−C14 1.356(6), C14−C10 1.464(6), C12−Si7 1.949(4), Hg1−Cl1 2.365(1), Hg1−Cl2 2.549(1), Hg1−Cl2a 2.946(1), Hg1−Hg1a 3.985(1), Hg1−C10 2.813(4), Hg1−C11 2.879(4); Cl1−Hg1−Cl2 113.1(1), Cl1−Hg1−Cl2a 88.9(1), Hg1−Cl2−Hg1a 92.70, N1−Hg1−Cl1 151.1(1)

A comparison of the positions of the $SiMe_3$ groups in the solid-state structures of **1**, **2** and **3** shows significant differences. The C_{Cp}−Si bond lengths become longer when going from **1** to **3** and to **2** [1.924(2), 1.949(4), 1.985(3), respectively]. The value for the zinc compound **2** is much larger than for a normal Si−C bond. In addition, the angles between the Si−C_{Cp} bonding vectors and the corresponding planes of the five-membered rings become larger in the same order (**1**: 62°, **3**: 71°, **2**: 76°). As other Lewis acids such as $TiCl_4$ react with **1** with substitution of the $SiMe_3$ group, the compounds **3** and **2** may be described as snapshots of this electrophilic substitution reaction where the metal fragment attacks from one face of the five-membered ring and the $SiMe_3$ group is released at the other face.

Experimental Section

All reactions were carried out under a nitrogen or argon atmosphere. Compound **1** was prepared by the reported procedure.[4]

2: A total of 300 mg (0.93 mmol) of the trimethylsilyl derivative **1** was added to a suspension of zinc(II)chloride (130 mg, 0.95 mmol) in 30 mL of toluene. The solution was stirred for 16 hours. The resulting yellow precipitate was separated by filtration and dried in vacuum. The solid was dissolved in dichloromethane and layered with 10 mL of hexane. Compound **2** crystallised from the hexane phase at −30 °C as yellow cubes, which were suitable for X-ray analysis. Dichloromethane, which is present in the single crystals, was removed by pulverising the solid and evaporation under vacuum. Yield 310 mg (0.68 mmol, 72%). ^{1}H NMR (300 MHz, CD_2Cl_2): δ = 0.12 [s, 18 H, $Si(CH_3)_3$], 1.83 (s, 6 H, Cp-CH_3), 1.99 (s, 6 H, Cp-CH_3), 7.66−7.75 (m, 3 H), 7.80−8.02 (m, 1 H), 8.57 (d, $J_{H,H}$ = 6.0 Hz, 1 H), 8.96 (d, $J_{H,H}$ = 3.2 Hz, 1 H). ^{13}C {^{1}H} NMR (75 MHz, CD_2Cl_2): δ = −2.53 [$Si(CH_3)_3$], 13.6 (Cp-CH_3), 14.0 (Cp-CH_3), 122.6, 128.5, 128.6, 133.0, 141.5, 151.3 ($CH_{quinoline}$). MS (EI): *m*/*z* (%) =322 (2) [$Cp^QSiMe_3^+$], 306 (5) [$Cp^QSiMe_2^+$], 249 (41) [Cp^QH^+], 108 (51) [$ClSiMe_3^+$], 93 (100) [$ClSiMe_2^+$], 74 (84) [$SiMe_3^+$], 65 (64) [Zn^+].

3: A total of 360 mg (1.12 mmol) of the trimethylsily-derivative **1** was added to a suspension of mercury(II)chloride (320 mg, 1.19 mmol) in 20 mL of toluene. The solution was stirred for 48 hours and the resulting orange solid was separated by filtration. The yellow solution was concentrated and layered with 10 mL of hexane. Compound **3** crystallised as bright yellow needles from the hexane phase, which were suitable for X-ray analysis; yield 320 mg (0.54 mmol, 48%). MS (FAB): *m*/*z* (%) = 558 (6) [M^+ − Cl], 322 (100) [$Cp^QSiMe_3H^+$], 248 (80) [Cp^{Q+}], 147 (55). $C_{21}H_{27}Cl_2HgNSi$ (593.03): calcd. C 42.53, H 4.59, N 2.36; found C 42.76, H 4.60, N 2.37.

Crystal Structure Determinations:

1: $C_{21}H_{27}NSi$, monoclinic, $P2_1/c$, a = 13.5835(9), b 16.3449(11), c = 8.6546(6) Å, β = 101.0150(10)°, V = 1886.1(2) Å^3, Z = 4, $d_{calcd.}$ = 1.132 g cm^{-3}, 4491 reflections, 316 parameters, $R1$ = 0.0445, $wR2$= 0.129.

2·1/2CH_2Cl_2: $C_{21.5}H_{28}Cl_3NSiZn$, monoclinic, $C2/c$, a = 34.954(17), b = 8.414(4), c = 17.501(9) Å, β = 113.07(2)°, V = 4735(4) Å^3, Z = 8, $d_{calcd.}$ = 1.403 g cm^{-3}, 4163 reflections, 361 parameters, $R1$ = 0.0285, $wR2$ = 0.0656.

3: $C_{21}H_{27}Cl_2HgNSi$, triclinic, $P\bar{1}$, a = 10.5069(2), b = 13.9186(2), c = 15.7285(3) Å, α= 85.213(1), β = 78.735(1), γ = 88.288(1)°, V = 2247.76(7) Å^3, $d_{calcd.}$ = 1.752 g cm^{-3}, 10594 reflections, 486 parameters, $R1$ = 0.0305, $wR2$ = 0.0791.

Data were collected on a Siemens Stoe AED2 (−70 °C, **2**) or on a Bruker AXS SMART1000 (−85 °C **1**, −100 °C **3**) diffractometer equipped with Mo-K_α radiation and in the ω-scan mode. An empirical absorption correction was applied. The structures were solved by direct methods (SHELXS-86 [7]) and refined by full-matrix least-squares techniques (SHELXL-93 [7]) based on F^2 using all

measured reflections and with anisotropic temperature factors for all non-hydrogen atoms. The hydrogen atoms were located and refined isotropically for **1** and **2**, for **3** they were inserted in their calculated positions.

Crystallographic data (excluding structure factors) for the structures reported in this paper have been deposited with the Cambridge Crystallographic Data Centre as supplementary publication nos. CCDC-168388 (**1**), -16389 (**2·1/2CH_2Cl_2**) and -168390 (**3**). Copies of the data can be obtained free of charge on application to CCDC, 12 Union Road, Cambridge CB2 1EZ, UK [Fax: (internat.) +44-1223/336-033; E-mail: deposit@ccdc.cam.ac.uk].

Acknowledgments

We thank Professor W. Siebert for his generous support over the years.

[1] Cationic metal carbonyls of group 11 and group 12 metals have been considered to be nonclassical because of some unusual properties, such as high ν(CO) values: [1a] S. H. Strauss, *J. Chem. Soc., Dalton Trans.* **2000**, 1−6. [1b] A. J. Lupinetti, G. Frenking, S. H. Strauss, *Angew. Chem.* **1998**, *110*, 2229−2232; *Angew. Chem. Int. Ed.* **1998**, *37*, 2113−2116.

[2] [2a] W. Lau, J. C. Huffman, J. K. Kochi, *J. Am. Chem. Soc.* **1982**, *104*, 5515−5517. [2b] W. Lau. J. K. Kochi, *J. Org. Chem.* **1986**, *51*, 1801−1811. [2c] M. A. Avales, R. Babiano, P. Cintas, C. J. Duran, F. J. Higes, J. L. Jimenez, I. Lopez, J. C. Palacios, *Tetrahedron* **1997**, *52*, 14463−14480. [2d] M. C. Corbeil, A. L. Beauchamp, *Can. J. Chem.* **1988**, *66*, 2458−2464. [2e] A. J. Canty, N. Chaichit, B. M. Gatehouse, *Acta Crystallogr., Sect. B* **1980**, *36*, 786−789.

[3] M. Enders, P. Fernández, M. Kaschke, G. Kohl, G. Ludwig, H. Pritzkow, R. Rudolph, *J. Organomet. Chem.* in press.

[4] M. Enders, R. Rudolph, H. Pritzkow, *Chem. Ber.* **1996**, *129*, 459−463.

[5] [5a] Cambridge Structural Database, Entries until April 2001. [5b] F. H. Allen, O. Kennard, *Chemical Design Automation News* **1993**, *8*, 31−37.

[6] P. H. M. Budzelaar, J. Boersma, G. J. M. Van der Kerk, A. L. Spek, A. J. M. Duisenberg, *J. Organomet. Chem.* **1985**, *281*, 123−130.

[7] G. M. Sheldrick, *SHELXS 86* **1986**, Universität Göttingen; G. M. Sheldrick, *SHELXL 97* **1997**, Universität Göttingen

Received October 4, 2001
[I01390]

Self-Assembly of a Chiral Three Dimensional Architecture Composed of Two Different Silver(I) Helical Chains Connected by Bitopic Tris(pyrazolyl)methane Ligands

Daniel L. Reger,*[a] Radu F. Semeniuc,[a] and Mark D. Smith[a]

Keywords: Helical structures / Ligand design / Silver / Self-assembly

The coordination polymer $\{p\text{-}C_6H_4[CH_2OCH_2C(pz)_3]_2\text{-}Ag_2(BF_4)_2\}_n$ contains two opposite chirality metallohelicates, formed by a κ^2, κ^1 bonding arrangement of each tris(pyrazolyl)methane unit, that are linked with the bitopic ligand into 2D sheets. The 3D supramolecular structure is formed by C–H···F weak hydrogen bonds that also order the solvent molecules.

Helical structures have received increasing attention because of their structural similarities to nucleic acids and proteins. Potential applications, such as asymmetric catalysis and nonlinear optical materials,[1] have also increased the interest in the synthesis and characterization of these types of structures. Helical organization has been driven by the formation of covalent bonds in metal complexes[1a,2] and intermolecular forces, mainly hydrogen bonding.[3] Most known structures consist of discrete molecules or ions,[1a,1b,4] although examples of coordination polymers with helical structures are also known.[2,5] We report here a unique supramolecular architecture formed by using a new bitopic ligand to link two different metallohelicates having opposite chirality.

We are developing supramolecular chemistry using a new class of multitopic ligands, formed from linking two or more tris(pyrazolyl)methane units[6] in a single molecule, a study made possible by our recent progress on the preparation and reaction chemistry of tris(pyrazolyl)methane ligands.[7] Our first example is $p\text{-}C_6H_4[CH_2OCH_2C(pz)_3]_2$ (**1**, Scheme 1). This ligand was designed to have the unique capability of linking metals into chiral polymer chains with a κ^2, κ^1 bonding arrangement while also linking these chains with the flexible side arms of a 1,4-bis(ethoxymethyl)benzene bridge.

The reaction of $p\text{-}C_6H_4[CH_2OCH_2C(pz)_3]_2$ with $AgBF_4$ in a 1:2 ratio in THF yields $\{p\text{-}C_6H_4[CH_2OCH_2C(pz)_3]_2Ag_2(BF_4)_2\}_n$ (**2**), a coordination polymer that contains two types of bridged helical chains. Crystals of **2** suitable for X-ray diffraction[8] were grown by vapor-phase diffusion of Et_2O into an acetonitrile solution. The left side of Figure 1 shows a drawing of one of the two polymer chains. Each Ag(1) is three-coordinate, κ^2-bonded to a tris(pyrazolyl)methane unit in one ligand and κ^1-bonded to a second from a different ligand, forming polymer chain **1**. The polyhedron involving the Ag(1) atom is a flattened trigonal pyramid [sum of the N–Ag(1)–N bond angles = 347°], with a significant distortion caused by the restricted angle [83.43(11)°] of the κ^2-bonded ligand.

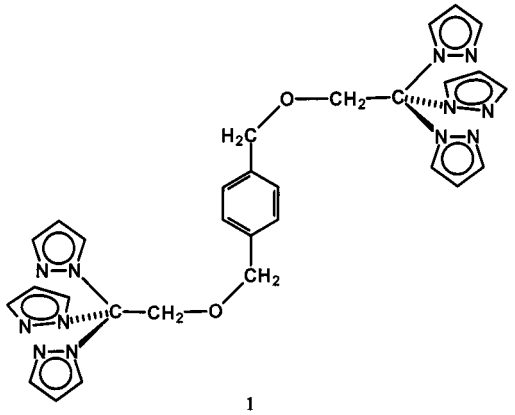

1

Scheme 1. 1,4-Bis[tris(pyrazolyl)ethoxymethyl]benzene

The right side of Figure 1 shows a drawing of the polymer chain formed by Ag(2). Each Ag(2) is four-coordinate. As with Ag(1), each silver(I) is κ^2-bonded to one tris(pyrazolyl)methane unit and κ^1-bonded to a second, forming polymer chain **2**. In addition, there is an acetonitrile molecule bonded to each Ag(2). The polyhedron involving the Ag(2) atom is a distorted tetrahedron with a large distortion caused by the restricted angle [77.40(11)°] of the κ^2-bonded ligand. The CH_3CN molecules bonded to the Ag(2) atoms are alternatively above and below the chain, as pictured (see also Figure 3b).

[a] Department of Chemistry and Biochemistry, University of South Carolina
Columbia, South Carolina 29208, USA
Fax: (internat.) +1-803/777-9521
E-mail: Reger@psc.sc.edu

 © WILEY-VCH Verlag GmbH, 69451 Weinheim, Germany, 2002 1434–1948/02/0303–0543 $ 17.50+.50/0

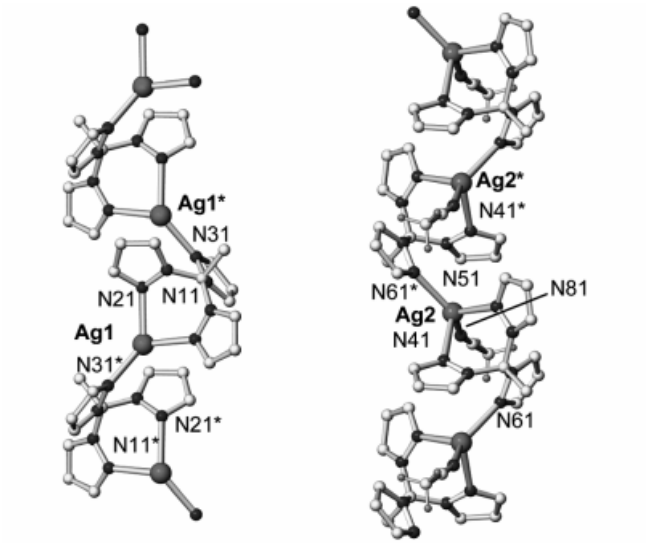

Figure 1. (a) Partial structure of **2** showing the polymeric chain formed by Ag(1); selected bonds (Å) and angles (deg.) are as follows: Ag(1)−N(11) 2.269(3), Ag(1)−N(21) 2.283(3), Ag(1)−N(31*) 2.196(4), N(11)−Ag(1)−N(21) 83.43(11), N(11)−Ag(1)−N(31*) 127.50(13), N(21)−Ag(1)−N(31*) 136.16(12); (b) the polymeric chain formed by Ag(2); selected bonds (Å) and angles (deg.) are as follows: Ag(2)−N(41) 2.405(3), Ag(2)−N(51) 2.380(3), Ag(2)−N(61*) 2.292(3), Ag(2)−N(81) 2.206(4), N(41)−Ag(2)−N(51) 77.40(11), N(41)−Ag(2)−N(61*) 107.07(11), N(41)−Ag(2)−N(81) 103.48(12), N(51)−Ag(2)−N(61*) 102.77(11), N(51)−Ag(2)−N(81) 124.19(13), N(61*)−Ag(2)−N(81) 128.28(12)

Figure 2 shows a space filling model of the backbone of both silver chains. In both cases the arrangement of the backbone is helical, but the chirality of each is opposite. Both helices are generated around crystallographic 2_1 screw axes along the *a* axis of the unit cell. For both, the distance between every other silver atom is equal and identical to the length of the *a* axis of the unit cell, 10.282 Å, making the pitches of both helicates identical.

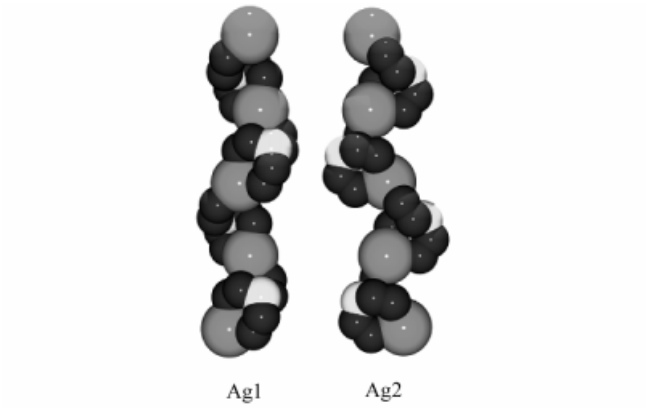

Figure 2. Space filling representation of the backbone of both silver chains, showing the helical arrangement; for the sake of clarity all atoms not directly related to the backbone chains have been omitted; the acetonitrile molecule is also excluded in the Ag(2) case

Figure 3a is a view perpendicular to the network formed by the alternating helical chains. The helical chains are connected by the 1,4-bis(ethoxymethyl)benzene bridging units with the ether groups in each ligand oriented on opposite sides of the aromatic ring. Although this part of the network is two dimensional, the structure has thickness. Figure 3b is the view in the same alignment of chains as in Figure 3a, viewed parallel to the network, showing two U-shape channels formed between the silver strands by the 1,4-bis(ethoxymethyl)benzene bridge. The dimensions of the channels are 5.8 × 3.6 Å, measured between the two methylene groups directly bonded to the phenyl ring and between these methylene groups and the central methine carbon atoms from the tris(pyrazolyl)methane units. There is also a cavity formed along the strand formed by the three-coordinate Ag(1) because of the parallel orientation of the flattened trigonal pyramids.

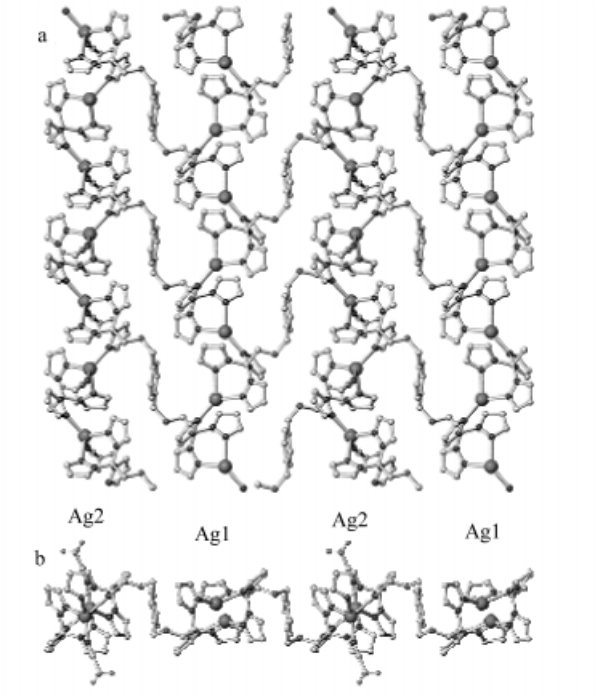

Figure 3. View perpendicular (a) and parallel (b) to the sheets formed by the alternating silver chains

Figure 4 shows that the 2D network (viewed as in Figure 3b) formed by the helical chains and the connecting organic bridges is arranged into a 3D supramolecular structure by weak C−H···F hydrogen bonds. One of the two nonequivalent BF_4^- ions makes four hydrogen bonds with two of the 2D sheets forming the 3D architecture. Two of the bonds, one to each sheet, are very short at 2.262 and 2.290 Å. The average C−H···F bond length of 2.326 Å is significantly shorter than the sum of the van der Waals radii for H and F atoms (2.54 Å)[9] and other known cases of this type of interaction,[10] where the reported values are close to 2.5 Å. The second BF_4^- ion makes two hydrogen bonds, one to each of two sheets, at a distance of 2.302 and 2.353 Å.

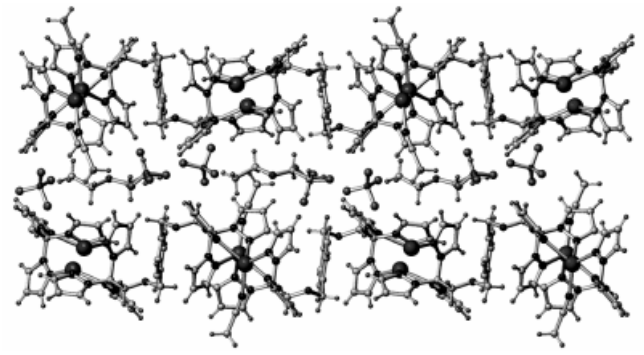

Figure 4. Two sheets held together through C−H···F bonds, forming a 3D architecture

An additional important structural feature is that the solvent molecules are held between the helical layers in a very ordered fashion by weak hydrogen bonds, an unusual observation for helical superstructures.[1a] As pictured in Figure 4, each diethyl ether molecule is bonded through one terminal methyl group to the BF_4 counter-ion that makes four hydrogen bonds (C−H···F separation is 2.362 Å, with the corresponding angle of 142.48°) and also through the ether oxygen atom to a coordinated acetonitrile (C−H···O separation is 2.557 Å with corresponding angle = 150.05°).

We plan to develop these chiral polymers as useful materials in the field of stereospecific synthesis or asymmetric catalysis.[11] The dual chiral material reported here is made using inexpensive and readily available materials. The potential applications of our compounds are increased by the observation of the ordered solvent molecules. Future work will determine the influence of the solvent and the counter-ion on the overall structure. We are also studying the diversity of the supramolecular structures that arise from small changes in the structure of the ligand (for example, by using *ortho*-xylene in the bridge instead of *para*-xylene).

Experimental Section

p-$C_6H_4[CH_2OCH_2C(pz)_3]_2$ (1): α,α′-Dibromo-*p*-xylene, *p*-$(BrCH_2)_2$-C_6H_4, (2.64 g, 0.010 mol) and tris-2,2,2-(1-pyrazoyl)ethanol,[7] HO-CH_2-$C(pz)_3$, (4.88 g, 0.020 mol) were dissolved in dry THF (125 mL). This solution was added dropwise to a suspension of NaH (1.5 g) in dry THF (300 mL) under an inert atmosphere. The mixture was stirred under reflux for 24 h and then allowed to cool at room temperature. Enough water (150 mL) was added dropwise to consume the excess NaH and dissolve the resulting NaBr and NaOH. The THF/water mixture was extracted with ethyl ether (3 × 100 mL), the combined organic extracts were washed with 100 mL saturated $NaHCO_3$ solution, with 100 mL saturated NaCl solution and finally with 100 mL water. The organic layer was dried over anhydrous Na_2SO_4, filtered and the solvent removed under vacuum to afford the desired compound as a white-yellow powder (5.38 g, 0.0091 mol, 91%). M.p. 128−129 °C. ^{1}H NMR (300 MHz, [D$_6$]acetone): δ = 7.59, 7.49 (m, 3,3 H, 3,5-H *pz*), 7.18 (s, 2 H, *C_6H_4*), 6.35 (m, 3 H, 4-H pz), 5.11 (s, 2 H, O*CH_2*Ph), 4.54 [s, 2 H, O*CH_2*C(pz)$_3$]. $C_{30}H_{30}N_{12}O_2$ (590.6): calcd. C 60.96, H 5.08; found C 61.06, H 4.98.

{p-$C_6H_4[CH_2OCH_2C(pz)_3]_2Ag_2(BF_4)_2$}$_n$ (2) $AgBF_4$ (0.195 g, 1.0 mmol) was dissolved in THF (15 mL) under an inert atmosphere. With vigorous stirring, a solution of *p*-$C_6H_4[CH_2OCH_2C(pz)_3]_2$ (0.295 g, 0.50 mmol) in THF (15 mL) was added dropwise during a 10 min period. A white precipitate appeared as the mixture was stirred for 3 h. The THF was removed by cannula filtration, the white precipitate washed with THF (2 × 10 mL) and then vacuum dried to afford 0.475 g of solid identified as {p-$C_6H_4[CH_2OCH_2C(pz)_3]_2Ag_2(BF_4)_2(THF)$}$_n$, m.p. 163−166 °C with decomposition. ^{1}H NMR ([D$_6$]acetone): δ = 7.82, 7.77 (m, 3,3 H, 3,5-H *pz*), 7.09 (s, 2 H, *C_6H_4*), 6.57 (m, 3 H, 4-H *pz*), 5.02 (s, 2 H, O*CH_2*Ph), 4.67 [s, 2 H, O*CH_2*C(pz)$_3$], 3.62 (m, 2 H, *CH_2*O THF), 1.92 (m, 2 H, *CH_2* THF). $C_{30}H_{30}Ag_2B_2F_8N_{12}O_2{\cdot}C_4H_8O$ (1051.1): calcd. C 38.81, H 3.64; found C 38.86, H 3.55. ES$^+$/MS: calcd. for $[C_{30}H_{30}N_{12}O_2Ag]^+$ 697.1666; found 697.1683.

Acknowledgments

The authors thank the National Science Foundation (CHE-0110493) for support. The Bruker CCD Single Crystal Diffractometer was purchased using funds provided by the NSF Instrumentation for Materials Research Program through Grant DMR:9975623.

[1] [1a] C. Piguet, G. Bernardinelli, G. Hopfgartner, *Chem. Rev.* **1997**, *97*, 2005−2062. [1b] P. Comba, A. Fath, T. W. Hambley, A. Kühner, D. T. Richens, A. Viefort, *Inorg. Chem.* **1998**, *37*, 4389−4401. [1c] P. N. Prasad, D. J. Williams, *Introduction to Non Linear Optical Effects in Molecules and Polymer*s, John Wiley & Sons, Chichester, **1991**.

[2] [2a] A. J. Blake, N. R. Champness, P. A. Cooke, J. E. B. Nicolson, *Chem. Commun.* **2000**, 665−666. [2b] L. Zhang, P. Cheng, L.-F. Tang, L.-H. Weng, Z.-H. Jiang, D.-Z. Liao, S.-P. Yan, G.-L. Wang, *Chem. Commun.* **2000**, 717−718. [2c] M. Munakata, G. L. Ning, Y. Suenaga, K. Sugimoto, T. Kuroda-Sowa, M. Maekawa, *Chem. Commun.* **1999**, 1545−1546. [2d] C. Kaes, M. W. Hosseini, C. E. F. Rickard, B. W. Skelton, A. H. White, *Angew. Chem.* **1998**, *110*, 970−973; *Angew. Chem. Int. Ed.* **1998**, *37*, 920−922.

[3] [3a] Y. Hamuro, S. J. Geib, A. D. Hamilton, *J. Am. Chem. Soc.* **1997**, *119*, 10587−10593. [3b] A. Tanatani, H. Kagechika, I. Azumaya, R. Fukutomi, Y. Ito, K. Yamaguchi, K. Shudo, *Tetrahedron Lett.* **1997**, *38*, 4425−4428. [3c] M. P. Lightfoot, F. S. Mair, R. G. Pritchard, J. E. Warren, *Chem. Commun.* **1999**, 1945−1946.

[4] [4a] E. C. Constable, M. D. Ward, D. A. Tocher, *J. Am. Chem. Soc.* **1990**, *112*, 1256−1258. [4b] M. J. Hannon, C. L. Painting, N. W. Alcock, *Chem. Commun.* **1999**, 2023−2024. [4c] K. M. Gardinier, R. G. Khoury, J.-M. Lehn, *Chem. Eur. J.* **2000**, *6*, 4124−4131. [4d] P. N. W. Baxter, J.-M. Lehn, G. Baum, D. Fenske, *Chem. Eur. J.* **2000**, *6*, 4510−4517. [4e] V. Berl, I. Huc, R. G. Khoury, M. J. Krische, J.-M. Lehn, *Nature* **2000**, *407*, 720−723.

[5] [5a] K. Biradha, C. Seward, M. J. Zaworotko, *Angew. Chem.* **1999**, *111*, 584−587; *Angew. Chem. Int. Ed.* **1999**, *38*, 492−495. [5b] M. Hong, W. Su, R. Cao, M. Fujita, J. Lu, *Chem. Eur. J.* **2000**, *6*, 427−431.

[6] [6a] D. L. Reger, *Comm. Inorg. Chem.* **1999**, *21*, 1−28. [6b] D. L. Reger, J. E. Collins, S. M. Myers, A. L. Rheingold, L. M. Liable-Sands, *Inorg. Chem.* **1996**, *35*, 4904−4909. [6c] D. L.

Reger, J. E. Collins, A. L. Rheingold, L. M. Liable-Sands, G. P. A. Yap, *Inorg. Chem.* **1997**, *36*, 345−351. [6d] D. L. Reger, J. E. Collins, D. L. Jameson, R. K. Castellano, *Inorg. Synth.* **1998**, *32*, 63−65. [6e] D. L. Reger, J. E. Collins, A. L. Rheingold, L. M. Liable-Sands, *Organometallics* **1996**, *15*, 2029−2032. [6f] D. L Reger, J. E. Collins, A. L. Rheingold, L. M. Liable-Sands, G. P. A. Yap, *Organometallics* **1997**, *16*, 349−353. [6g] D. L. Reger, J. E. Collins, R. Layland, R. D. Adams, *Inorg. Chem.* **1996**, *35*, 1372−1376. [6h] D. L. Reger, J. E. Collins, A. L. Rheingold, L. M. Liable-Sands, *Inorg. Chem.* **1999**, *38*, 3235−3237. [6i] D. L. Reger, J. E. Collins, M. A. Mathews, A. L. Rheingold, L. M. Liable-Sands, I. A. Guzei, *Inorg. Chem.* **1997**, *36*, 6266−6269. [6j] D. L. Reger, C. A. Little, A. L. Rheingold, K.-C. Lam, T. Concolino, A. Mohan, G. J. Long, *Inorg. Chem.* **2000**, *39*, 4674−4676. [6k] D. L. Reger, C. A. Little, A. L. Rheingold, M. Lam, L. M. Liable-Sands, B. M. Rhagitan, T. Concolino, A. Mohan, G. J. Long, V. Briois, F. Grandjean, *Inorg. Chem.* **2001**, *40*, 1508−1520.

[7] D. L. Reger, T. C. Grattan, K. J. Brown, C. A. Little, J. J. S. Lamba, A. L. Rheingold, R. D. Sommer, *J. Organomet. Chem.* **2000**, *607*, 120−128.

[8] *Crystal data* for **2**: $C_{36}H_{43}Ag_2B_2F_8N_{13}O_3$, M = 1095.19, orthorhombic, space group $P2_12_12_1$, a = 10.2820(7) Å, b = 20.2872(14) Å, c = 20.5518(14) Å, V = 4287.0(5) Å^3, T = 173(2) K, Z = 4, ρ = 1.697 Mg^{-3}, Mo-K_α radiation (λ = 0.71073 Å), μ = 1.002 mm^{-1}, 28911 reflections collected, 8758 independent (R_{int} = 0.0331), GOF = 1.010, final R indices [$I > 2\sigma(I)$], $R1$ = 0.0388, $wR2$ = 0.0913, R indices (all data), $R1$ = 0.0435, $wR2$ = 0.0933. Data were collected using 0.54 × 0.17 × 0.10 mm^3 colorless crystal and a Bruker SMART APEX CCD-based diffractometer and the structure was solved and refined using SAINT+ (Version 6.02a) and SHELXTL (Version 5.1). Crystallographic data (excluding structure factors) for the structure reported in this paper have been deposited with the Cambridge Crystallographic Data Centre as supplementary publication no. CCDC-166558. Copies of the data can be obtained free of charge on application to CCDC, 12 Union Road, Cambridge CB2 1EZ, UK [Fax (internat.) +44-1223/336-033; E-mail: deposit@ccdc.cam.ac.uk].

[9] [9a] A. Bondi, *J. Phys. Chem.* **1964**, *68*, 441−451. [9b] R. S. Rowland, R. Taylor, *J. Phys. Chem.* **1996**, *100*, 7384−7391.

[10] [10a] F. Grepioni, G. Cojazzi, S. M. Draper, N. Scully, D. Braga, *Organometallics* **1998**, *17*, 296−307. [10b] K. L. V. Mann, J. C. Jeffery, J. A. McCleverty, M. D. Ward, *J. Chem. Soc., Dalton Trans.* **1998**, 3029−3036. [10c] R. L. Paul, S. M. Couchman, J. C. Jeffery, J. A. McCleverty, Z. R. Reeves, M. D. Ward, *J. Chem. Soc., Dalton Trans.* **2000**, 845−851.

[11] [11a] F. A Rampf, M. Spiegler, W A. Herrmann, *J. Organomet. Chem.* **1999**, *582*, 204−210. [11b] M. E. Brown, M. D. Hollingsworth, *Nature* **1995**, *376*, 323−327. [11c] M. Sakamoto, *Chem. Eur. J.* **1997**, *3*, 684−689. [11d] H. Ito, T. Kusukawa, M. Fujita, *Chem. Lett.* **2000**, 598−599.

Received November 5, 2001
[I01389]

A New Family of Supramolecular Complexes with 3D Cationic Hg/Z Frameworks, SnX_3^- Guest Anions (Z = P, As, Sb; X = Cl, Br, I): Crystal Structures and Host−Guest Interactions

Andrei V. Olenev,[a] Alexei I. Baranov,[b] Andrei V. Shevelkov,*[a] and Boris A. Popovkin[a]

Keywords: Host-guest systems / Tin / Supramolecular chemistry / Mercury / Ab initio calculations / Pnicogens

Five new inorganic supramolecular complexes, $[Hg_6P_4Cl_3](SnCl_3)$ (**I**), $[Hg_6As_4Cl_3](SnCl_3)Hg_{0.13}$ (**II**), $[Hg_6As_4Br_3](SnBr_3)$ (**III**), $[Hg_6Sb_4I_3](SnI_3)Hg_{0.16}$ (**IV**), and $[Hg_7P_4Br_3](SnBr_3)$ (**V**), have been prepared and their structures determined by X-ray single crystal experiments. They all crystallize in the cubic space group $P2_13$ (No 198) with $Z = 4$, and unit cell parameters $a = 11.865(1)$ (**I**), 12.233(1) (**II**), 12.383(1) (**III**), 13.285(2) (**IV**), and 12.490(1) Å (**V**). The crystal structures of these compounds are composed of the 3D positively charged frameworks $[Hg_6Z_4X_3]^+$ (**I**–**IV**) or $[Hg_7P_4Br_3]^+$ (**V**), with SnX_3^- anions trapped in the larger cavities of the frameworks (X = Cl, Br, I; Z = P, As, Sb). In the structures of **II** and **IV** the smaller cavities are partly filled by mercury atoms. The structures of **I**–**V** and of previously reported $[Hg_7As_4I_3](SnI_3)$ (**VI**) are discussed with respect to the matching and mutual adjusting of the host frameworks and guest anions. A comparison of the observed and calculated (ab initio, RHF level) geometry of the SnX_3^- anions is used to analyze the weak host–guest interactions.

Introduction

Supramolecular inorganic compounds possess a huge variety of crystal structures and physical properties.[1] Among them a group of phases can be distinguished in which the three dimensional (3D) positively charged host framework is built up of linearly coordinated mercury and tetrahedrally coordinated pnicogen atoms.[2] Halometallate anions — guests of different shapes and sizes — reside in the cavities of the frameworks. These compounds may be exploited as convenient systems for the investigation of the role of the host-guest interactions in the formation and crystal structure organization of inorganic supramolecular architectures in which both host and guest fragments are electrically charged. For this purpose, a group of related phases with similar crystal structures should be used. In our previous work[2e] we reported on a novel supramolecular complex $[Hg_7As_4I_3](SnI_3)$ in which the cationic framework encapsulates the SnI_3^- anion. It therefore seemed obvious that different SnX_3^- anions (X = Cl, Br and I) may serve as templates for the formation of new Hg−Z (Z = P, As, Sb) cationic frameworks. We have performed a systematic search for such compounds, and here we report on the crystal structures of five new supramolecular phases: $[Hg_6P_4Cl_3](SnCl_3)$ (**I**), $[Hg_6As_4Cl_3](SnCl_3)Hg_{0.13}$ (**II**), $[Hg_6As_4Br_3](SnBr_3)$ (**III**), $[Hg_6Sb_4I_3](SnI_3)Hg_{0.16}$ (**IV**) and $[Hg_7P_4Br_3](SnBr_3)$ (**V**). The significant amounts of the materials isolated makes it possible to discuss the relationship between the structural organization of the title compounds and the host-guest complementarity.

[a] Inorganic Synthesis Laboratory, Department of Chemistry, Moscow State University,
Leninskie Gory, Moscow 119899, Russia
[b] Department of Materials Sciences, Moscow State University, Leninskie Gory, Moscow 119899, Russia

Results and Discussion

The new compounds were obtained by a standard ampoule technique (see Exp. Sect. for details) exploiting the synthetic conditions previously reported for a similar compound.[2e] As a result of a systematic search for new phases in the Hg−Z−Sn−X systems performed in this and our previous[2e] work, six supramolecular compounds have been prepared (Table 1).

Table 1. Host-guest phases in the Hg−Z−Sn−X systems (cubic cell parameter a in Å, space group $P2_13$)

	Cl	Br	I
P	$[Hg_6P_4Cl_3](SnCl_3)$ (**I**), Type 1[a] $a = 11.865(1)$	$[Hg_7P_4Br_3](SnBr_3)$ (**V**), Type 2[b] $a = 12.490(1)$	not found
As	$[Hg_6As_4Cl_3](SnCl_3)Hg_{0.13}$ (**II**), Type 1 $a = 12.233(1)$	$[Hg_6As_4Br_3](SnBr_3)$ (**III**), Type 1 $a = 12.383(1)$	$[Hg_7As_4I_3](SnI_3)$ (**VI**), Type 2 $a = 13.110(1)$
Sb	not found	not found	$[Hg_6Sb_4I_3](SnI_3)Hg_{0.16}$ (**IV**), Type 1 $a = 13.285(2)$

[a] Type 1 framework: $[Hg_6Z_4X_3]^+$. [b] Type 2 framework: $[Hg_7Z_4X_3]^+$.

The crystal structures of the five new phases prepared in this work were determined by means of single crystal X-ray diffraction (Table 2). Selected interatomic distances and bond angles are given in Table 3−7. All the reported compounds have a similar structural organization. Their crystal structures are composed of a 3D cationic host framework, built up of linearly coordinated mercury and tetrahedrally coordinated pnicogen atoms, and additional halogen atoms, and have two types of closed cavities of different sizes. The SnX_3^- guest anions are encapsulated in the larger cavities of the host framework (Figure 1). In all cases the separation between the halogen atoms of the guest anion and the mercury atoms of the host framework is much larger than the sum of the covalent radii of the respective elements — a feature that is characteristic of host-guest compounds. In the structures of **II** and **IV** the smaller cavities are partly filled by mercury atoms.

Despite the similarity of the reported compounds (the same $P2_13$ space group and the same type of guest anion) they possess two types of host frameworks with the general formulae $[Hg_6Z_4X_3]^+$ (**I**−**IV**) and $[Hg_7Z_4X_3]^+$ (**V**). The latter has the same structure as in the earlier reported compound $[Hg_7As_4I_3](SnI_3)$ (**VI**).[2e] The cationic framework of **V** contains two types of phosphorus atoms. While P(1) and P(2) are tetrahedrally coordinated by mercury atoms, P(3) and P(4) are joined into P_2^{4-} dumbbells, such that their nearest neighbors are one phosphorus and three mercury atoms. Compounds **I**−**IV** have frameworks of a different type, where all the pnicogen atoms are joined into Z_2^{4-} dumbbells. The structure of the host framework is closely related to that found in $[Hg_6As_4](HgBr_6)Hg_{0.4}$ [2b] and $[Hg_6As_4](M^{III}X_6)X$ (X = Cl, Br),[2f,2g] the only difference being that in the compounds reported here the additional halogen atoms modify the framework. The Hg−Z and Z−Z interatomic distances within the frameworks [d(Hg−P) = 2.37−2.45 Å; d(Hg−As) = 2.50−2.52 Å; d(Hg−Sb) = 2.67−2.69 Å; d(P−P) = 2.18 Å; d(As−As) 2.38−2.42 Å; d(Sb−Sb) = 2.76−2.80 Å] are in good agreement with those found in numerous mercury pnictide halides.[2,3]

Table 3. Selected interatomic distances and bond angles for **I**

Distances [Å]	
Sn−Cl(2)	2.615(10) ×3
P(1)−Hg(1)	2.447(6) ×3
P(2)−Hg(2)	2.436(6) ×3
P(3)−Hg(1)	2.443(7) ×3
P(4)−Hg(2)	2.424(6) ×3
P(1)−P(4)	2.18(2)
P(2)−P(3)	2.18(2)
Cl(1)−Hg(2)	2.814(11)
Cl(1)−Hg(1)	2.894(12)
Cl(2)−Hg(1)	2.947(9)
Cl(2)−Hg(2)	3.066(9)
Cl(2)−Hg(2)	3.177(9)
Cl(2)−Hg(2)	3.245(9)
Angles [°]	
Cl(2)−Sn−Cl(2)	86.5(3) ×3
P(3)−Hg(1)−P(1)	170.2(4)
P(4)−Hg(2)−P(2)	166.9(4)
P(4)−P(1)−Hg(1)	112.9(3) ×3
Hg(1)−P(1)−Hg(1)	105.9(4) ×3
P(3)−P(2)−Hg(2)	108.8(4) ×3
Hg(2)−P(2)−Hg(2)	110.1(4) ×3
P(2)−P(3)−Hg(1)	111.5(4) ×3
Hg(1)−P(3)−Hg(1)	107.3(4) ×3
P(1)−P(4)−Hg(2)	110.4(4) ×3
Hg(2)−P(4)−Hg(2)	108.5(4) ×3

The SnX_3^- anions residing in the larger cavities of the frameworks are formed by the unique tin and X(2) atoms and have the shape of a trigonal pyramid with the tin atom at the vertex. Such a geometry of the anions is in an agreement with the Gillespie−Nyholm rules:[4] the three halogen atoms and the lone electron pair of the Sn^{2+} cation form a pseudo-tetrahedron around the tin atom, the X−Sn−X angles being smaller than regular tetrahedral.

Table 2. Data collection and structure refinement parameters for **I**−**V**; space group $P2_13$, $Z = 4$, $\lambda = 0.71073$ (Mo-K_α)

	I	**II**	**III**	**IV**	**V**
Composition	$[Hg_6P_4Cl_3](SnCl_3)$	$[Hg_6As_4Cl_3](SnCl_3)Hg_{0.13(1)}$	$[Hg_6As_4Br_3](SnBr_3)$	$[Hg_6Sb_4I_3](SnI_3)Hg_{0.16(1)}$	$[Hg_7P_4Br_3](SnBr_3)$
a, Å	11.865(1)	12.233(1)	12.383(1)	13.285(2)	12.490(1)
V, Å^3	1670.3(2)	1830.6(3)	1898.8(3)	2344.7(6)	1948.4(3)
ρ (calcd.), Mg/m^3	6.596	6.751	7.351	7.373	7.248
μ, mm^{-1}	57.332	60.575	69.137	53.616	68.47
Theta range for data collection, deg.	2.43 to 27.96	2.35 to 26.98	2.33 to 25.98	2.17 to 25.97	2.31 to 27.87
Refl. collected/independ.	2302/771	2490/924	2330/870	2825/1052	2658/892
ref. parameters	54	57	53	57	56
R_1[a] ($F_0 > 4\sigma F_0$)	0.0620	0.0427	0.0553	0.0681	0.0560
wR_2[b] ($F_0 > 4\sigma F_0$)	0.1554	0.0916	0.1249	0.1424	0.1142
G-o-f on F^2	1.112	1.018	1.083	1.077	1.089
Largest diff. peak and hole, e Å^{-3}	5.256 and −4.282	1.702 and −1.724	3.197 and −2.508	3.522 and −2.764	6.084 and −5.145

[a] $R1 = \Sigma||F_o| - |F_c||/\Sigma|F_o|$. [b] $wR2 = [\Sigma w(F_0^2 - F_c^2)^2/\Sigma w(F_0^2)^2]^{1/2}$, $w = [\sigma^2(F_0^2) + A{\cdot}p^2 + B{\cdot}p]^{-1}$; $p = (F_0^2 + 2F_c^2)/3$; A = 0.0150 (**I**), 0.0309 (**II**), 0.0217 (**III**), 0.0561 (**IV**), 0.0556(**V**); B = 0 (**I**, **II**, **IV**, **V**), 76.6 (**III**).

Table 4. Selected interatomic distances and bond angles for **II**

Distances [Å]	
Sn−Cl(2)	2.626(6) ×3
As(1)−Hg(2)	2.496(1) ×3
As(2)−Hg(1)	2.495(1) ×3
As(3)−Hg(2)	2.494(1) ×3
As(4)−Hg(1)	2.497(1) ×3
As(1)−As(4)	2.403(6)
As(2)−As(3)	2.378(6)
Hg(1)−Cl(2)	3.162(6)
Hg(1)−Cl(2)	3.275(6)
Hg(1)−Cl(2)	3.412(6)
Hg(2)−Cl(1)	2.943(7)
Hg(2)−Cl(2)	3.008(6)
Hg(3)−Cl(1)	3.11(1) ×3
Hg(3)−As(4)	3.25(1)
Hg(3)−Hg(1)	3.50(1) ×3
Hg(3)−Cl(2)	3.633(8) ×3
Angles [°]	
Cl(2)−Sn−Cl(2)	87.6(2) ×3
As(4)−As(1)−Hg(2)	109.2(1) ×3
Hg(2)−As(1)−Hg(2)	109.67(9) ×3
As(3)−As(2)−Hg(1)	109.0(1) ×3
Hg(1)−As(2)−Hg(1)	109.90(9) ×3
As(2)−As(3)−Hg(2)	110.55(9) ×3
Hg(2)−As(3)−Hg(2)	108.4(1) ×3
As(1)−As(4)−Hg(1)	106.1(1) ×3
Hg(1)−As(4)−Hg(1)	112.59(9) ×3
As(2)−Hg(1)−As(4)	163.0(1)
As(3)−Hg(2)−As(1)	166.5(1)

Table 5. Selected interatomic distances and bond angles for **III**

Distances [Å]	
Sn−Br(2)	2.771(5) ×3
As(1)−As(4)	2.395(9)
As(1)−Hg(2)	2.523(3) ×3
As(2)−As(3)	2.416(9)
As(2)−Hg(1)	2.522(3) ×3
As(3)−Hg(2)	2.523(3) ×3
As(4)−Hg(1)	2.522(3) ×3
Hg(1)−Br(1)	3.047(5)
Hg(2)−Br(1)	2.926(5)
Hg1−Br(2)	3.049(4)
Hg2−Br(2)	3.180(4)
Hg2−Br(2)	3.306(4)
Hg2−Br(2)	3.402(4)
Angles [°]	
Br(2)−Sn−Br(2)	87.47(18) ×3
Hg(2)−As(1)−Hg(2)	109.69(14) ×3
As(4)−As(1)−Hg(2)	109.26(15) ×3
As(3)−As(2)−Hg(1)	109.58(15) ×3
Hg(1)−As(2)−Hg(1)	109.36(15) ×3
As(2)−As(3)−Hg(2)	107.24(15) ×3
Hg(2)−As(3)−Hg(2)	111.60(13) ×3
As(1)−As(4)−Hg(1)	111.07(14) ×3
Hg(1)−As(4)−Hg(1)	107.82(14) ×3
As(4)−Hg(1)−As(2)	168.0(1)
As(1)−Hg(2)−As(3)	164.66(15)

Table 6. Selected interatomic distances and bond angles for **IV**

Distances [Å]	
Sn−I(2)	2.992(5) ×3
Sb(1)−Hg(2)	2.678(3) ×3
Sb(1)−Sb(4)	2.762(8)
Sb(2)−Hg(2)	2.685(3) ×3
Sb(2)−Sb(3)	2.796(9)
Sb(3)−Hg(1)	2.690(3) ×3
Sb(4)−Hg(1)	2.671(3) ×3
Hg(1)−I(1)	3.261(5)
Hg(2)−I(1)	3.056(4)
Hg(1)−I(2)	3.203(4)
Hg(2)−I(2)	3.402(4)
Hg(2)−I(2)	3.572(4)
Hg(3)−Sb(2)	3.22(5)
Hg(3)−I(1)	3.31(3) ×3
Hg(3)−Hg(2)	3.64(3) ×3
Hg(3)−I(2)	3.792(14) ×3
Angles [°]	
I(2)−Sn−I(2)	88.0(1) ×3
Hg(2)−Sb(1)−Hg(2)	113.12(11) ×3
Hg(2)−Sb(1)−Sb(4)	105.51(13) ×3
Hg(2)−Sb(2)−Hg(2)	113.96(11) ×3
Hg(2)−Sb(2)−Sb(3)	104.49(14) ×3
Hg(1)−Sb(3)−Hg(1)	111.69(13) ×3
Hg(1)−Sb(3)−Sb(2)	107.15(14) ×3
Hg(1)−Sb(4)−Hg(1)	108.65(13) ×3
Hg(1)−Sb(4)−Sb(1)	110.28(13) ×3
Sb(4)−Hg(1)−Sb(3)	165.41(17)
Sb(1)−Hg(2)−Sb(2)	158.96(15)

The interesting feature of **II** and **IV** is that the additional mercury atoms partly occupy small cavities of the host framework. The coordination sphere of such a guest consists of 10 neighbors [3X(1), 1Z, 3Hg, and 3X(2) atoms]. The high coordination number of these mercury atoms, together with the large distances in their first coordination sphere (3.11−3.79 Å), indicate their low oxidation state. Mercury atoms serving as clathrated guests have already been observed in $[Hg_6As_4](HgCl_6)Hg_{0.4}$ [2a] where a zero oxidation state of the guest mercury was confirmed by means of solid state ^{199}Hg NMR spectroscopy.[5] It is not yet clear what factors control the population of mercury atoms in the smaller cavities of different frameworks. The results of this research suggest that the occupancies are only slightly different for **II** and **IV** (13 and 16%, respectively), the composition being confirmed by the stoichiometric synthesis of the phase-pure sample only in the former case, and differ significantly from the 40% population in $[Hg_6As_4](HgCl_6)Hg_{0.4}$ [2a] and 60% population in $[Hg_6As_4](FeBr_6)Hg_{0.6}$.[6] It could be that the population is sensitive both to the synthetic conditions and to the extent of the host-guest mismatch; this is currently being investigated.

As was described above, the SnX_3^- anions encapsulated in the framework cavities are not covalently bonded to the host structure (Figure 2), the host-guest interactions being limited to very weak electrostatic forces. Having a family of phases with similar crystal structures, we can now estimate

Table 7. Selected interatomic distances and bond angles for **V**

Distances [Å]	
Sn(1)−Br(2)	2.722(4) ×3
P(1)−Hg(1)	2.366(13)
P(1)−Hg(2)	2.414(2) ×3
P(2)−Hg(1)	2.385(15)
P(2)−Hg(3)	2.399(4) ×3
P(3)−P(4)	2.18(2)
P(3)−Hg(3)	2.422(5) ×3
P(4)−Hg(2)	2.428(4) ×3
Hg(2)−Br(1)	2.981(3)
Hg(3)−Br(1)	3.129(3)
Hg(2)−Br(2)	3.142(3)
Hg(2)−Br(2)	3.364(3)
Hg(3)−Br(2)	3.352(3)
Angles [°]	
Br(2)−Sn(1)−Br(2)	91.27(14) ×3
Hg(1)−P(1)−Hg(2)	98.5(3) ×3
Hg(2)−P(1)−Hg(2)	117.84(15) ×3
Hg(1)−P(2)−Hg(3)	107.0(3) ×3
Hg(3)−P(2)−Hg(3)	111.8(3) ×3
P(4)−P(3)−Hg(3)	110.7(3) ×3
Hg(3)−P(3)−Hg(3)	108.2(3) ×3
P(3)−P(4)−Hg(2)	108.4(3) ×3
Hg(2)−P(4)−Hg(2)	110.5(3) ×3
P(1)−Hg(1)−P(2)	180.0(2)
P(1)−Hg(2)−P(4)	166.6(4)
P(2)−Hg(3)−P(3)	176.0(3)

how these weak interactions influence the structural organization and formation of these compounds. As a first step, we shall discuss the problem of size matching between the cavity of the cationic framework and the guest anion, as well as the slight structural changes in the host structure that this mismatch may cause. Then we shall show how the cavity configuration influences the geometry of the guest anion through weak electrostatic forces. It should be noted that the quality of the structural data differs from one compound to another — as can be seen from Table 2 — the structures of the compounds **I** and **V** being less accurate. However, since the discussion of the host-guest interaction is semi-quantitative, the achieved accuracy of the structural data seems to be sufficient.

In the structures of **I** and **II**, the same $SnCl_3^-$ ion occupies the cavities of the $[Hg_6P_4Cl_3]^{1+}$ and $[Hg_6As_4Cl_3]^{1+}$ host frameworks. Evidently, the two frameworks possess cavities of different size (smaller in **I** than in **II**) to trap the same anion. This means that the size of the cavity may vary within a certain range, whilst still remaining appropriate for anions of the same size. Comparing **III** and **V**, one can see that the $SnBr_3^-$ anion fits into the cavity of the $[Hg_6As_4Br_3]^{1+}$ framework of **III**, but is too large if arsenic is replaced by phosphorus in the host structure (**V**). In the latter case the $SnBr_3^-$ anion requires a larger cavity in the host framework. Similarly, the SnI_3^- anion fits into the cavity of the $[Hg_6Sb_4I_3]^{1+}$ framework (**IV**), but becomes too large if antimony is replaced by arsenic in the framework (**VI**) and requires an expansion of the host structure. The

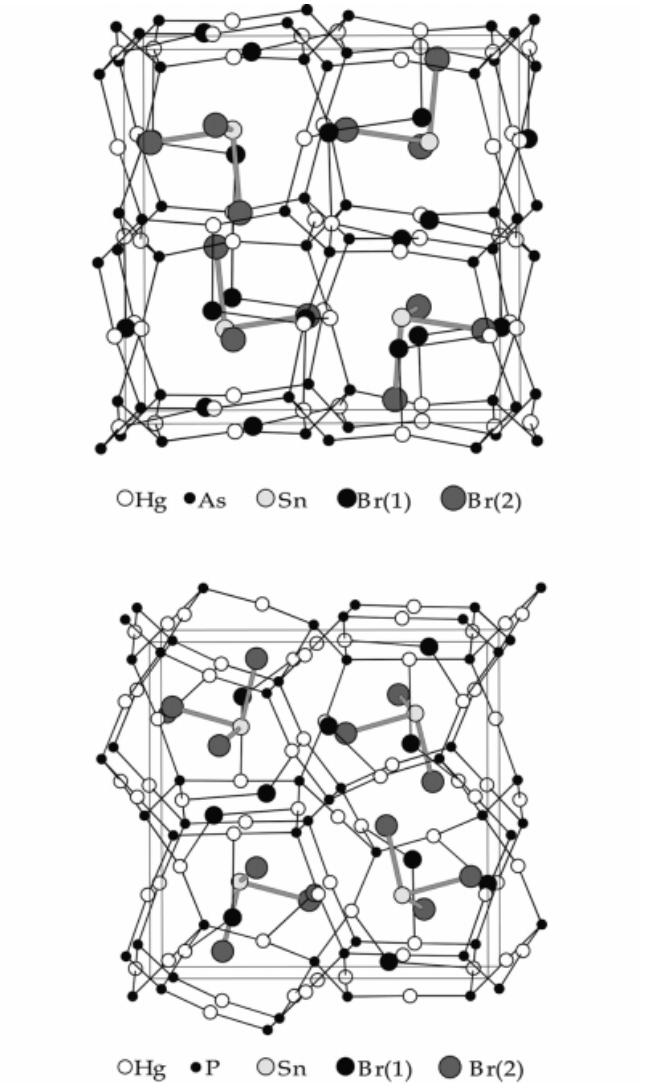

Figure 1. Unit cells of the crystal structures of $[Hg_6As_4Br_3](SnBr_3)$ (top) and $[Hg_7P_4Br_3](SnBr_3)$ (bottom)

expansion of the framework in **V** and **VI** occurs by the addition of an extra Hg^{2+} atom which "breaks" every second Z_2^{4-} dumbbell into two discrete Z^{3-} atoms (Figure 3). This leads to the formation of another type of host framework with larger cavities, $[Hg_7Z_4X_3]^{1+}$, and keeps the framework charge unchanged. Due to the severe size mismatch no SnX_3^--containing compounds have been found in the Hg/P/Sn/I, Hg/Sb/Sn/Cl, and Hg/Sb/Sn/Br systems. As is clear from Table 1, the $SnCl_3^-$ and $SnBr_3^-$ anions are too small for the antimony-containing frameworks, whereas the SnI_3^- anion is too large for the phosphorus-containing frameworks, be they of type 1 or 2 (Table 1). The above discussion leads to the following conclusion: the condition of the size matching of the guest anion and the host framework cavity is not too strict but is still important for the formation of the phases under consideration.

As has already been shown for **VI**,[2e] weak host-guest interactions influence the geometry of the SnI_3^- anion, and the calculated equilibrium geometry of the SnI_3^- anion appeared to differ from that observed in the crystal structure.

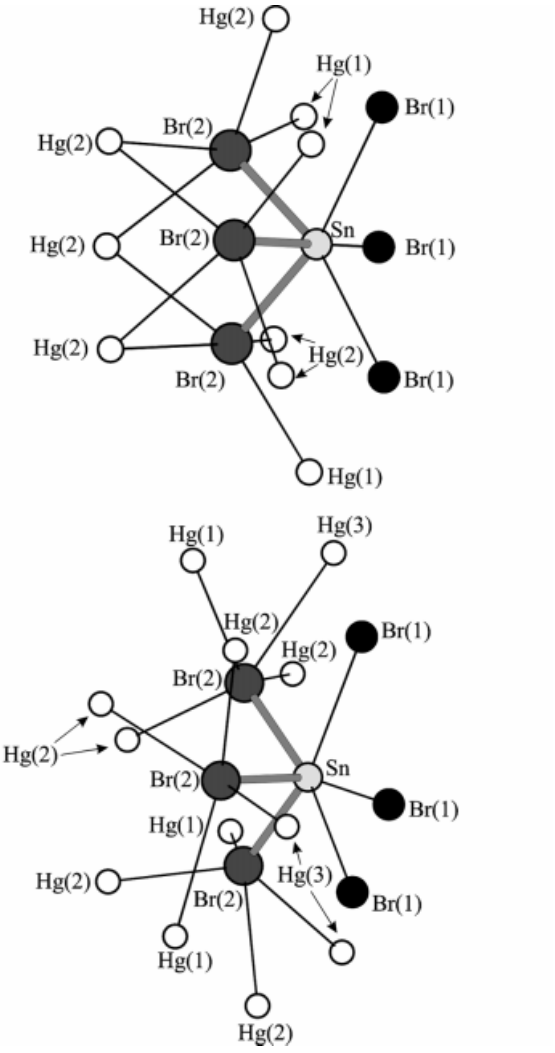

Figure 2. Coordination of the SnX_3^- anion by distant atoms of the host framework in **III** (top) and **V** (bottom)

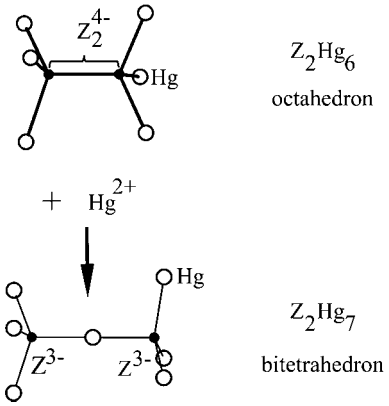

Figure 3. A scheme of the transition from the $[Hg_6Z_4X_3]^+$ framework to the $[Hg_7Z_4X_3]^+$ framework by breaking a Z_2^{4-} dumbbell with a Hg^{2+} cation

In this work we have performed the same level of ab initio calculations for the $SnCl_3^-$ and $SnBr_3^-$ guest anions (see Exp. Sect. for details). The geometry of the SnX_3^- anions found in the crystal structures of **I**−**V** and **VI**,[2e] and the corresponding calculated equilibrium values, are given in Table 8. It is clear that in all crystal structures the Sn−X separations are longer and the X−Sn−X angles are lower than the equilibrium values. A comparison of the observed geometry of the $SnBr_3^-$ guest anion in the structures of **III** and **V**, and of the SnI_3^- anion in **IV** and **VI** with the calculated ones shows that the same guest anion appears to be more distorted in **III** than in **V**, and in **IV** than in **VI**. The reason for such differences is quite apparent. The positive charge of the host cationic framework is "smeared" over the inner surface of the cavities. In **V** and **VI** the cavity has one additional mercury atom which expands its surface. Consequently, the "specific charge" of the cavity is smaller in **V** and **VI** than in the other four phases, and this is why the electrostatic interaction between the host and guest is weaker in **V** and **VI**. In turn, the weaker host-guest interaction causes a less-pronounced departure of the observed geometry from the equilibrium. A comparison of **I** and **II** shows that they possess an identical type of framework, and although the size of these frameworks is different, the observed geometry of the $SnCl_3^-$ anion they trap exhibits the same deviation from equilibrium in both structures. The above discussion leads to the conclusion that the weak electrostatic host-guest interactions primarily control the geometry of the guest SnX_3^- anion and the type of the host framework, provided that the size matching, which is not very strict, is achieved.

The nature of the weak electrostatic host-guest interaction is not discussed in this article. Recently[7] we showed that for similar supramolecular complexes containing d-metals as the centers of guest anions a host-guest charge transfer takes place.

Concluding Remarks

The above-described family of compounds illustrates features important for understanding the principles of the formation of solid state supramolecular complexes. Evidently, new compounds in the Hg/Z/Sn/X systems form only if the host-guest complementarity, which includes the geometry/topology matching and charge balance, is achieved. More important is that the mutual adjustment of the host and guest is possible. The supramolecular complexes discussed in this article show that the guest serves as a template for the construction of a host framework of the appropriate size, and changes its own geometry according to the "requirements" of the host. Weak electrostatic forces that exist between charged host and guest control their mutual adjustment.

Experimental Section

Starting Materials: Hg_2Cl_2, Hg_2Br_2, $HgBr_2$, HgI_2, red phosphorus, gray arsenic, antimony, tin powder, and mercury were used for the synthesis and single crystal growth of the reported compounds. All reagents were of high purity (> 99.99%), except for phosphorus (97%), which was purified as described elsewhere.[2e]

Table 8. Geometry of SnX_3^- as found and calculated

Anion	in compound		d(Sn−X)/Å and (X−Sn−X)/deg. from structure	calculated
$SnCl_3^-$	$[Hg_6P_4Cl_3]SnCl_3$	**(I)**	2.62 Å, 86.9°	2.49 Å, 96.6°
	$[Hg_6As_4Cl_3](SnCl_3)Hg_{0.13}$	**(II)**	2.63 Å, 87.7°	
$SnBr_3^-$	$[Hg_7P_4Br_3]SnBr_3$	**(V)**	2.71 Å, 91.5°	2.66 Å, 97.8°
	$[Hg_6As_4Br_3]SnBr_3$	**(III)**	2.77 Å, 87.5°	
SnI_3^-	$[Hg_7As_4I_3]SnI_3$	**(VI)**	2.95 Å, 90.9°	2.90 Å, 99.2°
	$[Hg_6Sb_4I_3](SnI_3)Hg_{0.16}$	**(IV)**	2.99 Å, 88.1°	

Synthesis: Compounds **I**, **II** and **III** were prepared from stoichiometric mixtures (approx. 1 g.) of the respective mercury(I) halide, pnicogen, and tin powder, which were heated for five days at 400 °C in vacuum-sealed silica tubes. The samples formed as yellow (**I**) or dark-red (**II** and **III**) air-stable polycrystalline powders, but did not contain single crystals suitable for a structure determination. A profile analysis of the diffraction patterns of the samples [STADI-P (STOE), Cu-$K_{\alpha 1}$ radiation] confirmed that they were phase-pure. For the X-ray crystal structure analysis, single crystals of **I**, **II**, and **III** were selected from the samples prepared from the mixtures of the respective mercury(I) halide, phosphorus (arsenic), tin powder, and mercury in a 3:4:1:1 molar ratio. The mixtures (total weight approx. 1 g) were vacuum-sealed in silica ampoules and heated at 400 °C for five days.

For the preparation of **IV**, mercury(II) iodide, antimony, tin powder, and mercury were mixed in a 3:4:1:4 ratio. Approximately 1 g of this mixture was heated for five days at 500 °C in an evacuated silica ampoule. The product formed as a mixture of a new black phase and liquid mercury, and contained single crystals suitable for a structure determination.

Compound **V** was prepared by heating a stoichiometric mixture of mercury(II) bromide, red phosphorus, tin powder, and mercury in a vacuum-sealed silica tube for two days at 400 °C. The sample appeared as a crop of yellow crystals of different shapes and sizes. Only a small admixture of unchanged starting materials was detected by X-ray powder diffraction.

No new compounds were obtained from the Hg/P/Sn/I, Hg/Sb/Sn/Cl and Hg/Sb/Sn/Br systems upon annealing samples with the composition $3HgI_2$:4P:1Sn, $3Hg_2Cl_2$:4Sb:1Sn, and $3Hg_2Br_2$:4Sb:1Sn for five days, and varying the temperature from 400 to 500 °C.

Crystal Structure Determinations: Suitable single crystals of **I**−**V** were mounted on a CAD-4 (Nonius) goniometer head. The cubic unit cell parameters were refined based on 24 well-centered reflections in the angular range $12° < \theta < 17°$. All data sets were collected at ambient temperature with the data collection parameters listed in Table 2. A semiempirical absorption correction was introduced based on azimuthal scans of not less than six reflections with χ angles close to 90°. Analysis of the systematic absences in the data sets revealed two possible space groups $P2_13$ (no. 198) and $P4_232$ (no. 208). For the structure solution, following the presumed analogy with the synthesized earlier compound $[Hg_7As_4I_3](SnI_3)$, the space group of lower symmetry was chosen in all cases. The atomic positions of mercury, iodine, antimony, tin, bromine and arsenic atoms in all the structures were estimated by direct methods (SHELXS-97).[8] The phosphorus and chlorine atoms were localized by a sequence of $\Delta\rho$(xyz) syntheses and least-squares cycles (SHELXL-97).[9] During the refinement of the crystal structures of **II** and **IV** an electron density peak was observed residing in the smaller cavity of the host framework. The position of this peak was refined as being partly occupied by mercury. Final anisotropic full-matrix refinement on F^2 led to satisfactory R_1 and wR_2 values as listed in Table 2. Attempts to solve the structures in the space group $P4_232$ did not lead to reasonable solutions.

It should be noted that the quality of the reflections that were used for the absorption correction procedure in the case of **I** was rather low. We consider this to be the reason why one of the phosphorus atoms has abnormally weak thermal displacement parameters. Unfortunately, due to the irregular shape of the crystal, the numerical absorption correction was unsuccessful.

Further details of the crystal structure determination may be obtained from Fachinformationszentrum Karlsruhe, 76344 Eggenstein-Leopoldshafen, Germany, on quoting the depository numbers CSD-411863 (**I**), -411862 (**II**), -411861 (**III**), -411859 (**IV**), and -411860 (**V**).

Computational Aspects: Ab initio RHF calculations were performed using the GAMESS-US[10] program. SBKJC effective core potentials were applied to all atoms and the SBKJC basis set[11] implemented in GAMESS was used. The starting geometry of the $SnCl_3^-$ and $SnBr_3^-$ anions was taken from the crystal structure refinement of **I** and **III**, respectively. The geometry of the SnX_3^- anions was optimized without any constraints (C_{3v} and C_s symmetries). Geometry optimizations were performed by the quasi-Newton algorithm[12] implemented in GAMESS. In all cases the optimized geometries did not depend on the point symmetry group applied to the SnX_3^- ion. The hessian computations and normal vibration analyses showed all stationary points located to be minima.

[1] A. Müller, H. Reuter, S. Dillinger, *Angew. Chem.* **1995**, *107*, 2505−2539; *Angew. Chem. Int. Ed. Engl.* **1995**, *34*, 2328−2361.
[2] [2a] A. V. Shevelkov, E. V. Dikarev, M. Yu. Mustiakimov, B. A. Popovkin, *J. Chem. Soc., Dalton Trans.* **1995**, 147−148. [2b] A. V. Shevelkov, E. V. Dikarev, B. A. Popovkin, *J. Solid State Chem.* **1996**, *126*, 324−327. [2c] A. V. Olenev, A. V. Shevelkov, B. A. Popovkin, *Zh. Neorg. Khim.* **1999**, *44*, 1911−1913; *Russ. J. Inorg. Chem.* **1999**, *44*, 1814−1816 (Engl. transl.). [2d] A. V. Olenev, A. V. Shevelkov, B. A. Popovkin, *Zh. Neorg. Khim.* **1999**, *44*, 1957−1965; *Russ. J. Inorg. Chem.* **1999**, *44*, 1853−1861 (Engl. transl.). [2e] A. V. Olenev, A. I. Baranov, A. V. Shevelkov, B. A. Popovkin, *Eur. J. Inorg. Chem.* **2000**, 265−270. [2f] J. Beck, U. Neisel, *Z. Anorg. Allg. Chem.* **2000**, *626*, 1620−1626. [2g] J. Beck, S. Hedderich, U. Neisel, *J. Solid State Chem.* **2000**, *154*, 350−355.
[3] [3a] Ph. Labbé, M. Ledésert, B. Raveau, A. Rebbah, *Z. Kristallogr.* **1989**, *187*, 117−123. [3b] A. V. Shevelkov, E. V. Dikarev, B. A. Popovkin, *J. Solid State Chem.* **1991**, *93*, 331−335. [3c] A. V. Olenev, A. V. Shevelkov, B. A. Popovkin, *J. Solid State Chem.* **1999**, *142*, 14−18.

[4] R. J. Gillespie, I. Hargittai, *The VSEPR Model of Molecular Geometry*, Allyn, Bacon, Boston, **1991**.
[5] A. V. Shevelkov, *6th European Conference on Solid State Chemistry*, September 17−20, 1997, Zürich, Switzerland. Book of Abstracts, vol. **I**, p. ML7.
[6] O. S. Zaikina, A. V. Olenev, A. V. Shevelkov, *6th International Workshop* "*High-temperature Superconductors, Novel Inorganic Materials Engineering*". June 24−30, 2001, Moscow − St. Petersburg, Russia. Book of Abstracts, PIII − 12.
[7] A. V. Olenev, A. V. Shevelkov, *J. Solid State Chem.* **2001**, *160*, 88−92.
[8] G. M. Sheldrik, SHELXS-97, (**1997**), *Program for crystal structure solution*, University of Göttingen, Germany.
[9] G. M. Sheldrik, SHELXL-97, (**1997**), *Program for crystal structure refinement*, University of Göttingen, Germany.
[10] M. W. Schmidt, K. K. Baldridge, J. A. Boatz, S. T. Elbert, M. S. Gordon, J. J. Jensen, S. Koseki, N. Matsunaga, K. A. Nguyen, S. Su, T. L. Windus, M. Dupuis, J. A. Montgomery, *J. Comput. Chem.* **1993**, *14*, 1347−1363.
[11] [11a] W. J. Stevens, H. Basch, M. Krauss, *J. Chem. Phys.* **1984**, *81*, 6026−6033. [11b] W. J. Stevens, H. Basch, M. Krauss, P. Jasien, *Can. J. Chem.* **1992**, *70*, 612−630. [11c] T. R. Cundari, W. J. Stevens, *J. Chem. Phys.* **1993**, *98*, 5555−5565.
[12] J. Baker, *J. Comput. Chem.* **1986**, *7*, 385−395.

Received April 27, 2001
[I01148]

Probing the Nature of the Redox Products and Lowest Excited State of $[(bpy)_2Ru(\mu\text{-}bptz)Ru(bpy)_2]^{4+}$: A Resonance Raman Study

Keith C. Gordon,*[a] Anthony K. Burrell,[b] Timothy J. Simpson,[a] Simon E. Page,[a] Geoffrey Kelso,[a] Matthew I. J. Polson,[a] and Amar Flood[a]

Keywords: Raman spectroscopy / Mixed-valent compounds / Ab initio calculations / Ruthenium(II) / Tetrazines

The resonance Raman and infrared spectra of the bridging ligand 3,6-bis(2-pyridyl)-1,2,4,5-tetrazine (bptz) have been studied. Ab initio calculations on bptz and the radical anion $bptz^{\cdot-}$ are able to predict the frequencies and intensities of the vibrational spectra. This analysis is used to interpret the vibrational spectroscopy of the bridged binuclear complexes $[(bpy)_2Ru(\mu\text{-}bptz)Ru(bpy)_2]^{4+}$ (**1**) and $[(PPh_3)_2Cu(\mu\text{-}bptz)Cu(PPh_3)_2]^{2+}$ (**2**) and their redox products. The resonance Raman spectroscopy of **1** reveals the bichromophoric nature of the complex, with bpy and bptz ligand modes being enhanced selectively as a function of excitation wavelength. The UV/Vis spectrum of $\mathbf{1}^+$ reveals a strong IVCT band suggesting the mixed-valent species is Class III in nature. This is consistent with findings for other metal moieties with the bptz ligand. The resonance Raman spectrum of $\mathbf{1}^+$ is also consistent with a Class III formulation. The resonance Raman spectrum of $\mathbf{2}^-$ is used to model $bptz^{\cdot-}$ and the ab initio calculations show some correlation with the observed spectrum. The excited-state resonance Raman spectra of **1**, generated with 532 and 633 nm excitation, show spectral features that are not strongly characteristic of $bptz^{\cdot-}$. This appears to be a consequence of the delocalised nature of the molecular orbitals involved in the excited-state of **1**.

Introduction

The extent to which different bridging ligands (BL) can facilitate coupling between adjacent metal-based moieties is an area of intense interest.[1−3] Mixed-valence complexes in which such metal coupling may occur are classified as Class I, II, or III. In a complex in which the BL provides no or little communication the resulting mixed-valent species would show Class I behaviour but when the communication is effective, Class II or III states may be formed.[4−8] Class III systems are completely delocalised such that the mixed-valence is equally shared by both metal centres. The Class II classification is intermediate between I and III, in which a barrier exists to moving charge between the adjacent centres. Studies of mixed-valence complexes may focus on the bridging ligand, by observing the properties of the π* MO.[9] The metal communication may be probed by creating mixed-valent species and observing inter-valence charge-transfer (IVCT) transitions, or by measuring the separation between metal-based oxidation for identical moieties such as $\{Fe(CN)_4\}^{2-}$ or $\{Ru(bpy)_2\}^{2+}$.[10−14] The electrochemical methods have been widely used to measure the comproportionation constant (K_c) for the mixed-valent species. Generally the mixed-valent species of interest is formed through chemical or electrochemical redox reactions.[15,16] However, it is possible to form mixed-valence species through photoexcitation of a binuclear metal complex:[17]

$$M-BL-M + h\nu \rightarrow M^+-BL^{\cdot-}-M \quad (1)$$

Fewer studies have addressed the nature of the mixed-valent state formed upon such excitation. Vibrational spectroscopy is a very powerful tool in this regard as reporter ligands may be used to provide vibrational signatures that are oxidation-state sensitive. The mixed-valent state may be accessed through electrochemistry[18−20] or photoexcitation.[17,21−26]

The aims of the present study are to probe the nature of the lowest excited state and the redox states of $[(bpy)_2Ru(\mu\text{-}bptz)Ru(bpy)_2]^{4+}$ (**1**) using resonance Raman spectroscopy. The structure of the bridging ligand, 3,6-bis(2-pyridyl)-1,2,4,5-tetrazine (bptz) is shown in Figure 1. The advantage of studying **1** is that the compound has a well-defined redox behaviour.[27,28] Thus the spectroscopic data obtained may

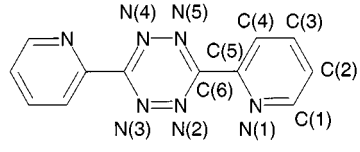

Figure 1. Structure and numbering system for bptz

[a] Chemistry Department, University of Otago, Union Place, Dunedin, New Zealand
Fax: (internat.) + 64-3/479-7906
E-mail: kgordon@alkali.otago.ac.nz
[b] IFS, Chemistry, Massey University, Palmerston North, Private Bag 11222, New Zealand

 © WILEY-VCH Verlag GmbH, 69451 Weinheim, Germany, 2002 1434−1948/02/0303−0554 $ 17.50+.50/0 *Eur. J. Inorg. Chem.* **2002**, 554−563

be related to a specific type of mixed-valent system, in this case Class III. The mixed-valent species formed by electrochemical oxidation is delocalised.[29] Furthermore the MO structure of the bridging ligand, bptz, has been studied experimentally[27] and through computational calculations.[30] These have found the redox MO for the reduced ligand and **1** to be strongly localised on the tetrazine portion of the bptz ligand. Complex **1** therefore provides a system in which each of the redox states that constitute an idealized model of the MLCT excited-state are known.

One of the disadvantages of using resonance Raman spectroscopy to probe the redox states and the lowest excited state of **1** is the presence of a number of overlapping chromophores in the visible region. In studying complexes with the $\{Ru(bpy)_2\}^{2+}$ moiety the strong enhancement of the bpy modes through the $Ru^{II} \rightarrow$ bpy MLCT transitions often conspire to obscure the resonance Raman spectral features from the other ligand present.[31–34] In order to obtain uncontaminated spectral signatures for bptz and bptz$^{\cdot-}$ the resonance Raman spectra of $[(PPh_3)_2Cu(\mu\text{-}bptz)Cu(PPh_3)_2]^{2+}$ (**2**) and **2**$^-$ were obtained. The $\{Cu(PPh_3)_2\}^+$ moiety possesses no additional chromophores in the visible region other than the $Cu^I \rightarrow$ bptz MLCT transition. Furthermore the $\{Cu(PPh_3)_2\}^+$ moiety causes only modest changes in the ligand structure and complexes with $\{Cu(PPh_3)_2\}^+$ may be used to obtain the radical anion spectra of ligands.[35–37] The crystal structures of **2**, reported herein, and **2**$^-$, previously published,[38] permit an analysis of the changes in the vibrational spectra in terms of the changes in bond lengths attendant upon reduction.

Results and Discussion

Electronic Spectroelectrochemistry

The electronic spectroscopic data for **1**, **2**, bptz, and their redox products are summarized in Table 1.

Table 1. Electronic absorption data for bptz, complexes, and their redox products

Compound	λ [nm] (ε [10^3 M^{-1}·cm^{-1}])				
bptz[a]	294 (19.6)				
bptz$^{\cdot-}$ [a]		368 (6.4)			
1[b]	281 (64.1)		404 (7.5)	688 (13.6)	
1$^+$ [b]			478 (4.6)	604 (12.2)	1483 (2.8)
1$^-$ [b]			434 (14.6)	491 (14.7)	
2[a]	258 (32.6)			707 (4.5)	
2$^-$ [a]			430 (3.7)		

[a] CH_2Cl_2 solution. [b] MeCN solution.

Reduction results in the depletion of ground state bands and the grow in of bptz$^{\cdot-}$ bands at approximately 400 to 450 nm. The spectra of **1**$^-$ and **2**$^-$ contain a bptz$^{\cdot-}$ band at ca. 430 nm. The spectrum of **1**$^-$ is also complicated by the red-shifting of $Ru^{II} \rightarrow$ bpy MLCT transitions as a consequence of the raising of dπ orbitals' energies because of the bptz reduction.[11] The spectrum of bptz$^{\cdot-}$ in solution shows a band at 368 nm. Recent studies of the spectroelectrochemistry for the mononuclear complex $[(bptz)Re(CO)_3Cl]^{\cdot-}$ reveals a band at 390 nm attributed to the bptz$^{\cdot-}$ species.[45a]

The absorption spectrum of **2** shows a strong MLCT transition at 707 nm. Reduction of **2** → **2**$^-$ results in the depletion of this band with the grow in of transitions at 430 and a shoulder at 520 nm, attributed to the radical anion of bptz. This is in good agreement with the reported UV/Vis spectrum of **2**$^-$ formed through comproportionation reaction,[38] which shows bands at 427 and 510 nm, and that observed for $[Cp^*ClIr(\mu\text{-}bptz)IrClCp^*]^+$ [39] which shows a band attributed to bptz$^{\cdot-}$ at 428 nm with ε = 4500 M^{-1} cm^{-1}.

The electrochemical oxidation of **1** → **1**$^+$ shows a reduction in the intensity of the MLCT band at 688 nm concomitant with the appearance of bands at 604 nm and 1483 nm (Figure 2). The intensity of the band in the NIR region is significantly greater than that observed for the related $[(NH_3)_4Ru(\mu\text{-}bptz)Ru(NH_3)_4]^{5+}$ (**3**$^+$).[30] In that case a band observed at 1453 nm (ε ≈ 500 M^{-1} cm^{-1}) was assigned as the IVCT transition. We propose that the feature observed at 1483 nm in **1**$^+$ is also of IVCT origin; however this band is more intense than that for the related **3**$^+$ complex. For both **1**$^+$ and **3**$^+$ the mixed-valent species formed are Class III in nature.[1,9] This may be established from the electrochemistry, the separation between metal-based oxidations being > 400 mV, and from the band shape of the IVCT band. In Class III systems the bandwidth ($\Delta\nu_{1/2}$) is less than that predicted by Hush theory.[7,8] In the Hush analysis the bandwidth is related to the transition wavenumber (ν) by $\Delta\nu_{1/2} = (2310\nu)^{1/2}$ cm^{-1}.

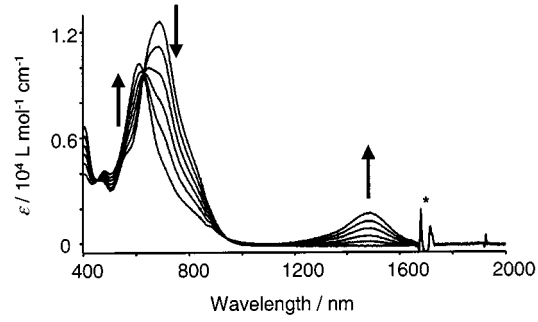

Figure 2. UV/Vis absorption spectra for **1** → **1**$^+$ (MeCN) electrochemical oxidation; arrows indicate the spectral changes occurring as the sample is oxidized; the asterisk * indicates overtone absorption bands of solvent (MeCN)

Compounds that show IVCT bands that fit this model are Class II in nature, whereas those which show much narrower transitions are Class III.[40]

For **1**$^+$ and **3**$^+$ the experimental values of $\Delta\nu_{1/2}$ are 1000 and 1600 cm^{-1},respectively, the values predicted through Hush theory would be 3960 and 3990 cm^{-1} for **1**$^+$ and **3**$^+$. They are therefore Class III systems. As **1**$^+$ and **3**$^+$ are Class III mixed-valence systems the amount of coupling may be parameterised by H_{ad}. This parameter represents the bonding interactions between the two identical Ru sites

directly and/or through superexchange pathways.[1,7,8] H_{ad} is related to the wavenumber of the IVCT transition (E_{op}) by $E_{op} = 2H_{ad}$.

In $\mathbf{1}^+$ and $\mathbf{3}^+$ H_{ad} is 3300 and 3440 cm^{-1}, respectively.

The upshot of this is that the μ-bptz ligand is allowing a similar level of coupling in the two complexes. The question arises as to why in $\mathbf{1}^+$ the IVCT transition is 5 times more intense than in $\mathbf{3}^+$. A similar phenomenon has been observed in mixed-valence complexes with 1,4-dicyanoamidobenzene.[41] In this case the peripheral ligands could tune the system between Class II and Class III behavior. The magnitude of the transition dipole moment (M) for the IVCT transition is dependent upon the overlap integral between the donor and acceptor wavefunctions (S_{ad}) and the dipole moment length (R).[40]

In the case of $\mathbf{3}^+$ the highly delocalised donor and acceptor wavefunction mean that R will be very small. This would result in a low ε for the IVCT band as is observed. In the case of $\mathbf{1}^+$ the dipole length is greater because of the inclusion of the bpy ligands in the donor and acceptor wavefunctions. Calculations on related Ru^{II} mononuclear complexes reveal that NH_3 ligands show less potential to mix with the dπ Ru^{II}-based HOMO than if bpy ligands are present.[42] In the case of $[Ru(bpy)_2L]^{2+}$ complexes the HOMO has ca. 70% dπ Ru character. In the case of $\mathbf{1}^+$ it is therefore reasonable to assume that the nature of the donor and acceptor MOs of the IVCT transition produce a greater dipole length than for $\mathbf{3}^+$.

Calculations of Structure and Crystal Structure Determination

The geometry of bptz was calculated by using HF and DFT (B3LYP) methods. In each case the ligand geometry was planar. Bond lengths and angles for the calculated and crystal structures are shown in Table 2. The notation is given in Figure 1. The result is surprising in view of the previously reported geometry optimization of bptz,[43] which reports a dihedral angle [as defined by N(1)−C(5)−C(6)−N(2)] of 19°. Furthermore, the crystal structure of the bptz contains a dihedral angle of 19°. In order to test our calculations we delibrately started the optimization with the structure having a significant dihedral angle. An analysis of the geometry optimization reveals that the major structural modification is in the dihedral angle − no other parameters show greater than 5% variation. Other than this discrepancy the bond lengths and angles we calculate are in good agreement with the crystal structure. Importantly the frequency calculations from these optimised structures show no imaginary frequencies, suggesting the geometries are at minimum energy.

An analysis of the bond lengths and angles reveals that the structure predicted at HF/6-31G(d) corresponds less closely to the crystal structure than the DFT (B3LYP) method. The average discrepancy in bond length for the HF calculation is 0.005 Å whereas for B3LYP it is 0.002 Å, for both basis sets used. The HF calculation generally does a poorer job with the C−N bond lengths and the N−N linkage is also too short. The increase in basis set in the B3LYP calculation does little to improve the predicted geometry.

Calculations were also carried out by using DFT methods on the radical anion of bptz. The spin expectation value, $<s^2>$, for the radical anion was 0.7501. This is very close to that for a pure doublet. We did not use HF methods to model the radical anion because they often give very poor $<s^2>$ values.[44] The calculated structure shows a lengthening of the N=N bond of the tetrazine. This is consistent with the population of a LUMO by the reducing electron that is based on the tetrazine and is antibonding with respect to the N=N bonds. It is consistent with the crystallographic data, vide infra.

The structure of **2** is similar to the previously described complexes, with the bptz acting as a linear bidentate ligand.[39,45] The structure confirms the presence of two $\{Cu(PPh_3)_2\}^+$ groups bound at a Cu−Cu distance of 6.78

Table 2. Bond lengths [Å] and angles [°] from calculations and crystallographic data

	bptz				**2**	$bptz^{\cdot-}$	$\mathbf{2}^-$
	Crystal structure[a]	HF/6-31G(d)	B3LYP/ 6-31G(d)	B3LYP/ 6-311G(d)	Crystal structure[b]	B3LYP/ 6-31G(d)	Crystal structure[c]
N(1)−C(1)	1.3326	1.316	1.333	1.330	1.350	1.340	1.338
C(1)−C(2)	1.388	1.382	1.398	1.396	1.376	1.400	1.385
C(2)−C(3)	1.381	1.386	1.393	1.391	1.372	1.400	1.375
C(3)−C(4)	1.387	1.384	1.393	1.390	1.400	1.393	1.381
C(4)−C(5)	1.3934	1.389	1.403	1.401	1.394	1.413	1.392
C(5)−N(1)	1.344	1.322	1.343	1.339	1.3495	1.361	1.353
C(5)−C(6)	1.4803	1.491	1.487	1.487	1.484	1.480	1.479
C(6)−N(5)	1.3416	1.323	1.348	1.345	1.3403	1.391	1.337
C(6)−N(2)	1.3426	1.323	1.348	1.345	1.3595	1.331	1.337
N(2)−N(3)	1.3198	1.285	1.315	1.311	1.334	1.399	1.393
C(4)−C(5)−N(1)	123.67	122.9	123.1	122.9	123.11	121.3	122.1
N(2)−C(6)−N(5)	124.77	123.1	124.1	123.9	125.1	127.0	129.9
N(1)−C(5)−C(6)−N(2)	19	0.00	0.00	0.00	9.72	0.00	0.00
Energy [Hartrees]		−785.68614	−790.51490	−790.68177		−790.55268	

[a] Ref.[43] [b] This work. [c] Ref.[38]

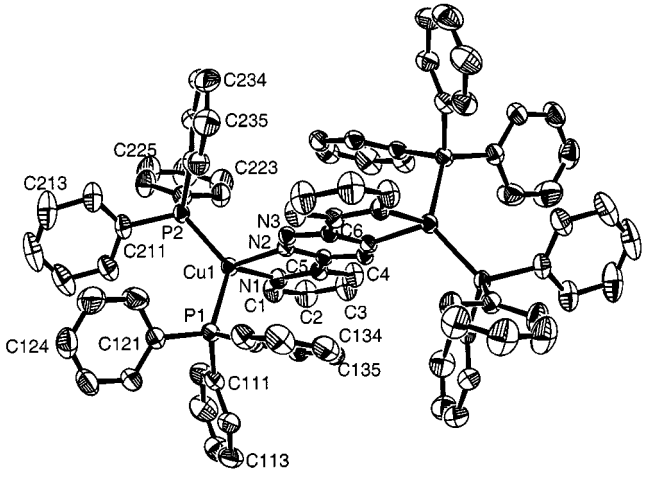

Figure 3. Molecular structure of **2** with thermal ellipsoids at 50% probability; selected bond lengths [Å]: Cu1−N2 2.0666(15), Cu1−N1 2.0957(17), Cu1−P2 2.2469(5), Cu1−P1 2.2760(5), N2−N3 1.329(2), N2−C6′ 1.355(2), N3−C6 1.341(2)

Å, Figure 3. The bond length and angles for the bptz moiety are presented in Table 2. The geometry about the copper is not completely tetrahedral with the small bite-angle of the bptz ligand and an axial-equatorial displacement of the PPh_3 groups. This displacement is not unusual in complexes of this type[46] and is driven by the π−π interactions between the tetrazine ring and one of the phenyl rings on each PPh_3. The distance from the tetrazine to the phenyl range from 3.3−3.7 Å.

The structure of the reduced complex has been previously reported and it is useful to compare the two structures in some detail. The structural details for bptz in **2** and $\mathbf{2}^-$ are given in Table 2.[38] The most important area for comparison is the bond lengths in the tetrazine ring. The study by Kaim and co-workers indicated that the reducing electron was located in the π* orbital of the N=N bond. The structure of **2** helps support this proposal; the N=N distance [1.329(2) Å] is significantly shorter than that observed in $\mathbf{2}^-$ [1.394(5) Å]. The other distances in the tetrazine ring of **2** do not vary significantly from those described in $\mathbf{2}^-$ (see Table 2). The bptz ligand in **2** is slightly more distorted than its anion radical form $\mathbf{2}^-$. The twist angle between the pyridyl groups and the tetrazine ring in **2** is 7.69°, whereas it is only 5.8° in $\mathbf{2}^-$. Another notable distortion is caused by the coordination of Cu^I. The ligand gains a slight distortion which can be seen in the relative distances between N1−N2 (2.66 Å) and N4−C4 (2.98 Å). The Cu−N distances show the same trend for **2** as noted for $\mathbf{2}^-$ with the Cu−N(1) pyridyl bond [2.0957(17) Å] being longer than the Cu−N(2) tetrazine [2.0666(15) Å] bond. The Cu−P distances in **2** at 2.2469(5) and 2.2760(5) Å are relatively similar, whereas in $\mathbf{2}^-$ they differ significantly [2.0297(12) and 2.2873(12) Å].

Frequency Calculations and Resonance Raman Spectroscopy

The frequency calculations were performed on bptz within a C_{2h} point group. The energy difference between the bptz with no symmetry and that with C_{2h} is less than $1.2\cdot10^{-7}$ Hartrees ($3.1\cdot10^{-1}$ J·mol^{-1}). Essentially the structures are equivalent.[47]

The frequencies calculated at HF/6-31G(d) were empirically scaled by 0.87 according to the findings of Radom et al.[48] The IR intensities and Raman activites were also obtained. Frequencies were also calculated using the DF hybrid method [B3LYP with a 6-31G(d) basis set, frequencies were scaled by 0.96].[48] The IR and Raman intensities were also calculated.

The HF and DFT calculations show reasonably good agreement with the IR data. The difference between the frequency calculations at HF and DFT/B3LYP level in the 1100 to 1700 cm^{-1} region are that the HF calculation poorly predicts the intensities of the Raman spectrum. It also places more a_g modes above 1500 cm^{-1} than the DFT calculation and has only two modes in the 1400 to 1500 cm^{-1} region. The Raman spectrum of bptz clearly shows 3 bands in the 1400 to 1500 cm^{-1} region. Furthermore the intensities calculated from HF predict strong Raman bands in the 1530 and 1600 cm^{-1}. This is not observed in the experimental spectra. For these reasons the HF calculations are not used in our subsequent analyses.

A listing of modes, their symmetries and wavenumbers for the DFT calculation and experimental data are given in Table 3.

The measured IR spectrum of bptz shows strong transitions at 1586, 1387, and 1130 cm^{-1} (Table 3). These correspond to modes 64, 54, and 45, respectively, from the DFT calculation. These modes are depicted in Figure 4 and can be best described as being pyridine ring (mode 64) and tetrazine ring (modes 54 and 45) stretches.

The Raman activity is related to the intensity of Raman bands as a function of the excitation wavelength and the wavenumber of the Raman photon.[49] It should be noted that the spectrum of bptz is a resonance Raman spectrum and this affords enhancement of band intensities not simply related to the Raman scattering cross section as calculated in the simulated spectrum. A detailed quantitative analysis is therefore inappropriate. It should, however, be noted that a_g modes are enhanced in resonance Raman spectra.[50] The predicted modes that should show large Raman scattering cross section are at 1599 (mode number 63), 1461 (mode 57), 1322 (mode 52), and 1278 cm^{-1} (mode 49). Modes 57 and 52 are almost exclusively tetrazine based stretches (Figure 4).

The calculated spectra of $bptz^{\cdot-}$ were only run using DFT methods. The predicted frequencies and intensities for $bptz^{\cdot-}$ are presented in Table 4. The Raman spectrum in the 1100 to 1700 cm^{-1} is dominated by mode 56 at 1380 cm^{-1}. This mode corresponds to mode 57 for the neutral ligand. A number of other weak a_g modes are also Raman-active in the 1100 to 1700 cm^{-1} region. It is interesting to note that those bands that are associated with normal modes of pyridine-ring character, such as modes 64 and 63, are predicted not to shift much upon reduction. However, the tetrazine modes, such as 57, 54, and 52, are predicted to shift significantly. Mode 57 (1461 cm^{-1} for bptz) is pre-

Table 3. Wavenumbers [cm^{-1}] of experimental and calculated bands for bptz in the 1000 to 1650 cm^{-1} region

bptz B3LYP/6-31G(d) calculated			bptz experimental data	
Mode number	Mode symmetry	ν [cm^{-1}][a]	IR ν [cm^{-1}][b]	Raman ν [cm^{-1}][c]
38	b_u	995 (9, 0)	993 (17)	
39	a_g	1034 (0, 1)		
40	b_u	1042 (2, 0)	1042 (8)	
41	b_u	1052 (6, 0)		
42	a_g	1067 (0, 0)		
43	b_u	1097 (2, 0)	1092 (5)	
44	a_g	1099 (0, 0)		
45	b_u	1132 (32, 0)	1130 (36)	
46	b_u	1156 (0, 0)	1152 (27)	
47	a_g	1156 (0, 1)		
48	b_u	1256 (1, 0)	1241 (7)	
49	a_g	1278 (0, 25)		1266
50	b_u	1291 (22, 0)	1255 (1)	
51	a_g	1291 (0, 0)		
52	a_g	1322 (0, 14)		1314
53	b_u	1339 (2, 0)		
54	b_u	1388 (100, 0)	1387 (100)	
55	a_g	1430 (0, 5)		1447
56	b_u	1448 (6, 0)	1444 (10)	
57	a_g	1461 (0, 100)		1462
58	a_g	1471 (0, 1)		1476
59	b_u	1485 (1, 0)		
60	a_g	1495 (0, 0)		
61	b_u	1589 (12, 0)	1576 (10)	
62	a_g	1590 (0, 0)		1576
63	a_g	1599 (0, 26)		1591
64	b_u	1599 (7, 0)	1586 (19)	

[a] Relative intensities of IR and Raman bands, respectively, are given in parentheses. The band intensities are normalized so that the strongest band in the reported region has an intensity of 100. [b] Relative intensities given in parentheses; normalized to 100 for the strongest band in the region. [c] These data pertain to a resonance Raman spectrum. The intensities are modulated by the resonance effect, hence they are not comparable to the predicted spectra and are not given.

dicted to shift to 1380 cm^{-1} in $bptz^{\cdot -}$ (corresponding to mode 56). Mode 54 shifts from 1388 to 1328 cm^{-1} and mode 52 from 1322 to 1280 cm^{-1}. These shifts are consistent with population of a tetrazine-based MO in $bptz^{\cdot -}$ and the concomitant weakening of the N−N linkages.

The resonance Raman spectra (RRS) of the complexes are presented in Figure 5.

The Raman spectrum of the bptz ligand (Figure 5, bptz) shows strong bands at around 1447 cm^{-1} and at 1591 and 1576 cm^{-1}. The 1447 cm^{-1} group of modes are assigned as predominantly tetrazine ring stretch, those at higher frequency are pyridyl ring stretches. If the excitation wavelength is changed from 457.9 nm to 514.5 nm the relative intensity of the 1447 cm^{-1} is diminished suggesting resonance enhancement of these spectra. All of the observed bands are polarised and are thus from modes of a_g symmetry.

The binding of the two $\{Ru(bpy)_2\}^{2+}$ moieties results in more complex resonance Raman spectra (Figure 5; **1**). The complex has two sets of chromophores in the visible region; these are Ru(dπ) → bpy(π*) MLCT transitions and Ru(dπ) → bptz(π*) MLCT transitions. From electrochemical studies the bptz-terminated MLCT transition should lie at lower energy than the bpy-based MLCT band. This is borne out in the resonance Raman spectra where bpy modes at 1605, 1566, 1499, 1317, and 1172 cm^{-1} are very strong with 457.9 nm excitation (Figure 5; **1**, 457 nm).[33] Modes associated with the bptz ligand lie at 1503 and 1366 cm^{-1} and are attributed to modes 60 and 53. The intensity of the 1366 cm^{-1} is convoluted with the solvent band; it is therefore difficult to assign. The observed bptz bands of **1** are significantly shifted from the bands in the free ligand. This may be due to the electronic effect of the $\{Ru(bpy)_2\}^{2+}$ distorting the ligand, or its steric effect. The relative intensity of the bpy modes is depleted as the excitation wavelength is tuned from 488.0 to 514.5 to 632.8 nm. With the red excitation wavelength no bpy modes are observed suggesting the Ru → bpy MLCT transition has negligible intensity at this wavelength.

The RRS of **2** (Figure 5) shows the enhancement of modes at 1488, 1459, 1437, 1305, and 1290 cm^{-1} assigned as modes 60, 57, 55, 52, and 51. For bptz they are shifted slightly from the Raman bands of the free ligand.

The RRS of **1** and **2** are generally similar with 632.8 nm excitation; they both show a strong band at about 1490 cm^{-1}, 1488 for **2** and 1503 cm^{-1} for **1**, and a group of vibrations at about 1300 cm^{-1}. The wavenumbers are shifted significantly for each. Structural data are not available for **1** but recent detailed calculations on related Pt^{II} complexes reveal significant perturbation of the electronic structure of bptz by the bound metals.[43] It is known that the $\{Ru(bpy)_2\}^{2+}$ moiety is a stronger π-acid than $\{Cu(PPh_3)_2\}^{+}$ and this may lead to perturbations of the ring structure and thus the vibrational spectra of the ligand.

Resonance Raman Spectroelectrochemistry

Resonance Raman spectroelectrochemistry offers a vibrational spectroscopic probe of the mixed-valent state, with oxidation, and of the bptz radical anion species, with reduction. The latter has already been thoroughly studied using ESR spectroscopy.[51] Such studies revealed that most of the electron density in the MO populated in the reduced species is localised at the tetrazine ring.

The resonance Raman spectrum of $\mathbf{1}^{+}$ was measured using 457.9, 488.0, 514.5, and 632.8 nm excitation wavelengths (Figure 5). In ascertaining the electron density changes about a metal upon oxidation, reporter groups are often utilised. These may be CO or CN^{-} ligands; both show a sensitivity of wavenumber of the stretch vibration to the oxidation state of the metal atom.[17,21−23] However, the bpy vibrations are also frequency dependent on the oxidation state of the metal atom.[33,34] For $[Ru(bpy)_3]^{3+}$ the bpy modes lie approximately 3−5 cm^{-1} higher in frequency than observed in the vibrational spectrum of $[Ru(bpy)_3]^{2+}$.[52] The spectra observed for $\mathbf{1}^{+}$ show bpy bands that are slightly shifted from that of **1**. This is most readily observed in the spectrum generated with 457.9 nm excitation; the bpy band at 1605 cm^{-1} in **1** is shifted to 1608 cm^{-1} in $\mathbf{1}^{+}$. Although this is a small shift it is not negligible

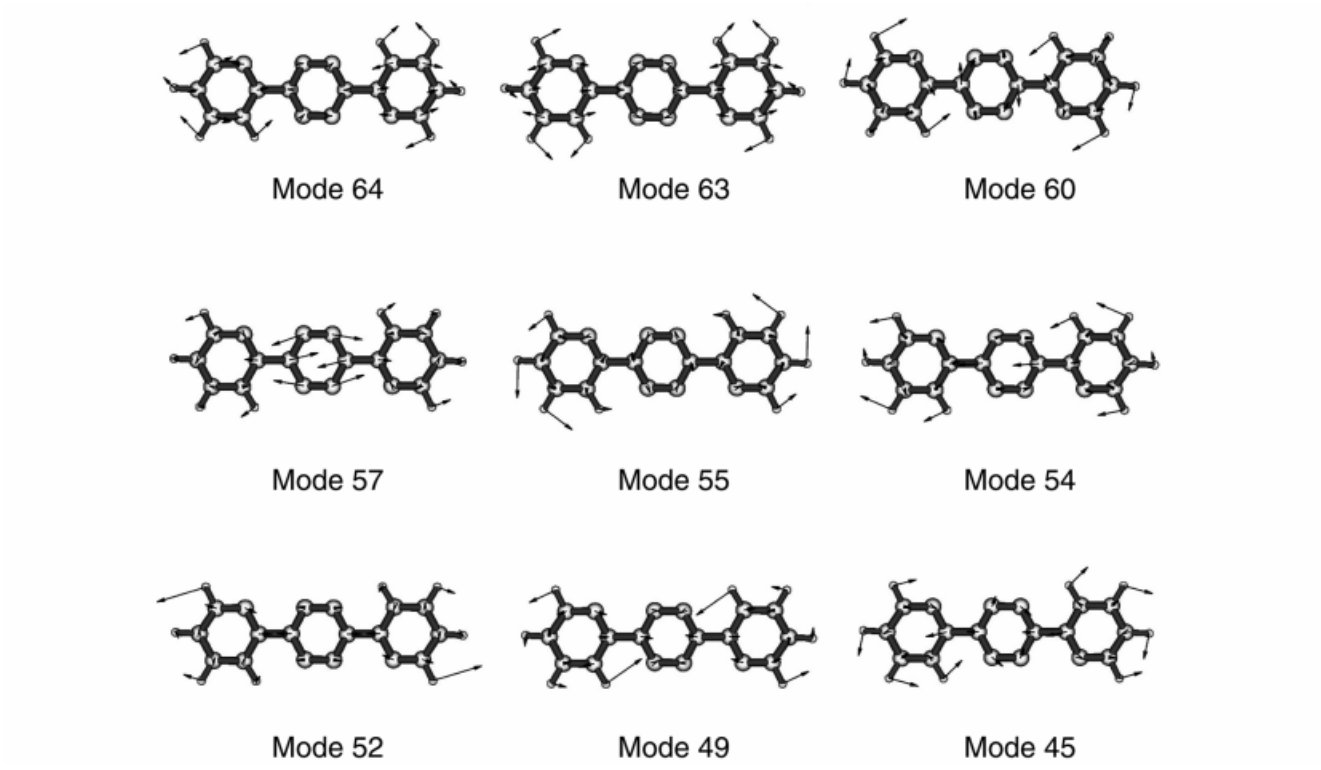

Figure 4. Selected normal modes calculated for bptz. Modes 64 and 63 are pyridine-based, 57, 54, and 52 are tetrazine-based

and is consistent with oxidation of a metal site or sites. The largest frequency shift observed in comparing **1** and $\mathbf{1}^+$ is the bptz band at 1503 and 1513 cm^{-1} respectively. This is most readily seen in the spectra generated with 632.8 nm excitation. The significance of these data are as follows: (1) The larger shift for the bptz vibrational transition is consistent with significant perturbation at the bridging ligand relative to the peripheral bpy ligands. (2) The shift of the bpy mode upon oxidation is consistent with a perturbation of electron density at *both metal sites*; an unperturbed Ru^{II} centre would retain bpy signatures at 1605 cm^{-1}. This is perhaps unsurprising in view of the strong coupling between the metal sites.[45a] Oxidation is likely to create an $\{Ru^{+2.5}(\mu\text{-bptz})Ru^{+2.5}\}$ species; thus the electron density change on the metal atoms is delocalised and changes in the bonding of the bpy ligands is delocalised over both metal centres.

The 10 cm^{-1} frequency shift of the bptz band, in relation to point (1) above, provides support for the presence of a superexchange contribution to the production of a Class III species. Consequently, the HOMO has some bptz π-character, in which the $\mathbf{1}^+$ formulation $\{Ru^{+2.4}(bptz^{+0.2})Ru^{+2.4}\}$ may be more truthfully representative. That is, the 10 cm^{-1} frequency shift of the bptz band is a direct result of the depopulation of the HOMO which is constituted by some% of bptz π-character.

In summary, the resonance Raman spectroscopy of $\mathbf{1}^+$ is consistent with a Class III species.

The electrochemical reduction of $\mathbf{2} \rightarrow \mathbf{2}^-$ results in significant spectral changes; firstly, the RRS of $\mathbf{2}^-$ is much more intense than that of **2** generated with 457.9 nm excitation. A new set of bands are observed at 1406, 1313, 1274, 1027, and 1002 cm^{-1}. These may be assigned to modes 56, 53, 51 43, and 40, respectively. The correlation is based on: (1) the fact that this is a resonance Raman spectrum, thus a_g modes will be enhanced; (2) the calculation predicts some intensity for each. The strongest of these bands lie at 1406 and 1274 cm^{-1}. The crystal structure of $\mathbf{2}^-$, and calculations on $bptz^{\cdot -}$, reveal that the N=N bond is 1.39 Å in $\mathbf{2}^-$ and 1.32 Å in **2**. The shift to lower frequencies is most prevalent for the tetrazine modes as predicted by calculation.

The resonance Raman spectra of $\mathbf{1}^-$ show significant changes to those of the parent complex at all 4 excitation wavelengths (Figure 5). The spectrum of $\mathbf{1}^-$ generated with 457.9 nm excitation shows bands at 1506 cm^{-1} that may be assigned as a $bptz^{\cdot -}$ feature; other bands at 1605, 1486 and 1317 cm^{-1} are bpy modes. Complete conversion from the parent species is confirmed by the absence of any residual 1494 cm^{-1} band. The band at 1559 cm^{-1} (mode 62, Table 4) is rather interesting; it appears to be composed of bpy and $bptz^{\cdot -}$ vibrations. The spectrum at 488.0 nm excitation shows similar bands with the bpy-modes reduced in intensity. However, their relative intensity is greater in the spectrum of $\mathbf{1}^-$ than in that of **1** at the same excitation wavelength. This is consistent with a destabilisation of the metal t_{2g} MOs upon reduction at the ligand site. This effect redshifts the $Ru(d\pi) \rightarrow bpy(\pi^*)$ MLCT transitions causing them to become resonant at 488.0 and 514.5 nm.[33,34,53]

The resonance Raman spectrum of $\mathbf{1}^-$ observed with 632.8 nm excitation shows a very different intensity pattern than that observed at the other excitation wavelengths. Firstly, no bpy modes are observed. This is consistent with

Table 4. Wavenumbers [cm^{-1}] of calculated bands for bptz$^{\cdot-}$, and experimental bands of $\mathbf{2}^-$ in the 1000 to 1650 cm^{-1} region

bptz$^{\cdot-}$ B3LYP/6-31G(d) calculated data			Resonance Raman data for $\mathbf{2}^-$
Mode number	Mode symmetry	ν [cm^{-1}][a]	ν [cm^{-1}][b]
41	b_u	1043 (51, 0)	
42	b_u	1049 (2, 0)	
43	a_g	1049 (0, 1)	1027
44	b_u	1083 (16, 0)	
45	a_g	1088 (0, 1)	
46	b_u	1134 (90, 0)	
47	a_g	1141 (0, 0)	
48	b_u	1143 (32, 0)	
49	a_g	1230 (0, 2)	
50	b_u	1261 (29, 0)	
51	a_g	1280 (0, 1)	1274
52	b_u	1283 (17, 0)	
53	a_g	1303 (0, 0)	1313
54	b_u	1328 (20, 0)	
55	b_u	1361 (34, 0)	
56	a_g	1380 (0, 1000)	
57	a_g	1435 (0, 3)	1406
58	b_u	1435 (70, 0)	
59	a_g	1477 (0, 0)	
60	b_u	1477 (66, 0)	
61	b_u	1574 (37, 0)	
62	a_g	1575 (0, 3)	
63	b_u	1593 (100, 0)	
64	a_g	1593 (0, 4)	

[a] Relative intensities of IR and Raman bands, respectively, are given in parentheses. The band intensities are normalized so that the strongest band in the reported region has an intensity of 100 for IR and 1000 for Raman. [b] These data pertain to a resonance Raman spectrum. The intensities are modulated by the resonance effect, hence they are not comparable to the predicted spectra and are not given.

the fact that at 632.8 nm there are no electronic transitions involving the bpy ligands. Secondly, the bptz$^{\cdot-}$ mode at 1559 cm^{-1} is absent and bands appear at 1005, 1257, and 1308 cm^{-1} in a pattern completely different from that observed at the other excitation wavelengths. The frequency calculation predicts modes at 996, 1280, and 1303 cm^{-1} which correspond to modes 40, 51, and 53, respectively. The enhancement of these modes is quite different from that observed for $\mathbf{2}^-$ (Figure 5; $\mathbf{2}^-$, 457 nm) and this suggests that the bptz$^{\cdot-}$ species has a number of transitions in the visible region that involve quite different portions of the bptz$^{\cdot-}$ radical anion ligand. This is also supported by the fact that the resonance Raman spectra of **2** show strong variations in intensity for bands at 1488 and 1305 cm^{-1} with λ_{exc} (Figure 5).

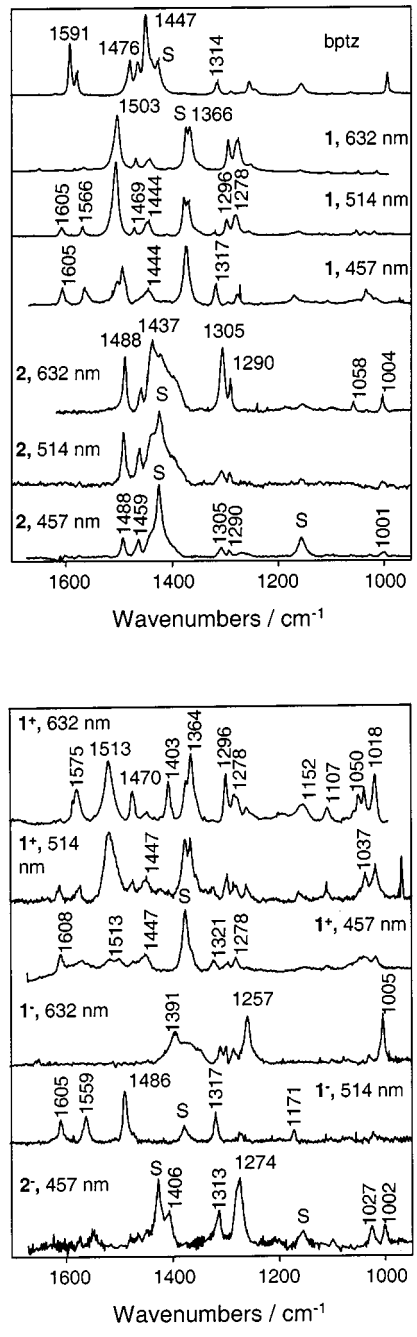

Figure 5. Resonance Raman spectra of **1** (3 mM MeCN), **2** (3 mM CH_2Cl_2), $\mathbf{1}^+$ (3 mM MeCN), $\mathbf{2}^-$ (3 mM CH_2Cl_2), $\mathbf{1}^-$ (3 mM MeCN); **S** represents a solvent band; all λ_{exc} = 15 mW at sample

Excited-State Resonance Raman Spectra

The excited-state lifetime of **1** has not been reported; the lack of any emission in fluid media suggests it is < 5 ns. It is possible to probe such short-lived species using nanosecond pulsed laser excitation at sufficient pump powers.[37,54–56] The RRS of **1** generated using 532 and 633 nm pulsed excitation are shown in Figure 6. As the pulse energy is increased a number of bands become stronger; these are assigned to the excited state (**1***). They lie at 988, 1100, 1120, 1161, 1568, and 1608 cm^{-1}. In a simple fashion the spectrum of **1*** can be thought of as a combination of the spectra of $\mathbf{1}^+$ and $\mathbf{1}^-$. The 1568 and 1608 cm^{-1} bands may be attributed to bpy vibrational bands of a Ru→bpy MLCT transition from an Ru centre. None of the other excited-state features present are bptz-associated marker bands for $\mathbf{1}^+$ or bptz$^{\cdot-}$ as probed in $\mathbf{1}^-$ or even $\mathbf{2}^-$.[57] This is in contrast to what is normally observed in the spectra of mononuclear polypyridylmetal complexes.[21,22] A plausible explanation for this discrepancy is that there is strong mixing

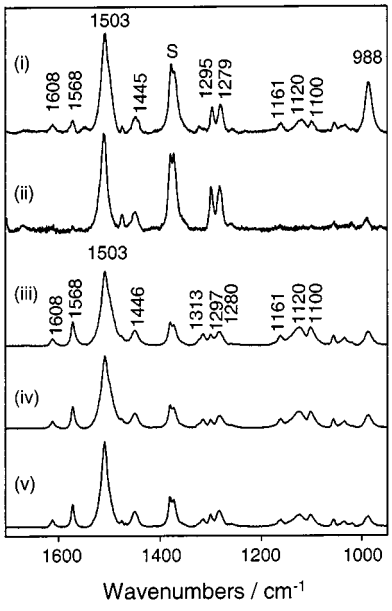

Figure 6. Resonance Raman spectra of **1** (2 mM MeCN) with pulsed laser excitation: (i) λ_{exc} = 633 nm, pulse energy 2 mJ; (ii) λ_{exc} = 633 nm, pulse energy 0.4 mJ; (iii) λ_{exc} = 532 nm, pulse energy 4 mJ; (iv) λ_{exc} = 532 nm, pulse energy 2 mJ; (v) λ_{exc} = 532 nm, pulse energy 0.5 mJ

(superexchange pathway) between the dπ and bptz π* MOs such that both the acceptor and donor orbital in the excited state are delocalised over the two Ru centres and bptz. Consequently, the bptz vibrational band positions will reflect the bonding changes due to the acceptor *and* donor orbitals and not solely the acceptor orbital as is the case for mononuclear metal polypyridyl complexes or Class I/II binuclear polypyridylmetal complexes. Therefore, the excited-state resonance Raman spectra of **1** are not inconsistent with a Class III formulation of the $\mathbf{1}^+$ mixed-valent state in which the Class III state is produced from a superexchange pathway via bptz.

Conclusion

Ab initio calculations can provide useful insight into the structure and vibrational spectra of ligands and their radical anions. In this case DFT calculations modelled the IR spectrum of bptz very well. The frequency calculation also allowed for a clear picture of the resonance Raman spectra of **1** and **2**.

The calculations on the $bptz^{\cdot-}$ predict a significant lengthening of the N=N linkage from 1.31 to 1.40 Å. This is the largest structural change predicted from the calculations. The crystal structure of $\mathbf{2}^-$ shows this predicted effect. The frequencies calculated for $bptz^{\cdot-}$ predict significant shifting of tetrazine modes from 1461 cm^{-1} in bptz (mode 57) to 1380 cm^{-1} in $bptz^{\cdot-}$ (mode 56). This may be correlated with bands of **2** at 1462 cm^{-1} shifting to 1406 cm^{-1} in $\mathbf{2}^-$.

The UV/Visible spectra of the oxidised complex, $\mathbf{1}^+$, shows a distinct and narrow IVCT transition at 1483 nm. This is somewhat more intense than that observed for other mixed-valent species with the bptz bridging ligand. We attribute the increased intensity to the ability of the $\{Ru(bpy)_2\}^{2+}$ moiety to mix bpy character into the wavefunction of the donor MO in the IVCT transition. This has the effect of increasing the dipole length of the transition and thus its intensity. The resonance Raman spectra of $\mathbf{1}^+$ reveal small shifts in the bpy bands consistent with metal oxidation. The absence of a discrete set of bpy bands for Ru^{II} and Ru^{III} centres suggests a Class III mixed-valent formulation for $\mathbf{1}^+$; consistent with previous findings.

The resonance Raman spectra of the complexes **1** and **2** are consistent with the UV/Vis spectral assignments. The resonance Raman spectra of **1** show enhancement of bpy modes at blue excitation wavelengths with bptz modes being enhanced with red excitation. This is consistent with Ru→bpy MLCT and Ru→bptz MLCT transitions. For **2** only bptz modes are enhanced with visible excitation. The change in relative intensities for the bptz bands suggest the presence of two Cu→bptz MLCT transitions in the visible region. This is exemplified by the increased resonance enhancement of the 1305 cm^{-1} band relative to 1488 cm^{-1} on going from 457.9 to 632.8 nm excitation.

The UV/Vis spectrum of $\mathbf{1}^-$ shows chromophores associated with the Ru→bpy MLCT and $bptz^{\cdot-}$ π→π* transitions. The spectra generated with 457.9, 488.0, and 514.5 nm excitation are dominated by bpy bands but at 632.8 nm excitation $bptz^{\cdot-}$ bands are evident. The signature for the $bptz^{\cdot-}$ comes from the spectrum of $\mathbf{2}^-$ which shows the vibrational signature of $bptz^{\cdot-}$ and reveals the π→π* transition to lie at ca. 430 nm.

The excited-state resonance Raman spectra of **1*** show spectral features that are not a simple linear combination of the oxidised metal centre and ligand radical anion. This is consistent with a pair of acceptor and donor orbitals that are delocalised over the two Ru centres and the bptz ligand. A delocalised donor orbital is consistent with a Class III mixed-valent species. It may also be due to the differing probe wavelengths employed in the excited-state spectra of **1** over the spectroelectochemical spectra of $\mathbf{2}^-$.

Experimental Section

Complex Synthesis: $[(bpy)_2Ru(\mu\text{-bptz})Ru(bpy)_2](PF_6)_4$ [**1**·$(PF_6)_4$] and $[(PPh_3)_2Cu(\mu\text{-bptz})Cu(PPh_3)_2](BF_4)_2$ [**2**·$(BF_4)_2$] were prepared by literature procedures.[58−60] Purity was confirmed by microanalysis. **1** can exist in a number of diastereoisomers; no attempt was made to separate them.

Physical Measurements: Electronic absorption spectra were measured using a Perkin−Elmer λ-19 spectrometer. Electrochemical and spectroscopic measurements used solvents of spectroscopic grade. These were further purified by distillation and were stored over 5-Å molecular sieves. The supporting electrolytes used in the electrochemical measurements were tetrabutylammonium perchlorate (TBAP) and tetrabutylammonium hexafluorophosphate (TBAH). These were purified by repeated recrystallizations from ethanol/water, for TBAP, or ethyl acetate/ether, for TBAH.[61] Cyclic voltammograms (CVs) were obtained from argon-purged degassed so-

lutions of compound (ca. 1 mM) with 0.1 M concentration of TBAP or TBAH present. The electrochemical cell consisted of a 1.6 mm diameter platinum working electrode embedded in a Kel-F cylinder with a platinum auxiliary electrode and a saturated potassium chloride calomel reference electrode. The CV was calibrated against ferrocene/ferrocenium couple by addition of ferrocene to the sample cell and the running of a calibration CV. The potential of the cell was controlled by an EG&G PAR 273A potentiostat with Model 270 software. Resonance Raman spectra, generated with continuous wave excitation, were obtained using an air-cooled argon ion laser (Melles−Griot Omnichrome 543-MAP) or helium-neon laser (Oplectra). Plasma emission lines were removed from the exciting beam using bandpass filters or a wavelength-specific holographic laser bandpass filter (Kaiser Optical Systems, Inc.). Spectra were analysed by using GRAMS 5.0 (Galactic Industries). The cell used for Raman spectroelectrochemistry was an OTTLE cell.[62] The sample was held in a spinning NMR tube or OTTLE cell and Raman photons were imaged into the spectrograph (SPEX 750M) with a 135° backscattering arrangement. The spectrograph was equipped with an 1800 g/mm holographic grating; detection was achieved using a CCD (Princeton Instruments 1152 EUV LN_2 cooled with CSMA version 2.3 software). Calibration of Raman spectra were achieved with neon or argon ion emission lines. Spectral calibrations were checked against solvent spectra.[63] This revealed that peak reproducibility was accurate to 1.5 cm^{-1} across differing excitation wavelengths. For electronic absorption spectroelectrochemistry spectra were acquired at a series of applied potentials stepping through the oxidation or reduction of interest. For Raman studies the applied potential was set beyond the $E^{0\prime}$ value of the electrochemical process, and data were collected after sufficient time that the probed volume contained only the reduced or oxidised product. The frequency-doubled output from an Nd:YAG (Continuum Surelite I-10) pulsed laser (5−7 ns pulse width, operating at 10 Hz) was used to generate excited-state resonance Raman (ESRR) spectra at 532 nm, it was also used to provide stimulated Raman scattering[64,65] for the ESRR experiments with 633 nm excitation. The 532 nm output from the Nd:YAG laser was focused into a 10-cm cell filled with spectrophotometric grade acetonitrile. A quartz Pellin−Broca prism was used to separate the co-linear partially depleted pump beam and four Stokes orders of stimulated Raman scattering. The first Stokes output from the Raman shifter was directed onto the sample in the same manner as the continuous-wave Raman experiments. Typically a 532 nm, 7−40 mJ pump pulse was used, generating 0.5−4.5 mJ of the second Stokes-shifted line at 633 nm. Beam diameter at sample was 300 μm. The geometry and vibrational frequencies of the bptz ligand and its radical anion were obtained using HF and DFT-HF hybrid calculations implemented with the Gaussian98 and -94 program packages.[66,67] Visualization of the MOs and vibrational modes was provided by the Molden package.[68]

X-ray Crystallographic Study: Crystal data for **2**·$(BF_4)_2$·CH_2Cl_2: $C_{85}H_{68}B_2Cl_2Cu_2F_8N_6P4$, M = 1668.93, triclinic, a = 13.2173(2), b = 13.2183(2), c = 14.70050(10) Å, α = 87.8200(10), β = 69.1300(10), γ = 64.0130(10)°, V = 2135.72(5) $Å^3$, T = 175 K, space group $P\bar{1}$, Z = 1, μ(Mo-K_α) = 0.699 mm^{-1}, d = 1.298 Mg/m^3. Data collection: Siemens SMART CCD area detector, graphite monochromator, 0.38 × 0.22 × 0.14 mm, 20511 reflections measured, 9168 unique (R_{int} = 0.0173) which were used in all calculations. The final $Rw(F_o^2)$ = 0.0983 [$R(F_o)$ = 0.0383] $Rw(F_o^2)$ = $[\{w(F_o^2 - F_c^2)^2\}]/\{w(F_o^2)^2\}]^{1/2}$ where w^{-1} = $[\sigma^2(F_o^2) + (aP)^2 + bP]$ (a = 0.0498; b = 1.20) and P = $[\max(F_o^2,0) + 2F_c^2]/3$. All other aspects of data collection, reduction, solution and refinement were performed as previously described.[62][69] Crystallographic data (excluding structure factors) for the structure(s) reported in this paper have been deposited with the Cambridge Crystallographic Data Centre as supplementary publication no. CCDC-166062. Copies of the data can be obtained free of charge on application to CCDC, 12 Union Road, Cambridge CB2 1EZ, UK [Fax: (internat.) + 44-1223/336-033; E-mail: deposit@ccdc.cam.ac.uk].

Acknowledgments

Support from the New Zealand Lottery Commission and the University of Otago Research Committee is gratefully acknowledged. A. F. would like to acknowledge the Alliance Group for a postgraduate scholarship.

[1] S. F. Nelsen, *Chem. Eur. J.* **2000**, *6*, 581−588.
[2] K. D. Demadis, G. A. Neyhart, E. M. Kober, T. J. Meyer, *J. Am. Chem. Soc.* **1998**, *120*, 7121−7122.
[3] K. D. Demadis, E.-S. El-Samanody, G. M. Coia, T. J. Meyer, *J. Am. Chem. Soc.* **1999**, *121*, 535−544.
[4] M. B. Robin, P. Day, *Adv. Inorg. Radiochem.* **1967**, *10*, 247−422.
[5] J. H. Elias, R. S. Drago, *Inorg. Chem.* **1972**, *11*, 415−418.
[6] R. W. Callahan, G. M. Brown, T. J. Meyer, *Inorg. Chem.* **1975**, *14*, 1443−1453.
[7] N. S. Hush, *Prog. Inorg. Chem.* **1967**, *8*, 391−444.
[8] N. S. Hush, *Coord. Chem. Rev.* **1985**, *64*, 135−157.
[9] C. Creutz, *Prog. Inorg. Chem.* **1983**, *30*, 1−73.
[10] H. Hartmann, T. Scheiring, J. Fiedler, W. Kaim, *J. Organomet. Chem.* **2000**, *604*, 267−272.
[11] T. Scheiring, W. Kaim, J. A. Olabe, A. R. Parise, J. Fiedler, *Inorg. Chim. Acta* **2000**, *300*, 125−130.
[12] M. Glockle, W. Kaim, *Angew. Chem. Int. Ed.* **1999**, *38*, 3072−3074.
[13] M. Ketterle, W. Kaim, J. A. Olabe, A. R. Parise, J. Fiedler, *Inorg. Chim. Acta* **1999**, *291*, 66−73.
[14] M. Ketterle, J. Fiedler, W. Kaim, *Chem. Commun.* **1998**, 1701−1702.
[15] S. D. Ernst, V. Kasack, W. Kaim, *Inorg. Chem.* **1988**, *27*, 1146−1148.
[16] S. Barlow, D. O'Hare, *Chem. Rev.* **1997**, *97*, 637−669.
[17] M. W. George, F. P. A. Johnson, J. J. Turner, J. R. Westwell, *J. Chem. Soc., Dalton Trans.* **1995**, 2711−2718.
[18] C. G. Atwood, W. E. Geiger, *J. Am. Chem. Soc.* **2000**, *122*, 5477−5485.
[19] T. Ito, T. Hamaguchi, H. Nagino, T. Yamaguchi, J. Washington, C. P. Kubiak, *Science* **1997**, *277*, 660−663.
[20] T. Ito, T. Hamaguchi, H. Nagino, T. Yamaguchi, H. Kido, I. S. Zavarine, T. Richmond, J. Washington, C. P. Kubiak, *J. Am. Chem. Soc.* **1999**, *121*, 4625−4632.
[21] J. R. Schoonover, G. F. Strouse, *Chem. Rev.* **1998**, *98*, 1335−1355.
[22] J. R. Schoonover, C. A. Bignozzi, T. J. Meyer, *Coord. Chem. Rev.* **1997**, *165*, 239−266.
[23] J. R. Schoonover, G. F. Strousse, R. B. Dyer, W. D. Bates, T. J. Meyer, *Inorg. Chem.* **1996**, *35*, 273−274.
[24] L. C. Abbott, C. J. Arnold, T.-Q. Ye, K. C. Gordon, R. N. Perutz, R. E. Hester, J. N. Moore, *J. Phys. Chem. A.* **1998**, *102*, 1252−1260.
[25] J. R. Schoonover, K. C. Gordon, R. Argazzi, W. H. Woodruff, K. A. Peterson, C. A. Bignozzi, R. B. Dyer, T. J. Meyer, *J. Am. Chem. Soc.* **1993**, *115*, 10996−10997.
[26] J. R. Schoonover, G. F. Strouse, K. M. Omberg, R. B. Dyer, *Comments Inorg. Chem.* **1996**, *18*, 165−188.
[27] W. Kaim, S. Kohlmann, *Inorg. Chem.* **1986**, *25*, 3442−3448.
[28] W. Kaim, S. Ernst, S. Kohlmann, P. Welkerling, *Chem. Phys. Lett.* **1985**, *118*, 431−434.
[29] J. Poppe, M. Moscherosch, W. Kaim, *Inorg. Chem.* **1993**, *32*, 2640−2643.

[30] S. D. Ernst, W. Kaim, *Inorg. Chem.* **1989**, *28*, 1520−1528.
[31] S. M. Scott, A. K. Burrell, P. A. Cocks, K. C. Gordon, *J. Chem. Soc., Dalton Trans.* **1998**, 3679−3684.
[32] C. A. Bignozzi, J. R. Schoonover, F. Scandola, *Prog. Inorg. Chem.* **1997**, *44*, 1−95.
[33] J. Sherborne, S. M. Scott, K. C. Gordon, *Inorg. Chim. Acta* **1997**, *260*, 199−205.
[34] J. Sherborne, K. C. Gordon, *Asian J. Spectrosc.* **1998**, *2*, 137−148.
[35] K. C. Gordon, J. J. McGarvey, *Inorg. Chem.* **1991**, *30*, 2986−2989.
[36] S. M. Scott, A. K. Burrell, K. C. Gordon, *J. Chem. Soc., Dalton Trans.* **1998**, 2873−2877.
[37] K. C. Gordon, J. J. McGarvey, *Chem. Phys. Lett.* **1989**, *162*, 117−122.
[38] M. Schwach, H. D. Hausen, W. Kaim, *Inorg. Chem.* **1999**, *38*, 2242−2243.
[39] W. Kaim, S. Berger, S. Greulich, R. Reinhardt, J. Fielder, *J. Organomet. Chem.* **1999**, *582*, 153−159.
[40] R. J. Crutchley, *Adv. Inorg. Chem.* **1994**, *41*, 273−325.
[41] C. E. G. Evans, M. L. Naklicki, A. R. Rezvani, C. A. White, V. V. Kondratiev, R. J. Crutchley, *J. Am. Chem. Soc.* **1998**, *120*, 13096−13103.
[42] H. Masui, A. L. Freda, M. C. Zerner, A. B. P. Lever, *Inorg. Chem.* **2000**, *39*, 141−152.
[43] A. Klein, E. J. L. McInnes, T. Scheiring, S. Zalis, *J. Chem. Soc., Faraday Trans.* **1998**, *94*, 2979−2984.
[44] N. H. Damrauer, B. T. Weldon, J. K. McCusker, *J. Phys. Chem. A* **1998**, *102*, 3382−3397.
[45] [45a] T. Scheiring, J. Fiedler, W. Kaim, *Organometallics* **2001**, *20*, 1437−1441. [45b] C. S. Campos-Fernandez, R. Clerac, J. M. Koomen, D. H. Russell, K. R. Dunbar, *J. Am. Chem. Soc.* **2001**, *123*, 773−774. [45c] X.-H. Bu, K. Tanaka, M. Shionoya, K. Biradha, H. Morishita, S. Furusho, *Chem. Commun.* **2000**, 971−972. [45d] C. S. Campos-Fernandez, R. Clerac, K. R. Dunbar, *Angew. Chem. Int. Ed.* **1999**, *38*, 3477−3479. [45e] M. Gloeckle, W. Kaim, N. E. Katz, M. G. Posse, E. H. Cutin, J. Fiedler, *Inorg. Chem.* **1999**, *38*, 3270−3274. [45f] P. N. Preston, S. J. Rettig, A. STorr, J. Trotter, *Can. J. Chem.* **1998**, *76*, 1800−1804. [45g] A. Klein, S. Hasenzahl, W. Kaim, J. Fiedler, *Organometallics* **1998**, *17*, 3532−3538. [45h] S. Roche, J. A. Thomas, L. J. Yellowlees, *Chem. Commun.* **1998**, 1429−1430. [45i] W. Kaim, R. Reinhardt, J. Fiedler, *Angew. Chem. Int. Ed. Engl.* **1997**, *36*, 2493−2495. [45j] J. Poppe, M. Moscherosch, W. Kaim, *Inorg. Chem.* **1993**, *32*, 2640−2643. [45k] T. S. Akasheh, Z. M. Al-Ahmad, *Dirasat − Univ. of Jordan, Ser. B* **1990**, *17*, 98−105. [45l] J. G. H. Du Preez, T. I. A. Gerber, M. L. Gibson, *J. Coord. Chem.* **1990**, *22*, 33−42.[45m] W. Kaim, V. Kasack, *Inorg. Chem.* **1990**, *29*, 4696−4699.
[46] S. E. Page, K. C. Gordon, A. K. Burrell, *Inorg. Chem.* **1998**, *37*, 4452−4459.
[47] A. M. Brouwer, R. Wilbrandt, *J. Phys. Chem.* **1996**, *100*, 9678−9688.
[48] A. P. Scott, L. Radom, *J. Phys. Chem.* **1996**, *100*, 16502−16513.
[49] G. A. Guirgis, Y. E. Nashed, J. R. Durig, *Spectrochim. Acta, Part A* **2000**, *56*, 1065−1078.
[50] R. J. H. Clark, T. J. Dines, *Angew. Chem. Int. Ed. Engl.* **1986**, *25*, 131−160.
[51] A. -L. Barra, L. -C. Brunel, F. Baumann, M. Scwach, M. Moscherosch, W. Kaim, *J. Chem. Soc., Dalton Trans.* **1999**, 3855−3857.
[52] P. G. Bradley, N. Kress, B. A. Hornberger, R. F. Dallinger, W. H. Woodruff, *J. Am. Chem. Soc.* **1981**, *103*, 7441−7446.
[53] R. J. Donohoe, C. D. Tait, M. K. DeArmond, D. W. Wertz, *Spectrochim. Acta, Part A* **1986**, *42*, 233−240.
[54] T. G. Spiro, D. S. Caswell, *Inorg. Chem.* **1987**, *26*, 18−19.
[55] K. C. Gordon, J. J. McGarvey, *Chem. Phys. Lett.* **1990**, *173*, 443−448.
[56] J. H. Perng, J. I. Zink, *Inorg. Chem.* **1988**, *27*, 1403−1406.
[57] One pragmatic possibility for the absence of $bptz^{\cdot-}$ features is that the bands observed in **1*** are $bptz^{\cdot-}$ in nature but differ from those seen in $\mathbf{2}^-$ because of the differing λ_{exc} used. The UV/Vis spectroelectrochemistry of $\mathbf{2} \rightarrow \mathbf{2}^-$ reveals that $bptz^{\cdot-}$ is not highly absorbing at 532 or 633 nm.
[58] S. Kohlmann, S. Ernst, W. Kaim, *Angew. Chem.* **1985**, *97*, 698−699; *Angew. Chem. Int. Ed. Engl.* **1985**, *24*, 684−685.
[59] Q. Jaradat, K. Barqawi, T. S. Akasheh, *Inorg. Chim. Acta* **1986**, *116*, 63−73.
[60] W. Kaim, S. Kohlmann, *Inorg. Chem.* **1987**, *26*, 1469−1470.
[61] H. O. House, E. Feng, N. P. Peet, *J. Org. Chem.* **1971**, *36*, 2371−2375.
[62] M. R. Waterland, T. J. Simpson, K. C. Gordon, A. K. Burrell, *J. Chem. Soc., Dalton Trans.* **1998**, 185−192.
[63] The ASTM subcommitte on Raman spectroscopy has adopted eight materials as Raman shift standards (ASTM E 1840). The band wavenumbers for these standards are available at: http://chemistry.ohio-state.edu/~rmccreer/shift.html
[64] R. P. Van Duyne, K. D. Parks, *Chem. Phys. Lett.* **1980**, *76*, 196−200.
[65] C. A. Grant, J. L. Hardwick, *J. Chem. Ed.* **1997**, *74*, 318−321.
[66] M. J. Frisch, G. W. Trucks, H. B. Schlegel, P. M. W. Gill, B. G. Johnson, M. A. Robb, J. R. Cheeseman, T. Keith, G. A. Petersson, J. A. Montgomery, K. Raghavachari, M. A. Al-Laham, V. G. Zakrzewski, J. V. Ortiz, J. B. Foresman, J. Cioslowski, B. B. Stefanov, A. Nanayakkara, M. Challacombe, C. Y. Peng, P. Y. Ayala, W. Chen, M. W. Wong, J. L. Andres, E. S. Replogle, R. Gomperts, R. L. Martin, D. J. Fox, J. S. Binkley, D. J. Defrees, J. Baker, J. P. Stewart, M. Head-Gordon, C. Gonzalez, J. A. Pople, *Gaussian 94, Revision D.4*, Gaussian, Inc., Pittsburgh PA, **1995**.
[67] M. J. Frisch, G. W. Trucks, H. B. Schlegel, G. E. Scuseria, M. A. Robb, J. R. Cheeseman, V. G. Zakrzewski, J. A. Montgomery, Jr., R. E. Stratmann, J. C. Burant, S. Dapprich, J. M. Millam, A. D. Daniels, K. N. Kudin, M. C. Strain, O. Farkas, J. Tomasi, V. Barone, M. Cossi, R. Cammi, B. Mennucci, C. Pomelli, C. Adamo, S. Clifford, J. Ochterski, G. A. Petersson, P. Y. Ayala, Q. Cui, K. Morokuma, D. K. Malick, A. D. Rabuck, K. Raghavachari, J. B. Foresman, J. Cioslowski, J. V. Ortiz, A. G. Baboul, B. B. Stefanov, G. Liu, A. Liashenko, P. Piskorz, I. Komaromi, R. Gomperts, R. L. Martin, D. J. Fox, T. Keith, M. A. Al-Laham, C. Y. Peng, A. Nanayakkara, C. Gonzalez, M. Challacombe, P. M. W. Gill, B. Johnson, W. Chen, M. W. Wong, J. L. Andres, C. Gonzalez, M. Head-Gordon, E. S. Replogle, J. A. Pople, *Gaussian 98*, *Revision A.7*, Gaussian, Inc., Pittsburgh PA, **1998**.
[68] G. Schaftenaar, J. H. Noordik, *J. Comput.-Aided Mol. Design* **2000**, *14*, 123−134.
[69] Computations were performed with the Enraf−Nonius Structure Determination Package, *SDP*, Enraf−Nonius, Delft, **1985**.
[70] G. M. Sheldrick, *SHELXL-95*, Institut für Anorganische Chemie der Universität Göttingen, Germany, **1993**.

Received July 10, 2001
[I01255]

Trichlorohydroxyphosphonium Hexafluorometallate — Synthesis, Spectroscopic Characterization and Crystal Structure of $Cl_3POH^+AsF_6^-$

Rolf Minkwitz*[a] and Markus Dzyk[a]

Keywords: Phosphonium salts / Superacidic systems / Structure elucidation / Vibrational spectroscopy

The reaction of trichlorophosphane oxide with the superacidic systems XF/MF_5 (X = H, D; M = As, Sb) leads to trichlorophosphonium hexafluorometallates. The structure of trichlorophosphonium hexafluoroarsenate was successfully determined. $Cl_3POH^+AsF_6^-$ crystallises in the orthorhombic space group *Pnma* (No. 53) with four formula units per unit cell with the dimensions a = 1286.7(1) pm, b = 842.2(1)pm and c = 822.2(1) pm. The Raman, IR, ^1H and ^{31}P NMR spectra of $Cl_3POX^+MF_6^-$ (X = H, D; M = As, Sb) are reported.

Introduction

The behaviour of trichlorophosphane oxide in strongly acidic solvents has been studied by various techniques since 1966.[1−8] Gillespie et al. found $POCl_3$ to be a non-electrolyte in 100% H_2SO_4, while Paul and co-workers, using mainly cryoscopy and conductance techniques, concluded that $POCl_3$ is incompletely protonated in HSO_3F, but completely protonated by $H_2S_2O_7$ to Cl_3POH^+.[1−4] Partial protonation of $POCl_3$ by chlorosulfuric acid has been reported by Zaidi et al.[5] Dillon et al. and Hibbert et al. used ^{31}P NMR spectroscopy to investigate the behaviour of $POCl_3$ in different acidic media.[6,7] Their studies suggested that an increase of the acidic strength leads to an increase in the degree of protonation of $POCl_3$ in the different acids. Dillon et al. observed the formation of the Cl_3POH^+ cation as an intermediate in the reaction of PCl_3 or PCl_5 with acidic solvents like H_2SO_4 (100%), oleum or HSO_3Cl.[6,8] No attempts were made to isolate the Cl_3POH^+ cation in the form of a phosphonium salt.

In recent years our research group has been successful in the isolation and characterisation of such unstable onium salts by protonation of various precursors at low temperature in the superacidic system HF/MF_5 (M = As, Sb).[9−11] Within the scope of our investigations of the behaviour of phosphorus compounds in the superacidic systems HF/MF_5 (M = As, Sb) we isolated a series of $Cl_3POX^+MF_6^-$ salts (X = H, D; M = As, Sb) and characterised them by X-ray diffraction, and vibrational and NMR spectroscopy.[12−14]

[a] Anorganische Chemie, Fachbereich Chemie der Universität Dortmund
44221 Dortmund, Germany

Results and Discussion

Formation of $Cl_3POX^+MF_6^-$ Salts (X = H, D; M = As, Sb)

The salts are prepared by protonation of trichlorophosphane oxide in superacidic media XF/MF_5 (X = H, D; M = As, Sb) [Equation (1)].

$$Cl_3PO + XF + MF_5 \rightarrow Cl_3POX^+MF_6^- \quad (X = H, D; M = As, Sb) \qquad (1)$$

The colourless solids are stable for several months at −70 °C under nitrogen atmosphere, decomposing at −30 °C in the case of the hexafluoroarsenates and at −5 °C in the case of the hexafluoroantimonates. The salts are slightly soluble in sulfur dioxide at −60 °C and HF at −78 °C.

X-ray Crystal Structure of $Cl_3POH^+AsF_6^-$

Trichlorohydroxyphosphonium hexafluoroarsenate crystallises in the orthorhombic space group *Pnma* (No. 53) with a = 1286.7(1) pm, b = 842.2(1) pm, c = 822.2(1) pm and four formula units per unit cell. The crystal structure was solved by applying the Patterson method and successive difference Fourier syntheses. For refinement full-matrix least-square methods were applied. The hydrogen atom was taken from Fourier maps and refined with isotropic displacement parameters; all non-hydrogen atoms were refined with anisotropic displacement parameters. For the data reduction, structure solution, and refinement, programs in the SHELXTL package, PLATON, MISSYM, and PARST were used.[16−18] The crystal data are summarised in Table 1.[19] The cation has C_s symmetry and the anion a distorted octahedral structure. Bond lengths and selected angles are shown in Table 2. The structure of the trichlorohydroxyphosponium cation with a hydrogen bond

 © WILEY-VCH Verlag GmbH, 69451 Weinheim, Germany, 2002 1434−1948/02/0303−0564 $ 17.50+.50/0 *Eur. J. Inorg. Chem.* **2002**, 564−568

[O···F(2): 249.5(9) pm] and weak interionic contacts to the nearest fluorine atoms of the anions is shown in Figure 1. Figure 2 shows a section of the crystal structure. The hydrogen bond and the strongest interionic Cl···F contact result in the formation of chains parallel to the *ac* plane, and the other weaker Cl···F contacts lead to a linkage of these chains. One of the chlorine atoms [Cl(1)] forms more contacts to fluorine atoms than the others. This different environment of the Cl atoms correlates with more vibrational modes for the PCl_3 group in the IR and Raman spectra (see below). The PO bond length of 150.6(7) pm is lengthened relative to the precursor [$POCl_3$: 145.6(1) pm] and lies in the range between typical single and double bonds.[20,21] In comparison to the precursor the phosphorus-chlorine bond lengths are equal and shortened [$POCl_3$: 196.6(1) pm to 199.0(1) pm].[20] The phosphorus has a distorted tetrahedral environment with angles between 107.4(2)° and 111.9(3)°.

Table 1. Crystal data and structure refinement for $Cl_3POH^+AsF_6^-$

	$Cl_3POH^+AsF_6^-$
Space group (no.)	*Pnma* (53)
Crystal system	Orthorhombic
a [pm]	1286.7(1)
b [pm]	841.2(1)
c [pm]	822.2(1)
V [nm^3]	0.8899(4)
Density (calcd.) [g cm^{-3}]	2.562
Z	4
Formula mass [g mol^{-1}]	343.2
Absorption coefficient [mm^{-1}]	4.947
T [K]	173
F(000)	648
Wavelength [pm]	71.069
Theta range for data collection [°]	2.94 to 30.53
Index range	$-18 \le h \le 18$ $-11 \le k \le 11$ $-11 \le l \le 11$
Reflections collected/independent	7937/1430
Parameters	71
Goodness-of-fit on F^2	1.167
R [$I > 2\sigma(I)$]	$R1$ = 0.0626; $wR2$ = 0.1492
R (all data)	$R1$ = 0.0743; $wR2$ = 0.1527
Largest diff. Peak and hole [e nm^3]	1145/−1077
Refinement method	Full-matrix, least-squares on F^2

Table 2. Bond lengths [pm] and selected angles [deg] for $Cl_3POH^+AsF_6^-$

P−O	150.6(7)	O−P−Cl(1)	111.9(3)
P−Cl(1)	193.6(4)	O−P−Cl(2)	109.4(2)
P−Cl(2)	193(1)	Cl(2)−P−Cl(1)	109.3(1)
As−F(1)	171.6(6)		
As−F(2)	175.7(7)	F(1)−As−F(2)	86.9(3)
As−F(3)	169.2(8)	F(1)−As−F(3)	92.5(4)
As−F(4)	169.6(6)	F(1)−As−F(4)	176.3(3)
As−F(5)	169.6(6)	F(1)−As−F(5)	89.4(2)
F(2)···O	249(1)	F(2)−As−F(3)	179.3(4)
Cl(1)···F(1)	294.3(7)	F(2)−As−F(4)	89.4(3)
Cl(1)···F(4)	310.6(7)	F(2)−As−F(5)	89.2(3)
Cl(1)···F(5)	311.6(6)	F(3)−As−F(4)	91.3(4)
Cl(2)···F(1)	306.9(3)		

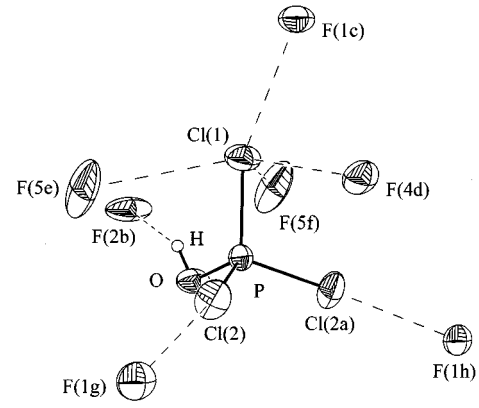

Figure 1. Fragment of the structure of $Cl_3POH^+AsF_6^-$, showing the Cl_3POH^+ cation with interionic contacts (50% probability ellipsoids for the non hydrogen atoms); symmetry operations: a = $x, -0.5 - y, 1 + z$; b = $-0.5 + x, y, -0.5 - z$; c = $-0.5 + x, y, 1.5 - z$; d = $x, +y, 1 + z$; e = $0.5 - x, y, 0.5 + z$; f = $0.5 - x, 0.5 + y, 0.5 + z$

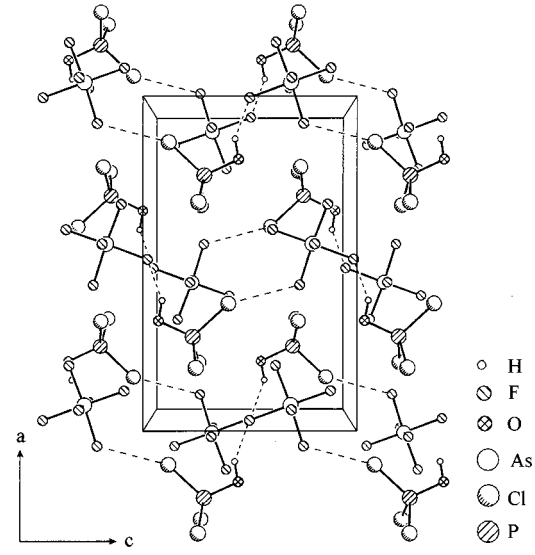

Figure 2. Structure of $Cl_3POH^+AsF_6^-$, showing the arrangement in the crystal lattice

The As−F bond lengths of the anion that is involved in the hydrogen bond and the short Cl···F contacts are longer than the other As−F lengths. A distorted octahedral structure is found for the AsF_6^- anions in the $Cl_3POH^+AsF_6^-$ salt, with deviations from an ideal octahedron of up to 3.3°.

Vibrational Spectra

The Raman and IR spectra of $Cl_3POD^+AsF_6^-$ are shown in Figure 3 and all observed wavenumbers of the salts are summarised in Table 3. The vibrational spectra are assigned according to C_s symmetry for the Cl_3POX^+ cation (X = H, D) and by comparison with the precursor and IR matrix spectra of the isoelectronic trichlorohydroxysilane.[22−24] The cation has twelve fundamental modes consisting of eight A_1 vibrations and four A_2 vibrations. All vibration modes are active in both the Raman

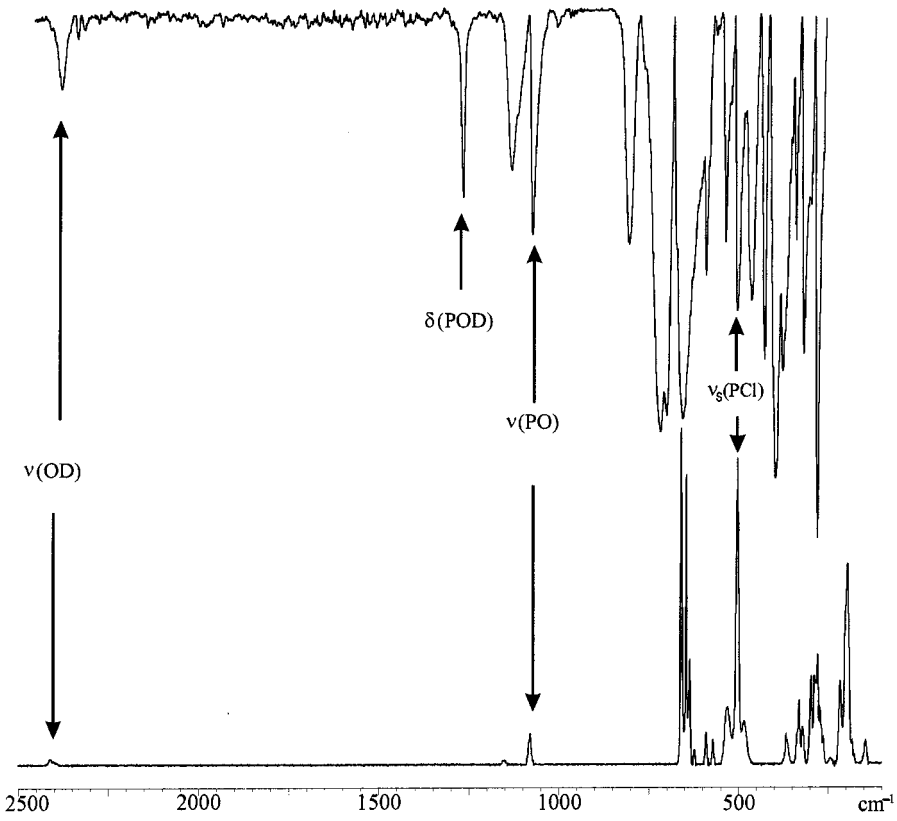

Figure 3. IR and Raman spectra of $Cl_3POD^+AsF_6^-$

and IR spectra. Due to the different interactions between the chlorine and fluorine atoms (see above) we observed more vibrational modes for the PCl_3 group than would have been expected without the X-ray studies. Altogether fifteen vibrational modes for the Cl_3POX^+ cation (X = H, D) were detected. Vibrational modes below 220 cm^{-1} were not detectable on account of the window material used in the low temperature cuvette for IR measurements (CsBr). The fifteen detected modes can be divided into four modes which are associated with the OH and PO modes, with the remaining modes being considered as motions of the PCl_3 group.

The OH and OD stretching modes are found at 3135 cm^{-1} and 2410 cm^{-1}, respectively. The corresponding POX (X = H, D) deformation modes were only observed by IR spectroscopy (at 1280 cm^{-1}) due to their low Raman intensity. The position of the PO stretching mode is important for the spectroscopic confirmation of the Cl_3POX^+ cation. The PO stretching mode is shifted to lower wavenumbers by 200 cm^{-1}, relative to the precursor, corresponding to protonation of Cl_3PO at the O atom.[22] The PCl stretching modes are observed in the range of 501 to 667 cm^{-1}. They are shifted by up to 80 cm^{-1} to higher wavenumbers relative to the analogous vibrations in trichlorophosphane oxide.[22] The PCl_3 deformation modes are found between 193 and 430 cm^{-1}. Two OPCl deformation modes are detected at 800 cm^{-1} and 1150 cm^{-1}, respectively, due to the interionic interactions between the Cl atoms and the F atoms of the anions.

Because of cation−anion interactions, the MF_6^- ions (M = As, Sb) do not show ideal O_h symmetry. This lowered symmetry causes a splitting of the anion vibrational modes.[25]

^1H and ^{31}P NMR Spectra of $Cl_3POH^+MF_6^-$ (M = As, Sb)

The ^1H NMR spectra of freshly prepared $Cl_3POH^+MF_6^-$ (M = As, Sb) dissolved in SO_2 with TMS as external standard at −60 °C show a singlet at δ = 10.7 (AsF_6^-) and δ = 10.8 (SbF_6^-) for the hydroxyl group. In the ^{31}P NMR spectra a singlet at δ = 55.5 for the arsenate and δ = 55.2 for the antimonate are observed. These signals are shifted to lower field by more than 51 ppm relative to the precursor. This result is similar to the results of Dillon and Hibbert (Table 4).[6,7]

Experimental Section

Caution: *Avoid contact with these compounds and note that the hydrolysis of AsF_6^- and SbF_6^- salts forms HF, which burns the skin and causes irreparable damage. Safety precautions should be taken when using and handling these materials!*

General: All synthetic work and sample handling was conducted by standard Schlenk techniques on a standard vacuum line (stainless steel or glass). Drying of HF was carried out with Fluorine (1.5 bar) in a stainless steel bomb. AsF_5 was synthesised from As and F_2.[26] SbF_5 (Merck) and $POCl_3$ (Merck) were distilled repeat-

Table 3. Vibrational wavenumbers of trichlorohydroxyphosphonium salts and their possible assignments[a]

$Cl_3POD^+AsF_6^-$		$Cl_3POD^+SbF_6^-$		$Cl_3POH^+AsF_6^-$		$Cl_3POH^+SbF_6^-$		Cl_3SiOH[23][24]	Possible Assignment
IR −50 °C	Raman −78 °C	Raman −78 °C	IR −50 °C	IR −50 °C	Raman −78 °C	IR −50 °C	Raman −78 °C	IR −253 °C	
2427 w	2410(3)	2407(2)	2426 w	3135 vs	n. o.	3120 s	n. o.	3693	ν(OX)
1283 m	n. o.	n. o.	1291 w	1289 m	n. o.	1252 w	n. o.	1330	δ(POX)
1149 m	1150 (3)	n. o.	n.o.	1159 w	n. o.	1152 w	n. o.		δ(OPCl)
1086 m	1078 (10)	1088 (9)	1077 m	1020 m	n. o.	1014 m	1026 (10)	960	ν(PO)
813 m	n. o.	n. o.	811 m	886 m	n. o.	868 m	n. o.	798	δ(OPCl)
657 vs	635 (32)	646 (10)	655 vs	667 s	655 (15)	645 vs	660 (55)		$\nu_{as}(PCl_3)$
592 m	589 (8)	592 (15)	588 m	593 m	593 (15)	585 s	591(10)	621	$\nu_{as}(PCl_3)$
535 m	530 (16)	531 (17)	536 m	534 m	529 (29)	532 s	531		δ(POX)
501 s	502 (83)	502 (100)	508 s	504 m	502 (100)	504 m	505 (100)	462	$\nu_s(PCl_3)$
424 s	n. o.	423 (6)	451 m	430 m	428 (7)	427 m	n. o.		$\rho(PCl_3)$
372 s	365 (10)	376 (38)	366 s	367 m	376 (38)	n. o.	378 (10)		$\rho(PCl_3)$
314 s	319 (13)	314 (24)	317 s	317 m	317 (35)	n. o.	324 (12)		$\delta(PCl_3)$
274 vs	279 (35)	273 (42)	289 vs	276 s	275 (58)	n. o.	277 (30)		$\delta_s(PCl_3)$
n. o.	217 (24)	211 (58)	n. o.	n. o.	212 (68)	n. o.	220 (25)		$\delta_{as}(PCl_3)$
n. o.	195 (58)	193 (55)	n. o.	n. o.	194 (50)	n. o.	197 (40)		$\delta_{as}(PCl_3)$
725 vs				723 s					MF_6^-
704 vs				705 s	703 (70)		700 (15)		MF_6^-
		700 (55)					685 (15)		MF_6^-
		673 (61)	660 vs		673 (83)	661 vs			MF_6^-
	659 (100)	661 (16)	631 s		662 (16)	630 s			MF_6^-
	645 (84)								MF_6^-
	570 (7)				569 (8)				MF_6^-
463 s	483 (12)			392 s		400 w			MF_6^-
394 vs									MF_6^-
335 m	331 (20)	337 (15)	333 m	346 m	347 (6)				MF_6^-
292 m	297 (31)							299 (25)	MF_6^-

[a] n. o. = not observed; vs = very strong; s = strong; m = medium; w = weak; X = H, D; M = As, Sb.

Table 4. ^1H and ^{31}P NMR spectroscopy data for $Cl_3POH^+MF_6^-$ (M = As, Sb) and literature data for Cl_3PO in acidic media

	$\delta(^{31}P)$[a]	$\delta(^1H)$
$Cl_3POH^+AsF_6^-$ [b]	55.5 (s)	10.7 (s)
$Cl_3POH^+SbF_6^-$ [b]	55.2 (s)	10.8 (s)
Cl_3PO in H_2SO_4 + 65% SO_3 [6][7]	55. 9 (s)	−
Cl_3PO in H_2SO_4 + 25% SO_3 [6][7]	35.3 (s)	−
Cl_3PO in H_2SO_4 [6], [7]	20.1 (s)	−
Cl_3PO [6], [7]	3.6 (s)	−

[a] (s) = Singlet. [b] Measured in SO_2 at −60 °C.

edly before use. Reactions in HF were carried out in a KEL-F reactor fitted with a KEL-F valve. The Raman spectra were recorded on a Jobin Yvon T64000 spectrometer using an Ar^+ laser (514.5 nm) from Spectra Physics. The spectra were obtained in a glass cell cooled with solid CO_2.[27] Infrared spectra were recorded on a Bruker ifs 113v spectrophotometer. Spectra were obtained from a coated CsBr plate in a low-temperature cuvette.[28] NMR spectra were recorded with a Bruker DPX spectrometer and referenced to either TMS (^1H) or 85% H_3PO_4 (^{31}P) in SO_2 at −60 °C. Single crystals for the crystallographic studies were placed in Lindemann capilllaries in a cooled stream of dry nitrogen, and an X-ray diffraction study was carried out at −100 °C using a Nonius Kappa CCD (1152 × 1242 Pixel) diffractometer.

Preparation of $Cl_3POX^+MF_6^-$ (X = H, D; M = As, Sb): In a typical reaction, 5 mL of XF (X = H, D) was distilled into the Kel-F reactor at −196 °C, followed by 0.2 mmol of MF_5 (M = As, Sb). The mixture was warmed to 20 °C to form the superacid. The reactor was then cooled to −196 °C, and $POCl_3$ (0.2 mmol) was added. The mixture was warmed to −78 °C. After removing the volatile compounds at −78 °C during 7 days colourless solids, stable up to −30 °C (arsenate) and −5 °C (antimonate) were obtained.

$Cl_3POH^+AsF_6^-$: ^1H NMR: δ = 10.7 (s). ^{31}P NMR: δ = 55.5(s).

$Cl_3POH^+SbF_6^-$: ^1H NMR: δ = 10.8 (s). ^{31}P NMR: δ = 55.2(s).

[1] R. J. Gillespie, R. Kapoor, A. Robinson, *Can. J. Chem.* **1966**, *44*, 1203−1210.
[2] R. C. Paul, V. P. Kapila, K. C. Malhotra, *J. Chem. Soc. (A)* **1970**, 2267−2273.
[3] R. C. Paul, V. P. Kapila, K. Puri, K. C. Malhotra, *J. Chem. Soc. (A)* **1971**, 2132−2137.
[4] R. C. Paul, K. K. Paul, K. C. Malhotra, *J. Inorg. Nuclear. Chem.* **1972**, *34*, 2523−2533.
[5] S. A. A. Zaidi, Z. A. Siddiqi, *Acta Chim. Acad. Sci. Hung.* **1977**, *92*, 57−64.
[6] K. B. Dillon, M. P. Nisbet, T. C. Waddington, *J. Chem. Soc., Dalton Trans.* **1978**, 1455−1460.
[7] R. C. Hibbert, N. Logan, *J. Chem. Soc., Dalton Trans.* **1985**, 865−866.
[8] K. B. Dillon, M. P. Nisbet, T. C. Waddington, *J. Chem. Soc., Dalton Trans.* **1979**, 883−890.

[9] R. Minkwitz, S. Schneider, *Angew. Chem. Int. Ed.* **1999**, *38*, 714−716.
[10] R. Minkwitz, C. Hirsch, H. Hartl, *Angew. Chem. Int. Ed.* **1998**, *37*, 1681−1684.
[11] R. Minkwitz, S. Schneider, H. Preut, *Angew. Chem. Int. Ed.* **1998**, *37*, 494−496.
[12] R. Minkwitz, S. Schneider, *Angew. Chem. Int. Ed.* **1999**, *38*, 210−212.
[13] R. Minkwitz, S. Schneider, A. Kornath, *Inorg. Chem.* **1998**, *37*, 4662−4665.
[14] R. Minkwitz, B. Bäck, *Z. Naturforsch., Teil B* **1994**, *49*, 221−224.
[15] G. M. Sheldrick, SHELXTL PLUS *An Integrated System for Solving, Refining and Displaying Structures from Diffraction Data*,. Universität of Göttingen, Germany, **1987.**
[16] A. L. Spek, The EUCLID Package, in *Computional Crystallography* (Ed.: D. Sayre), Claredon Press, Oxford, **1982**, 528.
[17] Y. Le Page, *J. Appl. Crystallogr.* **1987**, *20*, 264−269.
[18] M. Nardelli, *Comput. Chem.* **1983**, *7*, 95−98.
[19] Crystallographic data for the structure reported in this paper have been deposited at the Fachinformationszentrum Karlsruhe, Gesellschaft für wissentschaftlich−technische Information mbH, 76344 Eggenstein−Leopoldhafen, under the number CSD-412034.
[20] K. Olie, *Acta Crystallogr.*, **1971**, *B 27*, 1459−1460.
[21] D. E. C. Corbridge, *Phosphorus: An Outline of its Chemistry, Biochemistry, and Technology*, Elsevier, Amsterdam, **1980**.
[22] R. A. Nyquist, *App. Spec.* **1987**, *41*, 272−279.
[23] H. Niki, P. D. Maker, C. M. Savage, L. P. Breitenbach, M. D. Hurley, *J. Phys. Chem.* **1985**, *89*, 3725−3729.
[24] A. E. Shirk, J. S. Shirk, *J. Mol. Spectrosc.* **1982**, *92*, 218−228.
[25] A. A. A. Emara, G. J. Schrobilgen, *Inorg. Chem.* **1992**, *31*, 1323−1332.
[26] O. Ruff, W. Menzel, H. Plaut, *Z. Anorg. Allg. Chem.* **1931**, *206*, 61−64.
[27] A. Werner, *Dissertation*, University of Dortmund, **1988**.
[28] L. Bayersdorfer, R. Minkwitz, J. Jander, *Z. Anorg. Allg. Chem.* **1972**, *392*, 137−142.

Received August 9, 2001
[I01303]

The Crystal Structures of the Trihalogenphosphonium Salts $X_3PH^+As_2F_{11}^-$ (X = Cl, Br)

Rolf Minkwitz*[a] and Markus Dzyk[a]

Keywords: Phosphonium salts / Protonation / X-ray diffraction / Phosphorus / Main group elements

The X_3PH^+ ions (X = Cl, Br) were prepared as their $X_3PH^+As_2F_{11}^-$ salts by protonation of PX_3 with HF/AsF_5 at low temperature in anhydrous HF. Single crystals were obtained directly from this solvent. $Cl_3PH^+As_2F_{11}^-$ crystallises in the orthorhombic space group *Pnma* (No. 53) with a = 2350.6(1) pm, b = 837.7(1) pm, c = 1179.9(1) pm and eight formula units per cell. $Br_3PH^+As_2F_{11}^-$ crystallises in the monoclinic space group $P2_1/m$ (no. 14) with a = 617.7(1) pm, b = 872.4(2) pm, c = 1182.5(2) pm, β = 94.68(3)° and two formula units per cell.

Introduction

Salts with the phosphonium ion PR_4^+ are very well known, and R can be an organic or an inorganic group like hydrogen or halogen, amongst others. In contrast to phosphonium ions with organic groups relatively little is known about halogenated phosphonium salts. Only the fluorinated salts $F_{4-n}PH_n^+A^-$ (n = 0−3, A^- = anion) have been characterised by NMR and vibrational spectroscopy.[1−5] Recently Seppelt at al. prepared the salt $F_3PH^+SbF_5^-$ from a $PF_3/HF/SbF_5$ solution and determined its crystal structure by X-ray diffraction.[6]

Most of the corresponding chlorine and bromine compounds are not yet known. A few years ago our research group prepared a series of $X_3PH^+AsF_6^-$ salts (X = Cl, Br; M = As, Sb) by protonation of phosphorus trihalides with HF/MF_5.[7] The compounds were characterised by vibrational and NMR spectroscopy. Due to the negligible solubility no single crystals of these compounds were available. Within the scope of further investigations of the behaviour of phosphorus trihalides in the superacidic system HF/AsF_5 we have isolated single crystals of $X_3PH^+As_2F_{11}^-$ salts (X = Cl, Br) and determined their structures by X-ray diffraction.

Results and Discussion

Formation of $X_3PH^+As_2F_{11}^-$ (X = Cl, Br)

Protonation of phosphorus trichloride or phosphorus tribromide by the superacidic system HF/AsF_5 gives the corresponding phosphonium undecafluorodiarsenates [Equation (1)]:

$$X_3P + HF + 2AsF_5 \rightarrow X_3PH^+As_2F_{11}^- \quad (X = Cl, Br) \qquad (1)$$

The resulting colourless, moisture-sensitive salts decompose in the case of the trichlorophosphonium salt above −25 °C, and in the case of the bromine compound above −45 °C. They can be stored for several months without decomposition under inert conditions at −70 °C.

X-ray Crystal structure of $Cl_3PH^+As_2F_{11}^-$

Trichlorophosphonium undecafluorodiarsenate crystallises in the orthorhombic space group *Pnma* (no. 53) with eight units per cell (see Table 1).[8] For data collection and reduction, a semi-empirical correction determined from single ψ-scan data, and programs in the SHELXL package, PLATON, MISSYM and PARST, were used.[9−12] The solution of the crystal structure was done by the Patterson method with a subsequent difference Fourier synthesis. A final refinement with anisotropic (except H atoms) thermal parameters gave a value of R = 0.0314.

The orthorhombic unit cell contents two crystallographically independent anions and cations. Table 2 lists important bond lengths and angles. Figure 1 shows a trichlorophosphonium cation with weak interionic contacts to the nearest atoms of the anions and Figure 2 a section of the crystal structure. The cation has the shape of a trigonal pyramid and the anion has a distorted edge-linked dioctahedral structure. The P−Cl bond lengths [192.9(1)−193.6(1) pm] show no significant differences and they are shortened by about 10 pm relative to the precursor PCl_3 [PCl_3: P−Cl = 203.9(1) pm].[13] The Cl−P−Cl angles of 109.5(1)° to 110.1(5)° are wider than in phosphorus trichloride [PCl_3: Cl−P−Cl = 100.07(7)−100.19(7)°].[13]

The two independent cations form the same kind of interionic contacts to the fluorine atoms of neighbouring an-

[a] Anorganische Chemie, Fachbereich Chemie der Universität Dortmund
44221 Dortmund, Germany

 © WILEY-VCH Verlag GmbH, 69451 Weinheim, Germany, 2002 1434−1948/02/0303−0569 $ 17.50+.50/0

Table 1. Crystal data and structure refinement for $Cl_3PH^+As_2F_{11}^-$ and $Br_3PH^+As_2F_{11}^-$

	$Cl_3PH^+As_2F_{11}^-$	$Br_3PH^+As_2F_{11}^-$
Space group (no.)	*Pnma* (53)	$P2_1/m$ (14)
Crystal system	Orthorhombic	Monoclinic
a [pm]	2350.6(1)	6177.0(1)
b [pm]	837.7(1)	872.4(2)
c [pm]	1179.9(1)	1182.5(2))
β [°]	–	94.68(3)
Volume [nm^3]	2.3233(4)	0.6351(2)
Density (calcd.) [g cm^{-3}]	2.843	3.297
Z	8	2
Formula mass [g mol^{-1}]	497.15	630.49
Absorption coefficient [mm^{-1}]	6.698	14.932
Temperature [K]	173	173
F(000)	1856	572
Wavelength [pm]	71.069	71.069
Theta range for data collection [°]	1.73 to 28.78	2.90 to 25.56
Index range	$-31 \le h \le 31$	$-4 \le h \le 6$
	$-10 \le k \le 10$	$-10 \le k \le 10$
	$-15 \le l \le 15$	$-14 \le l \le 8$
Reflections collected/independent	16177/2949	1490/998
Parameters	187	94
Goodness-of-fit on F^2	0.977	1.013
R [$I > 2\sigma(I)$]	$R = 0.031$; $wR2 = 0.0572$	$R = 0.050$; $wR2 = 0.1160$
R (all data)	$R = 0.065$; $wR2 = 0.0622$	$R = 0.061$; $wR2 = 0.1199$
Largest diff. Peak and hole[e nm^3]	704/−495	897/−1596
Refinement method	Full-matrix, least-squares on F^2	Full-matrix, least-squares on F^2

Table 2. Bond lengths [pm], selected angles [°] and contacts [pm] for $Cl_3PH^+As_2F_{11}^-$[a]

P(1)−Cl(11)	192.9(1)	Cl(11)−P(1)−Cl(12)	109.9(9)
P(1)−Cl(12)	193.6(2)	Cl(11a)−P(1)−Cl(12)	109.9(5)
P(2)−Cl(21)	193.6(1)	Cl(22)−P(2)−Cl(21)	110.1(5)
P(2)−Cl(22)	193.1(2)	Cl(21)−P(2)−Cl(21a)	109.5(1)
As(1)−F(11)	168.4(3)		
As(1)−F(12)	169.6(2)	As(1)−F(14)−As(2)	145.6(2)
As(1)−F(13)	167.7(2)	F(14)−As(1)−F(11)	178.1(4)
As(1)−F(14)	193.7(3)	F(12)−As(1)−F(13)	89.7(1)
As(2)−F(21)	168.4(3)		
As(2)−F(22)	169.2(3)	As(3)−F(32)−As(4)	148.3(2)
As(2)−F(23)	169.5(2)	F(32)−AS(3)−F(34)	177.9(1)
As(2)−F(24)	170.2(3)	F(35)−As(3)−F(33)	89.2(7)
As(2)−F(14)	190.2(3)		
As(3)−F(31)	169.4(3)	Cl(21)···F(13)	302.0(2)
As(3)−F(32)	182.3(2)	Cl(22)···F(11)	280.4(3)
As(3)−F(33)	171.8(3)	P(2)···F(33)	300.4(2)
As(3)−F(34)	169.9(2)		
As(3)−F(35)	170.5(2)	Cl(11)···F(31)	308.7(2)
As(4)−F(41)	168.1(3)	Cl(12)···F(41)	312.5(3)
As(4)−F(42)	165.8(2)	P(1)···F(23)	321.9(2)
As(4)−F(43)	166.2(2)		
As(4)−F(32)	205.9(2)		

[a] Symmetry operation: a = x, $-y$, 0.5 + z.

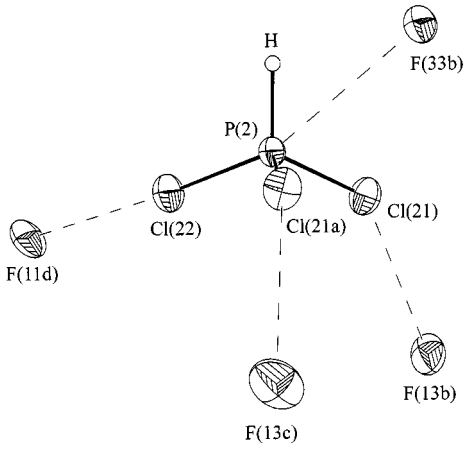

Figure 1. Fragment of the structure of $Cl_3PH^+As_2F_{11}^-$, showing the Cl_3PH^+ cation of the crystallographically independent unit 2 with interionic contacts (50% probability ellipsoids for the non-hydrogen atoms); symmetry operations: a = x, 0.5 − y, z; b = 0.5 − x, $-y$, $-0.5 + z$; c = 0.5 − x, 0.5 + y, $-0.5 + z$; d = $-0.5 + x$, y, 2.5 + z

ions, but with different strengths. There are chlorine-fluorine contacts of between 280.4(3) and 312.5(3) pm and P−F contacts of 300.4(2) pm and 321.9(2) pm, respectively. There are no contacts between hydrogen and fluorine atoms that are significantly below the sum of the van der Waals radii of 267 pm. The interionic contacts result in the formation of a three-dimensional linkage of anions and cations.

The anion consists of two distorted octahedra which are linked at one corner. The As−F bond lengths involving the "bridging" fluorine atom are 205.9(2) pm and are thus significantly longer than the other As−F bond lengths of between 167.7(2) and 170.5(2) pm, which are in the normal range of As−F bond lengths of hexafluoroarsenate anions.[14−16] These unusually long As−F bonds are in the same range as in the other known $As_2F_{11}^-$ salts.[14−16] In both anions the two octahedral AsF_6 units are in a gauche arrangement. The average torsion angles F−As−As−F of

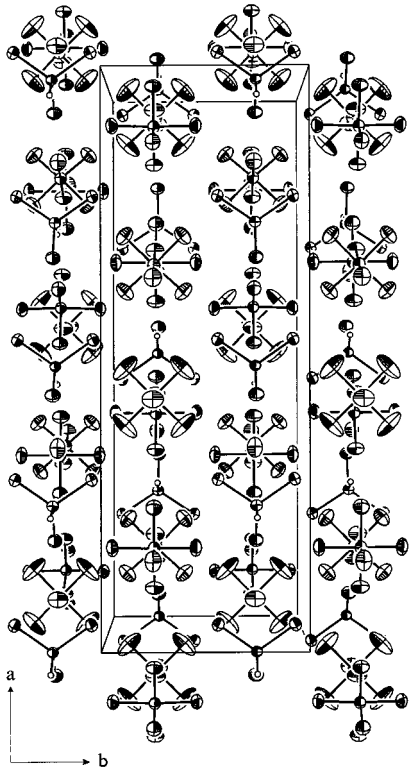

Figure 2. Projection of the $Cl_3PH^+As_2F_{11}^-$ salt

45.3° and 45.6° and the As−F−As bridge angles of 145.6(2)° and 148.3(2)° are similar to those found in other $As_2F_{11}^-$ salts.[14−16]

X-ray Crystal structure of $Br_3PH^+As_2F_{11}^-$

$Br_3PH^+As_2F_{11}^-$ crystallises in the monoclinic space group $P2_1/m$ (No. 14) with a = 617.7(1) pm, b = 872.4(2) pm, c = 1182.5(2) pm, β = 94.68(3)° and two formula units per unit cell.[17] The crystal structure was solved by direct methods and successive difference Fourier syntheses. For refinement full-matrix least-squares methods were applied. A final refinement with anisotropic (except H atoms) thermal parameters gave a value of R = 0.0504. For data reduction, structure solution, and refinement the same programs were used as for the structure solution of $Cl_3PH^+As_2F_{11}^-$.[9−12]

The crystal data are summarised in Table 1 and bond lengths and selected angles are shown in Table 3.

Table 3. Bond lengths [pm], selected angles [°] and contacts [pm] for $Br_3PH^+As_2F_{11}^-$[a]

Br(1)−P	211.1(2)	Br(1)−P−Br(2)	110.8(1)
Br(2)−P	211.1(4)	Br(1a)−P−Br(1)	110.3(2)
As(1)−F(11)	170.1(5)		
As(1)−F(12)	170.0(7)	As(1)−F(15)−As(2)	145.9(4)
As(1)−F(13)	171.0(6)	F(11)−As(1)−F(12)	89.8(2)
As(1)−F(14)	172.9(6)	F(13)−As(1)−F(14)	174.9(4)
As(1)−F(15)	183.6(6)		
As(2)−F(21)	168.5(5)	Br(1)·····F(13)	306.1(3)
As(2)−F(22)	168.5(7)	Br(1)·····F(21)	325.1(2)
As(2)−F(23)	167.8(6)	Br(2)·····F(22)	300.8(7)
As(2)−F(15)	202.0(6)		

[a] Symmetry operation: a = x, y − 1.5, z.

The phosphorus−bromine bond lengths are equal and shorter by about 10 pm than in the precursor [PBr_3: P−Br = 221.2(3) pm].[18] The Br−P−Br angles of 110.3(2)° and 110.8(1)° are wider than in phosphorus tribromide [PBr_3: Br−P−Br = 99.0(2)−101.3(2)°].[18]

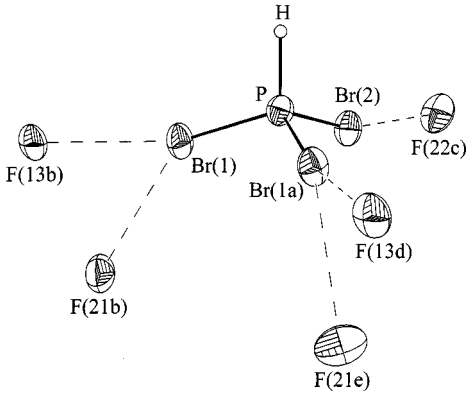

Figure 3. Fragment of the structure of $Br_3PH^+As_2F_{11}^-$, showing the Br_3PH^+ cation with interionic contacts (50% probability ellipsoids for the non-hydrogen atoms); symmetry operations: a = x, y − 1.5, z; b = 1 + x, 1 + y, z; c = −x, 1 − y, 1 − z; d = 1 − x, −y, −z; e = 1 + x, 0.5 − y, z

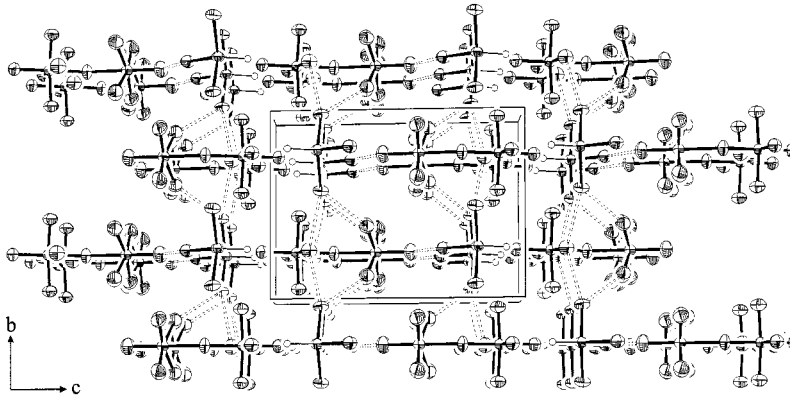

Figure 4. Projection of the $Br_3PH^+As_2F_{11}^-$ salt with interionic contacts

The cations form interionic contacts of different strengths to fluorine atoms of neighbouring anions (Figure 3). Two weak fluorine−bromine contacts of 300.8(7) pm and 325.1(2) pm result in the formation of chains in the *bc* plane. The chains of different *bc* planes are connected along the *c* axes by further weak fluorine−bromine contacts of 321.8(7) pm (Figure 4).

The undecafluorodiarsenate anion has the same distorted edge-linked dioctahedral structure as the anion in the $Cl_3PH^+As_2F_{11}^-$ salt. All bond lengths and angles of the anion (Table 3) are of the same order as the previous salt and similar to the other known $As_2F_{11}^-$ salts.[14−16]

Experimental Section

All synthetic work and sample handling was conducted by standard Schlenk techniques on a standard vacuum line (stainless steel or glass). Drying of HF was carried out with Fluorine (1.5 bar) in a stainless steel bomb. AsF_5 was synthesised from As and F_2.[19] The synthesis of PBr_3 was carried out by a known literature method from Br_2 (Riedel de Haen) and red phosphorous (Fluka).[20] PBr_3 and PCl_3 (Riedel de Haen) were distilled repeatedly before use. Reactions in HF were carried out in a KEL-F reactor fitted with a KEL-F valve. Single crystals were placed in Lindemann capillaries in a cooled stream of dry nitrogen, and an X-ray diffraction study was carried out at −100 °C using a Nonius Kappa CCD-(1152 × 1242 Pixel) diffractometer.

Preparation of $X_3PH^+As_2F_{11}^-$ (X = Cl, Br):

Caution! Avoid contact with these compounds and note that hydrolysis of $As_2F_{11}^-$salts forms HF, which burns the skin and causes irreparable damage. Safety precautions should be taken when using and handling these materials!

In a typical experiment AsF_5 (1 g, 5.9 mmol) was dissolved in HF (10 g) in a 50 mL KEL-F reactor. The solution was frozen at −196 °C and PX_3 (X = Cl, Br; 0.01 mmol) was added under an inert atmosphere (N_2). The mixture was warmed to −78 °C and kept for 30 minutes. The excess HF and AsF_5 were very slowly removed during 5 days under dynamic vacuum at −78 °C. The remaining colourless salts contained crystals suitable for X-ray diffraction studies and can be stored under inert conditions at −70 °C without decomposition.

[1] R. Minkwitz, D. Lennhoff, W. Sawodny, H. Härtner, *Z. Naturforsch., Teil B* **1992**, *47*, 1661−1666.
[2] R. Minkwitz, A. Liedke, *Z. Naturforsch., Teil B* **1989**, *44*, 679−682.
[3] H. W. Roesky, K. L. Weber, J. Schimkowiak, *Angew. Chem.* **1981**, *93*, 1017; *Angew. Chem. Int. Ed. Engl.* **1981**, *20*, 937.
[4] G. S. H. Chen, J. Passmore, *J. Chem. Soc., Chem. Commun.* **1973**, 559.
[5] J. F. Brazier, D. Hovalla, M. Loenig, R. Wolf, *Top. Phosphorous Chem.* **1976**, *8*, 99−193.
[6] R. Küster, T. Drews, K. Seppelt, *Inorg. Chem.* **2000**, *39*, 2784−2786.
[7] R. Minkwitz, B. Bäck, *Z. Naturforsch., Teil B* **1994**, *49*, 221−224.
[8] Crystallographic data for the structure of $Cl_3PH^+As_2F_{11}^-$ have been deposited at the Fachinformationszentrum Karlsruhe, 76344 Eggenstein-Leopoldshafen, Germany,under the number CSD-412036.
[9] G. M. Sheldrick, SHELXTL PLUS *An Integrated System for Solving, Refining and Displaying Structures from Diffraction Data*, Universität Göttingen, Germany, **1987**.
[10] A. L. Spek, The EUCLID Package, in *Computational Crystallography* (Ed.: D. Sayre), Claredon Press, Oxford, **1982**, 528.
[11] Y. Le Page, *J. Appl. Crystallogr.* **1987**, *20*, 264−269.
[12] M. Nardelli, *Comput. Chem.* **1983**, *7*, 95−98.
[13] H. Hartl, M. Rama, *Z. Naturforsch., Teil B* **1979**, *34*, 1035−1036.
[14] K. O. Christe, Submitted communication
[15] R. Minkwitz, F. Neikes, *Inorg. Chem.* **1999**, *38*, 5960−5963.
[16] R. Minkwitz, C. Hirsch, *Eur. J. Inorg. Chem.* **1999**, 2249−2254.
[17] Crystallographic data for the structure of $Br_3PH^+As_2F_{11}^-$ have been deposited at the Fachinformationszentrum Karlsruhe, 76344 Eggenstein-Leopoldshafen, Germany, under the number CSD-412035.
[18] P. R. Enjalbert, J. Galy, *Acta Crystallogr., Sect. B* **1979**, *35*, 546−550.
[19] O. Ruff, W. Menzel, H. Plaut, *Z. Anorg. Allg. Chem.* **1931**, *206*, 61−64.
[20] A. C. Christomanos, *Z. Anorg. Chem.* **1904**, *41*, 277−289.

Received August 9, 2001
[I01304]

High Molecular Weight Cu^{II} Coordination Polymers and Their Characterisation by Electrospray Mass Spectrometry (ESMS)

Hélène Nierengarten,[a] Javier Rojo,[b] Emmanuelle Leize,*[a] Jean-Marie Lehn,[b] and Alain Van Dorsselaer[a]

Keywords: Supramolecular chemistry / Copper / Polymers / Mass spectrometry / Self-assembly

The ligands L and ligand L* self-assemble with Cu^{II} in different solvents to give a mixture of coordination polymers. These artificial nanostructures have been characterised with the help of ESMS, the only analytical tool that allows their unambiguous characterisation. Kinetic and thermodynamic ESMS studies have excluded the possibility that these compounds form aggregates during the ES process.

Introduction

The self-assembly of suitably designed organic ligands with transition-metal ions allows the generation of a wide range of polymetallic complexes possessing a variety of well-defined architectures (racks, ladders, grids, rings, etc.).[1,2] These organised entities, and especially coordination polymers, may present interesting physical and chemical properties and are of much current interest within metallosupramolecular chemistry due to their potential applications in materials science.[3] One of the challenges in this field resides in the preparation of high molecular weight coordination polymers that may possess good solubilities in order to characterise their properties in solution as well as in the solid state. Unfortunately, an unequivocal structural analysis of these metallosupramolecular compounds is often missing. Indeed, because of the complexity of the NMR spectra and because of the recurrent presence of paramagnetic metals, NMR spectroscopy is often unusable. In the same way, X-ray suitable crystals of sufficient quality are often difficult to obtain; the use of X-ray crystallography is therefore limited. The other classical analytical tools able to give any information are in most cases inconclusive with respect to the formulation (e.g., UV/Vis absorption and emission spectroscopy, infrared, etc.). An unambiguous characterisation is therefore highly compromised. Despite the problems and difficulties that often occur during the development of this chemistry (especially due to the increasing size of such molecules), encouraging perspectives are offered by the use of electrospray mass spectrometry (ESMS)[4] for an unequivocal characterisation. ESMS has been proven to be a very useful technique for the characterisation of biological[5] and chemical[6] assemblies. Moreover, this analytical method is particularly suitable for large, noncovalent species with high molecular masses. Indeed, when several parameters are carefully controlled, ESMS is a mild method, which causes minimum fragmentation and therefore allows molecular mass determination.

We describe here the characterisation in solution by ESMS of the largest reported Cu^{II} coordination polymers stable in solution up to a concentration of 10^{-4} M and soluble in common organic solvents (acetonitrile, methanol, nitromethane). In this present case, ESMS was the only analytical tool allowing an unambiguous characterisation. Therefore, kinetic and thermodynamic studies have been undertaken in order to exclude the possibility that these coordination polymers are aggregates resulting from the ES process.[7]

Results and Discussion

The ligand **L** was synthesised following the procedure outlined in Scheme 1. The self-assembly reaction to obtain the Cu^{II} coordination polymers was carried out as follows: an equimolar amount of the ligand **L** and $Cu(CF_3SO_3)_2$ were mixed together in anhydrous acetonitrile (ca. 10^{-4} M), the mixture was stirred at room temperature for five minutes and a clear blue solution was obtained.

The analysis of this solution by ESMS immediately after preparation has shown the presence of coordination complexes of general formula $[LCu(CF_3SO_3)_2]_n$, M_n, in equilibrium in solution (Figure 1). Ions observed in the ES mass spectrum (M_n^{x+}; $1 \leq n \leq 47$ and $1 \leq x \leq 4$) are interpreted

[a] Laboratoire de Spectrométrie de Masse Bio-Organique, Université Louis Pasteur, CNRS UMR 7509, ECPM, 25 rue Becquerel, 67087 Strasbourg cedex 2, France
Fax: (internat.) +33-(0)3/9024-2781
E-mail: leize@chimie.u-strasbg.fr
[b] Laboratoire de Chimie Supramoléculaire, ISIS, Université Louis Pasteur, ESA CNRS 7006, 4 rue Blaise Pascal, 67000 Strasbourg cedex, France

 © WILEY-VCH Verlag GmbH, 69451 Weinheim, Germany, 2002 1434–1948/02/0303–0573 $ 17.50+.50/0

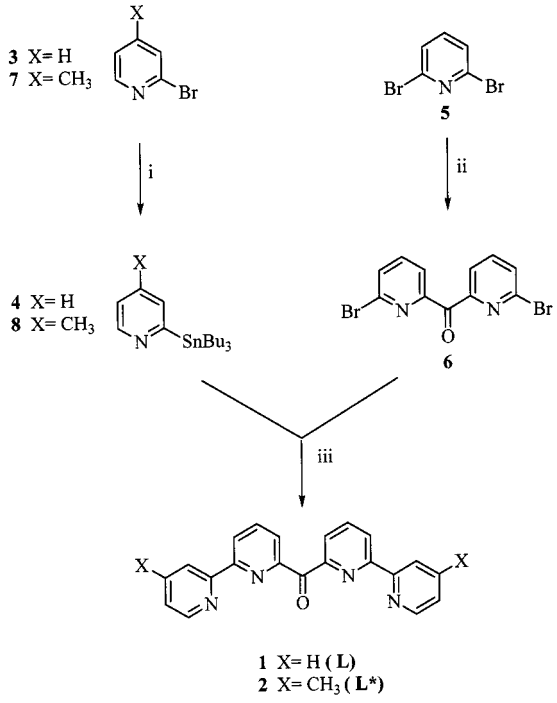

Scheme 1. i, *n*BuLi, THF, −78 °C; Bu_3SnCl, −78 °C, 96%; ii, *n*BuLi, ether, −90 °C; $ClCO_2Et$, 47%; iii, $Pd(PPh_3)_4$, toluene, 110 °C, 50−76%

as the successive loss of *x* counter anions $CF_3SO_3^-$ ($^-$OTf), leading to multiply charged ions, and correspond to molecular masses up to 32901.4 Da ($n = 47$).

The charge states of these ions were unambiguously determined owing to the high-resolution capability of a time of flight analyser (Figure 2). Charge states of these ions range from $x = 1+$ to $x = 4+$. The largest polymer ($n = 47$) has been identified owing to its 4+ charged ion at $m/z = 8076.0$ (see the ES mass spectra, Figure 1). The ES mass spectra obtained were reproducible (±10%) and identical in terms of relative intensities of the different peaks on four different instruments [Quattro II, LC-Tof, Q-Tof (Micromass, Altrincham, UK) and ESQUIRE-LC (Bruker-Franzen Analytik GmbH, Bremen, Germany)]. All the ions observed were interpreted and are summarised with their *m*/*z* values and their charge states in Table 1.

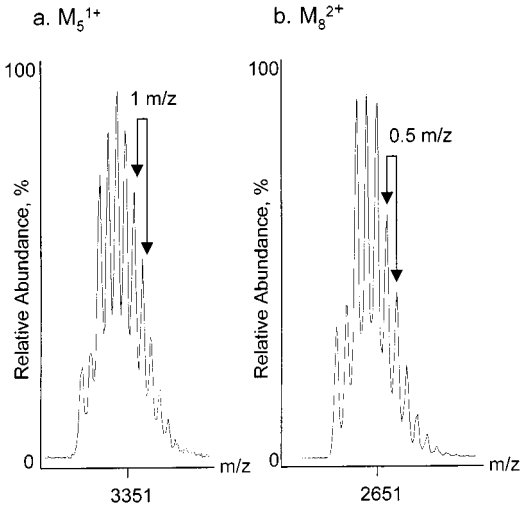

Figure 2. High resolution spectrum, obtained on an LC-Tof spectrometer

These ESMS results in acetonitrile and the stoichiometries determined suggest that in all complexes four nitrogen donor atoms coordinate one Cu^{II}. The IR analysis showed only a slight change in the C=O vibration frequency between the ligand and the mixture of complexes — from 1686 cm^{-1} to 1679 cm^{-1} — suggesting that the carbonyl group does not participate in the coordination with Cu^{II}. Since Cu^{II} is normally pentacoordinated, if we assume

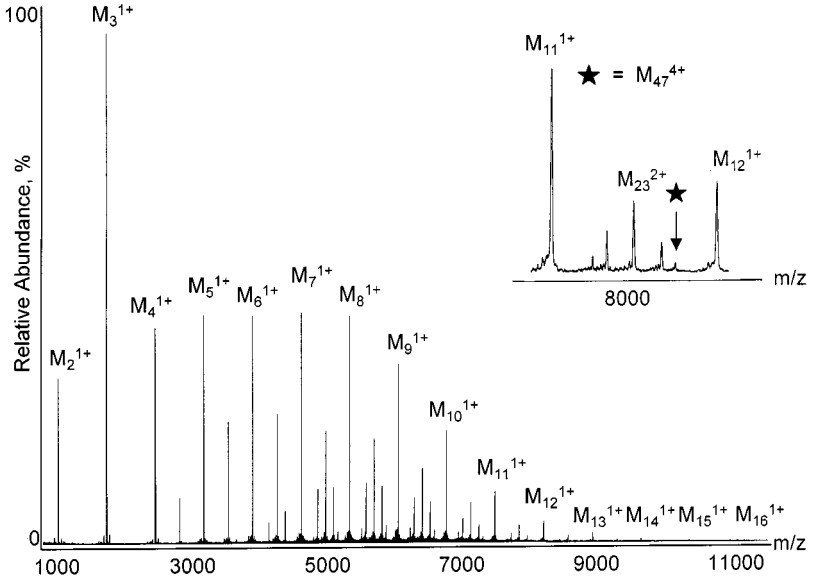

Figure 1. ES mass spectrum (obtained on an LC-Tof spectrometer) of an equimolar mixture of L and $Cu(CF_3SO_3)_2$ in anhydrous acetonitrile at 10^{-4} M

Table 1. Identification of the M_n ($1 < n < 47$) ions detected by ESMS[a]

M_1	M_2	M_3	M_4	M_5	M_6	M_7	M_8	M_9	M_{10}
551.0 (1+)	1250.9 (1+)	1950.9 (1+)	2650.9 (1+)	3351.3 (1+)	4050.9 (1+)	4751.1 (1+)	5451.2 (1+)	6150.3 (1+)	6851.9 (1+)
550.97	*1251.0*	*1951.03*	*2651.06*	*3351.09*	*4051.12*	*4751.15*	*5451.18*	*6151.21*	*6851.24*
							2650.9 (2+)	3000.8 (2+)	3351.3 (2+)
							2651.06	*3001.08*	*3351.10*
M_{11}	M_{12}	M_{13}	M_{14}	M_{15}	M_{16}	M_{17}	M_{18}	M_{19}	M_{20}
7550.6 (1+)	8250.9 (1+)	8949.8 (1+)	9650.1 (1+)	10353.1 (1+)	11048.1 (1+)	5801.1 (2+)	6150.3 (2+)	6500.3 (2+)	6851.9 (2+)
7551.27	*8251.30*	*8951.33*	9651.36	*10351.39*	*11051.42*	*5801.19*	*6151.21*	*6501.22*	*6851.24*
3700.7 (2+)	4050.9 (2+)	4400.4 (2+)	4751.1 (2+)	5100.6 (2+)	5451.2 (2+)	3817.5 (3+)	4050.9 (3+)	4284.6 (3+)	4517.4 (3+)
3701.91	*4051.12*	*4401.14*	*4751.15*	*5101.16*	*5451.18*	3817.77	4051.12	*4284.46*	*4517.80*
M_{21}	M_{22}	M_{23}	M_{24}	M_{25}	M_{26}	M_{27}	M_{28}	M_{29}	M_{30}
7200.0 (2+)	7550.6 (2+)	7901.0 (2+)	8250.9 (2+)	8601.1 (2+)	8949.8 (2+)	9300.6 (2+)	9650.1 (2+)	10001.9 (2+)	10353.1 (2+)
7201.25	*7551.27*	*7901.28*	*8251.30*	*8601.31*	*8951.33*	*9301.34*	*9651.36*	*10001.37*	*10351.39*
4751.1 (3+)	4984.4 (3+)	5217.2 (3+)	5451.2 (3+)	5684.2 (3+)	5917.0 (3+)	6150.3 (3+)	6384.0 (3+)	6617.9 (3+)	6851.9 (3+)
4751.15	*4984.49*	*5217.83*	*5451.18*	*5684.52*	*5917.86*	*6151.21*	*6384.55*	*6617.89*	*6851.24*
M_{31}	M_{32}	M_{33}	M_{34}	M_{35}	M_{36}	M_{37}	M_{38}	M_{39}	M_{40}
7084.58 (3+)	7317.8 (3+)	7550.6 (3+)	7784.5 (3+)	8017.8 (3+)	8250.9 (3+)	8485.5 (3+)	8717.0 (3+)	8949.8 (3+)	6851.9 (4+)
7085.0	*7317.92*	*7551.27*	*7784.61*	*8017.95*	*8251.30*	*8484.64*	*8717.98*	*8951.33*	*6851.24*
5276.2 (4+)	5451.2 (4+)	5626.2 (4+)	5801.1 (4+)	5976.6 (4+)	6150.3 (4+)	6326.6 (4+)	6500.3 (4+)	6676.2 (4+)	
5276.17	*5451.18*	*5626.18*	*5801.19*	*5976.20*	*6151.21*	*6326.21*	*6501.22*	*6676.23*	
M_{31}	M_{32}	M_{33}	M_{34}	M_{35}	M_{36}	M_{37}	M_{38}	M_{39}	M_{40}
7084.58 (3+)	7317.8 (3+)	7550.6 (3+)	7784.5 (3+)	8017.8 (3+)	8250.9 (3+)	8485.5 (3+)	8717.0 (3+)	8949.8 (3+)	6851.9 (4+)
7085.0	*7317.92*	*7551.27*	*7784.61*	*8017.95*	*8251.30*	*8484.64*	*8717.98*	*8951.33*	*6851.24*
5276.2 (4+)	5451.2 (4+)	5626.2 (4+)	5801.1 (4+)	5976.6 (4+)	6150.3 (4+)	6326.6 (4+)	6500.3 (4+)	6676.2 (4+)	
5276.17	*5451.18*	*5626.18*	*5801.19*	*5976.20*	*6151.21*	*6326.21*	*6501.22*	*6676.23*	
M_{41}	M_{42}	M_{43}	M_{44}	M_{45}	M_{46}	M_{47}			
7026.1 (4+)	7200.0 (4+)	7376.2 (4+)	7550.6 (4+)	7726.1 (4+)	7901.0 (4+)	8076.0 (4+)			
7026.24	*7201.25*	*7376.26*	*7551.27*	*7726.27*	*7901.28*	8076.29			

[a] Measured *m/z* (charge state) and calculated *m/z* in italics.

that four nitrogen donor atoms coordinate one Cu^{II}, the fifth coordination position is probably occupied by a molecule of solvent in order to complete the metal coordination sphere. In fact an acetonitrile molecule is probably coordinated to the Cu^{II} in solution but is lost in the gas phase.

To confirm this possible coordination cell, ESMS studies in anhydrous MeOH have been undertaken. Indeed, it has already been observed in the case of metallic complexes that MeOH is a better coordinating solvent than acetonitrile in the gas phase.[8] The ES mass spectrum (Figure 3) obtained in [D_4]MeOH has confirmed the presence of solvent molecules attached to these high-molecular-weight complexes. [D_4]MeOH was used in this case instead of MeOH to facilitate the resolution of the different adducts. In these conditions, for small oligomers (M_n, $n = 1$ to $n = 5$), the addition of one molecule of [D_4]MeOH to each Cu^{II} atom is observed from the *m/z* difference of 36 for singly charged peaks and 18 for doubly charged peaks. Unfortunately, for higher oligomers (M_n, $n > 5$) the ES mass spectrum is too complex at the resolution available (R = 8000) and no information could be obtained on the number of molecules of solvent attached to these large ions.

Slow crystallisation of these oligomers was unsuccessful and only crystals corresponding to the monomer (M_1) structure were found. Thanks to the ESMS and IR data a possible structure was deduced for these polymers in solution (Figure 4). Obviously, a cyclic form cannot be distinguished from a linear structure by mass measurement in our case. However, the 1:1:1 (L:Cu^{II}:MeOH) stoichiometry obtained for small oligomers (M_n, $n = 1$ to $n = 5$), suggests the formation of cyclic compounds in solution. On the other hand, considering the number of units, high polymers (M_n, $n > 5$) should be present as open structures (linear polymers). At both extremities the coordination sphere of Cu^{II} would be completed in solution by acetonitrile molecules, which are lost in the gas phase and not detected in the ESMS.

Considering that ESMS is the only analytical tool allowing an unambiguous characterisation in this case, kin-

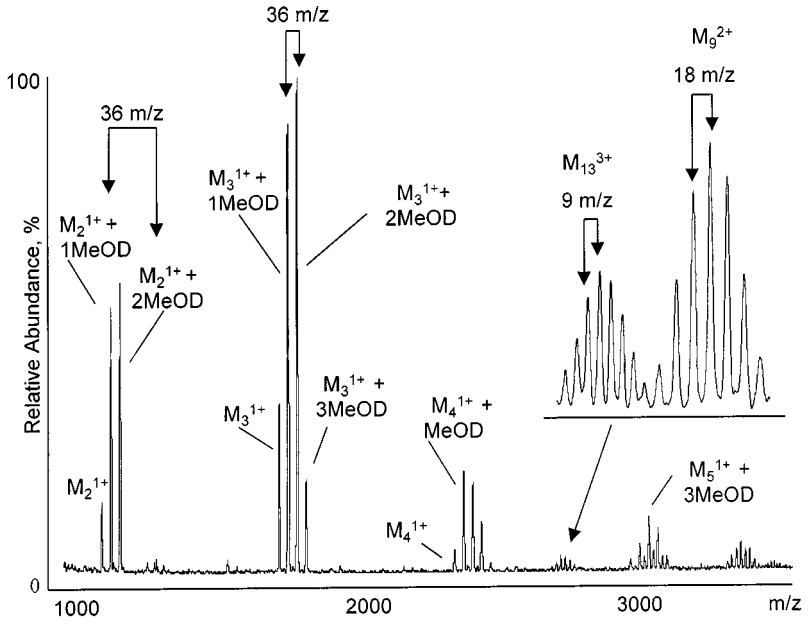

Figure 3. ES mass spectrum of an equimolar mixture of L and $Cu(CF_3SO_3)_2$ in $[D_4]MeOH$

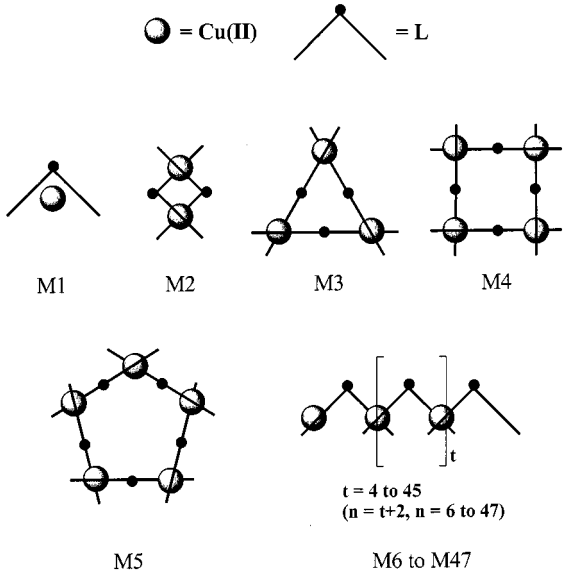

Figure 4. Possible structure of the coordination polymers $[LCu(CF_3SO_3)_2]_n$ deduced from ESMS and IR data (solvent adducts are omitted for clarity)

etic and thermodynamic studies were necessary in order to exclude the possibility of these oligomers being artefacts resulting from the ES process.

Kinetic Studies

The stability of the polymers in solution was tested during 40 days in several anhydrous solvents (acetonitrile, nitromethane, and methanol). ES mass spectra obtained from the same sample immediately after mixing (5 minutes) and after 40 days were found to be the same, showing the high stability of these compounds in solution. In the same way, when 5% water was added to one of these solutions, the ES analysis after 5 minutes was unchanged. Later, peaks corresponding to the higher oligomers progressively disappeared and after 24 hours only one peak corresponding to the monomer complex (M_1^{1+}) was observed in the ES mass spectrum (Figure 5a, b, c).

The observation of this progressive dissociation is the definitive piece of evidence which shows that these high molecular weight coordination complexes are formed in solution and not during the ES process. Hence, the possibility for these polymers of being artefacts of the ES process can be definitely rejected.

Thermodynamic Studies

Attempts to isolate some of the oligomers using size exclusion sephadex chromatography (by classical column or by HPLC) were fruitless and unfortunately only the monomer (M_1) was obtained. This result indicates that all these components are in equilibrium in solution. In order to determine if ligand exchange took place in this high-molecular-weight system, the ligand L was first mixed with a stoichiometric amount of $Cu(OTf)_2$ in anhydrous acetonitrile (ca. 10^{-4} M). Then, after stirring for 5 minutes, one equivalent of the methylated ligand L* (Scheme 1) was added to this mixture. The resulting solution was stirred for 5 minutes at room temperature and analysed immediately. The ES mass spectrum (Figure 6) showed that all possible combinations of oligomers M_aM_b* ($0 < a, b < 9$) of general formula L_aL_b*$[Cu(CF_3SO_3)_2]_{a+b}$ were obtained statistically in solution. This observation clearly indicates that ligand exchange occurred in solution, and confirms that these coordination polymers are in equilibrium in solution. Interestingly, the methylated ligand L* yielded a mixture of oligomers with $Cu(OTf)_2$ in anhydrous acetonitrile in the same manner as obtained with the ligand L.

To complete the study of these compounds, other thermodynamic experiments were carried out. In order to obtain more information about the stability of the complexes in solution, five solutions containing an equimolar amount of $Cu(OTf)_2$ and the ligand L in anhydrous acetonitrile at different concentrations (10^{-3}, 10^{-4}, 10^{-5}, 10^{-6} and 10^{-7} M) were analysed by ESMS. The ES mass spectra obtained showed the presence of the oligomeric mixture for a concentration down to 10^{-4} M. For lower concentrations, these high-molecular-weight complexes disappear and only the monomer ion (M_1^{1+}) is detected, indicating that dissociation processes occur below a concentration of 10^{-4} M (Figure 7a, b).

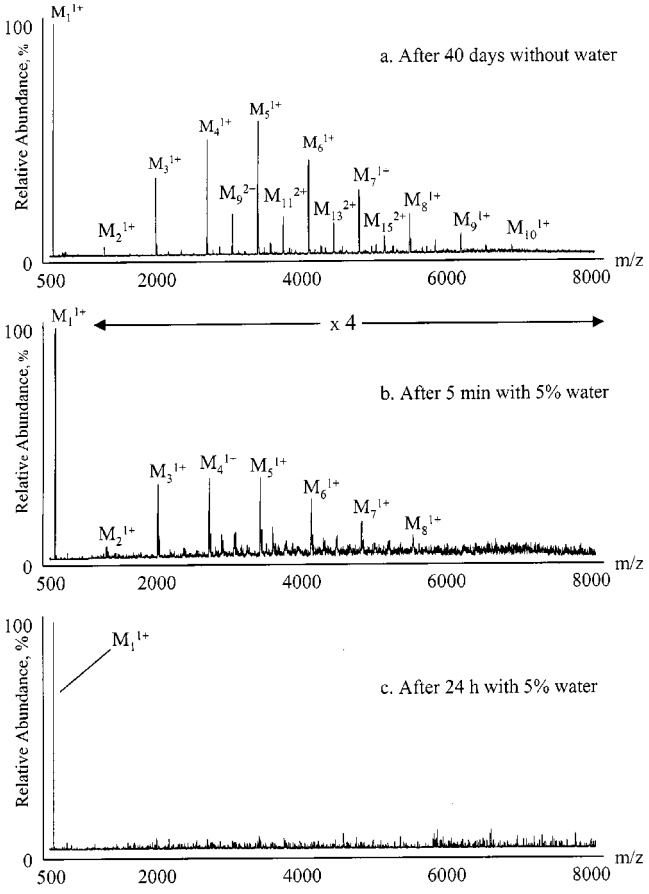

Figure 5a, b, c. Kinetic study: a. in anhydrous acetonitrile after 40 days; b. in acetonitrile with 5% water after 5 min; c. in acetonitrile with 5% water after 24 h; this study addresses the possibility that the compounds are ES process artefacts

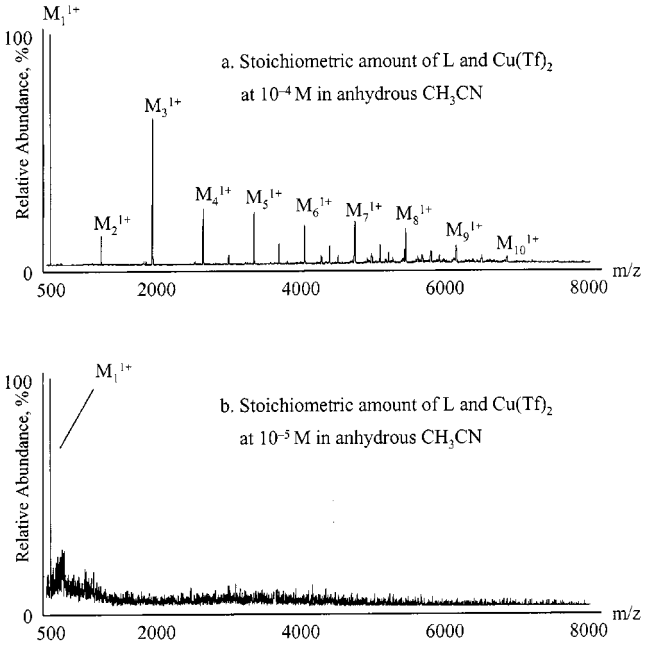

Figure 7a, b. Evaluation of the stability in solution of the coordination polymers at different concentrations

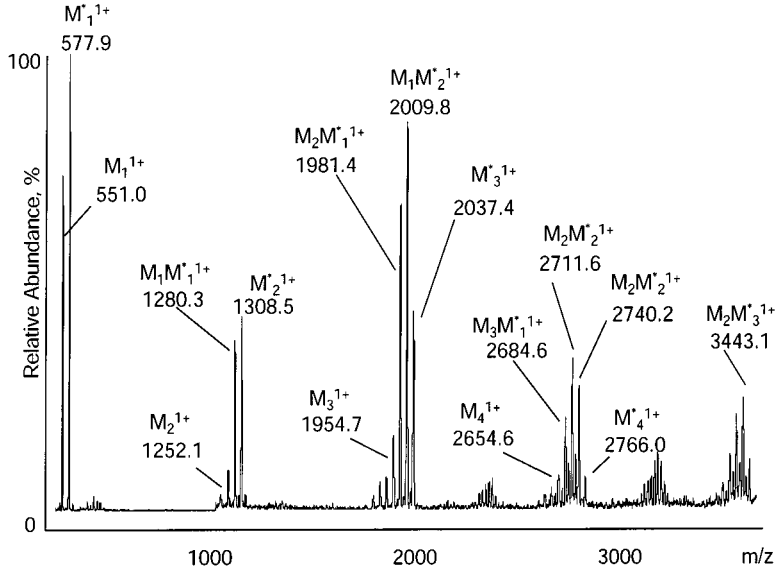

Figure 6. ES mass spectrum of an equimolar mixture of L and $Cu(CF_3SO_3)_2$ with one equivalent of L* in anhydrous acetonitrile at 10^{-4} M

Conclusion

We have shown that ligand L and $Cu(CF_3SO_3)_2$ in a 1:1 ratio in anhydrous solvents generate a mixture of high molecular weight coordination polymers of general formula $[LCu(CF_3SO_3)_2]_n$ by self-assembly. The largest oligomer clearly identified contains 47 units and weighs 32901.4 Da. The structure (cyclic for small oligomers and linear for the highest one) has been deduced from the IR and the ESMS data.

The kinetic decomplexation observed in the presence of 5% water shows that these self-assembled polymeric species are formed in solution and are not artefacts due to the ES process. To complete this study, ESMS thermodynamic experiments have been carried out and have demonstrated that these oligomers are in equilibrium in solution, are stable over time and can be observed down to a concentration of 10^{-4} M.

ESMS may therefore be regarded as an extremely valuable tool to prove the existence of very large polynuclear transition metal complexes in solution, and encouraging perspectives are offered for the characterisation of species of nanometric dimensions.

Experimental Section

Materials: Unless otherwise noted, ^{1}H NMR spectra were measured at 200 MHz with a Bruker AC 200 spectrometer in $CDCl_3$ and referenced to the residual solvent peak. Melting points were obtained with a digital Thomas Hoover (Electrotherma) apparatus. Infrared absorption spectra were recorded on a Perkin−Elmer 1600 series FTIR spectrometer in KBr, and electronic absorption spectra on a Cary 219 spectrometer in $CHCl_3$ with λ_{max} in nm and ε ($\times 10^4$) in M^{-1} cm^{-1}. Fast atom bombardment mass spectrometry (FAB-MS) was performed on a ZAB-HF VG spectrometer with *m*-nitrobenzyl alcohol as the matrix. Spectroscopic studies were performed in spectroscopic-grade solvents. All solvents were reagent-grade and used without further purification. The Cu^{II} triflate was purchased from Fluka (Buchs, Switzerland).

ESMS: Positive ES mass spectra were mainly obtained on an ES triple quadrupole mass spectrometer Quattro II with an *m*/*z* range extended to 8000 (Micromass, Altrincham, UK). The electrospray source was heated to 70 °C. The sampling cone voltage (V_c) was set to 70 V and the skimmer Lens Offset to 0 V to allow the transmission of ions with $m/z > 4000$ without fragmentation processes. Sample solutions were introduced into the mass spectrometer source with a syringe pump (Harvard type 55 1111: Harvard Apparatus Inc., South Natick, MA, USA) with a flow rate of 5 $\mu L \cdot min^{-1}$. Calibration was performed using protonated horse myoglobin. Scanning was performed from $m/z = 500$ to 8000 in 20 s, and several scans were summed to obtain the final spectrum. ES mass spectra at higher resolution were obtained on an LC-Tof mass spectrometer (Micromass, Altrincham, UK).

Samples for ESMS were prepared by mixing the corresponding ligand and $Cu(CF_3SO_3)_2$ in a 1:1 ratio to achieve a concentration of 10^{-3}, 10^{-4}, 10^{-5}, 10^{-6} or 10^{-7} M in anhydrous acetonitrile and a concentration of 10^{-4} M in $[D_4]$MeOH. After stirring at room temperature for 1 min, the clear blue solution was analysed directly by ESMS.

Synthesis of the Ligands L and L*: The ligands were prepared as shown in Scheme 1. The stannylation of 2-bromopyridine (**3**) with butyllithium and tributylstannyl chloride gave 2-tributylstannylpyridine (**4**).[9] The ketone **6** was prepared from 2,6-dibromopyridine (**5**) by monolithiation and reaction with ethylchloroformate as previously described.[10] The cross coupling reaction between **4** and **6** or **8** and **6** in the presence of $Pd(PPh_3)_4$ yielded ligand **1 (L)** or ligand **2 (L*)** which were completely characterised.

2-Tributylstannylpyridine (4): A 1.6 M solution of *n*-butyllithium in hexane (39.2 mL, 0.062 mol) was slowly added to a solution of 2-bromopyridine (**3**; 6 mL, 0.062 mol) in THF (120 mL) cooled to −78 °C under argon. After 30 min, Bu_3SnCl (16.8 mL, 0.062 mol) was added to give a dark solution which was stirred at −78 °C for one more hour. The solution was allowed to warm to room temperature and a saturated aqueous solution of NH_4Cl (60 mL) was added. The aqueous phase was extracted with ether (3 × 100 mL) and the combined organic layers were washed with brine (100 mL) and dried (Na_2SO_4). The solvent was removed under reduced pressure to give a yellow oil. The crude product was purified by chromatography on alumina (EtOAc/hexane 1:20) to obtain a pale yellow oil (22.1 g, 96%).[9] ^{1}H NMR: δ = 8.73 (ddd, *J* = 4.9, 1.9, 1.0 Hz, 1 H, H_6), 7.48 (dt, *J* = 7.4, 1.8 Hz, 1 H, H_5), 7.39 (dt, *J* = 7.4, 1.6 Hz, 1 H, H_3), 7.10 (ddd, *J* = 6.9, 4.9, 1.7 Hz, 1 H, H_4), 1.70−1.05 (m, 18 H, CH_2), 0.85 (t, 9 H, *J* = 7.3 Hz, CH_3).

Bis(6-bromo-2-pyridyl)ketone (6): 1.1 Equiv. of *n*-butyllithium in hexane (29 mL, 0.046 mol) was added dropwise under argon to a solution of 2,6-dibromopyridine (**5**; 10 g, 0.042 mol) in diethyl ether (200 mL) cooled to −90 °C. After stirring vigorously for 20 min, a solution of ethyl chloroformate (2.02 mL, 0.021 mol) in diethyl ether (50 mL) was added. The deep blue solution was stirred for one hour and warmed to −40 °C for 30 min. Then, the reaction was quenched successively with methanol (50 mL) and water (50 mL). The organic phase was removed under vacuum and the aqueous layer was extracted with chloroform (3 × 50 mL). The combined organic layers were dried (Na_2SO_4) and the solvent was removed under low pressure. The residue was purified by flash chromatography on silica gel using EtOAc/hexane (1:6) as eluent to give a white solid (3.4 g, 47%). M.p. 159−160 °C (ref.[10] 155−156.5 °C). ^{1}H NMR: δ = 8.08 (dd, *J* = 7.1, 1.4 Hz, 2 H, H_3), 7.76 (dd, *J* = 8.0, 7.2 Hz, 2 H, H_4), 7.69 (dd, *J* = 8.0, 1.5 Hz, 2 H, H_5). ^{13}C NMR: δ = 189.5, 154.0, 141.5, 138.9, 131.4, 124.3.

2-Tributylstannyl-4-picoline (8): 1 Equiv. of a 1.6 M solution of *n*-butyllithium in hexane (18.15 mL, 29.066 mmol) was added at −78 °C under argon to a solution of 2-bromopicoline (**7**; 5 g, 29.066 mmol) in tetrahydrofuran (100 mL). After 30 min, Bu_3SnCl (7.9 mL, 29.066 mmol) was added and the reaction was monitored by TLC. The reaction was allowed to rise to room temperature and after 30 min a saturated aqueous solution of NH_4Cl was added (100 mL). The organic layer was separated and the aqueous layer was extracted with diethyl ether (3 × 100 mL). The combined organic layers were dried (Na_2SO_4) and the solvent was removed under low pressure. The residue was purified by chromatography on alumina using EtOAc/hexane (1:20) as eluent to obtain a pale yellow oil (11.1 g, 78%). B.p. 144 °C (0.6 Torr). ^{1}H NMR: δ = 8.58 (d, *J* = 5.0 Hz, 1 H, H_6), 7.22 (s, 1 H, H_3), 6.94 (d, *J* = 5.0 Hz, 1 H, H_5), 2.32 (s, 3 H, CH_3), 1.70−1.05 (m, 18 H, CH_2), 0.85 (t, *J* = 7.2 Hz, 9 H, CH_3). ^{13}C NMR: δ = 173.1, 150.2, 143.9, 133.4, 123.0, 29.1, 27.3, 13.7, 9.7, 8.7. EI-MS: *m*/*z* (%) = 383 (5) [M + 1], 326 (85) [M − Bu], 268 (45) [M − 2Bu], 212 (100) [M − 3Bu].

L [Bis(2,2′-bipyrid-6′-yl)ketone]: Toluene (20 mL) was added to a mixture of compound **4** (2.15 g, 5.84 mmol), the dibromo com-

pound **6** (0.50 g, 1.46 mmol) and tetrakis(triphenylphosphane)palladium (0.34 g, 20% mol) and the resulting mixture was stirred at 110 °C under argon for 24 hours. The toluene was then evaporated and the residue was chromatographed on silica gel eluting with acetone/hexane (2:5). The pale yellow solid was triturated with hexane to afford a white solid (0.38 g, 77%). M.p. 171−172 °C. ^{1}H NMR: δ = 8.68 (m, 2 H, H_3), 8.66 (dd, J = 7.8, 1.3 Hz, 2 H, $H_{3'}$), 8.33 (dt, J = 7.9, 1.0 Hz, 2 H, H_6), 8.16 (dd, J = 7.6, 1.3 Hz, 2 H, $H_{5'}$), 8.04 (t, J = 7.7 Hz, 2 H, $H_{4'}$), 7.70 (dt, J = 7.7, 1.8 Hz, 2 H, H_5), 7.30 (ddd, J = 7.5, 4.8, 1.2 Hz, 2 H, H_4). ^{13}C NMR: δ = 192.8, 144.4 (2C), 153.7, 149.1, 137.3, 136.9, 125.0, 124.0, 123.4, 121.4. FAB-MS: *m*/*z* (%) = 339.1 (100) [M + 1], 155 (7) [M − 183 (bipy)]. $C_{21}H_{14}N_4O$ (338.4): calcd. C 74.53, H 4.17, N 16.57; found C 74.45, H 4.41, N 16.68. IR (KBr): $\tilde{\nu}$ = 1686, 1581, 1430, 1320, 1258, 1097, 992, 752, 667 cm^{-1}. UV/Vis: λ (ε_{max}) = 230 (1.0), 279 (0.9).

L* [Bis(2,2′-bipyrid-4-methyl-6′-yl)ketone]: Toluene (5 mL) was added to a mixture of compound **8** (0.17 g, 0.442 mmol), dibromo compound **6** (0.063 g, 0.184 mmol) and tetrakis(triphenylphosphane)palladium (0.043 g, 20% mol) and the resulting mixture was stirred at 110 °C under argon for 17 hours. The toluene was then evaporated and the residue was chromatographed on silica gel eluting with acetone/hexane (2:5). The pale yellow solid was triturated with hexane to afford a white solid (0.040 g, 59%). M.p. 149−150 °C. ^{1}H NMR: δ = 8.64 (dd, J = 1.2, 7.8 Hz, 2 H), 8.54 (d, J = 4.7 Hz, 2 H), 8.20−8.15 (m, 4 H), 8.03 (t, J = 7.8 Hz, 2 H), 7.12 (dq, J = 0.6, 6.1 Hz, 2 H), 2.25 (s, 3 H). FAB-MS: *m*/*z* (%)= 367.1 (100) [M + 1]. $C_{23}H_{18}N_4O$ (366.4): calcd. C 75.39, H 4.95, N 15.29; found C 74.3, H 4.95, N 15.5.

Synthesis of the Cu^{II} Coordination Polymers: The Cu^{II} coordination polymers were obtained by mixing the ligand **L** or **L*** and Cu^{II} triflate [$Cu(CF_3SO_3)_2$] in a 1:1 ratio in anhydrous acetonitrile or in [D_4]MeOH. The resulting clear blue solution was stirred at room temperature for 1 min.

Acknowledgments

H. N., E. L. and A. V. D. thank the TMR-Project EU Nr. ERBFMRXCT980226 on Nanometer Size Metallic Complexes for the financial support of the ESMS work. H. N. thanks the Laboratoire P. Fabre for financial support. J. R. thanks the French Government for a postdoctoral fellowship. Finally, the authors thank Dr. N. Potier for the LC-Tof analysis.

[1] [1a] J.-M. Lehn, *Supramolecular Chemistry: Concepts and Perspectives*, VCH, Weinheim, **1995**. [1b] *Comprehensive Supramolecular Chemistry* (Eds.: J. L. Atwood, J. E. D. Davies, D. D. MacNicol, F. Vögtle and J.-M. Lehn), Pergamon, Oxford, **1996**.

[2] [2a] J.-M. Lehn, *Angew. Chem.* **1990**, *102*, 1347; *Angew. Chem. Int. Ed. Engl.* **1990**, *29*, 1304−1319. [2b] E. C. Constable, *Tetrahedron* **1992**, *48*, 10013−10069. [2c] P. Baxter, J.-M. Lehn, A. Decian, J. Fischer, *Angew. Chem.* **1993**, *105*, 92−96; *Angew. Chem. Int. Ed. Engl.* **1993**, *32*, 69−71. [2d] J. Rojo, J.-M. Lehn, G. Baum, D. Fenske, O. Waldmann, P. Müller, *Eur. J. Inorg. Chem.* **1999**, 517−522. [2e] A. M. Garcia, F. J. Romero-Salguero, D. M. Bassani, J.-M. Lehn, G. Baum, D. Fenske, *Chem. Eur. J.* **1999**, *5*, 1803−1808. [2f] A. M. Garcia, D. M. Bassani, J.-M. Lehn, G. Baum, D. Fenske, *Chem. Eur. J.* **1999**, *5*, 1234−1238.

[3] [3a] P. Losier, M. J. Zaworotko, *Angew. Chem. Int. Ed. Engl.* **1996**, *35*, 2779−2781. [3b] U. Velten, M. Rehahn, *Chem. Commun.* **1996**, 2639−2641. [3c] R. Knapp, A. Schott, M. Rehahn, *Macromolecules* **1996**, *29*, 478−480. [3d] S. R. Batten, P. jansen, B. Moubaraki, K. S. Murray, R. Robson, *Chem. Commun.* **1998**, 439−441. [3e] F. P. Gabbaï, A. Schier, J. Riede, *Angew. Chem. Int. Ed.* **1998**, *37*, 622−624. [3f] S.-M. Kuang, Z.-Z. Zhang, Q.-G. Wang, T. C. W. Mark, *Chem. Commun.* **1998**, 581−583. [3g] K. N. Power, T. L. Hennigar, M. J. Zaworotko, *Chem. Commun.* **1998**, 595−597. [3h] C. Kaes, M. W. Hosseini, C. E. F. Rickard, B. W. Skelton, A. H. White, *Angew. Chem. Int. Ed.* **1998**, *37*, 920−922.

[4] [4a] M. Yamashita, J. B. Fenn, *J. Phys. Chem.* **1984**, *88*, 4451−4459. [4b] M. Yamashita, J. B. Fenn, *J. Phys. Chem.* **1984**, *88*, 4671−4675.

[5] [5a] J. A. Loo, *Mass Spectrom. Rev.* **1997**, *16*, 1−23. [5b] N. Potier, P. Barth, D. Tritsch, J. F. Biellmann, A. Van Dorsselaer, *Eur. J. Biochem.* **1997**, *243*, 274−282. [5c] H. Rogniaux, A. Van Dorsselaer, P. Barth, J. F. Biellmann, J. Barbanton, M. van Zandt, B. Chevrier, E. Howard, A. Mitschler, N. Potier, L. Urzhumtseva, D. Moras, A. Podjarny, *J. Am. Soc. Mass Spectrom.* **1999**, *10*, 635−647.

[6] [6a] E. Leize, A. Van Dorsselaer, R. Krämer, J.-M. Lehn, *J. Chem. Soc., Chem. Commun.* **1993**, 990−993. [6b] K. C. Russel, E. Leize, A. Van Dorsselaer, J.-M. Lehn, *Angew. Chem. Int. Ed. Engl.* **1994**, *34*, 209−213. [6c] C. Garcia, J. Guyot, G. Jeminet, E. Leize, H. Nierengarten, A. Van Dorsselaer, *Tetrahedron Lett.* **1999**, *40*, 4997−5000. [6d] E. Leize, A. Jaffrezic, A. Van Dorsselaer, *J. of Mass Spectrometry* **1996**, *31*, 537−544. [6e] C. Piguet, G. Bernardinelli, G. Hopfgartner, *Chem. Rev.* **1997**, *97*, 2005−2062.

[7] P. Kebarle, L. Tang, *Anal. Chem.* **1993**, *65*, 972A−986A.

[8] F. M. Romero, R. Ziessel, A. Dupont-Gervais, A. Van Dorsselaer, *Chem. Commun.* **1996**, 551−553.

[9] C. Bolm, M. Ewald, M. Felder, G. Schingloff, *Chem. Ber.* **1992**, *125*, 1169−1173.

[10] J. E. Parks, B. E. Wagner, R. H. Holm, *J. Organomet. Chem.* **1973**, *56*, 53−69.

Received August 24, 2001
[I01328]

Five-Coordination and Adduct Formation in Co^{III}−Corrinoids Dissecting Ligand Substitution into Its Component Steps

Mohamed S. A. Hamza,[a,c] Rudi van Eldik,*[a] Pascal L. S. Harper,[b] John M. Pratt,*[b] and Eric A. Betterton[d]

Keywords: Adduct formation / Reaction mechanisms / Cobalt / Equilibrium / Ligand substitution / High-pressure chemistry / Kinetics

The equilibria between the five- and six-coordinate species of alkylcobinamide and cobalamin (base-off) have been studied using high-pressure spectroscopic techniques. The addition of a water molecule to the five-coordinate complex is accompanied by a volume decrease of 12 $cm^3 \cdot mol^{-1}$.

Introduction

The mechanisms of ligand substitution reactions can be divided into the two extremes of limiting dissociative (D) and associative (A) mechanisms, linked by a broad range of interchange (I) mechanisms involving the formation of some weak, non-bonded "outer-sphere" (OS) adduct or intermediate between the entering and/or leaving ligand and the complex,[1] but few such adducts have been reported.[2] Good evidence for several such OS intermediates has recently been obtained from kinetic studies of both ligand substitution[3] in the six-coordinate Co^{III}−corrinoids (derivatives of vitamin B_{12})[4] and of the methylation of five-coordinate Co^{II}−corrinoids by MeI in the presence of thiols.[5] As will be shown here, the Co^{III}−corrinoids also offer an unusual opportunity to observe analogues of the five-coordinate intermediate of the limiting D mechanism, and of adducts with both five- and six-coordinate forms under equilibrium (i.e. non-reacting) conditions. In addition they offer the opportunity to establish a link between kinetically deduced transient intermediates and directly observable stable species.

Co−corrinoids with only amide side-chains are termed *cobinamides* (Cbi), those with the attached nucleotide (as in B_{12} itself) *cobalamins* (Cbl), and those where the amides have been esterified (usually as the Me ester) *cobesters* (Cbs); protonation and displacement of the coordinated nucleotide base in a Cbl gives a coordination sphere identical to that of a Cbi. UV/Vis spectrophotometry provides the main tool for kinetic and other studies.[4b] Both axial sites are surrounded by a hydrophobic cylinder of the exocyclic substituents, projecting roughly normal to the corrin ring, and an outer ring of hydrophilic amide groups. Comparing a Cbi with the analogous Cbs provides a test for possible involvement of the side-chains in, e.g. adduct formation. Co^{III}−corrinoids with the more typical axial ligands used in kinetic studies are red and six-coordinate. There is, however, good evidence that Cbi's (and protonated Cbl's) with stronger donor ligands (e.g. vinyl, methyl, sulfite, or dialkyl phosphite) exist as temperature-dependent mixtures of yellow five-coordinate and red six-coordinate aqua (solvato) forms based on UV/Vis, EXAFS, and NMR measurements.[4a,6] No other explanation for the available data has been put forward. Increasing temperature favours the yellow five-coordinate form, and with diethyl phosphite[7] as ligand it has also been shown qualitatively that increasing pressure favours the red six-coordinate form. No structural data on the yellow forms have yet been reported and more evidence for the reversible coordination of H_2O is clearly desirable.

We have now quantitatively studied the pressure dependence (up to 150 MPa) of the spectra of both vinyl-Cbi (VCbi, $4 \cdot 10^{-5}$ M, pH = 7, unbuffered solution) and protonated methyl-Cbl ($3 \cdot 10^{-5}$ M MeCbl/0.5 M $HClO_4$) in aqueous solution, which contain 70 and 90%, respectively, of the yellow form at ambient pressure and 20 °C,[6a] in order to determine the reaction volumes for conversion of the yellow to red forms according to Equation (1).

[a] Institute for Inorganic Chemistry, University of Erlangen-Nürnberg,
Egerlandstraße 1, Erlangen 91058, Germany
[b] Department of Chemistry, Imperial College of Science, Technology and Medicine,
London SW1 2AY, UK
[c] Department of Chemistry, Faculty of Science, Ain Shams University,
Abbassia, Cairo, Egypt
[d] Department of Atmospheric Science, University of Arizona, Tucson, AZ 85721-0081, USA

 © WILEY-VCH Verlag GmbH, 69451 Weinheim, Germany, 2002 1434−1948/02/0303−0580 $ 17.50+.50/0 *Eur. J. Inorg. Chem.* **2002**, 580−583

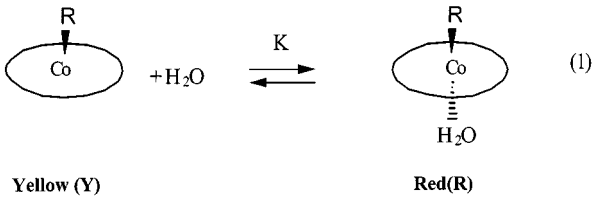

Calculations[8] suggest a volume of activation ($\Delta V^{\#}$) of $+13.1$ cm^3·mol^{-1} for a limiting D mechanism of ligand substitution involving the loss of coordinated H_2O in an octahedral complex and such a value may be taken as diagnostic of the loss of coordinated H_2O in the conversion of the red to yellow forms. In addition, possible adduct formation has been studied with the five-coordinate VCbi and vinyl-Cbs (VCbs), and the six-coordinate dicyano-Cbi (DCCbi) and dicyano-Cbs (DCCbs).

Results and Discussion

Increasing pressure p displaces the observed equilibrium from the yellow (Y) towards the red (R) form both for VCbi and MeCbl/H^+, as shown in Figures 1 and 2. Figure 1 shows distinct isosbestic points at 372, 447, and 536 nm, and a significant absorbance increase at the shoulder at 482 nm in the case of Vcbi. In addition, distinct isosbestic points at 385, 473, and 584 nm, and a significant increase in the absorbance at 490 nm were observed in the case of MeCbl/H^+ (Figure 2). The effect of pressure on the UV/Vis spectra suggests the formation of a six-coordinate species, since it is known that these (assumed) five-coordinate corrinoids exhibit maxima at 451 and 458 nm, respectively, and their six-coordinate corrinoid forms at ca. 495 and 503 nm, respectively.[6a] Values of the equilibrium constant (K = [R]/[Y]) as a function of p were calculated from the increase in absorbance at 490 nm using the optical density ratio of the two bands for the fully formed R and Y derived from the temperature-dependence studies as described in the literature.[6a] The slopes of the plots of ln K versus p (see Figures 3 and 4) gave values (in duplicate experiments) for the reaction volume $\Delta V = -12.4 \pm 1.0$ and -12.5 ± 1.2 cm^3·mol^{-1} for the conversion of Y to R in VCbi and MeCbl/H^+, respectively. Their identical values underline the close parallel between Cbi's and protonated Cbl's, and their agreement with the theoretical value of -13.1 cm^3·mol^{-1} (see above) confirms that conversion of the Y to R form involves the coordination of one molecule of H_2O by the five-coordinate Y form. Formation of the R form is therefore favoured both by increasing pressure ($\Delta V \approx -12.5$ cm^3·mol^{-1}) and by decreasing temperature ($\Delta S = -22 \pm 2$ e.u. reported for (diethyl phosphito)Cbl in aqueous acidic solution).[7]

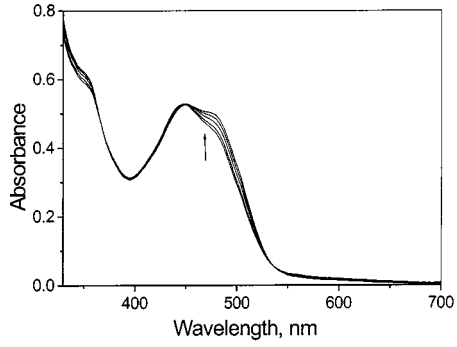

Figure 1. UV/Vis spectra of vinylcobinamide, recorded as a function of pressure (0.1, 30, 70, 110, and 150 MPa, accompanied by an increase in absorbance around 490 nm)

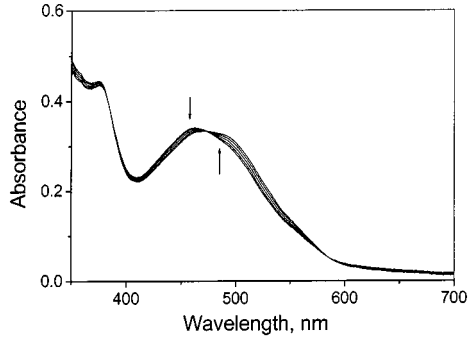

Figure 2. UV/Vis spectra of methylcobalamin (base-off form), recorded as a function of pressure (0.1, 30, 70, 110, and 150 MPa, accompanied by an increase in absorbance around 500 nm)

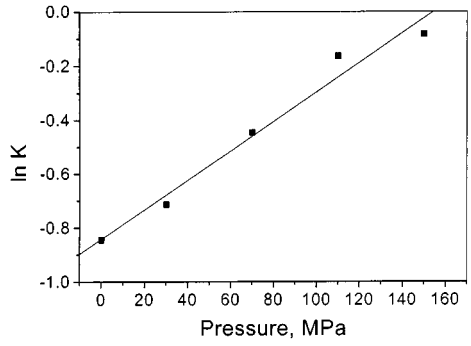

Figure 3. ln K versus pressure for the equilibrium between the five- and six-coordinate species of vinylcobinamide according to Equation (1); the best fit of the data (solid line) gives $\Delta V = -12.4 \pm 1.0$ cm^3·mol^{-1}

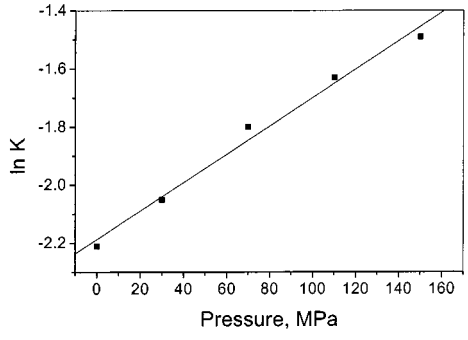

Figure 4. ln K versus pressure for the equilibrium between the five- and six-coordinate species of methylcobalamin (base-off) according to Equation (1); the best fit of the data (solid line) gives $\Delta V = -12.5 \pm 1.2$ cm^3·mol^{-1}

Initial experiments on adduct formation by VCbi showed that the addition of the structure-breakers[9] KI and $NaClO_4$ (but not the structure-makers[9] NaCl and NaF), of sodium iodoacetate (but not sodium acetate), and of MeI all caused an immediate and significant change in the spectrum, indicating a shift from the R to the Y form, with distinct isosbestic points observed at least in the case of $NaClO_4$. A similar positive result was obtained for VCbs with KI and $NaClO_4$ (a negative result was obtained with NaCl). All these observations suggest that the solute (as adduct or ion-pair) binds in the hydrophobic cavity close enough to the Co metal centre to destabilise the coordinated H_2O and favour the five-coordinate form. By contrast, hydroxide (as well as imidazole, etc.) forms a red six-coordinate complex.[10] Binding constants of $K = 3.0 \pm 0.4$ M^{-1} and 1.5 ± 0.5 M^{-1} were obtained for VCbi with iodide (phosphate buffer pH = 7.25, up to 0.4 M KI) and perchlorate (unbuffered solution, up to 2 M $NaClO_4$), respectively.

Comparison of the spectrum of DCCbi (with a slight excess of cyanide to suppress ligand substitution) in 1 M solutions of a range of solutes showed no detectable difference (from that in water alone) with urea, NH_2OH, ethylene glycol (i.e. very hydrophilic compounds), NaOH, NaF, and sodium acetate (structure-making anions), KF or Me_4NF. Differences, however, were observed in the presence of imidazole, pyridine, 2,6-dimethylpyridine, NaBr and NaI (structure-breaking anions), sodium iodoacetate, and MeI. These changes were not reversed by adding more cyanide (i.e. do not involve displacement of coordinated cyanide) and, at least with iodide, did not vary with the Co concentration (i.e. not due to aggregation). All the observed changes were characterised by a similar broadening of both the α, β and γ bands (at 580, 540, and 367 nm, respectively) with a decrease in absorbance but no significant shift in λ_{max}, an increase in the 400−450 nm region and a cross-over (or even an isosbestic point) at ca. 460 and 600 nm; cf. the so-called Ham effect.[11] Similar experiments with DCCbs showed changes with both pyridine and KI in aqueous solution but no change with urea or ethylene glycol, while no changes were observed even with pyridine or KI in methanol or with pyridine in chloroform. The tests for solute, solvent and side-chains all suggest that the solute interacts with some hydrophobic part of the corrin structure, which is probably (as with VCbi) the cavity around one or both of the axial coordination sites, but interaction with its external walls cannot be excluded. Binding constants could not reliably be determined from the small changes in spectra. On re-examining the reported failure of cyano-Cbl (vitamin B_{12} itself) and dicyano-Cbl (nucleotide base displaced from coordination by cyanide) to fluoresce,[12] however, it was found that DCCbi in methanol fluoresces in the visible region with a maximum at 603 nm (when excited at 500 nm) but that this is quenched by adding imidazole or benziminazole (modelling the 3,5-dimethylbenzimidazole present in the Cbl's) and not restored by adding more cyanide (i.e. quenching does not involve displacement of coordinated cyanide). A binding constant K of ca. 14 M^{-1} for DCCbi with imidazole was calculated from the decreasing emission at 603 nm with increasing imidazole concentration in unbuffered methanol (containing ca 10^{-3} M KCN). This is comparable to the value of $K = 12$ to 16 M^{-1} for aquapentaammineruthenium(II) with the incoming methylpyrazinium ion.[2]

The close agreement between our experimentally determined volumes of reaction and the calculated value provides strong evidence that the equilibrium of interest involves the simple coordination of H_2O by the yellow five-coordinate corrinoid to produce the red six-coordinate form. Conversely, it provides the first experimental value for (and support for the calculated value of) the limiting volume of activation required in discussing D and I_d mechanisms of ligand substitution. Our results also demonstrate that both the five-coordinate VCbi and the six-coordinate DCCbi can form directly observable stable adducts and ion-pairs; the solutes are probably located within the hydrophobic cylinder surrounding the Co ion which, in effect, acts like a calixarene. The qualitatively similar behaviour of iodide, iodoacetate, and MeI demonstrates that the corrin ring can promote the formation of adducts as potential intermediates in reactions ranging from nucleophiles with Co^{III} to electrophiles (such as MeI) with Co^{II} and Co^{I}. The Co^{III}−corrinoids offer a unique opportunity to see how, as the donor power of one axial ligand is increased in the established order of the *trans* effect [e.g. H_2O < DMB (nucleotide base) < OH^- < CN^- < acetylide < vinyl < methyl < ethyl],[4a] the unstable five-coordinate intermediate for ligand substitution in the other axial position will become the stable yellow five-coordinate form, a transient OS intermediate will become a stable adduct, and the observed low volumes of activation ($\Delta V^{\#} = +4$ to $+8$ cm^3 mol^{-1}),[3c−3d,13] typical of an I_d mechanism, will increase to the reaction volume ($\Delta V = +12.5$ cm^3·mol^{-1}), denoting a limiting D mechanism.

Experimental Section

The pH of the solutions was measured using a Mettler Delta 350 pH meter. It was calibrated with standard buffer solutions at pH = 4 and 7. UV/Vis spectra were recorded with Shimadzu UV-2101 or Cary 5 spectrophotometers. UV/Vis spectra under high pressure were recorded with the Shimadzu spectrophotometer utilizing a home-made high-pressure unit.[14] Emission spectra of degassed methanolic solutions were recorded with a Spex Fluorimax 2. All the instruments used in this work were thermostated to 25 °C. Values of ΔV were calculated from the slope (= $-\Delta V/RT$) of plots of ln K versus pressure. Methylcobalamin was purchased from Sigma. Dicyanocobinamide was prepared as described in the literature[15] by treating cyanocobalamin with trifluoromethanesulfonic acid and then adding cyanide. Dicyanocobester was prepared by heating cyanocobalamin under reflux in a solution of methanol containing 1 M H_2SO_4 under N_2 for 4 d, and then adding cyanide.[16] Vinylcobinamide was prepared by treating Co^{I}−cobinamide with acetylene and vinylcobester by an analogous reaction.[17] The purity of the prepared complexes was checked by UV/Vis spectroscopy and thin layer chromatography, and the results were found to be in excellent agreement with data reported in the literature. The preparation of solutions and measurements were carried out

in diffuse light since all the alkylcobalamins are known to be very light-sensitive.

Acknowledgments

The authors gratefully acknowledge financial support from the Deutsche Forschungsgemeinschaft, the Fonds der Chemischen Industrie, and the Alexander von Humboldt Foundation for a fellowship to M. S. A. H.

[1] R. G. Wilkins, *Kinetics and Mechanism of Reactions of Transition Metal Complexes*, 2nd ed., VCH, Weinheim, Germany, **1991**.

[2] The first reported example of an OS intermediate appears to have been between the aquapentaammineruthenium(II) cation and the incoming *N*-methylpyrazinium ion: [2a] H. E. Toma, J. M. Malin, *J. Am. Chem. Soc.* **1972**, *94*, 4039. [2b] R. E. Shepherd, H. Taube, *Inorg. Chem.* **1973**, *12*, 1392.

[3] [3a] H. M. Marques, J. C. Bradley, L. A. Campbell, *J. Chem. Soc., Dalton Trans.* **1992**, 2019. [3b] H. M. Marques, J. C. Bradley, K. L. Brown, H. Brooks, *J. Chem. Soc., Dalton Trans.* **1993**, 3475. [3c] M. Meier, R. van Eldik, *Inorg. Chem.* **1993**, *32*, 2635. [3d] F. F. Prinsloo, M. Meier, R. van Eldik, *Inorg. Chem.* **1994**, *33*, 900.

[4] For an introduction to some of the structures, equilibria and UV/Vis spectra exhibited by the Co−corrinoids see: J. M. Pratt, in: *Chemistry and Biochemistry of B_{12}* (Ed: R. Banerjee), John Wiley & Sons, New York, **1999**; [4a] pp. 73−112; [4b] pp. 113−164.

[5] J. M. Pratt, M. S. A. Hamza, G. J. Buist, *J. Chem. Soc., Chem. Commun.* **1993**, 701.

[6] [6a] R. A. Firth, H. A. O. Hill, B. E. Mann, J. M. Pratt, R. G. Thorp, R. J. P. Williams, *J. Chem. Soc. A* **1968**, 2419. [6b] M. D. Wirt, M. R. Chance, *J. Inorg. Biochem.* **1993**, *49*, 265. [6c] K. L. Brown, G.-Z. Wu, *Inorg. Chem.* **1994**, *33*, 4122.

[7] S. M. Chemaly, *J. Inorg. Biochem.* **1991**, *44*, 1.

[8] [8a] T.W. Swaddle, *Rev. Phys. Chem. Jpn.* **1980**, *50*, 230. [8b] R. van Eldik, T. Asano, W. J. le Noble, *Chem. Rev.* **1989**, *89*, 549. [8c] A. Drljaca, C. D. Hubbard, R. van Eldik, T. Asano, M. V. Basilevsky, W. J. Noble, *Chem. Rev.* **1998**, *98*, 2167.

[9] [9a] F. Franks (Ed.), *Water*, Plenum Press, London, New York, **1975**, vols. 2, 4. [9b] M. H. Abraham, J. Liszi, E. Papp, *J. Chem. Soc., Faraday Trans. 1* **1982**, *78*, 197.

[10] D. A. Baldwin, E. A. Betterton, J. M. Pratt, *J. Chem. Soc., Dalton Trans.* **1983**, 225.

[11] [11a] M. Koyanagi, Y. Kanda, *Spectrochim. Acta* **1964**, *20*, 993. [11b] G. Durocher, C. Sandorfy, *J. Mol. Spectr.* **1966**, *20*, 410. [11c] M. Koyanagi, *J. Mol. Spectr.* **1968**, *25*, 273.

[12] [12a] A. J. Thomson, *J. Am. Chem. Soc.* **1969**, *91*, 2780. [12b] A. Vogler, R. Hirschmann, H. Otto, H. Kunkely, *Ber. Bunsen-Ges. Phys. Chem.* **1976**, *80*, 420.

[13] [13a] B. B. Hasinoff, *Can. J. Chem.* **1974**, *52*, 910. [13b] G. Stochel, R. van Eldik, H. Kunkely, A. Vogler, *Inorg. Chem.* **1989**, *28*, 4314. [13c] G. Stochel, R. van Eldik, *Inorg. Chem.* **1990**, *29*, 2075. [13d] F. F. Prinsloo, E. L. J. Breet, R. van Eldik, *J. Chem. Soc., Dalton Trans.* **1995**, 685.

[14] R. van Eldik, W. Gaede, S. Wieland, J. Kraft, M. Spitzer, D. A. Palmer, *Rev. Sci. Instrum.* **1993**, *64*, 1355.

[15] X. Zou, D. R. Evans, K. L. Brown, *Inorg. Chem.* **1995**, *34*, 1634.

[16] [16a] Y. Murakami, Y. Hisaeda, T. Ohno, *Bull. Chem. Soc. Jpn.* **1984**, *57*, 2091. [16b] A. J. Markwell, J. M. Pratt, M. S. Shaikjee, J. G. Toerien, *J. Chem. Soc., Dalton Trans.* **1987**, 1349. [16c] L. Werthemann, Abhandlung, Eidgnössische Technische Hochschule (ETH), Zürich, **1968**.

[17] A. W. Johnson, L. Mervyn, N. Shaw, E. L. Smith, *J. Chem. Soc.* **1963**, 4146.

Received August 31, 2001
[I01337]

Synthesis and Structure of Novel Complexes of Gallium

Eva Leiner,[a] Oliver Hampe,[b] and Manfred Scheer*[a]

Dedicated to Prof. G. Schmid on the occasion of his 60th birthday

Keywords: Metathesis / Iron / Gallium / Cobalt / Cyclopentadienyl ligands

$[Cp^*GaCl_2]$ ($Cp^* = \eta^1$-C_5Me_5) reacts with $K[Co(CO)_4]$ with elimination of KCp^* and KCl to form the novel ionic complexes $[K(toluene)_2][Ga\{Co_2(CO)_6(\mu\text{-}CO)\}_2]$ (**1**) and $K[GaCl\{Co_2(CO)_6(\mu\text{-}CO)\}\{Co(CO)_4\}]$ (**2**), where the gallium atoms possess the coordination number four. The reaction of $[\{Co(CO)_4\}_2GaCl(THF)]$ with $LiCp^*$ leads to the ionic product $[Li(THF)][Ga\{Co_2(CO)_6(\mu\text{-}CO)\}_2]$ (**3**). The $[Ga\{Co_2(CO)_6(\mu\text{-}CO)\}_2]^-$ anions of **1** and **3** represent the first homoleptic spirocyclic coordination mode of gallium. The reaction of $GaCl_3$ with $Na_2[Fe(CO)_4]$ leads to the ionic compound $[Na(OEt_2)_2][Fe(CO)_4(GaCl_3)_2]$ (**4**). Complexes **1**, **2**, **3** and **4** were characterised by X-ray structure analysis and IR spectroscopy. Additionally, ESI mass spectra of **1** were recorded at different cone voltages, where the molecular ion peak of the anion $[Ga\{Co_2(CO)_6(\mu\text{-}CO)\}_2]^-$ as well as the peaks resulting from sequential loss of CO ligands until the formation of the naked $[Co_4Ga]^-$ cluster are observed. The ionic complexes **1**, **2**, **3** and **4** form polymeric networks through coordination of their cations. In **2** a three-dimensional polymeric network is formed by coordination of the Co_3Ga units and their K counterions, whereas in **1** the K ions are additionally coordinated by toluene molecules to form dimeric macrocyclic motifs by coordination of two of the anionic Co_4Ga units. In **3** a zigzag chain is formed by coordination of the Co_4Ga units through their Li cations. In the crystal packing of complex **4** the $FeGa_2$ moieties form zigzag chains, coordinating through their Na counterions.

Introduction

Metathesis reactions of group 13 element halides with carbonyl metalates represent a useful method to synthesise compounds with covalent transition metal-main group bonds. The majority of complexes thereby obtained possesses coordination numbers (CN) of three and four with exclusively trigonal planar and tetrahedral coordination modes, respectively. Depending on the reaction conditions competing reactions occur, for example the formation of anionic complexes of CN 4.[1] Among complexes of CN 4 of the general type $E(ML_n)_4^-$ (E = Al, Ga, In, Tl; ML_n = transition metal fragment), which can alternatively be regarded as Lewis base adducts of the type $E(ML_n)_3$, the coordination modes **A**, **B** and **C** are possible.

For complexes of type **A**, examples exist for E = In and Tl, such as $[In\{Co(CO)_4\}_4]^-$,[2] whereas for **B** the indium complexes $[In\{Fe_2(CO)_8\}_2]^-$,[3] $[\{(\mu\text{-}H)Mn_3(CO)_{12}\}_2(\mu_4\text{-}In)]$[4] and $[\{Re(CO)_3(\mu\text{-}I)_2Re(CO)_3\}In\{Re(CO)_4(\mu\text{-}I)Re(CO)_4\}]$[5] are the only known representatives. For gallium only $[Re_3(CO)_9(Ph_3P)_3(\mu\text{-}Cl)_3(\mu_3\text{-}\{GaRe(CO)_4(Ph_3P)\})]$ and the Re_4Ga_4 cluster $[Re_4(CO)_{12}\{\mu_3\text{-}\{GaRe(CO)_5\}_4]$[6] are known for type **C**; examples of the coordination modes **A** and **B** are as yet unknown for gallium. We report herein on the synthesis of the first examples for gallium with the coordination mode **B**.

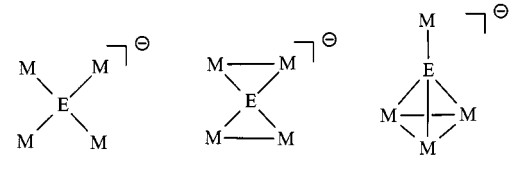

Results and Discussion

The reaction of Cp^*GaCl_2 ($Cp^* = \eta^1$-C_5Me_5) with $K[Co(CO)_4]$ in Et_2O or THF results in the formation of the ionic heteronuclear clusters $[K(toluene)_2][Ga\{Co_2(CO)_6(\mu\text{-}CO)\}_2]$ (**1**) and $K[GaCl\{Co_2(CO)_6\}(\mu\text{-}CO)\}\{Co(CO)_4\}]$ (**2**), respectively, in high yields [Equation (1) and (2)]. Although the workup of **2** was carried out by extraction with toluene, as was the case for **1**, no solvated toluene was found in the crystal lattice of **2**. The results show that besides the KCl elimination, Cp* removal also occurs as a competing reac-

[a] Institut für Anorganische Chemie der Universität Karlsruhe, 76128 Karlsruhe, Germany
Fax: (internat.) +49-(0)721/608-7021
E-mail: mascheer@chemie.uni-karlsruhe.de
[b] Institut für Nanotechnologie des Forschungszentrums Karlsruhe
76021 Karlsruhe, Germany
Fax: (internat.) +49-(0)7247/82-6416

 © WILEY-VCH Verlag GmbH, 69451 Weinheim, Germany, 2002 1434−1948/02/0303−0584 $ 17.50+.50/0 *Eur. J. Inorg. Chem.* **2002**, 584−590

tion. Furthermore, the reaction in donor solvents seems to favour the formation of ionic complexes. Complex **2** can be regarded as a formal precursor molecule of **1**, from which Cl substitution by $Co(CO)_4^-$ leads to the formation of the spirocyclic complex **2**.

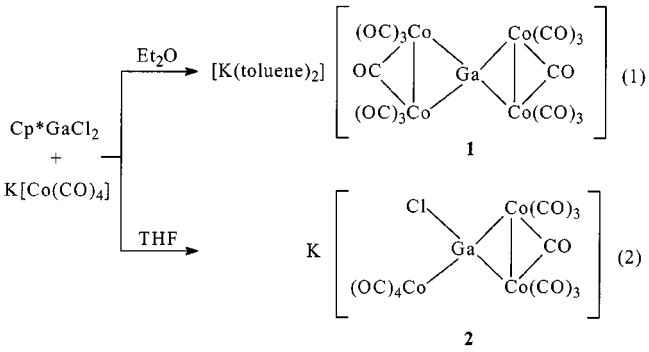

Surprisingly, we found that the reaction of $[\{Co(CO)_4\}_2GaCl(THF)]$ with LiCp* in toluene at −78 °C leads to the ionic product $[Li(THF)][Ga\{Co_2(CO)_6(\mu\text{-}CO)\}_2]$ **3** [Equation (3)].

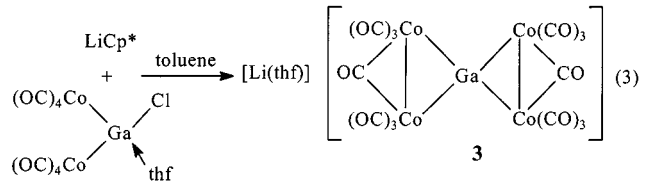

Complexes **1** and **3** represent the first examples of the coordination mode **B** where the Ga atom is additionally homoleptically coordinated by metal atoms.

Complexes **1** and **3** are orange and **2** red-brown crystalline compounds, which are readily soluble in toluene, THF and CH_2Cl_2. In their IR spectra, CO stretching frequencies for terminal and bridging CO ligands are observed.

The ionic complex **1** crystallises in the triclinic space group $P\bar{1}$ with two independent molecules (A and B) in the asymmetric unit, which reveal similar structural features.[7] Each of the K counterions possesses two coordinated toluene molecules. Figure 1 shows the molecular structure of the anion $[Ga\{Co_2(CO)_6(\mu\text{-}CO)\}_2]^-$ of one of the independent molecules (molecule A) of **1**. The gallium atom is bound side-on to two $[\{Co(CO)_3\}_2\{\mu\text{-}CO\}]$ groups to form a spirocyclic compound containing two Co−Ga−Co three membered rings. These rings are bent by 82.55(4)° (molecule A) and 87.58(4)° (molecule B). Alternatively, the structure of **1** can be described as a distorted Co_4 tetrahedron centred by a Ga atom.

The Co−Co bond lengths in both independent molecules [2.560(1) to 2.588(1) Å] are similar to the Co−Co bond length in $Co_2(CO)_8$ [2.528(1)−2.530(1) Å];[8] the Co−Ga bonds [2.395(1)−2.454(1) Å] are in the range of known Co−Ga bond lengths as in, for example, $[(CO)_3Co\{\mu\text{-}(\eta^5\text{-}Cp^*Ga)\}_2Co(CO)_3]$ [2.3784(5)−2.3959(5) Å].[9] In addition to the molecular structure of anion **1** described above, the location of the K atom and its coordinated toluene molecules are depicted in the crystal lattice in Figure 2. Both independent $GaCo_4$ units of **1** are bridged through their K counterions to form a dimer in which each K atom is coordinated by four CO ligands (a terminal and a bridging CO moiety of each anion of **1**) and two molecules of toluene. The macrocycle thus formed contains eight heavier atoms (gallium, cobalt and potassium), and two such macrocycles form the unit cell. The formation of the macrocyclic dimer of **1** in the crystal leads to the small structural

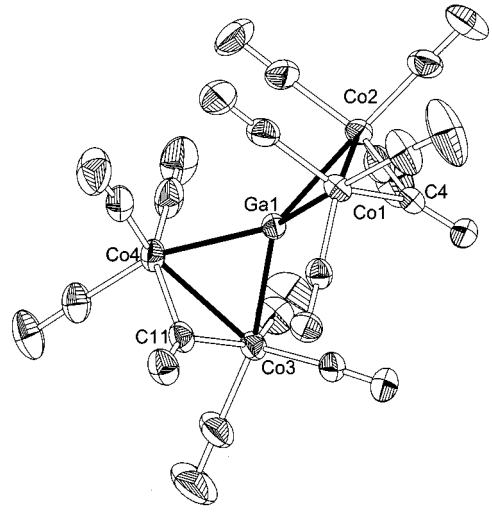

Figure 1. Molecular structure of the $[Ga\{Co_2(CO)_6(\mu\text{-}CO)\}_2]^-$ anion of one of the independent molecules (molecule A) of **1** in the crystal (showing 30% probability ellipsoids); selected bond lengths [Å] and angles [°]: Ga1−Co1 2.442(1), Ga1−Co2 2.397(1), Ga1−Co3 2.396(1), Ga1−Co4 2.451(1), Co1−Co2 2.588(1), Co3−Co4 2.562(1), Co1−C4 1.907(4), Co2−C4 1.925(4), Co3−C11 1.925(4), Co4−C11 1.904(4); Co1−Ga1−Co2 64.66(3), Co3−Ga1−Co4 63.78(3)

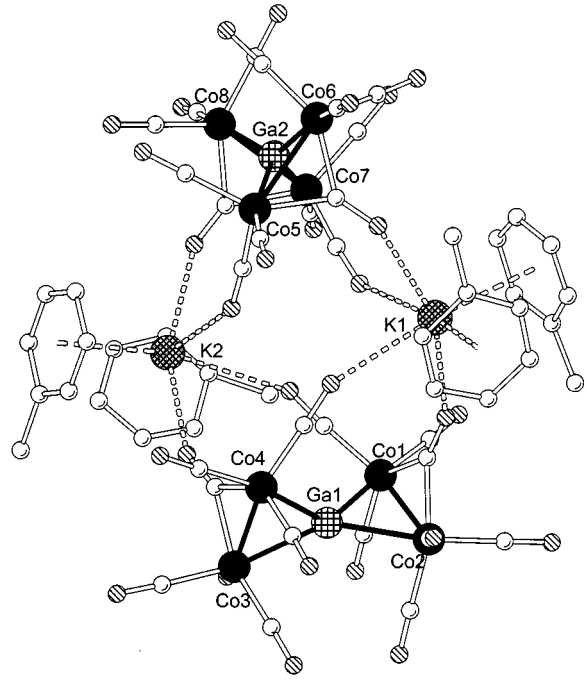

Figure 2. Formation of macrocyclic dimers in the crystal lattice of **1** (H atoms of the toluene molecules are omitted for clarity)

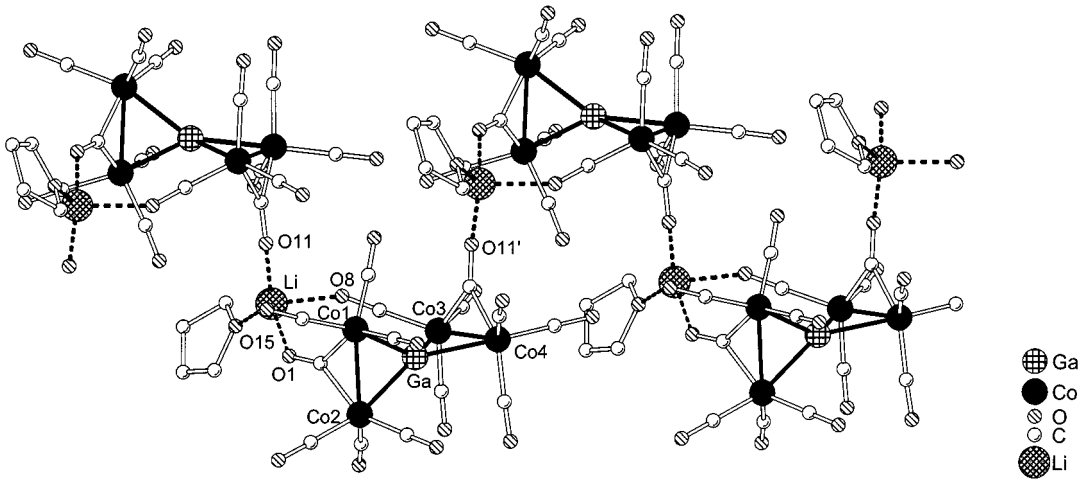

Figure 3. Structure of **3** in the crystal lattice; selected bond lengths [Å] (H atoms of the toluene molecules are omitted for clarity): Ga−Co1 2.439(1), Ga−Co2 2.398(1), Ga−Co3 2.453(1), Ga−Co4 2.398(1), Co1−Co2 2.557(1), Co3−Co4 2.576(1), Li−O1 1.946(13), Li−O8 2.17(2), Li−O11 1.904(13), Li−O15 1.807(13)

differences between the independent molecules of **1**. Thus, the Co−Ga−Co bond angles in molecule B are very similar [63.72(4)° and 63.96°], whereas those in molecule A differ slightly more [64.66(3)° and 63.78(3)°].

Complex **3** crystallises as one enantiomer in the orthorhombic space group $P2_12_12_1$, with four formula units in the asymmetric unit cell. The molecular structure of the anion of **3** is similar to the structure of the anion of **1** (Figure 1), where similar bond lengths and angles are observed. In contrast to **1**, **3** possesses Li counterions, which are coordinated by THF molecules. A view of the packing of **3** in the crystal lattice is shown in Figure 3, and is clearly different to that of **1**. Each of the $GaCo_4$ moieties in **3** is connected by two Li cations to the next molecular units establishing an overall zigzag chain forming a chiral helix. The Li counterions are fourfold coordinated by three O atoms of the CO ligands and the O atom of a THF molecule.

The existence of the $[Ga\{Co_2(CO)_6(\mu\text{-}CO)\}_2]^-$ anions of **1** and **3** in solution was further proved by Electrospray-Ionisation (ESI) mass spectrometry using a high resolution FT-ICR mass spectrometer.[10] Figure 4a shows the observed molecular ion peak of the anion $[Ga\{Co_2(CO)_6(\mu\text{-}CO)\}_2]^-$ of **1** (cone voltage = 20 V), which, as can clearly be seen from Figure 4b, is in good agreement with the simulated mass distribution at m/z = 696 $[^{69}Ga(^{12}CO)_{14}Co_4]$. The mass spectrum of the cation of **1** shows only the peak for the K^+ cation. In further experiments the fragmentation behaviour of the anion of **1** at continuously increasing cone voltages was investigated. A stepwise elimination of CO was found with a steadily increasing voltage, and all the fragments up to the naked $[Co_4Ga]^-$ cluster (cone voltage of 240 V) were detected. This result shows the exceptional stability of the $GaCo_4$ cluster core.

The ionic complex **2** crystallises in the monoclinic space group $P2_1/n$ with four molecules in the unit cell. The molecular structure of the $[GaCl\{Co_2(CO)_6\}(\mu\text{-}CO)\}\{Co(CO)_4\}]^-$ anion of **2** is depicted in Figure 5. The gallium atom is in a distorted tetrahedral geometry surrounded by one Cl and three Co atoms. The metal-metal bond between the Co1 and Co2 atoms is bridged by a CO ligand. The Co−Co [2.595(1) Å] and the Co−Ga bond lengths [2.419(1), 2.441(1) and 2.448(1) Å] of **2** are similar to those observed in **1** [2.396(1)−2.451(1) Å]. The angle between the planes formed by the atoms Co1−Ga−Co2 and Cl−Ga−Co3 is 83.96(3)°. In contrast to the macrocyclic

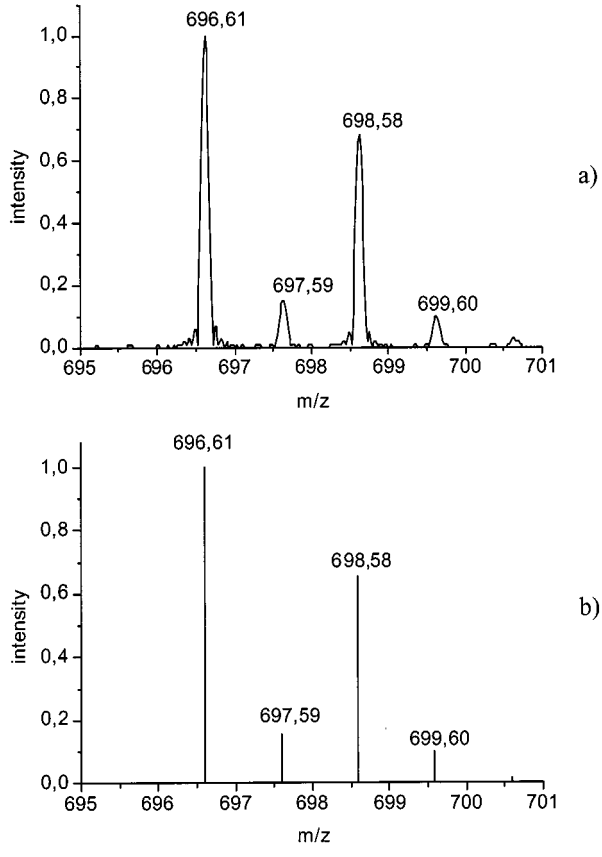

Figure 4. ESI mass spectrum of **1**: a) experimental at a cone voltage of 20 V; b) calculated

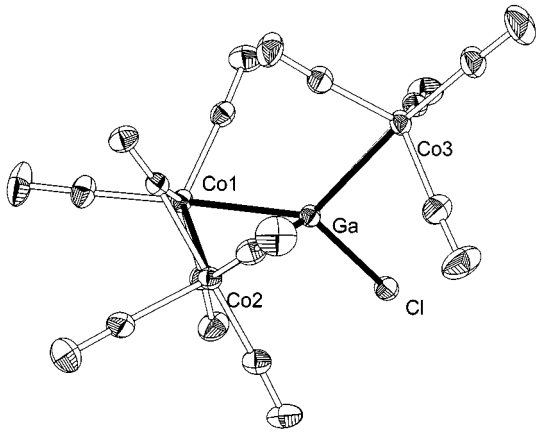

Figure 5. Molecular structure of the $[GaCl\{Co_2(CO)_6\}(\mu\text{-}CO)\}\{Co(CO)_4\}]^-$ anion of **2** in the crystal (showing 30% probability ellipsoids); selected bond lengths [Å] and angles [°]: Ga−Co1 2.441(1), Ga−Co2 2.419(1), Ga−Co3 2.448(1), Co1−Co2 2.595(1), Ga−Cl 2.304(1); Co1−Ga−Co2 64.54(2), Cl−Ga−Co2 118.66(3), Cl−Ga−Co1 112.34(3), Cl−Ga−Co3 102.30(3), Co2−Ga−Co3 125.71(2), Co1−Ga−Co3 131.00(3)

dimeric structure in the crystal lattice of **1** and the zigzag-chain of **3**, the $GaCo_3$ clusters of **2** coordinate to the unsolvated K atoms to form a three-dimensional network. A view of a layer along the crystallographic *c* axis of the crystal packing structure of **2** is depicted in Figure 6. The $GaCo_3$ units of **2** are similarly oriented along the crystallographic *a* axis, whereas they are alternately twisted along the *b* axis. Each of the K atoms is ninefold coordinated by seven O atoms of the CO ligands (terminal as well bridging CO) and by two Cl atoms. The K atoms along the *a* axis are oriented above and below the presented plane, and each are coordinated by five $GaCo_3$ moieties, three of which are shown in Figure 6.

The reaction of $GaCl_3$ with $Na_2[Fe(CO)_4]$ in Et_2O at 0 °C leads to the ionic addition product $[Na(OEt_2)]_2[Fe(CO)_4(GaCl_3)_2]$ **4** [Equation (4)], which was isolated as colourless crystals. Complex **4** is readily soluble in donor solvents like Et_2O and THF. In the IR spectrum of **4**, only bands for terminal CO groups are found.

$$2\ GaCl_3 + Na_2[Fe(CO)_4] \xrightarrow{Et_2O} [Na(OEt)]_2\left[\begin{array}{c} Cl_3Ga \quad GaCl_3 \\ \diagdown \quad \diagup \\ Fe(CO)_4 \end{array}\right] \quad (4)$$

4

Complex **4** crystallises in the monoclinic space group $P2_1/c$ with four formulae units in the asymmetric unit cell. The molecular structure of the anion of **4** is depicted in Figure 7. The central Fe atom is octahedrally surrounded by four CO ligands and two *cis*-oriented $GaCl_3$ moieties. The axial carbonyl ligands of the $Fe(CO)_4$ unit are unexpectedly strongly bent towards the $GaCl_3$ groups, probably due to the Lewis acid character of the group 13 atoms. The Ga−Fe bond lengths [2.409(1) and 2.411(1) Å, respectively] are slightly longer than in $[(CO)_4FeGaCl_2(tmeda)]$ [2.338(1) Å].[11]

A view of the packing of **4** in the crystal lattice is shown in Figure 8. Each of the $GaCl_3$ moieties in **4** is connected via two Na cations to the next molecular unit establishing

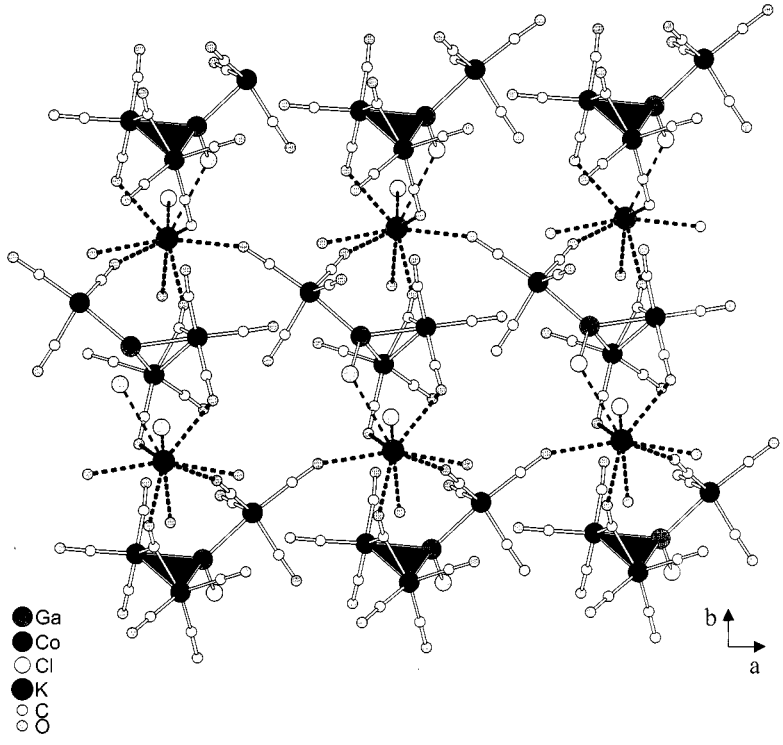

Figure 6. View along the crystallographic *c* axis in the crystal lattice of **2** (the Co_2Ga planes are marked); the coordinating O and Cl atoms of the K atoms above and below the *a*,*b* plane are depicted without their connecting cluster units for clarity

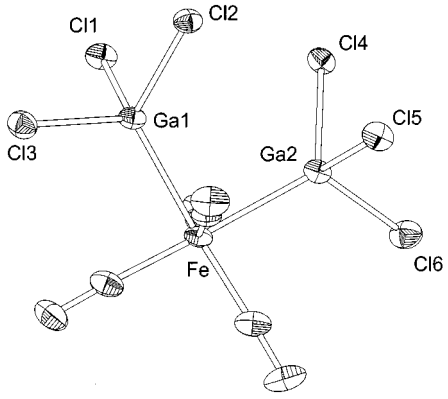

Figure 7. Molecular structure of the $[Fe(CO)_4(GaCl_3)_2]^{2-}$ anion of **4** in the crystal (showing 30% probability ellipsoids); selected bond lengths [Å] and angles [°]: Ga1−Fe 2.409(1), Ga2−Fe 2.411(1); Ga1−Fe−Ga2 90.74(3)

out identically, the coordination of the toluene molecules in **1** seems to be the determining factor for the formation of macrocycle **1**.

Experimental Section

General Techniques: All manipulations were performed under an atmosphere of dry N_2 using standard Schlenk techniques. All solvents were dried by common methods and freshly distilled prior to use. Gallium trichloride was obtained commercially and used without further purification. The starting materials Cp^*GaCl_2 [12] and the compounds $K[Co(CO)_4]$[13] and $Na_2[Fe(CO)_4]$[14] were prepared according to literature methods. The ESI mass spectra were recorded on a Bruker APEX II Fourier-Transform-ICR mass spectrometer and the IR spectra on a Bruker IFS 28.

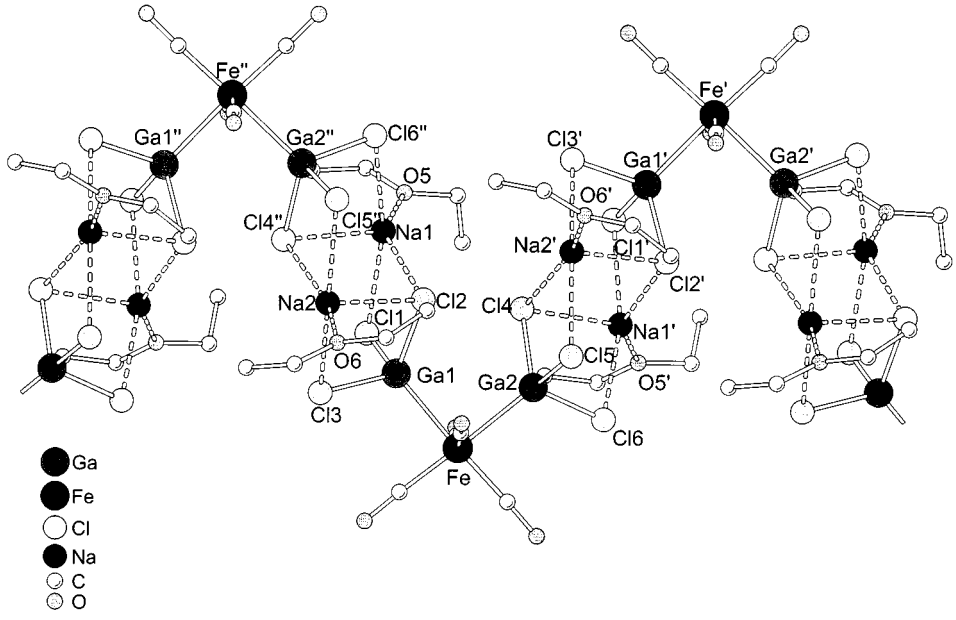

Figure 8. Structure of **4** in the crystal lattice; selected bond lengths [Å] and angles [°] (H atoms of the toluene molecules are omitted for clarity): Na1···Cl1 2.789(2), Na1···Cl2 2.818(2), Na1···Cl4 2.883(2), Na1···Cl6 2.799(2), Na2···Cl2 2.853(2), Na2···Cl3 2.779(2), Na2···Cl4 2.877(2); Cl5···Na2···C12 95.19(6), Cl3···Na2···Cl4 95.19(6).

an overall zigzag chain. The Na ions are fivefold coordinated by four Cl atoms and an O atom of the coordinated ether molecule.

Conclusions

We have shown that the reaction of Cp^*GaCl_2 and $GaCl_3$ with transition metal metalates leads to the formation of ionic compounds forming polymeric structures in the crystal lattice. Whereas the solvation of the K counterion in **1** by toluene leads to a macrocyclic dimer, the Li counterion in **3**, due to its lower coordination number, leads to a chiral zigzag chain-like structure. The absence of solvent molecules in **2** leads to the formation of a 3D polymeric network. The degree of aggregation is strongly determined by the coordination of the counterions and the coordinated solvent molecules. Since the workup of **1** and **2** was carried

$[K(toluene)_2][Ga\{Co_2(CO)_6(\mu\text{-}CO)\}_2]$ (1): A solution of Cp^*GaCl_2 (0.138 g, 0.5 mmol) in Et_2O (10 mL) was slowly added at −78 °C to a solution of $K[Co(CO)_4]$ (0.231 g, 1.1 mmol) in 10 mL Et_2O. The reaction mixture was stirred for 14 h and was then allowed to warm to room temperature. The resulting yellow solution was filtered through silica and all of the solvent was removed in vacuum. The yellow residue was extracted with 20 mL toluene and the solution was reduced to 2 mL. At −30 °C orange crystals of $[K(toluene)_2][Ga\{Co_2(CO)_6(\mu\text{-}CO)\}_2]$ (**1**) were formed (244 mg, 70%). IR (KBr): $\tilde{\nu}$ = 1968(s) cm^{-1}, 1764(m) ν(CO). MS (ESI): *m*/*z* = 696 $[M^-]$.

$K[GaCl\{Co_2(CO)_6\}(\mu\text{-}CO)\}\{Co(CO)_4\}]$ (2): A solution of Cp^*GaCl_2 (0.138 g, 0.5 mmol) in 15 mL THF was slowly added at −78 °C to a solution of $K[Co(CO)_4]$ (0.231 g, 1.1 mmol) in 15 mL THF. The solution was stirred for 14 h and was then allowed to warm to room temperature. Et_2O (2 mL) was added, and after two hours stirring the colour of the solution turned to red-brown and a white precipitate appeared. All volatiles were removed in vacuum, and

Table 1. Crystallographic data for **1**−**4**

	1·2C_7H_8	**2**	**3**·OC_4H_8	**4**·2OC_4H_{10}
Empirical formula	$C_{28}H_{16}Co_4GaKO_{14}$	$C_{11}ClCo_3GaKO_{11}$	$C_{18}H_8Co_4GaLiO_{15}$	$C_{12}H_{20}Cl_6FeGa_2Na_2O_6$
M_r	920.95	629.17	776.62	714.25
T [K]	210(2)	200(1)	200(1)	190(1)
Crystal size	0.40 × 0.24 × 0.06	0.14 × 0.06 × 0.02	0.20 × 0.10 × 0.04	0.50 × 0.20 × 0.10
Space group	$P\bar{1}$	$P2_1/n$	$P2_12_12_1$	$P2_1/c$
Crystal system	triclinic	monoclinic	orthorhombic	monoclinic
a [Å]	14.328(3)	9.777(2)	11.558(2)	13.427(3)
b [Å]	14.533(3)	15.587(3)	12.415(3)	16.778(3)
c [Å]	20.020(4)	13.594(3)	18.681(4)	12.675(3)
α [°]	101.85(3)	90	90	90
β [°]	94.79(3)	102.32(3)	90	108.61(3)
γ [°]	116.93(3)	90	90	90
V [A^{-3}]	3562.5(12)	2024.0(7)	2680.5(9)	2706.2(9)
Z	4	4	4	4
d_c [g cm^{-3}]	1.717	2.065	1.924	1.753
μ_c [mm^{-1}]	1.431[c]	4.119[d]	1.154[c]	3.154[d]
2θ range [°]	3.20 ≤ 2θ ≤ 43.22	4.02 ≤ 2θ ≤ 51.94	3.10 ≤ 2θ ≤ 41.67	4.56 ≤ 2θ ≤ 51.80
hkl range	−18 ≤ h ≤ 18, −17 ≤ k ≤ 19, −26 ≤ l ≤ 26	−10 ≤ h ≤ 11, −14 ≤ k ≤ 19, −16 ≤ l ≤ 16	−14 ≤ h ≤ 14, −15 ≤ k ≤ 15, −23 ≤ l ≤ 21	−16 ≤ h ≤ 16, −19 ≤ k ≤ 20, −14 ≤ l ≤ 15
Data/restraints/parameters	15978/1/864	3799/0/253	5691/0/352	5142/0/266
No. of unique data	15978 (R_{int} = 0.0383)	3799 (R_{int} = 0.0387)	5691 (R_{int} = 0.0592)	5142 (R_{int} = 0.0779)
Independent reflections [$I > 2\sigma(I)$]	11045	2920	4553	3655
Goodness-of fit on F^2	1.006	0.913	1.013	0.901
R_1[a], wR_2[b] [$I > 2\sigma(I)$][a]	0.0411, 0.0965	0.0274, 0.0610	0.0377, 0.0727	0.0346, 0.0748
R_1[a], wR_2[b] [all data]	0.0687, 0.1081	0.0416, 0.0642	0.0574, 0.0790	0.0549, 0.0799
Largest diff. peak/hole [e·$Å^{-3}$]	0.806, −0.408	0.340, −0.745	0.447, −0.392	0.428, −0.727

[a] $R = \Sigma||F_0| - |F_c||/\Sigma|F_0|$. [b] $wR_2 = [\Sigma\omega(F_0^2 - F_c^2)^2]/[\Sigma(F_0^2)^2]^{1/2}$. [c] μ(Ag-$K_\alpha$). [d] μ(Mo-$K_\alpha$).

the oily residue was extracted with about 50 mL toluene. After filtration over silica gel, the volume of the solution was reduced to 2 mL and at −20 °C red-brown crystals of K[GaCl{$Co_2(CO)_6$}(μ-CO)}{$Co(CO)_4$}] (**2**) were obtained (177 mg, 60%). IR (KBr): $\tilde{\nu}$ = 2062(s) cm^{-1}, 2039(s), 1987(s), 1969(s), 1765(m) ν(CO).

[Li(THF)][Ga{$Co_2(CO)_6$(μ-CO)}$_2$] (3): A solution of [{$Co(CO)_4$}$_2$GaCl(THF)] (0.154 g, 0.3 mmol) in 5 mL toluene was slowly added at −78 °C to a slurry of LiCp* (0.063 g, 0.3 mmol) in 5 mL toluene. The reaction mixture was allowed to warm to room temperature and stirred for three days. After filtration over silica gel, the volume of the orange solution was reduced to 2 mL and at −30 °C orange crystals of [Li(THF)][Ga{$Co_2(CO)_6$(μ-CO)}$_2$] (**3**) were obtained (0.167 g, 70%). IR (KBr): $\tilde{\nu}$ = 1968(s) cm^{-1}, 1764(m) ν(CO). MS (ESI): m/z = 696 [M^-].

[Na(OEt$_2$)]$_2$[Fe(CO)$_4$(GaCl$_3$)$_2$] (4): A solution of $GaCl_3$ (0.088 g, 0.5 mmol) in 5 mL Et_2O at 0 °C was slowly added to a suspension of $Na_2[Fe(CO)_4]$ (0.216 g, 1 mmol) in 20 mL Et_2O. The colour changed to yellow, and after stirring for 3 h at room temperature, the colour changed again to yellow-red. Addition of *n*-hexane led to colourless crystals of [Na(OEt$_2$)]$_2$[Fe(CO)$_4$(GaCl$_3$)$_2$] (**4**) (126 mg, 70%, based on $GaCl_3$). IR (KBr): 2082(s, br) cm^{-1}, 2042(s), 2035(s), 2025(s), 2000(m), 1978(s, br) ν(CO).

X-ray Structure Determination and Details of Refinement. Data were collected on a STOE IPDS area-detector diffractometer using Ag-K_α radiation (λ = 0.56087 Å) for complex **1** and Mo-K_α radiation (λ = 0.71069 Å) for **2**, **3** and **4**. Machine parameters, crystal data and data collection parameters are summarised in Table 1. The structures were solved by direct methods using SHELXS-86,[15a] and refined by full-matrix least-squares methods on F^2 in SHELXL-97[15b] with anisotropic displacement for non-H atoms (except for atom C50 of **1**, due to the limited crystal quality of this complex). Hydrogen atoms were placed in idealised positions and refined isotropically according to the riding model. The Flack-parameter of the chiral space group of **3** comes to −0.01(3).

Crystallographic data (excluding structure factors) for the structures reported in this paper have been deposited with the Cambridge Crystallographic Data Centre as supplementary publication nos. CCDC-170990 (**1**), -170991 (**2**), -170992 (**3**) and -170993 (**4**). Copies of the data can be obtained free of charge on application to CCDC, 12 Union Road, Cambridge CB2 1EZ, UK [Fax: (internat.) +44-1223/336-033; E-mail: deposit@ccdc.cam.ac.uk].

Acknowledgments

The authors thank the Deutsche Forschungsgemeinschaft and the Fonds der Chemischen Industrie for comprehensive financial support. E. Leiner is grateful to the Fonds der Chemischen Industrie for a PhD fellowship.

[1] R. A. Fischer, J. Weiß, *Angew. Chem.* **1999**, *111*, 3002−3022; *Angew. Chem. Int. Ed.* **1999**, *38*, 2831−2850.
[2] W. R. Robinson, D. P. Schussler, *J. Organomet. Chem.* **1971**, *30*, C5−C7.
[3] C. C. Chieh, G. Kong, H. Cho, B. R. Whittlesey, *Inorg. Chem.* **1993**, *32*, 2705−2710.

[4] W. Schatz, H. P. Neumann, B. Nuber, B. Kanellakopulos, M. L. Ziegler, *Chem. Ber.* **1991**, *12*, 453−463.
[5] H. J. Haupt, U. Floerke, *Acta Crystallogr., Sect. C* **1989**, *45*, 1718−1721.
[6] H. Haupt, P. Balsaa, B. Schwab, *Z. Anorg. Allg. Chem.* **1985**, *521*, 15−22.
[7] Complex **1** was independently obtained in the reaction of GaBr with $K[Co(CO)_4]$ and crystallises with THF as macrocycles containing six $GaCo_4$ moieties connected via K atoms: A. Donchev, PhD thesis, University of Karlsruhe (TH), **2000**.
[8] P. C. Leung, P. Coppens, *Acta Crystallogr., Sect. B* **1983**, *39*, 535−542.
[9] P. Jutzi, B. Neumann, G. Reumann, H.-G. Stammler, *Organometallics* **1998**, *17*, 1305−1314.
[10] Fourier-Transform-Ion-Cyclotron-Resonance (FT-ICR) mass spectrometry: A. G. Marshall, P. B. Großhans, *Anal. Chem.* **1991**, *63*, 215A−229A.
[11] G. Linti, G. Li, H. Pritzkow, *J. Organomet. Chem.* **2001**, *626*, 82−91.
[12] O. T. Beachley Jr., R. B. Hallock, H. M. Zhang, J. L. Atwood, *Organometallics* **1985**, *4*, 1675−1680.
[13] J. E. Ellis, E. A. Flom, *J. Organomet. Chem.* **1975**, *99*, 263−268.
[14] H. Strong, P. J. Krusic, J. San Filippo Jr., *Inorg. Synth.* **1986**, *24*, 157−161.
[15] [15a] G. M. Sheldrick, *SHELXS-86*, University of Göttingen, **1986**. [15b] G. M. Sheldrick, *SHELXL-97*, University of Göttingen, **1997**.

Received September 20, 2001
[I01371]

Synthesis, Structure, and Thermoelectric Properties of the New Antimonide Sulfide $MoSb_2S$

Chi-Shen Lee[a] and Holger Kleinke*[a]

Keywords: Antimony / Sulfur / Materials science / Chalcogens / Molybdenum

The structure of a new ternary compound, $MoSb_2S$, was identified by single-crystal X-ray diffraction. The title compound was synthesized by heating the elements in stoichiometric ratios in sealed silica tubes at 600–800 °C using small amounts of I_2 as a mineralizator. The compound crystallizes in a new structure type in the monoclinic space group *C*2/*m* [*a* = 36.157(3) Å, *b* = 6.3823(5) Å, *c* = 6.5379(5) Å, β = 95.093(2)°, *Z* = 16, *R*1/*wR*2 = 0.035/0.059]. Its crystal structure contains CdI_2-related layers (MoSbS) and Sb columns, namely a zigzag (*cis-trans*) chain and an equidistant ladder, both of which are located between the MoSbS layers. The results of thermoelectric measurements and electronic structure calculations indicate metallic properties.

Introduction

Thermoelectric materials exhibit a unique property, namely the conversion of heat into electrical energy and vice versa. Such materials, which are usually small-gap semiconductors, have been utilized in applications like refrigerators and power generators. Commercial materials include semiconductors based on Bi_2Te_3, $Si_{0.7}Ge_{0.3}$, and PbTe.[1] Extensive research activities were carried out with investigations of new thermoelectric materials, including the filled skutterudites LnM_4Sb_{12} (Ln = lanthanoid; M = Fe, Co, Ni, ...) and most recently the ternary telluride $CsBi_4Te_6$.[2–5] Good thermoelectric materials have a high *figure-of-merit* that combines a high Seebeck coefficient, low thermal conductivity, and high electrical conductivity. To approach the goal of preparing new thermoelectrics, heavy main group metalloid elements such as antimony, selenium or tellurium may be used as the common element.

Our group has focused on the syntheses and characterizations of new materials in the ternary M–Sb–Q systems (M = transition metal atoms; Q = S, Se, Te). During the course of this study, a new ternary compound, $MoSb_2Se$, was identified.[6] The structure of $MoSb_2Se$ can be treated as the combination of a CdI_2-related layer structure (MoSbSe layer) with interstitial Sb chains binding the Sb atoms of MoSbSe layers. A similar structure is realized in the Mo–Sb–S system; the structure of $MoSb_2S$ exhibits topologically equivalent MoSbS layers, yet significant differences in the Sb atom substructure. With this contribution, the synthesis, characterization and electronic structure studies of $MoSb_2S$ are presented.

[a] Department of Chemistry, University of Waterloo
Waterloo, ON, N2L 3G1, Canada,
Fax: (internat.) + 1-519/746-0435
E-mail: kleinke@uwaterloo.ca

Results and Discussion

Structure

$MoSb_2S$ crystallizes in the space group *C*2/*m*, with six independent positions for Sb, three for Mo, and three for S atoms. The perspective view of the $MoSb_2S$ crystal structure along [010] is illustrated in Figure 1. In general, the structure of $MoSb_2S$ contains a CdI_2-related layer of the composition MoSbS and two types of columnar Sb atom substructures, which bind the Sb atoms of the two surrounding MoSbS layers. Pseudo-octahedral voids remain present in the interlayer Sb atom substructure.

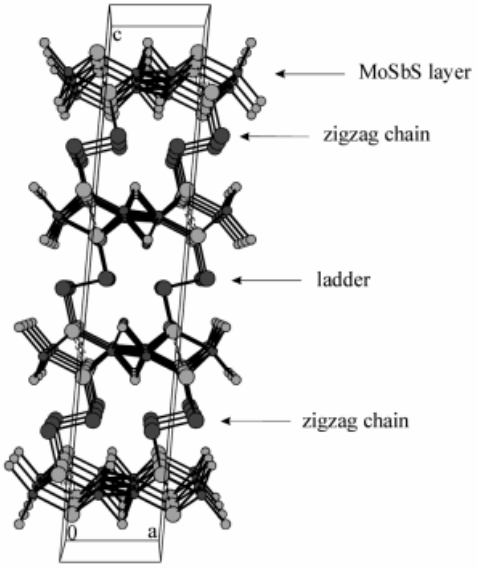

Figure 1. The three-dimensional structure of $MoSb_2S$ projected along [010]; dark circles: Mo; small gray circles: S; large circles: Sb, with dark circles representing interlayer and bright circles intralayer atoms

The Mo atoms are sandwiched between the approximately closed packed Sb and S atom layers, forming MoSbS layers that are reminiscent of the $MoTe_2$ layers of the monoclinic β-$MoTe_2$ [7] structure. Each Mo is coordinated by three Sb and three S atoms in a distorted octahedral coordination. The averaged Mo−Sb and Mo−S distances are 2.83 and 2.38 Å, respectively. This may be compared to the corresponding interatomic distances in Mo_3Sb_7 (d_{Mo-Sb} = 2.77 and 2.85 Å)[8] and MoS_2 (d_{Mo-S} = 2.41 Å).[9]

The Mo atoms in $MoSb_2S$ are connected to form zigzag chains along the *b* axis, as is the case for the β-$MoTe_2$ structure. The shortest Mo−Mo distances are 2.76−2.77 Å, shorter than that of the topologically equivalent chains of $MoSb_2Se$ (2.81 Å) and β-$MoTe_2$ (2.89−2.90 Å). The Mo−Mo bonds in elemental molybdenum (cubic body-centered packing, W type) are 8 × 2.73 and 6 × 3.15 Å per Mo atom. Thus, the Mo−Mo interactions in $MoSb_2S$ have significant bonding character.

The Sb−Sb distances within the MoSbS layer are between 3.18 and 3.33 Å. While these distances are larger than a typical Sb−Sb single bond (2.80−2.90 Å), they are shorter than the weak bond in elemental antimony (d = 3.35 Å). Interactions like these are typically weakly bonding.[10] The averaged S−S and S−Sb distances are 3.19 and 3.64 Å, respectively. These presumably nonbonding contacts are much longer than the sums of the covalent radii (r_S = 1.02, r_{Sb} = 1.40 Å).[11] A detailed discussion of the bonding character of these interactions will be given in the electronic structure section.

Chains comprising Sb atoms are running along the *b* axis between the MoSbS layers. Two types of interlayer Sb−Sb chains exist in the structure of $MoSb_2S$. The first type (located at *x* close to 1/4 and 3/4 as shown in Figure 2a) is a zigzag chain with Sb−Sb bonds of 2.84 (parallel to *b*) and 2.88 Å (approximately parallel to *c*), which are both in the range of the Sb−Sb single bond lengths, as comparisons with KSb (2.83 and 2.85 Å),[12] *cyclo*-Sb_5^{5-} (2.81−2.91 Å),[13] and Sb_{11}^{3-} (2.76−2.85 Å) reveal.[14] Short (2.84 Å) and long (3.54 Å) Sb−Sb distances alternate along [010]. This type of *cis-trans* chain is also found in the structure of $MoSb_2Se$ (Figure 2b). Furthermore, each Sb atom of the zigzag chain binds an Sb atom of the MoSbS layer (d = 2.84 Å). Thus, each Sb atom of the zigzag chain takes part in three Sb−Sb interactions described best as single bonds.

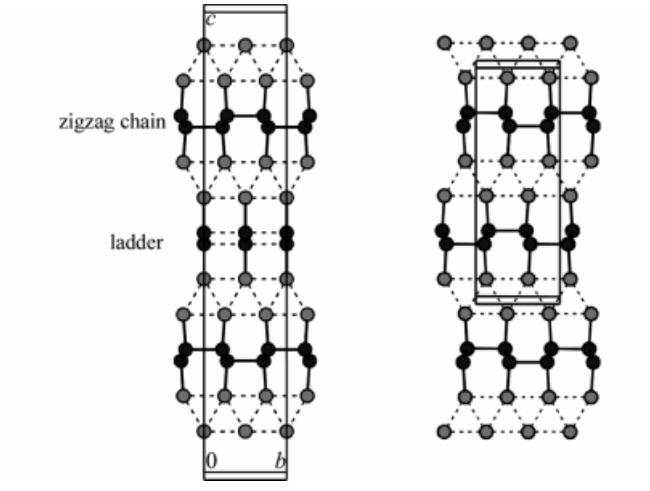

Figure 2. The pseudo two-dimensional Sb atom network of a) $MoSb_2S$ and b) $MoSb_2Se$; solid lines: short Sb−Sb contacts (2.8−2.9 Å); dash lines: long Sb−Sb contact (3.1−3.4 Å)

The second type is an Sb ladder at *x* close to 1/2. Each ladder contains two parallel Sb atom columns with equidistant Sb−Sb contacts of 3.19 Å parallel to the *b* axis. These two columns are interconnected to form the ladder by Sb−Sb bonds of 2.85 Å, and to the Sb atoms of the MoSbS layer by a second Sb−Sb single bond of 2.84 Å. This particular Sb atom substructure is not observed in the $MoSb_2Se$ structure, but the Sb atom ladder compares well to that found in $FeSb_2$ with Sb−Sb distances of 3.20 Å in the columns and 2.89 Å for the bonds connecting the columns to the ladder.[15] Figure 3 illustrates the different columnar Sb atom substructures of $MoSb_2S$, namely the *cis-trans* chain and the ladder.

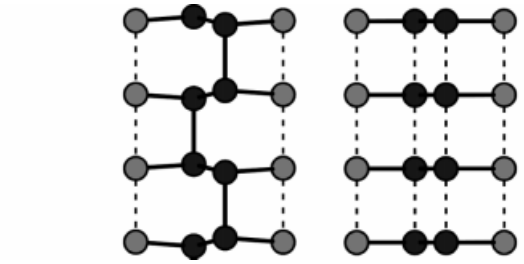

Figure 3. The columnar Sb atom substructure of $MoSb_2S$: a) zigzag chain; b) ladder

Sb−Sb bonds of 3.0−3.2 Å are usually identified as half bonds.[16−21] Instead of forming three full Sb−Sb bonds like the Sb atoms of the zigzag chain, each Sb atom of the ladder forms two full and two half Sb−Sb bonds. This bonding situation resembles those of the $FeSb_2$ structure and of the Li_2Sb structure. In the latter, two different linear Sb atom chains occur; one comprises equidistant Sb−Sb distances of 3.26 Å, and the second one has alternating short and long distances of 2.97 and 3.56 Å.[22]

The question remains, why two different columnar Sb atom substructures occur in $MoSb_2S$, but not in $MoSb_2Se$. In general, the presence of one full bond is preferred over two half bonds (Peierls distortion). However, the Li_2Sb structure proves that the energetic differences may be very small, since both alternatives exist in this same structure − as they do in $MoSb_2S$. Also, the differences between $MoSb_2S$ (one linear equidistant, thus an undistorted chain is present) and $MoSb_2Se$ are reminiscent of those between the high- and low-temperature form of $LaSiAs_3$.[23] In this arsenide, an almost square-planar, i.e. undistorted, As layer (with intermediate As−As bonds of 3.01 and 3.05 Å) is present in the high-temperature modification, resembling the $MoSb_2S$ case. This As layer is transformed into zigzag chains in the low-temperature modification (thus resembling the $MoSb_2Se$ case), with short and long As−As distances of alternating 2.56 and 3.52 Å along [100] and 2.76

and 3.29 Å along [010]. In analogy, one can consider $MoSb_2Se$ as the distorted variant of $MoSb_2S$.

However, even if the differences are subtle, why is there no undistorted Sb chain in $MoSb_2Se$, but one in $MoSb_2S$? We speculate that this is due to the matrix effect imposed by the larger chalcogen atom Se, which would make the half bonds longer than in $MoSb_2S$ as reflected in the longer *b* axis of $MoSb_2Se$, namely 3.25 Å compared to 3.19 Å.

The formal charges of each atom in $MoSb_2S$ may be assigned qualitatively based on the Zintl−Klemm concept.[24,25] Among these elements, the electronegativity of sulfur is the largest on any electronegativity scale, and the distances between two nearest S atoms fall in the range of 3.2−3.5 Å, which are normal van der Waals distances. Then, the S atom can be treated as S^{2-} ions. The short Mo−Mo contacts in the Mo zigzag chain suggest a d^2 configuration, that is Mo^{4+}, which is the preferred valence-electron configuration for the transition metal atom zigzag chain. The analogous assignments for MoS_2 and $MoTe_2$ result in $(Mo^{4+})(S^{2-})_2$ and $(Mo^{4+})(Te^{2-})_2$, respectively. The formal charge of each Sb atom is assigned based on the $(8 - N)$ rule, with N = number of full Sb−Sb bonds. Therefore, the Sb atom on the MoSbS layer is Sb^{2-} (one full bond, thus $N = 1$, ergo $8 - N = 7$ valence electrons), and the Sb atom of the zigzag chain is Sb^0 (three full bonds, $N = 3$). The Sb atom from the ladder carries the same charge (i.e. 0), since it comprises two full and two half bonds. We therefore arrive at an electron-precise formula, that is $Mo^{4+}Sb^0Sb^{2-}S^{2-}$, which in general implies that semiconducting properties are possible. In this case, however, semiconducting properties are unlikely due to the presence of other intermediate Sb−Sb interactions (3.18−3.20 Å) within the MoSbS layer. These increase N of the intralayer Sb atom, and thus decrease the formal charge to $(2 - x)-$ with $x < 1$, resulting in the more accurate formulation $Mo^{4+}Sb^0Sb^{(2-x)-}S^{2-}(e^-)_x$ that hints towards metallic properties.

Electronic Structure

Theoretical band calculations using the LMTO method were carried out to study the electronic structure of $MoSb_2S$. The band structure of $MoSb_2S$ is illustrated in Figure 4. Bands cross the Fermi level along each direction, which strongly suggests three-dimensional metallic property. The different orbital contributions can be evaluated by the *fat band* analyses.[26] The results indicate that the orbital contributions near the Fermi level stem mostly from Mo $d_{x^2-y^2}$ and Sb p orbitals from the interlayer Sb atoms (Sb1, Sb5 and Sb6, as emphasized by the fat band representations). The contributions from the S atom are near zero at the Fermi level. Thus, the Mo−Mo and Sb−Sb interactions are likely responsible for the metallic behavior of $MoSb_2S$.

Density of states (DOS) curves for $MoSb_2S$ and the partial projections onto the Mo and Sb atoms are illustrated in Figure 5. The s block of sulfur occurs in the energy window of −13 to −15 eV, and the broad peak between −13 eV and the Fermi level at 0 eV mainly comprises S p, Sb p and Mo d orbitals. There is no band gap, but a pronounced local minimum in the densities of states at the Fermi level.

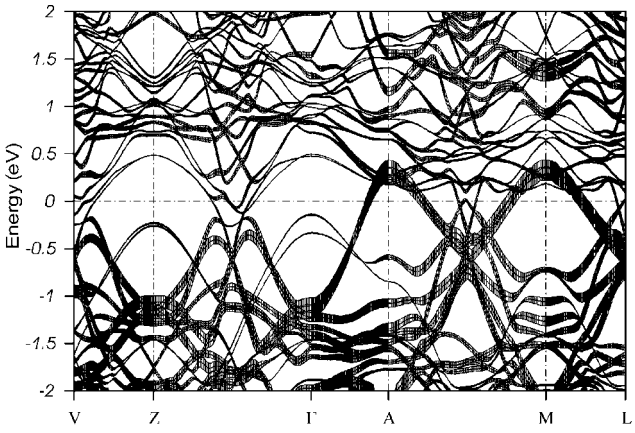

Figure 4. Band structure of $MoSb_2S$; the dashed line denotes the Fermi energy; the interlayer Sb contributions are emphasized

The interatomic interactions in $MoSb_2S$ were analyzed by integrating the area of the COHP curves, resulting in ICOHP values. This is a similar procedure to obtaining the widely used Mulliken overlap populations (MOPs)[27] from the Crystal Orbital Overlap Population (COOP) curves[28] calculated with the Extended Hückel method.[29,30] In contrast to the MOPs, bonding character is reflected in negative ICOHPs. Mo−Mo COHP curves (solid line in Figure 5b) are nearly optimized at the Fermi level E_F (ICOHP = −1.16 eV per bond). A small gap at E_F separates weak antibonding from strong antibonding Mo−Mo states, which suggests that the Mo−Mo bonding will be destabilized by small changes in the valence-electron concentration. The COHP curves of the Mo−S (dotted) and Mo−Sb (dashed) interactions also exhibit a nearly maximized bonding interaction at the Fermi level (ICOHP: Mo−Sb = −1.69; Mo−S = −2.93 eV per bond). All three kinds of interactions shown in Figure 5b comprise zero contributions directly at the Fermi level.

The Sb−Sb interactions are illustrated in Figure 5c for two kinds of Sb−Sb contacts. The first COHP curve (solid line, I) represents the shorter Sb−Sb contacts < 2.9 Å. Almost no antibonding states are filled, the interactions are almost optimized at the Fermi level with an averaged ICOHP value of −1.66 eV per bond. The second COHP curve (dotted line, II) represents Sb−Sb contacts within the MoSbS layer ($3.18 < d_{Sb-Sb} < 3.33$ Å). These interactions exhibit antibonding characters at the Fermi level. The average ICOHP value for these Sb−Sb bonds is −0.31, indicating weaker yet still bonding character. The longer bond of the equidistant ladder of 319 Å (curve III, dashed line) was considered as a half bond, which is reflected in an intermediate ICOHP value of −0.63 eV per bond. These ICOHPs may be compared to those of the two different bonds in elemental antimony, which are −1.63 for the short one of 2.91 and −0.23 eV for the longer one (3.35 Å). For the Sb−Sb bonds of 2.91 and 3.10 Å in Mo_3Sb_7,[31] we calculated similar ICOHPs of −0.79 and −0.40, respectively.

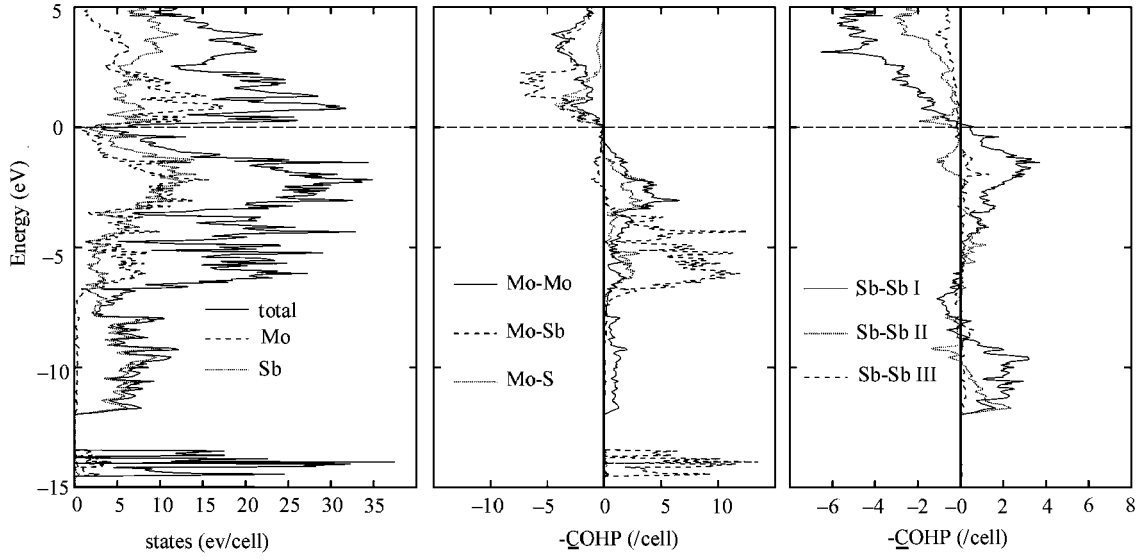

Figure 5. DOS and COHP curves for the $MoSb_2S$; the horizontal dashed line denotes the Fermi energy: a) total DOS (solid line), PDOS from Mo (dashed), Sb (dotted); b) COHP curves for Mo−Mo (solid line), Mo−Sb (dotted), Mo−S (dashed) interactions; c) Sb−Sb contacts (solid line: I, 2.83 < d_{Sb-Sb} < 2.88 Å; dotted line: II, intralayer 3.18 < d_{Sb-Sb} < 3.33 Å, dashed line: III, interlayer 3.19 Å)

Correspondingly, the half bond (3.11 Å) in $Zr_{11}Sb_{18}$ exhibits an ICOHP of −0.49, while the full bonds in KSb have larger ICOHPs of −2.29 and −1.87 eV per bond.[32]

Physical Properties

The temperature-dependent Seebeck coefficient measurement is shown in Figure 6. The Seebeck coefficient drops from −17 μV/K at 300 K to −30 μV/K at 600 K. The negative sign indicates that electrons are the main charge carriers. Typical magnitudes of Seebeck coefficients at 300 K range from a few μV/K for most metals to 10−20 μV/K for some transition metal elements.[1] The observed Seebeck coefficient of $MoSb_2S$ is at the upper end for metallic materials.

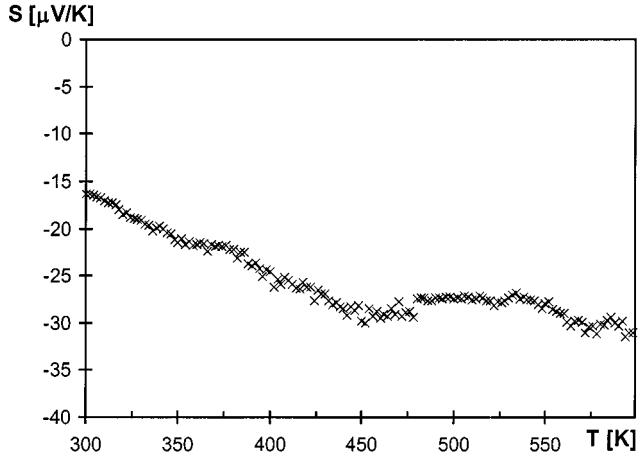

Figure 6. Temperature-dependent Seebeck coefficients of $MoSb_2S$

Conclusion

In summary, the synthesis and characterization of a new ternary compound, $MoSb_2S$, were presented. $MoSb_2S$ crystallizes in a new three-dimensional structure type exhibiting CdI_2-related layers (MoSbS) and Sb columns (*cis-trans* chains and equidistant ladders). The structure comprises strong heteronuclear Mo−S and Mo−Sb bonds, and additional Mo−Mo and Sb−Sb bonds. The Sb atom substructure of $MoSb_2S$ may be considered to be a partly undistorted variant of $MoSb_2Se$. Both antimonide chalcogenides can be formally derived from MoSbS layers topologically equivalent to the β-$MoTe_2$ layers, with additional interlayer Sb atoms. The (formal) intercalation of anionic Sb atoms actually enlarges the octahedral voids between the sheets, thereby rendering an additional intercalation of cations more facile.

$MoSb_2S$ exhibits metallic behavior as predicted by electron counting, electronic structure calculations and confirmed by physical property measurements (Seebeck coefficients). The results from the electronic structure calculations show the smallest number of states directly at the Fermi level; thus, changing the valence-electron concentration is likely to further increase the number of itinerant valence electrons, a disadvantage when looking for thermoelectric materials.

Experimental Section

Synthesis: All starting materials were stored in an Argon-filled glove box. The starting materials were molybdenum (Aldrich, 99.9%), antimony powder (Aldrich, 99.8%, melting point 903 K,

99.5%), sulfur (Aldrich, 99.98%), Mo_3Sb_7 and Sb_2S_3. Mo_3Sb_7 was synthesized by starting from the stoichiometric ratio of Mo/Sb = 3:7 and heating at 973 K for 3 d in an evacuated fused silica tube, whereas Sb_2S_3 was prepared at 773 K within 3 d in an evacuated fused silica tube. Initial reactions were carried out by preparing mixtures in stoichiometric ratios of the elements with a small amount of I_2 as the transport reagent, in a silica tube, sealed under vacuum ($< 10^{-3}$ mbar), and heated at 1073 K for 3 d. Black, needle-shaped crystals of $MoSb_2S$ and mixtures of Sb and binary phases (Mo_3Sb_7, MoS_2) were observed from these reactions. Pure $MoSb_2S$ can be synthesized either by heating stoichiometric amounts of the elements at 873 K for 3 d or annealing binary compounds Mo_3Sb_7 and Sb_2S_3 in a 1:1 ratio at 973 K for 2 d. The purity of $MoSb_2S$ was checked by powder X-ray diffraction and elemental analyses (EDS, see below). The second reaction route (Mo_3Sb_7 + Sb_2S_3) yielded $MoSb_2S$ and elemental antimony, that crystallized on different sides of the reaction container. Higher reaction temperatures (> 1123 K) for both reaction routes led to the disproportionation of $MoSb_2S$ into MoS_2, Mo and Sb. $MoSb_2S$ is stable in air for at least two weeks.

Structure Determination: Needle-shaped crystals for single-crystal X-ray diffraction experiments were selected under an optical microscope and then mounted on glass fibers. Single-crystal X-ray diffraction data were collected with the use of graphite-monochromatized Mo-K_α radiation (λ = 0.71073 Å) at 298(2) K with a Bruker APEX CCD diffractometer. The crystal-to-detector distance was 4.550 cm. Data were collected by a scan of 0.3° in ω groups of 606 frames each at φ settings of 0°, 60°, 120°. The exposure time was 120 s/frame. The 2θ values varied between 3° and 70°. The data were corrected for Lorentz and polarization effects. Absorption corrections were based on fitting a function to the empirical transmission surface as sampled by multiple equivalent measurements.[33] Diffraction peaks obtained from all frames of reciprocal space images were used to determine the unit cell parameters. Initially, the data revealed a primitive unit cell similar to the one of $MoSb_2Se$ and additional weak reflections, which suggested a supercell. The unit cell parameters of $MoSb_2S$ indicated monoclinic symmetry, as later proven by a comparison of symmetry-equivalent reflections (R_{int} = 0.043). The systematic absences revealed *C*-centering. Therefore, the space group *C*2/*m* was chosen for subsequent structural analyses. The structure model was obtained by direct methods and refined by full-matrix least-squares refinement based on F^2 with the SHELXTL5.12 package.[34] Table 1 summarizes the crystallographic data of $MoSb_2S$. Table 2 lists selected interatomic distances. Further details of the crystal-structure investigations may be obtained from the Fachinformationszentrum Karlsruhe, 76344 Eggenstein-Leopoldshafen, Germany, on quoting the depository number CSD-412092. All Mo and S atoms exhibit reasonable thermal displacement parameters. However, the Sb5 and Sb6 atoms show 2−3 times higher thermal displacement parameters along each main direction, which might suggest an even higher order of supercell or lower symmetry. However, lowering the symmetry, for example by refining in C_2 or *Cm*, did not result in any improvements. Also, we found no evidence for the existence of a higher superstructure.

Elemental Analysis: Energy dispersive spectroscopy (EDS, LEO 1050) was performed on the crystalline and powdered samples. The Mo/S ratio could not be determined due to the severe overlap of the peaks of Mo (L_α = 2.293 eV) and S (K_α = 2.307 eV). No impurities of other elements (like iodine, silicon or oxygen) were detected.

Table 1. Crystal data and conditions of data collection for $MoSb_2S$

Refined composition	$MoSb_2S$
Instrument	Smart APEX CCD
Molecular mass	371.5
Crystal size [mm]	0.16 × 0.04 × 0.01
Space group, *Z*	*C*2/*m*, 16
a [Å]	36.157(3)
b [Å]	6.3823(5)
c [Å]	6.5379(5)
β [°]	95.093(2)
V [Å^3]	1502.8(2)
$2\theta_{max}$	34.99°
Reflections collected	12316
Independent, observed reflections (R_{int})	3506, 1553 (0.043)
$d_{calcd.}$ [g/cm^3]	6.568
Absorption coeff. [mm^{-1}]	17.86
Transmission range	0.82−1.0
Temperature [K]	298(2)
$R1$[a], $wR2$ [$I > 2\sigma(I)$]	0.035, 0.059
Goodness-of-fit on F^2	0.80
Δρ(max/min) [e/Å^3]	2.54/−2.53

[a] $R1 = \Sigma||F_o| - |F_c||/\Sigma|F_o|$; $wR2 = [\Sigma[w(F_o^2 - F_c^2)^2]/\Sigma[w(F_o^2)^2]]^{1/2}$.

Table 2. Selected bond lengths [Å] for $MoSb_2S$

Sb1	Sb1	2.839(1)	Sb5	Sb5	2.853(4)
	Sb1	2.878(3)		Sb6	3.1912(3)
	Sb3	2.844(2)			
Sb2	Sb3	3.3294(7)	Mo1	Mo2	2.7650(9)
	Sb4	3.1912(2)		Mo3	3.1912(3)
	Sb5	2.841(2)		S2	2.382(4)
	Mo1	2.840(2)		S3	2.390(5)
	Mo2	2.823(2)	Mo2	Mo2	3.188(1)
Sb3	Mo1	2.826(2)		Mo2	3.194(1)
	Mo2	2.844(2)		Mo3	2.7596(9)
	Mo3	2.824(2)		S1	2.382(4)
	Sb3	3.1846(9)		S2	2.389(5)
	Sb3	3.1977(9)		S3	2.381(4)
	Sb4	3.3283(7)	Mo3	S1	2.388(5)
				S2	2.380(4)
Sb4	Sb6	2.842(2)	S1	S3	3.1912(3)
	Mo2	2.823(2)	S2	S2	3.188(3)
	Mo3	2.846(2)		S2	3.195(3)

Thermopower Measurements: Seebeck coefficients were determined on a cold-pressed bar by a commercial thermopower measurement apparatus (MMR Technologies) in the temperature range of 300 to 600 K, using Constantan as an internal standard. Silver paint (AMI DODUCO Technology) was used to create electric contacts.

Electronic Structure Calculations: The tight-binding LMTO (Linear Muffin Tin Orbitals)[35−37] band calculations were carried out in order to understand the electronic structure of $MoSb_2S$. The integration in *k* space was performed by an improved tetrahedron method[38] on a grid of 16 × 16 × 8 irreducible *k* points of the first Brillouin zone (i.e. 554 of 2048 *k* points). We analyzed the electronic structure by extracting information from the band structure, Densities of states (DOS), and Crystal Orbital Hamiltonian Population curves (COHP).[39]

Acknowledgments

Financial support from the Canadian Foundation for Innovation, the Ontario Innovation Trust, the Materials Manufacturing Ontario, the Province of Ontario, and the National Science and Engineering Research Council of Canada is appreciated.

[1] D. M. Rowe, *CRC Handbook of Thermoelectrics*, CRC Press, Boca Raton, FL, **1995**.
[2] D.-Y. Chung, T. Hogan, P. Brazis, M. Rocci-Lane, C. Kannewurf, M. Bastea, C. Uher, M. G. Kanatzidis, *Science (Washington, D. C.)* **2000**, *287*, 1024.
[3] T. M. Tritt, M. G. Kanatzidis, G. D. Mahan, H. B. J. Lyon, in *Materials Research Society Symposium Proceeding*, Materials Research Society, Warrendale, PA, **1999**, vol. 545.
[4] B. C. Sales, D. Mandrus, R. K. Williams, *Science* **1996**, *272*, 1325.
[5] F. J. DiSalvo, *Science* **1999**, *285*, 703.
[6] H. Kleinke, *Chem. Commun. (Cambridge)* **2000**, 1941.
[7] B. E. Brown, *Acta Crystallogr.* **1966**, *20*, 268.
[8] A. Brown, *Nature* **1965**, *206*, 502.
[9] K. D. Bronsema, J. L. De Boer, F. Jellinek, *Z. Anorg. Allg. Chem.* **1986**, *540*, 15.
[10] P. Villars, L. D. Calvert, *Pearson's Handbook of Crystallographic Data for Intermetallic Phases*, 2nd ed., ASM International, Metals Park, OH, **1991**.
[11] L. Pauling, *The Nature of the Chemical Bond*, 3rd ed., Cornell University, Ithaca, NY, **1948**.
[12] W. Hönle, H.-G. von Schnering, *Z. Kristallogr.* **1981**, *155*, 307.
[13] N. Korber, F. Richter, *Angew. Chem. Int. Ed. Engl.* **1997**, *36*, 1512.
[14] U. Bolle, W. Tremel, *J. Chem. Soc., Chem. Commun.* **1992**, 91.
[15] H. Holseth, A. Kjekshus, *Acta Chem. Scand.* **1969**, *23*, 3043.
[16] H. Kleinke, *Eur. J. Inorg. Chem.* **1998**, 1369.
[17] H. Kleinke, *Chem. Commun. (Cambridge)* **1998**, 2219.
[18] M. J. Ferguson, R. W. Hushagen, A. Mar, *J. Alloys Compd.* **1997**, *249*, 191.
[19] H. Kleinke, *Chem. Soc. Rev.* **2000**, *29*, 411.
[20] G. Papoian, R. Hoffmann, *J. Am. Chem. Soc.* **2001**, *123*, 6600.
[21] G. A. Papoian, R. Hoffmann, *Angew. Chem. Int. Ed.* **2000**, *39*, 2409.
[22] W. Müller, *Z. Naturforsch., Teil B* **1977**, *32*, 357.
[23] H. Hayakawa, S. Ono, *J. Less-Common Met.* **1988**, *144*, 177.
[24] W. Klemm, *Z. Anorg. Allg. Chem.* **1941**, *247*, 1.
[25] E. Zintl, *Angew. Chem.* **1939**, *1*, 52.
[26] O. Jepsen, O. K. Andersen, *Z. Phys.* **1995**, *97*, 25.
[27] R. S. Mulliken, *J. Chem. Phys.* **1955**, *23*, 2343.
[28] T. Hughbanks, R. Hoffmann, *J. Am. Chem. Soc.* **1983**, *105*, 3528.
[29] R. Hoffmann, *J. Chem. Phys.* **1963**, *39*, 1397.
[30] M.-H. Whangbo, R. Hoffmann, *J. Am. Chem. Soc.* **1978**, *100*, 6093.
[31] E. Dashjav, A. Szczepenowska, H. Kleinke, *J. Mater. Chem.*, in press.
[32] I. Elder, C.-S. Lee, H. Kleinke, *Inorg. Chem.*, in press.
[33] *SAINT Version 4*, Siemens Analytical X-ray Instruments Inc., Madison, WI., **1995**.
[34] *SHELXTL Version 5.12, Reference Manual*, Siemens Analytical X-ray Systems, Inc, Madison, WI, **1996**, **1995**.
[35] U. van Barth, L. Hedin, *J. Phys. C* **1971**, *4*, 2064.
[36] O. K. Andersen, *Phys. Rev. B* **1975**, *12*, 3060.
[37] H. L. Skriver, *The LMTO Method*, Springer, Berlin, **1984**.
[38] P. E. Blöchl, O. Jepsen, O. K. Andersen, *Phys. Rev. B: Condens. Matter* **1994**, *49*, 16223.
[39] R. Dronskowski, P. E. Blöchl, *J. Phys. Chem.* **1993**, *97*, 8617.

Received September 13, 2001
[I01360]

The Cationic Rearrangement of (3-Hydroxy-1-propenyl)tris(trimethylsilyl)-silanes into (1-Trimethylsilyl-2-propenyl)bis(trimethylsilyl)silanols – Experimental and Theoretical Studies

Kathleen Schmohl,[a] Dirk Wandschneider,[a][‡] Helmut Reinke,[a] Andreas Heintz,*[a] and Hartmut Oehme*[a]

Keywords: Alcohols / Rearrangements / Silanes / Silicon

(3-Hydroxy-1-propenyl)tris(trimethylsilyl)silanes $(Me_3Si)_3SiCH{=}CHCR_2OH$ (**8b,c**) (**b:** R = Me; **c:** R = Ph) undergo a rapid rearrangement involving a 1,2-Si,C migration of one trimethylsilyl group from the central silicon atom to a cationic neighboring carbon atom and a shift of the olefinic double bond, in the presence of acid, to afford (1-trimethylsilyl-2-propenyl)bis(trimethylsilyl)silanols $(Me_3Si)_2Si(OH)CH(SiMe_3)CH{=}CR_2$ (**13b,c**). Treatment of **8b,c** with sulfuric acid in methanol gives the methoxysilanes $(Me_3Si)_2Si(OMe)CH(SiMe_3)CH{=}CR_2$ (**14b,c**). In a related reaction, **8b,c** are converted by boron trifluoride into the fluorosilanes $(Me_3Si)_2SiFCH(SiMe_3)CH{=}CR_2$ (**15b,c**). A possible mechanism of the isomerization reaction, involving the rearrangement of the silylcarbenium ions $[(Me_3Si)_3SiCH{=}CHCR_2]^+$ into the silylium ions $[(Me_3Si)_2SiCH(SiMe_3)CH{=}CR_2]^+$, is proposed. This is supported by calculations, which indicate the higher stability of the silylium ion **10b** compared with the isomeric silylcarbenium cation **9b**. For **14c** the results of an X-ray structural analysis are given.

Introduction

Recently we found that 1-hydroxyalkyltris(trimethylsilyl)-silanes (**1**) undergo a rapid isomerization in the presence of strong acids into 1-trimethylsilylalkylbis(trimethylsilyl)silanols (**6**) (Scheme 1).[1] The reaction path was interpreted in terms of a cationic rearrangement initiated by an acid-catalyzed elimination of water from the alcohol **1** and formation of the carbenium ion **2**. The subsequent 1,2-Si,C migration of one trimethylsilyl group, and attack of X^-, the conjugate base of the acid used as the catalyst, at the central silicon atom produces the intermediate **5**, which after hydrolytic workup affords the silanol **6**. A decision as to whether the reaction involves a synchronous nucleophilic attack by X^- on the central silicon atom and migration of one trimethylsilyl group from silicon to carbon (**3**) or, alternatively, proceeds through a silylium ion intermediate **4**, could not be made. It is very likely that the isomerization is facilitated by the greater stability of the silylium ion **4** than the carbenium cation **2**, and we consider the crucial step of the conversion **1**→**6** to be the isomerization of the silyl-substituted carbenium ion into the silylium ion by 1,2-migration of one $SiMe_3$ group from the tetracoordinated silicon center to the neighboring carbon atom. Some reactions of this type have recently been described,[2,3] and confirm expectations from theoretical work, according to which α-silyl carbenium ions should generally be less stable than the isomeric silylium ions.[4]

Continuing these studies we extended our experiments to vinylogous derivatives of the alcohols **1**, and in the present paper we report on the related behavior of (3-hydroxy-1-propenyl)tris(trimethylsilyl)silanes **8**, which rearrange in the presence of acid to give the (1-trimethylsilyl-2-propenyl)bis-(trimethylsilyl)silanols **13**.

Results and Discussion

The aim of the studies described in this paper was to examine whether tris(trimethylsilyl)silyl-substituted carbenium ions with a delocalized positive charge also undergo 1,2-Si,C trimethylsilyl migrations as discussed above for the isomerization of **2** into **5**. As model compounds we have chosen tris(trimethylsilyl)silylcarbocations, which were intended to be generated by the acid-induced elimination of water from the respective 3-hydroxy-1-propenylsilanes. For that purpose we prepared the alcohols **8a–c** by addition of tris(trimethylsilyl)silane (**7**) across the triple bonds of propargylic alcohol, 2-methyl-3-butyn-2-ol and 1,1-diphenyl-2-propyn-1-ol (Scheme 2). This method, and its application to the synthesis of **8a**, has already been described,[5] and proved to be suitable also for the reaction of **7** with the above-mentioned propynols.

[‡] Theoretical calculations
[a] Fachbereich Chemie der Universität Rostock
18051 Rostock, Germany
Fax: (internat.) +49-(0)381/498-6382
E-mail: hartmut.oehme@chemie.uni-rostock.de
andreas.heintz@chemie.uni-rostock.de

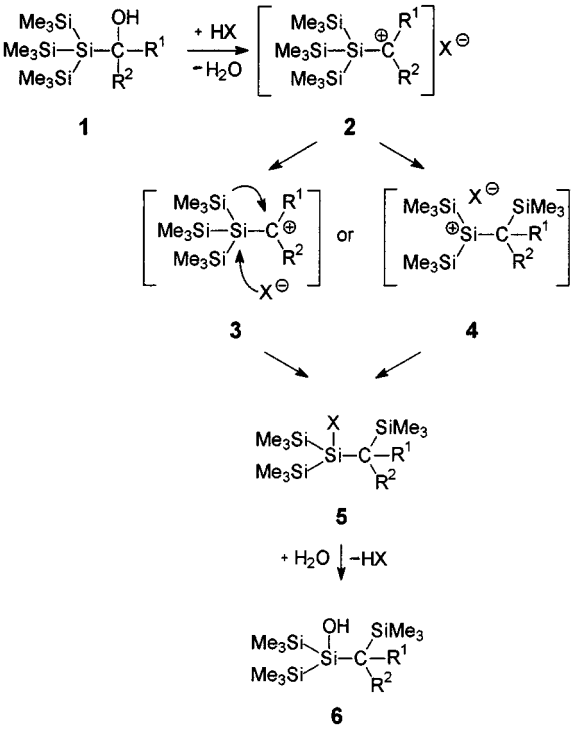

Scheme 1. The acid-induced rearrangement of 1-hydroxyalkyltris-(trimethylsilyl)silanes **1** into bis(trimethylsilyl)-1-trimethylsilylalkylsilanols **6**

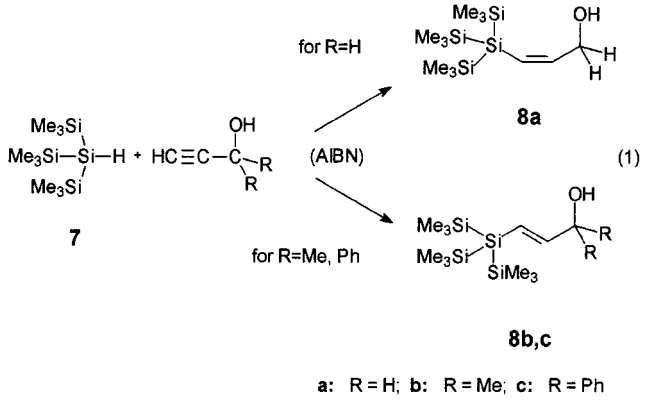

Scheme 2

In agreement with the literature data, the addition of **7** to the triple bond of propargylic alcohol led to the *Z*-olefin **8a**.[5] In contrast, the coupling constants of the olefinic protons in **8b** and **8c** unambiguously revealed an *E*-configuration for both olefins. This difference is due to the different space filling properties of the $C(OH)R_2$ substituents (R = Me, Ph) in **8b,c**.

The Acid-Induced Isomerization of the (3-Hydroxy-1-propenyl)tris(trimethylsilyl)silanes into (1-Trimethylsilyl-2-propenyl)bis(trimethylsilyl)silanols

The alcohols **8a−c**, dissolved in ether, were treated with hydrochloric acid or, alternatively, pentane solutions of **8a−c** were stirred with a few drops of sulfuric acid at room temperature. In all experiments with **8a** the alcohol was always recovered unchanged. Under the same conditions, however, **8b** and **8c** underwent rapid rearrangements and after aqueous workup of the reaction mixtures we obtained the silanols **13b** and **13c**, respectively. Sulfuric acid proved to be most effective for the acid-catalyzed isomerization of 1-hydroxyalkyl-tris(trimethylsilyl)silanes (**1**).[1] Therefore — and also because of the convenient experimental procedure — we used only this catalyst in all the studies described below.

The suggested mechanism of the reaction is outlined in Scheme 3. Protonation of **8b,c** and elimination of water leads to the carbenium ions **9b,c**. (3-Hydroxy-1-propenyl)-tris(trimethylsilyl)silane (**8a**) is reluctant to undergo the rearrangement. Obviously, elimination of water from the primary alcohol failed under our conditions and therefore no reaction occurs. Despite delocalization of the positive charge in **9b,c**, which is expected to enhance the stability of the carbocations, one trimethylsilyl group migrates from the central silicon atom to the adjacent carbon atom generating the transient silylium ions **10b,c**. As already mentioned, Apeloig et al. found that α-silyl-substituted carbenium ions are generally less stable than the isomeric silylium ions.[3,4] This is confirmed by ab initio calculations, described below, which indicate a significantly higher stability of the silylium ion **10b** than the carbenium ion **9b**; this energy difference is supposed to be the driving force of the rearrangement **9b,c→10b,c**. Addition of X^- to the silylium silicon atoms results in formation of the silanes **12b,c**, which during the aqueous workup hydrolyse to give the silanols **13b,c**. Of course, a synchronous process involving an attack of X^- at the central silicon atom of **9b,c** and a simultaneous shift of one Me_3Si group to the α-carbon atom of the alkyl substituent affording **12b,c** cannot be excluded.

For the reaction of **8c** with ethereal HCl the intermediate chlorosilane **12c** (R = Cl) was isolated; this compound can easily be converted into the silanol **13c** by addition of water. Attempts to isolate the silyl sulfates **12b,c** ($R = OSO_3H$) after reaction of **8b,c** with sulfuric acid failed. Due to rapid hydrolysis, the products obtained always contained considerable amounts of the silanols **13b,c**. When the isomerization of **8b,c** was carried out with sulfuric acid in methanol, solvolysis of the silylsulfates **12b,c** ($X = OSO_3H$) afforded the methoxysilanes **14b,c** (Scheme 3).

Of course, a 1,4-migration of one trimethylsilyl group of **9b,c** producing the silylium ions **11b,c** may be possible (Scheme 3), although products originating from conversions of **11b,c** were not observed. This is in agreement with the results of the calculations described below.

According to a related mechanism, treatment of **8b,c** with boron trifluoride produced the fluorosilanes **15b,c** (Scheme 4).

The structures of **8b,c** and **13b,c−15b,c** were elucidated by a full spectral analysis (^1H, ^{13}C and ^{29}Si NMR spectroscopy, IR spectroscopy, MS and elemental analysis). For the methoxysilane **14c** an X-ray structural analysis was performed, which confirmed the compound as a crowded silane (Figure 1). Thus, the Si1−C1 bond in **14c** is slightly elongated (1.906 Å) and the angle C1−Si1−Si3 (112.53 °)

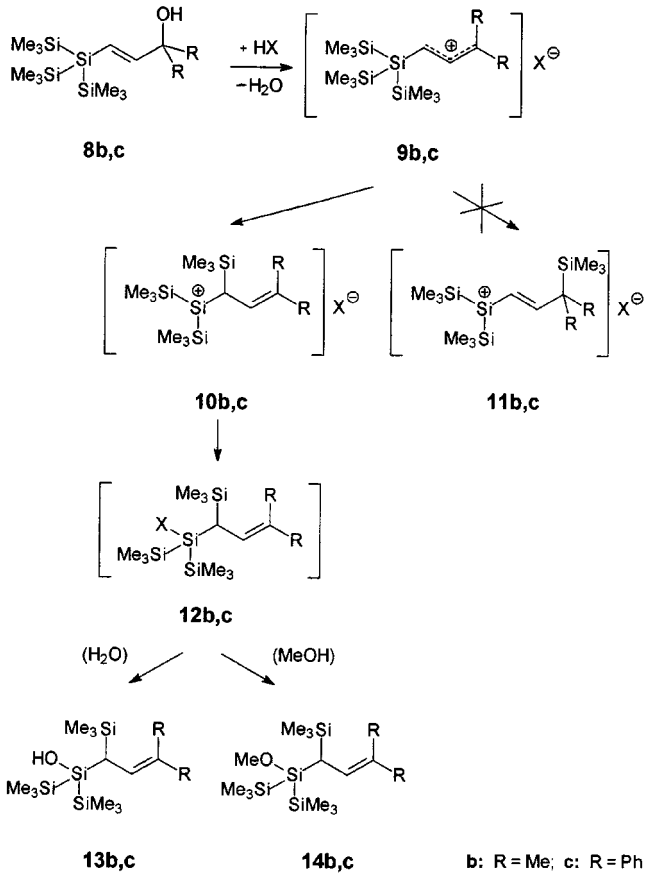

Scheme 3. The acid-induced conversion of the 3-hydroxy-1-propenyltris(trimethylsilyl)silanes **8b,c** into the silanols **13b,c** or the methoxysilanes **14b,c**

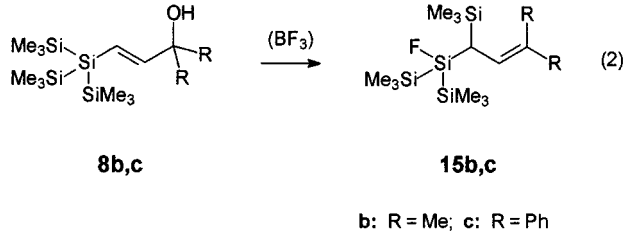

Scheme 4

is widened. The other bond lengths and angles are in the expected range.

The reaction sequence **8**→**10** can be considered to be possibly a useful method for the generation of sterically congested silylium ions just by operating in the unprotected periphery of the molecule.

Theoretical Studies

Since there is no direct experimental evidence that the rearrangement of **8b,c** → **13b,c** proceeds through the intermediates **9b,c** and **10b,c**, we have used ab initio calculations to predict the relative stabilities of the carbenium ion **9b** and the isomeric silylium ion **10b**. To estimate the probability of a 1,4-trimethylsilyl migration in **9b**, we also included the silylium ion **11b** in these studies (Scheme 3). The calculations were performed for isolated species using the Gaussian 98 program package.[6] The following procedure was applied. First, we made a geometry optimization of **9b, 10b** and **11b** at the HF/6-31G(d) level. Based on these geometric structures single point energy calculations were performed at the HF/6-31G(d) and MP2/6-31G(d) levels. Secondly, geometry optimizations with single point energy calculations were performed at the HF/6-31++G(d,p) level.[7] The values of the absolute energies obtained by these procedures are shown in Table 1. Table 2 shows the energy differences in kcal/mol. The differences of the absolute energies obtained at the different levels indicate a stabilization of **10b** of between 9.9 and 22.7 kcal·mol^{-1} compared with **9b** depending on the method indicated in Table 2. The values obtained are close to the stabilization energies of other silylium ions over their isomeric α-silyl-substituted carbenium ions reported by Apeloig.[4] The other possible intermediate **11b** is energetically disfavoured by between 3.6

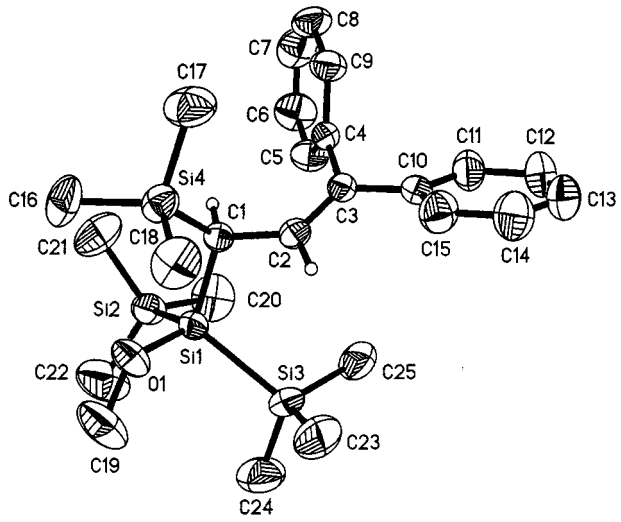

Figure 1. Molecular structure of **14c** in the crystal (H atoms omitted, except C1H and C2H, ORTEP plot with 30% probability of the thermal ellipsoids); selected bond lengths [A] and angles [°]: Si1−C1 1.906(4), Si1−Si2 2.3621(19), Si1−Si3 2.3630(18), Si1−O1 1.645(4), C1−Si4 1.898(4), C1−C2 1.496(5), C2−C3 1.338(5); Si2−Si1−Si3 111.27(7), Si1−C1−Si4 114.60(19), Si1−O1−C19 131.6(5), Si3−Si1−C1 112.53(13), Si2−Si1−C1 109.54(13), O1−Si1−C1 105.74(19)

Table 1. Sum of electronic energies and nuclear repulsion energies E [Hartrees][a] of isomers **9b**, **10b** and **11b**, without corrections due to zero-point energies, thermal energies and solute-solvent interactions

Method	E(**9b**)	E(**10b**)	E(**11b**)
HF/6-31G(d)	−1706.05509	−1706.07197	−1706.06543
MP2/6-31G(d)[b]	−1708.20490	−1708.24102	−1708.22252
HF/6-31++G(d,p)	−1706.12505	−1706.14087	−1706.13510

[a] 1 Hartree = 627.5095 kcal·mol^{-1}. [b] Single point energy calculation based on an HF/6-31G(d) geometry optimization.

kcal·mol^{-1} [HF/6-31++G(d,p)] and 11.6 kcal·mol^{-1} [MP2/6-31G(d)] compared with **10b**. These results clearly indicate a higher stability of **10b** compared with **9b** and **11b**, supporting the reaction mechanism suggested in Scheme 3.

Table 2. Differences in the total energies [kcal·mol^{-1}] of the three isomeric cations **9b**, **10b** and **11b**

Method	E(**9b**) − E(**10b**)	E(**11b**) − E(**10b**)
HF/6-31G(d)	10.6	4.1
MP2/6-31G(d)[a]	22.7	11.6
HF/6-31++G(d,p)	9.9	3.6

[a] Single point energy calculation based on a HF/6-31G(d) geometry optimization.

Experimental Section

General: All reactions involving organometallic reagents were carried out under purified argon. NMR: Bruker AC 250 or Bruker ARX 300, tetramethylsilane as internal standard. IR: Nicolet 205 FT-IR. MS: Intectra AMD 402. $(Me_3Si)_3SiH$ (**7**) was prepared using the method described by Marschner;[8] **8a** was synthesized following the procedure given by Utimoto,[5] but the reaction was induced by AIBN instead of triethylborane. Due to the formation of SiC, the results of the elemental analyses of some compounds were unsatisfactory. In these cases HRMS data are given.

(3-Hydroxy-3-methyl-1-butenyl)tris(trimethylsilyl)silane (8b): 2-Methyl-3-butyn-2-ol (1.2 g, 14.0 mmol) and AIBN (0.2 g) were gradually added at room temperature to a solution of **7** (3.0 g, 12.1 mmol) in toluene (30 mL). The mixture was heated under reflux for 5 h, and then water was added and the organic phase separated, dried and the solvents evaporated. The residue was purified by kugelrohr distillation at 75−100 °C/7·10^{-3} mbar to afford 3.0 g (74.7%) of **8b**. Colorless crystals, m.p. 58−63 °C. IR (nujol): $\tilde{\nu}$ = 3407 cm^{-1} (OH). ^{1}H NMR ([D$_6$]benzene): δ = 0.27 (s, 27 H, $SiCH_3$), 0.98 (s, 1 H, OH), 1.15 (s, 6 H, CCH_3), 5.92 (d, ^3J = 18.6 Hz, 1 H, CH), 6.29 (d, ^3J = 18.6 Hz, 1 H, CH). ^{13}C NMR ([D$_6$]benzene): δ = 0.9 ($SiCH_3$), 29.7 (CCH_3), 71.9 (COH), 115.4 and 156.9 (olef. C). ^{29}Si NMR ([D$_6$]benzene): δ = −85.5 (SiSiMe$_3$), −13.1 ($SiMe_3$). MS (70 eV): *m*/*z* (%) = 317 (3) [M − CH_3]$^+$, 315 (3) [M − OH]$^+$, 259 (12) [M − $SiMe_3$]$^+$, 73 (100) [$SiMe_3$]$^+$. $C_{14}H_{36}OSi_4$ (332.8): calcd. C 50.53, H 10.90; found C 50.79, H 10.85.

(3-Hydroxy-3,3-diphenyl-1-propenyl)tris(trimethylsilyl)silane (8c): Following the procedure given for **8b**, 3.0 g (12.1 mmol) of **7**, 2.50 g (12.1 mmol) of 1,1-diphenyl-2-propyn-1-ol and 0.2 g of AIBN gave 2.7 g (49%) of **8c** after kugelrohr distillation (200 °C/3·10^{-2} mbar). Colorless oil. IR (cap.): $\tilde{\nu}$ = 3462 cm^{-1} ($OH_{ass.}$), 3556 and 3601 cm^{-1} (OH_{free}). ^{1}H NMR ([D$_6$]benzene): δ = 0.23 (s, 27 H, $SiCH_3$), 1.84 (s, 1 H, OH), 6.12 (d, ^3J = 18.6 Hz, 1 H, CH), 6.82 (d, ^3J = 18.6 Hz, 1 H, CH), 7.03−7.49 (m, arom. 10 H, CH). ^{13}C NMR ([D$_6$]benzene): δ = 1.0 ($SiCH_3$), 81.0 (COH), 119.6 and 153.3 (olef. C), 127.3, 127.5 and 128.3 (arom. CH), 146.8 (arom. C). ^{29}Si NMR ([D$_6$]benzene): δ = −85.0 (SiSiMe$_3$), −12.8 ($SiMe_3$). MS (70 eV): *m*/*z* (%) = 456 (2) [M]$^+$, 441 (2) [M − CH_3]$^+$, 439 (2) [M − OH]$^+$, 383 (7) [M − $SiMe_3$], 73 (100) [$SiMe_3$]$^+$. $C_{24}H_{40}OSi_4$ (456.9): calcd. C 63.09, H 8.82; found 63.47, H 8.86.

Chloro(3,3-diphenyl-2-propenyl-1-trimethylsilyl)bis(trimethylsilyl)-silane (12c): Compound **8c** (0.5 g, 1.1 mmol) was dissolved in 30 mL of ether containing excess hydrogen chloride, and the solution was stirred at room temperature for 8 h. After addition of solid $NaHCO_3$ and filtration, the solution was evaporated. Chromatographic separation of the residue (silica gel, heptane/ethyl acetate 20:1) gave 0.14 g (26%) of the chlorosilane **12c** and 0.15 g (30%) of the silanol **13c**.

12c: Colorless oil. ^{1}H NMR ([D$_6$]benzene): δ = 0.18, 0.22 and 0.27 (3s, 3 × 9 H, $SiCH_3$). 2.51 (d, ^3J = 13.4 Hz, 1 H, SiCH), 6.43 (d, ^3J = 13.4 Hz, 1 H, olef. CH), 6.98−7.48 (m, arom. 10 H, CH). ^{13}C NMR ([D$_6$]benzene): δ = −0.9, −0.6 and 0.3 ($SiCH_3$), 22.8 (CH), 126.9, 127.1, 127.2, 127.4, 128.6, 128.7, 130.7, 139.4, 140.3 and 143.5 (arom. and olef. C). ^{29}Si NMR ([D$_6$]benzene): δ = −14.3 and −13.7 (SiSiMe$_3$), 3.3 ($CSiMe_3$), 9.6 (SiCl). MS (70 eV): *m*/*z* (%) = 474 (5) [M]$^+$, 459 (4) [M − CH_3]$^+$, 439 (1) [M − Cl]$^+$, 401 (2) [M − $SiMe_3$]$^+$, 73 (100) [$SiMe_3$]$^+$. $C_{24}H_{39}ClSi_4$ (475.4): calcd. C 60.64, H 8.27, Cl 7.46; found C 61.18, H 8.24, Cl 8.07. HRMS: calcd. 474.18173; found 474.18510.

(3-Methyl-1-trimethylsilyl-2-butenyl)bis(trimethylsilyl)silanol (13b): Concentrated sulfuric acid (0.15 g, 1.5 mmol) was added gradually to a solution of **8b** (0.5 g, 1.5 mmol) in pentane (30 mL) and the mixture was stirred at room temperature for 8 h. After neutralization with aqueous $NaHCO_3$ solution, washing with water and drying, the solvent was removed in vacuo and the residue purified by column chromatography (silica gel, heptane/ethyl acetate 20:1) to give 0.09 g (18%) of **13b**. Colorless oil. IR (nujol): $\tilde{\nu}$ = 3454 cm^{-1} ($SiOH_{ass.}$), 3649 cm^{-1} and 3677 cm^{-1} ($SiOH_{free}$). ^{1}H NMR ([D$_6$]benzene): δ = 0.19 (s, 18 H, $SiSiCH_3$), 0.24 (s, 9 H, $SCSiCH_3$), 0.52 (s, 1 H, OH), 1.54 and 1.70 (2d, ^4J = 1.2 Hz, 2 × 3 H, CCH_3), 1.97 (d, ^3J = 12.8 Hz, 1 H, SiCH), 5.24 (dpseudoquart, ^3J = 12.8, ^4J = 1.2 Hz, 1 H, olef.CH). ^{13}C NMR ([D$_6$]benzene): δ = −1.1, −0.3 and −0.1 ($SiCH_3$), 17.9 and 26.0 (CCH_3), 22.8 (CH), 121.6 and 127.8 (olef. C). ^{29}Si NMR ([D$_6$]benzene): δ = −19.4 and −19.6 (SiSiMe$_3$), 2.0 ($CSiMe_3$), 8.4 (SiSiMe$_3$). MS (70 eV): *m*/*z* (%) = 332 (2) [M]$^+$, 317 (4) [M − CH_3]$^+$, 259 (19) [M − $SiMe_3$]$^+$, 73 (100) [$SiMe_3$]$^+$. HRMS: calcd. 332.18433; found 332.18365.

(3,3-Diphenyl-1-trimethylsilyl-2-propenyl)bis(trimethylsilyl)silanol (13c): Following the procedure described above but using ether instead of pentane as the solvent, 0.5 g (1.1 mmol) of **8c** and 0.3 g (0.3 mmol) of sulfuric acid afforded 0.22 g (45%) of **13c**. Colorless crystals from heptane/ethyl acetate, m.p 96−98 °C. IR (nujol): $\tilde{\nu}$ = 3463 cm^{-1} ($SiOH_{ass.}$), 3646 and 3677 cm^{-1} ($SiOH_{free}$). ^{1}H NMR ([D$_6$]benzene): δ = 0.12, 0.21 and 0.23 (3s, 3 × 9 H, $SiCH_3$), 0.57 (s, 1 H, OH), 2.47 (d, ^3J = 13.4 Hz, 1 H, CH), 6.52 (d, ^3J = 13.4 Hz, 1 H, CH), 6.98−7.41 (m, arom. 10 H, CH). ^{13}C NMR ([D$_6$]acetone): δ = −1.0, −0.5 and 0.0 ($SiCH_3$), 25.8 (CH), 126.5, 127.0, 127.2, 128.6, 128.8, 129.7, 130.9, 137.2, 140.8 and 144.0 (arom. and olef. C). ^{29}Si NMR ([D$_6$]benzene): δ = −19.1 and −18.8 (SiSiMe$_3$), 2.1 ($CSiMe_3$), 8.8 (SiSiMe$_3$). MS (70 eV): *m*/*z* (%) = 456 (2) [M]$^+$, 441 (5) [M − CH_3]$^+$, 338 (20) [M − $SiMe_3$]$^+$, 73 (100) [$SiMe_3$]$^+$. $C_{24}H_{40}OSi_4$ (456.9): calcd. C 63.09, H 8.82; found C 62.92, H 8.88.

Methoxy(3-methyl-1-trimethylsilyl-2-butenyl)bis(trimethylsilyl)-silane (14b): Compound **8b** (0.5 g, 1.5 mmol) and sulfuric acid (0.4 g, 3.6 mmol) were dissolved in 30 mL of methanol. The solution was stirred at room temperature for 8 h, neutralized with solid $NaHCO_3$ and washed with cold water. The product was extracted with ether, the solution evaporated and the residue purified by chromatography (silica gel, heptane/ethyl acetate 20:1) to afford 0.21 g (40%) of **14b**. Colorless crystals, m.p. 54−58 °C. IR (nujol): $\tilde{\nu}$ = 1087 cm^{-1} (SiOC). ^{1}H NMR ([D$_6$]benzene): δ = 0.22, 0.24 and 0.29 (3s, 3 × 9 H, $SiCH_3$), 1.56 and 1.70 (2d, ^4J = 1.2 Hz, 2 × 3 H, CCH_3), 2.01 (d, ^3J = 12.8 Hz, 1 H, SiCH), 3.31 (s, 3 H, OCH_3), 5.25 (dpseudoquart, ^3J = 12.8, ^4J = 1.2 Hz, 1 H, olef.

CH). ^{13}C NMR ([D$_6$]benzene): δ = −0.2, −0.1 and 0.6 ($SiCH_3$), 17.9 and 26.0 (CCH_3), 21.3 (CH), 53.6 (OCH_3), 121.7 and 127.7 (olef. C). ^{29}Si NMR ([D$_6$]benzene): δ = −19.6 and −19.8 (Si*Si*Me$_3$), 2.4 ($CSiMe_3$), 12.2 (SiOMe). MS (70 eV): *m*/*z* (%) = 346 (2) $[M]^+$, 331 (7) $[M - CH_3]^+$, 273 (15) $[M - SiMe_3]^+$, 73 (100) $[SiMe_3]^+$. $C_{15}H_{38}OSi_4$ (346.8): calcd. C 51.95, H 11.04; found C 51.82, H 10.89. HRMS: calcd. 346.19998; found 346.19792.

Methoxy(3,3-diphenyl-1-trimethylsilyl-2-propenyl)bis(trimethylsilyl)silane (14c): As described for **14b**, 0.5 g (1.1 mmol) of **8c** gave 0.4 g (78%) of **14c** after treatment with H_2SO_4 in methanol. The purification was performed by chromatography (silica gel, heptane); single crystals were obtained by recrystallization from heptane, m.p. 83−87 °C. IR (nujol): $\tilde{\nu}$ = 1090 cm^{-1} (SiOC). ^{1}H NMR ([D$_6$]benzene): δ = 0.17, 0.24 and 0.29 (3s, 3 × 9 H, $SiCH_3$), 2.52 (d, ^3J = 13.4 Hz, 1 H, SiCH), 3.28 (s, OCH_3, 1 H), 6.54 (d, ^3J = 13.4 Hz, 1 H, olef. CH), 7.01−7.42 (m, 10 H, arom. CH). ^{13}C NMR ([D$_6$]benzene): δ = 0.1, 0.2 and 0.7 ($SiCH_3$), 24.9 (CH), 53.6 (OCH_3), 126.6, 127.0, 127.2, 128.5, 128.6, 128.9, 130.9, 137.9, 140.6 and 144.0 (arom. and olef. C). ^{29}Si NMR ([D$_6$]benzene): δ = −19.26 and −19.31 (Si*Si*Me$_3$), 2.7 ($CSiMe_3$), 13.2 (SiOMe). MS (70 eV): *m*/*z* (%) = 470 (2) $[M]^+$, 450 (10) $[M - CH_3]^+$, 397 (15) $[M - SiMe_3]^+$, 73 (100) $[SiMe_3]^+$. $C_{25}H_{42}OSi_4$ (471.0): calcd. C 63.76, H 8.99; found C 63.75, H 8.78.

Fluoro(3-methyl-1-trimethylsilyl-2-butenyl)bis(trimethylsilyl)silane (15b): Boron trifluoride diethyl ether complex (0.22 g, 1.6 mmol) was added gradually at −78 °C to a solution of **8b** (0.50 g, 1.5 mmol) in diethyl ether (30 mL) and the mixture was stirred for 2 h. After warming to room temperature stirring was continued for 4 h, water was added and the organic phase was separated, dried and the solvents evaporated. Column chromatography (silica gel, heptane) of the residue gave 0.40 g (79.5%) of **15b**. Colorless oil. IR (nujol): $\tilde{\nu}$ = 1011 cm^{-1} (SiF). ^{1}H NMR ([D$_6$]benzene): δ = 0.21 (s, 18 H, Si*Si*Me$_3$), 0.25 (s, 9 H, $CSiMe_3$), 1.51 and 1.67 (2d, ^4J = 1.53 Hz, 2 × 3 H, CCH_3), 2.18 (dd, ^3J = 5.8, ^3J = 12.8 Hz, 1 H, CH), 5.27 (dpseudoquart, ^3J = 12.8, ^4J = 1.53 Hz, olef. CH, 1 H). ^{13}C NMR ([D$_6$]benzene): δ = −1.5, −0.6 and −0.5 ($SiCH_3$), 17.8 and 25.9 (CCH_3), 22.9 (d, ^2J = 15.0 Hz, SiCH), 120.3 (d, ^3J = 4.7 Hz, olef. CH), 128.3 (olef. C). ^{29}Si NMR ([D$_6$]benzene): δ = −19.0 and −19.4 (Si*Si*Me$_3$), 2.6 ($CSiMe_3$), 33.5 (d, ^1J = 334 Hz, SiF). ^{19}F NMR ([D$_6$]benzene): δ = −198.1 (SiF). MS (70 eV): *m*/*z* (%) = 335 (5) $[M + H]^+$, 319 (5) $[M - CH_3]^+$, 261 (15) $[M - SiMe_3]^+$, 73 (100) $[SiMe_3]^+$. Due to the ease of fragmentation an HRMS could not be obtained.

Fluoro(3,3-diphenyl-1-trimethylsilyl-2-propenyl)bis(trimethylsilyl)-silane (15c): As described above, treatment of 0.50 g (1.1 mmol) of **8c** with 0.16 g (1.1 mmol) of boron trifluoride diethyl ether complex in ether (30 mL) afforded 0.22 g (43%) of colorless crystals, m.p. 76−79 °C. IR (nujol): $\tilde{\nu}$ = 1021 cm^{-1} (SiF). ^{1}H NMR ([D$_6$]benzene): δ = 0.13, 0.23 and 0.27 (3s, 3 × 9 H, $SiCH_3$), 2.57 (dd, ^3J = 8.8, ^3J = 13.4 Hz, 1 H, SiCH), 6.57 (d, ^3J = 13.4 Hz, 1 H, olef. CH), 7.01−7.39 (m, 10 H, arom. CH). ^{13}C NMR ([D$_6$]benzene): δ = −1.3, −0.7 and −0.3 ($SiCH_3$), 26.2 (d, ^2J = 15.9 Hz, CH), 126.8, 126.9, 127.2, 128.3, 128.7, 130.6, 138.8, 140.6, 143.3 and 148.7 (arom. and olef. C). ^{29}Si NMR ([D$_6$]benzene): δ = −18.6 (Si*Si*Me$_3$), 3.0 ($CSiMe_3$), 34.7 (d, ^1J = 334 Hz, SiF). ^{19}F NMR ([D$_6$]benzene): δ = −197.5 (SiF). MS (70 eV): *m*/*z* (%) = 458 (5) $[M]^+$, 443 (2) $[M - CH_3]^+$, 385 (2) $[M - SiMe_3]^+$, 73 (100) $[SiMe_3]^+$. $C_{24}H_{39}FSi_4$ (458.9): calcd. C 62.81, H 8.57; found C 62.82, H 8.50.

X-ray Structure Determination of 14c: X-ray diffraction data were collected with a Bruker P4 four-circle diffractometer, Mo-*Ka* radiation, graphite monochromator, crystal size 0.48 × 0.44 × 0.41 mm^3, *T* = 293(2)K, $C_{25}H_{42}OSi_4$, *M* = 470.95, colorless prism, monoclinic, *a* = 9.205(2), *b* = 12.684(7), *c* = 13.226(4) Å, β = 94.78(3)°, *V* = 1538.8(10) Å^3, *Z* = 2, space group *Pn*, ρ_{ber} = 1.016 Mg m^{-3}, μ = 0.206 mm^{-1}, *F*(000) = 512, data collection range: 4.46≤ 2Θ ≤ 44.00, −9 ≤ *h* ≤ 9, −13 ≤ *k* ≤ 13, −13 ≤ *l* ≤ 13, 4054 reflections collected, 3776 independent and 3156 observed [$I > 2\sigma(I)$], R_1 = 0.0452 (obs.), wR_2 = 0.1073 (obs.), GOF(F^2) = 1.033; max./min. residual electron density: +0.122/−0.105 e·Å^{-3}. The weighting scheme was calculated according to $w^{-1} = \sigma^2(F_0^2) + (0.0485P)^2 + 0.000\,P$ with $P = (F_0^2 + 2F_c^2)/3$. The structure was solved by direct methods (Bruker SHELXTL). All non-hydrogen atoms were refined anisotropically, with the hydrogen atoms introduced into theoretical positions and refined using a riding model.

Crystallographic data (excluding structure factors) for the structure in this paper have been deposited with the Cambridge Crystallographic Data Centre as supplementary publication no. CCDC-156379. Copies of the data can be obtained free of charge on application to CCDC, 12 Union Road, Cambridge CB2 1EZ, UK [Fax: (internat.) +44-1223/336-033; E-mail: deposit@ccdc.cam.ac.uk].

Acknowledgments

We gratefully acknowledge the support of our work by the Deutsche Forschungsgemeinschaft and the Fonds der Chemischen Industrie. We thank Prof. M. Michalik, Dr. W. Baumann and Prof. N. Stoll for recording the NMR and mass spectra.

[1] K. Sternberg, H. Oehme, *Eur. J. Inorg. Chem.* **1998**, 177−181.
[2] P. D. Lickiss, *J. Chem. Soc., Dalton Trans.* **1992**, 1333−1338; J. Chojnovski, W. Stancsyk, *Main Group Met. Chem.* **1994**, *2*, 6−15; J. B. Lambert, L. Kania, S. Zhang, *Chem. Rev.* **1995**, *95*, 1191−1201; R. Bakhtiar, C. M. Holznagel, D. B. Jacobson, *J. Am. Chem. Soc.* **1992**, *114*, 3227−3235 and references cited therein.
[3] Y. Apeloig, A. Stanger, *J. Am. Chem. Soc.* **1987**, *109*, 272−273.
[4] Y. Apeloig, A. Stanger, *J. Am. Chem. Soc.* **1985**, *107*, 2806−2807.
[5] K. Miura, K. Oshima, K. Utimoto, *Bull. Chem. Soc. Jpn.* **1993**, *66*, 2356−2364.
[6] Gaussian 98, Revision A.9; M. J. Frisch, G. W. Trucks, H. B. Schlegel, G. E. Scuseria, M. A. Robb, J. R. Cheeseman, V. G. Zakrzewski, J. A. Montgomery, Jr., R. E. Stratmann, J. C. Burant, S. Dapprich, J. M. Millam, A. D. Daniels, K. N. Kudin, M. C. Strain, O. Farkas, J. Tomasi, V. Barone, M. Cossi, R. Cammi, B. Mennucci, C. Pomelli, C. Adamo, S. Clifford, J. Ochterski, G. A. Petersson, P. Y. Ayala, Q. Cui, K. Morokuma, D. K. Malick, A. D. Rabuck, K. Raghavachari, J. B. Foresman, J. Cioslowski, J. V. Ortiz, A. G. Baboul, B. B. Stefanov, G. Liu, A. Liashenko, P. Piskorz, I. Komaromi, R. Gomperts, R. L. Martin, D. J. Fox, T. Keith, M. A. Al-Laham, C. Y. Peng, A. Nanayakkara, M. Challacombe, P. M. W. Gill, B. Johnson, W. Chen, M. W. Wong, J. L. Andres, C. Gonzalez, M. Head-Gordon, E. S. Replogle, and J. A. Pople, Gaussian, Inc., Pittsburgh PA, **1998**.
[7] Geometric data of the calculated structures are available on request.
[8] C. Marschner, *Eur. J. Inorg. Chem.* **1998**, 221−226.

Received May 7, 2001
[I01158]

Hydrazino Derivatives of Gallanes and Indanes − Synthesis and Structures

Heinrich Nöth*[a] and Thomas Seifert[a]

Dedicated to Prof. Dr. Marianne Baudler on the occasion of her 80th birthday

Keywords: Gallium / Indium / Cage compounds / Cleavage reactions / Hydrolysis

The reaction of Me_2GaCl with *t*BuHN–NH_2 proceeds with ligand exchange at the gallium atom leading to $MeCl_2Ga{\cdot}H_2N$–NH*t*Bu (**1**). On the other hand, only one methyl group of the trimethylgallium molecule reacts in refluxing toluene with anhydrous hydrazine in a 4:3 ratio to produce the bicyclic dimethylgallium hydrazide **3**. *N*-Lithio-*N*-trimethylsilyl-*N*′-2-naphthylhydrazine reacts with dimethylgallium chloride, not only by introducing a gallium atom into the hydrazine unit, but also by inducing CH activation at the 1-position of the naphthyl group with methane evolution. The main product isolated is the 2,3-dihydro-1*H*-naphtho[1,2-*d*][1,2,3]diazagallol **4** which proved to be dimeric. A 1:1 $GaMe_3$ adduct of Li(Me_3Si)N–NH*t*Bu (**5**) is the unexpected compound in the reaction of Me_2GaCl with Li(Me_3Si)N–NH*t*Bu. The expected substitution product $Me_2Ga(Me_3Si)$N–NH*t*Bu is not formed. Compound **5** is a dimer in the solid state. The products obtained from reactions of Li(Me_3Si)N–NH*t*Bu with Me_2InCl depend on the solvent. With hexane as a solvent the dimeric trimethylindium adduct of Li(Me_3Si)N–NH*t*Bu (**7**), is produced as the main species. In diethyl ether the cage compound **8** is isolated which can be regarded as an $(Me_3SiN{=}InMe)_2$ adduct with $[Li(Me_3Si)N–NHtBu]_2$. Moreover, the reaction of Me_2InCl in diethyl ether with the bulky lithium hydrazide $Li[Me_3SiN–N(SiMe_3)_2]$ leads not to the substitution product, but to the dimeric adduct **9** of a diindoxane, $Me_2In–O–InMe_2$ with Li(Me_3Si)N–N($SiMe_3$)$_2$. The formation of this product indicates that ether cleavage or hydrolysis (during crystallization) has occurred.

Introduction

Metal amides have not only become important reagents in synthesis,[1−3] but have also attracted interest due to unique structural patterns.[4−6] More recently, alkali metal hydrazides have been used in the synthesis of new non-metal hydrazides[7−13] and metal hydrazides.[14−16] Amongst the latter, those of group 13 are considered as being good single-source precursors in MOCVD processes (Metal Organic Chemical Vapor Deposition) for the preparation of AlN, GaN, and InN thin films, which are useful for the production of optoelectronic devices, particularly for light-emitting diodes.[17−23] In comparison to alkali metal organylamides, the molecular structure of the alkali metal hydrazides show additional features, particularly the *side-on* coordination of Li centers to the N−N bond.[13,24−26] The best studied class of group 13 hydrazides are the hydrazinoboranes that feature non-cyclic, cyclic, and cage arrangements as the molecular units.[27−30] Aluminum hydrazides have been reported only recently.[14,24,31−36] Information on hydrazides of gallium and indium is, so far, comparatively scanty.[37−40]

[a] Department of Chemistry, University of Munich, Butenandtstr. 5−13 (House D), 81377 München, Germany
E-mail: H.Noeth@lrz.uni-muenchen.de

Results

Gallium Hydrazides

Synthesis

Several routes to metallated hydrazines are known, and in this study only two have been employed, the reaction of dimethylgallium and dimethylindium chloride with monolithium hydrazides, and the reaction of trimethylgallium with anhydrous hydrazine.

It was expected that the reaction of dimethylgallium chloride with *tert*-butylhydrazine would first produce a 1:1 addition product followed by methane elimination either to give MeClGa−NH−NH*t*Bu or $(ClGa–NH–NtBu)_n$. However, in toluene solution no gas evolution was observed at ambient temperature. However, this gas evolution set in at 70 °C, and became rapid on heating the solution to reflux. Under these conditions a sparingly soluble product was formed, which showed two signals in the ^{1}H NMR spectrum in a 1:3 ratio, suggesting the formation of oligomeric $(MeGa–NH–NtBu)_n$ (**2**). From the solution the adduct $MeCl_2Ga{\cdot}H_2N$−NH*t*Bu (**1**) was isolated. This result suggests that under the conditions of the experiment Me_2-GaCl is subject to substituent exchange as shown in Equation (1). The Lewis acid $MeGaCl_2$ so formed added to the hydrazine [Equation (2)] while $GaMe_3$ reacted with the hy-

 © WILEY-VCH Verlag GmbH, 69451 Weinheim, Germany, 2002 1434−1948/02/0303−0602 $ 17.50+.50/0 *Eur. J. Inorg. Chem.* **2002**, 602−612

drazine $H_2N-NHtBu$ to produce methane and **2** [Equation (3)].

$$2\,Me_2GaCl \rightarrow Me_3Ga + MeGaCl_2 \quad (1)$$

$$MeGaCl_2 + H_2N{-}NHtBu \rightarrow \underset{\mathbf{1}}{MeCl_2Ga{-}NH_2{-}NHtBu} \quad (2)$$

$$Me_3Ga + H_2N{-}NHtBu \rightarrow {}^{1}/_{n}\,\underset{\mathbf{2}}{[MeGa{-}NH{-}NtBu]_n} + 2\,CH_4 \quad (3)$$

$$4\,GaMe_3 + 3\,H_2N{-}NH_2 \xrightarrow{\Delta} \underset{\mathbf{3}}{(Me_2Ga)_4(N_2H_2)(NH{-}NH_2)_2} + 4\,MeH \quad (4)$$

This result demonstrates the high reactivity of $GaMe_3$. Therefore, hydrazine was allowed to react with $GaMe_3$. In refluxing toluene, practically only compound **3** was formed, containing Me_2Ga and hydrazino units in a ratio of 4:3, irrespective of the molar ratio employed. In **3** there are two different hydrazino groups, one that is doubly metallated, and two hydrazino groups that are singly metallated [see Equation (4)].

Although one might expect that the reaction of Me_2GaCl with a lithiated disubstituted hydrazine would proceed in a more straightforward manner, a surprising reaction occurred between Me_2GaCl and *N*-lithio-*N′*-(2-naphthyl)-*N*-(trimethylsilyl)hydrazine in refluxing toluene, as depicted in Equation (5). The product was the 2,3-dihydro-1*H*-naphtho[1,2-*d*][1,2,3]diazagallol **4**.

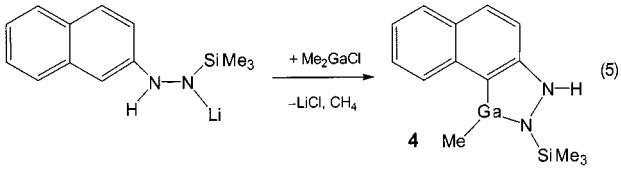

(5)

In the solid state **4** is present as a dimer (vide infra). Obviously, the hydrogen atom in position 1 of the 2-naphthyl group is more reactive than the hydrogen atom of the NH group of the hydrazide. Taking these results into account it was expected that a more bulky lithium hydrazide such as $Li(Me_3Si)N-NHtBu$ might react with Me_2GaCl by simple substitution as shown in Equation (6).

$$Me_2GaCl + LiNSiMe_3{-}NHtBu \rightarrow Me_2Ga{-}N(SiMe_3){-}NHtBu + LiCl \quad (6)$$

$$2\,Me_2GaCl + 2\,LiN(SiMe_3){-}NHtBu \rightarrow$$

$$\underset{\mathbf{5}}{LiN(SiMe_3){-}NHtBu{\cdot}GaMe_3} + \underset{\mathbf{6}}{MeClGa{-}N(SiMe_3){-}NHtBu} + LiCl \quad (7)$$

However, only a small amount of LiCl precipitated, and the product obtained was **5**. Obviously, Me_2GaCl again suffers substituent exchange as described by Equation (1), and $GaMe_3$ adds to the lithium hydrazide to form **5**. The second product of the reaction was expected to be $MeClGa-N(SiMe_3)-NHtBu$ (**6**), but this compound could not be isolated.

In summary, none of the reactions described above led to the anticipated product.

X-ray Structure Determinations

Compounds **1** and **3**−**5** were obtained as single crystals. This allowed the determination of their molecular structures in the solid state, and this knowledge was helpful for the assignment of signals obtained by NMR experiments.

The $MeGaCl_2$ adduct **1** crystallized in the tetragonal system, space group $I4_1/a$ with $Z = 16$. Figure 1 depicts the molecular structure of **1** ascertaining that the compound is the $MeGaCl_2$ adduct of the hydrazine $H_2N-NHtBu$. Its Ga−N distance [2.023(7) Å] correlates well with those found for $Cl_3Ga-NMe_2SiMe_2NMe_2$ [2.002(9) Å][41]or the dimeric gallium amides $[Me_2Ga-N(Ph)SiMe_3]_2$,[42] $[Me(Cl)Ga-NHSiMe_3]_2$,[43] and $(iPr_2Ga-NHNMe_2)_2$[44] [2.071(2), 2.012(8), and 2.031(2) Å, respectively]. The Ga−C bond in **1** [1.933(7) Å] lies in the range found for several amino(methyl)gallanes having tetracoordinated Ga atoms[33,42,43]. Both N atoms are in a non-planar situation, the coordination site at N1 corresponds with a distorted tetrahedral array (bond angles ranging from 104.3 to 113.8°) and a sum of bond angles of 656.6°, while that of the tricoordinated atom N2 is 320.1° slightly smaller than calculated for a pseudo-tetrahedral array (328.5°). Taking this into account, the N−N bond length of 1.446(9) Å in **1** corresponds with the N−N bond length of hydrazine (1.47 Å)[44] and of the methylhydrazinium cations $MeNH_2NH_2^+$ [1.445(1) Å][45] and $Me_3N-NH_2^+$ [1.457(1) Å].[46] The two amino groups are present in a staggered conformation. A *trans* conformation results for the Ga−N−N−C unit (τ = 175.5°).

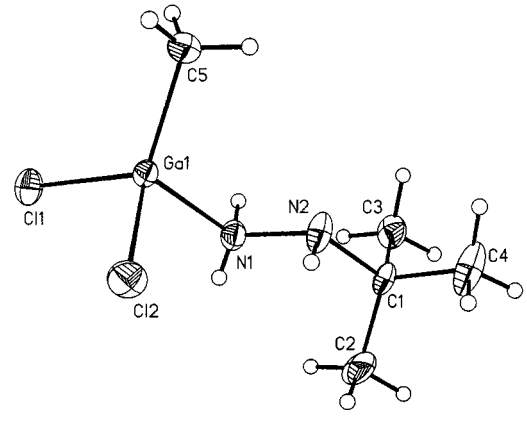

Figure 1. ORTEP representation of **1**; selected bond lengths [Å] and bond angles [°], esd values in parentheses: Ga1−N1 2.023(7), N1−N2 1.446(9), Ga1−C5 1.933(7), Ga1−Cl1 2.202(2), Ga1−Cl2 2.175(2), N1−H1A 0.72, N1−H1B 0.97; N1−Ga1−Cl2 100.8(2), N1−Ga1−C5 112.0(4), Cl1−Ga1−Cl2 105.62(8), Cl1−Ga1−C5 116.4(3), Cl2−Ga1−C5 118.9(3), Ga1−N1−N2 108.3(5), N1−N2−Cl 115.4(6), N1−N2−H2 115.4, Cll···H−N 2.5475(1), Cl2···H−N 2.88(1); angles at hydrogen bonds: N1−H1−Cl2A 160.7, N1−H1B−Cl1B 167.4; Cl···Cl contact: Cl1···Cl1B 3.556

The two Ga−Cl bond lengths differ significantly with Δ = 0.027 Å, and on first sight there is no reason why this should be so. One might suspect that the different Ga−Cl

bond lengths arise from different N−H···Cl hydrogen bonding. Hydrogen bonds indeed connect the molecules of **1** in the solid state, and only the H atoms of the NH_2 groups, which have ammonium-type character, are involved in hydrogen bonding, in contrast to the NH group. Bond angles at the H atoms of the bridging N−H···Cl units span a range from 160.7 to 167.4° with H···Cl distances between 2.547 to 2.878 Å. Tetrameric units result by these hydrogen bonds. Figure 2 depicts the association of four molecules of **1** in the crystal.

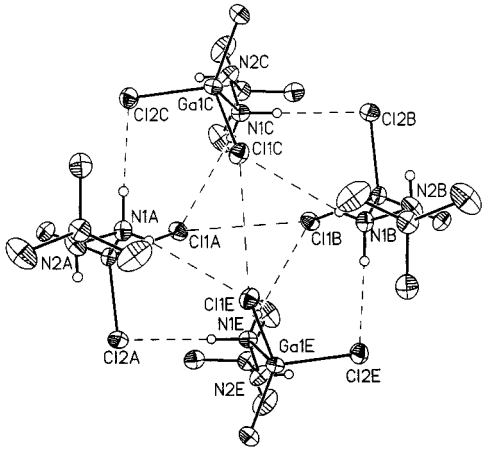

Figure 2. Tetrameric association of **1** formed by hydrogen bonds

The molecular structure of compound **3** is represented in Figure 3, showing a bicyclo[3.3.0]octane skeleton. Compound **3** crystallizes in the triclinic system in space group $P\bar{1}$.[47] The unit cell contains two independent molecules each having a crystallographically imposed center of symmetry lying at the midpoint of the central N−N vector, but these two N atoms are site-disordered with an SOF of 0.5. Therefore, the bicyclic system shows two conformations. In addition, there is a disordered toluene molecule in the unit cell with a center of inversion in the midpoint of the benzene unit. A consequence of this disorder is that the standard deviations particularly for the central N−N bond is fairly large, and this is also true for the *R* indices.

The structure of compound **3** can be considered to be composed of one dimetallated hydrazine unit, $Me_2Ga-NH-NH-GaMe_2$, and two $Me_2Ga-NH-NH_2$ units, which allows all Ga atoms to become tetracoordinated by two Me groups and two N atoms. Because the Ga atoms are part of a five-membered heterocycle the N−Ga−N angles are only 92.8(3) and 92.9(4)° while the C−Ga−C bond angles are 124.1(4)° at Ga1 and 123.8(4)° at Ga2. The Ga1−N2−Ga2 bond angle [107.7(3)°] is closer to the tetrahedral angle than the Ga1−N1−N1A and N1−N1A−Ga2 bond angles [111.7(11) and 111.5(11)°]. The two N−N bond lengths in the molecules with atoms Ga1 and Ga2 are 1.38(2) Å (N−N bridge of the bicycle) and 1.48(8) Å (for the exocyclic N−N bonds). However, these bonds are significantly different in the second independent molecule with 1.51(8) and 1.48(8) Å.

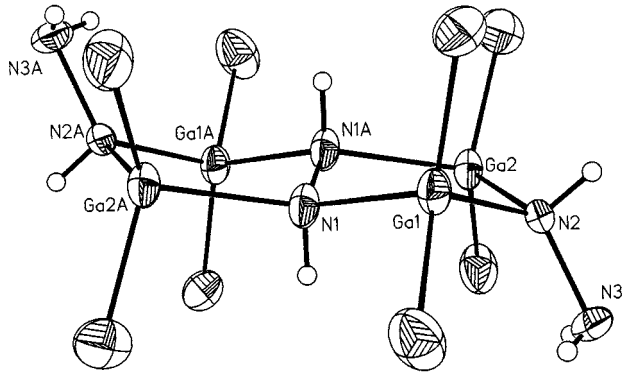

Figure 3. Molecular structure of one of the two independent molecules of **3** in ORTEP representation; *C*-bonded hydrogen atoms omitted; selected bond lengths [Å] and bond angles [°], esd values in parentheses: Ga1−C1 1.947(8), Ga1−C2 1.9478(8), Ga1−C2 1.947(7), Ga2−C3, 1.959(7), Ga1−C4 1.943(8), Ga1−N1 2.03(1), Ga1−N2 1.985(5), Ga2−N1A 2.05(1), Ga2−N2 2.000(5), N1−N1A 1.49(1), N2−N3 1.487(7); C1−Ga1−C2 124.1(4), C3−Ga2−C4 123.8(4), N1−Ga1−N2 92.9(4), N1A−Ga2−N2 96.4(4), Ga1−N2−Ga2 107.7(3), Ga1−N1−N1A 1112(1), Ga2−N1A−N1 112(1), H−N1−N2 104(2), H−N2−N3 106(2); sum of bond angles at N1 655.7, at N2 657.1, at N1A 655.1

While atoms Ga1, N2, Ga2, Ga1A, N2A, Ga2A lie almost in a plane, atom N1 is 0.65 Å apart from the Ga1−N2−Ga2−N1A plane (τ = 8.5°), e.g. the five-membered rings have an envelope conformation. Figure 4 shows the two conformations that result from the site disorder of the central N−N unit. These conformations result in an "up-and-down" arrangement for the central N−N groups.

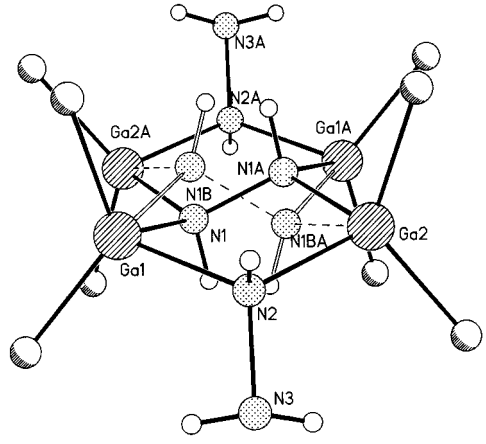

Figure 4. Representation of the disorder of the molecule **3**; methyl hydrogen atoms are removed for clarity

All N atoms in **3** are in a non-planar environment. They can be considered to be sp^3-hybridized. In the solid state, the molecules of **3** are interconnected by NH···N hydrogen bonding. These bridges are formed with the H atoms of the central N_2H_2 units, which bridge to NH_2 groups. This results in chains of interconnected molecules of **3** that extend parallel to the *c* axis of the crystal (Figure 5).

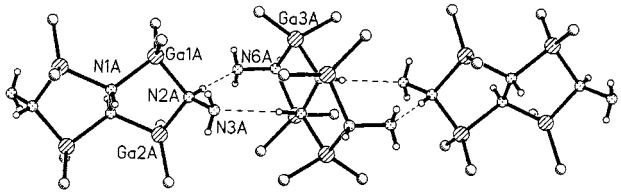

Figure 5. Association of the molecules of **3** in the solid; the chains extend parallel to the *z* axis; note that only N−H···NH_2 bridges are formed; the H atoms of the NH_2 groups are not involved in hydrogen bonds

Table 2. Population analysis and Wiberg bond orders

	Charges	Wiberg bond order	
Ga1	+0.66	N1−N1A	0.99
Ga2	+0.68	N2−N3	1.01
N1	−0.68	Ga1−N1	0.35
N2	−0.72	Ga1−N2	0.36
N3	−0.58	Ga2−N1A	0.35
C1−C4	−0.69	Ga−C	0.69

As indicated, the N−N bond and the corresponding bond angles of **3** could be determined only with large standard deviation and are, therefore, not very accurate due to the indicated disorder.[47] For this reason geometrical data for the molecule were calculated on the B3LYP/6-31* level.[48] The data for the geometry-optimized molecular structure of **3** and frequency analysis are compiled in Table 1 together with the data found in the X-ray structure determination. The calculated data correspond to the energy minimum.

Table 1 shows that the Ga−C distances comply well with the calculated bond lengths, while the calculated Ga−N bond lengths are shorter than the experimental values. More importantly, the calculated central N−N bond length is noticeably longer than the exocyclic N−N bonds. The average experimental value corresponds with the calculated bond length. On the other hand, the experimental bond angles differ by −2.5 to 3.4° from those calculated.

Data for the population analysis and the Wiberg bond orders are summarized in Table 2. These show that the N−N bonds are single bonds. A *trans* conformation for the central N−N unit also results for the calculated structure. In contrast to the experimental structure with its eclipsed conformation for the exocyclic hydrazino moiety (torsion angle Ga−N−N−H 3.9°), a *gauche* conformation results from the calculation as is well known for hydrazine itself[44] (torsion angle 34.7°). This discrepancy, however, can be easily resolved by considering the N−H···N hydrogen bonds that are present in the solid sate.

Yellow crystals of **4** are monoclinic, space group $P2_1/c$ with $Z = 4$ monomeric units; actually, $Z = 2$ because two molecules form a dimer via Ga−N coordinative bonds. The center of the Ga−Ga vector of the four-membered Ga_2N_2 ring coincides with a crystallographic inversion center. The molecular structure of $(\mathbf{4})_2$ is depicted in Figure 6.

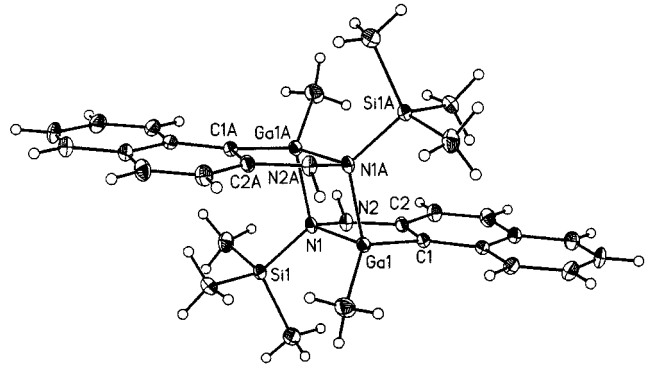

Figure 6. Molecular structure of dimeric **4** in the crystal; selected bond lengths [Å] and bond angles [°], esd values in parentheses: Ga1−C1 1.947(3), Ga1−C14 1.949(3), Ga1−N1 2.051(2), Ga1−N1A 2.031(2), N1−Si1 1.780(2), N1−N2 1.482(3), N2−C2 1.414(3), C1−C2 1.333(4), C1−C10 1.430(4), C2−C3 1.420(4), C3−C4 1.365(4), C4−C5 1.414(4), C5−C10 1.423(4); C1−Ga1−N1 110.98(9), C1−Ga1−C14 129.2(1), C1−Ga1−N1A 89.25(8), N2−N1−Si1 103.8(2), N2−N1−Ga1 112.5(2), Si1−N1−Ga1 123.5(1); interplanar angles: Ga1,N1,Ga1a,N1a/N1,N2,C1,C2,Ga1 110.1, N1,N2,C1,C2,Ga1/C1−C5,C10 6.5

Table 1. Experimental and calculated structural data for compound **3**

	Exp. values				Calcd. values
Ga1−C	1.947(8) C1	Ga3−C	1.95(1) C5	C1	1.997
	1.947(7) C2		1.960(1) C6	C2	1.997
Ga2−C	1.959(7) C3	Ga4−C	1.95(1) C7	C3	1.995
	1.943(8) C4		1.95(1) C8	C4	1.995
Ga1−N	2.03(1) N1	Ga3−N	1.96(1) N4A	N1	1.985
	1.985(5) N2		1.997(8) N5	N2	1.972
Ga2−N	2.05(1) N1A	Ga4−N	2.08(1) N4	N1A	1.996
	2.000(5) N2		1.992(7) N5	N2	1.984
N−N	1.49(1) N1	N−N	1.51(3) N4	N1	1.522
	1.481(7) N2		1.476(9)	N2	1.489
N1−Ga1−N2	92.8(3)	N5−Ga3−N4a	96.2(4)		95.3
Ga1−N2−Ga2	107.7(2)	Ga3−N5−Ga4	107.4((3)		108.3
N1−N1A−Ga2	107.3(9)	N4A−N4−Ga4	102(1)		110.7
N1A−N1−Ga1	109.7(9)				107.5

The two Ga−N bond lengths are significantly different, the shorter bond, Ga1−N1 [2.031(2) Å], is found in the five-membered ring, the longer one, Ga1−N1A [2.051(2) Å], in the four-membered ring. Inspection of the Ga−C bond lengths reveals an interesting and somewhat unusual feature, both are of equal lengths [Ga1−C1 1.949(3), Ga1−C14 1.947(3) Å] although C1 is of sp^2-type hybridization, and this should result in a shorter Ga−C distance as compared to the Ga1−C14 bond with an sp^3-C atom. Due to the situation that the Ga atom is both part of a four- and a five-membered ring system, the tetracoordinated Ga atom shows strong deviations from the tetrahedral bond angle. Even the C1−Ga1−N1 bond angle of the five-membered ring is only 87.4°, a consequence of the longer Ga1−C1 and Ga1−N1 bonds.

The molecular structure of **4** was of importance to unequivocally demonstrate that the Ga metallation of the naphthyl group occurred at the 1-position. An almost planar Ga−N−N−C−C five-membered ring is present with atoms N2 and C2 being 0.064 and −0.082 Å away from the best plane. The ring is almost coplanar with the naphthalene moiety, the angle between the two planes being only 7.2°. The Ga_2N_2 four-membered ring forms an angle of 113.6° with the five-membered GaN_2C_2 ring. Because both N atoms of the hydrazine moiety in compound **5** are sp^3-hybridized (sum of bond angles at N2 338.4°), a comparatively long N−N bond can be expected. The distance [1.482(3) Å], however, is typical for a simple hydrazine unit.

The needles of **5** proved to be monoclinic, space group $P2_1/n$ with $Z = 2$. Figure 7 shows that the molecule is dimeric. There is a crystallographic inversion center situated in the center of the six-membered Li_2N_4 ring. The $GaMe_3$ units are attached at the deprotonated side of the hydrazide units. Moreover, it can be noted that the hydrazine *t*BuNH−NHSiMe$_3$ is metallated at the silyl-group-carrying nitrogen atom. Both Li atoms of the Li_2N_4 ring are coordinated to two nitrogen atoms and, in addition, each one shows Li···H−C contacts with CH hydrogen atoms of the $GaMe_3$ units that add to the steric shielding of the Li centers [Li−H 2.20(1), 2.21(1) Å]. The Li−N bond lengths are found in the expected ranges,[49] actually both can be considered to be of equal length. Moreover, it should be noted that the Ga−N bond length is shorter than the Li−N distances.

It can be seen from Figure 7 that the Me groups are arranged in such a manner that a staggered orientation results, minimizing intramolecular repulsion of the methyl groups. Although the ring adopts no true chair conformation, the ring is, nevertheless, not planar. Bond angles for the ring atoms are: Li1−N2−N1 98.1(2), N1−N2−Li1A 108.6(2), and N2−Li1−N1A 124.8(2)°. The bond angles N2−N1−Si1 and N2−N1−Ga1 [119.5(1)° and 116.6(1)°, respectively] are wider than expected for a tetrahedral moiety at nitrogen atoms N1 and N2, and the angle Ga1−N1−Li1A is sharp with 80.5(1)°.

Two of the Ga−C bond lengths are almost of equal lengths considering the 3σ criterion. However, the Ga1−C9 distance is noticeably elongated; it is this atom of the CH_3 group that is involved in Li···H−C interactions. Consequently, the Li−C distance is short, 2.234(4) Å, a distance that is typical for organolithium compounds.[49,50] The N−N bond in **5** is fairly long, 1.496(2) Å. All N atoms are tetracoordinated.

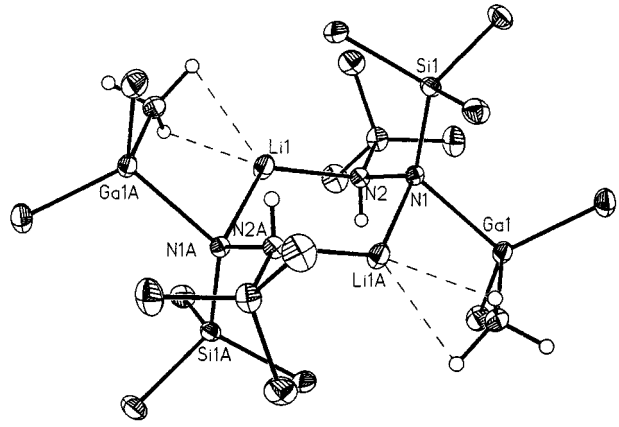

Figure 7. Molecular structure of **5** in the crystal; CH hydrogen atoms are omitted; selected atom distances [Å] and bond angles [°], esd values in parentheses: Ga1−N1 2.053(2), Ga1−C8 1.998(3), Ga1−C9 2.084(3), Ga1−C10 1.985(3), Li1−N1 2.093(4), Li1−N2 2.010(4), Li1···C9 2.234(4), N1−N2 1.496(2), N2−C4 1.514(3), N1−Si1 1.743(2), Li1···H9A 2.20(1); Li1···H9B 2.21(1); N1−Ga1−C8 108.7(1), N1−Ga1−C9 102.83(9), N1−Ga1−C10 113.0(1), N1A−Li1−C9 95.5(2), N2−Li1−N1A 124.8(2), N2−N1−Ga1 116.6(1), N2−N1−Si1 119.5(1), N2−N1−Li1A 108.6(2), N1−N2−Li1 98.1(2), Ga1−N1−Li1A 80.5(19); torsion angles: Li1A−N1−Ga1−C9 16.0, Li1−N2−N1−Li1A 49.0; sum of bond angles at N1 331.8, at N2 324.9

NMR Spectra

As expected, the ^{1}H and ^{13}C NMR spectra of the adduct **1** is simple. There are three signals of each kind. Those of the ^{1}H resonances are observed at δ = 0.33 (GaMe), 0.65 (CMe), and 4.15 (broad, NH) in a 1:3:1 ratio, while the ^{13}C signals are located at δ = −3.1 (GaMe), 25.6 (C*Me*), and 55.3 (*C*Me$_3$). It is well known that the shielding of the Ga*Me* group resonances depends on the nature of the substituents, the more electronegative the substituents the stronger the deshielding. For example, while the ^{1}H signal of $(Me_2GaCl)_2$ is found at δ = 0.12, it is observed for $(Me_2Ga{-}NMe_2)_2$ at δ = −0.4. The NH resonance signal is broad and not resolved, indicating rapid exchange of these protons.

In contrast, the signal for the *N*-bonded hydrogen atoms in the bicyclic compound **3** are well resolved. There are three signals at δ = 2.24, 2.35, and 2.72 in the correct intensity ratio. On the other hand, seven signals were observed in the region from δ = −0.4 to −0.1 for the Me groups attached to the Ga atoms. Complementary results were obtained in the ^{13}C NMR spectrum, which reveals 7 signals in the range δ = −11.2 to −7.1. The double envelope conformation of compound **3** should lead to four pairs of chemically equivalent methyl groups. In case of inversion at the N atoms two sets of four signals may results. That inversion takes place is ascertained by coalescence of the ^{13}C resonances at 80 °C. Using the Eyring equation[51] the

calculated activation energy is $\Delta G^* = 72.3$ kJ/mol. This corresponds with the activation energy of 73.9 kJ/mol[52] found for the six-membered hydrazinoalane $[Me_2Al-NSiMe_3-NCMe_3]_2$.[16]

Knowing the structure of compound **4**, only a single ^{29}Si resonance was expected and found at $\delta = -0.17$, apart from the ^1H and ^{13}C resonances of the $SiMe_3$ group. On the other hand, six ^1H signals for the naphthyl group were found, and this corresponds with a metallation of the naphthyl group at the 1-position, excluding the possibility of metallation at the 3-position. For this latter case, only three signals should be observable.

The ^1H and ^{13}C NMR spectra of compound **5** are in agreement with the X-ray structure. The GaMe protons are fairly well shielded with $\delta^1H = -0.08$. With $\delta = 7.00$ the ^{29}Si nucleus is better shielded compared with $\delta^{29}Si = 13.6$ for compound **4**, and this is most likely due to the negative charge at the Si bearing nitrogen atom of compound **5**.

Indium Hydrazides

Synthesis

In order to test whether Me_2InCl is also liable to substituent exchange on reactions with lithium hydrazides this indium chloride was allowed to react with $Li(Me_3Si)N-NHtBu$ in a 1:1 molar ratio in hexane. The indium homologue **7** of the gallium complex **5** was indeed formed as indicated in Equation (8).

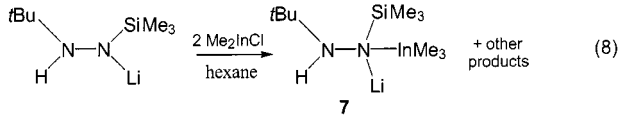

(8)

7

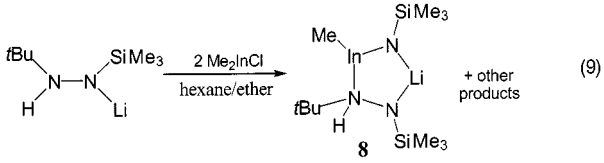

(9)

8

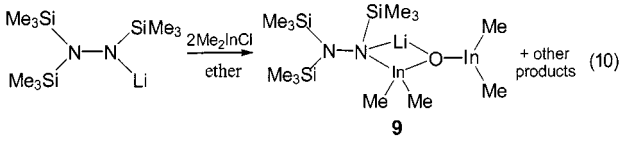

(10)

9

However, when the same reaction was performed in an ether/hexane mixture the reaction took a different course, as depicted in Equation (9). Only compound **8** and no by-products could be isolated and characterized. This would have been important to obtain an idea on the course of the redox reaction involved in the formation of compound **8**, which can be considered to be composed of the iminoindane $MeIn=NSiMe_3$ added to the lithium hydrazide used as a starting material. Assuming that the first step in the reaction is the expected substitution to give $Me_2In-N(SiMe_3)-NHtBu$, a methyl transfer to produce the amine $NHMe(tBu)$ may formally lead to the iminoindane. A similar reaction has not been observed in our experiments with gallium.

One might expect that by employing a sterically better shielded lithium hydrazide than $Li(Me_3Si)N-NHtBu$ could lead to anticipated products. For this reason Me_2InCl was treated with $Li(Me_3Si)N-N(SiMe_3)_2$. In nonpolar solvents such as hexane or toluene, the NMR spectra pointed to a very complex reaction, e.g. fifteen ^{29}Si NMR signals were detected in the range $\delta = 5.0-19.5$. However, when ether was employed as a solvent the situation changed drastically because compound **9** was formed as the main product. This compound was isolated and fully characterized. Nevertheless, it is once again an unexpected product, as shown in Equation (10). Compound **9** can be regarded as the adduct of a bis(dimethylindium) oxide (diindoxane) with lithium tris(trimethylsilyl)hydrazide. The X-ray structure determination shows that **9** is actually a dimer in the solid state.

Structures

Compound **7** crystallizes, like the trimethylgallane adduct **5**, in the monoclinic system, space group $P2_1/n$ (no figure is given because the structure of **7** is very similar to the structure of **5**). The molecular parameters for both compounds are listed in Table 3. The unit cells differ particularly with respect to the angle β. As far as the molecular parameters are concerned, there are no great differences except, of course, for the In−N and In−C bond lengths. The molecular symmetry is C_i. The equatorial positions of the chair-type six-membered ring are occupied by the *tert*-butyl and Me_3In groups while the Me_3Si groups are in axial positions. Li··H contacts complete the coordination sphere of the Li atom by two H atoms. The Li···C contact of Li1 to C10A [2.278(8) Å] is 0.04 Å longer than in compound **5**. This difference is probably due to the fact that there is only one Li···H contact while there are two Li···H contacts in compound **5**. The bond angles N2−N1−Si1 (120.4°) and N2−N1−In1 (116.0°) are quite open. This indicates that the Li−N bonds are highly polar.

Compound **8** is present as a dimer in the monoclinic crystal, space group $C2/m$. The molecular symmetry is, crystallographically imposed, C_2. Figure 8 shows the molecular structure with its cage-like arrangement of the core atoms. While we have previously discussed the compound as a formal adduct of an iminoindane with a lithium hydrazide, we now see that it is an adduct of a dimeric, tub-shaped six-membered lithium hydrazide with a four-membered 1,3,2,4-diazadiindetidine. The NH hydrogen atoms are present in axial positions, while the Me_3Si and MeIn groups are in equatorial positions. The four-membered In_2N_2 ring is only slightly bent (folding angle 13°) with endocyclic angles close to 90°. Due to the different atomic radii, one observes trapezoidal InN_2Li fragments. All indium atoms are tetracoordinated while the Li atoms are tricoordinated. The N atoms reside in a distorted tetrahedral environment.

The most interesting structural features are the In−N distances. These are short for the four-membered In_2N_2 ring [2.145, 2.178(4) Å], while those to the lithium hydrazide units are 2.223(3) Å. This latter bond length compares well with those found for $(Me_2N-InMe_2)_2$ (2.255 Å),[53]

Table 3. Structural parameters of the Me_3E adducts of Li(Me$_3$Si)N−NH*t*Bu (E = Ga, In); atom distances in Å, bond angles in °; standard deviations in parentheses

	E = Ga (**5**)	E = In (**7**)		E = Ga (**5**)	E = In (**7**)
E−N	2.053(2)	2.281(3)	N1−E−C10	102.83(9)	97.3(1)
E−C	1.998(3) C8	2.189(4) C8	N1−E−C8	113.0(1)	105.4(2)
	1.985(3) C10	2.242(3) C10	N1−E−C9	108.7(1)	112.9(1)
	2.048(3) C9	2.169(4) C9	N2−N1−E	116.6(1)	116.0(2)
N−N	1.492(2)	1.495(4)	N1−N2−Si	119.5(1)	120.4(2)
N−C	1.514(2)	1.503(5)	N2−Li1−Li1A	108.6(2)	109.9(3)
N−Li	2.093(4) N1	2.087(7)	N1−N2−Li1	98.1(2)	94.2(3)
	2.010(4) N2	2.008(6)	N1−Li1A−C10	95.5(3)	102.0(3)
N−Si	1.743(2)	1.744(3)			

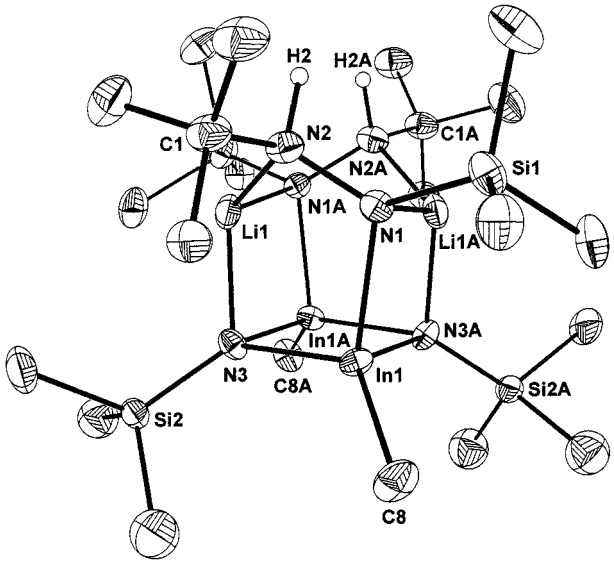

Figure 8. Molecular structure of **8**; hydrogen atoms are removed for clarity; selected atom distances [Å] and bond angles [°], esd values in parentheses: In1−N1 2.323(3), In1−N3 2.145(4), In1−N3A 2.178(3), Li1−N1A 2.165(8), Li1−N2 1.983(9), N1−N2 1.472(5), In1−C8 2.157(4), N1−Si1 1.752(7), N3−Si3 1.733(5); N3−In1−N3A 88.1(1), N3−In1−N1 99.8(1), In1−N1−Li1A 79.3(2), In1−N1−N2 1135.5(2), N2−N1−Li1A 107.3(3), N2−Li1−N3 114.1(4), N2−Li1−N1A 112.9(4), N3−Li1−N1A 101.9(3), N1−N2−Li1 103.0(3), Li1−N2−In1A 84.9(2), In1−N3−In1A 91.9(1), Li1−N3−In1 95.1(3); sum of bond angle at Li1 328.9, at N2 333.2

(*i*Pr$_2$In−NH*t*Bu)$_2$ (2.231 Å),[54] and various other aryl or Me$_3$Si substituted dimeric aminoindanes (up to 2.305 Å).[55,56] Shorter In−N bonds are observed for [Me$_2$In−N=CMe$_3$]$_2$ (2.195 Å)[57] or [Cl$_2$In−N=CPh$_2$]$_2$ (2.112 Å).[58] These latter distances fall into the range for the In$_2$N$_2$ unit of **8**.

The monoclinic compound **9**, which crystallizes in space group $P2_1/c$, displays a spirocyclic system (as depicted in Figure 9) featuring a central four-membered In$_2$O$_2$ ring. Its center coincides with a crystallographic inversion center. The interplanar angle between this ring and the neighboring LiN$_2$In ring is 67.1°, the latter ring is almost planar as demonstrated by an Li−N−In−N torsion angle of 4.3°. Both In atoms are tetra-coordinated with a very open C−In−C angle of 126.6(2)° at In1 and 131.4(2)° at In2.

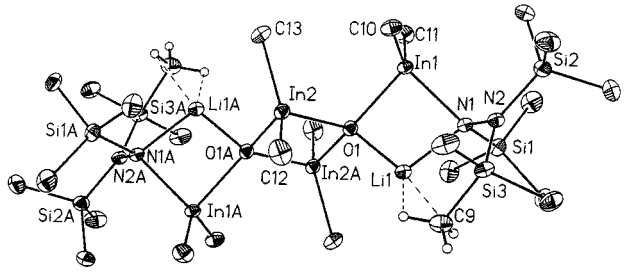

Figure 9. ORTEP plot of the molecular structure of **9**; selected atom distances [Å] and bond angles [°], esd values in parentheses: In1−N1 2.201(3), N1−N2 1.508(4), In1−O1 2.168(3), In2−O1 2.144(3), In2−O1A 2.162(3), N1−Si1 1.738(3), N2−Si2 1.738(4), N2−Si3 1.742(4), In1−C12 2.143(5), In1−C13 2.166(5), Li1−N1 2.036(9), Li1−O1 1.837(8), Li···H 2.03(1), 2.23(1);− O1−In1−N1 87.98(1), O1−In2−O1A 84.8(1), C11−In1−C12 126.6(2), C1−In2−C13 131.4(2), O1−Li1−N1 102.9(4), N1−Li1−C9 90.6(3), In2−O1In1 112.4(1)

The Li ions are formally two-coordinated with bonds to one O and one N atom, but the next shortest distances (2.03 and 2.23 Å) are found to H atoms of the Me$_3$Si groups. The N−N bond length is 1.508(4) Å. The sum of bond angles at atom N2 is 360°, and from this point of view, one has to regard the N−N bond as comparatively long. Once again, we take this as evidence for polar Li−N interactions due to a high negative charge at N2. The compound can be regarded an addition product of lithium tris(trimethylsilyl)hydrazide with bis(dimethylindium) oxide.

NMR Spectra

NMR spectroscopic data recorded for compound **7** are similar to those found for compound **5**. However, the ^{1}H and ^{13}C resonances for **7** are at slightly higher field due to the lower electronegativity of In. The ^{29}Si resonance is found at $\delta = 6.4$, shifted only by 0.6 ppm to higher field compared to **5**. On the other hand, the ^{7}Li chemical shift at $\delta = -1.0$ is the same as found for **5**.

Knowing the structure of compound **8**, it is not surprising to find its NMR spectroscopic data are close to those of **7**. Even δ^7Li = −0.9 is almost the same. As expected,

there are two ^{29}Si NMR signals, while the NH protons result in a broad signal.

In agreement with the structure of **9** there are four ^{1}H and ^{13}C signals in the NMR spectra for the MeIn groups and two signals each for the Me_3Si group in the ^{1}H, ^{13}C, and ^{29}Si NMR spectra. However, not having had available the X-ray structure result it would have been difficult to guess the presence of a bis(dimethylindium) oxide unit in the molecule.

Discussion

This study demonstrates that the reactions of Me_2GaCl with organylhydrazines and lithium organylhydrazides are characterized by a substituent exchange at Me_2GaCl, leading to $MeGaCl_2$ and $GaMe_3$. Most likely, the substituent exchange is induced by the base as depicted in Equation (11). Such exchange reactions are well know in the chemistry of organyl compounds of the heavier group 13 elements.[59] Nevertheless, reactions of lithium amides with dialkylaluminium chlorides or dialkylgallium chlorides lead to the expected dialkylmetal amides without ligand exchange.[60] However, reaction of tBu$_2$AlCl with $Li_2N_2(SiMe_3)_2$ produced $[t\text{BuAl}-N(SiMe_3)-N(SiMe_3)]_2$, indicating a similar ligand exchange at the metal atom as reported here.[14] Moreover, Uhl et al. found that the reaction of tBu$_2$AlCl with $H_2NNHSiMe_3$ produced $t\text{BuCl}_2\text{Al}\cdot NH_2-NHSiMe_3$, a compound that is analogous to compound **1**.[61]

It is interesting that the *tert*-butylhydrazine removes $MeGaCl_2$ from the equilibrium in Equation (1) while the lithium hydrazide $Li(Me_3Si)N-NH-t$Bu adds to trimethylgallium and not to a methylgallium chloride molecule. This can be rationalized as follows. The hydrazide is expected to be a stronger base than the hydrazine, and binds, therefore, to Me_3Ga because one can expect that $MeGaCl_2$ formed in the ligand exchange reaction has (most likely) reacted rapidly with the hydrazide by substitution as indicated in Equation (7).

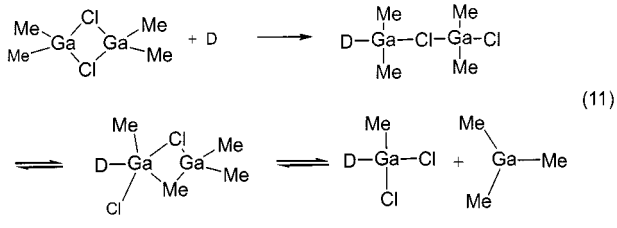

Trimethylgallium reacts with hydrazine (N_2H_4) readily with CH_4 evolution to produce a bicyclic compound **3** that may be a precursor for MOCVD of GaN. As far as we are aware, no such structure has been observed so far for group 13 hydrazides. So, in contrast, the reaction of tBu$_2$AlH with N_2H_4 leads, in a first step, to the six-membered $(t\text{Bu}_2\text{Al}-NH-NH_2)_2$, and in a second step to $(t\text{Bu}_2\text{Al}-NH-NH-\text{Al}t\text{Bu}_2)_2$ with retention of the six-membered ring structure.[62]

C-Metallation by Ga results when the reaction of Me_2GaCl with $Li(Me_3Si)N-NH$(naphth) is performed in refluxing toluene. The product **4** is a 2,3-dihydro-1*H*-naphtho[1,2-*d*][1,2,3]diazagallol, which dimerizes via Ga−N bonds generating a centrosymmetric Ga_2N_2 ring system. As far as we know, this is the first example of the gallation of a naphthalene ring.

Interestingly, Me_2InCl behaves in a manner similar to Me_2GaCl in its reactions with lithium organylhydrazides. However, the solvent seems to play a more important role than in the reactions with Me_2GaCl. Therefore, an unprecedented type of redox reaction occurs in the formation of compound **8**. And even the reaction shown in Equation (10) is unusual in the sense that the bulky $Li(Me_3Si)N-N(SiMe_3)_2$ is retained if the reaction is performed in ether. Whether dimethylindium chloride induces double ether cleavage or the formation of the diindoxane unit is a result of unintended slow hydrolyses during the crystallization process was not investigated. Ether cleavage by strong Lewis acidic group 13 halides is not unusual, but the cleavage reaction usually stops after the first step leading to alkoxides X_2EOR of group 13 compounds.[63] In−O−In structural units are well known e.g. in organylindium alkoxide or OH-bridged diorganylindium carboxylates.[64−66]

Experimental Section

General: All experiments were conducted using Schlenk techniques under a blanket of nitrogen or argon. Solvents used were rendered anhydrous by conventional methods and stored under nitrogen. NMR spectra were recorded using JEOL 270 and 400 instruments. X-ray diffraction data were obtained with a Siemens P4 instrument equipped with a CCD area detector and a low-temperature device LT2. Data collection was performed using Mo-K_α radiation. Commercial products were Me_2GaCl (1 M in hexane, checked for purity by NMR), $GaMe_3$ (neat), BuLi (1.5 M in hexane). Hydrazine hydrate was made anhydrous with activated BaO. The trimethylsilylhydrazines were prepared according to the literature.[67] Reaction with BuLi in hexane afforded the *N*-lithio derivatives. Me_2InCl was prepared from $InCl_3$ by methylation with an ether solution of MeLi in a 1:2 ratio. The sublimed product had a m.p. of 221−222 °C (ref. 222−225 °C[68]). ^{1}H NMR (C_6D_6): $\delta = 0.23$.

***tert*-Butylhydrazine−Dichloro(methyl)gallane (1):** To a stirred solution of $t\text{BuHN}-NH_2$ (1.24 g, 14.1 mmol), dissolved in toluene (30 mL), was added a solution of Me_2GaCl (1.91 g, 14.1 mmol) in 5 mL of toluene. No gas evolution occurred, which set in slowly at 70 °C and became rapid on heating the mixture to reflux for 3 h. A solid had formed that was removed by filtration and the filtrate was cooled to −20 °C. Within a few days crystals of **1** separated from the filtrate. These crystals were suitable for X-ray crystallography. Yield: 0.83 g (24%), m.p. 51−53 °C. The solid on dissolving in hot toluene showed ^{1}H NMR resonances in a 1:3 ratio for MeGa and tBu protons. This product, assumed to be **2**, was not further characterized. Yield: 0.84 g. NMR of **1** (C_6D_6): $\delta^{1}H = 0.33$ (s, 3 H, GaMe), 0.65 (s, 9 H, tBu), 4.15 (br., NH); $\delta^{13}C = -3.1$ (Ga*Me*), 25.6, 55.3 (tBu). $C_5H_{15}Cl_2GaN_2$ (243.81): calcd. C 24.63, H 6.20, N 11.49; found C 24.21, H 6.12, N 11.51.

3,7-Diamino-2,2,4,4,6,6,8,8-octamethyl-1,3,5,7-tetrazonia-2,4,6,8-tetragallatabicyclo[3.3.0]octane (3): $GaMe_3$ (5.85 g, 50.9 mmol) was condensed into a three-necked flask at −78 °C. It was diluted with toluene (40 mL). While stirring a solution of toluene (20 mL) containing N_2H_4 (1.63 g, 50.8 mmol), was added droppwise at −50 °C to the $GaMe_3$ solution. After slowly warming the reaction mixture to room temperature, gas evolution set in quickly and was rapid on heating the resulting suspension to reflux (2 h). The solid (5.68 g) that had formed was isolated by filtration and proved to be principally compound **3** (NMR). Single crystals separated from the filtrate kept at −20 °C. Yield after crystallization from toluene: 4.86 g of **3** (65% calcd. for $GaMe_3$), m.p. 62−63 °C. No explosive decomposition was observed on heating, but one should be careful in handling this compound because methylaluminium hydrazides are reported to be explosive. NMR (C_6D_6): δ^1H = 0.38 to −0.09 (7 signals, 24 H, Ga*Me*), 2.24 (br., 2 H, NH), 2.34 (br., 4 H, NH), 2.74 (br., 2 H, NH); at 80 °C: δ^1H = −0.32 (br. s, 24 H, Ga*Me*), 2.40 (br. s, 6 H, NH), 2.64 (br. s, 2 H, NH); $\delta^{13}C$ = −11.5, −10.6, −9.4, −7.3, −6.4, −5.9, −7.1 (Ga*Me*); at 80 °C: $\delta^{13}C$ = −9.0 (br., Ga*Me*). IR (hostaflon): $\tilde{\nu}$ = 3161 (br., νNH), 1613, 1601 cm^{-1} (δNH_2). $C_{15}H_{40}Ga_4N_6$ (583.40): calcd. C 30.88, H 6.91, N 14.41; found C 30.73, H 6.87, N 14.28.

1-Methyl-2-trimethylsilyl-2,3-dihydro-1*H*-naphtho[1,2-*d*]-[1,2,3]diazagallol (4): A stirred solution of naphth(H)N−$NHSiMe_3$ (2.01 g, 8.7 mmol) in toluene (40 mL) was metallated with a hexane solution of butyllithium (5.6 mL, 1.56 M, 8.7 mmol). After heating to reflux for 2 h, the solution was cooled to −30 °C. Then, a solution of Me_2GaCl (1.18 g, 8.7 mmol) in toluene (20 mL) was added dropwise. After addition, the suspension was allowed to attain room temperature. On heating to reflux for 2 h some gas evolution was noted. The solid that had formed was removed by filtration and the solvents evaporated in vacuo. The remaining oil was treated with hexane (10 mL) and the solution stored at −20 °C. Light yellow crystals separated within a few weeks. Yield: 1.56 g of **4** (57%), m.p. 113−115 °C. NMR (C_6D_6): δ^1H = −0.17 (s, 3 H, Ga*Me*), 0.30 (s, 9 H, *Me*Si), 5.71 (s, 1 H, NH), 6.7−7.8 (m, 6 H, naph*H*); $\delta^{13}C$ = −8.6 (Ga*Me*), 1.4 (Si*Me*), 114.8, 123.1, 126.9, 128.8, 130.0, 130.5, 130.8, 135.7, 139.9, 155.3 (arom. C); $\delta^{29}Si$ = 13.6. $C_{14}H_{19}GaN_2Si$ (313.12): calcd. C 53.70, H 6.12, N 8.95; found C 53.55, H 6.09, N 8.89.

Lithium *N*′-*tert*-Butyl-*N*-trimethylsilylhydrazide−Trimethylgallium (5): $Me_3Si(H)N-NHtBu$ (1.76 g, 11.0 mmol), dissolved in hexane (40 mL), was metallated by adding to the stirred solution BuLi in hexane (7.05 mL, 1.56 M, 11 mmol). The metallation was completed by heating to reflux for 2 h, followed by cooling to −40 °C. Addition of Me_2GaCl (1.54 g, 11.0 mmol), dissolved in hexane (20 mL), led to the formation of a precipitate that was removed by filtration after the suspension had been stirred for 12 h at ambient temperature. Cooling the filtrate to −78 °C yielded colorless needles of **5**, which separated within three weeks. Yield: 1.05 g (34%), m.p. 64−65 °C (dec.). NMR (C_6D_6): δ^1H = −0.08 (s, 9 H, Ga*Me*), 0.21 (s, 9 H, Si*Me*), 1.05 (br. s, 9 H, CMe_3), 3.6 (br. s, 1 H, NH); $\delta^{13}C$ = −2.7 (GaMe), 2.7 (SiMe), 29.0 (CMe_3); $\delta^{29}Si$ = 7.0; δ^7Li = −1.0 ($h_{1/2}$ = 19 Hz). $C_{10}H_{28}GaLiN_2Si$ (281.09): calcd. C 42.73, H 10.04, N 9.97; found C 41.85, H 9.87, N 9.73.

Lithium *N*′-*tert*-Butyl-*N*-trimethylsilylhydrazide−Trimethylindium (7): A stirred solution of $Me_3Si(H)N-NHtBu$ (1.68 g, 10.5 mmol) in 30 mL of toluene was treated with a 1.56 M solution of BuLi (6.7 mL, 10.5 mmol) in hexane. After heating to reflux for 4 h and cooling to ambient temperature, the solution was added dropwise to a stirred suspension of Me_2InCl (1.89 g, 10.5 mmol) in toluene (40 mL), kept at −60 °C. After addition, the mixture was allowed to attain room temperature followed by heating the orange mixture to reflux for 2.5 h. Then, the solids (0.15 g) were removed by filtration and the filtrate stored at −20 °C. Within three weeks small crystals had settled, suitable for X-ray diffraction analysis. Yield: 1.33 g of **6** (39%), m.p. 70−71 °C (dec.). NMR ([D_8]toluene): δ^1H = −0.18 (s, 9 H, InMe), 0.22 (s, 9 H, $SiMe_3$), 0.98 (s, 9 H, *t*Bu),3.4 (s br., 1 H, NH); $\delta^{13}C$ = −5.9 (InMe), 3.3 ($SiMe_3$), 28.3 (*t*Bu), 55.1 (*t*Bu); $\delta^{29}Si$ = 6.4; δ^7Li = −1.0 ($h_{1/2}$ = 18 Hz). $C_{10}H_{28}InLiN_2Si$ (326.19): calcd. C 36.82, H 8.65; N 8.59; found C 35.45, H 8.12, N 8.43.

Dimeric Lithium *N*′-*tert*-Butyl-*N*-trimethylsilylhydrazide−(Methylindyl)(trimethylsilyl)imide (8): A stirred solution of $Me_3Si(H)N-NHtBu$ (1.75 g, 10.9 mmol) in diethyl ether (40 mL) was deprotonated by adding a hexane solution of BuLi (1.56 M, 7.0 mL, 10.9 mmol). To complete the reaction the mixture was kept at reflux for 2 h. After cooling to ambient temperature, Me_2InCl (1.97 g, 10.9 mmol), dissolved in 40 mL of diethyl ether, was added. Small amounts of a solid were filtered off after 12 h. Then the solvents were removed from the filtrate in vacuo and the solid residue treated with hexane (40 mL). The solution was stored at −25 °C. Crystals of **8** separated within four weeks. Yield: 0.92 g of **8** (55%), m.p. 104−105 °C (dec.). NMR (C_6D_6 or [D_8]toluene): δ^1H = −0.10 (s, 3 H, InMe), 0.21 (s, 9 H, $SiMe_3$), 0.25 (s, 9 H, $SiMe_3$), 1.03 (s, 9 H, *t*Bu), 3.3 (br. s, 1 H, NH); $\delta^{13}C$ = −6.0 (InMe), 3.2 ($SiMe_3$), 4.4 ($SiMe_3$), 28.8 (*t*Bu), 55.2 (*t*Bu); $\delta^{29}Si$ = 3.5 ($NSiMe_3$), 6.5 ($NNSiMe_3$); δ^7Li = −0.9 ($\Delta h_{1/2}$ = 18 Hz). $C_{11}H_{31}InLiN_3Si_2$ (383.33): calcd. C 34.46, H 8.15, N 10.96; found C 33.98, H 7.85, N 11.21.

Lithium Tris(trimethylsilyl)hydrazide−Bis(dimethylindium) Oxide Dimer (9): To a stirred solution of Me_2InCl (0.83 g, 4.6 mmol) in ether (40 mL) was added a solution of $(Me_3Si)_2N-NLi(SiMe_3)$ (1.16 g, 4.6 mmol) in diethyl ether (20 mL). After 12 h, the insoluble material (0.10 g, 2.4 mmol LiCl) was removed by filtration. After all volatile components had been stripped off from the filtrate in vacuo, recrystallization of the residue from toluene produced colorless crystals of **9** within 2 weeks. Yield: 0.73 g (57%), m.p. 165 °C. NMR (C_6D_6): δ^1H = −0.03 (s, 3 H, InMe), 0.03 (s, 3 H, $SiMe_3$), 0.04 (s, 3 H, InMe), 0.08 (s, 3 H, InMe), 0.10 (s, 9 H, $SiMe_3$), 0.13 (s, 18 H, $SiMe_3$); $\delta^{13}C$ = −5.4, −3.4, −2.9, −0.6 (InMe), 0.9, 1.4 ($SiMe_3$); $\delta^{29}Si$ = 6.6, 12.1. $C_{13}H_{39}In_2Li-N_2OSi_3$(560.30): calcd. C 27.87, H 7.02, N 5.00; found C 27.79, H 7.05, N 4.98.

Crystal Structure Determinations: Single crystals were covered with a perfluoroether oil and a specimen selected, placed on the tip of a glass fiber and then mounted on the goniometer head. The crystal was then cooled to −80 °C. After alignment, the dimensions of the unit cell were determined from reflections on 5 sets of 15 frames each. Data were collected with the SMART program[69] in the hemisphere mode. An exposure time of 5 s/frames was chosen. Δφ was changed by 0.3° between two frames. Data on a total of 1240 frames were collected and reduced with the program SAINT[70] Absorption correction was employed (SADABS[71]). The structures were solved by direct methods and refined by using the programs SHELXTL and SHELX97.[72] Non-hydrogen atoms were refined with anisotropic thermal parameters. Hydrogen atoms were placed in calculated position and included in the final cycles of refinement as riding on the respective carbon atom. Table 4 contains relevant crystallographic data and data related to structure solution and refinement.[73] Thermal ellipsoids in the figures are depicted on a 25% probability level.

Table 4. Crystal data and data collection parameters

Compound	**1**	**3**	**4**	**5**	**7**	**8**	**9**
Empirical formula	$C_5H_{15}Cl_2GaN_2$	$C_{15}H_{40}Ga_4N_6$	$C_{14}H_{19}GaN_2Si$	$C_{10}H_{28}GaLiN_2Si$	$C_{10}H_{28}InLiN_2Si$	$C_{11}H_{31}InLiN_3Si_2$	$C_{13}H_{39}In_2LiN_2OSi_3$
Formula mass	243.81	583.41	313.12	281.09	326.19	383.33	560.31
Crystal size [mm]	0.20×0.30×0.50	0.20×0.30×0.40	0.09×0.10×0.20	0.10×0.10×0.30	0.07×0.1×0.3	0.1×0.2×0.3	0.10×0.20×0.20
Crystal system	tetragonal	triclinic	monoclinic	monoclinic	monoclinic	monoclinic	monoclinic
Space group	$I4(1)/a$	$P\bar{1}$	$P2_1/c$	$P2_1/n$	$P2_1/n$	$C2/c$	$P2_1/c$
a [Å]	21.0004(3)	9.831(5)	11.033(3)	8.9742(1)	12.453(4)	20.731(7)	18.111(4)
b [Å]	21.0004(3)	9.846(4)	13.678(4)	16.3792(2)	9.116(4)	10.066(3)	9.342(2)
c [Å]	9.9230(1)	14.862(5)	10.141(3)	10.7599(1)	14.648(5)	20.193(5)	15.539(3)
α [°]	90	98.08(1)	90	90	90	90	90
β [°]	90	98.40(1)	100.63(1)	97.877(1)	106.49(1)	115.63(1)	105.35(1)
γ [°]	90	111.552(9)	90	90	90	90	90
V [Å^3]	4376.2(1)	1293.7(9)	1504.0(7)	1566.68(3)	1594.5(10)	3798.9(19)	2535.3(9)
Z	16	2	4	4	4	8	4
ρ(calcd.) [Mg/m^3]	1.480	1.498	1.383	1.192	1.359	1.340	1.468
μ [mm^{-1}]	2.948	4.130	1.894	1.809	1.534	1.360	1.962
F(000)	1984	592	648	600	672	1584	1128
Index ranges	$-14 \le h \le 23$	$-11 \le h \le 11$	$-12 \le h \le 11$	$-11 \le h \le 10$	$-14 \le h \le 14$	$-25 \le h \le 25$	$-23 \le h \le 23$
	$-23 \le k \le 23$	$-11 \le k \le 11$	$-16 \le k \le 16$	$-20 \le k \le 20$	$-10 \le k \le 10$	$-12 \le k \le 12$	$-11 \le k \le 11$
	$-11 \le l \le 11$	$-17 \le l \le 13$	$-11 \le l \le 11$	$-12 \le l \le 13$	$-17 \le l \le 17$	$-21 \le l \le 23$	$-14 \le l \le 21$
2θ [°]	46.52	49.42	49.42	58.56	49.42	51.34	58.88
T [K]	193	193	193	193	193	193	193
Refl. collected	8870	6483	7090	8721	7607	9685	14106
Refl. unique	1503	3403	2251	3062	2205	2912	4362
Refl. observed (4σ)	1446	2500	1913	2676	1931	2554	3737
R(int.)	0.0245	0.0244	0.0259	0.0215	0.0261	0.0230	0.0279
No. of variables	107	253	171	248	171	257	223
Weighting scheme[a] x/y	0.0446/57.0488	0.1017/1.8549	0.0252/0.9647	0.0636/0.4699	0.0319/1.1868	0.0287/14.4461	0.0481/0.8766
GOOF	1.208	1.044	1.071	1.051	1.102	1.070	1.219
Final R(4σ)	0.0544	0.0608	0.0262	0.0321	0.0267	0.0306	0.0326
Final $wR2$	0.1378	0.1545	0.0577	0.0802	0.0599	0.0713	0.0771
Largest residual peak [e/Å^3]	1.154	0.736	0.256	0.736	0.419	1.065	0.479

[a] $w^{-1} = \sigma^2F_o^2 + (xP)^2 + yP$; $P = (F_o^2 + 2F_c^2)/3$.

Acknowledgments

We gratefully acknowledge the support of this work by Fonds der Chemische Industrie, Chemetall GmbH, Frankfurt as well as of the University of Munich.

[1] L. Fieser, *Reagents for Organic Synthesis*, John Wiley, Interscience Publ., New York, **1990**.
[2] K. W. Henderson, *Chem. Eur. J.* **2001**, *7*, 3430−3437.
[3] J. C. Stowell, *Carbanions in Organic Synthesis*, J. Wiley, Interscience Publ., New York, **1979**.
[4] *Lithium Chemistry* (Eds.: A. Sapse, P. von Rague-Schleyer), John Wiley & Sons, Inc., New York, Chichester, Brisbane, Toronto, Singapore, **1995**, chapter 5.
[5] R. E. Mulvey, *Chem. Soc. Rev.* **1991**, *20*, 167−209.
[6] K. Gregory, P. von Rague-Schleyer, R. Snaith, *Adv. Inorg. Chem.* **1991**, *37*, 48−142.
[7] N. Wiberg, M. Veith, *Chem. Ber.* **1971**, *104*, 3176−3190.
[8] C. Drost, U. Klingebiel, *Chem. Ber.* **1993**, *126*, 1413−1416.
[9] K. Bode, U. Klingebiel, M. Noltemeyer, H. Witte-Abel, *Z. Anorg. Allg. Chem.* **1995**, *421*, 500−505.
[10] W. Uhl, J. Molter, W. Saak, *Z. Anorg. Allg. Chem.* **1999**, *625*, 231−328.
[11] A. Heine, D. Stalke, *Angew. Chem.* **1992**, *104*, 941−942; *Angew. Chem. Int. Ed. Engl.* **1992**, *31*, 854−855.
[12] H. Hommer, H. Nöth, H. Sachdev, M. Schmidt, H. Schwenk, *Chem. Ber.* **1995**, *128*, 1187−1194;.
[13] R. J. Wehmschulte, P. P. Power, *Inorg. Chem.* **1996**, *35*, 2717−2718.
[14] W. Uhl, J. Molter, R. Koch, *Eur. J. Inorg. Chem.* **1999**, 2021−2028.
[15] D. A. Neumayer, A. H. Cowley, A. Decken, R. A. Jones, V. Lakkotia, J. G. Ekerdt, *Inorg. Chem.* **1995**, *14*, 4698−4700.
[16] H. Nöth, T. Seifert, *Eur. J. Inorg. Chem.* **1998**, 1931−1938.
[17] D. A. Neumayer, J. G. Ekerdt, *Chem. Mater.* **1996**, *8*, 9−25.
[18] V. Lakkotia, D. A. Neumayer, A. H. Cowley, R. A. Jones, J. G. Ekerdt, *Chem. Mater.* **1995**, *7*, 546−552.
[19] D. C. Boyd, R. T. Haasch, D. R. Mantell, R. K. Schulze, J. F. Evans, W. L. Gladfelter, *Chem. Mater.* **1989**, *1*, 119−124.
[20] A. Devi, W. Rogge, R. A. Fischer, F. Stowasser, H. Sussek, H. W. Becker, J. Wolfrum, *J. Phys. IV* **1999**, *9*, 589.
[21] M. A. Munoz-Hernandez, D. Rutherford, H. Tiaminen, D. A. Atwood, *J. Organomet. Chem.* **1999**, *582*, 103.
[22] J. McMurran, D. Dai, K. Balasubramanian, C. Steffek, J. Koutsetakis, J. L. Hubbard, *Inorg. Chem.* **1999**, *37*, 6638.
[23] A. Devi, H. Sussek, H. Pritzkow, M. Winter, R. A. Fischer, *Eur. J. Inorg. Chem.* **1999**, 2127−2134.
[24] N. Metzler, H. Nöth, H. Sachdev, *Angew. Chem.* **1994**, *106*, 1837−1839; *Angew. Chem. Int. Ed. Engl.* **1994**, *33*, 1746−1748.
[25] C. Drost, C. Jäger, U. Klingebiel, M. Noltemeyer, G. M. Sheldrick, *Chem. Ber.* **1994**, *621*, 290−847.
[26] B. Gemünd, H. Nöth, H. Sachdev, M. Schmidt, *Chem. Ber.* **1996**, *129*, 1335−1344.
[27] H. Nöth, W. Regnet, H. Rihl, R. Standfest, *Chem. Ber.* **1971**, *104*, 722−733.
[28] H. Fußstetter, H. Nöth, *Liebigs Ann. Chem.* **1981**, 633−641.
[29] S. Diemer, H. Nöth, W. Storch, *Eur. J. Inorg. Chem.* **1999**, 1765−1779.

[30] *Gmelin, Handbuch der Anorganischen Chemie, Ergänzungswerk zur 8. Auflage*, **1975**, vol. 22, pp. 249−257.
[31] N. R. Fetter, A. Bartocha, *Canad. J. Chem.* **1961**, *39*, 2001−2008.
[32] Y. Kim, J. H. Kim, J. E. Park, H. Hyunjoon, J. T. Park, *J. Organomet. Chem.* **1997**, 545−546, 99−103.
[33] D. W. Peters, M. P. Power, E. D. Bourret, J. Arnold, *Chem. Commun.* **1998**, 753−754.
[34] J. S. Silverman, C. D. Abernethy, R. A. Jones, A. H. Cowley, *Chem. Commun.* **1999**, 1645−1646.
[35] H. Nöth, T. Seifert, *Eur. J. Inorg. Chem.* **1998**, 1931−1938.
[36] W. Uhl, J. Molter, R. Koch, *Eur. J. Inorg. Chem.* **2000**, 2255−2262.
[37] D. W. Peters, E. D. Bourret, M. P. Power, J. Arnold, *J. Organomet. Chem.* **1999**, *582*, 108−115.
[38] D. A. Neumayer, A. H. Cowley, A. Decker, R. A. Jones, V. Lakhotia, J. Eckerdt, *Inorg. Chem.* **1995**, *34*, 4698−4700.
[39] D. W. Peters, M. P. Power, E. D. Blurret, J. Arnold, *Chem. Commun.* **1998**, 753−754.
[40] W. Uhl, F. Hannemann, *Eur. J. Inorg. Chem.* **1999**, 201−207.
[41] W. R. Null, J. S. Blanton, A. M. Boccanluso, L. A. Silks III, A. R. Garber, J. D. Odom, *Inorg. Chem.* **1991**, *30*, 4136.
[42] S. D. Waezsada, C. Rennekamp, H. W. Roesky, C. Röpken, E. Parsini, *Z. Anorg. Allg. Chem.* **1998**, *624*, 987−990.
[43] W. R. Nutt, R. E. Stimson, M. F. Leopold, B. H. Rubin, *Inorg. Chem.* **1982**, *21*, 1909−1921.
[44] A. Yamaguchi, I. Ichishima, T. Shimanouchi, S.-I. Mizushima, *J. Chem. Phys.* **1959**, *31*, 843
[45] T. M. Klapötke, H. Nöth, H. Schwenk-Kircher, W.-H. Walther, G. Holl, *Polyhehedron* **1999**, *18*, 717−719.
[46] T. Habereder, A. Hammerl, G. Holl, T. M. Klapötke, J. Knizek, H. Nöth, *Eur. J. Inorg. Chem.* **1999**, 849−852.
[47] The structural data are given for the triclinic unit cell, space group "$P\bar{1}$", The structure of **3** could also be solved in the monoclinic system, space group *C2/m.* In this case, two independent molecules were also found. However, the central N atom occupies a special position. This results in planar heterocycles. The model could be better refined by choosing split positions for this atom, however, the disorder for the toluene molecule could not be refined. Therefore the data are given here for a triclinic space group.
[48] M. J. Frisch, G. W. Trucks, H. B. Schlegel, G. E. Scuseria, M. A. Robb, J. R. Cheeseman, V. G. Zakrzewski, J. A. Montgomery, R. E. Stratmann, J. C. Burant, S. Dapprich, J. M. Millam, A. D. Daniels, K. N. Kudin, M. C. Strain, O. Farkas, J. Tomasi, V. Barone, M. Cossi, R. Cammi, B. Mennucci, C. Pomelli, C. Adamo, S. Clifford, J. Ochterski, G. A. Petersson, P. Y. Ayala, Q. Cui, K. Morokuma, D. K. Malick, A. D. Rabuck, K. Raghavachari, J. B. Foresman, J. Cioslowski, J. V. Ortiz, B. B. Stefanov, G. Liu, A. Liashenko, P. Piskorz, I. Komaromi, R. Gomperts, R. L. Martin, D. J. Fox, T. Keith, M. A. Al-Laham, C. Y. Peng, A. Nanayakkara, C. Gonzalez, M. Challacombe, P. M. W. Gill, B. G. Johnson, W. Chen, M. W. Wong, J. L. Andres, M. Head-Gordon, E. S. Replogle, J. A. Pople, *Gaussian 98 (Revision A.7)*, Gaussian, Inc., Pittsburgh, PA, **1998**.
[49] *Lithium Chemistry* (Eds.: M.-A. Sapse, P. von Rague-Schleyer), J. Wiley & Sons, New York, Chichester, Brisbane, Toronto, Singapore, **1995**.
[50] W. N. Setzer, P. v. R. Schleyer, *Adv. Organomet. Chem.* **1985**, *24*, 353−449.
[51] M. Hesse, H. Meier, B. Zech, *Spektroskopische Methoden in der organischen Chemie*, 4th ed., Georg Thieme, Stuttgart, New York, **1991**.
[52] T. Seifert, PhD Thesis, University of Munich, **2000**, p. 40.
[53] K. Mertz, W. Schwarz, F. Zettler, H.-D. Hausen, *Z. Naturforsch., Part B* **1975**, *30*, 159−161.
[54] B. Neumüller, *Chem. Ber.* **1989**, *122*, 2283−2287.
[55] O. T. Beachley, C. Bueno, M. R. Churchill, R. B. Hallock, R. G. Simmons, *Inorg. Chem.* **1981**, *20*, 2423−2428.
[56] K. Aitchison, J. D. J. Backer-Dirks, D. C. Bradley, M. Fator, D. M. Frigo, M. B. Hursthouse, B. Hussain, *J. Organomet. Chem.* **1989**, *366*, 11−23.
[57] F. Weller, U. Müller, *Chem. Ber.* **1979**, *112*, 2039−2044.
[58] H. W. Roesky, U. Seseke, M. Noltemeyer, G. M. Sheldrick, *Z. Naturforsch., Part B* **1988**, *43*, 1130−1136.
[59] J. R. Rice, J. P. Oliver, *J. Organomet. Chem.* **1977**, *133*, 183−188.
[60] M. R. Kopp, T. Kräuter, A. Dashti-Mommerz, B. Neumüller, *Z. Naturforsch., Teil B* **1999**, *54*, 627−631.
[61] W. Uhl, J. Molter, W. Saak, *Z. Anorg. Allg. Chem.* **1999**, *625*, 321−328.
[62] W. Uhl, J. Molter, B. Neumüller, *Inorg. Chem.* **2001**, *40*, 2011−2014.
[63] H. Reinheckel, K. Haage, D. Jahnke, *Organomet. Chem. Rev. A* **1969**, *4*, 47.
[64] U. Dembrowski, T. Pape, R. Herbst-Irmer, E. Pohl, H. W. Roesky, *Acta. Crystallogr., Sect.C* **1993**, *49*, 1309−1311.
[65] M. Häißlein, H.-D. Hausen, K. W. Klinkhammer, J. Weidlein, *Z. Anorg. Allg. Chem.* **1999**, *625*, 1608−1618.
[66] W. Uhl, R. Graupner, I. Hahn, *Z. Anorg. Allg. Chem.* **1997**, *623*, 565−572.
[67] K. B. Starowieyski, A. Bekalska, A. Okni′nski, *J. Organomet. Chem.* **1985**, *293*, 7.
[68] G. Brauer, *Handbuch der Präparativen Anorganischen Chemie*, 3rd ed., F. Enke, Stuttgart, **1990**, vol. 2.
[69] *SMART*, Siemens Analtyic Instruments, Madison, Version 5, **1996.**
[70] *SAINT*, Siemens Analytical Instruments, Madison, Version 5, **1996.**
[71] G. M. Sheldrick, *SADABS, A program for absorption correction for data obtained by the hemisphere mode, implemented in SAINTS*, Bruker Analytical Instruments, Madison, **1999**, version 6.05.
[72] G. M. Sheldrick, *SHELX97, programs for structure solution, refinement*, Göttingen, **1997**.
[73] Crystallographic Data for the structure reported in this paper have been deposited with the Cambridge Crystallographic Data Cenre as supplementary publication no. CCDC-165817 to -165823. Copies can be obtained free of charge on application to CCDC, 12 Union Road, Cambridge CB2 1EZ, U. K. [Fax: (internat.) + 44-1223/336-033; E-mail: deposit@ccdc.cam.ac.uk].

Received June 20, 2001
[I01225]

A Comparative Study of Cyclometallated Palladium(II) Compounds with Terdentate [C,N,S] Pincer Ligands − Crystal and Molecular Structure of [Pd{4-$MeC_6H_3C(Me)$=NNC(=S)NHMe}(PPh_3)] and [Pd{4-$MeOC_6H_3C(H)$=N[2-$(SMe)C_6H_4$]}(Cl)]

Adriana Amoedo,[a] María Graña,[a] Javier Martínez,[a] Teresa Pereira,[a] Margarita López-Torres,[b] Alberto Fernández,[b] Jesús J. Fernández,[b] and José M. Vila*[a]

Keywords: C−H activation / Palladium / S ligands / Schiff bases

Treatment of the thiosemicarbazone ligands 4-$MeC_6H_4C(Me)$=NN(H)C(=S)NHMe (**a**), 4-$MeC_6H_4C(Me)$=NN(H)C(=S)NHEt (**b**), and 4-$MeC_6H_4C(Me)$=NN(H)C(=S)NHPh (**c**) with $K_2[PdCl_4]$ produced the tetranuclear palladium(II) compounds [Pd{4-$MeC_6H_3C(Me)$=NNC(=S)-NHMe}]$_4$ (**1a**), [Pd{4-$MeC_6H_3C(Me)$=NNC(=S)NHEt}]$_4$ (**1b**), and [Pd{4-$MeC_6H_3C(Me)$=NNC(=S)NHPh}]$_4$ (**1c**) with deprotonation of the NH group. Treatment of thiosemicarbazones 4-$MeOC_6H_4C(H)$=NN(Me)C(=S)NH_2 (**d**) and 3-$MeOC_6H_4C(H)$=NN(Me)C(=S)NH_2 (**e**) with $K_2[PdCl_4]$ gave the mononuclear palladium(II) compounds [Pd{4-$MeOC_6H_3$-C(H)=NN(Me)C(=S)NH_2}(Cl)] (**1d**) and [Pd{3-$MeOC_6H_3$-C(H)=NN(Me)C(=S)NH_2}(Cl)] (**1e**). Treatment of the Schiff base 4-$MeOC_6H_4C(H)$=N[2-$(SMe)C_6H_4$] (**f**) with $Li_2[PdCl_4]$ afforded [Pd{4-$MeOC_6H_3C(H)$=N[2-$(SMe)C_6H_4$]}(Cl)] (**1f**). All the ligands are terdentate through the [C,N,S] atoms and the Pd–S bond formed is sufficiently strong to tolerate treatment with nucleophiles without bond cleavage. Treatment of **1a**, **1b**, and **1c** with triphenylphosphane gave the mononuclear species **2a**, **2b**, and **2c**, which upon treatment with hydrochloric acid resulted in the 1:1 electrolytes **3a**, **3b**, and **3c**, with NH and C=S groups. Coordination of PPh_3 to Pd in **1f** was achieved by treatment of the compound with sodium perchlorate, followed by the nucleophile in a 1:1 molar ratio, to yield **2f**. The crystal structures of compounds **2a** and **1f** are described.

Introduction

Cyclometallated compounds, as a class within the organometallic family, are quite numerous and they have been intensively studied.[1−7] This is due especially to the wide variety of organic ligands bearing an appropriate donor atom that may sustain metallation with formation of the stable five-membered ring. When the ligand to be metallated has more than one donor atom, a second ring, bonded to the metal ion through the corresponding non-carbon donor atoms, may be created, thus giving compounds with two fused rings at the metal center. We have previously met with this situation with terdentate [C,N,N] Schiff bases,[8−10] terdentate [C,N,O] semicarbazones,[11] and terdentate [C,N,S] thiosemicarbazones.[12] The last case is clearly distinct from the former two, in that the sulfur atom strongly binds to the metal ion, palladium(II) and platinum(II) in our case, thus making the ligands excellent pincer species that powerfully secure three of the four coordination positions of the metal ion, allowing only the fourth coordination site to undergo further reaction with nucleophiles such as tertiary phosphanes. Even with the use of strongly chelating diphosphanes, the palladium− or platinum−sulfur bond remains uncleaved, in contrast to the breakage of the oxygen− or nitrogen−metal bonds of the chelate ring found in the cases of semicarbazone or Schiff base ligands, respectively. Another interesting issue relating to these ligands is the tetrameric nature of the compounds obtained upon treatment of the ligand with the corresponding metal salt; these are cyclometallated thiosemicarbazone Pd_4 or Pt_4 clusters, which also form polymers through hydrogen bonds.[12] The outstanding question still to be answered is whether these findings are dependent on the structure of the −C(R)=N−X(R′)−C(S)−NH(R′′) chain (X = C, N; R, R′, R′′ = H, alkyl, aryl) that supports the rings at the metal atom and how modification of this chain may alter the nature of the resulting products and their properties. That is the purpose of this paper, and here we report results concerning ligands with three different chain se-

[a] Departamento de Química Inorgánica, Universidad de Santiago de Compostela,
15782 Santiago de Compostela, Spain
Fax: (internat.) + 34-981/595012
E-mail: qideport@usc.es
[b] Departamento de Química Fundamental, Universidad de La Coruña,
15071 La Coruña, Spain,
Fax: (internat.) + 34-981/167065
E-mail: qiluaafl@udc.es

 © WILEY-VCH Verlag GmbH, 69451 Weinheim, Germany, 2002 1434−1948/02/0303−0613 $ 17.50+.50/0

quences, −C(Me)=N−N(H)−C(NHR)−S (R = Me, Et, Ph), −C(H)=N−N(Me)−C(NH_2)−S, and −C(H)=N−C−C−SMe, in order to undertake a comparative study of the complexes.

Results and Discussion

The thiosemicarbazones **a**, **b**, **c**, **d**, and **e** were prepared by treatment of 4-methylthiosemicarbazide, 4-ethylthiosemicarbazide, 4-phenylthiosemicarbazide, or 2-methylthiosemicarbazide with 4-methylacetophenone, 4-methoxybenzaldehyde, or 3-methoxybenzaldehyde as appropriate, whilst ligand **f** was prepared by treatment of 4-methoxybenzaldehyde with 2-(methylthio)aniline (see Exp. Sect.). All the ligands showed the characteristic ν(C=N) stretch in their IR spectra, and ligands **a**−**e** also showed the ν(C=S) band (Exp. Sect.); although bands involving the C=S group are often difficult to assign, we have located the ν(C=S) mode in the free ligands in the 850−820 cm^{-1} range [for a more detailed study concerning the ν(C=S) mode, see ref.[12]]. The NH protons in **a**, **b**, and **c** showed signals at δ ≈ 8−9.5. From these ligands, new cyclometallated compounds were obtained, and these are shown in Schemes 1 and 2. In a typical experiment, a suspension of potassium tetrachloropalladate in ethanol/water was treated with the corresponding thiosemicarbazone ligand to give complexes [Pd{4-$MeC_6H_3C(Me)$=NNC(=S)NHMe}]$_4$ (**1a**), [Pd{4-$MeC_6H_3C(Me)$=NNC(=S)NHEt}]$_4$ (**1b**), and [Pd{4-$MeC_6H_3C(Me)$=NNC(=S)NHPh}]$_4$ (**1c**) as yellow, air-stable solids, with the ligand in the (*E*,*Z*) configuration.

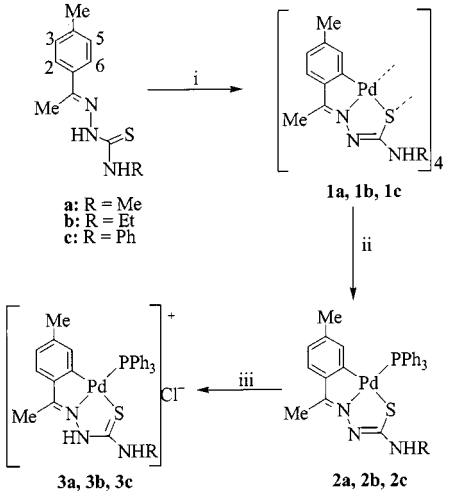

Scheme 1. (i) $K_2[PdCl_4]$/EtOH or $Pd(AcO)_2$/glacial acetic acid; (ii) PPh_3/Me_2CO (1:4); (iii) HCl(aq)

The products were characterized by elemental analysis (C, H, N) and IR and ^1H and ^{13}C {^1H} NMR spectroscopy. For complexes **1a**, **1b**, and **1c**, the mass spectra (FAB) showed peaks at *m*/*z* = 1302.9, 1359.0, and 1551.2, respectively, suggesting tetranuclear complexes similar to others obtained by us[12] and by others.[13−15] In addition, the absence of signals for the NH groups in the ^1H NMR spectra attested to deprotonation, as observed previously.[13,14,16,17]

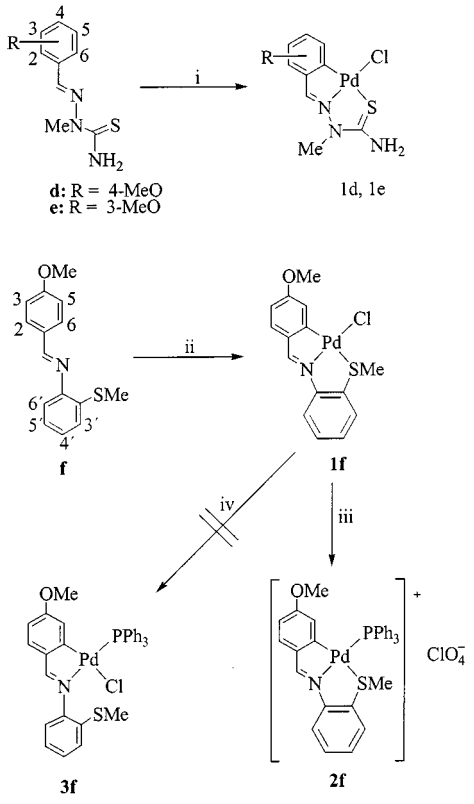

Scheme 2. (i) $K_2[PdCl_4]$/EtOH; (ii) $Li_2[PdCl_4]$/NaAcO/MeOH; (iii) $AgClO_4/PPh_3/Me_2CO$; (iv) PPh_3/Me_2CO

The metallation of the ligand was clear, from the absence of the AA′XX′ systems of the *para*-substituted phenyl rings, and the three remaining proton resonances were unequivocally assigned (see Exp. Sect.). The ^{13}C-{^1H} data confirmed metallation of the phenyl ring:[18] the C=N, C(1), and C(6) resonances were shifted to low field relative to those of the free ligands, whilst the N*C*S resonance was shifted upfield. The ν(C=N) band shifted to lower wavenumbers on complex formation,[19] contrary to the trend observed for other thiosemicarbazone complexes, which show a shift to higher wavenumbers.[20] The ν(C=S) band disappeared, in agreement with loss of the double bond character upon deprotonation of the NH group, which is necessary in order to preserve the electroneutrality of the tetranuclear complexes. In view of these results, we reasoned that, if deprotonation of the NH group could be hindered, then the N(H)−C=S moiety would not be able to adopt the N···C···S character needed for the tetrameric species. In order to achieve this, we synthesized ligands **d** and **e**, in which the chain sequence on the metallated aromatic ring was −C(H)=N−N(Me)−C(NH_2)−S. The stronger N−Me bond, in place of the N−H bond, should keep the −N(Me)−C=S moiety unaltered, providing a mononuclear compound. Thus, treatment of ligands **d** or **e** with potassium tetrachloropalladate in ethanol/water gave the complexes [Pd{4-$MeOC_6H_3C(H)$=NN(Me)C(=S)NH_2}(Cl)] (**1d**) and [Pd{3-$MeOC_6H_3C(H)$=NN(Me)C(=S)NH_2}(Cl)] (**1e**), as yellow, air-stable solids, which were fully characterized (see Exp. Sect.).

The ^{1}H and ^{13}C-{^{1}H} data showed metallation of the aromatic ring (vide supra). The mass spectra (FAB) in each case showed a peak at *m*/*z* = 364.2. The IR spectra showed ν(C=S) bands (absent in **1a**, **1b**, and **1c**) at 831 and 837 cm^{-1} for **1d** and **1e**, respectively, and ν(Pd−Cl) bands (also absent in **1a**, **1b**, and **1c**, in accordance with the absence of the chloride ligand in the palladium coordination environment) at 310 and 306 cm^{-1} for **1d** and **1e**, respectively. These findings are in good agreement with mononuclear species and establish that the −N(Me)−C=S group remains unchanged, confirming our initial assumption. Having established how modification of the chain alters the nature of the compounds synthesized, another issue to be considered was the reactivity of the complexes; that is, whether similar variations would influence the excellent pincer properties of the terdentate [C,N,S] ligands so far studied by us, the thiosemicarbazones, which strongly retain three metal coordination positions. For this purpose we included the sequence −C(H)=N−C=C−SMe (ligand **f**, in which the −C−C− group is part of an aryl ring) and synthesized compound **1f** for more detailed comparative study. Thus, treatment of 4-MeOC$_6$H$_4$C(H)=N[2-(SMe)C$_6$H$_4$] with lithium tetrachloropalladate in methanol gave compound [Pd{4-MeOC$_6$H$_3$C(H)=N[2-(SMe)C$_6$H$_4$]}(Cl)] as an air-stable, fully characterized solid (see Exp. Sect.). The shift of the ν(C=N) stretch towards lower wavenumbers[21] and the upfield shift of the HC=N resonance in the ^{1}H NMR spectrum supported nitrogen coordination to the metal center.[22] The metallated ligand showed the absence of the AA′XX′ system of the *para*-substituted phenyl ring (vide supra). The C=N, C(1), and C(6) resonances in the ^{13}C-{^{1}H} NMR spectrum were shifted downfield from those of the free ligand, in accordance with metallation and Pd−N coordination.[18] The S*Me* resonance was shifted downfield in both the ^{1}H and the ^{13}C-{^{1}H} NMR spectra, in agreement with Pd−S coordination. The crystal and the molecular structure of **1f** are described below.

Reactivity of the Complexes

For **1a**, **1b**, and **1c**, a reactivity pattern similar to that observed by us earlier[12] was found. Thus, treatment of **1a**, **1b**, and **1c** with triphenylphosphane in a 1:4 molar ratio gave compounds [Pd{4-MeC$_6$H$_3$C(Me)=NNC(=S)NHMe}(PPh$_3$)] (**2a**), [Pd{4-MeC$_6$H$_3$C(Me)=NNC(=S)NHEt}(PPh$_3$)] (**2b**), and [Pd{4-MeC$_6$H$_3$C(Me)=NNC(=S)NHPh}(PPh$_3$)] (**2c**), which were fully characterized (see Exp. Sect.). The ^{1}H NMR spectra showed the H(5) resonance shifted upfield and coupled to the phosphorus nucleus. The C=S, C=N, C(1), and C(6) signals in the ^{13}C-{^{1}H} spectra appeared shifted as shown above. The ^{31}P resonance was a singlet and the chemical shift values were consistent with a geometry with the phosphorus atom *trans* to the nitrogen atom.[23−26] Treatment of complexes **1a**, **1b**, and **1c** with hydrochloric acid gave compounds [Pd{4-MeC$_6$H$_3$C(Me)=NNC(=S)NHMe}(PPh$_3$)]$^+$Cl$^-$ (**3a**), [Pd{4-MeC$_6$H$_3$C(Me)=NNC(=S)NHEt}(PPh$_3$)]$^+$Cl$^-$ (**3b**), and [Pd{4-MeC$_6$H$_3$C(Me)=NNC(=S)NHPh}(PPh$_3$)]$^+$Cl$^-$ (**3c**) as fully characterized 1:1 electrolytes, as shown by electric conductivity measurements[27] (see Exp. Sect.). The most noticeable feature of these compounds is the protonation of their NC(=S) nitrogen atoms, as shown by the resonances at δ ≈ 9.0 in their ^{1}H NMR spectra, and bands attributable to ν(C=S) in the 840−820 cm^{-1} range. We then treated complex **1f** with triphenylphosphane to compare its behavior with that of the thiosemicarbazone complexes **1a**−**1c**, which did not show cleavage of the Pd−S bond even with a large excess of the triphenylphosphane ligand and use of prolonged reaction times (compounds **1d** and **1e** displayed similar behavior, and neither the Pd−S bond nor the Pd−Cl bond were cleaved). Under similar reaction conditions, the Pd−S bond in **1f** remained uncleaved and compound **3f** was not formed (Scheme 2). Triphenylphosphane could be coordinated to the metal atom only after abstraction of the chlorine ligand; this was achieved by treatment of compound **1f** with silver perchlorate, followed by addition of the phosphane ligand to give compound [Pd{4-MeOC$_6$H$_3$C(H)=N[2-(SMe)C$_6$H$_4$]}(PPh$_3$)](ClO$_4$) (**2f**) as a fully characterized (see Exp. Sect. and Scheme 2) 1:1 electrolyte. The removal of the chlorine ligand was confirmed by the absence of the ν(Pd−Cl) band. The H(5) resonance in the ^{1}H NMR spectrum showed an upfield shift and appeared as a multiplet, due to coupling to the ^{31}P nucleus, whilst the MeO resonance was shifted to lower frequency by 0.20 ppm, due to shielding by the phosphane phenyl ring.

Crystal and Molecular Structures of 2a and 1f

Suitable crystals were grown by slow concentration of chloroform solutions of complexes **2a** and **1f**. The labelling schemes for the complexes are shown in Figures 1 and 2, respectively. Both crystals consist of discrete molecules separated by normal van der Waals distances. Crystallographic data and selected interatomic distances and angles are listed in Tables 1 and 2.

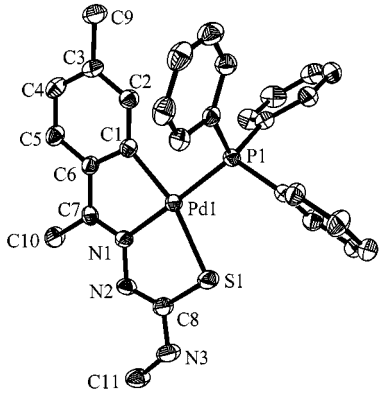

Figure 1. Molecular structure of complex [Pd{4-MeC$_6$H$_3$C(Me)=NNC(=S)NHMe}(PPh$_3$)] (**2a**), with labelling scheme; hydrogen atoms have been omitted for clarity

In compound **2a**, the structure comprises a molecule with the palladium(II) atom bonded in a slightly distorted square-planar environment to four different donor atoms, a terdentate thiosemicarbazone through the aryl C(1) carbon, the imine N(1) nitrogen, the thioamide S(1) sulfur atom,

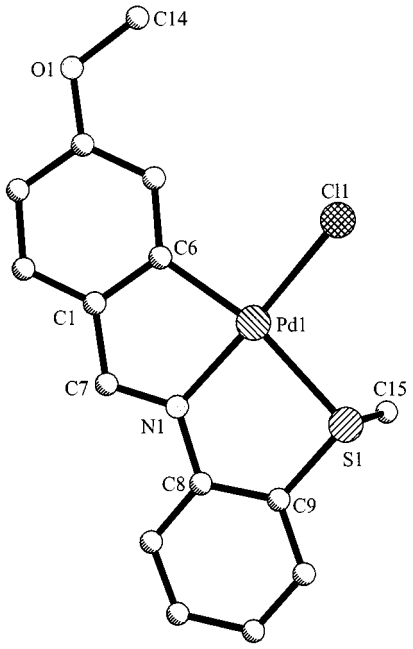

Figure 2. Molecular structure of complex [Pd{4-MeOC$_6$H$_3$C(H)=N[2-(SMe)C$_6$H$_4$]}(Cl)] (**1f**), with labelling scheme; hydrogen atoms have been omitted for clarity

Table 2. Selected bond lengths [Å] and angles [°] for complexes **2a** and **1f**

2a		**1f**	
Pd(1)−C(1)	2.044(4)	Pd(1)−C(6)	2.004(5)
Pd(1)−N(1)	2.024(3)	Pd(1)−N(1)	2.013(4)
Pd(1)−P(1)	2.2519(9)	Pd(1)−Cl(1)	2.303(4)
Pd(1)−S(1)	2.3419(11)	Pd(1)−S(1)	2.387(3)
S(1)−C(8)	1.757(4)	S(1)−C(9)	1.791(5)
N(1)−C(7)	1.290(4)	N(1)−C(7)	1.314(5)
N(1)−Pd(1)−C(1)	81.03(13)	N(1)−Pd(1)−C(6)	81.7(2)
N(1)−Pd(1)−P(1)	176.93(9)	N(1)−Pd(1)−S(1)	85.6(2)
C(1)−Pd(1)−P(1)	97.05(10)	C(6)−Pd(1)−Cl(1)	95.6(2)
N(1)−Pd(1)−S(1)	82.77(9)	S(1)−Pd(1)−Cl(1)	97.13(12)
C(1)−Pd(1)−S(1)	163.74(10)	C(6)−Pd(1)−S(1)	167.30(12)
P(1)−Pd(1)−S(1)	99.19(4)	N(1)−Pd(1)−Cl(1)	176.91(10)
C(7)−N(1)−Pd(1)	117.6(2)	C(1)−C(6)−Pd(1)	111.2(3)
C(6)−C(1)−Pd(1)	110.4(2)	C(6)−C(1)−C(7)	116.1(4)
C(1)−C(6)−C(7)	116.8(3)	C(1)−C(7)−N(1)	115.7(4)
N(1)−C(7)−C(6)	114.2(3)	C(7)−N(1)−Pd(1)	115.0(3)

Table 1. Crystal data for compounds **2a** and **1f**

	2a	**1f**
Empirical formula	$C_{29}H_{28}N_3PPdS$	$C_{15}H_{14}ClNOPdS$
Formula mass	587.97	398.18
T [K]	293(2)	150(2)
λ [Å]	0.71073	0.71073
Crystal system	triclinic	monoclinic
Space group	$P\bar{1}$	$P2_1/c$
Unit cell dimensions		
a [Å]	9.977(1)	8.117(10)
b [Å]	11.536(1)	11.814(13)
c [Å]	12.680(1)	15.69(2)
α [°]	93.214(1)	90
β [°]	108.285(1)	98.05(15)
γ [°]	108.000(1)	90
V [Å^3]	1298.8(1)	1490(3)
Z	2	4
Density (calcd.) [Mg/m^3]	1.503	1.775
μ [mm^{-1}]	0.880	1.558
Crystal size [mm]	0.20 × 0.10 × 0.05	0.34 × 0.21 × 0.21
θ range for data collection [°]	1.72 to 28.26	2.17 to 27.89
Reflections collected	8873	4021
Independent reflections	6173 (R_{int} = 0.0243)	2755 (R_{int} = 0.0209)
Final *R* indices [$I > 2.0\sigma(I)$]	R_1 = 0.0447, wR_2 = 0.0923	R_1 = 0.0350, wR_2 = 0.0747
R indices (all data)	R_1 = 0.0659, wR_2 = 0.1038	R_1 = 0.0527, wR_2 = 0.0810
Largest diff. peak and hole [eÅ^{-3}]	0.542 and −0.475	0.725 and −0.846

zone ligand. The angles N(1)−Pd(1)−C(1), at 81.03(3)°, and N(1)−Pd(1)−S(1), at 82.77(9)°, are less than 90°, whilst C(1)−Pd(1)−P(1), at 97.05(10)°, and S(1)−Pd(1)−C(1), at 99.19(4)°, are thus greater than 90°; the sum of angles at the palladium center in the equatorial plane is 360.04°. All and the phosphorus atom P(1) of the triphenylphosphane ligand.

The deviations from the mean plane are as follows: Pd −0.0096, C(1) −0.0320, N(1) 0.0403, P(1) 0.0282, S(1) −0.0269 Å. The angles between adjacent atoms in the coordination geometry of the metal atom are close to the expected value of 90°, in the 99.19(4) to 81.03(13)° range, with the most noticeable distortions being in the thiosemicarba-bond lengths are within the expected range, with allowance for the strong *trans* influence of the phosphorus donor ligand,[28] which is reflected in the Pd(1)−N(1) distance of 2.024(3) Å [a value larger than the sum of the covalent radii for Pd and N: 2.01 Å]. The Pd(1)−C(1) length, at 2.044(4) Å, and the Pd(1)−P(1) length, at 2.2519(9) Å, are shorter than the expected values of 2.081 Å and 2.41 Å,[29] respectively; this suggests some degree of multiple bond character

in the Pd−C(aryl)[30−32] and Pd−P linkages.[33] The S(1)−C(8) bond length, at 1.757(4) Å, and the N(2)−C(8) length, at 1.306(5) Å, are consistent with increased single- and double-bond character, respectively; the former is similar to that found for the Pd−S single bond in compound **1f** (vide infra). The metallacycle Pd, C(1), C(6) C(7), N(1) is planar, with mean deviations from the plane in the ±0.0113 Å range.

The crystal structure of **1f** consists of molecules with the palladium(II) atom bonded to a terdentate Schiff base system through the aryl C(6) carbon, the imine N(1) nitrogen, and the S(1) sulfur atoms, and also to the chlorine Cl(1) atom, thus yielding the palladium ion bonded to four different atoms.

The deviations from the mean plane are as follows: Pd −0.0088, C(6) −0.0162, N(1) 0.0218, S(1) −0.0127, and Cl(1) 0.0160 Å. The angles between adjacent atoms in the palladium coordination sphere show deviations from the ideal 90° similar to those described above for compound **2a**, with the most noticeable distortion in the N(1)−Pd(1)−C(6) angle of 81.7(2)°, a consequence of chelation; the sum of angles around the palladium atom is 360.03°. All bond lengths are within the expected ranges, with a shorter Pd(1)−C(aryl) linkage than in compound **2a** (vide supra). The Pd(1)−N(1) distance is also shorter in **1f** than in **2a**, reflecting the smaller *trans* influence of the chlorine atom in comparison with that of the phosphorus atom of the phosphane ligand. The metallacycle Pd, C(1), C(6), C(7), N(1) and the coordination ring Pd(1), N(1), C(8), C(9), S(1) are planar, with mean deviations from the plane in the ±0.0236 Å and ±0.0097 Å ranges, respectively, and they form angles with the Pd(1), C(6), N(1), S(1), Cl(1) palladium coordination plane of 2.63 and 0.72°, respectively.

Conclusion

We have shown that cyclometallation of organic ligands may be controlled, to provide different species through the introduction of appropriate changes in the chain bonded to the metallated aryl ring, and which contains the donor atoms that afford the metallated and coordination rings at the metal center. Thus, polynuclear metal compounds or mononuclear complexes may be synthesized by impeding cleavage of the N−H linkage on the hydrazine nitrogen atom. Furthermore, we have also demonstrated that the ligands discussed in this paper are good terdentate [C,N,S] pincer species that firmly sustain three metal coordination sites, allowing only one remaining position to undergo further reactions with nucleophiles, and they are therefore most suitable for providing a means to protect the metal ion against undesirable side reactions. Our goal now is to extend these findings to related ligands and also to examine their behavior in six-coordinate metals.

Experimental Section

General Remarks: Solvents were purified by standard methods.[34] Chemicals were reagent grade. Lithium tetrachloropalladate was prepared in situ by treatment of palladium(II) chloride with lithium chloride in methanol or ethanol. Palladium(II) acetate, potassium tetrachloropalladate, and palladium(II) chloride were purchased from Alfa Products, triphenylphosphane from Aldrich-Chemie. Microanalyses were carried out at the Servicio de Análisis Elemental at the University of Santiago, with a Carlo Erba Elemental Analyzer Model 1108. IR spectra were recorded as Nujol mulls or KBr discs with a Perkin−Elmer 1330 and with a Mattson spectrophotometer. NMR spectra were obtained as $CDCl_3$ solutions and referenced to $SiMe_4$ (^1H, ^{13}C) or 85% H_3PO_4 (^{31}P-{^1H}) and were recorded with Bruker WM250 and AMX 300 spectrometers. All chemical shifts are reported downfield from standards. The FAB mass spectra were recorded with a Fisons Quatro mass spectrometer with a Cs ion gun; 3-nitrobenzyl alcohol was used as the matrix.

CAUTION: Perchlorate salts of metal complexes are potentially explosive. Extreme caution should be exercised when handling these materials.

Synthesis of 4-$MeC_6H_4C(Me)$=NN(H)C(=S)NHMe (a): 4′-Methylacetophenone (650 mg, 4.84 mmol) and hydrochloric acid (35%, 0.65 mL) were added to a suspension of 4-methyl-3-thiosemicarbazide (510 mg, 4.84 mmol) in water (25 mL) to give a clear solution, which was stirred at room temperature for 4 h. The white solid that precipitated was filtered off, washed with cold water, and dried in air. Yield: 858 mg, 80%. $C_{11}H_{15}N_3S$ (221.3): calcd. C 59.7, H 6.8, N 19.0, S 14.5; found C 59.5, H 6.6, N 18.6, S 13.9. IR: $\tilde{\nu}$ = 1620 [s, ν(C=N)], 849 [m, ν(C=S)] cm^{-1}. ^1H NMR ($CDCl_3$): δ = 8.61 (s, 1 H, NH), 7.63 (br, 1 H, N*H*Me), 7.59 (d, 2 H, H2, H6, *N* = 8.3 Hz), 7.21 (d, 2 H, H3, H5, *N* = 8.3 Hz), 3.27 (d, 3 H, NMe, $^3J_{HH}$ = 4.9 Hz), 2.38 (s, 3 H, C4−Me), 2.25 (s, 3 H, =C−Me). ^{13}C-{^1H} NMR (62.46 MHz, $CDCl_3$): δ = 179.3 (C=S), 147.3 (C=N), 140.3 (C1), 135.0 (C4), 129.7 (C2, C6), 126.6 (C3, C5), 31.7 (NHMe), 21.7 (C4−Me), 13.9 (*Me*C=N).

Thiosemicarbazones b−e: These were prepared by similar procedures.

4-$MeC_6H_4C(Me)$=NN(H)C(=S)NHEt (b): Yield: 992 mg, 87%. $C_{12}H_{17}N_3S$ (235.4): calcd. C 61.2, H 7.3, N 17.9, S 13.6; found C 61.0, H 7.2, N 17.8, S 13.2. IR: $\tilde{\nu}$ = 1617 [m, ν(C=N)], 835 [m, ν(C=S)] cm^{-1}. ^1H NMR ($CDCl_3$): δ = 8.56 (s, 1 H, NH), 7.57 (d, 2 H, H2, H6, *N* = 8.5 Hz), 7.50 (br, N*H*Et), 7.21 (d, 2 H, H3, H5, *N* = 8.5 Hz), 3.77 (m, 2 H, N*CH*$_2$CH$_3$), 2.37 (s, 3 H, C4−Me), 2.24 (s, 3 H, =C−Me), 1.30 (t, 3 H, NCH$_2$*CH*$_3$, $^3J_{HH}$ = 7.1 Hz). ^{13}C {^1H} NMR (62.46 MHz, $CDCl_3$): δ = 178.1 (C=S), 147.3 (C=N), 140.3 (C1), 135.1 (C4), 129.7 (C2, C6), 126.6 (C3, C5), 39.8 (N*CH*$_2$CH$_3$), 21.7 (C4−Me), 14.9 (NCH$_2$*CH*$_3$), 14.0 (*Me*C=N).

4-$MeC_6H_4C(Me)$=NN(H)C(=S)NHPh (c): Yield: 1263 mg, 92%. $C_{16}H_{17}N_3S$ (283.4): calcd. C 67.8, H 6.0, N 14.8, S 11.3; found C 68.0, H 6.2, N 14.8, S 11.0. IR: $\tilde{\nu}$ = 1611 [s, ν(C=N)], 828 [m, ν(C=S)] cm^{-1}. ^1H NMR ($CDCl_3$): δ = 9.41 (s, 1 H, NH), 8.77 (br, N*H*Me), 7.63 (d, 2 H, H2, H6, *N* = 8.2 Hz), 7.23 (d, 2 H, H3, H5, *N* = 8.2 Hz), 2.39 (s, 3 H, C4−Me), 2.32 (s, 3 H, =C−Me).^{13}C-{^1H} NMR (62.46 MHz, $CDCl_3$): δ = 176.6 (C=S), 147.9 (C=N), 140.7 (C1), 138.4 (C4), 129.2 (C2, C6), 124.6 (C3, C5), 21.8 (C4−Me), 14.2 (*Me*C=N).

4-$MeOC_6H_4C(H)$=NN(Me)C(=S)NH_2 (d): Yield: 906 mg, 85%. $C_{10}H_{13}N_3OS$ (223.3): calcd. C 53.8, H 5.9, N 18.8, S 14.4; found C 53.4, H 6.0, N 18.5, S 15.3. IR: $\tilde{\nu}$ = 1619 [m, ν(C=N)], 836 [m, ν(C=S)] cm^{-1}. ^1H NMR ($CDCl_3$): δ = 8.27(s, 1 H, NH_2), 8.22 (s, 1 H, NH_2), 7.84 (s, 1 H, HC=N), 7.86 (d, 2 H, H2, H6, *N* = 8.6 Hz), 6.96 (d, 2 H, H3, H5, *N* = 8.6 Hz), 3.78 (s, 3 H, MeO),

3.74 (s, 1 H, NMe). ^{13}C {^1H} NMR (62.46 MHz, $CDCl_3$): δ = 180.5 (C=S), 161.0 (C4), 141.4 (C=N), 129.8 (C2, C6), 127.4 (C1), 114.4 (C3, C5), 55.6 (MeO), 33.1 (NMe).

3-MeOC$_6$H$_4$C(H)=NN(Me)C(=S)NH$_2$ (e): Yield: 906 mg, 85%. $C_{10}H_{13}N_3OS$ (223.3): calcd. C 53.8, H 5.9, N 18.8, S 14.4; found C 53.6, H 6.0, N 18.6, S 15.0. IR: $\tilde{\nu}$ = 1615 [m, ν(C=N)], 840 [m, ν(C=S)] cm^{-1}. ^1H NMR ($CDCl_3$): δ = 8.38 (s, 1 H, NH_2), 8.31 (s, 1 H, NH_2), 7.85 (s, 1 H, HC=N), 7.50 (s, 1 H, H2), 7.45 [d, 1 H, H6, ^3J(H5H6) = 7.5 Hz], 7.32 (t, 1 H, H5, $^3J_{H4H5}$ = 7.5 Hz), 6.96 (d, 1 H, H4), 3.79 (s, 3 H, MeO), 3.76 (s, 3 H, NMe). ^{13}C {^1H} NMR (62.46 MHz, $CDCl_3$): δ = 180.9 (C=S), 159.9 (C3), 141.5 (C=N), 136.2 (C1), 130.0, 121.2, 116.3, 112.4 (C2, C4, C5, C6), 55.6 (MeO), 33.2 (NMe).

Preparation of 4-MeOC$_6$H$_4$C(H)=N[2-(SMe)C$_6$H$_4$] (f): 4-Methoxybenzaldehyde (500 mg, 3.67 mmol) and 2-methylthioaniline (518 mg, 3.72 mmol) were heated together under reflux in a Dean−Stark apparatus. After the mixture had cooled to room temperature, the solvent was evaporated to dryness, and the residue was dried under vacuum to give an oily yellow product from which the desired ligand was obtained as a yellow solid. Yield: 785 mg, 83%. $C_{15}H_{15}NOS$ (257.4): calcd. C 70.0, H 5.9, N 5.4, S 12.5; found C 70.1, H 6.0, N 5.7, S 12.3. IR: $\tilde{\nu}$ = 1626 [s, ν(C=N)] cm^{-1}. ^1H NMR ($CDCl_3$): δ = 8.44 (s, 1 H, HC=N), 7.88 (d, 2 H, H2, H6, *N* = 8.0 Hz), 7.2 (m, 4 H), 7.07 (d, 2 H, H3, H5, *N* = 8.0 Hz), 3.82 (s, 3 H, MeO), 2.37 (s, 3 H, SMe). ^{13}C {^1H} NMR (62.46 MHz, $CDCl_3$): δ = 165.1 (C−SMe), 162.4 (C=N), 151.5 (C4), 137.0 (C−N), 133.6 (C2, C6), 132.0 (C1), 129.2, 128.0, 127.0, 120.4 (N-ring C atoms), 117.4 (C3, C5), 58.5 (MeO), 16.7 (SMe).

Preparation of [Pd{4-MeC$_6$H$_3$C(Me)=NNC(=S)NHMe}]$_4$ (1a). − Method 1: Ethanol (40 mL) was added to a stirred solution of potassium tetrachloropalladate (200 mg, 0.61 mmol) in water (6 mL). The obtained fine, yellow suspension of potassium tetrachloropalladate was treated with 4-MeOC$_6$H$_4$C(Me)=N(H)C(=S)NHMe (**a**) (148 mg, 0.67 mmol). The mixture was stirred for 48 h at room temperature. The yellow precipitate was filtered off, washed with ethanol, and dried. Yield: 178 mg, 89%. $C_{44}H_{52}N_{12}Pd_4S_4$ (1302.9): calcd. C 40.6, H 4.0, N 12.9, S 9.8; found C 40.1, H 3.8, N 12.3, S 9.5. IR: $\tilde{\nu}$ = 1590 [m, ν(C=N)] cm^{-1}. ^1H NMR ($CDCl_3$): δ = 7.27 (d, 1 H, H5, $^4J_{H3H5}$ = 1.3 Hz), 6.71 (dd, 1 H, H3, $^3J_{H2H3}$ = 7.8 Hz), 6.65 (d, 1 H, H2), 5.03 (q, 1 H, N*H*Me, $^3J_{HH}$ = 5.0 Hz), 2.98 (d, 3 H, NH*Me*), 2.30 (s, 3 H, C4−Me), 1.65 (s, 3 H, =C−Me). ^{13}C {^1H} NMR (62.46 MHz, $CDCl_3$): δ = 169.6 (C=S), 165.9 (C=N), 165.1 (C1), 147.2 (C6), 138.0 (C4), 134.2 (C2), 125.8, 125.0 (C3, C5), 33.1 (NHMe), 22.3 (C4−Me), 13.0 (*Me*C=N). − **Method 2:** Ligand **a** (201 mg, 0.91 mmol) and palladium(II) acetate (204 mg, 0.91 mmol) were added to glacial acetic acid (45 mL) to give a clear solution, which was heated to 60° C for 8 h. After this had cooled to room temperature, the yellow precipitate was filtered off, washed with ethanol, and dried. Yield: 169 mg, 57%.

[Pd{4-MeC$_6$H$_3$C(Me)=NNC(=S)NHEt}]$_4$ (1b). − Method 1: Analogous to **1a**. Yield: 181 mg, 87%. $C_{48}H_{60}N_{12}Pd_4S_4$ (1359.0): calcd. C 42.4, H 4.5, N 12.4, S 9.4; found C 41.9, H 3.6, N 11.8, S 8.7. IR: $\tilde{\nu}$ = 1586 [m, ν(C=N)] cm^{-1}. ^1H NMR ($CDCl_3$): δ = 7.30 (s, 1 H, H5), 6.71 (d, 1 H, H3, $^3J_{H2H3}$ = 7.4 Hz), 6.64 (d, 1 H, H2), 5.03 (m, 1 H, N*H*Et), 3.44 (m, 2 H, N*CH$_2$*CH$_3$), 2.29 (s, 3 H, C4−Me), 1.65 (s, 3 H, =C−Me), 1.26 (t, 3 H, NCH$_2$*CH$_3$*, $^3J_{HH}$ = 7.1 Hz). ^{13}C {^1H} NMR (62.46 MHz, $CDCl_3$): δ = 169.1 (C=S), 165.8 (C=N), 165.0 (C1), 147.5 (C6), 137.5 (C4), 134.3 (C2), 125.8, 125.0 (C3, C5), 41.4 (N*CH$_2$*CH$_3$), 22.2 (C4−Me), 15.0 (NCH$_2$*CH$_3$*), 13.0 (*Me*C=N). − **Method 2:** Ligand **b** (186 mg, 0.79 mmol) and palladium(II) acetate (177 mg, 0.79 mmol) were added to glacial acetic acid (40 mL) to give a clear solution, which was heated to 60° C for 8 h. After this had cooled to room temperature, the acetic acid was removed under vacuum. The residue was diluted with water and extracted with dichloromethane. The combined extracts were dried with anhydrous sodium sulfate, filtered, and concentrated in vacuo to give a yellow solid. This was chromatographed on a column packed with silica gel. Elution with dichloromethane/ethanol (1%) afforded product **1b** as a yellow solid after concentration. Yield: 169 mg, 63%.

[Pd{4-MeC$_6$H$_3$C(Me)=NNC(=S)NHPh}]$_4$ (1c): Compound **1c** was obtained through a similar procedure to that used for **1a** (method 1). Yield: 226 mg, 95%. $C_{64}H_{60}N_{12}Pd_4S_4$ (1551.2): calcd. C 49.6, H 3.9, N 10.8, S 8.3; found C 49.9, H 3.6, N 10.2, S 7.9. IR: $\tilde{\nu}$ = 1574 [m, ν(C=N)] cm^{-1}. ^1H NMR ($CDCl_3$): δ = 7.24 (br, 1 H, H5), 6.94 (s, 1 H, NHPh), 6.78 (br, 2 H, H2, H3), 2.16 (s, 3 H, C4−Me), 1.74 (s, 3 H, =C−Me).^{13}C {^1H} NMR (62.46 MHz, $CDCl_3$): δ = 172.1 (C=S), 166.5 (C=N), 161.0 (C1), 147.0 (C6), 139.4 (C4), 134.5 (C2), 126.5, 125.4 (C3, C5), 22.1 (C4−Me), 13.7 (*Me*C=N).

[Pd{4-MeC$_6$H$_3$C(Me)=NNC(=S)NHMe}(PPh$_3$)] (2a): Triphenylphosphane (40 mg, 0.152 mmol) was added to a suspension of complex **1a** (50 mg, 0.038 mmol) in acetone (15 mL). The mixture was stirred for 3 h and the resulting yellow solid was filtered off and dried. Yield: 55 mg, 61%. $C_{29}H_{28}N_3PPdS$ (588.0): calcd. C 59.2, H 4.8, N 7.1, S 5.5; found C 59.1, H 4.7, N 7.0, S 5.4. IR: $\tilde{\nu}$ = 1588 [m, ν(C=N)] cm^{-1}. ^{31}P {^1H} NMR ($CDCl_3$): δ = 36.7 (s). ^1H NMR ($CDCl_3$): δ = 6.95 (d, 1 H, H2, $^3J_{H2H3}$ = 7.7 Hz), 6.64 (d, 1 H, H3), 6.05 (d, 1 H, H5, $^4J_{PH5}$ = 4.3 Hz), 4.63 (m, 1 H, N*H*Me), 2.90 (d, 3 H, NH*Me*, $^3J_{HH}$ = 4.5 Hz), 2.35 (s, 3 H, C4−Me), 1.73 (s, 3 H, =C−Me).

Compounds 2b and 2c: These were synthesized by a similar procedure.

[Pd{4-MeC$_6$H$_3$C(Me)=NNC(=S)NHEt}(PPh$_3$)] (2b): Yield: 47 mg, 53%. $C_{30}H_{30}N_3PPdS$ (602.1): calcd. C 59.9, H 5.0, N 7.0, S 5.3; found C 59.8, H 4.9, N 6.9, S 5.1. IR: $\tilde{\nu}$ = 1588 [m, ν(C=N)] cm^{-1}. ^{31}P {^1H} NMR ($CDCl_3$): δ = 36.8 (s). ^1H NMR ($CDCl_3$): δ = 6.96 (d, 1 H, H2, $^3J_{H2H3}$ = 7.5 Hz), 6.65 (dd, 1 H, H3, $^4J_{H3H5}$ = 1.1 Hz), 6.07 (dd, 1 H, H5, $^4J_{PH5}$ = 3.5 Hz), 4.63 (m, 1 H, N*H*Et), 3.35 (m, 2 H, N*CH$_2$*CH$_3$), 2.35 (s, 3 H, C4−Me), 1.71 (s, 3 H, =C−Me), 1.12 (t, 3 H, NCH$_2$*CH$_3$*, $^3J_{HH}$ = 7.2 Hz).

[Pd{4-MeC$_6$H$_3$C(Me)=NNC(=S)NHPh}(PPh$_3$)] (2c): Yield: 48 mg, 57%. $C_{34}H_{30}N_3PPdS$ (650.1): calcd. C, 62.8, H 4.7, N 6.5, S 4.9; found C 62.5, H 4.6, N 6.3, S 4.7. IR: ν(C=N) 1577m, cm^{-1}. ^{31}P {^1H} NMR ($CDCl_3$): δ = 36.7 (s). ^1H NMR ($CDCl_3$): δ = 7.02 (d, 1 H, H2, $^3J_{H2H3}$ = 7.2 Hz), 6.68 (d, 1 H, H3), 6.63 (s, 1 H, NHPh), 6.10 (d, 1 H, H5, $^4J_{PH5}$ = 3.1 Hz), 2.46 (s, 3 H, C4−Me), 1.73 (s, 3 H, =C−Me).

[Pd{4-MeC$_6$H$_3$C(Me)=NNC(=S)NHMe}(PPh$_3$)]$^+$Cl$^-$ (3a): A suspension of complex **2a** (50 mg, 0.085 mmol) in ethanol (15 mL) was treated with three drops of concentrated hydrochloric acid (35%). The resulting mixture was stirred for 3 h and the yellow solid formed was filtered off and dried. Yield: 49 mg, 92%. $C_{29}H_{29}ClN_3PPdS$ (624.5): calcd. C 55.8, H 4.7, N 6.7, S 5.1; found C 55.6, H 4.6, N 6.7, S 4.9. IR: $\tilde{\nu}$ = 1574 [m, ν(C=N)], 840 [m, ν(C=S)] cm^{-1}. Λ_M (acetonitrile, 3×10^{-3} mol L^{-1}) = 97 Ω^{-1} cm^2 mol^{-1}. ^{31}P {^1H} NMR ($CDCl_3$): δ = 38.4 (s). ^1H NMR ($CDCl_3$): δ = 9.05 (s, 1 H, NH), 7.05 (d, 1 H, H2, $^3J_{H2H3}$ = 7.6 Hz), 6.68 (d, 1 H, H3), 6.09 (d, 1 H, H5, $^4J_{PH5}$ = 4.5 Hz), 5.9 (m, 1 H, N*H*Me), 3.05 (d, 3 H, NH*Me*, $^3J_{HH}$ = 4.0 Hz), 2.33 (s, 3 H, C4−Me), 1.93 (s, 3 H, =C−Me).

Compounds 3b and 3c: These were synthesized by a similar procedure.

[Pd{4-MeC$_6$H$_3$C(Me)=NNC(=S)NHEt}(PPh$_3$)]$^+$Cl$^-$ (3b): Yield: 49 mg, 93%. $C_{30}H_{31}ClN_3PPdS$ (638.5): calcd. C 56.4, H 4.9, N 6.6, S 5.0; found C 56.2, H 4.7, N 6.5, S 4.9. IR: $\tilde{\nu}$ = 1576 [m, ν(C=N)], 832 [m, ν(C=S)] cm^{-1}. Λ_M (acetonitrile, 3×10^{-3} mol L^{-1}) = 92 Ω^{-1} cm^2 mol^{-1}. ^{31}P {^{1}H} NMR ($CDCl_3$): δ = 38.5 (s). ^{1}H NMR ($CDCl_3$): δ = 9.07 (s, 1 H, NH), 7.03 (d, 1 H, H2, $^3J_{H2H3}$ = 7.1 Hz), 6.80 (dd, 1 H, H3, $^4J_{H3H5}$ = 7.0 Hz), 6.10 (dd, 1 H, H5, $^4J_{PH5}$ = 3.6 Hz), 6.12 (m, 1 H, N*H*Et), 3.45 (m, 2 H, N*CH$_2$*CH$_3$), 2.36 (s, 3 H, C4−Me), 1.91 (s, 3 H, =C−Me), 1.29 (t, 3 H, NCH$_2$*CH$_3$*, $^3J_{HH}$ = 7.0 Hz).

[Pd{4-MeC$_6$H$_3$C(Me)=NNC(=S)NHPh}(PPh$_3$)]$^+$Cl$^-$ (3c): Yield: 48 mg, 91%. $C_{34}H_{31}ClN_3PPdS$ (686.6): calcd. C, 59.5, H 4.6, N 6.1, S 4.7; found C 59.2, H 4.5, N 6.0, S 4.4. IR: $\tilde{\nu}$ = 1570 [m, ν(C=N)], 825 [m, ν(C=S)] cm^{-1}. Λ_M (acetonitrile, 3×10^{-3} mol L^{-1}) = 95 Ω^{-1} cm^2 mol^{-1}. ^{31}P {^{1}H} NMR ($CDCl_3$): δ = 38.6 (s). ^{1}H NMR ($CDCl_3$): δ = 9.04 (s, 1 H, NH), 7.6 (s, 1 H, NHPh), 7.18 (d, 1 H, H2, $^3J_{H2H3}$ = 7.0 Hz), 7.02 (d, 1 H, H3), 6.17 (d, 1 H, H5, $^4J_{PH5}$ = 3.4 Hz), 2.53 (s, 3 H, C4−Me), 1.92 (s, 3 H, =C−Me).

Compounds 1d and 1e: These were prepared in a similar fashion to **1a** (Method 1).

[Pd{4-MeOC$_6$H$_3$C(H)=NN(Me)C(=S)NH$_2$}(Cl)] (1d): Yield: 185 mg, 83%. $C_{10}H_{12}ClN_3OPdS$ (364.2): calcd. C 33.0, H 3.3, N 11.5, S 8.8; found C 31.9, H 3.3, N 11.1, S 9.2. IR: $\tilde{\nu}$ = 1589 [m, ν(C=N)], 309 [m, ν(Pd−Cl)], 834 [m, ν(C=S)] cm^{-1}. ^{1}H NMR ($CDCl_3$): δ = 8.14 (s, 1 H, HC=N), 7.24 (d, 1 H, H2, $^3J_{H2H3}$ = 8.4 Hz), 6.93 (d, 1 H, H5, $^4J_{H3H5}$ = 2.2 Hz), 6.53 (dd, 1 H, H3), 3.72 (s, 3 H, MeO), 3.46 (s, 3 H, NMe). ^{13}C {^{1}H} NMR (62.46 MHz, $CDCl_3$): δ = 189.1 (C=S), 163.5 (C4), 160.1 (C6), 157.6 (C=N), 139.6 (C1), 130.1 (C2), 118.6 (C3), 109.7 (C5), 55.4 (MeO), 35.4 (NMe).

[Pd{3-MeOC$_6$H$_3$C(H)=NN(Me)C(=S)NH$_2$}(Cl)] (1e): Yield: 185 mg, 83%. $C_{10}H_{12}ClN_3OPdS$ (364.2): calcd. C 33.0, H 3.3, N 11.5, S 8.8; found C 32.9, H 3.2, N 11.3, S 9.1. IR: $\tilde{\nu}$ = 1591 [m, ν(C=N)], 315 [m, ν(Pd-Cl)], 842 [m, ν(C=S)] cm^{-1}. ^{1}H NMR ($CDCl_3$): δ = 9.47 (s, 1 H, NH$_2$), 8.74 (s, 1 H, NH$_2$), 8.18 (s, 1 H, HC=N), 7.23 (d, 1 H, H5, $^3J_{H4H5}$ = 8.4 Hz), 6.94 (d, 1 H, H2, $^4J_{H2H4}$ = 2.7 Hz), 6.67 (dd, 1 H, H4), 3.68 (s, 3 H, MeO), 3.47 (s, 3 H, NMe). ^{13}C {^{1}H} NMR (62.46 MHz, $CDCl_3$): δ = 174.6 (C=S), 160.1 (C6), 157.8 (C=N), 157.1 (C3), 146.7 (C1), 133.2 (C2), 114.1 (C5), 113.4 (C4), 55.4 (MeO), 35.5 (NMe).

[Pd{4-MeOC$_6$H$_3$C(H)=N[2-(SMe)C$_6$H$_4$]}(Cl)] (1f): 4-MeOC$_6$H$_4$C(H)=N[2-(SMe)C$_6$H$_4$] (**f**) (217 mg, 0.84 mmol) and sodium acetate (500 mg, 6.1 mmol) were added to a stirred solution of palladium(II) chloride (135 mg, 0.76 mmol) and lithium chloride (65 mg, 1.53 mmol) in methanol (40 mL). The mixture was stirred for 48 h at room temperature under nitrogen. The yellow precipitate was filtered off, washed with ethanol, and dried. Yield: 252 mg, 83%. $C_{15}H_{14}ClNOPdS$ (398.18): calcd. C 45.2, H 3.5, N 3.5, S 8.1; found C 45.0, H 3.4, N 3.4, S 8.0. IR: $\tilde{\nu}$ = 1603 [m, ν(C=N)], 310 [m, ν(Pd−Cl)] cm^{-1}. ^{1}H NMR ($CDCl_3$): δ = 9.12 (s, 1 H, HC=N), 7.98 (d, 1 H, H6′, $^3J_{H5'H6'}$ = 8.4 Hz), 7.83 (d, 1 H, H3′, $^3J_{H3'H4'}$ = 7.9 Hz), 7.55 (t, 1 H, H4′, $^3J_{H4'H5'}$ = 8.0 Hz), 7.53 (d, 1 H, H2, $^3J_{H2H3}$ = 8.8 Hz), 7.44 (t, 1 H, H5′), 7.11 (d, 1 H, H5, $^4J_{H3H5}$ = 2.7 Hz), 6.71 (dd, 1 H, H3), 3.80 (s, 3 H, MeO), 2.75 (s, 3 H, SMe). ^{13}C {^{1}H} NMR (62.46 MHz, $CDCl_3$): δ = 169.7 (C=N), 168.0 (C−S), 167.1 (C4), 147.5 (C−N), 143.1 (C6), 133.2 (C1), 133.0 (C2), 135.3, 131.6, 129.9, 119.5 (N-ring C atoms), 118.3, 111.4 (C3, C5), 55.8 (MeO), 24.8 (SMe).

Synthesis of [Pd{4-MeOC$_6$H$_3$C(H)=N[2-(SMe)C$_6$H$_4$]}(PPh$_3$)](ClO$_4$) (2f): $AgClO_4$ (29 mg, 0.14 mmol) was added to compound **1f** (56 mg, 0.14 mmol) in acetone (15 mL). The resulting suspension was stirred for 3 h and filtered through Celite to remove the silver chloride precipitate. PPh_3 (37 mg, 0.14 mmol) was added to the filtrate and the solution was stirred for 3 h. The solvent was removed and the product was recrystallized from dichloromethane/hexane as a yellow solid. Yield: 84 mg, 83%. $C_{33}H_{29}ClNO_5PPdS$ (724.5): calcd. C 54.7, H 4.0, N 1.9, S 4.4; found C 54.2, H 3.9, N 1.8, S 4.7. IR: $\tilde{\nu}$ = 1607 [m, ν(C=N)] cm^{-1}. Λ_M (acetonitrile, 3×10^{-3} mol L^{-1}) = 91 Ω^{-1} cm^2 mol^{-1}.^{1}H NMR ($CDCl_3$): δ = 9.18 (d, 1 H, HC=N, $^4J_{PH}$ = 8.4 Hz), 8.06 (d, 1 H, H6′, $^3J_{H5'H6'}$ = 8.0 Hz), 7.86 [d, 1 H, H3′, $^3J_{H3'H4'}$ = 8.4 Hz), H4′, H2, H5′ (signals hidden by the phosphane resonances)], 6.57 (d, 1 H, H3, $^4J_{H3H5}$ = 2.7 Hz), 6.71 (dd, 1 H, H5, $^4J_{PH}$ = 5.5 Hz), 3.60 (s, 3 H, MeO), 2.75 (s, 3 H, SMe).

X-ray Crystallographic Study:[35] Crystals of complexes **2a** and **1f** were mounted on a glass fiber and transferred to the diffractometer. Three-dimensional, room-temperature X-ray data were collected with Siemens (**2a**) and Bruker (**1f**) SMART CCD diffractometers by the ω-scan method, using graphite-monochromated Mo-K_α radiation. All the measured reflections were corrected for Lorentz and polarization effects and for absorption by semiempirical methods based on symmetry-equivalent and repeated reflections [T_{max}/T_{min} = 0.9573/0.8437 (**2a**) and 0.7356/0.6194 (**1f**)]. The structure was solved by direct methods and refined by full-matrix, least squares on F^2. Hydrogen atoms were included in calculated positions (except H3 in **2a**, which was located from a Fourier-difference map) and refined in the riding mode. Refinement converged at a final R = 0.0447 (**2a**) and 0.0349 (**1f**) (observed data, F) and wR_2 = 0.1038 (**2a**) and 0.0811 (**1f**) (all unique data, F^2), with allowance for thermal anisotropy of all non-hydrogen atoms. Minimum and maximum final electron densities: −0.475 and 0.542 e Å^{-3} (**2a**), 0.726 and −0.839 e Å^{-3} (**1f**). The structure solutions and refinements were carried out with the SHELX-97 program package.[36]

Acknowledgments

We thank the Xunta de Galicia, Spain (Proyecto PGIDT99PXI20907B) and the DGES (Grant no. PB98-0638-C02-01/02) for financial support.

[1] S. Trofimenko, *Inorg. Chem.* **1973**, *12*, 1215−1221.
[2] M. I. Bruce, *Angew. Chem. Int. Ed. Engl.* **1977**, *16*, 73−86.
[3] I. Omae, *Chem. Rev.* **1979**, *79*, 287−321.
[4] I. Omae, *Coord. Chem. Rev.* **1988**, *83*, 137−167.
[5] I. Omae, *Organometallic Intramolecular-coordination Compounds*, Elsevier, Amsterdam, **1986**.
[6] V. V. Dunina, O. A. Zalevskaya, V. M. Potapov, *Russ. Chem. Rev.* **1988**, *57*, 250−269.
[7] G. R. Newkome, W. E. Puckett, W. K. Gupta, G. E. Kiefer, *Chem. Rev.* **1986**, *86*, 451.
[8] J. M. Vila, M. Gayoso, M. T. Pereira, A. Suárez, J. J. Fernández, J. M. Ortigueira, A. Fernández, M. López-Torres, *Trends Organomet. Chem.* **1997**, *2*, 21−37.
[9] J. M. Vila, M. Gayoso, M. T. Pereira, M. López-Torres, J. J. Fernández, J. M. Ortigueira, *J. Organomet. Chem.* **1997**, *532*, 171−180.
[10] J. M. Vila, M. T. Pereira, J. M. Ortigueira, D. Lata, M. López-Torres, J. J. Fernández, A. Fernández, H. Adams, *J. Organomet. Chem.* **1998**, *566*, 93−101.
[11] J. M. Vila, M. T. Pereira, J. M. Ortigueira, M. López-Torres, A. Castiñeiras, J. J. Fernández, A. Fernández, D. Lata, *J. Organomet. Chem.* **1998**, *556*, 21−30.
[12] J. M. Vila, M. T. Pereira, J. M. Ortigueira, M. Graña, D. Lata,

A. Suárez, J. J. Fernández, A. Fernández, M. López-Torres, H. Adams, *J. Chem. Soc., Dalton Trans.* **1999**, 4193−4201.
[13] T. Kawamoto, Y. Kushi, *Chem. Lett.* **1992**, 1057−1058.
[14] T. Kawamoto, Y. Nagasawa, H. Kuma, Y. Kushi, *Inorg. Chem.* **1996**, *35*, 2427−2432.
[15] A. G. Quiroga, J. M. Pérez, I. López-Solera, J. R. Masaguer, A. Luque, P. Román, A. Edwards, C. Alonso, C. Navarro-Ranninger, *J. Med. Chem.* **1998**, *41*, 1399−1408.
[16] F. Hueso-Ureña, N. A. Illán-Cabeza, M. Moreno-Carretero, A. L. Peñas-Chamorro, R. Faure, *Inorg. Chem. Commun.* **1999**, *2*, 323−326.
[17] D. Kovala-Demertzi, A. Domopoulou, M. A. Demertzis, C. P. Raptopoulou, A. Terzis, *Polyhedron* **1994**, *13*, 1917−1925.
[18] J. M. Vila, M. Gayoso, M. T. Pereira, M. López-Torres, J. Fernández, A. Fernández, J. M. Ortigueira, *J. Organomet. Chem.* **1996**, *506*, 165−174.
[19] D. X. West, J. S. Ives, G. A. Bain, A. E. Liberta, J. Valdés-Martínez, K. H. Ebert, S. Hernández-Ortega, *Polyhedron* **1997**, *16*, 1895−1905.
[20] T. S. Lobana, A. Sánchez, J. S. Casas, A. Castiñeiras, J. Sordo, M. S. García-Tasende, E. M. Vázquez-López, *J. Chem. Soc., Dalton Trans.* **1997**, 4289−4300.
[21] H. Onoue, Y. Moritani, *J. Organomet. Chem.* **1972**, *43*, 431−436.
[22] Y. Ustynyuk, V. A. Chertov, J. V. Barinov, *J. Organomet. Chem.* **1971**, *29*, C53−C54.
[23] P. S. Pregosin, R. W. Kuntz, *^{31}P and ^{13}C NMR of Transition Metal Phosphane Complexes* (Eds.: P. Diehl, E. Fluck, R. Kosfeld), Springer, Berlin, **1979**.
[24] J. Albert, M. Gómez, J. Granell, J. Sales, *Organometallics* **1990**, *9*, 1405−1413.
[25] R. Bosque, J. Granell, J. Sales, M. Font-Bardía, X. Soláns, *J. Organomet. Chem.* **1993**, *453*, 147−154.
[26] J. Albert, J. Granell, J. Sales, M. Font-Bardía, X. Soláns, *Organometallics* **1995**, *14*, 1393−1404.
[27] W. Geary, *Coord. Chem. Rev.* **1971**, *7*, 81−122.
[28] J. M. Vila, M. Gayoso, M. López-Torres, J. J. Fernández, A. Fernández, J. M. Ortigueira, N. A. Bailey, H. Adams, *J. Organomet. Chem.* **1996**, *511*, 129−138.
[29] L. Pauling, *The Nature of the Chemical Bond*, 3rd ed., Cornell University Press, Ithaca, New York, **1960**, pp.224.
[30] J. M. Vila, M. Gayoso, M. T. Pereira, A. Romar, J. J. Fernández, M. Thornton-Pett, *J. Organomet. Chem.* **1991**, *401*, 385−394.
[31] J. Selbin, K. Abboud, S. F. Watkins, M. A. Gutiérrez, F. R. Fronczek, *J. Organomet. Chem.* **1983**, *241*, 259−268.
[32] C. Navarro-Ranninger, I. López-Solera, A. Alvarez-Valdés, J. H. Rodríguez-Ramos, J. R. Masaguer, J. L. García-Ruano, *Organometallics* **1993**, *12*, 4104−4111.
[33] A. Suárez, J. M. Vila, E. Gayoso, M. Gayoso, W. Hiller, A. Castiñeiras, J. Strähle, *Z. Anorg. Allg. Chem.* **1986**, *535*, 213−218.
[34] D. D. Perrin, W. L. F. Armarego, D. L. Perrin, *Purification of Laboratory Chemicals*, 3rd ed., Pergamon, London, **1998**.
[35] Crystallographic data (excluding structure factors) for the structures reported in this paper have been deposited with the Cambridge Crystallographic Data Centre as supplementary publication nos. CCDC-167981 (**2a**) and -167980 (**1f**). Copies of the data can be obtained free of charge on application to CCDC, 12 Union Road, Cambridge CB2 1EZ, UK [Fax: (internat.) + 44-1223/336-033; E-mail: deposit@ccdc.cam.ac.uk].
[36] G. M Sheldrick, *SHELX-97*, *An Integrated System for Solving and Refining Crystal Structures from Diffraction Data*, University of Göttingen, Germany, **1997**.

Received July 31, 2001
[I01281]

New Neutral and Cationic Dialkylaluminium Complexes Bearing Imino-Amide or Imino-Phenoxide Ligands: Synthesis, Characterization and Reactivity With Olefins

Daniela Pappalardo,*[b] Consiglia Tedesco,[a] and Claudio Pellecchia[a]

Keywords: Alkenes / N ligands / N,O ligands / Polymerization / Aluminum

The synthesis and the characterization of some new aluminium complexes carrying bidentate monoanionic imino-amide or imino-phenoxide ligands are described. Reaction of 1-(*o*,*o*′-diisopropylphenylamino)-6-(*o*,*o*′-diisopropylphenylimino)cyclohexene with $AlMe_3$ proceeded by methane elimination to produce the yellow compound dimethylaluminium *N*-(*o*,*o*′-diisopropylphenyl)-6-[*N*-(*o*,*o*′-diisopropylphenyl)-imido]-1-cyclohexen-1-amide (**1**). In contrast, reaction of the same ligand with $AlEt_3$ under the same experimental conditions involved the 1,4-addition of $AlEt_3$ to the α,β-unsaturated imine, and led to the highly crystalline diethylaluminium *N*-(*o*,*o*′-diisopropylphenyl)-2-[(*o*,*o*′-diisopropylphenyl)amino]-3-ethyl-1-cyclohexen-1-amide (**2**). The structures of compounds **1** and **2** were determined by single-crystal X-ray diffraction. Thermolysis of **2** gave rise to ethane elimination, and led to the oily bis(amido) monoethyl derivative. Treatment of the salicylaldimine ligands 3-*t*Bu-2-(OH)C_6H_3CH=N–R with $AlMe_3$ yielded the dimethylaluminium compounds {3-*t*Bu-2-(O)C_6H_3CH=N–R}$AlMe_2$ [R = C_6H_5 (**3**); 2,6-*i*$Pr_2C_6H_3$ (**4**); and C_6F_5 (**5**)]. Compounds **1**, **3**, and **5** underwent methyl abstraction reactions with $B(C_6F_5)_3$; trapping of the cationic species was accomplished in the presence of THF in dichloromethane solution. Preliminary polymerization tests were carried out for the synthesized Al complexes. Toluene solutions of **3**, **4**, and **5**, when activated with 1 equiv. of $B(C_6F_5)_3$, polymerised ethylene (1 atm) to solid polyethylene with low activity.

Introduction

Since the disclosure by Ziegler of the "aufbau" reaction, alkylaluminium compounds have been known as olefin oligomerization catalysts, because of the displacement reaction competing with a "smooth stepwise addition of ethylene".[1] In 1992 Martin demonstrated that the growth reaction of ethylene at bis(dichloroaluminium)ethane and trialkylaluminium produces, with low activity, polyethylene of high molecular weight and thermoplastic character.[2] More recently, Sen et al. reported that simple alkylaluminium compounds, after reaction with the activators commonly used in the homogeneous olefin polymerization catalysis {i.e. $B(C_6F_5)_3$, $[(C_6H_5)_3C][B(C_6F_5)_4]$ or $[(C_6H_5)N(CH_3)_2H][B(C_6F_5)_4]$} are able to catalyse the polymerization of ethylene and propene, although with low activity.[3] The authors hypothesize that neutral aluminium species, such as $[(R)(C_6F_5)_2Al]_x$, are the active catalysts operating in these systems.[3] Actually, the reaction of $AlMe_3$ with $[(C_6H_5)_3C][B(C_6F_5)_4]$ gives the transient species $[AlMe_2]^+[B(C_6F_5)_4]^-$ which immediately decomposes by ligand exchange to $Al(C_6F_5)_3$ and BMe_3.[4,5] Trapping of the cationic alkylaluminium species was achieved in the presence of bases,[6] or using coordinating solvents such as diethyl ether and THF.[7] Base-free cationic species are expected to be highly electrophilic, and therefore more active as olefin polymerization catalysts.

The stability of base-free group-13 alkyl cations seems to be strongly dependent on the ancillary ligand and the kind of counter-anion. Bochmann described the bis(cyclopentadienyl)aluminium cation as an initiator for the carbocationic polymerization of isobutylene,[8] and Jordan reported the synthesis and characterization of several cationic aluminium complexes incorporating chelating nitrogen-based ligands, able to polymerise ethylene.[9] According to Jordan's results, a few related aluminium derivatives carrying chelating monoanionic ligands have also been shown to polymerise ethylene with comparably low activity.[10]

In this paper we report on the synthesis and the characterization of some new aluminium complexes carrying bidentate monoanionic imino-amide or imino-phenoxide ligands (Scheme 1) and some preliminary data on their reactivity with ion-generating activators and the subsequent reactivity in ethylene polymerization.[11]

[a] Dipartimento di Chimica, Università di Salerno,
84081 Baronissi, Salerno, Italy
Fax: (internat.) + 39-089/965296
E-mail: pappalardo@chem.unisa.it
[b] Facoltà di Scienze MM. FF. NN., Università del Sannio,
Via Port'Arsa 11, 82110, Benevento, Italy

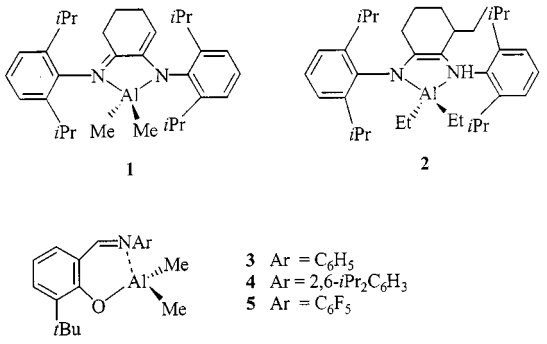

Scheme 1

Results and Discussion

Treatment of 1-(*o*,*o*′-diisopropylphenylamino)-6-(*o*,*o*′-diisopropylphenylimino)cyclohexene[12] with $AlMe_3$ in heptane at room temperature afforded the dimethyl complex **1** as a yellow solid in high yield. The disappearance of the N−*H* signal of the ligand in the ^1H NMR spectrum of **1** ([D_6]benzene, room temperature), and the appearance of a high-field signal (δ = −0.37, 6 H) compatible with Al*Me*$_2$ protons, reveal that the reaction proceeds by protodealumination of the Al−CH_3 bond with concomitant elimination of methane (Scheme 2). Although the molecule belongs to the C_1 symmetry group, the presence of only one signal for the Al*Me*$_2$ protons in the ^1H NMR spectrum, and the signals pattern in the ^{13}C NMR spectrum (i.e. 4 signals for the methyl groups of the isopropyl groups, 2 signals for C*H*Me$_2$) are compatible with the presence of a "pseudo" mirror symmetry passing through the Al and the two nitrogen atoms. This therefore indicates that, under the analysis conditions (i.e. room temperature, benzene solution), the change in conformation of the cyclohexene ring is fast on the NMR time scale.

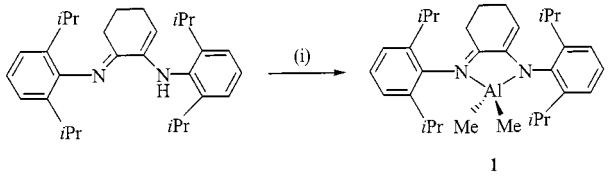

Scheme 2. Reaction conditions: (i) $AlMe_3$, heptane, room temperature

Crystals of **1** suitable for an X-ray structure determination were grown from toluene at −20 °C. The compound crystallized as prismatic crystals in the monoclinic space group $P2_1/n$, the asymmetric unit containing one discrete molecule of **1** and half of a centrosymmetric disordered toluene molecule. The molecular structure of **1** is shown in Figure 1; selected bond lengths and angles are given in Table 1. The coordination environment about the Al atom is approximately tetrahedral, with Al−CH_3 distances comparable to those observed in analogous β-diketiminato[13] and imino-amide complexes.[14] The Al−N distances differ slightly from each other [1.968(11) and 1.897(10) Å], suggesting a dative and a sigma bond, respectively, as already observed in the just cited imino-amide compounds.[14] Inspection of the bond lengths within the −N1−C1(C6)−C2(C3)−N2− moiety suggests the presence of a partial delocalization.[14,15] The puckering of the cyclohexene ring is described by the deviations of the atoms C3, C4, C5, and C6 from the least-square plane defined by N1, C1, C2, and N2 atoms (rmsd 0.005); these deviations are 0.01(2) Å, 0.45(3) Å, 0.25(3), and 0.02(2) Å, respectively. The Al atom lies under the previously defined plane and deviates by −0.22(2) Å. The aromatic rings C7···C12 and C19···C24 are planar with rmsd of 0.027 and 0.017, respectively, and are almost perpendicular to the Al−N1−C1−C2−N2 ring. The dihedral angles between the five-atom Al−N1−C1−C2−N2 plane and each aromatic ring are 87.8(4)° and 86.6(4)°.

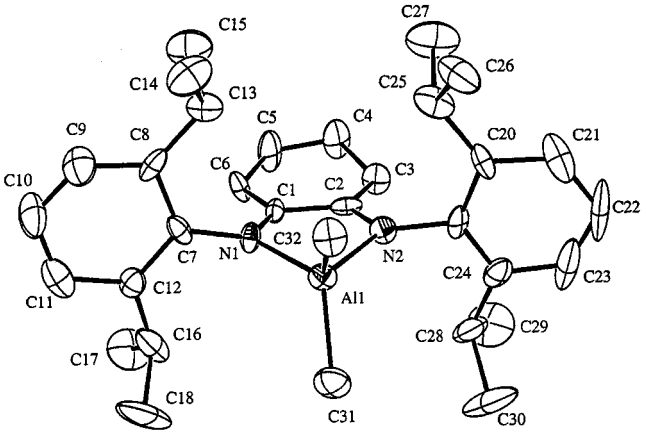

Figure 1. Molecular structure of **1**; thermal ellipsoids are drawn at 20% probability level; hydrogen atoms have been omitted for clarity

Table 1. Selected bond lengths [Å] and angles [°] for compounds **1** and **2**

1	**2**
Al−C31 1.968(12)	Al−C33 1.974(6)
Al−C32 1.961(12)	Al−C35 1.958(6)
Al−N1 1.968(11)	Al−N1 2.045(4)
Al−N2 1.897(10)	Al−N2 1.856(4)
N1−C1 1.344(14)	N1−C1 1.494(5)
N2−C2 1.333(14)	N2−C2 1.393(6)
C1−C2 1.434(15)	C1−C2 1.348(6)
C1−C6 1.385(15)	C1−C6 1.499(6)
C2−C3 1.49(2)	C2−C3 1.494(6)
C3−C4 1.44(2)	C3−C4 1.527(7)
C4−C5 1.43(2)	C4−C5 1.511(7)
C5−C6 1.47(2)	C5−C6 1.521(7)
C31−Al−C32 110.0(6)	C33−Al−C35 112.2(3)
N2−Al−N1 84.2(5)	N2−Al−N1 85.9(2)
N2−Al−C32 114.3(5)	N1−Al−C35 117.0(2)
N2−Al−C31 113.9(5)	N1−Al−C33 102.5(2)
C31−Al− N1 118.0(6)	C33−Al− N2 115.5(2)
C32−Al−N1 114.5(5)	C35−Al−N2 119.8(2)

Interestingly, the reaction of the same ligand with $AlEt_3$ under identical conditions did not afford the expected di-

ethylaluminium imino-amide derivative analogous to **1**, but an orange crystalline solid, characterized by X-ray diffraction and NMR spectroscopy as the diethylaluminium complex **2**, featuring a *C*-alkylated amino-amido ligand (Scheme 3). Particularly diagnostic in the ^{1}H NMR spectrum of **2** ([D$_6$]benzene, 25 °C) (Figure 2) is the broad singlet at δ = 6.55 (1 H, N*H*), indicating that the amine function is not deprotonated, while the signal of the unsaturation on the six-membered carbon ring of the ligand is absent, as a consequence of the ethyl addition. The ethyl groups bound to the aluminium atom are not equivalent, thus resulting in two well-defined patterns of signals at high field; in particular the methylene hydrogen atoms in each ethyl group are diastereotopic and appear as a double quadruplet (δ = 0.18, 2 H, AlCH_2CH$_3$) and two multiplets (δ = 0.52−0.28, 2 H, AlCH'_2CH$_3$).

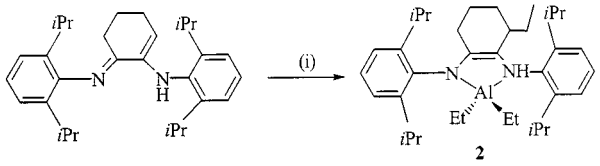

Scheme 3. Reaction conditions: (i) AlEt$_3$, heptane, room temperature

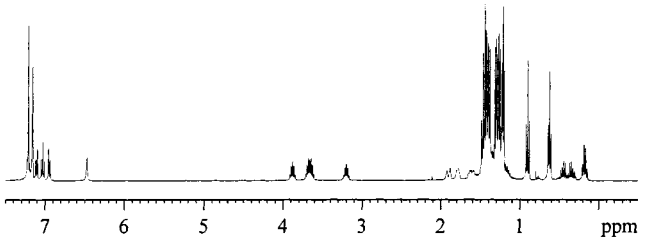

Figure 2. ^{1}H NMR spectrum of **2** (C$_6$D$_6$, room temperature)

This picture is consistent with a C_1 symmetry, that is confirmed by the number of signals in the ^{13}C NMR spectrum [i.e. 4 signals for *C*H(CH$_3$)$_2$, 8 signals for CH(*C*H$_3$)$_2$, 2 signals for AlCH$_2$*C*H$_3$ (δ = 9.6 and 9.0), and 2 broad signals for Al*C*H$_2$CH$_3$ (δ = 0.95 and −0.5)].

Complex **2** was crystallized from toluene at −20 °C. The molecular structure of **2** is shown in Figure 3; selected bond lengths and angles are given in Table 1. The coordination environment about the Al atom is almost tetrahedral with Al−Et bond lengths displaying usual values. The distances Al−N1 and Al−N2 are 2.045(4) Å and 1.856(4) Å, respectively, as observed in analogous aluminium compounds bearing a monoanionic chelating secondary amine-amido ligand.[16] The ligand bite angle N2−Al−N1 measures 85.9(2)° and differs significantly from the values previously observed in analogous secondary amine-amido compounds[16] [88.4(1)−93.6(3)°]. This feature can be ascribed to the different nature of the −N−C−C−N− backbone in compound **2**, which is the only one showing a central double bond. The five atom Al−N1−C1−C2−N2 ring is planar with rmsd = 0.034. The C3 and C6 atoms deviate from the plane by −0.025 and 0.190 Å, respectively. The aromatic rings C9···C14 and C21···C26 are planar with rmsd of 0.004 and 0.007, respectively. The C21···C26 ring lies perpendicularly to the five-atom Al−N1−C1−C2−N2 plane with a dihedral angle between the two mentioned planes of 89.3(1)°. The other aromatic ring cannot assume the same conformation with respect to the five-atom plane because of the steric hindrance of the ethyl group on the cyclohexene ring, thus resulting in a dihedral angle of 83.6(1)°.

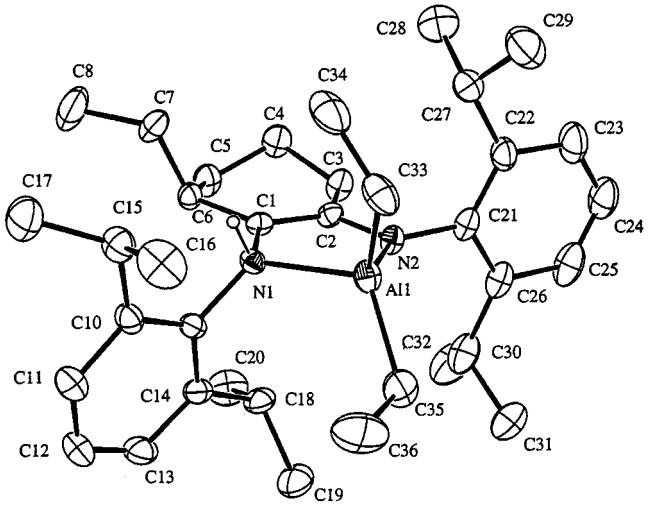

Figure 3. Molecular structure of **2**; thermal ellipsoids are drawn at 20% probability level; hydrogen atoms have been omitted for clarity, with the exception of the amine hydrogen atom

A reasonable reaction pathway leading to compound **2** involves 1,4-addition of AlEt$_3$ to the α,β-unsaturated imine, resulting in alkylation of the cyclohexene moiety of the ligand to give the diethylaluminium amido-amino complex **2**. Although we are not aware of similar reactions for α,β-unsaturated imines, there are many examples of this kind for α,β-unsaturated carbonyl derivatives. Addition of AlR$_2$I to enones, or addition of AlPh$_3$ to chalcone, for example, occurs in this manner almost quantitatively; with α,β-unsaturated ketones, in general, the 1,4-addition of AlR$_3$ can become the principal mode of reaction, and proceeds via initial coordination of the aluminium reagent at the carbonyl group.[17] We hypothesize that, also in our case, the coordination of the AlEt$_3$ is required prior to nucleophilic attack of the ethyl group to the ligand. Actually, the *pre*-coordination of the alkylaluminium compound to the iminic nitrogen atom should increase the electrophilic character of the β-unsaturated carbon atom on the cyclohexene ring, thus supporting the 1,4-addition. Moreover, it is well established that N,N-bidentate ligands, such as the closely related α-diimines, form initial complexes with trialkylaluminium in which only one N-atom is bonded to the aluminium centre.[18]

It is an open question why such a different behaviour is observed by just changing the alkyl group bound to Al from methyl to ethyl. It is, however, evident that the ligand can behave both as a Lewis acid and as a Brønsted acid, and actually nucleophilic addition is observed with AlEt$_3$, while AlMe$_3$ serves as a deprotonating agent.

With the aim of obtaining the protodealumination product analogous to **1**, we performed the reaction of the ligand with $AlEt_3$ in refluxing toluene. Removal of volatiles in vacuo left a red oil, that, on the basis of ^1H and ^{13}C NMR analysis, was identified as the bis(amido)monoethylaluminium derivative, possibly derived by thermolysis of **2** by ethane elimination (Scheme 4). Comparing the ^1H NMR spectrum ([D_6]benzene, 25 °C) of the thermolysis product with the ligand spectrum, we noticed the lack of both the resonances of N*H* and =C*H* of the cyclohexene ring. On the other hand, diagnostic signals are a quadruplet at $\delta = 0.33$ (2 H) and a triplet at $\delta = 0.85$ (3 H) attributable to one ethyl group bound to the aluminium atom, and a triplet at $\delta = 0.57$ (3 H) for the CH_3CH$_2$− on the cyclohexene ring. We suppose that, at higher temperatures, the reaction generates first the 1,4-addition product **2**, which rapidly decomposes by ethane elimination resulting in the monoethyl derivative. We cannot determine if the compound is a monomer or a dimer; unfortunately, ^{27}Al NMR experiments were precluded by the probe signal noise.

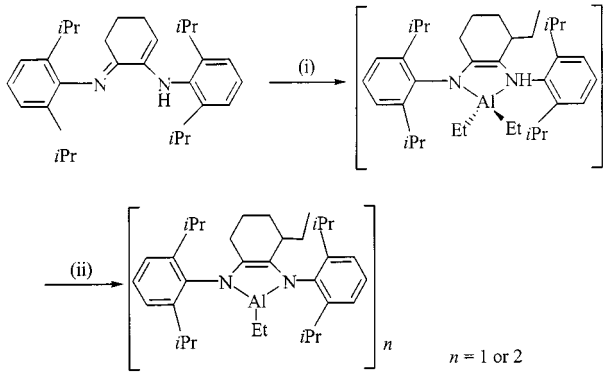

Scheme 4. Reaction conditions: (i) $AlEt_3$, refluxing toluene; (ii) − C_2H_6

While the five-coordinate alkyl(Salen)group-13 complexes have been largely studied and used in many catalytic reactions,[19] only a few reports concerning the related lower coordinate dialkyl(salicylaldiminato)aluminium compounds have appeared in the literature.[10b,11] We have synthesized the dimethyl(salicylaldiminato)aluminium compounds **3** and **4**, and the perfluoro derivative **5** with the aim to test their reactivity in olefin polymerization. Actually, recent reports by Coates[20a] and by Fujita[20b] described titanium complexes carrying salicylaldiminato ligands with electron-withdrawing substituents that show increased activity in the polymerization of olefins.

Compounds **3**−**5** were prepared in good yields as yellow solids by treating the related ligand with $AlMe_3$ (1:1 ratio) in heptane at room temperature (Scheme 5). Reactions cleanly proceed by protodealumination of the Al−CH_3 bond with concomitant elimination of methane. Products were characterized by ^1H and ^{13}C NMR (room temperature, C_6D_6 solution), revealing similar features. The methyl groups bound to the aluminium atom show characteristic resonances at $\delta \approx -0.30$ in the ^1H NMR spectrum, and between $\delta = -8$ and -9 in the ^{13}C NMR spectrum. No differences were observed for the resonances of the *tert*-butyl substituent on the phenoxy group; for all the complexes the C(CH_3)$_3$ signal appeared at $\delta \approx 1.5$ in ^1H NMR spectrum, while the ^{13}C NMR resonances for *C*Me$_3$ and C*Me*$_3$ are shown at $\delta = 35.7$ and 29.8, respectively. Diagnostic signals for the imine function appear at $\delta \approx 7.5$ in the ^1H NMR spectrum, and between $\delta = 170$ and 180 in the ^{13}C NMR spectrum. Interestingly, in the ^1H NMR spectrum of **5**, the Al*Me* resonance appears as a triplet ($J = 1.4$ Hz), which is probably due to the coupling with the α-fluorine atoms of the C_6F_5 group.

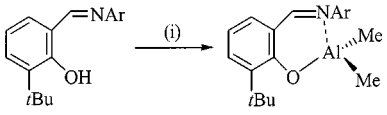

Scheme 5. Reaction conditions: (i) $AlMe_3$, heptane, room temperature

We have explored the generation of cationic complexes from the synthesized aluminium compounds by NMR tube reactions with $B(C_6F_5)_3$.

When **1** and $B(C_6F_5)_3$ are mixed in C_6D_6 at room temperature, a red oil precipitated, thus preventing NMR solution analysis. The reaction was consequently studied in CD_2Cl_2 solution. After in situ treatment of **1** with 0.5 equiv. of $B(C_6F_5)_3$, the ^1H NMR spectrum showed, in addition to the signals of the neutral dimethylaluminium starting compound, new resonances attributable to a mixture of organometallic species. Although the ^1H NMR spectrum's region relative to the ligand is quite complicated, the high-field region can be easily interpreted in terms of methyl abstraction by $B(C_6F_5)_3$. Diagnostic resonances are two singlets at $\delta = +0.45$ and -0.42, attributable, by comparison with the data reported in the literature, to the free anion $[MeB(C_6F_5)_3]^-$ [21] and to the methyl group bound to the aluminium cation $AlMe^+$, respectively.[9] Formation of $[MeB(C_6F_5)_3]^-$ was further confirmed by a resonance at $\delta = -15.4$ in the ^{11}B NMR spectrum. After addition of a further amount (0.5 equiv.) of $B(C_6F_5)_3$, the resonances of the neutral starting compound disappeared. Subsequently, ethylene was added to the NMR tube; monitoring of the reaction showed that ethylene was consumed. Attempts to isolate and better characterize the cationic species in the absence of bases were unsuccessful. Trapping of the cationic species was instead achieved in the presence of THF. When $B(C_6F_5)_3$ (1 equiv.) was added to a CD_2Cl_2 solution of **1** containing 1 equiv. of THF, the THF-coordinated methyl cation **1a** was formed (Scheme 6). Characteristic resonances are the signals at $\delta = -0.41$ for AlMe^+ (3 H) and at $\delta = 0.48$ (3 H) for B*Me* in the ^1H NMR spectrum; the corresponding ^{13}C NMR resonances appear at $\delta = -13.6$ and 10.3, respectively. As a consequence of the positive charge on the aluminium atom, the resonances of the ligand in the cationic species are shifted to lower field compared to the resonances of the neutral compound in the same solvent (CD_2Cl_2). For instance, the triplet of C*H*= in the cyclohex-

ene ring of the ligand moves from δ = 4.76 for compound **1** to δ = 5.61 for the cation **1a**. Moreover, a C_1 symmetry can be deduced by the number of signals relative to the isopropyl substituents on the aryl groups (i.e. four signals for C*H*Me$_2$ and eight doublets for CH*Me*$_2$). Ethylene (ca. 1.3 equiv.) was added in the NMR tube; reaction of the olefin with the cationic species did not take place under these conditions, as shown by the ^{1}H NMR spectrum. Further investigation is in progress to determine if polymerization of ethylene occurs under more severe conditions.

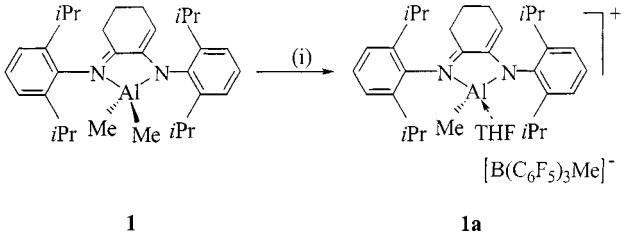

1 **1a**

Scheme 6. Reaction conditions: (i) B(C_6F_5)$_3$, THF in CD_2Cl_2

Attempts to generate clean cationic species from the amino-amide diethylaluminium compound **2** with B(C_6F_5)$_3$ were in vain; reactions always led to a mixture of species, even in the presence of THF.

Similar experiments were performed with the imino-phenoxide compounds **3** and **5**, giving analogous results. Thus, while reaction of **3** with B(C_6F_5)$_3$ in C_6D_6 gives a mixture of species, the cationic species {3-*t*Bu-2-(O)C_6H_3CH=N−C_6H_5}AlMe(THF)$^+$[MeB(C_6F_5)$_3$]$^-$ (**3a**) and {3-*t*Bu-2-(O)C_6H_3CH=N−C_6F_5}AlMe(THF)$^+$[MeB(C_6F_5)$_3$]$^-$ (**5a**) were instead obtained in the presence of THF in CD_2Cl_2 solution. The ^{1}H NMR spectrum of **3a** (CD_2Cl_2, room temperature) shows the Al*Me*$^+$ resonance at lower field in comparison with the resonance of the neutral one in the same solvent (δ = −0.15 vs. −0.82, respectively), as a consequence of the positive charge on the aluminium atom. Resonances relative to the imino-phenoxide ligand show an analogous shift; particularly, the C*H*=N signal moves from δ = 8.35 to 8.72. In addition, the aromatic hydrogen atom signals on the phenoxy group are split in a wider range (δ = 7.82−6.80). Signals for the THF coordinated to the aluminium atom appear at δ = 4.22 and 2.14 (OC*H*$_2$ and OCH$_2$C*H*$_2$, respectively). Our results parallel those of Gibson[11] for closely related (salicylaldiminato)aluminium compounds. As observed for the cationic complex **1a** (vide supra), ethylene does not polymerise appreciably under these conditions; aluminium species **3a** and **5a** are quite stable in CD_2Cl_2 solution.

It is worth noting that in all the examined cases, the broad ^{1}H NMR resonances for *Me*B(C_6F_5)$_3^-$ were observed in the range δ = 0.40−0.48, characteristic of the free anion,[21] thus suggesting that there are no relevant interactions between cation and anion, at least under the conditions used (this remark is further supported by the observed poor solubility of the cationic species in C_6D_6, compared to the high solubility of **1a**, **3a**, and **5a** in dichloromethane).

Preliminary polymerization tests were carried out for all the synthesized Al complexes. Toluene solutions of **3**, **4**, and **5**, when activated with 1 equiv. of B(C_6F_5)$_3$, polymerised ethylene (1 atm) to solid polyethylene with low activity [**3**: 400 g (PE) mol^{-1} h^{-1} atm^{-1}; **4**: 75 g (PE) mol^{-1} h^{-1} atm^{-1}; **5**: 200 g (PE) mol^{-1} h^{-1} atm^{-1}].

Compounds **1** and **2** were considerably less active; some solid polyethylene was obtained only in the presence of some added $AlMe_3$. A more detailed investigation of the polymerization activity of these Al derivatives after activation with different co-catalysts under more severe conditions is in progress.

Experimental Section

General: Manipulations of sensitive materials were carried out under dry nitrogen using Schlenk or glove-box techniques. Toluene, heptane, and THF were dried by reflux over sodium and benzophenone and distilled under nitrogen prior to use. $AlMe_3$ and $AlEt_3$ were purchased from Aldrich and used as received. The 1-(*o*,*o*′-diisopropylphenylamino)-6-(*o*,*o*′-diisopropylphenylimino)-cyclohexene,[12] the imino-phenoxide ligands,[22] and B(C_6F_5)$_3$ [21] were synthesized according to literature procedures. NMR spectra were recorded with a Bruker Advance 400 MHz spectrometer; chemical shifts were referenced to the residual protio impurities of the deuterated solvents. EI MS data were obtained with a Finnigan Thermoquest GCQ Plus 2000 spectrometer, using a direct exposure probe for compound **1** and **2**, and a direct insertion probe for compounds **3**, **4**, and **5**.

Preparation of Complexes

Complex 1: $AlMe_3$ (10.0 mL, 0.62 M in heptane, 6.2 mmol) was slowly added to a solution of 1-(*o*,*o*′-diisopropylphenylamino)-6-(*o*,*o*′-diisopropylphenylimino)cyclohexene (2.5 g, 6.8 mmol) in 20 mL of heptane at 0 °C with stirring. The orange solution was stirred at 0 °C for 1 h, at room temperature for additional 2 h and then was concentrated to 10 mL. Light orange crystals deposited overnight at −20 °C. Further crops were obtained by concentration and cooling of the mother liquor. Overall yield: 2.7 g (90%). Crystals of **1** suitable for an X-ray crystal structure determination were grown from toluene at −20 °C. ^{1}H NMR (400 MHz, C_6D_6, 293 K): δ = −0.37 [s, 6 H, Al(C*H*$_3$)$_2$], 0.96 [d, 6 H, CH(C*H*$_3$)$_3$], 1.27−1.28 [m, 14 H, CH(C*H*$_3$)$_2$ and N=C−CH$_2$C*H*$_2$CH$_2$)], 1.41 [d, 6 H, CH(C*H*$_3$)$_2$], 1.86 (q, 2 H, N=C−CH$_2$CH$_2$C*H*$_2$), 2.00 (t, 2 H, N=C−C*H*$_2$CH$_2$CH$_2$), 3.08 [sept, 2 H, C*H*(CH$_3$)$_2$], 3.68 [sept, 2 H, C*H*(CH$_3$)$_2$], 4.86 (t, 1 H, =C*H*), 7.03−7.28 (m, 6 H, Ar-*H*). ^{13}C NMR (C_6D_6, 293 K): δ = −8.0 [Al(*C*H$_3$)$_2$], 23.9 (N=C−CH$_2$*C*H$_2$CH$_2$), 25.4 (N=C−CH$_2$CH$_2$*C*H$_2$); 24.8, 25.3, 25.4, 26.2 [CH(*C*H$_3$)$_2$], 28.6, 28.8, [*C*H(CH$_3$)$_2$], 30.6 (N=C-*C*H$_2$CH$_2$CH$_2$); 113.8 (*C*H=C−N); 124.7, 125.2, 126.2, 128.4 (*meta* and *para* Ar), 146.8 (CH=*C*−N), 138.0, 141.5, 142.2, 147.6, (*ipso* and *ortho* Ar), 181.1 (*C*=N). Assignments were made using HMQC long-range experiments. EI MS (35 eV): *m*/*z* = 486, 487, 489 [M]$^+$, 471, 472, 473 [M − CH$_3$]$^+$.

Complex 2: $AlEt_3$ (6.0 mL, 1.1 M in heptane, 6.6 mmol) was slowly added to a solution of 1-(*o*,*o*′-diisopropylphenylamino)-6-(*o*,*o*′-diisopropylphenylimino)cyclohexene (2.5 g, 5.8 mmol) in 25 mL of heptane at 0 °C with stirring. The solution was stirred at 0 °C for 1 h and at room temperature for additional 3 h. The solvent was removed in vacuo, and the orange-red oil residue was dissolved in toluene (5 mL). Orange crystals deposited overnight at 0 °C. Yield: 2.4 g (75%). ^{1}H NMR (400 MHz, C_6D_6, 293 K): δ = 0.18 (dq, 2 H, $^3J_{H,H}$ = 8.1 Hz, CH$_3$C*H*$_2$Al), 0.28−0.52 (m, 2 H, CH′$_3$C*H*′$_2$Al),

0.62 (t, 3 H, $CHCH_2CH_3$), 0.90 (t, $^3J_{H,H}$ = 8.1 Hz, 3 H, CH_3CH_2Al), 1.2−1.6 [m, $CH(CH_3)_2$, $CH_2CH_2CH_2CHEt$, $CH_2CH_2CH_2CHEt$, $CHCH_2CH_3$ and $CH'_3CH'_2Al$ overlapping], 1.62−2.02 (m, br, 3 H, CHEt and $CH_2CH_2CH_2CHEt$), 3.27 [sept, 1 H, $CH(CH_3)_2$], 3.74 [sept, 2 H, $CH(CH_3)_2$], 3.96 [sept, 1 H, $CH(CH)_3$], 6.55 (s, 1 H, NH), 7.01−7.29 (m, 6 H, Ar-H). ^{13}C NMR (C_6D_6, 293 K): δ = −0.5 (br, $CH'_3CH'_2Al$ or CH_3CH_2Al), 0.9 (br, CH_3CH_2Al or $CH'_3CH'_2Al$), 9.0 ($CH'_3CH'_2Al$ or CH_3CH_2Al), 9.6 (CH_3CH_2Al or $CH'_3CH'_2Al$), 11.0 ($CHCH_2CH_3$), 18.9 ($CHCH_2CH_3$), 23.2, 24.3, 24.7, 25.0, 25.5, 25.6, 25.7, 26.1, $[CH(CH_3)_2]$, 26.0, 26.1, 26.4, (−CH_2− of cyclohexene), 26.9, 27.1, 27.9, 28.6, $[CH(CH_3)_3]$, 34.5 (CHEt), 108.9 (NC=CNH), 134.6 (NC=CNH), 123.8, 123.86, 123.91, 125.5, 126.0, 126.4 (*meta* and *para* Ar), 140.3, 140.8, 142.9, 147.4, 147.6, 147.8 (*ipso* and *ortho* Ar). Assignments were made using HMQC long-range experiments. EI MS (35 eV): *m*/*z* = 544, 545 $[M]^+$, 543, 544 $[M - H]^+$, 515, 516, 517 $[M - CH_3CH_2]^+$, 514, 515, 516 $[M - CH_3CH_3]^+$.

{[3-*t*Bu-2-(O)C_6H_3]CH=NC_6H_5}$AlMe_2$ (3): $AlMe_3$ solution (15.0 mL, 0.26 M in heptane, 4.0 mmol) was slowly added to a solution of 0.98 g of [3-*t*Bu-2-(OH)C_6H_3]CH=NC_6H_5 (3.9 mmol) in heptane (20 mL) at 0 °C. The reaction was allowed to warm to room temperature and stirred for 1 h. The solution was concentrated and stored at 0 °C, providing **3** as a yellow crystalline solid. Yield: 0. 85 g (71%). ^{1}H NMR (400 MHz, [D_8]toluene, 293 K): δ = −0.30 (s, 6 H, $AlCH_3$), 1.51 [(s, 9 H, $C(CH_3)_3$], 6.58 (t, 1 H, OAr-H), 6.62 (d, 1 H, OAr-H), 6.90−6.98 (m, 5 H, NAr-H), 7.38 (d, 1 H, OAr-H), 7.48 (s, 1 H, CH=N). ^{13}C NMR (C_6D_6, 293 K): δ = −8.4 (br, $AlCH_3$), 29.8 $[C(CH_3)_3]$, 35.7 $[C(CH_3)_3]$, 117.7, 120.4, 122.7, 130.1, 134.5, 135.3, 142.1, 147.4, 165.1, (Ar-C), 170.7 (CH=N). EI MS (35 eV): *m*/*z* = 294, 295 $[M - CH_3]^+$.

{[3-*t*Bu-2-(O)C_6H_3]CH=N(2,6-*i*$Pr_2C_6H_3$)}$AlMe_2$ (4): An $AlMe_3$ solution (10.0 mL, 0.25 M in heptane, 2.5 mmol) was slowly added to a solution of 0.75 g of [3-*t*Bu-2-(OH)C_6H_3]CH=N(2,6-*i*$Pr_2C_6H_3$) (2.2 mmol) in heptane (20 mL) at 0 °C. The reaction was allowed to warm to room temperature and stirred for 2 h. The volatiles were removed in vacuo affording a yellow oil that solidified upon standing one night at room temperature. Yield: 0.78 g (90%). ^{1}H NMR (400 MHz, C_6D_6, 293 K): δ = −0.27 (s, 6 H, $AlCH_3$), 0.81 [d, 6 H, $CH(CH_3)_2$], 1.19 [d, 6 H, $CH(CH_3)_2$], 1.54 [(s, 9 H, $C(CH_3)_3$], 3.13 [(sept, 2 H, $CH(CH_3)_2$], 6.60 (t, 1 H, OAr-H), 6.72 (d, 1 H, OAr-H), 7.00−7.12 (m, 3 H, NAr-H), 7.42 (d, 1 H, OAr-H), 7.82 (s, 1 H, CH=N). ^{13}C NMR (C_6D_6, 293 K): δ = −8.7 (br, $AlCH_3$), 23.0 and 26.2 $[CH(CH_3)_2]$, 28.8 $[CH(CH_3)_2]$, 29.8 $[C(CH_3)_3]$, 35.7 $[C(CH_3)_3]$, 118.1, 119.8, 124.9, 128.8, 134.1, 135.6, 142.4, 142.9, 143.1, 165.3, (Ar-C), 174.5 (CH=N). EI MS (35 eV): *m*/*z* = 393 $[M]^+$, 378, 379 $[M - CH_3]^+$.

{[3-*t*Bu-2-(O)C_6H_3]CH=NC_6F_5}$AlMe_2$ (5): This compound was prepared as above, using an $AlMe_3$ solution (10.0 mL, 0.25 M in heptane, 2.5 mmol) and 0.795 g of [3-*t*Bu-2-(OH)C_6H_3]CH=NC_6F_5 (2.3 mmol) in heptane (20 mL) at 0 °C. Yield: 0.79 g (86%). ^{1}H NMR (400 MHz, C_6D_6, 293 K): δ = −0.27 [t, 6 H, *J*(HF) = 1.4 Hz, $AlCH_3$], 1.46 [(s, 9 H, $C(CH_3)_3$], 6.53 (t, 1 H, OAr-H), 6.64 (d, 1 H, OAr-H), 7.28 (s, 1 H, CH=N), 7.40 (d, 1 H, OAr-H). ^{13}C NMR (C_6D_6, 293 K): δ = −9.74 (br, $AlCH_3$), 29.7 $[C(CH_3)_3]$, 35.7 $[C(CH_3)_3]$, 118.4, 119.7, 135.1, 137.5, 142.8, 166.8 (OAr-C), 177.3 (CH=N). EI MS (35 eV): *m*/*z* = 384 $[M - CH_3]^+$.

Thermolysis of Compound 2: $AlEt_3$ (10 mL, 0.22 M in heptane, 2.2 mmol) was quickly added to a solution of 1-(*o*,*o*′-diisopropylphenylamino)-6-(*o*,*o*′-diisopropylphenylimino)cyclohexene (0.800 g, 1.9 mmol) in 10 mL of toluene at room temperature and then heated under reflux for 2 h. Solvent and volatiles were removed in vacuo, leaving a red oil. ^{1}H NMR (400 MHz, C_6D_6, 293 K): δ = 0.33 (m, 2 H, CH_3CH_2Al), 0.57 (t, 3 H, CH_3CH_2−C), 0.84 (t, 3 H, CH_3CH_2Al), 1.10−1.30 [complex multiplet, $CH(CH_3)_2$ and CH_3CH_2C, overlapping, 26 H], 1.30−1.80 and 1.84−2.01 (three multiplets, CH_2 in the cyclohexene ring), 3.22 [sept, 1 H, $CH(CH_3)_2$], 3.48 [sept, 2 H, $CH(CH_3)_2$], 3.82 [sept, 1 H, $CH(CH_3)_2$], 7.16−7.18 (m, 6 H, Ar-H). ^{13}C NMR (C_6D_6, 293 K), selected resonances: δ = −0.4 (br, CH_3CH_2Al), 8.7 (CH_3CH_2Al), 12.8 ($CHCH_2CH_3$), 19.1 ($CHCH_2CH_3$), 22.7, 23.3, 23.4, 23.8, 25.8, 26.0, 26.9, 27.2 $[CH(CH_3)_2]$, 25.7, 26.4, 26.8 (−CH_2− of cyclohexene), 28.5, 28.8 $[CH(CH_3)_3]$, 34.1 (CHEt), 123.6, 123.9, 126.0, 126.3 (*meta* and *para* Ar), 140.2, 140.9 (NC=CN and NC=CN), 145.9, 146.6, 146.7, 147.2 (*ipso* and *ortho* Ar).

Generation of Cations

Complex 1a: Compound **1** (24 mg, 0.05 mmol) was dissolved in CD_2Cl_2 (0.5 mL). Dry THF (4.0 μL, 0.05 mmol) and $B(C_6F_5)_3$ (26 mg, 0.05 mmol) were sequentially added, and the resulting orange solution was analyzed by NMR spectroscopy at room temperature. ^{1}H NMR (400 MHz, 293 K): δ = −0.41 (s, 3 H, $AlCH_3$), 0.48 (br. s, 3 H, CH_3B), 0.83−1.38 [m, 24 H, $CH(CH_3)_2$], 1.72 −1.98 (m, 2 H, N=C−$CH_2CH_2CH_2$), 2.17 (m, br, 4 H, OCH_2CH_2), 2.50−2.60 [m, 5 H, N=C−$CH_2CH_2CH_2$, N=C−$CH_2CH_2CH_2$, $CH(CH_3)_2$, overlapping], 2.91 [sept, 1 H, $CH(CH_3)_2$], 3.11 [sept, 1 H, $CH(CH_3)_2$], 3.28 [sept, 1 H, $CH(CH_3)_2$], 4.25 (m, br, 4 H, OCH_2CH_2), 5.61 (t, 1 H, =CH), 7.15−7.50 (m, 6 H, Ar-H). ^{13}C NMR (293 K), selected resonances; cation: δ = −13.6 (br, $AlCH_3$), 23.6, 25.7, 30.7 (CH_2 of the cyclohexene ring), 23.7, 24.3, 24.5, 25.5, 25.9, 26.0 $[CH(CH_3)_2]$, 24.9, (OCH_2CH_2), 29.2, 29.6, 30.2 $[CH(CH_3)_2]$, 75.0 (OCH_2), 128.3 (CH=C−N), 123.9, 125.8, 126.0, 126.2, 127.6, 130.3 (*meta* and *para* Ar), 145.0 (CH=C−N), 134.7, 141.6, 142.3, 146.2, 147.0 (*ipso* and *ortho* Ar), 186.8 (C=N); anion: δ = 10.3 (br, BCH_3). Assignments were made using HMQC long-range experiments.

{[3-*t*Bu-2-(O)C_6H_3]CH=NC_6H_5}$AlMe(THF)^+[MeB(C_6F_5)_3]^-$ (3a): This compound was prepared as above by dissolving 15 mg of **5** (0.05 mmol) in CD_2Cl_2 (0.5 mL). Dry THF (4.0 μL, 0.05 mmol) and $B(C_6F_5)_3$ (26 mg, 0.05 mmol) were sequentially added, and the resulting yellow solution was analyzed by NMR spectroscopy at room temperature. ^{1}H NMR (400 MHz, 293 K): δ = −0.15 (s, 3 H, $AlCH_3$), 0.47 (br. s, 3 H, CH_3B), 1.51 [(s, 9 H, $C(CH_3)_3$], 2.14 (m, br, 4 H, OCH_2CH_2), 4.21 (m, br, 4 H, OCH_2CH_2), 7.06 (t, 1 H, OAr-H), 7.28 (d, 2 H, NAr-H), 7.45 (d, 1 H, OAr-H), 7.55−7.61 (m, 3 H, NAr-H), 7.81 (d, 1 H, OAr-H), 8.72 (s, 1 H, CH=N). ^{13}C NMR (293 K); cation: δ = −13.5 (br, $AlCH_3$), 25.9 (OCH_2CH_2), 29.6 $[C(CH_3)_3]$, 35.7 $[C(CH_3)_3]$, 75.8 (OCH_2), 120.0, 121.7, 122.3, 130.5, 131.7, 136.0, 139.1, 142.1, 144.3, 162.6 (all Ar-C), 175.8 (CH=N); anion: δ = 10.8 (br, BCH_3).

{[3-*t*Bu-2-(O)C_6H_3]CH=NC_6F_5}$AlMe(THF)^+[MeB(C_6F_5)_3]^-$ (5a): This compound was prepared as above by dissolving 20 mg of **5** (0.05 mmol) in CD_2Cl_2 (0.5 mL). Dry THF (4.0 μL, 0.05 mmol) and $B(C_6F_5)_3$ (26 mg, 0.05 mmol) were sequentially added, and the resulting yellow solution was analyzed by NMR spectroscopy at room temperature. ^{1}H NMR (400 MHz, 293 K): δ = −0.31 (s, 3 H, $AlCH_3$), 0.40 (br. s, 3 H, CH_3B), 1.45 [(s, 9 H, $C(CH_3)_3$], 2.21 (m, br, 4 H, OCH_2CH_2), 4.28 (m, br, 4 H, OCH_2CH_2), 7.12 (t, 1 H, OAr-H), 7.41 (d, 1 H, OAr-H), 7.93 (d, 1 H, OAr-H), 8.63 (s, 1 H, CH=N). ^{13}C NMR (293 K); cation: δ = −15.5 (br, $AlCH_3$), 25.8 (OCH_2CH_2), 29.7 $[C(CH_3)_3]$, 35.7 $[C(CH_3)_3]$, 76.0 (OCH_2), 118.4, 119.7, 135.1, 137.5, 142.8, 166.8, (OAr-C), 177.3 (CH=N); anion: δ = 10.2 (br, BCH_3).

Polymerization Tests: A typical polymerization test was carried out in a 100-mL glass flask charged under nitrogen with 20 mL of toluene and thermostated at 50 °C. The inert gas was replaced by ethylene at 1 atm, then 0.1 mmol of the proper aluminium complex and 0.1 mmol of $B(C_6F_5)_3$ (each dissolved in 2.0 mL of toluene) were injected into the flask. The flask was fed with constant monomer pressure, and after 15 min the reaction was stopped by injecting methanol. The mixture was poured into acidified methanol, and the polymer was recovered by filtration, washed with fresh methanol, and dried under vacuum.

X-ray Crystallography: Suitable crystals were selected and mounted in Lindemann capillaries under an inert gas. Diffraction data were measured at room temperature with a Rigaku AFC7S diffractometer using graphite-monochromated Mo-K_α radiation (λ = 0.71069 Å). Data reduction was performed with the crystallographic package TEXSAN.[23] No absorption correction was applied to the data. The structures were solved by direct methods using the program SIR92[24] and refined by means of full-matrix least squares based on F^2 using the program SHELXL93.[25] For compound **1**, half a molecule of toluene was located on an inversion centre. A rigid-body refinement was performed for the solvent molecule, assuming that two distinct molecules equally share the same site with opposite orientation, methyl group hydrogen atoms were assumed to be disordered over two sites rotated by 60° to each other. All non-hydrogen atoms excluding those belonging to the solvent molecule were refined anisotropically. For the disordered toluene molecule a unique displacement parameter was considered. Hydrogen atoms were positioned geometrically and included in structure factor calculations but not refined. Restraints were applied to the $CH-CH_3$ distance of the isopropyl groups. The presence of the disordered solvent molecule accounts for the low-quality structure refinements. For compound **2** all non-hydrogen atoms were refined anisotropically, hydrogen atoms were positioned geometrically and included in structure factor calculations but not refined. Crystal structures were drawn by means of the program ORTEP32.[26] Crystal data and refinement details for both compounds are reported in Table 2. Crystallographic data (excluding structure factors) for the structures reported in this paper have been deposited with the Cambridge Crystallographic Data Centre as supplementary publications no. CCDC-168133 (**1**) and -168132 (**2**). Copies of data may be obtained free of charge on application to CCDC, 12 Union Road, Cambridge CB2 EZ, UK [Fax: (internat.) + 44-1223/336-033; E-mail: deposit@ccdc.cam.ac.uk].

Table 2. Crystal data and structure refinement details for compounds **1** and **2**

	1	**2**
Empirical formula	$C_{32}H_{47}N_2Al{\cdot}0.5C_7H_8$	$C_{36}H_{57}N_2Al$
Formula mass	532.76	544.82
Crystal system	monoclinic	monoclinic
Space group	$P2_1/n$ (14)	$P2_1/n$ (14)
a [Å]	13.016(6)	9.868(8)
b [Å]	19.889(5)	18.595(8)
c [Å]	13.200(5)	19.365(8)
β [°]	91.20(4)	100.83(5)
V [Å^3]	3416(2)	3489(3)
Z	4	4
D_c [g cm^{-3}]	1.036	1.037
μ(Mo-K_α) [mm^{-1}]	0.08	0.08
F(000)	1164	1200
Indep. refl. measured	4452 (ω/2θ scans)	6134 (ω scans)
Param./restraints	323/7	352/0
$R1$ [$F_o > 4\sigma(F_o)$]	0.0913 [888 refl.]	0.0625 [1904 refl.]
R_w2 (all refl.)	0.3750	0.2513
GooF	1.276	1.073
Δρ(min) [eÅ^{-3}]	−0.33	−0.20
Δρ(max) [e Å^{-3}]	0.52	−0.20

Acknowledgments

The authors are grateful to Prof. A. Immirzi and to Dr. S. Milione for valuable discussions, to Dr. M. Fedrigo for some NMR experiments and to Mr. R. Miranda for EI MS measurements. This work was supported by the Italian Ministry of University and Research (PRIN 2000) and by the Italian National Council (CNR).

[1] K. Ziegler, H.-G. Gellert, K. Zosel, E. Holzkamp, J. Schneider, M. Söll, W.-R. Kroll, *Justus Liebigs Ann. Chem.* **1960**, *629*, 121−166.
[2] H. Martin, H. Bretinger, *Makromol. Chem.* **1992**, *193*, 1283−1288.
[3] J. S. Kim, L. M Wojieinski II, S. Liu, J. C. Sworen, A. Sen, *J. Am. Chem. Soc.* **2000**, *122*, 5668−5669.
[4] M. Bochmann, M. J. Sarfield, *Organometallics* **1998**, *17*, 5908−5912.
[5] The reaction between AlR_3 and $B(C_6F_5)_3$ proceeds in an analogous way, and was described in a patent application as a convenient approach to the synthesis of $Al(C_6F_5)_3$: P. Biagini, G. Lugli, L. Abis, P. Andreussi, *Eur. Patent Appl.* EP 0 694 548 A1, **1996**, 1−9 (Enichem Elastomeri S. r. l.).
[6] J. A. Jegier, D. A. Atwood, *Inorg. Chem.* **1997**, *36*, 2034−2039.
[7] G. Klosin, R. G. Roof, E. Y.-X. Chen, K. A Abboud, *Organometallics* **2000**, *19*, 4684−4686.
[8] M. Bochmann, D. M Dawson, *Angew. Chem. Int. Ed. Engl.* **1996**, *35*, 2226−2228.
[9] [9a] M. P. Coles, R. F. Jordan, *J. Am. Chem. Soc.* **1997**, *119*, 8125−8126. [9b] E. Ihara, V. G. Young, R. F. Jordan, Jr., *J. Am. Chem. Soc.* **1998**, *120*, 8277−8278. [9c] S. Dagorne, I. A. Guzei, M. P. Coles, R. F. Jordan, *J. Am. Chem. Soc.* **2000**, *122*, 274−289.
[10] [10a] M. Bruce, V. C. Gibson, C. Redshaw, G. A. Solan, A. J. P. White, D. J. Williams, *Chem. Commun.* **1998**, 2523−2524.,[10b] P. A. Cameron, V. C. Gibson, C. Redshaw, J. A. Segal, M. D. Bruce, A. J. P. White, D. J. Williams, *Chem. Commun.* **1999**, 1883−1884.
[11] After this work was completed, the synthesis of related iminophenoxide aluminium complexes was reported: P. A. Cameron, V. G. Gibson, C. Redshaw, J. A. Segal, G. A. Solan, A. J. P. White, D. J. Williams, *J. Chem. Soc., Dalton Trans.* **2001**, 1472−1476.
[12] D. P. Gates, S. A. Svejda, E. Oñate, C. M. Killian, L. K. Johnson, P. S. White, M. Brookhart, *Macromolecules* **2000**, *33*, 2320−2334.
[13] B. Qian, D. L. Ward, M. R. Smith III, *Organometallics* **1998**, *17*, 3070−3076.
[14] J. A. Kanters, G. P. M. van Mier, R. L. L. M. Nijs, F. van der Stehen, G. van Koten, *Acta Crystallogr., Sect. C* **1988**, *44*, 1391−1394.
[15] [15a] D. S. Brown, A. Decken, A. H. Cowley, *J. Am. Chem. Soc.* **1995**, *117*, 5421−5422. [15b] V. C. Gibson, C. Readshaw, A. J. P. White, D. J. Williams, *J. Organomet. Chem.* **1998**, *550*, 453−456.
[16] [16a] M. G. Gardiner, G. A. Koutsantonis, S. M. Lawrence, C. L. Raston, *Inorg. Chem.* **1996**, *35*, 5696−5702. [16b] M. G. Gar-

diner, S. M. Lawrence, C. L. Raston, *Inorg. Chem.* **1996**, *35*, 1349−1354. [16c] M. G. Gardiner, S. M. Lawrence, C. L. Raston, *Inorg. Chem.* **1995**, *34*, 465−46592. [16d] J. L. Atwood, S. M. Lawrence, C. L. Raston, *Chem. Commun.* **1994**, 73−74.
[17] J. J. Eisch, in *Comprehensive Organometallic Chemistry II* (Eds.: E. W. Abel, F. G. A. Stone, G. Wilkinson), Elsevier, Oxford, UK, **1995**, vol. 1, chapter 10, p. 494−495, and references therein.
[18] E. Wissing, J. T. B. H. Jastrzebski, J. Boersma, G. van Koten, *J. Organomet. Chem.* **1993**, *459*, 11−16 and references therein.
[19] For a recent review, see: D. A. Atwood, M. J. Harvey, *Chem. Rev.* **2001**, *101*, 37−52.
[20] [20a] J. Tian, D. Hustad, G. W. Coates, *J. Am. Chem. Soc.* **2001**, *123*, 5134−5135. [20b] J. Saito, M. Mitani, J.-i. Mohri, S.-i. Ishii, Y. Yoshida, T. Matsugi, S.-i. Kojoh, N. Kashiwa, T. Fujita, *Chem. Lett.* **2001**, 576−577.
[21] X. Yang, C. L. Stern, T. J. Marks, *J. Am. Chem. Soc.* **1994**, *116*, 10015−10031.
[22] T. Fujita, Y. Tohi, M. Mitani, M. Matsui, J. Saito, M. Nitabaru, K. Sugi, H. Makio, T. Tsutsui, *Eur. Patent Appl.* EP 0 874 005 A1, **1998** (Mitsui Chemicals, Inc., Tokyo 100−6070, JP).
[23] *TEXSAN*, Crystal Structure Analysis Package, Molecular Structure Corporation, The Woodlends, Texas, USA, **1985−1992**.
[24] A. Altomare, G. Cascarano, C. Giacovazzo, A. Guagliardi, M. C. Burla, G. Polidori, M. Camalli, *J. Appl. Crystallogr.* **1994**, *27*, 435
[25] G. M. Sheldrick, *SHELXL93, A program for refining crystal structures*, University of Göttingen, Germany, **1993**.
[26] L. J. Farrugia, *J. Appl. Crystallogr.* **1997**, *30*, 565.

Received August 3, 2001
[I01288]

Ring Closure Kinetics of Bidentate Hemilabile P,N and P,S Ligands on a Platinum(II) Complex

Raffaello Romeo,*[a] Luigi Monsu' Scolaro,[a,b] Maria Rosaria Plutino,[a] Andrea Romeo,[a] Francesco Nicolo',[a] and Alessandro Del Zotto[c]

Keywords: N,P ligands / Kinetics / Platinum / Hydrogen bonds / Chelate effect

Complexes of the type *cis*-[$PtPh_2(CO)(\eta^1$-P–N)] and *cis*-[$PtPh_2(CO)(\eta^1$-P–S)], where bidentate phosphorus–nitrogen and phosphorus–sulfur ligands are bound to the metal centre in a monodentate fashion [P–N = $Ph_2PC_5H_4N$ (Ph_2PPy), $Ph_2P(CH_2)_2C_5H_4N$ (ppye), $Ph_2P(o\text{-}C_6H_4)NMe_2$ ($PNMe_2$), $Ph_2P(CH_2)_nNMe_2$ (n = 2, 3, i.e., $peNMe_2$ and $ppNMe_2$) and P–S = $Ph_2P(CH_2)_2SEt$ (P–SEt), $Ph_2P(CH_2)_nSPh$ (n = 1, 2, i.e., P–CH_2SPh and P–SPh)], were prepared in situ by reaction of the hybrid ligands with *cis*-[$PtPh_2(CO)(SEt_2)$]. In each case, the first observed process was the fast substitution of diethyl sulfide by the phosphanyl group leading to the monosubstituted ring-open *cis*-[$PtPh_2(CO)(\eta^1$-P–X)] (X = N or S) complexes, which were characterised in solution by ^{1}H and $^{31}P\{^1H\}$ NMR spectroscopy. These initially formed species undergo a slow ring closure process with extrusion of carbon monoxide and formation of the chelate [$PtPh_2$(P–X)] products, except in the case of the short-bite Ph_2PPy and P–CH_2SPh ligands and of $ppNMe_2$, where ring closure was not observed. The chelate complexes were isolated as solids from the reaction of the ligands with *cis*-[$PtPh_2(Me_2SO)_2$]. A single-crystal X-ray diffractometric study of *cis*-[$PtPh_2$(P–SEt)] (**18**) was performed. The crystal packing showed linear chains originated by weak intermolecular Pt···H–C hydrogen bonding interactions. The chelation kinetics of P–X in the *cis*-[$PtPh_2(CO)(\eta^1$-P–X)] complexes have been monitored in [D]chloroform by ^{1}H and $^{31}P\{^1H\}$ NMR. The rates of ring closure were found to be strongly dependent on the nature (S or N) and steric hindrance of the chelating end of the monocoordinated bidentate P–X ligand, and on the size of the ring formed. In contrast, ring size plays a negligible role, if any, in the dechelation reactions of *cis*-[$PtPh_2$(S–S)] [S–S = 1,2-bis(phenylthio)ethane, dpte and 1,3-bis(phenylthio)propane, dptp] using diphosphanes (dppm and dppp) as reagents. These kinetic data, together with those of previous work, give useful insight into the factors controlling cyclisation reactions and the stability of the rings in square planar platinum(II) complexes.

Introduction

Factors affecting the ease of cyclisation of bifunctional organic chains, such as ring strain and the probability of end-to-end joining, have been well understood and recognised in physical organic chemistry, through detailed kinetic studies. At this stage they are at the basis of synthetic procedures in making rings of all sizes as well as macrocycles.[1,2] By contrast, in coordination or organometallic chemistry, kinetic studies on the formation of chelated rings are relatively scarce because of the difficulty of monitoring the rate of ring closure that, usually, is much faster than the rate of attack of the first end of the bidentate ligand on the metal centre. An old practice of overcoming this difficulty is to render the uncoordinated end of the ligand inactive by steric hindrance or protonation. This latter approach has been used with the formation of certain five- and six-membered chelated rings involving amino acids,[3] amino alcohols,[4] amino sulfides,[5] or diamines,[6−12] in platinum(II) complexes. The rate of ring closure can be modulated through an appropriate control of the acidity of the solution but, in most cases, it is not possible to separate the rate constant for ring closure from the acid dissociation constant of the protonated end of the ligand.

An alternative approach involves the generation in solution of coordinatively unsaturated species by photolysis, in the presence of a bidentate ligand L−L, as for $M(CO)_6$ (M = Cr, Mo, W) complexes.[13−18] The reaction involves photodissociation of one CO ligand to yield an extremely reactive $M(CO)_5$ species which captures L−L, leading to an $M(CO)_5(\eta^1$-L−L) intermediate with a monocoordinate bidentate ligand. Thereby, ring closure follows with loss of

[a] Dipartimento di Chimica Inorganica, Chimica Analitica e Chimica Fisica and ICTPN − CNR, Sezione di Messina, Università di Messina,
Salita Sperone, 31-Vill. S. Agata, 98166 Messina, Italy
Fax: (internat.) + 39-090/393756
E-mail: Raf.Romeo@chem.unime.it
[b] INFM, Unità di Messina
Salita Sperone, 31-Vill. S. Agata, 98166 Messina, Italy
[c] Dipartimento di Scienze e Tecnologie Chimiche − Università di Udine
Via Cotonificio, 108, 33100 Udine, Italy
Supporting information for this article is available on the WWW under http://www.eurjic.com or from the author.

 © WILEY-VCH Verlag GmbH, 69451 Weinheim, Germany, 2002 1434−1948/02/0303−0629 $ 17.50+.50/0

another CO ligand. If this latter process is too rapid, it is necessary to use flash photolysis techniques to initiate the kinetics.[19−24] In some cases the intimate nature of the thermal process was revealed by the determination of the volumes of activation.[20−24]

In the study of the reactivity of the complex *cis*-[$PtPh_2(CO)(SEt_2)$] (**1**) with pyridines[25] and amines[26] we became aware that this substrate contains a labile SEt_2 and a relatively inert CO ligand in the *trans* positions to the firmly bonded phenyl groups. The substrate showed a remarkable selectivity between the two nucleophilic ends of an unsymmetrical bidentate ligand, with a clear preference for the most basic and the less hindered end. Thus, we have exploited this property to prepare stable ring-open species such as *cis*-[$PtPh_2(CO)(\eta^1\text{-}NH_2(CH_2)_4NH_2)$] and *cis*-[$PtPh_2(CO)(\eta^1\text{-}NH_2(CH_2)_2NHPh)$] in solution, to intercept and characterise monocoordinate reaction intermediates of the type *cis*-[$PtPh_2(CO)(\eta^1\text{-}N-N)$] or *cis*-[$PtPh_2(CO)(\eta^1\text{-}P-P)$] in the reactions of this complex with diamines,[27] aminopyridines,[27] or diphosphanes,[28] and to identify the factors controlling the rates of their final conversion into the chelate products with extrusion of CO.

In this paper we have extended the study to so-called "hemilabile" ligands. New classes of unsymmetrical bidentate ligands (P−X) were recently developed and used in organometallic chemistry, which associate the phosphorus atom with donor atoms such as oxygen,[29] nitrogen[30] or sulfur.[31] Indeed it was expected, and it has often been observed, that the non-phosphorus donor X of the ligand is weakly coordinated in solution to the metal centre, generating potential catalytically active systems, by providing, under mild conditions, a vacant site for the coordination and activation of organic substrates. To complete the outline of reactivity of **1** we have chosen a series of hybrid ligands P−X of different chain length, bearing a diphenylphosphanyl group and a substituted sulfur or nitrogen atom of variable electronic and steric properties. The high lability of the SEt_2 group in the starting substrate, combined with the very high nucleophilic power of the phosphorus donor of the bidentate ligands, leads ineluctably to the rapid formation of *cis*-[$PtPh_2(CO)(\eta^1\text{-}P-X)$] and to a subsequent relatively slow ring closure to the final product [$PtPh_2(P-X)$]. The kinetics of ring closure of P−X ligands, together with those of dinitrogen and diphosphane ligands studied previously,[27,28] give a useful insight into the factors controlling these cyclization reactions and the stability of the rings in square-planar complexes.

thioether, a dimethylamino or a pyridyl function, characterised by different steric and electronic properties, and separated from the phosphorus atom by a backbone of variable length. The reaction takes place very rapidly at room temperature and produces the monosubstituted species in quantitative yield. The most interesting feature of this reaction concerns the selectivity of the nucleophilic site of attack of the unsymmetrical ligand that is invariably the phosphanyl group. The phosphorus atom enters the coordination sphere of the metal centre leaving the remaining nitrogen or sulfur atoms free. This is in line with the sequence of reactivity, phosphane[32] >> amine[26] > pyridine[25] of a monodentate ligand replacing SEt_2 from **1**, while the subsequent substitution of the carbonyl group takes place very slowly. Thus, the pattern of behaviour of the P−X ligands reflects the different nucleophilicity of the two donors (P and S or N) of the ligand. This peculiar selectivity of the substrate between the two ends of an unsymmetrical ligand was already shown in the reactions with dinitrogen ligands such as 2-(aminomethyl)pyridine and 2-(2-aminoethyl)-pyridine.[27]

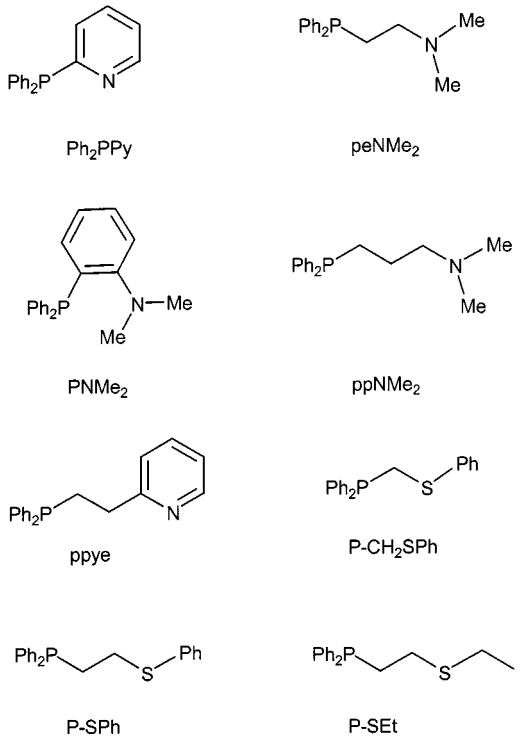

Scheme 1

Results and Discussion

Synthesis and Structural Characterisation of the Complexes

Complexes *cis*-[$Pt(Ph)_2(CO)(\eta^1\text{-}P-X)$] (**4−11**), in which P−X acts as a *P*-bound monodentate ligand, were prepared in situ by treating equimolar amounts of ligand and complex **1**. Sketches of the heteronuclear ligands used are given in Scheme 1. The P−X unsymmetrical species contain on one side a diphenylphosphanyl group and on the other a

The complexes [$PtPh_2(SEt_2)]_2$ (**2**) and *cis*-[$PtPh_2(Me_2SO)_2$] (**3**) proved to be very useful synthons for the synthesis of chelate complexes. The addition of an equimolar amount of a P−X ligand to a dichloromethane solution of **3**, according to Equation (1) leads to the rapid substitution of both sulfoxide ligands, yielding chelate compounds in a pure crystalline form and in almost quantitative yield.

$$cis\text{-}[PtPh_2(Me_2SO)_2] + P{-}X \rightarrow cis\text{-}[PtPh_2(P{-}X)] + 2\ Me_2SO \quad (1)$$

In a similar fashion, these compounds were formed starting from the dinuclear complex **2**, in the presence of a moderate excess of SEt_2.The cyclization reaction failed in the case of the short-bite Ph_2PPy and $P{-}CH_2SPh$ ligands and also $ppNMe_2$, but was successful for the formation of the chelate *cis*-$[PtPh_2(S{-}S)]$ complexes, containing the dithioether ligands dpte (**12**) and dptp (**13**). The isolation of the chelate complexes as solid compounds allowed for their complete characterisation through ^1H and $^{31}P\{^1H\}$ NMR spectroscopy. The complexes **14**–**18** are characterised by the presence, on the coordination plane, of two phenyl groups in the mutual *cis* position and of a 5- or 6-membered ring, arising from the coordination of the hybrid chelating ligand.

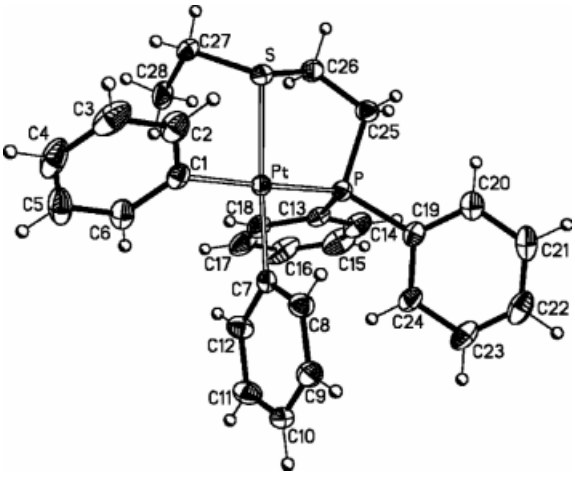

Figure 1. Perspective view and atom numbering scheme of one of the two equal complex units of compound **18**; thermal ellipsoids are drawn at 30% probability, while the H size is arbitrary

X-ray Structure of 18

The crystallographic asymmetric unit contains two independent molecules which are related by a pseudo two-fold screw axis 2_1 parallel to cell edge *a*. However, both are essentially identical structurally (Table 1) and one of them is illustrated in Figure 1. The main differences concern the arrangement of the phenyl groups. The η^1-phenyl rings are almost equally oriented with respect to the Pt coordination plane in the two complexes [53.1(2) vs. 52.8(2)° and 99.0(4) vs. 95.2(4)° for $C1_{Ph}$ and $C7_{Ph}$ planes, respectively] forming a reciprocal dihedral angle of 71.0(4) vs. 63.9(3)°. The same behaviour is exhibited by the phenyl groups of the diphenylphosphane fragment, with the $C13_{Ph}$ ring forming a dihedral angle of 79.2(2) vs. 66.1(3)° with the other $C19_{Ph}$ plane. The square-planar coordination around the two platinum atoms is almost identical and the geometric values are in agreement with those of other arylplatinum[26,33] and 1-(ethylthio)-2-(diphenylphosphanyl)ethane complexes.[31d,34] Both the two Pt–P and Pt–S bonds [mean length 2.280(3) and 2.352(2) Å, respectively] show a significant elongation caused by the strong *trans* influence of the η^1-phenyl acting as a powerful σ-donor, as already reported for the compound *cis*-$[PtPh_2(SMe_2)_2]$.[35] The chelating ligand forms a five-membered puckered ring with a bite angle of 85.97(7) vs. 86.30(8)°. The sulfur atoms display a tetrahedral arrangement acting as a stereogenic akyrotopic centre, but the solid state is a racemic mixture due to centrosymmetric space group.

The most interesting feature of the solid state is the presence of a weak nonconventional intermolecular hydrogen-bonding interaction between each platinum atom and the terminal methyl group of the diphenylphosphanyl ligand of the adjacent complexes (Figure 2). This interaction corresponds to a 3-centre-4-electron (3c-4e) model, the three centres being the C, H and Pt atoms and the four electrons belonging two each to the C–H bond and to the platinum d_z^2 orbital.[36] The two C–H···Pt interactions are almost equal [C(28)H···Pt = 2.94 vs. 2.88Å, C(28)···Pt = 3.68(1) vs. 3.680(8) Å, C(28)–H···Pt = 135 vs. 141°]. Despite the fairly high electron density available on the metal ion,[37] it seems that the Pt···H interaction is weak owing to the low electropositive character of the interacting hydrogen atom. This hydrogen interaction alternatively connects the two independent complexes of adjacent asymmetric units along the crystallographic axis *a*. The crystal packing is constituted by infinite columns parallel to *a* and interconnected by van der Waals interactions as a monodimensional polymer. The weakness of the hydrogen bond in the solid state precludes its existence in solution, as evidenced by the absence in the ^1H NMR spectrum of **18,** in $CDCl_3$, of upfield or downfield chemical shifts or of scalar ^1H-^{195}Pt couplings.

Table 1. Selected bond lengths [Å], bond and torsional angles [°] for the two independent molecules in the crystal unit

Pt–C(1)	2.069(8)	2.039(8)	P–C(13)	1.807(8)	1.813(9)
Pt–C(7)	2.033(7)	2.016(8)	P–C(19)	1.817(8)	1.800(9)
Pt–P	2.282(2)	2.277(2)	P–C(25)	1.841(7)	1.835(9)
Pt–S	2.353(2)	2.352(2)			
C(7)–Pt–C(1)	88.5(3)	90.6(3)	C(7)–Pt–P	94.2(2)	91.8(2)
P–Pt–S	85.97(7)	86.30(8)	C(1)–Pt–S	91.7(2)	91.9(2)
S–Pt–C(1)–C(2)	−51.6(6)	−50.3(6)	P–Pt–C(7)–C(8)	96.2(6)	95.9(6)
S–Pt–P–C(13)	−101.6(3)	−109.7(3)	S–Pt–P–C(19)	132.4(3)	125.5(3)
P–C(25)–C(26)–S	53.5(7)	37(1)	Pt–S–C(27)–C(28)	−40.8(8)	−43(1)

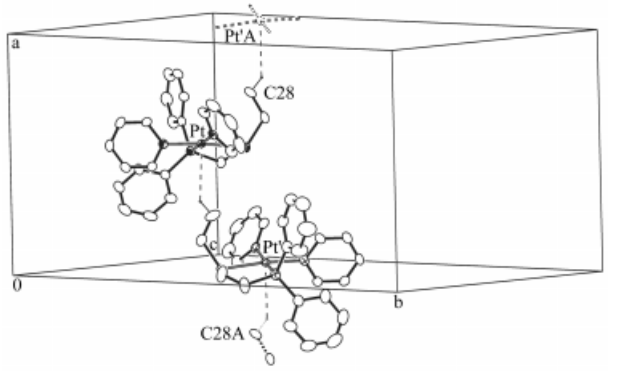

Figure 2. View of crystallographic asymmetric unit showing the intermolecular H bonds between the two independent complexes and the adjacent units translated along the crystallographic *a* axes ($x \pm 1$, y, z); shaded unit is the complex reported in Figure 1; thermal ellipsoids at the 10% probability level while the hydrogen size is arbitrary

NMR Characterisation

Selected ^{1}H and ^{31}P{^{1}H} NMR resonances for ring-open and chelate compounds are given in Table 2. Within the chelate compounds **14−18** the average value of $^1J_{PtP}$ for the ^{31}P{^{1}H} signal is found at 1885 Hz, typical for a phosphorus atom *trans* to a σ-Pt−C bond.[28,32] A remarkable decrease of the $^1J_{PtP}$ coupling constant is found for the ring-open derivatives **4−11** ($^1J_{PtP}$ average value 1603 Hz). For those ligands (peNMe$_2$, PNMe$_2$, P−SPh and P−SEt) which form a 5-membered ring upon chelation, the coordination of the N or S donor is confirmed by the marked downfield shift of the δ^{31}P values. In fact, an increase of ca. 20 ppm is observed for the P−N ligands (in complexes **15** and **16**), while a higher Δδ (ca. 30 ppm) is found for the P−S ligands (in complexes **17** and **18**). These features are in accordance with the criterion proposed by Garrou for assessing chelation in the case of P-containing potentially chelating ligands.[38] Furthermore, the chemical shift values reported here for the P−S species are very close to that found for other Pt^{II} derivatives with the same ligands.[31e] Finally, chelation in compound **14** (where the ligand ppye forms a six-membered ring) is proved on the basis of the existence of a ^{195}Pt-^{1}H scalar coupling between the metal and a proton of the "far-from-P" side of the ligand. In fact, the H^6 nucleus of the pyridine ring at δ = 8.55 exhibits a $^3J_{PtH}$ coupling of 23 Hz, while conversely the same proton in the corresponding ring-open complex **5** exhibits no coupling.

Ring Closure Reactions

As described above, the formation of the chelate complexes occurs in two steps, according to Equation (2): (i) a fast formation of the ring-open species, on mixing equivalent amounts of complex and ligand, (ii) a subsequent slow ring closure. The course of the reaction can be effectively monitored in [D]chloroform by ^{1}H or ^{31}P{^{1}H} NMR spectroscopy, through the changes in intensity of appropriate signals.

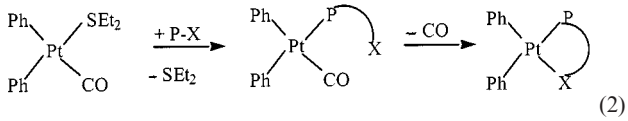

(2)

Typical time-resolved NMR spectra for a kinetic run with ppye are shown in Figure 3. The mol fraction F = [**A**]/([**A**] + [**B**]) of the unchanged complex **A** was obtained by integration of the signals and the first-order rate constant k_c [s^{-1}] for ring closure was obtained from a nonlinear least-squares fit of the experimental data to $F = c_1 + c_2 \exp(-k_c t)$, with c_1, c_2, and k_c as the parameters to be optimised. A similar analysis can be performed using the mol fraction of the chelate product **B**. In order to account for the possible re-entry of carbon monoxide into the coordina-

Table 2. Selected ^{1}H and ^{31}P NMR spectroscopic data for ring-open *cis*-[Pt(Ph)$_2$(CO){η^1-(P−X)}] (numbers in square brackets) and chelate [PtPh$_2$(P−X)] complexes[a]

No.	P−X	^{1}H	^{31}P
[4]	PPh$_2$Py	8.83 (*H*^{6}-py)	20.1 (1636)
[5]	ppye	2.74 (C*H*$_2$−P), 2.55 (C*H*$_2$−N), **8.39** (*H*^{6}-py)	12.9 (1592)
14	ppye	3.59 (C*H*$_2$−P), 2.36 (C*H*$_2$−N), **8.55** (23) (*H*^{6}-py)	16.4 (1886)
[6]	peNMe$_2$	2.01 (C*H*$_3$−N)	**9.8** (1585)
15	peNMe$_2$	2.72, 2.57 (18) (C*H*$_3$−N), 2.34	**31.0** (1915)
[7]	ppNMe$_2$	2.02 (C*H*$_3$−N), 1.94, 1.83, 1.43	13.8 (1598)
[8]	P−NMe$_2$	**2.71** (C*H*$_3$−N)	11.1 (1679)
16	P−NMe$_2$	**3.10** (17) (C*H*$_3$−N)	31.1 (1990)
[9]	P−CH$_2$SPh	3.37 (13.0) (C*H*$_2$−P)	12.9 (1593)
[10]	P−SPh	2.66, **2.26**	11.4 (1570)
17	P−SPh	2.99 (C*H*$_2$−P), **2.38** (C*H*$_2$−S)	41.6 (1803)
[11]	P−SEt	2.32, 2.24 (C*H*$_2$, CH$_3$−C*H*$_2$−S), **1.07** (C*H*$_3$−CH$_2$−S)	11.5 (1576)
18	P−SEt	2.80 (C*H*$_2$−P), 2.66 (CH$_3$−C*H*$_2$−S), 2.49 (C*H*$_2$−S), **1.20** (C*H*$_3$−CH$_2$−S)	40.2 (1832)

[a] In CDCl$_3$ at 298.2 K. Chemical shifts (δ) are reported in ppm downfield from TMS. Coupling constants with ^{195}Pt ($^3J_{PtH}$ and $^1J_{PtP}$) in Hz are given in parentheses. Peaks reported in bold were used for monitoring kinetics.

tion sphere of the metal ion, all the rate data were recalculated by using SCIENTIST[39] and the equation $-d[\mathbf{A}]/dt = k_c[\mathbf{A}] - k_2[\mathbf{B}][CO]$, where [**A**], [**B**] and [CO] are the concentrations of the ring-open complex, the chelate complex and carbon monoxide, respectively; k_c and k_2 are the rate constants for ring closure [s^{-1}] and ring opening [$M^{-1}\ s^{-1}$]. For the short-bite ligands Ph_2PPy (**4**), $P-CH_2SPh$ (**9**) as well as for $ppNMe_2$ (**7**) the only reaction observed was the fast formation of the ring-open species stable in solution for a long time before decomposition occurs. A summary of the relevant kinetic data for ring closure reactions are given in Table 3 together with data relative to diphosphanes and dinitrogen symmetrical and unsymmetrical ligands obtained in previous work.[27,28]

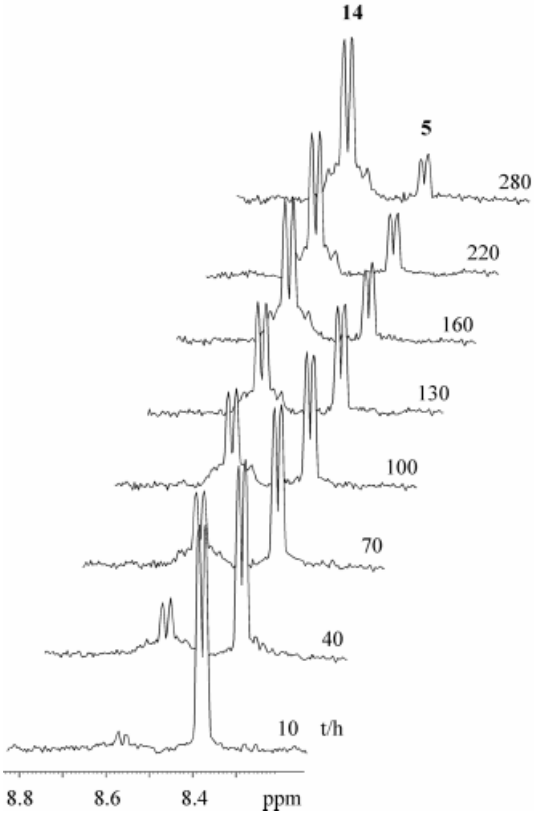

Figure 3. ^1H NMR spectral changes associated with ring closure on *cis*-[$PtPh_2$(CO)(η^1-ppye)] (**5**) in $CDCl_3$ at 298 K; the signals monitored are those of the H^6-py proton at $\delta = 8.39$ for the ring-open and at $\delta = 8.55$ for the chelate [$PtPh_2$(ppye)] (**14**) complex, respectively

Table 3. Summary of kinetic data for ring closure of dinitrogen, diphosphane and hybrid P−X (X = N, S) ligands[a]

	Ligand	Y	X	$10^5 k_c/s^{-1}$
4-membered rings	dppm	PPh_2	PPh_2	1980 ± 100[b]
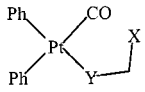	Ph_2PPy	PPh_2	py	0[c]
	$P-CH_2SPh$	PPh_2	SPh	0[c]
5-membered rings	dppe	PPh_2	PPh_2	very fast[b]
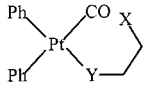	P–SEt	PPh_2	SEt	340 ± 10[c]
	P–SPh	PPh_2	SPh	0.65 ± 0.03[c]
	$peNMe_2$	PPh_2	NMe_2	18 ± 2[c]
	$PNMe_2$	PPh_2	NMe_2	6.9 ± 0.4[c]
	en	NH_2	NH_2	136 ± 3.2[d]
	2-ampy	NH_2	py	31.0 ± 0.55[d]
	N-(Ph)en	NH_2	NHPh	0[d]
6-membered rings	dppp	PPh_2	PPh_2	very fast[b]
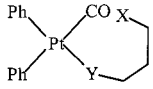	ppye	PPh_2	py	0.43 ± 0.02[c]
	$ppNMe_2$	PPh_2	NMe_2	0[c]
	dap	NH_2	NH_2	14.0 ± 0.34[d]
	2-aepy	NH_2	py	2.72 ± 0.34[d]
	dpy	py	py	4.16 ± 0.10[d]
	dps	py	py	18.8 ± 0.3[d]
7-membered rings	dppb	PPh_2	PPh_2	273[b]
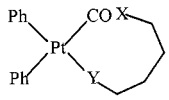	dab	NH_2	NH_2	0[d]

[a] In $CDCl_3$ at 298 K, unless otherwise mentioned. [b] From ref.[28] [c] This work. [d] From ref.[27], in CD_2Cl_2 as solvent. Abbreviations for ligands not encountered in the text: dppe = 1,2-bis(diphenylphosphanyl)ethane; en = 1,2-ethylenediamine; 2-ampy = 2-(aminomethyl)pyridine; *N*-(Ph)en = *N*-phenylethylendiamine; dap = 1,3-diaminopropane; 2-aepy = 2-(2-aminoethyl)pyridine; dpy = dipyrid-2-ylamine; dps = dipyrid-2-yl sulfide; dppb = 1,4-bis(diphenylphosphanyl)butane; dab = 1,4-diaminobutane

Dechelation Reactions

Complexes of the type [$PtPh_2$(S−S)] [S−S = dpte (**12**), dptp (**13**)] were easily prepared in high yield by reaction of **2** with the appropriate dithioether ligand S−S in dichloromethane at room temperature. Any attempt to prepare platinum(II) derivatives with shorter or longer S−S ligands [i.e. bis(phenylthio)methane and 1,4-bis(phenylthio)butane] failed, due to the instability of four- and seven-membered chelate rings. The analysis of the ^1H NMR spectral changes during the course of the reaction with diphosphane ligands (P−P = dppm, dppe, dppp) showed a single-stage conversion from the starting complex to the final chelate compound, according to Equation (3).

$$[PtPh_2(S\text{-}S)] \xrightarrow[+\ (P\text{-}P)]{k_{obs}} cis\text{-}[PtPh_2(\eta^1\text{-}S\text{-}S)(\eta^1\text{-}P\text{-}P)] \xrightarrow[-\ (S\text{-}S)]{fast} [PtPh_2(P\text{-}P)] \quad (3)$$

For example, the ^1H NMR spectrum of [$PtPh_2$(dpte)] in $CDCl_3$ at 298 K showed a broad singlet for the methylene protons (at $\delta = 3.03$; $^3J_{PtH} = 16.6$ Hz) and a doublet ($\delta = 7.38$; $^3J_{PtH} = 76$ Hz) in the aromatic region, relative to the *ortho*-protons of the coordinated phenyl rings. By addition of dppm, in an 1:1 ratio, these peaks begin to decrease in intensity and new signals appear which belong to [$PtPh_2$(dppm)] (methylene proton signals at $\delta = 4.36$), together with a sharp singlet at $\delta = 3.10$ of free dpte. The $^{31}P\{^1H\}$ NMR spectrum of the reaction product shows a singlet at $\delta = -37.6$ with platinum satellites of 1392 Hz, typical of the four-membered diphosphane chelate ring. The ^1H and $^{31}P\{^1H\}$ NMR spectra of the compound agree

with its formulation as a diaryl(phosphanyl)platinum chelate complex.[28] No intermediate species were detected in solution during the reaction and addition of excess dppm does not significantly affect the reaction. The same behaviour was observed using dppe or dppp as reagents, with formation of the phosphane-chelated derivatives [$PtPh_2$(dppe)] and [$PtPh_2$(dppp)], respectively.

Reaction according to Equation (3) (P−P = dppm, dppp) was carried out under pseudo-first-order conditions in dichloromethane at 298.2 K, using spectrophotometric techniques. The kinetics were monitored by repetitive scanning of the spectrum at suitable times in the wavelength range 315−350 nm, where the absorbance of the free diphosphane ligand is negligible. The reactions went to completion, the final spectra being identical to those of authentic samples of [$PtPh_2$(P−P)] complexes.[28] Abstract factor analysis[40] of the spectral changes confirmed the presence of only two absorbing species in solution, i.e. the starting complex [$PtPh_2$(S−S)] and the final diphosphane product [$PtPh_2$(P−P)]. The pseudo-first-order rate constants k_{obs} calculated from the kinetic traces, are listed in the Supporting Information (Table SI1, see footnote on the first page of this article). On plotting k_{obs} as a function of the entering diphosphane concentration straight lines were obtained with a y axis intercept different from zero. Linear regression analysis applied to the rate data and fitted with the simple two-term Equation (4) gave the following values of the rate constants for the two systems: (i) for [$PtPh_2$(dpte)], $k_1 = (0.004 \pm 0.0008)\ s^{-1}$, $k_2 = (1.04 \pm 0.03)\ M^{-1}s^{-1}$ in the reaction with dppm, and $k_1 = (0.007 \pm 0.0001)\ s^{-1}$, $k_2 = (1.86 \pm 0.05)\ M^{-1}s^{-1}$ with dppp; (ii) for [$PtPh_2$(dptp)] $k_1 = (0.004 \pm 0.0008)\ s^{-1}$, $k_2 = (1.00 \pm 0.03)\ M^{-1}s^{-1}$ in the reaction with dppm.

$$k_{obs} = k_1 + k_2\,[\text{P-P}] \quad (4)$$

We know from previous studies[37] that complexes containing ligands with an array of donor atoms of the type *cis*-[Pt(C,C)(S,S)] (C = alkyl or aryl; S = thioether or sulfoxide) show a great propensity to undergo substitution of one sulfur ligand through a dissociative mechanism. The reasons for the observed behaviour are a combination of (i) ground-state destabilisation (lengthening of the Pt−S bond), (ii) increase of electron density at the metal centre preventing the approach of weak nucleophiles, and (iii) stabilisation of the coordinatively unsaturated three-coordinated intermediate. The most likely mechanism that can be envisaged for substitution reactions of the chelated [$PtPh_2$(S−S)] complexes, on the basis of the behaviour of strictly similar substrates containing monodentate thioethers,[41] is depicted in Scheme 2, and involves: (i) dissociative opening of the chelate S−S ring (k_1 path) to yield a ring-open three-coordinated 14-electron intermediate, (ii) competition for it between ring closure (k_{-1} path) and the attack of one end of the diphosphane ligand (via k_3) to form a doubly ring-open species and, (iii) final fast ring closure of P−P to yield the observed products. The pathway via k_2 represents the usual direct bimolecular attack of the nucleophile on the substrate. The rate law derived for this mechanism obeys Equation (5) which reduces to $k_{obs} = k_1 + k_2\,[\text{P−P}]$, when $k_{-1} << k_3\,[\text{P−P}]$.

$$k_{obs} = k_1 k_3\,[\text{P−P}]/(k_{-1} + k_3\,[\text{P−P}]) + k_2\,[\text{P-P}] \quad (5)$$

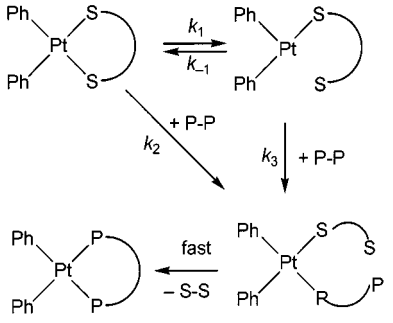

Scheme 2

Thus, the values derived for k_1 and k_2 represent the rate constants for ring opening upon dissociation of the Pt−S bond (k_1 [s^{-1}]) and upon bimolecular attack of the nucleophile (k_2 [$M^{-1}s^{-1}$]). The values of k_1 and k_2 derived for the two complexes do not show appreciable differences, indicating that both the pathways for dechelation (dissociative and associative) are hardly affected by the length of the ring (five- or six-membered).

The Chelate Effect

The formation constant of a metal−chelate complex is related to the rate constants of the separate bond-making and bond-breaking steps in Scheme 3 by the expression $K_f = k_1k_3/k_2k_4$. For octahedral systems, such as Co^{III} and Ni^{II} chelates, there is increasing evidence indicating that the processes of metal−ligand bond formation (k_1 and k_3) and loss of a monodentate ligand (k_2) hardly affect the stability of the chelate. An unexpected slowness of the ring-opening reaction (k_4) accounts for the high formation constant of the chelates,[42] while the effect has traditionally been associated with a high chelate ring-closing rate constant (k_3). Two different explanations have been given to account for the slowness of this dissociatively activated pathway (k_4). For ethylendiamine complexes of relatively small ions, Funahashi et al.[43] have proposed that the elongation of the M−N separation, along the coordinate reaction, forces the metal−nitrogen−carbon (M−N−C) angle to decrease, thus increasing the energy involved in the formation of the transition state. In the case of a monodentate amine such angular distortion around the leaving nitrogen donor is absent. Very recently, Blackman, Clark et al.[44] have given an alternative explanation for the much slower rate of chelate ring-opening in $[Co(cyclen)(diamine)]^{3+}$ compared to the loss of NH_3 from $[Co(cyclen)(NH_3)_2]^{3+}$, based on the reduced ability of the former system to allow the bond angle expansion required to produce the S_N1CB trigonal-bipyramidal intermediate. Formation of the latter from the conjugated base $[Co(cyclen\text{-}H)(diamine)]^{2+}$ requires expansion

of the bond angles in the equatorial plane from ca. 90° to 120°, and the in-plane bidentate ligand will hinder this expansion, while the loss of NH_3 from $[Co(cyclen-H)(NH_3)_2]^{2+}$ is not restricted in this way. Clearly, the energy barrier for the rate-determining Co−N bond cleavage and the formation of the dissociative five-coordinate intermediate is increased by the structural restriction imposed by the retention of the diamine chelate character.

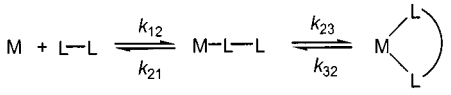

Scheme 3

The mechanistic picture for ring opening and closure in a square-planar complex appears to be much simpler than that of an octhaedral complex, since both processes (k_3 and k_4) are characterised by an associative mode of activation. We have shown above that the rates of dechelation of 5- and 6-membered rings in the complexes $[PtPh_2(S-S)]$ (S−S = dpte, dptp) have very similar values. This is in line with the results of previous studies showing that the rate constants for ring opening of complexes of the type $[Pt(Me_2SO)(N-N)Cl]^+$ (N−N = en, tn, bn) do not differ significantly from one complex to another.[10] The same complexes, in their ring-open $[Pt(Me_2SO)(N-NH)Cl_2]^+$ protonated forms, showed a marked dependence of the rate of ring closure on the ring size. The same strong dependence on ring size characterises the ring-closing kinetics of *trans*-$[PtCl_2(NH_3)(N-NH)]^+$.[12] Therefore, as for the relationships between the formation constant of square-planar complexes and the size of the chelate ring, it is possible to conclude that the rates of ring closure (k_3) have a dominant effect while ring opening (k_4) makes a relatively small contribution. The formation of 4-membered rings is hindered by ring strain and the formation of large rings (7- or 8-membered rings) must compete with other reaction pathways, in particular with the possibility of obtaining dinuclear or polynuclear species. In this context, it is interesting to mention the results of a recent work on chelation kinetics of bidentate phosphane ligands on five-coordinate $[Ru(CO)_4(\eta^1\text{-}P-P)]$ complexes, where the rates of ring closing (10^4 k_{obs}/s^{-1} at 60 °C, in *n*-heptane) are as follows: dppm (11.2), dppe (4.44), dppp (6.73), dppb (5.75). This stands in striking contrast with the strong dependence of the rates on ring size observed for the square-planar $[PtPh_2(CO)(\eta^1\text{-}P-P)]$ complexes (Table 3 and ref.[28]).

The nucleophilic power of the uncoordinated end of the chelating ligand is also a factor of major importance in controlling the rates of ring closure (k_3), as suggested by the data collected in Table 3. The differences in reactivity are the same as those found in the n^0_{Pt} nucleophilicity scale which controls the rates of bimolecular substitution reactions on platinum(II).[45] An attractive example comes from the comparison of the rates of ring closure by dppp, ppye, and $ppNMe_2$ with a 6-membered ring. As a matter of fact, the difference of velocity between dppp and ppye encompasses at least five orders of magnitude, in line with the much greater nucleophilicity of PPh_2 compared to pyridine. In the case of $ppNMe_2$, steric congestion brought about by alkyl substitution on the donor nitrogen atom impedes ring closure.

The opposite role of k_3 and k_4 in octahedral and square-planar complexes stems from the different mode of activation (dissociative vs. associative). In light of the above considerations, elongation of the ring combined with the use of a weak donor atom at one end of the chelating ligand, would be a way of increasing the "hemilability" of hybrid ligands in square-planar complexes and their possible efficiency as catalysts.

Experimental Section

General Procedures and Chemicals: All solvents were dried according to standard procedures by distillation under oxygen-free nitrogen from appropriate drying agents (i.e. dichloromethane from barium oxide and diethyl ether from sodium benzophenone ketyl). Spectrophotometric grade dichloromethane was dried by distillation, degassed by several freeze-pump-thaw cycles and then stored over activated 4-Å molecular sieves. $CDCl_3$ was purchased from Cambridge Isotopes Laboratories (D 99.8%). Solid phosphane ligands (Aldrich Chemical Co) triphenylphosphane (PPh_3), bis(diphenylphosphanyl)methane (dppm), and 1,3-bis(diphenylphosphanyl)propane (dppp) were recrystallized from ethanol. 1,2-Bis(phenylthio)ethane (dpte), and 1,3-bis(phenylthio)propane (dptp) were recrystallized from toluene before use. 2-(Diphenylphosphanyl)pyridine (PPh_2Py) was purchased from Aldrich. The other bidentate hybrid ligands P−X {1-(diphenylphosphanyl)-2-(pyrid-2-yl)ethane (ppye),[46] 1-(dimethylamino)-2-(diphenylphosphanyl)-ethane ($peNMe_2$),[47] 1-(dimethylamino)-3-(diphenylphosphanyl)-propane ($ppNMe_2$),[47] [*o*-(dimethylamino)phenyl]diphenylphosphane ($PNMe_2$),[48] 1-(diphenylphosphanyl)-2-(thioethyl)-ethane (P−SEt),[49] 1-(diphenylphosphanyl)-2-(thiophenyl)-ethane (P−SPh),[49] (diphenylphosphanyl)(thiophenyl)methane ($P-CH_2SPh$)[50]} were prepared according to published methods.

Instrumentation: ^1H and $^{31}P\{^1H\}$ NMR spectra were recorded at 298 K with a Bruker AMX R-300 spectrometer operating with a broad-band probe at 300.13 and 121.50 MHz for ^1H and ^{31}P nuclei, respectively. Chemical shifts (δ) refer to $SiMe_4$ for ^1H and to external H_3PO_4 (85%) for $^{31}P\{^1H\}$ NMR. The temperature within the NMR tube was calibrated by use of the ethylene glycole method.[51] UV/Vis data were collected with a rapid-scanning Hewlett−Packard Model 8452 A spectrophotometer. Infrared spectra were recorded in dichloromethane solution using a Perkin−Elmer FT-IR model 1730 spectrometer. Microanalysis was performed by Redox Analytical Laboratories, Milan, Italy.

X-ray Data Collection and Structure Refinement of 18: Crystal data: $C_{28}H_{29}PPtS$ (623.63), monoclinic, $P2_1/c$ (no. 14), a = 12.230(3), b = 24.911(3), c = 16.493(2) Å, β = 90.789(15)°, V = 5025(1) $Å^3$, Z = 8, $D_{calcd.}$ = 1.649 Mg/m^3, $F(000)$ = 2448, μ (Mo-K_α) = 5.745 mm^{-1}, $R1$ = 0.044/0.070 and $wR2$ = 0.098/0.112 for 7123/9763 observed [$I > 2\sigma(I)$]/all independent reflections, GOF = 1.024. Air-stable, pale yellow crystals of **18** were obtained by slow diffusion of *n*-hexane into a concentrated dichloromethane solution of the complex. For the data collection, a prismatic single crystal (0.33 × 0.25 × 0.10 mm) was mounted on a Siemens P4 automated four-circle single-crystal diffractometer and measured with graphite-monochromated Mo-K_α radiation (λ = 0.71073 Å). 12164

reflections were collected using the ω/2θ scan technique up to 2θ = 52°. No crystal decay was detected from the check reflections monitored every 197 measurements. Intensities were evaluated by profile fitting of a 96-steps peak scan among 2θ shells procedure[52] and then corrected for Lorentz polarisation effects. Absorption correction was applied by fitting a pseudo-ellipsoid to the azimuthal scan data of 20 suitable reflections with high χ angles.[53] Data collection and reduction were performed by XSCANS[54] and SHELXTL[55] packages. The accurate evaluation of the data set excluded the orthorhombic crystal system. The structure was solved by a combination of standard Direct Methods[56] and Fourier synthesis, and refined by minimising the function $\Sigma w(F_o^2 - F_c^2)^2$ with the full-matrix least-squares technique based on all 9763 independent F^2 [R(int) = 0.0284], by using SHELXL97.[57] All non-hydrogen atoms were refined anisotropically. Hydrogen atoms were included in the model refinement among the "riding model" method with the X−H bond geometry and isotropic displacement parameter depending on the parent atom X. An empirical extinction parameter was included in the last refinement cycles. The last difference map showed the largest electron density residuals within 1 Å from the platinum atoms (max/min values 1.657/−1.437 eÅ^{-3}). The final geometrical calculations and drawings were carried out with the PARST program[58] and the XPW utility of the Siemens package, respectively.[59]

Synthesis of Complexes: The complexes *cis*-[$PtPh_2(CO)(SEt_2)$] (**1**),[60] [$PtPh_2(SEt_2)]_2$ (**2**),[60] and *cis*-[$PtPh_2(dmso)_2$] (**3**),[61] were synthesised according to literature methods. Complexes in which the heteronuclear P−X ligands are bound to the metal ion in a monodentate fashion were formed upon mixing equimolar amounts of complex **1** and of the appropriate ligand in $CDCl_3$ solution, taking advantage of the slow rate of ring closure. These reaction intermediates have been characterised in situ by ^{1}H and $^{31}P\{^1H\}$ NMR spectroscopy (T = 298 K).

***cis*-[$PtPh_2(\eta^1$-$Ph_2PPy)$(CO)] (4):** ^{1}H NMR($CDCl_3$): δ = 6.57 (m, 1 H), 6.65 (m, 2 H), 6.83 (m, 1 H, H^3-py), 6.90 (m, 1 H), 7.04 (m, 2 H), 7.13 (m, 1 H, H^5-py), 7.27 (m, 1 H, H^4-py), 7.53−7.44 (m, 14 H), 8.83 (m, 1 H, H^6-py).$^{31}P\{^1H\}$ NMR ($CDCl_3$): δ = 20.1 ($^1J_{PtP}$ = 1636 Hz). IR: ν_{CO} = 2070 cm^{-1}.

***cis*-[$PtPh_2(\eta^1$-ppye)(CO)] (5):** ^{1}H NMR ($CDCl_3$): δ = 2.55 (m, 2 H, CH_2), 2.74 (m, 2 H, CH_2−P), 6.77 (m, 2 H), 6.89 (m, 3 H), 7.04 (m, 4 H), 7.50 (m, 8 H), 7.63 (m, 6 H), 8.39 (m, 1 H, H^6-py). $^{31}P\{^1H\}$ NMR ($CDCl_3$): δ = 12.9 ($^1J_{PtP}$ = 1592 Hz). IR: ν_{CO} = 2066 cm^{-1}.

***cis*-[$PtPh_2(\eta^1$-$peNMe_2)$(CO)] (6):** ^{1}H NMR ($CDCl_3$): δ = 2.01 (s, 6 H, CH_3−N). $^{31}P\{^1H\}$ NMR ($CDCl_3$): δ = 9.8 ($^1J_{PtP}$ = 1585 Hz). IR: ν_{CO} = 2062 cm^{-1}.

***cis*-[$PtPh_2(\eta^1$-$ppNMe_2)$(CO)] (7):** ^{1}H NMR ($CDCl_3$): δ = 1.43 (m, 2 H), 1.83 (m, 2 H), 1.94 (m, 2 H), 2.02 (s, 6 H, CH_3−N), 6.80 (m, 1 H), 7.05−6.90 (m, 7 H), 7.55−7.43 (m, 12 H). $^{31}P\{^1H\}$ NMR ($CDCl_3$): δ = 13.8 ($^1J_{PtP}$ = 1598 Hz). IR: ν_{CO} = 2071 cm^{-1}.

***cis*-[$PtPh_2(\eta^1$-$PNMe_2)$(CO)] (8):** ^{1}H NMR ($CDCl_3$): δ = 2.71 (s, 6 H, CH_3−N). $^{31}P\{^1H\}$ NMR ($CDCl_3$): δ = 11.1 ($^1J_{PtP}$ = 1679 Hz). IR: ν_{CO} = 2064 cm^{-1}.

***cis*-[$PtPh_2(\eta^1$-$PCH_2SPh)$(CO)] (9):** ^{1}H NMR ($CDCl_3$): δ = 3.37 (m, $^2J_{PH}$ = 6, $^3J_{PtH}$ = 13 Hz, 2 H, CH_2−P), 6.77 (m, 1 H), 6.89 (m, 4 H), 7.00 (m, 5 H), 7.14 (m, 3 H), 7.47 (m, 8 H), 7.60 (m, 4 H). $^{31}P\{^1H\}$ NMR ($CDCl_3$): δ = 12.9 ($^1J_{PtP}$ = 1593 Hz). IR: ν_{CO} = 2068 cm^{-1}.

***cis*-[$PtPh_2(\eta^1$-P−SPh)(CO)] (10):** ^{1}H NMR ($CDCl_3$):δ = 2.66 (m, 2 H), 2.26 (m, 2 H). $^{31}P\{^1H\}$ NMR ($CDCl_3$): δ = 11.4 ($^1J_{PtP}$ = 1570 Hz). IR: ν_{CO} = 2068 cm^{-1}.

***cis*-[$PtPh_2(\eta^1$- P−SEt)(CO)] (11):** ^{1}H NMR ($CDCl_3$): δ = 1.07 (t, 3 H, CH_3−CH_2−S), 2.24 (m, 4 H, CH_2 + CH_3−CH_2−S), 2.32 (m, 2 H). $^{31}P\{^1H\}$ NMR ($CDCl_3$): δ = 11.5 ($^1J_{PtP}$ = 1576 Hz). IR: ν_{CO} = 2066 cm^{-1}.

Chelate complexes with both dithioethers and hybrid P−X ligands were prepared by adding a stoichiometric amount of the ligand to compound **2** or **3** in dichloromethane solution. The compounds were precipitated in an almost quantitative yield by adding diethyl ether or *n*-hexane (1:1, v/v) and cooling to −30 °C. The off-white solids were washed with cold *n*-hexane and air-dried.

[$PtPh_2$(dpte)] (12): ^{1}H NMR ($CDCl_3$): δ = 3.03 (br. s, $^3J_{PtH}$ = 16.6 Hz, 4 H, CH_2−S), 6.81 (m, 2 H, H^4), 6.90 (dd, $^3J_{av}$ = 6.6, $^4J_{PtH}$ = 12.0 Hz, 4 H, $H^{3,5}$), 7.38 (d, $^3J_{H,H}$ = 6.6, $^3J_{PtH}$ = 76.0 Hz, 4 H, $H^{2,6}$), 7.41 (m, 6 H, $H^{m,m'}$ + H^p Ph−S), 8.00 (m, $^3J_{H,H}$ = 6.6, $^4J_{H,H}$ = 2.2 Hz, 4 H, $H_{o,o'}$ Ph−S). Yield: 95%. $C_{26}H_{24}PtS_2$ (595.68): calcd. C 52.42, H 4.06; found C 52.8, H 4.15.

[$PtPh_2$(dptp)] (13): ^{1}H NMR ($CDCl_3$): δ = 2.26 (m, 2 H, CH_2−CH_2−S), 3.28 (m, $^3J_{PtH}$ = 13.3 Hz, 4 H, CH_2−CH_2−S), 6.69 (m, 2 H, H^4), 6.78 (dd, $^3J_{av}$ = 7.1, $^4J_{PtH}$ = 11.5 Hz, 4 H, $H^{3,5}$), 7.23 (d, $^3J_{H,H}$ = 7.1, $^3J_{PtH}$ = 75.2 Hz, 4 H, $H^{2,6}$), 7.28 (m, 6 H, $H^{m,m'}$ + H^p Ph−S), 7.75 (m, $^3J_{H,H}$ = 7.1, $^4J_{H,H}$ = 2.7 Hz, 4 H, $H^{o,o'}$ Ph−S). Yield: 93%. $C_{27}H_{26}PtS_2$ (609.71): calcd. C 53.19; H 4.30; found C 53.6, H 4.27.

[$PtPh_2$(ppye)] (14): ^{1}H NMR ($CDCl_3$): δ = 2.36 (m, 2 H, CH_2), 3.59 (m, $^2J_{PH}$ = 25 Hz, 2 H, CH_2−P), 6.54 (m, 3 H), 6.85 (m, 1 H), 6.95 (m, 4 H), 7.08 (m, 2 H), 7.23 (m, 8 H), 7.40 (m, 4 H), 7.68 (m, 1 H), 8.55 (m, $^3J_{PtH}$ = 23 Hz, 1 H, H^6-py). $^{31}P\{^1H\}$ NMR ($CDCl^3$): δ = 16.4 ($^1J_{PtP}$ = 1886 Hz). Yield: 92%. $C_{31}H_{28}NPPt$ (640.61): calcd. C 58.12, H 4.41, N 2.19; found C 58.3, H 4.32, N 2.30.

[$PtPh_2$(peNMe$_2$)] (15): ^{1}H NMR ($CDCl_3$): δ = 2.34 (m, 2 H), 2.57 (s, $^3J_{PtH}$ = 18 Hz, 6 H, CH_3−N), 2.72 (m, 2 H), 6.60 (m, 1 H), 6.65 (m, 2 H), 6.82 (m, 1 H), 7.03 (m, 2 H), 7.20 (m, 2 H), 7.48−7.38 (m, 12 H). $^{31}P\{^1H\}$ NMR ($CDCl_3$): δ = 31.0 ($^1J_{PtP}$ = 1915 Hz). Yield: 89%. $C_{28}H_{30}NPPt$ (606.60): calcd. C 55.44, H 4.98, N 2.31; found C 55.6, H 5.07, N 2.42.

[$PtPh_2$(PNMe$_2$)] (16): ^{1}H NMR ($CDCl_3$): δ = 3.10 (s, $^3J_{PtH}$ = 17 Hz, 6 H, CH_3−N), 6.59 (m, 3 H), 6.85 (m, 1 H), 7.04 (m, 3 H), 7.14 (m, 2 H), 7.38 (m, 11 H), 7.53 (m, 2 H), 7.60 (m, 2 H). $^{31}P\{^1H\}$ NMR ($CDCl_3$): δ = 31.1 ($^1J_{PtP}$ = 1990 Hz). Yield: 90%. $C_{32}H_{30}NPPt$ (654.64): calcd. C 58.71, H 4.62, N 2.14; found C 58.8, H 4.70, N 2.21.

[$PtPh_2$(P−SPh)] (17): ^{1}H NMR ($CDCl_3$): δ = 2.38 (m, 2 H, CH_2−S), 2.99 (m, $^2J_{PH}$ = 24 Hz, 2 H, CH_2−P), 6.76 (m, 4 H), 6.92 (m, 2 H), 7.19 (m, $^3J_{PtH}$ = 76 Hz, 2 H, $H^{2,6}$ *trans* to S), 7.40 (m, 15 H), 7.99 (m, 2 H). $^{31}P\{^1H\}$ NMR ($CDCl_3$): δ = 41.6 ($^1J_{PtP}$ = 1803 Hz). Yield: 87%. $C_{32}H_{29}PPtS$ (671.69): calcd. C 57.22, H 4.35; found C 57.6, H 4.45.

[$PtPh_2$(P−SEt)] (18): ^{1}H NMR ($CDCl_3$): δ = 1.20 (t, $^3J_{H,H}$ = 7.5 Hz, 3 H, CH_3−CH_2−S), 2.49 (m, 2 H, CH_2−S), 2.66 (q, $^3J_{H,H}$ = 7.5 Hz, 2 H, CH_3−CH_2−S), 2.80 (m, 2 H, CH_2−P), 6.72 (m, 3 H), 6.86 (m, 1 H), 7.02 (m, 2 H), 7.19 (m, $^3J_{PtH}$ = 74 Hz, 2 H, $H^{2,6}$ *trans* to S), 7.49−7.34 (m, 12 H). $^{31}P\{^1H\}$ NMR ($CDCl_3$): δ = 40.2 ($^1J_{PtP}$ = 1832 Hz). Yield: 90%. $C_{28}H_{29}PPtS$ (623.65): calcd. C 53.92, H 4.69; found C 54.1, H 4.61.

Kinetics

NMR Measurements: The ring-closure reactions were initiated as follows: $6{\cdot}10^{-3}$ mmol of the hemilabile ligand was dissolved in $CDCl_3$ (0.3 mL) in a 5-mm NMR tube which was immersed in a liquid nitrogen bath. After a few minutes, a [D]chloroform solution of *cis*-[$PtPh_2(CO)(SEt_2)$] ($6{\cdot}10^{-3}$ mmol, 0.2 mL) was added over the frozen solution of the ligand and the NMR tube was cooled again to allow the complex solution to freeze over that of the ligand. Then, the NMR tube was rapidly inserted into the probe of the spectrometer thermostated at 298 K. ^1H or $^{31}P\{^1H\}$ NMR spectra were recorded, immediately after the sample temperature reached an equilibrium value (i.e. stable lock signal), and at subsequent appropriate time intervals. The first recorded spectrum only showed signals relative to free sulfide at $\delta = 2.57$ and 1.27 and to the ring-open *cis*-[$Pt(Ph)_2(CO)(\eta^1$-P−X)] complex, indicating that the displacement of SEt_2 from **1** by the phosphorus end of all the bidentate ligands is too fast at 298 K to be monitored by ^1H NMR spectroscopy. The ring-closure process was followed by monitoring the decrease in intensity of the ^1H or $^{31}P\{^1H\}$ signals associated with the amount of unchanged *cis*-[$PtPh_2(CO)(\eta^1$-P−X)] and the matching increase of the signals due to the final chelate [$PtPh_2$(P−X)] product. Care was taken to choose well-defined and not overlapping resonances for the kinetic analysis (selected values of the chemical shifts and of the ^{195}Pt coupling constants for ring-open and chelate complexes are reported in Table 2. The peaks monitored during the kinetic runs are marked in bold).

UV/Vis Measurements: The reactions of ring opening of the chelate complexes *cis*-[$Pt(Ph)_2$(S−S)] (S−S = dpte and dptb) by dppm and dppp were carried out in CH_2Cl_2 at 298 K, with various concentrations of diphosphane. The kinetics were started by mixing known pre-thermostated volumes of complex and diphosphane solutions, located in a tandem quartz cell (1 cm path length), in the cell compartment of the spectrophotometer. The use of at least a tenfold excess of nucleophile over the complex ensured pseudo-first-order kinetics in all runs. The kinetics were usually followed over four half-lives by monitoring the spectral changes at suitable times. Rate constants were determined using ProFit (Cherwell Scientific Publishing Limited) data analysis software by fitting absorbance data to $A_t = A_\infty + (A_0 - A_\infty)\exp(-k_{obs}\,t)$ with A_0, A_∞, and k_{obs} as the parameters to be optimized (A_0 = absorbance after mixing of reagents, A_∞ = absorbance at completion of the reaction).

Acknowledgments

We are grateful to the Ministero dell'Universitá e della Ricerca Scientifica e Tecnologica (MURST), Programmi di Ricerca Scientifica di Rilevante Interesse Nazionale, Cofinanziamento 2000−2002, to Messina and Udine Universities and CNR for funding this work.

[1] G. Illuminati, L. Mandolini, *Acc. Chem. Res.* **1981**, *14*, 95−102.
[2] L. Mandolini, *Adv. Phys. Org. Chem.* **1986**, *22*, 1−111.
[3] P. Carturan, P. Uguagliati, U. Belluco, *Inorg. Chem.* **1974**, *13*, 542−546.
[4] E. Rotondo, R. Pietropaolo, V. Marsala, F. Faraone, *J. Inorg. Nucl. Chem.* **1975**, *37*, 1465−1467.
[5] G. Albertin, A. Bordignon, A. A. Orio, B. Pavoni, H. B. Gray, *Inorg. Chem.* **1979**, *18*, 1451−1454.
[6] M. G. Carter, J. K. Beattie, *Inorg. Chem.* **1970**, *9*, 1233−1238.
[7] G. Natile, G. Albertin, E. Bordignon, A. A. Orio, *J. Chem. Soc., Dalton Trans.* **1976**, 626−631.
[8] G. Annibale, L. Maresca, L. Cattalini, G. Natile, *J. Chem. Soc., Dalton Trans.* **1982**, 1−7.
[9] R. Romeo, S. Lanza, M. L. Tobe, *Inorg. Chem.* **1977**, *16*, 785−790.
[10] R. Romeo, S. Lanza, D. Minniti, M. L. Tobe, *Inorg. Chem.* **1978**, *17*, 2436−2441.
[11] A. Schwab, M. L. Tobe, R. Romeo, *Inorg. Chim. Acta* **1981**, *58*, 161−165.
[12] M. L. Tobe, A. Schwab, R. Romeo, *Inorg. Chem.* **1982**, *21*, 1185−1190.
[13] D. J. Stufkens, *Coord. Chem. Rev.* **1990**, *104*, 39−112.
[14] D. E. Marx, A. J. Lees, *Organometallics* **1986**, *5*, 2072−2074.
[15] D. E. Marx, A. J. Lees, *Inorg. Chem.* **1987**, *26*, 620−622.
[16] D. E. Marx, A. J. Lees, *Inorg. Chem.* **1987**, *26*, 2254−2257.
[17] S. Oishi, *Organometallics* **1988**, *7*, 1237−1241.
[18] V. Zang, S. Zhang, C. B. Dobson, G. R. Dobson, R. van Eldik, *Organometallics* **1992**, *11*, 1154−1158.
[19] S. Zhang, V. Zang, G. R. Dobson, R. van Eldik, *Inorg. Chem.* **1991**, *30*, 355−356.
[20] K. Bal Reddy, E. M. Eyring, B. R. Brady, R. van Eldik, *J. Organomet. Chem.* **1992**, *440*, 113−117.
[21] K. Bal Reddy, R. Hoffmann, G. Konya, R. van Eldik, E. M. Eyring, *Organometallics* **1992**, *11*, 2319−2322.
[22] S. Cao, K. Bal Reddy, E. M. Eyring, R. van Eldik, *Organometallics* **1994**, *13*, 91−93.
[23] S. Cao, Y. Shi, J. Hollman, R. van Eldik, E. M. Eyring, *J. Chem. Soc., Dalton Trans.* **1996**, 1629−1635.
[24] C. Düker-Benfer, F. W. Grevels, R. van Eldik, *Organometallics* **1998**, *17*, 1669−1676.
[25] R. Romeo, A. Grassi, L. Monsù Scolaro, *Inorg. Chem.* **1992**, *31*, 4383−4390.
[26] R. Romeo, G. Arena, L. Monsù Scolaro, M. R. Plutino, G. Bruno, F. Nicolò, *Inorg. Chem.* **1994**, *33*, 4029−4037.
[27] R. Romeo, G. Alibrandi, G. Arena, L. Monsù Scolaro, M. R. Plutino, *Inorg. Chim. Acta* **1995**, *235*, 281−290.
[28] R. Romeo, L. Monsù Scolaro, M. R. Plutino, A. Del Zotto, *Transition Met. Chem.* **1998**, *23*, 789−793.
[29] For several recent examples, see: [29a] A. Bader, E. Lindner, *Coord. Chem. Rev.* **1991**, *108*, 27−110. [29b] H. Werner, A. Stark, M. Schulz, J. Wolf, *Organometallics* **1992**, *11*, 1126−1230. [29c] P. Braunstein, S. Coco Cea, M. I. Bruce, B. W. Skelton, A. H. White, *J. Chem. Soc., Dalton Trans.* **1992**, 2539−2542. [29d] P. Braunstein, Y. Chauvin, J. Nähring, Y. Dusausoy, D. Bayeul, A. Tiripicchio, F. Ugozzoli, *J. Chem. Soc., Dalton Trans.* **1995**, 851−862. [29e] P. Braunstein, Y. Chauvin, J. Nähring, A. DeCian, J. Fischer, *J. Chem. Soc., Dalton Trans.* **1995**, 863−873. [29f] Y. Uozumi, K. Kitayama, T. Hayashi, K. Yanagi, E. Fukuyo, *Bull. Chem. Soc. Jpn.* **1995**, *68*, 713−722. [29g] T. Braun, P. Steinert, H. Werner, *J. Organomet. Chem.* **1995**, *488*, 169−176. [29h] M. Martìn, O. Gevert, H. Werner, *J. Chem. Soc., Dalton Trans.* **1996**, 2275−2283. [29i] P. Crochet, B. Demerseman, C. Rocaboy, D. Schleyer, *Organometallics* **1996**, *15*, 3048−3061. [29j] E. T. Singewald, X. Shi, C. A. Mirkin, S. J. Shofer, C. L. Stern, *Organometallics* **1996**, *15*, 3062−3069. [29k] C. Bolzati, F. Tisato, F. Refosco, G. Bandoli, A. Dolmella, *Inorg. Chem.* **1996**, *35*, 6221−6229. [29l] P. Steinert, H. Werner, *Chem. Ber./Recueil* **1997**, *130*, 1591−1603. [29m] G. J. P. Britovsek, K. J. Cavell, M. J. Green, F. Gerhards, B. W. Skelton, A. H. White, *J. Organomet. Chem.* **1997**, *533*, 201−212. [29n] R. Kadyrov, J. Heinicke, M. K. Kindermann, D. Heller, C. Fischer, R. Selke, A. K. Fischer, P. G. Jones, *Chem. Ber./Recueil* **1997**, *130*, 1663−1670. [29o] E. Lindner, S. Pautz, R. Fawzi, M. Steimann, *J. Organomet. Chem.* **1998**, *555*, 247−253, and references therein.
[30] For several recent examples, see: [30a] G. R. Newkome, *Chem. Rev.* **1993**, *93*, 2067−2089. [30b] L. Costella, A. Del Zotto, A. Mezzetti, E. Zangrando, P. Rigo, *J. Chem. Soc., Dalton Trans.* **1993**, 3001−3008. [30c] A. Del Zotto, A. Mezzetti, P. Rigo, *J. Chem. Soc., Dalton Trans.* **1994**, 2257−2264. [30d] P. Barbaro, C. Bianchini, F. Laschi, S. Midollini, S. Moneti, G. Scapacci, P. Zanello, *Inorg. Chem.* **1994**, *33*, 1622−1630. [30e] H. Rieck, G. Helmchen, *Angew. Chem. Int. Ed. Engl.* **1995**, *34*,

2687−2689. [30f] A. Del Zotto, G. Nardin, P. Rigo, *J. Chem. Soc., Dalton Trans.* **1995**, 3343−3351. [30g] A. Habtemariam, P. J. Sadler, *Chem. Commun.* **1996**, 1785−1786. [30h] Z.-Z. Zhang, H. Cheng, *Coord. Chem. Rev.* **1996**, *147*, 1−39. [30i] A. Del Zotto, P. Rigo, G. Nardin, *Inorg. Chim. Acta* **1996**, *247*, 183−188. [30j] P. Wehman, H. M. A. van Donge, A. Hagos, P. C. J. Kamer, P. W. N. M. van Leeuwen, *J. Organomet. Chem.* **1997**, *535*, 183−193. [30k] P. Braunstein, J. Pietsch, Y. Chauvin, A. DeCian, J. Fischer, *J. Organomet. Chem.* **1997**, *529*, 387−393. [30l] U. Nagel, H. G. Nedden, *Chem. Ber./Recueil* **1997**, *130*, 989−1006, and references therein. [30m] A. Schnyder, A. Togni, U. Wiesli, *Organometallics* **1997**, *16*, 255−260. [30n] A. Del Zotto, E. Zangrando, *Inorg. Chim. Acta* **1998**, *277*, 111−117. [30o] L. Crociani, F. Tisato, F. Refosco, G. Bandoli, B. Corain, L. G. Venanzi, *J. Am. Chem. Soc.* **1998**, *120*, 2973−2974. [30p] A. Lightfoot, P. Schnider, A. Pfaltz, *Angew. Chem. Int. Ed.* **1998**, *37*, 2897−2899. [30q] S. Kudis, G. Helmchen, *Angew. Chem. Int. Ed.* **1998**, *37*, 3047−3050. [30r] X. Hu, H. Chen, X. Zhang, *Angew. Chem. Int. Ed.* **1999**, *38*, 3518−3521. [30s] J.-Y. Shen, C. Slugovc, P. Wiede, K. Mereiter, R. Schmid, K. Kirchner, *Inorg. Chim. Acta* **1999**, *268*, 69−76. [30t] A. Del Zotto, P. Di Bernardo, M. Tolazzi, P. L. Zanonato, *J. Chem. Soc., Dalton Trans.* **1999**, 979−986.

[31] For several recent examples, see: [31a] A. Del Zotto, P. Rigo, *J. Organomet. Chem.* **1986**, *315*, 165−169. [31b] A. Mezzetti, V. Novelli, A. Del Zotto, P. Rigo, *Acta Crystallogr., Sect. C* **1987**, *43*, 425−428. [31c] A. Del Zotto, P. Rigo, *Inorg. Chim. Acta* **1988**, *147*, 55−59. [31d] A. Del Zotto, A. Mezzetti, G. Dolcetti, P. Rigo, N. Bresciani Pahor, *J. Chem. Soc., Dalton Trans.* **1989**, 607−613. [31e] A. Del Zotto, A. Mezzetti, P. Rigo, M. Bressan, F. Morandini, A. Morvillo, *Inorg. Chim. Acta* **1989**, *158*, 151−158. [31f] P. Di Bernardo, P. Zanonato, M. Tolazzi, G. Tomat, *Inorg. Chim. Acta* **1990**, *177*, 25−29. [31g] E. W. Abel, D. Ellis, K. G. Orrell, V. Sik, *Polyhedron* **1991**, *10*, 1603−1609. [31h] P. Di Bernardo, M. Tolazzi, P. Zanonato, *Inorg. Chim. Acta* **1994**, *215*, 199−201. [31i] P. Di Bernardo, M. Tolazzi, P. Zanonato, *J. Chem. Soc., Dalton Trans.* **1995**, 1349−1355. [31j] P. Barbaro, A. Currao, J. Herrmann, R. Nesper, P. S. Pregosin, R. Salzmann, *Organometallics* **1996**, *15*, 1879−1888. [31k] A. Albinati, P. S. Pregosin, K. Wick, *Organometallics* **1996**, *15*, 2419−2421. [31l] A. J. Edwards, S. R. Mack, M. J. Mays, C.-Y. Mo, P. R. Raithby, M.-A. Rennie, *J. Organomet. Chem.* **1996**, *519*, 243−252. [31m] A. Del Zotto, B. Della Ricca, E. Zangrando, P. Rigo, *Inorg. Chim. Acta* **1997**, *261*, 147−159. [31n] E. I. Mastrosov, Z. A. Starikova, A. I. Yanovsky, D. I. Lobanov, I. M. Aladzheva, O. V. Bykhovskaya, Y. T. Struchkov, T. A. Mastryukova, M. I. Kabachnik, *J. Organomet. Chem.* **1997**, *535*, 121−127. [31o] N. Taguchi, K. Kashiwabara, K. Nakajima, H. Kawaguchi, K. Tatsumi, *J. Organomet. Chem.* **1999**, *587*, 290−298. [31p] O. Clot., M. O. Wolf, G. P. A. Yap, B. O. Patrick, *J. Chem. Soc., Dalton Trans.* **2000**, 2729−2737.

[32] R. Romeo, G. Arena, L. Monsù Scolaro, *Inorg. Chem.* **1992**, *31*, 4879−4884.

[33] Cambridge Structural Data Base, Cambridge Crystallographic Data Centre, 12 Union Road, Cambridge, UK, **1992−1997**.

[34] Y.-M. Hsiao, S. S. Chojnacki, P. Hinton, J. H. Reibenspies, M. Y. Darensbourg, *Organometallics* **1993**, *12*, 870−875.

[35] G. Alibrandi, G. Bruno, S. Lanza, D. Minniti, R. Romeo, M. L. Tobe, *Inorg. Chem.* **1987**, *26*, 185−190.

[36] [36a] A. Martin, *J. Chem. Educ.* **1999**, *76*, 578−583. [36b] A. J. Canty, G. van Koten, *Acc. Chem. Res.* **1995**, *28*, 406−413. [36c] G. Bruno, S. Lanza, F. Nicolò, *Acta Crystallogr., Sect. C* **1990**, *46*, 765−767. [36d] D. Braga, F. Grepioni, E. Tedesco, K. Biradha, G. R. Desiraju, *Organometallics* **1997**, *16*, 1846−1856. [36e] L. Brammer, D. Zhao, F. T. Ladipo, J. Braddock-Wilking, *Acta Crystallogr., Sect. B* **1995**, *51*, 632−640 and refs. therein. [36f] A. Albinati, F. Lianza, P. S. Pregosin, P. Müller, *Inorg. Chem.* **1994**, *33*, 2522−2526.

[37] M. R. Plutino, L. Monsù Scolaro, R. Romeo, A. Grassi, *Inorg. Chem.* **2001**, *39*, 2712−2720, and references therein.

[38] P. E. Garrou, *Chem. Rev.* **1981**, *81*, 229−266.

[39] *SCIENTIST*, Micro Math Scientific Software, Salt Lake City, UT, **1986−1995**.

[40] [40a] P. Uguagliati, A. Benedetti, S. Enzo, L. Schiffini, *Comput. Chem.* **1984**, *8*, 161−168. [40b] P. L. Sandrini, A. Mantovani, B. Crociani, P. Uguagliati, *Inorg. Chim. Acta* **1981**, *51*, 71−80. [40c] E. R. Malinowski, D. G. Hovery, *Factor Analysis in Chemistry*, Wiley-Interscience, New York, **1980**, pp. 159−161.

[41] [41a] D. Minniti, G. Alibrandi, M. L. Tobe, R. Romeo, *Inorg. Chem.* **1987**, *26*, 3956−3958. [41b] U. Frey, L. Helm, A. E. Merbach, R. Romeo, *J. Am. Chem. Soc.* **1989**, *111*, 8161−8165. [41c] D. Alibrandi, D. Minniti, L. Monsu′ Scolaro, R. Romeo, *Inorg. Chem.* **1989**, *28*, 1939−1943.

[42] R. B. Jordan, *Reaction Mechanisms of Inorganic and Organometallic Systems*, Oxford University Press, New York, **1991**, pp. 81−86.

[43] [43a] S. Aizava, K. Matsuda, T. Tajima, M. Maeda, T. Sugata, S. Funahashi, *Inorg. Chem.* **1995**, *34*, 2042−2047. [43b] S. Aizava, S. Iida, K. Matsuda, S. Funahashi, *Inorg. Chem.* **1996**, *35*, 1338−1342.

[44] A. J. Clarkson, D. A. Buckingham, A. J. Rogers, A. G. Blackman, C. R. Clark, *Inorg. Chem.* **2000**, *39*, 4769−4775.

[45] M. L. Tobe, J. Burgess, *Inorganic Reaction Mechanisms*, Addison Wesley Longman, Essex CM20 2JE, UK, **1999**, chapter 2, pp. 82−86.

[46] E. Uhlig, M. Maaser, *Z. Anorg. Allg. Chem.* **1966**, *344*, 205−213.

[47] D. W. Meek, P. E. Nicpon, V. I. Meek, *J. Am. Chem. Soc.* **1970**, *92*, 5351−5359.

[48] H. P. Fritz, I. R. Gordon, K. E. Schwarzhans, L. M. Venanzi, *J. Chem. Soc.* **1965**, 5210−5216.

[49] P. Rigo, M. Bressan, *Inorg. Chem.* **1975**, *14*, 1491−1494.

[50] A. R. Sanger, *Can. J. Chem.* **1983**, *61*, 2214−2219.

[51] [51a] A. L. Van Geet, *Anal. Chem.* **1968**, *40*, 2227−2229. [51b] A. L. Van Geet, *Anal. Chem.* **1970**, *42*, 679−680.

[52] R. Diamond, *Acta Crystallogr., Sect. A* **1969**, *25*, 43−55.

[53] G. Kopfmann, R. Huber, *Acta Crystallogr., Sect. A* **1968**, *24*, 348−351.

[54] Bruker, *XSCANS*, release 2.31, Bruker AXS Inc., Madison Wisconsin, **1999**.

[55] G. M. Sheldrick, *SHELXTL*, VMS version 5.05, Siemens Analytical X-ray Instruments Inc., Madison Wisconsin, **1991**.

[56] A. Altomare, O. Cascarano, C. Giacovazzo, A. Guagliardi, M. C. Burla, G. Polidori, M. Camalli, *J. Appl. Crystallogr.* **1994**, *27*, 435−436.

[57] G. M. Sheldrick, *SHELXL97, Program for Crystal Structure Refinement*, University of Göttingen, Germany, **1997**.

[58] M. Nardelli, *J. Appl. Chem.* **1995**, *28*, 659; version locally modified.

[59] Crystallographic data (excluding structure factors) for the structure reported in this paper have been deposited with the Cambridge Crystallographic Data Centre as supplementary publication no. CCDC-167054. Copies of the data can be obtained free of charge on application to CCDC, 12 Union Road, Cambridge CB2 1EZ, UK [Fax: (internat.) + 44-1223/336-033; E-mail: deposit@ccdc.cam.ac.uk].

[60] B. R. Steele, K. Vrieze, *Transition Met. Chem. (London)* **1977**, *2*, 140−144.

[61] S. Lanza, D. Minniti, P. Moore, J. Sachinidis, R. Romeo, M. L. Tobe, *Inorg. Chem.* **1984**, *23*, 4428−4433.

[62] Ligand concentration dependence of the pseudo-first-order rate constants (k_{obs}/s^{-1}) for the ring-opening reaction are available as Supporting Information (Table SI1; see footnote on the first page of this article).

Received August 3, 2001
[I01289]

Activation and Functionalization of Vinylic C−F Bonds by Transition Metal Compounds: The Factors Determining Reactions between Nucleophiles and a (Perfluorovinyl)diiron(I) Complex; Syntheses of Diiron Derivatives Containing New C−N, C−S, C−H and C−O Bonds

Karine Guennou de Cadenet,[a] René Rumin,[a] François Y. Pétillon,*[a] Dmitri S. Yufit,[b] and Kenneth W. Muir*[b]

Keywords: C−F activation / C−N, C−S coupling / Carbenes / Nucleophiles / Vinyl complexes

The reactions between alcohols ROH (R = Me, Et) and $RR(OH)_2$ (RR = CH_2–CH_2) and the [perfluoro(sulfanyl)vinyl]-diiron complex [{$Fe(CO)_3$}$_2${μ-C(SMe)(CF_3)$C_\beta C_\alpha F_2$}] (**1**) in THF at room temperature involve substitution at the C_α atom to give new (alkoxymethylene)thiaferracyclobutadiene compounds [{$Fe(CO)_3$}$_2${μ-S(Me)C(CF_3)$C_\beta C_\alpha$(OR)$_2$}] [R = Me (**2a**), Et (**2b**); RR = CH_2CH_2 (**2c**)]. Treatment of **1** with aniline and (methoxycarbonyl)hydrazine, bases of intermediate strength according to Pearson, produces α,β-substituted thiaferracyclopentadiene [{$Fe(CO)_3$}$_2${μ-S(Me)C(CF_3)C_β(NHR)C_α-(NHR)}] [R = Ph (**5a**), NHC(O)OMe (**5b**)] complexes. It is suggested that these compounds form through initial nucleophilic attack at C_α to give the zwitterionic intermediate [{$Fe(CO)_3$}$_2${μ-S(Me)C(CF_3)CC(NRH)$_2$}] (**f**). Thermally induced C–F bond activation is a feature of these reactions. When **1** reacts with thioamides containing three "hard" competitive primary and secondary amine functions and one "soft" thione function, the nucleophile first attacks at C_α through a secondary amine and, in a second step, at C_β through the thiol function to give α,β adducts [{$Fe(CO)_3$}$_2${μ-S(Me)C(CF_3)C_βSC(=NR^2)N(R^1)C_α(C_β–C_α)}] [R^1 = NH_2, R^2 = CH_3 (**6a**); R^1 = CH_3, R^2 = H (**6b**); R^1 = R^2 = CH_3 (**6c**)] possessing novel iminothiazolidine systems fused to the five-membered metallacyclic ring. Treatment of **1** with acetylhydrazine, which has three "hard" nucleophilic functions, results in the formation of the compound [{$Fe(CO)_3$}$_2${μ-S(Me)C(CF_3)C(H)$C_{(10)}$NNC(Me)O($C_{(10)}$–O)}] (**7a**), in which an oxadiazole function is fused to the thiaazaferracyclohexene ring. The position of the fluorine substituent on the $C_\alpha C_\beta C_\gamma$($CF_3$)S(Me) ring of ferracyclopentadiene complexes has been found to be the essential factor determining the specific activation of the C–F bond. A single fluoro substituent attached to the β-carbon atom of the chain can be activated by nucleophiles to give α,β adducts [{$Fe(CO)_3$}$_2${μ-S(Me)C(CF_3)C_β(X)C_α(NRR′)}] [X = OR″, R = R′ = R″ = Me (**3a**); X = OR″, R = R″ = Me, R′ = C(O)NMe_2 (**3b**); X = SR″ (**4**)]. In contrast, complexes in which a single fluorine atom is linked to the α-carbon atom do not undergo C–F bond cleavage reactions. X-ray structures of compounds **2a**, **3b**, **5a**, **5b**, **6a** and **7a** are reported.

Introduction

C−F activation reactions induced by transition metal compounds are of salient importance in organometallic chemistry. They are involved in many of the catalytic transformations that result in the formation of new carbon−heteroatom bonds and they are an essential feature of the synthesis of partially fluorinated molecules.[1] The recent upsurge of interest in (perfluorovinyl)metal complexes also stems from the observation that the chemical properties of these compounds differ substantially from those of their hydrocarbon analogues.[2] Although vinyl fluorides are normally inert, in some cases they undergo unexpected C−F cleavage reactions with nucleophilic agents to give either substituted vinyl derivatives[2] or new organofluorine compounds with unusual functional groups.[3,4]

In this context we have previously described the reaction between the [perfluoro(sulfanyl)vinyl]diiron(I) compound [{$Fe(CO)_3$}$_2${μ-C(SMe)(CF_3)$C_\beta C_\alpha F_2$}] (**1**) and primary and secondary amines, thiols, phosphanes and tertiary phosphanes. Analysis of the reaction products showed that soft nucleophiles (phosphanes, tertiary phosphanes, thiols) react at C_β to give thiaferracyclopentadiene compounds of types **D**, **E** or **F**[4b,4c] (Scheme 1), whereas hard nucleophiles (primary and secondary amines) react at C_α to give either monofluorothiaferracyclopentadiene complexes of type **A** when stoichiometric amounts of nucleophile are used, or thiaferracyclobutene compounds of type **C** when excess nucleophile is employed[4a,4d] (Scheme 1). These results imply

[a] UMR CNRS 6521, Laboratoire de Chimie, Electrochimie Moléculaires et Chimie Analytique, Faculté des Sciences et Techniques, Université de Bretagne Occidentale,
B. P. 809, 29285 Brest-cedex, France
Fax: (internat.) + 33-2/98017001
E-mail: francois.petillon@univ-brest.fr
[b] Department of Chemistry, University of Glasgow,
Glasgow G12 8QQ, UK
E-mail: ken@chem.gla.ac.uk

that soft nucleophiles activate only one C−F bond whereas hard bases activate both C−F bonds, resulting either in a 1,2-transfer of F onto C_β or in further addition of nucleophile.

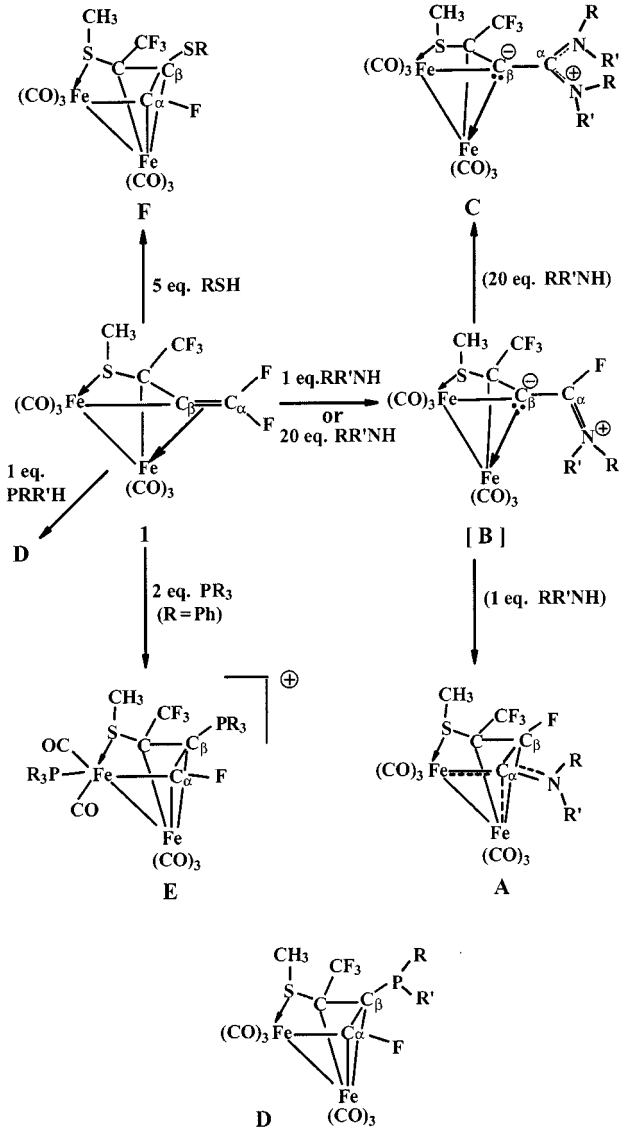

Scheme 1

Perhaps our most striking result from these earlier studies of the reactions of nucleophiles with **1** was that the C−F activation step depended on whether the attacking nucleophile was hard or soft.[4] We have therefore become interested in reactions between **1** and such nucleophiles as alcohols and aniline. These are still hard bases according to Pearson's concept,[5] but are nevertheless thought to be softer than most aliphatic amines. We have also investigated the addition of multifunctional amines to **1**, in order to see whether the reaction of the iron compound with one function influences the reactivity of the others. Moreover, as an extension of our earlier studies of the reactions between nucleophiles and **1**,[4] we have investigated the dependence of the C−F bond activation on the position of the fluorine atoms in the carbon chain of the vinylic ligand.[6] Here we report these various reactions and the characterisation of the resulting products.

Results and Discussion

Analytical data and mass, infrared and multinuclear (^{1}H, ^{19}F and ^{13}C) NMR spectroscopic data for all new compounds discussed in this paper are given in Table 1. Selected bond lengths for **2a**, **3b**, **5a**, **5b**, **6a** and **7a** are compared in Table 2. All these structures contain rather similar $Fe_2(CO)_6$ units, in which the single Fe−Fe bond is bridged in various ways by a six-electron donor $MeSC(CF_3)C_\beta C_\alpha$ ligand. Apart from **7a**, the Fe−Fe distances are in the narrow 2.60−2.65 Å range, with a mean of 2.634 Å. Further spectroscopic and structural details are presented in the Exp. Sect. and in figure captions.

1. Reactions between [{Fe(CO)$_3$}$_2${μ-C(SMe)(CF$_3$)C−CF$_2$}] (1) and Alcohols ROH (R = CH$_3$, C$_2$H$_5$) and RR(OH)$_2$ (RR = CH$_2$−CH$_2$)

Synthesis and Spectroscopic Characterisation

The reactions between **1** and alcohols depend markedly on the solvent. Treatment of **1** with a large excess of alcohol in THF at room temperature results in the quantitative formation of the (alkoxymethylene)thiaferracyclobutene compounds **2** (Scheme 2). When the reaction is carried out in CH_2Cl_2, it is necessary to heat the solution to 60 °C to obtain the same products. The regiochemistry observed in the reaction is consistent with the known hard base character of alcohols: they are expected to react at C_α like amines,[4d] which are even harder nucleophiles than alcohols.

The molecular structure of **2a** was established by X-ray diffraction (see below). It is clearly apparent from the NMR spectroscopic data in Table 1 that complexes **2a** and **2b** have the same basic structure. Both mass spectra have molecular ions corresponding to replacement of the two fluorine atoms of **1** by two alkoxide groups. The ^{13}C NMR spectra of **2a**, **2b** and the parent complex **1** are very similar, each showing two resonances at $\delta \approx 120$ and 160 in the range expected for vinylic carbon atoms σ- and π-bonded to metal atoms. The mass spectrum of **2c** shows a molecular ion peak corresponding to a complex in which two fluorine atoms have been replaced by one molecule of ethylene glycol. The most significant difference between **2c** and **2a** or **2b** occurs in the ^{13}C NMR spectra, and particularly in the region associated with the carbon atom (C_β) directly bound to the two iron atoms. The $^{13}C_\beta$ signal of **2c** appears at $\delta = 85.6$, whereas those of **2a** and **2b** occur at $\delta = 124.0$ and 116.2, respectively, indicating a difference in the bridging mode of the vinyl ligand. However, the ^{13}C NMR spectra of **2c** and **C**[4d] (Table 1) are very similar, strongly suggesting that **2c** in solution adopts mainly the zwitterionic form depicted in Scheme 2, whereas **2a** and **2b** adopt a neutral structure closely related to that of the parent compound **1**. The highfield shifting of the C_β resonance of **2c**

Table 1. Comparison of selected NMR chemical shift data (δ)[a] for neutral (**1**, **2a**, **b**) and zwitterionic (**2c**, [**f**], [**B**] and [**C**]) thiaferracyclobutene, thiaferracyclopentadiene (**3−6** and **A**) and thiaazaferracyclohexene (**7**) derivatives

Compd.	^{19}F			^{13}C{^{1}H}					
	CF_3	CF	SCH_3	C_β	C_α	CO [Fe(1)]	CO [Fe(1)]	CO [Fe(1)]	CO [Fe(2)]
1[c],[d]	−58.7 (d)	−59.2 (m) −81.2 (m)	32.5 (s)	127.7 (d)	152.6 (dd)				
2a	−57.9 (s)		32.4 (s)	124.0 (s)	161.8 (s)		209.5 (s)		210.3 (s, br)
2b	−57.6 (s)		32.4 (s)	116.2 (s)	165.4 (s)		209.9 (s)		211.0 (s, br)
2c	−58.8 (s)		32.4 (s)	85.6 (s)	171.9 (s)		211.7 (s)		210.0 (s, br)
[**f**][c]	−63.2 (s)		32.8 (s)	95.6 (s)	176.9 (s)	204.7 (s)	206.3 (s)	210.6 (s)	208.5 (s, br)
[**B**][c]	−63.35 (s)	−19.05 (s)	33.3 (s)	73.1 (d)	182.1 (d)	207.7 (s)	209.9 (s)	212.0 (s)	215.4 (s, br)
C[e][f]	−62.85 (s)		31.4 (s)	89.7 (s)	177.3 (s)		213.8 (s)		215.4 (s, br)
5a	−57.5 (s)		34.9 (s)	91.6 (s)	202.0 (q, $^4J_{CF}$ = 2)	206.5 (s)	208.6 (s)	210.5 (s)	210.1 (s, br)
5b	−56.6 (s)		34.7 (s)	93.5 (s)	210.7 (q, $^4J_{CF}$ = 2)	204.9 (s)	210.0 (s)	210.4 (s)	210.0 (s, br)
6a	−58.7 (s)		35.2 (s)	89.0 (s)	184.0 (s)	205.3 (s)	209.0 (s)	210.5 (s)	209.1 (s, br)
6b	−59.1 (s)		34.9 (s)	92.8 (s)	183.2 (s)	204.7 (s)	209.9 (s)	210.1 (s)	208.6 (s, br)
6c	−59.0 (s)		34.9 (s)	91.6 (s)	184.1 (s)	204.7 (s)	210.2 (s)	210.3 (s)	208.8 (s, br)
A[e][g]	−59.2 (d)	−152.65 (q)	34.4 (s)	120.0 (d)	190.75 (d)	205.0 (s)	210.7 (s)	211.2 (s)	210.2 (s, br)
3a	−58.4 (s)		34.5 (s)	122.5 (s)	189.1 (q, $^4J_{CF}$ = 2)	207.2 (s)	210.7 (s)	211.0 (s)	210.4 (s, br)
3b	−58.7 (s)		33.2 (s)	102.0 (s)	198.6 (q, $^4J_{CF}$ = 1.5)	205.2 (s)	210.8 (s)	211.5 (s)	210.5 (s, br)
F[h][i]	−58.6 (s)	−53.9 (s)	34.0 (s)	94.8 (d)	220.6 (q)	205.8 (d)	207.5 (d)	208.4 (d)	208.2 (s, br)
4a	−55.5 (s)		34.2 (s)	88.5 (s)	205.7 (s)	206.9 (s)	210.1 (s)	210.8 (s)	210.9 (s)
4b	−55.3 (s)		33.0 (s)	71.5 (s)	212.9 (m)	205.6 (s)	210.5 (s)	210.7 (s)	210.0.(s)
4c	−56.4 (s)		33.1 (s)	78.5 (s)	206.4 (m)	210.6 (s)	210.8 (s)	211.5 (s)	209.9 (s, br)
4d	−55.2 (s)		33.1 (s)	71.3 (s)	212.9 (q, $^4J_{CF}$ = 2)	205.6 (s)	210.5 (s)	210.9 (s)	210.0 (s, br)
4e	−54.9 (s)		33.3 (s)	65.4 (s)	206.3 (q, $^4J_{CF}$ = 2)	205.7 (s)	211.4 (s)	211.5 (s)	210.0 (s, br)
7a	− 62.6		30.1 (s)	24.4 (s)	175.9 (s)	198.3 (s)	211.1 (s)	215.6 (s)	207.6 (s) 214.0 (s, br) 219.4 (s, br)
7b	−62.4 (s)		25.4 (d^3, J_{CP} = 8)	24.8 (s)	176.5 (s)		216.2 (d, $^2J_{CP}$ = 7.5)[b]	219.6 (d, $^2J_{CP}$ = 2)[b]	207.9 (s, br)[b] 214.1 (s, br)[b] 222.8 (s, br)[b]
7c	−62.5 (s)		26.8 (d^3, J_{CP} = 6.5)	24.5 (s)	176.6 (s)		215.0 (d, $^2J_{CP}$ = 11.5)	220.4 (d, $^2J_{CP}$ = 4.5)	213.4 (s, br) 222.5 (s, br)

[a] Measured in $CDCl_3$ solution at 293 K unless stated otherwise, J in Hz. [b] At 240 K. [c] At 233 K. [d] From ref.[6] [e] From ref.[4d] [f] R−R′ = $(CH_2)_4$. [g] R = R′ = Me. [h] R = C_2H_5. [i] From ref.[4c]

Table 2. Selected bond lengths [Å] in $[Fe_2(CO)_6\{\mu\text{-}C_\alpha{-}C_\beta{-}C_\gamma(SMe)CF_3\}]$ complexes; Fe−CO distances are in the 1.763(6)−1.820(3) Å range, with a mean of 1.791 Å; except for **2a** the asymmetric unit of each structure contains two crystallographically independent molecules which are structurally indistinguishable

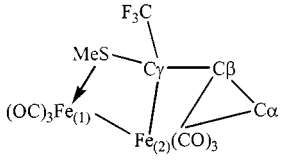

	2a	**3b**	**3b**	**5a**	**5a**	**5b**	**5b**	**6a**	**6a**	**7a**	**7a**	**Mean**
Fe1−C_β	1.963(2)											
Fe1−N										1.974(2)	1.964(2)	
Fe1−C_α		2.000(6)	1.997(6)	1.978(5)	1.966(5)	1.934(5)	1.947(5)	1.947(7)	1.936(7)			1.963
Fe1−S	2.307(1)	2.257(2)	2.246(2)	2.259(2)	2.276(2)	2.267(2)	2.266(2)	2.280(2)	2.282(2)	2.282(1)	2.276(1)	2.271
Fe−Fe	2.600(1)	2.649(1)	2.646(1)	2.634(1)	2.633(1)	2.651(1)	2.647(1)	2.640(2)	2.640(1)	2.794(1)[a]	2.799(1)[a]	2.634
Fe2−C_γ	2.039(2)	1.999(6)	2.016(6)	2.010(5)	2.008(5)	2.011(6)	2.000(6)	2.028(7)	2.028(7)	1.986(3)	1.983(3)	2.010
Fe2−C_β	1.973(2)	2.040(6)	2.043(5)	2.050(5)	2.064(5)	2.036(5)	2.026(5)	2.072(7)	2.060(7)	2.061(3)	2.063(3)	2.044
Fe2−C_α	2.347(2)	2.347(6)	2.397(5)	2.328(6)	2.335(5)	2.285(5)	2.292(5)	2.238(7)	2.229(7)			2.301
$C_\alpha{-}C_\beta$	1.384(3)	1.415(8)	1.428(8)	1.409(7)	1.440(7)	1.431(7)	1.430(7)	1.418(9)	1.416(9)	1.440(4)	1.424(4)	1.421
$C_\beta{-}C_\gamma$	1.441(3)	1.431(8)	1.469(8)	1.459(7)	1.441(7)	1.446(8)	1.440(8)	1.432(9)	1.442(9)	1.455(4)	1.463(4)	1.447
$C_\gamma{-}C_\delta$	1.501(3)	1.497(9)	1.499(9)	1.496(8)	1.487(7)	1.505(9)	1.500(8)	1.504(10)	1.500(11)	1.493(4)	1.489(4)	1.496

[a] Not included in the calculation of the mean.

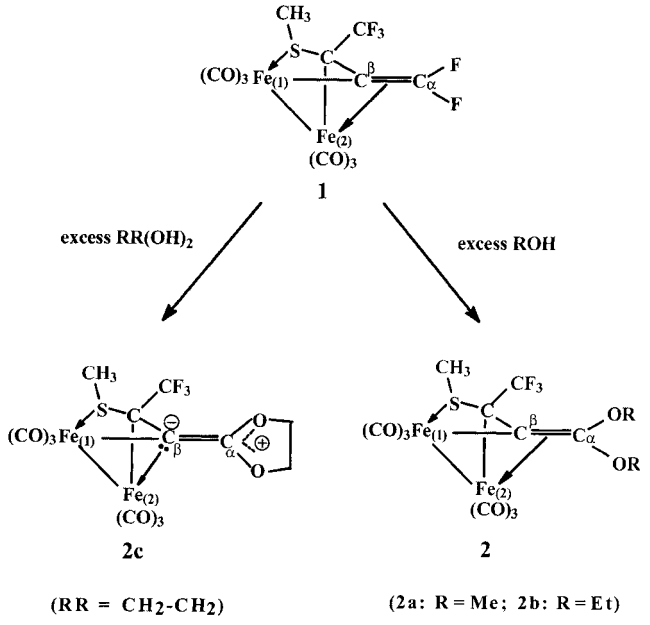

Scheme 2. Synthesis and proposed structures of complexes **2**

relative to that of **2a** and **2b** may be a consequence of the presence of negative charge on this carbon in **2c**.

Single-Crystal X-ray Analysis of 2a

Crystals suitable for X-ray diffraction were grown from a solution of **2a** in dichloromethane and hexane at −20 °C. The molecular structure of **2a** (Figure 1, Table 2) is broadly consistent with that deduced from the spectra (Scheme 2, Table 1). It is formally derived from **1** by replacement of both fluoro substituents by methoxide groups to give a six-electron donor $MeSC_\gamma(CF_3)C_\beta C_\alpha(OMe)_2$ ligand. This process obviously involves the cleavage of two C−F bonds. Iron atom Fe(1) is incorporated in an $Fe(1)S(1)C_\gamma C_\beta$ thiaferracyclobutene ring, linking to Fe(2) through a normal Fe−Fe bond. Fe(2) interacts weakly with C_α [Fe(2)−C(10) 2.347(2) Å], strongly with C_β [Fe(2)−C(9) 1.973(2) Å] and slightly less strongly with C_γ [Fe(2)−C(8) 2.039(2) Å]. Atom Fe(2) and the $C_\gamma-C_\beta-C_\alpha$ chain define a rather distorted (π-allyl)Fe substructure; this view is consistent with the $C_\delta-C_\gamma-C_\beta-C_\alpha$ and other torsion angles (Figure 1, caption) and with the $C_\alpha-C_\beta$ and $C_\beta-C_\gamma$ distances [1.384(3) and 1.441(3) Å], which may reflect the asymmetry in the Fe(2)−C distances [for comparison, average Fe−C(allyl) and C−C(allyl) distances are 2.07 and 1.404 Å and C−C bond lengths of 1.369(9) − 1.391(4) Å have been reported in μ_2-η^1:η^2-vinyl derivatives[7a,8]]. The Fe−C distances in **2a** are also broadly in agreement with those that we found in the C=C=CN*t*Bu derivative [{Fe(CO)$_3$}$_2$-{μ-C_β[C(CF$_3$)(SMe)]C_α(N*t*Bu)}] [Fe(2)−C_β 2.004(4), Fe(1)−C_β 1.970(3), Fe(2)−C_α 2.465(4) Å[4a]]. Finally, we note that C_β is nearly equidistant from the two metal atoms and that both Fe−C_β distances are within the range typical of iron−carbene bonds.[4b,4c,7b] The ^{13}C NMR spectrum of **2a** in solution shows a highfield resonance for the C_β carbon atom at δ = 124.0, in sharp contrast with the bridging C_α carbon atoms of thiaferracyclopentadiene compounds, which have carbene-like character and which give rise to lowfield resonances at δ ≈ 224.[4b,4c]

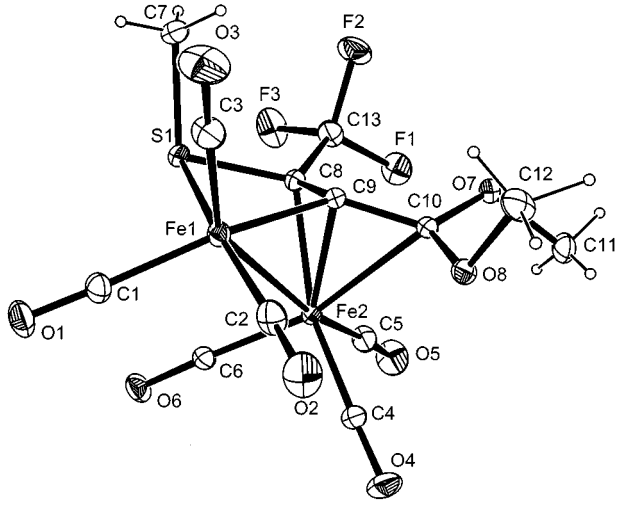

Figure 1. Molecular structure and numbering scheme of compound **2a** in the crystal; here and elsewhere 20% probability ellipsoids are shown for non-hydrogen atoms; selected bond lengths [Å] and angles [°]: O(7)−C(10) 1.352(3), O(7)−C(11) 1.437(3), O(8)−C(10) 1.356(3), O(8)−C(12) 1.446(3); C(8)−C(9)−C(10)−O(7) 38.8, C(8)−C(9)−C(10)−O(8) −161.7(2), and C(13)−C(8)−C(9)−C(10) −43.9(3)

Fluxional Behaviour of Compound 2 and Mechanistic Considerations

Spectroscopic data indicate that **2** is present as a single species in solution (Table 1 and Exp. Sect.). The fluxional solution behaviour of the ligands in **2a** and **2c** was examined by variable temperature $^{13}C\{^1H\}$ NMR studies, and typical results for **2a** in the OMe region between 195 and 270 K are presented in Figure 2. Limiting ^{13}C NMR spectra in the methyl or methylene regions consistent with structures **2a** and **2c** were obtained at 195 and 183 K, respectively. Two resonances in each spectrum are visible at these temperatures, indicating that the two OCH_3 (**2a**) and the two OCH_2 groups (**2c**) are inequivalent. As the temperature is raised from 183 to 270 K, these two signals broaden and coalesce into a single resonance, at 230 K (δ ≈ 59.3) for **2a** and 270 K (δ ≈ 68.9) for **2c**, the chemical shift of which is the weighted average of those of the two methyl or methylene groups in the limiting spectra. The activation barriers of the observed dynamic processes, estimated from the chemical shift difference ($\Delta\nu$) and coalescence temperature (T_c [9]) of the OCH_3 and CH_2 signals, are presented in Table 3. The most obvious route to high-temperature equivalence of the two OCH_3 or OCH_2 groups is rotary motion around the $C_\alpha-C_\beta$ axis. However, rotation about such a multiple bond [$C_\alpha-C_\beta$ 1.384(3) Å in **2a**] would seem at first sight to require an activation energy higher than those estimated for **2a** and **2c** (Table 3). A more elaborate explanation for the fluxionality involves a flip of the π-allyl system from Fe(2) to Fe(1). This would require simultaneous transfer of the Fe(1)−S bond to Fe(2) and of the Fe(2)−C_α and

Fe(2)−C_γ bonds to Fe(1). Both Fe−C_β bonds are conserved, so that C_β momentarily has sp^3 hybridisation (Scheme 3), which permits free rotation about C_α−C_β and averaging of the OR groups attached to C_α, as well as of the CO environments at Fe(1) and Fe(2).

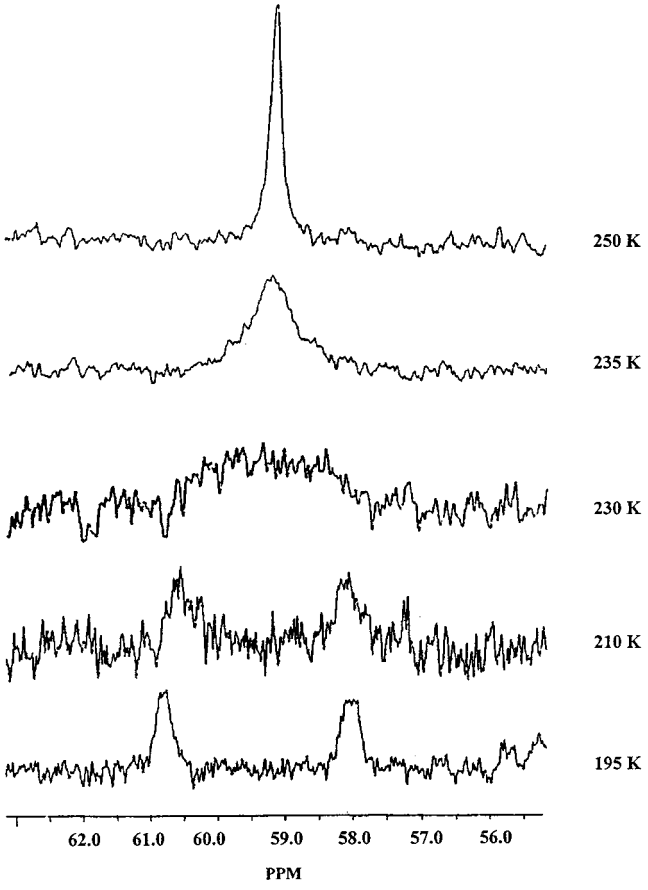

Figure 2. Variable-temperature $^{13}C\{^1H\}$ NMR spectra in the methyl region of **2a** in CD_2Cl_2

The $^{13}C\{^1H\}$ NMR spectra of **2a** and **2c** in the carbonyl region are also temperature-dependent; the low-temperature resonances are averaged as the temperature is increased. The spectrum of **2c** in the CO region between 183 and 298 K is presented in Figure 3 as an example. At 183 K, the spectra of **2a** and **2c** both show six singlets of equal intensity, but three of them are broad. On the basis of previous data for the parent fluorovinyl complex **1**,[6] we tentatively assign the broad resonances to the CO groups coordinated to Fe(1) and the three sharper singlets to the carbonyl groups attached to Fe(2). As the temperature is increased, the three signals assigned to the carbonyl groups bound to Fe(1) broaden still further and finally collapse at 213 and 250 K for **2c** and **2a**, respectively. At still higher temperatures, the signals for the three Fe(2)-bound carbonyl groups broaden and collapse, at about 240 K for **2a** and 270 K for **2c**, to a single broad resonance. Above 270 K the lines again sharpen, producing high-temperature spectra that consist of two singlets at 298 K. All these changes were found to be reversible. These observations indicate that all the carbonyl ligands take part in local CO exchange processes on the two iron atoms. The low values of the energy barriers associated with these site exchanges (Table 3) are roughly of the order expected for localised scrambling of the carbonyl groups on metal atoms.[10] The observed exchange of carbonyl groups at Fe(1) involves scission of only two bonds, whereas localised exchange at Fe(2) requires the rupture of at least three. Since Fe(2) is bonded to both C_α and C_β, it is perhaps to be expected that the energy barriers associated with scrambling of the R substituents in C_β−$C_\alpha(OR)_2$ and those associated with carbonyl exchange at Fe(2) are very similar (Table 3). It is also worth noting

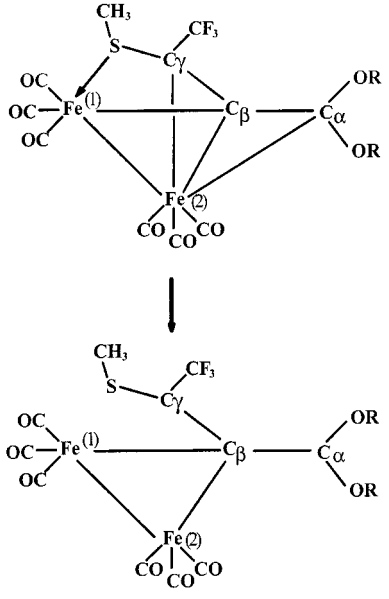

Scheme 3

Table 3. Dynamic $^{13}C\{^1H\}$ NMR spectroscopic data

Compd.	Resonance	T_c [K][a]	Δν [Hz][b]	$\Delta G^{\ddagger}_{T_c}$ [kJ mol^{-1}][c]
2a	$C_\alpha(OCH_3)_2$	230	203	44.1
	$Fe(1)(CO)_3$	250	193	48.3
	$Fe(2)(CO)_3$	240	442	44.6
2c	$C_\alpha(O-CH_2-CH_2-O)$	270	188	52.4
	$Fe(1)(CO)_3$	213	450	39.3
	$Fe(2)(CO)_3$	270	332	51.1

[a] Coalescence temperature. [b] Frequency difference between resonances of exchanging groups at low-temperature limit. [c] Highest error limit: ± 1 kJ mol^{-1}.

that the higher-energy process concerns CO movement at Fe(1) in **2a** but at Fe(2) in **2c**, which may indicate that the coordination modes of the $C_\beta-C_\alpha(OR)_2$ ligands to the iron atoms differ in **2a** and **2c**.

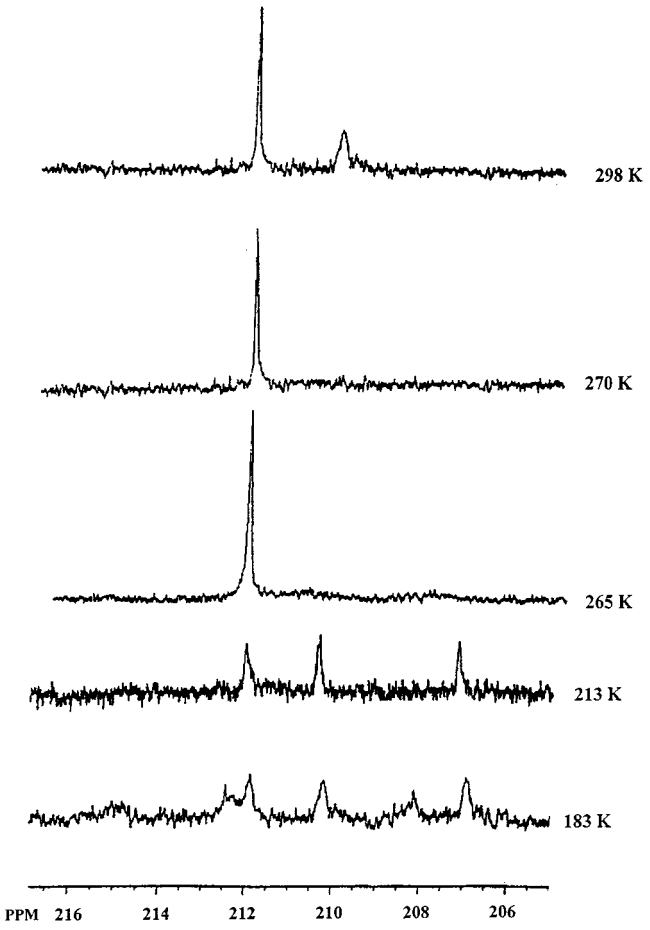

Figure 3. Variable-temperature $^{13}C\{^1H\}$ NMR spectra in the carbonyl region of **2c**, in CD_2C1_2

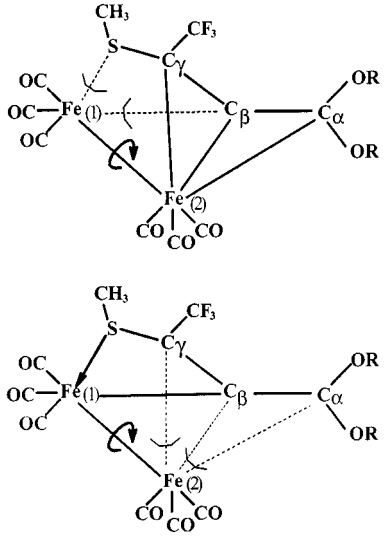

As mentioned above, the reactions between **1** and excess alcohol depend critically on the conditions; both the nature of the alcohol and that of the solvent greatly influence the reaction rates. Thus, in THF at room temperature, the reactions of **1** with methanol, ethanol and ethylene glycol were complete in 2, 3 and 5 h, respectively. The same reactions in dichloromethane were very slow at room temperature and heating was necessary to provide acceptable yields of **2**. Evidently, the solvent is involved in the mechanism of the reaction between **1** and a large excess of alcohol. Monitoring of the reaction of **1** with 40 equiv. of methanol in $[D_8]$THF by ^{19}F NMR at room temperature showed the gradual disappearance of **1** and the formation of several fluoro intermediates, **2a** being the last in this sequence. As the reaction proceeded, several fluoro complexes were present together in solution, giving rise to complicated ^{19}F NMR patterns from which it was difficult to identify the intermediates. Since the reaction depends markedly upon the nature of the solvent, it probably involves a transient, THF-containing intermediate. There is evidence that such a species plays a role in the reaction between **1** and Me_2NH.[4d]

2. Reactions between Monofluorothiaferracyclopentadiene Compounds of Types A, D and F and Nucleophiles

Synthesis and Spectroscopic Characterisation of Complexes 3 and 4

We have previously shown that hard nucleophiles (Nu) such as amines react with the (perfluorovinyl)diiron complex **1**, $[\{Fe(CO)_3\}_2\{\mu\text{-}CC(SMe)(CF_3)C_\beta C_\alpha F_2\}]$, by attack at C_α, activating both vinylic C−F bonds, to give only α adducts containing either a thiaferracyclopentadiene $Fe(1)C_\alpha(Nu)C_\beta(F)C(CF_3)S(Me)$ ring (compounds of type **A**) or a thiaferracyclobutene $Fe(1)S(Me)C(CF_3)C_\beta\text{-}\{C_\alpha(NRR')_2\}$ ring.[4d] In contrast, soft nucleophiles (Nu) (phosphanes, tertiary phosphanes, thiols) react only at C_β, activating only one vinylic C−F bond to give β adducts containing a thiaferracyclopentadiene $Fe(1)C_\alpha(F)C_\beta(Nu)\text{-}CCF_3)S(Me)$ ring (compounds of type **D** or **F**).[4c] It was therefore of interest to see how hard and soft nucleophiles activate the C−F bonds in monofluoro complexes of types **A**, **D** and **F**.

Accordingly, the aminofluorothiaferracyclopentadiene complex **A** (R = R′ = Me) in dichloromethane was treated with large excesses of either methanol or dimethylammonium dimethylcarbamate. The alkoxythiaferracyclopentadiene complexes **3a** and **3b** were formed quantitatively as red or orange microcrystalline solids, respectively (Scheme 4). Soft nucleophiles, such as thiols and dialkylammonium dialkyldithiocarbamates, also react with **A** in dichloromethane to afford high yields of new complexes **4a**−**4e** as orange or red crystalline solids (Scheme 4). Evidently, addition of both hard and soft nucleophiles to **A** results in activation and cleavage of the $C_\beta-F$ bond.

However, treatment of **D** and **F** with nucleophiles, both soft (thiols, phosphanes) and hard (methanol, primary and secondary amines), in dichloromethane produced no reac-

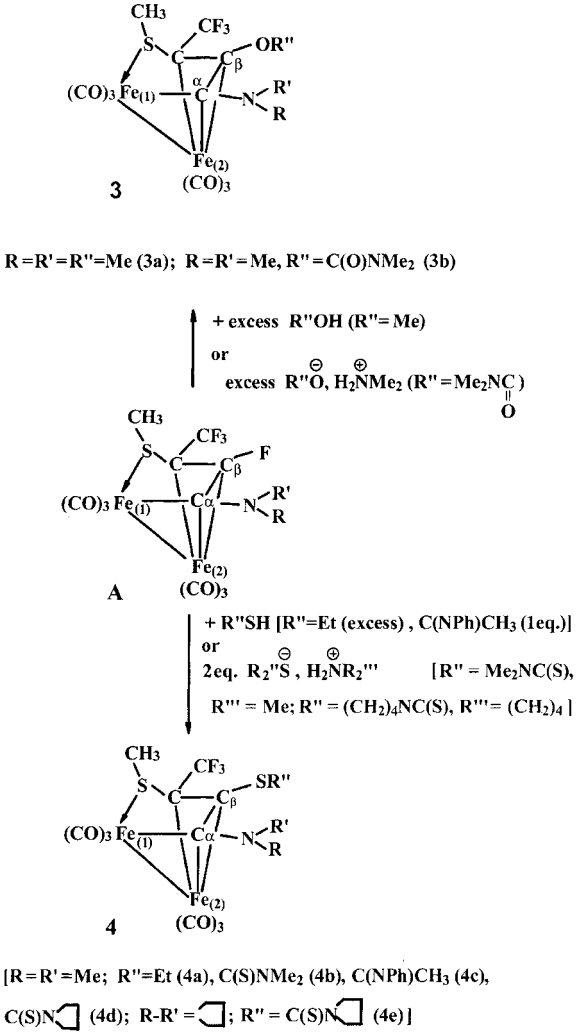

Scheme 4. Synthesis and proposed structures of complexes **3**−**4**

tion (Scheme 5). It thus appears that the vinylic C−F bond is unreactive towards nucleophiles when the fluorine atom is bound to C_α of a *mono*fluorothiaferracyclopentadiene derivative.

It is clearly apparent from the NMR spectroscopic data in Table 1 that the product compounds **3** have the same basic structure as their parent complex **A**. The ^{19}F and ^{13}C NMR spectra are consistent with the formation of **3** from **A** by rupture of the C_β−F bond and replacement of the fluorine atom by an alkoxy group. The $^{13}C\{^1H\}$ NMR spectra contain quadruplets indicative of coupling to a CF_3 group at δ = 189.1 (**3a**) and 198.6 (**3b**); these chemical shifts and the very small $^{13}C-^{19}F$ coupling constant, $^4J_{C,F}$ = 2 Hz, are consistent with the carbon atom responsible being positioned α to Fe(1) in the Fe(1)$C_\alpha C_\beta C_\gamma(CF_3)$S(Me) ring. The assignments of the other quaternary carbon atoms of the thiaferracyclopentadiene ring were then made on the basis of their observed $^{13}C-^{19}F$ coupling constants and chemical shifts. In the highfield regions of **3a** and **3b**, quadruplets at δ = 54.0 ($^2J_{C,F}$ = 34 Hz) and 51.9 ($^2J_{C,F}$ = 35 Hz) were found for the carbon atoms of the $C(CF_3)$ unit. The singlet resonances at δ = 122.5 (**3a**) and 102.0 (**3b**) are attributable to C_β, since a similar chemical shift was observed for the C_β atom (δ = 120.0) in the parent complex **A**. Signals due to the methoxide group were observed at δ = 59.9 in the ^{13}C NMR spectrum and δ = 3.66 in the ^1H NMR spectrum of **3a**. A lowfield resonance at δ = 154.7 in the ^{13}C NMR spectrum of **3b** was assigned to the carbonyl group of the dimethylcarbamoyl unit; the medium band at $\tilde{\nu}$ = 1725 cm^{-1} in the IR spectrum of **3b** is consistent with this attribution.

All compounds **4** may easily be identified from their mass and NMR spectra and elemental analyses. The upper parts of their mass spectra are characterised by the molecular ion peak $[M]^+$ and ion peaks of the sequence $[M^+ - nCO]$ (n = 1−6). The close similarities between the NMR spectra of **4** and those of complex **F**[4c] (Table 1) strongly suggest that all six compounds contain the same Fe(1)C(X)C(SR)$C(CF_3)$S(Me) ring (X = F or NRR′) π-bonded to an $Fe(CO)_3$. It is worth noting that in the ^{13}C NMR spectra the signals of the β-carbon atoms of the thiolato complexes **4** appeared at higher field ($\Delta\bar{\delta}$ = 37) than the corresponding signals from the alkoxo compounds **3**. This highfield shift is consistent with linkage of C_β to the "soft" polarizable sulfur atom rather than the "hard" oxygen nucleophile. In the lowfield part of the $^{13}C\{^1H\}$ NMR spectra of **4b**, **4d** and **4e**, resonances typical of the thiocarbamate groups occur at δ = 197.3, 192.6 and 194.9, respectively.

Single-Crystal X-ray Analysis of 3b

The solid-state structure of **3b** (Table 2, Figure 4) fully confirms the conclusions drawn from the solution spectra and is qualitatively similar to that of the parent complex **A**[4a] in that it contains a metallated, butadiene-like Fe(1)=C_α(11)−C_β(10)=C_γ(8) unit π-bonded to Fe(2), the Fe(2)−C_α bond being especially weak. However, as in the parent complex, there is extensive electron delocalization along the Fe(1)=C_α−C_β=C_γ chain, as shown by the sequence of distances [2.000(6), 1.415(8) and 1.431(8)/1.997(6), 1.428(8) and 1.469(8) Å] in the two independent molecules. The Fe(1)−C_α bonds in **3b** are the longest in Table 2, suggesting that C_α here has only a small amount of carbene-like character;[4b,4c,7] this is consistent with the comparatively highfield resonance (δ = 198.6) attributable to this carbon atom in the $^{13}C\{^1H\}$ NMR spectrum. The $C_\alpha-C_\beta-C_\gamma-C_\delta$ torsion angles in **3b** [−171.0(6) and −168.9(6)°] are typical of the values in thiaferracyclopentadiene complexes and contrast with that in **2a** [−43.9(3)°], which presumably resembles the value in the parent complex **1.**

3. Reactions between Compound 1 and Primary Aromatic and Multifunctional Amines

Synthesis of Complexes 5

We have shown that C−F bonds in **1** can be activated by primary[4a] and secondary[4b] monoamines, which have similar basicities according to Pearson.[5] These reactions

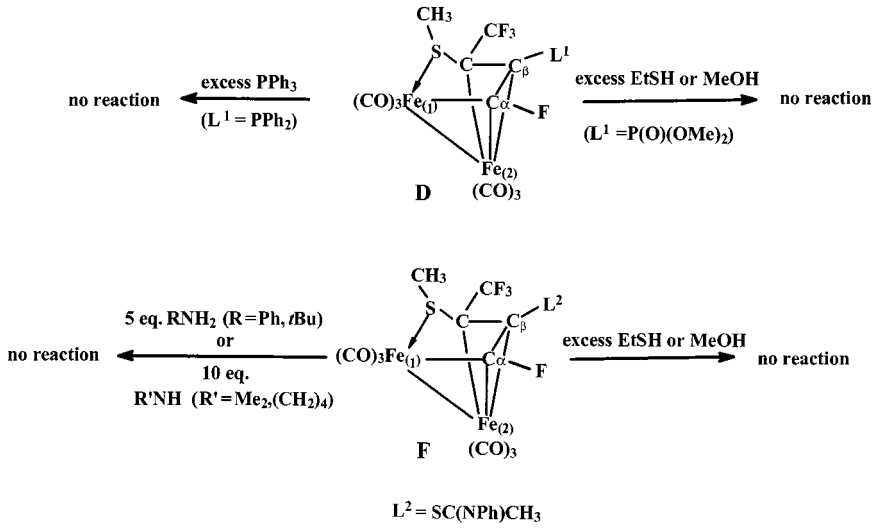

Scheme 5. Reaction of **D** and **F** species with nucleophiles

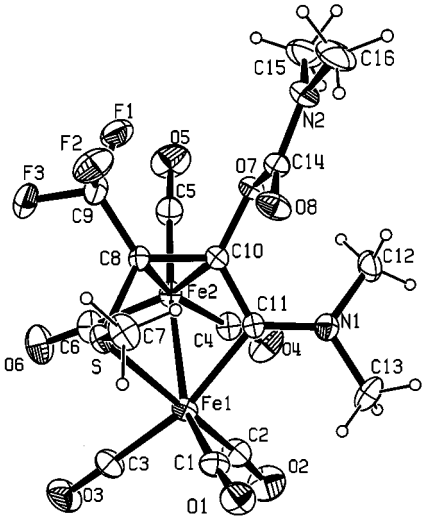

Figure 4. The structure of one of the two independent molecules of **3b** in the crystal; throughout this paper a common atom numbering system has been used for crystallographically independent molecules; selected bond lengths [Å] and angles [°]: O(7)−C(14) 1.369(8)/1.377(7), O(7)−C(10) 1.418(7)/1.405(6), O(8)−C(14) 1.217(8)/1.198(7), N(1)−C(11) 1.356(8)/1.345(7), N(1)−C(13) 1.448(8)/1.450(9), N(1)−C(12) 1.477(9)/1.478(8), N(2)−C(14) 1.332(9)/1.341(8), N(2)−C(15) 1.469(11)/1.441(9), N(2)−C(16) 1.462(10)/1.453(9); C(14)−O(7)−C(10)−C(11) 80.3(8)/75.2(8), C(12)−N(1)−C(11)−C(10) 20.8(10)/19.0(9), C(11)−C(10)−C(8)−C(9) −171.0(6)/−168.9(6)

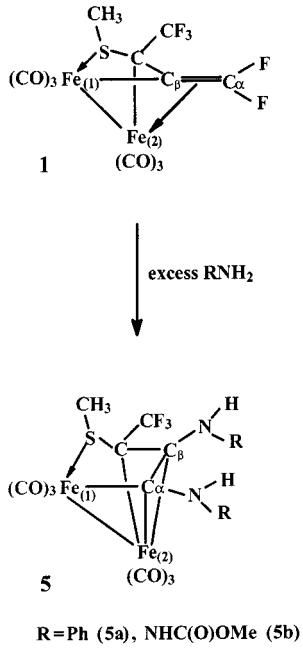

Scheme 6. Synthesis and proposed structures of complexes **5b**

give rise to substitution patterns that markedly depend on the strength of the attacking nucleophile in the carbon chain of the complex. We therefore decided to investigate the reaction between **1** and both aniline, a base of medium strength according to Pearson,[5] and also (methoxycarbonyl)hydrazine, $H_2NNHC(=O)OMe$, which contains potentially competitive primary and secondary amine functions. Compound **1** was treated with excess quantities (3−4 equiv.) of either aniline or (methoxycarbonyl)hydrazine in dichloromethane at room temperature. The α,β adducts **5a** and **5b** were formed as orange, microcrystalline solids in high yields (Scheme 6).

Elemental analysis, together with mass and NMR spectroscopy, indicated that the reaction of **1** with (methoxycarbonyl)hydrazine paralleled that with aniline. Both reactions gave thiaferracyclopentadiene products of the type $[\{Fe(CO)_3\}_2\{\mu\text{-}C(SMe)(CF_3)C(NHR)C(NHR)\}]$. Thus, in these reactions the (methoxycarbonyl)hydrazine behaves as a primary amine.

Single-crystal X-ray Analyses of Compounds 5a and 5b

The structures of **5a** and **5b** (Figures 5 and 6, Table 2) are based on an $Fe(1)S(1)C_\gamma C_\beta C_\alpha$ thiaferracyclopentadiene ring. The butadiene-like $Fe(1)=C_\alpha-C_\beta=C_\gamma$ unit π-bonds to

the $Fe(2)(CO)_3$ group. The bridging organic group is thus derived formally from the vinylic ligand in **1** through the loss of two fluorine atoms from C_α and the addition of a single NHR group to both C_α and C_β. Several diiron complexes containing the same $[\{(OC)_3Fe(1)S(Me)C_\gamma(CF_3)C_\beta(R^2)C_\alpha(R^1)\}Fe(2)(CO)_3]$ skeleton have now been characterised; they include **3b**, **6a**, and $[\{Fe(CO)_3\}_2\{\mu\text{-}C(SMe)(CF_3)C(PPh_2)CF\}]$ (**D**),[4c] as well as **5a** and **5b**. Some structural features characteristic of this group (see Table 2) are worth noting:

(a) The $Fe(1)S(Me)C_\gamma(CF_3)C_\beta C_\alpha$ rings are distorted envelopes with S at the flap, the S−Me bond axial, and the $C-CF_3$ bond equatorial, so that the $C_\alpha-C_\beta-C_\gamma-CF_3$ torsion angle is close to 180° (range 169−176°).

(b) Where possible, conjugation is maximised across $C_\alpha-R^1$ but minimised across $C_\beta-R^2$; in **5a**, for example, the C−C−N−Ph torsion angles are close to 180° across C7−N1, permitting π-overlap, but close to 90° across C8−N2, precluding it. This is consistent with the shortness of the C7−N1 bonds (1.35 Å) compared those across C8−N2 (1.41 Å). It can be argued that similar effects operate in **3b** and **5b**.

(c) Corresponding bond lengths are remarkably constant, except for the $Fe(1)-C_\alpha$ and $Fe(2)-C_\alpha$ distances (Table 2). Both of these bonds shorten as the substituent at C_α becomes more electron-withdrawing along the series NMe_2 (**3b**) < NHPh (**5a**) < $NHNHCO_2Me$ (**5b**) < $N(NH_2)R$ (**6a**) < F [**D**: $Fe(1)-C_\alpha$ = 1.918(3), $Fe(2)-C_\alpha$ = 2.073(3) Å]. The weak $Fe(2)-C_\alpha$ bonds shorten by 0.28 Å across this series. This can be explained in terms of the occurrence of two alternative structures, shown for **5a** in Scheme 7. Electron release by the substituent at C_α should stabilise the zwitterionic form **II** at the expense of the thiaferracyclopentadiene structure **I**, weakening $Fe(2)-C_\alpha$ but also discouraging $Fe(1)\rightarrow C_\alpha$ back-donation.

The structural features of the recently reported σ-η^3-allylic complex $[\{Fe(CO)_3\}(\mu\text{-}PPh_2)\{\mu\text{-}\eta^1(P):\eta^3(C)\text{-}(C)(Ph)C(Ph)C(H)C(=CH_2)PPh_2\}]$[11] are similar to those of the compounds discussed here.

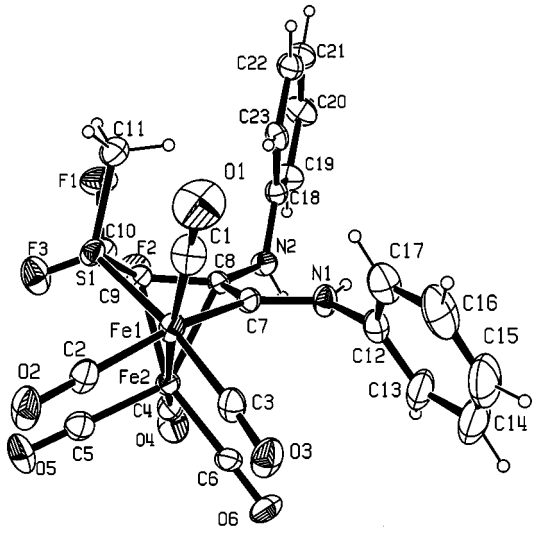

Figure 5. Molecular structure and numbering scheme of compound **5a** in the crystal; only one of the two independent molecules is shown; selected bond lengths [Å] and angles [°]: N(1)−C(7) 1.353(6)/1.353(6), N(1)−C(12) 1.420(8)/1.421(7), N(2)−C(18) 1.407(7)/1.412(6), N(2)−C(8) 1.443(6)/1.422(6), C(7)−C(8)−N(2)−C(18) −82.6(6)/−97.0(6), C(8)−C(7)−N(1)−C(12) −175.8(5)/− 172.1(6), C(7)−C(8)−C(9)−C(10) 172.2(5)/172.1(5)

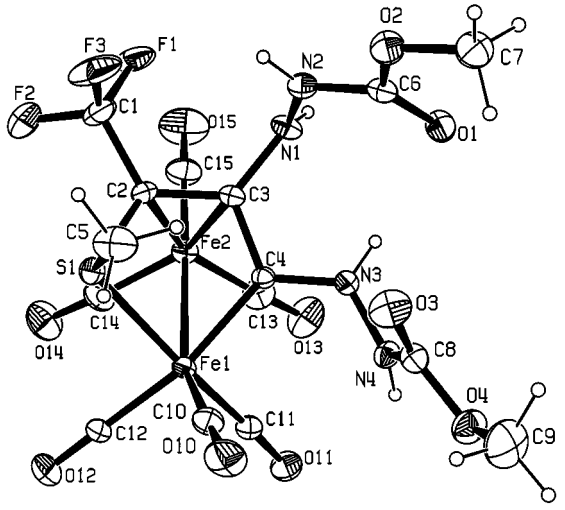

Figure 6. Molecular structure and numbering scheme of compound **5b** in the crystal; only one of the two independent molecules is shown; selected bond lengths [Å] and angles [°]: O(1)−C(6) 1.204(7)/1.202(7), O(2)−C(6) 1.336(7)/1.338(7), O(2)−C(7) 1.451(9)/1.429(9), O(3)−C(8) 1.197(8)/1.197(8), O(4)−C(8) 1.319(8)/1.349(8), O(4)−C(9) 1.447(11)/1.437(11), N(1)−N(2) 1.411(7)/1.405(8), N(1)−C(3) 1.440(7)/1.435(7), N(2)−C(6) 1.348(8)/1.351(9), N(3)−C(4) 1.370(7)/1.365(7), N(3)−N(4) 1.388(7)/1.383(7), N(4)−C(8) 1.371(8)/1.361(8); C(4)−C(3)−N(1)−N(2) −90.0(6)/−86.3(7), C(3)−C(4)−N(3)−N(4) 164.9(5)/168.0(5), C(4)−C(3)−C(2)−C(1) 173.2(6)/171.5(6)

Spectroscopic Characterisation of Complexes 5 and Mechanistic Considerations

The solid-state structures of **5a** and **5b** have definitively been shown to persist in solution by IR and NMR spectroscopy (see Table 1 and Exp. Sect.). The IR spectra in CH_2Cl_2 show four ν(CO) bands in the 2075−1950 cm^{-1} range, corresponding to the Fe-bound terminal carbonyl groups, along with a characteristic band at 1720 cm^{-1} (**5b**), which confirms the presence of the $NHNHC(O)OCH_3$ group. The ^{19}F and ^{13}C NMR spectra are also consistent with the structures proposed for **5a** and **5b**. In particular, the ^{19}F NMR spectra of **5a** and **5b** no longer contain the vinylic CF resonances typical of **1**, but do retain the peaks due to the CF_3 group. In the $^{13}C\{^1H\}$ NMR spectra, the quadruplets assigned to the metallated carbon atoms (C_α) appear at δ = 202.0 (**5a**) and 210.7 (**5b**), with C−F coupling constants (^4J) of about 2 Hz. These resonances are shifted to high field relative to that seen for the closely related phosphanyl complex $[\{Fe(CO)_3\}_2\{\mu\text{-}C_\alpha(F)C_\beta(PPh_2)\text{-}C_\gamma(CF_3)S(CH_3)\}]$ (**D**),[4c] indicating that C_α possesses a less carbene-like character in **5a** and **5b** than in the phosphanyl complex, in conformity with the trends in $Fe-C_\alpha$ bond lengths discussed in the preceding section. Atom C_β gives rise to singlets at δ = 91.6 for **5a** and δ = 93.5 for **5b**, and atom C_γ to quadruplets at δ = 53.4 for **5a** and δ = 52.5 for

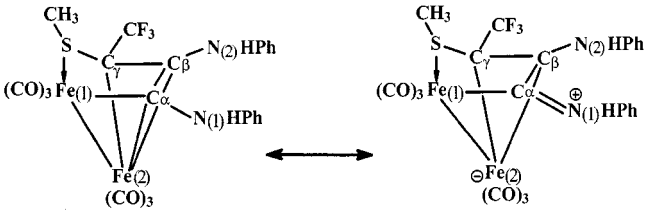

Scheme 7

5b, with C−F coupling constants (^2J) of about 33 Hz. The ^{1}H NMR spectra show lowfield resonances at δ = 8.50 (**5a**) and 9.46 (**5b**), characteristic of iminium protons, along with peaks at δ = 4.60 (**5a**) and 4.64 (**5b**), corresponding to the amino protons. In addition, the ^{1}H NMR spectrum of **5b** contains two broad singlets at δ = 6.55 and 6.85, attributable to the amino protons α to the methoxycarbonyl group. Thus, the ^{1}H NMR spectroscopic data clearly indicate that there is an iminium group at $C_α$ but an amino group at $C_β$ in **5a** and **5b**; in solution it is possible that there is an increased contribution from **II** to the overall structure (Scheme 7).

The reactions producing **5a** and **5b** were carried out at low temperature in order to detect possible intermediates. In the event, only one intermediate was found when either aniline or methyl hydrazinocarboxylate reacted with **1**. The reaction between **1** and aliphatic amines[4d] involves the initial formation of a stable fluoro−zwitterionic intermediate [**B**] (see Scheme 1). However, when **1** reacts with excess aniline (3 equiv.) or methyl hydrazinocarboxylate (4 equiv.), instead of [**B**] the only intermediate detected was the doubly substituted species [**f**] (Scheme 8). After 5 h, the relative amounts of [**f**], **1** and **5** were 47, 29 and 24%, respectively. The ^{19}F and ^{13}C{^{1}H} patterns of [**f**] are similar to those of neutral (alkoxymethylene)thiaferracyclobutene compounds (such as **2a**, **2b**; see Table 1) and to those of zwitterionic (diaminomethylene)thiaferracyclobutene derivatives such as **C**. Now, these species are mainly differentiated from one another by the $C_β$ atom resonances, which occur at δ = 70.0−90.0 for the zwitterionic complexes and at δ = 115.0−130.0 for neutral species (see Table 1). In view of this, a zwitterionic structure is proposed for [**f**], which has a chemical shift of δ = 95.6 for the $C_β$ atom (Scheme 8). Conversion of **f** into the final product requires the transfer of one amido group from $C_α$ to $C_β$. This probably occurs through a double intramolecular migration, from $C_α$ to the metal ion and from there to $C_β$, as postulated in Scheme 8.

4. Reactions between Compound 1 and Multifunctional Thioamines

Synthesis and Characterisation of Complexes 6

In the preceding section it was shown that methoxycarbonylhydrazine, although it contains three "hard" and potentially competitive base functions (carbonyl, primary amine and secondary amine), acts only as a primary amine to cleave both C−F bonds of **1**. We speculated that the choice of the nucleophile might be pivotal to the regiochemistry of the C−F activation. We therefore treated **1** with three thioamines containing competitive "hard" amine and "soft" thione functions, namely, MeNHC(S)NHR, R = NH_2, H and Me.

Treatment of **1** with equimolar amounts of 4-methyl-3-thiosemicarbazide in tetrahydrofuran at room temperature resulted in the formation, in high yields, of the N-α,S-β adduct **6a** (Scheme 9). Similar results were obtained with methyl- and dimethylthioureas; complexes **6b** and **6c** were isolated as orange powders (Scheme 9). All the complexes have been characterised by ^{1}H NMR, ^{19}F NMR, ^{13}C NMR and IR spectroscopy and by mass spectrometry and microanalysis (see Table 1 and Exp. Sect.) and, in addition, complex **6a** has been the subject of a single-crystal X-ray diffraction study.

It is immediately apparent from examination of the spectroscopic data that all the complexes **6** have the same basic structure. The close similarity of their ^{13}C NMR spectra with those of compounds **4** (see Table 1) strongly suggests that **4** and **6** contain similar five-membered rings [$FeC_α(NR)C_β(SR)C(CF_3)S(CH_3)$]. The ^{19}F NMR spectra showed only single trifluoromethyl resonances at δ ≈ − 59.0, confirming that the two vinylic C−F bonds had been cleaved. The ^{1}H NMR spectrum of **6a** displayed three singlets in a 2:3:3 ratio, two at δ = 4.67 and 3.18 corresponding to the amino[12] and the methylimino[13] groups, respectively, and the more upfield line (δ = 1.87) to the SMe ligand.[4d] The ^{1}H NMR spectrum of **6b** differs from that of **6c** only by the presence, in a 1:3 ratio, of a lowfield signal at δ = 7.59 for the C=NH imino group in **6b** versus a higher field peak at δ = 3.15 assignable to the methylimino function in **6c**.[14] Otherwise, complexes **6b** and **6c** showed similar ^{1}H NMR patterns, in particular they displayed two signals at δ ≈ 3.7 and 1.9, which were assigned to the methylamino[14] and SMe[4d] groups, respectively. The ^{1}H NMR spectroscopic data clearly indicated the presence in **6** of a $R^1NC(=NR^2)S$ unit (R^1 = NH_2 or CH_3, and R^2 = H or CH_3) derived from the parent thioamine, as depicted in Scheme 9. This was confirmed by the ^{13}C NMR spectra, in which typical C=N resonances were observed at δ ≈ 160, and by the IR spectra in which strong C=N stretching bands were seen at ca. 1625 cm^{-1}. To complete the characterisation, an X-ray diffraction study of **6a** was undertaken.

The structure of **6a** (Figure 7) is derived from **1** through the loss of two fluorine atoms from $C_α$; a new ring is formed by attachment of a hard N-donor function of the thioamide to $C_α$ and of the softer thione S atom to $C_β$. As in **3** and **5**, the Fe(1) atom is now bound to $C_α$, completing a $Fe(1)C_αC_βC(CF_3)S(CH_3)$ metallacycle. The short Fe(1)−$C_α$ bonds [1.947(7) and 1.936(7) Å] imply that $C_α$ has some carbene-like character,[4b,4c,7] and this conclusion is confirmed by the highfield resonance (δ = 205.3) attributable to this carbon atom in the ^{13}C{^{1}H} NMR spectrum. The C(4)N(1)C(5)S(2)C(3) heterocycle formed by coupling

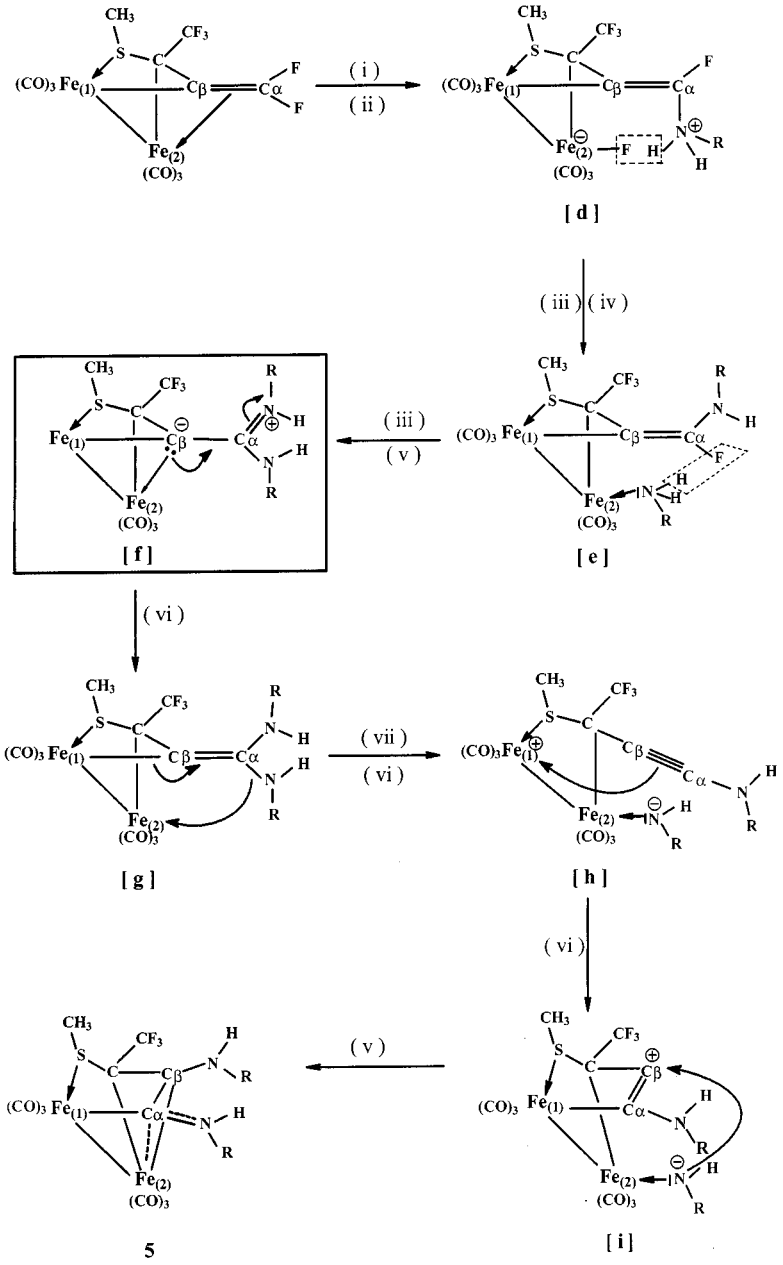

Scheme 8. Possible pathway to the formation of diaminothiaferracyclopentadiene derivatives **5**: (i) α-elimination of F; (ii) nucleophilic attack of RNH_2 at C_α; (iii) − HF; (iv) + RNH_2; (v) amino migration; (vi) internal rearrangement; (vii) α-elimination of NHR

of the 4-methyl-3-thiosemicarbazide to the coordinated $CCC(CF_3)SMe$ ligand is coplanar within ±0.03Å. The shortness of the C(5)−N(3) bonds [1.268(8) and 1.242(8) Å] compared to the C(13)−N(3) distances [1.471(9) and 1.469(9) Å] is consistent with the presence of a localised C(5)=N(3) double bond. The S(2)−C bond lengths (Figure 7, caption) suggest bonds of unit order, while the C_α−N(1) distances [1.382(8) and 1.361(8) Å], though longer than corresponding bonds in **5a** or **5b**, imply some multiple character.

Similar structural examples of diiron or diruthenium thiametallacyclic μ-C(R)C(R)C(R)S(R′) or phosphametallacyclic μ-C(R)C(R)C(R)P(R′)$_2$ ligands include [{$Fe(CO)_3$}$_2$-{μ-C(OEt)C(H)C(Ph)S(*t*Bu)}] (**I**)[15], [{$Fe(CO)_3$}$_2$(μ-C(Ph)-C(R)C(R′)P(Ph)$_2$}] (**J**)[16], [{$Ru_2(CO)_5X_2$}{μ-C(C_2H_5)-C(R)C(R′)S(C_2H_5)} (**K**)[17], as well as the complexes **3**−**5** and **A**, **D**−**F** that we have described previously.[4] The conformations of the μ-C(R)−C(R)−C(R)−X′(R_n) ligands [X′ = S (n = 1), P (n = 2)] in the complexes described by other authors[15−17] are very similar to those we have found in **6** and its close relatives.

Although two isomers, **6a$_1$** and **6a$_2$** (Scheme 10), could result from the reaction between 4-methyl-3-thiosemicarbazide and **1**, depending on whether the $NH(NH_2)$ or NHMe secondary amine function attacked the C_α atom, only one isomer is actually observed.

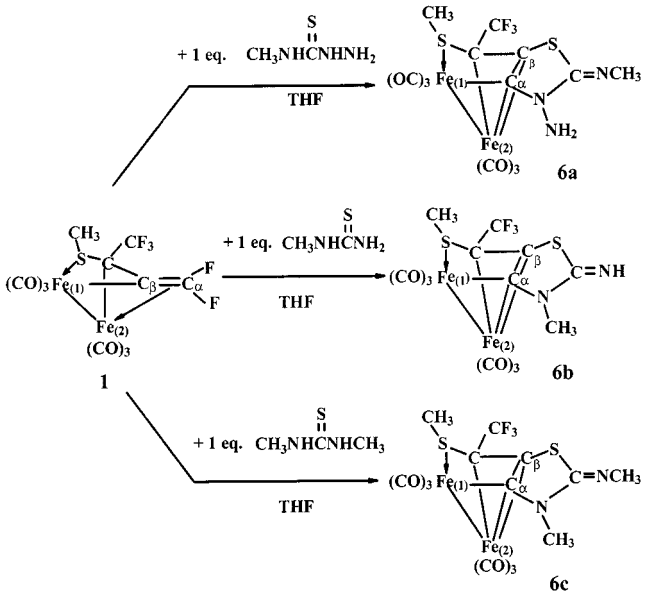

Scheme 9. Synthesis and proposed structures of complexes **6**

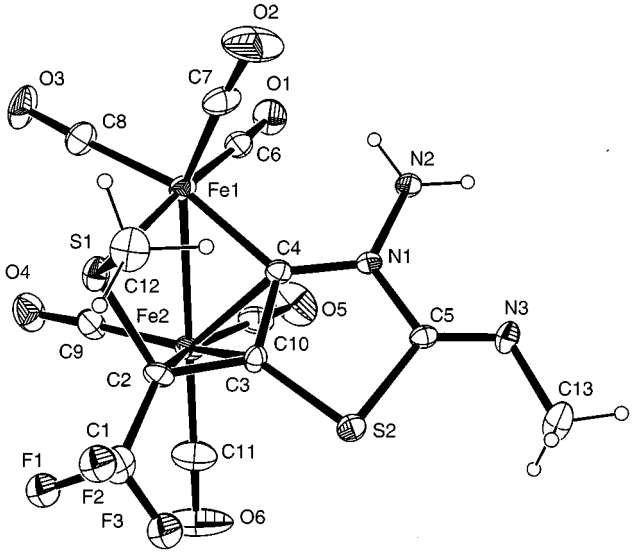

Figure 7. Molecular structure and numbering scheme of compound **6a** in the crystal; only one of the two independent molecules is shown; selected bond lengths [Å] and angles[°]: S(2)−C(3) 1.768(7)/1.762(7), S(2)−C(5) 1.776(7)/1.785(7), N(1)−C(4) 1.382(8)/1.361(8), N(1)−N(2) 1.397(7)/1.404(7), N(1)−C(5) 1.399(8)/1.407(8), N(3)−C(5) 1.268(8)/1.242(8), N(3)−C(13) 1.471(9)/1.469(9); C(4)−C(3)−C(2)−C(1) −176.3(7)/−175.9(7)

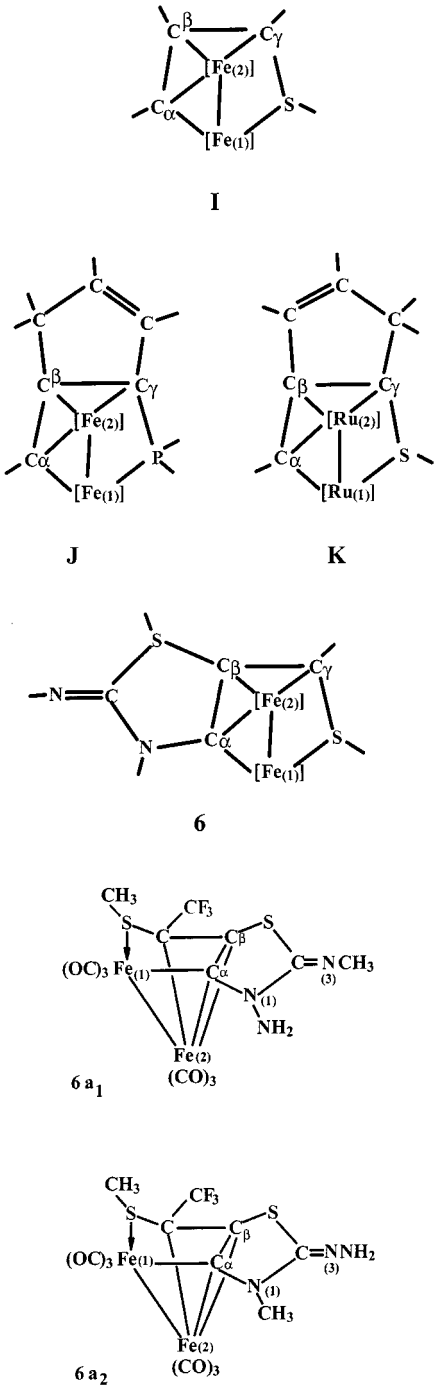

Scheme 10

The crystallographic study favours structure **6a$_1$**, but supporting evidence is desirable at this point, since **6a$_1$** and **6a$_2$** differ only in the positions of isoelectronic CH_3 and NH_2 groups. Accordingly, a ^{1}H-^{13}C 2D HMBC experiment was performed at room temperature. The carbon atom (δ = 159.4) of the imino group correlated ($^3J_{CH}$) with the hydrogen atoms of the methyl group (δ = 3.18), whereas the C_α atom (δ = 184.0) showed a correlation ($^3J_{CH}$) with the low-field resonance (δ = 4.61) due to the protons of the NH_2 group. This coupling pattern clearly showed that the amino group was attached to the nitrogen atom [N(1)], which was bound to C_α (**6a$_1$**). Similar experiments were undertaken for **6b** and revealed that the methyl group (δ = 3.71) correlated ($^3J_{CH}$) with both C_α (δ = 183.2) and the carbon atom of the imino group (δ = 166.0), thereby confirming the structure depicted in Scheme 9.

Mechanistic Considerations

It is likely that similar mechanisms are involved in the formation of **6a**−**6c**, and so we shall give only an illustrative

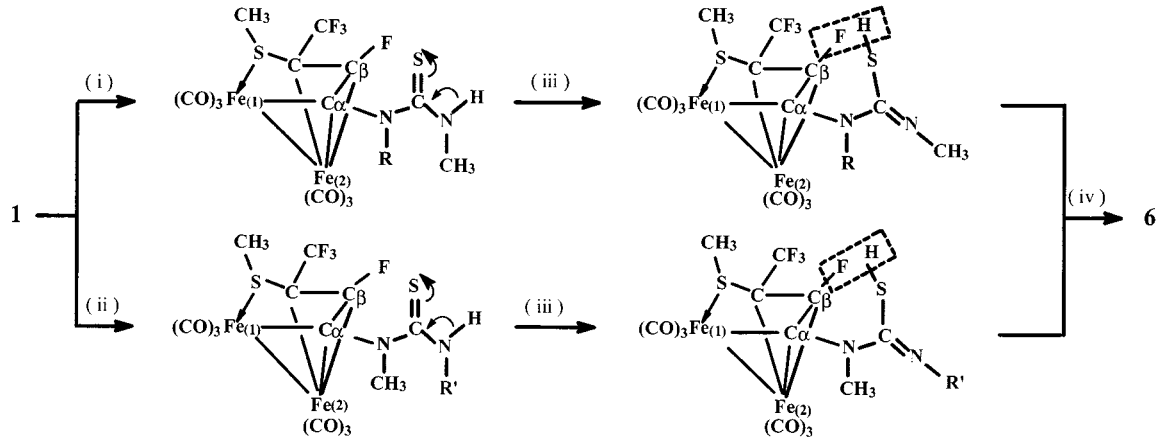

Scheme 11. Possible pathway to the formation of aminothiothiaferracyclopentadiene derivatives **6**: (i) nucleophilic attack of $CH_3-NH-C(S)-NHR$ at C_α; (ii) nucleophilic attack of $CH_3-NH-C(S)-NHR'$ (R′ = H, CH_3) at C_α; (iii) tautomerisation reaction; (iv) HF elimination

discussion of the pathway to **6a** (Scheme 11). Investigation of the reaction between **1** and 1 equiv. of thiosemicarbazide by NMR spectroscopy at low temperature did not result in the characterisation of any intermediate. However, the formation of **6a** is likely to resemble the well-established processes that produce the related thiaferracyclopentadiene derivatives of types **A**[4d] and **F**.[4c] Compound **6a** has some features in common with **A** and **F**, and all three complex types are obtained from the same parent compound **1**. The NH_2 function is preserved unchanged in **6a**, while the secondary amine and thiol functions of the thiosemicarbazide bind to the C_α and C_β atoms of **1**, respectively. If the thiol function initiated the attack, the expected product would be a ferracyclopentadiene intermediate of type **F**,[4c] which we have shown to be totally unreactive towards nucleophiles in Section 2 above. It is more likely then that **1** first reacts through a secondary amine function of the thiosemicarbazide to form a thiaferracyclopentadiene adduct of type **A**,[4d] which, as shown in Section 2, can give rise to intramolecular $C_\beta-F$ activation through a thione function tautomer of the coordinated 4-methyl-3-thiosemicarbazide, ultimately to afford complex **6a** (Scheme 11). A similar pathway to **6b** and **6c** is also summarized in Scheme 11. The main feature of these reactions is the successive activation of two C−F bonds by a nucleophile with both "hard" and "soft" functional groups, resulting in the formation of a five-membered heteroorganic ring fused to the cycloferrathiopentadiene unit.

5. Reactions between Compound 1 and Multifunctional Amides

Reaction between Compound 1 and Acetylhydrazine: Synthesis and Characterisation of Complex 7a

Since the perfluorovinyl complex **1** reacts with thioamides containing both "hard" and "soft" nucleophilic functions to give **6**, we also decided to investigate the behaviour of **1** toward multifunctional reagents containing only "hard" nucleophilic groups. On treatment of **1** with 3 equiv. of acetylhydrazine in CH_2Cl_2 at room temperature, the α,β adduct **7a** was formed (Scheme 12). It was isolated as red solid in 98% yield and has been characterised by ^1H NMR, ^{19}F NMR, ^{13}C NMR and IR spectroscopy and by mass spectrometry and microanalysis (see Table 1 and Exp. Sect.), as well as by a single-crystal X-ray diffraction study.

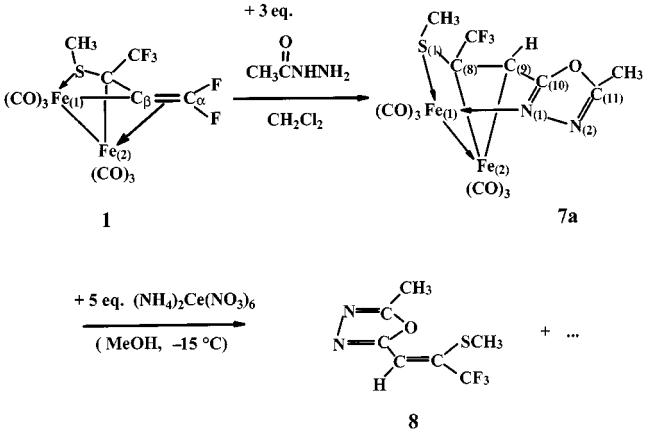

Scheme 12. Synthesis and proposed structures of compounds **7a** and **8**

Though the nucleophiles involved in the formation of **6a** and of **7a** are exact analogues, the molecular structure of **7a** (Figure 8, Table 2) is novel, differing significantly from that of **6a**. It consists of a dinuclear $Fe_2(CO)_6$ unit stabilized by an Fe−Fe bond and by a bridging organic group. This is derived *formally* from the vinylic ligand in **1** through the substitution of two fluorine atoms at C_α by O and N atoms of the deprotonated nucleophile and protonation of C_β. The result is a *six*-membered $Fe(1)-N(1)=C_\alpha(10)-C_\beta(9)=C(8)-S(1)$ metallacycle. There is extensive electron delocalization along the $Fe(1)-N(1)-C(10)-C(9)-C(8)$ chains, as shown by the bond length sequences [1.974(2), 1.288(3), 1.440(4) and 1.455(4) Å in molecule I and 1.964(2), 1.297(3), 1.424(4) and 1.463(4) Å in molecule II]. The

$Fe(2)(CO)_3$ unit is attached to the metallacycle through a π-interaction with the C(9)−C(8) double bond and through a direct bond to Fe(1). The Fe(1)−Fe(2) distances are long [2.794(1) and 2.799(1) Å], not unexpectedly since Fe(2) bridges across the six-membered Fe(1)-metalla ligand; shorter Fe−Fe distances of 2.591(1) and 2.643(1) Å are found in $[\{Fe(CO)_3\}_2\{\mu\text{-}S(Me)C(CF_3)C(CN\textit{t}Bu)\}]$ and $[\{Fe(CO)_3\}_2\{\mu\text{-}S(Me)C(CF_3)C(F)C(NMe_2)\}]$,[4a] in which the second $Fe(CO)_3$ group is attached to four- and five-membered ferracyclic bridging groups, respectively.

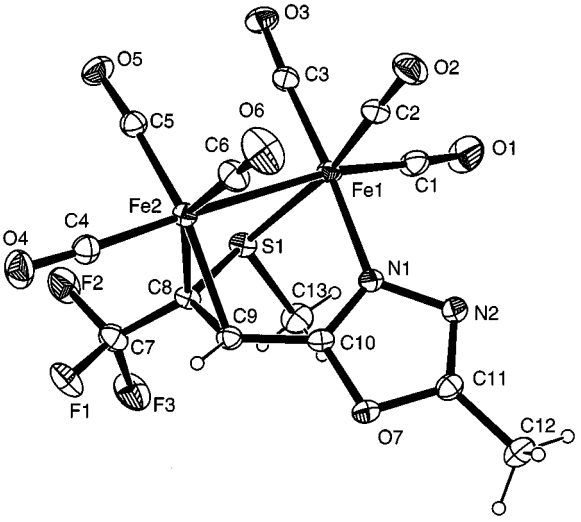

Figure 8. Molecular structure and numbering scheme of compound **7a** in the crystal; only one of the two independent molecules is shown; selected bond lengths [Å] and angles [°]: O(7)−C(10) 1.351(3)/1.359(3), O(7)−C(11) 1.368(3)/1.377(3), N(1)−C(10) 1.288(3)/1.297(3), N(1)−N(2) 1.401(3)/1.403(3), N(2)−C(11) 1.290(4)/1.282(4); C(4)−C(3)−C(2)−C(1) 140.3(3)/142.4(3)

Compound **7a** contains a planar 1,3,4-oxadiazole ring formed by cyclisation of the amide nucleophile with the vinylic C_α carbon atom of **1**. The shortness of the C(10)−N(1) and C(11)−N(2) bonds [1.282(4)−1.297(3) Å] indicates some multiple character.

The solution spectra of **7a** are consistent with the solid-state structure. Four strong to medium IR bands between 2072 and 1950 cm^{-1} can be attributed to carbonyl ν(CO) stretching vibrations. A single highfield signal (δ = −66.65) in the ^{19}F NMR spectrum, typical of a trifluoromethyl resonance, provided the first indication that both C−F bonds in **1** had been cleaved. In the $^{13}C\{^1H\}$NMR spectrum, the carbon atom of the trifluoromethyl group appeared as a quadruplet at δ = 128.6 ($^1J_{C,F}$ = 274 Hz). The assignments of the three carbon atoms of the thiaazaferracyclohexene ring were made on the basis of the observed ^{13}C-^{19}F coupling constants and chemical shifts. The highfield resonances at δ = 44.6 (quadruplet; $^2J_{C-F}$ = 36.5 Hz) and 24.4 (singlet) are attributable to C(8) and C(9). The chemical shifts of these two carbon atoms suggest that they form a $C(sp^3)-C(sp^3)$ single bond rather than a $C(sp^2)=C(sp^2)$ double bond; the C(8)−C(9) distances [1.455(4) and 1.463(4) Å] lie at the upper end of the range for alkenes π-bonded to transition metal ions. The lowfield signals at δ = 175.9 and 163.0 are typical of imino-substituted carbon atoms and are attributable to C(10) and C(11). The carbonyl region contains three singlets at δ = 198.3, 211.1 and 215.6 and three broader singlets at δ = 207.6, 211.0 and 219.4, which correspond to the $Fe(1)(CO)_3$ and $Fe(2)(CO)_3$ fragments, respectively. In the ^1H NMR spectrum there are three singlets at δ = 1.87, 2.49 and 2.86 with intensities in an integral ratio of 3:3:1. The first two resonances can be assigned to the C(12) oxadiazole and S−C(13) methyl groups and the third to the methine proton attached to C(9) of the bridging heteropolycarbon fragment.

Reactions between Compound 7a and Phosphanes and between Compound 7a and Oxidants

An attempt to liberate the bridging heteropolycarbon ligand of **7a** by treatment with an excess of either phosphane (PPh_2Me) or phosphite [$P(OMe)_3$] in CH_2Cl_2 at 60 °C was unsuccessful. However, it resulted in a carbonyl substitution reaction that gave high yields of the complexes $[\{Fe(CO)_2L\}\{\mu S(Me)C(CF_3)CHC_\alpha NNC(CH_3)O(C_\alpha\text{−}O)\}\text{-}\{Fe(CO)_3\}]$ [**7b**: L = PPh_2Me; **7c**: L = $P(OMe)_3$] as red solids. All complexes other than **7a** described in this work showed marked reluctance to undergo carbonyl substitution reactions. Microanalyses of **7b** and **7c** indicated that the two complexes had similar compositions. The mass spectrum of **7c** revealed a single molecular ion peak and fragmentation peaks corresponding to the sequential loss of five carbonyl ligands.

On the basis of the close similarity of their spectroscopic data (see Table 1), structures similar to **7a** are postulated for **7b** and **7c**, with phosphane bound to the iron atom Fe(1) as shown in Scheme 13. The ^{31}P NMR spectra each display only one signal, at δ = 29.12 (**7b**) and at 157.73 (**7c**), corresponding to the terminal PPh_2Me and $P(OMe)_3$ ligands, respectively.[16] The $^{13}C\{^1H\}$ NMR spectra of **7b** and **7c** contain only five distinct resonances in the carbonyl region, two doublets at δ ≈ 215.5 and 220.0, and three broad singlets at δ = 208.2−222.8. The singlets are associated with the $Fe(2)(CO)_3$ group and the two doublets with the carbonyl groups of the $Fe(1)L(CO)_2$ unit. The magnitude of $^2J_{C,P}$ (7.5−2.0 Hz) is consistent with a *cis* arrangement of the phosphane and carbonyl groups. In other respects, the magnitude of the splitting of the methyl resonance of the thiolato group ($^3J_{C,P}$ = 8 and 6.5 Hz) confirms that the phosphane ligand is located at Fe(1) and is *trans* to the SMe

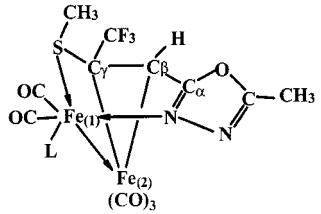

7b (L = PPh_2Me)

7c (L = $P(OMe)_3$)

Scheme 13

groups. The replacement of one carbonyl group in **7a** by an electron-releasing phosphane ligand to give **7b** or **7c** is accompanied by a shift of the resonances of the remaining carbonyl groups attached to Fe(1) to lower field compared with those attached to Fe(2). This observation confirms that the substitution reaction operated at Fe(1).

In a further attempt to decoordinate the bridging heteropolycarbon ligand, **7a** was treated at low temperature with excess ceric salt in methanol. The reaction resulted in the formation of **8** as a white solid in high yields (Scheme 12). The product was fully characterised by mass spectrometry and NMR spectroscopy (see Exp. Sect.). The mass spectrum exhibited a molecular ion, and sequential losses of methyl and oxadiazole fragments. The characterising NMR spectroscopic data of **8** were closely related to those of the parent heteropolycarbon ligand of **7a** and the ^{1}H, ^{19}F and ^{13}C NMR spectra showed the expected pattern of peaks for a 2-methyl-5-(3,3,3-trifluoro-2-methylthio-2-propenyl)-1,3,4-oxadiazole compound. Though unsubstituted and 2,5-dialkyl-1,3,4-oxadiazoles have long been known,[17] compound **8** has not previously been reported.

Conclusion

These investigations have shown that the (perfluorovinyl)-diiron complex [{$Fe(CO)_3$}$_2${μ-C(SMe)(CF_3)$C_\beta C_\alpha F_2$}] (**1**) reacts readily and cleanly with nucleophiles to give novel organometallic compounds through unusual C−F cleavage processes. This work confirms and extends our previous conclusion[4] that the pattern of reactivity depends strongly on the "hardness" or softness" of the nucleophile used in the reactions. Reactions between **1** and "hard" amines involve two C−F cleavages and migration of a fluorine atom from C_α to C_β to give exclusively α adducts with formation of Fe(1)−C_α(NR_2)−C_β(F)−C(CF_3)−S(Me) rings,[4d] while nucleophiles such as alcohol and aniline, thought to be less hard than aliphatic amines, afford either μ_2-η^1:η^2-vinyl complexes, [{Fe $(CO)_3$}$_2${μ-C(SMe)(CF_3)$C_\beta C_\alpha$($OR)_2$}] (**2**), or α,β adducts **5**, containing Fe(1)−C_α(NHR)−C_β-(NHR)−C(CF_3)−S(Me) rings. X-ray analysis of **2a** (R = Me) indicates that the μ_2-η^1:η^2-vinyl ligand [C(SMe)(CF_3)$C_\alpha C_\beta F_2$] present in **1** is maintained in **2** in the form of a dialkoxyvinyl ligand [C(SMe)(CF_3)$C_\beta C_\alpha$($OR)_2$], whereas X-ray analysis of **5** (R = Ph) demonstrates the transformation of the ligand in **1** into a new polycarbon [C(SMe)(CF_3)C_β(NHR)C_α(NHR)] chain by the action of aniline. The mechanisms proposed to account for the formation of complexes **2** and **5** both imply a double C−F bond cleavage. When **1** reacts with a thioamide containing three "hard" primary and secondary amine functions and one "soft" thiol function, the nucleophile attacks first at C_α with its secondary amine, while its primary amine function takes no part in the reaction. In a second step, the thiol function of the nucleophile attacks at C_β to give α,β adducts **6**, each containing a novel iminothiazolidine ring [C(SMe)(CF_3)C_βSC(=NR)N(R′)C_α(C_β−C_α)] fused to the five-membered metallacycle. Formation of the imino-thiazolidine ligand in **6** implies C−N and C−S couplings. When the nucleophile reacting with **1** contains only "hard" functions, namely a primary and secondary amine and a carbonyl group, the reaction involves attack by the primary amine and the carbonyl functions at C_α; two C−F bond cleavages and a 1,3-hydrogen shift from the nitrogen atom to the β-carbon atom of the vinyl ligand gives **7**. Compound **7** contains a thiaazaferracyclohexene ring to which is fused an oxadiazole fragment formed through a cyclisation reaction. Finally, it should be remarked that, while β-fluoro substituents on the $C_\alpha C_\beta C_\gamma$($CF_3$)S(Me) chain of thiaferracyclopentadiene (type **A**) complexes are readily activated by nucleophiles, α-fluoro substituents in compounds of type **D** and **F** are not cleaved by nucleophiles under the same conditions.

Experimental Section

General: All reactions were performed by Schlenk techniques under argon or nitrogen, and solvents were deoxygenated and dried by standard methods. Column chromatography was carried out with silica gel purchased from SDS and deoxygenated before use. The starting materials **1**,[18] **A**,[4d] **D**[4c] and **F**[4c] were prepared as described in the literature. All other reagents were purchased commercially. Yields are with respect to the starting clusters for the preparation of all the products. Infrared spectra were recorded with a Perkin−Elmer 1430 spectrophotometer on dichloromethane or hexane solutions. The mass spectra were measured with a GC/MS Hewlett−Packard 5595C or a GC/MS Ribermag R10−10 spectrometer at the "Laboratoire de Biochimie", Faculté de Médecine (Brest, France). Chemical analyses were performed by the "Centre de Microanalyses du CNRS de Lyon" or the "Laboratoire de Spectroscopie Atomique" at the University of Brest. The NMR spectra (^{1}H, ^{13}C, ^{19}F, ^{31}P), in $CDCl_3$ solutions, were recorded at room temperature with a Bruker AC 300 or DRX 400 spectrometer and were referenced to $SiMe_4$ (^{1}H, ^{13}C), $CFCl_3$ (^{19}F) and H_3PO_4 (^{31}P). Part of the NMR spectroscopic data for **2**−**7** and [**f**] are compared in Table 1; the remaining spectroscopic data of these complexes are reported in this section.

Synthesis of [{$Fe(CO)_3$}$_2${μ-S(Me)C(CF_3)CC($OR)_2$}] (2): A tetrahydrofuran (10 mL) solution of **1** (94.0 mg, 0.20 mmol) was treated at room temperature with 40 equiv. of alcohol (CH_3OH: 256.0 mg, 324 μL; C_2H_5OH: 369.0 mg, 542 μL). After it had been stirred for 3 h, the reaction mixture was filtered through Celite and the volatiles were removed under vacuum. The residue was then washed at −50 °C with pentane (10 mL) to give either **2a** (with CH_3OH) as an analytical pure red solid in 98% yield (97.0 mg) or **2b** (with C_2H_5OH) as an orange solid in 99% yield (103.0 mg). **2a:** $C_{13}H_9F_3Fe_2O_8S$ (493.96): calcd. C 31.6, H 1.8; found C 31.4, H 1.8. MS: *m*/*z* = 494 $[M]^+$, 466, 438, 410, 382, 354, 326 [M − *n* CO (*n* = 1−6)]$^+$, 232 [M − 6 CO − $FeFe_2$]$^+$. IR (hexane): ṽ =2077 m, 2062 w, 2032 s, 2004 s, 1983 m [ν(CO)] cm^{-1}. ^{1}H NMR ($CDCl_3$): δ = 2.2 (s, 3 H, SCH_3), 3.7 (s, 6 H, 2OCH_3). $^{13}C\{^{1}H\}$ NMR ($CDCl_3$): δ = 65.2 (q, $^{2}J_{C,F}$ = 38.0 Hz, CCF_3), 123.1 (q, $J_{C,F}$ = 278.0 Hz, CF_3). **2b:** $C_{15}H_{13}F_3Fe_2O_8S$ (522.01): calcd. C 34.5, H 2.5; found C 34.3, H 2.4. MS: *m*/*z* = 522 $[M]^+$, 507 $[M - CH_3]^+$, 466, 438, 410, 382, 354 [M − *n* CO (*n* = 2−6)]$^+$, 260 [M, 6 CO − FeF_2]$^+$. IR (CH_2Cl_2): ṽ = 2070 m, 1995 s, 1955 w, 1925 s [ν(CO)] cm^{-1}. ^{1}H NMR ($CDCl_3$): δ = 1.32 (t, 6 H, $^{3}J_{H,H}$ = 7.0 Hz, 2CH_3), 2.40 (s, 3 H, SCH_3), 3.98 (q, 2 H,^{3} $J_{H,H}$ = 7.0 Hz, CH_2), 4.02 (q,

$^3J_{H,H}$ = 7.0 Hz, 2 H, CH_2). $^{13}C\{^1H\}$ NMR ($CDCl_3$): δ = 14.2 (s, 2CH_2), 62.2 (q, $^2J_{C,F}$ = 38.5 Hz, CCF_3), 123.4 (q, $J_{C,F}$ = 277.5 Hz, CF_3). Similarly, a tetrahydrofuran (10 mL) solution of ethylene glycol (497.0 mg, 448 μL) and **1** (94.0 mg, 0.20 mmol) was stirred at room temperature for 5 h. After evaporation of the solvent, the residue was chromatographed on a silica gel column. Elution with hexane/CH_2Cl_2 (1:0.66) gave an orange band. After evaporation of the volatiles, **2c** was obtained as an analytical pure orange solid in 90% yield (88.5 mg). $C_{13}H_7F_3Fe_2O_8S$ (491.95): calcd. C 31.7, H 1.4; found C 31.5, H 1.3. MS: *m*/*z* = 492 $[M]^+$, 477 $[M - CH_3]^+$, 464, 436, 408, 380, 352, 324 $[M - n\ CO\ (n = 1-6)]^+$, 230 $[M - 6\ CO - FeF_2]^+$. IR (CH_2Cl_2): ν̃ =2070 m, 1995 s, 1960 w, 1928 s [ν(CO)] cm^{-1}. ^1H NMR ($CDCl_3$): δ = 2.3 (s, 3 H, SCH_3), 4.5 (s, 4 H, 2 CH_2). $^{13}C\{^1H\}$ NMR ($CDCl_3$): δ = 61.1 (q, $^2J_{C,F}$ = 39.0 Hz, CCF_3), 68.2 (s br, 2 CH_2), 123.5 (q, $J_{C,F}$ = 277.0 Hz, CF_3).

Synthesis of [{Fe(CO)$_3$}$_2${μ-S(Me)C(CF$_3$)C(OMe)C(NMe$_2$)}] (3a): A dichloromethane (5 mL) solution of methanol (128.0 mg, 162 μL, 0.4 mmol) and [{Fe(CO)$_3$}$_2${μ-S(Me)C(CF$_3$)C(F)C (NMe$_2$)}] (**A**: R = R′ = Me) (49.5 mg, 0.10 mmol) was stirred at 60 °C for 4 h. After evaporation of the solvent, column chromatography of the residue produced a red band of **3a** (49.7 mg, 98%) eluted with hexane/CH_2Cl_2 (1:0.2). $C_{14}H_{12}F_3Fe_2NO_7S$ (507.00): calcd. C 33.2, H 2.4, N 2.8; found C 33.3, H 2.4, N 2.7. MS: *m*/*z* = 507 $[M]^+$, 479, 451, 423, 395, 367, 339 $[M - n\ CO\ (n = 1-6)]^+$, 245 $[M - 6\ CO - FeF_2]^+$. IR (CH_2Cl_2): ν̃ =2065 m, 2025 s, 1995 s, 1966 sh [ν(CO)] cm^{-1}. ^1H NMR ($CDCl_3$): δ = 1.90 (s, 3 H, SCH_3), 3.10 [s, 6 H, N(CH_3)$_2$], 3.66 (s, 3 H, OCH_3). $^{13}C\{^1H\}$ NMR ($CDCl_3$): δ = 47.1 [s, N(CH_3)$_2$], 54.0 (q, $^2J_{C,F}$ = 34.0 Hz, CCF_3), 59.9 (s, OCH_3), 126.6 (q, $J_{C,F}$ = 274.0 Hz, CF_3).

Synthesis of [{Fe(CO)$_3$}$_2${μ-S(Me)C(CF$_3$)C[OC(O)NMe$_2$]-C(NMe$_2$)}] (3b): Carbon dioxide was bubbled at −50 °C for 5 min through a dichloromethane (10 mL) solution containing 49.5 mg (0.10 mmol) of **A** (R = R′ = Me). At −50 °C, 20 equiv. (90.0 mg, 132 μL) of Me_2NH was added. The mixture was warmed to 60 °C and stirred for 1 h. After evaporation of the solvent, the residue was chromatographed on deoxygenated silica gel. Elution with CH_2Cl_2/hexane (1:0.66) afforded an orange band, which gave **3b** as orange solid (98% yield). $C_{16}H_{15}F_3Fe_2N_2O_8S$ (564.04): calcd. C 34.1, H 2.7, N 5.0; found C 34.2, H 2.7, N 5.1. MS: *m*/*z* = 536, 508, 480, 452, 424, 396 $[M - n\ CO\ (n = 1-6)]^+$. IR (hexane): ν̃ =2066 m, 2020 s, 1998 m, 1990 sh, 1965 sh, 1725 m [ν(CO)] cm^{-1}. ^1H NMR ($CDCl_3$): δ = 2.18 (s, 3 H, SCH_3), 2.96 [s, 3 H, C(O)NCH_3], 2.99 (s, 3 H, C(O)NCH_3), 3.28 [s, 6 H, N(CH_3)$_2$]. $^{13}C\{^1H\}$ NMR ($CDCl_3$): δ = 36.15 [s, C(O)NCH$_3$], 36.8 [s, C(O)NCH$_3$)], 48.5 [s, N(CH_3)$_2$], 51.9 (q, $^2J_{C,F}$ = 35.0 Hz, CCF_3), 126.7 (q, $J_{C,F}$ = 274.0 Hz), 154.7 (s, *C*=O).

Synthesis of [{Fe(CO)$_3$}$_2${μ-S(Me)C(CF$_3$)C(SEt)C(NMe$_2$)}] (4a): Complex **A** (R = R′ = Me) (49.5 mg, 0.10 mmol) and 20 equiv. of ethanethiol were stirred in CH_2Cl_2 (5 mL) at 60 °C for 6 h. Compound **4a** was isolated as red solid (80% yield) by column chromatography on deoxygenated silica gel with hexane/dichloromethane (4:1). $C_{15}H_{14}F_3Fe_2NO_6S_2$ (537.08): calcd. C 33.5, H 2.6, N 2.6; found C 33.6, H 2.4, N 2.5. MS: *m*/*z* = 537 $[M]^+$, 509, 481, 453, 425, 397, 369 $[M - n\ CO\ (n = 1-6)]^+$. IR (CH_2Cl_2): ν̃ = 2065 s, 2022 s, 1988 sh, 1968 sh [ν(CO)] cm^{-1}. ^1H NMR ($CDCl_3$): δ =1.30 (t, $^3J_{H,H}$ = 7.5 Hz, 3 H, CH_3), 1.85 (s, 3 H, SCH_3), 2.60 (m, ABX_3, $^2J_{AB}$ = 11.5, $^3J_{H,H}$ = 7.5 Hz, CH_2), 3.00 (m, ABX_3, $^2J_{AB}$ = 11.5, $^3J_{H,H}$ = 7.5 Hz, CH_2), 3.19 [s, 6 H, N(CH_3)$_2$]. $^{13}C\{^1H\}$ NMR ($CDCl_3$): δ = 14.05 (s, CH_2CH_3), 30.2 (s, CH_2CH_3), 48.4 [s, N(CH_3)$_2$], 59.15 (q, $^2J_{C,F}$ = 32.0 Hz, CCF_3), 126.8 (q, $J_{C,F}$ = 274.0 Hz, CF_3).

Synthesis of [{Fe(CO)$_3$}$_2${μ-S(Me)C(CF$_3$)C[SC(S)NMe$_2$]C(NMe$_2$)}] (4b): Complex **A** (R = R′ = Me) (49.5 mg, 0.10 mmol) and 1 equiv. of dimethylammonium dimethylthiocarbamate were stirred in CH_2Cl_2 (5 mL) at room temperature for 1 h. The solution was then concentrated and chromatographed on a silica gel column. Elution with hexane/$CHCl_2$ (1:0.4) removed an orange band, which gave orange crystals of **4b** (53.5 mg, 90% yield). $C_{16}H_{15}F_3Fe_2N_2\ O_6S_3$ (596.16): calcd. C 33.2, H 2.5, Fe 18.7, N 4.8; found C 33.4, H 2.5, Fe 18.8, N 4.8. MS: *m*/*z* = 596 $[M]^+$, 568, 540, 512, 484, 456, 428 $[M - n\ CO\ (n = 1-6)]^+$, 334$[M - 6\ CO - FeF_2]^+$. IR (CH_2Cl_2): ν̃ = 2064 s, 2022 s, 1998 sh, 1970 sh [ν(CO)] cm^{-1}. ^1H NMR ($CDCl_3$): δ = 2.3 (s, 3 H, SCH_3), 3.4 (s, 9 H, 3 CH_3), 3.5 (s, 3 H, CH_3). $^{13}C\{^1H\}$ NMR ($CDCl_3$): δ = 42.0 (s, C(S)NCH_3), 45.3 (s, C(S)NCH_3), 49.8 [s, N(CH_3)$_2$], 59.7 (q, $^2J_{C,F}$ = 33.0 Hz, CCF_3), 127.0 (q, $J_{C,F}$ = 274.0 Hz, CF_3), 197.3 (s, *C*=S).

Synthesis of [{Fe(CO)$_3$}$_2${μ-S(Me)C(CF$_3$)C[SCMeNPh]C(NMe$_2$)}] (4c): This compound was prepared as described for **2a**, by using **A** (R = R′ = Me) (49.5 mg, 0.10 mmol) and *N*-phenylthioacetamide (15.2 mg, 0.10 mmol) as starting materials. Red crystals: yield 56.5 mg (90%). $C_{21}H_{17}F_3Fe_2N_2O_6S_2$ (626.16): calcd. C 40.3, H 2.7, N 4.5; found C 40.5, H 2.8, N 4.6. MS: *m*/*z* = 626 $[M]^+$, 598, 570, 542, 514, 486, 458 $[M - n\ CO\ (n = 1-6)]^+$. IR (CH_2Cl_2): ν̃ = 2065 s, 2022 s, 1990 sh, 1975 sh [ν(CO)] cm^{-1}. ^1H NMR ($CDCl_3$): δ = 2.02 (s, 3 H, CH_3 or SCH_3), 2.08 (s, 3 H, CH_3 or SCH_3), 3.3 [s, 6 H, N(CH_3)$_2$], 6.6−7.25 (m, 5 H, C_6H_5). $^{13}C\{^1H\}$ NMR ($CDCl_3$): δ = 20.3 (s, CCH_3), 33.1 (s, SCH_3), 49.1 [s, N(CH_3)$_2$], 59.3 (q, $^2J_{C,F}$ = 33.5 Hz, CCF_3), 119.7 (s, 2C, C_6H_5), 123.6 (s, *p*-*C* in C_6H_5), 126.8 (q, $J_{C,F}$ = 274.0 Hz, CF_3), 129.2 (s, 2 C, C_6H_5), 149.9 (s, quaternary C in C_6H_5), 167.4 [s, *C*(NPh)].

Synthesis of [{Fe(CO)$_3$}$_2${μ-S(Me)C(CF$_3$)C[SC(S)N(CH$_2$)$_4$]-C(NMe$_2$)}] (4d): A dichloromethane solution (5 mL) of **A** (R = R′ = Me) (49.5 mg, 0.10 mmol) and pyrrolidinium pyrrolidylthiocarbamate (43.6 mg, 0.20 mmol) was stirred at 60 °C for 2 h. The reaction mixture was then filtered through deoxygenated silica gel. After evaporation of the solvent, the residue was washed at −50 °C with pentane (5 mL) to afford **4d** as an analytically pure orange solid in 95% yield (59 mg). $C_{18}H_{17}F_3Fe_2N_2O_6S_3$ (622.19): calcd. C 34.7, H 2.8, N 4.5; found C 34.7, H 2.7, N 4.6. MS: *m*/*z* = 594, 566, 538, 510, 482, 454 $[M - n\ CO\ (n = 1-6)]^+$. IR (CH_2Cl_2): ν̃ = 2064 s, 2022 s, 1995 sh, 1966 sh [ν(CO)] cm^{-1}. ^1H NMR ($CDCl_3$): δ = 2.0 (m, 2 H, $C_\beta H_2$), 2.1 (m, 2 H, $C_\beta H_2$), 2.3 (s, 3 H, SCH_3), 3.4 [s, 6 H, N(CH_3)$_2$], 3.6 (m, 2 H, $C_\alpha H_2$), 3.9 (t, 2 H, $C_\alpha H_2$). $^{13}C\{^1H\}$ NMR ($CDCl_3$): δ = 24.3 (s, $C_\beta H_2$), 26.4 (s, $C_\beta H_2$), 49.8 [s, N(CH_3)$_2$], 51.1 (s, $C_\alpha H_2$), 54.9 (s, $C_\alpha H_2$), 59.7 (q, $^2J_{C,F}$ = 33.0 Hz, CCF_3), 126.8 (q, $J_{C,F}$ = 274.0 Hz, CF_3), 192.6 (s, *C*=S).

Synthesis of [{Fe(CO)$_3$}$_2${μ-S(Me)C(CF$_3$)C[SC(S)N(CH$_2$)$_4$]-C[N(CH$_2$)$_4$]}] (4e): This compound was prepared as described for **4d**, by using [{Fe(CO)$_3$}$_2${μ-S(Me)C(CF$_3$)C(F)C[N(CH$_2$)$_4$]}] [**A**: R−R′ = (CH$_2$)$_4$] (52.1 mg, 0.10 mmol) and pyrrolidinium pyrrolidylthiocarbamate (43.6 mg, 0.20 mmol) as starting materials. Orange crystals: yield 55.0 mg (85%). $C_{20}H_{19}F_3Fe_2N_2O_6S_3$ (648.23): calcd. C 37.1, H 2.9, N 4.3; found C 37.3, H 3.0, N 4.5. MS: *m*/*z*: 64 $[M]^+$, 592, 564, 536, 508, 480 $[M - n\ CO\ (n = 2-6)]^+$, 386 $[M - 6\ CO - FeF_2]^+$. IR (CH_2Cl_2): ν̃ = 2064 s, 2022 s, 1995 sh, 1966 sh [ν(CO)] cm^{-1}. ^1H NMR ($CDCl_3$): δ = 2.0 (t, 4 H, 2 $C_\beta H_2$), 2.05 (m, 4 H, 2 $C_\beta H_2$), 2.3 (s, 3 H, SCH_3), 3.7 (m, 2 H, $C_\alpha H_2$), 3.8 (t, 2 H, $C_\alpha H_2$), 3.9 (m, 4 H, 2 $C_\alpha H_2$). $^{13}C\{^1H\}$ NMR ($CDCl_3$): δ = 24.3 (s, $C_\beta H_2$), 26.2 (s, 2 $C_\beta H_2$), 26.4 (s, $C_\beta H_2$), 51.0 (s, $C_\alpha H_2$), 54.8 (s, $C_\alpha H_2$), 58.2 (s, 2 $C_\alpha H_2$), 61.3 (q, $^2J_{C,F}$ = 33.0 Hz, CCF_3), 127.0 (q, $J_{C,F}$ = 274.0 Hz, CF_3), 194.9 (s, *C*=S).

Treatment of [{Fe(CO)$_3$}$_2${μ-S(Me)C(CF$_3$)C(L1)C(F)}] [D: L$_1$ = PPh$_2$, P(O)(OMe)$_2$] and [{Fe(CO)$_3$}$_2${μ-S(Me)C(CF$_3$)C(L$_2$)C(F)}]

[F: L_2 = SC(NPh)CH_3] with Nucleophiles: Dichloromethane solutions of **D** (0.10 mmol) or **F** (0.10 mmol) and an excess of nucleophile {5 equiv. of RNH_2 (R = Ph, *t*Bu), 10 equiv. of R′NH [R′ = Me_2, $(CH_2)_4$], 10 equiv. of EtSH, 40 equiv. of MeOH, 5 equiv. of PPh_3} were stirred at 60 °C for 18 h. After this time the starting materials were wholly recovered. This was checked by IR analysis.

Synthesis of [{Fe(CO)$_3$}$_2${μ-S(Me)C(CF$_3$)C(NHPh)C(NHPh)}] (5a): A dichloromethane (10 mL) solution of **1** (94.0 mg, 0.20 mmol) and 3 equiv. of aniline (55.8 mg, 54.6 μL) was stirred at room temperature for 2 h. The reaction mixture was then filtered through deoxygenated silica gel. After evaporation of the solvent, the residue was crystallized from pentane (5 mL) at −60 °C to give **5a** as orange crystals in 95% yield (111.0 mg). $C_{23}H_{15}F_3N_2O_6S$ (616.11): calcd. C 44.8, H 2.45, Fe 18.1, N 4.5; found C 44.5, H 2.4, Fe 18.3, N 4.3. MS: *m*/*z* = 616 $[M]^+$, 588, 560, 532, 504, 476, 448 $[M - n\ CO\ (n = 1-6)]^+$, 354 $[M - 6\ CO - FeF_2]^+$. IR (CH_2Cl_2): $\tilde{\nu}$ = 2070 m, 2022 s, 2002 m, 1965 sh [ν(CO)] cm^{-1}. ^1H NMR ($CDCl_3$): δ = 2.0 (s, 3 H, SC*H*$_3$), 4.6 (s, 1 H, PhN*H*), 6.9−7.4 (m, 10 H, 2 C$_6$*H*$_5$), 8.5 (s, 1 H, PhN*H*). $^{13}C\{^1H\}$ NMR ($CDCl_3$): δ = 53.4 (q, $^2J_{C,F}$ = 33.0 Hz, *C*CF$_3$), 127.0 (q, $J_{C,F}$ = 273.5 Hz, *C*F$_3$), 110.0−150.0 (8 s, *C*$_6$H$_5$).

Synthesis of [{Fe(CO)$_3$}$_2${μ-S(Me)C(CF$_3$)C[NHNHC(O)OMe]C-[NHNHC(O)OMe)}] (5b): This compound was prepared as described for **5a**, by using **1** (94.0 mg, 0.20 mmol) and (methoxycarbonyl)hydrazine (72.0 mg, 0.80 mmol) as starting materials. Orange crystals: yield 112.3 mg (97%). $C_{15}H_{13}F_3Fe_2N_4O_{10}S$ (610.01): calcd. C 29.5, H 2.15, N 9.2; found C 29.8, H 2.2, N 9.1. IR (CH_2Cl_2): $\tilde{\nu}$ =2075 m, 2030 s, 1980 sh, 1950 sh, 1720 s [ν(CO)] cm^{-1}. ^1H NMR ($CDCl_3$): δ = 1.90 (s, 3 H, SC*H*$_3$), 3.78 (s, 3 H, OC*H*$_3$), 3.79 (s, 3 H, OC*H*$_3$), 4.74s (s br, 1 H, N*H*), 6.55 (s br, 1 H, N*H*), 6.85 (s br, 1 H, N*H*), 9.46 (s br, 1 H, N*H*). $^{13}C\{^1H\}$ NMR ($CDCl_3$): δ = 52.5 (m, *C*CF$_3$), 53.1 (s, OC*H*$_3$), 53.3 (s, OC*H*$_3$), 127.7 (q, $J_{C,F}$ = 273.5 Hz, *C*F$_3$), 156.8 (s, *C*(O)OMe), 158.8 (s, *C*(O)OMe).

Synthesis of [{Fe(CO)$_3$}$_2${μ-S(Me)C(CF$_3$)CC(NHPh)$_2$}] ([f]): The intermediate [**f**] was formed rapidly in the NMR tube on mixing **1** (23.5 mg, 0.05 mmol) with 3 equiv. of aniline (13.9 mg, 13.6μL) in $CDCl_3$ solution (at −10 °C). The reaction was monitored by ^{19}F NMR spectroscopy. When the yield of product [**f**] reached about 50%, a $^{13}C\{^1H\}$ (and ^1H) NMR analysis was undertaken at −40 °C in order to characterise this intermediate (see Table 1).

Synthesis of 6a: A tetrahydrofuran solution (10 mL) of **1** (94.0 mg, 0.20 mmol) and 1 equiv. of 4-methyl-3-thiosemicarbazide (21 mg) was stirred at room temperature for 3 h. After evaporation of the solvent, the residue was chromatographed on a deoxygenated silica gel column. Elution with ether/CH_2Cl_2 (1:4) gave an orange band. After evaporation of the volatiles, **6a** was obtained as an analytical pure orange solid in 86% yield (89.2 mg). $C_{13}H_8F_3Fe_2N_3O_6S_2$ (535.01): calcd. C 29.2, H 1.5, N 7.85; found C 29.5, H 1.5, N 7.7. MS: *m*/*z* = 535 $[M]^+$, 520 $[M - CH_3]^+$, 507, 479, 451, 423, 395, 367 $[M - n\ CO\ (n = 1-6)]^+$, 352 $[M - 6\ CO - CH_3]^+$, 273 $[M - 6\ CO - FeF_2]^+$, 258 $[M - 6\ CO - FeF_2 - CH_3]^+$. IR ($CH_2Cl_2$): $\tilde{\nu}$ = 2055 s, 2010 s, 1994 s, 1970 sh [ν(CO)], 1650 s [ν(C=N)] cm^{-1}. ^1H NMR ($CDCl_3$): δ = 1.87 (s, 3 H, SC*H*$_3$), 3.18 (s, 3 H, C*H*$_3$), 4.67 (s, 2 H, N*H*$_2$). $^{13}C\{^1H\}$ NMR ($CDCl_3$): δ = 40.9 (s, *C*H$_3$), 49.8 (q, $^2J_{C,F}$ = 37.0 Hz, *C*CF$_3$), 126.7 (q, $J_{C,F}$ = 274.0 Hz, *C*F$_3$), 159.4 (s, *C*=N).

Synthesis of 6b: This compound was prepared as described for **6a**, by using **1** (94.0 mg, 0.20 mmol) and 1 equiv. of *N*-methylthiourea (18.0 mg) as starting materials. The elution of product **6b** was performed with ether/dichloromethane (1:19) to give an orange solid in 88% yield (86.9 mg). $C_{13}H_7F_3Fe_2N_2O_6S_2$ (520.00): calcd. C 30.0, H 1.35, N 5.4; found C 30.2, H 1.4, N 5.7. MS: *m*/*z* = 520 $[M]^+$, 505 $[M - CH_3]^+$, 492, 464, 436, 408, 380, 352 $[M - n\ CO\ (n = 1-6)]^+$, 258 $[M - 6\ CO - FeF_2]^+$. IR (CH_2Cl_2): $\tilde{\nu}$ = 2075 s, 2035 s, 2005 s, 1998 sh [νCO), 1595 s [ν (C=N)] cm^{-1}. ^1H NMR ($CDCl_3$): δ = 1.90 (s, 3 H, SC*H*$_3$), 3.71 (s, 3 H, C$_α$N*H*$_3$), 7.59 (s br, 1 H, N*H*). $^{13}C\{^1H\}$ NMR ($CDCl_3$): δ = 35.7 (s, C$_α$NCH$_3$), 49.1 (q, $^2J_{C,F}$ = 37.5 Hz, *C*CF$_3$), 126.5 (q, $J_{C,F}$ = 27**1.0** Hz, *C*F$_3$), 166.0 (s, *C*=N).

Synthesis of 6c: A tetrahydrofuran solution (10 mL) of **1** (94.0 mg, 0.20 mmol) and 1 equiv. of *N*,*N*′-dimethylthiourea (20.8 mg) was stirred at room temperature for 2 h. The solvent was then removed under vacuum and **6c** was extracted with CH_2Cl_2/pentane (1:9) (10 mL) and then recrystallized at −60 °C in pentane (91.3 mg, 90% yield). $C_{14}H_9F_3Fe_2N_2O_6S_2$ (534.03): calcd. C 31.5, H 1.7, N 5.2; found C 31.9, H 1.8, N 5.2. MS: *m*/*z* = 534 $[M]^+$, 519 $[M - CH_3]^+$, 506, 478, 450, 422, 394, 366 $[M - n\ CO\ (n = 1-6)]^+$, 272 $[M - 6\ CO - FeF_2]^+$. IR (CH_2Cl_2): $\tilde{\nu}$ = 2075 s, 2032 s, 2004 s, 1980 sh [ν(CO)], 1630 s [ν(C=N)] cm^{-1}. ^1H NMR ($CDCl_3$): δ = 1.88 (s, 3 H, SC*H*$_3$), 3.15 (s, 3 H, C*H*$_3$ N=C), 3.68 (s, 3 H, C*H*$_3$NC$_α$). $^{13}C\{^1H\}$ NMR ($CDCl_3$): δ = 36.4 (s, *C*H$_3$NC$_α$), 41.4 (s, *C*H$_3$N=C), 49.5 (q, $^2J_{C,F}$ = 37.0 Hz, *C*CF$_3$), 126.7 (q, $J_{C,F}$ = 274.0 Hz, *C*F$_3$), 106.6 (s, *C*=N).

Synthesis of 7a: This compound was prepared as described for **5a**, by using **1** (94.0 mg, 0.20 mmol) and 3 equiv. of acetylhydrazine (44.4 mg) as starting materials. Red crystals: yield 93.8 mg (98%). $C_{13}H_7F_3Fe_2N_2O_7S$ (503.94): calcd. C 31.0, H 1.4, Fe 22.2, N 5.6; found C 31.1, H 1.4, Fe 21.8, N 5.5. MS: *m*/*z* = 504 $[M]^+$, 476, 448, 420, 392, 364, 336 $[M - n\ CO\ (n = 1-6)]^+$, 242 $[M - 6\ CO - FeF_2]^+$. IR (CH_2Cl_2): $\tilde{\nu}$ = 2072 m, 2022 s, 2002 m, 1950 sh [ν(CO)] cm^{-1}. ^1H NMR ($CDCl_3$): δ = 1.87 (s, 3 H, C*H*$_3$), 2.49 (s, 3 H, SC*H*$_3$), 2.86 (s, 1 H, C*H*). $^{13}C\{^1H\}$ NMR ($CDCl_3$): δ = 11.3 (s, *C*H$_3$), 24.4 (s, *C*H), 44.6 (q, $^2J_{C,F}$ = 36.5 Hz, *C*CF$_3$), 128.6 (q, $J_{C,F}$ = 274.0 Hz, *C*F$_3$), 163.0 (s, O*C*CH$_3$).

Synthesis of 7b: A dichloromethane solution (5 mL) of **7a** (50.4 mg, 0.10 mmol) and 2 equiv. of PPh_2Me (40.0 mg, 37.2 μL) was stirred at 60 °C for 1 h. The reaction mixture was then filtered through Celite and the volatiles were removed under vacuum. The residue was then washed at −50 °C with pentane (5 mL) to give **7b** as a red solid in 85% yield (57.5 mg). $C_{25}H_{20}F_3Fe_2N_2O_6PS$(676.14): calcd. C 44.4, H 3.0, Fe 16.5, N 4.1; found C 44.6, H 3.0, Fe 16.1, N 4.0. IR (CH_2Cl_2): $\tilde{\nu}$ = 2030 s, 1985 s, 1960 s [ν(CO)] cm^{-1}. ^1H NMR ($CDCl_3$): δ = 1.53 (s, 3 H, C*H*$_3$), 1.97 (d, $^2J_{PH}$ = 8.0 Hz, 3 H, PC*H*$_3$), 2.49 (s, 3 H, SC*H*$_3$), 2.74 (s, 1 H, C*H*), 7.5 (m, 10 H, 2 C$_6$*H*$_5$). ^{31}P NMR ($CDCl_3$): δ = 29.12 (s, *P*Ph$_2$Me). $^{13}C\{^1H\}$ NMR ($CDCl_3$): δ = 11.2 (s, *C*H$_3$), 15.6 (d, $J_{C,P}$ = 16.0 Hz, P*C*H$_3$), 42.1 (q, $^2J_{C,F}$ = 36.5 Hz, *C*CF$_3$), 129.0 (q, $J_{C,F}$ = 274.5 Hz, *C*F$_3$), 128.4 (s, *C*$_6$H$_5$), 128.6 (d, $J_{C,P}$ = 9.0 Hz, *C*$_6$H$_5$), 129.3 (d, $J_{C,P}$ = 9.0 Hz, *C*$_6$H$_5$), 129.9 (d, $J_{C,P}$ = 10.0 Hz, *C*$_6$H$_5$), 130.8 (s, *C*$_6$H$_5$), 132.3 (d, $J_{C,P}$ = 11.0 Hz, *C*$_6$H$_5$), 134.8 (d, $J_{C,P}$ = 33.0 Hz, *C*$_6$H$_5$), 138.5 (d, $J_{C,P}$ = 41.0 Hz, *C*$_6$H$_5$), 160.6 (s, O*C*CH$_3$).

Synthesis of 7c: This compound was prepared as for **7b**, by using **7a** (50.4 mg, 0.10 mmol) and 5 equiv. of $P(OMe)_3$ (62.0 mg, 59 μL) as starting materials. The stirring was undertaken for 20 h. Red solid: yield 58.8 mg (98%). $C_{15}H_{16}F_3Fe_2N_2O_9PS$ (600.01): calcd. C 30.0, H 2.7, Fe 18.6, N 4.7; found C 29.3, H 2.6, Fe 18.1, N 4.6. MS: *m*/*z* = 600 $[M]^+$, 572, 544, 516, 488, 460 $[M - n\ CO\ (n = 1-5)]^+$. IR (CH_2Cl_2): $\tilde{\nu}$ = 2036 s, 1990 s, 1968 s [ν(CO)] cm^{-1}. ^1H NMR ($CDCl_3$): δ = 1.88 (s, 3 H, C*H*$_3$), 2.44 (s, 3 H, SC*H*$_3$), 2.72 (s, 1 H, C*H*), 3.7 [d, $^3J_{PH}$ = 10.5 Hz, 9 H, P(OC*H*$_3$)$_3$]. ^{31}P NMR ($CDCl_3$): δ = 157.73 [s, *P*(OMe)$_3$]. $^{13}C\{^1H\}$ NMR ($CDCl_3$): δ = 11.2 (s, C*C*H$_3$), 42.9 (q, $^2J_{C,F}$ = 36.5 Hz, *C*CF$_3$), 52.25 [d, $^2J_{C,P}$ =

Table 4. Crystallographic data for **2a**, **3b**, **5a**, **5b**, **6a** and **7a**; data collected with Mo-K_α radiation (λ = 0.7073 Å) at 20 °C; structures refined by full-matrix least squares

	2a	**3b**	**5a**	**5b**	**6a**	**7a**
Empirical formula	$C_{13}H_9F_3Fe_2O_8S$	$C_{16}H_{15}F_3Fe_2N_2O_8S$	$C_{23}H_{15}F_3Fe_2N_2O_6S{\cdot}0.2CH_2Cl_2$	$C_{15}H_{13}F_3Fe_2N_4O_{10}S$	$C_{13}H_8F_3Fe_2N_3O_6S_2$	$C_{13}H_7F_3Fe_2N_2O_7S$
Formula mass	493.96	564.06	633.12	610.05	535.04	503.97
Crystal size [mm]	0.11 × 0.12 × 0.45	0.42 × 0.10 × 0.03	0.54 × 0.18 × 0.13	0.40 × 0.20 × 0.20	0.15 × 0.09 × 0.06	0.40 × 0.10 × 0.10
Crystal system	monoclinic	triclinic	triclinic	monoclinic	triclinic	triclinic
Space group	$P2_1/c$	$P\bar{1}$	$P\bar{1}$	Pn	$P\bar{1}$	$C\bar{1}$
a [Å]	9.757(2)	9.780(1)	11.451(2)	11.754(2)	9.535(2)	13.3286(10)
b [Å]	10.518(2)	15.671(1)	12.838(3)	11.613(2)	15.019(3)	13.5509(9)
c [Å]	18.437(4)	16.097(1)	19.367(5)	18.051(4)	15.306(3)	20.5896(13)
α [°]		70.031(5)	86.79(2)		114.92(3)	90.057(6)
β [°]	102.30(3)	87.141(6)	75.83(2)	108.87(3)	94.60(3)	104.456(7)
γ [°]		75.323(6)	78.48(2		91.47(3)	90.013(7)
V [Å^3]	1848.6(7)	2241.2(3)	2704.7(10)	2331.5(8)	1977.1(7)	3601.0(4)
Z	4	4	4	4	4	8
$D_{calcd.}$ [Mg/m^3]	1.775	1.672	1.555	1.738	1.797	1.859
μ [mm^{-1}]	1.749	1.456	1.249	1.415	1.741	1.797
θ_{max} (Mo-K_α) [°]	28.3	25.0	27.4	30.4	25.0	27.0
Index ranges	$-13 \le h \le 1$	$0 \le h \le 11$	$-14 \le h \le 13$	$-16 \le h \le 16$	$-11 \le h \le 11$	$-16 \le h \le 16 - 17 \le$
	$-1 \le k \le 14$	$-18 \le k \le 18$	$0 \le k \le 15$	$-2 \le k \le 16$	$-17 \le k \le 16$	$k \le 17$
	$-24 \le l \le 24$	$-19 \le l \le 19$	$-23 \le l \le 23$	$-2 \le l \le 25$	$0 \le l \le 18$	$0 \le l \le 26$
Reflections collected	5932	9337	10408	8801	7239	8132
Reflections unique	4594	7881	9933	7963	6951	7793
R(int.)	0.018	0.046	0.036	0.058	0.050	0.016
Reflections with $I > 2\sigma(I)$	3177	4629	5196	6243	2927	6251
Data/parameters	4594/244	7881/578	9933/667	7963/632	6951/517	7793/505
GoF on F^2	0.919	0.945	0.889	1.027	0.946	0.986
$R1$ [$I > 2\sigma(I)$]	0.030	0.065	0.055	0.050	0.043	0.033
$wR2$ [$I > 2\sigma(I)$]	0.072	0.161	0.123	0.125	0.090	0.081
$R1$ (all data)	0.058	0.116	0.141	0.073	0.177	0.046
$wR2$ (all data)	0.077	0.186	0.150	0.139	0.129	0.086
Δρ(max)/Δρ(min) [e/Å^3]	0.36/−0.32	0.91/−0.76	0.51/−0.39	1.80/−0.41	0.68/−0.55	0.43/−0.45

9.0 Hz, $P(OCH_3)_3$], 128.9 (q, $J_{C,F}$ = 274.0 Hz, CF_3), 160.9 (s, CCH_3).

Synthesis of 8: A solution of **7a** (50.4 mg, 0.10 mmol) in dichloromethane (2 mL) was added to a chilled solution (−15 °C) of $(NH_4)_2Ce(NO_3)_6$ (274 mg, 0.50 mmol) in methanol (2 mL). The reaction mixture was stirred at −15 °C for 45 min and was then slowly warmed to room temperature The volatiles were removed under vacuum and the product **8** was extracted with pentane (5 mL) and then recrystallized at −80 °C. White crystals were formed and filtered off to give 19.0 mg (85%) of **8**; m.p. 44 °C. $C_7H_7F_3N_2OS$ (224.18). MS: m/z = 224 $[M]^+$, 209 $[M - CH_3]^+$, 141 $[HCC(CF_3)SMe]^+$, 83 $[NNC(CH_3)OC]^+$. ^{1}H NMR ($CDCl_3$): δ = 2.54 (s, 3 H, CH_3), 2.60 (s, 3 H, SCH_3), 7.02 (s, 1 H, CH). ^{19}F NMR ($CDCl_3$): δ = −62.5 (s, CF_3). $^{13}C\{^1H\}$ NMR ($CDCl_3$): δ = 11.1 (s, CH_3), 15.9 (q, $^4J_{C,F}$ = 3.0 Hz, SCH_3), 111.5 (q, $^3J_{C,F}$ = 7.0 Hz, CH), 121.9 (q, $J_{C,F}$ = 276.0 Hz, CF_3), 137.5 (q, $^2J_{C,F}$ = 32.0 Hz, CCF_3), 161.7 (s, $NCCH$), 163.9 (s, $NCCH_3$).

Single-Crystal X-ray Analyses of 2a, 3b, 5a, 5b, 6a and 7a: Measurements were made with a Nonius CAD4 diffractometer. Subsequent calculations were performed with the WINGX system, the structures being refined with SHELXL97.[19] Crystallographic data for **2a**, **3b**, **5a**, **5b**, **6a** and **7a** are presented in Table 4. Full details of each structure have been deposited.[20] All the structures apart from **2a** involve asymmetric units that contain two independent molecules. Differences between these molecules are insignificant and are easily accounted for by packing forces. Crystals of **3b**, **5a** and **6a** are metrically triclinic. The collection of high-angle data for **5a** had to be abandoned when the crystal decomposed. The structure has two independent sites which contain disordered CH_2Cl_2 at about 20% occupancy. The scattering of the disordered CH_2Cl_2 was included by back-transformation of the difference map using the SQUEEZE facility of the PLATON program.[19] In **6a**, the CF_3 fluorine atoms are disordered equally over two sites. The structure of **5b** has several unusual features. It appears to be a distortion from space group $P2_1/n$ in that the two independent molecules are *roughly* related by the pseudo-screw operation $-x$, $-0.28 + y$, $-z$. The Laue symmetry is undoubtedly $2/m$, although it is possible to choose a centred orthorhombic cell. Four small residual peaks of 1.8−1.0 e/Å^3 suggest a very minor disorder of the O and OMe groups attached to C(8), but attempts to derive a satisfactory model of the disorder were unsuccessful. Compound **7a** is *metrically C*-centred monoclinic, although its Laue symmetry is that of a triclinic crystal.

Acknowledgments

We thank the CNRS, the EPSRC and the Universities of Brest and Glasgow for financial support. The Ministère de l'Enseignement Supérieur et de la Recherche is acknowledged for providing studentships (K. G.-d. C.).

[1] [1a] T. G. Richmond, *Angew. Chem. Int. Ed.* **2000**, *39*, 3241−3244. [1b] J. Burdeniuc, B. Jedlicka, R. H. Crabtree, *Chem. Ber./Recueil* **1997**, *130*, 145−154. [1c] T. Braun, L. Cronin, C. L. Higgit, J. E. McGrady, R. N. Perutz, M. Reinhold, *New J. Chem.* **2001**, *25*, 19−21. [1d] M. E. van der Boom, Y. Ben-David, D. Milstein, *J. Am. Chem. Soc.* **1999**, *121*, 6652−6656.

[2] [2a] T. H. Peterson, J. T. Golden, R. G. Bergman, *Organometallics* **1999**, *18*, 2005−2020. [2b] M. Fujiwara, J. Ichikawa, T. Okauchi, T. Minami, *Tetrahedron Lett.* **1999**, *40*, 7261−7265. [2c] J. L. Kiplinger, T. G. Richmond, C. E. Osterberg, *Chem. Rev.* **1994**, *94*, 373−431. [2d] P. J. Brothers, W. R. Roper, *Chem. Rev.* **1988**, *88*, 1293−1326.

[3] [3a] J. J. Bonnet, R. Mathieu, R. Poiblanc, J. A. Ibers, *J. Am. Chem. Soc.* **1979**, *101*, 7487−7496. [3b] L. Carlton, J. L. Davidson, P. Erwing, Lj. Manojlovic-Muir, K. W. Muir, *J. Chem. Soc., Chem. Commun.* **1985**, 1474−1476.

[4] [4a] R. Rumin, F. Y. Pétillon, Lj. Manojlovic-Muir, K. W. Muir, D. S. Yufit, *J. Chem. Soc., Chem. Commun.* **1995**, 1431−1432. [4b] R. Rumin, K. Guennou, F. Y. Pétillon, K. W. Muir, *J. Chem. Soc., Dalton Trans.* **1997**, 1381−1386. [4c] R. Rumin, K. Guennou, R. Pichon, F. Y. Pétillon, K. W. Muir, D. S. Yufit, *J. Organomet. Chem.* **1997**, *533*, 177−185. [4d] K. Guennou-de Cadenet, R. Rumin, F. Y. Pétillon, K. W. Muir, *Organometallics* **2000**, *19*, 1912−1926.

[5] R. G. Pearson, J. Songstad, *J. Am. Chem. Soc.* **1967**, *89*, 1827−1836.

[6] K. Guennou-de Cadenet, Ph. D Thesis, Université de Bretagne Occidentale, Brest, **1998**.

[7] [7a] *International Tables for Crystallography*, International Union of Crystallography, Kluwer, Dordrecht, **1992**, vol. C, p.723−791. [7b]P. E. Riley, R. E. Davis, N. T. Allison, W. M. Jones, *Inorg. Chem.* **1982**, *21*, 1321−1328.

[8] J. C. Daran, B. Heim, M. Gouygou, Y. Jeannin, *J. Organomet. Chem.* **1994**, *479*, 109−116.

[9] J. Sandström, *Dynamic NMR Spectroscopy*; Academic Press: London, New York, **1982**.

[10] R. Rumin, F. Robin-Le Guen, F. Y. Pétillon, R. Pichon, J. Talarmin, *Organometallics* **1993**, *12*, 1597−1607.

[11] S. Doherty, G. Hogarth, M. Waugh, W. Clegg, M. R. J. Elsegood, *Organometallics* **2000**, *19*, 4557−4562.

[12] K. Gruet, R. H. Crabtree, D-H. Lee, L. Liable-Sands, A. L. Rheingold, *Organometallics* **2000**, *19*, 2228−2232.

[13] W. P. Fehlhammer, T. Bliβ, W. Sperber, J. Fuchs, *Z. Naturforsch., Teil B* **1994**, *49*, 494−500.

[14] R. D. Adams, J. E. Babin, H. S. Kim, J. T. Tanner, T. A. Wolfe, *J. Am. Chem. Soc.* **1990**, *112*, 3426−3435.

[15] T. Fässler, G. Huttner, D. Günauer, S. Fielder, B. Eber, *J. Organomet. Chem.* **1990**, *381*, 409−428.

[16] M. Crutchfield, C. Dungan, J. Letcher, V. Mark, J. Van Wazer in *Topics in Phosphorus Chemistry*, Interscience Publishers, New York, **1967**, vol. 5.

[17] [17a] C. Ainsworth, *J. Am. Chem. Soc.* **1965**, *87*, 5800−5801. [17b] C. Ainsworth, R. E. Hackler, *J. Org. Chem.* **1966**, *31*, 3442−3444.

[18] R. Rumin, F. Y. Pétillon, L. Manojlovic-Muir, K. W. Muir, *Organometallics* **1990**, *9*, 944−952.

[19] SHELXS: G. M. Sheldrick, *Acta Crystallogr., Sect. A* **1990**, *46*, 467−473. G. M. Sheldrick, *SHELXL97*, University of Göttingen, Germany, **1997**. WINGX: L. J. Farrugia. *J. Appl. Crystallogr.* **1997**, *30*, 565.

[20] Crystallographic data for the structures reported in this paper have been deposited with the Cambridge Crystallographic Data Centre as supplementary publication of CCDC-168607 (**2a**), -168608 (**3b**), -168609 (**5a**), -168610 (**5b**), -168611 (**6a**) and -168612 (**7a**). Copies of the data can be obtained free of charge on applicaton to CCDC, 12 Union Road, Cambridge CB2 1EZ, UK [Fax: (internat.) + 44-1223/336-033; E-mail: deposit@ccdc.cam.ac.uk].

Received August 20, 2001
[I01318]

Transformations of Hydrazines $RNHNH_2$ (R = Me, Ph) at a Sulfur-Rich Bimetallic Site: Diazene−Diazenido−Isodiazene/Hydrazido(2−) Interconversions

Philippe Schollhammer,[a] Béatrice Didier,[a] Nathalie Le Grand,[a] François Y. Pétillon,*[a] Jean Talarmin,[a] Kenneth W. Muir,*[b] and Simon J. Teat[c]

Keywords: N ligands / S ligands / X-ray diffraction / Metal-metal interactions / Molybdenum

The bis(nitrile) compound $[Mo_2Cp_2(\mu\text{-}SMe)_3(MeCN)_2](BF_4)$ (**1**) (Cp = C_5H_5) reacted with substituted hydrazines $RNHNH_2$ (R = Me, Ph) in acetonitrile at room temperature to give the stable diazene species $[Mo_2Cp_2(\mu\text{-}SMe)_3(\mu\text{-}\eta^2\text{-}HN{=}NR)](BF_4)$ [R= Me (**2**), Ph (**3**)]. Compounds **2** and **3** could be readily deprotonated with BuLi to produce neutral diazenido species $[Mo_2Cp_2(\mu\text{-}SMe)_3(\mu\text{-}\eta^2\text{-}N{=}NR)]$ [R = Me (**4**), Ph (**5**)]. Photolysis of **4** in THF induced isomerization of the diazenide bridge, affording the complex $[Mo_2Cp_2(\mu\text{-}SMe)_3(\mu\text{-}\eta^1\text{-}N{=}NMe)]$ (**8**). This species underwent protonation at the outer nitrogen atom (N_β) to give the stable isodiazene/hydrazido(2–) complex $[Mo_2Cp_2(\mu\text{-}SMe)_3(\mu\text{-}\eta^1\text{-}N{=}NHMe)](BF_4)$ (**9**) which isomerised slowly back into **2** on warming. The molecular structure of the $\mu\text{-}\eta^2$-methyldiazenido complex **4** was established by an X-ray diffraction study.

Introduction

Transition metal complexes containing sulfur ligands have aroused much attention because of their biological and industrial potential.[1] We have been interested in making sulfur-rich dimolybdenum systems in order to relate their reactivity and electrochemical behaviour to their molecular structure.[2] Recently, we have investigated the chemistry of complexes with a tris-thiolato-bridged dimolybdenum(III) core $\{Mo_2Cp_2(\mu\text{-}SMe)_3\}^+$ (Cp = C_5H_5), and have shown that they are extremely suitable candidates for molecular activation.[3−5] In particular, the chloro-bridged complex $[Mo_2Cp_2(\mu\text{-}Cl)(\mu\text{-}SMe)_3]$ reacts with hydrazine and phenylhydrazine to give compounds containing nitrogenous functional groups: hydrazine yields the amido (NH_2)[4] group, while phenylhydrazine leads to the formation of diazenido ($N{=}N{-}Ph$)[5] ligands.

The mechanisms that give rise to these products are only poorly understood, but the products themselves are useful structural and chemical models of key intermediates in the reduction of dinitrogenous substrates to ammonia at a binuclear core.[6] In addition, we have demonstrated that the complex $[Mo_2Cp_2(\mu\text{-}SMe)_3(\mu\text{-}\eta^1\text{-}N_\alpha N_\beta Ph)]$ unexpectedly undergoes protonation at the outer nitrogen atom (N_β) to give the $\mu\text{-}\eta^1$-isodiazene derivative $[Mo_2Cp_2(\mu\text{-}SMe)_3(\mu\text{-}\eta^1\text{-}NNHPh)](BF_4)$, which, upon warming, readily isomerises into the more thermodynamically favoured $\mu\text{-}\eta^2$-diazene $[Mo_2Cp_2(\mu\text{-}SMe)_3(\mu\text{-}\eta^2\text{-}HN{=}NPh)](BF_4)$ species.[5] The molecular structure of this derivative showed that the *cis*-diazene Ph−N=N−H unit is stabilized by the $\{Mo_2Cp_2(\mu\text{-}SMe)_3^+\}$ dimolybdenum core.

In order to obtain more information on the interaction of hydrazines with Mo_2 systems we investigated the reactions of $RNHNH_2$ (R = Me, Ph) with another tris-thiolato-bridged compound, namely the bis-nitrile derivative $[Mo_2Cp_2(\mu\text{-}SMe)_3(MeCN)_2](BF_4)$ (**1**), in which the labile nitrile groups conferred a reactivity that was quite different from that of the chloride-bridged complex.[3a] We report here the ready formation of *cis*-diazene species $[Mo_2Cp_2(\mu\text{-}SMe)_3(\mu\text{-}\eta^2\text{-}HN{=}NR)](BF_4)$ [R= Me (**2**), Ph (**3**)] and their relationships with their η^1-, η^2-diazenido and η^1-isodiazene/hydrazido(2−) parent molecules. Moreover, we show multiple transformations of methyldiazene and methyldiazenido substrates at a bimetallic site and describe the solid-state structure of a rare η^2-methyldiazenido bridged complex.[7−9]

Results

Syntheses and Spectroscopic Characterisation of $[Mo_2Cp_2(\mu\text{-}SMe)_3(\mu\text{-}\eta^2\text{-}HN{=}NR)](BF_4)$ [R= Me (2), Ph (3)] and $[Mo_2Cp_2(\mu\text{-}SMe)_3(\mu\text{-}\eta^2\text{-}N{=}NR)]$ [R= Me (4), Ph (5)]

A red solution of $[Mo_2Cp_2(\mu\text{-}SMe)_3(MeCN)_2](BF_4)$ (**1**) in acetonitrile reacted with an excess of $MeNHNH_2$ at

[a] UMR CNRS 6521, Chimie, Electrochimie Moléculaires et Chimie Analytique, Faculté des Sciences, Université de Bretagne Occidentale,
BP 809, 29285 Brest-Cédex, France
[b] Department of Chemistry, University of Glasgow, Glasgow G 12 8QQ, UK
[c] CLRC Daresbury Laboratory, Daresbury, Warrington WA4 4AD, UK

 © WILEY-VCH Verlag GmbH, 69451 Weinheim, Germany, 2002 1434−1948/02/0303−0658 $ 17.50+.50/0 *Eur. J. Inorg. Chem.* **2002**, 658−663

room temperature within 1 h to give a mixture of the two compounds $[Mo_2Cp_2(\mu\text{-}SMe)_3(\mu\text{-}\eta^2\text{-}HN{=}NMe)](BF_4)$ (**2a**) and $[Mo_2Cp_2(\mu\text{-}SMe)_3(\mu\text{-}NH_2)]$ (**6**) [Equation (1)]. Precipitation of **6** from the cooled acetonitrile solution and subsequent workup permitted **2a** to be isolated as a spectroscopically and analytically pure brownish powder in 50−60% yields. Under the same conditions, $[Mo_2Cp_2(\mu\text{-}SMe)_3(\mu\text{-}\eta^2\text{-}HN{=}NPh)](BF_4)$ (**3a**) was the only product obtained with $PhNHNH_2$. The yields of **2a** and **3a** were occasionally lowered by the formation of a deactivated paramagnetic derivative of the bis-nitrile complex, namely $[Mo_2Cp_2(\mu\text{-}SMe)_3(\mu\text{-}\eta^2\text{-}NHCO(Me)](BF_4)$ (**7**), which was formed in low and varying yields and could also be detected in cyclic voltammetry experiments.[3b]

$$\underset{\mathbf{1}}{Mo_2Cp_2(\mu\text{-}SMe)_3(MeCN)_2](BF_4)} \xrightarrow[CH_3CN]{MeNHNH_2\ (excess)} \underset{\mathbf{2a}}{[Mo_2Cp_2(\mu\text{-}SMe)_3(\mu\text{-}NH{=}NMe)](BF_4)} + \underset{\mathbf{6}}{[Mo_2Cp_2(\mu\text{-}SMe)_3(\mu\text{-}NH_2)]} \quad (1)$$

Complexes **2a** and **3a** were unambiguously formulated as dimolybdenum species $[Mo_2Cp_2(\mu\text{-}SMe)_3(\mu\text{-}HN{=}NR)](BF_4)$ with R = Me and R = Ph, respectively. Their ^1H NMR ($CDCl_3$) spectra exhibit two inequivalent cyclopentadienyl resonances and three SMe resonances, indicating that the $\{Mo_2Cp_2(\mu\text{-}SMe)_3\}$ moiety has been retained. The presence of a H−N=N−R ligand is supported by the observation of a low-field signal (at about δ = 12) typical for the proton of the NH group and of the peaks expected for the R substituent.[7] Two-dimensional heteronuclear ^1H-^{15}N inverse-correlation experiments completed the characterisation of **2a**. The ^{15}N chemical shifts (relative to nitromethane) of the NH and NMe groups could be unambiguously assigned to peaks at δ = −18.5 and δ = −31.0, respectively.

On heating, **2a** and **3a** underwent a change in the orientation of the methyl group of one thiolate bridge [Equation (2)]. This isomerization reaction was complete within 24 h and afforded compounds **2b** and **3b**. Complex **2b** is new but it gives rise to ^1H NMR patterns that resemble those of **2a**, suggesting strongly that the two compounds have very similar structures. In particular, the ^1H NMR spectrum of **2b** shows a resonance at δ = 12.3 attributed to the NH group of the diazo bridge. Compound **3b** was identified by comparison of its ^1H NMR spectroscopic data with that of an authentic sample of the species obtained by protonation of the $\mu\text{-}\eta^2$-diazenido derivative $[Mo_2Cp_2(\mu\text{-}SMe)_3(\mu\text{-}\eta^2\text{-}N{=}NPh]$. X-ray analysis has established a *syn* orientation of the methyl groups borne by the two sulfur atoms that lie in the equatorial plane of this molecule.[5]

$$\underset{\text{R = Me 2a, Ph 3a}}{[Mo_2Cp_2(\mu\text{-}SMe)_3(\mu\text{-}NH{=}NR)](BF_4)} \xrightarrow{MeCN/\Delta} \underset{\text{R = Me 2b, Ph 3b}}{[Mo_2Cp_2(\mu\text{-}SMe)_3(\mu\text{-}NH{=}NR)](BF_4)} \quad (2)$$

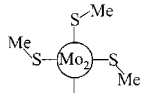

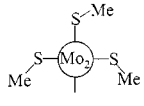

Deprotonation of **2a**−**b** and **3a**−**b** could readily be carried out with Et_3N or BuLi, and gave the η^2-diazenido species $[Mo_2Cp_2(\mu\text{-}SMe)_3(\mu\text{-}\eta^2\text{-}N{=}NR)]$ [R = Me (**4a**−**b**), R = Ph (**5a**−**b**)] [Equation (3)]. Likewise, complexes **4**−**5** could readily be protonated to regenerate **2**−**3**. The absence of a resonance at about δ = 12 in the ^1H NMR spectra of **4a**−**b** and **5a**−**b** indicates loss of the NH proton. Complexes **5a**−**b** have been identified as a pair of isomers, which differ in the orientation of the *S*-methyl substituents, by comparison of their ^1H NMR spectra with those of a mixture of the two isomers of the compound $[Mo_2Cp_2(\mu\text{-}SMe)_3(\mu\text{-}\eta^2\text{-}N{=}NPh)]$, previously obtained from the reaction of the chloro-bridged derivative $[Mo_2Cp_2(\mu\text{-}Cl)(\mu\text{-}SMe)_3]$ with $PhNHNH_2$.[5]

$$\underset{\mathbf{2\text{-}3}}{[Mo_2Cp_2(\mu\text{-}SMe)_3(\mu\text{-}NH{=}NR)](BF_4)} \underset{HBF_4}{\overset{BuLi}{\rightleftharpoons}} \underset{\mathbf{4\text{-}5}}{[Mo_2Cp_2(\mu\text{-}SMe)_3(\mu\text{-}\eta^2\text{-}N{=}NR)]} \quad (3)$$

Molecular Structure of $[Mo_2Cp_2(\mu\text{-}SMe)_3(\mu\text{-}\eta^2\text{-}N{=}NMe)]$ (4b)

Various bonding modes have been observed for the diazenido ligand.[7,8,10] Sutton et al have recently given a helpful summary of these, and we use their terminology in the following discussion.[8] However, very few of the available structural examples relate to the methyldiazenido ligand.[7−9,11−14]

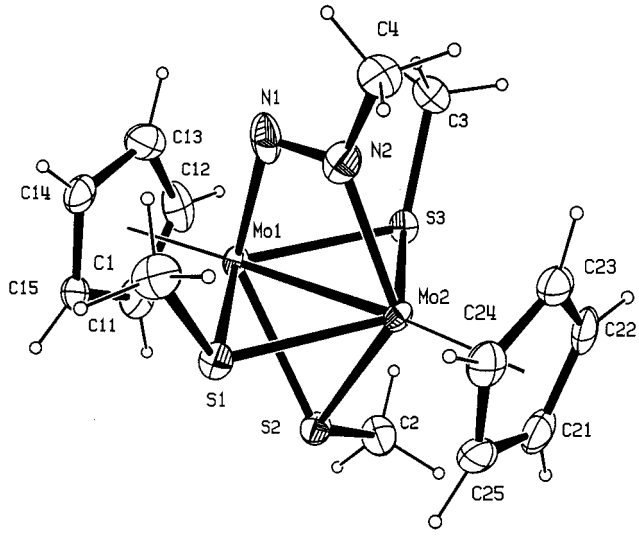

Figure 1. Molecular structure of $[Mo_2Cp_2(\mu\text{-}SMe)_3(\mu\text{-}\eta^2\text{-}N{=}NMe)]$ **4b** showing 20% probability ellipsoids; selected bond lengths [Å] and angles [°]: Mo(1)−Mo(2) 2.613(1), Mo(1)−N(1) 2.058(5), Mo(2)−N(2) 2.096(4), N(1)−N(2) 1.202(5), N(2)−C(4) 1.490(6), Mo(1)−S(1) 2.419(1), Mo(1)−S(2) 2.453(1), Mo(1)−S(3) 2.406(1), Mo(2)−S(1) 2.429(1), Mo(2)−S(2) 2.451(1), Mo(2)−S(3) 2.423(1); Mo(1)−S(1)−Mo(2) 65.2(1), Mo(2)−S(2)−Mo(1) 64.4(1), Mo(1)−S(3)−Mo(2) 65.5(1), N(2)−Mo(2)−Mo(1) 68.1(1), N(1)−Mo(1)−Mo(2) 72.2(1), N(2)−N(1)−Mo(1) 107.1(4), N(1)−N(2)−Mo(2) 112.5(4), N(1)−N(2)−C(4) 115.4(4), C(4)−N(2)−Mo(2) 132.0(3)

The structure of **4b** (Figure 1) consists of a tris(μ-thiolato)dimolybdenum unit $\{Mo_2Cp_2(\mu\text{-}SMe)_3\}$ bridged by a

bidentate, doubly bent N=N−Me group, which is σ-bonded to the Mo_2 unit through both nitrogen atoms [Mo(1)−N(1) = 2.058(5), Mo(2)−N(2) = 2.096(4) Å]. These Mo−N distances differ only slightly from one another. They are shorter than the Mo−NH_2 bonds in the amido complex [$Mo_2Cp_2(\mu\text{-}SMe)_3(\mu\text{-}NH_2)$] (**6**) [2.151(2) Å],[4] but not nearly as short as the terminal Mo−NNMe distance of 1.809(3) Å in [Mo{$N(CH_2CH_2S)_3$}(NNMe)], where the Mo−N=N angle is nearly linear.[14] In **4b** the N−N and Mo−Mo bonds are virtually coplanar [N(1)−Mo(1)−Mo(2)−N(2) = 0.1(2)°] and the N(1)−N(2) bond length of 1.202(5) Å is nearly equal to the corresponding value of 1.213(4) Å in [Mo{$N(CH_2CH_2S)_3$}(NNMe)], where the metal-bound N atom is *sp* rather than sp^2-hybridised. The N=N bond lengths in N_2Me ligands in general seem insensitive to the bonding mode of the diazenide: a value of 1.224(11) Å was found in the triply bridging diazenido compound [{$Mn(CO)_4$}$_3$(μ_3-N_2Me)],[11] 1.247(4) Å in the bridging singly bent diazo complex [$CpW(CO)_2(\mu_2\text{-}\eta^2\text{-}N_2Me)Cr(CO)_5$],[12] and values of 1.215(5) and 1.199(4) Å in the singly bent N_2Me mononuclear complexes [$CpW(CO)_2(N_2Me)$][13] and [$ReCl(N_2Me)(MeNHNH_2)${$PPh(OEt)_2$}$_3$][BPh_4], respectively.[9]

The endocyclic angles in the Mo_2N_2 ring [72.2(1) and 68.1(1)° at Mo, 107.1(4) and 112.5(4)° at N(1) and N(2)] resemble those in related strained four-membered M_2N_2 ring derivatives such as [{$C_5Me_5Ir(CO)$}$_2$($\mu\text{-}\eta^2$-*p*-$N_2C_6H_4OMe$)][8] and [$Os_3(CO)_{10}(\mu\text{-}H)(\mu\text{-}\eta^2\text{-}N_2C_6H_5)$].[10] The Mo(1)−Mo(2) distance [2.613(1) Å] is typical for a quadruply bridged {$Mo_2Cp_2(\mu\text{-}SMe)_3$} dimolybdenum(III) compound and indicates the bond of unit order required by electron counting rules.[2]

Synthesis and Spectroscopic Characterisation of [$Mo_2Cp_2(\mu\text{-}SMe)_3(\mu\text{-}\eta^1\text{-}N{=}NMe)$] (8) and [$Mo_2Cp_2(\mu\text{-}SMe)_3(\mu\text{-}\eta^1\text{-}N{=}NHMe)$]($BF_4$) (9)

Photolysis of a red solution of **4** in THF afforded an orange solution of the complex [$Mo_2Cp_2(\mu\text{-}SMe)_3(\mu\text{-}\eta^1\text{-}N{=}NMe)$] (**8**) (Scheme 1). Conversion of **4** into **8** was complete within 48 h. ^{1}H NMR analysis of **8** revealed the presence of two isomeric species, which are believed to differ only in the orientation of a single SMe group. The ^{1}H NMR spectrum shows two similar sets of resonances: two peaks between δ = 6 and δ = 5, a single signal at about δ = 3.4 and three peaks between δ = 2 and δ = 1, which can be assigned to inequivalent cyclopentadienyl ligands, the NMe end of the diazo bridge, and the three SMe groups, respectively.

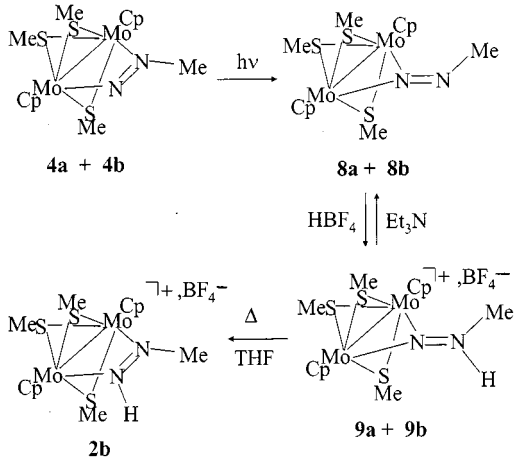

Scheme 1

The mode of coordination of the diazenido bridge in **8** is preserved in the orange cationic complex **9**, which is formed by addition of HBF_4 to a solution of **8** (Scheme 1). Compound **9** could be identified without any ambiguity by ^{1}H NMR spectroscopy. Its ^{1}H NMR spectrum displays two sets of characteristic resonances assigned to the {$Mo_2Cp_2(\mu\text{-}SMe)_3$} cores of two isomers. In addition, two similar patterns consisting of a doublet ($J_{H,H}$ = 4.0 Hz) at δ = 3.56 and 3.64, and a single broad resonance at δ = 11.98 and 12.64 can be attributed to an H−N−CH_3 group. Irradiation of the signals at δ = 11.98 and 12.64 gave two singlets at δ = 3.56 and 3.64, which confirms the $^3J_{H,H}$ coupling. Furthermore, variable-temperature ^{1}H NMR experiments (between 293 and 340 K) show that the line shape is temperature dependent, suggesting that isomer **9a** is fluxional. On warming to 330 K in CD_3CN, broadening and coalescence of the cyclopentadienyl signals of **9a** occurred. The activation barrier of the resulting dynamic process, estimated from the chemical shift difference Δν and the coalescence temperature of the Cp signals in the ^{1}H NMR spectrum [$\Delta G^{\neq} = 4.575T_c(9.972 + \log_{10}T_c - \log_{10}\Delta\nu)$], is 71 ± 1 kJ·mol^{-1}.[15] A similar behaviour ($\Delta G^{\neq}$ = 61 ± 1 kJ·mol^{-1}) has previously been reported for the analogous phenyl derivative [$Mo_2Cp_2(\mu\text{-}SMe)_3(\mu\text{-}\eta^1\text{-}N{=}NHPh)$]($BF_4$) (**10**), in which the methyl groups of the equatorial thiolate bridges are in an *anti* configuration.[5] The dynamic behaviour of **9** and **10** is attributable to rotation of the NHR group around the N=N bond axis.

Compound **9** was easily deprotonated to regenerate **8** (Scheme 1), and thermolysis of a mixture of **9a** and **9b** afforded complex **2b** exclusively (Scheme 1).

Discussion

Protic diazenes, RN=NH, are reactive species that readily decompose into RH by an N_2 extrusion process.[7,16] Such molecules may be stabilized through coordination to one or two metal centres. There are several reports of the formation of protic diazene complexes by insertion of aryldiazonium reagents ArN_2^+ into a metal-hydride bond or by oxidation of a suitable hydrazine $RNHNH_2$ (R = aryl, alkyl or H), previously coordinated to a metal centre.[7,9,17−19] The latter route has been used to effect the synthesis of methyldiazene derivatives.[9,19] However, it remains unclear precisely how substituted hydrazines $RNHNH_2$ (R = Me, Ph) undergo dehydrogenation upon treatment with [$Mo_2Cp_2(\mu\text{-}SMe)_3(MeCN)_2$]($BF_4$) (**1**). It has not been possible to detect the loss of H_2 or the formation of any other side products arising from the eventual disproportionation

or deprotonation of hydrazines.[20] The formation of the amido derivative $[Mo_2Cp_2(\mu\text{-}SMe)_3(\mu\text{-}NH_2)]$ (**6**) from methylhydrazine indicates that the reagent does undergo disproportionation, but **6** has not been isolated from the analogous reaction with phenylhydrazine. We assume that **6** can be formed by reaction of **1** with ammonia at room temperature, but that has no bearing on the formation of **2**−**3** through a disproportionation mechanism.[21] However, the hydrido complex $[HOs(CO)_{10}(\mu\text{-}\eta^2\text{-}N_2Ph)]$ was formed by reaction of phenylhydrazine with the triosmium derivative $[Os_3(CO)_{10}(MeCN)_2]$.[10] This suggests that the protons of the hydrazine can add to a metal centre and that subsequent elimination of H_2 or deprotonation may afford diazenido or diazene species.

The deprotonation of the diazene species **2a** allowed us to compare the behaviour of methyldiazene and methyldiazenido substrates at a bimetallic site with that of the related phenyl ligands that we have described previously.[5,6] $[Mo_2Cp_2(\mu\text{-}SMe)_3(\mu\text{-}\eta^2\text{-}N{=}NMe)]$ (**4**) was completely transformed by photolysis into its η^1 isomer $[Mo_2Cp_2(\mu\text{-}SMe)_3(\mu\text{-}\eta^1\text{-}N{=}NMe)]$ (**8**). It is worth noting that **8** was readily protonated at the outer nitrogen (N_β) atom and that the protonated product $[Mo_2Cp_2(\mu\text{-}SMe)_3(\mu\text{-}\eta^1\text{-}N{=}NHMe)](BF_4)$ (**9**) was easily isolated as a powder that could be stored for several weeks under a nitrogen atmosphere without isomerizing into **2**. Compound **9** is reasonably stable in solution, and its isomerization into the $\{\mu\text{-}\eta^2\text{-}HN{=}NMe\}$ species **2** was observed only after it had been kept for long periods in solution at ambient temperature (for example, during attempts at recrystallization) or when the solution had been heated. This contrasts with the behaviour of the phenyl analogue **10**, which isomerizes readily at room temperature, and which can be stored in solution only after cooling. The methyl group is evidently more effective than the phenyl group at stabilizing the $\{\mu\text{-}\eta^1\text{-}N{=}NHR\}$ system, and the outer nitrogen atom in $[Mo_2Cp_2(\mu\text{-}SMe)_3(\mu\text{-}\eta^1\text{-}N{=}NR)]$ complexes is obviously more basic when R = Me. Attempted protonation of the outer nitrogen atom in a doubly bent η^1-N=NR bridge has usually been unsuccessful.[8,10]

In mononuclear complexes containing a terminal doubly bent diazenido ligand it has been shown that the inner nitrogen atom (N_α) is more basic than the N_β atom, and is therefore more easily protonated to give diazene groups.[8] In complexes like $[Mo_2Cp_2(\mu\text{-}SMe)_3(\mu\text{-}\eta^1\text{-}N{=}NR)]$ the inner nitrogen atom is coordinated to both metal atoms and only the outer nitrogen can be protonated.

The facile $\mu\text{-}\eta^1 \rightarrow \mu\text{-}\eta^2$ rearrangement process observed in $[Mo_2Cp_2(\mu\text{-}SMe)_3(\mu\text{-}N_2HR)]^+$ species, with concomitant migration of the proton from the outer to the inner nitrogen atom to give an η^2-NH=NR species, reveals the flexible nature of the ($\mu\text{-}\eta^1\text{-}N_2HR$) bridge, especially when R= phenyl. The values of the energy barrier for rotation of the NHR group about the N−N axis in **9** and **10** are in agreement with a greater lability of the diazo bridge when R = Ph than when R = Me. Indeed, replacement of a phenyl by a methyl group increases the energy barrier ($\Delta G^{\neq}$) by about 10 kJ/mol. This suggests that the η^1-N_2HR bridging ligand is better described as an hydrazido(2−) limiting form when R = Ph (II in Scheme 2) and as an isodiazene form when R = Me (I in Scheme 2). The greater electron-withdrawing ability of Ph than Me is consistent with this suggestion. In addition, preliminary electrochemical experiments on the protonated diazenido complexes[22] show that oxidation, which can be compared with the electronic effect of replacing Me by Ph, favours the $\mu\text{-}\eta^1 \rightarrow \mu\text{-}\eta^2$ isomerisation. Moreover, in reactions with bases the cation $[Mo_2Cp_2(\mu\text{-}SMe)_3(MeCN)_2]^+$, (**1**$^+$), releases both of its terminal nitrile ligands more easily than $[Mo_2Cp_2(\mu\text{-}Cl)(\mu\text{-}SMe)_3]$ loses its bridging chloride group, thus explaining the formation of different products, η^2-diazene derivatives from **1**$^+$, but η^1-diazenido species from the μ-chloro complex.

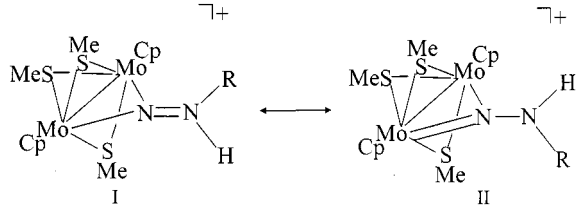

Scheme 2

Experimental Section

General Procedures: All the reactions were performed under nitrogen using standard Schlenk techniques. Solvents were deoxygenated and dried by standard methods. IR spectra were recorded on a Perkin−Elmer 1430 spectrophotometer from KBr pellets. Chemical analyses were performed by the Centre de Microanalyses du CNRS, Vernaison, France. ^{1}H NMR spectra were recorded on either a Bruker AC300 or AMX3 400 spectrometer and were referenced to $SiMe_4$. ^{1}H-^{15}N HMBC NMR spectra were recorded on a Bruker 500 and AMX3 400 spectrometer by R. Pichon and N. Kervarec. Literature methods were used for the preparation of $[Cp_2Mo_2(\mu\text{-}SMe)_3(CH_3CN)_2](BF_4)$ (**1**).[23]

Preparation of $[Mo_2Cp_2(\mu\text{-}SMe)_3(\mu\text{-}\eta^2\text{-}HN{=}NMe)](BF_4)$ (2a): An excess of methylhydrazine (72 μL, 1.36 mmol) was added to a solution of **1** (0.32 mmol, 200 mg) in 15 mL of acetonitrile. The mixture was stirred at room temperature for one hour, whereupon the colour of the mixture changed from red to orange and then a brown solid of $[Mo_2Cp_2(\mu\text{-}SMe)_3(\mu\text{-}NH_2)]$ (**6**) precipitated. Precipitation of **6** was completed by concentration and cooling of the solution (yields: 54 mg, 35%). The solution was then filtered off and the solvents evaporated under vacuum to afford a brown residue that was washed with pentane (2 × 10 mL). Complex **2a** was obtained as a brown powder (yield: 104 mg, 55%). $C_{14}H_{24}BF_4N_2Mo_2S_3$ (595.2): calcd. C 28.3, H 3.9, N 4.7; found C 28.1, H 4.3, N 5.3. Selected spectroscopic data for **2a**: ^{1}H NMR ($CDCl_3$, 298 K): δ = 1.54 (s, 3 H, SCH_3), 1.63 (s, 3 H, SCH_3), 1.77 (s, 3 H, SCH_3), 3.69 (s, 3 H, HN=NCH_3), 5.70 (s, 5 H, C_5H_5), 5.88 (s, 5 H, C_5H_5), 12.30 (s, 1 H, HN=NCH$_3$). IR (KBr): $\tilde{\nu}$ = 3160 cm^{-1} (w), [ν(N−H)], 1150−950 (s) [ν(B−F)].

Preparation of $[Mo_2Cp_2(\mu\text{-}SMe)_3(\mu\text{-}\eta^2\text{-}HN{=}NPh)](BF_4)$ (3a): An excess of phenylhydrazine (54 μL, 0.48 mmol) was added at room temperature to an acetonitrile (10 mL) solution of **1** (0.16 mmol, 100 mg). The mixture was stirred for one hour and the solution turned orange. The volume of the mixture was then reduced under vacuum and diethyl ether was added to precipitate the brown-or-

ange product **3a** (yield: 73 mg, 70%). $C_{19}H_{25}BF_4N_2Mo_2S_3$ (656.3): calcd. C 34.8, H 3.8, N 4.3; found C 35.3, H 4.2, N 4.3. Selected spectroscopic data for **3a**: ^{1}H NMR (CD_2Cl_2, 298 K): δ = 1.71 (s, 3 H, SCH_3), 1.73 (s, 3 H, SCH_3), 1.81 (s, 3 H, SCH_3), 5.85 (s, 5 H, C_5H_5), 6.03 (s, 5 H, C_5H_5), 7.32−6.79 (m, 5 H, HN=NC$_6H_5$), 12.0 (s, 1 H, HN=NC$_6$H$_5$). IR (KBr): ṽ = 3200 cm^{-1} (w) [ν(N−H)], 1200−900 (s), [ν(B−F)].

Preparation of [Mo_2Cp_2(μ-SMe)$_3$(μ-η^2-HN=NR)](BF$_4$) [R = Me (2b), R = Ph (3b)]: A solution of **2a** (0.17 mmol, 100 mg) in 10 mL of acetonitrile was warmed to 70 °C for 24 h. The solution turned green. The solution was then concentrated and addition of diethyl ether precipitated a green powder, which was washed twice with pentane (2 × 10 mL). Complex **2b** was obtained as a green powder (yield: 96 mg, 95%). $C_{14}H_{24}BF_4N_2Mo_2S_3$ (595.2): calcd. C 28.2, H 3.9, N 4.7; found C 28.0, H 4.2, N 5.3. Selected spectroscopic data for **2b**: ^{1}H NMR ($CDCl_3$, 298 K): δ = 1.45 (s, 3 H, SCH_3), 1.58 (s, 3 H, SCH_3), 1.63 (s, 3 H, SCH_3), 3.79 (s, 3 H, HN=NCH_3), 5.77 (s, 5 H, C_5H_5), 5.91 (s, 5 H, C_5H_5), 12.58 (s, 1 H, HN=NCH$_3$). IR (KBr): 3080 cm^{-1} (w), ṽ = [ν(N−H)], 1200−950 (s), [ν(B−F)].

In a similar manner, the complex **3b** was obtained as an orange powder (yield: 88 mg, 90%) upon warming **3a** (0.15 mmol, 98 mg). Selected spectroscopic data for **3b**:[5] ^{1}H NMR (CD_3CN, 298 K): δ = 1.52 (s, 3 H, SCH_3), 1.65 (s, 3 H, SCH_3), 1.72 (s, 3 H, SCH_3), 5.79 (s, 5 H, C_5H_5), 6.11 (s, 5 H, C_5H_5), 7.42−6.93 (m, 5 H, HN=NC$_6H_5$), 12.6 (s, 1 H, HN=NC$_6$H$_5$).

Preparation of [Mo_2Cp_2(μ-SMe)$_3$(μ-η^2-N=NMe)](BF$_4$) (4a−b): 100 μL of a 2.5 M solution of butyllithium in hexane (0.25 mmol) was added to a dichloromethane (10 mL) solution of **2a** or **2b** (100 mg, 0.17 mmol). The solution rapidly turned red. After stirring for a few minutes at ambient temperature, the solvent was evaporated. The residue was extracted with diethyl ether and the extract was purified by chromatography on a silica gel column. Elution with a mixture of THF/Et_3N (90:10) afforded compounds **4a** (yield: 60 mg, 70%) and **4b** (yield: 56 mg, 65%).
4a: ^{1}H NMR ($CDCl_3$, 298 K): δ = 1.29 (s, 3 H, SCH_3), 1.44 (s, 3 H, SCH_3), 1.69 (s, 3 H, SCH_3), 3.41 (s, 3 H, N=NCH_3), 5.44 (s, 5 H, C_5H_5), 5.67 (s, 5 H, C_5H_5).
4b: ^{1}H NMR ($CDCl_3$, 298 K): δ = 1.31 (s, 3 H, SCH_3), 1.38 (s, 3 H, SCH_3), 1.48 (s, 3 H, SCH_3), 3.45 (s, 3 H, N=NCH_3), 5.45 (s, 5 H, C_5H_5), 5.68 (s, 5 H, C_5H_5).

In similar manner, complexes **5a−b** were obtained as green powders (yield: **5a**: 55 mg, 65%; **5b**: 60 mg 70%) by reacting BuLi with **3a** or **3b** (0.15 mmol, 100 mg).
5a:[5] ^{1}H NMR ($CDCl_3$, 298 K): δ = 1.49 (s, 3 H, SCH_3), 1.50 (s, 3 H, SCH_3), 1.68 (s, 3 H, SCH_3), 5.31 (s, 5 H, C_5H_5), 5.85 (s, 5 H, C_5H_5), 7.13−6.59 (m, 5 H, HN=NC$_6H_5$).
5b:[5] ^{1}H NMR ($CDCl_3$, 298 K): 1.37 (s, 3 H, SCH_3), 1.45 (s, 3 H, SCH_3), 1.53 (s, 3 H, SCH_3), 5.44 (s, 5 H, C_5H_5), 5.89 (s, 5 H, C_5H_5), 7.20−6.61 (m, 5 H, HN=NC$_6H_5$).

Photolysis of [Mo_2Cp_2(μ-SMe)$_3$(μ-η^2-N=NMe)](BF$_4$) (4a−b): A mixture of **4a** and **4b** (100 mg, 0.20 mmol) was dissolved in 20 mL of THF and irradiated with UV light [Hanau TQ 150 mercury-vapour lamp (300−600 nm)] for 48 h at room temperature. The solution changed from red to orange during this time. THF was removed under vacuum and the residue was purified by chromatography on a silica gel column. Elution with THF/Et_3N (90:10) afforded an orange band containing **8a−b** (yields: 60 mg, 60%).
8a: (80%). ^{1}H NMR ($CDCl_3$, 298 K): δ = 1.20 (s, 3 H, SCH_3), 1.27 (s, 3 H, SCH_3), 1.90 (s, 3 H, SCH_3), 3.41 (s, 3 H, N=NCH_3), 5.35 (s, 5 H, C_5H_5), 5.53 (s, 5 H, C_5H_5).
8b: (20%). ^{1}H NMR ($CDCl_3$, 298 K): δ = 1.18 (s, 3 H, SCH_3), 1.46 (s, 3 H, SCH_3), 1.83 (s, 3 H, SCH_3), 3.43 (s, 3 H, N=NCH_3), 5.44 (s, 5 H, C_5H_5), 5.62 (s, 5 H, C_5H_5).

Preparation of Complexes [Mo_2Cp_2(μ-SMe)$_3$(μ-η^1-N=NHMe)](BF$_4$) (9a−b): 1 Equiv. of HBF_4·Et_2O was added to a solution of **8** (100 mg, 0.20 mmol) in Et_2O (10 mL). Orange solids of [Mo_2Cp_2(μ-SMe)$_3$(μ-η^1-N=NHMe)](BF$_4$) (**9**) precipitated from the solution and were collected by filtration and then washed with pentane (yields: 112 mg, 85%). $C_{14}H_{24}BF_4N_2Mo_2S_3$ (595.2): calcd. C 28.3, H 3.9, N 4.7; found C 29.0, H 4.1, N 4.7. Selected spectroscopic data for **9a**: ^{1}H NMR ($CDCl_3$, 298 K): δ = 1.51 (s, 3 H, SCH_3), 1.64 (s, 3 H, SCH_3), 2.08 (s, 3 H, SCH_3), 3.64 (d, $J_{H,H}$ = 4 Hz, 3 H, N=NHCH_3), 5.88 (s, 5 H, C_5H_5), 5.97 (s, 5 H, C_5H_5), 12.40 (s, 1 H, N=NHCH$_3$). Selected spectroscopic data for **9b**: ^{1}H NMR ($CDCl_3$, 298 K): δ = 1.47 (s, 3 H, SCH_3), 1.49 (s, 3 H, SCH_3), 1.98 (s, 3 H, SCH_3), 3.56 (d, $J_{H,H}$ = 4 Hz, 3 H, N=NHCH_3), 5.96 (s, 5 H, C_5H_5), 6.03 (s, 5 H, C_5H_5), 11.97 (s, 1 H, N=NHCH$_3$). IR (KBr): ṽ = 3220 cm^{-1} (w), [ν(N−H)], 1200−900 (s), [ν(B−F)].

Structure Analysis: Details of the structure analysis of **4b** are summarised in Table 1.[25] The crystals were very thin plates and it was necessary to use synchrotron radiation in conjunction with a Bruker SMART diffractometer to get measurable diffraction patterns. The structure was solved and refined by standard methods.[24] The cyclopentadienyl rings were treated as variable metric rigid groups.

Table 1. Crystallographic data for [Mo_2Cp_2(μ-SMe)$_3$(μ-η^2-N=NMe)] **4b**

	4b
Empirical formula	$C_{14}H_{22}Mo_2N_2S_3$
Fw	506.40
Temperature [K]	160(2)
Wavelength [Å]	0.68490
Cryst system	Orthorhombic
Space group	*Pbca*
a [Å]	11.9830(5)
b [Å]	16.1544(7)
c [Å]	17.5702(7)
V [Å^3]	3401.2(2)
Z	8
$D_{calcd.}$ [Mg/m^3]	1.978
μ [mm^{-1}]	1.837
F(000)	2016
Crystal size [mm]	0.52 × 0.18 × 0.01
θ range [deg]	2.23 to 23.0
Index ranges	$-13 \le h \le 14$ $-18 \le k \le 20$ $-23 \le l \le 22$
No. of rflns collected	14135
No. of indep rflns	2639 [R_{int} = 0.065]
Refinement method	Full-matrix least-squares on F^2
No. of data/params	2639/178
Goodness of fit on F^2	1.10
*R*1, w*R*2 [$I > 2\sigma(I)$]	0.038 0.062
*R*1, w*R*2 (all data)	0.054 0.065
Δρ range, e·A^{-3}	+1.13 to −0.75

Acknowledgments

We thank the CNRS, EPSRC, Glasgow University, and Brest University for financial support.

[1] [1a] *Transition Metal Sulfur Chemistry-Biological and Industrial Significance* (Eds.: E. I. Stiefel, K. Matsumoto), ACS Symposium Series, vol. 653, **1996**. [1b] D. Sellmann, J. Sutter, *Acc. Chem. Res.* **1997**, *30*, 460−469. [1c] D. Sellmann, J. Utz, N. Blum, F. W. Heinemann, *Coord. Chem. Rev.* **1999**, *190−192*, 607−627. [1d] R. L. Richards, *New J. Chem.* **1997**, *21*, 727−732. [1e] R. L. Richards, *Coord. Chem. Rev.* **1996**, *154*, 83−97. [1f] D. Coucouvanis, *J. Bio. Inorg. Chem.* **1996**, *1*, 594−600. [1g] M. Rakowski DuBois, *Polyhedron* **1997**, *16*, 3089−3098.[1h] M. Rakowski DuBois, *J. Cluster Sci.* **1996**, *7*, 293−315. [1i] S. Kuwata, M. Hidai, *Coord. Chem. Rev.* **2001**, *213*, 211−305.

[2] F. Y. Pétillon, P. Schollhammer, J. Talarmin, K. W. Muir, *Coord. Chem. Rev.* **1998**, *178−180*, 203−247.

[3] [3a] P. Schollhammer, N. Cabon, J-F. Capon, F. Y. Pétillon, J. Talarmin, K. W. Muir, *Organometallics* **2001**, *20*, 1230−1242. [3b] P. Schollhammer, M. Le Hénanf, C. Le Roy-Le Floch, F. Y. Pétillon, J. Talarmin, K. W. Muir, *J. Chem. Soc., Dalton Trans.* **2001**, 1573−1577.

[4] P. Schollhammer, F. Y. Pétillon, S. Poder-Guillou, J. Y. Saillard, J. Talarmin, K. W. Muir, *Chem. Commun.* **1996**, 2633−2634.

[5] P. Schollhammer, E. Guénin, F. Y. Pétillon, J. Talarmin, K. W. Muir, D. S. Yufit, *Organometallics* **1998**, *17*, 1922−1924.

[6] F. Y. Pétillon, P. Schollhammer, J. Talarmin, K. W. Muir, *Inorg. Chem.* **1999**, *38*, 1954−1955.

[7] [7a] D. Sutton, *Chem. Rev.* **1993**, *93*, 995−1022 and references therein. [7b] D. Sutton, *Chem. Soc. Rev.* **1975**, *4*, 443−470. [7c] R. B. King, *J. Organomet. Chem.* **1995**, *500*, 187−194. [7d] H. Zollinger, *Diazo Chemistry II*, VCH, Weinheim, Germany, **1995**.

[8] X. Yan, R. J. Batchelor, F. W. B. Einstein, D. Sutton, *Inorg. Chem.* **1996**, *35*, 7818−7828 and references therein.

[9] G. Albertin, S. Antoniutti, A. Bacchi, E. Bordignon, F. Miani, G. Pelizzi, *Inorg. Chem.* **2000**, *39*, 3283−3293 and references therein.

[10] D. E. Samkoff, J. R. Shapley, M. R. Churchill, H. J. Wasserman, *Inorg. Chem.* **1984**, *23*, 397−402.

[11] W. A. Herrmann, M. L. Ziegler, K. Wiedenhammer, *Angew. Chem. Int. Ed. Engl.* **1976**, *15*, 368−369.

[12] G. L. Hillhouse, B. L. Haymore, S. A. Bistram, W. A. Herrmann, *Inorg. Chem.* **1983**, *22*, 314−318 and references therein.

[13] G. L. Hillhouse, B. L. Haymore, W. A. Herrmann, *Inorg. Chem.* **1979**, *18*, 2423−2426.

[14] S. C. Davies, D. L. Hughes, R. L. Richards, J. R. Sanders, *J. Chem. Soc., Dalton Trans.* **2000**, 719−725.

[15] H. S. Gutowsky, C. H. Holm, *J. Chem. Phys.* **1956**, *25*, 1228−1234.

[16] [16a] M. R. Smith, G. L. Hillhouse, *J. Am. Chem. Soc.* **1988**, *110*, 4066−4068. [16b] M. R. Smith, G. L. Hillhouse, *J. Am. Chem. Soc.* **1989**, *111*, 3764−3765. [16c] M. R. Smith, T-Y. Cheng, G. L. Hillhouse, *Inorg. Chem.* **1992**, *31*, 1535−1538.

[17] H. Kisch, P. Holzmeier, *Adv. Organomet. Chem.* **1992**, *34*, 67−109.

[18] For example: [18a] D. Sellmann, J. Köppler, M. Moll, F. Knoch, *Inorg. Chem.* **1993**, *32*, 960−964. [18b] D. Sellmann, W. Soglowek, F. Knoch, M. Moll, *Angew. Chem. Int. Ed. Engl.* **1989**, *28*, 1271−1272. [18c] D. Sellmann, E. Böhlen, M. Waeber, G. Huttner, L. Zsolnai, *Angew. Chem. Int. Ed. Engl.* **1985**, *24*, 981−982. [18d] G. Huttner, W. Gartzke, K. Allinger, *Angew. Chem. Int. Ed. Engl.* **1974**, *13*, 822−823. [18e] M. R. Smith, T-Y. Cheng, G. L. Hillhouse, *J. Am. Chem. Soc.* **1993**, *115*, 8638−8642. [18f] T-Y. Cheng, A. Ponce, A. L. Rheingold, G. L. Hillhouse, *Angew. Chem. Int. Ed. Engl.* **1994**, *33*, 657−659. [18g] G. Albertin, S. Antoniutti, E. Bordignon, S. Pattaro, *J. Chem. Soc., Dalton Trans.* **1997**, 4445−4453. [18h] G. Albertin, S. Antoniutti, A. Bacchi, E. Bordignon, P. Matteo Dolcetti, G. Pelizzi, *J. Chem. Soc., Dalton Trans.* **1997**, 4435−4444. [18i] J. P. Collman, J. E. Hutchison, M. A. Lopez, R. Guilard, R. A. Reed, *J. Am. Chem. Soc.* **1991**, *113*, 2794−2796.

[19] [19a] M. R. Smith, R. L. Keys, G. L. Hillhouse, *J. Am. Chem. Soc.* **1989**, *110*, 8312−8314. [19b] G. Albertin, S. Antoniutti, A. Bacchi, M. Bergamo, E. Bordignon, G. Pelizzi, *Inorg. Chem.* **1998**, *37*, 479−489.

[20] [20a] W. J. Evans, G. Kociok-Köhn, V. S. Leong, J. W. Ziller, *Inorg. Chem.* **1992**, *31*, 3593−3600. [20b] T. E. Glassman, M. G. Vale, R. R. Schrock, *Inorg. Chem.* **1992**, *31*, 1985−1986. [20c] R. R. Schrock, T. E. Glassman, M. G. Vale, M. Kol, *J. Am. Chem. Soc.* **1993**, *115*, 1760−1772.

[21] P. Schollhammer, F. Y. Pétillon, J. Talarmin, K. W. Muir, unpublished results.

[22] J. Talarmin, unpublished results.

[23] F. Barrière, Y. Le Mest, F. Y. Pétillon, S. Poder-Guillou, P. Schollhammer, J. Talarmin, *J. Chem. Soc., Dalton Trans.* **1996**, 3967−3976.

[24] Programs used: SHELX97 − Programs for Crystal Structure Analysis (Release 97−2). G. M. Sheldrick, Institüt für Anorganische Chemie der Universität, Tammanstrasse 4, D-3400 Göttingen, Germany, 1998. WinGX − A Windows Program for Crystal Structure Analysis. L. J. Farrugia, *J. Appl. Crystallogr.* **1999**, *32*, 837.

[25] CCDC-170095 contains the supplementary crystallographic data for this paper. These data can be obtained free of charge at www.ccdc.cam.ac.uk/conts/retrieving.html [or from the Cambridge Crystallographic Data Centre, 12 Union Road, Cambridge CB2 1EZ, UK; fax: (internat.) + 44-1223/336-033; E-mail: deposit@ccdc.cam.ac.uk].

Received September 7, 2001
[I01347]

New Fluorenyl-Substituted Dioxotetraamine Ligands and Their Copper(II) Complexes − Crystal Structure and Fluorescent Sensing Properties in Aqueous Solution

Li-Jian Jiang,[a,b] Qin-Hui Luo,*[a] Qing-Xiang Li,[a] Meng-Chang Shen,[a] and Hong-Wen Hu[a]

Keywords: Copper / Dioxotetraamines / Fluorescence / N ligands

Two new ligands consisting of a fluorenyl and dioxotetraaza unit, namely, 2,10-diamino-6-(9*H*-fluoren-9-yl)-4,8-diazaundecane-5,7-dione (L^1) and 1-(9*H*-fluoren-9-yl)-1,4,7,10-tetraazadecane-5,6-dione (L^2) along with their copper(II) complexes have been synthesized. Their properties were examined by ES-MS and CV in aqueous solution and the crystal structure of the copper(II) complex of L^1 has also been determined. The recognition of the transition metal ions (Cu^{2+}, Ni^{2+}, etc.) by receptors has been studied in aqueous solutions using pH-potentiometric and fluorimetric titrations. The results show that the binding of Cu^{2+} or Ni^{2+} ion with L^1 leads to quenching of the fluorescence of the fluorenyl group, but on the contrary the fluorescence of L^2 is enhanced. The mechanisms are discussed.

Introduction

The phenomena of luminescence quenching and enhancement resulting from metal−ligand interactions have attracted much attention with regards to its application in sensing metal ions in solution.[1,2] The dioxotetraamine ligands are interesting because they coordinate metal ions with the release of two protons on the amide nitrogen atoms and are able to stabilize a +3 oxidation state of transition metal ions.[3] Recently, chemists have been devoted to append a luminophore to the framework of the dioxotetraamine ligands and to explore new fluorescent signaling systems.[4−6] Although many luminescent signaling systems have been presented,[7−9] to date, hydrophilic luminescent ligands used as receptors are still rarely reported.[1,10] In view of the high quantum yield and long fluorescent lifetime of fluorene, we linked it as a luminophore to the dioxotetraamine units and obtained two new water-soluble ligands, 2,10-diamino-6-(9*H*-fluoren-9-yl)-4,8-diazaundecane-5,7-dione (L^1) and 1-(9*H*-fluoren-9-yl)-1,4,7,10-tetraazadecane-5,6-dione (L^2) and synthesized their complexes $[Cu(H_{-2}L^1)]\cdot 2H_2O$ and $[Cu(H_{-2}L^2)]\cdot 4H_2O$ by the route shown in Scheme 1.

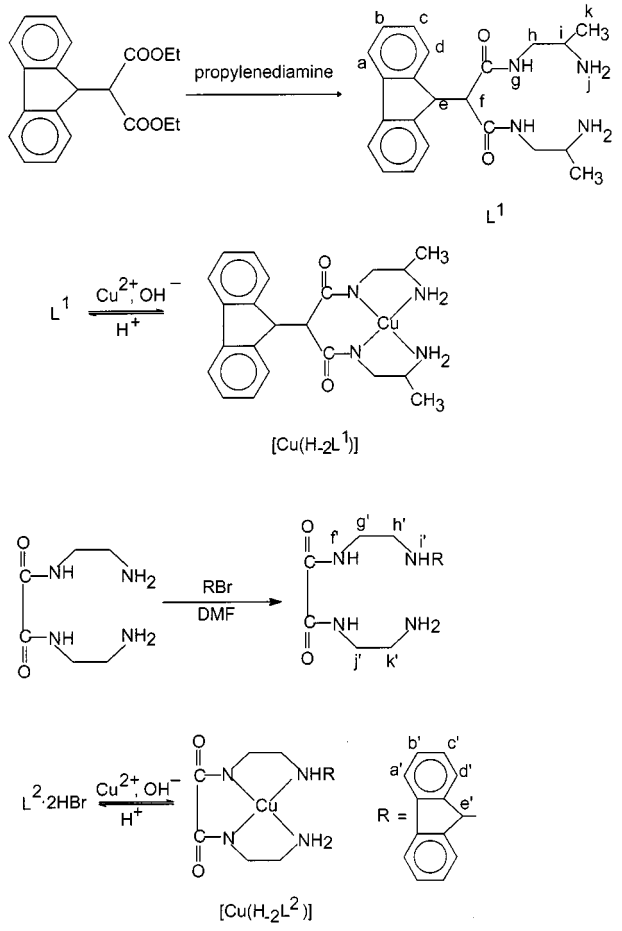

Scheme 1. Syntheses of ligands and complexes

[a] State Key Laboratory of Coordination Chemistry, Coordination Chemistry Institute, Nanjing University, Nanjing 210093, P. R. China
[b] Chemistry and Chemical Industry Department, Southeast University, Nanjing, 210009, P. R. China

 © WILEY-VCH Verlag GmbH, 69451 Weinheim, Germany, 2002 1434−1948/02/0303−0664 $ 17.50+.50/0 *Eur. J. Inorg. Chem.* **2002**, 664−670

It is interesting that L^1 and L^2 exhibit different fluorescent properties. The fluorescence of fluorenyl in L^1 is quenched by transfer of electrons from the metal center to the photoexcited state of fluorenyl during coordination of Cu^{II} or Ni^{II}. Conversely, fluorescence of L^2 is enhanced by coordination of transition metal ions. Their different fluorescent properties result from different positions of fluorenyl in the ligands. Because both ligands and complexes are water-soluble, they might have an application in biological analysis. To the best of our knowledge, the studies on enhancement of fluorescence of ligands by transition metal ions in aqueous solution are limited.[8]

Results and Discussion

Characterization

The values of molar conductivities of $[Cu(H_{-2}L^1)]\cdot 2H_2O$ and $[Cu(H_{-2}L^2)]\cdot 4H_2O$ in aqueous solution indicate that the amide protons are lost during coordination of the Cu^{2+} ion. In the IR spectra, both ligands exhibit two bands at about 760 and 740 cm^{-1} which are assigned to skeleton stretching vibration of the fluorene ring. The bands at 1660 cm^{-1} are assigned to the vibration of the carbonyl groups of L^1 or L^2 shifted by about 90 cm^{-1} during the coordination of Cu^{2+} ions. In the ^1H NMR spectrum of L^2 there are four groups of peaks at $\delta = 7.46-7.88$ assigned to the resonance absorption of protons of the fluorene ring, confirming linkage of the fluorenyl group to the dioxotetraamine unit. At $\delta = 2.96-3.62$ there are four groups of triple peaks assigned to the four methylene groups. The resonance absorption of protons on the nitrogen atoms disappeared due to exchange with heavy water. The ^1H NMR spectrum of the ligand L^1 is similar to that of L^2.

The ES-MS spectrum of L^2 that coexisted with the Cu^{2+} ion in methanol solution at pH = 9 is shown in Figure 1. The simplicity of the spectrum is attributed to the thermodynamic stability and kinetic inertness of the ligand. No obvious ligand fragmentation peaks were observed, showing that the ligand is quite stable under the ES-MS spectrum conditions.

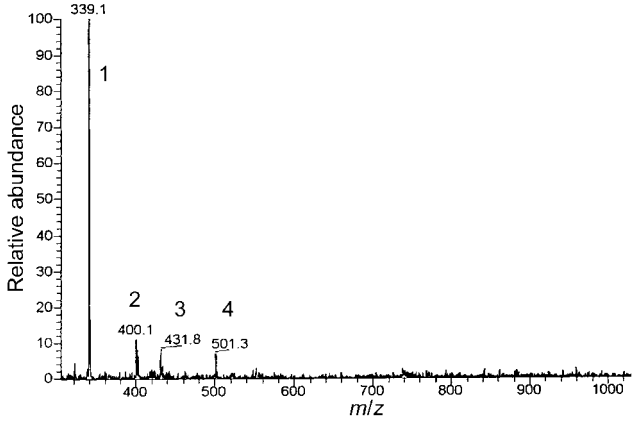

Figure 1. ES-MS spectrum of $L^2 + Cu^{2+}$ (1:1) system at pH = 9: 1. $[HL^2]^+$, 2. $[Cu(H_{-1}L^2)]^+$, 3. $[Cu(H_{-2}L^2)\cdot MeOH]^+$, 4. $[CuL^2(ClO_4)]^+$

Crystal Structure of $[Cu(H_{-2}L^1)]\cdot 2H_2O$

In Figure 2 the crystal structure of the copper(II) complex $[Cu(H_{-2}L^1)]\cdot 2H_2O$ is shown. Selected bond lengths and angles are listed in Table 1. From Figure 3 and Table 1 it can been seen that the copper(II) atom is situated in the center of a slightly distorted square composed of four nitrogen atoms. The distance between the plane and copper atom is 0.1628(4) Å. The distances of Cu−N are 1.941−2.022 Å. Two methyl groups are situated on the same side of the plane composed of four nitrogen atoms, and the carbon atoms (C-1, C-9) of the methyl groups deviate from the plane by 1.705(9) and 1.751(6) Å, respectively. The six-membered ring composed of N-2, Cu-1, N-3, C-6, C-5 and C-4 has a chair conformation. The fluorene ring is linked to the six-membered ring by the C-5 atom and forms a dihedral angle of 45.7 ° with the plane composed of N-2, N-3, C-6 and C-4. The complex was linked to the water molecules by the hydrogen bonds and formed a two-dimensional network structure.

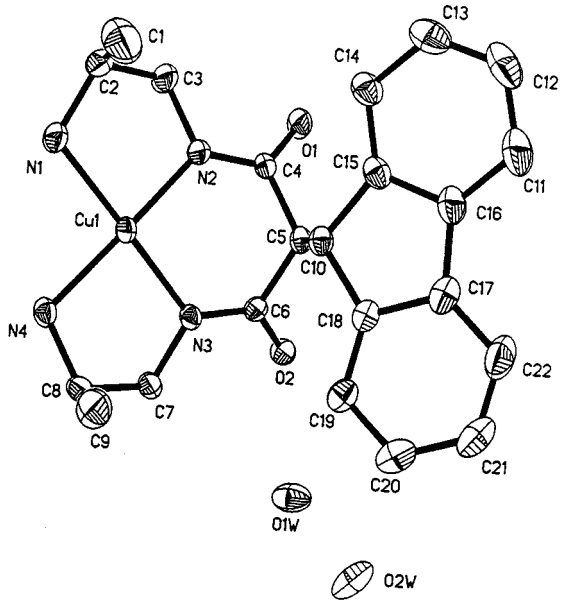

Figure 2. Crystal structure of $[Cu(H_{-2}L^1)]\cdot 2H_2O$

Table 1. Selected bond lengths [Å] and angles [°] of $[Cu(H_{-2}L^1)]$

Cu1−N1	2.012(4)	O1−C4	1.252(5)
Cu1−N2	1.941(3)	N1−C2	1.478(6)
Cu1−N3	1.955(3)	N2−C3	1.467(6)
Cu1−N4	2.022(3)	N2−C4	1.319(5)
N2−Cu1−N3	95.12(14)	C3−N2−Cu1	111.8(3)
N2−Cu1−N4	167.57(15)	C1−C2−N1	109.6(5)
N4−Cu1−N3	83.73(14)	N1−C2−C3	106.1(4)
N4−Cu1−N1	95.50(15)	C2−C3−N2	107.3(4)
N1−Cu1−N3	173.57(16)	C4−N2−C3	118.6(4)
C2−N1−Cu1	109.3(3)	O1−C4−N2	125.6(4)
C4−N2−Cu1	126.4(3)	O1−C4−C5	119.1(4)

Electrochemistry

The cyclic voltammetrical diagrams of $[Cu(H_{-2}L^1)]$ and $[Cu(H_{-2}L^2)]$ have similar features. During anodic scanning from 0−1.0 V, the ligands L^1 and L^2 do not show redox processes, but the two complexes display a pair of redox peaks. The separation between the anodic and cathodic peaks was 78−88 mV and the peak height ratio is near unit. A variation of the peak potential separation with scan rates (from 40 to 400 mVs^{-1}) was also observed. Furthermore, peak heights for the two complexes are proportional to the square roots of scan rates. The electron numbers of electrode oxidation reactions for $[Cu(H_{-2}L^1)]$ and $[Cu(H_{-2}L^2)]$ are 0.98 and 0.96 respectively, obtained by controlled potential analysis. These features are indicative of a one-electron quasi-reversible electrode process. Their values of $E_{1/2}$ are listed in Table 2.

Table 2. Half-wave potential $E_{1/2}$ (vs. SCE) for Cu^{III}/Cu^{II} redox process of $[Cu(H_{-2}L)]$ (L = L^1, L^2), pH = 9.8, scan rate 16 $mV{\cdot}s^{-1}$, Na_2SO_4 concentration = 0.5 $mol{\cdot}dm^{-3}$

	$[Cu(H_{-2}L^1)]$	$[Cu(H_{-2}L^2)]$
E_{pa} [V]	0.743	0.500
E_{Pc} [V]	0.655	0.422
ΔE [mV]	88	78
$E_{1/2}$ [V]	0.699	0.461

Stability of the Complexes

The pH-potentiometric titration curves of ligand L^1 and $L^2{\cdot}2HBr$ and that of the ligands plus metal ions(Cu^{2+}, Ni^{2+}, Co^{2+}, Zn^{2+}) are shown in Figure 3. In Figure 3 (a) all the curves 1−5 have two steps with defined inflection points. The first steps of all the curves are at $a = 2$ (a denotes the number of equivalents of base per mol of ligand), corresponding to free acid to be neutralized. The second step for the ligand L^1 (curve 1) is at $a \approx 4$, corresponding to protons of the amino cations to be neutralized. For the system of L^1 coexisting with the metal ions (curves 2−5), the second steps are at $a \approx 6$, corresponding to the formation of the predominant species $[M(H_{-2}L^1)]$.

The curves 6−8 in Figure 3 (b) are the titration curves of ligands L^2 and L^2 with the metal ions. At $a > 2$, the curves of the L^2 system are obviously different from those of the L^1 system. Curve 6 has two steps at $a = 3$ and $a = 4$, showing that the two amino nitrogen atoms have different abilities to bind protons. Two indistinct inflection points on curve 7 ($Cu^{2+} + L^2$) at $a = 4$ and $a = 5$ correspond to the formation of the dominant species $[CuL^2]^{2+}$ and $[Cu(H_{-1}L^2)]^{+}$, respectively. The obvious step of curve 8 at $a \approx 6$ shows that in the alkaline region $[Ni(H_{-2}L^2)]$ is the dominant species. Assuming that the above-mentioned species are formed, logarithms of the equilibrium constants, listed in Table 3, were obtained by curve fitting.

From Table 3 it can be seen that the stability sequence of the species [ML] and $[M(H_{-2}L)]$ (L = L^1 or L^2) is $Cu^{II} > Ni^{II} > Zn^{II} > Co^{II}$, being consistent with the Irving−Williams sequence. Stabilities of the complexes of L^2 in which an amino nitrogen atom is linked to a large fluorenyl group are lower than that of L^1. The species distribution curves of $L^1 + Cu^{2+}$ and $L^2 + Cu^{2+}$ systems are shown in Figure 4 and Figure 5, respectively.

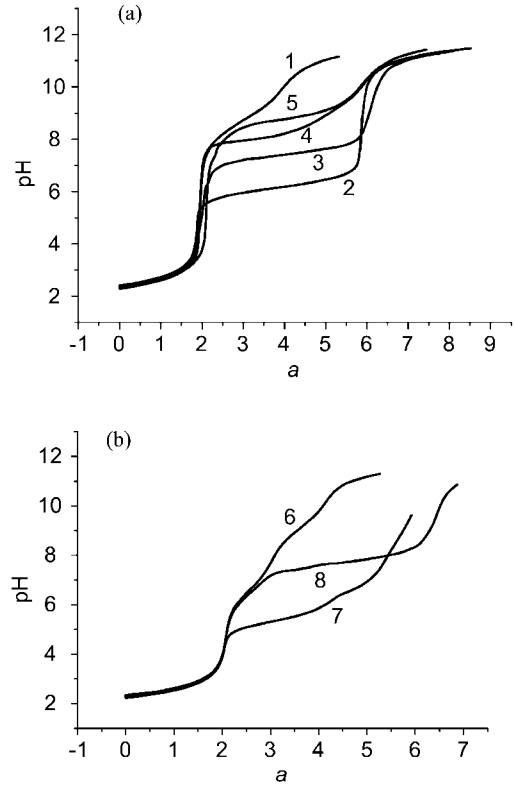

Figure 3. pH-potentiometric titration curves: (a) L^1 system, $L^1/M(NO_3)_2/HNO_3$ = 1:1:4; $L^1 = 1.8 \times 10^{-3}$ $mol{\cdot}dm^{-3}$: 1. M = none, 2. M = Cu^{2+}, 3. M = Ni^{2+}, 4. M = Zn^{2+}, 5. M = Co^{2+}; $L^2{\cdot}2HBr$ system, $L^2{\cdot}2HBr/HNO_3$ = 1:2; $L^2{\cdot}2HBr = 1.86 \times 10^{-3}$ $mol{\cdot}dm^{-3}$: 6. M = none, 7. $Cu^{2+} = 2.05 \times 10^{-3}$, 8. $Ni^{2+} = 2.08 \times 10^{-3}$ $mol{\cdot}dm^{-3}$

Fluorescent Properties of the Ligands in Aqueous Solution

The maximum fluorescence emission of L^1 in aqueous solution is located at 312 nm (pH = 9.0) by excitation of 280 nm. The intensity and position of the maximum emission remains constant at pH = 3−8. Figure 6 shows the dependence of the fluorescence intensity I_F (312 nm) and absorbance A (508 nm) of L^1 on the pH in the presence of Cu^{2+} ions. Both curves 1 and 2 show a typical sigmoidal shape. The dependence of the absorbance A on the pH is contrary to that of the fluorescence intensity. The curve of A vs. pH can be conveniently superimposed on the distribution diagram of $[Cu(H_{-2}L^1)]$ (Figure 4, curve 2), indicating that the formation of species $[Cu(H_{-2}L^1)]$ leads to quenching of the fluorescence by an electron transfer from the Cu^{II} center to the photoexcited state of the fluorenyl group Fl*. The fluorescent mechanism is similar to that of its analogs.[4,6] The electron-transfer process is described by Equation (1). The variation of potential of the electron transfer (ΔE_T) can be calculated by Equation (2).

Table 3. Logarithm of equilibrium constants of the ligands and complexes, 30±0.1 °C, KNO_3 concentration = 0.10 mol·dm^{-3}

Reaction[a]	H	Cu	Ni	Co	Zn[b]
$H^+ + L^1 \leftrightarrows (HL^1)^+$	9.11±0.01				
$2H^+ + L^1 \leftrightarrows (H_2L^1)^{2+}$	17.43±0.03				
$M^{2+} + L^1 \leftrightarrows [ML^1]^{2+}$		7.80±0.02	4.80±0.02		
$M^{2+} + L^1 \leftrightarrows [M(H_{-1}L^1)]^+ + H^+$		1.84±0.03		−5.85±0.02	−3.82±0.02
$M^{2+} + L^1 \leftrightarrows [M(H_{-2}L^1)] + 2\,H^+$		−4.12±0.03	−9.73±0.03	−14.39±0.03	−13.17±0.03
$H^+ + L^2 \leftrightarrows (HL^2)^+$	8.98±0.01				
$2H^+ + L^2 \leftrightarrows (H_2L^2)^{2+}$	15.51±0.03				
$M^{2+} + L^2 \leftrightarrows [ML^2]^{2+}$		7.68±0.02[b]	3.11±0.02[b]		
$M^{2+} + L^2 \leftrightarrows [M(H_{-1}L^2)]^+ + H^+$		1.68±0.03[b]			
$M^{2+} + L^2 \leftrightarrows [M(H_{-2}L^2)] + 2\,H^+$		−6.48±0.03[b]	−11.09±0.03[b]		

[a] For each system, two titrations were performed; during each titration more than 60 points were recorded. [b] At 25±0.1 °C.

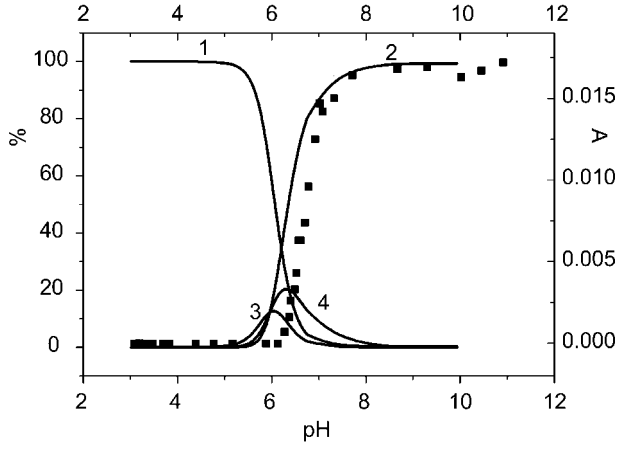

Figure 4. Species distribution curves and dependence of the absorbance A (■) on the pH for the $L^1 + Cu^{2+}$ system ($Cu^{2+} = L^1 = 2.6 \times 10^{-4}$ mol·dm^{-3}): 1. Cu^{2+}, 2. $[Cu(H_{-2}L^1)]$, 3. $[CuL^1]^{2+}$, 4. $[Cu(H_{-1}L^1)]^+$

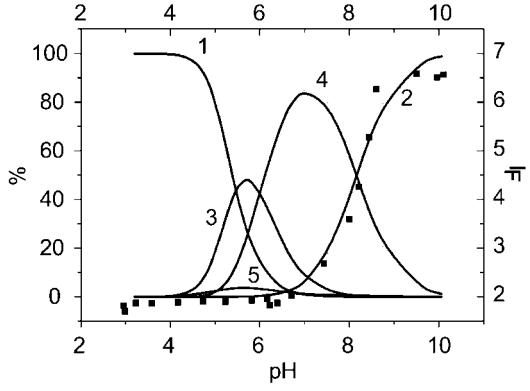

Figure 5. Species distribution curves and the dependence of the fluorescence intensity I_F (■) on the pH for the $L^2 + Cu^{2+}$ system ($Cu^{2+} = L^2 = 6.8 \times 10^{-5}$ mol·dm^{-3}): 1. Cu^{2+}, 2. $[Cu(H_{-2}L^2)]$, 3. $[CuL^2]^{2+}$, 4. $[Cu(H_{-1}L^2)]^+$, 5. $[HL^2]^+$

$$*Fl + [Cu^{II}(H_{-2}L^1)] \xrightarrow{\Delta E_T} Fl^- + [Cu^{III}(H_{-2}L^1)]^+ \quad (1)$$

$$\Delta E_T = E°(*Fl_{CT}) - E°(Cu^{III}/Cu^{II}) + E°(Fl/Fl^-) = 0.63\ V \quad (2)$$

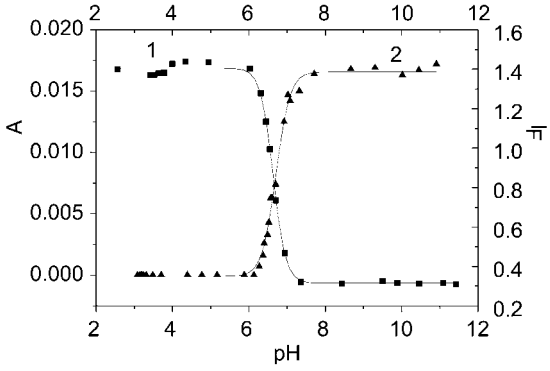

Figure 6. Dependence of fluorescence intensity I_F (1) and absorbance A (2) on the pH for an aqueous solution containing L^1 plus 1 equiv. Cu^{2+} ions

In Equation (2), the redox potential $E°(Fl/Fl^-)$ of the fluorenyl group linked to the dioxotetraaza moiety is −2.65 V, $E°(Cu^{III}/Cu^{II})$ is the redox potential obtained from cyclic voltammetrical experiments (0.699 V), and $E°(*Fl_{CT})$, the potential of the excited state, is 3.92 V, an approximation calculated from the energy of the emission band of the ligand.

The ΔE_T value of $[Cu(H_{-2}L^1)]$ is higher than that of $[Cu(H_{-2}L^3)]$[10b] (0.57 V) (L^3 denotes 6-(9*H*-fluoren-9-yl)-1,4,8,11-tetraazaundecane-5,7-dione), because in the former, two methyl groups that substituted two hydrogen atoms on the carbon atom of the ethylenediamine decreases the redox potential $E(Cu^{III}/Cu^{II})$ and increases the excited fluorescent potential of $[Cu(H_{-2}L^1)]$, thus favoring transfer of an electron from Cu^{II} to the fluorenyl group. The electron transfer behavior of L^1 in the presence of Ni^{2+} is similar to that in the presence of Cu^{2+}. For $[Ni(H_{-2}L^1)]$, ΔE_T (+0.57 V) was obtained by the same calculated method as that for $[Cu(H_{-2}L^1)]$. It is shown from Table 3 that the stability constants of the complexes of L^1 with Co^{II} and Zn^{II} are quite low, and the complexes $[M(H_{-2}L^1)]$ (M = Co, Zn) cannot be formed at pH ≤ 8.0, therefore the electron transfer cannot proceed. When the solution of ligand L^1 was adjusted to pH = 7.0 with NaOH and Ni^{2+} ions

were gradually added to it, no obvious decrease of I_F was observed (Figure 7). When Cu^{2+} ions were added to the same solution, I_F decreased linearly to a minimum value, corresponding to $n_{Cu}/n_L = 1$. Based on the above-mentioned results, L^1 could be employed as a fluorescent sensor to discriminate between Cu^{2+} and Ni^{2+}, as well as Cu^{2+} and Ni^{2+} ions from other divalent 3d metal ions.

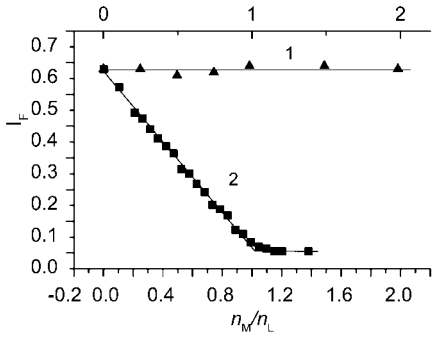

Figure 7. Plotting of I_F of H_2L^1 aqueous solution vs. n_M/n_L (M = Cu, Ni): 1. Ni^{2+} was added to a solution of H_2L^1 at pH = 7.0, 2. Cu^{2+} was added to the solution of 1.

Fluorescent properties of L^2 are different from L^1 and the fluorescent intensity of L^2 is low. A plot of I_F vs. pH in the presence of 1 equiv. of Cu^{2+} or Ni^{2+} ions is shown in Figure 8. In Figure 8, two systems display a similar fluorescent feature, when pH values of solutions are higher than 5.5. Fluorescence intensities increase with an increase of pH and reach a maximum value at pH $\approx$ 10. The curve of I_F vs. pH for systems of L^2 plus the Cu^{2+} ion can be superimposed on the distribution curve of $[Cu(H_{-2}L^2)]$ (Figure 5, curve 2), indicating that the formation of species $[Cu(H_{-2}L^2)]$ leads to an enhancement of the fluorescence. The distinction of the fluorescent properties between L^1 and of L^2 results from the difference of the structures. In L^2, a fluorenyl group substitutes a hydrogen atom of an amino group in the ligand and forms an imido group. The nitrogen atom of the imido group linked to the fluorenyl group can transfer its lone electron pair to a proximate excited fluorenyl group, quenching its fluorescence. When solutions of L^2 in the presence of metal ions were titrated with NaOH, an increase in the pH value led to binding of the metal ions. The electron transfer from the nitrogen atom to the fluorenyl group is suppressed, resulting in an enhancement of the fluorescence. The analogous mechanism has been reported by previous authors.[1,8,12] The detailed study on the fluorescence mechanism is in progress. Quantum yields of the ligand in the absence and presence of metal ions are listed in Table 4. From Table 4 it can be seen that L^2 has much lower quantum yields than L^1 in the absence of metal ions and the quantum yield of L^2 increases by about one order of magnitude upon binding of metal ions.

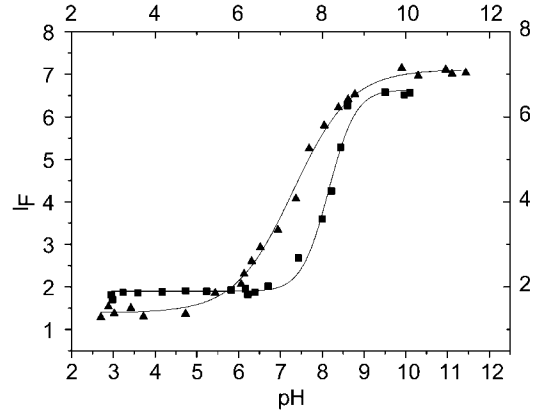

Figure 8. pH dependence of I_F for aqueous solutions containing L^2 plus metal ions; Cu^{2+} (■), Ni^{2+} (▲); $L^2 = Cu^{2+} = Ni^{2+} = 6.8 \times 10^{-5}$ mol·dm^{-3}

Table 4. Quantum yields of L^2 and L^2 plus metal ions (1:1) in aqueous solutions at 25 °C; $L^2 = Cu^{2+} = Ni^{2+} = 5 \times 10^{-5}$ mol·dm^{-3}

Sample	pH	Φ_u [a]
L^1	9.2	1.3×10^{-3}
L^2	9.2	2.0×10^{-4}
$Cu^{2+} + L^2$	5.0	5.2×10^{-4}
$Cu^{2+} + L^2$	9.2	2.7×10^{-3}
$Ni^{2+} + L^2$	5.0	2.6×10^{-4}
$Ni^{2+} + L^2$	9.2	3.4×10^{-3}
Trytophan[b]	7.2	0.14

[a] Deviation of measurement is ±15%. [b] Concentration of trytophan is 6.6×10^{-6} mol dm^{-3}.

It has been known for a long time that transition metal ions (especially Cu^{2+}) effectively quench the fluorescence of the systems by an electron transfer mechanism. Recently, Bharadwaj and co-workers[8] reported for the first time that Cu^{2+} and Ni^{2+} could enhance the fluorescence intensity of a ligand in THF/H_2O (9:1). In our systems, the enhancement of the fluorescence by Cu^{2+} and Ni^{2+} is carried out in aqueous solution. To the best of our knowledge, there are few reports[7] on enhancement of the fluorescence by transition metal ions in aqueous solution.

Experimental Section

Materials: Reagents and organic solvents were of reagent grade and purified prior to use. 9-Bromofluorene was prepared by literature methods.[13] Diethyl 2-(9*H*-fluoren-9-yl)malonate and *N*,*N*′-bis(2-aminoethyl)oxamide were synthesized by a method reported previously.[10b] Carbonate-free NaOH for pH titration was prepared by Powell's method.[14] $M(NO_3)_2 \cdot 6H_2O$ (M = Cu, Ni, Co, Zn) (reagent grade) were recrystallized from doubly distilled water and their stock solutions were standardized by titration with EDTA.

Spectral Measurements: IR spectra were measured as KBr discs with a Nicolet 5DX FT IR spectrophotometer. UV spectra were measured with an UV-3100 spectrophotometer. Luminescence spectra were recorded with an AB2 luminescence spectrometer.

Concentrations of metal ions and equivalent ligands in spectrophotometric titrations and in fluorimetric titrations were $2.6-4.3 \times 10^{-4}$ and $5.4-6.6 \times 10^{-5}$ mol·dm^{-3}, respectively. The solutions were deaerated for ca. 15 min before measurements. Quantum yields Φ of fluorescence were calculated by literature methods[15] using tryptophan as a standard. The quantum yield Φ_s of tryptophan is 0.14 in aqueous solution at 25 °C. Electrospray mass spectra (ES-MS) were obtained in positive mode with a Finnigan LCQ mass spectrograph. The diluted solutions were electrosprayed at a flow-rate of 2×10^{-4} dm^3·min^{-1} with a needle voltage of 4.5 kV. The mobile phase was a methanol solution. ^{1}H NMR spectroscopy was carried out with a Bruker AM500 spectrometer (TMS as internal reference).

Electrochemical Measurements: Cyclic voltammetry was carried out with a Model-270 electrochemical analysis system. A glassy carbon electrode was employed as working electrode, a saturated calomel electrode (SCE) as reference electrode and a platinum plate as auxiliary electrode. Experiments were performed under purified argon at 25 °C. Concentrations of the complexes were 1.0×10^{-3} to 1.0×10^{-4} mol·dm^{-3} in 0.2 mol·dm^{-3} potassium nitrate or in 0.5 mol·dm^{-3} sodium sulfate. The solutions were deaerated for ca. 15 min before applying the voltage. The half wave potentials $E_{1/2}$ were approximately calculated from $(E_{Pa} + E_{Pc})/2$. In a controlled potential coulometer, a platinum web electrode was employed as a working electrode instead of a glassy carbon.

pH Titration: The aqueous solutions containing L^1, $M(NO_3)_2$ and HNO_3 (1:1:4; M = Cu, Ni, Co, Zn) or L^2·2HBr, $M(NO_3)_2$ and HNO_3 (1:1:2; M = Cu, Ni) were titrated with carbonate-free 0.1598 mol·dm^{-3} NaOH using a microsyringe with a precision of ±2 μL in a sealed jacketed vessel at 30 °C under nitrogen. The pH values were measured with a Corning pH meter equipped with a glass/silver/silver chloride combination electrode with a precision of ±0.001 pH units. The combination electrode was standardized with buffer solutions of potassium hydrogen phthalate and sodium borate. The ionic strength was kept at 0.10 mol·dm^{-3} with KNO_3. The protonation constants of ligands were determined under the same conditions. The equilibrium constants were obtained by pH-potentiometric titrations. The protonation constants of the ligands were calculated by the PKAS program.[16] The equilibrium constants of complexes were calculated by using the program LEMIT,[17] which is based on the Newton−Raphson and Gauss−Newton method for minimizing U in Equation (3), where $C_{Hi}^{calcd.}$ and $C_{Hi}^{exp.}$ denote the calculated and experimental values of H^+ concentration at the ith point.

$$U = \sum_{i=1}^{n} (C_{Hi}^{\text{calcd.}} - C_{Hi}^{\text{exp.}})^2 \quad (3)$$

Preparation of Compounds

2,10-Diamino-6-(9*H*-fluoren-9-yl)-4,8-diazaundecane-5,7-dione (L^1): A mixture of diethyl 2-(9*H*-fluoren-9-yl)malonate (6.48 g, 0.02 mol) and freshly distilled propylenediamine (30 mL) was stirred at room temperature for two weeks. Excess propylenediamine was distilled off under reduced pressure. After cooling, the yellow residue was washed with ethanol and diethyl ether successively; L^1 (5.8 g, 76%) was obtained as a white solid. IR (KBr): ν_{max} = 3250 m (NH), 3030 w and 2930 w (CH), 1660 s (CO), 1540 s (NH), 760 m and 742 m cm^{-1} (C−C). UV (MeOH): λ_{max} (ε [dm^3·mol^{-1}·cm^{-1}]) = 266 (18700), 291 (4300) and 302 nm (4600). ^{1}H NMR (500 MHz, [D$_6$]DMSO, standard SiMe$_4$): δ = 0.92 (q, 6 H, *k*-CH$_3$), 2.91 (m, 2 H, *i*-CH), 2.98 (t, 4 H, *j*-NH$_2$), 3.06 (m, 7 H, *h*-CH$_2$, *f*-CH, *g*-CONH), 4.35 (d, 1 H, *e*-CH-Ar), 7.24 (m, 2 H, *c*-Ar-H), 7.39 (t, 2 H, *b*-Ar-H), 7.43 (d, 2 H, *d*-Ar-H), 7.86 (d, 2 H, *a*-Ar-H). $C_{22}H_{28}N_4O_2$ (380.5): calcd. C 69.45, H 7.42, N 14.72; found C 69.23, H 7.28, N 14.54.

1-(9*H*-Fluoren-9-yl)-1,4,7,10-tetraazadecane-5,6-dione Hydrogen Bromide (L^2·2HBr): To a solution of *N*,*N*′-bis(2-aminoethyl)oxamide (1.4 g, 0.008 mol) in DMF (30 mL), a solution of 9-bromofluorene (1.97 g, 0.008 mol) in DMF(20 mL) was added dropwise whilst stirring at 80 °C. After heating for 5 h at 80 °C, the mixture was cooled and filtered. The filtrate was added dropwise ice-cold water (400 mL). After filtering, the filtrate was concentrated to almost dryness and 30 mL of diethyl ether was added. The resultant product was separated and washed with diethyl ether, and 0.5 g of white solid was obtained. The white solid was recrystallized from 95% ethanol, and L^2·2HBr (0.4 g, 10.0%) was obtained. IR (KBr): ν_{max} = 3500 m to 2500 b (NH_3^+), 1660 s (CO), 1580 s (NH), 1520 s, 1440 s, 1070 m, 765 m and 745 m cm^{-1} (C−C). UV (MeOH): λ_{max} (ε [dm^3·mol^{-1}·cm^{-1}]) = 268 (15000), 294 (4130) and 304 (3730). ^{1}H NMR(500 MHz, D$_2$O, standard SiMe$_4$): δ = 2.96 (2 H, t, *j*′-CH$_2$NCO), 3.21 (2 H, t, *g*′-CH$_2$NCO), 3.51 (2 H, t, *h*′-CH$_2$-NAr), 3.62 (2 H, t, *k*′-CH$_2$N$^+$), 5.56 (1 H, s, *e*′-CH), 7.46 (2 H, t, *c*′-Ar-H), 7.59 (2 H, t, *b*′-Ar-H), 7.74 (2 H, d, *d*′-Ar-H), 7.88 (2 H, d, *a*′-Ar-H). $C_{19}H_{24}Br_2N_4O_2$ (500.2): calcd. C 45.62, H 4.84, N 11.20; found C 45.96, H 5.11, N 11.45.

[Cu(H$_{-2}$L^1)]·2H$_2$O: To a solution of L^1 (1.14 g, 3.0 mmol) in water (50 mL), $CuSO_4$·5H$_2$O (0.75 g, 3.0 mmol) was added. Whilst stirring, the mixture was adjusted to pH = 10 with dilute $Ba(OH)_2$ solution. After heating at 80 °C for 2 h, the mixture was filtered. The filtrate was concentrated and cooled; purple-red crystals of [Cu(H$_{-2}$L^1)]·2H$_2$O (0.32 g, 22.3%) were obtained. IR: ν_{max} = 3350 m (OH), 3200 m (NH), 3100 m, 2950 w and 2900 w (CH), 1570 vs (C=O), 760 w and 730 w cm^{-1}(C−C). UV (H$_2$O): λ_{max} (ε [dm^3·mol^{-1}·cm^{-1}]) = 265 (4280), 274 (3440), 291 (1210), 302 (1120) and 504 (69) nm. Λ_m (H$_2$O, 25 °C) = 68.75 S·cm^2·mol^{-1}. $C_{22}H_{30}CuN_4O_4$ (478.1): calcd. C 55.27, H 6.33, N 11.72, Cu 13.27; found C 55.61, H 6.25, N 11.57, Cu 13.13.

[Cu(H$_{-2}$L^2)]·4H$_2$O: L^2·2HBr (0.25 g, 0.5 mmol) and $CuSO_4$·5H$_2$O (0.125 g, 0.5 mmol) were dissolved in water (20 mL). The solution was adjusted to pH = 10 with a dilute solution of $Ba(OH)_2$ whilst stirring. After stirring for 1 h at 80 °C, the solution was cooled and filtered. The filtrate was concentrated and a purple solid of [Cu(H$_{-2}$L^2)]·4H$_2$O (0.12 g, 50.9%) was obtained. IR (KBr): ν_{max} = 3350 m (OH), 3200 m (NH), 2900 w (CH), 1651 s (CO), 1600 s (CO), 1100 m, 745 m and 620 cm^{-1} (C−C). UV (H$_2$O): λ_{max} (ε [dm^3·mol^{-1}·cm^{-1}]) = 268 (15000), 294 (4130), 304 (3730) and 536 (154). Λ_m (H$_2$O, 25 °C) = 69.10 S·cm^2·mol^{-1}. $C_{19}H_{28}CuN_4O_6$ (472.0): calcd. C 48.36, H 5.98, N 11.87; found C 48.54, H 6.08, N 11.57.

X-ray Structure Determination of [Cu(H$_{-2}$L^1)]·2H$_2$O: Crystal data: $C_{22}H_{30}CuN_4O_4$, M = 478.04, monoclinic, space group $P2_1/n$, a = 17.264(4) Å, b = 7.6627(16) Å, c =19.559(4) Å, β = 114.582(15) °, V = 2352.9(8) Å^3, $D_{calcd.}$ = 1.349 Mg·m^{-3}, F(000) = 1004, Z = 4, graphite-monochromated Mo-K radiation (λ = 0.71073 Å), μ = 0.962 mm^{-1}, T = 293(2) K. Data collection and processing: A crystal of [Cu(H$_{-2}$L)]·2H$_2$O with dimensions 0.40 × 0.30 × 0.30 mm, wrapped with resin, was mounted on a glass fiber and used for structure determination. The intensities were collected at 293 K with a Siemens *P*4 four-circle diffractometer with θ/2θ scan mode with a variable scan speed of 4.0−60.0 min^{-1} in ω. A total of 5316 reflections (4129 unique) were collected in the range of

$2.06° < \theta < 25.0°$. The data were corrected for Lorentz and polarization effects during data reduction using XSCANS.[18] Structure analysis and refinement: The structure was solved by direct methods. All non-hydrogen atoms were refinedanisotropically on F^2 by full-matrix least-squares methods. The hydrogen atoms were placed in calculated positions assigned fixed isotropic thermal parameters at 1.2 times the equivalent isotropic U of the atoms to which they are attached and allowed to ride on their respective parent atoms. The contributions of these hydrogen atoms were included in the structure-factor calculations. The final least-squares cycle gave $R = 0.0542$, $Rw = 0.1280$ and $GOF = 1.075$. The maximum and minimum peaks corresponded to $+0.665$ and -0.290 eÅ^{-3}, respectively. All computations were carried out using the SHELXTL PC program package.[19] Crystallographic data for the the crystal structure of $[Cu(H_{-2}L^1)]\cdot 2H_2O$ have been deposited with the Cambridge Crystallographic Data Centre as supplementary publication no. CCDC-163292. Copies of the data can be obtained free of charge on applicaton to CCDC, 12 Union Road, Cambridge CB2 1EZ, UK [Fax: (internat.) + 44-1223/336-033; E-mail: deposit@ccdc.cam.ac.uk].

Acknowledgments

The project was supported by the Natural Science Foundation of China and 211 Project of China.

[1] A. P. de Silva, H. Q. N. Gunaratne, T. Gunnlaugsson, A. J. M. Huxley, C. P. McCoy, J. T. Rademacher, T. E. Rice, *Chem. Rev.* **1997**, *97*, 1515.
[2] G. D. Santis, L. Fabbrizzi, M. Licchelli, A. Poggi, A. Taglietti, *Angew. Chem. Int. Ed. Engl.* **1996**, *35*, 202.
[3] [3a] E. Kimura, *Pure Appl. Chem.* **1986**, *58*, 1461. [3b] E. Kimura, *Pure Appl. Chem.* **1989**, *61*, 823. [3c] E. Kimura, T. Koike, *Chem. Soc. Rev.* **1998**, *27*, 179. [3d] G. E. Jackson, P. W. Linder, A. Voye, *J. Chem. Soc., Dalton Trans.* **1996**, 4605. [3e] Q. H. Luo, S. R. Zhu, M. C. Shen, S. Y. Yu, Z. Zhang, X. Y. Huang, Q. J. Wu, *J. Chem. Soc., Dalton Trans.* **1994**, 1873.
[4] L. Fabbrizzi, A. Poggi, *Chem. Soc. Rev.* **1995**, 197.
[5] L. Fabbrizzi, M. Licchelli, P. Pallavicini, D. Sacchi, A. Taglietti, *Analyst* **1996**, *121*, 1763.
[6] L. Fabbrizzi, M. Licchelli, P. Pallavicini, A. Perotti, D. Sacchi, *Angew. Chem. Int. Ed. Engl.* **1994**, *33*, 1975.
[7] F. Bolletta, I. Costa, L. Fabbrizzi, M. Licchelli, M. Montalti, P. Pallavicini, L. Prodi, N. Zaccheroni, *J. Chem. Soc., Dalton Trans.* **1999**, 1381.
[8] P. Ghosh, P.K. Bharadwaj, J. Roy, S. Ghosh, *J. Am. Chem. Soc.* **1997**, *119*, 11903.
[9] P. V. Bernhardt, B. M. Flanagan, M. J. Riley, *J. Chem. Soc., Dalton Trans.* **1999**, 3579.
[10] [10a] L. Fabbrizzi, I. Faravelli, G. Francese, M. Licchelli, A. Perotti, A. Taglietti, *Chem. Commun.* **1998**, 971. [10b] L. J. Jiang, Q. H. Luo, C. Y. Duan, M. C. Shen, H. W. Hu, Y. J. Liu, *Inorg. Chim. Acta* **1999**, *295*, 48.
[11] M. Kodama, E. Kimura, *J. Chem. Soc., Dalton Trans.* **1981**, 694.
[12] V. Amendola, L. Fabbrizzi, P. Pallavicini, L. Parodi, A. Perotti, *J. Chem. Soc., Dalton Trans.* **1998**, 2053.
[13] J. R. Sampey, E. E. Reid, *J. Am. Chem. Soc.* **1947**, *69*, 234.
[14] J. E. Powell, M. A. Hiller, *J. Chem. Educ.* **1957**, *34*, 330.
[15] D. F. Eaton, *Pure Appl. Chem.* **1988**, *60*, 1107.
[16] A. E. Martell, R. J. Motekaitis, *Determination and Use of Stability Constants*, 2nd ed., VCH Publishers, New York, **1992**, p. 129.
[17] Q. H. Luo, M. C. Shen, Y. Ding, X. L. Bao, A. B. Dai, *Talanta* **1990**, *37*, 357.
[18] Siemens, *XSCANS (Version 2.1)*, Siemens Analytical X-ray Instruments Inc. Madison USA, **1994**.
[19] Siemens, *SHELXTL (Version 5.0) Reference Manual*, Siemens Industrial Automation Inc. analytical Instrumentation, USA, **1995**.

Received August 21, 2001
[I01320]

Bis(pyrazol-1-yl)acetato Ligands in Ruthenium Chemistry: Syntheses and Structures of Ruthenium(II) and Ruthenium(III) Complexes with bpza and bdmpza

Alberto López-Hernández,[a] Rainer Müller,[a] Henning Kopf,[a] and Nicolai Burzlaff*[a]

Keywords: Ruthenium / N ligands / Scorpionates / Tripodal ligands / Structural chemistry

New ruthenium(II) and ruthenium(III) complexes with the ligands bis(pyrazol-1-yl)acetate (bpza) and bis(3,5-dimethylpyrazol-1-yl)acetate (bdmpza) are reported. The reaction of ruthenium trichloride hydrate, H[bpza], and excess PPh_3 yielded $[Ru(bpza)Cl(PPh_3)_2]$ as a racemic mixture of an unsymmetrical isomer with traces of a symmetrical isomer. Similar reaction conditions using the more bulky H[bdmpza] yielded $[Ru(bdmpza)Cl_2(PPh_3)]$. Reaction of K[bpza] with $[RuCl_2(PPh_3)_3]$ offered a second route to $[Ru(bpza)Cl(PPh_3)_2]$. Also, $[Ru(bdmpza)Cl(PPh_3)_2]$ was accessed by this synthetic approach. All three new complexes were characterized by X-ray structure determination.

Introduction

The cyclopentadienylruthenium(II) complex $[Ru(Cp)Cl(PPh_3)_2]$ has been used for more than 30 years as a versatile starting material in thousands of reactions in organometallics.[1−6] In the last ten years this chemistry has been extended to $[Ru(Cp^*)Cl(PPh_3)_2]$[7−9] and, due to the firmly established analogy between the cyclopentadienyl ligand and the hydrotris(pyrazol-1-yl)borato ligand (Tp), also to $[Ru(Tp)Cl(PPh_3)_2]$.[10,11] It is thought that the differences in the reactivity of these complexes are essentially determined by the cone angle of triphenylphosphane (145°) as well as the cone angles of the Cp (150°), Cp* (182°), and Tp (199°) ligands.[10−14] Structural data of the complexes, confirming these steric effects, have been available for a long time.[4−6,8−10] Therefore, these bulky ligands are an important factor in the chemistry of these complexes by inducing lability of one of the triphenylphosphane ligands.

Recently, bis(pyrazol-1-yl)acetato ligands, a new class of scorpionate ligands with binding properties similar to those of the cyclopentadienyl or the hydrotris(pyrazol-1-yl)borato ligand (Figure 1), have been introduced to organometallic and coordination chemistry.[15−20] The binding properties as well as the steric hindrance of the two new ligands bis(pyrazol-1-yl)acetate (bpza) and bis(3,5-dimethylpyrazol-1-yl)acetate (bdmpza) are between those of a Cp ligand and a Cp* ligand.

Recently, we studied iron(II) complexes with these ligands − although with our main focus on bioinorganic model complexes for iron enzymes.[17] Now we report on a route to ruthenium(II) and ruthenium(III) complexes with these new bis(pyrazol-1-yl)acetato ligands.

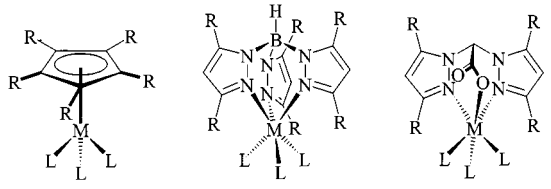

Figure 1. Metal complexes with Cp, Cp*, Tp, $Tp^{Me}{}_2$, bpza, and bdmpza ligands

Results and Discussion

First we investigated a one-step synthesis analogous to the synthesis of $[Ru(Cp)Cl(PPh_3)_2]$ reported by Bruce et al.[3] Reaction of $RuCl_3 \times nH_2O$ with bis(pyrazol-1-yl)acetic acid (H[bpza]) and an excess of PPh_3 in ethanol under refluxing conditions yielded $[Ru(bpza)Cl(PPh_3)_2]$ as the unsymmetrical isomer **1b** [Equation (1)].

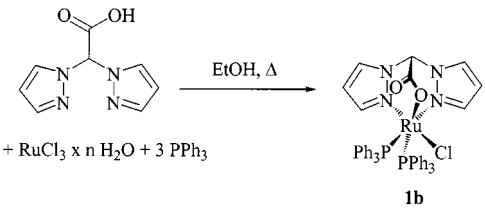

(1)

There are two possible isomeric products: (a) a symmetrical one (**1a**) with the chloride ion in *trans* position to the

[a] Fachbereich Chemie, Universität Konstanz, Fach M728, 78457 Konstanz, Germany
Fax: (internat.) + 49-(0)7531/88-3136
E-mail: nicolai@chemie.uni-konstanz.de

carboxylate group of the ligand and (b) an unsymmetrical one (**1b**) with the carboxylate group *trans* to a PPh_3 ligand. The main isomer **1b** obtained in this one-step synthesis is a racemic mixture of two enantiomers. The ^1H NMR spectra of the crude reaction product showed only traces of the symmetrical **1a**. Pure product **1b** could be obtained by column chromatography over silica followed by recrystallization in methanol. The solubility of **1b** in methanol is much lower than that of **1a**.

The coordination of the bpza ligand follows from the IR signal in KBr matrix $\nu_{asym}(CO_2^-) = 1653\ cm^{-1}$. The observation of two doublets in the ^{31}P NMR spectra [$\delta = 43.8$ ($^2J_{PP} = 31.0$ Hz), 49.5 ($^2J_{PP} = 31.0$ Hz)] and of two sets of signals for the pyrazolyl groups in the ^1H and ^{13}C NMR spectra indicates an unsymmetrical coordination of the triphenylphosphane ligands in **1b**. Finally, the molecular structure was proven by CHN analysis, mass spectra, and an X-ray structure determination (Figure 2) of crystals of **1b** obtained from a solution of **1b** in ethanol layered with diethyl ether. Selected bond lengths and angles are summarized in Tables 1 and 2.

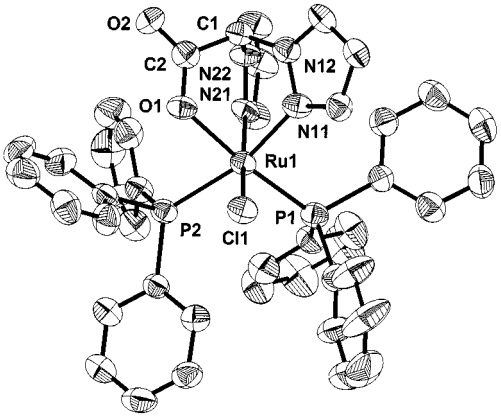

Figure 2. Molecular structure of [Ru(bpza)Cl(PPh_3)$_2$] (**1b**); thermal ellipsoids are shown at a 50% probability level; hydrogen atoms and co-crystallised solvent are omitted for clarity

Table 1. Selected distances of the complexes **1b**, **2**, and **3**

Distance [Å]	**1b**	**2**	**3**
Ru−N(11)	2.157(6)	2.109(3)	2.199(4)
Ru−N(21)	2.100(6)	2.184(3)	2.173(4)
Ru−O(1)	2.181(6)	2.045(3)	2.133(3)
Ru−Cl(1)	2.440(3)	2.346(2)	2.4157(17)
Ru−Cl(2)	−	2.3581(19)	−
Ru−P(1)	2.360(3)	2.3715(18)	2.3555(17)
Ru−P(2)	2.378(4)	−	2.3688(18)
O(2)−C(2)	1.241(9)	1.225(3)	1.241(5)
O(1)−C(2)	1.309(9)	1.298(3)	1.281(5)
C(1)−C(2)	1.566(10)	1.562(4)	1.539(6)

The molecular structure shows one PPh_3 ligand positioned *trans* to the carboxylate group of the bpza ligand and the other phosphane ligand *trans* to a pyrazolyl group. The distances of the bonds in the *cis* geometry [P(1)−Ru = 2.360(3) Å and N(21)−Ru = 2.100(6) Å] are slightly shorter than those in a *trans* geometry [P(2)−Ru = 2.378(4) Å and N(11)−Ru = 2.157(6) Å]. This might be due to the *trans* influence of the triphenylphosphane ligand and the pyrazolyl group.

Table 2. Selected angles of the complexes **1b**, **2**, and **3**

Angle [°]	**1b**	**2**	**3**
N(11)−Ru−N(21)	86.5(2)	84.05(9)	78.40(15)
O(1)−Ru−N(11)	82.1(2)	86.50(10)	88.23(14)
O(1)−Ru−N(21)	86.3(2)	87.73(10)	87.68(13)
O(1)−Ru−Cl(1)	87.79(14)	175.36(6)	170.52(9)
O(1)−Ru−P(1)	174.37(14)	85.45(8)	86.50(10)
O(1)−Ru−P(2)	81.58(15)	−	91.36(9)
N(11)−Ru−P(1)	93.07(19)	97.14(8)	169.31(11)
N(21)−Ru−P(1)	90.57(18)	172.99(6)	92.08(11)
N(11)−Ru−P(2)	163.46(18)	−	95.30(12)
N(21)−Ru−P(2)	95.07(18)	−	173.65(11)
N(11)−Ru−Cl(1)	85.35(17)	89.62(9)	84.92(12)
N(21)−Ru−Cl(1)	170.51(17)	89.34(9)	84.58(11)
Cl(1)−Ru−Cl(2)	−	90.90(6)	−
Cl(1)−Ru−P(1)	94.74(8)	97.57(6)	99.16(7)
Cl(1)−Ru−P(2)	91.36(10)	−	95.79(6)
Cl(2)−Ru−P(1)	−	88.27(5)	−
P(1)−Ru−P(2)	103.36(10)	−	94.12(6)

An analogous reaction of $RuCl_3$ with excess PPh_3 and bis(3,5-dimethylpyrazol-1-yl)acetic acid (H[bdmpza]) yielded [Ru(bdmpza)Cl_2(PPh_3)] (**2**) as an orange, air-sensitive complex [Equation (2)].

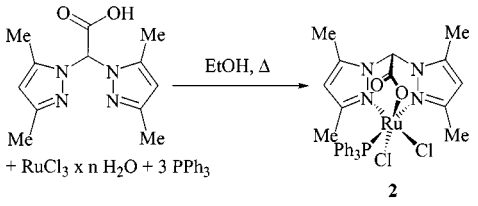

(2)

Complex **2** is paramagnetic, and therefore was only characterized by mass spectrometry, CHN analysis, and infrared spectroscopy (KBr matrix). The $\nu_{asym}(CO_2^-)$ at 1682 cm^{-1} established the coordination of bdmpza to the ruthenium ion. An X-ray structural analysis of **2** finally confirmed a constitution with the PPh_3 ligand *trans* to one of the pyrazolyl groups (Figure 3). Selected bond lengths and bond angles are summarised in Tables 1 and 2.

Apart from the distances Ru−N(21) [2.184(3) Å] and Ru−P(1) [2.3715(18) Å], all other distances Ru−O, Ru−N, and Ru−Cl are significantly shorter compared to those of **1b**. This is caused by the ruthenium(III) centre in **2** instead of ruthenium(II) in **1b**. These two significantly longer distances again imply a *trans* influence between the PPh_3 ligand and the pyrazolyl group of the bdmpza ligand.

In a second attempt to obtain the target molecule [Ru(bdmpza)Cl(PPh_3)$_2$], potassium bis(3,5-dimethylpyrazol-1-yl)acetate was allowed to react with [$RuCl_2$(PPh_3)$_3$] [Equation (3)].

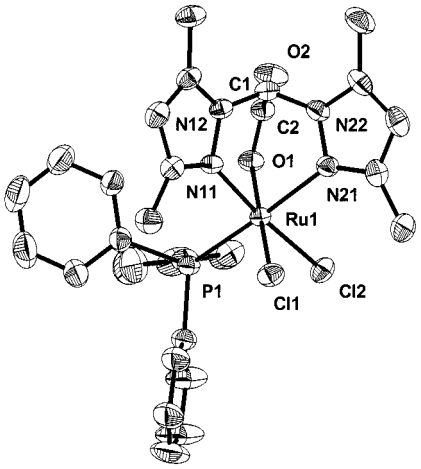

Figure 3. Molecular structure of $[Ru(bdmpza)Cl_2(PPh_3)]$ (**2**); thermal ellipsoids are shown at a 50% probability level; hydrogen atoms and co-crystallised solvent are omitted for clarity

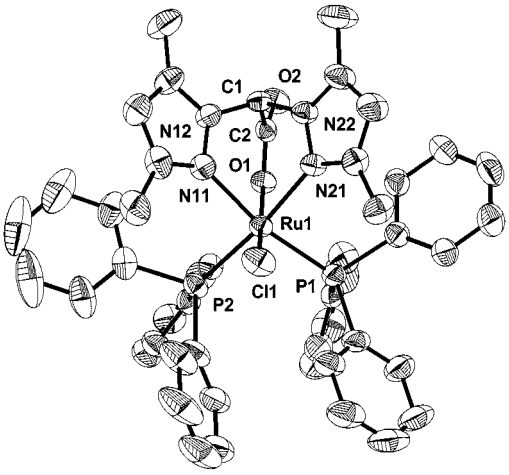

Figure 4. Molecular structure of $[Ru(bdmpza)Cl(PPh_3)_2]$ (**3**); thermal ellipsoids are shown at a 50% probability level; hydrogen atoms and co-crystallised solvent are omitted for clarity

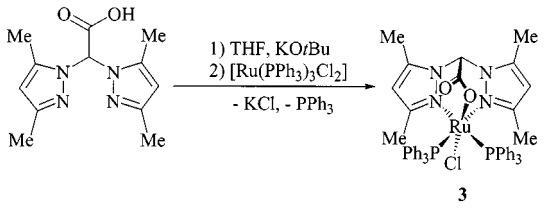

(3)

In an analogous reaction with potassium hydrotris(pyrazol-1-yl)borate and $[RuCl_2(PPh_3)_3]$ the complex $[Ru(Tp)Cl(PPh_3)_2]$ was obtained by Hill et al.[10] Very recently the complex $[RuCl(PPh_3)_2(TPM)]Cl$ was synthesized from tris(pyrazol-1-yl)methane (TPM) and $[RuCl_2(PPh_3)_3]$ by Field and Messerle.[21] $[Ru(bdmpza)Cl(PPh_3)_2]$ (**3**) was obtained in good yield after simply washing with degassed water and diethyl ether and was fully characterized. A single signal in the ^{31}P NMR spectrum as well as one set of signals for the pyrazolyl groups in the ^1H and ^{13}C NMR spectra indicate a symmetric geometry for **3**. Proton signals of **3** were assigned on the basis of cross-peaks observed in a rotating frame Overhauser spectroscopy (ROESY) experiment. The ^{13}C NMR resonances of the methyl groups were assigned by correlating them to the assigned proton resonances using a heteronuclear multiple quantum coherence (HMQC) experiment. The methyl group at position 3 of the pyrazolyl groups (Me^3) was found in the ^1H NMR spectra at $\delta = 1.72$ [^{13}C NMR: $\delta = 15.5$], the methyl group at position 5 (Me^5) at $\delta = 2.35$ [^{13}C NMR: $\delta = 11.1$]. A distinction of the quaternary pyrazolyl carbon resonances was possible with a heteronuclear multiple bond correlation (HMBC) experiment [^{13}C NMR: $\delta = 140.6$ (C^5), 157.3 (C^3)]. The assignment of the NMR signals is in good agreement with those reported by Otero for similar niobium complexes.[16] The symmetric structure was also proven by a single-crystal X-ray structure analysis of **3** (Figure 4). Selected bond lengths and bond angles of **3** are summarized in Tables 1 and 2.

The IR spectrum of **3** shows bands at 1668 and 1570 cm^{-1} [$\nu_{asym}(CO_2^-)$ and $\nu(C{=}N)$]. For all three complexes **1a/1b**, **2**, and **3** we were not able to assign $\nu_{sym}(CO_2^-)$ properly to one of the resonances in the region between 1400 and 1500 cm^{-1}. This was due to the weakness of the signals and several resonances of the PPh_3 ligand in that region.

Complex **3** is rather sensitive to oxygen (especially compared to the almost air-stable complexes **1a** or **1b**). This is caused by the bigger steric hindrance of **3**, causing a labilisation of the PPh_3 ligands. This hindrance is indicated by a much smaller angle N(11)−Ru−N(21) of 78.40(15)° compared to 86.5(2)° in **1b**. Another explanation might be, that bdmpza is a better donor ligand compared to bpza due to the four methyl groups in the pyrazolyl rings.

Also $[Ru(bpza)Cl(PPh_3)_2]$ could be obtained in good yield by reaction of potassium bis(pyrazol-1-yl)acetate with $[RuCl_2(PPh_3)_3]$. Both isomers **1a** and **1b** were formed [Equation (4)].

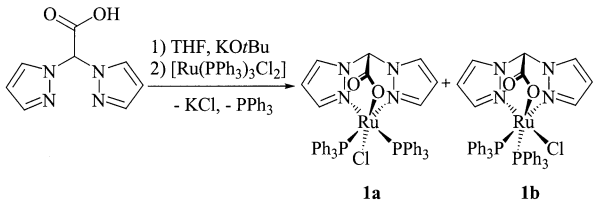

(4)

Due to the simple workup and high yield, we now favour this second synthetic route to **1a/1b**. Potassium chloride and traces of excess base are removed by washing with degassed water. Thus, ruthenium complexes with bis(pyrazol-1-yl)-

acetato ligands are stable against hydrolysis, an imminent advantage compared to hydrotris(pyrazolyl)borato ligands. In contrast to unsymmetrical **1b**, only a single ^{31}P NMR signal at $\delta = 40.4$ and one set of ^{1}H NMR signals is found for **1a**. Both isomers of **1a/1b** are rather stable and can be stored under air as a solid. Assignment of the proton signals of **1a/1b** was accomplished from the cross-peaks observed in correlation spectroscopy (COSY) experiments and ROESY experiments. HMQC experiments were used for correlation of these assigned proton resonances with ^{13}C NMR resonances. In the NMR spectra of the symmetrical isomer **1a** only three proton resonances [$\delta = 5.89$ (H^4), 6.87 (H^3), 7.55 (H^5)] and three carbon resonances [$\delta = 107.6$ (C^4), 132.6 (C^5), 146.6 (C^3)] were detected for the pyrazolyl groups. The pyrazolyl groups in **1b** are no longer spectroscopically equivalent causing six ^{1}H NMR signals [$\delta = 5.20$ (H^3), 5.46 (H^4), 5.97 ($H^{4'}$), 7.44 ($H^{3'}$), 7.79 ($H^{5'}$), 7.79 (H^5)] and six ^{13}C NMR signals [$\delta = 106.5$ (C^4), 107.4 ($C^{4'}$), 131.9 (C^5 or $C^{5'}$), 132.0 (C^5 or $C^{5'}$), 145.7 ($C^{3'}$), 147.9 (C^3)]. In the ROESY experiment of **1b** an NOE correlation was observed between a signal at $\delta = 7.84$ (six *ortho*-H of the PPh_3 ligand *trans* to the carboxylate donor group) and H^3 indicating a close spherical contact.

From the fact that the unsymmetrical isomer could be isolated by recrystallization, it follows that it is stable against conversion into **1a** at ambient temperature for a reasonable time. To investigate whether one of the isomers is thermodynamically favoured, a mixture of the isomers and PPh_3 in ethanol was heated under reflux. After 4 h in ethanol under refluxing conditions, surprisingly only traces of **1b** were detected by ^{1}H NMR spectroscopy besides **1a**. Since this formation of the symmetrical isomer **1a** seemed to be incompatible with the one-step synthesis of **1b**, a solution of **1a** with traces of **1b** and PPh_3 in ethanol was heated under reflux for 5 h. After this time **1b** was the main product and only traces of **1a** were left. Obviously, the ratio **1a/1b** depends on whether excess PPh_3 is present in the reaction mixture or not. Very likely, this is due to the intermediate formation of a cationic solvent complex. For alcoholic solutions of $[Ru(Cp)Cl(PPh_3)_2]$ dissociation of a chloride ligand and formation of a cationic alcohol complex is well known.[1,3] The most likely position of the ethanol ligand is the position *trans* to the carboxylate donor group. Exchange of the ethanol ligand by a chloride ion will therefore result in the symmetrical isomer **1a** (Scheme 1). With excess PPh_3 an intermediate cationic complex $[Ru(bpza)(PPh_3)_3]Cl$ might be formed. Similar complexes $[Ru(Cp)(dppm)(PPh_3)]PF_6$ and $[Ru(Cp^*)(PHPh_2)_3]Cl$ were recently reported.[22,23] Both PPh_3 ligands *trans* to pyrazolyl groups are more labile than the one *trans* to the carboxylate donor group because of the *trans* influence of the pyrazolyl groups. Therefore, in this case substitution for a chloride ion will result in formation of the unsymmetrical isomer **1b** (Scheme 1).

Finally, we observed that traces of alcohols or THF in NMR samples caused significant changes in the NMR spectra again indicating an interaction between **1a/1b** and traces of these donor solvents. In protic solvents the carboxylate group might also interact with protons and therefore be a less efficient donor, causing this behaviour. In future experiments we will concentrate on the question of whether such interactions of the carboxylate donor and protons, or even Lewis acids, could be used for changing the reactivity of the complexes.

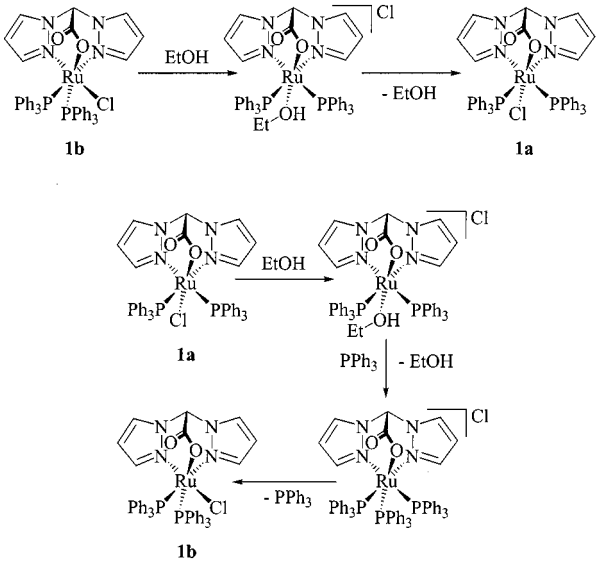

Scheme 1. Proposed mechanism for the conversion of **1b** in **1a** in ethanol and of **1a** in **1b** in ethanol with excess PPh_3

Conclusions

A simple synthetic route to the ruthenium(II) complexes $[Ru(bpza)Cl(PPh_3)_2]$ (**1a/1b**) and $[Ru(bdmpza)Cl(PPh_3)_2]$ (**3**) was established by reaction of the potassium bis(pyrazol-1-yl)acetates with $[RuCl_2(PPh_3)_3]$. Complex **3** seemed to be more active towards exchange of a PPh_3 ligand by another donor, whereas in **1a/1b** the ratio of the symmetrical isomer **1a** to the unsymmetrical isomer **1b** could be influenced by adding PPh_3 during heating under reflux. Thus, both complexes are promising starting complexes for future organometallic experiments.

Experimental Section

All experiments were carried out in Schlenk tubes under argon. The solvents were dried by standard procedures, distilled, and stored under argon. Microcrystalline precipitates were separated by filtration or centrifugation with a Hettich Rotina 46 R Schlenk tube centrifuge. IR: Biorad FTS 60, CaF_2 cuvettes (0.5 mm) or KBr matrix. ^{1}H NMR and ^{13}C NMR: Bruker WM 250, Bruker AC 250, δ values relative to TMS. ^{31}P NMR: JEOL GX 400. Two-dimensional NMR experiments: Bruker DRX 600 (Avance). EI-MS and FAB-MS: modified Finnigan MAT 312. Elemental analyses: Analytical Laboratory of the Fachbereich Chemie. A modified Siemens P4 diffractometer was used for X-ray structure determinations. Bis(pyrazol-1-yl)acetic acid and bis(3,5-dimethylpyra-

zol-1-yl)acetic acid were synthesised from pyrazole and 3,5-dimethylpyrazole as reported recently.[17,18] $[RuCl_2(PPh_3)_3]$ was prepared according to the literature.[24] Hydrated ruthenium trichloride (35−40% Ru) was used as purchased from Merck.

Synthesis of $[Ru(bpza)Cl(PPh_3)_2]$ (1a/1b). − Method A: A solution of $RuCl_3 \times n\ H_2O$ (670 mg, 2.65 mmol) and bis(pyrazol-1-yl)acetic acid (578 mg, 3.00 mmol) in EtOH (40 mL) was added over a period of 10 min to a refluxing solution of PPh_3 (2.09 g, 7.95 mmol) in EtOH (80 mL). The mixture was maintained under reflux for 3 h, cooled to ambient temperature and the solvent was evaporated. The crude product was loaded with CH_2Cl_2 on a short column of silica (length 6 cm, i.d. 4 cm). The column was washed with CH_2Cl_2 (150 mL). Finally, the pure product was recovered with MeOH. The dark yellow MeOH solution was concentrated in vacuo to 20 mL. The precipitated yellow product was filtered off and dried in vacuo. It was dissolved in CH_2Cl_2, precipitated with *n*-pentane, filtered off, and dried in vacuo. The unsymmetrical isomer **1b** was obtained as a yellow crystal powder. Suitable crystals of **1b** for X-ray structure analysis were obtained from a solution in EtOH layered with diethyl ether. Yield 1.23 g (1.44 mmol, 54%), m.p. 194−196 °C. − **Method B:** To a solution of bis(pyrazol-1-yl)acetic acid (200 mg, 1.04 mmol) in THF (25 mL) potassium *tert*-butoxide (117 mg, 1.04 mmol) was added and the mixture stirred for 1 h at ambient temperature. A white precipitate formed during this time indicated the formation of the potassium carboxylate. $[RuCl_2(PPh_3)_3]$ (1.00 g, 1.04 mmol) was added and the mixture was stirred at ambient temperature for 30 min, during which time the colour of the brown suspension changed to orange. The solvent was removed in vacuo and the residue was washed with degassed water (2 × 20 mL) and diethyl ether (2 × 20 mL) and dried in vacuo to yield a mixture of **1a/1b** as an orange crystal powder. Yield 760 mg (0.89 mmol, 86%), m.p. 188−192 °C. FAB-MS (NBOH matrix): *m/z* (%) = 853 (2) $[MH^+]$, 817 (4) $[(MH - Cl)^+]$, 590 (11) $[MH^+ - PPh_3]$, 555 (5) $[(MH - PPh_3 - Cl)^+]$. $C_{44}H_{37}ClN_4O_2P_2Ru \times H_2O \times EtOH$ (916.36): calcd. C 60.29, H 4.95, N 6.11; found C 60.58, H 4.73, N 6.00. − **1a:** ^1H NMR ($CDCl_3$, 250 MHz): δ = 5.89 (vt, $^3J_{H,H}$ = 2.3 Hz, 2 H, H^4), 6.61 (s, 1 H, CH), 6.87 (d, $^3J_{H,H}$ = 1.9 Hz, 2 H, H^3), 7.04 (m, 12 H, *m*-PPh_3), 7.21 (m, 6 H, *p*-PPh_3), 7.43(m, 12 H, *o*-PPh_3), 7.55 (d, $^3J_{H,H}$ = 2.5 Hz, 2 H, H^5). ^{13}C NMR ($CDCl_3$, 62.9 MHz): δ = 75.5 (CH), 107.6 (C^4), 127.1 (vt, $J_{C,P}$ = 3.7 Hz, *m*-PPh_3), 128.8 (*p*-PPh_3), 132.6 (C^5), 134.9 (vt, $J_{C,P}$ = 4.5 Hz, *o*-PPh_3), 135.0 (d, $J_{C,P}$ = 40.1 Hz, *i*-PPh_3), 146.6 (C^3), 166.1 (CO_2^-). ^{31}P NMR ($CDCl_3$, 161.8 MHz): δ = 40.4. IR (THF): $\tilde{\nu}$ = 1670 s (CO_2^-), 1653 m, 1507 w cm^{-1}. IR (KBr): $\tilde{\nu}$ = 1653 s (CO_2^-), 1482 w, 1433 m, 1408 w cm^{-1}. − **1b:** ^1H NMR ($CDCl_3$, 250 MHz): δ = 5.20 (s, 1 H, H^3), 5.46 (s, 1 H, H^4), 5.97 (s, 1 H, $H^{4'}$), 6.84 (s br, 6 H, *o*-PPh_3), 7.07 (m, 16 H, CH and *p*-PPh_3 and *m*-PPh_3), 7.26 (m, 3 H, *p*-PPh_3), 7.44 (s, 1 H, $H^{3'}$), 7.84(m, 8 H, *o*-PPh_3 and H^5 and $H^{5'}$). ^{13}C NMR ($CDCl_3$, 62.9 MHz): δ = 74.2 (CH), 106.5 (C^4), 107.4 ($C^{4'}$), 127.3 (d, $J_{C,P}$ = 9.1 Hz, *m*-PPh_3), 127.6 (d, $J_{C,P}$ = 9.0 Hz, *m*-PPh_3), 128.7 (*p*-PPh_3), 129.2 (*p*-PPh_3), 131.9 (C^5 or $C^{5'}$), 132.0 (C^5 or $C^{5'}$), 133.9 (d, $J_{C,P}$ = 9.0 Hz, *o*-PPh_3), 134.4 (d, $J_{C,P}$ = 9.4 Hz, *o*-PPh_3), 134.5 (d, $J_{C,P}$ = 40.4 Hz, *i*-PPh_3), 135.3 (d, $J_{C,P}$ = 40.5 Hz, *i*-PPh_3), 145.7 ($C^{3'}$), 147.9 (C^3), 166.6 (CO_2^-). ^{31}P NMR ($CDCl_3$, 161.8 MHz): δ = 43.8 ($^2J_{PP}$ = 31.0 Hz), 49.5 ($^2J_{PP}$ = 31.0 Hz). IR (CH_2Cl_2): $\tilde{\nu}$ = 1661 s (CO_2^-), 1481 w cm^{-1}. IR (KBr): $\tilde{\nu}$ = 1653 s (CO_2^-), 1482 w, 1433 m cm^{-1}.

Synthesis of $[Ru(bdmpza)Cl_2(PPh_3)]$ (2): A solution of $RuCl_3 \times n\ H_2O$ (383 mg, 1.52 mmol) in EtOH (20 mL) was added over a period of 10 min to a solution of bis(3,5-dimethylpyrazol-1-yl)-acetic acid (376 mg, 1.51 mmol) and PPh_3 (1.20 g, 4.57 mmol) in EtOH (30 mL). The mixture was heated under reflux for 1 h, cooled in an ice bath and the precipitate was collected by filtration. The brownish residue was washed with CH_2Cl_2 (30 mL) and the now orange residue was dried in vacuo. Crystals suitable for a X-ray structure determination were obtained from a solution of **2** in acetonitrile and also from a solution in $CHCl_3$. Yield 660 mg (0.97 mmol, 64%), m.p. 260−265 °C (dec.). FAB MS (NBOH matrix): *m/z* (%) = 722 (4) $[M^+ + CH_3CN]$, 681 (4) $[M^+]$, 646 (18) $[(M - Cl)^+]$, 611 (6) $[(M - Cl_2)^+]$, 566 (6) $[(M - Cl_2 - CO_2)^+]$. IR (KBr): $\tilde{\nu}$ = 1682 s (CO_2^-), 1560 w (C=N), 1482 w, 1458 w, 1436 w cm^{-1}. $C_{30}H_{30}Cl_2N_4O_2PRu \times CH_3CN$ (722.60): calcd. C 53.19, H 4.60, N 9.69; found C 53.32, H 4.23, N 9.83.

Synthesis of $[Ru(bdmpza)Cl(PPh_3)_2]$ (3): Reaction of bis(3,5-dimethylpyrazol-1-yl)acetic acid (248 mg, 1.00 mmol) in THF (25 mL) with potassium *tert*-butoxide (112 mg, 1.00 mmol) and $[RuCl_2(PPh_3)_3]$ (953 mg, 0.99 mmol) according to Method B yielded **3** as an orange crystal powder. Suitable crystals of **3** for X-ray structure analysis were obtained from a solution in $CHCl_3$. Yield 815 mg (0.90 mmol, 91%), m.p. 201−205 °C (dec.). ^1H NMR ($CDCl_3$, 250 MHz): δ = 1.72 (s, 3 H, Me^3), 2.35 (s, 3 H, Me^5), 5.42 (s, 2 H, H^4), 6.45 (s, 1 H, CH), 6.90 (m, 12 H, PPh_3), 7.04 (m, 6 H, PPh_3), 7.31 (m, 12 H, PPh_3). ^{13}C NMR ($CDCl_3$, 62.9 MHz): δ = 11.1 (Me^5), 15.5 (Me^3), 69.1 (CH), 109.3 (C^4), 126.5 (vt, $J_{C,P}$ = 4.2 Hz, *m*-PPh_3), 128.0 (*p*-PPh_3), 134.5 (vt, $J_{C,P}$ = 4.2 Hz, *o*-PPh_3), 136.2 (d, $J_{C,P}$ = 39.1 Hz, *i*-PPh_3), 140.6 (C^5), 157.3 (C^3), 168.2 (CO_2^-). ^{31}P NMR ($CDCl_3$, 161.8 MHz): δ = 35.3. FAB-MS (NBOH-matrix): *m/z* (%) = 908 (0.5) $[M^+]$, 873 (1) $[(M - Cl)^+]$, 648 (3) $[MH^+ - PPh_3]$, 611 (2) $[(MH - PPh_3 - Cl)^+]$. IR (THF): $\tilde{\nu}$ = 1672 s (CO_2^-), 1571 w (C=N) cm^{-1}. IR (CH_2Cl_2): $\tilde{\nu}$ = 1662 s (CO_2^-), 1571 w (C=N) cm^{-1}. IR (KBr): $\tilde{\nu}$ = 1668 s (CO_2^-), 1570 w (C=N), 1482 w, 1458 w, 1432 m cm^{-1}. $C_{48}H_{45}ClN_4O_2P_2Ru \times 3CHCl_3$ (1266.52): calcd. C 48.37, H 3.82, N 4.42; found C 48.50, H 3.98, N 4.21.

X-ray Structure Determinations: Single crystals of **1b**, **2**, and **3** were sealed in glass capillaries at room temperature. A modified Siemens P4-diffractometer was used for data collection (Wyckhoff technique, graphite monochromator, Mo-K_α radiation, λ = 0.71073 Å, scan rate 4−30 °min^{-1} in ω). The structures were solved and refined using the SHELX-97 program package (refined with full-matrix least squares against F^2).[25] A weighting scheme was applied in the last steps of the refinement with $w = 1/[\sigma^2(F_o^2) + (aP)^2 + bP]$ and $P = [2F_c^2 + \max(F_o^2,0)]/3$. Hydrogen atoms were included in their calculated positions and refined in a "riding model". One molecule of ethanol and water co-crystallised per asymmetric unit in **1b**, one molecule of $CHCl_3$ in **2**, and three molecules of $CHCl_3$ in **3**. The co-crystallised water in the structure of **1b** can be explained as being due to the crystallisation of **1b** in an open flask. Crystals of **2** were also obtained from a solution in acetonitrile. The X-ray structure determination of these crystals resulted in an almost identical structure model but with higher *R* factors. Therefore, this structure $\mathbf{2} \times CH_3CN$ is not discussed here although the data were deposited with CCDC (see below). Two of the $CHCl_3$ molecules in the structure of **3** are severely disordered causing relatively high *R* factors. All details and parameters of the measurements are summarised in Table 3. Crystallographic data (excluding structure factors) for the structures reported in this paper have been deposited with the Cambridge Crystallographic Data Centre as supplementary publication no. CCDC-168912 ($\mathbf{1b} \times H_2O \times EtOH$), -168913 ($\mathbf{2} \times CHCl_3$), -168914 ($\mathbf{2} \times CH_3CN$) and -168915 ($\mathbf{3} \times 3CHCl_3$). Copies of the data can be obtained free

Table 3. Structure determination details of compounds **1b**, **2**, and **3**

	1b	**2**	**3**
Empirical formula	$C_{44}H_{37}ClN_4O_2P_2Ru\times H_2O\times H_5C_2OH$	$C_{30}H_{30}Cl_2N_4O_2PRu\times CHCl_3$	$C_{48}H_{45}ClN_4O_2P_2Ru\times 3CHCl_3$
Formula mass	916.32	800.89	1266.44
Crystal colour/habit	yellow cube	orange cube	orange prism
Crystal system	monoclinic	triclinic	monoclinic
Space group	$P2_1/n$	$P\bar{1}$	$P2_1/c$
a [Å]	9.969(10)	10.113(7)	14.057(6)
b [Å]	19.37(3)	11.908(9)	31.792(19)
c [Å]	22.96(3)	15.583(10)	14.421(10)
α [°]	90	91.48(7)	90
β [°]	96.64(8)	108.59(3)	115.72(5)
γ [°]	90	103.07(6)	90
V [Å^3]	4405(10)	1723(2)	5806(6)
θ [°]	2.07−25.01	2.13−27.00	2.02−27.01
h	−11 to 11	−6 to 12	−17 to 0
k	−9 to 23	−15 to 14	−40 to 0
l	−27 to 27	−19 to 18	−16 to 18
F(000)	1888	810	2568
Z	4	2	4
μ(Mo-K_α) [mm^{-1}]	0.536	0.924	0.827
Crystal size [mm]	0.4 × 0.2 × 0.2	0.4 × 0.35 × 0.35	0.6 × 0.4 × 0.4
D_c [gcm^{-3}]	1.382	1.544	1.449
T [K]	239(2)	232(2)	242(2)
Reflections collected	10245	8278	13162
Independent reflections	7653	7482	12654
Observed reflections [$> 2\sigma(I)$]	3899	6311	9115
Parameter	530	397	703
Restraints	2	0	132
Wt. parameter a	0.0769	0.0437	0.0950
Wt. parameter b	2.4297	1.1694	10.8122
R_1 (obsd.)	0.0586	0.0354	0.0635
R_2 (overall)	0.1447	0.0462	0.0944
wR_1 (obsd.)	0.1328	0.0873	0.1660
wR_2 (overall)	0.1872	0.0934	0.1908
Diff. peak/hole [e/Å^3]	0.900/−1.022	0.757/−0.756	1.503/−1.121

of charge on application to CCDC, 12 Union Road, Cambridge CB2 1EZ, UK [Fax: (internat.) + 44-1223/336-033; E-mail: deposit@ccdc.cam.ac.uk]. Structure figures were prepared with the program Diamond 2.1c.[26]

Acknowledgments

N. B. thanks the Fonds der Chemie for a Liebig-Stipendium and Prof. Dr. H. Fischer for support and discussion. We are indebted to Mr. Hägele for recording mass spectra, Mr. Haunz for recording ^{31}P NMR spectra and Ms. Friemel for two-dimensional NMR experiments.

[1] Review: S. G. Davies, J. P. McNally, A. J. Smallridge, *Adv. Organomet. Chem.* **1990**, *30*, 1−76.
[2] T. Blackmore, M. I. Bruce, F. G. A. Stone, *J. Chem. Soc. A* **1971**, 2376−2382.
[3] M. I. Bruce, C. Hameister, A. G. Swincer, R. C. Wallis, *Inorg. Synth.* **1982**, *21*, 78−84.
[4] M. I. Bruce, F. S. Wong, B. W. Skelton, A. H. White, *J. Chem. Soc., Dalton Trans.* **1981**, 1398−1405.
[5] E. R. T. Tiekink, *Z. Kristallogr.* **1992**, *198*, 158−161.
[6] M. I. Bruce, H. Hinterding, E. R. T. Tiekink, *Z. Kristallogr.* **1993**, *205*, 287−290.
[7] M. S. Chinn, D. M. Heinekey, *J. Am. Chem. Soc.* **1990**, *112*, 5166−5175.
[8] D. C. Smith Jr., C. M. Haar, L. Luo, C. Li, M. E. Cucullu, C. H. Mahler, S. P. Nolan, W. J. Marshall, N. L. Jones, P. J. Fagan, *Organometallics* **1999**, *18*, 2357−2361.
[9] I. A. Guzei, M. A. Paz-Sandoval, R. Torres-Lubián, P. Juárez-Saavedra, *Acta Crystallogr., Sect. C* **1999**, *55*, 1090−1092.
[10] N. W. Alcock, I. D. Burns, K. S. Claire, A. F. Hill, *Inorg. Chem.* **1992**, *31*, 2906−2908.
[11] B. Buriez, I. D. Burns, A. F. Hill, A. J. P. White, D. J. Williams, J. D. E. T. Wilton-Ely, *Organometallics* **1999**, *18*, 1504−1516.
[12] L. E. Manzer, C. A. Tolman, *J. Am. Chem. Soc.* **1975**, *97*, 1955−1956.
[13] C. A. Tolman, *Chem. Rev.* **1977**, *77*, 313−348.
[14] N. Kitajima, W. B. Tolman, *Prog. Inorg. Chem.* **1995**, *43*, 419−531.
[15] A. Otero, J. Fernández-Baeza, J. Tejeda, A. Antiñolo, F. Carrillo-Hermosilla, E. Díez-Barra, A. Lara-Sánchez, M. Fernández-López, M. Lanfranchi, M. A. Pellinghelli, *J. Chem. Soc., Dalton Trans.* **1999**, 3537−3539.
[16] A. Otero, J. Fernández-Baeza, J. Tejeda, A. Antiñolo, F. Carrillo-Hermosilla, E. Díez-Barra, A. Lara-Sánchez, M. Fernández-López, *J. Chem. Soc., Dalton Trans.* **2000**, 2367−2374.

[17] A. Beck, B. Weibert, N. Burzlaff, *Eur. J. Inorg. Chem.* **2001**, 521−527.
[18] N. Burzlaff, I. Hegelmann, B. Weibert, *J. Organomet. Chem.* **2001**, *626*, 16−23.
[19] A. Otero, J. Fernández-Baeza, A. Antiñolo, F. Carrillo-Hermosilla, J. Tejeda, E. Díez-Barra, A. Lara-Sánchez, L. Sanchez-Barba, I. López-Solera, M. R. Ribeiro, J. M. Campos, *Organometallics* **2001**, *20*, 2428−2430.
[20] N. Burzlaff, I. Hegelmann, *Inorg. Chim. Acta*, submitted.
[21] L. D. Field, B. A. Messerle, L. Soler, I. E. Buys, T. W. Hambley, *J. Chem. Soc., Dalton Trans.* **2001**, 1959−1965.
[22] R. Torres-Lubián, M. J. Rosales-Hoz, A. M. Arif, R. D. Ernst, M. A. Paz-Sandoval, *J. Organomet. Chem.* **1999**, *585*, 68−82.
[23] J. Bezler, Dissertation, University of Würzburg, Germany, **1995**.
[24] P. S. Hallman, T. A. Stephenson, G. Wilkinson, *Inorg. Synth.* **1970**, *12*, 237−240.
[25] G. M. Sheldrick, *SHELX-97*, *Programs for Crystal Structure Analysis*, University of Göttingen, Germany, **1997**.
[26] K. Brandenburg, M. Berndt, *Diamond − Visual Crystal Structure Information System*, Crystal Impact GbR, Bonn, Germany, **1999**; for software review see: W. T. Pennington, *J. Appl. Crystallogr.* **1999**, *32*, 1028−1029.

Received August 24, 2001
[I01330]

Alkyl(amino)- and Alkyl(chloro)phosphanyl-Substituted Cyclopentadienyl Complexes of Titanium and Zirconium

Vasily V. Kotov,*[a][‡] Evgeni V. Avtomonov,*[b][‡‡] Jörg Sundermeyer,[c] Klaus Harms,[c] and Dmitry A. Lemenovskii[a]

Dedicated to Prof. Dr. J. Lorberth on the occasion of his 65th birthday

Keywords: Titanium / Zirconium / Cyclopentadienyl ligands / P ligands / Polymerisation

Phosphanyl-substituted cyclopentadienes of the type [R_nCp–PR(NR^1R^2/Cl)] (**1**–**22**) (R = Alk, Ar; R^1, R^2 = H, Alk, Ar, SiR_3; R_nCp = *t*BuCp, Me_4Cp, Ind, Me_6Ind, Flu) can be synthesised by reaction of alkyldichlorophosphanes and alkyl(amino)chlorophosphanes with alkali metal cyclopentadienides. The method used is a general one and provides high isolated yields of the target compounds. The phosphanylcyclopentadienes can easily be deprotonated by strong bases (e.g. *n*BuLi, $PhCH_2K$, Ph_2CHK) and the potassium salts [R_nCp–PR(NR^1R^2)]K (**25**–**28**) are efficiently transmetallated by Me_3SnCl. A subsequent reaction with $TiCl_4(L)_2$ and $ZrCl_4(L)_2$ (L = THF, tetrahydrothiophene, Me_3P) affords new half-sandwich complexes [{Me_4Cp–P*t*Bu(NEt_2)}$TiCl_3$] (**36**), [{Me_4Cp–P*t*Bu(NEt_2)}$TiCl_3$] (**37**) and [{*t*BuCp–P*t*Bu(NEt_2)}$TiCl_3$] (**38**) in moderate yields. The reaction of [*t*BuCp–P*t*Bu(Cl)] (**6**) with $TiCl_4$ in the presence of Et_3N at low temperature yields the half-sandwich complex [{*t*BuCp–P*t*Bu(Cl)}$TiCl_3$] (**39**) quantitatively; [(Cp–P*t*Bu(Cl)]$_2$-CMe_2] (**11**) reacts similarly and gives, dependent on the reagent ratio, either the homobimetallic derivative [{(Cp–P*t*Bu(Cl)$_2$$CMe_2$}{$TiCl_3$}$_2$] (**40**) (1:2 ratio) or the *ansa* complex [{(Cp–P*t*Bu(Cl)]$_2$$CMe_2$}$TiCl_2$] (**41**) (1:1 ratio). The scope of this reaction could not be extended to sterically more demanding cyclopentadienyl derivatives. Treatment of [{*t*BuCp–P*t*Bu(Cl)}$TiCl_3$] (**39**) by LiN(H)*t*Bu in the presence of Et_3N leads to the formation of the constrained geometry complex [{*t*BuCp–P*t*Bu(N*t*Bu)}$TiCl_2$] (**42**) in a high yield. All synthesised compounds were characterised by NMR spectroscopy, mass spectrometry and elemental analyses. The crystal structures of the ligand precursor [Me_6Ind–P*t*Bu(NH*t*Bu)] (**15**) and that of [{Me_4Cp–P*t*Bu(NEt_2)}$TiCl_3$] (**36**) have been determined by X-ray diffractometry. The complexes described in this work are active in the MAO-mediated polymerisation of ethylene.

Introduction

In the past three decades a variety of transition metal complexes have been developed and applied as catalysts for homogeneous polymerisation of α-olefins to form a wide number of polymers with unique properties.[1−3] The most famous of them are *ansa*-metallocenes **I**[4] and *C*onstrained *G*eometry *C*atalysts (CGC) **II** with ancillary cyclopentadienyl ligands first described by Bercaw,[5] Okuda[6] and later developed by researchers of Dow and Exxon.[7] At the same time other systems, having no cyclopentadienyl-type ligands at all[8−11] were successfully applied for the homogeneous polymerisation of alkenes and have promoted extensive studies focussed on the catalyst geometry,[12−20] and investigation of the relationship between the catalyst's structure and properties of the polymer produced.[21,22] As a consequence, a huge number of theoretical[23,24] and experimental studies of the mechanism of polymerisation have been reported to date.[25−29] There is still growing interest in substituted cyclopentadienylmetal compounds containing a terminal donor group in the side chain.[11−19] Due to the Lewis acidity of the metal centre in the postulated active species in the polymerisation reaction a coordination of the "pendant" donor functionality to the transition metal centre might be anticipated.

We were interested in novel ligand models and the synthesis of transition metal complexes on their basis. Recently,

[a] Department of Chemistry, M. V. Lomonosov Moscow State University,
Vorob'evy Gory, 119899 Moscow, Russian Federation
[b] A. N. Nesmeyanov Institute of Organoelement Compounds, Russian Academy of Sciences,
Vavilova str. 28, 117813 Moscow, Russian Federation
[c] Philipps-Universität Marburg, Fachbereich Chemie,
Hans-Meerwein-Strasse, 35032 Marburg, Germany
[‡] Present address: Organisch-Chemisches Institut,
Westfälische Wilhelms-Universität Münster,
Corrensstrasse 40, 48149 Münster, Germany
Fax: (internat.) + 49-(0)251/833-6503
E-mail: kww@uni-muenster.de
[‡‡] Present address: Bayer AG, Central Research & Development, Build. Q18,
Kaiser-Wilhelm-Allee, 51368 Leverkusen, Germany
Fax: (internat.) + 49-(0)214/302-4202
E-mail: evgueni.avtomonov.ea@bayer-ag.de

 © WILEY-VCH Verlag GmbH, 69451 Weinheim, Germany, 2002 1434−1948/02/0303−0678 $ 17.50+.50/0 *Eur. J. Inorg. Chem.* **2002**, 678−691

we have been exploring the synthesis of the ligands derived from phosphanyl-substituted cyclopentadienes [$R_nCp-PR(NR^1R^2)$] (**III**) (R_nCp = Cp, Ind, Flu; R, R^1, R^2 = Alk, Ar or H) in an attempt to probe this class of compounds in the organotransition metal chemistry. The choice of the [$R_nCp-PR(NR^1R^2)$] system was stimulated by the expectation that the presence of a σ-donating aminophosphanyl group in the periphery of the cyclopentadienyl ligand would have an impact on the catalytic properties of target complexes.

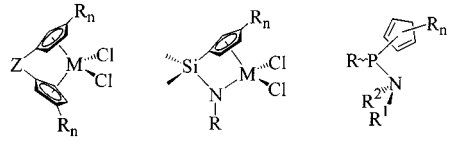

I **II** **III**

Z = carbon or silicon bridge; R_nCp = Cp, Ind, Flu; R, R^1, R^2 = Alk or Ar; M = Ti (IV), Zr (IV), Hf (IV).

There are two main synthetic approaches to these ligands of type **III** (Scheme 1) containing a three-coordinate phosphorus atom: ***A***) a stepwise nucleophilic substitution of the halogen atoms at the phosphorus centre of $RPCl_2$ by cyclopentadienyl-type carbanions [R_nCp]M (M = Li, Na, K) and amines HNR^1R^2 and ***B***) the reaction of cyclopentadienyl anions with (alkyl or aryl)chloro(dialkylamino)-phosphanes.

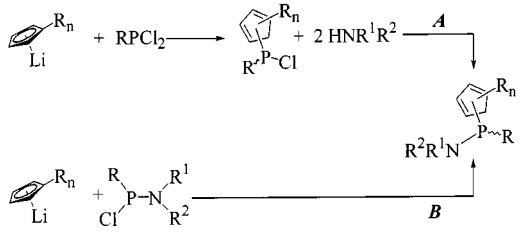

R_nCp = Cp, Ind, Flu; R = Alk, Ar; R^1 = H or R^2; R^2 = Alk or Ar.

Scheme 1

Route ***A*** is a common route to prepare alkyl(amino)-cyclopentadienylphosphanes and has been described previously in the literature for pentamethylcyclopentadienes.[30] The second approach ***B*** for which alkyl(or aryl)chloro(dialkylamino)phosphanes $RP(Cl)NR^1R^2$ are key starting compounds has recently been developed.[31] They could be advantageously used for the preparation of sterically less encumbered derivatives. Here we wish to report the synthesis of the new phosphanylcyclopentadienes **III**, using route ***A*** as a synthetic strategy, their transformations to group-4 transition metal complexes and our results of the polymerisation of ethylene by the catalysts obtained from the complexes and methylalumoxane (MAO).

Results and Discussion

Synthesis of the Ligand Precursors

Phosphanylcyclopentadienes of the type [$R_nCp-PR(Cl)$] can be prepared by nucleophilic substitution of a chlorine atom in dichlorophosphanes $RPCl_2$ (Scheme 1, route ***A***). In the 1980s this synthetic approach was applied for a variety of pentamethylcyclopentadienylphosphanes [$Me_4C_5-PR^3R^4$] (R^3, R^4 = C_5Me_5(Cp*), Alk, Ar, Cl, F, I, NMe_2) with the aim of studying isomerisation of the phosphanyl substituent around the Cp* ring.[32−36] Sterically crowded cyclopentadienes, indenes, fluorenes, or bulky phosphanes can also be utilised while cyclopentadienylphosphanes having less demanding substituents, e.g. Cp or MeCp, are a thermally labile class of compounds and readily undergo Diels−Alder reaction.[37] The most recent examples were reported by Alt and co-workers[38] and by researchers at Shell[39] as intermediate compounds in the synthesis of symmetrical and unsymmetrical *ansa*-metallocenes with the phenylphosphanylidene bridge. In both cases subsequent nucleophilic substitutions by different cyclopentadienyl-, indenyl- and fluorenyllithium salts have been carried out. According to a similar methodology we synthesised a number of alkylchloro(cyclopentadienyl-, indenyl- and fluorenyl)phosphanes [$R_nCp-PR(Cl)$] (**1**−**6**) and their bridged analogues [{$R_nCp-PR(Cl)$}$_2$Z] (**7**−**11**) (Scheme 2).

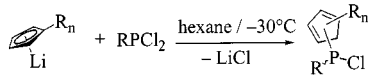

[R_nCp-PR(Cl)] = **1** [Ind-P*t*Bu(Cl)] 66%
2 [Flu-P*t*Bu(Cl)] 94%[40]
3 [Ind-PMes(Cl)] 82%
4 [Me_6Ind-P*t*Bu(Cl)] 85%
5 [Me_4Cp-P*t*Bu(Cl)] 73%
6 [*t*BuCp-P*t*Bu(Cl)] 95%

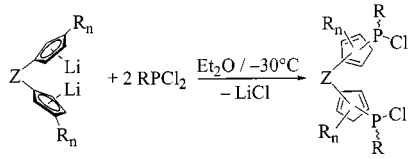

[{R_nCp-PR(Cl)}$_2$Z] = **7** [{Ind-P*t*Bu(Cl)}$_2$(CH_2)$_2$] 64%
8 [{Ind-P*t*Bu(Cl)}$_2$$CMe_2$] >95%
9 [{Ind-P*t*Bu(Cl)}$_2$$CEt_2$] 92%
10 [{Ind-P*t*Bu(Cl)}CMe_2{Cp-P*t*Bu(Cl)}] 50%
11 [{Cp-P*t*Bu(Cl)}$_2$$CMe_2$] 80%

Scheme 2

This method, however, has some drawbacks. In the case of monocyclopentadienyl-type carbanions the formation of by-products is observed, e.g. alkylbis(cyclopentadienyl)phosphane [$(R_nCp)_2PR$], as a result of the double substitution of the chlorine atoms at the phosphorus centre, when Et_2O was used as solvent. By-products can be avoided by the use of a nonpolar aliphatic solvent, e.g. hexane. Since many compounds derived from phosphanylcyclopentadienes [$R_nCp-PR(Cl)$] or [$R_nCp-PR(NR^1R^2)$] cannot be purified

by standard methods such as distillation or chromatography, pure starting materials have to be used in all stages of the preparation. The substances synthesised are highly soluble in aliphatic solvents and exist as expected as mixtures of isomers (see NMR spectroscopic data in the Exp. Sect.).

On the contrary, bis[*tert*-butylchloro(indenyl)phosphanes] [{Ind−P*t*Bu(Cl)}$_2$Z] (**7**−**9**) exist exclusively as allylic regioisomers. These compounds possess four stereogenic centres and hence consist of a complex set of stereoisomers. Eight diastereomeric pairs are theoretically possible. Four of them would exhibit an identical chemical environment around the phosphorus substituents and only four diastereomers could therefore be observed by conventional NMR techniques (three enantiomeric pairs and one *meso* form).[31] The ^{31}P NMR spectroscopic data confirm this assumption and demonstrate seven resonances, i.e. three pairs of nonequivalent phosphorus atoms in the racemic forms and one signal of the *meso* form, each part having different integral intensity (compare ref.[31]). For this reason we were not able to make a detailed assignment of the proton and carbon NMR spectra for compounds **6**,**7**−**11**. The structures of **10** and **11** were deduced solely on the basis of C,H,N analyses and ^{31}P NMR spectra.

The second step of method ***A*** is the reaction of [R$_n$Cp−PR(Cl)] (**1**−**11**) with amines. This transformation proceeds smoothly for **1**−**6** and affords aminophosphanyl derivatives **12**−**22** in high yields (Scheme 3). The structure of [Me$_6$Ind−P(*t*Bu)N(H)*t*Bu] (**15**) was determined by an X-ray analysis (Figure 1).

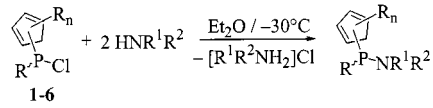

1-6

[R$_n$Cp-PR(NR^{1}R^2)] =
12 [Ind-P*t*Bu(NEt$_2$)] >95%
13 [Ind-P*t*Bu(NH*t*Bu)] >95%
14 [Ind-P*t*BuP(NHPh)] >95%
15 [Me$_6$Ind-P*t*Bu(NH*t*Bu)] 75%
16 [Ind-PMes(NH*t*Bu)] >95%
17 [Flu-P*t*Bu(NEt$_2$)] >95%
18 [Flu-P*t*Bu(NH*t*Bu)] >95%
19 [Me$_4$Cp-P*t*Bu(NH*t*Bu)] 78%
20 [Me$_4$Cp-P*t*Bu(NEt$_2$)] >95%
21 [*t*BuCp-P*t*Bu(NEt$_2$)] >95%
22 [*t*BuCp-P*t*Bu(NH*t*Bu)] >95%

Scheme 3

The geometry at the phosphorus atom that occupies the allylic position of the Me$_6$Ind group is trigonal-pyramidal. The bond angles range from 103 to 108°, indicating certain steric strain in the molecule. The P(1)−N(1) bond of 1.701(5) Å and the bond P(1)−C(11) of 1.899(5) Å are somewhat longer than typical P^{III}−N (ca. 1.65 Å) and P^{III}−C (1.83−1.87 Å) bond lengths for most substituted organophosphorus compounds,[41] which again confirms the steric congestion in **15**. All other structural fragments reveal no peculiarities.

To our surprise, for the bridged ligand precursors [{R$_n$Cp−P*t*Bu(Cl)}$_2$Z] (**7**−**10**), no nucleophilic substitution by secondary amines HNR^{1}R^2 takes place. The reaction affords oligomeric products which are difficult to analyse,

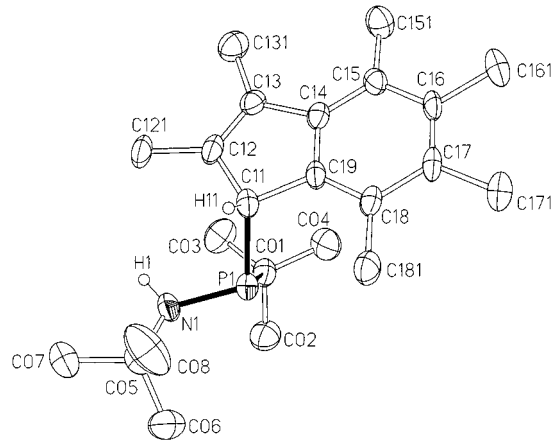

Figure 1. ORTEP diagram of the molecule of [Me$_6$Ind−P*t*Bu(NH*t*Bu)] (**15**); thermal ellipsoids are drawn at 50% probability level; hydrogen atoms except for H(1) and H(11) are omitted for the sake of clarity; selected bond lengths [Å]: P(1)−N(1) 1.701(5), P(1)−C(01) 1.880(6), P(1)−C(11) 1.899(5), C(11)−C(12) 1.504(8), C(11)−C(19) 1.518(7), C(12)−C(13) 1.350(8); selected bond angles [°]: N(1)−P(1)−C(01) 102.5(2), N(1)−P(1)−C(11) 103.3(2), C(01)−P(1)−C(11) 108.0(2), C(19)−C(11)−P(1) 112.7(3), C(13)−C(12)−C(11) 110.9(5)

probably stemming from the very reactive phosphafulvenes generated in situ by β-"HCl" elimination.[42] Thus, the elimination of HCl takes place faster than a nucleophilic substitution reaction (Scheme 4).

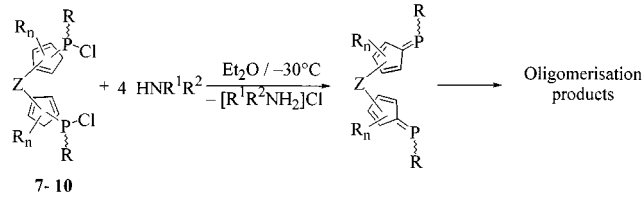

7- 10

HNR^{1}R^2 = HNMe$_2$, HNEt$_2$, HN(*i*Pr)$_2$, H$_2$N(*t*Bu); Z = -(CH$_2$)$_2$-, CMe$_2$.

Scheme 4

The result of the reaction is independent of the length of the bridge Z and the size of alkyl groups R^1 and R^2, which might be attributed to an exclusively allylic structure of the bis[alkylchloro(indenyl)phosphanes] [{R$_n$Cp−P*t*Bu(Cl)}$_2$Z] (**7**−**10**) and/or higher steric hindrance in these encumbered substrates. Bis[alkylchloro(indenyl)phosphane] **11**, isolated as a mixture of allylic and vinylic isomers, gave, after the addition of the amine HNR^{1}R^2 a mixture of the desired products formed from the vinylic isomer and oligomers derived from the allylic isomer. The attempts to separate these substances were unsuccessful. Luckily, such ligand precursors are available by synthetic route ***B*** and can readily be obtained in high yield.[31]

Syntheses of the Complexes

Taking into account the geometry of the prepared ligand precursors several types of transition metal complexes might be synthesised: half-sandwich, sandwich, CGC (**II**) and *ansa*-type (**I**) metallocenes. To date, a variety of methods for the preparation of such early transition metal complexes has been described in the literature.[43] The most

common synthetic approach to the desired compounds is the transmetallation reaction between transition metal halides and alkali metal derivatives of the ligands. The lithium salts **23** and **24** were prepared in order to be further treated with transition metal halides. After **13** and **18** have been treated with *n*BuLi in 2:1 and 1:1 ratios, respectively, the corresponding di- and monolithium salts are formed (Scheme 5).

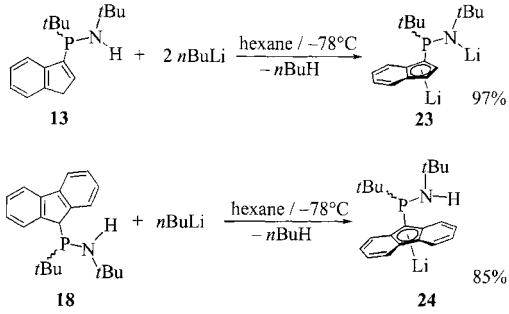

Scheme 5

The compounds **23** and **24** are soluble in aliphatic solvents, thus making purification difficult. Potassium salts are expected to be less soluble and a series was synthesised by the use of Ph_2CHK or $PhCH_2K$ as deprotonating agents in THF (Scheme 6).

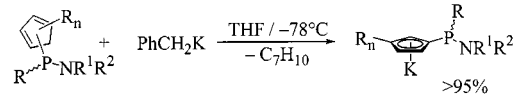

12, **17**, **18**, **20**, **21**

$[R_nCp\text{-}PR(NR^1R^2)]K$ = **25** [Me_4Cp-P*t*Bu(NEt_2)]K
26 [*t*BuCp-P*t*Bu(NEt_2)]K
27 [Ind-P*t*Bu(NEt_2)]K
28 [Flu-P*t*Bu(NEt_2)]K

$[\{R_nCp\text{-}PR(NR^1R^2)\}_2Z]K_2$ = **29** [$\{$Ind-P*t*Bu(NEt_2)$\}_2CEt_2]K_2(THF)_2$ 81%

Scheme 6

The salts **25**−**28** do not contain THF as a ligand and can be obtained free of any THF by washing with an aliphatic solvent. The alkali metal derivatives can then be transformed into the corresponding Me_3Si or Me_3Sn derivatives **30**−**34** (Scheme 7).

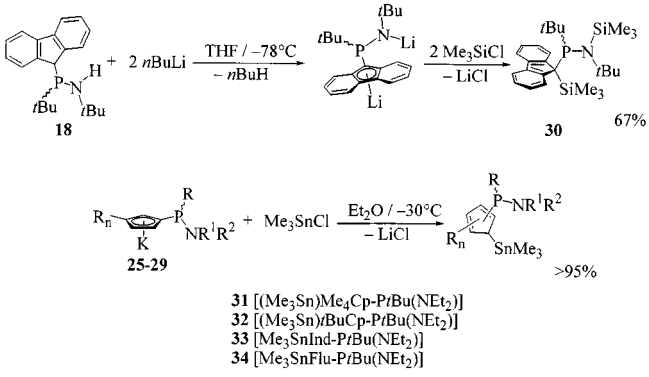

31 [(Me_3Sn)Me_4Cp-P*t*Bu(NEt_2)]
32 [(Me_3Sn)*t*BuCp-P*t*Bu(NEt_2)]
33 [Me_3SnInd-P*t*Bu(NEt_2)]
34 [Me_3SnFlu-P*t*Bu(NEt_2)]

Scheme 7

The reaction of the ligand precursors with trialkyltin amides proceeds smoothly and results in *C*-stannylated products, e.g. when **13** is treated with 1 equiv. of Me_3SnNMe_2, **35** is formed quantitatively (Scheme 8). At room temperature Me_3Si and Me_3Sn groups occupy allylic positions of the cyclopentadienyl ring.

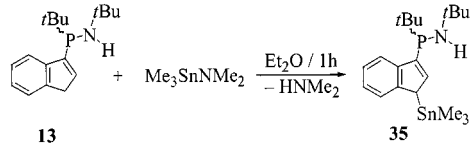

Scheme 8

Our numerous efforts to isolate desired complexes [half-sandwich, sandwich, CGC (**II**) and *ansa*-type (**I**)] of Ti^{IV} and Zr^{IV} from the reactions of homoleptic alkylmetal compounds (Alk = CH_2Ph), metal amides (NR_2 = NMe_2) of Ti^{IV}, Zr^{IV} and neutral ligand precursors **12**−**22** analogously to $R_nCpSiMe_2(NHtBu)$ (R_nCp = C_5H_5, Me_4C_5),[44] or between disilylated (**30**), dilithium/dipotassium (**23** and **29**), lithium/potassium (**24** and **25**−**28**) derivatives of the ligands and THF, THT (THT = tetrahydrothiophene) and Me_3P adducts of $TiCl_4$ and $ZrCl_4$, were unsuccessful. Either no reaction took place over rational periods of time, or complex mixtures of products were formed, which were difficult to separate and identify. The method of choice is the reaction of trimethyltin derivatives with $TiCl_4$ and $ZrCl_4$. Several substituted alkyl(amino)cyclopentadienylphosphanes [(Me_3Sn)R_nCp−P*t*Bu(NR^1R^2)] (**31**, **32**) and several Ti^{IV} (**36**, **38**) and Zr^{IV} (**37**) complexes have been synthesised in moderate yields (Scheme 9).

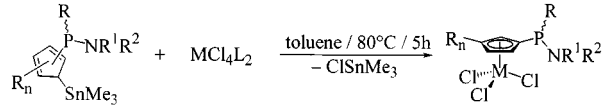

$[\{R_nCp\text{-}PR(NR^1R^2)\}MCl_3]$ = **36** [$\{Me_4Cp$-P*t*Bu(NEt_2)$\}TiCl_3$] 38%
37 [$\{Me_4Cp$-P*t*Bu(NEt_2)$\}ZrCl_3$] 25%
38 [$\{$*t*BuCp-P*t*Bu(NEt_2)$\}TiCl_3$] 30%
L = THF, THT, Me_3P.

Scheme 9

The main product of these reactions is a coordination polymer and the yield of the desired compound is not affected by donor molecules coordinated to the metal centre (THF, THT, Me_3P). In the case of indenyl- (**33**) and fluorenyltin (**34**) derivatives only ill-defined oligomeric products could be isolated. According to NMR spectroscopic data the oligomeric substance still contains the π-bound cyclopentadienyl ligand. The oligomeric products obtained from indenyl- and fluorenyl-containing phosphanes are soluble in polar solvents, e.g. CH_2Cl_2, toluene or THF, and decompose to $TiCl_3$ and presumably also the dimeric organic species formed from the ligand upon storage. Such behaviour is documented for situations when fluorenyltitanium complexes were attempted to be synthesised.[45] The complexes **36**−**38** are in turn very soluble in pentane and could be separated from the oligomers by extraction. Again, when a pentane solution of **36**−**38** was stored for several weeks at room temperature a precipitate containing decomposition products was formed.

Diffraction-quality crystals of [{$Me_4Cp-PtBu(NEt_2)$}$TiCl_3$] (**36**) and [{tBuCp−PtBu(NEt_2)}$TiCl_3$] (**38**) could be obtained from saturated *n*-pentane solutions at −80 °C, and a single-crystal X-ray structure of [{$Me_4Cp-PtBu(NEt_2)$}$TiCl_3$] (**36**) has been determined (Figure 2). The structure of **38** could not be solved due to twinning problems.

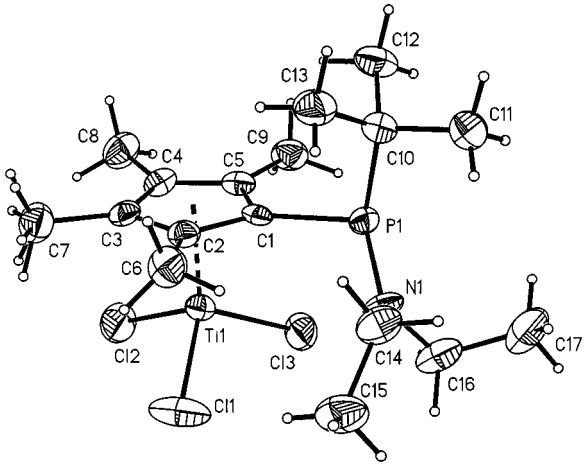

Figure 2. ORTEP diagram of the molecular structure of [{$Me_4Cp-PtBu(NEt_2)$}$TiCl_3$] (**36**); thermal ellipsoids are drawn at 50% probability level; selected bond lengths [Å]: Ti(1)−Cl(3) 2.232(2), Ti(1)−Cl(2) 2.235(2), Ti(1)−Cl(1) 2.235(2), Ti(1)−C(1) 2.328(5), Ti(1)−C(2) 2.352(5), Ti(1)−C(3) 2.368(5), Ti(1)−C(4) 2.379(5), Ti(1)−C(5) 2.339(5), P(1)−N(1) 1.691(4), P(1)−C(1) 1.862(6), P(1)−C(10) 1.897(6), N(1)−C(16) 1.465(7), N(1)−C(14) 1.479(7); selected bond angles [°]: Cl(1)−Ti(1)−Cl(2) 101.91(8), Cl(3)−Ti(1)−Cl(1) 104.47(8), Cl(3)−Ti(1)−Cl(2) 100.74(8), C(1)−P(1)−C(10) 100.3(2), N(1)−P(1)−C(1) 108.6(2), N(1)−P(1)−C(10) 110.4(2), C(16)−N(1)−C(14) 113.9(4), C(14)−N(1)−P(1) 128.7(4), C(16)−N(1)−P(1) 112.7(4); non-bonding distance [Å]: Ti(1)−N(1) 4.03

The racemic mixture of the chiral complex **36** crystallises in the centrosymmetric space group $P2_1/c$ building up non-chiral crystals. The coordination geometry at the titanium atom can be described as a piano-stool configuration typical for half-sandwich complexes, e.g. [$CpTiCl_3$].[46] The η^5-bound cyclopentadienyl ligand is practically planar with Ti−C bond lengths ranging from 2.332(2) to 2.379(5) Å and with C−C bond lengths of 1.407(8) to 1.438(8) Å. The deviations in the Ti−C distances indicate that the titanium atom is bonded somewhat more strongly to C(1), C(2) and C(5) atoms with average distances of 2.34 Å than to C(3) and C(4) atoms (2.37 Å), but the cyclopentadienyl fragment can be still regarded as η^5-coordinated. A different situation has been observed for the [$Ph_2PCpTiCl_3$] complex[47] in which the distance between the titanium atom and the phosphorus-substituted carbon atom is slightly elongated in comparison to the other carbon atoms of the cyclopentadienyl ligand. The bond angle C(1)−P(1)−C(10) at the phosphorus atom of 100.3(2)° is smaller than N(1)−P(1)−C(1) of 108.6(2)° and N(1)−P(1)−C(10) 110.4(2)°. This phenomenon may be attributed to a higher steric demand of a shorter bound nitrogen substituent at the phosphorus atom [1.691(4) Å], while the electronegative character of the Et_2N group should work in an absolutely opposite direction. This leads to a greater contribution of the 3p orbital of the phosphorus atom to the P−N bond and as a consequence more 3s character in the P−C bond according to the well-known "rehybridisation" effect, also referred to as Bent's rule.[48] Introduction of an electronegative substituent X (e.g. NR_2) in a compound X−EY_n (e.g. $R_2N-PR'_2$) develops more p-orbital character of the E−X (e.g. P−N) bond, leaving more s character for the bonds E−Y (e.g. P−C), thus shortening them and enhancing Y−E−Y angles. The Ti−Cl distances as well as Cl−Ti−Cl angles have values typical of other related cyclopentadienyltitanium trichlorides.[49−51] Although the Et_2N group is oriented towards the metal centre, the Ti(1)−N(1) distance of 4.03 Å is considerably longer than the sum of the van der Waals radii of 3.82 Å.[52]

When [tBuCp−PtBu(Cl)] (**6**) is treated with $TiCl_4$ in hexane at a low temperature in the presence of Et_3N [{tBuCp−PtBu(Cl)}$TiCl_3$] (**39**) is obtained in almost quantitative yield as estimated by ^1H and ^{31}P NMR spectroscopy(Scheme 10). Complex **39** is, however, very soluble in aliphatic solvents so that an analytically pure sample could be isolated with 40% yield.

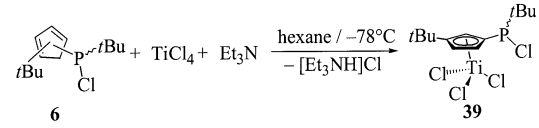

Scheme 10

Attempts to extend this synthetic strategy to other derivatives [$R_nCp-PtBu(Cl)$] (**1**−**3** and **5**) and [{$R_nCp-PtBu(Cl)$}$_2Z$] (**7**−**10**) failed. Only the sterically less encumbered [{$Cp-PtBu(Cl)$}$_2CMe_2$] (**11**) was successfully transformed into target complexes by the reaction with 1 and 2 equiv. of $TiCl_4$ to form complex isomeric mixtures of corresponding homobimetalic [{$(Cp-PtBu(Cl)]_2$-CMe_2}{$TiCl_3$}$_2$] (**40**) and *ansa*-[{$(Cp-PtBu(Cl)]_2$-CMe_2}$TiCl_2$] (**41**) compounds (Scheme 11).

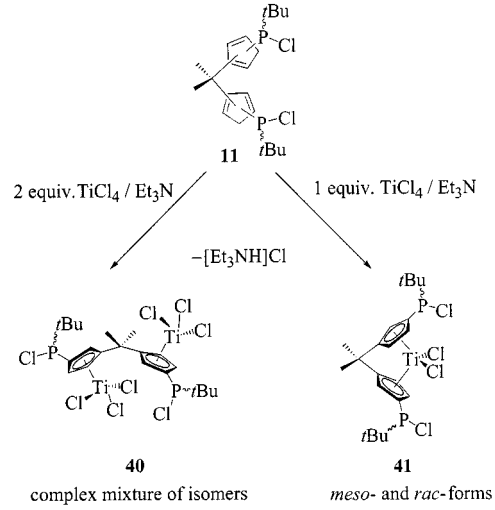

Scheme 11

According to ^1H and ^{31}P NMR spectroscopic data both complexes are formed in a high (ca. 90%) yield. The physical properties of **40** and **41** are totally different. **40** is only soluble in polar solvents, e.g. toluene, CH_2Cl_2, THF, and insoluble in aliphatic solvents, whereas the *ansa* complex **41** is practically unlimitedly soluble in aliphatic solvents. All of our efforts to purify these compounds by standard methods such as sublimation, liquid chromatography or recrystallisation have failed so far.

The fact that only sterically less demanding and more CH-acidic alkyl(chloro)cyclopentadienylphosphanes react with $TiCl_4$ in the presence of Et_3N to give complexes similar to **39** leads us to the hypothesis that in the mechanism of the reaction the key-step should be controlled by the acidity of the Cp protons. An analogous methodology has been used for the synthesis of [{Cp(CH$_2$)$_2$NR$_2$}TiCl$_3$] complexes by direct reaction of Cp ligand precursors and $TiCl_4$ in the presence of Et_3N as a base.[53,54]

The complex [{*t*BuCp−P*t*Bu(Cl)}TiCl$_3$] (**39**) is structurally related to [{R$_n$CpSiMe$_2$(Cl)}TiCl$_3$] derivatives bearing a reactive chlorine atom at the dimethylsilyl group that were then transformed into [{R$_n$CpSiMe$_2$(N*t*Bu)}TiCl$_2$] CGC-type of complexes.[55−58] Awarding all of our previous unsuccessful attempts to access this class of compounds with a phosphorus bridging group, the transformation of **39** (half-sandwich) into complex **42** of CGC-type proceeded in good yield (Scheme 12).

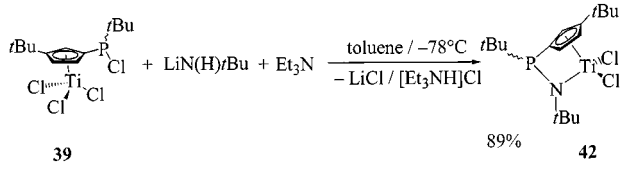

39 **42**

Scheme 12

The complex **42** is formed as a mixture of two diastereomers with respect to *syn* and *anti* orientation of the *t*Bu groups at the phosphorus atom and Cp ligand. Compound **42** was characterised by ^1H, ^{13}C, ^{31}P NMR spectroscopy and C,H,N elemental analyses.

Polymerisation of Ethylene

The preparative organotitanium chemistry described in the preceding sections was undertaken in part to provide precursors for an investigation of the catalytic polymerisation of ethylene in the presence of methylalumoxane (MAO), being suitable to roughly estimate the primary catalytic properties of the complexes.

Complexes **39** and **42** show moderate activities in the ethylene polymerisation at 20 and 80 °C (800 for **39** and 100 kg PE·mol^{-1}[Ti]·h^{-1}·bar^{-1} for **42**, MAO/[Ti] = 2000, T = 80 °C, p = 3 bar), while MAO-activated compounds **36**−**38** produce polyethylene with performances lower than 20 kg PE·mol^{-1}[M]·h^{-1}·bar^{-1} under the same polymerisation conditions. Related complexes [CpTiCl$_3$] (60), [Cp*TiCl$_3$] (600), [{Me$_4$CpCH$_2$CH$_2$NMe$_2$}TiCl$_3$] (200)[59] and [{Me$_4$CpSiMe$_2$N(*t*Bu)}TiCl$_2$] (950 kg PE·mol^{-1}·[Ti]·h^{-1}·bar^{-1})[60] show comparable and, under our experimental conditions, reproducible activities. The product is in all cases a highly linear polyethylene of high molecular weight ($10^5 < M_w < 1.4 \cdot 10^6$, determined viscosimetrically) having a melting point (DSC) in the range from 123 to 132 °C. Our main objective, however, was to compare the polymerisation activity of various organotitanium compounds and we have not investigated the morphology and the molecular weight distribution in detail. An investigation of the influence of the aminophosphanyl group attached to the cyclopentadienyl ligand on the catalytic behaviours of the complexes and the polymer properties is underway.

Conclusion

We have developed a new facile route to a class of P−N-functionalised phosphorylated cyclopentadienes, indenes and fluorenes **12**−**22**. Many attempts to obtain complexes **12**−**22** with group-4 transition metals Ti^{IV} and Zr^{IV} using classical procedures were, however, unsuccessful. We believe that the limiting factor is the high Lewis acidity of the Ti^{IV} and Zr^{IV} halides when they are treated with lithium and potassium salts of the ligand precursors giving complex mixtures of products. On the other hand, less Lewis-acidic Ti^{IV} and Zr^{IV} derivatives, e.g. Ti(NMe$_2$)$_4$, Zr(NMe$_2$)$_4$, do not react with the cyclopentadienylphosphanes under mild conditions due to a low CH acidity of these cyclopentadienes, while in the case of Ti(CH$_2$Ph)$_4$ or Zr(CH$_2$Ph)$_4$, again mixtures of products difficult to separate were formed at elevated temperatures. Several complexes could be synthesised only when trimethyltin-substituted amino(cyclopentadienyl)phosphane derivatives **31** and **32** were used as cyclopentadienylating agents. Surprising results have been obtained in the reaction of [*t*BuCp−P*t*Bu(Cl)] (**6**) with $TiCl_4$ in the presence of Et_3N at low temperature; the half-sandwich complex [{*t*BuCp−P*t*Bu(Cl)}TiCl$_3$] (**39**) was formed in a high yield. Compound **39** could be transformed into a CGC complex [{*t*BuCp−P*t*Bu(N*t*Bu)}TiCl$_2$] (**42**) by treatment with LiN(H)*t*Bu/Et_3N mixture in toluene. The isolated half-sandwich complexes [{R$_n$Cp−P*t*Bu(NEt$_2$)}TiCl$_3$] (**36**−**39** and **42**) were tested in the polymerisation of ethylene, some of them having activities comparable to known systems.[59][60]

Experimental Section

General Remarks: All manipulations involving air- and moisture-sensitive materials were carried out by standard Schlenk techniques under dry argon. Solvents were dried and distilled prior to use and stored under an inert gas. ^1H, ^{13}C and ^{31}P NMR spectra were recorded at 25 °C with Bruker AC250P, Bruker ARX300 and Varian VXR-400 spectrometers. Mass spectra (EI-MS) were recorded with a Varian CH-7a device using electron impact with an ionisation energy of 70 eV; all assignments were made with reference to the most abundant isotopes. C,H,N elemental analyses were carried out by the Microanalytical Division of Philipps-Universität Marburg. IR spectra were recorded with a Nicolet 510 FT-IR spectro-

meter. $[Cp_2CMe_2]$,[61] $[Ind_2CEt_2]$,[62] $[Ind_2(CH_2)_2]$ and $[IndCMe_2Cp]$,[63] $MesPCl_2$ (Mes = 2,4,6-$Me_3C_6H_2$) and $tBuPCl_2$,[64] Me_6IndH,[65] were prepared according to literature methods. Li salts of the cyclopentadienyl ligand precursors, indene and fluorene were obtained by deprotonation with a 1.6 M solution of *n*BuLi (purchased from Merck); $PhCH_2K$,[66] Ph_2CHK[67] by a standard procedure. MAO was used as 10% solution in toluene as received from Witco GmbH.

General Procedure for the Preparation of [$R_nCp-PR(Cl)$] (1−11): The total amount of dichlorophosphane ($RPCl_2$) (1 mol-equiv.; R = Alk or Ar) was added at once to a suspension of [R_nCp]Li (R_nCp = *t*BuCp, Me_4Cp, Ind, Flu) in hexane [in the case of bis(cyclopentadienyl) or bis(indenyl) diethyl ether had to be used] at −30 °C and the reaction mixture was stirred for 8 h, after warming to room temperature (1 h). Then the precipitated LiCl was removed by filtration. The filtrate was concentrated under vacuum (3 mbar) at room temperature to yield a product of an oily yellow liquid. Yield: 66−98%.

General Procedure for the Preparation of [$R_nCp-PR(NR^1R^2)$] (12−22): The total amount of HNR^1R^2 (2 mol) was immediately added to a solution of [$R_nCp-PR(Cl)$] (**1**−**6**) (1 mol) in diethyl ether at −20 °C and the reaction mixture was stirred for an additional 5 h at room temperature. Then the precipitated ammonium salt was removed by filtration. The filtrate was concentrated under vacuum at room temperature to yield a product of an oily yellow or red-yellow liquid. The yield, in all cases, was nearly quantitative.

General Procedure for the Preparation of [$R_nCp-PR(NR^1R^2)$]K (25−29): A solution of Ph_2CHK/$PhCH_2K$ (1 mol) was added slowly at −78 °C to a solution of [$R_nCp-PR(NR^1R^2)$] (**12**, **17**, **20** and **21**) (1 mol) in THF. The reaction mixture was stirred for 8 h, while warming to room temperature. The reaction mixture had a red colour except for the monoindenyl ligand derivatives that were green. Then the solvent was removed by evaporation under vacuum to give an oil. The oil solidified in pentane after several minutes to 2 d. Solvent-free potassium salts were isolated by filtration, washed twice with pentane and dried under vacuum. The yields, in all cases, were nearly quantitative.

General Procedure for the Preparation of [(Me_3Sn)-$R_nCp-PR(NR^1R^2)$] (31−34): A solution of Me_3SnCl (1 mol) in diethyl ether was added dropwise at −30 °C to a suspension of potassium salt [$R_nCp-PR(NR^1R^2)$]K (**25**−**28**) (1 mol) in diethyl ether. The reaction mixture was stirred for 8 h, while warming to room temperature. Then the precipitated KCl was removed by filtration. The filtrate was concentrated under vacuum at room temperature to yield a product of a white or pale yellow oil. The yield, in all cases, was nearly quantitative.

[Ind−P*t*Bu(Cl)] (1): Obtained from IndLi (3.54 g, 29.0 mmol) and $tBuPCl_2$ (4.77 g, 30.0 mmol). Isolated 4.61 g (19.3 mmol), yield 66%. *Isomer 1: tert*-Butylchloro(1*H*-inden-1-yl)phosphane (60%). ^1H NMR (300 MHz, [D_6]benzene): δ = 0.89 (d, 9 H, *t*Bu, $^3J_{HP}$ = 12.6 Hz), 3.99 (m, 1 H, Ind), 6.31−6.28 (dt, 1 H, Ind, $^3J_{H,H}$ = 4.2, $^3J_{HP}$ = 2.1 Hz), 6.66−6.64 (dt, 1 H, Ind, $^3J_{H,H}$ = 4.2 Hz), 7.13−7.01 (m, 2 H, Ind), 7.20−7.18 (d, 1 H, Ind), 7.81−7.78 (d, 1 H, Ind). $^{31}P\{^1H\}$ NMR (162 MHz, [D_6]benzene): δ = 132.0. *Isomer 2: tert*-Butylchloro(1*H*-inden-2-yl)phosphane (25%). ^1H NMR (300 MHz, [D_6]benzene): δ = 0.98 (d, $^3J_{HP}$ = 13.3 Hz, 9 H, *t*Bu), 3.62 (dt, 1 H, Ind), 6.42−6.38 (m, 1 H, Ind), 6.72−6.68 (m, $^3J_{H,H}$ = 8.1, $^3J_{HP}$ = 1.9 Hz, 1 H, Ind), 7.18−7.00 (m, 3 H, Ind), 7.59−7.57 (m, 1 H, Ind). *Isomers 1 and 2:* $^{13}C\{^1H\}$ NMR (75 MHz, [D_6]benzene): δ = 26.7 (d, $^2J_{C,P}$ = 9 Hz, CH_3, *t*BuP), 26.8 (d, $^2J_{C,P}$ = 9.3 Hz, CH_3, *t*BuP), 34.5 (d, $^1J_{C,P}$ = 35.9 Hz, C, *t*BuP), 35.3 (d, $^1J_{C,P}$ = 38.1 Hz, C, *t*BuP), 51.4 (d, $^1J_{C,P}$ = 47.2 Hz, CH, Ind), 54.8 (d, $^1J_{C,P}$ = 44.3 Hz, CH, Ind), 121.8 (CH, Ind), 121.9 (CH, Ind), 124.4 (d, $J_{C,P}$ = 9 Hz, CH, Ind), 125.2, 125.3, 125.4, 127.3, 127.4 (CH, Ind), 132.5 (d, $J_{C,P}$ = 5.2 Hz, CH, Ind), 132.8 (d, $J_{C,P}$ = 2.2 Hz, CH, Ind), 133.5 (d, $J_{C,P}$ = 3.7 Hz, CH, Ind), 133.6 (d, $J_{C,P}$ = 3.2 Hz, CH, Ind), 143.7 (d, $J_{C,P}$ = 11.3 Hz, C, Ind), 144.4 (d, $J_{C,P}$ = 22.5 Hz, C, Ind). $^{31}P\{^1H\}$ NMR (162 MHz, [D_6]benzene): δ = 127.2. *Isomer 3: tert*-Butylchloro(1*H*-inden-3-yl)phosphane (15%). ^1H NMR (300 MHz, [D_6]benzene): δ = 1.08 (d, $^3J_{HP}$ = 17.9 Hz, 9 H, *t*Bu), 3.00 (d, $^3J_{H,H}$ = 2 Hz, 2 H, Ind), 7.70−7.64 (m, 1 H, Ind), 6.79 (dt, $^3J_{H,H}$ = 2, $^3J_{HP}$ = 4.1 Hz, 1 H, Ind), 7.28−7.15 (m, 3 H, Ind). $^{13}C\{^1H\}$ NMR (75 MHz, [D_6]benzene): δ = 26.3 (d, $^2J_{C,P}$ = 18.1 Hz, CH_3), 35.3 (d, $^1J_{C,P}$ = 27.8 Hz, C, *t*Bu), 39.9 (CH, Ind), 122.3 (d, $J_{C,P}$ = 6 Hz, CH, Ind), 124.2, 125.4, 126.5 (CH, Ind), 141.0 (d, $^1J_{C,P}$ = 46.5 Hz, C, Ind), 144.2 (d, $^2J_{C,P}$ = 12.1 Hz, CH, Ind), 144.4 (d, $J_{C,P}$ = 3.7 Hz, C, Ind), 145.8 (d, $J_{C,P}$ = 21.3 Hz, C, Ind). $^{31}P\{^1H\}$ NMR (162 MHz, [D_6]benzene): δ = 102.4. EI-MS: *m*/*z* (%) = 238 (8) [M^+], 182 (9) [M^+ − *t*Bu], 115 (26) [Ind], 57 (100) [*t*Bu]. $C_{13}H_{16}PCl$ (238.70): calcd. C 65.41, H 6.76; found C 65.02, H 6.37.

[Flu−P*t*Bu(Cl)] (2):[40] Obtained from FluLi (2.61 g, 15.2 mmol) and $tBuPCl_2$ (2.41 g, 15.2 mmol). Isolated 4.13 g (14.3 mmol), yield 94%. ^1H NMR (300 MHz, [D_6]benzene): δ = 0.41 (d, $^3J_{HP}$ = 12.9 Hz, 9 H, *t*Bu), 7.98−7.90 (m, 1 H, Flu), 4.41 (s, 1 H, Flu), 7.18−6.95 (m, 4 H, Flu), 7.45−7.40 (m, 3 H, Flu). $^{13}C\{^1H\}$ NMR (75 MHz, [D_6]benzene): δ = 26.8 (d, $^2J_{C,P}$ = 16.7 Hz, CH_3, *t*BuP), 36.3 (d, $^1J_{C,P}$ = 40.7 Hz, C, *t*BuP), 51.2 (d, $^1J_{C,P}$ = 49.4 Hz, CH, Flu), 120.4, 120.5, 125.9, 126.1, 126.7, 126.8, 127.3, 127.8 (CH, Flu), 141.2 (d, $J_{C,P}$ = 15 Hz, C, Flu), 141.3 (C, Flu), 142.4 (d, $J_{C,P}$ = 15 Hz, C, Flu), 144.1 (C, Flu). $^{31}P\{^1H\}$ NMR (162 MHz, [D_6]benzene): δ = 132.0. EI-MS: *m*/*z* (%) = 288 (3) [M^+], 231 (1) [M^+ − *t*Bu], 165 (100) [Flu]. $C_{17}H_{18}ClP$ (288.76): calcd. C 70.71, H 6.28; found C 70.14, H 6.40.

[Ind−PMes(Cl)] (3): Obtained from IndLi (2.5 g, 20.5 mmol) and $MesPCl_2$ (4.53 g, 20.5 mmol). Isolated 5.07 g (16.9 mmol), yield 82%. *Mixture of Isomers:* ^1H NMR (300 MHz, [D_6]benzene): δ = 2.5−1.8 (several s and d, 9 H, CH_3), 5.3−4.5 (several m, 1 H, Ind), 7.5−6.2 (several m, 7 H, Ind and Mes). $^{13}C\{^1H\}$ NMR (75 MHz, [D_6]benzene): δ = 25.0−21.0 (10 resonances, CH_3), 56.0−39.0 (3 d, Ind), 126.0−120.0 (22 resonances, CH, Ind/Mes), 127.7 (CH, Ind/Mes), 131.0−129.0 (6 d, CH, Ind/Mes), 132.0 (3 d, C, Ind/Mes), 132.5 (2 d, C, Ind/Mes), 134 (d, C, Ind/Mes), 137.0−136.0 (2 d and 1 s, C, Ind/Mes), 142.0−141.0 (3 s, C, Ind/Mes), 145.0−144.5 (3 d, C, Ind/Mes). $^{31}P\{^1H\}$ NMR (162 MHz, [D_6]benzene): δ = 70.7, 83.5, 84.3. EI-MS: *m*/*z* (%) = 300 (25) [M^+], 265 (10), [M^+ − Cl], 185 (100), [M^+ − Ind], 119 (42) [Mes], 115 (56) [Ind]. $C_{18}H_{18}ClP$ (300.77): calcd. C 71.88, H 6.03; found C 71.21, H 5.87.

[Me_6C_9H−P*t*Bu(Cl)] (4): Obtained from [Me_6C_9H]Li (3.0 g, 14.5 mmol) and $tBuPCl_2$ (2.32 g, 14.5 mmol). Isolated 3.98 g (12.3 mmol), yield 85%. ^1H NMR (300 MHz, [D_6]benzene): δ = 0.81 (d, $^3J_{HP}$ = 12.9 Hz, 9 H, *t*Bu), 2.04 (s, 3 H, CH_3), 2.06 (s, 6 H, 2 CH_3), 2.20 (s, 3 H, CH_3), 2.32 (s, 3 H, CH_3), 2.45 (d, $^4J_{HP}$ = 2 Hz, 3 H, CH_3), 4.14 (s, 1 H, Me_6C_9H). $^{13}C\{^1H\}$ NMR (75 MHz, [D_6]benzene): δ = 15.1, 16.0 (CH_3), 16.2 (d, $^3J_{C,P}$ = 7.5 Hz, CH_3, Me_6C_9H), 16.3 (CH_3, Me_6C_9H), 18.9 (d, $^4J_{C,P}$ = 19.6 Hz, CH_3, Me_6C_9H), 24.5 (CH_3, Me_6C_9H), 26.6 (d, $^2J_{C,P}$ = 17.3 Hz, CH_3, *t*BuP), 36.2 (d, $^1J_{C,P}$ = 40.8 Hz, C, *t*BuP), 57.7 (d, $^1J_{C,P}$ = 52.1 Hz, C, Me_6C_9H), 126.7, 129.3, 131.4, 134.7, 135.2 (C, Me_6C_9H), 138.1 (d, $J_{C,P}$ = 8.5 Hz, C, Me_6C_9H), 140.0, 141.7 (C, Me_6C_9H). $^{31}P\{^1H\}$ NMR (162 MHz, [D_6]benzene): δ = 45.3. EI-MS: *m*/*z* (%) = 322

(3) [M^+], 199 (100) [Me_6C_9H]. $C_{19}H_{28}ClP$ (322.86): calcd. C 70.68, H 8.74; found C 70.05, H 8.49.

[Me_4C_5H-P*t*Bu(Cl)] (5): Obtained from [Me_4C_5H]Li (1.85 g, 14.5 mmol) and of *t*BuPCl_2 (2.76 g, 14.5 mmol). Isolated 2.49 g (10.6 mmol), yield 73%. *Isomer 1: tert*-butylchloro(2,3,4,5-tetramethylcyclopenta-2,4-dien-1-yl)phosphane. ^{1}H NMR (300 MHz, [D$_6$]benzene): δ = 0.92 (d, $^3J_{HP}$ = 13.1 Hz, 9 H, *t*BuP), 1.50 (s, 3 H, CH_3, Me_4C_5H), 1.52 (s, 3 H, CH_3, Me_4C_5H), 1.85 (s, 3 H, CH_3, Me_4C_5H), 2.01 (s, 3 H, CH_3, Me_4C_5H), 3.28 (d, $^2J_{HP}$ = 6.8 Hz, 1 H, Me_4C_5H). *Isomer 2: tert*-Butylchloro(1,2,4,5-tetramethylcyclopenta-2,4-dien-3-yl)phosphane. 1.05 (d, $^3J_{HP}$ = 13.9 Hz, 9 H, *t*BuP), 1.26 (d, 3 H, CH_3), 1.44 (m, 3 H, CH_3), 1.56 (d, 3 H, CH_3), 1.98 (d, 3 H, CH_3), 3.06 (m, 1 H, Me_4C_5H). *Both Isomers:* ^{13}C{^{1}H} NMR (75 MHz, [D$_6$]benzene): δ = 11.1, 11.3, 12.0, 13.9, 14.2, 15.2, 16.9 (CH_3), 26.7 (d, $^2J_{C,P}$ = 18.8 Hz, CH_3, *t*Bu, *isomer 2*), 27.0 (d, $^2J_{C,P}$ = 17.5 Hz CH_3, *t*Bu, *isomer 1*), 35.2 (d, $^1J_{C,P}$ = 37 Hz, C, *t*Bu, *isomer 2*), 36.4 (d, $^1J_{C,P}$ = 39.8 Hz, C, *t*Bu, *isomer 1*), 54.7 (CH, Me_4C_5H, *isomer 2*), 61.7 (d, $^1J_{C,P}$ = 49.2 Hz, CH, *isomer 1*, Me_4C_5H), 131.2, 134.1, 136.5, 137.6 150.1 (C, Me_4C_5H). ^{31}P{^{1}H} NMR (162 MHz, [D$_6$]benzene): δ = 34.5 (*isomer 2*; ca. 40%), 98.2 (*isomer 1*; ca. 60%). EI-MS: *m*/*z* (%) = 244 (12) [M^+], 187 (100) [M^+ − *t*Bu], 120 (65) [C_5Me_4]. $C_{13}H_{22}PCl$ (244): calcd. C 63.80, H 9.21; found C 63.41, H 9.22.

[*t*BuC_5H_4−P*t*Bu(Cl)] (6): Obtained from *t*BuCpLi (1.0 g, 7.81 mmol) and of *t*BuPCl_2 in hexane (9.6 mL, 7.81 mmol/0.81 M). Isolated 1.81 g (7.41 mmol), yield 95%. *Mixture of Isomers:* ^{1}H NMR (250 MHz, $CDCl_3$): δ = 1.2−1.0 (several d, 18 H, *t*Bu and *t*BuP), 3.25 (s, 1 H, *t*BuC_5H_4), 6.2 (several m, 1 H, *t*BuC_5H_4), 6.9 (several m, 1 H, *t*BuC_5H_4), 7.05 (several m, 1 H, *t*BuC_5H_4). ^{13}C{^{1}H} NMR (75 MHz, [D$_6$]benzene): δ = 12.1 (CH_3, *t*BuC_5H_4), 26.1−30.0 (several d, CH_3, *t*BuP), 32.1 (m, C, *t*Bu), 34.2 (m, C, *t*BuP), 43.9, 124.8, 144.9 (m, CH, *t*BuC_5H_4), 157.0 (d, C, *t*BuC_5H_4), 159.9 (m, CH, *t*BuC_5H_4). ^{31}P{^{1}H} NMR (162 MHz, $CDCl_3$): δ = 103.0, 106.9, 107.2. EI-MS: *m*/*z* (%) = 229 (24) [M^+ − CH_3], 211 (57) [M^+ − Et], 155 (19) [*t*Bu$C_5H_4PH_2$], 107 (37) [*t*BuC_5H_4 − Me], 57 (100) [*t*Bu], 35 (53) [Cl]. $C_{13}H_{22}ClP$ (244.74): calcd. C 63.80, H 9.06; found C 63.39, H 8.72.

[{Ind−P*t*Bu(Cl)}$_2$(CH_2)$_2$] (7): Obtained from [Ind(CH_2)$_2$Ind]Li_2 (2.0 g, 7.04 mmol) and *t*BuPCl_2 (18.1 mL, 14.08 mmol/0.81 M). Isolated 2.47 g (4.79 mmol), yield 64%. *Mixture of Isomers:* ^{1}H NMR (300 MHz, [D$_6$]benzene): δ = 0.9−1.1 (4 d, 18 H, *t*BuP), 2.75 and 2.85 (2 s, 4 H, −$CH_2$$CH_2$−), 4.1 (several m, 2 H, Ind), 6.1−6.4 (several m, 1 H, Ind), 7.64−7.7 (several m, 8 H, Ind), 7.99−7.91 (several m, 1 H, Ind). ^{13}C{^{1}H} NMR (75 MHz, [D$_6$]benzene): δ = 26.4−26.8 (CH_3, *t*BuP), 34.7−35.4 (−$CH_2$$CH_2$−), 50.0−50.5 (C, *t*BuP), 53.0−53.5, 119.7−119.8, 125.5−126.7, 127.2−127.3 (several resonances, CH, Ind), 144.6−145.1, 145.1, 145.8−146.2 (several resonances, C, Ind). ^{31}P{^{1}H} NMR (162 MHz, [D$_6$]benzene): δ = 127.7, 128.8, 128.9, 130.7, 131.3, 131.1, 131.3. EI-MS: *m*/*z* (%) = 253 (42) [MeInd(*t*Bu)P(Cl)H], 128 (100) [MeInd], 115 (38) [Ind], 57 (76) [*t*Bu]. $C_{28}H_{34}Cl_2P_2$ (502.15): calcd. C 66.80, H 6.81; found C 66.37, H 6.51.

[{Ind−P*t*Bu(Cl)}$_2$$CMe_2$] (8): Obtained from [(Ind)$_2$$CMe_2$]$Li_2$ (7.95 g, 18.44 mmol) and *t*BuPCl_2 (37.9 mL, 36.88 mmol/0.97 M). Isolated 9.43 g, yield > 95%. *Mixture of Isomers:* ^{1}H NMR (250 MHz, $CDCl_3$): δ = 1.0−1.5 (4 d, 18 H, *t*BuP), 1.8 (s, 6 H, CMe_2), 3.9−4.2 (m, 2 H, Ind), 6.6 (several m, 2 H, Ind), 7.1 (m, 4 H, Ind), 7.2−7.6 (several m, 2 H, Ind), 7.7 (m, 2 H, Ind). ^{13}C{^{1}H} NMR (125 MHz, $CDCl_3$): δ = 24.6 (CH_3, CMe_2), 25.7−26.8 (several resonances, CH_3, *t*BuP), 38.3−38.4 (several resonances, C, *C*Me_2), 48.5−48.8 (C, *t*BuP), 52.1−52.4, 121.8−122.4, 123.8−125.3, 125.4−127.0 (several resonances, CH, Ind), 143.0−144.9 (several resonances, C, Ind). ^{31}P{^{1}H} NMR (162 MHz, [D$_6$]benzene): δ = 130.1, 130.2, 130.3, 131.0, 131.2, 131.3, 131.4. $C_{29}H_{36}Cl_2P_2$ (516.16): calcd. C 67.31, H 7.01; found C 67.13, H 6.89.

[{Ind−P*t*Bu(Cl)}$_2$$CEt_2$] (9): Obtained from [(Ind)$_2$$CEt_2$]$Li_2$ (4.0 g, 12.85 mmol) and *t*BuPCl_2 (26.5 mL, 25.7 mmol/0.97 M). Isolated 6.48 g, yield 92%. *Mixture of Isomers:* ^{1}H NMR (400 MHz, $CDCl_3$): δ = 0.75−0.85 (m, 3 H, −$CH_2$$CH_3$), 1.3−1.5 (3 d, 9 H, *t*BuP), 2.23−2.27 (m, 2 H, −$CH_2$$CH_3$), 4.29 (s, 1 H, Ind), 6.56 (s, 1 H, Ind), 7.0−7.2 (m, 2 H, Ind), 7.58 (d, $J_{H,H}$ = 7.3 Hz, 1 H, Ind), 7.84 (d, $J_{H,H}$ = 7.3 Hz, 1 H, Ind). ^{31}P{^{1}H} NMR (162 MHz, $CDCl_3$): δ = 129.4 (br. s), 130.8 (br. m) and 131.0. $C_{31}H_{40}Cl_2P_2$ (545.51): calcd. C 68.26, H 7.39; found C 67.93, H 7.01.

[{Ind−P*t*Bu(Cl)}CMe_2{Cp−P*t*Bu(Cl)}] (10): Obtained from [IndCMe$_2$Cp]Li_2 (3.86 g, 16.5 mmol) and *t*BuPCl_2 (34.0 mL, 33.0 mmol/0.97 M). Isolated 3.9 g (8.4 mmol), yield 50%. *Mixture of Isomers:* ^{1}H NMR (400 MHz, [D$_6$]benzene): the spectrum is not informative, very complex set of partially low-resolved signals. ^{31}P{^{1}H} NMR (162 MHz, [D$_6$]benzene): δ = 106.7 (3 signals), 106.8, 124.6, 131.1, 131.7. $C_{25}H_{34}Cl_2P_2$ (467.39): calcd. C 64.24, H 7.33; found C 64.01, H 7.52.

[{Cp−P*t*Bu(Cl)}$_2$$CMe_2$] (11): Obtained from [Cp$_2$$CMe_2$]$Li_2$ (5.0 g, 27.20 mmol) and *t*BuPCl_2 (56.0 mL, 54.4 mmol/0.97 M). Isolated 9.26 g (22.2 mmol), yield 80%. *Mixture of Isomers:* ^{1}H NMR (250 MHz, $CDCl_3$): δ = 0.9−1.45 (several d, 18 H, *t*BuP), 1.45 (m, 6 H, CMe_2), 3.0−3.3 (s and several m, 2 H, Cp), 6.2−6.4 (several m, 2 H, Cp), 6.6−6.95 (m, 4 H, Cp). ^{13}C{^{1}H} NMR (125 MHz, $CDCl_3$): δ = 23.0−23.5 (2 resonances, CH_3, CMe_2), 25.5−26.3 (several resonances, CH_3, *t*BuP), 36.0−40.0 (several resonances, C, *C*Me_2), 43.5−46.0 (several resonances, C, *t*BuP), 51.0−55.0 (several resonances, CH, Cp), 129.0−133.0 (CH, Cp), 140.0−148.0 (several resonances, C, Cp). ^{31}P{^{1}H} NMR (162 MHz, [D$_6$]benzene): δ = 100.7, 101.0, 104.7, 104.8, 104.9, 105.0, 105.1 (2 signals), 105.2, 105.3, 105.4, 105.7, 105.8, 105.9, 106.0, 106.1. EI-MS: *m*/*z* (%) = 416 (1) [M^+], 187 (76) [Cp(*t*Bu)PCl], 172 (92) [Cp$_2$$CMe_2$], 170 (92) [$M^+$ − 2 *t*BuPCl], 57 (100) [*t*Bu]. $C_{21}H_{32}Cl_2P_2$ (416.13): calcd. C 60.44, H 7.73; found C 60.63, H 7.56.

[Ind−P*t*Bu(NEt_2)] (12): Obtained from [Ind−P*t*Bu(Cl)] (**1**) (2.39 g, 10.0 mmol) and Et_2NH (3.1 mL, > 20 mmol). Isolated 2.74 g (9.9 mmol), yield > 95%. IR (film): $\tilde{\nu}$ = 3000, 2950, 2875, 2864, 2396, 1558, 1457, 1180, 1093, 874, 773, 736 (P−N), 415 cm^{-1}. ^{1}H NMR (300 MHz, [D$_6$]benzene): δ = 0.83 (t, $^3J_{H,H}$ = 5.4 Hz, 6 H, −NCH_2CH_3), 1.19 (d, $^3J_{HP}$ = 12.9 Hz, 9 H, *t*Bu), 2.93 (m, 4 H, −NCH_2CH_3), 3.0−3.1 (m, 2 H, Ind), 6.43 (m, 1 H, Ind), 7.12 (m, 2 H, Ind), 7.18−7.23 (m, 1 H, Ind), 7.80 (m, 1 H, Ind). ^{13}C{^{1}H} NMR (75 MHz, [D$_6$]benzene): δ = 15.1 (d, $^3J_{C,P}$ = 3.2 Hz, −NCH_2CH_3), 28.1 (d, $^2J_{C,P}$ = 16.1 Hz, CH_3, *t*Bu), 33.65 (d, $^1J_{C,P}$ = 17.6 Hz, C, *t*Bu), 40.2 (CH, Ind), 46.5 (d, $^2J_{C,P}$ = 15.7 Hz, −NCH_2CH_3), 121.0 (d, $^3J_{C,P}$ = 7.4 Hz, CH, Ind), 123.6, 124.9, 126.4, 136.6 (CH, Ind), 142.3 (d, $^1J_{C,P}$ = 25.5 Hz, C, Ind), 143.4 (C, Ind), 148.0 (d, $^2J_{C,P}$ = 23.6 Hz, C, Ind). ^{31}P{^{1}H} NMR (162 MHz, [D$_6$]benzene): δ = 63.9. EI-MS: *m*/*z* (%) = 275 (7) [M^+], 218 (76) [M^+ − *t*Bu]. $C_{17}H_{28}NP$ (277.38): calcd. C 73.61, H 10.17, N 5.05; found C 73.32, H 9.74, N 4.91.

[Ind−P*t*Bu(NH*t*Bu)] (13): Obtained from [Ind−P*t*Bu(Cl)] (**1**) (2.39 g, 10 mmol) and *t*BuNH_2 (3.2 mL, > 20 mmol). Isolated 2.7 g (9.8 mmol), yield > 95%. IR (film): $\tilde{\nu}$ = 3000, 2961, 2771, 2380, 1635, 1578, 1540, 1192, 1180, 953, 736 (P−N), 656 cm^{-1}. ^{1}H NMR (300 MHz, [D$_6$]benzene): δ = 1.05 (d, $^3J_{HP}$ = 12.8 Hz, 9 H, *t*BuP), 1.15 (s, 9 H, *t*BuN), 1.68 (d, $^2J_{HP}$ = 11.9 Hz, 1 H, −NH), 3.07 (m,

2 H, Ind), 6.22 (m, 1 H, Ind), 7.12−7.18 (dt, 2 H, Ind), 7.24 (d, 1 H, Ind), 7.80 (d, 1 H, Ind). $^{13}C\{^1H\}$ NMR (75 MHz, [D$_6$]benzene): δ = 26.6 (d, $^2J_{C,P}$ = 15 Hz, CH_3, *t*BuP), 27.4 (d, $^1J_{C,P}$ = 16.4 Hz, CH_3, *t*BuP), 32.1 (d, $^3J_{C,P}$ = 8.3 Hz, C, *t*BuN), 39.4 (d, $^3J_{C,P}$ = 2.8 Hz, CH, Ind), 50.7 (d, $^2J_{C,P}$ = 17.2 Hz, C, *t*BuN), 122.4 (d, $^3J_{C,P}$ = 6.2 Hz, CH, Ind), 123.8, 125.0, 126.3, 141.1 (CH, Ind), 144.6 (C, Ind), 147.4 (d, $J_{C,P}$ = 32.4 Hz, C, Ind), 147.7 (d, $J_{C,P}$ = 23.6 Hz, C, Ind). $^{31}P\{^1H\}$ NMR (162 MHz, [D$_6$]benzene): δ = 21.7. EI-MS: *m*/*z* (%) = 275 (9) [M$^+$], 218 (65) [M$^+$ − *t*Bu], 162 (100) [M − 2 *t*Bu]. $C_{17}H_{28}NP$ (277.38): calcd. C 73.61, H 10.17, N 5.05; found C 73.19, H 9.77, N 4.89.

[Ind−P*t*Bu(NHPh)] (14): Obtained from [Ind−P*t*Bu(Cl)] (**1**) (2.9 g, 12.14 mmol) and $PhNH_2$. (2.2 mL, 24.28 mmol). Isolated 3.47 g (11.77 mmol), yield > 95%. ^1H NMR (200 MHz, [D$_6$]benzene): δ = 1.02 (d, $^3J_{HP}$ = 15.8 Hz, 9 H, *t*BuP), 1.33 (d, $^2J_{HP}$ = 13 Hz, 1 H, −NH), 3.01 (m, 2 H, Ind), 6.26 (m, 1 H, Ph and Ind), 6.76−7.24 (several m, 8 H, Ph and Ind), 7.97 (d, 1 H, Ind). $^{13}C\{^1H\}$ NMR (50.3 MHz, [D$_6$]benzene): δ = 25.0 (d, $^2J_{C,P}$ = 15.5 Hz, CH_3, *t*BuP), 31.0 (d, C, *t*BuP), 38.3 (d, $^3J_{C,P}$ =3 Hz, CH, Ind), 113.6, 115.4, 118.0, 122.5, 123.6, 123.7, 125.0, 128.1, 128.8 (CH, Ph/Ind), 137.1 (d, $^2J_{C,P}$ = 2.5 Hz, C, Ind), 140.0 (C, Ind), 143.0 (d, $^2J_{C,P}$ = 4.5 Hz, C, Ph), 145.2 (d, C, Ind), 146.5 (d, $J_{C,P}$ = 17.5 Hz, C, Ind). $^{31}P\{^1H\}$ NMR (81.0 MHz, [D$_6$]benzene): δ = 29.5. $C_{19}H_{24}NP$ (297.38): calcd. C 76.74, H 8.13, N 4.71; found C 76.10, H 8.25, N 4.63.

[Me$_6$C$_9$H−P*t*Bu(NH*t*Bu)] (15): Obtained from [Me$_6$C$_9$H−P*t*Bu(Cl)] (**4**) (3.44 g, 10.6 mmol) and *t*BuNH$_2$ (3.4 mL, >20 mmol). Isolated 2.85 g (7.94 mmol), yield 75%. ^1H NMR (200 MHz, [D$_6$]benzene): δ = 0.93 (d, $^3J_{HP}$ = 11.2 Hz, 9 H, *t*BuP), 1.31 (s, 9 H, *t*BuN), 1.98 (d, $^2J_{HP}$ = 2.5 Hz, 1 H, NH), 2.21 (s, 3 H, CH_3), 2.27 (s, 3 H, CH_3), 2.31 (s, 6 H, 2 CH_3), 2.57 (s, 3 H, CH_3), 2.80 (s, 3 H, CH_3), 3.85 (s, 1 H, Me$_6$C$_9$*H*). $^{13}C\{^1H\}$ NMR (50 MHz, [D$_6$]benzene): δ = 15.7, 16.5, 16.8, 19.4, 19.8, 26.0 (CH_3, Me$_6$C$_9$), 27.9 (d, $^2J_{C,P}$ = 16.1 Hz, CH_3, *t*BuP), 32.5 (d, $^3J_{C,P}$ = 7.8 Hz, CH_3, *t*BuN), 32.7 (d, CH, Me$_6$C$_9$H), 33.5 (d, $^1J_{C,P}$ = 16.9 Hz, C, *t*BuP), 51.3 (d, $^2J_{C,P}$ = 19.4 Hz, C, *t*BuN), 126.5, 133.5, 133.7, 140.8 (C, Me$_6$C$_9$H), 141.3 (d, $J_{C,P}$ = 6.9 Hz, C, Me$_6$C$_9$H). $^{31}P\{^1H\}$ NMR (162 MHz, [D$_6$]benzene): δ = 51.0. EI-MS: *m*/*z* (%) = 359 (2) [M$^+$], 302 (16) [M$^+$ − *t*Bu], 199 (34) [Me$_6$C$_9$H]. $C_{23}H_{38}NP$ (359.54): calcd. C 76.84, H 10.65, N 3.90; found C 76.43, H 10.47, N 3.81.

[Ind−PMes(NH*t*Bu)] (16): Obtained from [Ind−PMes(Cl)] (**3**) (3.01 g, 10 mmol) and *t*BuNH$_2$ (3.1 mL, > 20 mmol). Yield > 95%. ^1H NMR (200 MHz, [D$_6$]benzene): δ = 1.32 (s, 9 H, *t*BuN), 2.15 (s, 3 H, CH_3), 2.45 (d, $^2J_{HP}$ = 11.6 Hz, 1 H, -NH), 2.64 (s, 6 H, 2 CH_3), 3.20 (m, 1 H, Ind), 6.34 (m, 1 H, Ind), 6.47 (m, 1 H, Ind), 6.80 (s, 2 H, Mes), 7.11−7.24 (m, 2 H, Ind and Mes), 7.31−7.35 (m, 1 H, Ind and Mes), 7.4−7.6 (m, 1 H, Ind and Mes). $^{13}C\{^1H\}$ NMR (50 MHz, [D$_6$]benzene): δ = 19.7 (CH_3, Mes), 21.0 (d, $^3J_{C,P}$ = 23.2 Hz, CH_3, Mes), 30.65 (d, $^3J_{C,P}$ = 9 Hz, C, *t*BuP), 38.0 (CH, Ind), 49.9 (d, $^2J_{C,P}$ = 21.3 Hz, C, *t*BuN), 120.4, 122.4, 123.5, 124.9 (CH, Ind/Mes), 128.8 (d, $^3J_{C,P}$ = 12.5 Hz, CH, Ind/Mes), 133.3 (d, $J_{C,P}$ = 24.5 Hz, C, Ind/Mes), 133.9 (d, $^3J_{C,P}$ = 9.5 Hz, CH, Ind/Mes), 141.7 (d, $^2J_{C,P}$ = 17.5 Hz, CH, Ind/Mes), 143.0 (d, $J_{C,P}$ = 6.1 Hz, C, Ind/Mes), 143.8 (d, $J_{C,P}$ = 5.3 Hz, C, Ind/Mes), 144.7 (d, $J_{C,P}$ = 13.1 Hz, C, Ind/Mes), 146.0 (d, $J_{C,P}$ = 7 Hz, C, Ind/Mes). $^{31}P\{^1H\}$ NMR (162 MHz, [D$_6$]benzene): δ = 4.1. EI-MS: *m*/*z* (%) = 337 (1) [M$^+$], 265 (12) [M$^+$ − N(H)*t*Bu], 218 (34) [M$^+$ − Mes], 115 (100) [Ind]. $C_{22}H_{30}NP$ (339.46): calcd. C 77.84, H 8.91, N 4.13; found C 77.42, H 9.22, N 4.23.

[Flu−P*t*Bu(NEt$_2$)] (17):[31] Obtained from [Flu−P*t*Bu(Cl)] (**2**) (2.88 g, 10 mmol) and Et_2NH (1.0 mL, > 20 mmol). Isolated 3.20 g (9.8 mmol), yield 98%.

[Flu−P*t*Bu(NH*t*Bu)] (18): Obtained from 2.88 g (10 mmol) [Flu−P*t*Bu(Cl)] (**2**) and 1.0 mL (> 20 mmol) of *t*BuNH$_2$. Isolated 3.24 g (9.95 mmol), yield > 95%. ^1H NMR (200 MHz, [D$_6$]benzene): δ = 0.58 (s, 9 H, *t*BuN), 0.89 (d, $^3J_{HP}$ = 12.5 Hz, 9 H, *t*BuP), 1.56 (d, $^2J_{HP}$ = 10.3 Hz, 1 H, -NH), 3.84 (s, 1 H, Flu), 7.08−7.15 (m, 5 H, Flu), 7.23−7.27 (m, 1 H, Flu), 7.49−7.53 (m, 2 H, Flu). $^{13}C\{^1H\}$ NMR (50 MHz, [D$_6$]benzene): δ = 25.8 (d, $^2J_{C,P}$ = 16.5 Hz, CH_3, *t*BuP), 30.0 (d, $^1J_{C,P}$ = 13.6 Hz, C, *t*BuP), 30.4 (d, $^3J_{C,P}$ = 7.8 Hz, C, *t*BuN), 47.3 (d, $^1J_{C,P}$ = 39.2 Hz, C, Flu), 48.6 (d, $^2J_{C,P}$ = 18.2 Hz, C, *t*BuN), 118.5, 119.1, 124.1 (2 signals), 124.3, 124.9, 125.1, 125.7 (CH, Flu), 139.1 (d, $J_{C,P}$ = 3.3 Hz, C, Flu), 142.3, 140.8 (C, Flu), 147.0 (d, $J_{C,P}$ = 15.1 Hz, C, Flu). $^{31}P\{^1H\}$ NMR (162 MHz, [D$_6$]benzene): δ = 49.5. EI-MS: *m*/*z* = 325 (1) [M$^+$], 268 (5) [M$^+$ − *t*Bu], 212 (12) [M$^+$ − 2 *t*Bu+H], 165 (36) [Flu]. $C_{21}H_{28}NP$ (325.43): calcd. C 77.51, H 8.67, N 4.31; found C 77.10, H 8.13, N 4.17.

[Me$_4$C$_5$H−P*t*Bu(NH*t*Bu)] (19): Obtained from [Me$_4$Cp−P*t*Bu(Cl)] (**5**) (2.44 g, 10 mmol) and *t*BuNH$_2$ (3.1 mL, > 20 mmol). Isolated 2.2 g (7.8 mmol), yield 78%. ^1H NMR (300 MHz, [D$_6$]benzene): δ = 0.94 (d, $^3J_{HP}$ = 12.4 Hz, 9 H, *t*BuP), 1.03 (s, 9 H, *t*BuN), 1.64 (s, 6 H, 2 CH_3), 1.98 (s, 3 H, CH_3), 2.01 (s, 3 H, CH_3), 2.11 (br. s., 1 H, −NH), 2.6 (m, 1 H, Me$_4$C$_5$H). $^{13}C\{^1H\}$ NMR (75 MHz, [D$_6$]benzene): δ = 17.6 (CH_3), 27.2 (CH_3), 27.4 (d, $J_{C,P}$ = 3.8 Hz, CH_3), 27.7 (CH_3), 32.2 (d, $^3J_{C,P}$ = 6.2 Hz, C, *t*BuP), 54.2 (d, $^2J_{C,P}$ = 6.2 Hz, C, *t*BuN), 60.8 (d, $^1J_{C,P}$ = 36.9 Hz, CH, Me$_4$C$_5$H), 133.0, 136.6, 144.9 (C, Me$_4$C$_5$H), 152.3 (d, $J_{C,P}$ = 6.6 Hz, C, Me$_4$C$_5$H). $^{31}P\{^1H\}$ NMR (162 MHz, [D$_6$]benzene): δ = 21.3. EI-MS: *m*/*z* (%) = 281 (7) [M$^+$], 224 (100) [M$^+$ − *t*Bu], 168 (22) [M$^+$ − 2 *t*Bu]. $C_{17}H_{32}NP$ (281.42): calcd. C 72.56, H 11.46, N 4.98; found C 72.64, H 11.13, N 5.12.

[Me$_4$C$_5$H−P*t*Bu(NEt$_2$)] (20): Obtained from [Me$_4$Cp−P*t*Bu(Cl)] (**5**) (2.44 g, 10 mmol) and Et_2NH (3.3 mL, > 20 mmol). Isolated 2.79 g (9.9 mmol), yield > 95%. *Mixture of Isomers:* IR (film): $\tilde{\nu}$ = 3000, 2858, 2733, 2361, 1629, 1579, 1547, 1195, 1157, 958, 723 (P−N), 680. ^1H NMR (200 MHz, [D$_6$]benzene): δ = 0.87 (t, $^3J_{H,H}$ = 7.2 Hz, 6 H, $-NCH_2CH_3$), 1.19 (d, $^3J_{HP}$ = 13.2 Hz, 9 H, *t*BuP), 1.80 (s, 3 H, CH_3, Me$_4$C$_5$H), 1.87 (s, 3 H, CH_3, Me$_4$C$_5$H), 2.10 (s, 3 H, CH_3, Me$_4$C$_5$H), 2.21 (s, 3 H, CH_3, Me$_4$C$_5$H), 2.8−3.0 (m, 5 H, $-NCH_2CH_3$ and Me$_4$C$_5$H). $^{13}C\{^1H\}$ NMR (50 MHz, [D$_6$]benzene): δ = 11.1 ($-NCH_2CH_3$), 28.8−29.8 (several d, $J_{C,P}$ = 7.8 Hz, CH_3), 34.8−35.5 ($-NCH_2CH_3$), 46.6−47.6 (3 d, $^2J_{C,P}$ = 20.2 Hz, C, *t*BuP), 53.1 (d, $^2J_{C,P}$ = 3.6 Hz, C, *t*BuN), 61.2, 61.9, 62.8 (CH, Me$_4$C$_5$H), 151.9−133.6 (several resonances, C, Me$_4$C$_5$H). $^{31}P\{^1H\}$ NMR (162 MHz, [D$_6$]benzene): δ = 77.4, 86.4, 114.5. EI-MS: *m*/*z* (%) = 281 (2) [M$^+$], 224 (92) [M$^+$ − *t*Bu], 160 (38) [*t*BuPNEt$_2$], 153 (57) [Me$_4$C$_5$HP], 121 (19) [Me$_4$C$_5$H], 104 (100) [HPNEt$_2$], 72 (14) [NEt$_2$]. $C_{17}H_{32}NP$ (281.42): calcd. C 72.56, H 11.46, N 4.98; found C 72.17, H 11.33, N 5.10.

[*t*BuC$_5$H$_4$−P*t*Bu(NEt$_2$)] (21): Obtained from [*t*BuCp−P*t*Bu(Cl)] (**6**) (1.67 g, 10.51 mmol) and Et_2NH (2.5 mL, > 21 mmol). Yield > 95%. *Mixture of Isomers:* IR (film): $\tilde{\nu}$ = 3000, 2965, 1575, 1458, 1386, 922, 746 (P−N), 642 cm^{-1}. ^1H NMR (250 MHz, [D$_6$]benzene): δ = 0.9−1.3 (several m, 24 H, *t*Bu, *t*BuP and $-NCH_2CH_3$), 3.0 (m, 4 H, $-NCH_2CH_3$), 3.18 (s, 1 H, *t*BuC$_5$H$_4$), 6.1 (several m, 1 H, *t*BuC$_5$H$_4$), 6.35 (several m, 1 H, *t*BuC$_5$H$_4$), 6.6−6.75 (several m, 1 H, *t*BuC$_5$H$_4$). $^{13}C\{^1H\}$ NMR (50 MHz, [D$_6$]benzene): δ = 15.0 ($-NCH_2CH_3$), 28.8−28.9 (several d, CH_3, *t*BuP), 29.9, 31.0 ($-NCH_2CH_3$), 46.2−44.2 (several d, C, *t*BuN, *t*BuC$_5$H$_4$ and *t*BuP),

124.6, 124.7, 125.7 (CH, tBuC$_5$H$_4$), 133.7−162.7 (several resonances, CH, tBuC$_5$H$_4$). ^{31}P{^{1}H} NMR (162 MHz, [D$_6$]benzene): δ = 72.4, 74.9, 75.7. EI-MS: m/z (%) = 281 (3) [M$^+$], 224 (100) [M$^+$ − tBu], 160 (6) [tBuPNEt$_2$], 57 (68) [tBu]. C$_{17}$H$_{32}$NP (281.42): calcd. C 72.56, H 11.46, N 4.98; found C 72.34, H 11.01, N 5.32.

[tBuC$_5$H$_4$−PtBu(NHtBu)] (22): Obtained from [tBuCp−PtBu(Cl)] (**6**) (1.53 g, 6.26 mmol) and tBuNH$_2$ (2.0 mL, > 20 mmol). Yield > 95%. *Mixture of Isomers:* ^{1}H NMR (250 MHz, [D$_6$]benzene): δ = 1.16−1.31 (several m, 18 H, tBuN, tBuP), 2.9−3.20 (br. s, 1 H, tBuC$_5$H$_4$), 6.15−6.94 (several m, 3 H, tBuC$_5$H$_4$). ^{13}C{^{1}H} NMR (50 MHz, [D$_6$]benzene): δ = 26.3−26.8 (several d, CH$_3$), 41.0−44.1(d, C, tBuP, $^2J_{C,P}$ = 12.8 Hz), 50.77 (d, C, tBuN), 124.5, 124.7, 125.3 (CH, tBuC$_5$H$_4$), 133.9−162.2 (several resonances, CH, tBuC$_5$H$_4$). ^{31}P{^{1}H} NMR (162 MHz, [D$_6$]benzene): δ = 22.7, 26.1, 26.2. EI-MS: m/z (%) = 224 (100) [M$^+$ − tBu], 160 (4) [tBuPNH(tBu)]. C$_{17}$H$_{32}$PN (281.42): calcd. C 72.56, H 11.46, N 4.98; found C 72.61, H 11.21, N 5.13.

[Ind−PtBu(NtBu)]Li$_2$ (23): Obtained from [Ind−PtBu(NHtBu)] (**13**) (2.75 g, 10 mmol) and nBuLi (13.4 mL, 20 mmol/1.5 N). Isolated 3.26 g (9.7 mmol), yield 97%. ^{1}H NMR (200 MHz, [D$_8$]THF): δ = 0.91 (d, $^3J_{HP}$ = 12.1 Hz, 9 H, tBuP), 1.01 (s, 9 H, tBuN), 5.87 (m, 1 H, Ind), 6.28−6.35 (m, 2 H, Ind), 6.58 (m, 1 H, Ind), 7.15 (m, 1 H, Ind), 8.01 (m, 1 H, Ind). ^{13}C{^{1}H} NMR (50 MHz, [D$_8$]THF): δ = 26.9 (d, $^2J_{C,P}$ = 16.5 Hz, CH$_3$, tBuP), 32.0 (d, $^3J_{C,P}$ = 9.1 Hz, CH$_3$, tBuN), 35.6 (d, $^1J_{C,P}$ = 17.4 Hz, C, tBuP), 52.1 (d, $^2J_{C,P}$ = 16.5 Hz, C, tBuN), 91.2, 94.9, 112.7, 118.2, 119.4, 121.1 (CH, Ind); C (Ind) not observed.

[Flu−PtBu(NHtBu)]Li (24): Obtained from [Flu−PtBu(NHtBu)] (**18**) (0.35 g, 1.11 mmol) and nBuLi (0.75 mL, 1.12 mmol/1.5 N). Isolated 0.31 g (0.94 mmol), yield 85%. ^{1}H NMR (200 MHz, [D$_8$]THF): δ = 0.90 (d, $^3J_{HP}$ = 12 Hz, 9 H, tBuP), 0.96 (s, 9 H, tBuN), 2.75 (d, $^2J_{HP}$ = 9.7 Hz, 1 H, −NH), 6.3 (t, 2 H, Flu), 6.7 (t, 2 H, Flu), 7.11−8.21 (br. m, 4 H, Flu). ^{13}C{^{1}H} NMR (50 MHz, [D$_8$]THF): δ = 28.0 (d, $^2J_{C,P}$ = 16.5 Hz, CH$_3$, tBuP), 31.7 (d, $^3J_{C,P}$ = 9.8 Hz, tBuN), 34.4 (d, $^1J_{C,P}$ = 6.5 Hz, C, tBuP), 50.5 (d, $^2J_{C,P}$ = 18.1 Hz, C, tBuN), 108.9, 115.8, 117.4, 118.7, 119.3 (CH, Flu).

[Me$_4$C$_5$−PtBu(NEt$_2$)]K (25): Obtained from Ph$_2$CHK(THF) (4.26 g, 15.31 mmol) and [Me$_4$Cp−PtBu(NEt$_2$)] (**20**) (4.31 g, 15.31 mmol). The product was recrystallised from THF. Yield > 95%. ^{1}H NMR (200 MHz, [D$_8$]THF): δ = 0.93 (t, $^3J_{H,H}$ = 7 Hz, 6 H, −NCH$_2$*CH$_3$*), 1.08 (d, $^3J_{HP}$ = 12 Hz, 9 H, tBuP), 1.94, 2.22 (s, 6 H, CH$_3$, Me$_4$C$_5$), 2.94 (m, 4 H, −N*CH$_2$*CH$_3$). ^{13}C{^{1}H} NMR (50 MHz, [D$_8$]THF): δ = 11.9 (CH$_3$, Me$_4$C$_5$), 15.3 (d, $^3J_{C,P}$ = 7.2 Hz, CH$_3$, −NCH$_2$*CH$_3$*), 30.5 (d, $^2J_{C,P}$ = 18.6 Hz, CH$_3$, tBu), 33.5 (d, $^1J_{C,P}$ = 17.3 Hz, −N*CH$_2$*CH$_3$), 47.1 (d, $^2J_{C,P}$ = 17.8 Hz, C, tBuP), 108.3 (C, Me$_4$C$_5$), 112.3 (d, $J_{C,P}$ = 7.2 Hz, C, Me$_4$C$_5$), 128.9, 129.4 (C, Me$_4$C$_5$), 145.1 (d, $J_{C,P}$ = 19.7 Hz, C, Me$_4$C$_5$). ^{31}P{^{1}H} NMR (162 MHz, [D$_8$]THF, 25 °C): δ = 70.0. EI-MS: m/z (%) = 281 (2) [M$^+$ − K], 224 (78) [M$^+$ − tBuK], 153 (73) [Me$_4$C$_5$PH$_2$], 74 (23) [H$_2$NEt$_2$]. C$_{17}$H$_{31}$KNP (319.51): calcd. C 63.91, H 9.78, N 4.38; found C 63.78, H 9.63, N 4.20.

[tBuC$_5$H$_3$−PtBu(NEt$_2$)]K (26): Obtained from [tBuCp−PtBu(NEt$_2$)] (**21**) (3.48 g, 12.38 mmol) and Ph$_2$CHK(THF) (3.44 g, 12.38 mmol). Yield > 95%. ^{1}H NMR (200 MHz, [D$_8$]THF): δ = 0.93 (t, $^3J_{H,H}$ = 7.2 Hz, 6 H, −NCH$_2$*CH$_3$*), 1.0 (d, $^3J_{HP}$ = 12.5 Hz, 9 H, tBuP), 1.25 (d, $^5J_{HP}$ = 6.6 Hz, 9 H, tBuC$_5$H$_3$), 3.0 (m, 4 H, −N*CH$_2$*CH$_3$), 5.73 (m, 1 H, tBuC$_5$H$_3$), 6.55 (m, 1 H, tBuC$_5$H$_3$), 7.17 (m, 1 H, tBuC$_5$H$_3$). ^{13}C{^{1}H} NMR (50 MHz, [D$_8$]THF): δ = 12.3 (CH$_3$, tBuC$_5$H$_3$), 14.8 (d, $^3J_{C,P}$ = 3 Hz, −NCH$_2$*CH$_3$*), 28.3 (d, $^2J_{C,P}$ = 16 Hz, CH$_3$, tBuP), 43.6 (d, $^2J_{C,P}$ = 15.2 Hz, −N*CH$_2$*CH$_3$), 46.4 (C, tBu), 58.1 (d, $J_{C,P}$ = 28 Hz, C, tBuP), 125.8, 126.5, 127.9 (CH, tBuC$_5$H$_3$), 128.0, 129.5 (C, tBuC$_5$H$_3$). ^{31}P{^{1}H} NMR (162 MHz, [D$_8$]THF): δ = 76.0. EI-MS: m/z (%) = 281 (2) [M$^+$ − K], 224 (12) [M$^+$ − (K + tBu)], 153 (13) [tBuC$_5$H$_3$PH$_2$], 57 (5) [tBu]. C$_{17}$H$_{31}$KNP (319.51): calcd. C 63.91, H 9.78, N 4.38; found C 63.67, H 9.54, N 4.19.

[Ind−PtBu(NEt$_2$)]K (27): Obtained from [Ind−PtBu(NEt$_2$)] (**12**) (5.14 g, 18.68 mmol) and Ph$_2$CHK(THF) (5.2 g, 18.68 mmol). Yield > 95%. ^{1}H NMR (200 MHz, [D$_8$]THF): δ = 0.91 (t, $^3J_{H,H}$ = 7 Hz, 6 H, −NCH$_2$*CH$_3$*), 1.16 (d, $^3J_{HP}$ = 12 Hz, 9 H, tBuP), 3.1 (m, $^3J_{H,H}$ = 7 Hz, 4 H, −N*CH$_2$*CH$_3$), 6.11 (d, $J_{H,H}$ = 3.5 Hz, 1 H, Ind), 6.47 (q, $J_{H,H}$ = 4 Hz, 2 H, Ind), 7.0 (t, $J_{H,H}$ = 7 and 1.5 Hz, 1 H, Ind), 7.28 (d, $J_{H,H}$ = 7 Hz, 1 H, Ind), 7.78 (d, $J_{H,H}$ = 7 Hz, 1 H, Ind). ^{13}C{^{1}H} NMR (50 MHz, [D$_8$]THF): δ = 15.3 (d, $^3J_{C,P}$ = 3.7 Hz, −NCH$_2$*CH$_3$*), 29.4 (d, $^2J_{C,P}$ = 16.7 Hz, CH$_3$, tBuP), 33.9 (d, $^2J_{C,P}$ = 12.9 Hz, −N*CH$_2$*CH$_3$), 46.3 (d, $J_{C,P}$ = 16.2 Hz, C, tBuP), 98.0 (d, $^2J_{C,P}$ = 2.7 Hz, CH, Ind), 113.7 (d, $^3J_{C,P}$ = 1.4 Hz, CH, Ind), 113.8 (CH, Ind), 118.5 (d, $^3J_{C,P}$ = 1.8 Hz, CH, Ind), 119.0 (CH, Ind), 123.4 (d, $^2J_{C,P}$ = 2.7 Hz, C, Ind), 131.7 (d, $J_{C,P}$ = 8.3 Hz, C, Ind), 136.6 (CH, Ind), 137.3 (C, Ind). ^{31}P{^{1}H} NMR (162 MHz, [D$_8$]THF): δ = 60.1. EI-MS: m/z (%) = 146 (100), [tBuPN(CH$_3$)Et], 115 (41) [Ind], 74 (30) [H$_2$NEt$_2$], 58 (16) [tBuH], 39 (2) [K$^+$]. C$_{21}$H$_{33}$KNP (313.46): calcd. C 75.42, H 8.72, N 3.51; found C 75.05, H 8.81, N 3.50.

[Flu−PtBu(NEt$_2$)]K (28): Obtained from [Flu−PtBu(NEt$_2$)] **17** (4.15 g, 12.77 mmol) and PhCH$_2$K (1.66 g, 12.77 mmol). Yield > 95%. ^{1}H NMR (400 MHz, [D$_8$]THF): δ = 0.9 (t, $^3J_{H,H}$ = 7.0 Hz, 6 H, −NCH$_2$*CH$_3$*), 1.09 (d, $^2J_{HP}$ = 12.2 Hz, 9 H, tBuP), 3.03 (m, 4 H, −N*CH$_2$*CH$_3$), 6.55−8.39 (several m, 8 H, Flu). ^{13}C{^{1}H} NMR (75 MHz, [D$_8$]THF): δ = 14.1 (d, $^3J_{C,P}$ = 3 Hz, −NCH$_2$*CH$_3$*), 28.4 (d, $^1J_{C,P}$ = 22.3 Hz, CH$_3$, tBuP), 30.0 (d, $^1J_{C,P}$ = 27.3 Hz, C, tBuP), 34.7 (d, $^2J_{C,P}$ = 15 Hz, −N*CH$_2$*CH$_3$), 47.1 (d, $^1J_{C,P}$ = 40 Hz, C, Flu), 119.9, 120.0, 120.4 (CH, Flu), 121.2 (d, $J_{C,P}$ = 4.1 Hz, CH, Flu), 125.4 (d, $J_{C,P}$ = 6.5 Hz, CH, Flu), 125.5, 125.6, 126.2 (CH, Flu), 126.6 (C, Flu), 127.1 (d, $J_{C,P}$ = 2.7 Hz, C, Flu), 142.1 (d, $J_{C,P}$ = 7.9 Hz, C, Flu), 142.5 (d, $J_{C,P}$ = 4.1 Hz, C, Flu). ^{31}P{^{1}H} NMR (162 MHz, [D$_8$]THF): δ = 70.9. EI-MS: m/z (%) = 325 (35) [M$^+$ − KCH$_3$], 310 (83) [M$^+$ − (K + 2 CH$_3$)], 39 (46) [K$^+$]. C$_{22}$H$_{31}$NP (379.57): calcd. C 69.62, H 8.23, N 3.69; found C 69.24, H 8.11, N 3.52.

[{Ind−PtBu(NEt$_2$)}$_2$CEt$_2$]K$_2$(THF)$_2$ (29): Obtained from [{Ind−PtBu(NEt$_2$)}$_2$CEt$_2$][31] (3.63 g, 5.87 mmol) and Ph$_2$CHK(THF) (3.27 g, 11.74 mmol). Isolated 4.0 g, yield 81%. ^{1}H NMR (200 MHz, [D$_8$]THF): δ = 0.74−1.12 (several resonances, tBu and −NCH$_2$*CH$_3$*), 3.0 (m, 4 H, −N*CH$_2$*CH$_3$), 6.0−7.61 (several m, 6 H, Ind). ^{13}C{^{1}H} NMR (50 MHz, [D$_8$]THF): δ = 15.5 (d, $^3J_{C,P}$ = 3 Hz, −NCH$_2$*CH$_3$*), 29.7 (d, $^2J_{C,P}$ = 16.9 Hz, CH$_3$, tBu), 34.4 (d, $^2J_{C,P}$ = 15.9 Hz, −N*CH$_2$*CH$_3$), 46.4 (d, $^1J_{C,P}$ = 27.1 Hz, C, tBuP), 110.0−130.0 (C and CH resonances, Ind). ^{31}P{^{1}H} NMR (162 MHz, [D$_8$]THF): δ = 57.1. EI-MS: m/z (%) = 341 (16) [M$^+$ − MeInd(tBu)PNEt$_2$K], 160 (2) [tBuPNEt$_2$], 115 (87) [Ind], 57 (42) [tBu], 39 (100) [K$^+$]. C$_{47}$H$_{74}$KN$_2$O$_2$P$_2$ (839.26): calcd. C 67.26, H 8.89, N 3.34; found C 67.44, H 9.10, N 3.18.

[Me$_3$SiC$_{13}$H$_8$−PtBu(NSiMe$_3$$t$Bu)] (30): Obtained in situ from [Flu−PtBu(NHtBu)] (**18**) (1.44 g, 4.42 mmol) in THF, nBuLi (6 mL, 9 mmol) and Me$_3$SiCl (1.67 mL, 13.26 mmol). Isolated 1.41 g, yield 67%. ^{1}H NMR (200 MHz, [D$_6$]benzene): δ = −0.04 (s, 9 H, Me$_3$Si), 0.01 (s, 9 H, Me$_3$Si), 0.33 (d, $^3J_{HP}$ = 10.3 Hz, 9 H, tBuP), 0.47 (s, 9 H, tBuN), 7.05−7.44 (m, 4 H, Flu), 7.51 (m, 2 H, Flu), 7.94 (m, 2 H, Flu).

[(Me$_3$Sn)Me$_4$C$_5$−PtBu(NEt$_2$)] (31): Obtained from [Me$_4$Cp−PtBu(NEt$_2$)]K (**25**) (4.58 g, 14.36 mmol) and Me$_3$SnCl (2.9 g,

> 14.36 mmol). Yield > 95%. ^{1}H NMR (400 MHz, [D$_6$]benzene): δ = 0.08, 0.24, 0.26 (s, broad s, s, 9 H, Me_3Sn-), 1.04 (d, $^3J_{HP}$ = 10 Hz, 9 H, *t*BuP), 1.06 (t, $^3J_{H,H}$ = 8 Hz, 6 H, $-NCH_2CH_3$), 1.88 (s, 3 H, CH_3, Me_4C_5), 1.92 (s, 3 H, CH_3, Me_4C_5), 2.18 (s, 3 H, CH_3, Me_4C_5), 2.24 (s, 3 H, CH_3, Me_4C_5), 3.24 (m, $^3J_{HP}$ = 7.1 Hz, 4 H, $-NCH_2CH_3$). ^{13}C{^{1}H} NMR (75 MHz, [D$_6$]benzene): δ = −7.2 (d, $^5J_{C,P}$ = 2.7 Hz, CH_3, Me_3Sn-), 1.3 (CH_3, Me_3Sn-), 11.1 ($-NCH_2CH_3$), 11.5, 14.0, 14.2, 15.9 (CH_3, Me_4C_5), 29.6 (d, $^2J_{C,P}$ = 16.8 Hz, CH_3, *t*BuP), 38.4 (d, $^2J_{C,P}$ = 17.2 Hz, $-NCH_2CH_3$), 46.8 (d, C, *t*BuP, $^2J_{C,P}$ = 25.8 Hz), 48.0 (d, $J_{C,P}$ = 18.9 Hz, C, Me_4C_5), 130.9 (d, $J_{C,P}$ = 6 Hz, C, Me_4C_5), 131.3 (d, $J_{C,P}$ = 4.8 Hz, C, Me_4C_5), 132.9, 133.2 (C, Me_4C_5). ^{31}P{^{1}H} NMR (162 MHz, [D$_6$]benzene): δ = 85.0. EI-MS: *m*/*z* (%) = 254 (8) [$Me_2C_5SnMe_3$], 240 (46) [$Me_2C_5SnMe_2$], 121 (92) [Me_4C_5], 120 (100) [$Me_3C_5CH_2$], 72 (38) [NEt_2], 57 (46) [*t*Bu]. $C_{20}H_{40}NPSn$ (444.2): calcd. C 54.08, H 9.08, N 3.15; found C 54.19, H 8.92, N 3.01.

[(Me$_3$Sn)*t*BuC$_5$H$_3$−P*t*Bu(NEt$_2$)] (32): Obtained from [*t*BuCp−P*t*Bu(NEt$_2$)]K (**26**) (1.0 g, 3.12 mmol) and Me_3SnCl (0.7 g, 3.12 mmol). Yield > 95%. *Mixture of Isomers:* ^{1}H NMR (200 MHz, [D$_6$]benzene): δ = 0.15 (s, 9 H, Me_3Sn-), 0.92 (t, $^3J_{H,H}$ = 7 Hz, $-NCH_2CH_3$), 1.32 (d, $^3J_{HP}$ = 12.1 Hz, 9 H, *t*BuP), 2.98 (m, 4 H, $-NCH_2CH_3$), 4.28 (d, 1 H, *t*BuC$_5$H$_3$), 7.28−7.42 (m, 3 H, *t*BuC$_5$H$_3$), 6.3−7.1 (several m, 2 H, *t*BuC$_5$H$_3$). ^{13}C{^{1}H} NMR (50 MHz, [D$_6$]benzene): δ = −7.5 (d, $^3J_{C,P}$ = 5 Hz, CH_3, Me_3Sn-), 12.2 (CH_3, *t*BuC$_5$H$_3$), 14.8 (2 d, $^3J_{C,P}$ = 2.7 Hz, $-NCH_2CH_3$), 28.3 (2 d, $^2J_{C,P}$ = 16.1 Hz, CH_3, *t*BuP), 43.1 (C, *t*BuC$_5$H$_3$), 45.7 (d, $^2J_{C,P}$ = 15.6 Hz, $-NCH_2CH_3$), 61.0 (d, $J_{C,P}$ = 28.9 Hz, C, *t*BuP), 123.8, 124.9 (CH, *t*BuC$_5$H$_3$), 144.4, 152.1, 152.2 (C, *t*BuC$_5$H$_3$). ^{31}P{^{1}H} NMR (162 MHz, [D$_6$]benzene): δ = 71.8. EI-MS: *m*/*z* (%) = 445 (7) [M$^+$], 388 (29) [M$^+$ − *t*Bu], 317 (61) [M$^+$ − ($HNEt_2$ + *t*Bu)], 165 (100) [$SnMe_3$], 57 (43) [*t*Bu]. $C_{20}H_{40}NPSn$ (445.19): calcd. C 54.08, H 9.08, N 3.15; found C 54.16, H 8.84, N 3.20.

[Me$_3$SnC$_9$H$_6$−P*t*Bu(NEt$_2$)] (33): Obtained from [Ind−P*t*Bu(NEt$_2$)]K (**27**) (4.15 g, 13.24 mmol) and Me_3SnCl (2.7 g, 14.0 mmol). Yield > 95%. *Mixture of Isomers:* ^{1}H NMR (200 MHz, [D$_6$]benzene): δ = −0.13, −0.08 (2 s, 9 H, Me_3Sn-), 1.05 (t, $^3J_{H,H}$ = 5.7 Hz, $-NCH_2CH_3$), 1.36, 1.29 (d, $^3J_{HP}$ = 12.2 Hz, 9 H, *t*BuP), 3.25 (m, 4 H, $-NCH_2CH_3$), 4.27, 4.03 (d, 1 H, Ind), 7.06 (m, 1 H, Ind), 7.28−7.42 (m, 3 H, Ind), 8.55 (m, 1 H, Ind). ^{13}C{^{1}H} NMR (50 MHz, [D$_6$]benzene): δ = −9.1 (d, $^3J_{C,P}$ = 1.3 Hz, CH_3, Me_3Sn-), 15.3 (2 d, $^3J_{C,P}$ = 3.2 Hz, $-NCH_2CH_3$), 28.3 (2 d, $^1J_{C,P}$ = 16 Hz, CH_3, *t*BuP), 33.8 (d, $J_{C,P}$ = 17 Hz, C, *t*BuP), 45.8 (CH, Ind), 46.6, 46.3 (d, $^2J_{C,P}$ = 15.6 Hz, $-NCH_2CH_3$), 121.9 (CH, Ind), 122.1 (C, Ind), 123.7, 124.0, 134.9, 137.9, 145.2, 145.4, 145.5, 145.6 (CH, Ind), 145.7, 145.9, 146.0, 146.2 (C, Ind). ^{31}P{^{1}H} NMR (162 MHz, [D$_6$]benzene): δ = 63.2, 64.0. EI-MS: *m*/*z* (%) = 438 (5) [M$^+$], 382 (29) [M$^+$ − *t*Bu], 368.7 (1) [M$^+$ − NEt_2], 275 (9) [L$^+$], 202 (2) [L$^+$ − NEt_2], 165 (93) [$SnMe_3$], 161 (41) [*t*BuP(H)NEt_2]. $C_{20}H_{34}NPSn$ (438.16): calcd. C 54.82, H 7.82, N 3.20; found C 54.45, H 7.90, N 3.01.

[Me$_3$SnC$_{13}$H$_8$−P*t*Bu(NEt$_2$)] (34): Obtained from [Flu−P*t*Bu(NEt$_2$)]K (**28**) (0.5 g, 1.37 mmol) and Me_3SnCl (0.3 g, 1.5 mmol). Yield > 95%. ^{1}H NMR (200 MHz, [D$_6$]benzene): δ = 0.03 (s, 9 H, Me_3Sn-), 0.73 (d, $^3J_{HP}$ = 12.6 Hz, 9 H, *t*BuP), 1.11 (t, $^3J_{H,H}$ = 7.2 Hz, 6 H, $-NCH_2CH_3$), 3.36 (m, 4 H, $-NCH_2CH_3$), 7.29−7.37 (m, 4 H, Flu), 7.93−7.98 (br. m, 2 H, Flu), 8.2 (m, 2 H, Flu). ^{13}C{^{1}H} NMR (50 MHz, [D$_6$]benzene): δ = −8.15 (d, $^3J_{C,P}$ = 3.2 Hz, CH_3, Me_3Sn-), 15.18 ($-NCH_2CH_3$), 29.9 (d, $^2J_{C,P}$ = 16 Hz, CH_3, *t*BuP), 30.8 (d, $^2J_{C,P}$ = 15.1 Hz, $-NCH_2CH_3$), 39.0 (d, $J_{C,P}$ = 28.4 Hz, C, *t*BuP), 120.0, 120.5, 125.9, 126.0 (CH, Flu), 137.7, 139.0, 148.1, 148.7, 149.1 (C, Flu). ^{31}P{^{1}H} NMR (162 MHz, [D$_6$]benzene): δ = 102.9. $C_{20}H_{34}NPSn$ (488.22): calcd. C 59.04, H 7.43, N 2.87; found C 59.19, H 7.60, N 2.71.

[Me$_3$SnC$_9$H$_6$−P*t*Bu(NH*t*Bu)] (35): Me_3SnNEt_2 (2.36 g, 10.0 mmol) was added at 0 °C to a solution of [Ind−P*t*Bu(NH*t*Bu)] (**13**) (2.75 g, 10 mmol) in 100 mL of diethyl ether. Then the reaction mixture was stirred for 1 h, while warming to room temperature. The solvent and diethylamine were removed under vacuum. Yield > 95%. ^{1}H NMR (200 MHz, [D$_6$]benzene): δ = 0.03 (s, $^2J_{HSn}$ = 54 Hz, 9 H, Me_3Sn-),1.22 (d, $^3J_{HP}$ = 12.9 Hz, 9 H, *t*BuP), 1.35 (s, 9 H, *t*BuN), 1.96−1.90 (m, 1 H, −NH), 4.1 (s, 1 H, Ind), 6.79 (m, 1 H, Ind), 7.29−7.37 (m, 2 H, Ind), 7.39−7.48 (m, 1 H, Ind), 8.14−8.16 (m, 1 H, Ind). ^{13}C{^{1}H} NMR (50 MHz, [D$_6$]benzene): δ = −6.7 (CH_3, Me_3Sn-), 29.1 (d, $^2J_{C,P}$ = 15.3 Hz, *t*BuP), 34.2 (d, $^1J_{C,P}$ = 17.8 Hz, C, *t*BuP), 34.5 (d, $^3J_{C,P}$ = 8.8 Hz, *t*BuN), 47.7 (CH, Ind), 52.9 (d, $^2J_{C,P}$ = 15.9 Hz, C, *t*BuN), 123.6, 124.8, 126.1, 127.3, 127.7 (CH, Ind), 128.8, 139.9, 140.9 (C, Ind). ^{31}P{^{1}H} NMR (162 MHz, [D$_6$]benzene): δ = 22.3. $C_{20}H_{36}NPSn$ (440.17): calcd. C 54.57, H 8.24, N 3.18; found C 54.66, H 8.13, N 3.01.

[{Me$_4$C$_5$−P*t*Bu(NEt$_2$)}TiCl$_3$] (36): All of the $TiCl_4(THF)_2$ (0.64 g, 1.93 mmol) in 20 mL of toluene was immediately added to a solution of [(Me_3Sn)Me_4C_5−P*t*Bu(NEt_2)] (**31**) (0.86 g, 1.93 mmol) in 30 mL of toluene at −50 °C. The reaction mixture was then stirred for 3 h, while warming to room temperature. After that, the reaction mixture was additionally stirred for another 5 h at 80 °C. The solvent was removed under vacuum. The product was extracted with pentane. Isolated 0.31 g (0.7 mmol), deep red solid (yield 38%). ^{1}H NMR (250 MHz, CD_2Cl_2): δ = 1.11 (t, $^3J_{H,H}$ = 7.2 Hz, 6 H, $-NCH_2CH_3$), 1.14 (d, $^3J_{HP}$ = 14 Hz, 9 H, *t*BuP), 2.33 (s, 3 H, CH_3, Me_4C_5), 2.39 (d, $^4J_{HP}$ = 0.5 Hz, 3 H, CH_3, Me_4C_5), 2.61 (d, $^4J_{HP}$ = 0.7 Hz, 3 H, CH_3, Me_4C_5), 2.7 (s, 3 H, CH_3, Me_4C_5), 3.24 (m, 4 H, $-NCH_2CH_3$). ^{13}C{^{1}H} NMR (50 MHz, CD_2Cl_2): δ = 14.5 ($-NCH_2CH_3$), 15.0, 17.8, 18.1, 18.8 (CH_3, Me_4C_5), 29.7 (d, $J_{C,P}$ = 18.1 Hz, CH_3, *t*BuP), 37.7, 38.0 ($-NCH_2CH_3$), 47.4 (d, $J_{C,P}$ = 17.4 Hz, C, *t*BuP), 125.4 (d, $J_{C,P}$ = 23.5 Hz, C, Me_4C_5), 128.9 (d, $J_{C,P}$ = 32.9 Hz, C, Me_4C_5), 140.0 (d, $J_{C,P}$ = 4.5 Hz, C, Me_4C_5), 141.3 (d, $J_{C,P}$ = 2.2 Hz, C, Me_4C_5), 143.2 (C, Me_4C_5). ^{31}P{^{1}H} NMR (162 MHz, CD_2Cl_2): δ = 77.2. EI-MS: *m*/*z* (%) = 378 (3) [M$^+$ − (*t*Bu + H)], 187 (15) [$C_6H_{10}TiCl$], 153 (6) [$TiCl_3$], 121 (25) [Me_4C_5H], 73 (42) [$HNEt_2$], 58 (100) [*t*BuH]. $C_{17}H_{31}Cl_3NPTi$ (433.07): calcd. C 46.98, H 7.19, N 3.22; found C 46.88, H 7.24, N 3.15.

[{Me$_4$C$_5$−P*t*Bu(NEt$_2$)}ZrCl$_3$] (37): Obtained from [(Me_3Sn)-Me_4C_5−P*t*Bu(NEt_2)] (**31**) (0.57 g, 1.3 mmol) and $ZrCl_4(THF)_2$ (0.49 g, 1.3 mmol), using the same procedure as for the preparation of [{Me_4C_5−P*t*Bu(NEt_2)}$TiCl_3$] (**36**). Isolated 0.15 g (0.32 mmol), yellow solid (yield 25%). ^{1}H NMR (250 MHz, CD_2Cl_2): δ = 1.10 (t, $^3J_{H,H}$ = 7 Hz, 6 H, $-NCH_2CH_3$), 1.16 (d, $^3J_{HP}$ = 14.2 Hz, 9 H, *t*BuP), 2.15 (s, 3 H, CH_3, Me_4C_5), 2.16 (s, 3 H, CH_3, Me_4C_5), 2.45 (s, 3 H, CH_3, Me_4C_5), 2.52 (s, 3 H, CH_3, Me_4C_5), 3.19 (m, 4 H, $-NCH_2CH_3$). ^{13}C{^{1}H} NMR (50 MHz, CD_2Cl_2): δ = 12.8 ($-NCH_2CH_3$), 13.9, 15.7, 16.1, 17.5 (CH_3, Me_4C_5), 29.5 (d, $J_{C,P}$ = 18.9 Hz, CH_3, *t*BuP), 37.0, 37.5 ($-NCH_2CH_3$), 47.6 (d, $J_{C,P}$ = 17 Hz, C, *t*BuP), 128.4, 128.2 (C, Me_4C_5), 129.0 (br. resonance, C, Me_4C_5), 132.5 (d, $J_{C,P}$ = 3.8 Hz, Me_4C_5), 132.7 (br. resonance, C, Me_4C_5). ^{31}P{^{1}H} NMR (162 MHz, CD_2Cl_2): δ = 73.2. EI-MS: *m*/*z* (%) = 346 (1) [M$^+$ − $C_8H_{19}N$], 224 (27) [M$^+$ − $C_{12}H_{27}N$], 153 (40) [Me_4C_5P], 121 (100) [Me_4C_5H], 106 (7) [Me_4C_5H − Me], 73 (5) [$HNEt_2$] 57 (56) [*t*Bu]. $C_{17}H_{31}Cl_3NPZr$ (475.03): calcd. C 42.72, H 6.54, N 2.93; found C 42.57, H 6.33, N 2.81.

[{*t*BuC$_5$H$_3$−P*t*Bu(NEt$_2$)}TiCl$_3$] (38): Obtained from [(Me_3Sn)*t*BuC$_5$H$_3$−P*t*Bu(NEt_2)] (**32**) (0.57 g, 1.28 mmol) and

$TiCl_4(THF)_2$ (0.42 g, 1.28 mmol) using the same procedure as for the preparation of [{Me_4C_5−P*t*Bu(NEt$_2$)}$TiCl_3$] (**36**). Isolated 0.16 g (0.37 mmol), deep red solid (yield 30%). ^{1}H NMR (250 MHz, CD_2Cl_2): δ = 1.22 (t, $^3J_{H,H}$ = 7.1 Hz, 6 H, −NCH$_2$*CH$_3$*), 1.14 (d, $^3J_{HP}$ = 13.7 Hz, 9 H, *t*BuP), 1.40 (d, J_{HP} = 1 Hz, 9 H, CH_3, *t*BuC_3H_5), 3.16 (m, 4 H, −N*CH$_2$*CH$_3$), 6.93−7.30 (several m, 3 H, *t*BuC_3H_5). ^{13}C{^{1}H} NMR (50 MHz, CD_2Cl_2): δ = 15.5 (CH_3, −NCH$_2$*CH$_3$*), 15.7 (CH_3, *t*BuC_3H_5), 28.6 (d, $J_{C,P}$ = 17 Hz, CH_3, *t*BuP), 35.2, 35.3 (−N*CH$_2$*CH$_3$), 43.6 (C, *t*BuC_3H_5), 47.2 (d, $J_{C,P}$ = 15.5 Hz, C, *t*BuP), 125.1, 128.4, 129.2 (CH, *t*BuC_3H_5), 151.0 (d, $J_{C,P}$ = 21 Hz, C, *t*BuC_3H_5) 159.5 (C, *t*BuC_3H_5). ^{31}P{^{1}H} NMR (162 MHz, CD_2Cl_2): δ = 88.4, 88.5. EI-MS: *m*/*z* (%) = 361 (2) [M^+ − NEt_2], 304 (12) [M^+ − $C_8H_{19}N$], 281 (35) [$C_{15}H_{32}N$], 160 (4) [*t*BuPNEt$_2$], 121 (100) [*t*BuC_5H_3], 72 (54) [NEt_2], 57 (73) [*t*Bu]. $C_{17}H_{31}Cl_3NPTi$ (433.07): calcd. C 46.98, H 7.19, N 3.22; found C 47.11, H 7.29, N 3.05.

[{*t*BuC_5H_3−P*t*Bu(Cl)}$TiCl_3$] (39): $TiCl_4$ (0.45 mL, 4.09 mmol) was slowly added at −80°C to a solution of [*t*BuC_5H_3−P*t*Bu(Cl)] (**6**) (1.0 g, 4.1 mmol) in 30 mL of hexane; after 1 min of stirring, Et_3N (0.57 mL, 4.1 mmol) was added. The reaction mixture was stirred for 4 h, while warming to room temperature. The ammonium salt precipitate was removed by filtration. All volatiles were removed under vacuum to give the crude product. Yield according to ^{1}H and ^{31}P NMR spectra was 98%. An analytically pure product was obtained, after two times of washing with cold (−50 °C) pentane, as an orange solid with 40% yield. ^{1}H NMR (250 MHz, CD_2Cl_2): δ = 1.09, 1.05 (2 d, J_{HP} = 14.3 Hz, J_{HP} = 14.4 Hz, 9 H, *t*BuP), 1.4 (s, 9 H, *t*Bu), 7.0 (m, 6 H, *t*BuC_3H_5), 7.02−7.1 (2 m, CH, *t*BuC_3H_5), 7.25 (m, CH, *t*BuC_3H_5), 7.32 (m, CH, *t*BuC_3H_5). ^{13}C NMR (50 MHz, CD_2Cl_2): δ = 25.2 (CH_3, *t*BuC_3H_5), 30.8 (d, $^2J_{C,P}$ = 12.9 Hz, CH_3, *t*BuP), 35.2 (d, $^4J_{C,P}$ = 2.6 Hz, C, *t*Bu), 36.3 (d, $J_{C,P}$ = 25.4 Hz, C, *t*BuP), 122.3 (d, $^2J_{C,P}$ = 2.9 Hz, CH, *t*BuC_3H_5), 122.3 (d, $^2J_{C,P}$ = 2.9 Hz, CH, *t*BuC_3H_5), 125.4 (d, $J_{C,P}$ = 4.8 Hz, C, *t*BuC_3H_5), 125.9 (CH, *t*BuC_3H_5), 123.4 (d, $^2J_{C,P}$ = 3.3 Hz, CH, *t*BuC_3H_5), 126.3 (C, *t*BuC_3H_5). ^{31}P{^{1}H} NMR (162 MHz, CD_2Cl_2): δ = 105.4, 106.4. EI-MS: *m*/*z* (%) = 362 (1) [M^+ − Cl], 270 (2) [$C_9H_{13}Cl_2TiP$], 244 (3) [*t*BuC_5H_3(*t*Bu)PCl], 121 (10) [*t*BuC_5H_3], 57 (100) [*t*Bu]. $C_{13}H_{21}Cl_4PTi$ (397.37): calcd. C 39.23, H 5.32; found C 39.05, H 5.09.

[{(C_5H_4−P*t*Bu(Cl)]$_2$CMe$_2$}{$TiCl_3$}$_2$] (40): Obtained from [{C_5H_4−P*t*Bu(Cl)}$_2$CMe$_2$] (**11**) (3.98 g, 9.5 mmol), $TiCl_4$ (2.09 mL, 19.1 mmol) and Et_3N (2.66 mL, 19.1 mmol), using the same procedure as for the preparation of [{*t*BuC_5H_3−P*t*Bu(Cl)}$TiCl_3$] (**39**). According to ^{1}H and ^{31}P NMR spectra the yield was 90%. A product was isolated as a deep green solid. *Mixture of Isomers:* ^{1}H NMR (400 MHz, CD_2Cl_2): δ = 0.87−1.0 (several d, 9 H, *t*BuP),

Table 1. Crystal data and structure refinement for **15**

Empirical formula[a]	$C_{23}H_{38}NP$
Formula mass	359.51
Crystal size [mm]	0.40 × 0.20 × 0.15
Temperature [K]	223(2)
Wavelength [Å]	0.71073
Crystal system	monoclinic
Space group	$P2_1/c$
Unit cell dimensions [Å, °]	a = 7.768(1), b = 22.196(1), c = 12.8267(10), β = 91.14(1)
Volume [Å^3]	2211.2(3)
Z	4
Calculated density [g/cm^3]	1.080
Absorption coefficient [mm^{-1}]	0.130
F(000)	792
Θ-range for data collection [°]	2.43 to 23.41
Index ranges	$-8 \le h \le 0$, $-24 \le k \le 0$, $-14 \le l \le 14$
Reflections collected/unique	3502/3235, [R(int) = 0.0682]
Refinement method	Full-matrix least-squares on F^2
Data/restraints/parameters	3235/0/280
Goodness-of-fit on F^2	1.100
Final R indices [$I > 2\sigma(I)$]	$R1$ = 0.0754, $wR2$ = 0.2332
R indices (all data)	$R1$ = 0.1357, $wR2$ = 0.2678
Largest diff. peak and hole [e/Å^3]	0.454 and −0.489

[a] Data collection and cell refinement has been carried out with an Enraf Nonius CAD4 four-circle diffractometer using CAD4-EXPRESS software. Data reduction and Lorentz and polarisation corrections were undertaken using the XCAD4 programme (K. Harms, **1993**). For structure solution SHELXS-96 and structure refinement SHELXL-96 (both G. M. Sheldrick, **1996**) were used. Molecular graphics: ORTEP III. After data reduction the data set has been checked for systematic absence violations. Due to weak absence violations *h0l*: $l \neq 2n$ for compound **15** two space groups should be taken into account, $P2_1$ and $P2_1/c$. The structure was first solved by direct methods in the chiral space group $P2_1$ and a structural model including all non-hydrogen atoms was refined isotropically. A search for additional symmetry elements (PLATON: A. Speck, **1990**) showed that a slide mirror plane parallel to the crystallographic axis c exists. The "zero point" was placed in the centre of inversion and the structure was refined in the centrosymmetric space group $P2_1/c$, after all symmetrically dependent atoms had been eliminated. The hydrogen atoms were placed at a calculated position and refined in a riding model.

Table 2. Crystal data and structure refinement for **36**

Empirical formula[a]	$C_{17}H_{31}Cl_3NPTi$
Formula mass	434.65
Crystal size [mm]	0.36 × 0.21 × 0.12
Temperature [K]	203(2)
Wavelength [Å]	0.71073
Crystal system	monoclinic
Space group	$P2_1/c$
Unit cell dimensions [Å, °]	a = 9.351(2), b = 15.637(2), c = 14.732(1), β = 91.39(1)
Volume [Å^3]	2153.5(5)
Z	4
Calculated density [g/cm^3]	1.341
Absorption coefficient [mm^{-1}]	0.843
F(000)	912
Θ-range for data collection [°]	2.54 to 22.55
Index ranges	$0 \le h \le 10$, $-16 \le k \le 0$, $-15 \le l \le 15$
Reflections collected/unique	3007/2807, [R(int) = 0.0488]
Refinement method	Full-matrix least squares on F^2
Data/restraints/parameters	2807/0/217
Goodness-of-fit on F^2	1.022
Final R indices [$I > 2\sigma(I)$]	$R1$ = 0.0550, $wR2$ = 0.1168
R indices (all data)	$R1$ = 0.1007, $wR2$ = 0.1365
Largest diff. peak and hole [e/Å^3]	0.906 and −0.751

[a] Data collection and cell refinement has been carried out with an Enraf−Nonius CAD4 four-circle diffractometer using CAD4-EXPRESS software. Data reduction and Lorentz and polarisation corrections were undertaken using the XCAD4 programme (K. Harms, **1997**). For the structure solution SHELXS-97 and structure refinement SHELXL-97 (both G. M. Sheldrick, **1997**) were used. Molecular graphics: ORTEP III. An analytical absorption correction based on face indexing was applied to the data set. Hydrogen atoms were placed at calculated positions and refined in a riding model.

2.1 (s, 3 H, CH_3, CMe_2), 6.99−7.04 (several m, 1 H, Cp), 7.09−7.15 (several m, 1 H, Cp). $^{31}P\{^1H\}$ NMR (162 MHz, CD_2Cl_2): δ = 95.3, 94.4, 95.8, 101.3, 102.4, 102.5 (2 signals), 102.7, 103.0, 103.3(2 signals), 103.4, 103.5, 103.6, 104.0, 104.3. EI-MS: *m*/*z* (%) = 534 (12) [$M^+ - TiCl_4$], 442 (22) [$M^+ - TiCl_3 - t$BuPCl], 386 (30) [$M^+ - Cp(t\text{Bu})PTiCl_4$], 318 (92) [$Cp(t\text{Bu})PTiCl_3 - H$], 57 (100) [*t*Bu].

[{(C_5H_3−P*t*Bu(Cl)]$_2$$CMe_2$}$TiCl_2$] (41): Obtained from [{$C_5H_4$−P*t*Bu(Cl)}$_2$$CMe_2$] (**11**) (4.79 g, 11.5 mmol), $TiCl_4$ (1.25 mL, 11.5 mmol) and Et_3N (3.2 mL, 23.0 mmol) using the same procedure as for the preparation of [{*t*BuC_5H_3−P*t*Bu(Cl)}$TiCl_3$] (**39**). According to ^1H and ^{31}P NMR spectra the yield was 90%. A product was isolated as a deep red solid. *Mixture of Isomers:* ^1H NMR (400 MHz, CD_2Cl_2): δ = 0.85−1.5 (several m, *t*BuP), 1.7−1.9 (several m, CH_3, CMe_2), 5.3−5.92 (several m, Cp), 7.14−7.24 (several m, Cp). $^{31}P\{^1H\}$ NMR (162 MHz, CD_2Cl_2): δ = 96.2, 96.6, 96.8, 97.5, 101.7, 103.0, 103.2, 103.7.

[{*t*BuC_5H_3−P*t*Bu(N*t*Bu)}$TiCl_2$] (42): A suspension of Li[NH*t*Bu] (0.03 g, 0.37 mmol) and Et_3N (0.052 mL, 0.37 mmol) were immediately added, −78 °C, to a solution of [{*t*BuC_5H_3−P*t*Bu(Cl)}$TiCl_3$] (**39**) (0.15 g, 0.37 mmol) in 20 mL of toluene. The reaction mixture was stirred for 12 h, while warming to room temperature. Then the precipitated LiCl and Et_3NHCl were removed by filtration. The filtrate was concentrated under vacuum. The product was taken up in pentane. Isolated 0.13 g (0.33 mmol), deep red solid (yield 89%). *Mixture of 2 Isomers (1:3):* ^1H NMR (200 MHz, CD_2Cl_2): δ = 1.24 (*major*), 1.20 (*minor*) [2 d, $^3J_{HP}$ = 14.4 Hz (*both isomers*), 9 H, *t*BuP], 1.30 (*major*), 1.27 (*minor*) [2 d, $^6J_{HP}$ = 3.7 Hz (*major*), 3.5 Hz (*minor*), 9 H, CH_3, *t*BuC_5H_3], 1.45 (*minor*), 1.42 (*major*) [2 d, $^4J_{HP}$ = 0.7 Hz (*both isomers*), 9 H, *t*BuN], 6.95−7.85 (6 m, total 3 H, *t*BuC_5H_3). *Both Isomers:* $^{13}C\{^1H\}$ NMR (50 MHz, [D_6]benzene): δ = 15.0, 15.1, 15.2, 15.3 (CH_3, *t*BuN and *t*Bu), 29.0 (d, $J_{C,P}$ = 17 Hz, CH_3, *t*BuP), 29.6 (d, $J_{C,P}$ = 18.5 Hz, CH_3, *t*BuP), 47.0 (d, $J_{C,P}$ = 17 Hz, C, *t*BuP), 47.5 (d, $J_{C,P}$ = 16.1 Hz, C, *t*BuP), 53.1, 53.2 (C, *t*Bu), 61.9, 62.8 (C, *t*BuN), 134.6 (d, $J_{C,P}$ = 1.5 Hz, CH, *t*BuC_5H_3), 135.7 (d, $J_{C,P}$ = 1.5 Hz, CH, *t*BuC_5H_3), 135.8 (d, $J_{C,P}$ = 4.5 Hz, CH, *t*BuC_5H_3), 135.9 (d, $J_{C,P}$ = 4 Hz, CH, *t*BuC_5H_3), 141.7 (d, $J_{C,P}$ = 36 Hz, CH, *t*BuC_5H_3), 142.4 (d, $J_{C,P}$ = 34 Hz, CH, *t*BuC_5H_3), 145.1 (d, $J_{C,P}$ = 1.5 Hz, C, *t*BuC_5H_3), 145.3 (C, *t*BuC_5H_3), 150.5 (d, $J_{C,P}$ = 30 Hz, C, *t*BuC_5H_3), 151.5 (d, $J_{C,P}$ = 29 Hz, C, *t*BuC_5H_3). $^{31}P\{^1H\}$ NMR (162 MHz, CD_2Cl_2): δ = 45.9 (*major*), 51.1 (*minor*). EI-MS: *m*/*z* (%) = 340 (4) [$M^+ - t$Bu], 283 (15) [$M^+ - 2\ t$Bu], 226 (35) [$M^+ - 3\ t$Bu], 121 (100) [*t*BuC_5H_3], 57 (100) [*t*Bu]. $C_{17}H_{30}Cl_2NPTi$ (397.09): calcd. C 51.28, H 7.59, N 3.52; found C 51.13, H 7.68, N 3.44.

Polymerisation of Ethylene: A glass autoclave was charged with 50 mL of toluene and 0.5 mL of triisobutylaluminium, then thermostatted for 30 min and saturated with ethylene (3 bar) for another 30 min. The catalyst was generated by treatment of the corresponding complex with MAO [10% solution in toluene, Al/(Ti or Zr) ratio was either 500 or 2000] and preformed over 1 h in an ultrasonic bath. This toluene solution was injected into the autoclave. The reaction mixture was placed under 3 bar of ethylene for 30 min with rapid stirring. The polymerisation was stopped by quenching with 50 mL of aqueous HCl/methanol (1:5, v/v). The polymer was isolated by filtration, washed subsequently with HCl solution, water, methanol, acetone and dried at 60 °C to a constant weight. All polymerisation experiments were repeated at least twice, whereby no large deviations have been observed.

X-ray Crystallographic Study: Crystallographic data for the structures reported (Tables 1 and 2) in this paper have been deposited with the Cambridge Crystallographic Data Centre as supplementary publications nos. CCDC-162747 (**15**) and -162746 (**36**). Copies of the data can be obtained free of charge on application to CCDC, 12 Union Road, Cambridge CB2 1EZ, U.K. [Fax: (internat.) + 44-1223/336-033; E-mail: deposit@ccdc.cam.ac.uk].

Acknowledgments

We appreciate the help of, and many fruitful discussions with Prof. Dr. H.-H. Brintzinger (University of Konstanz) during the stay of K. V. V. in his research group. Financial support by the Deutscher Akademischer Austauschdienst (DAAD, research stay at the University of Konstanz) and the Deutsche Forschungsgemeinschaft (DFG, SFB 260, Graduiertenkolleg "Metallorganische Chemie", research stay at the University of Marburg) to K. V. V. is gratefully acknowledged.

[1] H.-H. Brintzinger, D. Fischer, R. Mülhaupt, B. Rieger, R. M. Waymouth, *Angew. Chem. Int. Ed. Engl.* **1995**, *34*, 1143−1170.
[2] G. J. P. Britovsek, V. C. Gibson, D. F. Wass, *Angew. Chem. Int. Ed.* **1999**, *38*, 428−447.
[3] C. Janiak in *Metallocenes: Synthesis, Reactivity, Applications* (Eds.: A. Togni, R. L. Haltermann), Wiley-VCH **1998**, vol. 2, p. 547−614.
[4] W. Kaminsky, K. Külper, H.-H. Brintzinger, F. R. W. P. Wild, *Angew. Chem. Int. Ed. Engl.* **1985**, *24*, 507−508.
[5] P. J. Shapiro, E. Bunel, W. P. Schaefer, J. E. Bercaw, *Organometallics* **1990**, *9*, 867−869.
[6] J. Okuda, *Chem. Ber.* **1990**, *123*, 1649−1651.
[7] A. L. McKnight, R. M. Waymouth, *Chem. Rev.* **1998**, *98*, 2587−2598.
[8] L. K. Johnson, C. M. Killian, M. Brookhart, *J. Am. Chem. Soc.* **1995**, *117*, 6414−6415.
[9] G. J. P. Britovsek, V. C. Gibson, B. S. Kimberley, P. J. Maddox, S. J. McTavish, G. A. Solan, A. J. P. White, D. J. Williams, *Chem. Commun.* **1998**, 849−850.
[10] J. D. Scollard, D. H. McConville, *J. Am. Chem. Soc.* **1996**, *118*, 10008−10009.
[11] K. H. A. Ostoja Starzewski, J. Witte, *Angew. Chem.* **1987**, *99*, 76−77.
[12] A. J. Ashe III, S. Al-Ahmad, X. Fang, J. W. Kampf, *Organometallics* **1998**, *17*, 3883−3888.
[13] D. W. Stephan, F. Guerin, R. E. v. Spence, L. Koch, X. Gao, S. J. Brown, J. W. Swabey, Q. Wang, W. Xu, P. Zoricak, D. G. Harrison, *Organometallics* **1999**, *17*, 2046−2048.
[14] C. H. Lee, Y.-H. La, J. W. Park, *Organometallics* **2000**, *19*, 344−351.
[15] E. J. Thomas, M. D. Rausch, J. C. W. Chien, *Organometallics* **2000**, *19*, 4077−4083.
[16] E. J. Thomas, M. D. Rausch, J. C. W. Chien, *Organometallics* **2000**, *19*, 5744−5749.
[17] P. N. Riley, P. E. Fanwick, I. P. Rothwell, *J. Chem. Soc., Dalton Trans.* **2001**, 181−186.
[18] M. Ganesan, S. Gambarotta, G. P. A. Yap, *Angew. Chem.* **2001**, *113*, 788−791; *Angew. Chem. Int. Ed.* **2001**, *40*, 766−769.
[19] J. D. Gardner, D. A. Robson, L. H. Rees, P. Mountford, *Inorg. Chem.* **2001**, *40*, 820−824.
[20] J. Kim, J.-W. Hwang, Y. Kim, M. H. Lee, Y. Han, Y. Do, *J. Organomet. Chem.* **2001**, *620*, 1−7.
[21] L. Resconi, L. Cavallo, A. Fait, F. Piemontesi, *Chem. Rev.* **2000**, *100*, 1253−1346.
[22] R. Schmid, T. Ziegler, *Organometallics* **2000**, *19*, 2756−2765.
[23] K. Vanka, T. Ziegler, *Organometallics* **2001**, *20*, 905−913.
[24] G. Lanza, I. L. Fragala, T. J. Marks, *J. Am. Chem. Soc.* **2000**, *122*, 12764−12777.
[25] J.-F. Carpentier, V. P. Maryin, J. Luci, R. F. Jordan, *J. Am. Chem. Soc.* **2001**, *123*, 898−909.
[26] R. Leino, F. J. Gomez, A. P. Cole, R. M. Waymouth, *Macromolecules* **2001**, *34*, 2072−2082.

[27] S. Lieber, M.-H. Prosenc, H.-H. Brintzinger, *Organometallics* **2000**, *19*, 377−387.
[28] N. Schneider, F. Schaper, K. Schmidt, R. Kirsten, A. Geyer, H.-H. Brintzinger, *Organometallics* **2000**, *19*, 3597−3604.
[29] S. D. Ittel, L. K. Johnson, M. Brookhart, *Chem. Rev.* **2000**, *100*, 1169−1203.
[30] D. Gudat, E. Niecke, B. Krebs, M. Dartmann, *Organometallics* **1986**, *5*, 2376−2377.
[31] V. V. Kotov, E. V. Avtomonov, N. A. Ustynyuk, D. A. Lemenovskii, *Z. Naturforsch., Teil B* **2001**, *56*, 812−822.
[32] P. Jutzi, H. Saleske, *Chem. Ber.* **1984**, *117*, 222−233.
[33] P. Jutzi, T. Wippermann, *J. Organomet. Chem.* **1985**, *287*, C5−C7.
[34] P. Jutzi, H. Saleske, D. Nadler, *J. Organomet. Chem.* **1976**, *118*, C8−C10.
[35] S. G. Baxter, A. H. Cowley, S. K. Mehrotra, *J. Am. Chem. Soc.* **1981**, *103*, 5572−5573.
[36] H. Lang, U. Eberle, M. Leise, L. Zsolnai, *J. Organomet. Chem.* **1996**, *519*, 137−145.
[37] P. Jutzi, *Chem. Rev.* **1986**, *86*, 983−996.
[38] H. G. Alt, M. Jung, *J. Organomet. Chem.* **1998**, *568*, 127−131.
[39] C. J. Schaverien, R. Ernst, W. Terlouw, P. Schut, O. Sudmeijer, P. H. M. Budyelaar, *J. Mol. Cat. A* **1998**, *128*, 245−256.
[40] O. I. Kolodyaznyi, I. V. Shevchenko, V. P. Kukhlar, A. N. Chernega, I. E. Boldeskul, M. Yu. Antipin, Yu. T. Struchkov, *Zh. Obshch. Khim.* **1983**, *53*, 1233−1237.
[41] *International Tables for Crystallography* (Ed.: A. J. C. Wilson), Kluwer Academic Publishers, London **1992**, vol. 2, p. 701, 704.
[42] G. Märkl, K. M. Raab, *Tetrahedron Lett.* **1989**, *30*, 1077−1080.
[43] Review of the literature **1982**−**1994**: *Comprehensive Organometallic Chemistry II* (Eds.: E. W. Abel, F. G. A. Stone, G. Wilkinson), Pergamon, **1995**, vol. 4, p. 273−433, 483−589.
[44] L. Jia, X. Yang, C. L. Stern, T. Marks, *Organometallics* **1997**, *16*, 842−857.
[45] S. Ya. Knjazhanski, G. Moreno, G. Cadenas, V. K. Belsky, B. M. Bulychev, *Tetrahedron* **1999**, *55*, 1639−1646.
[46] L. M. Engelhardt, R. I. Papasergio, C. L. Raston, A. H. White, *Organometallics* **1984**, *3*, 18−20.
[47] J. C. Flores, R. Hernandez, P. Royo, A. Butt, T. P. Spaniol, J. Okuda, *J. Organomet. Chem.* **2000**, *593*−*594*, 202−210.
[48] H. A. Bent, *Chem. Rev.* **1961**, *61*, 275−311.
[49] K. A. Rufanov, A. V. Churakov, N. B. Kazennova, G. P. Brusova, D. A. Lemenovskii, L. G. Kuźmina, *J. Organomet. Chem.* **1995**, *498*, 37−39.
[50] K. Kirschbaum, D. M. Giolando, *Acta Crystallogr., Sect. C* **1991**, *47*, 2216−2218.
[51] S. L. Hart, D. J. Duncaff, J. J. Hastings, A. McClay, P. C. Taylor, *J. Chem. Soc., Dalton Trans.* **1996**, 2843−2849.
[52] A. Bondi, *J. Phys. Chem.* **1964**, *68*, 441−451.
[53] P.-J. Sinnema, L. van der Veen, A. L. Spek, N. Veldman, J. H. Teuben, *Organometallics* **1997**, *16*, 4245−4247.
[54] P.-J. Sinnema, Dissertation, Netherlands Institute for Catalysis Research, Netherlands, **1999**.
[55] S. Ciruelos, C. P. Gomez-Sal, A. Manzanero, P. Royo, *Organometallics* **1995**, *14*, 177−185.
[56] S. Ciruelos, T. Cuenca, R. Gomez, C. P. Gomez-Sal, A. Manzanero, P. Royo, *Organometallics* **1996**, *15*, 5577−5585.
[57] G. Ciruelo, T. Cuenca, R. Gomez, P. Gomez-Sal, A. Martin, G. Rodriguez, P. Royo, *J. Organomet. Chem.* **1997**, *547*, 287−296.
[58] B. Royo, P. Royo, L. M. Cadenas, *J. Organomet. Chem.* **1998**, *551*, 293−297.
[59] J. C. Flores, J. C. W. Chien, M. D. Rausch, *Macromolecules* **1996**, *29*, 8030−8035.
[60] G. F. Schmidt, F. J. Timmers, G. W. Knight, S.-Y. Lai, P. N. Nickias, R. K. Rosen, J. C. Stevens, D. R. Wilson (Dow Chemical Company), *Eur. Patent Appl.* EP 0416815, March 13, **1991**.
[61] I. E. Nifant'ev, P. V. Ivchenko, M. V. Borzov, *J. Chem. Res. (S)* **1992**, 162.
[62] I. E. Nifant'ev, P. V. Ivchenko, L. G. Kuzmina, Yu. N. Luzikov, A. A. Sitnikov, O. E. Sizan, *Synthesis* **1997**, 469−474.
[63] Q. Yang, M. D. Jensen, *Synlett* **1996**, 147−148.
[64] K. Megges, Diploma Thesis, University of Marburg, Germany, **1995**.
[65] F. M. Alias, S. Barlow, J. S. Tudor, D. O'Hare, R. T. Perry, J. M. Nelson, I. Manners, *J. Organomet. Chem.* **1997**, *528*, 47−58.
[66] M. Schlosser, J. Hartmann, *Angew. Chem.* **1973**, *12*, 544; *Angew. Chem. Int. Ed. Engl.* **1973**, *12*, 508.
[67] D. R. Wilson, D. R. Neithamer, P. N. Nickias, W. J. Kruper (Dow Chemical Company), *Patent Appl.* WO 96/16094, May 30, **1996**.

Received September 3, 2001
[I01341]

Electrochemical and Complexation Studies of Ferrocenyl Complexes Bearing Terpyridine or Phenanthroline Ligands

Jean-Claude Moutet,*[a] Eric Saint-Aman,[a] Guy Royal,[a] Sophie Tingry,[a][‡] and Raymond Ziessel[b]

Keywords: N ligands / Sandwich complexes / Receptors / Cyclic voltammetry

The coordinative properties of 1,1′-bis(phen)- and bis(terpy)-carboxyester-bridged derivatives of ferrocene L^1 and L^2 (phen refers to 2,9-substituted-1,10-phenanthroline; terpy refers to 4′-substituted-2,2′:6′,2"-terpyridine) towards various transition metal cations have been investigated by a combination of cyclic voltammetry, mass spectrometry and ^1H NMR spectroscopy. These novel redox receptors form 1:1 ligand:metal complexes with all the surveyed metal cations (L^1: M = Cu^I, Ni^{II}, Fe^{II}, Hg^{II}; L^2: M = Ni^{II}, Fe^{II}, Hg^{II}). Particular attention was paid to the recognition properties of these redox-active ligands, as monitored by the modulation of the potential of the ferrocene/ferricinium (Fc/Fc^+) couple upon complexation. Complexation of L^1 gives rise to a new emerging Fc/Fc^+ redox peak system. In contrast, complexation of L^2 does not alter this redox process appreciably. In addition, decomposition of free L^2 occurs upon oxidation and causes the growth of a film of an Fe-bis(terpy) complex onto the electrode surface.

Introduction

Molecular structures comprising two or more coordinated metal cations are useful models for studying electronic coupling between metal centers in different oxidation states and for the coupling of a remote active metal centre to a putative catalytic site.[1] Ferrocenyl units are frequently employed as redox-active sites in supramolecular assemblies,[2] owing to their well-behaved redox activity as well as their synthetic versatility. A number of ferrocenyl-functionalized bipyridines,[3] terpyridines,[3c,4] quinquepyridines,[5] and sexipyridines[6] have been synthesized for these reasons.

In previous studies,[7] we reported that mono(bipy)- and bis(bipy)ester- and -carboxamide-bridged derivatives of ferrocene (bipy = 2,2′-bipyridine) present a very rich coordination chemistry and electrochemistry in the presence of various transition metal cations. The resultant di-, tri-,or tetranuclear complexes displayed significant levels of electronic coupling between the metal sites. Additionally, it was demonstrated that these redox ligands can be used for the electrochemical recognition of certain transition metal cations in both homogeneous[7a][7d] and polymeric[7b] phases by way of a large shift in the ferrocene/ferricinium (Fc/Fc^+) redox couple following the binding of a guest cation at the coordination site. Here we report on the electrochemical response of novel 1,1′-bis(phenanthroline) and bis(terpyridine) derivatives of ferrocene L^1 and L^2 (Figure 1) to various transition metal cations. Some particular spectral properties (^1H NMR, FT IR and electronic absorption spectra) of certain complexes are also described.

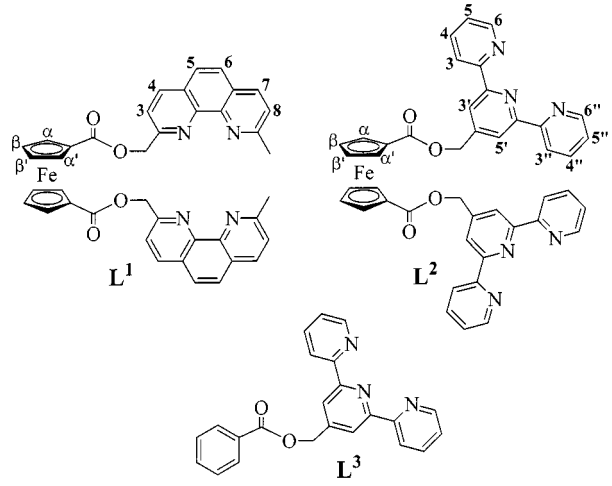

Figure 1. Chemical formula of ligands L^1, L^2 and L^3

Results and Discussion

Complexation of L^1 with Cu^I, Ni^{II}, Fe^{II} and Hg^{II}

The cyclic voltammetry (CV) curve for the free ferrocene-bis(phenanthroline) ligand L^1 in CH_3CN solution is characterized by a re-

[a] Laboratoire d′Electrochimie Organique et de Photochimie Rédox, UMR CNRS 5630, Université Joseph Fourier Grenoble 1,
BP 53, 38041 Grenoble Cédex 9, France
[b] Laboratoire de Chimie, d′Electronique et de Photonique Moléculaires, Ecole de Chimie, Matériaux et Polymères, Université Louis Pasteur,
25 rue Becquerel, 67087 Strasbourg Cédex 02, France
[‡] Current address: LMPM, UMR CNRS 5635,
1919 route de Mende, 34293 Montpellier Cédex 5, France

 © WILEY-VCH Verlag GmbH, 69451 Weinheim, Germany, 2002 1434−1948/02/0303−0692 $ 17.50+.50/0 *Eur. J. Inorg. Chem.* **2002**, 692−698

versible, one-electron wave corresponding to the Fc/Fc^+ couple ($E_{1/2}$ = 0.58 V; labeled I in Figure 2A and 2C, curves a). We have examined how complexation of L^1 by various transition metal cations (Cu^I, Ni^{II}, Fe^{II}, and Hg^{II}) affects the electrochemical features of the ferrocene centre. Metal cations were added as the salts $[Cu(CH_3CN)_4]ClO_4$, $[Ni(ClO_4)_2]$, $[Fe(ClO_4)_2]$ or $[Hg(CF_3SO_3)_2]$. The electrochemical data for L^1 and its metal complexes are summarized in Table 1.

Cu^IL^1 and $Ni^{II}L^1$ Complexes

The electrochemical behavior of L^1 in the presence of Cu^I and Ni^{II} ions is similar to that already observed with ferrocenyl receptors containing 2,2′-bipyridine ligands.[7] The progressive complexation of L^1 causes the emergence of a new redox peak system corresponding to the complexed Fc/Fc^+ redox couple (labeled II on Figure 2) at the expense of the original Fc/Fc^+ wave for the free ligand. It should be emphasized that oxidation of the ferrocene group occurs in the $[Cu^{II}L^1]^{2+}$ complex (see below). The new wave reaches full development at a metal cation:L^1 ratio of 1 (Figure 2A and 2C, curves c). These observations are in keeping with

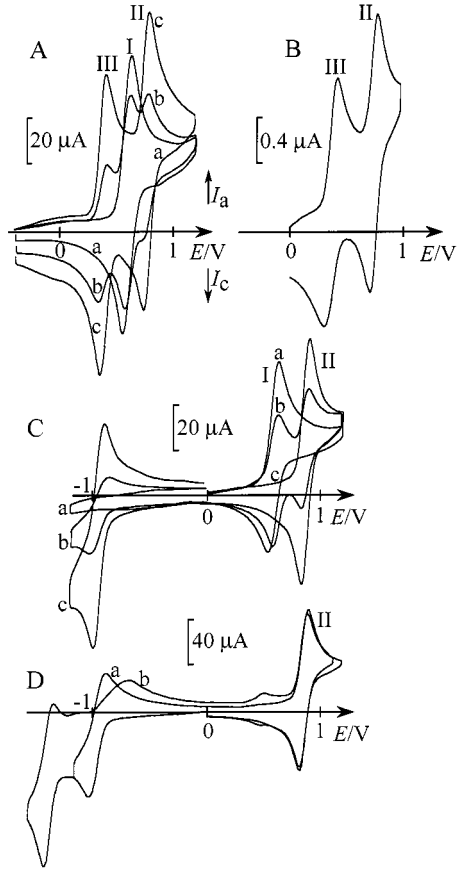

Figure 2. Cyclic voltammograms in CH_3CN + TBAP 0.1 M; (A): (a) free L^1 (2.9 mM), (b) L^1 + 0.4 $[Cu(CH_3CN)_4]ClO_4$, (c) L^1 + 1.0 $[Cu(CH_3CN)_4]ClO_4$, Pt disk (5 mm diameter); (B) $[CuL^1](ClO_4)$ 1 mM at a C disk (3 mm diameter); (C) (a) free L^1 (1.5 mM), (b) L^1 + 0.4 $Ni(ClO_4)_2$, (c) L^1 + 1.0 $Ni(ClO_4)_2$, Pt disk (5 mm diameter); (D) $[Ni\ L^1](ClO_4)_2$ 1 mM at a Pt disk (5 mm diameter); scan rate 0.1 Vs^{-1}

Table 1. Cyclic voltammetric data[a] for $[ML^1]$ complexes with M = Cu^I, Ni^{II}, Fe^{II}, Hg^{II}

Metal	Fc/Fc^+	Metal−centered redox systems
Free L^1	0.58	
Cu^I	0.74[b]	0.33($Cu^{I/II}$)
Ni^{II}	0.86	−0.96($Ni^{II/I}$),[c] −1.39($Ni^{I/0}$)[c] [d]
Fe^{II}	0.85	1.31($Fe^{II/III}$),[e] −1.33($Fe^{II/I}$)[c,e]
Hg^{II}	0.68	−0.75($Hg^{II/I}$)[c,e]

[a] $E_{1/2}$, V vs. $Ag/AgNO_3$ 0.01 M in CH_3CN + TBAP 0.1 M, determined by CV on Pt in CH_3CN + TBAP 0.1 M; ν = 0.1 Vs^{-1}. [b] Ferrocene oxidation occurs after copper oxidation, i.e. in the $[Cu^{II}L^1]^{2+}$ complex.[c] Formal oxidation states. [d] Poorly reversible system. [e] E_p; irreversible peak.

the formation of 1:1 $[CuL^1]^+$ and $[NiL^1]^{2+}$ complexes. This result is corroborated by electrochemical studies carried out with genuine samples of pure $[CuL^1](ClO_4)$ (Figure 2B) and $[NiL^1](ClO_4)_2$ (Figure 2D) complexes: when solubilized in CH_3CN + TBAP solution they display the same CV features as obtained by in situ complexation of L^1 with one mol equivalent of Cu^I (Figure 2A, curve c) or Ni^{II} (Figure 2C, curve c).

Complexation of L^1 with Cu^I causes the rise of a new redox peak system ($E_{1/2}$ = 0.33 V) attributed to the complexed Cu^I/Cu^{II} couple (labeled III on Figure 2A and 2B). The relatively high redox potential of the $Cu^{I/II}$ redox system is in good agreement with those previously reported for various polypyridyl copper complexes.[7a,8] The electrochemical behavior of $[CuL^1]^+$ is summarized in Equation (1):

$$[Cu^I\mathbf{L^1}]^+ \underset{+e}{\overset{0.33\ V\ -e}{\rightleftharpoons}} [Cu^{II}\mathbf{L^1}]^{2+} \underset{+e}{\overset{0.74\ V\ -e}{\rightleftharpoons}} [Cu^{II}(\mathbf{L^1})^+]^{3+} \quad (1)$$

Complexation of L^1 with Ni^{II} ions is also revealed by the appearance of two reversible one-electron reduction waves at −0.96 V and −1.39 V (Figure 2C and 2D). This behavior is reminiscent of that of the Ni^{II} complex of the 2,9-di-*p*-anisyl-1,10-phenanthroline.[8] However, the reduced $[NiL^1]^+$ complex is less stable, since the $Ni^{II/I}$ redox couple was found at a notably less negative potential in the nickel bis-(anisylphenanthroline) complex ($E_{1/2}$ = −0.18 V vs. SCE).[8] Furthermore, the second reduction of the nickel complex down to its $[NiL^1]^0$ form leads to some decomplexation, as shown by the appearance on the reverse scan of a weak Fc/Fc^+ peak system corresponding to the free ligand (Figure 2D, curve b). The redox behavior of $[NiL^1]^{2+}$ is summarized in Equation (2).

$$[Ni^0\mathbf{L^1}]^0 \underset{+e}{\overset{-1.39\ V\ -e}{\rightleftharpoons}} [Ni^I\mathbf{L^1}]^+ \underset{+e}{\overset{-0.96\ V\ -e}{\rightleftharpoons}} [Ni^{II}\mathbf{L^{1\bullet}}]^{2+} \underset{+e}{\overset{0.86\ V\ -e}{\rightleftharpoons}} [Ni^{II}(\mathbf{L^1})^+]^{3+} \quad (2)$$

Complexation of L^1 by Cu^I was further investigated by ^1H NMR titration. Addition of Cu^I cation to a solution of L^1 in CD_3CN produced significant perturbations in all ^1H

NMR resonances recorded at 273 K. Signals for both free and complexed ligand were observed at a substoichiometric level of copper salt. This fact reveals the inertness of this complex, i.e. intramolecular exchange is restricted on the NMR time scale. The ^{1}H NMR spectrum shows only resonances for the copper complex after the addition of one mol equivalent of Cu^I ions. In the copper complex, all the resonances of protons at the phenanthroline rings are shifted downfield (see the Experimental Section). As noticed in copper complexes of 1,1′-(bispyridyl) ferrocenes,[7a] ferrocene-proton pairs become nonequivalent in the $[CuL^1]^+$ complex; the α′-Cp resonances at δ = 4.91 in the free ligand are shifted upfield to δ = 4.72, whereas the α-Cp signal is found at δ = 3.66. The signal of the methylene protons changes from a singlet (δ = 5.52 in free L^1) to an AB system (H-exo: δ = 5.47, J = 12.0 Hz; H-endo: δ = 4.88, J = 12.0 Hz). The prochirality of the methylene protons is consistent with the fact that the 1,10-phenanthroline arms become more rigid upon coordination.

$Fe^{II}L^1$ Complex

Very recently,[7c] we found that L^1 forms a high spin 1:1 complex $[FeL^1]^{2+}$ with Fe^{II} ions. This unusual stoichiometry (two phen ligands per iron centre) was unambiguously established by FAB-MS data and X-ray structure analysis. The crystal structure of the complex revealed that the iron(II) coordination environment consists of four nitrogen atoms provided by the phenanthroline units and two oxygen atoms of the carbonyl groups, forming a distorted octahedral environment.

CV experiments show that the progressive complexation of L^1 with Fe^{II} ions leads to the growth of a new Fc/Fc^+ redox wave ($E_{1/2}$ = 0.85 V) at the expense of the original wave for free L^1 (Figure 3). However a weak oxidation peak for the uncomplexed ligand (labeled with an asterisk in Figure 3) is always seen even in the presence of an excess (e.g. 1.2 equivalent) of Fe^{II} ions. Obviously, the $[FeL^1]^{2+}$ complex is weaker than the copper and nickel complexes. Furthermore, oxidation of the ferrocene centre in the iron complex leads to partial decomplexation, as shown by the appearance on the reverse scan of a large reduction peak corresponding to the Fc/Fc^+ redox system in the free ligand (labeled with a double asterisk in Figure 3). Complexation of L^1 with Fe^{II} also gives rise to an irreversible oxidation wave (E_p = 1.31 V) at more positive potentials corresponding to the $Fe^{II/III}$ redox process in the $[FeL^1]^{2+}$ complex (Figure 3, curve b). The redox behavior of $[FeL^1]^{2+}$ is summarized in Equation (3).

$$[Fe^{II}(\mathbf{L^1})^-]^+ \xleftarrow[+e]{-1.33\ V} [Fe^{II}\mathbf{L^1}]^{2+} \underset{+e}{\overset{0.85\ V\ -e}{\rightleftharpoons}} [Fe^{II}(\mathbf{L^1})^+]^{3+} \xrightarrow[-e]{1.31\ V} [Fe^{III}(\mathbf{L^1})^+]^{4+} \quad (3)$$

The $Fe^{II/III}$ redox process in the $[FeL^1]^{2+}$ complex occurs at a potential close to that of free Fe^{2+} cations. In the presence of an excess of Fe^{II}, this last process (E_p = 1.44 V) is seen on the CV curve as a shoulder that appears at the positive foot of the complexed $Fe^{II/III}$ redox peak (Figure 3, curve b). The abnormally high intensity of the oxidation peak corresponding to the $Fe^{II/III}$ redox process in the $[FeL^1]^{2+}$ complex is probably due to its overlapping with the background current corresponding to some electrolyte oxidation that occurs at this potential. By comparing $[Fe^{II}L^1]^{2+}$ to a regular $[Fe(phen)_3]^{2+}$ complex (phen = 5,6-dimethyl-1,10-phenanthroline, for example; $E_{1/2}[Fe^{II/III}]$ = 0.62 V), it is obvious that the unusual coordination environment in the $[FeL^1]^{2+}$ complex strongly stabilizes the divalent state of the iron centre. It should be noted that stabilization of the Fe^{II} state in the $[Fe^{II}L^1]^{2+}$ complex based on phen binding sites is larger than in the corresponding Fe-bis(bipy) derivative of ferrocene ($E_{1/2}$ = 0.99 V).[7c]

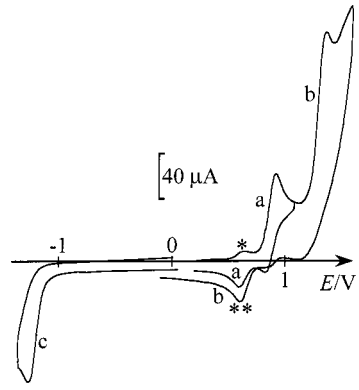

Figure 3. Cyclic voltammograms in CH_3CN + TBAP 0.1 M at a Pt disk electrode (5 mm diameter) of L^1 (2 mM) + 1.2 $Fe(ClO_4)_2$: (a) scan between 0 and 1 V; (b) scan between 0 and 1.5 V; (c) scan between 0 and −1.2 V; scan rate 0.1 Vs^{-1}

Oxidation of the iron centre in the $[Fe^{II}(L^1)^+]^{3+}$ complex (Figure 3, curve b) leads to an important degradation; on the reverse scan the complexed Fc/Fc^+ redox couple becomes less reversible and the intensity of the free Fc^+ reduction wave is twice that observed when the CV scan is restricted to the 0 to 1 V potential range. Since the iron-centered oxidation occurs after that of the ferrocenyl unit, decomplexation probably results from strong repulsive electrostatic forces between the Fc^+ and Fe^{III} centers in the fully oxidized $[Fe^{III}(L^1)^+]^{4+}$ complex.

CV curves recorded in the negative-potential region show a number of ill-behaved, irreversible reduction peaks between −1 V and −2 V; the first one appears at E_p = −1.33 V (Figure 3, curve c). Once again, the behavior of $[FeL^1]^{2+}$ contrasts with that for a regular Fe-tri(phen) complex, which is characterized by three ligand-centered, reversible reduction waves ($E_{1/2}$ = −1.85, −2.03, −2.25 V; phen = 5,6-dimethyl-1,10-phenanthroline).

$Hg^{II}L^1$ Complex

A mercury(II) complex was obtained from L^1 upon treatment with $Hg(CF_3SO_3)_2$. The FAB-mass spectra were identical when the complex was prepared using one or two molar equivalents of mercury salt and clearly show a 1:1 stoichiometry.

When investigated by NMR spectrometry, the progressive addition of Hg^{II} cations to a solution of L^1 in CD_3CN produces significant perturbations in all ^1H NMR resonances recorded at room temperature. The spectra are characterized by broad, unstructured peaks until one mol equivalent of metal cation had been added. The NMR spectra remained unresolved over the −20 °C to 40 °C temperature range and the solutions were EPR silent. These observations reveal that the intermolecular exchange is fast on the NMR time scale at substoichiometric levels of mercury salt. After the addition of more than one mol equivalent of Hg^{II} cations, well-behaved NMR signals for the Hg^{II} complex develop. As already noticed for the $[CuL^1]^+$ complex, the ferrocene-proton pairs become nonequivalent. The α-Cp and α′-Cp resonances are shifted downfield and upfield, respectively. The NMR signal of the methylene protons changes from a singlet to an AB system (see Figure 4 and the Exp. Sect.).

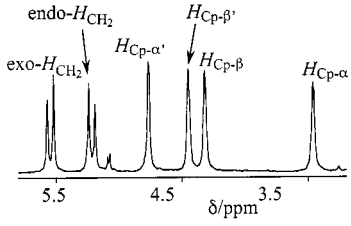

Figure 4. Methylene and cyclopentadienyl region of the ^1H NMR spectrum of $[HgL^1](CF_3SO_3)_2$ at room temperature in CD_3CN

CV experiments have confirmed that one Hg^{II} ion is complexed with one L^1 ligand. The addition of increasing amounts of $Hg(CF_3SO_3)_2$ to a solution of L^1 in acetonitrile results in the growth of a new Fc/Fc^+ wave ($E_{1/2}$ = 0.68 V) weakly separated from the original Fc/Fc^+ wave. This wave reaches full development after the addition of one mol equivalent of mercury salt and replaces the original Fc/Fc^+ wave in free L^1 (Figure 5A). In addition, the $[HgL^1]^{2+}$ complex presents an irreversible one-electron reduction wave (E_p = −0.75 V; Figure 5B), followed by several ill-behaved reduction peaks around −1.6 V. Reduction of the complex down to −2 V led to dissociation with formation of mercury metal, as evidenced on the reverse scan by the rise of a sharp mercury metal stripping peak (E_p = 0.42 V). The electrochemical behavior of $[HgL^1]^{2+}$ is summarized in Equation (4).

$$[Hg^{I}\mathbf{L^1}]^{+} \underset{+e}{\overset{-0.75\ V}{\rightleftharpoons}} [Hg^{II}\mathbf{L^1}]^{2+} \underset{+e}{\overset{0.68\ V}{\rightleftharpoons}} [Hg^{II}(\mathbf{L^1})^{+}]^{3-} \quad (4)$$

Electrochemical Behavior and Complexation of L^2 with Fe^{II}, Ni^{II} and Hg^{II}

Electrochemical Behavior and Polymerization of L^2

The CV behavior of L^2 in acetonitrile presents complex features. Repeated scans over the 0 to 1 V potential range (Figure 6A) leads to the progressive decrease of the Fc/Fc^+ redox wave ($E_{1/2}$ = 0.56 V) and to the rise of a large reversible peaks system ($E_{1/2}$ = 0.77 V; ΔE_p = 40 mV at ν = 0.1 Vs^{-1}). The new wave reaches full development when the original Fc/Fc^+ peak system has totally vanished (Figure 6A). This electroactivity is maintained after transfer of the electrode to clean CH_3CN + TBAP electrolyte and remains stable upon repeated scans (Figure 6B). This behavior is in accordance with the growth of an insoluble film of Fe-bis(terpyridine) complex onto the electrode surface. Indeed, the half wave potential of immobilized species is the same as that found for the $Fe^{II/III}$ couple in the $[Fe(L^2)]^{2+}$ complex ($E_{1/2}$ = 0.77 V; see Figure 6C and the discussion below) and is similar to that measured with the $[Fe(L^3)_2]^{2+}$ model complex ($E_{1/2}$ = 0.76 V) containing no ferrocenyl groups. The latter was obtained by in situ complexation of L^3 (Figure 1) with a half mol equivalent of Fe^{II}. Two broad, reversible waves (not shown in Figure 6) were also seen at −1.63 V and −1.82 V on the CV curve of the film, corresponding to ligand-localized reductions in the Fe-bis(terpyridine) moieties. These redox processes occur at −1.65 V and −1.80 V in the $[Fe(L^3)_2]^{2+}$ model complex.

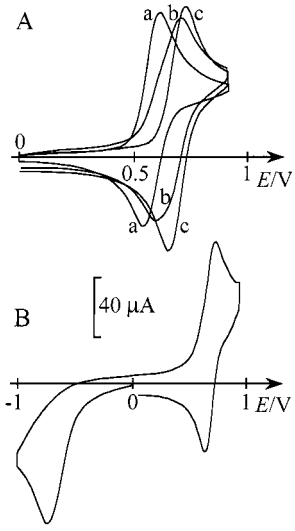

Figure 5. Cyclic voltammograms at a Pt disk electrode (5 mm diameter) in CH_3CN + TBAP 0.1 M: (A) (a) free L^1 (1.5 mM), (b) L^1 + 0.3 $Hg(CF_3SO_3)_2$, (c) L^1 + 1.0 $Hg(CF_3SO_3)_2$; (B) $[HgL^1](CF_3SO_3)_2$ 1.5 mM; scan rate 0.1 Vs^{-1}

The formation of Fe-bis(terpyridine) species upon oxidation of L^2 was corroborated by UV/Vis and FT-IR experiments. Around 40 scans have been performed in the 0 to 1 V potential range on a 1 cm^2 Pt electrode. The solution turned from orange to pink-violet and a dark-pink film covered the electrode surface. The visible spectrum of the electrolysis solution showed a new absorption peak at 557 nm, very close to that observed with the isolated $[FeL^2](ClO_4)_2$ complex (λ_{max} = 558 nm). Furthermore, the infrared spectrum of the film was characterized by strong bands at 1707 cm^{-1} (C=O stretching vibration) and 1628 cm^{-1} (terpyridine ring stretching vibration). These bands appear at 1708 and 1621 cm^{-1} in the $[FeL^2](ClO_4)_2$ complex.

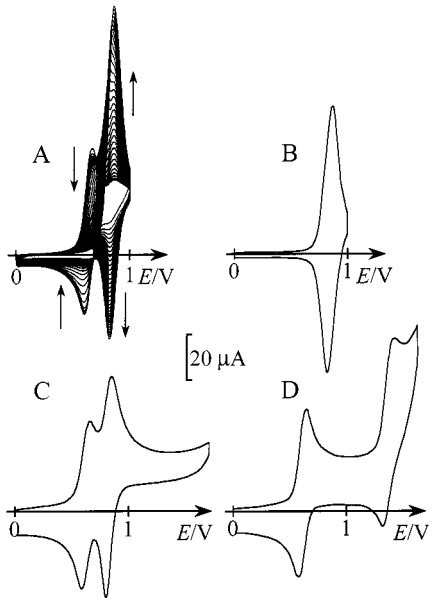

Figure 6. (A) Oxidative coating of a Pt disk electrode (5 mm diameter) with an Fe-bis(terpy) film, by repeated scans in a solution of L^2 (2.5 mM) in CH_3CN + TBAP 0.1 M; (B) modified electrode prepared in (A) and transferred to L^2-free CH_3CN + TBAP 0.1 M; (C) L^2 (2.5 mM) + 1 equiv. $Fe(ClO_4)_2$; (D) L^2 + 1 equiv. $Ni(ClO_4)_2$; scan rate 0.1 V

A similar behavior has already been observed with a ferrocenyl-substituted terpyridine containing an olefinic linkage.[4f] The formation of a polymer film containing iron centers in a terpyridine environment was attributed to the oxidative electropolymerization of the vinyl or vinyl-cyclopentadienyl backbone, followed by rupture of the ferrocenyl groups and complexation of iron cations. Since L^2 does not contain any olefinic group, the formation of a stable Fe-bis(terpyridine) material must be explained in a different way. Fe-bis(terpyridine) films are also obtained when the scan range is restricted to the Fc/Fc^+ redox couple. However, the films formed in these experimental conditions are of smaller size than those obtained when the potential scan range is extended up to 1 V. Electrode coating can thus be explained by considering the decomposition of the ferricinium groups in the presence of terpyridine ligands, to form poorly soluble Fe-bis(terpyridine) species, which precipitate onto the electrode surface. The high stability of the films upon cycling and their better growth when the scan range is increased up to 1 V could be due to some oxidative polymerization of free cyclopentadienyl groups released by decomposition of the ferricinium species.

The effect of added metal cations on film growth confirmed that this process is mainly due to the decomplexation of ferricinium groups by terpyridine ligands. The addition of small amounts (e.g. 0.2 mol equivalent) of Fe^{II}, Ni^{II} and Hg^{II} cations led to stabilization of the Fc/Fc^+ redox couple and slowed down the growth of the Fe-bis(terpyridine) films. This last process was fully inhibited in the presence of one mol equivalent of metal cation, suggesting the formation of 1:1 L^2 + M^{II} complexes (M = Fe, Ni, Hg).

The CV curves recorded in L^2 solutions containing one mol equivalent of metal cation show stable Fc/Fc^+ redox peak systems (Figure 6C and 6D). Complexation of L^2 with Fe^{II} ions is also revealed by the appearance of a $Fe^{II/III}$ redox wave ($E_{1/2}$ = 0.77 V; Figure 6C). The sharp and symmetrical shape of the Fe^{III} Fe^{II} reduction peak indicates that the oxidized form of the iron complex ($[FeL^2]^{4+}$) is poorly soluble in CH_3CN, adsorbs at the electrode surface during the scan towards positive potentials and dissolves upon reduction. No accumulation of complex onto the electrode surface was observed upon repeated scans. This observation confirms that the polymerization of free cyclopentadienyl groups is involved in the growth of films by oxidation of L^2.

Complexation of L^2 with Ni^{II} ions is also evidenced by the rise of a $Ni^{II/III}$ redox wave at 1.31 V (Figure 6D). This wave was found at 1.33 V for the $[Ni(L^3)_2]^{2+}$ model complex. No redox system concerning the metal centre could be found with the $[HgL^2]^{2+}$ complex. As already observed for other complexes of ferrocene-functionalized terpyridines,[4a,4f,4g] the potential of the Fc/Fc^+ process is slightly or not changed upon complexation of L^2 (+10 mV, +5 mV and 0 mV for Hg^{II}, Ni^{II} and Fe^{II} complexes, respectively). This behavior contrasts with that obtained upon complexation of the phen-based ligand L^1. As already found with iron,[7c] nickel and mercury complexes of L^1, the drop in the ν(CO) stretching vibration in L^2-based complexes (see the Exp. Sect.) indicates a coordination between the metal center and the oxygen atoms of the carbonyl groups. However, this interaction is not sufficient to produce an appreciable electronic coupling between the ferrocene group and the metal center in complexes of L^2. Although we have no clear explanation at the present time, this different behavior could be due to a structural effect, since the ferrocenyl group is linked to very different positions with regard to the complexing site in L^1 (2-position) and in L^2 (4′-position). Complexation of L^1 may lead to a non-coplanarity of the Cp rings in the complexes, which is known to result in marked positive potential shifts in strained ferrocene derivatives.[9,10]

Finally, the formation of 1:1 L^2 + M complexes (M = Fe, Ni, Hg) was confirmed by FAB-MS measurements. The spectra of the isolated complexes only displayed peaks corresponding to $[\{ML^2\}X]^+$ entities (Fe and Ni: X = ClO_4^-; Hg: X = $CF_3SO_3^-$), without any evidence for the presence of oligomeric species.

Conclusion

This study confirms the remarkable complexation and electrochemical properties of polypyridyl-ferrocene metallosynthons towards various transition metal cations. Complexation of the 1,1′-bis(phen) derivative of ferrocene (L^1) with Cu^I, Ni^{II}, Fe^{II} and Hg^{II} cations results in large potential shifts of the ferrocenyl-centered redox process. This redox ligand could thus be used for the electrochemical recognition of selected metal cations. In contrast, complexation of the ferrocene-bis(terpy) derivative L^2 does not

alter appreciably the electron density on the ferrocenyl groups. Additionally, we found that the oxidative decomposition of L^2 is a simple way to tailor stable polymer films of Fe-bis(terpyridine) complexes.

Experimental Section

Reagents, Instrumentation and Procedure: Acetonitrile (Rathburn, HPLC grade) was used as received. Dichloromethane was dried over neutral alumina (activity I) for at least six days before use. Tetra-*n*-butylammonium perchlorate (TBAP) was purchased from Fluka and dried under vacuum for three days at 80 °C. Electrochemical experiments were conducted in a conventional three-electrode cell under an argon atmosphere at 20 °C. The reference electrode was $Ag/AgNO_3$ (10 mM in CH_3CN containing 0.1 M TBAP). The ferrocene/ferricinium (Fc/Fc^+) redox couple was used as internal standard. FAB (positive mode) mass spectra were recorded with an AEI Kratos MS 50 spectrometer fitted with an Ion Tech Ltd. gun and using *m*-nitrobenzyl alcohol as matrix. Elemental analysis were performed by the Service Central d'Analyses, CNRS, Lyon.

Ligands: L^1 was synthesized as previously reported.[7c] ^1H NMR (250 MHz, CD_3CN): δ = 2.76 (s, 6 H, CH_3), 4.52 (t, 4 H, $H_{\beta\beta'}$), 4.91 (t, 4 H, $H_{\alpha\alpha'}$), 5.52 (s, 4 H, CH_2), 7.49 (d, J = 7.9 Hz, 2 H, H_8), 7.60−7.83 (m, 6 H, $H_{5,6,3}$), 8.13 (d, J = 7.9 Hz, 2 H, H_7), 8.23 (d, J = 7.9 Hz, 2 H, H_4). FAB-MS: m/z = 687 $[L^1 + H]^+$. UV/Vis (d-d band; CH_3CN): λ_{max} (ε/M^{-1} cm^{-1}) = 450 nm (300). FT-IR (KBr): ν(CO) = 1713 cm^{-1}. $C_{40}H_{30}FeN_4O_4$ (686.16): C 69.88, H 4.40, N 8.16; found C 69.26, H 4.89, N 8.36.

L^2 was prepared by the stoichiometric reaction of 4′-(hydroxymethyl)-2,2′:6′,2"-terpyridine[11] with 1 mmol of 1,1′-bis(chlorocarbonyl)ferrocene[12] in 10 mL of dried toluene containing 4 mmol of freshly distilled triethylamine. The reaction mixture was stirred overnight under an inert atmosphere, then filtered and the solvents evaporated to dryness. The crude product was extracted with CH_2Cl_2 and the organic phase was washed with H_2O. The solvent was removed in vacuo and the crude product was purified by column chromatography on neutral alumina eluting with CH_2Cl_2, to yield L^2 (70%) as an orange solid. ^1H NMR (250 MHz, CD_3CN): δ = 4.52 (t, 4 H, $H_{\beta\beta'}$), 5.08 (t, 4 H, $H_{\alpha\alpha'}$), 5.40 (s, 4 H, CH_2), 7.30 (dd, J = 7.5, 4.8 Hz, 4 H, $H_{5,5''}$), 7.79 (td, J = 7.7, 1.6 Hz, 4 H, $H_{4,4''}$), 8.45 (s, 4 H, $H_{3',5'}$), 8.55 (d, J = 7.9 Hz, 4 H, $H_{3,3''}$), 8.65 (m, 4 H, $H_{6,6''}$). FAB-MS: m/z = 765 $[L^2 + H]^+$. UV/Vis (d-d band; CH_2Cl_2): λ_{max} (ε/M^{-1} cm^{-1}) = 453 nm (310). FT-IR (KBr): ν(CO) = 1718 cm^{-1}. $C_{44}H_{32}FeN_6O_4{\cdot}H_2O$ (782.65): C 67.53, H 4.38, N 10.74; found C 67.51, H 4.34, N 10.24.

Complexes: The quantitative synthesis of metal complexes (yield 90%) was performed by the reaction of stoichiometric amounts of L^1 or L^2 and a metal salt {$[Cu(CH_3CN)_4]ClO_4$, $[Ni(ClO_4)_2{\cdot}xH_2O]$, $[Fe(ClO_4)_2{\cdot}6H_2O]$ and $[Hg(CF_3SO_3)_2]$} at room temperature in CH_2Cl_2. Products were precipitated by the addition of diethyl ether and collected by suction filtration. **Warning**! *Perchlorate salts are hazardous because of the possibility of explosion*. Characterization of the $[FeL^1](ClO_4)_2$ complex has already been reported.[7c]

$[CuL^1]ClO_4$: ^1H NMR (250 MHz, CD_3CN): δ = 2.56 (s, 6 H, CH_3), 3.66 (s, 2 H, H_α), 4.37 (s, 2 H, H_β), 4.43 (s, 2 H, $H_{\beta'}$), 4.72 (s, 2 H, $H_{\alpha'}$), 4.88 (d, J = 12.0 Hz, 2 H, CH_2-endo), 5.47 (d, J = 12.0 Hz, 2 H, CH_2-exo), 7.90 (d, J = 7.9 Hz, 2 H, H_8), 8.17 (d, J = 2.4 Hz, 4 H, $H_{5,6}$), 8.28 (d, J = 7.9 Hz, 2 H, H_3), 8.63 (d, J = 7.9 Hz, 2 H, H_7), 8.73 (d, J = 7.9 Hz, 2 H, H_4). FAB-MS: m/z = 749 $[CuL^1]^+$. UV/Vis (CH_3CN): λ_{max} (ε/M^{-1} cm^{-1}) = 444 nm (6975). FT-IR (KBr): ν(CO) = 1713 cm^{-1}. $C_{40}H_{30}ClCuFeN_4O_8{\cdot}H_2O$ (867.57): C 55.38, H 3.72, N 6.46; found C 55.45, H 3.54, N 6.76.

$[HgL^1](CF_3SO_3)_2$: ^1H NMR (250 MHz, CD_3CN): δ = 3.01 (s, 6 H, CH_3), 3.47 (s, 2 H, H_α), 4.32 (s, 2 H, H_β), 4.45 (s, 2 H, $H_{\beta'}$), 4.77 (s, 2 H, $H_{\alpha'}$), 5.22 (d, J = 12.0 Hz, 2 H, CH_2-endo), 5.54 (d, J = 12.0 Hz, 2 H, CH_2-exo), 8.21 (d, J = 7.9 Hz, 2 H, H_8), 8.35 (d, J = 2.2 Hz, 4 H, $H_{5,6}$), 8.46 (d, J = 7.9 Hz, 2 H, H_3), 8.92 (d, J = 7.9 Hz, 2 H, H_7), 9.06 (d, J = 7.9 Hz, 2 H, H_4). FAB-MS: m/z = 1037 $[\{HgL^1\}CF_3SO_3]^+$. UV/Vis (CH_3CN): λ_{max} (ε/M^{-1} cm^{-1}) = 454 nm (360). FT-IR (KBr): ν(CO) = 1710 cm^{-1}. $C_{42}H_{30}F_6FeHgN_4O_{10}S_2$ (1185.3): C 42.56, H 2.55, N 4.73; found C 42.43, H 2.37, N 4.33.

$[NiL^1](ClO_4)_2$: FAB-MS: m/z = 843 $[\{NiL^1\}ClO_4]^+$. UV/Vis (CH_3CN): λ_{max} (ε/M^{-1} cm^{-1}) = 454 nm (450). FT-IR (KBr): ν(CO) = 1664 cm^{-1}. $C_{40}H_{30}Cl_2FeN_4NiO_{12}{\cdot}H_2O$ (962.17): C 49.93, H 3.35, N 5.82; found C 49.23, H 3.28, N 6.06.

$[HgL^2](CF_3SO_3)_2$: FAB-MS: m/z = 1115 $[\{HgL^2\}CF_3SO_3]^+$. No correct elemental analysis for this compound could be obtained.

$[NiL^2](ClO_4)_2$: FAB-MS: m/z = 921 $[\{NiL^2\}ClO_4]^+$. UV/Vis (CH_3CN): λ_{max} (ε/M^{-1} cm^{-1}) = 452 nm (496). FT-IR (KBr): ν(CO) = 1666 cm^{-1}. $C_{44}H_{32}Cl_2FeN_6NiO_{12}{\cdot}H_2O$ (1040.2): C 50.08, H 3.29, N 8.08; found C 49.82, H 3.23, N 7.73.

$[FeL^2](ClO_4)_2$: FAB-MS: m/z = 919 $[\{FeL^2\}ClO_4]^+$. UV/Vis (CH_3CN): λ_{max} (ε/M^{-1} cm^{-1}) = 558 nm (2150), 510 (1050, sh). FT-IR (KBr): ν(CO) = 1708, 1621 cm^{-1}. $C_{44}H_{32}Cl_2Fe_2N_6O_{12}{\cdot}H_2O$ (1037.4): C 50.94, H 3.30, N 8.10; found C 50.75, H 3.25, N 8.01.

[1] A. Harriman, R. Ziessel, *Chem. Commun.* **1996**, 1707−1716.
[2] A. M. DeBlass, C. DeSantis, L. Fabbrizzi, M. Licchelli, P. Pallavicini, A. Poggi, in *Supramolecular Chemistry* (Eds.: V. Balzani, L. DeCola), Kluwer Academic Publishers, London **1995**, 87−103.
[3] [3a] P. D. Beer, O. Kocian, R. J. Mortimer, *J. Chem. Soc., Dalton Trans.* **1990**, 3283−3288. [3b] I. R. Butler, *Organometallics* **1992**, *11*, 74−83. [3c] I. R. Butler, N. Burke, L. J. Hobson, H. Findenegg, *Polyhedron* **1992**, *19*, 2435−2439. [3d] B. König, M. Nimtz, H. Zierg, *Tetrahedron* **1995**, *22*, 6267−6272. [3e] N. Sachsinger, C. D. Hall, *J. Organomet. Chem.* **1997**, *531*, 61−55. [3f] S. Achar, C. E. Immoos, M. G. Hill, V. J. Catalano, *Inorg. Chem.* **1997**, *36*, 2314−2320.
[4] [4a] J.-C. Chambron, C. Coudret, J.-P. Sauvage, *New. J. Chem.* **1992**, *16*, 361−367. [4b] B. Farlow, T. A. Nile, J. L. Walsh, A. T. McPhail, *Polyhedron* **1993**, *23*, 2891−2894. [4c] E. C. Constable, A. J. Andrews, M. D. Marcos, P. R. Raithby, R. Martínez-Máñez, M. J. L. Tendero, *Inorg. Chim. Acta* **1994**, *224*, 11−14. [4d] E. C. Constable, A. J. Andrews, R. Martínez-Máñez, P. R. Raithby, A. M. N. Cargill Thompson, *J. Chem. Soc., Dalton Trans.* **1994**, 645−650. [4e] I. R. Butler, S. J. McDonald, M. B. Hursthouse, K. M. Abdul Malik, *Polyhedron* **1995**, *14*, 529−539. [4f] M. E. Padilla-Tosta, R. Martínez-Máñez, J. Soto, J. M. Lloris, *Tetrahedron* **1998**, *54*, 12039−12046. [4g] U. Siemeling, U. Vorfeld, B. Neumann, H.-G. Stammler, P. Zanello, F. Fabrizi de Biani, *Eur. J. Inorg. Chem.* **1999**, 1−5.
[5] E. C. Constable, R. Martínez-Máñez, A. M. W. Cargill Thompson, J. V. Walker, *J. Chem. Soc., Dalton Trans.* **1994**, 1585−1594.
[6] E. C. Constable, A. J. Edwards, R. Martínez-Máñez, P. R. Raithby, *J. Chem. Soc., Dalton Trans.* **1995**, 3253−3261.

[7] [7a] M. Buda, J.-C. Moutet, E. Saint-Aman, A. De Cian, J. Fisher, R. Ziessel, *Inorg. Chem.* **1998**, *37*, 4146−4148. [7b] M. Buda, J.-C. Moutet, A. Pailleret, E. Saint-Aman, R. Ziessel, *J. Electroanal. Chem.* **2000**, *484*, 164−171. [7c] A. Ion, J.-C. Moutet, E. Saint-Aman, G. Royal, S. Tingry, J. Pécaut, S. Ménage, R. Ziessel, *Inorg. Chem.* **2001**, *40*, 3632−3636. [7d]A. Ion, M. Buda, J.-C. Moutet, E. Saint-Aman, G. Royal, I. Gauthier-Luneau, M. Bonin, A. Harriman, R. Ziessel, submitted for publication.

[8] C. Dietrich-Buchecker, J.-P. Sauvage, J.-M. Kern, *J. Am. Chem. Soc.* **1989**, *111*, 7791−7800 and references therein.

[9] J. C Medina, T. T. Goodnow, M. T. Rojas, J. L. Atwood, A. E. Kaifer, G. K. Gokel, *J. Am. Chem. Soc.* **1992**, *114*, 10583−10595.

[10] H. Scholl, K. Sochaj, *Electrochim. Acta* **1991**, *36*, 689−694.

[11] M. E. Padilla-Tosta, J. M. Lloris, R. Martínez-Máñez, A. Benito, J. Soto, T. Pardo, M. A. Miranda, M. Dolores-Marcos, *Eur. J. Inorg. Chem.* **2000**, 741−748.

[12] J.-C. Moutet, E. Saint-Aman, M. Ungureanu, T. Visan, *J. Electroanal. Chem.* **1996**, *41*, 79−85.

Received September 7, 2001
[I01348]

Two Ferromagnetic One-Dimensional Nickel(II) Complexes Containing the Diamagnetic $[Ni(CN)_4]^{2-}$ Group

Hui-Zhong Kou,[a][‡] Shu-Feng Si,[a] Song Gao,[b] Dai-Zheng Liao,*[a] Zong-Hui Jiang,[a] Shi-Ping Yan,[a] Yu-Guo Fan,[c] and Geng-Lin Wang[a]

Keywords: Cyanides / Bridging ligands / Nickel / Magnetic properties / Crystal structure

A cyano-bridged nickel(II) compound, $[NiL][Ni(CN)_4]\cdot 4H_2O$ (L = 3,10-diethyl-1,3,5,8,10,12-hexaazacyclotetradecane), was prepared and characterized. Single crystal X-ray analysis reveals that the compound assumes a cyano-bridged chain structure in which one nickel(II) ion is coordinated by four cyanide ligands and the other is coordinated by four nitrogen atoms of the macrocyclic ligand and two nitrogen atoms of the bridging cyanide ligands. The six-coordinate nickel(II) centres display an axially elongated octahedron, whereas the four-coordinate nickel(II) centres assume planar geometry. Magnetic investigations on $[NiL][Ni(CN)_4]\cdot 4H_2O$ and a similar chain-like compound $[Ni(TIM)][Ni(CN)_4]$ show the presence of weak intrachain ferromagnetic interactions between the paramagnetic nickel(II) ions through the diamagnetic $[Ni(CN)_4]^{2-}$ anions.

Introduction

During the last two decades, much attention has been directed to the synthesis of molecule-based magnets, especially to Prussian Blue analogues.[1] Prussian Blue, with the formula $Fe_4^{III}[Fe^{II}(CN)_6]_3\cdot 15H_2O$ is a ferromagnet with T_c = 5.6 K, in which the paramagnetic iron(III) ions are bridged in three-dimensions by the diamagnetic hexacyanoferrate(II) anion, with a shortest intermetallic $Fe^{III}\cdots Fe^{III}$ separation of 10.6 Å.[2] Recently, a series of three-dimensional bimetallic compounds $[Ni(L)_2]_3[Fe^{II}(CN)_6]X_2$ (L = en or tn, X = PF_6^- or ClO_4^-) and one two-dimensional copper(II)-iron(II) compound $[Cu(dmen)_2]_2[Fe^{II}(CN)_6]$ (dmen = dimethylaminoethylamine) were prepared and found to exhibit ferromagnetic interactions between the nearest nickel(II) or copper(II) ions through the diamagnetic $[Fe(CN)_6]^{4-}$ anions.[3] Nevertheless, antiferromagnetic coupling between paramagnetic transition metal ions is more often operative via diamagnetic building blocks, such as $[Co(CN)_6]^{3-}$, $[Ni(CN)_4]^{2-}$, $[Mo(CN)_8]^{4-}$ and $[W(CN)_8]^{4-}$.[4–6] In addition, the diamagnetic $[CrO_4]^{2-}$ group can mediate either ferromagnetic[7] or, in most cases, antiferromagnetic interactions.[8] We have been interested in magnetic interactions via cyanide-containing diamagnetic building blocks, and have found that the nitroprusside anion $[Fe(CN)_5(NO)]^{2-}$ can transmit weak antiferromagnetic interactions in $[Cu(en)][Fe(CN)_5(NO)]$,[9] as is also observed in $[Ni(en)_2][Fe(CN)_5(NO)]$.[10] Using the diamagnetic $[Ni(CN)_4]^{2-}$ building block, we prepared two one-dimensional chain complexes $[NiL][Ni(CN)_4]\cdot nH_2O$ [L = 2,3,9,10-tetramethyl-1,4,8,11-tetraazacyclotetradeca-1,3,8,10-tetraene abbreviated as TIM, n = 0 (**1**);[11] L = 3,10-diethyl-1,3,5,8,10,12-hexaazacyclotetradecane, n = 4 (**2**)]. Interestingly, a ferromagnetic interaction is observed in the two complexes. In the present paper, we report the synthesis, crystal structure and magnetic properties of **2** together with the magnetic behaviour of **1**.

Results and Discussion

The IR spectrum of **2** exhibits two strong bands at 2150 and 2120 cm^{-1}, which can be attributed to the C≡N stretching vibration. It is well-known that the formation of a cyanide bridge shifts ν(CN) towards higher frequencies.[1] The strong band at 2150 cm^{-1} may therefore be attributed to ν(CN) of the bridging cyanides and that at 2120 cm^{-1} to the terminal ones. The strong absorption at 1650 cm^{-1} indicates the presence of water in the molecule, which is consistent with the structural studies.

It has been shown that the four-coordinate nickel(II) macrocyclic complexes can accept donor atoms yielding six-coordinate nickel(II) geometries.[11,12] The cyano nitrogen

[a] Department of Chemistry, Nankai University, Tianjin 300071, P.R. China
E-mail: coord@nankai.edu.cn
[b] State Key Laboratory of Rare Earth Materials Chemistry and Applications, Peking University, Beijing 100871, P. R. China
[c] Laboratory of Supramolecular Structure and spectroscopy, Jilin University, Changchun 130023, P.R. China
[‡] Present address: Department of Chemistry, Tsinghua University, Beijing 100084, P.R. China

atom is a strong donor and easily coordinates to the nickel(II) ion to give rise to cyano-bridged complexes.

Crystal Structure

The structure of **2** consists of one *trans*-$[NiL]^{2+}$ cation and one $[Ni(CN)_4]^{2-}$ anion as illustrated in Figure 1. Selected bond lengths and angles are listed in Table 1. The coordination geometry about Ni(1) is nearly octahedral, with four secondary amine nitrogen atoms of the macrocyclic ligand L [$Ni-N_{eq}$ = 2.072(4) Å] occupying the equatorial plane and two nitrogen atoms of two bridging cyanide ligands situated at the axial sites [$Ni-N_{ax}$ = 2.137(2) Å]. The bridging cyanides coordinate to Ni(1) in a linear fashion [Ni(1)−N(1)−C(1) = 175.0(5)°], significantly different from the situation found in **1**[158.0(2)°].[11] The bond lengths and angles of [NiL] are similar to those in $[NiL]_3[Fe(CN)_6]_2\cdot 12H_2O$:[12a] each $[Ni(CN)_4]^{2-}$ unit uses two *trans* C≡N groups to connect to two *trans*-$[NiL]^{2+}$ moieties giving rise to one-dimensional Ni−C≡N−Ni linkages, whereas the two remaining *trans* CN^- groups are monodentate. The adjacent Ni···Ni distance is 5.094 Å, and the nearest interchain Ni(1)···Ni(1) distance is 9.337 Å. The water molecules are positioned in the vicinity of the chain and hydrogen-bonded to the nitrogen atoms of the nonbridging cyanides within the chain and to each other (Figure 2 top and bottom). No hydrogen-bonded two- or three-dimensional network is formed.

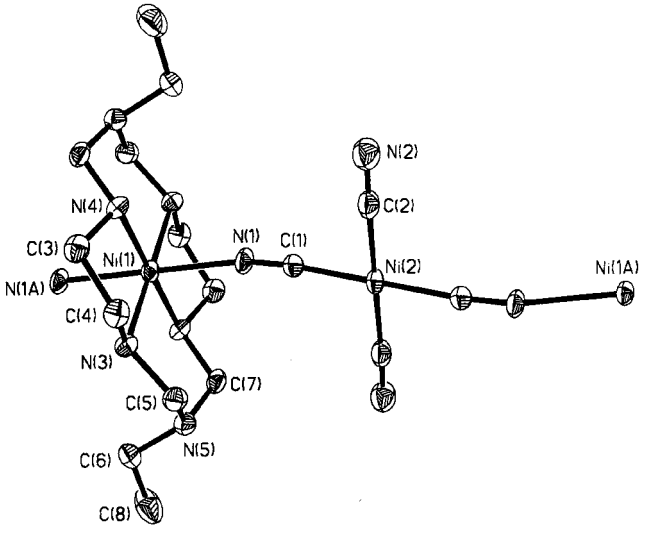

Figure 1.An ORTEP drawing of **2** with thermal ellipsoids drawn at the 30% probability level

Table 1. Bond lengths (Å) and angles (°) for **2**

Ni(1)−N(4)	2.070(4)	Ni(1)−N(3)	2.073(4)
Ni(1)−N(1)	2.137(5)	Ni(2)−C(2)	1.855(7)
Ni(2)−C(1)	1.871(6)	N(1)−C(1)	1.133(7)
N(2)−C(2)	1.148(7)		
C(1)−N(1)−Ni(1)	167.7(5)	C(4)−N(3)−Ni(1)	104.5(3)
N(1)−C(1)−Ni(2)	175.0(5)	N(2)−C(2)−Ni(2)	177.7(6)

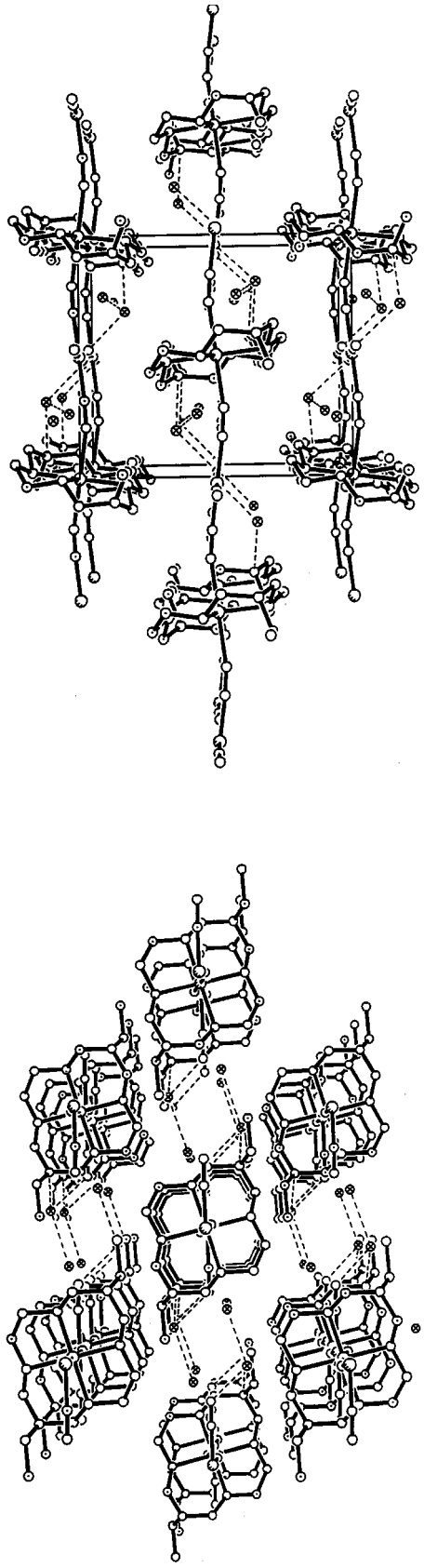

Figure 2. (top) Projection along the *c* axis, showing the polymeric chains including alternating nickel groups of **2**; (bottom) projection perpendicular to the *c* axis for **2**

Magnetic Properties

The magnetic susceptibilities of **1** and **2** have been measured in the temperature range 1.8−200 K. Plots of $\chi_m T$ and χ_m^{-1} vs. T for **1** and **2**, where χ_m is the magnetic susceptibility per Ni_2 unit, are shown below.

Complex 1

At 200 K, the $\chi_m T$ value is ca. 1.06 emu K mol^{-1} (2.91 μ_B), close to that (1.0 emu K mol^{-1}, 2.83 μ_B) of an isolated Ni^{II} ion ($S = 1$, $g = 2.0$) interacting with a diamagnetic Ni^{II} ion ($S = 0$). As the temperature decreases the $\chi_m T$ value increases slowly reaching a maximum value of 1.16 emu K mol^{-1} (3.05 μ_B) at 20.8 K and then decreases sharply reaching a minimum value of 0.53 emu K mol^{-1} (2.06 μ_B) at 1.8 K. Such a magnetic behaviour is characteristic of a dominant ferromagnetic interaction to which weak antiferromagnetic interactions are superimposed.[13] The lack of interchain intermolecular contacts in **1**[11] suggests the through-space magnetic coupling is weaker than that through the -NC−Ni−CN- pathway. Therefore, the dominant ferromagnetic interaction is due to the intrachain interaction, and the interchain interaction is antiferromagnetic. The magnetic susceptibility above 10 K obeys the Curie−Weiss law with a positive Weiss constant $\theta = +2.9$ K (Figure 3); this also proves the presence of ferromagnetic coupling within the Ni_2 chain of **1**.

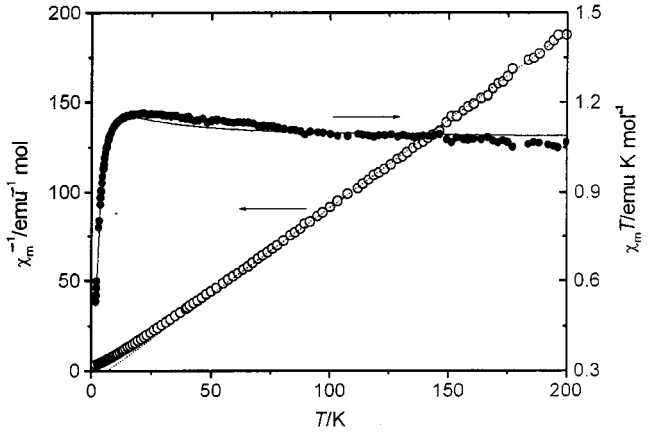

Figure 3. Temperature dependence of $\chi_m T$ and χ_m^{-1} for **1**; the solid line represents the theoretical values and the dotted line the fit to the Curie−Weiss law

We attempted to interpret the magnetic data using Fisher's model[14] for the classical spin chain system ($S = 1$ and $\boldsymbol{H}_{chain} = -J\Sigma \mathbf{S}_i\mathbf{S}_{i+1}$) neglecting zero-field splitting and the Haldane gap effect[15] and taking into consideration a mean-field correlation term.[7a,16] The magnetic susceptibility can be expressed by Equation (1), where N is Avogadro's number, β is the Bohr magneton, k is the Boltzmann constant and z is the number of nearest neighbours (two in this case). The least-squares fitting to the experimental data led to $J = +2.88$ cm^{-1}, $J' = -0.94$ cm^{-1} and $g = 2.08$. This result ($J = +2.88$ cm^{-1}) shows the presence of weak ferromagnetic interaction between the paramagnetic nickel ions within each chain through the diamagnetic $[Ni(CN)_4]^{2-}$ ions.

$$\chi_{chain} = \frac{Ng^2\beta^2}{3kT}\frac{1+u}{1-u} \times S(S+1)$$
$$u = \coth K - 1/K \text{ and } K = JS(S+1)/kT \quad (1)$$
$$\chi_m = \chi_{chain}/[1-\chi_{chain}(zJ'/Ng^2\beta^2)]$$

Complex 2

Complex **2** has a magnetic behaviour similar to that of **1** (Figure 4). At 200 K, the $\chi_m T$ value is ca. 1.25 emu K mol^{-1} (3.16 μ_B), larger than that (1.0 emu K mol^{-1}, 2.83 μ_B) of an isolated Ni^{II} ion ($S = 1$, g = 2.0) interacting with a diamagnetic Ni^{II} ion ($S = 0$). As the temperature decreases, the $\chi_m T$ value increases slightly reaching a maximum value of 1.29 emu K mol^{-1} (3.21 μ_B) at 16.6 K and then decreases sharply reaching a minimum value of 0.60 emu K mol^{-1} (2.2 μ_B) at 1.6 K. The magnetic susceptibility above 11 K obeys the Curie−Weiss law with a positive Weiss constant $\theta = +1.5$ K (Figure 4), which confirms the presence of ferromagnetic coupling within the Ni_2 chain of **2**. Similarly, the magnetic data can be analysed by Equation (1) giving the parameters $J = +2.19$ cm^{-1}, $J' = -0.92$ cm^{-1} and $g = 2.23$.

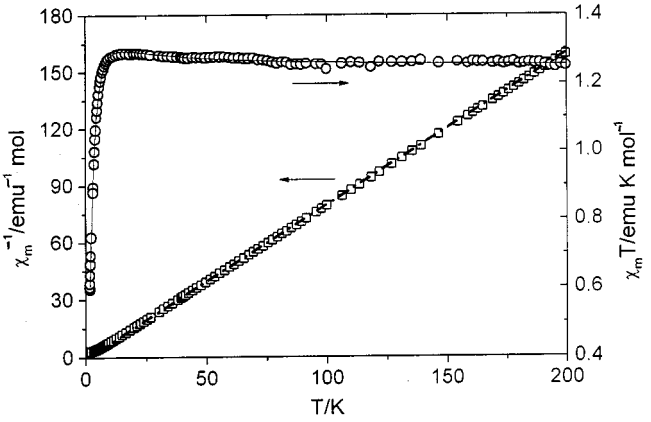

Figure 4. Plot of $\chi_m T$ and χ_m^{-1} vs. temperature for **2**; the solid line represents the theoretical values and the dashed line the fit to the Curie−Weiss law

The increase in $\chi_m T$ is due to a substantial contribution of ferromagnetic coupling, although the origin of this is not clear at this stage. Apparently, the ferromagnetic nature is not due to the orthogonality of the magnetic orbitals. One possibility is that it is due to a long-range interaction mediated through the empty d_σ orbital of the diamagnetic Ni^{II} ion. According to the Goodenogh−Kanamori rules for magnetic superexchange,[17] if a magnetic orbital overlaps an empty orbital the interaction between the two ions is ferromagnetic. This mechanism has recently been used to explain the ferromagnetic interaction between the nearest paramagnetic metal ions through the diamagnetic $[Fe(CN)_6]^{4-}$ or $[Co(CN)_6]^{3-}$ anions in $[Ni(en)]_3[Fe(CN)_6]PF_6$, $[NiL_2]_3[Fe(CN)_6]X_2$ (X = PF_6^- or ClO_4^-) and $[Ni(tn)_2]_2[Co(CN)_6]NO_3{\cdot}2H_2O$.[3a,18] For the present complexes, an electron spin of the same sign as that of the unpaired electron in the $d_{x^2-y^2}$ (paramagnetic Ni^{II}) orbital

(x axis is taken along the Ni−C≡N−Ni linkage) is polarized on the empty $d_{x^2-y^2}$ (diamagnetic Ni^{II}) orbital (x axis is taken perpendicular to the NiC_4 plane) through the filled orbital of the cyanide bridges, giving rise to a ferromagnetic coupling between the nearest intrachain paramagnetic nickel(II) ions.

If we compare the θ and J values of the two complexes, we see that the values for **1** are slightly larger indicating a stronger magnetic coupling in **1**. This is in good agreement with the increasing order of the Ni(2)−C(1) and Ni(1)−N(1) bond lengths (1.858, 2.123 Å for **1**, 1.871, 2.137 Å for **2**). Such an elongation indicates a decreasing overlap of the d_σ orbitals and is unfavourable for the magnetic interaction between paramagnetic Ni^{II} ions.

Experimental Section

Physical Measurements: Elemental analyses of carbon, hydrogen and nitrogen were carried out with a Perkin−Elmer analyzer model 240. Infrared spectroscopy on KBr pellets was performed on a Shimadzu IR-408 infrared spectrophotometer in the 4000−600 cm^{-1} region. Variable-temperature magnetic susceptibility measurements (1.8−200 K) of powder samples were performed in a field of 1 T on a model Maglab System^{2000} magnetometer. The experimental susceptibilities were corrected for the diamagnetism of the constituent atoms (Pascal's Tables).

Preparations: All reagents used in the syntheses were of analytical grade and were used without further purification. [Ni(TIM)][Ni(CN)$_4$] (**1**),[11] [Ni(TIM)](ClO$_4$)$_2$,[19] and [NiL](ClO$_4$)$_2$,[20] were prepared as described previously.

[NiL][Ni(CN)$_4$]·4H$_2$O (2): Two aqueous solutions of [NiL](ClO$_4$)$_2$ (0.25 mmol) and K$_2$[Ni(CN)$_4$] (0.25 mmol) were mixed to produce immediately a brown fine powder which was collected by suction filtration, washed with water and dried under vacuum over P_2O_5. Yield 125 mg (90%). $C_{16}H_{42}N_{10}Ni_2O_4$ (556.0): calcd. C 34.71, H 6.66, N 28.92; found C 34.87, H 6.48, N 28.95. IR: $\tilde{\nu}_{max}$ = 2150, 2130 and 2110 (C≡N) cm^{-1}. Well-shaped light-grey crystals suitable for an X-ray structure analysis were grown at room temperature by the slow mixing of an orange acetonitrile solution of [NiL](ClO$_4$)$_2$ and a colourless aqueous solution of K$_2$[Ni(CN)$_4$] in an H-tube.

Crystal Data for 2: $C_{16}H_{42}N_{10}Ni_2O_4$, M = 556.02, monoclinic, $P2_1/n$, a = 11.0104(8), b = 10.1878(4), c = 11.5099(10) Å, β = 91.980(10)°, U = 1290.3(2) Å^3, Z = 2, μ(Mo-K_α) = 1.500 mm^{-1}. F(000) = 592, 2263 unique reflections, 1265 observations ($I > 2.00\sigma(I)$] considered unique (R_{int} = 0.0295). The final R_{wF} was 0.129, with conventional R_F = 0.0401 for 148 parameters.

Crystallographic data (excluding structure factors) for the structures reported in this paper have been deposited with the Cambridge Crystallographic Data Centre as supplementary publication no. CCDC-152642. Copies of the data can be obtained free of charge on application to CCDC, 12 Union Road, Cambridge CB2 1EZ UK [Fax: (internat.) +44-1223/336-033; E-mail: deposit@ccdc.cam.ac.uk].

Acknowledgments

This work was supported by the National Natural Science Foundation of China (No. 20071019 and No. 20071020).

[1] [1a] V. Gadet, M. Bujoli-Doeuff, L. Force, M. Verdaguer, K. El Malkhi, A. Deroy, J. P. Besse, C. Chappert, P. Veillet, J. P. Renard, P. Beauvillain, in *Molecular Magnetic Materials* (Eds.: D. Gatteschi, O. Kahn, J. S. Miller, P. Palacio), NATO ASI Ser. 198, Kluwer, Dordrecht, **1990**, p. 281. [1b] W. R. Entley, G. S. Girolami, *Science* **1995**, *268*, 397−400. [1c] S. Ferlay, T. Mallah, R. Ouaches, P. Veillet, M. Verdaguer, *Nature* **1995**, *378*, 701−703. [1d] M. Verdaguer, *Science* **1996**, *272*, 698−699. [1e] O. Sato, T. Iyoda, A. Fujishima, K. Hashimoto, *Science* **1996**, *272*, 704−705.
[2] F. Herren, P. Fischer, A. Ludi, W. Hälg, *Inorg. Chem.* **1980**, *19*, 956−959.
[3] [3a] N. Fukita, M. Ohba, H. Okawa, K. Matsuda, H. Iwamura, *Inorg. Chem.* **1998**, *37*, 842−848. [3b] N. Mondal, M. K. Saha, B. Bag, S. Mitra, V. Gramlich, J. Ribas, M. S. Mallah, *J. Chem. Soc., Dalton Trans.* **2000**, 1601−1604.
[4] [4a] M. Ohba, N. Usuki, N. Fukita, H. Okawa, *Inorg. Chem.* **1998**, *37*, 3349−3354. [4b] M. Ohba, N. Fukita, H. Okawa, *J. Chem. Soc., Dalton Trans.* **1997**, 1733−1737. [4c] M. Ferbinteanu, S. Tanase, M. Andruh, Y. Journaux, F. Cimpoesu, I. Strenger, E. Riviere, *Polyhedron* **1999**, *18*, 3019−3025.
[5] H. Kitaguchi, S. Nagata, T. Watanabe, *J. Phys. Soc. Jpn.* **1975**, *38*, 998−1002. S.-Z. Zhan, D. Guo, X.-Y. Zhang, C.-X. Du, Y. Zhu, R.-N. Yang, *Inorg. Chim. Acta* **2000**, *298*, 57−62; Z. Smekal, F. Brezina, Z. Sindelar, R. Klicka, M. Nadvornik, *Chem. Pap.-Chem. Zvesti* **1997**, *51*, 95−98.
[6] B. Nowicka, M. Hagiwara, Y. Wakatsuki, H. Kisch, *Bull. Chem. Soc. Jpn.* **1999**, *72*, 441−445.
[7] [7a] H. Oshio, H. Okamoto, T. Kikuchi, T. Ito, *Inorg. Chem.* **1997**, *36*, 3201−3203. [7b] H. Oshio, T. Kikuchi, T. Ito, *Inorg. Chem.* **1996**, *35*, 4938−4941.
[8] P. Chaudhuri, M. Winter, K. Wieghardt, S. Gehring, J. Weiss, *Inorg. Chem.* **1988**, *27*, 1564−1569.
[9] [9a] H.-Z. Kou, H.-M. Wang, D.-Z. Liao, P. Cheng, Z.-H. Jiang, S.-P. Yan, X.-Y. Huang, G.-L. Wang, *Aust. J. Chem.* **1998**, *51*, 661−665. [9b] Z. Smekal, Z. Travnicek, J. Marek, M. Nadvornik, *Aust. J. Chem.* **2000**, *53*, 225−228.
[10] H. L. Shyu, H. H. Wei, Y. Wang, *Inorg. Chim. Acta* **1997**, *258*, 81−86.
[11] H.-Z. Kou, D.-Z. Liao, Z.-H. Jiang, S.-P. Yan, Q.-J. Wu, S. Gao, G.-L. Wang, *Inorg. Chem. Commun.* **2000**, *3*, 151−154.
[12] [12a] H.-Z. Kou, S. Gao, B.-Q. Ma, D.-Z. Liao, *Chem. Commun.* **2000**, 1309−1310. [12b] H.-Z. Kou, S. Gao, W.-M. Bu, D.-Z. Liao, B.-Q. Ma, Z.-H. Jiang, S.-P. Yan, Y.-G. Fan, G.-L. Wang, *J. Chem. Soc., Dalton Trans.* **1999**, 2477−2490. [12c] H.-Z. Kou, S. Gao, B.-Q. Ma, D.-Z. Liao, *Chem. Commun.* **2000**, 713−714. [12d] E. Colacio, J. M. Dominguez-Vera, M. Ghazi, R. Kivekas, F. Lloret, J. M. Moreno, H. Stoeckli-Evans, *Chem. Commun.* **1999**, 987−988. [12e] S. Ferlay, T. Mallah, J. Vaissermann, F. Bartolome, P. Veillet, M. Verdaguer, *Chem. Commun.* **1996**, 2481−2482.
[13] C. Michaut, L. Ouahab, P. Bergerat, O. Kahn, A. Bousseksou, *J. Am. Chem. Soc.* **1996**, *118*, 3610−3616.
[14] M. E. Fisher, *Am. J. Phys.* **1964**, *32*, 343−346.
[15] O. Kahn, *Molecular Magnetism*, VCH, Weinheim, Germany, **1993**, *Chapter II*, pp 251−263.
[16] H. J. Choi, M. P. Suh, *J. Am. Chem. Soc.* **1998**, *120*, 10622−10628.
[17] J. B. Goodenough, *Phys. Rev.* **1955**, *100*, 564−573; A. P. Ginsberg, *Inorg. Chim. Acta Rev.* **1971**, *5*, 45−68.; H. Weihe, H. Gudel, *Comments Inorg. Chem.* **2000**, *22*, 75−103.
[18] H.-Z. Kou, J.-K. Tang, D.-Z. Liao, S. Gao, P. Cheng, Z.-H. Jiang, S.-P. Yan, G.-L. Wang, B. Chansou, J.-P. Tuchagues, *Inorg. Chem.* **2001**, *40*, 4839−4844.
[19] A. M. Tait, D. H. Busch, *Inorg. Synth.* **1978**, *18*, 10−17.
[20] M. P. Suh, S.-G. Kang, *Inorg. Chem.* **1988**, *27*, 2544−2545.

Received June 15, 2001
[O01217]

Electrochemical Synthesis and X-ray Characterisation of Cadmium Complexes Containing 2,6-Bis(1-salicyloylhydrazonoethyl)pyridine − the Influence of the Supporting Electrolyte on the Nature of the Isolated Compounds

Matilde Fondo,[a] Antonio Sousa,*[a] Manuel R. Bermejo,[a] Ana García-Deibe,[a] Antonio Sousa-Pedrares,[a] Olga L. Hoyos,[b] and Madeleine Helliwell[c]

Keywords: N ligands / Cadmium / Electrochemistry

The influence of the supporting electrolyte and the solvent of crystallisation on the nature of cadmium complexes of 2,6-bis(1-salicyloylhydrazonoethyl)pyridine (H_4daps), obtained by an electrochemical procedure, has been investigated. [Cd(H_2daps)(H_2O)$_2$] (**1**), [Cd(H_2daps)(H_2O){(CH_3)$_2$CHOH}] (**2**), [Cd(H_3daps)Cl]·CH_3CN·0.25H_2O (**3**), [Cd(H_3daps)Cl-(CH_3OH)]·2H_2O·CH_3OH (**4**), and [Cd(H_2daps)Cl(H_2O)]N-(CH_3)$_4$ (**5**), have all been isolated and crystallographically characterised. X-ray diffraction studies show that the cadmium atom in **3** is in an unusual pentagonal pyramidal [CdN_3O_2Cl] geometry, while in the other compounds the cadmium atom is in a bipyramidal pentagonal environment. The organic ligand acts as a pentadentate dianionic ligand in **1**, **2**, and **5**, and as a pentadentate monoanionic ligand in **3** and **4**.

Introduction

The coordination chemistry of hydrazones has been extensively studied. The diversity seen in the structures of their metal complexes,[1−6] their pharmacological activity,[7−9] and magnetic properties[10−12] make these compounds of special interest.

Earlier studies of the coordination chemistry of hydrazone ligands have revealed some interesting aspects, such as their tendency to act as approximately planar pentadentate ligands in most complexes,[1−5,13,14] although an example of tridentate behaviour has recently been reported.[13] Furthermore, these ligands can coordinate in either the neutral,[2b−2d,14] monoanionic,[5,15] dianionic,[2a,16] or tetraanionic[17] form, giving rise to mononuclear or binuclear species. The type of complex obtained seems to be critically dependent on the reaction conditions employed.

We have recently reported that an electrochemical procedure can be used for the isolation of neutral hydrazone complexes that apparently cannot be prepared by other chemical methods.[18] For example, most nickel complexes with hydrazone ligands are mononuclear, while electrochemical synthesis yields a binuclear complex. As a continuation of this work, we have turned our attention to other metals such as cadmium. Although one chemical method for the synthesis of [Cd(H_2daps)(H_2O)] has been described,[2b] we were interested in studying the interaction of cadmium with H_4daps (Scheme 1) under an electrical current in the presence of different supporting electrolytes. The results of this study are described herein.

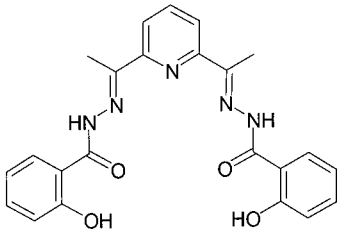

H_4daps

Scheme 1

Results and Discussion

The reaction of H_4daps with cadmium in an electrochemical cell in the presence of different electrolyte species yields a variety of complexes, as illustrated in Scheme 2. Thus, when a suspension of H_4daps in acetonitrile is electrolysed using [$N(CH_3CH_2)_4$]ClO_4 as the supporting electrolyte, the

[a] Departamento de Química Inorgánica, Facultade de Química, Universidade de Santiago de Compostela, 15706 Santiago de Compostela, Galicia, Spain
Fax: (internat.) +34-981/597-525
E-mail: qiansoal@usc.es
[b] Departamento de Química, Universidad del Cauca, Popayán, Colombia
[c] Department of Chemistry, University of Manchester, Oxford Road, Manchester M13 9PL, UK

 © WILEY-VCH Verlag GmbH, 69451 Weinheim, Germany, 2002 1434−1948/02/0303−0703 $ 17.50+.50/0

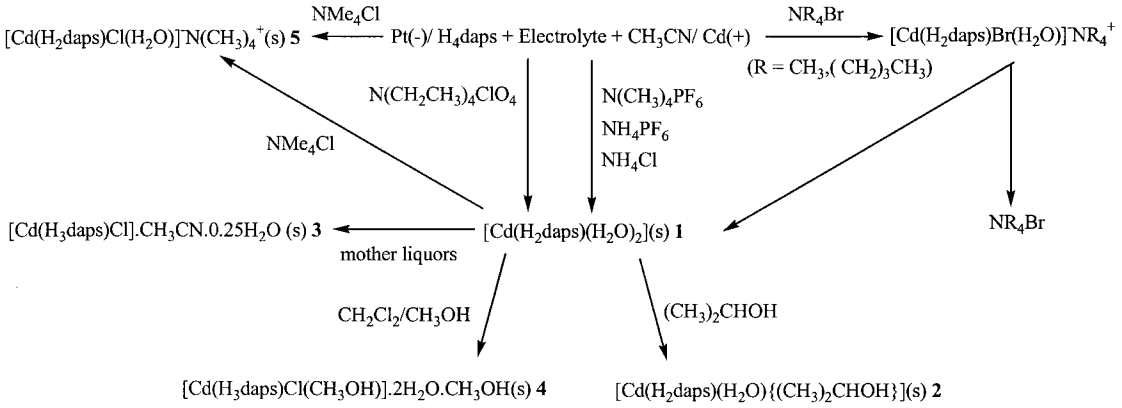

Scheme 2. Routes for the isolation of the metal complexes

insoluble complex $[Cd(H_2daps)(H_2O)_2]$ (**1**) is isolated as the main product. A similar complex, $[Cd(H_2daps)(H_2O)\{(CH_3)_2CHOH\}]$ (**2**), has been isolated and crystallographically characterised by recrystallisation of **1** from 2-propanol. Complex **1** is stable in air and thermally stable, melting above 300 °C without decomposition. The compound is insoluble or sparingly soluble in water and common organic solvents, but soluble in polar coordinating solvents such as DMF, DMSO, and pyridine.

Slow evaporation of the solvents from the mother liquors obtained following this electrochemical reaction allows the isolation of $[Cd(H_3daps)Cl]\cdot CH_3CN\cdot 0.25H_2O$ (**3**) as a secondary product, which has also been crystallographically characterised. It is clear that the chlorine ligand could only have come from the electrochemical reduction of the tetraethylammonium perchlorate used as the supporting electrolyte, as there is no other chlorine source in the reaction medium. This type of behaviour has been reported previously.[19]

Recrystallisation of **1** from CH_2Cl_2/CH_3OH yields a complex with the molecular formula $[Cd(H_3daps)Cl(CH_3OH)]\cdot 2H_2O\cdot CH_3OH$ (**4**). In this case, there are two possible sources of the chlorine ligand: (a) a slight impurity in **1**, arising from the reduction of the perchlorate electrolyte, or (b) the chlorine could have come from the dichloromethane used as solvent.

In an attempt to discern between these two possibilities, the perchlorate was replaced by a chlorine-free electrolyte, such as $[N(CH_3CH_2)_4]PF_6$. The electrochemical synthesis performed under these conditions again yielded complex **1**. Recrystallisation of the resulting powder from purified CH_2Cl_2/CH_3OH led to compound **4**, which was crystallographically characterised. This result demonstrates that the dichloromethane is the chlorine source. In view of this evidence, it was envisaged that electrolytes such as NH_4Cl or $N(CH_3)_4Cl$ might produce the same result. Therefore, the electrochemical synthesis in the presence of these chloride salts was investigated. Surprisingly, it was found that these two electrolytes play different roles in the reactions. NH_4Cl acts as a simple current carrier and leads to the isolation of the insoluble complex **1**, while the use of $N(CH_3)_4Cl$ produces the soluble complex $[Cd(H_2daps)Cl(H_2O)]N(CH_3)_4$ (**5**). Compound **5** was also obtained when a suspension of **1** in acetonitrile was treated with a stoichiometric amount of $N(CH_3)_4Cl$.

These results indicate that the cadmium centre is susceptible to nucleophilic attack, yielding ionic complexes. To verify this, the aforementioned electrochemical reaction was performed in the presence of other electrolytes, such as NH_4PF_6, $N(CH_3)_4Br$, or $N(CH_2CH_2CH_2CH_3)_4Br$. In the case of NH_4PF_6, the reaction yielded **1**, as one would expect in view of the poor nucleophilicity of PF_6^-. The use of the bromide electrolytes led to transparent yellow acetonitrile solutions, rather than to the insoluble complex **1**. When the solutions were left to stand, two different compounds could be identified. Thus, when $N(CH_3)_4Br$ was used, **1** and $N(CH_3)_4Br$ were identified by X-ray diffraction studies. A possible explanation for this could be the formation of $[Cd(H_2daps)Br(H_2O)]NR_4$, which reorganises when the solution is concentrated to give the final products **1** and NR_4Br, as shown in Scheme 3.

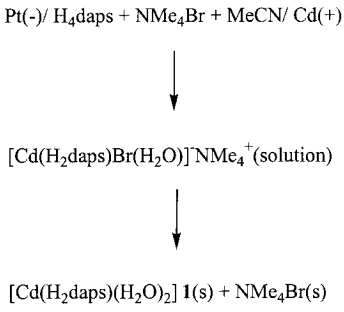

Scheme 3

Complexes **1** and **4** show very low conductivities in DMF (5.46 and 10.97 Ω^{-1} cm^2 mol^{-1}, respectively), in agreement with their nonelectrolyte natures.[20] This indicates that the chlorine ligand is coordinated to the metal in complex **4** and that it remains coordinated even after dissolution in a donor solvent. The conductivity of complex **5** in DMF (84.1 Ω^1 cm^2 mol^{-1}) is in the expected range for 1:1 electrolytes, in accordance with the proposed formulation.

X-ray Diffraction Studies

Pentagonal Bipyramidal Complexes $[Cd(H_2daps)(H_2O)_2]$ (1), $[Cd(H_2daps)(H_2O)\{(CH_3)_2CHOH\}]$ (2), $[Cd(H_3daps)Cl(CH_3OH)]\cdot 2H_2O\cdot CH_3OH$ (4), and $[Cd(H_2daps)Cl(H_2O)]N(CH_3)_4$ (5)

ORTEP views of **1**, **2**, **4**, and **5** are shown in Figures 1 to 4. Experimental details are given in Table 1 and selected bond lengths and angles are shown in Table 2.

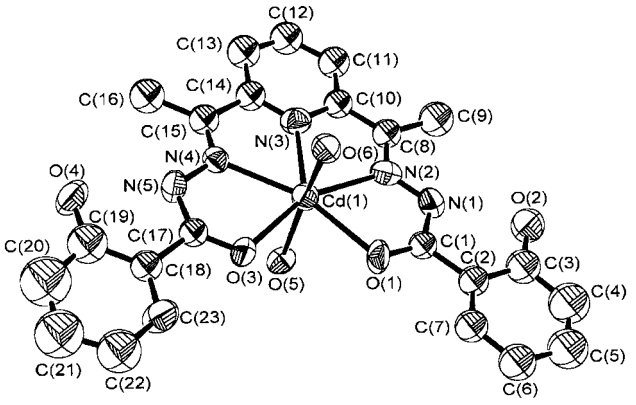

Figure 1. An ORTEP view of $[Cd(H_2daps)(H_2O)_2]$ (**1**) showing the atomic numbering scheme; ellipsoids are drawn at a 50% probability level

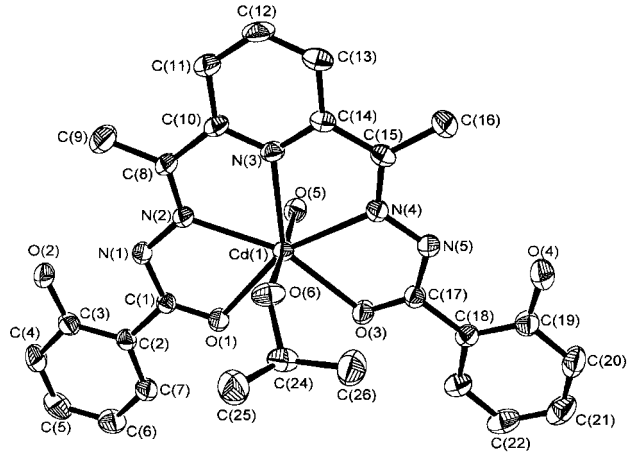

Figure 2. An ORTEP view of $[Cd(H_2daps)(H_2O)\{(CH_3)_2CHOH\}]$ (**2**) showing the atomic numbering scheme; ellipsoids are drawn at a 50% probability level

X-ray quality crystals of complex **4** proved to be extremely unstable under X-ray irradiation and we were unable to prevent them from decomposing (standard decay = 38%). This is the reason for the rather poor resolution of the structure. Therefore, only the general structural aspects will be discussed.

All the compounds are noncentrosymmetric, with the exception of **5**, which has a twofold crystallographic axis and hence the two halves of the hydrazone ligand are symmetry related. Complexes **1**, **2**, and **4** are neutral, while **5**, containing the $[Cd(H_2daps)Cl(H_2O)]^-$ anion, is ionic. This is remarkable, as all the previously reported ionic complexes

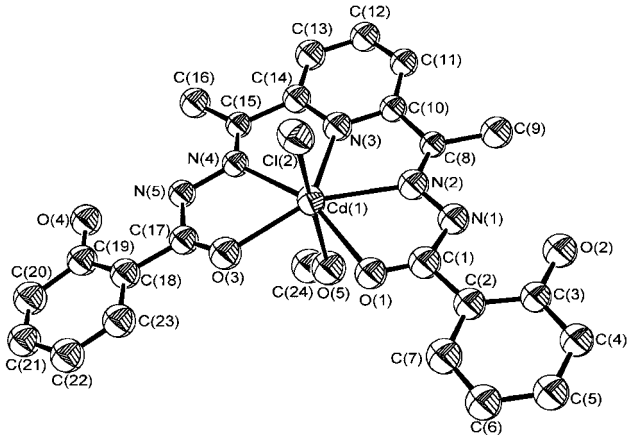

Figure 3. Molecular structure of $[Cd(H_3daps)Cl(CH_3OH)]\cdot 2H_2O\cdot CH_3OH$ (**4**) showing the atomic numbering scheme; solvent molecules are omitted for clarity; ellipsoids are drawn at a 30% probability level

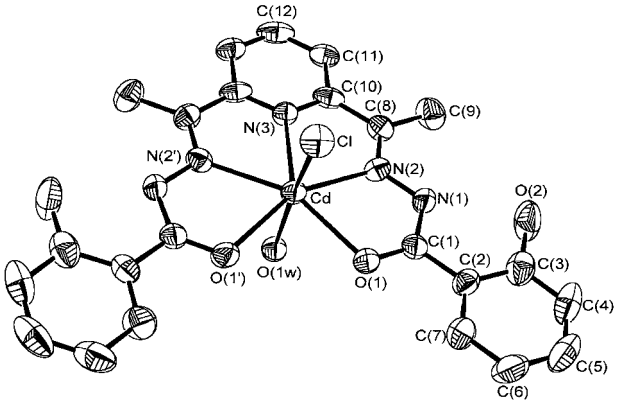

Figure 4. An ORTEP view of $[Cd(H_2daps)Cl(OH_2)]N(CH_3)_4$ (**5**) showing the complex anion; the $N(CH_3)_4^+$ cation is omitted for clarity; ellipsoids are drawn at a 50% probability level

derived from H_4daps or similar hydrazones contain a positively charged metallic fragment.

All the compounds exhibit a distorted pentagonal-bipyramidal environment around the Cd atom, with the hydrazone ligand being pentadentate. The N_3O_2 donor set of the dianionic (**1**, **2**, and **5**) or monoanionic (**4**) hydrazone occupies the equatorial plane of the bipyramid, while solvent molecules and/or chlorine atoms occupy the apical positions. All the distances around the cadmium atom are in the expected ranges for heptacoordinated cadmium,[21,22] although the interaxial and equatorial angles around the metal (Table 2) differ from the ideal values of 180° and 72°, respectively, for a pentagonal bipyramidal arrangement. Four of the five equatorial angles are smaller than the ideal value and the fifth $O_{carbonyl}-Cd-O_{carbonyl}$ angle is greater. These angles show the degree of distortion from the ideal polyhedron.

The N_3O_2 donor set is nearly planar in all cases, with the ionic complex **5** showing the least deviation from the N_3O_2 least-squares calculated plane (maximum deviation of any atom in **5**: 0.014 Å, with the cadmium atom lying 0.2251 Å below the plane).

Table 1. Crystal data and structure refinement for **1**−**5**

	1	**2**	**3**	**4**	**5**
Empirical formula	$C_{23}H_{19}N_5O_6Cd$	$C_{26}H_{29}N_5O_6Cd$	$C_{25}H_{23}N_6O_{4.25}CdCl$	$C_{25}H_{20}N_5O_8CdCl$	$C_{27}H_{33}N_6O_5CdCl$
Molecular weight	573.83	619.94	623.34	665.29	669.44
Crystal system	Tetragonal	Monoclinic	Monoclinic	Monoclinic	Orthorhombic
a (Å)	11.382(2)	10.556	11.556(3)	22.03(3)	11.7752(11)
b (Å)	11.382(2)	16.127	12.829(7)	7.531(5)	14.023(3)
c (Å)	35.874(3)	16.171	35.773(3)	36.66(3)	17.6946(8)
α (°)	90	90	90	90	90
β (°)	90	90.47	98.61(1)	97.73(8)	90
γ (°)	90	90	90	90	90
Volume (Å^3)	4647(1)	2582.1	5243(2)	6028(9)	2921.7(8)
Temperature (K)	296(1)	293(2)	296(1)	293(2)	293(2)
Space group	$P4_12_12$ (No. 92)	$P21/n$ (No. 14)	$C2/c$ (No. 15)	$C2/c$ (No. 15)	$Pnnm$
Z	8	4	8	8	4
Absorption coeff. (cm^{-1})	79.63	8.97	79.75	70.73	8.86
Reflections collected	2630	36217	5962	2211	3102
Independent reflections	2630	4306 [*R*(int) = 0.048]	5670 [*R*(int) = 0.039]	2107 [*R*(int) = 0.050]	3102
Final *R* indices [$I > 2\sigma(I)$] *R*1	0.0542	0.0291	0.0574	0.0994	0.0461
R indices (all data)	0.1120	0.0433	0.1477	0.2050	0.1910

Table 2. Selected bond lengths [Å] and angles [deg.] for [Cd(H_2daps)(H_2O)$_2$] (**1**), [Cd(H_2daps)(H_2O){$(CH_3)_2CHOH$}] (**2**), [Cd(H_3daps)Cl(CH_3OH)]·2H_2O·CH_3OH (**4**), and [Cd(H_2daps)Cl(OH_2)]-$N(CH_3)_4$ (**5**)

	1	**2**	**4**	**5**[a]
Cd(1)−O(1)	2.328(9)	2.3494(18)	2.438(17)	2.349(4)
Cd(1)−O(3)	2.346(10)	2.3334(18)	2.299(19)	–
Cd(1)−O(5)	2.382(7)	2.370(2)	2.36(2)	2.452(5)
Cd(1)−O(6)	2.362(8)	2.395(2)	–	–
Cd(1)−N(2)	2.362(10)	2.353(2)	2.39(2)	2.348(5)
Cd(1)−N(3)	2.359(9)	2.371(2)	2.43(2)	2.411(6)
Cd(1)−N(4)	2.347(10)	2.345(2)	2.42(2)	–
Cd(1)−Cl	–	–	2.559(8)	2.556(2)
O(1)−Cd(1)−O(3)	89.7(3)	89.83(6)	91.5(7)	89.98(19)
O(1)−Cd(1)−N(2)	67.7(3)	67.67(7)	64.7(8)	67.13(14)
O(3)−Cd(1)−N(4)	68.6(3)	67.79(7)	70.4(7)	–
N(2)−Cd(1)−N(3)	67.6(4)	67.36(7)	68.2(9)	66.92(10)
N(3)−Cd(1)−N(4)	66.4(4)	67.49(7)	63.7(8)	–
O(5)−Cd(1)−O(6)	164.5(3)	178.76(8)	–	–
O(5)−Cd(1)−Cl			168.7(5)	171.70(14)

[a] For **5**: O(5) = O(1w), O(3) = O(1′), and N(4) = N(2′).

In **1**, **2**, and **4**, the C−O_{phenol} distances are noticeably shorter than the ideal value of 1.36 Å, indicating some double character for this bond. This is consistent with the participation of the phenol oxygen atom in hydrogen-bonding interactions. In the case of complexes **1** and **4**, the hydrogen atoms bonded to oxygen were not included as they could not be unequivocally defined; they could not be located by difference Fourier methods and have more than one possibility for hydrogen bonding. However, the hydrogen atoms attached to oxygen could be located for **2** and **5**. Both complexes feature two types of hydrogen bond: intramolecular between the phenol oxygen and the hydrazide nitrogen atoms [O(2)···N(1) = 2.509(3) Å and O(4)···N(5) = 2.538(3) Å in **2**; O(2)···N(1) ≈ 2.516 Å in **5**], and intermolecular, involving solvent molecules. Thus, in complex **2**, the water molecule establishes two hydrogen bonds with the carbonyl oxygen atoms of another unit [O(5)···O(1′) = 2.781(3) Å and O(5)·O(3′) = 2.753(3) Å] and vice versa. The 2-propanol molecule also interacts through hydrogen bonding with a phenol oxygen atom of another unit [O(6)···O(2″) = 2.815(3) Å]. These contacts lead to shorter and longer Cd···Cd distances [Cd(1)···Cd(1′) = 5.1125(5) Å and Cd(1)···Cd(1″) = 8.981(5) Å].

In complex **5**, the water molecule of one unit establishes hydrogen bonds with the two carbonyl oxygen atoms of a neighbouring unit [O(1w)···O(1) distance ≈ 2.758 Å] and vice versa. Thus, two complex molecules interact through four hydrogen bonds, the shortest Cd···Cd distance being ca. 5.264 Å, with the structure resembling a weakly joined dimer (Figure 5).

Pentagonal Pyramidal Complex [Cd(H_3daps)Cl]·CH_3CN·0.25H_2O (3)

The X-ray crystal structure of **3** is shown in Figure 6 and selected bond lengths and angles are given in Table 3.

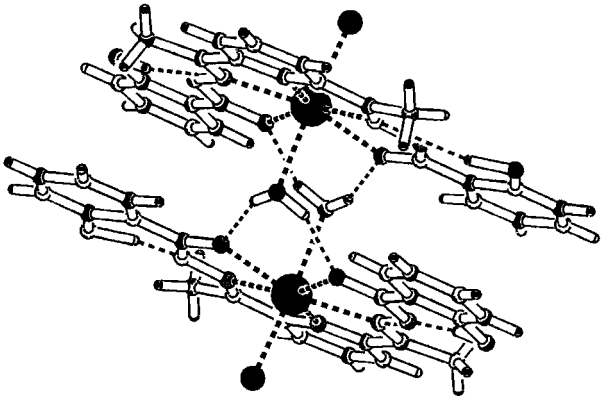

Figure 5. Part of the unit cell of **5** showing the association between two [Cd(H_2daps)Cl(H_2O)]$^-$ anions through hydrogen bonding

The crystal structure consists of discrete [Cd(H_3daps)Cl] molecules with acetonitrile and disordered water in the unit

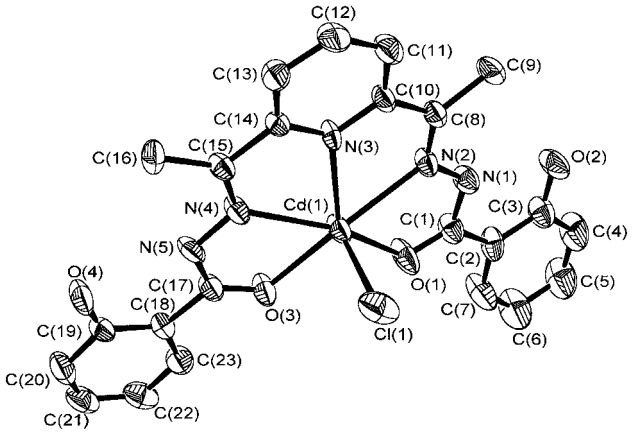

Figure 6. Molecular structure of $[Cd(H_3daps)Cl]\cdot CH_3CN\cdot 0.25H_2O$ (**3**); solvent molecules are omitted for clarity; ellipsoids are drawn at a 50% probability level

Table 3. Selected bond lengths [Å] and angles [deg] for $[Cd(H_3daps)Cl]\cdot CH_3CN\cdot 0.25H_2O$ (**3**)

Cd(1)−Cl(1)	2.497(3)	O(3)−Cd(1)−N(2)	152.0(2)
Cd(1)−O(1)	2.344(5)	O(3)−Cd(1)−N(3)	131.6(2)
Cd(1)−O(3)	2.374(4)	O(3)−Cd(1)−N(4)	68.0(2)
Cd(1)−N(2)	2.392(5)	N(2)−Cd(1)−N(3)	65.3(2)
Cd(1)−N(3)	2.403(6)	N(2)−Cd(1)−N(4)	129.3(2)
Cd(1)−N(4)	2.370(6)	N(3)−Cd(1)−N(4)	65.1(2)
		Cl(1)−Cd(1)−O(1)	95.6(2)
O(1)−Cd(1)−O(3)	89.2(2)	Cl(1)−Cd(1)−O(3)	97.1(1)
O(1)−Cd(1)−N(2)	67.9(2)	Cl(1)−Cd(1)−N(2)	100.8(2)
O(1)−Cd(1)−N(3)	132.4(2)	Cl(1)−Cd(1)−N(3)	101.1(1)
O(1)−Cd(1)−N(4)	154.3(2)	Cl(1)−Cd(1)−N(4)	98.7(2)

cell, these having occupancies of 0.25. The terminal carbon atom of the acetonitrile molecule is disordered over two sites with occupancies of 0.65 and 0.35.

The metal atom is in a hexacoordinate environment $[CdN_3O_2Cl]$. The seventh position is unoccupied, despite of the presence of acetonitrile in the unit cell. The Cd···N(6) distance, 2.739(10) Å, is too long to be considered a true coordinated bond and may be viewed as a secondary intramolecular interaction. Thus, the environment of the metal atom can be described as distorted pentagonal pyramidal, with the chlorine atom at the apex and the base formed by the N_3O_2 donor set of the pentadentate monoanionic $[H_3daps]^-$ ligand. The distortion from ideal geometry is clearly shown by the angles between chlorine, cadmium, and the donor set of the hydrazone ligand (Table 3). Moreover, four of the five angles subtended at Cd by adjacent equatorial atoms are slightly smaller than the value for an ideal pentagonal pyramidal arrangement, ranging from 65.1(2)° to 68.0(2)°, while the fifth angle, O(1)−Cd−O(3), is 89.2(2)°. The distortion of the polyhedron is further reinforced by the deviation of the donor set of the hydrazone ligand and the Cd atom from planarity. The maximum deviation from the N_3O_2 least-squares calculated plane is 0.044 Å, with the Cd atom lying 0.348 Å above this plane, giving rise to an "umbrella-like" distortion.

All the cadmium−donor distances are similar to those found in **1**−**3** and **5**, and the $C-O_{phenol}$ bond lengths (ca. 1.32 Å) also suggest hydrogen-bonding interactions. The short distances between phenol oxygen atoms of adjacent units [O(2)O(2′) = 2.446(9) Å and O(4)···O(4") = 2.505(9) Å] and the disposition of the molecules in the unit cell seem to indicate that every molecule establishes two intermolecular hydrogen bonds with neighbouring units. Thus, the unit cell shows a zigzag chain disposition of the molecules, with wide channels between layers of these chains (Figure 7).

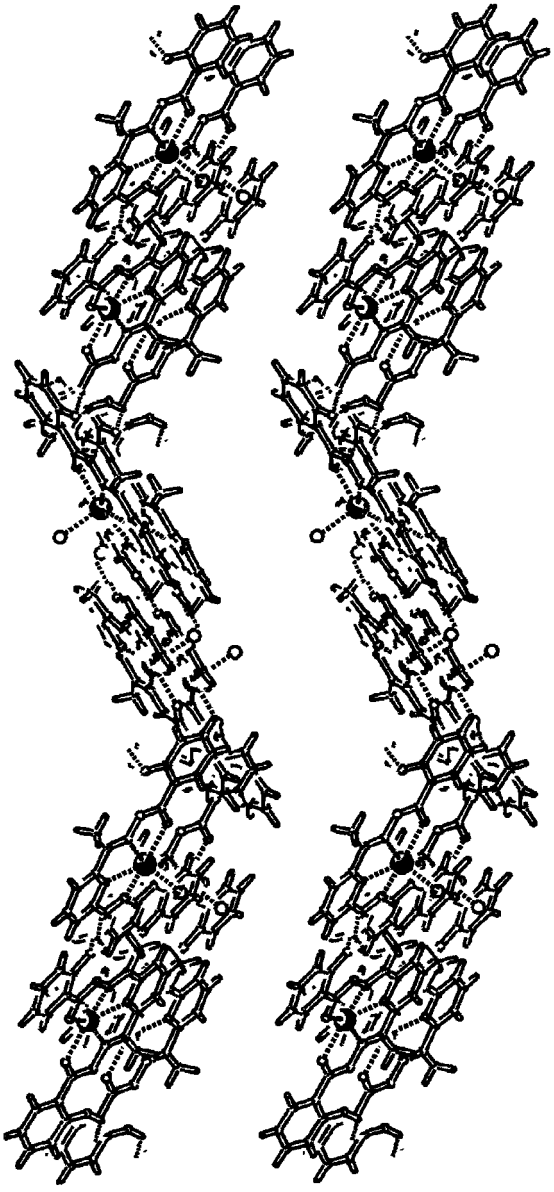

Figure 7. The unit cell of **3** showing the channels between the chains

It should be noted that the crystal structure of $[Cd(H_4daps)Cl_2]$, containing H_4daps as a neutral ligand, has been described previously.[2b] In this case, the complex has a pentagonal-bipyramidal geometry, characteristic of mononuclear compounds containing pentadentate hy-

Table 4. Comparison of bond lengths (Å) in **1**–**5** and similar related complexes

	1	**2**	**3**	**4**	**5**	**Cd(H_4daps)Cl_2** [a]
Cd–$O_{carbonyl}$	2.328(9)	2.3334(18)	2.344(5)	2.299(19)	2.349(4)	2.33(1)
	2.346(8)	2.3494(18)	2.374(4)	2.438(17)		2.35(1)
Cd–N_{imine}	2.347(10)	2.345(2)	2.370(6)	2.39(3)	2.348(5)	2.40(2)
	2.362(10)	2.353(2)	2.392(5)	2.42(2)		2.41(2)
Cd–$N_{pyridine}$	2.359(9)	2.371(2)	2.403(6)	2.43(2)	2.411(6)	2.42(2)
Cd–O_{water}	2.362(8)	2.370(2)	–	–	2.452(5)	–
	2.382(7)					
Cd–Cl	–	–	2.497(3)	2.559(8)	2.556(2)	2.565(7)
C–O_{phenol}	1.297(14)	1.343(4)	1.315(9)	1.27(3)	1.367(8)	1.36(2)
	1.319(17)	1.350(4)	1.325(9)	1.32(3)		1.36(2)
C–$O_{carbonyl}$	1.258(14)	1.267(3)	1.237(7)	1.18(3)	1.254(3)	1.20(2)
	1.273(14)	1.271(3)	1.241(7)	1.26(3)		1.27(2)
C–N_{imime}	1.283(15)	1.285(3)	1.260(8)	1.24(3)	1.309(6)	1.25(3)
	1.290(15)	1.286(3)	1.265(8)	1.28(3)		1.29(3)
O_{phenol}···$N_{hydrazine}$	2.485	2.503(3)	2.525	2.526	2.516(5)	2.67(2)
	2.494	2.538(3)	2.541	2.556		2.71(2)
Shortest Cd···Cd	5.258	5.1125(5)	8.225	8.216	5.264	

[a] See ref.[2b]

drazone ligands, as observed for **1**, **2**, **4**, and **5**. However, the geometry of **3** is quite unexpected, especially considering the presence of a possible donor molecule (acetonitrile) in the unit cell. The pentagonal pyramidal geometry is very unusual and, to the best of our knowledge, no other complexes containing hydrazone ligands have been reported with this structure. Some hydrazone complexes having the metal atom in a hexacoordinate environment have been published.[3,6,18,23–25] In all these cases, the metal atom resides in a distorted octahedral environment. On the other hand, although some examples of complexes with a pentagonal pyramidal geometry have been reported, mainly for metals of the s- or p-blocks,[26,27] to the best of our knowledge no cadmium complexes showing this type of geometry have hitherto been reported.

A comparison of the cadmium complexes described herein with [Cd(H_4daps)Cl_2] reveals some general trends (Table 4):

(i) Cadmium complexes with H_4daps contain the hydrazone ligand acting in a pentadentate manner and show a high preference for pentagonal-bipyramidal geometry.

(ii) The Cd–$O_{carbonyl}$ distances are more symmetric in those complexes in which the ligand is dianionic (**1**, **2**, **5**) or neutral {[Cd(H_4daps)Cl_2]} than in those in which the ligand is monoanionic (**3**, **4**).

(iii) The Cd–Cl distance in **3** is significantly shorter than those in **4**, **5**, and [Cd(H_4daps)Cl_2]. This reflects the lower coordination number for **3**.

(iv) The Cd–O_{water} distances in **1** and **2** are markedly shorter than those in **4**. This may be attributed to the stronger "*trans* effect" of the chlorine ligand. This pattern was also observed in previously reported pentagonal-bipyramidal cadmium complexes.[22]

(v) The C–O_{phenol} distances seem to reflect the deprotonation of the ligand in neutral complexes. Thus, complexes **1** to **4** show C–O_{phenol} distances that are shorter than the ideal value. However, anionic complexes do not seem to follow this pattern, as the C–O_{phenol} distance in **5** [1.367(8) Å] is typical of a single C–O bond.

(vi) A comparison of complexes **1** to **5** shows that when cadmium is coordinated by water, the shortest Cd···Cd distances have a lower value (ca. 5.26 Å for **1** and **5**; 5.11 Å for **2**) than in the remaining cases (ca. 8.2 Å for **3** and **4**).

IR and ^{1}H NMR Spectroscopy and Mass Spectrometry

The IR spectra of **1**, **4**, and **5** show a negative shift of the amide I and amide II bands, by 39–52 cm^{-1} and 59–64 cm^{-1}, respectively, compared with the values found in free H_4daps (see Exp. Sect.). This behaviour is indicative of the coordination of the ligand to the metal through the oxygen atoms of both carbonyl groups in all cases.[2] The spectra also show the absence of the ν(N–H) band for **1** and **5**, which appears at 3208 cm^{-1} in the free ligand. This situation is in accordance with the dianionic nature of the ligand in these cases. However, the IR spectrum of complex **4** features bands at 3200 and 3060 cm^{-1}, indicating that the hydrazide nitrogen atoms are not fully deprotonated.

The ^{1}H NMR spectra of **1** and **5** in [D_6]DMSO (see Exp. Sect.) show the absence of a resonance due to the NH protons, which appears at δ = 11.8 in the free ligand.[2] This is in agreement with the bis-deprotonation of the ligand. In the case of complex **4**, the resonance of the NH group is not observed either, in spite of the monoanionic nature of the ligand. This can be attributed to the fact that the hydrogen atom is in rapid exchange between the two nitrogen atoms. The signal due to the OH groups is strongly downfield shifted in each case (from δ = 11.51 to ca. δ = 14.5). This behaviour has been observed previously and was attributed to the participation of the OH groups in strong hydrogen bonds.[2b]

The ES mass spectra of **1**, **4**, and **5** are consistent with the isotopic simulated pattern, with peaks of maximum intensity at *m*/*z* = 544 attributable to the fragment $[CdL]^+$,

confirming the coordination of the ligand to the metal. In addition, it was possible to observe peaks at $m/z = 579$ for **4** and **5**, corresponding to the binding of the chlorine to the cadmium atom.

Conclusion

Electrolysis of a suspension of H_4daps in acetonitrile using a cadmium anode yields $[Cd(H_2daps)(H_2O)_2]$ (**1**) as the major product. Recrystallisation of this complex from 2-propanol gives $[Cd(H_2daps)(H_2O)\{(CH_3)_2CHOH\}]$ (**2**). Concomitant reduction of the perchlorate electrolyte during the electrochemical process produces $[Cd(H_3daps)Cl]\cdot CH_3CN\cdot 0.25H_2O$ (**3**) as a by-product. $[Cd(H_3daps)Cl(CH_3OH)]\cdot 2H_2O\cdot CH_3OH$ (**4**) and $[Cd(H_2daps)Cl(H_2O)]N(CH_3)_4$ (**5**) show that dichloromethane and tetramethylammonium chloride can also act as sources of chlorine. The five compounds are all monomers, but have different geometries. Complexes **1**, **2**, **4**, and **5** have pentagonal-bipyramidal environments, but **3** is a pentagonal-pyramidal complex and is, to the best of our knowledge, the first characterised example of an H_4daps metal complex showing this type of geometry. Therefore, this work further emphasises the variety of molecular structures that hydrazone ligands can produce. Moreover, the ability of H_4daps to behave as an anionic ligand has been demonstrated: monoanionic and dianionic forms are found in different complexes containing the same metal atom.

Experimental Section

General Remarks: Elemental analyses (C, H N) were performed on a Carlo Erba EA 1108 analyser. NMR spectra were recorded on a Bruker WM-250 spectrometer with samples in $[D_6]$DMSO solution. Infrared spectra were recorded from samples in KBr pellets on a Bio-Rad FTS 135 spectrophotometer in the range 4000−600 cm^{-1}. Electrospray mass spectra were obtained on a Hewlett−Packard LC/MS spectrometer, using methanol as solvent. Conductivities of 10^{-3} M solutions in DMF were measured using a Crison microCM 2200 conductivimeter.

Syntheses: All solvents, 2,6-diacetylpyridine, and salicyl hydrazide are commercially available and were used without further purification. Cadmium (Ega Chemie) was used in the form of ca. 2 × 2 cm^2 plates.

2,6-Bis(1-salicyloylhydrazonoethyl)pyridine (H_4daps) was synthesized as described previously[2a] and was satisfactorily characterised by elemental analysis, IR and ^{1}H NMR spectroscopy.

Syntheses of the Complexes: $[Cd(H_2daps)(H_2O)_2]$ (**1**) was obtained by electrochemical synthesis. A suspension of H_4daps (0.108 g, 2.5 × 10^{-4} mol) in acetonitrile (80 mL) containing tetraethylammonium perchlorate (ca. 10 mg) as a current carrier was electrolysed at 10 mA, 12 V for 1 h 20 min, using a platinum wire as the cathode and a cadmium plate as the anode. The cell system can be represented as Pt(−)/MeCN + H_4daps/Cd(+). At the end of the experiment, the insoluble yellow powder deposited was collected by filtration, washed with diethyl ether, and dried in air. Recrystallisation of the compound from CH_3CN and 2-propanol yielded crystals of $[Cd(H_2daps)(H_2O)_2]$ (**1**) and $[Cd(H_2daps)(H_2O)\{(CH_3)_2CHOH\}]$ (**2**), respectively, which were both suitable for X-ray diffraction studies.

$Cd(H_2daps)(H_2O)_2$: Yield: 85%. $C_{23}H_{23}N_5O_6Cd$ (577.4): calcd. C 47.8, H 4.0, N 12.1; found C 48.0, H 3.9, N 12.1. ES-MS (amu): $m/z = 544$ $[ML]^+$. Λ (Ω^{-1} cm^2 mol^{-1}) = 5.46. IR (KBr): $\tilde{\nu}$ = 1617 $\nu(am_1)$, 1530 $\nu(am_2)$, 3400 cm^{-1} ν(OH). ^{1}H NMR (250 MHz, $[D_6]$DMSO): δ = 14.65 (s, 2 H, OH), 6.83−8.15 (m, 11 H, H_{arom}), 2.45 (s, 6 H, CH_3).

Slow evaporation of the solvent from the mother liquor obtained following the electrochemical experiment led to the isolation of yellow crystals of $[Cd(H_3daps)Cl]CH_3CN\cdot 0.25H_2O$ (**3**), which were also suitable for X-ray diffraction analysis.

Slow recrystallisation of **1**, by diffusion of diethyl ether into a solution in dichloromethane/methanol, yielded crystals of $[Cd(H_3daps)Cl(CH_3OH)]\cdot 2H_2O\cdot CH_3OH$ (**4**), which loses solvent to generate $Cd(H_3daps)Cl(H_2O)_2$. Yield: 42%. $C_{23}H_{24}N_5O_6ClCd$ (613.9): calcd. C 44.9, H 3.9, N 11.4; found C 44.9, H 3.3, N 11.2. − ES-MS (amu): m/z = 544 $[ML]^+$, 579 $[MLCl]^+$. Λ (Ω^{-1} cm^2 mol^{-1}) = 10.97. IR (KBr): $\tilde{\nu}$ = 1595 $\nu(am_1)$, 1530 $\nu(am_2)$, 3417 cm^{-1} ν(OH). ^{1}H NMR (250 MHz, $[D_6]$DMSO): δ = 14.45 (s, 2 H, OH), 6.60−8.10 (m, 11 H, H_{arom}), 2.47 (s, 6 H, CH_3).

Compound **1** was also obtained when $[N(CH_2CH_3)_4]PF_6$, NH_4PF_6, or NH_4Cl was used as the supporting electrolyte instead of $[N(CH_2CH_3)_4]ClO_4$.

$[Cd(H_2daps)Cl(H_2O)]N(CH_3)_4$ (**5**) was obtained by two different methods:

Method A. Electrochemical Method: A suspension of H_4daps (0.108 g, 2.5 × 10^{-4} mol) in acetonitrile containing tetramethylammonium chloride (27.4 mg) was electrolysed at 10 mA, 9 V for 1 h 20 min, using a platinum wire as the cathode and a cadmium plate as the anode. Slow evaporation of the solvent from the resultant yellow solution yielded crystals of $[Cd(H_2daps)Cl(H_2O)]N(CH_3)_4$ (**5**), which proved suitable for X-ray diffraction studies. Yield: 76%. $C_{27}H_{33}N_6O_5ClCd$ (669.44): calcd. C 48.4, H 4.9, N 12.5; found C 47.2, H 4.0, N 12.1. ES-MS (amu): m/z = 544 $[ML]^+$, 579 $[MLCl]^+$. − Λ (Ω^{-1} cm^2 mol^{-1}) = 84.1. IR (KBr): $\tilde{\nu}$ = 1598 $\nu(am_1)$, 1530 $\nu(am_2)$, 3321 cm^{-1} ν(OH). ^{1}H NMR (250 MHz, $[D_6]$DMSO): δ = 14.63 (s, 2 H, OH), 6.78−8.20 (m, 11 H, H_{arom}), 2.45 (s, 6 H, CH_3), 3.36 [s, 12 H, $N(CH_3)_4$].

Method B. Chemical Method: Tetramethylammonium chloride (0.025 g, 2.3 × 10^{-4} mol) was added to a suspension of H_4daps (0.1 g, 2.3 × 10^{-4} mol) in acetonitrile. The suspension was stirred at room temperature until a yellow solution was obtained (ca. 1 h). The volume of the solution was reduced to ca. 10 mL, whereupon a yellow solid precipitated. This solid was collected by filtration, washed with diethyl ether, and dried in air.

X-ray Crystallographic Study: Crystal data and details of the refinement are given in Table 1.

$[Cd(H_2daps)(H_2O)_2]$ (1), $[Cd(H_3daps)Cl]\cdot'CH_3CN\cdot 0.25H_2O$ (3), and $[Cd(H_3daps)Cl(CH_3OH)]\cdot 2H_2O\cdot CH_3OH$ (4): Orange plate, orange prismatic, and yellow tabular crystals of **1**, **3**, and **4**, respectively, suitable for single-crystal X-ray studies, were obtained as described previously. The crystals were mounted on a glass fibre. Data were collected at 296 K on a Rigaku AFC5R diffractometer, employing graphite-monochromated Cu-K_α radiation (λ = 1.54178 Å) and a rotating anode generator. The structures were solved by and expanded using Fourier techniques.[28] An empirical absorption cor-

rection based on azimuthal scans of several reflections was applied for **1** and **3**. The data were corrected for Lorentz and polarisation effects. Some non-hydrogen atoms were refined anisotropically, while the rest were refined isotropically. The data for **1** and **4** were of rather low quality, hence only the Cd, N and O atoms were refined anisotropically in order to maintain a reasonable data-to-parameter ratio. Hydrogen atoms bonded to carbon were included in the structure factor calculation in idealised positions, but were not refined. Hydrogens attached to oxygen could not be located in the Fourier map and were not included (**1** and **4**) or were included with occupancies of 0.5 and refined isotropically (**3**), with the bond lengths restrained to 0.82 Å. All calculations were performed using the teXsan crystallographic software package from Molecular Structure Corporation.[29]

[Cd(H_2daps)(H_2O){(CH_3)$_2$CHOH}] (2) and [Cd(H_2daps)Cl(H_2O)]-N(CH_3)$_4$ (5): Yellow block and plate crystals of **2** and **5**, respectively, were obtained as detailed above. Data were collected using a CAD4 diffractometer or a Rigaku RAXIS diffractometer at 293(2) K employing Mo-K_α radiation (λ = 0.71073 Å). An absorption correction based on φ-scans was applied for **5**. Non-hydrogen atoms were refined anisotropically. Hydrogens attached to carbon atoms were included in idealised positions, but were not refined. Hydrogens bonded to oxygen atoms were located in the Fourier map and were refined isotropically. Data processing and computation were carried out using the SHELX-97 (**2** and **5**) program package[28] and the teXsan crystallographic software package (**2**).[29]

Crystallographic data (excluding structure factors) for the structures reported in this paper have been deposited with the Cambridge Crystallographic Data Centre as supplementary publication nos. CCDC-159081 (**1**), -159082 (**2**, -15983 (**3**), -15984 (**4**), -15985 (**5**). Copies of the data can be obtained free of charge on application to the CCDC, 12 Union Road, Cambridge CB2 1EZ, U.K. [Fax: (internat.) +44-(0)1223/336-033; E-mail: deposit@ccdc.cam.ac.uk].

Acknowledgments

The authors would like to thank the Xunta de Galicia (Spain) (grant nos. PGIDT99PXI20903B and PGIDT00PXI20910PR) and the Ministerio de Educación y Ciencia (Spain) (grant PB98-0600) for financial support.

[1] D. Wester, G. J. Palenik, *Inorg. Chem.* **1976**, *15*, 755−761.
[2] [2a] C. Pelizzi, G. Pelizzi, *J. Chem. Soc., Dalton Trans.* **1980**, 1970−1973. [2b] C. Pelizzi, G. Pelizzi, F. Vitali, *J. Chem. Soc., Dalton Trans.* **1987**, 177−181. [2c] C. Carini, G. Pelizzi, P. Tarasconi, C. Pelizzi, K. C. Molloy, P. C. Waterfield, *J. Chem. Soc., Dalton Trans.* **1989**, 289−291. [2d] A. Bonardi, C. Carini, C. Merlo, C. Pelizzi, G. Pelizzi, P. Tarasconi, F. Vitali, F. Cavatorta, *J. Chem. Soc., Dalton Trans.* **1990**, 2771−2777.
[3] E. C. Constable, in *Comprehensive Supramolecular Chemistry* (Eds.: J. L. Atwood, J. E. D. Davies, D. D. McNicol, F. Vögtle, J. P. Sauvage, M. W. Hosseini), Pergamon, Oxford, **1996**, vol. 9, p. 213−252.
[4] K. Andjelkovic, I. Ivanovic, B. Prelesnik, V. M. Leovac, D. Poketi, *Polyhedron* **1996**, *15*, 4361−4366.
[5] S. Abram, C. Maichle-Mössmer, U. Abram, *Polyhedron* **1998**, *17*, 131−143.
[6] G. Paolucci, S. Stelluto, S. Sitran, D. Ajo, F. Benetollo, A. Polo, G. Bombieri, *Inorg. Chim. Acta* **1992**, *193*, 57−75.
[7] M. Carcelli, P. Mazza, C. Pelizzi, G. Pelizzi, F. Zani, *J. Inorg. Biochem.* **1995**, *57*, 43−62 and references therein.
[8] A. Bacchi, A. Bonardi, M. Carcelli, P. Mazza, P. Pelagatti, C. Pelizzi, G. Pelizzi, C. Solinas, F. Zani, *J. Inorg. Biochem.* **1998**, *69*, 101−112.
[9] A. R. Todeschini, A. L. P. De Miranda, K. C. M. Da Silva, S. C. Parrini, E. J. Barreiro, *Eur. J. Med. Chem.* **1998**, *33*, 189−199.
[10] O. Kahn, *Angew. Chem.* **1985**, *97*, 837−853; *Angew. Chem. Int. Ed. Engl.* **1985**, *24*, 834−850.
[11] J. M. Williams, M. A. Beno, K. D. Carlson, U. Geiser, H. C. J. Kao, A. M. Kini, L. C. Porter, A. J. Schultz, R. J. Thorn, H. H. Wang, M.-H. Wanyho, M. Evain, *Acc. Chem. Res.* **1988**, *21*, 1−7.
[12] S. Rao, D. D. Mishra, R. V. Maurya, N. Nageswara, *Polyhedron* **1997**, *16*, 1825−1829.
[13] M. Carcelli, S. Ianelli, P. Pelagatti, G. Pelizzi, *Inorg. Chim. Acta* **1999**, *292*, 121−126.
[14] C. Pelizzi, G. Pelizzi, S. Porretta, F. Vitali, *Acta Crystallogr., Sect. C* **1986**, *C42*, 1131−1133.
[15] G. F. de Sousa, C. A. L. Filgueiras, A. Abras, S. S. Al-Juaid, P. B. Hitchcock, J. F. Nixon, *Inorg. Chim. Acta* **1994**, *218*, 139−142.
[16] K. Andjelkovic, I. Ivanovic, S. R. Niketic, B. Prelesnik, V. M. Leovac, *Polyhedron* **1997**, *16*, 4221−4228.
[17] A. Bonardi, C. Merlo, C. Pelizzi, G. Pelizzi, P. Tarasconi, F. Cavatorta, *J. Chem. Soc., Dalton Trans.* **1991**, 1063−1069.
[18] M. R. Bermejo, M. Fondo, A. M. González, O. L. Hoyos, A. Sousa, C. A. McAuliffe, W. Hussein, R. G. Pritchard, V. M. Novotorsev, *J. Chem. Soc., Dalton Trans.* **1999**, 2211−2217.
[19] J. A. Castro, J. Romero, J. A. García-Vázquez, A. Macías, A. Sousa, U. Englert, *Acta Crystallogr., Sect. C* **1994**, *50*, 369−370.
[20] W. J. Geary, *Coord. Chem. Rev.* **1971**, *7*, 81−122.
[21] [21a] H. Keypour, S. Salehzadeh, R. G. Pritchard, R. V. Parish, *Polyhedron* **2000**, *19*, 1633−1637. [21b] P. Arranz-Mascarós, R. López-Garzón, M. D. Gutierrez-Valero, M. L. Godino-Salido, J. M. Moreno, *Inorg. Chim. Acta* **2000**, *304*, 137−143.
[22] H. C. López-Sandoval, N. Barba-Behrens, S. Bernès, N. Farfán-García, H. Höpfl, *J. Chem. Soc., Dalton Trans.* **1997**, 3415−3420.
[23] [23a] C. Lorenzini, C. Pelizzi, G. Pelizzi, G. Predieri, *J. Chem. Soc., Dalton Trans.* **1983**, 2155−2158. [23b] S. Ianelli, G. Minardi, C. Pelizzi, G. Pelizzi, L. Reverberi, C. Solinas, P. Tarasconi, *J. Chem. Soc., Dalton Trans.* **1991**, 2113−2120. [23c] A. Bonardi, S. Ianelli, C. Pelizzi, C. Solinas, *Inorg. Chim. Acta* **1995**, *232*, 211−216.
[24] A. Bino, N. Cohen, *Inorg. Chim. Acta* **1993**, *210*, 11−16.
[25] M. R. Bermejo, A. Sousa, M. Fondo, A. M. González, O. L. Hoyos, R. Pedrido, M. A. Maestro, J. Mahia, *Z. Anorg. Allg. Chem.* **2000**, *626*, 506−513.
[26] [26a] C. A. Bayse, M. Couty, M. B. Hall, *J. Am. Chem. Soc.* **1996**, *118*, 8916−8919. [26b] J.-Y. Piquemal, H. Sabine, J.-M. Bregeault, *Angew. Chem. Int. Ed.* **1998**, *37*, 1146−1149.
[27] [27a] V. Venkatachalam, K. Ramalingam, U. Casellato, R. Graziani, *Polyhedron* **1997**, *16*, 1211−1221. [27b] J. D. Zubkowski, T. Hall, E. J. Valente, D. L. Perry, L. A. Feliu, J. Garmon, *J. Chem. Crystallogr.* **1997**, *27*, 251−255. [27c] H. Bock, R. Dienelt, C. Nather, Z. Havlas, *Chem. Ber. Recueil* **1997**, *130*, 1533−1537. [27d] M. Yamami, H. Furutachi, T. Yokoyama, H. Okawa, *Inorg. Chem.* **1998**, *37*, 6832−6838.
[28] G. M. Sheldrick, *SHELX-97: Programs for Crystal Structure Analysis*, Institut für Anorganische Chemie der Universität, Göttingen, Germany, **1998**.
[29] teXsan Structure Analysis Package, Molecular Structure Corp., The Woodlands, TX, **1985**.

Received June 25, 2001
[I01234]

Rhodium(I), Palladium(II), and Platinum(II) Complexes Containing New Mixed Phosphane−Phosphite Ligands − Effect of the Catalytic System Stability on the Enantioselective Hydroformylation of Styrene

Carmela G. Arena,[a] Felice Faraone,*[a] Claudia Graiff,[b] and Antonio Tiripicchio[b]

Keywords: Rhodium / Palladium / Platinum / Chirality / P ligands / Hydroformylation

The new mixed phosphane–phosphite ligands **1** and **2**, derived from 3,3′-di-*tert*-butyl-2,2′-dihydroxy-5,5′-dimethoxybiphenyl and (*S*)-binaphthol, respectively, reacted with $[Rh(COD)(THF)_2]CF_3SO_3$ to give the compounds $[Rh(COD)(\mathbf{1})]CF_3SO_3$ and $[Rh(COD)(\mathbf{2})]CF_3SO_3$ in which the ligands **1** and (*S*)-**2** are chelated to the rhodium centre. The reaction with $[Rh(CO)_2Cl]_2$ gave two different products, $[Rh(CO)_2(L)Cl]$ and [Rh(CO)(L)Cl] [L = **1** and (*S*)-**2**], containing L as a chelate. On the basis of the IR and NMR spectroscopic data, the proposed structure of the pentacoordinate species is a trigonal bipyramide in which the phosphane–phosphite ligand assumes an equatorial-axial coordination. The reactions of **1** and **2** with $[Pd(C_6H_5CN)_2Cl_2]$ and $[Pt(COD)I_2]$ gave the corresponding compounds $[Pd(L)Cl_2]$ and $[Pt(L)I_2]$ in which the ligands are chelated to the metal centre. The crystal structure of the chloroform solvate of $[Pd(L)Cl_2]$ was fully characterised by an X-ray study. The chiral ligands (*S*)-**2** and (*S*)-**3** [derived from the *ortho*-bis(trimethylsilyl)-substituted (*S*)-binaphthol] were tested in the hydroformylation of styrene. The results obtained were discussed in light of the catalytic system stability.

Introduction

In the last twenty years great efforts have been made in the design of chiral ligands due to their role in enantioselective catalysis.[1] Attempts have been made to correlate structural and electronic characteristics of the coordinated chiral ligands with catalytic regio- and enantioselectivity. The structural features of the coordinated ligands, viz. the geometry, rigidity, asymmetry, natural bite angle, presence of sterically hindered groups, type of chirality and distance of the chiral centre from the metal centre have been considered to be factors determining the asymmetric induction.[2] However, in spite of the number of works produced, the crucial factors in designing ligands able to induce high enantioselectivity are not clear. As concerns the electronic characteristics of bidentate ligands, the presence of donor atoms with different properties seems to afford an advantageous effect on the regio- and enantioselectivity of the catalytic process. For example, Takaya et al.[3] have reported excellent chemo- and regioselectivities in the rhodium(I)-catalysed hydroformylation of vinylarenes using the phosphane−phosphito mixed chiral ligand binaphos. Some of us,[4] using (R_a,S_C)-quinaphos, a phosphane−phosphoramidite ligand derived from quinoline, in the rhodium(I)-catalysed hydroformylation of styrene, obtained the branched aldehyde with 74% *ee* in the (*S*) form. Using the same ligand, in the (R_a,R_C) configuration, in the rhodium(I)-catalysed enantioselective hydrogenation of dimethyl itaconate and methyl 2-acetamidoacrylate the products have been obtained with a conversion higher than 99% and 98.8 and 97.8% of *ee*, respectively.

Recently we reported[5] on the synthesis of the new phosphane−phosphite ligands **1**−**3** and on their applications in the Pd-catalysed enantioselective allylic alkylation of 1,3-diphenyl-2-propen-1-yl acetate by dimethyl malonate. Using the complexes $[Pd(\eta^3\text{-}C_3H_5)(\mathbf{2})]CF_3SO_3$ and $[Pd(\eta^3\text{-}C_3H_5)(\mathbf{3})]CF_3SO_3$ as catalyst precursors, the allylic substitution product was obtained with up to 71% *ee*.

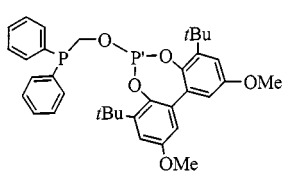

1

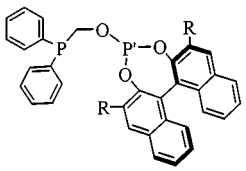

R = H (*S*)-**2**
R = $SiMe_3$ (*S*)-**3**

Here we describe the synthesis of rhodium(I), palladium(II) and platinum(II) complexes containing the ligands **1** and (*S*)-**2**, together with the X-ray structure of the compound $[Pd(\mathbf{1})Cl_2]$. The results obtained in the hydroformyl-

[a] Dipartimento di Chimica Inorganica, Chimica Analitica e Chimica Fisica, Università di Messina,
Salita Sperone, 31 Vill. S. Agata, 98166 Messina, Italy
Fax: (internat.) + 39-090/393756
E-mail: faraone@chem.unime.it
[b] Dipartimento di Chimica Generale ed Inorganica, Chimica Analitica, Chimica Fisica, Università di Parma, Centro di Studio per la Strutturistica Diffrattometrica del CNR,
Parco Area delle Scienze 17A, 43100 Parma, Italy

ation of styrene using ligands (*S*)-**2** and (*S*)-**3** are also briefly reported. This study stems from our interest in developing the synthesis of d^8-metal complexes able to act as efficient catalyst precursors in homogeneous catalysis.

Results and Discussion

As previously reported,[5] the ligands **1** and (*S*)-**2** have been easily prepared by treating (hydroxymethyl)diphenylphosphane (Ph_2PCH_2OH)[6] with 1 equiv. of 4,8-di-*tert*-butyl-6-chloro-2,10-dimethoxy-5,7-dioxa-6-phosphadibenzo[*a*,*c*]cycloheptene and (*S*)-4-chloro-3,5-dioxa-4-phosphacyclohepta[2,1-*a*:3,4-*a*′]dinaphthalene, respectively, in the presence of NEt_3 in toluene at 0 °C. They were obtained as white solids and are air-sensitive in both the solid state and in solution. The ligand (*S*)-**3** was used only in the hydroformylation.

Rhodium(I) Complexes

The addition of an equimolar THF solution of **1** or (*S*)-**2** to a solution of $[Rh(COD)(THF)_2]CF_3SO_3$ {prepared in situ by treating $[Rh(COD)Cl]_2$ in THF solution with $AgCF_3SO_3$ in a 1:2 molar ratio and filtration of AgCl precipitate} affords a yellow solution. Addition of hexane leads to the compounds $[Rh(COD)(\mathbf{1})]CF_3SO_3$ (**4**) and $[Rh(COD)(\mathbf{2})]CF_3SO_3$ (**5**). They are yellow solids that are soluble in chlorinated solvents, acetone, benzene and methanol; conductivity measurements performed on methanol solutions of **4** or **5** ($5\cdot10^{-4}$ to 10^{-3} M) are in accordance with their formulation as 1:1 electrolytes. As expected, the $^{31}P\{^1H\}$ NMR spectrum of **4** (C_6D_6 solution) shows two doublets of doublets at δ = 162.29 [J(RhP′) = 256.0 Hz; J(PP′) = 37.0 Hz] and δ = 63.89 [J_{RhP} = 148.0 Hz; J(PP′) = 37.0 Hz]. Analogously, compound **5** exhibits two doublets of doublets at δ = 167.0 [J(RhP′) = 260.0 Hz; J(PP′) = 41.3 Hz] and δ = 64.77 [J_{RhP} = 149.0 Hz; J(PP′) = 41.3 Hz]. The signals at higher frequencies are due to the phosphite moiety.[3] Of interest is that the phosphorus−phosphorus coupling constant appears in the $^{31}P\{^1H\}$ NMR spectra of **4** and **5**, but was not observed in the free ligands **1** and (*S*)-**2**. In the complexes containing **1** and **2**, the rigidity of the five-membered ring formed by chelation of the ligand to the rhodium centre promotes the coupling between the phosphorus atoms that are now only separated by the metal atom.

The slow addition of a hexane solution of the ligand **1** to a solution of $[Rh(CO)_2Cl]_2$ in the same solvent, in a 1:2 molar ratio, affords a yellow precipitate; its $^{31}P\{^1H\}$ NMR spectrum in $CDCl_3$ solution shows two signals as doublets of doublets of different intensity, centred at δ = 62.25 [J(RhP′) = 195 Hz, J(PP′) = 53.1 Hz] and δ = 84.5 [J_{RhP} = 133.5 Hz, J(PP′) = 49.1 Hz] for the phosphane group and two signals as doublets of doublets, centred at δ = 163.76 [J(RhP′) = 266.7 Hz, $J_{P'P}$ = 49.1 Hz] and 167.97 [J(RhP′) = 325.9 Hz, $J_{P'P}$ = 53.1 Hz] for the phosphite moiety. The IR spectrum of the solid in Nujol mull exhibits in the CO stretching region bands at 2001, 2008 and 2056 cm^{-1}. These spectroscopic data support the presence, in the crude product, of both the five-coordinated $[Rh(CO)_2(\mathbf{1})Cl]$ (**6**) and tetra-coordinated $[Rh(CO)(\mathbf{1})Cl]$ (**7**) species, containing ligand **1** as the chelate. When CO was bubbled for 10 min into a benzene solution of the yellow crude product, the $^{31}P\{^1H\}$ NMR spectrum only showed the signals centred at δ = 62.25 and 167.97. In the IR spectrum of the solution the ν(CO) bands occur at 2056 and 2008 cm^{-1}. This supports the presence in solution, under these conditions, of only the five-coordinated species **6** (Scheme 1). When argon was bubbled into the benzene solution containing **6**, the tetracoordinated square-planar species **7** was almost quantitatively formed; the ν(CO) at 2001 cm^{-1} is a high wave number value for a neutral rhodium(I) species and supports a structure in which the CO ligand is in the *trans* position to the phosphite moiety of **1**, with the phosphite group having a greater *trans* influence than the phosphane one.

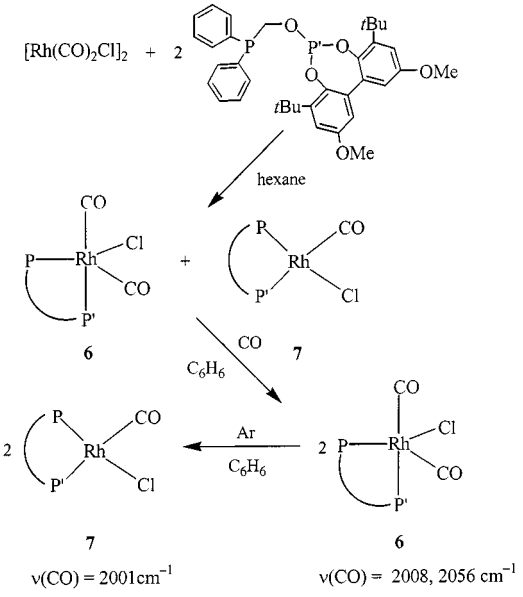

Scheme 1

The reaction of the ligand **1** with $[Rh(CO)_2Cl]_2$, in the molar ratio 2:1, was also undertaken in toluene solution; under these conditions the precipitate formed contained only the five-coordinated species **6**, while in solution both the tetra-coordinated **7** and five-coordinated species (the latter as minor product) were detected. By adding a solution of the ligand (*S*)-**2** in hexane dropwise to a solution of $[Rh(CO)_2Cl]_2$ in the same solvent, in a 2:1 molar ratio, a yellow precipitate was formed and the solution turned yellow. The solid, separated by filtration, on the basis of analytical data and spectroscopic properties, was formulated as the five-coordinated $[Rh(CO)_2(\mathbf{2})Cl]$ (**8**).

In accordance, the $^{31}P\{^1H\}$ NMR spectrum in C_6D_6 solution shows two signals as doublets of doublets at δ = 61.27 [J_{RhP} = 133 Hz, J(PP′) = 49.1 Hz] and δ = 177.34 [J(RhP′) = 266.7 Hz, $J_{P'P}$ = 49.1 Hz] and the IR spectrum (Nujol) exhibits two bands in the ν(CO) stretching region at 1998 and 2064 cm^{-1}. A yellow solid was recovered from

the mother liquor, the square-planar rhodium(I) species [Rh(CO)(**2**)Cl] (**9**). In accordance with its formulation the $^{31}P\{^{1}H\}$ NMR spectrum shows two signals as doublets of doublets at δ = 84.2 [J_{RhP} = 190 Hz, $J(PP')$ = 54.2 Hz] and δ = 170.75 [$J(RhP')$ = 325 Hz, $J_{P'P}$ = 54.2 Hz] and the IR spectrum (Nujol) exhibits a ν(CO) band at 2003 cm^{-1}. The ν(CO) value results are high for a neutral square-planar rhodium(I) species and supports a structure in which the CO ligand is in the *trans* position to a group with a high *trans* influence, such as the phosphite group.

For compounds **6** and **8**, the high values of the ν(CO) allows a trigonal bipyramide structure containing the CO and Cl ligands in the *trans* position to be ruled out and supports a structure in which the phosphite moiety of **1** or (*S*)-**2** and CO occupy the axial positions. The ligands **1** and (*S*)-**2** assume an equatorial-axial coordination as expected if their natural bite angle is nearly 90°.[3a] Moreover, the presence of two ν(CO) bands allowed us to rule out structures with both the CO ligands in the equatorial position.

The reactions of [Rh(acac)$(CO)_2$] with the ligands **1** and (*S*)-**2** in hexane afforded the complexes [Rh(acac)(**1**)] (**10**) and [Rh(acac)(**2**)] (**11**) as yellow solids. Compound **11** was not obtained in a pure form owing to the presence of a very minor unidentified carbonyl product. However, the IR spectra indicate that the reactions occur by displacement of the CO ligands. The $^{31}P\{^{1}H\}$ NMR spectra of **10** and **11** show the phosphorus resonances as two doublets of doublets. The observed $J(PP')$ coupling value supports for **10** and **11** structures in which the ligands **1** and **2** are chelated to the rhodium atom.

Palladium(II) and Platinum(II) Complexes

The reactions of [Pd$(C_6H_5CN)_2Cl_2$] with **1** and (*S*)-**2** in toluene solution afford the corresponding compounds [Pd(**1**)Cl_2] (**12**) and [Pd(**2**)Cl_2] (**13**) as pale yellow crystals, soluble in acetone and chlorinated solvents and slightly soluble in benzene. As expected the $^{31}P\{^{1}H\}$ NMR spectra of **12** and **13** in $CDCl_3$ solution show the phosphorus resonances as doublets at very different δ values [138.2 and 74.88, $J(PP')$ = 23.7 Hz for **12**; 134.48 and 74.71, $J(PP')$ = 25.0 Hz for **13**]. The crystal structure of the chloroform solvate of **12** was fully characterized by an X-ray study.

The reactions of [Pt(COD)I_2] with **1** and (*S*)-**2** in toluene solution afford the compounds [Pt(**1**)I_2] (**14**) and [Pt(**2**)I_2] (**15**), respectively, as white solids that are stable in air. In the $^{31}P\{^{1}H\}$ NMR spectra of **14** and **15** in $CDCl_3$ solution the phosphorus resonances appear as singlets at higher fields than those of **12** and **13** along with peaks due to $^{195}Pt-P$ coupling.

Description of the Crystal Structure of [Pd(1)Cl_2]·$CHCl_3$ (**12**·$CHCl_3$)

Chloroform molecules of solvation were found in the crystals. A view of the structure of complex **12** together with the atomic numbering system is shown in Figure 1. Selected bond lengths and angles are given in Table 1.

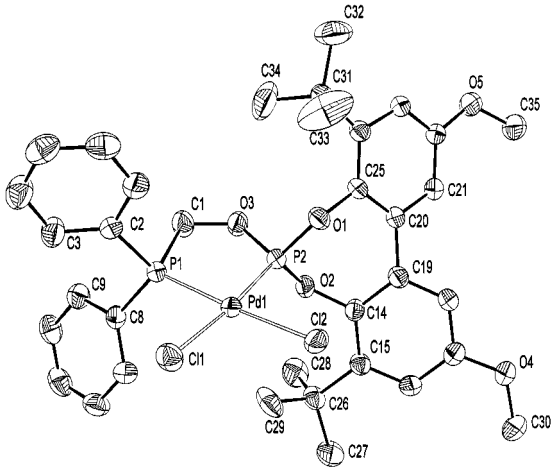

Figure 1. View of the molecular structure of complex **12** with the atomic numbering system; the ellipsoids are drawn at the 30% probability level

Table 1. Selected bond lengths [Å] and angles [°] for **12**·$CHCl_3$

Bond lengths	
Pd(1)−P(2) 2.192(1)	P(1)−C(1) 1.863(6)
Pd(1)−P(1) 2.227(1)	O(1)−C(25) 1.404(6)
Pd(1)−Cl(1) 2.341(2)	O(2)−C(14) 1.404(6)
Pd(1)−Cl(2) 2.354(1)	O(3)−C(1) 1.384(7)
O(1)−P(2) 1.573(4)	C(14)−C(19) 1.391(7)
O(2)−P(2) 1.585(4)	C(19)−C(20) 1.501(7)
O(3)−P(2) 1.590(4)	C(20)−C(25) 1.394(7)
Bond angles	
P(2)−Pd(1)−P(1) 85.95(5)	O(1)−P(2)−O(2) 106.3(2)
P(2)−Pd(1)−Cl(1) 173.39(5)	O(1)−P(2)−O(3) 107.3(2)
P(1)−Pd(1)−Cl(1) 87.47(6)	O(2)−P(2)−O(3) 96.2(2)
P(2)−Pd(1)−Cl(2) 90.87(6)	O(3)−C(1)−P(1) 113.4(4)
P(1)−Pd(1)−Cl(2) 176.43(5)	C(19)−C(14)−O(2) 117.8(5)
Cl(1)−Pd(1)−Cl(2) 95.69(6)	C(14)−C(19)−C(20) 124.1(5)
C(1)−O(3)−P(2) 122.9(4)	C(25)−C(20)−C(19) 124.1(5)
C(1)−P(1)−Pd(1) 105.8(2)	C(20)−C(25)−O(1) 118.2(4)
O(3)−P(2)−Pd(1) 111.6(1)	

The metal ion is square-planarly coordinated by two Cl atoms and two P atoms from the phosphane−phosphite chelating ligand **1** [maximum deviation from the mean plane through the five atoms 0.026(1) Å for Cl2]. The five-membered Pd1P1C1O3P2 ring [the P1−Pd1−P2 bite angle is 85.95(5)°] is roughly planar with only the Pd1 atom being significantly displaced from the mean plane [0.114(1) Å]. The two Pd1−P1 and Pd1−P2 bond lengths [2.227(1) and 2.192(1) Å] are comparable, as well as the two Pd1−Cl1 and Pd1−Cl2 ones [2.341(2) and 2.354(1) Å], as expected. The P and the N atoms are in the *trans* position.

In ligand **1** the P−O bond lengths are practically equal, in the range 1.573(4)−1.590(4) Å, whereas the O−P−O angles are in the range 96.2(2)−107.3(2)°. In the diphenyl moiety the C14−C19−C20−C25 torsion angle is +47.1(1)° with a C19−C20 bond length of 1.501(7) Å.

Catalysis

The catalytic systems formed by [Rh(acac)(CO)$_2$] and ligands (*S*)-**2** and (*S*)-**3** at variable ligand/metal ratios were used in the hydroformylation of styrene: The catalytic runs were carried out in benzene solution using an equimolar hydrogen/carbon monoxide mixture. The catalytic system with ligand (*S*)-**3** turned out to be the most efficient. Indeed, almost quantitative conversion (> 99%) of styrene could be attained within 66 h at 100 atm and 40 °C with a 1:4 Rh/ligand molar ratio. Also the chemo- and regioselectivity results are very high with the linear (L) and branched (B) aldehydes being about 99.9% of the reaction products with a B/L ratio of 32.3. Under these experimental conditions only a 20% *ee* of the branched aldehyde in the (*S*) form was obtained. No influence of the ligand/Rh ratio on the enantioselectivity was found. The stability of the catalytic system [Rh(acac)(CO)$_2$]/(*S*)-**2** was very low under the same experimental conditions.

The poor hydroformylation results are surprising in view of the high enantioselectivity reached by catalytic rhodium systems containing chiral diphosphites[2f] or phosphane−phosphite[3] mixed ligands in the styrene hydroformylation. However, in the literature examples of catalytic rhodium systems containing good ligands affording high conversion and chemo- and regioselectivity, but low or zero values of enantioselectivity from the styrene hydroformylation, have been reported.[7] Generally, these situations have been found when the chelate ligand is not strongly bonded to the rhodium centre. Thus, under elevated CO/H_2 pressure displacement of the chelate ligand by CO can take place to give [RhH(CO)$_4$] or [RhH(CO)$_3$L] (L = bidentate ligand acting as monodentate) as the catalytic species.[8] The use of a high ligand/Rh ratio can also modify the hydride−rhodium catalyst affording species containing two bidentate ligands which are monodentate or bridging (in a binuclear species) coordinated.

We attempted to obtain information about the catalytic system on leaving [Rh(acac){(*S*)-**3**}] to stand for36 h under CO/H_2 of 50 atm at 40 °C in C_6D_6. The resulting solution, transferred under H_2/CO to an NMR tube showed two doublets centred at δ = 120.1 (J_{RhP} = 193.6 Hz) and at δ = 11.7 in the $^{31}P\{^1H\}$ NMR spectrum along with some signals of low intensity in the δ = 12−18 region due to the presence of phosphane oxide.

The lack of the phosphorus−phosphorus coupling in the signal at δ = 120.1 supports the presence of a monodentate ligand coordinated to the rhodium(I) centre; the shift in the δ value from 169.7 as dd, to 120.1 is indicative of a modification at the phosphite group. Moreover the ^{31}P NMR ^1H-coupled spectrum showed the signal at δ = 11.7 as a doublet; the J_{PH} value of 729 Hz and the chemical shift values support the presence of a P−H bond of a phosphonate group.[9] This can be formed by hydrolysis of the ligand (*S*)-**3** in a tautomeric equilibrium, shifted towards the phosphonate, with the corresponding phosphite form. A similar process[9] was observed by hydrolysis of phosphite **15**.

Thus, considering the spectroscopic data and our previously reported results,[9] coordination of the hydrolysis product to the rhodium ion could occur in both phosphite and phosphonate forms affording a rhodium−phosphonate complex. This is further supported by the presence of the phosphorus signal at δ = 120.1 (J_{RhP} = 205 Hz) and of two ν(CO) bands at 2095 and 2050 cm^{-1}. We suggest that species **16** is prevalent in solution. This species can participate in a catalytic process affording the aldehydes but, since only monodentate ligands are present in the catalyst, it cannot bring about an asymmetric induction.

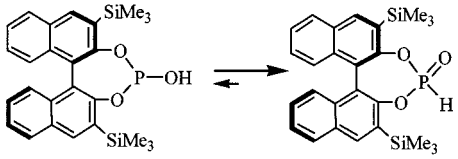

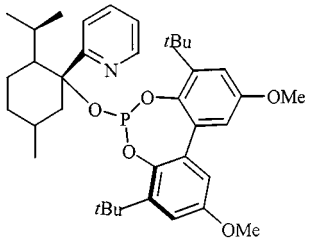

15

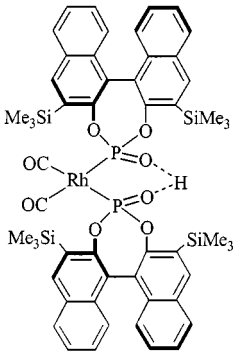

16

Experimental Section

General: All reagents were purchased and used as supplied. Solvents were dried by standard procedures. All experiments were performed under purified nitrogen. IR spectra were obtained as Nujol mulls on KBr plates using a Perkin−Elmer FT-IR 1720 spectrophotometer. ^1H, and $^{31}P\{^1H\}$ NMR spectra were recorded with a Bruker AMX R300. ^1H NMR spectra were referenced to internal tetramethylsilane and $^{31}P\{^1H\}$ spectra to external 85% H_3PO_4; positive chemical shifts for all nuclei are at higher frequencies. Elemental analyses were performed by Redox s.n.c., Cologno Monzese, Milano.

[Rh(COD)(1)]CF$_3$SO$_3$ (4): Solid AgCF$_3$SO$_3$ (0.063 g, 0.249 mmol) was added to a stirred solution of [Rh(COD)Cl$_2$]$_2$ (0.061 g, 0.124 mmol) in tetrahydrofuran (10 mL). After 10 min, the precipitate of AgCl was separated by filtration and ligand **1** (0.149 g, 0.248 mmol) was added to the filtrate. The yellow-orange solution

was stirred for 30 min and was then reduced to ca. 2 mL. On addition of 30 mL of hexane a yellow solid separated. It was removed by filtration, washed with hexane and vacuum-dried. Yield 85% (0.203 g, 0.211 mmol). $C_{44}H_{52}F_3O_8P_2RhS$ (962.8): calcd. C 54.89, H 5.44; found C 54.78, H 5.37. ^1H NMR ($CDCl_3$): δ = 1.58 [s, 18 H, $C(CH_3)_3$], 3.44 (s, 6 H, OCH_3), 4.35 [d, 2 H, $J_{P'H}$ = 22.4, CH_2], 5.35 (br. s, 2 H, CH), 5.62 (br. s, 2 H, CH), 6.76 [d, 2 H, J = 3.0 Hz, CH], 7.10 [d, 2 H, J = 3.0 Hz, CH], 7.25−7.62 (m, 10 H, CH). $^{31}P\{^1H\}$ NMR ($CDCl_3$): δ = 162.29 [dd, J(RhP′) = 256 Hz, $J_{P'P}$ = 37 Hz], 63.89 [dd, J_{RhP} = 148 Hz, J(PP′) = 37 Hz].

[Rh(COD)(2)]CF_3SO_3 (5): The yellow compound **5** was prepared from $[Rh(COD)Cl_2]_2$ (0.070 g, 0.142 mmol) and the ligand (*S*)-**2** (0.154 g, 0.284 mmol) as described above for the compound **4**. Yield 80% (0.202 g, 0.227 mmol). $C_{42}H_{36}F_3O_6P_2RhS$ (890.6): calcd. C 56.64, H 4.07; found C 56.49, H 4.15. ^1H NMR ($CDCl_3$): δ = 4.30 [d, 2 H, $J_{P'H}$ = 21, CH_2], 5.30 (br. s, 2 H, CH), 5.59 (br. s, 1 H, CH), 6.76 [d, 2 H, J = 3 Hz, CH], 7.01−7.95 (m, 22 H, CH). $^{31}P\{^1H\}$ NMR ($CDCl_3$): δ = 167 [dd, J(RhP′) = 260 Hz, $J_{P'P}$ = 41.3 Hz], 64.77 [dd, J_{RhP} = 149 Hz, J(PP′) = 41.3 Hz].

[$Rh(CO)_2$(1)Cl] (6) and [Rh(CO)(1)Cl] (7): To a stirred solution of $[Rh(CO)_2Cl]_2$ (0.080 g, 0.205 mmol) in hexane (30 mL) was added ligand **1** (0.247 g, 0.41 mmol). Immediately a yellow solid, containing both the products $[Rh(CO)_2$(**1**)Cl] and [Rh(CO)(**1**)Cl], precipitated. The solid was filtered, washed with hexane, and dried. Attempts to separate compounds **6** and **7** failed. Data for **7**: IR (KBr, Nujol): ν_{CO} = 2001 cm^{-1}. ^1H NMR ($CDCl_3$): δ = 1.65 [s, 18 H, $C(CH_3)_3$], 3.27 (s, 6 H, OCH_3), 4.12 [d, 2 H, $J_{P'H}$ = 20 Hz, CH_2], 6.67 [d, 2 H, J = 3.0 Hz, CH], 7.05 (m, 2 H, CH). $^{31}P\{^1H\}$ NMR ($CDCl_3$): δ = 163.76 [dd, J(RhP′) = 266.7 Hz, $J_{P'P}$ = 49.1], 84.5 [dd, J_{RhP} = 133.5 Hz, J(PP′) = 49.1 Hz].

[$Rh(CO)_2$(1)Cl] (6): Compound **6** was obtained by the following procedure: To a stirred solution of $[Rh(CO)_2Cl]_2$ (0.040 g, 0.103 mmol) in toluene (10 mL) was added dropwise a solution of **1** (0.124 g, 0.206 mmol) in the same solvent (2 mL). A yellow precipitate was deposited during the course of the addition. This was collected, washed with toluene (1 mL) and hexane, and then dried. Yield 87% (0.143 g, 0.179 mmol). $C_{37}H_{40}ClO_7P_2Rh$ (797.0): calcd. C 55.76, H 5.06, Cl 4.45; found C 55.69, H 5.10, Cl 4.39. IR (KBr, Nujol): ν_{CO} = 2033, 2072 cm^{-1}. ^1H NMR ($CDCl_3$): δ = 1.49 [s, 18 H, $C(CH_3)_3$], 3.30 (s, 6 H, OCH_3), 4.24 [d, 2 H, J(PH) = 20 Hz, CH_2], 6.71 [d, 2 H, J = 3.0 Hz, CH], 7.09 [d, 2 H, J = 3.0 Hz, CH], 7.83−7.90 (m, 10 H, CH). $^{31}P\{^1H\}$ NMR ($CDCl_3$): δ = 167.97 [dd, J(RhP′) = 325.9 Hz, $J_{P'P}$ = 53.1 Hz], 62.25 [dd, J_{RhP} = 195 Hz, J(PP′) = 53.1 Hz].

[$Rh(CO)_2$(2)Cl] (8) and [Rh(CO)(2)Cl] (9): A solution of ligand **2** (0.318 g, 0.6 mmol) in toluene (6 mL) was added dropwise to a stirred solution of $[Rh(CO)_2Cl]_2$ (0.120 g, 0.3 mmol) in hexane (30 mL). A yellow solid immediately precipitated. This was collected washed with toluene (1 × 1 mL) and hexane, and then dried. By IR and NMR spectroscopy the yellow solid was identified as $[Rh(CO)_2$(2)Cl] (**8**). Data of **8**: $C_{35}H_{24}ClO_5P_2Rh$ (724.8): calcd. C 57.99, H 3.34, Cl, 4.89; found C 57.78, H 3.29, Cl 4.93. IR (KBr, Nujol): ν_{CO} = 1995, 2064 cm^{-1}. ^1H NMR ($CDCl_3$): δ = 4.24 [d, 2 H, $J_{P'H}$ = 21 Hz, CH_2], 7.65−7.95 (m, 22 H, CH). $^{31}P\{^1H\}$ NMR ($CDCl_3$): δ = 177.34 [dd, J(RhP′) = 266.7 Hz, $J_{P'P}$ = 49.1 Hz], 61.27 [dd, J_{RhP} = 133 Hz, J(PP′) = 49.1 Hz]. Compound **9** was recovered, as a yellow powder, from the mother liquor by addition of hexane. Data of **9**: $C_{34}H_{24}ClO_4P_2Rh$ (708.9): calcd. C 58.60, H 3.47, Cl 5.09; found C 58.71, H 3.51; Cl 5.02. IR (KBr, Nujol): ν_{CO} = 2003 cm^{-1}. ^1H NMR ($CDCl_3$): δ = 4.20 [d, 2 H, $J_{P'H}$ = 21 Hz, CH_2], 7.62−7.94 (m, 22 H, CH). $^{31}P\{^1H\}$ NMR ($CDCl_3$): δ = 170.75 [dd, J(RhP′) = 325 Hz, $J_{P'P}$ = 54.2 Hz], 84.2 [dd, J_{RhP} = 190 Hz, J(PP′) = 54.2 Hz].

[Rh(acac)(1)] (10): A stirred solution of $[Rh(acac)(CO)_2]$ (0.050 g, 0.194 mmol) in hexane (15 mL) was added dropwise to a solution of **1** (0.117 g, 0.194 mmol) in the same solvent (10 mL). During the addition, a colour change from yellow to orange was observed. Monitoring the reaction by IR spectroscopy, a gradual disappearance of starting ν_{CO} bands was observed. After ca. 1 h, the solvent was removed to give an orange solid. It was washed twice with hexane and vacuum-dried. Yield 85% (0.133 g, 0.165 mmol). $C_{40}H_{47}O_7P_2Rh$ (801.7): C 59.71, H 5.89; found C 60.03, H 5.94. ^1H NMR (C_6D_6): δ = 1.25 (s, 3 H, acac-CH_3), 1.39 [s, 18 H, $C(CH_3)_3$], 1.60 (s, 3 H, acac-CH_3), 3.29 (s, 6 H, OCH_3), 4.22 (d, 2 H, $J_{P'H}$ = 20 Hz, CH_2), 5.03 (s, 1 H, acac-H), 6.61 (d, 2 H, J = 3.0 Hz, CH), 6.82 (d, 2 H, J = 3.0 Hz, CH), 7.04−7.99 (m, 10 H, CH). $^{31}P\{^1H\}$ NMR (C_6D_6): δ = 168.1 [dd, J(RhP′) = 308 Hz, $J_{P'P}$ = 77 Hz], 78.8 [dd, J_{RhP} = 188 Hz, J(PP′) = 77 Hz].

[Rh(acac)(2)] (11): This compound was obtained by an analogous procedure to **10** as yellow solid starting from $[Rh(acac)(CO)_2]$ (0.080 g, 0.310 mmol) and **2** (0.164 g, 0.310 mmol). Yield 80% (0.182 g, 0.248 mmol). $C_{38}H_{31}O_5P_2Rh$ (732.5): C 62.31, H 4.27; found C 62.81, H 4.29. ^1H NMR (C_6D_6): δ = 1.60 (s, 3 H, acac-CH_3), 4.22 [d, 2 H, $J_{P'H}$ = 20 Hz, CH_2], 5.03 (s, 1 H, acac-H), 7.04−7.99 (m, 10 H, CH). $^{31}P\{^1H\}$ NMR (C_6D_6): δ = 168.1 [dd, J(RhP′) = 308 Hz, $J_{P'P}$ = 77 Hz], 78.8 [dd, J_{RhP} = 188 Hz, J(PP′) = 77 Hz].

[$Pd(1)Cl_2$] (12): Solid ligand **1** (0.094 g, 0.156 mmol) was added to a stirred solution of $[Pd(PhCN)_2Cl_2]$ (0.060 g, 0.156 mmol) in toluene (10 mL). The resulting solution was stirred for ca. 30 min during which a colour change from red-orange to pale yellow occurred. The solution was reduced in volume (5 mL), and upon addition of hexane, compound **12** separated as a yellow solid. This was removed by filtration, washed with hexane and vacuum-dried. Yield 88% (0.107 g, 0.137 mmol). $C_{35}H_{40}Cl_2O_5P_2Pd$ (779.9): C 53.90, H 5.17, Cl 9.09; found C 53.65, H 5.22, Cl 9.23. ^1H NMR ($CDCl_3$): δ = 1.39 [s, 18 H, $C(CH_3)_3$], 3.81 (s, 6 H, OCH_3), 4.60 [dd, 2 H, $J_{P'H}$ = 26 Hz, J(PH) = 1 Hz, CH_2], 6.71 [d, 2 H, J = 3.0 Hz, CH], 6.99 [d, 2 H, J = 3.0 Hz, CH], 7.55−7.90 (m, 10 H, CH). $^{31}P\{^1H\}$ NMR ($CDCl_3$): δ = 138.2 [d, $J_{P'P}$ = 23.7 Hz], 74.88 [d, $J_{P'P}$ = 23.7 Hz].

[$Pd(2)Cl_2$] (13): This compound was obtained similarly to **12** as a yellow-orange solid by starting from $[Pd(PhCN)_2Cl_2]$ (0.070 g, 0.182 mmol) and ligand **2** (0.096 g, 0.182 mmol). Yield 83% (0.107 g, 0.151 mmol). $C_{33}H_{24}Cl_2O_3P_2Pd$ (707.8): C 56.00, H 3.42, Cl, 10.02; found C 56.15, H 3.46, Cl 10.16. ^1H NMR ($CDCl_3$): δ = 4.45 (m, 1 H, CH_2), 4.71 (m, 1 H, CH_2), 7.0−7.96 (m, 22 H, CH). $^{31}P\{^1H\}$ NMR ($CDCl_3$): δ = 144.4 [d, $J_{P'P}$ = 25 Hz], 74.71 [d, $J_{P'P}$ = 25 Hz].

[$Pt(1)I_2$] (14): Solid ligand **1** (0.064 g, 0.107 mmol) was added to a stirred solution of $[Pt(COD)I_2]$ (0.060 g, 0.107 mmol) in toluene (10 mL). Upon addition of **1** a white solid precipitated. This was removed by filtration, washed with toluene and hexane, and then vacuum-dried. Yield 90% (0.101 g, 0.096 mmol). $C_{35}H_{40}I_2O_5P_2Pt$ (1051): C 39.98, H 3.83, I 24.14; found C 39.89, H 3.87, I 24.20. ^1H NMR ($CDCl_3$): δ = 1.37 [s, 18 H, $C(CH_3)_3$], 3.82 (s, 6 H, OCH_3), 4.48 [dd, 2 H, $J_{P'H}$ = 22 Hz, J(PH) = 1 Hz, CH_2], 6.73 [d, 2 H, J = 3.0 Hz, CH], 6.99 [d, 2 H, J = 3.0 Hz, CH], 7.65−7.99 (m, 10 H, CH). $^{31}P\{^1H\}$ NMR ($CDCl_3$): δ = 123 [s, J(PtP′) = 5682 Hz], 52.28 [d, J_{PtP} = 3180 Hz].

[$Pt(2)I_2$] (15): This compound was obtained similarly to **14** as a yellow-orange solid by starting from $[Pt(COD)I_2]$ (0.100 g,

0.178 mmol) and ligand **2** (0.095 g, 0.178 mmol).Yield 89% (0.155 g, 0.158 mmol). $C_{33}H_{24}I_2O_3P_2Pt$ (979.4): C 40.47, H 2.47, I 25.92; found C 40.52, H 2.49, I 25.85. ^{1}H NMR ($CDCl_3$): δ = 4.37 (m, 1 H, CH_2), 4.55 (m, 1 H, CH_2), 7.1−7.95 (m, 22 H, CH). ^{31}P{^{1}H} NMR ($CDCl_3$): δ = 128.42 [s, J(PtP′) = 5621 Hz], 54.26 [d, J_{PtP} = 3180 Hz].

Crystal Structure Determination of [Pd(1)Cl$_2$]·CHCl$_3$ (12·CHCl$_3$): The intensity data of the complex was collected at room temperature with an Enraf Nonius CAD 4 single-crystal diffractometer using a graphite-monochromated Cu-K_α radiation and the θ/2θ scan technique. Crystallographic and experimental details for the structure are summarized in Table 2. A correction for absorption was made for the complex [maximum/minimum value for the transmission coefficient was 1.000/0.677].[10] The structure was solved by Patterson and Fourier methods and refined by full-matrix least-squares procedures (based on F_o^2) with anisotropic thermal parameters in the last cycles of refinement for all the non-hydrogen atoms. The hydrogen atoms were introduced into the geometrically calculated positions and refined *riding* on the corresponding parent atoms. In the final cycles of refinement a weighting scheme $w = 1/[\sigma^2F_o^2 + (0.1416\ P)^2]$, where $P = (F_o^2 + 2F_o^2)/3$, was used. All calculations were carried out with the DIGITAL AlphaStation 255 computers of the Centro di Studio per la Strutturistica Diffrattometrica del CNR, Parma, using the SHELX-97 systems of crystallographic computer programs.[11] Details of the crystal structure investigations are deposited at the Cambridge Crystallographic Data Centre as supplementary publication no. CCDC-166947. Copies of the data can be obtained free of charge on application to CCDC, 12 Union Road, Cambridge CB2 1EZ, UK [Fax: (internat.) + 44-1223/336-033, E-mail: deposit@ccdc.cam.ac.uk].

Table 2. Crystal data and structure refinement for **12**·$CHCl_3$; $R1 = \Sigma||F_o| - |F_c||/\Sigma|F_o|$ and $wR2 = \{\Sigma[w(F_o^2 - F_c^2)^2]/\Sigma[w(F_o^2)^2]\}^{1/2}$

Empirical formula	$C_{35}H_{40}Cl_2O_5P_2Pd{\cdot}CHCl_3$
Formula mass	899.28
Wavelength	1.54184 Å
Crystal system	triclinic
Space group	$P\bar{1}$
Unit cell dimensions	a = 13.474(4) Å
	b = 14.214(5) Å
	c = 10.424(3) Å
	α = 93.79(3)°
	β = 91.45(2)°
	γ = 97.27(3)°
V	1974.9(11) Å^3
Z	4
Density (calculated)	1.512 Mg/m^3
Absorption coefficient	79.95 cm^{-1}
F(000)	916
Crystal size	0.21 × 0.27 × 0.39 mm
θ range [°]	3−70
Index ranges	$-16 \le h \le 16$, $-17 \le k \le 17$, $0 \le l \le 12$
Reflections collected	7415
Independent reflections	7415 [R(int) = 0.0]
Observed reflections [$I > 2\sigma(I)$]	5953
Data/restraints/parameter	7415/0/451
Goodness-of-fit on F^2	1.067
Final R indices [$I > 2\sigma(I)$]	$R1$ = 0.0567, $wR2$ = 0.1777
R indices (all data)	$R1$ = 0.0676, $wR2$ = 0.1969

Hydroformylation Procedure: The air was evacuated from a 30-mL stainless steel autoclave and a benzene solution of [Rh(acac)(CO)$_2$], the ligand and the olefin were introduced by suction. The vessel was pressurised with CO/H$_2$ (1:1) at the required pressure at room temperature and thermostated. The conversion and the composition of the reaction products were determined by GLC with a Carlo Erba HRGC 5160 Mega Series apparatus (split/splitless injector, MEGA OV1 25-m column, film thickness 2 μm, carrier gas He, flame ionization detector). The enantiomeric excess was determined by the shift reagent Eu(hfc)$_3$.[12]

Acknowledgments

We thank MURST for financial support.

[1] [1a] *Applied Homogeneous Catalysis with Organometallic Compounds: A Comprehensive Handbook in Two Volumes* (Eds.: B. Cornils, W. A. Herrmann), VCH, New York, **1996**. [1b] G. W. Parshall in *Homogeneous Catalysis: The Applications and Chemistry of Catalysis by Soluble Transition-metal Complexes*, Wiley and Sons, New York, **1980**. [1c] *Catalytic Asymmetric Synthesis* (Ed: I. Ojima), VCH, Weinheim, **1995**. [1d]R. Noyori in *Asymmetric Catalysis in Organic Synthesis*, Wiley-Interscience Publications, New York, **1994**.

[2] [2a] C. P. Casey, G. T. Whiteker, M. G. Melville, L. M. Petrovich, J. A. Gavney, D. R. Powell, *J. Am. Chem. Soc.* **1992**, *114*, 5535. [2b] P. C. J. Kamer, J. N. H. Reek, P. W. N. M. van Leeuwen, *Chemtech* **1998**, *28*(9), 27 and references therein. [2c] G. Zhu, X. Zhang, *J. Org. Chem.* **1998**, *63*, 3133. [2d] A. Togni, C. Breutel, A. Schnyder, F. Spindler, H. Landert, A. Tijani, *J. Am. Chem. Soc.* **1994**, *116*, 4062. [2e] S. Cserépi, J. Bakos, *Chem. Commun.* **1997**, 635. [2f] G. J. H. Buisman, L. A. van der Veen, P. C. J. Kamer, P. W. N. M. van Leeuwen, *Organometallics* **1997**, *16*, 5681 and references therein. [2g] A. von Rooy, P. C. J. Kamer, P. W. N. M. van Leeuwen, K. Goubitz, J. Fraanje, N. Veldman, A. L. Spek, *Organometallics* **1996**, *15*, 835 and references therein. [2h] A. Togni, L. M. Venanzi, *Angew. Chem. Int. Ed. Engl.* **1994**, *33*, 497. [2i] K. Angermund, W. Baumann, E. Dinjus, R. Fornika, H. Gorls, M. Kessler, C. Kruger, W. Leitner, F. Lutz, *Chem. Eur. J.* **1997**, *3*, 755. [2l] B. M. Trost, B. Breit, S. Peukert, J. Zambrano, J. W. Ziller, *Angew. Chem. Int. Ed. Engl.* **1995**, *34*, 2386. [2m] M. P. T. Sjogren, S. Hansson, B. Akermark, A. Vitagliano, *Organometallics* **1994**, *13*, 1963. [2n] B. M. Trost, D. J. Murphy, *Organometallics* **1985**, *4*, 1143. [2o] P. W. N. M. van Leeuwen, G. J. H. Buisman, A. von Rooy, P. C. J. Kamer, *Recl. Trav. Chim. Pays-Bas* **1994**, *113*, 61.

[3] [3a] N. Sakai, S. Mano, K. Nozaki, H. Takaya, *J. Am. Chem. Soc.* **1993**, *115*, 7033. [3b] N. Sakai, K. Nozaki, H. Takaya, *J. Chem. Soc., Chem. Commun.* **1994**, 395. [3c] K. Nozaki, N. Sakai, T. Nanno, T. Higashijima, S. Mano, T. Horiuchi, H. Takaya, *J. Am. Chem. Soc.* **1997**, *119*, 4413.

[4] G. Franciò, F. Faraone, W. Leitner, *Angew. Chem. Int. Ed.* **2000**, *39*, 1428.

[5] C. G. Arena, D. Drommi, F. Faraone, *Tetrahedron: Asymmetry* **2000**, *11*, 2765.

[6] H. Helmann, J. Badu, H. Birkner, O. Schumacher, *Justus Liebigs Ann. Chem.* **1962**, *659*, 49.

[7] See for example: Z. Freisa, M. N. Pereira, A. C. Pais, J. C. Bayon, *J. Chem. Soc., Dalton Trans.* **1999**, 3245.

[8] R. Lazzaroni, R. Settambolo, G. Uccello-Baretta, *Organometallics* **1995**, *14*, 4644 and refs. therein.

[9] C. G. Arena, F. Nicolò, D. Drommi, G. Bruno, F. Faraone, *J. Chem. Soc., Dalton Trans.* **1996**, 4357.

[10] [10a] N. Walker, D. Stuart, *Acta Crystallogr., Sect. A* **1983**, *39*, 158. [10b] F. Ugozzoli, *Comput. Chem.* **1987**, *11*, 109.

[11] G. M. Sheldrick, *SHELX-97*, *Program for the Solution and the refinement of Crystal Structures*, Universität Göttingen, Germany, **1997**.

[12] G. Parrinello, J. K. Stille, *J. Am. Chem. Soc.* **1987**, *109*, 7122.

Received July 18, 2001
[I01266]

2,5-Bis(di-*tert*-butylhydroxysilyl)furan as a Host Molecule for Potassium Fluoride, H_2O, NH_3 and $MeNH_2$

Uwe Klingebiel,*[a] Peter Neugebauer,[a] Ilka Müller,[a] Mathias Noltemeyer,[a] and Isabel Usón[a]

Keywords: Silicon / Furan / Host-guest complexes / Structure elucidation

2,5-Bis(di-*tert*-butylfluorosilyl)furan reacts with potassium hydroxide in a 1:2 molar ratio to give 2,5-bis(di-*tert*-butylhydroxysilyl)furan, $O(CRCH)_2$ [R = $SiOH(CMe_3)_2$ (**1**)]. Compound **1** is very selective in its adduct formation and forms host-guest complexes in the presence of KF [**1**·1/2KF (**2**)], H_2O [**1**·H_2O (**3**)], NH_3 [**1**·NH_3 (**4**)] and $MeNH_2$ [**1**·2$MeNH_2$ (**5**)]. The host-guest complexes are stable at room temperature. Compound **4** is the first neutral ammonia cage that is stable up to 100 °C. The crystal structures of **2**, **3**, **4** and **5** have been determined.

Introduction

Heterocycles such as furan undergo electrophilic aromatic substitution reactions very readily and regioselectively, with the 2-position being more reactive than the 3-position. On particular such reaction is metallation, particularly lithiation of a C−H group next to the oxygen atom. These lithium compounds are very reactive and combine with electrophiles such as fluorosilanes.[1] Recently, 2,5-bis(di-*tert*-butylfluorosilyl)furan was obtained from the reaction of dilithiated furan and $F_2Si(CMe_3)_2$ in a 1:2 molar ratio.[1] Fluorosilyl compounds are, like other halosilanes, excellent precursors for the synthesis of silylamines or silanols.[2] In view of the high acidity and the relatively high basicity of silanols[2] is to be expected that they will form strong hydrogen bonds both with themselves[2−5] and with other suitable species.[2] The association of silanols in solution has been discussed previously and a wide range of hydrogen-bonded structures has been found in the solid state.[2−5] The crystal structure of triphenylsilanol, for example, has 16 molecules in the unit cell, arranged as two sets of two independent tetrameric hydrogen-bonded units.[2,6] This tetrameric structure is retained in the adduct with ethanol, $(Ph_3SiOH)_4$·EtOH, which has a cyclic network of hydrogen bonds. Silanol is very selective in its adduct formation and also forms adducts with MeOH, DMSO and ethers.[2,7,8] Host-guest complexes between silanols and many organic liquids and solids are nicely summarized in ref. 2.

In this paper we describe the preparation of 2,5-bis(di-*tert*-butylhydroxysilyl)furan and its application as a host molecule for the gases NH_3 and $MeNH_2$, the liquid H_2O and the salt KF.

Results and Discussion

2,5-Bis(di-*tert*-butylfluorosilyl)furan[1] reacts with KOH in a 1:2 molar ratio to give 2,5-bis(di-*tert*-butylhydroxysilyl)furan.[1]

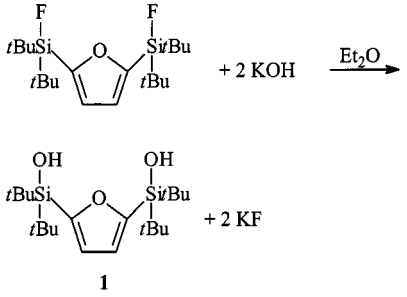

1

The reaction progress can be followed by ^{19}F NMR spectroscopy. Unreacted KF was separated by filtration and condensation of **1** into a cooled trap in vacuo (10^{-2} mbar) above 100 °C.

Attempts to crystallize **1** from the reaction mixture led to the isolation of the host-guest complex **2**, where two molecules of **1** coordinate one of KF.

Heating **2** in vacuo (10^{-2} mbar) above 100 °C leads to the condensation of **1** into the cold trap. The reaction is not reversible: we didn't succeed in preparing **2** from **1** and KF, perhaps because of the insolubility of KF in organic solvents.

[a] Institut für Anorganische Chemie der Georg-August-Universität Göttingen,
Tammannstraße 4, 37077 Göttingen, Germany
Fax: (internat.) +49-(0)551/393-373
E-mail: uklinge@gwdg.de

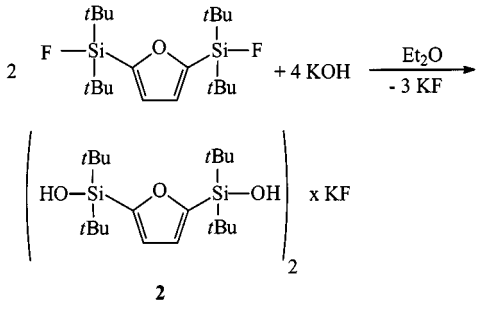

2

Crystal Structure of 2

Compound **2** crystallizes in the monoclinic space group $P2_1/c$ with one molecule of **1** and half a molecule of potassium fluoride in the asymmetric unit i.e. the potassium atom is coordinated by two disilanol molecules. In this dimer, the coordination sphere of the potassium is quite unusual: six oxygen atoms and one fluorine atom coordinate to the cation to form a distorted hexagonal pyramid with the fluorine atom, which forms hydrogen bonds with two hydroxyl groups, at the axial position (Figure 1).

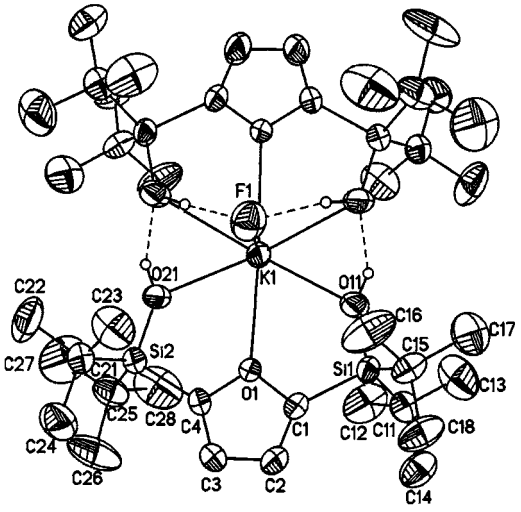

Figure 1. Structure of **2**

The potassium atom lies out of the base of the pyramid. This could be a result of the limited space in the dimer which does not allow the potassium and the fluoride atom to lie in the plane of the hydroxyl group. Another reason for the special arrangement of the potassium atom above the pyramid base could be the conflict between the attempts of the fluorine atom to build up hydrogen bonds and the minimum distance between the fluorine and potassium atoms.

As all oxygen atoms of the disilanol are coordinated to the potassium, the Si(1)−O(11) [Si(2)−O(21)] and the C(1)−O(1) [C(4)−O(1)] bonds are eclipsed. This induces stronger steric interactions between the methylene group C(2) and the *tert*-butyl substituents so that the Si(1)−C(1) and the Si(2)−C(4) bonds are lengthened.

Attempts to accelerate the formation of **1** by addition of water or to dissolve KF in order to purify **1** led to the formation of the host-guest complex **3**. Warming **3** in vacuo (10^{-2} mbar) up to 130 °C leads to the loss of water and reisolation of **1**. This process is reversible.

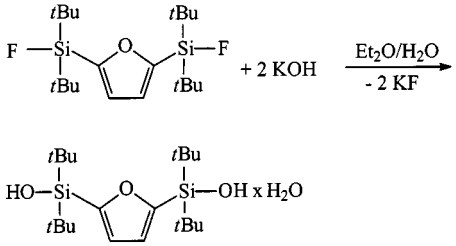

3

Crystal Structure of 3

In compound **3**, which crystallizes in the orthorhombic space group *F*dd2, one water molecule per disilanol molecule is incorporated in the crystal. One 2,5-bis(di-*tert*-butylsilyl)furan molecule and one water molecule form the asymmetric unit.

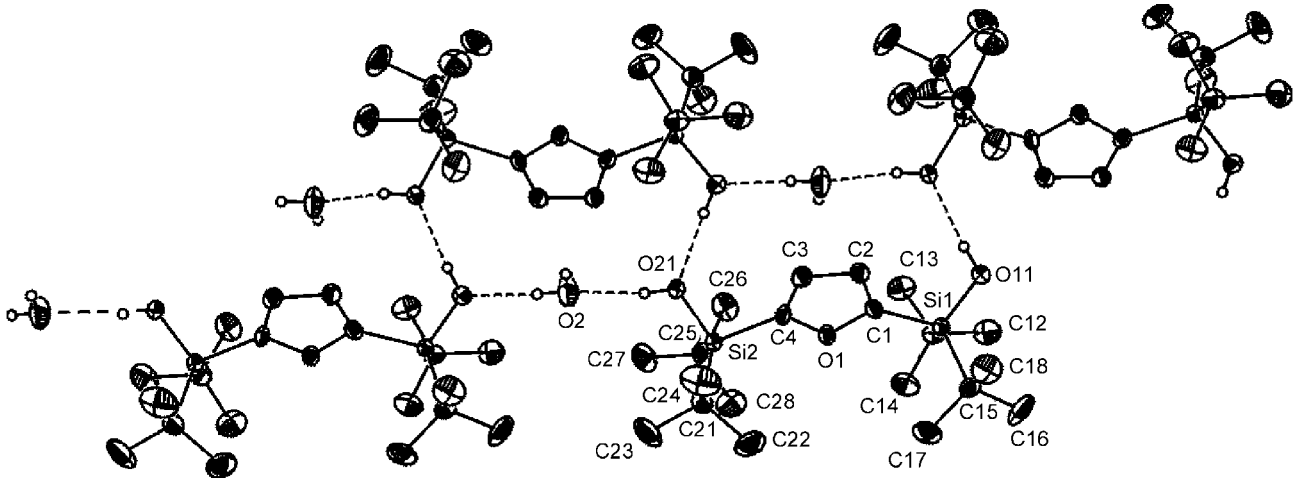

Figure 2. Structure of **3**

The disilanol molecules are arranged in zig-zag chains with hydrogen bonds between the hydroxyl groups. In these chains, a water molecule connects a monomer N, with monomer (N + 2), acting once as a hydrogen donor and once as an acceptor (Figure 2). One of the water hydrogen atoms is not involved in hydrogen bonding.

In order to minimize steric constraints, the distance between the *tert*-butyl groups at the silicon and the methylene groups of the furan is maximized. As a result, the Si(1)−O(11) [Si(2)−C(21)] and the C(1)−C(2) [C(4)−C(3)] bonds are arranged eclipsed. Due to this conformation, the oxygen atom that is part of the furan ring lies on the outer side of the zig-zag chain, and it does not form hydrogen bonds because of the shielding effect of the *tert*-butyl groups. In this way, the chains form tubes along the crystallographic *c*-axis with the hydrophobic groups on the outside and hydrophilic ones inside.

Ammonia and amines are well-known as ligands in complexes, where they generally undergo a formal Lewis acid-base interaction, with the nitrogen bound to the central metal atom or ion through its free electron pair.[10] The inclusion of gas molecules in salts or clathrates prepared under gas pressure or at low temperature has been reported,[11] although only one inclusion compound of dihydroxybinaphthyl containing ammonia and methanol as guest molecules is known.[12]

Having succeeded in isolating host-guest complexes of the bis(hydroxysilyl)furan **1** with the KF and water, we considered the possibility of the inclusion of gaseous amines such as NH_3 and $MeNH_2$. A solution of **1** in *n*-hexane was saturated with ammonia or methylamine at room temperature to give the host-guest compounds **4** or **5**, respectively. Compound **4** was obtained as colourless prisms with a melting point of 90 °C. TG and DTA studies show that **4** loses NH_3 above its melting point (90 °C), in two steps (at 100 °C and 110 °C), with reconversion of **1**.

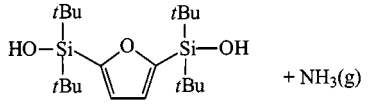

1

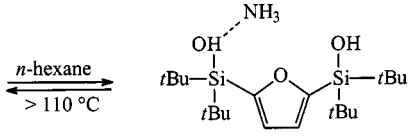

4

Crystal Structure of 4

Compound **4** crystallizes in the monoclinic space group $P2_1/c$ with one disilanol molecule and two ammonia molecules in the asymmetric unit. The hydroxyl groups of the disilanol monomers form hydrogen bonds with each other and with the ammonia molecules. Only two of the hydrogen atoms of each ammonia molecule participate in this hydrogen bonding (Figure 3). As in compound **2**, the Si1−O11 (Si2−O21) and the C1−O1 (C4−O1) bonds are eclipsed thus permitting formation of the dimer and causing the lengthening of the Si1−C1 (Si2−C4) bond.

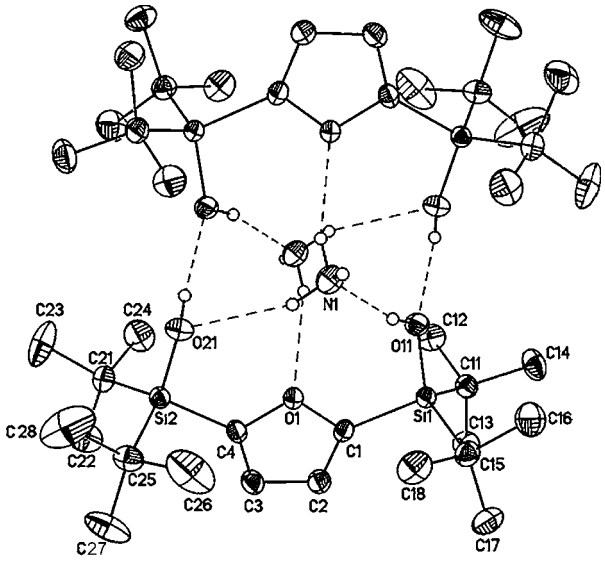

Figure 3. Structure of **4**

The host-guest complex **5**, obtained at room temperature, incorporates $MeNH_2$ in a molar ratio 1:2. It is far less stable than **4** and loses $MeNH_2$ when isolated from solution at room temperature.

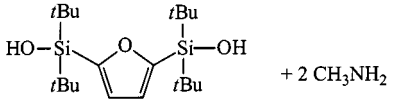

1

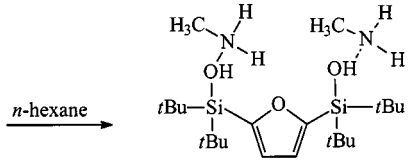

5

Crystal Structure of 5

Crystals of compound **5**, which were not stable out of the mother liquor at room temperature, belong to the triclinic space group $P\bar{1}$. They contain one 2,5-bis(di-*tert*-butylsilyl)-furan molecule and two methylamine molecules in the asymmetric unit (Figure). The disilanol monomers are connected to each other and the guest molecules through hydrogen bonds, forming a double chain. One of the methylamine molecules [$CH_3-N(1)H_2$] in the asymmetric unit connects opposite disilanol molecules through hydrogen bonds. The other one [$CH_3-N(2)H_2$] establishes these same contacts and an additional hydrogen bond to the next disilanol molecule along the chain. The hydrogen bonds

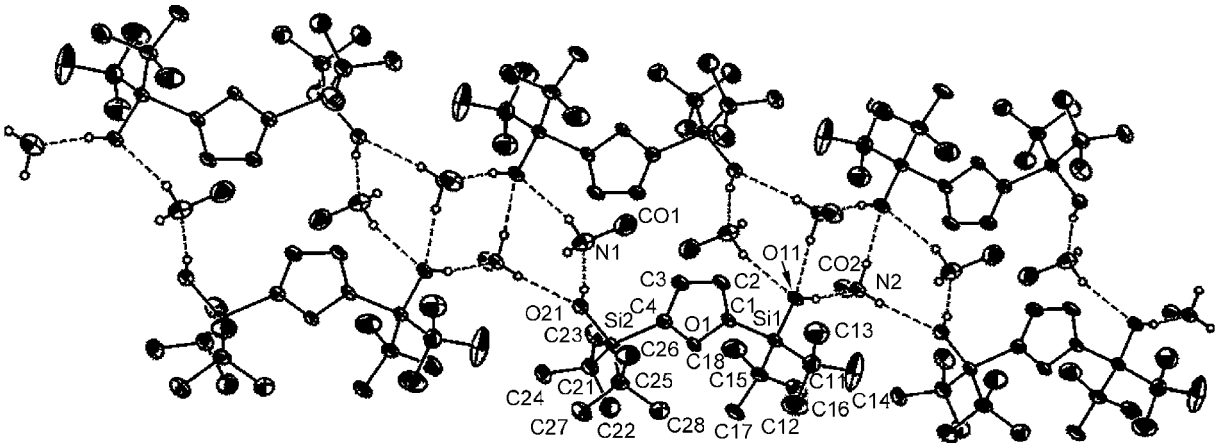

Figure 4. Structure of **5**

Table 1. Crystal data and data collections parameters for **2**, **3**, **4,** and **5**

	2	**3**	**4**	**5**
Empirical formula	$C_{40}H_{80}FKO_6Si_4$	$C_{20}H_{42}O_4Si_2$	$C_{40}H_{86}N_2O_6Si_4$	$C_{22}H_{50}N_2O_3Si_2$
Molecular weight	827.50	402.72	803.47	446.82
Temperature[K]	210(2)	150(2)	150(2)	133(2)
Wavelength [Å]	0.71073	0.71073	0.71073	0.71073
Crystal system	monoclinic	orthorhombic	monoclinic	triclinic
Space group	$P2_1/c$	$Fdd2$	$P2_1/c$	$P\bar{1}$
Unit cell dimensions [Å]	a = 8.6035(12)	a = 23.872(9)	a = 12.8380(15)	a = 9.0380(18)
	b = 23.927(8)	b = 32.482(3)	b = 15.459(3)	b = 12.529(3)
	c = 12.6008(18)	c = 12.834(3)	c = 12.9418(15)	c = 13.712(3)
	α = 90°	α = 90°	α = 90°	α = 64.31(3)°
	β = 104.771(13)°	β = 90°	β = 106.030(10)°	β = 80.20(3)°
	γ = 90°	γ = 90°	γ = 90°	γ = 88.36(3)°
Volume [Å^3]	2508.2(10)	9951(4)	2468.6(6)	1377(5)
Z	2	16	2	2
Density (calculated) [Mg/m^3]	1.096	1.075	1.081	1.078
Absorption coefficient [mm^{-1}]	0.243	0.162	0.161	0.151
F(000)	904	3552	888	496
Crystal size [mm^3]	0.70 × 0.50 × 0.30	1.00 × 0.70 × 0.60	1.00 × 1.00 × 1.00	0.40 × 0.30 × 0.10
θ range for data collection	3.54 to 22.45°	3.55 to 24.95°	3.49 to 24.88°	2.29 to 25.99°
Reflections collected	4099	3373	8926	17419
Independent reflections	3234 [R_{int} = 0.0436]	3163 [R_{int} = 0.0488]	4275 [R_{int} = 0.0663]	5386 [R_{int} = 0.058]
Refinement method	Full-matrix least-squares on F^2	Full-matrix least-squares on F^2	Full-matrix least-squares on F^2	Full-matrix least-squares on F^2
Data/restraints/parameters	3234/4/268	3163/5/259	4275/4/ 267	5386/6/294
Goodness-of-fit on F^2	1.065	1.050	1.073	1.065
Final R indices [$I > 2\sigma(I)$]	R1 = 0.0453	R1 = 0.0369	R1 = 0.0348	R1 = 0.0659
	wR2 = 0.1031	wR2 = 0.0958	wR2 = 0.0884	wR2 = 0.1703
R indices (all data)	R1 = 0.0594	R1 = 0.0390	R1 = 0.0380	R1 = 0.0808
	wR2 = 0.1148	wR2 = 0.0984	wR2 = 0.0907	wR2 = 0.1875
Largest diff. peak and hole [e·Å^{-3}]	0.259 and −0.202	0.272 and −0.189	0.274 and −0.228	0.836 and −0.736

formed by the first methylamine are longer than those formed by the4 ammonia molecule in compound **4**. The second methylamine molecule interacts more strongly with the disilanol than with the ammonia molecule (Table 2). The instability of the crystals of compound **5** could be a consequence of the formation of only two hydrogen bonds by one of the methylamine moieties instead of the three that are possible.

As in compound **2**, the Si(1)−O(11) and Si(2)−O(21) bonds are eclipsed to the C(1)−C(2) and C(4)−C(3) bonds, respectively, to avoid steric hindrance between the furan methylene groups and the *tert*-butyl groups. The difference between the Si(1)−O(11) and Si(2)−O(21) bond lengths is 0.01 Å, whereas the same bonds in compounds **2**−**4** are equal within the experimental error. As the oxygen atom O(11) is part of three hydrogen bonds and O(21) partici-

pates only in two hydrogen bonds, the Si(2)−O(21) bond is shorter than the corresponding Si(1)−O(11) bond.

Comparison of the Crystal structures of 2, 3, 4, and 5

The crystallographic data of compounds **2** to **5** are summarized in Table 1 and selected bond lengths and angles are given in Table 2.

Table 2. Comparison of selected bond lengths [Å] and angles [°] of **2**, **3**, **4** and **5**

	2	**3**	**4**	**5**
Si1−O11	1.618(2)	1.653(2)	1.6350(11)	1.6349(18)
Si2−O21	1.623(2)	1.652(2)	1.6304(11)	1.6246(18)
Si1−C11	1.890(3)	1.896(3)	1.8974(16)	1.898(3)
Si1−C15	1.891(3)	1.888(3)	1.9006(16)	1.897(3)
Si2−C21	1.890(3)	1.899(3)	1.8917(16)	1.891(3)
Si2−C25	1.884(3)	1.894(3)	1.8935(16)	1.896(3)
Si1−C1	1.875(3)	1.860(3)	1.8803(15)	1.861(2)
Si2−C4	1.878(3)	1.871(3)	1.8830(15)	1.867(2)
O11−Si1−C1	106.13(13)	105.08(12)	107.54(6)	101.33(10)
O11−Si1−C11	107.67(14)	109.06(11)	106.38(7)	108.89(11)
O11−Si1−C15	109.61(13)	106.95(12)	108.23(6)	110.41(11)
C11−Si1−C15	117.39(14)	116.88(12)	118.41(7)	116.33(12)
C11−Si1−C1	107.54(15)	110.34(13)	109.48(7)	108.40(11)
C15−Si1−C1	107.93(15)	107.84(12)	106.37(7)	110.41(11)
O21−Si2−C4	106.04(12)	100.07(12)	107.46(6)	107.84(10)
O21−Si2−C21	109.11(13)	111.30(12)	110.84(7)	104.60(11)
O21−Si2−C25	107.42(15)	108.35(13)	103.38(7)	110.49(10)
C21−Si2−C25	118.34(15)	117.36(12)	118.22(7)	117.20(12)
C21−Si2−C4	107.51(15)	107.12(12)	108.65(7)	108.96(11)
C25−Si2−C4	107.78(16)	111.28(13)	107.75(7)	106.45(11)
K1−F1	2.843(6)			
K1−O1	2.948(3)			
K1−O11	2.695(3)			
K1−O21	2.659(3)			
N1−C01				1.458(4)
N2−C02				1.463(4)

The X-ray analyses of **2**, **3**, **4**, and **5** show that the arrangement of the 2,5-bis(di-*tert*-butylhydroxysilyl)furan, which is the central structural element of all four structures, is mainly influenced by the guest molecule. In the case of compounds **2** and **4** the molecules form dimers that are held together by hydrogen bonds. Additionally, ionic interactions occur between potassium and the oxygen atoms of the disilanol in compound **2**. Again, hydrogen bonds between the guest molecules and the disilanol connect the monomers in compounds **3** and **5** to form long chains. Due to the arrangement of the silane molecules either as chains or as dimers in the crystals, the conformations of the silanol groups are different depending on the guest molecule.

Nevertheless, the bond lengths and angles of the disilanol molecules are very similar. The angles between the *tert*-butyl substituents at the silicon atoms are not tetrahedral but about 118° (**2:**118.34°; **3:** 116.88°; **4:** 118.41°; **5:** 116.33°) in all four structures to minimize steric hindrance. The geometry of the furan ring in these structures is identical within experimental error. As the four structures are not isostructural and the fixation of the different guest molecules is unique. Interatomic distances concerning hydrogen bonds between the monomers and guest molecules of **2** to **5** are given in Table 3.

Table 3. Interatomic distances concerning hydrogen bonds between the monomers and the guest molecules of compounds **2** to **5**

Compound **2**		
D−H···A	d(D···A)	<(DHA)
O(11)−H(11B)···O(21)#1	2.594(3)	147(8)
O(21)−H(21B)···O(11)#1	2.594(3)	142(8)
O(21)−H(21A)···F(1)#1	2.724(7)	170(7)
O(11)−H(11A)···F(1)#1	2.632(7)	172(8)
O(21)−H(21A)···O(1)	2.925(3)	110(6)
Symmetry transformations used to generate equivalent atoms: #1 $-x+1, -y+1, -z+2$		
Compound **3**		
O(11)−H(11)···O(21)#1	2.846(3)	171(3)
O(21)−H(21)···O(2)	2.759(4)	160(4)
O(2)−H(1)···O(11)#2	2.863(3)	175(4)
Symmetry transformations used to generate equivalent atoms: #1 $-x+1/2, -y, z+1/2$; #2 $x, y, z-1$		
Compound **4**		
O(11)−H(11)···N(1)	2.6539(18)	165(3)
N(1)−H(2)···O(21)	3.2326(19)	153(2)
N(1)−H(3)···O(1)#1	3.3228(18)	162(2)
O(21)−H(21)···O(11)#1	2.6935(16)	166(2)
Symmetry transformations used to generate equivalent atoms: #1 $-x, -y, -z+2$		
Compound **5**		
O(11)−H(11)···N(2)	2.667(3)	169(3)
O(21)−H(21)···N(1)	2.723(3)	169(3)
N(1)−H(2)···O(11)#1	3.265(3)	165(3)
N(2)−H(3)···O(11)#2	3.130(3)	169(2)
N(2)−H(4)···O(21)#3	3.116(3)	170(3)
Symmetry transformations used to generate equivalent atoms: #1 $-x+1, -y+1, -z$; #2 $-x+1, -y+2, -z$; #3 $x, y+1, z$		

Experimental Section

All experiments were performed under N_2. The NMR spectra were recorded in $CDCl_3$ with $SiMe_4$ as internal references. The mass spectrum of **1** was obtained with a Finnigan MAT 8200.

2,5-Bis(di-*tert*-butylhydroxysilyl)furan (1): 2,5-Bis(di-*tert*-butylfluorosilyl)furan (3.9 g, 0.01 mol) was added to a suspension of KOH (1.1 g, 0.02 mol) in Et_2O (200 mL) and the resulting mixture was stirred for 24 h. Separation of KF by filtration and condensation of the raw product into a cooled trap in vacuo (10^{-2} mbar) gave **1**. Yield: 98% (3.8 g), m.p. 95 °C. ^{1}H NMR ($CDCl_3$): δ = 1.04 (s, 36 H, CH_3), 1.63 (br. s, 2 H, OH), 6.78 (s, 2 H, 3-H, 4-H). ^{13}C NMR: δ = 20.00 [s, $C(CH_3)_3$], 27.29 [s, $C(CH_3)_3$], 121.16 (s, 3-H, 4-C), 161.0 (s, 2-C, 5-C). ^{29}Si NMR: δ = 1.08 (s). MS (EI): *m*/*z* (%) = 384 (15) $[M]^+$, 327 (100) $[M - C_4H_9]^+$. $C_{20}H_{40}O_3Si_2$ (384.70): calcd. C 62.96, H 10.48; found C 63.15, H 10.64.

2,5-Bis(di-*tert*-butylhydroxysilyl)furan Potassium Fluoride Adduct (2): The synthesis of **2** was performed analogously to the synthesis of **1**. Compound **2** crystallized out of the reaction mixture at room

temperature. Yield: 35% (1.4 g), m.p. > 260 °C (decomposition). $C_{40}H_{80}FKOSi_4$ (827.51): calcd. C 58.54, H 9.74; found C 59.02, H 10.05.

2,5-Bis(di-*tert*-butylhydroxysilyl)furan-hydrate (3): The synthesis of **3** was performed analogously to the synthesis of **2** in aqueous KOH solvent (5% H_2O in Et_2O). Compound **3** crystallized from the reaction solvent. Yield: 61% (2.5 g), m.p. 90 °C. $C_{20}H_{42}O_2Si_2$ (402.72): calcd. C 61.15, H 10.51; found C 61.02, H 10.38.

2,5-Bis(di-*tert*-butylhydroxysilyl)furan-ammoniate (4): A solution of **1** (1.9 g, 0.005 mol) in *n*-hexane (150 mL) was saturated with ammonia. Compound **4** crystallized as colourless prisms from the reaction mixture. Yield: 65% (2.6 g), m.p. 90 °C. $C_{20}H_{43}NO_3Si_2$ (401.73): calcd. C 60.29, H 10.79; found C 60.51, H 11.02.

2,5-Bis(di-*tert*-butylbutylhydroxysilyl)furan-methylamine (5): The synthesis of **5** was performed similarly to the synthesis of **4**, with $MeNH_2$ instead of NH_3. Yield: 20% (0.9 g). $C_{22}H_{50}N_2O_3Si_2$ (446.82): calcd. 59.14, H 11.28; found C 58.85, H 11.01.

X-ray Crystallographic Study: Crystals were mounted on a glass fibre in a rapidly cooled perfluoropolyether.[12] Data for compounds **3** and **4** were collected at 150(2) K, and data for compound **2** were collected at 210(2) K. The diffraction data of compounds **3** and **4** were collected on a Stoe AED2 four circle diffractometer with graphite-monochromated Mo-K_α radiation (λ = 0.71073 Å).

The diffraction data of compound **5** were collected on a Stoe−Siemens−Huber four-circle diffractometer coupled to a Siemens CCD area-detector at 133(2) K, with graphite-monochromated Mo-K_α radiation. The small, air-sensitive, plate-shaped crystals of **5** showed weaker diffraction than those of compounds **2**−**4**. This accounts for the somewhat higher values of the *R* factors obtained.

The structures were solved by direct methods using SHELXS-97[14] and refined against F^2 on all data by full-matrix least-squares with SHELXL-97.[15] All non-hydrogen atoms were refined anisotropically. The hydrogen atoms on the methyl groups of the *tert*-butyl ligands and the hydrogen atoms on the methylene groups of the furan ring were included in the model at geometrically calculated positions and refined using a riding model. The positions of the hydrogen atoms of the hydroxyl groups were located in the difference electron density map and the O−H bond lengths were restrained to be about 0.84 Å for compounds **3**, **4** and **5** and about 0.83 Å for compound **2**.

The structure of compound **3** is racemically twinned in the space group *Fdd*2.

In compound **2**, the position of the host molecule KF is only half occupied. Because of that the potassium fluoride molecule in the dimer is allowed to occupy one of two symmetry-related positions. As the formation of the hydrogen bonds depends on the orientation of the KF in the dimer, two half-occupied positions for the hydrogen atoms were refined as described above with an occupancy of 50%.

The unusual coordination sphere of the potassium atom (coordinated to the disilanol molecule and the fluorine atom, with the potassium above the base of a hexagonal pyramid) indicated the presence of a solvent molecule coordinated to the cation. However, residual electron density was not found near the cation and the packing of the dimers in the crystal does not allow enough space for additional ligands at the potassium.

CCDC-166872 (**2**), CCDC-166871 (**3**), CCDC-166873 (**4**) and CCDC-166874 (**5**) contain the supplementary crystallographic data for this paper. These data can be obtained free of charge at www.ccdc.cam.ac.uk/conts/retrieving.html [or from the Cambridge Crystallographic Data Centre, 12 Union Road, Cambridge CB2 1EZ, UK; Fax: (internat.) + 44-1223/336-033; E-mail: deposit@ccdc.cam.ac.uk].

Acknowledgments

We are grateful to the Fonds der Chemischen Industrie for financial support of this work.

[1] P. Neugebauer, U. Klingebiel, M. Noltemeyer, *Z. Naturforsch. B, Chem. Sci.* **2000**, *55*, 913.
[2] P. D. Lickiss, *Adv. Inorg. Chem.* **1995**, *42*, 14.
[3] L. King, A. C. Sullivan, *Coord. Chem. Rev.* **1999**, *6*, 1.
[4] U. Klingebiel, S. Schütte, D. Schmidt-Bäse, *The Chemistry of Inorganic Ring Systems* (Ed.: R. Steudel) Elsevier, Amsterdam, **1992**.
[5] R. Murugavel, M. Bhattacharjee, H. W. Roesky, *Appl. Organomet. Chem.* **1999**, *13*, 227.
[6] H. Puff, K. Braun, H. Reuter, *J. Organomet. Chem.* **1991**, *409*, 119.
[7] S. A. Bourne, L. R. Nassimbeni, K. Skobridis, E. Weber, *J. Chem. Soc., Chem. Commun.* **1991**, 228.
[8] E. Weber, K. Skobridis, I. Goldberg, *J. Chem. Soc., Chem. Commun.* **1989**, 1195.
[9] E. A. Babaian, M. Huff, F. A. Tibbals, D. C. Hrneir, *J. Chem. Soc., Chem. Commun.* **1990**, 306.
[10] C. Stanley, E. Livingstone, *Compr. Inorg. Chem.* **1973**, *3*, 1330.
[11] J. L. Atwood, J. E. D. Davies, D. D. Mac Nicol, *Inclusion Compounds, Vol. 1*, Academic Press Inc., London Ltd., **1984.**
[12] F. Toda, K. Tanaka, M. C. Wong, T. C. W. Mak, *Chem. Lett.* **1987**, 2069. D. J. Chadwick, C. Willbe, *J. Chem. Soc., Perkin Trans. 1*, **1977**, 887.
[13] T. Kottke, D. Stalke, *J. Appl. Cryst.* **1993**, *26*, 615.
[14] SHELXS-97, Program for structure solution. Release 97−2. © G. M. Sheldrick, **1986**−**1997**.
[15] SHELXL-97, Program for structure refinement. Release 97−2. © G. M. Sheldrick, **1986**−**1997**.

Received August 23, 2001
[I01326]

Interactions of Remote Alkyl Groups with Lanthanide Metal Centers: Synthesis, Characterization and Ligand Redistribution Reactions of Heterobimetallic Species Containing Trialkylaluminum Fragments

Garth R. Giesbrecht,[a] John C. Gordon,*[b] John T. Brady,[b] David L. Clark,[c] D. Webster Keogh,[b] Ryszard Michalczyk,[d] Brian L. Scott,[b] and John G. Watkin[b]

Keywords: Lanthanides / Samarium / Aluminum / O ligands / Agostic interactions

The reaction of $[Ln(OAr)_3]_2$ with four equivalents of trialkylaluminum leads to the formation of the bis-trialkylaluminum adducts $(ArO)Ln[(\mu\text{-}OAr)(\mu\text{-}R)AlR_2]_2$ [Ln = La, R = Me (**1**); Ln = La, R = Et (**3**); Ln = Sm, R = Et (**4**)]. The X-ray crystal structure of **1** reveals short La–C(bridging) distances of 2.800(5) and 2.759(5) Å. A reduced $^1J_{C\text{-}H}$ coupling constant of 110 Hz and a low energy ν(C–H) stretch in the solution and solid state IR spectra are consistent with a strong agostic La···H–C interaction in solution. Crystal data for **1**: a = 11.708(2) Å; b = 18.416(4) Å; c = 20.949(4) Å; α = 90°; β = 90°; γ = 90°; V = 4516.8(15) Å^3; Z = 4; $R1$ = 4.69%. The solid-state structure of the samarium ethyl derivative **4** reveals close contacts of 2.627(4) and 2.649(4) Å between the samarium center and the methylene carbons of the triethylaluminum groups. The room temperature ^{13}C NMR spectrum of **4** exhibits a $^1J_{C\text{-}H}$ coupling constant of 102 Hz; additionally, the fluxional process that exchanges methyl groups in **1** and **2** is slow enough on the NMR time scale to allow distinct methylene groups in **4** to be observed. Crystal data for **4**: a = 19.318(1) Å; b = 20.150(1) Å; c = 26.280(1) Å; α = 90°; β = 90°; γ = 90°; V = 10229.8(9) Å^3; Z = 8; $R1$ = 3.53%. Thermolysis of **1**–**4** results in ligand redistribution to form $[R_2Al(OAr)]_2$ [R = Me, Et (**5**)] and other unidentified species. Crystal data for **5**: a = 9.496(4) Å; b = 10.183(4) Å; c = 18.794(7) Å; α = 90.06(1)°; β = 92.394(7)°; γ = 114.976(6)°; V = 1645.6(11) Å^3; Z = 2; $R1$ = 10.13%.

Introduction

Aryloxide groups have proven to be suitable ancillary ligands in organolanthanide chemistry due in part to their ability to participate in π-bonding with electron-deficient metal centers.[1−3] Additionally, the coordination number and degree of oligomerization may be controlled through the use of bulky substituents on the arene ring. For example, use of the sterically demanding aryloxide ligand 2,6-di-*tert*-butyl-4-MeC_6H_2 leads to the formation of mononuclear complexes $Ln(OAr)_3$ for the entire lanthanide series.[4] Although these complexes are three-coordinate, they are essentially inert, with their reaction chemistry being limited to adduct formation with Lewis bases [i.e. $Ln(OAr)_3L$].[5] Previously, we demonstrated that the smaller 2,6-diisopropylphenoxide ligand bridges between metal centers in an unusual η^6-bridging mode to alleviate the steric unsaturation at the metal center.[1] Addition of a Lewis base to these complexes (e.g. THF, NH_3) leads to the formation of five-, six- or seven-coordinate species,[2] illustrating the large effect that a relatively small change in the steric bulk of the ancillary ligand may have upon a simple process such as adduct formation.

Recent studies of lanthanide alkoxide and aryloxide complexes have revealed that heterobimetallic complexes can often be obtained by utilizing the tendency of $^-$OR and $^-$OAr ligands to bridge two different metals.[6−10] Heterobimetallic complexes of the lanthanide metals (particularly when aluminum is one component) are of interest with respect to a) catalysis[11−13] and b) in the production of mixed-metal solid-state materials (e.g. lanthanide-doped ceramics) which may exhibit unusual and interesting physical properties.[14−18] In light of these reports, we were interested in exploring the reaction of these π-arene-bridged dimers with Lewis acids such as $AlMe_3$. Recently, we reported the solid state and solution properties of the mixed-metal complex $(ArO)Sm[(\mu\text{-}OAr)(\mu\text{-}Me)AlMe_2]_2$ (Ar = 2,6-*i*$Pr_2C_6H_3$) which maintains a strong agostic Sm···H−C interaction

[a] Nuclear Materials Technology Division, Los Alamos National Laboratory,
Los Alamos, New Mexico 87545, USA
[b] Chemistry Division, Los Alamos National Laboratory,
Los Alamos, New Mexico 87545, USA
Fax: (internat.) +1-505/667-9905
E-mail: jgordon@lanl.gov
[c] Glenn T. Seaborg Institute for Transactinium Science, Los Alamos National Laboratory,
Los Alamos, New Mexico 87545, USA
[d] Bioscience Division, Los Alamos National Laboratory,
Los Alamos, New Mexico 87545, USA

in solution.[19] However, the paramagnetism of trivalent samarium precluded a detailed study of this compound by ^1H and ^{13}C NMR spectroscopy. Thus, we sought to synthesize the diamagnetic lanthanum derivative in order to further investigate the nature of any fluxional processes that may be occurring in solution. Additionally, we were interested in the effect of introducing a larger Lewis acid into the coordination sphere (i.e. $AlEt_3$). Here we describe the synthesis and characterization of heterobimetallic complexes of lanthanum and samarium, and suggest that the solid-state structures of these agostic complexes may be viewed as potential "snapshots" of the intermediates present in the alkylation reaction of a lanthanide metal with trialkylaluminum reagents.

Results and Discussion

The addition of four equivalents of trimethyl- or triethylaluminum to a toluene solution of the π-arene bridged dimers $[Ln(OAr)_3]_2$ (Ar = 2,6-*i*$Pr_2C_6H_3$) (Ln = La, Sm)[1,2] yields the bis-trialkylaluminum adducts (ArO)Ln[(μ-OAr)(μ-R)$AlR_2]_2$ [Ln = La, R = Me (**1**); Ln = Sm, R = Me (**2**); Ln = La, R = Et (**3**); Ln = Sm, R = Et (**4**)] [Equation (1)].

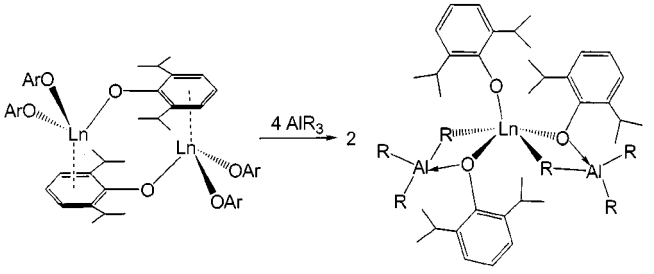

(1)

The trimethylaluminum adducts were isolated as colorless (La) and orange (Sm) solids in good yield. Complexes **1**−**4** are soluble in common organic solvents such as hexane and toluene. A measure of the crowding around the lanthanide center is given by the complexation of only two molecules of $AlMe_3$ or $AlEt_3$ per metal. In the reaction of $[Ln(OAr)_3]_2$ with six equivalents of AlR_3 only the bis-aluminum complex was isolated {and not Ln[(μ-OAr)(μ-R)-$AlR_2]_3$ as is observed for smaller alkoxide groups such as O*t*Bu (M = Y, Pr, Nd).[8,9]}

Single crystals of (ArO)La[(μ-OAr)(μ-Me)$AlMe_2]_2$ (**1**) were obtained by slow evaporation of a saturated toluene solution. An ORTEP view of the molecular structure is given in Figure 1; selected bond lengths and angles are given in Table 1. Complete details of the structural analyses of compounds **1**, **4** and $[Et_2Al(OAr)]_2$ (**5**) are presented in Table 4.

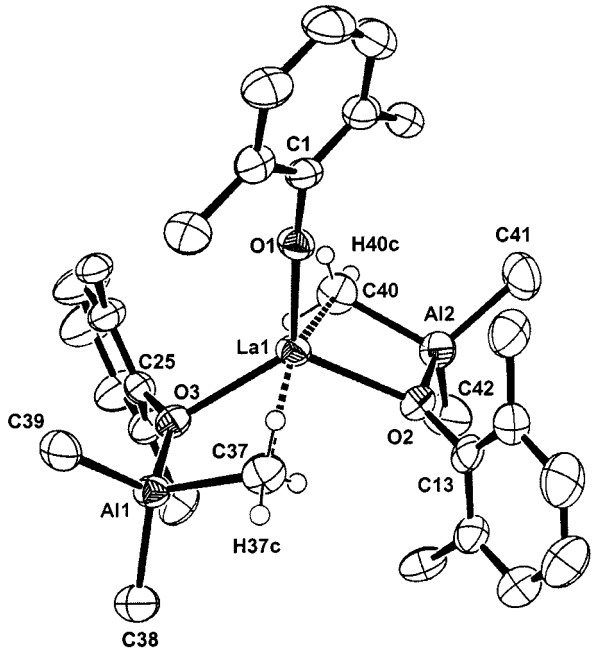

Figure 1. ORTEP view of (ArO)La[(μ-OAr)(μ-Me)$AlMe_2]_2$ (**1**) drawn with 30% probability ellipsoids; isopropyl methyl groups have been omitted for clarity

Table 1. Selected bond lengths (Å) and angles (deg) for (ArO)La-[(μ-OAr)(μ-Me)$AlMe_2]_2$ (**1**)

La1−O1	2.136(3)	La1−O2	2.387(3)
La1−O3	2.367(3)	La1−C37	2.800(5)
La1−C40	2.759(5)	O1−C1	1.369(5)
O2−C13	1.403(5)	O3−C25	1.386(4)
O2−Al2	1.864(3)	O3−Al1	1.848(3)
Al1−C37	2.040(5)	Al1−C38	1.969(5)
Al1−C39	1.967(5)	Al2−C40	2.053(6)
Al2−C41	1.964(6)	Al2−C42	1.963(6)
O1−La1−O2	116.16(11)	O1−La1−O3	120.72(11)
O1−La1−C37	99.27(15)	O1−La1−C40	102.87(16)
O2−La1−O3	122.01(10)	O2−La1−C37	93.70(13)
O2−La1−C40	69.82(15)	O3−La1−C37	67.56(12)
O3−La1−C40	106.43(14)	C37−La1−C40	156.62(16)
La1−O1−C1	175.2(3)	La1−O2−C13	125.4(2)
La1−O3−C25	108.1(2)	La1−O2−Al2	104.09(14)
La1−O3−Al1	107.31(12)	La1−C37−H37c	172(3)
La1−C40−H40c	177(4)		

The structure of **1** is isomorphous with that previously reported for the samarium derivative **2**. Both trimethylaluminum adducts crystallize in the orthorhombic space group $P2_12_12_1$ with equivalent unit cell parameters. As found for **2**, the geometry about the metal center is square-based pyramidal, with a terminal aryloxide ligand occupying the apical site and two [(μ-OAr)(μ-Me)$AlMe_2$] units in the basal plane of the molecule. The La−C distances of 2.800(5) and 2.759(5) Å are slightly longer than the Sm−C distances observed in **2** [2.620(5) and 2.632(5) Å] and reflect both the larger size of lanthanum and a weaker agostic Ln···H−C interaction.[20] By comparison, these bond lengths are longer than the La−C σ bonds in La[$CH(SiMe_3)_2]_3$

[2.515(9) Å][21] or (η^5-C_5Me_5)La[$CH(SiMe_3)_2$]$_2$ [2.537(5) and 2.588(4) Å][22] but similar to the Nd−C(bridging) distance reported in Nd[(μ-O*t*Bu)(μ-Me)$AlMe_2$]$_3$ (2.784 (11) Å].[9] A feature common to the crystal structures of **1**, **2** and **4** is the presence of two distinct types of lanthanide-oxygen bonds; the two longer bonds [2.387(3) and 2.367(3) Å in **1**] are a result of the interaction of the AlR_3 groups with the phenoxide oxygen atoms (i.e. there is a competition between two Lewis acid centers for the oxygen electron density). The third unique phenoxide ligand "compensates" for the electron-deficient nature of the lanthanide center by engaging in O→M π-bonding, as evidenced by the very short Ln−O distance [2.136(3) Å] and the almost linear La−O−C angle [175.2(3)°]. The hydrogen atoms on C37 and C40 were located and refined and define a trigonal bipyramidal geometry for these carbon atoms. The lanthanum center and H37c and H40c occupy the axial positions [La1−C37−H37c = 172(3)°, La1−C40−H40c = 177(4)°] with the aluminum center and the remaining hydrogen atoms in the equatorial positions. As was found for **2**, the hydrogen atoms do not point directly towards the lanthanide center, which supports a β-Al−C···La type of interaction in which electron density from the aluminum-carbon bond is donated to the metal center.[23,24] Consistent with this postulate is the observation of elongated $Al-C_{agostic}$ bonds [2.040(5) and 2.053(6) Å]; these bond lengths are about 0.1 Å longer than the remaining Al−C bonds in **1** [1.969(5) to 1.964(6) Å]. Overall, the metrical parameters of **1** are similar to those determined for the samarium derivative **2**, with the significant features of an agostic Ln···H−C interaction being present in both.

Orange crystals of (ArO)Sm[(μ-OAr)(μ-Et)$AlEt_2$]$_2$ (**4**) that were amenable to X-ray crystal diffraction were obtained by slow evaporation of a saturated hexamethydisiloxane solution. The molecular structure of **4** is shown in Figure 2 with a list of important bond lengths and angles available in Table 2.

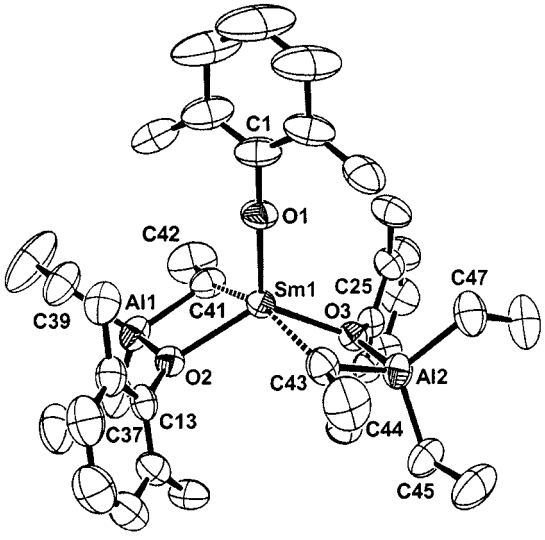

Figure 2. ORTEP view of (ArO)Sm[(μ-OAr)(μ-Et)$AlEt_2$]$_2$ (**4**) drawn with 30% probability ellipsoids; isopropyl methyl groups have been omitted for clarity

Table 2. Selected bond lengths (Å) and angles (deg) for (ArO)Sm[(μ−OAr)(μ-Et)$AlEt_2$]$_2$ (**4**)

Sm1−O1	2.060(2)	Sm1−O2	2.292(2)
Sm1−O3	2.295(2)	Sm1−C41	2.627(4)
Sm1−C43	2.649(4)	O1−C1	1.376(4)
O2−C13	1.404(4)	O3−C25	1.408(4)
O2−Al1	1.877(2)	O3−Al2	1.875(2)
Al1−C37	1.963(4)	Al1−C39	1.975(4)
Al1−C41	2.067(4)	Al2−C43	2.055(4)
Al2−C45	1.966(4)	Al2−C47	1.976(4)
O1−Sm1−O2	117.18(8)	O1−Sm1−O3	118.33(8)
O1−Sm1−C41	97.52(11)	O1−Sm1−C43	102.30(11)
O2−Sm1−O3	124.49(7)	O2−Sm1−C41	72.37(10)
O2−Sm1−C43	97.10(10)	O3−Sm1−C41	99.85(10)
O3−Sm1−C43	71.80(10)	C41−Sm1−C43	160.14(12)
Sm1−O1−C1	178.0(2)	Sm1−O2−C13	124.81(17)
Sm1−O3−C25	126.12(17)	Sm1−O2−Al1	103.60(9)
Sm1−O3−Al2	103.88(10)	Sm1−C41−C42	166.8(3)
Sm1−C43−C44	165.9(3)		

The structure of **4** is similar to that determined for **1** and **2**; however, in the case of **4**, the samarium center engages in agostic interactions with the methylene carbons of the triethylaluminum groups. The $Sm-C_{methylene}$ distances of 2.627(4) and 2.649(4) Å are similar to the Sm−C bond lengths to the bridging alkyl groups in **2** [2.620(5) and 2.632(5) Å]. The geometry about the agostic carbon atoms (C41, C43) is best described as trigonal bipyramidal, as are the agostic methyl carbons in **1** and **2**. In this case, the Sm−C−C bond angles are 166.8(3)° and 165.9(3)° (Sm1−C41−C42 and Sm1−C43−C44, respectively). The bond lengths and angles determined for the triethylaluminum derivative **4** are virtually identical to those observed for the trimethylaluminum analogue **2**. From this metric data, one would conclude that the substitution of a triethylaluminum group for a trimethylaluminum moiety has a negligible effect on steric congestion about the metal center. While the use of triethylaluminum does not result in longer $Sm-C_{agostic}$ bonds, the effect of using a larger Lewis acid on ligand dynamics in these complexes can be directly observed by ^{1}H NMR spectroscopy (vide supra).

We previously reported the ^{1}H and ^{13}C NMR spectra of (ArO)Sm[(μ-OAr)(μ-Me)$AlMe_2$]$_2$ (**2**); although the spectra were broadened by fluxional processes and the paramagnetism of Sm^{III}, we were able to extract a $^1J_{C\text{-}H}$ coupling constant of 106 Hz for the agostic methyl groups. Lowering the temperature to −90 °C did not result in decoalescence into separate methyl resonances as would be expected for a static structure. Thus, the coupling constant of 106 Hz may be viewed as an average of agostic and nonagostic coupling constants, indicating that the true $^1J_{C\text{-}H}$ coupling determined for the agostic methyl group would be significantly lower. This suggests a strong "classical" Sm···H−C agostic interaction, in which electron density from the C−H bond is donated to the electrophilic metal center.[25,26] This is supported by the infrared spectrum of **2**, which shows a weak intensity ν(C−H) stretch in the solid state and in solution (2728 cm^{-1}). It is possible that a number of different fluxional processes may give rise to the single aluminum-methyl

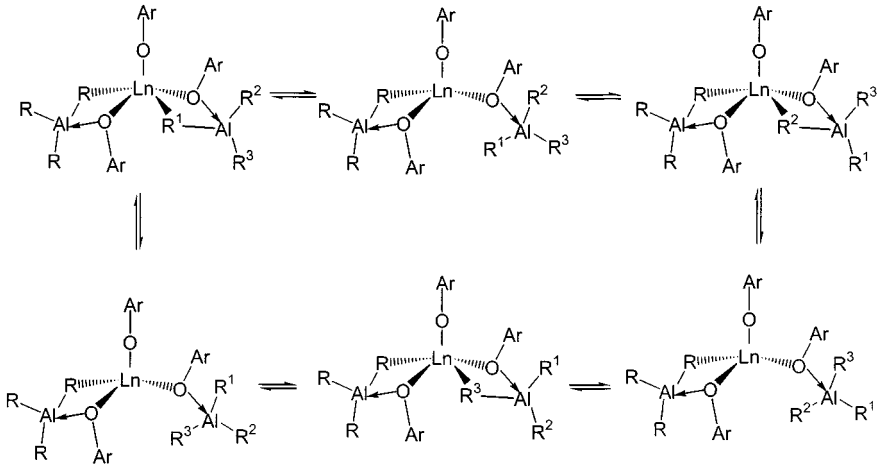

Scheme 1

resonance observed in the variable temperature NMR spectra of **2**: a) rotation about the O−Al bond may serve to average the three aluminum-methyl groups (Scheme 1), b) the trimethylaluminum units may remain fixed to their respective oxygen atoms, but flip between sides of the molecule, roughly defined by the three oxygens (Scheme 2), and c) the two trialkylaluminum moieties may rotate between the three oxygen sites (Scheme 3). In order to potentially distinguish between these three processes, we synthesized the diamagnetic lanthanum analogue in the hope of obtaining spectra that were not broadened by the presence of a paramagnetic metal center.

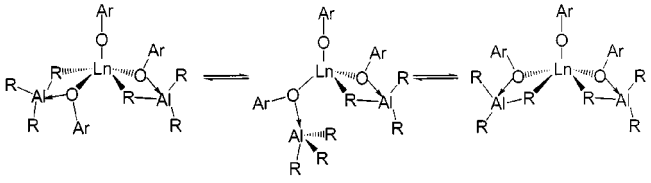

Scheme 2

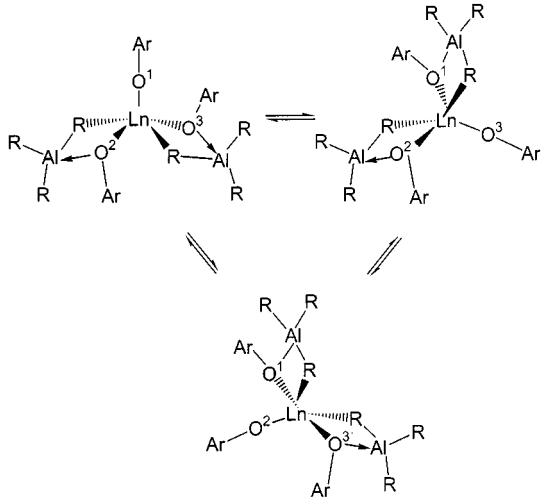

Scheme 3

The ambient temperature ^{1}H NMR spectrum of **1** exhibits a single sharp resonance for the aluminum-methyl groups ($\delta = -0.31$) consistent with rapid bridge-terminal exchange at room temperature (Scheme 1). Lowering the temperature to −90 °C ([D_8]toluene) causes a broadening of the resonance, but decoalescence into separate methyl signals was not observed. The isopropyl methine protons appear as septets in a 2:1 ratio at all temperatures ($\delta = 3.49$ and 3.36). This is consistent with a solution structure that retains the integrity of the aluminum-oxygen bonds at all temperatures, i.e. the trimethylaluminum groups do not exchange between all three aryloxides since this would result in an averaging of the methine proton signals into a single septet (Scheme 3). However, the observation of two methine signals does not allow one to assess whether the fluxional process detailed in Scheme 2 makes a significant contribution to the averaging of the aluminum methyl resonances in solution. In the solid state structure outlined in Figure 1, the four methine protons on the aryloxide ligands associated with the two coordinated trialkylaluminum groups are rendered equivalent both by symmetry (C_2) and by free rotation about the O−C_{ipso} bond; additionally, the two methine protons on the remaining aryloxide ligand are equivalent by symmetry. We note that the operation of a fluxional process such as that described in Scheme 2 would also result in the observation of two methine peaks in a 2:1 ratio, and therefore this piece of data alone does not allow us to determine whether the processes in Scheme 1, Scheme 2, or both, are operating. However, a study of the isopropyl group methyl resonances does allow a distinction to be made. The isopropyl methyl groups in **1** give rise to two doublets in a 2:1 ratio ($\delta = 1.29$ and 1.21); this is consistent with the fluxional process in Scheme 2 being operative at room temperature. Since the isopropyl methyl groups in **1** are diastereotopic in the case of a rigid solution structure, one would expect this region of the ^{1}H NMR spectrum to be more complicated. For example, the methyl groups of the uncomplexed aryloxide unit would result in two doublets of equal intensity. However, dissociation, rotation of the

[(μ-OAr)(μ-Me)AlMe$_2$] fragments about the La−O bonds, and reattachment to the other side of the molecule would generate two pseudo mirror planes (one roughly defined by the three oxygen atoms, and a second plane perpendicular to the first, containing La1, O1 and C1), allowing the four isopropyl methyl groups to appear as a single doublet. Cooling the sample to the low temperature limit (−90 °C) resulted in a loss of resolution such that only a single broad resonance was observed.

The room temperature $^{13}C\{^1H\}$ NMR spectrum of **1** displays a single resonance corresponding to the aluminum-bound methyl groups ($\delta = -0.6$). When the ^{13}C NMR spectrum is collected with proton coupling, a quadruplet is observed with a $^1J_{C\text{-}H}$ coupling constant of 110 Hz. This compares to a coupling constant of 106 Hz determined for the samarium analogue, (ArO)Sm[(μ-OAr)(μ-Me)AlMe$_2$]$_2$ (**2**). As for **2**, a single resonance was evident at all temperatures; thus the value of 110 Hz represents an average of agostic and nonagostic methyl groups. The slightly larger $^1J_{C\text{-}H}$ coupling constant for **1** is consistent with a weaker Ln···H−C agostic interaction and is reflected in the slightly longer Ln−C$_{agostic}$ bond lengths determined for **1**.

As observed previously for **2**, the ^1H NMR spectrum of the samarium triethylaluminum derivative, (ArO)Sm[(μ-OAr)(μ-Et)AlEt$_2$]$_2$ (**4**) consisted of broad, unassignable resonances due to the paramagnetism of samarium. However, in the $^{13}C\{^1H\}$ NMR spectrum, the aluminum-methylene resonances were upfield of the remaining resonances and could be identified by comparison with the spectrum of **2**. In contrast to **2**, the bridge-terminal exchange process is arrested at room temperature; the proton-coupled ^{13}C NMR spectrum displays two triplets in a 2:1 ratio ($\delta = 7.2$ and -5.3). The downfield resonance is twice the intensity of the upfield resonance, and exhibits a normal $^1J_{C\text{-}H}$ coupling constant of 126 Hz. Additionally, this resonance is only slightly broadened, indicating a limited direct contact with the paramagnetic metal center. Conversely, the upfield resonance is significantly broadened ($\Delta\nu_{1/2} = 150$ Hz vs. 50 Hz for **2**) suggesting a carbon atom that resides in a highly relaxed environment. The $^1J_{C\text{-}H}$ coupling constant of 102 Hz is lower than that determined for the agostic methyl groups in **1** or **2**; however, it should be noted that the coupling constant in **4** arises from a static structure, and indicates a weaker interaction than in **1** or **2**, where the $^1J_{C\text{-}H}$ coupling constants of 106 and 110 Hz, respectively, are the averaged values arising from agostic and nonagostic methyl groups. The infrared spectrum of **4** shows a low energy ν(C−H) stretch at 2727 cm^{-1}, which we have previously shown to be consistent with the presence of agostic Ln···C−H interactions in the solid state.[27] In the case of **4**, ^{13}C NMR spectroscopy provides direct evidence for the effect that small changes in sterics can have upon dynamic processes that occur in solution. Whereas X-ray crystallography suggests that the coordination sphere about the samarium center remains virtually unchanged upon going from trimethylaluminum to triethylaluminum, NMR spectroscopy indicates that the triethylaluminum group is sufficiently bulky to retard the fluxional processes postulated to be present in **1** and **2**.

In contrast to **1**, the ^1H and $^{13}C\{^1H\}$ NMR spectra of material isolated in an attempt to prepare (ArO)La[(μ-OAr)(μ-Et)AlEt$_2$]$_2$ (**3**) consist of a large number of resonances that are difficult to assign. From this data, it is evident that **3** is unstable and readily converts to other species in solution or in the solid state. If samples of **3** were left to stand at room temperature for several days, the formation of a dark brown oil and colorless crystals were observed. An X-ray crystallographic study of the crystals determined them to be the aluminum aryloxide species, [Et$_2$Al(OAr)]$_2$ (**5**). An ORTEP representation of the molecular structure of **5** is given in Figure 3. A partial list of bond lengths and angles is available in Table 3.

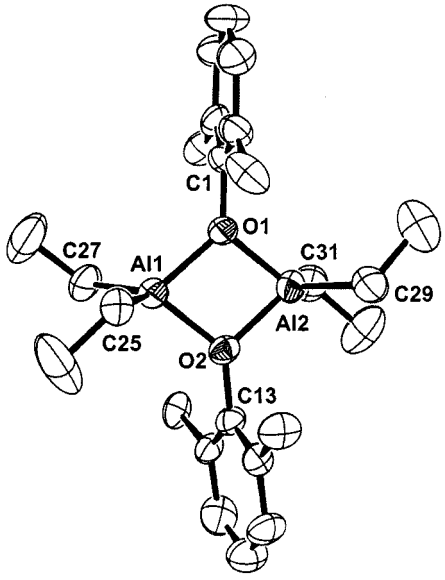

Figure 3. ORTEP view of [Et$_2$Al(OAr)]$_2$ (**5**) drawn with 30% probability ellipsoids; isopropyl methyl groups have been omitted for clarity

Table 3. Selected bond lengths (Å) and angles (deg) for [Et$_2$Al(OAr)]$_2$ (**5**)

Al1−O1	1.855(4)	Al1−O2	1.857(4)
Al1−C25	1.930(7)	Al1−C27	1.948(7)
Al2−O1	1.853(4)	Al2−O2	1.862(4)
Al2−C29	1.916(7)	Al2−C31	1.942(7)
O1−C1	1.420(7)	O2−C13	1.421(6)
O1−Al1−O2	79.65(18)	O1−Al1−C25	116.2(2)
O1−Al1−C27	112.1(3)	O2−Al1−C25	113.2(3)
O2−Al1−C27	116.2(3)	C25−Al1−C27	114.9(3)
O1−Al2−O2	79.56(17)	O1−Al2−C29	112.1(3)
O1−Al2−C31	117.2(3)	O2−Al2−C29	117.3(3)
O2−Al2−C31	112.1(2)	C29−Al2−C31	114.3(3)
C1−O1−Al1	130.5(4)	C1−O1−Al2	129.0(4)
Al1−O1−Al2	100.45(19)	C13−O2−Al1	134.0(4)
C13−O2−Al2	125.9(4)	Al1−O2−Al2	100.04(19)

The crystallographic analysis confirmed the dimeric nature of **5**, in which two aluminum centers are bridged by two phenoxide oxygen atoms. The structure of **5** is analogous to those determined for $[Me_2Al(\mu\text{-}O\text{-}2,6\text{-}i\text{Pr}_2C_6H_3)]_2$ [28] and $[Me_2Al(\mu\text{-}O\text{-}2,4,6\text{-}t\text{Bu}_3C_6H_2)]_2$ [29] and the Al−O and Al−C distances are similar in all three structures. Compound **5** was prepared independently and isolated as colorless crystals from the treatment of $AlEt_3$ with one equivalent of 2,6-diisopropylphenol in toluene after evaporation of the solvent. The isolation of the aluminum-aryloxide dimer **5** from a reaction mixture thought to contain the heterobimetallic species $(ArO)La[(\mu\text{-}OAr)(\mu\text{-}Et)AlEt_2]_2$ implies that aryloxide group transfer is relatively facile in these systems. Samples of $(ArO)La[(\mu\text{-}OAr)(\mu\text{-}Me)AlMe_2]_2$ (**1**) and $(ArO)Sm[(\mu\text{-}OAr)(\mu\text{-}Me)AlMe_2]_2$ (**2**) were re-examined by NMR spectroscopy and found to contain small amounts ($< 5\%$) of the previously reported aluminum phenoxide species, $[Me_2Al(\mu\text{-}O\text{-}2,6\text{-}i\text{Pr}_2C_6H_3)]_2$. Heating samples of **1** or **2** to 80 °C overnight resulted in an increase in the intensity of the signals due to $[Me_2Al(\mu\text{-}O\text{-}2,6\text{-}i\text{Pr}_2C_6H_3)]_2$, and the formation of a third, unidentified species (presumably a Ln dialkyl derivative). We suggest that a ligand redistribution reaction such as that detailed in Scheme 4 is occurring: original addition of four equivalents of trialkylaluminum to the π-arene-bridged dimers $[Ln(OAr)_3]_2$ results in the monomeric bis-trialkylaluminum adducts $(ArO)Ln[(\mu\text{-}OAr)(\mu\text{-}R)AlR_2]_2$ which are held together by dative O→Al bonds (I). Due to the steric constraints of the bulky aryloxide groups, only two trialkylaluminum groups per metal center are complexed. The electrophilic lanthanide center engages in further interactions to satisfy its Lewis acidity in the form of a π-bonding interaction with the remaining uncomplexed aryloxide group, and two agostic interactions with the methyl or methylene carbons of the trialkylaluminum units (II). Due to the oxophilicity of aluminum, and the weakened $Al-C_{agostic}$ bonds in II, an alkyl group from each aluminum atom is transferred to the lanthanide center as two formal aluminum-oxygen bonds are formed (III). The bis-trialkylaluminum adduct then separates into three discrete species (IV) which then recombine to form one equivalent of the dimeric aluminum-aryloxide species $[R_2Al(OAr)]_2$ (V) and a lanthanide dialkyl species (VI), which is most likely unstable and reacts further to form other unidentified decomposition products.

In the sense that II is an intermediate in the ligand redistribution reaction of $(ArO)Ln[(\mu\text{-}OAr)(\mu\text{-}R)AlR_2]_2$ to form $[R_2Al(OAr)]_2$ and "R_2LnOAr", the crystal structures of $(ArO)La[(\mu\text{-}OAr)(\mu\text{-}Me)AlMe_2]_2$ (**1**), $(ArO)Sm[(\mu\text{-}OAr)(\mu\text{-}Me)AlMe_2]_2$ (**2**) and $(ArO)Sm[(\mu\text{-}OAr)(\mu\text{-}Et)AlEt_2]_2$ (**4**) may be viewed as "snapshots" of these intermediates, where the migration of the methyl and/or ethyl groups from the aluminum to the metal center has been arrested.[30]

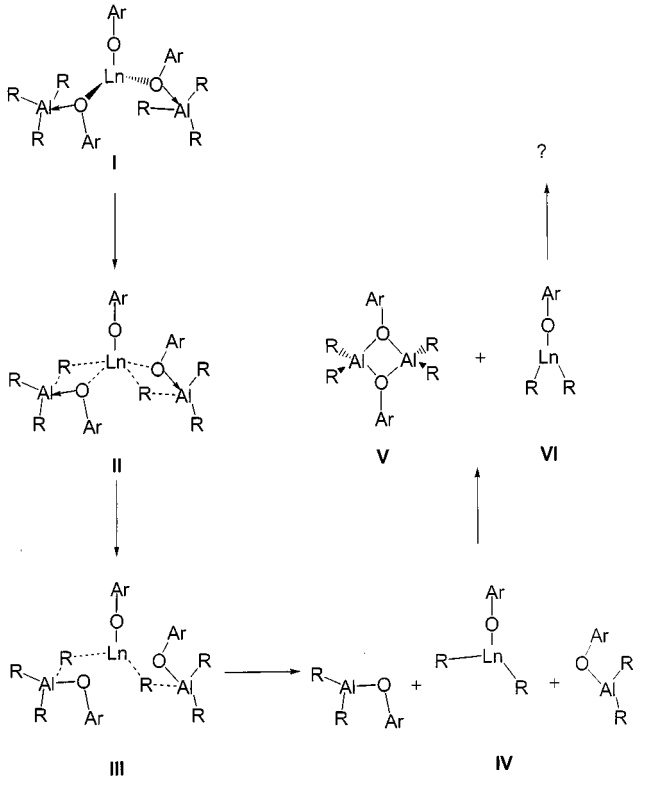

Scheme 4

Conclusions

The synthesis of heterobimetallic complexes of the lanthanides is easily achieved by the addition of trialkylaluminum reagents to the dimeric starting materials, $[Ln(OAr)_3]_2$. By utilizing the bulky 2,6-ddiisopropylphenoxide ligand, adduct formation stops after the addition of two trialkylaluminum units per metal center, which contrasts with trialkylaluminum adducts of the smaller alkoxide, $Ln[(\mu\text{-}Ot\text{Bu})(\mu\text{-}Me)AlMe_2]_3$. These heterobimetallic complexes appear to lie somewhere on a continuum between classical Ln···H−C interactions and Ln···C−X bonding modes which have recently been described. The staggered hydrogens on the five-coordinate agostic carbons and the elongated Al−C bonds in the crystal structures of **1** and **4** support the donation of electron density from the aluminum-carbon bond to the lanthanide center; however, the reduced C−H coupling constants and the lowered infrared stretching frequencies are consistent with a more conventional γ-C−H···Ln interaction. The averaging of the trialkylaluminum methyl groups in the ambient temperature NMR spectra of **1** is likely a result of two separate processes: 1) rotation about the O−Al bond, and 2) the flipping of trialkylaluminum units to opposite sides of the molecule while remaining bound to the aryloxide oxygen atoms. The effect of the larger trialkylaluminum group in **4** is evidenced by ^{13}C NMR spectroscopy, where the bridging and terminal methylene groups give rise to distinct resonances. These adducts readily undergo alkyl/aryloxide group transfer upon thermolysis; thus the crystals structures of **1** and **4** may not only be viewed as examples of lanthanide centers engaging in agostic interactions with remote alkyl groups, but also as intermediates in the transfer of alkyl groups from an aluminum atom to a highly electrophilic lanthanide center.

Experimental Section

General Remarks: All manipulations were carried out under an inert atmosphere of oxygen-free UHP grade argon using standard Schlenk techniques or under oxygen-free helium in a Vacuum Atmospheres glovebox. $AlMe_3$ (2.0 M hexane solution) and $AlEt_3$ (1.9 M toluene solution) were purchased from Aldrich and used as received. 2,6-diisopropylphenol was purchased from Aldrich, distilled over sodium and crystallized at −40 °C prior to use. $[Sm(OAr)_3]_2$,[1] $[La(OAr)_3]_2$ [2] and $[Me_2Al(OAr)]_2$ [28] were prepared according to literature procedures. Hexane and toluene were deoxygenated by passage through a column of supported copper redox catalyst (Cu-0226 S) and dried by passing through a second column of activated alumina. Hexamethyldisiloxane was distilled over sodium benzophenone and degassed prior to use. $[D_6]$benzene and $[D_8]$toluene were degassed, dried over Na-K alloy, and trap-to-trap distilled before use. ^{1}H NMR spectra were recorded on a Bruker AMX 500 spectrometer at ambient temperature; chemical shifts are given relative to residual $[D_5H]$benzene (δ = 7.15) or $[D_7H]$toluene (δ = 2.09). ^{13}C NMR chemical shifts are given relative to $[D_6]$benzene (δ = 128.39) or $[D_8]$toluene (δ = 20.4). Infrared spectra were recorded on a Nicolet Avatar 360 FT-IR spectrometer; solid-state spectra were taken as Nujol mulls between KBr plates, while solution spectra were recorded as benzene solutions vs. a solvent blank in KBr cells. Elemental analyses were performed on a Perkin−Elmer 2400 CHN analyzer. Elemental analysis samples were prepared and sealed in tin capsules in a glovebox prior to combustion.

(ArO)La[(μ-OAr)(μ-Me)AlMe$_2$]$_2$ (1): $AlMe_3$ (0.75 mL of a 2.0 M solution in hexane, 1.50 mmol) was added to a toluene solution of $[La(OAr)_3]_2$ (500 mg, 0.37 mmol). The mixture was stirred at room temperature for 30 minutes and then filtered through a Celite pad. The solvent was removed under vacuum and the sticky residue was washed with a minimum of hexane. Slow evaporation of a saturated toluene solution yielded waxy, colorless crystals (420 mg, 68% yield). ^{1}H NMR (500 MHz, $[D_8]$toluene): δ = −0.31 (s, 18 H, Al*Me$_3$*), 1.21 and 1.29 (2:1 d, $^3J_{H\text{-}H}$ = 6.6 Hz, 36 H, CH*Me$_2$*), 3.36 and 3.49 (1:2 sept, $^3J_{H\text{-}H}$ = 6.6 Hz, 6 H, C*H*Me$_2$), 6.70−7.20 (overlapping m, 9 H, *m,p*-H). ^{13}C{^{1}H} NMR (125 MHz, $[D_8]$toluene): δ = −0.6 (Al*Me$_3$*), 24.5, 24.8 and 24.9 (isopropyl methyl), 27.6 and 28.2 (isopropyl methine), 121.2, 123.0, 123.8 and 124.2 (phenyl *C*H), 136.7, 139.8, 147.0 and 159.1 (tertiary phenyl). Selected ^{13}C NMR spectroscopic data (125 MHz, $[D_8]$toluene): δ = −0.6 (q, $^1J_{C\text{-}H}$ = 110 Hz, Al*Me$_3$*). IR (Nujol): $\tilde{\nu}$ = 2783 cm^{-1} (m), 2725 (m), 1588 (m), 1364 (s), 1322 (s), 1252 (s), 1197 (s), 1097 (s), 1054 (m), 1041 (s), 933 (s), 886 (s), 835 (s), 797 (s), 758 (s), 703 (s), 628 (s). $C_{42}H_{69}Al_2LaO_3$ (814.9): calcd. C 61.91, H 8.53; found C 60.97, H 8.24.

(ArO)La[(μ-OAr)(μ-Et)AlEt$_2$]$_2$ (3): $AlEt_3$ (0.75 mL of a 1.9 M solution in toluene, 1.50 mmol) was added to a toluene solution of $[La(OAr)_3]_2$ (500 mg, 0.37 mmol). The mixture was stirred at room temperature for 90 minutes. The solvent was removed under vacuum and the residue was washed with a minimum of hexane to yield a colorless oil. Over a period of several days, the residue changed into a mixture of a dark red oil and large colorless crystals. X-ray crystallography indicated that the crystals consisted of $[Et_2Al(OAr)]_2$ (**5**). No discrete lanthanum-containing species were identified.

(ArO)Sm[(μ-OAr)(μ-Et)AlEt$_2$]$_2$ (4): $AlEt_3$ (0.47 mL of a 1.9 M solution in toluene, 0.91 mmol) was added to a toluene solution of $[Sm(OAr)_3]_2$ (310 mg, 0.23 mmol), causing an immediate color change from yellow to orange. The mixture was stirred at room temperature for 90 minutes. The solvent was removed under vacuum and the sticky residue was washed with a minimum of hexane. Slow evaporation of a saturated hexamethyldisiloxane solution yielded small orange crystals (340 mg, 80% yield). Selected ^{13}C NMR spectroscopic data (125 MHz, $[D_6]$benzene): δ = 7.2 (t, $^1J_{C\text{-}H}$ = 126 Hz, 4C, nonagostic Al*C*H$_2$), −5.3 (t, $^1J_{C\text{-}H}$ = 102 Hz, $\Delta\nu_{1/2}$ = 150 Hz, 2C, agostic Al*C*H$_2$). IR (Nujol): $\tilde{\nu}$ = 2785 cm^{-1} (w), 2727 (w), 1588 (m), 1424 (s), 1391 (s), 1317 (m), 1243 (m), 1186 (m), 1181 (m), 1088 (m), 1047 (w), 1030 (m), 965 (w), 948 (m), 924 (w), 883 (m), 855 (m), 825 (m), 785 (s), 735 (s), 686 (w), 673 (m), 654 (w). $C_{48}H_{81}Al_2O_3Sm$ (910.5): calcd. C 63.32, H 8.97; found C 61.69, H 9.36.

[Et$_2$Al(OAr)]$_2$ (5): $AlEt_3$ (1.00 mL of a 1.9 M solution in toluene, 1.90 mmol) was added to a toluene solution of 2,6-diisopropylphenol (340 mg, 1.90 mmol). Gas evolution was apparent immediately. The reaction mixture was stirred for 1 h, and the solvent removed under vacuum to yield a white, crystalline solid (420 mg, 84% yield). ^{1}H NMR (500 MHz, $[D_6]$benzene): δ = 0.41 (q, $^3J_{H\text{-}H}$ = 8.2 Hz, 8 H, CH$_3$C*H$_2$*Al), 1.01 (t, $^3J_{H\text{-}H}$ = 8.2 Hz, 12 H, C*H$_3$*CH$_2$Al), 1.30 (d, $^3J_{H\text{-}H}$ = 6.8 Hz, 24 H, CH*Me$_2$*), 3.72 (sept, $^3J_{H\text{-}H}$ = 6.8 Hz, 4 H, C*H*Me$_2$), 6.95−7.04 (overlapping m, 6 H, *m,p*-H). ^{13}C{^{1}H} NMR (125 MHz, $[D_6]$benzene): δ = 0.8 (CH$_3$*C*H$_2$Al), 10.6 (*C*H$_3$CH$_2$Al), 25.9 (*C*HMe$_2$), 27.2 (CH*Me$_2$*), 125.7 and 125.9 (phenyl *C*H), 141.0 (*o*-phenyl), 145.8 (*ipso*-phenyl). IR (Nujol): $\tilde{\nu}$ = 1445 cm^{-1} (s), 1411 (m), 1383 (m), 1377 (m), 1344 (w), 1320 (w), 1260 (m), 1245 (w), 1189 (m), 1162 (s), 1097 (s), 1054 (m), 1041 (w), 972 (m), 949 (m), 933 (m), 884 (m), 833 (s), 800 (m), 758 (s), 693 (s), 668 (s), 633 (s), 610 (s). $C_{32}H_{54}Al_2O_2$ (524.7): calcd. C 73.25, H 10.37; found C 72.31, H 11.04.

X-ray Crystallographic Studies: Crystals of **1**, **4**, and **5** were mounted on a thin glass fiber using a small dot of silicone grease. The crystals were then immediately placed on a Bruker P4/CCD/PC diffractometer, and cooled to 203 K using a Bruker LT-2 temperature device. The data were collected using a sealed, graphite monochromatized Mo-K_α X-ray source. A hemisphere of data was collected using a combination of and ω scans, with 30-second frame exposures and 0.3° frame widths. Data collection and initial indexing and cell refinement was handled using SMART[31] software. Frame integration and final cell parameter calculations were carried out using SAINT[32] software. The data were corrected for absorption using the SADABS[33] program. Decay of reflection intensity was not observed.

The structures were solved using Direct methods and difference Fourier techniques. The initial solution revealed all non-hydrogen atom positions. The methyl hydrogen atom positions for C37 and C40 (**1**) were found on the difference map and refined with their isotropic temperature factors set to 0.08 Å^2. The methylene hydrogen atom positions for C41 and C43 (**4**) were also found and refined as described above. All other hydrogen atoms positions were idealized, C−H = 0.93 Å (aromatic), 0.96 Å (methyl), 0.98 Å (methine) and 0.97 Å (methylene). The hydrogen atoms were refined using a riding model, with isotropic temperature factors fixed at 1.5 (methyl) or 1.2 (all others) times the equivalent isotropic U of the atom they are bonded to. The final refinement[34] included anisotropic temperature factors on all atoms. Structure solution, refinement, graphics, and creation of publication materials were performed using SHELXTL NT.[35] Additional details of data collection and structure refinement are listed in Table 4. Crystallographic data (excluding structure factors) for the structures reported in this paper have been deposited with the Cambridge Crystallographic Data Centre as supplementary publication nos. CCDC-171086 (**1**), CCDC-171087 (**4**) and CCDC-171088 (**5**). Cop-

Table 4. Crystallographic data

Compound	**1**	**4**	**5**
Formula	$C_{42}H_{69}Al_2LaO_3$	$C_{48}H_{81}Al_2O_3Sm$	$C_{32}H_{54}Al_2O_2$
Molecular Weight	814.84	910.44	524.71
Temperature, K	203(2)	203(2)	203(2)
Crystal System	Orthorhombic	Orthorhombic	Triclinic
Space Group	$P2_12_12_1$	*P*bca	$P\bar{1}$
Crystal Size, mm	0.16 × 0.16 × 0.12	0.12 × 0.12 × 0.31	0.28 × 0.20 × 0.12
a, Å	11.708(2)	19.318(1)	9.496(4)
b, Å	18.416(4)	20.150(1)	10.183(4)
c, Å	20.949(4)	26.280(1)	18.794(7)
α, °	90	90	90.06(1)
β, °	90	90	92.394(7)
γ, °	90	90	114.976(6)
V, Å^3	4516.8(15)	10229.8(9)	1645.6(11)
Z	4	8	2
D_{calc}, g/mL	1.198	1.182	1.059
Absorption coeffiecient, mm^{-1}	1.017	1.217	0.112
F(000)	1712	3848	576
Theta range, °	1.47 to 25.35	1.6 to 23.4	1.08 to 22.46
Total reflections	29540	36958	7343
Independent reflections	8251	7363	3969
GOF	1.103	1.439	1.334
R*1*	0.0469	0.0353	0.1013
*wR*2	0.0798	0.0719	0.2061

ies of the data can be obtained free of charge on application to CCDC, 12 Union Road, Cambridge CB2 1EZ, UK [Fax: (internat.) + 44-1223/336-033; E-mail: deposit@ccdc.cam.ac.uk].

Acknowledgments

We acknowledge the Office of Basic Energy Sciences, the Division of Chemical Sciences and the U. S. Department of Energy for funding (via the LDRD ER program). Los Alamos National Laboratory is operated by the University of California for the U.S. Department of Energy under Contract W-7405-ENG-36.

[1] D. M. Barnhart, D. L. Clark, J. C. Gordon, J. C. Huffman, R. L. Vincent, J. G. Watkin, B. D. Zwick, *Inorg. Chem.* **1994**, *33*, 3487−3497 and references therein.
[2] R. J. Butcher, D. L. Clark, S. K. Grumbine, R. L. Vincent-Hollis, B. L. Scott, J. G. Watkin, *Inorg. Chem.* **1995**, *34*, 5468−5476 and references therein.
[3] D. L. Clark, S. K. Grumbine, B. L. Scott, J. G. Watkin, *Organometallics* **1996**, *15*, 949−957 and references therein.
[4] P. B. Hitchcock, M. F. Lappert, A. Singh, *J. Chem. Soc., Chem. Commun.* **1983**, 1499−1501.
[5] G. H. Qi, Y. Lin, J. Hu, Q. Shen, *Polyhedron* **1995**, *14*, 413−415.
[6] K. G. Caulton, L. G. Hubert-Pfalzgraf, *Chem. Rev.* **1990**, *90*, 969−995.
[7] W. J. Evans, T. J. Boyle, J. W. Ziller, *J. Organomet. Chem.* **1993**, *462*, 141−148.
[8] W. J. Evans, T. J. Boyle, J. W. Ziller, *J. Am. Chem. Soc.* **1993**, *115*, 5084−5092.
[9] P. Biagini, G. Lugli, L. Abis, R. Millini, *J. Organomet. Chem.* **1994**, C16−C18.
[10] W. J. Evans, M. A. Ansari, J. W. Ziller, *Polyhedron* **1997**, *16*, 3429−3434.
[11] H. Sinn, W. Kaminsky, *Adv. Organomet. Chem.* **1980**, *18*, 99−149.
[12] G. Wilkinson, F. G. A. Stone, E. W. Abel, *Comprehensive Organometallic Chemistry, Vol. 3*, Pergamon Press, Oxford, **1982**, p. 475.
[13] L. Porri, A. Giarrusso, in *Comprehensive Polymer Science, Vol. 4* (Eds.: G. C. Eastmond, A. Ledwith, S. Russo, P. Sigwalt), Pergamon Press, Oxford, **1989**, p. 53.
[14] L. G. Hubert-Pfalzgraf, *New J. Chem.* **1987**, *11*, 663−675.
[15] D. C. Bradley, *Chem. Rev.* **1989**, *89*, 1317−1322.
[16] D. C. Bradley, *Polyhedron* **1994**, *13*, 1111−1121.
[17] L. G. Hubert-Pfaltzgraf, *New J. Chem.* **1995**, *19*, 727−750.
[18] R. C. Mehrotra, A. Singh, *Chem. Soc. Rev.* **1996**, 1−14.
[19] J. C. Gordon, G. R. Giesbrecht, J. T. Brady, D. L. Clark, D. W. Keogh, B. L. Scott, J. G. Watkin, *Organometallics* **2001**, in press.
[20] [20a] The difference in ionic radii between lanthanum (1.17 Å) and samarium (1.10 Å) is 0.07 Å. [20b] Taking this into account, the Ln−C distances in **1** are about 0.085 Å longer than those found in the samarium derivative **2**. [20b] R. D. Shannon, *Acta Crystallogr., Sect. A* **1976**, *32*, 751−767.
[21] P. B. Hitchcock, M. F. Lappert, R. G. Smith, R. A. Bartlett, P. P. Power, *Chem. Commun.* **1988**, 1007−1009.
[22] H. van der Heijden, C. J. Schaverien, A. G. Orpen, *Organometallics* **1989**, *8*, 255−258.
[23] C. J. Schaverien, G. J. Nesbitt, *J. Chem. Soc., Dalton Trans.* **1992**, 157−167.
[24] W. T. Klooster, L. Brammer, C. J. Schaverien, P. H. M. Budzelaar, *J. Am. Chem. Soc.* **1999**, 1381−1382.
[25] M. Brookhart, M. L. H. Green, L. L. Wong, *Prog. Inorg. Chem.* **1988**, *36*, 1−124.
[26] J. Eppinger, M. Spiegler, W. Hieringer, W. A. Herrmann, R. Anwander, *J. Am. Chem. Soc.* **2000**, *122*, 3080−3096.
[27] D. M. Barnhart, D. L. Clark, J. C. Gordon, J. C. Huffman, J.

G. Watkin, B. D. Zwick, *J. Am. Chem. Soc.* **1993**, *115*, 8461−8462.
[28] A. V. Firth, J. C. Stewart, A. J. Hoskin, D. W. Stephan, *J. Organomet. Chem.* **1999**, *591*, 185−193.
[29] B. Cetinkaya, P. B. Hitchcock, H. A. Jasim, M. F. Lappert, H. D. Williams, *Polyhedron* **1990**, *9*, 239−243.
[30] For a similar example of an arrested methyl-group migration, see: D. L. Clark, J. C. Gordon, J. C. Huffman, J. G. Watkin, B. D. Zwick, *Organometallics* **1994**, *13*, 4266−4270.
[31] SMART Version 4.210, **1996**, Bruker Analytical X-ray Systems, Inc., Madison, Wisconson, 53719.
[32] SAINT Version 4.05, **1996**, Bruker Analytical X-ray Systems, Inc., Madison, Wisconson, 53719.
[33] SADABS, first release, George Sheldrick, University of Göttingen, Germany.
[34] $R_1 = \Sigma||F_o|-|F_c||/\Sigma|F_o|$ and $R_{2w} = \{\Sigma[w(F_o^2 - F_c^2)^2]/\Sigma[\omega(F_o^2)^2]\}^{1/2}$; $w = 1/[\sigma^2(F_o^2) + (aP)^2]$, where $a = 0.0393(2)$, $0.0285(3)$, and $0.0719(4)$.
[35] SHELXTL NT Version 5.10, **1997**, Bruker Analytical X-ray Instruments, Inc., Madison, Wisconsin, 53719.

Received September 18, 2001
[I01367]

Synthesis and Reactivity of Group 6 and 10 Complexes of the Bis(dialkylaminophosphanyl)imine *i*PrN=C[$CH_2P(NiPr_2)_2$]$_2$

Françoise Dahan,[a] Philip W. Dyer,*[b] Martin J. Hanton,[b] Matthew Jones,[b] D. Michael P. Mingos,[c,d] Andrew J. P. White,[c] David J. Williams,[c] and Anna-Maria Williamson[c]

Keywords: P,N ligands / Chelates / Diaminophosphanes / Imines / Palladium

The coordination behaviour of the readily prepared, potentially ambidentate, bis(α,α′-phosphanyl)imine (iPr_2N)$_2$-PCH_2C(=N*i*Pr)$CH_2P(NiPr_2)_2$ (**1**, **PNP**) has been investigated. Treatment of palladium(II), platinum(II), chromium(0), and molybdenum(0) sources with ligand **1** afforded complexes in which **1** was coordinated solely in a bidentate *P,N*-chelating fashion with a non-coordinating bis(diisopropylamino)phosphanyl-substituted pendant arm. Ligand **1** and complexes [$PdCl_2$(**PNP**-κ^2*P,N*)] (**2**) and [$Mo(CO)_4$(**PNP**-κ^2*P,N*)] (**10**) were characterised in the solid state by X-ray crystallography. The preparation of cationic Pd^{II} derivatives of **PNP** is discussed.

Introduction

There is continued interest in hetero-bifunctional "hybrid" ligands, which possess two chemically distinct donor sites that are each able to interact to a different extent with a chelated metal centre (e.g. one soft and one hard donor).[1] The asymmetry present in systems of this type offers a degree of selectivity in reactions occurring at the metal centre, due to the electronic and steric disparity between the two different donor groups. In addition, it has been suggested that ligands of this type confer a "flexible" coordination environment at the metal centre, such that a vacant coordination site can be generated reversibly, without complete dissociation of the ligand (so-called "hemilability"). This feature is of considerable importance in catalysis and, since phosphanes are essential components in numerous industrially relevant catalytic processes, it is perhaps not surprising that many of the best-studied "hybrid" systems contain a *P*-donor constituent.

Currently there is a considerable resurgence in the use of heteroatom substituents at phosphorus to "tune" the steric demands and basicity of phosphane ligands.[2] This is due, in part, to the ease with which phosphorus−heteroatom bonds can be formed, as exemplified by *P*−*O* and *P*−*N* moieties. Diaminophosphanes have been targeted for study as they exhibit enhanced σ-donor strength (basicity) when compared with arylphosphanes and even triaminophosphanes, yet are often more easily prepared than strongly basic alkylphosphanes.[2h]

As the number of stoichiometric and catalytic applications involving hetero-bifunctional ligands increases,[3,4] simple, high-yielding syntheses of such species are of particular interest. Recently, we have reported the simple, "one-pot" synthesis of the bis(α,α′-phosphanyl)-substituted imines, e.g. **PNP** (**1**; Figure 1).[5] These compounds are rare examples of a potentially chelating diaminophosphane-containing "hybrid" ligand. However, the presence of one imino- and two phosphanyl-donor sites permits **1** to potentially adopt a number of different coordination modes, examples of which are outlined in Figure 1. Here we report preliminary studies of the coordination chemistry of this ligand, with particular emphasis placed on investigating its mode of binding.

Results and Discussion

Neutral Palladium(II) Derivatives

The dichloro complex [$PdCl_2$(**PNP**-κ^2*P,N*)] (**2**) is readily prepared through addition of **PNP** (**1**), prepared as reported previously,[5] to a dichloromethane solution of [$PdCl_2(NCPh)_2$] at ambient temperature, the reaction reaching completion within 1 h according to $^{31}P\{^1H\}$ NMR spectroscopy (Scheme 1). Removal of volatile components

[a] Laboratoire de Chimie de Coordination,
205 route de Narbonne, 31077 Toulouse, Cedex 4, France
[b] Department of Chemistry, University of Leicester,
University Road, Leicester, LE1 7RH, UK
Fax: (internat.) + 44-116/252-3789
E-mail: p.dyer@le.ac.uk
[c] Department of Chemistry, Imperial College,
Exhibition Road, South Kensington, London, SW7 2AY, UK
[d] Current address: St. Edmund Hall, University of Oxford,
Queens Lane, Oxford OX1 4AR, UK
Supporting information for this article is available on the WWW under http://www.eurjic.com or from the author.

 © WILEY-VCH Verlag GmbH, 69451 Weinheim, Germany, 2002 1434−1948/02/0303−0732 $ 17.50+.50/0 *Eur. J. Inorg. Chem.* **2002**, 732−742

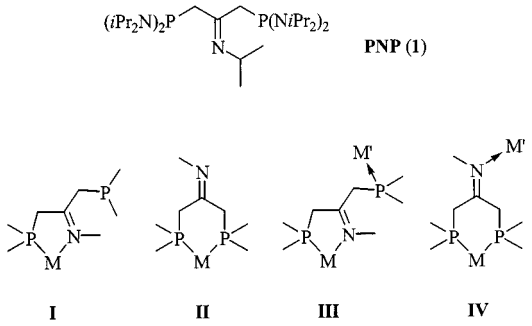

Figure 1. Ligand **1** and its potential binding modes

in vacuo, followed by washing with dry hexane affords **2** as a yellow, air-stable, analytically pure powder in 90% yield, which exhibits a fragment ion at *m*/*z* = 702 {[PdCl(**PNP**)]$^+$} by mass spectrometry.

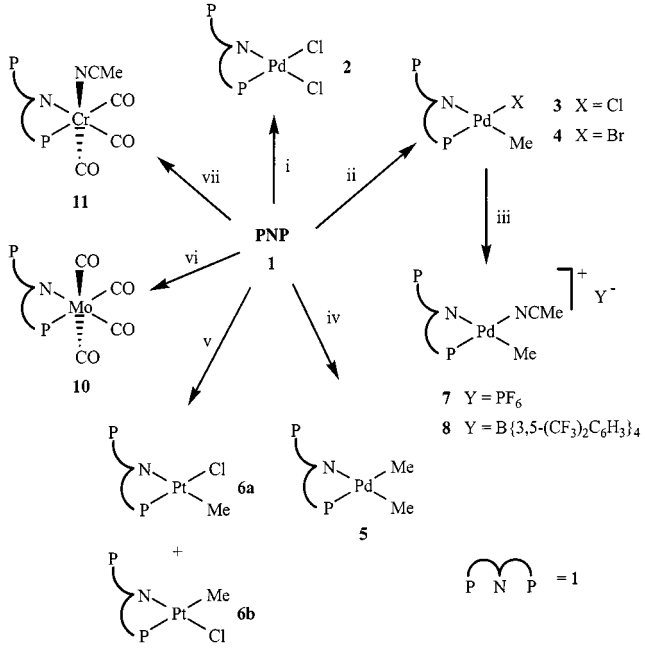

Scheme 1. Reagents and conditions: i: *trans*-[PdCl$_2$(NCPh)$_2$], CH$_2$Cl$_2$, room temp., 2 h; ii: [PdX(Me)(cod)] (X = Cl, Br), CH$_2$Cl$_2$, room temp., 1 h; iii: NaY {Y = PF$_6$, [B{3,5-(CF$_3$)$_2$C$_6$H$_3$}$_4$]}, CH$_3$CN, room temp., 3 d; iv: [PdMe$_2$(tmeda)], CH$_2$Cl$_2$, room temp., 2 d; v: [PtCl(Me)(cod)], CDCl$_3$, room temp., 3 d; vi: *cis*-[Mo(CO)$_4$(pip)$_2$], CH$_2$Cl$_2$, room temp., 18 h; vii: *fac*-[Cr(CO)$_3$(NCMe)$_3$], toluene, room temp., 2 d

The ^{31}P{^{1}H} NMR spectrum of complex **2** exhibits two sharp resonances at δ = +100.9 (s) and +51.9 (s). The considerable downfield shift of only one of the two resonances associated with **1** (Table 1) upon coordination (Δδ ≈ 50 ppm) suggests that in **2** the **PNP** ligand (**1**) is coordinated in a bidentate *P*,*N*-chelating bonding mode (**I**; Figure 1), with a pendant bis(diisopropylamino)phosphane arm.[6] The lack of any detectable $^4J_{PP}$ coupling constant for **2** could result either from an alteration in the angle between the two phosphorus centres or from the change in hybridization of the phosphorus atom upon coordination.[7] There is no evidence by NMR of any exchange between the free and bound phosphane components of **2** over the temperature regime −80 to +40 °C. The ^{1}H NMR spectroscopic data for the **PNP** moiety are little changed following its coordination to the palladium centre with the two methylene resonances being obtained at δ = 2.94 (s) and δ = 3.61 (d, $^2J_{PH}$ = 11.6, endocyclic C*H*$_2$), although the latter clearly exhibits a coupling to the phosphorus atom; both CH$_2$ groups appear as singlets in the ^{1}H NMR spectrum of **1**.[5] Similarly, ^{13}C NMR spectroscopy clearly distinguishes the two different CH$_2$ environments: δ = 54.4 (dd, $^1J_{PC}$ = 35.6, $^3J_{PC}$ = 10.8 Hz) and 38.5 (dd, $^1J_{PC}$ = 20.6, $^3J_{PC}$ = 9.8 Hz). The former has been assigned to the endocyclic methylene group based on its coordination chemical shift change (Δδ ≈ 10 ppm). As expected, the imine carbon atom appears as a doublet of doublets at δ = 176.6 ($^2J_{PC}$ = 16.5, 8.3 Hz), exhibiting a downfield shift compared with uncoordinated **1** [δ = 166.0 (dd, $^2J_{PC}$ = 15.0, 9.5 Hz)].

Table 1. ^{31}P NMR spectroscopic data for **PNP** (**1**) and its complexes

Compound	Solvent	^{31}P{^{1}H}
1	CDCl$_3$	+53.1 (d, $^4J_{PP}$ = 14.5 Hz), +46.2 (d, $^4J_{PP}$ = 14.5 Hz)[a]
2	CDCl$_3$	+100.9 (s), +51.9 (s)[b]
3	CDCl$_3$	+112.6 (s), +49.3 (s)[c]
4	CDCl$_3$	+114.5 (s), +49.8 (s)[c]
5	CDCl$_3$	+113. 2 (s), +48.9 (s)[b]
6	CDCl$_3$	+82.1 ($^1J_{PPt}$ = 6007.0), +49.0 (s) +70.2 ($^1J_{PPt}$ = 4565.0), +51.3 (s)
7	CDCl$_3$	+108.4 (s), +52.8 (s), −143.4 (sept, $^1J_{PF}$ = 706.5, PF$_6^-$)[c]
8	CDCl$_3$	+108.4 (s), +52.8 (s)[c]
9	CDCl$_3$	+108.4 (s), +52.9 (s)[c]
10	C$_6$D$_6$	+132.1 (s), +51.4 (s)[d]
11	CDCl$_3$	+158.3 (s), +50.3 (s)[d]

[a] 81.0 MHz. [b] 122.0 MHz. [c] 101.3 MHz. [d] 109.4 MHz.

Preparation of **2** through reaction of **1** with [PdCl$_2$(cod)] (cod = 1,5-cyclooctadiene) was considerably slower (ca. 2 d) than with [PdCl$_2$(NCPh)$_2$]. This observation is presumed to reflect the higher barrier to dissociation of the chelating cod ligand, compared with that for benzonitrile, and is consistent with the observation that [PdCl$_2$(tmeda)] does not react with **PNP**.

In contrast, **1** reacted rapidly at room temperature with dichloromethane solutions of [PdX(Me)(cod)] to afford [PdX(Me)(**PNP**-κ^2*P*,*N*)] [X = Cl (**3**), Br (**4**)] quantitatively within 1 h, according to ^{31}P NMR spectroscopy (Scheme 1). Complexes **3** and **4** could be isolated as air-stable, cream solids in 85 and 72% yields, respectively. The ^{31}P{^{1}H} NMR spectra suggest that ligand **1** again adopts a *P*,*N*-chelating bonding mode (**I**; Figure 1), with the formation of a single isomer in each case [e.g. **3**: δ: +112.6 (s), +49.3 (s)] (Table 1). In contrast with **2**, the endocyclic CH$_2$ resonance from **3** now displays both $^2J_{PH}$ and $^4J_{PH}$ couplings (overlapping resonances obscure the signal for **4**). The presence of one methyl ligand environment was confirmed

by both ^{1}H [e.g. **3**: δ = 0.71 (s)] and ^{13}C [e.g. **3**: δ = 0.8 (d)] NMR spectroscopy. The ^{1}H NMR chemical shifts associated with the methyl ligand are comparable to those observed for related [PdCl(Me)(*P′*,*N′*)] complexes (ca. 0.7 ppm).[8,9] Resonances corresponding to the exo- and endocyclic CH_2 groups are readily detected by ^{13}C NMR spectroscopy for **3** and **4**. Again, neither **3** nor **4** showed any evidence for exchange of the free and bound phosphane moieties.

The small magnitudes of the $^2J_{P-Pd-C}$ coupling constants associated with the methyl ligands (**3**: 7.3 Hz; **4**: 9.0 Hz) suggest that both complexes **3** and **4** adopt a structure in which the strongly *trans*-influencing methyl group lies *trans* to the weakly *trans*-influencing imine *N*-atom, i.e. the thermodynamically favoured form.[10] This is consistent with data from other palladium complexes possessing a *P*,*N*-ligand.[11] However, Boersma has indicated that caution must be used when spectroscopic methods are employed to assign *cis*/*trans* configurations about Pd for these types of complex.[8] The geometric assignment for complex **3** is strongly supported by a combination of COSY and NOE NMR experiments.

Attempts were made to prepare the corresponding dimethyl complex, [$PdMe_2$(**PNP**-κ^2*P*,*N*)], by methylation of complexes **2**, **3**, and **4** with Me_2LiCu, MeLi, or MeMgBr at low temperatures by analogy with previous work.[12] In each case, an inseparable mixture of products, including some resulting from deprotonation of the coordinated **PNP** ligand methylene backbone, was obtained on warming to room temperature. There was no evidence for the generation of any Pd−Me species.

In contrast, treating a dichloromethane solution of the known [$PdMe_2$(tmeda)] complex with 1 equiv. of ligand **1** cleanly afforded a single new product, which has tentatively been assigned as [$PdMe_2$(**PNP**-κ^2*P*,*N*)] (**5**), according to ^{31}P{^{1}H} NMR spectroscopy [δ = +113.2 (s), +48.9 (s)] in 77% yield (Scheme 1).[9] Complete displacement of tmeda by **PNP** occurred within 2 d at room temperature. The exchange is presumably aided by the strong *trans* influence of the two methyl groups that facilitate dissociation of the diamine.

Problems were encountered, however, with the ^{1}H and ^{13}C NMR spectra associated with **5**. In both cases, only a single resonance attributable to a palladium-bound methyl ligand could be detected [^{1}H: δ = 0.73 (d, $^3J_{PH}$ 0.9 Hz); ^{13}C: δ = −0.6 (d, $^2J_{PC}$ 7.8 Hz)]. Variable-temperature, T_1, and correlated ^{1}H/^{13}C NMR spectra were obtained but did not aid identification.

The correct formulation of **5** as [$PdMe_2$(**PNP**-κ^2*P*,*N*)] was suggested by mass spectrometry, which exhibited ions at *m*/*z* = 681 and 695 corresponding to the species [PdH(Me)(**PNP**)]$^+$ and [$PdMe_2$(**PNP**)]$^+$, respectively. Elemental analyses were irreproducible and inconclusive, possibly as a result of the lack of long-term thermal stability of the dimethyl complex. However, further support for the formation of the desired species was obtained by treating a sample of **5** with 1 equiv. of dppe in dichloromethane. This cleanly afforded the known [$PdMe_2$(dppe)] complex (δ = +55.7) with concomitant liberation of ligand **1**, according to ^{31}P{^{1}H} NMR spectroscopy.[12]

Neutral Platinum(II) Derivatives

Attempts were made to prepare the analogous platinum(II) complexes of **PNP**. Somewhat surprisingly, no reaction was observed between either [$PtCl_2$(cod)] or [$PtCl_2(NCR)_2$] (R = Me, Ph) and ligand **1** in chlorinated solvents even at elevated temperatures (under rigorously dry and anaerobic conditions). In each case, **1** could be recovered unchanged. However, displacement of cod from unsymmetrical [PtCl(Me)(cod)] by **1** proved more facile (vide supra). After 3 d at room temp., [PtCl(Me)(**PNP**-κ^2*P*,*N*)] (**6a**,**b**) was obtained as a mixture of *trans* and *cis* isomers according to ^{31}P NMR spectroscopy (20:1) in $CDCl_3$, the product in which the phosphorus atom lies *trans* to the chloride ion (**6a**) being the major species ($^1J_{PtP}$ = 6007.0 Hz). No interconversion of isomers was observed on prolonged heating.

Cationic Palladium(II) Derivatives

Part of our interest in group 10 complexes of the sterically demanding ligand **PNP**, arises from their potential to serve as precursors to the corresponding cationic Pd^{II} salts for application in olefin oligomerisation and polymerisation.[14,15] Initial, unsuccessful attempts to prepare the desired alkyl cations focussed on halide abstraction from acetonitrile solutions of the dichloro and chloro(methyl) complexes **2** and **3**, respectively, using a variety of silver salts. In each case, oxidation and subsequent decomposition of the *P*,*N*-ligand accompanied by precipitation of colloidal palladium was observed.

In contrast, halide abstraction from **3** using 1 equiv. of NaY (Y = PF_6, [B{3,5-$(CF_3)_2C_6H_3$}$_4$]) proceeded cleanly in acetonitrile at room temperature to afford the monocationic acetonitrile adducts [PdMe($NCCH_3$)(**PNP**-κ^2*P*,*N*)]Y {Y = PF_6 (**7**); Y = [B{3,5-$(CF_3)_2C_6H_3$}$_4$] (**8**)} (Table 1, Scheme 1), which could be isolated as moisture-sensitive, yellow/brown solids. Elemental analyses and variable-temperature ^{1}H NMR spectroscopy confirmed the presence of acetonitrile in both complexes. At 300 K complex **7** presents a broadened resonance at δ = 2.33 ($\nu_{1/2}$ = 11 Hz), which is replaced by two singlets (δ = 2.45 and 2.04) in a 50:1 ratio at 243 K, corresponding to bound and a trace of residual free CH_3CN, respectively. [Pure acetonitrile displays a single resonance at δ = 2.04 by ^{1}H NMR spectroscopy (400.1 MHz, $CDCl_3$) at 243 K.] This behaviour has been attributed to the CH_3CN ligand of **7** undergoing slow exchange with any residual CH_3CN at 300 K, a process that no longer occurs at lower temperatures. Similarly, complex **8** exhibits a single resonance at δ = 2.23 (300 K), which is resolved into two signals at 243 K (δ = 2.30 and 2.04) corresponding to bound and free CH_3CN, respectively.

Surprisingly, treatment of **3** with $NaBPh_4$ under identical reaction conditions resulted in the formation of the acetonitrile-free salt [PdMe($NCCH_3$)(**PNP**-κ^2*P*,*N*)][BPh_4] (**9**), as confirmed by both elemental analyses and variable-temper-

ature ^{1}H NMR spectroscopy. Indeed, the room-temperature ^{1}H NMR spectrum of a freshly prepared $CDCl_3$ solution of **9** shows no evidence of free or bound acetonitrile. On lowering the temperature to 243 K, a small resonance corresponding to a trace of residual unbound CH_3CN was detected (δ = 2.04), despite extended drying of the solid sample of **9** under high vacuum. There was no indication of bound acetonitrile. Addition of 1.1 equiv. of CH_3CN to this sample, followed by cooling to 243 K, merely increased the intensity of the signal corresponding to unbound CH_3CN.

The coordination of the tetraphenylborate anion to electron-deficient metal centres is now well documented.[16] Thus, it seems reasonable to suggest that the formation of complex **9** as a base-free species has to be attributed to the presence of the $[BPh_4]^-$ anion presumably as a result of ion pairing. However, variable-temperature ^{1}H NMR spectroscopy, over the temperature regime 243−300 K, could not establish the nature of the cation−anion interaction for **9**. The possibility of intermolecular coordination of the pendant diaminophosphane arm or a monomer/dimer equilibrium was, however, clearly ruled out by ^{31}P NMR spectroscopy (243−300 K).

Salts **7** and **8** are stable in acetonitrile solution and in the solid state under nitrogen (months). Complex **8** is also stable in $CDCl_3$ solution, but both **7** and **9** decompose slowly in dry chlorinated solvents (24 h at room temp.). Despite the differences in structure, complexes **7**−**9** exhibit virtually identical ^{31}P NMR spectra, in both CD_3CN and $CDCl_3$. As for the neutral Pd^{II} derivatives, ^{13}C NMR spectroscopy readily distinguishes two CH_2 environments for the cationic derivatives **7**−**9**. Just as was observed for **3** the ^{1}H NMR spectra of these complexes display both $^2J_{PH}$ and $^4J_{PH}$ couplings to the endocyclic CH_2 resonance.

In the olefin polymerisation arena, high catalytic activities have been achieved by combining sterically encumbered metal alkyl cations with a noncoordinating anion such as the perfluorinated analogue of BPh_4, $[B(C_6F_5)_4]^-$.[17] Hence, a number of attempts were made to prepare the palladium **PNP** salts of this anion. Both halide elimination from **3**, using $Li[B(C_6F_5)_4]$, and alkyl abstraction from the proposed dimethyl complex **5** by $[Ph_3C][B(C_6F_5)_4]$, led to intractable mixtures of largely unidentifiable but similar products according to NMR spectroscopy, when performed under rigorously dry and anaerobic conditions. However, for the latter reaction, the formation of Ph_3CH was evident presumably as a result of hydride abstraction by the trityl cation. There was no evidence of C_6F_5-group transfer to the metal centre.

Carbonylmetal Coordination Chemistry

The potential for ligand **1** to adopt a number of different coordination modes is readily apparent (Figure 1). Thus, in order to probe the coordination behaviour of **PNP** (**1**), substitution reactions between **1** and a number of group 6 carbonyl complexes were undertaken. Subsequently, examination of the metal−carbonyl stretching frequencies from the resulting complexes can be used to assess the relative basicity of the chelating ligand **1**, although some caution must be observed when comparing carbonyl stretching frequencies of unsymmetrical chelate complexes.[2c,2h]

Treating a dichloromethane solution of $[Mo(CO)_4(pip)_2]$ (pip = piperidine) with an equimolar amount of chelate **1** cleanly afforded the six-coordinate carbonylmolybdenum complex [*cis*-$Mo(CO)_4$(**PNP**-κ^2*P,N*)] (**10**) in 64% yield after 18 h at room temperature. The complex was isolated, after workup, as an air-stable crystalline solid. Data from both $^{31}P\{^1H\}$ NMR and infrared spectroscopy are consistent with ligand **1** being coordinated in a bidentate, *P,N* fashion [δ = +132.1 (s), +51.4 (s)] (mode **I**; Figure 1). A compound which possesses identical spectroscopic data to those obtained for **10** was isolated in low yield (28%) from the reaction of **1** with $[Mo(CO)_3(cht)]$ (cht = η^6-cycloheptatriene). In the latter case, the formation of **10** is believed to result from carbon monoxide scrambling.

As was observed for the palladium−**PNP** derivatives, complex **10** is rigid on the NMR timescale, with no interconversion of the free and bound phosphane components being detectable. The infrared spectroscopic data from complex **10** reveal that the presence of the diisopropylamino substituents on the phosphane component does render ligand **1** slightly more basic when compared with the values of the range of carbonyl stretching frequencies observed for similar *P,N*-ligands bearing a diphenylphosphane moiety bound to the $Mo(CO)_4$ fragment (Table 2). However, ligand **1** remains considerably less basic than the strongly σ-donating bis(pyrrolyl)-substituted diphosphane, $(pyrrolyl)_2P(CH_2)_2P(pyrrolyl)_2$ [$\tilde{\nu}_{CO}$ = 2044, 1970, 1916 cm^{-1}], which possesses related diaminophosphane components, as a result of aromatic delocalisation of the nitrogen lone pair in the latter.[2b]

Table 2. Representative metal−carbonyl stretching frequencies observed for $[Mo(CO)_4(\kappa^2P,N)]$ complexes

κ^2 ligand	$\tilde{\nu}_{CO}$	Ref.
1	2009, 1897, 1882, 1822	This work
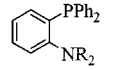 R = Me	2014, 1905, 1887, 1853	[18]
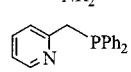 R = H	2020, 1910, 1870, 1843	[19]
	2018, 1911, 1897, 1850	[20]
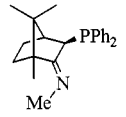	2020, 1905, 1850	[21]
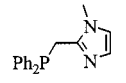	2013, 1909, 1878, 1820	[22]

Treatment of a toluene solution of *fac*-$[Cr(CO)_3(NCCH_3)_3]$ with 1 mol-equiv. of **1** afforded a single phosphorus-containing product according to $^{31}P\{^1H\}$ NMR spectroscopy [δ = +158.3 (s) and +50.3 (s)] after 2 d at room temp. Cooling (−30 °C, 12 h) of a concentrated

toluene/pentane solution of the crude mixture produced yellow/orange microcrystals in a low yield (23%).

The ^{31}P, ^{1}H, and ^{13}C NMR spectroscopic data are consistent with the formulation of this product as the mono(acetonitrile) adduct, *fac*-[$Cr(CO)_3(NCCH_3)$(**PNP**-κ^2*P*,*N*)] (**11**), with **1** again adopting a mode **I** coordination (Figure 1).

In the IR spectrum of **11**, recorded under rigorously dry, anaerobic conditions (KBr, Nujol), no C−N absorption corresponding to bound CH_3CN could be detected. For comparison, an IR spectrum of an authentic sample of *fac*-[$Cr(CO)_3(NCMe)_3$] [$C_9H_9N_3O_3Cr$ (259.18): calcd. C 41.71, H 3.50, N 16.21; found C 41.79, H 3.39, N 16.09] was recorded under identical conditions. In contrast to the original work,[40] no CN absorption was detectable at 2280 cm^{-1}, despite the carbonyl regions being identical [experimentally observed IR (Nujol): $\tilde{\nu}$ = 1915, 1782 cm^{-1}]. Neither decomposition nor the appearance of free CH_3CN was observed over a period of approximately 30 min.

The isolation of an octahedral group 6, tricarbonyl/mono(acetonitrile) complex bearing a bidentate ligand is not without precedent.[23] The formation of a bridged species of the type [{$Cr(CO)_5$}$_2$(**PNP**-κ^2*P*,*P*)], resulting from CO scrambling, is clearly ruled out by ^{31}P NMR spectroscopy.[24] Both the ^{1}H and ^{13}C NMR spectra show some line broadening, which appears temperature-independent (−45 to +40 °C). This suggests the presence of traces of a paramagnetic chromium species rather than any fluxionality associated with **11**. Such an explanation is reinforced by the broadened signals observed for the residual protio impurities of the deuterated NMR solvents. All attempts to further purify **11** were unsuccessful and resulted in decomposition. Prolonged cooling of the reaction mixture containing **11** eventually yielded inseparable mixtures of $Cr(CO)_6$ and **11**. Simply heating a toluene solution containing equimolar amounts of **1** and hexacarbonylchromium resulted in the formation of an intractable mixture of unidentified products with no evidence consistent with the formation of **11**.

Investigation of the Reactivity of the Pendant Diaminophosphane Arm

Since complexes **2**−**11** all possess a pendant, non-coordinating diaminophosphane moiety, it was of interest to investigate the reactivity of this group. Preliminary studies employing [$PdCl_2$(**PNP**-κ^2*P*,*N*)] (**2**) are somewhat surprising. In dry dichloromethane solution, no reaction was observed at either of the two phosphorus centres with molecular oxygen, sulfur, BH_3(THF), Me_3SiN_3, or [Mo(CO)$_5$(THF)]. In contrast, **1** reacted rapidly with elemental sulfur.[5] A similar lack of reactivity towards boranes or chalcogens was noted for the free phosphane arm of **10**.

It is noteworthy that despite the well-documented reactivity of P−N bonds towards protic reagents, complexes **2**, **3**, and **4** were found stable to alcoholysis, even in neat anhydrous methanol.[25] However, when solutions of complex **2** were treated with 1 equiv. of either methyl iodide or benzyl bromide (CH_2Cl_2, −30 °C), many unidentifiable products were observed by $^{31}P\{^{1}H\}$ NMR spectroscopy. Similar reactivity is observed when the oxidative addition of alkyl halides is attempted with **1**.

Molecular Structure Determinations

Surprisingly few metal complexes of chelating ligands bearing a diaminophosphane unit rather than a dialkyl- or diarylphosphane have been structurally characterised.[2c,26,27] This prompted an investigation of the molecular structures of ligand **1** and complexes **2** and **10** in the solid state.

The crystal structure of **1** revealed that the geometric parameters associated with the imine moiety [C=N 1.268(4) Å, C(3)−N(1)−C(4) 122.8(2)°, sum of angles about C(3) = 360.0°] are typical of this functionality (Figure 2, Table 3).[2c] A staggered conformation is adopted such that the lone pair of phosphorus atom P(1) is directed away from those on both the imine nitrogen N(1) and the second phosphorus atom P(2). As is observed for many aminophosphanes, the four P−N bond lengths are significantly shorter than that associated with a true P−N single bond, the sums of angles about nitrogen atoms N(2) to N(5) [358.4, 359.9, 360.0, 360.0°, respectively] indicating significant sp^2 character;[28] together this suggests there is a degree of lone pair donation from the nitrogen atom to the phosphorus atoms.

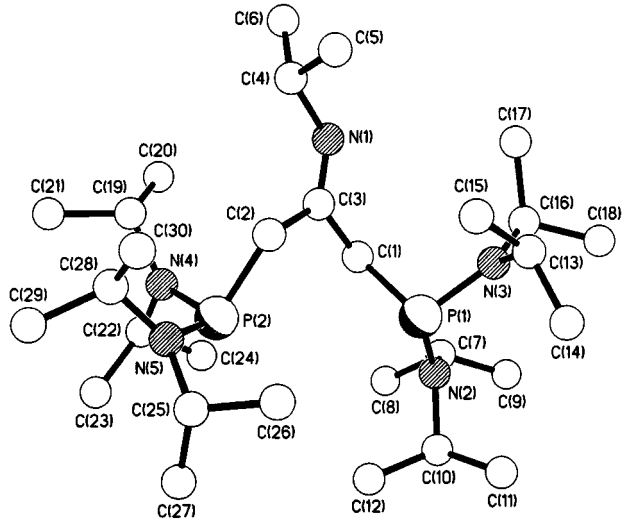

Figure 2. Molecular structure of **PNP** (**1**)

Table 3. Selected bond lengths [Å] and angles [°] for ligand **PNP** (**1**)

P(1)−N(3)	1.691(2)	P(1)−N(2)	1.698(2)
P(1)−C(1)	1.870(3)	P(2)−N(5)	1.703(2)
P(2)−N(4)	1.687(2)	P(2)−C(2)	1.857(3)
N(1)−C(3)	1.268(4)	C(1)−C(3)	1.502(4)
C(2)−C(3)	1.509(4)		
N(3)−P(1)−N(2)	110.0(1)	N(3)−P(1)−C(1)	102.6(1)
N(2)−P(1)−C(1)	99.5(1)	N(5)−P(2)−N(4)	109.7(1)
N(5)−P(2)−C(2)	100.7(1)	N(4)−P(2)−C(2)	102.3(1)
C(3)−N(1)−C(4)	122.8(2)	C(3)−C(1)−P(1)	114.8(2)
C(3)−C(2)−P(2)	117.1(2)	N(1)−C(3)−C(2)	126.9(2)
N(1)−C(3)−C(1)	117.0(2)	C(2)−C(3)−C(1)	116.1(2)

The molecular structure determination of complex **2** (Figure 3, Table 4) revealed a near square-planar geometry, the palladium centre and its four coordinated atoms being co-planar to within 0.049 Å, with a *cis*-$PdCl_2$ arrangement. No inter- or intramolecular interaction of the pendant phosphane P(2) was observed, the closest intermolecular contact being 4.93 Å to Cl(2). The P(1)−Pd and N(1)−Pd bond lengths of 2.197(2) and 2.112(7) Å, respectively, and the P(1)−Pd−N(1) angle of 81.7(2)° are entirely consistent with those reported for similar Pd^{II} complexes.[11,29] The non-equivalence observed for the two palladium−chlorine bond lengths Pd−Cl(1) and Pd−Cl(2) of 2.412(2) and 2.306(3) Å, respectively, reflects the larger *trans* influence of phosphorus compared to nitrogen.[30]

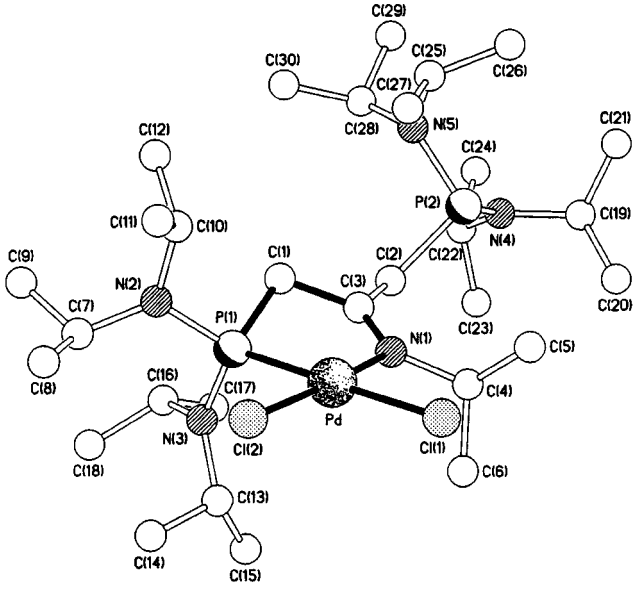

Figure 3. Molecular structure of [$PdCl_2$(PNP-κ^2*P*,*N*)] (**2**)

Table 4. Selected bond lengths [Å] and angles [°] for complex **2**

Pd−N(1)	2.112(7)	Pd−P(1)	2.197(2)
Pd−Cl(2)	2.306(3)	Pd−Cl(1)	2.412(2)
P(1)−N(3)	1.647(7)	P(1)−N(2)	1.669(6)
P(1)−C(1)	1.838(8)	P(2)−N(5)	1.690(8)
P(2)−N(4)	1.697(8)	P(2)−C(2)	1.880(8)
N(1)−C(3)	1.293(11)	C(1)−C(3)	1.518(10)
C(2)−C(3)	1.504(12)		
N(1)−Pd−P(1)	81.7(2)	N(1)−Pd−Cl(2)	171.4(2)
P(1)−Pd−Cl(2)	90.12(9)	N(1)−Pd−Cl(1)	100.8(2)
P(1)−Pd−Cl(1)	176.86(8)	Cl(2)−Pd−Cl(1)	87.51(9)
N(3)−P(1)−N(2)	109.5(4)	N(3)−P(1)−C(1)	109.0(4)
N(2)−P(1)−C(1)	104.1(4)	N(3)−P(1)−Pd	111.7(3)
N(2)−P(1)−Pd	121.7(3)	C(1)−P(1)−Pd	99.4(3)
N(5)−P(2)−N(4)	111.3(4)	N(5)−P(2)−C(2)	102.8(4)
N(4)−P(2)−C(2)	98.2(4)	C(3)−N(1)−C(4)	119.2(7)
C(3)−N(1)−Pd	119.6(5)	C(4)−N(1)−Pd	121.1(5)
C(3)−C(1)−P(1)	107.5(6)	C(3)−C(2)−P(2)	113.1(6)
N(1)−C(3)−C(2)	127.0(7)	N(1)−C(3)−C(1)	117.9(7)
C(2)−C(3)−C(1)	115.1(7)		

Following its complexation to the $PdCl_2$ fragment, ligand **1** adopts a folded envelope conformation with C(3) and C(1) lying 0.37 and 0.88 Å, respectively, "above" the coordination plane a geometry that results from the presence of the planar C=N moiety. There is little perturbation of the metrical parameters for the imine fragment [C(3)−N(1) 1.293(11) Å, C(3)−N(1)−C(4) 119.2(7)°, sums of angles at C(3) and N(1) 360.0 and 359.9°, respectively]. Similarly, the geometry around each of the four amino nitrogen atoms N(2) to N(5) remains essentially planar (sum of angles 359.4, 359.9, 359.5, and 359.3°, respectively). The P−N bond lengths in the non-coordinated aminophosphane moiety [P(2)−N(4) 1.697(8); P(2)−N(5) 1.690(8) Å] are both marginally longer than their counterparts [P(1)−N(2) 1.669(6), P(1)−N(3) 1.647(7) Å] in the metal-bound component. As in the free ligand **1**, these distances are significantly shorter than the values quoted for a P−N single bond,[28] but are in line with those of other structurally characterised coordinated aminophosphanes.[2c,26,27,31]

For comparison, the crystal structure of **10** was also determined and is presented in Figure 4 with selected bond lengths and angles given in Table 5. The comparatively small P−N "bite angle" [P(1)−Mo−N(1) 75.96(9)°] of ligand **1** results in a distorted octahedral geometry about the molybdenum centre. The metal atom lies only 0.011 Å from the equatorial plane formed by atoms P(1), N(1), and the two carbonyl ligands C(31) and C(32), which are coplanar to within 0.042 Å. The contracted geometry at the molybdenum centre caused by the small bite angle of the chelating ligand is compensated in the equatorial plane by an increase in both the adjacent angles P(1)−Mo−C(32) and N(1)−Mo−C(31) to 95.8(2) and 100.4(2)°, respectively. The two pseudo-axial carbonyl ligands bend slightly away from the chelating ligand [C(33)−Mo−C(34) 171.8(2)°]. As was observed for the palladium complex **2**, the P−N-metallacycle adopts a folded envelope conformation with C(3) and C(1) lying 0.25 and 0.77 Å, respectively, "above" the coordination plane. Again the metric parameters of the imine fragment [N(1)−C(3) of 1.287(5) Å, C(3)−N(1)−C(4) 117.9(4)°] differ little from those for the free ligand **1**, with both N(1) and C(3) remaining essentially planar (sums of angles around both atoms 360°). Similarly, the P(1)−N bond lengths, and the geometries about N(2) and N(3), show little alteration from those of the free ligand. The Mo−N(1) bond length [2.356(4) Å] is comparable with other Mo−N σ-donor bonds.[29,31] The greater *trans* influence of phosphorus over nitrogen is reflected in the molybdenum−carbonyl bond lengths of the equatorial carbonyl ligands with that to C(31) being significantly longer than that to C(32) [Mo−C(31) 1.987(6) Å, Mo−C(32) 1.940(6) Å]. The molybdenum−phosphorus bond length of 2.5367(11) Å [P(1)−Mo] is unremarkable.[22,29,33] There are no short inter- or intramolecular interactions involving the pendant phosphane P(2), the closest intermolecular contact being 5.46 Å to O(32).

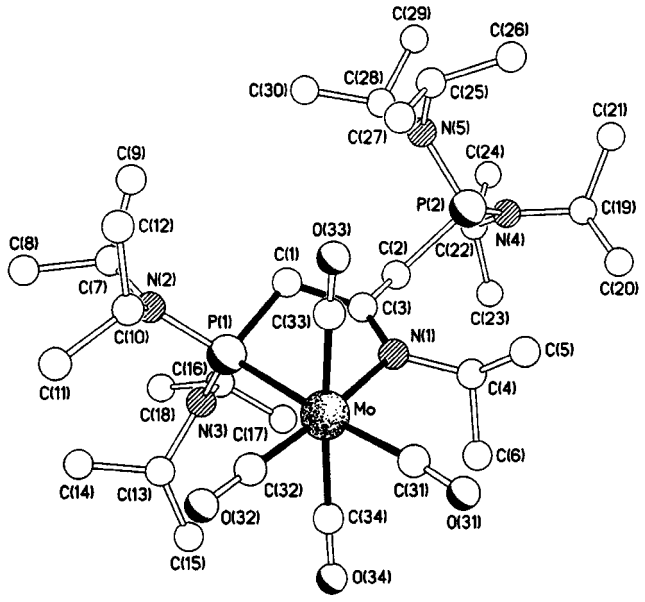

Figure 4. Molecular structure of $[Mo(CO)_4(PNP\text{-}\kappa^2P,N)]$ (**10**)

Table 5. Selected bond lengths [Å] and angles [°] for complex **10**

Mo−C(32)	1.940(6)	Mo−C(31)	1.987(6)
Mo−C(34)	2.026(5)	Mo−C(33)	2.052(5)
Mo−N(1)	2.356(4)	Mo−P(1)	2.5367(11)
P(1)−N(2)	1.687(4)	P(1)−N(3)	1.692(3)
P(1)−C(1)	1.843(4)	P(2)−N(5)	1.680(4)
P(2)−N(4)	1.694(4)	P(2)−C(2)	1.890(4)
N(1)−C(3)	1.287(5)	C(1)−C(3)	1.497(5)
C(2)−C(3)	1.516(5)		
C(32)−Mo−C(31)	87.9(3)	C(32)−Mo−C(34)	84.4(3)
C(31)−Mo−C(34)	84.0(3)	C(32)−Mo−C(33)	92.3(2)
C(31)−Mo−C(33)	88.4(3)	C(34)−Mo−C(33)	171.8(2)
C(32)−Mo−N(1)	171.3(2)	C(31)−Mo−N(1)	100.4(2)
C(34)−Mo−N(1)	93.8(2)	C(33)−Mo−N(1)	90.5(2)
C(32)−Mo−P(1)	95.8(2)	C(31)−Mo−P(1)	176.1(2)
C(34)−Mo−P(1)	97.8(2)	C(33)−Mo−P(1)	90.1(2)
N(1)−Mo−P(1)	75.96(9)	N(2)−P(1)−N(3)	108.2(2)
N(2)−P(1)−C(1)	104.0(2)	N(3)−P(1)−C(1)	104.8(2)
N(2)−P(1)−Mo	121.6(2)	N(3)−P(1)−Mo	118.20(14)
C(1)−P(1)−Mo	96.70(13)	N(5)−P(2)−N(4)	111.7(2)
N(5)−P(2)−C(2)	101.7(2)	N(4)−P(2)−C(2)	98.3(2)
C(3)−N(1)−C(4)	117.9(4)	C(3)−N(1)−Mo	121.2(3)
C(4)−N(1)−Mo	120.9(3)	C(3)−C(1)−P(1)	113.5(3)
C(3)−C(2)−P(2)	112.7(2)	N(1)−C(3)−C(1)	118.6(3)
N(1)−C(3)−C(2)	125.8(4)	C(1)−C(3)−C(2)	115.6(3)

Conclusion

Together, these observations suggest that the easily prepared, chelating *P,N*-ligand **1** makes an interesting partner for a range of metals. The straightforward synthesis and now predictable coordination geometry of bis(phosphanyl)-imine **1** offers considerable scope for further "tuning" the chemistry of **PNP**-containing complexes. The incorporation of amino rather than alkyl or aryl groups at the phosphorus atoms considerably facilitates greater variation of the steric and electronic properties of the ligand. X-ray crystallography clearly demonstrates the considerable steric demands of ligand **1**, the isopropyl substituents dominating the molecular structures of complexes **2** and **10**. Furthermore, the amino substituents at the phosphorus atoms that are simultaneously σ-electron-withdrawing but π-electron-donating, render the phosphane comparatively electron-rich. This is something that is likely to have a profound effect on the nature of the metal−phosphorus interaction and hence on the chemistry of the metal complexes.[2c][2h]

The apparent lack of reactivity of the pendant, non-coordinated, diaminophosphane unit warrants additional study. If the reactions at this site can be controlled, then this "arm" could be exploited as a means of "immobilising" these complexes on insoluble support materials such as silica or cross-linked polystyrenes. Further coordination chemistry and catalysis studies are on-going.

Experimental Section

All manipulations were performed under nitrogen using standard Schlenk and cannula techniques or in a conventional nitrogen-filled glove box. Solvents were freshly distilled under nitrogen from sodium/benzophenone (tetrahydrofuran, diethyl ether, toluene), from calcium hydride (dichloromethane, acetonitrile), from sodium (hexane, pentane), or from P_2O_5 (C_6D_6, CD_3CN, and $CDCl_3$) and degassed prior to use. Elemental analyses were performed by the microanalytical services of Imperial College or by S. Boyer at the University of North London. NMR spectra were recorded with a Bruker AC200, AM 250, AMX 300, AMX 400, or JEOL 270; chemical shifts were referenced to residual protio impurities in the deuterated solvent (^1H), to the deuterated solvent (^{13}C), external $CFCl_3$ (^{19}F), or to external aqueous 85% H_3PO_4 (^{31}P). All spectra were obtained at ambient probe temperatures unless stated otherwise. Infrared spectra were recorded [Nujol mulls (KBr windows), KBr discs, or in solution (KBr windows)] with either Perkin−Elmer 1600 or Mattson Research Series 1 spectrophotometers; Nujol was dried over sodium wire. Mass spectra were recorded with either Kratos Concept 1H or AutospecQ instruments and are reported in (*m/z*). **PNP (1)**,[5] *cis*-$[Mo(CO)_4(pip)_2]$,[34] *fac*-$[Cr(CO)_3(NCCH_3)_3]$,[35] *trans*-$[PdCl_2(NCPh)_2]$,[36] $[PdCl_2(cod)]$,[37] $[PdCl_2(tmeda)]$, $[PdMe_2(tmeda)]$,[9] [PdCl(Me)(cod)],[38] [PtCl(Me)-(cod)],[11b] and $Na[B\{3,5\text{-}(CF_3)_2C_6H_3\}_4]$[39] were prepared according to literature procedures. [PdBr(Me)(cod)] was prepared using a procedure based on that used for the preparation of [PdCl(Me)-(cod)] but starting with $[PdBr_2(cod)]$. All other chemicals were obtained commercially and used as received. Melting points were obtained in sealed glass tubes under nitrogen, using a Gallenkamp melting point apparatus and are uncorrected. A variable-temperature ^1H NMR study of the various cationic palladium systems reported is recorded in the electronic Supporting Information in addition to ORTEP views for each of the molecular structures determined by X-ray crystallography.

Synthesis of $[PdCl_2(PNP\text{-}\kappa^2P,N)]$ (2): A dichloromethane (10 mL) solution of **1** (0.32 g, 0.57 mmol) was added to a solution of $[PdCl_2(NCPh)_2]$ (0.22 g, 0.57 mmol) in dichloromethane (10 mL) at −30 °C. The mixture was allowed to warm to room temp. and

stirred for 2 h, affording a red-orange solution. Removal of solvent under reduced pressure gave a yellow-orange solid that was washed with Et_2O (3 × 10 mL) yielding a pale yellow analytically pure sample of **2** (0.38 g, 90% yield). Single crystals suitable for study by X-ray diffraction were obtained following prolonged cooling (−30 °C) of a concentrated CH_2Cl_2/Et_2O solution, m.p. > 225 °C (dec.). $C_{30}H_{67}Cl_2N_5P_2Pd$ (737.16): calcd. C 48.88, H 9.18, N 9.50; found C 49.02, H 9.02, N 9.48. MS (FAB$^+$, NBA matrix): *m*/*z* = 702 [M − Cl]. ^{1}H NMR (270.1 MHz, $CDCl_3$): δ = 1.08 [d, 12 H, $^3J_{H,H}$ = 6.7, PNCH(C*H*$_3$)$_2$], 1.16 [d, 12 H, $^3J_{H,H}$ = 6.7, PNCH(C*H*$_3$)$_2$], 1.28 [d, 12 H, $^3J_{H,H}$ = 6.9, PNCH(C*H*$_3$)$_2$], 1.45 [d, 12 H, $^3J_{H,H}$ = 6.9, PNCH(C*H*$_3$)$_2$], 1.65 [d, 6 H, $^3J_{H,H}$ = 6.7, C=NCH(C*H*$_3$)$_2$], 2.94 (s, 2 H, C*H*$_2$), 3.35 (m, 4 H, PNC*H*), 3.61 (d, 2 H, $^2J_{PH}$ = 11.6, C*H*$_2$), 4.07 (sept, 4 H, $^3J_{H,H}$ = 6.9, PNC*H*), 4.28 (sept, 1 H, $^3J_{H,H}$ = 6.7, C=NC*H*). ^{13}C {^{1}H} NMR (68.0 MHz, $CDCl_3$): δ = 23.1 [s, C=NCH(*C*H$_3$)$_2$], 24.4 [d, $^3J_{CP}$ = 6.2, PNCH(*C*H$_3$)$_2$], 25.2 [d, $^3J_{CP}$ = 7.2, PNCH(*C*H$_3$)$_2$], 25.7 [s, PNCH(*C*H$_3$)$_2$], 38.5 (dd, $^1J_{CP}$ = 20.6, $^3J_{CP}$ = 9.8, exocyclic P*C*H$_2$), 47.7 (d, $^2J_{CP}$ = 10.3, PN*C*H), 50.0 (d, $^2J_{CP}$ = 7.2, PN*C*H), 54.4 (dd, $^1J_{CP}$ = 35.6, $^3J_{PC}$ = 10.8, endocyclic P*C*H$_2$), 59.0 (s, C=N*C*H), 176.6 (dd, $^2J_{CP}$ = 8.3, 16.5, *C*=N).

Synthesis of [PdCl(Me)(PNP-κ^2*P*,*N*)] (3): A dichloromethane solution (10 mL) of **1** (0.72 g, 1.28 mmol) was added to a solution of [PdCl(Me)(cod)] (0.34 g, 1.28 mmol) in dichloromethane (10 mL) at −30 °C. The mixture was allowed to warm to room temp. and stirred for 1 h, affording a red solution. Removal of solvent under reduced pressure gave a yellow-orange solid that was washed with Et_2O (3 × 10 mL) yielding **3** as a cream powder that was used without further purification (0.78 g, 85% yield), m.p. > 200 °C (dec.). $C_{31}H_{70}ClN_5P_2Pd$ (716.74): calcd. C 54.64, H 10.38, N 10.28; found C 55.01, H 10.10, N 10.20. MS (FAB$^+$, NBA matrix): *m*/*z* = 717 [M$^+$], 702 [M$^+$ − Me], 681 [M$^+$ − Cl]. ^{1}H NMR (400.1 MHz, $CDCl_3$): δ = 0.71 (s, 3 H, Pd−C*H*$_3$), 1.11 [d, 12 H, $^3J_{H,H}$ = 6.6, PNCH(C*H*$_3$)$_2$], 1.20 [d, 12 H, $^3J_{H,H}$ = 6.7, PNCH(C*H*$_3$)$_2$], 1.30 [24 H, overlapping d, $^3J_{H,H}$ = 6.7, PNCH(C*H*$_3$)$_2$], 1.60 [d, 6 H, $^3J_{H,H}$ = 6.5, C=NCH(C*H*$_3$)$_2$], 2.85 (s, 2 H, C*H*$_2$), 3.31 (dd, 2 H, $^2J_{PH}$ = 10.0, $^4J_{PH}$ = 1.5, C*H*$_2$), 3.39 (septd, 4 H, $^3J_{H,H}$ = 6.7, $^3J_{PH}$ = 11.1, PNC*H*), 3.92 (sept, 4 H, $^3J_{H,H}$ = 6.7, PNC*H*), 4.10 (sept, 1 H, $^3J_{H,H}$ = 6.5, C=NC*H*). ^{13}C {^{1}H} NMR (100.6 MHz, $CDCl_3$): δ = 0.75 (d, $^2J_{CP}$ = 7.3, Pd-*C*H$_3$), 22.9 [s, C=NCH(*C*H$_3$)$_2$], 24.9 [d, $^3J_{CP}$ = 7.1, PNCH(*C*H$_3$)$_2$], 24.4 [d, $^3J_{CP}$ = 6.4, PNCH(*C*H$_3$)$_2$], 24.6 [d, $^3J_{CP}$ = 2.4, PNCH(*C*H$_3$)$_2$], 26.1 [d, $^3J_{CP}$ = 2.1, PNCH(*C*H$_3$)$_2$], 37.3 (dd, $^1J_{CP}$ = 19.7, $^3J_{CP}$ = 5.7, exocyclic P*C*H$_2$), 46.9 (d, $^2J_{CP}$ = 10.9, PN*C*H), 47.8 (d, $^2J_{CP}$ = 9.3, PN*C*H), 50.6 (dd, $^1J_{CP}$ = 26.5, $^3J_{CP}$ = 7.3, endocyclic P*C*H$_2$), 56.0 (s, C=N*C*H), 171.2 (dd, $^2J_{CP}$ = 5.7, 16.1, *C*=N).

Synthesis of [PdBr(Me)(PNP-κ^2*P*,*N*)] (4): In a similar manner to the above, reaction of **1** (0.132 g, 0.24 mmol) in dichloromethane (25 mL) with a solution of [PdBrMe(cod)] (0.073 g, 0.24 mmol) in dichloromethane (15 mL) at −30 °C afforded **4**. Recrystallisation from a mixture of ether and dichloromethane (1:1) and prolonged cooling to −30 °C afforded **4** as yellow-orange microcrystals (0.14 g, 72% yield). A small (50 mg) sample of **4** was recrystallised a second time using the same combination to afford a microcrystalline material that afforded correct elemental analyses, m.p. > 195 °C (dec.). $C_{31}H_{70}BrN_5P_2Pd$ (761.32): calcd. C 48.92, H 9.27, N 9.20; found C 48.95, H 9.20, N 9.19. MS (FAB$^+$, NBA matrix): *m*/*z* = 761 [M$^+$], 747 [M$^+$ − CH_2], 681 [M$^+$ − Br]. ^{1}H NMR (301.5 MHz, $CDCl_3$): δ = 0.71 (s, 3 H, Pd−C*H*$_3$), 1.08 [d, 12 H, $^3J_{H,H}$ = 6.7 Hz, PNCH(C*H*$_3$)$_2$], 1.18 [d, 12 H, $^3J_{H,H}$ = 6.7, PNCH(C*H*$_3$)$_2$], 1.28 [m, 24 H, PNCH(C*H*$_3$)$_2$], 1.60 [d, 6 H, $^3J_{H,H}$ = 6.4, C=NCH(C*H*$_3$)$_2$], 2.84 (s, 2 H, C*H*$_2$), 3.35 (m, 6 H, PNC*H* and C*H*$_2$), 3.90 (m, 4 H, PNC*H*), 4.08 (sept, 1 H, $^3J_{H,H}$ = 6.4, C=NC*H*). ^{13}C {^{1}H} NMR (75.8 MHz, $CDCl_3$): δ = −1.7 (d, Pd*C*H$_3$, $^3J_{PC}$ = 9.0), 21.9 [s, C=NCH(*C*H$_3$)$_2$], 23.0 [d, $^3J_{PC}$ = 6.6, PNCH(*C*H$_3$)$_2$], 23.2 (d, J_{PC} = 3.0), 23.5 [d, $^3J_{PC}$ = 7.2, PNCH(*C*H$_3$)$_2$], 24.5 [d, $^3J_{PC}$ = 3.0, PNCH(*C*H$_3$)$_2$], 36.4 (dd, $^1J_{PC}$ = 19.2, $^3J_{PC}$ = 4.5, exocyclic P*C*H$_2$), 46.1 (d, $^2J_{PC}$ = 10.8, PN*C*H), 47.0 (d, $^2J_{PC}$ = 9.0, PN*C*H), 49.2 (dd, $^2J_{PC}$ = 25.9, 7.2, endocyclic P*C*H$_2$), 54.7 (s, C=N*C*H), 170.4 (m, *C*=N).

[PdMe$_2$(PNP-κ^2*P*,*N*)] (5): To a mixture of [$PdMe_2$(tmeda)] (0.48 g, 1.9 mmol) and **1** (1.07 g, 1.9 mmol) was added dichloromethane (30 mL) at room temp. The yellow reaction mixture was stirred for 48 h at room temp. before volatile components were removed in vacuo. The resulting off white solid was washed with Et_2O (3 × 10 mL). Complex **5** was dried under vacuum (1.02 g, 77% yield), m.p. > 180 °C (dec.). $C_{32}H_{73}N_5P_2Pd$ (696.46): calcd. C 55.18, H 10.59, N 10.06; found C 49.27, H 10.67, N 10.18. MS (FAB$^+$, NBA matrix): *m*/*z* = 696 [M$^+$], 682 [M$^+$ − CH_2]. ^{1}H NMR (301.5 MHz, $CDCl_3$): δ = 0.73 (d, 3 H, $^3J_{PH}$ = 0.9, Pd−C*H*$_3$), 1.12 [d, 12 H, $^3J_{H,H}$ = 6.4, PNCH(C*H*$_3$)$_2$], 1.22 [d, 12 H, $^3J_{H,H}$ = 6.4, PNCH(C*H*$_3$)$_2$], 1.31 [d, 12 H, $^3J_{H,H}$ = 6.9, PNCH(C*H*$_3$)$_2$], 1.34 [d, 12 H, $^3J_{H,H}$ = 7.1, PNCH(C*H*$_3$)$_2$], 1.61 [d, 6 H, $^3J_{H,H}$ = 6.5, C=NCH(C*H*$_3$)$_2$], 2.87 (s, 2 H, C*H*$_2$), 3.33 (dd, 2 H, $^2J_{PH}$ = 13.7, $^4J_{PH}$ = 3.8, C*H*$_2$), 3.40 (sept, 4 H, $^3J_{H,H}$ = 6.7, PNC*H*), 3.94 (sept, 4 H, $^3J_{H,H}$ = 6.7, PNC*H*), 4.12 (sept, 1 H, $^3J_{H,H}$ = 6.5, C=NC*H*). ^{13}C {^{1}H} NMR (62.9 MHz, $CDCl_3$): δ = −0.6 (d, $^2J_{PC}$ = 7.8, Pd-*C*H$_3$), 22.7 [s, C=NCH(*C*H$_3$)$_2$], 24.3 [d, $^3J_{PC}$ = 6.6, PNCH(*C*H$_3$)$_2$], 24.4 [d, $^3J_{PC}$ = 3.0, PNCH(*C*H$_3$)$_2$], 24.7 [d, $^3J_{PC}$ = 7.2, PNCH(*C*H$_3$)$_2$], 25.9 [d, $^3J_{PC}$ = 2.4, PNCH(*C*H$_3$)$_2$], 37.4 (dd, $^1J_{PC}$ 19.0, $^3J_{PC}$ = 5.7, exocyclic P*C*H$_2$), 47.3 (d, $^2J_{PC}$ = 11.4, PN*C*H), 48.1 (d, $^2J_{PC}$ = 9.0, PN*C*H), 50.6 (dd, $^1J_{PC}$ = 27.1, $^3J_{PC}$ 8.4, endocyclic P*C*H$_2$), 55.8 (s, C=N*C*H), 171.3 (dd, $^2J_{PC}$ = 16.0, $^2J_{PC}$ = 5.7, *C*=N).

[PtCl(Me)(PNP-κ^2*P*,*N*)] (6): An NMR tube fitted with a J. Young's valve was charged with **1** (71 mg, 0.13 mmol), [PtCl(Me)(cod)] (45 mg, 0.13 mmol) and $CDCl_3$ (0.5 mL) under nitrogen. After 3 d at room temp., no further evolution was observed according to ^{31}P NMR spectroscopy. Removal of volatile components in vacuo, followed by washing with Et_2O (2 × 2 mL) afforded a mixture of both *cis* and *trans* isomers of **6** as a white powder (0.10 g, 98% yield), m.p. > 230 °C (dec.). $C_{31}H_{70}ClN_5P_2Pt$ (805.53) calcd. C 46.22, H 8.78, N 8.71; found C 46.24, H 8.73, N 8.68. MS (FAB$^+$, NBA matrix): *m*/*z* = 805 [M$^+$], 790 [M$^+$ − Me], 770 [M$^+$ − Cl]. ^{1}H NMR (301.5 MHz, $CDCl_3$), major isomer **6a** only: δ = 0.77 (d, 3 H, $^3J_{PH}$ = 2.0, Pt−C*H*$_3$), 1.12 [d, 12 H, $^3J_{H,H}$ = 6.7, PNCH(C*H*$_3$)$_2$], 1.22 [d, 12 H, $^3J_{H,H}$ = 6.7, PNCH(C*H*$_3$)$_2$], 1.31 [d, 12 H, $^3J_{H,H}$ = 7.0, PNCH(C*H*$_3$)$_2$], 1.32 [d, 12 H, $^3J_{H,H}$ = 7.0, PNCH(C*H*$_3$)$_2$], 1.64 [d, 6 H, $^3J_{H,H}$ = 6.4, C=NCH(C*H*$_3$)$_2$], 2.85 (s, 2 H, C*H*$_2$), 3.22 (dd, 2 H, $^2J_{PH}$ = 12.6, $^4J_{PH}$ = 1.5, C*H*$_2$), 3.40 (sept, 4 H, $^3J_{H,H}$ = 6.7, PNC*H*), 4.03 (sept, 4 H, $^3J_{H,H}$ = 6.7, PNC*H*), 4.63 (sept, 1 H, $^3J_{H,H}$ = 6.7, C=NC*H*). ^{13}C {^{1}H} NMR (75. 8 MHz, $CDCl_3$), major isomer **6a** only: δ = −15.4 (d, $^2J_{PH}$ = 4.8, Pt−*C*H$_3$), 22.5 [s, C=NCH(*C*H$_3$)$_2$], 24.2 [d, $^3J_{PC}$ = 6.0, PNCH(*C*H$_3$)$_2$], 24.5 [d, $^3J_{PC}$ = 3.0, PNCH(*C*H$_3$)$_2$], 24.7 [d, $^3J_{PC}$ = 7.2, PNCH(*C*H$_3$)$_2$], 25.7 [d, $^3J_{PC}$ = 2.4, PNCH(*C*H$_3$)$_2$], 38.0 (dd, $^1J_{PC}$ = 18.9, $^3J_{PC}$ = 6.6, exocyclic P*C*H$_2$), 47.3 (d, $^2J_{PC}$ = 10.8, PN*C*H), 47.8 (d, $^2J_{PC}$ = 8.4, PN*C*H), 51.0 (dd, $^1J_{PC}$ = 41.8, $^3J_{PC}$ = 9.3, endocyclic P*C*H$_2$), 57.2 (s, C=N*C*H), 173.6 (dd, $^2J_{PC}$ = 15.1 and 3.6, *C*=N).

Synthesis of [PdMe(NCCH$_3$)(PNP-κ^2*P*,*N*)][PF_6] (7): A Schlenk tube was charged with **3** (108 mg, 0.15 mmol), $NaPF_6$ (28 mg, 0.17 mmol), and CH_3CN (15 mL) under nitrogen. After stirring at room temp. for 3 d, the reaction mixture was filtered and all volatile components removed in vacuo to afford **7** as a yellow solid, which

was dried under high vacuum overnight (115 mg, 91% yield), m.p. > 109−110 °C (dec.). $C_{33}H_{73}F_6N_6P_3Pd$ (867.31) calcd. C 45.70, H 8.48, N 9.69; found C 45.78, H 8.32, N 9.56. MS (FAB$^+$, NBA matrix): *m*/*z* = 681 [M$^+$ − CH_3CN]. IR (KBr disc): $\tilde{\nu}$ = 2287 (C≡N), 2313 (C≡N). ^{1}H NMR (400.1 MHz, $CDCl_3$): δ = 0.50 (s, 3 H, Pd−C*H*$_3$), 1.12 [d, 12 H, $^3J_{H,H}$ = 6.6, PNCH(C*H*$_3$)$_2$], 1.23 [d, 12 H, $^3J_{H,H}$ = 6.8, PNCH(C*H*$_3$)$_2$], 1.32 [m, 30 H, PNCH(C*H*$_3$)$_2$ and C=NCH(C*H*$_3$)$_2$], 2.33 (br. s, $\nu_{1/2}$ 11 Hz, C*H*$_3$CN), 2.93 (s, 2 H, C*H*$_2$), 3.37 (d, 2 H, $^2J_{PH}$ = 11.5, C*H*$_2$), 3.43 (sept, 4 H, $^3J_{H,H}$ = 6.6, $^4J_{PH}$ = 1.6, PNC*H*), 3.86 (sept, 4 H, $^3J_{H,H}$ = 6.8, PNC*H*), 4.09 (sept, 1 H, $^3J_{H,H}$ = 6.6, C=NC*H*). ^{13}C NMR (62.9 MHz, CD_3CN): δ = 0.3 (d, $^2J_{PC}$ = 6.6, Pd-*C*H$_3$), 23.9 [d, $^3J_{PC}$ = 3.6, C=NCH(*C*H$_3$)$_2$], 24.5 [d, $^3J_{PC}$ = 3.6, PNCH(*C*H$_3$)$_2$], 24.9 [d, $^3J_{PC}$ = 6.6, PNCH(*C*H$_3$)$_2$], 25.2 [d, $^3J_{PC}$ = 7.1, PNCH(*C*H$_3$)$_2$], 26.1 [d, $^3J_{PC}$ = 3.1, PNCH(*C*H$_3$)$_2$], 39.2 (dd, $^1J_{PC}$ = 20.3, $^3J_{PC}$ = 6.6, exocyclic P*C*H$_2$), 48.2 (d, $^2J_{PC}$ = 11.7, PN*C*H), 49.5 (d, $^2J_{PC}$ = 8.1, PN*C*H), 53.4 (dd, $^1J_{PC}$ = 32.0, $^3J_{PC}$ 5.1, endocyclic P*C*H$_2$), 56.1 (d, $^3J_{PC}$ = 3.0, C=N*C*H), 176.3 (dd, $^2J_{PC}$ = 13.5, $^2J_{PC}$ = 4.8, *C*=N). ^{19}F (235.3 MHz, CD_3CN): δ = −73.3 (d, $^1J_{PF}$ = 706.5).

Synthesis of [PdMe(NCCH$_3$)(PNP-κ^2*P*,*N*)][B{3,5-(CF$_3$)$_2$C$_6$H$_3$}$_4$] (8): To a mixture of **3** (125 mg, 0.14 mmol) and Na[B{3,5-(CF$_3$)$_2$C$_6$H$_3$}$_4$] (100 mg, 0.14 mmol) was added acetonitrile (20 mL) at room temp. After 3 d at room temp., the solution was filtered to eliminate NaCl and the solvent subsequently removed under reduced pressure to afford a yellow solid of **8**, which was dried under high vacuum overnight (194 mg, 91% yield), m.p. 57−60 °C. $C_{65}H_{85}BF_{24}N_6P_2Pd$ (1585.35): calcd. C 49.24, H 5.42, N 5.30; found C 49.16, H 5.50, N 5.26. MS (FAB$^+$, NBA matrix): *m*/*z* = 681 (M$^+$ − CH_3CN). IR (KBr disc): $\tilde{\nu}$ = 2288 (C≡N), 2316 (C≡N). ^{1}H NMR (400.1 MHz, $CDCl_3$): δ = 0.50 (s, 3 H, PdC*H*$_3$), 1.11 [d, 12 H, $^3J_{H,H}$ = 6.6, PNCH(C*H*$_3$)$_2$], 1.23 [d, 12 H, $^3J_{H,H}$ = 6.6, PNCH(C*H*$_3$)$_2$], 1.30−1.37 [m, 30 H, C=NCH(C*H*$_3$)$_2$ and PNCH(C*H*$_3$)$_2$], 2.23 (s, 3 H, CH_3CN), 2.90 (s, 2 H, C*H*$_2$), 3.39−3.48 [m, 6 H, PNC*H*(CH$_3$)$_2$ and C*H*$_2$], 3.82 [sept, 4 H, $^3J_{H,H}$ = 6.6, PNC*H*(CH$_3$)$_2$], 4.08 [sept, 1 H, $^3J_{H,H}$ = 6.6, C=NCH(CH$_3$)$_2$], 7.54 (s, 4 H, *p*-C$_6$*H*$_3$), 7.71 (8 H, *o*-C$_6$*H*$_3$). ^{13}C NMR (62.9 MHz, CD_3CN): δ = 0.3 (d, $^2J_{PC}$ = 6.2, PdC*H*$_3$), 23.8 [d, $^4J_{PC}$ = 3.5, C=NCH(*C*H$_3$)$_2$], 24.5 [d, $^3J_{PC}$ = 3.5, PNCH(*C*H$_3$)$_2$], 24.8 [d, $^3J_{PC}$ = 6.9, PNCH(*C*H$_3$)$_2$], 25.2 [d, $^3J_{PC}$ = 7.6, PNCH(*C*H$_3$)$_2$], 26.1 [d, $^3J_{PC}$ = 2.8, PNCH(*C*H$_3$)$_2$], 39.1 (dd, $^1J_{PC}$ = 20.5, $^3J_{PC}$ = 6.6 exocyclic P*C*H$_2$), 48.2 [d, $^2J_{PC}$ = 11.8, PN*C*H(CH$_3$)$_2$], 49.4 [d, $^2J_{PC}$ = 8.3, PN*C*H(CH$_3$)$_2$], 53.3 (dd, $^1J_{PC}$ = 32.5, $^3J_{PC}$ = 4.8, endocyclic P*C*H$_2$), 56.0 [d, $^3J_{PC}$ = 2.8, C=N*C*H(CH$_3$)$_2$], 124.0 (s, *p*-C$_6$H$_3$), 127.6 (s, *m*-C$_6$H$_3$), 130.3 (m, *C*F$_3$), 136.0 (s, *o*-C$_6$H$_3$), 163.0 (q, $^1J_{BC}$ = 49.8, *ipso*-C$_6$H$_3$), 176.2 (dd, $^2J_{PC}$ = 12.9, $^2J_{PC}$ = 3.8, *C*=N). ^{19}F NMR (235.3 MHz, CD_3CN): δ = −63.8 (s, CF_3).

Synthesis of [PdMe(PNP-κ^2*P*,*N*)][BPh$_4$] (9): A Schlenk tube was charged with **3** (0.60 g, 0.84 mmol), $NaBPh_4$ (0.32 g, 0.93 mmol), and CH_3CN (80 mL) under nitrogen. The resulting suspension was stirred at room temp. for 3 d and subsequently filtered under nitrogen to give a clear yellow solution. Removal of solvent in vacuo afforded **9** as a brown/orange solid that was dried under high vacuum overnight (0.77 g, 92%), m.p. 100−102 °C. $C_{55}H_{90}BN_5P_2Pd$ (1000.52): calcd. C 66.02, H 9.07, N 7.00; found C 66.84, H 9.06, N 6.75. MS (FAB$^+$, NBA matrix): *m*/*z* = 681 [M$^+$]. ^{1}H NMR (400.1 MHz, $CDCl_3$): δ = 0.51 (s, 3 H, PdC*H*$_3$), 1.14 [d, 12 H, $^3J_{H,H}$ = 6.6, PNCH(C*H*$_3$)$_2$], 1.25 [d, 12 H, $^3J_{H,H}$ = 6.6, PNCH(C*H*$_3$)$_2$], 1.33 [m, 30 H, PNCH(C*H*$_3$)$_2$ and C=NCH(C*H*$_3$)$_2$], 2.90 (s, 2 H, C*H*$_2$), 3.36 (d, 2 H, $^2J_{PH}$ = 11.7, C*H*$_2$), 3.42 [sept, 4 H, $^3J_{H,H}$ = 6.6, $^4J_{PH}$ = 1.8, PNC*H*(CH$_3$)$_2$], 3.85 [4 H, sept, $^3J_{H,H}$ = 6.6, PNC*H*(CH$_3$)$_2$], 4.07 [sept, 1 H, $^3J_{H,H}$ = 6.7, C=NC*H*(CH$_3$)$_2$]; 6.91 (4 H, pseudo-t, $^3J_{H,H}$ = 7.3, *p*-C$_6$*H*$_5$), 7.07 (8 H, pseudo-t, $^3J_{H,H}$ = 7.3, *m*-C$_6$*H*$_5$), 7.48 (8 H, br. s, *o*-C$_6$*H*$_5$). ^{13}C NMR (62.9 MHz, CD_3CN): δ = 0.4 (s, PdC*H*$_3$), 23.9 [d, $^4J_{PC}$ = 4.1, C=NCH(*C*H$_3$)$_2$], 24.6 [d, $^3J_{PC}$ = 3.6, PNCH(*C*H$_3$)$_2$], 24.9 [d, $^3J_{PC}$ = 6.6, PNCH(*C*H$_3$)$_2$], 25.3 [d, $^3J_{PC}$ = 6.6, PNCH(*C*H$_3$)$_2$], 26.1 [d, $^3J_{PC}$ = 3.1, PNCH(*C*H$_3$)$_2$], 38.4 (dd, $^1J_{PC}$ = 20.7, $^3J_{PC}$ = 6.3, exocyclic P*C*H$_2$), 48.2 [d, $^2J_{PC}$ = 11.7, PN*C*H(CH$_3$)$_2$], 49.5 [d, $^2J_{PC}$ = 8.6, PN*C*H(CH$_3$)$_2$], 52.6 (d, $^1J_{PC}$ = 32.4, $^3J_{PC}$ = 4.7, endocyclic P*C*H$_2$), 123.2 (s, *p*-*C*$_6$H$_5$), 127.0 (m, *m*-*C*$_6$H$_5$), 137.1 (s, *o*-*C*$_6$H$_5$), 165.2 (q, $^1J_{BC}$ = 49.4, *ipso*-*C*$_6$H$_5$).

Synthesis of [Mo(CO)$_4$(PNP-κ^2*P*,*N*)] (10): To a cold (−30 °C) solution of [Mo(CO)$_4$(pip)$_2$] (0.15 g, 0.41 mmol) in CH_2Cl_2 (10 mL) was added dropwise a CH_2Cl_2 solution (10 mL) of **1** (0.23 g, 0.41 mmol). The solution became brown on warming to room temp. After stirring for 18 h, the volatile components were removed under reduced pressure. The resulting solid was dissolved in a minimum of CH_2Cl_2 (ca. 2 mL) and pentane added dropwise until the solution became turbid. Subsequent recrystallisation at −30 °C afforded **10** as yellow-orange single crystals (0.20 g, 64% yield) that were isolated by filtration, m.p. 172−174 °C. $C_{34}H_{67}N_5O_4P_2Mo$ (767.81): calcd. C 53.18, H 8.81, N 9.12; found C 53.23, H 8.53, N 9.12. MS (EI): *m*/*z* = 740 [M$^+$ − CO], 712 [M$^+$ − 2 CO]. IR (Nujol): $\tilde{\nu}$ = 2009 (CO), 1897 (CO), 1882 (CO), 1822 (CO). ^{1}H NMR (270.1 MHz, C_6D_6): δ = 1.01 [d, 12 H, $^3J_{H,H}$ = 6.4, PNCH(*C*H$_3$)$_2$], 1.08 [d, 12 H, $^3J_{H,H}$ = 6.4, PNCH(*C*H$_3$)$_2$], 1.27 (24 H, overlapping d, measurable coupling constants $^3J_{H,H}$ = 8.2 and 7.9 Hz), 1.48 [d, 6 H, $^3J_{H,H}$ = 6.2, C=NCH(C*H*$_3$)$_2$], 2.94 (s, 2 H, br, C*H*$_2$), 3.14 (m, 4 H, PNC*H*), 3.59 (s, 2 H, br, C*H*$_2$), 4.07 (m, 4 H, PNC*H*), 4.13 (sept, 1 H, $^3J_{H,H}$ = 6.4, C=NC*H*). ^{13}C NMR (100.6 MHz, C_6D_6): δ = 24.0 [d, $^3J_{PC}$ = 6.2, PNCH(*C*H$_3$)$_2$], 24.4 [d, $^3J_{PC}$ = 7.0, PNCH(*C*H$_3$)$_2$], 24.6 (br), 26.1 (s, br), 39.9 (dd, $^3J_{PC}$ = 3.2, $^1J_{PC}$ = 18.8, exocyclic *C*H$_2$), 47.3 (d, $^2J_{PC}$ = 11.1, PN*C*H), 50.3 (d, $^2J_{PC}$ = 10.7, PN*C*H), 51.5 (dd, $^3J_{PC}$ = 12.0, $^1J_{PC}$ 21.6, endocyclic *C*H$_2$), 56.2 (s, C=N*C*H), 176.1 (overlapping dd, measurable coupling constants $^2J_{CP}$ = 10.9 and 11.7 Hz, *C*=N), 210.1 (d, $^2J_{PC}$ = 8.4, *C*O), 218.5 (d, $^2J_{PC}$ = 42.9, *C*O), 221.8 (d, $^2J_{PC}$ = 9.1, *C*O).

Preparation of 10 from [Mo(cht)(CO)$_3$]: Toluene (10 mL) was added to a mixture of **1** (0.20 g, 0.36 mmol) and [Mo(cht)(CO)$_3$] (0.08 g, 0.36 mmol) at room temp. After stirring at room temp. for 2 d, the reaction mixture was heated to 70 °C for a further 3 d. Complex **10** was observed as the only phosphorus-containing product by ^{31}P NMR spectroscopy. Subsequent removal of all volatile components under reduced pressure afforded a brown waxy solid. Washing with ether (3 × 10 mL) afforded **10** as an orange-brown solid (0.08 g, 28% yield).

Synthesis of *fac*-[Cr(CO)$_3$(NCMe)(PNP-κ^2*P*,*N*)] (11): To a solution of *fac*-[Cr(CO)$_3$(NCMe)$_3$] (0.2 g, 0.8 mmol) in toluene (10 mL) was added a toluene (10 mL) solution of **1** (0.44 g, 0.8 mmol) at −30 °C. The solution slowly darkened from yellow to orange/brown upon stirring at room temp. for 2 d. Removal of solvent in vacuo afforded a dark brown waxy solid. The product was extracted into toluene (3 mL) and pentane (ca. 2 mL) added. After cooling at −30 °C for 12 h, yellow-orange microcrystals of **11** were isolated by filtration and dried in vacuo for 4 d, at room temp. (0.12 g, 23% yield). No reliable analyses could be obtained presumably due to subsequent decomposition. MS (FAB$^+$, NBA matrix): *m*/*z* = 639 [M$^+$ − CH_3CN − 2 CO], 611 [M$^+$ − CH_3CN − 3 CO]. IR (Nujol): $\tilde{\nu}$ = 1941 (w, CO), 1885 (s, CO), 1821 (s, CO). ^{1}H NMR (270.1 MHz, $CDCl_3$): δ = 1.25 (54H br. m), 2.28 (3 H, br. s, C*H*$_3$CN), 2.90 (2 H, br. s, CH$_2$), 3.39 (9 H, br. m, PNC*H*, C*H*$_2$, and C*H*$_3$CN), 3.97 (4 H, br. m, PNC*H*), 4.22 (1 H, br. m, C=

NC*H*). ^{13}C NMR (75.8 MHz, $CDCl_3$): δ = 22.6 (br, s, *C*H_3CN), 24.0 [br, C=NCH(*C*H_3)$_2$], 24.2 [br. d, $^3J_{PC}$ = 6.6, PNCH(*C*H_3)$_2$], 24.6 [br. d, $^3J_{PC}$ = 6.6, PNCH(*C*H_3)$_2$], 24.9 (br. s), 25.9 (br. s), 39.6 (br. d, $^1J_{PC}$ = 21.1, exocyclic *C*H_2), 47.3 (br. d, $^2J_{PC}$ = 10.8, PN*C*H), 49.4 (br. d, $^2J_{PC}$ = 9.0, PN*C*H), 52.8 (br. m, endocyclic P*C*H_2), 57.3 (br. s, C=N*C*H), 127.8 (br. s, CH_3*C*N), 176.3 (br. m, *C*=N*i*Pr), 219.5 (br. d, $^2J_{PC}$ = 14.5, *C*O), 227.9 (br. s, *C*O), 229.0 (br. d, $^2J_{PC}$ = 18.1, *C*O).

Reaction of [$PdMe_2$(PNP-κ^2*P*,*N*)] (5) with dppe: An NMR tube was charged under nitrogen with **5** (0.01 g, 0.01 mmol), dppe (0.005 g, 0.01 mmol), and dry $CDCl_3$ (0.5 mL). The reaction mixture was shaken and left to stand at room temp. for 30 min. ^{31}P NMR (101.3 MHz, $CDCl_3$): δ = +55.7 ($PdMe_2${dppe}), +53.1 (d, $^4J_{PP}$ = 14.5 Hz, [**PNP**]), +46.2 (d, $^4J_{PP}$ = 14.5 Hz, [**PNP**]).

X-ray Crystallographic Study: Crystal Data for **1**: $C_{30}H_{67}N_5P_2$, *M* = 559.8, orthorhombic, *Pbca* (no. 61), *a* = 17.888(1), *b* = 18.586(2), *c* = 21.924(2) Å, *V* = 7289(1) Å^3, *Z* = 8, D_c = 1.020 g·cm^{-3}, μ(Mo-$K_α$) = 1.40 cm^{-1}, *T* = 293 K, yellow/white blocks; 6404 independent measured reflections, *F* refinement, R_1 = 0.028, *Rw* = 0.029, 2743 independent observed absorption corrected reflections [$|F_o| > 4σ(|F_o|)$, 2θ ≤ 50°], 334 parameters. Crystal Data for **2**: $C_{30}H_{67}Cl_2N_5P_2Pd$, *M* = 737.1, monoclinic, $P2_1/c$ (no. 14), *a* = 14.617(1), *b* = 15.998(3), *c* = 18.323(3) Å, β = 109.44(1)°, *V* = 4040(1) Å^3, *Z* = 4, D_c = 1.212 g·cm^{-3}, μ(Cu-$K_α$) = 58.5 cm^{-1}, *T* = 293 K, yellow platy needles; 5989 independent reflections, F^2 refinement, R_1 = 0.066, wR_2 = 0.164, 4241 independent observed absorption corrected reflections [$|F_o| > 4σ(|F_o|)$, 2θ ≤ 120°], 362 parameters. Crystal Data for **10**: $C_{34}H_{67}MoN_5O_4P_2$, *M* = 767.8, monoclinic, $P2_1/n$ (no. 14), *a* = 13.722(1), *b* = 17.284(1), *c* = 19.098(2) Å, β = 109.19(1)°, *V* = 4278.0(6) Å^3, *Z* = 4, D_c = 1.192 g·cm^{-3}, μ(Mo-$K_α$) = 4.19 cm^{-1}, *T* = 293 K, yellow blocks; 7494 independent reflections, F^2 refinement, R_1 = 0.050, wR_2 = 0.106, 5006 independent observed reflections [$|F_o| > 4σ(|F_o|)$, 2θ ≤ 50°], 415 parameters. Crystallographic data (excluding structure factors) for the structures reported in this paper have been deposited with the Cambridge Crystallographic Data Centre as supplementary publication nos. CCDC-165966 to -165968. Copies of the data can be obtained free of charge on application to CCDC, 12 Union Road, Cambridge CB2 1EZ, UK [Fax: (internat.) + 44-1223/336-033; E-mail: deposit@ccdc.cam.ac.uk].

Electronic Supporting Information: Variable-temperature ^1H NMR spectra for complexes **7**–**9** together with ORTEP views of the molecular structures of ligand **1** and complexes **2** and **10** have been deposited (see also footnote on the first page of this article).

Acknowledgments

The Nuffield Foundation (Award to Newly Appointed Science Lecturers), The Royal Society, the Chemistry Departments of the Imperial College and the University of Leicester, the EPSRC and Lubrizol Ltd. (CASE award to M. J. H.) are gratefully acknowledged for funding. Johnson Matthey is thanked for a loan of palladium salts while Asahi Glass Corporation is thanked for gifts of $B(C_6H_5)_3$. Drs. G. Griffiths (Leicester), R. N. Shepherd (Imperial College), and P. Hammerton (Imperial College) are thanked for their help with NMR spectroscopy.

[1] P. Braunstein, F. Naud, *Angew. Chem. Int. Ed.* **2001**, *40*, 680–699.

[2] See for example: [2a] S. C. van der Slot, P. C. J. Kamer, P. W. N. M van Leeuwen, J. Fraanje, K. Goubitz, M. Lutz, A. L. Spek, *Organometallics* **2000**, *19*, 2504–2515. [2b] K. G. Moloy, J. L. Petersen, *J. Am. Chem. Soc.* **1995**, *117*, 7696–7710. [2c] A. Huang, J. E. Marcone, K. L. Mason, W. J. Marshall, K. G. Moloy, *Organometallics* **1997**, *16*, 3377–3380. [2d] S. M. Aucott, A. M. Z. Slawin, J. D. Woollins, *J. Chem. Soc., Dalton Trans.* **2000**, 2559–2575. [2e] H. Tye, D. Smyth, C. Eldred, M. Wills, *Chem. Commun.* **1997**, 1053–1054. [2f] D. E. C. Corbridge, *Phosphorus: An Outline of Its Chemistry, Biochemistry and Technology*, 5th ed., Elsevier, Amsterdam, **1995**, p. 51. [2g] J. M. Brunel, A. Heumann, G. Buono, *Angew. Chem. Int. Ed.* **2000**, *39*, 1946–1949. [2h] M. L. Clarke, D. J. Cole-Hamilton, A. M. Z. Slawin, J. D. Woollins, *Chem. Commun.* **2000**, 2065–2066. [2i] M. R. I. Zubiri, M. L. Clarke, D. F. Foster, D. J. Cole-Hamilton, A. M. Z. Slawin, J. D. Woollins, *J. Chem. Soc., Dalton Trans.* **2001**, 969–971.

[3] [3a] A. M. Z. Slawin, M. B. Smith, J. D. Woollins, *J. Chem. Soc., Dalton Trans.* **1996**, 1283–1293. [3b] E. Valls, J. Suades, R. Mathieu, *Organometallics* **1999**, *18*, 5475–5483. [3c] J. Andrieu, P. Braunstein, Y. Dusausoy, N. Germani, *Inorg. Chem.* **1996**, *35*, 7174–7180. – [3d] M. J. Baker, M. F. Giles, A. G. Orpen, M. J. Taylor, R. J. Watt, *J. Chem. Soc., Chem. Commun.* **1995**, 197–198. [3e] M. A. Jalil, S. Fujinami, H. Nishikawa, *J. Chem. Soc., Dalton Trans.* **2001**, 1091–1098.

[4] P. Braunstein, M. D. Fryzuk, M. Le Dall, F. Naud, S. J. Rettig, F. Speiser, *J. Chem. Soc., Dalton Trans.* **2000**, 1067–1074.

[5] A. Baceiredo, G. Bertand, P. W. Dyer, J. Fawcett, N. Griep-Raming, O. Guerret, M. J. Hanton, D. R. Russell, A. M. Williamson, *New J. Chem.* **2001**, *25*, 591–596.

[6] E. Lindner, H. A. Mayer, A. Möckel, in: *Phosphorus-31NMR Spectral Properties in Compound Characterization and Structural Analysis* (Eds.: L. D. Quin, J. G. Verkade), VCH, New York, **1994**, p. 215.

[7] A. L. Crumbliss, R. J. Topping, in: *Phosphorus-31 NMR Spectroscopy in Stereochemical Analysis* (Eds.: J. G. Verkade, L. D. Quin), VCH, Florida, **1987**, chapter 15.

[8] W. de Graaf, S. Harder, J. Boersma, G. van Koten, J. A. Kanters, *J. Organomet. Chem.* **1988**, *358*, 545–562.

[9] W. de Graaf, J. Boersma, W. J. J. Smeets, A. L. Spek, G. Van Koten, *Organometallics* **1989**, *8*, 2907–2917.

[10] P. S. Pregosin, R. W. Kunz, in: *^{31}P and ^{13}C NMR of Transition Metal Phosphane Complexes* (Eds.: P. Diehl, E. Fluck, R. Kosfeld), Springer, Berlin, Heidelberg, **1979**, vol. 16 ("NMR, Basic Principles and Progress").

[11] See for example: [11a] E. K. van den Beuken, W. J. J. Smeets, A. L. Spek, B. L. Feringa, *Chem. Commun.* **1998**, 223–224. [11b] G. P. C. M. Dekker, A. Buijs, C. J. Elsevier, K. Vrieze, P. W. N. M. van Leeuwen, W. J. J. Smeets, A. L. Spek, Y. F. Wang, C. H. Stam, *Organometallics* **1992**, *11*, 1937–1948. [11c] A. Pfaltz, *Acta Chem. Scand.* **1996**, *50*, 189–194. [11d] K. R. Reddy, C-L. Chen, Y-H. Liu, S-M. Peng, J-T. Chen, S-T. Liu, *Organometallics* **1999**, *18*, 2574–2576. [11e] A. Saitoh, M. Misawa, T. Morimotom, *Synlett* **1999**, *4*, 483–485.

[12] T. Schleis, J. Heinemann, T. P. Spaniol, R. Mulhaupt, J. Okuda, *Inorg. Chem. Commun.* **1998**, *1*, 431–434.

[13] ^{31}P NMR spectroscopic data for [$PdMe_2$(dppe)] were obtained from an authentic sample prepared according to ref.[9]

[14] [14a] L. K. Johnson, C. M. Killian, M. Brookhart, *J. Am. Chem. Soc.* **1995**, *117*, 6414–6415. [14b] G. J. P. Britovsek, V. C. Gibson, D. F. Wass, *Angew. Chem. Int. Ed.* **1999**, *38*, 428–447. [14c] S. D. Ittel, L. K. Johnson, M. Brookhart, *Chem. Rev.* **2000**, *100*, 1169–1203. [14d] Y-C. Chen, C-L. Chen, J-T. Chen, S-T. Liu, *Organometallics* **2001**, *20*, 1285–1286.

[15] For a review on palladium-catalysed polyketone synthesis see: E. Drent, P. H. M. Budzelaar, *Chem. Rev.* **1996**, *96*, 663–681.

[16] [16a] S. H. Strauss, *Chem. Rev.* **1993**, *93*, 927–942. [16b] M. Bochmann, *J. Chem. Soc., Dalton Trans.* **1996**, 255–270. [16c] M. Bochmann, A. J. Jaggar, J. C. Nicholls, *Angew. Chem. Int. Ed. Engl.* **1990**, *29*, 780–782.

[17] W. E. Piers, T. Chivers, *Chem. Soc. Rev.* **1997**, *26*, 345–354.

[18] L. Dahlenburg, K. Herbst, H. Berke, *J. Organomet. Chem.* **1999**, *585*, 225–233.

[19] L. Dahlenburg, K. Herbst, G. Liehr, *Acta Crystallogr., Sect. C: Cryst. Struct. Commun.* **1997**, *53*, 1545−1547.
[20] W. J. Knebel, R. J. Angelici, *Inorg. Chim. Acta* **1973**, *7*, 713−716.
[21] M. A. Jalil, S. Fujinami, H. Nishikawa, *J. Chem. Soc., Dalton Trans.* **1999**, 3499−3505.
[22] S. D. Perera, B. L. Shaw, M. Thornton-Pett, *J. Organomet. Chem.* **1992**, *428*, 59−67.
[23] B. P. Buffin, T. G. Richmond, *Polyhedron* **1990**, *9*, 2887−2893.
[24] E. W. Ainscough, A. M. Brodie, P. D. Buckley, A. K. Burrell, S. M. F. Kennedy, J. M. Waters, *J. Chem. Soc., Dalton Trans.* **2000**, 2663−2671.
[25] N. N. Greenwood, A. Earnshaw, *Chemistry of the Elements*, 2nd ed., Butterworth-Heinemann, Oxford, **1997**, pp. 532−533.
[26] I. C. F. Vasconcelos, G. K. Anderson, N. P. Rath, C. D. Spilling, *Tetrahedron: Asymmetry* **1998**, *9*, 927−935.
[27] L. Dahlenburg, S. Mertel, *Acta Crystallogr., Sect. C: Cryst. Struct. Commun.* **1999**, *55*, 347−349.
[28] [28a] P−N single bond: 1.8 Å: L. Pauling, in: *Nature of the Chemical Bond*, Cornell University Press, New York, **1960**. [28b] 1.76 Å: V. Schomaker, D. P. Stevenson, *J. Am. Chem. Soc.* **1941**, *63*, 37−40.
[29] S. D. Perera, B. L. Shaw, M. Thornton-Pett, *Inorg. Chim. Acta* **1995**, *236*, 7−12.
[30] W. L. Steffen, G. J. Palenik, *Inorg. Chem.* **1976**, *15*, 2432−2438.
[31] J. C. Clardy, R. L. Kolpa, J. G. Verkade, *Phosphorus* **1974**, *4*, 133−141; C. Rømming, J. Songstad, *Acta Chem. Scand.*, **1978**, *A32*, 689−699.
[32] S. Woodward, in: *Comprehensive Organometallic Chemistry II* (Eds.: E. W. Abel, F. G. A. Stone, G. Wilkinson), Elsevier, Oxford, **1995**, vol. 5, p. 226.
[33] I. Bernal, G. M. Reisner, G. R. Dobson, C. B. Dobson, *Inorg. Chim. Acta* **1986**, *121*, 199−206.
[34] M. A. Beckett, D. P. Cassidy, A. J. Duffin, *Inorg. Chim. Acta* **1991**, *189*, 229−232.
[35] G. R. Knox, D. G. Leppard, P. L. Pauson, W. E. Watts, *J. Organomet. Chem.* **1972**, *34*, 347−352.
[36] J. R. Doyle, P. E. Slade, H. B. Jonassen, *Inorg. Synth.* **1960**, *6*, 218.
[37] J. Chatt, L. M. Vallarino, L. M. Venanzi, *J. Chem. Soc.* **1957**, 3413−3416.
[38] R. E. Rülke, J. M. Ernsting, A. L. Spek, C. J. Elsevier, P. W. N. M. van Leeuwen, K. Vrieze, *Inorg. Chem.* **1993**, *32*, 5769−5778.
[39] H. Nishida, N. Takada, M. Yoshimura, T. Sonoda, H. Kobayashi, *Bull. Chem. Soc. Jpn.* **1984**, *57*, 2600−2604.
[40] B. L. Ross, J. G. Grasselli, W. M. Ritchey, H. D. Kaesz, *Inorg. Chem.* **1963**, *2*, 1023−1030.

Received July 3, 2001
[I01252]

Reduced Molybdovanadophosphates[‡]

Anna Selling,*[a] Ingegärd Andersson,[a] John H. Grate,[b] and Lage Pettersson[a]

Keywords: Polyoxometalates / NMR spectroscopy / Redox chemistry / Speciation / Formation constants

The equilibrium speciation in the aqueous $H^+/MoO_4^{2-}/HVO_4^{2-}/HPO_4^{2-}/e^-$ system, 0.600 M Na(Cl) medium at 25 °C, was characterised by potentiometric [H^+] (glass electrode) and {e^-} (platinum electrode) titration techniques as fundamental tools, complemented by $^{51}V^V$ NMR (131.6 MHz) and V^{IV} ESR spectroscopy. The study has been focused on solutions with the Keggin ratio, (Mo + V)/P = 12:1 and Mo/V > 5, in the pH range 1.4–4.5, where anions having the formula $[H_zMo_{12-x-y}V^V_xV^{IV}_yPO_{40}]^{(3+x+2y-z)-}$ are predominant species. Added numbers of electrons per vanadium(V) (e^-/V^V) have been kept less than one to exclude reduction of molybdenum(VI). Six reduced molybdovanadophosphate species have been identified. The $[Mo_{11}V^{IV}PO_{40}]^{5-}$ species [logβ = 154.15 ± 0.03 (3σ)] and the mixed-valence species $[Mo_{10}V^VV^{IV}PO_{40}]^{6-}$ (logβ = 155.84 ± 0.02) can both be monoprotonated. These species have pK_a values of 0.93 and 3.68, respectively. A "fully" reduced Keggin species, $[H_2Mo_{10}V^{IV}_2PO_{40}]^{5-}$ (logβ = 171.27 ± 0.06), and a lacunary $[H_4Mo_{10}V^{IV}PO_{39}]^{5-}$ species (logβ = 142.0 ± 0.2) were found as well. Except for the molybdovanadophosphate species, the only reduced species formed, in the present investigation, is the vanadyl ion, VO^{2+}. logK_{red} ($2H^+ + VO_2^+ + e \rightleftarrows VO^{2+} + H_2O$) was determined to 17.15 ± 0.01 (E^0 = 1014.5 ± 0.6 mV).

Introduction

Polyoxoanions are of considerable interest as redox catalysts, for they are easily reduced and can often be reoxidised by O_2. Molybdovanadophosphate complexes have for example been used as catalysts in the selective oxidation of olefins to carbonyl groups.[1] Studies of solutions containing vanadium(IV), tungsten, and phosphorus[2–7] or vanadium(IV), molybdenum, and phosphorus[3,8–12] are frequently reported in the literature. In both cases so-called mixed addenda Keggin species are formed. In most of these studies the experimental techniques used have been cyclic voltammetry, NMR, and ESR. Recently, results from investigations of solutions containing vanadium(IV), tungsten, molybdenum, and phosphorus, forming Keggin anions with three addenda atoms, have been reported.[13,14]

As a part of our studies of the equilibrium speciation in the aqueous molybdovanadophosphate system, the electron has been included as the fifth component. A complete study of this system can only be done when all the oxidised and reduced subsystems are known at the same experimental conditions. The oxidised subsystems are the three binary systems H^+/MoO_4^{2-},[15] H^+/HVO_4^{2-},[16–18] and H^+/HPO_4^{2-},[19] the three ternary systems $H^+/MoO_4^{2-}/HVO_4^{2-}$,[20,21] $H^+/MoO_4^{2-}/HPO_4^{2-}$,[22,23] and $H^+/HVO_4^{2-}/HPO_4^{2-}$,[19] and the quaternary system $H^+/MoO_4^{2-}/HVO_4^{2-}/HPO_4^{2-}$.[24,25] Within the concentration ranges of this study, it was found that the only reduced species, except for those with five components, was the vanadyl cation, VO^{2+}. The formation constant for VO^{2+} has already been determined,[17] but is redetermined here with more advanced equipment.

The present system has, like all the subsystems, been studied in 0.600 M Na(Cl) medium at 25 °C. Species and formation constants have been determined by using potentiometric [H^+] (glass electrode) and {e^-} (platinum electrode) titration techniques as fundamental tools, complemented by NMR and ESR spectroscopy. One prerequisite of working with complicated systems is to have access to a computer program, which can treat all kinds of data simultaneously. Therefore, all calculations for determining the formation constants were made with the calculation program LAKE,[26] which can treat both potentiometric (EMF) and NMR spectroscopic data simultaneously.

Notations and Designations

The formation constants are reported with H^+, MoO_4^{2-}, HVO_4^{2-}, HPO_4^{2-}, and e^- as components. The equilibria are written according to Equation (1).

[‡] Multicomponent Polyanions, 50. – Part 49: Ref.[25]

[a] Department of Chemistry, Inorganic Chemistry, Umeå University,
90187 Umeå, Sweden
Fax: (internat.) + 46-90/786-9195
E-mail: anna.selling@chem.umu.se
[b] Catalytica Inc.,
430 Ferguson Drive, Mountain View, California 94043, USA

$$p\,H^+ + q\,MoO_4^{2-} + r\,HVO_4^{2-} + s\,HPO_4^{2-} + t\,e^- \rightleftarrows [(H^+)_p(MoO_4^{2-})_q(HVO_4^{2-})_r(HPO_4^{2-})_s(e^-)_t]^{p-2(q+r+s)-t} \quad (1)$$

A species formed will, for brevity, sometimes be denoted by its (*p*,*q*,*r*,*s*,*t*) integers. The potentiometric data can only establish the composition and charge of the species formed, as water may be gained or lost relative to the components. However, when complementary structural information is available, the formula can be given. For example, since in the present study (23,11,1,1,1) is known to have the Keggin composition it can be written $[HMo_{11}V^{IV}PO_{40}]^{4-}$. The charge and number of oxygen atoms and protons are often omitted below, and species are instead written in the compact forms $Mo_{11}VP$ and $Mo_{10}V_2P$. Our definition of the degree of reduction, denoted z_e, is equivalents of electrons added per mol of vanadium(V). Thus, a z_e value of 0.25, means that 25% of the vanadium, initially of valence V, is reduced.

A 0.600 M Na(Cl) ionic medium is 0.600 M Na^+ with Cl^- providing counteranion balance not provided by the oxometalate anions. The acidity measurements are on the concentration scale, where pH = $-\log[H^+]$, and *not* on the activity scale, pH = $-\log\{a_{H+}\}$. For brevity, the total concentrations of molybdenum, vanadium, and phosphorus will be denoted Mo, V, and P.

Results and Discussion

To fully understand the reduced molybdovanadophosphate system, all subsystems, both oxidised and reduced, must be known at the same experimental conditions. All oxidised subsystems have already been determined and the only reduced non-Keggin vanadium species present in this study is VO^{2+}. It is formed when the $H_zMo_{12-x-y}V^V{}_xV^{IV}{}_yP$ species decompose in acidic solutions. In the decamolybdodivanadophosphate system it was found that the ^{51}V NMR signal disappears as soon as one electron is added to the complex. One would expect that the vanadium atom, well separated from the reduced vanadium atom, should not be affected, but due to an electron tunnelling effect even this signal disappears. Similar observations have been made in studies on the reduced molybdotungstohosphate system showing that tungsten atoms, not adjacent to the reduced molybdenum atom, are affected of the reduction.[27,28]

The Reduced Vanadate System

The $H^+/HVO_4^{2-}/e^-$ system had been studied earlier in acidic solutions and in the same medium [0.600 M Na(Cl)], but with rather simple equipment.[17] Therefore, a redetermination using more advanced equipment and a more sophisticated technique for working with air-sensitive solutions was found worthwhile. Since VO^{2+} is the only reduced non-Keggin vanadium species present, only one reaction and one equilibrium constant ($\log K_{red}$) has to be determined; $2\,H^+ + VO_2^+ + e^- \rightleftarrows VO^{2+} + H_2O$, $\log K_{red}$ = 17.15 ± 0.01 (E^0 = 1014.5 ± 0.6 mV), can be compared with the old result of 17.37. When the redox equilibrium is written with the components used in the study of the five component system, $5\,H^+ + HVO_4^{2-} + e^- \rightleftarrows VO^{2+} + 3\,H_2O$, the $\log\beta_{5,0,1,0,1}$ value is 32.03 ± 0.01. NMR and ESR spectra were recorded to establish that VO_2^+ and VO^{2+} are the only species formed in acidic solutions (pH < 2). ESR spectra of VO^{2+} reveal a typical vanadium(IV) signal, with 8 hyperfine lines arising from the unpaired electron (S = 1/2) with the nuclear spin (I = 7/2). ESR and NMR spectra recorded on the same solutions showed the 8-line ESR pattern for VO^{2+} increasing in proportion to the decrease of the VO_2^+ resonance in the NMR spectrum.

The Reduced Molybdovanadophosphate System

In the determination of formation constants of reduced molybdovanadophosphate species, both EMF and ^{51}V integral data were included. Calculations have been made stepwise by gradually decreasing the Mo/V ratio and expanding the pH range. Starting with different rather high Mo/V ratios (11−22), where only $Mo_{11}VP$ species and some MoP species are present, constants for the reduced $Mo_{11}V^{IV}P$ species could be determined. Once these constants were known, data from lower Mo/V ratios, down to 5.67, where also $Mo_{10}V_2P$ species are present in oxidised solutions, were included in the calculations. Different formulations for reduced species were systematically tested using LAKE. Table 1 shows the model that gave the best (lowest sum of squared errors) fit of data. Of the reduced species found, $[Mo_{11}V^{IV}PO_{40}]^{5-}$ can be monoprotonated (pK_a = 0.93), in contrast to the oxidised $[Mo_{11}V^{V}PO_{40}]^{4-}$ species.[25] The $Mo_{10}V_2P$ species with mixed valence states of vanadium, $Mo_{10}V^VV^{IV}P$, can also be monoprotonated, having a pK_a value of 3.68. A diprotonated doubly reduced species, $[H_2Mo_{10}V^{IV}{}_2PO_{40}]^{5-}$, is also found. An X-ray structure study on deep blue tabular crystals obtained when concentrating a fully reduced molybdovanadophosphate solution (Mo/V = 5.67; pH ≈ 4.8; z_e = 1.0), showed that the doubly reduced species have an α-Keggin structure.[29] One incomplete Keggin species, (20,10,1,1,1), an $Mo_{10}V^{IV}P$ species, is required in the model to explain data. Incomplete Keggin species (often called lacunary species e.g. with tungsten and Si,[30] B,[31] or P[32] as heteroatoms) are well known

Table 1. The equilibrium model obtained from calculations on data in the pH range 1.4 < pH < 4.5 and at Mo/V>5

(*p*,*q*,*r*,*s*,*t*)	Formula	$\log\beta \pm 3\sigma$	pK_a
22,11,1,1,1	$[Mo_{11}V^{IV}PO_{40}]^{5-}$	154.15 ± 0.03	
23,11,1,1,1	$[HMo_{11}V^{IV}PO_{40}]^{4-}$	155.08 ± 0.15	0.93
21,10,2,1,1	$[Mo_{10}V^VV^{IV}PO_{40}]^{6-}$	155.84 ± 0.02	
22,10,2,1,1	$[HMo_{10}V^VV^{IV}PO_{40}]^{5-}$	159.52 ± 0.04	3.68
23,10,2,1,2	$[H_2Mo_{10}V^{IV}{}_2PO_{40}]^{5-}$	171.27 ± 0.06	
20,10,1,1,1	$[H_4Mo_{10}V^{IV}PO_{39}]^{5-}$	142.04 ± 0.20	

in heteropoly anion systems. Such a lacunary species of a generalised polyhedral structure is shown in Figure 1. Accordingly, (20,10,1,1,1) most probably has the lacunary Keggin formula $[H_4Mo_{10}V^{IV}PO_{39}]^{5-}$. This lacunary species is most likely formed by dissociation of VO^{2+} from the double reduced divanadium Keggin species.

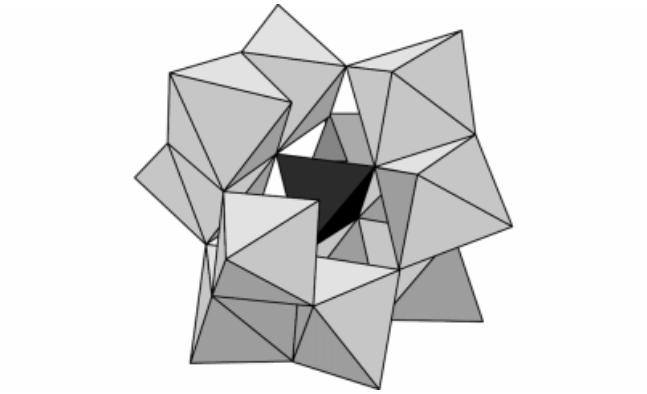

Figure 1. Polyhedral structure of an incomplete Keggin anion, a so-called lacunary species

Figure 2 shows distribution diagrams of a) vanadium and b) phosphorus for a solution where 50% of the vanadium(V) atoms are reduced to vanadium(IV). The fully oxidised solution had a composition of 20% $Mo_{11}VP$ and 80% $Mo_{10}V_2P$. The $(\alpha_i)_{V(P)}$ coordinate quantitates the fraction of every species *i* relative to the total V(P). Each species has its own region in the cumulative diagram, so that the fraction of the species is the region's vertical extent, at a given pH. A bold line separates reduced and oxidised species. In this figure, each protonation step is plotted individually with a dotted line and the solid line shows the sum of them. The symbols (O) in Figure 2 (a) represent experimental points (integral values) and show how the experimental NMR spectroscopic data fit the proposed model. The fit is within the evaluation error of the integrals.

In acidic solutions (pH < 2.5) there is considerable decomposition of reduced $Mo_{10}V_2P$ species to VO^{2+} and $Mo_{11}V^{IV}P$ species. Where VO^{2+} is the predominant reduced species, most of the phosphorus atoms are bound in oxidised species or present as phosphoric acid.

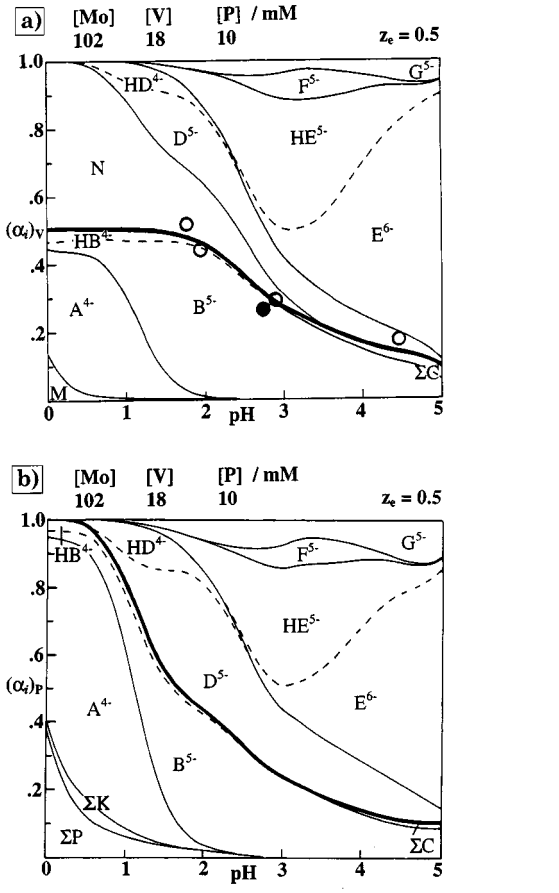

Figure 2. Distribution diagrams of a) vanadium and b) phosphorus at z_e = 0.5 and (Mo + V)/P = (102 + 18)/10 mM; oxidised and reduced species are separated with a bold line; each protonation step is plotted individually with a dotted line and the solid line shows the sum of them; symbols (O) represent ^{51}V integral data, and (●) is the integral value from the equilibrated, "aged", solution in Figure 5; A^{4-} = $Mo_{11}VP^{4-}$; B^{5-} = $Mo_{10}V_2P^{5-}$; HB^{4-} = $HMo_{10}V_2P^{4-}$; ΣC = ΣMo_9V_3P; M = VO_2^+; D^{5-} = $Mo_{11}V^{IV}P^{5-}$; HD^{4-} = $HMo_{11}V^{IV}P^{4-}$; E^{6-} = $Mo_{10}V^{V}V^{IV}P^{6-}$; HE^{5-} = $HMo_{10}V^{V}V^{IV}P^{5-}$; F^{5-} = $H_2Mo_{10}V^{IV}_2P^{5-}$; G^{5-} = $H_4Mo_{10}V^{IV}P^{5-}$; N = VO^{2+}; ΣP = ΣH_3PO_4; ΣK = ΣMo_xP_y

Comparison between Distribution Diagrams and NMR Spectra

^{51}V NMR spectra of acidic solutions (pH ≈ 2) containing 20% $Mo_{11}VP$ and 80% $Mo_{10}V_2P$ at different z_e values have been recorded on an absolute intensity mode, as shown in Figure 3. At this rather low pH value, the resonance arising from $Mo_{11}VP$ (a) decreases first when electrons are added, cf. spectra at z_e = 0 and 0.10. When almost all of the $Mo_{11}VP$ species has been reduced, the positional isomers of the $Mo_{10}V_2P$ (b−e) species start to reduce. In more acidic solutions (pH ≈ 1.5) the behaviour is different, the $Mo_{10}V_2P$ isomers are the first to be reduced. The redox reactions are thus very dependent upon the pH of the solutions. The simplified distribution diagram in Figure 4 shows the difference between the oxidised $Mo_{11}VP$ and $Mo_{10}V_2P$ species in solutions with z_e = 0.0 (full-drawn lines) and z_e = 0.10 (dashed lines). The $Mo_{11}VP$ species is present with approximately the same amount in oxidised and reduced solutions at pH ≈ 1.5, while it is almost completely reduced at pH ≈ 2.1. This was also experimentally observed in the NMR spectra recorded from such solutions.

To examine which one of the five positional $Mo_{10}V_2P$ isomers[24] is the first to be reduced, a ^{51}V NMR spectrum was recorded immediately after the electrons had been added from a potentiostat to z_e = 0.50 (fresh) and then at equilibrium 2 d later (aged), Figure 5. A comparison between the two spectra shows that the resonance from the α-1,4-$Mo_{10}V_2P$ isomer (b), where two vanadium octahedra share edges, decreases more than the others in fresh solution; but after equilibrium, the ratio between all the isomers

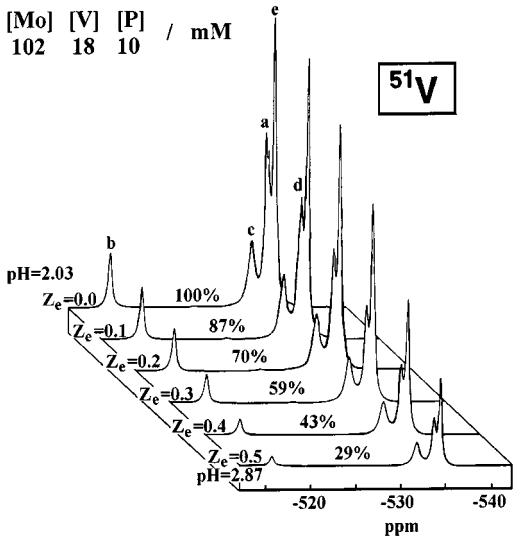

Figure 3. A set of ^{51}V NMR spectra of a solution containing 80% $Mo_{10}V_2P$ and 20% $Mo_{11}VP$ at different degrees of reduction recorded on an absolute intensity mode; resonance labelled **a** arise from the $Mo_{11}VP$ species and resonances **b**−**e** from the $Mo_{10}V_2P$ isomers; **b** = α-1,4; **c** = α-1,2; **d** = α-1,5; **e** = α-1,6 + α-1,11

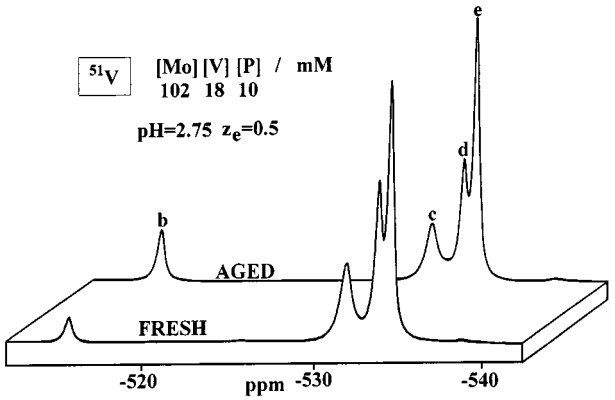

Figure 5. Two ^{51}V spectra recorded on the same $Mo_{10}V_2P$ solution; the front spectrum was recorded only a few minutes after the electrons were added with a potentiostat, and the rear spectrum after equilibration; resonances arising from the $Mo_{10}V_2P$ isomers are labelled **b**−**e**; **b** = α-1,4; **c** = α-1,2; **d** = α-1,5; **e** = α-1,6 + α-1,11

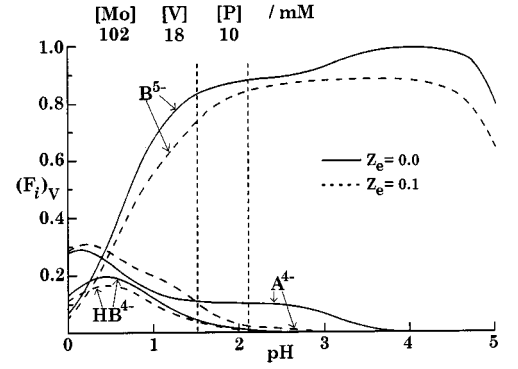

Figure 4. A simplified distribution diagram for a solution with (Mo + V)/P = (102 + 18)/10 mM, where only some oxidised species are shown at two different z_e values; full-drawn lines represent the distribution at z_e = 0.0 and dashed lines at z_e = 0.1; A^{4-} = $Mo_{11}VP^{4-}$; B^{5-} = $Mo_{10}V_2P^{5-}$; HB^{4-} = $HMo_{10}V_2P^{4-}$

are the same as in a fully oxidised solution. This means that the α-1,4-$Mo_{10}V_2P$ isomer (b) takes care of most of the added electrons in the start, but at equilibrium all isomers have the same amount of reduction. In non-aqueous solutions, a similar reduction pattern has been observed. The isomers with vicinal vanadium atoms seem to be the first to be reduced.[33] The distribution diagram in Figure 2 (a) shows that an equilibrated solution at z_e = 0.5 and pH = 2.75, should have 71% of the total vanadium in fully or partially reduced species. Experimentally, the equilibrated solution in Figure 5 has an integral value showing that 27% of the total vanadium is present in nonreduced species [marked with ● in Figure 2 (a)].

Comparison between Distribution Diagrams and ESR Spectra

In a solution with pH ≈ 2, containing both $Mo_{11}VP$ and $Mo_{10}V_2P$ species, the first species to be reduced when electrons are added is $Mo_{11}VP$, since its resonance disappears first, cf. Figure 3. A distribution diagram of a solution, where 10% of the total amount of vanadium is reduced is shown in Figure 6 (a). At pH = 2.1 the only reduced species is $[Mo_{11}V^{IV}PO_{40}]^{5-}$. An ESR spectrum [Figure 6 (b)] of the same solution indeed corresponds to the feature of $[Mo_{11}V^{IV}PO_{40}]^{5-}$ alone. The ESR spectrum of a solution with the ratio (Mo + V)/P = (110 + 10)/10 mM, reduced to z_e = 1.0 at pH = 1.0 is shown in Figure 7 (a). From our model, three reduced species should be present in such a solution, 42% $[Mo_{11}V^{IV}PO_{40}]^{5-}$, 40% $[HMo_{11}V^{IV}PO_{40}]^{4-}$, and 18% $[V^{IV}O]^{2+}$ [Figure 7 (b)]. Arrows in Figure 7 (a) mark peaks arising from VO^{2+}. Subtracting VO^{2+} from this spectrum gives the same pattern as in Figure 6 (b), which means that both the protonated and deprotonated $Mo_{11}V^{IV}P$ have the same ESR spectrum. Similar checks of the proposed model against ESR spectra were also made at different pH values and different Mo/V ratios and the agreement was good.

ESR spectra of the present system should be virtually the same as for the corresponding vanadotungstates, reported by Pope et al.[2] Five positional isomers of $W_{10}V_2P$ and $Mo_{10}V_2P$ occur in both systems. Two isomers have neighbouring vanadium atoms and in the remaining three isomers one or more tungsten/molybdenum atoms separate the two vanadium atoms. The relative statistical abundances are 12 + 12 = 24 and 12 + 24 + 6 = 42, respectively. These have been verified in solution by ^{31}P NMR for both $W_{10}V_2P$[2] and $Mo_{10}V_2P$.[24] The unpaired electron in the

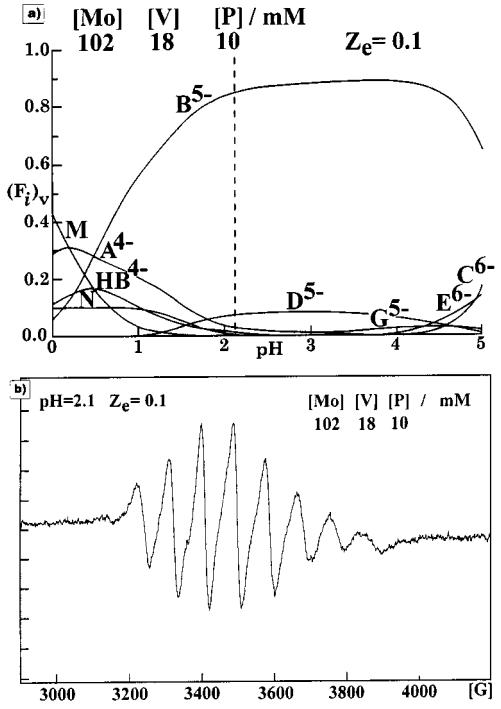

Figure 6. a) Distribution diagram of vanadium at z_e = 0.1 and (Mo + V)/P = (102 + 18)/10 mM; A^{4-} = $Mo_{11}VP^{4-}$; B^{5-} = $Mo_{10}V_2P^{5-}$; HB^{4-} = $HMo_{10}V_2P^{4-}$; C^{6-} = $Mo_9V_3P^{6-}$; M = VO_2^+; D^{5-} = $Mo_{11}V^{IV}P^{5-}$; E^{6-} = $Mo_{10}V^{V}V^{IV}P^{6-}$; G^{5-} = $H_4Mo_{10}V^{IV}P^{5-}$; N = VO^{2+}; b) ESR spectrum of the solution marked with a dashed line in a), showing the 8-line feature for $[Mo_{11}V^{IV}PO_{40}]^{5-}$

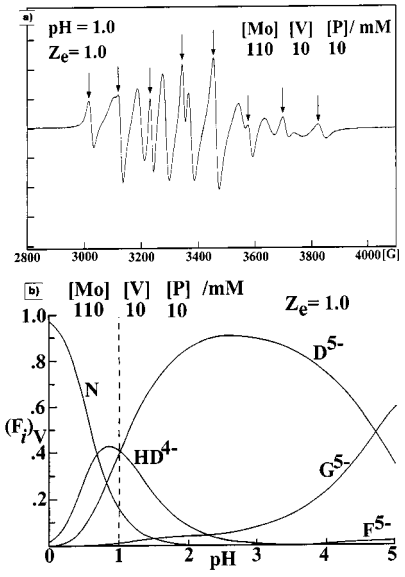

Figure 7. a) ESR spectrum of a solution with (Mo + V)/P = (110 + 10)/10 mM reduced to z_e = 1.0; arrows mark peaks arising from VO^{2+}; b) distribution diagram of vanadium for the same concentrations; dashed line marks the solution recorded on ESR in a); D^{5-} = $Mo_{11}V^{IV}P^{5-}$; HD^{4-} = $HMo_{11}V^{IV}P^{4-}$; F^{5-} = $H_2Mo_{10}V^{IV}{}_2P^{5-}$; G^{5-} = $H_4Mo_{10}V^{IV}P^{5-}$; N = VO^{2+}

two isomers with vicinal vanadium atoms, interacts with both vanadium nuclei through rapid intramolecular hopping to give a 15-line spectrum. In the remaining three isomers, where vanadium atoms are separated, the electron is effectively trapped by a single vanadium atom, thus giving an 8-line spectrum.[2] The relative intensity of the overlapping 15- and 8-line spectra in a mixed-valence vanadium solution should be 24:42 = 4:7. From our model, a solution with the ratio Mo/V = 102:18 = 5.7 and pH = 4.5 contains predominantly $Mo_{10}V^{V}V^{IV}P$ when z_e = 0.5. As expected, an ESR spectrum of the $Mo_{10}V^{V}V^{IV}P$ solution (Figure 8, bottom spectrum) shows a mixed 8- and 15-line pattern. The 8-line feature in the figure has, however, higher intensity than the 15-line, which means that the abundance observed by ESR is in accordance with the statistical prediction. In contrast, the doubly reduced $W_{10}V_2P$ species gives a spectrum with 15 equal lines, expected for the interaction of the unpaired electrons with two vanadium nuclei.[2] In the present work, a solution with the ratio Mo/V = 200:40 = 5 and pH = 4.5, which should contain 50% $Mo_{10}V^{V}V^{IV}P$ and 50% $Mo_{10}V^{IV}{}_2P$ species when z_e = 0.75, gave rise to the top 15-line spectrum shown in Figure 8. It has both the previous (8 + 15)-line component feature arising from $Mo_{10}V^{V}V^{IV}P$ species and also a 15-line component feature from $Mo_{10}V^{IV}{}_2P$ species, with an increase for the latter compared with the lower spectrum in Figure 8. This shows again that the proposed model is in good agreement with the experimental data.

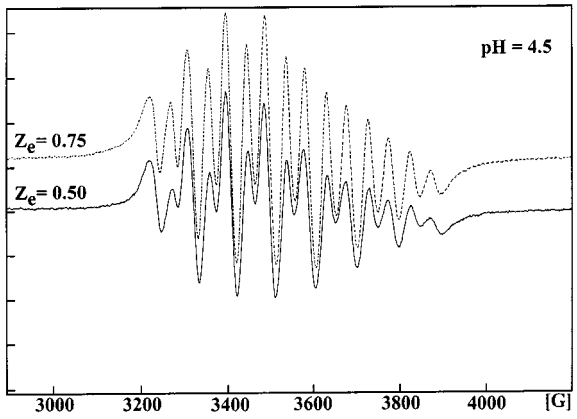

Figure 8. The bottom spectrum (z_e = 0.5) shows the (8 + 15)-line feature for the mixed valence state of the $Mo_{10}V^{V}V^{IV}P$ isomers; the top dashed spectrum (z_e = 0.75) shows how the 15-line pattern has increased when $Mo_{10}V^{IV}{}_2P$ also is present in the solution

Pourbaix Diagrams

The redox speciation in systems with few components is often illustrated in the literature by means of predominance diagrams, so-called Pourbaix diagrams [showing areas of predominant species as a function of *E* (or *pe*) and pH]. Numerous diagrams are needed to illustrate the speciation in the present 5-component system. The reason is that the speciation is not only dependent on the total concentrations, but also on the Mo/V/P ratios. Figure 9 shows a diagram of vanadium containing species at (Mo + V)/P = (105 + 15)/10 mM (equal amounts of $Mo_{11}VP$ and $Mo_{10}V_2P$). At high *E* values (oxidised solutions), $Mo_{11}VP$ is the predominant species at the pH range 0.2−1.3. In less acidic

solutions at this high E value, the deprotonated $Mo_{10}V_2P$ isomers are predominant. When the E value is lowered, i.e. electrons have been added, these species are reduced to VO^{2+} and the monoprotonated $Mo_{11}V^{IV}P$, respectively. As can be seen from the figure, additional reduced species appear as predominant species at pH values higher than 3.4.

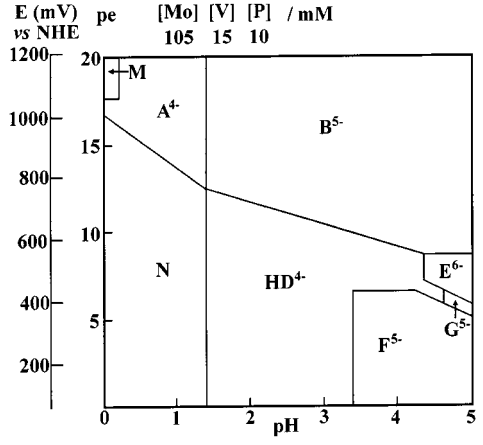

Figure 9. Predominance (Pourbaix) diagram of vanadium at (Mo + V)/P = (105 + 15)/10 mM; $A^{4-} = Mo_{11}VP^{4-}$; $B^{5-} = Mo_{10}V_2P^{5-}$; M = VO_2^+; $HD^{4-} = HMo_{11}V^{IV}P^{4-}$; $E^{6-} = Mo_{10}V^{V}V^{IV}P^{6-}$; $F^{5-} = H_2Mo_{10}V^{IV}{}_2P^{5-}$; $G^{5-} = H_4Mo_{10}V^{IV}P^{5-}$; N = VO^{2+}

Experimental Section

Solutions for Potentiometric, NMR, and ESR Studies: The oxidised solutions for potentiometric, NMR, and ESR studies were prepared as previously described.[24,25] Stock solutions of vanadium(IV) were prepared from vanadium(IV) oxide, V_2O_4 (Aldrich Chemical 99.9%), which was dried at 100 °C and then used without any further purification. V_2O_4 was dissolved in diluted hydrochloric acid and the absence of vanadium(V) as VO_2^+ was checked by ^{51}V NMR. The dissolution process is very slow, but can be speeded up in an ultrasound bath. To make sure that no reoxidation will occur, all glassware was filled with argon and all solutions bubbled with argon for at least 30−40 min before mixing.

Equilibria: Equilibria in the reduced molybdovanadophosphate system were attained within 2−48 h, and in the reduced vanadium system within 2−24 hours. No matter how the electrons were added, coulometrically or with a vanadium(IV) stock solution, the same results were obtained. Equilibrium was, however, reached more rapidly using a vanadium(IV) solution. The redox reactions of Keggin species were shown to be reversible.

EMF Measurements: EMF titrations were conducted at 25.0 ± 0.1 °C using an automated potentiometric titrator. Free H^+ concentrations were determined by measuring the EMF of the following cell, using an Ingold type 201-NS glass electrode, an Ag/AgCl reference electrode, prepared according to Brown,[34] and a Wilhelm bridge.[35]

− Ag, AgCl | 0.600 M NaCl ‖ equilibrium solution | measuring electrode +

The redox potential was measured between a small foil or spiral of platinum metal in the solution and the same reference electrode as for the measurements of free [H^+]. The free H^+ concentration and the electron activity were calculated from the measured EMF values E [mV] by Equation (2) and Equation (3), where the last term is the liquid junction potential for 0.6 M NaCl medium and the type of bridge used.

$$E = E_{0a} + 59.157\cdot\log[H^+] - 76\cdot[H^+] \quad (2)$$

$$E = E_{0b} - 59.157\cdot\log\{e^-\} - 76\cdot[H^+] \quad (3)$$

The electrons were added coulometrically at 800−250 mV vs. NHE using an automated potentiostat (developed at our department), or with a solution containing vanadium(IV) of known concentration. All titrations were performed under pure argon to prevent contamination by oxygen from the air. The argon was sparged through 10% NaOH solution to remove any acid impurities, 10% H_2SO_4 solution to remove any alkaline impurities, and, finally, 0.6 M NaCl medium before introduction to the titration vessel. Before each titration, the platinum electrode was rinsed in distilled water and heated in an ethanol flame. The constant E_{0a} was determined before and after each titration, using a separate solution of known [H^+]. In separate experiments, E_{0b} was determined to −250 mV in solutions with known {e^-}. Several experiments were performed and the variation in E_{0b} was negligible. The value −250 mV could thus be used for all titrations. Reduction constants are often reported with E^0 instead of $\log K_{red}$ values. The relation between them is described in Equation (4), where $g = (R\cdot T\cdot\ln 10)/F$ and n_e is the number of electrons in the redox reaction; at 25 °C, g = 59.157 mV.

$$E^0 = g/n_e\cdot\log K_{red} \quad (4)$$

EMF Data: In the determination of the formation constant of the vanadyl cation, VO^{2+}, 118 data points were collected from 12 different titrations in the concentration ranges 1.5 < pH < 2.1 and 4 < [V] < 10 mM. To ensure that no other species than the vanadyl ion was formed, the upper limit of the z_e value was 0.92. In the reduced molybdovanadophosphate system 44 titrations were performed on Keggin ratio solutions, (Mo + V)/P = 12, with 5 < Mo/V < 22 and 10 < Mo/P < 11. The concentration ranges 1.38 < pH < 5.49, 100 < [Mo] < 200 mM, 5 < [V] < 40 mM, and 10 < [P] < 20 mM have been covered. In the calculations, data were restricted to the pH and z_e ranges 1.38 < pH < 4.5 and 0.0 < z_e < 0.9 giving in total 322 data points. To confirm that the same result is achieved both when electrons are added to an oxidised solution and when an oxidised solution is added to a reduced, titrations were made in both directions and they coincide. Since the present study has been focused on $Mo_{11}VP$ and $Mo_{10}V_2P$ species and to avoid the formation of Mo_9V_3P species, no Mo/V ratio lower than 5 was allowed. The upper limit of z_e was set at 0.9 to avoid the reduction of molybdenum(VI).

NMR Measurements: The ^{51}V and ^{31}P NMR measurements were obtained by using a Bruker AM500 spectrometer at 131.6 and 202.5 MHz, respectively. The probe temperature was thermostatted at 25.0 ± 0.5 °C. The field frequency stabilisation was locked to deuterium by placing the 8-mm sample tubes into 10-mm tubes containing D_2O. The samples were spinning in all experiments. All NMR samples were transferred from the titration solution to the sample tubes with a Hamilton® gas syringe. Commercial stainless steel needles could not be used since the steel was found to reduce oxidised MoVP solutions. Instead, specially prepared titanium needles were used. The NMR tubes used were of septa type and were "rinsed" with argon for about 45 min, to avoid oxidation of

the reduced solutions by oxygen in the air. The spin-lattice relaxation time (T_1) was just a few ms for ^{51}V, so by having a relaxation delay of 1 s the spectra were quantitatively recorded. The free induction decay (FID) was multiplied by an exponential line-broadening function (LB = 1), using the Bruker software, to improve the signal/noise ratio. A Gaussian−Lorentzian double apodization was sometimes applied to the FID, also by using the Bruker software, to enhance resolution to obtain more accurate chemical shifts of overlapping resonances. $VOCl_3$ and 85% H_3PO_4 were used as external shift standards. Positive chemical shifts (δ) correspond to higher frequency. For an exact shift scale, a solution of α-$[Mo_{11}VPO_{40}]^{4-}$ = 10 mM in 0.600 M Na(Cl) medium was used as external ^{51}V and ^{31}P chemical shift standards.[24] When studying reduced solutions, the absolute intensity (AI) mode was used and spectra recorded with exactly the same experimental parameters as for a spectrum of a fully oxidised solution with known concentration of vanadium(V) and phosphorus.

NMR Spectroscopic Data: Integral values from 42 different ^{51}V spectra in the pH range 1.51−4.42 were included in the calculations. By working in an AI mode, it was possible from the total integral value to determine how much of the total vanadium is bound in oxidised and reduced species, since species containing vanadium(IV) are NMR-silent. A set of ^{51}V NMR spectra recorded in AI mode is shown in Figure 3, and the total integral values (sum of vanadium in oxidised species) of each spectrum decreases when z_e increases. ^{31}P NMR spectroscopic data have not been included in any of the calculations. Spectra were recorded only to find out if the resonances of oxidised species decrease at the same rate as for vanadium when electrons were added. When this was shown to be the case, only ^{51}V NMR spectroscopic data were recorded, since quantitative data of high quality could be obtained in much shorter time.

ESR Measurements and Data: ESR measurements on vanadium(IV) were carried out with a Bruker ESP 300E X-band spectrometer. Aqueous samples were contained in 115 μL sealed capillary tubes, and spectra scanned from 2800 G to 4200 G. The microwave power was 5 mW. No ESR data have been included in the calculations. ESR was used to (i) obtain "fingerprints" of reduced species and (ii) verify that the proposed model fitted to experimental reduced data.

Computer Programs: Resonance intensities were computed by integration using the Bruker software. By using the least-square program LAKE,[26] mathematical analysis of combined $[H^+]$ and $\{e^-\}$ data, and ^{51}V NMR integral data was accomplished. Multimethod data can be treated simultaneously in LAKE, which considerably refines the equilibrium analysis. This is the greatest advantage of the program. Calculation and plotting of distribution and predominance diagrams were performed using the program SOLGASWATER.[36]

Acknowledgments

We want to thank Drs. Oliver Howarth and Masato Hashimoto for valuable comments on the manuscript. Financial support by Catalytica Inc. and the Swedish Natural Science Research Council (NFR) for research at the Umeå University is gratefully acknowledged.

[1] J. H. Grate, D. R. Hamm, S. Mahajan, in *Polyoxometallates: From Platonic Solids to Antiretroviral Activity* (Eds.: M. T. Pope, A. Müller), Kluwer Academic Publishers, Dordrecht, The Netherlands, **1994**, pp. 281−305.
[2] M. T. Pope, S. E. O'Donell, R. A. Prados, *Adv. Chem. Ser.* **1976**, *150*, 85−94.
[3] J. J. Altenau, M. T. Pope, R. A. Prados, H. So, *Inorg. Chem.* **1975**, *14*, 417−421.
[4] D. D. Smith, M. T. Pope, *Inorg. Chem.* **1973**, *12*, 331−336.
[5] D. D. Smith, H. So, J. Bender, M. T. Pope, *Inorg. Chem.* **1973**, *12*, 685−688.
[6] H. So, C. W. Lee, *Bull. Korean Chem. Soc.* **1990**, *11*, 115−118.
[7] R. Murugesan, P. Sami, T. Jeyabalan, A. Shunmugasundaram, *Trans. Met. Chem.* **1998**, *23*, 583−588.
[8] M. Otake, Y. Komiyama, T. Otaki, *J. Phys. Chem.* **1973**, *77*, 2896−2903.
[9] R. Fricke, H.-G. Jerschkewitz, G. Öhlmann, *J. Chem. Soc., Faraday Trans. 1* **1986**, *82*, 3491−3499.
[10] M. S. Freund, N. S. Lewis, *Inorg. Chem.* **1994**, *33*, 1638−1643.
[11] V. F. Odyakov, E. G. Zhizhina, K. I. Matveev, *J. Mol. Catal. A* **2000**, *158*, 453−456.
[12] D. V. Evtuguin, C. Pascoal Neto, J. Rocha, J. D. Pedrosa de Jesus, *Appl. Catal. A* **1998**, *167*, 123−139.
[13] E. Cadot, M. Fournier, A. Tézé, G. Hervé, *Inorg. Chem.* **1996**, *35*, 282−288.
[14] L. David, C. Cracium, M. Rusu, D. Rusu, O. Cozar, *J. Chem. Soc., Dalton Trans.* **2000**, 4374−4378.
[15] A. Yagasaki, I. Andersson, L. Pettersson, *Inorg. Chem.* **1987**, *26*, 3926−3933.
[16] L. Pettersson, B. Hedman, I. Andersson, N. Ingri, *Chem. Scr.* **1983**, *22*, 254−264.
[17] L. Pettersson, B. Hedman, A.-M. Nenner, I. Andersson, *Acta Chem. Scand., Ser. A* **1985**, *39*, 499−506.
[18] K. Elvingson, M. Fritzsche, D. Rehder, L. Pettersson, *Acta Chem. Scand.* **1994**, *48*, 878−885.
[19] A. Selling, I. Andersson, L. Pettersson, C. M. Schramm, L. D. Shannan, J. H. Grate, *Inorg. Chem.* **1994**, *33*, 3141−3150.
[20] O. W. Howarth, L. Pettersson, I. Andersson, *Chem. Soc. Dalton Trans.* **1991**, 1799−1812.
[21] O. W. Howarth, L. Pettersson, I. Andersson, *Chem. Soc. Dalton Trans.* **1989**, 1915−1923.
[22] L. Pettersson, I. Andersson, L.-O. Öhman, *Inorg. Chem.* **1986**, *25*, 4726−4733. This study was made in 3.0 M $Na(ClO_4)$, but the speciation is essentially the same as in 0.6 M Na(Cl) medium (ref.[23]).
[23] L. Pettersson, I. Andersson, manuscript in preparation.
[24] L. Pettersson, I. Andersson, A. Selling, J. H. Grate, *Inorg. Chem.* **1994**, *33*, 982−993.
[25] A. Selling, I. Andersson, J. H. Grate, L. Pettersson, *Eur. J. Inorg. Chem.* **2000**, *7*, 1509−1521.
[26] N. Ingri, I. Andersson, L. Pettersson, A. Yagasaki, L. Andersson, K. Holmström, *Acta Chem. Scand.* **1996**, *50*, 717−734.
[27] M. Kozik, C. F. Hammer, L. C. W. Baker, *J. Am. Chem. Soc.* **1986**, *108*, 2748−2749.
[28] M. Kozik, C. F. Hammer, L. C. W. Baker, *J. Am. Chem. Soc.* **1986**, *108*, 7627−7630.
[29] M. Hashimoto, A. Selling, L. Pettersson, M. Hakansson, *Acta Chem. Scand.* **1999**, *53*, 305−313.
[30] K. Y. Matsumoto, Y. Sasaki, *Bull. Chem. Soc. Jpn.* **1976**, *49*, 156−158.
[31] F. Guoyi, W. Enbo, L. Jingfu, *Chin. J. Appl. Chem.* **1989**, *6*, 16−20.
[32] J. Fuchs, A. Thiele, R. Palm, *Z. Naturforsch., Teil B* **1981**, *36*, 544−550.
[33] A. M. Khenkin, A. Rosenberger, R. Neumann, *J. Catal.* **1999**, *182*, 82−91.
[34] A. S. Brown, *J. Am. Chem. Soc.* **1934**, *56*, 646−647.
[35] W. Forsling, S. Hietanen, L.-G. Sillén, *Acta Chem. Scand.* **1952**, *8*, 901−909.
[36] G. Eriksson, *Anal. Chim. Acta* **1979**, *112*, 375−383.

Received June 25, 2001
[I01268]

A Study of the Interactions in an Extended Unsupported Gold-Silver Chain

Eduardo J. Fernández,[a] Antonio Laguna,*[b] José M. López-de-Luzuriaga,[a] Miguel Monge,[a] Pekka Pyykkö,*[c] and Nino Runeberg[c]

Keywords: Gold / Silver / Ab initio calculations / N ligands

The complex $[Ag(Py)_3][Au(C_6F_5)_2]\cdot Py$ (**1**) (Py = pyridine) has been prepared by the reaction of $NBu_4[Au(C_6F_5)_2]$ with $AgClO_4$ in the presence of pyridine. The crystallographic measurements indicate the presence of an extended unsupported one-dimensional chain of alternating gold and silver atoms. This arrangement is due to the formation of molecular Au–Ag ion pairs, to the π-stacking of C_6F_5 and pyridine arene ligands and to the packing effects that lead to molecular ion pairs at short distance. Theoretical calculations based on approximate experimental distances and angles reveal the presence of both metallophilic Au^I–Ag^I and aromatic C_6F_5-pyridine interactions. From a theoretical point of view the nature of the intermetallic attraction arises from both an ionic contribution and from dispersion-type correlation effects; the aromatic interaction is mainly due to dispersion-type correlation effects.

Introduction

The tendency of gold centers to aggregate has been termed "aurophilicity" by Schmidbaur.[1] Many research groups have been involved in an exhaustive search for structural information concerning such systems. The results have encouraged the theorists to construct theoretical models whose results could be compared with the experimental data. These models lead one to conclude that these interactions arise from correlation and relativistic effects.[2,3] The attraction due to electron correlation is dominated by dispersion, with a significant contribution from the recently identified ionic-type excitations.[4] These studies are nowadays being extended to other metals with closed shell configurations in theoretical models of systems with the same or different centers. Previous studies carried out in our group of heteropolynuclear metallacycles of the type $[AuM(HSCH_2PH_2)_2]^{2+}$ (M = Ag, Cu) concluded that the presence of only one gold atom is enough to induce metallophilic attractions in the group congeners and that this effect could be modulated depending on the gold ligand.[5] We also performed a detailed analysis of the d^8-d^{10} interaction between Pd^{II} and Au^I in the model complex $[AuPdCl_3(HSCH_2PH_2)_2]$ showing a dominant dispersion effect, some ionic contributions and no net charge transfer between the metals.[6] In both cases a bidentate ligand acts as a bridge between the metallic centers and its contribution to the close approach of the metal atoms cannot be neglected.

In contrast, the anionic complex $[Au(C_6F_5)_2]^-$ has been found to be a very valuable agent in the preparation of heteropolynuclear complexes in which the metal-metal interactions are not imposed by the ligand architecture.[7–10] Accordingly, we report here the synthesis, characterization and theoretical study of the complex $[Ag(Py)_3][Au(C_6F_5)_2]\cdot Py$ (**1**) (Py = pyridine), which shows an extended unsupported one-dimensional chain formed by repetition of gold-silver ion pairs that, in addition, displays π-stacking interactions[11–14] between C_6F_5 and pyridine arene ligands supporting the formation of the infinite chains.

Results and Discussion

Compound **1** was synthesized according to Equation (1). An ionic formulation could be proposed in solution based on the molar conductivity measurement in acetone solution (Λ_M = 110 Ω^{-1} cm^2 mol^{-1}, $5\cdot10^{-4}$ M) assigned to a 1:1 electrolyte. The IR spectrum shows, amongst others, the absorptions of the C_6F_5 ligands at 783, 963 and 1500 cm^{-1} [15] and pyridine ligands in the range 617–651 cm^{-1}.[16] Moreover, the ^{19}F NMR chemical shifts of δ = −114.60, −162.07 and −163.87 are similar to the values observed for the $[Au(C_6F_5)_2]^-$ fragment in solution. The separation of compound **1** into ionic components in solution is also confirmed by the mass spectrometry measurements (electrospray) in which we observe, depending on the experiment, the $[Au(C_6F_5)_2]^-$ anion at m/z = 541 (ES^-) and the

[a] Departamento de Química. Universidad de la Rioja-UA-CSIC
Madre de Dios, 51, 26004 Logroño, Spain
[b] Departamento de Química Inorgánica, Instituto de Ciencia de Materiales de Aragón, Universidad de Zaragoza-CSIC
50009 Zaragoza, Spain
E-mail: alaguna@posta.unizar.es
[c] Department of Chemistry. University of Helsinki,
P. O. B. 55 (A. I. Virtasen aukio 1), 00014 Helsinki, Finland
E-mail: pekka.pyykko@helsinki.fi

 © WILEY-VCH Verlag GmbH, 69451 Weinheim, Germany, 2002 1434–1948/02/0303–0750 $ 17.50+.50/0 *Eur. J. Inorg. Chem.* **2002**, 750–753

$[Ag(Py)_2]^+$ cation at $m/z = 266$ or the $[Ag(Py)]^+$ cation at $m/z = 187$ (ES^+).

$$NBu_4[Au(C_6F_5)_2] + AgClO_4 + C_5H_5N_{(excess)} \xrightarrow[-\,NBu_4ClO_4]{CH_2Cl_2} [Ag(C_5H_5N)_3][Au(C_6F_5)_2]\cdot C_5H_5N \quad (1)$$

A single-crystal X-ray diffraction study has been carried out for compound **1**. The silver atom is found to be disordered over two positions (50% each one), which makes the results of this study not completely valid. Despite this, the molecular structure can be described as being formed by $[Au(C_6F_5)_2]^-$ units and tricoordinate $[Ag(Py)_3]^+$ cations giving rise to a molecular ion-pair model (Figure 1). The molecular Au−Ag ion pairs are repeated in one dimension forming a chain due to the presence of π-stacking interactions between C_6F_5 and pyridine rings and packing effects,. Because of the disorder, any comment about bond lengths and angles is inappropriate, but nevertheless, the singular structural disposition could be used as a basis for a theoretical study.

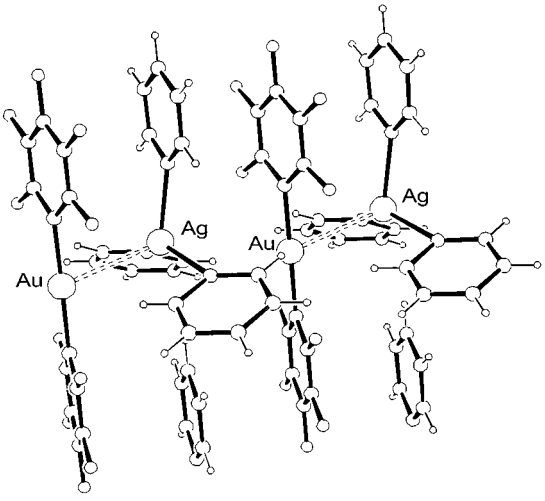

Figure 1. Structure of complex **1**; two molecular Au−Ag ion pairs and C_6F_5-pyridine π-stacking are shown

The structural arrangement of complex **1** shows some interesting features from a theoretical point of view. First, a short distance between the Au^I and Ag^I atoms is observed. Secondly, two C_6F_5···Py aromatic interactions could be proposed in the formula unit $[Ag(Py)_3][Au(C_6F_5)_2]\cdot Py$, one between a free pyridine molecule and one of the C_6F_5 rings and the other between a pyridine ligand bonded to silver and the other C_6F_5 ring. A theoretical study of these secondary interactions has been carried out separately on three different model systems (Figure 2) using two levels of theory based on Hartree−Fock (HF) and Local second order Møller−Plesset perturbation (LMP2) theory. The LMP2 approach, which is the simplest of the local correlation methods,[17−19] is analogous to the traditional MP2 but is performed using localized occupied and local virtual orbitals. The virtual space is spanned by nonorthogonal atomic orbitals (AOs), which are projected against the occupied space in order to ensure orthogonality between the occupied and virtual spaces. These nonorthogonal projected orbitals are inherently localized. The *orbital domain* [i] is that part of the virtual space assigned to an individual LMO (i), consisting only of those basis functions that are centered on the atoms involved in that particular LMO. The orbital domains [i] are kept orthogonal to the occupied space by projecting out the LMOs. Double excitations from an orbital pair (ij) are only allowed into the *pair domain* [ij], which is spanned by the union of the corresponding orbital domains [i] and [j]. The introduction of this physically appealing restriction in which electron pairs are only interacting in the vicinity of either electron, gives rise to the significant reduction of the computational cost as well as a diminished basis-set supposition error (BSSE). On the other hand the use of localized orbitals makes it possible to decompose the correlation contribution into the interaction energy of a complex according to different classes of double excitations. The two most important contributions arise from the dispersion class, in which one electron is excited from each subsystem into its own virtual space, and the ionic class, in which one of the electrons is excited from one of the subsystems to the virtual space of the other subsystem. In addition to the partition of the correlation contribution of the interaction energy, we can assume that the major part of the electrostatic interaction is already described at the uncorrelated HF level. Hence, we can theoretically study in great detail the forces that are responsible for the one dimensional disposition of complex **1** in the solid state.

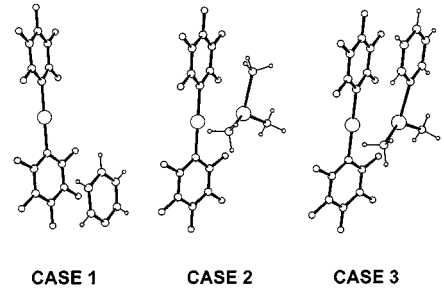

Figure 2. The assumed structures of the theoretical models, (a): $[Au(C_6F_5)_2]$···Py **CASE 1**; (b): $[Ag(NH_3)_3]$···$[Au(C_6F_5)_2]$ **CASE 2**; (c): $[Ag(NH_3)_2(Py)]$···$[Au(C_6F_5)_2]$ **CASE 3**

Finally, we emphasize that the role of dynamic correlation effects in transition-metal chemistry is well-known. The particular correlation effects leading to the R^{-6} dispersion forces involve dipole-allowed virtual excitations at the two centers involved ($A \rightarrow A'$, $B \rightarrow B'$). The "ionic correlation" mentioned above means ($A \rightarrow A'$, $B \rightarrow A'$). These interaction can only be reproduced by explicitly correlated methods.

One advantage of the LMP2 method is that it has almost no BSSE. Thus, no counterpoise corrections are needed.

In principle one should simulate the entire crystal structure but we have only considered particular contributions using cluster models.

In case 1 (Figure 2a) we have studied the interaction between $[Au(C_6F_5)_2]^-$ and a free pyridine molecule present in the crystal structure. The results of this interaction are given in Table 1 and the calculated interaction energy curves are shown in Figure 3. The HF curve is repulsive, whereas the LMP2 curve is attractive. The calculated $[Au(C_6F_5)_2]\cdots$Py distance, defined as the distance between the virtually parallel Py and C_6F_5 units, is 344.7 pm for our simplified model system and the interaction energy is 36.5 kJ/mol at the equilibrium distance. Thus, we can assume that the aromatic interaction between a C_6F_5 group from the $[Au(C_6F_5)_2]^-$ unit and the free pyridine molecule is due to dispersion-type correlation effects, since a stabilization energy is observed when these effects are included at the LMP2 level of theory and a repulsion between the rings at HF level is found.

Table 1. Optimized distance (R_e) and interaction energy (E_e) for the three model systems at HF and LMP2 levels (distances in pm and energy in kJ/mol)

	R_e (SCF)	E_e (SCF)	R_e (LMP2)	E_e (LMP2)
CASE 1	REPULSIVE	−0.44[a]	317.8[b]	36.5
CASE 2	312.3	160	284.3	234
CASE 3	323.2	143	289.4	239

[a] At the LMP2 optimized distance. [b] Referred to the Au−Ag distance.

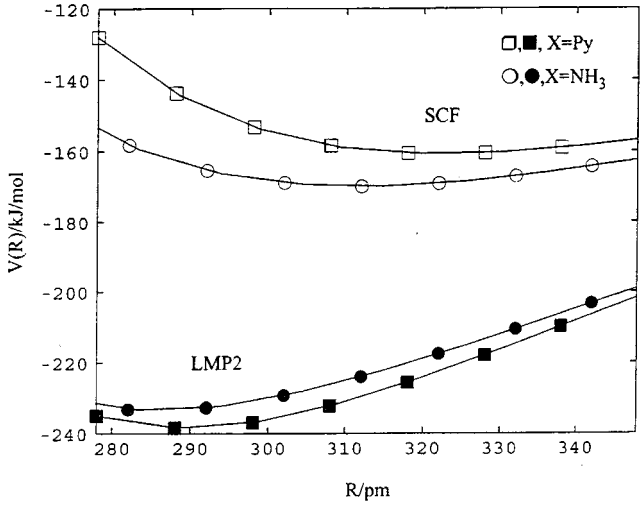

Figure 3. Interaction energy curves for the $[Au(C_6F_5)_2]\cdots[XAg(NH_3)_2]$ (X = NH_3, Py) interaction calculated at the SCF and LMP2 levels

Many earlier examples of coplanar "π-stacks" between aromatic rings are known. A typical ring-ring distance is 350 pm.[13] If the two rings have opposite electric quadrupole moments, like C_6H_6 and C_6F_6, the electric quadrupole-quadrupole interactions already yield an attraction of about 6 kJ/mol.[20] Examples of π-stacks in organometallic chemistry are also known.[14] For further information on this subject see ref.[21]

In case 2 (Figure 2b) we have proposed a model system $[Ag(NH_3)_3]\cdots[Au(C_6F_5)_2]$ in order to study only the intermetallic Au−Ag interaction. The results of the interaction energies at the theoretically predicted equilibrium distance are given in Table 1 and the calculated interaction energy curves are shown in Figure 3. In this case, the HF curve is attractive with a minimum corresponding to the equilibrium distance at 312.3 pm and an attractive interaction energy of 160 kJ/mol compared to the ionic dissociation limit. Regarding the LMP2 curve we also obtain an attractive behavior with an interaction energy at the equilibrium distance (284.3 pm) of 234 kJ/mol. In this case, in which only the Au···Ag interaction is studied, both electrostatic attraction and dispersion-type correlation effects are responsible for this interaction. The electrostatic interaction is responsible for the attractive behavior obtained at the HF level since dispersion-type correlation effects are not included. The additional stabilization obtained at the LMP2 level is due to the introduction of these correlation effects, which include dispersion.

Going from case 2 to case 3, we exchange one of the NH_3 ligands bonded to silver for one pyridine ligand that is parallel and at a short distance from one of the C_6F_5 rings bonded to gold (Figure 2c). In this case we study the influence of the presence of two interactions, the intermetallic Au−Ag and the aromatic $C_6F_5\cdots$Py (Ag-bonded), at the equilibrium distances and at the interaction energy values. For this case we obtain an $Au^I\cdots Ag^I$ equilibrium distance at the HF level of 323.2 pm and of 289.4 pm at the LMP2 level. The equilibrium distance at both levels of theory is accompanied by interaction energy values of 143 kJ/mol at the HF level and 239 kJ/mol at the LMP2 level (see Table 2 and Figure 3). Thus, this comparison allows us, if we make the simplified conclusion that HF covers electrostatic interactions and the correlation energy (the difference between LMP2 and HF) covers the dispersion contribution, to establish that the overall interaction is very similar for both cases 2 and 3, in terms of the LMP2 equilibrium distance and the interaction energy (284.3 pm and 234 kJ/mol for case 2 and 289.4 pm and 239 kJ/mol for case 3). However, the contributions are different. The pyridine ligand in case 3 introduces electrostatic repulsion since the electrostatic interaction diminishes from 160 kJ/mol in case 2 to 143 kJ/mol in case 3, but it also introduces attractive dispersion interactions (74 kJ/mol in case 2 to 96 kJ/mol in case 3), as occurs in case 1. In Table 2 we compare the results for cases 2 and 3 at the LMP2 optimized distances, which are quite similar in both cases (284 vs. 289 pm respectively).

Table 2. Electrostatic (HF) and dispersion (LMP2) contributions to the intermetallic Au−Ag interaction (kJ/mol) at the LMP2 optimized distance

	Electrostatic	Correlation Energy	Total
CASE 2	160	74	234
CASE 3	143	96	239

The partitioning of the correlation contribution to the $[Ag(NH_3)_3]\cdots[Au(C_6F_5)_2]$ (case 2) and $[Ag(NH_3)_2(Py)]\cdots[Au(C_6F_5)_2]$ (case 3) interaction energies based on the obtained experimental distances are given in Table 3. The introduction of the pyridine ring into the model system in case 3 gives, as we have commented above, a net enhancement of the correlation energy and, looking at the partition of this correlation energy, the dispersion (van der Waals) contribution increases with respect to the ionic correlation contribution seen as the charge transfer.

Table 3. LMP2 correlation energy partitioning at the experimental geometry (kJ/mol)

	Ex-dispersion	Dispersion	Ionic	Ag→Au	Au→Ag
CASE 2	0.0	29	16	4	12
CASE 3	−0.1	45	20	6	14

Conclusions

1) An ionic, Coulomb attraction obviously exists between the $[Au(C_6F_5)_2]^-$ anions and the $[Ag(Py)_3]^+$ cations. This is an important contribution behind the infinite chains.

2) In addition, dispersion-type correlation effects lead to attractions both between Ag^I and Au^I and between C_6F_5 and pyridine moieties.

3) Looking at the detailed correlation energy partitioning, the most important contributions are the normal dispersion (van der Waals) terms. Charge-transfer-type contributions are about one third as important and, of them, the Au→Ag virtual excitation is more important than the Ag→Au one.

Experimental Section

General: All experiments were performed under argon by using standard Schlenk techniques. Solvents were dried and distilled under argon. ^1H and ^{19}F NMR spectra were recorded on a Bruker ARX 300. Elemental analyses were carried out with a C.E. instrument EA-1110 CHNS-O microanalyzer. Infrared spectrum was recorded in the 4000−200 cm^{-1} range on a Perkin−Elmer FT-IR Spectrum 1000 spectrophotometer as nujol mulls between polyethylene sheets. Mass spectra were recorded on a HP-5989B Mass Spectrometer API-Electrospray with interface 59987A.

$[Ag(Py)_3][Au(C_6F_5)_2]\cdot Py$ (1): The reaction between $NBu_4[Au(C_6F_5)_2]$ (200 mg, 0.258 mmol), $AgClO_4$ (54 mg, 0.258 mmol) and an excess of pyridine in CH_2Cl_2 leads, after a slow crystallization process (24 h) at low temperature, to compound **1** as colorless crystals. Yield: 47%. ^1H NMR [$(CD_3)_2CO$]: δ = 7.52 (dd, 2 H, -CH-), 7.96 (t, 1 H, -CH-), 8.67 (d, 2 H, -CH-). $C_{32}H_{20}AgAuF_{10}N_4$ (955.4): calcd. C 40.23, H 2.18, N 5.86; found C 39.92, H 2.25, N 5.41.

Computational Details: All calculations were performed as implemented in the MOLPRO program package. For the metals, the 19 valence electron pseudopotentials from Stuttgart and the corresponding basis sets[22a] augmented with two f polarization functions were used.[22b] For the lighter atoms the cc-pVDZ basis sets were used.[22c] The LMOs were obtained through a Pipek−Mezey localization procedure.[22d]

Acknowledgments

This work was supported by the Spanish DGES (BQU2001-2409) and the U.R. API-01/B14. P. Pyykkö and N. Runeberg are supported by The Academy of Finland.

[1] F. Scherbaum, A. Grohmann, B. Huber, C. Krüger, H. Schmidbaur, *Angew. Chem. Int. Ed. Engl.* **1988**, *27*, 1544−1546.
[2] P. Pyykkö, Y.-F. Zhao, *Angew. Chem. Int. Ed. Engl.* **1991**, *30*, 604−605.
[3] P. Pyykkö, T. Tamm, *Organometallics* **1998**, *17*, 4842−4852.
[4] N. Runeberg, M. Schütz, H.-J. Werner, *J. Chem. Phys.* **1999**, *110*, 7210−7215.
[5] E. J. Fernández, J. M. López-de-Luzuriaga, M. Monge, M. A. Rodríguez, O. Crespo, M. C. Gimeno, A. Laguna, P. G. Jones, *Chem. Eur. J.* **2000**, *6*, 636−644.
[6] O. Crespo, A. Laguna, E. J. Fernández, J. M. López-de-Luzuriaga, P. G. Jones, M. Teichert, M. Monge, P. Pyykkö, N. Runeberg, M. Schütz, H.-J. Werner, *Inorg. Chem.* **2000**, *39*, 4786−4792.
[7] R. Usón, A. Laguna, M. Laguna, P. G. Jones, G. M. Sheldrick, *J. Chem. Soc., Chem. Commun.* **1981**, 1097−1098.
[8] R. Usón, A. Laguna, M. Laguna, B. R. Manzano, P. G. Jones, G. M. Sheldrick, *J. Chem. Soc., Dalton Trans.* **1984**, 285−292.
[9] O. Crespo, E. J. Fernández, P. G. Jones, A. Laguna, J. M. López-de-Luzuriaga, A. Mendía, M. Monge, E. Olmos, *Chem. Commun.* **1998**, 2233−2234.
[10] E. J. Fernández, M. C. Gimeno, A. Laguna, J. M. López-de-Luzuriaga, M. Monge, P. Pyykkö, D. Sundholm, *J. Am. Chem. Soc.* **2000**, *122*, 7287−7293.
[11] W. L. Jorgensen, D. L. Severance, *J. Am. Chem. Soc.* **1990**, *112*, 4768−4774.
[12] D. D. Graf, J. P. Campbell, L. L. Miller, K. R. Mann, *J. Am. Chem. Soc.* **1996**, *118*, 5480−5481.
[13] D. D. Graf, R. G. Duan, J. P. Campbell, L. L. Miller, K. R. Mann, *J. Am. Chem. Soc.* **1997**, *119*, 5888−5899.
[14] G. Ujaque, F. Maseras, A. Lledós, *J. Am. Chem. Soc.* **1999**, *121*, 1317−1323.
[15] R. Usón, A. Laguna, J. García, M. Laguna, *Inorg. Chim. Acta* **1979**, *37*, 201−207.
[16] K. Nakamoto, *Infrared and Raman Spectra of Inorganic and Coordination Compounds*, 4th Edition, John Wiley & Sons, **1986**. p. 206.
[17] P. Pulay, *Chem. Phys. Lett.* **1983**, *100*, 151−154.
[18] S. Saebø, P. Pulay, *Annu. Rev. Phys. Chem.* **1993**, *44*, 213−236.
[19] C. Hampel, H.-J. Werner, *J. Chem. Phys.* **1996**, *104*, 6286−6297.
[20] N. J. Heaton, P. Bello, B. Herradón, A. del Campo, J. Jiménez-Barbero, *J. Am. Chem. Soc.* **1998**, *120*, 12371−12384.
[21] D. Sundholm, M. R. Sundberg, R. Uggla, *J. Phys. Chem. A* **1998**, *102*, 7137−7142.
[22] [22a] D. Andrae, U. Häusserman, M. Dolg, H. Stoll, H. Preuss, *Theor. Chim. Acta* **1990**, *77*, 123−141. [22b] P. Pyykkö, N. Runeberg, F. Mendizabal, *Chem. Eur. J.* **1997**, *3*, 1451−1457. [22c] T. H. Dunning, Jr., *J. Chem. Phys.* **1989**, *90*, 1007−1023. [22d] J. Pipek, P. G. Mezey, *J. Chem. Phys.* **1989**, *90*, 4916−4926.

Received August 2, 2001
[I01285]

Anionic Poly(pyrazolyl)borate Ligands Obtained from 3,5-Dimethylpyrazole and 3,5-Diphenylpyrazole and Their Cobalt(II) Complexes − X-ray Crystallographic and ^{1}H NMR Studies[‡]

Tomasz Ruman,[a] Zbigniew Ciunik,[b] Jaroslaw Mazurek,[b] and Stanislaw Wolowiec*[a]

Keywords: Cobalt / Borates / X-ray diffraction / NMR spectroscopy / N ligands

Synthesis of poly(pyrazolyl)borate anionic ligands composed of 3,5-dimethyl- and 3,5-diphenylpyrazoles and their bis(ligand) high-spin cobalt(II) complexes are described. The molecular structures of [dihydrobis(3,5-diphenylpyrazolyl)borato][hydrobis(3,5-dimethylpyrazolyl)(3,5-diphenylpyrazolyl)borato]cobalt(II) and bis[dihydro(3,5-dimethylpyrazolyl)(3,5-diphenylpyrazolyl)borato]cobalt(II) complexes were established by X-ray crystallography. The cobalt center is hexacoordinate in the former with five Co–N_2(pyrazolyl) bonds and short Co–H [attached to the boron atom of bis(pyrazolyl)borate] bond (2.03 Å), whereas a distorted tetrahedral geometry was found for the latter due to four Co–N_2(pyrazolyl) bonds. Additionally, the pentacoordinate homoscorpionate [tris(3,5-diphenylpyrazolyl)borato]cobalt(II) nitrate side product was obtained from the reaction and characterized structurally. It contains a κ^3-coordinated Tp′ ligand and a κ^2-bound nitrate anion.

Introduction

Heteroscorpionate tris(pyrazolyl)borate anions (Tp′) − tripodal ligands containing two or more substituted pyrazol-1-yl moieties − provide a unique opportunity to construct transition metal complexes of low symmetry. Early work by Trofimenko demonstrated that some homoscorpionate Tp′ ligands undergo intramolecular rearrangement into heteroscorpionate ones in their transition metal complexes by borotropic rearrangement of the 3-R-pyrazolyl residue of Tp′ into the 5-R-pyrazolyl one (R = isopropyl or neopentyl).[1,2] Recently, we reported that 3(5)-methyl-5(3)-phenylpyrazole (Ph,MepzH) gave two Tp′ ligands upon condensation of Ph,MepzH with borohydride anion: the homoscorpionate [hydrotris(5-methyl-3-phenylpyrazolyl)borate]$^-$ and the heteroscorpionate [hydrobis(5-methyl-3-phenylpyrazolyl)(3-methyl-5-phenylpyrazolyl)-borate]$^-$, which were characterized structurally in the solid state by X-ray crystallography and in solution by ^{1}H NMR spectroscopy as high-spin cobalt(II) complexes of the general formula Tp′Co(NCS).[3,4]

Continuing our efforts to synthesize a chiral Tp′ ligand with boron-centered chirality we have applied two independent routes to reach the target: a stepwise synthetic approach, in which dihydro(3,5-dimethylpyrazolyl)(3,5-diphenylpyrazolyl)borate was synthesized in the first step, dihydrobis(pyrazolyl)borate (Bp′) being a convenient substrate for conversion into chiral Tp′ by condensation of NaBp′ with another substituted pyrazole, and a more promising and less laborious method based on a one-step condensation of 2 equiv. of Ph,MepzH and 1 equiv. of 3,5-diMepzH with sodium borohydride.[4] This first-step condensation led to the isolation of a mixture of Tp′ and Bp′ products, some of which were converted into high-spin cobalt(II) complexes, characterized structurally by X-ray crystallography in the solid state and ^{1}H NMR spectroscopy in solution.

Chiral Tp ligands of C_3 symmetry based on pyrazoles derived from camphor and menthone[5] and potentially hexacoordinate hydrotris[3-{2-(pinene[4,5]pyridyl)}pyrazolyl]borate[6] were synthesized recently and used to construct metal complexes of catalytic activity.

Results and Discussion

Synthetic Procedures and Distribution of Products

The synthesis of poly(pyrazolyl)borate anions by condensation of sodium (or potassium) borohydride with pyrazoles in the melt can be controlled exclusively by the appropriate choice of stoichiometry of substrates and often leads to a nonstatistical distribution of products due to inhomogeneity of the reaction mixture. A typical example of this phenomenon is represented by synthetic route (1) (see Exp. Sect.), in which the condensation of KBH_4 (or $NaBH_4$)

[‡] Complexes of Heteroscorpionate Tris(pyrazolyl)borate Anionic Ligands, IV. − Part III: Ref.[4]

[a] Faculty of Chemistry, Rzeszów University of Technology, 6 Powstanców Warszawy Ave., 35-959 Rzeszów, Poland
[b] Faculty of Chemistry, University of Wroclaw, 14 Joliot-Curie Str., 50-383 Wroclaw, Poland

 © WILEY-VCH Verlag GmbH, 69451 Weinheim, Germany, 2002 1434−1948/02/0303−0754 $ 17.50+.50/0 *Eur. J. Inorg. Chem.* **2002**, 754−760

with 1 equiv. of 3,5-diphenylpyrazole and 1 equiv. of 3,5-dimethylpyrazole led to the formation of a mixture of potassium (or sodium) dihydrobis(pyrazolyl)borates (Bp′) and hydrotris(pyrazolyl)borates (Tp′), i.e. dihydro(3,5-diphenylpyrazolyl)(3,5-dimethylpyrazolyl)borate, dihydrobis(3,5-diphenylpyrazolyl)borate, dihydrobis(3,5-dimethylpyrazolyl)borate, hydrobis(3,5-dimethylpyrazolyl)(3,5-diphenylpyrazolyl)borate, hydrobis(3,5-diphenylpyrazolyl)-(3,5-dimethylpyrazolyl)borate, and hydrotris(3,5-diphenylpyrazolyl)borate. The anionic products were identified as their high-spin cobalt(II) complexes. This method was proven to be particularly useful[1−4,7] because it allows for both the isolation of the anionic poly(pyrazolyl)borate ligands and their identification by ^{1}H NMR spectroscopy. This method is effective in the case of tris(pyrazolyl)borate ligands (Tp′) with large or intermediate steric hindrance imposed by substituents placed at the 3- and/or 5-positions on the pyrazolyl moiety, which can be isolated as Tp′Co(X) complexes, where X = NCS^-, Cl^-, or CO_2^-. The Bp′ and Tp′ ligands obtained in the synthesis described here gave bis(ligand) complexes of the type Bp′$_2$Co, Bp′CoTp′, and Tp′$_2$Co along with Tp′Co(X). We have isolated three complexes, containing different Bp′ and Tp′ ligands and found other ligands coordinated to the cobalt(II) ion in the mixture of products. The pyrazoles used for the construction of the Bp′ and Tp′ ligands have small (3,5-dimethylpyrazole) and intermediate (3,5-diphenylpyrazole) steric hindrance. The isolation procedure applied for the separation of cobalt(II) complexes was based on fractional crystallization from THF/hexane solvent mixtures: the least soluble product, the hydrotris(3,5-diphenylpyrazolyl)boratocobalt(II) nitrate complex [$Tp^{Ph_2}Co(NO_3)$, **1**], was isolated as a pure crystalline product in the first instance, although the synthetic yield of the ligand was only 1%. Deliberate synthesis of this ligand and conversion into the $Tp^{Ph_2}Co(NCS)$ complex **1′** gave the analytically pure product, which was completely insoluble in all common organic solvents, analogously to **1**. Similar $Tp^{Ph_2}Zn(OOCCH_3)$ and $Tp^{Ph_2}NiCl$ complexes have been synthesized before and characterized crystallographically.[8] The purple $Tp^{Ph_2}NiCl$ complex with the ligand κ^3-bound in the solid state was found to be diamagnetic in [D$_6$]DMSO solution as was concluded from its ^{1}H NMR spectrum.

Even though we observed the formation of only two of the three expected Bp′ ligands in the synthetic route (1) (Exp. Sect.), the conversion of the mixture of anionic ligands into cobalt(II) complexes gave the pink crystalline product Bp′CoTp′ (**2**) in 12% yield. Surprisingly, the Tp′ ligand trapped in this heteroleptic complex is the hydrobis(3,5-dimethylpyrazolyl)(3,5-diphenylpyrazolyl)borate {[HB(3,5-diMepz)$_2$(3,5-diPhpz)]$^-$} with intermediate steric hindrance, while the Bp′ ligand turned out to be the symmetrical dihydrobis(3,5-diphenylpyrazolyl)borate {[H_2B-(3,5-diPhpz)$_2$]$^-$) instead of the statistically more probable [H_2B(3,5-diMepz)(3,5-diPhpz)]$^-$ ligand. Although the new heteroscorpionate Tp′ ligand was itself interesting for us from a structural point of view, the synthetic procedure, which was designed to synthesize [H_2B(3,5-diMepz)(3,5-diPhpz)]$^-$, had to be modified. We therefore performed the condensation of $NaBH_4$ with one equivalent each of 3,5-diMepzH and 3,5-diPhpzH in refluxing tetradecane. The reaction at 254° C allowed for better control and thus optimization of the reaction conditions for the desired unsymmetrical Bp′ ligand. The [H_2B(3,5-diMepz)(3,5-diPhpz)]$^-$ ligand was thus isolated as the complex Bp′$_2$Co (**3**) and characterized structurally in the solid state by single-crystal X-ray diffraction measurements. The isolated yields of **2** and **3** are rather low, although we observed the formation of other Tp′Co(NO_3) and Bp′CoTp′ complexes containing other heteroscorpionate Tp′ and unsymmetrical Bp′ ligands, which were later identified. We were therefore able to determine the composition of the crude reaction mixture obtained in the synthesis of KBp′ (NaBp′) and KTp′ (NaTp′) salts on the basis of the integration of the corresponding resonances in the ^{1}H NMR spectrum of a mixture composed of Tp′Co(NO_3), Bp′CoTp′, and Bp′CoBp′′ complexes.

X-ray Crystallographic Studies of the Co Complexes

Structure of $Tp^{Ph_2}Co(NO_3)$ (1)

A view of the molecule of **1** is presented in Figure 1, along with selected bond lengths and angles. The cobalt-centered bite angle is 133.1°, which is much lower than those found in tetracoordinate $Tp^{Ph_2}Cu(CO)$ (145.5°)[9] and pentacoordinate $Tp^{Ph_2}Fe(OOCC(O)Ph)$ (139.6°).[10] It is noteworthy that an increasing steric hindrance at *C*-5(pyrazole) in the order H < CH_3 < Ph causes a tightening of the bite angle from 142.0° [5-H in $Tp^{Ph}Co(NCS)(pzH)$],[7] through 140.3° [5-CH_3 in $Tp^{PhMe}Co(NCS)(THF)$][4] to

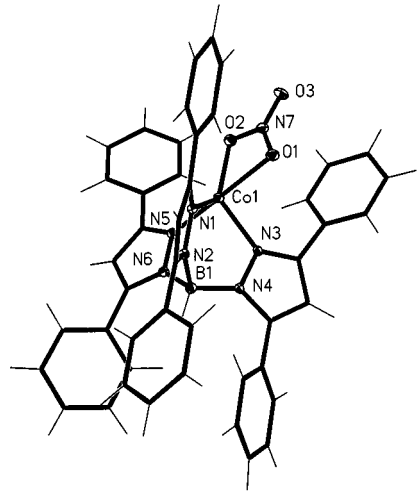

Figure 1. Molecular structure of **1** with crystallographic numbering; selected bond lengths (Å) and angles (°): Co(1)−N(1) 2.038(2), Co(1)−N(3) 2.030(2), Co(1)−N(5) 2.059(2), Co(1)−O(1) 2.230(2), Co(1)−O(2) 2.008(2); N(1)−Co(1)−N(3) 96.18(7), N(1)−Co(1)−N(5) 93.23(7), N(3)−Co(1)−N(5) 89.83(8), O(2)−Co(1)−O(1) 60.67(6), O(1)−N(7)−O(2) 114.15(17), O(1)−N(7)−O(3) 124.2(2), O(2)−N(7)−O(3) 121.68(19)

133.1° [5-Ph in $Tp^{Ph_2}Co(NO_3)$] in pentacoordinate Tp′Co(XY) complexes.

Structure of [Dihydrobis(3,5-diphenylpyrazolyl)borato]-[hydrobis(3,5-dimethylpyrazolyl)(3,5-diphenylpyrazolyl)-borato]cobalt(II) (2)

The cobalt(II) center in **2** is surrounded by five nitrogen donors from the pyrazolyl moieties of the Tp′ and Bp′ ligands (Figure 2). The sixth coordination site is occupied by the boron-bonded hydrogen of the Bp′ ligand. The two shortest Co−N(pz) bonds were found for the 3,5-di-Mepz(Tp′) moieties, whereas the longest Co−N(Tp′) bond was observed for the 3,5-diPhpz moiety, presumably because of steric clashes between 3,5-diPhpz(Tp′) and one of the 3,5-diPhpz(Bp′) ligands. The distance between the cobalt center and hydrogen (Bp′) (2.03 Å) is the shortest amongst this type of complexes. This distance was found to be equal to 2.26 Å in $[H_2B(3\text{-}Phpz)_2]Co[HB(3\text{-}i\text{Pr},4\text{-}Brpz)_3]$,[1] 2.69 Å in $[H_2B(3,5\text{-}diMepz)_2]Cd[HB(3\text{-}Phpz)_3]$,[11] 2.84 Å in BpSmTp,[12] and 2.26 Å and 2.17 Å in hexacoordinate $[\kappa^3\text{-}H,N,N(Tp')]$ $[(\kappa^3\text{-}N,N,N(Tp''))]Co^{II}$ complexes, where Tp′ = Tp^{Ph}, $Tp^{iPr,4Br}$ [1] and Tp′ = Tp′′ = Tp^{Ph}.[13]

Structure of $[H_2B(3,5\text{-}diMepz)(3,5\text{-}diPhpz)]_2Co$ (3)

A view of the molecule of **3** is presented in Figure 3 with selected bond lengths and angles. An almost isostructural complex (Bp'_2Zn) has been synthesized previously.[14] In both complexes the M−N(3,5-diMepz) distances are shorter (1.98−1.99 Å) than the M−N(3,5-diPhpz) ones (2.01−2.02 Å). The Co−N(pz) distances are slightly shorter in the Bp_2Co complex (1.93−1.98 Å).[15] In all cases there is no Co−H(Bp′) contact; the Co−H distances increase from 2.93 Å (2.96 Å) for **3** through 3.00 Å (3.06 Å) for Bp_2Co up to 3.26 Å (3.28 Å) for Bp'_2Zn. The closest distance between the metal ion and the boron-bound hydrogen in tetracoordinate complexes with Bp′ ligands was found in the complex $Bp^{tBu}Zn(t\text{Bu})$ (2.47 Å)[16] whereas in other cases it falls in the range 2.9−3.1 Å.[17−23]

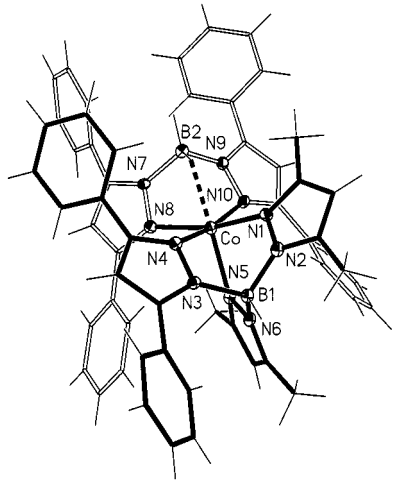

Figure 2. Molecular structure of **2** with crystallographic numbering; selected bond lengths (Å) and angles (°): Co(1)−N(1) 2.091(3), Co−N(4) 2.153(3), Co−N(5) 2.103(3), Co−N(8) 2.113(3), Co−N(10) 2.140(3); N(1)−Co−N(5) 91.00(13), N(1)−Co−N(4) 81.91(12), N(5)−Co−N(4) 90.03(12), N(8)−Co−N(10) 89.91(12)

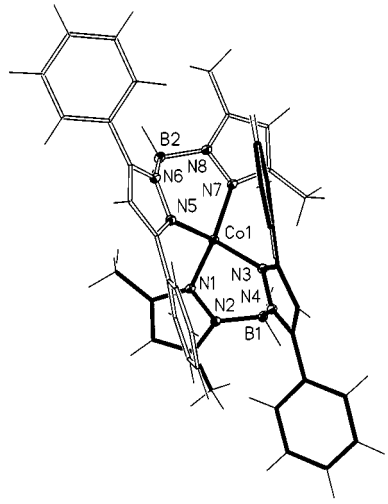

Figure 3. Molecular structure of **3** with crystallographic numbering; selected bond lengths (Å) and angles (°): Co(1)−N(1) 1.985(2), Co(1)−N(3) 2.008(2), Co(1)−N(5) 2.015(2), Co(1)−N(7) 1.987(2), N(1)−Co(1)−N(3) 100.72(7), N(5)−Co(1)−N(7) 101.05(7), N(1)−Co(1)−N(5) 109.11(7), N(1)−Co(1)−N(7) 128.10(7), N(3)−Co(1)−N(5) 106.65(7), N(3)−Co(1)−N(7) 109.89(7)

Spectral Studies

The pink color of **2** is characteristic of pentacoordinate complexes of Tp′Co(XY), which can be produced either by coordination of a neutral ligand, such as a methanol solvent molecule, to Tp′CoX (X = NCS^-, N_3^-, Cl^-), or by chelation of an anionic carboxylate with an additional donor atom (lactate). The most characteristic feature of the ^1H NMR spectra of the high-spin Tp′Co(XY) complexes is the chemical shift of the B−H proton, which depends on the coordination number of the cobalt ion center. Thus, the B−*H* resonances can be found between δ = 0 and −20 for tetracoordinate Tp′Co(X) complexes,[1−3,7,24] between δ = 83 and 130 for hexacoordinate complexes,[1,3,7,24−28] and between δ = 40 and 90 for pentacoordinate complexes, the latter depending on the nature of the fifth donor.[3,7]

There are two interesting features in the ^1H NMR spectrum of **2**: i) the low symmetry of the complex found in the solid state is preserved in solution at room temperature; consequently all the pyrazole proton resonances can be distinguished, and ii) the chemical shift of B−*H* from the Tp′ ligand (δ = 61.3) is rather low in comparison with other typical pentacoordinate Tp′Co(XY) complexes (XY = lactate).[3,7] This low symmetry is even preserved at 383 K (in $[D_8]$toluene) indicating that the mutual rotation of the Tp′ and Bp′ ligands at this temperature is still slow on the timescale of this method. The 2-D ^1H COSY spectrum of **2** taken at 372 K (Figure 4) allowed us to unambiguously identify the *o*-, *m*-, and *p*-H resonances from the three 5-Ph

substituents of the Bp′ and Tp′ ligands due to the presence of scalar cross-peaks (lower left inset at Figure 4). These resonances are paramagnetically shifted downfield, as was observed previously for [HB(3-Ph,5-Mepz)2(3-Me,5-Phpz)]Co(NCS)(CD_3OD) and [HB(3-Ph,5-Mepz)(3-Me,5-Phpz)2]Co(NCS)(CD_3OD) complexes.[4,7] Three cross-peaks between the *m*- and *p*-H of the 3-Ph substituents of the Tp′ and Bp′ ligands were also observed, although the scalar connectivity pattern within the 3-Ph substituents was broken due to the short relaxation times of the *ortho* hydrogens (right inset of Figure 4). We were also unable to observe the appropriate NOE cross-peaks between 3-CH_3(Tp′) and *o*-H(Bp′) which would have allowed us to assign all the resonances. Nevertheless, the resonances for *o*-H(3-Ph,Bp′) are shifted upfield considerably less than those of *o*-H(3-Ph,Tp′) which is consistent with the static geometry of the molecule (see above). Very broad resonances at $\delta = 9$ and 10, which can be tentatively assigned to the H-B(Bp′) protons, were observed in the spectrum. One of the resonances for 5-CH_3 (Tp′) is also extremely broad and is placed within the diamagnetic envelope.

The UV/Vis spectra of **2** and **3** are characteristic of high-spin cobalt(II) in octahedral and tetrahedral environments, respectively.[29] Two bands centered at 498 and 538 nm for **2**, which can be assigned to a $^4T_{1g}(P) \leftarrow {}^4T_{1g}$ transition, have extinction coefficients near 60 mol^{-1} dm^3 cm^{-1}. This slightly higher than the corresponding band observed for Tp_2Co,[30] and is probably due to the higher coordination geometry in **2**. In the case of **3** the position and extinction coefficient of the three observed bands are close to those found for Bp_2Co,[30] and can be assigned to a $^4T_1(P) \leftarrow {}^4A_2$ transition.[29]

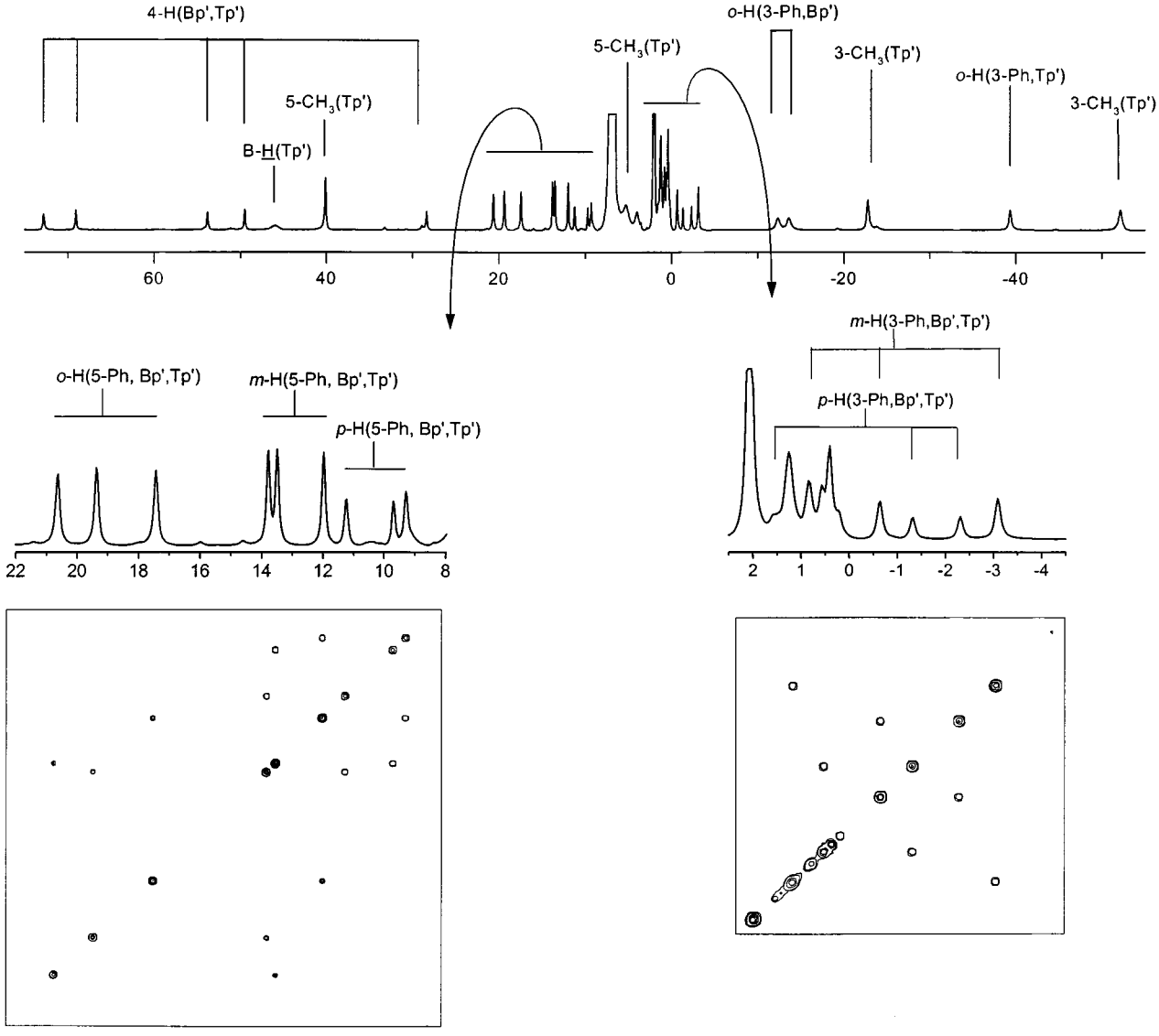

Figure 4. The ^1H NMR spectrum of **2** in [D_8]toluene at 373 K; the two lower insets demonstrate the relevant fragments of the COSY map

Experimental Section

Methods: ^{1}H NMR spectra were obtained with a Bruker AMX300 spectrometer operating in the quadrature mode at 300 MHz. The residual peaks of the deuterated solvents were used as internal standards. The 2-D ^{1}H COSY spectrum was obtained with a repetition time of 0.2 s. The magnetic moments of **2** and **3** were measured on the same instrument in $CDCl_3$ at 298 K. The IR and UV/Vis spectra were recorded on a Perkin−Elmer 1725X and a HP 8453 diode-array spectrophotometer, respectively. Elemental analyses were performed with an EA 1108 apparatus (Carbo Erba) at Department of Organic Chemistry, Faculty of Chemistry, Rzeszów University of Technology.

Crystal data for **1**−**3** are given in Table 1, together with refinement details. All measurements were performed on a Kuma KM4CCD κ-axis diffractometer with graphite-monochromated Mo-K_α radiation. The crystals were positioned 65 mm from the KM4CCD camera. 612 frames were measured at 0.75° intervals with a counting time of 20 sec. The data were corrected for Lorentz and polarization effects. An absorption correction based on least-squares fitted against $|F_c| - |F_o|$ differences was also applied for **1**.[31] No absorption corrections were applied for **2** and **3**. Data reduction and analysis were carried out with the Kuma Diffraction (Wroclaw) programs. Structures were solved by direct methods (program SHELXS-97)[32] and refined by the full-matrix least-squares method on all F^2 data using the SHELXL-97[33] program suite. Non-hydrogen atoms were refined with anisotropic thermal parameters; hydrogen atoms were included from the geometry of the molecules and Δρ maps, and refined with isotropic thermal parameters for **1** only.

Crystallographic data for the structures reported in this paper have been deposited with the Cambridge Crystallographic Data Centre as supplementary publication nos. CCDC-160912 (**1**), CCDC-160913 (**2**), and CCDC-160914 (**3**). Copies of the data can be obtained free of charge on applicaton to The Director, CCDC, 12 Union Road,m Cambridge CB2 1EZ, UK [Fax: (internat.) + 44-1223/336-033; E-mail: deposit@ccdc.cam.ac.uk].

Condensation of 3,5-Dimethylpyrazole and 3,5-Diphenylpyrazole with Potassium Borohydride. Route (1): The one-step condensation of KBH_4 (0.818 g, 15.2 mmol) with 3,5-diphenylpyrazole (3.304 g, 15.0 mmol) and 3,5-dimethylpyrazole (1.35 g, 14.1 mmol) was done by heating the reagents in melted pyrazoles at 165−225° C until 725 cm^3 hydrogen had been evolved. The crude reaction mixture was washed with hot heptane (100 cm^3), then petroleum ether (50 cm^3) and dried in air to give 3.131 g of crude product [as a mixture of potassium poly(pyrazolyl)borate salts] in approximately 56% yield.

Route (2): The one-step condensation of $NaBH_4$ (0.352 g, 9.31 mmol) with 3,5-diphenylpyrazole (1.640 g, 7.45 mmol) and 3,5-dimethylpyrazole (0.716 g, 7.45 mmol) was performed by heating the mixture in tetradecane 50 (cm^3) under reflux (254 °C) until 340 cm^3 hydrogen had been evolved. The crude reaction mixture was cooled to about 80° C, filtered to remove unchanged pyrazoles, washed with hot heptane (100 cm^3) and petroleum ether (50 cm^3). The solid residue was dried, crushed into pieces, suspended in 50 cm^3 heptane, boiled, filtered and washed with petroleum ether. A dry mixture of sodium salts of anionic poly(pyrazolyl)borates (1.85 g) was obtained (approximately 57% yield).

Synthesis of Cobalt(II) Complexes with Poly(pyrazolyl)borate Ligands: 1.21 g of potassium salts [approx. 3.3 mmol of crude reac-

Table 1. Crystal data and structure refinement

Compound	**1**	**2**	**3**
Empirical formula	$C_{45}H_{34}BN_7O_3Co$	$C_{58}H_{57}B_2N_{10}Co$	$C_{40}H_{40}B_2N_8Co$
Formula mass	790.53	974.69	713.35
T /K	100(1)	100(2)	100(2)
λ /Å	0.71073	0.71073	0.71073
Crystal system	Monoclinic	Triclinic	Monoclinic
Space group	$P2_1/c$	$P\bar{1}$	$P2_1/n$
a /Å	13.6260(10)	13.326(2)	9.907(2)
b /Å	16.4753(13)	13.713(2)	18.300(4)
c /Å	17.4850(13)	14.721(2)	19.869(4)
α /°	−	85.00(2)	−
β /°	109.086(7)	81.38(2)	99.20(3)
γ /°	−	71.76(2)	−
V /Å^3	3709.5(5)	2523.8(6)	3555.9(13)
Z	4	2	4
D_c /Mg·m^{-3}	1.416	1.283	1.332
μ /mm^{-1}	0.517	0.390	0.525
F(000)	1636	1024	1492
Crystal size /mm	0.23 × 0.17 × 0.15	0.18 × 0.15 × 0.15	0.15 × 0.10 × 0.10
Diffractometer	Kuma KM4CCD	Kuma KM4CCD	Kuma KM4CCD
θ range for data collection, °	3.24−30.00	3.24−25.00	3.33−28.81
Ranges of h,k,l	−12→19, −22→22, −13→13	−14→15, −15→16, −17→15	−13→9, −24→23, −25→26
Reflections collected	41509	14645	25246
Independent reflections (R_{int})	7894 (0.0518)	8665 (0.0493)	8564 (0.0450)
Data/parameters	7894/650	8665/652	8564/460
Absorption coefficients min./max.	0.78279−1.09435	−	−
Goodness-of-fit (F^2)	1.100	1.079	1.112
Final R_1/wR_2 indices ($I > 2\sigma_I$)	0.0516/0.0958	0.0786/0.1913	0.0539/0.0947
Largest diff. peak/hole /e·Å^{-3}	0.309/−0.291	0.850/−0.601	0.306/−0.426

tion mixture obtained in route (1), vide supra] was dissolved in tetrahydrofuran (THF, 150 cm^3) and into this solution a stock solution of cobalt(II) nitrate in THF [1.5 equivalents of cobalt(II) calculated for potassium dihydro(3,5-dimethylpyrazolyl)(3,5-diphenylpyrazolyl)borate] was added dropwise, with vigorous stirring. The resulting pink-violet solution was concentrated to a volume of 30 cm^3, then 150 cm^3 of methylene dichloride was added and the organic phase was twice extracted rapidly with 150 cm^3 of water. The organic phase was separated and the solvents removed on a rotary evaporator. The solid obtained was dissolved in THF, passed through a short bed of celite and the solution layered with heptane. After two days, 25 mg of deep-violet crystals deposited from the mixture. These crystals were separated and their composition was determined by elemental analysis and X-ray diffraction as hydrotris(3,5-diphenylpyrazolyl)boratocobalt(II) nitrate [Tp^{Ph_2}-$Co(NO_3)$ (**1**)]. The complex was totally insoluble in most organic solvents and water. Yield: approx. 1%.

For comparison we also synthesized potassium hydrotris(3,5-diphenylpyrazolyl)borate KTp^{Ph_2} by the standard procedure[8] and $Tp^{Ph_2}Co(NCS)$ complex (**1′**) by addition of KTp^{Ph_2} in THF to an excess of cobalt(II) thiocyanate, as described previously.[7]

After separation of **1**, crystallization of the cobalt(II) complexes was continued and the mixture of products was examined by ^1H NMR spectroscopy. The major product in the mixture was finally separated after four recrystallizations from THF/heptane as pink crystals (160 mg) and identified by elemental analysis, ^1H NMR spectroscopy, and X-ray crystallography as [dihydrobis(3,5-diphenylpyrazolyl)borato][hydrobis(3,5-dimethylpyrazolyl)(3,5-diphenylpyrazolyl)borato]cobalt(II) (**2**). Yield: approx. 12%.

In a separate synthesis, 1.85 g (approx. 5.3 mmol) of the mixture of poly(pyrazolyl)borate sodium salts obtained from route (2) (vide supra) was converted into a mixture of bis(ligand) cobalt(II) complexes as described above. Fractional crystallization of the complexes from THF/hexane mixture gave pink crystals of a mixture of Bp′CoTp′ compounds and another Tp′$Co(NO_3)$ complex in the first instance (220 mg), whereas the desired Bp′CoBp′′ complexes remained in solution. The complex [H_2B(3,5-diMepz)(3,5-diPhpz)]$_2$Co (**3**; 385 mg, 0.54 mmol, yield approx. 18%) was obtained from the filtrate as burgundy red crystals and identified by means of an X-ray crystallographic analysis.

1: $C_{45}H_{34}BCoN_7O_3$ (790.53): calcd. C 68.37, H 4.35, N 12.40; found C 68.43, H 4.41, N 12.32.

1′: $C_{46}H_{34}BCoN_7S$ (786.63): calcd. C 70.24, H 4.36, N 12.46; found C 69.99, H 4.51, N 12.24. IR (KBr): $\tilde{\nu}$ = 2065 ν(NCS), 2495 cm^{-1} ν(BH).

2: $C_{58}H_{57}B_2CoN_{10}$ (974.69): C 71.47, H 5.89, N 14.37; found C 71.29, H 5.71, N 14.42. ^1H NMR ($CDCl_3$, 293 K): δ = −68.3 [3 H, CH_3 (*3*,5-diMepzTp′)], −55.1 [2 H, *o*-H (*3*,5-diPhpzTp′)], −32.0 [3 H, CH_3 (*3*,5-diMepzTp′)], −20.9 [2 H, *o*-H (*3*,5-diPhpzBp^{Ph_2})], −19.3 [2 H, *o*-H (*3*,5-diPhpzBp^{Ph_2})], −6.2 [2 H, *m*-H (*3*,5-diPhpz of Tp′ or Bp^{Ph_2})], −5.2 [1 H, *p*-H (*3*,5-diPhpz of Tp′ or Bp^{Ph_2})], −3.9 [1 H, *p*-H (*3*,5-diPhpz of Tp′ or Bp^{Ph_2})], −3.2 [2 H, *m*-H (*3*,5-diPhpz of Tp′ or Bp^{Ph_2})], −1.7 [2 H, *m*-H (*3*,5-diPhpz of Tp′ or Bp^{Ph2})], −0.2 [1 H, *p*-H (*3*,5-diPhpz of Tp′ or Bp^{Ph_2})], 7.9 [3 H, CH_3 (*3*,5-diMepz2Tp′)], 10.2 [1 H, *p*-H (*3*,5-diPhpz of Tp′ or Bp^{Ph_2})], 10.8 [1 H, *p*-H (*3*,5-diPhpz of Tp′ or Bp^{Ph_2})], 12.8 [1 H, *p*-H (*3*,5-diPhpz of Tp′ or Bp^{Ph_2})], 13.6 [2 H, *m*-H (*3*,5-diPhpz of Tp′ or Bp^{Ph_2})], 15.6 [2 H, *m*-H (*3*,5-diPhpz of Tp′ or Bp^{Ph_2})], 16.0 [2 H, *m*-H (*3*,5-diPhpz of Tp′ or Bp^{Ph_2})], 20.9 [2 H, *o*-H(*3*,5-diPhpz3 of Tp′ or Bp^{Ph_2})], 23.1 [2 H, *o*-H(*3*,5-diPhpz3 of Tp′ or Bp^{Ph_2})], 25.3 [2 H, *o*-H(*3*,5-diPhpz of Tp′ or Bp^{Ph_2})], 31.5 [1 H, 4-H (pz of Tp′ or Bp^{Ph_2})], 51.3 [3 H, CH_3 (*3*,5-diMepzTp′)], 59.3 [1 H, 4-H (pz of Tp′ or Bp^{Ph_2})], 61.3 [1 H (broad), B-*H* of Tp′], 65.2 [1 H, 4-H (pz of Tp′ or Bp^{Ph_2})], 83.3 [1 H, 4-H (pz of Tp′ or Bp^{Ph_2})], 88.2 [1 H, 4-H (pz of Tp′ or Bp^{Ph_2})]. IR (KBr): $\tilde{\nu}$ = 2501 (m) ν[BH (Tp′)], 2275 (w) ν[BH (Bp′)], 2190 cm^{-1} (m). Magnetic moment (Evans method): μ = 4.53 B.M. UV/Vis (CH_2Cl_2): λ_{max} (ε [mol^{-1} dm^3 cm^{-1}]) = 498 (61.2), 538 nm (64.2).

3: $C_{40}H_{40}B_2CoN_8$ (713.35): calcd. C 67.33, H 5.65, N 15.71; found C 67.53, H 5.63, N 15.68.

IR (KBr): $\tilde{\nu}$ = 2493 (m) ν(BH), 2400 cm^{-1} (m). Magnetic moment (Evans method): μ = 3.9 B.M. UV/Vis: λ_{max} (ε [mol^{-1} dm^3 cm^{-1}]) = 580 (510), 555 (640), 512 nm (356).

Acknowledgments

T. Ruman, Z.Ciunik, and S.Wolowiec kindly acknowledge financial support from the State Committee for Scientific Research KBN (Poland, Grant number 3 T09A 05219).

[1] J. C. Calabrese, P. J. Domaille, J. S. Thompson, S. Trofimenko, *Inorg. Chem.* **1990**, *29*, 4429−4437.
[2] J. C. Calabrese, S. Trofimenko, *Inorg. Chem.* **1992**, *31*, 4810−4814.
[3] M. Lukasiewicz, Z. Ciunik, T. Ruman, M. Skóra, S. Wolowiec, *Polyhedron* **2001**, *20*, 237−244.
[4] T. Ruman, M. Lukasiewicz, Z. Ciunik, S. Wolowiec, *Polyhedron* **2001**, *20*, 2551−2558.
[5] M. C. Chisholm, N. W. Eilerts, J. C. Huffman, S. S. Iyer, M. Pacold, K. Phomphrai, *J. Am. Chem. Soc.* **2000**, *122*, 11845−11854 and ref. 17 cited therein.
[6] G. R. Motson, O. Mamula, J. C. Jeffery, J. A. McCleverty, M. D. Ward, A. von Zelewsky, *J. Chem. Soc., Dalton Trans.* **2001**, 1389−1391.
[7] M. Lukasiewicz, Z. Ciunik, S. Wolowiec, *Polyhedron* **2000**, *19*, 2119−2125.
[8] S. Guo, E. Ding, Y. Yin, K. Yu, *Polyhedron* **1998**, *17*, 3841−3849.
[9] S. Imai, K. Fujisawa, K. Kobayashi, N. Shirasawa, H. Fuji, T. Yoshimura, N. Kitajima, Y. Moro-oka, *Inorg. Chem.* **1998**, *37*, 3066−3070.
[10] E. L. Hegg, R. Y. N. Ho, L. Que, Jr, *J. Am. Chem. Soc.* **1999**, *121*, 1972−1973.
[11] D. L. Reger, S. M. Myers, S. S. Mason, A. L. Rheingold, B. S. Hagerty, P. D. Ellis, *Inorg. Chem.* **1995**, *34*, 4996−5002.
[12] M. Onishi, K. Itoh, K. Hiraki, R. Oda, K. Aoki, *Inorg. Chim. Acta* **1998**, *277*, 8−13.
[13] A. Kremer-Aach, W. Klaui, R. Bell, A. Sterath, H. Wunderlich, D. Mootz, *Inorg. Chem.* **1997**, *36*, 1552−1563.
[14] M. V. Capparelli, G. Agrifolio, *J. Crystallogr. Spectrosc. Res.* **1992**, *22*, 651−657.
[15] L. J. Guggenberger, C. T. Prewitt, P. Meakin, S. Trofimenko, J. P. Jesson, *Inorg. Chem.* **1973**, *12*, 508−515.
[16] I. B. Gorrell, A. Looney, G. Parkin, A. L. Rheingold, *J. Am. Chem. Soc.* **1990**, *112*, 4068−4069.
[17] P. Ghosh, T. Hascall, C. Dowling, G. Parkin, *J. Chem. Soc., Dalton Trans.* **1998**, 3355−3357.
[18] H. M. Echols, D. Dennis, *Acta Crystallogr., Sect. B* **1976**, *32*, 1627−1630.
[19] D. A. Clemente, M. Cigni-Biagini, *Inorg. Chem.* **1987**, *26*, 2350−2359.

[20] C. M. Dowling, G. Parkin, *Polyhedron* **1999**, *18*, 3567−3571.
[21] D. L. Reger, S. J. Knox, A. L. Rheingold, B. S. Haggerty, *Organometallics* **1990**, *9*, 2581−2587.
[22] D. L. Reger, M. J. Pender, D. L. Caulder, L. B. Reger, A. L. Rheinhold, L. M. Liable-Sands, *J. Organomet. Chem.* **1996**, *512*, 91−96.
[23] A. Beheshti, W. Clegg, M. H. Sadr, *Polyhedron* **2001**, *20*, 179−183.
[24] S. Trofimenko, J. C. Calabrese, P. J. Domaille, S. Thompson, *Inorg. Chem.* **1989**, *28*, 1091−1101.
[25] J. C. Calabrese, P. J. Domaille, S. Trofimenko, G. J. Long, *Inorg. Chem.* **1991**, *30*, 2795−2801.
[26] A. I. Rheingold, R. L. Ostrander, B. S. Haggerty, S. Trofimenko, *Inorg. Chem.* **1994**, *33*, 3666−3676.
[27] A. I. Rheingold, G. Yap, S. Trofimenko, *Inorg. Chem.* **1995**, *34*, 759−760.
[28] A. I. Rheingold, G. Yap, L. Liable-Sands, I. A. Guzel S. Trofimenko, *Inorg. Chem.* **1997**, *36*, 6261−6265.
[29] A. B. P. Lever, in *Inorganic Electronic Spectroscopy*, Chapter 9, 318−333.
[30] J. P. Jesson, S. Trofimenko, D. R. Eaton, *J. Am. Chem. Soc.* **1967**, *89*, 3148−3158.
[31] P. Starynowicz, *COSABS99, Program for absorption correction*, University of Wroclaw, **1999**.
[32] G. M. Sheldrick, *SHELXS97, Program for solution of crystal structures*, University of Göttingen, **1997**.
[33] G. M. Sheldrick, SHELXL97, *Program for crystal structure refinement*, University of Göttingen, **1997**.

Received August 8, 2001
[I01301]

Dipeptides Made up Solely from Histidine: Solution Behaviour and Zinc Complexation[‡]

Raphael Vogler[a] and Heinrich Vahrenkamp*[a]

Keywords: Zinc / Peptides / Histidine / Complex stabilities

The acid/base chemistry and the zinc complexation of the four dipeptides H-HisHis-OH, H-HisHis-OEt, Ac-HisHis-OH and Ac-HisHis-OEt were investigated by potentiometric methods. 1:1 (zinc:dipeptide) complexes prevail in solution, and those complexes that could be isolated on a preparative scale also have 1:1 compositions. The stability data confirm that exclusive zinc-imidazole(histidine) coordination is weak, and additional effects are essential to effect the high preference of zinc for histidine in proteins. A comparison of the stability data for zinc complexes of all dipeptides made up solely from histidine and/or cysteine reveals systematic trends and allows a parameterization of the log β values.

Introduction

Both catalytic and structural zinc in enzymes are always coordinated by at least one cysteine or histidine donor, and specifically in hydrolytic zinc enzymes a $(histidine)_3Zn-X$ coordination is typical.[2,3] This is the reason why we have focused heavily on peptides containing cysteine or histidine in our series of studies on zinc peptide complexes. Prior and parallel to our investigations there were relatively few reports in the literature on the zinc coordination of small peptides dominated by these two amino acids. The main reason for this is the great effort which is necessary for the synthesis of peptides that are rich in cysteine or histidine.

This paper completes our work on the zinc complexation of peptides containing two cysteine and/or histidine units. Previously we have reported on HisCys[4] and CysCys[1] dipeptides, on cyclic dipeptides,[5] and on tri- and tetrapeptides with cysteine and/or histidine at both termini and referenced the related literature.[6−8] The missing part — the HisHis dipeptides — is reported here.

In principle simple unprotected peptides are not suitable as representatives of the related proteins. They offer additional donor functions by their amino and carboxylate termini, and they lack the geometrical effects resulting from folding and helix formation. This disadvantage is compensated, however, by the basic information obtainable from them. When they have unprotected termini, the effect of those on complex formation can be quantified; when they offer only their side-chain donors the strength of the zinc−side-chain interactions can be evaluated free from the influences of protein preorganization. Being inorganic and not protein chemists we see our justification in providing this basic information.

For the present study the four possible HisHis dipeptides listed below were chosen. They represent the various stages of reduction of the donor functionality to exclusive imidazole donation. They were subjected to potentiometric titrations in the absence and presence of zinc nitrate, and they were treated with zinc salts on a preparative scale. The data obtained from them have enabled a comprehensive comparison of zinc complex stabilities for all small peptides with two closely spaced histidine and/or cysteine units.

H-HisHis-OH H-HisHis-OEt
Ac-HisHis-OH Ac-HisHis-OEt

Results and Discussion

Synthesis of the Peptides

The preparation of HisHis dipeptides requires the heavy use of protective groups due to the trifunctional nature of histidine itself. Such dipeptides have been reported in the literature,[9] and H-HisHis-OH is commercially available. We chose to prepare the four dipeptides by the methods used in our laboratory. As outlined in the Exp. Sect., Boc protection of the amino terminus and ethyl ester protection of the carboxylate terminus were used. The imidazole function was protected either by the Boc or the Trt groups. Peptide coupling was effected either by the CAIBE or by the DCC methods, and the standard procedures were applied to remove the protective groups as necessary. Final purification by preparative HPLC yielded the TFA adducts of the

[‡] Zinc Complexes of Amino Acids and Peptides, 15. − Part 14: Ref.[1]

[a] Institut für Anorganische und Analytische Chemie der Universität Freiburg,
Albertstr. 21, 79104 Freiburg, Germany
Fax: (internat.) +49-(0)761/203-6001
E-mail: vahrenka@uni-freiburg.de

 © WILEY-VCH Verlag GmbH, 69451 Weinheim, Germany, 2002 1434−1948/02/0303−0761 $ 17.50+.50/0

four peptides in gram quantities as analytically pure solids which are very hygroscopic.

Isolated Zinc Complexes

All four peptides were treated in a 1:1 and a 2:1 ratio with zinc perchlorate, nitrate, trifluoroacetate, chloride and iodide. Solid products containing zinc and the peptide could be obtained in all cases, but only some of the 1:1 reactions yielded complexes with simple compositions. It must be concluded that the formation of coordination polymers prevails. As observed by us before[1,4,5] the odd zinc:peptide ratios of these compounds make it difficult to assign constitutions or structures to them.

Those 1:1 reactions that were successful yielded 1:1 complexes in water or ethanol/water. The fully unprotected peptide could be combined with zinc trifluoroacetate to form **1**. Likewise, Ac-HisHis-OH yielded the trifluoroacetate **2**. Zinc chloride could be combined with Ac-HisHis-OH to form **3**, and with the fully protected peptide to form **4**. After slow crystallization these complexes were analytically pure but not suited for crystal structure determinations. Once crystallized they were not soluble enough for NMR measurements. Thus, although they seem to be mononuclear in solution (as is also evident from potentiometry, see below) they must be coordination polymers in the solid state. Counting the number of donor functions available for the zinc ions in the observed compositions allows the conclusion that zinc is tetrahedrally coordinated both in the monomers and the polymers. While none of our zinc complexes of bis(histidine) oligopeptides[1,6,8] has formed crystals suitable for X-ray analysis, we could confirm the tetrahedral coordination by an EXAFS analysis for $Zn(Ac\text{-}His\text{-}GlyGlyHis\text{-}NH_2)_2Zn(ClO_4)_2$.[6]

(H-HisHis-O)Zn-OCOCF$_3$ **1**

(Ac-HisHis-O)Zn-OCOCF$_3$ **2**

(Ac-HisHis-O)Zn-Cl **3**

(Ac-HisHis-OEt)ZnCl$_2$ **4**

Potentiometric Titrations

The acid/base titrations of the peptides themselves initially determined the amount of trifluoroacetic acid contained in them, as given in the Exp. Sect. Then they yielded the pK_a values which are listed in Table 1.

Table 1. Acid dissociation constants (pK_a) of the peptides (standard deviations in parentheses)

	COOH	ImH$^+$(1)	ImH$^+$(2)	NH_3^+
H-HisHis-OH	2.58(9)	5.72(1)	6.83(1)	8.04(4)
H-HisHis-OEt		5.47(1)	6.63(2)	7.86(3)
Ac-HisHis-OH	2.68(8)	6.40(6)	7.60(7)	
Ac-HisHis-OEt		5.96(11)	6.89(17)	

The carboxylate and amine pK_a's of the dipeptides can simply be referenced against those of histidine itself [pK(COOH) = 1.77, pK(NH_3^+) = 9.24].[9] The insertion of the second histidine unit between the carboxylate and ammonium functions, i.e. increasing their distance, eliminates completely their mutual influence. As a result the carboxylic pK_a rises and the ammonium pK_a decreases by about one unit. For histidine itself the imidazole pK_a (6.14) rises when the amino function is blocked and decreases when the carboxylate function is blocked;[10] these are basically charge effects. This can also be seen when comparing H-HisHis-OH with both H-HisHis-OEt and Ac-HisHis-OH in terms of the first imidazole pK_a. It seems that a mutual compensation of these two effects moves the first imidazole pK_a of Ac-HisHis-OEt back to the value of H-HisHis-OH.

In terms of exclusive histidine coordination, like in the proteins themselves the imidazole pK_a's of the fully protected histidine peptides are relevant. While the fully protected histidine Ac-His-NH_2 (pK = 7.07)[11] and isolated histidine in the peptide Ac-HisVal-OH (pK = 6.84)[12] have the typical pK_a for histidine near 7, the first histidine pK_a for all four dipeptides in this study is roughly one unit lower. This again is a charge effect: the positive charge on the second imidazolium function makes the deprotonation of the first one easier. The two pK_a values for Ac-HisHis-OEt are almost identical to those for the two histidine units in fully protected His-X-His tripeptides with X = Gly, Pro, Val and Apa.[8] This indicates that the distances between the two imidazolium functions has no pronounced effect. On the other hand, cyclo-HisHis shows pK_a's of 5.53 and 6.61[5] which are significantly lower than the others, and which may be correlated with the highly polar nature of this diketopiperazine derivative. One feature is common for all the bis(histidine) peptides mentioned here: their two imidazole pK_a's are all 1.1 ± 0.1 units apart.

The titrations in the presence of zinc nitrate did not suffer from the problem of precipitation which is a common one for cysteine-containing peptides. The rich species distributions exemplified by Figures 1 and 2 could be analyzed and correlated with the complex stabilities listed in Table 2.

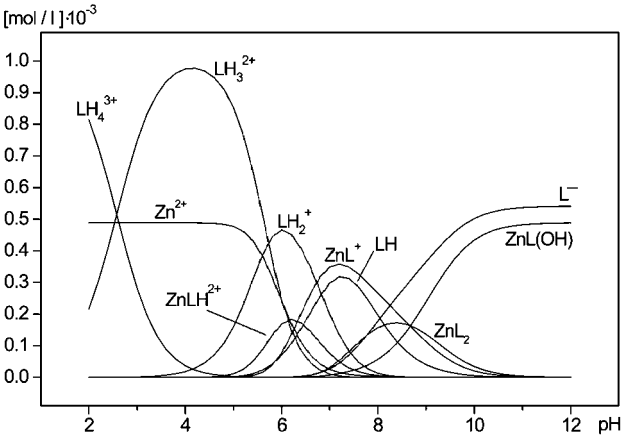

Figure 1. Species distribution in a solution of H-HisHis-OH and $Zn(NO_3)_2$ in a ratio of 2.1:1

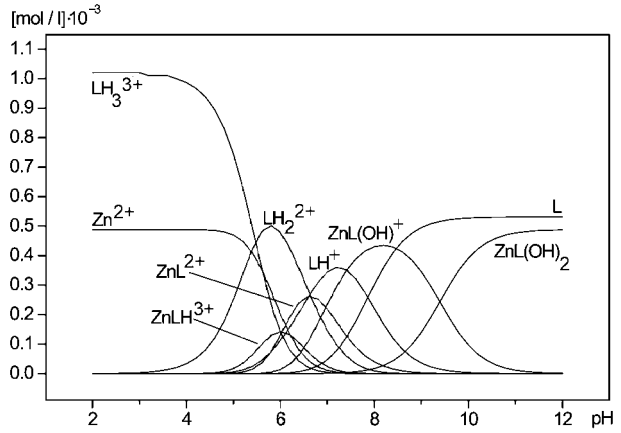

Figure 2. Species distribution in a solution of H-HisHis-OEt and $Zn(NO_3)_2$ in a ratio of 2:1

Table 2. Stability constants for the zinc complexes (log β) in solutions of the peptides (σ values in parentheses)

	ZnLH	ZnL	ZnL(OH)	$ZnL(OH)_2$	ZnL_2
H-HisHis-OH	12.02(6)	5.79(13)	−3.18(18)	−	9.18(6)
H-HisHis-OEt	11.70(2)	5.70(6)	−1.20(9)	−10.62(8)	−
Ac-HisHis-OH	−	3.35(15)	−3.74(18)	−	−
Ac-HisHis-OEt	10.05(4)	4.19(11)	−2.31(11)	−	−

As a rule only three complex species were necessary to fit the data: ZnLH, ZnL and ZnLOH, which are all 1:1 complexes. Of these, ZnLH represents a complex with a protonated peptide ligand, and ZnLOH represents a complex with a deprotonated water ligand, and hence ZnL is the only relevant species. Only in the case of H-HisHis-OH is a ZnL_2 complex observed, which must have to do with the fact that this ZnL_2 complex is uncharged and there is good chelation involving the imidazole and amino nitrogen donors.[10]

The stability constants for the four ZnL species have characteristic and very informative values. First and most important, they underline that the complex stability provided by exclusive Zn-imidazole(histidine) coordination is unusually small. Even two such interactions, as for Ac-HisHis-OEt, yield only a moderate stability of the ZnL species. This is also evident from the data for ZnL complexes of fully protected His-X-His peptides (X = Gly, Val, Apa), whose log β values are 3.4 ± 0.1.[8] Even the presumed preorganization of the two imidazole donors in cyclo-HisHis yields the very poor log β for ZnL of 2.55.[5] Reference compounds with a single and exclusive imidazole(histidine) donor are Ac-His-NH_2 (log β for ZnL = 1.96)[11] and cyclo-GlyHis (log β for ZnL = 1.71).[5]

This situation only gets better when additional donors of the dipeptides are involved. The best combination is that with the amino function, which forms a six-membered chelate ring. As Table 2 shows by the comparison of the H-HisHis with the Ac-HisHis dipeptides, this combination accounts for 2−2.5 log units in stability. This increase of stability is larger than the one resulting from the combination of one imidazole(histidine) donor with a second, neighbouring one (see above). The same observation also results from a comparison of the mono-histidine reference compounds H-His-OMe/Ac-His-NH_2 (log β = 4.45/1.96)[10] or H-ValHis-OEt/Ac-HisVal-OH (log β = 4.20/2.89).[12]

The effect of using the carboxylate function as an additional donor is small. The log β values for ZnL of H-HisHis-OH and H-HisHis-OEt are virtually identical, and that of Ac-HisHis-OH is even smaller than that of Ac-HisHis-OEt. For the simpler reference compounds the effect is noticeable: ZnL of Ac-His-OH (log β = 2.91)[10] is more stable than that of Ac-His-NH_2 (log β = 1.96),[11] and that of H-HisCys-OEt (log β = 8.36) is more stable than that of Ac-HisCys-OEt (log β = 6.17).[4]

The latter two values are again reminiscent of the low donor strength of the histidine-imidazole function relative to that of the cysteine-thiolate function. For all pairs of peptide derivatives X-His-Y/X-Cys-Y that form ZnL complexes in solution, the Cys compound is more stable than

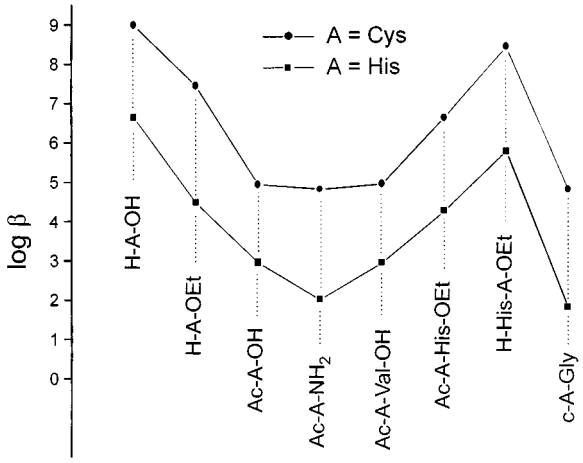

Figure 3. Stabilities of ZnL complexes for amino acid and peptide derivatives with one histidine (A = His) or cysteine (A = Cys) unit

the His compound by roughly 2.5 log β units. Figure 3 visualizes this for all available data for ZnL complexes. A similar relation holds for ZnL complexes of peptide ligands representing pairs of comparable His_2 and Cys_2 derivatives. As Figure 4 shows, the difference of the stabilities amounts to roughly six log β units, i.e. twice the amount of the mono-His/mono-Cys pairs.

This latter observation points to a further generalization, namely the possibility of expressing the stabilities of all ZnL complexes mentioned in this paper by parameters for the donors involved. It seems that this can be done with a satisfactory degree of precision in the ± 0.2 log β range of total stabilities for ZnL complexes with exclusive Cys or His coordination. Table 3 demonstrates this in section (a), based on log β parameters of 4.7 for Cys and 2.1 for His. Serious deviations from this approximation occur only for cyclo-HisHis, the unusually low log β value of which has already been discussed before,[5] and for Ac-CysCys-OEt for which the calculated log β is 0.8 units off.

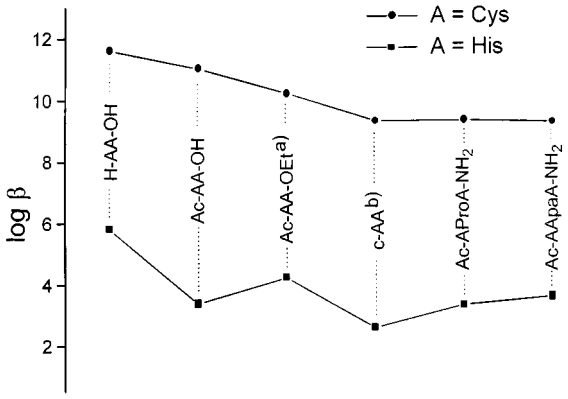

Figure 4. Stabilities of ZnL complexes for peptide derivatives with two histidine (A = His) or cysteine (A = Cys) units
[a] Data for Ac-LCys-DCys-OEt. [b] Estimated value for cyclo-CysCys[5]

Table 3. Comparison of observed log β values for ZnL complexes with calculated ones, using log β parameters of 2.1 for imidazole-(histidine), 4.7 for thiolate(cysteine), 2.2 for amine adjacent to Cys or His and 0.5 for carboxylate adjacent to Cys or His

L	log β (obs)	log β (calc)
(a) exclusive imidazole or thiolate coordination		
Ac-His-NH_2	2.0	2.1
Ac-Cys-NH_2	4.8	4.7
cyclo-GlyHis	1.7	2.1
cyclo-GlyCys	4.7	4.7
Ac-HisHis-OEt	4.2	4.2
Ac-HisCys-OEt	6.6	6.8
Ac-CysCys-OEt	10.2	9.4
cyclo-HisHis	2.5	4.2
cyclo-HisCys	6.6	6.8
cyclo-CysCys	9.3[a]	9.4
Ac-HisApaHis-NH_2	3.6	4.2
Ac-CysApaCys-NH_2	9.3	9.4
(b) with additional amine or carboxylate coordination		
H-His-OMe	4.5	4.3
H-Cys-OEt	7.4	6.9
Ac-His-OH	2.9	2.6
Ac-Cys-OH	4.9	5.2
H-HisHis-OEt	5.7	6.2
H-HisCys-OEt	8.4	8.8
H-CysCys-OEt	n.o.	11.4
Ac-HisHis-OH	3.4	4.7
Ac-CysCys-OH	11.0	9.9
(c) with additional amine and carboxylate coordination		
H-His-OH	6.6	4.8
H-Cys-OH	9.0	7.4
H-HisHis-OH	5.8	6.9
H-Cys-His-OH	9.4	9.5
H-CysCys-OH	11.6	12.1

[a] Estimated value from ref.[5]

The parameterization works less satisfactorily for the amine and carboxylate donors, cf. parts (b) and (c) of Table 3. As mentioned above the effect of chelation involving the amino function is strong, accounting for a log β contribution of more than two units. However, it is obviously variable, depending on whether the amino group is part of histidine or cysteine and on the number of amino acid building blocks. Likewise the contribution of the carboxylate function cannot be accounted for by a fixed parameter. Thus the agreement between observed and calculated log β values is not so good in section (b) of Table 3, and in section (c), where four parameters are involved, the disagreement amounts to 0.1−1.8 log β units. Nevertheless the given parameters should be good enough to estimate the stabilities of ZnL complexes of peptides containing two cysteine and/or histidine units, either in adjacent positions or separated by one or two nonligating amino acid constituents.

Conclusions

This paper has completed our studies of the acid/base chemistry and zinc complexation of small peptides rich in cysteine and histidine. The four possible His-His dipeptides (unprotected, partly and fully protected) were employed. Their 1:1 zinc complexes are of moderate stability. Even for two imidazole(histidine) donor functions there is no stabilization which could compete with that of a single thiolate-(cysteine) donor, and the complex stability for a chelating coordination of the imidazole and a terminal amino function surpasses that for a bis(imidazole) coordination. Furthermore, conformational effects due to the position of histidine in a peptide are not evident: compared to the ZnL complex of Ac-HisHis-OEt both the ZnL complexes of cyclo-HisHis or Ac-HisApaHis-NH_2, whose imidazole donors should be positioned more favourably, are less stable. All this underlines the notion that the frequent occurrence of Zn-histidine coordination in proteins reflects a very efficient tuning of preorganization of the donors by the polypeptide backbone.

Our accumulated data for zinc complexes of peptides with one or two cysteine and/or histidine constituents has allowed a comparative discussion of their stabilities. As Table 3 shows, this has enabled a parameterization of the contributions of the individual donors to the stability of 1:1 complexes in terms of log β increments. The agreement between calculated and observed complex stabilities is quite satisfying for the systems with exclusive histidine and/or cysteine coordination. When additional carboxylate or amine coordination is involved the parameterization for these donors works less satisfactorily. However, as cysteine and histidine are the natural donors and terminal amino or carboxylate functions do not coordinate in proteins, the stability parameters should be valuable for estimating the strength of zinc-peptide interactions for new or hitherto uninvestigated peptides containing cysteine and/or histidine.

Experimental Section

General: For general working and measuring procedures, see ref.[13] The histidine derivatives Boc-His(Boc)-OH, H-His-OEt, Ac-His-OH and Ac-His(Trt)-OH were obtained commercially. The detailed procedures of peptide coupling by the CAIBE and the DCC method as well as for the removal of the protective groups Boc and

Trt[8] have been described by us before. Purifications by HPLC were performed with a Merck−Hitachi system using Nucleosil 7C18 from Macherey−Nagel. The flow rate was 6 mL/min. The eluents always contained 0.1% of trifluoroacetic acid which thereby became a constituent of the isolated peptides. The specific HTFA content of each peptide was determined by potentiometric titration.

H-HisHis-OH: Boc-His(Boc)-OH (10.00 g, 28.14 mmol) and H-His-OEt·3*p*-TosOH (19.69 g, 28.14 mmol) were coupled by the CAIBE method resulting in 4.42 g (30%) of Boc-His(Boc)-His-OEt as a colourless solid. 2.15 g (4.13 mmol) of this in a mixture of 25 mL of methanol and 25 mL of 1 M NaOH was stirred at 50 °C for 30 min. After cooling to room temp. the solution was brought to pH 2 with 1 M HCl. All volatiles were removed in vacuo, the residue was suspended in 30 mL of dry methanol, filtered, and the filtrate evaporated to dryness again. The residue was washed three times with 15 mL of diethyl ether and dried in vacuo to give of Boc-His(Boc)-His-OH (1.99 g, 98%) as a pale yellow solid. This solid was treated with trifluoroacetic acid as described previously[8] to remove the Boc groups, giving H-HisHis-OH·4HTFA (2.10 g, 82%) as a yellow oil. Preparative HPLC with water and freeze-drying yielded the analytically pure product as a colourless, very hygroscopic solid, m.p. 63 °C. $C_{12}H_{16}N_6O_3·4C_2HF_3O_2$ (292.30 + 456.09): calcd. C 32.10, H 2.69, N 11.23; found C 31.82, H 2.71, N 11.27. IR (KBr): $\tilde{\nu}$ = 3436 bs, (OH), 3156 bs, (NH), 1676 vs (amide I), 1559 m, 1540 m (amide II), 1205 vs (CF). ^{1}H NMR: ([D$_6$]DMSO): δ = 2.92−3.31 (m, 4 H, H$_\beta$), 4.19−4.25 (m, 1 H, H$_\alpha$), 4.59−4.69 (m, 1 H, H$_\alpha$), 4.91−5.58 (m, 3 H, NH_3^+), 7.40 (s, 1 H, im), 7.42 (s, 1 H, im), 8.92−9.00 (m, 1 H, amide), 8.98 (s, 1 H, im), 8.99 (s, 1 H, im).

H-HisHis-OEt: Boc-His(Boc)-His-OEt (2.17 g, 4.17 mmol; see above) was treated with trifluoroacetic acid as described previously[8] to remove the Boc groups, giving H-HisHis-OEt·4HTFA (2.57 g, 93%) as a yellow oil. Preparative HPLC with water/acetonitrile (98:2) and subsequent freeze-drying yielded the analytically pure product as a colourless, very hygroscopic solid, m.p. 59 °C. $C_{14}H_{20}N_6O_3·4C_2HF_3O_2·2H_2O$ (320.35 + 456.09 + 36.03): calcd. C 32.52, H 3.47, N 10.34; found C 32.69, H 3.07, N 10.60. IR (KBr): $\tilde{\nu}$ = 3442 m, 3385 m (NH), 1672 vs (amide I), 1559 m (amide II), 1203 vs (CF). ^{1}H NMR ([D$_6$]DMSO): δ = 1.14 (t, *J* = 7.4 Hz, 3 H, Et), 3.00−3.29 (m, 4 H, H$_\beta$), 4.09 (q, *J* = 7.4 Hz, 2 H, Et), 4.20−4.26 (m, 1 H, H$_\alpha$), 4.65−4.76 (m, 1 H, H$_\alpha$), 7.40 (s, 1 H, im), 7.44 (s, 1 H, im), 8.99 (s, 1 H, im), 9.00 (s, 1 H, im), 9.12 (d, *J* = 6.3 Hz, 1 H, amide).

Ac-HisHis-OEt: Ac-His(Trt)-OH (8.79 g, 20.0 mmol) and H-His-OEt·3*p*-TosOH (14.00 g, 20.0 mmol) were coupled by the DCC method to give Ac-His(Trt)-His-OEtr (9.89 g, 82%) as a colourless solid. 3.98 g of this were treated with ethanethiol as described previously[8] to remove the Trt group, yielding Ac-HisHis-OEt·2.4HTFA (1.63 g, 42%) as a colourless solid. Preparative HPLC with water which was gradually replaced by acetonitrile, and subsequent freeze-drying, yielded the analytically pure product as a colourless, very hygroscopic solid, m.p. 48 °C. $C_{16}H_{22}N_6O_4·2.4C_2HF_3O_2$ (362.39 + 273.65): calcd. C 39.28, H 3.87, N 13.21; found C 39.18, H 3.85, N 13.41. IR (KBr): $\tilde{\nu}$ = 3424 bs, 3148 m (NH), 1672 vs (amide I), 1541 m (amide II), 1204 vs (CF). ^{1}H NMR ([D$_6$]DMSO): δ = 1.14 (t, *J* = 7.0 Hz, 3 H, Et), 1.82 (s, 3 H, Ac), 2.78−3.23 (m, 4 H, H$_\beta$), 4.08 (q, *J* = 7.0 Hz, 2 H, Et), 4.48−4.65 (m, 2 H, H$_\alpha$), 7.31 (s, 1 H, im), 7.38 (s, 1 H, im), 8.25 (d, *J* = 8.0 Hz, 1 H, amide), 8.58 (d, *J* = 7.6 Hz, 1 H, amide), 8.95 (s, 1 H, im), 8.97 (s, 1 H, im).

Ac-HisHis-OH: Ac-HisHis-OEt·2.4HTFA (2.01 g, 3.40 mmol; see above) was treated with NaOH as described above for H-HisHis-OH to remove the ethyl group, giving Ac-HisHis-OH·2HCl (1.28 g, 93%) as a colourless solid. Preparative HPLC with water/acetonitrile (95:5) and subsequent freeze-drying yielded the analytically pure product as a colourless, very hygroscopic solid, m.p. 144 °C. $C_{14}H_{18}N_6O_4·4C_2HF_3O_2·5H_2O$ (334.33 + 456.09 + 90.08): calcd. C 30.01, H 3.66, N 9.54; found C 29.63, H 3.72, N 9.87. IR (KBr): $\tilde{\nu}$ = 3437 vs, b (OH), 1659 s (amide I), 1641 s, 1548 s (amide II), 1206 s (CF). ^{1}H NMR ([D$_6$]DMSO): δ = 1.83 (s, 3 H, Ac), 2.76−3.33 (m, 4 H, H$_\beta$), 4.42−4.62 (m, 2 H, H$_\alpha$), 7.33 (s, 1 H, im), 7.43 (s, 1 H, im), 8.38 (d, *J* = 8.0 Hz, 1 H, amide), 8.61 (d, *J* = 7.8 Hz, 1 H, amide), 8.99 (s, 1 H, im), 9.01 (s, 1 H, im).

1: A solution of $Zn(TFA)_2$ (13.2 mg, 0.045 mmol) in 10 mL of water was added to a solution of H-HisHis-OH·4HTFA (34.0 mg, 0.045 mmol) in 10 mL of ethanol. Triethylamine (31.7 μL, 23.0 mg, 0.23 mmol) was then added with vigorous stirring, and the solution was reduced in vacuo to 5 mL. The resulting precipitate was filtered off, washed twice with 5 mL of dry ethanol and dried in vacuo to give **1**·EtOH (11.0 mg, 47%) as a colourless solid, m.p. 270 °C (dec.). $C_{16}H_{21}F_3N_6O_6Zn$ (515.76): calcd. C 37.26, H 4.10, N 16.29, Zn 12.68; found C 37.23, H 3.99, N 17.04, Zn 12.09. IR (KBr): $\tilde{\nu}$ = 3415 vs, b (OH), 3274 vs, b, 3133 s (NH), 1669 vs (amide I), 1507 s (amide II), 1204 s (CF).

2: A solution of $Zn(TFA)_2$ (55.0 mg, 0.19 mmol) in 10 mL of water was added to a solution of Ac-HisHis-OH·4HTFA·5H$_2$O (166 mg, 0.19 mmol) in 10 mL of water. The reaction flask was attached to a second flask containing triethylamine (132 μL, 96 mg, 0.95 mmol) which diffused into the reaction solution. After two days the resulting precipitate was filtered off, washed three times with 5 mL of dry ethanol and dried in vacuo to give **2**·2H$_2$O (22.5 mg, 43%) as a colourless solid, m.p. 280 °C (dec.). $C_{16}H_{21}F_3N_6O_8Zn$ (547.76): calcd. C 35.08, H 3.86, N 15.34, Zn 11.94; found C 35.21, H 3.61, N16.31, Zn 12.50. IR (KBr): $\tilde{\nu}$ = 3416 vs, b (OH), 3282 s, 3135 s (NH), 1646 vs (amide I), 1540 s (amide II), 1203 s (CF).

3: Prepared as for **2** from of $ZnCl_2$ (38.5 mg, 0.28 mmol), Ac-HisHis-OH·4HTFA·5H$_2$O (249 mg, 0.28 mmol) and triethylamine (197 μL, 143 mg, 1.41 mmol). Yield 81.0 mg (63%) of **3**·H$_2$O as a colourless solid, m.p. 280 °C (dec.). $C_{14}H_{19}ClN_6O_5Zn$ (452.18): calcd. C 37.19, H 4.24, N 18.59, Zn 14.46; found C 36.90, H 3.74, N 17.72, Zn 14.12. IR (KBr): $\tilde{\nu}$ = 3291 vs, b (OH), 3131 s (NH), 1650 vs (amide I), 1536 s (amide II).

4: Prepared as for **2** from $ZnCl_2$ (23.2 mg, 0.17 mmol), Ac-HisHis-OEt·2.4HTFA (108 mg, 0.17 mmol) and triethylamine (119 μL, 0.85 mmol). Yield 46.3 mg (55%) of **4** as a colourless solid, m.p. 260 °C (dec.). $C_{16}H_{22}Cl_2N_6O_4Zn$ (498.68): calcd. C 38.54, H 4.45, N 16.85, Zn 13.11; found C 38.82, H 4.23, N 17.21, Zn 13.65. IR (KBr): $\tilde{\nu}$ = 3378 bs, 3285 bs, 3134 s (NH), 1654 vs (amide I), 1539 s (amide II).

Potentiometric Titrations: The apparatus used, the experimental details, the calibration techniques and the titration procedure were as described before.[8,10] The common anion in all solutions was ni-

Table 4. Starting concentrations (× 10^{-3} M) of the regents for the potentiometric titrations

Peptide	c(peptide)	c(acid)	c(Zn)
H-HisHis-OH	0.890−1.030	0.602−1.082	0.235−0.940
H-HisHis-OEt	1.001−1.020	1.331−1.405	0.240−0.977
Ac-HisHis-OH	0.860−1.741	0.013−1.716	0.250−1.038
Ac-HisHis-OEt	0.707−0.778	0.827−1.573	0.309−0.865

trate [KNO_3, $Zn(NO_3)_2$, HNO_3]. Zuberbühler's TITFIT program[14] was used for the computations. The ionic strength was 0.1. All measurements were done at 25.0 ± 0.1 °C. The starting concentrations of peptides, acid and zinc nitrate are given in Table 4.

Acknowledgments

This work was supported by the Fonds der Chemischen Industrie. We thank Mrs. F. Bitgül for technical assistance.

[1] R. Vogler, M. Gelinsky, L. F. Guo, H. Vahrenkamp, *Inorg. Chim. Acta* **2002**, in press.
[2] D. W. Christianson, *Adv. Protein Chem.* **1991**, *42*, 281−355.
[3] B. L. Vallee, D. S. Auld, *Acc. Chem. Res.* **1993**, *26*, 543−551.
[4] P. Gockel, R. Vogler, H. Vahrenkamp, *Chem. Ber.* **1996**, *129*, 887−895.
[5] P. Gockel, R. Vogler, M. Gelinsky, A. Meißner, H. Albrich, H. Vahrenkamp, *Inorg. Chim. Acta* **2001**, in press.
[6] M. Förster, I. Brasack, A. K. Duhme, H. F. Nolting, H. Vahrenkamp, *Chem. Ber.* **1996**, *129*, 347−353.
[7] A. Meißner, W. Haehnel, H. Vahrenkamp, *Chem. Eur. J.* **1997**, *3*, 261−267.
[8] P. Gockel, M. Gelinsky, R. Vogler, H. Vahrenkamp, *Inorg. Chim. Acta* **1998**, *272*, 115−124.
[9] T. Brown, J. H. Jones, J. D. Richards, *J. Chem. Soc., Perkin Trans. 1* **1982**, 1553−1562.
[10] P. Gockel, H. Vahrenkamp, A. D. Zuberbühler, *Helv. Chim. Acta* **1993**, *76*, 511−520.
[11] P. Gockel, R. Vogler, H. Vahrenkamp, unpublished results.
[12] P. Gockel, H. Vahrenkamp, *Chem. Ber.* **1996**, *129*, 1243−1249.
[13] M. Förster, R. Burth, A. K. Powell, T. Eiche, H. Vahrenkamp, *Chem. Ber.* **1993**, *126*, 2643−2648.
[14] A. D. Zuberbühler, T. A. Kaden, *Talanta* **1982**, *29*, 201−206.
Received September 14, 2001
[I01372]

EurJIC
European Journal of Inorganic Chemistry

April 2002
Issue 4
Pages 767–990

COVER PICTURE

The cover picture shows the electron diffraction pattern, high resolution electron microscopy and a structural model of $Ba_9Rh_{7.92}O_{24}$, the $\alpha = 3$, $\beta = 6$ member of the one-dimensional $(A_3B_2O_6)_\alpha(A_3B_3O_9)_\beta$ homologous series. Seven octahedra sharing faces alternate with a trigonal prism defining chains of Rh atoms running parallel to the *c* axis of a rhombohedral unit cell ($R\bar{3}c$), separated by Ba atoms. Electron diffraction allows the direct observation of the α and β structural blocks forming such a commensurate modulated structure as well as the superstructure direction. Details are discussed in the article by J. M. González-Calbet et al. on p. 805 ff.

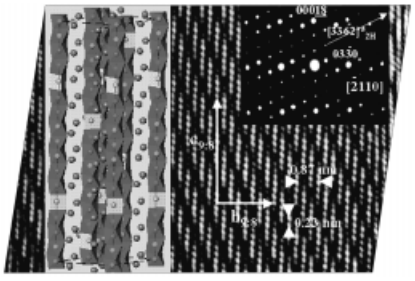

MICROREVIEW

Contents

783 **V. Guerchais**

Electrophilic Half-Sandwich (Carbene)metal (Metal = Fe, Ru, Os) Complexes: Recent Developments in Synthesis and Applications

Keywords: Carbene complexes / Catalysis / C–C bond formation / Diazo compounds

 © WILEY-VCH Verlag GmbH, 69451 Weinheim, Germany, 2002 1434–1948/02/0404–0771 $ 17.50+.50/0

SHORT COMMUNICATIONS

797 **C.-D. Wu, C.-Z. Lu,* W.-B. Yang, S.-F. Lu, H.-H. Zhuang, J.-S. Huang**

The Structure and Physical Properties of a Novel Three-Dimensional Zeolite-Like Nanoporous Architecture Formed by Two Different Polymeric Layers: $[Eu_2(btc)(H_2btc)(H_2O)]\cdot 4H_2O$

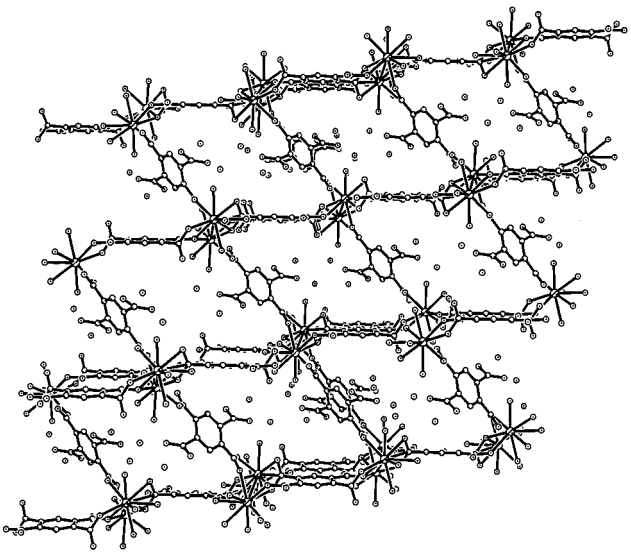

Keywords: Hydrothermal synthesis / Nanostructures / Materials science / Europium / Organic-inorganic hybrid composites

801 **M. Zablocka, K. Owsianik, A. Igau, A. Skowronska, J.-P. Majoral***

From *P*-Metalated *trans*-Iminodiphosphanes to *N*-Metalated *cis*-Iminodiphosphanes: An Unprecedented Rearrangement

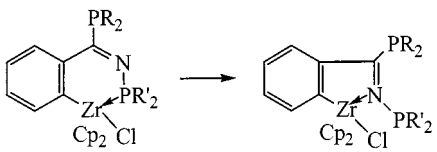

Keywords: Phosphanes / Zirconium / N ligands

FULL PAPERS

805 **K. Boulahya, M. Hernando, A. Varela, J. M. González-Calbet,* M. Parras, U. Amador, J. L. Martínez**

Structure Determination of the α = 3, β = 6 Term of the $(A_3B_2O_6)_\alpha(A_3B_3O_9)_\beta$ Homologous Series (A = Ba, B = Rh) by a Combination of Powder X-ray Diffraction and Electron Microscopy

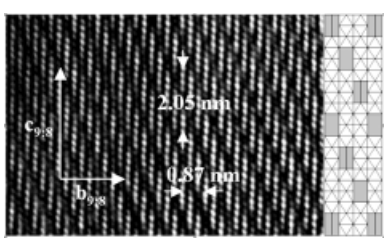

Keywords: One-dimensional oxides / X-ray diffraction / Electron diffraction / Electron microscopy

811 **M. Abul Haj, M. Quirós,* J. M. Salas, J. A. Dobado, J. M. Molina, M. G. Basallote, J. A. Mánez**

Structurally Different Dinuclear Copper(II) Complexes with the Same Triazolopyrimidine Bridging Ligand

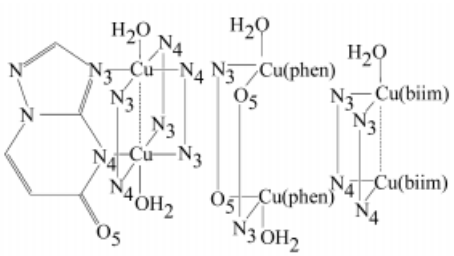

Keywords: Copper / N,O ligands / Metal-metal interactions / Structure elucidation

819 **M. Biruš,* R. van Eldik,* M. Gabričević, A. Zahl**

^{139}La NMR Kinetic Study of Lanthanum(III) Complexation with Acetohydroxamic Acid

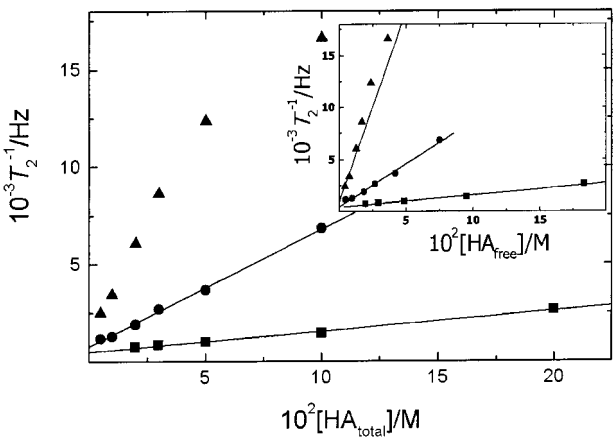

Keywords: Lanthanum / NMR spectroscopy / Kinetics / Reaction mechanisms

826 **E. Cerrada, L. R. Falvello, M. B. Hursthouse, M. Laguna,* A. Luquin, C. Pozo-Gonzalo**

PPh(2-$C_6H_4S)_2$ as a Pincer Ligand in Nickel(II) and Palladium(II) Complexes − X-ray Structure of [Ni{PPh($C_6H_4S)_2$}(PPh_2Me)], [Pd_2(μ-dppe)-{PPh($C_6H_4S)_2$}$_2$] and [Ni{PPh($C_6H_4S)_2$}]$_2$

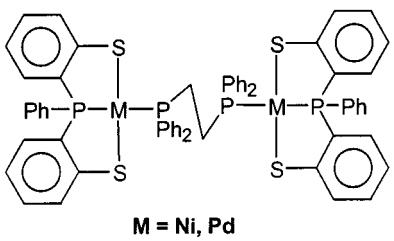

Keywords: Nickel / Palladium / P ligands / S ligands

834 **A. Hammerl, G. Holl, T. M. Klapötke,* P. Mayer, H. Nöth, H. Piotrowski, M. Warchhold**

Salts of 5,5′-Azotetrazolate

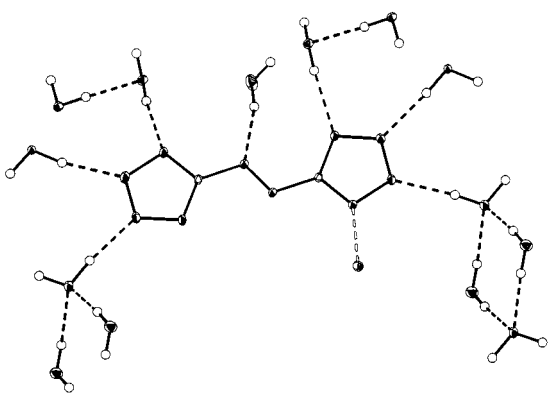

Keywords: Azo compounds / Hydrates / Nitrogen heterocycles / Tetrazoles / Highly energetic materials

846 **H. M. Burke, J. F. Gallagher, M. T. Indelli, F. Scandola, J. G. Vos***

Rhodium Mediated N−O Bond Formation

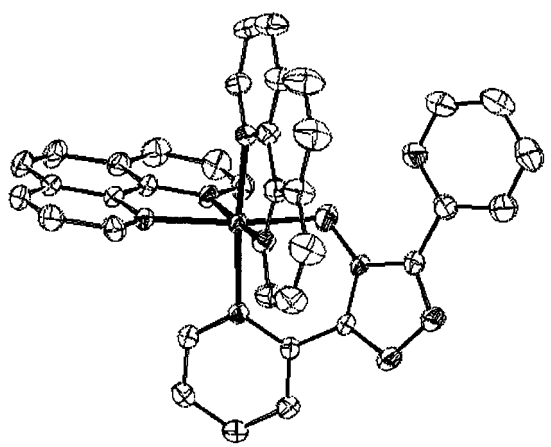

Keywords: Rhodium / N ligands / Oxygen / Insertion / Crystal structure

850 **J. C. Berthet,* M. Nierlich, M. Ephritikhine**

Synthesis of Organouranium(IV) Triflates from $U(OTf)_4$ or from Alkyl or Amide Precursors

Keywords: Uranium / Triflate complexes / Cyclopentadienyl complexes / Cyclooctatetraenyl complexes

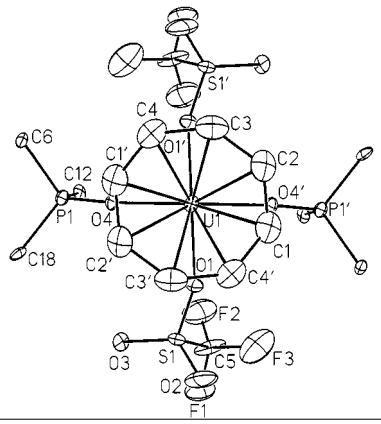

859 **D. S. Marlin, M. M. Olmstead, P. K. Mascharak***

Spin States and Stability of Fe^{III} Complexes of Ligands with Carboxamido Nitrogen and Phenolato Oxygen Donors

Keywords: Iron / N ligands / O ligands / Spin states

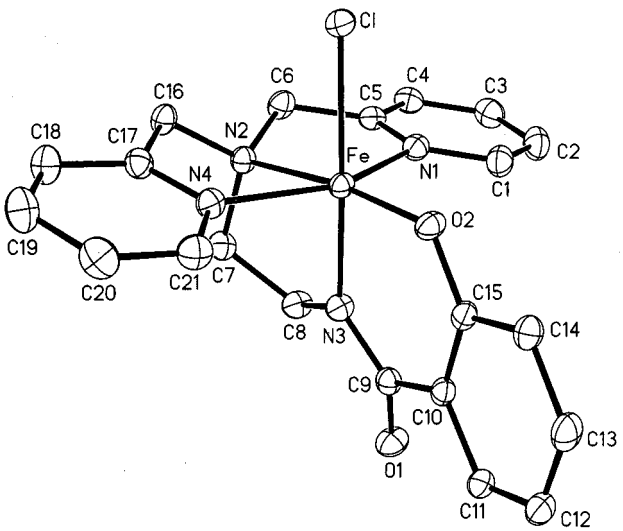

866 **F. Sancenon, A. Benito, F. J. Hernández, J. M. Lloris, R. Martínez-Máñez,* T. Pardo, J. Soto**

Difunctionalised Chemosensors Containing Electroactive and Fluorescent Signalling Subunits

Keywords: Ferrocene / Anthracene / Fluorescence / Chemosensors

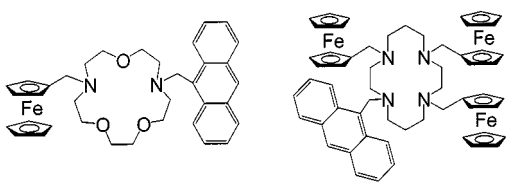

876 **S. Schmatz,* F. Diedrich, C. Ebker, U. Klingebiel***

Thermal Isomerisation of Tris(silyl)hydroxylamines to Silylaminodisiloxanes − Experimental and Quantum Chemical Results

Keywords: Silicon / Hydroxylamines / Isomerisation / Ab initio calculations / Transition states

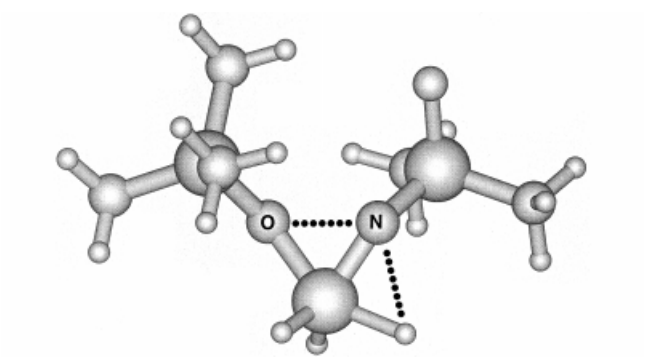

886 **M. Ogita, Y. Yamamoto, T. Suzuki, S. Kaizaki***

Syntheses, Structures, and Spectroscopic Properties of Cobalt(III) Complexes Containing 3- or 4-Pyridyl-Substituted Nitronyl and Imino Nitroxide Ligands

Keywords: Nitroxides / Radicals / Cobalt / NMR spectroscopy / Deoxygenation

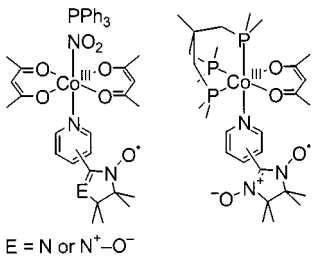

895 **J.-M. Rueff, S. Pillet, N. Claiser, G. Bonaventure, M. Souhassou, P. Rabu***

Synthesis, Crystal Structure and Magnetic Properties of the Helical-Chain Compounds $[M_2(O_2CC_{12}H_8CO_2)_2(H_2O)_8]$ [M = Cobalt(II), Nickel(II)]

Keywords: Carboxylate ligands / Hydrothermal synthesis / Nickel / Cobalt / Magnetic properties

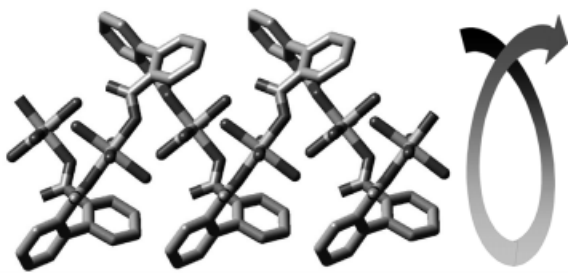

901 **J.-O. Dalbavie, J.-B. Regnouf-de-Vains,* R. Lamartine, M. Perrin, S. Lecocq, B. Fenet**

A Calix[4]arene-Based Bipyridine Podand as Versatile Ligand for Transition Metal Cations

Keywords: Calixarenes / Bipyridines / Podands / Cobalt / Nickel / Zinc / Copper

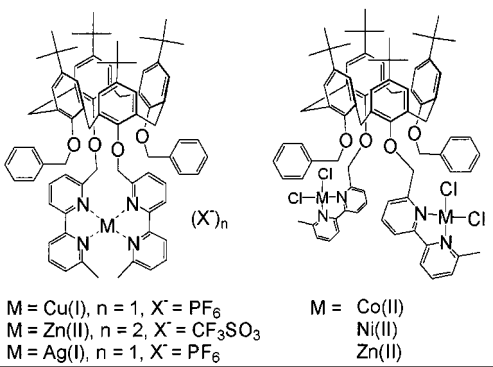

910 **M. Bröring,* C. D. Brandt, J. Bley-Escrich, J.-P. Gisselbrecht***

Structural and Spectroelectrochemical Studies on (2,2′-Bidipyrrinato)copper(II) and -palladium(II) Complexes

Keywords: Porphyrinoids / N ligands / Copper / Palladium / Electrochemistry

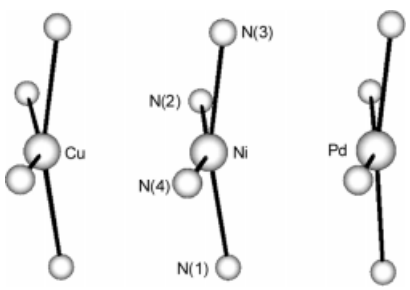

918 **M. Tamm,* K. Baum, T. Lügger, R. Fröhlich, K. Bergander**

Chelate Complexes of Functionalized Cycloheptatrienyl Ligands: 17- and 18-Electron Molybdenum Complexes with Linked Cycloheptatrienyl−Phosphane Ligands and Their Use in Transition Metal Catalysis

Keywords: Cycloheptatrienyl complexes / Molybdenum / Ligand functionalization / Ring-opening polymerization / Metathesis

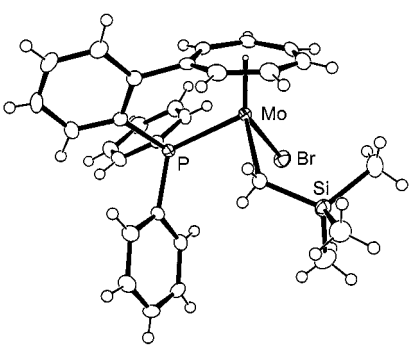

929 **N. Wiberg,* T. Blank, H. Nöth, M. Suter, M. Warchhold**

Octagallane $(t\mathrm{Bu_3Si})_6\mathrm{Ga_8}$ and Its Reduction to $(t\mathrm{Bu_3Si})_6\mathrm{Ga_8}^{2-}$ − On the Existence of Isomeric Gallium Clusters

Keywords: Clusters / Gallium / Isomers / Silicon

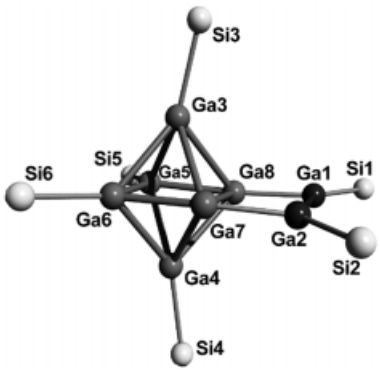

935 **J.-L. Fillaut,* I. de los Rios, D. Masi, A. Romerosa, F. Zanobini, M. Peruzzini***

Synthesis and Structural Characterization of (Carbene)ruthenium Complexes Binding Nucleobases

Keywords: Carbenes / Ruthenium / Adenine / Uracil / X-ray crystallography / Aminophosphanes

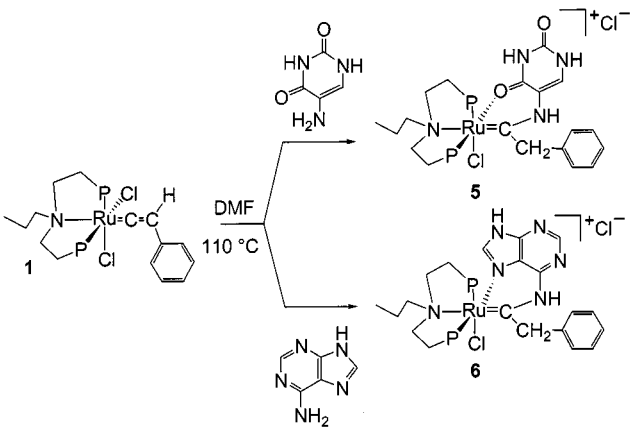

943 **P. S. Mukherjee, T. K. Maji, A. Escuer,* R. Vicente, J. Ribas, G. Rosair, F. A. Mautner, N. R. Chaudhuri***

Three Novel End-to-End Single Azido-Bridged Ferromagnetic Copper(II) Chains: Synthesis, Crystal Structure, and Magnetic Behavior

Keywords: Copper / N ligands / Azido bridge / Magnetic properties

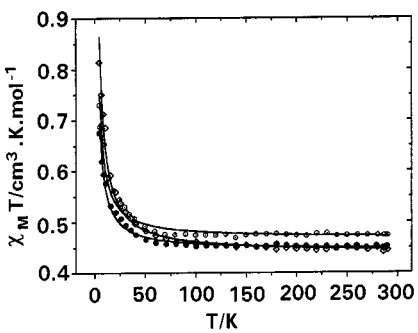

950 **N. C. Mösch-Zanetti,* M. Ferbinteanu, J. Magull**

A New μ_4-Oxo Tetranuclear Magnesium Compound: Coordination Effects of the Azolato Ligands

Keywords: N ligands / Magnesium / Coordination modes

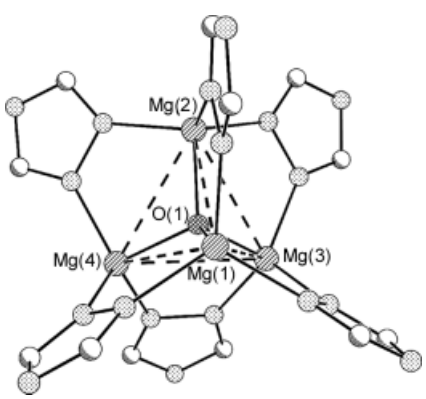

957 **R. Streubel,* N. Hoffmann, H.-M. Schiebel, F. Ruthe, P. G. Jones**

Synthesis of the First 2*H*-1,2-Azaphosphole Complexes with P,C and P,N Ylide Functional Groups

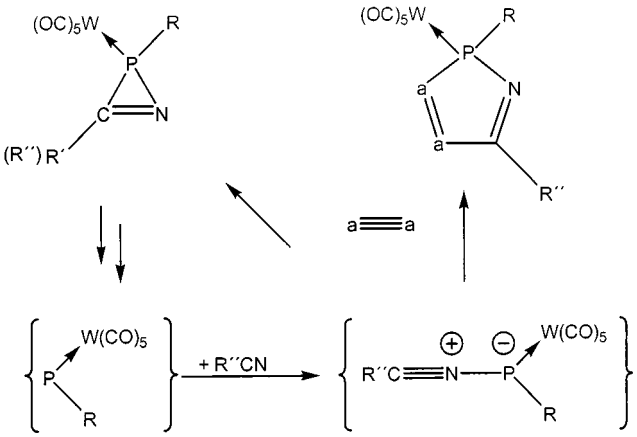

Keywords: Ylides / Phosphorus heterocycles / Tungsten / Cyclization

968 **B. M. Alzoubi, M. S. A. Hamza, C. Dücker-Benfer, R. van Eldik***

Equilibrium, Kinetic and Leaving Group Effect Studies on Ligand Substitution Reactions of a Simple Model for Coenzyme B_{12}

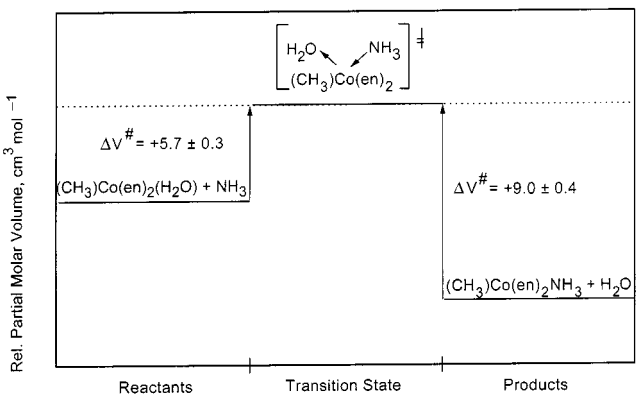

Keywords: Enzyme models / Equilibrium / Kinetics / Ligand effects / Leaving group effect / Volume profile

975 **L. Ruhlmann, L. Nadjo,* J. Canny, R. Contant, R. Thouvenot***

Di- and Tetranuclear Dawson-Derived Sandwich Complexes: Synthesis, Spectroscopic Characterization, and Electrochemical Behavior

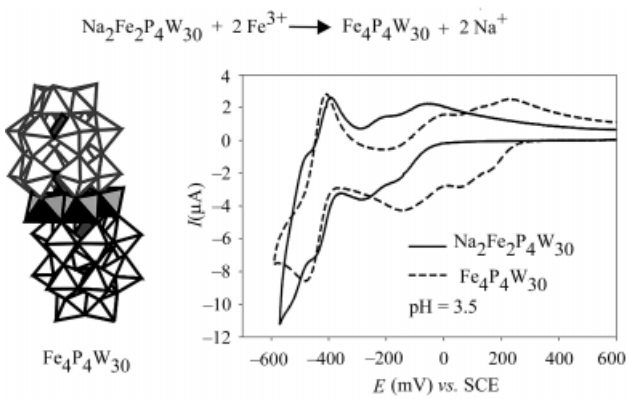

Keywords: Polyoxometalates / Sandwich complexes / Synthesis / NMR spectroscopy / Electrochemistry

987 **V. Fusi,* A. Llobet,* J. Mahia, M. Micheloni, P. Paoli, X. Ribas, P. Rossi**

A New Cu^{I} Complex that Mimics the Cresolase Reaction of Tyrosinase and the Crystal Structure of its Oxygenated Cu^{II} Complex

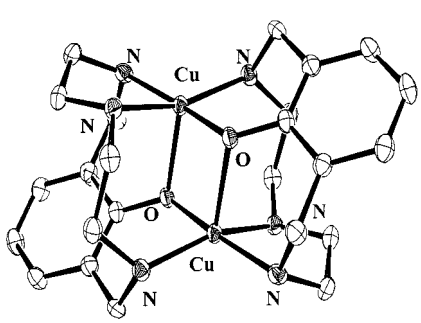

Keywords: Bioinorganic chemistry / Copper / Macrocyclic ligands / O-O activation / Tyrosinase

Electrophilic Half-Sandwich (Carbene)metal (Metal = Fe, Ru, Os) Complexes: Recent Developments in Synthesis and Applications

Véronique Guerchais[a]

Keywords: Carbene complexes / Catalysis / C−C bond formation / Diazo compounds

This review covers synthetic and structural aspects of electrophilic half-sandwich (carbene)metal complexes of Group-8 metals as well as the use of these complexes in transformations of organic molecules. These species, including chelate complexes, are involved in C–C bond-forming reactions in stoichiometric or catalytic processes.

Contents

1. Introduction
2. Preparation and Structural Characterisation
2.1. Iron Complexes
2.2. Ruthenium and Osmium Complexes
2.3. Conformational and Structural Features
3. Reactivity of Carbene Complexes in Stoichiometric Reactions
3.1. Chelated Carbene Complexes: Bond Activation and Formation Reactions
3.2. Transient Carbene Species: Cyclopropanation and Intramolecular C−H Insertion Reactions
4. Carbene Complexes as Intermediates in Catalysis
4.1. Oxidative Cycloisomerisation of Homopropargyl Alcohols
4.2. Reactions Involving Diazo Compounds
5. Concluding Remarks

1. Introduction

The chemistry of electrophilic (carbene)metal complexes is an area of current interest because of the wide applications in organic synthesis.[1,2] Their potential to mediate novel C−C bond-forming reactions has generated the development of new synthetic methodologies. In this context, the (carbene)ruthenium complexes, that are highly active metathesis catalysts able to generate polymeric materials and five-, six-, seven-, and eight-membered carbocycles or heterocycles, have seen rapid developments.[3] In addition, (carbene)metal complexes attract considerable attention since they offer the possibility of the development of new types of organometallic intermediates that may have unusual reactivity.

This review deals with electrophilic half-sandwich complexes of iron, ruthenium, and osmium containing the C_5R_5 (R = H, Me, Ph), $C_9H_4R_3$ (R = H, Me), or Tp [Tp = hydrotris(pyrazolyl)borate] ligand and covers the literature from January 1995 up to June 2001. We will focus our attention on the synthesis, the structural features, and the role of these carbene complexes in C−C bond-forming reactions. The discussion will emphasise our ongoing research on chelate (carbene)iron derivatives that are involved in bond-activation reactions. We are interested in investigating the chemistry of electrophilic (carbene)iron complexes containing a labile or hemi-labile ligand. The presence of a potential vacant coordination site allows the introduction of a substrate capable of reacting with the carbene ligand within the coordination sphere of the metal centre. Finally,

[a] Institut de Chimie de Rennes, UMR 6509 CNRS-Université de Rennes 1 "Organométalliques et Catalyse",
Campus de Beaulieu, 35042 Rennes Cedex, France

Véronique Guerchais is a CNRS researcher at the Institut de Chimie de Rennes, unit "Organometallics and Catalysis". She received her PhD under the supervision of Prof. D. Astruc on "electron reservoir" complexes. She carried out postdoctoral studies on the activation of alkynes at diruthenium centres at the University of Bristol (U. K.) with Prof. S. A. R. Knox. Her current research interests are focused on iron complexes, including carbene species, for bond activation and C−C bond formation.

MICROREVIEWS: This feature introduces the readers to the authors' research through a concise overview of the selected topic. Reference to important work from others in the field is included.

we will describe the catalytic reactions of (carbene)-ruthenium complexes.[4] Cyclopentadienyl complexes $[Ru(C_5R_5)(L)_2Cl]$ and related species were found to be effective catalyst precursors in C−C coupling reactions involving diazo compounds,[5] including insertion, carbene dimerisation, and carbene transfer reactions to alkenes and alkynes.

2. Preparation and Structural Characterisation

2.1. Iron Complexes

The reaction of an acyl complex with an electrophile is a common route to alkoxycarbene complexes of iron $[Fe(C_5R_5)(CO)_2\{C(OR^2)R^1\}]^+$ (R = H, Me). The required alkyl- and aryl-substituted acyl derivatives $[Fe(C_5R_5)(CO)_2\{C(O)R^1\}]$ are in turn accessible by the reaction of the ferrate complex $[M][Fe(C_5R_5)(CO)_2]$ (M = Na, K) with the appropriate acyl chloride.[6]

ortho-Substituted arylcarbene complexes are good precursors of chelate carbene species.[7] Thus, the cationic κ^2-(*C*,*X*) chelate complexes $[Fe(C_5R_5)(CO)\{C(OMe)C_6H_4$-*o*-$X\}(Fe-X)][OTf]$ (**3**) (R = Me; **a**: X = Cl; **b**: X = OMe)[7a] and **4** (R = H; X = OMe)[7b] are obtained upon irradiation of the corresponding dicarbonyl species in a non-coordinating solvent such as CH_2Cl_2 (Scheme 1). In contrast with the C_5Me_5 analogue, coordination of the chlorine atom of **2a** does not take place. When irradiation of **2a** is performed in CH_3CN, the stable acetonitrile complex $[Fe(C_5H_5)(CO)(CH_3CN)\{C(OMe)C_6H_4$-*o*-$Cl\}][OTf]$ (**5**) is obtained (Scheme 2). Substitution of one carbonyl ligand by PPh_3 allows the isolation of the κ^2-(*C*,*Cl*) chelated derivative **6** (Scheme 2).[7b] The phosphane ligand has the same effect on the nature of the product as the permethylation of the C_5 ring. The formation of the chelate structure can easily be established by ^{13}C NMR spectroscopy. The signal of the aryl carbon atom which bears the heteroatom is shifted downfield upon coordination of the *ortho* substituent X. There is a marked shift difference of 20 ppm in both the C_5H_5 and C_5Me_5 series, in agreement with a decrease in electronic density. The chlorine and the oxygen atoms act as neutral two-electron donor ligands allowing the formation of a five-membered metallacycle. This has been confirmed by the crystallographic analyses of **3a** and **4**.

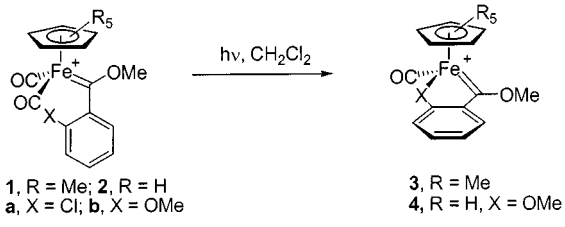

Scheme 1. Synthesis of chelate arylcarbene complexes

The neutral iodo derivatives **7a**,**b** are obtained on treating **3a**,**b** with $[nBu_4N][I]$, due to the lability of the chelating group X (Scheme 3). In contrast with the dicarbonyl species, the competitive *O*-demethylation reaction that leads to the acyl complex and methyl iodide does not take place.[8]

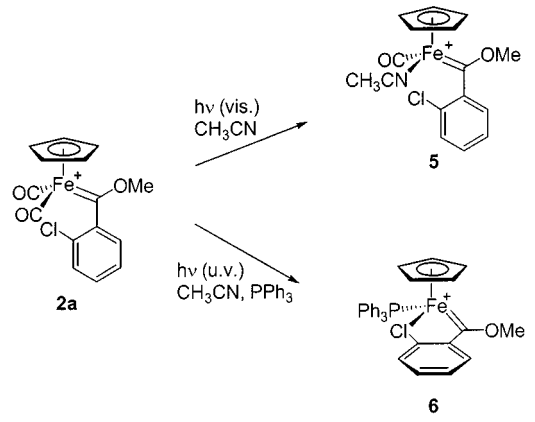

Scheme 2. Synthesis of (chloroaryl)carbene complexes containing a labile or hemi-labile ligand

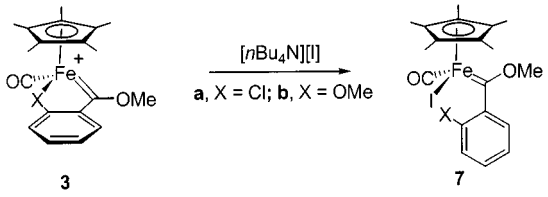

Scheme 3. Synthesis of iodo carbene complexes **7**

Carbene complexes containing two labile ligands can also be obtained. For example, UV irradiation of **3a** gives **8**, and then addition of dppm [dppm = bis(diphenylphosphanyl)-methane] provides **9** (Scheme 4).

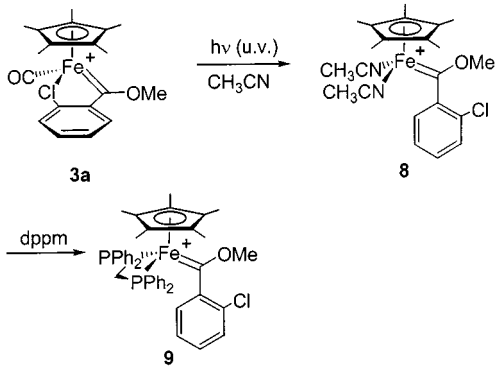

Scheme 4. Ligand exchange reactions of **3a**

The presence of a labile or hemi-labile ligand in carbene complexes **4** and **5** allows the chelation of the C−C double bond of an allyloxy group, and the chelate (allyloxy)carbene complexes **10** and **11** are thus accessible (Scheme 5).[9] They are prepared in a two-step one pot procedure, by treating **4** or **5** with the appropriate allyl oxide followed by protonation. This sequence conveniently gives access to various substituted complexes. The iron moiety, which is sterically not encumbered, is able to coordinate a di- and trisubstituted C−C double bond. We found that this preparation

requires pre-coordination of the allyloxy group, otherwise the synthesis fails.

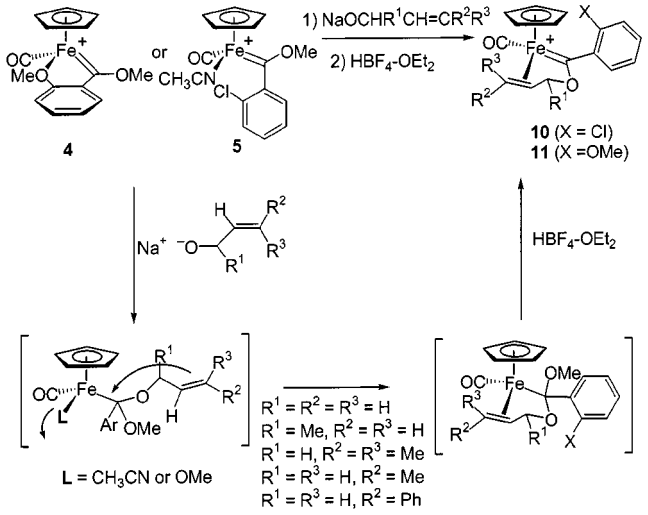

Scheme 5. Synthesis of chelate (allyloxy)carbene complexes **10** and **11**

The preparation of the alkynyl-substituted acyl complexes **12** has been achieved by using mixed anhydrides [*i*PrCH$_2$OC(O)OC(O)C≡CR] (Scheme 6).[10] Compounds **12** are obtained in high yields and can be converted into the respective methoxy- and aminocarbene complexes **13** and **14** (Scheme 6). Some of the methoxycarbene complexes **13** undergo a Michael-type addition of aniline at room temperature to give the (2-aminoethenyl)methoxycarbene complexes **15** (Scheme 7).[10d]

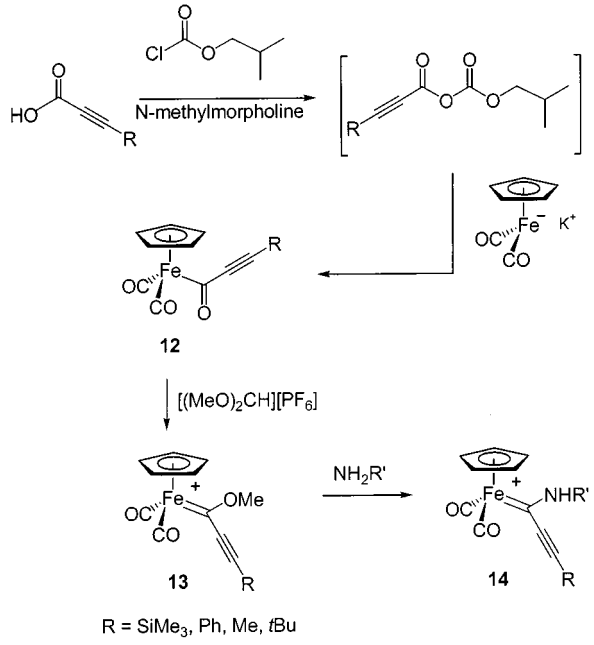

Scheme 6. Synthesis of (alkynyl)acyl complexes and the corresponding methoxy- and aminocarbene complexes

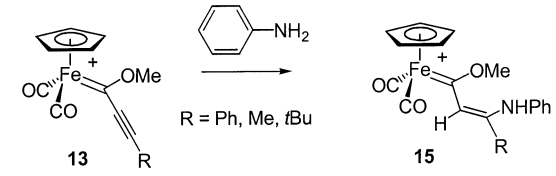

Scheme 7. Synthesis of (2-aminoethenyl)methoxycarbene complexes **15**

We have found that the activation of propargylic alcohols by [Fe(C$_5$Me$_5$)(CO)$_2$(H$_2$O)][BF$_4$] in the presence of methanol leads to the isolation of the α,β-unsaturated acyl complexes **16** or the Michael adducts **17** (Scheme 8).[11] The expected methoxycarbene complexes [Fe(C$_5$Me$_5$)(CO)$_2${=C(OMe)CH=CR^{1}R^2}] (**18**) are not obtained directly, and *O*-alkylation of **16** or **17** with methyl triflate generates **18**. This may be due to a spontaneous demethylation reaction of methoxycarbene complexes in solution, a feature already described.[8]

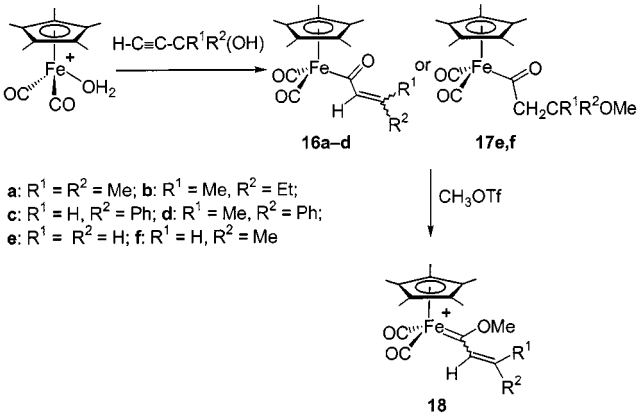

Scheme 8. Synthesis of (alkenyl)carbene complexes **18** by activation of propargylic alcohols

Alkylation of formyl transition metal complexes constitutes a route to secondary alkoxycarbene complexes. Thus, methylation of the stable formyl complex [Fe(C$_5$Ph$_5$)(CO)(PMe$_3$)(CHO)] and addition of [NH$_4$][PF$_6$] afford the secondary methoxycarbene complex [Fe(C$_5$Ph$_5$)(CO)(PMe$_3$)(=CHOMe)][PF$_6$] in high yield.[12]

Dinuclear bis(carbene) complexes have been synthesised from mononuclear species through a carbon−carbon ligand coupling.[13] The 18-electron (vinyl)iron(II) derivatives **19** undergo oxidative coupling via 17-electron **19**$^+$ (Fe^{III}) to produce [μ-bis(methoxycarbene) or μ-bis(ethylidene)]diiron

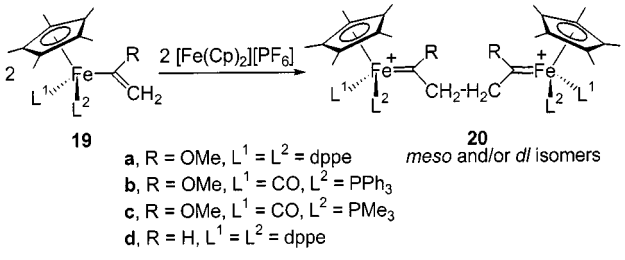

Scheme 9. Synthesis of bridged bis(carbene) complexes

complexes **20** in good yields (Scheme 9). The coupling reaction is sensitive to steric effects of the ancillary ligands at the metal centre, and the *meso* and *dl* couples of the bis(carbene) dimers are formed with good diastereoselectivities.

The dinuclear butadienediyl-bridged bis(carbene) complex **21** is then accessible through deprotonation of **20a**, followed by a two-electron oxidation with 2 equiv. of ferricenium (Scheme 10).[14] Complex **21** is diamagnetic in solution. However, variable-temperature Mössbauer spectroscopy allows the observation of the singlet and triplet spin isomers and their interconversion (Scheme 11).[14,15]

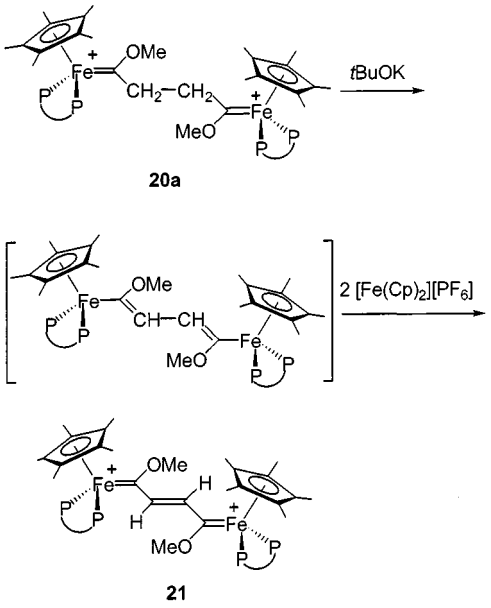

Scheme 10. Synthesis of the butadienediyl-bridged bis(carbene) complex **21**

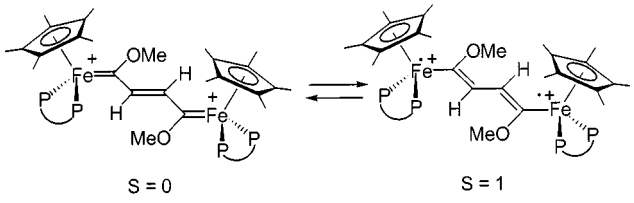

Scheme 11. Interconversion of the singlet and triplet spin isomers of **21**

2.2. Ruthenium and Osmium Complexes

(Carbene)ruthenium complexes are accessible from vinylidene and allenylidene precursors but the formation of the carbene ligand depends on both the ligand sphere of the metal centre and on the nature of the substituents of the unsaturated ligand.[16]

For instance, the methoxycarbene complex [Ru(Tp)(dippe){=C(OMe)CH_2CO_2Me}][BPh_4] (**22**) [dippe = bis(diisopropylphosphane)ethane] is formed by the addition of MeOH to the corresponding vinylidene complex [Ru(Tp)(dippe)(=C=$CHCO_2$Me)][BPh_4].[17] Similar alkoxycarbene complexes have not been obtained from [Ru(Tp)(dippe)(=C=CHR)][BPh_4] when R is different from CO_2Me. Complex [Ru(Tp)(Haapy)(Cl)] (Haapy = 2-acetamido-4-methylpyridine) reacts with HC≡CR to give the cyclic amidocarbene complexes [Ru(Tp)(Cl)(=CCH_2R-aapy)] (**23**) (**a**: R = Ph; **b**: R = *n*Bu).[18] The formation of **23** presumably proceeds via vinylidene intermediates. Although such intermediates could not be isolated or detected spectroscopically, such a process would be facile when the nucleophilic attack occurs in an intramolecular, chelate-assisted fashion. This can explain the addition of the weakly nucleophilic nitrogen atom of the amide. Similarly, addition of allyl alcohol to terminal alkynes mediated by [Ru(Tp)$(dmso)_2$(Cl)] gives the (allyloxy)carbene complexes **24** (Scheme 12).[19]

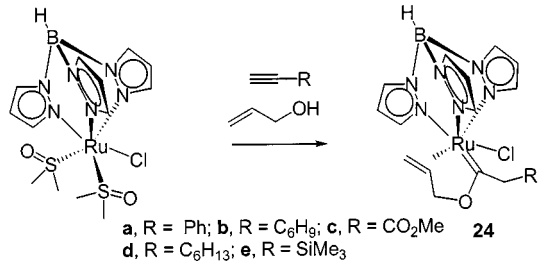

Scheme 12. Synthesis of (allyloxy)carbene complexes **24**

Addition of nucleophiles to allenylidene complexes is a general route to Fischer-type α,β-unsaturated carbene complexes of ruthenium. The reactivity of allenylidene complexes has recently been reviewed.[20] For example, the addition of methanol or ethanol to the trimethylindenyl complex [Ru(η^5-1,2,3-$Me_3C_9H_4$)(L^1)(L^2){=C=C=CPh_2}][BF_4] (L^1 = CO and L^2 = PPh_3, P*i*Pr_3, PCy_3) takes place to afford the corresponding alkoxy derivatives **25** (Scheme 13).[20,21] Unstable allenylidene derivatives can be trapped in situ by methanol, and this allows the complexes [Ru(η^5-C_9H_7)(L^1)(L^2){=C(OMe)−CH=CHR}][PF_6] (R = Ph, L^1 = L^2 = dppe, dppm; R = H, L^1 = L^2 = dppm) to be isolated.[22] By contrast, the bis(triphenylphosphane)-substituted carbene derivatives are not formed, presumably because the PPh_3 ligands offer a steric protection of the allenylidene group towards nucleophilic addition.

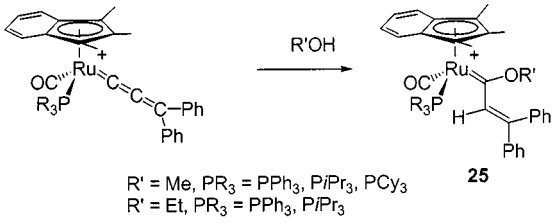

Scheme 13. Synthesis of alkoxy(alkenyl)carbene complexes **25**

The acetone complex [Ru(C_5H_5)(CO)(P*i*Pr_3){OC-$(CH_3)_2$}][BF_4] reacts with 1,1-diphenyl-2-propyn-1-ol to afford the allenylidene derivative [Ru(C_5H_5)(CO)(P*i*Pr_3){C=C=CPh_2}][BF_4] (**26**) which adds water, alcohols, and thiols, at the $C_\alpha-C_\beta$ double bond of the allenylidene group to afford diphenyl-α,β-unsaturated-hydroxycarbene, -alkoxycar-

bene, and -(alkylthio)carbene complexes, respectively.[23] Complex **26** reacts with alcohols such as allyl alcohol (without pre-coordination of the olefinic moiety) and propargyl alcohol affording $[Ru(C_5H_5)(CO)(P\mathit{i}Pr_3)\{C(OCH_2CH{=}CH_2)CH{=}CPh_2\}][BF_4]$ (**27**)[24] and $[Ru(C_5H_5)(CO)(P\mathit{i}Pr_3)\{C(OCH_2C{\equiv}CH)CH{=}CPh_2\}][BF_4]$ (**28**),[25] respectively. Treatment of **26** with secondary and primary amines affords azoniabutadienyl derivatives $[Ru(C_5H_5)(CO)(P\mathit{i}Pr_3)\{C(CH{=}CPh_2){=}NR^1R^2\}][BF_4]$ (**29**).[26] Addition of ethyl diazoacetate to **26** affords the cyclic carbene complex $[Ru(C_5H_5)(CO)(P\mathit{i}Pr_3)\{{=}[-CCH{=}C(OEt)-O-C(=CPh_2)-]\}][BF_4]$ (**30**), which results from a formal 1,3-addition of the organic reagent at the $C_\alpha-C_\beta$ double bond (Scheme 14).[27]

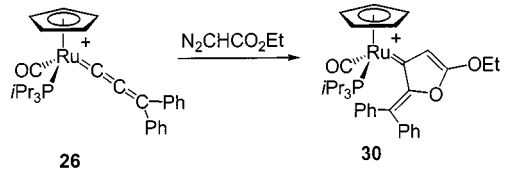

Scheme 14. Synthesis of the cyclic carbene complex **30**

The common approach to cyclic Fischer-type carbene complexes is the metal-assisted cycloisomerisation of ω-alkynols to oxacycloalkylidenes.[28] Such a reaction has been used for the preparation of $[Ru(C_5Me_5)(\kappa^1\text{-DPVP})_2\{{=}C^a(CH_2)_3O(C^a{-}O)\}][PF_6]$ (DPVP = diphenylvinylphosphane) starting from $[Ru(C_5Me_5)(\kappa^1\text{-DPVP})(\kappa^3\text{-DPVP})][PF_6]$.[29] In contrast, the formation of $[Ru(C_5Me_5)(\kappa^3\text{-ADPP})\{{=}C^a(CH_2)_3O(C^a{-}O)\}][PF_6]$ (**32**) (ADPP = allyldiphenylphosphane) from $[Ru(C_5Me_5)(\kappa^1\text{-ADPP})(\kappa^3\text{-ADPP})][PF_6]$ is accompanied by the loss of one phosphane ligand (Scheme 15).[30]

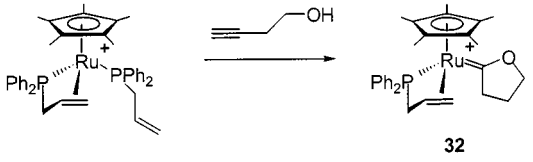

Scheme 15. Synthesis of cyclic oxycarbene complex **32**

The synthesis of (alkenyl)carbene complexes **33** has been achieved by protonation of the readily available (vinyl)alkenyl derivatives $[Ru(\eta^5\text{-}C_9H_7)(dppm)\{CHCH{=}CR^1R^2\}]$ (Scheme 16).[31] The formation of these α,β-unsaturated alkylidene complexes proceeds through regioselective protonation at either the C_γ or C_δ atom revealing the high electron density on these positions of the vinylalkenyl ligand.

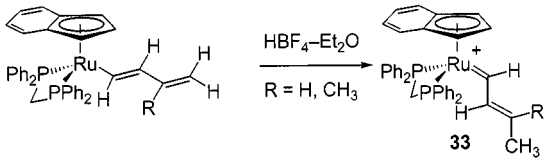

Scheme 16. Synthesis of vinylcarbene complexes **33**

(Allyl)carbene complexes are accessible through alkyne coupling reactions. The labile complexes $[Ru(C_5H_5)(PR_3)(CH_3CN)_2][PF_6]$ (**37**) (R = Me, Ph, Cy) react with alkynes HC≡CR′ and 1,6-heptadiyne to afford the (allyl)carbene complexes **38** and $[Ru(C_5H_5)\{{=}CH\text{-}\kappa^3\text{-}C(CH_2)_3CCHPR_3\}][PF_6]$ in high yields.[32] For the substituted derivatives, the substituents are exclusively in the 1- and 3-positions (Scheme 17).

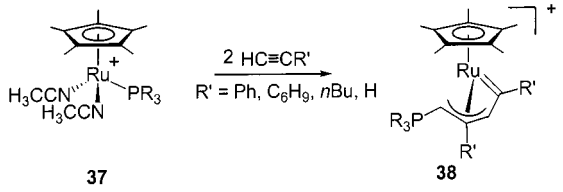

Scheme 17. Synthesis of the (allyl)carbene complexes **38** from **37**

A possible mechanism may involve a metallacyclopentatriene intermediate, from which subsequent migration of the phosphane to one of the electrophilic carbene carbon atoms occurs to give the observed carbene complex. This proposal is supported by the formation of **40** by treating the isolated ruthenacyclopentatriene **39** with PMe_3.[33] Addition of the phosphane occurs at the electrophilic α-carbon atom. Note that the substituents of **40** are located on the 1,4-positions due to a head-to-head coupling of the alkynes (Scheme 18). The ruthenacyclopentatriene complexes are prepared from $[Ru(C_5Me_5)(Cl)(TMEDA)]$ [34] or $[Ru(C_5Me_5)(cod)(Cl)]$ [33] in the presence of alkynes.

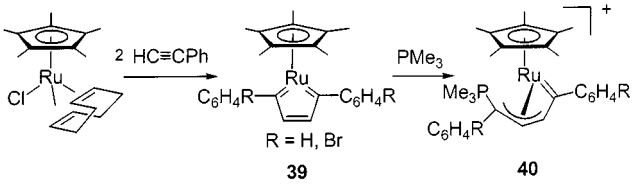

Scheme 18. Synthesis of (allyl)carbene complex **40** via **39**

The complex $[Ru(Tp)(PCy_3)(Cl)(=CHPh)]$ (**41**) has been synthesised by the reaction of $[Ru(PCy_3)_2(Cl)_2(=CHPh)]$ and KTp (Scheme 19).[35] The cationic species **42** are then obtained by treatment of **41** with $AgBF_4$ or $AgSbF_6$ in the presence of various coordinating solvents L (L = H_2O, CH_3CN, pyridine).

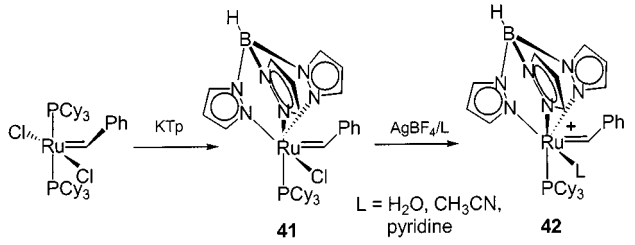

Scheme 19. Synthesis of benzylidene complexes **41** and **42**

The synthesis of alkoxycarbenes **43** from an acetal derivative has been described.[36] Heating the acetal complexes

$[Ru(C_5H_5)(CH_3CN)_2\{\kappa^1\text{-}Ph_2PCH(OR)_2C_6H_4\}][OTf]$ (R = Me, Et) at 60−95 °C results in loss of one CH_3CN ligand and the alcohol ROH resulting from C−O bond cleavage, leading to carbene complex **43** in high yield (Scheme 20).

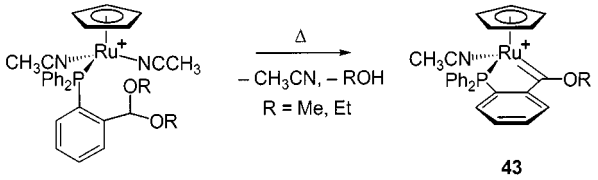

Scheme 20. Synthesis of alkoxycarbene complexes **43** from an acetal derivative

The diarylcarbene complexes $[Ru(C_5H_5)(PPh_3)(Cl)(=CRR')]$ (**45**) (**a**: R = Ph, R′= Ph; **b**: R = Ph, R′= *p*-C_6H_4Me; **c**: R = *p*-C_6H_4Cl, R′= *p*-C_6H_4Cl; **d**: R = *p*-C_6H_4OMe, R′= *p*-C_6H_4OMe) can be readily prepared by reaction of the acetato complex $[Ru(C_5H_5)(\kappa^2\text{-}O_2CMe)(PPh_3)]$ (**44**) with diaryldiazomethanes N_2CRR', followed by treatment with Et_3NHCl (Scheme 21).[37]

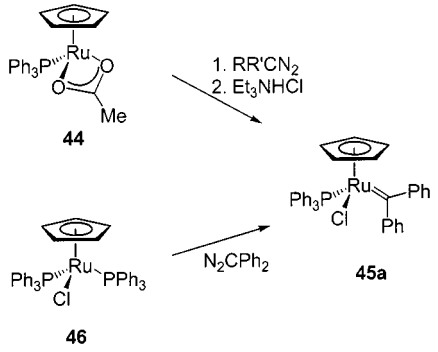

Scheme 21. Synthesis of the (diphenylcarbene)Ru complex **45a**

Complex **45a** is also obtained from $[Ru(C_5H_5)(PPh_3)_2(Cl)]$ (**46**) by direct reaction with diphenyldiazomethane. The dissociation of one triphenylphosphane ligand from **46** occurs at 65 °C in a non-polar solvent such as toluene (Scheme 21).[38] An excess of N_2CPh_2 has to be added during the reaction to obtain complete conversion of **46** into **45a**, because of the slow decomposition of N_2CPh_2. Similarly, facile displacement of one phosphane ligand in $[Ru(C_5H_5)\{PPh_2(2\text{-}MeC_6H_4)\}_2(Cl)]$ leads to the formation of $[Ru(C_5H_5)\{PPh_2(2\text{-}MeC_6H_4)\}(Cl)(=CPh_2)]$.[38] The (methyl-substituted aryl)phosphane appears to be more weakly bound to the ruthenium centre compared to PPh_3 and therefore more prone to dissociation. Complex **46** is also a good precursor for the aminocarbene complex $[Ru(C_5H_5)(PPh_3)_2(=CNHPh-CH_2Ph)]$ via the vinylidene complex $[Ru(C_5H_5)(PPh_3)_2(=C=CHPh)]$[40] by addition of benzylamine.[39]

Well-characterised examples of methylidene complexes remain relatively rare. One example has recently been described; complex **48** is obtained by treatment of the osmium hydride **47** with 2 equiv. of methyl triflate (Scheme 22).[41] The mechanism depicted in Scheme 23 is proposed to account for the formation of **48**. Methylation of the hydride precursor **47** generates the methyl/hydride intermediate, which then undergoes reductive elimination of methane. Attack of a second molecule of methyl triflate would give a methyl dication that provides **48** by loss of a proton.

Scheme 22. Synthesis of the (methylidene)osmium complex **48**

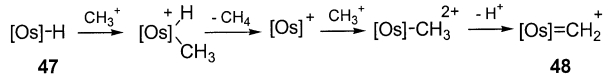

Scheme 23. Proposed mechanism for the formation of **48**

2.3. Conformational and Structural Features

Table 1 lists the M=C and C−X (X = O, N) bond lengths of structurally characterised (carbene)metal complexes (M = Fe, Ru, Os). These piano-stool complexes adopt a classical pseudo-octahedral geometry around the metal centre. The carbene ligand of such piano-stool complexes is generally oriented perpendicular to the plane of the C_5 ligand, the so-called "upright" conformation. This is for example the case for the ethylidene complex $[Fe(C_5Me_5)(dppe)(=CHMe)][CF_3SO_3]$ (**49**) in which the hydrogen atom is directed towards the C_5 ring.[13] The aminocarbene complex **14a** was found to exist in an "upright" conformation, whereas the related derivative **14b** shows an "orthogonal" conformation.[10b] Moreover, it has been shown that **14a** and **14b** exist in the solid state as *anti* isomers with respect to the C−N bond.

In solution, dynamic studies show that the arylcarbene complex **50** exists as two isomers in solution at −80 °C. Since the rotation around the Fe−C_α bond usually cannot be frozen out in such complexes, this feature most likely arises from restricted rotation about the C_α−C_{ipso} bond. Therefore, these two geometric isomers differ from each other in the orientation of the anisyl group [$\Delta G^{\ddagger}$ = 9.7 kcal·mol^{-1}, T_C(300 MHz) = 211 K].[7a] The conformation in which the aryl group is aligned with the Fe−C_α−C_{ipso} plane (rotamer **A**) provides the better electronic delocalisation of the positive charge (Scheme 24). On the basis of the NMR spectroscopic data of the carbonyl ligands, we assume that conformation **B** is preferred for the methoxycarbene derivatives **1**, **2**, and **9**; steric interactions appear to govern the carbene conformation. A twisted orientation of the carbene ligand is expected for the unsymmetrically substituted carbene complex **2a**.

X-ray structures of (alkylidene)iron complexes are scarce. The only complex that has been structurally characterised is the ethylidene complex **49**. The Fe−C_α bond length [1.787(8) Å] reflects the double-bond character of the iron−carbon bond.[13] The Fe−C bond lengths of het-

Table 1. Selected bond lengths [Å] of (carbene)metal complexes (M = Fe, Ru, Os)

Complex	$M-C_{carbene}$	$C_\alpha-X$ (X = O, N)	Ref.
$[Fe(C_5Me_5)(CO)(\kappa^2\text{-}C(OMe)\text{-}o\text{-}C_6H_4Cl][OTf]$ (**3a**)	1.857(6)	1.304(7)	[7a]
$[Fe(C_5H_5)(CO)\{\kappa^2\text{-}C(OMe)\text{-}o\text{-}C_6H_4OMe\}][OTf]$ (**4**)[a]	1.859(6)	1.299(7)	[7b]
	1.879(5)	1.303(6)	
	1.870(5)	1.299(7)	
$[Fe(C_5H_5)(CO)\{\kappa^3\text{-}C(OCH_2CH{=}CMe_2)\text{-}o\text{-}C_6H_4Cl\}][BF_4]$ (**10c**)	1.828(11)	1.344(14)	[51]
$[Fe(C_5H_5)(CO)_2\{C(OMe)CH{=}CRNHR'\}][PF_6]$ (**15**)			[10d]
a: R = Me, R′ = $CH(CH_3)CO_2tBu$	1.961(7)	1.361(10)	
b: R = *t*Bu, R′ = Ph	1.968(6)	1.336(7)	
c: R = Me, R′ = Ph	1.960(4)	1.323(5)	
$[Fe(C_5H_5)(CO)_2\{C(NHR')C{\equiv}CR\}][PF_6]$ (**14**)			[10b]
a: R = $SiMe_3$, R′ = C_6H_5	1.928(4)	1.305(6)	
b: R = $SiMe_3$, R′ = $p\text{-}C_6H_5CH_3$	1.940(5)	1.303(6)	
$[Fe(C_5Me_5)(dppe)(=CHMe)][OTf]$ (**49**)	1.787(8)		[13]
$[Ru(C_5H_5)(CO)(PiPr_3)\{C(OCH_2C{\equiv}CH)CH{=}CPh_2\}][BF_4]$ (**28**)	1.965(4)	1.321(4)	[25]
$[Ru(C_5H_5)(CO)(PiPr_3)(C{=}CH{=}(OEt)OC{=}CPh_2)][BF_4]$ (**30**)	2.017(6)		[27]
$[Ru(C_5H_5)(CO)(PiPr_3)(C{=}CH{=}(Me)OC{=}CPh_2)][BF_4]$ (**31**)	2.010(6)		[27]
$[Ru(C_5Me_5)(\kappa^3\text{-}ADPP)\{{=}C(CH_2)_3O\}][PF_6]$ (**32**)	1.956(4)		[29]
$[Ru(Tp)(dippe)\{{=}C(OMe)CH_2CO_2Me\}][BPh_4]$ (**22**)	1.86(2)	1.43(2)	[17]
$[Ru(Tp)(Cl)\{{=}CCH_2Ph(aapy)]$ (**23a**)	1.897 2)	1.387(3)	[18]
$[Ru(Tp)(Cl)\{\kappa^3\text{-}C(OCH_2CH{=}CH_2)(CH_2Hex)]$ (**24d**)	1.928(2)	1.329(3)	[19]
$[Ru(Tp)(Cl)\{\kappa^3\text{-}C(OCH_2CH{=}CH_2)(CH_2SiMe_3)]$ (**24e**)	1.918(7)	1.331(8)	[19]
$[Ru(Tp)(PCy_3)_2(H_2O)(=CHPh)][BF_4]$ (**42**)	1.878(4)		[35]
$[Ru(C_5H_5)\{{=}CH\text{-}\kappa^3\text{-}C(CH_2)_3CCHPMe_3\}][PF_6]$ (**38**)	1.897(2)		[32]
$[Ru(C_5H_5)\{{=}C(C_6H_5)\text{-}\kappa^3\text{-}CHCHC(C_6H_5)PMe_3\}][PF_6]$ (**40**)	1.934(3)		[33]
$[Ru(C_5H_5)\{{=}C(p\text{-}C_6H_4Br)\text{-}\kappa^3\text{-}CHCHC(pC_6H_4Br)P(OMe_3\}][PF_6]$	1.928(2)		[33]
$[Os(C_5Me_5)(dppm)(=CH_2)]$ (**48**)	1.926(9)		[41]

[a] Three independent molecules per unit cell.

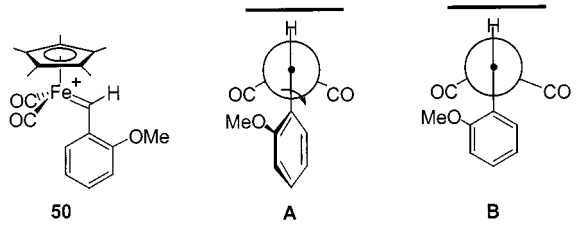

Scheme 24. Conformers of complex **50**

eroatom-stabilised carbene complexes are typically in the range 1.83−1.97 Å. We can note that the Fe−C bond lengths are shorter in the case of chelated structures (Table 1, complexes **3a** and **4**). The $C_{carbene}-O$ bond length ranges from 1.30 to 1.36 Å. In the case of chelated complexes, the C−O bond lengths are shortened. Similarly, the C−N bond lengths of aminocarbene complexes of iron reflect the π-bonding between the amino substituent and the carbene carbon atom.

The chelate κ^2-(*C*,*Cl*) complex **3a** is characterised by an Fe−Cl bond length of 2.310(2) Å.[7a] The Fe−O bonds [2.045(5), 2.043(4), 2.043(4) Å, three independent molecules][7b] in κ^2-(*C*,*O*) complex **4** are similar to those found for other oxygen-containing iron complexes,[42] such as $[Fe(C_5Me_5)(dppe)(O{=}CMe_2)][OTf]$[42a] [2.031(4) Å] and $[Fe(C_5Me_4Et)(CO)_2(H_2O)][BF_4]$ [2.022(8), 2.043(9) Å, two independent molecules].[42c]

For ruthenium complexes, the bond lengths Ru−C(carbene) are typically in the range 1.90−1.97 Å. The $Ru-C_\alpha$ bond length in **22** is rather short,[17] compared with that of other (alkoxycarbene)Ru complexes, and found to be even shorter than that of the benzylidene complex **42**.[35] The longest bond length was found in the cyclic carbene complexes $[Ru(C_5H_5)(CO)(PiPr_3)\{{=}C^aCH{=}C(R)\text{-}OC^b(=CPh_2)(C^\alpha\text{-}C^b)\}][BF_4]$ (R = OEt, Me),[27] for which the Ru−C bond order is between that of a single and double bond. This suggests a significant contribution of the alkenyl resonance form.

X-ray diffraction studies and calculations on $[Ru(C_5H_5)(CO)(PiPr_3)\{C(CH{=}CPh_2){=}NEt_2\}][BF_4]$ (**29a**) show that the contribution of the carbene form is not relevant.[26] The $Ru-C_\alpha$ [2.063(6) Å] and the $C_\alpha-N$ [1.306(7) Å] bond lengths correspond rather to an Ru−C single bond and a C=N double bond, respectively. Complexes **29** can be considered as azoniabutadienyl rather than carbene complexes.

3. Reactivity of Carbene Complexes in Stoichiometric Reactions

3.1. Chelated Carbene Complexes: Bond-Activation and -Formation Reactions

Hemilabile ligands in carbene complexes may stabilize reactive intermediates or influence catalytic activity. For instance, the importance of chelated carbene complexes has been pointed out for diastereoselective cyclopropanation reactions of electronically neutral alkenes with chromium

complexes.[43] The chelate isopropoxy derivative $[Ru(Cl)_2(PCy_3)(\kappa^2\text{-CH-}o\text{-}C_6H_4OiPr)]$ was found to be efficient in Ring Closing Metatheses (RCM) reactions for the formation of five- to eight-membered carbo- and heterocycles and it can be recovered through simple chromatography in high yield.[44] The importance of the chelated structure was also found for arylcarbene complexes **3a**,**b** which are involved in bond-activation and -formation reactions.

Nucleophilic attack of Lewis bases at the halocarbon atom gives rise to substitution reactions.[45] However, addition of stabilized carbanions $NaCH(CO_2Me)(COR)$ (R = OMe, Me) to **3a** affords oxametallacycles **51** (Scheme 25).[46] The substitution of the chlorine atom does not take place in these cases. The formation of **51** results from an α-attack by the nucleophile to give the C−C-bonded adduct, followed by displacement of the chlorine ligand by the coordinating carbonyl group to form a new five-membered ring. Eventually, spontaneous elimination of MeOH produces a more stable conjugated ring in the final product.

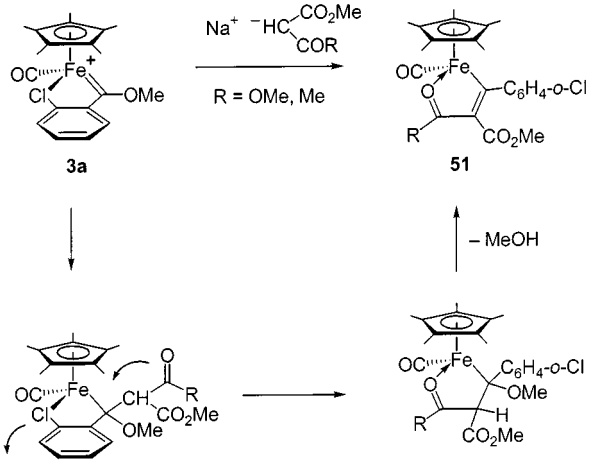

Scheme 25. Formation of oxametallacycles **51**

The chelated chloro derivative **3a** cleanly reacts with ethoxide or methoxide affording **52** which contains a chelated orthoester group (Scheme 26).[47] Similarly, complex **53** is formed upon treatment of **5** with EtONa (Scheme).[7b] The formation of **52**−**53** involves the cleavage of the Ar−Cl bond, which can be promoted by the coordination of the chlorine atom or the presence of a vacant coordination site. In contrast, the Ar−Cl bond cleavage does not occur for the dicarbonyl(carbene) complex **1a**. The reaction with RO^- affords the ketal derivatives $[Fe(C_5Me_5)(CO)_2\{C(OMe)(OR)(C_6H_4\text{-}o\text{-Cl}\}]$ by addition at the electrophilic carbene centre. Although the formation of an orthoester group from a carbene species has already been reported,[27] such a rearrangement process is without precedent.

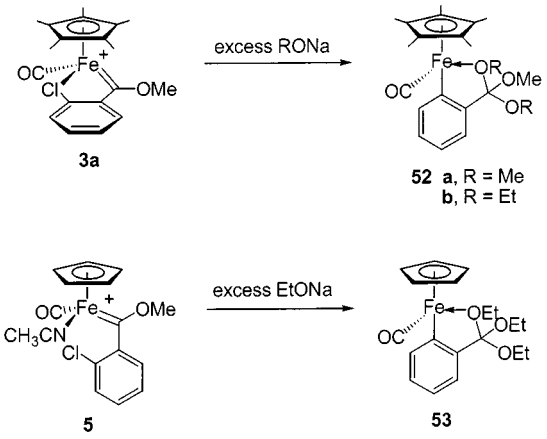

Scheme 26. Activation of the Ar−Cl bond of (chloroaryl)carbene complexes

The related anisyl derivative $[Fe(C_5Me_5)(CO)\{\kappa^2\text{-C-}(OMe)C_6H_4\text{-}o\text{-}O^aMe\}(Fe-O^a)][OTf]$ (**3b**) affords the bis-(ethoxy)carbene complex **54** upon treatment with ethoxide (Scheme 27).[47] The Lewis base interaction in **3b** appears not to weaken the Ar−OMe bond to the same extent as the Ar−Cl bond in the chloroaryl derivative **3a**. Therefore, a different rearrangement process takes place. We assume that the formation of **54** results from an initial formation of the chelate ketal intermediate $[Fe(C_5Me_5)(CO)\{C(OMe)(OEt)\text{-}(C_6H_4\text{-}o\text{-}O^aMe)\}(Fe-O^a)]$ followed by deinsertion/migration of the anisyl substituent to the metal centre. This final step is promoted by the presence of a labile ligand. Such migrations of alkyl or aryl groups to give carbenes are rare,[48,49] and are relevant to C−C bond activation. The C−C bond formation corresponds to the insertion/migration of an alkyl or aryl group to a carbene ligand (Scheme 28).

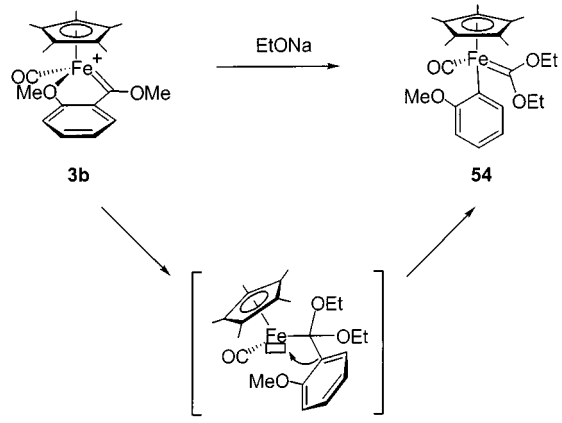

Scheme 27. C−C bond cleavage of complex **3b**

Scheme 28. Alkyl migration in carbene complexes

In this system, the Me−O bond is cleaved in the presence of halide anions.[7a] The (anisylcarbene)iodo complex **7b** spontaneously rearranges in dichloromethane or chloroform solution into the chelate aryloxy complex **55** along with the formation of methyl iodide (Scheme 29). We assume that the neutral iodo complex **7b** is in equilibrium with the cationic chelated form. The iodide counter-anion reacts as a demethylation reagent. The organometallic fragment plays the role of a Lewis acid to activate the C−O bond. Related sp^3-sp^3 C−O bond cleavage has previously been reported in the case of a palladium complex.[50]

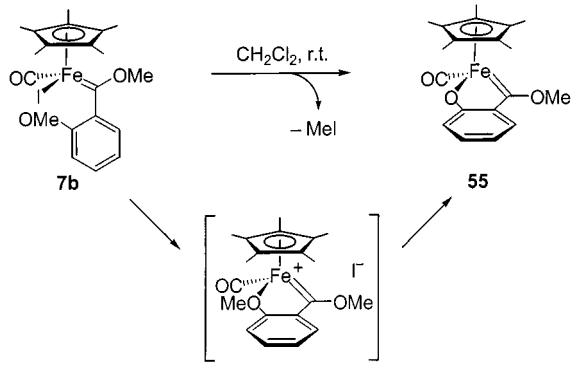

Scheme 29. Formation of the (aryloxy)carbene complex **55**

We found that chelate [(allyloxy)carbene]iron complexes **10** are involved in regioselective C−C bond-coupling reactions. Complex **10** reacts with [*n*Bu$_4$N][I] to give the corresponding β,γ-unsaturated ketones **56** (Scheme 30).[51] The organometallic fragment is recovered as the iodo derivative [Fe(C$_5$H$_5$)(CO)$_2$(I)] when the reaction is carried out under CO. Remarkably, no rearrangement of the initial allyl substituent is observed. Moreover, the C−C coupling is regioselective, since the carbon atom that is involved in the C−O bond cleavage recombines to form the new C−C bond.

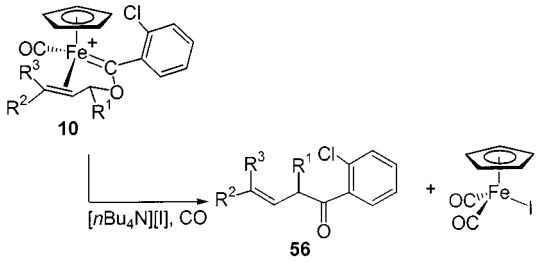

Scheme 30. Formation of β,γ-unsaturated ketones **56** from (allyloxy)carbene complexes **10**

We propose that the formation of **56** results from an initial nucleophilic attack of the iodide, the rupture of the C−O bond thus leads to a coordinated η^2-(*C*,*C*)-allyl iodide. Oxidative addition of the latter and decoordination of the olefinic unit provide a transient Fe^{IV} species. Reductive elimination of the acyl and allyl ligands affords the observed ketone (Scheme 31).

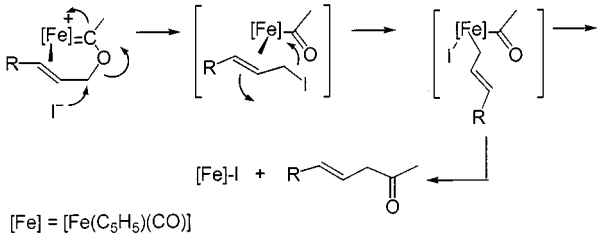

Scheme 31. Postulated mechanism for the formation of **56** showing the participation of the iodide anion

This study provides the direct evidence of the formation of unsaturated ketones from *chelate* (allyloxy)carbene complexes by an intramolecular regioselective C−C coupling reaction. Such (allyloxy)carbene complex intermediates have been postulated in the Ru-catalysed synthesis of β,γ-unsaturated ketones from terminal alkynes and allyl alcohols.[52,53]

The β,γ-unsaturated ketone complex [Ru(Tp)(Cl)(κ^3-C$_7$H$_{15}$C(O)CH$_2$CH=CH$_2$)] (**57**) as well as the free ketone 4-dodec-1-enone (**58**) are formed during the synthesis of the chelate carbene complex [Ru(Tp)(Cl){κ^3-C(OCH$_2$CH=CH$_2$)(C$_7$H$_{15}$)}] (**24d**).[19] Although this result is also in agreement with the proposed intermediary of chelate (allyloxy)carbene complexes, it is only observed for **58**, and the yields of **57** and **58** are low.

We attempted to synthesise the parent (carbene)(C$_5$Me$_5$)Ru complex **59** from the acetonitrile derivative [Ru(C$_5$Me$_5$)(PPh$_3$)$_2$(CH$_3$CN)][PF$_6$] in the presence of PhC≡CH and CH$_2$=CH−CH$_2$OH, but a mixture of the expected (allyloxy)carbene complex **59** [Ru(C$_5$Me$_5$)(PPh$_3$){(κ^3-*C*,*C*,*C*)-C(OCH$_2$CH=CH$_2$)CH$_2$Ph}][PF$_6$] and the allylphosphonium salt [CH$_2$=CH−CH$_2$PPh$_3$][PF$_6$] was obtained (Scheme 32).[54] The formation of the latter results from nucleophilic attack of free PPh$_3$ at the terminal carbon atom of the coordinated olefinic fragment, precluding the isolation of the pure carbene complex.

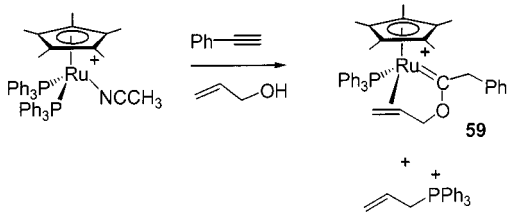

Scheme 32. Synthesis of the [(allyloxy)carbene]ruthenium complex **59**

When the allyloxy group is not coordinated to the metal fragment such as in **27**, it can be involved in an intramolecular reaction. The phenylallene fragment of the deprotonated complex [Ru(C$_5$H$_5$)(CO)(P*i*Pr$_3$){C(OCH$_2$CH=CH$_2$)=C=CPh$_2$}] (**60**) reacts with the free C=C double bond (Scheme 33).[25] In solution at room temperature, **60** isomerised into the tricyclic tetraenyl complex **61** by an intramolecular Diels−Alder reaction where the C$_\beta$−C$_\gamma$ double bond and one of the two phenyl groups of the al-

lenyl unit acts as an inner-outer sphere diene and the CH=CH_2 double bond of the alkoxy fragment act as a dienophile.

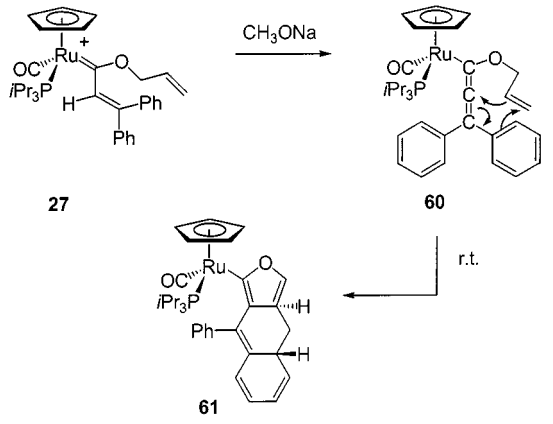

Scheme 33. Intramolecular Diels–Alder reaction involving a free allyloxy group

3.2. Transient Carbene Species: Cyclopropanation and Intramolecular C–H Bond-Insertion Reactions

Non-heteroatom-stabilised carbene complexes of iron are good cyclopropanating agents of alkenes.[55,56] These transient species can be generated from (α-siloxyalkyl)iron derivatives [Fe(η^5-ligand)$(CO)_2${CH(OSiMe)R}] (η^5-ligand = C_5H_5, C_9H_7). They are readily accessible from saturated or unsaturated aldehydes RCHO (R = Ph, CH_3, *p*-C_6H_4OMe, *p*-C_6H_4Cl, *p*-C_6H_4Me, *p*-$C_6H_4CF_3$, *o*-C_6H_4OMe, CH=CMe_2) by addition to the iron metallate [Na][Fe(η^5-ligand)$(CO)_2$] and subsequent capture with $ClSiMe_3$.[57]

Asymmetric cyclopropanation reactions involving a chiral carbene ligand have been performed using the dimetallic Fe/Cr complex **63** (Scheme 34).[58] Reaction with styrene affords the corresponding cyclopropanes in a 10:1 *cis*/*trans* ratio. The origin of diastereoselectivity has been investigated. The Cr participation that stabilises the (carbene)iron was expected to induce a *trans* selectivity. However, when aromatic alkenes are used, a π-stacking effect leads to *cis* selectivity.[59]

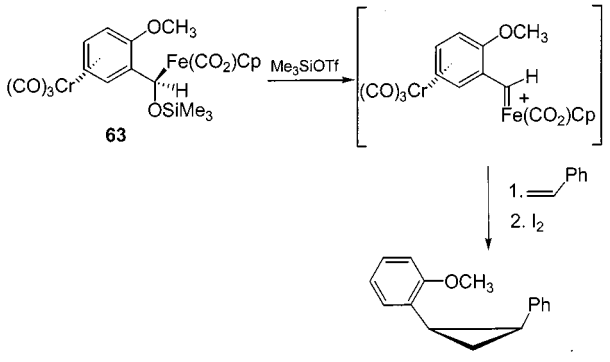

Scheme 34. Cyclopropanation of styrene by **63**

(Carbene)metal complexes are also known to insert into X–H bonds (X = Si, C). Examples of Si–H insertion reactions from alkylidene and benzylidene complexes [Fe(C_5H_5)(CO)(PR_3)(=CHR′)]$^+$ (R = Ph, Et) have been described.[60] With regards to the C–H bond, an intramolecular procedure from (carbene)iron complexes has been developed as a highly stereoselective route to cyclopentanes (Scheme 35).[61] The carbene complexes **65** are generated by *S*-methylation of thiophenyl derivatives **64** and loss of thioanisole. Intramolecular C–H insertion affords the fused cyclopentanes **66**. The main stereochemical features of the cyclisation have been investigated. In agreement with the observed diastereoselectivities, the reaction may proceed through a one-step, concerted insertion of a (carbene)iron complex into a properly situated C–H bond, namely via the chair-like cyclic transition state **67** (Scheme 36).

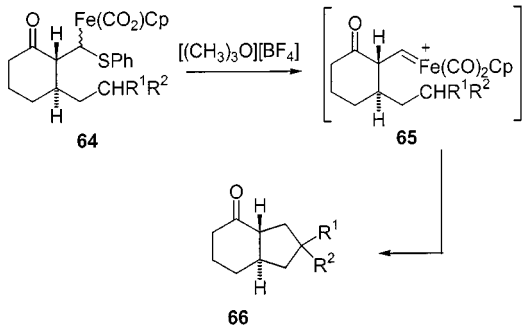

Scheme 35. Intramolecular C–H insertion reactions involving transient (carbene)iron complexes

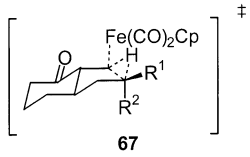

Scheme 36. Chair-like cyclic transition state

4. Carbene Complexes as Intermediates in Catalysis

4.1. Oxidative Cycloisomerisation of Homopropargyl Alcohols

Homopropargyl alcohols react with Ru complexes to form oxycarbene species via hydroxyvinylidenes.[28] This approach was used to convert homopropargyl alcohols into γ-butyrolactones through a mild oxidative cycloisomerisation process catalysed by **46** (Scheme 37).[62] *N*-Hydroxyimides are used as oxidants which do not affect the catalytic activity. The proposed mechanism involves initial formation of the (oxycarbene)metal intermediate **68** followed by nucleophilic attack of *N*-hydroxyimide (Scheme 38). Eventually, the lactone **69** is released along with the imide.

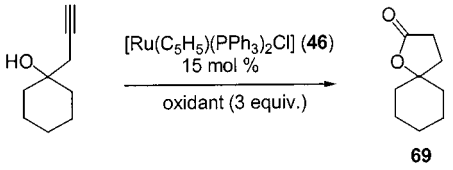

Scheme 37. Ru-catalysed synthesis of γ-butyrolactones **69**

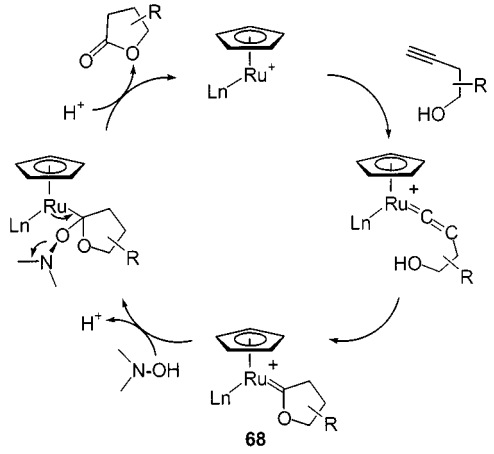

Scheme 38. Proposed catalytic cycle for oxidative cycloisomerisation of homopropargyl alcohols

4.2. Reactions Involving Diazo Compounds

It is generally agreed that carbene species are key intermediates in transition-metal-catalysed C−C bond-forming reactions involving diazo compounds. However, the catalytically active (carbene)Ru species have rarely been isolated or detected during these processes.[3,63] Complex **46** was found to be a catalyst for carbene−carbene coupling, insertion reactions into X−H bonds (X = N, S), cyclopropanation of olefins, and carbene transfer reactions. The formation of neutral carbene intermediates from the 16-electron species $[Ru(C_5H_5)(PR_3)(Cl)]$ is a key step in all these catalytic reactions involving diazo compounds and **46** as a catalyst.

Stereoselective decomposition of α-diazo carbonyl compounds N_2CHCOR [R= Me, *n*Pr, *i*Pr, $(CH_2)_{10}CH_3$] catalysed by **46** affords the corresponding ene-diones RCOCH=CHCOR, the *cis* isomers being formed in 95−97% yield (Scheme 39).[64]

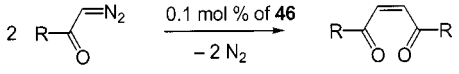

Scheme 39. Formation of *cis*-enediones from α-diazo carbonyl compounds

Under the same conditions, ethyl diazoacetate (EDA) is converted into diethyl maleate (DEM). The observed stereoselectivity (95−99%) may be due to steric factors. A detailed study suggests that the less crowded (*cis*-π-olefin)metal intermediate **71** is formed (Scheme 40). The proposed mechanism involves the carbene complex $[Ru(C_5H_5)(PR_3)(Cl)\{=CHCO_2Et\}]$ (**70**) (Scheme 39). The latter would be formed by dissociation of a PPh_3 ligand from **46**, a key step of the catalytic process. The highly reactive species **70** was spectroscopically not detected in the reaction mixture but has been independently prepared from the Ru acetate precursor **44** and characterised in solution (Scheme 41). Addition of equimolar amounts of EDA to **44** gives the metallacycle derivative **73**. Its formation arises from nucleophilic addition of the κ^1-acetate group at the electrophilic carbene carbon atom. Complex **73** is then converted at −40 °C to the expected carbene derivative **70** by displacement of the acetato group using Me_2SiCl_2. Finally, the DEM complex **71** is formed upon addition of another equivalent of EDA. The reactions have been monitored by NMR spectroscopy allowing all of the intermediates to be characterised.

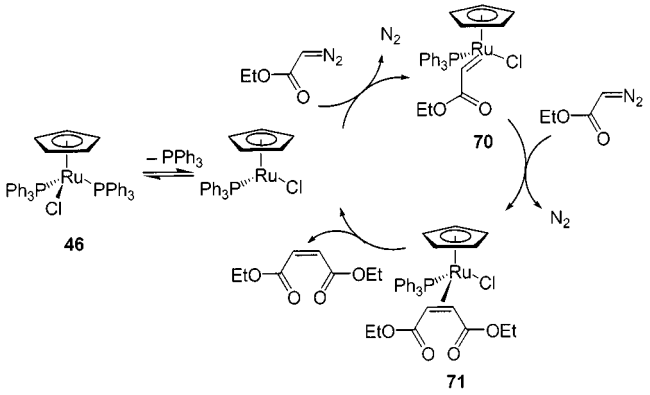

Scheme 40. Proposed mechanism for EDA dimerisation

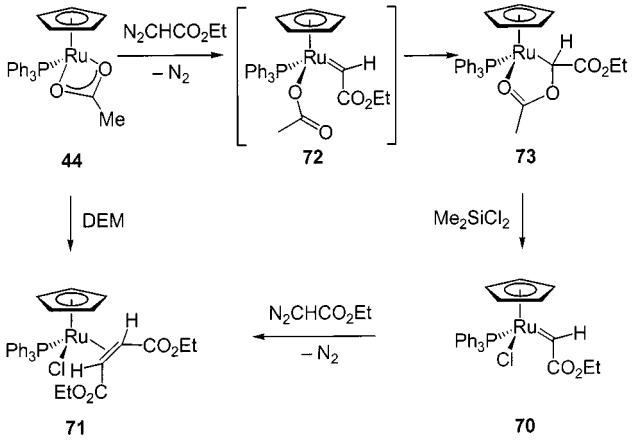

Scheme 41. Independent synthesis of the carbene intermediate **70** and the DEM complex **71**

Complex **46** also catalyses chemoselective insertion reactions of α-diazo carbonyl compounds $N_2CHC(O)R$ [R = CH_3, *n*Pr, *i*Pr, $(CH_2)_{10}CH_3$, $(CH_2)_{14}CH_3$, Ph] into N−H and S−H bonds.[65] This procedure affords α-oxo amines and α-oxo thioethers in very good yields (Scheme 42). As proposed for the synthesis of *cis*-enediones, a (carbene)ruthenium complex $[Ru(C_5H_5)(PR_3)(Cl)\{=CHC(O)R\}]$ is in-

volved in the catalytic process. Nucleophilic attack by amine or thiol (X−H) gives the product $RC(O)CH_2X$.

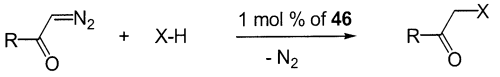

Scheme 42. Insertion reactions of diazo carbonyl compounds into X−H (X = N, S) bonds catalysed by **46**

Selective catalytic carbene transfer reactions from diazo compounds to terminal alkenes have been reported. Complex **46** is an efficient catalyst for cyclopropanation of styrene with EDA (Scheme 43).[38] The catalytic activity of Ru derivatives of general formula $[Ru(\eta^5\text{-ligand})(PR_3)_2(X)]$ have also been investigated. The reaction is performed in pure alkene solvent, in order to avoid dimerisation of EDA. The cyclopropane products are readily obtained in high yields and with significant *cis* stereoselectivity. For instance, in the case of **46**, optimum conditions gave rise to a 95% yield of ethyl 2-phenylcyclopropanecarboxylate with a stereoselectivity of 67% *cis* versus 33% *trans*. As above, the reaction is likely to proceed via the carbene derivative **70** that would account for the observed stereoselectivity (Scheme 44). However, no spectroscopic evidence for the formation of this intermediate in the reaction mixture was obtained.

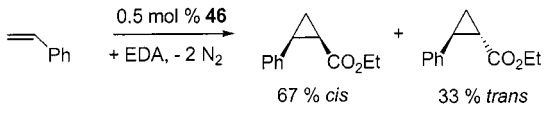

Scheme 43. Ru-catalysed cyclopropanation of styrene with EDA

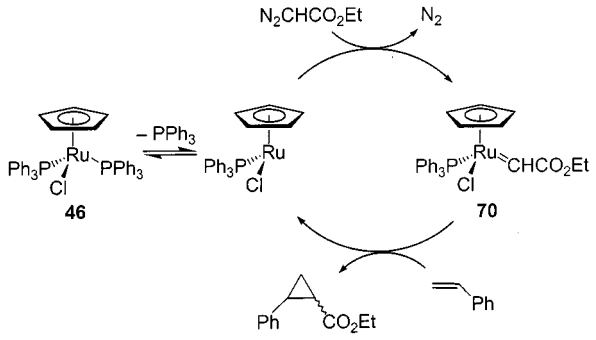

Scheme 44. Proposed mechanism of cyclopropanation of styrene with EDA catalysed by **46**

When diphenyldiazomethane is used, an unusual C−C coupling reaction takes place (Scheme 45).[38] The reaction with styrene in the presence of **46** (1 mol %), affords mainly 1,1,3-triphenylpropene (**75**) (58%), together with a 1:1 mixture of 1,1-diphenylethene (**76**) (17%), and 1,2-diphenylcyclopropanes **77a**,**b** (16%). Only 9% of the expected cyclopropyl derivative **74** is present, the product is actually formed in a thermal side reaction from styrene and diphenyldiazomethane without involvement of **46**. The carbene intermediate **45a** has been spectroscopically identified during catalysis. In a stoichiometric reaction, complex **45a** can transfer its carbene ligand to styrene to give the compounds **75**, **76**, and **77**, formed with a distribution comparable to that of the catalytic reaction.

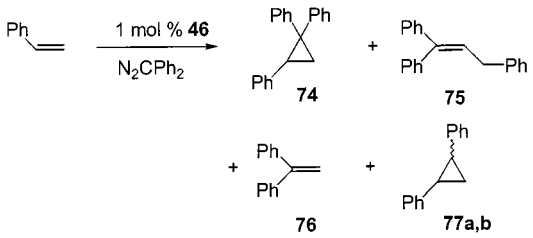

Scheme 45. Ru-catalysed C−C bond-forming reactions from styrene and diphenyldiazomethane

On the basis of the mechanism suggested for (sulfonato)rhodium complexes,[66] the formation of compound **75** results from a formal $:CPh_2$ and $:CHCH_2Ph$ coupling (Scheme 46). In the first stage, the carbene derivative **B** is generated from **A**. Coordination of styrene and coupling with the carbene ligand affords a metallacyclobutane intermediate **C**. Then, **C** rearranges into the π-allyl complex **D** by a β-H elimination. Reductive elimination affords the observed propene derivative **75**. Note that the metallacycle **C** is postulated in olefin metathesis reactions and can account for the formation, in a side reaction, of 1,1-diphenylethene (**76**). Thus, this second competitive reaction would lead to the formation of a benzylidene complex **E**. Carbene transfer to styrene provides the cyclopropanes **77** and regenerates **A**.

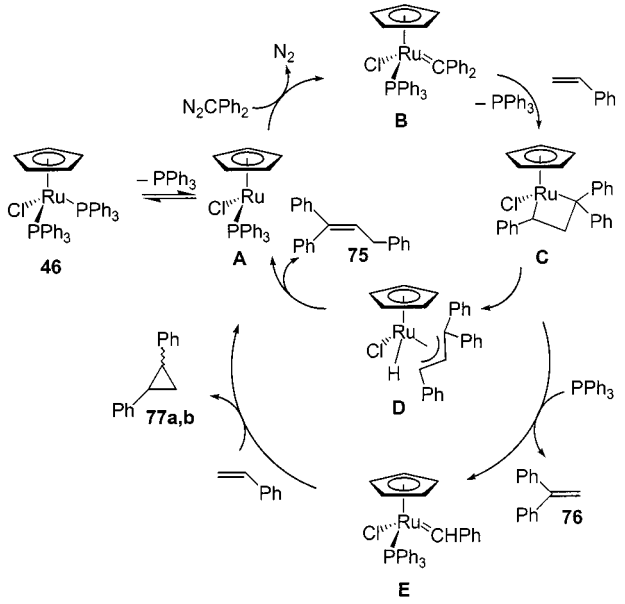

Scheme 46. Proposed mechanism for the formation of **75**, **76**, and **77**

The above results suggest that complex **46** and related complexes constitute a promising class of catalysts for chemo-, regio-, and stereoselective processes involving diazo compounds. A wide range of synthetically useful trans-

formations have been developed. In another example, the ruthenium-catalysed addition of diazo compounds to alkynes has been reported.[67] This double addition is catalysed by [Ru(C_5Me_5)(cod)(Cl)] (**78**) allowing, for example, the access to 1,4-bis(trimethylsilyl)buta-1,3-dienes, by combination of two molecules of trimethylsilyldiazomethane and one of alkyne (Scheme 47).

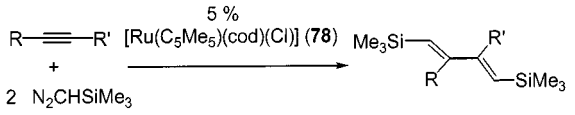

Scheme 47. Synthesis of 1,4-bis(trimethylsilyl)butadiene catalysed by **78**

A plausible mechanism for this selective process has been proposed (Scheme 48). Displacement of the cod ligand by one molecule of alkyne and trimethyldiazomethane to the ruthenium centre provides the (carbene)ruthenium intermediate **B′**. The intramolecular C−C coupling leads to **C′** which then rearranges into the unsaturated vinylcarbene derivative **D′**. Addition of a second molecule of diazomethane leads to the bis(carbene) **E′**. Finally, coupling of the two carbene ligands affords the observed diene. This reaction constitutes an unusual 2:1 coupling between diazoalkanes and a wide range of alkynes, demonstrating that it is possible to selectively create two C=C double bonds.

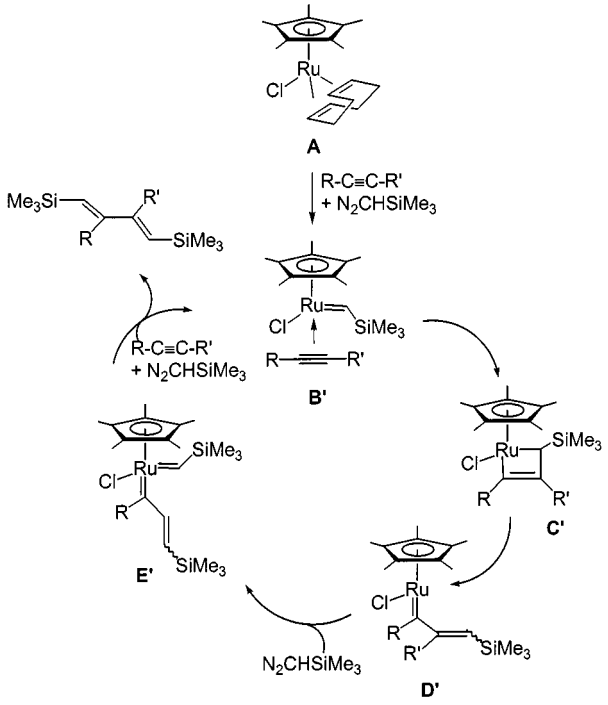

Scheme 48. Proposed mechanism for the catalytic formation of functional conjugated dienes

5. Concluding Remarks

The importance of the carbene complexes is reflected by their widespread use in synthesis. In stoichiometric reactions, electrophilic iron complexes are involved in diastereoselective syntheses of fused cyclopentanes. The development of enantioselective methodologies is an important challenge in organic synthesis. In catalysis, most of the (carbene)ruthenium complexes are generated from diazo compounds. An alternative pathway is via vinylidene complexes. The intermediary of allenylidene complexes is still rare. Condensation of the Ru=C double bond with unsaturated substrates appears to be a promising new field. The search for new catalysts is highly desirable, and then carbene complexes could become standard tools in synthesis provided that these species are readily accessible and easily handled.

Acknowledgments

I would like to thank my co-workers who have contributed to this project. Their names are mentioned in the references. I am indebted to the CNRS and the University of Rennes 1 for generous support of this work.

[1] [1a] R. C. Kerber, in: *Comprehensive Organometallic Chemistry II*, vol. 7 (Eds.: D. F. Shriver, M. I. Bruce), Pergamon, New York, **1995**, pp. 176−181. [1b] A. F. Hill, in: *Comprehensive Organometallic Chemistry II*, vol. 7 (Eds.: D. F. Shriver, M. I. Bruce), Pergamon, New York, **1995**, pp. 336−362. [1c] M. Sierra, *Chem. Rev.* **2000**, *100*, 3591−3637.

[2] F. Zaragoza Dörwald, *Metal Carbenes in Organic Synthesis*, Wiley-VCH, Weinheim, **1999**.

[3] For recent reviews concerning metathesis reactions, see inter alia: [3a] R. H. Grubbs, S. Chang, *Tetrahedron* **1998**, *54*, 4413−4450. [3b] *Alkene Metathesis in Organic Synthesis* (Ed.: A. Fürstner), Springer-Verlag, Berlin, **1999**. [3c] A. J. Phillips, A. D. Abell, *Aldrichim. Acta* **1999**, *32*, 75−89. [3d] A. Fürstner, *Angew. Chem. Int. Ed.* **2000**, *39*, 3012−3043. [3e] A. H. Hoveyda, R. R. Schrock, *Chem. Eur. J.* **2001**, *7*, 945−950.

[4] For reviews on ruthenium-catalysed reactions, see: [4a] T. Naota, H. Takaya, S.-I. Murahashi, *Chem. Rev.* **1998**, *98*, 2599−2660. [4b] C. Bruneau, P. H. Dixneuf, *Acc. Chem. Res.* **1999**, *32*, 311−323. [4c] B. M. Trost, D. Toste, A. B. Pinkerton, *Chem. Rev.* **2001**, *101*, 2067−2096.

[5] M. P. Doyle, M. A. McKervey, T. Ye, *Modern catalytic methods for organic synthesis with diazo compounds: from cyclopropanes to ylides*, Wiley, New York, **1998**.

[6] K. Ruck-Braun, M. Mikulas, P. Amrhein, *Synthesis* **1999**, 727−744.

[7] [7a] G. Poignant, S. Nlate, V. Guerchais, A. J. Edwards, P. R. Raithby, *Organometallics* **1997**, *16*, 124−132. [7b] K. Ferré, G. Poignant, L. Toupet, V. Guerchais, *J. Organomet. Chem.* **2001**, *629*, 19−27.

[8] A. R. Cutler, *J. Am. Chem. Soc.* **1979**, *101*, 604−606.

[9] C. Schulz, M. Tohier, S. Sinbandhit, V. Guerchais, *Inorg. Chim. Acta* **1999**, *291*, 449−451.

[10] [10a] K. Rück-Braun, J. Kühn, *Synlett* **1995**, 1194−1196. [10b] K. Rück-Braun, J. Kühn, D. Schollmeyer, *Chem. Ber.* **1996**, *129*, 937−944. [10c] K. Rück-Braun, J. Kühn, *Chem. Ber.* **1996**, *129*, 1057−1059. [10d] J. Kühn, D. Schollmeyer, K. Rück-Braun, *Chem. Ber./Recueil* **1997**, *130*, 1647−1654.

[11] G. Poignant, F. Martin, V. Guerchais, *Synlett* **1997**, 913−914.

[12] M.-A. Guillevic, P. Brégaint, C. Lapinte, *J. Organomet. Chem.* **1996**, *514*, 157−162.

[13] V. Mahias, S. Cron, L. Toupet, C. Lapinte, *Organometallics* **1996**, *15*, 5399−5408.

[14] V. Guillaume, V. Mahias, A. Mari, C. Lapinte, *Organometallics* **2000**, *19*, 1422−1426.

[15] For a review focusing on dimetallic complexes containing a carbon bridge, see: F. Paul, C. Lapinte, *Coord. Chem. Rev.* **1998**, *178−180*, 427−509.

[16] M. I. Bruce, *Chem. Rev.* **1998**, *98*, 2797−2858.
[17] M. A. J. Tenorio, M. J. Tenorio, M. C. Puerta, P. Valerga, *Organometallics* **1997**, *16*, 5528−5535.
[18] C. Slugovc, K. Mereiter, R. Schmid, K. Kirchner, *Organometallics* **1998**, *17*, 827−831.
[19] E. Rüba, C. Gemel, C. Slugovc, K. Mereiter, R. Schmid, K. Kirchner, *Organometallics* **1999**, *18*, 2275−2280.
[20] V. Cadierno, M. P. Gamasa, J. Gimeno, *Eur. J. Inorg. Chem.* **2001**, 571−591.
[21] M. P. Gamasa, J. Gimeno, C. Gonzalez-Bernado, J. Borge, S. Garcia-Granda, *Organometallics* **1997**, *16*, 2483−2485.
[22] V. Cadierno, M. P. Gamasa, J. Gimeno, M. Gonzalez-Cueva, E. Lastra, J. Borge, S. Garcia-Granda, E. Perez-Carreno, *Organometallics* **1996**, *15*, 2137−2147.
[23] M. A. Esteruelas, A. V. Gomez, F. J. Lahoz, A. M. Lopez, E. Onate, L. A. Oro, *Organometallics* **1996**, *15*, 3423−3435.
[24] M. A. Esteruelas, A. V. Gomez, A. M. Lopez, E. Onate, N. Ruiz, *Organometallics* **1998**, *17*, 2297−2306.
[25] M. A. Esteruelas, A. V. Gomez, A. M. Lopez, M. Olivan, E. Onate, N. Ruiz, *Organometallics* **2000**, *19*, 4−14.
[26] D. J. Bernad, M. A. Estuerelas, A. M. Lopez, J. Modrego, M. C. Puerta, P. Valerga, *Organometallics* **1999**, *18*, 4995−5003.
[27] M. A. Esteruelas, A. V. Gomez, A. M. Lopez, M. C. Puerta, P. Valerga, *Organometallics* **1998**, *17*, 4959−4965.
[28] The cycloisomerisation of alkynols by Group-6 to -10 metals has been reviewed, see: B. Weyershausen, K. H. Dötz, *Eur. J. Inorg. Chem.* **1999**, 1057−1066.
[29] L. P. Barthel-Rosa, K. Maitra, J. Fischer, J. H. Nelson, *Organometallics* **1997**, *16*, 1714−1723.
[30] L. P. Barthel-Rosa, K. Maitra, J. H. Nelson, *Inorg. Chem.* **1998**, *37*, 633−639.
[31] M. P. Gamasa, J. Gimeno, B. M. Martin-Vaca, *Organometallics* **1998**, *17*, 3707−37015.
[32] K. Mauthner, K. M. Sodouzi, K. Mereiter, R. Schmid, K. Kirchner, *Organometallics* **1999**, *18*, 4681−4683.
[33] C. Ernst, O. Walter, E. Dinjus, *J. Organomet. Chem.* **2001**, *627*, 249−254.
[34] C. Gemel, A. La Pensée, K. Mauthner, K. Mereiter, R. Schmid, K. Kirchner, *Monasth. Chem.* **1997**, *128*, 1189−1199.
[35] M. S. Sanford, L. M. Henling, R. H. Grubbs, *Organometallics* **1998**, *17*, 5384−5389.
[36] D. B. Grotjahn, H. C. Lo, *Organometallics* **1996**, *15*, 2860−2862.
[37] T. Braun, O. Gevert, H. Werner, *J. Am. Chem. Soc.* **1995**, *117*, 7291−7292. H. Werner, T. Braun, T. Daniel, O. Gevert, M. Schulz *J. Organomet. Chem.* **1997**, *541*, 127−141.
[38] W. Baratta, W. A. Herrmann, R. M. Kratzer, P. Rigo, *Organometallics* **2000**, *19*, 3664−3669.
[39] W. Baratta, A. Del Zotto, E. Herdtweck, S. Vuano, P. Rigo, *J. Organomet. Chem.* **2001**, *617−618*, 511−519.
[40] For the related vinylidene C_5Me_5 analog, see: C. S. Yi, N. Liu, A. L. Rheingold, M. Liable-Sands, I. A. Guzei, *Organometallics* **1997**, *17*, 3729−3731.
[41] J. Brumaghi, G. S. Girolami, *Chem. Commun.* **1999**, 953−954.
[42] [42a] P. Hamon, L. Toupet, J.-R. Hamon, C. Lapinte, *J. Chem. Soc., Chem. Commun.* **1994**, 931−932. [42b] P. Hamon, L. Toupet, J.-R. Hamon, C. Lapinte, *Organometallics* **1996**, *15*, 10−12. [42c] M. Akita, M. Terada, M. Tanaka, Y. Morooka, *J. Organomet. Chem.* **1996**, *510*, 255−261. [42d] M. B. Humphrey, W. M. Lammana, M. Brookhart, G. R. Husk, *Inorg. Chem.* **1983**, *22*, 3355−3358.
[43] J. Barluenga, S. Lopez, A. A. Trabanco, A. Fernandez-Acebes, J. Florez, *J. Am. Chem. Soc.* **2000**, *122*, 8145−8154.
[44] J. S. Kingsbury, J. P. A. Harrity, P. J. Bonitatebus, Jr., A. H. Hoveyda, *J. Am. Chem. Soc.* **1999**, *121*, 791−799. S. B. Garber, J. S. Kingsbury, B. L. Gray, A. H. Hoveyda, *J. Am. Chem. Soc.* **2000**, *122*, 8168−8179.
[45] R. J. Kulawiec, R. H. Crabtree, *Coord. Chem. Rev.* **1990**, *99*, 89−115.
[46] G. Poignant, S. Sinbandhit, L. Toupet, V. Guerchais, *Eur. J. Inorg. Chem.* **1998**, 1387−1389.
[47] G. Poignant, S. Sinbandhit, L. Toupet, V. Guerchais, *Angew. Chem. Int. Ed.* **1998**, *37*, 963−965.
[48] [48a] Y. Stenstrom, W. M. Jones, *Organometallics* **1986**, *5*, 178−180. [48b] J. Yang, J. Yin, K. A. Abboud, W. M. Jones, *Organometallics* **1994**, *13*, 971−978.
[49] For examples of carbene migratory insertion reactions, see: [49a] J. Yang, W. M. Jones, J. K. Dixon, N. T. Allison, *J. Am. Chem. Soc.* **1995**, *117*, 9776−9777. [49b] J. F. Hoover, J. M. Stryker, *J. Am. Chem. Soc.* **1990**, *112*, 464−465. [49c] D. L. Thorn, T. H. Tulip, *J. Am. Chem. Soc.* **1981**, *103*, 5984−5986. [49d] J. E. Muir, A. Haynes, M. J. Winter, *Chem. Commun.* **1996**, 1765−1766. [49e] F. M. Alias, M. L. Poveda, M. Sellin, E. Carmona, *J. Am. Chem. Soc.* **1998**, *120*, 5816−5817. [49f] T. Braun, O. Gevert, H. Werner, *J. Am. Chem. Soc.* **1995**, *117*, 7291−7292.
[50] For selective activation of the ArO−Me bond controlled by the choice of the metal complex, see: [50a] M. E. van der Boom, S.-Y. Liou, Y. Ben-David, A. Vigalok, D. Milstein, *Angew. Chem. Int. Ed. Engl.* **1997**, *36*, 625−626. [50b] M. E. van der Boom, S.-Y. Liou, Y. Ben-David, L. J. W. Shimon, D. Milstein, *J. Am. Chem. Soc.* **1998**, *120*, 6531−6541.
[51] K. Ferré, P. Le Mignot, S. Sinbandhit, L. Toupet, V. Guerchais, *Chem. Commun.* **2000**, 1405−1406.
[52] B. M. Trost, R. J. Kulawiec, *J. Am. Chem. Soc.* **1992**, *114*, 5579−5584 and references therein.
[53] [53a] For asymmetric reactions, see: B. M. Trost, B. Vidal, M. Thommen, *Chem. Eur. J.* **1999**, *5*, 1055−1069. [53b] Y. Nishibayashi, I. Takei, M. Hidai, *Organometallics* **1997**, *16*, 3091−3093.
[54] V. Guerchais, K. Ferré, unpublished results.
[55] M. Brookhart, W. B. Studabaker, *Chem. Rev.* **1987**, *87*, 411−432.
[56] The iron Lewis acid $[Fe(C_5H_5)(CO)_2(THF)]^+$ was found to catalyse the formation of aziridines and epoxides in the presence of diazo compounds, but no carbene intermediates were operative.[56a] S. J. Mahmood, A. K. Saha, M. M. Hossain, *Tetrahedron* **1998**, *54*, 349−358. [56b] M. F. Mayer, M. M. Hossain, *J. Org. Chem.* **1998**, *63*, 6839−6844.
[57] R. D. Theys, R. M. Vargas, Q. Wang, M. M. Hossain, *Organometallics* **1998**, *17*, 1333−1339.
[58] R. D. Theys, M. M. Hossain, *Tetrahedron Let.* **1995**, *36*, 5113−5116.
[59] Q. Wang, M. Hossain, *J. Organomet. Chem.* **2001**, *617−618*, 751−754.
[60] For examples of Si−H insertion reactions, see: E. Scharrer, M. Brookhart, *J. Organomet. Chem.* **1995**, *497*, 61−71.
[61] [61a] S. Ishii, S. Zhao, P. Helquist, *J. Am. Chem. Soc.* **2000**, *122*, 5897−5898. [61b] S. Ishii, P. Helquist, *Synlett* **1997**, 508−510.
[62] B. M. Trost, Y. H. Rhee, *J. Am. Chem. Soc.* **1999**, *121*, 11680−11683.
[63] For examplexes of isolated active (carbene)Ru complexes, see: [63a] H. M. Lee, C. Bianchini, G. Jia, P. Barbaro, *Organometallics* **1999**, *18*, 1961−1966. [63b] S.-B. Park, N. Sakata, H. Nishiyama, *Chem. Eur. J.* **1996**, *2*, 303−306.
[64] [64a] W. Baratta, A. Del Zotto, P. Rigo, *Organometallics* **1999**, *18*, 5091−5096. [64b] W. Baratta, A. Del Zotto, P. Rigo, *Chem. Commun.* **1997**, 2163−2164.
[65] A. Del Zotto, W. Baratta, P. Rigo, *J. Chem. Soc., Perkin Trans. 1* **1999**, 3079−3081.
[66] H. Werner, M. Bosch, M. E. Schneider, C. Hahn, F. Kukla, M. Manger, B. Windmüller, B. Weberndörfer, M. Laubender, *J. Chem. Soc., Dalton Trans.* **1998**, 3549−3558.
[67] J. Le Paih, S. Derien, I. Ozdemir, P. H. Dixneuf, *J. Am. Chem. Soc.* **2000**, *122*, 7400−7401.

Received August 20, 2001
[I01316]

The Structure and Physical Properties of a Novel Three-Dimensional Zeolite-Like Nanoporous Architecture Formed by Two Different Polymeric Layers: $[Eu_2(btc)(H_2btc)(H_2O)]\cdot 4H_2O$

Chuan-De Wu,[a] Can-Zhong Lu,*[a] Wen-Bin Yang,[a] Shao-Fang Lu,[a] Hong-Hui Zhuang,[a] and Jin-Shun Huang[a]

Keywords: Hydrothermal synthesis / Nanostructures / Materials science / Europium / Organic-inorganic hybrid composites

The open framework of $[Eu_2(btc)(H_2btc)(H_2O)]\cdot 4H_2O$ (**1**), prepared by hydrothermal reaction of $EuCl_3$ with 1,2,4,5-benzenetetracarboxylic anhydride in acidified aqueous solution, is built up from two types of polymeric layers with $[EuO_6(H_2O)]_n$ units as tethers, resulting in nanoporous channels that host water molecules through complex hydrogen bonding. Crystallographic data for **1**: monoclinic, $P2_1/n$, with a = 10.7562(2) Å, b = 7.2075(2) Å, c = 17.2180(5) Å, β = 97.072(2)° and Z = 2. A study of the temperature dependence of the magnetic susceptibility data reveals that the paramagnetic behavior of **1** is mainly due to the effective spin-orbital coupling between the ground and exited states through the Zeeman perturbation; the magnetic interaction between europium(III) centers is very weak. A study of the electronic properties demonstrates that compound **1** is a semiconductor. A TGA analysis between 30 and 600 °C for **1** suggests that when the lattice water molecules are removed from the network, the skeleton of the network still remains stable up to 150 °C; this is also confirmed by XRPD.
(© Wiley-VCH Verlag GmbH, 69451 Weinheim, Germany, 2002)

Introduction

In the past few years, the construction of inorganic coordination networks, especially of zeolite-like microporous materials, has attracted much attention[1−4] not only because of their intriguing architectures, but also because of their promising potential applications.[5−7] The design and synthesis of new frameworks containing large pores that can facilitate the removal/adsorption of guest molecules is a continuing challenge.

We are currently interested in pursuing synthetic strategies that use lanthanide ions as nodes for the construction of three-dimensional microporous frameworks. Such structures are more difficult to control than those of d-block transition metal analogues due to the higher coordination numbers of lanthanide ions and the inherent flexibility of their coordination geometries, which could lead to unprecedented topological architectures. Recent reports have demonstrated that some organic ligands have a dramatic impact on structures, and consequently on their properties, and are therefore very useful for the control of the architectures of coordinated polymers.[8−11] The 1,2,4,5-Benzenetetracarboxylic (pyromellitic) acid (H_4btc) ligand,[12] which has eight (btc) or four (H_2btc) potential donor oxygen atoms, is a rather versatile ligand for the synthesis of polymeric complexes with metal cations.[13] However, examples of H_4btc-bridged metal-organic frameworks that can maintain their structural integrity upon the removal of guest molecules are still rare. In the course of our investigations on the synthesis of btc- and/or H_2btc-bridged f-block lanthanide metal-based materials, we realized that the unique lanthanide nature, the H_4btc ligand and the reaction conditions could work synergistically to produce new 3D porous open frameworks. Here we report the synthesis and crystal structure of $[Eu_2(btc)(H_2btc)(H_2O)]\cdot 4H_2O$ (**1**), as well as some new phenomena observed during the course of investigations of its physical properties.

Results and Discussion

The hydrothermal reaction of an acidified aqueous solution of $EuCl_3$ with 1,2,4,5-benzenetetracarboxylic anhydride gives rise to **1** as colorless crystals. A single crystal X-ray analysis revealed that the three-dimensional microporous framework of compound **1** is built by linking one crystallographically independent nine-coordinate Eu^{III} subunit through its btc and H_2btc ligands. Each nine-coordinated Eu^{III} unit is a distorted tricapped trigonal prism, of which eight oxygen atoms belong to six different carboxylate groups of btc or H_2btc and the other one to a water molec-

[a] The State Key Laboratory of Structural Chemistry, Fujian Institute of Research on the Structure of Matter, the Chinese Academy of Sciences,
Fuzhou, Fujian 350002, P. R. China
Fax: (internat.) + 86-0591/371-4946
E-mail: czlu@ms.fjirsm.ac.cn
Supporting information for this article is available on the WWW under http://www.eurjic.com or from the author.

ule, with the $Eu^{III}-O$ bond lengths ranging from 2.353(4) to 2.581(4) Å.

Interestingly, there are two types of coordination modes for the H_4btc ligands in compound **1** (I and II). In mode I, each H_4btc unit acts as a dodecadentate ligand coordinating six europium(III) atoms, that is, each of the four carboxylate groups chelates to one Eu^{III} center, while every two adjacent oxygen atoms of the nearest carboxylate groups coordinate to one more europium(III) atom (Figure 1). In mode II, only two of the four carboxylate groups of an H_4btc ligand coordinate to europium(III) centers and each carboxylate group coordinates to two different Eu^{III}, thus, each ligand coordinates to four europium(III) centers (Figure 2). The H_4btc ligand links europium(III) atoms in very different ways to produce two different infinite network layers. The layers of these two types interlock with each other with a fold of about 60° to form a unique three-dimensional microporous framework with channels (dimensions about 10.331 × 11.201 Å). The zigzag $[EuO_6(H_2O)]_n$ tethers, which are built up from nine-coordinate europium(III) atoms with Eu−Eu distances of about 3.950(1) Å, are bridged by carboxyl oxygen atoms and the carboxylate groups of H_4btc. The channels are filled with eight water molecules per unit cell, which can be replaced by other suitable molecules under certain conditions (Figure 3). Finally, it should also be pointed out that the distances between guest water oxygen atoms are about 2.83(1) Å, while those between the water oxygen atoms and the oxygen atoms of the carboxylate groups range from 2.65(1) to 3.08(1) Å. Additionally, the distances between the oxygen atoms of coordinated water molecules and guest water molecules or carboxylate groups are also within the hydrogen bonding ranges [2.75(1) to 2.97(1) Å], indicating a complex hydrogen bonding network in the packing of compound **1**.

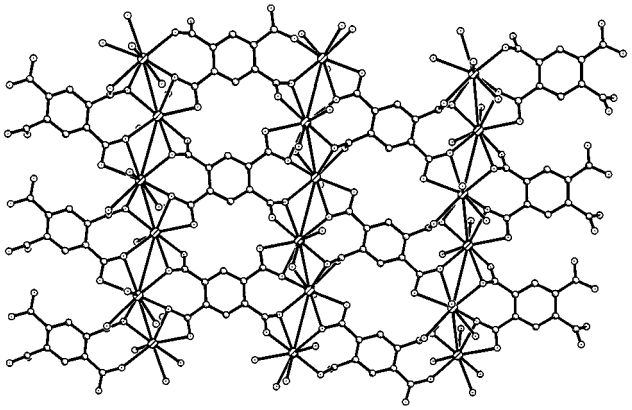

Figure 1. View of an intralamellar structure down the *a* axis for **1**, showing the environments of Eu^{III} atoms and one of the coordination modes for H_4btc

The variation of the molar magnetic susceptibility χ_M was investigated for compound **1** in the temperature range from 5.0 to 300 K in a 10 KG applied field. Figure 4 shows

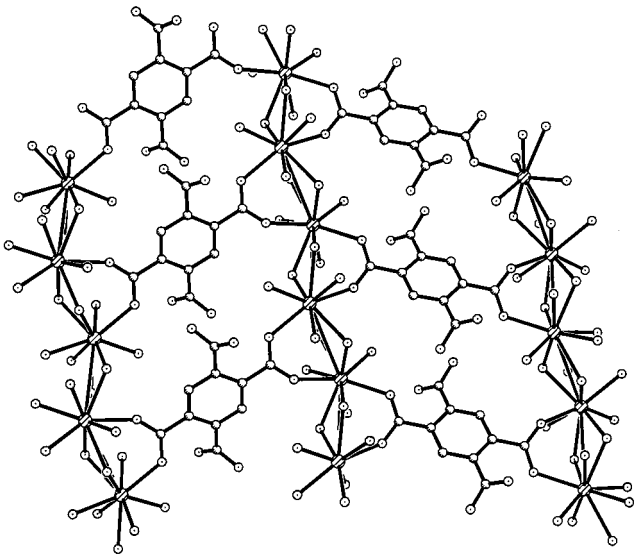

Figure 2. Side view of another intralamellar structure of **1**, showing the environments of the Eu^{III} atoms and the second coordination mode for H_4btc

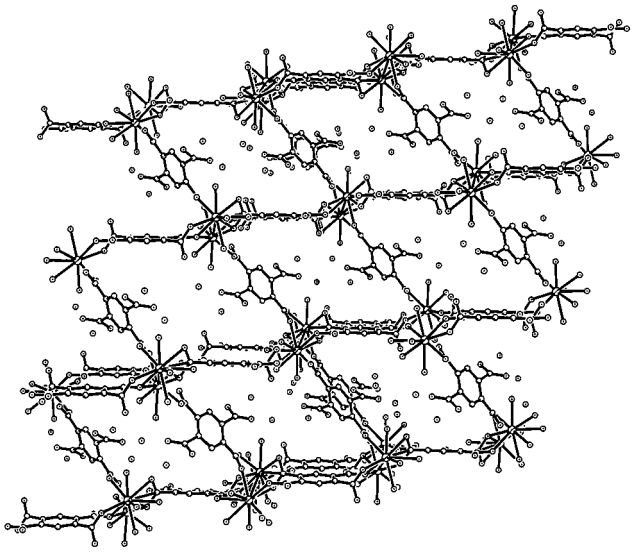

Figure 3. View down the *b* axis showing the channels that are occupied by water molecules in **1**

the magnetic behavior of **1** in the form of $\chi_M T$ vs. T and χ_M vs. T plots. At 299.2 K, the $\chi_M T$ value is 1.262 emu·K·mol^{-1} per Eu^{III}, and upon cooling to 5.0 K the $\chi_M T$ values decrease gradually to 0.0288 emu·K·mol^{-1}, indicating the presence of a strong paramagnetic coupling in compound **1**.

In contrast with transition metal compounds, the magnetic properties of rare earth metal compounds, even of mononuclear species, have not yet been fully understood. According to the literature,[14] the effect of the crystal field is not easily calculated, while the angular momentum often plays a key role in the magnetic susceptibilities of rare earth metal compounds. For the trivalent europium ion, the ^7F ground term is split by the spin orbit coupling into seven

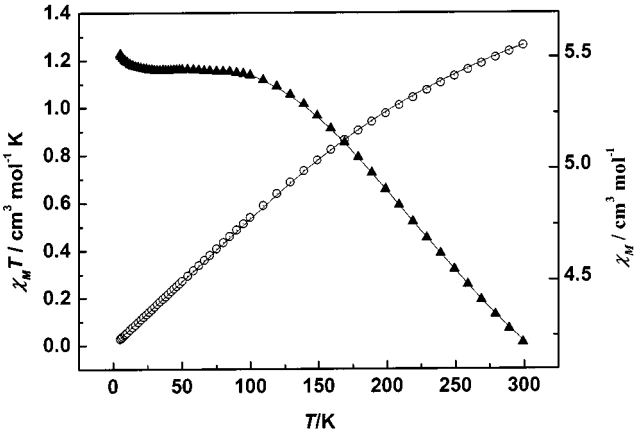

Figure 4. The $\chi_M T$ vs. T and χ_M vs. T plots for compound **1**

states, ^7F_J ($J = 0, 1, 2, \ldots 6$). Thus, the removal of the $2J + 1$ degeneracy of the ground state at zero field and the thermal population of the free-ion exited states must be considered in this case for Eu^{III}; these factors obviously cause the deviation from normal Curie−Weiss behavior. Based upon the above discussion, the magnetic susceptibility data were quantitatively analyzed using Equation (1):

$$\chi_M = N\beta^2/3k(T-\theta)x[24 + (27x/2 - 3/2)e^{-x} + (135x/2 - 5/2)e^{-3x} + (189x - 7/2)e^{-6x} + (405x - 9/2)e^{-10x} + (1485x/2 - 11/2)e^{15x} + (2457x/2 - 13/2)e^{-21x}]/[1 + 3e^{-x} + 5e^{-3x} + 7e^{-6x} + 9e^{-10x} + 11e^{-15x} + 13e^{-21x}] \quad (1)$$
with $x = \lambda/kT$

In this case, λ is the spin-orbit coupling parameter between ground and exited states through the Zeeman perturbation, while θ is the Curie−Weiss temperature. A least-squares fitting of all experimental data leads to λ and θ values of 393.99 cm^{-1} and 0.897 K with an agreement factor R of 2.0×10^{-5} ($R = \Sigma[(\chi_M)_{obs} - (\chi_M)_{calcd}]^2/\Sigma[(\chi_M)^2_{obs}]$). These results demonstrate that all of the europium(III) ions are well isolated from each other in the magnetic molecular field, even if the Eu−Eu distance is rather short [3.950(1) Å]. The paramagnetic behavior is mainly due to the spin-orbital coupling and weak ferromagnetic interactions between Eu^{III} centers transferred through oxygen atoms and the ligands.

Determination of the conductivity (powder sample from ground crystals) gives a value of 3.01×10^{-7} Scm^{-1} at 303 K for **1**, and it increases as the temperature rises, indicating that **1** is a semiconductor. This semiconducting behavior of **1**, which demonstrates the existence of either Eu−Eu or Eu−L−Eu interactions, is probably due to the unique structural feature whereby the arrays of Eu^{III} atoms are coordinated by bridging oxygen atoms, and to the short Eu−Eu distance [3.950(1) Å].

The overall neutral three-dimensional framework of **1** shows clearly the presence of large channels, which are occupied by water molecules. These guest molecules can be removed to generate nanoporous solids with retention of the framework skeleton. The thermogravimetric analysis (TGA) data graph shows a four-stage weight loss for compound **1**. The first stage, which occurs from 30−190 °C, is attributed to the loss of the four crystal water molecules per formula unit. The observed weight loss (7.3%) is in agreement with the calculated value (7.0%). The second stage occurs between 190−230 °C, with a weight loss corresponding to one aqua ligand per empirical formula (calcd. 2.0%; found 1.7%). The weight of the molecule remains almost unchanged in the third stage (230−410 °C). At 410 °C, the product begins to lose btc and H_2btc ligands and then to decompose.

A sample of **1** was ground and heated at 150 °C for 24 h at 10^{-2} Torr and then an XRPD spectrum was recorded of the remains. The characteristic peaks are almost identical to those of freshly prepared sample of **1**, which suggests that the hybrid organic-inorganic skeleton is retained. This result demonstrates clearly that the unique framework of **1** is rather stable and its application as a nanoporous material is very promising.

Conclusion

In summary, it is well-known that hydrothermal reactions often produce unprecedented complexes with interesting properties.[15] However, to produce novel complexes with desirable properties under mild reaction conditions is still the preferred option for most chemists. The successful isolation of complex **1** is an example of how to carry out hydrothermal reactions at relatively low temperatures (100 °C). Our strategy not only yields a novel architecture, but also allows us to understand more about whether the reactions are controlled by thermodynamic or by kinetic factors. Although the Eu−Eu distance in the $[EuO_6(H_2O)]_n$ chain is rather short [3.950(3) Å], the magnetic study reveals that the paramagnetic behavior of **1** is mainly due to the coupling among the populated free-ion states, which causes the magnetic behavior to deviate from the Curie−Weiss law. This work provides very important evidence that shows that the free-ion approximation is also appropriate for the interpretation of the magnetic properties of polynuclear rare earth metal species, while the contribution from the overlap of the magnetic orbitals can be almost ignored. The semiconducting behavior of **1** demonstrates the existence of metal-metal interactions. Based upon the TGA and XRPD analyses, the structure is rather stable, and this is undoubtedly due to the multidentate ligands forming a rigid framework for **1**. Moreover, from these studies, compound **1** is one of the few compounds that maintains its structural integrity after the removal of guest molecules. We have reasons to believe that it has potential applications for shape-selective reactions[16] or solvent-exchange process,[17] and these are now under investigation.

Experimental Section

Synthesis of 1: The pH of a mixture of $EuCl_3$ (0.68 mmol) (prepared from Eu_2O_3 dissolved in 35% HCl) and 1,2,4,5-benzenetetra-

carboxylic anhydride (0.22 g, 1.0 mmol) in H_2O (18 mL) was adjusted to 1.22 whilst stirring vigorously and the resulting mixture was then heated at 100 °C for twelve days under autogenous pressure in a sealed 30 mL Teflon-lined stainless steel vessel. Colorless crystals were isolated after the reaction solution was cooled down gradually and washed with water and ethanol. Yield: 0.239 g (76.8%, based on Eu). $C_{20}H_{18}Eu_2O_{22}$ (914.26): calcd. C 26.27, H 1.98; found C 26.19, H 1.96. IR (KBr pellet): $\tilde{\nu}$ = 1878w cm^{-1}, 1659s, 1610s, 1579s, 1554s, 1498s, 1429sh, 1387s, 1336m, 1323m, 1294s, 1269s, 1142w, 1124s, 849m, 933m, 881s, 849m, 835s, 816m, 775m, 754m, 658m, 590s, 521s, 442m. FT-Raman (solid, λ = 1064 nm): $\tilde{\nu}$ = 1677m cm^{-1}, 1633sh, 1594s, 1579s, 1459s, 1440sh, 1419sh, 1390sh, 1278m, 1253m, 1187s, 973s, 898s, 848s, 825m, 794s, 682s, 597w, 489m, 478m, 456m, 399m, 331m, 304w, 250m, 215m, 179m, 165m, 138m, 119m.

X-ray Crystallography: The determination of the unit cell and the data collection for a colorless crystal of compound **1** were performed on a Siemens SMART CCD, and the data were collected using graphite-monochromated Mo-K_α radiation (λ = 0.71073 Å) at 293 K in the range of $2.12 < \theta < 25.05°$. The data set was corrected with the SADABS program.[18] The structure was solved by direct methods and refined by full-matrix least-squares methods, which were performed using the SHELXL-97 software package.[19] All non-hydrogen atoms were refined anisotropically. Crystal data: $C_{20}H_{18}Eu_2O_{22}$, M_r = 914.26, monoclinic, space group $P2_1/n$, a = 10.7562(2), b = 7.2075(2), c = 17.2180(5) Å, β = 97.072(2)°, U = 1324.68(6) $Å^3$, Z = 2, D_c = 2.292 gcm^{-3}, μ = 4.795 mm^{-1}, $F(000)$ = 880, crystal size = 0.30 × 0.06 × 0.04 mm^3. $R1$ = 0.0289, $wR2$ = 0.0613 and S =1.077 for 1943 reflections with $F_o > 4\sigma(F_o)$ and 216 parameters ($R1$ = 0.0414 and $wR2$ = 0.0681 for all 2316 data). CCDC-160794 contains the supplementary crystallographic data for this paper. These data can be obtained free of charge at www.ccdc.cam.ac.uk/conts/retrieving.html [or from the Cambridge Crystallographic Data Centre, 12, Union Road, Cambridge CB2 1EZ, UK; fax: (internat.) +44-1223/336-033; E-mail: deposit@ccdc.cam.ac.uk].

Acknowledgments

We are grateful to the State Education Ministry, the State Personal Ministry, the National Natural Science Foundation of China (20073048), the NSF of Fujian and the Chinese Academy of Sciences for financial support.

[1] W. F. Hölderich, H. van Bekkum, in *Introduction to Zeolite Science and Practice* (*Stud. Surf. Sci. Catal.* **1991**, *58*, 631−727).
[2] S. M. Csicsery, *Zeolites* **1984**, *4*, 202−213.
[3] S. S.-Y. Chui, S. M.-F. Lo, J. P. H. Charmant, A. G. Orpen, L. D. Willians, *Science* **1999**, *283*, 1148−1150.
[4] M. J. Zaworotko, *Angew. Chem.* **2000**, *112*, 3180−3182; *Angew. Chem. Int. Ed.* **2000**, *39*, 3052−3054.
[5] H. Li, M. Eddaoudi, T. L. Groy, O. M. Yaghi, *J. Am. Chem. Soc.* **1998**, *120*, 8571−8572.
[6] C. Janiak, *Angew. Chem.* **1997**, *109*, 1499−1502; *Angew. Chem. Int. Ed. Engl.* **1997**, *36*, 1431−1434.
[7] G. B. Gardner, D. Venkataraman, J. S. Moore, S. Lee, *Nature* **1995**, *374*, 792−795.
[8] M. L. Occelli and H. C. Robson, in *Zeolite Synthesis*, American Chemical Society, Washington DC, **1989**.
[9] C. T. Kresge, M. E. Leonowicz, W. J. Roth, J. C. Vartuli, J. S. Beck, *Nature* **1992**, *359*, 710−712.
[10] L. L. Hench, *Inorganic Biomaterials*, in *Materials Chemistry, an Emerging Discipline*, (Eds.: L. V. Interrante, L. A. Caspar and A. B. Ellis), ACS Ser. 245, **1995**, ch. 21, pp. 523−547.
[11] P. J. Hagrman, D. Hagrman, J. Zubieta, *Angew. Chem.* **1999**, *111*, 2798−2848; *Angew. Chem. Int. Ed.* **1999**, *38*, 2638−2684.
[12] F. Takusagawa, K. Hirotsu, A. Shimada, *Bull. Chem. Soc. Jpn.* **1971**, *44*, 1274−1278.
[13] For several examples, see: [13a] A. Nectoux, H. Abazli, J. Jove, A. Cousson, M. Pages, M. Gasperin, G. Choppin, *J. Less-Common Met.* **1984**, *97*, 1−10. [13b] A. Cousson, B. Stout, F. Nectoux, M. Pages, *J. Less-Common Met.* **1986**, *125*, 111−115. [13c] C. Robl, *Z. Anorg. Allg. Chem.* **1987**, *554*, 79−86. [13d] Y. Xing, Z.-S. Jin, Z.-B. Duan, J.-Z. Ni, *Acta Chim. Sinica* **1987**, *45*, 1044−1047. [13e] O. M. Yaghi, H. Li, T. L. Groy, *Z. Kristallogr.-New Crystal Structures* **1997**, *212*, 457. [13f] B. T. Usubaliev, A. N. Shnulin, Kh. S. Mamedov, *Koord. Khim.* **1982**, *8*, 1532−1538. [13g] C. Robl, S. Hentschel, *Mater. Res. Bull.* **1991**, *26*, 1355−1362. [13h] F. Jaber, F. Charbonnier, R. Faure, *J. Chem. Cryst.* **1997**, *27*, 397−400. [13i] C. Robl, *Mater. Res. Bull.* **1992**, *27*, 99−107. [13j] F. R. Rochon, G. Massarweh, *Inorg. Chim. Acta* **2000**, *304*, 190−198.
[14] [14a] M. Andruh, E. Bakalbasis, O. Kahn, J. C. Trombe, P. Porcher, *Inorg. Chem.* **1993**, *32*, 1616−1622. [14b] E. Bakalbasis, O. Kahn, J. Sainton, J. C. Trombe, J. Gaiy, *J. Chem. Soc., Chem. Commun.* **1991**, 755−756.
[15] [15a] J. Gopalakrishnan, *Chem. Mater.* **1975**, *7*, 1265. [15b] A. Rabenau, *Angew. Chem.* **1985**, *97*, 1017−1031; *Angew. Chem. Int. Ed. Engl.* **1985**, *24*, 1026−1040. [15c] R. A. Ludise, *Chem. Eng. News* **1987**, *65*(40), 30−43. [15d] J. Y. Lu, M. L. Lawandy, J. Li, T. Yuen, C. L. Lin, *Inorg. Chem.* **1999**, *38*, 2695−2704.
[16] M. Hölscher, U. Englert, B. Zibrowins, W. F. Hölderich, *Angew. Chem.* **1994**, *106*, 2552−2554; *Angew. Chem. Int. Ed. Engl.* **1994**, *33*, 2491−2493.
[17] [17a] M. Fujita, O. Sasaki, K. Watanabe, K. Ogura, K. Yamaguchi, *New. J. Chem.* **1998**, *22*, 189. [17b] L. Carlucci, G. Liani, D. M. Proserpio, S. Rizzato, *Angew. Chem.* **2000**, *112*, 1566−1570; *Angew. Chem. Int. Ed.* **2000**, *39*, 1506−1510.
[18] G. M. Sheldrick. SADABS; Siemens Analytical X-ray Instrument Division: Madison, WI, **1995**.
[19] G. M. Sheldrick, Universität Göttingen, Germany, **1997**.

Received September 21, 2001
[I01374]

From *P*-Metalated *trans*-Iminodiphosphanes to *N*-Metalated *cis*-Iminodiphosphanes: An Unprecedented Rearrangement

Maria Zablocka,[a] Krzysztof Owsianik,[a] Alain Igau,[b] Aleksandra Skowronska,[a] and Jean-Pierre Majoral*[b]

Keywords: Phosphanes / Zirconium / N ligands

The reaction of chlorophosphanes with azazirconacyclopentenes provides an unique way to cyclic *P*-metalated *trans*-iminodiphosphanes, which rearrange to give unprecedented *N*-metalated *cis*-iminodiphosphanes.

(© Wiley-VCH Verlag GmbH, 69451 Weinheim, Germany, 2002)

Introduction

The search for new derivatives incorporating phosphorus and nitrogen continues to receive considerable attention due to the versatility of these ligands (combination of hard and soft donor atoms) towards complexation. Classical nitrogen ligands (amine, pyridine, oxazoline, quinoline, pyrazole etc.) and classical phosphanes constitute the coordinating skeleton of the majority of these P,N species.[1] Similarly, β- or γ-iminophosphanes in which the imine acts as a weak π-acceptor and the phosphane as a good σ-donor are also being used more and more frequently. Palladium(II) complexes of these phosphorus-nitrogen mixed donors ligands have been found, for example, to be efficient catalysts for the Heck reaction,[2] for the carbostannylation of alkynes,[3] for the copolymerisation of CO/ethylene and CO/norbornylene[4] or for allylic alkylation.[5]

In contrast, very few iminodiphosphanes, namely the linear *trans*-*C*-phosphanyl, *N*-phosphanyl imines **I**, are known[6] and no complexes of this potential ligand or free or complexed *trans* or *cis* cyclic analogs of these derivatives have been described.

We report herein a powerful and versatile one-pot synthesis of cyclic *P*-metalated *trans*-iminodiphosphanes from azazirconacyclopentenes and chlorophosphanes and the quite unusual rearrangement of the former derivatives to cyclic *N*-metalated *cis*-iminodiphosphanes.

[a] Centre of Molecular and Macromolecular Studies, Polish Academy of Sciences,
Sienkiewicza 112, 90-362, Lodz, Poland
[b] Laboratoire de Chimie de Coordination, CNRS,
205 route de Narbonne, 31077 Toulouse cedex 4, France
Fax: (internat.) + 33-5/6155-3003
E-mail: majoral@lcc-toulouse.fr

Results and Discussion

We have already reported that the thermolysis of diphenylzirconocene in the presence of bis(amino)cyanophosphane leads to the formation of the azazirconacyclopentenes **1** and **1′**. These complexes can then be reacted with various dichlorophosphanes to give the 1,2-azaphosphindoles **2** and Cp_2ZrCl_2 (Scheme 1).[7] The same reaction performed with chlorophosphanes R'_2PCl (**3a−c: a** R′ = Me, **b** R′ = Et, **c** R′ = Ph) instead of dichlorophosphanes proceeds differently. In this case no exchange reaction takes place. Indeed, the addition of chlorophosphanes **3a−c** to **1** (R = N*i*Pr$_2$) in toluene at −20 °C affords the unexpected cyclic *P*-metalated *trans* (the two phosphanyl groups) iminodiphosphanes **4a−c** (Scheme 2). The reaction can be monitored by ^{31}P NMR spectroscopy which shows the disappearance of the signal due to **1** (δ = 45) and the appearance of two doublets at δ = 74.0 [P(NiPr$_2$)$_2$] and 67.5 (PMe$_2$) ($J_{P,P}$ = 6.9 Hz) for **4a**, δ = 78.4 (PEt$_2$) and 74.1 [P(NiPr$_2$)$_2$] ($J_{P,P}$ = 8 Hz) for **4b** and δ = 78.8 [P(NiPr$_2$)$_2$] and 63.3 (PPh$_2$) ($J_{P,P}$ = 8.6 Hz) for **4c**. The direct complexation of the R$_2$P phosphanyl group to the 16e$^-$ zirconium moiety is shown in the ^{1}H NMR spectrum by the presence of two doublets for the Cp groups due to the coupling between phosphorus and the Cp protons ($1.9 < J_{H,P} < 2.2$ Hz). Such $J_{H,P}$ values are characteristic of compounds with a P→ZrCp$_2$ dative bond.[8] The formation of **4a−c** can be viewed as the 1,2-addition of the chlorophosphane to the zirconium-nitrogen covalent bond of **1** initiated by the halophilicity of the zirconium moiety and the nucleophilicity of the cyclic imino-nitrogen bond, followed by direct complexation of the phosphanyl group at zirconium. However, the resulting *P*-metalated *trans*-iminodiphosphanes appear to be the kinetic products of the reaction. In solution at room temperature, **4a−b** afford the thermodynamically favored complexes **5a−b** (Scheme 2). Such an evolution de-

pends strongly on the nature of the phosphanyl group linked to zirconium: it takes 24 h for the transformation **4a** → **5a** and 24 days for **4b** → **5b**. The evolution of **4c** gave numerous unidentified products.

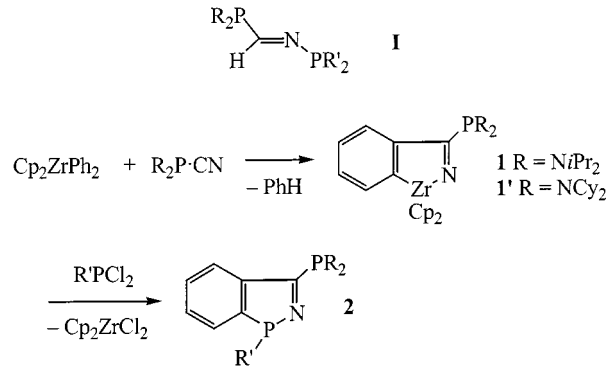

Scheme 1

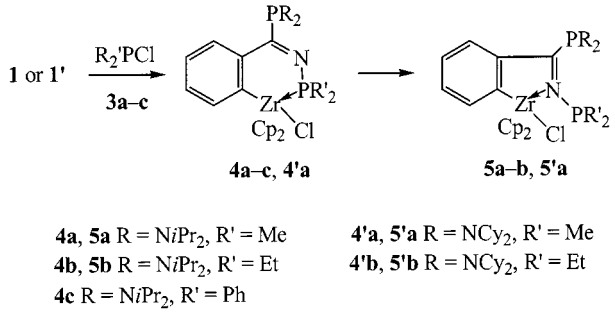

Scheme 2

These transformations can be monitored by ^{31}P NMR spectroscopy. As an example, the two doublets for **4a** disappeared and two new doublets appeared at δ = 74.0 (PMe_2) and 41.7 [$P(NiPr_2)_2$] ($J_{P,P}$ = 6.2 Hz) for **5a**. As expected, only a singlet is detected for the Cp groups in the ^1H NMR spectrum, strongly indicating that the phosphanyl group is not linked to the Cp_2Zr unit. A similar observation can be made for the evolution of **4b** into **5b**, with an analogous characteristic shielding effect in the ^{31}P NMR spectrum for the $P(NiPr_2)_2$ group (Δδ = 30.1 ppm).

The stability of *P*-metalated *trans*-iminodiphosphanes and their transformation to the corresponding *N*-metalated *cis*-iminodiphosphanes depends also on the nature of the substituents directly linked to the exocyclic phosphorus atom. Thus, treatment of the azazirconacyclopentene **1′** with chlorodimethylphosphane **3a** at −20 °C leads to the unstable *P*-metalated *trans*-iminodiphosphane **4′a** which was only characterized by ^{31}P NMR spectroscopy {doublets at δ = 81.3 [$P(N(Cy)_2$] and 64.9 (PMe_2) with $J_{P,P}$ = 7.0 Hz}. The evolution of **4′a** is fast (a few hours at room temperature) and leads to the thermodynamically stable complex **5′a** which was fully characterized by NMR spectroscopy, mass spectrometry and elemental analysis. In marked contrast the same reaction performed with **1′** and **3b** allowed us to isolate the *P*-metalated iminodiphosphane **4′b** {$\delta^{31}P$ = 80.7 [$P(N(Cy)_2]_2$ and 77.1 (PEt_2) ($J_{P,P}$ = 8.5 Hz)}. The formation of a dative bond between the Et_2P group and Zr is again confirmed by the presence in the ^1H NMR spectrum of the characteristic two doublets for the Cp groups at δ = 5.87 and 6.25 with $J_{H,P}$ = 2.0 and 1.9 Hz. The full transformation of **4′b** to **5′b** occurs at room temperature after 6 h (Scheme 2). Here again a typical shielding effect is observed for the $P[N(Cy)_2]_2$ group when moving from the six- to the five-membered ring (Δδ = 34.6 ppm).

Attempts to grow suitable crystals for an X-ray diffraction study have so far been unsuccessful.

Conclusion

The treatment of cyanophosphanes successively with diphenylzirconocene and then a chlorophosphane allows the clean reduction of the cyano group to an imino group, the formation of cyclic *P*-metalated *trans*-iminodiphosphanes and their unprecedented rearrangement to cyclic *N*-metalated *cis*-iminodiphosphanes. Such a sequence of reactions can be performed as a one-pot process.

Investigations concerning the generality of this unique synthetic methodology, studies concerning the complexation of the *N*-metalated *cis*-iminodisphosphanes and the use of the resulting complexes in catalytic processes are currently underway.

Experimental Section

General: All reactions were carried out under argon using standard Schlenk techniques and vacuum-line manipulations. All solvents were dried degassed and distilled before use. A Perkin−Elmer 1725X spectrometer was used to record the FT-IR spectra. NMR spectra were recorded on Bruker AC80, AC200, or AM250 spectrometers for ^1H, ^{13}C and ^{31}P NMR, with $SiMe_4$ and H_3PO_4, as references. The assignment of the signals in the ^{13}C NMR spectrum was done using Jmod, two dimensional HMBC and HMQC, broad band or CW ^{31}P decoupling experiments when necessary.

Compound 4a: Chlorodimethylphosphane (0.079 g, 64.8 μL, 0.82 mmol) was added to a solution of azazirconacyclopentene **1** (0.455 g, 0.82 mmol) in toluene at −20 °C. The mixture was stirred at room temperature for 30 min, and then evaporated to dryness. The resulting solid residue was extracted with pentane (2 × 20 mL) and filtered. The volatiles were removed from the solution to give **4a** as a yellow solid in 92% yield (0.491 g). ^1H NMR (C_6D_6): δ = 0.62 (d, $J_{H,P}$ = 5.7 Hz, 3 H, CH_3), 1.01 (d, $J_{H,H}$ = 6.7 Hz, 12 H, CH_3), 1.14 (d, $J_{H,H}$ = 6.7 Hz, 12 H, CH_3), 1.31 (d, $J_{H,P}$ = 4.2 Hz, 3 H, CH_3), 3.4 (sept, $J_{H,H}$ = 6.7 Hz, 4 H, CH), 5.74 (d, $J_{H,P}$ = 2.0 Hz, 5 H, CH_{Cp}), 6.09 (d, $J_{H,P}$ = 1.9 Hz, 5 H, CH_{Cp}), 7.14 (m, 1 H, CH_{arom}), 7.53 (m, 1 H, CH_{arom}), 7.89 (d, $J_{H,P}$ = 1.1 Hz, $J_{H,H}$ = 7.7 Hz, CH_{arom}), 8.5 (d, $J_{H,H}$ = 7.7 Hz, CH_{arom}). $^{13}C\{^1H\}$ NMR (C_6D_6): δ = 15.4 (d, $J_{C,P}$ = 16.7 Hz, CH_3P), 17.7 (d, $J_{C,P}$ = 16.6 Hz, CH_3P), 25.4 (d, $J_{C,P}$ = 11.1 Hz, CH_3), 26.6 (d, $J_{C,P}$ = 8.5 Hz, CH_3), 26.8 (d, $J_{C,P}$ = 10.6 Hz, CH_3), 51.4 (d, $J_{C,P}$ = 8 Hz, CH), 58.4 (d, $J_{C,P}$ = 11.9 Hz, CH), 109.8 (s, CH_{Cp}), 109.9 (s, CH_{Cp}), 124.1, 125.2, 137.6 (s, CH_{arom}), 156.1 (dd, $J_{C,P}$ = 7.5 Hz, $J_{C,P}$ = 20.9 Hz, C_{arom}), 172.9 (dd, $J_{C,P}$ = 26.9 Hz, C_{arom}), 204.3 (dd, $J_{C,P}$ = 12.2 Hz, $J_{C,P}$ = 8.9 Hz, C=N). $^{31}P\{^1H\}$ NMR (C_6D_6): δ = 74.0 [d, $J_{P,P}$ = 6.9 Hz, $P(NiPr_2)_2$], 67.5 (d, $J_{P,P}$ = 6.9 Hz,

PMe_2). $C_{31}H_{48}ClN_3P_2Zr$ (651.36): calcd. C 57.16, H 7.42, N 6.45; found C 57.01, H 7.38, N 6.39.

Compound 4b: Same experimental procedure as for **4a** starting from **1** (0.416 g, 0.75 mmol) and chlorodiethylphosphane (0.094 g. 91 μL, 0.75 mmol); **4b** was obtained in 88% yield (0.484 mg). ^1H NMR (C_6D_6): δ = 0.65 (dt, $J_{H,H}$ = 7.5 Hz, $J_{H,P}$ = 18.8 Hz, 3 H, CH_3, Et), 0.68 (dt, $J_{H,H}$ = 7.7 Hz, $J_{H,P}$ = 13.3 Hz, 3 H, CH_3, Et), 1.10 (d, $J_{H,H}$ = 6.7 Hz, 12 H, CH_3), 1.20 (d, $J_{H,H}$ = 6.7 Hz, 12 H, CH_3), 2.20 (m, 4 H, CH_2), 3.50 (sept, $J_{H,H}$ = 6.7 Hz, 4 H, CH), 5.94 (d, $J_{H,P}$ = 2.0 Hz, 5 H, $CH_{C,P}$), 6.17 (d, $J_{C,P}$ = 2.2 Hz, 5 H, CH_{Cp}), 7.30 (m, 1 H, CH_{arom}), 8.00 (dd, $J_{H,P}$ = 1.2 Hz, $J_{H,H}$ = 7.7 Hz, 1 H, CH_{arom}), 8.21 (d, $J_{H,H}$ = 7.9 Hz, 1 H, CH_{arom}), 8.64 (d, $J_{H,H}$ = 7.6 Hz, 1 H, CH_{arom}). $^{13}C\{^1H\}$ NMR (C_6D_6): δ = 8.2 (d, $J_{C,P}$ = 8.1 Hz, CH_2CH_3), 18.5 (d, $J_{C,P}$ = 8.8 Hz, CH_2CH_3), 25.5 (d, $J_{C,P}$ = 12.1 Hz, CH_3), 27.6 (d, $J_{C,P}$ = 12.1 Hz, CH_3), 51.5 (d, $J_{C,P}$ = 8.9 Hz, CH), 58.7 (d, $J_{C,P}$ = 12.6 Hz, CH), 110.5 (s, CH_{Cp}), 109.8 (s, CH_{Cp}), 124.2, 126.6, 128, 146.5 (s, CH_{arom}), 146.2 (d, $J_{C,P}$ = 3.5 Hz, CH), 173.7 (d, $J_{C,P}$ = 27.1 Hz, C_{arom}), 205.1 (dd, $J_{C,P}$ = 10.0 Hz, $J_{C,P}$ = 9.8 Hz, C=N). $^{31}P\{^1H\}$ NMR (C_6D_6): δ = 78.4 (d, $J_{P,P}$ = 8.0 Hz, PEt_2), 74.1 [d, $J_{P,P}$ = 8.0 Hz, $P(NiPr_2)_2$]. $C_{33}H_{52}ClN_3P_2Zr$ (679.4): calcd. C 58.34, H 7.71, N 6.18; found C 58.16, H 7.60, N 6.04.

4c: ^1H NMR (C_6D_6): δ = 1.09 (d, $J_{H,H}$ = 6.7 Hz, 12 H, CH_3), 1.20 (d, $J_{H,H}$ = 6.7 Hz, 12 H, CH_3), 3.40 (sept $J_{H,H}$ = 6.7 Hz, 4 H, CH), 6.12 (d, $J_{H,P}$ = 1.9 Hz, 5 H, Cp), 6.17 (d, $J_{H,P}$ = 2.1 Hz, 5 H, Cp), 7.1−7.6 (m, 12 H, CH_{arom}), 8.22 (m, 1 H, CH_{arom}), 8.83 (d, $J_{H,H}$ = 6.9 Hz, 1 H, CH_{arom}). $^{13}C\{^1H\}$ NMR (C_6D_6): δ = 23.4 (d, $J_{C,P}$ = 5.7 Hz, CH_3), 24.2 (d, $J_{C,P}$ = 5.8 Hz, CH_3), 49.5 (d, $J_{C,P}$ = 12.0 Hz, CH), 111.6 (s, CH, Cp), 124.4 (d, $J_{C,P}$ = 24.3 Hz, C_{ipso}), 124.9 (d, $J_{C,P}$ = 23.8 Hz, C_{ipso}), 127.6, 127.8, 128.0, 128.4 (s, CH_{arom}, PPh), 124.1, 126.7, 138.6 (s, CH_{arom}), 178.9 (s, *C*−C=N), 199.9 (dd, $J_{C,P}$ = 12 Hz, $J_{C,P}$ = 9 Hz, C=N). $^{31}P\{^1H\}$ NMR (C_6D_6): δ = 78.8 [d, $J_{P,P}$ = 8.6 Hz, $P(NiPr_2)_2$], 63.3 (d, $J_{P,P}$ = 8.6 Hz, PPh_2). $C_{41}H_{52}ClN_3P_2Zr$ (775.50): calcd. C 63.50, H 6.76, N 5.42; found C 63.31, H 6.51, N 5.34.

Compound 5a: Evolution of **4a** at room temperature in toluene for 24 h gave rise quantitatively to **5a**. ^1H NMR (C_6D_6): δ = 1.20 (d, $J_{H,H}$ = 6.6 Hz, 12 H, CH_3), 1.24 (d, $J_{H,H}$ = 6.6 Hz, 12 H, CH_3), 1.27 (d, $J_{H,P}$ = 3.0 Hz, 6 H, CH_3P), 3.30 (m, 4 H, CH), 5.80 (s, 10 H, CH_{Cp}), 7.0−7.2 (m, 2 H, CH_{arom}), 7.52 (m, 1 H, CH_{arom}), 8.41 (dd, $J_{H,H}$ = 7.8 Hz, $J_{H,P}$ = 0.9 Hz, 1 H, CH_{arom}). $^{13}C\{^1H\}$ NMR (C_6D_6): δ = 14.0 (dd, $J_{C,P}$ = 5 Hz, $J_{C,P}$ = 23.0 Hz, CH_3), 24.3 (d, $J_{C,P}$ = 5.4 Hz, CH_3), 24.5 (d, $J_{C,P}$ = 5.8 Hz, CH_3), 48.1 (d, $J_{C,P}$ = 10.4 Hz, CH), 112.2 (s, CH_{Cp}), 112.6 (s, CH_{Cp}), 124.9, 125.7, 126.8, 139.0 (s, CH_{arom}), 145.1 (dd, $J_{C,P}$ = 41.9 Hz, $J_{C,P}$ = 17.8 Hz, *C*−C=N), 156.1 (dd, $J_{C,P}$ = 4.6 Hz, $J_{C,P}$ = 17.8 Hz, C-Zr), 185.8 (dd, $J_{C,P}$ = 15.7 Hz, $J_{C,P}$ = 15.7 Hz, C=N). $^{31}P\{^1H\}$ NMR (C_6D_6): δ = 74.0 (d, $J_{P,P}$ = 6.2 Hz, PMe_2), 41.7 [d, $J_{P,P}$ = 6.2 Hz $P(NiPr_2)_2$]. $C_{31}H_{48}ClN_3P_2Zr$ (651.4): calcd. C 57.16, H 7.42, N 6.45; found C 56.97, H 7.35, N 6.31.

Compound 5b: The evolution of **4b** to **5b** was very slow (24 days) and the formation of **5b** (NMR yield: 60%) was accompanied by that of numerous unidentified by-products. **5b** was only characterized by ^{31}P NMR [δ = 86.9 (d, $J_{P,P}$ = 6.5 Hz), 43.9 (d, $J_{P,P}$ = 6.5 Hz)].

Compounds 4′a and 5′a: Chlorodimethylphosphane (0.068 g, 56 μL, 0.7 mmol) was added to a solution of azazirconacyclopentene **1′** (0.364 g, 0.7 mmol) in toluene at −20 °C. The mixture was stirred at room temperature for 15 min and then evaporated to dryness. The resulting solid residue was extracted with pentane (20 mL) and filtered. The volatiles were removed from the solution to give a mixture of **4′a** and **5′a** in a 4:1 ratio. Compound **4′a** was only characterized by ^{31}P NMR: δ = 81.3 (d, $J_{P,P}$ = 7.0 Hz, $P(NCy_2)_2$, 64.9 (d, $J_{P,P}$ = 7.0 Hz, PMe_2). Evolution of **4′a** to **5′a** is fast and complete within 24 h at room temperature.

5′a: ^1H NMR (C_6D_6): δ = 1.06 (d, $J_{H,P}$ = 3.2 Hz, 3 H, CH_3), 1.29 (d, $J_{H,P}$ = 3.2 Hz, 3 H, CH_3), 1.39−2.11 (m, 40 H, CH_2), 3.21−3.30 (m, 4 H, CHN), 6.00 (s, 10 H, CH_{Cp}), 6.45−7.20 (m, 2 H, CH_{arom}), 7.51 (d, $J_{H,H}$ = 6.5 Hz, 1 H, CH_{arom}), 8.51 (d, $J_{H,H}$ = 5.5 Hz, 1 H, CH_{arom}). $^{13}C\{^1H\}$ NMR (C_6D_6): δ = 13.6 (d, $J_{C,P}$ = 23.6 Hz, CH_3), 13.7 (d, $J_{C,P}$ = 23.6 Hz, CH_3), 26.0, 26.8, 27.0 (s, CH_2), 35.0 (br. s, CH_2), 57.6 (d, $J_{C,P}$ = 9.4 Hz, CH), 57.9 (d, $J_{C,P}$ = 8.5 Hz, CH), 113.8 (s, CH, C_{Cp}), 125.6, 125.8, 126.7, 138.6 (s, CH_{arom}), 145.3 (dd, $J_{C,P}$ = 43.4 Hz, $J_{C,P}$ = 21.8 Hz, CCN), 155.5 (dd, $J_{C,P}$ = 3.7 Hz, $J_{C,P}$ = 17.7 Hz, C-Zr), 185.6 (dd, $J_{C,P}$ = 17.4 Hz, $J_{C,P}$ = 17.4 Hz, C=N). $^{31}P\{^1H\}$ NMR (C_6D_6): δ = 70.2 (d, $J_{P,P}$ = 8.4 Hz, PMe_2), 40.3 [d, $J_{P,P}$ = 8.4 Hz, $P(NCy_2)_2$]. $C_{43}H_{64}ClN_3P_2Zr$ (811.6): calcd. C 63.63, H 7.95, N 5.18; found C 63.41, H 7.89, N 5.09.

Compound 4′b: Chlorodiethylphosphane (0.077 g, 76 μL, 0.62 mmol) was added to a solution of azazirconacyclopentene **1′** (0.323 g, 0.62 mmol) in toluene at −20 °C. The mixture was stirred at room temperature for 20 min and then the solvents evaporated to dryness. The resulting solid residue was extracted with pentane (2 × 20 mL) and filtered. The volatiles were removed from the solution to give **4′b** as an orange-yellow solid in 68% yield (0.272 mg). ^1H NMR (C_6D_6): δ = 1.57 (t, $J_{H,H}$ = 3.1 Hz, 3 H, CH_3), 1.64 (t, $J_{H,H}$ = 3.1 Hz, 3 H, CH_3), 2.15 (dq, $J_{H,P}$ = $J_{H,H}$ = 3.1 Hz, 4 H, CH_2), 1.20−2.10 (m, 40 H, CH_2), 2.95 (br. s, 4 H, CHN)5.87 (d, $J_{H,P}$ = 2.0 Hz, 5 H, CH_{Cp}), 6.25 (d, $J_{H,P}$ = 1.9 Hz, 5 H, CH_{Cp}), 7.02−7.40 (m, 2 H, CH_{arom}), 7.70 (m, 1 H, CH_{arom}), 8.50 (d, $J_{H,H}$ = 9.2 Hz, 1 H, CH). $^{13}C\{^1H\}$ NMR (C_6D_6): δ = 10.3 (s, CH_3), 10.6 (s, CH_3), 20.9 (d, $J_{C,P}$ = 11.7 Hz, CH_2), 26.4, 27.5, 27.7 (s, CH_2), 35.7 (br. s, CH_2), 56.6 (d, $J_{C,P}$ = 9.2 Hz, CHN), 58.5 (d, $J_{C,P}$ = 8.2 Hz, CHN), 59.6 (d, $J_{C,P}$ = 8.3 Hz, CHN), 62.0 (d, $J_{C,P}$ = 8.4 Hz, CHN), 110.2 (s, CH_{Cp}), 110.4 (s, CH_{Cp}), 124.7, 125.6, 126.0, 137.4 (s, CH_{arom}), 147.1 (s, C_{arom}), 172.8 (d, $J_{C,P}$ = 25.7 Hz, C_{arom}), 205.0 (dd, $J_{C,P}$ = 12.73 Hz, $J_{C,P}$ = 9 Hz, C=N). $^{31}P\{^1H\}$ NMR (C_6D_6): δ = 80.7 (d, $J_{P,P}$ = 8.5 Hz, PEt_2), 77.1 [d, $J_{P,P}$ = 8.5 Hz, $P(NCy_2)_2$]. $C_{45}H_{68}ClN_3P_2Zr$ (839.67): calcd. C 64.37, H 8.16, N 5.00; found C 64.21, H 7.98, N 4.92.

Compound 5′b: Compound **4′b** evolves quickly (6 h, room temperature) to give **5′b**. ^1H NMR (C_6D_6): δ = 0.92 (t, $J_{H,H}$ = 7.5 Hz, 3 H, CH_3), 0.99 (t, $J_{H,H}$ = 7.4 Hz, 3 H, CH_3), 1.31−1.95 (m, 40 H, CH_2), 3.25 (q, $J_{H,H}$ = 7.0 Hz, 4 H, CH_2), 3.15−3.35 (m, 4 H, CH), 5.81 (s, 10 H, CH_{Cp}), 7.02−7.20 (m, 2 H, CH_{arom}), 7.60 (d, $J_{H,H}$ = 6.8 Hz, 1 H, CH_{arom}), 8.55 (d, $J_{H,H}$ = 8.7 Hz, 1 H, CH_{arom}). $^{13}C\{^1H\}$ NMR (C_6D_6): δ = 10.1 (d, $J_{C,P}$ = 14.0 Hz, CH_3), 21.0 (d, $J_{C,P}$ = 12.7, CH_2), 26.7, 27.5, 27.7, 35.7 (s, CH_2), 58.5 (br. s, CH), 114.6 (s, CH_{Cp}), 125.4, 125.6, 126.4, 138.2, (s, CH_{arom}), 146.0 (dd, $J_{C,PN}$ = 41.6 Hz, $J_{C,PEt}$ = 21.4 Hz, C_{arom}), 154.1 (dd, $J_{C,P}$ = 5.3 Hz, $J_{C,P}$ = 19.2 Hz, C_{arom}), 186.8 (dd, $J_{C,P}$ = 17.4 Hz, C=N). $^{31}P\{^1H\}$ NMR (C_6D_6): δ = 83.2 (d, $J_{P,P}$ = 6.9 Hz, PEt_2), 42.5 (d, $J_{P,P}$ = 6.9 Hz, $P(NCy_2)_2$. $C_{45}H_{68}ClN_3P_2Zr$ (839.67): calcd. C 64.37, H 8.16, N 5.00; found C 64.17, H 7.82, N 4.86.

Acknowledgments

This work was performed with the support of the European Associate Laboratory financed by CNRS (France) and the Polish Committee for Scientific Research (KBN grant 3TO9A03619).

[1] F. Y. Kwong, K. S. Chan, *Organometallics* **2001**, *20*, 2570−2578 and references therein.
[2] K. R. Reddy, K. Surekka, G.-H. Lee, S.-M. Peng, S.-T. Liu, *Organometallics* **2000**, *19*, 2637−2639.
[3] [3a] E. Shirakawa, H. Yoshida, T. Kurahashi, Y. Nakao, T. Hiyama, *J. Am. Chem. Soc.* **1998**, *120*, 2975−2976. [3b] T. Hiyama, *J. Organomet. Chem.* **1999**, *576*, 169−178. [3c] E. Shirakawa, K. Yamasaki, H. Yoshida, T. Hiyama, *J. Am. Chem. Soc.* **1999**, *121*, 10221−10222.
[4] K. R. Reddy, C. L. Chen, Y.-H. Liu, S.-M. Peng, J.-T. Chen, S.-T. Liu, *Organometallics* **1999**, *18*, 2574−2576.
[5] R. J. van Haaren, C. J. M. Druijven, G. P. F. van Strijdonck, H. Oevering, J. N. H. Reek, P. C. J. Kamer, P. W. N. M. van Leeuwen, *J. Chem. Soc., Dalton Trans.* **2000**, 1549−1554.
[6] F. Boutonnet, N. Dufour, T. Straw, A. Igau, J.-P. Majoral, *Organometallics* **1991**, *10*, 3939−3941.
[7] V. Cadierno, B. Donnadieu, A. Igau, J.-P. Majoral, *Eur. J. Inorg. Chem.* **2000**, 417−421.
[8] See for example: A. Igau, N. Dufour, A. Mahieu, J. P. Majoral, *Angew. Chem. Int. Ed. Engl.* **1993**, *32*, 95−97.

Received October 10, 2001
[I01403]

Structure Determination of the α = 3, β = 6 Term of the $(A_3B_2O_6)_\alpha(A_3B_3O_9)_\beta$ Homologous Series (A = Ba, B = Rh) by a Combination of Powder X-ray Diffraction and Electron Microscopy

Khalid Boulahya,[a] María Hernando,[a] Aurea Varela,[a] José M. González-Calbet,*[a] Marina Parras,[a] Ulises Amador,[b] and José L. Martínez[c]

Keywords: One-dimensional oxides / X-ray diffraction / Electron diffraction / Electron microscopy

The α = 3, β = 6 term of the series $(A_3B_2O_6)_\alpha$ $(A_3B_3O_9)_\beta$ has been synthesized in polycrystalline form. The structural characterization by powder X-ray diffraction, electron diffraction and high-resolution electron microscopy indicates that this material is isostructural with $Ba_9Co_8O_{24}$. In the structure, seven face-sharing octahedra alternate with a trigonal prism defining chains running parallel to the *c* axis of a rhombohedral unit cell ($R\bar{3}c$), with parameters a = 1.00766(4) nm and c = 4.1571(2) nm. The structural refinement shows the presence of a small percentage of Rh vacancies leading to the composition $Ba_9Rh_{7.92}O_{24}$. Pauli paramagnetic behaviour is observed.
(© Wiley-VCH Verlag GmbH, 69451 Weinheim, Germany, 2002)

Introduction

Recently, a great deal of interest has been devoted to a family of pseudo-monodimensional oxides structurally related to the 2H-hexagonal perovskite ABO_3.[1] This structure and the K_4CdCl_6 structure type[2] constitute the two end-members of this family. The main feature of both structures is that they are formed by a hexagonal array of isolated chains of face-sharing polyhedra running parallel to the *c* axis. In the hexagonal 2H-ABO_3 perovskite, the polyhedral rows are built up by $[BO_6]$ octahedra (O_h), while in the K_4CdCl_6 halide, or $A_3A'BO_6$ oxide,[3] one $[BO_6]$ octahedron and one $[A'O_6]$ trigonal prism (TP) alternate in an ordered 1:1 sequence. An unlimited number of closely related structures can be generated by varying the ratio of the octahedral and trigonal prisms.

There are several ways to describe this family of materials. Darriet et al.[4] provide a structural systematisation of these phases based on the stacking of $[A_3O_9]$ and $[A_3A'O_6]$ layers. The B and A′ cations fill the generated O_h and TP sites, respectively. Different sequences of both layer types lead to different stoichiometries that can be expressed by the general formula $A_{3n+3m}A'_nB_{3m+n}O_{9m+6n}$. Besides this generic formulation, several general formulas have been proposed to denote this homologous series, and different approaches to describe their structures have been reported.[5−7] A very useful approach is to consider these structures as formed by the ordered intergrowth of the structural units building up the two end-members. This building principle gives rise to the $(A_3A'BO_6)_\alpha(A_3B_3O_9)_\beta$ general formula,[8] where α and β denote the number of $A_3A'BO_6$ and 2H-ABO_3 structural blocks in each member, respectively.

A large number of one-dimensional oxides have been obtained by varying the chemical nature of A, A′ and B cations in the above family, due to the ability of these structures to accommodate any value of α and β blocks. So far, when A′ = B, few oxides have been reported and members belonging to this family have been only described in the A-(A′ = B)-O (A = Ca, Sr, Ba; B = Co, Ni, Rh) systems. Among them, the A-Co-O system has proven to be the most fruitful one: at least twelve members of the above series have been stabilized by varying the chemical nature of the alkaline-earth metal between the two limiting structures $Ca_3Co_2O_6$ (α = 3,β = 0)[9] and 2H-$BaCoO_3$ [10] (α = 0, β = 3).[8,11,12] In all of them, cobalt atoms occupy both the TP and the O_h sites. It is worth mentioning that $Ba_9Co_8O_{24}$,[11] the α = 3, β = 6 member, is, apart from the end-member of this series, the largest member of this one-dimensional family stabilized until now. In this phase, seven octahedra and one trigonal prism constitute the polyhedral chains by sharing faces.

When Ni occupies the polyhedral chains, the stabilized phases are much less numerous. The α = 3, β = 1 term $Sr_4Ni_3O_9$,[13] the α = 2, β = 1 term $Sr_9Ni_7O_{21}$,[14] and the

[a] Departamento de Química Inorgánica, Facultad de Químicas, Universidad Complutense
28040 Madrid, Spain
E-mail: jgcalbet@quim.ucm.es
[b] Departamento de Química Inorgánica y Materiales, Facultad de Ciencias Experimentales y Técnicas, Universidad San Pablo, Urb. Montepríncipe, Boadilla del Monte
28668 Madrid, Spain
[c] Instituto Ciencia de Materiales, CSIC, Cantoblanco, 28049, Madrid, Spain

$\alpha = 3$, $\beta = 3$ term $Ba_6Ni_5O_{15}$ [15] have been synthesised and structurally characterized.

Finally, when $A' = B = Rh$, only a 1D-oxide has been described: Zur Loye et al.[16] reported the stabilization of the $Sr_6Rh_5O_{15}$ phase, closely related to $Sr_6Co_5O_{15}$,[17] the $\alpha = 3$, $\beta = 3$ member of the above series. In fact, the main structural features of the latter are maintained in the Sr-Rh oxide, i.e. the polyhedral rows are also constituted by four face-sharing RhO_6 octahedra linked by one RhO_6 trigonal prism. However, when Rh occupies these polyhedra, the authors propose, from X-ray diffraction data, a new unit cell doubling the basal plane with respect to the $Sr_6Co_5O_{15}$ oxide. This superstructure seems to originate from a distortion of the strontium chains. The microstructural characterization[18] of such a member shows that it actually presents a complex stoichiometry, $Sr_{30}Rh_{23}O_{75}$, which results from the presence of empty Rh sites in the polyhedral chains. This feature leads to a fivefold superstructure along the *c* axis with respect to the $Sr_6Co_5O_{15}$ unit cell.

In the Ba-Rh-O system, several well-known ABO_3-hexagonal polytypes have been described. The hexagonal 4H[19] and 18R-$BaRhO_3$ [20] phases can be stabilized under oxidising conditions. These hexagonal phases, which always present the Ba/Rh = 1:1 cationic ratio, can be structurally considered as intermediates between the cubic-ABO_3 perovskite and the 2H-type, hexagonal-ABO_3 perovskite. The latter structure therefore provides the link between these phases and the monodimensional oxides belonging to the $(A_3A'BO_6)_\alpha(A_3B_3O_9)_\beta$ family. Much less information on these rhodium-containing phases is available, since only the synthesis of a non-commensurate $Ba_{1.06}RhO_3$ single crystal has been reported, and no structural data were provided.[21]

In a systematic characterization of powdered samples in the A-Rh-O system (A = Sr, Ba),[22,23] preliminary data from selective area electron diffraction (SAED) and high-resolution electron microscopy (HREM) give evidence of a commensurate one-dimensional Ba-Rh oxide belonging to the $(A_3A'BO_6)_\alpha(A_3B_3O_9)_\beta$ family with the composition $Ba_9Rh_8O_{24}$. We describe in this paper its synthesis and structural characterization by means of X-ray and electron diffraction and HREM. This study reveals that this new oxide adopts the structure corresponding to the $\alpha = 3$, $\beta = 6$ member of the series and, therefore, that it is isostructural to $Ba_9Co_8O_{24}$. $Ba_9Rh_8O_{24}$ is therefore the second such example reported, expanding the range of elements that can be incorporated into this structure. (NB During the writing of this paper, Slitzer et al.[24] reported the structure determination of a $Ba_9Rh_8O_{24}$ single crystal. Both powder and single crystal X-ray diffraction data provide structural models that are coincident in the main features.)

Results and Discussion

Chemical and Structural Characterization

The sample of nominal composition $Ba_9Rh_8O_{24}$ was confirmed to be a single phase by X-ray diffraction (XRD). The average Ba:Rh ratio, as determined by ICP, is close to 0.90(5) along the whole sample, in good agreement with the nominal metallic ratio. It is worth emphasizing that energy dispersive spectroscopy (EDS) analyses performed on numerous crystallites suggest that the sample is very homogeneous, since all of them exhibit the same Ba/Rh ratio of close to 0.9, confirming the ICP results. The anionic composition, as determined from TGA data, is in agreement with 24 oxygen atoms per formula unit, indicating that the anionic sublattice is complete.

The whole XRD pattern of $Ba_9Rh_8O_{24}$ (Figure 1) can be indexed within a hexagonal unit cell of parameters $a = 1.00755(7)$ nm and $c = 4.1572(3)$ nm, corresponding to the $\alpha = 3$, $\beta = 6$ member of the $(A_3B_2O_6)_\alpha(A_3B_3O_9)_\beta$ family.

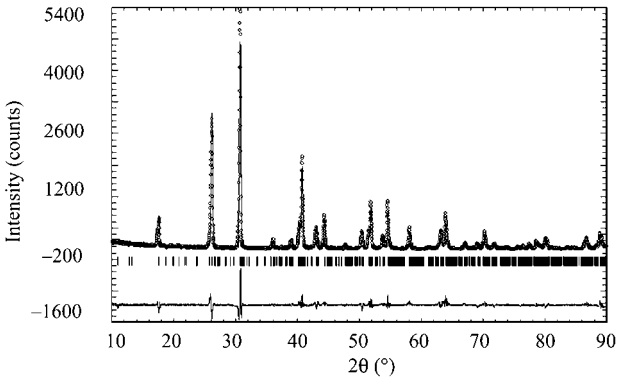

Figure 1. Results of the fitting of the powder XRD data of $Ba_9Rh_{7.92}O_{24}$: experimental (points), calculated (solid line) and difference (bottom)

Microstructural characterization by SAED and HREM confirms the XRD results. The most relevant SAED patterns, taken along the $[\bar{2}110]$, [0001] and $[1\bar{1}00]$ zone axes are shown in Figure 2a, 2b and 2c, respectively. Among them, the $[\bar{2}110]$ reciprocal plane provides the most valuable structural information. In fact, this SAED pattern allows us to obtain directly the values of α and β structural blocks forming the corresponding structure, and, thus, to identify the different members of the $(A_3B_2O_6)_\alpha(A_3B_3O_9)_\beta$ series. For this purpose, it is useful to describe this SAED pattern on the basis of the 2H-hexagonal subcell by differencing two sets of maxima. The more intense spots (referred to as subindex 2H in Figure 2a) correspond to the hexagonal 2H planes, while the least intense ones can be considered as satellite reflections with a modulation vector $\mathbf{k} = (a^*_{2H} + b^*_{2H})/3 + m\,2c^*_{2H}$. The *z* component (*m*) of this vector is related to the α and β values according to the expression $m = \alpha/(3\alpha + 3\beta)$. Besides, and taking into account that such a modulation is commensurate, the studied $Ba_9Rh_8O_{24}$ phase can also be regarded as a 2H superstructure, the 2H superstructure direction being $[\alpha+\beta\ \alpha+\beta\ i\ 2\alpha]^*_{2H}$. In this case, as can be observed in Figure 2a, this direction corresponds to $[33\bar{6}2]_{2H}$, and the *m* value is 1/9, therefore the $\alpha = 3$, $\beta = 6$ values are obtained, which indicates the stabilization of such a member in the Ba-Rh-O system. Furthermore, the observed reflection conditions, (*hkl*), $-h+k+l = 3n$, (000*l*) $l = 6n$ and (*h*00) $h = 3n$, are in agreement with

the rhombohedral $R\bar{3}c$ space group previously proposed for the $Ba_9Co_8O_{24}$ oxide.[11]

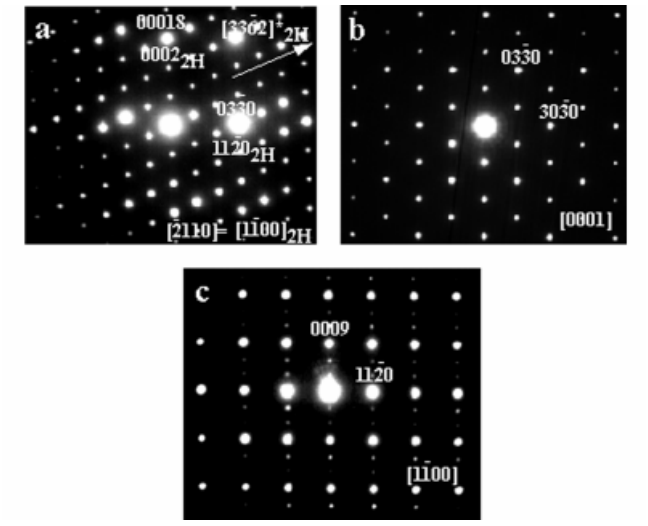

Figure 2. SAED patterns corresponding to $Ba_9Rh_{7.92}O_{24}$ along the [$\bar{2}$110] (a), [0001] (b) and [1$\bar{1}$00] (c) zone axes

The SAED patterns shown in Figure 2b and 2c confirm this result. In the first one, along the [0001] reciprocal plane, the reflections are distributed in a hexagonal array corresponding to a lattice parameter close to 1.0 nm. Only the (*h00*), *h* = *3n* reflections are visible according to the $R\bar{3}c$ space group. Furthermore, the [1$\bar{1}$00] reciprocal plane is also in agreement with the rhombohedral unit cell of this phase, although (*000l*), *l* = 3n reflections appear due to the dynamical diffraction effect.

The polyhedral sequence along the *c* axis, i.e. the arrangement of the blocks building the structure, can be deduced from the contrast variation observed in the experimental HREM. Figure 3 shows the high-resolution micrograph of the $Ba_9Rh_8O_{24}$ compound along the [$\bar{2}$110] zone axis. An apparently well-ordered material is observed with d-spacings close to 2.05 and 0.87 nm, corresponding to d_{002} and d_{100} of the hexagonal unit cell obtained by XRD. The image features are very close to those found in $Ba_9Co_8O_{24}$ and can be interpreted in a similar way. The sequence of bright dots of different contrast is due to rhodium columns. The two brightest dots correspond to the Rh prisms that are aligned following the diagonal cell, according to the rhombohedral symmetry proposed for this phase. The less intense dots could be due to Rh in an octahedral environment, leading to the -1TP-7O_h- polyhedra sequence characteristic of this structure. From this ideal model, the image has been calculated using the MacTempas package. The simulated image (inset in Figure 3) fits well with the experimental one for Δf = −95 nm and a sample thickness of 6 nm.

These results when taken together allow us to conclude that $Ba_9Rh_8O_{24}$ is isostructural to $Ba_9Co_8O_{24}$ and, therefore, that rhodium metal can also be incorporated into the metal-oxygen structure framework of the α = 3, β = 6 member of the one-dimensional $(A_3B_2O_6)_\alpha(A_3B_3O_9)_\beta$ family.

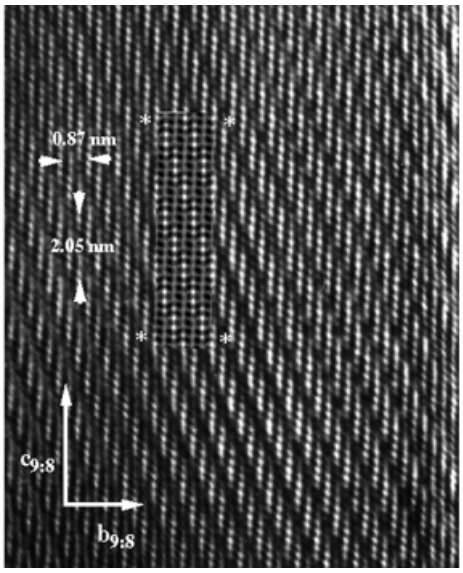

Figure 3. HREM image of $Ba_9Rh_{7.92}O_{24}$ along the [$\bar{2}$110] axis; the simulated image (Δf = −95 nm, Δf = 6 nm) is shown at the inset

Structural Refinement

Since the previous structural results obtained from SAED and HREM data suggested that the title compound is isostructural to $Ba_9Co_8O_{24}$, the structure of the latter was used as the starting model for the refinement of the XRD data of $Ba_9Rh_8O_{24}$. Figure 1 shows the graphic result of the fitting of the experimental X-ray diffraction pattern for $Ba_9Rh_8O_{24}$ and the difference between observed and calculated data. The final structural parameters are collected in Table 1; Table 2 shows some selected interatomic distances. A schematic representation of the structure is depicted in Figure 4a.

Table 1. Final structural parameters of $Ba_9Rh_{7.92}O_{24}$ [a]

Atom	x/a	y/b	z/c	Occ.
Ba(1)	0.3232(9)	−0.007(1)	0.0264(1)	1.000(2)
Ba(2)	0.351(1)	0	1/4	1.000(1)
Rh(1)	0	0	1/4	1.000(2)
Rh(2)	0	0	0.1826(3)	1.000(1)
Rh(3)	0	0	0.1206(4)	0.999(1)
Rh(4)	0	0	0.0618(4)	0.96(1)
Rh(5)	0	0	0	1.000(2)
O(1)	0.171(5)	0.178(5)	0.029(2)	1
O(2)	0.682(6)	0.177(5)	0.049(1)	1
O(3)	0.507(6)	0.353(6)	0.245(2)	1
O(4)	0.364(5)	0.517(6)	0.012(1)	1

[a] Space group $R\bar{3}c$ (167), *a* = 1.00766(4) nm, *c* = 4.1571(2) nm, *V* = 3.6556(2) nm^3, $B_{overall}(A^2)$ = 0.97(4), R_B = 0.075, R_{exp} = 0.086, R_{wp} = 0.16, χ^2 = 3.4.

As is well-known, X-ray diffraction is not the best technique to study structural effects related to light atoms such as oxygen in a "matrix" of heavy metallic atoms, as is the case with our material. In the diffraction pattern of these

Table 2. Selected inter-atomic distances (Å) in $Ba_9Rh_{7.92}O_{24}$

Ba(1)−O(1)	2.95(6)	Rh(1)−O(1)	2.18(5) × 6
Ba(1)−O(1)′	2.76(6)		
Ba(1)−O(1)"	2.77(8)	Rh(2)−O(2)	2.16(5) × 3
Ba(1)−O(2)	3.00(4)	Rh(2)−O(4)	2.04(5) × 3
Ba(1)−O(3)	2.72(6)		
Ba(1)−O(3)′	3.00(7)	Rh(3)−O(3)	2.19(7) × 3
Ba(1)−O(4)	2.74(6)	Rh(3)−O(4)	2.19(6) × 3
Ba(1)−O(4)′	2.42(5)		
		Rh(4)−O(1)	2.22(7) × 3
Ba(2)−O(1)	2.72(8) × 2	Rh(4)−O(3)	2.03(6) × 3
Ba(2)−O(2)	2.36(6) × 2		
Ba(2)−O(3)	2.59(7) × 2	Rh(5)−O(1)	2.13(6) × 6
Ba(2)−O(3)′	3.10(6) × 2		
Rh(1)−Rh(2)	2.80(1)		
Rh(2)−Rh(3)	2.58(2)		
Rh(3)−Rh(4)	2.45(2)		
Rh(4)−Rh(5)	2.57(2)		

one-dimensional materials, a strong preferred orientation effect is usually present because of the pronounced hexagonal shape of the crystallites. This is an additional problem when it comes to solving and refining the structure of these materials from powder diffraction data. In spite of this, the refinement was stable and it was possible to refine the positions of the oxygen atoms, provided an overall temperature factor was used. Any attempt to use individual temperature factors yielded unstable refinements, probably due to the very large volume of the cell and the limited number of observed reflections. Thus, the metal−oxygen distances in Table 2 should be considered with some care, although the metallic coordination, i.e. the polyhedron defined by the closest oxygen atoms around a given metal, is undoubtedly correct. According to that, both Ba atoms are coordinated to eight oxygen atoms at distances in the range 2.36−3.02 Å. Rh(1) occupies a regular trigonal prism, while the other Rh atoms (2, 3, 4 and 5) are octahedrally coordinated by nearby oxygen atoms at the distances reported in Table 2. The obtained values for all M−O distances are reasonable and consistent with previously reported bond lengths in comparable Ba/Rh oxides.[20,21]

Inside the chains, the inter-octahedral Rh(2)−Rh(3) and Rh(4)−Rh(5) distances are very close to those found in 4H or 18H-$BaRhO_3$ (2.5−2.6 Å). However, the Rh(3)−Rh(4) distance (2.45 Å) is significantly shorter and this could be due to the presence of some Rh vacancies in the Rh(4) octahedral site. On the other hand, the distance between Rh(1) in a trigonal prism and Rh(2) in a neighbouring octahedron sharing a triangular face is larger than the other Rh−Rh distances (2.81 Å). Although there is no comparable data for Rh ions in a similar oxygen environment, the enlargement of the distance between TP-O_h metals compared to that shown by O_h-O_h metals is also observed in other similar one-dimensional oxides such as $Ba_6Ni_5O_{15}$ [16] and $Sr_6Co_5O_{15}$.[17]

It is worth mentioning that we found some degree of metal vacancies (4%) in one of the rhodium positions. According to this, the actual composition of the title material

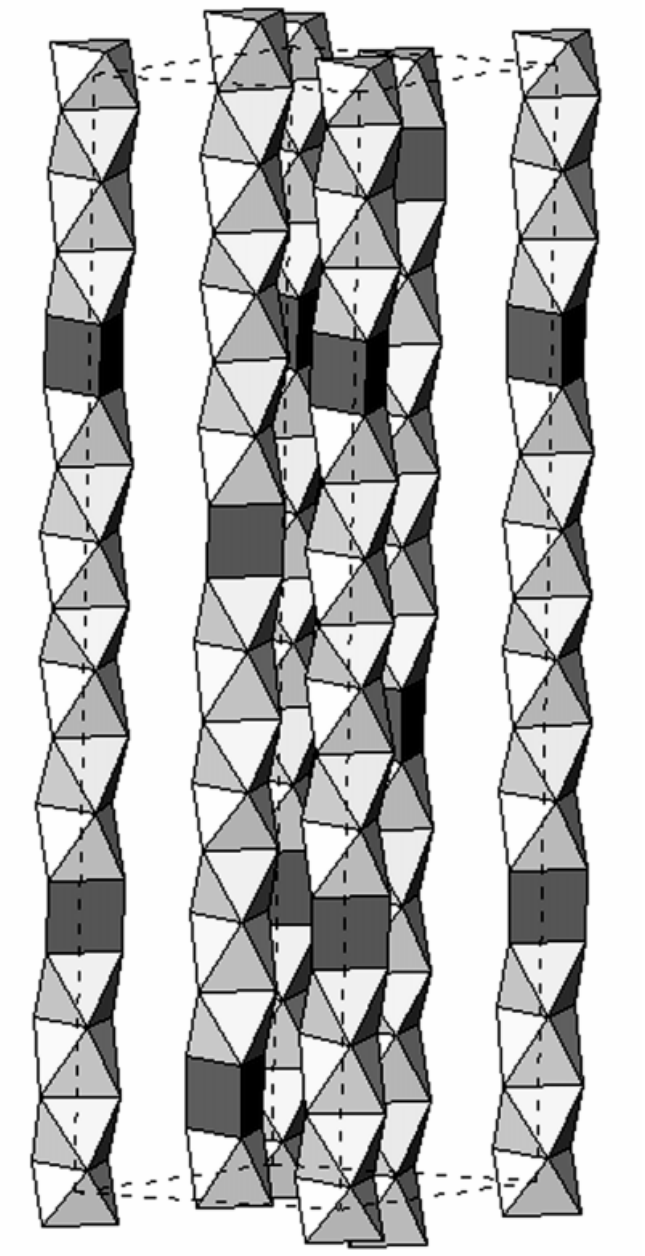

Figure 4. Schematic representation of the $Ba_9Rh_{7.92}O_{24}$ structure; Ba atoms have been omitted for clarity

obtained from the refinement of XRD data is $Ba_9Rh_{7.92(2)}O_{24}$. Assuming the usual valences for Ba and O, then the average Rh oxidation state is +3.78, indicating the presence of both Rh^{IV} and Rh^{III} in the polyhedra chains. However, Bond Valence Sums (BVS) calculations[25] give inappropriate values of the actual oxidation states of rhodium atoms.

The presence of vacancies at rhodium positions seems to play an important role in the stabilisation of the structures. In fact, as we have mentioned above, the $\alpha = 3$, $\beta = 3$ member of this series, stabilised when Sr fully occupies the A-sublattice, is characterized by the presence of one empty position every ten Rh sites in the polyhedra rows. The or-

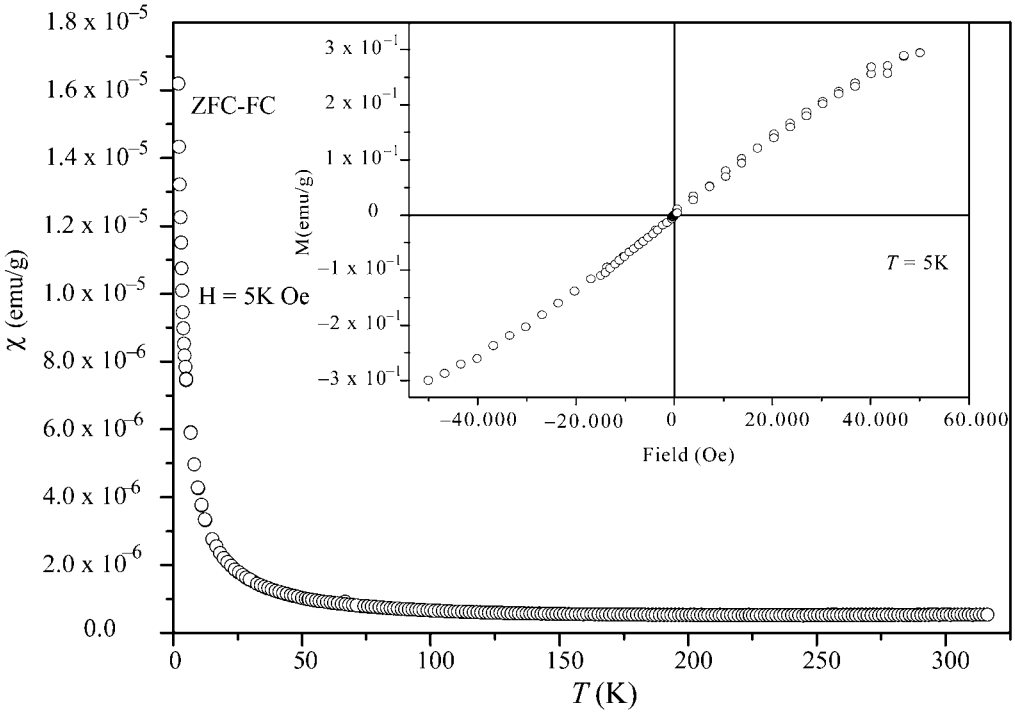

Figure 5. Magnetic susceptibility versus temperature plot for polycrystalline $Ba_9Rh_{7.92}O_{24}$; the susceptibility variation as a function of the applied field is shown as the inset

dered distribution of empty and full sites along the crystal is clearly seen in both the SAED patterns and the HREM study. Interestingly enough, the Rh vacancy concentration in $Ba_9Rh_{7.92}O_{24}$ is considerably lower, and it is not detected either by SAED or HREM. Apparently, the substitution of Sr by Ba causes an increase of the polyhedra average volume in such a way that Rh^{III} can also be accommodated into the structure and, therefore, the number of empty sites decreases considerably.

Magnetic Behaviour

Figure 5 shows the variation of the magnetic susceptibility versus temperature for $Ba_9Rh_{7.92}O_{24}$. The magnetic susceptibility of this oxide presents a Pauli-type behaviour, with an almost temperature independent susceptibility in a wide temperature range from 100 K to 350 K. At low temperature, the susceptibility shows a Curie tail which may be due to a small paramagnetic contribution. A low temperature isotherm until 5T (inset of Figure 5) shows an almost linear behaviour as expected for a Pauli-like system. From the magnetic point of view the system appears to be a linear chain of Rh^{IV} atoms with uncoupled electrons.

Experimental Section

Polycrystalline $Ba_9Rh_8O_{24}$ was prepared by a solid-state reaction with stoichiometric amounts of $BaCO_3$ (Merck, 99.9%) and RhO_2 (Aldrich, 99.8%). The mixture was initially calcined at 900 °C for 12 hours, and then heated at 1050 °C for three days.

The average cationic composition was determined by Inductively Coupled Plasma (ICP) while the local composition in every crystal was analysed by X-ray Energy Dispersive Spectroscopy (EDS). For this purpose, a JEOL 2000 FX electron microscope equipped with a LINK ISIS 300 analyser system was employed. The oxygen content was determined by thermogravimetric analysis (TGA) by using a thermobalance based on a CAHN D-200 electrobalance. The sample (about 100 mg) was reduced in a platinum crucible at 700 °C under $0.2H_2/0.3He$ atmosphere.

Powder X-ray diffraction (XRD) patterns were collected at room temperature on a PHILIPS X′PERT diffractometer equipped with a graphite monochromator and Cu-K_α radiation. The diffraction data were analysed by the Rietveld method[26] using the Fullprof program.[27]

Selected Area Electron Diffraction (SAED) was carried out using a JEOL 2000FX electron microscope fitted with a double-tilting goniometer stage (±45°). High Resolution Electron Microscopy (HREM) was performed on a JEOL 4000EX electron microscope fitted with a double-tilting goniometer stage (±25°). Simulated HREM images were calculated by the multi-slice method using the MacTempas software package.

Magnetic behaviour was measured by a SQUID magnetometer in a temperature range from 5 to 350 K, with a maximum applied magnetic field of 5T.

Acknowledgments

Financial support through research project MAT98-0648 (CICYT, Spain) is acknowledged.

[1] J. J. Lander, *Acta Crystallogr.* **1951**, *4*, 148−156.
[2] G. Bergerhoff, O. Schmitz-Dumont, *Z. Anorg. Allg. Chem.* **1956**, *284*, 10−14.
[3] J. J. Randall, L. Katz, *Acta Crystallogr.* **1959**, *12*, 148−151.
[4] J. Darriet, M. A. Subramanian, *J. Mater. Chem.* **1995**, *5*, 543−552.
[5] M. Evain, F. Boucher, O. Gourdon, V. Petricek, M. Dusek, P. Bezdicka, *Chem. Mater.* **1998**, *10*, 3068−76.
[6] J. M. Perez-Mato, M. Zakhour-Nakhl, F. Weill, J. Darriet, *J. Mater. Chem.* **1999**, *9*, 2795−2808.
[7] K. Ukey, A. Yamamoto, Y. Watanabe, T. Shishido, T. Fukuda, *Acta Crystallogr., Sect. B* **1993**, *49*, 67−72.
[8] K. Boulahya, M. Parras, J. M. González-Calbet, *Chem. Mater.* **2000**, *12*, 25−32.
[9] H. Fjellvag, E. Gulbrandsen, S. Aasland, A. Olsen, B. Hauback, *J. Solid State Chem.* **1996**, *124*, 190−194.
[10] H. Taguchi, Y. Takeda, F. Kanamara, M. Shimada, M. Kaizumi, *Acta Crystallogr., Sect. B* **1977**, *33*, 1299−1301.
[11] K. Boulahya, M. Parras, J. M. González-Calbet, *J. Solid State Chem.* **1999**, *142*, 419−427.
[12] K. Boulahya, M. Parras, J. M. González-Calbet, *J. Solid State Chem.* **1999**, *145*, 116−127.
[13] M. Huvé, C. Renard, F. Abraham, G. Van Tendeloo, S. Amelinckx, *J. Solid State Chem.* **1998**, *135*, 1−16.
[14] J. Campá, E. Gutierrez-Puebla, A. Monge, I. Rasines, C. Ruiz-Valero, *J. Solid State Chem.* **1996**, *126*, 27−32.
[15] J. Campá, E. Gutierrez-Puebla, A. Monge, I. Rasines, C. Ruiz-Valero, *J. Solid State Chem.* **1994**, *108*, 230−235.
[16] J. B. Claridge, H.-C. zur Loye, *Chem. Mater.* **1998**, *10*, 2320−2322.
[17] W. T. A. Harrison, S. L. Hagwood, A. J. Jacobson, *J. Chem. Soc., Chem. Commun.* **1995**, 1953−1954.
[18] A. Varela, K. Boulahya, M. Parras, J. M. Gonzalez-Calbet, *Chem. Mater.* **2000**, *12*, 3237−3239.
[19] B. L. Chamberland, J. B. Anderson, *J. Solid State Chem.* **1981**, *39*, 114−119.
[20] T. Siegrist, E. M. Larson, B. L. Chamberland, *J. Alloys Comp.* **1994**, *210*, 13−17.
[21] W. H. Henley, J. B. Claridge, P. L. Smallwood, H.-C. Zur Loye, *J. Cryst. Growth* **1999**, *204*, 122−127.
[22] A. Varela, K. Boulahya, M. Parras, J. M. Gonzalez-Calbet, T. Vogt, D. J. Buttrey, *Chem. Eur. J.* **2001**, *7*, 1444−1449.
[23] [23a] J. M. Gonzalez-Calbet, A. Varela, K. Boulahya, M. Parras. *Proceedings of 8th European Conference on Solid State Chemistry*, Oslo, **2001**.[23b] J. M. Gonzalez-Calbet, A. Varela, K. Boulahya, M. Parras, *Proceedings of Microscopy*, Barcelona, **2001**, (Ed.: University of Barcelona, 13-36560-2001), p.480.
[24] K. E. Stitzer, M. D. Smith, J. Darriet, H.-C. zur Loye, *Chem. Commun.* **2001**, 1680−1681.
[25] D. Altermatt, I. D. Brown, *Acta Crystallogr., Sect. B* **1985**, *41*, 240−244.
[26] H. M. Rietveld, *J. Appl. Crystallogr.* **1969**, *2*, 65−71.
[27] J. Rodríguez-Carvajal, *J. Physica* **1993**, *B192*, 55−69.

Received October 8, 2001
[I01396]

Structurally Different Dinuclear Copper(II) Complexes with the Same Triazolopyrimidine Bridging Ligand

Mohammad Abul Haj,[a] Miguel Quirós,*[a] Juan M. Salas,[a] José A. Dobado,[b] José Molina Molina,[b][†] Manuel G. Basallote,[c] and M. Ángeles Máñez[c]

Keywords: Copper / N,O ligands / Metal-metal interactions / Structure elucidation

Four binuclear copper(II) compounds with the anionic form of the ligand 4,5-dihydro-5-oxo[1,2,4]triazolo[1,5-*a*]pyrimidine ($5tpO^-$) have been isolated, their formulae being $[Cu_2(5tpO)_4(H_2O)_2]\cdot 2H_2O$ (**1**), $[Cu_2(phen)_2(5tpO)_2(H_2O)_2](NO_3)_2\cdot 4H_2O$ (**2**), $[Cu_2(biim)_2(5tpO)_2(H_2O)](ClO_4)_2\cdot 5.5H_2O$ (**3**), and $[Cu_2(CH_3CO_2)_2(5tpO)_2(H_2O)_2]$ (**4**) (phen = 1,10-phenanthroline, biim = bisimidazole). A related mononuclear complex, $[Cu(phen)_2(5HtpO)_2](NO_3)_2$ (**5**), has also been prepared. The crystal structure of compounds **1**–**3** has been determined by X-ray diffraction, showing their binuclear nature with four (**1**) or two (**2**, **3**) bridging $5tpO^-$ moieties. The triazolopyrimidine ligand binds the copper atoms through N3 and N4 in compounds **1** and **3**, whereas a novel binding mode through N3 and the exocyclic oxygen atom has been found in **2**. The study of the solution behaviour of **2** and **5** shows the important role of the solvent in the formation of the mono or binuclear complex. The reduction of the metal centres to Cu^I has been observed by electrochemical methods, demonstrating that this ligand stabilizes this oxidation state. Magnetic susceptibility measurements and electronic paramagnetic resonance (EPR) spectra seem to indicate a dimeric nature also for compound **4**. The antiferromagnetic interaction between the copper atoms inside the dimer is very strong for **4** ($2J = -221.3\ cm^{-1}$) and **1** ($2J = -104.9\ cm^{-1}$), fairly strong for **3** ($2J = -21.6\ cm^{-1}$), and very weak or non-existent for **2**. The nature of the copper–copper interaction in compound **1** has been analyzed by using molecular orbital calculations.

Introduction

The study of dinuclear complexes of copper(II) is a very active research field and more than nine hundred of such complexes have been structurally characterized, according to a recent review.[1] The interaction between the spins of both metal atoms leads to the existence of two states with different energy, one with a total spin of zero (singlet) and the other with a total spin of one (triplet). This difference of energy ($2J$) is experimentally observable by means of magnetic susceptibility measurements. The value of $2J$ depends on many structural features and the Cu−Cu distance does not seem to be the key parameter. This dependence is far from being fully understood in the general case, but useful correlations, more empirical than theoretical, have been formulated for a few types of bridging ligands: hydroxo,[2] halides,[3,4] carboxylates,[5] azide and thiocyanate,[6] or even purine bases.[7]

The work presented here follows the research line that has been carried out in the last few years by our group on the interaction of 1,2,4-triazolo[1,5-*a*]pyrimidine ligands with metal ions; a review about the subject has been recently published by us.[8] These compounds present several positions in their molecules for binding metal ions making them suitable for building dinuclear or polynuclear compounds. The interactions between the metal centres have been studied by means of molecular orbital (MO) calculations in dimeric compounds of silver(I)[9] and platinum(II),[10] but dinuclear copper(II) complexes with bridging triazolopyrimidine ligands have not been described previously to this article, despite the structural and theoretical interest of copper dinuclear compounds and their magnetic properties.

We describe here the synthesis and characterization of several copper(II) dinuclear complexes with the ligand 4,5-dihydro-5-oxo[1,2,4]triazolo[1,5-*a*]pyrimidine in its anionic form ($5tpO^-$) bridging the metal centres. The aim of this work is to characterize the bridging coordination behaviour of the ligand towards Cu^{II}, studying the relationship between the structure and the experimental properties of the isolated compounds. The role of the ligand has been determined by X-ray diffraction, an unexpected binding mode having been found in the compound with phenanthroline as

[a] Departamento de Química Inorgánica, Facultad de Ciencias, Universidad de Granada,
18071 Granada, Spain
Fax: (internat.) + 34-958/248526
E-mail: mquiros@ugr.es
[b] Grupo de Modelización y Diseño Molecular, Instituto de Biotecnología, Facultad de Ciencias, Universidad de Granada, 18071 Granada, Spain
[c] Departamento de Ciencia de los Materiales e Ingeniería Metalúrgica y Química Inorgánica, Facultad de Ciencias, Universidad de Cádiz,
Apartado 40, 11510 Puerto Real, Cádiz, Spain
[†] Professor José Molina Molina passed away on June 13, 2000.

an auxiliary ligand. The way in which the structural features influence the redox properties (observed by electrochemical measurements) and the intermetallic interaction (observed by magnetic susceptibility and EPR measurements) has been studied. The nature of this interaction has been theoretically analyzed by means of MO calculations for the compound with a quadruple bridge. The study of the formation process in solution of the related mono- and dinuclear complexes containing phenanthroline as an auxiliary ligand has revealed the role of the solvent.

Results and Discussion

The compounds described in this work are the following: $[Cu_2(5tpO)_4(H_2O)_2]\cdot 2H_2O$, (**1**) $[Cu_2(phen)_2(5tpO)_2(H_2O)_2](NO_3)_2\cdot 4H_2O$ (**2**), $[Cu_2(biim)_2(5tpO)_2(H_2O)](ClO_4)_2\cdot 5.5H_2O$ (**3**), $[Cu_2(CH_3CO_2)_2(5tpO)_2\ (H_2O)_2]$ (**4**), and $[Cu(phen)(5HtpO)_2](NO_3)_2$ (**5**), 5HtpO being the ligand 4,5-dihydro-5-oxo[1,2,4]triazolo[1,5-*a*]pyrimidine and phen and biim representing respectively the auxiliary chelating ligands 1,10-phenanthroline and bisimidazole.

Description of the Structures

The crystal structures of compounds **1**, **2**, and **3** have been determined from single-crystal X-ray diffractometry. The molecular structure of these compounds is depicted in Figures 1, 2, and 3. The three complexes are dinuclear with the anionic form of ($5tpO^-$) acting as the bridging ligand; four such bridges are present in compound **1** and two in compounds **2** and **3**. Attached to each copper atom in the two latter compounds, there is a bidentate aromatic amine (1,10-phenanthroline or 2,2′-bisimidazole) acting as an auxiliary ligand. A typical 4+1 square pyramidal environment (not considering the other copper atom) is completed by a water molecule at a longer distance (see Table 1) at the apical position, except for one of the metal atoms (Cu2) in compound **3**, which is square planar. Copper atoms are, in all cases, deviated from the corresponding basal planes

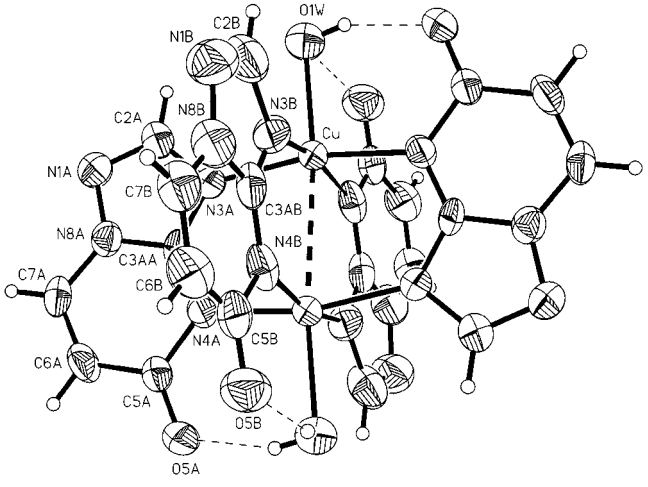

Figure 1. View of the molecular structure of compound **1**; atoms are represented as 50% probability thermal ellipsoids

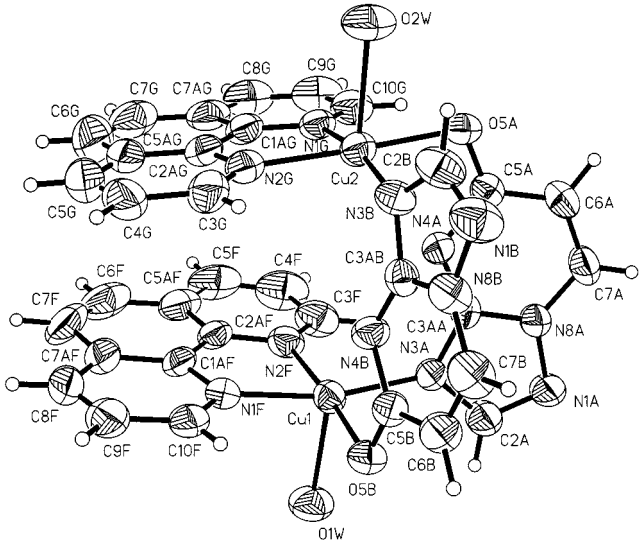

Figure 2. View of the molecular structure of compound **2**; atoms are represented as 50% probability thermal ellipsoids

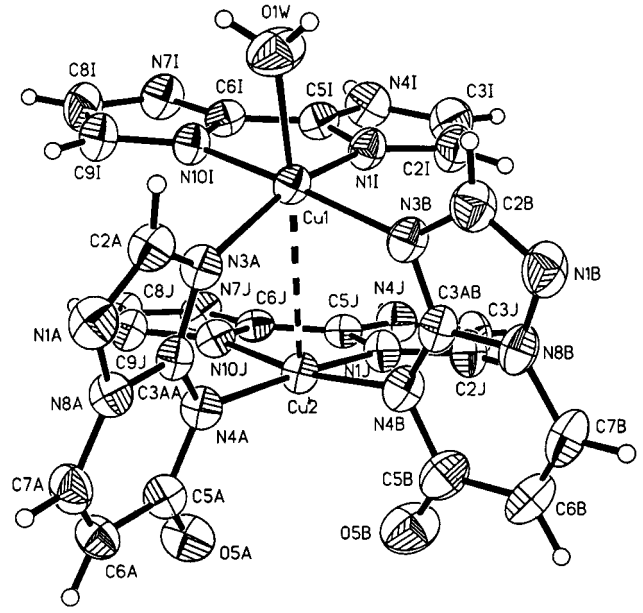

Figure 3. View of the molecular structure of compound **3**; atoms are represented as 50% probability thermal ellipsoids

away from their counterparts: the corresponding distances (also included in Table 1) seem to be influenced both by the presence of the water molecule in the fifth position (the deviation is almost zero for the square planar Cu atom and is higher when the $Cu-OH_2$ distance is shorter) and also by the proximity of the other metal atom. Nitrate **2** or perchlorate **3** ions balance the charge and non-coordinated water molecules complete the crystal structures.

The most outstanding feature of these structures is the different coordinating behaviour of the ligand. In **1** and **3**, the $5tpO^-$ entities bridge the metal atoms through the nitrogen atoms at positions 3 and 4; such a binding mode is

Table 1. Selected distances [Å] and angles [°]

	1	2	3
Cu−Cu	2.891(2)	4.610(1)	3.1968(7)
Cu−N3	2.000(8)	2.004(6)	1.994(3)
	1.985(9)	1.997(6)	2.001(3)
Cu−N4	2.036(7)	−	1.987(3)
	2.080(9)		2.003(3)
Cu−O5	−	2.005(5)	−
		1.993(5)	
Cu−N(amine)	−	2.009(6)	2.005(3)
		2.012(6)	2.020(3)
		2.010(6)	1.995(3)
		2.028(7)	2.018(3)
Cu−O(water)	2.207(7)	2.287(5)	2.193(3)
		2.345(6)	
C5−O5	1.242(11)	1.273(8)	1.249(5)
	1.217(13)	1.280(8)	1.240(6)
Cu−N_4/N_3O plane	0.2523(13)	0.088(3)	0.2599(10)
		0.080(3)	0.0051(10)
N3−Cu−N3	87.0(4)	−	91.30(13)
N4−Cu−N4	90.3(3)	−	93.11(13)
N3−Cu−N4 *cis*	88.4(3)	−	−
	90.7(3)		
N3−Cu−N4 *trans*	165.5(3)	−	−
	165.4(3)		
N3−Cu−O5	−	91.1(2)	−
		92.5(2)	
C3A−N4−C5	118.1(8)	116.4(6)	118.2(3)
	115.5(9)	116.7(6)	118.5(4)
N4−C3A−N8	123.6(8)	123.6(7)	122.6(4)
	124.0(10)	123.9(7)	122.7(4)
N4−C5−O5	120.5(8)	117.0(7)	119.1(4)
	117.3(11)	116.8(7)	118.9(4)

common for triazolopyrimidine ligands and has been observed for Cu^{I},[11] Ag^{I},[9,12] Pd^{II},[13] Pt^{II} [10] and heterometallic $Pt^{II}-Pd^{II}$ compounds,[14] but it was observed first for Cu^{II}, although other ligands such as purines interact with Cu^{II} in a similar fashion.[15] The coordination behaviour of the ligand in **2**, is much more unusual, however, in using the exocyclic oxygen atom (instead of N4) together with N3 to bridge the metal atoms (Figure 2). We have not found any other example in the bibliography of this binding mode for any metal and any bicyclic aromatic heterocycle containing an exocyclic oxygen atom, apart from a compound with a single xanthinato ion bridging three titanium atoms in a disposition that is, however, rather different to that in our compound.[16]

The versatility of triazolopyrimidine ligands for binding metal ions has been well established in previous works[8] and the possible involvement of the exocyclic oxygen atom in coordination was predicted for $5tpO^{-}$ from theoretical calculations.[17] However, it is quite unexpected to find such different ligand binding modes for compounds that are otherwise so similar, and we cannot see a clear reason for this behaviour. Perhaps it is just a matter of crystal packing optimization or small differences between the stacking properties (or even just the steric demands) of both auxiliary ligands. These are not parallel but convergent in **2** and divergent in **3** as we move away from the metal atoms (angles between the average planes are 10.7 and 11.7°, respectively). Stacking interactions are possibly responsible for this, since the optimum stacking distance between parallel aromatic rings is around 3.4 Å,[18] intermediate between the intermetallic distance in compounds **2** and **3**.

There are also differences in the relative disposition of the ligands: it is head-head-tail-tail for **1**, head-tail for **2**, and head-head for **3**. The molecular symmetry is then C_{2h} for **1**, C_2 for **2**, and C_s for **3**. This symmetry is only local, however: the only exact crystallographic symmetry present in the dimers is the inversion centre in **1**. The relative disposition of the ligands in **1** is stabilized by the presence of the coordinated water molecule (see Figure 1) which forms strong hydrogen bonds with the carbonyl oxygen atoms of the ligands [distances O1W···O5, 2.651(10) and 2.689(12) Å] and is the same as that found in the analogous Pt^{II} compound with 4,7-dihydro-5-methyl-7-oxopyrimidine.[10] Compounds analogous to **1** have been reported with purine ligands[15,19,20] and 7-azaindolate[21] and all of them present the C_{2h} atropisomer. We have not found any example of a copper(II) compound similar to **3,** but the analogous Pd^{II} complexes with 4,7-dihydro-5-methyl-7-oxopyrimidine[13] display head-tail geometry.

Bond lengths within the ligands are not significantly different from those in free 5HtpO,[17] except for the C5−O5 bond in **2**, which is somewhat longer as a consequence of O5 binding to the metal [1.236(3) Å for 5HtpO]. The bond angles within the ligands are very similar in the three compounds and differ from the values in free 5HtpO mainly in the angles around N4, C3A−N4−C5 being closed and N4−C3A−N8 being open [the angles in the free ligand are 122.6(2) and 118.8(2)° respectively].

The structures are stabilized by extensive hydrogen bonding, with water molecules being the donors towards carbonyl oxygen atoms, oxygen atoms of the anions and other water molecules. The nitrogen atoms of bisimidazole away from the copper atoms in **3** remain protonated and form hydrogen bonds in a "chelating" way towards the oxygen atom of a water molecule (N4I and N7I) and a neighbouring carbonyl oxygen (N4J and N7J). This suggests that these couples of atoms, if deprotonated, could act as new chelating binding sites for metal atoms.

Infrared Spectra

The infrared spectrum of **5**, with the ligand in neutral form, is almost identical to that of the free ligand, displaying an intense band in the C=O region at 1684 cm^{-1}, with two shoulders at 1711 and 1738 cm^{-1}. The spectra of the other compounds, with the ligand in anionic form, display the expected shift of this band to lower wavenumber. The spectrum shows a single narrow band at 1649 cm^{-1} for **1** and **3** and 1637 cm^{-1} for **2**, this extra shift being perhaps due to the involvement of O5 in coordination. For compound **4**, the C=O band seems to overlap with a band of the acetate anion, giving rise to a broader band centred at 1640 cm^{-1}. The presence of the anions is indicated by the typical stretching vibrations of nitrate (**2** and **5**) and perchlorate (**3**) at 1385 and 1107 cm^{-1} respectively. Assignment of other bands is quite uncertain.

Studies in Solution of Compounds 2 and 5

The behaviour in solution of compound **2** and the related mononuclear compound **5** has been studied. Compound **2** has been chosen because of its greater solubility in water and the possibility of making useful comparisons with **5**. The visible spectrum of a 10^{-3} M aqueous solution of **2** presents a band centred at 670 nm ($\varepsilon = 72$) whereas for **5** the maximum appears at 710 nm ($\varepsilon = 38$). The spectra of the latter are identical to those of solutions containing Cu^{II}, 5HtpO, and phen in 1:1:1 molar ratio. These results seem to indicate that the dimeric structure of **2** is kept in solution or, at least, that **5** is not its decomposition product.

In order to explore the formation process of compounds **2** and **5**, kinetic studies were carried out using a stopped-flow apparatus. In these studies two solutions were mixed, one containing Cu^{II} and phenanthroline at 10^{-3} M concentration each, and the other containing 5HtpO in concentrations ranging from $5\cdot10^{-3}$ to 10^{-2} M. When water or acetonitrile were used as the solvent, the mononuclear complex $[Cu(5HtpO)_2(phen)]^{2+}$ was generated within the stopped-flow mixing time without further spectral changes. Formation of the binuclear complex **2** was only observed if a mixed solvent (water/acetonitrile, 1:1) was used; in that case, the absorbance changes last for ca. 2 seconds. These results reveal an important effect of the solvent on the course of the reaction, in agreement with the synthetic procedures of **2** and **5** (see below), despite the fact that compound **2**, once obtained, seems to be stable in solution (see above). Unfortunately, a more detailed kinetic study of the formation of **2** was not possible because of the small absorbance changes and the overlap with the deviations of the stopped-flow baseline caused by the use of the mixed solvent.

Electrochemical Studies

The electrochemical properties of complexes **1**, **2**, **3**, and **5** were studied by measuring their cyclic voltammograms (CV) and square-wave voltammograms (SWV) in aqueous solution. Solubility of compounds **1** and **3** in water is quite low, just enough to record the voltammograms; the even lower solubility of compound **4** precluded reliable measurements. Despite their binuclear nature, a single reduction signal is observed in the CV of **1**, **2**, and **3**. The corresponding reduction potentials are 0.49 V (**1**), 0.24 V (**2**), 0.20 V (**3**), and 0.27 V (**5**). The same is observed in the SWV of **1** and **3**, a single signal at the same potentials as the CV. On the other hand, the SWV of **2** shows two overlapping peaks at 0.239 and 0.293 V, which can be considered as indicative of the presence of two copper centres and as evidence that the binuclear structure is maintained in solution, as was also suggested by visible spectroscopy. In contrast, both the mononuclear compound **5** and the solution containing Cu^{II}, 5HtpO, and phen (1:1:1) show a single reduction peak close to 0.28 V. Controlled-potential coulometry confirmed that this signal corresponds to a single electron process. The possibility of a breakage of the dimeric compound to generate a mononuclear compound analogous to the cationic complex of **5** and a species of the type $[Cu(phen)(H_2O)_n]^{2+}$ can be ruled out by the absence of a reduction peak around 0.174 V in the voltammograms of **2**, which is what is observed in solutions containing only Cu^{II} and phenanthroline.[22]

A comparison of the redox potential of the complexes $[Cu_2(5tpO)_2(phen)_2]$ or $[Cu(5HtpO)_2(phen)]^{2+}$ with those found for binary copper–phenanthroline complexes[22] indicates that the triazolopyrimidine ligand stabilizes Cu^{I}, probably by the generation of dimeric species analogous to the very stable ones formed by Ag^{I} with these types of ligands.[12] This stabilization is corroborated by the quite high potential value obtained for **1** and for solutions containing Cu^{II} and a great excess of 5HtpO (also 0.49 V).

Magnetic Susceptibility Measurements and EPR Spectra

The magnetic susceptibility of the four compounds has been measured in the range 5–300 K. In this range, **2** behaves as a magnetically diluted compound obeying the Curie law with a constant effective magnetic moment of 1.86 BM. Thus, no interaction between the two copper atoms in the dimer is observed. As expected, the same happens for the mononuclear compound **5** with $\mu_{eff} = 1.95$ BM.

On the other hand, **1**, **3**, and **4** present a χ vs. T curve with a maximum (Figure 4), indicative of antiferromagnetic interactions between the metal atoms. In the three cases, the data fit very well to the Bleaney–Bowers equation for copper(II) dimers.[23] The values of g and $2J$ (energy gap between the singlet and the triplet state) obtained from this fit are shown in Table 2. The interaction is very strong for compounds **1** and **4** and fairly strong for **3**. The trend in the strength of the interaction **1** >> **3** >> **2** is the expected one according to the number of bridging ligands, the length of the path across the ligand and the Cu–Cu distance.

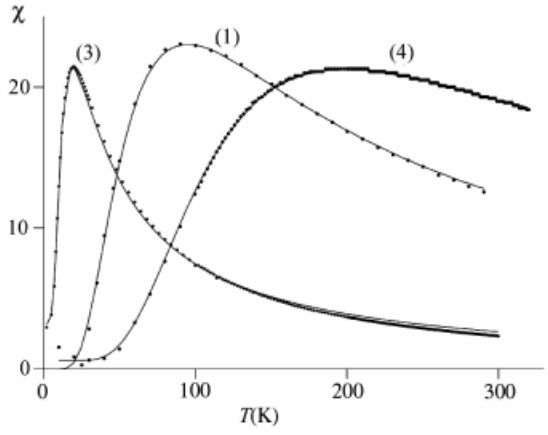

Figure 4. Magnetic susceptibility of compounds **1**, **3**, and **4** as a function of temperature; data (in emu/mol) have been multiplied by $5\cdot10^3$ (**1**), by 10^3 (**3**), or by 10^4 (**4**); solid lines represent the Bleaney–Bowers equation with the parameters indicated in Table 2

Table 2. Data from magnetic susceptibility measurements and EPR spectra

	1	3	**4**
From χ measurements			
g	2.148	2.081	2.117
$2J$ [cm^{-1}]	−104.9	−21.6	−221.3
From EPR spectra:			
$g_{\|}$	2.28	ca. 2.3	2.36
$g_{\perp}$	2.05	2.05	2.06
D [cm^{-1}]	0.161	0.095	0.247

The value of $2J$ in **1** is, however, considerably smaller than those found in compounds with quadruple purine bridges,[7] including that with the adeninate anion,[24] which is the most similar one. The wide range of values found for these compounds indicate how sensitive $2J$ is to subtle changes in the structure. We have not been able to find a clear and unambiguous relationship between $2J$ and any structural parameter.

The interaction in **4** is even stronger than in **1**, the value of $2J$ being intermediate between that of the latter and that of the copper acetate dimer ($2J = -305$ cm^{-1}).[25] We have not been able to grow crystals of compound **4** large enough to undergo X-ray determination, but these data allow us to propose a molecular dimeric structure with two acetate and two $5tpO^-$ bridging ligands, with the two water molecules occupying apical positions.

X-band EPR spectra have been recorded for the polycrystalline powdered samples at room temperature. Compound **2** presents a spectrum made up by a single very broad asymmetric band with an average g value of 2.11, which could be attributed to an unresolved anisotropic triplet or doublet spectrum. No half-field transition is detected for this compound. The mononuclear compound **5** presents a normal axial spectrum with $g_{\|} = 2.25$ and $g_{\perp} = 2.08$.

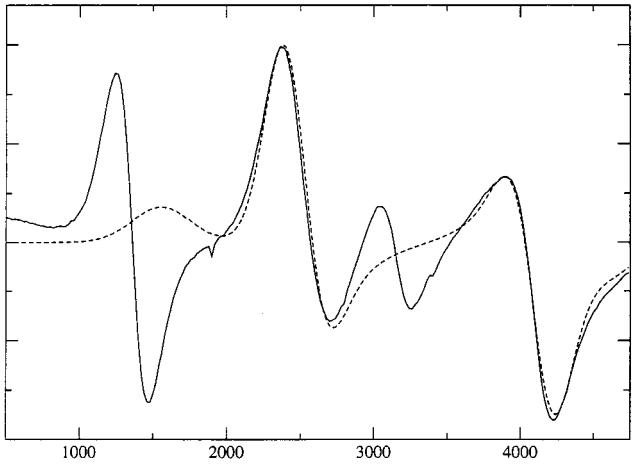

Figure 5. Experimental (− − −) and simulated (- - -) X-band EPR spectra of **1**; the simulation does not include the $S = 1/2$ and the half-field transitions (features at 3200 and 1400 G); simulation parameters, collected in Table 2, also reproduce well the Q-band spectrum; the spectrum of compound **4** is analogous to this

The other three spectra are quite complex and their main features have been assigned to ($S = 1$, $\Delta M_S = 1$) transitions with axial symmetry, although the parallel components in the spectrum of **3** are quite broad and difficult to identify. Together with these, strong signals also appear assignable to $S = 1/2$ transitions and, in the case of **1** and **4**, there is also a quite strong half-field ($S = 1$, $\Delta M_S = 2$ transition) band. As all these features overlap, the Q-band spectrum was also recorded for **1** to help in the assignments. Using computer simulation by means of the WINEPR program,[26] the values in Table 2 were finally obtained. Figure 5 displays the experimental and the calculated X-band spectra for **1**, only the ($S = 1$, $\Delta M_S = 1$) transitions are included in the simulation, which easily explains the differences between both. It is noteworthy that, comparing the zero-field splitting parameters of these compounds, we find the same trend as when comparing the $2J$ values.

Theoretical Studies

In order to analyze the Cu···Cu interaction in **1**, theoretical calculations have been performed for the singlet state of this compound. Its geometry was optimized and constrained to C_{2h} symmetry (thus, keeping a mirror plane that relates "head" with "head" and "tail" with "tail" and a binary axis perpendicular to it, so that the four ligands are equivalent). A very good agreement between the experimental and theoretical geometries was obtained; in particular, the theoretical Cu···Cu distance obtained was 2.893 Å. As in previous work by our group,[27] the hybrid density functional method with a large basis set (B3LYP/6-311G*) has been demonstrated to be accurate for describing large transition-metal complexes.

The topology of the electron charge density $\rho(r)$ was analyzed by means of the "Atoms in Molecules" (AIM) theory.[28,29] This analysis revealed the presence of a bond critical point (BCP) between the metal atoms, showing that the corresponding atomic basins share a common surface, and thus supporting the existence of a direct metal−metal interaction. As a consequence, four ring critical points (RCP) also appear at the middle of the Cu−Cu−C−N−C irregular pentagons. The $\rho(r)$ value at the Cu−Cu BCP is 0.012 ea_o^{-3}, only about one eighth of the corresponding values at the Cu−N bonds (0.085 and 0.081 ea_o^{-3}); this value may be taken as a rough estimation of the strength of the interaction. The Laplacian of the electron density [$\nabla^2(\rho)$] is positive at both Cu−Cu and Cu−N BCP (with values 0.054, 0.344, and 0.302 ea_o^{-5} for Cu−Cu, Cu−N3, and Cu−N4 respectively), as expected for closed-shell types of interactions, which are always found in coordination bonds and metal-metal interactions.

It is interesting to have a look at the shape of the calculated MO of the compound, particularly the HOMO and the LUMO, which are displayed in Figure 6. Looking only at one half of these orbitals, they resemble the antibonding combination of the $d_{x^2-y^2}$ orbital of the metal atom and the proper symmetry adapted combination of the orbitals of the ligands, as expected from textbook simple MO theory for metal complexes. These two halves mix with each other

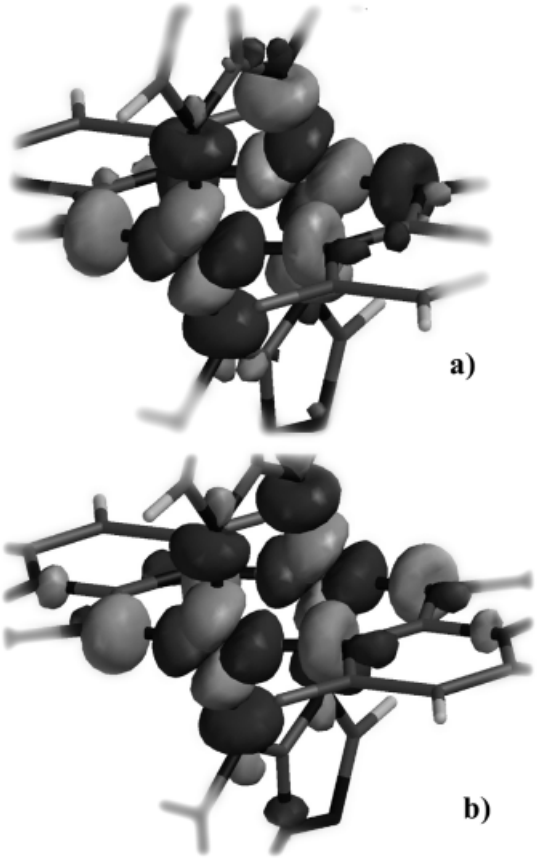

Figure 6. Calculated (B3LYP/6-311G*) HOMO (a) and LUMO (b) of **1**

giving rise to a "same-phase" (b_g) and to a "opposite-phase" (a_u) combination, the latter (HOMO) with less energy than the former (LUMO). The fact that the lobes of the HOMO on one copper atom have opposite signs to those on the other copper atom indicates that this orbital is antibonding (Δ antibonding) for the Cu−Cu union. This result, surprising at first sight, indicates that the stabilization of the HOMO with respect to the LUMO does not come from the direct intermetallic interaction, but from energetically more favourable electronic distribution within the ligands.

The calculated energy gap between these two orbitals is 1.095 eV, which of course cannot be regarded, not even as a first approximation, as the energy difference between the singlet and the triplet state. This latter value (2*J*) can only be theoretically obtained by performing separate calculations for both states (singlet and triplet) and subtracting the corresponding total energies. Extremely accurate methods must be applied for this since the goal is to get a small number by subtracting another two, very similar to each other and several orders of magnitude larger. Nevertheless, a method for calculating 2*J* in copper(II) dimers has been developed by Ruiz et al.,[30] which implies performing a so-called "broken-symmetry" calculation for the singlet state without geometry optimization (that is, keeping the geometry observed by X-ray data). This method has yielded good results for some systems[31] but the assumption that the energy of the singlet is well represented by the broken-symmetry model has been criticized by several authors.[32,33] Nevertheless, we have tested the method with our compound but the results do not reproduce, even qualitatively, the experimental data.

Conclusions

In this work, we have demonstrated the ability of the ligand 4,5-dihydro-5-oxo[1,2,4]triazolo[1,5-*a*]pyrimidinate ($5tpO^-$) to bridge copper(II) atoms to form dimeric species. Four such compounds have been isolated, three of them having been structurally characterized by single-crystal X-ray diffraction: compound **1** with a quadruple bridge and compounds **2** and **3** with a double bridge, and containing phenanthroline or bisimidazole, respectively, as auxiliary ligands. The bridging mode of the ligand in **1** and **3** is the one most usually found in the triazolopyrimidine ligand through the nitrogen atoms in positions 3 and 4, whereas compound **2** displays an unprecedented binding mode trough N3 and the exocyclic oxygen atom. The dimeric nature of compound **4**, for which X-ray structural data are not available, is indicated by its magnetic behaviour and EPR spectrum, which allow us to tentatively propose the presence of two $5tpO^-$ and two acetate bridges.

The structural features of these compounds clearly influence their electrochemical, magnetic and EPR properties. Thus, the ligand ability for stabilizing lower oxidation states is indicated by the reduction potentials, which increase with the number of $5tpO^-$ ligands attached to the metal. The dimeric nature of **1**, **3**, and **4** is shown by their strong antiferromagnetic behaviour as well as by their triplet EPR spectra, these methods not showing clearly the interaction for the compound with the longer bite (**2**). Opposite to this, the SWV of **2** display a double peak, probably revealing its dimeric nature in solution, whereas the reduction of Cu^{II} to Cu^{I} seems to be simultaneous for both metal atoms in **1** and **3**.

The strength of the intermetallic interaction, measured as the 2*J* parameter, is clearly correlated with the number and nature of bridging ligands and with the length of the bite, following the order: **4** > **1** > **3** > **2**. For compound **1**, an unsuccessful attempt has been made for calculating this parameter theoretically. The zero-field splitting of the triplet state, as deduced from the EPR spectra, follows the same trend as 2*J*.

A theoretical analysis has been performed by means of MO calculations for compound **1**. The calculated geometry fits well with the experimental one and the Bader analysis indicates the existence of a direct contact between the metal basins (the BCP). The topology of the HOMO of the compound indicates that its stabilization with respect to the LUMO comes from the electronic structure within the ligands rather than from the direct intermetallic interaction.

Lastly, it is interesting to note the need for a mixed solvent for the formation of compound **2**, revealed by kinetic measurements, in agreement with the synthetic procedure.

Experimental Section

Synthesis of the Compounds

4,5-dihydro-5-oxo[1,2,4]triazolo[1,5-*a*]pyrimidine (5HtpO) was synthesized as indicated in a previous work.[17] Bisimidazole was also synthesized according to the literature.[34] Copper salts, other reagents and solvents were obtained from standard commercial suppliers.

$[Cu_2(5tpO)_4(H_2O)_2]\cdot 2H_2O$ (1): A suspension was made with 80 mg (0.24 mmol) of copper basic carbonate and 200 mg (1.47 mmol) of 5HtpO in 20 mL of water, the mixture being stirred at room temperature for 30 min. After this, a dark blue precipitate was obtained, which was dissolved by adding 10 mL of acetonitrile to the mixture. Unchanged copper carbonate was then filtered off and, after two days of keeping the solution at room temperature, dark blue crystals of **1** were obtained. Yield: 40 mg (7.4%). $C_{20}H_{20}Cu_2N_{16}O_8$: calcd. C 32.48, H 2.71, N 30.31; found C 32.68, H 2.79, N 30.52%.

$[Cu_2(phen)_2(5tpO)_2(H_2O)_2](NO_3)_2\cdot 4H_2O$ (2): 240 mg (1 mmol) of copper(II) nitrate trihydrate and 180 mg (1 mmol) of 1,10-phenanthroline (phen) were dissolved in 20 mL of methanol. This solution was mixed with another one containing 136 mg (1 mmol) of 5HtpO in 20 mL of water/acetonitrile 2:1. After one week, blue crystals of the compound appeared. Yield: 300 mg (30%). $C_{34}H_{34}Cu_2N_{14}O_{14}$: calcd. C 41.25, H 3.43, N 19.82; found C 41.45, H 3.23, N 19.96%.

$[Cu_2(biim)_2(5tpO)_2(H_2O)](ClO_4)_2\cdot 5.5H_2O$ (3): The same procedure was followed as for compound **2**, using copper(II) perchlorate hexahydrate instead of copper(II) nitrate and 2,2′-bisimidazole (biim) instead of 1,10-phenanthroline. Yield: 50 mg (5.2%). $C_{22}H_{29}Cl_2Cu_2N_{16}O_{15.5}$: calcd. C 27.47, H 3.04, N 23.31; found C 27.66, H 3.09, N 23.50%.

$[Cu_2(CH_3CO_2)_2(5tpO)_2(H_2O)_2]$ (4): The procedure starts as for compound **1**, but the dark blue solid initially obtained is treated with 20 mL of a 10% solution of acetic acid in ethanol instead of acetonitrile, which dissolves it completely. After two days, a blue microcrystalline solid was obtained. Yield: 50 mg (12.5%). $C_{14}H_{16}Cu_2N_8O_8$: calcd. C 30.49, H 2.92, N 20.32; found C 30.62, H 3.13, N 20.21%.

$[Cu(phen)(5HtpO)_2](NO_3)_2$ (5): 240 mg (1 mmol) of copper(II) nitrate trihydrate and 180 mg (1 mmol) of 1,10-phenanthroline (phen) were dissolved in 20 mL of acetonitrile. 272 mg (2 mmol) of 5HtpO were then added and the suspension was refluxed for 30 min, after which the product was obtained as a blue powder. Yield: 500 mg (78%). $C_{22}H_{16}CuN_{12}O_8$: calcd. C 41.31, H 2.52, N 26.29; found C 41.34, H 2.44, N 26.54%.

Instrumental Work: Microanalysis of C, H and N were performed in a Fisons Instruments EA-1008 analyzer, X-band EPR spectra were recorded in a X-band Bruker ESP-300 apparatus (all this equipment sited at the Centre of Scientific Instrumentation of the University of Granada). The Q-band spectrum of **1** was recorded on a Q-band Bruker ESP-300 apparatus. IR spectra were obtained using a FT MIDAC Prospect 1 spectrophotometer with samples dispersed in KBr pellets. Magnetic susceptibility measurements were made in a SQUID MPMS-XL Quantum Design magnetometer. Solution electronic spectra were obtained using a Perkin−Elmer Lambda 3B spectrophotometer, whereas the stopped-flow experiments were carried out using an Applied Photophysics SX 17MV instrument.

X-ray Crystallography: X-ray work was carried out at room temperature on a Stoe Stadi4 (**1** and **2**) or Siemens P4 (**3**) diffractometer with Mo-K_α radiation. The dimensions of the chosen crystals were (in mm) 0.6 × 0.3 × 0.1 (**1**), 0.45 × 0.3 × 0.15 (**2**), and 0.5 × 0.4 × 0.3 (**3**). Data collections were performed in 2Θ/ω scan mode. The number of independent reflections collected were, after averaging, 3908, 7333, and 4640 for **1**, **2**, and **3**, respectively. Data were corrected for Lorentz and polarization effects and empirically (psi-scans) for absorption (transmission ranges: 0.5888−0.6927 for **1**, 0.6456−0.7601 for **2**, and 0.6471−0.7750 for **3**). The structures were solved by standard Patterson methods and refined by full-matrix least-squares using the SHELXL-93[35] (**1**, **2**) or SHELXL-97[36] (**3**) programs. One of the nitrate ions and two water molecules in **2** were found to be disordered over two positions, as well as two water molecules in compound **3**; another water molecule in this compound was refined with an occupancy of 1/2. Fixed N−O distances (1.19 Å) were imposed to the disordered nitrate. Atoms with an occupancy of less than one were refined isotropically, all other non-hydrogen atoms were refined anisotropically. Hydrogen atoms of the organic residues were introduced in their ideal positions, those of water molecules were found and refined with a fixed O−H distance (0.86 Å) in

Table 3. Crystal and refinement data for compounds **1**, **2**, and **3**

	1	**2**	**3**
Empirical formula	$C_{20}H_{20}Cu_2N_{16}O_8$	$C_{34}H_{34}Cu_2N_{14}O_{14}$	$C_{22}H_{29}Cl_2Cu_2N_{16}O_{15.5}$
Molecular mass	739.60	989.83	963.59
Space group	Pbca	$P2_1/c$	$P\bar{1}$
a [Å]	10.2473(5)	11.957(2)	11.6132(9)
b [Å]	16.1318(8)	14.422(3)	12.2274(8)
c [Å]	16.2087(12)	23.888(4)	14.7856(12)
α [deg]	−	−	97.278(7)
β [deg]	−	104.13(1)	108.381(6)
γ [deg]	−	−	110.615(6)
V [Å^3]	2679.4(3)	3994.5(12)	1796.8(2)
Z	4	4	2
$\rho_{calcd.}$ [g/cm^3]	1.833	1.646	1.781
μ [mm^{-1}]	1.67	1.15	1.43
R_1(F) [$F_o^2 > 2\sigma(F_o^2)$]	0.1138	0.0718	0.0391
$R_w(F_o^2)$ (all data)	0.2631	0.1879	0.1062
CCDC deposition number	160636	160637	160638

compounds **1** and **3** and were not found in compound **2**. An isotropic thermal parameter was applied to all hydrogen atoms 1.2 times those of their parent atoms. The full sets of crystal data (excluding structure factors) for these compounds have been deposited with the Cambridge Crystallographic Data Centre (CCDC, 12 Union Road, Cambridge CB2 1EZ, UK, E-mail: deposit@ccdc.cam.ac.uk), the corresponding deposition numbers are indicated in Table 3, together with selected crystal data.

Electrochemical Measurements: The electrochemical measurements were carried out using an EG&G PARC model 163A potentiostat provided with a Pt disk working electrode and a Pt wire auxiliary electrode. A Ag/AgCl electrode was used as reference for the measurements in water and the measured potentials were referenced to the normal hydrogen electrode by adding 0.222 V.[37] The complex solutions for electrochemical measurements (1−2 mM) contained 0.10 M KNO_3 and were purged with N_2 and thermostated at 25.01°C before measurement. The CVs were recorded at a scan rate of 50 mV/s and the SWVs with a frequency of 5 Hz.

MO and Electronic Charge Density Calculations: Density functional theory (B3LYP) calculations were performed with the Gaussian 98 package of programs.[38] The singlet state of structure **1** was fully optimized at the B3LYP/6-311G* level, with constrained C_{2h} symmetry and tested with frequency calculations (no imaginary frequencies). The Bader analysis was made by using the AIMPAC series of programs,[39] with the DFT density as input as described in the AIM theory.[28,29]

Calculations at the B3LYP/6-31G* level without geometry optimization have also been performed for both the singlet and the triplet state, including for the singlet state the "broken-symmetry" procedure that has been described elsewhere[30] in order to get an estimate for the 2*J* value.

Acknowledgments

This work was supported by a DGES project (PB 97-0786-CO3) from Ministerio de Educación y Cultura. Computing time was provided by the Universidad de Granada. We are grateful to Professor R. F. W. Bader for a copy of the AIMPAC package of programs. We acknowledge Professors T. Rojo and J. L. Lezama (Universidad del País Vasco) for collecting the Q-band spectrum of compound **1** and help with its assignment. We are also grateful to Professor R. Sáez (Universidad Autónoma de Madrid) for the magnetic measurements. M. Abul Haj acknowledges UNESCO for a PEACE grant.

[1] M. Melník, M. Kabešová, M. Koman, L. Macášková, J. Garaj, C. E. Holloway, A. Valent, *J. Coord. Chem.* **1998**, *45*, 147−359.
[2] V. H. Crawford, H. W. Richardson, J. R. Wasson, D. J. Hodgson, W. E. Hatfield, *Inorg. Chem.* **1976**, *15*, 2107−2110.
[3] W. E. Marsh, K. C. Patel, W. E. Hatfield, D. J. Hodgson, *Inorg. Chem.* **1983**, *22*, 511−515.
[4] M. A. Romero, J. M. Salas, M. Quirós, M. P. Sánchez, J. Romero, D. Martín, *Inorg. Chem.* **1994**, *33*, 5477−5481.
[5] E. Colacio, M. Ghazi, R. Kivekäs, J. M. Moreno, *Inorg. Chem.* **2000**, *39*, 2882−2890.
[6] J. A. R. Navarro, M. A. Romero, J. M. Salas, M. Quirós, E. R. T. Tiekink, *Inorg. Chem.* **1997**, *36*, 4988−4991.
[7] D. Sonnenfroh, R. W. Kreilick, *Inorg. Chem.* **1980**, *19*, 1259−1262.
[8] J. M. Salas, M. A. Romero, M. P. Sánchez, M. Quirós, *Coord. Chem. Rev.* **1999**, *193*, 1119−1142.
[9] M. A. Romero, J. M. Salas, M. Quirós, M. P. Sánchez, J. Molina, J. El Bahraoui, R. Faure, *J. Mol. Struct.* **1995**, *354*, 189−195.
[10] J. A. R. Navarro, M. A. Romero, J. M. Salas, M. Quirós, J. El Bahraoui, J. Molina, *Inorg. Chem.* **1996**, *35*, 7829−7835.
[11] J. G. Haasnoot, T. L. F. Favre, W. Hinrichs, J. Reedijk, *Angew. Chem. Int. Ed. Engl.* **1988**, *27*, 856−857.
[12] J. A. R. Navarro, J. M. Salas, M. A. Romero, R. Faure, *J. Chem. Soc., Dalton Trans.* **1998**, 901−904.
[13] J. A. R. Navarro, M. A. Romero, J. M. Salas, *J. Chem. Soc., Dalton Trans.* **1997**, 1001−1005.
[14] J. A. R. Navarro, M. A. Romero, J. M. Salas, M. Quirós, *Inorg. Chem.* **1997**, *36*, 3277−3283.
[15] A. Terzis, A. L. Beauchamp, R. Rivest, *Inorg. Chem.* **1973**, *12*, 1166−1170.
[16] A. L. Beauchamp, F. Belanger-Gariepy, A. Mardhy, D. Cozak, *Inorg. Chim. Acta* **1986**, *124*, L23−L24.
[17] M. Abul Haj, J. M. Salas, M. Quirós, J. Molina, R. Faure, *J. Mol. Struct.* **2000**, *519*, 165−172.
[18] W. Saenger, *Principles of Nucleic Acid Structure*; Springer-Verlag; New York, **1984**.
[19] P. de Meester, A. C. Skapski, *J. Chem. Soc. A* **1971**, 2167−2169.
[20] E. Sletten, *Acta Crystallogr., Sect. B* **1970**, *26*, 1609−1614.
[21] S. M. Peng, Y. N. Lin, *Acta Crystallogr., Sect. C* **1986**, *42*, 1725−1731.
[22] C. J. Hawkins, D. D. Perrin, *J. Chem. Soc.* **1962**, 1351−1357.
[23] B. Bleaney, K. D. Bowers, *Proc. Royal Soc. London Ser. A* **1952**, 451−465.
[24] R. W. Duerst, S. J. Baum, G. F. Kokoszka, *Nature* **1969**, *222*, 665−666.
[25] R. J. Doedens, *Prog. Inorg. Chem.* **1976**, *21*, 209−231.
[26] *WINEPR SimFonia*, version 1.25 (shareware version). Bruker Analytische Messtechnick GmbH, **1996**.
[27] J. A. Dobado, R. Uggla, M. R. Sundberg, J. Molina, *J. Chem. Soc., Dalton Trans.* **1999**, 489−496.
[28] R. F. W. Bader, *Atoms in Molecules: a Quantum Theory*; Clarendon Press: Oxford, 1990.
[29] R. F. W. Bader, *Chem. Rev.* **1991**, *91*, 893−928.
[30] E. Ruiz, P. Alemany, S. Álvarez, J. Cano, *J. Am. Chem. Soc.* **1997**, *119*, 1297−1303.
[31] I. Castro, M. L. Calatayud, J. Sletten, F. Lloret, J. Cano, M. Julve, G. Seitz, K. Mann, *Inorg. Chem.* **1999**, *38*, 4680−4687.
[32] R. Caballol, O. Castell, F. Illas, P. R. Moreira, J. P. Mabrieu, *J. Phys. Chem. A* **1997**, *101*, 7860−7866.
[33] C. Adam, V. Barone, A. Bencini, F. Totti, I. Ciofini, *Inorg. Chem.* **1999**, *38*, 1996−2004.
[34] F. Holmes, K. M. Jones, E. G. Torrible, *J. Chem. Soc.* **1961**, 4790−4795.
[35] G. M. Sheldrick, SHELXL 93. *Program for the Refinement of Crystal Structures.* University of Göttingen, Germany, **1993**.
[36] G. M. Sheldrick, SHELXL 97. *Program for the Refinement of Crystal Structures.* University of Göttingen, Germany, **1997**. Available at http://shelx.uni-ac.gwdg.de/SHELX/.
[37] N. Navon, G. Golub, H. Cohen, P. Paoletti, B. Valtancoli, A. Bencini, D. Meyerstein, *Inorg. Chem.* **1999**, *38*, 3484−3488.
[38] M. J. Frisch, G. W. Trucks, H. B. Schlegel, G. E. Scuseria, M. A. Robb, J. R. Cheeseman, V. G. Zakrzewski, J. A. Montgomery, Jr., R. E. Stratmann, J. C. Burant, S. Dapprich, J. M. Millam, A. D. Daniels, K. N. Kudin, M. C. Strain, O. Farkas, J. Tomasi, V. Barone, M. Cossi, R. Cammi, B. Mennucci, C. Pomelli, C. Adamo, S. Clifford, J. Ochterski, G. A. Petersson, P. Y. Ayala, Q. Cui, K. Morokuma, D. K. Malick, A. D. Rabuck, K. Raghavachari, J. B. Foresman, J. Cioslowski, J. V. Ortiz, B. B. Stefanov, G. Liu, A. Liashenko, P. Piskorz, I. Komaromi, R. Gomperts, R. L. Martin, D. J. Fox, T. Keith, M. A. Al-Laham, C. Y. Peng, A. Nanayakkara, C. González, M. Challacombe, P. M. W. Gill, B. Johnson, W. Chen, M. V. Wong, J. L. Andrés, C. González, M. Head-Gordon, E. S. Replogle, J. A. Pople, *GAUSSIAN 98*, *revision A.4*. Gaussian, Inc., Pittsburgh PA, **1998**.
[39] F. W. Biegler-König, R. F. W. Bader, T.-H. Tang, *J. Comput. Chem.* **1982**, *3*, 317−328.

Received April 17, 2001
[I01133]

^{139}La NMR Kinetic Study of Lanthanum(III) Complexation with Acetohydroxamic Acid

Mladen Biruš,*[a] Rudi van Eldik,*[b] Mario Gabričević,[a] and Achim Zahl[b]

Keywords: Lanthanum / NMR spectroscopy / Kinetics / Reaction mechanisms

The application of ^{139}La NMR spectroscopy to kinetic and equilibrium studies of the substitution of coordinated water by acetohydroxamic acid (HA) is described. The reaction of La^{3+} with HA can be represented by the following equation (with equilibrium constant K_1): $La^{3+} + HA \rightleftarrows La(A)^{2+} + H^+$ (1). The following equilibrium parameters were calculated from the ^{139}La NMR chemical shift of the equimolar reactants measured as a function of acidity and temperature: $K_1(298) = 2.36(8)\cdot10^{-4}$, $\Delta_rH_1 = -28(1)$ kJ·mol^{-1}, $\Delta_rS_1 = -162(4)$ J·K^{-1}·mol^{-1}. The kinetics of the reaction between La^{3+} and HA can be represented by the following equations: $La^{3+} + HA \rightleftarrows La(A)^{2+} + H^+$ (11) and $La^{3+} + A^- \rightleftarrows La(A)^{2+}$ (12). The complexation rate constants were calculated from the line widths of the corresponding signals as a function of acidity and temperature: $k_{11}(298\ K) = 1.54(4)\cdot10^6$ M^{-1}·s^{-1}, $\Delta H^{\ddagger}_{11} = 70(14)$ kJ·mol^{-1} and $\Delta S^{\ddagger}_{11} = +108(47)$ J·K^{-1}·mol^{-1}, k_{12} (298 K) = 1.6 10^{10} M^{-1}·s^{-1}, $\Delta H^{\ddagger}_{12} = 35(6)$ kJ·mol^{-1} and $\Delta S^{\ddagger}_{12} = +68(20)$ J·K^{-1}·mol^{-1}. The spin-spin relaxation times of La^{III} in the aqua ion and the hydroxamato complex are 4.36(4) ms and 54(1) μs at 298 K, respectively.

Introduction

The rare earth metal cations are widely used in industry[1] and medicine.[2] Due to the "hard" character of the lanthanum(III) ion, it is capable of forming stable complexes with "hard" ligands that contain oxygen electron-donor atom(s) within their functional groups. It also forms stable complexes with hydroxamic acids [$R^1C(=O)N(OH)R^2$], coordinating in a bidentate manner through the two oxygen atoms of the hydroxamate group.[3] Hydroxamic acids are weak organic acids with $pK_a \approx 9$, which release one proton per coordinated hydroxamato group as shown in the following reaction.

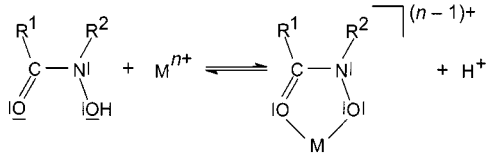

Hydroxamic acids are believed to exist in the two forms shown below, evidence for the presence of these forms and their isomerization is confirmed by NMR spectroscopic data.[4–6]

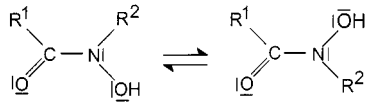

cis *trans*

The room-temperature isomerization of *N*-methylacetohydroxamic acid (≡ NMHA; $R^1 = R^2 = CH_3$) from the *trans* to the (chelation kinetically appropriate) *cis* form is characterized by a rate constant of ca. 3 s^{-1}. The magnitude of this rate constant indicates a partial double bond character of the hydroxamate C–N bonds, which can be explained by the two extreme resonance structures of the hydroxamic acids shown by structures **Ia** and **Ib**.[7–9]

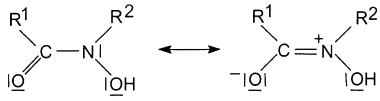

Ia **Ib**

As the electron-donor capability of R^2 increases, the form **Ib** predominates. This form bears a partial negative charge on the carbonyl oxygen atom, which results in an increased stability of the formed metal complex. The crystallographic data show that the more stable the ferric hydroxamate complex, the shorter the Fe–O(C) bond in the complex, probably due to the emerging negative charge on the carbonyl oxygen atom.[10]

[a] Faculty of Pharmacy and Biochemistry, University of Zagreb, A. Kovačića 1, 10000 Zagreb, Croatia
E-mail: birus@nana.pharma.hr
[b] Institute for Inorganic Chemistry, University of Erlangen–Nürnberg, 91058 Erlangen, Germany
E-mail: vaneldik@chemie.uni-erlangen.de

Supporting information for this article is available on the WWW under http://www.eurjic.com or from the author.

To date, only two papers (from our laboratories) have been devoted to the kinetics of the complexation of La^{III} with hydroxamic acids.[5,6] We have recently proposed that a slow *trans*→*cis* isomerization of *N*-alkylhydroxamic acids is the rate-determining step for their chelation to La^{3+} ions. The observed complexation processes were followed on the same time scale as was the isomerization of the free ligands. On the other hand, when R^2 is an H atom, as in HA, the complexation rate was found to be extremely fast, exceeding the limits of the stopped-flow mixing time. In order to investigate the complexation of La^{3+} with HA, it was necessary to utilize a kinetic technique that is not limited to such a long time-scale. ^{139}La NMR has already been successfully used as a tool for determining rate constants in kinetic studies involving complex-formation reactions.[11] In this study, we extend our previous investigations by presenting kinetic and equilibrium studies of the complexation of La^{3+} with HA ($R^1 = CH_3$; $R^2 = H$) in aqueous medium. The study was accomplished by observing ^{139}La NMR line-broadening and the chemical-shift change as a function of temperature, acidity and concentration of the reactants.

Results and Discussion

Figure 1(a) shows the ^{139}La NMR spectra of 0.2 M solutions of $La(ClO_4)_3$ and acetohydroxamic acid at 298 K as a function of $p[H^+]$. The recorded spectra are characterized by a one-resonance peak, which broadens as the $p[H^+]$ increases.[12] The spectra also exhibit a temperature dependence, which is shown for the same reactants at $p[H^+] = 3.71$ in Figure 1(b).

Since the UV-spectroscopic data under the employed conditions indicate a complexation reaction, the occurrence of only one peak in the recorded spectra reveals that lanthanum nuclei exchange fast on the NMR time-scale between two different environments, i.e. the aqualanthanum(III) ion and mono(acetohydroxamato)lanthanum(III) complex. In other words, reaction (1) lies in the so-called "fast-exchange region".

In the acidity range used, neither the hydrated La^{3+} ions nor HA deprotonate considerably in aqueous solutions; for both reactants $pK_a \geq 9$.[13,14] In equimolar solutions of the reactants, the only expected species formed is a monohydroxamato complex in which acetohydroxamate is chelated in a bidentate manner through two oxygen atoms of hydroxamate.[3] The formation of such a complex is represented by Equation (1), which is related to the equilibrium constant, $K_1 = [La(A)^{2+}]\cdot[H^+]\cdot[La^{3+}]^{-1}\cdot[HA]^{-1}$, where the terms in brackets represent the molar concentrations, HA is $CH_3C(=O)N(H)OH$ and $La(A)^{2+}$ is $La[CH_3C(=O)N(H)O]^{2+}$ (coordinated water molecules are omitted for clarity).

$$La^{3+} + HA \rightleftarrows La(A)^{2+} + H^+ \quad (1)$$

The modified Bloch equation for a two-site exchange has been solved by Leigh[15], and for the reaction system

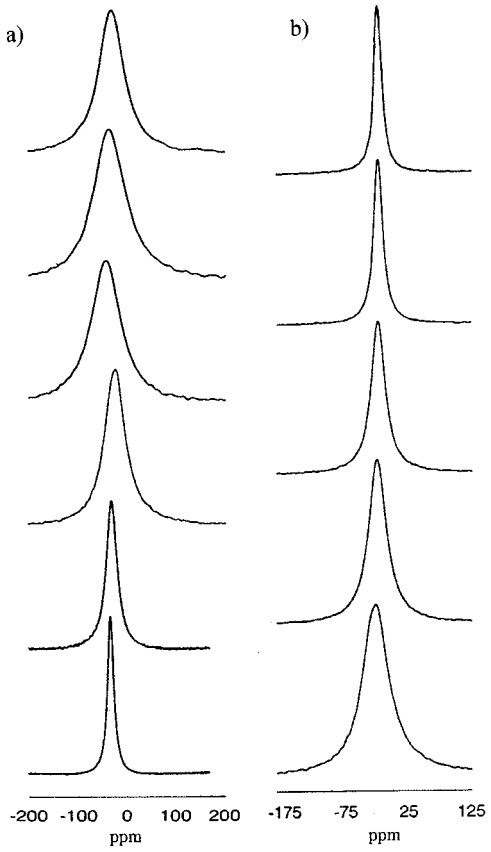

Figure 1. (a) ^{139}La NMR spectra of 0.2 M $La(ClO_4)_3$ and 0.2 M acetohydroxamic acid in 20% (w/w) D_2O at 298 K at $p[H^+] = 2.48$ (bottom), 3.49, 3.99, 4.47, 4.89, and 5.46 (top); (b) ^{139}La NMR spectra of 0.2 M $La(ClO_4)_3$ and 0.2 M acetohydroxamic acid in 20% (w/w) D_2O ($p[H^+] = 3.71$) at 278 K (bottom), 288 K, 298 K, 328 K, and 338 K (top)

studied, the relaxation rate ($1/T_2$) is described by Equations (2) to (9).

$$1/T_2 = A_2 \pm \{[G + (G^2 + H^2)^{1/2}]/2\}^{1/2} \quad (2)$$

$$A_2 = (1/\tau_{2a} + 1/\tau_{2b})/2 \quad (3)$$

$$G = (1/\tau_{2a} - 1/\tau_{2b})^2/4 + 1/\tau_A\tau_B - (\Delta\omega_{AB}/2)^2 \quad (4)$$

$$H = 0.5\cdot(1/\tau_{2a} - 1/\tau_{2b})\,\Delta\omega_{AB} \quad (5)$$

$$1/\tau_{2a} = 1/T_{2A} + 1/\tau_A \quad (6)$$

$$1/\tau_{2b} = 1/T_{2B} + 1/\tau_B \quad (7)$$

$$\Delta\omega_{AB} = \Delta\nu_{La^{3+}} - \Delta\nu_{La(A)^{2+}} \quad (8)$$

$$p_A = \tau_A/(\tau_A + \tau_B) = p_{La^{3+}}; p_B = \tau_B/(\tau_A + \tau_B) = p_{La(A)^{2+}} \quad (9)$$

In these equations, A and B are the above-mentioned two different environments, $1/T_{2A}$ and $1/T_{2B}$ are the intrinsic relaxation rates in the absence of the exchange, τ_A and τ_B are the residence times and p_A and p_B are the molar fractions

of lanthanum in the sites A and B, respectively; $\Delta\omega_{AB}$ is the difference in chemical shift of the two sites in the absence of exchange, i.e. $\Delta\nu_A - \Delta\nu_B$. Since the observed relaxation rate ($1/T_2$) was found to depend linearly on the "free" ligand concentration, as shown in Figure 2, Equation (6) had to be modified to include the first-order term with respect to the concentration of HA, $\tau_A^{-1} = k$ [HA].

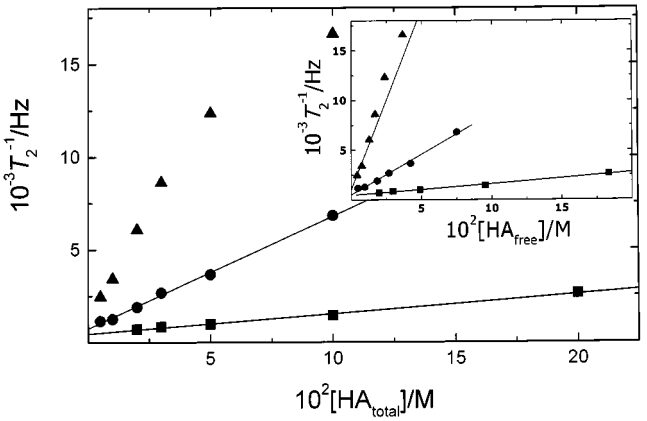

Figure 2. The observed ($1/T_2$) as a function of the total HA concentration at: − solid squares − p[H$^+$] = 3.74(2), − solid circles − p[H$^+$] = 4.85(2), − solid triangles − p[H$^+$] = 5.74(1); conditions: temperature 298 K, ionic strength 1.2 M (perchlorate), equimolar [La(ClO$_4$)$_3$]$_{total}$ and [HA]$_{total}$ = 0.005−0.2 M; the inset shows the observed ($1/T_2$) as a function of the calculated "free" HA concentration, under the same experimental conditions

The above equations show that in order to calculate the kinetic parameters for the La^{III} complexation reaction, it is necessary to accurately estimate p_A, p_B, and the concentration of free HA under the experimental conditions employed. The estimates were made using the equilibrium parameters for reaction (1) obtained from the experimentally determined temperature and p[H$^+$] dependent ^{139}La chemical shift, seen in Figure 3. The chemical shift of the ^{139}La NMR resonance for equimolar solutions containing lanthanum perchlorate and acetohydroxamic acid is mainly determined by temperature and by the composition of the La^{III} inner coordination sphere, which depends on p[H$^+$]. The observed chemical shift in the reaction mixture can be regarded as a weighted average of the shifts related to the La^{3+} and $La(A)^{2+}$ species, using the mol fractions as a weighting factor for each species.

$$\Delta\nu_{obs.} = \Delta\nu_{La}{}^{3+}\cdot p_{La}{}^{3+} + \Delta\nu_{La(A)}{}^{2+}\cdot p_{La(A)}{}^{2+} \quad (10)$$

For each experimental data point the species concentrations were calculated from the known total concentration of each reactant and the value of K_1 in the temperature range used. A nonlinear least-square fitting procedure[16] was applied for the optimization of the parameters defined in Equation (10) to the experimental data points shown in Figure 3, taking into account the temperature dependent behavior of both the chemical shifts and the equilibrium constant. The following equation $K_1(T) = K_1(298) \times \exp[\Delta_r H_1(T - 298)/298RT]$ describes the relationship between temperature and the equilibrium constant, where

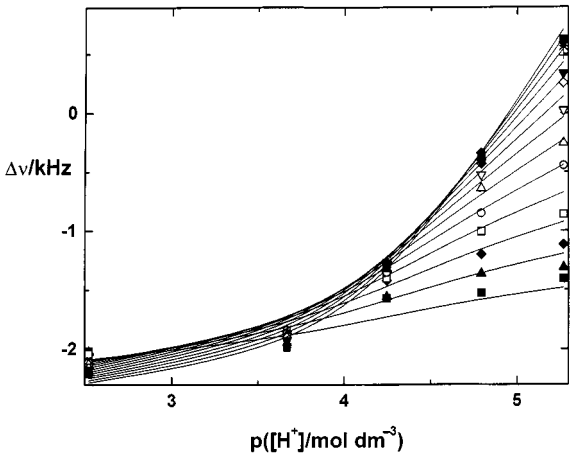

Figure 3. The temperature and p[H$^+$] dependencies of the ^{139}La chemical shift of 0.2 M La(ClO$_4$)$_3$ and 0.2 M acetohydroxamic acid in 20% (w/w) D$_2$O; the lines drawn are the theoretical ones calculated using the optimized parameters of Equation (10); the temperature increment between the experimental series is 5 K, the solid squares corresponding to the lowest temperature, 278 K

$\Delta_r H_1$ is the reaction enthalpy for reaction (1). During the fitting procedure, the distribution of species was calculated simultaneously for each experimental point by a Newton−Raphson algorithm[17] used for solving a set of homogeneous differential equations. The temperature dependence of the chemical shift for the La^{3+} ion was found to be concentration-independent. Within the temperature range used, the experimentally determined $\Delta\nu_{La}{}^{3+}$ is found to be satisfactorily described by the linear relationship $\Delta\nu_{La}{}^{3+}(T)$ Hz = $-2.18(2)\cdot10^3$ Hz − 3.3(3) Hz·K^{-1} × (T − 298) K (see Supporting Information, Figure S1).[18] Under the experimental conditions used, full complexation could not be achieved (see Supporting Information, Figure S2), hence, the experimental determination of the temperature-dependent nature of $\Delta\nu_{La(A)}{}^{2+}$ is impossible.[19] Therefore, the parameters describing the dependence had to be adjusted during the fitting procedure. For the La^{3+} ion, a linear temperature dependence of $\Delta\nu_{La(A)}{}^{2+}$ within the temperature range used, is proposed,. Fitting Equation (10) to 87 data points collected at various temperatures and proton concentrations resulted in the following parameters: $\Delta\nu_{La(A)}{}^{2+}(T)$ Hz = $2.5(3)\cdot10^2$ Hz + $7.9(2)\cdot10^1$·Hz·K^{-1} × (T − 298) K, $K_1(298) = 2.36(8)\cdot10^{-4}$, $\Delta_r H_1 = -28(1)$ kJ·mol^{-1}, and $\Delta_r S_1 = -162(4)$ J·K^{-1}·mol^{-1}.

From these parameters a chemical shift of $\delta = 44$ is calculated for ^{139}La in the $La(A)^{2+}$ complex relative to the aqua ion at 298 K. This is within the range expected for the coordination of the hydroxamate oxygen atoms to the central lanthanum ion.[20] The $K_1(298)$ value obtained, which was confirmed by potentiometric titration under the same experimental conditions, differs from the reported value of $6.17\cdot10^{-5}$ determined at 20 °C and $I = 0.1$.[3] The observed discrepancy can be attributed to the difference between the reactant concentrations and activities used in our and the reported study. For the same reason our calculated values of the thermodynamic functions do not represent the standard

values, and possibly a larger negative value of the reaction entropy than expected is calculated. As expected, the K_1 value obtained is slightly smaller than that reported for the complexation of La^{III} with *N*-methylacetohydroxamic acid.[6]

The ^{139}La ($I = {}^{7}/_{2}$) nuclear spin-spin relaxation is governed by the quadrupolar interaction, for which it was shown that the extreme narrowing is valid above 278 K.[11] The intrinsic relaxation time in the absence of the exchange for the aqualanthanum(III) ion (T_{2A}) was determined from the NMR spectra of 0.2 M $La(ClO_4)_3$ in 20% D_2O (w/w), collected as a function of concentration and temperature. Figure S3 shows that in the temperature range 278−338 K, the observed relaxation time of the $La(ClO_4)_3$ solution, which was found to be concentration-independent, depends almost linearly on the temperature according to the following equation: $T_{2La}{}^{3+}(T) = -0.00758$ (s) + $3.009 \cdot 10^{-5}$ ($s \cdot K^{-1}$) × T (K). At 298 K, the spin-spin relaxation time $T_{2La}{}^{3+} = 4.36(4)$ ms compares reasonably well with the reported values,[11,20] taking into account the slightly different experimental conditions employed in these studies. Since full complexation of La^{3+} was impossible to achieve under our experimental conditions, T_{2B} and its temperature dependence were refined during the fitting procedure (vide infra). The optimized spin-spin relaxation times of lanthanum in the hydroxamato complex at 298 K, $T_{2B}(298) = 54(1)$ μs, is within the range reported for other complexes.[20] For a quadrupolar nucleus such as ^{139}La, besides the exchange broadening effect, the line-width variation should result essentially from two factors, a change in the symmetry of the first coordination shell, and a change in the size of the La^{III} species. The larger the size and the lower the species symmetry, the broader the resonance will be. The substitution of two coordinated water molecules by one acetohydroxamato ligand in the inner sphere of La^{III} should slightly increase the size of the complex, as expected from the reaction molar volume determined for the complexation of iron with HA.[21] This, along with the lower symmetry of the monohydroxamato complex, accounts for a much broader resonance observed for the complex than for the aqua species.

Two essentially different reaction models could be considered as the operative reaction mechanism for the complexation of the lanthanum ion by acetohydroxamic acid. The rate-determining step should be characterized by the energetics of either (*i*) the water exchange on the aquated lanthanum ions, or (*ii*) the ring-closure reaction of the mono-coordinated ligand. For the former process either a dissociative or an associative mode of activation can be proposed, whereas for the latter one the rate-determining step may involve a slow proton transfer from the −NO*H* group or a slow *trans*→*cis* isomerization of the attached hydroxamato ligand.

Besides the proton, four different reactants can be considered to participate in the complexation kinetics, i.e. La^{3+}, $La(OH)^{2+}$, HA, and A^-. Accordingly, the studied reaction can be plausibly represented by Equations (11) to (14).

$$La^{3+} + HA \rightleftarrows La(A)^{2+} + H^+ \quad (11)$$

$$La^{3+} + A^- \rightleftarrows La(A)^{2+} \quad (12)$$

$$La(OH)^{2+} + HA \rightleftarrows La(A)^{2+} \quad (13)$$

$$La(OH)^{2+} + A^- \rightleftarrows La(A)(OH)^+ \quad (14)$$

Since the pK_a values of both reactants are > 9,[13,22] reaction path (14) results in a calculated microscopic rate constant for the complexation, that would greatly exceed the rate of the diffusion-controlled processes. The reaction paths (12) and (13) are kinetically indistinguishable from each other, but the contribution of the latter path could be excluded for the following reasons. Due to the difference in electric charge of La^{3+} and $La(OH)^{2+}$, the ion−dipole attractive coulombic force between the reactants of path (11) must be more than doubled in comparison with path (13). Furthermore, even at the lowest acidity used, the concentration of La^{3+} was more than 10^3 times that of $La(OH)^{2+}$. Therefore, for a notable contribution of path (13) HA would have to react at least 10^3 times faster with $La(OH)^{2+}$ than with La^{3+}. However, the latter ion exchanges water on a time-scale shorter than 10 ns.[23]

Taking into account the above arguments, Equations (2) to (9) were fitted to the experimental data, but k in Equation (6) was substituted by $k_{11} + k_{12}K_a[H^+]^{-1}$ (the subscripts of the rate constants are related to the equation numbers, whereas K_a stands for the ionization constant of HA). Figure 4 shows the experimentally determined $\Delta\nu_{1/2}$ of 0.2 M reactants plotted as a function of p[H^+] at various temperatures. The lines drawn are the theoretical ones calculated using the optimized parameters of Equations (2) to (9), obtained by a non-linear least-squares fit[16] in which

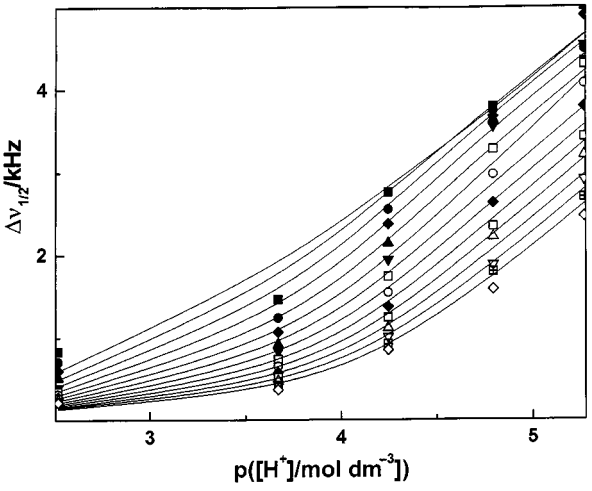

Figure 4. The observed $\Delta\nu_{1/2}$ of 0.2 M $La(ClO_4)_3$ and 0.2 M acetohydroxamic acid in 20% (w/w) D_2O plotted vs. p[H^+] at various temperatures; the lines drawn are the theoretical ones calculated using the optimized parameters of Equations (2) to (9); the temperature increment between the experimental series is 5 K, the open diamonds corresponding to lowest temperature, 278 K

τ_B was substituted for $\tau_A p_B/p_A$ in order to reduce the number of variables. The theoretical values follow a general trend delineated by the observed values. A slight disagreement seems acceptable considering the complexity of the expression describing $\Delta\nu_{1/2}$ and the number of parameters that had to be adjusted during the fitting procedure. The necessary equilibrium concentration of free HA for each data point was calculated simultaneously during the iteration procedure, as well as the difference in chemical shift of the two sites in the absence of exchange, $\Delta\omega_{AB}(T) = \Delta\nu_{La}{}^{3+}(T) - \Delta\nu_{La(A)}{}^{2+}(T)$. The values of the kinetic parameters for the formation of $La(A)^{2+}$ are calculated as: $k_{11}(298\ K) = 1.54(4)\cdot10^6\ M^{-1}\cdot s^{-1}$, $\Delta H^{\ddagger}_{11} = 70(14)\ kJ\cdot mol^{-1}$ and $\Delta S^{\ddagger}_{11} = +108(47)\ J\cdot K^{-1}\cdot mol^{-1}$, $k_{12}K_a(298\ K) = 1.5(5)\cdot10^1\ s^{-1}$, $(\Delta H^{\ddagger}_{12} + \Delta_r H_a) = 53(5)\ kJ\cdot mol^{-1}$ and $(\Delta S^{\ddagger}_{12} + \Delta_r S_a) = -45(17)\ J\cdot K^{-1}\cdot mol^{-1}$. From the calculated values and the published thermodynamic parameters for the ionization of HA,[23] the following values can be calculated: $k_{12}(298\ K) = 1.5\cdot10^1/K_a = 1.6\cdot10^{10}\ M^{-1}\cdot s^{-1}$, $\Delta H^{\ddagger}_{12} = 53 - \Delta_r H_a = 35(6)\ kJ\cdot mol^{-1}$ and $\Delta S^{\ddagger}_{12} = -45 - \Delta_r S_a = +68(20)\ J\cdot K^{-1}\cdot mol^{-1}$. The kinetic parameters for the backward reaction are calculated from the forward reaction and the equilibrium parameters: $k_{-11}(298\ K) = 6.75\cdot10^9\ M^{-1}\cdot s^{-1}$, $\Delta H^{\ddagger}_{-11} = 98(14)\ kJ\cdot mol^{-1}$, $\Delta S^{\ddagger}_{-11} = +270(47)\ J\cdot K^{-1}\cdot mol^{-1}$, $k_{-12}(298\ K) = 6.48\cdot10^4\ s^{-1}$, $\Delta H^{\ddagger}_{-12} = 82(8)\ kJ\cdot mol^{-1}$, and $\Delta S^{\ddagger}_{-12} = +121(24)\ J\cdot K^{-1}\cdot mol^{-1}$.

From the calculated values of k_{11} and k_{12}, and the estimated outer-sphere association constants for $\{La^{3+}\cdots AH\}$ and $\{La^{3+}\cdots A^-\}$ with concentrations of ca. 10^{-1} M^{-1} and ca. $5\cdot10^2$ M^{-1},[24] respectively, the inner-sphere reorganization rate constants for reactions (11) and (12) can be calculated as $1.5\cdot10^7\ s^{-1}$ ($= 1.54\cdot10^6\ M^{-1}\cdot s^{-1}/10^{-1}\ M^{-1}$) and $3\cdot10^7\ s^{-1}$ ($= 1.6\cdot10^{10}\ M^{-1}\cdot s^{-1}/5\cdot10^2\ M^{-1}$), respectively. Both constants appear to be an order of magnitude smaller than the water exchange rate constants for the La^{3+} and $La(OH)^{2+}$ ions.[25] However, two factors could easily increase these rate constants to values similar to that of the water exchange rate constant. Participation of the *trans* isomer in free HA increases their values, as well as the inner-sphere reorganization rate constants by a factor of ca. 10, as a statistical correction for the outer-sphere water molecules.

A value of k_{-11} that is larger than the estimated water exchange rate constant by an order of magnitude indicates that this rate constant is not strictly related to the inner-sphere reorganization of the complex, but possibly encompasses protonation of the coordinated hydroxamate according to Equations (15) and (16).[26]

$$La(CH_3C(=O)N(H)O)^{2+} + H^+ \underset{k_{-2}}{\overset{k_2}{\rightleftharpoons}} La(CH_3C(=O)N(H)OH)^{3+} \quad K_2 \tag{15}$$

$$La(CH_3C(=O)N(H)OH)^{3+} \xrightarrow{k_{-HA}} La^{3+} + CH_3C(=O)N(H)OH \tag{16}$$

A lack of spectroscopic evidence for $La(AH)^{3+}$, even at the highest proton concentration used (0.003 M), indicates that $K_2 \leq 3\cdot10^1\ M^{-1}$. This results in a decreased protonation constant of $La(A)^{2+}$, by ca. 7 orders of magnitude, in comparison with free A^-. This favorably compares with a decreased protonation constant of the hydroxo ligand coordinated to La^{3+} by ca. $6^1/_2$ orders of magnitude compared with free OH^-. Assuming that $La(AH)^{3+}$ is formed by a fast pre-equilibrium protonation of $La(A)^{2+}$, the inverse of the mean residence time of lanthanum in the mono complexes can be expressed by Equation (17).

$$1/\tau_B = k_{-11}[H^+] + k_{-12} = \frac{k_{-HA}K_2[H^+]}{1+K_2[H^+]} + k_{-12} \tag{17}$$

For $K_2[H^+] << 1$, the equation reduces to a simpler form: $\tau_B{}^{-1} = k_{-HA}K_2[H^+] + k_{-12}$ (the plots of calculated $\tau_B{}^{-1}$ vs. $[H^+]$ at various temperatures show linearity with significant intercepts, Figure S4). Therefore, k_{-11} could be considered as a product of the equilibrium constant for the protonation of $La(A)^{2+}$ and the first order dissociation rate constant of HA from the $La(AH)^{3+}$ complex, and a minimum value of k_{-HA} can be estimated as $7\cdot10^8\ s^{-1}$. The closeness of this value to the water-exchange rate constant seems reasonable considering that both ligands are uncharged, i.e. H_2O and HA molecules, and considering the electrostatic nature of the ligand−La^{III} bond,[27] which also accounts for a much smaller value calculated for k_{-12} than k_{-11}.

Despite the uncertainty in its determination from a far-removed intercept in the Eyring plot, the activation entropy has frequently been used as a useful criterion for distinction between possible mechanisms. The value $\Delta S^{\ddagger} = -100\ J\cdot K^{-1}\cdot mol^{-1}$ reported for the second-order complexation of Fe^{3+} with HA[7] was taken as evidence for an associative mechanism for this reaction. Similarly, the negative activation entropies determined for water exchange on a series of lanthanide ions were interpreted in terms of an associative mechanism.[23] Therefore, considering an associative mechanism for the studied reaction, negative activation entropies would be expected. The reliability of the activation entropies is made more dubious when obtained by such a complex iterative procedure as presented in this study, since mutual compensations between the activation parameters and the natural line broadening for the observed temperature effects are possible. Nevertheless, we believe that for the deduction of the reaction mechanism at least the signs of calculated entropies could be used. Therefore, the positive signs obtained could be indicative of a dissociative mode of activation for the studied reaction. The activation entropies for the backward reactions show that the dechelation of $La(A)^{2+}$ is also accompanied by a large increase in disorder. The proton assisted aquation exhibits an additional 149 $J\cdot K^{-1}\cdot mol^{-1}$ increase in entropy compared with the spontaneous aquation. The additional increase in activation entropy is very similar to the reaction entropy for the proton dehydration in water, viz. $\Delta S = +130\ J\cdot K^{-1}\ mol^{-1}$.[28]

All the above arguments speak in favor of a dissociative reaction mechanism and indeed no other mechanism is necessary to be invoked to rationalize the results obtained.

Furthermore, Crumbliss and Garrison[29] have shown that for Fe^{3+} and Al^{3+} ions, the ring-closure step is fast enough not to interfere with the complexation rate, but the water-exchange rate constants for those metal ions are much smaller than for the La^{3+} ion.

Nevertheless, it must also be mentioned that the chelation of HA was indeed proposed as the rate-determining step for its complexation to Fe^{2+}, Co^{2+}, and Ni^{2+}. Ring closure was assumed to be sufficiently retarded by slow proton dissociation from mono-coordinated hydroxamic acid to become the rate-limiting step. However, the value for k_{11} we obtained is more than three orders of magnitude larger than the rate constant for the proton dissociation from free HA in 55 M water at 25 °C, which was estimated as $1.4 \cdot 10^3$ $M^{-1} \cdot s^{-1}$.[30] The metal ion−proton repulsion and the inductive electron flow into the electron-deficient metal ion center could enhance the proton loss from $La(AH)^{3+}$ relative to the free acid, but for the above-mentioned ions the metal ion−proton repulsion was not the dominant factor.

Obviously, the proton exchange limited chelation could not be the rate-determining step for the reaction according to Equation (12) since the entering ligand had already been deprotonated. On the other hand, if the rate-determining chelation step was limited by the *trans*→*cis* isomerization of mono-coordinated HA, approximately equal rates would be expected for paths (11) and (12), which is not the case based on our results. These arguments indicate that the isomerization rate constant for HA exceeds the reported isomerization rate constant for *N*-alkyl derivatives by at least a factor of ca. 10^5 [$= 1.54 \cdot 10^6$ $M^{-1} \cdot s^{-1} \times 0.3$ M (HA)/($\approx$ 3) s^{-1}].

Experimental Section

General Remarks: A stock solution of $La(ClO_4)_3$ was prepared by mixing equivalent amounts of $Ba(ClO_4)_2$ (Merck) and $La_2(SO_4)_3$ (Fluka), dissolved in distilled water, followed by the centrifugation of precipitated $BaSO_4$. The concentration of La^{3+} was determined by titration with EDTA. Acetohydroxamic acid (98%) from Aldrich was used without further purification. Doubly distilled water was used in the preparation of all solutions. The ionic strength was 1.2 M in all the experiments, maintained by the addition of La/Na/H/ClO_4 ions. The pH of the solutions was adjusted with 2 M NaOH. The ^{139}La NMR measurements were performed at 56.52 MHz with a Bruker Avance 400 DRX spectrometer equipped with an 89-mm wide-bore magnet. The temperature was kept constant within ±0.1 K by means of a Bruker BVT 3000 digital temperature control unit, which was tested for the absolute temperature-scale reading. The spectral width of the spectra varied between $\delta = 200$ and 800, according to the changing La linewidth (11.3−45.2 kHz), and 128 up to 8000 data points were collected with a 90° pulse duration of about 18 μs. The half width ($\Delta\nu_{1/2}$), related to the relaxation times T_2 ($= 1/\pi\Delta\nu_{1/2}$), were calculated by fitting a single Lorentzian function to the recorded spectroscopic data. Chemical shifts were measured relative to external 0.2 M $La(ClO_4)_3$ in 20% (w/w) D_2O keeping the frequency of the external lanthanum fixed at 298 K, i.e. $\Delta\nu_{La^{3+}}(298) = -2187$ Hz. The observed temperature dependence of the ^{139}La NMR line widths were within the experimental error limits. A Mettler Toledo MP230 research digital pH meter equipped with a Schott N 6480 combination electrode, containing saturated NaCl solution, was used for pH measurements. The pH readings in H_2O/D_2O = 4:1 (w/w) solutions were converted into the $p[H^+]$ ($\equiv -\log([H^+]/mol \cdot dm^{-3})$ values by means of a linear function experimentally determined by the titration of $HClO_4$ with NaOH in the same solvent mixture at an ionic strength of 1.2 M (H/Na perchlorate) and at various temperatures. The results revealed that the slope and intercept of the function are temperature-independent within the experimental error limits. In order to exclude hydrolysis of lanthanum ions, experiments were performed in solutions of $p[H^+] < 6$.

Acknowledgments

This work has received financial support from the Croatian Ministry of Science and Technology through Grant Number 006141. M. G. thanks the DAAD for a scholarship that enabled him to perform experimental work at the University of Erlangen−Nürnberg. R. v. E. gratefully acknowledges financial support from the Deutsche Forschungsgemeinschaft and the Fonds der Chemischen Industrie.

[1] *Industrial Application of the Rare Earth Elements* (Eds.: L. W. Riker, K. A. Gschneider), Am. Chem. Soc., Washington, DC, **1981**.
[2] C. H. Evans, *Biochemistry of the Lanthanides*, Plenum Press, New York, **1990**.
[3] G. Schwarzenbach, K. Schwarzenbach, *Helv. Chim. Acta* **1963**, *46*, 1090.
[4] M. T. Caudle, A. L. Crumbliss, *Inorg. Chem.* **1985**, *24*, 2198.
[5] M. Biruš, M. Gabričević, O. Kronja, B. Klaić, *Inorg. Chem.* **1995**, *34*, 3110.
[6] M. Biruš, M. Gabričević, O. Kronja, B. Klaić, R. van Eldik, A. Zahl, *Inorg. Chem.* **1999**, *38*, 4064.
[7] B. Monzyk, A. L. Crumbliss, *J. Am. Chem. Soc.* **1979**, *101*, 6203.
[8] C. P. Brink, A. L. Crumbliss, *Inorg. Chem.* **1984**, *104*, 4708.
[9] L. L. Fish, A. L. Crumbliss, *Inorg. Chem.* **1985**, *24*, 2198.
[10] D. van der Helm, M. A. F. Jalal, M. B. Hossian, in *Iron Transport in Microbes, Plants, and Animals* (Eds.: G. Winkelmann, D. van der Helm, J. B. Nielands), VCH, New York, **1987**, chapter 9.
[11] Y. Ducommun, L. Helm, G. Laurenczy, A. E. Merbach, *Magn. Reson. Chem.* **1988**, *26*, 1023.
[12] Above 293 K, as the $p[H^+]$ increases the peak strongly shifts to the lower fields, but below that temperature the $p[H^+]$ increase above 5.27 reverses the direction of the shift towards the upper field. However, since at the latter acidity a weak opalescence appears slowly, the spectra were collected only at $p[H^+] \leq 5.27$. The same $p[H^+]$ increase at the lowest used temperature does not reverse the direction of the peak shift of 0.2 M $La(ClO_4)_3$.
[13] C. F. Baes, Jr., R. E. Mesmer, *The Hydrolysis of Cations*, John Wiley & Sons, New York, **1976**.
[14] B. Monzyk, A. L. Crumbliss, *J. Org. Chem.* **1980**, *45*, 4670.
[15] J. S. Leigh Jr., *J. Magn. Reson.* **1971**, *4*, 315.
[16] P. R. Bevington, *Data Reduction and Error Analysis for the Physical Scinces*, McGraw-Hill, **1969**.
[17] W. H. Press, S. A. Teukolsky, W. T. Vetterling, B. P. Flannery, *Numerical Recipes in Fortran, The Art of Scientific Computing*, 2nd ed., Cambridge University Press, **1992**.
[18] Hereafter, the number in brackets represent the uncertainty quoted as a single standard deviation for the particular parameter expresed in terms of the last significant digit reported for the parameter.

[19] A large fraction of the complex is achievable by increasing p[H^+], but then the bis and tris complexes would form if HA was in excess over La^{III}, whereas the hydrolyzed lanthanum(III) species would interfere if hydroxamic acid was not in a large excess.
[20] D. F. Evans, P. H. Missen, *J. Chem. Soc., Dalton Trans.* **1982**, 1929.
[21] M. Biruš, R. van Eldik, *Inorg. Chem.* **1991**, *30*, 4559.
[22] B. Monzyk, A. L. Crumbliss, *J. Org. Chem.* **1980**, *45*, 4670.
[23] C. Cossy, L. Helm, A. E. Merbach, *Inorg. Chem.* **1989**, *28*, 2699.
[24] R. M. Fuoss, *J. Am. Chem. Soc.* **1958**, *80*, 5059.
[25] It should be noted that the calculated value of an outer-sphere association equilibrium constant remarkably depends on the arbitrary choice of the ion-pair radius. An experimentally determined value of the ion-pair equilibrium constant for association of aquapentaamminecobalt(III) with azide at 25 °C and 3.5 M ionic strength was reported as low as 0.18 M^{-1} in: T. W. Swaddle, G. Guastalla, *Inorg. Chem.* **1969**, *8*, 1604.
[26] In the protonated complex species, $La(CH_3C(=O)N(H)OH)^{3+} \equiv La(AH)^{3+}$, a molecule of hydroxamic acid could be coordinated to the La^{3+} ion either bidentately through carbonyl and hydroxy oxygen atoms, or monodentately through the carbonyl oxygen atom alone. In any case this species is expected to be much more reactive than the $La(A)^{2+}$ species.
[27] E. N. Rizkalla, *Radiochim. Acta* **1993**, *61*, 181.
[28] B. E. Conway, *Ionic Hydration in Chemistry and Biophysics*, Elsevier Scientific Publishing Company, Amsterdam − Oxford − New York, **1981**, chapter 16.
[29] A. L. Crumbliss, J. M. Garrison, *Comments Inorg. Chem.* **1988**, *8*, 1.
[30] L. A. Dominey, K. Kustin, *Inorg. Chem.* **1984**, *23*, 103.

Received July 10, 2001
[I01256]

$PPh(2\text{-}C_6H_4S)_2$ as a Pincer Ligand in Nickel(II) and Palladium(II) Complexes — X-ray Structure of $[Ni\{PPh(C_6H_4S)_2\}(PPh_2Me)]$, $[Pd_2(\mu\text{-dppe})\{PPh(C_6H_4S)_2\}_2]$ and $[Ni\{PPh(C_6H_4S)_2\}]_2$

Elena Cerrada,[a] Larry R. Falvello,[a] Michael B. Hursthouse,[b] Mariano Laguna,*[a] Asunción Luquín,[a] and Cristina Pozo-Gonzalo[a]

Keywords: Nickel / Palladium / P ligands / S ligands

The phosphanylthiol $PPh(2\text{-}C_6H_4SH)_2$ reacts with the Ni^{II} and Pd^{II} complexes $[MCl_2L_2]$ in the presence of NaOEt to give the mononuclear derivatives $[M\{PPh(C_6H_4S)_2\}L]$ [M = Ni, L = PPh_3 (**1**), PPh_2Me (**2**); M = Pd, L = PPh_3 (**3**)]. The analogous reaction starting with complexes containing bidentate ligands $[MX_2(L\text{-}L)]$ produces different results depending on the ligand used. The complexes $[M\{PPh(C_6H_4S)_2\}(dppm)]$ [M = Ni (**4**), Pd (**5**)], with an unligated phosphorus atom in the diphosphane are obtained with bis(diphenylphosphanyl)methane (dppm), while the dinuclear complexes $[M_2(\mu\text{-dppe})\{PPh(C_6H_4S)_2\}]$ [M = Ni (**6**), Pd (**7**)] are isolated in the case of 1,2-bis(diphenylphosphanyl)-ethane (dppe). With 1,10-phenanthroline (phen), the complexes $[M\{PPh(C_6H_4S)_2\}(phen)]$ [M = Ni (**8**), Pd (**9**)] are obtained, but when 2,2′-bipyridine is used the dinuclear compounds $[M\{PPh(C_6H_4S)_2\}]_2$ [M = Ni (**10**), Pd (**11**)] are isolated instead. Complexes **10** and **11**, which can be obtained starting from $NiCl_2$ or $[PdCl_2(NCPh)_2]$ respectively, afford complexes **1**–**7** when treated with the respective phosphanes in the appropriate stoichiometries. The structures of **2**, **7** and **10** have been confirmed by X-ray analysis.

Introduction

Transition metal chemistry involving sulfur donor groups is of current interest because of its relevance in biology, because of its many industrial applications, and because of its importance in the area of novel complex synthesis.[1] Thus, sulfur-ligated transition metal complexes form the inorganic parts of the biologically active centres of some metalloproteins and enzymes. Consequently, some of these have found applications in pharmacology,[2−4] and industrial chemistry.[5−7] As for synthetic chemistry as such, transition metal thiolate complexes have received special interest because of their ability to adopt different structures and nuclearities.[8]

It is fairly common that these thiolate complexes contain phosphane moieties which, operating as ancillary ligands, are able to enhance the properties of interest. For this reason the chemistry of polydentate ligands with sulfur and phosphorus donor atoms in their frameworks has attracted increasing interest, augmented by the observation of unusual structures and reactivities in the resulting transition metal complexes.[9] In this regard, the systems most studied have been the proligands $PR_2(CH_2SH)$, $PR_2(CH_2CH_2SH)$ and $PR_2(C_6H_4SH)$.[10−16]

Species with more than two donor atoms — $PR(CH_2CH_2SH)_2$, $PR(C_6H_4SH)_2$, $P(CH_2CH_2SH)_3$ and $P(C_6H_4SH)_3$ — have received much less attention,[17−20] although they possess intrinsic interest in as much as they stably occupy three or more coordination sites, thus permitting more specific chemistry to be performed at the remaining sites. Such is the case for $PPh(C_6H_4S)_2^{2-}$, which possesses a three-donor set "PS_2" and can be described as a pincer ligand similar to van Koten's[21] $[C_6H_3(CH_2NMe_2)_2]^-$ and $[2,6\text{-}(Ph_2PCH_2)_2C_6H_3)]^-$, Milstein's[22] $[C_6H_3(CH_2PBu_2)_2]^-$ and $[C_6H_4(CH_2PPr_2)_2]$ or to Sellmann's [bis(2-mercaptophenyl)sulfide^{2-}].[23]

In this paper we describe some mono- and dinuclear complexes of Ni^{II} and Pd^{II}, with $PPh(C_6H_4S)_2^{2-}$ acting as a pincer ligand in an *S,S′,P* coordination mode, as confirmed by the X-ray structures of $[Ni\{PPh(C_6H_4S)_2\}(PPh_2Me)]$, $[Pd_2(\mu\text{-dppe})\{PPh(C_6H_4S)_2\}_2]$ and $[Ni\{PPh(C_6H_4S)_2\}]_2$.

Results and Discussion

The reaction of a solution of $PPh(C_6H_4SH)_2$ and sodium ethoxide with the nickel(II) and palladium(II) species MCl_2L_2 (L = monodentate phosphane; step *i,* Scheme 1), yields the mononuclear derivatives $[M\{PPh(C_6H_4S)_2\}(L)]$

[a] Departamento de Química Inorgánica, Instituto de Ciencia de Materiales de Aragón, Universidad de Zaragoza-C.S.I.C, 50009 Zaragoza, Spain
E-mail: mlaguna@posta.unizar.es
[b] Department of Chemistry, University of Southampton, Highfield, Southampton, SO17 1BJ, UK

 © WILEY-VCH Verlag GmbH, 69451 Weinheim, Germany, 2002 1434−1948/02/0404−0826 $ 17.50+.50/0 *Eur. J. Inorg. Chem.* **2002**, 826−833

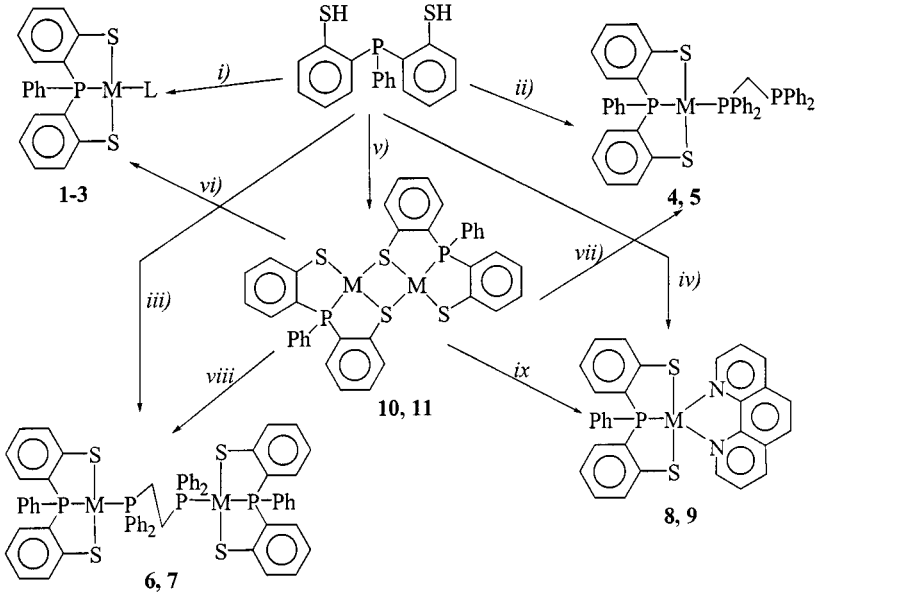

i) EtONa, $[MCl_2L_2]$; *ii)* EtONa, $[MCl_2(dppm)]$; *iii)* EtONa, $[MCl_2(dppe)]$; *iv)* $[MCl_2(phen)]$
v) EtONa, $MCl_2{\cdot}6H_2O$ or $[PdCl_2(PhCN)_2]$; *vi)* 2L; *vii)* 2 dppm; *viii)* dppe; *ix)* phen

Scheme 1. Synthesis of complexes **1−11**

[M = Ni, L = PPh_3 (**1**), PPh_2Me (**2**); M = Pd, L = PPh_3 (**3**)]. This process can be described as the result of deprotonation of the starting phosphanylthiol ligand at room temperature, followed by coordination to the metal centre with the concomitant dissociation of one monodentate phosphane. To date the most common synthetic routes to complexes with these ligands have involved electrochemical procedures[24] or reflux conditions in the presence of NEt_3 as a base. The preparation of **1−3** occurs under milder conditions than those reported for related complexes.

The IR spectra of complexes **1−3** do not show the ν(S−H) band, which appears at 2495 cm^{-1} in the free ligand. This fact, and the absence of the S−*H* signal in the ^1H NMR spectrum, indicates the presence of the anionic form of the ligand. The ^1H NMR spectra exhibit multiplets in the aromatic region and, for **2**, a doublet at δ = 1.93 due to the methyl group of the PPh_2Me ligand. The ^{31}P NMR spectra of the complexes show two doublets due to the two nonequivalent phosphorus atoms. The phosphanylthiolate resonance, which appears at δ = −19.4 in the free ligand, is shifted to about δ = 85 in complexes **1−3**. This downfield shift could be considered as being due to the coordination of the phosphorus atom to the metal. The second doublet appears at higher field: δ = 26.0 (**1**), 9.4 (**2**) and 22.6 (**3**). The $LSIMS^+$ mass spectra show the parent peak at *m/z* = 644 (**1**), 582 (**2**) and 692 (**3**), with appropriate isotope distributions, in agreement with the mononuclear description of the three products. Electrovoltammetry studies show a nonreversible one-electron oxidation at 0.412 V only in the case of $[Ni\{PPh(C_6H_4S)_2\}(L)]$ (**1**).

When the same reaction as described in *i)* is carried out in the presence of a nickel or palladium complex with a bidentate phosphane $[MCl_2(L\text{-}L)]$ (steps *ii* and *iii*, Scheme 1), the results obtained are different depending on the diphosphane used. Thus, in the case of bis(diphenylphosphanyl)methane (dppm) the mononuclear complexes **4** and **5** are isolated, whereas the dinuclear species **6** and **7** are formed when 1,2-bis(diphenylphosphanyl)ethane (dppe) is used instead.

The complexes $[M\{PPh(C_6H_4S)_2\}dppm]$ [M = Ni (**4**), Pd (**5**)] show IR spectra similar to those of compounds **1−3**, with the S−H vibration absent and the phosphane bands present. The ^1H NMR spectra show multiplets in the aromatic region, and broad signals centred at δ = 3.17 (**4**) and 3.33 (**5**), even at low temperature, due to the -CH_2- group of dppm. The room temperature ^{31}P NMR spectrum of **4** shows a triplet at δ = 85 assignable to the P atom of the phosphanylthiolate, although no signal was observed for the phosphorus atoms of dppm. A new broad signal appears in the negative region upon lowering the sample temperature that could be attributed to the dppm ligand. Decoalescence occurs at 283 K and a pattern corresponding to an AMX spin system becomes well-resolved at 223 K with the parameters δ_A = 85.9 (d, J_{AM} = 284 Hz), δ_M = 18.6 (dd, J_{MX} = 77.4 Hz) and δ_X = −27.1 (d). The high-field signal at δ = −27 is indicative of a free P-atom in the diphosphane. At 283 K $\Delta G^{\neq}$ has a value of 12.18 kcal/mol.[25] Complex **5** exhibits a similar three-resonance pattern at room temperature. The $LSIMS^+$ spectra show the parent peaks at *m/z* = 766 (**4**) and 813 (**5**) with the appropriate isotope distribution, again in agreement with the proposed formulation.

When the diphosphane 1,2-bis(diphenylphosphanyl)-ethane (dppe) is used instead of dppm, the dinuclear derivatives $[Pd_2(\mu\text{-}dppe)\{PPh(C_6H_4S)_2\}_2]$ [M = Ni (**6**), Pd (**7**)] can be isolated as air stable solids (step *iii*, Scheme 1). The ^1H NMR spectra in $CDCl_3$ solution display the resonances characteristic of the phosphanyldithiolate ligand in the aro-

matic region, as well as those of the dppe. The ^{31}P NMR spectra reveal AA′XX′ systems for both complexes: **6** (δ_A = 87.46, δ_X = 22.47, $J_{AA'}$ = 21.32, J_{AX} = 234.13, $J_{XX'}$ = 21.60 Hz), **7** (δ_A = 84.8, δ_X = 20.85, $J_{AA'}$ = 23.7, J_{AX} = 414.2, $J_{XX'}$ = 25.1 Hz). This is consistent with a dinuclear formulation. The mass spectrum (LSIMS$^+$) does not show the molecular peak for **6** and shows only weak intensity for **7** (*m*/*z* = 1258, 5%).

The reaction of [MCl_2(N-N)] [N-N = 2,2′-bipyridine (bipy), 1,10-phenanthroline (phen)] with $PPh(C_6H_4SH)_2$ in the presence of sodium ethoxide, depends on the N-containing ligand. This ligand remains bound to the metal only in the case of 1,10-phenanthroline, yielding [M{$PPh(C_6H_4S)_2$}(phen)] [M = Ni (**8**), Pd (**9**); process *iv*, Scheme 1]. Curiously, the nickel complex is soluble in conventional solvents, while the palladium-containing product is not soluble enough, so that no solution data could be measured for complex **9**. The ^{31}P NMR spectrum of **8** shows a singlet at δ = 75.4, as a consequence of the coordination of the P atom to the metal centre, meaning that complex **8** is in all likelihood pentacoordinated. With bipy present as the auxiliary ligand, the reaction proceeds with the formation of the dinuclear species [M{$PPh(C_6H_4S)_2$}]$_2$ [M = Ni (**10**) and Pd (**11**)].

The dinuclear derivatives **10** and **11** can also be obtained from the reaction between $PPh(C_6H_4SH)_2$ in NaOEt, and $NiCl_2{\cdot}6H_2O$ or [$PdCl_2(PhCN)_2$], in which PhCN serves as a leaving group (step *v*, Scheme 1). The ^1H NMR spectra show only signals in the aromatic region, while the ^{31}P NMR spectra display the expected singlets at δ = 72.7 and 76.9, respectively, due to the equivalent phosphorus donors in each complex. The mass spectra show the molecular peaks at *m*/*z* = 764 (45%) (**10**) and 861 (12%) (**11**), in agreement with a dinuclear formulation.

Complexes **10** and **11** react readily with mono- and bidentate phosphanes in dichloromethane in the appropriate stoichiometries, to give mixtures of products in which complexes **1**−**9** are the major products, as shown by ^1H and ^{31}P NMR spectroscopic data. This fact is in agreement with the dinuclear formulation of **10** and **11**. [M{$PPh(C_6H_4S)_2$}(bipy)] complexes are again inaccessible by this route, and when the corresponding reaction was attempted the starting materials were recovered unchanged.

Crystal Structures of [Ni{$PPh(C_6H_4S)_2$}(PPh_2Me)] (2), [Pd_2(μ-dppe){$PPh(C_6H_4S)_2$}$_2$] (7) and [Ni{$PPh(C_6H_4S)_2$}]$_2$ (10)

Zubieta et al.[20] have previously reported a complex similar to **1**, and described it as a dinuclear derivative. Because the data for complexes **1**−**5**, and particularly the mass spectra, point more to them being mononuclear, we undertook the X-ray analysis of one of these complexes, namely [Ni{$PPh(C_6H_4S)_2$}(PPh_2Me)] (**2**), which yielded the most suitable crystals for X-ray studies. Figure 1 shows a view of the molecule, a mononuclear, distorted square planar *trans*-P,P and *trans*-S,S nickel complex with the Ni atom 0.031 Å out of the plane formed by S(1), P(1), S(2) and P(2) (planar within 0.208 Å). The main distortion from square-planar geometry arises from closure of the S(2)−Ni−S(1) angle [166.22(4)°], and to a much lesser extent, of the angles S(1)−Ni−P(2) and S(2)−Ni−P(2) [87.05(3)° and 88.66(3)°, respectively] most likely imposed by the rigidity of the phosphanyldithiolate ligand. The two Ni−P distances are quite different from each other. The Ni−P(1) distance of 2.2054(8) Å is similar to that found for Ni−PPh_3 bonds such as that found in [Ni(S_3)PPh_3] [S_3^{2-} = bis(2-mercaptophenyl)sulfide, 2.197(1) Å].[23] However, the Ni−P(2) bond

Table 1. Summary of crystallographic data for complexes [Ni{$PhP(C_6H_4S)_2$}(PPh_2Me)] (**2**), [Pd_2(μ-dppe){$PPh(C_6H_4S)_2$}$_2$] CH_2Cl_2 (**7**) and [Ni{$PhP(C_6H_4S)_2$}]$_2$ (**10**)

	2	**7**	**10**
Empirical formula	$C_{31}H_{26}NiP_2S_2$	$C_{64}H_{52}Cl_4P_4Pd_2S_4$	$C_{18}H_{13}NiPS_2$
Molecular mass	583.29	1427.78	383.08
Temperature	295(2) K	293(2) K	301(2) K
Crystal system	Monoclinic	Triclinic	Monoclinic
Space group	$P2_1/n$	$P\bar{1}$	$P2_1/n$
a, Å	9.8082(6)	9.648(2)	16.645(7)
b, Å	28.9852(19)	10.858(2)	11.073(15)
c, Å	9.9463(6)	15.054(3)	18.24(3)
α, deg	90	97.99(3)	90
β, deg	104.5850(10)	98.78(3)	107.80(8)
γ, deg	90	100.31(3).	90
V, Å^3	2736.5(3)	1510.8(5)	3201(7)
Z	4	1	8
D_c (Mg/m^3)	1.416	1.569	1.590
μ, mm^{-1}	0.998	1.057	1.564
Crystal size (mm)	0.28 × 0.25 × 0.18	0.2 × 0.2 × 0.12	0.18 × 0.17 × 0.01
θ range	1.41 to 25.00°	2.36 to 25.02°	2.18 to 22.99°
*R*1,[a] *wR*2[b] [$I > 2\sigma(I)$]	0.0530, 0.1621	0.0344, 0.0941	0.1491, 0.2748
Residual ρ, e Å^3	0.252, −0.425	0.821, −0.720	1.215, −1.133

[a] $R1 = ||F_o| - |F_c||/|F_o|$. [b] $wR2 = \{[w(F^2_o - F^2_c)]/[w(F^2_o)^2]\}^{1/2}$.

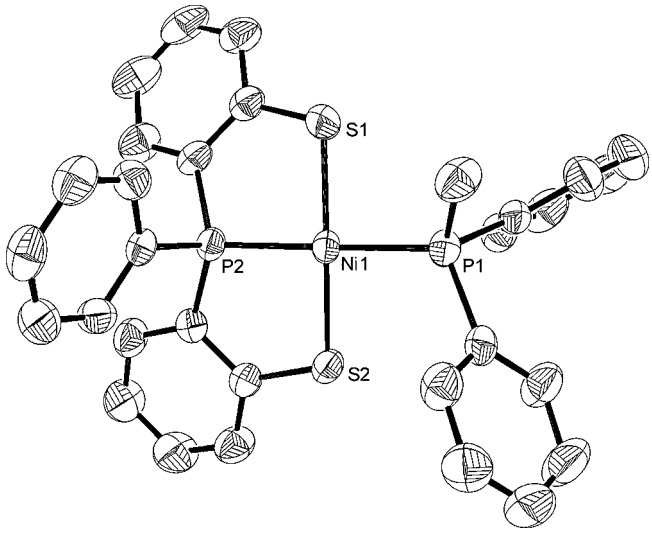

Figure 1. Compound **2** in the crystal; displacement parameter ellipsoids represent 50% probability surfaces; H atoms are omitted for clarity

Table 2. Selected bond lengths [Å] and angles [°] for **2**

Ni(1)−P(2)	2.1186(8)	Ni(1)−S(1)	2.1756(9)
Ni(1)−S(2)	2.1630(8)	Ni(1)−P(1)	2.2054(8)
P(2)−Ni(1)−S(2)	88.66(3)	C(4)−P(1)−Ni(1)	113.55(11)
P(2)−Ni(1)−S(1)	87.05(3)	C(1)−P(1)−Ni(1)	112.37(12)
S(2)−Ni(1)−S(1)	166.22(4)	C(10)−P(1)−Ni(1)	115.74(10)
P(2)−Ni(1)−P(1)	170.41(3)	C(16)−S(1)−Ni(1)	104.97(11)
S(2)−Ni(1)−P(1)	94.18(3)	C(32)−P(2)−C(21)	115.43(14)
S(1)−Ni(1)−P(1)	92.19(3)	C(32)−P(2)−Ni(1)	109.63(10)
C(4)−P(1)−C(1)	105.50(16)	C(21)−P(2)−Ni(1)	108.97(10)
C(4)−P(1)−C(10)	105.42(13)	C(31)−S(2)−Ni(1)	105.83(10)
C(1)−P(1)−C(10)	103.21(15)		

length of 2.1186(8) Å is shorter than the former and shorter than other Ni-phosphanylthiolate complexes:[26] [$Ni(PS)_2$] with PS = $PPh_2(C_6H_4S)$ and $PPh_2[C_6H_3(SiMe_3)S]$, 2.181(2) and 2.172(3) Å, respectively. The Ni−P(2) bond is similar to that found in the binuclear compound [$Ni_2\{P(C_6H_4S)_3\}_2$][27] [2.109(4) Å]. This short distance is again consistent with the constraints imposed by the PS_2 ligand. The Ni−S distances, which average 2.1693(8) Å, are in the range reported for terminal nickel-thiolate bonds[23] and lie in the range found for [$Ni(PS)_2$]:[25,26] PS = $PPh_2(C_6H_4S)$, 2.180(2); $PPh_2(C_6H_3(SiMe_3)S)$, 2.151(3) Å. Moreover, the Ni−S distances are similar to those found for other phosphanylthiolate derivatives.[28−30] Complexes **1**, **3**, **4** and **5** presumably adopt similar mononuclear dispositions.

The crystal structure of **7**, which includes an interstitial molecule of CH_2Cl_2, was also determined by X-ray diffraction. The structure (Figure 2) displays two Pd-phosphanylthiolate units connected to each other by the dppe ligand. The geometry around each palladium centre, *trans*-P,P and -S,S, is close to square planar, as was the case in **2**, and

Table 3. Selected bond lengths [Å] and angles [°] for **7**·CH_2Cl_2

Pd (1)−P(1)	2.2265(10)	Pd(1)−S(2)	2.3316(10)
Pd(1)−S(1)	2.3137(9)	Pd(1)−P(2)	2.3402(11)
P(1)−Pd(1)−S(1)	86.78(4)	C(13)−P(1)−C(7)	108.41(14)
P(1)−Pd(1)−S(2)	84.24(4)	C(6)−P(1)−Pd(1)	109.03(11)
S(1)−Pd(1)−S(2)	164.93(3)	C(13)−P(1)−Pd(1)	105.78(10)
P(1)−Pd(1)−P(2)	171.77(3)	C(7)−P(1)−Pd(1)	115.55(10)
S(1)−Pd(1)−P(2)	93.79(4)	C(20)−P(2)−Pd(1)	104.99(10)
S(2)−Pd(1)−P(2)	93.39(4)	C(1)−S(1)−Pd(1)	103.97(11)
C(6)−P(1)−C(13)	113.20(14)	C(18)−S(2)−Pd (1)	101.51(11)
C(6)−P(1)−C(7)	105.08(13)		

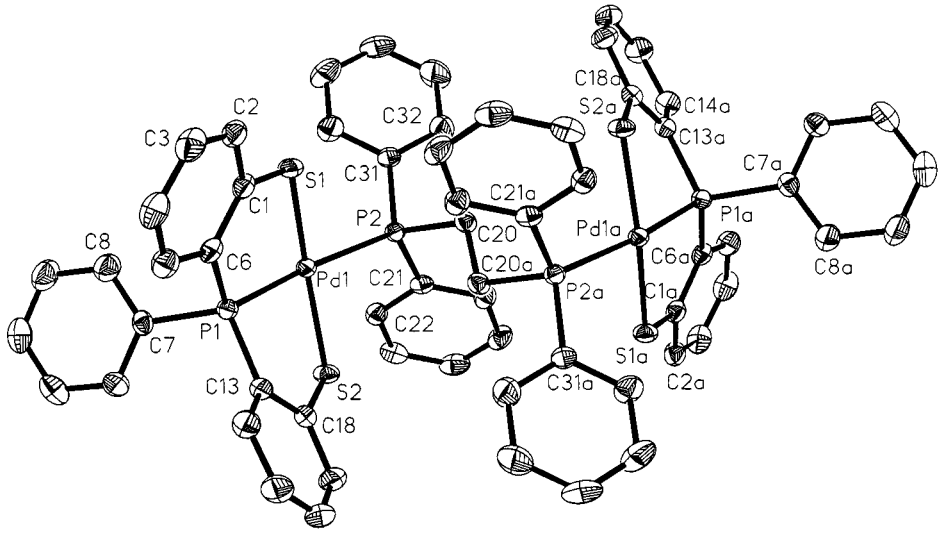

Figure 2. Compound **7** in the crystal; displacement parameter ellipsoids represent 50% probability surfaces; H atoms are omitted for clarity

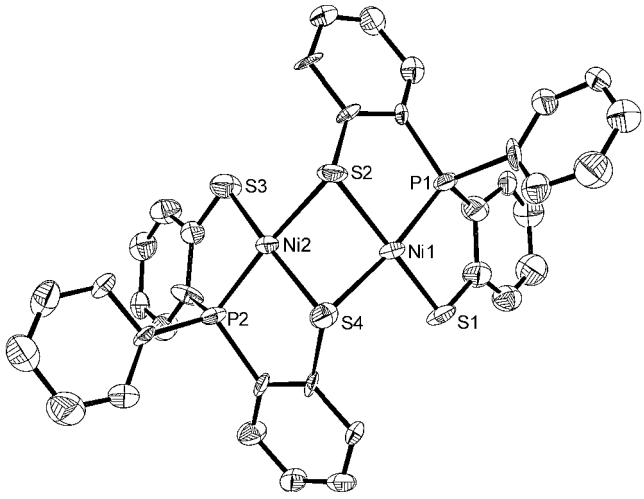

Figure 3. Compound **10** in the crystal; displacement parameter ellipsoids represent 50% probability surfaces; H atoms are omitted for clarity

Table 4. Selected bond lengths [Å] and angles [°] for **10**

Ni(1)−P(1)	2.078(10)	Ni(2)−P(2)	2.088(10)
Ni(1)−S(1)	2.147(11)	Ni(2)−S(3)	2.168(11)
Ni(1)−S(4)	2.215(11)	Ni(2)−S(4)	2.201(10)
Ni(1)−S(2)	2.229(10)	Ni(2)−S(2)	2.257(10)
Ni(1)−Ni(2)	2.714(6)		
P(1)−Ni(1)−S(1)	89.0(4)	S(3)−Ni(2)−Ni(1)	120.8(3)
P(1)−Ni(1)−S(4)	171.4(4)	S(4)−Ni(2)−Ni(1)	52.3(3)
S(1)−Ni(1)−S(4)	99.4(4)	S(2)−Ni(2)−Ni(1)	52.3(3)
P(1)−Ni(1)−S(2)	86.9(4)	C(1)−P(1)−Ni(1)	109.7(12)
S(1)−Ni(1)−S(2)	170.0(4)	C(7)−P(1)−Ni(1)	117.4(13)
S(4)−Ni(1)−S(2)	84.5(4)	C(13)−P(1)−Ni(1)	110.2(11)
P(1)−Ni(1)−Ni(2)	122.1(3)	C(2)−S(1)−Ni(1)	106.6(14)
S(1)−Ni(1)−Ni(2)	122.5(3)	C(14)−S(2)−Ni(1)	102.1(11)
S(4)−Ni(1)−Ni(2)	51.8(3)	C(14)−S(2)−Ni(2)	112.3(12)
S(2)−Ni(1)−Ni(2)	53.2(3)	Ni(1)−S(2)−Ni(2)	74.5(3)
P(2)−Ni(2)−S(3)	88.9(4)	C(19)−P(2)−Ni(2)	109.9(11)
P(2)−Ni(2)−S(4)	88.5(4)	C(25)−P(2)−Ni(2)	115.1(11)
S(3)−Ni(2)−S(4)	167.9(4)	C(31)−P(2)−Ni(2)	106.6(11)
P(2)−Ni(2)−S(2)	172.2(4)	C(20)−S(3)−Ni(2)	105.2(13)
S(3)−Ni(2)−S(2)	98.8(4)	C(32)−S(4)−Ni(2)	101.5(11)
S(4)−Ni(2)−S(2)	84.2(4)	C(32)−S(4)−Ni(1)	111.7(11)
P(2)−Ni(2)−Ni(1)	124.3(3)	Ni(2)−S(4)−Ni(1)	75.8(3)

the Pd atom lies out of the plane by 0.167 Å, with the main deviations due to contraction of the S(2)−Pd−S(1) [164.93(3)°], S(1)−Pd−P(1) [86.78(4)°], and S(2)−Pd−P(1) [84.24(4)°] angles. The two Pd−P distances are different from each other, as in **2**. The Pd−P(phosphanylthiolate) bond [Pd(1)−P(1) = 2.2265(10) Å] is shorter than that in Pd−P(dppe) [Pd(1)−P(2) = 2.3402(10) Å]. This reinforces the notion that the shorter bond distance from Pd to the phosphanylthiolate phosphorus atom results from constraints imposed by the ligand. Accordingly, several systems with palladium coordinated by less restrictive P,S ligands show larger Pd−P distances, such as in $[Pd\{PPh_2(CH_2CH_2S)\}Cl(PPh_3)]$ [2.280(2) Å],[31] *trans*-$[Pd\{PPh_2(C_6H_4S)\}_2]$ [2.291(1) Å][32] or *cis*-$[Pd\{PPh_2(C_6H_4S)\}_2]$ [2.2845(8) and 2.2802(8) Å].[33] The Pd−P bonds involving the dppe ligand are slightly longer [2.3402(11) Å] than in other derivatives with this diphosphane.[34] The Pd−S bond lengths [average value 2.3227(10) Å] are similar to those found in the complexes mentioned above and in other bisdithiolene derivatives.[35−37]

The structure determination of **10** was undertaken in order to establish the chemical connectivity, although it was clear from the outset that the data would not be of high quality. The analysis reveals (Figure 3) a dinuclear complex consisting of two Ni-phosphanyldithiolate units linked by a double sulfur bridge. Although the accuracy of the structure determination does not permit a systematic comparison of distances, the Ni−P and Ni−S(terminal) distances are similar to those found in complex **2**; the Ni−S(bridging) distances are greater than those for Ni−S(terminal) as is the case in other systems with terminal and bridging sulfur atoms, such as $[Ni(S_3)]_3$ [S_3^{2-} = bis(2-mercaptophenyl)sulfide][23] and $[Ni_2\{P(C_6H_4S)_3\}_2]$.[27] It is worth noting that the Ni−Ni distance of 2.714(6) Å is rather short, which could be indicative of some degree of metal-metal interaction.[27,38,39]

Experimental Section

General Procedures: All reactions were performed under argon using standard Schlenk techniques, although the products are air stable. $[MCl_2L_2]$ (M = Ni, Pd; L = PPh_3, PPh_2Me),[40,41] and $[MCl_2(L\text{-}L)]$ (M = Ni, Pd; L-L = dppm, dppe,[42,43] bipy, phen[44]) were prepared by established procedures. All other reagents were used as supplied. The synthesis of $PPh(2\text{-}C_6H_4SH)_2$ was carried out using the standard literature procedure.[45] IR spectra were recorded on a Perkin−Elmer 883 spectrophotometer, over the range 4000−200 cm^{-1}, using Nujol mulls between polyethylene sheets. ^1H and ^{31}P NMR spectra were measured on a Varian UNITY 300 or Bruker 300 spectrometer in $CDCl_3$ or CD_2Cl_2 solution; chemical shifts are quoted relative to $SiMe_4$ (^1H) or H_3PO_4 (external, ^{31}P). The C, H N and S analyses were performed with a Perkin−Elmer 2400 microanalyser. Mass spectra were recorded on a VG Autospec, by liquid secondary ion mass spectrometry (LSIMS+) using nitrobenzyl alcohol as matrix and a cesium gun.

Preparation of the Phosphanyldithiolate Complexes [Ni{PPh($C_6H_4S)_2$}PPh_3] (1), [Ni{PPh($C_6H_4S)_2$}PPh_2Me] (2), and [Pd{PPh($C_6H_4S)_2$}PPh_3] (3): A solution of 0.1 M NaOEt (3 mL, 0.3 mmol) and $[NiCl_2(PPh_3)_2]$ (0.098 g, 0.15 mmol), $[NiCl_2(PPh_2Me)_2]$ (0.079 g, 0.15 mmol) or $[PdCl_2(PPh_3)_2]$ (0.105 g, 0.15 mmol) was added, over a period of 10 minutes, to a suspension of $PPh(C_6H_4SH)_2$ (0.048 g, 0.15 mmol) in 10 mL of ethanol. After 5 h of stirring, green (**1,2**) or brown (**3**) solids precipitated; these were filtered off, washed with ethanol and dried in vacuo.

1: Yield: 73 mg (75%). $C_{36}H_{28}NiP_2S_2$ (645.4): calcd. C 66.99, H 4.37, S 9.93; found C 66.45, H 4.20, S 9.50. ^1H NMR ($CDCl_3$): δ = 6.69 (m, 2 H, Ph), 7.18 (m, 2 H, Ph), 7.62−7.26 (m, 24 H, Ph). $^{31}P\{^1H\}$ NMR ($CDCl_3$): δ = 86.2 (d, $J_{P\text{-}P}$ = 270 Hz), 26 (d). MS: *m*/*z* (%) = 644 (100) $[M]^+$.

2: Yield: 62 mg (70%). $C_{31}H_{26}NiP_2S_2$ (583.3): calcd. C 63.83, H 4.49, S 10.99; found C 63.42, H 4.21, S 10.38. ^1H NMR ($CDCl_3$): δ = 1.93 (d, $^2J_{P\text{-}H}$ = 8.3 Hz, 3 H, Me), 7.0 (m, 2 H), 7.64−7.22 (m, 21 H, Ph). $^{31}P\{^1H\}$ NMR ($CDCl_3$): δ = 87.4 (d, $J_{P\text{-}P}$ = 280 Hz), 9.4 (d). MS: *m*/*z* (%) = 582 (100) $[M]^+$, 382 (60) $[M - PPh_2Me]^+$.

3: Yield: 94 mg (90%). $C_{36}H_{28}P_2PdS_2$ (693.1): calcd. C 62.38, H 4.07, S 9.25; found C 61.95, H 4.21, S 8.69. ^1H NMR ($CDCl_3$): δ = 6.99 (m, 2 H, Ph), 7.21 (m, 2 H, Ph), 7.62−7.27 (m, 24 H, Ph).

$^{31}P\{^1H\}$ NMR ($CDCl_3$): δ = 85.2 (d, $J_{P\text{-}P}$ = 406 Hz), 22.6 (d). MS: *m/z* (%) = 692 (100) $[M]^+$, 430 (55) $[M - PPh_3]^+$.

[Ni{PPh($C_6H_4S)_2$}(dppm)] (4) and [Pd{PPh($C_6H_4S)_2$}(dppm)] (5): A solution of 0.1 M NaOEt (3 mL, 0.3 mmol) and either [$NiCl_2$dppm] (0.077 g, 0.15 mmol) or [$PdCl_2$dppm] (0.084 g, 0.15 mmol) was added, over a period of 10 minutes, to a suspension of PPh($C_6H_4SH)_2$ (0.048 g, 0.15 mmol) in 10 mL of ethanol. Green (**4**) or orange (**5**) solids precipitated immediately, and were filtered off, washed with ethanol and dried in vacuo.

4: Yield: 80 mg (70%). $C_{43}H_{35}NiP_3S_2$ (767.5): calcd. C 67.29, H 4.59, S 8.35; found C 66.96, H 4.35, S 7.85. ^1H NMR ($CDCl_3$): δ = 3.17 (br. s, 2 H, CH_2), 6.95 (m, 2 H), 7.45−7.14 (m, 29 H, Ph), 7.54 (m, 2 H, Ph). $^{31}P\{^1H\}$ NMR (CD_2Cl_2): δ = (−50 °C): δ_A = 85.9 (d, J_{AM} = 284 Hz), δ_M = 18.6 (dd, J_{MX} = 77.4 Hz), δ_X = −27.1 (d). MS: *m/z* (%) = 766 (100) $[M]^+$, 383 (70) $[M - dppm]^+$.

5: Yield: 107 mg (88%). $C_{43}H_{35}P_3PdS_2$ (815.2): calcd. 63.35, H 4.3, S 7.85; found C 62.94, H 3.92, S 7.71. ^1H NMR ($CDCl_3$): δ = 3.33 (br. s, 2 H, CH_2), 6.95 (m, 2 H, Ph), 7.71−7.15 (m, 31 H, Ph). $^{31}P\{^1H\}$ NMR ($CDCl_3$): δ = 83.2 (d, $J_{P\text{-}P}$ = 399 Hz), 11.3 (d), −26.1 (br. s,). MS: *m/z* (%) = 813 (100) $[M]^+$, 430 (70) $[M - dppm]^+$.

[Ni_2(μ-dppe){PPh($C_6H_4S)_2$}$_2$] (6) and [Pd_2(μ-dppe){PPh($C_6H_4S)_2$}$_2$] (7): The procedure followed was similar to that described for **4** and **5**, using [$NiCl_2$dppe] (0.078 g, 0.15 mmol) or [$PdCl_2$dppe] (0.085 g, 0.15 mmol). Green (**6**) or brown (**7**) solids precipitated from the reaction media, and were filtered off and washed with EtOH.

6: Yield: 123 mg (70%). $C_{62}H_{50}Ni_2P_4S_4$ (1164.6): calcd. C 63.94, H 4.32, S 11.01; found C 63.55, H 4.15, S 10.52. ^1H NMR ($CDCl_3$): δ = 2.74 (br. s, 4 H, CH_2-CH_2), 7.61−6.66 (m, 46 H, Ph). $^{31}P\{^1H\}$ NMR ($CDCl_3$): AA′XX′: $\delta_A = \delta_{A'}$ = 87.46, $\delta_X = \delta_{X'}$ = 22.47, $J_{AA'}$ = 21.32 Hz, J_{AX} = 234.13 Hz, $J_{AX'} = J_{A'X}$ = 0 Hz, $J_{XX'}$ = 21.60 Hz. MS: *m/z* (%) = 780 (30) $[M - Ni(PPh(C_6H_4S)_2]^+$.

7: Yield: 123 mg (65%). $C_{62}H_{50}P_4Pd_2S_4$ (1260.0): calcd. C 59.09, H 3.99, S 10.17; found C 58.82, H 3.81, S 9.85. ^1H NMR ($CDCl_3$): δ = 3.33 (br. s, 4 H, CH_2-CH_2), 7.0 (m, 4 H), 7.61−7.17 (m, 42 H, Ph). $^{31}P\{^1H\}$ NMR ($CDCl_3$): AA′XX′: $\delta_A = \delta_{A'}$ = 84.8, $\delta_X = \delta_{X'}$ = 20.85, $J_{AA'}$ = 23.7 Hz, J_{AX} = 414.2 Hz, $J_{AX'} = J_{A'X}$ = 0 Hz, $J_{XX'}$ = 25.1 Hz. MS: *m/z* (%) = 1258 (5) $[M]^+$, 780 (30) $[M - Ni(PPh(C_6H_4S)_2]^+$.

[Ni{PPh($C_6H_4S)_2$}(phen)] (8) and [Pd{PPh($C_6H_4S)_2$}(phen)] (9): A 0.1 M solution of NaOEt (3 mL, 0.3 mmol) was added over a period of 10 minutes to a suspension of PPh($C_6H_4SH)_2$ (0.048 g, 0.15 mmol) in 10 mL of ethanol, and then [$NiCl_2$phen] (0.046 g, 0.15 mmol) or [$PdCl_2$phen] (0.054 g, 0.15 mmol) was added. After stirring overnight brown solids precipitated, which were filtered off, washed with ethanol and dried in vacuo.

8: Yield: 55 mg (65%). $C_{30}H_{21}N_2NiPS_2$ (563.3): calcd. C 64.06, H 3.76, N 4.98, S 11.40; found C 63.65, H 3.35, N 4.52, S 10.98. ^1H NMR ($CDCl_3$): δ = 7.58−6.79 (m, 14 H, Ph), 7.62 (m, 2 H, phen), 7.78 (s, 2 H, phen), 8.23 (m, 2 H, phen), 9.72 (m, 1 H, phen). $^{31}P\{^1H\}$ NMR ($CDCl_3$): δ = 4.5(s). MS: *m/z* (%) = 562 (5) $[M]^+$, 780 (30) $[M - Ni(PPh(C_6H_4S)_2]^+$.

9: Yield: 64 mg (70%). $C_{30}H_{21}PPdN_2S_2$ (611.0): calcd. C 58.97, H 3.46, N 4.58, S 10.49; found C 58.75, H 3.5, N 4.35, S 11.05.

[Ni{PPh($C_6H_4S)_2$}]$_2$ (10) and [Pd{PPh($C_6H_4S)_2$}]$_2$ (11): a) Following the same procedure as described for the previous complexes, using $NiCl_2{\cdot}6H_2O$ (0.036 g, 0.15 mmol) or [$PdCl_2$(PhCN)$_2$] (0.057 g, 0.15 mmol), afforded green or brown solids which precipitated from their respective reaction media and were filtered off and washed with EtOH.

10: Yield: 40 mg (70%). $C_{36}H_{26}Ni_2P_2S_4$ (766.2): calcd. C 56.43, H 3.42, S 16.73; found C 56.10, H 3.21, S, 16.25. ^1H NMR (CD_2Cl_2): δ = 6.99 (m, 4 H), 7.22 (m, 4 H), 7.49−7.19 (m, 10 H), 7.56 (m, 4 H), 7.76 (m, 4 H, Ph). $^{31}P\{^1H\}$ NMR (CD_2Cl_2): δ = 72.7 (s). MS: *m/z* (%) = 764 (65) $[M]^+$.

11: Yield: 56 mg (87%). $C_{36}H_{26}P_2Pd_2S_4$ (861.6): calcd. C 50.18, H 3.04, S 14.88; found 50.45, H 3.14, S 15.26. ^1H NMR (CD_2Cl_2): δ = 7.61−7.17 (m). $^{31}P\{^1H\}$ NMR (CD_2Cl_2): δ = 76.9 (s). MS: *m/z* (%) = 861 (15) $[M]^+$.

b) A 0.1 M solution of NaOEt (3 mL, 0.3 mmol) was added, over a period of 10 minutes, to a suspension of PPh($C_6H_4SH)_2$ (0.048 g, 0.15 mmol) in 10 mL of ethanol. Then, [$NiCl_2$·bipy] (0.042 g, 0.15 mmol) or [$PdCl_2$·bipy] (0.050 g, 0.15 mmol) was added. After stirring overnight green (**10**) or brown (**11**) solids precipitated, which were filtered off, washed with ethanol and dried in vacuo. Yields: **10:** 42 mg (73%); **11:** 55 mg (85%).

Reaction of [Ni{PPh($C_6H_4S)_2$}]$_2$ (10) and [Pd{PPh($C_6H_4S)_2$}]$_2$ (11) with Ligands: 0.1 mmol of L (L= PPh_3, PPh_2Me, dppm, or phen), or 0.05 mmol of dppe was added to a suspension of [Ni{PPh($C_6H_4S)_2$}]$_2$ (**10**; 0.076 g, 0.05 mmol) or [Pd{PPh($C_6H_4S)_2$}]$_2$ (**11**; 0.086 g, 0.05 mmol) in dichloromethane (30 mL) and stirred for 6 hours to give clear solutions. Partial evaporation of the solvents and addition of ethanol (20 mL) afford complexes **1**−**8**. Complex [Pd{PPh($C_6H_4S)_2$}(phen)] (**9**) was obtained as a brown insoluble solid from dichloromethane.

X-ray Crystallography: Single crystals of [Ni{PPh-($C_6H_4S)_2$}(PPh_2Me)] (**2**) and of [Pd_2(μ-dppe){PPh($C_6H_4S)_2$}$_2$] CH_2Cl_2 (**7**) were grown by slow diffusion of hexane into dichloromethane solutions of the complexes. Data collection[46] at low temperature was carried out on a Bruker SMART diffractometer for **2** and on a Nonius−KappaCCD diffractometer for **7**. Crystal parameters and experimental details are summarised in Table 1. The structures were solved by direct methods for **2**[47] and for **7**,[48] and refined on F_0^2 by full-matrix least-squares using the program SHELXL-97.[49] Data were corrected for absorption using SADABS[50] for **2** and SORTAV[51] for **7**. All hydrogen atoms were included at idealised positions. Selected bond lengths and angles are given in Table 2 and 3. The details of the crystal structures have been deposited at the Cambridge Crystallographic Data Center as supplementary publication nos. CCDC-162696, CCDC-162697 and CCDC-162698 for complexes **2**, **7** and **10** respectively. Copies of the data can be obtained free of charge on application to the CCDC, 12 Union Road, Cambridge UK CB2 1EZ [E-mail: deposit@ccdc.cam.ac.uk, Fax: (internat.) +44-1223/336-033].

A very thin plate-like crystal of **10**, suffering from severe anisotropic mosaicity, was used for X-ray measurements. An initial, slow reflection search yielded 12 reflections, which were indexed to a primitive monoclinic cell.[52] Preliminary data collection between 26 and 32° (2θ) was used in an attempt to obtain better reflections for cell determination and for ψ-scans, but the results were not satisfactory. The positions of 13 reflections with lower values of 2θ were used to calculate the unit cell parameters reported. Accurate centring of reflections in the higher 2θ range was rendered difficult because of the mosaic spread of the crystal. As for the ψ-scans, in addition to producing low signal-to-noise ratios, they also suffered from the effects of mosaicity; this compromises the validity of the absorption corrections so obtained, and so absorption corrections were not applied.

Intensity data were gathered in the 2θ range of 4.0−46.0°. Omega-scans were used, with the ω scan speed set for each reflection on the basis of a preliminary measurement made at a speed of 4°/min. The weakest data were gathered at the slowest speed; no reflection was skipped on the basis of a poor showing on the initial scan. The

maximum scan time for any reflection was limited to 270 sec, and most reflections were measured for that amount of time. The photon count for the preliminary scan was added to that of the final scan to give the datum. A single monitor reflection was measured after every 30 min of accumulated beam time, as a check on experimental stability. An orientation check was made after every 1000 intensity measurements. In all, 5630 intensity measurements were made, in a single quadrant of reciprocal space.

Following data reduction,[53] the structure was solved by direct methods, which yielded the positions of all of the non-hydrogen atoms in the asymmetric unit. The hydrogen atoms, all of which are in phenyl groups, were placed at calculated positions and refined as riders, with isotropic displacement parameters set to 1.2-times the equivalent isotropic displacement parameters of their respective parent carbon atoms. All non-hydrogen atoms were refined anisotropically, but it was necessary to apply both rigid bond restraints and restraints to isotropic behavior to the anisotropic displacement parameters of the carbon atoms. The isotropic restraints had one-quarter the relative weight of the rigid bond restraints. The heavier atoms were refined freely.

In all, 397 parameters were adjusted to all 4437 unique data (used as F_0^2) and to 288 restraints in the full-matrix least-squares calculation, giving an observation-to-parameter ratio of 11.9:1. The final residuals are shown in Table 1.

The diffraction data were weak, with mean $I/\sigma(I) = 1.45$ in the data set before averaging of equivalents. Only 16% of the data had $I > 3\sigma(I)$. Consequently, the standard uncertainties in the derived bond distances and angles are high, and we emphasize that it would not be useful to try to derive conclusions beyond the connectivity from this structure determination.

As already mentioned, the results reported here are based on data without correction for absorption. We also performed a separate refinement of the structure with data that had been treated with an *a posteriori* calculated absorption correction.[54] The residual $R1$ was found to be lowered by only slightly more than 0.01, and it was still necessary to apply restraints to the anisotropic displacement parameters of the carbon atoms to avoid having the large majority of them emerge nonpositive definite. The results of this second refinement are available from the authors upon request. Selected bond lengths and angles are given in Table 4.

Acknowledgments

We thank the Spanish Directorate General for Higher Education and Scientific Research Grants PB98-0542 and PB98-1593 for financial support. M.B.H. thanks the Engineering and Physical Sciences Research Council for support of the X-ray facilities. We thank Dr. Milagros Tomás and Dr. Antonio Martín for assistance with the X-ray data collection.

[1] E. I. Stiefel, *Transition Metal Sulfur Chemistry* (Eds.: E. I. Stiefel, K. Matsumoto), ACS Symposium Series, 653, American Chemical Society, Washington DC, **1995**.
[2] R. Hille, *Chem. Rev.* **1996**, *96*, 2757−2826.
[3] E. I. Stiefel, *Molybdenum Enzymes, Cofactors, and Model Systems* (Eds.: E. I. Stiefel, D. Coucouvanis, W. E. Newton), ACS Symposium Series, 535, American Chemical Society, Washington, D.C., **1993**.
[4] R. H. Holm, J. A. Ibers, *Science* **1980**, *209*, 223.
[5] Y. Yamamoto, S. Gondo, *Tribology Trans.* **1989**, *32*, 251−257
[6] P. C. H. Mitchell, *Wear* **1984**, *100*, 281−300.
[7] H. Topsöe, B. S. Clausen, F. E. Massoth, *Hydrotreating Catalysis: Science and Technology*, Springer Verlag, Berlin **1996**.
[8] P. J. Blower, J. R. Dilworth, *Coord. Chem. Rev.* **1987**, *76*, 121−185.
[9] J. R. Dilworth, N. Wheatley, *Coord. Chem. Rev.* **2000**, *199*, 89−158.
[10] D. Morales, R. Poli, P. Richard, J. Andrieu, E. Collange, *J. Chem. Soc., Dalton Trans.* **1999**, 867−873.
[11] J. R. Dilworth, D. V. Griffiths, S. J. Parrott, Y. F. Zheng, *J. Chem. Soc., Dalton Trans.* **1997**, 2931−2936.
[12] S.-T. Liu, D.-R. Hou, T.-C. Cheng, S.-M. Peng, *Organometallics* **1995**, *14*, 1529−1532.
[13] J. R. Dilworth, J. R. Miller, N. Wheatley, M. J. Baker, J. G Sunle, *Chem. Commun.* **1995**, 1579−1581.
[14] J. S. Kim, J. H. Reibenspies, M. Y. Darensbourg, *J. Am. Chem. Soc.* **1996**, *118*, 4115−4123.
[15] E. J. Fernández, M. B. Hursthouse, M. Laguna, R. Terroba, *J. Organomet. Chem.* **1999**, *574*, 207−212.
[16] J. Aznar, E. Cerrada, M. B. Hursthouse, M. Laguna, C. Pozo, M. P. Romero, *J. Organomet. Chem.* **2001**, *622*, 274−279.
[17] K. Ortner, L. Hilditch, Y. Zheng, J. R. Dilworth, U. Abram, *Inorg. Chem.* **2000**, *39*, 2801−2806 and references therein
[18] K. Ortner, L. Hilditch, J. R. Dilworth, U. Abram, *Inorg. Chem. Commun.* **1998**, *1*, 469−471.
[19] H-F. Hsu, S. A. Koch, C. V. Popescu, E. Munck, *J. Am. Chem. Soc.* **1997**, *119*, 8371−8372.
[20] J. R. Dilworth, A. J. Hutson, J. S. Lewis, J. R. Miller, Y. Zheng, Q. Chen, J. Zubieta, *J. Chem. Soc., Dalton Trans.* **1996**, 1093−1104.
[21] [21a] M. H. P. Rietveld, D. M. Grove, G. van Koten, *New. J. Chem.* **1997**, *21*, 751−771. [21b] P. Dani, T. Karlen, R. A. Gossage, W. J. J. Smeets, A. L. Spek, G. van Koten, *J. Am. Chem. Soc.* **1997**, *119*, 11317−11318.
[22] [22a] M. E. Vanderboom, C. L. Higgitt, D. Milstein, *Organometallics* **1999**, *18*, 2413−2419. [22b] R. M. Gavin, H. Rozenberg, L. J. V. Simon, D. Milstein, *Organometallics* **2001**, *20*, 1719−1724.
[23] D. Sellmann, F. Geipel, F. W. Heinemann, *Eur. J. Inorg. Chem.* **2000**, 271−279.
[24] [24a] P. Perez-Lourido, J. Romero, J. García-Vazquez, A. Sousa, K. P. Maresca, D. R. Rose, J. Zubieta, *Inorg. Chem.* **1998**, *37*, 3331−3336. [24b] P. Perez-Lourido, J. Romero, J. García-Vazquez, A. Sousa, K. P. Maresca, D. R. Rose, J. Zubieta, *Inorg. Chem.* **1999**, *38*, 3709−3715.
[25] J. S. Ström, *Dynamic NMR Spectroscopy*, Academic Press, London, **1982**.
[26] [26a] R. Castro, J. Romero, J. García-Vazquez, J. A. Sousa, I. D. Chang, J. Zubieta, *Inorg. Chim. Acta* **1996**, *245*, 119−124. [26b] P. Perez-Lourido, J. Romero, J. García-Vazquez, J. A: Sousa, J. Zubieta, K. Mareska, *Polyhedron* **1998**, *17*, 4457−4462.
[27] J. D. Franolic, W. Y. Wang, M. Millar, *J. Am. Chem. Soc.* **1992**, *114*, 6587−6588.
[28] G. S. White, D. W. Stephan, *Organometallics* **1988**, *7*, 903−910.
[29] M. Che, J. Sletten, S. Critchlow, J. A. Kovacs, *Inorg. Chim. Acta* **1997**, *263*, 153−159.
[30] S. S. Chojnacki, Y-M. Hsiao, M. Y. Darensbourg, J. H. Reibenspies, *Inorg. Chem.* **1993**, *32*, 3573−3576.
[31] N. Brugat, A. Polo, A. Álvarez-Larena, J. F. Piniella, J. Real, *Inorg. Chem.* **1999**, *38*, 4829−4837.
[32] A. Benefiel, D. M. Roundhill, W. C. Fultz, A. L. Rheingold, *Inorg. Chem.* **1984**, *23*, 3316−3321.
[33] J. Real, E. Prat, A. Polo, A. Álvarez-Larena, J. F. Piniella, *Inorg. Chem. Commun.* **2000**, *3*, 221−223.
[34] M. Capdevilla, W. Clegg, P. Gonzalez-Duarte, B. Harris, Y. Mira, J. Sola, I. C. Taylor, *J. Chem. Soc., Dalton Trans.* **1992**, 2817−2826.
[35] S. Takemoto, S. Kuwata, Y. Nishibayashi, M. Hidai, *Inorg. Chem.* **1998**, *37*, 6428−6434.
[36] E. M. Padilla, J. H. Yamamoto, C. M. Jensen, *Inorg. Chim. Acta* **1990**, *174*, 209−215.
[37] R. L. Cowan, D. B. Pourreau, A. L. Rheingold, S. J. Geib, W. C. Trogler, *Inorg. Chem.* **1987**, *26*, 259−264.

[38] F. A. Cotton, M. Matusz, R. Poly, X. Feng, *J. Am. Chem. Soc.* **1988**, *110*, 1144−1149.
[39] E. Erkizia, R. R. Conry, *Inorg. Chem.* **2000**, *39*, 1674−1679.
[40] R. G. Hayter, F. S. Humic, *Inorg. Chem.* **1965**, *4*, 170−173.
[41] D. C. Goodall, *J. Chem. Soc. (A)* **1968**, 887−890.
[42] G. Booth, J. Chatt, *J. Chem. Soc.* **1965**, 3238−3241.
[43] W. L. Steffen, G. J. Palenik, *Inorg. Chem.* **1976**, *15*, 2432−2439.
[44] F. L. Wimmer, S. Wimmer, P. Castain, *Inorg. Synth.* **1991**, *29*, 185−190.
[45] E. Bloch, G. Ofori-Okai, J. Zubieta, *J. Am. Chem. Soc.* **1989**, *111*, 2327−2329.
[46] SMART V5.05 (c) 1997−98, Bruker AXS; SAINT V5.05 (c) 1997−98, Bruker AXS; Z. Otwinowski, W. Minor, *Methods in Enzymology* **1997**, *276*, 307−326. *Macromolecular Crystallography*, part A
[47] SHELXS-97: Fortran *Program for Crystal Structure Solution.* ©**1997**, George M. Sheldrick
[48] SIR92 − A *program for crystal structure solution*, A. Altomare, G. Cascarano, C. Giacovazzo, A. Guagliardi, *J. Appl. Crystallogr.* **1993**, *26*, 343−350.
[49] SHELXL-97: Fortran *Program for Crystal Structure Refinement.* ©**1997**, G. M. Sheldrick.
[50] SADABS: "Bruker Area Detector Absorption Corrections".
[51] R. H. Blessing, *Acta Crystallogr., Sect. A* **1995**, *51*, 33−38; R. H. Blessing, *J. Appl. Cryst.* **1997**, *30*, 421−425.
[52] Diffractometer control program: CAD4/PC Version 2.0, © **1996** Nonius bv, Delft, The Netherlands
[53] Data were processed on an AlphaStation 200 4/166 (OpenVMS/Alpha V6.2), with the program XCAD4B (K. Harms, 1996) and with the commercial package SHELXTL Rel. 5.05/VMS: ©**1996**, Siemens Analytical X-ray Instruments, Inc., Madison, Wisconsin. Further processing was done under Windows98 with WinGX: WinGX − A Windows Program for Crystal Structure Analysis. L. J. Farrugia, University of Glasgow, Glasgow, **1998**.
[54] SHELXA: Fortran program for *a posteriori* absorption corrections to single-crystal diffraction data, distributed with SHELX-97.

Received July 17, 2001
[I01264]

Salts of 5,5′-Azotetrazolate

Anton Hammerl,[a] Gerhard Holl,[b] Thomas M. Klapötke,*[a] Peter Mayer,[a] Heinrich Nöth,[a] Holger Piotrowski,[a] and Marcus Warchhold[a]

Keywords: Azo compounds / Hydrates / Nitrogen heterocycles / Tetrazoles / Highly energetic materials

Salts of 5,5′-azotetrazolate with alkali metal, alkaline earth metal and several trivalent cations were synthesized as potential initial explosives. The synthesis in water yields hydrates of these salts that were studied by NMR and vibrational spectroscopy as well as X-ray diffraction. Their thermal properties were studied by DSC and TG.

Introduction

Thiele first prepared sodium 5,5′-azotetrazolate (**2**), which is the starting material for all other 5,5′-azotetrazolate compounds, from the oxidation of aminotetrazole with potassium permanganate [Equation (1)].[1]

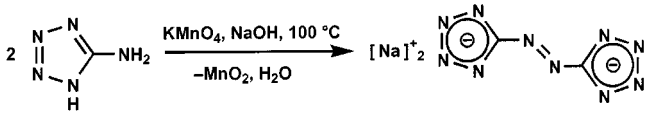

(1)

He prepared several salts with metal cations (K^+, Ca^{2+}, Ba^{2+}, Ag^+, Hg^+, Pb^{2+}) and salts of protonated nitrogen bases (NH_4^+, NH_3OH^+, $N_2H_6^+$). 5,5′-Azotetrazolate salts decompose in mineral acid solution to form hydrazinotetrazole, dinitrogen and formic acid [Equation (2)].

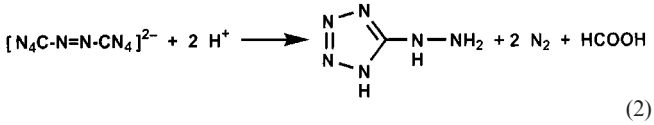

(2)

Azidotetrazole,[2] 5-azo(diazomethano)tetrazole hydrate[3] and other compounds[4] were recovered as intermediates from the decomposition reaction of 5,5′-azotetrazolate salts in acidic media. Salts of 5,5′-azotetrazolate with protonated nitrogen bases (e.g. guanidinium, triaminoguanidinium and hydrazinium 5,5′-azotetrazolate) are powerful gas generation agents and can be used in gas generators for airbags and fire extinguishing systems.[5] Heavy metal salts of 5,5′-azotetrazolate, especially $Pb_2(OH)_2C_2N_{10}$, which consists of PbO ladders with a pyramidal coordination of the lead atom,[6] have been used as initiators.[7] Anhydrous sodium and potassium 5,5′-azotetrazolate are very sensitive to shock and friction.[5e,7f] 1,1′-Dimethyl-5,5′-azotetrazole, first studied by Stolle,[8] has been used as an additive in solid rocket propellants.[9] Although some of the alkali- and alkaline earth metal salts of 5,5′-azotetrazolate have been known since 1898, no data on these compounds have been reported. We therefore investigated these salts as potential initiators. We also investigated the 5,5′-azotetrazolate salts of trivalent and tetravalent cations. All 5,5′-azotetrazolate salts include water of crystallisation. We also examined the thermal properties of the compounds and determined the temperatures of water loss. For a better understanding of the decomposition of 5,5′-azotetrazolate we synthesized the free acid 5,5′-azotetrazole. The tetraphenylarsonium salt and the covalent 2,2′-dimethyl-5,5′-azotetrazolate were synthesized to investigate 5,5′-azotetrazolate units that have no interactions with cations in the solid state. The quality of all elemental analyses suffers because of the difficulty of obtaining correct values for compounds with extremely high nitrogen content.[9]

Results and Discussion

Syntheses and properties

Sodium 5,5′-azotetrazolate (**2**) was used as starting material and was synthesized according to Thiele [see Equation (1)].[1d] Strontium (**8**) and barium 5,5′-azotetrazolate (**9**) were prepared from solutions of **2** and the respective

[‡] Crystal structure analyses

[a] Department of Chemistry, Ludwig-Maximilians-Universität München,
Butenandtstr. 5–13, 81377 München, Germany
Fax: (internat.) +49-(0)89/2180 7492
E-mail: Thomas.M.Klapoetke@cup.uni-muenchen.de
[b] Wehrwissenschaftliches Institut für Werk-, Explosiv- und Betriebsstoffe,
Großes Cent, 53913 Swisstal, Germany

 © WILEY-VCH Verlag GmbH, 69451 Weinheim, Germany, 2002 1434–1948/02/0404–0834 $ 17.50+.50/0 *Eur. J. Inorg. Chem.* **2002**, 834–845

metal chlorides [Equation (3)]. Both compounds are almost insoluble in water and precipitated after the solutions were mixed.

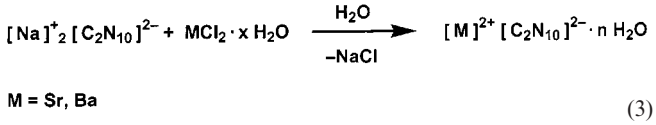

(3)

All other metal salts were obtained from the respective metal sulfates and barium 5,5-azotetrazolate [Equation (4)−(6)]. After barium sulfate had been filtered off and the water evaporated, yellow crystals of the salts were obtained. During the reaction of $Ce(SO_4)_2$ with barium 5,5′-azotetrazolate (**9**) a gas was evolved and no 5,5′-azotetrazolate salt of Ce^{IV} could be isolated. The Ce^{III} salt **13** does not show this decomposition.

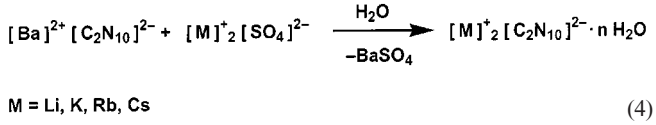

(4)

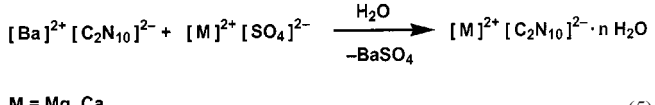

(5)

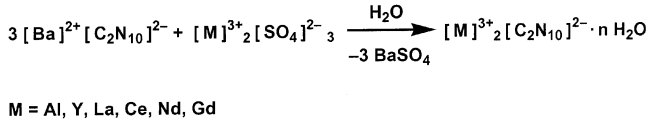

(6)

All compounds contain water of crystallisation (see Table 1). For the heavier elements the deviation of the elemental analysis is too big to calculate the exact number of water molecules present. During storage all compounds lose water; this takes place over a period of hours for the lithium **1** and potassium salt **3** as well as the salts of the trivalent cations **10**−**15**. The water loss from the other compounds takes between days and weeks. Upon loss of water, the salts of the trivalent cation **10**−**15** decompose to colourless substances. The magnesium salt **6** shows a similar behaviour. This decomposition is the reason for the low yields in the syntheses of these compounds, and it occurs due to the acidity of the metal-water complexes of the trivalent cations [cf. the decomposition of 5,5′-azotetrazolate in acidic medium, Equation (1)].

The free acid 5,5′-azotetrazole **16** was synthesized from the sodium salt **1** and $HBF_4{\cdot}Et_2O$ at −30 °C in methanol [Equation (7)] in order to gain an insight into its decomposition.

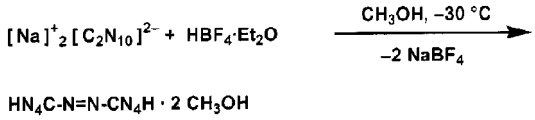

(7)

A crystal structure analysis showed the presence of two methanol molecules. The free acid is a yellow solid that can be stored for several months at −80 °C without decomposition.[10] At 0 °C, however, it decomposes in an hour to form tetrazolhydrazine, and at room temperature this decomposition takes only a few seconds.

Tetraphenylarsonium 5,5′-azotetrazolate (**17**) was synthesized from the sodium salt **2** and tetraphenylarsonium chloride [Equation (8)]. The cations in this compound do not interact with the 5,5′-azotetrazole units.

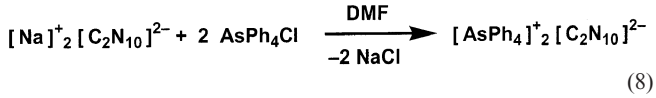

(8)

We also synthesized 2,2′-dimethyl-5,5′azotetrazolate from silver 5,5′-azotetrazolate and iodomethane [Equation (9)].

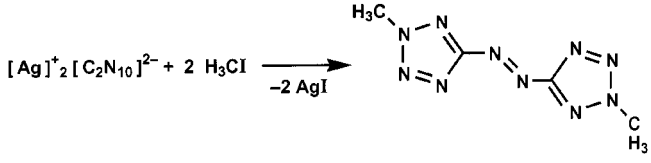

(9)

NMR Properties

The ^1H NMR spectrum of **1** shows water at δ = 4.1; the carbon atom of the 5,5′-azotetrazolate ion appears in the ^{13}C NMR spectrum at δ = 173.1. The ^{14}N NMR spectrum of **1** in [D_6]DMSO displays no absorptions: only very concentrated solutions in D_2O (sample amount 3.5 g) show absorptions. The same sample was used for the recording of a ^{15}N NMR spectrum. Figure 1 shows the broad ^{14}N NMR

Table 1. Numbering scheme for metal salt hydrates of 5,5′-azotetrazolate

1	**2**	**3**	**4**	**5**
$Li_2[C_2N_{10}](H_2O)_6$	$Na_2[C_2N_{10}](H_2O)_5$	$K_2[C_2N_{10}](H_2O)_5$	$Rb_2[C_2N_{10}](H_2O)$	$Cs_2[C_2N_{10}](H_2O)_2$
6	**7**	**8**	**9**	**10**
$Mg[C_2N_{10}](H_2O)_8$	$Ca[C_2N_{10}](H_2O)_8$	$Sr[C_2N_{10}](H_2O)_6$	$Ba[C_2N_{10}](H_2O)_5$	$Al_2[C_2N_{10}]_3(H_2O)_x$
11	**12**	**13**	**14**	**15**
$Y_2[C_2N_{10}]_3(H_2O)_{22}$	$La_2[C_2N_{10}]_3(H_2O)_x$	$Ce_2[C_2N_{10}]_3(H_2O)_x$	$Nd_2[C_2N_{10}]_3(H_2O)_x$	$Gd_2[C_2N_{10}]_3(H_2O)_x$

signals (due to the quadrupole moment of ^{14}N)[11] in comparison to the sharp signals in the ^{15}N NMR spectrum.

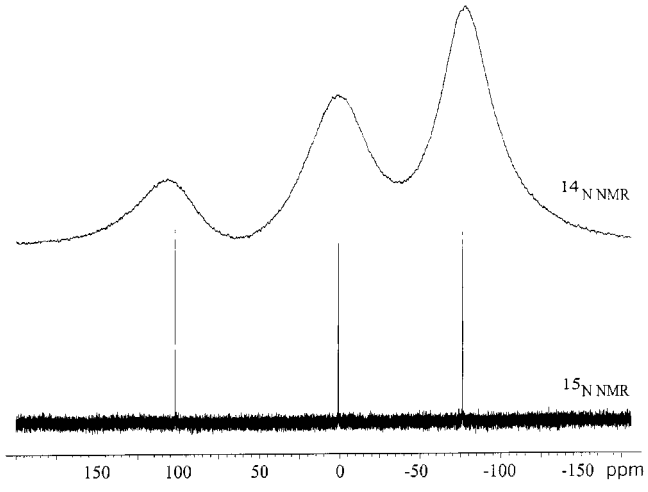

Figure 1. $^{14/15}N$ NMR spectra of **2**

The signal of the C−N nitrogen atoms of the tetrazole ring system appears at δ = 2/0.6 ($^{14}N/^{15}N$), and the signal of the other two tetrazole nitrogen atoms at δ = −77/−76.2 ($^{14}N/^{15}N$). The diazo nitrogen signal appears at δ = 105/102.0 ($^{14}N/^{15}N$). Since the ^{1}H and ^{13}C NMR spectrum are the same for all 5,5′-azotetrazolate salts and the sample amount needed to record a ^{14}N NMR spectrum is very high, the NMR spectra of the other salts were not recorded. The signals of the tetraphenylarsonium salt **17** in the ^{1}H and ^{13}C NMR spectra have the same chemical shifts as for the starting material. The signal of the methyl group of dimethylated **18** in the ^{1}H NMR is found at δ = 4.47 (^{13}C: δ = 40.5), with the NH signal of the acid **16** at δ = 5.68. The signals of the azotetrazolate carbon atoms of **16** and **18** are shifted to higher field than in the ionic compounds [δ = 168.6 (**16**) and 171.5 (**18**)]. No absorptions were detected in the ^{14}N NMR spectra of **16** and **18**, the same as for the ionic compounds.

Vibrational Spectra

The most intense absorptions in the IR spectra (see Table 2) are an asymmetrical $C-N_3$ stretching mode around 1390 cm^{-1} and an asymmetrical $C-N_2$ stretching mode around 735 cm^{-1}. For several compounds two bands are detected in this region. In the Raman spectra the most intense bands are a symmetrical $C-N_{azo}$ stretching mode around 1384 cm^{-1} and the N−N stretching mode of the diazo group around 1480 cm^{-1}. Again, for several compounds two signals are observed for these modes. The $C-N_{azo}$ stretching mode and the N−N stretching mode of the covalent compounds **16** and **18** are shifted slightly to higher wavenumbers relative to the 5,5′-azotetrazolate salts. Some absorptions were assigned according to a calculation of the 5,5-azotetrazolate dianion at the B3LYP level of theory,[5d] although, due to the large number of combination modes, especially in the IR spectra, not all modes could be assigned.

Table 2. Characteristic data for 5,5′-azotetrazolate salts (wavenumbers in cm^{-1}, Temperatures and DSC peaks in °C)

	IR	Raman	$T_{Dec.}$	DSC
1	1399, 733	1484, 1387	335	64, 109, 134
2	1401, 732	1480, 1386	248	116, 159
3	1390, 727	1482, 1378	243	41, 70, 144
4	1395, 736	1494, 1386	239	97
5	1389/1382 728	1494, 1381	237	40
6	1393/1386 736	1499, 1375	239	–
7	1398 735	1496/1479 1394/1377	221	–
8	1396/1384 734	1488, 1382	238	76, 133
9	1399, 735	1488, 1391	211	129
10	1398, 738	1488, 1399	–	–
11	1403, 727	1487, 1388	–	–
12	1398/1384 730	1479, 1390	–	–
13	1408/1394, 744	1476, 1396/1388	–	–
14	1404/1396, 743	1477, 1394	–	–
15	1416, 730	1477, 1390	–	–
16	1383, 735	1483, 1361	–	–
17	1373, 742	1466, 1361	–	–
18	1375	1503, 1393	170	–

Thermal Properties

The temperature for the loss of different water molecules depends on their coordination. DSC measurements (Table 2) show endotherms at temperatures between 41 °C and 144 °C. Compounds that have water molecules bound by hydrogen bonds lose these water molecules faster than those with the water molecules included in the coordination sphere of the cation. Slow heating (1 °C/min) of the alkali- and alkaline earth metal salt hydrates results in an explosion at a specific decomposition temperature. The lithium salt **1** has the highest decomposition temperature of 335 °C. The other alkali and alkaline earth metal salts have decomposition temperatures in the range between 211 °C and 248 °C, with the barium salt **9** having the lowest decomposition temperature. The salts of the trivalent cations decompose slowly at temperatures higher than room temperature: the tetraphenylarsonium salt **17** decomposes slowly at temperatures higher than 180 °C and the dimethylated **18** explodes at170 °C. It is not possible to dry the compounds at higher temperatures in vacuo. All attempts resulted in explosions.

Crystal Structures

The bonding parameters of the 5,5′-azotetrazolate anions in **1**, **2**, **4**, **7**, **9**, **11** and **15** are very similar (see Table 3) and are in agreement with the theoretical values calculated at the B3LYP/6-31+G(2df) level of theory. In the reported

Table 3. Bond lengths and angles of the 5,5′-azotetrazolate ions

	1	**2**	**4**	**7**	**9**	**11 (a)**	**11 (b)**	**17**	**18**
N(11)−N(12)	1.269(2)	1.258(3)	1.259(7)	1.255(3)	1.251(7)	1.263(4)	1.255(6)	1.081(8)	1.256(3)
								1.274(5)	
N(21)−N(31)	1.332(2)	1.342(3)	1.353(5)	1.336(3)	1.335(5)	1.338(4)	1.331(4)	1.324(6)	1.321(2)
N(22)−N(32)	1.336(2)	1.334(3)		1.337(3)		1.337(4)		1.340(4)	
N(31)−N(41)	1.317(2)	1.311(3)	1.319(5)	1.327(3)	1.311(6)	1.325(4)	1.322(4)	1.317(6)	1.321(2)
N(32)−N(42)	1.316(2)	1.318(3)		1.331(3)		1.326(4)		1.319(4)	
N(41)−N(51)	1.334(2)	1.344(3)	1.343(5)	1.336(3)	1.343(6)	1.332(4)	1.342(4)	1.320(6)	1.322(2)
N(42)−N(52)	1.336(2)	1.347(3)		1.334(3)		1.336(4)		1.331(4)	
N(11)−C(11)	1.398(3)	1.412(3)	1.413(5)	1.406(3)	1.414(5)	1.404(4)	1.415(4)	1.598(7)	1.411(3)
N(12)−C(12)	1.400(3)	1.406(3)		1.412(3)		1.404(4)		1.403(3)	
N(21)−C(11)	1.338(2)	1.333(3)	1.328(5)	1.341(3)	1.327(5)	1.332(4)	1.336(4)	1.322(6)	1.324(3)
N(22)−C(12)	1.345(2)	1.333(3)		1.332(3)		1.331(4)		1.343(4)	
N(51)−C(11)	1.337(2)	1.327(3)	1.336(5)	1.338(3)	1.328(5)	1.334(4)	1.329(4)	1.310(6)	1.344(3)
N(52)−C(12)	1.335(2)	1.332(3)		1.343(3)		1.332(4)		1.329(5)	
N(12)−N(11)−C(11)	112.7(2)	112.0(2)	112.7(4)	115.7(2)	112.8(4)	114.0(3)	113.1(3)	98.1(4)	112.2(2)
N(11)−N(12)−C(12)	113.3(2)	114.6(2)		112.2(2)		114.7(3)		113.0(3)	
N(21)−N(31)−N(41)	110.0(2)	109.3(2)	109.8(3)	108.9(2)	109.2(4)	120.5(3)	119.6(3)	109.6(5)	114.1(2)
N(22)−N(32)−N(42)	110.0(2)	109.2(2)		109.0(2)		120.3(3)		109.4(3)	
N(31)−N(41)−N(51)	109.4(2)	110.3(2)	109.6(3)	110.3(2)	109.8(4)	109.4(2)	110.0(3)	109.6(5)	106.4(2)
N(32)−N(42)−N(52)	109.7(2)	110.5(2)		109.9(2)		109.5(2)		110.3(3)	
N(11)−C(11)−N(21)	128.2(2)	120.6(2)	128.1(4)	117.8(2)	112.4(4)	109.6(2)	109.1(3)	111.7(4)	118.4(2)
N(12)−C(12)−N(22)	127.9(2)	118.4(2)		119.6(2)		109.4(2)		118.1(3)	
N(11)−C(11)−N(51)	120.1(2)	126.1(2)	118.3(4)	130.1(2)	128.2(4)	127.1(3)	127.9(3)	135.4(5)	127.8(2)
N(12)−C(12)−N(52)	120.0(2)	128.1(3)		128.1(2)		127.0(3)		129.0(3)	
N(21)−C(11)−N(51)	111.8(2)	113.2(2)	113.5(3)	112.13(2)	112.4(4)	112.4(3)	112.5(3)	112.9(4)	113.8(2)
N(22)−C(12)−N(52)	112.0(2)	113.4(2)		112.3(2)		112.7(3)		112.9(3)	
C(11)−N(21)−N(31)	104.3(2)	103.8(2)	103.3(3)	104.7(2)	104.7(3)	104.1(2)	104.6(3)	103.8(4)	100.9(2)
C(12)−N(22)−N(32)	104.0(2)	104.1(2)		104.8(2)		104.2(2)		103.5(3)	
C(11)−N(51)−N(41)	104.6(2)	103.3(2)	103.7(3)	104.0(2)	103.9(4)	104.5(2)	103.8(3)	104.5(5)	104.8(2)
C(12)−N(52)−N(42)	104.4(2)	102.8(2)		104.0(2)		104.2(2)		103.9(3)	

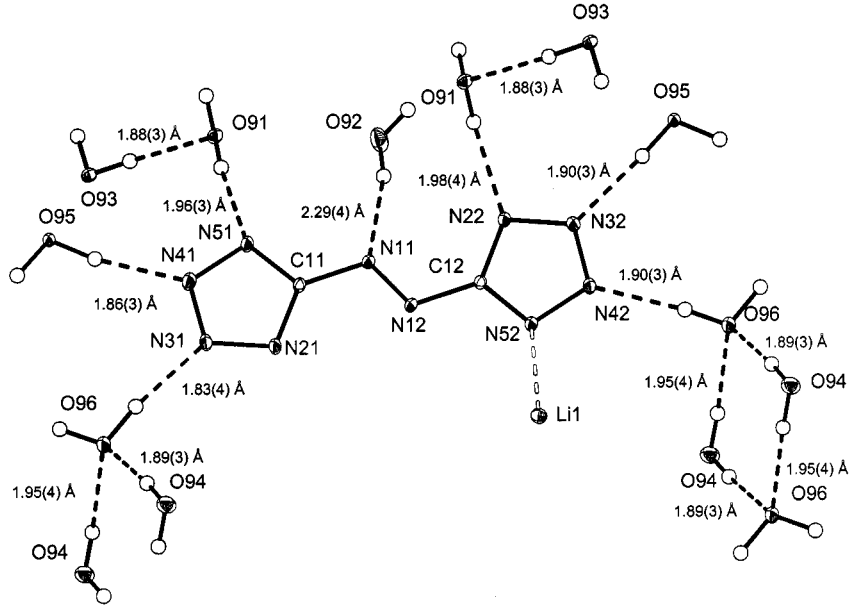

Figure 2. Coordination of the 5,5′-azotetrazolate ions in **1** (thermal ellipsoids represent 25% probability); selected bond lengths [Å]: Li(1)−O(91) 1.951(4), Li(1)−O(92) 1.951(4), Li(1)−O(93) 1.969(4), Li(1)−N(52) 2.077(4), Li(2)−O(93) 1.972(4), Li(2)−O(94) 1.910(4), Li(2)−O(95) 1.955(3), Li(2)−O(95) 1.980(4), Li(2)-0(95A) 1.955(3); hydrogen bonds: O−N distances [Å] (OHN angles [°]), N···H distances are given in the figure: O(91)−H(911)···N(51) 2.805(3) [171(3)], O(91)−H(912)···N(22) 2.830(3) [162(2)], O(92)−H(921)···N(11) 3.188(3) [167(3)], O(93)−H(931)···O(91) 2.778(2) [176(3)], O(93)−H(932)···N(21) 2.787(3) [166(3)], O(94)−H(941)···O(96) 2.760(3) [163(3)], O(94)−H(942)···O(96) 2.700(2) [172(4)], O(95)−H(951)···N(41) 2.798(2) [169(3)], O(95)−H(952)···N(32) 2.826(3) [175(3)], O(96)−H(961)···N(42) 2.783(2) [172(3)], O(96)−H(962)···N(31) 2.793(3) [172(3)]

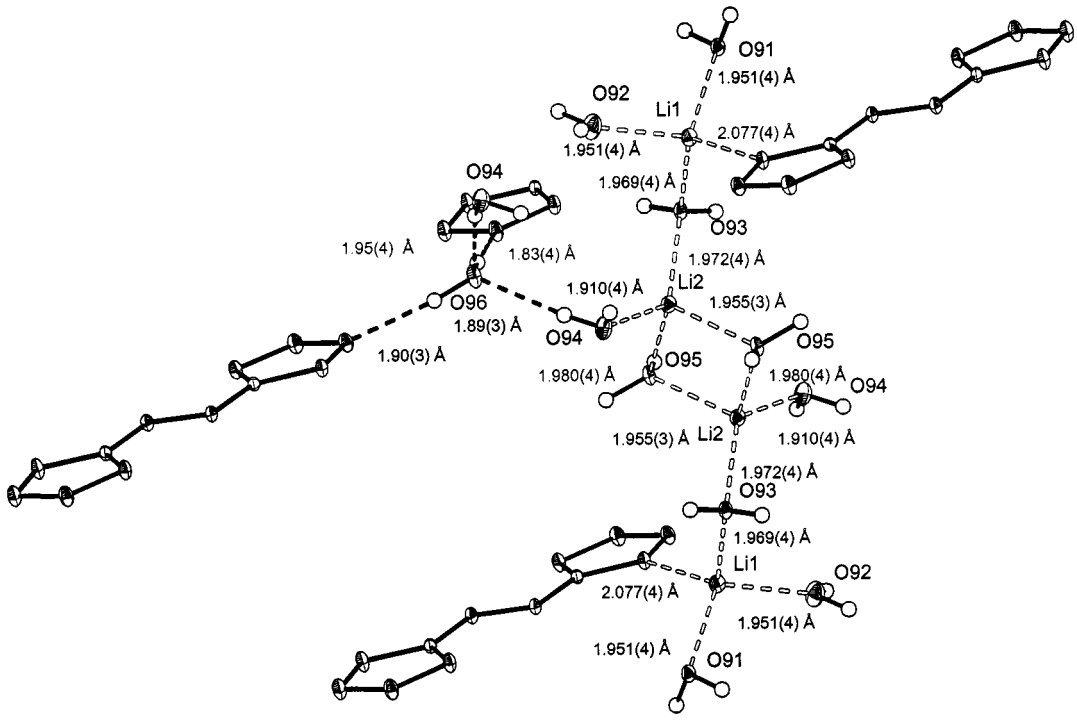

Figure 3. Coordination of the lithium ions in **1** (thermal ellipsoids represent 25% probability); parts of the 5,5′-azotetrazolate ions have been omitted for clarity

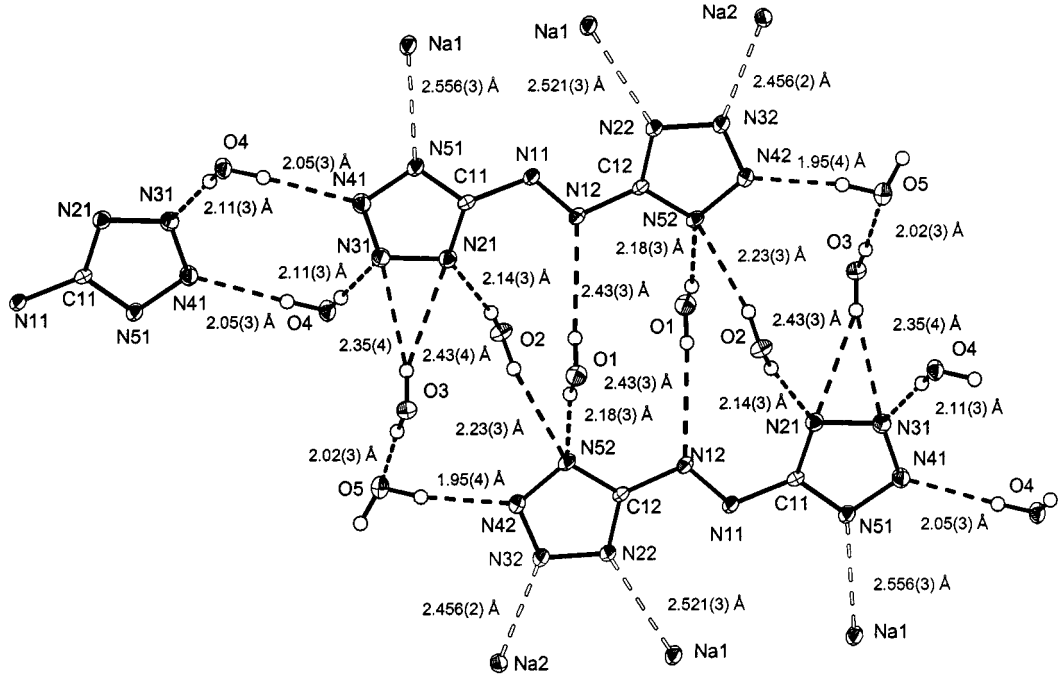

Figure 4. Coordination of the 5,5′-azotetrazolate ions in **2** (thermal ellipsoids represent 25% probability); selected bond lengths [Å]: Na(1)−O(1) 2.427(2), Na(1)−O(1A) 2.465(2), Na(1)−O(2) 2.483(2), Na(1)−O(3) 2.414(2), Na(1)−N(22) 2.521(2), Na(1)−N(51) 2.556(3), Na(2)−O(2) 2.466(2), Na(2)−O(3) 2.405(2), Na(2)−O(4) 2.376(2), Na(2)−O(4B) 2.369(2), Na(2)−O(5) 2.380(2), Na(2)−N(32) 2.456(2); symmetry operations for equivalent atoms: A: $-x + 1, -y, -z + 1$; B: $-x, -y, -z + 2$; hydrogen bonds: O−N and O−O distances [Å] (OHN/OHO angles [°]), N···H distances are given in the figure: O(1)−H(1A)···N(12) 3.219(3) [163(4)], O(1)−H(1B)···N(52) 2.973(3) [167(3)], O(2)−H(2A)···N(21) 2.939(3) [170(3)], O(2)−H(2B)···N(52) 3.039(3) [169(4)], O(3)−H(3A)···N(21) 3.216(3) [160(3)], O(3)−H(3A)···N(31) 3.156(4) [165(4)], O(4)−H(4A)···N(31) 2.923(3) [175(3)], O(4)−H(4B)···N(41) 2.859(3) [170(3)], O(5)−H(5A)···N(31) 3.342(3) [150(3)], O(5)−H(5B)···N(42) 2.776(3) [171(4)], O(3)−H(3B)···O(5) 2.826(3) [177(3)]

structure of dihydroxylead 5,5′-azotetrazolate[6] the N−N bond length of the diazo group is 1.20(3) Å shorter, otherwise the bonding parameters agree with the new structures.

The 5,5′-azotetrazolate ions of the lithium salt **1** are connected to water molecules through seven hydrogen bonds (see Figure 2). N(21) and N(12) are not connected to other molecules; N(52) is coordinated to a lithium ion. All other nitrogen atoms take part in hydrogen bonding to the water molecules. The hydrogen bonds to the ring nitrogen atoms have O−N distances of between 2.783(2) and 2.830(3) Å. The hydrogen bond to the N(11) nitrogen atom of the diazo group is, at 3.188(3) Å, longer. There are also hydrogen bonds between water molecules, with O−O distances of between 2.700(2) and 2.778(2) Å.

Compound **1** contains two different lithium atoms with tetrahedral coordination (Figure 3). The Li(2) atom is surrounded only by water molecules, whereas the Li(1) atom is coordinated to three water molecules and the N(52) nitrogen atom. Lithium has been reported to show tetrahedral, octahedral and sometimes fivefold coordination when surrounded by oxygen atoms.[12] The lithium-oxygen distances [1.910(4) to 1.980(4) Å] compare well with the reported values of 1.94−1.99 Å for tetrahedrally coordinated lithium ions. The lithium-nitrogen distance [2.077(4) Å] is also in the expected range (2.06−2.08 Å).[13] The coordination tetrahedra of two Li(2) atoms share an edge with each other and a corner with the coordination tetrahedron of Li(1) atom. The O(96) oxygen atom is not coordinated to a lithium ion, although it is bound by hydrogen bonds. The weak bonding of the O(96) oxygen atom explains the rapid loss of water from **1**.

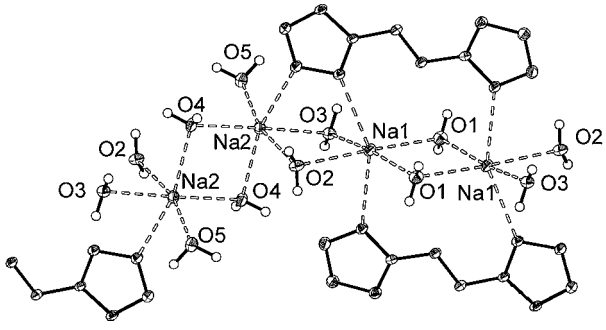

Figure 5. Coordination of the sodium ions in **2** (thermal ellipsoids represent 25% probability); parts of the 5,5′-azotetrazolate ions have been omitted for clarity

The 5,5′-azotetrazolate ions of **2** are coordinated to three sodium ions and eight water molecules (4). The hydrogen bonds have O−N distances of between 2.776(3) and 3.342(3) Å, the longest distances belonging to the bridging hydrogen bonds of the hydrogen atoms of O(3) with N(21) and N(31). The O−N distance to the N(12) nitrogen atom of the diazo group is also longer, and there is only one hydrogen bond between water molecules [O−O distance 2.826(3) Å].

The sodium ions in **2** have different surroundings (Figure 5). They all have a distorted octahedral coordination geometry, with the Na(1) atom connected to four water molecules and the N(22) and N(51) nitrogen atoms, and the Na(2) atom to five water molecules and the N(32) nitrogen atom. The Na−O distances [2.369(2) and 2.483(2) Å][14] as well as the Na−N distances [2.456(2) to 2.556(3) Å][15] are in the expected range. The coordination octahedra of the sodium ions are connected edgewise. The aquated sodium ions form chains, and the 5,5′-azotetrazolate ions form stacks between these chains.

Compound **4** has an inversion centre (Figure 6) and the water molecules are hydrogen bonded to the N(3) and N(4)

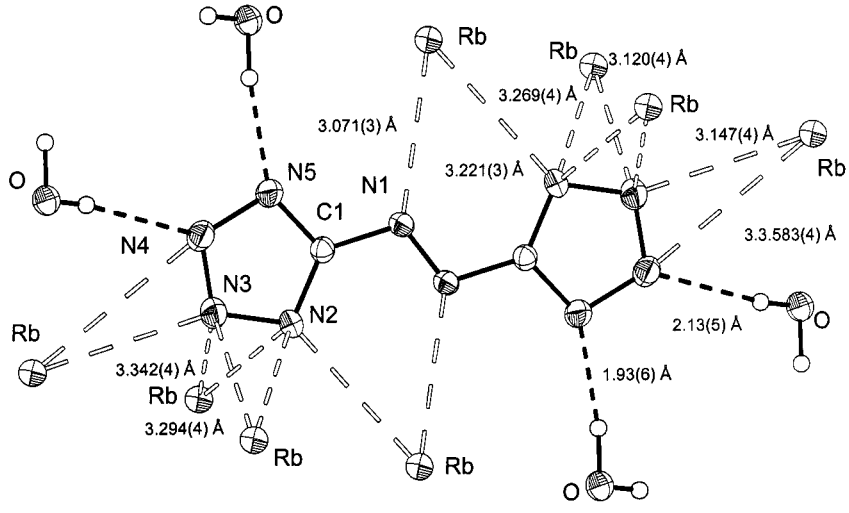

Figure 6. Coordination of the 5,5′-azotetrazolate ions in **4** (thermal ellipsoids represent 25% probability); selected bond lengths [Å]: Rb−O 2.964(3), Rb−O(B) 3.080(3), Rb−O(D) 3.125(3), Rb−O(F) 3.080(3), Rb−N(1A) 3.071(3), Rb−N(2) 3.221(3), Rb−N(2B) 3.294(4), Rb−N(2C) 3.269(4), N(2)−Rb(F) 3.294(3), Rb−N(3B) 3.342(4), Rb−N(3C) 3.120(4), Rb−N(3E) 3.147(4), N(3)−Rb(F) 3.342(4), Rb−N(4E) 3.583(4); symmetry operations for equivalent atoms: A: $-x + 1, -y + 1, -z + 1$; B: $x + 1, y, z$; C: $-x + 1, -y + 1, -z + 2$; D: $-x + 1, -y, -z + 2$; E: $-x, -y + 1; -z + 2$; F: $x - 1, y, z$; hydrogen bonds: O−N distances [Å] (OHN angles [°]), N···H distances are given in the figure: O−H(1)···N(5) 2.875(4) [161(5)], O−H(2)···N(4) 2.823(5) [172(6)]

nitrogen atoms [O−N distances 2.875(4) and 2.823(5) Å]. The 5,5′-azotetrazolate ions are coordinated to eight rubidium ions, with every nitrogen atom either being hydrogen bonded to a water molecule or coordinated to rubidium.

The rubidium ions in **4** are tenfold coordinated to three oxygen atoms and seven nitrogen atoms (Figure 7). The coordination polyhedra of the rubidium ions form face-sharing layers that are separated by layers of 5,5′-azotetrazolate ions. The Rb−O distances [2.964(3) to 3.125(3) Å][16] and the Rb−N distances [3.071(3) to 3.583(4) Å][17] agree with literature values.

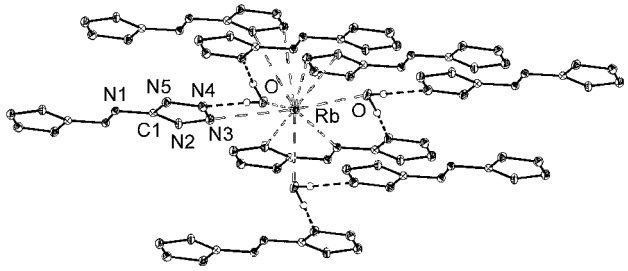

Figure 7. Coordination of the rubidium ions in **4** (thermal ellipsoids represent 25% probability); parts of the 5,5′-azotetrazolate ions have been omitted for clarity

The calcium ions of **7** are not coordinated to any nitrogen atoms (Figure 8). They are surrounded by eight water molecules in the form of a slightly distorted, bi-capped trigonal prism. Two coordination polyhedra share an edge. The bridging water molecules have longer Ca−O distances [2.613(2) and 2.639(2) Å] than the other water molecules [2.369(2) to 2.480(2) Å]. Calcium coordinated by eight water molecules is well-known in the literature, and the distances of the bridging and nonbridging oxygen atoms found here agree well with the previously reported values.[18] One water molecule is not connected to calcium but is hydrogen bonded to the other water molecules and to the 5,5′-azotetrazolate ions. The 5,5′-azotetrazolate ions have hydrogen bonds to eleven water molecules [O−N distances 2.787(3) to 3.226(3) Å].

The 5,5′-azotetrazolate ions of **9** are connected to six water molecules with hydrogen bonds to the N(2) and N(3) nitrogen atoms [Figure 9; O−N distances 2.791(4) to 3.158(5) Å]. The N(4) and N(5) nitrogen atoms are coordin-

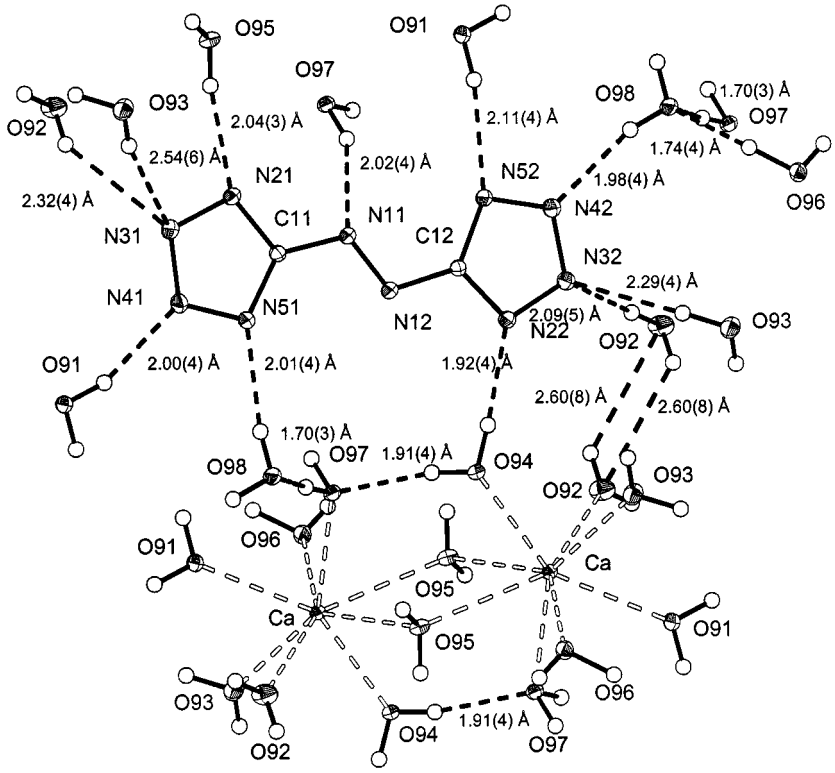

Figure 8. Structure of **7** (thermal ellipsoids represent 25% probability); selected bond lengths [Å]: Ca−O(91) 2.384(2), Ca−O(92) 2.422(2), Ca−O(93) 2.480(2), Ca−O(94) 2.369(2), Ca−O(95) 2.639(2), Ca−O(95A) 2.613(2), Ca−O(96) 2.455(2), Ca−O(97) 2.426(2); symmetry operations for equivalent atoms: A: $-x + 1, -y + 1, -z$; hydrogen bonds: O−N and O−O distances [Å] (OHN/OHO angles [°]), N···H distances are given in the figure: O(91)−H(911)···N(52) 2.944(3) [170(4)], O(91)−H(912)···N(41) 2.831(3) [161(3)], O(92)−H(921)···N(32) 2.960(3) [177(4)], O(92)−H(922)···O(92) 3.145(3) [129(7)], O(92)−H(922)···N(31) 3.226(3) [148(8)], O(93)−H(931)···N(32) 3.190(3) [171(4)], O(93)−H(932)···N(31) 3.047(3) [161(4)], O(94)−H(941)···N(22) 2.787(3) [177(3)], O(94)−H(942)···O(97) 2.745(3) [169(4)], O(95)−H(951)···N(21) 2.856(3) [170(3)], O(95)−H(952)···O(96) 2.901(3) [156(4)], O(96)−H(961)···O(94) 2.959(3) [139(3)], O(96)−H(962)···O(98) 2.708(3) [164(4)], O(97)−H(971)···N(11) 2.814(3) [154(4)], O(97)−H(972)···O(98) 2.654(3) [171(3)], O(98)−H(981)···N(42) 2.804(3) [161(3)], O(98)−H(982)···N(51) 2.827(3) [166(4)]

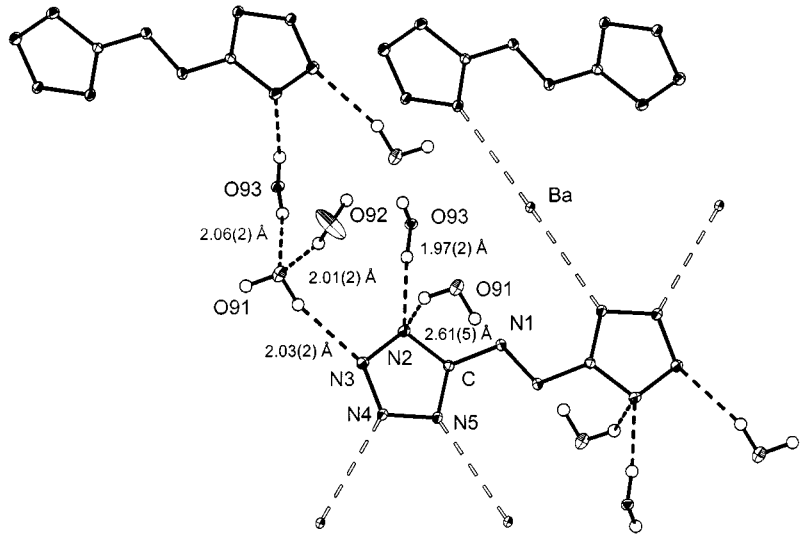

Figure 9. Structure of **9** (thermal ellipsoids represent 25% probability); selected bond lengths [Å]: Ba−O(92) 2.799(6), Ba−O(93) 2.840(3), Ba−O(93) 2.867(3), Ba−N(4) 3.046(4), Ba−N(5) 2.935(4); hydrogen bonds: O−N and O−O distances [Å] (OHN/OHO angles [°]), N···H distances are given in the figure: O(91)−H(911)−N(3) 2.834(6) [162(6)], O(91)−H(912)−N(2) 3.158(5) [124(5)], O(93)−H(932)−N(2) 2.791(4) [171(6)], O(92)−H(92)−O(91) 2.823(6) [167(10)], O(93)−H(931)−O(91) 2.873(4) [168(7)]

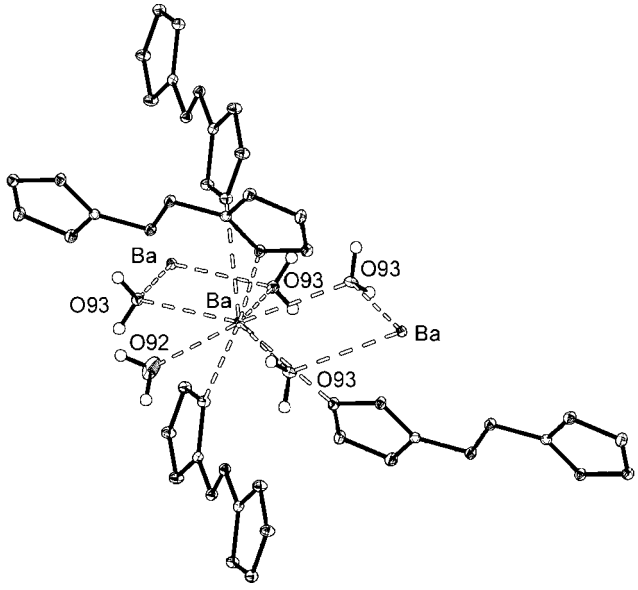

Figure 10. Coordination of the barium ions in **9** (thermal ellipsoids represent 25% probability); parts of the 5,5′-azotetrazolate ions have been omitted for clarity

ated to barium. The O(91) water molecule is not coordinated to barium, but has hydrogen bonds to the O(93) and O(92) oxygen atoms [O−O distances 2.283(6) to 2.873(4) Å], which are themselves coordinated to barium.

The barium atoms of **9** are coordinated to five water molecules and four nitrogen atoms to form a distorted, capped quadratic antiprism (Figure 10). The coordination polyhedra share faces. The Ba−O [2.799(6) to 2.867(3) Å] and Ba−N [2.935(4) and 3.046(4) Å] bond lengths agree with the values for barium azide hydrate.[19] The structure consists of layers of hydrated barium atoms and a layer of stacks of 5,5′-azotetrazolate ions. The layers are connected by Ba−N interactions, explaining the greater insolubility of this compound compared to the calcium salt **7**. The insolubility of the strontium salt is probably also due to Sr−N interactions.

Compound **11** contains two different 5,5′-azotetrazolate ions, one with and one without an inversion centre (Figure 11). The bonding parameters of the two ions are identical within the standard deviation (see Table 3, **11a** and **11b**). The yttrium ions of **11**, like the calcium ions of **7**, are coordinated to eight water molecules in the form of a threefold capped, trigonal prism. In contrast to **7**, however, the coordination polyhedra are not connected. The Y−O distances [2.322(2) to 2.450(2) Å] agree with those of known compounds.[20] Three further water molecules are bound with hydrogen bonds. The O−N distances of the hydrogen bonds between the water molecules and the ring nitrogen atoms of the 5,5′-azotetrazolate ions [2.722(3) and 2.973(3) Å] are shorter than the hydrogen bonds to the diazo nitrogen atoms [3.323(3) and 3.376(3) Å]. The hydrogen bonds between the water molecules have O−O distances of between 2.683(3) and 2.975(3) Å.

The bonding parameters of the tetraphenylarsonium ions of **17** agree with the literature data.[21] The cations have no interactions with the 5,5′-azotetrazolate ions. Figure 12 shows stacks of 5,5′-azotetrazolate ions between the tetraphenylarsonium ions. The orange colour of **17** and **18**, in contrast to the yellow colour of all the other compounds, is probably due to the lack of interactions with the 5,5′-azotetrazolate unit.

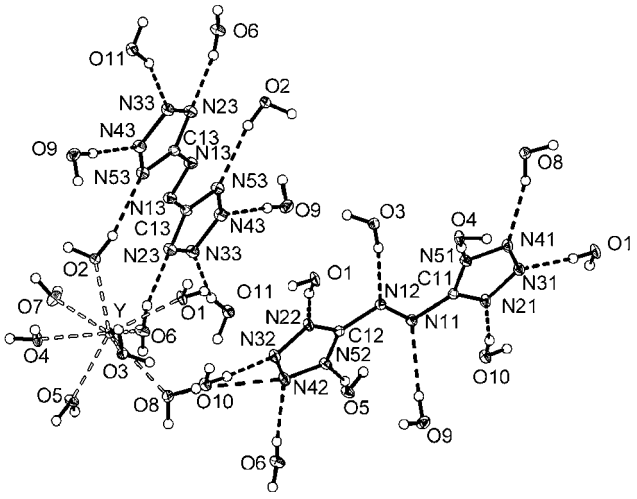

Figure 11. Structure of **11** (thermal ellipsoids represent 25% probability); selected bond lengths [Å]: Y−O(1) 2.327(2), Y−O(2) 2.361(2), Y−O(3) 2.395(2), Y−O(4) 2.351(2), Y−O(5) 2.322(2), Y−O(6) 2.340(2), Y−O(7) 2.332(2), Y−O(8) 2.450(2); symmetry operations for equivalent atoms: A: $-x$, $-y+1$, $-z+1$; hydrogen bonds: O−N and O−O distances [Å] (NHN angles [°]): O1−H11···N22 2.845(3) [169(3)], O1−H21···N31 2.795(3) [176(4)], O2−H22···N53 2.797(3) [166(3)], O3−H23···N12 2.845(3) [173(3)], O4−H24···N51 2.820(3) [172(4)], O5−H25···N52 2.747(3) [167(4)], O6−H16···N23 2.722(3) [168(2)], O6−H26···N42 2.882(3) [163(3)], O6−H26···N52 3.323(3) [136(3)], O8−H18···N42 3.376(4) [170(3)], O8−H28···N41 2.903(3) [164(3)], O9−H19···N11 2.973(3) [162(3)], O9−H29···N43 2.773(4) [177(4)], O10−H110···N21 2.863(3) 169(3), O10−H210···N32 2.797(3) [176(4)], O11−H211···N33 2.846(3) [159(4)], O2−H12···O9 2.757(3) [158(4)], O3−H13···O10 2.683(3) [170(3)], O4−H14···O11 2.723(3) [177(3)], O5−H15···O3 2.975(3) [173(3)], O7−H17···O11 2.747(3) [168(2)], O7−H27···O9 2.726(3) [161(3)], O11−H111···O10 2.782(3) [161(3)]

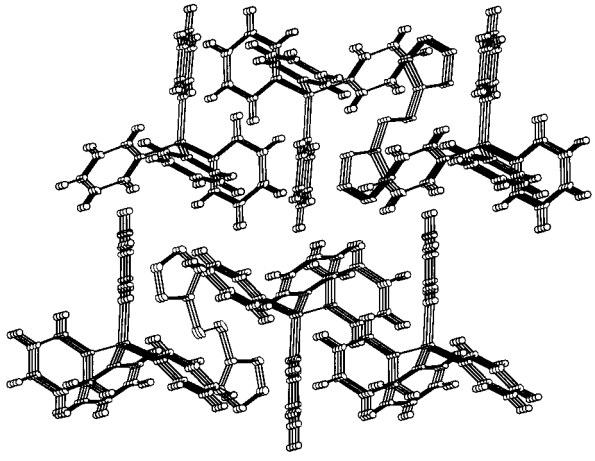

Figure 12. Stacks of 5,5′-azotetrazolate ions in **17**

The bonding parameters of **18** are in good agreement with the bonding parameters of 2-methyl-5-aminotetrazole.[22] As in **17**, the 5,5′-azotetrazole units form stacks (Figure 13).

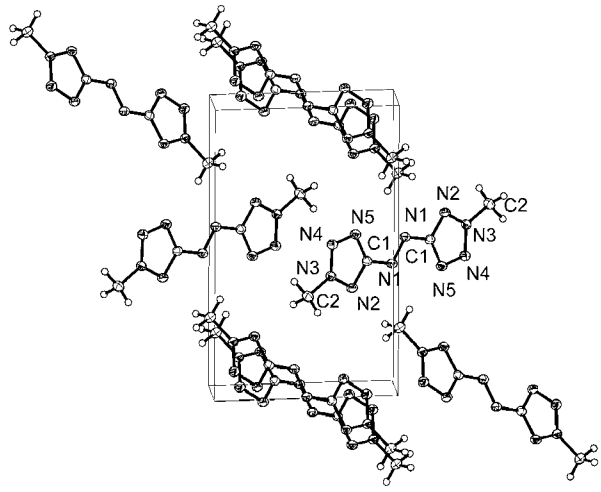

Figure 13. ORTEP plot of the unit cell of 2,2′-dimethyl-5,5′-azotetrazole **18** (thermal ellipsoids represent 25% probability); selected bond lengths [Å] and angles [°]: N(3)−C(2) 1.464(3); C(2)−N(3)−N(2) 123.0(2), C(2)−N(3)−N(4) 122.9(2)

Conclusion

Salts of the 5,5′-azotetrazole dianion with different metal cations were examined. These salts include different amounts of water molecules that are either in the coordination sphere of the cation or bound by hydrogen bonds. The azotetrazolate ion is not connected to harder cations (calcium, yttrium), and these salts decompose, due to their acidity in water, to form tetrazolhydrazine, with evolution of nitrogen. The free acid 5,5′-azotetrazole, which was synthesized from sodium 5,5′-azotetrazolate and HBF_4 decomposes within seconds at room temperature, but can be handled at −30 °C. The loss of water from the 5,5′-azotetrazolate salts occurs at different temperatures depending on how the water molecule is bound in the compound. Upon loss of water, the sensitivity of the compounds toward shock and friction increase drastically. During drying under dynamic vacuum many explosions occurred.

Experimental Section

CAUTION: While all hydrates of 5,5′-azotetrazolate salts are insensitive to shock and friction, the anhydrous 5,5′-azotetrazolate salts and silver 5,5′-azotetrazolate are very sensitive. Safety equipment such as leather gloves, face shields and ear plugs are necessary.

General Remarks: All chemicals were used as provided from the chemical store of the Department of Chemistry. Silver 5,5′-azotetrazolate was prepared from sodium 5,5′azotetrazolate (**2**) and silver nitrate.[1d] NMR: Jeol EX 400, ^{1}H (400.0 MHz), ^{13}C (100.0 MHz): chemical shifts referenced to TMS δ = 0.00; ^{14}N (28.6 MHz), ^{15}N (40.5 MHz): shifts referenced to external CH_3NO_2. IR: Nicolet 520 FT−IR (as KBr pellets). Raman: Perkin−Elmer FTIR−2000 spectrometer (Nd−Yag Laser:

1064 nm, Laser power: 100 mW). CHN analyses: Elementar Vario EL analysator. DSC: Setaram DSC 141. TG: Setaram DTA−TG 92. MS: Balzers QMS 420.

General Procedure: Sodium 5,5′-azotetrazolate (**2**) was prepared following a literature synthesis.[1d] Barium (**9**) and strontium 5,5′-azotetrazolate (**8**) were synthesized by adding the respective chloride to a solution of sodium 5,5′-azotetrazolate (**2**). After stirring for 30 minutes a yellow precipitate was separated and recrystallized from water. All other 5,5′-azotetrazolate salts were obtained from the reaction of barium 5,5′-azotetrazolate (**9**) with the respective metal sulfates in water. After stirring for 30 minutes a yellow solution was obtained after filtration. The water was allowed to evaporate from this solution to give respective 5,5′-azotetrazolate salts as yellow crystals that were then recrystallized from water.

Lithium 5,5′-Azotetrazolate Hexahydrate (1): Yield: 92%. $T_{Dec.}$ = 335 °C. DSC: 64.0 °C (44.0 J/g), 109.2 °C (25.0 J/g), 133.9 °C (581.9 J/g). IR: $\tilde{\nu}$ = 3425 cm^{-1} m, 3183 m, 1625 w, 1399 s, 1211 m, 1180 m, 1096 m, 1046 m, 891 m, 760 m, 733 s, 693 m, 602 w, 564 w. Raman: $\tilde{\nu}$ = 1484 cm^{-1} m, 1420 w, 1387 s, 1108 m, 1080 w, 926 w, 111 w. $C_2H_{12}Li_2N_{10}O_6$ (286.06): calcd. C 8.4, H 4.2, N 49.0; found C 11.6, H 4.1, N 82.6.

Sodium 5,5′-Azotetrazolate Pentahydrate (2): $T_{Dec.}$ = 248 °C. DSC: 115.6 °C (355.5 J/g), 159.3 °C (306.1 J/g). ^1H NMR ([D$_6$]DMSO): δ = 4.1 (H_2O). ^{13}C NMR ([D$_6$]DMSO): δ = 173.1 ([$N_4C-N=N-CN_4$]$^{2-}$). ^{14}N NMR (D_2O): δ = −77 (CN_β), 2 (CN_α), 105(-*N*=*N*-). ^{15}N NMR (D_2O): δ = −76.2 (CN_β), 0.6 (CN_α), 101.8 (-*N*=*N*-). IR: = $\tilde{\nu}$ = 3612 cm^{-1} s, 3544 s, 3435 s, 3389 s, 3248 s, 2443 w, 2257 w, 2216 w, 2152 w, 2106 m, 1685 m, 1628 s, 1401 s, 1165 m, 1096 w, 1082 w, 1065 m, 1044 m, 776 s, 741 s, 732 s, 566 s, 526 s, 398 s. Raman: $\tilde{\nu}$ = 1480 cm^{-1} m, 1420 w, 1386 s, 1088 m, 1058 m, 926 w, 383 w, 223 w, 123 w. $C_2H_{10}N_{10}Na_2O_5$ (300.14): calcd. C 8.0, H 3.4, N 46.7; found C 8.1, H 3.3, N 46.6.

Potassium 5,5′-Azotetrazolate Pentahydrate (3): Yield: 93%. $T_{Dec.}$ = 243 °C. DSC: 40.5 °C (49.1 J/g), 107.5 °C (70.1 J/g), 144.1 °C (326.3 J/g). IR: $\tilde{\nu}$ = 3647 cm^{-1} m, 3265 w, 2921 m, 2851 w, 2415 m, 2355 m, 2319 m, 2097 m, 1960 w, 1668 w, 1488 w, 1447 m, 1390 m, 1380 m, 1185 m, 1153 m, 1058 w, 1033 w, 866 m, 846 m, 822 m, 772 m, 727 s, 667 m. Raman: $\tilde{\nu}$ = 1482 cm^{-1} m, 1416 w, 1378 s, 1189 w, 1155 w, 1079 w, 1065 w, 1053 w, 1041 w, 925 w, 736 w, 340 w, 104 w. $C_2H_{10}K_2N_{10}O_5$ (278.32): calcd. C 7.2, H 3.0, N 42.1; found C 7.5, H 2.6, N 42.8.

Rubidium 5,5′-Azotetrazolate Dihydrate (4): Yield: 90%. $T_{Dec.}$ = 239 °C. DSC: 96.9 °C (200.5 J/g). IR: $\tilde{\nu}$ = 3440 cm^{-1} s. 3281 s, 2550 w, 2509 w, 2442 w, 2103 w, 2062 w, 1981 w, 1887 w, 1791 w, 1710 m, 1519 w, 1453 w, 1395 m, 1292 w, 1199 w, 1156 m, 1073 w, 1056 w, 1033 m, 933 w, 847 w, 773 w, 736 m, 666 m, 565 m. Raman: $\tilde{\nu}$ = 1494 cm^{-1} s, 1418 w, 1386 s, 1361 w, 1200 w, 1155 w, 1082 m, 1059 m, 1036 w, 924 w, 348 w, 104 w. $C_2H_4N_{10}O_2Rb_2$ (371.05): calcd. C 6.4, H 1.1, N 37.7; found C 6.4, H 0.9, N 38.0.

Caesium 5,5′-Azotetrazolate Dihydrate (5): Yield: 91%. $T_{Dec.}$ = 237 °C. DSC: 40.3 °C. IR: $\tilde{\nu}$ = 3314 cm^{-1} m, 3244 m, 2924 s, 2853 m, 1742 w, 1593 w, 1463 w, 1389 m, 1382 m, 1195 w, 1179 w, 1146 w, 1064 w, 1052 w, 1039 w, 773 w, 728 s, 661 w, 559 w. Raman: $\tilde{\nu}$ = 1494 cm^{-1} s, 1467 w, 1413 w, 1381 s, 1356 w, 1313 w, 1197 w, 1154 w, 1080 w, 1068 m, 1057 m, 1035 w, 923 w, 340 w, 98 w. $C_2H_4Cs_2N_{10}O_2$ (465.93): calcd. C 5.2, H 0.9, N 30.1; found C 5.3, H 0.8, N 29.9.

Magnesium 5,5′-Azotetrazolate Octahydrate (6): Yield: 15%. $T_{Dec.}$ = 231 °C. IR: $\tilde{\nu}$ = 3256 cm^{-1} s, 2881 w, 2832 w, 1668 m, 1639 m, 1529 w, 1428 w, 1393 m, 1386 m, 1323 w, 1199 w, 1053 w, 767 w, 736 m, 657 m. Raman: $\tilde{\nu}$ = 1499 cm^{-1} m, 1452 w, 1416 w, 1375 s, 1200 w, 1086 w, 1062 m, 932 w, 112 w. $C_2H_{16}MgN_{10}O_8$ (332.5): calcd. C 7.2, H 4.8, N 42.1; found C 7.5, H 4.4, N 34.3.

Calcium 5,5′-Azotetrazolate Octahydrate (7): Yield: 74%. $T_{Dec.}$ = 221 °C. IR: $\tilde{\nu}$ = 3513 cm^{-1} s, 3425 s, 3250 s, 2950 s, 2925 s, 2850 s, 2251 w, 2093 w, 1659 m, 1619 m, 1510 w, 1463 w, 1398 s, 1375 m, 1201 m, 1193 w, 1063 m, 1042 w, 943 w, 821 w, 772 w, 734 m, 672 w, 614 w, 563 w, 444 w. Raman: $\tilde{\nu}$ = 1496 cm^{-1} m, 1479 w, 1435 w, 1416 w, 1394 s, 1377 s, 1202 w, 1089 w, 1070 s, 1051 w, 929 w, 336 w, 143 w. $C_2H_{16}CaN_{10}O_8$ (348.29): calcd. C 6.9, H 4.6, N 40.2; found C 6.6, H 4.4, N 40.2.

Strontium 5,5′-Azotetrazolate Hexahydrate (8): Yield: 80%. $T_{Dec.}$ = 238 °C. DSC: 76.2 °C (51.7 J/g), 130.3 °C (132.7 J/g), 139.3 °C (285.6 J/g). IR: $\tilde{\nu}$ = 3378 cm^{-1} s, 3225 s, 2967 m, 2926 m, 2844 m, 2439 m, 1651 m, 1468 wm 1396 m, 1384 s, 1258 w, 1203 w, 1161 w, 1083 w, 1068 w, 1039 w, 855 w, 802 w, 760 w, 734 w, 662 w, 554 w. Raman: $\tilde{\nu}$ = 1488 cm^{-1} m, 1420 w, 1382 s, 1203 w, 1165 w, 1094 m, 1071 m, 1042 w, 918 w, 336 w. $C_2H_{12}N_{10}O_6Sr$ (359.80): calcd. C 6.7, H 3.4, N 38.9; found C 6.7, H 3.2, N 38.6.

Barium 5,5′-Azotetrazolate Pentahydrate (9): Yield: 90%. $T_{Dec.}$ = 211 °C. DSC: 129.1 °C (265.2 J/g). IR: $\tilde{\nu}$ = 3401 cm^{-1} m, 3276 m, 3142 m, 2954 m, 2926 m, 2446 w, 2220 w, 2037 w, 1609 m, 1504 w, 1450 w, 1399 s, 1199 m, 1161 m, 1061 w, 1039 w, 805 m, 774 w, 735 m, 675 w, 562 m. Raman: $\tilde{\nu}$ = 1488 cm^{-1} m, 1428 w, 1391 s, 1365 w, 1163 w, 1090 w, 1068 m, 1044 w, 922 w, 357 w, 206 w, 111 w. $C_2H_{10}BaN_{10}O_5$ (391.49): calcd. C 6.1, H 2.6, 35.8 N; found C 6.3, H 3.0, N 35.3.

Aluminium 5,5′-Azotetrazolate Hydrate (10): IR: $\tilde{\nu}$ = 2956 cm^{-1} s, 2845 s, 2405 m, 2400 m, 2321 m, 1601 m, 1505 w, 1489 w, 1464 w, 1442 w, 1409 m, 1398 s, 1381 w, 1228 w, 1213 w, 1190 w, 1121 w, 1085 w, 950 w, 869 w, 797 m, 738 s, 725 m, 667 w, 613 w, 553 m. Raman: $\tilde{\nu}$ = 1488 cm^{-1} m, 1399 s, 1385 s, 1124 m, 1110 m, 1089 m, 931 w. $C_6Al_2N_{30}\cdot(16-18)H_2O$: found C 8.8, H 3.7, N 46.1.

Yttrium 5,5′-Azotetrazolate Docosahydrate (11): Yield: 24%. IR: $\tilde{\nu}$ = 3598 cm^{-1} m, 3542 m, 3191 s, 2391 m, 1649 m, 1629 m, 1448 w, 1403 s, 1207 m, 1172 w, 1083 w, 1061 w, 1043 w, 951 w, 770 s, 727 s, 667 s, 575 m. Raman: $\tilde{\nu}$ = 1487 cm^{-1} m, 1453 w, 1424 w, 1388 s, 1365 w, 1209 w, 1177 w, 1103 w, 1085 w, 1076 w, 1062 w, 926 w, 734 w, 356 w, 206 w, 124 w. $C_6H_{44}N_{30}O_{22}Y_2$ (1066.53): calcd. C 6.8, H 4.2, 40.2 N; found C 8.1, H 4.2, N 40.2.

Lanthanum 5,5′-Azotetrazolate Hydrate (12): IR: $\tilde{\nu}$ = 2954 cm^{-1} m, 2925 s, 2854 m, 2148 w, 1623 w, 1535 w, 1512 w, 1459 m, 1398 m, 1384 m, 1259 w, 1228 w, 1096 w, 1032 w, 968 w, 879 w, 799 w, 730 m, 630 w, 563 w. Raman: $\tilde{\nu}$ = 1479 cm^{-1} m, 1429 w, 1390 s, 1109 w, 1088 w, 1074 w, 931 w. $C_6N_{30}La_2\cdot(20-24)H_2O$: found C 6.1, H 3.8, N 34.7.

Cerium 5,5′-Azotetrazolate Hydrate (13): IR: $\tilde{\nu}$ = 3129 cm^{-1} m, 1624 m, 1550 w, 1529 w, 1452 w, 1408 m, 1394 m, 1361 m, 1208 w, 1184 w, 1169 w, 1048 m, 768 s, 743 s, 650 s, 627 s, 570 s. Raman: $\tilde{\nu}$ = 1478 cm^{-1} m, 1437 w, 1396 s, 1388 m, 1110 w, 1090 w, 1073 m, 1053 w, 934 w. $C_6N_{30}Ce_2\cdot(14-18)H_2O$: found C 6.8, H 2.8, N 36.6.

Neodymium 5,5′-Azotetrazolate Hydrate (14): IR: $\tilde{\nu}$ = 3138 cm^{-1} s, 2946 m, 2880 m, 2811 m, 2346 w, 2148 w, 1626 w, 1498 w, 1442 w, 1404 s, 1396 m, 1332 w, 1203 w, 1182 w, 1064 w, 771 m, 743 s, 730 m, 673 m. Raman: $\tilde{\nu}$ = 1477 cm^{-1} m, 1426 w, 1394 s, 1111 w, 1091 w, 1067 m, 929 w.

Gadolinium 5,5′-Azotetrazolate Hydrate (15): IR: $\tilde{\nu}$ = 3173 cm^{-1} m, 2894 w, 2146 w, 1656 w, 1541 s, 1454 s, 1416 m, 1345 m, 1221

w, 1049 w, 1022 w, 962 w, 941 w, 730 w, 681 m. Raman: $\tilde{\nu}$ = 2935 cm^{-1} w, 1488 m, 1477m, 1424 w, 1390 s, 1084 w, 1066 m, 967 w, 943 w, 680 w.

Reaction of $Ce(SO_4)_2$ with Barium 5,5′-Azotetrazolate: $Ce(SO_4)_2$ (1.00 g, 3.0 mmol) and barium 5,5′-azotetrazolate (1.81 g, 6.0 mmol) were stirred in 30 mL of water. During stirring gas evolved and a brown precipitate was formed.

5,5′-Azotetrazole-dimethanol (16): $HBF_4{\cdot}Et_2O$ (0.26 g, 1.6 mmol) was added to a suspension of sodium 5,5′-azotetrazolate (**2**; 0.17 g, 0.8 mmol) in methanol. After stirring for 2 h a yellow solution was formed. The solvent was then removed in vacuo at −30 °C to give yellow needles of **16**, which were dried under oil-pump vacuum at −30 °C. ^{1}H NMR (CD_3CN, −30 °C): δ = 3.34 (s, 6 H, CH_3), 5.68 (s, 4 H, NH, OH). ^{13}C NMR (CD_3CN, −30 °C): δ = 49.9 (CH_3), 168.6 ($[N_4C{-}N{=}N{-}CN_4]^{2-}$). IR: $\tilde{\nu}$ = 3518 cm^{-1} m, 3224 m, 2956 m, 2923 m, 2852 m, 1687 w, 1630 w, 1467 w, 1436 w, 1383 m, 1056 s, 735 m, 666 w. Raman (100 mW, −30 °C): $\tilde{\nu}$ = 2970 cm^{-1} w, 1542 m, 1483 s, 1463 w, 1361 m, 1208 m, 1122 w, 1061 w, 1003 w, 913 w, 785 w, 330 w, 180 w, 141 w, 101 w.

Bis-tetraphenylarsonium 5,5′-Azotetrazolate (17): Sodium 5,5′-azotetrazolate (**2**; 0.13 g (0.62 mmol) and tetraphenylarsonium chloride (0.52 g, 1.24 mmol) were stirred in 20 mL DMF for two weeks. The resulting orange solution was isolated by filtration, the DMF removed in vacuo, and the remaining orange crystals recrystallized from DMF. Yield: 435 mg (76%). ^{1}H NMR ([D$_6$]DMSO): δ = 7.77−7.92 (m, PhH). ^{13}C NMR ([D$_6$]DMSO): δ = 121.0 (C-As), 130.9 (C_α), 133.1 (C_β), 134.3 (C_γ). IR: $\tilde{\nu}$ = 3421 cm^{-1} m, 3158 m, 3085 m, 3047 m, 3011 m, 2228 m, 2189 w, 2158 w, 2130 s, 2101 w, 2037 m, 1998 s, 1660 m, 1578 m, 1480 s, 1438 s, 1373 m, 1338 m, 1308 m, 1282 w, 1184 m, 1171 w, 1162 w, 1081 s, 1022 w, 997 s, 931 w, 855 w, 752 s, 742 s, 723 m, 690 s, 612 w, 557 w, 521 w, 478 s, 467 s, 363 m, 351 m. Raman: $\tilde{\nu}$ = 3061 cm^{-1} m, 1578 m, 1466 m, 1397 m, 1361 s, 1019 m, 1001 m, 913 w, 672 m, 240 w, 108 w. $C_{50}H_{40}As_2N_{10}$ (930.76): calcd. C 64.52, H 4.3, N 15.0; found C 65.8, H 4.6, N 11.1.

2,2′-Dimethyl-5,5′-azotetrazole (18): Iodomethane (6.05 g, 4.1 mmol) was added to a suspension of silver 5,5′-azotetrazolate (0.50 g, 1.3 mmol) in 20 mL water. The reaction mixture was stirred for three days in a closed vessel. The unreacted iodomethane was then removed in vacuo, and the reaction mixture was extracted three times with chloroform and dried with magnesium sulfate. Recrystallisation from chloroform gave 89 mg (34%) of an orange solid. $T_{Dec.}$: 170 °C. ^{1}H NMR (CD_3CN): δ = 4.47 (s, 6 H, CH_3). ^{13}C NMR (CD_3CN): δ = 40.5 (CH_3), 171.5 ($[N_4C{-}N{=}N{-}CN_4]^{2-}$). IR: $\tilde{\nu}$ = 2928 cm^{-1} m, 2857 m, 2356 w, 2347 w, 1745 w, 1457 w, 1420 w, 1375 m, 1346 m, 1316 m, 1266 w, 1189 w, 1157 w, 1094 w, 1036 w, 831 w, 774 s, 701 w, 649 w, 569 m, 556 w, 532 w, 349 m, 326 w. Raman: $\tilde{\nu}$ = 2961 cm^{-1} w, 1503 s, 1433 m, 1393 s, 1354 s, 1277 w, 1235 w, 1196 m, 1102 w, 1014 m, 914 w, 713 w. $C_4H_6N_{10}$ (374.33): calcd. C 24.7, H 3.1, N 72.1; found C 25.0, H 3.0, 70.9 N.

X-ray Structure Determination: Data were collected with graphite monochromated Mo-K_α radiation (λ = 0.71073 Å). Data collection for **2** was performed on a Siemens P4 diffractometer, for **1**, **16** and **17** on a Stoe IPDS diffractometer equipped with an image-plate area detector and for **4**, **7**, **9** and **11** on a Nonius Kappa CCD diffractometer. All data refinement was performed using SIR97[23] and SHELXL-97.[24] Acquisition and refinement data are shown in Table 4.

Crystallographic data (excluding structure factors) for the structure(s) reported in this paper have been deposited with the Cambridge Crystallographic Data Centre as supplementary publication nos. CCDC-169910 (**1**), -169906 (**2**), -169907 (**4**), -169908 (**7**), -169911 (**9**), -169909 (**11**), -169912 (**17**), -169913 (**18**). Copies of the data can be obtained free of charge on application to CCDC, 12

Table 4. Crystallographic data and data related to data acquisition and refinement

	1	**2**	**4**	**7**	**9**	**11**	**17**	**18**
Chem. Formula	$C_2H_{12}Li_2N_{10}O_6$	$C_2H_{10}N_{10}Na_2O_5$	$C_2H_4N_{10}O_2Rb_2$	$C_2H_{16}CaN_{10}O_8$	$C_2H_{10}BaN_{10}O_5$	$C_6H_{44}N_{30}O_{22}Y_2$	$C_{50}H_{40}N_{10}As_2$	$C_4H_6N_{10}$
Molecular weight	286.10	300.18	371.09	348.33	391.492	1066.53	930.763	194.158
Color, Habit	yellow prism	yellow prism	yellow prism	yellow prism	yellow block	yellow prism	Orange, irregular	orange, irregular
Crystal size [mm]	0.25 × 0.13 × 0.10	0.4 × 0.4 × 0.2	0.25 × 0.12 × 0.06	0.26 × 0.22 × 0.16	0.35 × 0.18 × 0.10	0.30 × 0.09 × 0.04	0.28 × 0.15 × 0.09	0.30 × 0.15 × 0.06
Crystal system	triclinic	triclinic	triclinic	triclinic	monoclinic	triclinic	triclinic	monoclinic
Space group	$P\bar{1}$	$P\bar{1}$	$P\bar{1}$	$P\bar{1}$	$C2/c$	$P\bar{1}$	$P\bar{1}$	$P2_1/c$
a [Å]	8.852(2)	7.1239(8)	4.41100(1)	6.52990(1)	16.3414(2)	10.1262(1)	9.4125(7)	4.5638(9)
b [Å]	8.883(2)	7.5783(8)	7.7298(2)	10.05040(1)	9.4086(2)	10.3796(2)	13.509(1)	12.126(4)
c [Å]	9.119(2)	12.055(1)	7.7716(2)	11.2142(2)	8.5886(2)	10.4524(1)	18.487(2)	7.807(2)
α [°]	88.32(2)	79.756(2)	80.780(1)	70.1999(8)	90	73.0015(9)	78.05(1)	90
β [°]	82.48(2)	81.105(2)	84.569(1)	89.9935(7)	121.0060(9)	78.6168(9)	76.618(9)	99.97(3)
γ [°]	61.07(2)	68.230(2)	80.303(1)	85.4095(7)	90	74.7266(6)	72.51(1)	90
V [Å^3]	621.7(2)	592.0(1)	257.10(1)	689.95(2)	1131.81(4)	1004.84(2)	2157.3(3)	425.5(2)
Z	2	2	1	2	4	1	2	2
ρ(calcd.) [mg/m^3]	1.528	1.684	2.396	1.677	2.29755	1.762	1.433	1.515
μ [mm^{-1}]	0.137	0.209	9.521	0.516	3.547	2.985	1.598	0.116
F(000)	296	308	176	364	752	544	952	200
θ range [°]	2.25 bis 28.11	3.44 bis 57.98	2.66 bis 27.44	1.93 bis 27.97	0.999 bis 27.49	2.05 bis 27.48	1.82 bis 25.91	3.14 bis 25.82
Temp. [K]	200(2)	193(2)	200(3)	200(3)	200(2)	200(2)	200(3)	200(3)
Index range	$-11 \le h \le 11$	$-8 \le h \le 8$	$-5 \le h \le 5$	$-8 \le h \le 8$	$-21 \le h \le 20$	$-13 \le h \le 13$	$-10 \le h \le 16$	$-5 \le h \le 4$
	$-11 \le k \le 11$	$-8 \le k \le 9$	$-10 \le k \le 10$	$-13 \le k \le 13$	$-12 \le k \le 12$	$-13 \le k \le 13$	$-16 \le k \le 16$	$-10 \le k \le 14$
	$-11 \le l \le 11$	$-15 \le l \le 15$	$-10 \le l \le 9$	$-14 \le l \le 14$	$-11 \le l \le 10$	$-13 \le l \le 12$	$-22 \le l \le 22$	$-9 \le l \le 9$
Refl. collected	5327	3456	3993	13112	8907	16144	17080	1570
Refl. unique	2761	1822	1161	3160	1303	4534	7814	782
Refl. observed (4σ)	1918	1510	1088	2766	1246	3972	5502	500
R (int.)	0.0971	0.0196	0.0388	0.0346	0.0482	0.0402	0.1096	0.0455
Data/restraints/parameters	2761/0/229	1822/9/204	1161/0/81	3160/1/254	1303/7/103	3972/33/338	7814/0/559	782/0/76
GOOF	0.985	1.065	1.294	1.206	1.364	1.201	0.880	0.863
R_1, wR_2 [$I > 4\sigma(I)$]	0.0524, 0.1113	0.0431, 0.1194	0.0279, 0.0924	0.0345, 0.0986	0.0211, 0.0572	0.0310, 0.0846	0.0463, 0.0862	0.0398, 0.0776
R_1, wR_2 (all data)	0.0754, 0.1314	0.0532, 0.1265	0.0314, 0.1122	0.0425, 0.1144	0.0260, 0.0959	0.0426, 0.1138	0.0679, 0.0920	0.0736, 0.0835
Larg. res. peak [e/Å^3]	0.357/−0.357	1.079/−0.206	0.667/−0.731	0.452/−0.349	1.609/−1.585	0.982/−0.739	1.204/−1.051	0.150/−0.171

Union Road, Cambridge CB2 1EZ, UK [Fax: (internat.) + 44-1223/336-033; E-mail: deposit@ccdc.cam.ac.uk].

Acknowledgments

Financial support by the Deutsche Forschungsgemeinschaft (DFG, KL 636/7−1), the Fonds der Chemischen Industrie (FCI) and the German Federal Office for Defence Technology and Procurement (BWB) is gratefully acknowledged. The NMR spectra were measured by Dr. B. Krumm, the IR spectra by Mrs. Kiesewetter, the Raman spectra by Mr. G. Spiess the DSC measurements were performed by Mr. W. Wünschheim. We also want to acknowledge Mrs. A. Burdzy for help with the experimental work.

[1] [1a] J. Thiele, *Justus Liebigs Ann. Chem.* **1892**, *270*, 54−63. [1b] J. Thiele, J. T. Marais, *Justus Liebigs Ann. Chem.* **1893**, *273*, 144−160. [1c] J. Thiele, *Ber.* **1893**, *26*, 2645−2646. [1d] J. Thiele, *Justus Liebigs Ann. Chem.* **1898**, *303*, 57−75.

[2] A. J. Barrat, L. R. Bates, J. M. Jenkins, J. R. White, *Govt. Rep. Announce. (U. S.)* **1973**, *73(2)*, 70.

[3] A. G. Mayants, V. N. Vladimirov, N. M. Razumov, V. A. Shlyapochnikov, *J. Org. Chem. USSR (Engl. Transl.)* **1991**, *27*, 2177−2181; *Zh. Org. Kim.* **1991**, *27*, 2450−2455.

[4] A. G. Mayants, V. N. Vladimirov, V. A. Shlyapochnikov, L. M. Tischenko, S. S. Gordeichuk, S. V. Mikhailova, *Khim. Geterotsikl. Soedin.* **1993**, *4*, 468−475; *Chem. Abstr.* **1994**, *120*, 164064w.

[5] [5a] M. A. Hiskey, N. Goldman, J. R. Stine, *J. Energ. Mat.* **1998**, *16*, 119−127. [5b] A. Hammerl, G. Holl, M. Kaiser, T. M. Klapötke, H. Nöth, U. Ticmanis, M. Warchhold, *Inorg. Chem.* **2001**, *40*, 3570−3575. [5c] A. Hammerl, G. Holl, M. Kaiser, T. M. Klapötke, P. Mayer, H. Piotrowski, M. Vogt, *Z. Naturforsch. B*, in press. [5d] A. Hammerl, G. Holl, M. Kaiser, T. M. Klapötke, P. Mayer, H. Nöth, H. Piotrowski, M. Suter, *Z. Naturforsch. B*, in press. [5e] T. Matsuzawa, M. Itoh, M. Arai, M. Tamura, *Proc. Int. Pyrotech Semin.* **1996**, *22nd*, 317−324.

[6] M. A. Pierce-Butler, *Acta Crystallogr., Sect. B* **1982**, *38*, 2681−2683.

[7] [7a] M. M. Chaudhri, *Nature* **1976**, *263*, 121−122. [7b] G. O. Reddy, A. K. Chatterjee, *Thermochim. Acta* **1983**, *66*, 231−244. [7c] D. J. Whelan, R. J. Spear, R. W. Read, *Thermochimica Acta* **1984**, *80*, 149−163. [7d] M. M. Chaudhri, *J. Mater. Sci. Lett.* **1984**, *3*, 565−568. [7e] M. M. Chaudhri, *J. Mat. Sci.* **1984**, *19*, 3028−3042. [7f] V. K. Mohan, T. B. Tang, *J. Chem. Phys.* **1983**, *79*, 4271−4278.

[8] [8a] R. Stolle, K. Ehrmann, D. Rieder, H. Wille, H. Winter, F. Henke-Stark, *J. Prakt. Chem.* **1932**, *134*, 282−309. [8b] R. Stolle, O. Orth, *Ber.* **1925**, *58B*, 2100−2105. [8c] R. Stolle, A. Netz, O. Kramer, S. Rothschild, H. Erbe, O. Schick, *J. Prakt. Chem.* **1933**, *138*, 1−17.

[9] [9a] M. M. Williams, W. S. McEwan, R. A. Henry, *J. Phys. Chem.* **1957**, *61*, 261−267. [9b] W. Pan, *Int. Annu. Conf. ICT* **1994**, *24th*, 77.

[10] M.-X. Zhang, P. E. Eaton, R. Gilardi, *Angew. Chem.* **2000**, *112*, 422; *Angew. Chem. Int. Ed. Engl.* **2000**, *39*, 401−404.

[11] A. Hammerl, T. M. Klapötke, H. Nöth, M. Warchhold, unpublished results.

[12] J. Mason, *Multinuclear NMR* **1987**, Plenum Press, New York, 335−362.

[13] K. Hermansson, J. O. Thomas, I. Olovsson, *Acta Crystallogr., Sect. B* **1977**, *33*, 2857−2861.

[14] W. Klein, M. Jansen, *Z. Naturforsch., Teil B* **1999**, *54*, 1345−1349.

[15] [15a] B. Klewe, B. Pedersen, *Acta Crystallogr., Sect. B* **1970**, *30*, 2363−2371. [15b] W. R. Haaf, G. B. Carpenter, *Acta Crystallogr.* **1964**, *17*, 730−732.

[16] I. Olovsson, *Acta Crystallogr.* **1965**, *18*, 879−889.

[17] H. Jacobs, T. Tacke, J. Kockelkorn, *Z. Anorg. Allg. Chem.* **1984**, *516*, 67−78.

[18] U. Müller, *Z. Anorg. Allg. Chem.* **1972**, *392*, 159−166.

[19] [19a] G. Thiele, D. Putzas, *Z. Anorg. Allg. Chem.* **1984**, *519*, 217−224. [19b] P. A. Leclaire, M. M. Borel, J. C. Monier, *Acta Crystallogr., Sect. B* **1980**, *36*, 2757−2759.

[20] E. M. Walitzi, H. Kirschner, *Z. Kristallogr.* **1973**, *137*, 368−379.

[21] B. Eriksson, *Acta Chem. Scand., Ser. A* **1982**, *36*, 186−188.

[22] T. M. Klapötke, H. Nöth, T. Schütt, M. Warchhold, *Angew. Chem.* **2000**, *112*, 2197−2199; *Angew. Chem. Int. Ed.* **2000**, *39*, 2108−2109.

[23] J. H. Bryden, *Acta Crystallogr.* **1956**, *9*, 874−878.

[24] G. Cascarano, *Acta Crystallogr., Sect. A* **1996**, C79.

[25] G. M. Sheldrick, SHELXL-97, *Program for Crystal Structure Refinement*, Universität Göttingen, **1997**.

Received August 27, 2001
[I01332]

Rhodium Mediated N−O Bond Formation

Helen M. Burke,[a] John F. Gallagher,[b] Maria T. Indelli,[c] Franco Scandola,[c] and Johannes G. Vos*[a]

Keywords: Rhodium / N ligands / Oxygen / Insertion / Crystal structure

Reaction of $[Rh(phen)_2Cl_2]Cl$ (phen = 1,10-phenanthroline) with the ligand 3,5-bis(pyridin-2-yl)-1,2,4-triazole (Hbpt) in H_2O at pH 9 gives rise to the formation of a single stable compound. Single-crystal X-ray analysis of this material reveals that in the product obtained an oxygen atom has been inserted between the $Rh(phen)_2$ moiety and the triazole ring of the bpt ligand yielding a compound of the type $[Rh(phen)_2(Obpt)](PF_6)_2 \cdot 0.767CH_3CN \cdot 0.28H_2O$. Insertion of oxygen in this manner has not been reported previously.

(© Wiley-VCH Verlag GmbH, 69451 Weinheim, Germany, 2002)

Introduction

A considerable amount of research has been dedicated to the study of ligand-bridged polynuclear transition metal complexes.[1] This particular class of complexes has been used as a basis for studying electron transfer processes with the aim of creating multicomponent systems (supramolecular systems) capable of effecting useful light- and/or redox-induced functions. Most of the initial systems developed incorporated ruthenium(II) polypyridine compounds, although systems incorporating other transition metals such as rhodium(III), osmium(II) and iridium(III) have also been investigated.[2−5]

We have recently started a systematic investigation into the photophysical properties of mixed ligand rhodium(III) complexes. These studies are aimed at achieving a better understanding of the way in which the excited states of rhodium(III) complexes are affected by the introduction of ligands other than polypyridyl ligands. In these studies the ligands investigated are based on substituted 1,2,4-triazole moieties. Through well-established synthetic routes both π accepting and σ donating groupings can be introduced and these triazole based ligands have been shown to promote interactions between metal centres in dinuclear structures via deprotonation of the triazole ring. As a result a wide range of both mononuclear and dinuclear complexes of ruthenium(II) and osmium(II) incorporating these ligands has been reported.[6] An additional interest in these ligands is due to their asymmetry, which allows for different coordination modes. Of particular interest are ligands such as 3,5-bis(pyridin-2-yl)-1,2,4-triazole (Hbpt) (for structure see Figure 1) for which mononuclear and dinuclear Ru^{II} and Os^{II} complexes have been reported.[5] Orthometallated Rh^{III} complexes with Hbpt and the related ligand 4-amino-3,5-bis(2-pyridyl)-4*H*-1,2,4-triazole ($bptNH_2$) have also been reported,[7−9] as have Rh^{I} complexes with the ligands Hbpt and $bptNH_2$.[10−11] In this paper we wish to report on a very unusual reaction product obtained when a rhodium(III) precursor is reacted with Hbpt. In the compound obtained an oxygen atom has inserted into the Rh^{III}-nitrogen bond. To the best of our knowledge this is the first time that such an insertion reaction has been observed.

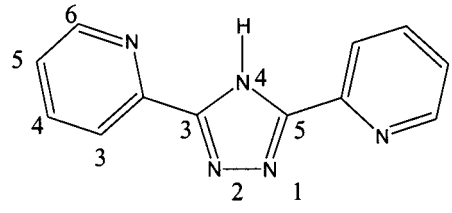

Figure 1. 3,5-bis(pyridin-2-yl)-1,2,4-triazole (Hbpt)

Results and Discussion

$[Rh^{III}$ bis(1,10-phenanthroline)$Cl_2]Cl$ was reacted with Hbpt in aqueous solution at pH 9. The product obtained was purified by column chromatography and precipitated

[a] National Centre for Sensor Research, School of Chemical Sciences, Dublin City University,
Dublin 9, Ireland
Fax: (internat.) + 353-1/700-5503
E-mail: johannes.vos@dcu.ie
[b] School of Chemical Sciences, Dublin City University,
Dublin 9, Ireland
Fax: (internat.) + 353-1/700-5503
E-mail: john.gallagher@dcu.ie
[c] Dipartimento di Chimica dell'Universita, Universita di Ferrara, 44100 Ferrara, Italy
Fax: (internat.) + 39-0532/240-709
E-mail: snf@unife.it

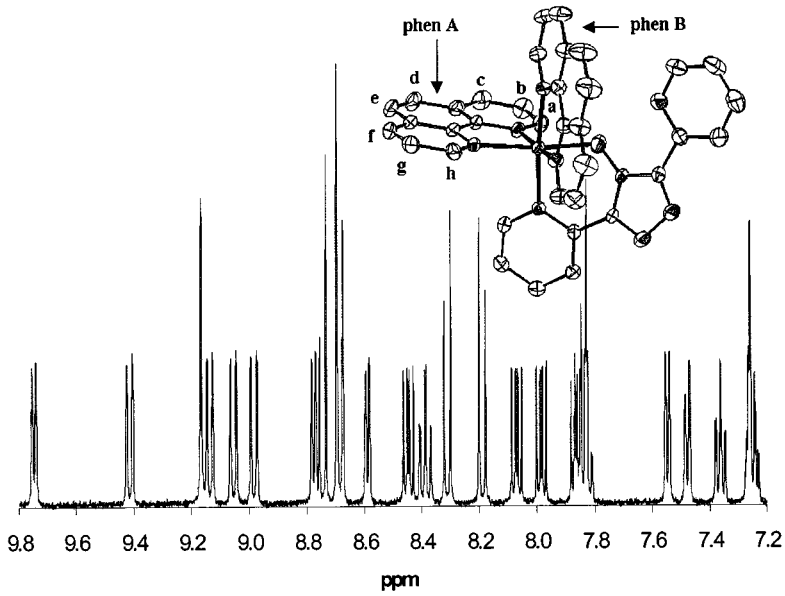

Figure 2. ^{1}H NMR spectrum $[Rh(phen)_2(Obpt)](PF_6)_2$ in $[D_6]$DMSO

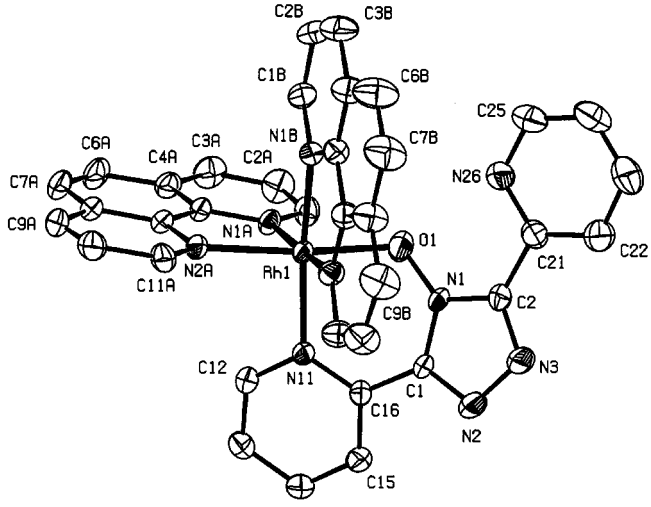

Figure 3. Molecular structure of the cation in $[Rh(phen)_2(Obpt)](PF_6)_2$; hydrogen atoms, counterions and the solvent molecules have been omitted for clarity

as a PF_6^- salt. NMR spectroscopy shows the presence of a single product (see Figure 2). Upon further recrystallisation of the product from acetonitrile/toluene (7:3) yellow needles were obtained. A single crystal X-ray investigation yielded the molecular structure, the cation of which is depicted in Figure 3. X-ray collection parameters are listed in Table 1 and selected bond lengths and angles are given in Table 2 and Table 3, respectively.

The most striking feature of the molecular structure is the presence of an oxygen atom between the metal centre and the triazole nitrogen atom. The rhodium centre is further surrounded by the two 1,10-phenanthroline ligands and the sixth coordination site is taken up by a pyridine ring of the bpt ligand. Two disordered PF_6^- counterions

Table 1. Crystallographic data for $[Rh(phen)_2(Obpt)](PF_6)_2\cdot0.767CH_3CN\cdot0.28H_2O$

Chem formula	$C_{36}H_{26}F_{12}N_9OP_2Rh\cdot0.767CH_3CN\cdot0.28H_2O$
Mol. wt.	1029.05
a (Å)	13.2334(12)
b (Å)	20.507(3)
c (Å)	16.0732(15)
β (°)	103.620(6)
Z	4
Volume (Å^3)	4239.3(8)
System, space group	monoclinic, $P2_1/m$
Crystal size	0.43 × 0.10 × 0.08
Temperature	297(2) K
F(000)	2059
Radiation, λ (Å)	Mo-K_α, 0.71073
D_{cald}, g·cm^{-3}	1.612
Abs coeff, μ (mm^{-1})	0.577
Abs corr T (min, max)	0.791, 0.958
θ range for data collection	2 to 26°
Reflections collected	8528
Unique, $>2\sigma(I)$	8164, 5460
Parameters	709
Restraints	288
R (F_o)	0.062
R_w (F_o)	0.149
Residual electron density	+0.76, −0.68

Table 2. Selected bond lengths (Å) for $[Rh(phen)_2(Obpt)](PF_6)_2\cdot0.767CH_3CN\cdot0.28H_2O$

Rh1−O1	2.016(4)	Rh1−N11	2.086(5)
Rh1−N1A	2.034(4)	Rh1−N2A	2.105(4)
Rh1−N2B	2.035(5)	N1−O1	1.406(6)
Rh1−N1B	2.039(5)	N1−C1	1.342(7)
		N1−C2	1.372(7)

Table 3. Selected bond angles (°) for $[Rh(phen)_2(Obpt)](PF_6)_2 \cdot 0.767CH_3CN \cdot 0.28H_2O$

O1−Rh1−N1A	91.5(2)	N1A−Rh1−N2B	174.2(2)
O1−Rh1−N2A	171.4(2)	N1A−Rh1−N1B	93.6(2)
O1−Rh1−N1B	88.2(2)	N1B−Rh1−N2B	81.4(2)
O1−Rh1−N2B	91.4(2)	N1B−Rh1−N11	174.8(2)
O1−Rh1−N11	87.2(2)	N1−O1−Rh1	110.1(3)
Rh1−O1−N1−C1	56.3(6)		

and partial site occupancy acetonitrile (0.767) and water solvent molecules (0.28) complete the crystal structure (not depicted). The Rh−O bond length is 2.016(4) Å, in the range expected for Rh−O bond lengths. For example, in the diacetyl monooxime Rh^{III} complex reported by Moszner et. al., typical Rh−O bond lengths are 2.028Å and 2.023Å.[12] The N−O bond length is 1.406(6) Å and typical of an N−O single bond. The presence of the oxygen atom causes a substantial *trans* effect. The Rh−N distance *trans* to the oxygen atom is 2.105(4) Å, which is about 0.07 Å longer than the other three rhodium-nitrogen distances. A number of other rhodium polypyridyl crystal structures have been reported. Paul et al. have reported Rh−N bond lengths of 1.990(5), 2.059(5) and 2.036(5) Å in a rhodium(II) complex with the ligand 2,4,6-tris(2-pyridyl)-1,3,5-triazine and bond lengths of 2.027(10), 2.031(10), 2.083(9) and 2.071(9) Å were found by Brewer et al. in the case of the rhodium(III) complex with the ligand 2,3-bis(2-pyridyl)quinoxaline.[13,14] The X-ray structure of a ruthenium(II) complex with the ligand Hbpt has also been reported.[15]

The NMR spectrum shown in Figure 2 clearly indicates the presence of only one species, indicative of the absence of linkage isomers. This is in contrast with the behaviour of most common triazole complexes.[16,17] 2-D COSY spectroscopic techniques were used to assign the ^1H resonances where possible. The doublets observed at $\delta = 9.75$ and 9.42 can be attributed to the protons at positions **a** and **c** of the phenanthroline ring **A** respectively. These resonances are downfield with respect to the resonances observed for the equivalent protons in the $[Rh(phen)_3]^{3+}$ complex and this can be attributed to the influence of the oxygen in the rhodium complex.[18] The source of the singlet at $\delta = 9.17$ has yet to be determined. Deuteration of the $[Rh(phen)_2(Obpt)](PF_6)_2$ is currently being undertaken in order to unambiguously assign all of the resonances.

The emission spectrum obtained at 77 K in a 4:1 ethanol/methanol glass for $[Rh(phen)_2(Obpt)](PF_6)_2$ can be seen in Figure 4. This structured emission, with maxima at 453 nm, 482 nm and 513 nm, is typical of ligand-centred (LC) phosphorescence of rhodium(III) phenanthroline complexes.[19] This indicates that the lowest LC excited state in this heteroleptic complex lies on the phen ligands.

An insertion of oxygen, as observed in this case, has not been reported previously. The only slightly related compound reported in the literature is a Rh^I complex with the ligand $bptNH_2$.[11] In the complex [Rh(NHbpt)(diolefin)], where the diolefin is for example 2,2,2-octatriene, NMR spectroscopy and elemental analysis suggest that an isoelectronic Rh−NH−N-triazole bond is formed. The mechanism responsible for the formation of $[Rh(phen)_2(Obpt)](PF_6)_2$ can at present only be tentatively formulated. The fact that the reaction described here is carried out in basic solution may indicate that a rhodium hydroxy intermediate is formed by replacement of the chloride atom by water and subsequent deprotonation [Equation (1)]. Interaction between the OH group and the triazole ring may then result in the formation of the N−O bond. In order to account for the oxidative nature of this step, a likely mechanism is the formation of an intermediate Rh^I complex [Equation (2)] which is subsequently reoxidised by oxygen [Equation (3)]. The overall reaction would then amount to a rhodium-mediated oxidation of the ligand by molecular oxygen [Equation (4)].

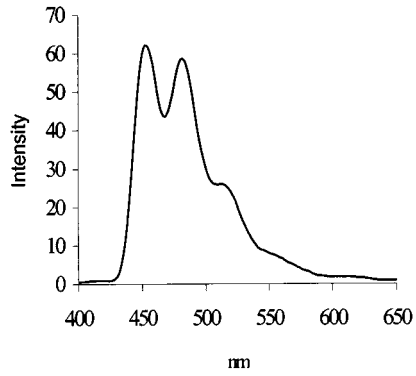

Figure 4. Emission spectra of $[Rh(phen)_2(Obpt)](PF_6)_2$ obtained in an ethanol/methanol 4:1 glass at 77 K

$$[Rh^{III}(phen)_2Cl_2]^+ + Hbpt + H_2O \rightarrow [Rh^{III}(phen)_2(OH)bpt]^+ + 2H^+ + 2Cl^- \quad (1)$$

$$[Rh^{III}(phen)_2(OH)bpt]^+ \rightarrow [Rh^{I}(phen)_2(Obpt)] + H^+ \quad (2)$$

$$[Rh^{I}(phen)_2(Obpt)] + 2H^+ + 1/2O_2 \rightarrow [Rh^{III}(phen)_2(Obpt)]^{2+} + H_2O \quad (3)$$

$$[Rh^{III}(phen)_2Cl_2]^+ + Hbpt + 1/2O_2 \rightarrow [Rh^{III}(phen)_2(Obpt)]^{2+} + 2Cl^- + H^+ \quad (4)$$

Interestingly no *N*-hydroxytriazoles have been reported in the literature. The formation of this N−O bond is therefore clearly dependent on the presence of the rhodium centre. Recently the formation of Rh^I−O−C bond via a Rh-hydroxy intermediate has been reported for the compound $[C_5(CH_3)_5]RhO(C_6F_4)CF_2]$.[20]

Conclusion

The reaction product reported upon reaction of $[Rh(phen)_2Cl_2]Cl$ and Hbpt is a very unusual one. In the complex obtained an oxygen atom has been inserted between the rhodium centre and the triazole ring. We are at present engaged in a systematic study of the interaction be-

tween rhodium polypyridyl centres and triazole type ligands. In this investigation we aim to further develop this chemistry and to determine the factors that control this unusual behaviour.

Experimental Section

Materials: Rhodium(III) chloride hydrate and 1,10-phenanthroline were purchased from Aldrich. $[Rh(1,10\text{-phenthroline})_2Cl_2]Cl$ and 3,5-bis(pyridin-2-yl)-1,2,4-triazole (Figure1) were prepared by previously reported procedures.[21,22]

Instrumentation: NMR spectra were obtained on a Bruker AC 400 MHz spectrometer. The peak positions are relative to TMS and the spectra were converted from their FID profiles using a Bruker WINNMR software package. Low temperature emission spectra were obtained at 77 K in a 4:1 ethanol/methanol glass using a Perkin−Elmer LS50B instrument. Elemental analysis on C, H and N was carried out at the Microanalytical Laboratory at University College Dublin (UCD) using an Exador analytical CE440.

Preparation of the Complex: Hbpt (0.3 mmol) was dissolved in H_2O at pH 9. $[Rh(phen)_2Cl_2]Cl$ (0.1 mmol) was then added and the reaction mixture was refluxed for 8 hours. Purification was carried out using a Sephadex C-25 column. Unreacted ligand was removed with distilled water and the product was eluted using 0.1 M NaCl. The complex was precipitated by the addition of a saturated aqueous solution of NH_4PF_6 to the required fraction. Yield: 0.033 g, 32%. Crystals were obtained by recrystallisation from a minimum amount of acetonitrile/toluene (7:3). ^1H NMR spectroscopy was carried in $[(CD_3)_2SO]$ and the resonances observed have been tentatively assigned as follows: **phenanthroline A:** δ = 9.75 (d, 1Ha), 8.45 (dd, 1Hb), 9.41 (d, 1Hc), 8.74 (d, 1Hd), 8.68 (d, 1He), 9.13 (d, 1Hf), 7.98 (dd, 1Hg), 8.59 (d, 1Hh); **phenanthroline B:** δ = 8.98 (d, 1Ha), 8.07 (dd, 1Hb), 8.78 (d, 1Hc), 8.31 (d, 1Hd), 8.19 (d, 1He); **bpt:** δ = 8.68 (d, 1H6), 8.39 (dd, 1H5), 7.36 (dd, 1H4), 7.48 (d, 1H3). It was not possible to assign the resonances at δ = 9.17 (s, 1 H), 9.05 (d, 1 H), 7.9−7.8 (m, 3 H), 7.55 (d, 1 H), 7.26 (m, 2 H) unambiguously. $[Rh(phen)_2(Obpt)](PF_6)_2{\cdot}H_2O$: calcd. C 42.83, H 2.60, N 12.49; found C 42.24, H 2.63, N 12.97. It should be noted that the sample for elemental analysis was recrystallised from ethanol/water.

CCDC-168699 contains the supplementary crystallographic data for this paper. These data can be obtained free of charge at www.ccdc.cam.ac.uk/conts/retrieving.html [or from the Cambridge Crystallographic Data Centre, 12, Union Road, Cambridge CB2 1EZ, UK; fax: (internat.) +44-1223/336-033; E-mail: deposit@ccdc.cam.ac.uk].

Acknowledgments

The authors thank the EU under the TMR programme for financial assistance under contract CT96-0076.

[1] V. Balzani, A. Juris, M. Venturi, S. Campagna, S. Serroni, *Chem. Rev.* **1996**, *96*, 759−833.
[2] J.-P. Sauvage, J.-P. Collin, J.-C. Chambron, S. Guillerez, C. Coudret, V. Balzani, F. Barigelletti, L. De Cola, L. Flamigni, *Chem. Rev.* **1994**, *94*, 993−1019.
[3] M. T. Indelli, C. A. Bignozzi, A. Harriman, J. R. Schnoonover, F. Scandola, *J. Am. Chem. Soc.* **1994**, *116*, 3768−3779.
[4] L. Flamigni, F. Barigelletti, N. Armaroli, J-P. Collin, I. M. Dixon, J.-P. Sauvage, J. A. G. Williams, *Coord. Chem. Rev.* **1999**, *190−192*, 671−682.
[5] R. Hage, J. G. Haasnoot, H. A Nieuwenhuis, J. Reedijk, D. J. A. De Ridder, J. G. Vos, *J. Am. Chem. Soc.* **1990**, *112*, 9245−9251.
[6] J. G. Haasnoot, *Coord. Chem. Rev.* **2000**, *200−202*, 131−185.
[7] J. H. van Diemen, R. Hage, J. G. Haasnoot, H. E. B. Lempers, J. Reedijk, J. G. Vos, L. De Cola, F. Barigelletti, V. Balzani, *Inorg. Chem.* **1992**, *31*, 3518−3522.
[8] J. H. van Diemen, J. G. Haasnoot, R. Hage, J. Reedijk, J. G. Vos, R. J. Wang, *Inorg. Chem.* **1991**, *30*, 4038−4043.
[9] G. Calogero, G. Giuffrida, S. Serroni, V. Ricevuto, S. Campagna, *Inorg. Chem.* **1995**, *34*, 541−545.
[10] M. P. Garcia, M. Martin, L. A. Oro, *Inorg. Chim. Acta* **1992**, *191*, 221−225.
[11] M. P. Garcia, J. A. Manero, L. A. Oro, M. C. Apreda, F. H. Cano, C. Foces-Foces, J. G. Haasnoot, R. Prins, J. Reedijk, *Inorg. Chim. Acta* **1986**, *122*, 235−241.
[12] M. Moszner, T. Glowiak, M. Kubiak, J. J. Ziolkowski, G. Costa, C. Tavagnacco, *Polyhedron* **1997**, *16*, 307−313.
[13] P. Paul, B. Tyagi, A. K. Bilakhiya, M. M. Bhadbhade, E. Suresh, *J. Chem. Soc., Dalton Trans.* **1999**, 2009−2014.
[14] S. C. Rasmussen, M. M. Richter, E. Yi, H. Place, K. Brewer, *Inorg. Chem.* **1990**, *29*, 3926−3932.
[15] R. Hage, R. A. G. de Graaff, J. G. Haasnoot, J. P. Turkenburg, J. Reedijk, J. G. Vos, *Acta Crystallogr., Sect. C* **1989**, *45*, 381−383.
[16] B. E. Buchanan, R. Wang, J. G. Vos, R. Hage, J. G. Haasnoot, J. Reedijk, *Inorg. Chem.* **1990**, *29*, 3263−3265.
[17] B. E. Buchanan, E. McGovern, P. Harkin, J. G. Vos, *Inorg. Chim. Acta* **1988**, *154*, 1−4.
[18] H. M. Burke, J. G. Vos, to be published.
[19] M. T. Indelli, F. Scandola, *Inorg. Chem.* **1990**, *29*, 3056−3058.
[20] R. P. Hughes, D. C. Lindner, L. M. Liable-Sands, A. L Rheingold, *Organometallics* **2001**, *20*, 363−366.
[21] P. M. Gidney, R. D. Gillard, B. T. Heaton, *J. Chem. Soc., Dalton Trans.* **1972**, 2621−2628.
[22] J. F. Geldard, F. Lions, *J. Org. Chem.* **1965**, *30*, 318−319.

Received September 12, 2001
[I01357]

Synthesis of Organouranium(IV) Triflates from $U(OTf)_4$ or from Alkyl or Amide Precursors

Jean Claude Berthet,*[a] Martine Nierlich,[a] and Michel Ephritikhine[a]

Keywords: Uranium / Triflate complexes / Cyclopentadienyl complexes / Cyclooctatetraenyl complexes

The uranium(IV) triflate $[U(OTf)_4]$ (**1**) (OTf = OSO_2CF_3) gives stable adducts with Lewis bases, such as $[U(OTf)_4(py)]$ (**2**) (py = pyridine). The crystal structure of a solvate of $[U(OTf)_4(OPPh_3)_3]$ (**3**), which exhibits a bidentate OTf group, has been determined. Substitution of the triflate ligands of **1** with $LiNEt_2$, Kacac (acac = MeCOCHCOMe), KCp (Cp = η-C_5H_5), and K_2COT (COT = η-C_8H_8) has led to the formation of $[U(NEt_2)_4]$, $[U(acac)_4]$, $[U(Cp)_3(OTf)]$ (**4**), and $[U(COT)(OTf)_2(py)]$ (**5**), respectively. However, the bis(cyclopentadienyl) compounds $[U(Cp^*)_2(OTf)_2]$ (**6**) (Cp^* = η-C_5Me_5) and $[U(Cp)_2(OTf)_2(py)]$ (**7**) could not be prepared from **1**. Complexes **4**–**7** have been isolated in good yields from the protonolysis reactions of the corresponding alkyl or amide precursors by means of pyridinium triflate. Compound **5** has also been prepared by treating $[U(COT)_2]$ with either [pyH][OTf] or **1** in pyridine. The crystal structures of $[U(Cp)_2(OTf)_2(py)_2]$ (**8**) and $[U(COT)(OTf)_2(OPPh_3)_2]\cdot0.5py$ (**9**) have been determined.

Introduction

The growing interest in metal triflates (trifluoromethanesulfonates), which proved to be effective Lewis acid catalysts in a number of organic reactions[1] and valuable precursors in inorganic and organometallic syntheses,[2] prompted us to study the preparation and properties of such complexes of uranium. In a preliminary communication,[3] we described the synthesis of $[U(OTf)_4(py)]$ (OTf = OSO_2CF_3; py = pyridine) and some organouranium(IV) triflates using the pyridinium salt [pyH][OTf] as a novel reagent for the protonolysis of U−C and U−N bonds. Following these initial results, we found that the base-free uranium(IV) triflate $[U(OTf)_4]$ (**1**) could be prepared in a more expeditious and simple way by treatment of U, UH_3, UCl_3, or UCl_4 with pure triflic acid.[4] The uranium(III) triflate $[U(OTf)_3]$ has also been obtained in a good yield by performing the reactions with U, UH_3, or UCl_3 at a lower temperature. These large-scale preparations of **1** allowed us to consider it as a possible good precursor for the syntheses of the derivatives. Here we present some reactions of $[U(OTf)_4]$, with special attention to those leading to organouranium(IV) triflate complexes. These preparations are compared with the alternative synthetic routes starting from the parent chloride, alkyl or amide compounds. The X-ray crystal structures of $[U(OTf)_4(OPPh_3)_3]\cdot0.5py\cdot0.5Et_2O$, $[U(Cp)_2(OTf)_2(py)_2]$ (Cp = η-C_5H_5), and $[U(COT)(OTf)_2(OPPh_3)_2]\cdot0.5py$ (COT = η-C_8H_8) are also described.

[a] Service de Chimie Moléculaire, DSM, DRECAM, CNRS URA 331, CEA Saclay,
91191 Gif sur Yvette, France
Fax: (internat.) + 33-1/69086640
E-mail: berthet@drecam.cea.fr

Results and Discussion

Reactions of $[U(OTf)_4]$ − X-ray Crystal Structure of $[U(OTf)_4(OPPh_3)_3]\cdot0.5py\cdot0.5Et_2O$

The uranium(IV) triflate $[U(OTf)_4]$ (**1**) is a strong Lewis acid and is quite soluble in coordinating solvents giving stable adducts. Thus, $[U(OTf)_4(py)]$ (**2**) was isolated from the reaction of the metallacycle $[U(N\{SiMe_3\}\{CH_2SiMe_2\})(N\{SiMe_3\}_2)_2]$ with [pyH][OTf] in pyridine [Equation (1)]. It is worth noting that similar treatment of $[U(NEt_2)_4]$ gave a mixture of unidentified amide products; this difference is not understood as the NEt_2 group, which is sterically less demanding and has a more basic character than $N(SiMe_3)_2$, is expected to be more easily protonated.[5]

$$[U(N\{SiMe_3\}\{CH_2SiMe_2\})(N\{SiMe_3\}_2)_2] + 4\,[pyH][OTf] \xrightarrow{py} [U(OTf)_4(py)]\ (\mathbf{2}) + 3\,HN(SiMe_3)_2 \quad (1)$$

In the presence of 2 equiv. of $OPPh_3$, **1** was transformed into $[U(OTf)_4(OPPh_3)_2]$ in pyridine or dimethoxyethane,[4] while green crystals of a solvate of $[U(OTf)_4(OPPh_3)_3]$ (**3**) were obtained by slow diffusion of diethyl ether into a pyridine solution of **1** and excess $OPPh_3$. Complex **3** is the first actinide tetratriflate to have been crystallographically characterized. Such metal complexes with four coordinated OTf ligands are not common and to the best of our knowledge, only the crystal structures of the neutral chromium compound $[Cr(OTf)_4(C_6H_4\{NH_2\}_2)]$,[6] and of the anionic species $[Fe(OTf)_4]^{2-}$ [7] and $[Na(OTf)_4]^{3-}$ [8] have been determined. The crystal structure of **3** is shown in Figure 1; selected bond lengths and angles are listed in Table 1. The

 © WILEY-VCH Verlag GmbH, 69451 Weinheim, Germany, 2002 1434−1948/02/0404−0850 $ 17.50+.50/0 *Eur. J. Inorg. Chem.* **2002**, 850−858

uranium atom is surrounded by eight oxygen atoms in a dodecahedral arrangement defined by the two trapezia O(1)O(2)O(13)O(14) and O(3)O(4)O(7)O(10) intersecting at an angle of 90.4(4)°. The most salient feature of the structure is the presence of the η^2-O,O′ triflate ligand. This mode of ligation of the OTf group remains rare in d-transition metal complexes,[9] as well as in the f-block element compounds where only the two trivalent lanthanum and uranium complexes $[La(OTf)_2(HMPA)_4][OTf]$ (HMPA = hexamethylphosphoramide)[10] and $[U(OTf)_2(OPPh_3)_4][OTf]$[4] exhibit such a bidentate triflate ligand in their crystal structure. The U−O(η^2-OTf) bond lengths of 2.563(3) and 2.593(3) Å are ca 0.2 Å longer than the three U−O(η^1-OTf) distances which average 2.39(2) Å. Such a difference between the metal−oxygen bond lengths of the mono- and bidentate OTf ligands has been previously observed, in particular in the aforementioned uranium(III) compound.[4] The lengths of the U−O($OPPh_3$) bonds have an average value of 2.26(7) Å.

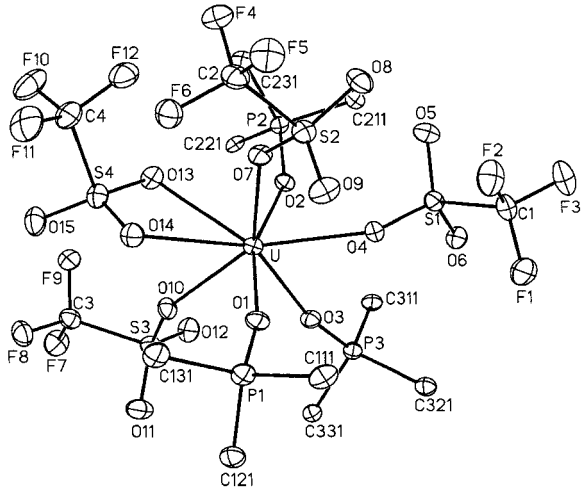

Figure 1. X-ray crystal structure of $[U(OTf)_4(OPPh_3)_3]$ with displacement ellipsoids at the 30% probability level; for clarity, only the *ipso*-carbon atoms of the phenyl rings are represented

Table 1. Selected bond lengths [Å] and angles [°] for $[U(OTf)_4(OPPh_3)_3]$

U−O(1)	2.207(3)	U−O(2)	2.252(3)
U−O(3)	2.318(3)	U−O(4)	2.403(3)
U−O(7)	2.371(3)	U−O(10)	2.418(3)
U−O(13)	2.563(3)	U−O(14)	2.593(3)
O(1)−U−O(2)	161.1(1)	O(3)−U−O(4)	74.9(1)
O(7)−U−O(10)	138.3(1)	O(13)−U−O(14)	54.5(1)

Homoleptic triflate complexes, like their halide counterparts, have been commonly used as starting materials for the synthesis of inorganic and organometallic derivatives;[2] in this context, it was of interest to evaluate the potential of **1**. The triflate groups of **1** can easily be substituted with anionic ligands (Scheme 1). For example, treatment of **1** with a slight excess of $LiNEt_2$ or Kacac (acac = MeCOCHCOMe) in tetrahydrofuran (THF) gave $[U(NEt_2)_4]$ or $[U(acac)_4]$ in almost quantitative yields (NMR experiments). In these syntheses, **1** proved to be as good a starting material as UCl_4.

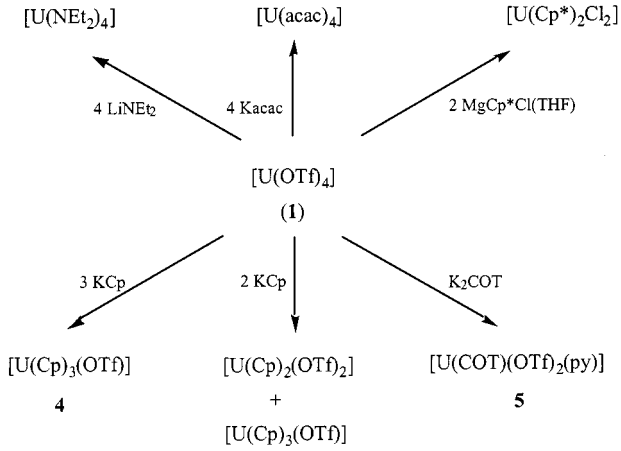

Scheme 1. Reactions of $[U(OTf)_4]$

Attempts to prepare new organouranium(IV) triflates from **1** have been moderately successful. Reaction of **1** with 2 equiv. of KCp* in THF, pyridine, or toluene gave some unidentified products, while its treatment with MgCp*Cl(THF) in refluxing toluene afforded only the dichloride $[U(Cp^*)_2Cl_2]$ ($Cp^* = \eta$-C_5Me_5).[11] Tris(cyclopentadienyl)-uranium(IV) triflate $[U(Cp)_3(OTf)]$ (**4**) was synthesized in an almost quantitative yield by treatment of **1** with 3 equiv. of KCp in THF, followed by extraction with diethyl ether. However, a similar reaction of **1** with 2 equiv. of KCp afforded a mixture of $[U(Cp)_3(OTf)]$ and $[U(Cp)_2(OTf)_2]$ in a ratio of 73:27. Thus, pure bis(cyclopentadienyl)uranium(IV) compounds $[U(Cp^*)_2(OTf)_2]$ and $[U(Cp)_2(OTf)_2]$ could not be obtained by substitution of the triflate ligands of **1**.

Addition of 1 equiv. of $K_2C_8H_8$ to **1** in pyridine led to the immediate precipitation of a green powder, presumably $[U(COT)_2]$. The reaction mixture was heated under reflux for 15 h affording the (cyclooctatetraenyl)uranium(IV) triflate $[U(COT)(OTf)_2(py)]$ (**5**). In agreement with this observation, compound **5** was synthesized in an almost quantitative yield by direct comproportionation of **1** and $[U(COT)_2]$ in pyridine [Equation (2)]. Most notably, this ligand exchange reaction proceeded much less rapidly in THF. Such a remarkable solvent effect was also observed in the synthesis of $[U(COT)(BH_4)_2]$ from $[U(COT)_2]$ and $[U(BH_4)_4]$, which was effective in toluene but not in THF.[12] These results led us to re-examine the comproportionation reaction of UCl_4 and $[U(COT)_2]$ which, in refluxing pyridine, was found to readily afford the (cyclooctatetraenyl)uranium(IV) dichloride $[U(COT)Cl_2(py)_2]$ [Equation (3)].[13] It is ironical that this complex could so easily be obtained in pyridine whilst its synthesis in THF was difficult. This was a major obstacle in the development of the chemistry of mono(cyclooctatetraenyl) uranium compounds for a long time.[13] However, this situation favored the design of several $[U(COT)X_2]$ complexes (X = I,[14] BH_4,[12] NEt_2[15]) which were useful precursors for the synthesis of alkyl,[14b] alkoxide,[16] or thiolate[17] derivatives.

$$[U(OTf)_4] + [U(COT)_2] \xrightarrow{py} 2\,[U(COT)(OTf)_2(py)] \quad (2)$$
(1) (5)

$$UCl_4 + [U(COT)_2] \xrightarrow{py} 2\,[U(COT)Cl_2(py)_2] \quad (3)$$

Synthesis of Organouranium(IV) Triflates from Alkyl or Amide Precursors − X-ray Crystal Structures of $[U(Cp)_2(OTf)_2(py)_2]$ and $[U(COT)(OTf)_2(OPPh_3)_2]\cdot 0.5py$

The lack of success in the preparation of $[U(Cp^*)_2(OTf)_2]$ and $[U(Cp)_2(OTf)_2]$ from **1** forced us to envisage other synthetic routes. We first tried to prepare these complexes by treating chloride, alkyl or amide precursors with classical reagents like AgOTf, Me_3SiOTf, or TfOH that proved to be effective in the synthesis of main-group and d-transition metal triflates.[2] While reaction of $[U(Cp)_3X]$ (X = Cl, *n*Bu) with AgOTf in THF or toluene cleanly afforded **4**, similar treatment of $[U(Cp^*)_2X_2]$ (X = Cl, Me, NMe_2) failed to give any tractable product, and polymerization of THF was sometimes observed. Compounds **4** and **5** were prepared in quantitative yields by immersing the parent chlorides in pure Me_3SiOTf at 110 °C, but the same reaction with $[U(Cp^*)_2Cl_2]$ gave a mixture of unidentified products. Reactions of $[U(Cp)_3(NEt_2)]$ or $[U(Cp^*)_2Me_2]$ with stoichiometric amounts of triflic acid in benzene effectively produced the expected compounds **4** and $[U(Cp^*)_2(OTf)_2]$ (**6**). The X-ray crystal structures of the Lewis base adducts $[U(Cp)_3(OTf)(CN\textit{t}Bu)]$ and $[U(Cp^*)_2(OTf)_2(H_2O)]$ have been described in the preliminary communication.[3] However, difficulties were encountered when the above reactions were performed on a preparative scale; products resulting from protonation of the cyclopentadienyl ligands were also formed in variable yields, apparently depending on the concentration of the acid. Similar observations have previously been seen in the reaction of $[Zr(Cp)_4]$ and triflic acid.[2e]

The pyridinium triflate was then considered as a milder and more selective acidic reagent than triflic acid. Its use in the synthesis of uranium triflates was inspired by our previous studies on the protonolysis reactions of U−C and U−N bonds by means of the ammonium salt $[NHEt_3][BPh_4]$, which constitute an efficient route to cationic complexes.[18] Treatment of $[U(Cp)_3(NEt_2)]$ with [pyH][OTf] afforded **4** which was isolated with a 93% yield; **4** was similarly obtained from the alkyl precursor $[U(Cp)_3\textit{n}Bu]$. This synthetic method was found to have a general applicability, since **5** was prepared in a 92% yield from $[U(COT)(NR_2)_2]$ (R = Et, $SiMe_3$) and, most notably, the bis(cyclopentadienyl) complexes **6** and $[U(Cp)_2(OTf)_2(py)]$ (**7**) were obtained from $[U(Cp^*)_2X_2]$ (X = Me, NMe_2) and $[U(Cp)_2(NEt_2)_2]$ in a 78 and 60% yield, respectively. These syntheses, depicted in Equations (4) to (7), were reproducible.

$$[U(Cp)_3(NEt_2)] + [pyH][OTf] \xrightarrow{THF} [U(Cp)_3(OTf)] + HNEt_2 + py \quad (4)$$
(4)

$$[U(COT)(NR_2)_2] + 2\,[pyH][OTf] \xrightarrow{THF} [U(COT)(OTf)_2(py)] + 2\,HNR_2 + py \quad (5)$$
R = Et, $SiMe_3$ (5)

$$[U(Cp^*)_2Me_2] + 2\,[pyH][OTf] \xrightarrow{THF} [U(Cp^*)_2(OTf)_2] + 2\,CH_4 + 2\,py \quad (6)$$
(6)

$$[U(Cp)_2(NEt_2)_2] + 2\,[pyH][OTf] \xrightarrow{THF} [U(Cp)_2(OTf)_2(py)] + 2\,HNEt_2 + py \quad (7)$$
(7)

The synthesis of **7** from $[U(Cp)_2(NEt_2)_2]$ [Equation (7)] indicates that the formation of the tris(cyclopentadienyl) compound **4** as the major product in the reaction of **1** with 2 equiv. of KCp most likely occurs as a result of kinetic factors, and is not due to the decomposition of **7**, which is stable in coordinating solvents. This behavior of **7** is in contrast with that of the Lewis base adducts of $[U(Cp)_2Cl_2]$, which could not be isolated because of their rapid rearrangement into the equimolar mixture of $[U(Cp)_3Cl]$ and $[U(Cp)Cl_3L_2]$ (L = Lewis base or solvent).[19] As this disproportionation reaction was explained in terms of the great electron-rich nature of $[U(Cp)_2Cl_2L_x]$,[20] the stability of **7**, like that of the cationic complex $[U(Cp)_2(NEt_2)(THF)_x]^+$,[18a][18c] can clearly be related to the greater Lewis acidity of the metal center.

The acidic reagent [pyH][OTf] was also effective in the protonation of the aromatic ligand in $[U(COT)_2]$, since **5** was quantitatively obtained in refluxing THF or pyridine [Equation (8)]. Such syntheses of mono(cyclooctatetraenyl)-uranium complexes by protonolysis of uranocene are not common; they are limited to the preparation of $[U(COT)(acac)_2]$ by reaction of $[U(COT)_2]$ with Hacac,[21] and to the non-selective formation of $[U(COT)Cl_2(THF)_x]$ by treatment of $[U(COT)_2]$ with HCl.[13] It is likely that the driving force of reaction (8) is the formation of a uranium−oxygen σ-bond, since $[U(COT)_2]$ failed to react with $[pyH][BPh_4]$ to give the dication $[U(COT)(THF)_x]^{2+}$.[22] A reaction was not observed between $[U(COT)_2]$ and NaOTf, while the uranocene was easily transformed into the anion $[U(COT)(O\textit{i}Pr)_3]^-$ in the presence of NaO*i*Pr;[23] this difference would simply reflect the weaker nucleophilic character of the triflate ligand.

$$[U(COT)_2] + 2\,[pyH][OTf] \xrightarrow{py\ or\ THF} [U(COT)(OTf)_2(py)] + C_8H_{10} \quad (8)$$
(5)

The pyridinium triflate thus proved to be very useful in the synthesis of organouranium(IV) triflates by protonolysis of alkyl or amide precursors. In addition to its selectivity and efficiency, this commercial reagent presents many advantages over triflic acid since it can be used in a greater variety of organic solvents, is not corrosive, can be stored for a long time and is easy to handle. Trialkylammonium triflates can also be used in such protonolysis reactions, as shown recently by the synthesis of (cyclopentadienyl)zirconium triflates by treatment of $[Zr(Cp)_4]$ with $[NBu_3H][OTf]$.[2e]

Compounds **2**−**7** were characterized by elemental analyses and ^1H NMR spectroscopy. Brown crystals of $[U(Cp)_2(OTf)_2(py)_2]$ (**8**) and orange crystals of a pyridine solvate of $[U(COT)(OTf)_2(OPPh_3)_2]$ (**9**) were obtained by slow diffusion of diethyl ether into a pyridine solution of **7**, or into a pyridine solution of **5** and excess $OPPh_3$. These crystals were suitable for X-ray diffraction analysis.

Other than the uranium borohydride $[U(Cp)_2(BH_4)_2]$[24] and the thorium complexes $[Th(Cp)_2X_2(DMPE)]$ (X = Cl, Me,[25a] CH_2Ph;[25b] DMPE = $Me_2PCH_2CH_2PMe_2$), **8** is one of the few mononuclear bis(cyclopentadienyl)actinide(IV) compounds to have been crystallographically characterized. The crystal structure is shown in Figure 2 and selected bond lengths and angles are listed in Table 2. The stereochemistry of this six-coordinate complex (if the Cp ring centroid is considered as occupying a single coordination site) strongly resembles that of the thorium derivatives $[Th(Cp)_2X_2(DMPE)]$; the two *cis* pyridine ligands can be thought of as replacing the bidentate phosphane ligand and the two *trans* monodentate triflate ligands can be thought of as replacing the X groups. The geometrical parameters of the $U(Cp)_2(py)_2$ and $Th(Cp)_2(DMPE)$ fragments are very similar, with the ring centroid−metal−ring centroid angles equal to 113.8(1) and 115(1)° (mean value) and the N(1)−U−N(2) and P−Th−P angles equal to 65.5(1) and 64.3(2)° (mean value), respectively. However, the O(1)−U−O(4) angle of 153.1(1)° is much greater than the C−Th−C or Cl−Th−Cl angles which average 140(1)°; this difference most likely reflects the greater steric size of the triflate ligands. The U−C bond lengths are unexceptional, with an average value of 2.73(4) Å, and the U−N bond lengths of 2.614(5) and 2.685(5) Å compare with those in $[U(SiPr)_2I_2(py)_3]$[26] and $[U(COT)Cl_2(py)_2]$[13] [2.56(9) and 2.64(1) Å, respectively]. The U−O(1) and U−O(4) distances [2.395(4) and 2.385(4) Å, respectively] are similar to those found in the other uranium(IV) triflate compounds (vide infra).

Table 2. Selected bond lengths [Å] and angles [°] for $[U(Cp)_2(OTf)_2(py)_2]$

U−O(1)	2.395(4)	U−O(4)	2.385(4)
U−N(2)	2.685(5)	U−Cp(1)[a]	2.454(5)
U−N(1)	2.614(5)	U−Cp(2)[a]	2.466(5)
O(1)−U−O(4)	153.1(1)	N(1)−U−N(2)	65.5(1)
Cp(1)−U−Cp(2)	113.8(1)	Cp(1)−U−N(1)	155.5(1)
Cp(2)−U−N(2)	155.3(1)	Cp(1)−U−O(1)	94.1(1)
Cp(2)−U−O(1)	99.3(1)	Cp(1)−U−O(4)	98.5(1)
Cp(2)−U−O(4)	97.1(1)		

[a] Cp(1) and Cp(2) are the centroids of the C(1)−C(5) and C(6)−C(10) cyclopentadienyl rings.

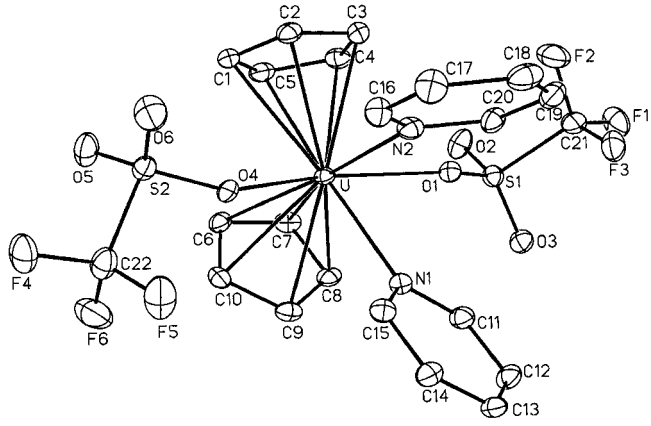

Figure 2. X-ray crystal structure of $[U(Cp)_2(OTf)_2(py)_2]$ with displacement ellipsoids at the 30% probability level

The crystal structure of one of the two independent and identical molecules of **9** is shown in Figure 3, and selected bond lengths and angles are listed in Table 3. The complex adopts a perfect square-pyramidal configuration, if the COT ligand is considered to be monodentate. The square base is defined by the oxygen atoms of the two $OPPh_3$ and the two monodentate OTf ligands, which are mutually in the *trans* positions; in the quadrilateral O(1)O(4)O(1′)O(4′), the O(1)−O(4) and O(1)−O(4′) distances are 2.923(4) and 2.763(4) Å, respectively, and the angles O(4)−O(1)−O(4′) and O(1)−O(4)−O(1′) have a value of 88.3(4) and 91.6(4)°, respectively. The square base is almost parallel to the planar COT ring, with a dihedral angle of 1.8(4)°, and the two planes are perpendicular to the two-fold axis. The U atom is 1.202(4) and 1.957(4) Å away from the square base and the COT ring, respectively. The COT ligation is similar to that found in uranocene and other mono(cyclooctatetraenyl)uranium(IV) compounds, with an average U−C bond length of 2.66(2) Å.[5a,13,27] The U−O($OPPh_3$) distances of 2.304(4) Å are unexceptional and the U−O(OTf) distances of 2.433(4) Å are within the range of the U−O bond lengths found in uranium(IV) monodentate triflates. These distances, which are equal to 2.371(3), 2.404(3) and 2.418(3) Å in $[U(OTf)_4(OPPh_3)_3]$ (vide supra), 2.36(1) and 2.40(1) Å in $[U(Cp^*)_2(OTf)_2(H_2O)]$,[3] 2.395(4) and 2.385(4) Å in $[U(Cp)_2(OTf)_2(py)_2]$ (vide supra), and 2.485(9) Å in $[U(Cp)_3(OTf)(NCtBu)]$,[3] are significantly longer than the typical U−O bond length of the alkoxide ligand (2.0−2.3 Å),[28] thus indicating the much lower nucleophilic character of the OTf group. However, no dissociation and substitution of the triflate ligands were found to occur in these uranium(IV) compounds, even in the presence of strongly coordinating ligands like $OPPh_3$. In particular, it is worth noting that such a dissociation was not observed in $[U(OTf)_4(OPPh_3)_3]$, in contrast to the U^{III} derivative $[U(OTf)_2(OPPh_3)_4][OTf]$ which is composed of discrete

cation−anion pairs in the solid state.[4] These features indicate that the uranium triflate bond is not as weak as is expected.

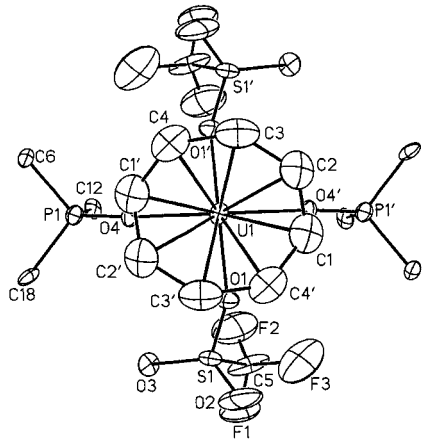

Figure 3. X-ray crystal structure of one of the two independent molecules of $[U(COT)(OTf)_2(OPPh_3)_2]$ with displacement ellipsoids at the 30% probability level; view along the two-fold axis; for clarity, only the *ipso*-carbon atoms of the phenyl rings are represented; atoms labeled prime are related to the non-labeled ones by the two-fold axis (symmetry code: 0.75 − *x*, 1.75 − *y*, *z*)

Table 3. Selected bond lengths [Å] and angles [°] for $[U(COT)(OTf)_2(OPPh_3)_2]$

U(1)−O(1)[a]	2.382(4)	U(2)−O(5)[a]	2.433(4)
U(1)−O(4)	2.304(4)	U(2)−O(8)	2.296(4)
U(1)−COT[b]	1.957(4)	U(2)−COT	1.938(4)
O(1)−U(1)−O(1′)[c]	117.8(2)	O(5)−U(2)−O(5′)	117.4(2)
O(4)−U(1)−O(4′)	118.7(2)	O(8)−U(2)−O(8′)	116.5(2)
COT−U(1)−O(1)	121.2(2)	COT−U(2)−O(5)	121.3(2)
COT−U(1)−O(4)	120.7(2)	COT−U(2)−O(8)	121.7(2)

[a] The corresponding values in the two independent molecules [U(1) and U(2)] are given. [b] COT is the centroid of the cyclooctatetraenyl ring. [c] Atoms labeled prime are related to the non-labeled ones by the two-fold axis.

Conclusion

The uranium(IV) triflate $[U(OTf)_4]$ (**1**) can be considered, like UCl_4, as a useful starting material for the synthesis of uranium complexes. We think that the preparation of **1**, although requiring the use of triflic acid, is more convenient and less hazardous than that of UCl_4 which necessitates the handling of harmful and volatile chlorinating agents.[29] However, there are some limitations associated with the use of **1** for the synthesis of organometallic compounds since the bis(cyclopentadienyl) complexes $[U(Cp^*)_2(OTf)_2]$ (**6**) and $[U(Cp)_2(OTf)_2(py)]$ (**7**) could not be obtained by substitution of the triflate ligands. These compounds, as well as $[U(Cp)_3(OTf)]$ (**4**) and $[U(COT)(OTf)_2(py)]$ (**5**), the most representative examples of organouranium(IV) triflates, were prepared in good yields by protonolysis of the corresponding alkyl or amide precursors by means of pyridinium triflate. This synthetic method appears to have a general applicability, and [pyH][OTf] is a practical, effective and selective reagent which can be favorably used in place of TfOH or AgOTf. Of special interest is the synthesis of **5**, which was alternatively prepared by treatment of $[U(COT)_2]$ with either [pyH][OTf] or $[U(OTf)_4]$; the solvent plays a major role in the comproportionation reactions of $[U(COT)_2]$ and UX_4 (X = OTf, Cl), which were found to occur easily in pyridine. These results provide new and convenient findings for the chemistry of monocyclooctatetraenyl uranium compounds.

Experimental Section

General: All preparations were carried out under argon (less than 2 ppm of oxygen and water) using standard Schlenk vessel and vacuum-line techniques or in a glove box. Solvents were thoroughly dried and deoxygenated by standard methods and distilled before use. $[D]_8$THF was dried with Na/K alloy. The ^{1}H NMR spectra were recorded with a Bruker DPX 200 instrument and were referenced internally using the residual protio solvent resonances relative to tetramethylsilane (δ = 0). Elemental analyses were performed by Analytische Laboratorien at Lindlar (Germany). TfOH and Me_3SiOTf (Aldrich) were distilled before use, AgOTf (Aldrich) was used without purification, and the white powder of [pyH][OTf] was obtained by addition of pyridine to a solution of TfOH in diethyl ether. The uranium compounds UCl_4,[29] $[U(OTf)_4]$,[4] $[U(NEt_2)_4]$,[30] $[U(N\{SiMe_3\}\{CH_2SiMe_2\})(N\{SiMe_3\}_2)_2]$,[31] $[U(Cp)_3X]$ (X = Cl,[32] *n*Bu,[33] NEt_2[34]), $[U(Cp^*)_2X_2]$ (X = Cl,[11] Me,[35] NMe_2[36]), $[U(Cp)_2(NEt_2)_2]$,[37] $[U(COT)_2]$,[38] and $[U(COT)(NR_2)_2]$ (R = Et,[18c] $SiMe_3$[39]) were synthesized as previously reported.

Syntheses of the Complexes

$[U(OTf)_4(py)]$ (2): A 100-mL round-bottom flask was charged with $[U(N\{SiMe_3\}\{CH_2SiMe_2\})(N\{SiMe_3\}_2)_2]$ (250 mg, 0.35 mmol) and [pyH][OTf] (319.1 mg, 1.39 mmol), and pyridine (20 mL) was condensed into it under vacuum at −78 °C. The reaction mixture was heated for 20 h at 110 °C. After filtration, the volume of the green solution was reduced to 10 mL, and addition of pentane or diethyl ether (30 mL) led to the precipitation of a green powder of **2** which was filtered off, washed with diethyl ether and dried under vacuum (244 mg, 76%). ^{1}H NMR (200 MHz, $[D_8]$THF): δ = 7.3, 7.85, and 8.8 (py). $C_9H_5F_{12}NO_{12}S_4U$ (913): calcd. C 11.83, H 0.55, N 1.55; found C 12.07, H 0.72, N 1.59.

$[U(NEt_2)_4]$: An NMR tube was charged with $[U(OTf)_4]$ (10.0 mg, 0.012 mmol) and $LiNEt_2$ (3.9 mg, 0.049 mmol) in $[D_8]$THF (0.4 mL). The tube was immersed in an ultrasound bath (80 W, 40 kHz) for 1.5 h, and the spectrum showed the quantitative formation of $[U(NEt_2)_4]$.

$[U(acac)_4]$: An NMR tube was charged with $[U(OTf)_4]$ (10.0 mg, 0.012 mmol) and Kacac (6.6 mg, 0.048 mmol) in $[D_8]$THF (0.4 mL). The tube was immersed in an ultrasound bath (80 W, 40 kHz) for 30 min, and the spectrum showed the quantitative formation of $[U(acac)_4]$.

$[U(Cp)_3(OTf)]$ (4)

From $[U(Cp)_3(NEt_2)]$ and [pyH][OTf]: A 50-mL round-bottom flask was charged with $[U(Cp)_3(NEt_2)]$ (209 mg, 0.41 mmol), and THF (20 mL) was condensed into it under vacuum at −78 °C. At 20 °C, a solution of [pyH][OTf] (95 mg, 0.41 mmol) in THF (15 mL) was

slowly added to the red solution of the uranium complex, which rapidly turned orange. After 45 min, the solution was filtered and its volume was reduced to 10 mL. Addition of pentane (20 mL) led to the precipitation of a brown powder of **4** which was filtered off, washed with pentane and dried under vacuum (225 mg, 93%). ^{1}H NMR (200 MHz, [D$_8$]THF): δ = −2.45 (s, Cp). $C_{16}H_{15}F_3O_3SU$ (582): calcd. C 32.99, H 2.60; found C 32.86, H 2.70.

From [U(Cp)$_3$*n*Bu] and [pyH][OTf]: An NMR tube was charged with [U(Cp)$_3$*n*Bu] (10.0 mg, 0.02 mmol) and [pyH][OTf] (4.7 mg, 0.02 mmol) in [D$_8$]THF. After 15 h at 20 °C, the spectrum showed the quantitative formation of **4**.

From [U(Cp)$_3$X] (X = Cl, *n*Bu) and AgOTf: An NMR tube was charged with [U(Cp)$_3$Cl] (10.0 mg, 0.021 mmol) and AgOTf (6.6 mg, 0.025 mmol) in [D$_8$]THF (0.4 mL). The tube was immersed in an ultrasound bath for 10 min; the color of the solution turned brown and precipitation of AgCl was observed. The spectrum showed the quantitative formation of **4**. The same reaction with [U(Cp)$_3$*n*Bu] also gave **4** in a quantitative yield, with the precipitation of metallic silver.

From [U(Cp)$_3$Cl] and Me$_3$SiOTf: An NMR tube was charged with [U(Cp)$_3$Cl] (10.0 mg, 0.021 mmol) and Me$_3$SiOTf (0.1 mL, 0.55 mmol). The tube was immersed in an ultrasound bath for 1 h and left at 20 °C for 15 h. After concentration to dryness, the brown residue was washed with diethyl ether, dried under vacuum and dissolved in [D$_8$]THF. The spectrum showed the quantitative formation of **4**.

From [U(Cp)$_3$(NEt$_2$)] and TfOH: An NMR tube was charged with [U(Cp)$_3$(NEt$_2$)] (10.0 mg, 0.021 mmol) in benzene (0.4 mL), and TfOH (1.7 μL, 0.02 mmol) was added via a microsyringe. After vigorous shaking by hand, a brown powder was deposited from the red solution. After concentration to dryness, the residue was dissolved in [D$_8$]THF and the spectrum showed the formation of the unique product **4**.

From [U(OTf)$_4$] and KCp: An NMR tube was charged with [U(OTf)$_4$] (10.0 mg, 0.012 mmol) and KCp (3.8 mg, 0.036 mmol) in [D$_8$]THF (0.4 mL). After 1 h at 20 °C, the spectrum showed a large signal at δ = −4.7. The solvent was evaporated and the residue extracted with diethyl ether. After concentration to dryness, the spectrum of the brown powder in [D$_8$]THF showed the formation of the unique product **4**.

[U(COT)(OTf)$_2$(py)] (5)

From [U(COT)(N{SiMe$_3$}$_2$)$_2$] and [pyH][OTf]: A 50-mL round-bottom flask was charged with [U(COT)(N{SiMe$_3$}$_2$)$_2$] (250 mg, 0.38 mmol), and THF (20 mL) was condensed into it under vacuum at −78 °C. At 20 °C, a solution of [pyH][OTf] (174 mg, 0.76 mmol) in THF (15 mL) was introduced and the resulting dark red solution was stirred for 30 min. After filtration and concentration to dryness, the residue was extracted with diethyl ether or toluene (30 mL). The solvent was evaporated and the brown powder of **5** was dried under vacuum (250 mg, 92%). ^{1}H NMR (200 MHz, [D$_8$]THF): δ = −37.5 (s, 8 H, COT), 6.9, 7.4 and 7.6 (s, 5 H, py). $C_{15}H_{13}F_6NO_6S_2U$ (719): calcd. C 25.04, H 1.82, N 1.94; found C 24.98, H 1.92, N 2.08. Complex **5** was similarly prepared in an almost quantitative yield from [U(COT)(NEt$_2$)$_2$] (10.0 mg, 0.02 mmol) and [pyH][OTf] (9.3 mg, 0.04 mmol).

From [U(COT)$_2$] and [pyH][OTf]: An NMR tube was charged with [U(COT)$_2$] (10.0 mg, 0.022 mmol) and [pyH][OTf] (10.3 mg, 0.45 mmol) in [D$_8$]THF (0.4 mL). After 15 min at 80 °C, the spectrum of the red solution showed the quantitative formation of **5**. The same reaction in refluxing pyridine required 15 h to go to completion.

From [U(COT)Cl$_2$(py)$_2$] and Me$_3$SiOTf: An NMR tube was charged with [U(COT)Cl$_2$(py)$_2$] (25 mg, 0.044 mmol) (prepared from [U(COT)$_2$] and UCl$_4$, see below) and Me$_3$SiOTf (0.4 mL, 2.2 mmol). The suspension was heated for 15 h at 110 °C, and after concentration to dryness, the brown residue was dissolved in [D$_8$]THF. The spectrum showed the formation of [U(COT)(OTf)$_2$(THF)$_x$] (δ = 37.3) and [PySiMe$_3$][OTf].

From [U(OTf)$_4$] and K$_2$C$_8$H$_8$: An NMR tube was charged with [U(OTf)$_4$] (10.0 mg, 0.012 mmol) and K$_2$C$_8$H$_8$ (2.2 mg, 0.012 mmol) in pyridine. Precipitation of a green powder of [U(COT)$_2$] was immediately observed. After heating at 110 °C for 15 h, the dark green solution was concentrated to dryness and the residue dissolved in [D$_8$]THF. The spectrum showed the formation of **5** as a unique product.

From [U(OTf)$_4$] and [U(COT)$_2$]: A 50-mL round-bottom flask was charged with [U(OTf)$_4$] (100 mg, 0.12 mmol) and [U(COT)$_2$] (53.5 mg, 0.12 mmol), and pyridine (20 mL) was condensed into it under vacuum at −78 °C. The mixture was heated at 110 °C for 20 h and the resulting dark green solution was concentrated to dryness. The residue was extracted with diethyl ether and the brown powder of **5** was obtained after evaporation of the solvent (155 mg, 90%). Under the same conditions, reaction of **2** and [U(COT)$_2$] in [D$_8$]THF did not reach completion, as only ca. 20% of the green crystalline powder of uranocene was transformed into **5**.

[U(COT)Cl$_2$(py)$_2$]: A 25-mL round-bottom flask was charged with [U(COT)$_2$] (50 mg, 0.11 mmol) and UCl$_4$ (42.5 mg, 0.11 mmol) in pyridine (10 mL). The mixture was heated for 24 h at 110 °C; the color of the solution turned from green to red. The solvent was evaporated and the residue extracted with THF (10 mL). After concentration to dryness, the product was dissolved in pyridine (5 mL) and was then precipitated on addition of diethyl ether (10 mL). The red powder was filtered, washed with toluene (10 mL) and dried under vacuum (88 mg, 70%).

[U(Cp*)$_2$(OTf)$_2$] (6)

From [U(Cp*)$_2$X$_2$] (X = Me, NMe$_2$) and [pyH][OTf]: A 100-mL round-bottom flask was charged with [U(Cp*)$_2$Me$_2$] (257 mg, 0.47 mmol), and THF (20 mL) was condensed into it under vacuum at −78 °C. A solution of [pyH][OTf] (219 mg, 0.95 mmol) in THF (20 mL) was slowly added to the solution of the uranium complex at −70 °C; vigorous evolution of gas was observed. After 1 h at 20 °C, the brown solution was concentrated to dryness and the residue extracted with toluene (30 mL). The solvent was evaporated and a red brown powder of **6** was washed with pentane and dried under vacuum (300 mg, 78%). ^{1}H NMR (200 MHz, [D$_8$]THF): δ = 20.1 (s, Cp*). $C_{22}H_{30}F_6O_6S_2U$ (806): calcd. C 32.75, H 3.75, S 7.95; found C 32.81, H 3.73, N 7.84. An NMR tube was charged with [U(Cp*)$_2$(NMe$_2$)$_2$] (10.0 mg, 0.017 mmol) and [pyH][OTf] (7.7 mg, 0.034 mmol) in [D$_8$]THF (0.4 mL). The tube was immersed in an ultrasound bath and after 30 min, the spectrum showed that **6** was formed in an almost quantitative yield.

From [U(Cp*)$_2$Me$_2$] and TfOH: An NMR tube was charged with [U(Cp*)$_2$Me$_2$] (10.0 mg, 0.018 mmol) in [D$_8$]toluene (0.4 mL), and TfOH (1.6 μL, 0.018 mmol) was introduced via a microsyringe. Evolution of gas was immediately observed and the spectrum showed the formation of **6** with variable amounts of side products.

[U(Cp*)$_2$Cl$_2$]: An NMR tube was charged with **1** (10.0 mg, 0.012 mmol) and MgCp*Cl(THF) (6.4 mg, 0.024 mmol) in [D$_8$]tol-

uene (0.4 mL). After 3 h at 110 °C, the spectrum of the red solution showed the formation of $[U(Cp^*)_2Cl_2]$ as the unique product.

$[U(Cp)_2(OTf)_2(py)]$ (7)

From $[U(Cp)_2(NEt_2)_2]$ and [pyH][OTf]: A 100-mL round-bottom flask was charged with $[U(Cp)_2(NEt_2)_2]$ (300 mg, 0.58 mmol), and THF (20 mL) was condensed into it under vacuum at −78 °C. A solution of [pyH][OTf] (268 mg, 1.17 mmol) in THF (20 mL) was slowly added into the solution of the uranium compound at −40 °C. After stirring for 1 h at −30 °C and 3 h at 20 °C, the orange solution was filtered, concentrated to dryness and the orange powder of **7** was washed with diethyl ether and dried under vacuum (260 mg, 60%). Compound **7** may be contaminated with traces (2−3%) of **4**. ^{1}H NMR (200 MHz, $[D_8]$THF): δ = 6.9, 8.8 and 8.85 (s, 5 H, py), 11.2 (s, 10 H, Cp). $C_{17}H_{15}F_6NO_6S_2U$ (745): calcd. C 27.39, H 2.02, N 1.88; found C 26.66, H 1.99, N 2.05.

From $[U(OTf)_4]$ and KCp: An NMR tube was charged with $[U(OTf)_4]$ (10.0 mg, 0.012 mmol) and KCp (2.5 mg, 0.024 mmol) in $[D_8]$THF (0.4 mL). After 12 h at 20 °C, the spectrum of the yellow solution showed the formation of **4** and **7** in a ratio of 73:27.

X-ray Crystallography of $[U(OTf)_4(OPPh_3)_3]\cdot 0.5py\cdot 0.5Et_2O$: Diffraction data collection was carried out with a Nonius diffractometer equipped with a CCD detector. The lattice parameters were determined from ten images recorded with 2° Φ-scans and later refined on all data. A 180° Φ-range was scanned with 2° steps with a crystal-to-detector distance fixed at 30 mm. Data were corrected for Lorentz polarization and absorption[40] effects. The structure was solved by the heavy-atom method and refined by full-matrix least squares on F^2 with anisotropic thermal parameters for all non-solvent atoms. H atoms were introduced at calculated positions and constrained to ride on their parent C atom with an isotropic displacement parameter equal to 1.2 (CH, CH_2) or 1.5 (CH_3) times that of the parent atom. One pyridine and one diethyl ether solvent molecules were found on the same position and were refined disordered on two positions with 0.5 occupation factor. All calculations were performed with an O2 Silicon Graphics Station using the SHELXTL package.[41] Crystal data and summary of data collection and refinement are given in Table 4. Crystallographic data (excluding structure factors) for the structure reported in this paper have been deposited with the Cambridge Crystallographic Data Centre as supplementary publication no. CCDC-171474. Copies of the data can be obtained free of charge on application to CCDC, 12 Union Road, Cambridge CB2 1EZ, UK [Fax: (internat.) + 44-1223/336-033; E-mail: deposit@ccdc.cam.ac.uk].

X-ray Crystallography of $[U(Cp)_2(OTf)_2(py)_2]$: Diffraction collection was carried out with a Nonius diffractometer equipped with a CCD detector. The lattice parameters were determined from ten images recorded with 2° Φ-scans and later refined on all data. A 180° Φ-range was scanned with 2° steps with a crystal-to-detector distance fixed at 30 mm. Data were corrected for Lorentz polarization and absorption[40] effects. The structure was solved by the heavy-atom method and refined by full-matrix least squares on F^2 with anisotropic thermal parameters for all non-hydrogen atoms. H atoms were introduced at calculated positions and constrained

Table 4. Crystal data and structure refinement for the complexes

	3·0.5py·0.5Et_2O	**8**	**9**·0.5py
Empirical formula	$C_{62.5}H_{52.5}F_{12}N_{0.5}O_{15.5}P_3S_4U$	$C_{22}H_{20}F_6N_2O_6S_2U$	$C_{48.5}H_{40.5}F_6O_8P_2S_2U$
M [g·mol^{-1}]	1745.73	824.55	1229.40
Crystal system	triclinic	monoclinic	orthorhombic
Space group	$P\bar{1}$	$P2_1/n$	$Fddd$
a [Å]	12.879(3)	10.804(2)	13.376(3)
b [Å]	13.475(3)	9.924(2)	45.169(9)
c [Å]	19.917(4)	24.660(5)	66.273(13)
α [°]	84.78(3)	90	90
β [°]	88.31(3)	99.95(3)	90
γ [°]	79.35(3)	90	90
V [Å^3]	3382.6(12)	2604.2(9)	40041(14)
Z	2	4	32
$\rho_{calcd.}$ [g·cm^{-3}]	1.714	2.103	1.632
μ(Mo-K_α) [mm^{-1}]	2.693	6.478	3.463
Crystal size [mm]	0.20 × 0.15 × 0.10	0.15 × 0.10 × 0.10	0.20 × 0.15 × 0.10
T_{min}/T_{max}	0.633/0.766	0.830/0.974	0.550/0.698
F(000)	1728	1568	19312
2θ range [°]	4−50	4−50	4−46
T [K]	123(2)	123(2)	123(2)
No. of data collected	18318	16307	26890
No. of unique data	10662	4378	6152
Observed data [$I > 2\sigma(I)$]	9700	3677	3275
R_{int}	0.036	0.052	0.084
No. of parameters	903	352	596
R_1[a]	0.031	0.033	0.064
wR_2[b]	0.072	0.073	0.120
S	1.008	1.015	0.972
$\Delta\rho_{min}$ [e·Å^{-3}]	−1.341	−1.288	−0.786
$\Delta\rho_{max}$ [e·Å^{-3}]	0.668	0.726	0.654

[a] $R_1 = \Sigma||F_o| - |F_c||/|F_o|$ (observed reflections). [b] $wR_2 = [\Sigma w(|F_o^2| - |F_c^2|)^2/\Sigma(w|F_o^2|)^2]^{1/2}$ (observed reflections).

to ride on their parent C atom with an isotropic displacement parameter equal to 1.2 (CH) times that of the parent atom. All calculations were performed with an O2 Silicon Graphics Station using the SHELXTL package.[41] Crystal data and summary of data collection and refinement are given in Table 4. Crystallographic data (excluding structure factors) for the structure reported in this paper have been deposited with the Cambridge Crystallographic Data Centre as supplementary publication no. CCDC-171475. Copies of the data can be obtained free of charge on application to CCDC, 12 Union Road, Cambridge CB2 1EZ, UK [Fax: (internat.) + 44-1223/336-033; E-mail: deposit@ccdc.cam.ac.uk].

X-ray Crystallography of $[U(COT)(OTf)_2(OPPh_3)_2]\cdot 0.5py$: Diffraction collection was carried out with a Nonius diffractometer equipped with a CCD detector. The lattice parameters were determined from ten images recorded with 2° Φ-scans and later refined on all data. A 180° Φ-range was scanned with 2° steps with a crystal-to-detector distance fixed at 35 mm. Data were corrected for Lorentz polarization and absorption[40] effects. The structure was solved by the heavy-atom method and refined by full-matrix least squares on F^2 with anisotropic thermal parameters for all non-hydrogen atoms. Two independent and similar molecular complexes were found in the unit cell, with the two uranium atoms lying on a two-fold axis. H atoms (except those of the solvent molecules) were introduced at calculated positions and constrained to ride on their parent C atom with an isotropic displacement parameter equal to 1.2 (CH) times that of the parent atom. The pyridine solvent molecule lies on a two-fold axis and all atoms were assigned as C atoms. All calculations were performed with an O2 Silicon Graphics Station using the SHELXTL package.[41] Crystal data and summary of data collection and refinement are given in Table 4. Crystallographic data (excluding structure factors) for the structure reported in this paper have been deposited with the Cambridge Crystallographic Data Centre as supplementary publication no. CCDC-171476. Copies of the data can be obtained free of charge on application to CCDC, 12 Union Road, Cambridge CB2 1EZ, UK [Fax: (internat.) + 44-1223/336-033; E-mail: deposit@ccdc.cam.ac.uk].

[1] [1a] T. Imamoto, *Lanthanides in Organic Synthesis*, Academic Press, London, **1994**. [1b] S. Kobayashi, *Synlett* **1994**, 689−701. [1c] H. Yasuda, E. Ihara, *Bull. Chem. Soc. Jpn.* **1997**, *70*, 1745−1767. [1d] S. Kobayashi, M. Moriwaki, I. Hachiya, *Bull. Chem. Soc. Jpn.* **1997**, *70*, 267−273. [1e] B. E. Woodworth, Z. Metzner, K. Matyjaszewski, *Macromolecules* **1998**, *31*, 7999−8004. [1f] B. Bosnich, *Aldrichim. Acta* **1998**, *31*, 76−83. [1g] H. C. Aspinall, J. L. M. Dwyer, N. Greeves, E. G. McIver, J. C. Woolley, *Organometallics* **1998**, *17*, 1884−1888.

[2] [2a] G. A. Lawrance, *Chem. Rev.* **1986**, *86*, 17−33. [2b] F. T. Edelmann, *Angew. Chem. Int. Ed. Engl.* **1995**, *34*, 2466−2488. [2c] H. Schumann, J. A. Meese-Marktcheffel, L. Esser, *Chem. Rev.* **1995**, *95*, 865−986. [2d] C. D. Sofield, R. A. Andersen, *J. Organomet. Chem.* **1995**, *501*, 271−276. [2e] G. A. Luinstra, *J. Organomet. Chem.* **1996**, *517*, 209−215. [2f] P. Poremba, U. Reißmann, M. Noltemeyer, H. G. Schmidt, W. Brüser, F. T. Edelmann, *J. Organomet. Chem.* **1997**, *544*, 1−6. [2g] F. Calderazzo, U. Englert, G. Pampaloni, G. Tripepi, *J. Organomet. Chem.* **1998**, *555*, 49−56. [2h] K. S. Hagen, *Inorg. Chem.* **2000**, *39*, 5867−5869.

[3] J. C. Berthet, M. Lance, M. Nierlich, M. Ephritikhine, *Chem. Commun.* **1998**, 1373−1374.

[4] J. C. Berthet, M. Lance, M. Nierlich, M. Ephritikhine, *Eur. J. Inorg. Chem.* **1999**, 2005−2007.

[5] [5a] C. Boisson, J. C. Berthet, M. Ephritikhine, M. Lance, M. Nierlich, *J. Organomet. Chem.* **1996**, *522*, 249−257. [5b] C. Boisson, J. C. Berthet, M. Ephritikhine, M. Lance, M. Nierlich, *J. Organomet. Chem.* **1997**, *533*, 7−11.

[6] C. Redshaw, G. Wilkinson, B. Hussain-Bates, M. B. Hursthouse, *J. Chem. Soc., Dalton Trans.* **1992**, 1803−1811.

[7] L. Busetto, V. Zanotti, S. Bordoni, L. Carlucci, V. G. Albano, D. Braga, *J. Chem. Soc., Dalton Trans.* **1992**, 1105−1109.

[8] G. H. Rawji, V. M. Lynch, *Acta Crystallogr., Sect. C* **1992**, *48*, 1667−1669.

[9] [9a] H. Plenio, R. Diodone, *Chem. Ber.* **1997**, *130*, 963−968. [9b] J. G. Donkervoort, J. T. B. H. Jastrzebski, B. J. Deelman, H. Kooijman, N. Veldman, A. L. Spek, G. van Koten, *Organometallics* **1997**, *16*, 4174−4184. [9c] L. Giannini, A. Caselli, E. Solari, C. Floriani, A. Chiesi-Villa, C. Rizzoli, N. Re, A. Sgamellotti, *J. Am. Chem. Soc.* **1997**, *119*, 9198−9210. [9d] G. A. van Albada, W. J. J. Smeets, A. L. Spek, J. Reedijk, *Inorg. Chim. Acta* **1997**, *260*, 151−161. [9e] D. Gudat, M. Schrott, V. Bajorat, M. Nieger, S. Kotila, R. Fleischer, D. Stalke, *Chem. Ber.* **1996**, *129*, 337−345.

[10] T. Imamoto, M. Nishiura, Y. Yamanoi, H. Tsuruta, K. Yamaguchi, *Chem. Lett.* **1996**, 875−876.

[11] J. M. Manriquez, P. J. Fagan, T. J. Marks, *J. Am. Chem. Soc.* **1978**, *100*, 3939−3941.

[12] D. Baudry, E. Bulot, M. Ephritikhine, M. Nierlich, M. lance, J. Vigner, *J. Organomet. Chem.* **1990**, *388*, 279−287.

[13] T. R. Boussie, R. M. Moore, A. Streitwieser, A. Zalkin, J. Brennan, K. A. Smith, *Organometallics* **1990**, *9*, 2010−2016.

[14] [14a] J. C. Berthet, J. F. Le Maréchal, M. Ephritikhine, *J. Organomet. Chem.* **1990**, *393*, C47−C48. [14b] J. C. Berthet, J. F. Le Maréchal, M. Ephritikhine, *J. Organomet. Chem.* **1994**, *480*, 155−161

[15] C. Boisson, J. C. Berthet, M. Lance, J. Vigner, M. Nierlich, M. Ephritikhine, *J. Chem. Soc., Dalton Trans.* **1996**, 947−953.

[16] T. Arliguie, D. Baudry, M. Ephritikhine, M. Nierlich, M. Lance, J. Vigner, *J. Chem. Soc., Dalton Trans.* **1992**, 1019−1024.

[17] P. C. Leverd, T. Arliguie, M. Lance, M. Nierlich, J. Vigner, M. Ephritikhine, *J. Chem. Soc., Dalton Trans.* **1994**, 501−504.

[18] [18a] J. C. Berthet, M. Ephritikhine, *Coord. Chem. Rev.* **1998**, *178/180*, 83−116. [18b] J. C. Berthet, C. Boisson, M. Lance, J. Vigner, M. Nierlich, M. Ephritikhine, *J. Chem. Soc., Dalton Trans.* **1995**, 3019−3025. [18c] J. C. Berthet, C. Boisson, M. Lance, J. Vigner, M. Nierlich, M. Ephritikhine, *J. Chem. Soc., Dalton Trans.* **1995**, 3027−3033.

[19] R. D. Ernst, W. J. Kennely, C. S. Day, V. W. Day, T. J. Marks, *J. Am. Chem. Soc.* **1979**, *101*, 2656−2664.

[20] C. Baudin, D. Baudry, M. Ephritikhine, M. Lance, A. Navaza, M. Nierlich, J. Vigner, *J. Organomet. Chem.* **1991**, *415*, 59−73.

[21] J. C. Berthet, M. Ephritikhine, unpublished results.

[22] S. M. Cendrowski-Guillaume, M. Lance, M. Nierlich, M. Ephritikhine, *Organometallics* **2000**, *19*, 3257−3259.

[23] C. Boisson, J. C. Berthet, M. Lance, J. Vigner, M. Nierlich, M. Ephritikhine, *J. Chem. Soc., Dalton Trans.* **1996**, 947−953.

[24] P. Zanella, G. De Paoli, G. Bombieri, G. Zanotti, R. Rossi, *J. Organomet. Chem.* **1977**, *142*, C21−C24.

[25] [25a] A. Zalkin, J. G. Brennan, R. A. Andersen, *Acta Crystallogr., Sect. C* **1987**, *43*, 418−420. [25b] A. Zalkin, J. G. Brennan, R. A. Andersen, *Acta Crystallogr., Sect. C* **1987**, *43*, 421−423.

[26] P. C. Leverd, M. Lance, J. Vigner, M. Nierlich, M. Ephritikhine, *J. Chem. Soc., Dalton Trans.* **1995**, 237−244.

[27] A. Streitwieser, T. R. Boussie, *Eur. J. Solid State Inorg. Chem.* **1991**, *28*, 399- 410.

[28] [28a] F. A. Cotton, D. O. Marler, W. Schwotzer, *Inorg. Chem.* **1984**, *23*, 4211−4215. [28b] W. G. Van Der Sluys, A. P. Sattelberger, *Chem. Rev.* **1990**, *90*, 1027−1040. [28c] M. Ephritikhine, O. Maury, C. Villiers, M. Lance, M. Nierlich, *J. Chem. Soc., Dalton Trans.* **1998**, 3021−3027.

[29] J. A. Hermann, J. F. Suttle, *Inorg. Synth.* **1957**, *5*, 143−145.

[30] J. G. Reynolds, A. Zalkin, D. H. Templeton, N. M. Edelstein, L. K. Templeton, *Inorg. Chem.* **1976**, *15*, 2498−2502.

[31] S. J. Simpson, H. W. Turner, R. A. Andersen, *Inorg. Chem.* **1981**, *20*, 2991−2995.
[32] L. T. Reynolds, G. Wilkinson, *J. Inorg. Nucl. Chem.* **1956**, *2*, 246−253.
[33] T. J. Marks, A. M. Seyam, J. R. Kolb, *J. Am. Chem. Soc.* **1973**, *95*, 5529−5539.
[34] G. Paolucci, G. Rossetto, P. Zanella, R. D. Fischer, *J. Organomet. Chem.* **1985**, *284*, 213−228.
[35] P. J. Fagan, J. M. Manriquez, E. A. Maatta, A. M. Seyam, T. J. Marks, *J. Am. Chem. Soc.* **1981**, *103*, 6650−6667.
[36] P. J. Fagan, J. M. Manriquez, S. H. Vollmer, C. S. Day, V. W. Day, T. J. Marks, *J. Am. Chem. Soc.* **1981**, *103*, 2206−2220.
[37] A. L. Arduini, N. M. Edelstein, J. D. Jamerson, J. G. Reynolds, K. Schmid, J. Takats, *Inorg. Chem.* **1981**, *20*, 2470−2474.
[38] A. Streitwieser, U. Müller-Westerhoff, *J. Am. Chem. Soc.* **1968**, *90*, 7364.
[39] T. M. Gilbert, R. R. Ryan, A. P. Sattelberger, *Organometallics* **1988**, *7*, 2514−2518.
[40] A. L. Spek, MULABS, *PLATON*, University of Utrecht, The Netherlands, **1997**.
[41] G. Sheldrick, *SHELXTL*, Bruker-AXS, Madison, WI, USA, **1999**.

Received October 1, 2001
[I01384]

Spin States and Stability of Fe^{III} Complexes of Ligands with Carboxamido Nitrogen and Phenolato Oxygen Donors

Dana S. Marlin,[a] Marilyn M. Olmstead,[b] and Pradip K. Mascharak*[a]

Keywords: Iron / N ligands / O ligands / Spin states

As part of our attempts to prepare Fe^{III} complexes with "tunable" spin states, we have synthesized three novel six-coordinate Fe^{III} complexes containing both carboxamido nitrogen (N_{amido}) and phenolato oxygen (O_{phen}) donors in their ligand framework. Since it has already been shown that carboxamido nitrogen donors usually stabilize Fe^{III} in a low spin configuration, while phenolato oxygens tend to stabilize Fe^{III} in a high spin state, we have incorporated both donor groups in our designed ligands. The syntheses and structures of Fe^{III} complexes with either one or two N_{amido} and O_{phen} donors are reported in this paper. The properties of these complexes have been compared with the properties of analogous Fe^{III} complexes. The competing effects of N_{amido} and O_{phen} on the spin state of the Fe^{III} center are discussed in terms of the stabilities of the overall complexes.

(© Wiley-VCH Verlag GmbH, 69451 Weinheim, Germany, 2002)

Introduction

Monomeric complexes with stable Fe^{III} centers are attractive synthetic targets to inorganic chemists for their use, among other things, as catalysts, enzyme mimics, or as model complexes that allow for detailed study of the electronic properties of the Fe^{III} center.[1−4] Recent work from this laboratory in conjunction with the work of others has shown that coordination of a carboxamido nitrogen (N_{amido}) to an Fe^{III} center makes it resistant toward hydrolytic decomposition.[5] Furthermore, the reduction potential of the Fe^{III} center is shifted toward more negative values by approximately −0.5 V per N_{amido} to a maximum of about −1.10 V.[5,6] In addition, the majority of the six-coordinate Fe^{III} complexes with one, two, and four N_{amido} donors possess low spin (LS) ground states.[3,5,6] Wieghardt and coworkers have performed extensive studies to evaluate the electronic and physical properties of mononuclear Fe^{III} complexes with $Fe^{III}-O_{phen}$ (O_{phen} = phenolato O) bonds.[7−8] They have pointed out that the majority of these complexes tend to have high spin (HS) Fe^{III} centers (with a $t_{2g}^3e_g^2$ electronic configuration) and that $Fe^{III}-O_{phen}$ bonds are often short, indicating considerable double bond character with ligand-to-metal d_π-p_π back bonding.[9] We decided to combine both $Fe^{III}-N_{amido}$ and $Fe^{III}-O_{phen}$ interactions within the same Fe^{III} complex with the intention of obtaining Fe^{III} complexes with "tunable" spin states. In the long term, we intend to gain control over (a) the redox potential, (b) stability and (c) the spin state of the Fe^{III} center, all of which influence its reactivity. Here we report the results of our initial effort toward this goal.

Previously, we have described the structure and chemistry of Fe^{III} complexes of the pentadentate ligand *N*,*N*′-bis(2-hydroxyphenyl)-pyridine-2,6-dicarboxamide ($POPYH_4$) (Figure 1).[10] When deprotonated, this ligand becomes planar and coordinates to the Fe^{III} center in the basal plane of a pentagonal bipyramid. The HS Fe^{III} complexes of this ligand namely, $[Fe(POPY)(L)_2]^{n-}$ (L = SCN^-, *N*-methylimidazole), were the first examples of structurally characterized species in which both N_{amido} and O_{phen} donors are coordinated to the Fe^{III} center in the same complex. We have now prepared additional six-coordinate complexes with similar ligands in order to explore the properties of these types of complexes in more detail. The two designed ligands that have been employed in this study are the tridentate ligand *N*-(2-hydroxyphenyl)-2-pyridinecarboxamide ($PypepOH_2$) and the pentadentate ligand *N*,*N*-bis(2-pyridylmethyl)amine-*N*-ethyl-2-hydroxyphenyl-2-carboxamide ($Papy_2OH_2$) (Figure 1). In both $PypepOH_2$ and $Papy_2OH_2$, the H's represent dissociable phenolic and carboxamide hydrogens. In the deprotonated forms, these ligands coordinate to Fe^{III} to afford stable HS six-coordinate complexes $Na[Fe(PypepO)_2]$ (**1**), and $[Fe(Papy_2O)(L)]$ (**2** L = Cl^-; **3** L = SCN^-). These complexes represent only the second and third set of examples of structurally characterized complexes with Fe^{III} centers coordinated to both N_{amido} and O_{phen} donors. They are also the first such examples of six-coordinate Fe^{III} complexes. The structural and spectro-

[a] Department of Chemistry and Biochemistry, University of California, Santa Cruz,
Santa Cruz, CA 95064, USA
Fax: (internat.) + 1-831/459-2935
E-mail: pradip@chemistry.ucsc.edu
[b] Department of Chemistry, University of California, Davis
Davis, CA 95616, USA

scopic properties of these complexes (with both $Fe^{III}-N_{amido}$ and $Fe^{III}-O_{phen}$ bonds) have been compared with Fe^{III} complexes with either $Fe^{III}-O_{phen}$ or $Fe^{III}-N_{amido}$ bonds.

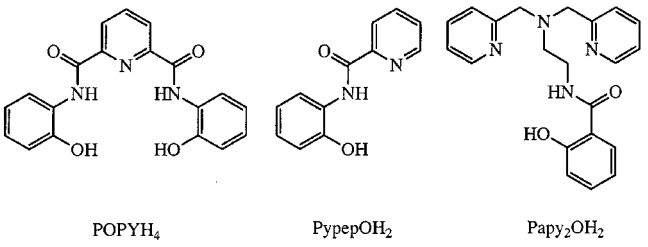

Figure 1. Ligands that contain both N_{amido} and O_{phen} donors used in previous ($POPYH_4$) and the present study ($PypepOH_2$ and $Papy_2OH_2$); the H's in $POPYH_4$, $PypepOH_2$ and $Papy_2OH_2$ represent dissociable phenolate and carboxamide hydrogens

Results and Discussion

The tridentate ligand $PypepOH_2$ was prepared by reacting 2-aminophenol with 2-pyridinecarbonyl chloride (the latter prepared from 2-picolinic acid and thionyl chloride) in tetrahydrofuran (THF). The acetate-protected derivative of the pentadentate ligand $Papy_2OH_2$, namely $Papy_2OCOCH_3$, was synthesized from (2-aminoethyl)bis(2-pyridylmethyl)amine and 2-acetylphenylcarbonyl chloride (the latter prepared from 2-acetylsalicylic acid and oxalyl chloride). Pure $Papy_2OH_2$ was obtained in good yield following deprotection of $Papy_2OCOCH_3$ with NaOH and neutralization with HCl. For ease of handling, $Papy_2OH_2$ was converted into the mono-sodium salt $NaPapy_2OH$ by reaction of $Papy_2OH_2$ with NaOMe in MeOH. Reaction of $[Fe(DMF)_6](ClO_4)_3$ with two equiv. of $PypepOH_2$ and four equiv. of NaH (both relative to iron) in DMF afforded the Fe^{III} complex $Na[Fe(PypepO)_2]$ (**1**). The dark red complex $[Fe(Papy_2O)(Cl)]$ (**2**) was synthesized by reacting $(Et_4N)[FeCl_4]$ with $NaPapy_2OH$ plus one equiv. of NaH in DMF. Reaction of $[Fe(DMF)_6](ClO_4)_3$ with one equiv. of $Papy_2O^{2-}$ in DMF followed by one equiv. of NaSCN resulted in the formation of $[Fe(Papy_2O)(NCS)]$ (**3**) in high yield.

Molecular Structure of Na[Fe(PypepO)2] (1)

X-ray quality crystals of **1**·2.5CH_3CN were grown from a saturated solution of **1** in CH_3CN, upon cooling to −20 °C. The structure of the complex shows two deprotonated $PypepO^{2-}$ ligands coordinated to an Fe^{III} center in a *mer* geometry (Figure 2a). In the solid state, **1**·2.5CH_3CN forms an elaborate network of $[Fe(Pypep)_2]^-$ and Na^+ ions bridged through carbonyl and phenolato oxygens with additional coordination of CH_3CN to the Na^+ center. The lattice structure is built up of dimeric $[Fe(PypepO)_2]^-\cdots Na^+\cdots[Fe(PypepO)_2]^-\cdots Na^+$ units which in turn are connected together into an extended network with large pockets formed by four such dimeric units (Figure 2b). This arrangement creates small pockets at the center of each dimer and large pockets by the four-dimer clusters. Some of the large pockets are occupied by uncoordinated CH_3CN molecules (Figure 2b).

It is interesting to note that like complex **1**, $Na[Fe(POPY)(N\text{-}MeIm)_2]\cdot 3CH_3CN$ also forms an extended structure in the solid state with Na^+ bonded to phenolate and carbonyl oxygen donors from the $POPY^{4-}$ ligand and lattice CH_3CN molecules.[10] However, in the case of $Na[Fe(POPY)(N\text{-}MeIm)_2]\cdot 3CH_3CN$, polymeric chains form between monomeric $Na^+\cdots[Fe(POPY)(N\text{-}MeIm)_2]^-$ units in the lattice, which differs considerably from the elaborate porous network seen in **1**·2.5CH_3CN. Also, the bond lengths for **1** $Fe^{III}-N_{amido}$ [av. 2.064(4) Å] and $Fe^{III}-O_{phen}$ [av. 1.962(4) Å] as well as $Fe^{III}-N_{py}$ [av. 2.178(5) Å] (py = pyridine) are substantially shorter than analogous bond lengths in $Na[Fe(POPY)(N\text{-}MeIm)_2]$ (av. 2.228 Å, 2.045 Å, and 2.221 Å respectively) due to the ligand strain imposed by the pentadentate planar $POPY^{4-}$ ligand in the latter complex.

Molecular Structures of [Fe(Papy2O)(Cl)] (2) and [Fe(Papy2O)(SCN)] (3)

X-ray quality crystals of **2**·2CH_3CN were grown from CH_3CN at −20 °C while a toluene/CH_2Cl_2 (3:1) mixture was used to obtain single crystals of **3**·toluene. Both **2** and **3** are monomeric and the coordination geometry is octahedral with the deprotonated $Papy_2O^{2-}$ ligand coordinated to five of the six sites of the Fe^{III} center in both complexes. In **2**, a Cl^- ion occupies the sixth site (Figure 3) while in **3**, the sixth site is occupied by a SCN^- ion (Figure 4).

Since these complexes are neutral, there is no extended structure in solid state. The bond lengths of **2** and **3** are similar (Table 1). The $Fe^{III}-N_{amido}$ [av. 2.0157(14) Å] and $Fe^{III}-N_{py}$ [av. 2.1511(15) Å] bond lengths of **2** and **3** compare well with those noted for **1** while the $Fe^{III}-O_{phen}$ distance [av. 1.8781(12) Å] is slightly shorter. The $N_{amido}-Fe-O_{phen}$ angles in both **2** and **3** are larger (91°, six-membered rings) than the same angles in **1** (av. 80°, five-membered rings, Table 1).

Stability and Spectroscopic Properties

The EPR spectra of **1**, **2**, and **3** in DMF glass clearly indicate that the Fe^{III} centers in these complexes exist as HS. During the past few years, we have synthesized several similar Fe^{III} complexes that contain one, two or four $Fe^{III}-N_{amido}$ bonds in addition to $Fe^{III}-N_{py}$ and/or $Fe^{III}-S_{thio}$ (thio = thiophenolato) bonds.[5,11−14] All these complexes are consistently LS (Table 2). The obvious difference between the present set of complexes (**1**, **2**, and **3**) and the rest of the entries in Table 2 is the fact that complexes **1**, **2**, and **3** contain $Fe^{III}-O_{phen}$ bonds. In general, mononuclear Fe^{III} complexes with either one,[7,15,16] two,[17] three[8,18] or four[10,19] $Fe^{III}-O_{phen}$ bonds all tend to possess HS ($t_{2g}^3e_g^2$) Fe^{III} centers. The $Fe^{III}-O_{phen}$ bond in the majority of these complexes has been described as more than a single bond with additional d_π-p_π back-bonding.[9] Wiegh-

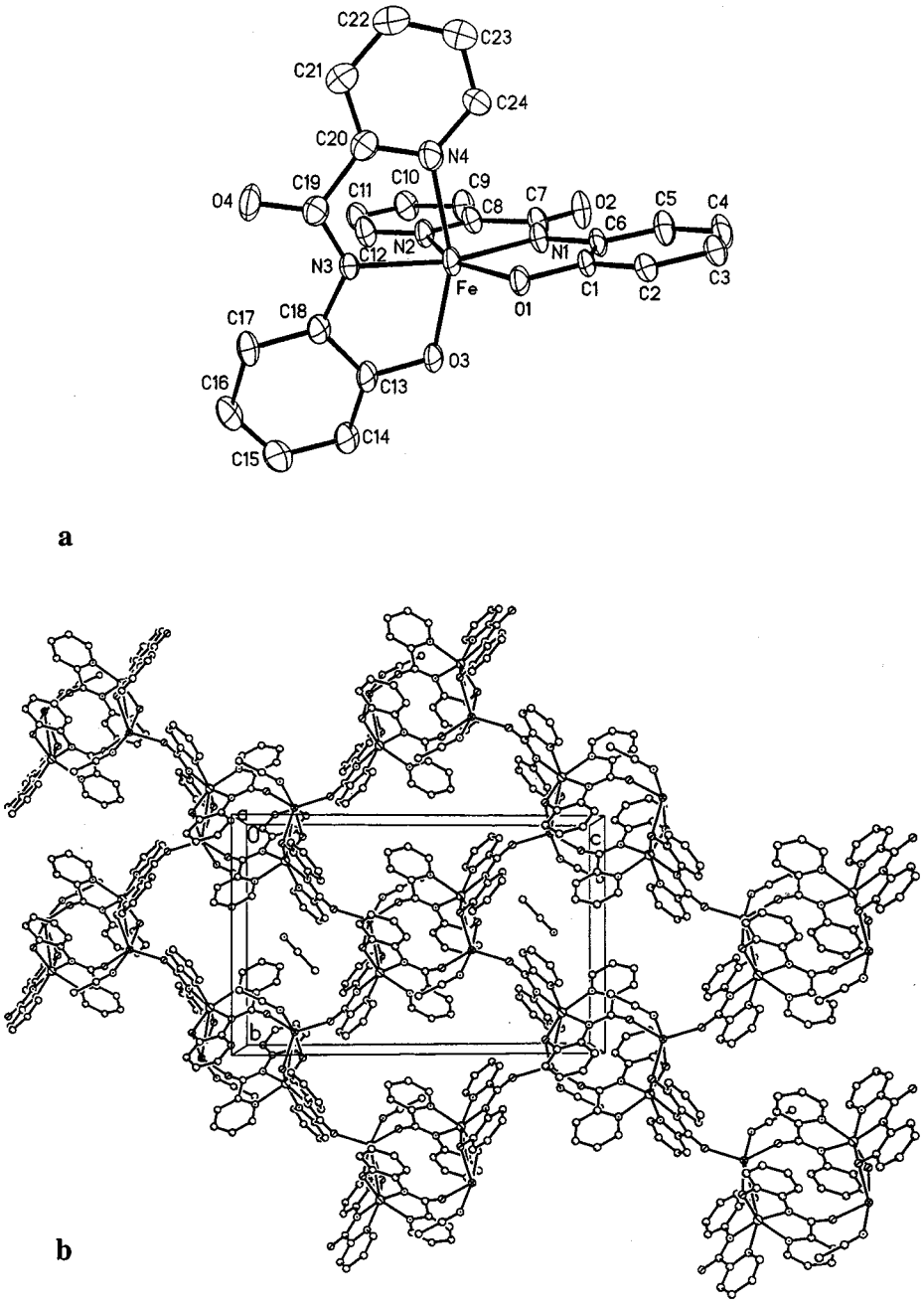

Figure 2. (a) Thermal ellipsoid plot of $[Fe(PypepO)_2]^+$ (at the 35% probability level); (b) extended structure of $Na[Fe(PypepO)_2]\cdot 2.5CH_3CN$ showing the small and large pockets formed in the solid state

ardt and co-workers have suggested that the HS configuration of the Fe^{III} center facilitates such a d_π-p_π interaction.[9] Since the $Fe^{III}-O_{phen}$ distances in complexes **1**, **2**, and **3** (Table 1) compare well with the "short" $Fe^{III}-O_{phen}$ distances reported so far (range = 1.85−1.97 Å),[7−10,15−19] it is evident that the $Fe^{III}-O_{phen}$ bonds in **1**, **2**, and **3** are of a similar nature, and hence these complexes prefer a HS configuration. Taken together, these facts indicate that when the Fe^{III} center is coordinated to both carboxamido nitrogen(s) and phenolato oxygen(s) (like **1**, **2**, and **3**), the $Fe^{III}-O_{phen}$ interaction dominates and the resultant complexes are HS.

A change in spin state occurs when the Cl^- ligand of $[Fe(Papy_2O)(Cl)]$ (**2**) is replaced with CN^-. The HS complex **2** is converted into a LS cyanide adduct $[Fe(Papy_2O)(CN)]$ upon addition of one equiv. of $(Et_4N)(CN)$ to a solution of **2** in DMF (EPR data, Figure 5). This change in spin state on going from **2** to $[Fe(Papy_2O)(CN)]$ supports the notion that the spin state of the Fe^{III} center is controlled by the $Fe^{III}-N_{amido}$ and $Fe^{III}-O_{phen}$ interactions *which*

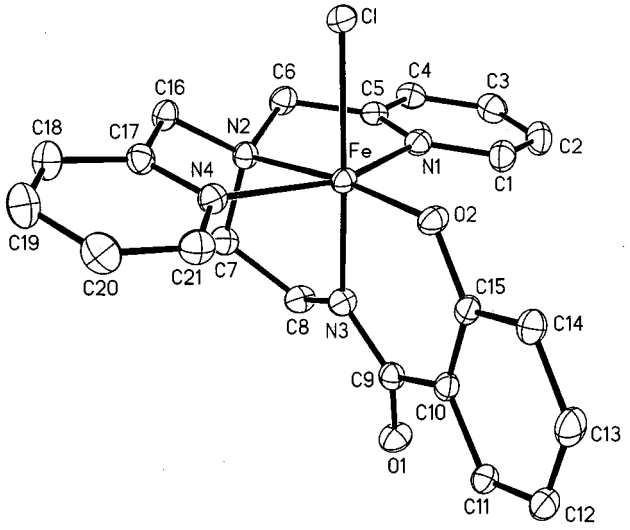

Figure 3. Thermal ellipsoid plot of **2** (at the 50% probability level)

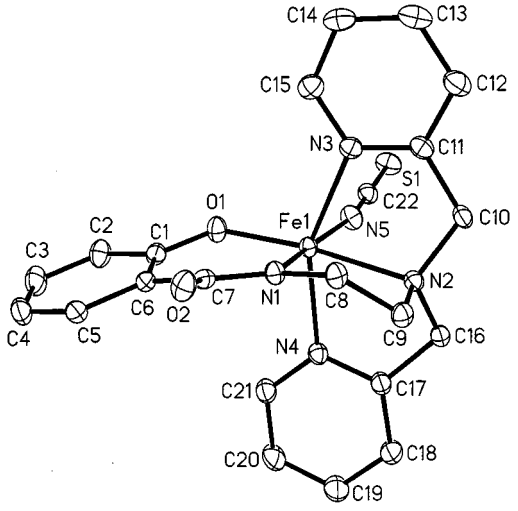

Figure 4. Thermal ellipsoid plot of **3** (at the 50% probability level)

compete against each other. The competing effect of these two interactions appears to be similar enough so that addition of a strong sixth ligand like CN^- results in a switch in the spin state during the [Fe(Papy$_2$O)(Cl)] → [Fe(Papy$_2$O)(CN)] transformation.

At this point it is also important to note that the LS species [Fe(Papy$_2$O)(CN)] is quite unstable and can only be studied by low temperature spectroscopy. All attempts to isolate this complex as a solid product have failed so far. In contrast, the analogous CN^- adduct $[Fe(Papy_3)(CN)]^+$ (a similar complex with *no* $Fe^{III}-O_{phen}$ bond) is LS and very stable.[6] Clearly, the change in spin state converts a stable complex **2** into an unstable species [Fe(Papy$_2$O)(CN)]. Since HS complexes with $Fe^{III}-O_{phen}$ bonds are usually very stable, it is quite evident that forcing the HS complex **2** (with $Fe^{III}-O_{phen}$ bond) into a LS ($t_{2g}^5e_g^0$) configuration in [Fe(Papy$_2$O)(CN)] reduces its stability, presumably by minimizing the d_π-p_π bonding interaction. Reduction of the $M^{III}-O_{phen}$ bonding interaction has been noted for Co^{III} complexes with phenolate ligands in which the t_{2g}^6 configuration of the Co^{III} center eliminates any d_π-p_π bonding.[9] Our work thus far indicates that LS complexes with $Fe^{III}-N_{amido}$ and $Fe^{III}-O_{phen}$ bonds are inherently unstable. We must comment here that our conclusion regarding weakening of the $Fe^{III}-O_{phen}$ interaction in LS complexes is preliminary and the final word on the stability of LS versus HS Fe^{III} complexes with both $Fe^{III}-N_{amido}$ and $Fe^{III}-O_{phen}$ coordination will require more in-depth studies. Such studies are in progress in this laboratory at the present time.

Finally, we like to point out that complexes **2** and **3** are quite stable toward hydrolysis and do not give rise to species with a (μ-oxo)diiron(III) core. For some time now we have maintained that the presence of an $Fe^{III}-N_{amido}$ bond stabilizes the Fe^{III} center to a great extent and prevents both

Table 1. Selected bond lengths [Å] and angles[°] for complexes **1**, **2** and **3**

Complex **1**			
Fe−N(1)	2.069(4)	Fe−N(4)	2.164(5)
Fe−N(2)	2.192(5)	Fe−O(1)	1.964(4)
Fe−N(3)	2.059(4)	Fe−O(3)	1.959(4)
C(19)−N(3)	1.311(7)	C(19)−O(4)	1.243(7)
C(7)−N(1)	1.307(7)	C(7)−O(2)	1.229(7)
O(3)−Fe−O(1)	92.91(16)	O(3)−Fe−N(3)	79.79(17)
O(1)−Fe−N(3)	113.73(17)	O(3)−Fe−N(1)	107.98(18)
O(1)−Fe−N(1)	80.15(17)	N(3)−Fe−N(1)	164.22(19)
O(3)−Fe−N(4)	155.35(18)	O(1)−Fe−N(4)	92.40(18)
N(3)−Fe−N(4)	76.04(19)	N(1)−Fe−N(4)	96.6(2)
O(3)−Fe−N(2)	94.06(18)	O(1)−Fe−N(2)	154.92(17)
N(3)−Fe−N(2)	91.23(18)	N(1)−Fe−N(2)	74.77(18)
N(4)−Fe−N(2)	91.23(19)		
Complex **2**			
Fe−N(1)	2.1449(12)	Fe−N(4)	2.1489(12)
Fe−N(2)	2.2065(11)	Fe−O(2)	1.8745(9)
Fe−N(3)	2.0172(12)	Fe−Cl	2.3822(4)
C(9)−N(3)	1.3472(17)	C(9)−O(1)	1.2532(17)
O(2)−Fe−N(3)	91.08(4)	N(1)−Fe−N(2)	77.61(4)
O(2)−Fe−N(1)	104.91(4)	N(4)−Fe−N(2)	75.33(4)
N(3)−Fe−N(1)	85.98(5)	O(2)−Fe−Cl	95.99(3)
O(2)−Fe−N(4)	102.47(4)	N(3)−Fe−Cl	171.52(4)
N(3)−Fe−N(4)	94.65(5)	N(1)−Fe−Cl	87.68(3)
N(1)−Fe−N(4)	152.60(5)	N(4)−Fe−Cl	88.40(3)
O(2)−Fe−N(2)	172.92(4)	N(2)−Fe−Cl	90.70(3)
N(3)−Fe−N(2)	82.45(4)		
Complex **3**			
Fe−N(1)	2.0142(14)	Fe−N(4)	2.1553(15)
Fe−N(2)	2.2171(14)	Fe−N(5)	2.0478(16)
Fe−N(3)	2.1551(15)	Fe−O(1)	1.8816(12)
O(1)−Fe−N(1)	90.29(6)	N(3)−Fe−N(4)	152.41(6)
O(1)−Fe−N(5)	96.87(6)	O(1)−Fe−N(2)	170.35(5)
N(1)−Fe−N(5)	171.20(6)	N(1)−Fe−N(2)	81.01(5)
O(1)−Fe−N(3)	106.93(6)	N(5)−Fe−N(2)	92.18(6)
N(1)−Fe−N(3)	86.78(6)	N(3)−Fe−N(2)	76.93(5)
N(5)−Fe−N(3)	86.23(6)	N(4)−Fe−N(2)	76.01(5)
O(1)−Fe−N(4)	100.64(6)	N(5)−Fe−N(4)	89.49(6)
N(1)−Fe−N(4)	94.23(6)	Fe−N(5)−C(22)	169.33(15)

Table 2. Comparison of $Fe^{III}-N_{amido}$ and $Fe^{III}-O_{phen}$ (or S_{thio}) bond lengths, with spin state (on Fe^{III}) and half wave reduction potential (vs. SCE) for six coordinate Fe^{III} complexes

Complex	No. of $Fe^{III}-N_{amido}$ bonds	$Fe^{III}-N_{amido}$ (Å)[a]	$Fe^{III}-O_{phen}$ (or S_{thio})[a] (Å)	Spin state of Fe^{III}	$E_{1/2}$ (V) (DMF)	Reference
$[Fe(Papy_3)(Cl)]^+$	1	1.8559(17)		LS	−0.03	6
$[Fe(Papy_3)(CN)]^+$	1	1.858(2)		LS	−0.01	6
$[Fe(Papy_2O)(Cl)]$ (**2**)	1	2.0172(12)	1.8745(9)	HS	−0.51	this work
$[Fe(Papy_2O)(NCS)]$ (**3**)	1	2.0142(14)	1.8816(12)	HS		this work
$[Fe(Prpep)_2]^+$	2	1.955(2)		LS	−0.10	12
$[Fe(Pypep)_2]^+$	2	1.957(4)		LS	−0.31	11
$[Fe(PypepS)_2]^-$	2	1.954(2)	2.2291(11)	LS	−1.12	14
$[Fe(PypepO)_2]^-$ (**1**)	2	2.064(4)	1.962(4)	HS	−1.08	this work
$[Fe(Py_3P)_2]^-$	4	1.962(2)		LS	−0.95	13
$[Fe(MePy_3P)_2]^-$	4	1.955(3)		LS	−1.05	13

[a] Average bond length when more than one bond is present.

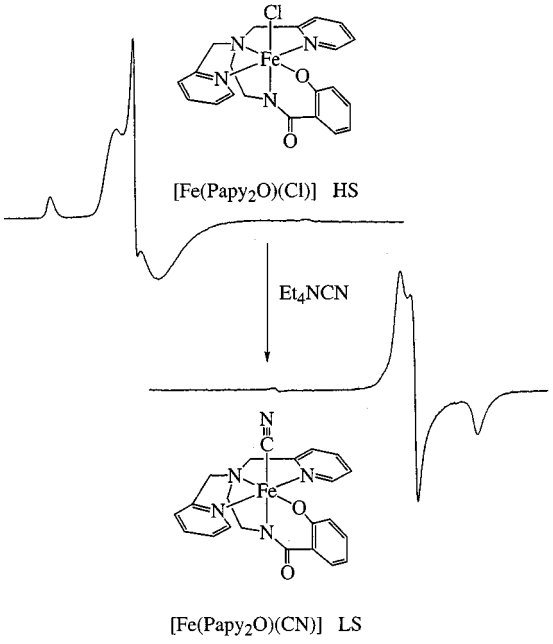

Figure 5. Conversion of HS $[Fe(Papy_2O)(Cl)]$ (**2**) to LS $[Fe(Papy_2O)(CN)]$ upon addition of $(Et_4N)(CN)$; EPR settings: DMF/MeOH (10:1) glass, T = 80 K, microwave power 13 mW, microwave frequency 9.43 GHz, modulation frequency 100 KHz, modulation amplitude 2 G; the *g* values for **2** are 9.05, 4.22 and 4.17, and for $[Fe(Papy_2O)(CN)]$ g = 2.39, 2.27 and 1.87

hydrolytic decomposition and formation of oxo- or hydroxo-bridged iron species which are often the thermodynamic end products in iron chemistry.[10,13] Since the complexes with the $Papy_2O^{2-}$ ligand contain only one $Fe^{III}-N_{amido}$ bond, we have attempted to synthesize directly the corresponding (μ-oxo)diiron(III) complex. However, addition of 2 equiv. of $Papy_2O^{2-}$ to $(Et_4N)_2[Fe_2OCl_6]$ [a pre-formed (μ-oxo)diiron(III) synthon] resulted in the isolation of complex **2** rather than the expected μ-oxo species $[\{Fe(Papy_2O)\}_2O]$. This further supports our previous remarks that complexes with $Fe^{III}-N_{amido}$ bonds do not form oxo-bridged dimers (or polymers), which translates into an enhanced stability of these complexes towards hydrolytic decomposition.

Conclusion

In conclusion, we have prepared and structurally characterized three stable complexes that contain both $Fe^{III}-N_{amido}$ and $Fe^{III}-O_{phen}$ bonds. In previous studies, it has been shown that carboxamido nitrogens (N_{amido}) are strong donors and their coordination to iron usually results in LS Fe^{III} complexes. Previous studies have also shown that complexes with O_{phen} comprise HS Fe^{III} centers. The complexes reported herein now indicate that these two donor atoms in the same molecule influence the spin state of the Fe^{III} center in the opposite sense. Overall, the resulting complexes are HS and so far, no LS complex with both $Fe^{III}-N_{amido}$ and $Fe^{III}-O_{phen}$ bonds has been isolated. It thus appears that the effect of the phenolato oxygen to afford HS Fe^{III} species overrides the spin-pairing trend of the carboxamido nitrogen in Fe^{III} complexes. In the case of Fe^{III} complexes of the $Papy_2O^{2-}$ ligand (which has one N_{amido} and one O_{phen} donor), the overriding effect of O_{phen} can just be compensated by adding a strong sixth ligand (like CN^-). The resulting LS complex $[Fe(Papy_2O)(CN)]$ is, however, unstable. Since similar LS Fe^{III} complexes with no $Fe^{III}-O_{phen}$ bond(s) are stable entities, it now appears that $Fe^{III}-O_{phen}$ bonds impart instability to LS Fe^{III} complexes.

Experimental Section

Physical Measurements: A Perkin−Elmer 1600 FTIR spectrophotometer was used to monitor the IR spectra. ^1H NMR spectra were recorded on a Bruker 250 MHz spectrometer. EPR spectra were monitored at X-band frequencies on a Bruker ESP-300 spectrometer. Electrochemical measurements were performed with standard Princeton Applied Research instrumentation and a Pt inlay electrode. Potentials were measured at 25 °C versus an aqueous saturated calomel electrode (SCE) as reference.

Materials and Methods: All manipulations were carried out in air. (2-Aminoethyl)bis(2-pyridylmethyl)amine was prepared following a published procedure.[20] 2-Aminophenol, 2-picolinic acid, 2-acetylsalicyclic acid, thionyl chloride ($SOCl_2$), oxalyl chloride, sodium hydroxide (NaOH), sodium hydride (NaH), and sodium thiocyanate (NaSCN) were purchased from Aldrich Chemical Company

and used without further purification. $(Et_4N)[FeCl_4]$[21] and $[Fe(DMF)_6](ClO_4)_3$ [22] were prepared by following published procedures. *N*,*N*′-dimethylformamide (DMF) was distilled from BaO while tetrahydrofuran (THF) and toluene were distilled from Na/benzophenone prior to use. Dichloromethane (CH_2Cl_2) and acetonitrile (CH_3CN) were distilled from CaH_2 prior to use.

Preparation of $PypepOH_2$: 2-picolinic acid (5.00 g, 41 mmol) was dissolved in neat $SOCl_2$ (10−20 mL) and warmed to 50 °C until a clear deep purple solution remained (approx. 1 h). The excess $SOCl_2$ was removed under vacuum and the purple residue was triturated twice with THF to remove traces of HCl. The purple solid was then redissolved in THF (30 mL) and added to a solution of 2-aminophenol (4.40 g, 41 mmol) and Et_3N (6.30 g, 62 mmol) in THF (50 mL) at 0 °C. The mixture was then heated to reflux for 5 h. Following a brief cooling period, triethylamine hydrochloride was filtered off, and the volatiles were removed by rotary evaporation. The remaining residue was triturated twice with THF and recrystallized from $MeOH/H_2O$ (1:10 v/v) (6.90 g, 78% yield). ^1H NMR (250 MHz, $CDCl_3$): δ = 6.85 (t, 1 H, ArH), 7.00 (d, 1 H, ArH), 7.08 (t, 2 H, ArH), 7.47 (t, 1 H, ArH), 7.87 (t, 1 H, ArH), 8.23 (d, 1 H, ArH), 8.58 (d, 1 H, ArH), 10.16 (s, 1 H, NH). Selected FTIR absorption bands (KBr pellet): $\tilde{\nu}$ = 3308 (m, N−H), 3072 (m, O−H), 1653 (s, C=O), 1593 (s), 1543 (s), 1458 (s), 1434 (m), 1370 (m), 1284 (m), 1230 (m), 1098 (w), 1038 (w), 932 (w), 852 (w), 757 (s), 738 (s), 691 (s), 618 (w), 594 (w) cm^{-1}.

$NaPapy_2OH$: 2-Acetylsalicyclic acid (1.40 g, 7.5 mmol) was dissolved in neat oxalyl chloride (10−20 mL) and warmed to 40 °C until a clear solution remained (approx. 1 h). Excess oxalyl chloride was removed under vacuum and the clear oil was triturated twice with THF to remove traces of HCl. The residue was then redissolved in THF (10 mL) and added dropwise to a solution of (2-aminoethyl)bis(2-pyridylmethyl)amine (1.80 g, 7.5 mmol) and triethylamine (0.90 g, 9.0 mmol) in THF (25 mL) at 0 °C. The mixture was warmed to room temperature and allowed to stir for 12 h, at which point 6 M NaOH (20 mL) was added. Volatiles were removed by rotary evaporation, the residue was made neutral with 12 M HCl, and extracted with CH_2Cl_2 (3 × 20 mL). The combined extracts were dried over $MgSO_4$ and volatiles were removed under vacuum to yield a gummy yellow residue (crude $Papy_2OH_2$: 2.30 g, 6.2 mmol). Sodium metal (0.14 g, 6.2 mmol) was dissolved in methanol (10 mL) and added to the residue. The solution was stirred for 1 h and then the solvent was removed under vacuum. The remaining yellow solid, $NaPapy_2OH$, was used without further purification (2.40 g, 83% yield). ^1H NMR (250 MHz, $[D_6]DMSO$): δ = 2.56 (t, 2 H, CH_2), 3.40 (m, 2 H, CH_2), 3.78 (s, 4 H, CH_2), 6.08 (t, 1 H, ArH), 6.36 (d, 1 H, ArH), 6.87 (t, 1 H, ArH), 7.19 (t, 2 H, ArH), 7.63 (m, 5 H, ArH), 8.44 (d, 2 H, ArH). Selected FTIR absorption bands (KBr pellet): $\tilde{\nu}$ = 3051 (w), 2933 (w), 1625 (s), 1594 (s), 1466 (s), 1438 (s), 1390 (m), 1342 (m), 1256 (m), 1150 (m), 860 (w), 758 (s), 704 (m), 567 (w), 543 (w) cm^{-1}.

$Na[Fe(PypepO)_2]$ (1): $PypepOH_2$ (0.24 g, 1.1 mmol) was dissolved in DMF (25 mL) and to this was added solid NaH (0.05 g, 2.2 mmol). The mixture was stirred for 2 h and then a batch of $[Fe(DMF)_6](ClO_4)_3$ (0.43 g, 0.55 mmol) dissolved in DMF (5 mL) was added to it. The resultant deep green solution was allowed to stir for 2 h at 25 °C. Next, the solvent was removed under vacuum and the residue was dissolved in CH_3CN (10 mL). The solution was then stored at −20 °C for 3 days. The dark green microcrystalline solid thus obtained was collected by filtration (0.27 g, 42% yield). $C_{29}H_{23.5}FeN_{6.5}NaO_4$ (605.58 for $Na[Fe(PypepO)_2]\cdot 2.5\,CH_3CN$): calcd. C 57.47, H 3.91, N 15.03; found C 57.21, H 3.85, N 15.21. Selected FTIR absorption bands (KBr pellet): $\tilde{\nu}$ = 1670 (s), 1614 (s), 1593 (s, C=O), 1567 (s), 1464 (s), 1388 (m), 1274 (s), 1248 (m), 1098 (m), 1020 (w), 937 (w), 863 (w), 803 (w), 754 (m), 742 (m), 692 (w), 642 (w), 611 (w), 575 (w), 562 (w), 501 (w) cm^{-1}.

$[Fe(Papy_2O)(Cl)]$ (2): A portion of solid NaH (0.01 g, 0.43 mmol) was added to $NaPapy_2OH$ (0.16 g, 0.43 mmol) dissolved in DMF (10 mL) and the mixture was stirred for 2 h. To this solution was added a solution of $(Et_4N)[FeCl_4]$ (0.14 g, 0.43 mmol) dissolved in DMF (5 mL) and the resultant deep red solution was allowed to stir for an additional 1 h. The DMF solvent was then removed under vacuum and the residue was dissolved in CH_3CN (20 mL). The red solution was stored at −20 °C overnight. The resultant deep red microcrystalline solid was then filtered off and dried under

Table 3. Crystallographic data for $Na[Fe(PypepO)_2]\cdot 2.5CH_3CN$ (**1**·2.5CH_3CN), $[Fe(PapyO)(Cl)]\cdot 2CH_3CN$ (**2**·2CH_3CN), and [Fe(PapyO)(NCS)]·toluene (**3**·toluene)

	1·2.5CH_3CN	**2**·2CH_3CN	**3**·toluene
Empirical formula	$C_{29}H_{23.5}FeN_{6.5}NaO_4$	$C_{25}H_{26}ClFeN_6O_2$	$C_{29}H_{28}FeN_5O_2S$
Molecular weight	605.88	533.82	566.47
a [Å]	10.7660(10)	15.3649(7)	9.4884(4)
b [Å]	13.0305(12)	11.3058(5)	22.1746(10)
c [Å]	20.5973(19)	15.8124(8)	12.9277(6)
β [°]	95.239(2)	115.7740(10)	94.1370(10)
V [$Å^3$]	2877.4(5)	2473.5(2)	2712.9(2)
Z	4	4	4
Crystal system	monoclinic	monoclinic	monoclinic
Space group	$P2_1/n$	$P2_1/c$	$P2_1/n$
ρ [$g\cdot cm^{-3}$]	1.399	1.433	1.387
T [K]	90(2)	90(2)	90(2)
abs coeff, μ, mm^{-1}	0.585	0.753	0.669
GOF[a] on F^2	0.961	0.960	1.019
R_1 [b]	6.23	3.26	4.12
R_{w2} [c]	15.26	7.77	9.13

[a] $GOF = [\Sigma[w(F_0^2 - F_c^2)^2][M - N]]^{1/2}$ (*M* = number of reflections, *N* = number of parameters refined). [b] $R_1 = \Sigma||F_o| - |F_c||/\Sigma|F_o|$. [c] $R_{w2} = [\Sigma[w(F_0^2 - F_c^2)^2]/\Sigma[w(F_0^2)^2]]^{1/2}$.

vacuum (0.16 g, 70% yield). $C_{25}H_{26}ClFeN_6O_2$ (533.55 for [Fe(Papy$_2$O)(Cl)]·2CH_3CN): calcd. C 56.23, H 4.91, N 15.75; found C 56.19, H 4.96, N 15.28. Selected FTIR absorption bands (KBr pellet): $\tilde{\nu}$ = 1597 (m, C=O), 1571 (s), 1533 (s), 1444 (s), 1360 (s), 1290 (w), 1244 (w), 1102 (w), 1024 (w), 895 (w), 768 (s,), 704 (w), 658 (w) cm^{-1}.

[Fe(Papy$_2$O)(NCS)] (3): To a solution of NaPapy$_2$OH (0.21 g, 0.55 mmol) in DMF (10 mL) was added a batch of solid NaH (0.013 g, 0.55 mmol) and the mixture was allowed to stir for 2 h. To this solution was then added a batch of $[Fe(DMF)_6](ClO_4)_3$ (0.43 g, 0.55 mmol) dissolved in DMF (5 mL) and the purple/red solution was stirred for an additional 1 h. At this point, a solution of NaSCN (0.067 g, 0.83 mmol) in DMF (1 mL) was added and the color of the solution changed to red/brown. The DMF solvent was removed under vacuum and the residue was dissolved in THF (30 mL). The solution was stored at −20 °C overnight. The deep red needles were collected by filtration (0.15 g, 50% yield). $C_{26}H_{28}FeN_5O_3S$ (546.17 for [Fe(Papy$_2$O)(NCS)]·THF): calcd. C 57.13, H 5.17, N 12.82; found C 57.27, H 5.19, N 12.74. Selected FTIR absorption bands (KBr pellet): $\tilde{\nu}$ = 2046 (s, SCN), 1594 (m, C=O), 1570 (m), 1534 (m), 1445 (m), 1352 (m), 1103 (w), 1024 (w), 763 (m,) cm^{-1}.

Crystal Structure Analysis: Deep black/green crystals of Na[Fe(PypepO)$_2$]·2.5CH_3CN (**1**·2.5CH_3CN) and dark red crystals of [Fe(Papy$_2$O)(Cl)]·2CH_3CN (**2**·2CH_3CN) were each grown from CH_3CN at −20 °C. Black/red X-ray quality plates of [Fe(Papy$_2$O)(NCS)]·toluene (**3**·toluene) were grown from toluene/CH_2Cl_2 (3:1). Diffraction data for all complexes were collected at 90 K on Bruker SMART 1000 diffractometer. Mo-K_α (0.71073 Å) radiation was used in all cases and the data were corrected for absorption. The structures were solved using the standard SHELXS-97 package. Machine parameters, crystal data, and data collection parameters for **1**·2.5CH_3CN, **2**·2CH_3CN, and **3**·toluene are summarized in Table 3, while selected bond lengths and angles are listed in Table 1.

CCDC-166560, -166561 and -166552 contain the supplementary crystallographic data for complexes **1**·2.5CH_3CN, **2**·2CH_3CN, and **3**·toluene, respectively. These data can be obtained free of charge at www.ccdc.cam.ac.uk/conts/retrieving.html [or from the Cambridge Crystallographic Data Centre, 12, Union Road, Cambridge CB2 1EZ, UK; Fax: (internat.) +44-1223/336-033; E-mail: deposit@ccdc.cam.ac.uk].

Acknowledgments

Financial support from NSF (CHE-9818492) and NIH (GM 61636) is gratefully acknowledged. The Bruker SMART 1000 diffractometer was funded in part by an NSF Instrumentation Grant CHE-9808259.

[1] E. I. Solomon, T. C. Brunold, M. I. Davis, J. N. Kemsley, S. -K. Lee, N. Lehnert, F. Neese, A. J. Skulan, Y. -S. Yang, J. Zhou, *Chem. Rev.* **2000**, *100*, 235−350.
[2] *Biomimetic Oxidations Catalyzed by Transition Metal Complexes* (Ed.: B. Meunier), Imperial College Press, London, **1999**.
[3] D. S. Marlin, P. K. Mascharak, in *Encyclopedia of Catalysis: Biomimetic Catalysis by Models of Non-Heme Iron Enzymes* (Ed.: I. T. Horváth), John Wiley & Sons, Inc. New York, in press.
[4] T. J. Collins, S. W. Gordon-Wylie, M. J. Bartos, C. P. Horwitz, C. G. Woomer, S. A. Williams, R. E. Patterson, L. D. Vuocolo, S. A. Paterno, S. A. Strazisar, D. K. Peraino, C. A. Dudash, in *Green Chemistry: Frontiers in Benign Chemical Syntheses and Processes* (Eds.: P. T. Anastas and T. C. Williamson), Oxford University Press, Oxford, **1998**, 46.
[5] D. S. Marlin, P. K. Mascharak, *Chem. Soc. Rev.* **2000**, *29*, 69−74.
[6] J. M. Rowland, M. M. Olmstead, P. K. Mascharak, *Inorg. Chem.* **2001**, *40*, 2810−2817.
[7] C. Stockheim, L. Hoster, T. Weyhermüller, K. Wieghardt, B. Nuber, *J. Chem. Soc., Dalton Trans.* **1996**, 4409−4416.
[8] U. Auerbach, U. Eckert, K. Wieghardt, B. Nuber, J. Weiss, *Inorg. Chem.* **1990**, *29*, 938−944.
[9] U. Auerbach, T. Weyhermüller, K. Wieghardt, B. Nuber, E. Bill, C. Butzlaff, A. X. Trautwein, *Inorg. Chem.* **1993**, *32*, 508−519.
[10] D. S. Marlin, M. M. Olmstead, P. K. Mascharak, *Inorg. Chim. Acta* **2000**, *297*, 106−114.
[11] X. Tao, D. W. Stephan, P. K. Mascharak, *Inorg. Chem.* **1987**, *26*, 754−759.
[12] S. J. Brown, M. M. Olmstead, P. K. Mascharak, *Inorg. Chem.* **1990**, *29*, 3229−3234.
[13] D. S. Marlin, M. M. Olmstead, P. K. Mascharak, *Inorg. Chem.* **1999**, *38*, 3258−3260.
[14] J. C. Noveron, M. M. Olmstead, P. K. Mascharak, *Inorg. Chem.* **1998**, *37*, 1138−1139.
[15] S. Kimura, E. Bill, E. Bothe, T. Weyhermüller, K. Wieghardt, *J. Am. Chem. Soc.* **2001**, *123*, 6025−6039.
[16] S. Wang, L. Wang, X. Wang, Q. Luo, *Inorg. Chim. Acta* **1997**, *254*, 71−77.
[17] K. Ramesh, R. Mukherjee, *J. Chem. Soc., Dalton Trans.* **1992**, 83−89.
[18] J. W. Hwang, K. Govindaswamy, S. A. Koch, *Chem. Commun.* **1998**, 1667−1669.
[19] S. A. Koch, M. Millar, *J. Am. Chem. Soc.* **1982**, *104*, 5255−5257.
[20] G. S. Matouzenko, A. Bousseksou, S. Lecocq, P. J. Van Koningsbruggen, M. Perrin, O. Kahn, A. Collet, *Inorg. Chem.* **1997**, *36*, 2975−2981.
[21] A. P. Ginsberg, M. B. Robin, *Inorg. Chem.* **1963**, *2*, 817−822.
[22] J. Hodgkinson, R. B. Jordan, *J. Am. Chem. Soc.* **1973**, *95*, 763−768.

Received July 18, 2001
[I01267]

Difunctionalised Chemosensors Containing Electroactive and Fluorescent Signalling Subunits

Félix Sancenon,[a] Angel Benito,[a] Francisco J. Hernández,[a] José M. Lloris,[a] Ramón Martínez-Máñez,*[a] Teresa Pardo,[a] and Juan Soto[a]

Keywords: Ferrocene / Anthracene / Fluorescence / Chemosensors

The new ligands 13-anthrylmethyl-7-ferrocenylmethyl-1,4,10-trioxa-7,13-diaza-cyclopentadecane (L^1) and 1-anthrylmethyl-4,8,11-ferrocenylmethyl-1,4,8,11-tetraaza-cyclotetradecane (L^2) have been synthesised, characterised, and their potential activity as chemosensors towards the metal cations Ni^{2+}, Cu^{2+}, Zn^{2+}, Cd^{2+}, Hg^{2+} and Pb^{2+} studied in 1,4-dioxane/water (70:30, v/v). Both ligands L^1 and L^2 are difunctionalised receptors containing redox-active (ferrocene) and fluorescent (anthracene) signalling subunits. The crystal structures of $[H_2L^1][PF_6]_2$ and $[CuL^2][PF_6]_2$ were determined by single-crystal X-ray procedures. Potentiometric experiments in dioxane/water (70:30, v/v; 0.1 M KNO_3; 25.0 ± 0.1 °C) for L^1 and L^2 allowed the determination of protonation constants and complex stability constants with the Cu^{2+} and Pb^{2+} metal ions. They form stable complexes with both ligands and show stability constants with values close to those reported for similar complexes. The electrochemical and fluorescence behaviour of L^1 and L^2 was studied as a function of the pH and in the presence of the Ni^{2+}, Cu^{2+}, Zn^{2+}, Cd^{2+}, Hg^{2+}, and Pb^{2+} metal cations. The fluorescence and electrochemical response of L^1 and L^2 is pH-dependent. Ligand L^1 was able to electrochemically and selectively sense Pb^{2+} whereas L^2 sensed Cu^{2+}, Zn^{2+}, and Cd^{2+} using electrochemical techniques. The maximum electrochemical shift (ca. 57 mV) was found for L^2 in the presence of Cu^{2+} at pH = 8. Fluorescence studies showed that the emission intensities of L^1 and L^2 were selectively enhanced in the presence of Cu^{2+}. Additionally, the $[Cu(L^2)]^{2+}$complex acted as anion-sensing receptor in acetonitrile. The oxidation potential of the ferrocenyl group of the $[Cu(L^2)]^{2+}$complex was cathodically shifted upon addition of anions. The largest electrochemical shift was observed in the presence of fluoride (210 mV). The fluorescence emission of the anthracene groups in $[Cu(L^2)]^{2+}$ was enhanced in the presence of fluoride, nitrate, and dihydrogenophosphate.

Introduction

The design of functionalised receptors for the development of potential chemosensors is a field of active research. Of especial interest is the synthesis of molecules capable of amplifying microscopic events (for instance the presence of a target guest in a certain solution) to macroscopic levels.[1] This sensing function is generally achieved by the coupling of two well-defined parts, (i) selective binding sites and (ii) signalling subunits. This second component can be classified by the type of signal output; colour changes,[2] redox shifts,[3] and fluorescence quenching or enhancement[4] are among some commonly observed signals. Sensing molecules showing those changes can be built by attaching chromogenic units,[5] redox-active groups,[6] or fluorescent signalling subunits,[7] respectively, near the binding sites. Whereas the ligand−guest interaction is controlled by well-known binding rules (this is particularly true for ligand−cation interactions) the communication with the signalling subunit is more subtle. In some cases this is even unpredictable due to the competition of several processes, namely changes in photoelectron transfer or energy transfer paths, changes in redox properties of the receptor, etc. These new molecules are important because they will surely be the chemical active part of new sensing devices. For instance, receptors able to change spectroscopic properties (colour or fluorescence) in the presence of target substrates are of application in optical fibre devices,[8] whereas changes in redox potential upon addition of certain guests could be of application in the development of amperometric sensing devices.[9]

Despite the development of these individual areas, there are very few examples of molecules containing more than one type of signalling unit.[10] These systems can be important in the development of a new family of ion chemosensors that can either be able to sense different guests or display two or more macroscopic observable events upon addition of a certain analyte. Towards this goal, we have synthesised macrocyclic polyaza or oxaaza components and have functionalised them with both ferrocenyl and anthryl groups. Ferrocene is a well-known electro-active signalling subunit. Anthracene can act as either an electro- or photo-active

[a] Departamento de Química, Universidad Politécnica de Valencia,
Camino de Vera s/n, 46071 Valencia, España
Fax: (internat.) + 34-96/387-7349
E-mail: rmaez@qim.upv.es
Supporting information for this article is available on the WWW under http://www.eurjic.com or from the author.

 © WILEY-VCH Verlag GmbH, 69451 Weinheim, Germany, 2002 1434−1948/02/0404−0866 $ 17.50+.50/0 *Eur. J. Inorg. Chem.* **2002**, 866−875

group. Moreover, we have used the anthracene group because of its photophysical properties, and therefore we will refer to it as a fluorescent signalling subunit.

Results and Discussion

The new ligands L^1 and L^2 (Scheme 1) were synthesised according to a two-step reaction. Thus, reaction of 9-(chloromethyl)anthracene and the corresponding macrocycle (1:1 molar ratio) allowed isolation of the anthrylmethyl-functionalised derivatives that were further treated with an excess of (ferrocenylmethyl)trimethylammonium iodide in acetonitrile to give L^1 and L^2 in rather good yield. ^1H and ^{13}C NMR and mass spectra of L^1 and L^2 were consistent with the proposed formulation. Additionally, the crystal structures of the protonated form of L^1 and the Cu^{2+} complex of L^2 were determined using single-crystal X-ray procedures (see below).

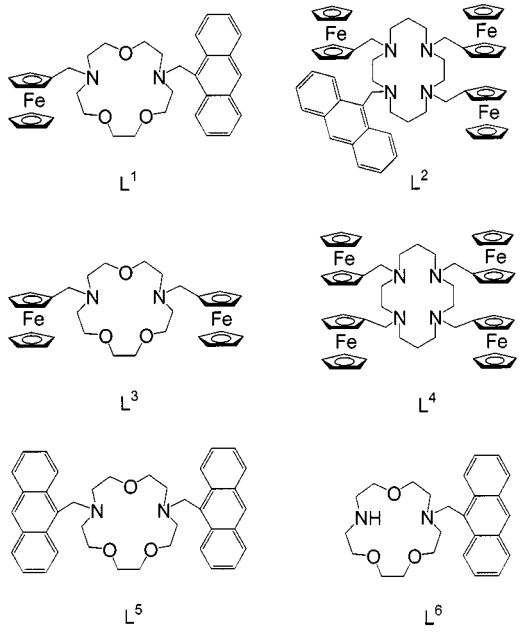

Scheme 1

L^1 and L^2 are rare examples of molecules containing redox-active and fluorescence signalling subunits. The following work has been devoted to characterise the ligands, their solution behaviour and their electrochemical and emission properties in the presence of transition metal ions and anions.

Crystal Structure of $[H_2L^1][PF_6]_2$

Addition of aqueous $[NH_4][PF_6]$ to acetonitrile solutions of L^1 allowed us to isolate the $[H_2L^1][PF_6]_2$ salt as a yellow solid. Suitable crystals of this compound for single-crystal X-ray diffraction techniques were obtained by slow diffusion of ether into dichloromethane solutions of $[H_2L^1][PF_6]_2$. The molecular structure consists of $[H_2L^1]^{2+}$ cations and PF_6^- anions linked ionically. The anthryl and cyclopentadienyl groups are planar within the experimental error and the ferrocenyl moiety adopts a nearly eclipsed conformation. The Fc−Cp(centroid) distances are 1.631 and 1.639 Å. A view of the $[H_2L^1]^{2+}$ cation and selected bond lengths and angles have been included as Supporting Information (see footnote on the first page of this article).

Crystal Structure of $[CuL^2][PF_6]_2 \cdot CH_2Cl_2$

The $[CuL^2][PF_6]_2$ complex was obtained by reaction of L^2 with copper(II) nitrate in acetonitrile and further addition of aqueous $[NH_4][PF_6]$. Suitable crystals for X-ray diffraction were obtained by diffusion of ether into dichloromethane solutions of the complex. Table 1 gives selected bond lengths and angles. Figure 1 shows a view of the compound. The molecular structure consists of cationic $[CuL^2]^{2+}$ and PF_6^- anions as counterions. Molecules of dichloromethane complete the packing. The Cu^{2+} atom is coordinated by the four nitrogen atoms of the macrocycle, giving a distorted square-planar geometry. Three nitrogen atoms are also covalently bonded to three ferrocenylmethyl centres, whereas one nitrogen atom is attached to an anthrylmethyl group. The Cu−N distances range from 2.116(7) to 2.152(7), averaging 2.127 Å. Some bond angles around Cu^{2+} are far from the ideal square-planar geometry, for instance N(3)−Cu(1)−N(2), N(3)−Cu(1)−N(1), and N(4)−Cu(1)−N(1) are 86.8(3), 151.2(3), and 85.7(3), respectively. The four nitrogen atoms define a plane within ±

Table 1. Selected distances and angles for compound $[CuL^2][PF_6]_2$

Distances [Å]			
Cu(1)−N(1)	2.152(7)	Cu(1)−N(2)	2.123(7)
Cu(1)−N(3)	2.116(7)	Cu(1)−N(4)	2.116(7)
N(1)−C(10)	1.465(11)	N(1)−C(1)	1.511(10)
N(1)−C(44)	1.510(11)	N(2)−C(3)	1.492(11)
N(2)−C(4)	1.498(12)	N(2)−C(11)	1.499(11)
N(3)−C(6)	1.454(11)	N(3)−C(5)	1.47(11)
N(3)−C(22)	1.532(11)	N(4)−C(9)	1.472(12)
N(4)−C(8)	1.483(11)	N(4)−C(33)	1.534(8)
Angles (°)			
N(3)−Cu(1)−N(4)	93.4(3)	N(3)−Cu(1)−N(2)	86.8(3)
N(4)−Cu(1)−N(2)	176.0(3	N(3)−Cu(1)−N(1)	151.2(3)
N(4)−Cu(1)−N(1)	85.7(3)	N(2)−Cu(1)−N(1)	92.2(3)
C(10)−N(1)−C(44)	112.7(6)	C(10)−N(1)−C(1)	107.2(7)
C(44)−N(1)−C(1)	112.6(7)	C(10)−N(1)−Cu(1)	101.5(5)
C(44)−N(1)−Cu(1)	111.7(5)	C(1)−N(1)−Cu(1)	110.5(5)
C(3)−N(2)−C(4)	107.7(6)	C(3)−N(2)−C(11)	112.4(7)
C(4)−N(2)−C(11)	107.1(7)	C(3)−N(2)−Cu(1)	110.4(5)
C(4)−N(2)−Cu(1)	103.6(5)	C(11)−N(1)−Cu(1)	114.9(5)
C(6)−N(3)−C(5)	109.0(6)	C(6)−N(3)−C(22)	111.3(7)
C(5)−N(3)−C(22)	109.1(7)	C(6)−N(3)−Cu(1)	113.6(6)
C(5)−N(3)−Cu(1)	103.9(6)	C(22)−N(3)−Cu(1)	109.5(5)
C(9)−N(4)−C(8)	108.7(7)	C(9)−N(4)−C(33)	107.7(6)
C(8)−N(4)−C(33)	110.6(6)	C(9)−N(4)−Cu(1)	104.6(5)
C(8)−N(4)−Cu(1)	111.3(5)	C(33)−N(4)−Cu(1)	113.5(4)
C(2)−C(1)−N(1)	117.1(8)	C(1)−C(2)−C(3)	114.6(8)
N(2)−C(3)−C(2)	114.9(7)	N(2)−C(4)−C(5)	110.6(7)
N(3)−C(5)−C(4)	111.3(7)	N(3)−C(6)−C(7)	116.4(7)
C(6)−C(7)−C(8)	114.6(8)	N(4)−C(8)−C(7)	115.2(7)
N(4)−C(9)−C(10)	110.8(7)	N(1)−C(10)−C(9)	112.4(7)

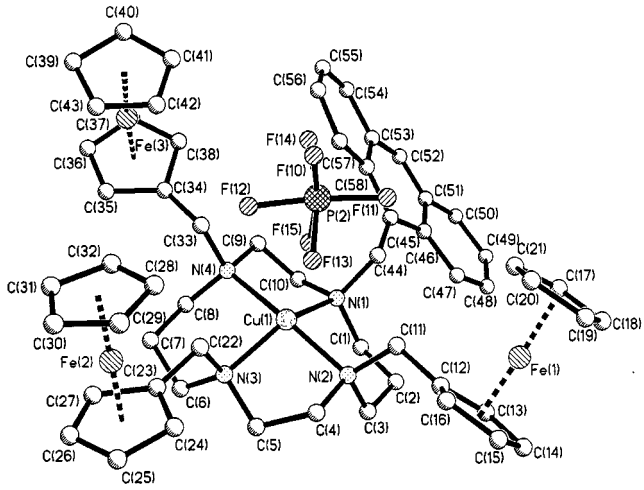

Figure 1. Molecular structure of the $[CuL^2]^{2+}$ cation

0.23 Å and the copper atom is out-of-plane by ± 0.30 Å. The deviation from the ideal geometry is mainly induced by the cyclam unit that adopts a configuration with the four nitrogen atoms pointing above the N4 plane. This has been reported to be the thermodynamically less favourable isomer.[11] However, the conformation of tetrafunctionalised cyclam derivatives containing the four groups above the N4 plane is not unusual and has also been found in complexes such as $[Ni(Me_4cyclam)]^{2+}$, Me_4cyclam = 1,4,8,11-tetramethyl-1,4,8,11-tetraazacyclotetradecane, and in the nickel(II) complex of L^4.

It is remarkable that the molecular assembly of Cu^{2+} and the ligand L^2 leads to the formation of a host molecule containing a cavity built with three ferrocenylmethyl groups and one anthrylmethyl group. In the crystal structure this cavity is filled by one PF_6^- counterion. In fact, there is a very close contact between the Cu^{2+} and the F(15) atom [Cu^{2+}···F(15) 2.47 Å]. Figure 2 also shows as an alternative view, with the space-filling representation emphasising the electro-photo-active cavity and the host−guest association.[12] No significant distortions were found in the ferrocenylmethyl and anthrylmethyl groups. The ferrocenyl units adopt the usual sandwich conformation with the cyclopentadienyl rings parallel within the experimental error. Fe-Cp(centroid) distances range from 1.621 to 1.659, averaging 1.637 Å.

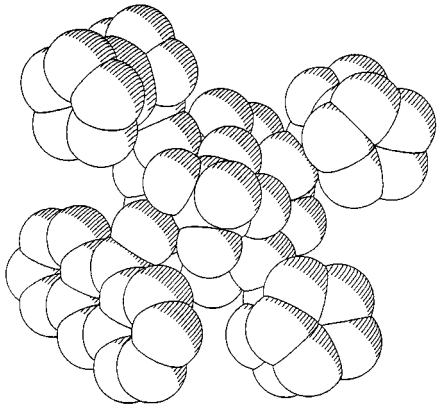

Figure 2. the space-filling representationof the $[CuL^2]^{2+}$ cation

Potentiometric Studies

Protonation constants determined potentiometrically in 1,4-dioxane/water (70:30 v/v; 25 °C; 0.1 M potassium nitrate) are shown in Table 2. As expected, L^1 and L^2 show two and four protonation processes, respectively. Ligand L^1 displays stepwise protonation constants close to those reported[13] for L^3. Ligand L^4 is a cyclam derivative, and it shows the two first protonations being much more basic than the last two. A similar behaviour was found for cyclam itself and other cyclam derivatives.[14] Figure 3 shows the distribution diagram of the L^1/H^+ and L^2/H^+ systems.

Table 2. Stepwise protonation constants for L^1 and L^2 in dioxane/water (70:30 v/v; 25 °C; 0.1 M potassium nitrate)

Reaction	L^1	L^2
$L + H^+ = [HL]^+$	8.14(2)	8.91(2)
$[HL]^+ + H^+ = [H_2L]^{2+}$	5.80(2)	6.56(1)
$[H_2L]^{2+} + H^+ = [H_3L]^{3+}$		2.71(3)
$[H_3L]^{3+} + H^+ = [H_4L]^{4+}$		2.36(1)

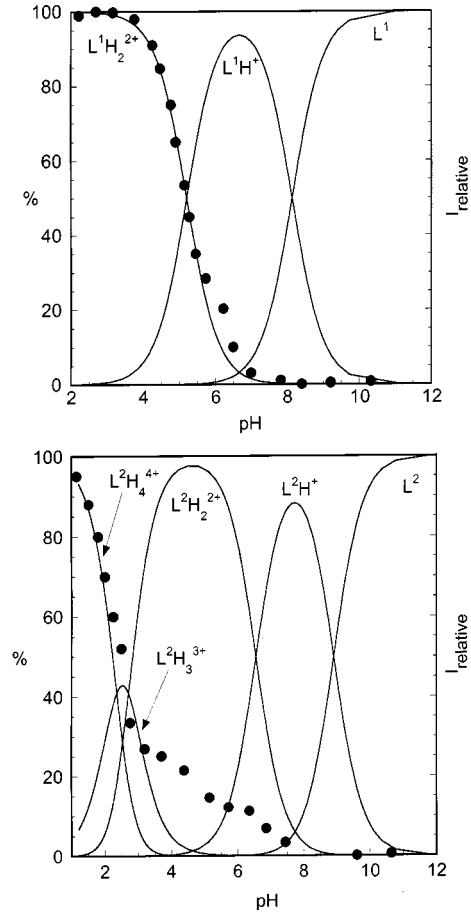

Figure 3. Distribution diagrams of the species for a) L^1/H^+ and b) L^2/H^+ (full line) and the fluorescence emission titration curves (•) for those systems

Stability constants for the formation of complexes of L^1 and L^2 with Cu^{2+}, Pb^{2+} in dioxane/water (70:30, v/v) mixtures are shown in Table 3. Both metal ions form with the receptors here considered stable $[ML]^{2+}$ complexes. Figures 4 and 5 show the distribution diagram of the $L/Cu^{2+}/H^+$ and $L/Pb^{2+}/H^+$ systems (L = L^1 or L^2). In general, the formation stability constants obtained are in line with those reported for related complexes.[14] Receptor L^2 is a tetraaza macrocycle, and displays larger stability constants with Cu^{2+} than with Pb^{2+}. In fact, the stability constant of the $L^2 + M^{2+} = [M(L^2)]^{2+}$ process is 10^3 times larger for Cu^{2+} than for Pb^{2+}. In contrast, when the N-donor atoms are partially replaced with O-donor atoms the affinity for Cu^{2+} is considerably reduced and the stability constants for the formation of the $[M(L^1)]^{2+}$ complexes are similar for Cu^{2+} and Pb^{2+} (log$K$ = 5.23 for copper and log$K$ = 5.12 for lead). These stability constants are not very different to those found for L^3 with the same metal ions {log$K$ = 6.27 and log$K$ = 6.43, for the formation of the $[M(L^3)]^{2+}$ complexes with Cu^{2+} and Pb^{2+}, respectively}.[13]

Table 3. Stability constants (log K) for the formation of Cu^{2+} and Pb^{2+} complexes of L^1 and L^2 in dioxane/water (70:30, v/v; 25 °C; 0.1 M potassium nitrate)

Reaction	L^1	L^2
$Cu^{2+} + L + H^+ = [Cu(HL)]^{3+}$	12.85(4)	14.05(4)
$Cu^{2+} + L = [Cu(L)]^{2+}$	5.23(2)	9.67(1)
$Cu^{2+} + L + H_2O = [Cu(L)(OH)]^+ + H^+$	−1.84(2)	0.56(4)
$Cu^{2+} + L + 2H_2O = [Cu(L)(OH)_2] + 2H^+$	−13.13(3)	−9.34(3)
$Pb^{2+} + L + H^+ = [Pb(HL)]^{3+}$	11.15(3)	13.45(4)
$Pb^{2+} + L = [Pb(L)]^{2+}$	5.12(1)	6.31(3)
$Pb^{2+} + L + H_2O = [Pb(L)(OH)]^+ + H^+$	−2.72(1)	−0.70(3)
$Pb^{2+} + L + 2H_2O = [Pb(L)(OH)_2] + 2H^+$	−12.81(3)	−10.12(4)

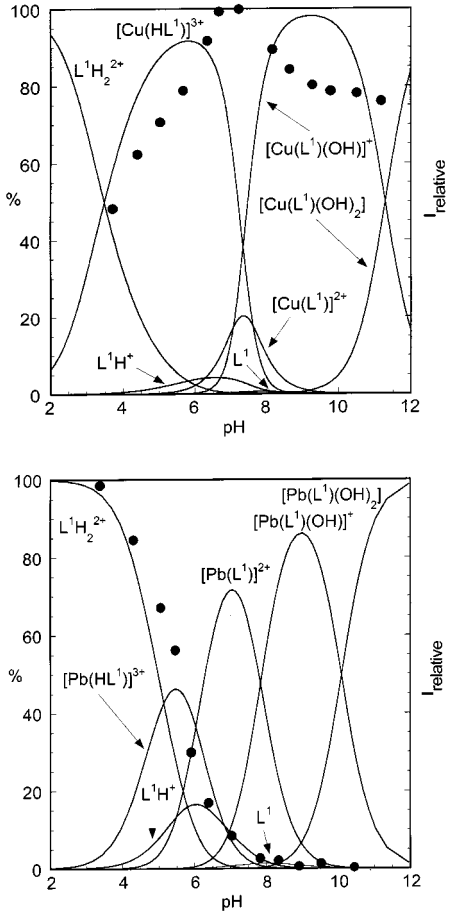

Figure 4. Distribution diagrams of the species for a) $L^1/Cu^{2+}/H^+$ and b) $L^1/Pb^{2+}/H^+$ (full line) and the fluorescence emission titration curves (•) for those systems

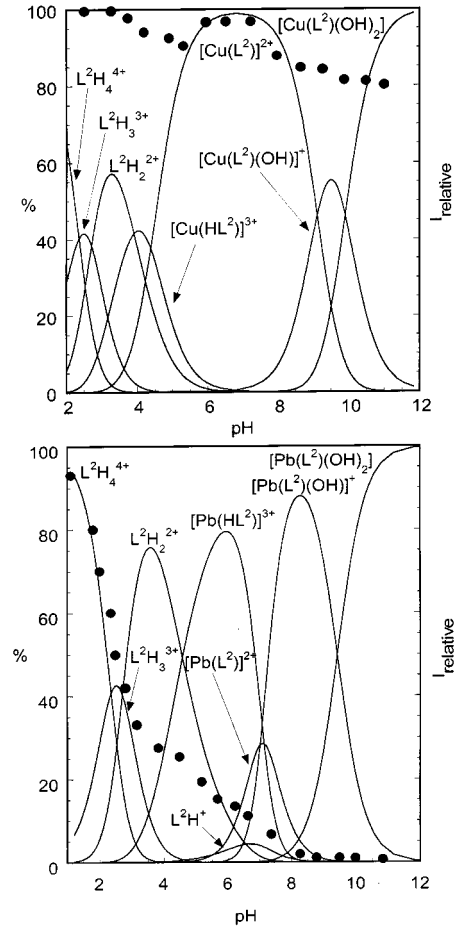

Figure 5. Distribution diagrams of the species for a) $L^2/Cu^{2+}/H^+$ and b) $L^2/Pb^{2+}/H^+$(full line) and the fluorescence emission titration curves (•) for those systems

Cation Sensing

Electrochemical Behaviour

The redox potentials of both L^1 and L^2 are pH-dependent. When basic solutions of L^1 and L^2 are acidified a steady displacement of $E_{1/2}$ ($E_{1/2}$ = half-wave potential) to more anodic potentials was observed. This is a known behaviour, attributed to the protonation of the amino groups and therefore to the formation of positively charged species that are more difficult to be oxidised.[15] The difference found between the oxidation potential under basic (pH ≈ 12) and acidic (pH ≈ 2) conditions was 140 and 110 mV for L^1 and L^2, respectively. We have also electrochemically

studied the variation of $E_{1/2}$ versus pH for the $L/H^+/M^{2+}$ systems (L = L^1 or L^2; M = Ni^{2+}, Cu^{2+}, Zn^{2+}, Cd^{2+}, Hg^{2+} or Pb^{2+}; M^{2+}/L molar ratio = 1). In order to rationalise those data the difference between $E_{1/2}$ for the receptor/metal system and that for the free receptor [$\Delta E_{1/2}$ = $E_{1/2}$(receptor/metal) − $E_{1/2}$(receptor)] was monitored at different pH values from 2 to 12. Figure 6 (top) shows $\Delta E_{1/2}$ versus pH for L^1 in the presence of Pb^{2+}. For other metal ions (Ni^{2+}, Cu^{2+}, Zn^{2+}, Cd^{2+}, and Hg^{2+}) $\Delta E_{1/2}$ is less than 5 mV (not shown). Ligand L^1 was able to electrochemically recognise Pb^{2+} over other common, typically present (in water samples) metal ions in the pH range of 5 to 7.5, although the maximum shift found of 25 mV at pH = 6.5 is rather small. Figure 6 (bottom) displays the electrochemical response found for L^2 as a function of the pH in the presence of Cu^{2+}, Zn^{2+}, and Cd^{2+}. No electrochemical shift was induced for Ni^{2+}, Hg^{2+}, and Pb^{2+}. The Cu^{2+}, Cd^{2+}, and Zn^{2+} ions change the oxidation potential of the L^2 ligand in a wide pH range, the maximum shift being observed for Cu^{2+} at pH = 8 (ca. 57 mV).

Comparison between the electrochemical response in Figure 6 and the distribution diagrams in Figures 4 and 5 allows a determination of the species responsible for the electrochemical shift. Thus, the $[Pb(L^1)]^{2+}$ complex exists in the pH range 6−8, at which the redox potential of the ferrocenyl groups suffer an anodic shift of ca. 25 mV with respect to that of the L^1 ligand. Comparison between Figure 5 (top) and Figure 6 (bottom) also suggests that it is the existence in solution of the $[Cu(L^2)]^{2+}$ complex that induces anodic shifts of up to 60 mV. It seems that there is a correlation between the presence, in solution, of the $[M(L)]^{2+}$ species and the electrochemical response. In this sense the absence of an electrochemical signal for the L^1/Cu^{2+} and L^2/Pb^{2+} systems might be related to the appearance of the $[Cu(L^1)]^{2+}$ and $[Pb(L^2)]^{2+}$ complexes as minor species [see Figure 4 (top) and Figure 5 (bottom)].

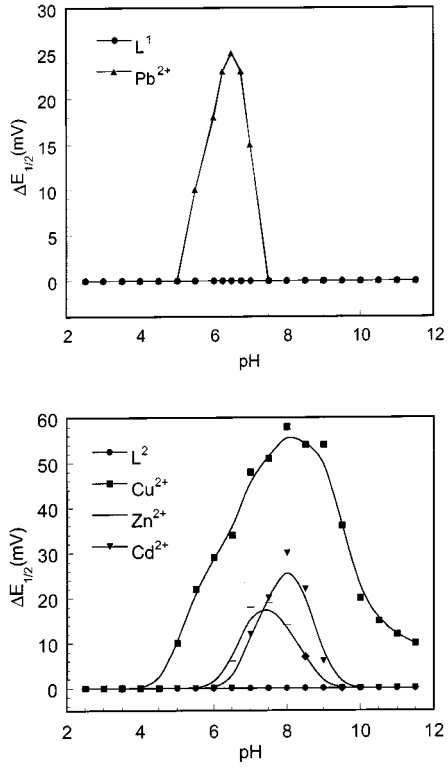

Figure 6. Oxidation potential shift ΔE [defined as $E_{1/2}$(receptor + metal ion) − $E_{1/2}$(receptor)] of a) L^1 and b) L^2 as a function of the pH in the presence of certain metal ions

At this point, it might be interesting to compare the electrochemical response of L^1 and L^2 with that previously reported for the L^3 and L^4 ferrocene-functionalised ligands. L^3 displays a large electrochemical recognition for Pb^{2+} (ca. −60 mV), although other heavy metal ions such as Cd^{2+} and Hg^{2+} also produce significant shifts (ca. −35 mV).[13] Additionally, the electrochemical shift in the presence of Pb^{2+} for L^1 is anodic but was reported to be cathodic for L^3. We have recently pointed out that in these systems, where there is no electronic communication through the bond between the metal centre and the signalling subunits, the electrochemical shift is mainly controlled by the nature of the complex formed at a certain pH and the distance between the positively charged metal centre and the ferrocenyl unit. The significant difference between the electrochemical response of L^1 and L^3 shows how subtle differences in the receptor (one or two ferrocenyl units) have significant influence in the electrochemical response. The receptor L^4 is able to electrochemically detect Cu^{2+}, Zn^{2+}, and Cd^{2+} in a wide pH range over Ni^{2+} and Pb^{2+}. This is a similar response to that observed for L^2. However, the maximum shift for L^2 in the presence of Cu^{2+} is ca. 60 mV at pH = 8, whereas for L^4 the maximum electrochemical shift was ca. 100 mV for Cu^{2+} at the same pH.[14] In conclusion, L^1 and L^2 are redox-active functionalised molecules that can electrochemically sense Pb^{2+} (L^1) and Cu^{2+}, Zn^{2+}, and Cd^{2+} (L^2) using electrochemical methods.

Fluorescence Behaviour

The study of the fluorescence behaviour of the L^1 and L^2 ligands was also carried out in dioxane/water (70:30) mixtures and with modulation of the pH. The ligands L^1 and L^2 show typical structured anthracene-like absorption and emission spectra with a maximum in the absorption band at 366 nm for L^1 and 367 nm for L^2, and with maximum emission wavelengths at 412 and 414 nm, respectively (see photophysical data in Table 4). The fluorescence intensity of L^1 and L^2 shows the typical behaviour of anthrylmethyl-substituted polyamines with maximum fluorescence at acidic pH and decrease of fluorescence at basic pH (see Figure 3 for the fluorescence emission titration curves of L^1 and L^2). This pH-dependent emission behaviour is well

Table 4. Photophysical parameters

	λ_{exc}	λ_{emi}	φ[a]
L^1	366	412	0.0030
L^5	366	410	0.0080
L^6	366	411	0.0055

[a] Quantum yield relative to anthracene in acetonitrile (φ = 0.36).

known and attributed to the existence of electron-transfer paths from the lone pair of the amine to the photo-excited state of the anthracene at basic pH that is not operative upon amine protonation.[16] From Figure 3 it can be observed that the fully protonated species of H_2L^1 are fluorescent, whereas deprotonation of at least one nitrogen atom gave species showing a much weaker emission intensity. In line with this behaviour, the species L^2 and L^2H^+ display low fluorescence; $L^2H_2^{2+}$ and $L^2H_3^{3+}$ induce some fluorescence enhancement, but the emission enhancement is at a maximum with the fully protonated $L^2H_4^{4+}$ species.

Figures 4 and 5 show the fluorescent emission titration curves for L^1 and L^2 in the presence of Cu^{2+} and Pb^{2+} (1:1 metal/ligand ratio). In both cases, Cu^{2+} is the only metal ion able to produce a considerable modification of the emission intensity versus pH profile of the free ligand. In contrast, Pb^{2+} [shown in Figure 4 (bottom) and Figure 5 (bottom)] and the cations Ni^{2+}, Zn^{2+}, Cd^{2+}, and Hg^{2+} (not shown) do not change significantly the fluorescence emission versus pH curves of the free receptors. Figure 4 (top) shows that all four complexes $[Cu(HL^1)]^{3+}$, $[Cu(L^1)]^{2+}$, $[Cu(L^1)(OH)]^+$, and $[Cu(L^1)(OH)_2]$ induce enhancement of the emission fluorescence intensity. The quantum yield of L^1 at pH = 7 is 0.050, whereas in the presence of Cu^{2+} the quantum yield at the same pH is 0.10. Figure 5 (top) also shows that all the Cu^{2+} complexes induce fluorescence emission enhancement.

The fluorescence curve in the presence of Pb^{2+} is very close to that found for the free receptors. At this point it has to be noted that a similar effect has been observed for instance in zinc(II) complexes of *N*,*N*-dibenzylated- or *N*-(anthrylmethyl)polyazaalkanes; that is, despite the formation of stable complexes the fluorescence behaviour versus pH of the free ligand and in the presence of Zn^{2+} is very similar.[17] From Figure 4 (bottom) and Figure 5 (bottom) it can be deduced that, except for the $[Pb(HL)]^{3+}$ complex (L = L^1 or L^2), that slightly enhances the fluorescence, the remaining species, $[Pb(L)]^{2+}$, $[Pb(L)(OH)]^+$, and $[Pb(L)(OH)_2]$, do not increase the emission intensity of the free L^1 receptor. This indicates that the coordination of Pb^{2+} to the nitrogen atoms is less effective than protonation in preventing photo-induced electron-transfer processes, and that the Pb^{2+} cation has little effect on the fluorescence behaviour despite the formation of stable complexes. One possible explanation of this observed behaviour could be related to the strength of the coordination between the nitrogen atoms and the Pb^{2+} cation, a poor coordination with at least one nitrogen atom will not hinder the photo-electron transfer from the lone pair of the nitrogen atom to the excited fluorophore. In this sense the effect is similar to that observed with protons; only when the L^1 or L^2 molecules are fully protonated there is an emission enhancement, whereas partial protonations have a lesser effect or no effect at all.

The fluorescent response of L^1 and L^2 in the presence of Cu^{2+} is remarkably different to the response observed for Cu^{2+} for similar receptors. The usual behaviour observed with anthrylaza macrocycles in the presence of Cu^{2+} is a fluorescence quenching upon complexation.[18] The chelation-enhanced quenching (CHEQ) has been reported to occur with copper and also with other open-shell paramagnetic or easily reducible metal cations. In fact, for the receptor 1,4,8,11-tetrakis(naphthylmethyl)-1,4,8,11-tetraazacyclotetradecane (containing four naphthylmethyl groups attached to the four N-donor atoms of the cyclam unit) the presence of Cu^{2+} (and also Hg^{2+}) produces a noticeable quenching of the emission fluorescent intensity at acidic pH.[19] A similar effect, the quenching of the emission fluorescence, is observed for cyclam functionalised with $Ru(tpy)_2^{2+}$ groups in the presence of Cu^{2+}.[20] All these reported data contrast with the fluorescence enhancement observed for L^1 and L^2 upon complexation of Cu^{2+}. This result could be of interest because in sensing processes fluorescence enhancement rather than quenching is usually preferred in order to observe a high signal output. However, it has to be pointed out that there are a few papers reporting enhancement of the fluorescence upon copper(II) complexation.[21] This has been achieved for instance by controlling either the interaction of the metal ion with the receptor in order to reduce the metal−fluorophore interaction or acting directly modifying the nature of the fluorophore. Thus, Bharadwaj has reported that the use of preorganised cryptands can induce unusual geometries that suppress the redox activity of the coordinated Cu^{II} cation, inhibiting the interaction between the copper(II) and the photo-excited state of anthryl fluorescent groups.[21a] In a recent paper Samanta reports the development of a receptor that suffers enhancement upon addition of metal ions by simply using electron-deficient fluorophores.[21b]

In our case we believe that the anomalous behaviour observed for Cu^{2+} could be ascribed to the presence of the ferrocenyl groups (see below). It is well known that ferrocene is an efficient fluorescence quencher via both energy-transfer and reductive quenching processes.[10d] In our case, the occurrence of an electron-transfer mechanism is thermodynamically favourable as it can be demonstrated from electrochemical and photophysical data. The free energy of the process (anthracene + Fc = anthracene$^-$ + Fc$^+$) in which the ferrocene is acting as reductive quencher can be calculated by the equation of Rehm-Weller, where $E^0_{Fc^+/Fc}$ and E^0_{fl/fl^-} are the redox potentials of the processes $Fc^+ + 1e^- \rightarrow Fc$ and $fl + 1e^- \rightarrow fl^-$ (fl = fluorophore), respectively, and λ can be obtained from the emission fluorescence spectrum.[22]

$$\Delta G = -\frac{hcN_A}{\lambda} + F\left[E^o_{Fc^+/Fc} - E^o_{fl/fl^-}\right]$$

Redox potentials were measured in dry acetonitrile (0.1 M tetrabutylammonium perchlorate; 25 °C). The ligand L^2 shows a reversible oxidation process at 450 mV and a reduction irreversible wave at −2.2 V versus SCE, which have been ascribed to the oxidation of the ferrocenyl and to the reduction of the anthryl groups, respectively. Taking into account these data, ΔG is −33.6 kJ/mol indicating that photo-induced electron transfer from the ferrocene to the anthryl fluorophore can occur. Additionally, an energy-

transfer quenching mechanism could also be possible.[10d] The quenching induced by the ferrocenyl group is supported by experimental data, thus the quantum yield of the ferrocene-containing ligand L^1 in acetonitrile ($\varphi = 0.0030$) is lower than that of L^6 ($\varphi = 0.0055$) or L^5 ($\varphi = 0.0080$). This difference in quantum yield is ascribed to the presence of ferrocenylmethyl groups in L^1. In fact, when stoichiometric amounts of H_2O_2 were added to L^1, the solution turned green-blue (due to the oxidation of ferrocene) and there was a fluorescence enhancement (quantum yield of ca. 0.0042).

As stated above, Cu^{2+} is also a well-known quencher. From a thermodynamic point of view both energy-transfer or electron-transfer processes are possible when Cu^{2+} ions are added to L^1 or L^2 solutions. Bearing this in mind, one would expect that the presence of Cu^{2+} would reduce even more the emission intensity of the receptors. In contrast, an enhancement of the fluorescence is observed. However, it has to be taken into account that, although the presence of Cu^{2+} gives new quenching routes, it might also inhibit some. Namely, strong coordination to nitrogen atoms can inhibit the photo-electron transfer from the lone pair of the amine to the fluorophore. Additionally, it might also happen that the presence of Cu^{2+} hinders the energy-transfer quenching process from the ferrocene to the anthracene due to the increase of the rigidity of the receptor upon coordination, thereby disfavouring the nonradiative decay processes. Furthermore, and especially for L^2, the cation Cu^{2+} induces a significant cathodic electrochemical shift of the ferrocenyl redox potential of ca. 60 mV in dioxane/water and of ca. 100 mV in acetonitrile making electron transfer from the ferrocene to the anthracene thermodynamically less favourable. In resume, although Cu^{2+} itself might introduce energy- and electron-transfer quenching paths it also inhibits other quenching mechanisms, the overall effect being an emission fluorescence enhancement.

Anion Sensing

The free receptors L^1 and L^2 are anion-insensitive. Thus, addition of different anions such as phosphate, sulfate, nitrate, fluoride, chloride, bromide, etc. to solutions of these receptors in acetonitrile or dioxane/water resulted in no variation of either electrochemical or photochemical properties. This contrasts with the anion-sensing ability found for the $[Cu(L^2)]^{2+}$complex (see below). In this sense it is noticeable that one of the most interesting features in the crystallographic characterisation of the $[Cu(L^2)]^{2+}$ complex is the formation of a host molecule containing a Cu^{2+} ion surrounded by a cavity built with three ferrocenylmethyl and one anthrylmethyl group. This is a peculiar topology. The interaction (either covalent or electrostatic) of anions with the Cu^{2+} charged cation might allow a close proximity between the guest (anion) and the electro-active ferrocenyl or the photo-active anthryl signalling units. In order to check this possible co-operative effect, the anion-sensing properties of the $[Cu(L^2)]^{2+}$complex was investigated electrochemically and by fluorescence studies. Table 5 summarises the electrochemical data in acetonitrile. The most remarkable effect is the very large cathodic shift of 210 mV observed upon fluoride addition. Other halide anions such as chloride and bromide gave much lower cathodic shifts (ca. 20 mV). Thus, the $[Cu(L^2)]^{2+}$complex is able to selectively and electrochemically sense fluoride over other halide anions.[23] The $H_2PO_4^-$ anion also induces an important electrochemical cathodic shift of 150 mV whereas the response in the presence of HSO_4^-, and NO_3^- is remarkably lower.[24] Fluorescence studies on the $[Cu(L^2)]^{2+}$complex upon addition of anions in acetonitrile were also carried out. Table 5 summarises the anion response. The addition of Cl^-, Br^-, I^-, and HSO_4^- had no effect, whereas nitrate, fluoride and $H_2PO_4^-$ induced an enhancement of the fluorescence intensity of the $[Cu(L^2)]^{2+}$ complex of 26%, 20%, and 17%, respectively. From fluorimetric/spectroscopic titration well-defined isosbestic points were observed indicating the formation of 1:1 complexes. The logarithms of the stability constants obtained by least-squares analysis of the titration curves were 4.5 ± 0.2; 4.2 ± 0.1, and 4.4 ± 0.3 for nitrate, fluoride, and dihydrogenophosphate, respectively.[25]

Table 5. Photophysical and electrochemical anion response of $[Cu(L^2)]^{2+}$ upon addition of 10 equiv. of the corresponding anion in acetonitrile

Electrochemical							
Receptor	$H_2PO_4^-$	HSO_4^-	NO_3^-	F^-	Cl^-	Br^-	
$[Cu(L^2)]^{2+}$	150[a]	55	< 5	210	24	20	
Photophysical							
Receptor	$H_2PO_4^-$	HSO_4^-	NO_3^-	F^-	Cl^-	Br^-	I^-
$[Cu(L^2)]^{2+}$	17%[b]	< 5%	26%	20%	< 5%	< 5%	< 5%

[a] ΔE_{pa} calculated as E_{pa} of the receptor $-E_{pa}$ of the receptor anion in mV for $[Cu(L^2)]^{2+}$ in 0.1 M tetrabutylammonium perchlorate. Iodide has an oxidation potential in acetonitrile similar to that of ferrocene and was not studied. [b] Enhancement of the fluorescence intensity of the 412-nm emission band.

Conclusions

We can conclude that L^1 and L^2 are rare receptors, containing two signalling subunits whose response against metal cations can be controlled by the type of output signal (electrochemical shift or changes in fluorescence emission) used to trace information from the solution. This is resumed in Table 6 that shows the selective response obtained by the oxaaza ring 1,4,10-trioxa-7,13-diazacyclopentadecane or the polyaza ring 1,4,8,11-tetraazacyclotetradecane depending on their functionalisation. Difunctionalised systems could have advantages over monofunctionalised ones because the former might act as multiple-sensing receptors. Thus, L^1 responds to Pb^{2+} using electrochemical methods, but is a Cu^{2+} chemosensor if emission intensity is used as output signal. In a similar way, L^2 electrochemically responds to Cu^{2+}, Zn^{2+}, and Cd^{2+} but it only gives emission response against Cu^{2+}. A similar control effect on the sens-

Table 6. Electrochemical and photophysical response against certain transition metal ions by the functionalised binding domains 1,4,10-trioxa-7,13-diazacyclopentadecane and 1,4,8,11-tetraazacyclotetradecane functionalised with ferrocene and anthracene

	Ferrocene	Anthracene	Ferrocene and Anthracene
1,4,10-Trioxa-7,13-diazacyclopentadecane	Pb^{2+}, Cd^{2+}, Hg^{2+}	Hg^{2+}	Electrochemical: Pb^{2+} Photophysical: Cu^{2+}
1,4,8,11-Tetraazacyclotetradecane	Cu^{2+}, Zn^{2+}, Cd^{2+}	–	Electrochemical: Cu^{2+}, Zn^{2+}, Cd^{2+} Photophysical: Cu^{2+}

ing process depending on the output signal, is observed for the $[Cu(L^2)]^{2+}$complex in its interaction with anions. Thus, the maximum electrochemical shift is observed in the presence of fluoride, whereas the largest emission fluorescence enhancement was observed upon addition of the poorly coordinating anion nitrate.

Experimental Section

General Remarks: All commercially available reagents were used without further purification. Air/water-sensitive reactions were performed in flame-dried glassware under argon. Dioxane and acetonitrile were dried with CaH_2 and distilled prior to use.

L^1: The free base 1,4,10-trioxa-7,13-diazacyclopentadecane (400 mg, 1.832 mmol) was heated under reflux in dry dichloromethane with 9-(chloromethyl)anthracene (410 mg, 1.805 mmol) in the presence of triethylamine (560 mg, 5.5 mmol). After 6 h, the mixture was cooled to room temperature, basic water was added and the organic phase separated, dried with anhydrous magnesium sulfate, filtered, and concentrated to dryness. The resulting oil was dissolved in dichloromethane and purified by chromatography on alumina using dichloromethane/ethanol (100:1, v/v) as eluent. This allowed us to isolate the compound 7-anthracenylmethyl-1,4,10-trioxa-7,13-diazacyclopentadecane. Yield 450 mg, 56%. This compound (415 mg, 1.015 mmol) was heated under reflux in dry acetonitrile with (ferrocenylmethyl)trimethylammonium iodide (508 mg, 1.32 mmol) in the presence of potassium carbonate. After 24 h, the reaction mixture was filtered and the orange solution concentrated to dryness. The product L^1 was obtained after chromatography on alumina using dichloromethane/ethanol (100:1, v/v) as eluent. Yield 615 mg, 67%. ^{1}H NMR ($CDCl_3$): δ = 2.65 (dt, 4 H, CH_2), 2.81 (t, 2 H, CH_2), 2.96 (t, 2 H, NCH_2), 3.55 (m, 14 H, CH_2), 4.09 (t, 2 H, C_5H_4), 4.10 (s, 5 H, C_5H_5), 4.14 (t, 2 H, C_5H_4), 4.55 (s, 2 H, CH_2), 7.48 (m, 4 H, CH_{anthr}), 8.00 (d, 2 H, CH), 8.40 (s, 1 H, CH), 8.55 (d, 2 H, CH_{anthr}). ^{13}C {^{1}H} NMR ($CDCl_3$): δ = 52.1, 53.2, 53.5, 53.6, 54.2, 55.5 (CH_2), 67.9, 68.4, 69.1 (CH, Cp), 70.1, 70.3, 70.4 (CH_2O), 124.7, 125.2, 125.5, 127.3, 128.8, 130.3, 131.3, 131.3 (CH_{anthr}). MS (FAB): *m*/*z* = 607 [M^+]. $C_{36}H_{42}FeN_2O_3{\cdot}3H_2O$ (660): calcd. C 65.5, H 6.4, N 4.3; found C 65.5, H 6.3, N 4.2.

L^2: The polyazacycloalkane 1,4,8,11-tetraazacyclotetradecane (520 mg, 2.6 mmol) was heated under reflux in absolute ethanol with 9-(chloromethyl)anthracene (560 mg, 2.6 mmol) in the presence of triethylamine. After 16 h, the mixture was cooled to room temperature and the solvent was removed. To the residue basic water and dichloromethane were added and the organic phase was separated, dried with anhydrous magnesium sulfate, filtered, and concentrated to dryness. The resulting oil was dissolved in dichloromethane and purified by chromatography on alumina using dichloromethane/ethanol (100:3, v/v) as eluent. This allowed us to isolate the compound 1-anthrylmethyl-1,4,8,11-tetraazacyclotetradecane. Yield 280 mg, 28%. This compound (280 mg, 0.717 mmol) was heated under reflux in dry acetonitrile with (ferrocenylmethyl)trimethylammonium iodide (1103 mg, 2.868 mmol) in the presence of potassium carbonate. After 24 h, the reaction mixture was filtered and the orange solution concentrated to dryness. The product L^2 was obtained after column chromatography on alumina using dichloromethane/ethanol (100:1, v/v) as eluent. Yield 565 mg, 80%. ^{1}H NMR ($CDCl_3$): δ = 1.55 (q, 2 H, $CH_2CH_2CH_2$), 1.75 (q, 2 H, $CH_2CH_2CH_2$), 2.00 (t, 4 H, N$CH_2CH_2CH_2$N), 2.28−2.70 (m, 12 H, NCH_2CH_2N), 3.36, 3.28, 3.15 (s, 6 H, CH_2), 3.84 (t, 2 H, C_5H_4), 3.90 (t, 2 H, C_5H_4), 3.93 (s, 5 H, C_5H_5), 3.99 (t, 2 H, C_5H_4), 4.01 (s, 5 H, C_5H_5), 4.02 (t, 4 H, C_5H_4), 4.05 (s, 5 H, C_5H_5), 4.07 (t, 2 H, C_5H_4), 4.31 (s, 2 H, CH_2), 7.48 (m, 4 H, CH_{anthr}), 8.00 (d, 2 H, CH), 8.40 (s, 1 H, CH), 8.55 (d, 2 H, CH_{anthr}).^{13}C {^{1}H} NMR ($CDCl_3$): δ = 24.1, 24.8 ($CH_2CH_2CH_2$), 47.0, 49.0, 49.6, 49.7, 50.3, 50.4, 51.0, 51.3, 51.4, 53.3, 53.4, 54.1 (CH_2N), 67.6, 67.7, 68.2, 68.3, 68.4, 70.1, 70.2, 70.3 (CH, Cp), 124.8, 125.1, 126.1, 127.0, 128.7, 131.2, 131.4, 131.5 (CH_{anthr}). MS (FAB): 985 [M^+]. $C_{56}H_{64}Fe_3N_4{\cdot}3H_2O$ (1014): calcd. C 67.0, H 6.6, N 5.2; found C 67.1, H 6.7, N 5.4.

Structure Determination of $[H_2L^1][PF_6]_2{\cdot}0.5CH_2Cl_2{\cdot}H_2O$: $C_{36.5}H_{44}ClF_{12}FeN_2O_4P_2$, M = 955.98, triclinic, space group $P\bar{1}$, a = 12.176(2), b = 12.787(2), c = 15.589(2) Å, α = 95.716(11), β = 110.088(12), γ = 106.236(12) °, Z = 2, V = 2136.1(5) Å^3, $D_{calcd.}$ = 1.486 g cm^{-3}, λ(Mo-K_α) = 0.71069 Å, T = 293(2) K, μ(Mo-K_α) = 0.583 mm^{-1}. Measurements were carried out using a Siemens P4 diffractometer with graphite-monochromated Mo-K_α radiation on a yellow crystal of dimensions 0.10 × 0.20 × 0.27 mm. A total of 5844 reflections was collected of which 5532 were independent (R_{int} = 0.0143). Lorentz, polarisation and absorption (ψ-scan, max. and min. transmission 0.541 and 0.014) corrections were applied. The structure was solved by direct methods (SHELXTL)[26] and refined by full-matrix least-squares analysis on F^2 (SHELXTL). The refinement converged at $R1$ = 0.084 [$F > 4\sigma(F)$] and $wR2$ = 0.249 (all data). Largest peak and hole in the final difference map +0.75 and −0.41 e Å^{-3}.

Structure Determination of $[CuL^2][PF_6]_2{\cdot}CH_2Cl_2$: $C_{59}H_{66}Cl_2CuF_{12}Fe_3N_4P_2$, M = 1423.09, monoclinic, space group $P2_1/c$, a = 14.419(5), b = 35.644(9), c = 13.282(4) Å, β = 104.20(3) °, Z = 4, V = 6618(3) Å^3, $D_{calcd.}$ = 1.428 g cm^{-3}, λ(Mo-K_α) = 0.71069 Å, T = 293(2) K, μ(Mo-K_α) = 1.163 mm^{-1}. Measurements were carried out using a Siemens P4 diffractometer with graphite-monochromated Mo-K_α radiation on a yellow crystal of dimensions 0.15 × 0.15 × 0.23 mm. A total of 9086 reflections was collected of which 8645 were independent (R_{int} = 0.0985). Lorentz, polarisation and absorption (ψ-scan, max. and min. transmission 0.3133 and 0.2912) corrections were applied. The structure was solved by direct methods (SHELXTL) [26] and refined by full-matrix least-squares analysis on F^2 (SHELXTL). The refinement converged at $R1$ = 0.1008 [$F > 4\sigma(F)$] and $wR2$ = 0.3609 (all data). Largest peak and hole in the final difference map +0.78 and −0.63 e Å^{-3}.

Crystallographic data for the structures reported in this paper have been deposited with the Cambridge Crystallographic Data Centre as supplementary publication no. CCDC-158668 ($[H_2L^1][PF_6]_2 \cdot 0.5CH_2Cl_2 \cdot H_2O$) and -158669 ($[CuL^2][PF_6]_2 \cdot CH_2Cl_2$). Copies of the data can be obtained free of charge on application to CCDC, 12 Union Road, Cambridge CB2 1EZ, UK [Fax: (internat.) + 44-1223/336-033; E-mail: deposit@ccdc.cam.ac.uk].

Physical Measurements: The fluorescence behaviour was studied with a FS900CDT Steady State T-Geometry Fluorimeter, Edinburgh Analytical Instruments. All solutions for photophysical studies were previously degassed. The concentration of ligands and metal ions were ca. 1.0×10^{-4} M in dioxane/water (the metal ions were perchlorate or nitrate salts of Ni^{2+}, Cu^{2+}, Zn^{2+}, Cd^{2+}, Hg^{2+}, and Pb^{2+}). The fluorescence quantum yield of anthracene [27] in acetonitrile was used as standard and taken to be 0.36. In order to obtain the quantum yield of the new ligands, those were dissolved in acetonitrile, their absorbance adjusted to ca. 0.15 and then compared to the standard. The ^1H NMR spectra were recorded with a Varian Gemini spectrometer. Chemical shifts are reported in ppm downfield from the TMS signal. Spectra taken in $CDCl_3$ were referenced to residual $CHCl_3$. Potentiometric titrations were carried out in 1,4-dioxane/water (70:30, v/v; 0.1 M KNO_3) using a reaction vessel that was thermostatically controlled using water at 25.0 ± 0.1 °C under nitrogen. The titrant was added by a Crison microburete 2031. The potentiometric measurements were made using a Crison 2002 pH-meter and a combined glass electrode. The titration system was automatically controlled using a PC. The electrode was calibrated as a hydrogen concentration prove by titration of well-known amounts of HCl with CO_2-free KOH solution and determining the equivalent point by the Gran's method which gives the standard potential E'° and the ionic product of water ($K'_w = [H^+][OH^-]$). The concentration of the metal ions was determined using standard methods. The computer program SUPERQUAD [28] was used to calculate the protonation and stability constants. The titration curves for each system (ca. 250 experimental points corresponding to at least three titration curves, pH = −log [H] range investigated 2.2−10.3, concentration of the ligand and metal ion being ca. 1.2×10^{-3} M) were treated either as a single set or as separated entities without significant variations in the values of the stability constant. Finally, the data sets were merged and treated simultaneously to give the stability constant. Electrochemical data were carried out in 1,4-dioxane/water (70:30, v/v) and in dry acetonitrile, with a programmable function generator Tacussel IMT-1, connected to a Tacussel PJT 120−1 potentiostat. The concentration of ligands and metal ions were ca. 1.0×10^{-3} M in dioxane/water (the metal ions were perchlorate or nitrate salts of Cu^{2+} and Pb^{2+}; metal-to-ligand ratio 1:1). The working electrode was platinum with a saturated calomel reference electrode separated from the test solution by a salt bridge containing the solvent/supporting electrolyte. The auxiliary electrode was platinum wire. $E_{1/2}$ values were measured by rotating-disc electrode experiments (scan speed 10 mVs^{-1}, rotating speed 7000 revolutions min^{-1}).

Acknowledgments

We thank the DGICYT (proyectos PB98−1430-C02−02, 1FD97−0508-C03−01 and AMB99−0504-C02−01) for support. F. S. also thanks the Ministerio de Ciencia y Tecnología for a Doctoral Fellowship.

[1] [1a] J.-M. Lehn, *Supramolecular Chemistry: Concept and Perspective*, VCH Verlagsgesellschaft, **1996**, Weinheim. [1b] E. C. Constable, *Comprehensive Supramolecular Chemistry* (Ed: J.-M. Lehn), Pergamon, Oxford, **1996**, vol. 9.

[2] [2a] M. Takagi, K. Ueno, *Top. Curr. Chem.* **1984**, *121*, 39−65. [2b] H. G. Löhr, F. Vögtle, *Acc. Chem. Res.* **1985**, *18*, 65−72.

[3] See for example: [3a] F. C. J. M. van Veggel, W. Verboom, D. N. Reinhoudt, *Chem. Rev.* **1994**, *94*, 279−299. [3b] R. Martínez-Mañez, J. Soto, J. M. Lloris, T. Pardo, *Trends Inorg. Chem.* **1998**, *5*, 183−203. [3c] P. D. Beer, *Acc. Chem. Res.* **1998**, *31*, 71−80.

[4] See for example: [4a] A. P. de Silva, H. Q. N. Gunaratne, T. Gunnlaugsson, A. J. M. Huxley, C. P. McCoy, J. T. Rademacher, T. E. Rice, *Chem. Rev.* **1997**, *97*, 1515−1566. [4b] A. W. Czarnik, *Acc. Chem. Res.* **1994**, *27*, 302−308. [4c] Special Issue on Luminescent Sensors of *Coord. Chem. Rev.* **2000**, *205*, 1−232.

[5] See for example: [5a] O. Brümmer, J. J. La Clair, K. D. Janda, *Org. Lett.* **1999**, *1*, 415−418. [5b] H. Miyaji, J. L. Sessler, *Angew. Chem. Int. Ed.* **2001**, *40*, 154−157. [5c] H. Miyaji, W. Sato, J. L. Sessler, *Angew. Chem. Int. Ed.* **2000**, *39*, 1777−1780. [5d] F. Sancenón, A. B. Descalzo, R. Martínez-Máñez, M. A. Miranda, J. Soto, *Angew. Chem. Int. Ed.* **2001**, *40*, 2640−2643.

[6] See for example: [6a] P. D. Beer, J. Cadman, J. M. Lloris, R. Martínez-Máñez, J. Soto, T. Pardo, M. D. Marcos, *J. Chem. Soc., Dalton Trans.* **2000**, 1805−1812. [6b] J. M. Lloris, R. Martínez−Máñez, T. Pardo, J. Soto, M. E. Padilla-Tosta, *Chem. Commun.* **1998**, 837−838. [6c] H. Plenio, C. Aberle, Y. Al Shihadeh, J. M. Lloris, R. Martínez-Máñez, T. Pardo, J. Soto, *Chem. Eur. J.* **2001**, *7*, 2848−2861.

[7] See for example: [7a] H. F. Ji, R. Dabestani, G. M. Brown, *J. Am. Chem. Soc.* **2000**, *122*, 9306−9307. [7b] K. Rurack, W. Rettig, U. Resch-Geuger, *Chem. Commun.* **2000**, 407−408. [7c] T. Hirano, K. Kikuchi, Y. Urano, T. Higuchi, T. Nagano, *Angew. Chem. Int. Ed.* **2000**, *39*, 1052−1054. [7d] E. Kimura, T. Koike, *Chem. Soc. Rev.* **1998**, *27*, 179−184. [7e] L. Fabbrizzi, M. Licchelli, P. Pallavicini, L. Prodi, *Angew. Chem. Int. Ed.* **1998**, *37*, 800−802.

[8] See for example: [8a] B. L. Feringa, W. F. Jager, B. De Lange, *Tetrahedron* **1993**, *49*, 8267−8310. [8b] D. R. Walt, *Acc. Chem. Res.* **1998**, *31*, 267−278. [8c] M. Ahmad, H. Hamzah, E. S. Marsoun, *Talanta* **1998**, *47*, 275−283.

[9] See for example: [9a] A. Doron, E. Katz, M. Portnoy, I. Willner, *Angew. Chem. Int. Ed. Engl.* **1996**, *35*, 1535−1537. [9b] G. Zotti, G. Schiavon, S. Zecchin, *Langmuir* **1998**, *14*, 1728−1733. [9c] G. Zotti, G. Schiavon, S. Zecchin, A. Berlin, G. Pagani, A. Canavesi, *Langmuir* **1997**, *13*, 2694−2698.

[10] [10a] P. D. Harvey, L. Gan, C. Aubry, *Can. J. Chem.* **1990**, *68*, 2278−2288. [10b] P. D. Harvey, L. Gan, *Inorg. Chem.* **1991**, *30*, 3239−3241. [10c] B. Delavaux-Nicot, S. Fery-Forgues, *Eur. J. Inorg. Chem.* **1999**, 1821−1825. [10d] P. D. Beer, F. Szemes, V. Balzani, C. M. Salà, M. G. B. Drew, S. W. Dent, M. Maestri, *J. Am. Chem. Soc.* **1997**, *119*, 11864−11875. [10e] U. Siemeling, U. Vorfeld, B. Neumann, H. G. Stammler, P. Zanello, F. F. De Biani, *Eur. J. Inorg. Chem.* **1999**, 1−5.

[11] L. F. Lindoy, *The Chemistry of Macrocyclic Ligand Complexes*, Cambridge University Press, Cambridge, **1989**.

[12] M. J. L. Tendero, A. Benito, J. Cano, J. M. Lloris, R. Martínez-Máñez, J. Soto, A. J. Edwards, P. R. Raithby, M. A. Rennie, *J. Chem. Soc., Chem. Commun.* **1995**, 1643−1644.

[13] J. M. Lloris, R. Martínez-Máñez, M. E. Padilla-Tosta, T. Pardo, J. Soto, P. D. Beer, J. Cadman, D. K. Smith, *J. Chem. Soc., Dalton Trans.* **1999**, 2359−2369.

[14] J. M. Lloris, R. Martínez-Máñez, T. Pardo, J. Soto, M. E. Padilla−Tosta, *J. Chem. Soc., Dalton Trans.* **1998**, 2635−2641.

[15] [15a] A. Benito, R. Martínez-Máñez, J. Payá, J. Soto, M. J. L. Tendero, E. Sinn, *J. Organomet. Chem.* **1995**, *503*, 259−263. [15b] M. J. L. Tendero, A. Benito, R. Martínez-Máñez, J. Payá, A. J. Edwards, P. R. Raithby, *J. Chem. Soc., Dalton Trans.* **1996**, 343−351.

[16] [16a] A. P. de Silva, T. Gunnlaugsson, T. E. Rice, *Analyst* **1996**, *121*, 1759−1762. [16b] L. Fabbrizzi, M. Licchelli, P. Pallavicini, D. Sacchi, A. Taglietti, *Analyst* **1996**, *121*, 1763−1768.

[17] [17a] F. Pina, M. A. Bernardo, E. García-España, *Eur. J. Inorg. Chem.* **2000**, 2143−2157. [17b] S. Alves, F. Pina, M. T. Albelda, E. García-España, C. Soriano, S. V. Luis, *Eur. J. Inorg. Chem.* **2001**, 405−412.

[18] [18a] L. Fabbrizzi, M. Licchelli, P. Pallavicini, A. Perotti, D. Sacchi, *Angew. Chem. Int. Ed. Engl.* **1994**, *33*, 1975−1977. [18b] G. De Santis, L. Fabbrizzi, M. Licchelli, C. Mangano, D. Sacchi, N. Sardone, *Inorg. Chim. Acta.* **1997**, 69−76. [18c] J. Yoon, N. E. Ohler, D. H. Vance, W. D. Aumiller, A. W. Czarnik, *Tetrahedron Lett.* **1997**, *38*, 3845−3848. [18d] L. Fabbrizzi, M. Licchelli, L. Parodi, A. Poggi, A. Taglietti, *Eur. J. Inorg. Chem.* **1999**, 35−39.

[19] Y. Al Shihadeh, A. Benito, J. M. Lloris, R. Martínez-Máñez, T. Pardo, J. Soto, M. D. Marcos, *J. Chem. Soc., Dalton Trans.* **2000**, 1199−1205.

[20] M. E. Padilla-Tosta, J. M. Lloris, R. Martínez-Máñez, A. Benito, J. Soto, T. Pardo, M. A. Miranda, M. D. Marcos, *Eur. J. Inorg. Chem.* **2000**, 741−748.

[21] [21a] P. Ghosh, P. Bharadwaj, S. Mandal, S. Ghosh, *J. Am. Chem. Soc.* **1996**, *118*, 1553−1554. [21b] B. Ramachandram, A. Samanta, *Chem. Commun.* **1997**, 1037−1038. [21c] M. Narita, Y. Higuchi, F. Hamada, H. Kumagai, *Tetrahedron Lett.* **1998**, *39*, 8687−8690. [21d] K. Kubo, T. Sakurai, A. Mori, *Talanta* **1999**, *50*, 73−77. [21e] K. Rurack, M. Kollmannsberger, U. Resch-Genger, J. Daub, *J. Am. Chem. Soc.* **2000**, *122*, 968−969.

[22] D. Rehm, A. Weller, *Isr. J. Chem.* **1970**, *8*, 259.

[23] See for example: [23a] M. Staffilani, K. S. B. Hancock, J. W. Steed, K. T. Holman, J. L. Atwood, R. K. Junega, R. S. Burkhalter, *J. Am. Chem. Soc.* **1997**, *119*, 6324−6335. [23b] C. Dusemund, K. R. A. S. Sandanayake, S. Shinkai, *J. Chem. Soc., Chem. Commun.* **1995**, 333−334.

[24] See for example: [24a] P. D. Beer, M. G. B. Drew, A. R. Graydon, D. K. Smith, S. E. Stokes, *J. Chem. Soc., Dalton Trans.* **1995**, 403−408. [24b] P. D. Beer, J. Cadman, J. M. Lloris, R. Martínez-Máñez, J. Soto, T. Pardo, M. D. Marcos, *J. Chem. Soc., Dalton Trans.* **2000**, 1805−1812. [24c] P. D. Beer, J. Cadman, J. M. Lloris, R. Martínez-Máñez, M. E. Padilla, T. Pardo, D. K. Smith, J. Soto, *J. Chem. Soc., Dalton Trans.* **1999**, 127−133. [24d] C. Valério, J.-L. Fillaut, J. Ruíz, J. Guittard, J.-C. Blais, D. Astruc, *J. Am. Chem. Soc.* **1997**, *119*, 2588−2589.

[25] J. Bourson, J. Pouget, B. Valeur, *J. Phys. Chem.* **1993**, *97*, 4552−4557.

[26] SHELXTL, Version 5.03, Siemens Analytical X-ray Instruments, Madison, WI, **1994**.

[27] I. B. Berlman, *Handbook of Fluorescence Spectra of Aromatic Molecules*, Academic Press, New York, **1971**.

[28] P. Gans, A. Sabatini, A. Vacca, *J. Chem. Soc., Dalton Trans.* **1995**, 1195−1200.

Received July 13, 2001
[I01271]

Thermal Isomerisation of Tris(silyl)hydroxylamines to Silylaminodisiloxanes – Experimental and Quantum Chemical Results

Stefan Schmatz,*[a] Friedhelm Diedrich,[b] Christina Ebker,[b] and Uwe Klingebiel*[b]

Keywords: Silicon / Hydroxylamines / Isomerisation / Ab initio calculations / Transition states

O-Lithio-*N*,*N*-bis(trimethylsilyl)hydroxylamide, LiO–N-$(SiMe_3)_2$, reacts with $ClSiMe_2H$ to give $HMe_2Si–O–N(SiMe_3)_2$ (**1**), while $LiO–N(SiMe_2CMe_3)_2$ reacts with $C_6H_5SiF_3$ to give $C_6H_5SiF_2–O–N(SiMe_2CMe_3)_2$ (**2**). **2** isomerises in solution to give *N*,*O*-bis(*tert*-butyldimethylsilyl)-*N*-[difluoro(phenyl)silyl]hydroxylamine (**3**). Boiling of **1** leads to the structurally isomeric silylaminodisiloxane, $Me_3Si–O–SiMe_2–NH–SiMe_3$ (**4**), while boiling of **3** leads to the isomeric $Me_3CSiMe_2–O–Si(Me)CMe_3–NMe–SiF_2C_6H_5$ (**5**). Quantum chemical calculations (B3LYP) on the thermal rearrangement of tris(silyl)hydroxylamines to silylaminodisiloxanes for the model compounds $H_3Si–O–N(SiMe_3)_2$ (**A**), $Me_3Si–O–N(SiH_3)_2$ (**B**), $Me_3Si–O–N(SiH_3)SiMe_2F$ (**C**), and $Me_3Si–O–N(SiMe_2F)SiMeF_2$ (**D**) demonstrate that *N*-bonded silyl units, e.g. SiH_2 in model compound **B** or SiFMe in model compound **D**, preferentially insert into the N–O bond. The reaction mechanisms and the structures of the transition states are discussed in detail.
(© Wiley-VCH Verlag GmbH, 69451 Weinheim, Germany, 2002)

Introduction

The most dramatic difference between the chemistry of silylhydroxylamines and that of organylhydroxylamines is the ability of the former to undergo anionic, radical, and thermal intramolecular rearrangements.[1–7] The first example of a 1,2-anionic rearrangement of a silyl group from an oxygen atom to a nitrogen atom was observed for lithiated *N*,*O*-bis(silyl)hydroxylamines.[1,2,8] Although lithiobis(silyl)hydroxylamines have been successfully used in the synthesis of tris(silyl)hydroxylamines since the end of the 1960s, the first crystal structures of these compounds were described only two years ago.[6,7] It was found that lithium derivatives of *N*,*O*-bis(silyl)hydroxylamines form *O*-lithio-*N*,*N*-bis(silyl)hydroxylamides in the solid state.

Depending on the bulkiness of the silyl groups and on the solvent used, $(Li–O)_{2,3,4}$ four-, six-, or eight-membered rings were formed,[6,7] and dimeric, trimeric, or tetrameric *O*-lithio-*N*,*N*-bis(silyl)hydroxylamides could be isolated. This indicated that silyl group migration from the oxygen atom to the nitrogen atom had occurred. In the reactions of halosilanes with these lithium salts, the new silyl group is attached to the oxygen atom in each case [Equation (1)].

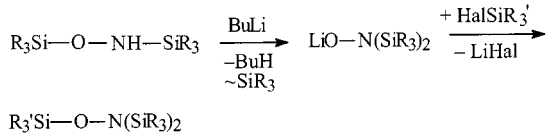

(1)

R, R' = alkyl, aryl

1,2-Silyl shifts in *neutral* organosilylhydroxylamines have been known since 1973,[1,2,9] when Frainnet and Nowakowski described an exchange of trialkylsilyl groups in bis(organosilyl)hydroxylamines.[9] Later, West and co-workers found a reversible rearrangement involving positional exchange between the organosilicon groups on the oxygen and the nitrogen atom in tris(silyl)hydroxylamines, which they suggested to proceed via a dyotropic transition state[1,2,10,11] [Equation (2)].

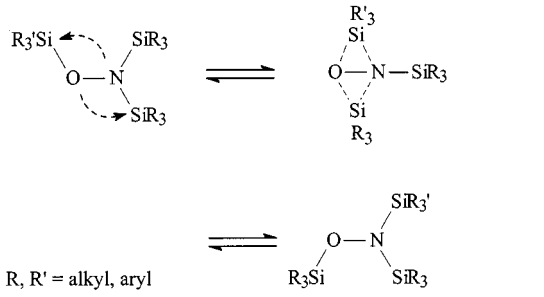

(2)

R, R' = alkyl, aryl

In 1998, we studied the rearrangement of *O*-(fluorosilyl)-*N*,*N*-bis(trimethylsilyl)hydroxylamines to the isomeric *N*-

[a] Institut für Physikalische Chemie der Universität Göttingen, Tammannstraße 6, 37077 Göttingen, Germany
E-mail: sschmat@gwdg.de
[b] Institut für Anorganische Chemie der Universität Göttingen, Tammannstraße 4, 37077 Göttingen, Germany
E-mail: uklinge@gwdg.de

(fluorosilyl)-*N*,*O*-bis(trimethylsilyl)hydroxylamines and found it to be irreversible.[5] Ab initio and density functional calculations were consistent with the dyotropic course of the isomerisation.

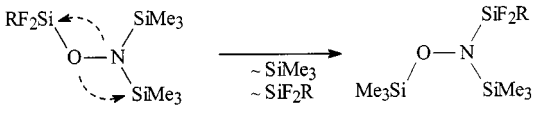

(3)

R = alkyl, aryl

In a thermal rearrangement, which proceeds at temperatures up to 200 °C, tris(organosilyl)hydroxylamines undergo an intramolecular isomerisation involving the insertion of a silicon moiety into the bond between the nitrogen and the oxygen atom and the transfer of an organyl group from the silicon to the nitrogen atom, thereby forming silylaminodisiloxanes.[1,2,6,12]

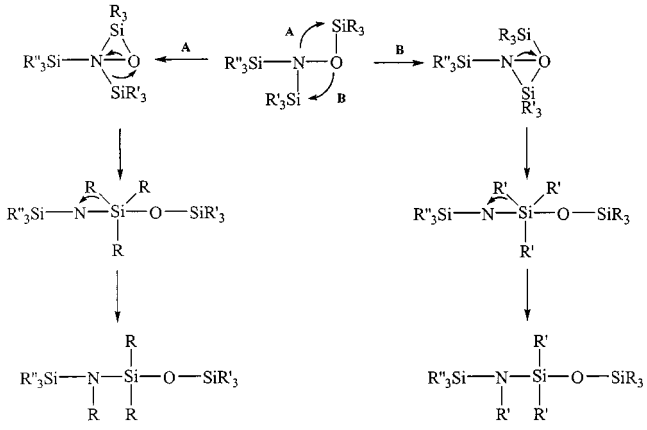

(4)

This conversion occurs in high yields. We studied rearrangements of *N*-(fluorosilyl)-*N*,*O*-bis(organylsilyl)hydroxylamines and found that the insertion of a silicon moiety into the N−O bond exclusively involves the silicon moiety that was bonded to the nitrogen atom. The insertion of an SiF_2 unit into the N−O bond has not been observed.

For a better understanding of our results, we report herein on quantum chemical investigations of the isomerisations of tris(silyl)hydroxylamines based on several model compounds and the thermal rearrangements of two *N*,*N*,*O*-tris(silyl)hydroxylamines with formation of the isomeric silylaminodisiloxanes.

Results and Discussion

Experimental

O-Lithio-*N*,*N*-bis(trimethylsilyl)hydroxylamide reacts with $ClSiMe_2H$ to give *O*-(dimethylsilyl)-*N*,*N*-bis(trimethylsilyl)hydroxylamine (**1**) [Equation (5)].

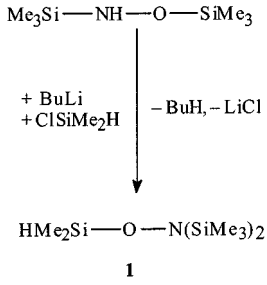

(5)

The lithium salt of *N*,*O*-bis(*tert*-butyldimethylsilyl)hydroxylamine crystallises from THF as dimeric *N*,*N*-bis(*tert*-butyldimethylsilyl)hydroxylamide[7] and reacts with trifluoro(phenyl)silane at 0 °C with formation of *N*,*N*-bis(*tert*-butyldimethylsilyl)-*O*-[difluoro(phenyl)silyl]hydroxylamine (**2**).

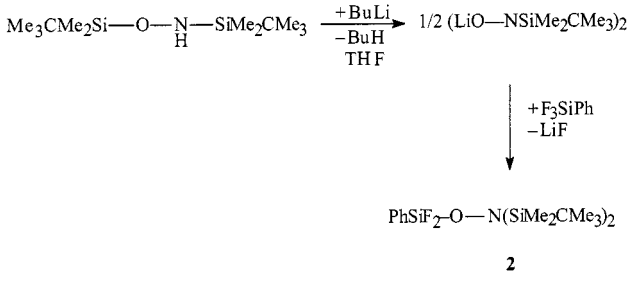

(6)

Product **2** could be isolated following the removal of LiF in a centrifuge by virtue of the low reaction temperature and the bulky $SiMe_2CMe_3$ groups. In solution, even at room temperature, the onset of the dyotropic rearrangement of **2** into the isomeric *N*,*O*-bis(*tert*-butyldimethylsilyl)-*N*-difluorophenylsilyl)hydroxylamine (**3**) can be observed by means of NMR spectroscopy. The conversion of **2** to **3** is found to be quantitative within a few hours in boiling THF. The softer Lewis acid F_2SiPh migrates to the softer Lewis base nitrogen, while the harder Lewis acid $SiMe_2CMe_3$ migrates to the harder Lewis base oxygen.

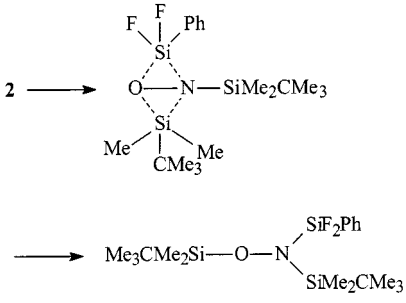

(7)

When heated under reflux for 3 d, **1** and **3** undergo a thermal rearrangement to form the silylaminodisiloxanes **4** and **5**, respectively. The conversion of **1** to **4** was monitored by ^1H NMR spectroscopy. It was found that a structural isomer of **1**, namely *N*-(dimethylsilyl)-*N*,*O*-bis(trimethylsilyl)hydroxylamine, was formed initially, which could not be isolated under the given reaction conditions.

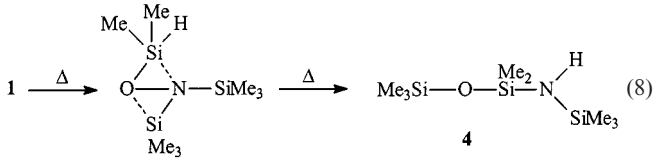

(8)

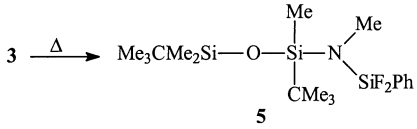

(9)

The formation of **4** involves the insertion of an $SiMe_2$ moiety into the N−O bond and a hydrogen atom transfer from the silicon to the nitrogen atom, whereas the formation of **5** involves the insertion of an $SiMeCMe_3$ moiety into the N−O bond and the migration of a CH_3 group from the silicon to the nitrogen atom.

Quantum Chemical Study on the Isomerisation of Tris(silyl)hydroxylamines

In order to gain more insight into the mechanisms governing the thermal isomerisation reactions of tris(silyl)hydroxylamines, quantum chemical calculations have been carried out.

Methodology

The program package GAUSSIAN-98[13] was employed throughout. The geometries of the minima and first-order saddle points on the potential energy surfaces (PES) were calculated using the density functional variant B3LYP, which is a hybrid method employing Becke's exchange functional[14] and the Lee, Yang, and Parr correlation functional.[15] The 6-31G* basis set was used. The calculated stationary points on the PES were characterised by the Hessian matrices. The obtained harmonic vibrational frequencies were used to calculate the zero-point energy contributions. The saddle points were further characterised using the TS routine in GAUSSIAN-98 (intrinsic reaction coordinate method).[16]

Using the B3LYP/6-31G* methodology, we have recently studied various isomerisation reactions in silylhydrazine chemistry.[17−21] The calculated structures were compared with available X-ray diffraction data and good agreement was found throughout.

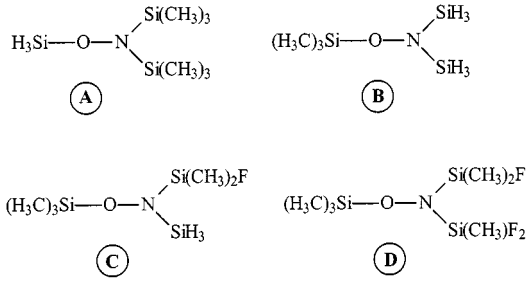

Here, four different model compounds are investigated in detail: *N*,*N*-bis(trimethylsilyl)-*O*-(silyl)hydroxylamine (**A**), *N*,*N*-bis(silyl)-*O*-(trimethylsilyl)hydroxylamine (**B**), *N*-(fluorodimethylsilyl)-*N*-silyl-*O*-(trimethylsilyl)hydroxylamine (**C**), and *N*-(fluorodimethylsilyl)-*N*-(difluoromethylsilyl)-*O*-(trimethylsilyl)hydroxylamine (**D**).

In all four cases, insertion of a silicon atom initially located at the nitrogen atom into the N−O bond occurs. For **A** and **B**, only one product (**PA** and **PB**, respectively) is possible for symmetry reasons. However, **A** and **B** can undergo a dyotropic rearrangement yielding structures **A1** and **B1**. Starting from these isomers, a silicon atom from the nitrogen site can be inserted into the N−O bond yielding products **PA1** and **PB1**, respectively.

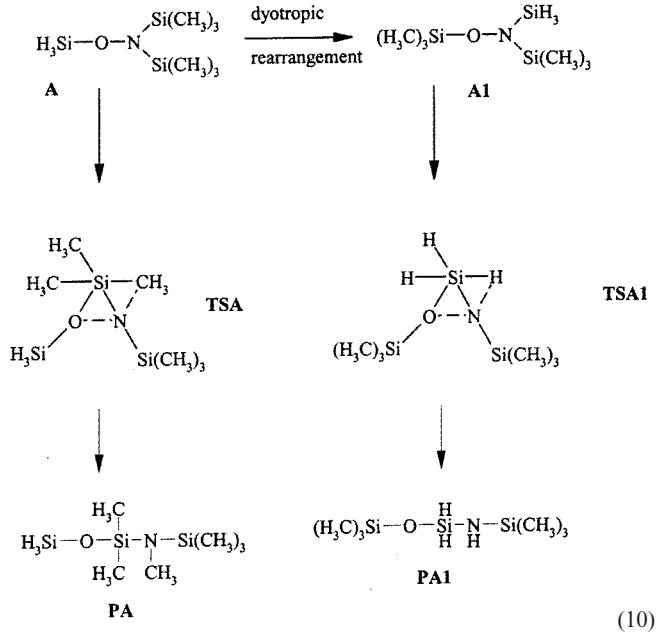

(10)

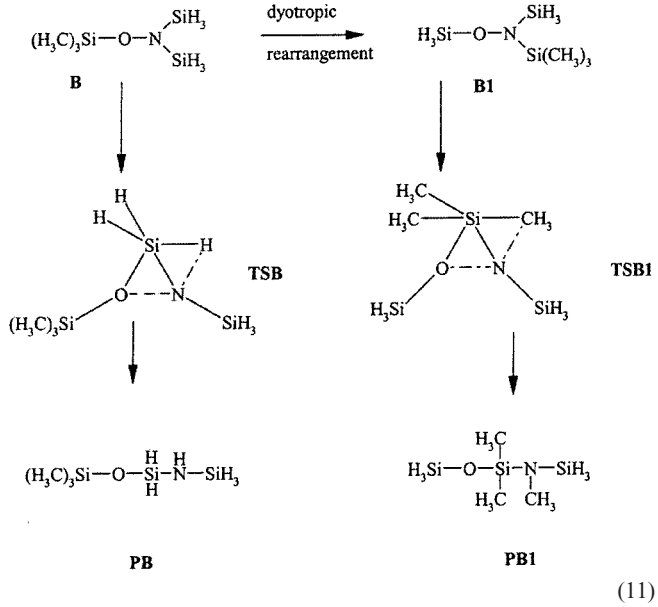

(11)

For **C** and **D**, two different reaction pathways are possible, yielding products **PC1/PC2** and **PD1/PD2**, respectively.

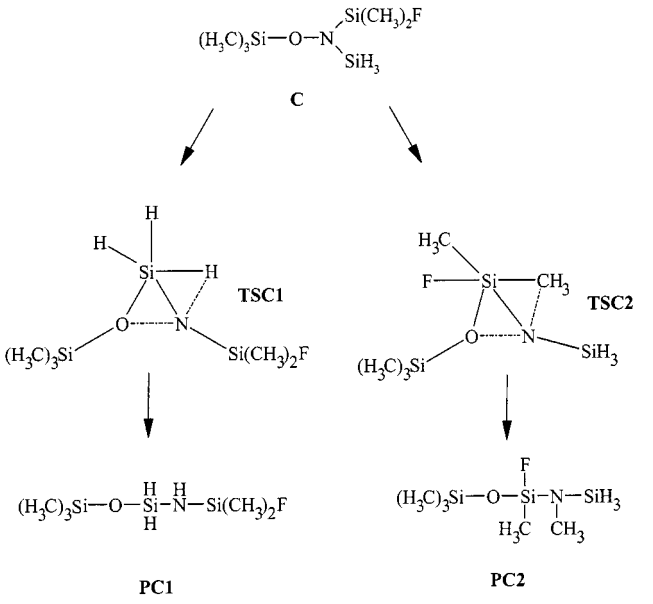

(12)

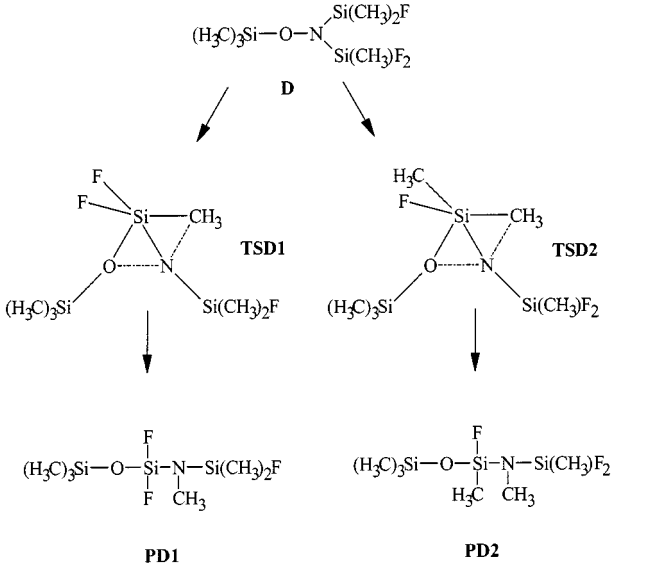

(13)

The transition states corresponding to these reactions are denoted as follows: **TSdA** and **TSdB** are the dyotropic transition states in the isomerisations **A** → **TSdA** → **A1** and **B** → **TSdB** → **B1**. The transition states leading to the silylaminodisiloxanes **PA**, **PA1**, **PB**, **PB1**, **PC1**, **PC2**, **PD1**, and **PD2** are denoted by **TSA**, **TSA1**, **TSB**, **TSB1**, **TSC1**, **TSC2**, **TSD1**, and **TSD2**, respectively.

Structures

In Table 1, the B3LYP/6-31G* equilibrium geometries for the hydroxylamines **A**, **A1**, **B**, **B1**, **C**, and **D** are given. **A** and **B** exhibit C_s symmetry with the Si−O−N chain contained in the symmetry plane. The O−N bond length is calculated to be within the range 147−150 pm. Electron-withdrawing (e.g. fluorosilyl) groups shorten the O−N bond. Depending on the substituents at the silicon atom, the Si−O bond lengths range from 169 to 172 pm and the Si−N bond lengths from 173 to 179 pm. The Si−O−N angles are in the range 109 to 118°, indicating pure sp^3 to sp^2 hybridisation of the oxygen atom. The angles O−N−Si, on the other hand, clearly show that the nitrogen atom is sp^3-hybridised. Depending on the steric demand of the silyl groups, the Si−N−Si angles are between 122 and 129°. As can be seen from the torsional angles Si−O−N−Si, all hydroxylamines adopt a *trans* conformation.

Table 1. B3LYP/6-31G(d) equilibrium geometries of the tris(silyl)hydroxylamines (reactants **A**, **A1**, **B**, **B1**, **C**, and **D**); bond lengths in pm, angles in °; bond angles are denoted by α, torsional angles by θ; **A** and **B** exhibit C_s symmetry; values in parentheses give the equilibrium geometry of structure **B** obtained at the B3LYP/6-31+G(d) level of theory; **C**: Si′ = $SiMe_2F$; **D**: Si′ = $SiMeF_2$

	A	**A1**	**B**	**B1**	**C**	**D**
r(SiO)	168.5	170.8	171.3 (171.7)	169.0	170.9	172.0
r(ON)	149.8	148.4	147.7 (147.6)	149.2	147.6	146.6
r(NSi′)	178.8	176.0	176.1 (176.4)	178.9	176.2	173.1
r(NSi′′)	178.8	178.8	176.1 (176.4)	176.1	176.6	175.7
α(SiON)	110.2	117.0	114.8 (115.0)	108.5	116.2	117.6
α(ONSi′)	105.4	107.7	108.2 (108.2)	108.6	111.2	108.4
α(Si′NSi′′)	127.5	123.4	125.0 (125.1)	126.9	122.2	128.9
θ(SiONSi′)	111.0	121.9	111.0 (110.9)	115.2	118.4	117.4

The geometries of the two saddle points corresponding to the dyotropic transition states **TSdA** and **TSdB** are given in Table 2. The structure of **TSdB** is shown graphically in Figure 1. The steric demand of the bicyclic structures is considerable because both three-membered rings exhibit acute O−Si−N angles of ca. 45° and thus underlie strong ring tension. It should be noted that the first calculations on dyotropic transition states in silylhydroxylamines were carried out by Müller.[5] Compared to the reactants **A** and **B**, the O−N bonds are only slightly longer by 4.6 and 5.3 pm, respectively. In both transition states, the hydroxylamine Si−O bonds are considerably stretched (by 39.7 pm and 46.1 pm for **TSdA** and **TSdB**, respectively). The original and the newly formed Si−O bonds are almost

Table 2. B3LYP/6-31G(d) geometries of the dyotropic transition states **TSdA** and **TSdB**; bond lengths in pm, angles in °; bond angles are denoted by α, torsional angles by θ

	TSdA	TSdB
r(ON)	154.4	153.0
r(Si′O)	208.2	217.4
r(Si′N)	181.4	180.8
r(Si′′O)	206.5	212.4
r(Si′′N)	188.6	187.8
r(NSi)	183.5	180.2
α(OSi′N)	46.0	44.0
α(OSi′′N)	45.7	44.4
α(Si′NSi)	118.7	118.4
θ(Si′ONSi′′)	122.1	123.3
θ(Si′ONSi)	115.6	117.0

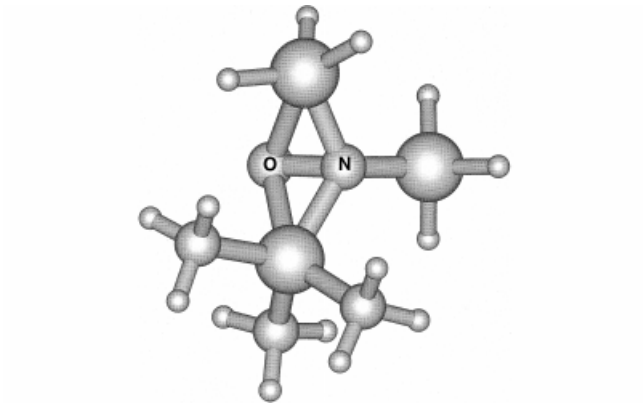

Figure 1. Structure of saddle point **TSdB** (bicyclic dyotropic transition state; see text for details)

equal in length. On the contrary, the hydroxylamine Si−N bonds are stretched by only ca. 10 pm, and the newly formed endocyclic Si−N bond lengths are 7 pm longer that the original ones. The exocyclic Si−N bond is slightly elongated in the dyotropic TS compared to the Si−N bonds in hydroxylamines. The angle between the two three-membered rings is given by the torsional angle $\theta(Si_1ONSi_2)$, which is calculated to be 122 and 123° in **TSdA** and **TSdB**, respectively. The geometries are in very good agreement with the results for $H_3SiO-N(SiH_3)_2$ reported in ref.[5]

In Table 3, the equilibrium structures of the eight silylaminodisiloxanes **PA**, **PA1**, **PB**, **PB1**, **PC1**, **PC2**, **PD1**, and **PD2** are given. These structures may be compared with the structures of the diazasilacyclopropanes discussed in refs.[17,18] The triangular O−Si−N structural motif is analogous to the SiN_2 ring; however, the N−O bond is broken (distance 272 to 286 pm) and the nitrogen atom bears an additional substituent. The O−Si bonds are considerably shortened compared to those in the hydroxylamines, on average by 4 pm. The shortest O−Si bond length is calculated to be only 162 pm. The Si−N bonds are also slightly shorter in the disiloxanes, but the effect is less pronounced compared to the situation with the Si−O bonds. The central silicon atom is clearly sp^3-hybridised (as is the case for the diazasilacyclopropanes[17,18]). The Si−O−Si angles, however, are between 138 and 153°, and indicate sp^2 hybridisation of the oxygen atom with a tendency towards sp hybridisation. The Si−N−Si angles are in the range 124 to 132°. The sum of the angles at the nitrogen centre amounts to almost 360° throughout, clearly indicating sp^2 hybridisation.

Table 3. B3LYP/6-31G(d) equilibrium geometries of the silylaminodisiloxanes (products **PA**, **PA1**, **PB**, **PB1**, **PC1**, **PC2**, **PD1**, and **PD2**); bond lengths in pm, angles in °; bond angles are denoted by α, torsional angles by θ; R = H for **PA1**, **PB** and **PC2**; R = Me otherwise values in parentheses give the equilibrium geometry of structure **PB** obtained at the B3LYP/6-31+G(d) level of theory

	PA	PA1	PB	PB1	PC1	PC2	PD1	PD2
r(SiO)	164.4	166.7	166.8 (166.3)	164.9	167.9	167.0	168.0	169.1
r(OSi)	167.6	165.1	164.4 (163.9)	167.2	163.9	164.5	163.8	162.1
r(SiN)	174.3	173.1	173.9 (173.9)	174.9	172.8	174.0	174.0	170.3
r(NSi)	176.9	176.3	174.4 (174.7)	174.3	174.6	173.7	171.8	175.0
r(NO)	278.7	285.8	285.6 (283.9)	280.6	272.4	283.6	271.7	275.7
r(NR)	147.8	101.7	101.6 (101.7)	148.0	147.9	101.8	148.4	148.4
α(SiOSi)	148.9	150.3	153.3 (178.4)	144.3	142.5	150.6	142.2	138.3
α(OSiN)	109.2	115.3	115.1 (114.3)	110.2	107.9	113.8	107.0	112.1
α(SiNSi)	126.0	131.8	129.1 (129.2)	128.5	124.6	130.8	123.8	126.0
θ(SiOSiN)	179.2	65.8	40.3 (174.8)	49.5	148.2	58.4	146.5	154.1
θ(OSiNSi)	55.8	78.1	83.8 (84.1)	113.0	170.1	115.0	175.6	35.3

Table 4. B3LYP/6-31G(d) equilibrium geometries of the transition states for Si insertion into the N−O bond (**TSA**, **TSA1**, **TSB**, **TSB1**, **TSC1**, **TSC2**, **TSD1** and **TSD2**); bond lengths in pm, angles in °; bond angles are denoted by α, torsional angles by θ; R = H for **TSA1**, **TSB** and **TSC2**; R = Me otherwise; values in parentheses give the equilibrium geometry of structure **TSB** obtained at the B3LYP/6-31+G(d) level of theory

	TSA	TSA1	TSB	TSB1	TSC1	TSC2	TSD1	TSD2
r(SiO)	166.3	169.7	169.9 (170.4)	166.6	169.9	170.2	170.5	169.1
r(OSi)	192.1	183.0	182.4 (183.5)	193.2	183.6	181.8	185.3	176.7
r(SiN)	170.5	171.6	171.5 (171.6)	170.5	170.0	170.4	168.6	169.1
r(NSi)	178.0	178.8	177.1 (177.4)	176.7	176.4	176.5	174.8	177.9
r(NO)	206.4	207.1	205.2 (205.5)	204.6	205.6	206.7	203.2	211.9
r(SiR)	208.4	160.5	161.0 (160.9)	209.8	206.1	162.2	207.3	202.0
r(NR)	248.0	212.7	210.5 (210.3)	245.4	248.5	208.4	245.6	247.4
α(SiOSi)	135.8	134.7	141.6 (138.9)	137.7	135.3	137.7	135.9	139.9
α(OSiN)	69.1	71.4	70.8 (70.7)	68.1	71.0	71.8	69.9	75.5
α(SiNSi)	139.7	131.6	131.0 (131.9)	131.2	133.8	136.5	137.1	133.9
θ(SiOSiN)	94.2	100.8	100.8 (97.7)	87.8	99.5	92.2	95.6	111.4
θ(OSiNSi)	89.5	92.7	88.0 (89.5)	87.8	90.3	89.7	84.2	84.3

Table 4 gives the geometrical parameters of the saddle points corresponding to transition states **TSA**, **TSA1**, **TSB**, **TSB1**, **TSC1**, **TSC2**, **TSD1**, and **TSD2**. As an example, the structure **TSC1** is shown graphically in Figure 2. The O−N bonds (between 203 and 212 pm) are markedly elongated (by more than 30 pm) compared with the corresponding bonds in the reactant structures. The exocyclic Si−O bond length is only slightly greater than the corresponding bond length in the products. The newly formed O−Si bond is relatively long (up to 20 pm longer than that in the silylaminodisiloxanes). The exocyclic N−Si bond length is slightly greater than the corresponding bond length in the product. The Si−N bond bridging to the oxygen atom is only slightly shorter than that in the silylaminodisiloxanes, and much shorter than that in the hydroxylamines. The acute central

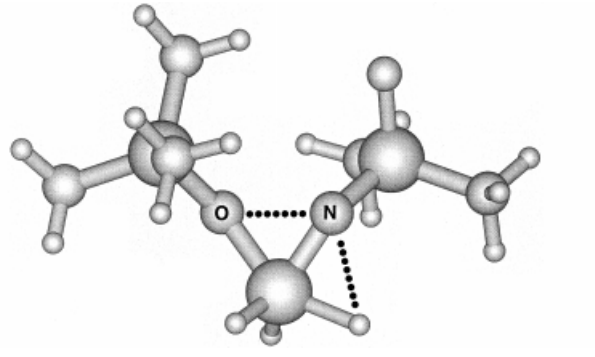

Figure 2. Structure of the saddle point **TSC1** (SiH_3 insertion into the O−N bond; see text for details)

O−Si−N angle is between 68 and 76°. The Si−O−Si and Si−N−Si angles are between 131 and 142°.

The transition states are bicyclic structures with the first ring formed by the NO moiety and the inserting silicon atom, while the second ring is formed by the central silicon atom, the nitrogen atom, and the group R transferred from the silicon atom to the nitrogen atom (see Figure 2). The transferred group (R) is either a hydrogen atom or a methyl group. The silicon, the oxygen, the nitrogen, and the hydrogen atom (or the methyl carbon atom) are almost coplanar. At the saddle point, the reacting Si−R bonds are considerably stretched. Thus, the reacting Si−C bond in **TSA** is 19.2 pm longer than the other two Si−C bonds (198.2 pm) at the same silicon atom. The Si−H bond in **TSA1** is 11.7 pm longer compared to the other two Si−H bond lengths (148.8 pm). However, the new bond to the nitrogen atom has yet to be formed at the saddle point. The N−C distance in **TSA** is 248.0 pm and the N−H distance in **TSA1** amounts to 212.7 pm; these are much longer than the corresponding distances in the silylaminodisiloxanes (Table 3). Thus, the saddle points reported in Table 4 may be classified as *early* transition states. The N−O bond is not yet fully broken and the interaction between the nitrogen atom and the transferred moiety is only weak. The bicyclic first-order saddle point structures for silicon insertion into the N−O bond are analogous to the dyotropic transition states **TSdA** and **TSdB** (the bond between the central silicon atom and the nitrogen atom adopts the role of the N−O bond in the dyotropic TS). The B3LYP/6-31G(d) structures of all compounds described in this quantum chemical study can be obtained from one of the authors (sschmat@gwdg.de).

The influence of diffuse basis functions [6-31+G(d) basis set] on the geometries of the stationary points was investigated for structures **B**, **PB**, and **TSB** (see Tables 1, 3, and 4). The only remarkable deviation from the B3LYP/6-31G(d) results was found for the Si−O−Si angle in the silylaminodisiloxane **PB**, which is widened by 25°. The Si−O−Si unit becomes almost linear (178.4°) when the additional diffuse functions are taken into account. However, the energetics are hardly affected. The saddle point **TSB** is found at 38.3 kcal·mol^{-1} above **B** [38.2 kcal·mol^{-1} with 6-31G(d)], whereas the product **PB** is located at 84.9 kcal·mol^{-1} below **B** [83.8 kcal·mol^{-1} with 6-31G(d)].

Energetics

In Table 5, the energetics of the dyotropic transition state **TSdA** and silylhydroxylamine **A1** relative to species **A** are given. **A1** is more stable than **A** by ca. 3 kcal·mol^{-1}, and zero-point energy effects enhance its stability. Energetically, the dyotropic TS is located at 33 kcal·mol^{-1} above the reactant. This is of the same order of magnitude as reported by Wolfgramm et al.[5] The dyotropic **TSdB** is calculated to be 36 kcal·mol^{-1} above the reactant **B** (Table 6). The isomer **B1** is 1.5 kcal·mol^{-1} higher in energy than **B**. This indicates that configurations with silyl groups at the nitrogen atom and trimethylsilyl groups at the oxygen site are energetically favoured.

In Figures 3−6, the potential energy profiles of the isomerising tris(silyl)hydroxylamines **A**, **B**, **C**, and **D** are displayed graphically as functions of the reaction coordinate. Note that the stationary points are connected by a smooth curve; the "reaction coordinate" in Figures 3−6 does not have any quantitative physical significance. The influence of zero-point vibrational energy (at the harmonic level; reaction coordinate at saddle points not included) is given in Tables 5−8. The effect of finite temperature (298 K) is also highlighted in these tables (reaction enthalpies $\Delta_R H°$). As can be seen from Figure 3, the insertion of an SiH_3 group into the N−O bond is favoured compared to $SiMe_2$ insertion. In addition to the thermodynamic control ($|\Delta E_{\mathbf{PA1}}| > |\Delta E_{\mathbf{PA}}|$), the reaction is also kinetically controlled (by the barriers to isomerisation $\Delta E_{\mathbf{TSA1}} < \Delta E_{\mathbf{TSA}}$). Silylhydroxylamine **A** first has to undergo isomerisation via the dyotropic transition state **TSdA**, for which the activation energy (barrier height $\Delta E_{\mathbf{TSdA}}$) is very similar to the corresponding value for the silyl group insertion ($\Delta E_{\mathbf{TSA1}}$). The larger reaction enthalpy and the lower isomerisation barrier determine the course of the reaction (**A** → **PA1**).

A similar conclusion can be drawn from Figure 4. Here, reaction **B** → **PB** (SiH_3 insertion) is favoured both thermodynamically and kinetically. The barrier $\Delta E_{\mathbf{TSdB}}$ for the dyotropic rearrangement **B** → **B1** is smaller than the barrier $\Delta E_{\mathbf{TSB1}}$ for $SiMe_3$ insertion **B1** → **PB1**.

In Figure 5, insertion of a silyl group is compared with that of a fluorodimethylsilyl group. Again, SiH_3 insertion (**C** → **PC1**) is favoured both thermodynamically and kinetically (Table 7).

Table 5. Energetics of the reactions involving tris(silyl)hydroxylamine **A** (energies in kcal·mol^{-1} with respect to the starting material); E_{zp} denotes the zero-point energy contribution

		A	**TSdA**	**A1**	**TSA1**	**PA1**	**TSA**	**PA**
ΔE	B3LYP/6-31G(d)	0.0	31.2	−2.6	31.7	−87.7	41.2	−65.9
$\Delta(E+E_{zp})$	B3LYP/6-31G(d)	0.0	30.7	−2.9	29.2	−86.1	39.1	−64.5
$\Delta_R H°$(298 K)	B3LYP/6-31G(d)	0.0		−2.8		−85.7		−64.3
ΔE	B3LYP/6-311+G(2d,p)[a]	0.0	32.8	−2.6	30.9	−91.7	40.0	−66.1
ΔE	MP2/6-31G(d)[a]	0.0	26.5	−1.1	48.4	−90.0	55.9	−69.6
ΔE	MP2/6-31+G(d,p)[a]	0.0	26.6	−0.7	50.2	−90.9	55.3	−69.2

[a] At B3LYP/6-31G(d) geometry.

Table 6. Energetics of the reactions involving tris(silyl)hydroxylamine **B** (energies in kcal·mol^{-1} with respect to the starting material); E_{zp} denotes the zero-point energy contribution

		B	TSdB	B1	TSB1	PB1	TSB	PB
ΔE	B3LYP/6-31G(d)	0.0	35.7	1.5	46.4	−65.1	38.2	−83.8
$\Delta(E+E_{zp})$	B3LYP/6-31G(d)	0.0	35.3	1.5	44.5	−63.5	35.9	−81.8
$\Delta_R H°$(298 K)	B3LYP/6-31G(d)	0.0		1.5		−63.3		−81.5
ΔE	B3LYP/6-311+G(2d,p)[a]	0.0	35.7	1.3	44.6	−65.5	36.9	−87.6
ΔE	MP2/6-31G(d)[a]	0.0	30.8	0.4	58.3	−70.2	53.1	−88.5
ΔE	MP2/6-31+G(d,p)[a]	0.0	30.4	0.2	57.4	−70.0	53.8	−89.8

[a] At B3LYP/6-31G(d) geometry.

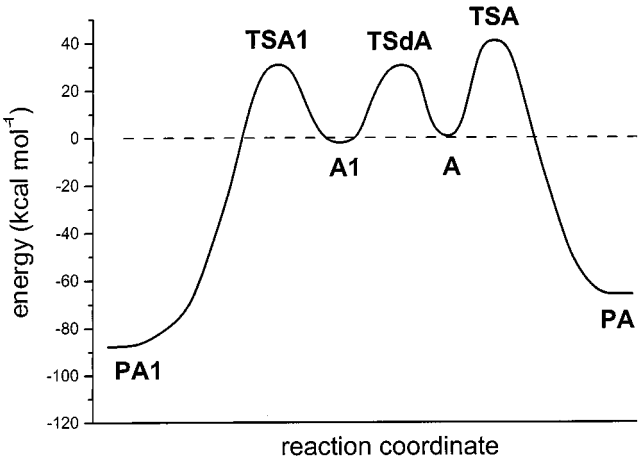

Figure 3. Potential energy diagram for reaction **A** (schematic)

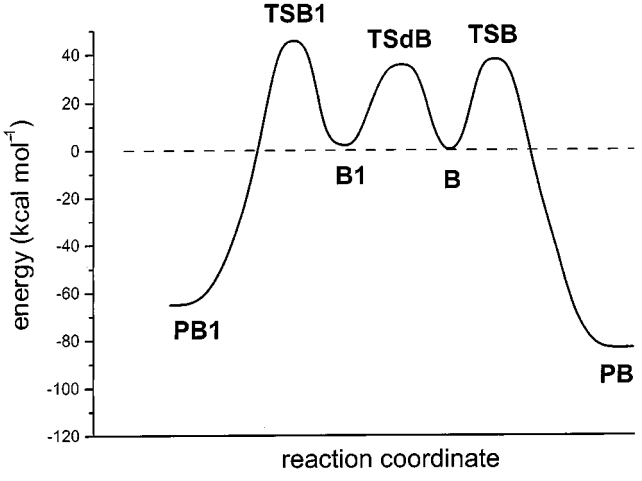

Figure 4. Potential energy diagram for reaction **B** (schematic)

Figure 6 shows the thermal rearrangement of *N*-(difluoromethyl)-*N*-(fluorodimethylsilyl)-*O*-(trimethylsilyl)-hydroxylamine. Insertion of the difluorosilyl group has a slightly smaller associated barrier height ΔE_{TSD1} than insertion of the monofluorosilyl group. However, the product **PD2** is energetically favoured by 1.3 kcal·mol^{-1} (Table 8). The reaction is clearly subject to thermodynamic control. This is in keeping with the conditions of preparation of the silylaminodisiloxane, i.e. heating of a fluoro-substituted tris(silyl)hydroxylamine up to 200 °C and keeping it at this temperature for several hours.

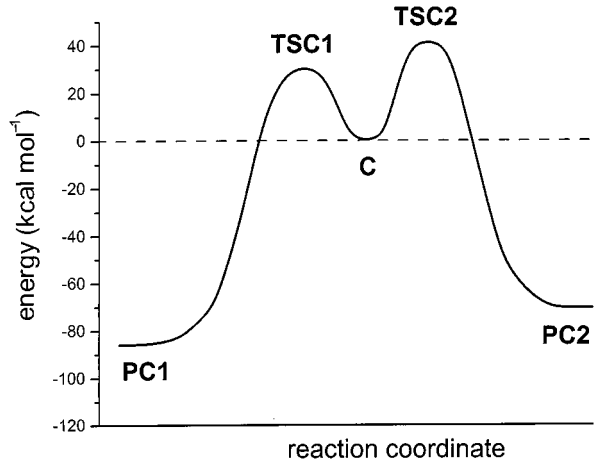

Figure 5. Potential energy diagram for reaction **C** (schematic)

It should be noted that the theoretical results are in nice agreement with the experimental finding that during the conversion of **1** to **4** a structural isomer of **1** was monitored. This isomer is formed by a dyotropic rearrangement. After this step, the $SiHMe_2$ group inserts instead of the $SiMe_3$ group.

It remains to be considered how well hybrid DFT methods, e.g. B3LYP, can predict transition-state geometries and barrier heights. Hybrid DFT involves mixing various amounts of the Hartree−Fock non-local exchange operator with DFT exchange-correlation functionals, and it has been observed that the fraction needed for an accurate prediction of thermochemical data differs from the optimal fraction for predicting accurate barrier heights. Recently, Lynch and Truhlar[22] reported DFT calculations of barrier heights in 22 reactions and found a mean unsigned error of 3.4−4.2 kcal·mol^{-1} (depending on the basis set) in comparison with best estimates derived from experimental data. Møller−Plesset second-order perturbation theory (MP2) performed slightly less well. Lynch and Truhlar recommend their own hybrid method MPW1K,[23] which gave a mean unsigned error of only 1.5 kcal·mol^{-1}. However, all of the 22 reactions involve free radicals and the transfer of a hydrogen atom, and all but one are bimolecular reactions. Since the empirical data are as yet only limited, and since, in the present work, we focus on the energetic *differences* between several reaction pathways, we are confident that the B3LYP method yields reliable results.

Table 7. Energetics of the reactions involving tris(silyl)hydroxylamine **C** (energies in kcal·mol^{-1} with respect to the starting material); E_{zp} denotes the zero-point energy contribution

		C	TSC1	PC1	TSC2	PC2
ΔE	B3LYP/6-31G(d)	0.0	36.4	−85.9	41.7	−70.4
$\Delta(E+E_{zp})$	B3LYP/6-31G(d)	0.0	34.0	−83.6	39.5	−68.8
$\Delta_R H°$(298 K)	B3LYP/6-31G(d)	0.0		−83.5		−68.7
ΔE	B3LYP/6-311+G(2d,p)[a]	0.0	35.0	−90.1	41.6	−70.8
ΔE	MP2/6-31G(d)[a]	0.0	51.1	−90.3	55.7	−74.6
ΔE	MP2/6-31+G(d,p)[a]	0.0	51.6	−91.6	56.0	−73.8

[a] At B3LYP/6-31G(d) geometry.

Table 8. Energetics of the reactions involving tris(silyl)hydroxylamine **D** (energies in kcal·mol^{-1} with respect to the starting material); E_{zp} denotes the zero-point energy contribution

		D	TSD1	PD1	TSD2	PD2
ΔE	B3LYP/6-31G(d)	0.0	43.5	−68.6	45.6	−69.9
$\Delta(E+E_{zp})$	B3LYP/6-31G(d)	0.0	41.6	−66.7	43.7	−68.0
$\Delta_R H°$(298 K)	B3LYP/6-31G(d)	0.0		−66.8		−68.1
ΔE	B3LYP/6-311+G(2d,p)[a]	0.0	43.0	−69.2	45.2	−71.1
ΔE	MP2/6-31G(d)[a]	0.0	59.6	−71.9	57.6	−74.1
ΔE	MP2/6-31+G(d,p)[a]	0.0	60.0	−71.0	57.6	−73.3

[a] At B3LYP/6-31G(d) geometry.

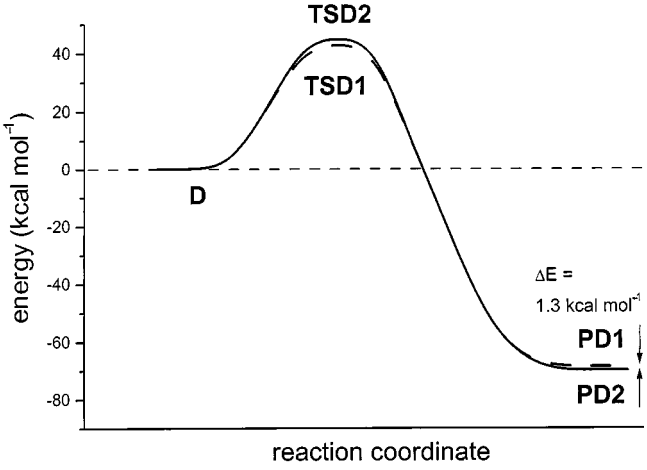

Figure 6. Potential energy diagram for reaction **D** (schematic)

In order to study the influence of polarization and diffuse basis functions on the energetics of the four systems, we performed B3LYP/6-311+G(2d,p) calculations on the B3LYP/6-31G(d) geometries (see Tables 5−8). Overall, the results are in good agreement with those obtained employing the smaller basis set. The products **PA1**, **PB**, and **PC1** are lowered in energy because the additional diffuse and polarization functions allow for a better description of the SiH_2−NH unit in these cases.

We also carried out MP2 calculations with the 6-31G(d) and 6-31+G(d,p) basis sets at the optimized B3LYP geometries (see Tables 5−8). The energetic differences between reactants and products are very close to the DFT results. The two saddle points describing the dyotropic transition states are slightly lower in energy than the corresponding saddle points from the MP2 calculations. However, all other MP2 saddle points are much higher in energy. This can be explained by the fact that the dyotropic transition states (TS) can be classified as "tight" TS, whereas the other TS (Table 4) are "loose" TS with considerably stretched bonds. MP2 does not include a major fraction of the non-dynamical correlation energy and is not capable of describing such loose structures. In particular, the order of the two saddle points in reaction according to eq. 13 is reversed at the MP2 level of theory.

Normal Modes of Transition States

The harmonic vibrational frequencies ω_{TS} of the reactive normal modes Q_{TS} at the various saddle points are given in Table 9. The two dyotropic transition states have rather similar imaginary frequencies and corresponding reduced masses μ_{TS}. In both cases, a silyl group and a trimethylsilyl group undergo simultaneous migration. However, the motion along Q_{TS} is governed by the oxygen atom, which is much lighter than the heavy silyl groups (see Figure 7). From the viewpoint of reaction dynamics, the term "silyl group migration" is somewhat misleading.

Table 9. Harmonic vibrational frequencies in cm^{-1} of the reactive normal coordinates Q_{TS} of the transition states; the corresponding reduced mass in a.m.u. is denoted by μ_{TS}

	TSdA	TSA	TSA1	TSdB	TSB	TSB1	TSC1	TSC2	TSD1	TSD2
ω_{TS}	278*i*	558*i*	505*i*	267*i*	559*i*	617*i*	613*i*	527*i*	509*i*	546*i*
μ_{TS}	8.96	2.78	8.46	8.04	7.04	2.48	2.40	7.04	8.99	8.80

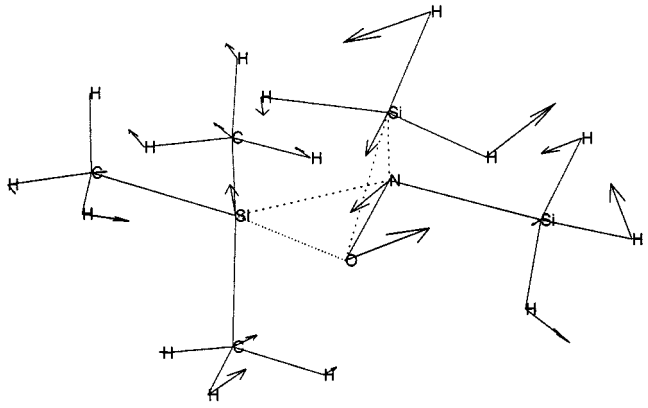

Figure 7. The reaction coordinate Q_{TS} at the saddle point **TSdB**, i.e. the normal coordinate of the mode with the imaginary vibrational frequency ω_{TS}

The transition states for SiH_3 group insertion into the N−O bond (**TSA**, **TSB1**, and **TSC1**) exhibit very similar characteristic ω_{TS} and μ_{TS} data for the reactive normal modes Q_{TS}. Inspection of the remaining saddle points (**TSA1**, **TSB**, **TSC2**, **TSD1**, and **TSD2**) reveals that substitution of an $SiMe_3$ group by $SiMe_2F$ or $SiMeF_2$ has only a small influence on the nuclear dynamics in the saddle-point region of the PES (the curvature of the saddle point, given by $\mu_{TS}\,\omega_{TS}^2$, is relatively similar). The reactive motion is described by the fission of the N−O bond and the insertion of the silicon atom (see Figure 8). The bond between the transferred group (H or CH_3) is considerably stretched. The nitrogen atom moves towards the transferred group and forms a new bond.

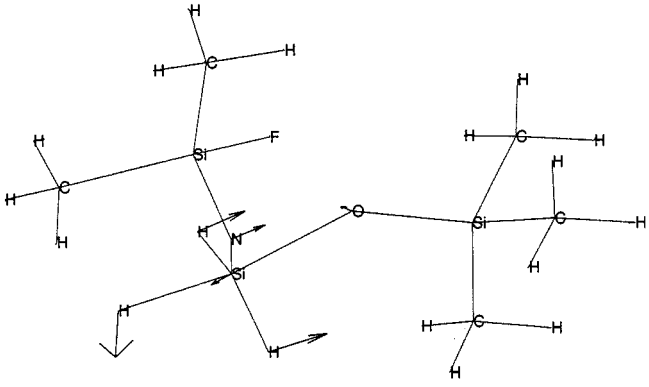

Figure 8. The reaction coordinate Q_{TS} at the saddle point **TSC2**, i.e. the normal coordinate of the mode with the imaginary vibrational frequency ω_{TS}

In summary, it has been shown that the insertion of a silyl group into the N−O bond is energetically favoured if it occurs from the nitrogen atom. Furthermore, a monofluorosilyl group inserts into the N−O bond whereas the difluorosilyl group does not. Insertion of SiH_2 stabilises the product by 86 kcal·mol^{-1} whereas insertion of $SiMe_2$, SiMeF, or SiF_2 yields a stabilisation of 66, 70, and 69 kcal·mol^{-1}, respectively. The transition state for SiH_2 insertion is located at 35±3 kcal·mol^{-1} above the tris(silyl)hydroxylamines, whereas the transition state for insertion of $SiMe_2$, SiMeF, and SiF_2 is ca. 10 kcal·mol^{-1} higher (44±3 kcal·mol^{-1}).

Experimental Section

General: All experiments were performed in oven-dried glassware using standard inert gas and vacuum-line techniques. NMR spectra were recorded from samples in $CDCl_3$ with $SiMe_4$ and C_6F_6 (^{1}H, ^{13}C, ^{19}F, ^{29}Si) as internal and $MeNO_2$ (^{15}N) as external references. Mass spectral data are reported in mass-to-charge units (*m*/*z*). The progress of the reactions was monitored by ^{19}F NMR spectroscopy. The compounds were obtained in analytically pure form.

***O*-(Dimethylsilyl)-*N*,*N*-bis(trimethylsilyl)hydroxylamine (1):** To a solution of *N*,*N*-bis(trimethylsilyl)hydroxylamine (8.8 g, 0.05 mol) in *n*-hexane (70 mL), *n*BuLi (1.6 M solution in *n*-hexane, 0.05 mol) was slowly added. After heating under reflux for 2 h, the reaction mixture was cooled to room temperature, whereupon $ClSiMe_2H$ (0.05 mol, 4.7 g) was added. LiCl was removed on a frit and **1** was purified by distillation; yield 73%; b.p. 63 °C/0.01 mbar. ^{1}H NMR ($CDCl_3$): δ = 0.11 [s, 18 H, $Si(CH_3)_3$], 0.22 [d, $^3J_{H,H}$ = 2.9 Hz, 6 H, $Si(CH_3)_2$], 4.7 (sept, $^3J_{H,H}$ = 2.9 Hz, 1 H, SiH). ^{13}C NMR ($CDCl_3$): δ = −1.22 (SiC_3), 0.76 (SiC_2). ^{29}Si NMR ($CDCl_3$): δ = 8.27 [$Si(CH_3)_3$], 13.43 (SiH). MS (EI): *m*/*z* (%) = 235(21) $[M]^+$, 220(8) $[M - CH_3]^+$. IR: $\tilde{\nu}$ = 2131.6 cm^{-1} (SiH). $C_8H_{25}NOSi_3$ (235.55): calcd. C 40.79, H 10.70; found C 40.53, H 10.32.

***N*,*N*-Bis(*tert*-butyldimethylsilyl)-*O*-(difluorophenylsilyl)hydroxylamine (2):** F_3SiPh (8.1 g, 0.05 mol) was added to *N*,*N*-bis(*tert*-butyldimethylsilyl)-*O*-lithiohydroxylamine[6] (13.0 g, 0.5 mol) at 0 °C and the mixture was slowly allowed to warm to room temperature. **2** was freed of LiF by centrifugation; yield 76%; b.p. 100 °C/0.05 mbar. ^{1}H NMR ($CDCl_3$): δ = 0.23 (t, $^6J_{HF}$ = 0.56 Hz, 12 H, $NSiCH_3$), 1.01 [s, 18 H, $NSiC(CH_3)_3$], 7.0−7.2 (C_6H_5). ^{13}C NMR ($CDCl_3$): δ = −2.91 (t, $^5J_{C,F}$ = 1.51 Hz, NSiC), 20.03 ($NSiCC_3$), 27.89 ($NSiCC_3$), 125.04 (t, $^2J_{C,F}$ = 26.7 Hz, C-1 of Ph), 128.47 (t, $^4J_{C,F}$ = 0.7 Hz, C-3,5 of Ph), 132.25 (C-4 of Ph), 134.72 (t, $^3J_{C,F}$ = 119 Hz, C-2,6 of Ph). ^{19}F NMR ($CDCl_3/C_6F_6$): δ = 29.5. ^{29}Si NMR ($CDCl_3$): δ = −65.02 (t, J_{SiF} = 278.7 Hz, OSiF), 14.85 (NSi). MS (EI): *m*/*z* (%) = 388(8) $[M - CH_3]^+$, 346(100) $[M - C(CH_3)_3]^+$.

***N*,*O*-Bis(*tert*-butyldimethylsilyl)-*N*-(difluorophenylsilyl)hydroxylamine (3):** A solution of **2** (20.2 g, 0.05 mol) in THF (50 mL) was refluxed for 3 d (^{19}F NMR control). Thereafter, the **3** obtained was distilled in vacuo. yield 67%. ^{1}H NMR ($CDCl_3$): δ = 0.12 (s, 6 H, $OSiCH_3$), 0.16 (s, 6 H, $NSiCH_3$), 0.28 [s, 9 H, $OSiC(CH_3)_3$], 0.88 [s, 9 H, $NSiC(CH_3)_3$], 7.2−7.8 (m, 5 H, C_6H_5). ^{13}C NMR ($CDCl_3$): δ = −6.37 ($NSiCH_3$), −5.49 ($OSiCH_3$), 17.82 [$NSiC(CH_3)_3$], 18.12 [$OSiC(CH_3)_3$], 25.84 [$NSiC(CH_3)_3$], 26.39 [$OSiC(CH_3)_3$]. ^{19}F NMR ($CDCl_3$): δ = 27.19 (OSiF). ^{29}Si NMR ($CDCl_3$): δ = −51.02 (t, $^1J_{SiF}$ = 271.19 Hz, NSiF), 15.49 (NSi), 24.56 (OSi). MS (EI): *m*/*z* (%) = 403(2) $[M]^+$, 388(8) $[M - CH_3]^+$, 346(100) $[M - CMe_3]^+$. $C_{18}H_{35}F_2NOSi_3$ (403.20): calcd. C 53.62, H 8.75; found C 53.16, H 8.49.

Compounds 4 and 5: The respective tris(silyl)hydroxylamine **1** or **3** (0.03 mol) was heated under reflux without a solvent for 3 d. Compounds **4** and **5** produced were purified by distillation in vacuo.

1,1,1,3,3-Pentamethyl-3-[(trimethylsilyl)amino]-1,3-disiloxane (4): Yield 82%; b.p. 63 °C/10 mbar. ^{1}H NMR ($CDCl_3$): δ = 0.04

[$Si(CH_3)_2$], 0.06 [$NSi(CH_3)_3$], 0.07 [$OSi(CH_3)_3$], 0.42 (NH). ^{13}C NMR ($CDCl_3$): δ = 1.97 [$OSi(CH_3)_3$], 2.30 [$NSi(CH_3)_3$], 2.46 [$Si(CH_3)_2$]. ^{15}N NMR ($CDCl_3$): δ = −344.71 (NH). ^{29}Si NMR ($CDCl_3$): δ = −11.24 (NSi), 2.12 (OSiN), 6.08 (SiO). MS (EI): *m*/*z* (%) = 235(4) $[M]^+$, 220(100) $[M - CH_3]^+$. $C_8H_{25}NOSi_3$ (235.55): calcd. C 40.79, H 10.70; found C 40.31, H 10.35.

1,3-Di-*tert*-butyl-3-[(difluorophenylsilyl)methylamino]-1,1,3-trimethyl-1,3-disiloxane (5): Yield 67%; b.p. 101 °C/0.05 mbar. ^1H NMR ($CDCl_3$): δ = 0.14 (3 H, $OSiCH_3$), 0.15 (3 H, $OSiCH_3$), 0.36 (3 H, $SiCH_3$), 0.97 [9 H, $SiC(CH_3)_3$], 1.04 [9 H, $SiC(CH_3)_3$], 2.68 (t, $^4J_{HF}$ = 1.15 Hz, 9 H, NCH_3), 7.4−7.8 (m, 5 H, C_6H_5). ^{13}C NMR ($CDCl_3$): δ = −2.92 ($OSiCH_3$), −2.90 ($OSiCH_3$), −5.66 (t, $^4J_{HF}$ = 2.53 Hz, $SiCH_3$), 18.27 [$SiC(CH_3)_3$], 18.37 [$SiC(CH_3)_3$], 25.84 [$SiC(CH_3)_3$], 26.67 [$SiC(CH_3)_3$], 33.72 (t, $^3J_{C,F}$ = 2.45 Hz, NCH_3), 128.04 (C-1 of Ph), 128.27 (C-3,5 of Ph), 131.57 (C-4 of Ph), 134.72 (t, $^3J_{C,F}$ = 1.26 Hz, C-2,6 of Ph). ^{19}F NMR ($CDCl_3$): δ = 24.71−26.55 (NSiF). ^{29}Si NMR ($CDCl_3$): δ = −47.22 (t, $^1J_{SiF}$ = 268.35 Hz, NSiF), 8.95 (t, $^3J_{SiF}$ = 1.53 Hz, NSiO), 11.62 (OSi). MS (EI): *m*/*z* (%) = 403(2) $[M]^+$, 388(8) $[M - CH_3]^+$, 346(100) $[M - CMe_3]^+$. $C_{18}H_{35}F_2NOSi_3$ (403.20): calcd. C 53.62, H 8.75; found C 53.74, H 8.92.

Acknowledgments

S. S. is indebted to Professor Peter Botschwina for continuous support. We would like to thank Dr. Rainer Oswald for his help with Figures 7 and 8. Helpful discussions with Dr. Thomas Müller (University of Frankfurt/Main) are gratefully acknowledged. Most of the calculations were carried out on workstations of the Gesellschaft für wissenschaftliche Datenverarbeitung Göttingen (GWDG). Support through Sonderforschungsbereich 357 "Molekulare Mechanismen unimolekularer Prozesse" is gratefully acknowledged. We are grateful to the Deutsche Forschungsgemeinschaft and Fonds der Chemischen Industrie for support of this work.

[1] P. Boudjouk, R. West, *Intra-Sci. Chem. Rep.* **1973**, *7*, 65.
[2] R. West, *Adv. Organomet. Chem.* **1977**, *16*, 1.
[3] R. Wolfgramm, U. Klingebiel, *Z. Anorg. Allg. Chem.* **1998**, *624*, 1031.
[4] R. Wolfgramm, U. Klingebiel, M. Noltemeyer, *Z. Anorg. Allg. Chem.* **1998**, *624*, 865.
[5] R. Wolfgramm, T. Müller, U. Klingebiel, *Organometallics* **1998**, *17*, 3222.
[6] F. Diedrich, U. Klingebiel, M. Schäfer, *J. Organomet. Chem.* **1999**, *588*, 242.
[7] F. Diedrich, U. Klingebiel, F. Dall′Antonia, C. Lehmann, M. Noltemeyer, T. R. Schneider, *Organometallics* **2000**, *19*, 5376.
[8] R. West, P. Boudjouk, T. A. Matuszko, *J. Am. Chem. Soc.* **1969**, *91*, 5184.
[9] E. Frainnet, F. Duboudin, F. Dabescat, G. C. Vincon, *C. R. Acad. Sci., Ser. C* **1973**, *276*, 1469.
[10] C. Trindle, D. D. Schillady, *J. Am. Chem. Soc.* **1973**, *95*, 703.
[11] M. T. Reetz, *Adv. Organomet. Chem.* **1977**, *16*, 33−65.
[12] R. Wolfgramm, U. Klingebiel, *Z. Anorg. Allg. Chem.* **1998**, *624*, 1035−1040.
[13] M. J. Frisch, G. W. Trucks, H. B. Schlegel, G. E. Scuseria, M. A. Robb, J. R. Cheeseman, V. G. Zakrzewski, J. A. Montgomery, R. E. Stratmann, J. C. Burant, S. Dapprich, J. M. Millam, A. D. Daniels, K. N. Kudin, M. C. Strain, O. Farkas, J. Tomasi, V. Barone, M. Cossi, R. Cammi, B. Mennucci, C. Pomelli, C. Adamo, S. Clifford, J. Ochterski, G. A. Petersson, P. Y. Ayala, Q. Cui, K. Morokuma, D. K. Malick, A. D. Rabuck, K. Raghavachari, J. B. Foresman, J. Cioslowski, J. V. Ortiz, A. G. Baboul, B. B. Stefanov, G. Liu, A. Liashenko, P. Piskorz, I. Komaromi, R. Gomberts, R. L. Martin, D. J. Fox, T. Keith, M. A. Al-Laham, C. Y. Peng, A. Nanayakkara, C. Gonzales, M. Challacombe, P. M. W. Gill, B. Johnson, W. Chen, M. W. Wong, J. L. Andres, C. Gonzales, M. Head-Gordon, E. S. Replogle, J. A. Pople, *GAUSSIAN-98, Revision A.7*, Gaussian, Inc., Pittsburgh PA, **1998**.
[14] A. D. Becke, *J. Chem. Phys.* **1993**, *98*, 5648.
[15] C. Lee, W. Yang, R. G. Parr, *Phys. Rev. B* **1988**, *37*, 785.
[16] C. Gonzales, H. B. Schlegel, *J. Chem. Phys.* **1989**, *90*, 2154; *J. Chem. Phys.* **1990**, *94*, 5523.
[17] E. Gellermann, U. Klingebiel, M. Noltemeyer, S. Schmatz, *J. Am. Chem. Soc.* **2001**, *123*, 378.
[18] S. Schmatz, *J. Phys. Chem. A* **2001**, *105*, 3875.
[19] U. Klingebiel, S. Schmatz, E. Gellermann, C. Drost, M. Noltemeyer, *Monatsh. Chem.* **2001**, *132*, 1105.
[20] E. Gellermann, U. Klingebiel, T. Pape, F. Dall'Antonia, T. R. Schneider, S. Schmatz, *Z. Anorg. Allg. Chem.* **2001**, *627*, 2581.
[21] S. Schmatz, *Organometallics*, in press.
[22] B. J. Lynch, D. G. Truhlar, *J. Phys. Chem. A* **2001**, *105*, 2936.
[23] B. J. Lynch, P. L. Fast, K. Harris, D. G. Truhlar, *J. Phys. Chem. A* **2000**, *104*, 21.

Received August 6, 2001
[I01298]

Syntheses, Structures, and Spectroscopic Properties of Cobalt(III) Complexes Containing 3- or 4-Pyridyl-Substituted Nitronyl and Imino Nitroxide Ligands

Masahiro Ogita,[a] Youhei Yamamoto,[a] Takayoshi Suzuki,[a] and Sumio Kaizaki*[a]

Keywords: Nitroxides / Radicals / Cobalt / NMR spectroscopy / Deoxygenation

Several new cobalt(III) complexes incorporating 4,4,5,5-tetramethyl-2-(3- or 4-pyridyl)imidazolin-1-oxyl 3-oxide (NIT*n*py) (*n* = 3 or 4) or 4,4,5,5-tetramethyl-2-(3- or 4-pyridyl)-imidazolin-1-oxyl (IM*n*py) have been prepared. The X-ray crystallographic analyses and the spectroscopic investigations have revealed that the nitronyl or imino nitroxides with the radical character are bound through the pyridyl-N atom to a Co^{III} center. There are some influences from the radical unpaired electron toward the Co^{III} complex moiety and those from the coordination of the Co^{III} ion toward the nature of these radicals which can be detected by ^{59}Co NMR and UV/Vis spectroscopy. Such observed changes coincide with the proposed spin density on the N atom of the pyridyl substituent. Furthermore, it was found that *trans*-[Co(acac)$_2$(PPh$_3$)(NIT4py)]$^+$ in methanol was gradually converted into the corresponding IM4py complex, while free NIT4py is stable in methanol. The Co^{II} species formed on the partial decomposition of the NIT4py complex in methanol seems to catalyze the deoxygenation of NIT4py to IM4py.

Introduction

In the last two decades, the chemistry and magnetic properties of transition metal complexes containing imidazolin-1-oxyl 3-oxide (abbreviated as nitronyl nitroxide; NIT) or imidazolin-1-oxyl (imino nitroxide; IM) radicals have been examined extensively.[1−11] These studies have been aimed mainly at investigating the magnetic exchange interactions between the metal d (or f) and the radical unpaired electrons, and at designing and synthesizing molecular ferro/ferrimagnets. Therefore, most of the complexes studied were of paramagnetic metal ions such as Mn^{II}, Cu^{II}, Ni^{II},[1−5] Cr^{III},[5a] Co^{II},[6−8] and lanthanide(III).[9] Among the nitronyl or imino nitroxide radicals, the pyridyl-substituted derivatives are especially attractive and are utilized successfully, because the auxiliary donor ability of the pyridyl-N atom tends to assemble extended coordination compounds by binding to metal ions.[2a,10] The suitability of such pyridyl-substituted nitroxides with the metal ions has afforded new aspects of their paramagnetic and diamagnetic metal complexes. In our previous papers concerning paramagnetic metal radical complexes, we have reported on the structures, magnetic, and spectroscopic (UV/Vis absorption, MCD, resonance Raman, NMR) properties of the 2-pyridyl-substituted nitronyl nitroxide (NIT2py) or imino nitroxide (IM2py) complexes of Cr^{III}, Ni^{II}, Co^{II}, and Mn^{II}.[5,6] For diamagnetic metal complexes Oshio et al. have observed a large ferromagnetic or antiferromagnetic interaction between the two imino nitroxides through a diamagnetic metal center in tetrahedral Cu^{I}, Ag^{I} and square-planar Pd^{II} complexes.[11] Wei et al. have found a fairly large antiferromagnetic interaction in a polymeric Hg^{II} chain compound.[10] Recently, we described the X-ray structures and magnetic properties of the IM2py Zn^{II} complex and related complexes.[6] On the other hand, substitution-inert Co^{III} complexes incorporating the pyridyl-substituted nitronyl or imino nitroxides (NIT*n*py or IM*n*py) would exhibit a variety of coordination modes of the 3- or 4-pyridyl-substituted nitroxide radicals, or exert an influence from nonradical coligands. Such nitroxide radical Co^{III} complexes are expected to afford moderately or slightly magnetically coupled systems, where the spectroscopic properties could be regulated, as observed for the Ni^{II} and Cr^{III} complexes.[5] This is in contrast to semiquinone radical Co^{III} complexes, which are susceptible to reduction to Co^{II}.[12] Here, we report on the synthesis and structural characterization of *trans*-[Co(acac)$_2$(NO$_2$-κ*N*)(L)], *trans*-[Co(acac)$_2$(PPh$_3$)(L)]PF$_6$, and [Co(acac)(tdmme)(L)](PF$_6$)$_2$ [acac = pentane-2,4-dionate; tdmme = 1,1,1-tris(dimethylphosphanylmethyl)-ethane; L = NIT4py, NIT3py, IM4py, and IM3py] (Scheme 1). We also report on the novel deoxygenation reaction of NIT4py in *trans*-[Co(acac)$_2$(PPh$_3$)(NIT4py)]PF$_6$, and on the attempts to prepare the bis(nitroxide) Co^{III} complexes.

[a] Department of Chemistry, Graduate School of Science, Osaka University,
Toyonaka 560-0043, Japan
Fax: (internat.) + 81-6/6850-5408
E-mail: kaizaki@chem.sci.osaka-u.ac.jp

Supporting information for this article is available on the WWW under http://www.eurjic.com or from the author.

 © WILEY-VCH Verlag GmbH, 69451 Weinheim, Germany, 2002 1434−1948/02/0404−0886 $ 17.50+.50/0 *Eur. J. Inorg. Chem.* **2002**, 886−894

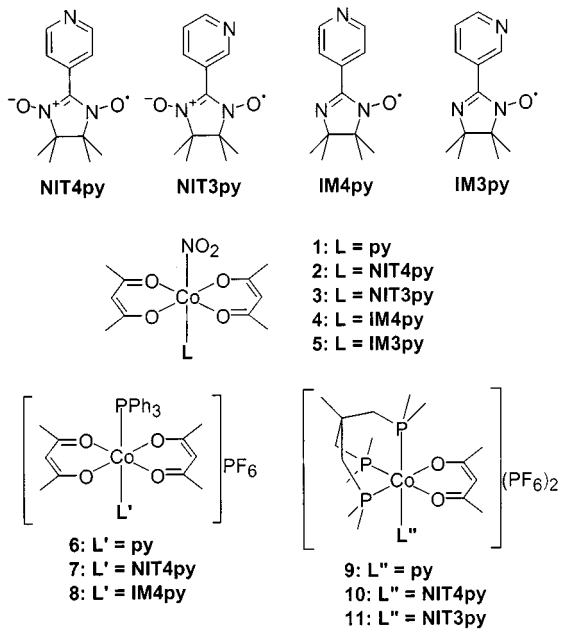

Scheme 1. The nitronyl and imino nitroxides and their Co^{III} complexes, together with the reference pyridine complexes, prepared in this study

Results and Discussion

Bis(pentane-2,4-dionato)(nitrito-κ*N* or triphenylphosphane) Complexes

Although both 4- and 3-pyridyl-substituted nitroxide complexes, *trans*-$[Co(acac)_2(NO_2\text{-}\kappa N)(L)]$ [L = NIT4py (**2**), IM4py (**4**), NIT3py (**3**), and IM3py (**5**)], were prepared from *trans*-$Na[Co(acac)_2(NO_2\text{-}\kappa N)_2]$, the reaction of *trans*-$[Co(acac)_2(PPh_3)_2]PF_6$ with the nitroxides gave only the 4-pyridyl-substituted complexes, *trans*-$[Co(acac)_2(PPh_3)(L')]PF_6$ [L′ = NIT4py (**7**) and IM4py (**8**)]. The formation of the 3-pyridyl-substituted nitroxide (NIT3py or IM3py)/PPh_3 complexes was not observed due to steric factors (vide infra). The *trans* geometry of the nitroxide complexes, as well as of the corresponding pyridine complexes of **1** and **6** was determined by ^1H NMR spectroscopy in $CDCl_3$. The spectra showed only one methyl and one methine proton resonances of the acac moiety with an intensity ratio of 6:1 (Table 1).

Table 1. ^1H NMR chemical shifts of the acac moiety in the Co^{III} complexes **1**−**8**

Compound	$-CH_3$[a]	$=CH-$[a]
1	2.12	5.33
2	2.11	5.33
3	2.19	5.35
4	2.12	5.33
5	2.12	5.32
6	1.78	4.89
7	1.74	4.91
8	1.79	4.90

[a] In $CDCl_3$. Chemical shifts (δ scale) are relative to TMS. For all compounds listed the intensity ratio of $-CH_3$ to $=CH-$ was found to be 6:1.

The structures of complexes **5**, **7**, and **8** were confirmed by X-ray analysis. The molecular structures of *trans*-$[Co(acac)_2(NO_2\text{-}\kappa N)(IM3py)]$ (**5**) and *trans*-$[Co(acac)_2(PPh_3)(NIT4py)]^+$ in **7**·CH_2Cl_2 are shown in Figure 1. The crystal of **8**·CH_2Cl_2 is isomorphous to that of **7**·CH_2Cl_2 and the molecular structure of *trans*-$[Co(acac)_2(PPh_3)(IM4py)]^+$ in **8**·CH_2Cl_2 (Figure S1, Supporting Information) is very similar to that of the NIT4py complex, except for the absence

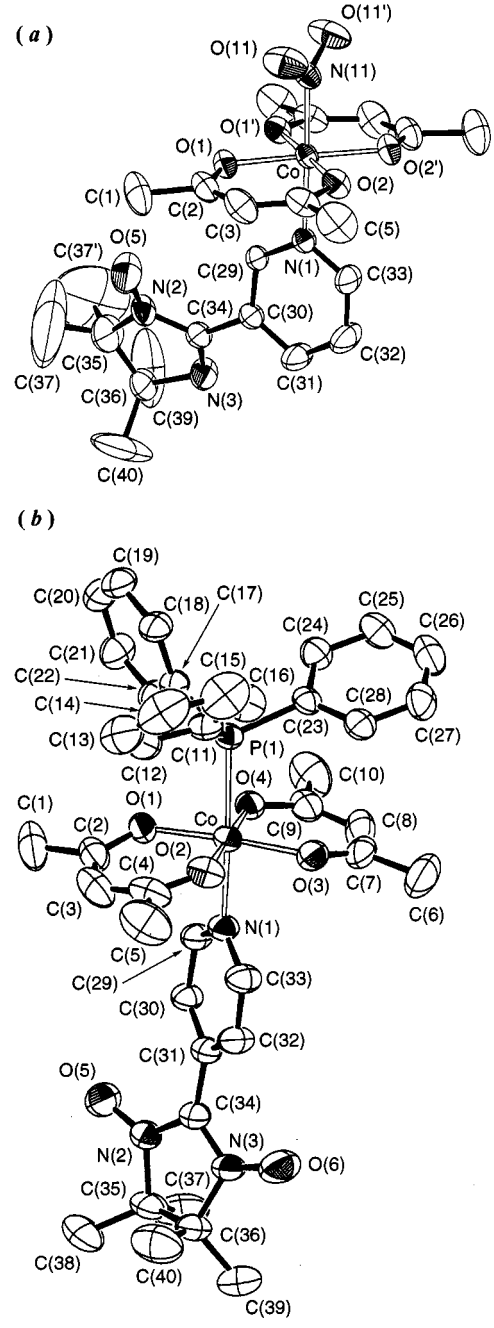

Figure 1. Perspective views of (*a*) *trans*-$[Co(acac)_2(NO_2\text{-}\kappa N)(IM3py)]$ (**5**) (40% probability level) and (*b*) *trans*-$[Co(acac)_2(PPh_3)(NIT4py)]^+$ in **7**·CH_2Cl_2 (50% probability level); hydrogen atoms are omitted for clarity

of one O atom from the nitronyl nitroxide moiety. The pyridyl-substituted nitronyl or imino nitroxide is bound to a Co^{III} center via a pyridyl-N atom at the position *trans* to NO_2-κ*N* or PPh_3.

Selected bond lengths, bond angles, and dihedral angles between the least-squared planes are listed in Table 2. The structural parameters of the NIT4py moiety in **7** are similar to those of free NIT4py,[7b,13] and those of the other complexes containing monodentate pyridyl-N donating NIT4py.[1,2b,2c] The dihedral angle between the nitronyl nitroxide mean plane and the pyridyl ring in **7** [28.8(1)°] is slightly larger than those in free NIT4py (24.7°[7b] or 22.8°[13]). The N−O bond lengths in **7** [1.276(3) and 1.260(3) Å] are close to the typical bond lengths in the free nitronyl nitroxides.[7b,13,14] In contrast, the structural parameters of IM4py in **8**, IM3py in **5**, and the free 5-pyrimidyl or *m*-nitrophenyl imino nitroxide (IM5pym or IM*m*NP)[14a,15] are fairly different from one another. For example, the N−O bond length becomes shorter in the order **8** [1.295(6) Å] > **5** [1.273(6) Å] > IM5pym [1.268(4) Å] > IM*m*NP (average 1.246 Å). The dihedral angle between the imino nitroxide mean plane and the pyridyl ring is 29.2(2) and 22.5(2)° for **5** and **8**, respectively, 19.1° for IM5pym,[14a] and 44.7 and 13.0° for two crystallographically independent IM*m*NP molecules.[15]

Table 2. Selected bond lengths [Å], bond angles [°], and dihedral angles [°] between the least-squared planes for the complexes

Compound[a]	**5**	**7**	**8**
Co−P(1)	−	2.2723(7)	2.269(1)
Co−O(1)	1.879(2)	1.873(2)	1.876(3)
Co−O(2)	1.889(2)	1.885(2)	1.880(3)
Co−O(3)	−	1.888(2)	1.882(3)
Co−O(4)	−	1.879(2)	1.882(3)
Co−N(1)	1.996(3)	2.021(2)	2.019(3)
Co−N(11)	1.902(3)	−	−
N(2)−O(5)	1.273(6)	1.276(3)	1.295(6)
N(3)−O(6)	−	1.260(3)	−
N(2)−C(34)	1.348(5)	1.347(4)	1.343(5)
N(3)−C(34)	1.306(5)	1.348(4)	1.306(5)
P(1)−Co−N(1)	−	175.47(6)	175.11(9)
N(1)−Co−N(11)	178.3(1)	−	−
O(1)−Co−O(2)	95.73(8)	94.59(9)	94.5(1)
O(3)−Co−O(4)	−	94.95(9)	95.0(1)
C(34)−N(2)−O(5)	125.2(4)	127.1(2)	127.5(4)
C(34)−N(3)−O(6)	−	126.3(2)	−
C(35)−N(2)−O(5)	127.2(4)	121.4(2)	121.5(4)
C(36)−N(3)−O(6)	−	122.3(3)	−
C(34)−N(2)−C(35)	107.6(3)	111.4(2)	110.0(4)
C(34)−N(3)−C(36)	109.4(4)	111.2(2)	108.2(4)
plane(Co−4O) vs. plane(acac 1)	4.0(1)	14.9(1)	16.5(2)
plane(Co−4O) vs. plane(acac 2)	−	9.5(1)	10.3(2)
plane(acac 1) vs. plane(acac 2)	−	24.3(1)	26.8(2)
plane(Co−4O) vs. plane(py)	90	84.53(9)	83.5(1)
plane(Co−4O) vs. plane(phenyl 1)	−	40.1(1)	40.8(2)
plane(Co−4O) vs. plane(phenyl 2)	−	72.7(1)	69.0(1)
plane(Co−4O) vs. plane(phenyl 3)	−	23.5(1)	22.8(1)
plane(py) vs. plane(nitroxide)	29.2(2)	28.8(1)	22.5(2)

[a] Plane(Co−4O) was defined by O(1), O(2), O(3 or 1′) and O(4 or 2′); plane(acac 1) by O(1), O(2), and C(2)−C(4); plane(acac 2) by O(3), O(4), and C(7)−C(9); plane(py) by N(1) and C(29)−C(33); plane(phenyl 1) by C(11)−C(16); plane(phenyl 2) by C(17)−C(22); plane(phenyl 3) by C(23)−C(28).

The structures of the *trans*-$Co(acac)_2(PPh_3)$ moiety in **7** and **8** are similar to those in *trans*-$[Co(acac)_2(PPh_3)(H_2O)]PF_6$[16a] and *trans*-$[Co(acac)_2(PPh_3)(atmp)]PF_6$ (atmp = 4-amino-2,2,6,6-tetramethylpiperidine-κN^4).[16b] In particular, the acac ligands in the equatorial positions bend away from the axial PPh_3 group, due to the steric effects presented by the bulky axial PPh_3 group. The dihedral angle between the two acac planes are 24.3(1) and 26.8(2)° in **7** and **8**, respectively. The Co−P bond lengths, 2.2723(7) in **7** and 2.269(1) Å in **8**, are similar to those in *trans*-$[Co(acac)_2(PPh_3)(H_2O)]PF_6$ [2.243(1) Å] and *trans*-$[Co(acac)_2(PPh_3)(atmp)]PF_6$ [2.295(2) Å].

The pyridyl ring of NIT4py or IM*n*py in **5**, **7**, and **8** is oriented toward the cleft between the two equatorial acac ligands (Figure 1 and Figure S1). This orientation would minimize the sterically repulsive interaction between the planar pyridyl moiety of the nitroxide and the equatorial acac planes. Comparison with the structures of complexes **5**, **7**, and **8** suggests that in the hypothetical complex, *trans*-$[Co(acac)_2(PPh_3)(NIT3py \text{ or } IM3py)]^+$, severe steric interaction exists between the nitroxide part of the coordinated NIT3py or IM3py and the equatorial acac planes which would bend away from the axial PPh_3 group due to steric hindrance. This seems to be the reason for the unsuccessful syntheses of the 3-pyridyl-substituted nitroxide complexes for PPh_3 derivatives.

(Tripodal tridentate phosphane)(pentane-2,4-dionato) Complexes

For spectroscopic purposes (vide infra), we have also attempted to prepare the NIT4py and NIT3py complexes which incorporates tripodal tridentate phosphane,

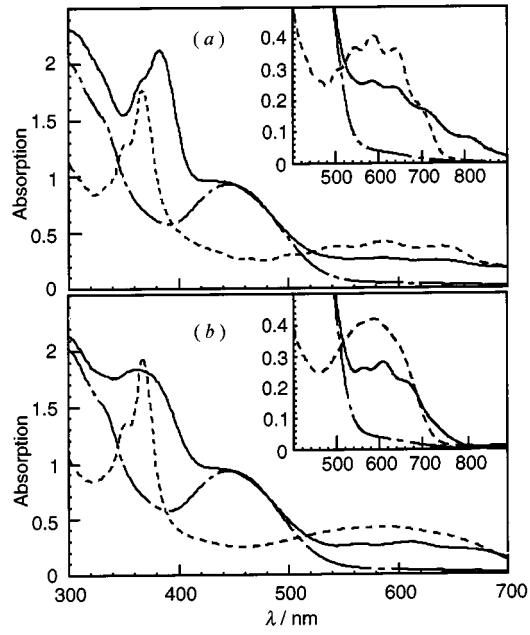

Figure 2. UV/Vis spectra in the solid state: (*a*) complex **9** (− · −), complex **10** (——), and NIT4py (− − − −); (*b*) complex **9** (− · −), complex **11** (——), and NIT3py (− − − −)

tdmme.[17] The reaction of [Co(acac)(tdmme)-(CH_3CN)](PF_6)$_2$ (**12**) and L′′ (L′′ = py, NIT4py, or NIT3py) in methanol afforded powder products of [Co(acac)(tdmme)(L′′)](PF_6)$_2$ (**9**−**11**). The UV/Vis spectra of the products in the solid state showed distinct changes from the superimposed spectra of the starting materials (Figure 2 and Table 3). These compounds were insoluble in dichloromethane, chloroform, and methanol, and fairly soluble in acetonitrile. However, the absorption spectra of compounds **9**−**11** in acetonitrile showed apparent shifts from those in the solid, and coincided with the superimposed spectra of complex **12** and free L′′. These facts indicate that in acetonitrile NIT*n*py (or py) dissociates from the Co^{III} center giving a mixture of the acetonitrile complex **12** and free L′′. This lability is probably due to the strong *trans* influence of tdmme.[17]

Deoxygenation of NIT4py to IM4py in the PPh_3 Complex

Ullman reported that heating nitronyl nitroxides with PPh_3 in benzene affords the corresponding imino nitroxides in high yields.[18] In view of this fact, the successful synthesis of complex **7** from *trans*-[Co(acac)$_2$(PPh_3)$_2$]PF_6 seems to be strange since free PPh_3 is produced in the reaction mixture. Under the experimental conditions employed (in dichloromethane at room temperature for several hours), detectable deoxygenation of NIT*n*py to IM*n*py was not observed. Further, refluxing NIT4py with PPh_3 in dichloromethane, chloroform, or methanol for several hours did not result in any UV/Vis spectral change. The isolated complex **7** was also stable on refluxing in dichloromethane or chloroform for several hours. However, when a methanol solution of **7** was allowed to stand at room temperature for 1 d, the UV/Vis and ESR spectra of the solution changed to those corresponding to the IM4py complex **8**. On refluxing the methanol solution, deoxygenation of NIT4py in complex **7** was completed within 10 min (Figure 3). A prolonged reaction in boiling methanol resulted in the decomposition of IM4py; a very weak ESR signal of IM4py was seen after 1 d.

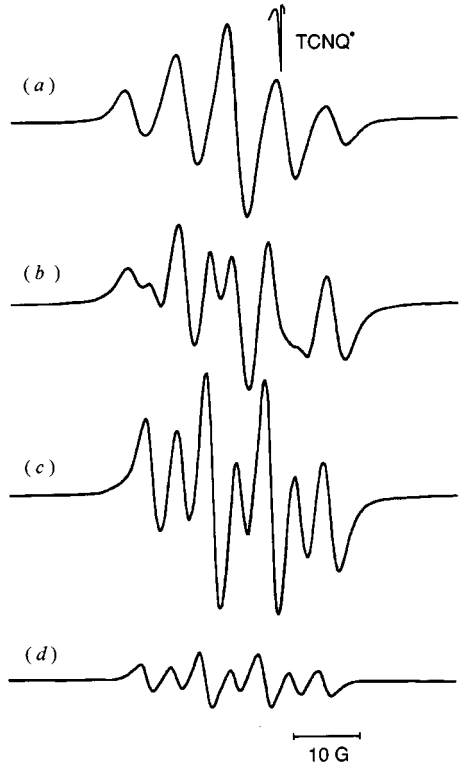

Figure 3. The ESR spectra of complex **7** (*a*) in dichloromethane, (*b*) in methanol, (*c*) in refluxing methanol for 10 min, and (*d*) in refluxing methanol for 24 h

The reagent that is responsible for the deoxygenation of NIT4py in complex **7** was investigated. As described above, a methanol solution of NIT4py alone, or together with PPh_3, did not result in such a deoxygenation reaction. The following Sephadex LH-20 chromatographic behavior in methanol suggests that complex **7** exists as a dissociated equilibrium mixture. Of the two bands separated from the

Table 3. Absorption spectroscopic data of the free nitroxides and the Co^{III} complexes

Compounds	Solvent	10^{-3} σ [cm^{-1}] (ε [dm^3 mol^{-1} cm^{-1}])
NIT4py	CH_2Cl_2	14[a] (80), 15.5[a] (175), 16.8 (230), 18[a] (180), 19.5[a] (80), 27.3 (16300), 28.5[a] (7400), 35.7[a] (8500), 38.2[a] (8800)
NIT3py	CH_2Cl_2	14.5[a] (190), 16.1 (476), 17.1 (489), 18.5[a] (300), 27.3 (17600), 28.5[a] (9600), 37.8 (10600), 40[a] (10000)
IM4py	CH_2Cl_2	17.8[a] (50), 19.5[a] (120), 21.1[a] (240), 22.4 (315), 23.5 (300), 25[a] (260), 33.3 (4400), 34.8[a] (3900), 37.4[a] (3800)
IM3py[b]	CH_2Cl_2	17.8[a], 19.7[a], 21.3[a], 22.6, 23.8[a], 25.1[a], 33[a], 37.5[a]
1	CH_2Cl_2	18.8 (157), 29.5 (8500)
2	CH_2Cl_2	12.5[a] (40), 14.3[a] (75), 16[a] (150), 18.4 (227), 26.5 (17600), 27.6[a] (13000)
3	CH_2Cl_2	14.4[a] (80), 15.8[a] (260), 17.3 (364), 18.3[a] (345), 27.0 (12000), 28.7 (12400)
4	CH_2Cl_2	18.5[a] (280), 20.0 (360), 29.5 (10800), 37.5 (33500)
5	CH_2Cl_2	17.8[a] (150), 19.5 (270), 21.0[a] (420), 29.5 (9200), 37.5 (29400)
6	CH_2Cl_2	18.7[a] (267), 30.3 (16000)
7	CH_2Cl_2	12.2[a] (50), 14[a] (80), 18.6[a] (370), 26.4 (19446), 27.8[a] (17000), 30.0 (22500), 33.8[a] (26500)
8	CH_2Cl_2	16.2[a] (180), 18.2[a] (430), 30.5 (20300)
9[b]	solid	22.5, 33.7[a]
10[b]	solid	14.9[a], 16.5, 17.8, 22.8[a], 27.8, 33.3[a], 38.3
11[b]	solid	12.5[a], 14.2[a], 15.8, 17.2, 22.9[a], 26.3, 33.7, 38.2
12	py	22.4 (910), 30.2[a] (3140)
	CH_3CN	23.1 (835), 30.7[a] (3200), 34.1 (10800), 39.4[a] (24700)

[a] Shoulder. [b] These data were measured qualitatively.

adsorbed products, the faster developing green band was a mixture of complex **7** and *trans*-[Co(acac)$_2$(PPh$_3$)(H$_2$O)]PF$_6$,[16a] whereas the slower developing blue eluate was free NIT4py. Thus, the aquated complex, [Co(acac)$_2$(PPh$_3$)(H$_2$O)]$^+$ would mainly contribute to the deoxygenation of NIT4py. In fact, NIT4py itself is catalyzed to form deoxygenated IM4py by a methanol solution of the triphenylphosphane complex *trans*-[Co(acac)$_2$(PPh$_3$)(H$_2$O)]PF$_6$, but not by a methanol solution of the dimethylphenylphosphane complex *trans*-[Co(acac)$_2$(PMe$_2$Ph)(H$_2$O)]PF$_6$ and the Co^{II} complex [Co^{II}(acac)$_2$(H$_2$O)$_2$]. The Co^{III}−PPh$_3$ complex, *trans*-[Co(acac)$_2$(PPh$_3$)(H$_2$O)]PF$_6$ slowly decomposes to give Co^{II} species, while *trans*-[Co(acac)$_2$(PMe$_2$Ph)(H$_2$O)]PF$_6$ is stable in methanol.[16a,19] Thus, the decomposed, yet uncharacterized Co^{II} products may be a catalyst for the deoxygenation process.

Attempts to Prepare Bis(nitronyl or imino nitroxide)bis(pentane-2,4-dionato) Complexes

Although the reaction of *trans*-[Co(acac)$_2$(PPh$_3$)$_2$]PF$_6$ with NIT3py in dichloromethane did not proceed, a similar reaction with twice the equimolar amounts of NIT3py in methanol showed a gradual change in color from dark red to brown. The elemental analysis and the spectroscopic data of the brown product indicate the formation of a complicated mixture of bis(NIT3py)-, (NIT3py)(IM3py)-, and bis(IM3py)-bis(acac)cobalt(III) complexes (Figure S2, Supporting Information), as suggested from the reaction conditions for the deoxygenation of NIT3py to IM3py as described above. The formation of IM3py could not be avoided under these reaction conditions.

An attempt to oxidize an ethanolic solution of *trans*-[Co^{II}(acac)$_2$(NIT*n*py or IM*n*py)$_2$][7b] with acidic PbO$_2$ resulted in the formation of a mixture of bis(NIT*n*py or IM*n*py) complexes (Figure S2), as in the case started from the Co^{III} complex. It is noted that in the reactions with PbO$_2$, NIT*n*py still deoxygenates to give IM*n*py.

ESR Spectra and Magnetic Properties

The ESR spectra of the Co^{III} NIT*n*py (**2**, **3**, **7**) and IM*n*py (**4**, **5**, **8**) complexes give a well-resolved quintuplet and septuplet signal, respectively (Figure S3, Supporting Information), as observed for free NIT*n*py and IM*n*py.[1,21] The *g* and *A* values of the Co^{III} complexes are close to those of the free nitroxide (Table 4). This fact indicates that the radical unpaired electron of the nitroxide is not significantly influenced by the coordination to a diamagnetic Co^{III} ion through the substituted pyridyl-N atom. This is also suggested by the variable-temperature magnetic measurements in the solid state, the overall profiles of the temperature dependence of the molar magnetic susceptibilities of the Co^{III} complexes are found to be similar to those of the free nitroxides (Figure S4, Supporting Information).

NMR Spectra

The ^{1}H NMR signals of the acac or PPh$_3$ moiety in the Co(acac)$_2$(NO$_2$-κ*N* or PPh$_3$) unit of **2**, **3**, **7**, and **8** were found to become broad. Since the observed broad signals did not show any shift from those of the parent complexes (Table 1), the line-broadening on coordination of NIT*n*py or IM*n*py via the pyridyl-N atom results from the dipolar relaxation (through space) mechanism, but not from the contact (through bond) mechanism. This is also related to the difference in broadening between the NIT3py and NIT4py complexes, the former being larger than the latter. The distance from the radical moiety in NIT3py to the protons in the coligands is shorter than for NIT4py, and accounts for the difference in line broadening in terms of the dipolar relaxation.

Table 4. ESR spectral parameters

Compounds[a]	Solvent	*g*	A_1	A_2
NIT4py	H_2O	2.007	8.2	–
2	CH_2Cl_2	2.007	7.3	–
7	CH_2Cl_2	2.007	7.3	–
NIT3py	H_2O	2.006	7.9	–
3	CH_2Cl_2	2.006	7.2	–
IM4py	H_2O	2.005	9.4	4.2
4	CH_2Cl_2	2.006	9.0	4.4
8	CH_2Cl_2	2.006	9.2	4.4
IM3py	H_2O	2.006	9.4	4.2
5	CH_2Cl_2	2.006	9.2	4.3

[a] H_0 = 3360 Gauss, 9.45 GHz, room temp., A_1, A_2 in Gauss.

Table 5. ^{59}Co NMR spectroscopic data

Compound[a]	Solvent	δ	$\Delta_{1/2}$ [Hz]
1	$CDCl_3$	10633	1200
2	$CDCl_3$	10700	11000
3	$CDCl_3$	10585	2600
4	$CDCl_3$	10624	4500
5	$CDCl_3$	10606	2000
6	$CDCl_3$	9800	2000
7	$CDCl_3$	9837	12000
8	$CDCl_3$	9780	5900
trans-[Co(acac)$_2$(py)$_2$]PF$_6$	CD_3CN	13260	
trans-[Co(acac)$_2$(NIT4py)$_2$]BF$_4$[b]	CD_3CN	13352	
trans-[Co(acac)$_2$(NIT4py)(IM4py)]BF$_4$[b]	CD_3CN	13284	
trans-[Co(acac)$_2$(IM4py)$_2$]BF$_4$[b]	CD_3CN	13231	

[a] Chemical shifts (δ scale) are relative to K$_3$[Co(CN)$_6$]. [b] Could not be isolated.

Table 5 presents the ^{59}Co NMR parameters of the pyridine and nitroxide complexes. The ^{59}Co NMR chemical shifts of the PPh$_3$ complexes with py, NIT4py, and IM4py are located at a higher field than those of the corresponding NO$_2$-κ*N* complexes. The ^{59}Co NMR resonances of the nitroxide complexes are relatively broader as compared with the py complexes. For the NIT*n*py complexes **2**, **3**, and **7**, the ^{59}Co NMR signals on coordination of NIT3py and NIT4py shift to a higher and lower field, respectively, from those of the corresponding py complexes. The line-broadening for the NIT3py complex is small and considerably larger for the NIT4py complex (Figure S5, Supporting Information). These observations coincide with the ^{1}H

NMR behavior of the *meta*- and *para*-protons in the phenyl group of NITPh[22] and NITPhOH,[23] and also with the experimental and theoretical spin density (and sign) at these positions.[14,24]

The ^{59}Co NMR resonances of the IM*n*py complexes **3**, **4**, and **8** show slightly higher field shifts with less broadening than the corresponding NIT*n*py complexes. This also coincides with the difference in the spin density between the imino and nitronyl nitroxides.[14,15] Thus, the ^{59}Co NMR chemical shifts reflect the spin density and sign on the pyridyl-N atom of NIT*n*py or IM*n*py, although the shift values are relatively small, in accordance with the small spin density on the N atom.

UV/Vis Absorption Spectra

The UV/Vis spectra of complexes **2**−**5**, **7**, and **8** give a complicated pattern due to the overlap with the intraligand bands for the nitroxides and the Co(acac)$_2$(NO$_2$-κ*N* or PPh$_3$) moieties (Figure S6, Supporting Information). Thus, it is difficult to evaluate the coordination effect on the ligand-field d−d transitions of the Co^{III} ion and on the intraligand transitions of the radical moiety in these complexes by comparison with the spectra of the py complexes **1** and **6**. This difficulty may be overcome if the d−d bands are shifted to a shorter wavelength where the nitronyl nitroxides are transparent. This can be achieved with the use of a tripodal tridentate phosphane tdmme instead of PPh$_3$ and one acac ligand, since the ligand-field strength of tdmme is much larger than that of PPh$_3$ and acac.[17] Since the complexes [Co(acac)(tdmme)(L′′)](PF$_6$)$_2$ (**9**−**11**) are unstable in acetonitrile, the following UV/Vis spectra were measured in the solid state. The ligand-field d−d band of the py complex **9** appears at 22200 cm^{-1}, as expected from the difference in the ligand-field strengths between tdmme and (acac)(PPh$_3$). It is noted that the d−d transition of the NIT*n*py complex **10** or **11** is observed at the same position as that of the py complex **9** (Figure 2). Therefore, the radical unpaired electron of NIT*n*py exerts no influence on the d−d transition energy of the Co^{III} complexes. However, there are explicit perturbations for the broad vibronic band at 15000−18000 cm^{-1} upon coordination, and a very sharp strong band following the higher energy component around 27000 cm^{-1}, due to the n→π* and π→π* transitions of the nitronyl nitroxide moiety, respectively.[1] In the NIT4py complex **10** [Figure 2 (*a*)], the n→π* and π→π* bands are red-shifted by 1300 and 1100 cm^{-1}, respectively. In contrast, the NIT3py complex **11** [Figure 2 (*b*)] gives a slightly red-shifted (500 cm^{-1}) n→π* transition band, however, the π→π* band is shifted by a negligible amount, but is remarkably broad.

This perturbation is confirmed by subtracting the UV/Vis spectra of the NIT*n*py complexes from the py complex, which gives the spectrum of the perturbed nitroxide in the complex. For the NIT*n*py complexes, comparisons of both the difference spectra of complexes **2** (subtracted from **1**) and **3** (subtracted from **1**) with the spectra of free nitroxides (Figure 4) gives a similar result as the above tdmme complexes. Further, the difference spectrum of the PPh$_3$ complex **7** (subtracted from **6**) gives the same result (Figure S7, Supporting Information). Thus, it is concluded that the n→π* and π→π* transition bands are red-shifted (by ca. 800 cm^{-1}) on coordination of NIT4py to the Co^{III} ion via the pyridyl-N atom, while these bands show a slight shift and band-broadening when NIT3py is coordinated. These differences in perturbation between the NIT4py and NIT3py complexes may result from the difference in spin density (and sign) at the pyridyl-N atom, as found in the ^{59}Co NMR chemical shifts of complexes **2** and **3** (vide supra). Another reason is considered to be related to the difference in perturbation on the NIT*n*py SOMO π* orbitals through π-back-bonding from the Co^{III} t_{2g} orbital to the pyridyl π* orbital, in view of the plausible inherent interaction of the π-systems between the NIT*n*py and the pyridyl group. This interaction is suggested by the lower frequency shift of both the n→π* and π→π* transitions by 1000−2000 cm^{-1}, on going from NITMe to NIT*n*py.[1]

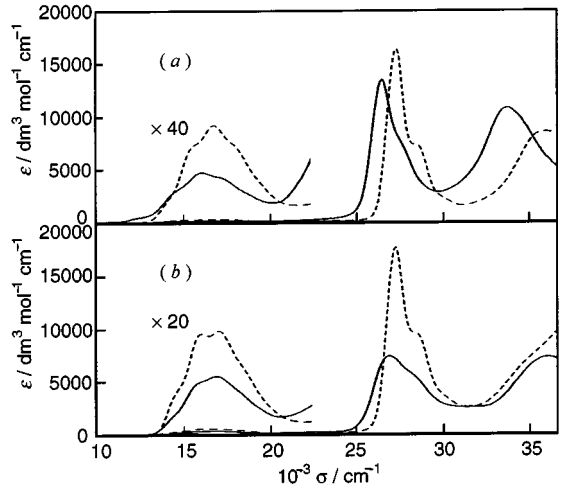

Figure 4. The difference absorption spectra of (*a*) complex **2** − complex **1** and (*b*) complex **3** − complex **1** (——), together with the UV/Vis spectra of NIT4py and NIT3py (− − − −), respectively

We have also made a similar analysis for the IM*n*py complexes (Figure S8, Supporting Information). Although the n(N−O)→π* transition band in the IM4py complexes **4** and **8** shows a distinct red-shift and that in the IM3py complex **5** does not shift, the results are not so clear, because the absorption spectra are much more complicated.

The intensity enhancement of the spin-forbidden $^1A_1 \rightarrow {}^3T_2$, $^3T_1$ ligand-field transitions is expected as a result of the magnetic exchange coupling with the doublet ground state of the nitroxide radical and the triplet excited state of Co^{III}. This intensity enhancement is also found for the intraligand singlet−triplet transition in diamagnetic bipyridine, due to the nearby paramagnetic Cr^{III} ion in [Cr(mal)$_2$(bpy)]$^-$.[25] However, in the predicted region for the $^1A_1 \rightarrow {}^3T_2$, $^3T_1$ transitions, only one shoulder is observed for complexes **2**, **7**, and **11** near 12500 cm^{-1}, which belongs to the lowest frequency vibronic component of the n→π* NIT*n*py intraligand transition, in terms of the above difference spectra. It is seen that the magnetic exchange coupling

in this kind of nitroxide complex is not large enough to observe the spin-forbidden transition intensity enhancement. The chelated NIT2py or IM2py Co^{III} complexes may be such a candidate to give observable intensity enhancement. The research in this direction is currently under way in our laboratory.

Conclusion

Explicit perturbations are found in the ^{59}Co NMR chemical shifts resulting from the radical unpaired electron, and on the n→π* and π→π* transition bands of the nitroxide moieties as a result of coordination to the Co^{III} center, in several newly prepared Co^{III} complexes bearing 3- or 4-pyridyl-substituted nitronyl or imino nitroxides. The structural and magnetic properties do not show any significant changes from the corresponding pyridine complexes and/or from the free nitroxides. These perturbed properties reflect the radical spin density and sign on the pyridyl-N atom of NIT*n*py or IM*n*py and/or the π-back bonding which is fine-tuned by coordination. Attempts to prepare bis(NIT*n*py or IM*n*py) Co^{III} complexes resulted in the formation of a mixture of the NIT*n*py and IM*n*py complexes, due to the deoxygenation of NIT*n*py to IM*n*py, and the decomposition of the IM*n*py radicals.

Experimental Section

General Remarks: The nitronyl and imino nitroxides, NIT4py, NIT3py, IM4py, and IM3py,[18,20,21a,26] and the starting Co^{III} complexes, *trans*-Na[Co(acac)$_2$(NO$_2$-κ*N*)$_2$],[27a] *trans*-[Co(acac)$_2$(PPh$_3$)$_2$]PF$_6$,[19a] and [CoCl(acac)(tdmme)]PF$_6$,[17a] and the pyridine (py) complex, *trans*-[Co(acac)$_2$(NO$_2$-κ*N*)(py)] (**1**),[27b] were prepared by the literature methods. UV/Vis spectra were measured with a Perkin−Elmer Lambda 19 spectrophotometer at room temperature. The solid-state spectra in the form of Nujol mulls were obtained according to the method described by Lee et al.[28] The ^1H and ^{59}Co NMR spectra were recorded with a JEOL EX-270 or Lambda 500 spectrometer at 30 °C. The ^{59}Co chemical shifts were referenced from external [Co(acac)$_3$] (in CDCl$_3$; δ = 12625).[16a,29] The ESR spectra were obtained with a JEOL JES-FE or JES RE1X spectrometer at ambient temperature. The magnetic susceptibility data were collected with a SQUID-based sample magnetometer using a QUANTUM Design model MPMS instrument. Data were corrected for the magnetization of the sample holder and for the diamagnetic contributions, which were estimated from Pascal's constants.

***trans*-[Co(acac)$_2$(NO$_2$-κ*N*)(L)] {L = NIT4py (2), NIT3py (3), IM4py (4), and IM3py (5)}:** A methanol solution (10 mL) of **L** (1.00 mmol) was added to an aqueous solution (50 mL) of *trans*-Na[Co(acac)$_2$(NO$_2$-κ*N*)$_2$] (1.00 mmol). The mixture was stirred at 30 °C for 10 min, and then cooled in an ice bath. The resulting red-brown precipitate was collected by filtration, and washed with a small amount of methanol and with diethyl ether. The crude product was recrystallized from chloroform/diethyl ether. **2**: Dark red-brown prismatic crystals, yield 0.38 g (70%). $C_{22}H_{30}CoN_4O_8$ (537.4): calcd. C 49.17, H 5.63, N 10.42; found C 48.09, H 5.50, N 10.20. **3**: Dark red-brown needle crystals, yield 0.27 g (50%). $C_{22}H_{30}CoN_4O_8$ (537.4): calcd. C 49.17, H 5.63, N 10.42; found C 48.15, H 5.65, N 10.24. **4**: Red powder, yield 0.42 g (80%). $C_{22}H_{30}CoN_4O_7$ (521.4): calcd. C 50.68, H 5.80, N 10.74; found C 49.90, H 5.66, N 11.15. **5**: Red columnar crystals, yield 0.26 g (50%). $C_{22}H_{30}CoN_4O_7$ (521.4): calcd. C 50.68, H 5.80, N 10.74; found C 49.92, H 5.66, N 10.68.

***trans*-[Co(acac)$_2$(PPh$_3$)(L′)]PF$_6$·*x*CH$_2$Cl$_2$ {L′ = py (6): *x* = 0, NIT4py (7): *x* = 1, and IM4py (8): *x* = 1}: L′** (1.00 mmol) was added to a red-purple dichloromethane solution (100 mL) of *trans*-[Co(acac)$_2$(PPh$_3$)$_2$]PF$_6$ (1.00 mmol) while stirring; the color of the mixture turned brown immediately. The solution was concentrated to dryness under reduced pressure, and the residue was thoroughly washed with diethyl ether (100 mL). The obtained brown solid was recrystallized either from dichloromethane/hexane or from dichloromethane/diethyl ether. **6**: Dark brown columnar crystals from CH$_2$Cl$_2$/C$_6$H$_{14}$, yield 0.67 g (90%). $C_{33}H_{34}CoF_6NO_4P_2$ (743.5): calcd. C 53.31, H 4.61, N 1.88; found C 52.98, H 4.52, N 2.10. **7**: Dark brown trigonal columnar crystals from CH$_2$Cl$_2$/Et$_2$O, yield 0.88 g (90%). $C_{41}H_{47}Cl_2CoF_6N_3O_6P_2$ (983.6): calcd. C 50.07, H 4.82, N 4.27; found C 49.54, H 4.80, N 4.42. **8**: Red plate crystals from CH$_2$Cl$_2$/C$_6$H$_{14}$, yield 0.87 g (90%). $C_{41}H_{47}Cl_2CoF_6N_3O_5P_2$ (967.6): calcd. C 50.89, H 4.90, N 4.34; found C 50.65, H 4.80, N 4.74.

[Co(acac)(tdmme)(L′′)](PF$_6$)$_2$·*x*H$_2$O {L′′ = py (9): *x* = 0, NIT4py (10): *x* = 1, and NIT3py (11): *x* = 1}: A methanol solution (15 mL) of AgPF$_6$ (1.61 mmol) was added to a solution of [Co(acac)Cl(tdmme)]PF$_6$ (1.60 mmol) in a mixture of methanol and acetonitrile (1:1, 50 mL) while stirring. The mixture was stirred in the dark for 2 h at room temperature, and the resulting white precipitate was filtered off. The precipitate was washed with acetonitrile (10 mL × 2), and the filtrate and washings were combined and concentrated to ca. 5 mL under reduced pressure. Diethyl ether vapor was diffused into the filtered concentrate in a desiccator, depositing red prismatic crystals of [Co(acac)(tdmme)(CH$_3$CN)](PF$_6$)$_2$ (**12**), yield 1.08 g (91%). $C_{18}H_{37}CoF_{12}NO_2P_5$ (741.3): calcd. C 29.17, H 5.03, N 1.89; found C 29.11, H 4.95, N 1.84. Compound **12** (1.00 mmol) was dissolved in acetonitrile (40 mL), and ligand **L′′** (4.00 mmol of py or 1.00 mmol of NIT*n*py) was added to the solution. After stirring for 20 min at room temperature, the solvents were evaporated to dryness under reduced pressure. The residue was thoroughly washed with methanol (10 mL) and dried in vacuo. **9**: Red powder, yield 0.38 g (95%). $C_{21}H_{39}CoF_{12}NO_2P_5$ (779.3): calcd. C 32.37, H 5.04, N 1.80; found C 32.21, H 4.95, N 1.85. **10**: Green powder, yield 0.89 g (96%). $C_{28}H_{52}CoF_{12}N_3O_5P_5$ (952.5): calcd. C 35.31, H 5.50, N 4.41; found C 35.29, H 5.32, N 4.36. **11**: Green powder, yield 0.90 g (96%). $C_{28}H_{52}CoF_{12}N_3O_5P_5$ (952.5): calcd. C 35.31, H 5.50, N 4.41; found C 34.82, H 5.33, N 4.23.

***trans*-[Co(acac)$_2$(py)$_2$]PF$_6$:** The bis(pyridine) complex *trans*-[Co(acac)$_2$(py)$_2$]PF$_6$ was prepared as follows. Acetic acid (1 mL) and PbO_2 (7.78 mmol) were added to an ethanol solution (200 mL) of *trans*-[Co^{II}(acac)$_2$(py)$_2$] (3.05 mmol). The mixture was stirred for 2 h at room temperature, and then filtered. The filtrate was concentrated to ca. 50 mL under reduced pressure, and an excess amount of solid NH_4PF_6 was added to the concentrate with vigorous stirring. The resulting pale brown precipitate was collected by filtration, and recrystallized from acetone/diethyl ether, affording red-brown needle crystals, yield 0.51 g (30%). $C_{20}H_{24}CoF_6N_2O_4P$ (560.3): calcd. C 42.87, H 4.32, N 5.00; found C 43.33, H 4.34, N 5.02.

Table 6. Crystallographic data for compounds **5**, **7**·CH_2Cl_2, and **8**·CH_2Cl_2

Compound	**5**	**7**·CH_2Cl_2	**8**·CH_2Cl_2
Empirical formula	$C_{22}H_{30}CoN_4O_7$	$C_{41}H_{47}Cl_2CoF_6N_3O_6P_2$	$C_{41}H_{47}Cl_2CoF_6N_3O_5P_2$
M	521.43	983.59	967.59
Crystal size [mm]	0.80×0.28×0.26	0.50×0.30×0.30	0.46×0.35×0.12
Crystal system	orthorhombic	triclinic	triclinic
Space group	*Pnma* (no. 62)	$P\bar{1}$ (no. 2)	$P\bar{1}$ (no. 2)
a [Å]	13.892(2)	13.558(2)	13.371(3)
b [Å]	14.790(2)	14.654(2)	14.520(4)
c [Å]	12.889(2)	13.174(2)	13.148(6)
α [°]	90	103.35(1)	101.76(4)
β [°]	90	94.46(1)	93.41(4)
γ [°]	90	65.41(1)	68.27(2)
V [Å^3]	2648.3(6)	2315.2(6)	2321(1)
Z	4	2	2
D_c [Mg m^{-3}]	1.308	1.411	1.384
μ(Mo-K_α) [mm^{-1}]	0.693	0.626	0.622
F(000)	1092	1014	998
Transmission factors	0.967−1.000	0.883−1.000	0.832−1.000
Reflns/param ratio	3999/201	13503/558	13554/551
$R1$ [$\|F_o\| > 2\sigma(\|F_o\|)$]	0.049	0.054	0.077
wR (all reflns.)	0.153	0.170	0.254

Attempts To Prepare Bis(nitroxide) Complexes. − Method A: NIT*n*py (2.00 mmol) was added to a green methanol solution (150 mL) of *trans*-[$Co(acac)_2(PPh_3)_2$]PF_6 (1.00 mmol). The mixture was stirred at room temperature for 1 d, and the solvents evaporated to dryness under reduced pressure. The residue was extracted with a minimum amount of methanol, and diethyl ether was added to the filtered extract. The resulting precipitate was collected by filtration and washed with diethyl ether. − **Method B:** Acetic acid (1 mL) and PbO_2 (1.00 mmol) were added to an ethanol solution (150 mL) of *trans*-[$Co^{II}(acac)_2(L)_2$] (1.00 mmol), which was prepared from [$Co(acac)_2(H_2O)_2$] and **L** in methanol in a molar ratio of 1:2.[7b] The mixture was stirred for 2 h in an ice bath and then filtered. The filtrate was concentrated to ca. 30 mL under reduced pressure, mixed with an excess amount of a saturated ethanol solution of $NaBPh_4$ or $LiBF_4$, and stored in a refrigerator overnight. The crystalline product deposited was collected by filtration, and recrystallized either from acetone/diethyl ether (BPh_4 salt) or from acetonitrile/diethyl ether (BF_4 salt).

X-ray Crystallographic Study:[30] A suitable crystal of each compound **5**, **7**·CH_2Cl_2, **8**·CH_2Cl_2 was coated with enamel and used for an X-ray diffraction study. The X-ray intensities were measured with an automated Rigaku four-circle diffractometer AFC-5R or -7R [23 °C, graphite-monochromated Mo-K_α radiation (λ = 0.71073 Å), 2 θ_{max} = 60°]. Absorption corrections were made by an empirical Ψ-scan method.[30a] The structures were solved by the usual heavy-atom method using the SHELXS-86 program,[30b] and refined on F^2 by full-matrix least squares with all independent reflections using the SHELXL-97 program.[30c] All non-hydrogen atoms were refined anisotropically, and hydrogen atoms were treated by riding models. All calculations were carried out using the teXsan software package.[30d] Selected crystallographic data are summarized in Table 6. The structures of **7**·CH_2Cl_2 and **8**·CH_2Cl_2 were successfully solved on the assumption of a centrosymmetric space group $P\bar{1}$. For the analysis of **8**·CH_2Cl_2, there is no electron density (larger than 1 e·Å^{-3}) around the imino-N, N(3), site of IM4py, although from the crystal packing point of view there is no difference between the O(5) and O(6) sites of the NIT4py group in **7**·CH_2Cl_2. For **5**, the Laue symmetry check and systematic absences (0kl, $k + l$ = odd; hk0, h = odd) indicated the space group was either *Pnma* or *Pn*2_1a. Initially the structure was solved based on the centrosymmetric space group *Pnma* with Z = 4. It was suggested that the complex possessed a crystallographically imposed plane of symmetry, on which Co, N(11) of nitrito-κ*N*, all atoms [N(1) and C(29)−C(33)] of the pyridyl ring, atoms C(34) and C(35) were located. The imino nitroxide moiety of IM3py was almost planar, but the plane was twisted against the pyridyl ring; this twist forces the N(2), N(3), O(5), C(36), C(39) and C(40) atoms to be positionally disordered over two positions related to the symmetry plane. Even though the space group was deduced to be the non-centrosymmetric *Pn*2_1a, such disorders could not be resolved. Consequently, the space group *Pnma* was adapted. The O atom of the nitroxide group was located at the *endo* position [N(2) site] relative to the Co atom, no electron-density (larger than 1 e·Å^{-3}) was observed at the corresponding *exo* position [N(3) site]. CCDC-168533 to -168535 (**5**, **7**·CH_2Cl_2, **8**·CH_2Cl_2) contain the supplementary crystallographic data for this paper. These data can be obtained free of charge at www.ccdc.cam.ac.uk/conts/retrieving.html or from the Cambridge Crystallographic Data Centre, 12 Union Road, Cambridge CB2 1EZ, UK [Fax: (internat.) + 44-1223/336-033; E-mail: deposit@ccdc.cam.ac.uk].

Acknowledgments

We gratefully acknowledge support of this research by Grant-in-Aids for Scientific Research (nos. 10304056 and 09740489) from the Ministry of Education, Science and Culture, Japan.

[1] A. Caneschi, D. Gatteschi, P. Rey, *Prog. Inorg. Chem.* **1991**, *39*, 331−429; and references therein.
[2] [2a] F. L. de Panthou, E. Belorizky, R. Calemczuk, D. Luneau, C. Marcenat, E. Ressouche, P. Turek, P. Rey, *J. Am. Chem. Soc.* **1995**, *117*, 11247−11253. [2b] A. Caneschi, F. Ferraro, D. Gatteschi, P. Rey, R. Sessoli, *Inorg. Chem.* **1990**, *29*, 1756−1760. [2c] A. Caneschi, F. Ferraro, D. Gatteschi, P. Rey, R. Sessoli, *Inorg. Chem.* **1990**, *29*, 4217−4223. [2d] A. Caneschi, D. Gatteschi, R. Sessoli, P. Rey, *Inorg. Chim. Acta* **1991**, *184*, 67−71. [2e] D. Luneau, G. Risoan, P. Rey, A. Grand, A. Caneschi, D. Gatteschi, J. Laugier, *Inorg. Chem.* **1993**, *32*, 5616−5622.
[3] [3a] D. Luneau, P. Rey, J. Laugier, P. Fries, A. Caneschi, D.

Gatteschi, R. Sessoli, *J. Am. Chem. Soc.* **1991**, *113*, 1245−1251. [3b] D. Luneau, P. Rey, J. Laugier, E. Belorizky, A. Conge, *Inorg. Chem.* **1992**, *31*, 3578−3584. [3c] K. E. Vostrikova, D. Luneau, W. Wernsdorfer, P. Rey, M. Verdaguer, *J. Am. Chem. Soc.* **2000**, *122*, 718−719.

[4] [4a] P. F. Richardson, R. W. Kreilick, *J. Am. Chem. Soc.* **1977**, *99*, 8183−8187. [4b] P. F. Richardson, R. W. Kreilick, *J. Phys. Chem.* **1978**, *82*, 1149−1151.

[5] [5a] T. Yoshida, K. Kanamori, S. Takamizawa, W. Mori, S. Kaizaki, *Chem. Lett.* **1997**, 603−604. [5b] T. Yoshida, S. Kaizaki, *Inorg. Chem.* **1999**, *38*, 1054−1058. [5c] T. Yoshida, T. Suzuki, K. Kanamori, S. Kaizaki, *Inorg. Chem.* **1999**, *38*, 1059−1068.

[6] [6a] Y. Yamamoto, T. Suzuki, S. Kaizaki, *J. Chem. Soc., Dalton Trans.* **2001**, 1566−1572. [6b] Y. Yamamoto, T. Yoshida, T. Suzuki, S. Kaizaki, *Inorg. Chim. Acta* **2001**, *325*, 187−192. [6c] Y. Yamamoto, T. Suzuki, S. Kaizaki, *J. Chem. Soc., Dalton Trans.* **2001**, 2943−2950.

[7] [7a] C.-F. Huang, H.-H. Wei, *J. Chin. Chem. Soc. (Taipei)* **1997**, *44*, 439−443. [7b] H.-H. Wei, H.-Y. Wong, G.-H. Lee, Y. Wang, *J. Chin. Chem. Soc. (Taipei)* **1996**, *43*, 253−259.

[8] [8a] B.-W. Sun, Q.-H. Zhao, D.-Z. Liao, Z.-H. Jiang, S.-P. Yan, G.-L. Wang, X.-K. Yao, H.-G. Wang, *Can. J. Chem.* **2000**, *78*, 322−327. [8b] A. Caneschi, D. Gatteschi, J. Laugier, P. Rey, R. Sessoli, *Inorg. Chem.* **1988**, *27*, 1553−1557.

[9] [9a] C. Benelli, A. Caneschi, D. Gatteschi, L. Pardi, P. Rey, *Inorg. Chem.* **1990**, *29*, 4223−4228. [9b] C. Benelli, A. Caneschi, D. Gatteschi, L. Pardi, *Inorg. Chem.* **1992**, *31*, 741−746. [9c] C. Benelli, A. Caneschi, D. Gatteschi, R. Sessoli, *Inorg. Chem.* **1993**, *32*, 4797−4801. [9d] J.-P. Sutter, M. L. Kahn, S. Golhen, L. Ouahab, O. Kahn, *Chem. Eur. J.* **1998**, *4*, 571−576. [9e] C. Lescop, D. Luneau, G. Bussière, M. Triest, C. Reber, *Inorg. Chem.* **2000**, *39*, 3740−3741.

[10] C.-J. Lee, C.-H. Huang, H.-H. Wei, Y.-H. Liu, G.-H. Lee, Y. Wang, *J. Chem. Soc., Dalton Trans.* **1998**, 171−176.

[11] [11a] H. Oshio, T. Watanabe, A. Ohto, T. Ito, T. Ikoma, S. Tero-Kubota, *Inorg. Chem.* **1997**, *36*, 3014−3021. [11b] H. Oshio, T. Watanabe, A. Ohto, T. Ito, U. Nagashima, *Angew. Chem. Int. Ed. Engl.* **1994**, *33*, 670−671. [11c] H. Oshio, A. Ohto, T. Ito, *Chem. Commun.* **1996**, 1541−1542.

[12] L. I. Simándi, T. Barna, G. Argay, T. L. Simándi, *Inorg. Chem.* **1995**, *34*, 6337−6340.

[13] K. Awaga, T. Inabe, Y. Maruyama, *Chem. Phys. Lett.* **1992**, *190*, 349−352.

[14] [14a] F. L. de Panthou, D. Luneau, J. Laugier, P. Rey, *J. Am. Chem. Soc.* **1993**, *115*, 9095−9100. [14b] F. M. Romero, R. Ziessel, M. Bonnet, Y. Pontillan, E. Ressouche, J. Schweizer, B. Delley, A. Grand, C. Paulsen, *J. Am. Chem. Soc.* **2000**, *122*, 1298−1309. [14c] A. Zheludev, V. Barone, M. Bonnet, B. Delley, A. Grand, E. Ressouche, P. Rey, R. Subra, J. Schweizer, *J. Am. Chem. Soc.* **1994**, *116*, 2019−2027. [14d] A. Zheludev, M. Bonnet, E. Ressouche, J. Schweizer, M. Wan, H. Wang, *J. Magn. Magn. Mater.* **1994**, *135*, 147−160.

[15] A. Zheludev, M. Bonnet, B. Delley, A. Grand, D. Luneau, L. Örström, E. Ressouche, P. Rey, J. Schweizer, *J. Magn. Magn. Mater.* **1995**, *145*, 293−305.

[16] [16a] T. Suzuki, S. Kaizaki, K. Kashiwabara, *Inorg. Chim. Acta* **2000**, *298*, 131−140. [16b] T. Suzuki, M. Ogita, S. Kaizaki, *Acta Crystallogr., Sect. C* **2000**, *56*, 532−533.

[17] [17a] T. Suzuki, T. Imamura, S. Kaizaki, K. Kashiwabara, *Polyhedron*, in press. [17b] T. Ando, M. Kita, K. Kashiwabara, J. Fujita, S. Kurachi, S. Ohba, *Bull. Chem. Soc. Jpn.* **1992**, *65*, 2748−2755.

[18] E. F. Ullman, L. Call, J. H. Osiecki, *J. Org. Chem.* **1970**, *35*, 3623−3631.

[19] [19a] K. Katoh, H. Sugiura, K. Kashiwabara, J. Fujita, *Bull. Chem. Soc. Jpn.* **1984**, *57*, 3580−3586. [19b] K. Kashiwabara, K. Katoh, T. Ohishi, J. Fujita, M. Shibata, *Bull. Chem. Soc. Jpn.* **1982**, *55*, 149−155.

[20] T. Akita, Y. Mazaki, K. Kobayashi, N. Koga, H. Iwamura, *J. Org. Chem.* **1995**, *60*, 2092−2098.

[21] [21a] E. F. Ullman, J. H. Osiecki, D. G. B. Boocock, R. Darcy, *J. Am. Chem. Soc.* **1972**, *94*, 7049−7059. [21b] J. N. Helbert, P. W. Kopt, E. H. Poindexter, B. E. Wagner, *J. Chem. Soc., Dalton Trans.* **1975**, 998−1006.

[22] M. S. Davis, K. Morokuma, R. W. Kreilick, *J. Am. Chem. Soc.* **1972**, *94*, 5588−5592.

[23] H. Heise, F. H. Köhler, F. Mota, J. J. Novoa, J. Veciana, *J. Am. Chem. Soc.* **1999**, *121*, 9659−9667.

[24] [24a] S. Yamanaka, T. Kawakami, S. Yamada, H. Nagao, M. Nakano, K. Yamaguchi, *Chem. Phys. Lett.* **1995**, *240*, 268−277. [24b] K. Yamaguchi, M. Okuyama, J. Maki, T. Noro, H. Namimoto, M. Nakano, T. Fueno, K. Nakasuji, *Chem. Phys. Lett.* **1992**, *190*, 353−360.

[25] T. Ohno, S. Kato, S. Kaizaki, I. Hanazaki, *Inorg. Chem.* **1986**, *25*, 3853−3858.

[26] [26a] M. Lamchen, T. W. Mittag, *J. Chem. Soc., C* **1966**, 2300−2303. [26b] J. H. Osiecki, E. F. Ullman, *J. Am. Chem. Soc.* **1968**, *90*, 1078−1079. [26c] G. Ulrich, R. Ziessel, *Tetrahedron Lett.* **1994**, *35*, 1215−1218. [26d] G. Ulrich, R. Ziessel, D. Luneau, P. Rey, *Tetrahedron Lett.* **1994**, *35*, 1211−1214.

[27] [27a] L. J. Boucher, J. C. Bailar, Jr., *J. Inorg. Nucl. Chem.* **1965**, *27*, 1093−1097. [27b] L. J. Boucher, N. G. Paez, *Inorg. Chem.* **1970**, *9*, 418−421.

[28] R. H. Lee, E. Griswold, J. Kleinberg, *Inorg. Chem.* **1964**, *3*, 1278−1283.

[29] A. Yamazaki, *J. Coord. Chem.* **1991**, *24*, 211−260.

[30] [30a] A. C. T. North, D. C. Phillips, F. S. Mathews, *Acta Crystallogr., Sect. A* **1968**, *24*, 351−359. [30b] G. M. Sheldrick, *Acta Crystallogr., Sect. A* **1990**, *46*, 467−473. [30c] G. M. Sheldrick, *SHELXL-97*, Universität Göttingen, **1997**. [30d] *teXsan*, Single Crystal Structure Analysis Software, Molecular Structure Corporation and Rigaku Corporation, MSC, The Woodlands, TX, USA, and Rigaku, Akishima, Tokyo, Japan, **1999**, ver. 1.10.

Received August 14, 2001
[I01309]

Synthesis, Crystal Structure and Magnetic Properties of the Helical-Chain Compounds $[M_2(O_2CC_{12}H_8CO_2)_2(H_2O)_8]$ [M = Cobalt(II), Nickel(II)]

Jean-Michel Rueff,[a] Sébastien Pillet,[b] Nicolas Claiser,[b] Gautier Bonaventure,[a] Mohamed Souhassou,[b] and Pierre Rabu*[a]

Keywords: Carboxylate ligands / Hydrothermal synthesis / Nickel / Cobalt / Magnetic properties

New 1D complexes are obtained from the reaction of 1,1′-biphenyl-2,2′-dicarboxylic acid (diphenic acid) with KOH and $[Co(NO_3)_2{\cdot}6H_2O]$ or $[Ni(NO_3)_2{\cdot}6H_2O]$ under hydrothermal conditions. Compounds **1** and **2** are isostructural and their structure consists of stacked helical chains of octahedral metal(II) ions. Magnetic measurements show that the Co^{II} atoms in compound **1** are quasi-isolated. In compound **2**, the Ni^{II} chains exhibit a ferromagnetic behaviour. From a simple model derived from the scaling theory of phase transition, the exchange coupling between neighbouring Ni^{II} atoms is evaluated at $J = +1.06$ K. A zero-field splitting effect is observed below 16 K.

Introduction

Low-dimensional magnetism (1D, 2D) is an important research field for chemists interested in the design of new magnetic materials and a better understanding of the mechanisms responsible for their magnetic behaviours.[1−4] Correlations between the magnetic properties of molecule-based solids and their structure or the nature of the chemical bond is largely used for the design of new materials, including high T_C magnets.[5−8] In this context, helicate structures are of current interest in supramolecular coordination chemistry, mainly for their similarity with the structure of the DNA molecule.[9−11] Very few of these studies discuss the effect of the helical arrangement of spin carriers on the magnetic properties[12−14] even though chirality is known to induce photo-magnetic effects.[15] For the design of new coordination compounds with extended structures, the solvo- or hydrothermal route is currently being developed by several research teams involved in solid-state coordination chemistry,[16,17] and organic-inorganic materials,[18−20] including helical chain compounds[21,22] and mesoporous (possibly magnetic) materials.[23−25] In this approach, the organic ligand acts as a template, the structure of the product being closely related to the geometry and the number of coordination sites provided by the ligand. Important results have recently been obtained in the field of low dimensional magnetic materials exhibiting unusual behaviours.[26−29]

The present paper describes the crystal structure and the magnetic properties of new Ni^{II} and Co^{II} coordination polymers synthesised by using self-assembly in hydrothermal conditions and exhibiting helical chains based on an inexpensive ligand, the 1,1′-biphenyl-2,2′-dicarboxylate.

Results and Discussion

Compounds **1** and **2** were synthesised by the hydrothermal method from cobalt(II) nitrate, and nickel(II) nitrate, respectively, with diphenic acid, potassium hydroxide and water in a 2:3:8:120 ratio, at 170 °C during 72 h (see Exp. Sect.). The title compounds are obtained in good yields, and crystallise as large (mm size), thin platelets. In the case of compound **1**, another phase is also observed as purple needle-shaped crystals, whose structure and properties will be reported elsewhere. The synthetic conditions can be optimised in order to favour compound **1**, and pure compound **1** is easily obtained by manual separation of the largest crystals. The formula of both compounds **1** and **2** has been checked by chemical analysis, and ancillary characterisation techniques, and their structure has been determined by single crystal X-ray diffraction at room and low temperature (see Exp. Sect.). The principal distances are reported in Table 1.

[a] Institut de Physique et Chimie des Matériaux de Strasbourg, UMR 75040 du CNRS,
23 rue du Loess, 67037 Strasbourg, France
Fax: (internat.) +33-3/8810-7247
E-mail: pierre.rabu@ipcms.u-strasbg.fr
[b] Laboratoire de Cristallographie et Modélisation des Matériaux Minéraux et Biologiques, Faculté des Sciences, UHP BP239, 54506 Vandoeuvre-les-Nancy Cedex, France

Table 1. Selected bond lengths (Å) and angles (°); symmetry codes: (i) $1/2 - x$, $1/2 + y$, $1/2 - z$, (ii) $-x$, $2 - y$, $-z$, (iii) $x - 1$, $y + 1$, z, (iv) $x - 1/2$, $3/2 - y$, $z + 1/2$

Compound **1**			
Co−O1	2.0989(13)	Co−O4	2.1216(13)
Co−O2	2.1727(16)	Co−O5	2.0462(12)
Co−O3	2.1066(14)	Co−O6	2.0632(11)
O8...O3(H14)	2.618(2)	$O8^{ii}$...O4(H8)	2.645(1)
O8···H14	1.90(3)	$O8^{ii}$···H8	1.83(2)
O7...O4(H15)	2.612(2)	$O6^{i}$...O1(H6)	2.705(2)
O7···H15	1.83(3)	$O6^{i}$···H6	1.96(2)
$C6^{iv}$...C11	3.734(4)	$C4^{iii}$...C13	3.875(4)
O1−Co−O3	177.60(6)	O1−Co−O6	87.73(5)
O1−Co−O2	92.58(6)	O5−Co−O6	177.07(5)
O1−Co−O4	87.36(5)	O2−Co−O4	178.42(7)
O1−Co−O5	90.12(5)		
O8···H14−O3	160(3)	$O8^{ii}$···H8−O4	174(2)
O7···H15−O4	160(3)	$O6^{i}$···H6−O1	162(2)
Compound **2**			
Ni−O1	2.0713(11)	Ni−O4	2.0652(11)
Ni−O2	2.1105(12)	Ni−O5	2.0257(10)
Ni−O3	2.0641(13)	Ni−O6	2.0407(10)
O8...O3(H14)	2.598(2)	$O8^{ii}$...O4(H8)	2.635(2)
O8···H14	1.82(3)	$O8^{ii}$···H8	1.81(2)
O7...O4(H15)	2.592(2)	$O6^{i}$...O1(H6)	2.684(2)
O7···H15	1.74(3)	$O6^{i}$···H6	1.94(2)
$C6^{iv}$...C11	3.689(3)	$C4^{iii}$...C13	3.839(4)
O1−Ni−O3	176.68(5)	O1−Ni−O6	87.86(4)
O1−Ni−O2	92.58(5)	O5−Ni−O6	176.41(4)
O1−Ni−O4	86.89(4)	O2−Ni−O4	177.61(5)
O1−Ni−O5	89.41(4)		
O8···H14−O3	160(3)	$O8^{ii}$···H8−O4	170(2)
O7···H15−O4	162(2)	$O6^{i}$···H6−O1	161(2)

Compounds **1** and **2** are isostructural. The crystal cell parameters of **2** are slightly smaller than for **1**[30] in agreement with the smaller metal−oxygen bond lengths for the nickel(II) ions compared to cobalt(II) as also found in aqua complexes and η^1-carboxylates.[31] The molecular structure consists of divalent metal atoms, located in slightly distorted octahedral sites (Figure 1 and Table 1). Water molecules (O1 to O4) are located at the four basal positions [mean Co−O = 2.1249(14) Å, mean Ni−O = 2.0778(13) Å] whereas the apical ones [mean Co−O = 2.0547(12) Å, mean Ni−O = 2.0332(10) Å] are occupied by oxygen atoms of carboxylate groups (O5 and O6). Only one oxygen of each carboxylate group is coordinated to a metal atom, the other one being involved in short hydrogen bonds with hydrogen atoms of the neighbouring water molecules [O8···O3(H14), $O8^{ii}$···O4(H8), in Table 1 (A in Figure 2), and O7···O4(H15) (B in Figure 3)]. The M^{2+} ions form helical chains running along the *b* axis (Figure 3). These ions

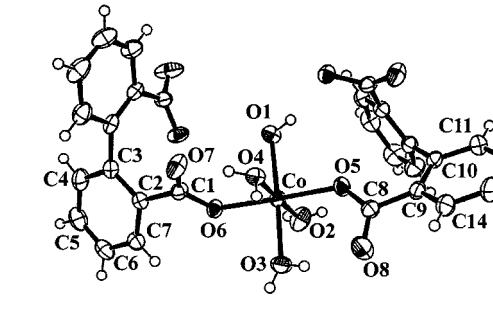

Figure 1. Molecular structure and atomic labels (asymmetric unit only) of the non-H atoms for compound **1**; both biphenyldicarboxylate ligands have been completed using the $1/2 - x$, $y - 1/2$, $1/2 - z$ symmetry element; compound **2** exhibits the same structure, with Ni instead of Co

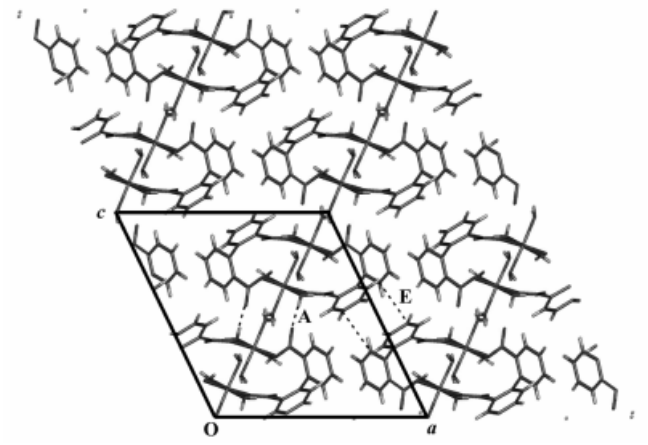

Figure 2. Perspective view of the molecular packing along the *b* axis, showing the helical stacking (H atoms omitted for clarity); inter-chain hydrogen bonds between $O8^{ii}$ and H8 [$O8^{ii}$···O4(H8)] are drawn as dashed lines (label A); inter-chain short $C6^{iv}$···C11 interactions are drawn as dashed lines (label E); symmetry codes given in Table 1

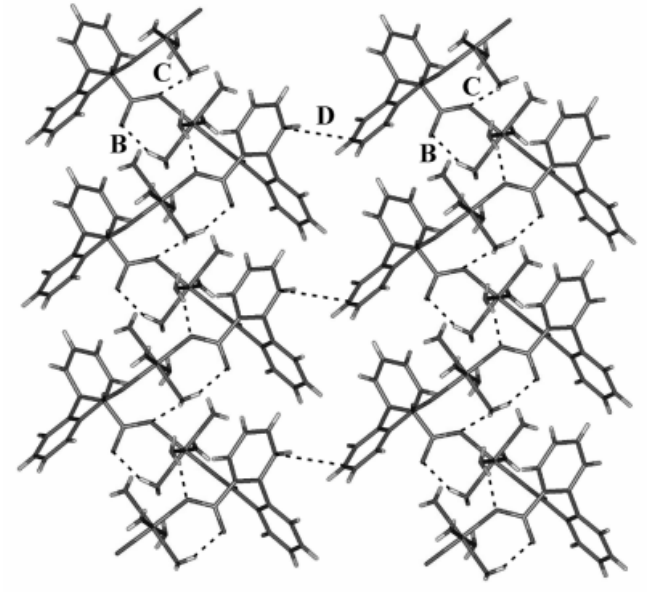

Figure 3. View of two neighbouring M^{II} helical chains; in one chain, the shortest M−M distance is 4.9981(3) Å for M = Co, and 4.9373(3) Å for M = Ni; intra-chain short hydrogen bonds between O7 and H15 [O7···O4(H15)] and between $O6^{i}$ and H6 [$O6^{i}$···O1(H6)] are drawn as dashed lines (B and C respectively); inter-chain short $C4^{iii}$···C13 contacts are drawn as dashed lines (D); symmetry codes given in Table 1

are connected through the biphenyldicarboxylate ligand, the shortest M···M distance along the chain being 4.9981(3) Å and 4.9373(3) Å, for Co and Ni, respectively. The shortest exchange pathway involves a short intra-chain hydrogen bond (C in Figure 3) between $O6^{i}$ and H6 [$O6^{i}$···O1(H6) = 2.705(2) Å in **1** and $O6^{i}$···O1(H6) = 2.684(2) Å in **2**]. The two aromatic rings of each ligand are tilted around the C3−C10 bond by 85.96(8)° and 87.2(1)° for **1** and **2**, respectively. Moreover, the chains are connected by inter-chain hydrogen bonds (A in Figure 2) to form planes quasi perpendicular to the [1 0 $\bar{1}$] direction. The metal atoms are arranged in a zigzag manner between the planes. Phenyl-phenyl contacts in a T-shape arrangement (cf. D,E in Figure 2 and 3, and $C6^{iv}$···C11, $C4^{iii}$···C13 distances in Table 1) ensure inter-plane connections. In E contacts, the corresponding aromatic rings stack almost perpendicular to each other, the dihedral angle between the best planes corresponding to the two rings is 86.10(6)° for **1** and 85.46(6)° for **2**. Contacts D involve similar inter-plane contacts, the corresponding dihedral angles being 115.47(6)° and 113.82(4)° for **1** and **2**, respectively. In each of these inter-plane contacts, the positively charged C−H groups of one aromatic ring probably interact with the negatively charged π-electron cloud of the other aromatic ring.[32] No parallel π−π stacking of the phenyl rings results from the present geometrical configuration.

The IR spectra of both compounds exhibit the same features, as would be expected from their structural homology. The frequency difference between the symmetric and antisymmetric carboxylate vibrations, $\Delta\nu$ = 141 cm^{-1}, is small but in agreement with the unidentate coordination mode of the carboxylate groups;[33] this small value can be explained by the occurrence of hydrogen bond involving the oxygen atom that is not linked to the metal atom, thus giving a bidentate character to the carboxylate groups. The presence of two broad ν(O−H) bands in the range 3200−3400 cm^{-1} is due to the two hydrogen-bonded *aqua* ligands. As for the UV spectra shown in Figure 4, it corroborates the octahedral geometry of Co^{II} and Ni^{II} ions.[34,35] The values of *Dq* (1050 cm^{-1} for **1** and 877 cm^{-1} for **2**) and Racah's parameter *B* (862 cm^{-1} for **1** and 1005 cm^{-1} for **2**), deduced from the transitions observed, agree with a low crystal field (Dq/B = 1.2 for **1** and Dq/B = 0.9 for **2**) and an octahedral high-spin configuration for the metal centres, which can also be inferred from the magnetic findings (see below).

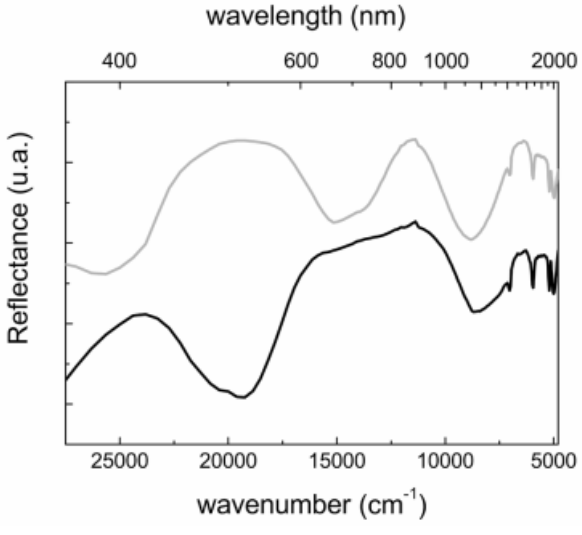

Figure 4. UV spectra of compounds **1** (below) and **2** (upper curve)

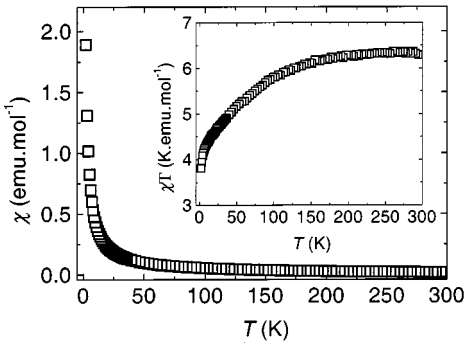

Figure 5. Magnetic susceptibility and χT product of compound **1**

The magnetic properties of **1** and **2** were investigated as described in the Exp. Sect.. The temperature variation of the magnetic susceptibilities χ of **1** is shown in Figure 5, after correction for diamagnetic contributions. Upon cooling down, $\chi = f(T)$ increases continuously up to a maximum of 1.9 emu·mol^{-1} at 2 K. The χT product exhibits a regular decrease from 6.36 emu·K·mol^{-1} at 300 K to 3.81 emu·K·mol^{-1} at 2 K. The inverse susceptibility varies linearly with the temperature in the high temperature regime ($T > 180$ K) and is well fitted in this region by using the Curie−Weiss law, giving C = 6.55 emu·K·mol^{-1} and θ = −8.63 K. The calculated effective moment per metal ion, $\mu_{eff} = (8 \times 1/2 \times C)^{1/2}$ = 5.12 μ_B/Co, agrees with that expected for octahedral high spin Co^{II} ions.[36,37] In accordance with this, the magnetisation vs. field curve at 2 K is characteristic of a paramagnetic phase, with a saturation moment per cobalt(II) ion of Ms = 2.5 $\mu_B mol^{-1}$ (expected, 2−3 μ_B per cobalt ion).[36,37]

The decrease of the χT product together with the negative value of θ are well explained by the effect of the spin-orbit coupling for isolated Co^{II} ions in an octahedral crystal field, which results in the splitting of the energy levels arising from the $^4T_{1g}$ ground term, stabilising the $J = \pm 1/2$ doublet that is well separated from the excited states.[36] An antiferromagnetic coupling could also contribute, although this is expected to be very small since the value measured at 2 K (1.9 emu·K per Co^{II} mol) is close to that expected for isolated metal ions in an O_h crystal field (≈1.8 emu·K per Co^{II}).[36] An analytical expression of the susceptibility for isolated Co^{II} ions is reported in the literature,[36] but corresponds to the particular case of a cubic crystal field and it is stated that the magnetic behaviour of such an ion is highly sensitive to site distortion and crystal field variations. Attempts to use this expression for the present compound give not particularly satisfactory results. Likewise no expression is available for Co^{II} chains taking into account the spin-orbit coupling. Thus the fitting of the experimental

data to an appropriate model is rather complex for compound **1**, although its behaviour is qualitatively very well explained on the basis of quasi-isolated magnetic centres.

The magnetic behaviour of compound **2** is presented in Figure 6. The $1/\chi = f(T)$ curve fits well the Curie−Weiss law at high temperature ($T > 100$ K) with $C = 2.289$ emu·K·mol^{-1}, in agreement with the value expected for isolated Ni^{II} ions in an octahedral ligand field (giving $\mu_{eff} = 3.03\ \mu_B$/Ni), and $\theta = +1.08$ K, pointing to weak ferromagnetic interactions. Accordingly, the χT product is almost constant from ambient temperature down to about 150 K at a value of approximately 2.3 emu·K·mol^{-1}. Below 150 K, a slight increase up to a maximum of 2.49 emu·K·mol^{-1} at 16 K and a drop down to 1.69 emu·K·mol^{-1} at 2 K are observed. Zero-field splitting is known to occur for nickel(II) ions, and for isolated ions may induce either an increase or a decrease of χT, at very low temperature, depending on the site distortion.[4] It cannot give rise to both at the same time however. The observed behaviour is thus characteristic of the occurrence of ferromagnetic interactions within the chains. The drop to zero below 16 K can be related to antiferromagnetic coupling between the chains together with the effect of zero-field splitting. The absence of any maximum in the χ vs. T curve is rather in favour of the latter mechanism. Moreover, the magnetisation versus field measurement exhibits a paramagnetic-like behaviour. As expected for divalent metal ions, the saturation magnetisation at 2 K is 2 μ_B per nickel, and neither metamagnetic nor spin-flop transitions are observed, suggesting that no 3D antiferromagnetic order is reached at this temperature.

In order to evaluate the exchange interaction between neighbouring nickel(II) atoms, the susceptibility measurements were fitted in the high temperature region by using a simple model for Heisenberg $S = 1$ ferromagnetic regular chains. In this approach, the zero-field splitting for nickel(II) is not taken into account, assuming that its effect is significant only at low temperatures ($T < 16$ K).[38]

The spin-exchange Hamiltonian of the system [Equation (1)] can be solved numerically only for ring chains involving a limited number of spins N. The study of the variation of the susceptibility as a function of the reduced temperature $T_r = T/[S(S + 1)J]$, for chains of various size (up

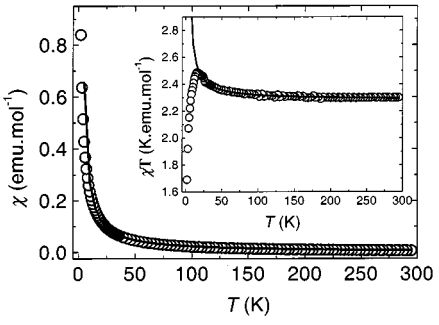

Figure 6. Magnetic susceptibility and χT product of compound **2**; the full line corresponds to the best fit to the expression calculated for a ferromagnetic Heisenberg chain of $S = 1$ spins

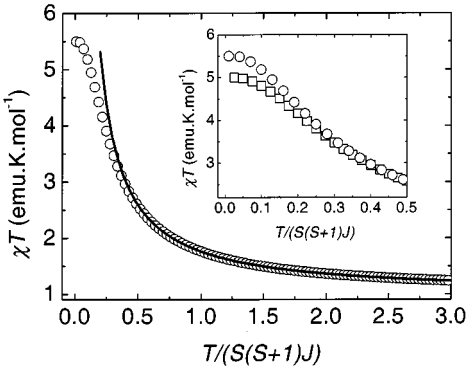

Figure 7. Variation of the χT product as a function of reduced temperature for a Heisenberg chain of 10 (square) and 9 (circle) $S = 1$ spins; the full line corresponds to the best fit of the $N = 10$ system to the power law expression given in the text; the inset is a zoom at low temperature showing the discrepancy between $N = 9$ and $N = 10$ spin chains

to $N = 10$) shows that data corresponding to N and $N + 1$ chains coincide in a wide range down to a limiting value at low temperatures (inset in Figure 7). This value decreases when N increases and corresponds to the temperature limit above which the calculation for N spins is the exact solution for the infinite chain. Moreover, following the approach developed within the frame of the scaling theory by Soulétie,[39,40] the χT product for a regular ferromagnetic $S = 1$ chain can be described in the high temperature range by the power law[41] shown in Equation (2):

$$\hat{H}_{ex} = -J\sum_{i=1}^{N}\hat{S}_i\hat{S}_{i+1} - g\mu_B\sum_{i=1}^{N}\hat{S}_i\vec{H} \quad (1)$$

$$\chi T = C(1 - T_c/T_r)^{-\gamma} \quad (2)$$

where C is the Curie constant $[g^2\mu_B^2S(S + 1)/3k]$, T_c the reduced critical temperature and γ is a critical exponent. With this relation, the $\chi T = f(T_r)$ data for $N = 10$ have been fitted from high temperatures down to the limit ($T_r \approx 0.6$) where it does not coincide with the $N = 9$ calculation (Figure 7) giving the general relation for $S = 1$ Heisenberg ferromagnetic chains shown in Equation (3):

$$\chi T = (g^2\mu_B^2S(S + 1)/3k)(1 - 0.59679/T_r)^{-1.2322} \quad (3)$$

Finally, this simple expression fits very well with the experimental susceptibility of compound **2** (Figure 6), giving $g = 2.13$, and $J = +1.06$ K, which is weak and in agreement with the value of θ deduced above.

The crystal structure of the present compounds indicates that the exchange pathways between neighbouring magnetic centres involve the biphenyldicarboxylate ligands and hydrogen bonds. Both are known to promote weak exchange interactions. Indeed, the binuclear 1,1′-biphenyl-2,2′-dicarboxylate transition metal complexes reported in the literature[42] exhibit a quasi-paramagnetic behaviour, and the coupling through hydrogen bonds in molecular materials is

likewise very weak.[43] The low efficiency of these exchange pathways explains this behaviour of **1** and also the weak ferromagnetic behaviour observed for **2**, although the magnetic centres are relatively close to each other.

Conclusion

New one-dimensional cobalt(II) and nickel(II) compounds have been synthesised as large single crystals by hydrothermal methods. Their structures have been solved and consist of stacked helical chains, which are generated by using the simple 1,1′-biphenyl-2,2′-dicarboxylate ligand as an efficient template. From the magnetic point of view this ligand appears to be fairly poor for magnetic exchange coupling, as shown by the results obtained for compound **1** where the cobalt(II) ions are quasi-isolated. Nevertheless, in the isostructural compound **2**, the nickel(II) ions are coupled and form ferromagnetic $S = 1$ chains. The present compounds are not chiral since both right hand and left hand orientations of the helical chain are present in the structure. Further work is in progress on related systems in order to isolate enantiomerically pure forms. The purple phase obtained as needle crystals with the compound **1** is currently under investigation.

Experimental Section

General Remarks: Thermogravimetric experiments were performed using a Setaram TG92 instrument (heating rate of 2 °C/min, air stream). FT-IR studies were performed with an ATI Mattson Genesis computer-driven instrument (0.1 mm thick powder samples in KBr). UV/Vis-NIR studies were performed with a Perkin−Elmer Lambda 19 instrument (spectra recorded by reflection with a resolution of 4 nm and a sampling rate of 480 nm/min). Magnetic studies were carried out using a (Quantum Design XMPMS) SQUID magnetometer. Susceptibilities were measured at H = 2000 Oe, in the field range of the linear variation of magnetization versus H.

Bis{cobalt(II)-tetraaqua-biphenyl-2,2′-η¹,η¹-dicarboxylate} (1): $C_{28}H_{32}Co_2O_{16}$ (**1**) was synthesised by the hydrothermal method from $[Co(NO_3)_2{\cdot}6H_2O]$ (98% Aldrich), diphenic acid (1,1′-Biphenyl-2,2′-dicarboxylic acid, 98% Acros), and KOH (85%, SDS). The starting mixture corresponding to the molar composition 2:3:8:120 of $[Co(NO_3)_2{\cdot}6H_2O]$, $C_{14}H_{10}O_4$, KOH and H_2O was homogenised and transferred (170 °C, 72 h, autogenous pressure) to a sealed hydrothermal bomb (23 cm^3 bomb volume) walled with a Teflon liner. Pink plates were obtained, washed and rinsed with deionised water (18.2 MΩcm) and absolute ethyl alcohol (Carlo Erba) (yield > 60% on the basis of $[Co(NO_3)_2{\cdot}6H_2O]$). The purity was confirmed by elemental analysis (EA) {$C_{28}H_{32}Co_2O_{16}$ (742.4): calcd. C 44.6, H 7.5; found C 44.3, H 7.5}, oxidising pyrolysis (OP) {heating in air from 20 to 700 °C at 2 °C/min, 30 min at 700 °C to transform cobalt into Co_3O_4,[44−45] and cooling to 20 °C at 10 °C/min: calcd. Co 15.88; found 15.64}, and ATG weight loss at 172 °C titration of water {calcd. 19.4; found 19.2 }. IR (KBr pellet): $\tilde{\nu}$ = 3612 cm^{-1} (ν OH), 3440 (ν OH−O), 3197 (ν OH−Co), 1598 (ν C−C), 1576 (ν C−C), 1539 (ν_{as} C=O), 1496 (ν C−C), 1440 (ν C−C), 1398 (ν_s C−O), 1267 (in plane δ_b C−H), 1151 (in plane δ_b C−H), 1108 (in plane δ_b C−H), 1049 (in plane δ_b C−H). UV/Vis (reflectance for octahedral coordination of Co^{II}): λ = 1190 nm ($^4T_{1g} \rightarrow {}^4T_{2g}$), 520 nm ($^4T_{1g} \rightarrow {}^4T_{1g}(P)$].

Bis{nickel(II)-tetraaqua-biphenyl-2,2′-η¹,η¹-dicarboxylate} (2): $C_{28}H_{32}Ni_2O_{16}$ (**2**) was synthesised by the hydrothermal method from $[Ni(NO_3)_2{\cdot}6H_2O]$ (98% Aldrich), diphenic acid (1,1′-Biphenyl-2,2′-dicarboxylic acid, 98% Across), and KOH (85%, SDS). The starting mixture corresponding to the molar composition 2:3:8:120 of $[Ni(NO_3)_2{\cdot}6H_2O]$, $C_{14}H_{10}O_4$, KOH and H_2O was homogenised and transferred (170 °C, 72 h, autogenous pressure) to a sealed hydrothermal bomb (23 cm^3 bomb volume) walled with a Teflon liner. Pale green plate crystals were obtained (yield > 90% on the basis of $[Ni(NO_3)_2{\cdot}6H_2O]$), washed and rinsed with deionised water (18.2 MΩcm) and absolute ethyl alcohol (Carlo Erba). The purity was confirmed by elemental analysis (EA) {$C_{28}H_{32}Ni_2O_{16}$ (742.0): calcd. C 45.33, H 4.35; found C 45.3, H 4.35}, oxidising pyrolysis (OP) {heating in air from 20 to 700 °C at 2 °C/min, 30 min at 700 °C to transform nickel into NiO,[44] and cooling to 20 °C at 10 °C/min: calcd. Ni 15.82; found 16.0}, and ATG titration of water {weight loss (%) at 200 °C: calcd. 19.41; found 19.32}. IR (KBr pellet): $\tilde{\nu}$ = 3608 cm^{-1} (ν OH), 3432 (ν OH−O), 3180 (ν OH−Ni), 1598 (ν C−C), 1575 (ν C−C), 1539 (ν_{as} C=O), 1496 (ν C−C), 1442 (ν C−C), 1398 (ν_s C−O), 1269 (in plane δ_b C−H), 1151 (in plane δ_b C−H), 1109 (in plane δ_b C−H), 1049 (in plane δ_b C−H). UV/Vis (reflectance for octahedral coordination of Ni^{II}): λ = 1140 nm ($^3T_{2g} \rightarrow {}^3A_{2g}$), 720 nm ($^1E_g \rightarrow {}^4A_{2g}$), 653 nm ($^3T_{1g}(F) \rightarrow {}^3A_{2g}$), 391 nm ($^3T_{1g}(P) \rightarrow {}^3A_{2g}$).

X-ray Crystallographic Study: $C_{28}H_{32}Co_2O_{16}$, (**1**), M_r = 742.40, monoclinic, $P2_1/n$ (No. 14), a = 14.3800(4) Å, b = 7.5373(2) Å, c = 15.6142(5) Å, β = 115.3850(10)°, V = 1528.96(8) $Å^3$, Z = 2, D_x = 1.613 g cm^{-3}, μ (Mo-K_α) = 1.155 mm^{-1}, F(000) = 764, T = 293(2) K. A total of 5173 independent reflections (N_{tot} = 36455, R_{int} = 4.70%) were measured on a Nonius Kappa CCD. Absorption corrections were performed by Gaussian integration (ABSORB, DeTitta, 1985[46]) using the crystal shape (T_{min} = 0.688, T_{max} = 0.850), $R[F^2 > 2\sigma(F^2)]$ = 0.056, $wR(F^2)$ = 0.083. The structure was solved by direct methods (SHELXS, Sheldrick 1997[47]) and refined on F^2 by using full-matrix least-squares techniques (SHELXL, Sheldrick 1997[48]). All H atoms were located in the difference Fourier map and refined isotropically, all non-H atoms were refined anisotropically.

$C_{28}H_{32}Ni_2O_{16}$, (**2**), M_r = 741.96, monoclinic, $P2_1/n$ (No. 14), a = 14.3092(4) Å, b = 7.4605(2) Å, c = 15.4260(5) Å, β = 115.4540(10)°, V = 1486.93(8) $Å^3$, Z = 2, D_x = 1.612 g cm^{-3}, μ (Mo-K_α) = 1.345 mm^{-1}, F(000) = 768, T = 110(2) K. A total of 8129 independent reflections (N_{tot} = 48871, R_{int} = 4.80%) were measured on a Nonius Kappa CCD. Absorption corrections were performed by Gaussian integration (ABSORB, DeTitta, 1985) using the crystal shape (T_{min} = 0.701, T_{max} = 0.908), $R[F^2 > 2\sigma(F^2)]$ = 0.042, $wR(F^2)$ = 0.091. The structure was solved by direct methods (SHELXS, Sheldrick 1997[47]) and refined on F^2 using full-matrix least-squares techniques (SHELXL, Sheldrick 1997[48]). All H atoms were located in the difference Fourier map and refined isotropically, all non-H atoms were refined anisotropically.

CCDC-158624 (**1**) and -168731 (**2**) contain the supplementary crystallographic data for this paper. These data can be obtained free of charge at www.ccdc.cam.ac.uk/conts/retrieving.html [or from the Cambridge Crystallographic Data Centre, 12, Union Road, Cambridge CB2 1EZ, UK; fax: (internat.) +44-1223/336-033; E-mail: deposit@ccdc.cam.ac.uk].

Acknowledgments

We thank Dr. M. Drillon, Institut de Physique et Chimie des Matériaux de Strasbourg, France, and Pr C. Lecomte, Laboratoire de Cristallographie et Modélisation des Matériaux Minéraux et Biologiques, Nancy, France, for helpful discussion.

[1] *Research Frontiers in Magnetochemistry* (Ed.: C. O'Connor), World Scientific Publishers, **1993**.
[2] *Magnetic Properties of Layered Transition Metal Compounds* (Ed.: L. J. de Jongh), *Physics and Chemistry of Materials with Low-dimensional Structures 9A*, Kluwer Academic Publishers: Dordrecht, **1990**.
[3] *Magnetic Molecular Materials* (Eds.: D. Gatteschi, O. Kahn, J. S. Miller, F. Palacio), Kluwer, Dordrecht, **1991**.
[4] O. Kahn *Molecular Magnetism*, VCH Verlagsgesellschaft, Weinheim, **1993**.
[5] D. Babel, *Comments Inorg. Chem.* **1986**, *5*, 285−320.
[6] M. Verdaguer, *Science* **1996**, *272*, 698−699.
[7] O. Sato, T. Iyoda, A. Fujishima, K. Hashimoto, *Science* **1996**, *272*, 704−705.
[8] O. Hatlevik, W. E. Buschmann, J. Zhang, J. L. Manson, J. S. Miller, *Adv. Mater.* **1999**, *11*, 914−918.
[9] J.-M. Lehn, *Supramolecular Chemistruy − Concepts and Perspectives*, VCH Verlagsgesellschaft, Weinheim, **1995**.
[10] E. C. Constable, in *Comprehensive Supramolecular Chemistry*, vol. 9 (Eds.: J. P. Sauvage, M. W. Hosseini), Pergamon Press, Oxford, **1996**, 213.
[11] C. R. Rice, S. Wörl, J. C. Jeffery, R. L. Paul, M. Ward, *Chem. Commun.* **2000**, 1529−1530, and references therein.
[12] H. Kumagai, K. Inoue, *Angew. Chem. Int. Ed.* **1999**, *38*, 1601−1603.
[13] H. Kumagai, A. S. Markoshian, K. Inoue, *Mol. Cryst. Liq. Cryst.* **2000**, *343*, 97−102.
[14] M. Vazquez, M. R. Bermejo, M. Fondo, A. M. Gonzalez, J. Mahia, L. Sorace, D. Gatteschi, *Eur. J. Inorg. Chem.* **2001**, 1863−1868.
[15] L. D. Barron, *Nature* **2000**, *504*, 895−896. G. L. Rikken, E. Raupach, *Nature* **2000**, *405*, 932−935.
[16] P. J. Hagrman, J. Zubieta, *Inorg. Chem.* **2000**, *39*, 5218−5224.
[17] R. P. Hammond, D. J. Chesnut, J. Zubieta, *J. Solid State Chem.* **2001**, *158*, 55−60.
[18] Y. Zhou, L. Zhang, H.-K. Fun, X. You, *Inorg. Chem. Commun.* **2000**, *3*, 114−116.
[19] J. Tao, X.-M. Zhang, M.-L. Tong, X.-M. Chen, *J. Chem. Soc., Dalton Trans.* **2001**, 770−771.
[20] B. Bazan, J. L. Mesa, J. L. Pizzaro, L. Lezama, M. I. Arriortura, T. Rojo, *Inorg. Chem.* **2001**, *40*, 5691−5694; P. J. Zapf, R. C. Haushalter, J. Zubieta, *Chem. Mater.* **1997**, *9*, 2019−2024.
[21] L.-M. Zheng, T. Whitfield, X. Wang, A. J. Jacobson, *Angew. Chem. Int. Ed.* **2000**, *39*, 4528−4531.
[22] Z. Shi, S. Feng, S. Gao, L. Zhang, G. Yang, J. Hua, *Angew. Chem. Int. Ed.* **2000**, *39*, 2325−2327.
[23] C. Livage, C. Egger, G. Férey, *Chem. Mater.* **2001**, *13*, 410−414, and references therein.
[24] A. Rujiwatra, C. J. Kepert, M. J. Rosseinsky, *Chem. Commun.* **1999**, 2307−2308.
[25] S. Fernandez, J. L. Mesa, J. L. Pizzaro, L. Lezama, M. I. Arriortura, R. Olazcuaga, T. Rojo, *Chem. Mater.* **2000**, *12*, 2092−2098.
[26] P. Rabu, P. Janvier, B. Bujoli, *J. Mater. Chem.* **1999**, *9*, 1323−1326.
[27] Z.-L. Huang, M. Drillon, N. Masciocchi, A. Sironi, J.-T. Zhao, P. Rabu, P. Panissod, *Chem. Mater.* **2000**, *12*, 2805−2812.
[28] S. O. H. Gutschke, D. J. Price, A. K. Powell, P. T. Wood, *Angew. Chem. Int. Ed.* **2001**, *40*, 1920−1023.
[29] D. J. Price, S. Tripp, A. K. Powell, P. T. Wood, *Chem. Eur. J.* **2001**, *7*, 200−208.
[30] For comparison, the cell parameters at room temperature for compound **2** are: a = 14.342 Å, b = 7.502 Å, c =15.612 Å, and β = 115.808°.
[31] F. H. Allen, O. Kennard, D. G. Watson, L. Brammer, A. G. Orpen, R. Taylor, in *International Tables for Crystallography*, vol. C (Ed A. J. C. Wilson), Kluwer Academic Publishers, Dordrecht 1995, 750−757.
[32] C. Janiak, *J. Chem. Soc., Dalton Trans.* **2000**, 3885−3896.
[33] K. Nakamoto, *Infrared and Raman Spectra of Organic and Coordination Compounds*, 4th ed., Wiley Interscience Publication, New York, **1986**, 231.
[34] A. B. P. Lever, *Inorganic Electronic Spectroscopy*, 2nd Ed., Elsevier, Amsterdam **1984**.
[35] L. Banci, A. Bencini, C. Benelli, D. Gatteschi and C. Zanchini, *Structure and Bonding*, **1982** *52*, 37−86.
[36] F. E. Mabbs, D. J. Machin, *Magnetism and Transition Metal Complexes*, Chapman and Hall Ltd., London, **1973**.
[37] R. L. Carlin, *Magnetochemistry*, Springer-Verlag, Berlin, Heidelberg, **1986**.
[38] O. Castillo, A. Luque, P. Romá, F. Lloret, M. Julve, *Inorg. Chem.* **2001**, *40*, 5526−5535.
[39] P. Rabu, J.-M. Rueff, Z. L. Huang, S. Angelov, J. Souletie, M. Drillon, *Polyhedron* **2001**, *20*, 1677−1685.
[40] J. Souletie, *J. Phys. (France)* **1988**, *49*, 1211−1217.
[41] J. Souletie, P. Rabu, M. Drillon, article to be published.
[42] J. Gao, S.-L. Ma, C.-Y. Jin, D.-Z. Liao, *Polyhedron* **1996**, *15*, 2633−2639.
[43] B. N. Figgis, E. S. Kucharski, M. Vrtis, *J. Am. Chem. Soc.* **1993**, *115*, 176−181.
[44] J. Amiel, J. Besson, *Nouveau Traité de Chimie Minérale* (Ed.: P. Pascal), Masson, Paris, **1963**, 17.
[45] M. A. Mohamed, S. A. Halawy, M. M. Ebrahim, *J. Thermal Anal.* **1994**, *41*, 387−404.
[46] G. T. DeTitta, *J. Appl. Cryst.* **1985**, *18*, 75−79.
[47] G. M. Sheldrick, SHELXS97. Program for structure solution. University of Göttingen, Germany, **1997**.
[48] G. M. Sheldrick, SHELXL97. Program for the refinement of crystal structures. University of Göttingen, Germany, **1997.**

Received August 22, 2001
[I01321]

A Calix[4]arene-Based Bipyridine Podand as Versatile Ligand for Transition Metal Cations

Jean-Olivier Dalbavie,[a] Jean-Bernard Regnouf-de-Vains,*[a] Roger Lamartine,[b] Monique Perrin,[b] Sylvain Lecocq,[b] and Bernard Fenet[c]

Keywords: Calixarenes / Bipyridines / Podands / Cobalt / Nickel / Zinc / Copper

The calix[4]arene-based podand **1** which incorporates two 2,2′-bipyridine units and two benzyl units in alternate positions at the lower rim has been subjected to complexation studies with copper(I), copper(II), cobalt(II), nickel(II), and zinc(II). The reaction of **1** with $Cu(MeCN)_4PF_6$ afforded the expected mononuclear Cu^I complex. With cobalt(II), nickel(II), and zinc(II) chloride, **1** gave dinuclear tetrahedral complexes in which each bipyridine unit is associated to two chlorine atoms around the metal centre. With Zn^{II}, replacing the chloride ion for the trifluoromethanesulfonate ion resulted in the formation of the mononuclear complex species. The complexes thus obtained were fully characterised, notably by NMR techniques and, for the dinuclear cobalt, nickel and zinc species, by X-ray crystal structure analyses.
(© Wiley-VCH Verlag GmbH, 69451 Weinheim, Germany, 2002)

1. Introduction

The abundant literature related to calixarenes illustrates their important role in supramolecular chemistry,[1] and particularly, as recently reviewed by Asfari et al.[2] or by Matt et al. or Roundhill et al.,[3] as ligands for metal cations. Their complexation properties are attractive in the development of selective extracting agents for metallic cations, notably for rare metals. This can be accomplished through their own binding sites (oxygen atoms, aryl rings), or by their ability to act as carriers and spatial organisers of various types of chelating agents, such as ethers, esters, amides and their thio analogues, ketones, alkenes, ammonium species, amino acids, phosphanes, or heterocycles.

Among these chelating subunits, introduced at the upper or lower rims at the calix[4]arene platform, the biheterocyclic systems have been moderately studied, with a major attention brought to the 2,2′-bipyridine group,[4] and to the corresponding Ru^{II}, Cu^I, and Ag^I complexes. Other contributions have been devoted to ligands incorporating 2,2′-bithiazole[5] or 2,2′-bipyrazine,[6] and their Cu^I complexes.

Depending on the nature, the number and the position of the chelating units, such podands should be able to provide different coordination geometries. We thus attempted to employ this behaviour in a selective metal extraction process based on the use of the tetrahedral geometry. In this sense, we have recently demonstrated the interest of such kinds of complexing structures with the bis(bipyridyl) ligand **1** displaying in alternate positions two opposing 2,2′-bipyridyl chelating subunits and two opposing lipophilic pendant benzyl groups. Complex **1** showed a very interesting selective and quantitative extraction behaviour towards Ag^I against Pb^{II} from neutral aqueous media.[7]

The objective of the present report was to verify the complexing behaviour of **1** toward various transition metal cations. We found this necessary because, on the one hand, except for the above-mentioned metallic cations, the coordinating behaviour of such ligands towards transition metal species has not been reported until now, and on the other hand our extraction study necessitated a better knowledge of the other available complexes.

As assessed by X-ray crystallographic study of its picolyl parent compound **A**,[8] complex **1** should give a mononuclear Cu^I pro-helicoidal tetrahedral complex, which should also be encountered with Ag^I in complex **B**.[7,9] With $CoCl_2$, we recently reported the synthesis and X-ray crystal structure determination of a mononuclear complex involving a calix[4]arene podand at the upper rim by a 2,2′-bipyridyl unit, and in which the metal centre was coordinated in a tetrahedral mode by the two chloride ions and the two bipyridyl nitrogen atoms.[4f] This structure was proposed some years ago by Newkome et al. for 6,6′-dimethyl-2,2′-bipyridine and $CoCl_2$, $NiCl_2$, $ZnCl_2$, $CuCl_2$, as well as less common metal species.[10] With the two close bipyridyl units of

[a] GEVSM, UMR 7565 CNRS-UHP, Faculté de Pharmacie, 5, rue Albert Lebrun, 54001 Nancy Cedex, France
Fax: (internat.) + 33-3/83179057
E-mail: jean-bernard.regnouf@pharma.u-nancy.fr
[b] SROMB, UMR 5078 CNRS-UCBL, 43 Bd. du 11 Novembre 1918, 69622 Villeurbanne Cedex, France
[c] Centre Commun de RMN, UCBL-CPE, 43 Bd. du 11 Novembre 1918, 69622 Villeurbanne Cedex, France

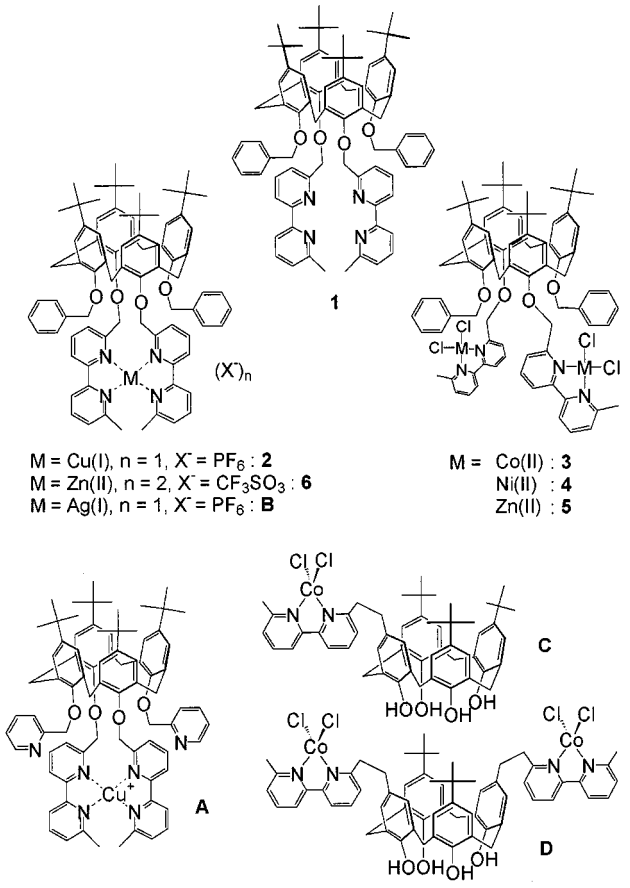

1, one may expect the two coordinating chlorine atoms to be replaced by the second bipyridine unit, thus affording mononuclear complexes with Co^{II}, Ni^{II}, Zn^{II}, and Cu^{II}; however, dinuclear complexes could be obtained.

2. Synthesis and Analysis of Complexes

The bis(benzyl) bis(bipyridyl) podand **1** was prepared as previously reported.[7] The air-stable orange copper(I) complex, **2**, was synthesised by mixing stoichiometric amounts of ligand **1** and $Cu(CH_3CN)_4PF_6$ in CH_3CN. It was obtained in a pure state with a yield of 90% after chromatography on alumina with CH_2Cl_2 as eluent. The ML stoichiometry was preliminarily determined by UV titration, with the appearance of the characteristic MLCT (Metal-to-Ligand Charge Transfer) band at 447 nm; the ε value of 5500 $dm^3 \cdot mol^{-1} \cdot cm^{-1}$, measured with a CH_2Cl_2 solution of **2**, is similar to those of the parent complexes.[4b,4e] Electrospray mass spectrometry (positive mode, 60 V) showed the presence of the monocharged 1:1 adduct [**1** + Cu]$^+$, characterised by a base peak at 1257.7 amu, and elemental analysis was consistent with the proposed formula. ^{1}H NMR study of **2** (Figure 1) showed strong similitude with parent species,[4e] and with its picolyl analogue **A**,[8] for which the racemic pro-helicoidal metal-centred structure was demonstrated by X-ray analysis. More particularly, the helicoidal arrangement of the two bipyridine units was evident by the presence of an AB system at δ = 5.00, 6.35, attributed to the two corresponding anchoring methylene groups. In the grooves thus generated, the benzyl groups should have place, resulting in the discrimination of the two enantiotopic OCH_2 protons, characterised by a strong AB system at δ = 3.82, 4.01.

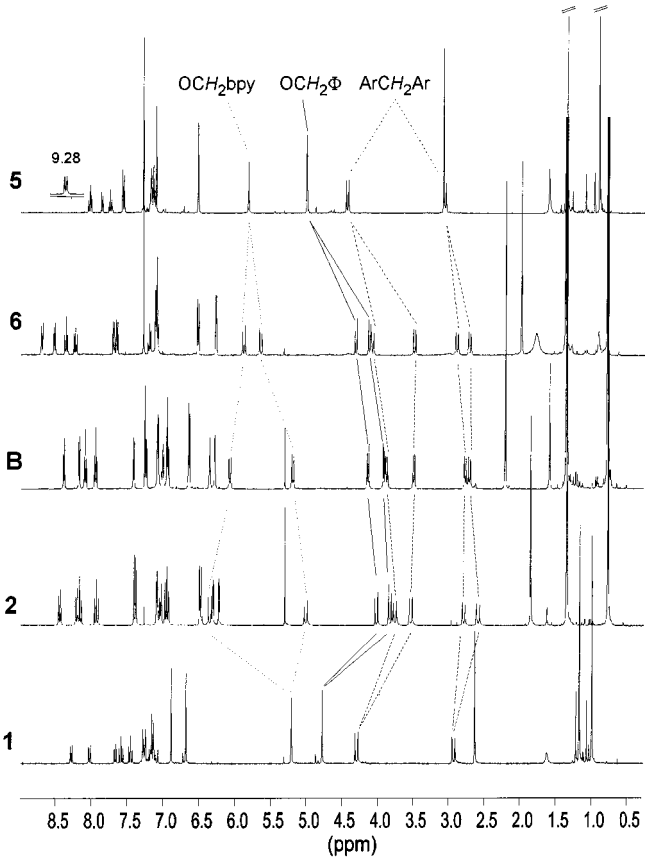

Figure 1. ^{1}H NMR spectra of **1**, **2**, **B**, **6** and **5** (500 MHz, $CDCl_3$, room temp.)

As previously experienced at the upper rim of the calix[4]arene (complexes **C** and **D**) and assessed by a crystal structure (complex **C**),[4f] the cobalt(II) chloride can be complexed by a bipyridine unit in a tetrahedral mode involving two chloride ions and the two bipyridyl nitrogen atoms.[10]

The blue-green complex **3** was prepared by adding an excess of $CoCl_2$ to **1** in a mixture of CH_3CN and CH_2Cl_2 at room temperature; due to its good solubility in CH_2Cl_2, **3** was easily separated from excess $CoCl_2$ in a highly pure form. The dinuclear nature of **3** was indicated by UV/Vis spectroscopy, which showed the presence of the expected metal-centred transition at 658 cm^{-1}, with a molar extinction coefficient of ca. 1000 $dm^3 \cdot mol^{-1} \cdot cm^{-1}$, twice the value reported for complex **C**, and identical to that of complex **D**. Elemental analysis was consistent with the formula $C_{82}H_{88}Co_2Cl_4N_4O_4$. Electrospray mass spectrometry (positive mode, 252 V) showed notably the presence of the expected mono-charged species [**1** + 2 $CoCl_2$ − Cl]$^+$ at 1417.5 amu (10%), accompanied by the "decomplexed" species, such as [**1** + $CoCl_2$ − Cl]$^+$ at 1287.5 amu (40%), [**1** + Na]$^+$

at 1216.7 amu (100%), $[\mathbf{1} + H]^+$ at 1193.7 amu (60%), and by various fragmentation products.

In the standard ^1H NMR spectrum of **3** ($\delta = 0-15$), the absence of some resonance signals confirmed the paramagnetic nature of the [Co/bpy] subunit, as was previously observed.[4f] Recording data in a larger frequency domain (65000 Hz; $\delta = 216$ at 300 MHz, $\delta = 130$ at 500 MHz) showed 11 new resonance signals that were correlated by a COSY experiment (Figure 2): two groups of three singlets integrating 2 H each at $\delta = 72.93$ ($\Delta\nu_{1/2} = 32$ Hz), 42.28 ($\Delta\nu_{1/2} = 34$ Hz), −6.75 (s, $\Delta\nu_{1/2} = 77$ Hz), and $\delta = 72.72$ (s, $\Delta\nu_{1/2} = 25$ Hz), 49.18 (s, $\Delta\nu_{1/2} = 28$ Hz), −14.76 (s, $\Delta\nu_{1/2} = 21$ Hz) were attributed to the bipyridyl groups; one group of two singlets integrating 4 H each at $\delta = -9.70$ (s, $\Delta\nu_{1/2} = 40$ Hz) and $\delta = -3.05$ (s, $\Delta\nu_{1/2} = 22$ Hz) was attributed to the Ar-CH_2-Ar protons. No correlation was found between the groups of bipyridyl aromatic protons and signals corresponding to the OCH_2 and CH_3 groups. Nevertheless, due to their chemical shifts and their integration values, the large singlets found at $\delta = -42.49$ (br. s, $\Delta\nu_{1/2} = 317$ Hz, 4 H) and −22.60 (br. s, $\Delta\nu_{1/2} = 196$ Hz, 6 H) were assigned to the latter, respectively. Finally, the sharp singlet ($\Delta\nu_{1/2} = 4$ Hz) found at $\delta = -1.72$ and integrating 18 H was assigned to two of the four *tert*-butyl groups.

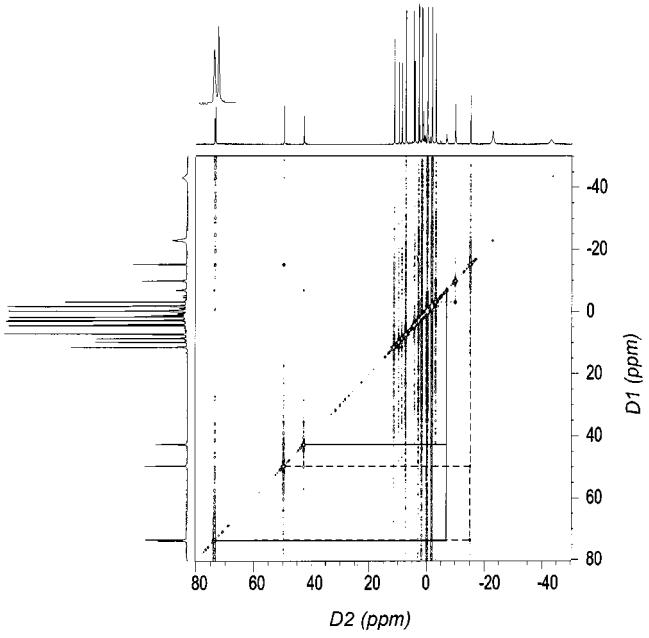

Figure 2. 2D COSY spectrum of cobalt complex **3** (500 MHz, 298 K, $CDCl_3$)

A preliminary study of the complexation of the nickel(II) cation was conducted in solution by UV/Vis titration of **1** with $NiCl_2{\cdot}6H_2O$ in CH_3CN/CH_2Cl_2 (95:5) (Figure 3). The new ligand-centred absorption band that appeared at 318 nm upon complexation increased, up to exactly 2 equiv. of the metal ion, confirming the formation of a dinuclear complex. Two close isosbestic points (offset) were observed at 300.5 nm (curves a−d; 0.0−0.8 equiv. of $NiCl_2{\cdot}6H_2O$) and 295.5 nm (curves f−i; 1.2−2.0 equiv. of $NiCl_2{\cdot}6H_2O$), which correspond to the formation of the mono- and the dinuclear species, respectively. Attempts to isolate the former have failed until now.

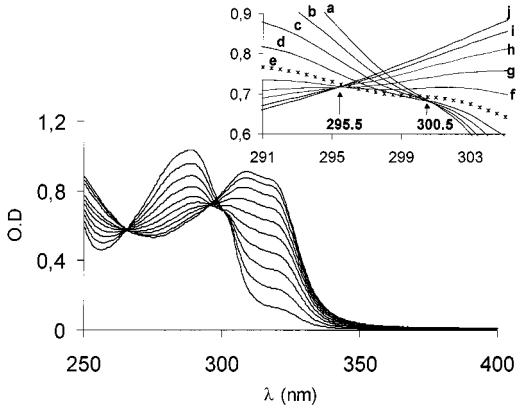

Figure 3. UV/Vis titration of **1** by $NiCl_2{\cdot}6H_2O$ [CH_3CN/CH_2Cl_2 (95:5); a−d: 0.0−0.8 equiv. of $NiCl_2{\cdot}6H_2O$; f−i: 1.2−2.0 equiv. of $NiCl_2{\cdot}6H_2O$]

The reaction of **1** with 2 equiv. of $NiCl_2{\cdot}6H_2O$ at room temp., followed by evaporation of solvents, re-dissolution in $CHCl_3$ and precipitation with hexane, afforded **4** as a salmon-pink microcrystalline solid. Elemental analysis was consistent with the formula $C_{82}H_{88}Cl_4N_4Ni_2O_4{\cdot}0.5CHCl_3$. Electrospray mass spectrometry (positive mode, 234 V) showed, as for the cobalt complex **3**, the presence of the expected mono-charged species $[\mathbf{1} + 2\ NiCl_2 - Cl]^+$ at 1413.5, 1415.5, 1416.5, 1417.5, 1419.5 amu (10%), accompanied by the "decomplexed" species, such as $[\mathbf{1} + NiCl_2 - Cl]^+$ at 1285.5, 1287.5 amu (30%), $[\mathbf{1} + Na]^+$ at 1216.7 amu (100%), $[\mathbf{1} + H]^+$ at 1193.7 amu (80%), and by various fragmentation products. Expecting that, as for the cobalt complex **3**, the paramagnetic nature of the nickel(II) ion should only influence the bipyridine unit resonance signals, **4** was analysed by NMR at 500 MHz. The ^1H NMR spectrum, recorded in a large frequency domain ($\delta = 0-85$) showed the presence of 18 resonance signals with $\Delta\nu_{1/2}$ varying from 9 to 392 Hz. Among them, two sharp singlets ($\Delta\nu_{1/2} = 9$ Hz) integrating 18 H each at $\delta = 1.97$ and 2.03 were attributed to the *tert*-butyl groups; four singlets integrating 2 H each located at $\delta = 58.22$ ($\Delta\nu_{1/2} = 46$ Hz), 63.80 ($\Delta\nu_{1/2} = 38$ Hz), 80.41 ($\Delta\nu_{1/2} = 80$ Hz), and 84.72 ($\Delta\nu_{1/2} = 90$ Hz) were suspected to be bipyridyl resonance signals. A 2D COSY experiment (Figure 4) confirmed this hypothesis, allowing us to build in two groups of three singlets at $\delta = 84.72$ ($\Delta\nu_{1/2} = 90$ Hz), 58.22 ($\Delta\nu_{1/2} = 46$ Hz), 16.75 ($\Delta\nu_{1/2} = 87$ Hz), and $\delta = 80.41$ ($\Delta\nu_{1/2} = 80$ Hz), 63.80 ($\Delta\nu_{1/2} = 38$ Hz), 22.50 ($\Delta\nu_{1/2} = 26$ Hz). Another correlation was found between two signals located at $\delta = 10.75$ (s, $\Delta\nu_{1/2} = 57$ Hz) and 5.60 (s, $\Delta\nu_{1/2} = 50$ Hz), integrating 4 H each,

which were attributed to the Ar-CH_2-Ar groups (Figure 4, offset). The residual signals were not precisely assigned.

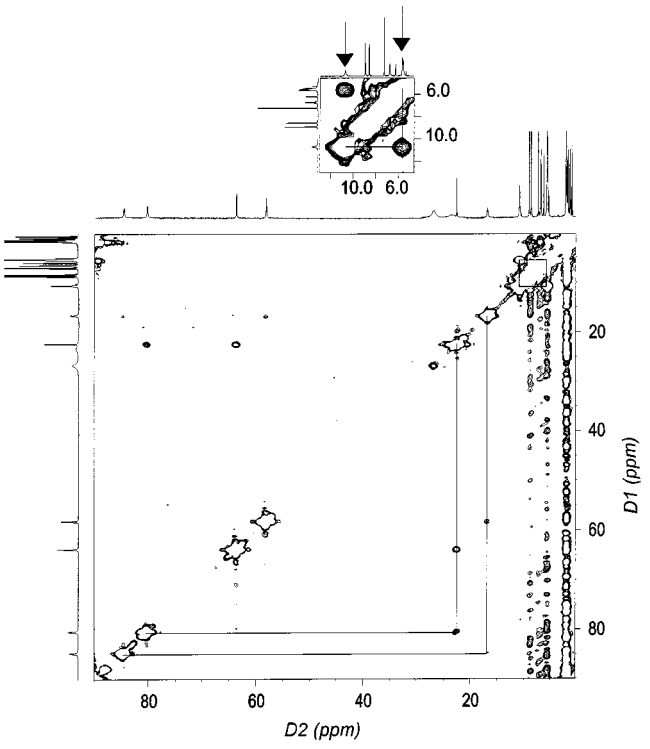

Figure 4. 2D COSY spectrum of nickel complex **4** (500 MHz, 298 K, $CDCl_3$)

Since zinc(II) accepts a tetrahedral geometry with 6,6′-dimethyl-2,2′-bipyridine,[10] we attempted to prepare the dinuclear complex **5**, in which, as for its cobalt and nickel parents **3** and **4**, each metallic centre should be coordinated to one bipyridine unit and to two chloride ions. The complexation of $ZnCl_2$ by ligand **1** was studied by UV/Vis titration, which showed the presence of two close isosbestic points at 299.4 and 303 nm. The two new ligand-centred absorption bands that appeared at 310 and 321 nm upon addition of $ZnCl_2$ increased, up to exactly 2 equiv. of metal ion, confirming the formation of the expected dinuclear species **5**. The latter was prepared as a white microcrystalline solid by mixing the ligand **1** and an excess of $ZnCl_2$ in MeOH and CH_2Cl_2 at room temp., followed by filtration of unchanged $ZnCl_2$ and slow concentration of the filtrate. Surprisingly, with regards to complexes **3** and **4**, electrospray mass spectrometry (positive mode, 80 V) gave poor information on the complex composition, with the presence of one partially "decomplexed" species at 1255.8, 1258.7, and 1259.8 amu [**1** + Zn^{2+} − H^+]$^+$, and the presence of a fragment of ligand at 1032.9, 1033.8, and 1034.9 amu [**1** − 2 ($CH_2C_6H_5$) + Na^+]$^+$. Elemental analysis was consistent with the formula $C_{82}H_{88}Cl_4N_4O_4Zn_2{\cdot}0.5CH_2Cl_2$. Due to its diamagnetism, complex **5** gave a perfectly well-resolved ^{1}H NMR spectrum (Figure 1) between δ = 0 and 10, displaying notably an AB system at δ = 3.12, 4.48 (J_{AB} = 12.9 Hz) assigned to the Ar-CH_2-Ar groups. Both benzyl and bipyridyl methylene groups appear as singlets at δ = 5.02 and 5.81, respectively, indicating the absence of conformational constraint on these pendant arms. All the resonance signals were attributed with the help of a COSY experiment. ^{13}C NMR Ar-*C*H_2-Ar resonance signal was found at δ = 31.56, in the range accepted for the cone conformation.[11]

With the aim of preparing a mononuclear zinc(II) complex displaying structural features equivalent to the above-mentioned copper(I) and silver(I) complexes **2** and **B**, we changed the chloride ions to the noncoordinating trifluoromethanesulfonate ion. UV/Vis titration of **1** by $Zn(Tfo)_2$ (Tfo = $CF_3SO_3^-$) in CH_2Cl_2 resulted in the bathochromic shift of the ligand-centred transition from 288 to 317 nm, and confirmed the formation of the expected mononuclear species. Complex **6** was thus prepared by mixing **1** and 1 equiv. of $Zn(Tfo)_2$ in CH_2Cl_2 and methanol at room temperature. Evaporation of the solvents and dissolution of the residue in $CHCl_3$, followed by filtration and addition of hexane afforded **6** as a white precipitate, in a yield of 90%. Electrospray mass spectrometry (positive mode, alcohol-free CH_2Cl_2, +90 V) showed the presence of the expected mono-charged mononuclear species at 1405.7, 1409.6, 1410.7, and 1413.9 amu ([**1** + Zn + Tfo]$^+$), accompanied by a fragment resulting from the loss of one $C_6H_5CH_2O$ group at 1301.8, 1303.8, 1304.8, and 1306.8 amu ([**1** + Zn + Tfo − $C_6H_5CH_2O$ + H]$^+$); working at a lower voltage (45 V) resulted in the appearance of a base peak at 628.5, 629.4, and 630.0 amu attributed to the doubly-charged species ([**1** + Zn]$^{2+}$/2. Elemental analysis was consistent with the formula $C_{82}H_{88}N_4O_4{\cdot}(CF_3SO_3)_2{\cdot}Zn{\cdot}CHCl_3$. The two Ar-C$H_2$-Ar ^{13}C NMR resonance signals located at δ = 32.37 and 32.87 indicated that **6** was in a distorted cone conformation.[11] A ^{1}H NMR 2D COSY experiment allowed the full assignment of the resonance signals of **6**. As for the tetrahedral species **2** and **B** (Figure 1), the Ar-CH_2-Ar resonance signals appear as two AB systems at δ = 2.67, 3.40 and 2.84, 4.02, indicating a distortion of the conic calixarene platform; the benzyl methylene groups also appear as an AB system at δ = 4.06, 4.21, resulting from an environmental difference generated by the helicoidal complex substructure. The latter is also characterised by a strong AB system located at δ = 5.55, 5.78, attributed to the OCH_2-bpy groups. All attempts to obtain crystals suitable for a convenient X-ray analysis have failed until now.

In parallel, attempts to prepare, on the base of the results obtained with zinc(II), the mononuclear cobalt(II) and nickel(II) species by anion metathesis were unsuccessful.

On the other hand, the different experiments performed to obtain a di- or mononuclear copper(II) complex species resulted in the slow partial to full formation of red copper(I) species. This phenomenon had been previously observed, but as a spontaneous reaction, during the study of **A**[8] and was explained by an oxido reduction process involving an oxidisable substrate and a base in the presence of

copper(II) and the bipyridyl calixarene podand. This particular reactivity is currently under investigation.

3. X-ray Crystal Structure Analyses

At the end of the above-mentioned investigations developed in solution, we obtained single crystals suitable for X-ray analysis with the dinuclear cobalt, nickel and zinc complexes **3**, **4** and **5**. In each case the results of the X-ray crystal structure analyses confirmed that two divalent metal ions are complexed by a podand unit in the expected, more or less distorted, tetrahedral mode,[4f,10] with the participation of the two nitrogen atoms of each bipyridine unit and two coordinating chloride ions.

The study of the calixarene platform subunit shows that the three compounds display a similar cone conformation. The inclination angles versus the mean plane of the methylene groups are very similar: two of the phenolic rings are near 90° (values between 90.8 and 98.5°) and the two others carrying the bipyridine units lie outside (values between 129.9 and 135.7°; Figure 5, ORTEP view of nickel complex **4**).

The bipyridine units are very planar (χ^2 from 0.01 to 0.08), but the angles between their planes are different, increasing from 24.8(1)° for **3**, to 31.65(7)° for **5** and 47.39(9)° for **4**. Distances from the metal ion to the mean plane of each bipyridine unit vary from 0.006 Å to 0.103 Å, while the chloride distances vary from 1.626 Å to 2.311 Å.

Distances and angles have been calculated around each metal ion (Tables 1 and 2). The geometry is very similar with a mean angle value N−metal−N of 81.6°. Mean distances metal−N have values of 2.033 Å in **3**, 2.005 Å in **4** and 2.050 Å in **5**, while the mean value for metal−Cl is 2.21 Å for the 3 compounds.

Comparison of cobalt complex subunits in **C** and **3** shows a high similarity in the coordination mode; in **3**, the Co1 coordination appears less distorted than that of Co2 and that in **C**. A similar difference in distortion is also observed between the two complex subunits in **4** and in **5**.

In each compound, one of the benzyl groups (E) is always found in the same position, in such a way that the benzene ring is almost parallel to the corresponding phenolic ring of the calixarene. The second benzyl group (F) is oriented out of the cone (Figure 6).

In the study of the packing of the zinc complex **5**, we can note some π−π interactions between one ring of a bipyridine unit (B) and another one (D) of the macrocycle obtained by a 2_1 axis (Figure 7). The same situation is found in **3**.

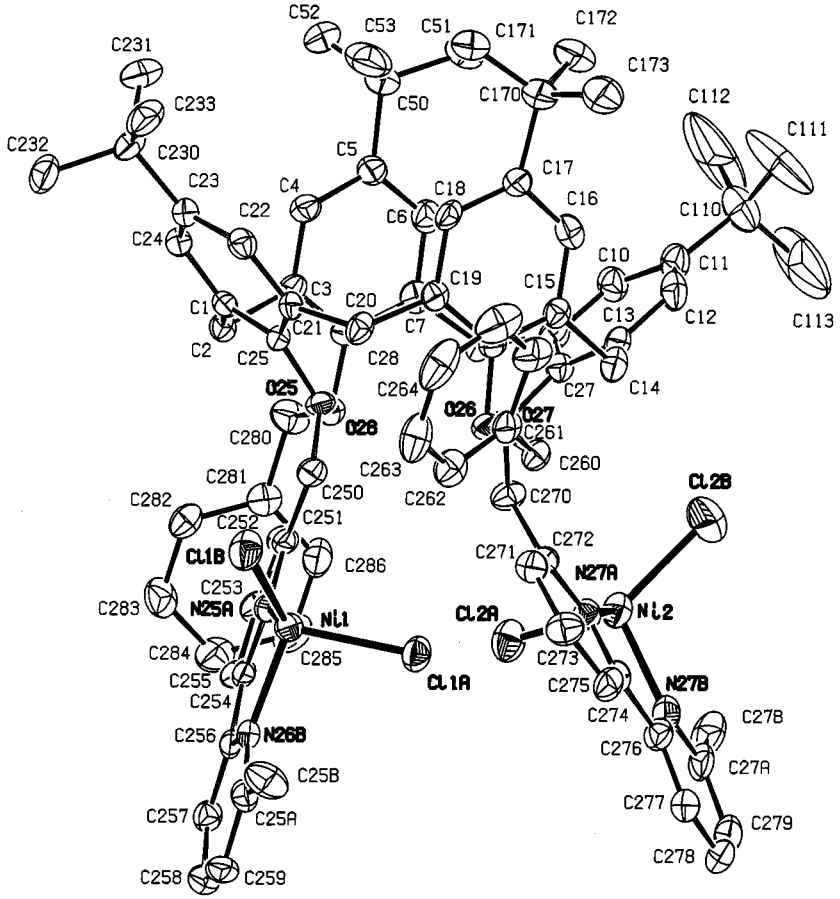

Figure 5. ORTEP side-view and numbering scheme of complex **4** (carbon atoms 8, 9, 26, 225 and 226 are omitted for clarity)

Table 1. Selected geometric parameters around the cobalt centres in complexes **C** and **3**

C		**3**			
Bond angles [°]					
Cl2−Co−Cl3	118.4(9)	Cl10−Co1−Cl11	115.2(9)	Cl20−Co2−Cl21	119.3(1)
N52−Co−N6	182.3(2)	N27M−Co1−N27F	82.3(3)	N25B−Co2−N25M	80.8(3)
N52−Co−Cl2	119.6(2)	N27M−Co1−Cl11	114.4(2)	N25B−Co2−Cl20	119.2(2)
N52−Co−Cl3	108.7(2)	N27F−Co1 −Cl11	111.7(2)	N25B−Co2−Cl21	113.9(2)
N61−Co−Cl2	112.0(2)	N27M−Co1−Cl10	116.0(2)	N25M−Co2−Cl20	110.1(2)
N61−Co−Cl3	110.1(2)	N27F−Co1−Cl10	112.9(2)	N25M−Co2−Cl21	115.3(2)
Bond lengths [Å]					
Co−Cl2	2.2213(2)	Co1−Cl11	2.201(2)	Co2−Cl20	2.210(3)
Co−Cl3	2.222(2)	Co1−Cl10	2.225(2)	Co2−Cl21	2.212(3)
Co−N52	2.021(5)	Co1−N27F	2.029(6)	Co2−N25M	2.050(7)
Co−N61	2.027(6)	Co1−N27M	2.015(6)	Co2−N25B	2.036(6)

Table 2. Selected geometric parameters around the metal centres in complexes **4** and **5**

4		**5**	
Bond angles [°]			
Cl1B−Ni1−Cl1A	118.6(5)	Cl3−Zn1−Cl4	116.95(5)
N26B−Ni1−N25A	82.0(2)	N261−Zn1−N266	81.6(2)
N26B−Ni1−Cl1B	126.7(1)	N261−Zn1−Cl4	114.9(1)
N25A−Ni1−Cl1B	123.1(1)	N261 −Zn1−Cl3	110.7(1)
N26B−Ni1−Cl1A	98.0(1)	N266−Zn1−Cl4	120.9(1)
N25A−Ni1−Cl1A	100.1(1)	N266−Zn1−Cl3	106.5(1)
Cl2B−Ni2−Cl2A	133.0(7)	Cl5−Zn2−Cl6	118.01(6)
N27B−Ni2−N27A	82.1(2)	N281−Zn2−N286	80.9(2)
N27B−Ni2−Cl2B	110.5(1)	N281−Zn2−Cl6	105.7(1)
N27A−Ni2−Cl2B	109.2(1)	N281−Zn2−Cl5	116.4(1)
N27B−Ni2−Cl2A	105.3(1)	N286−Zn2−Cl6	113.6(1)
N27A−Ni2−Cl2A	104.9(1)	N286−Zn2−Cl5	116.2(1)
Bond lengths [Å]			
Ni1−Cl1A	2.240(1)	Zn1−Cl3	2.222(1)
Ni1−Cl1B	2.180(2)	Zn1−Cl4	2.196(1)
Ni1−N25A	2.010(4)	Zn1−N261	2.051(4)
Ni1−N26B	2.003(4)	Zn1−N266	2.038(4)
Ni2−Cl2A	2.228(1)	Zn2−Cl5	2.204(2)
Ni2−Cl2B	2.188(2)	Zn2−Cl6	2.236(2)
Ni2−N27A	2.002(4)	Zn2−N281	2.070(4)
Ni2−N27B	2.003(4)	Zn2−N286	2.041(4)

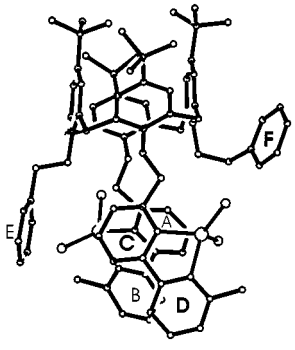

Figure 6. Side views of complex **4** and labelling of pendant bipyridyl and benzyl arms[14]

The nickel complex **4**, which crystallises in the triclinic system, shows interactions between bipyridine units A and B on one part, and pyridine rings C and D on another part.

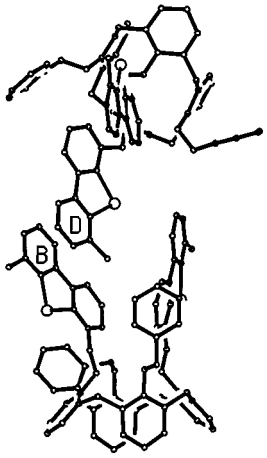

Figure 7. Interactions between rings B and D in complex **5** (*tert*-butyl groups and chlorine atoms were omitted for clarity

The corresponding calixarenes are obtained both by the centre of symmetry and by translation along *b* axis (Figure 8).

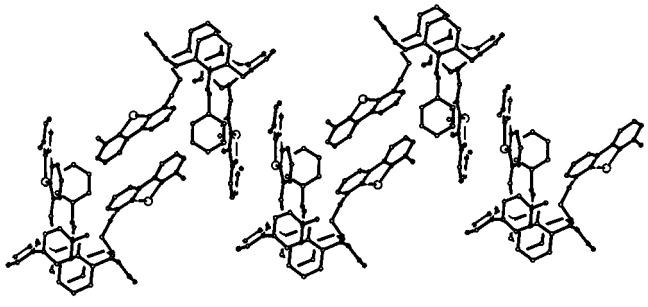

Figure 8. Interactions between the bipyridine units A and B, and C and D in nickel complex **4** (solvent atoms, *tert*-butyl groups and chlorine atoms are omitted for clarity)

Each complex crystallises with solvents which are not shown in the figures: **4** with three molecules of toluene, **3** with one molecule of dichloromethane, and **5** with two molecules of dichloromethane and two of ethanol. For the latter, one of the ethanol molecules displays a short contact

with a chlorine atom of one dichloromethane molecule (Cl···O = 3.208 Å).

Conclusion

The bipyridyl-containing calix[4]arene podand **1** described in this report shows interesting versatile complexing properties towards various common transition metal cations, giving in all cases complexes with tetrahedral coordination geometry. Depending on the nature of the cation, but also of the coordinating ability of the counter-anion, these complexes are of the L/M or L/M_2 stoichiometry, as demonstrated by UV/Vis spectroscopy, high resolution NMR spectroscopy and X-ray diffraction analysis. This versatile behaviour is currently the subject of competitive extraction studies, which necessitates developing in parallel the synthesis of the corresponding heterodinuclear complexes.

Experimental Section

General: Melting points (°C, uncorrected values) were determined with an Electrothermal 9100 (capillary apparatus). ^1H and ^{13}C NMR spectra were recorded with a Bruker AM 300 or DRX 300 and DRX 500 ($CDCl_3$, TMS as internal standard, chemical shifts in ppm). Mass spectra (electrospray, ES) were recorded with a Platform Micromass apparatus at the Service Central d'Analyse du CNRS, Solaize. Infrared spectroscopy was performed with a Mattson 5000 FT apparatus (KBr, ν in cm^{-1}) and UV spectra were recorded with a Shimadzu UV 2401 PC or a SAFAS UV mc^2 apparatus, λ_{max} in nm, ε in $dm^3 \cdot mol^{-1} \cdot cm^{-1}$. Elemental analyses were performed at the Service Central de Microanalyse, Ecole Supérieure de Chimie, Montpellier. Macherey−Nagel TLC plates were used for chromatography analysis (SiO_2, Polygram SIL G/UV254, ref. no. 805021). All commercially available products were used without further purification unless otherwise specified.

Mononuclear Copper(I) Hexafluorophosphate Complex 2: A solution of 0.0156 g of $Cu(CH_3CN)_4PF_6$ ($4.2\ 10^{-5}$ mol) in 5 mL of acetonitrile was added to a suspension of 0.05 g of **1** ($4.2\ 10^{-5}$ mol) in 20 mL of acetonitrile. Upon complexation, **1** was dissolved, giving an orange-coloured solution. The solvent was evaporated to dryness and the residue was chromatographed (Al_2O_3, CH_2Cl_2) to give **2** (0.055 g, 90%). Orange powder. M.p. 308 °C. IR: $\tilde{\nu}$ = 1570 (C−N), 2960 (C−H). UV/Vis (CH_2Cl_2): λ = 266 (29900), 302 (34700), 447 (5500, MLCT). ^1H NMR (300 MHz, $CDCl_3$): δ = 0.76 (s, 18 H, *Me*$_3$C), 1.34 (s, 18 H, *Me*$_3$C), 1.85 (s, 6 H, *Me*bpy), 2.58, 3.75 ("q", AB, J_{AB} = 13.3, 4 H, Ar-C*H*$_2$-Ar), 2.78, 3.53 ("q", AB, J_{AB} = 12.6, 4 H, Ar-C*H*$_2$-Ar), 3.82, 4.01 ("q", AB, J_{AB} = 11.5, 4 H, OC*H*$_2$C$_6$H$_5$), 5.00, 6.35 ("q", AB, J_{AB} = 12.9, 4 H, OC*H*$_2$bpy), 6.22, 6.30 (AB, J_{AB} = 2.0, 4 H, Ar*H*), 6.47 (dd, *J* = 7.7 *J* = 1.4, 4 H, C$_6$*H*$_5$), 7.02, 7.09 (AB, J_{AB} = 2.0, 4 H, Ar*H*), 7.06−7.29 (m, 6 H, C$_6$*H*$_5$), 7.39 (d, *J* = 7.7, 4 H, bpy), 7.93 (t, *J* = 8.1, 2 H, bpy), 8.16 (t, *J* = 8.1, 2 H, bpy), 8.19 (d, *J* = 8.1, 2 H, bpy), 8.44 (d, *J* = 8.1, 2 H, bpy). ^{13}C NMR (75 MHz, $CDCl_3$): δ = 23.7 (*Me*bpy), 31.8, 32.4 (Ar-C*H*$_2$-Ar), 31.1, 31.7 (*Me*$_3$C), 33.6, 34.2 (Me$_3$*C*), 77.4 (OCH$_2$C$_6$H$_5$), 79.3 (O*C*H$_2$bpy), 119.8, 121.9, 124.1, 124.54, 125.50, 126.7, 126.9, 127.8, 127.9, 128.9, 138.7, 139.0 (aromatic *C*H), 131.1, 131.4, 134.8, 135.8, 137.0, 144.5, 145.9, 151.96, 151.98, 152.1, 154.0, 157.7, 157.8 (aromatic *C*). ES-MS (pos. mode): *m*/*z* = 1255.6 [**1** + Cu^I]$^+$. $C_{82}H_{88}CuF_6N_4O_4P \cdot 0.8CH_2Cl_2$ (1470.09): calcd. C 68.30, H 6.08, N 3.77; found C 68.06, H 6.03, N 3.86.

Dinuclear Cobalt(II) Chloride Complex 3: A solution of 0.016 g of $CoCl_2$ ($1.26\ 10^{-4}$ mol) in 5 mL of acetonitrile was added to a solution of 0.05 g of **1** ($4.2\ 10^{-5}$ mol) in 10 mL of CH_2Cl_2. The resulting blue-green solution was stirred at room temp. during 1 h and then concentrated to dryness. The residue was treated with 5 mL of CH_2Cl_2 and the excess of $CoCl_2$ was removed by filtration. Slow concentration of the filtrate gave blue-green crystals of **3** (0.060 g, 98%). M.p. 235 °C. IR: $\tilde{\nu}$ = 1570, 1601 (C−N), 2956 (C−H). UV/Vis (CH_2Cl_2): λ = 317 (30700), 568 (550), 658 (1000). ^1H NMR (500 MHz, $CDCl_3$): δ = −42.49 (br. s, $\Delta\nu_{1/2}$ = 317 Hz, 4 H, OC*H*$_2$bpy), −22.60 (br. s, $\Delta\nu_{1/2}$ = 196 Hz, 6 H, *Me*bpy), −14.76 (s, $\Delta\nu_{1/2}$ = 21 Hz, 2 H, bpy), −9.70 (s, $\Delta\nu_{1/2}$ = 40 Hz, 4 H, 2 Ar-C*H*$_2$-Ar), − 6.75 (s, $\Delta\nu_{1/2}$ = 77 Hz, 2 H, bpy), −3.05 (s, $\Delta\nu_{1/2}$ = 22 Hz, 4 H, 2 Ar-C*H*$_2$-Ar), −1.72 (s, $\Delta\nu_{1/2}$ = 4 Hz, 18 H, *Me*$_3$C), −0.13 (s, $\Delta\nu_{1/2}$ = 6 Hz, 18 H, *Me*$_3$C), 1.75 (s, $\Delta\nu_{1/2}$ = 6 Hz, 4 H, Ar*H*), 1.78 (s, $\Delta\nu_{1/2}$ = 6 Hz, 4 H, Ar*H*), 4.17 (s, $\Delta\nu_{1/2}$ = 18 Hz, 4 H, 2 OC*H*$_2$C$_6$H$_5$), 8.63 (s, $\Delta\nu_{1/2}$ = 22 Hz, 4 H, C$_6$*H*$_5$), 9.77 (s, $\Delta\nu_{1/2}$ = 12 Hz, 2 H, C$_6$*H*$_5$), 11.38 (s, $\Delta\nu_{1/2}$ = 22 Hz, 4 H, C$_6$*H*$_5$), 42.28 (s, $\Delta\nu_{1/2}$ = 34 Hz, 2 H, bpy), 49.18 (s, $\Delta\nu_{1/2}$ = 28 Hz, 2 H, bpy), 72.72 (s, $\Delta\nu_{1/2}$ = 25 Hz, 2 H, bpy), 72.93 (s, $\Delta\nu_{1/2}$ = 32 Hz, 2 H, bpy). ES-MS (pos. mode, 252 V): *m*/*z* = 1417.5 [**1** + 2 ($CoCl_2$) − Cl^-]$^+$, 1288.5 [**1** + $CoCl_2$ − Cl^-]$^+$, 1215.7 [**1** + Na]$^+$, 1193.7 [**1** + H]$^+$. $C_{82}H_{88}Cl_4Co_2N_4O_4$ (1453.32): calcd. C 67.77, H 6.10, N 3.86; found C 68.00, H 6.25, N 3.65.

Dinuclear Nickel(II) Chloride Complex 4: A solution of 0.020 g of **1** ($1.67\ 10^{-5}$ mol) and 0.0081 g of $NiCl_2 \cdot 6H_2O$ ($3.35\ 10^{-5}$ mol) in a mixture of CH_2Cl_2 (1 mL), acetonitrile (10 mL) and methanol (1 mL) was stirred at room temp. during 1 h. The resulting salmon-pink solution was concentrated to dryness; the residue was dissolved in $CHCl_3$ and the addition of 10 mL of hexane resulted in the precipitation of **4** as a pink microcrystalline solid (0.017 g; 71%). M.p. 295 °C. IR: $\tilde{\nu}$ = 2957 (CH), 1574, 1603 (C−N). UV/Vis (CH_2Cl_2): λ = 310 (40200), 488 (325). ^1H NMR (500 MHz, $CDCl_3$): δ = 1.97 (s, $\Delta\nu_{1/2}$ = 9 Hz, 18 H, *Me*$_3$C), 2.03 (s, $\Delta\nu_{1/2}$ = 9 Hz, 18 H, *Me*$_3$C), 5.60 (s, 4 H, Ar-C*H*$_2$-Ar), 10.75 (s, $\Delta\nu_{1/2}$ = 57 Hz, 4 H, Ar-C*H*$_2$Ar), 16.75 [s, $\Delta\nu_{1/2}$ = 87 Hz, 2 H, bpy(1)], 22.50 [s, $\Delta\nu_{1/2}$ = 26 Hz, 2 H, bpy(2)], 58.22 [s, $\Delta\nu_{1/2}$ = 46 Hz, 2 H, bpy(1)], 63.80 [s, $\Delta\nu_{1/2}$ = 38 Hz, 2 H, bpy(2)], 80.41 [s, $\Delta\nu_{1/2}$ = 80 Hz, 2 H, bpy(2)], 84.72 [s, $\Delta\nu_{1/2}$ = 90 Hz, 2 H, bpy(1)],1.72 (s, $\Delta\nu_{1/2}$ = 28 Hz, 6 H), 5.32 (s, 4 H), 5.67 (s, 4 H), 6.25 (s, $\Delta\nu_{1/2}$ = 16 Hz, 2 H), 6.77 (s, $\Delta\nu_{1/2}$ = 28 Hz, 4 H), 8.60 (s, $\Delta\nu_{1/2}$ = 14 Hz, 4 H), 8.94 (s, $\Delta\nu_{1/2}$ = 12 Hz, 4 H), 26.82 (s, $\Delta\nu_{1/2}$ = 392 Hz, 4 H) (*Me*bpy, OC*H*$_2$C$_6$H$_5$, C$_6$*H*$_5$, Ar*H*, OC*H*$_2$bpy). ES-MS (pos. mode, 234 V): *m*/*z* = 1417.5 [**1** + 2 ($NiCl_2$) − Cl^-]$^+$, 1287.5 [**1** + ($NiCl_2$) − Cl^-]$^+$, 1215.7 [**1** + Na]$^+$. $C_{82}H_{88}Cl_4N_4Ni_2O_4 \cdot 0.5CHCl_3$ (1512.52): calcd. C 65.51, H 5.90, N 3.70; found C 65.48, H 6.15, N 3.64.

Dinuclear Zinc(II) Chloride Complex 5: A solution of 0.030 g of $ZnCl_2$ ($22.0\ 10^{-5}$ mol) in 5 mL of methanol was added to a solution of 0.060 g of **1** ($5.0\ 10^{-5}$ mol) in 10 mL of CH_2Cl_2. The solution was stirred at room temp. during 1 h, and the excess of $ZnCl_2$ which precipitated was removed by filtration. Slow concentration of the filtrate afforded **5** as white crystals (0.068 g, 90%). M.p. 245 °C. IR: $\tilde{\nu}$ = 1576, 1601 (C−N). UV/Vis (CH_2Cl_2): λ = 321 (32400), 310 (36500). ^1H NMR (500 MHz, CD_2Cl_2): δ = 0.93 (s, 18 H, *Me*$_3$C), 1.38 (s, 18 H, *Me*$_3$C), 3.05 (s, 6 H, *Me*bpy), 3.12, 4.48 ("q", AB, J_{AB} = 12.9, 8 H, Ar-C*H*$_2$-Ar), 5.02 (s, 4 H, OC*H*$_2$C$_6$H$_5$), 5.81 (s, 4 H, OC*H*$_2$bpy), 6.60 (s, 4 H, ArH), 7.11−7.22 (m, 10 H, C$_6$*H*$_5$), 7.21 (s, 4 H, ArH), 7.64 (d, *J* = 8.1, 2 H, bpy), 7.67 (d, *J* = 7.4, 2 H,

bpy), 7.71 (t, J = 7.7, 2 H, bpy), 7.96 (d, J = 8.1, 2 H, bpy), 8.11 (t, J = 7.9, 2 H, bpy), 9.24 (d, J = 7.9, 2 H, bpy). ^{13}C NMR (125.75 MHz, CD_2Cl_2): δ = 24.7 (*Me*bpy), 31.4, 31.8 (*Me*$_3$C), 31.6 (Ar-*C*H$_2$-Ar), 34.1, 34.4 (Me$_3$*C*), 75.7 (O*C*H$_2$C$_6$H$_5$), 78.9 (O*C*H$_2$bpy), 119.3, 120.0, 125.2, 126.88, 126.94, 127.7, 128.2, 128.4, 130.6, 142.0 (aromatic *C*H), 132.6, 134.9, 137.1, 145.5, 146.9, 147.9, 149.2, 150.7, 154.8, 160.2, 160.9 (aromatic *C*). ES-MS (pos. mode, 80 V): *m*/*z* = 1255.8, 1258.7, 1259.8 [**1** + Zn^{2+} − H^+]$^+$, 1032.9, 1033.8, 1034.9 [**1** − 2 $CH_2C_6H_5$ + Na^+]$^+$. $C_{82}H_{88}Cl_4N_4O_4Zn_2$·0.5$CH_2Cl_2$ (1508.69): calcd. C 65.68, H 5.95, N 3.71; found C 65.63, H 6.18, N 3.82.

Mononuclear Zinc(II)trifluoromethanesulfonate Complex 6: A solution of 0.019 g of $Zn(CF_3SO_3)_2$ (5.0 10^{-5} mol) in 10 mL of CH_2Cl_2/methanol was added to a solution of 0.060 g of **1** (5.0 10^{-5} mol) in 20 mL of CH_2Cl_2. The solution was stirred at room temp. during 1 h, and the solvent was evaporated to dryness. The residue was dissolved in 4 mL of $CHCl_3$ and 20 mL of hexane was added, affording **6** as a white precipitate (0.076 g, 90%). M.p. 202 °C. UV/Vis (CH_2Cl_2): λ = 317 (31700). ^{1}H NMR (300 MHz, $CDCl_3$): δ = 0.76 (s, 18 H, *Me*$_3$C), 1.34 (s, 18 H, *Me*$_3$C), 1.91 (s, 6 H, *Me*bpy), 2.67, 3.40 ("q", AB, J_{AB} = 12.9, 4 H, Ar-C*H*$_2$-Ar), 2.84, 4.02 ("q", AB, J_{AB} = 13.6, 4 H, Ar-C*H*$_2$-Ar), 4.06, 4.21 ("q", AB, J_{AB} = 11.8, 4 H, OC*H*$_2$C$_6$H$_5$), 5.55, 5.78 ("q", AB, J_{AB} = 14.0, 4 H, OC*H*$_2$bpy), 6.24 (s, 4 H, Ar*H*), 6.48 (d, J = 7, 4 H, C$_6$*H*$_5$), 7.09(s, 4 H, Ar*H*), 7.04−7.17 (m, 6 H, C$_6$*H*$_5$), 7.60 (d, J = 7.7, 2 H, bpy), 7.62 (d, J = 7.7, 2 H, bpy), 8.18 (t, J = 7.9, 2 H, bpy), 8.36 (t, J = 7.9, 2 H, bpy), 8.60 (d, J = 8.1, 2 H, bpy), 8.81 (d, J = 8.1, 2 H, bpy). ^{13}C NMR (75 MHz, $CDCl_3$): δ = 23.7 (*Me*bpy), 31.4, 32.0 (*Me*$_3$C), 32.4, 32.9 (Ar-C*H*$_2$-Ar), 33.9, 34.6 (Me$_3$*C*), 78.1 (O*C*H$_2$C$_6$H$_5$), 78.2 (O*C*H$_2$bpy), 122.2, 124.4, 124.6, 125.0, 126.2, 128.0, 128.5, 128.6, 128.8, 129.2, 129.5, 130.0, 144.1, 144.6 (aromatic *C*H), 128.05, 128.2, 131.2, 131.3, 134.8, 135.8, 136.8, 145.3, 147.1, 148.9, 149.6, 152.0, 153.7, 159.9, 161.0 (aromatic *C*). ES-MS (pos. mode, 90 V): *m*/*z* = 1405.7, 1409.6, 1410.7, 1413.9 [**1** + Zn(Tfo)$_2$ − Tfo$^-$]$^+$; (45 V): *m*/*z* = 628.5, 629.4, 630.0 [**1** + Zn]$^{2+}$/2. $C_{84}H_{88}F_6N_4O_{10}S_2Zn$·$CHCl_3$ (1676.55): calcd. C 60.89, H 5.35, N 3.34; found C 60.80, H 5.62, N 3.38.

X-ray Crystallographic Study of Complexes 3, 4 and 5: The data were collected with a Nonius Kappa CCD diffractometer using monochromated Mo-K_α radiation. Structures were solved by direct methods and refined using full-matrix least squares with SHELXS97 [12] and SHELXL97 programmes.[13] All non-H atoms were refined anisotropically. Hydrogen atoms were calculated at their idealised positions and refined isotropically riding on previous atoms. Details for the experimental conditions, cell data, structure and refinement data are given in Table 3. CCDC-167144 (**3**), -167143 (**4**) and -167145 (**5**) contain the supplementary crystallographic data for this paper. These data can be obtained free of charge at www.ccdc.cam.ac.uk/conts/retrieving.html or from the Cambridge Crystallographic Data Centre, 12, Union Road, Cambridge CB2 1EZ, UK [Fax: (internat.) + 44-1223/336-033; E-mail: deposit@ccdc.cam.ac.uk].

Acknowledgments

We are grateful to the MRES for financial support, especially J.-O. D. for a PhD fellowship; to SAFAS (Monaco) and BRUKER S. A. for UV spectroscopy and WinNMR facilities, respectively. The authors thank Mrs. Nicole Marshall for correcting the manuscript.

Table 3. Crystal data and structure refinement of **3**, **4** and **5**

	3	**4**	**5**
Empirical formula	$C_{83}H_{90}Cl_{8.5}Co_2N_4O_4$	$C_{103}H_{112}Cl_9N_4O_4Ni_2$	$C_{87}H_{102}Cl_7N_4O_6Zn_2$
Formula mass	1538.15	1729.19	1685.63
Temperature [K]	293	293	123
Crystal system, space group	monoclinic, *C*2/*c*	triclinic, $P\bar{1}$	monoclinic, *C*2/*c*
Unit cell dimensions			
a [Å]	45.852(9)	11.691(2)	48.501(9)
b [Å]	15.054(3)	17.225(3)	14.798(3)
c [A]	23.798(5)	24.510(5)	24.082(5)
α [°]	90	92.94(3)	90
β [°]	91.78(3)	94.08(3)	92.019(3)
γ [°]	90	105.98(3)	90
V [Å ^{3}]	16419(6)	4719.8(16)	17273.2(4)
Z	8	2	8
$D_{calcd.}$ [Mgm^{-3}]	1.244	1.217	1.291
Absorption coefficient [mm^{-1}]	0.648	0.564	0.825
F(000)	804	914	883
Crystal size [mm]	0.35 × 0.30 × 0.25	0.35 × 0.30 × 0.04	0.44 × 0.30 × 0.18
θ range for data collection [°]	2.07 to 25.63	2.83 to 28.16	1.02 to 23.26
Limiting indices	$0 \le h \le 50$	$0 \le h \le 15$	$0 \le h \le 53$
	$0 \le k \le 18$	$-21 \le k \le 21$	$-16 \le k \le 16$
	$-27 \le l \le 27$	$-31 \le l \le 31$	$-26 \le l \le 26$
Reflections collected/unique	12921/12921	18423/18423	117262/12367
Max./min. transmission	0.8547 and 0.8049	0.9778 and 0.8270	0.866 and 0.712
Data/restraints/parameters	12921/0/892	18423/1/1041	12367/2/964
Goodness-of-fit on F^2	0.961	0.952	1.080
Final *R* indices [$I > 2\sigma(I)$]	*R*1 = 0.0882, *wR*2 = 0.2433	*R*1 = 0.0748, *wR*2 = 0.1362	*R*1 = 0.0620, *wR*2 = 0.1506
R indices (all data)	*R*1 = 0.1731, *wR*2 = 0.2960	*R*1 = 0.1907, *wR*2 = 0.1669	*R*1 = 0.0798, *wR*2 = 0.1590
Densities (max./min.) [e·Å^{-3}]	0.894 and −1.084	0.534 and −0.520	1.00 and −0.82

[1] [1a] C. D. Gutsche, *Calixarenes*, Monographs in Supramolecular Chemistry, Series (Ed.: J. F. Stoddart), Royal Society of Chemistry, Cambridge, **1989**. [1b] *Calixarenes. A Versatile Class of Macrocyclic Compounds* (Eds.: J. Vicens, V. Böhmer), Kluwer Academic Publishers, Dordrecht, **1991**. [1c] *Calixarenes, Macrocycles with (Almost) Unlimited Possibilities:* V. Böhmer, *Angew. Chem. Int. Ed. Engl.* **1995**, *34*, 713. [1d] C. D. Gutsche, *Calixarenes Revisited*, Royal Society of Chemistry, Cambridge, **1998**.

[2] *Calixarenes 2001* (Eds.: Z. Asfari, V. Böhmer, J. Harrowfield, J. Vicens), Kluwer, Dordrecht, The Netherlands, **2001**.

[3] [3a] C. Wieser, D. B. Dieleman, D. Matt, *Coord. Chem. Rev.* **1997**, *165*, 93−161. [3b] A. T. Yordanov, D. M. Roundhill, *Coord. Chem. Rev.* **1998**, *170*, 93−124.

[4] For example: [4a] P. D. Beer, J. P. Martin, M. G. B. Drew, *Tetrahedron* **1992**, *48*, 9917−9928. [4b] J.-B. Regnouf-de-Vains, R. Lamartine, *Helv. Chim. Acta* **1994**, *77*, 1817−1825. [4c] R. Grigg, J. M. Holmes, S. K. Jones, W. D. Amilaprasadh Norbert, *J. Chem. Soc., Chem. Commun.* **1994**, 185−187. [4d] G. Ulrich, R. Ziessel, *Tetrahedron Lett.* **1994**, *35*, 6299−6302. [4e] J.-B. Regnouf-de-Vains, R. Lamartine, B. Fenet, *Helv. Chim. Acta* **1998**, *81*, 661−669. [4f] J.-O. Dalbavie, J.-B. Regnouf-de-Vains, R. Lamartine, S. Lecocq, M. Perrin, *Eur. J. Inorg. Chem.* **2000**, *4*, 683−691.

[5] [5a] S. Pellet-Rostaing, J.-B. Regnouf-de-Vains, R. Lamartine, *Tetrahedron Lett.* **1996**, *37*, 5889−5892. [5b] S. Pellet-Rostaing, J.-B. Regnouf-de-Vains, R. Lamartine, P. Meallier, S. Guittonneau, B. Fenet, *Helv. Chim. Acta* **1997**, *80*, 1229−1243. [5c] S. Pellet-Rostaing, J.-B. Regnouf-de-Vains, R. Lamartine, B. Fenet, *Inorg. Chem. Commun.* **1999**, *2*, 4−7.

[6] [6a] S. Pellet-Rostaing, Thèse d'Université, Université Claude Bernard-Lyon I, **1996**. [6b] S. Pellet-Rostaing, J.-B. Regnouf-de-Vains, A. Marsura, manuscript in preparation.

[7] J.-B. Regnouf-de-Vains, J.-O. Dalbavie, R. Lamartine, B. Fenet, *Tetrahedron Lett.* **2001**, *42*, 2681−2684.

[8] J.-B. Regnouf-de-Vains, R. Lamartine, B. Fenet, C. Bavoux, A. Thozet, M. Perrin, *Helv. Chim. Acta* **1995**, *78*, 1607−1619.

[9] For example: [9a] P. D. Beer, J. W. Wheeler, C. P. Moore, *J. Chem. Soc., Dalton Trans.* **1992**, 2667−2673. [9b] M. D. Ward, S. M. Couchman, J. C. Jeffrey, *Acta Crystallogr., Sect. C: Cryst. Struct. Commun.* **1998**, *54*, 1820−1823. [9c] A. M. W. Cargill Thompson, I. Blandford, H. Readfearn, J. C. Jeffery, M. D. Ward, *J. Chem. Soc., Dalton Trans.* **1997**, 2661−2666. [9d] T. M. Garrett, U. Koert, J.-M. Lehn, A. Rigault, D. Meyer, J. Fisher, *J. Chem. Soc., Chem. Commun.* **1990**, 557−558.

[10] G. R. Newkome, D. C. Pantaleo, W. E. Puckett, P. L. Ziefle, W. A. Deutsch, *J. Inorg. Nucl. Chem.* **1981**, *43*, 1529−1531.

[11] [11a] C. Jaime, J. de Mendoza, P. Prados, P. M. Nieto, C. Sanchez, *J. Org. Chem.* **1991**, *56*, 3372−3376. [11b] J. O. Magrans, J. de Mendoza, M. Pons, P. Prados, *J. Org. Chem.* **1997**, *62*, 4518−4520.

[12] G. M. Sheldrick, *SHELXS97, Programme for Crystal Structure Determination*, University of Göttingen, Germany, **1997**.

[13] G. M. Sheldrick, *SHELXL97, Programme for Refinement of Crystal Structures*, University of Göttingen, Germany, **1997**.

[14] A. L. Spek, *PLATON, A Multipurpose Crystallographic Tool*, University of Utrecht, The Netherlands, **1999**.

Received September 7, 2001
[I01346]

Structural and Spectroelectrochemical Studies on (2,2′-Bidipyrrinato)copper(II) and -palladium(II) Complexes

Martin Bröring,*[a] Carsten D. Brandt,[a] Jordi Bley-Escrich,[b] and Jean-Paul Gisselbrecht*[b]

Keywords: Porphyrinoids / N ligands / Copper / Palladium / Electrochemistry

Copper(II) and palladium(II) complexes of two 2,2′-bidipyrrin ligands were prepared and examined, in comparison with the known nickel(II) complexes of these ligands, by means of X-ray crystallography, cyclic voltammetry, and spectroelectrochemistry. All compounds are of helical geometry with coordination environments of the metal centres displaying very small tetrahedral distortions for palladium and very large ones for copper complexes. Porphyrinoid behaviour was found for the one- and two-electron oxidations of all complexes studied, as well as for the reductions of the Pd^{II} species. On the other hand, the reduction of the Cu^{II} complexes shows some special features, which may be explained from the results of spectroelectrochemical studies as related to the particular non-planarity of these compounds.
(© Wiley-VCH Verlag GmbH, 69451 Weinheim, Germany, 2002)

Introduction

As part of an ongoing project to study the coordination chemistry of open-chain oligopyrrolic ligands, we recently became interested in the tetrapyrrolic 2,2′-bidipyrrins.[1,2] Topologically, 2,2′-bidipyrrins resemble the porphyrins both in their build-up (from two connected dipyrrin units) and their expected dianionic character when serving as ligands in metal complexes.[3] Our initial studies on a set of (2,2′-bidipyrrinato)nickel(II) complexes showed that this tetrapyrrole formed conformatively stable helicates, which may be resolved chromatographically into the separate enantiomers. In addition to this, the delocalized π system of 2,2′-bidipyrrin ligands largely determines the electrochemical behaviour of the Ni^{II} complexes, in that only ligand centred oxidation and reduction steps could be observed. This finding, in particular, qualifies 2,2′-bidipyrrins as open-chain analogues of the porphyrins.[4]

The higher flexibility of the 2,2′-bidipyrrin ligand with respect to the porphyrins, however, has tremendous impact on its coordination chemistry, as was recently shown by the X-ray crystallographic characterization of two non-porphyrinoid coordination modes (Scheme 1).[5,6] Therefore, a prediction of how this tetrapyrrole would interact with a given metal ion is not trivial. In the early 1960s, the Johnson group reported the first palladium and copper complexes of 2,2′-bidipyrrins. From molecular mass determination, the latter were deduced to exist in two different, interchangeable forms, namely the coordination modes displayed by **1** and **2** (Scheme 1).[7]

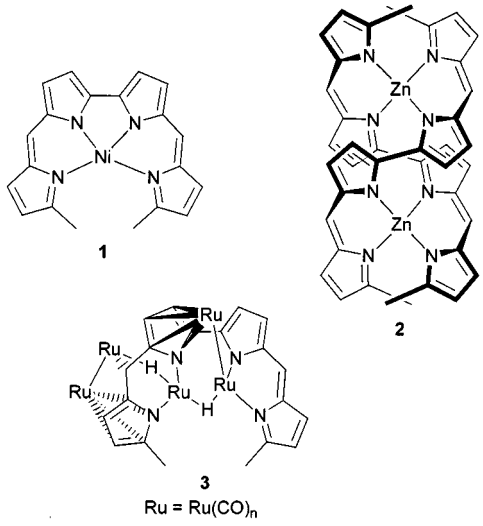

Scheme 1. Coordination modes of 2,2′-bidipyrrins

In this context, we had two important questions. Firstly, what is the impact of elongated M−N bonds of e.g. Pd^{II} vs. Ni^{II} complexes of 2,2′-bidipyrrins on the stability of the helical conformation? Secondly, how does the typical structural lability for Cu^{II} complexes influence the coordination mode, the ligand structure, and the redox behaviour of these complexes? In this paper we try to answer these questions using structural and electrochemical arguments.

[a] Institut für Anorganische Chemie, Universität Würzburg, Am Hubland, 97074 Würzburg, Germany;
E-mail: martin.broering@mail.uni-wuerzburg.de
[b] UMR 7512 C.N.R.S. Université Louis Pasteur, 4 rue Blaise Pascal, 67000 Strasbourg, France

Results and Discussion

Preparation and Characterization of Complexes 6−9

The copper(II) and palladium(II) complexes **6−9** were prepared from the 2,2′-bidipyrrins **4** and **5** by treatment with a methanolic solution of excess metal acetate (Scheme 2). The complexation reactions were complete after 30 min at room temperature. The copper complexes **6** and **7** were purified by several washings of the resulting solutions with water, and recrystallization from dichloromethane/*n*-hexane. In the case of the palladium complexes **8** and **9**, convenient purification could be achieved by chromatographic filtration through silica and subsequent recrystallization from the above solvent mixture. The observed yields were good (78−92%). Only one copper(II) complex was formed from either ligand by this method, namely the M_1L_1 compound of type **1**.

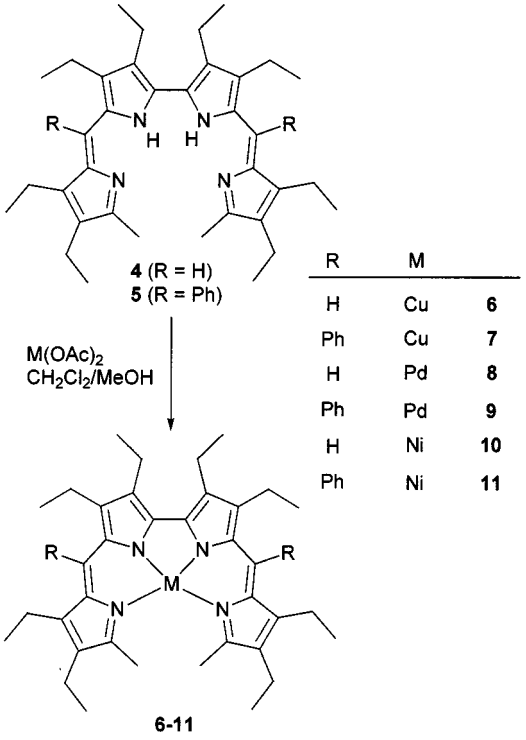

R	M	
H	Cu	**6**
Ph	Cu	**7**
H	Pd	**8**
Ph	Pd	**9**
H	Ni	**10**
Ph	Ni	**11**

Scheme 2. Syntheses of (2,2′-bidipyrrinato)metal(II) complexes

All new compounds gave correct analyses, and were further characterized by EIMS. In addition, proton and carbon NMR measurements were carried out on the palladium derivatives **8** and **9**, showing the expected sharp signals for **8** and broadened resonances for **9** due to the steric encumbrance of the peripheral substituents. The same line broadening was observed earlier on a set of related (2,2′-bidipyrrinato)nickel(II) complexes like **11**.[3] The splitting of the signals of the *meso*-phenyl substituents indicates the expected helical conformation of **9** in solution at room temperature.

Molecular Structures of 6 and 8

Crystals of **6** and **8** were obtained from slow concentration of the respective solutions in dichloromethane/*n*-hexane. As in the case of the nickel(II) complex **10** of the same ligand, complexes **6** and **8** crystallized in the monoclinic system, space group $P2_1/c$, with $Z = 4$. Both compounds show helically distorted ligand frameworks in the solid, and both enantiomers co-crystallize in the same unit cell. Figures 1 and 2 show the molecular structures of **8** and **6**, and Table 1 summarizes structural parameters of **6**, **8**, and **10**.

For the palladium derivative **8**, the Pd−N bond lengths of 1.956(3)−2.045(3) Å appear in the range found for other (tetrapyrrole)palladium(II) complexes,[8−12] and indicate a larger N_4 core as compared with the Ni^{II} derivative **10**. As a consequence of these elongations, the coordination sphere of the metal ion becomes significantly more trapezoidal. This is clearly visible in the reduced internal N−M−N angles (by 1.37−2.05° with respect to **10**), and a widened N(1)−Pd−N(4) angle of 105.44°. The ligand itself was found to expand upon coordination of the Pd^{II} ion. This

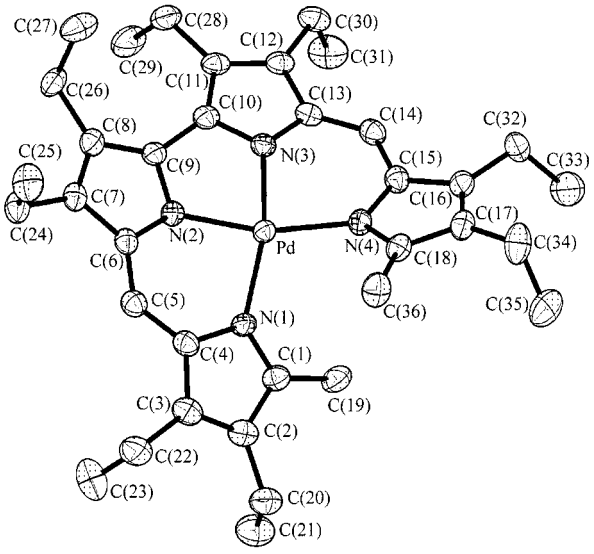

Figure 1. ORTEP plot of the molecular structure of **8** (50% probability)

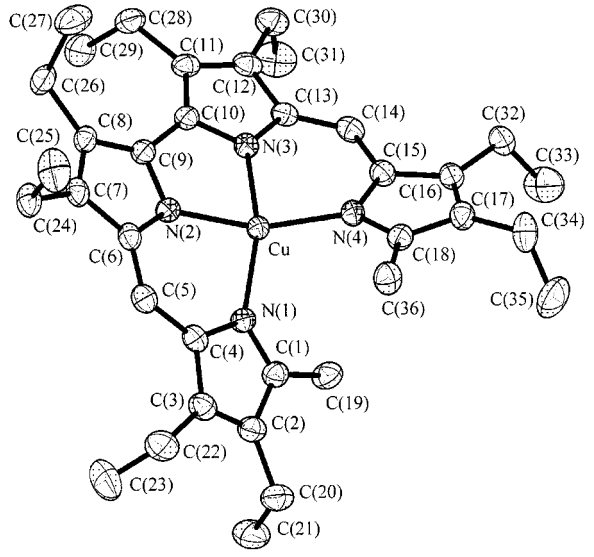

Figure 2. ORTEP plot of the molecular structure of **6** (50% probability)

Table 1. Selected bond lengths, distances [Å] and angles [°] for **6**, **8**, and **10**

	M = Cu (**6**)	M = Pd (**8**)	M = Ni (**10**)
M−N(1)	1.9782(16)	2.044(3)	1.9088(15)
M−N(2)	1.9291(16)	1.959(3)	1.8451(15)
M−N(3)	1.9250(17)	1.956(3)	1.8498(14)
M−N(4)	1.9794(16)	2.045(3)	1.9068(15)
N(1)−C(1)	1.332(3)	1.337(4)	1.341(2)
N(1)−C(4)	1.407(3)	1.404(4)	1.409(2)
N(2)−C(6)	1.366(3)	1.372(4)	1.371(2)
N(2)−C(9)	1.348(3)	1.356(4)	1.349(2)
N(3)−C(10)	1.349(3)	1.351(4)	1.353(2)
N(3)−C(13)	1.360(3)	1.360(4)	1.373(2)
N(4)−C(15)	1.405(3)	1.407(4)	1.409(2)
N(4)−C(18)	1.340(3)	1.338(4)	1.340(2)
C(1)−C(2)	1.429(3)	1.432(5)	1.432(3)
C(2)−C(3)	1.370(3)	1.372(5)	1.372(3)
C(3)−C(4)	1.433(3)	1.432(5)	1.432(3)
C(4)−C(5)	1.392(3)	1.388(5)	1.380(3)
C(5)−C(6)	1.393(3)	1.390(5)	1.391(3)
C(6)−C(7)	1.429(3)	1.430(5)	1.426(3)
C(7)−C(8)	1.385(3)	1.387(5)	1.386(3)
C(8)−C(9)	1.430(3)	1.427(5)	1.428(3)
C(9)−C(10)	1.464(3)	1.463(5)	1.457(3)
C(10)−C(11)	1.435(3)	1.430(5)	1.425(3)
C(11)−C(12)	1.389(3)	1.387(5)	1.382(3)
C(12)−C(13)	1.427(3)	1.425(5)	1.430(3)
C(13)−C(14)	1.397(3)	1.398(5)	1.386(3)
C(14)−C(15)	1.389(3)	1.378(5)	1.383(3)
C(15)−C(16)	1.435(3)	1.444(5)	1.435(3)
C(16)−C(17)	1.379(3)	1.364(5)	1.365(3)
C(17)−C(18)	1.430(3)	1.434(5)	1.427(3)
$C_{term}\cdots C_{term}$	3.58	3.48	3.34
N(1)−M−N(2)	88.92(7)	89.02(11)	90.39(7)
N(1)−M−N(3)	159.28(7)	164.02(11)	161.72(7)
N(1)−M−N(4)	107.69(7)	105.44(11)	101.76(7)
N(2)−M−N(3)	78.86(8)	78.73(12)	80.72(7)
N(2)−M−N(4)	157.97(7)	162.69(11)	163.08(7)
N(3)−M−N(4)	88.80(7)	88.50(11)	90.55(6)
N(2)−C(9)−C(10)	111.15(16)	111.8(3)	109.57(15)
N(3)−C(10)−C(9)	110.75(17)	111.2(3)	109.99(15)
C(4)−C(5)−C(6)	126.22(19)	127.9(3)	125.45(18)
C(13)−C(14)−C(15)	126.03(19)	127.0(3)	125.33(17)

was deduced from the fact that the inner bond angles of the bipyrrole linkage N(2)−C(9)−C(10) and N(3)−C(10)−C(9) as well as those at the *meso* carbon atoms C(4)−C(5)−C(6) and C(13)−C(14)−C(15) became larger. In summary, the changes result in reduced overlap of the terminal methyl groups, and thus in diminished helicity of the ligand and enhanced planarity of the metal centre {rms deviation of MN_4 fragments from planarity: Pd 0.151 Å, Ni 0.203 Å; angle between the planes [N(2),N(3),M] and [N(1),N(4),M]: for **8** 14.0°, for **10** 19.9°; angles N(1)−M−N(3) and N(2)−M−N(4): Pd 164.02(11) and 162.69(11)°, Ni 161.72(7) and 163.08(7)°; Figure 3}. The distance between the terminal methyl groups, however, increased in the Pd^{II} complex from 3.34 to 3.48 Å. Obviously, this value is not a good indicator for the helical topology of the tetrapyrrole perimeter in chelates with different metal ions. Despite the more open structure of **8** with respect to **10**, the helical arrangement is still quite pronounced and

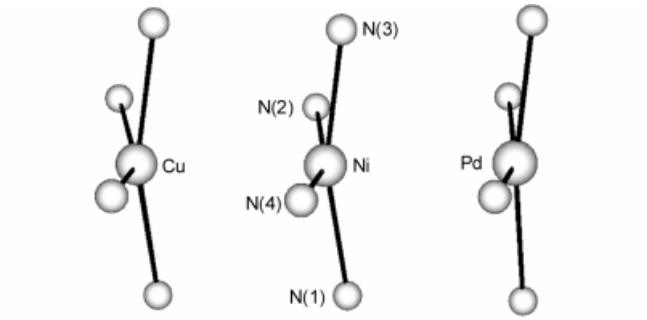

Figure 3. Comparison of coordination geometries found in **6**, **8**, and **10**

stable. Further support to this statement is provided by the fact, that the diphenyl derivative **9** of (2,2′-bidipyrrinato)-palladium(II) could be separated into the enantiomers by HPLC on an analytical scale, and by the observation, that in the ^1H NMR spectrum the splitting of the signals of the *meso*-phenyl groups of **9** remained unchanged up to 90 °C.

The Cu−N bond lengths of the copper(II) complex **6** of 1.9250(17)−1.9794(16) Å are normal for copper(II) complexes of tetrapyrrolic ligands,[9,13−16] and are therefore again longer than the Ni−N bond length of **10**. The same conclusions as with the palladium derivative **8** above can thus be drawn concerning the changes found for the inner bond angles and the overlap of the terminal methyl groups of the tetrapyrrole ligand. In contrast to **8**, however, the more open structure of complex **6** results in enhanced helicity of the ligand and reduced planarity of the metal coordination sphere. This difference is caused by the pronounced tetrahedral distortion imposed by the metal centre as measured by the N(1)−Cu−N(3) and N(2)−Cu−N(4) angles of 159.28(7) and 157.97(7)°, respectively. The difference could be monitored in the enlarged deviation of the CuN_4 fragment from planarity (0.234 Å) as well as in the angle between the planes [N(2),N(3),Cu] and [N(1),N(4),Cu] of 22.0° (Figure 3). The flexibility of 2,2′-bidipyrrin ligands thus allows different metal centres to accommodate the coordination geometry within some range, even if the same coordination mode is established.

Cyclic Voltammetry

As we have shown earlier, the redox characteristics of (2,2′-bidipyrrinato)nickel(II) complexes resemble those of porphyrinoid nickel(II) complexes. In both cases, two one-electron transfer steps occurred upon oxidation or reduction, and all could be shown to be ligand centred.[4] The values detected for the potentials of (2,2′-bidipyrrinato)-nickel(II) complex oxidations and reductions, however, are more closely related to those of the chlorinato- and bacteriochlorinato complexes than to the metalloporphyrins themselves.[17,18]

Cu^{II} and Pd^{II} complexes **6**−**9** were studied in benzonitrile with 0.1 M $n Bu_4NPF_6$, and gave well-defined signals (Fig-

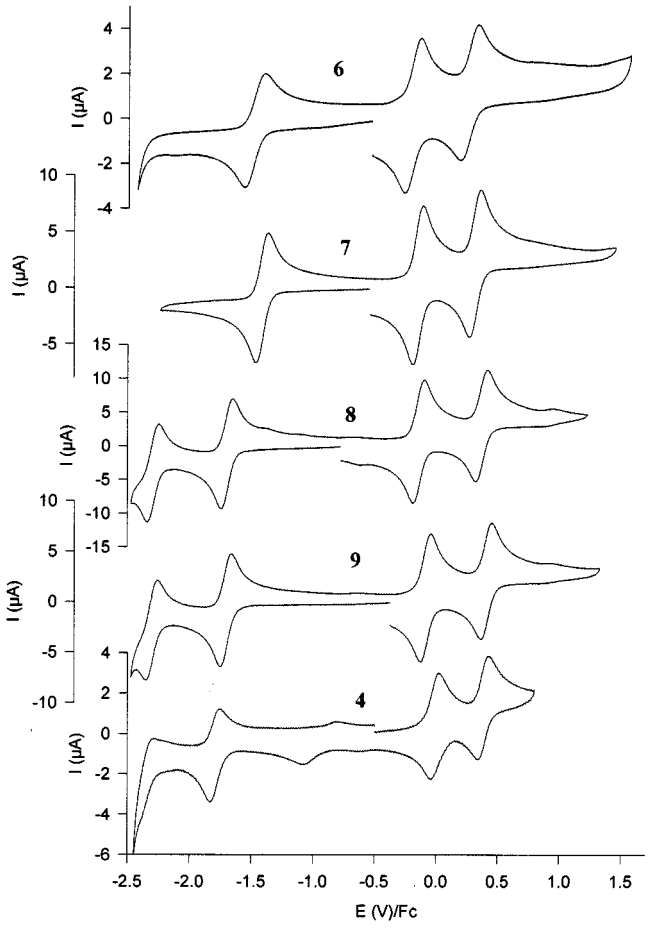

Figure 4. Cyclic voltammetry of **4**, **6**, **7**, **8**, and **9** in PhCN with 0.1 M Bu_4NPF_6 on a platinum working electrode; sweep rate: v = 0.2 V s^{-1}

ure 4). All derivatives underwent two reversible one-electron oxidations at rather low potentials. In reduction, the first reduction step (one-electron reversible step) was well resolved, whereas the second reduction step occurred close to the electrolyte discharge for the Pd^{II} complexes and could not be observed for the Cu^{II} complexes. The potentials of all accessible electron transfers are collected in Table 2.

Table 2. Electrochemical data for free base **4** and complexes **6**−**11**

Compound[a]	Red. 2	Red. 1	Ox. 1	Ox. 2	HLG[b]	EN[c]
4 (H_2, R = H)	−2.37	−1.82	−0.02	0.37	1.80	−
6 (Cu, R = H)	−[d]	−1.50	−0.22	0.25	1.28	1.9
7 (Cu, R = Ph)	−[d]	−1.42	−0.15	0.31	1.27	1.9
8 (Pd, R = H)	−2.30	−1.70	−0.15	0.32	1.55	2.2
9 (Pd, R = Ph)	−2.30	−1.71	−0.08	0.41	1.63	2.2
10 (Ni, R = H)	−2.35	−1.71	−0.18	0.31	1.53	1.8
11 (Ni, R = Ph)	−2.36	−1.75	−0.13	0.36	1.62	1.8

[a] Measured on a platinum electrode in PhCN solution with 0.1 M nBu_4NPF_6. Values are given in V relative to the Fc^+/Fc couple. [b] HOMO−LUMO gap (= $E_{Ox.\ 1} - E_{Red.\ 1}$). [c] Electronegativity values taken from ref.[19] [d] Not observed.

The redox behaviour of the palladium complexes **8** and **9** is similar to that of the respective nickel complexes **10** and **11**, and all four redox waves were in analogy assigned to ligand-centred electron transfer processes. The phenyl substituents of **9** and **11** shifted the oxidation potentials to more positive values, whereas the first reduction became slightly more negative. Such shifts are not expected for donor substitution. It seems much more likely that the electronic effect of the phenyl moiety is superimposed by a structural one. X-ray crystallographic work on *meso*-aryl-substituted nickel(II) complexes shows a reduced bite angle of both dipyrrin units due to the higher congested periphery. This structural difference may be responsible for the effect in **9** and **11**.

For the two one-electron oxidation steps of the copper(II) derivatives **6** and **7**, the above discussion still holds true, and both electron transfers are therefore assigned to ligand-centred processes. The interpretation of the reduction behaviour of **6** and **7**, however, is more difficult. A comparison of the obtained data clearly shows, that the potentials of the first reduction step of the copper complexes are at less negative values than those of the nickel and palladium species. However, even if the first reduction is facilitated, the second reduction step is not observed in the available potential range. This peculiar behaviour is again probably due to geometric reasons, since Cu^{II} can more easily adopt and support the non-planar coordination geometry imposed by the ligand, in contrast to Ni^{II} or Pd^{II}, which prefer square-planar environments. The easier reduction of the copper complexes **6** and **7** is most likely a consequence of strain release, and does not seem to result from a possible reduction of the metal ion. Spectroelectrochemical studies discussed below further strengthen this conclusion.

Since structural effects have a strong impact on the redox characteristics of 2,2′-bidipyrrinato complexes, it is obvious that metal-dependent trends known from metalloporphyrin electrochemistry cannot be expected to hold true for the open-chain analogues. Correlations like the potential evolution vs. metal electronegativity,[19] or the energy of the HOMO−LUMO gap vs. the potential difference between the first oxidation and first reduction potential,[20−22] which are typical for metalloporphyrins and other rigid porphyrinoid complexes, strongly depend on structural factors and are therefore not valid for complexes **6**−**11** (Table 2).

Spectroelectrochemical Investigations

Spectroelectrochemical studies were carried out on the complexes **7**, **9**, and **11**, as well as on the free base **4**. The time-resolved UV/Vis spectra recorded during spectroelectrochemical studies are given in Figures 5 and 6, and the UV/Vis data for all species are summarized in Table 3. It has to be mentioned that in all cases after the first reduction, as well as after the first oxidation, the initial spectrum could be recovered quantitatively. After the second oxidation step, the reduction to regenerate the radical cation was not quantitative, and only 60 to 75% of the radical cation could be recovered for the studied complexes. The second oxidation step of the free base was irreversible on the time scale of spectroelectrochemistry.

Table 3. UV/Vis data from spectroelectrochemical studies on **4**, **7**, **9**, and **11**

Compound	
4 (H_2)	336, 600, 628 sh
7 (Cu)	310, 422, 495, 842
9 (Pd)	347, 436, 528, 843
11 (Ni)	310, 356, 436, 545, 630, 894
$\mathbf{4}^{+\cdot}$	434, 629, 718 sh, 972
$\mathbf{7}^{+\cdot}$	308, 348, 464, 820
$\mathbf{9}^{+\cdot}$	342, 418, 482, 830
$\mathbf{11}^{+\cdot}$	356, 439, 567, 843, 887 sh
$\mathbf{4}^{2+}$	447, 599
$\mathbf{7}^{2+}$	403, 689, 788
$\mathbf{9}^{2+}$	344, 861
$\mathbf{11}^{2+}$	348, 516, 609
$\mathbf{4}^{-\cdot}$	553, 637, 696, 772
$\mathbf{7}^{-\cdot}$	319, 448, 524 sh, 556, 706, 973
$\mathbf{9}^{-\cdot}$	332, 478, 502, 821 sh, 899
$\mathbf{11}^{-\cdot}$	339, 487, 635, 713, 932

Since the UV/Vis spectra and redox potentials of free base 2,2′-bidipyrrins **4** differ significantly from those of the respective metal complexes, the spectroelectrochemical data of **4** are only of limited value as a reference. One important trend, however, is easily seen in Figure 5: the one-electron oxidised and reduced ligand species are both characterized by new and quite narrow bands in the optical spectra. For the two-electron oxidised species, on the other hand, only broad absorptions were detected.

The UV/Vis spectra of the metal complexes **7**, **9**, and **11** also changed dramatically upon reduction or oxidation, and the different electrogenerated species show the same trends within the series (Figure 6). As for the free base ligand **4**, rather sharp absorptions were found after one-electron oxidation and reduction, and only broad bands were observed for the two-electron oxidised members. These similarities are best explained by the assumption of ligand-centred redox reactions throughout the series. The reduction of the copper(II) complex **7**, however, produced an extra distinct band at 706 nm, which was missing in the spectra of the other chelates. This band inhibits a simple comparative analysis of the data. We believe that a ligand-centred one-electron step occurs also in the case of Cu^{II} rather than a reduction to Cu^{I}, since upon reduction of **7** the other bands evolve in a similar fashion to those of **9** and **11**, and because these bands obviously belong to transitions of the tetrapyrrole ligand π system.

In order to identify the site of the one-electron reduction of the copper complexes **6** and **7**, further electrochemical experiments were performed. Upon changing the solvent from benzonitrile to dichloromethane very similar results were obtained for **6**, and all redox processes remained perfectly reversible. On the time scale of spectroelectrochemistry (i.e. ca. 20 min), however, the one-electron reduced $\mathbf{6}^{-\cdot}$ reacted irreversibly with the solvent, leading to a different UV/Vis spectrum with respect to the one obtained in benzonitrile. In fact, by cyclic voltammetry, in the presence of a large excess of the better electrophile *n*-propyl bromide (1000 equiv.), the first reduction step of **6** remained reversible at sweep rates higher than 1 V/s and became irreversible, and dielectronic at sweep rates lower than 0.1 V/s. Such a behaviour is characteristic for an ECE mechanism (*E*lectrochemical *C*hemical *E*lectrochemical) in the presence of a sufficient amount of an electrophile. The generated anion (electrochemical step) is reacting with *n*-propyl bromide (chemical step) to generate a new species, which is again one-electron reduced in another electrochemical step. Since four-coordinate Cu^{I} is a poor nucleophile, the outcome of this experiment strongly supports the hypothesis of a ligand radical anion character of $\mathbf{6}^{-\cdot}$. Similar experiments have been performed before on metalloporphyrins.[23]

In addition to the electrochemical investigations, chemical reduction of **6** using NaHg was attempted and was monitored by proton NMR and EPR spectroscopy. In THF (or [D_8]THF) the one-electron reduction of **6** proceeded slowly at room temperature and could be conveniently followed through the colour change from orange-red to red-violet. In NMR spectroscopy, the reduction of **6** was accompanied by an additional line broadening and the entire loss of any residual signal fine structure, which was detected even in the spectrum of **6** for the most distant CH_3 groups only.[24] This observation is again indicative of the presence of a π-radical on $\mathbf{6}^{-\cdot}$ that has no magnetic coupling with the

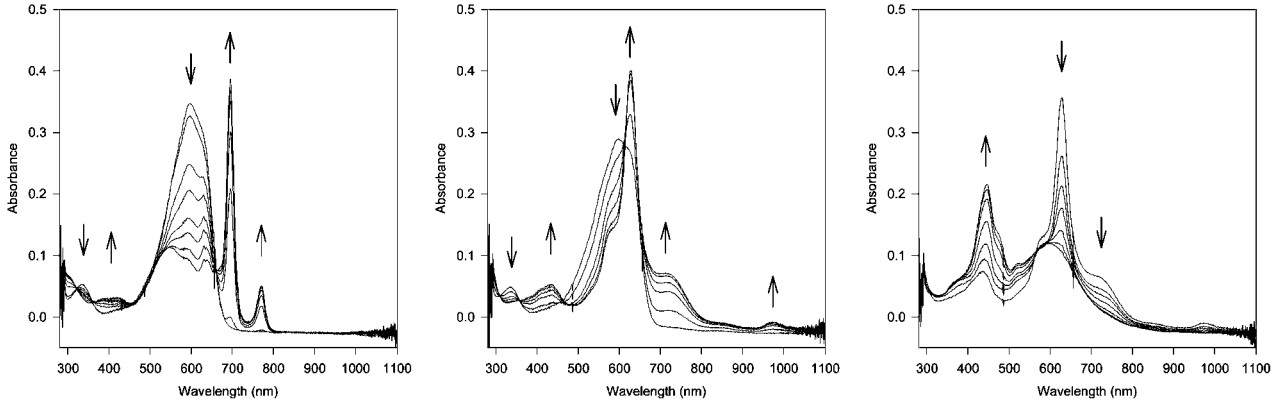

Figure 5. Time-resolved UV/Vis spectroelectrochemical measurements of free base 2,2′-bidipyrrin **4** in PhCN with 0.1 M Bu_4NPF_6; first column: Red. 1, second column Ox. 1, third column Ox. 2

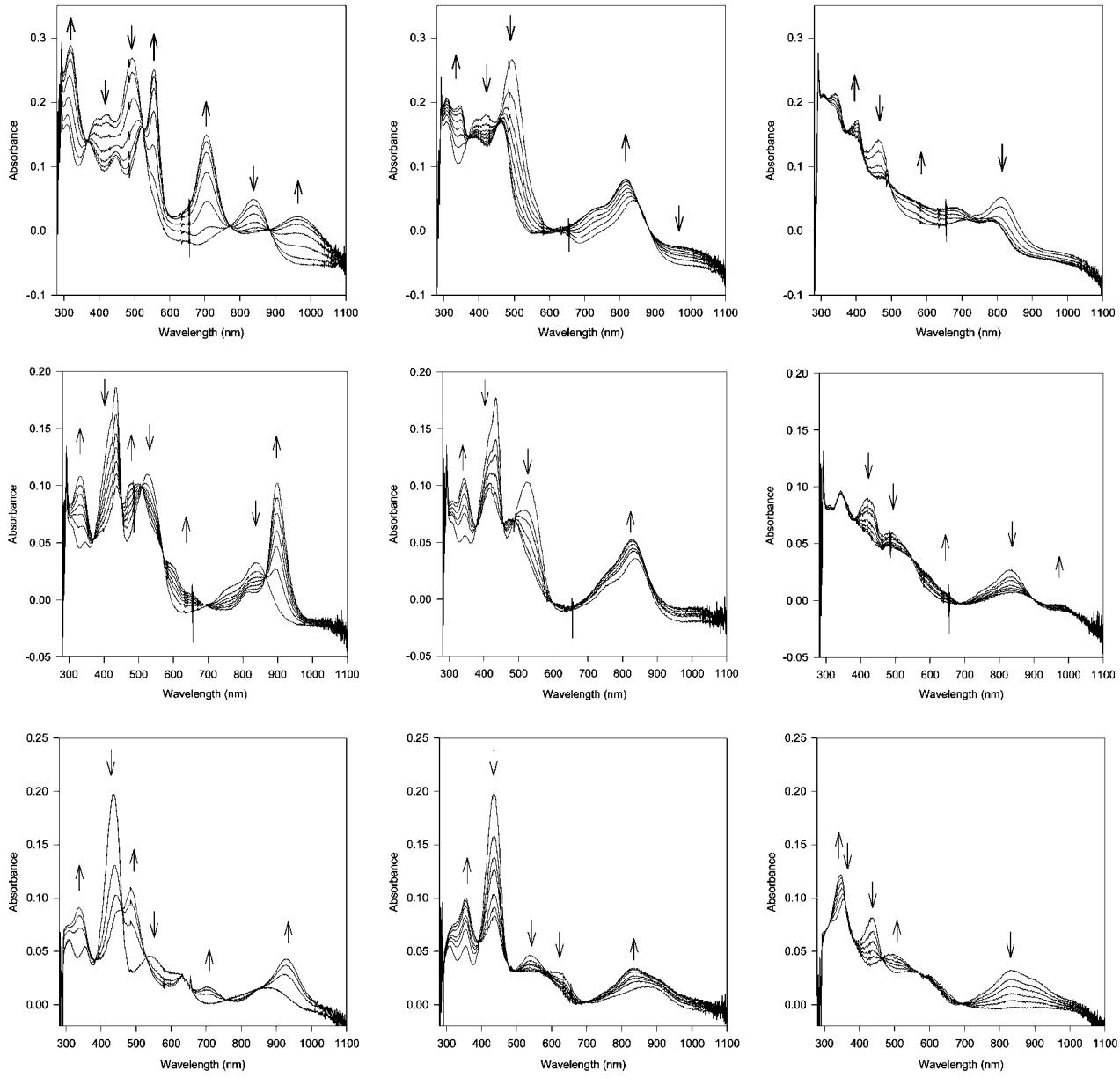

Figure 6. Time-resolved UV/Vis spectroelectrochemical measurements of 2,2′-bidipyrrinato complexes **7** (first row), **9** (second row), and **11** (third row) in PhCN with 0.1 M Bu_4NPF_6; first column: Red. 1, second column Ox. 1, third column Ox. 2

d-electron of the metal centre.[25] The EPR spectroscopic investigation of the reduction of **6** (X-band at 9.76 GHz, room temperature) gave the spectra depicted in Figure 7. Complex **6** shows an EPR spectrum similar to that of a related (porphyrinato)copper(II) complex,[26] with a g_0 value of 2.092 and a Cu hyperfine splitting of 82.6 G. The expected splitting of the signals by the nitrogen donors was not resolved. After chemical reduction, the signal for the Cu^{II} ion was still present and found shifted to $g_0 = 2.073$ with an enlarged splitting of 104.6 G. For $\mathbf{6}^{-\cdot}$ the hyperfine splitting by the nitrogen atoms is well resolved (line distance 16.6 G), and the theoretically possible nine lines (assuming, that all four nitrogen atoms are equivalent) can be found in two overlapping sets. The signal for the π-radical, however, is broad and heavily obscured by the signals of the single 3d-electron. The *g* value for this electron of ca. 2.00 is close to that of a free electron, which is expected for a porphyrinoid π-radical.[27]

Conclusion

(2,2′-Bidipyrrinato)copper(II) and -palladium(II) complexes belong to the same structural type as the respective nickel(II) complexes. The porphyrinoid M_1L_1 coordination mode generally leads to a helical distortion of the ligand scaffold, which is stable to helix inversion in all cases studied. The open-chain tetrapyrrolic ligand, however, is sufficiently flexible to accommodate different bonding situ-

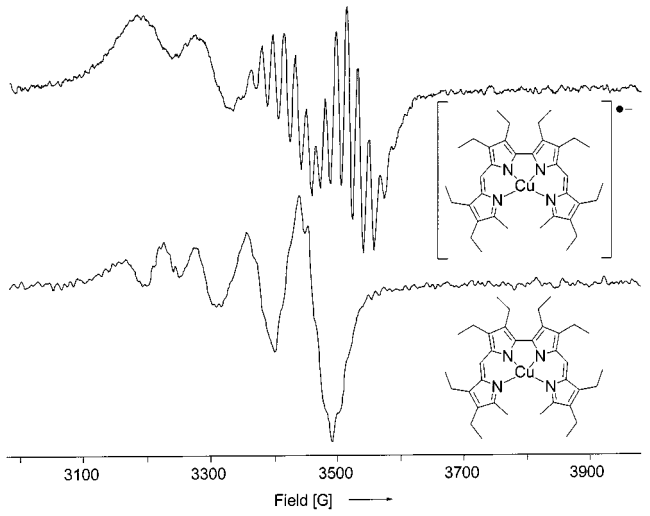

Figure 7. Solution EPR spectra of **6** and $\mathbf{6}^{-\cdot}$ in THF at X-band (9.76 GHz)

ations for metal ions with square-planar or distorted tetrahedral coordination preferences. Electrochemically, 2,2′-bidipyrrinato complexes are enormously robust, so that even spectroelectrochemical analyses of electrogenerated oxidised and reduced species could be performed. The electrochemical behaviour of these complexes is strongly dependent on structural parameters, which almost always superimpose the electronic effects typical for the electrochemistry of metalloporphyrins.

Experimental Section

General: All reagents and solvents were purchased from commercial sources and used as received. NMR spectra were obtained in $CDCl_3$ solution with a Bruker AC 200 spectrometer. Chemical shifts (δ) are given in ppm relative to residual protio solvent resonances (^1H spectra) or to chloroform (^{13}C). Mass spectra (EI, 70 eV or FAB) were recorded with a Finnigan 90 MAT instrument; *m*/*z* values are given for the most abundant isotopes only. Melting points were measured by DTA with a Thermoanalyzer DuPont 9000. Elemental analyses (C, H, N) were effected at the microanalytical laboratory of the Institut für Anorganische Chemie, Universität Würzburg. Solution EPR spectra were measured in THF at ambient temperature with a Bruker ESP 300 spectrometer at X-band (9.76 GHz). Chiral HPLC was performed with a Pirkle-type column (D-phenylglycine on spherical silica gel; 25 cm × 4.6 mm, 5 μ particle size), using a Latek P402 chromatographic system and 2% acetone in *n*-hexane as the eluent. The fractions were detected by single point UV absorption at 400 nm. Electrochemical studies were carried out in benzonitrile containing nBu$_4$NPF$_6$ as supporting electrolyte (0.1 M). Benzonitrile (Aldrich) was dried with anhydrous $CaCl_2$ for 2 d, and further distilled from P_2O_5 under a reduced pressure of argon. nBu$_4$NPF$_6$ (Fluka, electrochemical grade) was dried under vacuum at 65 °C. Before use, the 0.1 M solution of nBu$_4$NPF$_6$ in benzonitrile was purified in a glove box on activated neutral alumina (Merck). The measurements were carried out in the glove box using a classical three-electrode cell. The working electrode was a platinum disk (2 mm in diameter), the pseudo reference electrode and the counter electrode being platinum wires. All potentials are given against the ferrocene/ferrocenium couple used as internal standard. The cell was connected to an EG&G PAR potentiostat (Model 273) interfaced with a computer (type PC). The studies were carried out by cyclic voltammetry (CV), at sweep rates ranging from 0.02 to 5 V/s, and by steady state voltammetry (SSV), on a platinum rotating disk electrode. Spectroelectrochemical measurements were performed in an air-tight closed quartz cell (1 mm) through an optically transparent thin-layer electrode (OTTLE) made of a Pt mini-grid (1000 mesh). The auxiliary electrode and the pseudo-reference electrode were Pt wires placed in separate compartments. The cell was filled with the electrolyte and the species to be studied, and hermetically closed in the glove-box. The cell was then removed from the glove-box and placed in a Hewlett Packard diode-array UV/Vis spectrometer model 8453. The OTTLE cell was connected to a Bruker potentiostat (model EI30M) for control and measurement of the electrochemical parameters.

Preparation of Complexes

(2,2′-Bisdipyrrinato)copper Complexes 6 and 7. − General Procedure: 2,2′-Bidipyrrin **4** or **5** (0.1 mmol) in 30 mL of dichloromethane was treated with a solution of copper(II) acetate hydrate (399 mg, 2 mmol) in 30 mL of methanol, and the resulting solution was stirred for 30 min (colour change from deep blue to brownish-orange). The reaction mixture was extracted four times with 100 mL of water, dried with sodium sulfate, and the solvent removed in vacuo. Recrystallization from dichloromethane/methanol yielded the title compounds as dark green, shiny crystals.

(3,3′,4,4′,8,8′,9,9′-Octaethyl-10,10′-dimethyl-2,2′-bidipyrrinato)copper (6): Yield 48.6 mg (81%); m.p. 192 °C (decomp.). MS (70 eV, EI): m/z = 599 [M^+]. $C_{36}H_{48}CuN_4$ (600.34): C 72.02, H 8.06, N 9.33; found C 71.88, H 8.04, N 9.20.

Crystallographic Data for 6: $C_{36}H_{48}CuN_4$, green plates obtained by slow concentration of a CH_2Cl_2/*n*-hexane solution, crystal size: 0.40 × 0.40 × 0.20 mm, monoclinic, space group $P2_1/c$, a = 12.580(3), b = 20.030(4), c = 13.316(3) Å, β = 108.721(4)°, V = 3177.8(11) Å^3, $\rho_{calcd.}$ = 1.255 g cm^{-3}, Z = 4, $2\theta_{max}$ = 50°, Mo-K_α radiation, λ = 0.71073 Å, scan mode: ω-scans, T = 173(2) K, 44776 measured, 5576 independent reflections, 5019 reflections observed for $I > 2\sigma(I)$, μ = 0.718 mm^{-1}, solved by Patterson method (SHELXS-97: G. Sheldrick, University of Göttingen), refined with full-matrix least squares on F^2 (SHELXL-97: G. Sheldrick, University of Göttingen), 380 parameters, H atoms refined with isotropic temperature factors. R = 0.0379, wR = 0.0964, residual electron density ρ = 0.438/−0.207 e Å^{-3}. CCDC-170387 (**6**) contains the supplementary crystallographic data for this paper. These data can be obtained free of charge at www.ccdc.cam.ac.uk/conts/retrieving.html or from the Cambridge Crystallographic Data Centre, 12, Union Road, Cambridge CB2 1EZ, UK [Fax: (internat.) + 44-1223/336-033; E-mail: deposit@ccdc.cam.ac.uk].

(3,3′,4,4′,8,8′,9,9′-Octaethyl-10,10′-dimethyl-6,6′-diphenyl-2,2′-bidipyrrinato)copper (7): Yield 58.7 mg (78%); m.p. 249 °C (decomp.). MS (70 eV, EI): m/z = 751 [M^+]. $C_{48}H_{56}CuN_4$ (752.54): C 76.61, H 7.50, N 7.45; found C 76.28, H 7.29, N 7.19.

(2,2′-Bisdipyrrinato)palladium Complexes 8 and 9. − General Procedure: 2,2′-Bidipyrrin **4** or **5** (0.1 mmol) in 30 mL of dichloromethane was treated with a solution of palladium(II) acetate (80 mg, 0.4 mmol) in 30 mL of methanol, and the resulting solution was stirred for 30 min (colour change from deep blue to deep red). The reaction mixture was extracted with 100 mL of water, dried with sodium sulfate, and the solvent removed in vacuo. Chromato-

graphic filtration with dichloromethane on silica gave the product as a red, major band. Recrystallization from dichloromethane/methanol yielded the title compounds as green, shiny crystals.

(3,3′,4,4′,8,8′,9,9′-Octaethyl-10,10′-dimethyl-2,2′-bidipyrrinato)-palladium (8): Yield 59.2 mg (92%); m.p. 212 °C. ^{1}H NMR (200 MHz, $CDCl_3$): δ = 0.90 (t, 6 H, ^3J = 7.5 Hz, 2×CH_3), 1.03 (t, 6 H, ^3J = 7.5 Hz, 2×CH_3), 1.06 (t, 6 H, ^3J = 7.5 Hz, 2×CH_3), 1.08 (t, 6 H, ^3J = 7.5 Hz, 2×CH_3), 2.11 (q, ^3J = 7.5 Hz, 4 H, 2×CH_2CH$_3$), 2.31−2.39 (m, 12 H, 6×CH_2CH$_3$), 2.59 (s, 6 H, terminal CH_3), 6.18 (s, 2 H, H_{meso}). ^{13}C NMR (50.3 MHz, $CDCl_3$): δ = 14.3, 16.7, 16.8, 17.2, 17.3, 17.6, 17.7, 18.1, 18.4, 120.1, 128.1, 130.9, 131.6, 136.1, 138.5, 148.0, 150.1, 165.8. MS (70 eV, EI): *m*/*z* = 642 [M$^+$]. $C_{36}H_{48}N_4Pd$ (643.22): C 67.22, H 7.52, N 8.71; found C 67.21, H 7.50, N 8.51.

Crystallographic Data for 8: $C_{36}H_{48}N_4Pd$, green plates obtained by slow concentration of a CH_2Cl_2/*n*-hexane solution, crystal size: 0.40 × 0.40 × 0.24 mm, monoclinic, space group $P2_1/c$, a = 12.6786(19), b = 19.954(3), c = 13.3074(19) Å, β = 108.546(3)°, V = 3191.8(8) Å^3, $\rho_{calcd.}$ = 1.338 g cm^{-3}, Z = 4, $2\theta_{max}$ = 50°, Mo-K_α radiation, λ = 0.71073 Å, scan mode: ω-scans, T = 173(2) K, 45066 measured, 5603 independent reflections, 5351 reflections observed for $I > 2\sigma(I)$, μ = 0.612 mm^{-1}, solved by direct methods (SHELXS-97: G. Sheldrick, University of Göttingen), refined with full-matrix least squares on F^2 (SHELXL-97: G. Sheldrick, University of Göttingen), 380 parameters, H atoms refined with isotropic temperature factors. R = 0.0456, wR = 0.1012, residual electron density ρ = 0.872/−0.900 e Å^{-3}. CCDC-170388 (**8**) contains the supplementary crystallographic data for this paper. These data can be obtained free of charge at www.ccdc.cam.ac.uk/conts/retrieving.html or from the Cambridge Crystallographic Data Centre, 12, Union Road, Cambridge CB2 1EZ, UK [Fax: (internat.) + 44-1223/336-033; E-mail: deposit@ccdc.cam.ac.uk].

(3,3′,4,4′,8,8′,9,9′-Octaethyl-10,10′-dimethyl-6,6′-diphenyl-2,2′-bidipyrrinato)palladium (9): Yield 69.2 mg (87%); m.p. 267 °C. ^{1}H NMR (200 MHz, $CDCl_3$): δ = 0.55 (t, 6 H, ^3J = 7.5 Hz, 2×CH_3), 0.58 (t, 6 H, ^3J = 7.5 Hz, 2×CH_3), 0.83 (t, 6 H, ^3J = 7.5 Hz, 2×CH_3), 0.96 (t, 6 H, ^3J = 7.5 Hz, 2×CH_3), 1.04−1.36 (m, 8 H, 4×CH_2CH$_3$), 2.01, 2.26 (2×br.s, 14 H, terminal CH_3 and 4×CH_2CH$_3$), 7.19−7.61 (m, 10 H, H_{phenyl}). ^{13}C NMR (50.3 MHz, $CDCl_3$): δ = 13.9, 16.2, 17.0, 17.1, 17.6, 17.8, 18.0, 18.5, 19.5, 127.4, 127.5, 128.1, 129.7, 130.1, 132.1, 137.9, 141.1, 142.0, 149.7, 151.3, 151.9, 165.6. MS (70 eV, EI): *m*/*z* = 794 [M$^+$]. $C_{48}H_{56}N_4Pd$ (795.41): C 72.48, H 7.10, N 7.04; found C 72.33, H 7.18, N 6.96.

Acknowledgments

This work was funded by the Deutsche Forschungsgemeinschaft (DFG; Emmy−Noether−Programm), the Fonds der Chemischen Industrie (FCI) and by the Centre National de la Recherche Scientifique (C. N. R. S). The assistance of Stefan Marquardt and Sascha Stellwag with the EPR experiments is gratefully acknowledged. We thank Professor H. Werner (Würzburg) for his continued support.

[1] M. Bröring, *Synthesis* **2000**, 1291−1294.
[2] M. Bröring, D. Griebel, C. Hell, A. Pfister, *J. Porph. Phthal.* **2001**, *5*, 708−714.
[3] A. W. Johnson, R. Price, *J. Chem. Soc.* **1960**, 1649−1653.
[4] M. Bröring, C. D. Brandt, J. Lex, H.-U. Humpf, J. Bley-Escrich, J.-P. Gisselbrecht, *Eur. J. Inorg. Chem.* **2001**, 2549−2556.
[5] Y. Zhang, A. Thompson, S. J. Rettig, D. Dolphin, *J. Am. Chem. Soc.* **1998**, *120*, 13537−13538; for related structures, see also: R. G. Khoury, L. Jaquinod, K. M. Smith, *Tetrahedron* **1998**, *54*, 2339−2346.
[6] M. Bröring, A. Pfister, K. Ilg, *Chem. Commun.* **2000**, 1407−1408.
[7] D. Dolphin, R. L. N. Harris, J. L. Huppatz, A. W. Johnson, I. T. Kay, J. Leng, *J. Chem. Soc. C* **1966**, 98−106.
[8] P. A. Lord, M. M. Olmstead, A. L. Balch, *Inorg. Chem.* **2000**, *39*, 1128−1134.
[9] R. G. Khoury, M. O. Senge, J. E. Colchester, K. M. Smith, *J. Chem. Soc., Dalton Trans.* **1996**, 3937−3950.
[10] A. J. Golder, K. B. Nolan, D. C. Povey, L. R. Milgrom, *Acta Crystallogr., Sect. C* **1988**, *44*, 1916−1917.
[11] M. Currie, J. D. Dunitz, *Helv. Chim. Acta* **1971**, *54*, 98−112.
[12] E. B. Fleischer, C. K. Miller, L. E. Webb, *J. Am. Chem. Soc.* **1964**, *86*, 2342−2347.
[13] R. Koerner, M. M. Olmstead, A. Ozarowski, S. L. Phillips, P. M. Van Calcar, K. Winkler, A. L. Balch, *J. Am. Chem. Soc.* **1998**, *120*, 1274−1284.
[14] A. L. Balch, M. Mazzanti, B. C. Noll, M. M. Olmstead, *J. Am. Chem. Soc.* **1993**, *115*, 12206−12207.
[15] L. D. Sparks, C. J. Medforth, M.-S. Park, J. R. Chamberlain, M. R. Ondrias, M. O. Senge, K. M. Smith, J. A. Shelnutt, *J. Am. Chem. Soc.* **1993**, *115*, 581−592.
[16] M. O. Senge, C. J. Medforth, L. D. Sparks, J. A. Shelnutt, K. M. Smith, *Inorg. Chem.* **1993**, *32*, 1716.
[17] G. Peychal-Heiling, G. S. Wilson, *Anal. Chem.* **1971**, *43*, 550−556.
[18] D. Chang, T. Malinski, A. Ulman, K. M. Kadish, *Inorg. Chem.* **1984**, *23*, 817−824.
[19] J.-H. Fuhrhop, K. M. Kadish, D. G. Davis, *J. Am. Chem. Soc.* **1973**, *95*, 5140−5147.
[20] K. M. Barkigia, M. W. Renner, L. R. Furenlid, C. J. Medforth, K. M. Smith, J. Fajer, *J. Am. Chem. Soc.* **1993**, *113*, 3627−3635.
[21] C. Bernard, J.-P. Gisselbrecht, M. Gross, E. Vogel, M. Lausmann, *Inorg. Chem.* **1994**, *33*, 2393−2401.
[22] J. Wytko, V. Berl, M. McLaughlin, R. R. Tykwinski, M. Schreiber, F. Diederich, C. Boudon, J.-P. Gisselbrecht, M. Gross, *Helv. Chim. Acta* **1998**, *81*, 1964−1977.
[23] Y. J. Deng, X. H. Mu, P. Tagliatesta, K. M. Kadish, *Inorg. Chem.* **1991**, *30*, 1957−1960.
[24] G. M. Godziela, H. M. Goff, *J. Am. Chem. Soc.* **1986**, *108*, 2237−2243.
[25] For a discussion, see: A. L. Balch, *Coord. Chem. Rev.* **2000**, *200−202*, 349−377; L. Latos-Grazynski, J. Wojaczynski, R. Koerner, J. J. Johnson, A. L. Balch, *Inorg. Chem.* **2001**, *40*, 4971−4977.
[26] E. M. Roberts, W. S. Koski, *J. Am. Chem. Soc.* **1960**, *82*, 3006−3010.
[27] J. Seth, D. F. Bocian, *J. Am. Chem. Soc.* **1994**, *116*, 143−153.

Received September 12, 2001
[I01355]

Chelate Complexes of Functionalized Cycloheptatrienyl Ligands: 17- and 18-Electron Molybdenum Complexes with Linked Cycloheptatrienyl−Phosphane Ligands and Their Use in Transition Metal Catalysis

Matthias Tamm,*[a] Kim Baum,[a] Thomas Lügger,[a] Roland Fröhlich,[b] and Klaus Bergander[b]

Keywords: Cycloheptatrienyl complexes / Molybdenum / Ligand functionalization / Ring-opening polymerization / Metathesis

The synthesis of *P*-functionalized molybdenum chelate complexes incorporating the linked cycloheptatrienyl–phosphane ligand [2-(diphenylphosphanyl)phenyl]cycloheptatrienyl, *o*-$Ph_2P–C_6H_4–C_7H_6$, is described. The air-stable ligand precursor [2-(cyclohepta-2,4,6-trienyl)phenyl]diphenylphosphane (**2**) can be obtained in large quantities by addition of lithiated 2-$BrC_6H_4PPh_2$ (**1**) to the tropylium cation $C_7H_7^+$. Hydride abstraction employing the trityl cation, Ph_3C^+, results in the formation of the tricyclic phosphonium salt **3**. The *P*-functionalized cycloheptatriene **2** acts as an eight-electron ligand on reaction with $Mo(CO)_6$ to afford the cycloheptatriene–phosphane complex [(*o*-$Ph_2PC_6H_4$-η^6-C_7H_7)$Mo(CO)_2$(*P–Mo*)] (**4**) as a single, chiral regioisomer, which undergoes clean hydride abstraction on treatment with $(Ph_3C)BF_4$. The resulting cationic cycloheptatrienyl–phosphane complex **5** reacts with sodium bromide to yield the uncharged "chiral-at-metal" complex [(*o*-$Ph_2PC_6H_4$-η^7-C_7H_6)Mo(CO)Br(*P–Mo*)] (**6**). This 18-electron complex can be oxidized with 0.5 equiv. of Br_2 to give the paramagnetic dibromo complex **7**, which is a versatile starting material for the preparation of the 17-electron mono- and dialkyl complexes [(*o*-$Ph_2PC_6H_4$-η^7-C_7H_6)$Mo(CH_2SiMe_3)$X(*P–Mo*)] (X = Br, **8**; X = CH_2SiMe_3, **9**). In combination with Me_3SiCH_2MgCl, complexes **7** and **9** prove to be active catalysts for the ring-opening metathesis polymerization of norbornene. In addition, the X-ray crystal structures of **2**, **4**, **5**·CH_2Cl_2, **7**·$CHCl_3$, **8**, and **9**·C_6H_{14} are reported.

Introduction

η-Cyclopentadienyl complexes, (η-C_5R_5)M, as well as η-arene complexes, (η-C_6R_6)M, are among the most important classes of compounds in organotransition metal chemistry.[1] In particular, the widespread use of cyclopentadienes as organometallic ligands is due to the large number of ring-substituted derivatives, which have been synthesized since the serendipitous synthesis and discovery of ferrocene. Successive replacement of hydrogen atoms by alkyl or aryl substituents alters the steric and electronic properties of the Cp ring and gives rise to increased steric bulk, solubility and stability of the resulting complexes.[2] Numerous routes to ring-substituted Cp derivatives are known to date, and stable cyclopentadienyl complexes of almost any element have been synthesized. It has recently been estimated that about 80% of all organometallic compounds of the transition metals are cyclopentadienyl complexes.[2a] Consequently, cyclopentadienyl complexes are now ubiquitous and indispensable in research areas such as homogeneous catalysis,[3] organic synthesis[4] and materials science.[5] In contrast, η-cycloheptatrienyl transition metal complexes, (η-C_7R_7)M, have been much less thoroughly studied, and with a few exceptions, the use of cycloheptatrienyl ligands had been confined to the parent C_7H_7 system.[6] Only recently have we been able to report on the syntheses and properties of the first heptamethylcycloheptatrienyl (CHT*) complexes[7] and of complexes derived from sterically demanding tropylium salts of the type (1,3,5-$C_7H_4R_3$)BF_4 (R = *tert*-butyl, $SiMe_3$).[8]

Another concept, which has been extremely successful, in particular in cyclopentadienyl chemistry, is ligand functionalization, whereby an additional coordinating site is linked to the periphery of the five-membered ring via a suitable bridging moiety. This prospering area has produced a large number of novel cyclopentadienyl ligands bearing pendant *N*-,[9,10] *O*-,[11] *P*-, *As*-, and *S*-donor groups.[12] If properly designed, these ligands can coordinate to a transition metal center in a chelating η^5:η^1-fashion, and several of these complexes have played a key role in homogeneous catalysis as so-called constraint-geometry catalyst sys-

[a] Anorganisch-Chemisches Institut, Westfälische Wilhelms-Universität,
Wilhelm-Klemm-Straße 8, 48149 Münster, Germany
Fax: (internat.) + 49-(0)251/833-3108
E-mail: mtamm@uni-muenster.de
[b] Organisch-Chemisches Institut, Westfälische Wilhelms-Universität,
Corrensstraße 40, 48149 Münster, Germany

 © WILEY-VCH Verlag GmbH, 69451 Weinheim, Germany, 2002 1434−1948/02/0404−0918 $ 17.50+.50/0 *Eur. J. Inorg. Chem.* **2002**, 918−928

tems.[3] In cycloheptatrienyl transition metal chemistry on the other hand, ligand functionalization is an almost unknown concept, and we have recently started to apply this concept to the preparation of cycloheptatrienyl complexes bearing pendant phenolate,[13] amine, and phosphane donor groups (Figure 1). The reasons for our interest in the development of such ligand systems are twofold. Firstly, donor-functionalization can in general lead to the formation of chelate complexes of significantly enhanced stability, which can allow the preparation and isolation of complexes of previously unknown structural types and reactivities. For instance, since the coordination of the cycloheptatrienyl ring to a transition metal center is often much more difficult than the introduction of a cyclopentadienyl group, the donor group can serve as a *Trojan horse*, which binds to a metal ion first followed by the formation of the metal−carbon bonds. Secondly, some of the donor groups might only coordinate in a labile fashion or could be converted into hemilabile groups, which offers the possibility of reversibly providing free coordination sites for other molecules or substrates.

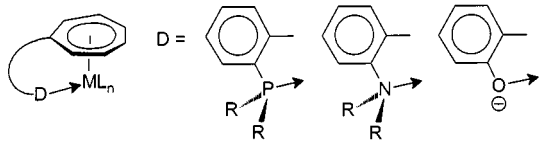

Figure 1. Cycloheptatrienyl complexes bearing pendant *P*-, *N*-, and *O*-donors

To the best of our knowledge, no complexes with donor-functionalized cycloheptatrienyl ligands coordinating in a chelating η^7:η^1-fashion have been reported prior to our work,[13] whereas a few examples are known, in which the functional group is directly attached to the seven-membered ring allowing the cycloheptatrienyl ligand to only bridge two different metal centers.[14−16] For instance, lithiation of [(η-C_7H_7)Ti(η-C_5H_5)] with *n*BuLi occurs preferentially at the seven-membered ring,[14] and the consecutive reaction with chlorodiphenylphosphane allows the selective functionalization of the cycloheptatrienyl ring to yield [(η^7-$C_7H_6PPh_2$)Ti(η-C_5H_5)], which has been used as a monodentate phosphane ligand forming bimetallic complexes.[15] Dimetalation of [(η-C_7H_7)Ti(η-C_5H_5)] can also be achieved, and the reaction with $ClPR_2$ (R = Me, Ph) produces [(η^7-$C_7H_6PR_2$)Ti(η^5-$C_5H_4PR_2$)], which can react with various carbonylmetal complexes to produce a series of complexes with the bifunctionalized sandwich unit acting as a chelating or bridging diphosphane ligand.[16] In this respect, bimetallic sesquifulvalene derivatives can also be regarded as complexes containing cyclopentadienyl-functionalized cycloheptatrienyl ligands, and various complexes have been reported, in which the five- and seven-membered rings are coordinated in a bridging μ-η^7:η^5-mode.[17,18]

With this contribution, we introduce, for the first time, phosphorus-functionalized cycloheptatrienyl ligands, which are capable of binding the metal center in a chelating η^7:η^1-fashion (Figure 1), and we wish to report on the syntheses of a series of molybdenum complexes of the type [(*o*-$Ph_2PC_6H_4$-η^7-C_7H_6)$MoLL'(P-Mo)$] containing a cycloheptatrienyl ligand with a linked 2-(diphenylphosphanyl)-phenyl substituent. The *ortho*-phenylene moiety had been chosen as the bridging unit between the seven-membered ring and the *P*-donor group, as it will lead to the formation of complexes with a very rigid, C_s-symmetric ligand backbone and will additionally allow the alteration of their steric and electronic properties by modification of the aryl fragment. Furthermore, the synthesis and use of 17-electron complexes of the type [(*o*-$Ph_2PC_6H_4$-η^7-C_7H_6)-$MoX_2(P-Mo)$] (X = Br, CH_2SiMe_3) for the ring-opening metathesis polymerization of norbornene will be described, which is among the first reports on the application of cycloheptatrienyl complexes to homogeneous transition metal catalysis.

Results and Discussion

Ligand Synthesis

Although a large number of phosphorus-functionalized cyclopentadienyl systems are known,[12] we are only aware of a few related cyclopentadienyl complexes, in which the phosphane group is attached to the five-membered ring via a bridging *ortho*-phenylene moiety.[19−21] For instance, Trost and co-workers have obtained the ligand precursor [2-(diphenylphosphanyl)phenyl]cyclopentadiene by the reaction of (2-bromophenyl)diphenylphosphane (**1**) with 1 equiv. of *n*-butyllithium followed by addition of 2-cyclopentenone.[19] Similarly, one should be able to obtain the related cycloheptatriene−phosphane ligand precursor **2** (Scheme 1) by addition of 2-(diphenylphosphanyl)phenyllithium[22] to the tropylium cation $C_7H_7^+$.[23] In fact, careful monolithiation of 1,2-dibromobenzene and reaction with $ClPPh_2$ led to 2-$BrC_6H_4PPh_2$ (**1**),[22,24] which was successively treated with *n*BuLi and (C_7H_7)BF_4 to afford the air-stable ligand precursor [2-(cyclohepta-2,4,6-trienyl)phenyl]diphenylphosphane (**2**) in large quantities.

The ^{31}P NMR spectrum of **2** exhibits one single resonance at δ = −15.9, which is about 10 ppm up-field from the resonance observed for triphenylphosphane under identical conditions.[25] The molecular structure of **2** could be established by X-ray diffraction (Figure 2, top) confirming the *ortho* linkage between the phosphorus atom and the cycloheptatriene moiety, which bears the PPh_2 residue in the allylic 1-position. As anticipated,[26] the seven-membered ring adopts a boat conformation, and all bond lengths and angles fall in the expected ranges.

As we have recently developed a method for the quantitative complexation of tropylium salts by an arene exchange reaction employing [(η-*p*-xylene)$Mo(CO)_3$],[8,18a] we sought for the synthesis of a phosphanyl-functionalized tropylium salt by hydride abstraction using triphenylcarbenium tetrafluoroborate, (Ph_3C)BF_4. The direct reaction of **2** with (Ph_3C)BF_4, however, did not result in a clean reaction, presumably due to steric hindrance at the allylic position of the seven-membered ring created by the 2-(diphenylphos-

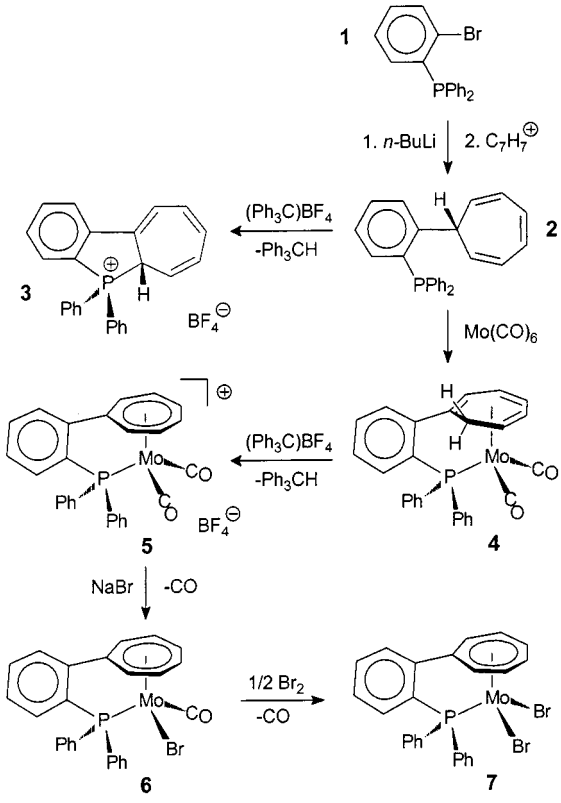

Scheme 1

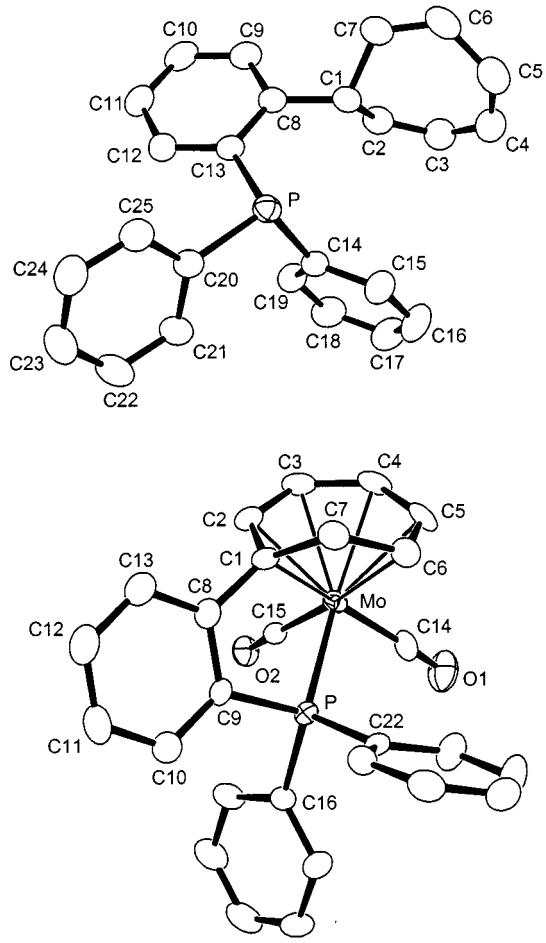

Figure 2. ORTEP drawings of **2** (top) and **4** (bottom) with thermal ellipsoids drawn at 50% probability

phanyl)phenyl substituent. Therefore, **2** was heated in DMF at 150 °C to undergo a thermal rearrangement through consecutive 1,5-sigmatropic hydrogen migrations.[18b,27] The resulting isomeric mixture was treated with $(Ph_3C)BF_4$ to afford Ph_3CH and a colorless tetrafluoroborate salt, which turned out to be the tricylic phosphonium salt **3**, formed by intramolecular nucleophilic attack of the tethered phosphane group at the seven-membered ring in the intermediate [2-(diphenylphosphanyl)phenyl]cycloheptatrienylium tetrafluoroborate (Scheme 1). A similar ring-closure has been observed for a linked cycloheptatrienyl−phenolate system.[13] As expected for asymmetric **3**, the ^1H NMR spectrum exhibits six different resonances for the allylic and vinylic cycloheptatrienyl protons, and the ^{31}P NMR spectrum displays a resonance at $\delta = 43.8$ indicative of a deshielded phosphonium center.[25]

Synthesis of 18-Electron Cycloheptatrienyl−Phosphane Complexes

Attempts to use **3** for the direct synthesis of the linked cycloheptatrienyl−phosphane complex **5** were unsuccessful, and the reaction with various $Mo(CO)_3$ transfer reagents such as $[(CH_3CN)_3Mo(CO)_3]$ or $[(\eta\text{-}p\text{-xylene})Mo(CO)_3]$ did not result in ring-opening of the phosphonium salt and insertion of the molybdenum complex fragment into the P−CH bond. More conveniently, the cycloheptatriene−phosphane ligand can be used as a multidentate ligand, and the reaction with $Mo(CO)_6$ in refluxing methylcyclohexane leads to the substitution of four carbonyl groups and the formation of cycloheptatriene−phosphane complexes of the type $[(o\text{-}Ph_2PC_6H_4\text{-}\eta^6\text{-}C_7H_7)Mo(CO)_2(P\text{−}Mo)]$. In comparison to the reaction of cycloheptatriene, C_7H_8, with $Mo(CO)_6$, the reaction described here proceeds much faster and no sublimation of hexacarbonylmolybdenum out of the flask into the reflux condenser was observed indicating that the phosphane group adds rapidly to the molybdenum center to form an involatile material followed by coordination of the cycloheptatriene moiety. If the reaction mixture is kept at 100 °C overnight, complex **4** crystallizes from the solution, upon cooling with dry ice, as the only detectable regioisomer (Scheme 1). The formation of **4** must have resulted from thermal rearrangement of the coordinated cycloheptatriene ring involving, in principle, two consecutive 1,5-hydrogen shifts.[28] In its ^1H NMR spectrum **4** exhibits five resonances due to the vinylic protons and two resonances due to the allylic *exo* and *endo* protons (Figure 3). The ^{31}P NMR resonance is observed at $\delta = 64.5$ revealing that the phosphorous atom is coordinated to the metal center. As **4** is obtained as a racemic mixture of two enantiomers, two different sets of resonances are observed for the diastereotopic phenyl groups in the ^{13}C NMR spectrum. Accordingly, two doublets are found for the ^{13}CO

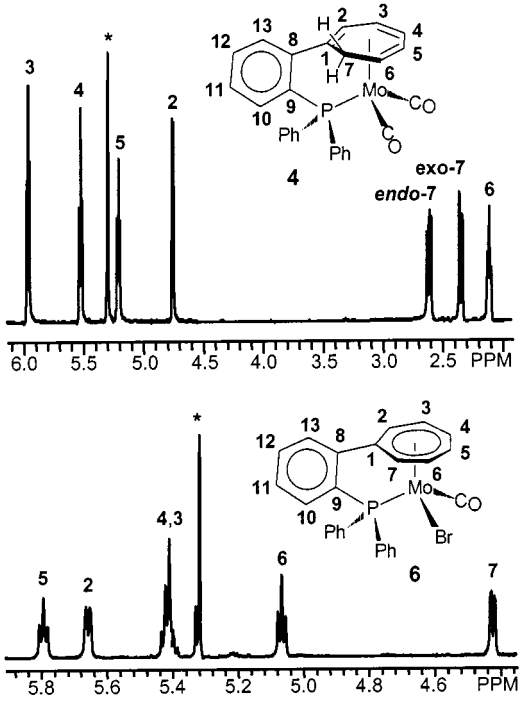

Figure 3. Selected parts of the ^{1}H NMR spectra (600 MHz, CD_2Cl_2) of **4** (top) and **6** (bottom)

carbonyl resonances at δ = 227.2 ($^2J_{C,P}$ = 10 Hz) and 223.9 ($^2J_{C,P}$ = 12 Hz), respectively.

In order to confirm the spectroscopic results, the molecular structure of **4** was established by X-ray diffraction analysis, and Figure 2 (bottom) shows an ORTEP diagram of one enantiomer. The 2-(diphenylphosphanyl)phenyl substituent is indeed attached to the vinylic carbon atom C1, which is next to the CH_2 group, and the cycloheptatriene−phosphane ligand binds to the metal center in a chelating η^6:η^1 fashion. If compared to the molecular structures of related (cycloheptatriene)molybdenum complexes, e.g. [(η^6-C_7H_8)Mo(CO)$_3$][29] and [(η^6-C_7H_8)Mo(CRR′)(CO)$_2$] (R = OEt, R′ = *o*-tolyl),[30] the bond lengths and angles within the seven-membered ring fall in the expected ranges (Table 1). The distances between the molybdenum atom and the cycloheptatriene carbon atoms, however, differ significantly with the shortest bond to C3 [2.296(3) Å] and the longest bond to C6 [2.468(3) Å], which is probably due to the asymmetry of the linked cycloheptatriene−phosphane ligand as well as the mixed set of co-ligands (one phosphane and two carbonyl ligands) about the molybdenum center.[30]

In **4** the *exo* hydrogen atom is accessible to the trityl cation for hydride abstraction, and the cycloheptatrienyl−phosphane complex [(*o*-$Ph_2PC_6H_4$-η^7-C_7H_6)Mo(CO)$_2$(*P*−*Mo*)]BF_4 (**5**) is formed almost quantitatively upon treatment with $(Ph_3C)BF_4$ (Scheme 1). With removal of the hydrogen atom from the CH_2 group, **5** becomes C_s-symmetric and exhibits three cycloheptatrienyl resonances in its ^{1}H NMR spectrum at δ = 6.06, 6.00, and 5.59 in a 2:2:2 ratio. Accordingly, the ^{13}C NMR spectrum displays four resonances for the C_7H_6 carbon atoms together with ten resonances for the phenyl and phenylene carbon atoms. The ^{13}CO resonance for the magnetically equivalent carbonyl groups is observed as a doublet at δ = 212.7 ($^2J_{P,C}$ = 25 Hz), and the ^{31}P resonance at 59.9 is slightly shifted to higher field in comparison with **4**. To unambiguously confirm the formation of the first cycloheptarienyl−phosphane chelate complex, a single-crystal of **5**·CH_2Cl_2 was subjected to X-ray diffraction analysis, and the molecular structure of the cation in **5** is depicted in Figure 4 (top). One recognizes that the ligand does indeed act as a chelate ligand in an η^7:η^1 fashion with almost perfectly perpendicularly oriented six- and seven-membered rings (interplanar angle of 85.8°). The molybdenum atom is symmetrically η^7-coordinated with the shortest bond to C1 [2.262(2) Å] and the longest bond to C6 [2.323(2) Å] (Table 1). On average, these distances are similar to those found for [(η-C_7H_7)Mo(CO)$_3$]BF_4 (mean 2.31 Å),[31] [(η-C_7H_7)Mo(CO)$_2$X] (X = Cl, mean 2.31 Å; X = Br, mean = 2.32 Å)[32] and [(η-C_7H_7)Mo(CO)$_2$(C_6F_5)] (mean = 2.32 Å).[33] No significant deviation from planarity can be observed for the seven-membered ring in **5**, and the mean and maximum deviations from the least-squares plane (C1−C7) are 0.028 and −0.058 Å (for C1), respectively. In order to allow chelate formation, the six-membered ring bends slightly down towards the metal center, and the angle between the centroid of the seven-membered ring, C1 and C8 deviates by 10.3° from a perfectly linear orientation. On the other hand, this out-of-plane displacement observed for C8 could also be attributed to a reorientation of the large seven-membered ring favoring a better metal overlap (vide infra). In addition, the phenylene bridge also leads to a somewhat distorted tetrahedral environment about the phosphorous atom with the angle Mo−P−C13 [105.95(8)°] being smaller than the adjacent angles Mo−P−C16 [116.53(7)°] and Mo−P−C22 [119.12(7)°].

It has previously been demonstrated that monophosphane complexes of the type [(η-C_7H_7)M(CO)X(PR_3)] (M = Mo, W; X = halide) allow the introduction of various nucleophiles by halide substitution reactions and are suitable precursors for studying organometallic transformations supported by the (cycloheptatrienyl)molybdenum and -tungsten fragments.[34] Therefore, **5** was treated with an excess of NaBr in THF at elevated temperature leading to the direct, high-yield formation of [(*o*-$Ph_2PC_6H_4$-η^7-C_7H_6)Mo(CO)Br(*P*−*Mo*)] (**6**). Due to chelation by the linked cycloheptatrienyl−phosphane ligand, complex **6** seems to be significantly more stable than related unbridged phosphane halide complexes, and chromatographic purification is possible under ambient conditions using alumina (4% H_2O). In **6**, the pseudotetrahedrally coordinated molybdenum center has four different ligands, and the complex is thus obtained as a racemic mixture of two enantiomers. Since this new representative of so-called "chiral-at-metal" half-sandwich compounds[35,36] is configurationally stable, the diastereotopic cycloheptatrienyl hydrogen atoms give rise to six different ^{1}H NMR resonances. This portion of

Table 1. Selected bond lengths [Å] and angles [°] for **2**, **4**, **5**·CH_2Cl_2, **7**·$CHCl_3$, **8**, and **9**·C_6H_{14}

	2	**4**	**5**·CH_2Cl_2	**7**·$CHCl_3$	**8**	**9**·C_6H_{14}
C1−C2	1.509(2)	1.395(4)	1.423(3)	1.415(5)	1.417(4)	1.429(3)
C2−C3	1.334(2)	1.418(4)	1.406(3)	1.390(5)	1.409(5)	1.401(4)
C3−C4	1.436(3)	1.419(4)	1.413(4)	1.418(5)	1.407(5)	1.418(4)
C4−C5	1.346(3)	1.419(4)	1.399(3)	1.395(5)	1.402(5)	1.387(4)
C5−C6	1.437(3)	1.381(4)	1.418(4)	1.409(5)	1.415(4)	1.418(4)
C6−C7	1.338(2)	1.505(4)	1.398(4)	1.396(4)	1.399(4)	1.387(4)
C1−C7	1.5083(19)	1.526(4)	1.427(3)	1.429(4)	1.431(4)	1.422(4)
C1−C8	1.516(2)	1.490(4)	1.497(3)	1.500(4)	1.494(4)	1.495(4)
Mo−C1		2.365(3)	2.262(2)	2.239(3)	2.234(3)	2.261(2)
Mo−C2		2.314(3)	2.321(2)	2.273(3)	2.261(3)	2.319(2)
Mo−C3		2.296(3)	2.320(2	2.257(3)	2.266(3)	2.294(2)
Mo−C4		2.322(3)	2.320(2)	2.310(3)	2.306(3)	2.289(3)
Mo−C5		2.350(3)	2.319(2)	2.292(3)	2.300(3)	2.302(3)
Mo−C6		2.468(3)	2.323(2)	2.281(3)	2.361(3)	2.312(2)
Mo−C7			2.321(2)	2.271(3)	2.303(3)	2.324(2)
Mo−C14/C26		1.985(3)	2.033(2)		2.211(3)	2.225(2)
Mo−C15/C18		1.951(3)	2.044(3)			2.228(2)
Mo−P		2.4343(8)	2.4813(6)	2.5763(9)	2.5484(8)	2.5427(7)
Mo−Br1				2.5834(5)	2.5865(4)	
Mo−Br2				2.5806(6)		
C14−O1		1.155(4)	1.137(3)			
C15−O2		1.167(3)	1.132(3)			
mean/max. dev.[a]			0.028/−0.058 (at C1)	0.012/−0.020 (at C2)	0.030/−0.045 (at C1)	0.027/0.054 (at C1)
Mo−C14−O1		177.2(3)	177.9(2)			
Mo−C15−O2		175.4(2)	179.4(2)			
centroid (C1−C7)−C1−C8			169.7	169.4	169.1	170.4
(C1−C7)−(C8−C13)[b]			85.5	78.2	71.5	85.4

[a] Minimum and maximum deviations from the least-squares plane containing C1−C7. [b] Interplanar angles.

the 600-MHz NMR spectrum is shown in Figure 3. Accordingly, seven ^{13}C NMR resonances are observed for the C_7H_6 carbon atoms together with six resonances for the phenylene bridge and eight resonances for the diastereotopic phenyl groups. The assignment of all ^1H and ^{13}C NMR resonances in **6** is supported by two-dimensional NMR spectroscopy (COSY and NOE experiments). The ^{13}CO carbonyl resonance in **6** is observed as a doublet at $\delta = 232.3$ ($^2J_{C,P} = 15.6$ Hz), and one single ^{31}P NMR resonance is found at $\delta = 49.1$. As expected, the IR spectrum of **6** exhibits one CO absorption at 1946 cm^{-1}, which is in good agreement with the stretching frequency of 1944 cm^{-1} reported for the closely related, unbridged analogue [(η-C_7H_7)Mo(CO)Br(PPh_3)].[34a] Single crystals of **6**·$CHCl_3$ could be obtained by recrystallization from a $CHCl_3$ solution allowing the molecular structure of **6** to be established by X-ray crystal structure determination.[37]

Synthesis of 17-Electron Cycloheptatrienyl−Phosphane Complexes

Ng et al. have recently reported on the ring-opening metathesis polymerization of norbornene promoted by (η-cycloheptatrienyl)molybdenum and -tungsten complexes of the type [(η-C_7H_7)MLI_2] (M = Mo, W; L = CH_3CN, PPh_3).[38] This is one of the first reports on the application of cycloheptatrienyl complexes to homogeneous transition metal catalysis.[6] Activated by Me_3SiCH_2MgCl, these 17-electron complexes give high molecular weight poly(1,3-cyclopentylenevinylene). The synthesis of such complexes has been developed by Green and co-workers, during the last decade, employing the sandwich compound [(η-C_7H_7)M(η^5-C_7H_9)] (M = Mo, W), which can be obtained in a one-pot reaction from cycloheptatriene, sodium amalgam and $MoCl_5$ or WCl_6, respectively. Treatment of these complexes with chlorine, bromine or iodine in the presence of Lewis bases provides a convenient route to half-sandwich derivatives such as [(η-C_7H_7)MLX_2] (M = Mo, W; L = CH_3CN, THF, PPh_3, PMe_3; X = Cl, Br, I).[39,40] Moreover, the magnetic properties of several of these paramagnetic compounds have been studied in detail.[41]

Herein, we present a new route to analogous 17-electron complexes containing linked cycloheptatrienyl−phosphane ligands. If [(*o*-$Ph_2PC_6H_4$-η^7-C_7H_6)Mo(CO)Br(*P−Mo*)] (**6**) is treated with 0.5 equiv. of bromine in CH_2Cl_2 a rapid color change from green to brown-red is observed together with the evolution of gas. After stirring for 1 h at ambient temperature, paramagnetic [(*o*-$Ph_2PC_6H_4$-η^7-C_7H_6)-$MoBr_2$(*P−Mo*)] (**7**) can be isolated as an air-stable brown dichloromethane adduct after precipitation with hexane (Scheme 1). The formation of **7** is obtained by oxidation of **6** with 0.5 equiv. of bromine to give the labile odd-electron intermediate [(*o*-$Ph_2PC_6H_4$-η^7-C_7H_6)Mo(CO)Br(*P−Mo*)]-

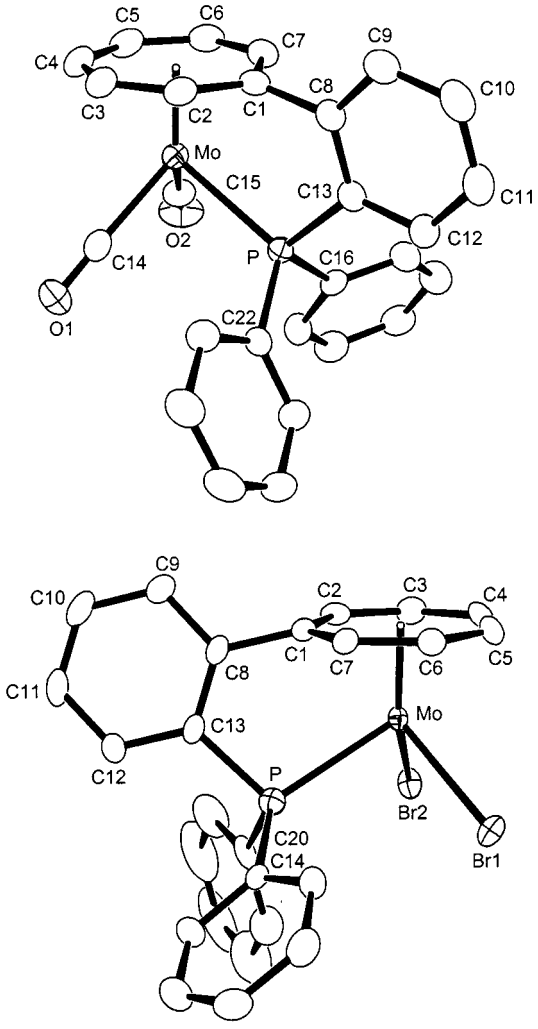

Figure 4. ORTEP drawings of the cation in **5**·CH_2Cl_2 (top) and of **7** in **7**·CH_2Cl_2 (bottom) with thermal ellipsoids drawn at 50% probability

Br, which rapidly undergoes carbonyl substitution by bromide to give complex **7** in high yield. Due to the unpaired electron in **7**, the compound was only characterized by mass spectrometry and by ^{31}P NMR spectroscopy revealing a resonance at $\delta = 38.5$, and the purity was additionally checked by elemental analysis.

Recrystallization from chloroform afforded single crystals of **7**·$CHCl_3$, which were suitable for structure determination by X-ray diffraction. The molecular structure is shown in Figure 4 (bottom). The Mo−C distances range from 2.239(3) to 2.310(3) Å (mean 2.27 Å, Table 1), which are similar to those in the 17-electron complexes [(η-C_7H_7)Mo(CH_3CN)I_2] [2.258(5)−2.280(5), mean 2.27 Å][41] and [(η-C_7H_7)Mo(THF)I_2] [2.23(2)−2.29(2), mean 2.25 Å],[42] and they are, on average, shorter than the corresponding values observed in 18-electron complexes such as **5** [2.262(2)−2.323(2), mean 2.31 Å] (vide supra). In contrast, the Mo−P bond length of 2.5763(9) Å is significantly longer than that in **5** [2.4183(6) Å]. Again, the cycloheptatrienyl ring in **7** is almost perfectly planar, and the mean and maximum deviations from the least-squares plane (C1−C7) are 0.012 and −0.020 Å (for C2), respectively. The structural features of the ligand backbone are quite similar to those found for the molecular structure of **5**, with an interplanar angle between the least-squares planes containing C1−C7 and C8−C13 of 78.2° and an angle between the centroid of the seven-membered ring, C1 and C8 of 169.4°.

As indicated above, it has been observed that, on activation with Me_3SiCH_2MgCl, molybdenum complexes such as [(η-C_7H_7)MoLI_2] (M = Mo, W; L = CH_3CN, PPh_3) catalyze the ring-opening metathesis polymerization of norbornene. It was concluded that these reactions presumably involve the intermediate carbene complexes [(η-C_7H_7)Mo(=$CHSiMe_3$)L], which could have been generated by α-deprotonation of the initially formed dialkyl complexes [(η-C_7H_7)Mo(CH_2SiMe_3)$_2$L].[38] Although precedents for similar reaction sequences can be found in the literature,[43] the formation of 17-electron dialkyl(cycloheptatrienyl) complexes has not yet been confirmed. As the formation of metal−alkyl bonds is essential for most industrially important catalytic processes[3,4] and since cycloheptatrienyl complexes bearing alkyl ligands are generally a rare class of compounds,[6,44] we sought to isolate the first 17-electron alkyl(cycloheptatrienyl) complexes by the reaction of the dibromide [(*o*-$Ph_2PC_6H_4$-η^7-C_7H_6)MoBr_2(*P*−*Mo*)] (**7**) with Me_3SiCH_2MgCl (1.0 M solution in diethyl ether). Treatment of **7** with 2 equiv. of the Grignard reagent resulted, after extraction with hexane, in a mixture of two compounds as indicated by the observation of two ^{31}P NMR resonances. Recrystallization from hexane afforded orange crystals of [(*o*-$Ph_2PC_6H_4$-η^7-C_7H_6)Mo(CH_2SiMe_3)Br(*P*−*Mo*)] (**8**), which contains only one trimethylsilylmethyl group, in moderate yield (Scheme 2). Transfer of the mother liquor to a chromatography column (SiO_2) and elution with diethyl ether/petroleum ether (1:1) led to the collection of an orange-yellow fraction, from which the dialkyl complex [(*o*-$Ph_2PC_6H_4$-η^7-C_7H_6)Mo(CH_2SiMe_3)$_2$(*P*−*Mo*)] could be isolated in low yield. Presumably, the introduction of the second alkyl substituent to form **9** is obstructed by steric hindrance produced by the first neosilyl (CH_2SiMe_3) group in **8**. In order to selectively prepare the monoalkyl derivative, the dibromide **7** can be treated with just 1 equiv. of the Grignard reagent to obtain **8** in about 60% yield. Complete dialkylation can be achieved by employing a large excess (about tenfold based on **7**) of the Grignard solution to afford excellent yields of the dialkyl complex **9**. The purity of the two paramagnetic compounds was only checked by elemental analysis and by ^{31}P NMR spectroscopy to reveal one resonance each at $\delta = 51.9$ for **8** and at $\delta = 54.6$ for **9**. Both compounds are air-stable and highly soluble in nonpolar solvents such as hexane or toluene as well as in THF and diethyl ether. As indicated above, **9** can even be purified by chromatography on silica without any significant loss of material by decomposition.

The molecular structures of both complexes could additionally be established by means of X-ray diffraction. **9** crystallizes with one molecule of hexane per formula unit,

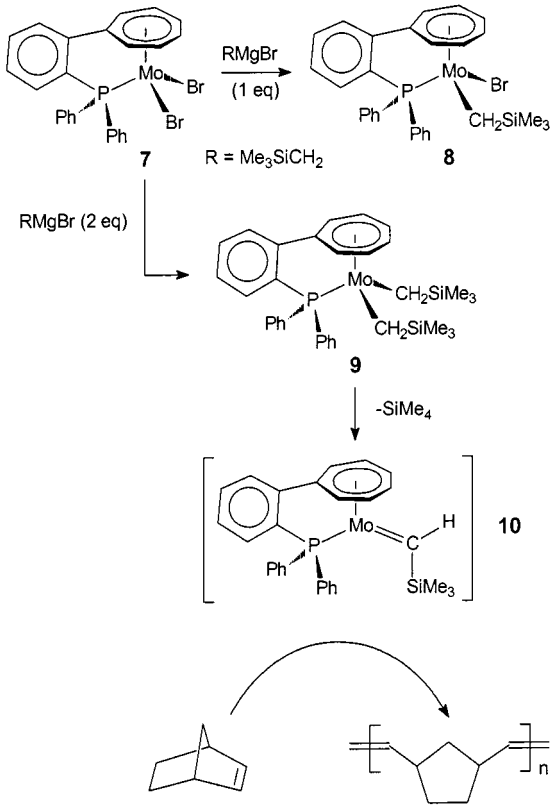

Scheme 2

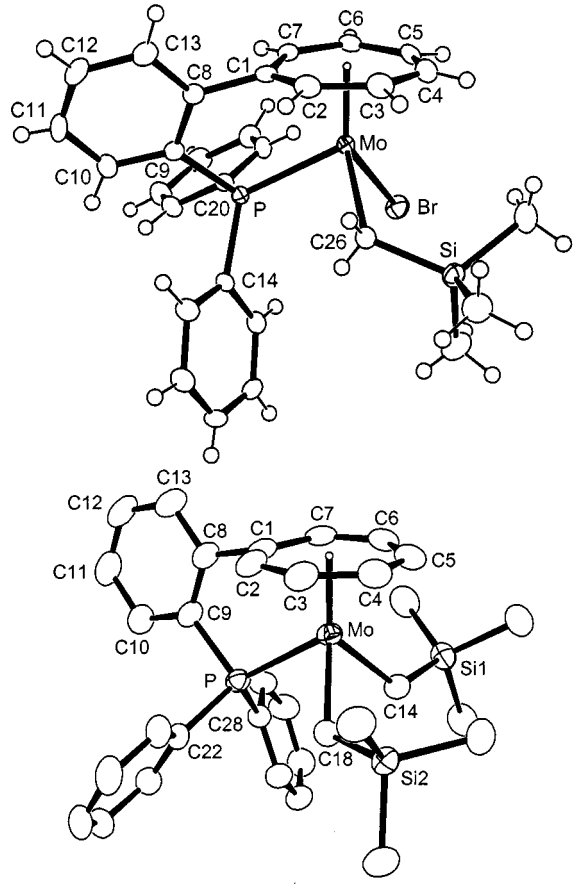

Figure 5. ORTEP drawings of the cation in **8** (top) and **9** in **9**·C_6H_{14} (bottom) with thermal ellipsoids drawn at 50% probability

and Figure 5 shows ORTEP presentations of **8** (top) and of **9** in **9**·C_6H_{14} (bottom). Successive substitution of the two bromine atoms in **7** by the sterically more demanding Me_3SiCH_2 group does not seem to have great consequences on the structural parameters of the cycloheptatrienyl−phosphane scaffold in **8** and **9**. Thus, the Mo−C distances range from 2.234(3) to 2.361(3) Å (mean 2.29 Å) in **8** and from 2.261(2) to 2.324(4) Å (mean 2.30 Å) in **9** and are only slightly elongated in comparison to those in **7** [2.239(3)−2.310(3) Å (mean 2.27 Å] (Table 1). In contrast, the Mo−P bond length slightly decreases on going from **7** [2.5763(9) Å] to **8** [2.5484(8) Å] and **9** [2.5427(7) Å]. The cycloheptatrienyl rings in **8** and **9** remain planar, and the mean and maximum deviations from the least-squares plane (C1−C7) together with the dihedral angle between the best planes containing C1−C7 and C8−C13 are summarized in Table 1. The metal-to-alkyl carbon distances observed for compounds **8** [2.211(3) Å] and **9** [2.225(2), 2.228(2) Å] are rather large but still comparable to those found in other alkylmolybdenum complexes, which lie in the range 2.08−2.20 Å.[45] The bond angles Mo−C−Si of 121.71(16)° in **8** and 124.62(13) and 129.34(12)° in **9** are significantly larger than expected for sp^3-hybridized carbon atoms, although similar bond angles have also been found in neosilylmolybdenum(VI) and -tungsten(VI) complexes.[43,45] It should be noted that the positions of all hydrogen atoms could be refined for **8**. Therefore, it is possible to establish the angles between the centroid of the cycloheptatrienyl ring, the C_7 carbon atoms and the adjacent hydrogen atoms revealing a significant out-of-plane displacement for the C_7 hydrogen atoms. The average bending is about 9° toward the molybdenum center, and such a deviation has been attributed to a reorientation of the large seven-membered ring for a better metal overlap.[6,46]

Ring-Opening Metathesis Polymerization (ROMP) of Norbornene

Homogeneous metathesis polymerization is dominated by well-defined alkylidene complexes of group-VI and group-VIII transition metals,[47,48] some of which have been neosilyl (M−CH_2SiMe_3) or neosilylidene complexes (M=$CHSiMe_3$), respectively.[43,45] Encouraged by the report on the ability of complexes of the type [(η-C_7H_7)MLI_2] (M = Mo, W; L = CH_3CN, PPh_3) to promote the ring-opening metathesis polymerization of norbornene,[38] we were prompted to test the ROMP activity of our 17-electron cycloheptatrienyl−phosphane complexes. Hence, the dibromo complex **7** was treated with 300 equiv. of norbornene in toluene. After addition of an excess amount of Me_3SiCH_2MgCl (6 equiv. of a 1.0 M solution in diethyl ether), the reaction mixture, which gradually became viscous, was heated for 12 h at 40 °C to ensure completion of the polymerization. The formed poly(1,3-cyclopentylenevinylene) was obtained as a colorless, fibrous material after

quenching with a few drops of benzaldehyde and dropwise addition of the hot solution to vigorously stirred methanol. Initial ^{13}C NMR and IR spectroscopic studies show in comparison with the literature data,[49,50] that about 80% of the double bonds in the polymer are in the *trans* configuration.

As we have demonstrated, that [(*o*-$Ph_2PC_6H_4$-η^7-C_7H_6)Mo(CH_2SiMe_3)$_2$(*P*−*Mo*)] (**9**) is actually formed by the reaction of Me_3SiCH_2MgCl with **7**, we anticipated that **9** might be an active single-source catalyst, from which the active species [(*o*-$Ph_2PC_6H_4$-η^7-C_7H_7)Mo=$CHSiMe_3$-(*P*−*Mo*)] (**10**) could be generated by intramolecular α-deprotonation and elimination of Me_4Si (Scheme 2). The formation of this alkylidene complex would then allow the course of the metathesis polymerization to be described by the Chauvin mechanism.[51] Treatment of **9** with norbornene in different solvents at various temperatures, however, did not give detectable amounts of polymer. On the other hand, addition of 1 equiv. of Me_3SiCH_2MgCl to such a reaction mixture resulted in a rapid and quantitative formation of medium molecular weight polynorbornene (M_n = $2.6 \cdot 10^4$ g/mol, PDI = M_w/M_n = 6.7, approx. 80% *trans* double bonds). A standard procedure is described in the Exp. Sect. It should be noted, that we have ruled out the possibility of the Grignard reagent alone reacting as a ROMP catalyst by independent control experiments, and at this stage, the mechanism as well as the active catalyst in our system remains unclear. Further work will be directed toward the synthesis and isolation of paramagnetic alkylidene complexes such as **10**, which might then dimerize to form interesting bis(μ-alkylidene) species containing metal−metal bonds. Substitution of the neosilyl by other alkyl groups, e.g. by neopentyl groups, as well as modification of the residues of the R_2P donor moiety will allow fine tuning of the activity of this catalyst system and adjustment of the electronic and steric requirements of the resulting complexes according to future challenges.

Conclusion

With this contribution, chelate complexes of functionalized cycloheptatrienyl ligands bearing a pendant phosphane donor group have been reported for the first time, and we have presented a high-yielding protocol for the synthesis of a series of 17- and 18-electron molybdenum complexes containing linked cycloheptatrienyl−phosphane ligands. These complexes are archetypal for the new class of donor-functionalized cycloheptatrienyl complexes,[13] that will emerge from our laboratory in the near future. Although the preliminary results on the use of the 17-electron complexes presented herein as catalyst systems for olefin metathesis polymerization are by no means spectacular, these findings indicate that cycloheptatrienyl complexes can be potentially useful for applications in homogeneous transition metal catalysis. Hence, we are currently pursuing a general study on the utilization of these systems in various areas of application in view of our general objectives in order to extend the chemistry of cycloheptatrienyl complexes and to raise their level of significance in comparison with that of cyclopentadienyl and benzene complexes.

Experimental Section

General: All operations were performed in dry argon by using Schlenk and vacuum techniques. Solvents were dried by standard methods and distilled prior to use. (2-bromophenyl)diphenylphosphane (**1**),[24] tropylium tetrafluoroborate,[52] and triphenylcarbenium tetrafluoroborate,[53] were prepared according to published procedures. Elemental analyses (C, H, N) were performed with a Heraeus CHNO-Rapid elemental analyzer. EI and ESI mass spectra were recorded with a Varian MAT 212 or with a Micromass Quattro LCZ mass spectrometer, respectively. ^1H and ^{13}C NMR spectra were measured with Bruker AC 200, Bruker AMX 400 or Varian U 600 spectrometers using the solvent as internal standard, whereas ^{31}P NMR spectroscopic measurements were run with a Bruker AC 200 spectrometer using aqueous H_3PO_4 (85%) as an external reference. IR spectra were recorded with a Bruker Vector 22 instrument. The assignment of all ^1H and ^{13}C NMR resonances has been supported by two-dimensional NMR spectroscopy (COSY and NOE experiments). For the atomic numbering schemes used in the Exp. Sect., see Figure 3.

[2-(Cyclohepta-2,4,6-trienyl)phenyl]diphenylphosphane (2): A solution of **1** (9.62 g, 28.20 mmol) in THF (140 mL) was treated with *n*-butyllithium (12.2 mL of a 2.5 M solution in hexane, 30.5 mmol). After stirring for 45 min, solid (C_7H_7)BF_4 (5.01 g, 28.16 mmol) was added at −78 °C, and the resulting reaction mixture was slowly warmed to room temperature (3 h). It was then diluted with a saturated aqueous NH_4Cl solution (100 mL) and extracted with diethyl ether (100 mL) and dichloromethane (2 × 50 mL). The combined organic extracts were dried with $MgSO_4$. Evaporation of the solvents and purification by column chromatography on silica using petroleum ether/dichloromethane (1:1) as eluent afforded **2** as a colorless, crystalline solid. Yield: 7.41 g (75%). ^1H NMR ($CDCl_3$, 400 MHz): δ = 7.66 (dd, 1 H, 13-H), 7.49 (t, 1 H, 12-H), 7.40−7.28 (m, 10 H, C_6H_5), 7.24 (t, 1 H, 11-H), 6.98 (dd, 1 H, 10-H), 6.65 (t, 2 H, 4,5-H), 6.11 (m, 2 H, 3,6-H), 5.26 (dd, 2 H, 2,7-H), 3.66 (m, 1 H, 1-H). ^{31}P NMR ($CDCl_3$, 81 MHz): δ = −15.9. MS (EI): *m*/*z* (%) = 352 (100) [M^+], 351 (94) [M − H]$^+$, 262 (25) [PPh_3]$^+$. $C_{25}H_{21}P$ (352.42): calcd. C 85.20, H 6.01; found C 84.93, H 6.27.

Phosphonium Salt 3: Prior to hydride abstraction, the phosphane **2** was thermally rearranged by heating in *N*,*N*-dimethylformamide at 150 °C overnight. After evaporation of the solvent, the mixture was purified by chromatography as described above. A solution of this isomeric mixture (0.82 g, 2.33 mmol) in acetonitrile (35 mL) was treated with (Ph_3C)BF_4 (0.69 g, 2.09 mmol) at 0 °C. After it was warmed to room temperature, the reaction mixture was warmed to reflux for 2 h. The solvent was removed by evaporation, and the residue was washed with diethyl ether to remove Ph_3CH and recrystallized from dichloromethane/petroleum ether at 0 °C to afford **3** as a yellow, crystalline solid. Yield: 0.64 g (70%). ^1H NMR (CD_2Cl_2, 400 MHz): δ = 8.02−7.66 (m, 14 H, C_6H_5 + 10,11,12,13-H), 7.28 (m, 1 H, C_7 ring: CH), 6.98 (dd, 1 H, C_7 ring: CH), 6.85 (dd, 1 H, C_7 ring: CH), 6.43 (m, 1 H, C_7 ring: CH), 4.89 (m, 1 H, C_7 ring: CH), 3.89 (m, 1 H, C_7 ring: CHP). ^{31}P NMR (CD_3CN, 81 MHz): δ = 43.8. MS (ESI): *m*/*z* (%) = 351 (100) [M − BF_4]$^+$. $C_{25}H_{20}BF_4P$ (438.21): calcd. C 68.52, H 4.60; found C 68.24, H 4.70.

[(*o*-$Ph_2PC_6H_4$-η^6-C_7H_7)Mo(CO)$_2$(*P*−*Mo*)] (4): The phosphane **2** (9.72 g, 28.58 mmol) and $Mo(CO)_6$ (7.65 g, 28.98 mmol) were dissolved in methylcyclohexane (250 mL) and slowly heated to 120 °C within 2 h. Heating was continued at this temperature while stirring for 10 h. The solvent and unchanged $Mo(CO)_6$ were removed in vacuo, and the residue was recrystallized from dichloromethane/hexane at 0 °C. After 12 h, **4** was isolated as a red crystalline solid by filtration. Yield: 8.84 g (64%) − ^{1}H NMR (CD_2Cl_2, 600 MHz): δ = 7.66 (m, 2 H, *o*-C_6H_5), 7.47 (dd, 1 H, 13-H), 7.42 (m, 6 H, C_6H_5), 7.38 (m, 3 H, C_6H_5 + 12-H), 7.31 (t, 1 H, 11-H), 7.27 (t, 1 H, 10-H), 5.97 (t, 1 H, 3-H), 5.53 (t, 1 H, 4-H), 5.22 (t, 1 H, 5-H), 4.77 (d, 1 H, 2-H), 2.62 (dd, 1 H, 7-*endo*-CH_2), 2.35 (dd, 1 H, 7-*exo*-CH_2), 2.12 (tt, 1 H, 6-H). ^{13}C NMR (CD_2Cl_2, 150.7 MHz): δ = 227.2 (d, $^2J_{C,P}$ = 10.2 Hz, CO), 223.9 (d, $^2J_{C,P}$ = 12.1 Hz, CO), 153.6 (d, $^2J_{C,P}$ = 27.5 Hz, C-8), 151.3 (d, $^1J_{C,P}$ = 40.9 Hz, C-9), 142.0 (d, $^1J_{C,P}$ = 36.4 Hz, *i*-C_6H_5), 138.1 (d, $^1J_{C,P}$ = 40.2 Hz, *i*-C), 133.4 (s, C-10), 133.1 (d, $^2J_{C,P}$ = 12.8 Hz, *o*-C), 132.8 (d, $^2J_{C,P}$ = 11.5 Hz, *o*-C), 130.3 (s, C-12), 129.8 (s, *p*-C), 129.6 (s, *p*-C), 128.7 (d, ^3J = 9.6 Hz, *m*-C), 128.4 (d, ^3J = 10.1 Hz, *m*-C), 127.4 (d, ^3J = 12.8 Hz, C-13), 127.3 (d, ^3J = 5.8 Hz, C-11), 104.7 (s, C-5), 98.8 (s, C-2), 90.9 (s, C-3), 86.3 (s, C-4), 86.0 (s, C-1), 54.8 (s, C-6), 33.6 (s, CH_2-7). ^{31}P NMR ($CDCl_3$, 81 MHz): δ = 64.5. MS (EI): *m*/*z* (%) = 504 (12) [M^+], 476 (4) [M − CO]$^+$, 448 (100) [M − 2 CO]$^+$. IR (KBr): ν(CO) = 1905 (shoulder), 1889, 1873, 1816 cm^{-1}. $C_{27}H_{21}MoO_2P$ (504.38): calcd. C 64.30, H 4.20; found C 64.90, H 4.30.

[(*o*-$Ph_2PC_6H_4$-η^7-C_7H_6)Mo(CO)$_2$(*P*−*Mo*)]BF_4 (5): A solution of **4** (8.84 g, 17.53 mmol) in dichloromethane (200 mL) was treated with $(Ph_3C)BF_4$ (5.20 g, 15.75 mmol) at 0 °C, and the resulting mixture was subsequently heated to reflux for 30 min. The solution was reduced in volume to about 50 mL and added dropwise to rapidly stirred diethyl ether at 0 °C to precipitate **5**, which was isolated as an orange crystalline solid by filtration, washing with diethyl ether and drying in vacuo. Yield: 8.34 g (90%). ^{1}H NMR (CD_2Cl_2, 600 MHz): δ = 7.88 (dd, 1 H, 13-H), 7.71 (t, 1 H, 12-H), 7.59 (t, 1 H, 11-H), 7.55−7.59 (m, 6 H, *p*- + *m*-C_6H_5), 7.43−7.39 (m, 4 H, *o*-C_6H_5), 7.38 (t, 1 H, 10-H), 6.06 (m, 2 H, 3,6-H), 6.00 (m, 2 H, 4,5-H), 5.59 (dd, 2 H, 2,7-H). ^{13}C NMR (CD_2Cl_2, 150.7 MHz): δ = 212.6 (d, $^2J_{C,P}$ = 25.3 Hz, CO), 146.7 (d, $^2J_{C,P}$ = 25.5 Hz, C-8), 141.5 (d, $^1J_{C,P}$ = 47.3 Hz, C-9), 133.3 (s, C-10), 132.8 (d, $^4J_{C,P}$ = 2.6 Hz, C-12), 132.3 (d, $^2J_{C,P}$ = 12.1 Hz, *o*-C), 132.1 (d, $^1J_{C,P}$ = 47.2 Hz, *i*-C), 132.0 (d, $^4J_{C,P}$ = 2.6 Hz, *p*-C), 131.0 (d, $^3J_{C,P}$ = 6.4 Hz, C-11), 129.9 (d, $^3J_{C,P}$ = 10.9 Hz, *m*-C), 127.3 (d, $^3J_{C,P}$ = 11.5 Hz, C-13), 126.7 (d, $^3J_{C,P}$ = 3.2 Hz, C-1), 98.2 (s, C-3,6), 96.0 (s, C-4,5), 94.7 (d, $^4J_{C,P}$ = 3.6 Hz, C-2,7). ^{31}P NMR ($CDCl_3$, 81 MHz): δ = 59.9. MS (ESI): *m*/*z* (%) = 503 (100) [M − BF_4]$^+$. IR (KBr): ν(CO) = 2032, 1988 cm^{-1}. IR (CH_2Cl_2): ν(CO) = 2035, 1994 cm^{-1}. $C_{27}H_{20}BF_4MoO_2P$ (590.17): calcd. C 54.95, H 3.42; found C 54.16, H 3.48.

[(*o*-$Ph_2PC_6H_4$-η^7-C_7H_6)Mo(CO)Br(*P*−*Mo*)] (6): A solution of **5** (2.40 g, 4.07 mmol) in acetone (160 mL) was treated with NaBr (3.04 g, 29.55 mmol), and the resulting mixture was subsequently heated to reflux for 14 h. After evaporation of the solvent, the residue was transferred to a silica chromatography column. Elution with dichloromethane produced a green band that was collected to give **6** as a green, crystalline solid. Yield: 0.72 g (35%). ^{1}H NMR (CD_2Cl_2, 600 MHz): δ = 7.79 (dd, 1 H, 13-H), 7.71 (dd, 2 H, *o*-C_6H_5), 7.53 (t, 1 H, 12-H), 7.47 (t, 1 H, 11-H), 7.44 (t, 1 H, 10-H), 7.43−7.33 (m, 6 H, *p*- + *m*-C_6H_5), 7.20 (dd, 2 H, *o*-C_6H_5), 5.80 (t, 1 H, 5-H), 5.66 (d, 1 H, 2-H), 5.42 (t, 1 H, 4-H), 5.40 (t, 1 H, 3-H), 5.07 (t, 1 H, 6-H), 4.42 (d, 1 H, 7-H). ^{13}C NMR (CD_2Cl_2, 150.7 MHz): δ = 232.3 (d, $^2J_{C,P}$ = 15.6 Hz, CO), 150.4 (d, $^2J_{C,P}$ = 29.4 Hz, C-8), 141.5 (d, $^1J_{C,P}$ = 45.3 Hz, C-9), 134.5 (d, $^1J_{C,P}$ = 42.1 Hz, *i*-C), 134.2 (d, $^2J_{C,P}$ = 12.1 Hz, *o*-C), 132.7 (d, $^1J_{C,P}$ = 37.7 Hz, *i*-C), 132.2 (s, C-10), 131.6 (d, $^2J_{C,P}$ = 12.1 Hz, *o*-C), 130.6 (d, $^4J_{C,P}$ = 1.9 Hz, C-12), 130.5 (d, $^4J_{C,P}$ = 2.6 Hz, *p*-C), 129.8 (d, $^4J_{C,P}$ = 1.9 Hz, *p*-C), 129.1 (d, $^3J_{C,P}$ = 5.8 Hz, C-11), 128.5 (d, $^3J_{C,P}$ = 9.6 Hz, *m*-C), 128.3 (d, $^3J_{C,P}$ = 10.2 Hz, *m*-C), 127.5 (d, $^3J_{C,P}$ = 9.6 Hz, C-13), 107.3 (d, $^3J_{C,P}$ = 2.2 Hz, C-1), 99.4 (d, $J_{C,P}$ = 1.3 Hz, C-3), 99.2 (s, C-2), 98.5 (d, $J_{C,P}$ = 5.3 Hz, C-4), 93.6 (d, $J_{C,P}$ = 5.1 Hz, C-5), 89.5 (s, C-7), 80.9 (s, C-6). ^{31}P NMR ($CDCl_3$, 81 MHz): δ = 49.1. MS (EI): *m*/*z* (%) = 527 (11) [M − CO]$^+$, 447 (9) [M − CO − Br]$^+$. IR (KBr): ν(CO) = 1946 cm^{-1}. IR (CH_2Cl_2): ν(CO) = 1956 cm^{-1}. $C_{26}H_{20}BrMoOP$ (555.26): calcd. C 56.24, H 3.63; found C 55.30, H 3.64.

[(*o*-$Ph_2PC_6H_4$-η^7-C_7H_6)$MoBr_2$(*P*−*Mo*)] (7): A solution of **6** (4.92 g, 8.86 mmol) in dichloromethane (120 mL) was treated with a solution of bromine (0.24 mL, 4.68 mmol) in dichloromethane (10 mL) at 0 °C, and the resulting mixture was subsequently stirred for 1 h at ambient temperature. The solution was reduced in volume to about 50 mL and added dropwise to rapidly stirred hexane to precipitate **7**, which was isolated as a brown, crystalline solid by filtration, washing with hexane and drying in vacuo. Purification was possible by recrystallization from dichloromethane to afford crystals of **7**·CH_2Cl_2. Yield: 5.30 g (86%). ^{31}P NMR ($CDCl_3$, 81 MHz): δ = 38.5. MS (EI): *m*/*z* (%) = 607 (16) [M^+], 527 (68) [M − Br]$^+$, 448 (21) [M − 2 Br]$^+$. $C_{26}H_{22}Br_2Cl_2MoP$ (692.09): calcd. C 45.12, H 3.20; found C 45.72, H 3.13.

[(*o*-$Ph_2PC_6H_4$-η^7-C_7H_6)Mo(CH_2SiMe_3)Br(*P*−*Mo*)] (8): A solution of **7**·CH_2Cl_2 (200 mg, 0.29 mmol) in THF (20 mL) was treated with Me_3SiCH_2MgCl (0.3 mL of a 1.0 M solution in diethyl ether, 0.3 mmol) at −78 °C, and the resulting mixture was allowed to warm to room temperature and was subsequently stirred for 12 h at ambient temperature. The solvent was evaporated, and the residue was extracted with hexane (20 mL). Keeping the filtrate in the refrigerator for 24 h at 0 °C afforded orange crystals of **8**. Yield: 110 mg (62%). ^{31}P NMR ($CDCl_3$, 81 MHz): δ = 51.9. $C_{29}H_{31}BrMoPSi$ (614.47): calcd. C 56.69, H 5.09; found C 56.97, H 5.11.

[(*o*-$Ph_2PC_6H_4$-η^7-C_7H_6)Mo(CH_2SiMe_3)$_2$(*P*−*Mo*)] (9): A solution of **7**·CH_2Cl_2 (500 mg, 0.72 mmol) in THF (20 mL) was treated with a large excess of Me_3SiCH_2MgCl (7.2 mL of a 1.0 M solution in diethyl ether, 7.2 mmol) at −78 °C, and the resulting mixture was allowed to warm to room temperature and was subsequently stirred for 12 h at ambient temperature. The solvent was evaporated, and the residue was extracted with hexane (20 mL). Purification was possible by column chromatography on silica using diethyl ether/petroleum ether (1:1) as eluent to isolate **8** as an orange-yellow, crystalline solid. Yield: 420 mg (93%). ^{31}P NMR ($CDCl_3$, 81 MHz): δ = 54.6. $C_{33}H_{42}MoPSi_2$ (621.78): calcd. C 63.75, H 6.81; found C 63.35, H 6.74.

X-ray Crystallography:[37,54] Data sets were collected at −75 °C (for **2**, **4**, and **5**) with an Enraf−Nonius KappaCCD or at −120 °C (for **6**−**9**) with a Bruker AXS APEX diffractometer both equipped with a rotating anode using Mo-K_α radiation (λ = 0.71073 Å). Empirical absorption correction with SORTAV[55] (for **2**, **4**, and **5**) or SADABS[56] (for **6**−**9**) was applied to the raw data. Structure solution was performed in all cases with SHELXS[57] and refinement with SHELXL[58] with anisotropic thermal parameters for all atoms. Hydrogen atoms were added to the structure models on calculated positions and were refined as riding atoms (**2**, **4**, and **5**) or are unrefined for **6**, **7**, and **9**. Hydrogen atoms for **8** were located in the difference Fourier map and were refined with isotropic ther-

Table 2. Crystallographic Data for **2**, **4**, **5**·CH_2Cl_2, **7**·$CHCl_3$, **8**, and **9**·C_6H_{14}

	2	**4**	**5**·CH_2Cl_2	**7**·$CHCl_3$	**8**	**9**·C_6H_{14}
Empirical formula	$C_{25}H_{21}P$	$C_{27}H_{21}MoO_2P$	$C_{28}H_{22}BCl_2F_4MoO_2P$	$C_{26}H_{21}Br_2Cl_3MoP$	$C_{29}H_{31}BrMoPSi$	$C_{39}H_{56}MoPSi_2$
Formula mass	352.39	504.35	675.08	726.51	614.45	707.93
a [Å]	7.0168(1)	13.933(1)	10.3457(2)	8.364(1)	14.6027(13)	15.3044(7)
b [Å]	11.1396(2)	12.979(1)	10.8398(2)	27.749(5)	18.5103(17)	16.0758(7)
c [Å]	25.0062(4)	24.305(1)	12.8623(2)	11.225(2)	19.3375(18)	15.5570(7)
α [°]	90	90	90.474(1)	90	90	90
β [°]	91.689(1)	90.14(1)	105.434(1)	92.643(4)	90	97.925(1)
γ [°]	90	90	92.154(1)	90	90	90
V [Å^3]	1953.74(5)	4395.2(5)	1389.20(5)	2602.3(7)	5226.9(8)	3790.9(3)
$d_{calcd.}$ [g cm^{-1}]	1.198	1.524	1.614	1.854	1.562	1.240
Crystal system	monoclinic	monoclinic	triclinic	monoclinic	orthorhombic	monoclinic
Space group	$P2_1/n$ (no. 14)	$C2/c$ (no. 15)	$P\bar{1}$ (no. 2)	$P2_1/c$ (no. 14)	*Pbca* (no. 61)	$P2_1/n$ (no. 14)
Z	4	8	2	4	8	4
μ [mm^{-1}]	1.45	6.91	7.74	3.959	2.15	0.476
Unique data	4586	5052	6341	5978	8307	11750
Observed data [$I > 2\sigma(I)$]	3555	3539	5438	4538	6307	7265
*R*1 (obs. data) [%]	3.93, w*R*1 = 9.01	4.01, w*R*1 = 7.02	3.28, w*R*1 = 7.29	3.59, w*R*1 = 6.86	5.44, w*R*1 = 8.95	4.76, w*R*1 = 8.86
*R*2 (all data) [%]	5.80, *w*R2 = 9.93	7.68, *w*R2 = 8.48	4.30, *w*R2 = 7.76	5.35, *w*R2 = 7.17	7.95, *w*R2 = 9.55	9.21, *w*R2 = 9.84
GoF	1.030	1.011	1.043	0.939	1.076	0.917
No. of variables	235	280	352	298	422	381
Res. electr. dens. [e/Å^3]	0.22/−0.24	0.42/−0.48	0.51/−0.51	0.94/−0.55	1.10/-0.88	0.81/-0.44

mal parameters. ORTEP[59] was used for all drawings. Additional crystallographic data are listed in Table 2 and in ref.[37]

Metathesis Studies: A solution of norbornene (750 mg, 7.97 mmol) and the bis(neosilyl) complex **9** (16.5 mg, 26.5 μmol) in chlorobenzene (60 mL) was treated with Me_3SiCH_2MgCl (30 μL of a 1.0 M solution in diethyl ether, 30 μmol), and the resulting mixture was heated at 40 °C for 12 h. After quenching with a few drops of benzaldehyde, the viscous mixture was heated to 80 °C and then added dropwise to rapidly stirred methanol (400 mL) to precipitate a white, fibrous material, which was collected by filtration and dried in vacuo. Yield: 650 mg (87%). The molecular weights of the poly(1,3-cyclopentylenevinylene) samples thus obtained were determined by GPC with THF as eluent using refraction index detection and polystyrene as standard ($M_n = 2.6 \cdot 10^4$ g/mol, PDI = $M_w/M_n = 6.7$, approx. 80% *trans* double bonds as indicated by ^{13}C NMR[49] and IR[50] measurements).

Acknowledgments

This work was financially supported by the Deutsche Forschungsgemeinschaft, the Fonds der Chemischen Industrie and the government of North Rhine-Westphalia (Bennigsen-Foerder-Preis 2000 to M. T.). We are indepted to Tania Pape for excellent technical assistance and to Dr. Victoria Urban and to Bernd Dreßel for considerable support during the preparation of the manuscript.

[1] [1a] *Comprehensive Organometallic Chemistry* (Eds.: G. Wilkinson, F. G. A. Stone, E. W. Abel), Pergamon Press, Oxford, **1982**. [1b] *Comprehensive Organometallic Chemistry II* (Eds.: E. W. Abel, F. G. A. Stone, G. Wilkinson), Chapman and Hall, Oxford, **1995**. [1c] *Metallocenes* (Eds.: A. Togni, R. L. Halterman), Wiley-VCH, Weinheim, **1998**.

[2] [2a] C. Janiak, H. Schumann, *Adv. Organomet. Chem.* **1991**, *33*, 331. [2b] J. Okuda, *Top. Curr. Chem.* **1991**, *160*, 99. [2c] N. J. Coville, K. E. du Plooy, W. Pickl, *Coord. Chem. Rev.* **1992**, *116*, 1. [2d] R. L. Halterman, *Chem. Rev.* **1992**, *92*, 965. [2e] M. L. Hays, T. P. Hanusa, *Adv. Organomet. Chem.* **1996**, *40*, 117.

[3] [3a] *Applied Homogenous Catalysis with Organometallic Compounds* (Eds.: B. Cornils, W. A. Herrmann), Wiley-VCH, Weinheim, **1996**. [3b] W. A. Herrmann, B. Cornils, *Angew. Chem.* **1997**, *109*, 1074; *Angew. Chem. Int. Ed. Engl.* **1997**, *36*, 1048. [3c] G. J. P. Britovsek, V. C. Gibson, D. F. Wass, *Angew. Chem.* **1999**, *111*, 448; *Angew. Chem. Int. Ed.* **1999**, *38*, 428. [3d] *Chem. Rev.* **2000**, vol. 100, issue 4, Special Issue "Frontiers in Metal-Catalyzed Polymerisation".

[4] [4a] L. S. Hegedus, *Transition Metals in the Synthesis of Complex Organic Molecules*, University Science, California, **1994**. [4b] *Transition Metals for Organic Synthesis* (Eds.: M. Beller, C. Bolm), Wiley-VCH, Weinheim, **1998**.

[5] *Inorganic Materials* (Eds.: D. W. Bruce, D. O'Hare), Wiley, Chichester, **1992**.

[6] M. L. H. Green, D. K. P. Ng, *Chem. Rev.* **1995**, *95*, 439.

[7] [7a] M. Tamm, B. Dreßel, R. Fröhlich, K. Bergander, *Chem. Commun.* **2000**, 1731. [7b] M. Tamm, B. Dreßel, R. Fröhlich, *J. Org. Chem.* **2000**, *65*, 6795.

[8] M. Tamm, T. Bannenberg, B. Dreßel, R. Fröhlich, D. Kunz, *Organometallics* **2001**, *20*, 900.

[9] [9a] J. Okuda, T. Eberle, in: *Metallocenes* (Eds.: A. Togni, R. L. Halterman), Wiley-VCH, Weinheim, **1998**, vol. 1, p. 415. [9b] J. Okuda, *Comments Inorg. Chem.* **1994**, *16*, 185.

[10] P. Jutzi, T. Redeker, *Eur. J. Inorg. Chem.* **1998**, 663.

[11] U. Siemeling, *Chem. Rev.* **2000**, *100*, 1495.

[12] H. Butenschön, *Chem. Rev.* **2000**, *100*, 1527.

[13] M. Tamm, T. Bannenberg, B. Dreßel, R. Fröhlich, C. Holst, *Inorg. Chem.*, accepted.

[14] C. J. Groenenboom, H. J. de Liefde Meijer, F. Jellinek, *J. Organomet. Chem.* **1974**, *69*, 235.

[15] B. Demerseman, P. H. Dixneuf, J. Douglade, R. Mercier, *Inorg. Chem.* **1982**, *21*, 3942.

[16] [16a] L. B. Kool, M. Ogasa, M. D. Rausch, *Organometallics* **1989**, *8*, 1785. [16b] M. Ogasa, M. D. Rausch, R. D. Rogers, *J. Organomet. Chem.* **1991**, *403*, 279. [16c] M. D. Rausch, M. Ogasa, M. A. Ayers, R. D. Rogers, A. N. Rollins, *Organometallics* **1991**, *10*, 2481.

[17] [17a] J. Heck, T. Meyer-Friedrichsen, *Coord. Chem. Rev.* **1999**, *190–192*, 1217. [17b] U. Behrens, H. Brussard, U. Hagenau, J. Heck, E. Hendrickx, J. Körnich, J. G. M. van der Linden, A.

Persoons, A. L. Spek, N. Veldman, B. Voss, H. Wong, *Chem. Eur. J.* **1996**, *2*, 98.
[18] [18a] M. Tamm, K. Baum, R. Fröhlich, P. Saarenketo, *Organometallics* **2001**, *20*, 1376. [18b] M. Tamm, T. Bannenberg, K. Baum, R. Fröhlich, T. Steiner, T. Meyer-Friedrichsen, J. Heck, *Eur. J. Inorg. Chem.* **2000**, 1161. [18c] M. Tamm, A. Grzegorzewski, T. Steiner, *Chem. Ber./Recueil* **1997**, *130*, 225.
[19] B. M. Trost, B. Vidal, M. Thommen, *Chem. Eur. J.* **1995**, *5*, 1055.
[20] [20a] M. I. Bruce, R. C. F. Gardner, B. L. Goodall, F. G. A. Stone, R. J. Doedens, J. A. Moreland, *J. Chem. Soc., Chem. Commun.* **1974**, 185. [20b] J. A. Moreland, R. J. Doedens, *Inorg. Chem.* **1976**, *15*, 2486. [20c] M. I. Bruce, R. C. F. Gardner, F. G. A. Stone, *J. Chem. Soc., Dalton Trans.* **1976**, 81.
[21] For a recent publication describing the syntheses of related complexes bearing tethered homoallylic phosphanes, see: C. Wippert Rodrigues, B. Antelmann, C. Limberg, E. Kaifer, H. Pritzkow, *Organometallics* **2001**, *20*, 1825.
[22] S. Harder, L. Brandsma, J. A. Kanters, A. Duisenberg, J. H. van Lenthe, *J. Organomet. Chem.* **1991**, *420*, 143.
[23] C. Jutz, F. Voithenleitner, *Chem. Ber.* **1964**, *97*, 29.
[24] V. Ravindar, H. Hemling, H. Schumann, J. Blum, *Synth. Commun.* **1992**, *22*, 1453.
[25] M. Hesse, H. Meier, B. Zeeh, *Spektroskopische Methoden in der organischen Chemie*, Georg Thieme Verlag, Stuttgart, **1995**.
[26] M. Traetteberg, *J. Am. Chem. Soc.* **1964**, *86*, 4265.
[27] [27a] P. Bönzil, M. Neuenschwander, P. Engel, *Helv. Chim. Acta* **1990**, *73*, 1685. [27b] G. Cavicchio, G. Gaudiano, P. P. Ponti, *Tetrahedron Lett.* **1980**, *21*, 2333.
[28] [28a] A. Roberts, M. W. Whiteley, *J. Organomet. Chem.* **1993**, *458*, 131. [28b] H. Wadepohl, W. Galm, H. Pritzkow, *Organometallics* **1996**, *15*, 570 and references cited therein.
[29] J. D. Dunitz, P. Pauling, *Helv. Chim. Acta* **1960**, *43*, 2188.
[30] C. Jiabi, Y. Jiengo, L. Guixin, X. Weihua, S. Meicheng, Z. Zeying, T. Youqi, *J. Organomet. Chem.* **1987**, *329*, 69.
[31] G. R. Clark, G. J. Palenik, *J. Organomet. Chem.* **1973**, *50*, 185.
[32] M. L. Ziegler, H. E. Sasse, B. Nuber, *Z. Naturforsch., Teil B* **1975**, *30*, 26.
[33] M. D. Rausch, A. K. Ignatowicz, M. R. Churchill, T. A. O'Brien, *J. Am. Chem. Soc.* **1968**, *90*, 3242.
[34] [34a] R. W. Grime, M. W. Whiteley, *J. Chem. Soc., Dalton Trans.* **1994**, 1671. [34b] E. Schwed, H.-U. Hund, W. Bosch, H. Berke, *Helv. Chim. Acta* **1991**, *74*, 189.
[35] [35a] H. Brunner, *Eur. J. Inorg. Chem.* **2001**, 905. [35b] H. Brunner, *Angew. Chem.* **1999**, *111*, 1248; *Angew. Chem. Int. Ed.* **1999**, *38*, 1194.
[36] H. Brunner, M. Muschiol, I. Bernal, G. M. Reisner, *J. Organomet. Chem.* **1980**, *198*, 169.
[37] Crystal data for **6**·$CHCl_3$: a = 8.5415(10), b = 27.360(3), c = 11.2183(13) Å, β = 93.934(2)°, Z = 4, monoclinic, space group $P2_1/c$ (no. 14), final R value = 4.78% based on 5256 observed structure factors [$I \geq 2\,\sigma(I)$].
[38] Y.-O. Yeung, A. C. H. Ng, D. K. P. Ng, *Inorg. Chim. Acta* **1999**, *288*, 226.
[39] [39a] M. L. H. Green, D. K. P. Ng, R. C. Tovey, *J. Chem. Soc., Chem. Commun.* **1992**, 918. [39b] M. L. H. Green, D. K. P. Ng, R. C. Tovey, A. N. Chernega, *J. Chem. Soc., Dalton Trans.* **1993**, 3203.
[40] [40a] M. L. H. Green, D. K. P. Ng, *J. Chem. Soc., Chem. Commun.* **1992**, 1116. [40b] M. L. H. Green, D. K. P. Ng, H.-V. Wong, *J. Chem. Soc., Dalton Trans.* **1993**, 3213.
[41] M. L. H. Green, A. Harrison, P. Mountford, D. K. P. Ng, *J. Chem. Soc., Dalton Trans.* **1993**, 2215.
[42] A. Gourdon, K. Prout, *Acta Crystallogr., Sect. B* **1982**, *38*, 1596.
[43] [43a] P. A. van der Schaaf, W. J. J. Smeets, A. L. Spek, G. van Koten, *J. Chem. Soc., Chem. Commun.* **1992**, 717. [43b] P. A. van der Schaaf, R. A. T. M. Abbenhuis, D. M. Grove, W. J. J. Smeets, A. L. Spek, G. van Koten, *J. Chem. Soc., Chem. Commun.* **1993**, 504. [43c] P. A. van der Schaaf, R. A. T. M. Abbenhuis, W. P. A. van der Noort, R. de Graaf, D. M. Grove, W. J. J. Smeets, A. L. Spek, G. van Koten, *Organometallics* **1994**, *13*, 1433.
[44] [44a] C. E. Davies, I. M. Gardiner, J. C. Green, M. L. H. Green, N. J. Hazel, P. D. Grebenik, V. S. B. Mtetwa, K. Prout, *J. Chem. Soc., Dalton Trans.* **1985**, 669. [44b] J. C. Green, M. L. H. Green, N. M. Walker, *J. Chem. Soc., Dalton Trans.* **1991**, 173.
[45] J. A. M. Brandts, J. Boersma, A. L. Spek, G. van Koten, *Eur. J. Inorg. Chem.* **1999**, 1727, and references cited therein.
[46] M. Elian, M. M. L: Chen, D. M. P. Mingos, R. Hoffmann, *Inorg. Chem.* **1976**, *15*, 1148.
[47] M. R. Buchmeiser, *Chem. Rev.* **2000**, *100*, 1565.
[48] [48a] T. M. Trnaka, R. H. Grubbs, *Acc. Chem. Res.* **2001**, *34*, 18. [48b] A. Fürstner, *Angew. Chem.* **2000**, *112*, 3140; *Angew. Chem. Int. Ed.* **2000**, *39*, 3012. [48c] R. R. Schrock, *Tetrahedron* **1999**, *55*, 8141.
[49] K. J. Ivin, D. T. Laverty, J. J. Rooney, *Makromol. Chem.* **1977**, *178*, 1545.
[50] T. Oshika, H. Tabuchi, *Bull. Chem. Soc. Jpn.* **1968**, *41*, 211.
[51] J.-L. Hérrison, Y. Chauvin, *Makromol. Chem.* **1970**, *141*, 161.
[52] T. Asao, M. Oda, in: *Methoden der Organischen Chemie (Houben-Weyl)* **1985**, vol. V/2c, p. 49.
[53] H. J. Dauben, L. R. Lewis, R. Honnen, K. M. Harmon, *J. Org. Chem.* **1960**, *25*, 1442.
[54] CCDC-171207 to -171213 (**2**, **4**−**9**) contain the supplementary crystallographic data for this paper. These data can be obtained free of charge at www.ccdc.cam.ac.uk/conts/retrieving.html or from the Cambridge Crystallographic Data Centre, 12 Union Road, Cambridge CB2 1EZ, UK [Fax: (internat.) + 44-1223/336-033; E-mail: deposit@ccdc.cam.ac.uk].
[55] *SORTAV*: R. H. Blessing, *J. Appl. Crystallogr.* **1997**, *30*, 421.
[56] *SMART*, Bruker AXS, **2000**.
[57] *SHELXS-97*: G. M. Sheldrick, *Acta Crystallogr., Sect. A* **1990**, *46*, 467.
[58] *SHELXL-97*: G. M. Sheldrick, Universität Göttingen, **1997**.
[59] *ORTEP-3*: L. J. Farrugia, University of Glasgow, **1999**.

Received September 26, 2001
[I01378]

Octagallane (tBu$_3$Si)$_6$Ga$_8$ and Its Reduction to (tBu$_3$Si)$_6$Ga$_8^{2-}$ – On the Existence of Isomeric Gallium Clusters[‡]

Nils Wiberg,*[a] Thomas Blank,[a] Heinrich Nöth,[a][‡‡] Max Suter,[a][‡‡] and Markus Warchhold[a][‡‡]

Keywords: Clusters / Gallium / Isomers / Silicon

Thermolysis of the trigallanyl radical R*$_4$Ga$_3^{\cdot}$ in heptane at 60 °C leads to the dark blue octagallane R*$_6$Ga$_8$ (R* = supersilyl SitBu$_3$), as well as the digallanyl radical R*$_3$Ga$_2^{\cdot}$ and the *tetrahedro*-tetragallane R*$_4$Ga$_4$. In addition, supersilyl radicals R*$^{\cdot}$ are formed which stabilize themselves either by dimerization or by addition of hydrogen atoms. R*$_6$Ga$_8$ can be reduced in THF with NaC$_{10}$H$_8$ to the dark-red octagallanediide Na$_2$Ga$_8$R*$_6$·2THF. According to an X-ray structure analysis of R*$_6$Ga$_8$ and R*$_6$Ga$_8^{2-}$ one finds that the Ga atoms of four R*Ga moieties, together with two "naked" Ga atoms, occupy the corners of a distorted octahedron; the "naked" Ga atoms themselves are located, along with Ga atoms of two further R*Ga moieties, at the corners of a distorted square. The reduction of R*$_6$Ga$_8$ leads only to a negligible shortening of the Ga–Ga distances from 2.64 to 2.61 Å (mean values) in R*$_6$Ga$_8^{2-}$. Both the octagallanes possess Ga$_8$ frameworks previously unknown for group 13 clusters. They are isomeric to the recently described Ga$_8$ framework of the octagallane Tsi$_6$Ga$_8$ [Tsi = trisyl C(SiMe$_3$)$_3$]. Hence, not only boron but also the heavier group 13 atoms form isomeric clusters.

Introduction

Cluster compounds R$_m$E$_n$ of the heavier group 13 metals Al, Ga, In, Tl — unlike those of B — became accessible only recently when it was realized that the tendency of R$_m$E$_n$ to disproportionate into R$_3$E and E (or R$_2$ and E) can be stopped by employing bulky substituents such as trisyl (Tsi) [C(SiMe$_3$)$_3$], hypersilyl (Hsi) [Si(SiMe$_3$)$_3$] or supersilyl (R*) [Si(CMe$_3$)$_3$]. In fact, numerous clusters of Ga — the subject of this publication — have been isolated within the last few years (for more than 30 gallium cluster compounds see ref.[1]).

Schnöckel and co-workers[2] recently reported the preparation of hexatrisyloctagallane Tsi$_6$Ga$_8$ (**1**) with a framework of two *tetrahedro*-tetragallanyl moieties connected by a Ga–Ga bond (see Scheme 1). We now report the isolation of hexasupersilyloctagallane R*$_6$Ga$_8$ (**3**) as well as its reduction product disodium hexasupersilyloctagallanediide-tetrahydrofuran(1/2) Na$_2$Ga$_8$R*$_6$·2THF (**4**), the Ga$_8$ frameworks of which are isomeric with the Ga$_8$ cluster of Tsi$_6$Ga$_8$ (Scheme 1). It is worth mentioning here that the In$_8$ framework of hexasupersilyloctaindane R*$_6$In$_8$ (**2**; Scheme 1), reported some years ago by us,[3] has a structure different to the structures of Tsi$_6$Ga$_8$ and R*$_6$Ga$_8$.

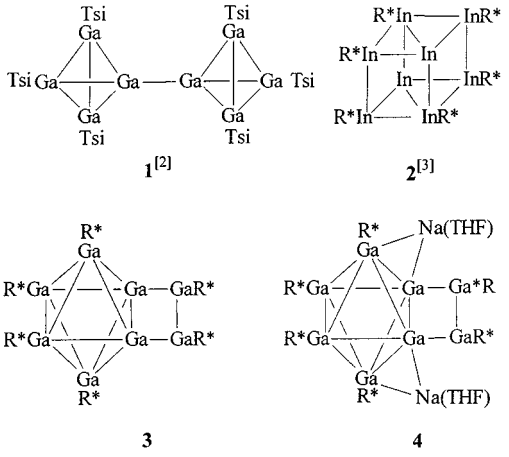

Scheme 1. Compounds with isomeric group 13 E$_8$ cluster frameworks [Tsi = C(SiMe$_3$)$_3$, R* = SitBu$_3$]

Results and Discussion

Syntheses of R*$_6$Ga$_8$ (3) and Na$_2$Ga$_8$R*$_6$·2THF (4)

The dark green radical R*$_4$Ga$_3^{\cdot}$ (**5**), which may be synthesized, via isolable intermediates, from gallium trichloride GaCl$_3$, supersilyl sodium NaR*, and supersilyl bromide R*Br,[4] slowly decomposes in heptane at 40 °C with formation of the dark blue radical R*$_3$Ga$_2^{\cdot}$ (**6**) and the dark violet *tetrahedro*-tetragallane R*$_4$Ga$_4$ (**7**) [see Scheme 2, Equation

[‡] Compounds of Silicon and Homologues, 152; Compounds of Boron and Homologues, 19. – Parts 151 and 18: Ref.[7]
[‡‡] X-ray structure analyses
[a] Department Chemie der Universität München, Butenandtstraße 5–13 (Haus D), 81377 München, Germany

(a); for the structures see Scheme 3].[4] The radical **6** transforms quantitatively at 100 °C in heptane into the tetrahedrane **7** [Scheme 2, Equation (c)] which decomposes as a solid at 322 °C and in solution at 140 °C to metallic gallium [Scheme 2, Equation (e)].[5] The supersilyl radicals R*· obtained in reactions (c) and (e) dimerize to give superdisilane molecules R^*_2, which at higher temperatures transform via R*· into supersilane R*H.[6]

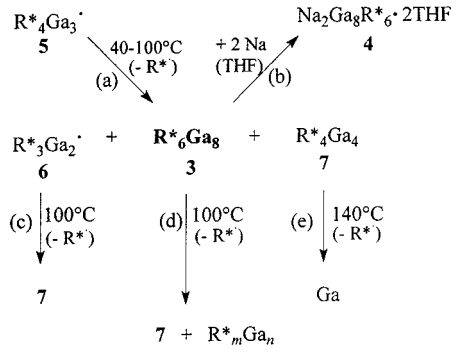

Scheme 2. Decomposition of **5** (the produced supersilyl radical R* stabilizes with formation of R^*_2 and/or R*H; R* = Si*t*Bu$_3$)

The thermolysis of **5** in addition leads to the octagallane $R^*_6Ga_8$ (**3**) [Scheme 2, Equation (a); maximum yields at about 60 °C], which itself decomposes in benzene at 100 °C to give the tetrahedrane **7** (main product) as well as unidentified cluster compounds R_mGa_n [Scheme 2, Equation (d)]. The octagallane **3** can be reduced in THF with $NaC_{10}H_8$ to give the octagallanediide $Na_2Ga_8R^*_6$·2THF (**4**) [Scheme 2, Equation (b)]. Reduction of the tetragallane **7** in THF with sodium occurs analogously to produce the tetragallanediide $Na_2Ga_4R^*_4$·2THF.[7]

To date our insight into the pathways of the formation and thermolysis of **3** is still incomplete. It is possible that compounds **8**−**13**, which are shown in Scheme 3 along with the isolated products **3**−**7**, may play the role of intermediates (cf. ref.[4] for formation of **3**, and the following for thermolysis of **3**). Radical **5** can react with cleavage of Ga−Ga bonds to form **6** and **9**, as well as **8** and **10**, and with cleavage of a Ga−Si bond to form **11** and R*·; radical **8**, after dimerization and R* elimination, transforms into isolable **6** (cf.[4]), and radical **6**, after elimination of R*, into non-isolable **10**. The formed gallylene **9** and the digallene **10** tetramerize and dimerize, respectively, to give isolable **7**. It is also possible that the cyclotrigallane **11** may eliminate R* and then dimerize with formation of the hitherto non-isolated hexagallane **13** which, on adding **10**, might form the isolable octagallane **3**. This compound decomposes on gentle heating to give the isolable tetrahedrane **7** and the non-isolable tetragallane **12** which possibly stabilizes with formation of unidentified oligogallanes (see above). Support for this suggestion is based on the formation of decagallanide $R^*_6Ga_{10}^-$ [8] as an isolable adduct of **12** and **13** [see also Hsi_6Ga_{10}, Hsi = Si(SiMe$_3$)$_3$ [8]] as well as the formation of dodecaindane $R^*_8In_{12}$ [9] from two molecules of the In analog of **13** (Hexaindane $R^*_4In_6$ — an obvious intermediate in the formation of $R^*_8In_{12}$ — has been observed by NMR spectroscopy[9].) In addition, a cluster formed from two equivalents of **12** with In/Dmp instead of Ga/R* has been synthesized[10] (Dmp = 2,6-Mes*$_2$C$_6$H$_3$ with Mes* = 2,4,6-*t*Bu$_3$C$_6$H$_2$). The preparation and isolation of hexagallane **13** is the next challenge for group 13 cluster chemists.

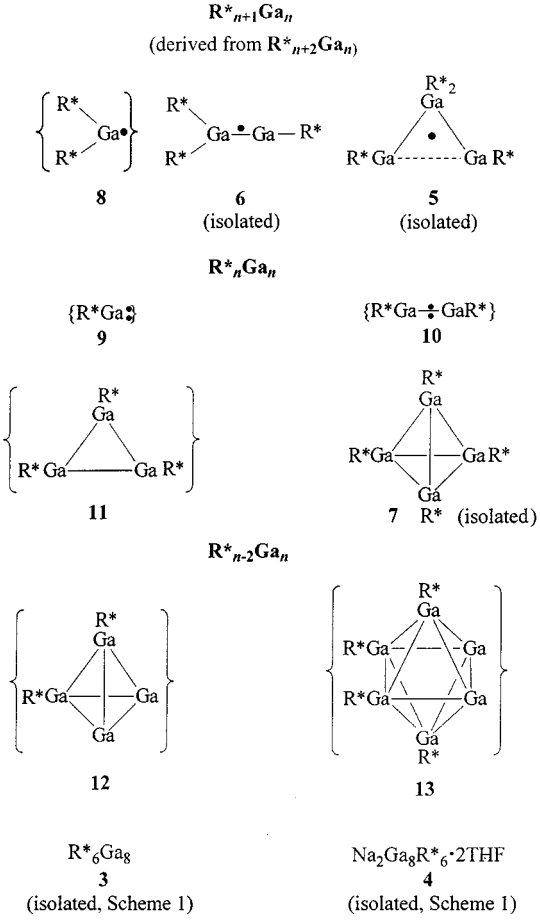

Scheme 3. Isolated and postulated products of the thermolysis of **5** as well as the reduction product **4** of **3** (R* = Si*t*Bu$_3$)

Characterization and Structures of $R^*_6Ga_8$ (3) and $Na_2Ga_8R^*_6$·2THF (4)

Hexasupersilyloctagallane (**3**) crystallizes from benzene as water- and air-sensitive dark blue prisms (monoclinic, space group $P2_1/c$) which are thermolabile at elevated temperatures. Disodium hexasupersilyloctagallanediide-tetrahydrofuran(1/2) (**4**) crystallizes from benzene as extremely water- and air-sensitive dark red prisms (triclinic, space group $P\bar{1}$).

The molecular structures of the molecules **3** and **4** in the crystal are shown in Figure 1 and 2, respectively. In both compounds the Ga atoms of four R*Ga moieties occupy the corners of a distorted octahedron together with two "naked" Ga atoms. The "naked" Ga atoms are located next to each other, along with the Ga atoms of two further R*Ga moieties, at the corners of a distorted square. The Ga

atoms that form the Ga_6 octahedron and the anellated Ga_4 square lie almost in a plane together with the Si atoms of the four connected R* groups. All quadrangle surfaces Ga1Ga2Ga7Ga8/Ga5Ga6Ga7Ga8/Ga3Ga5Ga4Ga7/Ga3Ga6Ga4Ga8 in **3** and **4** are planar (angles sum ca. 360°). The Si atoms connected at the apices of the Ga_6 octahedron are tilted towards the square. The two Na(THF) moieties of **4** bridge opposite edges between the Ga atoms of the apex and the central plane of the Ga_6 octahedron. Surprisingly, Na(THF) is not located above and below the Ga_4 square, probably due to steric reasons. $(Hsi)_6Ga_{10}$, which is derived from **4** after exchange of supersilyl for the sterically less crowded hypersilyl $Si(SiMe_3)_3$ and $Na(THF)^+$ by "isoelectronic" Ga^+, shows a Ga_{10} framework built from two anellated Ga_6 octahedrons. Scheme 4 shows the structural relationships between the octagallanediide $R_6Ga_8^{2-}$ (isolated as **4**) and the decagallane R_6Ga_{10} [isolated as $(Hsi)_6Ga_{10}$][8] via the nonagallanide $R_6Ga_9^-$ {isolated as $[Na(THF)_6]^+(Hsi)_6Ga_9^-$},[8] which are formally derived from $R_6Ga_8^{2-}$ by successive "neutralization" of the dianion with Ga^+ cations (it remains to be seen whether $R^*_6Ga_8^{2-}$ is transformed in the presence of a Ga^I compound into $R^*_6Ga_{10}$ via $R^*_6Ga_9^-$).

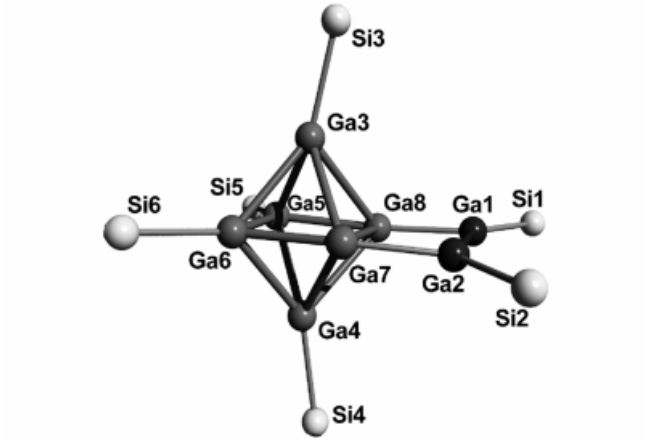

Figure 1. View of a molecule of **3** in the crystal (tBu groups excluded for clarity); for bond lengths and angles see Table 1

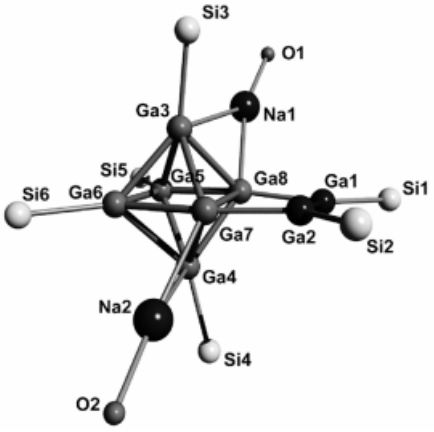

Figure 2. View of a molecule of **4** in the crystal (tBu and CH_2 groups excluded for clarity); for bond lengths and angles see Table 1

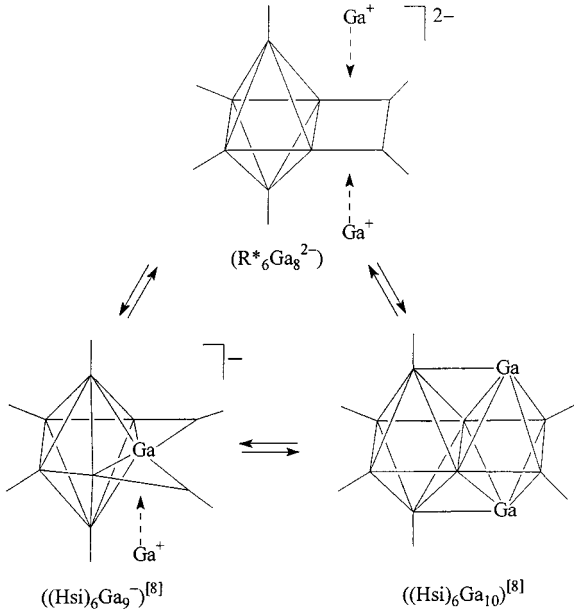

Scheme 4. Topological relation between $R^*_6Ga_2^{2-}$, $(Hsi)_6Ga_9$, and $(Hsi)_6Ga_{10}$ [R* = SitBu$_3$, Hsi = Si(SiMe$_3$)$_3$]

Table 1 presents selected bond lengths [Å] and angles [°] of **3** and **4**. The Ga−Ga distances (2.41−2.93 Å for **3** and 2.45−2.76 for **4**) lie in the typical range observed in other gallium cluster compounds such as $R^*_4Ga_4$ [5] and $R^*_8Ga_{18}/R^*_8Ga_{22}$.[1] On reduction of **3** to **4** some of the Ga−Ga bonds lengthen and some shorten, but on average they remain practically constant (mean bond length of 2.64 Å in **3** and 2.61 Å in **4**). Although the reductions of **3** and **7** with sodium in THF formally proceed in the same manner ($R^*_6Ga_8/R^*_4Ga_4$ + 2 Na + 2 THF → $Na_2Ga_8R^*_6$·2THF/$Na_2Ga_4R^*_4$·2THF), in the first case very little structural change is observed, whereas in the second case a drastic structure change and significant Ga−Ga bond shortening occurs.[7] The Ga_8 framework of **3** is less symmetric than that of **4** (cf. Ga−Ga distances). The Na−GaR*, Na−Ga, and Na−O distances are 3.52 Å (mean value), 2.99 Å, and 2.31 Å (angles sum at Na 357°, mean value of the Ga−Na−Ga angles 46°), respectively.

Compounds **3** and **4** possess a framework of eight Ga atoms that was previously unknown for clusters of the group 13 elements B − Tl. The isolation of $R^*_6Ga_8$ (**3**) and Tsi_6Ga_8 (**1**)[2] shows for the first time that the heavier group 13 elements can also form isomeric clusters that hitherto were thought to be restricted to boron.

Compound **3** can be described as a *conjuncto*-octagallane, based on hexagallane $R^*_4Ga_6$ (**13**) and digallene $R^*_2Ga_2$ (**10**). Considering the Wade−Mingos rules[11] compound **13** may therefore be classified as a doubly capped *tetrahedro*-tetragallane, that is a *hypoprecloso*-hexagallane [**13** possesses 10 cluster electrons ($2n$ − 2 with n = number of cluster atoms), giving 1 electron for Ga and two electrons for GaR*], although this description does not agree at all with the structure obtained for **3** by X-ray crystallography (see Table 1).

Table 1. Selected bond lengths and angles of the molecules **3** and **4** in the crystal

Bond lengths [Å][a]	**3**	**4**
Ga7−Ga8	2.782(3)	2.678(1)
Ga1−Ga2/Ga5−Ga6	2.519(2)/2.561(3)	2.535(1)/2.685(1)
Ga1−Ga8/Ga2−Ga7	2.406(3)/2.446(3)	2.466(1)/2.453(1)
Ga5−Ga8/Ga6−Ga7	2.638(3)/2.502(3)	2.630(1)/2.561(1)
Ga3−Ga5/Ga3−Ga6	2.652(2)/2.713(2)	2.757(1)/2.641(1)
Ga3−Ga7/Ga3−Ga8	2.647(2)/2.849(2)	2.551(1)/2.592(1)
Ga4−Ga5/Ga4−Ga6	2.614(2)/2.731(2)	2.612(1)/2.761(1)
Ga4−Ga7/Ga4−Ga8	2.638(2)/2.925(2)	2.628(1)/2.536(1)
Ga−Si / Si−C (av.)	2.50/1.95	2.51/1.96
Ga4−Na1/Ga7−Na1	−	3.491(3)/2.983(2)
Ga3−Na2/Ga8−Na2	−	3.544(3)/2.989(2)
Na1−O1/Na2−O1	−	2.308(4)/2.308(5)
Bond angles [°] in quadrangles		
Ga1/Ga2/Ga7/Ga8	76.60(4)/109.36(4)/ 71.16(3)/102.44(4)	92.00(3)/90.93(3)/ 88.94(3)/87.38(3)
Ga5/Ga6/Ga7/Ga8	98.55(4)/85.97(4)/ 96.29(5)/79.11(4)	89.04(3)/90.76(3)/ 90.67(3)/89.44(2)
Ga3/Ga5/Ga4/Ga7	81.34(7)/98.46(7)/ 82.22(7)/97.98(7)	89.35(2)/87.56(2)/ 90.90(2)/91.70(3)
Ga3/Ga6/Ga4/Ga8	90.18(7)/94.19(7)/ 88.25(7)/87.36(7)	90.81(2)/86.92(2)/ 89.32(2)/92.88(3)
Bond angles [°] in triangles[b] and at other positions		
Ga(base)−Ga(apex)−Ga(base) (av.)	57.45	60.08
Ga(apex)−Ga(base)−Ga(base) (av.)	61.28	59.96
Ga1−Ga8−Ga5/Ga2−Ga7−Ga6	175.70(4)/167.11(4)	175.59(3)/174.32(3)
C−Si−C (av.)	111.1	109.9
O1−Na1−Ga4/Ga7	−	144.0(2)/163.4(2)
O2−Na2−Ga3/Ga8	−	148.0(2)/165.6(2)
Ga−Na−Ga (av.)	−	46.44
Torsion angles		
Ga5−Ga8−Ga7−Ga2	0.96	3.49
Ga6−Ga7−Ga8−Ga1	2.01	0.88
Si1−Ga1−Ga2−Si2	3.34	0.42
Si5−Ga5−Ga6−Si6	11.39	5.30

[a] Compound numbering from Figures 1 and 2. [b] Apex = Ga3, Ga4; basis = Ga5, Ga6, Ga7, Ga8.

However, **3** may also be derived from the hexagallane $R^*_6Ga_6$ − that should not be preparable for steric reasons − by substituting two neighbouring R* groups for digallanediyl -R*Ga−GaR*-. According to its 12 ($2n$) cluster electrons, $R^*_6Ga_6$ should be classified as a monocapped trigonal-bipyramidal *closo*-Ga_5 cluster, that is a *pre-closo*-hexagallane. This description agrees with the solid-state structure found for **3** (Table 1). The long Ga8−Ga3/Ga4/Ga7 distances of the $R^*_4Ga_6$ moiety of **3** suggest that $R^*_4Ga_6$ contains a trigonal-bipyramidal Ga3Ga4Ga5-Ga6Ga7 cluster with Ga8 as the edge-bridging atom. By the same reasoning, the octagallanediide **4** may be described as a derivative of the *closo*-octagallanediide $R^*_6Ga_6^{2-}$ [14 ($2n + 2$) cluster electrons] by substituting two neighbouring R* groups for -R*Ga−GaR*-, and in fact the $R^*_4Ga_6^{2-}$ moiety of **4** shows a more regular (octahedral) Ga_6 framework than the $R^*_4Ga_6$ moiety of **3** (Table 1).

Information about the structures of **3** and **4** in solution is still limited. Only one (broad) NMR signal is found for the six R* groups of **3** in benzene, whereas three NMR signals (ratio of areas 1:1:1) are found for **4** in benzene. This either means that **3** gives equal NMR shifts for the nonequivalent R* groups, or that it is fluxional. Low temperature NMR studies of **3** in solution are planned. In addition, NMR studies of **4** in donor solvents D may confirm the expected dissociation of the cluster into $Na(D)_n^+$ and $R^*_6Ga_8^{2-}$ ions.

Experimental Section

All experiments were carried out in flame-dried glass apparatus with standard Schlenk techniques under dry argon or nitrogen. Air and moisture were strictly excluded. The solvents (heptane, ben-

zene, THF) were dried with sodium plumbide or sodium in the presence of benzophenone. Available for use: C_6D_6. The following compounds were synthesized according to literature procedures: R*$_4$Ga$_3$ (**3**),[4] $NaC_{10}H_8$ in THF.[12]

NMR Spectra: Jeol GX-270 (^{1}H/^{13}C/^{29}Si: 270.17/67.94/53.67 MHz), Jeol EX-400 (^{1}H/^{13}C/^{29}Si: 399.78/100.54/79.43 MHz). The NMR spectra were recorded with the INEPT and DEPT pulse sequences using empirically optimized parameters for the mentioned groups.

Synthesis of R*$_6$Ga$_8$ (3): A solution of **5** (0.151 g, 0.130 mmol) in 5 mL of heptane was kept 25 h at 60 °C, after which time it had quantitatively decomposed into R*H,[13] R*$_2$,[13] **6**,[4] **7**,[5] and **3** (ratio of ^{1}H NMR signal areas of the R* groups of molecules R*H, R*$_2$, **7**, **3** about 1:1:5:3, corresponding to a mol ratio of the compounds of about 4:2:5:2) according to ESR, and ^{1}H, ^{13}C and ^{29}Si NMR spectroscopy. After the removal of all volatile compounds under vacuum and dissolving the residue in 2 mL of benzene, compound **3** (0.115 g, 0.066 mmol, 15%) was obtained after eight days at 8 °C as water- and air-sensitive dark-blue crystals. ^{1}H NMR (C_6D_6): δ = 1.28 (broad, 162 H, 6 SitBu$_3$). ^{13}C{^{1}H} NMR (C_6D_6): δ = 25.6/33.6 (broad/broad, 18 C/54 C, 18 CMe$_3$/18 CMe_3). ^{29}Si NMR (C_6D_6): δ = 58.7 (broad, 6 Si, 6SitBu$_3$). X-ray structure analysis: see Figure 1 (blue prisms from benzene). *Note*: The relative yields of **6** (seen only by ESR spectroscopy), **7** and **3** (seen only by NMR spectroscopy) depend, amongst others, on the reaction temperature. According to the NMR spectra, **7** and **3** are formed from **5** in heptane after 25 h at 40 or 60 or 100 °C in the mol ratio of about 99:1 or 71:29 or 100:0 (**3** is thermolabile at 100 °C).

Thermolysis of R*$_6$Ga$_8$ (3): A solution of **3** (0.073 g, 0.042 mmol) in 0.6 mL of C_6D_6 was kept for 14 h at 100 °C. After this time, according to the ^{1}H/^{13}C/^{29}Si NMR spectra, **3** had quantitatively decomposed into R*H,[13] R*$_2$,[13] **7**,[5] and an unidentified compound R$_m$Ga$_n$ (ratio of ^{1}H NMR signal areas of the R* groups of molecules R*H, R*$_2$, **7**, R$_m$Ga$_n$ about 2:1:10:(4+2), corresponding to a mol ratio of R*H, R*$_2$ and **7** of about 4:1:5). In addition, an insoluble product was formed (oligogallane ?). Characterization of the dissolved R$_m$Ga$_n$: ^{1}H NMR (C_6D_6): δ = 1.39 (broad). ^{13}C{^{1}H} NMR (C_6D_6): δ = 25.59/26.01 (s/s, 2x C/x C, 2x CMe$_3$/x CMe$_3$), 30.27/33.45 (s/s, 6x C/3x C, 2x CMe_3/x CMe_3). ^{29}Si NMR (C_6D_6): δ = 43.28/56.70 (s/s, 2x Si/x Si, 2x SitBu$_3$/x SitBu$_3$). *Note*: Octagallane R*$_6$Ga$_8$ with the structure of R*$_6$In$_8$ (**2**) should give a ratio of SitBu$_3$ NMR signal areas of 2:1).

Synthesis of Na$_2$Ga$_8$R*$_6$·2THF (4): A solution of $NaC_{10}H_8$ (0.11 mmol) in 1.5 mL of THF was added dropwise to a solution of **3** (0.05 mmol) in 10 mL of THF at −78 °C. After 5 h stirring at −78 °C all volatile components were removed from the reaction mixture under vacuum at −45 °C and the residue was dissolved in 3 mL of C_6D_6. This solution was concentrated to 0.8 mL and water- and air-sensitive red crystals of **4** were obtained after two months at 5 °C. ^{1}H NMR (C_6D_6): δ = 1.289/1.367/1.380 (s/s/s, 54 H/54 H/54 H, 2 SitBu$_3$/2 SitBu$_3$/2 SitBu$_3$), 1.124/3.325 (m/m, 8 H/8 H, 4 CH$_2$/4 CH$_2$O). ^{29}Si{^{1}H} NMR (C_6D_6): δ = 43.8/47.1/51.2 (s/s/s, 2Si/2Si/2Si, 2 SitBu$_3$/2 SitBu$_3$/2 SitBu$_3$). X-ray structure analysis: see Figure 2 (red prisms from benzene).

X-ray Structure Determinations: Data collection was performed with a Siemens P4 diffractometer equipped with an area-detector (Mo-K_α radiation λ = 0.71073 Å). Crystals were mounted in perfluoropolyether oil and data collected at T = 188(2) (**3**) and 193(2) K (**4**). The structures were solved by direct methods (SHELXS-97) and refined with full-matrix procedures against F^2 for all observed reflections. All non-hydrogen atoms were refined anisotropically and H atoms were included in the final refinement at calculated positions using a riding model and fixed isotropic U$_i$ values. A semiempirical absorption correction was applied by using the program SADABS. The structures of **3** and **4** are shown in Figure 1 and 2, crystallographic details are summarized in Table 2.
CCDC-165237 (**3**) and CCDC-165238 (**4**) contain the supplementary crystallographic data for this paper. These data can be obtained free of charge at www.ccdc.cam.ac.uk/conts/retrieving.html [or from the Cambridge Crystallographic Data Centre, 12 Union Road, Cambridge CB2 1EZ, UK; fax: (internat.) + 44-1223/336-033; E-mail: deposit@ccdc.cam.ac.uk].

Table 2. Selected parameters of the X-ray structure analyses of the compounds **3** and **4**

	3	**4**
Empirical formula	$C_{72}H_{162}Ga_8Si_6$	$C_{92}H_{190}Ga_8Na_2O_2Si_6$
M_r	1754.32	2100.72
System	monoclinic	triclinic
Space group	$P2_1/c$	$P\bar{1}$
a [Å]	25.02(2)	16.641(2)
b [Å]	16.18(2)	16.717(2)
c [Å]	25.53(3)	21.589(2)
α [°]	90	91.996(2)
β [°]	118.195(1)	90.194(2)
γ [°]	90.000	113.033(2)
V [Å^3]	9110(2)	5525(1)
Z	4	2
D [Mg m^{-3}]	1.279	1.263
μ [mm^{-1}]	2.441	2.032
F(000)	3704	2224
2θ [°]	3.10−46.50	1.88−58.26
Ranges [°]	$-21 \le h \le 22$	$-20 \le h \le 20$
	$-17 \le k \le 17$	$-20 \le k \le 22$
	$-28 \le l \le 28$	$-27 \le l \le 28$
All reflections	37958	32188
Independent	10435	16939
Observed[a]	7428	10368
R_{int}	0.0496	0.0495
x/y[a]	0.8372/0.5403	0.6946/0.6205
R_1 [$F > 4\sigma(F)$]	0.0706	0.0439
wR_2[a] [$F > 4\sigma(F)$]	0.0965	0.0878
GOOF(F^2)	0.980	0.951
Max./min. electron density[e·Å^{-3}]	0.8372/−0.5403	0.6946/−0.6205

[a] $w^{-1} = \sigma^2F_0^2 + (xP)^2 + yP$ with $P = (F_0^2 + 2F_c^2)/3$.

Acknowledgments

We thank the Deutsche Forschungsgemeinschaft and the Fonds der Chemischen Industrie for support of our research.

[1] A. Donchev, A. Schnepf, G. Stößer, E. Baum, H. Schnöckel, T. Blank, N. Wiberg, *Chem. Eur. J.* **2001**, 3348−3353.
[2] A. Schnepf, R. Köppe, H. Schnöckel, *Angew. Chem.* **2001**, *113*, 1287−1290; *Angew. Chem. Int. Ed.* **2001**, *40*, 1241−1244.
[3] N. Wiberg, T. Blank, A. Purath, G. Stößer, H. Schnöckel, *Angew. Chem.* **1999**, *111*, 2745−2748; *Angew. Chem. Int. Ed.* **1999**, *38*, 2563−2565.
[4] N. Wiberg, T. Blank, K. Amelunxen, H. Nöth, J. Knizek, T.

Habereder, W. Kaim, M. Wanner, *Eur. J. Inorg. Chem.* **2001**, 1719−1725.
[5] N. Wiberg, K. Amelunxen, H.-W. Lerner, H. Nöth, W. Ponikwar, H. Schwenk, *J. Organomet. Chem.* **1999**, *574*, 246−251.
[6] N. Wiberg, *Coord. Chem. Rev.* **1997**, *163*, 217−252.
[7] N. Wiberg, T. Blank, M. Westerhausen, S. Schneiderbauer, H. Schnöckel, I. Krossing, A. Schnepf, *Eur. J. Inorg. Chem.* **2002**, 351−356.
[8] M. Kehrwald, W. Köster, A. Rodig, G. Linti, T. Blank, N. Wiberg, *Organometallics* **2001**, *20*, 860−868.
[9] N. Wiberg, T. Blank, H. Nöth, W. Ponikwar, *Angew. Chem.* **1999**, *111*, 887−890; *Angew. Chem. Int. Ed.* **1999**, *38*, 839−841.
[10] B. E. Eichler, N. J. Hardmann, P. P. Power, *Angew. Chem.* **2000**, *112*, 391−393; *Angew. Chem. Int. Ed.* **2000**, *39*, 383−385.
[11] See standard text books on inorganic chemistry, for example N. Wiberg, *Inorganic Chemistry*, 1st English ed., Academic Press, **2001**.
[12] J. L. Wardell, in *Comprehensive Organometallic Chemistry* (Eds.: G. Wilkinson, F. G. Stone), Vol. 1, Pergamon, Oxford, **1982**, 109−111.
[13] N. Wiberg, K. Amelunxen, H.-W. Lerner, H. Schuster, H. Nöth, I. Krossing, M. Schmidt-Amelunxen, T. Seifert, *J. Organomet. Chem.* **1997**, *542*, 1−18.

Received October 2, 2001
[I01386]

Synthesis and Structural Characterization of (Carbene)ruthenium Complexes Binding Nucleobases

Jean-Luc Fillaut,*[a] Isaac de los Rios,[b] Dante Masi,[b] Antonio Romerosa,[c] Fabrizio Zanobini,[b] and Maurizio Peruzzini*[b]

Keywords: Carbenes / Ruthenium / Adenine / Uracil / X-ray crystallography / Aminophosphanes

The new (carbene)ruthenium(II) nucleobase derivatives *fac*,*cis*-[(PNP)RuCl{C($NHC_4H_3N_2O_2$)(CH_2Ph)}]Cl (**5**) and *fac*,*cis*-[(PNP)RuCl{C($NHC_5H_3N_4$)(CH_2Ph)}]Cl (**6**) [PNP = $CH_3CH_2CH_2N(CH_2CH_2PPh_2)_2$] were synthesised by treating (vinylidene)ruthenium(II) complex *fac*,*cis*-[(PNP)$RuCl_2${C=C(H)Ph}] (**1**) with 5-aminouracil or adenine, respectively. Both complexes were characterized by spectroscopic techniques (IR and NMR) and elemental analyses, which confirmed the formation of the aminocarbene moieties incorporating 1 equiv. of the nucleobase in the complex framework. Crystal and molecular structure determination by X-ray diffraction analysis of the uracil derivative **5** revealed a very unusual *O*-coordination of the exocyclic C=O group on the C(4) atom of the uracil ring to the ruthenium atom leading to an unprecedented six-membered aminocarbene metallacycle.
(© Wiley-VCH Verlag GmbH, 69451 Weinheim, Germany, 2002)

Introduction

The chemistry of organotransition metal complexes containing biologically important molecules as ligands constitutes a recent research field of general interest relevant to aspects such as DNA condensation,[1] heavy metal toxicity and mutagenicity,[2] and, in a broader sense, to topics related to the subject of supramolecular architectures where metal-to-ligand coordination bonds are intimately combined with H-bonding interactions. These supramolecular bio-organometallic aggregates have potential implications for the design of new metal-based drugs[3] as well as in material chemistry.[4]

The presence of metal ions in these systems introduces additional variables, whose effects remain largely to be explored in detail. These include inter alia the overall charge of the complex, the oxidation state of the metal atom, the electronic and steric properties of the coligands and also, in charged compounds, the nature of the counterion.[5] Among transition metal ions, ruthenium has unique properties making it particularly useful in drug design.[6] A ruthenium anticancer agent showing promising activity against otherwise resistant tumours and a low systemic toxicity has recently entered clinical trials.[7] Remarkably, bio-organometallic compounds conjugating nucleobases with typical metal−carbon multiple bond species such as carbenes and carbynes have not yet been described in spite of the enormous interest in this class of compounds[8] and the steadily increasing attention paid to the search of new routes to ruthenium species bio-conjugated with nucleobases.

Herein, we wish to report on our results in this area describing the first examples of transition metal carbenes incorporating nucleobases in their molecular structure. Noticeably, an unprecedented bonding mode of the uracil moiety to a transition metal ion has been ascertained by X-ray analysis.

[a] Institut de Chimie de Rennes, UMR 6509 CNRS − Université de Rennes 1,
35042 Rennes, France
Fax: (internat.) + 33-2/99286939
E-mail: jean-luc.fillaut@univ-rennes1.fr
[b] ISSECC CNR,
Via Jacopo Nardi, 39, 50132 Firenze, Italy
Fax: (internat.) + 39-055/247-8366
E-mail: peruz@fi.cnr.it
[c] Área de Química Inorgánica, Facultad de Ciencias, Universidad de Almería,
Almería, Spain

Results and Discussion

Synthesis and Characterization of the (Carbene)ruthenium Nucleobase Derivatives *fac*,*cis*-[(PNP)RuCl{C($NHC_4H_3N_2O_2$)-(CH_2Ph)}]Cl (5) and *fac*,*cis*-[(PNP)RuCl{C($NHC_5H_3N_4$)(CH_2Ph)}]Cl (6)

In recent years, some of us reported that the reaction of the (vinylidene)ruthenium(II) complex *fac*,*cis*-[(PNP)-$RuCl_2${C=C(H)Ph}] (**1**) [PNP = $CH_3CH_2CH_2N$-$(CH_2CH_2PPh_2)_2$] with a variety of primary amines is a simple general method to synthesising the neutral aminocarbene complexes *fac*,*cis*-[(PNP)$RuCl_2${C(NHR)(CH_2Ph)}]

(**2**) in excellent yields via the intermediary aminoalkynyl compounds **3**.[9] The aminocarbene complexes are air- and thermally stable in the solid state but slowly decompose in boiling THF eliminating toluene and forming the corresponding isocyanide complexes *fac*,*cis*-[(PNP)$RuCl_2$-(C≡NR)] (**4**) (Scheme 1).

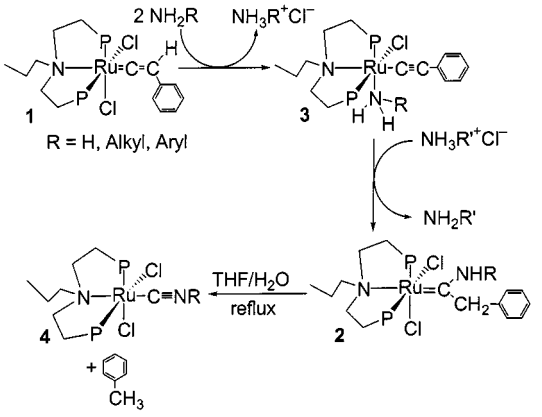

Scheme 1

We were intrigued by the generality of the reaction of **1** with primary amines, and so decided to investigate the possibility of introducing biologically relevant molecules such as 5-aminouracil and adenine into the skeleton of the ruthenium−carbene moiety. The incorporation of both 5-aminouracil and adenine in the ruthenium complex would lead to the building of bifunctional organometallic moieties that could exploit their potential to act as ligands capable of recognising complementary nucleobases trough hydrogen bond interactions.

With these ideas in mind, we have examined the reactivity of the vinylidene complex **1** with a slight excess of 5-aminouracil or adenine. This was done by adapting our general preparation of the aminocarbene complexes **2** for both the insolubility of these nucleobases in common organic solvents and the reluctance of these weak bases to interact with the Ru=C=C fragment under less forceful conditions. A straightforward reaction was obtained by allowing **1** to react with an excess of either 5-aminouracil or adenine in distilled dimethylformamide at ca. 110 °C where both the nucleobases and the ruthenium precursors are soluble enough. Concentration of the hot solution to dryness under vacuum left a yellowish residue which was taken up with a mixture of dichloromethane/ethanol to yield, after workup, a crop of light-yellow microcrystals of *fac*,*cis*-[(PNP)-$RuCl\{C(NHC_4H_3N_2O_2)(CH_2Ph)\}]Cl$ (**5**) or orange platelets of *fac*,*cis*-[(PNP)$RuCl\{C(NHC_5H_3N_4)(CH_2Ph)\}]Cl$ (**6**), respectively (Scheme 2). The uracil derivative could be recrystallized in air as lemon-yellow needles suitable for an X-ray diffraction study from dichloromethane/petroleum ether mixtures. In contrast, several attempts to grow crystals of **6** (either as chloride or tetraphenylborate salt) were unsuccessful.

Apart from conventional spectroscopic techniques (IR and NMR spectroscopy) and elemental analysis (see Exp. Sect.), which confirmed the incorporation of one equiv. of

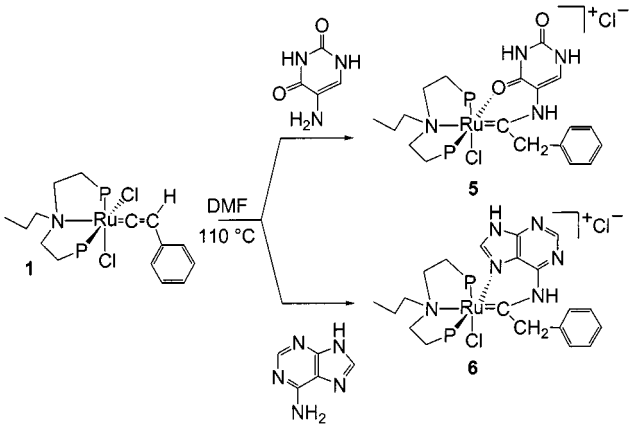

Scheme 2

nucleobase and the formation of the expected aminocarbene moiety in the complex framework of both **5** and **6**, precious information that shed light on their structures was inferred from chemical tests. A complete X-ray diffraction analysis was also obtained for **5** (see below).

Unambiguous evidence for the presence of the aminocarbene ligands in **5** and **6** was provided by NMR spectroscopy ([D_6]DMSO) that showed the typical ^{13}C NMR absorptions of the aminocarbene carbon atom at $\delta = 257.9$ (t, $^2J_{C,P} = 13.9$ Hz) for **5** and $\delta = 284.5$ (t, $^2J_{C,P} = 19.2$ Hz) for **6**. The magnitude of the coupling constants, which are in the expected range for Fischer-type (carbene)ruthenium(II) complexes points to a *trans* disposition of the carbene ligand and the nitrogen donor atom of the PNP ligand. The IR spectra contained a broad absorption in the N−H stretching region (3500−3400 cm^{-1}), while the uracil derivative, in addition, exhibited medium-to-strong bands at 1720, 1643 and 1621 cm^{-1}, which were assigned to the stretching of the oxo groups in position 2 and 4 and to the C(5)−C(6) double bond in the uracil residue, respectively. In the ^1H NMR spectra, the hydrogen atoms of the benzyl substituents are diastereotopic and thus give rise to an AB multiplet, whereas the NH proton of the aminocarbene moiety appears as a very broad singlet at $\delta = 11.70$ (**5**) and $\delta = 13.90$ (**6**) due to the presence of the quadrupolar ^{14}N-nucleus.

In keeping with a *facial* arrangement of the PNP ligand and an inequivalent chemical environment of the two phosphane ends, the $^{31}P\{^1H\}$ NMR spectra in [D_6]DMSO showed slightly perturbed second-order AB splitting patterns with homonuclear geminal coupling constants $^2J_{P,P}$ equal to 32.5 and 27.5 Hz, respectively. The inequivalence of the two P-donor atoms in both **5** and **6** was quite unexpected in view of the *facial* geometry adopted by the aminodiphosphane ligand ($\delta_P > 39$)[10] and of the absence of any chiral element in the frame of the nucleobases incorporated in the complexes.[9] While a ^{31}P NMR singlet could be anticipated for a *fac*,*cis*-PNP(carbene)Ru complex, the occurrence of an AB system could not be simply explained. On the basis of the elemental analysis, confirming two chloride ligands for each ruthenium atom, a reasonable structural

hypothesis suggested that one of the two chloride ligands was no longer coordinated to the metal centre, therefore acting as the counteranion in a charged complex. In agreement with this hypothesis, both **5** and **6** readily exchanged one of the two chloride ions with tetraphenylborate when their solutions in CH_2Cl_2/EtOH were treated with excess $NaBPh_4$. Elemental analysis, IR and NMR spectroscopy, as well as solution conductivities (1,2-dichloroethane) clearly indicated that the tetraphenylborate complexes *fac*,*cis*-[(PNP)RuCl{C($NHC_4H_3N_2O_2$)(CH_2Ph)}]BPh_4 (**5-BPh$_4$**) and *fac*,*cis*-[(PNP)RuCl{C($NHC_5H_3N_4$)(CH_2Ph)}]BPh_4 (**6-BPh$_4$**), were quantitatively produced by metathetical chloride substitution.

Crystal Structure of *fac,cis*-[(PNP)RuCl{C($NHC_4H_3N_2O_2$)(CH_2Ph)}]Cl·CH_3OH·H_2O (5·CH_3OH·H_2O)

The easy formation of the tetraphenylborate salts of **5** and **6** raised the question of which structure is attributed to carbenes **5** and **6** where a nucleobase is incorporated with a (carbene)ruthenium moiety. This makes it of paramount importance to attain single crystals suitable for an X-ray diffraction analysis. While for **6** we were unable to grow well-shaped crystals, the thermal and air robustness of the uracil derivative makes it feasible to grow crystals of **5** for the diffraction study from a saturated dichloromethane/methanol solution in air. Thus, in order to collect geometrical information on this class of aminocarbenes, an X-ray analysis was carried out on a single crystal of **5**. An ORTEP drawing of the complex is shown in Figure 1 with the adopted atomic numbering scheme. A list of selected bond lengths and angles is given in Table 1.

In the structure of *fac*,*cis*-[(PNP)RuCl{C($NHC_4H_3N_2O_2$)(CH_2Ph)}]Cl·CH_3OH·H_2O (**5·CH_3OH·H_2O**), formed by *fac*,*cis*-[(PNP)RuCl{C($NHC_4H_3N_2O_2$)(CH_2Ph)}]$^+$ cations, chloride anions and interspersed solvate molecules of methanol and water in a 1:1:1:1 ratio, the arrangement of the non-hydrogen atoms about the metal atom in the cation is approximately octahedral with the aminodiphosphane ligand occupying three facial coordination sites. A chloride ligand and one aminocarbene group incorporating the 5-aminouracil fragment and located *trans* to the PNP nitrogen donor, are also coordinated to the metal centre. The coordination polyhedron about the ruthenium atom is completed by O-coordination from the exocyclic C=O group on the C(4) atom of the uracil ring. The arrangement found in **5** does not significantly differ from that established in the related aminocarbene derivative *fac*,*cis*-[(PNP)$RuCl_2${C[NH(*S*)-(−)-CH(Me)(1-naphthyl)](CH_2Ph)}], which was also authenticated by X-ray methods,[9] as well as in other PNPruthenium(II) complexes.[10,11] Bond lengths and angles match well with the data reported for other (aminocarbene)ruthenium complexes.[9,12] Cocrystallised molecules of methanol and water, the latter likely taken from the air, contribute to the stability of the crystal lattice. As a matter of fact, a net of hydrogen bonding interactions involves the uracil N(4), the methanol O(3) and the water O(4) atoms, the most important contacts being N(4)···O(3) 2.79 Å and O(3)···O(4) 2.72 Å. Additionally, the O(4) water atom shows weak interactions

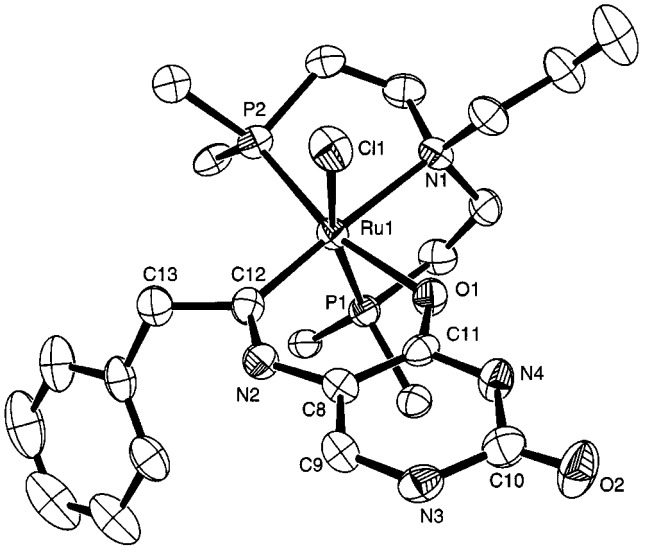

Figure 1. ORTEP drawing of the complex cation *fac*,*cis*-[(PNP)RuCl{C($NHC_4H_3N_2O_2$)(CH_2Ph)}]$^+$; only the *ipso*-carbon atoms of the PNP phenyl substituents are shown for the sake of clarity

Table 1. Selected bond lengths [Å] and angles [°] for *fac*-[(PNP)RuCl{C($NHC_4H_3N_2O_2$)(CH_2Ph)}]Cl·CH_3OH·H_2O (**5**·CH_3OH·H_2O)

Ru(1)−C(12)	1.956(6)	C(12)−Ru(1)−O(1)	91.99(19)
Ru(1)−O(1)	2.126(4)	C(12)−Ru(1)−P(2)	100.27(17)
Ru(1)−P(2)	2.2792(17)	O(1)−Ru(1)−P(2)	165.25(11)
Ru(1)−P(1)	2.2847(17)	C(12)−Ru(1)−P(1)	98.58(17)
Ru(1)−N(1)	2.352(5)	O(1)−Ru(1)−P(1)	85.37(11)
Ru(1)−Cl(1)	2.4631(17)	P(2)−Ru(1)−P(1)	100.71(6)
O(1)−C(11)	1.240(6)	C(12)−Ru(1)−N(1)	176.0(2)
O(2)−C(10)	1.203(7)	O(1)−Ru(1)−N(1)	84.19(15)
N(2)−C(12)	1.349(7)	P(2)−Ru(1)−N(1)	83.33(12)
N(2)−C(8)	1.415(7)	P(1)−Ru(1)−N(1)	82.42(12)
N(3)−C(10)	1.368(8)	C(12)−Ru(1)−Cl(1)	86.94(17)
N(3)−C(9)	1.372(7)	O(1)−Ru(1)−Cl(1)	81.15(11)
N(4)−C(11)	1.371(7)	P(2)−Ru(1)−Cl(1)	91.28(6)
N(4)−C(10)	1.386(7)	P(1)−Ru(1)−Cl(1)	165.61(6)
C(8)−C(9)	1.352(7)	N(1)−Ru(1)−Cl(1)	91.20(12)
C(8)−C(11)	1.430(8)	C(11)−O(1)−Ru(1)	124.2(4)
C(12)−C(13)	1.528(8)	C(12)−N(2)−C(8)	128.6(5)
C(13)−C(1*5)	1.518(6)	C(10)−N(3)−C(9)	123.9(5)
		C(11)−N(4)−C(10)	127.5(5)
		C(9)−C(8)−N(2)	118.0(5)
		C(9)−C(8)−C(11)	118.3(5)
		N(2)−C(8)−C(11)	123.7(5)
		C(8)−C(9)−N(3)	121.7(5)
		O(2)−C(10)−N(3)	124.3(6)
		O(2)−C(10)−N(4)	123.0(6)
		N(3)−C(10)−N(4)	112.6(5)
		O(1)−C(11)−N(4)	117.5(5)
		O(1)−C(11)−C(8)	126.6(5)
		N(4)−C(11)−C(8)	115.9(5)
		N(2)−C(12)−C(13)	107.5(5)
		N(2)−C(12)−Ru(1)	123.1(4)
		C(13)−C(12)−Ru(1)	128.8(4)
		C(1*5)−C(13)−C(12)	118.6(5)

with both chlorine atoms [3.24 Å with Cl(1), 3.31 Å with Cl(2)].

The most notable feature of the crystal structure of **5** is the unexpected metallation of the C=O group at the 4-position of the uracil moiety, that, therefore, behaves as an η^1-monodentate ligand through the exocyclic oxygen atom. The complexation of one of the carbonyl groups of the uracil ligand to the ruthenium centre was quite surprising and has no precedents in this series of PNP(carbene)Ru derivatives. In this regard, it is remarkable to underline that the reaction of **1** with several α,ω-diamines parallels that established for simple monoamines and resulted in the synthesis of (aminocarbene)ruthenium complexes with a pendant, noncoordinated, amino arm.[13]

Although few examples of transition metal complexes containing uracil residues have been described so far,[5a,14a] the arrangement found in **5**, where the nucleobase metallates through one carbonyl group, is unprecedented.[14] The C(11)−O(1) bond length [1.240(6) Å] of the carbonyl group involved in the intramolecular interaction with the ruthenium atom [the O(1)−Ru separation is 2.126(4) Å], even if longer than in free uracil [1.227(2) Å],[15] does not significantly differ from that observed in the known uracil derivatives containing metal complexes.[5a,14a] This points to a weak interaction between the uracil moiety and the ruthenium centre. The two rings deriving from the adopted geometry of the (aminocarbene)ruthenium complex with 5-aminouracil are virtually planar. In order to analyse the influence of the coordination of one uracil carbonyl group to the ruthenium centre, the bond lengths of the uracil ring in **5** have been compared with those determined for the free ligand.[15] Five different valence isomers may be drawn in which the positive charge is moved from the metal atom to the nitrogen atoms N(3) and N(4) (Scheme 3).

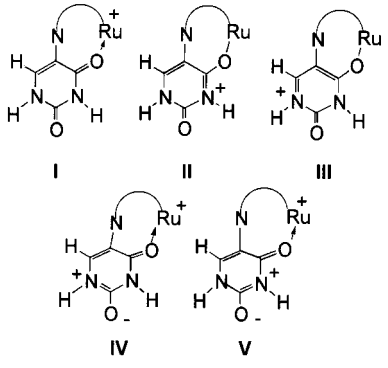

Scheme 3. Structure of the possible valence isomers for the metal modified uracil ring in **5**

A perusal of the bond lengths listed in Table 1, suggests that both **IV** and **V**, in which the oxygen atom O(2) bears a negative charge, do not provide a major contribution to the representation of **5**, and, in keeping with this hypothesis, the "distal" C(10)−O(2) separation (1.203 Å), which is typical of a C=O double bond, is shorter in **5** than in the free uracil molecule [1.218(2) Å].[15] In contrast, the C(10)−N(4) bond length is definitely longer than all the other C−N distances pertaining to the uracil residue in **5**, which rules out the occurrence of a ketoimine equilibrium involving N(4) and O(2). The closeness of two positive charges in **V** also agrees with this observation. In accordance with a significant contribution from the structures **II** and **III**, both C(9)−N(3) and C(11)−N(4) bond lengths are slightly shorter in **5** than in the free uracil while the separations C(9)−C(8) and C(8)−C(11) are longer and shorter, respectively, with respect to the free nucleobase. On the basis of all these findings, it is conceivable that form **I** corresponds to the closest representation of the cationic complex **5**.

Although one of the two carbonyl groups of the uracil moiety is blocked by coordination to the ruthenium centre, preventing H-bonding, **5** still presents a potential hydrogen bond donor/hydrogen bond acceptor/hydrogen bond donor arrangement (DAD),[16] capable of forming hydrogen bonds with molecules containing complementary ADA or AD ends (Scheme 4).

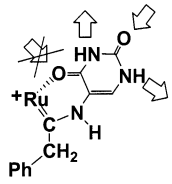

Scheme 4

The formation of centrosymmetric [2+2] "dimer pairs" by association of N−H···O hydrogen bonds between an amide N−H group of one molecule of **5** with the "free" carbonyl oxygen atom of a second molecule of **5** and vice versa could be expected. Actually, the analysis of the crystal packing of **5** does not permit us to detect any links via hydrogen bonds between independent molecules, even if geometrical complementarity is unaltered.

NMR Spectroscopic Studies of the H-Binding Properties of the (Aminocarbene)ruthenium Complexes 5 and 6

Because of coordination to the metal centre in **5** (and **6**), it is evident that the "usual" H bonding at the uracil (or adenine) fragment is not possible. Nevertheless, the new aminocarbenes **5** and **6** bear appropriate hydrogen bonding molecular recognition sites, which could, in principle, still form non-covalent host-guest assemblies with suitable substrates.[5a,17] Therefore, in order to assess this property, we decided to study how the ^{1}H NMR chemical shift of the N−H protons of **5** and **6** change as a function of the sample concentration and of the presence of substrates with complementary hydrogen-bonding recognition sites.[18] At first, we noticed that, independently from the solvent used, (CD_2Cl_2 or CD_3CN), the N−H chemical shift of both **5** and **6** is not concentration-dependent. Whereas this fact is quite intriguing and suggests that dimerisation of these nucleobase aminocarbenes does not occur through hydrogen bonding, it can be related with the information derived from the X-ray study of **5**. This behaviour does not have a clear explanation as electrostatic repulsions between cationic organometallic species, steric hindrance due to the

presence of bulky ancillary ligands,[19] or even changes in the electronic distribution in the metal-bounded nucleobases,[20] could be responsible. In order to understand better this piece of evidence, we unsuccessfully attempted to detect by ^{1}H NMR spectroscopy the formation of hydrogen bonding adducts of **5** in the presence of adenine. The latter could indeed act as a neutral sterically nondemanding molecule with a DA (DA = donor/acceptor)[16] motif capable of utilising only one hydrogen bond acceptor and donor motif of the uracil derivative **5** in a Watson−Crick manner.[16,17] This negative result could suggest that either electrostatic repulsions or steric hindrance at the approaching of a complementary motif to the metal-modified uracil are not decisive. In any case, it can be anticipated that O-binding of the uracil ring to a metal ion significantly disturbs its electronic complementarity with the adenine partner.

Mechanism of the Formation of the Nucleobase Carbene Complexes

The mechanism accounting for the formation of the vast family of PNP aminocarbene derivatives by nucleophilic attack of primary amines to the (vinylidene)ruthenium complex **1** encompasses a well-established pathway requiring 2 equiv. of amine.[9,10] In summary, the first amine equivalent deprotonates the vinylidene C_β carbon atom, while the second one coordinates the metal centre prior to be transferred, by an intramolecular nucleophilic attack, on the C_α carbon atom of the alkynyl intermediate (Scheme 1).

The synthetic route to both **5** and **6** most likely goes through a related pathway with the obvious changes expected by the formation of the metallated aminocarbenes. In the case of **6**, the N(7) atom of the adenine is responsible for chelation at the ruthenium centre affording the unprecedented cyclic adeninylcarbene **6**. Remarkably, once formed, **5** is much more robust than **6** indicating that the Ru−O=C interaction involving the uracil system is much more stable than the Ru−N(7) interaction of the aminocarbene deriving from adenine.

Monitoring the reaction between **1** and adenine in an NMR tube via ^{1}H and ^{31}P NMR spectroscopy is a straightforward method to providing experimental evidence for the proposed mechanism as well as confirming that for **6,** the final reaction product is an N(7)-metallated adeninylcarbene (Scheme 5). In the case at hand, when 2 equiv. of adenine are dissolved in a 5-mm NMR tube containing a solution of **1** in [D_6]DMSO and the solution is monitored by ^{31}P NMR spectroscopy, a neat reaction takes place at room temperature affording a single compound displaying a well-resolved AB spin system at δ = 53.90 and 52.01 with $J_{P,P}$ = 35.2 Hz. The latter derives from the chemical inequivalence of the two PPh_2 groups in the adenine complex *fac*,*cis*-[(PNP)RuCl(C≡CPh)($NH_2C_5H_3N_4$)] (**7**) that forms after the substitution of one chloride ligand by an amine. Attempts to isolate **7** by stripping off DMSO at room temperature leave a yellowish residue whose ^{31}P NMR spectrum denies a simple analysis owing to the accompanying presence of several unidentified products. Nevertheless, the IR spectrum of this solid species exhibits a sharp IR absorption at 2050 cm^{-1} assigned to the phenylethynyl ligand in **7**. Heating the [D_6]DMSO solution of **7** at 65 °C turns the light yellow colour to greenish yellow as **7** transforms into a new compound still exhibiting an AB spin system in the phosphorus NMR spectrum. The formation of this latter species, assigned to the nonmetallated neutral (aminocarbene)ruthenium complex *fac*,*cis*-[(PNP)$RuCl_2${C($NHC_5H_3N_4$)(CH_2Ph)}] (**8**), is accompanied by the appearance of the final metallated derivative **6**. In keeping with the accepted mechanistic hypothesis, on transforming **7** into **8** (and then into **6**), the informative AB system of the diastereotopic benzylic CH_2 protons and the featureless NH signal of the aminocarbene (δ = 11.91) rises in the ^{1}H NMR spectrum indicating that the intramolecular ruthenium-mediated attack of the adenine-NH_2 end has just occurred along the C=C moiety of the vinylidene ligand. The conversion of **8** into **6** is not completed at 65 °C in 1 d and goes to completion only after prolonged heating at 95 °C. A perusal of the collected pieces of evidence makes it reasonable to assign **6** to a structure similar to that ascertained in **5** by X-ray methods.

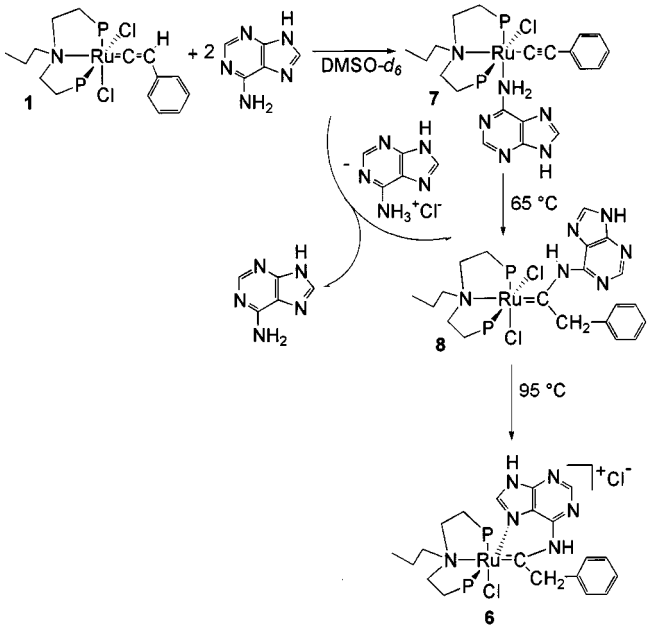

Scheme 5

Conclusions

In this paper we have described the first examples of transition metal carbenes incorporating nucleobases such as adenine and 5-aminouracil. Surprisingly these novel bio-organometallic derivatives exploit a new coordination mode towards a ruthenium centre. Thus, in the 5-aminouracil derivative a six-membered ring is closed by metallation of the oxo group on C(4) while in the adenine complex the aminocarbene uses the nitrogen atom N(7) to coordinate the ruthenium atom. This behaviour is quite surprising and has no precedents either in the series of PNP(carbene)Ru

derivatives, or, to the best of our knowledge, in the coordination chemistry of these nucleobases. As a final consideration, it can be stressed that the present coordination mode of the two nucleobases has an important influence on their hydrogen-bonding pattern.

Experimental Section

General Procedures: Dimethylformamide (DMF), *n*-hexane and dichloromethane were purified by distillation under nitrogen over molecular sieves, sodium and P_2O_5, respectively. Adenine and 5-aminouracil were purchased from Aldrich and used as received. All the other reagents and chemicals were reagent grade and, unless otherwise stated, were used as received from commercial suppliers. All reactions and manipulations were routinely performed under dry nitrogen by using standard Schlenk-tube techniques. The solid complexes were collected on sintered glass-frits and washed with light petroleum ether (b.p. 40−60 °C) before being dried in a stream of nitrogen. The ligand $CH_3CH_2CH_2N(CH_2CH_2PPh_2)_2$ (PNP)[21] and the vinylidene complex *fac*,*cis*-[(PNP)RuCl$_2${C=C(H)Ph}] (**1**),[10b] were prepared as described in the literature. [D$_6$]DMSO for NMR measurements (Aldrich) was dried with molecular sieves (0.4 nm). ^{1}H and ^{13}C{^{1}H} NMR spectra were recorded with Varian VXR 300 or Bruker AC200 spectrometers operating at 299.94 or 200.13 MHz (^{1}H) and 75.42 or 50.32 MHz (^{13}C), respectively. Peak positions are relative to tetramethylsilane and were calibrated against the residual solvent resonance (^{1}H) or the deuterated solvent multiplet (^{13}C). ^{13}C-DEPT-135 experiments were run with the Bruker AC200 spectrometer. ^{31}P{^{1}H} NMR spectra were recorded with the same instruments operating at 121.42 and 81.01 MHz, respectively. Chemical shifts were measured relative to external 85% H_3PO_4 with downfield values taken as positive. Infrared spectra were recorded as Nujol mulls with a Perkin−Elmer 1600 series FT-IR spectrometer between KBr plates. The molar conductivities were measured with an AMEL model 134 conductance cell connected with a model 101 conductivity meter. The conductivity data were obtained at sample concentration of 10^{-3} M in 1,2-dichloroethane solution at room temperature (22 °C). Elemental analyses (C,H,N) were performed using a Carlo Erba model 1106 elemental analyser.

Synthesis of *fac*,*cis*-[(PNP)RuCl{C(NHC$_4$H$_3$N$_2$O$_2$)(CH$_2$Ph)}]Cl (5): A fourfold excess of 5-aminouracil (0.27 g, 2.12 mmol) was added in small portions at room temperature to a stirred suspension of the vinylidene complex **1** (0.40 g, 0.53 mmol) in 30 mL of dichloromethane. The reaction mixture was stirred for 30 min and then DMF (15 mL) was added and the temperature gently raised to evaporate all the dichloromethane and then to about 110 °C. Heating was continued for 30 min to afford a light yellow solution, which was concentrated to dryness under vacuum. The crude yellowish material was taken with two portions (10 mL each) of a 1:2 mixture of ethanol and dichloromethane and the excess of unchanged 5-aminouracil was separated by filtration of the hot solutions. The filtered yellow solutions were collected in an Erlenmeyer flask and concentrated to ca. 5 mL. Addition of petroleum ether (3 mL) and slow concentration in air gave lemon-yellow crystals of the aminocarbene complex **5** that were recrystallised from dichloromethane and methanol in air to yield the solvate salt **5·CH$_3$OH·H$_2$O**. Yield ca. 82%. $C_{44}H_{49}Cl_2N_4O_4P_2Ru$ (931.16): calcd. C 56.72, H 6.01, N 5.30; found C 56.39, H 5.89, N 6.10. IR: $\tilde{\nu}$ = 3400 (br, m, ν_{NH}), 1720 (s, $\nu_{C=O}$), 1643 (s, $\nu_{C=O-Ru}$), 1621 (sh, $\nu_{C=C}$) cm^{-1}. ^{31}P{^{1}H} NMR (22 °C, [D$_6$]DMSO, 121.42 MHz): AB system: δ_A = 55.24, δ_B = 50.14, $^2J(P_A,P_B)$ = 32.5 Hz. ^{1}H NMR (22 °C, [D$_6$]DMSO, 299.94 MHz): δ = 12.4 [br, 2 H, NH(uracil)], 11.70 [s, 1 H, NH(aminocarbene)], 8.04 [s, 6-H, 1 H, CH(uracil)], 5.13 (CH_2Ph), 4.75 [AB system, $^3J_{H,H}$ = 16.9 Hz, 2 H]. ^{13}C{^{1}H} NMR (22 °C, [D$_6$]DMSO, 75.42 MHz): δ = 257.9 [t, $^2J_{C,P}$ = 13.9 Hz, Ru=*C*], 161.3 [*C*=O(uracil)], 149.1 (s, C-2 and C-4), 118.0 [s, C-6, C=*C*H(uracil)], 66.0 [br d, $^3J_{C,P}$ = 2.2 Hz, *C*H$_2$Ph].

Synthesis of *fac*,*cis*-[(PNP)RuCl{C(NHC$_5$H$_3$N$_4$)(CH$_2$Ph)}]Cl (6): A threefold excess of adenine (0.22 g, 1.63 mmol) was added at room temperature to a stirred suspension of the vinylidene complex **1** (0.40 g, 0.53 mmol) in 20 mL of DMF. The reaction mixture was stirred for 10 min and then gently heated to about 110 °C. Heating was continued for 30 min to afford a light orange solution, which was concentrated to dryness under vacuum. The crude orange material was combined with two portions (10 mL each) of hot dichloromethane and the excess of unchanged adenine was separated by filtration through a cotton plug. Addition of *n*-hexane (8 mL) and concentration of the orange solution under nitrogen gave orange yellowish crystals of the aminocarbene complex **6** that were recrystallised from dichloromethane/*n*-hexane (2:1). Yield ca. 74%. $C_{44}H_{46}Cl_2N_6P_2Ru$ (892.81): calcd. C 59.19, H 5.19, N 9.41; found C 58.87, H 5.20, N 9.22. IR: $\tilde{\nu}$ = 3480−3350 cm^{-1} (br, ν_{NH}). ^{31}P{^{1}H} NMR (22 °C, [D$_6$]DMSO, 81.01 MHz): AB system: δ_A 47.74, δ_B 39.21, $^2J(P_A,P_B)$ = 27.5 Hz. ^{1}H NMR (22 °C, [D$_6$]DMSO, 299.94 MHz): δ = 13.9 [br. d, $J_{H,P}$ = 12.4 Hz, 1 H, NH(aminocarbene)], 8.75 [s, 1 H, NH(adenine)], 8.62 [CH(adenine)], 7.90 (s, 2 H, 2-H + 8-H), 5.88 (CH_2Ph), 5.25 [AB system, $^3J_{H,H}$ = 16.8 Hz, 2 H]. ^{13}C{^{1}H} NMR (22 °C, [D$_6$]DMSO, 75.42 MHz): δ = 284.5 [t, $^2J_{C,P}$ = 19.2 Hz, Ru=*C*], 154.7 [s, C-5(adenine)], 152.6 [s, C-2(adenine)], 146.8 [s, C-4(adenine)], C-8(adenine) not observed, likely masked by aromatic resonances, 56.3 (s, *C*H$_2$Ph).

Synthesis of *fac*,*cis*-[(PNP)RuCl{C(NHC$_4$H$_3$N$_2$O$_2$)(CH$_2$Ph)}](BPh$_4$) (5-BPh$_4$) and *fac*,*cis*-[(PNP)RuCl{C(NHC$_5$H$_3$N$_4$)(CH$_2$Ph)}](BPh$_4$) (6-BPh$_4$): Metathetical reaction of **5** or **6** with $NaBPh_4$ (2 equiv.) in CH_2Cl_2/EtOH (2:1) yielded the tetraphenylborate salts *fac*,*cis*-[(PNP)RuCl{C(NHC$_4$H$_3$N$_2$O$_2$)(CH$_2$Ph)}](BPh$_4$) **(5-BPh$_4$)** and *fac*,*cis*-[(PNP)RuCl{C(NHC$_5$H$_3$N$_4$)(CH$_2$Ph)}](BPh$_4$) **(6-BPh$_4$)** in almost quantitative yields. **5-BPh$_4$:** $C_{67}H_{63}BClN_4O_2P_2Ru$ (1165.54): calcd. C 69.04, H 5.45, N 4.81; found C 69.67, H 5.65, N 4.59. **6-BPh$_4$:** $C_{68}H_{66}BClN_6P_2Ru$ (1176.59): calcd. C 69.42, H 5.65, N 7.14; found C 69.56, H 5.42, N 6.84. $\Lambda_{M(5\text{-}BPh4)}$ = 26 Ω^{-1} cm^2 mol^{-1} (295 K, in 1,2-dichloroethane). $\Lambda_{M(6\text{-}BPh4)}$ = 24 Ω^{-1} cm^2 mol^{-1} (295 K, in 1,2-dichloroethane).[22] IR: $\tilde{\nu}$ = 612 cm^{-1} (m, ν_{BC}).

In situ NMR Spectroscopic Study of the Reaction of 1 and Adenine: A 5-mm NMR tube was filled under nitrogen with **1** (20 mg, 0.026 mmol), adenine (7 mg, 0.052 mmol) and [D$_6$]DMSO (0.8 mL). ^{31}P{^{1}H} NMR monitoring of the reaction showed the fast and complete conversion of **1** into *fac*,*cis*-[(PNP)RuCl(C≡CPh)(NH$_2$C$_5$H$_3$N$_4$)] (**7**). After 2 h, when **7** was the only ruthenium complex, the temperature of the probehead was raised to 65 °C and the NMR analysis showed a slow conversion of **7** into a mixture of *fac*,*cis*-[(PNP)RuCl$_2${C(NHC$_5$H$_3$N$_4$)(CH$_2$Ph)}] (**8**) and **6** {after 12 h: **8** (68%), **6** (30%), *mer*,*trans*-[(PNP)RuCl$_2$(CO)] (2%)}. Heating to 95 °C completed the transformation of **8** into **6** in 24 h, but caused the formation of several unidentified compounds {after 24 h at 95 °C: **6** (81%), **8** (5%), *mer*,*trans*-[(PNP)RuCl$_2$(CO)] (3%), *fac*,*cis*-[(PNP)RuCl$_2$(CO)] (2%), unidentified compounds (9%, δ = 46.9, 36.5, 34.9 all singlets)}.

***fac*,*cis*-[(PNP)RuCl(C≡CPh)(NH$_2$C$_5$H$_3$N$_4$)] (7):** ^{31}P{^{1}H} NMR (22 °C, [D$_6$]DMSO, 121.42 MHz): AB system: δ_A 53.90, δ_B 52.01,

$^2J(P_A,P_B)$ = 35.2 Hz. ^1H NMR (22 °C, [D$_6$]DMSO, 299.94 MHz): δ = 3.21 (br. s, 2 H, NH_2, superimposed to aliphatic resonances of PNP ligand), , 8.60 [NH(adenine) and CH(adenine)], 8.52, 7.85 (all s, NH, 2-H, 8-H, 3 H).

***fac*,*cis*-[(PNP)RuCl$_2${C(NHC$_5$H$_3$N$_4$)(CH$_2$Ph)}] (8):** $^{31}P\{^1H\}$ NMR (22 °C, [D$_6$]DMSO, 121.42 MHz): AB system: δ_A 49.69, δ_B 37.99, $^2J(P_A,P_B)$ = 28.0 Hz. ^1H NMR (22 °C, [D$_6$]DMSO, 299.94 MHz): 11.91 [br. s, 1 H, NH(aminocarbene)], , 8.88 [NH(adenine) + CH(adenine)], 8.56, 8.21 (all s, NH, 2-H, 8-H, 3 H), 5.04 (CH_2Ph), 4.87 [AB system, $^3J_{H,H}$ = 17.1 Hz, 2 H]. $^{13}C\{^1H\}$ NMR (22 °C, [D$_6$]DMSO, 75.42 MHz): 279.9 [t, $^2J_{C,P}$ = 13.6 Hz, Ru=*C*], 163.7 [s, C-5(adenine)], 156.1 [s, C-2(adenine)], 141.3 [s, C-4(adenine)], C-6(adenine) and C-8(adenine) not observed, likely masked by aromatic resonances, 62.6 [t, $^3J_{C,P}$ = 1.9 Hz, *C*H$_2$Ph].

X-ray Diffraction Study of *fac*,*cis*-[(PNP)RuCl{C(NHC$_4$H$_3$N$_2$O$_2$)(CH$_2$Ph)}]Cl·CH$_3$OH·H$_2$O (5·CH$_3$OH·H$_2$O): A lemon-yellow crystal of **5·CH$_3$OH·H$_2$O** was chosen for an X-ray analysis. A summary of crystal and intensity data for the compound is presented in Table 2. Experimental data were recorded at room temperature with an ENRAF-NONIUS CAD4 diffractometer using graphite-monochromated Mo-K_α radiation. A set of 25 carefully centred reflections in the range 7.5° ≤ θ ≤ 9° was used for determining the lattice constants. As a general procedure, the intensity of three standard reflections was measured periodically every 2 h for orientation and intensity control. This procedure did not reveal any decay of intensities. The data were corrected for Lorentz and polarisation effects. Atomic scattering factors were those tabulated by Cromer and Waber[23] with anomalous dispersion corrections taken from ref.[24] An empirical absorption correction was applied via Ψ scan with transmission factors in the range 1.0−0.9. All the calculations were performed using the WINGX package[25] SIR97,[26] SHELX97[27] and ORTEP-III.[28] Final atomic coordinates with equivalent isotropic thermal parameters of all atoms and structure factors are available as supplementary material. All the non-hydrogen atoms were found through a series of F_0 Fourier maps. Refinement was done by full-matrix least-squares calculations, initially with isotropic thermal parameters, and then, in the last least-squares cycle, with anisotropic thermal parameters for all atoms, except the solvents ones. All of the phenyl rings were treated as rigid bodies with D_{6h} symmetry and C−C distances fixed at 1.39 Å. Hydrogen atoms of the PNP ligand were introduced in calculated positions, but not refined. At an advanced stage of the refinement, two solvent molecules, one of methanol and the other of water, were located in the Fourier map and successfully refined. CCDC-172155 (**5·CH$_3$OH·H$_2$O**) contains the supplementary crystallographic data for this paper. These data can be obtained free of charge at www.ccdc.cam.ac.uk/conts/retrieving.html or from the Cambridge Crystallographic Data Centre, 12, Union Road, Cambridge CB2 1EZ, UK [Fax: (internat.) + 44-1223/336-033; E-mail: deposit@ccdc.cam.ac.uk].

Table 2. Crystal data and structure refinement for *fac*-[(PNP)RuCl{C(NHC$_4$H$_3$N$_2$O$_2$)(CH$_2$Ph)}]Cl·CH$_3$OH·H$_2$O (**5**·CH$_3$OH·H$_2$O)

Empirical formula	$C_{44}H_{49}Cl_2N_4O_4P_2Ru$
Formula mass	931.16
Temperature	293(2) K
Wavelength	0.71069 Å
Crystal system, space group	monoclinic, $P2_1/n$
Unit cell dimensions	a = 15.682(9) Å b = 14.273(5) Å, β = 102.79(3) ° c = 19.748(2) Å
Volume	4311(3) Å^3
Z, calculated density	4, 1.447 Mg/m^3
Absorption coefficient	0.609 mm^{-1}
F(000)	1952
Crystal size	0.30 × 0.25 × 0.55 mm
θ range for data collection	1.51−22.48 °
Limiting indices	−16 ≤ h ≤ 16, 0 ≤ k ≤ 15, 0 ≤ l ≤ 21
Reflections collected/unique	5788/5596 [R(int) = 0.0401]
Completeness to θ	22.48 99.6%
Refinement method	Full-matrix least squares on F^2
Data/restraints/parameters	5596/0/443
Goodness-of-fit on F^2	1.016
Final R indices [$I > 2\sigma(I)$]	$R1$ = 0.0455, $wR2$ = 0.1012
R indices (all data)	$R1$ = 0.0962, $wR2$ = 0.1167
Largest diff. peak and hole	0.893 and −0.484 eÅ^{-3}

Acknowledgments

The authors wish to thank the COST Action D17/003 of the European Community for promoting this scientific activity and for a travel grant to J. L. F. to Florence. This work was also supported by the bilateral program "Azione Integrata" between the Universities of Ferrara (Italy) and Almeria (Spain) and NATO (project PST.CLG.978521). Thanks are expressed to Dr. Annabella Orlandini (ISSECC CNR, Florence, Italy) for helpful discussions.

[1] J. G. Duguid, V. A. Bloomfield, *Biophys. J.* **1995**, *69*, 2642.
[2] L. J. N. Bradley, K. J. Yarema, S. J. Lippard, J. M. Essigman, *Biochemistry* **1993**, *32*, 982.
[3] [3a] G. Jaouen, A. Vessières, I. S. Butler, *Acc. Chem. Res.* **1993**, *26*, 361. [3b] C. D. Garner, *J. Chem. Soc., Dalton Trans.* **1997**, 3903−3908
[4] [4a] J. M. Lehn, *Supramolecular Chemistry: Concepts and Perspectives*, VCH, Weinheim, Germany, **1995**. [4b] D. Braga, F. Grepioni, *Coord. Chem. Rev.* **1999**, *183*, 19.
[5] [5a] A. D. Burrows, D. M. P. Mingos, A. J. P. White, D. J. Williams, *J. Chem. Soc., Dalton Trans.* **1996**, 149. [5b] C. Price, M. A. Shipman, S. L. Gummerson, A. Houlton, W. Clegg, M. J. Elsegood, *J. Chem. Soc., Dalton Trans.* **2001**, 353.
[6] M. J. Clarke, F. Zhu, D. R. Frasca, *Chem. Rev.* **1999**, *99*, 2511.
[7] [7a] G. Sava, E. Alessio, A. Bergamo, G. Mestroni, *Topics in Biological Inorganic Chemistry*, vol. I ("Metallo-pharmaceuticals") (Eds.: M. J. Clarke, P. J. Sadler), Springer, Berlin, Germany, **1999**, pp. 143−169. [7b] Z. Guo, P. J. Sadler, *Angew. Chem. Int. Ed.* **1999**, *38*, 1512.
[8] [8a] K. H. Dötz, H. Fischer, P. Hoffmann, F. R. Kreissl, U. Schubert, K. Weiss, *Transition Metal Carbene Complexes*; Verlag Chemie, Weinheim, Germany, **1983**. [8b] F. Zaragoza Dörwald in *Metal Carbenes in Organic Synthesis*, Wiley-VCH, Weinheim, Germany, **1999**.
[9] C. Bianchini, D. Masi, A. Romerosa, F. Zanobini, M. Peruzzini, *Organometallics* **1999**, *18*, 2376.
[10] [10a] C. Bianchini, J. A. Casares, M. Peruzzini, A. Romerosa, F. Zanobini, *J. Am. Chem. Soc.* **1996**, *118*, 4585. [10b] C. Bianchini, P. Innocenti, M. Peruzzini, A. Romerosa, F. Zanobini, *Organometallics* **1996**, *15*, 272.
[11] C. Bianchini, D. Masi, M. Peruzzini, A. Romerosa, F. Zanobini, *Acta Crystallogr.* **1996**, *52*, 1973.
[12] H. Adams, N. A. Bailey, C. Ridgway, B. F. Taylor, S. J. Walters, M. J. Winter, *J. Organomet. Chem.* **1990**, *394*, 349.
[13] C. Bianchini, A. Romerosa, M. Peruzzini, unpublished observations.
[14] [14a] F. Huesco-Ureña, N. A. Illan-Cabeza, M. N. Moreno-Carretero, A. L. Peñas-Chamorro, R. Faure, *Polyhedron* **2000**, *19*, 689. [14b] F. Huesco-Ureña, N. A. Illan-Cabeza, M. N. Moreno-Carretero, A. L. Peñas-Chamorro, *Acta Chim. Slov.* **2000**, *47*, 481.

[15] R. Taylor, O. Kennard, *J. Am. Chem. Soc.* **1982**, *104*, 3209.
[16] J. Pranata, S. G. Wierschke, W. L. Jorgensen, *J. Am. Chem. Soc.* **1991**, *113*, 2810.
[17] B. Lippert, *J. Chem. Soc., Dalton Trans.* **1997**, 3971.
[18] C. Wilcox, in *Frontiers of Supramolecular Organic Chemistry and Photochemistry*, (Eds.: H.-J. Schneider, H. Dürr), VCH, Weinheim, Germany, **1990**.
[19] S. L. James, D. M. Mingos, X. Xu, A. J. P. White, D. J. Williams, *J. Chem. Soc., Dalton Trans.* **1998**, 1335.
[20] J. E. McGrady, D. M. P. Mingos, *J. Chem. Soc., Perkin Trans. 2* **1996**, 355.
[21] L. Sacconi, R. Morassi, *J. Chem. Soc. A* **1969**, 2904.
[22] W. J. Geary, *Coord. Chem. Rev.* **1971**, *7*, 81.
[23] D. Cromer, J. Waber, *Acta Crystallogr.* **1965**, *18*, 104.
[24] A. J. C. Wilson (Ed.), *International Tables for X-ray Crystallography*, vol. C, Kluwer Academic Press, Dordrecht, The Netherlands, **1992**, p. 219.
[25] L. J. Farrugia, *J. Appl. Crystallogr.* **1999**, *32*, 837.
[26] A. Altomare, M. C. Burlla, M. Cavalli, G. L. Cascarano, G. Giacovazzo, A. Guagliardi, A. G. C. Moliterni, G. Polidori, R. Spagna, *J. Appl. Crystallogr.* **1999**, *32*, 115.
[27] G. M. Sheldrick, *SHELX97, Program for crystal structure refinement*, University of Göttingen, Germany, **1997**.
[28] M. N. Burnett, C. K. Johnson, Report ORNL-6895, Oak Ridge National Laboratory: Oak Ridge, TN, USA, **1996**.

Received October 9, 2001
[I01400]

Three Novel End-to-End Single Azido-Bridged Ferromagnetic Copper(II) Chains: Synthesis, Crystal Structure, and Magnetic Behavior

Partha Sarathi Mukherjee,[a] Tapas Kumar Maji,[a] Albert Escuer,*[b] Ramon Vicente,[b] Joan Ribas,[b] Georgina Rosair,[c] Franz A. Mautner,[d] and Nirmalendu Ray Chaudhuri*[a]

Keywords: Copper / N ligands / Azido bridge / Magnetic properties

Three new single end-to-end azido-bridged copper(II) chains $[Cu(L1)(N_3)]_n(ClO_4)_n$ (**1**), $[Cu(L2)(N_3)]_n(ClO_4)_n$ (**2**), and $[Cu(L3)(N_3)]_n(ClO_4)_n$ (**3**) using three different tridentate Schiff bases L1, L2, and L3, obtained from condensation of pyridine-2-carbaldehyde with *N*,*N*-dimethylethane-1,2-diamine, *N*,*N*-diethylethane-1,2-diamine, and 4-(2-aminoethyl)morpholine, respectively, have been synthesized, and their crystal structures have been determined by X-ray diffraction methods. Complex **1**, $C_{10}H_{15}CuN_6ClO_4$, crystallizes in an orthorhombic system, space group $P2_12_12_1$, with a = 7.434(3), b = 12.047(4), c = 17.404(6) Å, and Z = 4; complex **2**, $C_{12}H_{19}CuN_6ClO_4$, crystallizes in an orthorhombic system, space group $Pna2_1$, with a = 14.723(5), b = 13.829(5), c = 8.002(5) Å, and Z = 4 and complex **3**, $C_{12}H_{17}CuN_6ClO_5$, crystallizes in an orthorhombic system, space group $Pna2_1$, with a = 13.837(15), b = 14.804(2), c = 8.050(4) Å, and Z = 4. Each structure consists of a single end-to-end azido-bridged copper(II) 1D chain where each copper(II) center possesses a square pyramidal geometry. Magnetic susceptibility data, measured from 4 to 300 K, show weak ferromagnetic interaction through the end-to-end bridging azido pathway in all the complexes. The magnetic data were fitted to a high temperature series-expansion for a one-dimensional system with $S = {}^1/_2$ local spin based on the Hamiltonian $H = -J\Sigma S_i \cdot S_{i+1}$ for all the complexes**,** giving the parameters J = +2.15 cm^{-1}, g = 2.23 for **1**, J = +3.61 cm^{-1}, g = 2.16 for **2**, and J = +2.06 cm^{-1}, g = 2.17 for **3**. This unusual magnetic behavior through the end-to-end bridging azido pathway has been correlated to the structural parameters.

(© Wiley-VCH Verlag GmbH, 69451 Weinheim, Germany, 2002)

Introduction

Recently, chemists as well as physicists have concentrated their efforts on the study of multinuclear molecular-based magnetic materials from the need to understand the fundamental science associated with magnetic interactions between the paramagnetic metal ions and the bridging ligands to develop the magneto-structural correlation enabling the design synthesis of interesting magnetic materials.[1−4] These molecular-based magnets can be designed to yield dimer, tetramer, mono-, bi-, and three-dimensional extended structures[5−8] with the paramagnetic metal ions using suitable bridging ligands which act as a superexchange pathway between paramagnetic centers and determine the strength of magnetic interactions i.e., the coupling parameter (J). The construction of molecular-based magnetic materials with ferromagnetic ordering is one of the major challenges in magneto-chemistry. The proper choice of the bridging ligand, which determines the magnetic behavior of the molecule, is an important task to the chemist for synthesizing such type of materials.

The azido ligand is an efficient superexchange pathway for propagating magnetic interaction between the paramagnetic centers such as copper(II), giving dimeric, tetranuclear, cubane, 1D, 2D, and 3D complexes.[9−17] The versatility of this ligand is due to its diverse binding modes leading to a variation in the magnetic properties that depend on its orientation with respect to the magnetic centers.[18] In general, the bridging modes observed for the azido group are end-to-end with anti-ferromagnetic interaction[19,20] and end-on with ferromagnetic interaction.[21] However, the magnetism of the latter is dependent on the M−N−M angle.[22−27] For copper(II) systems, ferromagnetic interaction is observed for complexes having Cu−N−Cu angles less than 108°. For angles above this value, molecules show antiferromagnetic interaction.[27] Hoffmann et al.[28] and later Ribas et al.[29] showed the possibility of even ferro-

[a] Department of Inorganic Chemistry, Indian Association for the Cultivation of Science,
Kolkata-700032, India
E-mail: icnrc@mahendra.iacs.res.in
Fax: (internat.) + 91-33/473-2805
[b] Departament de Química Inorgànica, Universitat de Barcelona, Diagonal 647, 08028 Barcelona, Spain
[c] Department of Chemistry, Heriot Watt University, Edinburgh EH 144AS, UK
[d] Institut für Physikalische und Theoretische Chemie, Technische Universität Graz,
8010 Graz, Austria

magnetic interaction through an end-to-end azido pathway on the basis of theoretical calculations. This theory has been successfully tested in a scarce number of complexes. Only a few structurally solved M^{II} systems, showing weak ferromagnetic interaction through the end-to-end bridging azido pathway have recently been reported in the literature.[30−33] One of them is a 1D chain of Ni^{II} with an end-to-end azido-bridge using a nonchelating capping co-ligand[30] and the second one is a dimer of Ni^{II} using a chelating co-ligand.[31] Recently this laboratory reported the first observation of a ferromagnetic interaction through end-to-end azido pathways in a copper(II) system.[32,33] This unusual result prompted us to synthesize more and more such complexes types. In the present paper we report on the synthesis, X-ray crystal structures of three new 1D single azido-bridged copper(II) chains, $[Cu(L1)(N_3)]_n(ClO_4)_n$ (**1**), $[Cu(L2)(N_3)]_n(ClO_4)_n$ (**2**), and $[Cu(L3)(N_3)]_n(ClO_4)_n$ (**3**) where L1, L2, and L3 are three different Schiff bases obtained from the condensation of pyridine-2-carbaldehyde with *N*,*N*-dimethylethane-1,2-diamine, *N*,*N*-diethylethane-1,2-diamine, and 4-(2-aminoethyl)morpholine, respectively, and observation of unusual ferromagnetic interaction through the end-to-end azido pathway.

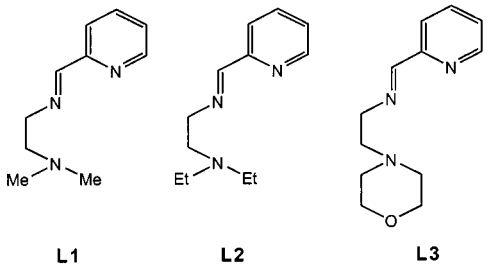

L1 L2 L3

Results and Discussion

IR Spectroscopy

The presence of strong bands at 2062, 2075, and 2070 cm^{-1} in the IR spectrum of complexes **1**, **2**, and **3,** respectively, are due to asymmetric stretching of azide. Peaks at 1662, 1659, and 1674 cm^{-1} in the IR spectrum of **1**, **2**, and **3**, respectively, are due to the stretching of the C=N group in these complexes.

Description of the Structures

All the structures consist of 1D copper(II)-azido chain isolated by a ClO_4^- anion. In the chain structures, each copper(II) atom is coordinated by one tridentate (NNN donor) Schiff base ligand and two bridging azido ligands in a square pyramidal geometry.

$[Cu(L1)(N_3)]_n(ClO_4)_n$ (1)

A labeled scheme of **1** is shown in Figure 1. The main bond lengths and angles are listed in Table 1. Other distances and angles may be found in the deposited information (Cambridge database; see reference at the end of the

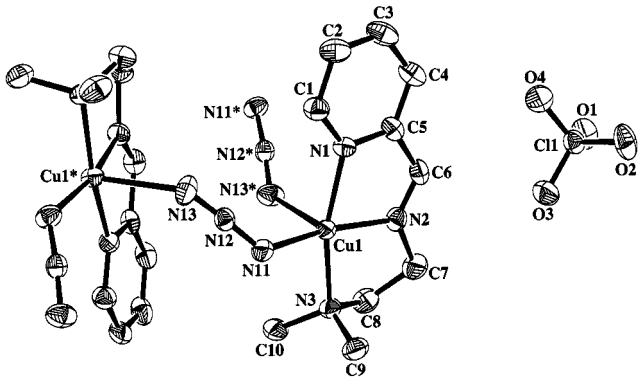

Figure 1. View of the $[Cu(L1)(N_3)]_n(ClO_4)_n$ (**1**) with atom labeling scheme showing 50% probability thermal ellipsoids for all non-hydrogen atoms

Exp. Sect.). The structure of **1** consists of copper $Cu(L1)(N_3)$ units bridged by an end-to-end azido resulting in a chain system with perchlorate counter anions. The basal plane of each copper atom consists of one tridentate L1 ligand, Cu(1)−N(1) 2.051(4), Cu(1)−N(2) 1.953(4), Cu(1)−N(3) 2.058(3) Å, and one nitrogen atom N(11) of the azido ligand *trans* to N(2) with a Cu(1)−N(11) distance of 1.947(3) Å and the apical coordination site occupied by the N(13)* atom from another azido-bridging ligand, Cu(1)−N(13)* 2.355(4) Å. One oxygen atom from the perchlorate counter anion weakly interacts with the copper atom, Cu(1)−O(1) 2.914(4) Å in a *trans* position to N(13)*. The L1 ligand is roughly planar, with N(2) and N(3) displaced 0.120(1) and 0.036(4) Å from the mean plane defined by the aromatic ring. Bond angles between N(2)−Cu(1)−N(11) and N(1)−Cu(1)−N(3) are 168.2(2)° and 163.3(2)° and the bond angles between the apical equatorial coordination sites are greater than 90°, suggesting a square pyramidal arrangement. Azido ligand acts as a single end-to-end bridge between the copper atoms, showing the Cu(1)−N(11)−N(12) and Cu(1)−N(13)* −N(12)* bond angles of 126.5(3)° and 131.2(4)°. The torsion angle Cu(1)−N(11)−N(12)−N(13)−Cu(1)* has a value of 97.8(4)° and the CuN_4 neighboring mean planes an angle of 34.6(1)°.

$[Cu(L2)(N_3)]_n(ClO_4)_n$ (2) and $[Cu(L3)(N_3)]_n(ClO_4)_n$ (3)

The labeled scheme of complexes **2** and **3** are shown in Figures 2 and 3, respectively. The main bond lengths and angles of complexes **2** and **3** are listed in Tables 2 and 3, respectively. Other distances and angles may be found in the deposited information (Cambridge database). The structures of **2** and **3** consist of $Cu(L2)(N_3)$ and $Cu(L3)(N_3)$ units, respectively, bridged by end-to-end azido resulting in a 1D coordination chain and perchlorate counter anions. Each copper atom in the polymeric chain is in a square pyramidal geometry. The local environment of the copper atoms in both the complexes consists of one tridentate Schiff base ligand and the two azido-bridging ligand. In both the complexes all three nitrogen atoms of the tridentate ligands (L2 and L3) are occupied in the basal plane of

Table 1. Selected bond lengths [Å] and angles [°] for $[Cu(L1)(N_3)]_n(ClO_4)_n$ (**1**) (symmetry codes: $i = x + 1/2, -y + 1/2, -z$; $ii = x - 1/2, -y + 1/2, -z$)

Cu(1)−N(11)	1.947(3)	Cu(1)−N(2)	1.953(4)
Cu(1)−N(1)	2.051(4)	Cu(1)−N(3)	2.058(3)
Cu(1)−N(13)*_*i*	2.355(4)	N(11)−N(12)	1.181(5)
N(12)−N(13)	1.158(5)		
N(11)−Cu(1)−N(2)	168.2(2)	N(11)−Cu(1)−N(1)	102.7(2)
N(2)−Cu(1)−N(1)	80.4(2)	N(11)−Cu(1)−N(3)	93.4(2)
N(2)−Cu(1)−N(3)	83.0(2)	N(1)−Cu(1)−N(3)	163.3(2)
N(11)−Cu(1)−N(13)*_*i*	95.7(2)	N(2)−Cu(1)−N(13)*_*i*	95.8(2)
N(1)−Cu(1)−N(13)*_*i*	89.3(2)	N(3)−Cu(1)−N(13)*_*i*	93.4(2)
Cu(1)−N(11)−N(12)	126.5(3)	N(13)−N(12)−N(11)	176.0(4)
Cu(1)*_*ii*−N(13)−N(12)	131.2(4)		

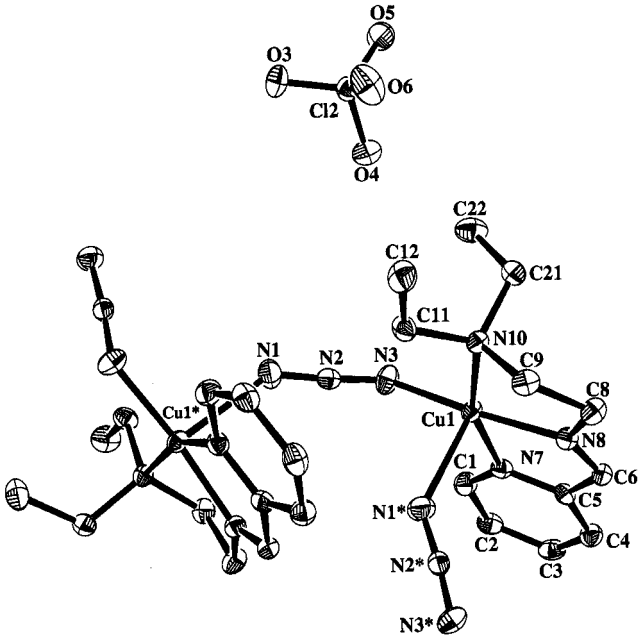

Figure 2. View of the $[Cu(L2)(N_3)]_n(ClO_4)_n$ (**2**) chain with atom labeling scheme showing 50% probability thermal ellipsoids for all non-hydrogen atoms

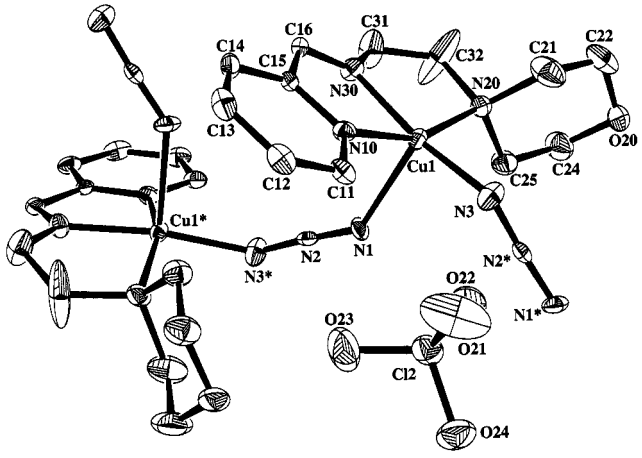

Figure 3. View of the $[Cu(L3)(N_3)]_n(ClO_4)_n$ (**3**) chain with atom labeling scheme showing 50% probability thermal ellipsoids for all non-hydrogen atoms

the square pyramid. In the case of complex **2** the bond lengths in the basal plane are Cu(1)−N(8) 1.961(3), Cu(1)−N(7) 2.039(3), Cu(1)−N(10) 2.068(3), and Cu(1)−N(3) 1.965(3) Å. The axial position of Cu(1) is occupied by N(1)* of the azido of the neighboring $[Cu(L2)(N_3)](ClO_4)$ moiety with a Cu(1)−N(1)* distance of 2.311(3) Å for **2**. While for complex **3** the basal plane bond lengths are Cu(1)−N(30) 1.939(7), Cu(1)−N(20) 2.064(6), Cu(1)−N(10) 2.030(6), and Cu(1)−N(3) 1.951(7) Å which is in a *trans* position to N(30) and the axial position of Cu(1) is occupied by N(1) of the azido of the neighboring $[Cu(L3)(N_3)](ClO_4)$ moiety with a Cu(1)−N(1) distance of 2.270(5) Å. The Cu(1)−N(3)−N(2)−N(1)−Cu(1)* torsion angle is 50.0(4)° and the normals to the two copper equatorial coordination planes are inclined at 15.9(1)° for **2**. For complex **3** the Cu(1)−N(1)−N(2)−N(3)*−Cu(1)* torsion angle is 40.4(8)° and the normals to the two copper equatorial coordination planes are inclined at 14.2(2)°. The intrachain copper−copper distance is 5.630(2) and 5.540(2) Å for complexes **2** and **3,** respectively, and each copper(II) in the chain has square pyramidal geometry with the Cu atom displaced towards the axial azide ligand by 0.1681(15) and 0.241(3) Å out of the equatorial plane. One of the perchlorate oxygen atoms has an intermolecular contact to copper approximately *trans* to N(1)* with a Cu(1)−O(3) distance of 3.405(5) Å in **2** and the similar contact distance in **3** is 3.398(6) Å. Such long Cu−O contact distances are beyond the bonding region.

Magnetic Results

The variable temperature magnetic susceptibility data for complexes **1−3** were recorded between 300 and 4 K. Plots of $\chi_M T$ versus T for compounds **1−3** are similar (Figure 4), showing a constant increase of the $\chi_M T$ when the temperature decreases, reaching $\chi_M T$ values between 0.68 and 0.86 $cm^3 \cdot K \cdot mol^{-1}$ per copper atom respectively, suggesting ferromagnetic interactions. On the basis of structural features of complexes **1−3** the magnetic data were fitted as chains using the one-dimensional $S = {}^1/_2$ expression based on the Hamiltonian $H = -J\Sigma S_i \cdot S_{i+1}$. A high-temperature series-

Table 2. Selected bond lengths [Å] and angles [°] for $[Cu(L2)(N_3)]_n(ClO_4)_n$ (**2**) (symmetry codes: $i = -x + 1, -y + 2, z + 1/2$, $ii = -x + 1, -y + 2, z - 1/2$)

Cu(1)−N(8)	1.961(3)	Cu(1)−N(1)*_*i*	2.311(3)
Cu(1)−N(10)	2.068(3)	Cu(1)−N(7)	2.039(3)
Cu(1)−N(3)	1.965(3)	N(2)−N(3)	1.161(4)
N(1)−N(2)	1.181(4)		
N(8)−Cu(1)−N(1)*_*i*	91.43(11)	N(8)−Cu(1)−N(7)	79.94(11)
N(1)*_*i*−Cu(1)−N(7)	92.04(11)	N(8)−Cu(1)−N(10)	82.90(10)
N(1)*_*i*−Cu(1)−N(10)	101.62(12)	N(7)−Cu(1)−N(10)	160.11(11)
N(8)−Cu(1)−N(3)	170.40(12)	N(1)*_*i*−Cu(1)−N(3))	96.24(11)
N(7)−Cu(1)−N(3)	93.99(11)	N(10)−Cu(1)−N(3)	101.60(11)
Cu(1)−N(3)−N(2)	131.2(3)	Cu(1)*_*ii*−N(1)−N(2)	139.1(3)
N(1)−N(2)−N(3)	175.0(3)		

Table 3. Selected bond lengths [Å] and angles [°] for $[Cu(L3)(N_3)]_n(ClO_4)_n$ (**3**) (symmetry codes: $i = -x, -y, z - 1/2$, $ii = -x, -y, z + 1/2$)

Cu(1)−N(30)	1.939(7)	Cu(1)−N(3)	1.951(7)
Cu(1)−N(10)	2.030(6)	Cu(1)−N(1)	2.270(5)
Cu(1)−N(20)	2.064(6)	N(1)−N(2)	1.144(9)
N(2)−N(3)*_*i*	1.193(9)		
N(30)−Cu(1)−N(3)	167.5(2)	N(30)−Cu(1)−N(10)	80.4(2)
N(3)−Cu(1)−N(10)	93.6(3)	N(30)−Cu(1)−N(20)	83.6(3)
N(3)−Cu(1)−N(20)	99.1(3)	N(10)−Cu(1)−N(20)	158.4(2)
N(30)−Cu(1)−N(1)	91.6(3)	N(10)−Cu(1)−N(1)	95.3(2)
N(3)−Cu(1)−N(1)	99.9(3)	Cu(1)−N(1)−N(2)	139.0(5)
N(20)−Cu(1)−N(1)	99.6(2)	Cu(1)−N(3)−N(2)*_*ii*	132.2(5)
N(1)−N(2)−N(3)*_*i*	176.1(7)		

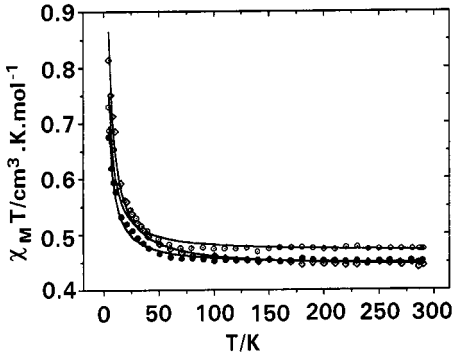

Figure 4. Plots of $\chi_M T$ vs. T (K) data for **1** (open circles), **2** (open rhombus), and **3** (filled circles); the solid lines correspond to the best fit obtained

expansion, valid for both positive and negative J values, has been proposed.[41−42] The results of the best fit, shown as the solid lines in Figure 4, were $J = +2.15$ cm^{-1}, $g = 2.23$, $R = 1.5 \cdot 10^{-4}$ for complex **1**; $J = +3.61$ cm^{-1}, $g = 2.16$, $R = 1.3 \cdot 10^{-4}$ for complex **2**; and $J = +2.06$ cm^{-1}, $g = 2.17$, $R = 1.3 \cdot 10^{-4}$ for complex **3**. These J values are of the same order as that of previously reported results for a similar compound with a tridentate Schiff base.[32]

From the EPR spectra, the g values for complexes **1**−**3** are (at 4 K): $g_{\|} = 2$, 19, 2.22, 2.22 and $g_{\perp} = 2.08$, 2.12, 2.07, respectively. The three spectra are very similar as may be expected from structural data. On cooling from room temperature down to 4 K the g values are practically constant, but the line-width becomes larger due to dipolar effects along the ferromagnetic chain for all of them.

Superexchange Mechanism

Ferromagnetic interactions for azido-bridged metal complexes are generally associated with an end-on coordination mode whereas end-to-end coordination modes of the azido bridge generally allows antiferromagnetic coupling for a large number of Cu^{II}, Ni^{II}, Co^{II}, or Mn^{II} systems reported to date.[41,43] For copper systems, the magnitude of the antiferromagnetic component of the superexchange parameter J is strongly dependent on two main factors, i.e. the atomic orbitals of the copper atoms involved in the superexchange pathway and on the M−N−N angle α and on the M−N_3−M torsion angle θ in the bridging region.

The coupling may be strongly AF when the end-to-end azido ligands are bonded to the equatorial coordination sites of the two copper atoms, in which case the atomic orbitals involved in the superexchange mechanism are the two $d_{x^2-y^2}$ orbitals. In contrast, very low coupling interactions should be expected when the interaction is between axial-equatorial coordination sites and the atomic orbitals involved are the $d_{x^2-y^2}$ and d_{z^2} respectively. The different magnetic behavior is related to the low unpaired electronic density found in the d_{z^2} atomic orbital in the square pyramidal or octahedrally coordinated copper atoms. Classical attempts to relate the magnitude of the superexchange coupling and the structural data for the axial-equatorial case conclude a greater anti-ferromagnetic coupling for the trigonal bipyramidal arrangement in agreement with the greater mixing of the $d_{x^2-y^2}$ and d_{z^2} atomic orbitals.[44] In our case, complexes **1**−**3** exhibit a square pyramidal geometry of the copper(II) with one nitrogen of the bridging azido linked to the equatorial position of one copper(II) whereas the other end nitrogen of the same azide is linked to the axial site of the neighboring copper(II) center, indicating that the spin unpaired electron is mainly located in the basal $d_{x^2-y^2}$ orbital whereas the d_{z^2} orbital contains spin paired electrons. The consequence is that there is a good delocalization of the electron density of one of the copper(II) atoms towards the bridging azido, while the delocalization from the second copper is poor because azide

Table 4. Crystal data and structure refinement for $[Cu(L1)(N_3)]_n(ClO_4)_n$ (**1**), $[Cu(L2)(N_3)]_n(ClO_4)_n$ (**2**), and $[Cu(L3)(N_3)]_n(ClO_4)_n$ (**3**)

	1	**2**	**3**
Empirical formula	$C_{10}H_{15}ClCuN_6O_4$	$C_{12}H_{19}ClCuN_6O_4$	$C_{12}H_{17}ClCuN_6O_5$
Formula mass	382.27	410.32	424.31
Space group	$P2_12_12_1$	$Pna2_1$	$Pna2_1$
a [Å]	7.434(3)	14.723(5)	13.837(15)
b [Å]	12.047(4)	13.829(5)	14.804(2)
c [Å]	17.404(6)	8.002(5)	8.050(4)
α, β, γ [°]	90, 90, 90	90, 90, 90	90, 90, 90
V [Å^3]	1558.7(10)	1629.2(13)	1649.0(8)
Z	4	4	4
T [°C]	20(2)	20(2)	20(2)
λ(Mo-K_α) [Å]	0.71069	0.71069	0.71069
$\rho_{calcd.}$, g cm^{-1}	1.629	1.673	1.709
μ(Mo-K_α) [mm^{-1}]	1.599	1.536	1.525
R[a]	0.0426	0.0341	0.0469
$R^2\omega$[b]	0.0862	0.0770	0.1200

[a] $R = \|\|F_o\| - |F_c\|\|/\Sigma|F_o|$. [b] $R_w = [\Sigma\{w(F_o^2 - F_c^2)^2\}/\Sigma\{w(F_o^2)^2\}]^{1/2}$.

occupies an apical position with a longer distance and so, a weak interaction should be expected, which is also observed experimentally.[8]

The nature of this low interaction may be ferro or antiferromagnetic, as a function of the bond parameters in the bridging region. The AF component of the superexchange may be drastically reduced for large M−N−N bond angles or large M−N_3−M torsion angles.[29] The effect of the M−N−N bond angle is not determinant in our case because the Cu−N−N bond angles, in all cases, lie below 140°, but the effect of the θ torsion angles should be considered. The maximum antiferromagnetic component is found for θ = 180 or 0° and quickly diminishes with an increase in θ and becomes zero (accidental orthogonality) for θ = 90°.[29] In compound **1** the Cu−N−N angles are 126.6 and 131.3° and the torsion angle defined by the Cu(1)−N(11)−N(12)−N(13) and the N(11)−N(12)−N(13)−Cu(1)* mean planes is 97.8°. In compound **2** the Cu−N−N angles are 131.2(3) and 139.1(3)° and the Cu−N_3−Cu torsion angle is 50.4(4)°. In compound **3** the Cu−N−N angles are 132.2(5) and 139.0(5)° and the Cu−N_3−Cu torsion angle θ is 40.4(8)°. The large Cu−N_3−Cu torsion angles, along with the axial-equatorial bridging mode of the azido ligand and the square-pyramid geometry in all these complexes orient the magnetic orbitals in almost orthogonal fashion to nullify the antiferromagnetic component of the superexchange resulting in a net weak ferromagnetic interaction.

Conclusions

We have presented here the synthesis, single crystal structure and magneto-structural correlation of three novel end-to-end single azido-bridged 1D copper(II) chains, using three different tridentate (NNN-donor) Schiff base ligands and the observation of unusual ferromagnetic interaction through end-to-end azido pathways in a copper(II) system. Fitting of the $\chi_M T$ versus T data in the temperature range between 300 and 4 K using a high temperature series-expansion for $S = {}^1/_2$ local spin lead to the coupling parameters, $J = +2.15$ cm^{-1} for **1**, $J = +3.61$ cm^{-1} for **2**, and $J = +2.06$ cm^{-1} for **3**. Positive J values as well as the nature of $\chi_M T$ versus T plot clearly indicate the existence of an intrachain ferromagnetic interaction in all of the complexes **1**−**3**. Such an unusual magnetic behavior through an end-to-end azido pathway is explained on the basis of the axial-equatorial bridging mode as well as the bond parameters like the Cu−N_3−Cu torsion angle.

Experimental Section

Caution! Perchlorate and azido complexes of metal ions in the presence of organic ligands are potentially explosive. Only a small amount of the materials should be prepared, and it should be handled with care.

Synthesis

L1, L2, and L3 Ligands: The three Schiff bases were prepared by reflux of 2 mmol of pyridine-2-carbaldehyde and 2 mmol of *N*,*N*-dimethylethane-1,2-diamine, or *N*,*N*-diethylethane-1,2-diamine, or 4-(2-aminoethyl)morpholine, respectively, in 10 mL of methanol, according to the literature methods.[34−35]

$[Cu(L1)(N_3)]_n(ClO_4)_n$ (1): A methanolic solution (10 mL) of copper(II) perchlorate hexahydrate (2 mmol) was added to the hot methanolic solution (10 mL) of the L1 (2 mmol) ligand. To the resulting deep blue cold solution, an aqueous solution (5 mL) of sodium azide (2 mmol) was added dropwise with continuous stirring and filtered. Suitable single crystals for structure determination were obtained by slow evaporation of this solution in air. Yield ca. 60%. $C_{10}H_{15}ClCuN_6O_4$: calcd. C 31.4, H 4.0, N 22.0; found C 32.0, H 4.1, N 22.3%.

$[Cu(L2)(N_3)]_n(ClO_4)_n$ (2): A methanolic solution (10 mL) of copper(II) perchlorate hexahydrate (2 mmol) was added to the hot methanolic solution (10 mL) of the L2 ligand (2 mmol). To the resulting bluish-green cold solution, an aqueous solution (5 mL) of

sodium azide (2 mmol) was added dropwise with continuous stirring. Suitable green single crystals for structure determination were obtained after a few days by slow evaporation of this dark green solution in air. Yield ca. 80%. $C_{12}H_{19}ClCuN_6O_4$: calcd. C 35.0, H 4.7, N 20.5; found C 35.2, H 4.6, N 20.2%.

$[Cu(L3)(N_3)]_n(ClO_4)_n$ (3): This complex was synthesized following the strategy adopted for complexes (**1**) and (**2**) using the ligand L3. Suitable single crystals for X-ray diffraction were obtained by slow evaporation of the final solution in a refrigerator. Yield ca. 75%. $C_{12}H_{17}ClCuN_6O_5$: calcd. C 33.9, H 4.0, N 19.8; found C 34.2, H 4.2, N 19.5%.

Crystallographic Data Collection and Refinement: The X-ray single-crystal data for compound **1** was collected on a modified STOE four-circle diffractometer. While the crystals of **2** and **3** were covered in nujol and mounted with vacuum grease on a glass fiber and transferred to a Bruker AXS P4 diffractometer[36] and data were measured at 293 K. The crystallographic data, the conditions for the intensity data collection and some features of the structure refinements are listed in Table 4. Graphite-monochromatized Mo-K_α radiation ($\lambda = 0.71069$ Å) and the ω-scan technique for **1** and ψ- scan technique for **2** and **3** were used to collect the data sets. The accurate unit-cell parameters were determined from automatic centering of 54 reflections ($9.4° < \theta < 13.7°$) for **1**, 37 reflections ($2.76° < \theta < 20.82°$) for **2** and 30 reflections ($4.75° < \theta < 12.49°$) for **3** and refined by least-squares method. A total of 2755 reflections (2709 independent reflections, $R_{int} = 0.0238$) for **1**; 3244 reflections (2740 independent reflections, $R_{int} = 0.0323$) for **2**; and 1960 reflections (1707 independent reflections, $R_{int} = 0.0221$) for **3**,were collected in the range $2.89° < \theta < 30.00°$, $2.02° < \theta < 25.00°$, and $2.75° < \theta < 25.00°$ for **1**, **2**, and **3** respectively. The structures were solved by direct methods using the SHELXS-86[37] computer program, and refined by full-matrix least-squares methods on F^2, using the SHELXL-93[38] program incorporated in the SHELXTL/PC V 5.03[39] program library and the graphics program PLATON.[40] All non-hydrogen atoms were refined anisotropically. The hydrogen atoms were located on calculated positions by use of the HFIX utility of the SHELXL-93 program. For complexes **1**, **2**, and **3,** respectively, the final *R* indices for all observed reflections are 0.0426, 0.0341, and 0.0469. Maximum and minimum peaks in the final difference Fourier syntheses were 0.29 and −0.44 e·Å^{-3} for **1**, 0.31 and −0.30 e·Å^{-3} for **2**, and 0.53 and −0.84 e·Å^{-3} for **3**. Significant bond parameters are given in Tables 1−3.

Physical Measurements: IR spectra (4000−400 cm^{-1}) were recorded from KBr pellets on a Nicolet 520 FT-IR spectrometer. Magnetic measurements were carried out with a DSM8 pendulum susceptometer equipped with a helium continuous-flow cryostat, working in the temperature range 300−4 K. The applied external magnetic field was 1.5 T. Diamagnetic corrections were estimated from Pascal constants. Electronic Spin Resonance spectra of the polycrystalline samples have been recorded at X-band frequency by using a Bruker ESP 300 E automatic spectrometer from room temperature to 4 K.

CCDC-168803, -168804, and -168805 for complexes **1**, **2**, and **3**, respectively, contain the supplementary crystallographic data for this paper. These data can be obtained free of charge at www.ccdc.cam.ac.uk/conts/retrieving.html [or from the Cambridge Crystallographic Data Centre, 12, Union Road, Cambridge CB2 1EZ, UK; fax: (internat.) + 44-1223/336-033; E-mail: deposit@ccdc.cam.ac.uk].

Acknowledgments

Funding for the work described here is provided by the Council of Scientific and Industrial Research (New Delhi) Grants Scheme (Granted to NRC) and is gratefully acknowledged. This research was also partially supported by CICYT (Spanish Government; Grant BQU2000-0791) and OENB (grant 6630). F. A. Mautner thanks Prof. C. Kratky and Dr. F. Belaj (University of Graz) for use of experimental equipment.

[1] J. S. Miller, A. J. Epstein, *Angew. Chem. Int. Ed. Engl.* **1994**, *33*, 385.
[2] A. Caneschi, D. Gatteschi, R. Sessoli, P. Rey, *Acc. Chem. Res.* **1989**, *22*, 392.
[3] D. Gatteschi, *Adv. Mater.* **1994**, *6*, 635.
[4] J.S. Miller, A. J. Epstein, W. M. Reiff, *Science* **1988**, *240*, 40.
[5] A. Escuer, R. Vicente, J. Ribas, X. Solans, *Inorg. Chem.* **1995**, *34*, 1793.
[6] J. Ribas, M. Monfort, C. Diaz, C. Bastos, X. Solans, *Inorg. Chem.* **1994**, *33*, 484.
[7] A. Escuer, R. Vicente, M. A. S. Goher, F. A. Mautner, *Inorg. Chem.* **1996**, *35*, 6386.
[8] P. S. Mukherjee, T. K. Maji, G. Mostafa, T. Mallah, N. Ray Chaudhuri, *Inorg. Chem.* **2000**, *39*, 5147.
[9] J. Ribas, M. Monfort, C. Diaz, C. Bastos, X. Solans, *Inorg. Chem.* **1993**, *32*, 3557.
[10] J. Ribas, M. Monfort, R. Costa, X. Solans, *Inorg. Chem.* **1993**, *32*, 695.
[11] M. A. Halcrow, J. C. Huffman, G. Christou, *Angew. Chem. Int. Ed. Engl.* **1995**, *35*, 971.
[12] A. Escuer, R. Vicente, J. Ribas, M. S. El Fallah, X. Solans, M. Font-Bardia, *Inorg. Chem.* **1994**, *33*, 1842.
[13] R. Vicente, A. Escuer, J. Ribas, M. S. El Fallah, X. Solans, M. Font Bardia, *Inorg. Chem.* **1995**, *34*, 1278.
[14] J. Ribas, M. Monfort, B. K. Ghosh, R. Cortes, X. Solans, M. Font Bardia, *Inorg. Chem.* **1996**, *35*, 864.
[15] M. Monfort, J. Ribas, X. Solans, *J. Chem. Soc., Chem. Commun.* **1993**, 350.
[16] M. Monfort, I. Resino, J. Ribas, H. Stoeckli-Evans, *Angew. Chem. Int. Ed.* **2000**, *39*, 191.
[17] F. A. Mautner, R. Cortes, L. Lezema, T. Rojo, *Angew. Chem. Int. Ed. Engl.* **1996**, *35*, 96.
[18] J. Ribas, M. Monfort, I. Resino, X. Solans, P. Rabu, F. Maingot, M. Drillon, *Angew. Chem. Int. Ed. Engl.* **1996**, *35*, 2671.
[19] C. G. Pierpont, D. N. Hendrickson, D. M. Duggan, F. Wanger, E. K. Barefield, *Inorg. Chem.* **1975**, *14*, 604.
[20] A. Escuer, R. Vicente, J. Ribas, M. S. El Fallah, X. Solans, *Inorg. Chem.* **1993**, *32*, 1033.
[21] P. Chaudhuri, M. Guttmann, D. Ventur, K. Weighardt, B. Nuber, J. Weiss, *J. Chem. Soc., Chem. Commun.* **1985**, 1618.
[22] M. I. Arriortua, A. R. Cortes, L. Lezema, T. Rojo, X. Solans, *Inorg. Chim. Acta* **1990**, *174*, 263.
[23] A. Escuer, R. Vicente, J. Ribas, *J. Magn. Magn. Mater.* **1992**, *110*, 181.
[24] A. Escuer, R. Vicente, J. Ribas, X. Solans, *Inorg. Chem.* **1995**, *34*, 1793.
[25] J. Comarmond, P. Plumere, J. M. Lehn, Y. Agnus, R. Louis, R. Weiss, O. Kahn, I. Morgesten-badarau, *J. Am. Chem. Soc.* **1982**, *104*, 6330.
[26] O. Kahn, S. Sikorav, J. Gouteron, S. Jeannin, Y. Jeannin, *Inorg. Chem.* **1983**, *22*, 2877.
[27] S. S. Tandon, L. K. Thompson, M. E. Manuel, J. N. Bridson, *Inorg. Chem.* **1994**, *33*, 5555.
[28] P.J. Hay, J. C. Thibeault, R. Hoffmann, *J. Am. Chem. Soc.* **1975**, *97*, 4884.
[29] A. Escuer, R. Vicente, J. Ribas, M. S. El Fallah, X. Solans, M. Font-Bardia, *Inorg. Chem.* **1993**, *32*, 3727.
[30] C. S. Hong, Y. Do, *Angew. Chem. Int. Ed.* **1999**, *38*, 193.
[31] A. Escuer, C. J. Harding, Y. Dussart, J. Nelson, V. McKee, R. Vicente, *J. Chem. Soc., Dalton Trans.* **1999**, 223.

[32] T. K. Maji, P. S. Mukherjee, G. Mostafa, T. Mallah, J. Cano-Boquera, N. Ray Chaudhuri, *Chem. Commun.* **2001**, 1012.
[33] P. S. Mukherjee, S. Dalai, G. Mostafa, T. H. Lu, E. Rentschler, N. Ray Chaudhuri, *New J. Chem.* **2001**, *25*, 1203.
[34] G. Zakrzewski, L. Sacconi, *Inorg. Chem.* **1968**, *7*, 1034.
[35] P. Bamfield, R. Price, R. G. J. Miller, *J. Chem. Soc. (A)* **1969**, 1447.
[36] *XSCANS*, **1994**, Data Collection and Reduction Program, Version 2.2, Bruker AXS., Madison, Wisconsin, USA.
[37] G. M. Sheldrick, *SHELXS-86*, Program for the Solution of Crystal Structure. University of Gottingen, Germany, **1986**.
[38] G. M. Sheldrick, *SHELXL-93*, Program for the Refinement of Crystal Structure. University of Gottingen, Germany, **1993**.
[39] *SHELXTL 5.03* (PC-Version), Program library for the Solution and Molecular Graphics. Siemens Analytical Instruments Division, Madison, WI, **1995**.
[40] A. L. Spek, *PLUTON-92*, University of Utrecht, 3584, CH Utrecht, The Netherlands **1992**.
[41] O. Kahn, *Molecular Magnetism*, VCH, **1993**, Chap. 6.
[42] G. A. Baker, G. S. Rushbrooke, H. E. Gilbert, *Phys. Rev.* **1964**, *135*, A1272
[43] J. Ribas, A. Escuer, M. Monfort, R. Vicente, R. Cortés, L. Lezama, T. Rojo, *Coord. Chem. Rev.* **1999**, *193*, 1027.
[44] T. R. Felthouse, D. N. Hendrickson, *Inorg. Chem.* **1978**, *17*, 444.

Received August 15, 2001
[I01315]

A New μ_4-Oxo Tetranuclear Magnesium Compound: Coordination Effects of the Azolato Ligands

Nadia C. Mösch-Zanetti,*[a] Marilena Ferbinteanu,[b] and Jörg Magull[a]

Keywords: N ligands / Magnesium / Coordination modes

The μ_4-oxo tetranuclear magnesium compound $[Mg_4(\mu_4\text{-oxo})(\mu\text{-tz})_6]$ **1** (tz = 3,5-*i*Pr_2-1,2,4-triazolato) with six η^1-η^1-bridging triazolato ligands was prepared in a one-step reaction between $MgBr_2$ and tzK. The solid state structure was determined by X-ray diffraction analysis showing the tetrahedral arrangement of the Mg_4O core. The reaction of $MgBr_2$ with pzK and pzH gave $[Mg(pz)_2(pzH)_2]$ **2** (pz = 3,5-*t*Bu_2-pyrazolato), which contains hydrogen bonds between two different ligands, as established by X-ray crystal structure analysis. In solution, compound **2** shows a dynamic behavior involving two different processes. Line shape analysis of variable temperature NMR experiments suggests that the interconversion occurs via an η^2-coordination of the pyrazolato ligand.
(© Wiley-VCH Verlag GmbH, 69451 Weinheim, Germany, 2002)

Introduction

The structural chemistry of magnesium amido and imido compounds is becoming an increasingly active area of research. The main reason for this recent interest is their use as reagents in numerous organic transformations.[1−7] Stimulated by the desire to elucidate the mechanisms of such reactions, several magnesium bisamido species have been structurally characterized as dimeric units of the type $[R_2NMg(\mu\text{-}NR_2)_2MgNR_2]$;[8−10] monomeric compounds are formed in the presence of sterically demanding amido ligands or additional donors.[11−14] However, polynuclear species with a higher magnesium atom count are still relatively limited. The rather unusual nitrogen-centered hexameric amido species $[Mg_6(\mu_6\text{-}N)(NHtBu)_9]$ was reported as early as 1980.[15] More than 10 years later, hexameric[16] and trimeric arrangements[17,18] were found with bifunctional amido ligands. With imido ligands, hexagonal prismatic structures of the type $[\{(THF)MgNR\}_6]$ (R = Ph, 1-naphthyl) have been reported.[19,20] In addition to these pure magnesium species a nice series[21,22] of mixed alkali metal magnesium compounds including oxide-captured examples such as $[Li_2Mg_2\{N(SiMe_3)_2\}_4(O_2)_x(O)_y]$[23] and $[K_2Mg_2[N(SiMe_3)_2]_4(O_2)\}_8]$[24] has been reported by Mulvey and co-workers. In addition to these amido species, the oxo-centered lithium magnesium cresylate cage $[LiMg_4OR_7\cdot 4THF]$ [R = *o*-$Me(C_6H_4)O^-$] has been reported.[25]

Pyrazolates and triazolates are known to be good bridging ligands for the synthesis of polynuclear complexes[26] and have proven to coordinate to magnesium in a μ_2-bridging mode[27,28] as well as an η^2-fashion[29] forming dimeric units. This prompted us to investigate whether these ligands are suitable for the construction of unusual polynuclear magnesium species. Herein, we present the synthesis and X-ray crystal structure determination of the μ_4-oxo tetranuclear magnesium compound $[Mg_4(\mu_4\text{-oxo})(\mu\text{-tz})_6]$ **1** (tz = 3,5-*i*Pr_2-1,2,4-triazolato) with six η^1-η^1-bridging triazolato ligands. Due to a structural pattern similar to those known for divalent transition metal ions, compound **1** is an appropriate model for the investigation of structural factors that are independent of the *d*-electron configuration. The second compound $[Mg(pz)_2(pzH)_2]$ **2** (pz = 3,5-*t*Bu_2-pyrazolato) employing a more sterically demanding pyrazolato ligand features both protonated and deprotonated ligands allowing an in-depth study of the coordination capabilities of these versatile ligands.

Results and Discussion

The general route for the synthesis of the triazole ligand starts from 4-NH_2-3,5-*i*Pr_2-1,2,4-triazole[30] (4-NH_2-tz) followed by diazotization to produce, after standard workup, tzH in high yield (Scheme 1). Sublimation under reduced pressure at 110 °C gave the analytically pure ligand. The analogous triazole ligand with *tert*-butyl substituents was not accessible since its higher steric demand prevents the formation of the heterocycle. The deprotonation of tzH was achieved with stoichiometric amounts of elemental potas-

[a] Institut für Anorganische Chemie der Georg-August-Universität Göttingen,
Tammannstrasse 4, 37077 Göttingen, Germany
Fax: (internat.) +49-0551/393-373
E-mail: nmoesch@gwdg.de
[b] University of Bucharest, Faculty of Chemistry, Inorg. Chem. Dept.,
Dumbrava Rosie 23, 70254 Bucharest, Romania

sium in refluxing THF. The white powders of tzK thus obtained were analytically pure and used without further purification. The potassium salt is slightly soluble in THF, readily soluble in acetonitrile and insoluble in hydrocarbon solvents. The ^{1}H NMR spectrum of the dried compound in CD_3CN shows no coordinated THF molecules.

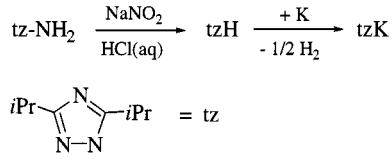

Scheme 1

The reaction of magnesium bromide with two equivalents of tzK in THF at room temperature for 48 h afforded **1** in moderate yield (Scheme 2). The compound is only soluble in polar solvents such as THF, and can be separated from the finely dispersed KBr precipitate by centrifugation. Recrystallization from cold THF gave **1** as large colorless crystals. The NMR spectroscopic data in CD_3CN show signals for one kind of ligand coordinated in a symmetric fashion.

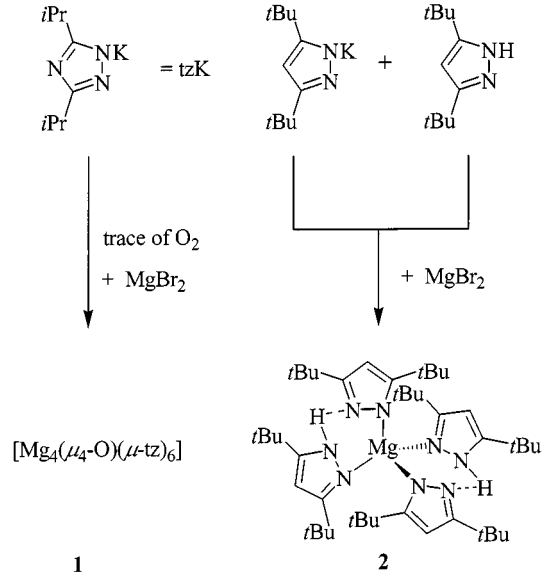

Scheme 2

The source of the oxygen anion cannot be unambiguously identified although several experiments along this line have been carried out. Repeated syntheses under more rigorous anhydrous conditions always led to the isolation of **1** arguing against the source being adventitious water. To avoid contamination with water due to residual $MgBr_2{\cdot}H_2O$, the magnesium bromide was prepared from the elements according to literature procedures.[31] The incorporation of oxygen due to a reaction with the employed grease could be ruled out by using commercially available non-silicon grease (Lithelen, Leybold Vakuum GmbH). Such a reaction is not unprecedented, although entire $O-SiMe_3$ or $O-SiMe_2$ units are usually transferred.[32–34] The cleavage of THF, which cannot be replaced due to insolubility in hydrocarbon solvents, seems unlikely. Cleavage of alkyl aryl ethers by Grignard reagents has been reported but usually requires drastic conditions,[35,36] except for certain crown ethers, where cleavage of an O–Me bond was found within 1 h at room temperature.[37] In addition, an NMR experiment in [D_8]THF ($MgBr_2$, 2 equiv. tzK and 10 equiv. THF) did not show any by-products of the cleavage. Replacement of the ethereal solvent by acetonitrile led to unidentified reaction mixtures, from which no uniform product crystallized. Incorporation of KOH remains a possibility, since the parent triazole is deprotonated by the reaction with elemental potassium. However, the yield of **1** argues against it since the potassium metal was freshly cut inside a well-maintained glove box prior to use. Finally, molecular oxygen might be a possible source as its complete exclusion is difficult to accomplish by routine Schlenk techniques. Reactions of organomagnesium compounds with oxygen are known to give peroxide[23,24] and oxide species.[38] Although this is a hint for a reaction with O_2, the oxygen source cannot be pinned down conclusively to one of the above reasons.

A structural analysis of **1** reveals a slightly distorted tetrahedral oxo-centered arrangement of four Mg atoms bridged by six η^1-η^1-triazolato ligands. Figure 1 shows an ORTEP view of **1**, crystallographic data are given in Table 1 and selected bond lengths and angles in Table 2. The Mg_4O unit is embedded in a matrix of 10 disordered molecules of THF, none of which is coordinated to a metal atom. This is consistent with the NMR spectroscopic data of the isolated and dried material in CD_3CN, where no THF signals are detectable. This is similar to the situation with the structures of proteins surrounded by disordered water molecules. Therefore, the structural parameters of the THF molecules were only approximately refined. The geometry at the four-coordinate Mg atoms is distorted tetrahedral, unlike the trigonal-bipyramidal geometry in the inorganic species [$Mg_4(\mu_4\text{-}O)(\mu\text{-}Br)_6{\cdot}4Et_2O$] published in 1964 by Stucky and Rundle,[38] where each Mg atom is additionally coordinated by an Et_2O molecule. The smaller coordination number in **1** apparently does not influence the Mg–O bond lengths {1.937(2)–1.950(2) Å in **1**; 1.95 Å in [$Mg_4(\mu_4\text{-}O)(\mu\text{-}Br)_6{\cdot}4Et_2O$][38]}. Similar structural features are exhibited by complexes of beryllium in the basic acetates [$Be_4(\mu_4\text{-}O)(RCO_2)_6$],[39] for example, and even in well-known transition metal systems such as [$Co_4(\mu_4\text{-}O)(\mu\text{-}pz)_6$],[40,41] suggesting that the formation of **1** arises from geometrical packing and ionic effects rather than from the electronic configuration of the metal. The structure of **1** should also be compared with that of the cresylate species [$LiMg_4(\mu_5\text{-}O)R_7{\cdot}4THF$] (R = *o*-Me($C_6H_4$)$O^-$),[25] where a $Mg_4(\mu_4\text{-}O)$ core is additionally coordinated by a lithium cresylate. This leads to an oxo-centered, trigonal bipyramidal $LiMg_4(\mu_5\text{-}O)$ core. Unlike in **1**, all the Mg atoms are coordinated by one molecule of THF. The Mg–O(central) bonds are slightly longer [2.002(4) to 2.041(2) Å], presumably due to the higher coordination number.

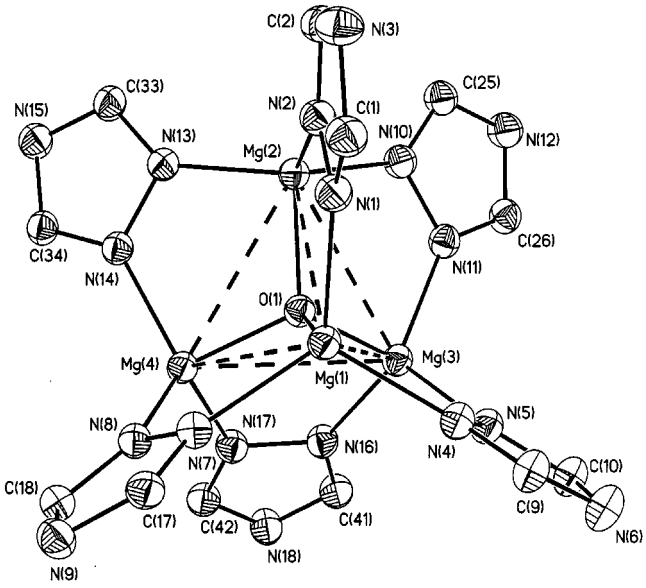

Figure 1. Molecular view of $[Mg_4(\mu_4\text{-oxo})(\mu\text{-tz})_6]$ (**1**); *iso*-propyl groups have been omitted for clarity

The $MgON_3$ tetrahedra show a pronounced trigonal distortion with the Mg atom lying almost within the N_3 plane [O(1)−Mg(1)−N(1) = 100.71°]. This structure ensures a perfect alignment of the lone pairs of the N atoms toward the metal and, in addition, obeys Bent's rules:[42,43] the hybrid orbitals pointing towards the less electronegative atom acquire a higher *s* character and therefore increased angles [N(1)−Mg(1)−N(4) = 117.16°]. The $MgON_3$ tetrahedron can be modeled with $s^{1+x/3}p^{3-x/3}$ hybrid orbitals in the Mg−N directions and with $s^{1-x}p^{3+x}$ orbitals for the Mg−O axis. From this, the N−Mg−N bond angles are arccos[−(1 + *x*/3)/(3 − *x*/3)]. Thus, the experimental angles yield an estimation of $x = 0.73$, showing a distinct redistribution of *s* vs. *p* character compared to the sp^3 reference.

Compound **2** may be prepared by two different routes. The more straightforward method involves the addition of two equiv. of pzH[44] and pzK[45] each to $MgBr_2$ in THF (Scheme 2). The product is soluble in most organic solvents, including hexane and toluene. Compound **2** may also be prepared by the addition of water to a hexane solution containing $[\{Mgpz_2\}_2]$, a species recently reported by Winter.[29] During the reaction with water, a white precipitate is formed and **2** is found exclusively in solution. Evaporation of the solvent gave pure **2** in 40% yield (based on the amount of pzK). The ^{1}H NMR spectrum in C_6D_6 of the precipitate shows six different signals in the *t*Bu region pointing to a mixture of compounds. At this point it is unclear whether one of these species is the compound $[Mg_4(\mu_4\text{-O})(\mu\text{-pz})_6]$, similar to **1**, although mass spectrometry points to its existence.[46] An interesting experiment would be a similar reaction with the triazolato ligand to find out whether water is the oxo anion source; however tzK and $MgBr_2$ do not react at all in toluene or hexane due to their insolubility in these solvents.

The solid state structure of **2** determined by X-ray crystallography shows the magnesium atom tetrahedrally surrounded by two η^1-coordinated pyrazole and two pyrazolato ligands. Figure 2 shows an ORTEP view of **2**, crystallographic data are given in Table 1 and selected bond lengths and angles in Table 2. A particular feature are the intramolecular hydrogen bonds between two pairs of different ligands [N(4)−H(4)···N(2) 2.7448(17) Å, 153(3)°] preventing the possibility of η^2-coordination [Mg(1)−N(1) 2.038(1) Å vs. Mg(1)−N(2) 2.737(1) Å] although a preference for such a coordination even in a sterically congested six-coordinate species has been previously found.[29]

Table 1. Experimental crystallographic data for **1** and **2**

	1	**2**
Empirical formula	$C_{48}H_{84}MgN_{18}O\cdot 10THF$	$C_{44}H_{78}MgN_8$
Mol. wt.	1747.61	743.45
Crystal system	monoclinic	monoclinic
Space group	$P2_1/c$	$C2/c$
a (Å)	24.9166(9)	23.4784(17)
b (Å)	16.6528(6)	11.0558(9)
c (Å)	25.7123(9)	19.2892(15)
β (deg)	106.737(3)	112.149(6)
V (Å^3)	10216.9(6)	4637.5(6)
Z	4	4
T (K)	133(2) K	133(2)
Density $\rho_{calcd.}$ (Mg/m^3)	1.136	1.065
Absorption coefficient (mm^{-1})	0.097	0.076
F(000)	3816	1640
Reflections collected	167504	11682
Reflection unique	17573 (R_{int} = 0.0828)	3884 (R_{int} = 0.0731)
Final *R* indices [$I > 2\sigma(I)$][a]	$R1 = 0.0727$	$R1 = 0.0471$
	$wR2 = 0.2048$	$wR2 = 0.1256$
Goodness-of-fit on F^2 [b]	1.037	1.039

[a] $R1 = \Sigma|F_o - F_c|/\Sigma|F_o|$; $wR2 = [\Sigma w(F_0^2 - F_c^2)^2/\Sigma wF_o^4]^{1/2}$. [b] $S = [\Sigma w(F_0^2 - F_c^2)^2/\Sigma(n - p)]^{1/2}$.

Table 2. Selected bond lengths (Å) and angles (deg) for **1** and **2**

Complex **1**			
Mg(1)−O(1)	1.950(2)	Mg(2)−O(1)	1.941(2)
Mg(3)−O(1)	1.937(2)	Mg(4)−O(1)	1.944(2)
Mg(1)−N(1)	2.065(3)	Mg(1)−N(4)	2.058(3)
Mg(1)−N(7)	2.062(3)	Mg(1)−Mg(2)	3.167(2)
Mg(1)−O(1)−Mg(2)	108.97(10)	Mg(1)−O(1)−Mg(2)	108.62(10)
O(1)−Mg(1)−N(1)	100.71(11)	O(1)−Mg(1)−N(4)	98.90(10)
O(1)−Mg(1)−N(7)	100.42(10)	N(1)−Mg(1)−N(4)	117.16(12)
Complex **2**			
Mg(1)−N(1)	2.038(1)	Mg(1)−N(2)	2.737(1)
Mg(1)−N(3)	2.202(1)	Mg(1)−N(4)	2.957(1)
N(2)···H(4)−N(4)	2.7448(17)	N(2)···H(4)−N(4)	154(3)
N(1)−Mg(1)−N(3)	105.77(5)	N(1)−Mg(1)−N(1A)[a]	118.24(8)
N(1)−Mg(1)−N(3A)[a]	103.39(5)		

[a] Equivalent atoms "A" generated with: $-x$, y, $-z + 1/2$.

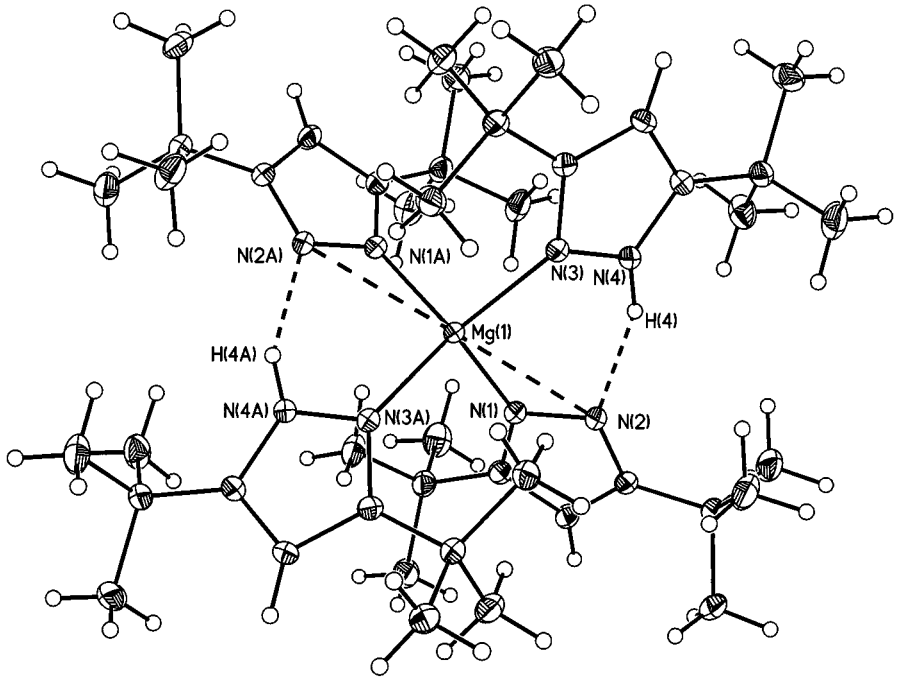

Figure 2. Molecular view of $[Mg(pz)_2(pzH)_2]$ (**2**)

The ^{1}H NMR spectrum of **2** at room temperature shows broad resonances for one kind of ligand, indicating a dynamic process. As the sample was cooled to 183 K the individual resonances of the four *t*Bu, two CH and one NH protons appeared, consistent with the structure in the solid state at 133 K (Figure 3). The temperature dependent behavior of the *t*Bu region can be modeled with two separate exchanges $A_1 \rightleftarrows B_1$ with rate constant k_τ (coalescence temperature ≈243 K) as well as $A_1(B_1) \rightleftarrows A_2(B_2)$ with rate constant k_H (coalescence temperature ≈290 K) (Figure 3). This is consistent with a rapid interchange of the A_1 and B_1 signals of the deprotonated ligand. The process coalescing at higher temperatures corresponds to the exchange of the bridging proton between different ligands interchanging A_1 in A_2 and parallel B_1 in B_2 (with equal rate constant k_H).

The rates were measured by line shape analysis by solving the following matrix:[47−49]

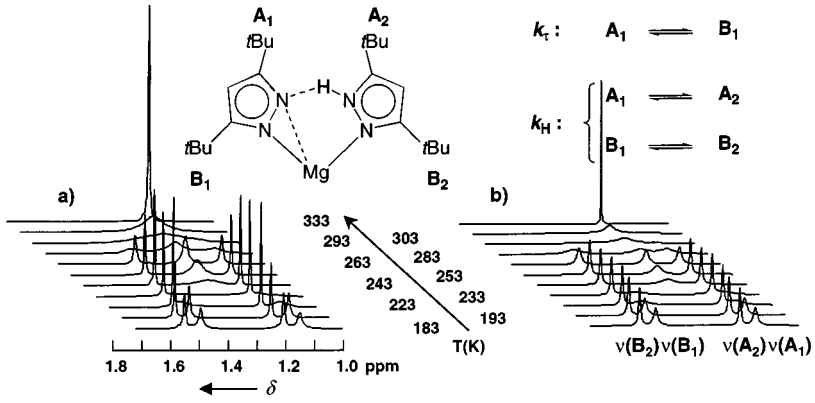

Figure 3. a) Variable temperature ^{1}H NMR spectra (500 MHz, [D$_8$]toluene) of **2** showing the *t*Bu resonances; b) computer simulated spectra and proposed kinetic processes

$$\begin{pmatrix} \nu(A_1)+\alpha T+ik_\tau(T)+ik_H(T) & 0 & -ik_\tau(T) & 0 \\ -ik_H(T) & \nu(A_2)+\alpha T+ik_H(T) & 0 & 0 \\ -ik_\tau(T) & 0 & \nu(B_1)+\alpha T+ik_\tau(T)+ik_H(T) & -ik_H(T) \\ 0 & 0 & -ik_H(T) & \nu(B_2)+\alpha T+ik_H(T) \end{pmatrix}$$

where ν denotes the chemical shift of the four types of protons.

The real part of the eigenvalues corresponds to the position of the peaks, while the imaginary part corresponds to their bandwidths. The solutions of this matrix were used to form the spectrum as the sum of four Lorentzian peaks. In addition, a slight shift of the barycenter of the experimental signals with temperature required a linear adjustment αT, which was added to each diagonal element. This is probably due to a general modification of the average Mg−N bond lengths with temperature. Targeting only a qualitative simulation, kinetic terms corresponding to spin-lattice relaxation were not ascribed. Both the chemical shift ν and the rate constant *k* have the common meaning of a frequency and therefore, in this case, *k* is defined in units of the chemical shifts. The coalescence appears when the frequency of the chemical exchange becomes similar to those of the magnetic resonance.

A fit of the chemical rate constants to the Arrhenius equation yielded activation energies of E_τ = 8.3 kcal/mol and E_H = 15.2 kcal/mol; use of the Eyring form gave similar results (E_τ = 8.0 kcal/mol and E_H = 14.7 kcal/mol). The low value of E_τ points to an interchange of the two N atoms of the deprotonated ligand via η^2-coordination. Surprisingly, in previously reported magnesium η^2-pyrazolato complexes dynamic processes were proposed, but seem to be faster than the NMR time scale.[29] The value of E_H is consistent with a facile exchange of the proton between two ligands favored by an N−H···N hydrogen bond established in the low temperature structure. These intramolecular rearrangements are complex processes at the quantum level. However, the employed classical rate laws allow a semi-quantitative statement that, due to the possible η^1- and η^2-coordination modes, the pseudo-rotation of the deprotonated ligand is more rapid than the intramolecular proton exchange.

Conclusion

Here, we present a μ_4-oxo tetranuclear main group metal compound with azolato ligands. Due to the lack of *d*-electrons, compound **1** represents a model for this structural prototype allowing the conclusion that the forces to build this structure pattern are mainly of an ionic nature and that *d-d* electron interactions seem not to play a role. In addition, our investigations of **2** offer an illustration for the paradigm used in supramolecular concepts stating that hydrogen bonds and coordination effects compete in the same range of bonding energies.

Experimental Section

General Remarks: All preparations were carried out under an atmosphere of dry nitrogen. All common reagents and solvents were purchased from commercial suppliers and used without further purification unless otherwise indicated. Melting points were determined on a Büchi B-540 melting point apparatus in sealed glass tubes and are uncorrected. NMR spectra were recorded on Bruker Avance 200 or Bruker Avance 500 spectrometers. The chemical shifts are referenced to external $SiMe_4$.

tzH: 4-NH_2-3,5-*i*Pr_2-triazole was synthesized according to a published method from *i*PrCOOH and hydrazine hydrate at 180 °C. Subsequently, a solution of 4-NH_2-3,5-*i*Pr_2-triazole (4.28 g, 0.025 mol) in aqueous HCl (6 M, 5.5 mL) was treated with a solution of $NaNO_2$ (2.01 g, 0.029 mol) in 30 mL of water and stirred until evolution of N_2 ceased. The temperature was kept in the range 20−30 °C by occasional cooling with an ice bath. After neutralization, extraction with CH_2Cl_2 and evaporation of the solvent the pure product was obtained as colorless crystals (3.42 g, 88%). m.p. 154 °C. ^{1}H NMR (C_6D_6, 200.1 MHz):δ = 12.98 (br. s, NH, 1 H), 3.19 [hept, C*H*$(CH_3)_2$, 2 H], 1.35 [d, CH$(CH_3)_2$, 12 H]. ^{13}C NMR (C_6D_6, 125.8 MHz):δ = 164.0 (C ring), 27.6 [*C*H$(CH_3)_2$], 21.5

[$CH(CH_3)_2$]. $C_8H_{15}N_3$ (153.2): calcd. C 62.71, H 9.87, N 27.42; found C 62.79, H 9.61, N 27.23.

tzK: A solution of tzH (1.65 g, 10.8 mmol) in 60 mL of THF was treated with one equivalent of potassium metal (0.43 g). The solution was stirred under reflux for 5 h after which all the metal had reacted. The solvent was removed under reduced pressure to give the product as a white powder that was pure enough for further reactions (1.92 g, 93%). m.p. > 300 °C ^{1}H NMR (CD_3CN, 200.1 MHz):δ = 2.84 [hept, 2 H, C*H*(CH_3)$_2$], 1.18 [d, 12 H, CH(C*H*$_3$)$_2$]. $C_8H_{14}KN_3$ (191.3): calcd. C 50.22, H 7.38, N 20.44; found C 49.88, H 7.29, N 20.42.

[Mg_4(μ_4-oxo)(μ-tz)$_6$] (1): Freshly distilled THF (20 mL) was added to a mixture of $MgBr_2$ (0.21 g, 1.14 mmol) and tzK (0.43 g, 2.25 mmol). The resulting suspension was stirred for 48 h at room temp. The fine precipitate was then centrifuged and the solution decanted. After evaporation of the solvent to a volume of approximately 10 mL, colorless crystals of **1** formed overnight (0.11 g, 38% based on Mg). ^{1}H NMR (CD_3CN, 200.1 MHz, room temp.): δ = 3.07 [sept, $^3J_{H,H}$ = 7 Hz, 2 H, C*H*(CH_3)$_2$], 1.16 [d, $^3J_{H,H}$ = 7, 12 Hz, CH(C*H*$_3$)$_2$]. ^{13}C NMR (CD_3CN, 125.8 MHz, room temp.): δ = 171.11 (C ring), 29.71 [*C*H(CH_3)$_2$], 23.13 [CH(*C*H$_3$)$_2$]. $C_{48}H_{84}Mg_4N_{18}O$ (1026.5): calcd. C 56.16, H 8.25, N 24.56; found C 55.78, H 8.41, N 24.03.

[Mg(pz)$_2$(pzH)$_2$] (2): Freshly distilled THF (20 mL) was added to a mixture of $MgBr_2$ (0.16 g, 0.87 mmol), pzK (0.38 g, 1.74 mmol) and pzH (0.31 g, 1.72 mmol). The resulting suspension was stirred for 48 h at room temp. The solvent was then removed under reduced pressure and the resulting white residue was extracted with hexane. After removal of hexane, the powder was recrystallized from toluene at −25 °C to give **2** as colorless crystals (0.21 g, 32%). ^{1}H NMR (C_6D_6, 500.1 MHz, 193 K): δ = 13.22 (s, 1 H, NH), 6.15 (s, 1 H, CH), 6.05 (s, 1 H, CH), 1.60 [s, 9 H, C(CH_3)$_3$], 1.54 [s, 9 H, C(CH_3)$_3$], 1.22 [s, 9 H, C(CH_3)$_3$], 1.16 [s, 9 H, C(CH_3)$_3$].). ^{13}C NMR (C_6D_6, 125.8 MHz, room temp.): δ = 159.57 (CH ring), 98.72 (C ring), 31.76 [*C*(CH_3)$_3$], 30.991 [C(*C*H$_3$)$_3$]. $C_{44}H_{78}MgN_8$ (743.5): calcd. C 70.25, H 10.54, N 14.90; found C 70.70, H 10.52, N 14.96.

X-ray Crystal Structure Analysis: The data were collected on a Stoe IPDS II-array detector system instrument with graphite-monochromated Mo-K_α radiation (λ = 0.71073 Å). The structures were solved by direct methods and refined against F^2 on all data by full-matrix least-squares procedures with SHELX-97.[50]
1: To verify the complex composition of **1**·10THF and especially the connectivity in the 10 solvent molecules, complete crystal structure determinations were carried out with five different crystals. The best results are presented in this paper. All THF molecules are disordered and refined with restraints. In the Mg_4 unit two *i*Pr groups are disordered.

CCDC-166225 (**1**) and CCDC-166226 (**2**) contain the supplementary crystallographic data for this paper. These data can be obtained free of charge at www.ccdc.cam.ac.uk/conts/retrieving.html [or from the Cambridge Crystallographic Data Centre, 12, Union Road, Cambridge CB2 1EZ, UK; fax: (internat.) +44-1223/336-033; E-mail: deposit@ccdc.cam.ac.uk].

Acknowledgments

Generous support from Prof. H. W. Roesky and the Alexander-von-Humboldt-Foundation (M. F.) is gratefully acknowledged.

[1] K. W. Henderson, W. J. Kerr, J. H. Moir, *Chem. Commun.* **2000**, 479−480.
[2] K. W. Henderson, J. F. Allan, A. R. Kennedy, *Chem. Commun.* **1997**, 1149−1150.
[3] D. A. Evans, S. A. Nelson, *J. Am. Chem. Soc.* **1997**, *119*, 6452−6453.
[4] K. Kobayashi, M. Kawakita, H. Akamatsu, O. Morikawa, H. Konishi, *Bull. Chem. Soc. Jpn.* **1996**, *69*, 2645−2647.
[5] Y. Kondo, A. Yoshida, T. Sakamoto, *J. Chem. Soc., Perkin Trans. 1* **1996**, 2331−2332.
[6] W. Schlecker, A. Huth, E. Ottow, J. Mulzer, *J. Org. Chem.* **1995**, *60*, 8414−8416.
[7] P. E. Eaton, C.-H. Lee, Y. Xiong, *J. Am. Chem. Soc.* **1989**, *111*, 8016−8018.
[8] M. Westerhausen, W. Schwarz, *Z. Anorg. Allg. Chem.* **1992**, *609*, 39−44.
[9] W. Clegg, K. W. Henderson, R. E. Mulvey, P. A. O'Neil, *J. Chem. Soc., Chem. Commun.* **1994**, 769−770.
[10] M. M. Olmstead, W. J. Grigsby, D. R. Chacon, T. Hascall, P. P. Power, *Inorg. Chim. Acta* **1996**, *251*, 273−284.
[11] D. C. Bradley, M. B. Hursthouse, A. A. Ibrahim, K. M. A. Malik, M. Motevalli, R. Möseler, H. Powell, J. D. Runnacles, A. C. Sullivan, *Polyhedron* **1990**, *9*, 2959−2964.
[12] L. M. Englehardt, P. C. Junk, W. C. Patalinghug, R. E. Sue, C. L. Raston, B. W. Skelton, A. H. White, *J. Chem. Soc., Chem. Commun.* **1991**, 930−932.
[13] R. A. Bartlett, M. M. Olmstead, P. P. Power, *Inorg. Chem.* **1994**, *33*, 4800−4803.
[14] J. L. Sebestl, T. T. Nadasdi, M. J. Heeg, C. H. Winter, *Inorg. Chem.* **1998**, *37*, 1289−1294.
[15] G. Dozzi, G. Del Piero, M. Cesari, S. Cucinella, *J. Organomet. Chem.* **1980**, *190*, 229−236.
[16] W. Clegg, M. Frank, R. E. Mulvey, P. A. O′Neil, *J. Chem. Soc., Chem. Commun.* **1994**, 97−98.
[17] W. Clegg, L. Horsburgh, R. E. Mulvey, R. Rowlings, *Chem. Commun.* **1996**, 1739−1740.
[18] M. Veith, A. Spaniol, J. Pöhlmann, F. Gross, V. Huch, *Chem. Ber.* **1993**, *126*, 2625−2635.
[19] T. Hascall, K. Ruhlandt-Senge, P. P. Power, *Angew. Chem.* **1994**, *106*, 350−351; *Angew. Chem. Int. Ed. Engl.* **1994**, *33*, 356−357.
[20] W. J. Grigsby, T. Hascall, J. J. Ellison, M. M. Olmstead, P. P. Power, *Inorg. Chem.* **1996**, *35*, 3254−3261.
[21] R. E. Mulvey, *Chem. Commun.* **2001**, 1049−1056.
[22] P. C. Andrews, A. R. Kennedy, R. E. Mulvey, C. L. Raston, B. A. Roberts, R. B. Rowlings, *Angew. Chem.* **2000**, *112*, 2036−2038; *Angew. Chem. Int. Ed.* **2000**, *39*, 1960−1962.
[23] A. R. Kennedy, R. E. Mulvey, R. B. Rowlings, *J. Am. Chem. Soc.* **1998**, *120*, 7816−7824.
[24] A. R. Kennedy, R. Mulvey, C. L. Raston, B. A. Roberts, R. B. Rowlings, *Chem. Commun.* **1999**, 353−354.
[25] K. W. Henderson, R. E. Mulvey, F. B. M. Reinhard, *J. Am. Chem. Soc.* **1994**, *116*, 10777−10778.
[26] G. La Monica, G. A. Ardizzoia, *Prog. Inorg. Chem.* **1997**, *46*, 151−238.
[27] D. A. Atwood, A. H. Cowley, R. A. Jones, *Organometallics* **1993**, *12*, 236−238.
[28] C.-C. Chang, T.-Y. Her, F.-Y. Hsieh, C.-Y. Yang, M. Y. Chiang, G.-H. Lee, Y. Wang, S.-M. Peng, *J. Chin. Chem. Soc. (Taipei)* **1994**, *41*, 783−789.
[29] D. Pfeiffer, M. J. Heeg, C. H. Winter, *Angew. Chem.* **1998**, *110*, 2674−2676; *Angew. Chem. Int. Ed.* **1998**, *37*, 2517−2519.
[30] R. M. Herbst, J. A. Garrison, *J. Org. Chem.* **1953**, *18*, 872−877.
[31] *Gmelins Handbuch der anorganischen Chemie, Magnesium, Teil B, die Verbindungen des Magnesiums*; Verlag Chemie: Berlin, 1939.
[32] H. Bock, M. Sievert, C. L. Bogdan, B. O. Kolbesen, A. Wittershagen, *Organometallics* **1999**, *18*, 2387−2389.
[33] T. I. Gountchev, T. D. Tilley, *Organometallics* **1999**, *18*, 2896−2905.

[34] C. N. McMahon, S. G. Bott, L. B. Alemany, H. W. Roesky, A. R. Barron, *Organometallics* **1999**, *18*, 5395−5408.
[35] E. Müller, *Methoden der Organischen Chemie (Houben Weyl)*; 4th Ed.; Thieme Verlag: Stuttgart, **1973**, Vol. XIII/2a.
[36] H. Meerwein, *Methoden der Organischen Chemie (Houben Weyl)*; Thieme Verlag: Stuttgart, **1965**, Vol. VI/3.
[37] G. J. M. Gruter, G. P. M. van Klink, O. S. Akkerman, F. Bickelhaupt, *Organometallics* **1993**, *12*, 1180−1188.
[38] G. Stucky, R. E. Rundle, *J. Am. Chem. Soc.* **1964**, *86*, 4821−4825.
[39] A. Tulinsky, *Acta Crystallogr.* **1959**, *12*, 634−637.
[40] I. G. Dance, *Comprehensive Coordination Chemistry*; (Eds.: G. Wilkinson, R. D. Gillard, J. A. McCleverty) Pergamon Press: Oxford, **1987**, Vol. 1, pp 135.
[41] M. K. Ehlert, S. J. Rettig, A. Storr, R. C. Thompson, J. Trotter, *Acta Crystallogr., Sect. C* **1994**, *50*, 1023−1026.
[42] H. A. Bent, *Chem. Rev.* **1961**, *61*, 275−311.
[43] N. Fröhlich, G. Frenking, *Chem. Rev.* **2000**, *100*, 717−774.
[44] J. Elguero, E. Gonzalez, R. Jacquier, *Bull. Soc. Chim. Fr.* **1968**, 707−713.
[45] C. Yélamos, M. J. Heeg, C. H. Winter, *Inorg. Chem.* **1998**, *37*, 3892−3894.
[46] We thank the referees for their helpful comments and suggestions.
[47] C. P. Poole, *Theory of Magnetic Resonance*; 2nd ed.; John Wiley & Son: New York, 1987, pp 171.
[48] G. Binsch, *J. Am. Chem. Soc.* **1969**, *91*, 1304−1309.
[49] The formation of the matrix can be intuitively described as follows: i) The real part of the matrix elements corresponds to the spin Hamiltonian; the diagonal elements contain only chemical shifts without coupling between different types of protons. ii) The imaginary part is related to the kinetic equations; nondiagonal elements -*ik*H or -*ik*t are added at intersections between the lines and columns of the corresponding interchange. iii) The sum of the imaginary parts on each diagonal element must contain all the rate constants that affect a given species. iv) The sum of the imaginary terms of each row or column must be zero.
[50] G. M. Sheldrick, Universität Göttingen, **1997**.

Received August 23, 2001
[I01323]

Synthesis of the First 2*H*-1,2-Azaphosphole Complexes with P,C and P,N Ylide Functional Groups

Rainer Streubel,*[a] Nils Hoffmann,[a] H.-M. Schiebel,[a] Frank Ruthe,[a] and Peter G. Jones[a]

Dedicated to Professor Wolfgang W. Schoeller on the occasion of his 60th birthday

Keywords: Ylides / Phosphorus heterocycles / Tungsten / Cyclization

The first C^5-functionalized 2*H*-1,2-azaphosphole complexes have been obtained by the reactions of P,C and P,N ylide substituted carbonitriles and terminal phosphanediyl complexes involving transiently formed nitrilium phosphanylide complexes.

(© Wiley-VCH Verlag GmbH, 69451 Weinheim, Germany, 2002)

Introduction

The transition metal promoted synthesis of P-heterocycles is of current interest because of the frequently observed outstanding reaction selectivities and product yields.[1] Recently, we presented a new concept in phosphorus heterocycle synthesis, which relies on the use of short-lived 1,3-dipole species that are stabilized through metal coordination, viz. nitrilium phosphanylide complexes **II**.[2] Complexes **II** may be formed by 1,1-addition of thermally generated terminal phosphanediyl complexes **I**[2,3] to carbonitriles, which is a weakly exothermic reaction according to theoretical calculations,[4] or by ring-opening of 2*H*-azaphosphirene complexes **III** (Scheme 1).[2,4] To date, the 1,1-addition of terminal phosphanediyl complexes **I** to carbonitriles has been demonstrated using two different precursor systems for **I**, namely 2*H*-azaphosphirene complexes **III**[2] and 7-phosphanorbornadiene complexes **IV**.[3,5] The former is especially useful for the transient formation of bulky *P*-substituted derivatives of **I** having a bis(trimethylsilyl)methyl (**1a**) or pentamethylcyclopentadienyl group (**1b**) attached to the phosphorus atom, whereas the latter can be employed to generate derivatives of **I** with small and/or functional substituents at the phosphorus atom.

Only two different intramolecular trapping reactions of transient nitrilium phosphanylide complexes **II** have hitherto been observed, which were shown to be very sensitive to the substituent at the phosphorus atom. For example, complex **2a** isomerized to the 2*H*-azaphosphirene complex **4a**[6] while complex **3** led to the C,N,P cage complex **5**[7] through an intramolecular [2+1] cycloaddition of the phosphanediyl phosphorus center of **3** to the Cp* π-system (Scheme 2).

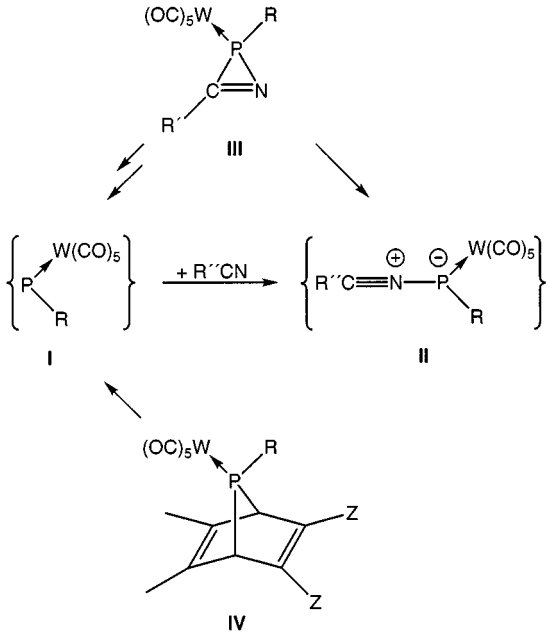

Scheme 1. Generation of terminal phosphanediyltungsten complexes **I** and (nitrilium phosphanylide)tungsten complexes **II** using precursors **III** and **IV**

Furthermore, we showed that *C*-dialkylamino-, *C*-alkyl-, or *C*-aryl-substituted nitrilium phosphanylide complexes **II** reacted with electron-deficient alkynes such as dimethylacetylene dicarboxylate (DMAD) to furnish 2*H*-1,2-azaphosphole complexes through [3+2]-cycloaddition reactions.[2,8,9] It is noteworthy that only complex **2b**, which has

[a] Institut für Anorganische und Analytische Chemie der Technischen Universität Braunschweig,
P. O. Box 3329, 38023 Braunschweig, Germany

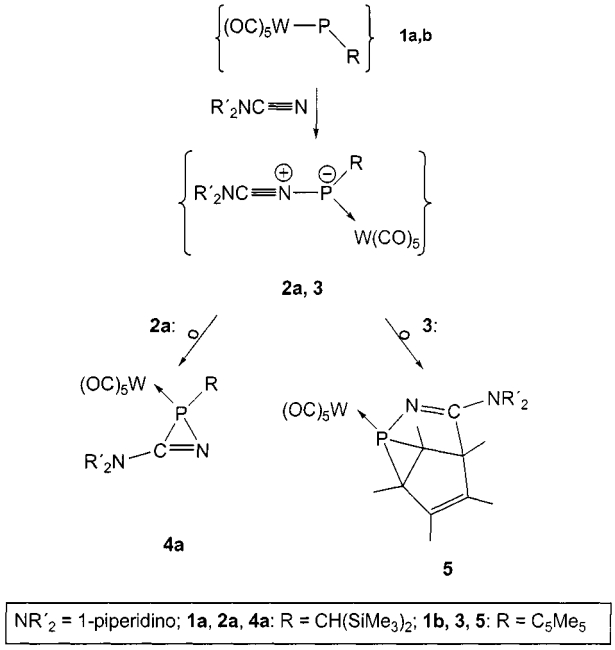

Scheme 2. Generation and intramolecular reactions of (nitrilium phosphanylide)tungsten complexes **2a** and **3**

the dimethylamino group at the carbon atom and a bulky substituent at the phosphorus atom, reacted with DMAD (**6**) to give both the Δ^3-1,3,2-oxazaphospholene complexes **7a**,**b** and the 2*H*-1,2-azaphosphole complex **8a** (Scheme 3).[10]

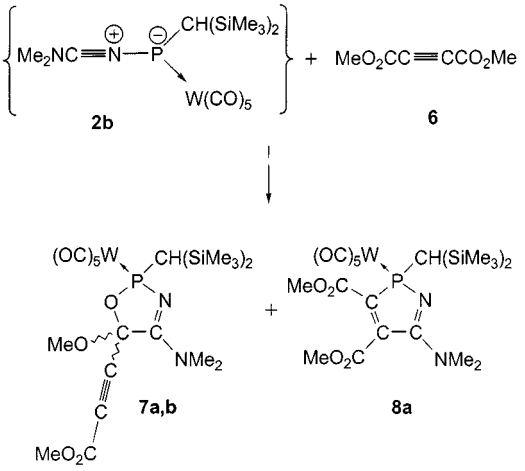

Scheme 3. Reaction modes of transiently formed (nitrilium phosphanylide)tungsten complex **2b** towards DMAD

We report herein on a comparative study of the stereoelectronic effects of various strong π-donor *C*-substituents of transiently formed [nitrilium bis(trimethylsilyl)methylphosphanylide]tungsten complexes **II** on ring-closure reactions of **II** to **III** (e.g. **1a** → **3**) and on the reactivity of **II** towards electronically activated alkynes. In view of the known electronic stabilizing effect of P,C ylide substituents in low-coordinated phosphorus compounds such as thioxophosphanes or selenoxophosphanes of the formula RPX [R = $Ph_3PC(R')$; X = S, Se[11]] we decided to include $Ph_3PC(H)CN$[12] and Ph_3PNCN[13] in this study, the latter for comparison purposes. Furthermore, we have also sought an optimized synthesis of 2*H*-1,2-azaphosphole complexes, whereby such systems can be obtained bearing new P,C and P,N ylide functional groups. The first results concerning new three-component reactions are reported herein.

Results and Discussion

Thermal reaction of the (2*H*-azaphosphirene)tungsten complex **4b**[14] with piperidinocarbonitrile (**9a**) and DMAD (**6**) furnished the Δ^3-1,3,2-oxazaphospholene complexes **10a**,**b** and the 2*H*-1,2-azaphosphole complex **8b** in a 1:1:1 ratio as the phosphorus-containing products. Although only complexes **10a** and **8b** could be isolated by column chromatography, complex **10b** was readily identified by its ^{31}P NMR spectroscopic data (δ = 191.8, $^1J_{W,P}$ = 305.7 Hz) (Scheme 4).

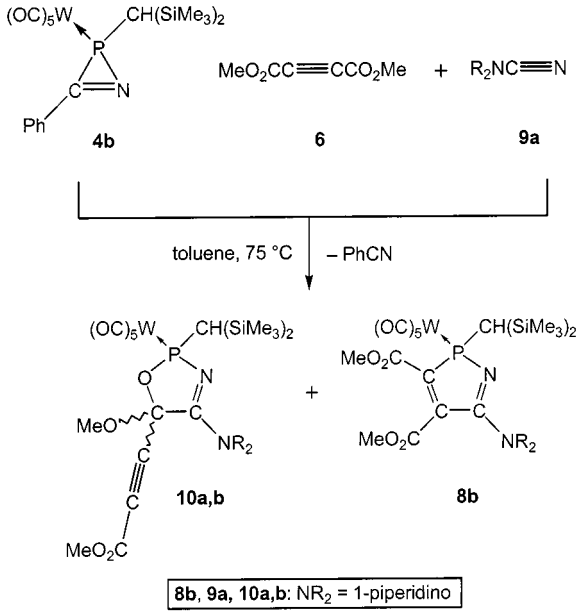

Scheme 4. Three-component reaction of 2*H*-azaphosphirene complex **4b** with DMAD and 1-piperidinocarbonitrile (**9a**)

Very selective reactions were observed with **4b**, 2-furylcarbonitrile (**9b**) or 2-thienylcarbonitrile (**9c**), and **6**. In this case, we obtained exclusively the 2*H*-1,2-azaphosphole complexes **8c**,**d** and no side-reactions leading to Δ^3-1,3,2-oxazaphospholene complexes were observed; complexes **8c**,**d** were isolated and fully characterized (Scheme 5).

To our surprise, reaction of the 2*H*-azaphosphirene complex **4b** (1 equiv.) with the pyrrolyl-substituted carbonitrile **9d** (2 equiv.) and DMAD (2 equiv.) led exclusively to the 2*H*-azaphosphirene complex **4c** (**i**). Even more surprising was that we had to change the ratio of 2*H*-azaphosphirene complex **4b**/pyrrolyl-substituted carbonitrile **9d**/DMAD to 1:4:2 in order to obtain the 2*H*-azaphosphirene complex **4c** and the 2*H*-1,2-azaphosphole complex **8e** in a 1:10 ratio (**ii**) (Scheme 6). This finding was completely counterintuitive. It was also very remarkable that a 2*H*-azaphosphirene complex was formed in a three-component reaction with DMAD; this had not been observed previously. This points

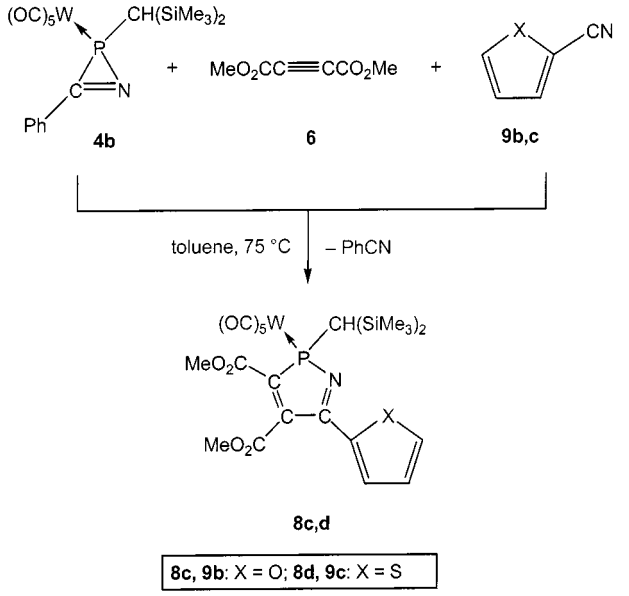

Scheme 5. Three-component reactions of 2*H*-azaphosphirene complex **4b** with DMAD and hetarene-substituted carbonitriles (**9b**,**c**)

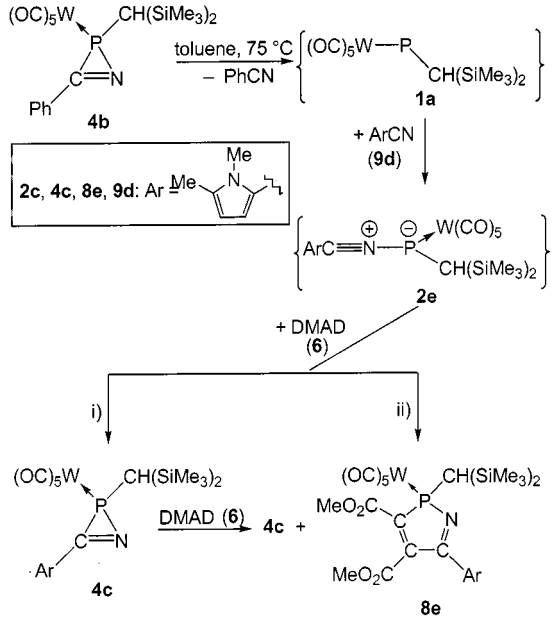

Scheme 6. Two- and three-component reactions of 2*H*-azaphosphirene complex **4b** with DMAD and pyrrolecarbonitrile (**9d**) (for explanations of **i** and **ii**, see text)

to an increased tendency of nitrilium phosphanylide complex **2e** to isomerize to **4c**, even under such conditions. Furthermore, the pure complex **4c** displayed an enhanced thermal stability in solution and underwent rapid ring-opening to transient **2c** only beyond 78 °C to yield complex **8e** with DMAD (Scheme 6).

The course of the reaction of the 2*H*-azaphosphirene complex **4b** with $Ph_3PC(H)CN$ (**9e**) and DMAD appeared to be more complicated under the same reaction conditions, although the outcome was in some respects not very surprising. Primarily, and at ambient temperature, rapid formation of the carbonitrile derivative **9f** was observed.[15] Nevertheless, this nitrile then selectively led to the 2*H*-1,2-azaphosphole complex **8f** (Scheme 7). Neither formation of Δ^3-1,3,2-oxazaphospholene complexes nor of a 2*H*-azaphosphirene complex was observed.

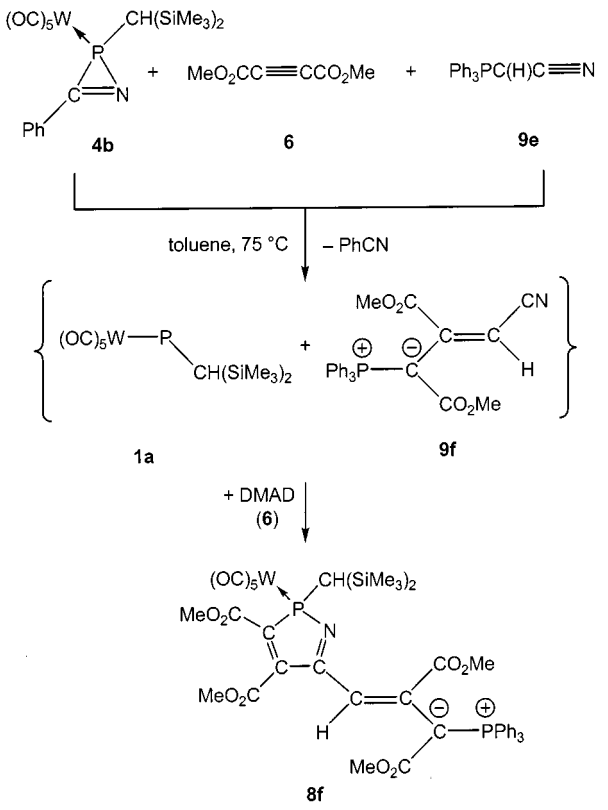

Scheme 7. Three-component reaction of 2*H*-azaphosphirene complex **4b** with DMAD and $Ph_3PC(H)CN$ (**9e**)

Also very selective was the reaction of the 2*H*-azaphosphirene complex **4b** with Ph_3PNCN (**9g**) and DMAD (1:1:1 ratio). ^{31}P NMR spectroscopic monitoring of the reaction showed exclusively the formation of the 2*H*-1,2-azaphosphole complex **8g** as the sole phosphorus-containing product, which was isolated in good yields by column chromatography (Scheme 8).

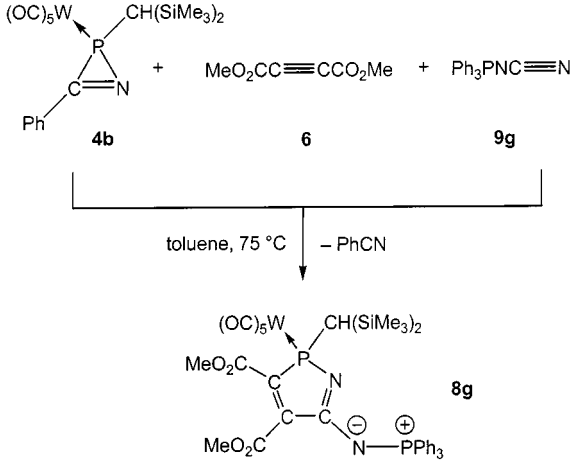

Scheme 8. Three-component reaction of 2*H*-azaphosphirene complex **4b** with DMAD and Ph_3PNCN (**9g**)

As our former studies on the regioselectivity of reaction of transiently generated nitrilium phosphanylide complexes

2a,**b**[8] and **2c**−**e**[9] with ethyl acetylenecarboxylate (**11**) showed, these highly reactive species always yield two regioisomeric 2*H*-1,2-azaphosphole complexes, with formation of the 4-ethoxycarbonyl-substituted 2*H*-1,2-azaphosphole complexes being favored. This was established by X-ray crystal structure analysis of a 5-(1,5-dimethylpyrrol-2-yl)-substituted 2*H*-1,2-azaphosphole complex.[9] Furthermore, we found that the regioisomer ratios showed a marked dependence on the C^5 substituent, e.g., 2-furanyl (3:1 ratio), 2-thienyl (5:1 ratio), and 2-(1,5-dimethylpyrrolyl) (8:1 ratio). Therefore, we were interested in examining the regioselectivity of transiently generated nitrilium phosphanylide complexes **2f**,**g** of the general formula RCNP[CH(SiMe$_3$)$_2$]W(CO)$_5$ [**2f**: R = Ph$_3$PC(H); **2g**: R = Ph$_3$PN] towards the terminal alkyne derivative **11**. Applying the aforementioned reaction protocols to the reactions of 2*H*-azaphosphirene complex **4b** with the carbonitriles **9e**,**h** and **11** led to the exclusive formation of only one regioisomer in each case, namely the 4-ethoxycarbonyl-substituted 2*H*-1,2-azaphosphole complexes **8h** and **8j**, which, in the case of **8h**, partially underwent subsequent reaction with the alkyne **11** to additionally yield complex **8i** (Scheme 9). All complexes were isolated in pure form by column chromatography. Related reactions of phosphonium ylides with activated alkynes have been reported previously and were interpreted as [2+2] cycloadditions with subsequent electrocyclic ring-opening, thus leading to new acyclic phosphonium ylides.[15,16]

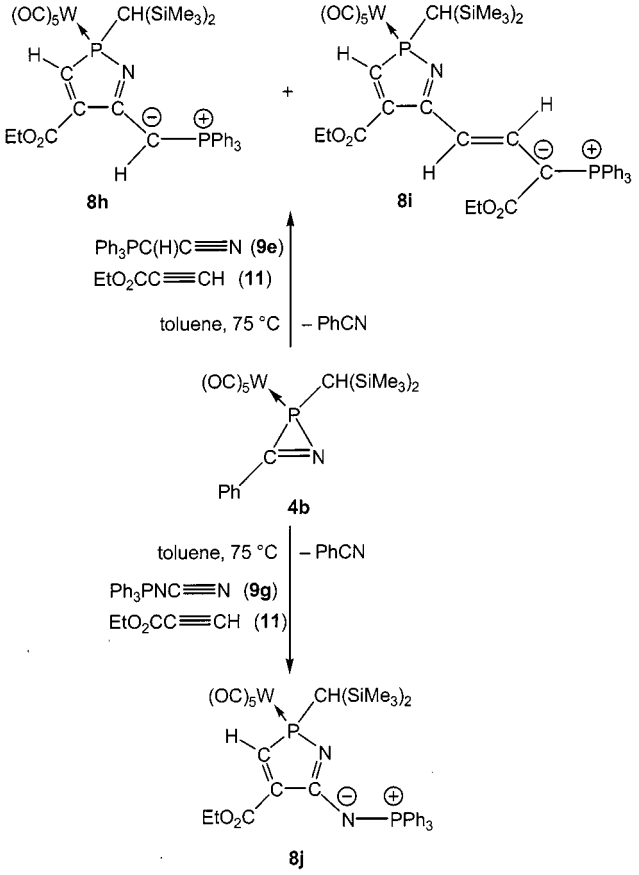

Scheme 9. Three-component reactions of 2*H*-azaphosphirene complex **4b** with carbonitriles **9e**/**9g** and ethyl acetylenecarboxylate (**11**)

Although spectroscopic data for 1*H*-1,2-azaphosphole derivatives are available in the literature,[17,18] we will not make any comparisons with these because of the significantly different bonding situations. 1*H*-1,2-azaphosphole derivatives can be regarded as 6π-heteroaromatic systems,[19] whereas 2*H*-1,2-azaphosphole derivatives can be expected to have no such aromaticity.[20] The salient NMR spectroscopic data of the 2*H*-1,2-azaphosphole ring atoms of complexes **8b**−**8j** are collected in Table 1. Besides the typical chemical shifts of the ^{31}P NMR resonances, which are associated with the nature of the element directly bonded to the C^5 ring atom, the resonances show tungsten−phosphorus couplings but no phosphorus−phosphorus couplings. The $^{13}C\{^1H\}$ NMR spectra each feature three resonances due to the 2*H*-1,2-azaphosphole ring with different phosphorus−carbon coupling constant magnitudes. The assignments of the resonances and thus the regiochemistry of the rings of **8g**−**8j** were unambiguously established by means of DEPT experiments. Besides the typical small $|J(^{31}P,^{13}C)|$ values for the C^5 atoms, we observed that the magnitudes of the phosphorus−carbon coupling constants of the C^4 atoms were always greater than those of the C^3 atoms, even though the latter are directly bonded to the phosphorus atoms. This means that the $|^{2+3}J(^{31}P,^{13}C)|$ values are considerably larger than the $|^{1+4}J(^{31}P,^{13}C)|$ values! In the case of complexes **8g**,**h** and **8j**, the proposed constitutions were also established through additional phosphorus−carbon couplings of the C^4 atom with the ylide phosphorus atom of about 40 to 50 Hz, which were absent in complexes **8f** and **8i** as a consequence of the greater distances of the through-bond coupling pathways.

The ^{1}H NMR spectra of **8h**−**8j** show the typical parameters for the protons bonded to the C^3 atoms with chemical shifts of $\delta \approx 8.1$ and phosphorus−proton couplings $|^2J(^{31}P,^1H)|$ of ca. 31 Hz. In the case of complexes **8h** and **8j**, long-range couplings $|^5J(^{31}P,^1H)|$ of ca. 3−4 Hz are also seen, but these are absent in the case of complex **8i**. Selected NMR parameters of the ylide functional groups are collected in Table 2; further confirmation of the proposed structures comes from the fact that the $^{13}C\{^1H\}$ NMR spectroscopic data of the side-chain and ylide functionalities are all as expected.[15] The UV/Vis spectra lend further support to the constitutions of **8f**−**8j** by displaying additional absorptions for complexes **8g**, **8h**, and **8j** at $\lambda \approx 420-430$ nm ($\lg \varepsilon \approx 3.8$) and for complexes **8f** and **8i** at $\lambda = 470-510$ nm ($\lg \varepsilon \approx 4.1$), and an additional broad band at $\lambda = 558$ nm ($\lg \varepsilon \approx 3.8$) for complex **8f** (Figure 1). These bands additionally show the existence of more elongated π-systems.[16]

EI mass spectrometric experiments revealed that all of these 2*H*-1,2-azaphosphole complexes lose carbon monoxide following the ionization process as one important fragmentation pathway. Apart from this, other fragmentation pathways can occur, which are highly dependent on the C^5 substituent, e.g. cleavage of the tungsten−phosphorus bond in the case of complex **8g**. In this case, the initially formed

Table 1. Selected NMR spectroscopic data of the 2*H*-1,2-azaphosphole complexes **8b**−**8j**

Compd.[a]	δ(^{31}P)	$^{1}J_{W,P}$	δ(^{13}C^{3})	^{1+4}J(P,C^{3})	δ(^{13}C^{4})	^{2+3}J(P,C^{4})	δ(^{13}C^{5})	^{2+3}J(P,C^{5})
8b	84.5	250.1	158.0	5.9	139.2	21.4	161.5	6.8
8c	103.4	239.8	155.5	9.0	141.8	25.0	160.8	[b]
8d	100.6	239.9	159.4	10.0	138.8	19.3	161.6	[b]
8e	100.9	244.3	157.3	8.6	145.9	27.0	157.1	[b]
8f	102.8	241.3	162.2	12.6	145.6	28.7	157.6	[b]
8g	85.8	249.6	163.1	14.0	149.0[c]	25.8	153.3	[b]
8h	75.9	237.2	158.3	8.5	138.5[c]	16.5	169.3[d]	4.8
8i	82.8	230.2	160.5	[b]	139.6	27.6	163.6	[b]
8j	72.2	236.1	157.0	8.1	140.3	17.4	167.0	[b]

[a] In $CDCl_3$; δ in ppm and *J* in Hz. [b] Not resolved. [c] **8g**: ^{3}J(P,C^{4}) = 48.1 Hz; **8h**: ^{3}J(P,C^{4}) = 44.3 Hz. [d] **8h**: ^{2}J(P,C^{5}) = 11.3 Hz.

Table 2. Selected NMR spectroscopic data of the P,C and P,N ylide functional groups of 2*H*-1,2-azaphosphole complexes **8f**−**8j** (**8f**: R = R′ = CO_2Me; **8g**: R = R′ = CO_2Me, E = N; **8h**: R = H, R′ = CO_2Et; E = CH; **8i**: R = H, R′ = CO_2Et; **8j**: R = H, R′ = CO_2Et; E = N)

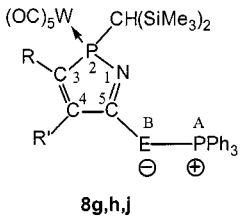

8g,h,j

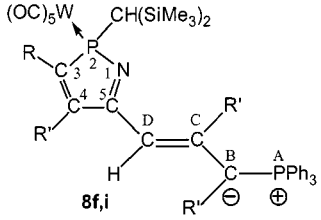

8f,i

Compd.[a]	δ(^{31}P)	δ(^{13}C^{B})	^{1}J(P,C^{B})	δ(^{13}C^{C})	^{2+4}J(P,C^{C})	δ(^{13}C^{D})	^{3}J(P,C^{D})	^{3}J(P,C^{D})	δ(^{1}H$^{D/E}$)	^{4}J(P,H^{D})
8f	18.7	61.2	116.2	149.2	9.6	108.3	7.4	17.6	5.11	1.8
8g	14.7	–	–	–	–	–	–	–	–	–
8h	15.0	47.6[b]	113.3	–	–	–	–	–	4.61	[b]
8i	25.3	63.9	117.2	144.4	15.5	106.2	15.7	18.5	3.80	10.2[c]
8j	15.0	–	–	–	–	–	–	–	–	–

[a] In $CDCl_3$; δ in ppm and *J* in Hz. [b] **8h**: ^{3}J(P^{2},C) = 22.7, $^{2}J_{P,H}$ = 21.3, $^{3}J_{P,H}$ = 15.7 Hz. [c] $^{3}J_{H,H}$ = 7.1 Hz

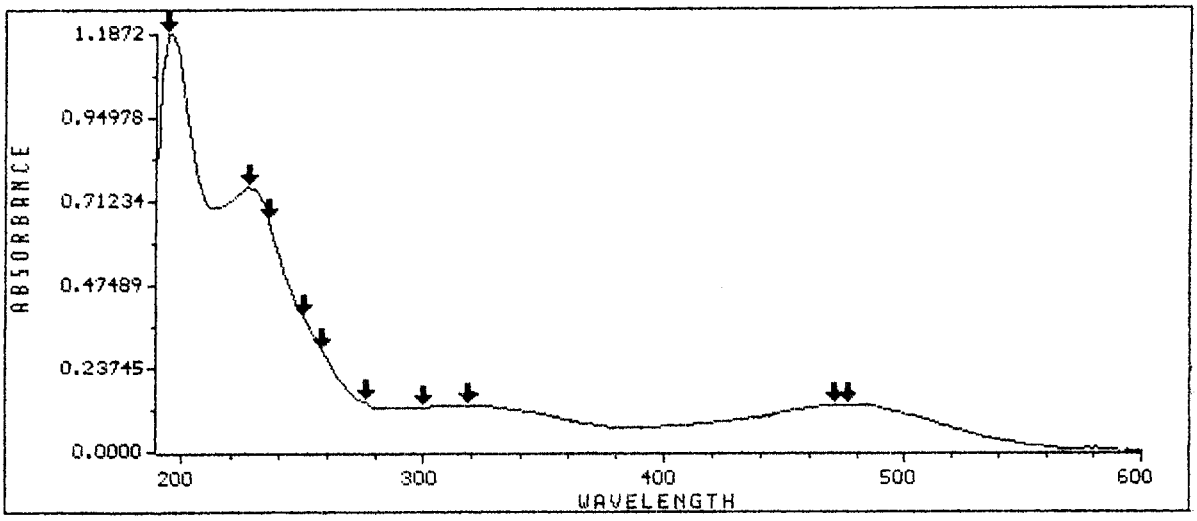

Figure 1. UV/Vis spectrum of 2*H*-1,2-azaphosphole complex **8i** (acetonitrile, c = 9.50 mg dm^{-3})

radical cation **12** undergoes C−Si bond cleavage to yield **13** (Scheme 10). Furthermore, the complexes **8g**−**8j** were seen to undergo cleavage of the P−C or P−N ylide bonds of the C^{5} substituent, e.g. in the case of complex **8g**, thus generating $[Ph_3P]^{+\cdot}$ (**14**) and neutral species such as carbenes and nitrenes. The further degradation of **14** to $[Ph_2P]^{+}$ (**15**) and **16** has been reported previously.[21]

We were able to confirm the constitutions of complexes **4c** (Figure 2, Table 3), **8d**,**8e**, and **8g** by single-crystal X-ray structure analyses (Figure 3, Figure 4, and Figure 5 and

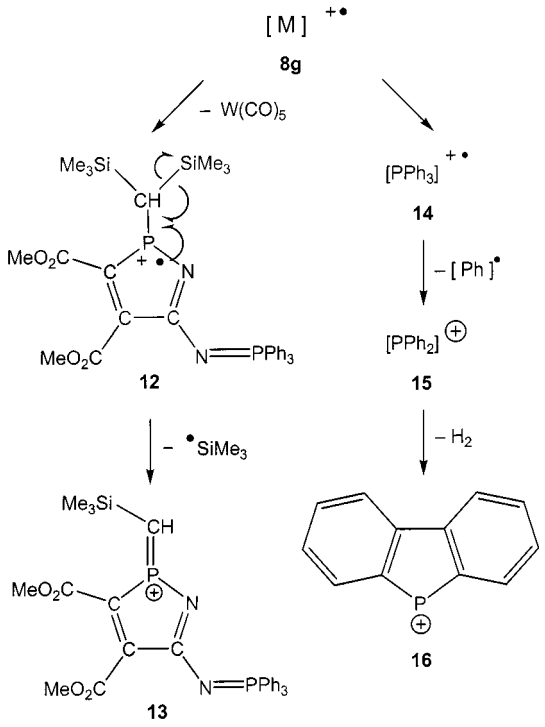

Scheme 10. Fragmentation pathway of complex **8g**

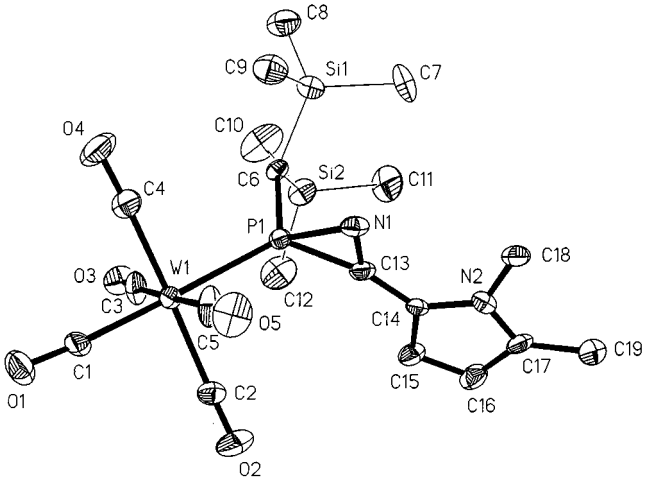

Figure 2. Molecular structure of one of the two independent molecules of **4c** in the crystal (ellipsoids represent 30% probability levels; hydrogen atoms are omitted for clarity); selected bond lengths [Å] and angles [°] (values for both molecules are given): W1−C1 1.980(13), 1.977(14), W1−P1 2.485(3), 2.488(3), P1−N1 1.800(10), 1.785(11), N1−C13 1.313(14), 1.307(14), C13−C14 1.411(16), 1.403(16); W1−P1−C6 120.8(4), 120.7(4), N1−C13−P1 70.7(7), 69.5(7), C13−C14−C15 126.0(12), 126.4(11)

Table 3 and Table 4). The molecular structure of complex **4c** shows an approximately coplanar arrangement of the two ring systems (interplanar angles 12.0° and 6.0° in two independent but closely similar molecules), thus enabling effective electronic interactions between the two rings. This is manifested in a shortened C(13)−C(14) bond of 1.411(16) Å, 1.403(16) Å and an elongated C(13)−N bond of 1.313(14) Å, 1.307(14) Å [compared to analogous C−C and C−N bond lengths of 1.457(7) Å and 1.272(7) Å in the C^3-phenyl-substituted (2*H*-azaphosphirene)tungsten complex].[14] It is also noteworthy that the NMe group adopts a position below the C−N double bond, thus pointing away from the phosphorus atom. This is interesting in the light of the observation that two alternative orientations seem to exist in *ortho*-substituted phenyl derivatives, depending on the *ortho* substituent.[22,23] We are currently trying to understand and exploit this aspect of the stereochemistry of 2*H*-azaphosphirene complexes.

The 2*H*-1,2-azaphosphole rings of complexes **8d**, **8e** and **8g** showed no unusual interatomic distances between the ring atoms, nor to the externally bonded atoms (Table 4). In all cases, the 2*H*-1,2-azaphosphole rings are approximately planar (largest mean deviation 0.014 Å in **8e**) and the bis-(trimethylsilyl)methyl group adopts the same preferred relative orientation towards the tungsten center and thus towards the ring as reported previously for other structures of related phosphorus heterocycle complexes. A further common structural motif is that the ester groups bonded to the C^{13} atoms adopt an approximately in-plane orientation, whereas the ester groups bonded to the C^{14} atoms adopt an out-of-plane orientation. The interplanar angles in **8d**, **8e** (22.3° and 24.6°, respectively) and the torsion angle of N(1)−C(15)−N(2)−P(2) of −18.9° in **8g** should, in all cases, enable electronic interactions between the two ring systems or the substituent. It is also noteworthy that in **8g** the $NPPh_3$ group adopts an *s-cis* configuration with respect to the C(15)−N(2) bond and seems to induce a slight elongation of the phosphorus−tungsten bond.

The following short contacts are observed: **8d**: S···O9 3.312 Å (operator $1 + x, y, z$); **8e**: C24−H24···O9 2.39 Å (angle at H 147°, operator $1 + x, y, z$); **8g**: C17−H17···O9 2.34 Å (angle at H 162°, operator $-x, 2 - y, -z$).

Concluding Remarks

We have shown that the chemistry of transiently generated nitrilium phosphanylide complexes can be further exploited, especially by using reactions of P,C and P,N ylide substituted carbonitriles and terminal phosphanediyl complexes, ultimately leading to the first C^5-functionalized 2*H*-1,2-azaphosphole complexes. It is also remarkable that no products were observed that may conceivably have arisen from initial attack of the transiently formed electrophilic terminal phosphanediyl complex at the nucleophilic ylide carbon or nitrogen atoms, which can probably be attributed to steric shielding of these centers. Therefore, the carbonitrile nitrogen atoms are predisposed to act exclusively as efficient donor centers towards the phosphorus atom of the electrophilic terminal phosphanediyl complex. In view of the lack of diazaphosphole complex formation, we conclude that the nitrile/nitrile exchange is a dissociative process (cf. ref.[6]) and, therefore, that the generation of the nitrilium phosphanylide complexes has to be described as 1,1-addition (cf. ref.[3]). With regard to the possible competition of the trapping reagents, nitriles and alkynes, the selectivity of the P,N ylide substituted nitrilium phosphanylide complexes towards alkynes is remarkable. Furthermore, the

Table 3. Crystal data and structure refinement of complexes **4c**, **8d**, **8e**, and **8g**

Complex	**4c**	**8d**	**8e**	**8g**
Empirical formula	$C_{19}H_{27}N_2O_5PSi_2W$	$C_{23}H_{28}NO_9PSSi_2W$	$C_{25}H_{33}N_2O_9PSi_2W$	$C_{37}H_{33}N_2O_9P_2Si_2W$
M_r	634.43	765.52	776.53	958.68
Crystal size [mm]	0.40 × 0.24 × 0.20	0.26 × 0.23 × 0.07	0.25 × 0.24 × 0.09	0.38 × 0.28 × 0.13
Crystal system	triclinic	monoclinic	monoclinic	triclinic
Space group	$P\bar{1}$	$P2_1/n$	$P2_1/n$	$P\bar{1}$
Unit cell dimensions				
a [Å]	9.374(2)	10.2984(8)	10.5410(10)	12.0023(8)
b [Å]	11.485(2)	21.6888(14)	21.9904(10)	12.8064(8)
c [Å]	24.547(4)	13.5948(10)	13.7490(12)	13.7749(8)
α [°]	99.963(15)	90	90	88.298(3)
β [°]	93.937(15)	101.802(3)	102.540(2)	89.684(3)
γ [°]	94.955(15)	90	90	74.802(3)
V [Å^3]	2583.9(8)	2972.3(4)	3111.0(4)	2042.3(2)
Z	4	4	4	2
D_x [Mg m^{-3}]	1.631	1.711	1.658	1.559
μ [mm^{-1}]	4.655	4.139	3.892	3.018
Transmissions	0.601−0.980	0.482−0.746	0.694−0.949	0.656−0.928
F(000)	1248	1512	1544	960
T [K]	173(2)	143(2)	143(2)	133(2)
$2\theta_{max}$ [°]	50	60	57	60
No. of reflections				
measured	9679	64172	48722	44213
unique	9008	8699	7914	11907
R_{int}	0.0715	0.0559	0.0572	0.0459
Parameters	541	350	371	486
Restraints	220	19	194	73
wR (F^2, all reflns.)	0.1288	0.0516	0.0445	0.0504
R [F, $I > 2\sigma(I)$]	0.0536	0.0213	0.0203	0.0250
S	0.781	1.011	0.981	1.027
Max. Δρ [e Å^{-3}]	2.161	1.153	0.759	1.272

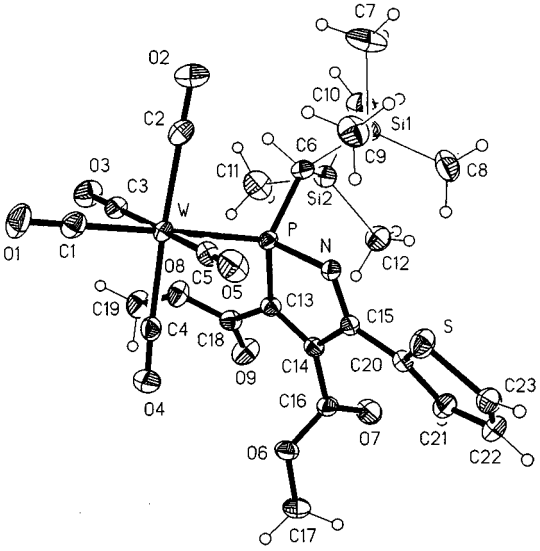

Figure 3. Molecular structure of **8d** in the crystal (ellipsoids represent 50% probability levels); selected angles [°]: W−P−C6 119.08(7), N−P−C13 92.03(9), P−N−C15 112.50(14), N−C15−C14 115.22(17), C13−C14−C15 112.23(17), C14−C13−P 107.87(15)

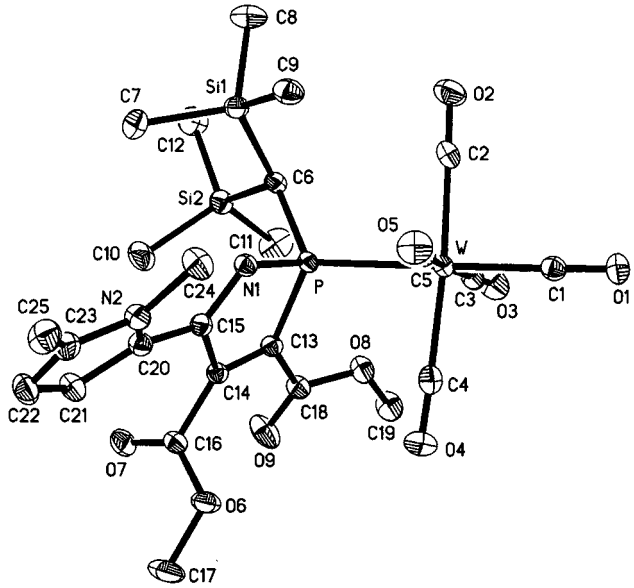

Figure 4. Molecular structure of **8e** in the crystal (ellipsoids represent 50% probability levels; hydrogen atoms are omitted for clarity); selected angles [°]: W−P−C6 117.95(6), N−P−C13 92.14(8), P−N−C15 112.60(13), N−C15−C14 114.69(16), C13−C14−C15 112.06(15), C14−C13−P 108.48(13)

finding that such 1,3-dipoles do not tend to form 2*H*-azaphosphirene complexes is very interesting, and, although no calculations were carried out on such systems, one may assume that the $Ph_3PC(H)$ and Ph_3PN ylide substituents stabilize nitrilium phosphanylide complexes more effectively than 2*H*-azaphosphirene complexes.[4,24] It is also remarkable that no cross-reactions and/or side-reactions of the transiently formed nitrilium phosphanylide complexes were detected, i.e. cycloaddition reactions involving the P−C and/or P−N bond − common organic 1,3-dipoles show

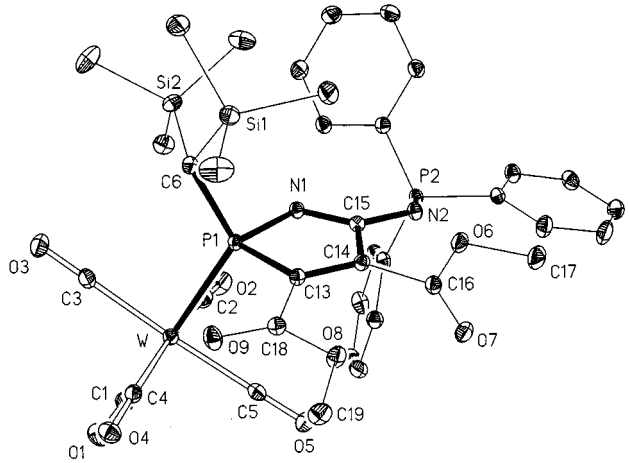

Figure 5. Molecular structure of **8g** in the crystal (ellipsoids represent 30% probability levels; hydrogen atoms are omitted for clarity); selected angles [°]: W−P1−C6 121.36(5), N−P−C13 93.69(7), P−N−C15 110.85(11), N−C15−C14 115.69(13), C13−C14−C15 112.26(14), C14−C13−P 107.41(11)

Table 4. Selected bond lengths [Å] in 2*H*-1,2-azaphosphole complexes **8d**, **8e** and **8g**

	8d	**8e**	**8g**
W−C(1)	1.997(2)	2.007(2)	2.0024(19)
W−P	2.5062(5)	2.5135(5)	2.5384(4)
P−C(13)	1.843(2)	1.8382(18)	1.8345(16)
P−N(1)	1.7063(17)	1.7079(16)	1.7005(14)
C(13)−C(14)	1.348(3)	1.346(2)	1.345(2)
N(1)−C(15)	1.297(2)	1.307(2)	1.311(2)
C(14)−C(15)	1.492(3)	1.503(3)	1.502(2)
C(15)−C(20)/C(15)−N(2)	1.459(3)	1.446(3)	1.347(2)

such cycloaddition reactions with phosphorus ylides such as $Ph_3PC(H)CN$.[16] Overall, very bulky ylide-substituted carbonitriles seem to be very interesting candidates for the generation of stable nitrilium phosphanylide complexes.

We are currently trying to exploit such ylide-substituted carbonitriles in other three-component reactions and to use the ylide functionalities in 2*H*-1,2-azaphosphole complexes to construct more extended N,P-heterocycle ligand structures, e.g. by using Wittig and aza-Wittig reactions.

Experimental Section

General Procedures: All reactions and manipulations were carried out under deoxygenated dry nitrogen in conventional glassware using standard Schlenk techniques. Solvents were dried according to standard procedures. NMR spectra were recorded with a Bruker AC-200 spectrometer (200 MHz for ^1H; 50.3 MHz for ^{13}C; 81.0 MHz for ^{31}P) using [D]chloroform or [D_6]benzene as solvent and internal standard; shifts are given relative to external tetramethylsilane (^1H, ^{13}C) or 85% H_3PO_4 (^{31}P); only coupling constant magnitudes are given. Electron impact (EI) (70 eV), chemical ionization (CI) (ammonia), and fast atom bombardment (FAB) (xenon) mass spectra were recorded with a Finnigan MAT-8430 double-focusing mass spectrometer. Infrared spectra were recorded with a Biorad FT-IR 165 spectrometer (selected data given). UV/Vis spectra were recorded with a Hewlett Packard HP 8452 spectrophotometer. Melting points were obtained with a Büchi 535 capillary apparatus. Elemental analyses were performed using a Carlo Erba analytical gas chromatograph. The *κP* notation in the nomenclature is intended to differentiate between P and N coordination of the relevant heterocycle to the metal ion.

{2-[Bis(trimethylsilyl)methyl]-3-(1,5-dimethylpyrrol-2-yl)-2*H*-azaphosphirene-*κP*}pentacarbonyltungsten(0) (4c): A solution of the (2*H*-azaphosphirene)tungsten complex **4b** (0.62 g, 1 mmol) and 1,5-dimethyl-2-pyrrolecarbonitrile **(9d)** (0.617 g, 5 mmol) in toluene (10 mL) was heated at 72 °C for 2 h with slow stirring. Thereafter, the solvent was removed in vacuo (ca. 0.01 mbar) and the product was separated by low-temperature column chromatography (SiO_2, −15 °C, 10 × 2 cm, *n*-pentane/diethyl ether, 70:30). Evaporation of the solvents from the second fraction yielded **4c** as a yellow solid. Yield 220 mg (36%); m.p. 131 °C (decomp.). ^1H NMR ($CDCl_3$): δ = 0.07 (s, 9 H, $SiMe_3$), 0.15 (s, 9 H, $SiMe_3$), 0.33 [d, $^2J_{P,H}$ = 1.3 Hz, 1 H, C*H*($SiMe_3$)$_2$], 2.23 (s, 3 H, CH_3), 3.60 (s, 3 H, NCH_3), 5.89 (d, $^3J_{H,H}$ = 3.4 Hz, 1 H, 3-H), 6.66 (d, $^3J_{H,H}$ = 3.9 Hz, 1 H, 4-H). $^{13}C\{^1H\}$ NMR ($CDCl_3$): δ = 1.2 (d, $^3J_{P,C}$ = 3.2 Hz, $SiMe_3$), 2.0 (d, $^3J_{P,C}$ = 3.1 Hz, $SiMe_3$), 12.4 (s, C*C*H_3), 27.0 [d, $^1J_{P,C}$ = 24.3 Hz, *C*H($SiMe_3$)$_2$], 32.1 (s, NCH_3), 110.8 (s, $C5_{aryl}$), 119.2 (d, $^2J_{P,C}$ = 19.4 Hz, $C2_{aryl}$), 122.0 (s, $C3_{aryl}$), 135.4 (s, $C4_{aryl}$), 177.4 (d, $^{1+2}J_{P,C}$ = 8.5 Hz, PCN), 196.0 (d, $^2J_{P,C}$ = 9.0 Hz, *cis*-CO), 198.1 (d, $^2J_{P,C}$ = 35.2 Hz, *trans*-CO). $^{31}P\{^1H\}$ NMR ($CDCl_3$): δ = −131.4 (s, $^1J_{P,W}$ = 294.2 Hz). MS (pos. CI, ^{184}W): *m/z* = 634 (1) $[M]^{+\cdot}$.

General Procedure for the Preparation of Complexes 8b−8e: To a solution of the (2*H*-azaphosphirene)tungsten complex **4b** (0.62 g, 1 mmol) in toluene (10 mL), the respective carbonitrile **9b−9e** (4 mmol) and dimethyl acetylenedicarboxylate (**6**; 0.245 mL, 2 mmol) were added and the resulting mixture was heated at 75 °C for 3.5 h with slow stirring. Thereafter, all volatile components were removed in vacuo (ca. 0.01 mbar) and the products were separated by low-temperature column chromatography (SiO_2, −10 °C, 10 × 2 cm, *n*-pentane/diethyl ether, 70:30). Evaporation of the solvents from the respective second fractions yielded **10a** and **8b** as yellow solids and **8c−8e** as red solids.

{2-[Bis(trimethylsilyl)methyl]-4-methoxy-4-(2-methoxycarbonylethynyl)-5-piperidino-Δ^3-1,3,2-oxazaphospholene-*κP*}pentacarbonyltungsten(0) (10a,b): Yield 84 mg (11%); m.p. 144 °C (decomp.). ^1H NMR ($CDCl_3$): δ = 0.01 (s, 9 H, $SiMe_3$), 0.15 (s, 9 H, $SiMe_3$), 1.49 [s, 1 H, C*H*($SiMe_3$)$_2$], 1.54 (m_c, 6 H, $NCH_2CH_2CH_2$), 3.44 (m_c, 4 H, $NCH_2CH_2CH_2$), 3.63 (s, 3 H, OCH_3), 3.80 (s, 3 H, OCH_3). $^{13}C\{^1H\}$ NMR ($CDCl_3$): δ = 2.0 (d, $^3J_{P,C}$ = 2.4 Hz, $SiMe_3$), 2.3 (s, $SiMe_3$), 24.3 (s, $NCH_2CH_2CH_2$), 24.7 (s, $NCH_2CH_2CH_2$), 36.8 [d, $^1J_{P,C}$ = 5.9 Hz, *C*H($SiMe_3$)$_2$], 48.1 (s, $NCH_2CH_2CH_2$), 52.8 (s, OCH_3), 53.2 (s, OCH_3), 77.2 (s, C*C*CO_2Me), 79.9 (s, *C*CCO_2Me), 99.0 (d, $^{2+3}J_{P,C}$ = 7.2 Hz, POC), 152.7 (s, PNC), 156.7 (s, *C*O_2Me), 197.2 (d, $^2J_{P,C}$ = 8.6 Hz, *cis*-CO), 201.1 (d, $^2J_{P,C}$ = 28.4 Hz, *trans*-CO). $^{31}P\{^1H\}$ NMR ($CDCl_3$): δ = 198.3 (s, $^1J_{P,W}$ = 300.9 Hz). IR (KBr): $\tilde{\nu}$ = 2070 (s), 1990 (s), 1951 (vs), 1935 (vs), 1900 cm^{-1} (vs) (CO), 1602 cm^{-1} (s) (CO_2). MS (EI, ^{184}W): *m/z* = 766 (48) $[M]^{+\cdot}$, 626 (100) $[M - 5CO]^{+\cdot}$. $C_{24}H_{35}N_2O_9PSi_2W$ (766.5): calcd. C 37.61, H 4.60, N 3.65; found C 39.22, H 4.94, N 3.58.

{2-[Bis(trimethylsilyl)methyl]-3,4-bis(methoxycarbonyl)-5-piperidino-2*H*-1,2-azaphosphole-*κP*}pentacarbonyltungsten(0) (8b): Yield 107 mg (14%); m.p. 112 °C (decomp.). ^1H NMR ($CDCl_3$): δ = 0.01 (s, 9 H, $SiMe_3$), 0.26 (s, 9 H, $SiMe_3$), 1.07 [d, $^2J_{P,H}$ = 6.2 Hz, 1 H, C*H*($SiMe_3$)$_2$], 1.57 (m_c, 2 H, $NCH_2CH_2CH_2$), 3.45 (m_c, 4 H, $NCH_2CH_2CH_2$), 3.77 (s, 3 H, OCH_3), 3.81 (s, 3 H, OCH_3), 4.05

(m_c, 4 H, $NCH_2CH_2CH_2$). $^{13}C\{^1H\}$ NMR ($CDCl_3$): δ = 2.7 (d, $^3J_{P,C}$ = 2.0 Hz, $SiMe_3$), 3.3 (d, $^3J_{P,C}$ = 2.5 Hz, $SiMe_3$), 22.1 [s, *C*H($SiMe_3$)$_2$], 24.4 (s, $NCH_2CH_2CH_2$), 25.9 (s, $NCH_2CH_2CH_2$), 48.6 (s, $NCH_2CH_2CH_2$), 52.6 (s, OCH_3), 53.2 (s, OCH_3), 139.2 (d, $^{2+3}J_{P,C}$ = 21.4 Hz, PC*C*), 158.0 (d, $^{1+4}J_{P,C}$ = 5.9 Hz, P*C*C), 161.5 (d, $^{2+3}J_{P,C}$ = 6.8 Hz, PNC), 163.3 (d, $^3J_{P,C}$ = 10.3 Hz, *C*O_2Me), 165.7 (d, $^3J_{P,C}$ = 14.7 Hz, *C*O_2Me), 197.5 (d, $^2J_{P,C}$ = 7.2 Hz, *cis*-CO), 199.6 (d, $^2J_{P,C}$ = 23.0 Hz, *trans*-CO). $^{31}P\{^1H\}$ NMR ($CDCl_3$): δ = 84.5 (s, $^1J_{P,W}$ = 250.1 Hz). MS (EI, ^{184}W): *m*/*z* = 766 (12) $[M]^{+\cdot}$, 598 (100) $[M - 5CO - CO]^{+\cdot}$. $C_{24}H_{35}N_2O_9PSi_2W$ (766.5): calcd. C 37.61, H 4.60, N 3.65; found C 38.94, H 4.49, N 3.50.

{2-[Bis(trimethylsilyl)methyl]-3,4-bis(methoxycarbonyl)-5-furyl-2*H*-1,2-azaphosphole-κ*P*}pentacarbonyltungsten(0) (8c): Yield 240 mg (32%); m.p. 136 °C (decomp.). ^1H NMR ($CDCl_3$): δ = 0.21 (s, 9 H, $SiMe_3$), 0.78 (s, 9 H, $SiMe_3$), 1.14 [d, $^2J_{P,H}$ = 6.4 Hz, 1 H, C*H*($SiMe_3$)$_2$], 3.73 (s, 3 H, OCH_3), 3.81 (s, 3 H, OCH_3), 6.41 (m_c, 1 H, CH_{aryl}), 7.09 (m_c, 1 H, CH_{aryl}), 7.41 (m_c, 1 H, CH_{aryl}). $^{13}C\{^1H\}$ NMR ($CDCl_3$): δ = 2.7 (d, $^3J_{P,C}$ = 1.7 Hz, $SiMe_3$), 3.2 (d, $^3J_{P,C}$ = 2.2 Hz, $SiMe_3$), 20.0 [s, *C*H($SiMe_3$)$_2$], 52.8 (s, OCH_3), 53.2 (s, OCH_3), 113.0 (s, C^3_{aryl}), 117.0 (s, C^4_{aryl}), 141.8 (d, $^{2+3}J_{P,C}$ = 25.0 Hz, PC*C*), 146.7 (s, C^5_{aryl}), 149.2 (d, $^3J_{P,C}$ = 21.7 Hz, C^2_{aryl}), 155.5 (d, $^1J_{P,C}$ = 9.0 Hz, P*C*C), 160.8 (s, PNC), 162.5 (d, $^2J_{P,C}$ = 12.9 Hz, *C*O_2Me), 164.7 (d, $^3J_{P,C}$ = 13.6 Hz, *C*O_2Me), 196.7 (d, $^2J_{P,C}$ = 6.7 Hz, *cis*-CO), 198.3 (d, $^2J_{P,C}$ = 23.0 Hz, *trans*-CO). $^{31}P\{^1H\}$ NMR ($CDCl_3$): δ = 103.4 (s, $^1J_{P,W}$ = 239.8 Hz). UV/Vis (CH_3CN): λ (lg ε) = 234 (4.86), 268 (4.30), 278 (4.15), 286 (4.09), 346 (4.04), 400 (3.46). IR (KBr): $\tilde{\nu}$ = 2076 (s, CO), 2001 (s, CO), 1937 (vs, CO), 1909 (vs, CO), 1745 (s, CO_2), 1714 cm^{-1} (s, CO_2). MS (EI, ^{184}W): *m*/*z* = 749 (7) $[M]^{+\cdot}$, 581 (100) $[M - 5CO - CO]^{+\cdot}$. $C_{23}H_{28}NO_{10}PSi_2W$: calcd. C 36.86, H 3.77, N 1.87; found C 35.99, H 3.80, N 1.94.

{2-[Bis(trimethylsilyl)methyl]-3,4-bis(methoxycarbonyl)-5-thienyl-2*H*-1,2-azaphosphole-κ*P*}pentacarbonyltungsten(0) (8d): Yield 260 mg (33%); m.p. 150 °C (decomp.). ^1H NMR ($CDCl_3$): δ = 0.08 (s, 9 H, $SiMe_3$), 0.38 (s, 9 H, $SiMe_3$), 1.31 [d, $^2J_{P,H}$ = 6.3 Hz, 1 H, C*H*($SiMe_3$)$_2$], 3.90 (s, 3 H, OCH_3), 3.98 (s, 3 H, OCH_3), 7.10 (m_c, 1 H, CH_{aryl}), 7.54 (m_c, 1 H, CH_{aryl}), 7.61 (m_c, 1 H, CH_{aryl}). $^{13}C\{^1H\}$ NMR ($CDCl_3$): δ = 2.6 (d, $^3J_{P,C}$ = 2.1 Hz, $SiMe_3$), 3.1 (d, $^3J_{P,C}$ = 2.7 Hz, $SiMe_3$), 20.0 [d, $^2J_{P,C}$ = 1.4 Hz, *C*H($SiMe_3$)$_2$], 52.9 (s, OCH_3), 53.4 (s, OCH_3), 133.3 (s, C^3_{aryl}), 134.9 (s, C^4_{aryl}), 138.8 (d, $^{2+3}J_{P,C}$ = 19.3 Hz, PC*C*), 139.7 (s, C^5_{aryl}), 141.9 (d, $^3J_{P,C}$ = 24.6 Hz, C^2_{aryl}), 159.4 (d, $^{1+4}J_{P,C}$ = 10.0 Hz, P*C*C), 161.6 (s, PNC), 162.7 (d, $^2J_{P,C}$ = 12.4 Hz, *C*O_2Me), 165.3 (d, $^3J_{P,C}$ = 13.8 Hz, *C*O_2Me), 196.7 (d, $^2J_{P,C}$ = 6.4 Hz, *cis*-CO), 198.3 (d, $^2J_{P,C}$ = 22.9 Hz, *trans*-CO). $^{31}P\{^1H\}$ NMR ($CDCl_3$): δ = 100.6 (s, $^1J_{P,W}$ = 239.9 Hz). UV/Vis (CH_3CN): λ (lg ε) = 232 (4.84), 264 (4.34), 284 (4.11), 348 (4.01), 394 (3.53), 404 (3.39), 420 (3.34), 440 (3.33). IR (KBr): $\tilde{\nu}$ = 2075 (s, CO), 1999 (s, CO), 1935 (vs, CO), 1909 (vs, CO), 1744 (s, CO_2), 1716 cm^{-1} (s, CO_2). MS (EI, ^{184}W): *m*/*z* = 765 (5) $[M]^{+\cdot}$, 597 (100) $[M - 5CO - CO]^{+\cdot}$. $C_{23}H_{28}NO_9PSSi_2W$: calcd. C 36.09, H 3.69, N 1.83, S 4.19; found C 35.19, H 3.65, N 1.82, S 4.38.

{2-[Bis(trimethylsilyl)methyl]-3,4-bis(methoxycarbonyl)-5-(1,5-dimethylpyrrol-2-yl)-2*H*-1,2-azaphosphole-κ*P*}pentacarbonyltungsten(0) (8e): Yield 700 mg (89%); m.p. 143 °C (decomp.). ^1H NMR ($CDCl_3$): δ = 0.03 (s, 9 H, $SiMe_3$), 0.31 (s, 9 H, $SiMe_3$), 1.19 [d, $^2J_{P,H}$ = 6.0 Hz, 1 H, C*H*($SiMe_3$)$_2$], 2.25 (s, 3 H, C_{aryl}-CH_3), 3.82 (s, 3 H, NCH_3), 3.88 (s, 3 H, OCH_3), 3.89 (s, 3 H, OCH_3), 5.93 (d, $^3J_{H,H}$ = 4.1 Hz, 1 H, CH_{aryl}), 6.65 (d, $^3J_{H,H}$ = 4.2 Hz, 1 H, CH_{aryl}). $^{13}C\{^1H\}$ NMR ($CDCl_3$): δ = 2.6 (d, $^3J_{P,C}$ = 2.0 Hz, $SiMe_3$), 3.2 (d, $^3J_{P,C}$ = 2.8 Hz, $SiMe_3$), 12.3 (s, C*C*H_3), 20.1 [s, *C*H($SiMe_3$)$_2$], 32.1 (s, NCH_3), 52.5 (s, OCH_3), 53.1 (s, OCH_3), 109.4 (s, C^3_{aryl}), 118.4 (s, C^4_{aryl}), 126.7 (d, $^2J_{P,C}$ = 17.3 Hz, C^2_{aryl}), 135.5 (s, C^5_{aryl}), 145.9 (d, $^{2+3}J_{P,C}$ = 27.0 Hz, PC*C*), 157.1 (s, PNC), 157.3 (d, $^{1+4}J_{P,C}$ = 8.6 Hz, P*C*C), 162.5 (d, $^2J_{P,C}$ = 13.1 Hz, *C*O_2Me), 166.0 (d, $^3J_{P,C}$ = 14.6 Hz, *C*O_2Me), 197.1 (d, $^2J_{P,C}$ = 6.8 Hz, *cis*-CO), 198.7 (d, $^2J_{P,C}$ = 23.1 Hz, *trans*-CO). $^{31}P\{^1H\}$ NMR ($CDCl_3$): δ = 100.9 (s, $^1J_{P,W}$ = 244.3 Hz). UV/Vis (CH_3CN): λ (lg ε) = 222 (4.70), 232 (4.78), 248 (4.59), 254 (4.54), 262 (4.45), 276 (4.31), 412 (4.05). IR (KBr): $\tilde{\nu}$ = 2070 (s, CO), 1985 (s, CO), 1951 (vs, CO), 1926 (vs, CO), 1913 (s, CO), 1743 (s, CO_2), 1718 cm^{-1} (s, CO_2). MS (EI, ^{184}W): *m*/*z* = 776 (6) $[M]^{+\cdot}$, 608 (100) $[M - 5CO - CO]^{+\cdot}$, (neg. CI, ^{184}W): *m*/*z* = 776 (2) $[M]^{-\cdot}$, 617 (100) $[M - C_7H_{19}Si_2]^-$; (pos. CI, ^{184}W): *m*/*z* = 777 (100) $[M + H]^+$. $C_{25}H_{33}N_2O_9PSi_2W$: calcd. C 38.67, H 4.28, N 3.61; found C 38.32, H 4.33, N 3.46.

General Procedure for the Preparation of Complexes 8f−8j: To a solution of the 2*H*-azaphosphirene complex **4b** (0.62 g, 1 mmol) in toluene (6 mL), the appropriate carbonitrile **9e** or **9h** (1 mmol) and the appropriate alkyne **6** or **11** (1 mmol) were added and the resulting mixture was heated at 75 °C for 2 h with slow stirring. Thereafter, all volatile components were removed in vacuo (ca. 0.01 mbar) and the products were separated by low-temperature column chromatography (SiO_2, −10 °C, 10 × 2 cm, *n*-pentane/diethyl ether, 70:30). Evaporation of the solvents from the respective second fractions yielded **8f** and **8i** as red solids, **8g** and **8h** as yellow solids, and **8j** as a pale-brown solid.

{2-[Bis(trimethylsilyl)methyl]-3,4-bis(methoxycarbonyl)-5-[2,3-bis(methoxycarbonyl)-3-(triphenylphosphonio)propenylidyl]-2*H*-1,2-azaphosphole-κ*P*}pentacarbonyltungsten(0) (8f): Yield 452 mg (41%); m.p. 58 °C (decomp.). ^1H NMR ($CDCl_3$): δ = 0.01 (s, 9 H, $SiMe_3$), 0.50 (s, 9 H, $SiMe_3$), 1.19 [d, $^2J_{P,H}$ = 5.3 Hz, 1 H, C*H*($SiMe_3$)$_2$], 3.35 (s, OCH_3), 3.38 (s, OCH_3), 3.86 (s, OCH_3), 4.04 (s, OCH_3), 5.11 (d, $^4J_{P,H}$ = 1.8 Hz, 1 H, HC=C), 7.64 (m_c, 5 H, Ph), 7.70 (m_c, 3 H, Ph), 7.89 (m_c, 7 H, Ph), $^{13}C\{^1H\}$ NMR ($CDCl_3$): δ = 2.7 (d, $^3J_{P,C}$ = 1.9 Hz, $SiMe_3$), 3.1 (d, $^3J_{P,C}$ = 2.7 Hz, $SiMe_3$), 21.1 [s, *C*H$Si(Me_3)_2$], 50.3 (s, OCH_3), 52.1 (s, OCH_3), 52.2 (s, OCH_3), 53.0 (s, OCH_3), 61.2 (d, $^1J_{P,C}$ = 116.2 Hz, *C*PPh_3), 108.3 (dd, $^3J_{P,C}$ = 7.4, $^3J_{P,C}$ = 17.6 Hz, H*C*C*C*PPh_3), 123.9 (d, $^1J_{P,C}$ = 91.2 Hz, *ipso*-Ph), 129.0 (d, $^3J_{P,C}$ = 12.5 Hz, *meta*-Ph), 132.6 (d, $^4J_{P,C}$ = 3.0 Hz, *para*-Ph), 133.8 (d, $^2J_{P,C}$ = 9.7 Hz, *ortho*-Ph), 145.6 (d, $^2J_{P,C}$ = 28.7 Hz, PC*C*), 149.2 (d, $^2J_{P,C}$ = 9.6 Hz, HC*C*CPPh_3), 157.6 (s, PNC), 162.2 (d, $^1J_{P,C}$ = 12.6 Hz, P*C*C), 163.2 (d, $^3J_{P,C}$ = 13.1 Hz, *C*O_2Me), 164.5 (d, $^2J_{P,C}$ = 14.8 Hz, *C*O_2Me), 167.1 (d, $^2J_{P,C}$ = 15.1 Hz, *C*O_2Me), 168.9 (d, $^3J_{P,C}$ = 14.6 Hz, *C*O_2Me), 197.1 (d, $^2J_{P,C}$ = 6.8 Hz, *cis*-CO), 199.4 (d, $^2J_{P,C}$ = 22.4 Hz, *trans*-CO). $^{31}P\{^1H\}$ NMR ($CDCl_3$): δ = 102.8 (s, $^1J_{P,W}$ = 241.3 Hz), 18.7 (s). UV/Vis (CH_3CN): λ (lg ε) = 230 (4.91), 242 (4.75), 260 (4.40), 284 (4.08), 324 (4.08), 428 (3.84), 478 (4.23), 500 (4.28), 558 (3.81). IR (KBr): $\tilde{\nu}$ = 2068 (s, CO), 1983 (vs, CO), 1930 (s, CO), 1731 (vs, CO_2), 1721 (vs, CO_2), 1675 cm^{-1} (vs, CO_2). MS (pos. FAB, *m*-NBA, ^{184}W): *m*/*z* = 1100 (7) $[M + H]^+$, 776 (100) $[M + H - W(CO)_5]^+$. $C_{44}H_{47}NO_{13}P_2Si_2W$: calcd. C 48.05, H 4.31, N 1.27; found C 47.09, H 4.35, N 1.30.

{2-[Bis(trimethylsilyl)methyl]-3,4-bis(methoxycarbonyl)-5-[(triphenylphosphonio)imido]-2*H*-1,2-azaphosphole-κ*P*}pentacarbonyltungsten(0) (8g): Yield 610 mg (64%); m.p. 68 °C (decomp.). ^1H NMR ($CDCl_3$): δ = 0.01 (s, 9 H, $SiMe_3$), 0.06 (s, 9 H, $SiMe_3$), 0.94 [d, $^2J_{P,H}$ = 5.7 Hz, 1 H, C*H*($SiMe_3$)$_2$], 3.88 (s, OCH_3), 4.02 (s, OCH_3), 7.48 (m_c, 5 H, Ph), 7.58 (m_c, 3 H, Ph), 7.79 (m_c, 7 H, Ph). $^{13}C\{^1H\}$ NMR ($CDCl_3$): δ = 2.8 (d, $^3J_{P,C}$ = 1.8 Hz, $SiMe_3$), 3.0 (d, $^3J_{P,C}$ = 2.9 Hz, $SiMe_3$), 20.8 [s, *C*H($SiMe_3$)$_2$], 52.2 (s, OCH_3), 52.5 (s, OCH_3), 127.8 (d, $^1J_{P,C}$ = 101.4 Hz, *ipso*-Ph), 128.8 (d, $^3J_{P,C}$ = 12.5 Hz, *meta*-Ph), 132.4 (d, $^4J_{P,C}$ = 2.9 Hz, *para*-Ph), 133.2 (d, $^2J_{P,C}$ = 10.2 Hz, *ortho*-Ph), 149.0 (dd, $^{2+3}J_{P,C}$ = 25.8,

$^3J_{P,C}$ = 48.1 Hz, PC*C*), 153.3 (s, PNC), 163.1 (d, $^1J_{P,C}$ = 14.0 Hz, P*C*C), 164.9 (d, $^2J_{P,C}$ = 9.3 Hz, *C*O$_2$Me), 166.0 (d, $^3J_{P,C}$ = 14.5 Hz, *C*O$_2$Me), 197.9 (d, $^2J_{P,C}$ = 7.3 Hz, *cis*-CO), 200.0 (d, $^2J_{P,C}$ = 22.7 Hz, *trans*-CO). ^{31}P{^{1}H} NMR (CDCl$_3$): δ = 85.8 (s, $^1J_{P,W}$ = 249.6 Hz), 14.7 (s). UV/Vis (CH$_3$CN): λ (lg ε) = 230 (4.94), 244 (4.75), 248 (4.68), 254 (4.59), 258 (4.51), 264 (4.35), 330 (3.83), 344 (3.85), 356 (3.81). IR (KBr): ṽ = 2068 (vs, CO), 1984 (vs, CO), 1933 (w, CO), 1909 (w, CO), 1744 (vs, CO$_2$), 1718 (vs, CO$_2$) cm^{-1}. MS (EI, ^{184}W): *m*/*z* = 958 (1) [M]$^{+\cdot}$, 634 (100) [M − W(CO)$_5$]$^{+\cdot}$. MS (neg. CI, ^{184}W): *m*/*z* = 958 (18) [M]$^{-\cdot}$, 475 (100) [M − C$_7$H$_{19}$Si$_2$ − W(CO)$_5$]$^-$. MS (pos. CI, ^{184}W): *m*/*z* = 959 (36) [M + H]$^+$, 263 (100) [PPh$_3$ + H]$^+$. C$_{37}$H$_{40}$N$_2$O$_9$P$_2$Si$_2$W: calcd. C 46.35, H 4.21, N 2.92; found C 45.96, H 4.31, N 2.88.

{2-[Bis(trimethylsilyl)methyl]-4-(ethoxycarbonyl)-5-[(triphenylphosphonio)methylidyl]-2*H*-1,2-azaphosphole-κ*P*}pentacarbonyltungsten(0) (8h): Yield 220 mg (32%); m.p. 52 °C (decomp.). ^{1}H NMR (CDCl$_3$): δ = 0.00 (s, 9 H, SiMe$_3$), 0.16 (s, 9 H, SiMe$_3$), 0.88 [d, $^2J_{P,H}$ = 8.1 Hz, 1 H, C*H*(SiMe$_3$)$_2$], 1.28 (t, $^3J_{H,H}$ = 7.1 Hz, 3 H, CH$_2$C*H*$_3$), 4.23 (q, $^3J_{H,H}$ = 7.1 Hz, 2 H, C*H*$_2$CH$_3$), 4.61 (dd, $^3J_{P,H}$ = 21.3, $^2J_{P,H}$ = 15.7 Hz, 1 H, C*H*PPh$_3$), 7.37 (m$_c$, 5 H, Ph), 7.47 (m$_c$, 3 H, Ph), 7.62 (m$_c$, 7 H, Ph), 8.15 (dd, $^2J_{P,H}$ = 30.8, $^5J_{P,H}$ = 3.3 Hz, 1 H, PCH). ^{13}C{^{1}H} NMR (CDCl$_3$): δ = 2.2 (d, $^3J_{P,C}$ = 2.6 Hz, SiMe$_3$), 2.5 (d, $^3J_{P,C}$ = 2.2 Hz, SiMe$_3$), 14.2 (s, CH$_2$*C*H$_3$), 24.8 [s, *C*H(SiMe$_3$)$_2$], 47.6 (dd, $^1J_{P,C}$ = 113.3, $^3J_{P,C}$ = 22.7 Hz, *C*HPPh$_3$), 60.9 (s, *C*H$_2$CH$_3$), 127.0 (d, $^1J_{P,C}$ = 91.0 Hz, *ipso*-Ph), 128.7 (d, $^3J_{P,C}$ = 12.2 Hz, *meta*-Ph), 132.2 (d, $^4J_{P,C}$ = 2.8 Hz, *para*-Ph), 133.4 (d, $^2J_{P,C}$ = 10.2 Hz, *ortho*-Ph), 138.5 (dd, $^{2+3}J_{P,C}$ = 16.5, $^3J_{P,C}$ = 44.3 Hz, PC*C*), 158.3 (d, $^1J_{P,C}$ = 8.5 Hz, P*C*C), 164.3 (d, $^3J_{P,C}$ = 17.2 Hz, *C*O$_2$Et), 169.3 (dd, $^{2+3}J_{P,C}$ = 4.8, $^2J_{P,C}$ = 11.3 Hz, PNC), 198.1 (d, $^2J_{P,C}$ = 7.4 Hz, *cis*-CO), 201.4 (d, $^2J_{P,C}$ = 18.8 Hz, *trans*-CO). ^{31}P{^{1}H} NMR (CDCl$_3$): δ = 75.9 (s, $^1J_{P,W}$ = 237.2 Hz), 15.0 (s). UV/Vis (CH$_3$CN): λ (lg ε) = 228 (4.87), 242 (4.75), 256 (4.56), 300 (4.02), 364 (3.83), 380 (3.80), 416 (3.84), 424 (3.84), 432 (3.83). IR (KBr): ṽ = 2063 (vs, CO), 1970 (vs, CO), 1926 (s, CO), 1899 (s, CO), 1718 cm^{-1} (vs, CO$_2$). MS (EI, ^{184}W): *m*/*z* = 913 (12) [M]$^{+\cdot}$, 698 (100) [M − C$_7$H$_{19}$Si$_2$]$^+$. C$_{37}$H$_{41}$NO$_7$P$_2$Si$_2$W: calcd. C 48.64, H 4.52, N 1.53; found C 47.90, H 4.60, N 1.56.

{2-[Bis(trimethylsilyl)methyl]-4-(ethoxycarbonyl)-5-[*trans*-2-(ethoxycarbonyl)-3-(triphenylphosphonio)propenylidyl]-2*H*-1,2-azaphosphole-κ*P*}pentacarbonyltungsten(0) (8i): Yield 600 mg (66%); m.p. 51 °C (decomp.). ^{1}H NMR (CDCl$_3$): δ = 0.00 (s, 9 H, SiMe$_3$), 0.07 (s, 9 H, SiMe$_3$), 0.81 (t, $^3J_{H,H}$ = 7.2 Hz, 3 H, C*H*$_3$CH$_2$), 0.99 [d, $^2J_{P,H}$ = 8.2 Hz, 1 H, C*H*(SiMe$_3$)$_2$], 1.35 (t, $^3J_{H,H}$ = 7.2 Hz, 3 H, CH$_2$C*H*$_3$), 3.80 (dd, $^4J_{P,H}$ = 10.2, $^3J_{H,H}$ = 7.1 Hz, 1 H, C*H*CHCPPh$_3$), 3.87 (dd, $^3J_{P,H}$ = 26.2, $^3J_{H,H}$ = 7.2 Hz, 1 H, C*H*CPPh$_3$), 3.88 (dq, $^4J_{P,H}$ = 4.9, $^3J_{H,H}$ = 7.1 Hz, 2 H, Ph$_3$PCCO$_2$C*H*$_2$CH$_3$), 4.30 (q, $^3J_{H,H}$ = 7.2 Hz, 2 H, PCCCO$_2$C*H*$_2$CH$_3$), 7.41 (m$_c$, 10 H, Ph), 7.49 (m$_c$, 5 H, Ph), 8.15 (d, $^2J_{P,H}$ = 31.8 Hz, 1 H, PCH). ^{13}C{^{1}H} NMR (CDCl$_3$): δ = 2.3 (d, $^3J_{P,C}$ = 2.4 Hz, SiMe$_3$), 2.5 (d, $^3J_{P,C}$ = 2.2 Hz, SiMe$_3$), 13.8 (s, CH$_2$*C*H$_3$), 14.1 (s, CH$_2$*C*H$_3$), 21.5 [d, $^1J_{P,C}$ = 3.7 Hz, *C*H(SiMe$_3$)$_2$], 58.8 (s, *C*H$_2$CH$_3$), 61.0 (s, *C*H$_2$CH$_3$), 63.9 (d, $^1J_{P,C}$ = 117.2 Hz, *C*PPh$_3$), 106.2 (dd, $^3J_{P,C}$ = 15.7, $^3J_{P,C}$ = 18.5 Hz, *C*CCPPh$_3$), 124.8 (d, $^1J_{P,C}$ = 102.1 Hz, *ipso*-Ph), 128.9 (d, $^3J_{P,C}$ = 12.4 Hz, *meta*-Ph), 132.5 (d, $^4J_{P,C}$ = 2.7 Hz, *para*-Ph), 133.5 (d, $^2J_{P,C}$ = 9.7 Hz, *ortho*-Ph), 139.6 (d, $^2J_{P,C}$ = 27.6 Hz, PC*C*), 144.4 (d, $^2J_{P,C}$ = 15.5 Hz, C*C*CPPh$_3$), 160.5 (s, P*C*C), 163.6 (d, $^3J_{P,C}$ = 18.3 Hz, PCC*C*O$_2$Et), 167.5 (d, $^2J_{P,C}$ = 14.8 Hz, Ph$_3$PC*C*O$_2$Et), 169.3 (d, $^2J_{P,C}$ = 10.9 Hz, PNC), 197.1 (d, $^2J_{P,C}$ = 7.0 Hz, *cis*-CO), 200.4 (d, $^2J_{P,C}$ = 19.3 Hz, *trans*-CO). ^{31}P{^{1}H} NMR (CDCl$_3$): δ = 82.8 (s, $^1J_{P,W}$ = 230.2 Hz), 25.3 (s). UV/Vis (CH$_3$CN): λ (lg ε) = 228 (4.86), 236 (4.80), 250 (4.57), 258 (4.44), 276 (4.13), 300 (4.09), 318 (4.10), 470 (4.10), 476 (4.10). IR (KBr): ṽ = 2066 (vs, CO), 1979 (vs, CO), 1929 (s, CO), 1722 (vs, CO$_2$), 1671 cm^{-1} (vs, CO$_2$). MS (pos. FAB, *m*-NBA, ^{184}W): *m*/*z* = 1012 (38) [M + H]$^+$, 688 (100) [M + H − W(CO)$_5$]$^+$. C$_{42}$H$_{47}$NO$_9$P$_2$Si$_2$W: calcd. C 49.86, H 4.68, N 1.38; found C 49.13, H 4.66, N 1.49.

{2-[Bis(trimethylsilyl)methyl]-4-(ethoxycarbonyl)-5-[(triphenylphosphonio)imido]-2*H*-1,2-azaphosphole-κ*P*}pentacarbonyltungsten(0) (8j): Yield 200 mg (22%); m.p. 52 °C (decomp.). ^{1}H NMR (CDCl$_3$): δ = 0.00 (s, 9 H, SiMe$_3$), 0.15 (s, 9 H, SiMe$_3$), 0.85 [d, $^2J_{P,H}$ = 7.8 Hz, 1 H, C*H*(SiMe$_3$)$_2$], 1.30 (t, $^3J_{H,H}$ = 7.0 Hz, 3 H, CH$_2$C*H*$_3$), 4.31 (q, $^3J_{H,H}$ = 7.0 Hz, 2 H, C*H*$_2$CH$_3$), 7.36 (m$_c$, 5 H, Ph), 7.45 (m$_c$, 3 H, Ph), 7.72 (m$_c$, 7 H, Ph), 8.03 (dd, $^2J_{P,H}$ = 29.8, $^5J_{P,H}$ = 4.0 Hz, 1 H, PCH). ^{13}C{^{1}H} NMR (CDCl$_3$): δ = 2.2 [d, $^3J_{P,C}$ = 2.5 Hz, Si(CH$_3$)$_3$], 2.5 [d, $^3J_{P,C}$ = 2.2 Hz, Si(CH$_3$)$_3$], 14.3 (s, CH$_2$*C*H$_3$), 22.3 [s, *C*H(SiMe$_3$)$_2$], 61.0 (s, *C*H$_2$CH$_3$), 128.3 (d, $^1J_{P,C}$ = 100.9 Hz, *ipso*-Ph), 128.6 (d, $^3J_{P,C}$ = 12.4 Hz, *meta*-Ph), 132.2 (d, $^4J_{P,C}$ = 2.7 Hz, *para*-Ph), 133.4 (d, $^2J_{P,C}$ = 10.1 Hz, *ortho*-Ph), 140.3 (d, $^{2+3}J_{P,C}$ = 17.4 Hz, PC*C*), 157.0 (d, $^1J_{P,C}$ = 8.1 Hz, P*C*C), 164.6 (d, $^3J_{P,C}$ = 19.8 Hz, *C*O$_2$Et), 167.0 (s, PNC), 197.5 (d, $^2J_{P,C}$ = 7.2 Hz, *cis*-CO), 200.6 (d, $^2J_{P,C}$ = 19.9 Hz, *trans*-CO). ^{31}P{^{1}H} NMR (CDCl$_3$): δ = 72.2 (s, $^1J_{P,W}$ = 236.1 Hz), 15.0 (s). UV/Vis (CH$_3$CN): λ (lg ε) = 228 (4.82), 238 (4.76), 244 (4.65), 250 (4.57), 256 (4.47), 268 (4.21), 316 (4.00), 340 (3.92), 364 (3.72). IR (KBr): ṽ = 2066 (s, CO), 1973 (s, CO), 1933 (w, CO), 1902 (w, CO), 1716 cm^{-1} (vs, CO$_2$). MS (EI, ^{184}W): *m*/*z* = 914 (8) [M]$^{+\cdot}$, 858 (100) [M − 2CO]$^{+\cdot}$.

X-ray Crystallography: The structure of **4c** was determined with a Siemens P4 diffractometer, while the structures of **8d**, **8e**, and **8g** were determined with a Bruker SMART 1000 CCD diffractometer. The structures were solved by the heavy atom method and refined anisotropically by full-matrix least-squares on F^2.[25] CCDC-168172 (**4c**), -168173 (**8d**), -168174 (**8e**), and -168175 (**8g**) contain the supplementary crystallographic data for this paper. These data can be obtained free of charge at www.ccdc.cam.ac.uk/conts/retrieving.html or from the Cambridge Crystallographic Data Centre, 12, Union Road, Cambridge CB2 1EZ, U.K. [Fax: (internat.) + 44-1223/336-033; E-mail: deposit@ccdc.cam.ac.uk].

Acknowledgments

We are grateful to the Deutsche Forschungsgemeinschaft and the Fonds der Chemischen Industrie for financial support.

[1] K. B. Dillon, F. Mathey, J. F. Nixon, *Phosphorus: The Carbon Copy*, Wiley, Chichester, **1998**.
[2] [2a] R. Streubel, H. Wilkens, A. Ostrowski, C. Neumann, F. Ruthe, P. G. Jones, *Angew. Chem.* **1997**, *109*, 1549−1550; *Angew. Chem. Int. Ed. Engl.* **1997**, *36*, 1492−1493. [2b] U. Rohde, F. Ruthe, P. G. Jones, R. Streubel, *Angew. Chem.* **1999**, *111*, 158−160; *Angew. Chem. Int. Ed.* **1999**, *38*, 215−217.
[3] R. Streubel, U. Schiemann, P. G. Jones, N. H. Tran Huy, F. Mathey, *Angew. Chem.* **2000**, *112*, 3845−3847; *Angew. Chem. Int. Ed.* **2000**, *39*, 3686−3688.
[4] A. Alijah, S. Grigoleit, R. Streubel, W. W. Schoeller, *J. Organomet. Chem.*, in press.
[5] R. Streubel, U. Schiemann, N. H. Tran Huy, F. Mathey, *Eur. J. Inorg. Chem.*, **2001**, 3175−3179.
[6] H. Wilkens, F. Ruthe, P. G. Jones, R. Streubel, *Chem. Eur. J.* **1998**, *4*, 1542−1553.
[7] R. Streubel, U. Schiemann, N. Hoffmann, Y. Schiemann, P. G. Jones, D. Gudat, *Organometallics* **2000**, *19*, 475−481.

[8] H. Wilkens, A. Ostrowski, J. Jeske, F. Ruthe, P. G. Jones, R. Streubel, *Organometallics* **1999**, *18*, 5627−5642.
[9] R. Streubel, N. Hoffmann, F. Ruthe, P. G. Jones, *Polyhedron*, in press.
[10] H. Wilkens, F. Ruthe, P. G. Jones, R. Streubel, *Chem. Commun.* **1998**, 1529−1530.
[11] G. Jochem, A. Schmidpeter, F. Kulzer, S. Dick, *Chem. Ber.* **1995**, *128*, 1207.
[12] E. Ciganek, *J. Org. Chem.* **1970**, *35*, 1723−1729.
[13] S. Bittner, M. Pomerantz, Y. Assaf, P. Krief, S. Xi, M. K. Witczak, *J. Org. Chem.* **1988**, *53*, 1−5. Comment: Because of the fact that the bonding situations in both P,C ylides *and* σ^4,λ^5-phosphorane imines, R_3PNR, are ylidic, the latter are referred to herein as P,N ylides.
[14] R. Streubel, A. Ostrowski, S. Priemer, U. Rohde, J. Jeske, P. G. Jones, *Eur. J. Inorg. Chem.* **1998**, 257−261.
[15] J. Barluenga, F. Lopez, F. Palacios, F. Sánchez-Ferrando, *Tetrahedron Lett.* **1988**, *29*, 381−384.
[16] O. I. Kolodiazhnyi, *Phosphorus Ylides*, Wiley-VCH, Weinheim, **1999**.
[17] K. Karaghiosoff, H. Klehr, A. Schmidpeter, *Chem. Ber.* **1986**, *119*, 410−419.
[18] C. Peters, F. Tabellion, M. Schröder, U. Bergsträßer, F. Preuss, M. Regitz, *Synthesis* **2000**, *3*, 417−428.
[19] A. Schmidpeter, in *Comprehensive Heterocyclic Chemistry II* (Eds.: A. R. Katritzky, C. W. Rees, E. F. V. Scriven), Pergamon, Oxford, **1996**, vol. 3, p. 709−714.
[20] L. Nyulászi, *Chem. Rev.* **2001**, *101*, 1229−1246.
[21] J. M. Miller, Ph.D. Thesis, Cambridge University, **1966**.
[22] C. Neumann, E. Ionescu, U. Schiemann, M. Schlenker, M. Bode, F. Ruthe, P. G. Jones, R. Streubel, *J. Organomet. Chem.*, in press.
[23] R. Streubel, S. Priemer, J. J. Jeske, P. G. Jones, unpublished results.
[24] W. Schoeller, A. B. Rozhenko, *Eur. J. Inorg. Chem.* **2001**, 845−850.
[25] G. M. Sheldrick, *SHELXL-97, Program for crystal structure refinement*, Universität Göttingen, **1997**.

Received August 30, 2001
[I01335]

Equilibrium, Kinetic and Leaving Group Effect Studies on Ligand Substitution Reactions of a Simple Model for Coenzyme B_{12}

Basam M. Alzoubi,[a] Mohamed S. A. Hamza,[a][‡] Carlos Dücker-Benfer,[a] and Rudi van Eldik*[a]

Keywords: Enzyme models / Equilibrium / Kinetics / Ligand effects / Leaving group effect / Volume profile

The ligand substitution reactions of *trans*-$[Co^{III}(en)_2(Me)H_2O]^{2+}$ and *trans*-$[Co^{III}(en)_2(Me)NH_3]^{2+}$ were studied for CN^-, SCN^-, N_3^-, and NH_3 as entering nucleophiles. These nucleophiles displace the coordinated H_2O and NH_3 molecules *trans* to the methyl group and form the six-coordinate complex *trans*-$[Co(en)_2(Me)L]$. The complex-formation constant for the displacement of H_2O by NH_3 was found to be 17.4 ± 1.1 M^{-1} at 20 °C, and those for the displacement of NH_3 by SCN^- and N_3^- were found to be 4.4 ± 1.5 and 3.1 ± 0.4 at 10 °C, respectively. From temperature and pressure dependence studies, activation parameters ($\Delta H^{\neq}$, $\Delta S^{\neq}$ and $\Delta V^{\neq}$) for the reaction of *trans*-$[Co^{III}(en)_2(Me)H_2O]^{2+}$ with NH_3 were found to be 62 ± 1 kJ mol^{-1}, $+3 \pm 5$ J K^{-1} mol^{-1} and $+5.7 \pm 0.3$ cm^3 mol^{-1}, respectively, compared to 79 ± 2 kJ mol^{-1}, $+40 \pm 6$ J K^{-1} mol^{-1} and $+9.0 \pm 0.4$ cm^3 mol^{-1} for the reverse aquation reaction of *trans*-$[Co^{III}(en)_2(Me)NH_3]^{2+}$. Based on the reported kinetic and activation parameters, the substitution of coordinated H_2O by NH_3 follows an I_d mechanism in which the entering nucleophile participates in the transition state. The substitution of NH_3 by SCN^-, N_3^- and CN^- proceeds via the intermediate aqua complex such that aquation of the amine complex becomes the rate-determining step at high entering ligand concentration. A detailed comparison with available data in the literature is made.

Introduction

Model complexes for vitamin B_{12} have played an important role in understanding the behavior of the ligand substitution reactions of vitamin B_{12} and the role of the Co−C bond in the coenzyme vitamin B_{12}.[1,2] Many octahedral organometallic complexes of Co^{III}, such as cobaloxime[2−10] and Costa's complex[11] (a mixed Schiff base/oxime complex with a uni-negative N_4 equatorial ligand), those with a Schiff base,[12,13] *N*,*N*′-ethylenebis(actylacetoneiminato),[14] *N*,*N*′-ethylenebis(salicylideneiminato)[15] and the dianion of disalicylidene-*O*-phenylenediamine[15] as ligands, have been suggested as models for the vitamin B_{12} coenzyme, to mimic either the nature of the active site or a specific function of the enzyme. These model complexes have shown that the ligand in the *trans* position to the Co−C bond can affect the kinetics and thermodynamic stability of this bond.[16] We recently studied the reaction of cyanide with different alkylcobalamins (RCbl, where R = CF_3, CF_3CH_2, CF_2H, CH_3, CH_2Br) and found that the nature of the alkyl group has an influence on the thermodynamic equilibrium constants, kinetics and mechanism of the substitution reactions of the axial ligand *trans* to the alkyl group.[17]

The simplest model for coenzyme B_{12} was synthesized by Kofod in 1995[18] and consists of a Co^{III} metal center surrounded by five ammine groups and one methyl group as ligands. This complex is only stable in aqueous solution in the presence of a high ammonia concentration (ca. 3 M). We recently suggested that the $[Co(NH_3)_5(Me)]^{2+}$ cation is not favored in being used as a model for vitamin B_{12} due to the necessary presence of a high ammonia concentration and the unfavorable pH.[19] $[Co(NH_3)_5(Me)]^{2+}$ undergoes a rapid ligand substitution reaction with ethylenediamine (en) to form *cis*-$[Co(en)_2(Me)NH_3]^{2+}$, which slowly isomerizes to the more stable and isolable *trans* isomer.[19] The kinetic and activation parameters for the displacement of the four ammonia ligands by two ethylenediamine (en) chelates confirmed the operation of a limiting dissociative reaction mechanism under limiting concentration conditions. The activation parameters also confirmed the operation of a dissociative mechanism for the subsequent *cis* to *trans* isomerization reaction.

A potential advantage of the planar bis(ethylenediamine) arrangement around the Co^{III} center is the flexibility of the chelates, an aspect that has been suggested to be important for the biological activity of the coenzyme.[20] We studied the ligand substitution reactions of *trans*-$[Co^{III}(en)_2(Me)H_2O]^{2+}$ with CN^- and imidazole. Activation parameters ($\Delta H^{\neq}$, $\Delta S^{\neq}$ and $\Delta V^{\neq}$) for the reaction of *trans*-$[Co^{III}(en)_2(Me)H_2O]^{2+}$ with cyanide were found to be 49 ± 4 kJ mol^{-1}, -38 ± 15 J K^{-1} mol^{-1} and $+7.0 \pm 0.6$

[‡] On leave from the Department of Chemistry, Faculty of Science, Ain Shams University, Abbassia, Cairo, Egypt.
[a] Institute for Inorganic Chemistry, University of Erlangen−Nürnberg, Egerlandstraße 1, 91058 Erlangen, Germany
Supporting information for this article is available on the WWW under http://www.eurjic.com or from the author.

 © WILEY-VCH Verlag GmbH, 69451 Weinheim, Germany, 2002 1434−1948/02/0404−0968 $ 17.50+.50/0 *Eur. J. Inorg. Chem.* **2002**, 968−974

$cm^3\ mol^{-1}$, respectively, compared to 53 ± 2 kJ mol^{-1}, −22 ± 7 J K^{-1} mol^{-1} and +4.7 ± 0.1 $cm^3\ mol^{-1}$ for the reaction with imidazole.[21] Based on the reported activation volumes, these reactions follow a dissociative (interchange dissociative, I_d, or limiting dissociative, D) mechanism in which the entering nucleophile could be weakly bound in the transition state.[21] By way of comparison, ligand substitution reactions of vitamin B_{12} in general follow a dissociative (I_d or D) type of mechanism.[22−36] In the case of the coenzyme, however, evidence for an associative substitution mode was reported.[37] In order to gain further insight into the reasons for this unexpected mechanistic changeover, we have now investigated substitution reactions of *trans*-$[Co(en)_2(Me)H_2O]^{2+}$ and *trans*-$[Co(en)_2(Me)NH_3]^{2+}$ to study the effect of the leaving group on the axial ligand substitution mechanism of these model complexes that include a cobalt−carbon σ-bond. These complexes allow us to mimic the active site of the coenzyme since the ammine ligand *trans* to the Co−Me bond represents the dimethylbenzimidazole moiety in the coenzyme.

Results and Discussion

As mentioned before, the pK_a value of coordinated water in *trans*-$[Co(en)_2(Me)H_2O]^{2+}$ is higher than 12, since there was no change observed in the pH titration curve up to that pH.[21] Furthermore, it was found that *trans*-$[Co(en)_2(Me)H_2O]^{2+}$ decomposes upon exposure to UV light, suggesting that the Co−C bond can be cleaved photochemically. This was observed for most of the Co^{III} complexes containing alkyl groups coordinated to the cobalt atom in the axial position.[16] Preliminary experiments showed that decomposition of this complex by the light beam of the spectrophotometer was negligible. Despite the lower light sensitivity of this complex as compared to other alkylcobalamins, special care was taken to protect this complex from photochemical decomposition.

In the present study, we investigated the displacement of the axial H_2O molecule in *trans*-$[Co(en)_2(Me)H_2O]^{2+}$ by NH_3 in order to make comparisons with our earlier study on the reactions of cyanide and imidazole with this complex.[21] Subsequently, we investigated the displacement of NH_3 in *trans*-$[Co(en)_2(Me)NH_3]^{2+}$ by SCN^-, N_3^- and CN^-, in order to obtain more information on leaving group effects in such systems. The investigated reaction is shown in Equation (1), where X = H_2O for L = NH_3, and X = NH_3 for L = CN^-, SCN^-, N_3^-.

$$\textit{trans}\text{-}[Co(en)_2(Me)X]^{2+} + L \underset{k_b}{\overset{k_a}{\rightleftharpoons}} \textit{trans}\text{-}[Co(en)_2(Me)L]^{2+} + X \quad (1)$$

Reaction of *trans*-$[Co(en)_2(Me)H_2O]^{2+}$ with NH_3

Equilibrium Measurements

The UV/Vis spectrum of *trans*-$[Co(en)_2(Me)H_2O]^{2+}$ in buffers at pH = 11 shows characteristic bands at 364 (125 $M^{-1}\ cm^{-1}$) and 472 nm (74 $M^{-1}\ cm^{-1}$). Addition of NH_3 shifts the bands to 354 (133 $M^{-1}\ cm^{-1}$) and 464 nm (67 $M^{-1}\ cm^{-1}$) with a shoulder at 290 nm (166 $M^{-1}\ cm^{-1}$). These changes in the UV/Vis spectra are accompanied by distinct isosbestic points, indicating that a simple equilibrium exists under these conditions. These observations suggest that the aqua ligand in the *trans* position to the methyl group is displaced by ammonia to form the six-coordinate *trans*-$[Co(en)_2(Me)NH_3]^{2+}$ complex.

Preliminary experiments in which the UV/Vis spectrum was scanned in the range 250 to 600 nm, showed that at pH = 11, NH_3 reacts rapidly with *trans*-$[Co(en)_2(Me)H_2O]^{2+}$. Equilibrium (1) was established within the time required for mixing the solutions and recording the spectra. The values of the overall equilibrium constant K were determined spectrophotometrically (in duplicate experiments) by titrating ca. 3×10^{-3} M *trans*-$[Co(en)_2(Me)H_2O]^{2+}$ (I = 0.1 M, $NaClO_4$) with a concentrated stock solution of NH_3 to minimize dilution effects.

The spectrophotometric titration of NH_3 was monitored by following the increase in absorbance at 326 nm or the decrease in absorbance at 380 nm, where the largest change in absorbance occurred. Typical data for the reaction with NH_3 are shown in Figure 1. The solid line represents the fit of the experimental data to Equation (2), where A_o and A_∞ represent the absorbance at 0 and 100% formation of *trans*-$[Co(en)_2(Me)L]^{2+}$, respectively, and A_x is the absorbance at any given ligand concentration [L].

$$A_x = A_o + A_\infty K[L]/(1 + K[L]) \quad (2)$$

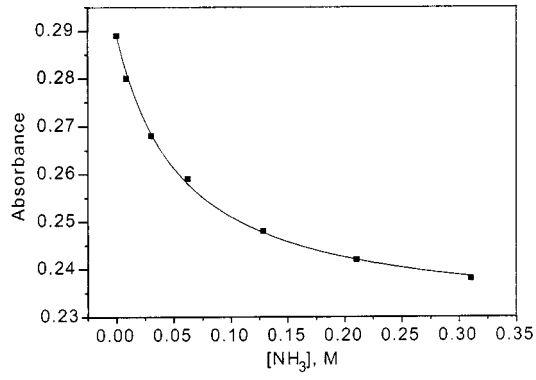

Figure 1. Changes in absorbance at 380 nm on addition of NH_3 to *trans*-$[Co(en)_2(Me)H_2O]^{2+}$; the solid line is a fit of the data to Equation (2) in the text

The values of K and A_∞ were calculated from a non-linear least-squares fit of the data to Equation (2). The data were subsequently also analyzed by plotting log $(A_x - A_o)/(A_\infty - A_x)$ versus log[L], which resulted in a linear plot with slope of 0.99 ± 0.06 for NH_3, indicating that only one ligand (L) is coordinated to the cobalt complex. The intercept of the linear plot gives the value of log K, which is in excellent agreement with the directly determined value described above.

The value of $K(NH_3)$ was found to be 17.4 ± 1.1 M^{-1} at 20 °C. The value of K for the binding of NH_3 to $[Co(corrin)(Me)H_2O]^{2+}$ was reported to be 0.1 M^{-1},[38] from which it follows that the affinity of NH_3 for *trans*-$[Co(en)_2(Me)H_2O]^{2+}$ is almost 200 times higher than for $[Co(corrin)(Me)H_2O]^{2+}$. This comparison demonstrates the *cis* effect, i.e. the influence of the equatorial ligand on the substitution reaction of the axial ligand *trans* to the alkyl group. The observed trend in the formation constants for the equatorial ligands is corrin < $(en)_2$.

Kinetic Measurements

The reaction between *trans*-$[Co(en)_2(Me)H_2O]^{2+}$ and excess NH_3 at pH = 11 ($[NH_3]$ = 0.1 to 1.25 M, I = 0.1 M using $NaClO_4$) was studied at different temperatures. The results are shown in Figure 2, from which it follows that good linear plots with significant intercepts are obtained within the experimental error limits. Furthermore, the plots do not indicate any saturation at high $[NH_3]$ values. This behavior can be expressed by the rate law given in Equation (3), where k_a and k_b represent the rate constants for the forward and reverse reactions in Equation (1), respectively, L represents NH_3 and X is H_2O (the concentration of water is a constant and taken into k_b). It should be noted that the intercepts in Figure 2 are subjected to large error limits and an alternative procedure was used to determine the rate constant for the reverse reaction more accurately (see further Discussion). The values of k_a and k_b as a function of temperature, along with the corresponding activation parameters are summarized in Table 1.

$$k_{obs} = k_a[L] + k_b \quad (3)$$

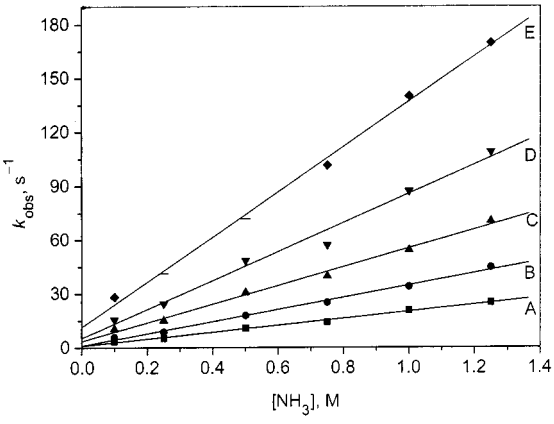

Figure 2. Plot of k_{obs} versus $[NH_3]$ for the reaction between *trans*-$[Co(en)_2(Me)H_2O]^{2+}$ and NH_3 as a function of temperature; experimental conditions: $[Co^{III}]$ = 0.0045 M, pH = 11, I = 0.1 M $NaClO_4$ and temperature = 5.0 (A), 10.0 (B), 15.0 (C), 20.0 (D) and 25.0 °C (E)

The values of $\Delta H^{\neq}$ and $\Delta S^{\neq}$ for the forward reaction (k_a) were found to be 62 ± 1 kJ mol^{-1} and 3 ± 5 J K^{-1} mol^{-1}, respectively, whereas those for the reverse reaction (k_b) were found to be 85 ± 13 kJ mol^{-1} and 60 ± 43 J K^{-1} mol^{-1}, respectively.

Table 1. Kinetic data for the reaction of *trans*-$[Co(en)_2(Me)H_2O]^{2+}$ with NH_3 as a function of temperature (experimental conditions see footnotes)

T [°C]	k_a [M^{-1} s^{-1}][a]	k_b [s^{-1}][b]	k_b [s^{-1}][c]
5.0	19.1 ± 0.8	1.0 ± 0.6	1.33 ± 0.03
10.0	33.6 ± 1.3	1.1 ± 1.0	2.28 ± 0.06
15.0	51.8 ± 2.1	3.5 ± 1.6	4.45 ± 0.04
20.0	82.2 ± 5.4	4.7 ± 4.1	7.5 ± 0.6
25.0	125.5 ± 3.7	11.5 ± 2.8	13.8 ± 0.9
$\Delta H^{\neq}$ [kJ mol^{-1}]	62 ± 1	85 ± 13	79 ± 2
$\Delta S^{\neq}$ [J K^{-1} mol^{-1}]	+3 ± 5	+60 ± 43	+40 ± 6

[a] $[Co(en)_2(Me)H_2O]$ = 4.5 × 10^{-3} M, pH = 11, I = 0.1 M $NaClO_4$. [b] Values were calculated from the intercepts in Figure 2. [c] Values were calculated from the direct reaction of 9 × 10^{-3} M $[Co(en)_2(Me)NH_3]^{2+}$ in the presence of 0.3 M NH_3, at pH = 11 and 0.1 M $NaClO_4$, with 0.5 M HCl.

We determined the rate and activation parameters for the aquation (k_b) of *trans*-$[Co(en)_2(Me)NH_3]^{2+}$ (in the presence of 0.3 M NH_3) directly by treating this amine complex with 0.5 M HCl to protonate ammonia to form *trans*-$[Co(en)_2(Me)H_2O]^{2+}$. This reaction was found to be independent of the acid concentration as long as the acid is in excess under the selected conditions, and the results for k_b are included in Table 1. The values of $\Delta H^{\neq}$ and $\Delta S^{\neq}$ were found to be 79 ± 2 kJ mol^{-1} and 40 ± 6 J K^{-1} mol^{-1}, respectively, and are more accurate than those determined from the intercepts of Figure 2.

The values of k_a and k_b can be used to calculate K (= k_a/k_b), which turns out to be 11.0 ± 1.6 M^{-1} at 20 °C. The kinetically determined value of K is in close agreement with that obtained spectrophotometrically at the same temperature, viz. 17.4 ± 1.1 M^{-1}.

The high lability of coordinated water in *trans*-$[Co(en)_2(Me)H_2O]^{2+}$ is also seen in the relatively low activation enthalpy for the substitution by NH_3, as compared to the higher activation enthalpy for the aquation reaction of the ammonia complex (i.e. back reaction). The value of the activation enthalpy for the reaction with NH_3 (63 ± 1 kJ mol^{-1}) is close to that obtained previously[21] for the reaction with CN^- and imidazole (50 ± 4 kJ mol^{-1} and 53 ± 2 kJ mol^{-1}, respectively). The activation entropy for the formation of *trans*-$[Co(en)_2(Me)NH_3]^{2+}$ was found to be close to zero, compared to a significantly positive value for the back reaction. It is known that $\Delta S^{\neq}$ is usually subjected to large error limits because of the intrinsic extrapolation involved in its determination, such that small absolute numbers are not very significant in terms of the assignment of a mechanism.[39] The significantly positive value found for the reverse aquation reaction, points to a dissociatively activated transition state.

The pressure dependence of the reaction of *trans*-$[Co(en)_2(Me)H_2O]^{2+}$ with NH_3 was investigated and the data are summarized in Table 2. Plots of ln k_a versus pressure gave a good linear plot from which $\Delta V^{\neq}$ was found to be +5.7 ± 0.3 cm^3 mol^{-1}. The pressure dependence of the aquation reaction of *trans*-$[Co(en)_2(Me)NH_3]^{2+}$ (in the

Table 2. Kinetic data for the reaction of *trans*-$[Co(en)_2(Me)H_2O]^{2+}$ with NH_3 as a function of pressure at 5 °C (experimental conditions see footnotes)

p [MPa]	k_a [M^{-1} s^{-1}][a][b]	k_b [s^{-1}][c]
10	3.88 ± 0.16	1.74 ± 0.04
50	3.43 ± 0.22	1.50 ± 0.01
90	3.08 ± 0.12	1.25 ± 0.02
130	2.73 ± 0.22	1.10 ± 0.04
$\Delta V^{\neq}$ [cm^3 mol^{-1}]	+5.7 ± 0.3	+9.0 ± 0.4

[a] $[Co(en)_2(Me)H_2O] = 4.5 \times 10^{-3}$ M, $[NH_3] = 1.5$ M, pH = 11, 5 °C, $I = 0.1$ M $NaClO_4$. [b] Calculated from the equation: $k_{obs} = k_b + k_a[NH_3]$. [c] Determined from the reaction of 1.8×10^{-2} M $[Co(en)_2(Me)NH_3]^{2+}$ in the presence of 0.3 M NH_3 at pH = 11, 0.1 M $NaClO_4$ and 5 °C, with 0.5 M HCl.

presence of 0.3 M NH_3) was also investigated by the direct reaction of 1.8×10^{-2} M $[Co(en)_2(Me)NH_3]^{2+}$ with 0.5 M HCl to protonate the ammonia. A plot of ln k_b versus pressure gave a good linear relationship, from which $\Delta V^{\neq}$ was calculated to be +9.0 ± 0.4 cm^3 mol^{-1} (the data are summarized in Table 2; see Supporting Information, Figure S-1). From the values of $\Delta V^{\neq}$ it is possible to construct a volume profile for the substitution of *trans*-$[Co(en)_2(Me)H_2O]^{2+}$ by NH_3 (see Figure 3), from which it can be concluded that the substitution process is dissociatively activated, since the transition state has a significantly higher partial molar volume than the reactant state. Similar results were reported for reactions of *trans*-$[Co(en)_2(Me)H_2O]^{2+}$ with CN^- and imidazole[21] and also for the reaction of aquacobalamin with different ligands such as HN_3, N_3^-, pyridine and its derivatives, and thiourea and its derivatives.[30–32] In all these cases, $\Delta V^{\neq}$ was found to be in the range of +4 to +8 cm^3 mol^{-1}, i.e. similar to the value found for the reaction of NH_3 with *trans*-$[Co(en)_2(Me)H_2O]^{2+}$ in this study, and was interpreted in terms of an I_d mechanism. These values are significantly smaller than those reported for substitution reactions of (porphyrin)cobalt(III) systems. There it was found that $\Delta V^{\neq}$ for ligand substitution on $[Co(TMPP)(H_2O)_2]^{5+}$ and $[Co(TPPS)(H_2O)_2]^{3-}$, where TMPP = *meso*-tetrakis(4-*N*-methylpyridyl)porphine and TPPS = *meso*-tetrakis(*p*-sulfonatophenyl)porphine, are +14.4 and +15.4 cm^3 mol^{-1}, respectively,[40,41] and these were assigned to a limiting D mechanism. It follows from this comparison that the introduction of a single cobalt–carbon bond significantly labilizes the coordinated water molecule in *trans*-$[Co(en)_2(Me)H_2O]^{2+}$, as reflected by its high pK_a value, but apparently does not induce a limiting D mechanism on the basis of the reported $\Delta V^{\neq}$ data.

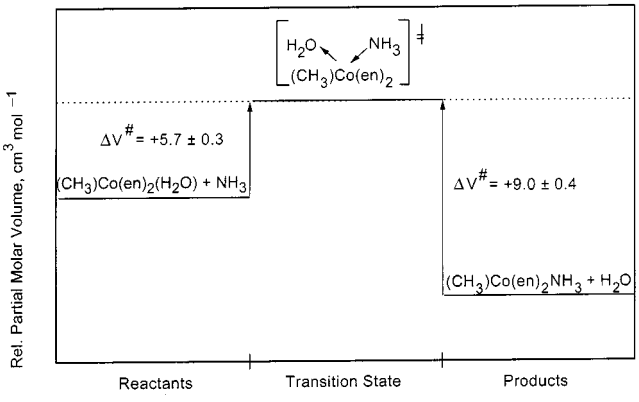

Figure 3. Volume profile for the reaction *trans*-$[Co(en)_2(Me)H_2O]^{2+}$ + NH_3 ⇄ *trans*-$[Co(en)_2(Me)NH_3]^{2+}$ + H_2O

On the basis of the volume of activation data and the constructed volume profile, it is reasonable to conclude that the reaction of *trans*-$[Co(en)_2(Me)H_2O]^{2+}$ with NH_3 follows an I_d mechanism, where the entering nucleophile partially participates in the transition state. The volume changes during the complex-formation reaction are controlled by the lengthening of the Co–OH_2 bond that should be independent of the nature of L.

Reaction of *trans*-$[Co(en)_2(Me)NH_3]^{2+}$ with CN^-, SCN^- and N_3^-

The UV/Vis spectrum of *trans*-$[Co(en)_2(Me)NH_3]^{2+}$, dissolved in buffers at pH = 11 in the presence of 1 M NH_3, showed bands at 354 (133 M^{-1} cm^{-1}) and 464 nm (67 M^{-1} cm^{-1}) with a shoulder at 290 nm (166 M^{-1} cm^{-1}). Addition of SCN^- shifts the UV/Vis bands to 356 (208 M^{-1} cm^{-1}) and 464 nm (97 M^{-1} cm^{-1}), whereas addition of N_3^- shifts the UV/Vis bands to 364 (182 M^{-1} cm^{-1}) and 472 nm (98 M^{-1} cm^{-1}).

Spectrophotometric titrations for the reactions with SCN^- and N_3^- were performed in the presence of 1 M NH_3 at 10 °C, and monitored by the increase in absorbance at 461 and 467 nm, respectively. The values of K were calculated from a non-linear least-squares fit of the data to Equation (2) and found to be 4.4 ± 1.5 and 3.0 ± 0.4, respectively. The data were also analyzed by plotting log $(A_x - A_o)/(A_\infty - A_x)$ versus log[L], which resulted in linear plots with slopes of 0.99 ± 0.04 and 0.99 ± 0.09 for SCN^- and N_3^-, respectively, indicating that only one ligand (L) is coordinated to the cobalt complex.

Figure 4 shows a plot of k_{obs} versus $[CN^-]$ for the reaction of *trans*-$[Co(en)_2(Me)NH_3]^{2+}$ (in the presence of 1 M NH_3) with CN^- at pH = 11 ($[CN^-] = 0.05$ to 1 M), $I = 1$ M ($NaClO_4$) and 10 °C. This plot shows saturation kinetics (a limiting value of k_{obs} (= k_3) is reached at high $[CN^-]$ values) and exhibits no intercept, indicating that the reverse reaction does not contribute significantly. The suggested mechanism in reaction (4) involves the dissociative formation of a six-coordinate aqua intermediate, followed by the reaction with the entering ligand L. The data in Figure 4 were fitted to Equation (5), and resulted in $k_3 = 2.79 \pm 0.02$ s^{-1}, $k_{-4} \approx 0$ and $k_4/k_{-3} = 73 \pm 3$. The value of k_{obs} increases with increasing cyanide concentration due to the fact that $k_3 >> k_{-4}$. The value of k_4/k_{-3} represents the efficiency of CN^- compared with NH_3 to scavenge the six-coordinate aqua intermediate. The rate law is presented in Equation (5)

$$\begin{aligned} &trans\text{-}[Co(en)_2(Me)NH_3]^{2+} + H_2O \rightleftarrows \\ &\quad trans\text{-}[Co(en)_2(Me)H_2O]^{2+} + NH_3 \quad k_3,k_{-3} \\ &trans\text{-}[Co(en)_2(Me)H_2O]^{2+} + L \rightleftarrows \\ &\quad trans\text{-}[Co(en)_2(Me)L]^{+} + H_2O \quad k_4,k_{-4} \end{aligned} \tag{4}$$

$$k_{obs} = \{k_3k_4[L] + k_{-3}k_{-4}[NH_3]\}/\{k_4[L] + k_{-3}[NH_3]\} \tag{5}$$

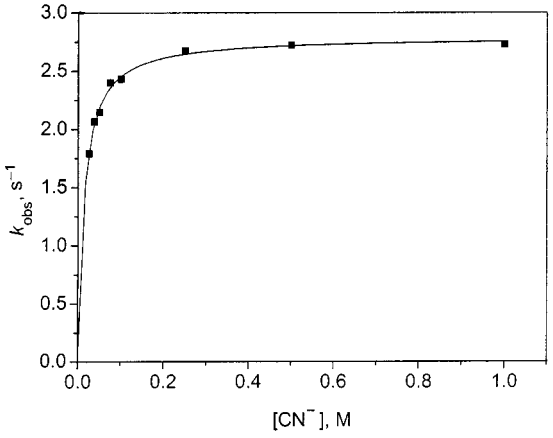

Figure 4. k_{obs} versus $[CN^-]_{total}$ for the reaction between *trans*-$[Co(en)_2(Me)NH_3]^{2+}$ and CN^- at pH = 11, $[NH_3]$ = 1 M, 10 °C and I = 1 M ($NaClO_4$); the best fit of the data (solid line) to Equation (5) gives $k_3 = 2.79 \pm 0.02$ s^{-1}, $k_4/k_{-3} = 73 \pm 3$

The reactions of SCN^- and N_3^- with *trans*-$[Co(en)_2(Me)NH_3]^{2+}$ were studied at 10 °C, using a buffer at pH = 9 and I = 1 M $NaClO_4$. Interestingly, the plot of k_{obs} versus $[SCN^-]$ results in a decrease of k_{obs} with increasing ligand concentration presumably due to the fact that $k_3 << k_{-4}$ as shown in Figure 5. A Similar plot was obtained for the reaction with N_3^- (see Supporting Information, Figure S-2). This is characteristic for the dissociative formation of an intermediate and the occurrence of an efficient back reaction. A similar nucleophile concentration dependence was reported for several reversible dissociative ligand substitution reactions, such as the reaction of $[Co(NH_3)_5(Me)]^{2+}$ with ethylenediamine,[19] the reaction of (*N*-methylimidazole)cobalamin with *N*-methylimidazole,[27] and other reactions reported in the literature.[42–46] A nonlinear least-squares fit of the data for SCN^-, revealed that $k_3 = 3.1 \pm 0.2$ s^{-1}, $k_{-4} = 19 \pm 4$ s^{-1} and $k_4/k_{-3} = 34 \pm 13$, and those obtained for N_3^- are $k_3 = 3.1 \pm 0.3$ s^{-1}, $k_{-4} = 23 \pm 5$ s^{-1} and $k_4/k_{-3} = 16 \pm 7$. The values of k_4/k_{-3} represent the efficiency of SCN^- and N_3^- compared with NH_3 to scavenge the six-coordinate intermediate. The complex-formation constant $K = k_3k_4/k_{-3}k_{-4}$ obtained from the kinetic data for the reaction with SCN^- and N_3^- are 5.6 ± 0.5 and 2.2 ± 0.5, respectively, which are in good agreement with the thermodynamically determined values of 4.4 ± 1.5 and 3.0 ± 0.4, respectively.

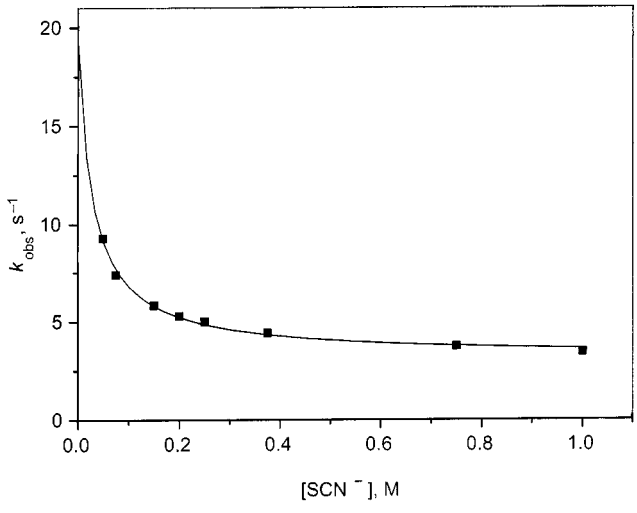

Figure 5. k_{obs} versus $[SCN]_{total}$ for the reaction between *trans*-$[Co(en)_2(Me)NH_3]^{2+}$ and SCN^- at pH = 9, $[NH_3]$ = 1 M, 10 °C and I = 1 M $NaClO_4$; the best fit of the data (solid line) to Equation (5) gives $k_3 = 3.1 \pm 0.2$ s^{-1}, $k_{-4} = 19 \pm 4$ M^{-1} s^{-1}, $k_4/k_{-3} = 34 \pm 13$

By way of comparison, the value of k_3 for the reaction of *trans*-$[Co(en)_2(Me)NH_3]^{2+}$ with $[CN^-]$ (2.79 ± 0.02 s^{-1}) is close to that obtained when L is SCN^- and N_3^-, viz. 3.1 ± 0.2 and 3.1 ± 0.3 s^{-1}, respectively, and also in agreement with that obtained for the aquation of *trans*-$[Co(en)_2(Me)NH_3]^{2+}$ (viz. 2.28 ± 0.06 s^{-1}) at 10 °C. This suggests that the limiting rate constant reached at high nucleophile concentration for all these reactions, is for aquation of the ammine complex that is controlled by the release of NH_3 (i.e., k_3), for which the mechanism has been discussed above.

The value of k_{-4} for the reaction of $[Co(en)_2(Me)CN]^+$ with NH_3 is close to zero. However, k_{-4} for the reaction of the SCN^- and N_3^- complexes with NH_3 is 19 ± 4 and 23 ± 5 M^{-1} s^{-1}, respectively. These values indicate that the back reaction contributes significantly in the case of the weaker nucleophiles SCN^- and N_3^-, and that the reaction is irreversible in the case of the stronger nucleophile CN^-.

The ratio of k_4/k_{-3} for the reaction of CN^- with $[Co(en)_2(Me)NH_3]^{2+}$ was found to be 73 ± 3, significantly higher than for the reactions with SCN^- and N_3^-, viz. 34 ± 13 and 16 ± 7, respectively. The higher ratio in the case of CN^- is due to its stronger nucleophilicity than SCN^- and N_3^-, and is therefore a better scavenger for the six-coordinate aqua intermediate in its competition with NH_3 as nucleophile. We conclude that aquation of the ammine complex controls the ligand substitution reactions with the studied nucleophiles and proceeds according to the mechanism outlined in Equation (4).

Experimental Section

Materials: All chemicals were of p.a. grade and used as received. Taps buffer (pH = 9) and Caps buffer (pH = 11) were purchased from Sigma. $NaClO_4$ was purchased from Fluka. NaSCN, NaN_3, NH_3 and NaCN were purchased from Merck. Ultra pure water

was used for all measurements. All preparations and measurements were carried out in diffuse light since the complexes were found to be light sensitive. *trans*-$[Co(en)_2(Me)NH_3]S_2O_6$ was prepared as described by Kofod[47] by treating Co^{II} nitrate with methylhydrazine in the presence of NH_3 to give $[Co(NH_3)_5Me](NO_3)_2$. This complex was treated with ethylenediamine to give *cis*-$[Co(en)_2(Me)NH_3]^{2+}$, followed by a slow isomerization to give *trans*-$[Co(en)_2(Me)NH_3]^{2+}$, which can be isolated in the solid form; *trans*-$[Co(en)_2(Me)H_2O]^{2+}$ was prepared by dissolving *trans*-$[Co(en)_2(Me)NH_3]S_2O_6$ in water at 60 °C for 2 h as previously described. The complexes were characterized by elemental analyses, UV/Vis and NMR spectroscopy, and the results were in agreement with literature data.[47]

Instrumentation: The pH of the solution was measured using a Mettler Delta 350 pH meter. The pH meter was calibrated with standard buffer solutions at pH = 7 and 10. UV/Vis spectra were recorded with Shimadzu UV-2101 and Cary 5 spectrophotometers. Kinetic measurements were carried out with an Applied Photophysics SX 18MV stopped-flow instrument coupled to an online data acquisition system. At least eight kinetic runs were recorded under all conditions, and the reported rate constants represent the mean values. All kinetic measurements were carried out under pseudo-first order conditions, i.e. the ligand concentration was in at least tenfold excess. Measurements at high pressure were carried out using a homemade high-pressure stopped-flow unit.[48] Kinetic data were analyzed with the OLIS KINFIT (Bogart, GA, USA) program. All instruments used were thermostated to the desired temperature (± 0.1 °C). Equilibrium measurements: $3-5 \times 10^{-3}$ M *trans*-$[Co(en)_2(Me)NH_3]S_2O_6$ or *trans*-$[Co(en)_2(Me)H_2O]S_2O_6$, dissolved in Taps buffer pH = 9 or caps buffer pH = 11 (I = 0.1 M using $NaClO_4$), was placed in a 1.0-cm path length cuvette in the thermostated cell block of the spectrophotometer for ca. 20 min. This solution was titrated by addition of small volumes of a concentrated stock solution of the ligand, using a Hamilton syringe. The ligand solution was prepared in the same buffer and the ionic strength was also adjusted to 0.1 M using $NaClO_4$. The titrations were carried out in duplicate and were monitored at several wavelengths where the largest change in absorbance occurred. The values of the equilibrium constant, K, were obtained by fitting the absorbance versus concentration curve to the appropriate equation, after correction for dilution (see further Discussion).

Acknowledgments

The authors gratefully acknowledge financial support from the Deutsche Forschungsgemeinschaft, a fellowship from the Alexander von Humboldt Foundation (MSAH), and sabbatical leave from the Ain Shams University, Cairo (MSAH).

[1] J. Halpern, *Science* **1985**, *227*, 869.
[2] [2a] N. Bresciani-Pahor, M. Forcolin, L. G. Marzilli, L. Randaccio, M. F. Summers, P. J. Toscano, *Coord. Chem. Rev.* **1985**, *63*, 1. [2b] L. G. Marzilli, M. F. Summers, E. Zangrando, N. Bresciani-Pahor, L. Randaccio, *J. Am. Chem. Soc.* **1986**, *108*, 4830. [2c] L. Randaccio, N. Bresciani-Pahor, E. Zangrando, L. G. Marzilli, *Chem. Soc. Rev.* **1989**, *18*, 225. [2d] S. M. Polson, L. Hansen, L. G. Marzilli, *Inorg. Chem.* **1997**, *36*, 307.
[3] A. L. Crumbliss, W. K. Wilmarth, *J. Am. Chem. Soc.* **1970**, *92*, 2593.
[4] K. L. Brown, S. Satyanarayana, *J. Am. Chem. Soc.* **1992**, *114*, 5674.
[5] K. L. Brown, R. G. Kallen, *J. Am. Chem. Soc.* **1972**, *94*, 1894.
[6] L. G. Marzilli, P. J. Toscano, L. Randaccio, N. Bresciani-Pahor, M. Calligaris, *J. Am. Chem. Soc.* **1979**, *101*, 6754.
[7] L. Randaccio, N. Bresciani-Pahor, P. J Toscano, L. G. Marzilli, *J. Am. Chem. Soc.* **1980**, *102*, 7372.
[8] N. Bresciani-Pahor, L. Randaccio, P. J. Toscano, A. Sandercock, L. G. Marzilli, *J. Chem. Soc., Dalton Trans.* **1982**, 129.
[9] M. F. Summers, P. J. Toscano, N. Bresciani-Pahor, G. Nardin, L. Randaccio, L. G. Marzilli, *J. Am. Chem. Soc.* **1983**, *105*, 6259.
[10] N. Bresciani-Pahor, L. G. Marzilli, L. Randaccio, P. J. Toscano, E. Zangrando, *J. Chem. Soc., Chem. Commun.* **1984**, 1508.
[11] G. Costa, G. Mestroni, E. de Savorgnani, *Inorg. Chim. Acta.* **1969**, *3*, 323.
[12] G. Costa, A. Puxeddu, E. Reisenhofer, *Collect. Czech. Chem. Commun.* **1971**, *36*, 1065.
[13] G. Costa, *Coord. Chem. Rev.* **1972**, *8*, 63.
[14] G. Costa, G. Mestroni, G. Tauzher, L. Stefani, *J. Organomet. Chem.* **1966**, *6*, 181.
[15] [15a] G. Costa, G. Mestroni, L. Stefani, *J. Organomet. Chem.* **1967**, *7*, 493. [15b] A. Bigotto, G. Costa, G. Mestroni, G. Pellizer, A. Puxeddu, E. Reisenhofer, L. Stefani, G. Tauzher, *Inorg. Chim. Acta Rev.* **1970**, 41.
[16] J. M. Pratt, *Inorganic Chemistry of Vitamin B_{12}, Academic Press, London, **1972**.*
[17] M. S. A. Hamza, X. Zou, K. L. Brown, R. van Eldik, *Inorg. Chem.* **2001**, *40*, 5440.
[18] P. Kofod, *Inorg. Chem.* **1995**, *34*, 2768.
[19] C. Dücker-Benfer, M. S. A. Hamza, C. Eckhardt, R. van Eldik, *Eur. J. Inorg. Chem.* **2000**, 1563.
[20] L. M. Hansen, P. N. V. Pavan Kumar, D. S. Marynick, *Inorg. Chem.* **1994**, *33*, 728.
[21] M. S. A. Hamza, C. Dücker-Benfer, R. van Eldik, *Inorg. Chem.* **2000**, *39*, 3777, 6145.
[22] D. Thusius, *J. Am. Chem. Soc.* **1971**, *93*, 2629.
[23] F. Nome, J. H. Fendler, *J. Chem. Soc., Dalton Trans.* **1976**, 1212.
[24] D. A. Baldwin, E. A. Betterton, J. M. Pratt, *S. Afr. J. Chem.* **1982**, *35*, 173.
[25] G. Stochel, R. van Eldik, *Inorg. Chem.* **1990**, *29*, 2075.
[26] G. Stochel, R. van Eldik, H. Kunkely, A. Vogler, *Inorg. Chem.* **1989**, *28*, 4314.
[27] A. G. Cregan, N. E. Brasch, R. van Eldik, *Inorg. Chem.* **2001**, *40*, 1430.
[28] W. C. Randall, R. A. Alberty, *Biochemistry* **1967**, *6*, 1520.
[29] W. W. Reenstra, W. P. Jencks, *J. Am. Chem. Soc.* **1979**, *101*, 5780.
[30] F. F. Prinsloo, M. Meier, R. van Eldik, *Inorg. Chem.* **1994**, *33*, 900.
[31] M. Meier, R. van Eldik, *Inorg. Chem.* **1993**, *32*, 2635.
[32] F. F. Prinsloo, E. L. J. Breet, R. van Eldik, *J. Chem. Soc., Dalton Trans.* **1995**, 685.
[33] H. M. Marques, *J. Chem. Soc., Dalton Trans.* **1991**, 339.
[34] H. M. Marques, J. C. Bradley, L. A. Campbell, *J. Chem. Soc., Dalton Trans.* **1992**, 2019.
[35] H. M. Marques, O. Q. Munro, B. M. Cumming, C. Denysschen, *J. Chem. Soc., Dalton Trans.* **1991**, 297.
[36] H. M. Marques, J. C. Bradley, K. L. Brown, H. Brooks, *J. Chem. Soc., Dalton Trans.* **1993**, 3475.
[37] N. E. Brasch, M. S. A. Hamza, R. van Eldik, *Inorg. Chem.* **1997**, *36*, 3216.
[38] W. H. Pailes, H. P. C. Hogenkamp, *Biochemistry* **1968**, *7*, 4160.
[39] [39a] R. van Eldik, A. E. Merbach, *Comments Inorg. Chem.* **1992**, *12*, 341. [39b] R. van Eldik, in *Perspectives in Coordination Chemistry* (Eds.: A. F. Williams, C. Floriani, A. E. Merbach), VCH, Weinheim, ***1992***, p. 55.
[40] S. Funahashi, M. Inamo, K. Ishihara, M. Tanaka, *Inorg. Chem.* **1982**, *21*, 447.

[41] J. G. Leipoldt, R. van Eldik, H. Kelm, *Inorg. Chem.* **1983**, *22*, 4146.
[42] H. E. Toma, J. M. Malin, E. Giesbrech, *Inorg. Chem.* **1973**, *12*, 2084.
[43] J. M. Malin, H. E. Toma, E. Giesbrech, *J. Chem. Educ.* **1977**, *54*, 385.
[44] W. Byers, J. A. Cossham, J. O. Edwards, A. T. Gordon; J. G. Jones, E. T. P. Kenny, A. Mahamed, J. McKnight, D. A. Sweigart, G. A. Tondreau, T. Wright, *Inorg. Chem.* **1986**, *25*, 4767.
[45] K. J. Schneider, R. van Eldik, *Organometallics* **1990**, *9*, 92.
[46] R. A. Henderson, K. E. Oglieve, *J. Chem. Soc., Chem. Commun.* **1994**, 1961.
[47] P. Kofod, P. Harris, S. Larsen, *Inorg. Chem.* **1997**, *36*, 2258.
[48] R. van Eldik, D. A. Palmer, R. Schmidt, H. Kelm, *Inorg. Chim. Acta* **1981**, *50*, 131.

Received September 7, 2001
[I01352]

Di- and Tetranuclear Dawson-Derived Sandwich Complexes: Synthesis, Spectroscopic Characterization, and Electrochemical Behavior

Laurent Ruhlmann,[a] Louis Nadjo,*[a] Jacqueline Canny,[b] Roland Contant,[b] and René Thouvenot*[b]

Keywords: Polyoxometalates / Sandwich complexes / Synthesis / NMR spectroscopy / Electrochemistry

The reaction of α-$[P_2W_{15}O_{56}]^{12-}$ with divalent cations M^{2+} leads to sandwich complexes of the formula $[M_4(H_2O)_2(P_2W_{15}O_{56})_2]^{16-}$ ($M_4P_4W_{30}$) where M = Mn^{II}, Co^{II}, Ni^{II}, Cu^{II}, Zn^{II}, or Cd^{II}. An Fe^{III} tetranuclear sandwich complex has also been obtained. Full details are reported concerning procedures by which the pure sandwich complexes can be obtained in good yield. A pure dinuclear trivalent Dawson-derived sandwich complex of the formula $[(H_2O)_2Na_2Fe^{III}_2(P_2W_{15}O_{56})_2]^{16-}$ has also been prepared as a water-soluble sodium salt. All the compounds have been characterized by IR spectroscopy, elemental analysis, and ^{31}P NMR spectrometry. The acid-base equilibria of the $M_4P_4W_{30}$ series have been studied. The electrochemical behavior of this series of sandwich complexes in aqueous solution has been investigated and systematic comparisons have been made. All these compounds exhibit successive reduction processes of the W atoms in a negative potential range, but in some cases the electrochemistry also involves redox reactions originating from the substituent transition metal (M), such as the reduction of Fe^{III} and Cu^{II} and the oxidation of Mn^{II}.
(© Wiley-VCH Verlag GmbH, 69451 Weinheim, Germany, 2002)

Introduction

The possibility of modifying the redox and chemical properties of heteropolyanions by replacing one or many elements renders them particularly attractive for catalytic and electrocatalytic applications.[1] For instance, a cluster such as $[P_2W_{18}O_{62}]^{6-}$ may be modified under hydrolytic conditions to give lacunary complexes containing one, three, or more vacant sites.[2] The action of metallic cations on the trivacant heteropoly ligand $[P_2W_{15}O_{56}]^{12-}$ (derived from the Dawson structure $[P_2W_{18}O_{62}]^{6-}$; Scheme 1) leads to metal-heteropolyanions that can be formulated as $[M_4(H_2O)_2(P_2W_{15}O_{56})_2]^{n-}$ (where M = Mn^{II}, Fe^{III}, Co^{II}, Ni^{II}, Cu^{II}, Zn^{II}, or Cd^{II}, and n = 16, except in the case of Fe^{III}, where n = 12). These constitute an extensive series of compounds in which a tetranuclear cluster $M_4O_{14}(H_2O)_2$ is encapsulated between two trivacant fragments.[3] Of the four metal atoms, two reside in a pseudooctahedral environment with one coordination site occupied by a labile water molecule, which can be replaced by other ligands.

This series of sandwich polyoxoanions with four d-electron transition metal cations appears quite promising as a potential class of catalysts because both the four central metal ions and, in principle, the heteroatoms in the trivacant polyoxoanions units can be varied considerably. Thus, they can be used in catalytic reactions as inorganic analogues of porphyrins with the advantage of being more robust and inert toward an oxidizing environment and more thermally stable than systems based on organic ligands.[4]

We report herein on a new route for the synthesis of a tetranuclear Co Dawson-derived sandwich complex as well as of a dinuclear Fe Dawson-derived sandwich complex[3i,3j] of the formula $[(H_2O)_2Na_2Fe_2(P_2W_{15}O_{56})_2]^{16-}$, which have been obtained when operating in acidic media.

We also present in the following a systematic spectroscopic investigation by ^{31}P NMR of the para- and diamagnetic sandwich complexes of the composition $[M_4(H_2O)_2(P_2W_{15}O_{56})_2]^{16-}$, as well as a study of their electrochemical behavior.

These sandwich complexes exhibit at least three consecutive processes involving oxo-tungsten based reduction in a negative potential range, but in some cases the electrochemistry also involves redox reactions originating from the substituent transition metal (M), such as the reduction of Fe^{III} and Cu^{II} and the oxidation of Mn^{II}.

Interestingly, for the compounds $[Fe_4(H_2O)_2P_4W_{30}O_{112}]^{12-}$ and $[(H_2O)_2Na_2Fe_2P_4W_{30}O_{112}]^{16-}$, the Fe-centered redox processes are fully reversible prior to reduction of the polyanions. Splitting of this wave is often seen.

[a] Laboratoire de Chimie Physique, Equipe d'Electrochimie et de Photoélectrochimie, UMR 8000, CNRS, Université Paris XI, Bâtiment 420,
91405 Orsay Cedex, France
E-mail: louis.nadjo@lcp.u-psud.fr
[b] Laboratoire de Chimie Inorganique et Matériaux Moléculaires, UMR 7071, CNRS, case courrier 42, Université Pierre et Marie Curie,
4, place Jussieu, 75252 Paris Cedex 05, France
E-mail: rth@ccr.jussieu.fr
Supporting information for this article is available on the WWW under http://www.eurjic.com or from the author.

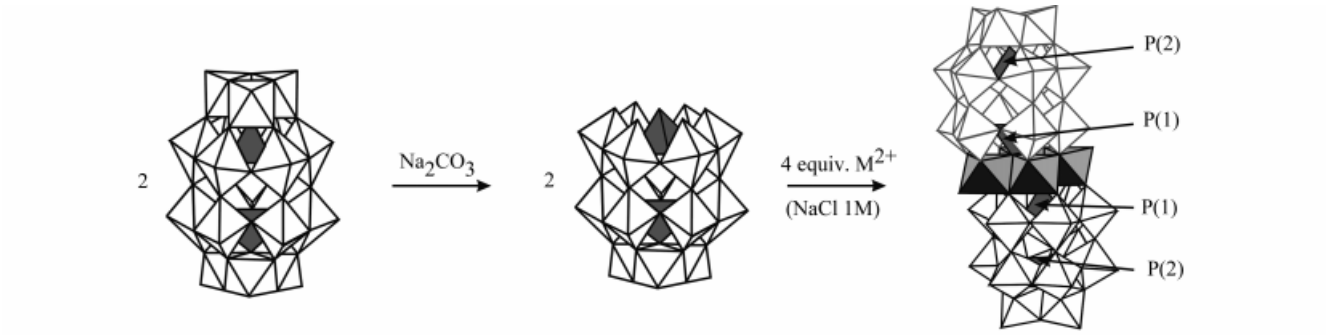

Scheme 1

Intriguingly, the Fe^{III}/Fe^{II} couples in $[(H_2O)_2Na_2Fe_2P_4W_{30}O_{112}]^{16-}$ ($Fe_2P_4W_{30}$) were found to be pH dependent; this is rather unusual for Fe-centered redox processes, for which the redox potential is usually almost pH-independent at low pH.[5] Assuming that $Fe_2P_4W_{30}$ has the molecular structure recently reported by Hill et al.,[3i,3j] with the two external sites of the sandwich structure occupied by Na^+ cations, the unusual pH dependence can be tentatively explained in terms of a stepwise exchange of the Na^+ cations by H^+ during the consecutive reduction of the two Fe^{III} centers.

To the best of our knowledge, such a complete investigation of Dawson sandwich species has not been published previously.

Results and Discussion

Synthesis

The first objective of this work was the large-scale, high-yielding preparation of very pure tetranuclear sandwich complexes of the composition $[M_4(H_2O)_2(P_2W_{15}O_{56})_2]^{16-}$. This polyanion consists of an oxo-aqua tetranuclear metal core, $M_4O_{14}(H_2O)_2$, sandwiched by two trivacant α-Dawson moieties, α-$[P_2W_{15}O_{56}]^{12-}$. The polyanion has C_{2h} symmetry (see Scheme 1).

Key factors in the strategy that led to the results described below included: (i) use of the pure lacunary precursor α-$[P_2W_{15}O_{56}]^{12-}$, (ii) extensive use of ^{31}P NMR spectroscopy to survey different conditions in optimizing the route to pure $[M_4(H_2O)_2(P_2W_{15}O_{56})_2]^{16-}$ products, (iii) careful control of the solution pH, and (iv) control of the stoichiometry of M^{n+} vs. α-$[P_2W_{15}O_{56}]^{12-}$ in order to obtain pure compounds.

The complexes were readily prepared in ca. 50−90% isolated yields and in high purity. The best preparation is similar to that cited in the literature for sandwich polytungstophosphate complexes $[M_4(H_2O)_2(P_2W_{15}O_{56})_2]^{16-}$, where M = Mn^{II}, Zn^{II}, or Cd^{II}.

However, to obtain pure $[Co_4(H_2O)_2(P_2W_{15}O_{56})_2]^{16-}$ it is necessary to operate in an acidic medium. Actually, as is evident from Figure 1, which shows the ^{31}P NMR spectra of $Co_4P_4W_{30}$ prepared by the literature method (neutral medium) and at ca. pH 3, the best preparation of pure $Co_4P_4W_{30}$ is undoubtedly achieved at pH 3. From the ^{31}P analysis, it appears that the preparation in neutral media, as described in the literature, invariably gives a mixture of several species, and that two different types of crystals, one green-brown and the other gray, are deposited from such solutions on crystallization. In contrast, the synthesis in acidic solution (ca. pH 3) leads exclusively to one major species as green-brown crystals with a purity of 95% (A in Figure 1).

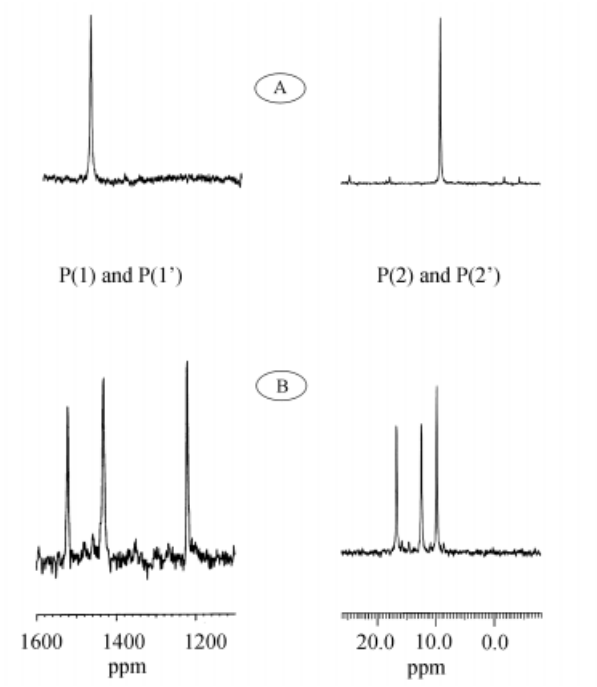

Figure 1. 121.5 MHz ^{31}P NMR spectra of $Co_4P_4W_{30}$ (0.02 M in 0.5 M aqueous LiCl): (A) sample prepared at pH 3; (B) sample prepared in neutral medium; left part: P(1) region; experimental conditions: spectral width 125 kHz; pulse width 2 μs (ca. 40° flip angle); 8K data points; acquisition time 33 ms; ca. 10K transients acquired without relaxation delay; line-broadening factor 40 Hz; right part: P(2) region; experimental conditions: spectral width 9 kHz; pulse width 2 μs (ca. 40° flip angle); 4K data points; acquisition time 0.23 s; ca. 1000 transients acquired without relaxation delay; line-broadening factor 4 Hz

The ^{31}P NMR spectrum of the mixture obtained following the synthesis in a neutral medium exhibits three "pairs"

Table 1. ^{31}P NMR data for α-P_2W_{15} and the sandwich species

Compound[a] δ≅[c]	P(1)[b] Δν[d]	δ[c]	P(2)[b] Δν[d]	
α-P_2W_{15}	+0.5	< 3	−13.8	< 3
$Mn_4P_4W_{30}$	[e]	130	−12.3	130
$Fe_2P_4W_{30}$	[e]	–	−11.2	220
$Fe_4P_4W_{30}$	+915	2500	−11.7	55
sym-$Co_4P_4W_{30}$	+1483	420	+9.9	20
sym-$Co_4P_4W_{30}$ [f]	+1459	420	+9.8	20
disym-$Co_4P_4W_{30}$ [f]	+1551	420	+16.7	20
	+1242	420	+12.3	20
sym-$Co_4P_4W_{30}$ [g]	+1473	1400	+8.8	25
disym-$Co_4P_4W_{30}$ [g]	+1590	1250	+16.7	30
	+1201	950	+10.1	40
$Ni_4P_4W_{30}$	+460	3400	−14.2	15
$Cu_4P_4W_{30}$	[e]	–	−16.2	60
$Zn_4P_4W_{30}$	−3.92	< 3	−13.95	< 3
$Cd_4P_4W_{30}$	−3.60	< 5	−14.36	< 3

[a] Unless otherwise noted, 0.02 M solution in 0.5 M LiCl. [b] P(1) and P(2) in the PW_6 and PW_9 subunits, respectively. [c] In ppm with respect to 85% H_3PO_4. [d] In Hz. [e] Not observed. [f] In a mixture as obtained from the synthesis medium (see text). [g] As for f, but in 0.1 M AcONa/AcOH buffer (pH 4.7).

of resonances (see Table 1 and B in Figure 1). The pair at δ = 1459 and 9.8 correspond to the two resonances of the pure $Co_4P_4W_{30}$ synthesized at pH 1 (see A in Figure 1). The four other signals will be considered below.

In more acidic solution (0.1 M AcONa/AcOH buffer), the ^{31}P NMR spectrum evolves by a concomitant decrease in the four resonances (at δ = 1590, 1201, 16.7, and 10.1). After one day, only the two peaks at δ = 1473 and 8.8 remain, which are characteristic of the pure $Co_4P_4W_{30}$ compound.

The chemical shift variations observed between neutral and acidic solutions can be attributed to deprotonation of the aqua ligands in neutral media (see below).

Because they disappear simultaneously at the expense of the $Co_4P_4W_{30}$ signals, the four resonances (at δ = 1590, 1201, 16.7, and 10.1) are most probably due to a single species, which contains four non-equivalent P atoms and should be structurally related to the symmetrical sandwich compound $Co_4P_4W_{30}$ (C_{2h}). Two unsymmetrical structural isomers of $Co_4P_4W_{30}$, both of C_s symmetry, can be considered, resulting from either (i) the formal π/3 rotation of the polar cap of one P_2W_{15} moiety, leading to a β-P_2W_{15} subunit (see Scheme 1) or (ii) the formal rotation of a whole α-P_2W_{15} subunit leading to both α-type and β-type junctions at the Co_4 tetrad.

Thus, in neutral solution, the synthesis of the Dawson sandwich species gives a mixture of symmetrical (δ = 1459 and 9.8) and unsymmetrical (δ = 1551, 1242, 16.7 and 12.3) complexes in relative proportions of 38 and 62% (by integration of the NMR resonances).

In acidic solution, only the symmetrical isomer is formed, which suggests that this isomer is the thermodynamic product obtained at pH 3 and that slow transformation occurs on decreasing the pH. Finke et al.[3b] described a similar behavior for $[Zn_4(H_2O)_2P_4W_{30}O_{112}]^{16-}$, where thermal isomerization was observed with the appearance of additional ^{31}P resonances. On the other hand, the temperature is not a factor in the present isomerization since the same temperature is used for the syntheses in acidic and neutral solutions. This result may suggest a control of the isomerization by the pH of the medium.

Di- and tetrairon sandwich polyoxoanions were prepared in 67% and 52% isolated yields, respectively, using essentially the same procedure. Actually, powdered α-$Na_{12}[P_2W_{15}O_{56}]$ dissolves readily at room temperature in an aqueous solution of iron(III) chloride (pH 3) without the formation of any insoluble intermediate. However, the optimal synthetic conditions were found when operating in more acidic media (pH 1) at high temperature (80 °C) and under vigorous stirring. With only one equivalent of α-P_2W_{15} added to the iron(III) solution, i.e. with one equivalent of Fe^{3+}, the diiron sandwich complex is obtained and can be isolated in high purity.

Conversely, with a stoichiometry of one equivalent of α-P_2W_{15} to two equivalents of Fe^{3+}, only the tetrairon sandwich compound is obtained as a pure species. This suggests an equilibrium between the di- and tetrairon sandwich polyoxoanions [Equation (1)]:

$$(H_2O)_2Na_2Fe^{III}_2(P_2W_{15}O_{56})_2^{16-} + 2\,Fe^{3+} \rightleftarrows Fe^{III}_4(H_2O)_2(P_2W_{15}O_{56})_2^{12-} + 2\,Na^+ \quad (1)$$

Accordingly, the "unsaturated" diiron species must be formed first and exists predominantly at low Fe^{3+}/α-P_2W_{15} ratios. It is converted to the "saturated" tetrairon species in the presence of an excess of iron.

IR Characterization

The IR spectrum of $Zn_4P_4W_{30}$ is shown Figure 2 and is compared with those of the parent anions α-P_2W_{15} and α-P_2W_{18}.

Apart from the W−O bands, which appear at low wavenumbers (< 1000 cm^{-1}), the IR spectra of phosphorus-centered polyoxotungstates are characterized by well-separated P−O stretching vibrations between 1200 and 1000 cm^{-1}.[6]

According to the local symmetry of the PO_4 group, the triply-degenerate mode F_2 (for T_d symmetry) may split into two or three absorption bands for C_{3v} or C_s symmetry, respectively; the splitting depends on the deviation from ideal symmetry. Hence, for the lacunary anions $[PMo_{11}]$ and $[PW_{11}]$, and for the substituted metallophosphates $[PMMo_{11}]$ and $[PMW_{11}]$ (M = first row transition metal), it was shown that the splitting Δν decreases when the metal M interacts more strongly with the oxygen atom of the PO_4 tetrahedron.[7] For lacunary or substituted unsymmetrical Dawson species, the situation is more intricate due to the overlap of vibrational absorption bands arising from two different PO_4 tetrahedra; in favorable cases, however, it is possible to discriminate between the bands arising from the unperturbed subunit PW_9 and those arising from the PW_xM_y moiety.[8] For example, α-P_2W_{15}, like α-P_2W_{18}, ex-

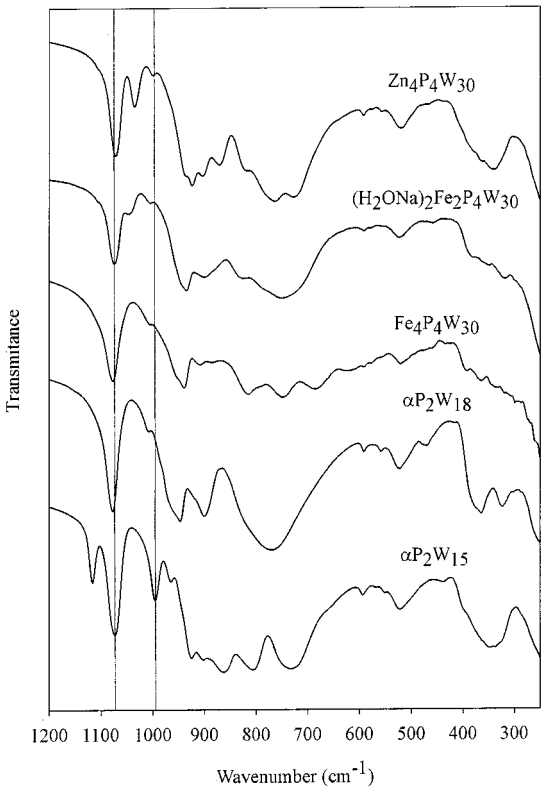

Figure 2. Comparison of the IR spectra (KBr) of the hydrated sandwich compounds $Zn_4P_4W_{30}$, $Fe_2P_4W_{30}$, $Fe_4P_4W_{30}$, and of their precursors

hibits two bands at around 1080 and 1010 cm^{-1} (assigned to PW_9), as well as an additional band at high wavenumbers (1131 cm^{-1}), which can be attributed to the PW_6 subunit. The corresponding vibrational mode may be described as a stretching of the $P-O_{ter}$ bond along the ternary axis (A_1-type in the C_{3v} point group) and the relatively high frequency is related to the large force constant of this bond, which has some P=O double bond character. This band is not observed for the sandwich compounds $M_4P_4W_{30}$, in agreement with the fact that the oxygen atom has contracted bonds with some M atoms, which results in a decrease of the k_{P-O} force constant. Actually, it appears that the band associated with the PW_6 subunit is correspondingly shifted to low wavenumbers and all of the tetrametallic sandwich compounds, except for $Fe_4P_4W_{30}$, exhibit a band at about 1055 cm^{-1}. The IR spectra of the Mn, Co, Ni, Cu, Zn, and Cd derivatives are nearly identical, which indicates a structural similarity throughout the whole $M_4P_4W_{30}$ series. Finally, we note that terminal W−O and bridging W−O−W stretching bands are located in the range 970−700 cm^{-1}, at lower wavenumbers than for the parent saturated α-P_2W_{18} anion.

Let us return to the case of the iron compounds: in the phosphate stretching region, the IR spectrum of $Fe_4P_4W_{30}$ exhibits the same pattern as that of P_2W_{18}, and no band is present at around 1060 cm^{-1} (Figure 2). This indicates that both PO_4 groups in the PW_6 and PW_9 moieties are becoming nearly equivalent, most probably because of the stronger M−O interaction exerted by the trivalent Fe^{3+} ions as compared with those of the divalent Mn^{2+}, Co^{2+}, Ni^{2+}, Cu^{2+}, Zn^{2+}, and Cd^{2+} cations. For $[Fe_2P_4W_{30}]$, however, only two iron atoms may interact with the oxygen atom of the phosphate, which is insufficient to restore the equivalence of the two PO_4 groups belonging to the two subunits; this accounts for the presence of the small absorption band at almost the same wavenumber as seen for the $M_4^{II}P_4W_{30}$ species.

^{31}P NMR Characterization

^{31}P NMR spectroscopy is particularly well-suited for checking the purities of polyoxometallate species and for characterizing the nature of the substituting elements. The ^{31}P NMR spectroscopic data for the sandwich complexes $[M_4(H_2O)_2(P_2W_{15}O_{56})_2]^{16-}$ (M = Mn^{2+}, Co^{2+}, Ni^{2+}, Cu^{2+}, Zn^{2+}, and Cd^{2+}), $[Fe_4^{III}(H_2O)_2(P_2W_{15}O_{56})_2]^{12-}$ and $[(H_2O)_2Na_2Fe_2^{III}(P_2W_{15}O_{56})_2]^{16-}$ ($Fe_2P_4W_{30}$), and their parent compounds are reported in Table 1. The ^{31}P NMR spectra of the diamagnetic species $Cd_4P_4W_{30}$ and $Zn_4P_4W_{30}$ show two lines, consistent with the presence of a single isomer (Figure 3); the most shielded line, at about $\delta = -14$, is assigned to P(2) of the PW_9 unit. The deshielded line, at about $\delta = -4$, corresponds to P(1) in the PW_6M_3 unit; its integrated intensity appears smaller than that of P(2) because of a slow relaxation rate (large T_1).

In comparison with the diamagnetic complexes, the spectra of the paramagnetic compounds are characterized by broad signals and large frequency shifts. For paramagnetic species, the signals can be assigned according to the following rule: the most broadened and shifted resonances correspond to the atoms nearest to the paramagnetic centers. Then, for each sandwich compound, the sharper line, with a chemical shift close to those seen for diamagnetic metallophosphates (between $\delta = +20$ and $\delta = -20$) is assigned to P(2), the P atom furthest from the M^{n+} ions. The P(1) atom, which is very close to the paramagnetic elements, is responsible for the broad and strongly deshielded resonances. For $Ni_4P_4W_{30}$, the broadening of the P(1) signal makes the line difficult to discern accurately from base-line artifacts. Figures 1, 3, and 4 show typical ^{31}P NMR spectra of $M_4P_4W_{30}$ and $Fe_2P_4W_{30}$ Dawson sandwich complexes.

For the series of sandwich complexes, the observed line widths, $\Delta\nu_{1/2}$, for the P(1) resonance are as follows: for the diamagnetic Zn^{2+} and Cd^{2+} complexes the signal is very narrow ($\Delta\nu_{1/2} < 5$ Hz); for Co^{2+} complexes it is relatively narrow ($\Delta\nu_{1/2} = 420$ Hz), while for tetrametallic Fe^{3+} and Ni^{2+} complexes it is very broad ($\Delta\nu_{1/2} = 2500$ Hz and 3400 Hz, respectively). In the case of Cu^{2+} and Mn^{2+}, as well as for the diiron species, the signals from P(1) are probably too broad to be observed. As a consequence, the spectra of these complexes feature only one resonance, corresponding to the P(2) atom.

The same trend in line width is also observed for the P(2) signal (the P atom furthest from the M^{n+} ions). The line width $\Delta\nu_{1/2}$ for P(2) varies as follows: for the diamagnetic Zn^{2+} and Cd^{2+} complexes the signal is very narrow ($\Delta\nu_{1/2} < 3$ Hz), it remains relatively narrow for Co^{2+} and Ni^{2+} (in

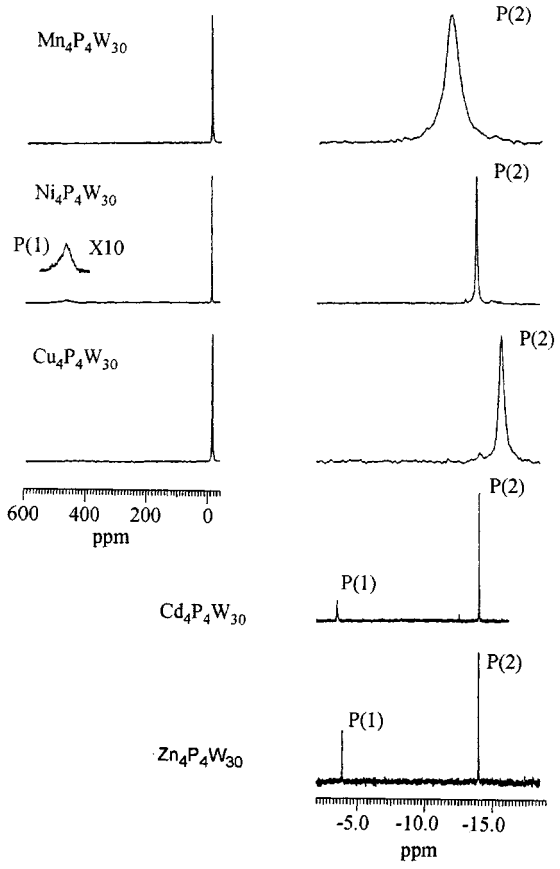

Figure 3. 121.5 MHz ^{31}P NMR spectra of various $M_4P_4W_{30}$ species (0.02 M in 0.5 M aqueous LiCl); experimental conditions for the left part: spectral width 166 kHz; pulse width 2 μs (ca. 40° flip angle); 4K data points; acquisition time 13 ms; ca. 70K transients acquired without relaxation delay; line-broadening factor 80 Hz; experimental conditions for the right part: $Cd_4P_4W_{30}$ and $Zn_4P_4W_{30}$: spectral width 2.5 kHz; 8K data points; acquisition time 1.6 s; ca. 300 transients acquired without relaxation delay; line-broadening factor 0.6 Hz; $Mn_4P_4W_{30}$, $Ni_4P_4W_{30}$, and $Cu_4P_4W_{30}$: spectral width 6 kHz; 4K data points; acquisition time 0.3 s; ca. 2000 transients acquired without relaxation delay; line-broadening factor 20 Hz (Mn), 3 Hz (Ni), and 10 Hz (Cu)

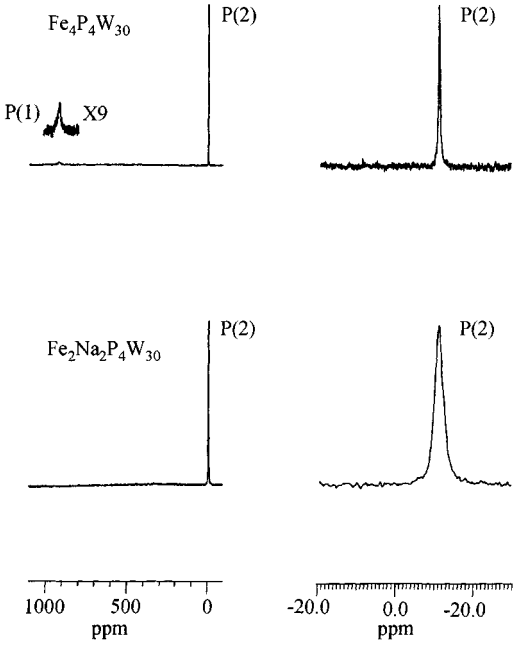

Figure 4. 121.5 MHz ^{31}P NMR spectra of $Fe_4P_4W_{30}$ and $Na_2Fe_2P_4W_{30}$ (0.02 M in 0.5 M aqueous LiCl); experimental conditions for the left part: spectral width 166 kHz; pulse width 2 μs (ca. 40° flip angle); 4K data points; acquisition time 13 ms; ca. 70K transients acquired without relaxation delay; line-broadening factor 80 Hz; experimental conditions for the right part: spectral width 10 kHz; 4K data points; acquisition time 0.2 s; ca. 3000 transients acquired without relaxation delay; line-broadening factor 10 Hz ($Fe_4P_4W_{30}$) and 10 Hz ($Na_2Fe_2P_4W_{30}$)

the range 15−20 Hz), but is markedly broadened for Mn^{2+} ($\Delta\nu_{1/2}$ = 130 Hz) and for the diiron species ($\Delta\nu_{1/2}$ = 220 Hz). For Cu^{2+} and for the tetrairon species, the signal is of intermediate width ($\Delta\nu_{1/2}$ = 60 Hz and 55 Hz, respectively).

A similar variation in ^{31}P line width has previously been observed by Baker et al. for Keggin and Dawson monosubstituted polytungstates.[9] Baker noted that complexes containing paramagnetic ions with orbitally nondegenerate ground states (i.e. Mn^{2+}, $^6A_{1g}$) are those giving very broad ^{31}P signals. Orbitally nondegenerate states have long electronic relaxation times, which lead to very fast nuclear relaxation of the nearby nuclei (short T_1 and T_2). Therefore, in accordance with the relationship $\Delta\nu_{1/2} = 1/\pi T_2$, the NMR resonances are very broad. On the contrary, for orbitally degenerate ground states, such as Co^{2+} ($^4T_{1g}$), the fast electronic relaxation rate leads to relatively slow nuclear relaxation, which explains the relatively narrow NMR lines.[9]

pK_a Determination

In the sandwich compounds, the sixth coordination position of the external metal atoms is occupied by a labile water molecule. According to the pH, this aqua ligand can be easily deprotonated, successively giving the hydroxo-aqua and the dihydroxo forms [Equations (2) and (3)].

$$M_4^{II}(H_2O)_2P_4W_{30}O_{112}^{16-} + H_2O \rightleftarrows M_4^{II}(H_2O)(OH)P_4W_{30}O_{112}^{17-} + H_3O^+ \quad pKa_1 \tag{2}$$

$$M_4^{II}(H_2O)(OH)\,P_4W_{30}O_{112}^{17-} + H_2O \rightleftarrows M_4^{II}(OH)_2P_4W_{30}O_{112}^{18-} + H_3O^+ \quad pKa_2 \tag{3}$$

The dihydroxo forms of the M^{II} sandwich complexes were obtained directly from their syntheses in neutral solutions, except in the case of the Co^{II} species. For the titration, the hydroxo-aqua form of $Co_4P_4W_{30}$, as obtained from the synthesis at ca. pH 3, was initially converted to its dihydroxo form by adding a stoichiometric amount of NaOH.

Acidification curves of the dihydroxo complexes do not depend on the concentration and show the successive protonation of the two hydroxo groups. Actually, the diacid character of the sandwich complex could be confirmed by a pH jump in the presence of two equivalents of HNO_3.

The titration curves are characteristic of diacid behavior where pK_{a1} and pK_{a2} are close.

K_{a1} and K_{a2} were calculated from experimental points using the following relationship (A):

$$[H_3O^+] = \frac{-(1-x)Ka_1 + \sqrt{Ka_1^2(1-x)2 + 4xKa_1Ka_2(2-x)}}{2(2-x)} \quad (A)$$

where x is the number of mol of HNO_3 per mol of complex. The values of pK_{a1} and pK_{a2} are reported in Table 2.

Table 2. Acidity constants for the sandwich species $M_4P_4W_{30}$ and $Fe_2P_4W_{30}$

Compound	pK_{a1}	pK_{a2}
$Mn_4P_4W_{30}$	3.5 ± 0.1	5.3 ± 0.1
$Fe_4P_4W_{30}$	3.6 ± 0.1	5.6 ± 0.1
$Fe_2P_4W_{30}$	3.6 ± 0.1	5.6 ± 0.1
$Co_4P_4W_{30}$	3.5 ± 0.1	5.3 ± 0.1
$Ni_4P_4W_{30}$	—[a]	—[a]
$Cu_4P_4W_{30}$	3.2 ± 0.1	5.0 ± 0.1
$Zn_4P_4W_{30}$	3.2 ± 0.1	5.2 ± 0.1
$Cd_4P_4W_{30}$	3.6 ± 0.1	5.4 ± 0.1

[a] Degradation occurred during the titration.

In the case of iron(III) complexes, as their syntheses were conducted in acidic solutions, they were obtained as diaqua species. Therefore, their acidity constants were determined from the titration of their diaqua forms with NaOH. This corresponds to the successive deprotonation of the two aqua ligands. pK_{a1} and pK_{a2} were obtained by analysis of the basification curves using the following relationship (B):

$$[H_3O^+] = \frac{(1-x)Ka_1 + \sqrt{Ka_1^2(1-x)2 + 4xKa_1Ka_2(2-x)}}{2x} \quad (B)$$

where x is the number of mol of NaOH per mol of complex.

Electrochemistry

General Electrochemical Behavior

The electrochemical behavior of sandwich complexes of the composition $[M_4(H_2O)_2(P_2W_{15}O_{56})_2]^{16-}$ ($M_4P_4W_{30}$) was mainly studied in aqueous solutions by cyclic voltammetry (CV). $M_4P_4W_{30}$ complexes are stable in aqueous media in the pH range 1−6 (with the exception of the $Ni_4P_4W_{30}$ sandwich, for which slow degradation was observed during the titration).

Beyond this pH range, the complexes become unstable due to hydrolytic decomposition.

These sandwich complexes exhibit at least three successive processes involving W in a negative potential range. Some of them also undergo redox reactions originating from the substituent transition metal (M), such as the reduction of Fe^{III} and Cu^{II} at less negative potentials and the oxidation of Mn^{II} at a more positive potential. In general, the reduction of heteropolyanions is accompanied by protonation at low pH, and hence the pH of the solution has a great effect on the electrochemical behavior of the sandwich. For the three couples corresponding to oxo W-based reduction, the cathodic peak currents are almost proportional to the square root of the scan rate up to 500 mV s^{-1}, which indicates that the electrode reaction of $M_4P_4W_{30}$ is diffusion controlled.

All electrochemical data acquired at pH 2.52 are gathered in Table 3 and typical cyclic voltammograms are presented in Figures 5−9.

$M_4P_4W_{30}$ Complexes with Electrochemically Silent Heterometallic Ions, M = Co^{2+}, Ni^{2+}, Zn^{2+}, Cd^{2+}

The electrochemical behavior of all $M_4P_4W_{30}$ complexes with M = Co^{2+}, Ni^{2+}, Zn^{2+}, or Cd^{2+} is very similar. Therefore, only the characteristics of the Co compound will be described in detail. CVs of $Co_4P_4W_{30}$ in aqueous solutions at pH 2.52 are presented in Figure 5. $Co_4P_4W_{30}$ is stable in aqueous solution in the pH range 1−6. At pH > 6, the cyclic voltammogram becomes ill-defined and the peak current is much smaller; such an observation has previously been reported by Dong et al. in relation to Keggin-type polyoxometallates;[10] this behavior may be due to a repulsion of the 18^- charge of $Co_4P_4W_{30}$ at the glassy carbon electrode surface.

In the pH range 1−6, three well-defined redox waves originating from the oxo-tungsten framework are seen between −0.30 and −0.95 V. These three redox couples with equal heights all relate to four-electron reaction processes, as determined by coulometry. At more acidic pH (in the range 1−3), the redox potentials of the three four-electron waves become more negative; the first and the last four-electron waves for M = Co^{2+} or Ni^{2+} split into two two-electron waves (see B in Figure 5). Thus, in the pH range 1−3, the formal potentials of all three pairs of waves are pH dependent; the slopes of plots of the formal potentials vs. pH lie in the range 80−95 mV per pH unit, which indicates the addition of two or four H^+ ions to the reduced form of each redox couple. Above pH 3, the formal potentials for the two first redox couples are influenced by pH to a lesser degree, and they are shifted only slightly to more negative values with increasing pH. On the contrary, the formal potential of the third redox process is shifted slightly in the positive direction at pH > 3. These results show that H^+ does not participate in the redox reaction at pH > 3.

In addition, a fourth reduction wave is observed in the more negative range, between −1.00 and −1.20 V. It is an irreversible multi-electron wave that overlaps with the hydrogen evolution, and is not shown in the figure. In the more positive potential range between +1.60 and −0.30 V, however, no redox waves are observed, suggesting that the four sandwich complexes with Co, Ni, Zn, and Cd divalent

Table 3. Electrochemical data for the sandwich species $M_4P_4W_{30}$ and $Fe_2P_4W_{30}$

Compound[a]	W(1)	W(2)	W(3)	$Fe^{III/II}$	$Mn^{IV/II}$	$Mn^{IV/III}$	$Mn^{III/II}$	Cu(ox)	Cu(red)
$Mn_4P_4W_{30}$	−0.404 (4e)	−0.533 (4e)	−0.733 (4e)	−	1.000 (8e)	0.800 (4e)	0.004 (4e)	−	−
$Fe_4P_4W_{30}$	−0.352 (2e)	−0.517 (4e)	−0.735 (4e)	0.187 (1e)	−	−	−	−	−
	−0.403 (2e)			0.110 (1e)					
				−0.028 (2e)					
$Fe_2P_4W_{30}$	−0.350 (2e)	−0.530 (4e)	−0.755 (4e)	−0.060 (1e)	−	−	−	−	−
	−0.407 (2e)			−0.164 (1e)					
$Co_4P_4W_{30}$	−0.354 (2e)	−0.534 (4e)	−0.788 (2e)	−	−	−	−	−	−
	−0.416 (2e)		−0.837 (2e)						
$Ni_4P_4W_{30}$	−0.366 (4e)	−0.472 (4e)	−0.755 (4e)	−	−	−	−	−	−
$Cu_4P_4W_{30}$	−0.295[b]	−	−	−	−	−	−	$E_{pa} = -0.004$	$E_{pc} = -0.150$
	−0.353[b]								
$Zn_4P_4W_{30}$	−0.358 (4e)	−0.583 (4e)	−0.748 (4e)	−	−	−	−	−	−
$Cd_4P_4W_{30}$	−0.400 (4e)	−0.703 (4e)	−0.779 (4e)	−	−	−	−	−	−
αP_2W_{15}	−0.590 (4e)[c]	−0.812 (2e)[c]							
	−0.52 (4e)[d]	−0.78 (2e)[d]							

[a] All redox potentials $E^{\circ\prime}$, approximated by $(E_{pa} + E_{pc})/2$ for the reversible steps, are given in V vs. SCE as obtained from cyclic voltammetry ($v = 20\ mV\ s^{-1}$) in 0.5 M $Na_2SO_4 + H_2SO_4$ (pH 2.52). [b] Irreversible. [c] In 0.1 M acetic acid/lithium acetate buffer, GC electrode. [d] In 1 M acetic acid/lithium acetate buffer, Hg electrode.

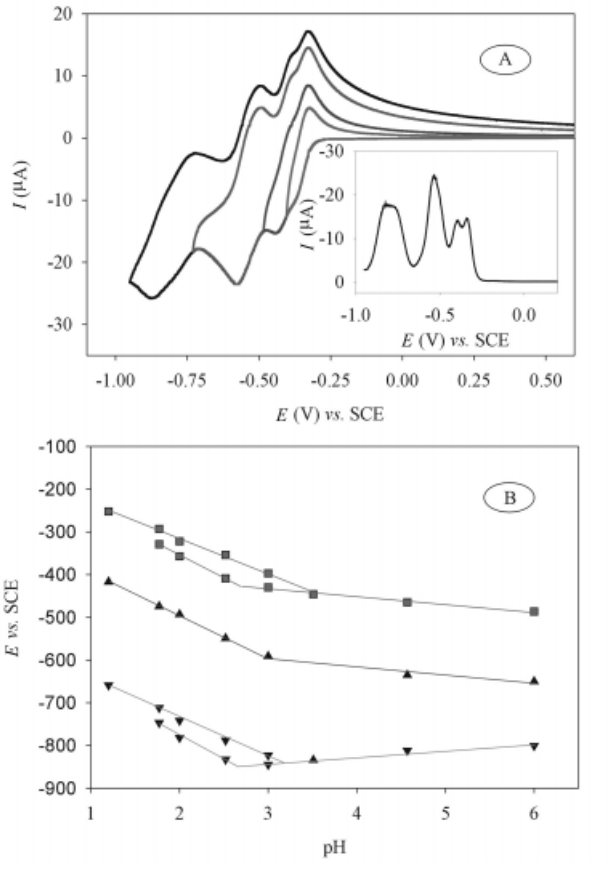

Figure 5. (A) Cyclic voltammograms of 1 mM $Co_4P_4W_{30}$ in 0.5 M $Na_2SO_4 + H_2SO_4$ at pH 2.52 with different negative potential limits: −0.30 V, −0.45 V, −0.70 V, and −0.90 V; scan rate 20 mV s^{-1}; inset: differential pulse voltammetry; scan rate 25 mV s^{-1}; (B) half-wave potential vs. pH plots for the first (■), second (▲), and third tungsten redox couples (▼)

transition metal cations are not electroactive under our experimental conditions.

$Fe_2P_4W_{30}$ and $M_4P_4W_{30}$ Complexes with Electroactive Substituent Metals, M = Mn^{2+}, Cu^{2+}, Fe^{3+}

$[Mn_4(H_2O)_2(P_2W_{15}O_{56})_2]^{16-}$ ($Mn_4P_4W_{30}$): CVs of the compound ($Mn_4P_4W_{30}$) at pH 2.52 are shown in Figure 6.

Three couples of oxo-tungsten based reduction processes can be seen at negative potentials in Figure 6, close to those of other $M_4P_4W_{30}$ species (M = Co, Ni, Zn, and Cd). The fourth reduction wave is a multi-electron wave that overlaps with the hydrogen evolution and is not shown in the figure. A new pair of redox process is observed at positive potentials of 1.00 V for oxidation and 0.80 V for reduction, which must correspond to the Mn-centered reaction (see B in Figure 6).[11] Controlled-potential electrolysis oxidation at +1.20 V (pH 2.52) resulted in the passage of 8.2 electrons per molecular anion, whereas subsequent reduction at +0.60 V consumes 4.2 electrons. These results show that the Mn-centered anodic peak corresponds to an eight-electron process, which suggests simultaneous oxidation of the four Mn^{II} heterometals to Mn^{IV} at +1.00 V and reduction of Mn^{IV} to Mn^{III} at 0.80 V. When the pH is increased, the peak potentials of both W- and Mn-centered redox waves of $Mn_4P_4W_{30}$ shift in the negative direction, indicating that they are all accompanied by protonation. Additionally, a new cathodic peak appears at −0.08 V.

Figure 6 (A) shows that the appearance of the new cathodic peak is closely related to the Mn oxidation state. This new cathodic peak appears in the CVs only after the Mn-centered redox wave. It can be seen that as the preconditioning time at +1.00 V increases, the new cathodic peak at −0.08 V grows gradually, the peak current of the first Mn-centered reduction at 0.80 V increases simultaneously, while the W-based peak currents remain unchanged.

Similar results have also been obtained for α_2-MnP_2W_{17} and $ZnW_{11}Mn$ polyanions.[10] The present results suggest the oxidation of Mn^{II} to Mn^{IV} at ca. 1.00 V followed by the

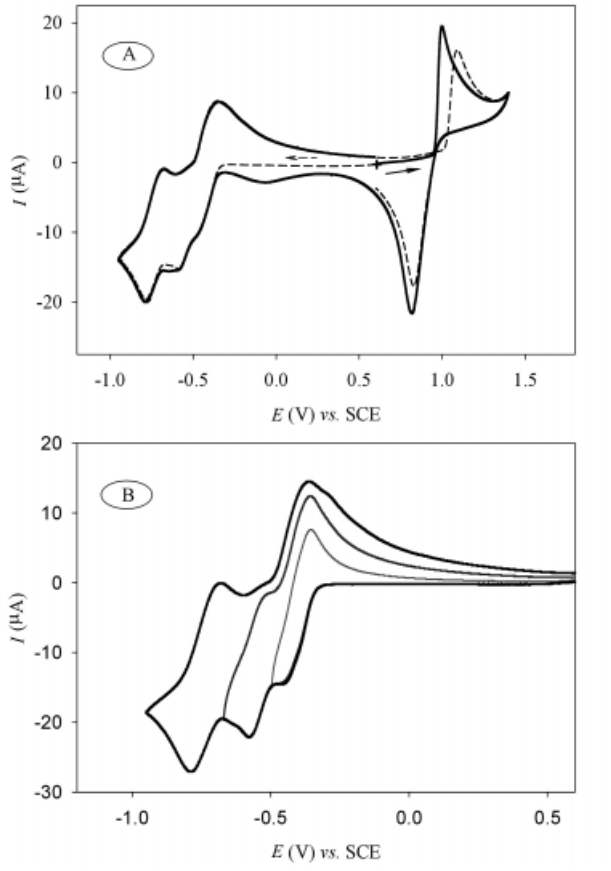

Figure 6. (A) Cyclic voltammograms of 1 mM $Mn_4P_4W_{30}$ in 0.5 M Na_2SO_4 + H_2SO_4 at pH 2.52; scan rate 10 mV s^{-1}; the arrows indicate the sweep direction; (B) cyclic voltammograms of 1 mM $Mn_4P_4W_{30}$ in 0.5 M Na_2SO_4 + H_2SO_4 at pH 2.52 with different negative potential limits: −0.45 V, −0.65 V, and −0.95 V; scan rate 10 mV s^{-1}

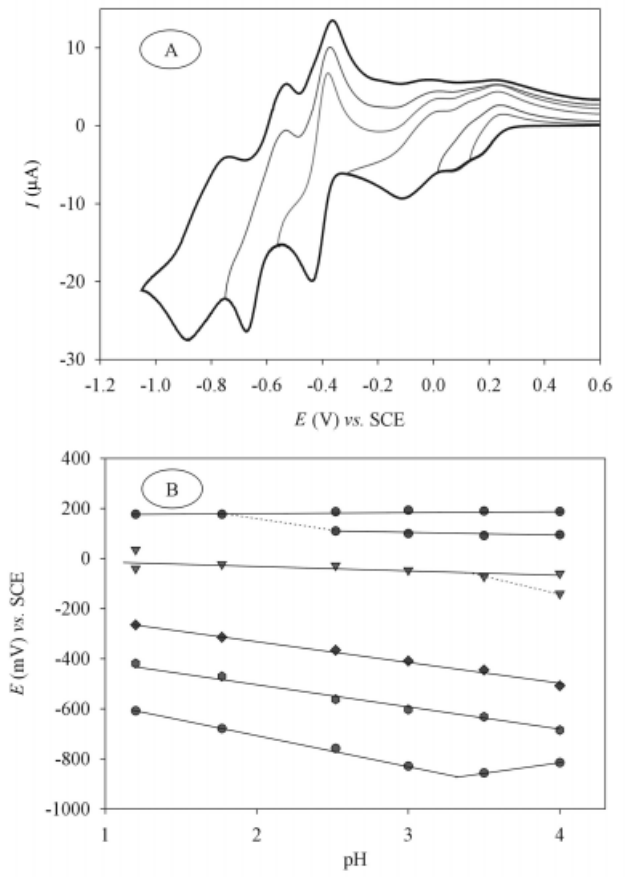

Figure 7. (A) Cyclic voltammograms of 1 mM $Fe_4P_4W_{30}$ in 0.5 M Na_2SO_4 + H_2SO_4 at pH 2.52 with different negative potential limits: −0.13 V, −0.30 V, −0.39 V, −0.47 V, −0.69 V, and −0.95 V; scan rate 20 mV s^{-1}; inset: differential pulse voltammetry; scan rate 25 mV s^{-1}; (B) half-wave potential vs. pH plots for the $Fe^{III/II}$ redox couples (● and ▼) and the first (◆), second (■), and third tungsten redox couples (●)

reduction of Mn^{IV} to Mn^{III} at ca. 0.80 V and reduction of Mn^{III} to Mn^{II} at ca. −0.08 V on the reverse scan.

$[Fe_4^{III}(H_2O)_2(P_2W_{15}O_{56})_2]^{12-}$ ($Fe_4P_4W_{30}$): This species is stable in aqueous solution in the pH range 0.24−6.0, but at pH > 4 the cyclic voltammogram becomes ill-defined and the peak current is much smaller. No redox process is seen between 0.30 and 1.60 V; on the cathodic part, three or (depending on the pH) four $Fe^{III/II}$ reduction waves and three W reduction waves are observed. The positions of these three tungsten oxo reduction waves were studied as a function of pH; the formal potentials were found to shift by 87−95 mV per pH unit, which indicates the addition of one or two protons to the reduced forms of each redox couple.

In contrast, the three Fe-centered waves are almost pH independent. These results show that H^+ does not participate in the Fe-centered redox reaction in the pH range 0.24−6.00. At pH 2.52, two reversible one-electron and one reversible two-electron waves appear (Figure 7) with $E^{\circ\prime}$ values of +0.187 V, +0.110 V, and −0.028 V (ΔE_p = 74, 68, and 112 mV, respectively). Controlled potential electrolysis at −0.20 V in a medium at pH 2.52 and under continuous argon bubbling indicated the involvement of 4.10 electrons per molecule.

The reduction processes of $Fe_4P_4W_{30}$ can be represented as follows [Equations (4)−(6)].

$$[Fe_4^{III}(H_2O)_2(P_2W_{15}O_{56})_2]^{12-} + e^- \leftrightharpoons [Fe_3^{III}Fe^{II}(H_2O)_2(P_2W_{15}O_{56})_2]^{13-} \quad (4)$$

$$[Fe_3^{III}Fe^{II}(H_2O)_2(P_2W_{15}O_{56})_2]^{13-} + e^- \leftrightharpoons [Fe_2^{III}Fe_2^{II}(H_2O)_2(P_2W_{15}O_{56})_2]^{14-} \quad (5)$$

$$[Fe_2^{III}Fe_2^{II}(H_2O)_2(P_2W_{15}O_{56})_2]^{14-} + 2e^- \leftrightharpoons [Fe_4^{II}(H_2O)_2(P_2W_{15}O_{56})_2]^{16-} \text{ (at pH} < 3.5) \quad (6)$$

$[(H_2O)_2Na_2Fe_2(P_2W_{15}O_{56})_2]^{16-}$ ($Fe_2P_4W_{30}$): This species is stable in aqueous solution in the pH range 0.24−7.00. As shown in Figure 8, at pH 2.52 it also exhibits three four-electron waves at negative potentials close to those of $M_4P_4W_{30}$ (M = Co, Ni, Zn, and Cd). The positions of these three tungsten oxo reduction waves were found to be pH dependent. The slopes of plots of the formal potential vs. pH vary in the range 55−80 mV per pH unit. This is indicative of the addition of four protons to the reduced forms of each redox couple.

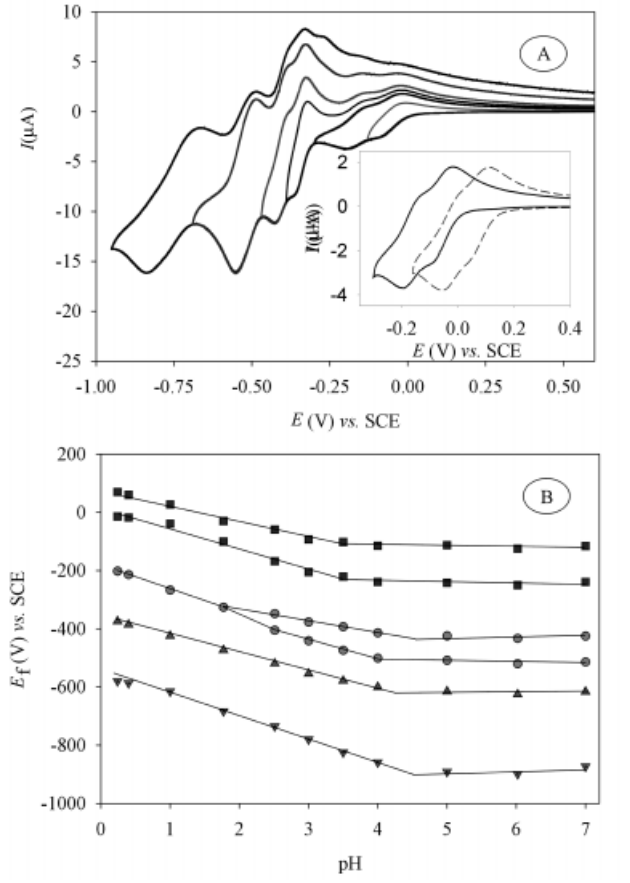

Figure 8. (A) Cyclic voltammograms of 1 mM $Na_2Fe_2P_4W_{30}$ in 0.5 M Na_2SO_4 + H_2SO_4 at pH 2.52 with different negative potential limits: −0.13 V, −0.30 V, −0.39 V, −0.47 V, −0.69 V, and −0.95 V; scan rate 20 mV s^{-1}; (B) half-wave potential vs. pH plots for the $Fe^{III/II}$ redox couples (■), and the first (●), second (▲), and third tungsten redox couples (▼); inset: the voltammograms are restricted to the first waves of the cathodic patterns, which corresponds to the $Fe^{III/II}$ couples; solid line: pH 2.52; dotted line: pH 0.24

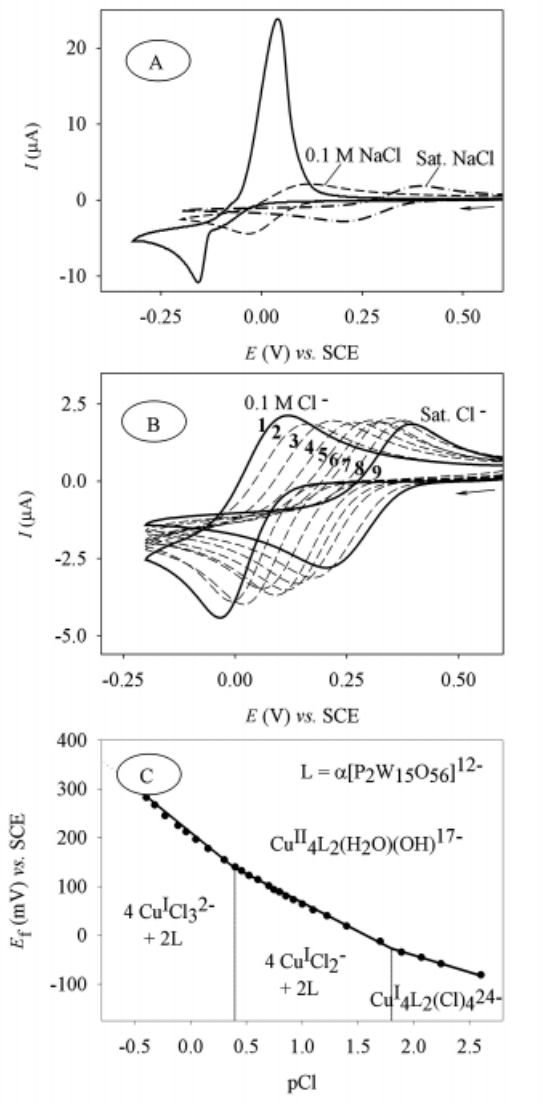

Figure 9. (A) Cyclic voltammograms of 1 mM $Cu_4P_4W_{30}$ in 0.5 M Na_2SO_4 + H_2SO_4 at pH 4.57; scan rate 20 mV s^{-1}; (1) without NaCl (—), (2) in the presence of 0.1 M NaCl (----), and (3) in the presence of saturated NaCl (-.-); (B) evolution of the voltammograms (Cu-centered reduction, Cu^{II}/Cu^{I}) with increasing chloride ion concentration: **1**. 0.1 M NaCl; **2**. 0.2 M NaCl; **3**. 0.4 M NaCl; **4**. 0.8 M NaCl; **5**. 1.2 M NaCl; **6**. 1.6 M NaCl; **7**. 2.0 M NaCl; **8**. 2.8 M NaCl; **9**. saturated solution of NaCl; scan rate 20 mV s^{-1}; pH 4.57; (C) plot of $E_f = (E_{pa} + E_{pc})/2$ vs. pCl (scan rate 20 mV s^{-1}, pH 4.57)

As for $Mn_4P_4W_{30}$, other redox processes can be identified at more positive potentials: at pH 2.52, two reversible one-electron waves are observed at −0.060 V and −0.164 V (ΔE_p = 66 and 68 mV, respectively). Controlled-potential coulometry at −0.245 V in a medium at pH 2.52 and under continuous argon bubbling and stirring consumes 2.10 electrons per molecule, consistent with the reduction of the two Fe^{III} cations.

These waves must thus be attributed to the successive reduction of both Fe^{3+} cations.[12] The couple Fe^{III}/Fe^{II} in $Fe_2P_4W_{30}$ remains fully reversible in the pH range 0.24−7.00, as shown in the inset of Figure 9 and the *E* vs. pH diagram (B in Figure 8). The stability of $Fe_2P_4W_{30}$ was checked by comparison of the CVs obtained immediately after the preparation of the solution and after it had been set aside for at least 4 hours. No variation in current intensities or in the potentials of the different waves was observed; this reproducibility was considered as a sufficient test of the stability of $Fe_2P_4W_{30}$ complexes in these media. The peak currents for the tungsten-based reduction waves and the metal-based reduction waves were seen to vary linearly with the square root of the scan rate up to 500 mV s^{-1} at pH 2.52, which indicates that the electrode reaction is a diffusion-controlled process.

At more acidic pH, i.e. in the pH range 0.24−3.50, Fe-centered redox waves show a negative shift, indicating that they are all accompanied by protonation. It could be shown that the variations in the potentials were of the order of 50−55 mV per pH unit (B in Figure 8), which corresponds to the exchange of one proton.

This result is rather unusual in the case of the Fe-centered redox processes, for which, at low pH, the redox potential is generally almost pH independent.[12c,13]

Assuming that $Fe_2P_4W_{30}$ has the molecular structure recently reported by Hill et al.,[3i,3j] with the two external sites of the sandwich structure occupied by Na^+ cations, the unusual pH dependence can be tentatively explained as follows [Equation (7)−(8)].

At pH < 3.50:

$$[(H_2O)_2Na_2Fe^{III}_2(P_2W_{15}O_{56})_2]^{16-} + e^- + H^+ \leftrightarrows [(H_2ONa)(H_3O)Fe^{III}Fe^{II}(P_2W_{15}O_{56})_2]^{17-} + Na^+ \quad (7)$$

$$[(H_2ONa)(H_3O)Fe^{III}Fe^{II}(P_2W_{15}O_{56})_2]^{17-} + e^- + H^+ \leftrightarrows [(H_3O)_2Fe^{II}_2(P_2W_{15}O_{56})_2]^{18-} + Na^+ \quad (8)$$

$[Cu_4(OH)_2(P_2W_{15}O_{56})_2]^{18-}$ ($Cu_4P_4W_{30}$): Figure 9 shows CVs of 1 mM $Cu_4P_4W_{30}$ at pH 4.57. An irreversible broad peak is observed at −0.15 V, along with an unusual sharp redox anodic peak at about 0.04 V. Similar results have been reported elsewhere for Dawson-type α_2-$P_2W_{17}Cu$ and $ZnW_{11}Cu$.[10]

The sharp anodic peak current increases with the preconditioning time at −0.20 V vs. SCE and with the scan rate. This redox wave is assigned to reduction and oxidation of the transition metal Cu. It is reasonable to expect that both the Cu^{II} and Cu^{I} cations within $Cu_4P_4W_{30}$ will be destabilized by the six-coordinate geometry imposed by the polyoxometallate framework, favoring reduction to Cu^0. In fact, upon reduction, deposition of metallic Cu is observed on the glassy carbon electrode surface, which demonstrates the irreversible dissociation of the complex into α-P_2W_{15}. The anodic peak at 0.04 V should correspond to the reoxidation of Cu^0 to Cu^{2+}. The α-P_2W_{15} anion is not stable in this medium and therefore further decomposition occurs. This accounts for the fact that the W-based waves are irreversible and ill-defined.

Addition of chloride ions to the solution leads to dramatic changes in the electrochemical behavior of $Cu_4P_4W_{30}$, as shown in Figure 9 (B,C). The irreversible cathodic peak at −0.15 V becomes reversible. As this wave, corresponding to copper reduction, is well-separated from the tungsten waves, it is reasonable to assume that this redox process is associated with a $Cu^{II}/Cu^{I}(Cl)_n^{(n-1)}$ couple. The redox potential becomes more negative on increasing the chloride ion concentration. Figure 9 (C) shows a plot of the formal potential vs. pCl. The slopes amount to 64 mV per pCl unit above pCl = 1.8, 121 mV per pCl unit between 1.8 and 0.4, and 177 mV for pCl < 0.4. These results suggest that the Cu-centered reaction mechanism in presence of chloride can be described by Equations (9)−(11).

$$[Cu^{II}_4(H_2O)(OH)(P_2W_{15}O_{56})_2]^{17-} + 4e^- + 4\,Cl^- \leftrightarrows [Cu^{I}_4Cl_4(P_2W_{15}O_{56})_2]^{24-} + OH^- + H_2O\,E_1^{0'}$$
$$[Cu^{I}_4Cl_4(P_2W_{15}O_{56})_2]^{24-} \leftrightarrows 4Cu^{I}Cl(s) + 2\,\alpha\text{-}[P_2W_{15}O_{56}]^{12-} \quad (9)$$

$$[Cu^{II}_4(H_2O)(OH)(P_2W_{15}O_{56})_2]^{17-} + 4e^- + 8\,Cl^- \leftrightarrows 4Cu^{I}Cl_2^- + 2\,\alpha\text{-}[P_2W_{15}O_{56}]^{12-} + OH^- + H_2O\,E_2^{0'} \quad (10)$$

$$[Cu^{II}_4(H_2O)(OH)(P_2W_{15}O_{56})_2]^{17-} + 4e^- + 12\,Cl^- \leftrightarrows 4Cu^{I}Cl_3^{2-} + 2\,\alpha\text{-}[P_2W_{15}O_{56}]^{12-} + OH^- + H_2O\,E_3^{0'} \quad (11)$$

The six-coordinate geometry imposed by the polyoxoanion framework might favor the extraction of the stable $Cu^{I}Cl_n^{(n-1)}$ complex, where n = 1, 2, or 3.

Apparent standard potentials can be calculated from the E_f vs. pCl plot: $E_1^{0'}$ = −0.217 V, $E_2^{0'}$ = −0.109 V, and $E_3^{0'}$ = −0.086 V.

Summary and Concluding Remarks

It is well-known from the literature that the reaction of α-$[P_2W_{15}O_{56}]^{12-}$ with divalent cations M^{2+} leads to sandwich complexes of the general formula $[M_4(H_2O)_2(P_2W_{15}O_{56})_2]^{16-}$ ($M_4P_4W_{30}$). However, in the case of the Fe^{III} and Co^{II} complexes, preparations according to the literature methods, that is in neutral media, invariably give a mixture of several species. In contrast, we have shown that performing the synthesis at low pH leads exclusively to one major isomer with high purity.

The electrochemical behavior of the $M_4P_4W_{30}$ compounds has been investigated systematically at various pH values. All the compounds exhibit three couples due to W-centered reduction processes with slightly different peak potentials from one complex to the next. Two types of sandwich complexes can be distinguished:

(i) For those with Co^{II}, Ni^{II}, Zn^{II}, and Cd^{II}, the metallic centers are electrochemically silent in the potential domains explored in this work.

(ii) For those with Mn^{II}, Fe^{III}, and Cu^{II}, redox reactions originating at the metals M are seen.

The Mn^{II} complex shows an oxidation and two reduction processes, which correspond to oxidation of Mn^{II} to Mn^{IV}, followed, in the reverse scan, by the reduction of Mn^{IV} to Mn^{III} and reduction of Mn^{III} to Mn^{II}. The compound $Cu_4P_4W_{30}$ exhibits a deposition process accompanied by decomposition of the copper complex. Extraction of the copper(I) complexes $Cu^{I}Cl_n^{(n-1)}$ (n = 1−3) can also be observed upon reduction of the polyoxoanions in the presence of chloride ions.

Finally, the compounds $[Fe_4(H_2O)_2(P_2W_{15}O_{56})_2]^{12-}$ and $[(H_2O)_2Na_2Fe_2(P_2W_{15}O_{56})_2]^{16-}$ both exhibit Fe-centered redox processes prior to reductions of the polyanions. Splitting of this wave often occurs.

This series of sandwich polyoxoanion complexes would appear to be quite promising in relation to electrocatalytic reactions; in particular, the Mn^{II} sandwich complex is a potential candidate for both oxidative and reductive catalysis. $[(H_2O)_2Na_2Fe_2(P_2W_{15}O_{56})_2]^{16-}$ also appears to be quite promising and may find application in the preparation of pure mixed sandwich complexes of the type $[M^{II}_2Fe^{III}_2(H_2O)_2(P_2W_{15}O_{56})_2]^{14-}$.

Electrocatalytic processes of this type, both in aqueous solution and in organic media, and the preparation of new $[M^{II}_2Fe^{III}_2(H_2O)_2(P_2W_{15}O_{56})_2]^{14-}$ complexes are currently under investigation.

Experimental Section

General: Most common laboratory chemicals were reagent grade, as purchased from commercial sources, and were used without further purification.

Preparation of the Compounds: The potassium salt of α-$[P_2W_{18}O_{62}]^{6-}$ and the sodium salt of α-$[P_2W_{15}O_{56}]^{12-}$ were prepared by published methods.[2] An extensive series of tetranuclear divalent Dawson-derived sandwich complexes of the formula $[M_4(H_2O)_2(P_2W_{15}O_{56})_2]^{16-}$ (where M = Mn^{II}, Ni^{II}, Zn^{II}, Cd^{II}) were prepared as described elsewhere.[3] All samples were recrystallized as described in the original procedures and were characterized by IR spectroscopy and ^{31}P NMR spectrometry.

$Na_{16}[(H_2O)_2Na_2Fe_2(P_2W_{15}O_{56})_2]\cdot 53H_2O\cdot 4NaCl$: $FeCl_3\cdot 6H_2O$ (0.34 g, 1.25 mmol) was dissolved in 1 M aq. NaCl/0.1 M aq. HCl (pH 1) (50 mL) with stirring. α-$Na_{12}P_2W_{15}O_{56}\cdot 24H_2O$ (5.00 g, 1.13 mmol) was then added under vigorous stirring. The solution was heated at 80 °C until the volume had been reduced to ca. 12.5 mL. It was then filtered hot and the filtrate was left to stand in air. After evaporation of the solvent, 1 M aq. NaCl (5 mL) was added with stirring. A yellow solid was precipitated, which was collected by filtration and dried in air; yield 3.49 g (0.38 mmol; 67%). $Cl_4Fe_2Na_{22}O_{112}P_4W_{30}\cdot 55H_2O$: calcd. Fe 1.22, P 1.35, W 60.08, H_2O 10.79; found Fe 1.24, P 1.35, W 59.89, H_2O 10.76.

The purity of the compound was checked by ^{31}P NMR in D_2O, which showed a single resonance [P(2)] at δ = −11.2 ($\Delta\nu_{1/2}$ = 220 Hz). The signal of the phosphorus atom nearest to the paramagnetic Fe^{III} ions [P(1)] was not observed.

$Na_{11}H[Fe^{III}_4(H_2O)_2(P_2W_{15}O_{56})_2]\cdot 45H_2O$: This complex was prepared as follows by a modification of the literature method:[3i] $FeCl_3\cdot 6H_2O$ (0.82 g, 3.01 mmol) was dissolved in 1 M NaCl/0.1 M HCl (pH ≈ 1) (40 mL) with stirring. α-$Na_{12}P_2W_{15}O_{56}\cdot 24H_2O$ (6.00 g, 1.36 mmol) was then slowly added under vigorous stirring. The solution was heated at 80 °C until the volume had been reduced to ca. 12.5 mL. It was then filtered hot and the filtrate was left to stand in air. After evaporation of the solvent, 1 M aq. NaCl (5 mL) was added with stirring. A yellow solid precipitated, which was collected by filtration, dried in air, and recrystallized from 2 M aq. NaCl; yield: 3.09 g (0.35 mmol; 52%). $Fe_4Na_{11}HO_{112}P_4W_{30}\cdot 47H_2O$: calcd. Fe 2.55, P 1.41, W 63.00, H_2O 9.67; found Fe 2.69, P 1.38, W 62.98, H_2O 9.78.

The purity of the compound was checked by ^{31}P NMR, which showed two resonances at δ = −11.7 [P(2); $\Delta\nu_{1/2}$ = 55 Hz] and δ = +915 [P(1); $\Delta\nu_{1/2}$ = 2500 Hz].

$Na_{17}[Co_4(H_2O)(OH)(P_2W_{15}O_{56})_2]\cdot 51H_2O\cdot 2NaCl$: $Co(NO_3)_2\cdot 6H_2O$ (0.73 g, 2.25 mmol) was dissolved in 1 M aq. NaCl/0.1 M aq. HCl (50 mL) with stirring. α-$Na_{12}P_2W_{15}O_{56}\cdot 24H_2O$ (5.00 g, 1.13 mmol) was then slowly added under vigorous stirring. The solution was heated at 40 °C for 15 min (pH 3), then filtered hot and the filtrate was left to stand in air. After evaporation of the solvent, 1 M aq. NaCl (5 mL) was added with stirring. A pale green-brown solid was precipitated, which was collected by filtration and dried in air; yield 3.99 g (0.44 mmol, 78%). $Cl_2Co_4Na_{18}P_4W_{30}O_{112}\cdot OH\cdot 52H_2O$: calcd. Co 2.59, P 1.35, W 60.34, H_2O 10.87; found Co 2.77, P 1.30, W 60.10, H_2O 11.16.

The purity of the compound was checked by ^{31}P NMR, which showed two resonances at δ = 9.9 [P(2); $\Delta\nu_{1/2}$ = 20 Hz] and δ = 1483 [P(1); $\Delta\nu_{1/2}$ = 420 Hz].

$Na_{16}Cu[Cu_4(OH)_2(P_2W_{15}O_{56})_2]\cdot 53H_2O$: This complex was prepared, as follows, by a method slightly different from that reported elsewhere:[3c] $CuCl_2$ (0.35 g, 2.50 mmol) was dissolved in 1 M aq. NaCl (50 mL) with stirring. α-$Na_{12}P_2W_{15}O_{56}\cdot 24H_2O$ (5.00 g, 1.13 mmol) was then slowly added under vigorous stirring. The solution was heated at 40 °C until the P_2W_{15} had completely dissolved. It was then filtered hot and the filtrate was left to stand in air for one day at room temperature and then cooled to 5 °C. Pale-green crystals were deposited after two days, which were collected by filtration and dried in air; yield (3.20 g, 0.35 mmol, 62%). $Cu_5Na_{12}O_{112}P_4W_{30}\cdot 2(OH)\cdot 53H_2O$: calcd. Cu 3.52, P 1.37, W 60.87, H_2O 10.58; found Cu 3.43, P 1.37, W 60.88, H_2O 10.26.

The purity of the compound was checked by ^{31}P NMR, which showed a single resonance at δ = −16.2 ($\Delta\nu_{1/2}$ = 60 Hz). This line was assigned to P(2), the more distant P atom from the Cu^{II} center. The signal from the phosphorus atom designated P(1) nearest to the paramagnetic Cu^{II} ions was not observed.

NMR, IR, and Potentiometric Measurements: ^{31}P NMR spectra were recorded from sample solutions in 5 mm o.d. tubes on a Bruker AC 300 spectrometer operating at 121.5 MHz in Fourier-transform mode (equipped with a QNP probe for ^{31}P NMR). The ^{31}P chemical shifts were measured at 300 K using 0.02 M solutions of the polyanions in 0.5 M aqueous LiCl (50% D_2O) solutions and were referenced to external 85% H_3PO_4 (IUPAC convention) by the substitution method.

IR spectra were recorded on a Bio-Rad FTS 165 FTIR spectrophotometer from samples in KBr pellets.

Potentiometric measurements were made on a Tacussel PHN330T pH meter. Constant ionic strength (μ = 0.1 M, $NaNO_3$) was used in the titrations. In potentiometric titrations, the dilution was less than 2%.

Electrochemical Experiments

Chemicals, Equipment, and Apparatus: Pure water was used throughout. It was obtained by passing water through a Milli-RO_4 unit and subsequently through a Millipore Q water purification set. H_2SO_4 and Na_2SO_4 were commercial products (Prolabo). The pH 2 electrolyte was made up from 0.5 M Na_2SO_4 and the pH was adjusted by the addition of 0.5 M (H_2SO_4 + Na_2SO_4). Other pHs were obtained by the addition of H_2SO_4 or NaOH (Prolabo) as appropriate. The solutions were thoroughly deaerated for at least 30 min by bubbling pure argon and were kept under argon pressure during the experiments.

The source, mounting, and polishing of glassy carbon (GC, Tokai, Japan) have been described previously.[14] The glassy carbon samples for use as electrodes had a diameter of 3 mm. The electrochemical set-up consisted of an EG&G 273 A potentiostat driven by a personal computer with 270 software. Potentials are quoted with respect to a saturated calomel electrode (SCE). The counter-electrode was a platinum gauze of large surface area. All voltammetric experiments were carried out at room temperature.

Analyses: Elemental analyses were performed by classical gravimetric, potentiometric, and spectrophotometric methods.

The anions were first decomposed in boiling concentrated hydrochloric acid solution. Tungsten and phosphorus were then precipitated together by adding cinchonium hydrochloride. They were determined simultaneously as WO_3 and P_2O_5 by gravimetry after calcination of the cinchonium salt. Cobalt, which remained in the filtrate, was complexed with ammonia and then titrated as hexacyanocobaltate(III) complex by potentiometry. Phosphorus was determined by spectroscopy of the molybdovanadophosphate.[15] Water content was determined by thermogravimetric analysis. The other metallic elements (Fe, Cu) were analyzed by atomic absorption spectroscopy.

Supporting Information (see footnote on the first page of this article): Comparison of the IR spectra (KBr) of the hydrated sandwich heteropolyanion series.

Acknowledgments

This work was supported by the CNRS and by the Universities Paris XI and Paris VI. We are also grateful to Martine Richet for performing the microanalyses.

[1] [1a] B. Keita, L. Nadjo, R. Contant, M. Fournier, G. Hervé, French Patent (CNRS) 8911, 728; February 10, **1989**. [1b] B. Keita, L. Nadjo, R. Contant, M. Fournier, G. Hervé, Eu. Patent (CNRS), Appl. EP 382,644; *Chem. Abstr.* **1991**, *114*, 191882u. [1c] B. Keita, A. Belhouari, L. Nadjo, R. Contant, *J. Electroanal. Chem.* **1995**, *181*, 243−250. [1d] M. Abbessi, R. Contant, R. Thouvenot, G. Hervé, *Inorg. Chem.* **1991**, *30*, 1695−1702. [1e] B. Keita, K. Eassadi, L. Nadjo, R. Contant, Y. Justun, *J. Electroanal. Chem.* **1996**, *404*, 271−279. [1f] J. F. Garvey, M. T. Pope, *Inorg. Chem.* **1978**, *17*, 1115−1118. [1g] B. Keita, Y. W. Lu, L. Nadjo, R. Contant, M. Abbessi, J. Canny, M. Richet, *J. Electroanal. Chem.* **1999**, *477*, 146−157.

[2] [2a] J.-P. Ciabrini, R. Contant, J.-M. Fruchart, *Polyhedron* **1983**, *2*, 1229−1233. [2b] R. Contant, J.-P. Ciabrini, *J. Chem. Res.* **1977**, (S) 222, (M) 2601−2609. [2c]R. Contant, *Inorg. Synth.* **1990**, *27*, 104−109.

[3] [3a] R. G. Finke, M. W. Droege, *Inorg. Chem.* **1983**, *22*, 1006−1008. [3b] R. G. Finke, M. W. Droege, P. J. Domaille, *Inorg. Chem.* **1987**, *26*, 3886−3896. [3c] T. J. R. Weakley, R. G. Finke, *Inorg. Chem.* **1990**, *29*, 1235−1241. [3d] J.-P. Ciabrini, R. Contant, *J. Chem. Res.* **1993**, *(S) 391*, (M) 2719−2744. [3e] C. J. Gómez-García, J. J. Borrás-Almenar, E. Coronado, L. Ouahab, *Inorg. Chem.* **1994**, *33*, 4016−4022. [3f] R. G. Finke, T. J. R. Weakley, *J. Chem. Cryst.* **1994**, *24*, 123−128. [3g] J. F. Kirby, L. C. W. Baker, *J. Am. Chem. Soc.* **1995**, *117*, 10010−10016. [3h] N. J. Crano, R. C. Chambers, V. M. Lunch, M. A. Fox, *J. Mol. Cat. A: Chem.* **1996**, *114*, 65−75. [3i] X. Zhang, D. C. Duncan, C. F. Campana, C. L. Hill, *Inorg. Chem.* **1997**, *36*, 4208−4215. [3j] X. Zhang, T. M. Anderson, Q. Chen, C. L. Hill, *Inorg. Chem.* **2001**, *40*, 418−419. [3k] A. Müller, F. Peter, M. Pope, D. Gatteschi, *Chem. Rev.* **1998**, *98*, 239−271. [3l] L. Meng, J. F. Liu, *Chem. Res. in Chinese Universities* **1998**, *14*, 1−5. [3m] X. Zhang, C. L. Hill, *Chem. Ind.* **1998**, *75*, 519−524.

[4] [4a] L. C. W. Baker, *Plenary Lecture, Proc. XV Int. Conf. Coord. Chem. 15th*, Moscow, **1973**. [4b] D. K. Lyon, W. K. Miller, T. Novet, P. J. Domaille, E. Evitt, D. C. Johnson, R. G. Finke, *J. Am. Chem. Soc.* **1991**, *113*, 7209−7221.

[5] R. Contant, M. Abbessi, J. Canny, A. Belhouari, B. Keita, L. Nadjo, *Inorg. Chem.* **1997**, *36*, 4961−4967.

[6] C. Rocchiccioli-Deltcheff, R. Thouvenot, R. Franck, *Spectrochim. Acta* **1976**, *22A*, 587−597.

[7] C. Rocchiccioli-Deltcheff, R. Thouvenot, *J. Chem. Res.* **1977**, (S) *46−47*, (M) 549−571.

[8] C. Rocchiccioli-Deltcheff, R. Thouvenot, *Spectrosc. Lett.* **1979**, *12*, 127−138.

[9] T. L. Jorris, M. Kozik, N. Casañ-Pastor, P. J. Domaille, R. G. Finke, W. K. Miller, L. C. W. Baker, *J. Am. Chem. Soc.* **1987**, *109*, 7402−7408.

[10] [10a] L. Cheng, H. Seen, J. Liu, S. Dong, *J. Chem. Soc., Dalton Trans.* **1999**, 2619−2625. [10b] B. Keita, E. Abdeljalil, L. Nadjo, B. Avisse, R. Contant, J. Canny, M. Richet, *Electrochem. Commun.* **2000**, *2*, 145−149.

[11] [11a] D. E. Katsoulis, M. T. Pope, *J. Chem. Soc., Dalton Trans.* **1989**, 1483−1489. [11b] C. L. Hill, R. B. Brown, *J. Am. Chem. Soc.* **1986**, *108*, 536−538. [11c] D. Mansuy, J. F. Bartoli, D. K. Lyon, R. C. Finke, *J. Am. Chem. Soc.* **1991**, *113*, 7222−7226. [11d] C. M. Tourné, G. F. Tourné, S. M. Malik, T. J. R. Weakley, *J. Inorg. Nucl. Chem.* **1970**, *32*, 3875−3890. [11e] X. Y. Zhang, M. T. Pope, M. R. Chance, G. B. Jameson, *Polyhedron* **1995**, *14*, 1381−1392. [11f] X. Y. Zhang, G. B. Jameson, C. J. O'Connor, M. T. Pope, *Polyhedron* **1996**, *15*, 917−922. [11g] X. Y. Zhang, C. J. O'Connor, G. B. Jameson, M. T. Pope, *Inorg. Chem.* **1996**, *35*, 30−34. [11h] M. Sadakane, E. Steckhan, *J. Mol. Catal. A.* **1996**, *114*, 221−228. [11i] A. Muller, L. Dloczik, E. Diemann, M. T. Pope, *Inorg. Chim. Acta* **1997**, *257*, 231.

[12] [12a] S. Dong, M. J. Liu, *J. Electroanal. Chem.* **1994**, *372*, 95−100. [12b] B. Fabre, G. Bidan, M. Lapkowski, *J. Chem. Soc., Faraday Trans.* **1997**, 591−601. [12c] T. McCormac, B. Fabre, G. Bidan, *J. Electroanal. Chem. Interfacial Electrochem.* **1997**, *425*, 49−54. [12d] T. McCormac, B. Fabre, G. Bidan, *J. Electroanal. Chem. Interfacial Electrochem.* **1997**, *427*, 155−159. [12e] J. E. Toth, F. C. Anson, *J. Electroanal. Chem. Interfacial Electrochem.* **1988**, *256*, 361−370. [12f] J. E. Toth, F. C. Anson, *J. Am. Chem. Soc.* **1989**, *111*, 2444−2451. [12g] J. E. Toth, J. D. Melton, D. Cabelli, B. H. J. Bielski, F. C. Anson, *Inorg. Chem.* **1990**, *29*, 1952−1957. [12h] K. K. Shiu, F. C. Anson, *J. Electroanal. Chem. Interfacial Electrochem.* **1991**, *309*, 115−119.

[13] B. Keita, A. Belhouari, L. Nadjo, R. Contant, *J. Electroanal. Chem.* **1998**, *442*, 49−57.

[14] B. Keita, K. Essaadi, L. Nadjo, *J. Electroanal. Chem. Interfacial. Electrochem.* **1989**, *259*, 127−146.

[15] B. Cherreton, F. Chauveau, G. Bertho, P. Courtin, *Chim. Anal.* **1965**, *47*, 17.

Received August 13, 2001
[I01305]

A New Cu^{I} Complex that Mimics the Cresolase Reaction of Tyrosinase and the Crystal Structure of its Oxygenated Cu^{II} Complex

Vieri Fusi,*[a] Antoni Llobet,*[b] José Mahía,[c] Mauro Micheloni,[a] Paola Paoli,[d] Xavi Ribas,[b] and Patrizia Rossi[d]

Keywords: Bioinorganic chemistry / Copper / Macrocyclic ligands / O-O activation / Tyrosinase

A new dinuclear Cu^{II} complex with a unique structural arrangement and containing a doubly bridged macrocyclic ligand has been prepared from two different routes, one of which involves the reaction of oxygen and a Cu^{I} precursor, thus mimicking the cresolase activity of tyrosinase

Introduction

The synthesis, structural elucidation and characterization of the reactivity of copper-dioxygen compounds obtained from the interaction of molecular oxygen with Cu^{I} complexes is an important goal in the comprehension of the fundamental chemistry involved in oxidase and oxygenase reactions of synthetic and biological copper-containing catalysts.[1] Within this context, tyrosinase is a monooxygenase enzyme with a binuclear copper active-site and is responsible for the *ortho* hydroxylation of the existing hydroxyl group of substrates as shown in Equation (1).[2–5]

$$\text{R-Ph-OH} \xrightarrow[O_2]{\text{tyrosinase}} \text{R-Ph-(OH)}_2 \qquad (1)$$

A number of xylene-substituted ligands, including amines[6–11] and imines,[12,13] have been used to prepare binuclear Cu^{I} complexes that successfully mimic this reaction. The ligand influence in the modelling of such reactions is of great importance in order to elucidate the detailed pathways that can lead to the activation of the Cu complex towards the oxidation of C–H bonds, and therefore has implications in the understanding of metalloenzymes and other catalysts.[14,15]

[a] Institute of Chemical Sciences, University of Urbino
Piazza Rinascimento 4, 61029 Urbino, Italy
Fax: (internat.) +39-0722/350-032
E-mail: vieri@chim.uniurb.it
[b] Departament de Química, Universitat de Girona
Campus de Montilivi, 17071, Girona, Spain
Fax: (internat.) +34-972/418-150
E-mail: antoni.llobet@udg.es
[c] Servicios Xerais de Apoio A Investigación, Universidade da Coruña
15071, A Coruña, Spain
Fax: (internat.) +34-981/167-068
E-mail: sxaixs@udc.es
[d] Department of Energetics "S. Stecco", University of Florence
Via S. Marta 3, 50139 Florence, Italy

In this paper we present a new example of a Cu^{I} complex that is capable of producing an intramolecular hydroxylation reaction. We also report an alternative synthesis directly from the hydroxylated ligand and Cu^{II} that generates the same final complex. Furthermore, this oxygenated complex constitutes the first example of a macrocyclic ligand that does not contain pendant arms, and that doubly bridges the Cu metal[16–18] with an unusual geometry.[19]

Results and discussion

The synthetic strategy for the preparation of the new ligands L-H and L-OH is outlined in Scheme 1, and in both cases is based on the condensation of the protected triamine

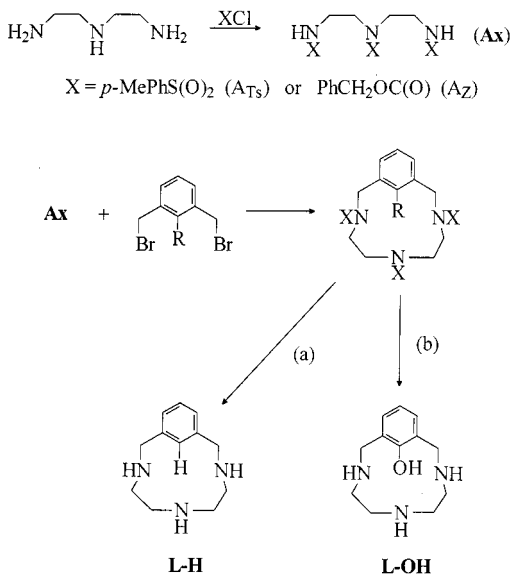

(a) R = H, X = Z : H_2 (Pd/C); (b) R = OMe, X = Ts : Li/NH_3 (l)

Scheme 1. Synthetic strategy

 © WILEY-VCH Verlag GmbH, 69451 Weinheim, Germany, 2002 1434–1948/02/0404–0987 $ 17.50+.50/0

with 1,3-dibromoxylene or 1,3-dibromoanisole. The L-OH ligand was isolated after simultaneous deprotection of the amine and phenol groups with lithium in liquid ammonia.

The reaction of stoichiometric amounts of L-H and $[Cu^{I}(MeCN)_4](PF_6)$ in acetonitrile presumably produces a dinuclear complex $[Cu_2(L\text{-}H)_2]^{2+}$ in equilibrium with different conformers, as seen by variable temperature ^1H NMR and ESI spectroscopy. Molecular models clearly show that the monomeric species $[Cu(L\text{-}H)]^+$ contains two fused five-membered rings highly constrained due to the rigidity imposed by the *meta*-substituted phenyl group. On the other hand, the dimer contains only one five-membered ring per ligand and thus the steric strain is much lower. Solution equilibrium studies with Cu^{II} and the L-OH ligand, performed by potentiometric methods, are also in agreement with this behaviour.[20]

The formation constant value of this dinuclear complex [Equation (2)] is $\log K = 38.47$, more than twice that of the mononuclear species ($\log K = 17.53$), indicating that the association process of two mononuclear species is highly favoured.

$$2\,Cu^{2+} + 2\,L\text{-}OH \longrightarrow [Cu_2(L\text{-}O)_2]^{2+} \quad (2)$$

Bubbling oxygen through an acetonitrile solution of the colourless complex $[Cu^{I}_2(L\text{-}H)_2]^{2+}$ at low temperatures (−40 °C) generates a blue intermediate, whose nature is currently under investigation, which upon warming to room temperature turns green [Equation (3)]. Addition of ether to this solution and cooling to 5 °C overnight produces green crystals of the binuclear Cu^{II} bisphenolate complex $[Cu^{II}_2(L\text{-}O)_2]^{2+}$ in 22% isolated yield.

$$[Cu_2(L\text{-}H)_2]^{2+} + O_2 \rightleftharpoons [Cu_2(L\text{-}O)_2]^{2+} + 2\,H^+ + 2\,e^- \quad (3)$$

Exactly the same dicationic complex can be obtained in quantitative yield by the direct reaction of the L-OH ligand and $CuCl_2$ or $Cu(ClO_4)_2$.

The crystal structure of $[Cu_2(L\text{-}O)_2](PF_6)_2$ was determined by X-ray crystallography and its ORTEP diagram is shown in Figure 1.

The molecule sits on a centre of symmetry that transforms one macrocyclic ligand into the other. The Cu_2O_2 core atoms lie in a plane forming a rhomboidal arrangement. Each copper atom has a slightly distorted square-pyramidal geometry (with a τ factor of 0.21).[21] The base of the pyramid is occupied by two N atoms from one of the macrocyclic ligands together with a third N atom and a phenoxo O atom from the other macrocyclic ligand. The apical position is occupied by a phenoxo O atom from the former macrocyclic ligand and therefore the copper centres become doubly bridged by each macrocyclic ligand. The oxygen atoms of the phenoxo groups bridge the copper centres so that the apical oxygen atom from one pyramid is also the base of the other pyramid. As a result, the geometry of the complex consists of two square pyramids sharing a base-to-apex edge with the bases nearly parallel to one another. The constraint imposed by the macrocyclic ligand in this bis(μ-phenoxo)dicopper complex gives rise to long Cu−O [1.927(2) Å, 2.201(2) Å], Cu−Cu [2.864(1) Å] and O−O [2.988(1) Å] distances relative to unconstrained systems.[14]

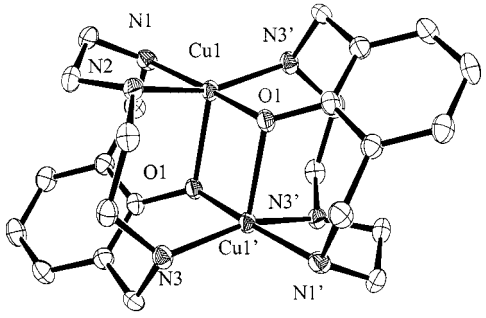

Figure 1. ORTEP view of the molecular structure of complex $[Cu_2(L\text{-}O)_2]^{2+}$ (ellipsoids at 50% probability); H atoms are omitted for clarity; selected bond lengths (Å) and angles (°): Cu1−N1 2.026(3), Cu1−N2 20142(3), Cu1−N3′ 2.044(3), Cu1−O1′ 1.927(2), Cu1−O1 2.201(2), Cu1−Cu1′ 2.864(1), O1−O1′ 2.988(1); Cu1−O1′−Cu1′ 92.44(9), O1−Cu1−O1′ 87.56(9), N1−Cu1−N2 85.13(11), N1−Cu1−N3′ 99.53(11), N2−Cu1−O1′ 86.41(10), O1−Cu1−N3′ 87.97(10), N2−Cu1−N3′158.78(11), N1−Cu1−O1′ 171.48(10), N1−Cu1−O1 89.51(10), N2−Cu1−O1 96.17(11), N3′−Cu1−O1 104.51(11)

The complex $[Cu_2(L\text{-}O)_2]^{2+}$ constitutes the first example of a complex bearing a macrocyclic ligand that does not contain pendant arms, and that doubly bridges the Cu centres. In the structure the Cu pyramids have an unusual parallel bases type of relative arrangement due to the constraints imposed by the macrocyclic ligand. The driving force for the doubly bridged disposition of $L\text{-}O^-$ is due to both the tendency of phenoxo groups to act as bridging ligands and to the release of steric strain that would otherwise exist if the $L\text{-}O^-$ ligand had all three N atoms coordinating to the same Cu metal centre. Molecular models clearly show that the corresponding oxygenated dinuclear Cu^{I} complex has the adequate geometry, thanks to the specific coordination of the macrocyclic ligand, to undergo oxygen insertion into the aromatic C−H bond, as indeed occurs in our case. This reaction is of importance since it results in a low molecular weight complex capable of mimicking the reactivity exhibited by tyrosinase in its cresolase activity.

Experimental Section

Materials and Instruments: All reagents used in the present work were obtained from Aldrich Chemical Co. and were used without further purification. Reagent-grade organic solvents were obtained from SDS. IR spectra were recorded with a Mattson Satellite FT-IR spectrometer on KBr pellets. UV/Vis spectroscopy was performed with a Cary 50 Scan (Varian) UV/Vis spectrophotometer with 1-cm quartz cells. The ^1H-NMR spectroscopy was performed with a Bruker DPX 200 MHz or a Bruker 400 MHz. Samples were

run in $CDCl_3$, CD_2Cl_2 or deuterium oxide with internal references (residual protons and/or tetramethylsilane). Elemental analyses were performed using a CHNS-O Elemental Analyzer EA-1108 from Fisons. FAB-MS experiments were run with a Fisons VG-Quattro and the ESI-MS experiments with a Navigator LC/MS chromatography from ThermoQuest. X-ray analyses were carried out using a Siemens Smart CCD diffractometer.

Ligand L-H: The protected linear amine A_z (1.75 g, 3.46 mmol), Cs_2CO_3 (2.82 g, 8.66 mmol) and α,α′-dibromo-*m*-xylene (0,.914 g, 3.46 mmol) were heated to reflux in CH_3CN (180 mL) under a N_2 atmosphere for 14 h. After cooling to room temperature, the mixture was filtered and the solvent removed under reduced pressure. The protected triazamacrocycle was then purified by column chromatography using silica as the chromatographic support and CH_2Cl_2/EtOAc (98:2) as the eluting agent to give the protected amine (0.469 g, 0.73 mmol, 22.3% isolated yield). Deprotection was achieved by hydrogenation with H_2/Pd(C) in methanol at 0 °C. The product was then purified by column chromatography using silica as the chromatographic support and CH_2Cl_2/MeOH/NH_4OH (75:25:7) as the eluting agent to obtain ligand L-H in 62.3% yield. ^1H NMR (200 MHz, $CDCl_3$, 298 K, TMS): δ = 2.01 (s, 3 H), 2.08 (m, 4 H), 2.71 (t, *J* = 3.0 Hz, 4 H), 3.90 (s, 4 H), 6.99−7.26 (m, 3 H), 8.26 (s, 1 H). MS (FAB): *m*/*z* = 206 [M + H^+]. $C_{12}H_{19}N_3$ (205.3): C 70.2, H 9.3, N 20.3; found C 69.9, H 9.4, N 20.1.

Ligand L-OH·3HCl: This ligand was prepared according to a published synthetic procedure.[22] ^1H NMR (200 MHz, D_2O, pH 3, 298 K, HOD): δ = 3.22 (t, *J* = 12.4 Hz, 4 H), 3.32 (t, *J* = 12.4, 4 H), 4.44 (s, 4 H), 7.04 (t, *J* = 7.3, 1 H), 7.53 (d, *J* = 7.3, 2 H). MS (FAB): *m*/*z* = 222 [M + H^+]. $C_{12}H_{22}Cl_3N_3O$ (330.7): C 43.6, H 6.7, N 12.7; found C 43.5, H 6.7, N 12.6.

$[Cu_2(L\text{-}H)_2(MeCN)_2](PF_6)_2$: L-H (21.6 mg, 0.105 mmol) and [Cu(MeCN)$_4$](PF_6) (39.2 mg, 0.105 mmol) were placed in a Schlenk tube under an argon atmosphere, 2 mL of CH_2Cl_2 were added and the solution stirred for 5 min. Addition of Et_2O (approx. 5 mL) to the resulting light yellow solution produced a white solid which was filtered, and dried under vacuum (38.3 mg, 80.0%). ^1H NMR (200 MHz, CD_2Cl_2, 300 K): δ = 1.50 (br. s, 2 H), 2.22 (br. s, 2 H), 2.49 (br. s, 2 H), 2.76 (br. s, 2 H), 3.50 (br. s, 2 H), 4.25 (br. s, 2 H), 7.1−7.3 (m, 3 H), 8.78 (s, 1 H). The resonances in the aromatic region were sharp with a clear hyperfine structure whereas the other resonances were broad. Upon lowering the temperature all resonances progressively broadened but no splitting was observed even at 210 K. FT-IR (KBr): $\tilde{\nu}$ = 2253cm^{-1} (C≡N), 846 (PF_6^-), 559 (PF_6^-).

Complex $[Cu_2(L\text{-}O)_2](PF_6)_2$: The ligand L-H (0.02 g, 0.097 mmol) and $[Cu^I(CH_3CN)_4]PF_6$ (0.036 g, 0.097 mmol) were dissolved in 1 mL of degassed, anhydrous CH_3CN under an argon atmosphere. The resulting colorless solution was cooled to −20 °C and O_2 was bubbled through at this temperature for 10min, during which time the solution turned blue. The mixture was then warmed to room temp. whilst stirring overnight. Slow diffusion of diethyl ether into the resulting solution allowed the formation of green crystals of the final product in 20% yield (0.0084 g, 0.010 mmol). FT-IR (KBr): $\tilde{\nu}$ = 3337 cm^{-1} (NH), 3291 (NH), 1595 (Ph-O), 1455 (C=C), 1297 (O-Ph), 843 (PF_6^-), 559 (PF_6^-). UV/Vis (CH_3CN): λ_{max} (ε) = 406 nm (542), 578 (323). ESI-MS (CH_3CN): *m*/*z* = 711 $[Cu_2(L\text{-}O)_2(PF_6)]^+$, 283 $[(L\text{-}O)Cu^{II}]^+$. $C_{24}H_{36}Cu_2F_{12}N_6O_2P_2$ (857.6): C 33.6, H 4.2, N 9.8; found C 34.0, H 4.5, N 9.7.

Crystal Data for $[Cu_2(L\text{-}O)_2](PF_6)_2$: $C_{24}H_{36}Cu_2F_{12}N_6O_2P_2$, *M* = 857.61, green crystals, triclinic, space group $P\bar{1}$ (no. 2), *a* = 8.818(4), *b* = 9.696(3), *c* = 10.801(6) Å, *Z* = 1, α = 113.89(5)°, β = 113.20(2)°, γ = 90.28(3)°, *V* = 761.0(6) Å^3, D_c = 1.871 g cm^{-3}, *T* = 173(2) K, Mo-K_α radiation (λ = 0.71073 Å), 4306 reflections measured, 3653 unique (R_{int} = 0.0212) which were used in all calculations. *R* = 0.0429, *Rw* = 0.0954.

CCDC-137239 contains the supplementary crystallographic data for this paper. These data can be obtained free of charge at www.ccdc.cam.ac.uk/conts/retrieving.html [or from the Cambridge Crystallographic Data Centre, 12 Union Road, Cambridge CB2 1EZ, UK; fax: (internat.) + 44-1223/336-033; E-mail: deposit@ccdc.cam.ac.uk].

Acknowledgments

This research has been financed by the MICYT of Spain through project PBQ2000-0548 and with support from CIRIT Generalitat de Catalunya, Spain (SGR-3102-UG-01). X. Ribas is grateful for the award of a doctoral grant from CIRIT.

[1] S. Fox, K. D. Karlin, in *Active Oxygen in Biochemistry* (Eds.: J. S. Valentine, C. S. Foote, A. Greenberg, J. F. Liebman), Blackie Academic and Professional, Chapman & Hall, Glasgow, Scotland **1995**, pp. 188−231.
[2] E. I. Solomon, U. M. Sundaram, T. E. Machonkin, *Chem. Rev.* **1996**, *96*, 2563−2605.
[3] V. Mahadevan, R. J. M. K. Gebbink, T. D. P. Stack, *Curr. Opin. Chem. Biol.* **2000**, 228−234.
[4] H. Decker, R. Dillinger, F. Tuczek, *Angew. Chem. Int. Ed.* **2000**, *39*, 1591−1595.
[5] N. N. Murthy, M. Mahor-Tahir, K. D. Karlin, *Inorg. Chem.* **2001**, *40*, 628−635.
[6] S. Ryan, H. Adams, D. E. Fenton, M. Becker, S. Schindler, *Inorg. Chem.* **1998**, *37*, 2134−2140.
[7] S. Mahapatra, S. Kaderli, A. Llobet, M. Y. Neuhold, T. Palanche, V. G. Young, T. A. Kaden, L. Que, Jr., A. D. Zuberbühler, W. B. Tolman, *Inorg. Chem.* **1997**, *36*, 6343−6356.
[8] K. D. Karlin, P. L. Dahlstrom, S. N. Cozzette, P. M. Scensny, J. Zubieta, *J. Chem. Soc., Chem. Commun.* **1981**, 881−882.
[9] T. N. Sorrell, M. L. Garrity, *Inorg. Chem.* **1991**, *30*, 210−215.
[10] T. N. Sorrell, V. A. Vankai, M. L. Garrity, *Inorg. Chem.* **1991**, *30*, 207−210.
[11] L. Santagostini, M. Gullotti, E. Monzani, L. Casella, R. Dillinger, F. Tuczek, *Chem. Eur. J.* **2000**, *6*, 519−522.
[12] R. Menif, A. E. Martell, P. J. Squatritto, A. Clearfield, *Inorg. Chem.* **1990**, *29*, 4723−4729.
[13] L. Casella, M. Gullotti, M. Bartosek, G. Pallanza, L. Rigoni, E. Laurenti, *J. Chem. Soc., Chem. Commun.* **1991**, 1611−1612.
[14] S. Mahapatra, V. G. Young, S. Kaderli, A. D. Zuberbühler, W. B. Tolman, *Angew. Chem. Int. Ed. Engl.* **1997**, *36*, 130−133.
[15] P. L. Holland, K. R. Rodgers, W. B. Tolman, *Angew. Chem. Int. Ed.* **1999**, *38*, 1139−1142.
[16] R. P. Houser, J. A. Halfen, V. G. Young, N. J. Balckburn, W. B. Tolman, *J. Am. Chem. Soc.* **1995**, *117*, 10745−10746.
[17] P. V. Bernhardt, E. J. Hayes, *Inorg. Chem.* **1998**, *37*, 4214−4219.
[18] G. Wei, C. C. Allen, T. W. Hambley, G. A. Lawrence, M. Maeder, *J. Chem. Soc., Dalton Trans.* **1995**, 2541−2547.
[19] In Cu^{II} complexes with a Cu_2O_2 core, the metal atoms generally adopt a square-based pyramid geometry and the pyramids are arranged so that their bases are coplanar sharing a basal edge. Here the bases are parallel as is the case for the following examples: [19a] R. Hämäläinen, M. Ahlgrén, U. Turpeinen, *Acta Crystallogr., Sect. B* **1982**, *38*, 1577−1580. [19b] A. Odani, T. Maruyama, O. Yamauchi, T. Fujiwara, K. Tomita, *J. Chem.*

Soc., Chem. Commun. **1982**, 646−647. [19c] Y. Boukari, A. Busnot, F. Busnot, A. Leclaire, M. A. Bernard, *Acta Crystallogr., Sect. B* **1982**, *38*, 2458−2461.

[20] Stability constants of the Cu^{II} complex with **L-OH** (0.15 mol dm^{-3} NMe_4Cl aqueous solution, 298.1 K): $2Cu^{2+} + 2\ L\text{-}O^- = [Cu_2(L\text{-}O)_2]^{2+}$, log K = 38.47(2); $Cu^{2+} + L\text{-}O^- = [Cu(L\text{-}O)]^+$, log K = 17.47(2); $Cu^{2+} + L\text{-}OH = [Cu(L\text{-}OH)]^{2+}$, log K = 12.70(2); $Cu^{2+} + HL\text{-}OH^+ = [Cu(HL\text{-}OH)]^{3+}$, log K = 4.70(3). The values in parenthesis are the standard deviation in the last significant figure. Ligand and metal concentration: 0.5 $\times 10^{-3}$ M. Potentiometric measurements were carried out in the pH range 2−7 due to the precipitation of the dinuclear species at higher pH.

[21] A. W. Addison, T. N. Rao, J. Reedijk, J. V. Rijn, G. C. Verschoor, *J. Chem. Soc., Dalton Trans.* **1984**, 1349−1356.

[22] C. Bazzicalupi, A. Bencini, A. Bianchi, V. Fusi, E. Garcia-Espana, P. Paoletti, P. Paoli, B. Valtancoli, *Inorg. Chem.* **1993**, *32*, 4900−4908.

Received October 5, 2001
[I01395]

EurJIC
European Journal of Inorganic Chemistry

May 2002
Issue 5
Pages 991–1240

COVER PICTURE

The cover picture shows the structure of the bis[citrato(3−)]-silicate dianion, a hexacoordinate silicon species with two tridentate ligands derived from citric acid. This complex has been synthesized and structurally characterized in context with studies on silica biomineralization. Details are discussed in the Short Communication by R. Tacke et al. on p. 1025 ff.

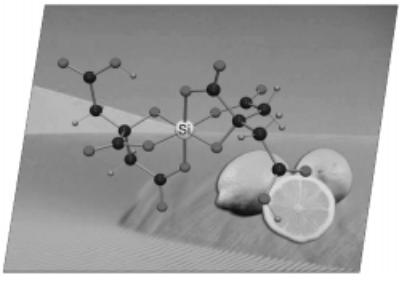

MICROREVIEW

Contents

1009 **H. Suzuki**

Activation of Organic Substrates on Multi-Metallic Sites of Transition Metal Polyhydride Clusters Having C_5Me_5 Groups as Auxiliary Ligands

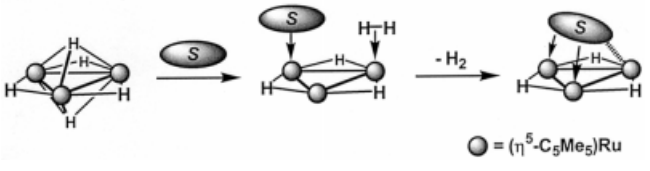

Keywords: Cluster compounds / Hydride ligands / Iron / Ruthenium

 © WILEY-VCH Verlag GmbH, 69451 Weinheim, Germany, 2002 1434–1948/02/0505–0995 $ 20.00+.50/0

SHORT COMMUNICATIONS

1025 **R. Tacke,* M. Penka, F. Popp, I. Richter**

Bis[citrato(3−)-O^1,O^3,O^6]silicate: A Dianionic Complex with Hexacoordinate Silicon(IV) and Two Tridentate Dioato(2−)olato(1−) Ligands

Keywords: Silicon / Silicates / Coordination modes / Biomineralization

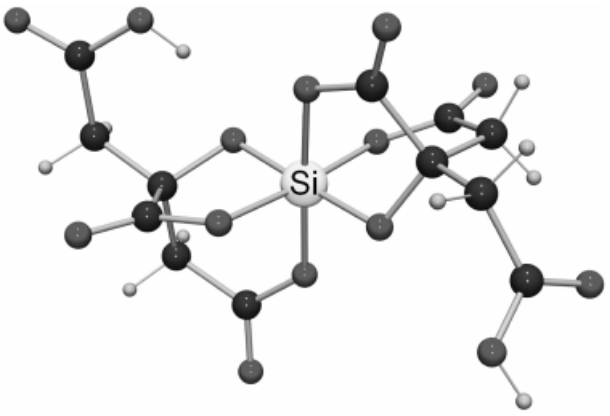

1029 **Y. K. Gun'ko,* U. Cristmann, V. G. Kessler**

Synthesis and Structure of the First Fe^{II} Heterometallic Alkoxide $[(THF)NaFe(OtBu)_3]_2$ − a Possible Precursor for New Materials

Keywords: Iron / O ligands / Heterometallic complexes / Alkali metals / Materials science

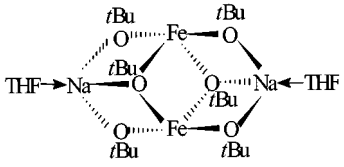

1032 **Y. Chen, L. R. Subramanian, M. Barthel, M. Hanack***

Synthesis and Characterization of Soluble Axially Substituted Tetra-(*tert*-butyl)gallium-(III)phthalocyanines

Keywords: Gallium / Nitrogen heterocycles / Nonlinear optics / Phthalocyanines

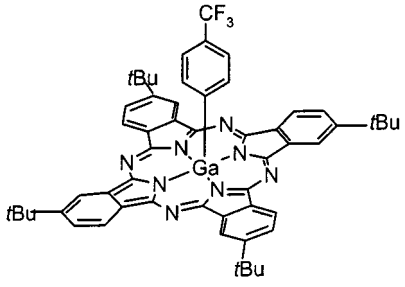

1035 **A. C. G. Hotze, Y. Chen, T. W. Hambley, S. Parsons, N. A. Kratochwil, J. A. Parkinson, V. P. Munk, P. J. Sadler***

cis-$[PtCl_2(NH_3)\{2\text{-}(2\text{-hydroxyethyl})pyridine\}]$ − an Analogue of the Anticancer Drug AMD473: Unusual Hydrolysis Rates and pK_a Values for the Diaqua Adduct

Keywords: Platinum / Antitumor agents / Hydrolysis / Molecular modelling

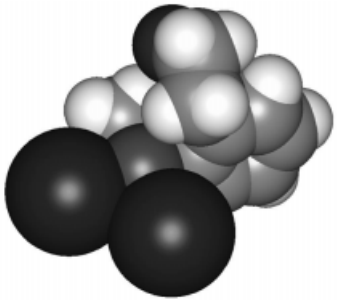

1040 **C. Neumann, A. Schulz, T. Seifert, W. Storch,* M. Vosteen**

N,*N*-Dilithioarylamines as New Building Blocks in Amide Chemistry; the Structure of a Carbanion-Stabilized $[C_2N_5Li_{10}]^{2-}$ Cluster

Keywords: Amines / Tin / Lithium / Clusters / Structure elucidation

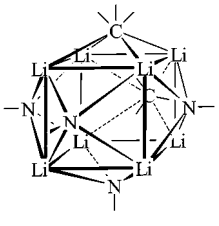

1046 **G. Aromí, P. Gamez, O. Roubeau, P. Carrero-Berzal, H. Kooijman, A. L. Spek, W. L. Driessen, J. Reedijk***

The First Case of Local *cis* versus *trans* Coordination as the Controlling Factor for the Overall Structure in Dinuclear Assemblies

Keywords: Stereochemistry / Self assembly / O ligands / Manganese / Nickel

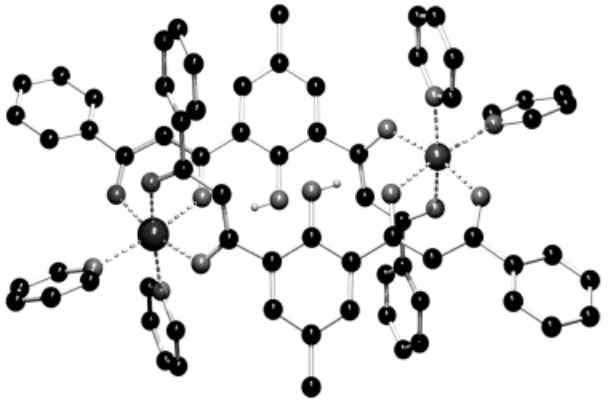

FULL PAPERS

1049 **S. Lanza,* F. Nicolò, G. Tresoldi**

Synthesis, Stereochemistry and Ligating Properties of Tetraalkyl-Substituted Ethanedithioamides − Evidence for the Lowering of High-Energy Rotation Barriers under the *trans* Influence of Pt-σ-Bonded Aryl Groups

Keywords: C−C hindered rotation / C−N hindered rotation / (*E*)/(*Z*) isomerisation / Tetraalkylethanedithioamides

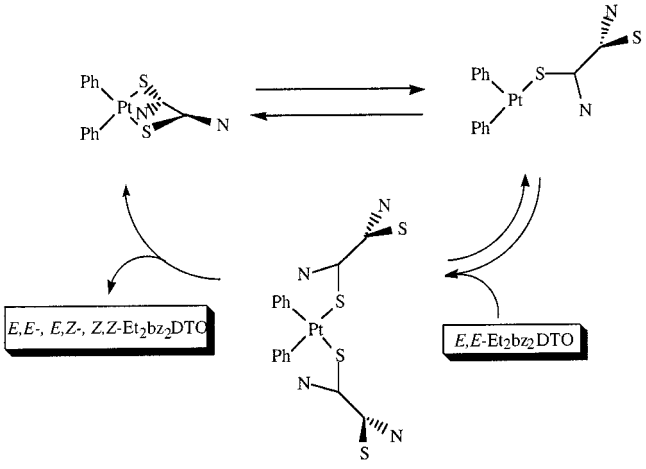

1056 **W. Zheng, H. W. Roesky,* N. C. Mösch-Zanetti, H.-G. Schmidt, M. Noltemeyer**

Synthesis and Characterization of Derivatives of a Chelating Aluminum Dichloride Complex Containing a 3,5-Di-*tert*-butylpyrazolato Unit

Keywords: Aluminum / N ligands / Pyrazolato ligands / Structural elucidation

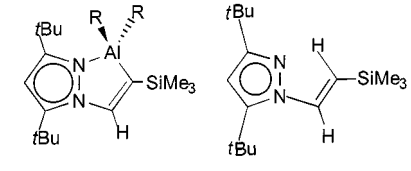

R = Me (**2**), H (**3**), I (**4**) **5**

1060 **H. Hao, S. Bhandari, Y. Ding, H. W. Roesky,* J. Magull, H.-G. Schmidt, M. Noltemeyer, C. Cui**

Pyrrolylaldiminato Complexes of Zn, Mg and Al

Keywords: Zinc / Magnesium / Aluminum / N ligands

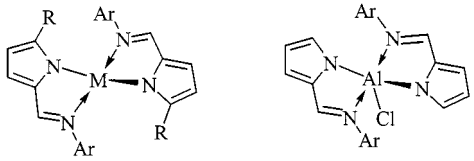

R = H, L^1_2 Zn (**1**)
R = *t*Bu, L^2_2 Zn (**2**)
R = *t*Bu, L^2_2 Mg (**3**)

L^1_2 AlCl (**8**)

Ar = 2,6-*i*-$Pr_2C_6H_3$

1066 N. Wiberg,* W. Niedermayer, G. Fischer, H. Nöth, M. Suter

Synthesis, Structure and Dehalogenation of the Disilene RClSi=SiClR [R = $(t\mathrm{Bu_3Si})_2\mathrm{MeSi}$]

Keywords: Disilene / Disilyne / Silicon / Silylene / X-ray structure analysis

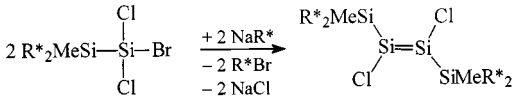

1071 A. I. Ruiz,* J. Campo, M. L. López, J. L. Martínez Peña, C. Pico, M. L. Veiga

Magnetic Behaviour in the System $La_{1.33}$-$Na_xMn_xTi_{2-x}O_6$

Keywords: Perovskite phases / Neutron diffraction / Magnetic properties

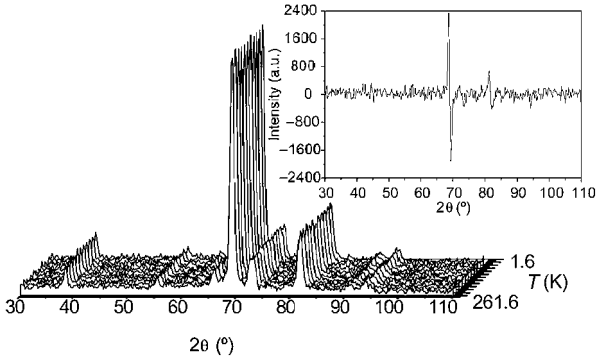

1076 H. Werner,* W. Stüer, S. Jung, B. Weberndörfer, J. Wolf

Preparation of Trifluorophosphaneruthenium-(II) Complexes from η^3:η^3-Cyclooctadienediyl-ruthenium(IV) Compounds as Precursors

Keywords: Allyl complexes / Carbene complexes / Hydrido complexes / P ligands / Ruthenium

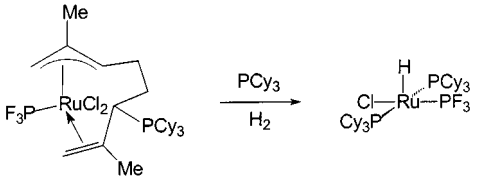

1081 B. Hasenknopf, R. Delmont, P. Herson, P. Gouzerh*

Anderson-Type Heteropolymolybdates Containing Tris(alkoxo) Ligands: Synthesis and Structural Characterization

Keywords: Coordination modes / Molybdenum / Polyoxometalates / Tridentate ligands

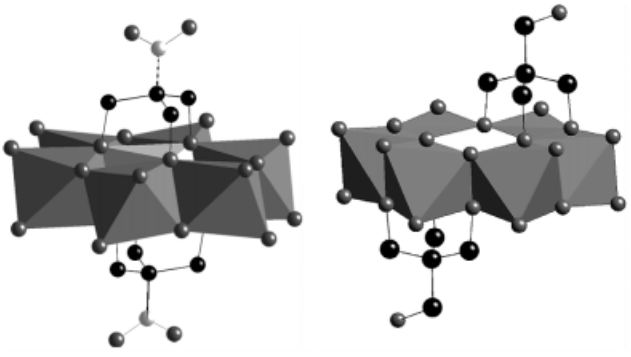

1088 R. Frantz,* J.-O. Durand, G. F. Lanneau, J.-C. Jumas, J. Olivier-Fourcade, M. Cretin, M. Persin

Studies of Phosphonic Acids Containing a π-Conjugated Ferrocenyl Unit Grafted on Metal Oxides − Mössbauer and Electrochemical Behaviour

Keywords: Mössbauer spectroscopy / Electrochemistry / Phosphorus / Sandwich complexes

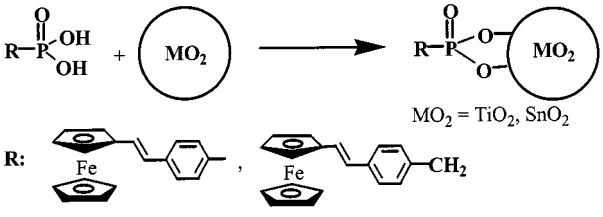

1094 **M. M. Dell'Anna, P. Mastrorilli, F. Muscio, C. F. Nobile,* G. P. Suranna**

A Polymer-Supported β-Ketoesterate Complex of Palladium as an Efficient, Phosphane-Free, Air-Stable, Recyclable Catalyst for the Heck Reaction

Keywords: Heck reaction / Supported catalysts / Palladium

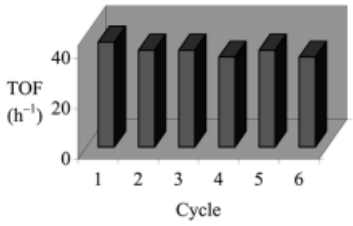

1100 **C. D. Nunes, M. Pillinger, A. A. Valente, I. S. Gonçalves,* J. Rocha, P. Ferreira, F. E. Kühn***

Synthesis and Characterization of Methyltrioxorhenium(VII) Immobilized in Bipyridyl-Functionalized Mesoporous Silica

Keywords: Rhenium / Supported catalysts / Mesoporous materials / Lewis base adducts

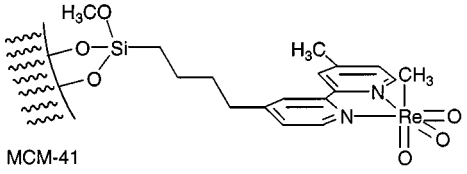

1108 **A. Perner,* K. Holl, D. Ilic, M. Wohlfahrt-Mehrens**

A New MnO_x Cathode Material for Rechargeable Lithium Batteries

Keywords: Lithium batteries / Manganese oxides / Cathode materials

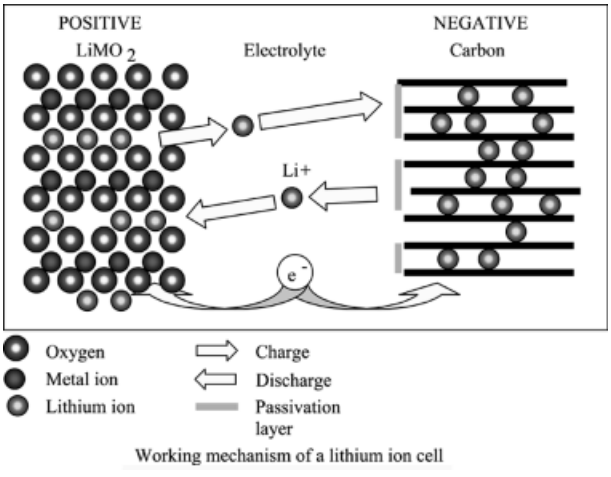

Working mechanism of a lithium ion cell

1115 **R. Diniz, H. A. de Abreu, W. B. de Almeida, M. T. C. Sansiviero, N. G. Fernandes***

X-ray Crystal Structure of Triaquacopper(II) Dihydrogen 1,2,4,5- Benzenetetracarboxylate Trihydrate and Raman Spectra of Cu^{2+}, Co^{2+}, and Fe^{2+} Salts of 1,2,4,5-Benzenetetracarboxylic (Pyromellitic) Acid

Keywords: Hydrogen bonds / X-ray diffraction / Raman spectroscopy / Transition metals

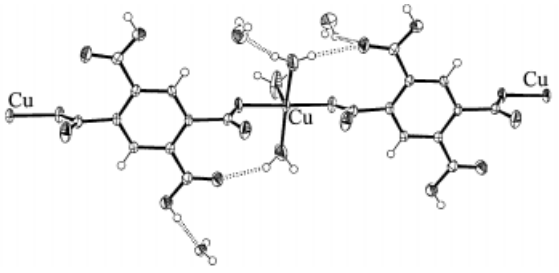

1124 **P. K. Santra, P. Byabartta, S. Chattopadhyay, L. R. Falvello, C. Sinha***

Coupling of Arylamines with Coordinated Arylazopyrimidines in Palladium(II) Complexes

Keywords: Nitrogen heterocycles / Palladium / N ligands / Aminations / X-ray structure / EHMO calculation

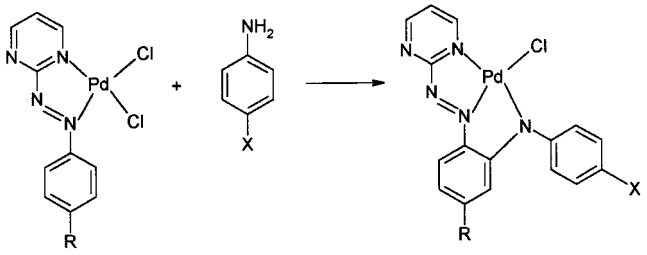

1132 **U. Braun, T. Habereder, H. Nöth,* H. Piotrowski, M. Warchhold**

Triaminoboranes and Their Metallation to *N*-Lithiotriaminoboranes

Keywords: Boranes / Deprotonation / Lithium / Nitrogen / X-ray diffraction

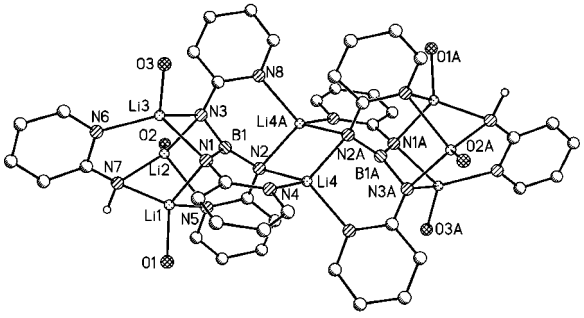

1146 **A. Papakyriakou, A. Anagnostopoulou, A. Garnier-Suillerot, N. Katsaros***

Interaction of Uranyl Ions with Daunorubicin and Adriamycin

Keywords: Antibiotics / Antitumor agents / Anthracyclines / O ligands / Uranium

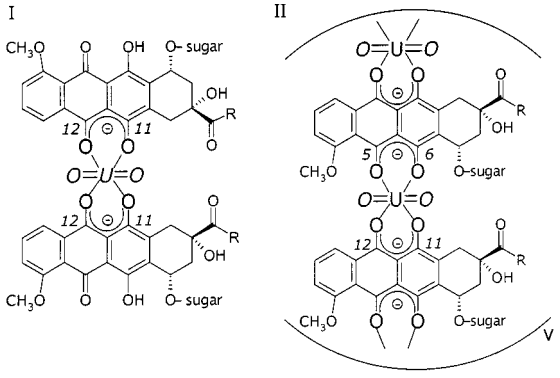

1155 **M. Bianchi, P. Frediani,* F. Piacenti, L. Rosi, A. Salvini**

Influence of an Additional Gas on the Hydroformylation and Related Reactions

Keywords: Hydroformylation / Carbonyl ligands / Cobalt / Carbonylation / Dinitrogen complexes / Argon / Xenon

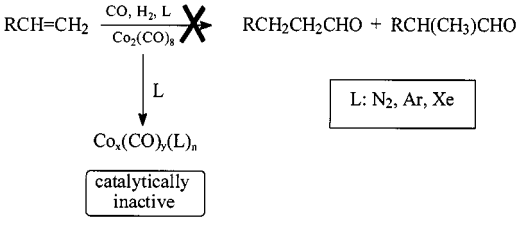

1162 **S. Giroux, S. Aury, B. Henry, P. Rubini***

Complexation of Lanthanide(III) Ions with Polyhydroxy Carboxylic Acids in Aqueous Solutions

Keywords: Lanthanides / Cations / Acidity / Complexation / NMR spectroscopy

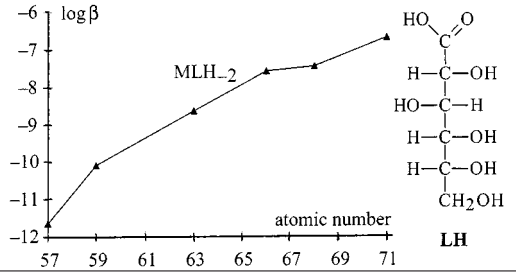

1169 E. Eskelinen, T.-J. J. Kinnunen, M. Haukka,* T. A. Pakkanen

Photochemical Studies of *cis*(CO),*trans*(Cl)-[Ru(bpy)$(CO)_2Cl_2$] (bpy = 2,2′-bipyridine): Ligand Exchange Reactions in Methanol

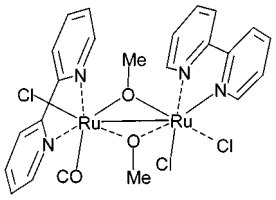

Keywords: Photochemistry / Ruthenium / Cyclic voltammetry / N ligands / O ligands

1174 T. Höcher, S. Blaurock, E. Hey-Hawkins*

Novel Ferrocene Derivatives with PH-Functionalized Phosphanylalkylcyclopentadienyl Ligands: Syntheses and Molecular Structures of *rac*-[Fe{(η^5-C_5H_4)CMe_2PHR}$_2$] (R = Ph, Mes) and *rac*-[Fe{(η^5-C_5H_4)CMe_2PHPh(Cp*$TaCl_4$)}$_2$]

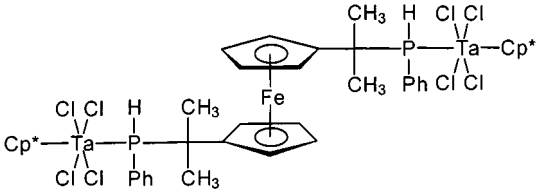

Keywords: Metallocenes / P ligands / Bridging ligands / Secondary phosphanes / Tantalum

1181 N. C. Mösch-Zanetti,* M. Hewitt, T. R. Schneider, J. Magull

Titanium Complexes Containing Bulky η^2-1,2,4-Triazolato Ligands

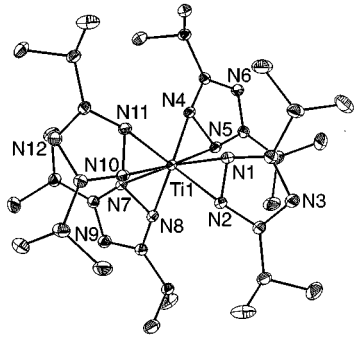

Keywords: N ligands / Titanium / Structure elucidation

1186 O. Horner,* C. Jeandey, J.-L. Oddou, P. Bonville, J.-M. Latour

A Mössbauer Study of [Fe(edta)(O_2)]$^{3-}$Agrees with a High-Spin Fe^{III} Peroxo Complex

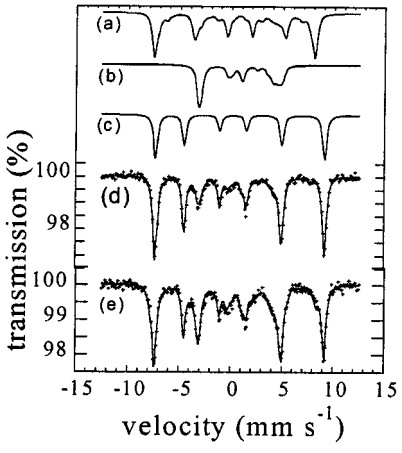

Keywords: Iron / Peroxo ligands / Mössbauer spectroscopy / N ligands

1190 **D. L. Reger,* C. A. Little, M. D. Smith, A. L. Rheingold, K.-C. Lam, T. L. Concolino, G. J. Long,* R. P. Hermann, F. Grandjean**

Synthetic, Structural, Magnetic, and Mössbauer Spectral Study of $\{Fe[HC(3,5\text{-}Me_2pz)_3]_2\}I_2$ and Its Spin-State Crossover Behavior

Keywords: Iron / N ligands / Spin crossover / Magnetic properties / Mössbauer spectroscopy

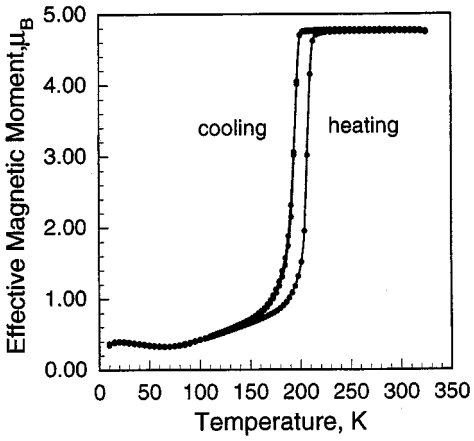

1198 **S. B. Artemkina, N. G. Naumov,* A. V. Virovets, O. Oeckler, A. Simon, S. B. Erenburg, N. V. Bausk, V. E. Fedorov**

Two Molecular-Type Complexes of the Octahedral Rhenium(III) Cyanocluster Anion $[Re_6Se_8(CN)_6]^{4-}$ with M^{2+} (Mn^{2+}, Ni^{2+})

Keywords: Rhenium / Cluster compounds / Structure elucidation / Cyanide ligands / XANES

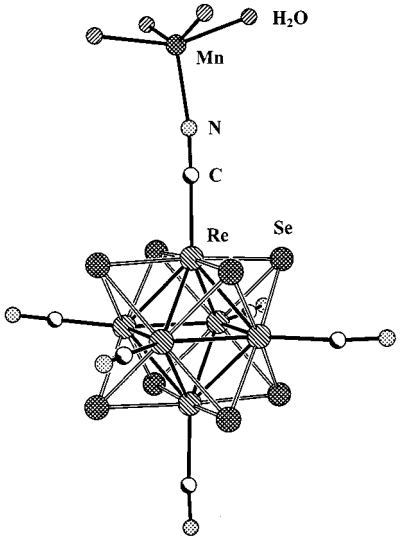

1203 **L. Kloo,* J. Rosdahl, P. H. Svensson**

On the Intra- and Intermolecular Bonding in Polyiodides

Keywords: Iodine / Polyhalides / Bond theory

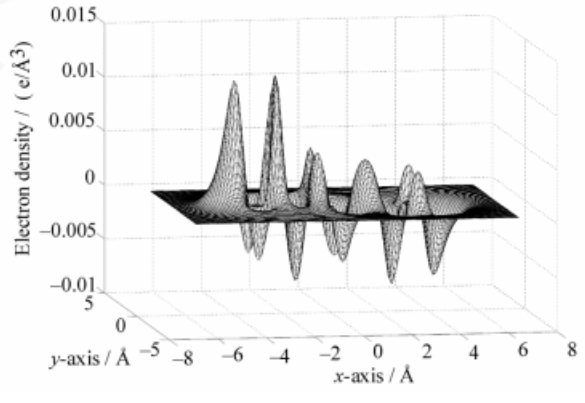

1210 **P. Mastrorilli,* C. F. Nobile, F. P. Fanizzi, M. Latronico, C. Hu, U. Englert**

(Phosphido)platinum Complexes by Sodium-Promoted Reaction of *cis*-$PtCl_2(PHCy_2)_2$ – Synthesis and Crystal Structure of [*trans*-$Pt(PCy_2H)_2(PCy_2)Cl$], a Rare Example of a Terminal (Phosphido)platinum(II) Complex

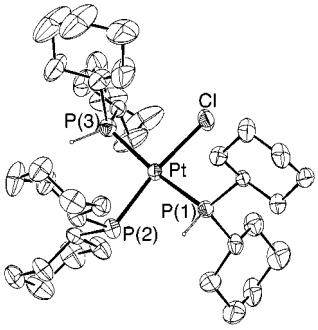

Keywords: Platinum / P ligands / Terminal phosphides / Hydrides / Small ring systems

1219 **C. M. Jung, W. Kraus, P. Leibnitz, H.-J. Pietzsch, J. Kropp, H. Spies***

Syntheses and First Crystal Structures of Rhenium Complexes Derived from ω-Functionalized Fatty Acids as Model Compounds of Technetium Tracers for Myocardial Metabolism Imaging

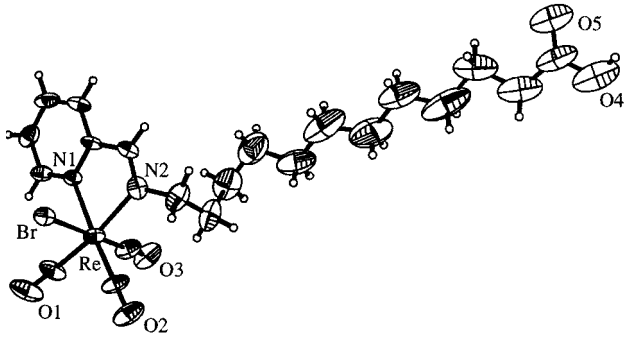

Keywords: Rhenium / Technetium / Fatty acids / Drug research / Radiopharmaceuticals

1226 **M. Saphier,* A. Masarwa, H. Cohen, D. Meyerstein**

Copper(I) as a Homogeneous Catalyst for the Ullmann Reaction in Aqueous Solutions – The Transformation of 2-Bromobenzoate into Salicylate

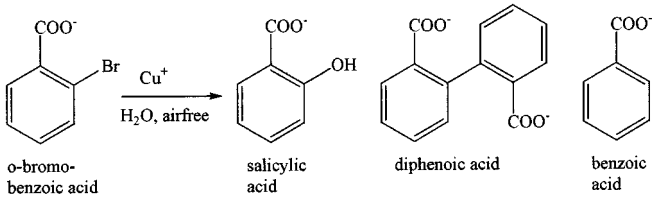

Keywords: Copper(I) / Aromatic compounds / Catalysis / Ullmann reaction

1235 **I. Cassidy, M. Garner, A. R. Kennedy, G. B. S. Potts, J. Reglinski,* P. A. Slavin, M. D. Spicer***

The Preparation and Structures of Group 12 (Zn, Cd, Hg) Complexes of the Soft Tripodal Ligand Hydrotris(methimazolyl)borate (Tm)

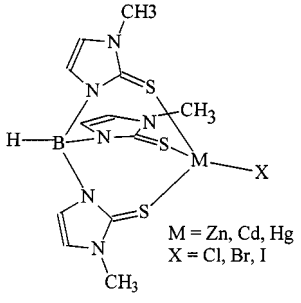

Keywords: Tripodal ligands / N ligands / S ligands / Group 12 complexes

Activation of Organic Substrates on Multi-Metallic Sites of Transition Metal Polyhydride Clusters Having C_5Me_5 Groups as Auxiliary Ligands

Hiroharu Suzuki[a]

Keywords: Cluster compounds / Hydride ligands / Iron / Ruthenium

An overview of the chemistry of the di- and trinuclear transition metal polyhydride complexes containing only C_5Me_5 groups as auxiliary ligands is presented. The synthesis of a series of η^5-C_5Me_5 polyhydride clusters and their reactivities centered about some typical examples of "multi-metallic activation" including the cleavage of carbon–hydrogen bonds of alkanes, carbon-carbon bond of cyclopentadiene, and carbon–carbon double bond of 1,1-disubstituted alkenes, achieved on the reaction site of the polyhydride-bridged clusters, are reported.
(© Wiley-VCH Verlag GmbH, 69451 Weinheim, Germany, 2002)

1. Introduction

The reactivity of transition metal cluster complexes has been of special interest recently, in the area of organometallic chemistry, because of their potential applicability to organic synthesis.[1] The advantageous properties of multi-metallic systems over a mono-metallic ones in the substrate activation step are their capability for multiple coordination of the substrate to the metal clusters, and the multi-electron transfer between the substrate and the cluster. Transition metal clusters have therefore been intensively investigated, in the quest to develop new and effective organic transformations achieved by the synergetic effect of the metal centers. A large number of studies on the reaction chemistry of clusters have been reported, to date using mostly carbonylmetal clusters. However, most of the metal clusters used in these studies have been binary carbonylmetal complexes or clusters directly derived from them, $M_m(CO)_n$ or $L_kM_m(CO)_n$, and it is hard to say that the reactions developed are really characteristic of the metal cluster. Although selectivity and efficiency of the reactions are modified in some cases, the mode of the reaction is sometimes similar to that achieved by using mononuclear metal complexes. In contrast, there have been a relatively small number of reported examples of metal polyhydride clusters – probably due to their instability. Furthermore, an effective synthetic method for obtaining polyhydride clusters that is applicable to the many ligand/metal combinations has not been developed thus far.

Electron density at the metal centers in the metal hydride cluster is most certainly higher than that in the polycarbonylmetal or polycarbonylmetal hydride clusters. The metal polyhydride clusters are, therefore, expected to be much more active than the carbonylmetal clusters toward oxidative addition of substrates. In addition, a metal polyhydride cluster, particularly a polyhydride-bridged cluster, is considered to be a suitable and versatile precursor of the active species for multi-metallic activation. We have used the term

[a] Department of Applied Chemistry, Graduate School of Science and Engineering, Tokyo Institute of Technology and CREST, Japan Science and Technology Corporation (JST), O-okayama, Meguro-ku, 152-8552 Tokyo, Japan

Hiroharu Suzuki was born in Gifu, Japan, in 1948 and studied chemistry at Nagoya University. In 1976, he obtained his Ph.D. degree from Nagoya University on a study on organometal–nitrogen bonds, under the supervision of Prof. Yoshio Ishii. Upon graduation, he moved to the Research Laboratory of Resources Utilization at Tokyo Institute of Technology and was offered a position of Assistant Professor. After a post-doctoral stay with Prof. Tobin J. Marks at Northwestern University (1982–1983), he returned to Tokyo and became Associate Professor in 1984. In 1991, he was promoted to his current position of Professor. He is concurrently serving as Research Director of the "CREST Molecular Architecture of Metal Hydride Cluster" Project of Japan Science and Technology Corporation (JST). His research interests are concentrated on the chemistry of transition metal polyhydride clusters, in particular development of new synthetic methods for polyhydride clusters, and activation of unreactive substrates such as alkanes and dinitrogen on multimetallic sites.

MICROREVIEWS: This feature introduces the readers to the authors' research through a concise overview of the selected topic. Reference to important work from others in the field is included.

"multi-metallic activation" to refer to a mode of activation achieved as a result of cooperative action of many metal centers. Liberation of bridging hydride ligands from the metal cluster gives rise, spontaneously, to vacant coordination sites on the adjacent metal centers, and the substrate taken in the reaction site likely interacts with the resulting vacant metal centers all together. In such a situation, the metal centers probably cooperate in activating the substrate as a binding site and an activation site. This must be the origin of the cluster effect in the substrate activation.

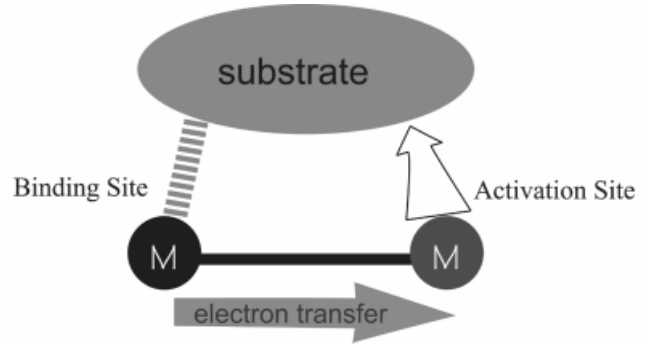

There had been several reported examples of multinuclear polyhydride-bridged complexes having tertiary phosphanes as auxiliary ligands,[2] while no polyhydride clusters having only cyclopentadienyl ligands as auxiliaries were known at the end of the 1980s. Unfortunately, the reaction chemistry of the phosphane polyhydride clusters is not as remarkable or unique as that of a polycarbonylmetal cluster.

A cyclopentadienyl ligand, especially the C_5Me_5 ligand, is strongly electron-releasing and almost inert towards substitution, unlike tertiary phosphanes. Introduction of C_5Me_5 groups into the cluster framework, therefore, increases the electron density at the metal centers and, as a result, makes the cluster much more reactive to oxidative addition. Even carbonyl clusters become highly reactive and therefore often reveal really unique reactivity when cyclopentadienyl ligands are introduced into the cluster framework.[3] Introduction of cyclopentadienyl ligands affects not only the activity but also the selectivity. An empty space surrounded by the C_5Me_5 ligands becomes a reaction site in which substrates are activated in a shape-selective manner, due to the steric repulsion among the substrates and the C_5Me_5 groups.

We now describe the synthesis of a series of η^5-C_5Me_5 polyhydride clusters and some typical examples of "bi- and trimetallic activation" achieved on the reaction site of the polyhydride-bridged clusters.

2. Synthesis of Transition Metal Polyhydride Clusters Having C_5Me_5 Groups

2.1 Synthesis and Structure of a Dinuclear Tetrahydride Complex of Ruthenium

Ruthenium is a fascinating metal from the standpoint of electron transfer between the substrate and the metal atom because of its wide diversity of oxidation states, from −2 (d^{10}) to +8 (d^0). We therefore attempted to synthesize a new class of polyhydride complex having only C_5Me_5 groups as the auxiliary ligands.

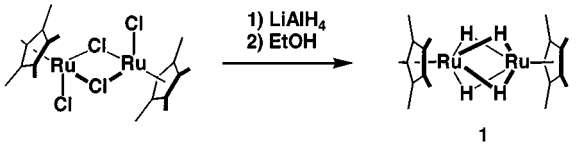

1 (1)

A dinuclear tetrahydride-bridged complex of ruthenium $\{(C_5Me_5)Ru\}_2(\mu\text{-}H)_4$ (**1**) was synthesized by treatment of $\{(C_5Me_5)RuCl_2\}_2$ [4] with $LiAlH_4$ followed by workup with ethanol [Equation (1)].[5] To the best of our knowledge, only two examples have been reported for the dinuclear tetrahydride-bridged complexes $L_mM(\mu\text{-}H)_4ML_n$,[6] while related trihydride-bridged complexes such as $[\{(C_6Me_6)Ru\}_2(\mu\text{-}H)_3]^+$ are known.[7] Complex **1** is the first dinuclear tetrahydride-bridged complex having no phosphane or arsane ligands.

An X-ray diffraction study of **1** showed that the four hydride ligands were essentially arrayed at the vertices of an approximate square, and were placed perpendicularly to the Ru−Ru vector (Figure 1). The average H−H distance of 1.46 Å and the T_1 value of 2.28 s were deemed to be sufficient to characterize the complex as a classical metal polyhydride.[8] Although the short Ru−Ru distance [2.463(1) Å] and the 18-electron rule applied to the dimer **1** require a triple bond between the ruthenium atoms, a theoretical study performed by Morokuma et al. showed the absence of a direct metal−metal bond.[9] The short Ru−Ru distance is most likely due to four 3c-2e M−H−M bonds.

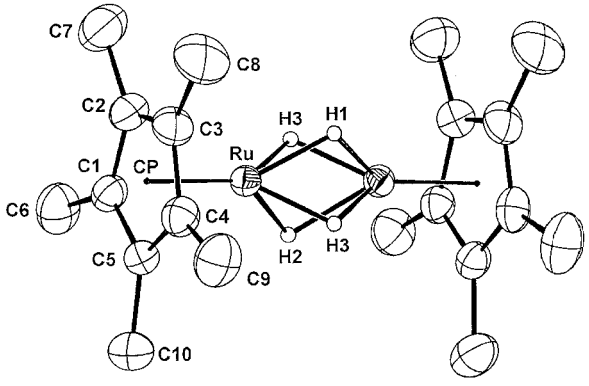

Figure 1. Molecular structure of $\{(C_5Me_5)Ru\}_2(\mu\text{-}H)_4$ (**1**)

The hydride ligands of **1** undergo an intermolecular exchange reaction with dihydrogen under mild conditions. Exposure of a toluene solution of an isotopomer **1**-d_4 to an atmospheric pressure of dihydrogen resulted in the quantitative exchange of the deuteride ligands for hydride, affording **1**-h_4 [Equation (2)].

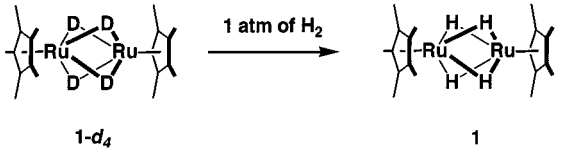

(2)

The mechanism shown in Scheme 1 possibly accounts for the H/D exchange reaction of **1** with H_2, which presumably involves a dihydride/dihydrogen equilibrium (step A and step B). With regard to the chemistry of η^2-dihydrogen complexes, such an equilibrium is proposed on the basis of VT-^{1}H NMR studies.[10]

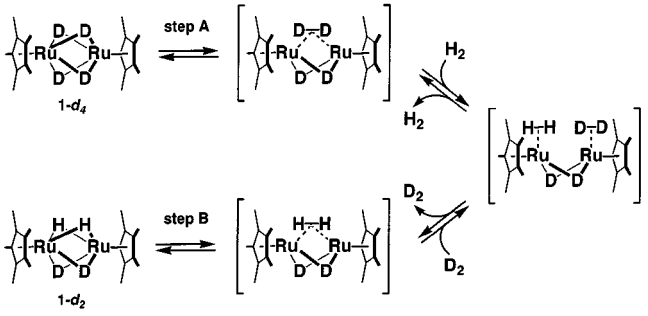

Scheme 1

2.2 Synthesis and Structure of Dinuclear Tetrahydride Complex of Iron

According to the vertical trends associated with the transition elements, the metal−metal and metal−ligand bond enthalpies decrease up a period and the complexes become substitutionally active. The iron analogue of diruthenium tetrahydride **1** is, therefore, expected to be much more reactive than **1**.

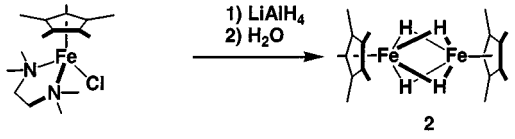

(3)

Treatment of $(C_5Me_5)FeCl(tmeda)$[11] with $LiAlH_4$, followed by workup with H_2O, gave the dinuclear iron tetrahydride $\{(C_5Me_5)Fe\}_2(\mu\text{-}H)_4$ (**2**) [Equation (3)].[12] The X-ray analysis clearly showed structural identity between **1** and **2**. The presence of four bridging hydride ligands are probably responsible for the short Fe−Fe distance of 2.202(1) Å.

We concluded that compound **2** was a classical metal hydride similar to **1** on the basis of the long H−H distance (av. 1.60 Å) and the large T_1 value of 0.63 s (−80 °C) for the hydride ligands. The iron tetrahydride **2** has also been shown to undergo H/D exchange between hydride ions and added dihydrogen. As anticipated, the reaction proceeded much faster than that of the corresponding ruthenium analogue. Since tetrahydride **2** is stable enough in solution not to release dihydrogen even under reduced pressure, the H/D exchange must be an associative process.

2.3 Dinuclear Polyhydride Clusters Bridged by a Ligand Containing a Heteroatom

Introduction of a bridging ligand containing a heteroatom into a dinuclear complex possibly affects the electronic and steric environment of the bimetallic reaction sites and, therefore, modifies the complex with regard to both reactivity and selectivity.

A dinuclear μ-alkylideneamide complex $\{(C_5Me_5)Ru\}_2(NC{-}R)_2(\mu\text{-}N{=}CHR)$ (**3**) was exclusively generated in the reaction of **1** with R−CN in diethyl ether, as a result of insertion of the nitrile into an Ru−H bond (Scheme 2).[13] The coordinated nitrile molecule in **3** was readily replaced with arene to form an (alkylideneamide)(η^2:η^2-arene) complex $\{(C_5Me_5)Ru\}_2(\mu\text{-}\eta^2\text{:}\eta^2\text{-arene})(\mu\text{-}N{=}CHR)$ (**4**). Complex **4** was directly synthesized by the reaction of **1** with nitrile in an appropriate arene solution.

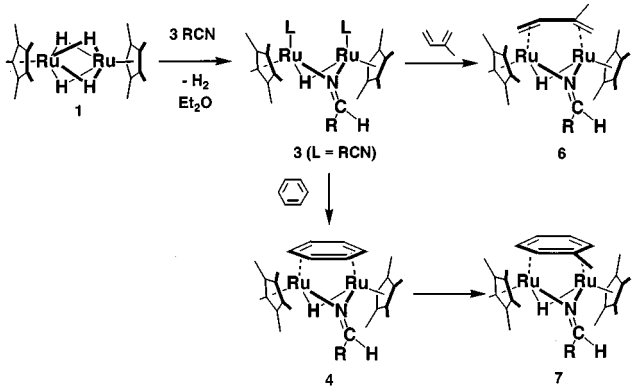

Scheme 2

A phosphide-bridged dinuclear complex $\{(C_5Me_5)Ru\}_2(\mu\text{-}\eta^2\text{:}\eta^2\text{-}C_6H_6)(\mu\text{-}PPh_2)$ (**5**) was prepared by applying a P−C(aromatic) bond cleavage reaction to PPh_3. Treatment of **1** with PPh_3 in toluene led to the formation of **5** as a result of the P−C bond cleavage [Equation (4)].[14]

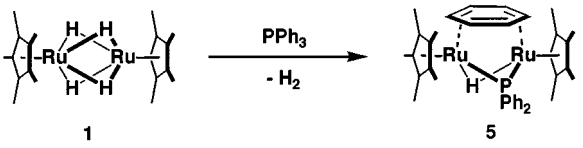

(4)

The formation of **5** is reasonably elucidated by a sequence of reactions depicted in Scheme 3. Coordination of PPh_3 and reductive elimination of H_2 would form an intermediary (dihydrido)(monophosphane) complex $\{(C_5Me_5)Ru\}_2(H)_2(PPh_3)$. Cleavage of a P−C bond of the coordinated PPh_3 ligand by one of the ruthenium centers would be expected to yield a μ-phosphido species that would then undergo reductive elimination of benzene and subsequent coordination of the benzene molecule in a $\mu\text{-}\eta^2\text{:}\eta^2$ mode to give **5**. For the cluster-mediated P−C bond cleavage of tertiary phosphane, a similar mechanism has been proposed.[15]

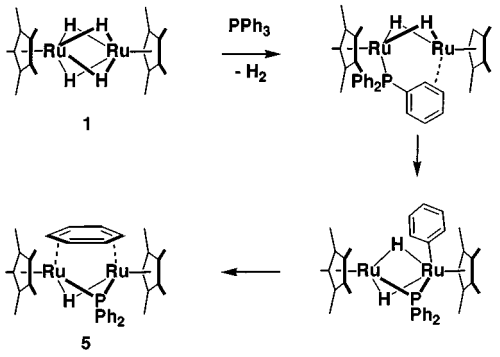

Scheme 3

A series of dinuclear μ-phosphido complexes $\{(C_5Me_5)Ru\}_2(\mu\text{-}\eta^2\text{:}\eta^2\text{-}C_6H_6)(\mu\text{-}PRR')$ were synthesized in a similar manner.[16] As a result, modification of the electronic environment of the bimetallic reaction sites might be achieved by changes in the substituents on the bridging phosphido ligand. It is noteworthy that arene molecules coordinated both in **4** and **5** were readily replaced by the added organic substrates and therefore, they are considered to be a suitable precursor of the active species for bimetallic activation. For example, addition of isoprene to a solution of **4** in tetrahydrofuran resulted in the exclusive formation of a (μ-alkylideneamide)(η^2:η^2-isoprene) complex $\{(C_5Me_5)Ru\}_2(\mu\text{-}\eta^2\text{:}\eta^2\text{-isoprene})(\mu\text{-N=CHR})$ (**6**). Similarly, the coordinated benzene was substituted with toluene to yield $\{(C_5Me_5)Ru\}_2(\mu\text{-}\eta^2\text{:}\eta^2\text{-toluene})(\mu\text{-N=CHR})$ (**7**) when **5** was heated at 60 °C in toluene.

2.4 Synthesis of Heterobimetallic Polyhydride Complexes

As an extension to multimetallic activation by homonuclear cluster complexes, we focused our attention on the synthesis of a heterometallic polyhydride cluster, thereby making the reaction sites electronically anisotropic. Enhancement of the anisotropic character of the reaction sites likely causes changes in regioselectivity at the stage of substrate activation. Although a number of heterobimetallic polyhydride cluster complexes have been synthesized,[17] there have only been a few reported examples of successful achievement of heterobimetallic activation of organic substrates.[18]

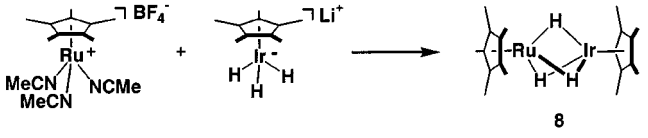

(5)

The reaction of $[(C_5Me_5)Ru(CH_3CN)_3](BF_4)$[19] with an anionic iridium hydride complex $Li[(C_5Me_5)IrH_3]$[20] led to a new heterobimetallic hydride cluster $(C_5Me_5)Ru(\mu\text{-}H)_3Ir(C_5Me_5)$ (**8**) [Equation (5)].[21]

The longitudinal relaxation time T_1 for the hydride ligands was determined to be 3.34 s at −80 °C, which is sufficient to characterize the complex as a classical trihydride complex. The hydride ligands of **8**, as well as the methyl group of the C_5Me_5 ligand coordinated to iridium, underwent an intermolecular H/D exchange reaction with C_6D_6. Interestingly, the H/D exchange of the bridging hydride ions preceded that of the methyl hydrogen atoms of the C_5Me_5 group, and the H/D exchange of the methyl hydrogen atoms selectively occurred on the C_5Me_5 ligand bound to the iridium center. The H/D exchange between the bridging hydride ions and that of the methyl hydrogen atoms on the C_5Me_5 group likely proceed via an intermediary η^2-C_6D_6 complex and an η^6-1,2,3,4-tetramethylfulvene or η^1:η^6-tetramethylcyclopentadienylmethyl intermediate, respectively. The latter process is proposed for the reversible hydrogen shift from a ring methyl group to the titanium center in $(C_5Me_5)_2Ti$.[22]

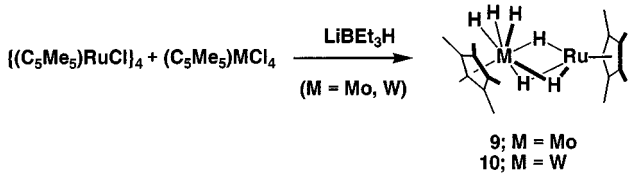

(6)

Heterobimetallic polyhydride complexes containing ruthenium and electron-deficient group-6 metal atoms, $(C_5Me_5)MH_3(\mu\text{-}H)_3Ru(C_5Me_5)$ (**9**: M = Mo; **10**: M = W), were obtained by the treatment of a 1:1 mixture of $\{(C_5Me_5)RuCl\}_4$ [19] and $(C_5Me_5)MCl_4$ [23] with $LiBEt_3H$ [Equation (6)].[24]

The X-ray diffraction studies of **9** and **10** clearly establish the dinuclear structure with 3 terminal hydride ions and the three bridging hydride ions. The signals for the six hydride ions of **10** were observed to be equivalent above −40 °C due to a rapid exchange of the hydride ions among the terminal sites on the molybdenum center and the bridging sites. The hydride ligands of **9** were more mobile than those of the tungsten analogue **10**, and the signal for the terminal and the bridging hydride ions de-coalesced at −110 °C. On the basis of the T_1 value, both **9** and **10** were concluded to be the classical hydride complexes.

Heterobimetallic polyhydride clusters with different metal/metal combinations, such as Ru/Rh,[25] Ru/Os,[26] and Ru/Re[27] were also synthesized and characterized.

2.5 Synthesis of a Trinuclear Polyhydride Cluster of Ruthenium

The reactivity of a cluster complex most probably depends on the ease of the electron transfer between complex and substrate. The number of transferable electrons between the cluster complex and the substrate must be changed by the nuclearity of the cluster: the more nuclei there are in the cluster, the more effectively electrons are transferred. As an extension of bimetallic activation, the trimetallic polyhydride cluster has attracted some attention.

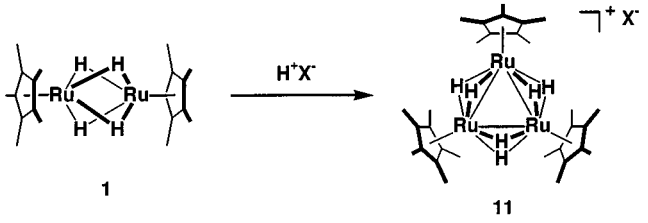

(7)

A cationic triruthenim hexahydride cluster $[\{(C_5Me_5)Ru(\mu\text{-}H)_2\}_3](X)$ (**11**) was obtained by the reaction of **1** with an acid HX in excellent yields [Equation (7)].[28,29] Compound **11** is stable enough to be stored in chloroform for several hours without decomposition.

The T_1 value of 0.387 s for the hydride resonance of **11** lies within the range of those for the classical hydride complexes. This result is consistent with the relatively long distance (average 1.81 Å) between the two hydrogen atoms bridging the same Ru−Ru bond observed in the X-ray structure.

Treatment of the cationic cluster **11** with an appropriate base such as sodium methoxide afforded a neutral pentahydride cluster $\{(C_5Me_5)Ru\}_3(\mu\text{-}H)_3(\mu_3\text{-}H)_2$ (**12**) [Equation (8)].[29]

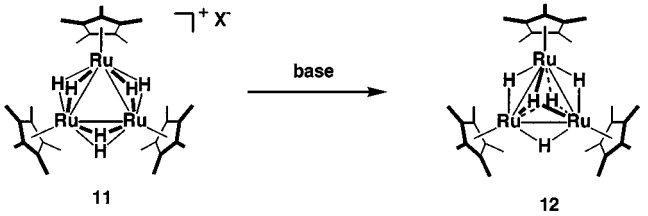

(8)

The VT-^{1}H NMR study has shown the rapid exchange of the hydride ions among the coordination sites, on an NMR timescale in the temperature range from 20 to −120 °C. The T_1 value of 2.55 s (−80 °C) for the hydride signal of **12** is significantly large in comparison with that of the hydride signal of the cationic cluster **11**. Cluster **12** was also concluded to be a classical hydride complex based on this T_1 value.

Triruthenium pentahydride **12** is an unsaturated 44-electron cluster and is able to capture a weakly coordinating substrate such as dihydrogen or benzene in a triangular reaction site. As a result, **12** readily underwent an H/D exchange reaction between the hydride ligands and D_2 or C_6D_6.

Unlike the cationic cluster **11**, the neutral cluster **12** is much more reactive because of high electron density at the metal center to activate even a chemically inert alkane molecule (vide infra).

2.6 Trinuclear Polyhydride Clusters with a Triply Bridged Ligand Containing a Heteroatom

Introduction of a triply bridging ligand on to the Ru_3 core allowed control over the reactivity of the cluster due to change in the electronic environment of the reaction site. It is of utmost importance to introduce one bridging ligand onto one side of the Ru_3 core. If both faces of the Ru_3 plane are covered with the two bridging ligands, there is no space for the substrate activation on the Ru_3 plane. Cluster **12** is stable enough not to undergo fragmentation of the Ru_3 framework even in the reaction with various reactive small molecules such as dioxygen and pressurized dihydrogen. A new class of trinuclear polyhydride cluster with a triply bridging ligand has therefore been synthesized by using pentahydride **12** as the starting material.

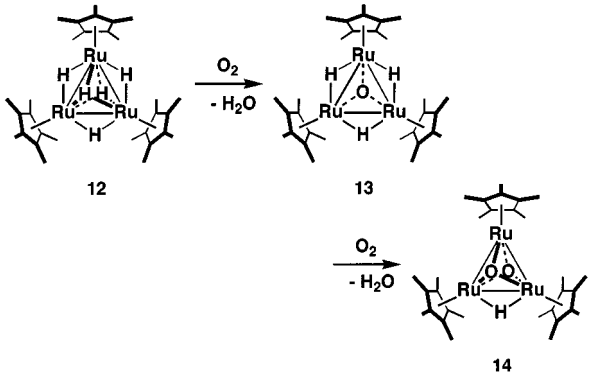

(9)

Cluster **12** was converted into a mono-μ_3-oxo complex $\{(C_5Me_5)Ru\}_3(\mu_3\text{-}O)(\mu\text{-}H)_3$ (**13**) and a di-μ_3-oxo complex $\{(C_5Me_5)Ru\}_3(\mu_3\text{-}O)_2(\mu\text{-}H)$ (**14**), successively, by the reaction with dioxygen at low temperature [Equation (9)].[29] The mono-μ_3-oxo complex was isolated in high yield by controlling the reaction conditions such as the O_2/**12** ratio and the temperature.

The sulfur analogue of **13**, $\{(C_5Me_5)Ru\}_3(\mu_3\text{-}S)(\mu\text{-}H)_3$ (**15**), was selectively synthesized by the reaction of **12** with an equimolar amount of thiophenol or diphenyl sulfide [Equation (10)].[30] An intermediary μ-(phenyl sulfide) complex $\{(C_5Me_5)Ru\}_3(\mu\text{-}SPh)(\mu\text{-}H)_4$ (**16**) was isolated in the reaction, which underwent S−C(aromatic) bond cleavage to afford **15**.

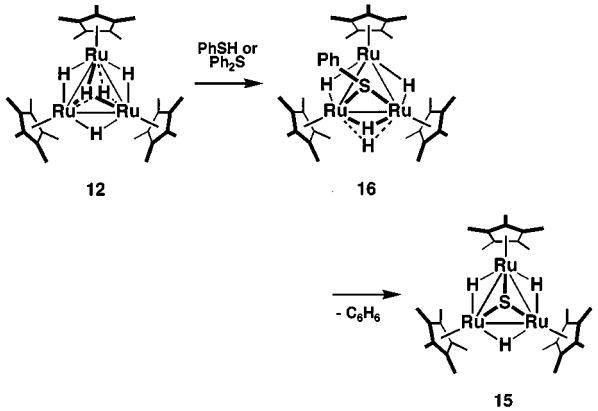

(10)

Reaction of **12** with excess diphenyl sulfide yielded a bi-capped cluster $\{(C_5Me_5)Ru\}_3(\mu_3\text{-}S)_2(\mu\text{-}H)$, which was almost inactive toward various unsaturated hydrocarbons because both faces of the Ru_3 core were covered with the μ_3-S groups.

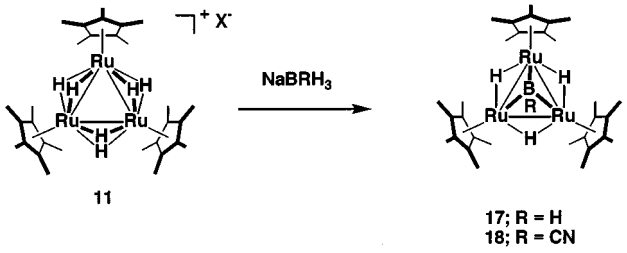

(11)

Bridging ligands containing not only an electronegative element but also an electropositive one were introduced into the Ru_3 core. The reaction of a cationic polyhydride cluster **11** with $NaBH_4$ resulted in the exclusive formation of $\{(C_5Me_5)Ru\}_3(\mu_3\text{-}BH)(\mu\text{-}H)_3$ (**17**) [Equation (11)].[31] A cluster having a μ_3-BCN ligand, $\{(C_5Me_5)Ru\}_3(\mu_3\text{-}BCN)(\mu\text{-}H)_3$ (**18**), was similarly prepared by using $NaB(CN)H_3$.[31] Complexes **17** and **18** are both an unprecedented type of a μ_3-borylene cluster, namely, "single-faced μ_3-borylene cluster", having a spacious reaction site on the reverse side of the μ_3-borylene ligand with respect to the Ru_3 plane.

3 Multimetallic Activation of Hydrocarbon Molecules on the Reaction Site of a Polyhydride Cluster

3.1 Reactions of a Dinuclear Polyhydride Cluster with Ethylene and Diphenylacetylene

The reaction of **1** with ethylene under atmospheric pressure proceeded at ambient temperature to form a dinuclear di-μ-η^1:η^2-vinyl complex $\{(C_5Me_5)Ru\}_2(CH_2CH_2)(\mu\text{-}CHCH_2)_2$ (**19**) in excellent yield [Equation (12)].[5b] The GLC analysis of the gas phase of the reaction revealed the formation of ca. 270% of ethane together with a small amount of 1-butene. This result suggests that the coordinatively unsaturated sites are generated on **1** by way of a hydride transfer from the ruthenium center to the ethylene ligand, i.e., hydrogenation of ethylene.

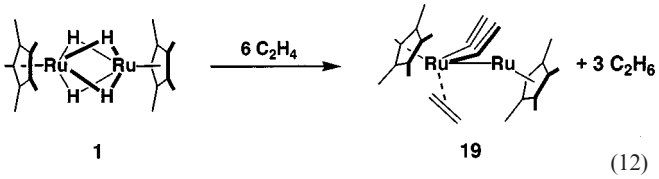

(12)

Monitoring the reaction by NMR spectroscopy showed the formation of an intermediary mono-μ-vinyl complex $\{(C_5Me_5)Ru\}_2(CH_2CH_2)(\mu\text{-}CHCH_2)(\mu\text{-}H)$ (**20**). Monovinyl complex **20** was highly reactive owing to coordinative unsaturation at the metal centers and could be readily converted into **19** in the presence of excess amounts of ethylene (Scheme 4).

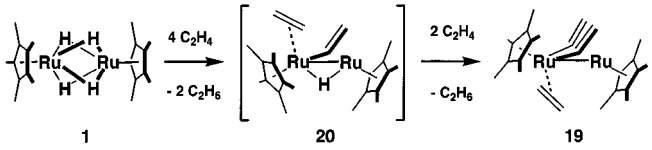

Scheme 4

Subsequent reaction proceeded to yield a 2,5-dimethylruthenacyclopentadiene complex **21** when **19** was heated in the presence of ethylene under atmospheric pressure [Equation (13)]. Ruthenacycle **21** was further converted into a μ-η^2:η^2:η^2-5-methylhepta-2,4,6-trien-2-yl complex **22** (Scheme 5). The formation of **22** is reasonably elucidated by the mechanism involving an insertion of the coordinated ethylene ligand into one of the Ru−C σ bonds of **21**. Subsequent β-H elimination from the resulting intermediary ruthenacycloheptadiene would yield **22**.

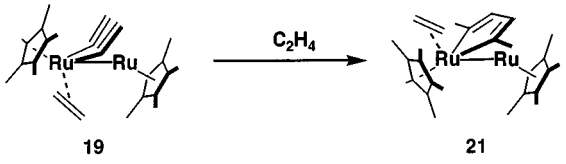

(13)

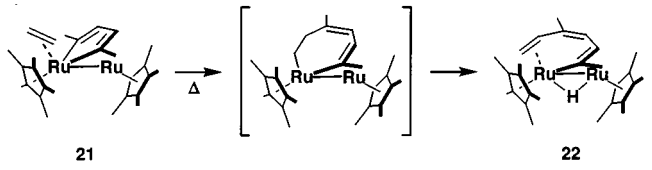

Scheme 5

Interestingly, dinuclear divinyl complex **19** underwent dehydrogenative C−C coupling between the terminal carbon atoms of the bridging vinyl groups to generate a ruthenacyclopentadiene complex **23** upon heating in the presence of trimethylphosphane (Scheme 6).[32]

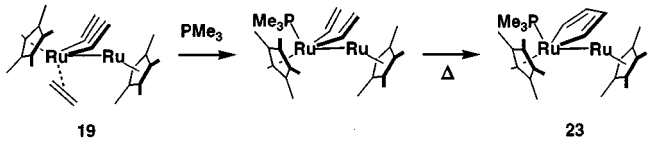

Scheme 6

Introduction of a bridging ligand onto the bimetallic reaction site caused changes in reactivity due to changes in the electronic and steric environment around the metal centers. The (μ-alkylidene)(amide) complex **4** could easily open a pair of vacant coordination sites in solution to generate an active species for bimetallic activation. The reaction of **4** with 1 atm of ethylene proceeded at ambient temperature

to give a bis(η^2-ethylene)ruthenium complex **24**.[13] When **24** was heated at 80 °C, a μ-η^2:η^2-*s*-*cis*-butadiene complex **25** was exclusively formed by a dehydrogenative coupling of the coordinated ethylene molecule (Scheme 7).

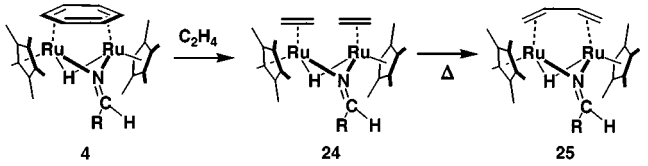

Scheme 7

The butadiene complex **25** could be directly synthesized from **4** by treatment with 1 atm of ethylene in refluxing toluene.

The reaction of the heterobimetallic complex **8** with ethylene revealed the site selectivity of the heterobimetallic system toward an organic substrate. The reaction of **8** with ethylene led to the exclusive formation of a di-μ-η^1:η^2-vinyl complex **26** [Equation (14)].[21] A notable feature of this reaction is the site selectivity in which C−H bond cleavage exclusively took place at the iridium center. The ruthenium center most likely plays the role of a coordination site.

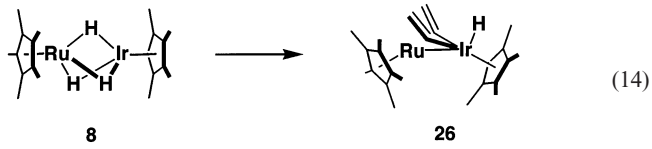

(14)

The reactivity of the heterobimetallic cluster **8** is significantly different from that observed for homonuclear cluster **1**. While the reaction of **1** with diphenylacetylene resulted in the formation of a dinuclear complex bridged by a perpendicularly coordinated diphenylacetylene, {(C_5Me_5)Ru}$_2$(μ-η^2:η^2-PhCCPh)(μ-H)$_2$ (**27**) [Equation (15)],[33] complex **8** smoothly reacted with diphenylacetylene to produce a μ-η^1:η^2-alkenyl complex, (C_5Me_5)Ir{μ-η^1:η^2-(*Z*)-CPh=CHPh}(μ-H)$_2$Ru(C_5Me_5) (**28**) (Scheme 8).[21] The formation of **28** is most likely due to an initial μ-η^2:η^2-alkyne coordination perpendicular to the Ir−Ru vector and subsequent *trans*-addition of Ir and a hydride ion to the carbon−carbon triple bond. The bridging alkenyl complex **28** was quantitatively converted into a dinuclear benzoiridacyclopentadiene complex **29**, as a result of intramolecular activation of the C(*ortho*)−H bond, upon heating at 80 °C.

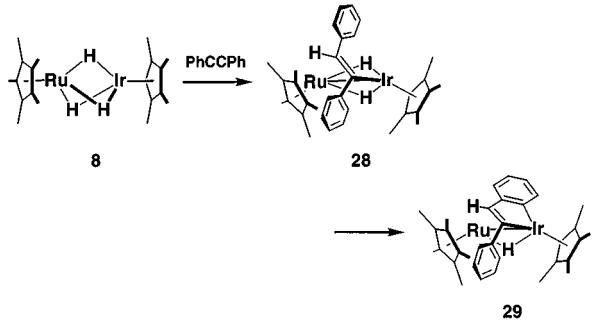

Scheme 8

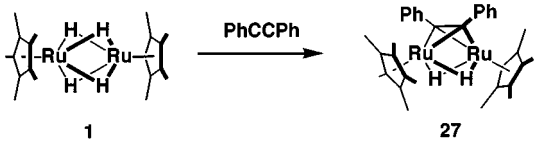

(15)

The reaction of **1** with various organosilanes provided evidence for the concerted activation of the Si−C and Si−H bonds, in which the two ruthenium atoms cooperatively affect the silane molecule. In the reaction of **1** with secondary silanes, a stepwise transformation of the silane from the μ-silane complex to a μ-silylene complex by way of the μ-silyl complex was observed, and each metal center mutually took the role of a binding site and an activation site (Scheme 9).[12,34]

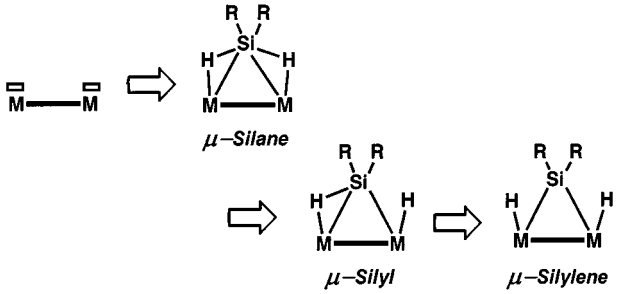

Scheme 9

3.2 Reactions of a Trinuclear Polyhydride Cluster with Acyclic 1,3-Dienes

The reaction of **12** with acyclic conjugated dienes such as butadiene and isoprene affords a novel trinuclear μ_3-η^2:η^2-*s*-*cis*-1,3-diene complexes having an agostic Ru−H−C interaction.

Treatment of **12** with excess butadiene (1 atm) in tetrahydrofuran led to the formation of a trinuclear 1-methyl-1,3-dimetalloallyl complex {(C_5Me_5)Ru}$_3$(H)$_4$(μ_3-η^3-C(Me)-CHCH} (**30**).[35] The reaction of **12** with isoprene proceeded in a similar manner at ambient temperature to form the corresponding μ_3-dimetalloallyl complex **31** [Equation (16)].

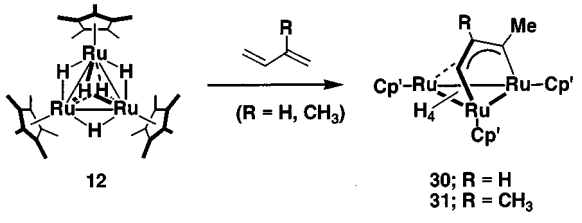

(16)

The molecular structure of **30** was proven by X-ray crystallography. Monitoring the reaction of **12** with 1 equiv. of isoprene in [D_6]benzene at room temperature by ^{1}H and ^{13}C NMR spectroscopy showed the formation of an intermediary trinuclear μ_3-η^2:η^2-*s*-*cis*-isoprene complex **33** in the initial stage of the reaction. Complex **33** involved an agostic interaction among the terminal carbon and hydrogen atoms and one of the ruthenium atoms. The small C(sp^2)−H

coupling constant (J_{CH} = 107 Hz) and the upfield shift (δ = −9.33) of the resonance for the terminal methylene proton of the diene ligand in **33** lie within the range of structurally well-established agostic complexes and unambiguously indicate the presence of a three-center two-electron Ru−H−C interaction.[18d,36] An intermediary agostic complex **32** was similarly detected in the reaction of **12** with butadiene by means of NMR spectroscopy.

The intermediates **32** and **33** underwent activation of the agostic C−H bond to ultimately form the 1,3-dimetalloallyl complexes **30** and **31**, respectively. These results show that 2 of the 3 ruthenium centers in **12** act as coordination sites, and the third metal atom takes the role of an activation site by agostic interaction in the reaction with 1,3-diene. This is a typical example showing the activation process performed by the concerted action of three metal centers.

Formation of the μ_3-η^2:η^2-*s*-*cis*-1,3-diene complexes **32** and **33** suggests the mechanism shown in Scheme 10 for the reaction of **12** with acyclic conjugated dienes leading to the exclusive formation of the μ_3-1,3-dimetalloallyl complexes. When the 1,3-diene is incorporated into the triangular reaction site, the diene ligand is forced to adopt the *s*-*cis* conformation to minimize the steric repulsion between the substrate and the C_5Me_5 groups. The agostic intermediate likely undergoes activation of the carbon−hydrogen bond to form a μ_3-η^1:η^2:η^2-dienyl complex. Insertion of the terminal carbon−carbon double bond into an adjacent Ru−H bond followed by carbon−hydrogen cleavage at the allylic position of the resulting dimetallocyclopentene would give the μ_3-1,3-dimetalloallyl complex as a final product.

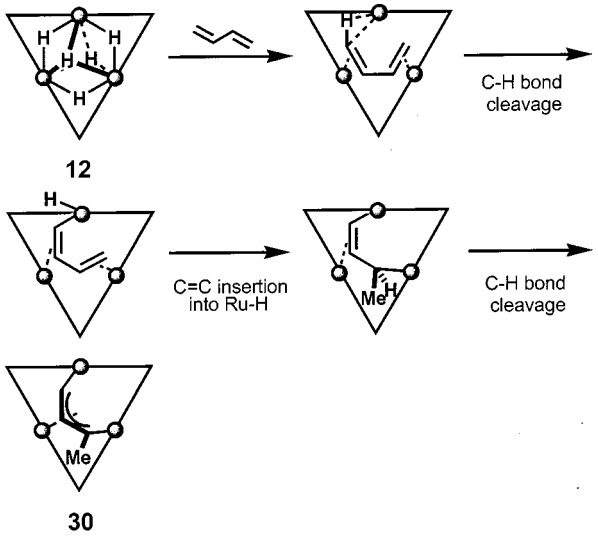

Scheme 10

As the trimetallic reaction site of **12** is surrounded by the three C_5Me_5 groups, steric repulsion between the C_5Me_5 ligand and the substrate strongly influences the incorporation step of the substrate into the trimetallic site. As a result, remarkable shape selectivity for the incorporation of the substrate was observed in the reaction of **12** with a series of substituted 1,3-diene. While complex **12** readily reacted with monosubstituted 1,3-butadienes such as isoprene, 1,3-pentadiene, and 1,3-hexadiene to generate the corresponding μ_3-1,3-dimetalloallyl complexes exclusively, the reaction of **12** with disubstituted butadiene such as 2,3-dimethyl-1,3-butadiene, 2-methyl-1,3-pentadiene, 3-methyl-1,3-pentadiene, and 2,4-hexadiene resulted in the recovery of the starting complex **12** and the diene.

3.3 Reactions of a Trinuclear Polyhydride Cluster with Cyclic 1,3-Dienes

The size and shape of cyclopentadiene fit well with those of the reaction site of **12**. Whereas C−H bond cleavage took place at the terminal carbon atom of the diene in the reaction of **12** with acyclic 1,3-diene, the reaction of **12** with cyclopentadiene resulted in selective C−C bond cleavage in cooperation with the three metal centers.

The reaction of **12** with cyclopentadiene in tetrahydrofuran at room temperature led to the quantitative formation of the trinuclear 2-methylruthenacyclopentadiene $\{(C_5Me_5)Ru\}_3(\mu\text{-}H)_3\{\mu_3\text{-}\eta^4\text{-}C(Me)=CHCH=CH\}$ (**34**) as a result of the $C(sp^2)-C(sp^3)$ bond cleavage of the cyclopentadiene [Equation (17)].[37] To the best of our knowledge, this is the first example of the selective activation of an unactivated carbon−carbon bond in cooperation with three metal centers. Kinetic parameters of $\Delta H^{\ddagger}$ = 12.7(3) kcal mol^{-1} and $\Delta S^{\ddagger}$ = −30.0(10) cal mol^{-1} K^{-1} for this reaction indicate that incorporation of the cyclopentadiene into the trimetallic reaction site is the rate-determining step.

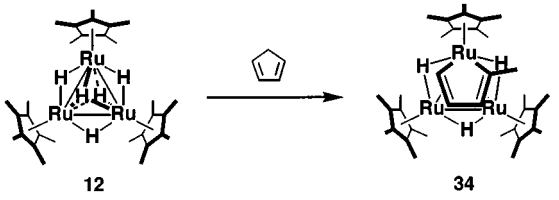

(17)

Monitoring the reaction of **12** with 5 equiv. of cyclopentadiene in [D_8]tetrahydrofuran at room temperature by ^{1}H NMR spectroscopy showed the formation of an intermediary ruthenacyclohexadiene **35** during the initial stage of the reaction. Although **35** could not be isolated, it was unambiguously characterized by means of NMR spectroscopy.

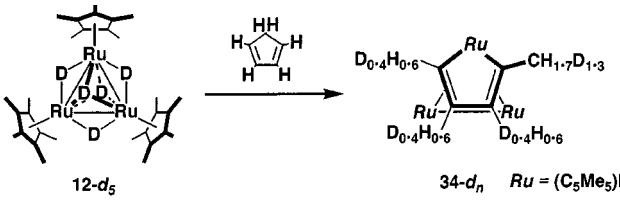

(18)

To elucidate the reaction mechanism, a labeling experiment was performed by use of triruthenium pentadeuteride complex **12**-d_5. The reaction of **12**-d_5 with cyclopentadiene-h_6 smoothly proceeded at room temperature to give an iso-

topomer of the 2-methylruthenacyclopentadiene **34**-d_n, in which the deuterium atoms were uniformly scrambled over the ruthenacycle [Equation (18)]. This result indicates that the activation of the carbon−hydrogen bond at the allylic position of cyclopentadiene leading to a μ_3-cyclopentadienyl intermediate takes place prior to the carbon−carbon bond cleavage.

One plausible reaction mechanism involving a pre-equilibrium between a μ_3-η^2:η^2-cyclopentadiene complex and a μ_3-η^5-cyclopentadienyl complex is illustrated in Scheme 11. Cyclopentadiene incorporated into the Ru_3 core is bound to two of the three ruthenium centers of **12** through μ-η^2:η^2 coordination to form the μ_3-cyclopentadiene complex. In the intermediary μ_3-cyclopentadiene complex, both the allylic C−H bond and the C(sp^3)−C(sp^2) bond are nicely oriented towards the third metal atom for the bond cleavage. Ruthenacyclohexadiene formed as a result of the C(sp^3)−C(sp^2) bond cleavage is in equilibrium with a μ_3-penta-1,4-diene-1,3-diyl complex, which undergoes insertion of the carbon−carbon double bond into Ru−H to yield a μ_3-5-methylruthenacyclopent-2-ene complex.

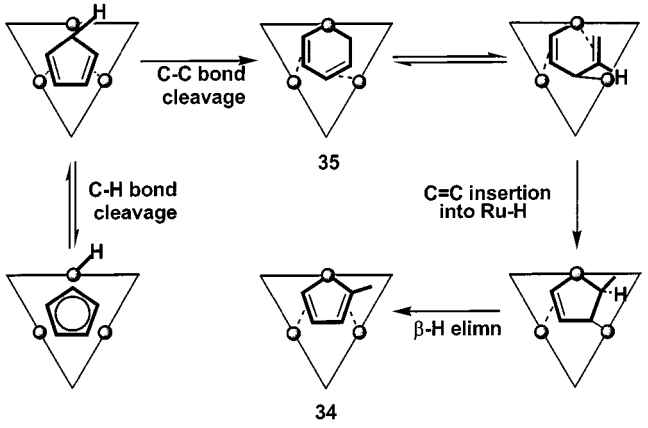

Scheme 11

The space of the triangular reaction site in **12** is large enough to accommodate a C_6-ring compound. The reaction of **12** with 5 equiv. of 1,3-cyclohexadiene in tetrahydrofuran resulted in the quantitative formation of a face-capping benzene complex $\{(C_5Me_5)Ru)_3(\mu\text{-}H)_3(\mu_3\text{-}\eta^2\text{:}\eta^2\text{:}\eta^2\text{-}C_6H_6)$ (**36**) by C−H bond cleavage at the allylic carbon atoms [Equation (19)].[38]

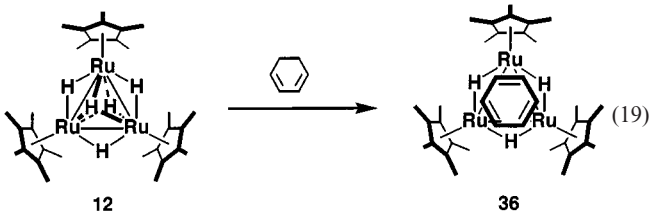

(19)

The shift of the ^1H and ^{13}C NMR resonances for the coordinated benzene ligand, respectively, are much higher than those observed in the carbonyl clusters $Ru_3(CO)_9(\mu_3\text{-}\eta^2\text{:}\eta^2\text{:}\eta^2\text{-}C_6H_6)$[39] and $Os_3(CO)_9$ (μ_3-η^2:η^2:η^2-C_6H_6).[40]

The μ_3-η^2:η^2:η^2 coordination of the benzene ring was unequivocally confirmed by an X-ray diffraction study. The reaction of **12** with 1,3-cyclohexadiene to give **36** is first-order in both **12** and cyclohexadiene [$k_{obs} = 2.7(1) \times 10^{-3}$ mol^{-1} s^{-1} at 66 °C] with $\Delta H^{\ddagger} = 13.5(8)$ kcal mol^{-1} and $\Delta S^{\ddagger} = -30.6(3)$ cal mol^{-1} K^{-1}. The value of the activation entropy is similar to that for the reaction of **12** with cyclopentadiene, as mentioned above. The negative large value of $\Delta S^{\ddagger}$ and the relatively small value of $\Delta H^{\ddagger}$ indicate that fitting into the size and shape between the substrate and the reaction site surrounded by the three C_5Me_5 groups is essential for the progress of the reaction.

In an attempt to observe intermediates by NMR spectroscopy, the reaction was performed in an NMR tube at 0 °C. Although no resonance signal except for those attributable to **12**, **36**, and H_2 was observed, the reaction most likely proceeds via an intermediary μ_3-η^2:η^2-cyclohexadiene complex. One plausible reaction mechanism for the reaction of **12** with cyclohexadiene leading to the μ_3-η^2:η^2-cyclohexadiene complex **37** is illustrated in Scheme 12. In the present reaction, two of the three metal centers in **12** act as coordination sites, and the third metal atom plays the role of an activation site to cleave an allylic C−H bond as observed in the reaction of **12** with butadiene or isoprene.

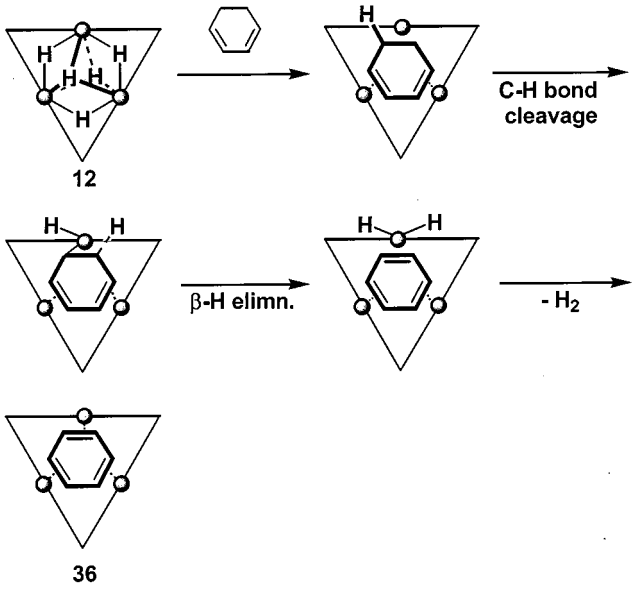

Scheme 12

In the trimetallic reaction site of the triruthenium pentahydride **12**, conjugated dienes with the appropriate size and shape could be effectively activated due to the concerted action of the three metal centers. The reaction of **12** with 1,4-cyclohexadiene or 1,3-cycloheptadiene, however, required heating at 60−100 °C to complete, because the orientation of two carbon−carbon double bonds or the ring size of the substrate is not suitable for the coordination to the Ru_3 site.

It is noteworthy that oxidation of the face-capping C_6H_6 complex **36** induces change in the coordination mode of the benzene ligand. The electrochemistry of **36** displays two

reversible one-electron oxidations at −490 and −224 mV vs. Ag/AgCl. To examine changes in the coordination mode of the face-capping benzene ligand due to changes in the oxidation state, oxidation of **36** with a ferricinium salt was examined (Scheme 13).

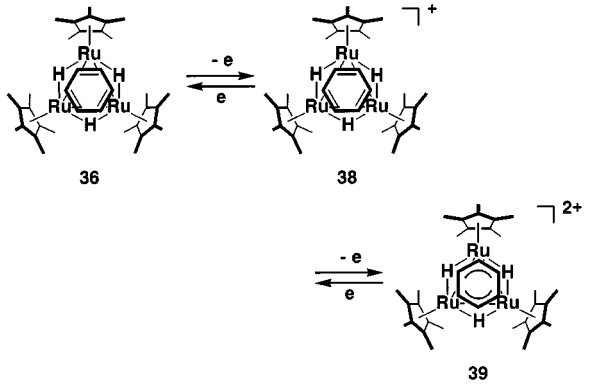

Scheme 13

Treatment of **36** with 1 equiv. of $[(C_5H_5)_2Fe]PF_6$ in toluene quantitatively yielded a paramagnetic monocationic complex $[\{(C_5Me_5)Ru\}_3(\mu\text{-}H)_3(\mu_3\text{-}\eta^2\text{:}\eta^2\text{:}\eta^2\text{-}C_6H_6)]PF_6$ (**38**). The X-ray diffraction study established the μ_3-η^2:η^2:η^2 coordination of benzene in **38**. As was anticipated from the electrochemical study, a diamagnetic complex $[\{(C_5Me_5)Ru\}_3(\mu\text{-}H)_3(\mu_3\text{-}\eta^3\text{:}\eta^3\text{-}C_6H_6)](PF_6)_2$ (**39**) was obtained by two-electron oxidation of **36**. The most striking structural feature of **39** is the μ_3-η^3:η^3 coordination of the C_6 ring (Figure 2). Thus far, there have been a few precedents of trinuclear μ_3-η^3:η^3-C_6H_6 complexes.[41] Complex **36** is, however, the first example that exhibits the hapticity change in the face-capping benzene ligand induced by a redox process.

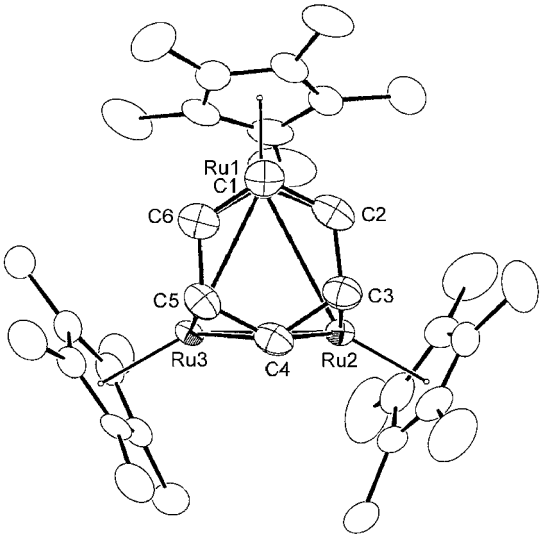

Figure 2. Molecular structure of $[\{(C_5Me_5)Ru\}_3(\mu\text{-}\eta^3\text{:}\eta^3\text{-}C_6H_6)]^{2+}$ (**39**)

3.4 Reactions of a Trinuclear Polyhydride Cluster with Benzothiophene and Dibenzothiophene

Cleavage of the C−S bond of thiophenes by transition metal complexes has attracted the attention of many inorganic and organometallic chemists in connection with hydrodesulfurization (HDS) from petroleum feedstock. While there is a vast chemistry of organosulfur−transition metal complexes, successful examples of C−S bond cleavage of benzothiophene and dibenzothiophene by mono- and dinuclear transition metal complexes have been limited.[42]

Interestingly, the trimetallic hydride cluster **12** could effectively activate benzothiophene and dibenzothiophene to cleave their C−S bonds selectively. The reaction of **12** with benzothiophene in toluene quantitatively afforded a (μ_3-phenethylidyne)(μ_3-sulfido) complex $\{(C_5Me_5)Ru\}_3(\mu\text{-}H)_2(\mu_3\text{-}S)(\mu_3\text{-}CCH_2Ph)$ (**41**) as a result of the successive cleavage of two C−S bonds (Scheme 14).[43]

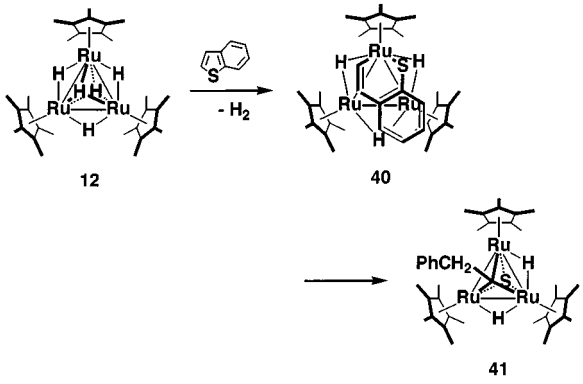

Scheme 14

Monitoring the reaction by means of ^{1}H NMR spectroscopy revealed formation of an intermediary thiaruthenacyclohexadiene complex **40**, which was isolated from the resulting mixture at −30 °C. The structure of the intermediary thiaruthenacyclohexadiene **40** was confirmed in comparison with that of the analogous thiaruthenacycle derived by the reaction of μ_3-borylene complex **17** with benzothiophene.[31] Complex **41** underwent hydrogenolysis by treatment of **41** with dihydrogen (7.2 atm) to produce ethylbenzene and the μ_3-sulfido complex **15** [Equation (20)].

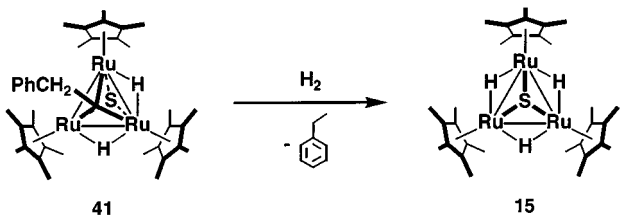

(20)

Complex **12** shows reactivity for the cleavage of the C−S bonds in dibenzothiophene. The reaction of **12** with dibenzothiophene proceeded at 110 °C to form **15** and biphenyl in high yield [Equation (21)].

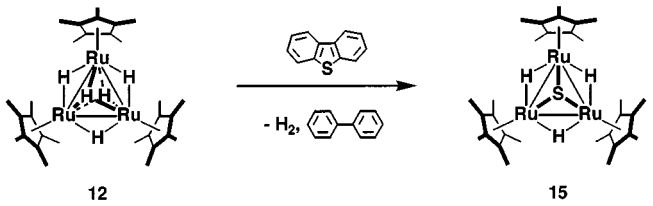

(21)

3.5 Reactions of a Trinuclear Polyhydride Cluster with Alkanes

Activation of an alkane C−H bond mediated by late transition metal complexes has been the focus of recent studies in organometallic chemistry because of its potential applicability to the functionalization of alkanes.[44] We have dealt with C−H bond activation of alkanes on the multimetallic site and found that trinuclear clusters **12** and **15** effectively activated alkanes in a thermal reaction.

Heating a solution of **12** in various alkanes at 170 °C resulted in the formation of novel trinuclear *closo*-ruthenacyclopentadiene complexs **42** (**a**: R = Me; **b**: R = Et; **c**: R = Pr; **d**: R = Bu; **e**: R = Am; **f**: R = Hx) in reasonable yield [Equation (22)].[45]

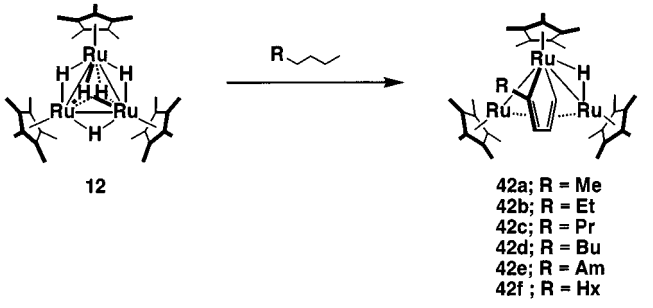

(22)

It is clear that the carbon framework of 2-alkylruthenacyclopentadiene in **42** originates from the *n*-alkane used as the solvent. In this reaction, six C−H bonds of the alkanes were successively cleaved on the trimetallic site, and these results strongly suggest the potential applicability of transition metal cluster complexes, especially polyhydrido metal clusters, to the functionalization of alkanes.

The *n*-alkane molecule is most likely incorporated into the triangular reaction site from one of the methyl termini at the initial stage of the reaction. This was confirmed through the H/D exchange between the hydride ligands in **12** and the deuterated methyl group in octane-d_{18} observed in the temperature range of 140−160 °C.

Monitoring the reaction by means of ^{1}H NMR spectroscopy showed signals for several reaction intermediates. They finally converged into thermodynamically stable products **42**. When the reaction of **12** with hexane was monitored at 170 °C by ^{1}H NMR spectroscopy, formation of an equilibrated mixture of perpendicularly coordinated μ_3-hexyne complexes, $\{(C_5Me_5)Ru\}_3(\mu\text{-}H)_3\{\mu_3\text{-}\eta^1\text{:}\eta^2\text{:}\eta^2\text{-}HCCC_4H_9\}$ (**43**-*in*) and $\{(C_5Me_5)Ru\}_3(\mu\text{-}H)_3\{\mu_3\text{-}\eta^1\text{:}\eta^2\text{:}\eta^2\text{-}C_4H_9CCH\}$ (**43**-*out*), was detected in a complex mixture of intermediates (Scheme 15). The intermediacy of the alkyne complex **43** was confirmed by use of an authentic complex independently prepared by treatment of **12** with 1-hexyne.

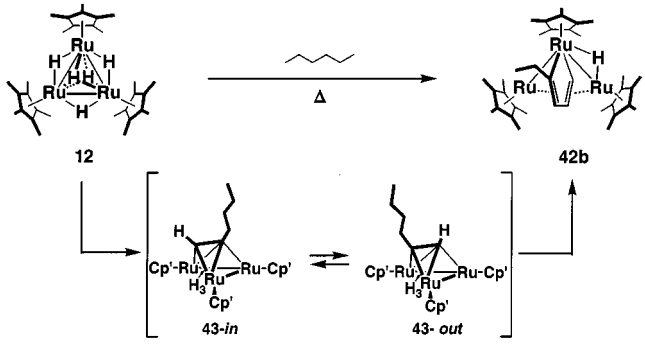

Scheme 15

To modify the regioselectivity of the triruthenium cluster mediated alkane C−H bond activation, a triply bridging sulfido ligand was introduced into the Ru_3 core by the reaction of **12** with thiophenol. The μ_3-sulfido group introduced was expected to reinforce the Ru_3 framework and to prevent Ru−Ru bond cleavage in the course of the reaction with the alkane.

Heating a solution of **15** in hexane at 170 °C for 107 h led to the quantitative formation of a μ_3-hexylidyne complex $\{(C_5Me_5)Ru\}_3(\mu_3\text{-}S)(\mu\text{-}H)_2\{\mu_3\text{-}C(CH_2)_4CH_3\}$ (**44b**) as a result of C−H bond cleavage at the terminal carbon atom while the reaction of **12** with hexane afforded a *closo*-ruthenacyclopentadiene complex **42**.[46] The results of the reactions of **15** with a series of alkanes are summarized in Scheme 16.

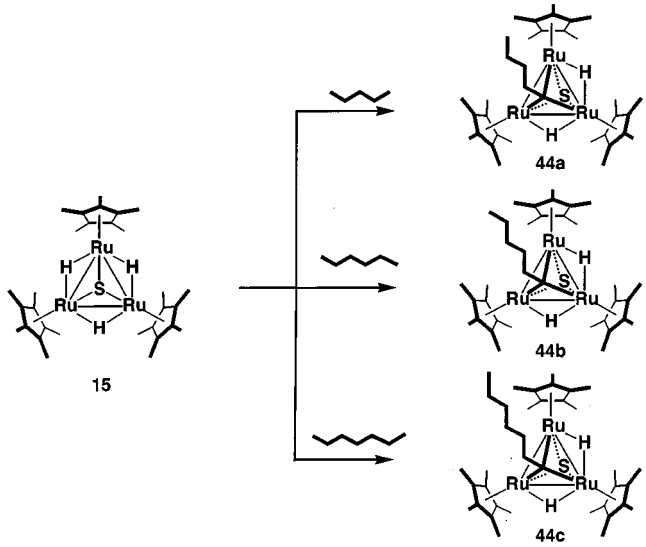

Scheme 16

A notable feature of the reaction is its regioselectivity such that no metal insertion products into the secondary C−H bonds were detected in spite of the clear advantage

over that of the primary C−H bonds, judging from the bond dissociation energy, ca. 95 kcal/mol vs. ca. 98 kcal/mol. The steric repulsion between the substrates and the C_5Me_5 fences surrounding the reaction site would be responsible for the highly primary-selective C−H bond activation because it impedes the access of the secondary C−H bonds to the metal center. The oxidative addition of the C−H bond at the less-hindered methyl group exclusively took place in the reaction with a 5-methylhexane to yield a 5-methylhexylidyne complex despite the statistical disadvantage.

Complex **15** was active toward cleavage of both aromatic and benzylic C−H bonds of toluene. When complex **15** was heated in [D_8]toluene at 130 °C, H/D exchange took place among the hydride ligands of **15** and the aromatic C−D bonds of [D_8]toluene. However, a tolyl intermediate resulting from the aromatic C−D bond cleavage could not be detected because it is presumably unstable due to the steric repulsion with the C_5Me_5 group. Heating a toluene solution of **15** at 170 °C, however, led to the exclusive formation of a thermally stable μ_3-benzilidyne complex $\{(C_5Me_5)Ru\}_3(\mu_3\text{-}S)(\mu\text{-}H)_2(\mu_3\text{-}CC_6H_5)$ (**46**) as a result of C−H bond cleavage at the benzylic carbon.

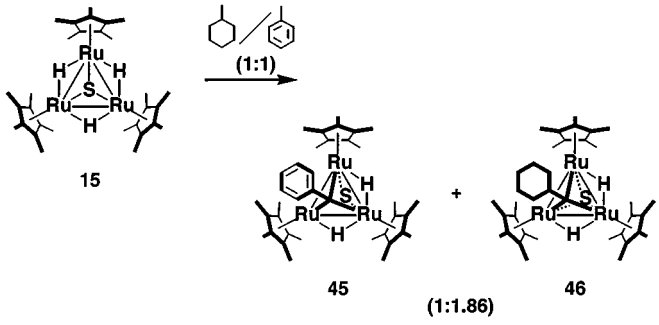

(23)

A competition experiment with a 1:1 mixture of toluene and methylcyclohexane was carried out to elucidate the mechanism. While the accessibility of the methyl group of these two substrates to the reaction site seem to be of similar extent in terms of the steric bulk of the substrate, the C(methyl)−H bond dissociation energy of toluene (ca. 88 kcal/mol) is much smaller than that of methylcyclohexane (ca. 98 kcal/mol). From a thermodynamic point of view, the μ_3-benzylidyne complex should be exclusively formed if the reaction proceeded via homolysis of the C−H bond. In spite of this, heating a solution of **15** in the mixed solvent at 170 °C for 142 h resulted in the formation of **45** and **46** in the ratio of 1:1.86 [Equation (23)]. This result implies that a radical mechanism seems unlikely for these reactions.

3.5 Reactions of a Trinuclear Polyhydride Cluster with 1,1-Disubstituted Alkenes

In comparison with the C−H bond cleavage reaction, there have been a relatively small number of successful examples of C−C bond cleavage mediated by mononuclear transition metal complexes.[44h,47] However, the remarkable properties of a multimetallic system, namely its capability of multiple coordination and multi-electron transfer, enabled us to activate not only a C−C single bond[37,48] but also a double bond.

The reaction of **12** with excess methyl methacrylate at 80 °C resulted in the quantitative formation of $\{(C_5Me_5)Ru\}_3(\mu_3\text{-}\eta^2\text{:}\eta^2\text{-}CH{=}CCO_2Me)(\mu_3\text{-}CH)(\mu\text{-}H)_2$ (**47a**) [Equation (24)].[49] The reaction of **12** with a 1,1-disubstituted alkene such as α-methylstyrene, methylenecyclopentane, methylenecyclohexane, and α-methylene-γ-butyrolactone proceeded similarly, leading to the exclusive formation of the corresponding (μ_3-alkyne)(μ_3-methylidyne) complexes **47b**−**47e**.

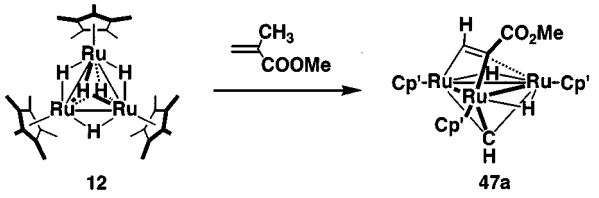

(24)

Formation of **47** evidently shows that the C−C double bond is cleaved, and the resulting two fragments are converted into the μ_3-methylidyne and the μ_3-alkyne moieties. When the reaction of **12** with the alkene was conducted under milder conditions, formation of an intermediary μ_3-vinylidene complex **48** was detected. Interestingly, heating a solution of the dimetalloallyl complex **31** derived from isoprene resulted in the formation of a 1:1 mixture of **47f** and **47g** by way of the μ_3-vinylidene complex. These observations are consistent with the reaction path involving a reversible isomerization between the μ_3-vinylidene complex and the μ_3-1,3-dimetalloallyl complex, followed by C−C bond cleavage that is likely associated with metal−metal bond cleavage and recombination (Scheme 17).

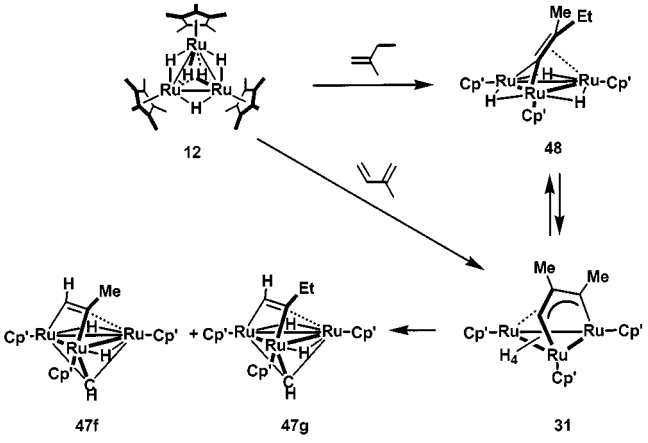

Scheme 17

4. Conclusion

The reaction chemistry of metal polyhydride clusters has been a relatively unexplored field in comparison with that

of polycarbonyl clusters. However, the newly developed cyclopentadienylmetal polyhydride system has brought about several great changes in the reactivity of the clusters. Metal polyhydride clusters, especially those having C_5Me_5 groups, reveal remarkable reactivity, that is, an unprecedented mode of C−C bond cleavage, C−C double bond cleavage of terminal alkenes, alkane C−H bond cleavage, and so on.

Among the intrinsic properties of metal clusters, their capability of multi-electron transfer and multiple coordination discriminate their reactivity from that of mononuclear metal complexes. Particularly, the latter is most probably essential for the multimetallic activation. The metal−metal distances of the polyhydride clusters appearing in this review are in the range of 2−3 Å, and these metal−metal separations would be suitable for cooperation of multiple metal atoms in the activation step of the substrate. In the above-mentioned polyhydride clusters, metal centers are tightly bound to each other by multiple bridging hydride ions and, therefore, the clusters are stable enough not to undergo fragmentation during the reaction. As a result, each metal center mutually takes the role of a binding site and an activation site and activates the substrate concertedly.

We are now exploring the following three subjects: (1) synthesis of clusters with higher nuclearity, (2) modification of the electronic and steric environment of the reaction site by introducing a variety of bridging ligands into the core of the cluster, and (3) synthesis of heterometallic polyhydride clusters.

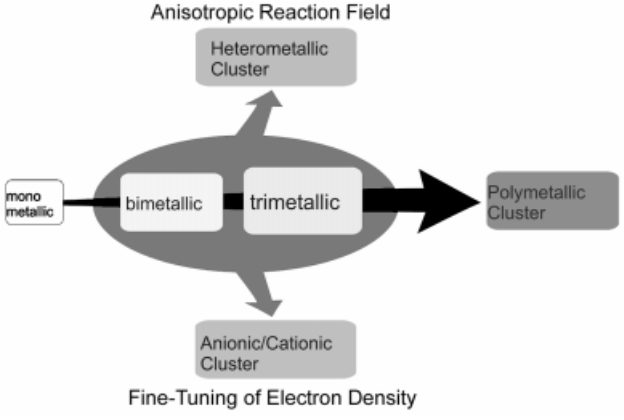

Systematic, namely both experimental and theoretical studies of the multimetallic activation would be a shortcut to the successful development of really new and versatile methods of transformation of the organic substrates.

[1] For example: [1a] J. Feng, M. Garland, *Organometallics* **1999**, *18*, 417−427. [1b] M. Castiglioni, S. Deabate, R. Giordano, P. J. King, S. A. R. Knox, E. Sappa, *J. Organomet. Chem.* **1998**, *571*, 251−260. [1c] T. A. Bazhenova, M. A. Bazhenova, S. A. Mironova, G. N. Petrova, A. K. Shilova, N. I. Shuvalova, A. E. Shilov, *Inorg. Chem. Acta* **1998**, *270*, 221−226. [1d] G. Suess-Fink, G. Meister, *Adv. Organomet. Chem.* **1993**, *35*, 41−134. [1e] B. C. Gates, L. Guzci, V. H. Knozinger (Eds.), *Metal Clusters in Catalysis*, Elsevier, Amsterdam, **1986**. [1f] R. D. Adams, F. A. Cotton (Eds.), *Catalysis by Di- and Polynuclear Metal Cluster Complexes*, Wiley-VCH, New York, **1998**, and references cited therein.

[2] For example: [2a] P. Dapporto, S. Midollini, L. Sacconi, *Inorg. Chem.* **1975**, *14*, 1643−1650. [2b] H. H. Wang, L. H. Pignolet, *Inorg. Chem.* **1980**, *19*, 1470−1480. [2c] R. A. Jones, G. Wilkinson, I. J. Colquhoun, W. McFarlane, A. M. R. Galas, M. B. Hursthouse, *J. Chem. Soc., Dalton Trans.* **1980**, 2480−2487. [2d] I. R. Butler, W. R. Cullen, T.-J. Kim, F. W. B. Einstein, T. Jones, *J. Chem. Soc., Chem. Commun.* **1984**, 719−721. [2e] J. W. Bruno, J. C. Huffman, M. A. Green, J. D. Zubokowski, W. E. Hatfield, K. G. Caulton, *Organometallics* **1990**, *9*, 2556−2567. [2f] M. D. Fryzuk, J. B. Ng, J. Rettig, J. H. Huffman, K. Jonas, *Inorg. Chem.* **1991**, *30*, 2437−2431. [2g] I. Moldes, B. Delavaux-Nicot, N. Lugan, R. Mathieu, *Inorg. Chem.* **1994**, *33*, 3510−3514. [2h] I. Moldes, S. Nefedov, N. Lugan, R. Mathieu, *J. Organomet. Chem.* **1995**, *490*, 11−19. [2i] F. Bachechi, *J. Organomet. Chem.* **1994**, *474*, 191−197. [2j] P. Berno, S. Gambarotta, *Angew. Chem. Int. Engl.* **1995**, *34*, 822−824. [2k] R. C. Schnabel, P. S. Carrol, D. M. Roddick, *Organometallics* **1996**, *15*, 655−662. [2l] W.-Q. Weng, A. M. Arif, R. D. Ernst, *J. Cluster Sci.* **1996**, *7*, 629−641. [2m] M. H. Drabnis, R. Bau, S. A. Mason, J. E. Freeman, R. D. Ernst, *Eur. J. Inorg. Chem.* **1998**, 851−854.

[3] For example: [3a] E. Roland, W. Bernhardt, H. Vahrenkamp, *Chem. Ber.* **1985**, *118*, 2858−2873. [3b] C. E. Barnes, J. A. Orvis, G. M. Finniss, *Organometallics* **1990**, *9*, 1695−1697. [3c] C. P. Casey, E. A. Austin, A. L. Rheingold, *Organometallics* **1987**, *6*, 2157−2164. [3d] E. N. Jacobsen, R. G. Bergman, *Organometallics* **1984**, *3*, 329−331. [3e] K. H. Theopold, R. G. Bergman, *J. Am. Chem. Soc.* **1983**, *105*, 464−475. [3f] N. M. Doherty, J. A. K. Howard, S. A. R. Knox, N. J. Tevrill, M. I. Yates, *J. Chem. Soc., Chem. Commun.* **1989**, 638−640. [3g] N. J. Forrow, S. A. R. Knox, *J. Chem. Soc., Chem. Commun.* **1984**, 679−681. [3h] A. F. Dyke, S. A. R. Knox, M. J. Morris, P. J. Naish, *J. Chem. Soc., Dalton Trans.* **1983**, 1417−1426. [3i] R. E. Colborn, D. L. Davis, A. F. Dyke, S. A. R. Knox, K. A. Mead, A. G. Orpen, *J. Chem. Soc., Dalton Trans.* **1989**, 1799−1805. [3j] J. A. Beck, S. A. R. Knox, G. H. Riding, G. E. Taylor, M. J. Winter, *J. Organomet. Chem.* **1980**, *202*, C49−C52. [3k] R. E. Colborn, A. F. Dyke, B. P. Gracey, S. A. R. Knox, K. A. Macpherson, K. A. Mead, A. G. Orpen, *J. Chem. Soc., Dalton Trans.* **1990**, 761−771. [3l] L. A. Brady, A. F. Dyke, S. E. Garner, V. Guerchais, S. A. R. Knox, J. P. Maher, S. M. Nicholls, A. G. Orpen, *J. Chem. Soc., Chem. Commun.* **1992**, 310−312. [3m] P. Brun, G. M. Dawkins, M. Green, R. M. Mills, J. Y. Salaun, F. G. A. Stone, P. Woodward, *J. Chem. Soc., Chem. Commun.* **1981**, 966−968. [3n] N. J. Forrow, S. A. R. Knox, M. J. Morris, A. G. Orpen, *J. Chem. Soc., Chem. Commun.* **1983**, 234−235. [3o] H. Wadepohl, T. Borchert, K. Buchner, H. Rritzkow, *Chem. Ber.* **1993**, *126*, 1615−1618. [3p] H. Bantel, A. K. Powell, H. Vahrenkamp, *Chem. Ber.* **1990**, *123*, 1607−1616. [3q] K. J. Adams, J. J. Baker, S. A. R. Knox, A. G. Orpen, *J. Chem. Soc., Dalton Trans.* **1996**, 975−988.

[4] [4a] N. Oshima, H. Suzuki, Y. Moro-oka, *Chem. Lett.* **1984**, 1161−1164. [4b] T. D. Tilley, R. H. Grubbs, J. E. Bercaw, *Organometallics* **1984**, *3*, 274−278.

[5] [5a] H. Suzuki, H. Omori, D. H. Lee, Y. Yoshida, Y. Moro-oka, *Organometallics* **1988**, *7*, 2243−2245. [5b] H. Suzuki, H. Omori, D. H. Lee, Y. Yoshida, M. Fukushima, M. Tanaka, Y. Moro-oka, *Organometallics* **1994**, *13*, 1129−1146.

[6] [6a] R. Bau, W. E. Carrol, R. G. Teller, T. F. Koetzle, *J. Am. Chem. Soc.* **1977**, *99*, 3872−3874. [6b] R. B. Wilson, Jr., A. P. Sattelberger, J. C. Huffman, *J. Am. Chem. Soc.* **1982**, *104*, 858−860.

[7] [7a] M. A. Bennett, J. P. Ennett, K. I. Gell, *J. Organomet. Chem.* **1982**, *233*, C17−C20. [7b] M. A. Bennett, J. P. Ennett, *Inorg. Chem. Acta* **1992**, *198*, 583−592. [7c] M. Jahncke, A. Neels, H. Stoeckli-Evans, G. Suess-Fink, *J. Organomet. Chem.* **1998**, *561*, 227−235.

[8] D. G. Hamilton, R. H. Crabtree, *J. Am. Chem. Soc.* **1988**, *110*, 4126−4133.
[9] N. Koga, K. Morokuma, *J. Mol. Struct.* **1993**, *300*, 181−189.
[10] [10a] G. J. Kubas, R. R. Ryan, D. A. Wrobleski, *J. Am. Chem. Soc.* **1986**, *108*, 1339−1341. [10b] M. Bautista, K. A. Earl, R. H. Morris, A. Sella, *J. Am. Chem. Soc.* **1987**, *109*, 3780−3782. [10c] T. Arliguie, B. Chaudret, *J. Chem. Soc., Chem. Commun.* **1989**, 155−157. [10d] M. S. Chinn, D. M. Heinekey, *J. Am. Chem. Soc.* **1990**, *112*, 5166−5175. [10e] R. H. Crabtree, M. Lavin, L. Bonneviot, *J. Am. Chem. Soc.* **1986**, *108*, 4032−4037. [10f] C. Bianchini, C. Mealli, M. Peruzzini, F. Zanobini, *J. Am. Chem. Soc.* **1987**, *109*, 5548−5549.
[11] K. Jonas, P. Klusmann, R. Goddard, *Z. Naturforsch., Teil B* **1995**, *50*, 394−404.
[12] Y. Ohki, H. Suzuki, *Angew. Chem. Int. Ed.* **2000**, *39*, 3120−3122.
[13] K. Tada, M. Oishi, H. Suzuki, *Organometallics* **1996**, *15*, 2422−2424.
[14] H. Omori, H. Suzuki, Y. Take, Y. Moro-oka, *Organometallics* **1989**, *8*, 2270−2272.
[15] R. A. Dubois, P. E. Garrou, *Organometallics* **1986**, *5*, 466−473.
[16] Y. Ohki, H. Suzuki, to be published.
[17] [17a] D. Michos, X. L. Luo, R. H. Crabtree, *Inorg. Chem.* **1993**, *32*, 2118−2122. [17b] N. S. Radu, P. K. Grantzel, T. D. Tilley, *J. Chem. Soc., Chem. Commun.* **1994**, 1175−1176. [17c] M. L. H. Green, A. K. Hughes, D. M. Michaelidou, P. Mountford, *J. Chem. Soc., Chem. Commun.* **1993**, 591−593. [17d] D. W. Stephan, *Coord. Chem. Rev.* **1989**, *95*, 41−107. [17e] S. F. Amevor, H. U. Hund, A. Salzer, *J. Organomet. Chem.* **1996**, *520*, 79−84. [17f] J. T. Poulton, K. Folting, K. G. Caulton, *Organometallics* **1992**, *11*, 1364−1372. [17g] D. Alvarez, Jr., E. G. Lundquist, J. W. Ziller, W. J. Evans, K. G. Caulton, *J. Am. Chem. Soc.* **1989**, *111*, 8392−8398. [17h] D. Alvarez, Jr., K. G. Caulton, W. J. Evans, J. W. Ziller, *Inorg. Chem.* **1992**, *31*, 5500−5508. [17i] D. Alvarez, Jr., K. G. Caulton, *J. Am. Chem. Soc.* **1990**, *112*, 5674−5676. [17j] Z. He, S. Nefedov, N. Lugan, D. Neibecker, R. Mathieu, *Organometallics* **1993**, *12*, 3837−3845. [17k] Z. He, D. Neibecker, N. Lugan, R. Mathieu, *Organometallics* **1992**, *11*, 817−821.
[18] [18a] A. M. Baranger, R. G. Bergman, *J. Am. Chem. Soc.* **1994**, *116*, 3822−3835. [18b] R. M. Bullock, C. P. Casey, *Acc. Chem. Res.* **1987**, *20*, 167−173. [18c] T. Nakajima, I. Shimizu, K. Kobayashi, H. Koshino, Y. Wakatsuki, *Inorg. Chem.* **1997**, *36*, 6440−6442. [18d] Z. He, L. Plasseraud, I. Moldes, F. Dahan, D. Neibecker, M. Etienne, R. Mathieu, *Angew. Chem. Int. Ed. Engl.* **1995**, *34*, 916−917.
[19] P. Fagan, D. W. Michael, J. C. Calabrese, *J. Am. Chem. Soc.* **1989**, *111*, 1698−1719.
[20] T. M. Gilbert, F. J. Hollander, R. G. Bergman, *J. Am. Chem. Soc.* **1985**, *107*, 3508−3516.
[21] T. Shima, H. Suzuki, *Organometallics* **2000**, *19*, 2420−2422.
[22] J. E. Bercaw, *J. Am. Chem. Soc.* **1974**, *96*, 5087−5095.
[23] R. C. Murray, L. Blum, A. H. Liu, R. R. Schrock, *Organometallics* **1985**, *4*, 953−954.
[24] T. Shima, J. Ito, H. Suzuki, *Organometallics* **2001**, *20*, 10−12.
[25] T. Shima, Y. Sugimura, H. Suzuki, to be published.
[26] T. Shima, H. Suzuki, to be published.
[27] T. Shima, J. Ito, H. Suzuki, to be published.
[28] H. Suzuki, T. Kakigano, M. Igarashi, M. Tanaka, Y. Moro-oka, *J. Chem. Soc., Chem. Commun.* **1991**, 283−285.
[29] H. Suzuki, T. Kakigano, K. Tada, M. Igarashi, K. Matsubara, A. Inagaki, M. Ohshima, M. Tanaka, to be published.
[30] K. Matsubara, H. Suzuki, to be published.
[31] R. Okamura, K. Tada, K. Matsubara, M. Oshima, H. Suzuki, *Organometallics* **2001**, *20*, 4772−4774.
[32] H. Omori, H. Suzuki, Y. Moro-oka, *Organometallics* **1989**, *8*, 1576−1578.
[33] H. Omori, H. Suzuki, T. Kakigano, Y. Moro-oka, *Organometallics* **1992**, *11*, 989−992.
[34] [34a] H. Suzuki, T. Takao, M. Tanaka, Y. Moro-oka, *J. Chem. Soc., Chem. Commun.* **1992**, 476−478. [34b] T. Takao, H. Suzuki, *Organometallics* **1994**, *13*, 2554−2556. [34c] T. Takao, S. Yoshida, H. Suzuki, M. Tanaka, *Organometallics* **1995**, *14*, 3855−3868. [34d] Y. Ohki, T. Kojima, M. Oshima, H. Suzuki, *Organometallics* **2001**, *20*, 2654−2656. [34e] T. Takao, M. Amako, H. Suzuki, *Organometallics* **2001**, *20*, 3406−3422. [34f] T. Takao, M. Amako, H. Suzuki, *Chem. Lett.* **2001**, 1100−1101.
[35] T. Takemori, H. Suzuki, M. Tanaka, *Organometallics* **1996**, *15*, 4346−4348.
[36] [36a] G. Erker, W. Froemberg, K. Angermund, R. Schlund, C. Krueger, *J. Chem. Soc., Chem. Commun.* **1986**, 1629−1630. [36b] I. Hylakryspin, R. Gleiter, C. Krueger, R. Zwettler, G. Erker, *Organometallics* **1990**, *9*, 517−523. [36c] F. R. Lemke, D. J. Szalda, R. M. Bullock, *J. Am. Chem. Soc.* **1991**, *113*, 8466−8477. [36d] M. Brookhart, M. L. H. Green, *J. Organomet. Chem.* **1983**, *250*, 395−408.
[37] H. Suzuki, Y. Takaya, T. Takemori, *J. Am. Chem. Soc.* **1994**, *116*, 10779−10780.
[38] A. Inagaki, Y. Takaya, T. Takemori, H. Suzuki, M. Tanaka, M. Haga, *J. Am. Chem. Soc.* **1997**, *119*, 625−626.
[39] B. F. G. Johnson, J. Lewis, M. Martinelli, A. H. Wright, D. Braga, F. Grepioni, *J. Chem. Soc., Chem. Commun.* **1990**, 364−366.
[40] M. A. Gallop, M. P. Gomez-Sal, C. E. Housecroft, B. F. G. Johnson, J. Lewis, S. M. Owen, P. R. Raithby, A. H. Wright, *J. Am. Chem. Soc.* **1992**, *114*, 2502−2509.
[41] [41a] S. I. Troyanov, V. B. Rybakov, *Organomet Chem. USSR* **1988**, 579−583. [41b] S. I. Troyanov, *J. Organomet. Chem.* **1994**, *475*, 139−147.
[42] For example: [42a] A. E. Ogilvy, M. Draganjac, T. B. Rauchfuss, S. R. Wilson, *Organometallics* **1988**, *7*, 1171−1177. [42b] W. D. Jones, L. Dong, *J. Am. Chem. Soc.* **1991**, *113*, 559−564. [42c] W. D. Jones, R. M. Chin, *J. Am. Chem. Soc.* **1992**, *114*, 9851−9858. [42d] D. A. Vicic, W. D. Jones, *Organometallics* **1997**, *16*, 1912−1919. [42e] C. Bianchini, A. Meli, M. Peruzzini, F. Vizza, P. Frediani, V. Herrera, R. A. Sanchez-Delgado, *J. Am. Chem. Soc.* **1993**, *115*, 7505−7506. [42f] C. Bianchini, A. Meli, M. Peruzzini, F. Vizza, S. Moneti, V. Herrera, R. A. Sanchez-Delgado, *J. Am. Chem. Soc.* **1994**, *116*, 4370−4381. [42g] C. Bianchini, A. Meli, *J. Chem. Soc., Dalton Trans.* **1996**, 801−814. [42h] J. J. Garcia, B. E. Mann, H. Adams, N. A. Bailey, P. M. Maitlis, *J. Am. Chem. Soc.* **1995**, *117*, 2179−2186. [42i] C. A. Dullaghan, S. Sun, G. B. Carpenter, B. Weldon, D. A. Sweigart, *Angew. Chem. Int. Ed. Engl.* **1996**, *35*, 212−214. [42j] M. D. Curtis, S. H. Drucker, *J. Am. Chem. Soc.* **1997**, *119*, 1027−1036.
[43] K. Matsubara, R. Okamura, M. Tanaka, H. Suzuki, *J. Am. Chem. Soc.* **1998**, *120*, 1108−1109.
[44] For example: [44a] A. H. Janowicz, R. G. Bergman, *J. Am. Chem. Soc.* **1982**, *104*, 352−354. [44b] J. K. Hoyano, W. A. G. Graham, *J. Am. Chem. Soc.* **1982**, *104*, 3723−3725. [44c] A. H. Janwicz, R. G. Bergman, *J. Am. Chem. Soc.* **1983**, *105*, 3929−3939. [44d] P. L. Watson, *J. Am. Chem. Soc.* **1983**, *105*, 6491−6493. [44e] W. D. Jones, F. J. Feher, *Organometallics* **1983**, *2*, 562−563. [44f] C. M. Fendrick, T. J. Marks, *J. Am. Chem. Soc.* **1984**, *106*, 2214−2216. [44g] R. G. Bergman, *Science* **1984**, *223*, 902−908. [44h] R. H. Crabtree, *Chem. Rev.* **1985**, *85*, 245−269. [44i] B. A. Arndtsen, R. G. Bergmann, *Science* **1995**, *270*, 1970−1973. [44j] G. Suess-Fink, S. Stanislas, G. B. Shulpin, G. V. Nizova, H. Stoeckli-Evans, A. Neels, C. Bobillier, S. Claude, *J. Chem. Soc., Dalton Trans.* **1999**, 3169−3175.
[45] A. Inagaki, T. Takemori, M. Tanaka, H. Suzuki, *Angew. Chem. Int. Ed.* **2000**, *39*, 404−406.
[46] K. Matsubara, A. Inagaki, M. Tanaka, H. Suzuki, *J. Am. Chem. Soc.* **1999**, *121*, 7421−7422.
[47] For example: [47a] J. W. Kang, R. Moseley, P. M. Maitlis, *J. Am. Chem. Soc.* **1969**, *91*, 5970−5977. [47b] R. B. King, A. Efraty, *J. Am. Chem. Soc.* **1972**, *94*, 3773−3779. [47c] F. W. S. Benfield,

M. L. H. Green, *J. Chem. Soc., Dalton Trans.* **1974**, 1324−1331. [47d] R. H. Crabtree, R. P. Dion, *J. Chem. Soc., Chem. Commun.* **1984**, 1260−1261. [47e] J. W. Suggs, C.-H. Jun, *J. Am. Chem. Soc.* **1986**, *108*, 4679−4681. [47f] E. Bunel, B. J. Burger, J. E. Bercaw, *J. Am. Chem. Soc.* **1988**, *110*, 976−978. [47g] J. F. Hartwig, R. A. Andersen, R. G. Bergman, *J. Am. Chem. Soc.* **1989**, *111*, 2717−2719. [47h] M. Gozin, A. Weisman, Y. Ben-David, D. Milstein, *Nature* **1993**, *364*, 699−701.

[48] Y. Ohki, H. Suzuki, *Angew. Chem. Int. Ed.* **2000**, *39*, 3463−3465.

[49] T. Takemori, A. Inagaki, H. Suzuki, *J. Am. Chem. Soc.* **2001**, *123*, 1762−1763.

Received September 2, 2001
[I01388]

Bis[citrato(3−)-O^1,O^3,O^6]silicate: A Dianionic Complex with Hexacoordinate Silicon(IV) and Two Tridentate Dioato(2−)olato(1−) Ligands

Reinhold Tacke,*[a] Martin Penka,[a] Friedrich Popp,[a] and Ingo Richter[a]

Keywords: Silicon / Silicates / Coordination modes / Biomineralization

Simple preparative methods for the synthesis of a hexacoordinate silicate dianion with two tridentate citrato(3–) ligands have been developed. Thus, treatment of tetramethoxysilane with two molar equivalents of citric acid and two molar equivalents of tri(*n*-butyl)amine in tetrahydrofuran yielded tri(*n*-butyl)ammonium bis[citrato(3–)-O^1,O^3,O^6]silicate (**10**). Alternatively, **10** was prepared by treatment of tetrachlorosilane with two molar equivalents of citric acid and six molar equivalents of tri(*n*-butyl)amine in acetonitrile. Compound **10** was characterized by elemental analyses (C,H,N), solid-state ^{29}Si VACP/MAS NMR studies, solution NMR experiments (^{1}H, ^{13}C; CD_3CN), and a crystal structure analysis.
(© Wiley-VCH Verlag GmbH, 69451 Weinheim, Germany, 2002)

Introduction

In recent years, biochemistry and molecular biology have made significant contributions to the understanding of silica biomineralization.[1] However, almost nothing is known about how silicon acts in biological systems at the molecular level. Two decades ago it was speculated that organosilicates with chelate ligands derived from organic hydroxy compounds may play a role in silicon chemistry in the biosphere, controlling the transport of silicon, its concentration as a soluble silicon pool, and its deposition as silica.[2] In this context, chelate complexes with tetra-, penta-, or hexacoordinate silicon(IV) may be promising candidates.[3] In continuation of our studies on penta- and hexacoordinate silicates with bidentate ligands derived from organic dihydroxy compounds (mono- or dianionic complexes, such as **1**,[3c] **2**,[3d] **3**,[4,5] **4**,[4,5] and **5**[5]), we have attempted to synthesize the tris[citrato(2−)]silicate dianion **6**.[6]

Results and Discussion

To prepare the hexacoordinate silicate dianion **6** according to the strategy applied to the synthesis of **1**−**5**, tetramethoxysilane or tetrachlorosilane were treated with three molar equivalents of citric acid in acetonitrile in the presence of a tertiary amine. However, to our great surprise we did not observe the formation of **6**, but instead obtained the dianionic bis[citrato(3−)-O^1,O^3,O^6]silicate **7** in which two tridentate dioato(2−)olato(1−) ligands are bound to the silicon(IV) center. It is interesting to note that the reaction of

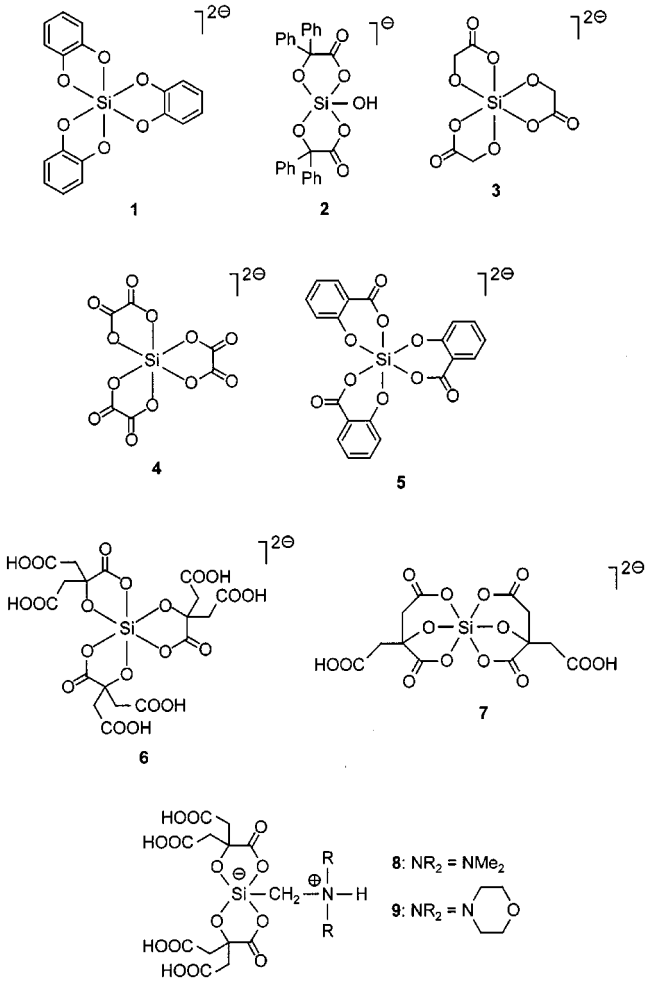

$(MeO)_3SiCH_2NR_2$ (NR_2 = NMe_2 or morpholino) with two molar equivalents of citric acid leads to the zwitterionic sil-

[a] Institut für Anorganische Chemie, Universität Würzburg,
Am Hubland, 97074 Würzburg, Germany
Fax: (internat.) +49-931/888-4609
E-mail: r.tacke@mail.uni-wuerzburg.de

icates **8**[3a] and **9**,[7] with two bidentate citrato(2−) ligands that exhibit chelating properties as in the hypothetical dianion **6**.

We report here on the synthesis of tri(*n*-butyl)ammonium bis[citrato(3−)-O^1,O^3,O^6]silicate (**10**), starting from tetramethoxysilane or tetrachlorosilane (Scheme 1). Compound **10** was isolated in 93% and 40% yield, respectively, as a colorless crystalline solid. To the best of our knowledge, complexes with hexacoordinate silicon(IV) and two tridentate dioato(2−)olato(1−) ligands have not yet been described in the literature.[8]

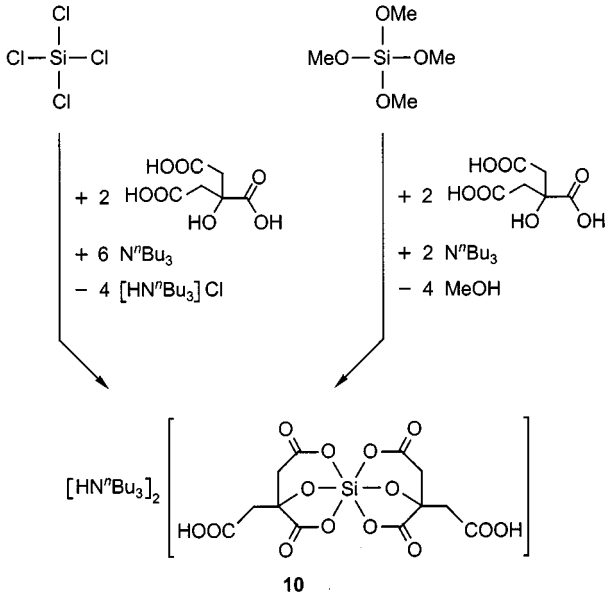

Scheme 1. Synthesis of compound **10**

As shown by single-crystal X-ray diffraction, the Si-coordination polyhedron of **10** is a distorted octahedron, with maximum deviations of 3.41(5)° and 5.59(5)° from the ideal 90° and 180° O−Si−O angles, respectively (Figure 1). The two tridentate citrato(3−) ligands are coordinated to the silicon atom each with two carboxylato oxygen atoms (O2/O3, O5/O6) and one alcoholato oxygen atom (O1, O4), forming two bicyclic moieties each with a five-, six-, and seven-membered ring. The Si−O(carboxylato) distances are in the range 1.7952(10)−1.8151(10) Å, whereas the Si−O(alcoholato) distances amount to 1.7163(10) Å (Si−O1) and 1.7330(10) Å (Si−O4). The carbon atoms C1 and C7 are stereogenic centers with identical absolute configurations (chiral dianion), and compound **10** crystallizes as a racemate (space group $P2_1/n$). It is interesting to note that related mononuclear hexacoordinate aluminum(III)[9,10] and gallium(III)[10] complexes with two tridentate citrato(3−) or citrato(4−) ligands crystallize as *meso* isomers (achiral dianion, center of inversion).

The isotropic ^{29}Si chemical shift ($\delta = -167.4$) determined by solid-state ^{29}Si VACP/MAS NMR experiments and the ^{13}C VACP/MAS NMR spectroscopic data of compound **10** are in excellent agreement with its crystal structure. However, the situation in solution (solvent: CD_3CN) appears to be more complicated since the ^{1}H and ^{13}C NMR

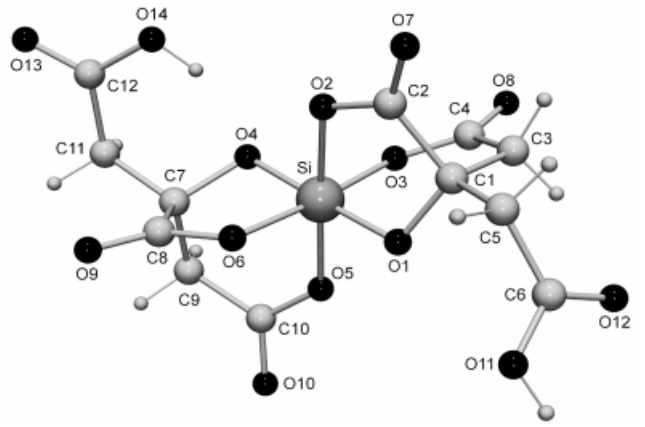

Figure 1. Structure of the silicate dianion in the crystal of **10**; selected bond lengths [Å] and angles [°]: Si−O1 1.7163(10), Si−O2 1.8151(10), Si−O3 1.8001(10), Si−O4 1.7330(10), Si−O5 1.7952(10), Si−O6 1.8116(10); O1−Si−O2 88.49(5), O1−Si−O3 92.78(5), O1−Si−O4 178.56(5), O1−Si−O5 88.25(5), O1−Si−O6 92.76(5), O2−Si−O3 90.62(5), O2−Si−O4 90.22(5), O2−Si−O5 176.62(5), O2−Si−O6 88.74(5), O3−Si−O4 86.59(5), O3−Si−O5 90.41(5), O3−Si−O6 174.41(5), O4−Si−O5 93.05(5), O4−Si−O6 87.85(5), O5−Si−O6 90.54(5), Si−O1−C1 109.95(8), Si−O2−C2 112.92(8), Si−O3−C4 127.73(9), Si−O4−C7 109.80(8), Si−O5−C10 127.71(9), Si−O6−C8 113.37(9); hydrogen-bonding system in the crystal: intermolecular bifurcate N1−H···O3/O8 and N2−H···O5/O10 hydrogen bonds; intermolecular O11−H···O12 interaction; intramolecular bifurcate O14−H···O2/O4 hydrogen bond[11]

spectroscopic data (^{1}H,^{1}H and ^{1}H,^{13}C correlation experiments) point to the existence of more than one silicate species. The ^{1}H and ^{13}C NMR spectra of the major species are in accordance with the crystal structure of **10**, and the solution and solid-state ^{13}C NMR spectroscopic data show an excellent agreement. However, the solution NMR spectra do not allow a differentiation between C_2 symmetry (chiral silicate dianion) and C_i symmetry (achiral silicate dianion). All attempts to record a solution ^{29}Si NMR spectrum of **10** have failed so far.

Upon dissolution of **10** in water, spontaneous hydrolysis occurred, meaning that the expected chelation effect of the two tridentate ligands of the bis[citrato(3−)]silicate complex is not strong enough to stabilize this species in water.[12] Starting from a 0.2 M aqueous solution of **10** (pH 3.6, 20 °C), gel formation was observed after a period of two weeks. In this context it is interesting to note that the zwitterionic pentacoordinate silicon compounds **8**,[3a] **9**,[3a] **11**,[13] **12**,[13] and **15**[14] could be recovered almost quantitatively from aqueous solutions by crystallization at room temperature. Taking into account all these findings, it remains an open question as to whether or not α-hydroxycarboxylic acids (including citric acid) have any potential relevance for silicon biochemistry.

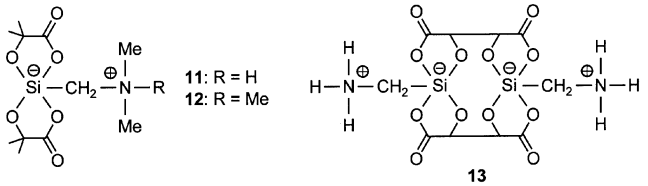

Experimental Section

General: All syntheses were carried out under dry nitrogen. The organic solvents used were dried and purified according to standard procedures and stored under nitrogen. Melting points were determined with a Büchi Melting Point B-540 apparatus using samples in sealed capillaries. The ^{1}H, ^{13}C, and ^{29}Si solution NMR spectra were recorded at 22 °C on a Bruker DRX-300 NMR spectrometer (^{1}H: 300.1 MHz; ^{13}C: 75.5 MHz; ^{29}Si: 59.6 MHz). CD_3CN was used as solvent. Chemical shifts (ppm) were determined relative to internal CHD_2CN (^{1}H: δ = 1.94), internal CD_3CN (^{13}C: δ = 1.27), and external TMS (^{29}Si: δ = 0). Assignment of the ^{13}C NMR spectroscopic data was supported by DEPT 135 experiments. Solid-state ^{29}Si VACP/MAS NMR spectra were recorded at 22 °C on a Bruker DSX-400 NMR spectrometer with bottom layer rotors of ZrO_2 (diameter 7 mm) containing ca. 300 mg of sample [79.5 MHz; TMS as external standard (δ = 0); spinning rate, 5 kHz; contact time, 5 ms; 90° ^{1}H transmitter pulse length, 3.6 μs; repetition time, 4 s].

Synthesis of Tri(*n*-butyl)ammonium Bis[citrato(3−)-*O*^{1},*O*^{3},*O*^{6}]silicate (10). Method 1: Tetramethoxysilane (1.00 g, 6.57 mmol) and tri(*n*-butyl)amine (2.43 g, 13.1 mmol) were added one after another at 20 °C to a solution of citric acid (2.52 g, 13.1 mmol) in THF (10 mL). The mixture was stirred for 2 min and then kept undisturbed for 2 days at 20 °C. The resulting crystalline product was isolated by filtration, washed with diethyl ether (10 mL), and then dried in vacuo (0.01 Torr, 20 °C, 1 h). Yield: 4.73 g (6.07 mmol, 93%). M.p. 188 °C (dec.). ^{1}H NMR (CD_3CN): δ = 0.89−0.99 (m, 18 H, CH_3), 1.28−1.43 (m, 12 H, CH_2), 1.55−1.69 (m, 12 H, CH_2), 2.46−2.81 (m, 8 H, CH_2), 3.02−3.12 (m, 12 H, NCH_2), 8.0 (br. s, 2 H, NH), 11.6 (br. s, 2 H, OH). ^{13}C NMR (CD_3CN):[15] δ = 13.8 (CH_3), 20.4 (CH_2CH_3), 26.0 ($NCCH_2$), 41.2 (CH_2CO), 44.0 (CH_2CO), 53.3 (NCH_2), 74.0 (OCC_3), 171.3 (C=O), 172.5 (C=O), 178.2 (C=O). ^{13}C VACP/MAS NMR: δ = 13.8 (CH_3), 13.9 (CH_3), 14.8 (CH_3), 15.0 (CH_3), 15.2 (CH_3), 15.4 (CH_3), 19.0 (CH_2CH_3), 20.0 (CH_2CH_3), 20.3 (CH_2CH_3), 20.5 (CH_2CH_3), 20.6 (CH_2CH_3), 21.4 (CH_2CH_3), 24.4 ($NCCH_2$), 26.4 ($NCCH_2$), 27.8 ($NCCH_2$), 27.9 (2 C) ($NCCH_2$), 29.1 ($NCCH_2$), 39.3 (CH_2CO), 41.2 (CH_2CO), 42.5 (CH_2CO), 44.2 (CH_2CO), 45.6 (NCH_2), 53.8 (NCH_2), 54.2 (2 C) (NCH_2), 56.3 (NCH_2), 57.8 (NCH_2), 74.1 (2 C) (OCC_3), 171.8 (C=O), 176.4 (2 C) (C=O), 177.0 (C=O), 178.0 (C=O), 181.5 (C=O). ^{29}Si VACP/MAS NMR: δ = −167.4. $C_{36}H_{66}N_2O_{14}Si$ (779.01): calcd. C 55.51, H 8.54, N 3.60; found C 55.4, H 8.1, N 3.6.

Method 2: Tri(*n*-butyl)amine (2.89 g, 15.6 mmol) was added at 20 °C to a stirred suspension of citric acid (1.00 g, 5.20 mmol) in acetonitrile (20 mL) (formation of a clear solution), followed by addition of tetrachlorosilane (442 mg, 2.60 mmol) over a period of 10 min. The mixture was stirred at 20 °C for 1 day, the solvent removed in vacuo, and acetone (15 mL) added to the stirred oily residue. The resulting solid was isolated by filtration and then purified by twofold recrystallization from acetonitrile/diethyl ether [1:1 (v/v); addition of diethyl ether to a solution of **10** in acetonitrile at 20 °C]. Yield: 807 mg (1.04 mmol, 40%). M.p. 188 °C (dec.). Identical NMR spectroscopic data as described above. $C_{36}H_{66}N_2O_{14}Si$ (779.01): calcd. C 55.51, H 8.54, N 3.60; found C 55.4, H 8.1, N 3.6.

Crystal Structure Analysis of 10: A suitable single crystal was mounted in inert oil (perfluoroalkyl ether, ABCR) on a glass fiber and then transferred to the cold nitrogen gas stream of the diffractometer (Stoe IPDS; graphite-monochromated Mo-K_α radiation, λ = 0.71073 Å). The structure was solved by direct methods (SHELXS-97) and refined by full-matrix least-squares on F^2 with all unique reflections (SHELXL-97).[16] For the CH hydrogen atoms, a riding model was employed. The positions of the NH and OH hydrogen atoms were localized in difference Fourier syntheses and refined freely. Selected data: single crystal (0.5 × 0.5 × 0.4 mm) obtained by recrystallization from acetonitrile/diethyl ether (see synthesis), $C_{36}H_{66}N_2O_{14}Si$, M_r = 779.00, analysis at 173(2) K, monoclinic, space group $P2_1/n$, a = 10.647(2), b = 15.612(3), c = 24.923(5) Å, β = 96.11(3)°, V = 4119.1(14) Å^3, Z = 4, $\rho_{calcd.}$ = 1.256 g cm^{-3}, μ = 0.122 mm^{-1}, $F(000)$ = 1688, $2\theta_{max}$ = 49.46°, 51175 collected reflections, 7033 unique reflections (R_{int} = 0.0597), 496 parameters, R_1 = 0.0305 [$I > 2\sigma(I)$], wR_2 (all data) = 0.0757, S = 1.013, largest difference peak and hole +0.404/−0.194 e Å^{-3}. CCDC-175178 contains the supplementary crystallographic data for this paper. These data can be obtained free of charge at www.ccdc.cam.ac.uk/conts/retrieving.html [or from the Cambridge Crystallographic Data Centre, 12, Union Road, Cambridge CB2 1EZ, UK; fax: (internat.) +44−1223/336−033; E-mail: deposit@ccdc.cam.ac.uk].

Acknowledgments

This work was supported by the Deutsche Forschungsgemeinschaft and the Fonds der Chemischen Industrie.

[1] [1a] R. Tacke, *Angew. Chem.* **1999**, *111*, 3197−3200; *Angew. Chem. Int. Ed.* **1999**, *38*, 3015−3018. [1b] N. Kröger, M. Sumper, in *Biomineralization* (Ed.: E. Baeuerlein), Wiley-VCH, Weinheim, **2000**, pp. 151−170. [1c] M. Hildebrand, in *Biomineralization* (Ed.: E. Baeuerlein), Wiley-VCH, Weinheim, **2000**, pp. 171−188. [1d] R. Wetherbee, S. Crawford, P. Mulvaney, in *Biomineralization* (Ed.: E. Baeuerlein), Wiley-VCH, Weinheim, **2000**, pp. 189−206. [1e] K. Shimizu, D. E. Morse, in *Biomineralization* (Ed.: E. Baeuerlein), Wiley-VCH, Weinheim, **2000**, pp. 207−220.

[2] [2a] R. K. Iler, in *The Chemistry of Silica: Solubility, Polymerization, Colloid and Surface Properties, and Biochemistry*, Wiley, New York, **1978**, pp. 783−784. [2b] P. B. Kaufman, P. Dayanandan, Y. Takeoka, W. C. Bigelow, J. D. Jones, R. Iler, in *Silicon and Siliceous Structures in Biological Systems* (Eds.: T. L. Simpson, B. E. Volcani), Springer-Verlag, New York, **1981**, pp. 442−446. [2c] C. W. Sullivan, in *Silicon Biochemistry* (Eds.: D. Evered, M. O'Connor), Wiley, Chichester, UK, **1986**, pp. 70−73.

[3] [3a] M. Mühleisen, R. Tacke, *Chem. Ber.* **1994**, *127*, 1615−1617. [3b] K. Benner, P. Klüfers, J. Schuhmacher, *Z. Anorg. Allg. Chem.* **1999**, *625*, 541−543. [3c] R. Tacke, A. Stewart, J. Becht, C. Burschka, I. Richter, *Can. J. Chem.* **2000**, *78*, 1380−1387. [3d] R. Tacke, C. Burschka, I. Richter, B. Wagner, R. Willeke, *J. Am. Chem. Soc.* **2000**, *122*, 8480−8485. [3e] S. D. Kinrade, R. J. Hamilton, A. S. Schach, C. T. G. Knight, *J. Chem. Soc., Dalton Trans.* **2001**, 961−963. [3f] S. D. Kinrade, A. S. Schach, R. J. Hamilton, C. T. G. Knight, *Chem. Commun.* **2001**, 1564−1565.

[4] A. Biller, I. Richter, O. Seiler, R. Tacke, *The 9th International Conference on Inorganic Ring Systems*, Saarbrücken, Germany, July 23−28, **2000**, Abstract P-111.

[5] O. Seiler, I. Richter, C. Burschka, M. Penka, R. Tacke, *34th Organosilicon Symposium*, White Plains, NY/USA, May 3−5, **2001**, Abstract PS1-8.

[6] Citric acid is ubiquitous in nature; its chelating properties have been reviewed: J. P. Glusker, *Acc. Chem. Res.* **1980**, *13*, 345−352.

[7] R. Tacke, J. Heermann, M. Pülm, *Organometallics* **1997**, *16*, 5648−5652.

[8] Selected reviews dealing with higher-coordinate silicon compounds: [8a] S. N. Tandura, M. G. Voronkov, N. V. Alekseev,

Top. Curr. Chem. **1986**, *131*, 99−189. [8b] W. S. Sheldrick, in *The Chemistry of Organic Silicon Compounds*, Part 1 (Eds.: S. Patai, Z. Rappoport), Wiley, Chichester, **1989**, pp. 227−303. [8c] C. Chuit, R. J. P. Corriu, C. Reyé, J. C. Young, *Chem. Rev.* **1993**, *93*, 1371−1448. [8d] R. R. Holmes, *Chem. Rev.* **1996**, *96*, 927−950. [8e] D. Kost, I. Kalikhman, in *The Chemistry of Organic Silicon Compounds*, Vol. 2, Part 2 (Eds.: Z. Rappoport, Y. Apeloig), Wiley, Chichester, **1998**, pp. 1339−1445.

[9] M. Matzapetakis, C. P. Raptopoulou, A. Terzis, A. Lakatos, T. Kiss, A. Salifoglou, *Inorg. Chem.* **1999**, *38*, 618−619.

[10] M. Matzapetakis, M. Kourginatakis, M. Dakanali, C. P. Raptopoulou, A. Terzis, A. Lakatos, T. Kiss, I. Banyai, L. Iordanidis, T. Mavromoustakos, A. Salifoglou, *Inorg. Chem.* **2001**, *40*, 1734−1744.

[11] The hydrogen-bonding system was analyzed by using the program PLATON: A. L. Spek, PLATON, University of Utrecht, The Netherlands, **1998**.

[12] Immediately after dissolution of **10** in water (D_2O) or in an aqueous KOH solution (80 mg KOH/700 μL D_2O; pH ca. 14), the bis[citrato(3−)]silicate complex could no longer be detected (^1H and ^{13}C NMR studies; comparison with the NMR spectroscopic data obtained in CD_3CN). All attempts to record an ^{29}Si NMR spectrum in D_2O have failed so far.

[13] R. Bertermann, R. Tacke, *The 12th International Symposium on Organosilicon Chemistry*, Sendai, Japan, May 23−28, **1999**, Abstract P59.

[14] R. Tacke, M. Mühleisen, P. G. Jones, *Angew. Chem.* **1994**, *106*, 1250−1252; *Angew. Chem. Int. Ed. Engl.* **1994**, *33*, 1186−1188.

[15] The values for the ^{13}C NMR shifts given for the citrato(3−) ligands correspond to the more intense (well resolved) resonance signals. In addition, there are some significantly less intense (poorly resolved) signals that point to the presence of another silicate species in solution.

[16] [16a] G. M. Sheldrick, SHELXS-97, University of Göttingen, Germany, **1997**; G. M. Sheldrick, *Acta Crystallogr., Sect. A* **1990**, *46*, 467−473. [16b] G. M. Sheldrick, SHELXL-97, University of Göttingen, Germany, **1997**.

Received January 16, 2002
[I02026]

Synthesis and Structure of the First Fe^{II} Heterometallic Alkoxide $[(THF)NaFe(O\mathit{t}Bu)_3]_2$ – a Possible Precursor for New Materials

Yurii K. Gun'ko,*[a] Ute Cristmann,[a] and Vadim G. Kessler[b]

Keywords: Iron / O ligands / Heterometallic complexes / Alkali metals / Materials science

The reaction of $FeBr_2$ with three equivalents of $NaO\mathit{t}Bu$ in THF affords the first heterometallic Fe^{II} alkoxide, $[(THF)NaFe(O\mathit{t}Bu)_3]_2$ (**1**), to be structurally characterised. The central core of the structure is an $M_2O_6M'_2$ fragment with C_2 symmetry. The compound is shown to be promising as a new precursor for magnetic iron oxide Fe_3O_4.
(© Wiley-VCH Verlag GmbH, 69451 Weinheim, Germany, 2002)

Introduction

Iron(III) alkoxides have been studied quite extensively. They show a quite unusual structural diversity and possess many interesting physical properties.[1] In contrast, the chemistry of Fe^{II} alkoxides is very poorly developed,[2,3] even though Fe^{II} complexes might be very promising precursors for the preparation (by MOCVD or sol-gel technology) of important iron-based compounds and materials. Here we report the synthesis, structure, and some selected reactions of the first Fe^{II} heterometallic alkoxide $[(THF)NaFe(O\mathit{t}Bu)_3]_2$.

Results and Discussion

The reaction of $FeBr_2$ with three equivalents of $NaO\mathit{t}Bu$ in THF at ambient temperature proceeds with the precipitation of NaBr to afford the heterometallic Fe^{II} alkoxide $[(THF)NaFe(O\mathit{t}Bu)_3]_2$ (**1**). The preparation of **1** and further reactions are summarised in Scheme 1. Compound **1** gave a satisfactory C, H, N analysis and was characterised by IR and ^1H NMR spectroscopy. The structure of **1** was also studied by X-ray single crystal diffraction.

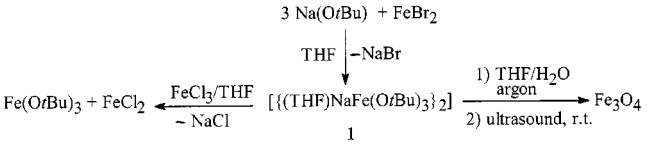

Scheme 1. Synthesis and selected reactions of $[\{(THF)NaFe(O\mathit{t}Bu)_3\}_2]$ (**1**)

[a] The Department of Chemistry, Trinity College Dublin, Dublin 2, Ireland
[b] Department of Chemistry, Swedish University of Agricultural Sciences, Box 7015, 75007 Uppsala, Sweden

The IR spectrum of **1** in nujol shows the characteristic C–O stretching bands for metal alkoxides at 1286, 1227 and 1195 cm^{-1} and M–O stretching bands at 618, 574 and 538 cm^{-1}. The ^1H NMR spectrum of **1** in C_6D_6 displays broad, paramagnetically shifted signals for the bridging $O\mathit{t}Bu$ groups (δ = 11.71 and −4.08) and THF (δ = 12.90 and 6.27).

X-ray quality crystals of **1** were crystallised from a concentrated solution in THF at ambient temperature. The central fragment of the molecule **1** (Figure 1) is an $Na_2O_6Fe_2$ cage-like unit with C_2 symmetry. A similar fragment (Figure 2) is found in several heterometallic alkoxides, for example in $[LiNbO(OEt)_4(EtOH)]_2$,[4] $[NaWO(OEt)_5(EtOH)_2]_2$,[5] $[MSn(O\mathit{t}Bu)_3]_2$ (M = Li, Na),[6] $[LiTi(O\mathit{i}Pr)_5]_2$,[7] $[KTi(O\mathit{t}Bu)_5]_2$,[8] and $[LiHf(O\mathit{i}Pr)_5]_2$.[9] In **1** the M positions in the central metal-oxygen core, which are occupied by alkali metals in the majority of above-mentioned complexes (Figure 2), are occupied by Fe atoms, and the M′ positions, which are occupied by Sn or multivalent transition metals (e.g. Ti, Hf, Zr, Mo, W) in the previously reported compounds, are occupied by alkali metal (Na) atoms. Such an uncommon arrangement of metal atoms has earlier been observed in the structures of, for example, $[LiNbO(OEt)_4(EtOH)]_2$,[4] $[NaMoO_2(OC_2H_4OMe)_3]_2$,[10] and $[NaWO_2(OC_2H_4OMe)_3]_2$.[11] In **1** each of the Fe atoms is coordinated by two μ_2- and two μ_3-$O\mathit{t}Bu$ bridging groups with O–Fe–O angles that vary between 78.0(7)° and 150.7(9)°. Because of this the coordination polyhedron around the Fe atom could be described as either a very distorted tetrahedron or, alternatively, as an octahedron in which *cis* apices are missing. A similar geometry around the Fe^{II} atom has been observed before in $[Fe(OCPh_3)_2(THF)_2]$.[2] As expected, the Fe–O(μ_3) bond lengths [2.074(16) and 2.061(14) Å] are longer than the Fe–O(μ_2) ones [1.923(14) and 1.829(19) Å]. There is an asymmetry in the Fe–O bond lengths, which is particularly significant for the Fe–O(μ_2) bonds [Δ(Fe–O) = 0.094 Å].

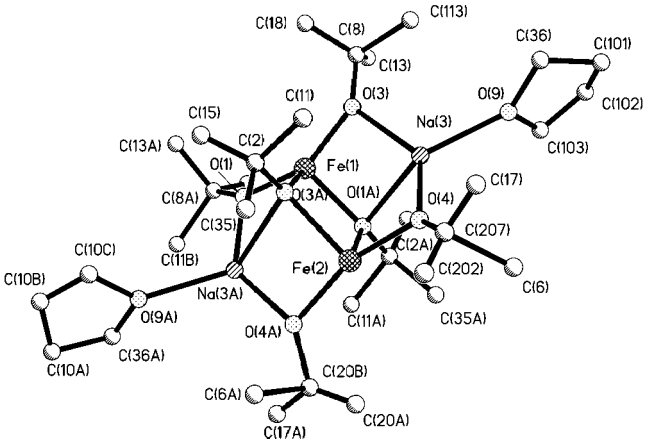

Figure 1. X-ray crystal structure of [{(THF)NaFe(O*t*Bu)$_3$}$_2$] (**1**); selected bond lengths (Å) and angles (°): Fe(1)−O(3) 1.923(14), Fe(1)−O(3A) 1.923(14), Fe(1)−O(1A) 2.074(16), Fe(1)−O(1) 2.074(16), Fe(1)−Na(3) 2.988(7), Fe(1)−Na(3A) 2.988(7), Fe(2)−O(4) 1.829(19), Fe(2)−O(4A) 1.829(19), Fe(2)−O(1A) 2.061(14), Fe(2)−O(1) 2.061(14), Fe(2)−Na(3A) 3.114(8), Fe(2)−Na(3) 3.114(8), Na(3)−O(3) 2.138(18), Na(3)−O(10) 2.370(11), Na(3)−O(4) 2.425(19), Na(3)−O(1A) 2.468(8); O(3)−Fe(1)−O(3A) 150.7(9), O(3)−Fe(1)−O(1A) 195.2(5), O(3A)−Fe(1)−O(1A) 1107.6(4), O(3)−Fe(1)−O(1) 107.6(4), O(3A)−Fe(1)−O(1) 95.2(5), O(1A)−Fe(1)−O(1) 78.0(7), O(4)−Fe(2)−O(4A) 150.0(10), O(4)−Fe(2)−O(1A) 99.1(5), O(4A)−Fe(2)−O(1A) 104.1(6), O(4)−Fe(2)−O(1) 104.1(6), O(4A)−Fe(2)−O(1) 99.1(5), O(1A)−Fe(2)−O(1) 78.5(8), O(3)−Na(3)−O(10) 112.4(10), O(3)−Na(3)−O(4) 132.2(5), O(10)−Na(3)−O(4) 114.6(11), O(3)−Na(3)−O(1A) 79.4(6), O(10)−Na(3)−O(1A)134.3(4), O(4)−Na(3)−O(1A) 74.5(6); Fe(1)−O(1)−Fe(2) 101.8(3)

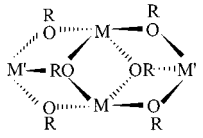

Figure 2. Schematic presentation of the M′$_2$O$_6$M$_2$ unit in heterometallic alkoxides (R = *t*Bu or *i*Pr)

In general the Fe−O(*t*Bu) bond lengths in **1** are similar to the corresponding ones in other Fe^{II} alkoxy derivatives: [Fe(OCPh$_3$)$_2$(THF)$_2$] [1.883(1) Å],[2] [Fe$_4$(DBCat)$_4$(py)$_6$] [from 1.974(6) to 2.236(5) Å] and [Fe$_2$(DBCat)$_2$(py)$_n$] [from 1.936(4) to 2.326(4) Å] (DBCat = 3,5-di-*tert*-butylcatechol, n = 4, 6).[3] The Fe···Fe distance of 3.208 Å is also quite close to those in the tetranuclear Fe^{II} complex [Fe$_4$(DBCat)$_4$(py)$_6$] [from 3.079(2) to 3.481(2) Å] and in the binuclear complex [Fe$_2$(DBCat)$_2$(py)$_n$] [3.223(3) and 3.195(3) Å].[3] The sodium atom in **1** is coordinated by the oxygen atoms of two μ_2- and one μ_3-O*t*Bu groups and one THF molecule, in a distorted tetrahedral arrangement. The O−Na−O angles vary between 74.5(6)° and 132.2(5)° and the Na−O(*t*Bu) bond lengths between 2.138(18) Å (μ_2-O) and 2.468(8) Å (μ_3-O). Surprisingly, one of the Na−O(μ_2) bonds is substantially longer, at 2.425(19) Å, than the other one, and is in fact very close to an Na−O(μ_3) bond length; this causes a significant asymmetry in the molecule. The observed structure can also be considered as a dimer of [(THF)Na(O*t*Bu)$_2$Fe(O*t*Bu)$_2$Na(THF)] held together by additional metal/O*t*Bu bonds.

It was of great interest to us to investigate the chemical properties of **1** as a potential precursor for other iron-containing compounds and materials. The reaction of **1** with two equivalents of FeCl$_3$ in THF at ambient temperature (24 h) gave FeCl$_2$ and Fe(O*t*Bu)$_3$, which were separated by fractional crystallisation and clearly identified by elemental analysis (Scheme 1). This reaction demonstrates the labile nature of **1**.

Fe^{II} compounds have recently been reported to be very good precursors for the preparation of Fe$_3$O$_4$ nanoparticles by sol-gel and sonochemical methods.[12−14] For this reason a solution of **1** in THF was hydrolysed with doubly distilled water under argon, followed by ultrasonic treatment (Scheme 1). The black product was characterised by X-ray powder diffraction (XRD). The reflections of the XRD patterns (2θ from 5 to 70°) for the sample show d spacing values and relative intensities of the peaks that coincide exactly with the JCPDS data of magnetite (Fe$_3$O$_4$). The product was also characterised by Mössbauer spectroscopy at room temperature. The Mössbauer spectrum of the Fe$_3$O$_4$ sample shows combined magnetic and quadrupole splittings. A least-squares fit to the experimental data indicates that the lines are characteristic of nonstoichiometric magnetite, with a small line-broadening due to a distribution of hyperfine magnetic fields caused by the different iron environments in the structure, and a small contribution from paramagnetic Fe^{3+}. The most plausible mechanism of the magnetite formation in this reaction involves an oxidation of Fe^{II} into Fe^{III} by oxygen from the water during the hydrolysis and subsequent ultrasonic treatment. Ultrasonically generated radical and peroxide species from water might also contribute to the oxidation of Fe^{II}, as has been reported recently.[13,14]

The above reactions demonstrate that the new iron(II) alkoxide **1** can be used as a promising precursor for the facile preparation of magnetite. Work on the further development of this research is currently in progress.

Experimental Section

General: All manipulations were carried out under vacuum or dry argon by Schlenk techniques. Solvents were purified and degassed by standard procedures. FeBr$_2$ and NaO*t*Bu were obtained from Aldrich. Microanalyses were carried out by Medac Ltd. The ^{1}H NMR spectra were recorded using a Varian-400 (^{1}H, 400 MHz) instrument. Deuteriated benzene was dried with a K metal mirror and distilled prior to use. IR spectra (500−4000 cm^{-1}) were recorded in Nujol, using KBr discs and a Perkin Elmer instrument.

[(THF)NaFe(O*t*Bu)$_3$]$_2$ (1): NaO*t*Bu (5.27 g, 54.9 mmol) was added to FeBr$_2$ (3.95 g, 18.3 mmol) in THF (300 mL) at ca. 0 °C. The mixture was stirred for 24 h at ambient temperature and was then filtered. The filtrate was concentrated in vacuo to give grey crystals of **1**. Yield: 4.27 g (64%). C$_{32}$H$_{70}$Fe$_2$Na$_2$O$_8$ (740.6): calcd. C 51.8, H 9.45; found C 51.7, H 9.39. ^{1}H NMR (400 MHz, C$_6$D$_6$, 22 °C): δ = −4.08 (v. br., 18 H, μ_3-O*t*Bu), 6.27 (br, 8 H, THF), 11.71 (v.

br., 36 H, μ_2-O*t*Bu), 12.90 (br, 8 H, THF). IR (Nujol): $\tilde{\nu}$ = 2709 (s), 1657 (w), 1570 (w), 1356 (w), 1286 (w), 1227 (s), 1195 (w), 1055 (s), 968 (w), 775 (w), 618 (w), 574 (w) 538 (w) cm^{-1}.

Fe_3O_4: A solution of **1** (2.3 g, 3.1 mmol) in THF (100 cm^3) was carefully hydrolysed with doubly distilled water (40 cm^3) under argon. The resultant mixture was then ultrasonically (Ultrasonic bath Grant XB6, 30 kHz, 130 W) irradiated at ambient temperature for one hour under argon. The dark precipitate was filtered and washed five times with distilled water. The product was then dried in vacuum for five hours at room temperature giving a black powder of Fe_3O_4 (0.44 g, 92%) characterised by X-ray powder diffraction (XRD) and Mössbauer spectroscopy.

X-ray Crystallography

A single crystal of **1** was placed in a glass capillary and sealed under vacuum. Data were measured on a SMART CCD 1 K diffractometer using monochromated Mo-K_α radiation. Corrections for absorption were made using the Bruker SADABS program.[15] The crystal was found to be a merohedral twin, with the centre of symmetry as an external symmetry element not belonging to the true symmetry group. Structure solutions were made using the SHELXTL program package Version 5.3. The structure was solved by direct methods and was refined first in an isotropic and then an anisotropic (all non-hydrogen atoms) approximation. The positions of the hydrogen atoms were calculated geometrically and included in the final cycles of the refinement in an isotropic approximation.

Crystal Data for 1: $C_{32}H_{70}Fe_2Na_2O_8$, M = 740.56, monoclinic, a = 18.822(7), b = 12.516(5), c = 9.262(3) Å, β = 91.179 (6)°, U = 2181.4(14) $Å^3$, T = 295(2) K, space group $C2$, Z = 2, ρ = 1.127 Mg/m^3, μ(Mo-K_α) = 0.723 mm^{-1}, 3446 reflections collected, 1675 independent reflections [R(int) = 0.0870], R_1 = 0.0815 for reflections with $I > 2\sigma(I)$, wR_2 = 0.2191 (all data). CCDC 170603 contains the supplementary crystallographic data for this paper. These data can be obtained free of charge at www.ccdc.cam.ac.uk/conts/retrieving.html [or from the Cambridge Crystallographic Data Centre, 12 Union Road, Cambridge CB2 1EZ, UK; Fax: (internat.) + 44-1223/336-033; E-mail: deposit@ccdc.cam.ac.uk].

Acknowledgments

The authors express their gratitude to the Swedish Council for Scientific Research and Trinity College Dublin for their financial support of this work.

[1] [1a] K. L. Taft, S. Lippard, *J. Am. Chem. Soc.* **1990**, *112*, 9629−9630. [1b] K. Hegetschweiler, H. W. Schmalle, H. M. Streit, V. Gramlich, H. U. Hund, I. Erni, *Inorg. Chem.* **1992**, *31*, 1299−1302. [1c] A. Caneschi, A. Cornia, S. J. Lippard, *Angew. Chem. Int. Ed. Engl.* **1995**, *34*, 467−469. [1d] H. K. Chae, C. Hwang, Y. Dong, H. Yun, H. G. Jang, *Chem. Lett.* **2000**, 992−993. [1e] M. Veith, F. Grätz, V. Huch, *Eur. J. Inorg. Chem.* **2001**, 367−368.

[2] R. A. Bartlett, J. J. Ellison, P. P. Power, S. C. Shoner, *Inorg. Chem.* **1991**, *30*, 2888−2894.

[3] S. C. Shoner, P. P. Power, *Inorg. Chem.* **1992**, *31*, 1001−1010.

[4] A. I. Yanovsky, E. P. Turevskaya, N. Ya. Turova, Yu. T. Struchkov, *Koord. Khimija.* **1985**, *11*, 110−114.

[5] A. I. Yanovsky, V. G. Kessler, N. Ya. Turova, Yu. T. Struchkov, *Koord. Khimija.* **1991**, *17*, 54−58.

[6] M. Veith, R. Rosler, *Z. Naturforsch., Teil B* **1986**, *41*, 1071−1072.

[7] M. J. Hampden-Smith, D. S. Williams, A. L. Rheingold, *Inorg. Chem.* **1990**, *29*, 4076−4081.

[8] D. J. Teff, J. J. C. Huffman, K. G. Caulton, *Inorg. Chem.* **1994**, *33*, 6289−6292.

[9] M. Veith, S. Mathur, C. Mathur, V. Huch, *J. Chem. Soc., Dalton Trans.* **1997**, 2101−2108.

[10] N. Y. Turova, V. G. Kessler, S. I. Kucheiko, *Polyhedron* **1991**, *10*, 2617−2628

[11] V. G. Kessler, D. E. Chebukov, N. Ya. Turova, *Zh. Neorg. Khim.* **1993**, *38*, 27−28.

[12] X. Cao, Yu. Koltypin, G. Katabi, R. Prozorov, I. Felner, A. Gedanken, *J. Mater. Chem.* **1997**, *7*, 1007−1009.

[13] R. Vijayakumar, Yu. Koltypin, I. Felner, A. Gedanken, *Mater. Sci. and Eng. A* **2000**, *286*, 101−105.

[14] R. Vijayakumar, Yu. Koltypin, Y. S. Cohen, Y. Cohen, D. Aurbach, O. Palchik, I. Felner, A. Gedanken, *J. Mater. Chem.* **2000**, *10*, 1125−1129.

[15] SAINTPLUS and SHELXTL-NT reference manuals, Bruker AXS, 1997.

Received October 19, 2001
[I01413]

Synthesis and Characterization of Soluble Axially Substituted Tetra-(*tert*-butyl)gallium(III)phthalocyanines

Yu Chen,[a] Lakshminarayanapuram R. Subramanian,[a] Markus Barthel,[a] and Michael Hanack*[a]

Keywords: Gallium / Nitrogen heterocycles / Nonlinear optics / Phthalocyanines

The synthesis and characterization of the highly soluble tetra(*tert*-butyl)gallium(III) phthalocyanines (tBu)$_4$PcGaCl (**2**) and (tBu)$_4$PcGa(*p*-TMP) (**3**) is described. They were characterized by IR, UV/Vis, MS, and ^{1}H, ^{13}C, and ^{19}F NMR spectroscopy.

(© Wiley-VCH Verlag GmbH, 69451 Weinheim, Germany, 2002)

Introduction

Phthalocyanines (Pcs) and their analogs have been intensively investigated for many technological applications due to their remarkable photophysical, optoelectronic, conductive properties, and biological activities, as well as their wide variety of architectural flexibility.[1−3] In recent years we have concentrated our efforts on studying the influence of different axial substituents on the nonlinear optical (NLO) properties, particularly on the optical limiting (OL) properties of soluble peripherally alkyl-substituted phthalocyaninato-and naphthalocyaninatoindium(III) complexes. We have synthesized, for example, a series of soluble axially substituted indium(III)phthalocyanines (tBu)$_4$PcInX with X = Cl, Br, I, *p*-trifluoromethylphenyl (*p*-TMP), *m*-TMP, *p*-fluorophenyl, and pentafluorophenyl, amongst others.[4−6]

In comparison to the chloro compounds, each of the (phthalocyaninato)indium complexes studied showed very promising results, such as higher nonlinear absorption coefficients, lower limiting thresholds, and an earlier onset of the optical limiting behavior.[5,7,8] Furthermore, soluble axially substituted indium naphthalocyanines have been prepared[9] that show a similar optical limiting behavior.[10]

Peripherally unsubstituted gallium phthalocyanines with an axial chloro, fluoro or hydroxy ligand (PcGaX, X = Cl, F, OH) were the first phthalocyanines to be investigated for their third order (χ^3) nonlinear behavior;[11] values of the order of 10^{-11} esu were found. The greatest disadvantage of peripherally unsubstituted phthalocyanines is their poor solubility in organic solvents. For this reason, we report here the synthesis of the highly soluble chlorogallium(III) 2,(3)-tetra(*tert*-butyl)phthalocyanine [(tBu)$_4$PcGaCl] (**2**), and its reaction with R′MgBr (R′ = *p*-TMP) leading to the σ-bonded aryl(phthalocyaninato)gallium(III) complex (tBu)$_4$PcGa(*p*-TMP) (**3**). The aryl substituent should introduce greater steric crowding than the chloro ligand and should reduce the tendency, which is common in Pc's, to form aggregates.[12]

[a] Institut für Organische Chemie, Universität Tübingen,
Auf der Morgenstelle 18, 72076 Tübingen, Germany
E-mail: hanack@uni-tuebingen.de
http://www.uni-tuebingen.de/hanack/index.html

Results and Discussion

The synthetic pathway to **2** and **3**, together with the numbering of the atoms of the macrocycles and the axial *p*-TMP ligand, is shown in Scheme 1. Compound **2** was obtained by the reaction of 4-*tert*-butylphthalonitrile with anhydrous $GaCl_3$ (molar ratio, 4:1.05) in doubly distilled, deoxygenated quinoline at 180 °C in the presence of catalytic amounts of the nonnucleophilic base 1,8-diazabicyclo-[5.4.0]undec-7-ene (DBU). Compound **3** was synthesized by the reaction of a freshly prepared 10-fold excess of *p*-TMP Grignard reagent with (tBu)$_4$PcGaCl. Products **2** and **3** were further purified by column chromatography and recrystallization; they are highly soluble in common organic solvents.

The UV/Vis spectra of **2** and **3** in $CHCl_3$ are shown in Figure 1; it can clearly be seen that they are almost identical. The introduction of electron-donating *tert*-butyl groups in the periphery of the macrocycle of **2** leads to a red-shift of about 8 nm of the Q-band maximum with respect to the unsubstituted PcGaCl (Fluka product). The axial *p*-TMP ligand has little influence on the position of the Q-band maximum in comparison with compound **2**. The observed red-shift is only of the order of 1.5 nm. Similar results with (tBu)$_4$PcInCl and (tBu)$_4$PcIn(*p*-TMP) have been reported by us earlier.[4] The UV/Vis spectra of (tBu)$_4$PcGaCl (**2**) and (tBu)$_4$PcInCl are almost identical, with a $\Delta\lambda$ value of 2−3 nm. (tBu)$_4$PcIn(*p*-TMP), on the

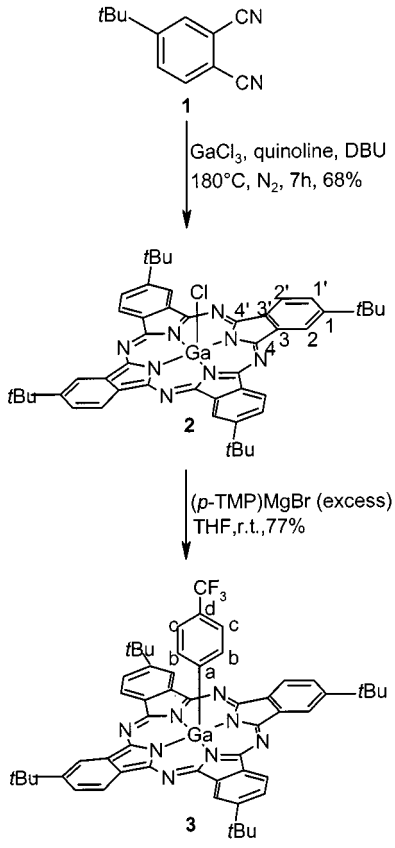

Scheme 1

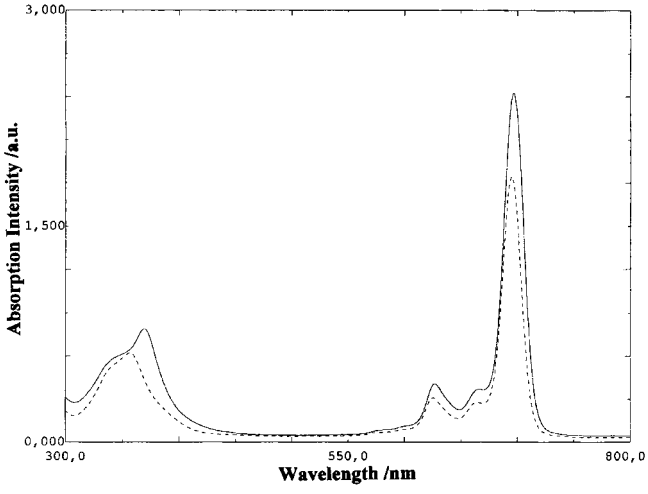

Figure 1. The UV/Vis spectra of $(t\text{Bu})_4$PcGaCl (dashed line) and $(t\text{Bu})_4$PcGa(*p*-TMP) (solid line) in $CHCl_3$.

other hand, shows a bathochromically shifted Q-band (1.5 nm) relative to the gallium compound **3**.

The greater solubility of compound **3** than of the chloro analog **2** shows that the usual tendency of phthalocyanines to form aggregates can be effectively suppressed by axial substitution.[4] Similar to the aryl axially substituted indium(III)phthalocyanines,[5] the shape of the UV/Vis spectrum of **3** is almost independent of the concentration of the solution and shows no aggregation. However, for the chlorogallium phthalocyanine **2**, a concentration-dependent increase of the absorption on the red side of the Q-band indicates a somewhat larger degree of aggregation. A comparison of the UV/Vis absorption spectra of thin film and dilute solutions of **2** and **3** in $CHCl_3$ shows that the absorption spectra of thin films of **2** and **3** are broader. Upon comparing the thin film and dilute solution UV/Vis spectra of **2**, it is observed that the position of the Q-band maximum is shifted slightly by about 2.5 nm towards longer wavelength. In the case of **3**, the same comparison shows that the position of the Q-band maximum is almost unchanged, which is consistent with relatively weak aggregation of **3** in solution.

The field desorption (FD) mass spectrum of **2** shows a cluster of peaks centered at *m*/*z* (%) = 842.3 (100), assigned to the molecular peak, which is almost identical to the calculated intensity pattern for **2** [*m*/*z* (%) = 840.3 (90), 841.3 (50), 842.3 (100), 843.3 (52), 844.3 (33) and 845.3 (12)]. Likewise, the molecular peak of **3** at *m*/*z* (%) = 951.4 (100) is also detected in the FD mode. The mass spectrum of **3** measured in the FAB modes shows a peak at *m*/*z* = 958 which is assigned to an $[M^+ + Li]$ peak.

The IR spectrum of **2** is similar to that of $(t\text{Bu})_4$PcInCl.[4] The Ga−Cl stretching vibration is shifted from 431 cm^{-1} in unsubstituted PcGaCl[13] to 351 cm^{-1} in **2**, while the ν_{In-Cl} band in $(t\text{Bu})_4$PcInCl appears at 336 cm^{-1}.[4] For **3**, some new absorption bands, which do not appear in the spectrum of $(t\text{Bu})_4$PcGaCl (**2**), were observed (see Exp. Sect.).

The ^{1}H NMR spectra of **2** and **3** in $CDCl_3$ confirm the presence of the expected mixtures of structural isomers of tetrasubstituted phthalocyanines. The numbering of the atoms of the macrocycle and the axial *p*-TMP ligand is shown in Scheme 1. In **2** the aromatic signals appear as two broad multiplets [δ = 9.4−8.9 (8 H, H-2,2′) and δ = 8.4−8.2 (4 H, H-1)], the singlet of the *tert*-butyl group appears at δ = 1.9 (36 H) and is split because of the structural isomers; the signals are located almost in the same range as those of $(t\text{Bu})_4$PcInCl.[4,5] For compound **3**, the σ-bonded *p*-TMP ligand causes a slightly stronger deshielding of the aromatic protons, especially those closer to the heteroaromatic 18-π-electron system (H-2,2′), than does the chloro ligand in **2**. The proton signals of the *p*-TMP ligand are shifted upfield due to the diamagnetic ring-current of the phthalocyanine macrocycle. They appear at δ = 7.1 (d, ^3J = 8.9 Hz, 2 H, H-c,c′) and 6.8 (d, ^3J = 8.7 Hz, 2 H, H-b,b′), compared to δ = 7.5(H-c,c′) and 7.6 (H-b,b′) in pure *p*-trifluoromethylphenyl bromide (*p*-TMPBr). This is a smaller upfield shift than in $(t\text{Bu})_4$PcIn(*p*-TMP) due to the different central metal atom.[4,5]

The ^{13}C NMR spectra of **2** and **3** are also similar to the ^{13}C NMR spectra of $(t\text{Bu})_4$PcInCl and $(t\text{Bu})_4$PcIn(*p*-TMP),[4] and show seven signals for the aromatic carbon atoms and two signals for the *tert*-butyl group. The aromatic signals are broadened due to the structural isomers,

and the carbon signals of the *p*-TMP ligand are split on account of C−F coupling and are of very low intensity. However, additional signals can be observed at δ = 113.9, 127.5−127.8 and 133.3, and are assigned to C-d, C-c,c′ and C-a of the axial ligand, respectively.

The ^{19}F NMR spectrum of **3** provides evidence for the attachment of the *p*-TMP ligand at the gallium atom: only one narrow singlet at δ = −62.8 was observed for the axial ligand, whereas the ^{19}F signal of pure α,α,α-trifluorotoluene appears at δ = −63.9.[5] Similarly to **3**, the ^{19}F signal of (tBu)$_4$PcIn(*p*-TMP) appears at δ = −64.1.[4,5] The difference in chemical shifts of the fluorine atoms in (tBu)$_4$PcIn(*p*-TMP) and (tBu)$_4$PcGa(*p*-TMP) **3** is due to the different electronic effects of indium(III) and gallium(III).

Experimental Section

General: The operations for synthesis prior to the termination reaction were carried out under purified dry nitrogen. Solvents were purified, dried and distilled under dry nitrogen. FT-IR: Perkin−Elmer Spectrum 1000. UV/Vis: Shimadzu UV-365. MS: Varian Mat 711(FD: temperature of the ion source 30 °C; FAB: temperature of the ion source 50 °C); ^1H,^{13}C NMR: Bruker AC 250 (^1H: 250.131 MHz, ^{13}C: 62.902 MHz). ^{19}F NMR: Bruker Avance DRX 250 (235.334 MHz); elemental analyses: Carlo−Erba Elemental Analyser 1104, 1106.

Chlorogallium(III) 2,(3)-Tetra(*tert*-butyl)phthalocyanine [(tBu)$_4$PcGaCl] (2): A mixture of anhydrous gallium(III) chloride (0.75 g, 4.26 mmol), 4-*tert*-butylphthalonitrile (**1**; 3 g, 16.3 mmol), quinoline (15 mL, doubly distilled over CaH_2), and DBU (1 mL) was stirred at 180 °C for 7 h. The solvent was then removed by distillation under reduced pressure, leaving a dark green residue, which was chromatographed on silica gel using a gradient of toluene and chloroform 100:0 to 0:100 in order to remove metal-free phthalocyanine and a large portion of polar impurities. The blackish green fraction ($R_f \geq 0$) was collected, the solvent evaporated, and the crude compound recrystallized from a mixture of CH_2Cl_2/MeOH (v/v 4:3) by slowly evaporating the more volatile dichloromethane in a rotary evaporator at 40−60 °C under slightly reduced pressure. To complete the crystallization, the mixture was kept in a refrigerator overnight. The complex was collected by filtration, washed twice with methanol and dried at 80 °C in vacuum for 10 h. Yield 2.35 g (68.5%) of **2** as a blackish green powder. FD-MS ($C_{48}H_{48}ClGaN_8$): calcd. 842.14; found 842.3(100). UV/Vis ($CHCl_3$): λ_{max} (nm) = 695, 664.5 (sh), 625, 356. FT-IR (KBr): $\tilde{\nu}$ = 3068 cm^{-1} vw, 2958 s, 2866 m, 1734 w, 1682 w, 1615 m, 1507 m, 1483 m, 1406 m, 1394 m, 1364 m, 1334 vs, 1281 m, 1258 s, 1201 m, 1149 m, 1087 vs, 1052 m, 1024 w, 967 w, 929 s, 895 w, 831 m, 765 m, 750 s, 694 m, 670 m, 602 vw, 566 vw, 532 m, 444 vw, 350.5 w [ν(Ga-Cl)]. ^1H NMR ($CDCl_3$): δ = 1.9 (m, 36 H, tBu), 8.2−8.4 (m, 4 H, H-1), 8.9−9.4 (m, 8 H, H-2, -2′). ^{13}C NMR ($CDCl_3$): δ = 31.1−32.1 (tBuCH$_3$), 36.2 (CMe$_3$), 119.1−119.6 (C-2′), 122.6−122.9 (C-2), 128.5−128.6 (C-1), 133.7−133.9 (C-3), 135.9−136.2 (C-3′), 150.4−151.1 (C-4, -4′), 154.2−154.6 (C-1′). $C_{48}H_{48}ClGaN_8$ (842.1): calcd. C 68.46, H 5.74, N 13.31, Cl 4.21; found C 66.50, H 5.63, N 12.36, Cl 4.15.

***p*-(Trifluoromethyl)phenylgallium(III) 2,(3)-Tetra(*tert*-butyl)phthalocyanine [(tBu)$_4$PcGa(*p*-TMP)] (3):** A freshly prepared solution of R′MgBr (R′ = *p*-trifluoromethylphenyl) in THF (20 mL, 0.18 M R′MgBr) was added dropwise to a stirred solution of (tBu)$_4$PcGaCl (**2**; 300 mg, 0.356 mmol) in dry THF (25 mL). The reaction was monitored by TLC and stopped when all of the chloro complex **2** had been consumed. The deep green mixture was poured onto ice and then extracted several times with diethyl ether. The combined organic layers were washed with water and dried with $MgSO_4$. After evaporation of the solvent, the residue was rapidly subjected to column chromatography (silica gel/toluene). Light was strictly excluded during this step. Further purification of the complex was achieved by recrystallization from a mixture of CH_2Cl_2/MeOH (v/v 1:1) by slowly evaporating the more volatile dichloromethane in a rotary evaporator at 40−60 °C under slightly reduced pressure. To complete crystallization, the mixture was kept in a refrigerator overnight. The complex was collected by filtration, washed twice with methanol and dried at 70 °C in vacuum for 6 h. Yield 260 mg (77%) of **3** as a green powder. FD-MS ($C_{52}H_{52}F_3GaN_8$): calcd. 951.14; found 951.4 (100). FAB-MS (*m*/*z*): 958 [M$^+$ + Li], 864, 857, 842, 823, 805 [(tBu)$_4$PcGa$^+$], 789, 749, 637, 539, 489, 481, 469, 385, 342, 281, 269, 253. UV/Vis ($CHCl_3$): λ_{max} (nm) = 696.5, 666 (sh), 626.5, 369.5. FT-IR (KBr): $\tilde{\nu}$ = 2962 cm^{-1} s, 2870 m, 1737 m, 1668 m, 1617 m, 1548 s,1516 vs, 1486 m, 1465 m, 1399 w, 1376 m, 1365 m, 1325 s (C−F), 1284 w, 1258 m, 1233 w, 1199 w, 1163 m (C−F), 1146 vw, 1123 ms, 1088 m, 1067 m, 1048 m, 1037 m, 1017 m, 929 w, 902 w, 842 m, 796 w, 750 m, 697 w, 687 w, 665 w, 521 w. ^1H NMR ($CDCl_3$): δ = 1.9 (m, 36 H, tBu), 6.8 (d, ^3J = 8.7 Hz, 2 H, H-b,b′), 7.1 (d, ^3J = 8.9 Hz, 2 H, H-c,c′), 8.2−8.3 (m, 4 H, H-1), 9.0−9.4 (m, 8 H, H-2,2′). ^{13}C NMR ($CDCl_3$): δ = 31.0−33.3 (tBuCH$_3$), 36.2 (CMe$_3$), 113.9 (-c-d), 119.2−119.6 (C-2′), 122.8 −123.0 (C-2), 127.5−127.8 (C-c,c′), 128.6 (C-1), 133.3 (C-a), 133.9−134.3 (C-3), 136.5−136.8 (C-3′), 151.7 (C-4,4′), 154.4−154.6 (C-1′). ^{19}F NMR($CDCl_3$): δ = −62.8. $C_{52}H_{52}F_3GaN_8$ (915.8): calcd. C 69.41, H 5.51, N 11.77, F 5.99; found C 68.95, H 5.34, N 10.44, F 8.31.

Acknowledgments

This research was supported by the Alexander von Humboldt Foundation of Germany, and Deutsche Forschungsgemeinschaft (Projekt Ha 280/165−1).

[1] *Phthalocyanines: Properties and Applications* (Eds.: C. C. Leznoff, A. B. P. Lever), VCH Publishers, Inc., New York, **1989−1996**, Vols. 1−4.
[2] C. G. Claessens, W. J. Blau, M. Cook, M. Hanack, R. J. M. Nolte, T. Torres, D. Wöhrle, *Monatsh. Chem.* **2001**, *132*, 3−11.
[3] M. Hanack, M. Lang, *Adv. Mater.* **1994**, *6*, 819−833.
[4] M. Hanack, H. Heckmann, *Eur. J. Inorg. Chem.* **1998**, 367−373.
[5] H. Heckmann, *PhD Thesis*, University of Tübingen, Germany, **1999**.
[6] T. Schneider, *PhD Thesis*, University of Tübingen, Germany, **2000**.
[7] G. Rojo, G. Martin, F. Agullo-Lopez, T. Torres, H. Heckmann, M. Hanack, *J. Phys. Chem. B* **2000**, *104*, 7066−7070.
[8] J. S. Shirk, R. G. S. Pong, S. R. Flom, H. Heckmann, M. Hanack, *J. Phys. Chem. A* **2000**, *104*, 1438−1449.
[9] T. Schneider, H. Heckmann, M. Barthel, M. Hanack, *Eur. J. Org. Chem.* **2001**, 3055−3065.
[10] D. Dini, M. Barthel, M. Hanack, *Eur. J. Org. Chem.* **2001**, 3759−3769.
[11] Z. Z. Ho, C. Y. Ju, W. M. Hetherington III, *J. Appl. Phys.* **1987**, *62*, 716−718.
[12] M. Hanack, T. Schneider, M. Barthel, J. S. Shirk, S. R. Flom, R. G. S. Pong, *Coord. Chem. Rev.* **2001**, *219−221*, 235−258.
[13] T. D. Sims, J. E. Pemberton, P. Lee, N. R. Armstrong, *Chem. Mater.* **1989**, *1*, 26−34.

Received November 16, 2001
[I01462]

cis-[$PtCl_2(NH_3)$\{2-(2-hydroxyethyl)pyridine\}] − an Analogue of the Anticancer Drug AMD473: Unusual Hydrolysis Rates and pK_a Values for the Diaqua Adduct

Anna C. G. Hotze,[a] Yu Chen,[a] Trevor W. Hambley,[b] Simon Parsons,[a] Nicole A. Kratochwil,[a] John A. Parkinson,[a] Vivienne P. Munk,[a] and Peter J. Sadler*[a]

Keywords: Platinum / Antitumor agents / Hydrolysis / Molecular modelling

The X-ray crystal structure of *cis*-[$PtCl_2(NH_3)$\{2-(2-hydroxyethyl)pyridine\}] shows that it has similar structural features to the 2-picoline analogue, the anticancer drug AMD473 (ZD0473), but undergoes aquation much more rapidly. The diaqua adduct has unusually low pK_a values which have been rationalised by molecular modelling.
(© Wiley-VCH Verlag GmbH, 69451 Weinheim, Germany, 2002)

Introduction

cis-[$PtCl_2(NH_3)$(2-picoline)] (AMD473) is a new anticancer drug which entered phase I clinical trials in 1997.[1,2] It is active against cisplatin-resistant cell lines, and appears to circumvent thiol-mediated resistance mechanisms whilst still maintaining the ability to form cytotoxic lesions with DNA.[2,3] In reactions of cisplatin with DNA, hydrolysis is known to be the rate-limiting step. The steric influence of 2-picoline plays an important role in decreasing the rates of hydrolysis and substitution reactions of AMD473,[4,5] and also in promoting high stereoselectivity in the formation of a GG intrastrand adduct with a 14-mer DNA duplex.[6] In order to elucidate further the role of pyridine substituents in determining the reactivity of platinum(II) picoline complexes, we have studied the hydrolysis rates of the AMD473 analogue *cis*-[$PtCl_2(NH_3)$\{2-(2-hydroxyethyl)pyridine\}] (**1**) and determined the pK_a values of its monoaqua and diaqua adducts by [^1H,^{15}N] NMR studies of complex **1** labelled with $^{15}NH_3$. The side-chain hydroxyl group introduces the potential for second coordination sphere interactions which may affect both the rate of hydrolysis and the acidity of the mono and diaqua adducts. Molecular mechanics modelling was therefore used to investigate possible hydrogen bonding between the side-chain hydroxyl group and am(m)ine or aqua ligands. The results show how both first and second coordination sphere interactions can have a major influence on the kinetic and thermodynamic properties of Pt^{II} complexes. These interactions probably also affect their anticancer activities.

[a] Department of Chemistry, University of Edinburgh, King's Buildings,
West Mains Road, Edinburgh EH9 3JJ, UK
Fax: (internat.) +44-131/650-6452
E-mail: P.J.Sadler@ed.ac.uk
[b] Department of Chemistry, the University of Sydney
NSW 2006, Australia
Supporting information for this article is available on the WWW under http://www.eurjoc.com or from the author.

Results and Discussion

X-ray Structure

cis-[$PtCl_2(NH_3)$\{2-(2-hydroxyethyl)pyridine\}] (**1**) was synthesised using a procedure reported previously for mixed am(m)ine complexes. The crystal structure of **1** (Figure 1) shows a square-planar complex with angles close to the ideal values of 90° and 180°. The angle between the two planes defined by Cl(1)−Pt−Cl(2) and N(1)−Pt−N(2) is 4.1°. The pyridine ring of complex **1** is nearly perpendicular to the platinum plane (76°) and the α-CH_2 group is very close to the platinum atom (H_2C···Pt 3.16 Å). These structural features are similar to those of the 2-picoline complex AMD473 (103° and H_3C···Pt 3.22 Å).[4] The Pt−N1 distance (2.028 Å) is also similar to that of the 2-picoline complex (2.017 Å). No intramolecular hydrogen bonding is observed between the hydroxyl group and the two Cl ligands. The 2-hydroxyethyl group is rotated away from the Pt atom, probably due to crystal packing effects. The pattern of intermolecular hydrogen bonding observed in the crystal packing of complex **1** (Supplementary Figure S1) is different from that observed previously for AMD473. For complex **1**, the packing is dominated by intermolecular NH_3···Cl hydrogen bonding [e.g. NH(2A)···Cl(1) 2.54 Å]. Additional intermolecular hydrogen bonding involves NH_3···OH [NH(2C)···O(23) 2.20 Å], and the OH group and a Cl ligand [OH(23)···Cl(1) 2.33 Å]. The X-ray diffraction data for the diiodo analogue **6** were of much poorer quality but were sufficient to define the connectivities. The complex

is again almost square-planar, with a slight lengthening of the Pt−N bonds to 2.08 and 2.10 Å due to the stronger *trans* influence of I versus Cl. There is no significant H-bonding to the coordinated halide, and interactions involving the side-chain OH are much weaker. This demonstrates the flexibility of the side-chain and that the conformation is determined by both inter- and intramolecular interactions. An overlay of the structures of complexes **1** and **6** is shown in Supplementary Figure S2.

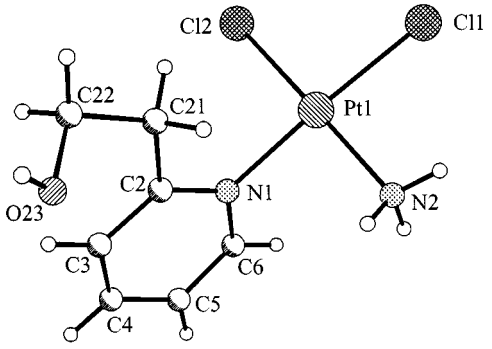

Figure 1. X-ray crystal structure of complex **1**

Hydrolysis and pK_a Values

2D [^{1}H, ^{15}N] HSQC NMR spectroscopy was used to monitor the hydrolysis of $^{15}NH_3$-labelled **1** in 0.1 M $NaClO_4$ for a period of 16 h at 298 K. Four major cross-peaks were observed in the first 2D NMR spectrum, recorded after 15 min. The assignments of the cross-peaks are based on the ^{15}N chemical shifts, which are diagnostic of the *trans* ligands,[4] and the time-dependent intensity changes of the cross-peaks. The assignments are consistent with the reaction pathway summarised in Scheme 1. The cross-peak at δ = 4.22 (^{1}H)/−65.59 (^{15}N) gradually decreased in intensity, and was assigned to the starting complex **1**. The intensity of the cross-peak at δ = 4.48/−63.30 was significantly lower than that of the cross-peak at δ = 4.40/−86.47. The ^{15}N chemical shift of the former is consistent with the assignment to the mono-aqua complex **2a** with a ^{15}N atom *trans* to Cl, while the latter peak is assignable to the monoaqua complex with the ammine trans to water (**2b**). The fourth peak at δ = 4.47/−78.07, assignable to the diaqua complex **3**, has a ^{15}N chemical shift typical of $^{15}NH_3$ *trans* to O. These shifts are similar to those observed for the 2-picoline complex AMD473.[4]

Two minor additional cross-peaks at δ = 4.34/−68.70 (complex **4**, NH_3 *trans* to N or Cl) and δ = 4.65/−82.60 (complex **5**, NH_3 *trans* to O) were present during the later stages of the aquation reaction. However, they disappeared when the pH of the solution was lowered and were therefore assigned to hydroxy-bridged species. These species were ignored in the kinetic calculations. The possibility of the formation of species containing a chelate ring by deprotonation of the hydroxyethyl side-chain and ring closure of complex **2b** was considered. Such a chelated complex would, however, contain high levels of steric strain on account of the severe steric clash between the pyridine *ortho* protons and the protons of the *cis* ammonia ligand.

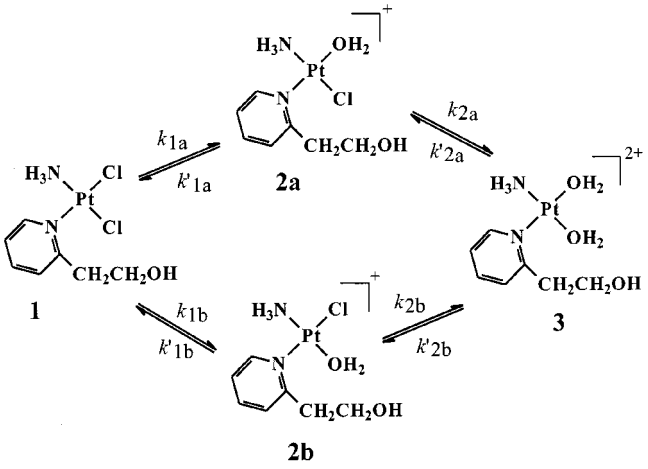

Scheme 1

The time-dependence of the concentrations of species detected during hydrolysis of complex **1** (as determined by integration of NMR cross-peaks) is shown in Figure 2. Remarkably, the cross-peak for the diaqua adduct was already intense after 15 min, and the shape of the signal was very distorted in the early stages of the hydrolysis due to the lowering of pH which accompanied the hydrolysis. The percentages of the species present after ca. 16 h at 298 K were **1**: 26.4%, **2a**: 15.5%, **2b**: 30.1%, **3**:23.1%, **4**:4.6% and **5**:0.3%. The diaqua adduct is formed much faster than for the analogous 2-picoline complex. For the latter it appears only after 2.5 h even at the higher temperature of 310 K, and less than half as much is formed after 16 h.[4]

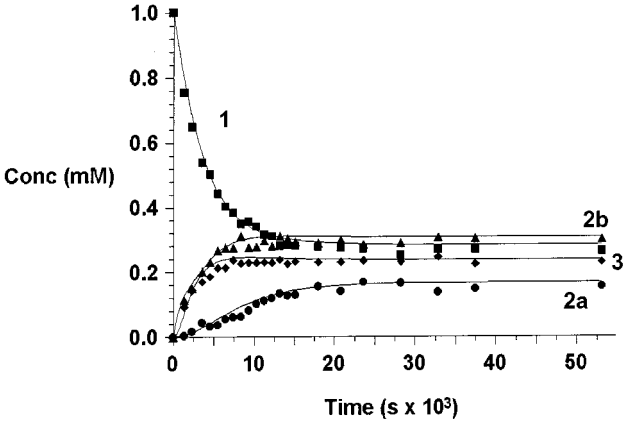

Figure 2. Dependence of the concentrations of complex **1** and its hydrolysis products on time as determined by NMR spectroscopy; labels: complex **1** (■), monoaqua complexes **2a** (•) and **2b** (▲), and diaqua complex **3** (◆); the curves represent the calculated best fits based on the rate constants given in Table 2 (see Scheme 1)

The assignments of the peaks for the mono- and diaqua complexes were further confirmed by pH titrations (Figure 3). As expected, the ^{1}H and ^{15}N chemical shift changes during the pH titration are larger for an ammine ligand

trans to an aqua ligand than when *trans* to a chloride ligand. The pK_a values of the mono- and diaqua complexes obtained by fitting the titration curves are listed in Table 1 and compared with those for the analogous 2-picoline and 3-picoline complexes, and with cisplatin.

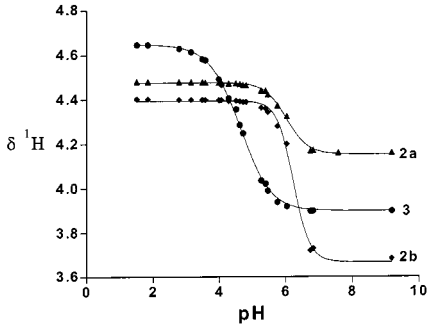

Figure 3. Dependence of the ^{1}H NMR chemical shifts of the NH_3 ligand in the monoaqua complexes **2a** and **2b** and diaqua complex **3** on pH; the curves represent best fits based on the pK_a values listed in Table 1

The rate of aquation for the chloride ligand *cis* to the pyridine ligand is much faster for complex **1** than for the 2-picoline complex AMD473 (8 × even at a temperature 12 K lower: k_{1b}, Scheme 1, Table 2). Since the X-ray crystal structures suggest that the steric effects of the pyridine side-chains are similar in the ground states of complex **1** and the 2-picoline analogue, the faster hydrolysis must arise from a lowering of the energy of the five-coordinate transition state. This may arise from H-bonding between the 2-hydroxyethyl side-chain and an incoming water ligand. The slower rate of aquation for the Cl ligand *trans* to the pyridine ligand in complex **1** in the first step of the aquation reaction (k_{1a}, Scheme 1, Table 2) is slower than for the ammine, 2-picoline or 3-picoline analogues in line with the basicities of the *trans* ligand, for which the pK_a values are in the order: NH_3 (9.29)[7] > 2-picoline (6.1), 3-picoline (6.0) > 2-(2-hydroxyethyl)pyridine (4.52).[8]

The pK_a values of the two monoaqua species of complex **1** (6.01, 6.23) are similar to those of the 2- and 3-picoline complexes (Table 1). However, the pK_a values for the diaqua adduct of complex **1** (3.90, 4.78) are significantly lower than those of the 2- and 3-picoline analogue complexes. It seems likely that a cooperative interaction between the hydroxyethyl side-chain and the H_2O/OH ligands in the diaqua complex is involved since the pK_a values for the monoaqua complexes are normal.

Molecular Modelling

The potential for hydrogen-bonding between the hydroxyl side-chain and am(m)ine or aqua ligands and its possible influence on the deprotonation of the aqua ligands was investigated by molecular mechanics modelling. A view of a molecular model of *cis*-[$Pt(NH_3)${2-(2-hydroxyethyl)pyridine}$(H_2O)_2$]·H_2O is shown in Figure 4A. The planar picoline ligand adopts an orientation perpendicular to the coordination plane. The first methylene of the hydroxyethyl side chain is necessarily disposed toward the Pt atom, but the remainder of this chain is free to adopt orientations that map out an arc lying above the coordination plane. At the two extremes of this arc, close contacts with the ligands *cis* to the picoline ligand occur and, depending on the orientation of the hydroxyl group, this contact can take the form of a hydrogen bond. The hydroxyl group can act as a hydrogen bond acceptor or hydrogen bond donor, and in the latter role would stabilise a hydroxo

Table 1. Values of pK_a for the mono- and diaqua adducts of *cis*-[$PtCl_2(NH_3)${2-(2-hydroxyethyl)pyridine}] (**1**), *cis*-[$PtCl_2(NH_3)$(2-picoline)], *cis*-[$PtCl_2(NH_3)$(3-picoline)] and cisplatin[4,23]

Adduct	**1**	*cis*-[$PtCl_2(NH_3)$(2-picoline)]	*cis*-[$PtCl_2(NH_3)$(3-picoline)]	cisplatin
Monoaqua	6.01[a]	6.13[a]	5.98[a]	6.41
Monoaqua[b]	6.23[b]	6.49[b]	6.26[b]	6.41
Diaqua	3.90, 4.78[c]	5.22, 7.16	5.07, 6.94	5.37, 7.21

[a] H_2O *trans* to picoline ligand. [b] H_2O *trans* to NH_3 ligand. [c] Average of values obtained from fits to ^{1}H NMR spectroscopic data (3.89, 4.79) and ^{15}N NMR spectroscopic data (3.91, 4.76).

Table 2. Rate constants determined for the hydrolysis of platinum complexes at 298 K (I = 0.1 M), unless otherwise stated (see Scheme 1); the errors represent one standard deviation

Complex	Rate constant (x 10^{-6} s^{-1}) (Anation rate constants × 10^{-3} M^{-1} s^{-1})[a]			
Complex **1**	k_{1a} 8.6 ± 4.5 (k'_{1a} 55.7 ± 50.3)	k_{1b} 167.9 ± 6.1 (k'_{1b} 144.1 ± 27.5)	k_{2a} 89.8 ± 58.3 (k'_{2a} 95.9 ± 26.8)	k_{2b} 737.9 ± 120.4 (k'_{2b} 95.5 ± 17.4)
AMD473[b]	k_{1a} 31.9 ± 1.5	k_{1b} 22.1 ± 1.4	k_{2a} 73.0 ± 14.0	k_{2b} 3.5 ± 2.5
3-picoline[b]	k_{1a} 44.7 ± 1.9	k_{1b} 103.0 ± 4.0	k_{2a} 35.0 ± 1.7	k_{2b} 78.0 ± 60.0
Cisplatin[c]	k_{1a} 51.8 ($k1$)	-	-	-

[a] Obtained from best fits to the curves shown in Figure 2 (see Scheme 1). The anation rates are subject to large errors because the reverse reactions are relatively fast. [b] Ref.[4] 310 K. [c] Ref.[24]

ligand in the *cis* position. Thus, it has the potential to promote deprotonation of the *cis* aqua ligand and contribute to the unusually low pK_a value. No stable orientation of the hydroxyethyl side chain resulted in a close contact with the ligand lying *trans* to the picoline ligand, primarily because of the unfavourably short contacts between the side-chain and the Pt atom that result from any disposition toward the *trans* ligand. Therefore an alternative explanation for its low pK_a was sought. A water molecule, added to the second coordination sphere close to the coordination plane and in a position to form hydrogen bonds with both aqua ligands, moved away from this plane toward the hydroxyethyl side chain on energy minimisation. In the final model (Figure 4B), this water molecule acts as a hydrogen bond acceptor to the aqua ligand *cis* to the picoline ligand and a hydrogen bond donor to both the hydroxyethyl group and the aqua ligand *trans* to the picoline. This is but one of many arrangements that might be considered, but it shows that the 2-hydroxyethyl side chain can be viewed as providing an environment conducive to the close association of a water molecule with the *cis*-[Pt{2-(2-hydroxyethyl)-pyridine}$(NH_3)(OH_2)_2]^{2+}$ complex. The Pt···OH_2 interaction is long (3.33 Å) but may provide an additional electrostatic contribution to bonding, as previously described for other Pt^{II} ammine complexes.[9,10] Hydrogen bonding between the Pt and a water molecule would be expected to stabilise the hydroxo form of the aqua ligands. In addition, the hydrophilic environment created by the 2-hydroxyethyl side chain would promote deprotonation of the aqua ligands and so contribute to their unusually low pK_a values.

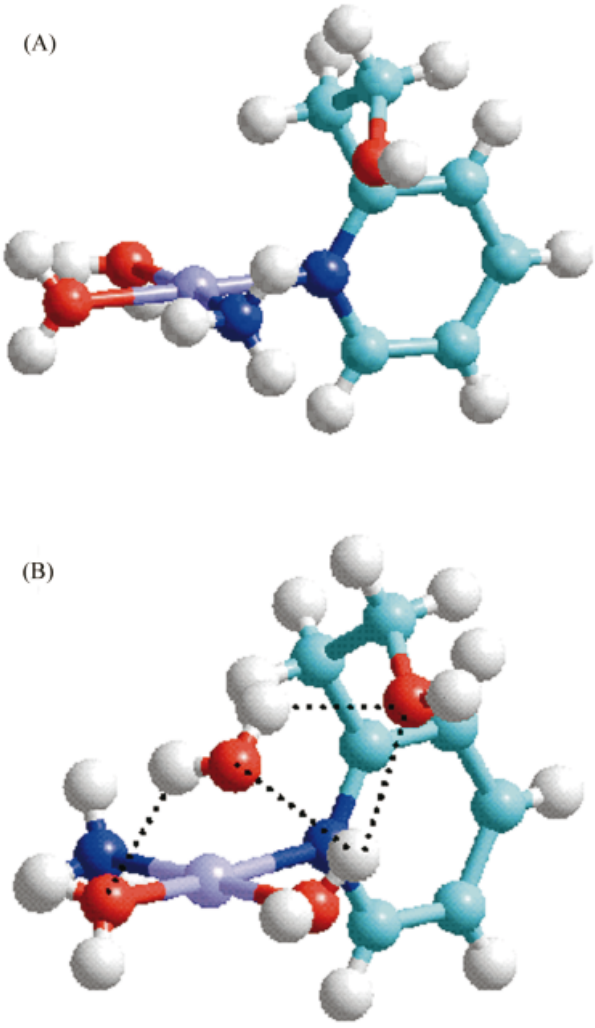

Figure 4. (A) A ball and stick view of a molecular model of *cis*-[Pt(NH_3)\{2-(2-hydroxyethyl)pyridine\}$(OH_2)_2]^{2+}$; colour code: H (white), C (cyan), O (red), Pt (dark blue), N (blue); (B) energy-minimised model of [Pt(NH_3)\{2-(2-hydroxyethyl)-pyridine\}$(OH_2)_2]^{2+}\cdot H_2O$, showing that the water molecule acts as a hydrogen bond acceptor to the aqua ligand *cis* to the picoline ligand and a hydrogen bond donor to both the hydroxyethyl group and the aqua ligand *trans* to the picoline ligand; colour code: H (white), C (green), O (red), Pt (light blue), N (dark blue)

In conclusion, complex **1** is an interesting new analogue of the anticancer drug AMD473, and it will now be interesting to investigate the effects of the rapid hydrolysis of complex **1** and low pK_a values of the diaqua adduct on its biological activity in comparison with AMD473.

Experimental Section

Materials and Preparations: 2-(2-Hydroxyethyl)pyridine was purchased from Aldrich. *cis*-[$PtCl_2(^{15}NH_3)$\{2-(2-hydroxyethyl)-pyridine\}] (**1**) and the iodide analogue **6** were prepared by a similar procedure to that described in the literature for natural abundance, mixed-ligand am(m)ine Pt^{II} complexes.[11] Crystals suitable for X-ray diffraction were obtained by recrystallisation from water, in the case of **1** by very slow evaporation of solvent in the presence of 0.5 M NaCl.

pH Measurements: These were obtained on a Corning 145 pH meter equipped with an Aldrich micro combination electrode calibrated with Aldrich buffer solutions of pH 4, 7 and 10. The values of pH were adjusted with 1 M $HClO_4$ or NaOH as appropriate.

NMR Spectroscopy: NMR spectra were recorded on a Bruker DMX500 instrument using 5 mm tubes, as described previously.[4] The chemical shift references were sodium trimethylsilyl[D_4]propionate for ^1H, and $^{15}NH_4Cl$ in 1.5 M HCl for ^{15}N (external).

X-ray Crystallography

Crystal Data for Complex 1: $C_7H_{12}Cl_2N_2OPt$, M = 406.18, monoclinic, space group $P2_1/c$; a = 9.608(5), b = 10.722.(6), c = 10.608(5) Å, β = 100.72(5)°, V = 1073.8(9) $Å^3$, Z = 4, ρ_c = 2.512 g cm^{-3}, $F(000)$ = 752, μ(Mo-K_α) = 13.53 mm^{-1}, yellow block 0.38 × 0.24 × 0.12 mm^3. Data were collected to 2θ = 50° at 220 K in the manner described above. An absorption correction was applied by Gaussian integration following refinement of the crystal dimensions and face indices against a set of ψ-scans (Stoe X-SHAPE;[12] range of T: 0.364−0.737). The structure was solved by Patterson methods (DIRDIF)[13] and refined against F^2 using SHELX-97. H-atoms were treated as described above. The refinement converged to $R1$ = 2.98% [for 1552 data with $F > 4\sigma(F)$], $wR2$ = 6.36% (for all 1908 unique data), S = 1.021. The final difference map extremes were +1.39 and −1.02 $eÅ^{-3}$.

Crystal Data for Complex 6: $C_7H_{12}I_2N_2OPt$, M = 589.08, monoclinic; space group $P2_1/c$; a = 7.253(4), b = 20.702.(9), c = 8.834(5) Å, β = 113.68(4)°, V = 1213.4 $Å^3$, Z = 4, ρ_c = 3.225 g cm^{-3}, $F(000)$ = 1040, μ(Mo-K_α) = 16.62 mm^{-1}, yellow lath 0.43 × 0.18 × 0.10 mm^3. Data were collected to 2θ = 50° in ω-θ mode at 220 K

on a Stoe Stadi-4 diffractometer equipped with an Oxford Cryosystems low-temperature device. The diffraction peaks had irregular profiles and high, uneven backgrounds; perhaps for this reason, intensity versus ψ plots derived from azimuthal scans showed significantly different intensities for reflections differing in ψ by 180°. Not surprisingly, an attempt to perform an absorption correction based on these was unsuccessful, and so a DIFABS[14] correction was applied during refinement at isotropic convergence (T = 0.129−0.599). Therefore, while these data establish chemical connectivity, the displacement parameters are liable to be systematically in error as a result of the absorption correction procedure. The structure was solved by direct methods and refined by full-matrix least-squares against F^2 (SHELX-97).[15] The OH and NH_3 groups were treated as rotating rigid groups, while other H-positions were calculated and treated using a riding model. Anisotropic displacement parameters were refined for all non-H atoms, similar restraints being applied to those of directly-bonded light atoms. The refinement converged to $R1$ = 5.96% [for 1434 data with $F > 4\sigma(F)$], $wR2$ = 14.71% (for all 2149 unique data), S = 1.045. The final difference map extremes were +2.18 and −2.12 e·Å^{-3}.

CCDC-136876 (**1**) and -136877 (**6**) contains the supplementary crystallographic data for this paper. These data can be obtained free of charge at www.ccdc.cam.ac.uk/conts/retrieving.html [or from the Cambridge Crystallographic Data Centre, 12, Union Road, Cambridge CB2 1EZ, UK; fax: (internat.) +44-1223/336-033; E-mail: deposit@ccdc.cam.ac.uk].

Molecular Mechanics Modelling: The starting models were generated using the HyperChem program[16] and energy minimised using the MOMECPC-95[17] program and a force field based on one described elsewhere.[18−22] All models were subjected to energy minimisation using MOMECPC-95 until convergence (all shifts < 0.001 Å) was achieved.

Kinetic Measurements: Peak volumes and relative concentrations from the NMR spectra recorded during the hydrolysis of complex **1** were calculated for each time point. Appropriate differential equations were integrated numerically. A nonlinear optimisation procedure using the program SCIENTIST® (version 2.01, MicroMath Inc) was employed to determined the rate constants. The errors represent one standard deviation.

Acknowledgments

We thank the EPSRC, BBSRC, Wolfson Foundation and Royal Society for their support for this work. We thank Professor Jan Reedijk (Leiden) and other members of EC COST D8/D20 for encouragement and stimulating discussions.

[1] F. I. Raynaud, F. E. Boxall, P. M. Goddard, M. Valenti, M. Jones, B. A. Murrer, M. Abrams, L. R. Kelland, *Clin. Cancer Res.* **1997**, *3*, 2063−2074.
[2] J. Holford, S. Y. Sharp, B. A. Murrer, M. Abrams, L. R. Kelland, *Br. J. Cancer* **1998**, *77*, 366−373.
[3] J. Holford, F. Raynaud, B. A. Murrer, K. Grimaldi, J. A. Hartley, M. Abrams, L. R. Kelland, *Anti-Cancer Drug Design* **1998**, *13*, 1−18.
[4] Y. Chen, Z. Guo, S. J. Parsons, P. J. Sadler, *Chem. Eur. J.* **1998**, *4*, 672−676.
[5] Y. Chen, Z. Guo, J. A. Parkinson, P. J. Sadler, *J. Chem. Soc., Dalton Trans.* **1998**, 3577−3585.
[6] Y. Chen, J. A. Parkinson, Z. Guo, P. J. Sadler, *Angew. Chem. Int. Ed.* **1999**, *38*, 2060−2063.
[7] G. Pettit and L. D. Pettit, *IUPAC Stability Constants Database*, IUPAC and Academic Software, Otley (UK), **1993**.
[8] T. Lane, A. Kandathil, S. Rosalie, *Inorg. Chem.* **1964**, *3*, 487−490.
[9] M. Krauss, H. Basch, K. J. Miller, *J. Am. Chem. Soc.* **1988**, *110*, 4517−4521.
[10] K. J. Barnham, C. J. Bauer, M. I. Djuran, M. A. Mazid, T. Rau, P. J. Sadler, *Inorg. Chem.* **1995**, *34*, 2826−2832.
[11] S. J. Barton, K. J. Barnham, A. Habtemariam, P. J. Sadler, R. E. Sue, *Inorg. Chim. Acta* **1998**, *273*, 8−13.
[12] Stoe X-Shape, Stoe & Cie, Darmstadt, Germany, **1998**.
[13] P. T. Beurskens, G. Beurskens, W. P. Bosman, R. de Gelder, S. García-Granda, R. O. Gould, R. Israel and J. M. M. Smits, DIRDIF, Crystallography Laboratory, University of Nijmegen, The Netherlands, **1996**.
[14] N. Walker, D. Stuart, *Acta Crystallogr., Sect. A* **1983**, *39*, 158−166.
[15] G. M. Sheldrick, SHELX-97, University of Gottingen, Germany, **1997**.
[16] HYPERCHEM, Hypercube Inc., Ontario, Canada.
[17] T. W. Hambley, P. Comba, and N. Okon, MOMECPC-95, A Strain Energy Minimization Package adapted to HyperChem; University of Sydney and University of Heidelberg, **1995**.
[18] T. W. Hambley, *Inorg. Chem.* **1988**, *30*, 1073−1079.
[19] T. W. Hambley, *Inorg. Chem.* **1991**, *30*, 937−942.
[20] E. C. L. Ling, G. W. Allen, T. W. Hambley, *J. Chem. Soc., Dalton Trans.* **1993**, 3705−3710.
[21] S. J. Weiner, P. A. Kollman, D. A. Case, U. C. Singh, C. Ghio, G. Alagona, S. Profeta Jr., P. Weiner, *J. Am. Chem. Soc.* **1984**, *106*, 765−784.
[22] T. W. Hambley, *Inorg. Chem.* **1998**, *37*, 3767−3774.
[23] S. J. Berners-Price, T. A. Frenkiel, U. Frey, J. D. Ranford, P. J. Sadler, *J. Chem. Soc., Chem. Commun.* **1992**, 789−791.
[24] K. Hindmarsh, D. A. House, M. M. Turnbull, *Inorg. Chim. Acta* **1997**, *257*, 11−18.

Received October 22, 2001
[I01415]

N,*N*-Dilithioarylamines as New Building Blocks in Amide Chemistry; the Structure of a Carbanion-Stabilized $[C_2N_5Li_{10}]^{2-}$ Cluster

Christine Neumann,[a] Axel Schulz,[a] Thomas Seifert,[a] Wolfgang Storch,*[a] and Martina Vosteen[a]

Keywords: Amines / Tin / Lithium / Clusters / Structure elucidation

2-Biphenylamine reacts with (dimethylamino)trimethylstannane in a 2:1 molar ratio, undergoing transamination to the distannylamine **1a**. The extremely air and moisture sensitive (2-biphenyl)-*N*,*N*-dilithium amide **2a** is obtained by the stannazane cleavage reaction of **1a** with *n*BuLi in MeO*t*Bu. Compound **2a** is the first example of a highly reactive, doubly metallated amine that can be used as a precursor in inorganic synthesis under fairly mild conditions. For example, both lithium atoms can be substituted by boryl or silyl groups, which cannot be introduced using other routes. Amide **2a** crystallizes as a cluster containing five $RNLi_2$ units, and is unexpectedly stabilized by two methanide anions. When the methanide ions are included, the lattice of the central $C_2N_4Li_8$ unit represents a section of the antiisomorphic lattice of the CaF_2-type. DFT (B3LYP) calculations and population analysis (NBO) have been carried out to get further insights into the thermodynamics of several dilithioamines $(RNLi_2)_n$ (R = H, CH_3, Ph; n = 1–6).
(© Wiley-VCH Verlag GmbH, 69451 Weinheim, Germany, 2002)

Introduction

Lithium amides are of widespread importance as precursors in the synthesis of novel main group element-nitrogen compounds and as deprotonating agents.[1] Their synthesis from secondary amines and alkyllithium compounds,[1] as well as their structural features in solution and the solid state, have been documented in numerous examples.[2] In contrast, little information is available about synthetic routes to doubly lithiated primary amines and the molecular structures of these compounds. Apart from powder diffraction studies on $LiNH_2/Li_2NH$ in the early fifties,[3] only the complex structure of the dilithiated α-naphthylamine has been reported.[4] This metal amide crystallizes as a cyclo-oligomeric aggregate containing ten molecular units with intermolecular Li−N bridging bonds. Dilithiated species have been postulated as intermediates in the decomposition of metallated amines, although their existence has not yet been confirmed.[5]

Recently we reported the synthesis and structures of monometallated organostannylamides of the type $RN(SnMe_3)M$.[6] In this paper we want to describe the synthesis of the first example of a highly reactive dilithiated primary amine, its unexpected molecular structure and its promising use as a building block.

[a] Department Chemie der Ludwig-Maximilians-Universität München,
Butenandtstrasse 5−13, Haus D, 81377 München, Germany
Fax: (internat.) + 49-(0)89/2180-7407
E-mail: wst@cup.uni-muenchen.de

Results and Discussion

The dilithium organylamides **2** are obtained by stannazane cleavage reactions of the distannylamines **1** with lithium alkyls in a 1:2 molar ratio according to Equation (1) and (2) under kinetically controlled conditions in good yield.[7] The deprotonation reaction of primary amines with metal alkyls does not lead to dimetallated amides. These reactions are usually not straightforward and lead to a mixture of products owing to unintentional C−H bond-cleavage reactions.

$$R\text{–}NH_2 \xrightarrow[-\ 2\ Me_2NH]{+\ 2\ Me_3SnNMe_2} \underset{\mathbf{1}}{R\text{–}N(SnMe_3)_2} \quad (1)$$

$$R\text{–}N(SnMe_3)_2 \xrightarrow[-2\ Me_3SnR']{+\ 2\ R'Li} \underset{\mathbf{2}}{1/n\ [R\text{–}NLi_2]_n} \quad (2)$$

The distannazanes **1** can be obtained from the transamination of Me_3SnNR_2 (R = Me, Et) with primary amines [Equation (1)] according to well-known procedures.[8a,8b] The progress of the reaction [Equation (2)] can be monitored by ^1H and ^{119}Sn NMR spectroscopy by following the change of the signal intensity of the cleavage product tetraalkylstannane as well as of the signal of **1**.

The extremely air- and moisture-sensitive dilithium amides **2** can only be isolated as colorless powders when butyllithium is used as the metalating agent in a 1:1 mixture of hexane and diethyl ether. Monomeric species of **2** could

not be detected in solution even when temperature-dependent NMR spectroscopy methods were applied. In most cases complex multiplet signals (^{7}Li or ^{13}C NMR) were detected, or the low concentration of compounds remaining in solution after cooling the reaction mixture did not allow the detection of nuclei with low natural abundance. This holds particularly for ^{15}N NMR studies, which are essential for the elucidation of structural features in solution. The signal pattern and the chemical shift of the nuclei measured (^{1}H, ^{7}Li, ^{13}C, ^{14}N) point to aggregation even in the presence of chelating amine ligands (pmdta, tmeda) for complexation of the lithium ions. These findings are in contrast to the properties of the respective precursors, the monolithium stannylamides.[6] Depending on the reaction conditions mono- or dinuclear units can be detected in solution, confirmed by their excellent resolved spin-spin coupling pattern of $^{1}J(^{6}Li,^{15}N)$ and $^{2}J(^{6}Li,^{119}Sn)$ and by an X-ray structure determination in the solid state. Although the predominant ionic character of the Li−N bond is indisputable, the values of the coupling constants mentioned above indicate a significant degree of covalency in that bond. Previous theoretical investigations of the hypothetical structure of the monomeric $HNLi_2$ [2d] suggested a considerable amount of p_π overlap in the Li−N bond, which has not been proved to be a good description.

The tendency of metal amides to form polynuclear aggregates should increase on going from mono- to dilithiated amides owing to the increase of electron density at the nitrogen center and the change of the ionic character in the Li−N bonds. To obtain an insight into the aggregation of dilithioamines, several species of the type $(RNLi_2)_n$ (R = H, CH_3, Ph; n = 1−6) have been studied by DFT (B3LYP)[9] calculations and population analysis (NBO).[10] These results are summarized in Table 1. They confirm that all the examined aggregation reactions are exothermic. For each substituent R attached to the nitrogen atom the calculated reaction enthalpy reveals the same trend. Starting with the dimer up to the hexamer, with R = H, the reaction enthalpy is smallest (largest stability) for the formation of the trimer (**C** in Figure 1).

The energy values of the exothermic oligomerization for different reactions decrease along the series R = H > CH_3 > Ph (Table 1).[11] According to NBO analysis the Li−N bonds are highly polar with significant amounts of covalent bonding [e.g. in the trimer (**C**): only 90% of the σ(Li−N) orbital is localized at the N atom]. In general, the polarity of the Li−N bonds increases with growing cluster size. In all cluster units each nitrogen atom interacts with four lithium centers. The lithium atoms, however, show a strong

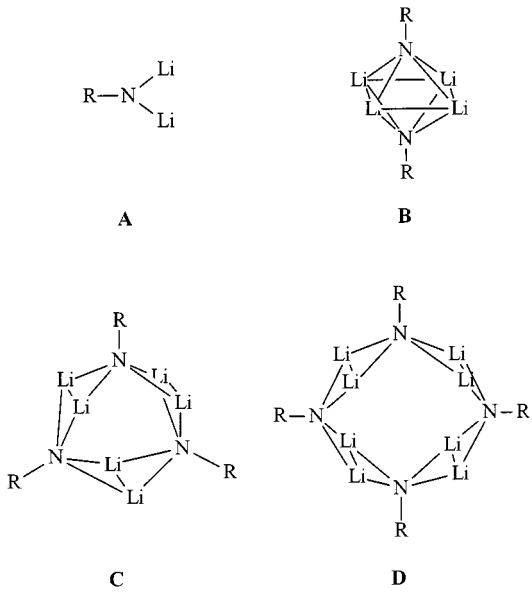

Figure 1. Schematic representation of di-, tetra-, hexa- and octanuclear Li clusters of the type ($[RNLi_2]_n$ for n = 1−4)

interaction with one adjacent lithium center and two weak interactions with two additional lithium centers [e.g. **C**: d(Li−Li) = 2.11 Å vs. 2.63 Å]. The calculated covalent (atom-atom NLMO) bond orders for this type of Li···Li interaction lie in the range between 0.03 and 0.04. Consequently, edge-linked square pyramids, containing four lithium atoms in the square positions and a nitrogen in the apical position, represent the predominant structural element (**B**−**D** in Figure 1). It therefore becomes evident that there is a positively charged area perpendicular to the rings formed by linked pyramids (see **C** and **D)** which is suitable for the attack of Lewis bases. The title molecule **2a**, the *N*-arylated species 2-dilithioaminobiphenyl, represents the product of such a formal Lewis acid-base reaction.

The X-ray structure determination of **2a** revealed an overall composition of $(C_{12}H_9NLi_2)_5{\cdot}2LiCH_3{\cdot}5OEt_2$ with a central $Li_8N_4C_2$ unit (Figure 2).[12] This structural feature is nicely in agreement with our theoretical prediction that the formation of oligomeric species (trimers and tetramers, respectively) is energetically preferred to the formation of monomeric or polymeric entities. Large R values are obtained due to the disorder of ether molecules in the crystal and the insufficient reflection properties of such a light atom cluster compound.[13] A detailed discussion of bond lengths and bond angles must therefore be carried out with care. However, the topological framework and the peculiar-

Table 1. Reaction enthalpies [B3LYP/6-31G(d,p); kcal mol^{-1}] for the successive aggregation of $n(RNLi_2) \rightarrow (RNLi_2)_n$

Reaction type[9]	**A** + **A** → **B**	**B** + **A** → **C**	**C** + **A** → **D**	**D** + **A** → **E**	**E** + **A** → **F**
R = H	−61.9	−91.1	−76.3	−68.9	−63.9
R = CH_3	−54.3	−82.5	−68.5	−	−
R = Ph	−40.9	−74.9	−	−	−

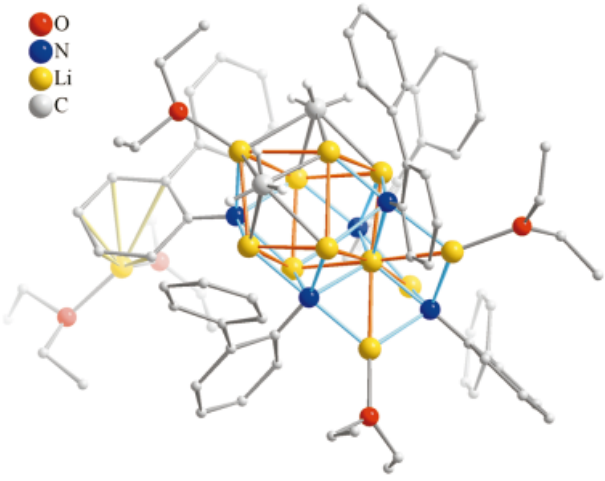

Figure 2. Molecular structure of [(2-Biphenyl-NLi_2)$_5$·2MeLi·5Et_2O] **2a**; the hydrogen atoms attached to the aryl groups are omitted for clarity, and the size of the carbon atoms of the aryl groups has been decreased.

ities of the cluster structure could be determined unambiguously. We should stress here that the results of the X-ray structure determination have been reproduced by the investigation of different single crystals deriving from several experiments. The most striking structural feature is the peculiar stabilization of the central Li_8N_4 aggregate (Figure 3) by the introduction of two methanide ions, each of them coordinating to four lithium centers. The eight lithium ions occupy the corners of a cube. The four organyl nitrogen and the two methanide anions compensate the positive charge of the cube by occupying the apical positions of six square pyramids. The six squares of the pyramids composed of lithium atoms form a cube as shown in Figure 3b. The two reactive sites in the tetrameric aggregate **D** are no longer available for further attack of the Biph-NLi_2 moiety, which would lead to the formation of larger aggregates, because of the introduction of the two methanide ions. However, the large biphenyl group of the amide center cannot prevent one additional BiphNLi_2 species from attaching itself to the periphery of the polyhedron stabilized by a lithium ion originally belonging to one of the methanide groups. Consequently the coordination number of three nitrogen centers of the polyhedron is extended to six. The Li cation of the second methanide ion is attached to a peripheral phenyl group of the biphenyl substituent by an η^6 π-

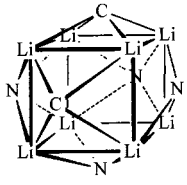

Figure 3. Central entity of the molecular structure of **2a** [without substituents R at the nitrogen atoms, the fifth $RNLi_2$ unit and the coordinating ether molecules]

interaction and additionally coordinates to two ether molecules. The lithium centers are three- and four-coordinate. The fourth position is predominantly occupied by an η^2 π-coordination with the aryl ligands (not shown in Figure 2)

When the methanide ions are included, the arrangement of the atoms in the central cluster unit represents a section of the antiisomorphic lattice of the CaF_2-type (Figure 3).[14] The positions of the fluoride ions at the corners of the cube are occupied by the lithium ions and the calcium positions above the centers of the edges of the cube are filled with $(R\text{-}N)^{2-}$ and CH_3^- ions. The same arrangement of atoms is found in the lattice of Li_2O. The bond lengths in the cluster **2a** are summarized in Table 2. With the reservations mentioned above they can be compared to the interatomic distances of already known lithium amides and alkyllithium compounds to see if there is a small or large deviation from normal values. The Li−N bond lengths of 1.942(5)−2.149(6) Å are in the range of the values determined by ab initio calculations of the mono lithiated $(LiNH_2)_4$ [$d_{(LiN)}$: 1.99−2.06 Å].[2b] The structural features of the latter are similar to the cluster of $(MeLi)_4$, where the positions of the methyl groups are occupied by the amino groups instead. In general the Li−N distances are significantly shorter in **2a**, probably due to the change of the electron density at the doubly metallated nitrogen atom. The Li−C bond lengths of 2.156(6)−2.445(7) Å of the methyl carbanions are similar to the values determined for tetrameric MeLi {$d_{(LiC)}$: 2.36 Å[15] and 2.236 Å according to recent ab initio studies[2b]}. Moreover, the Li−Li distances of 2.329(7)−2.611(7) Å are in good agreement with the values of 2.420 Å calculated by ab initio studies of $(MeLi)_4$.[15] Finally, the sufficient agreement of the bond lengths in **2a** with those in similar compounds confirms the topology of this unusual cluster.

Table 2. Range of selected bond lengths [Å] of the cluster **2a**

Li−N	1.942(5)−2.149(6)	Li−Li	2.329(7)−2.611(7)
Li−O	1.921(6)−1.992(6)	Li−CH_3	2.156(6)−2.445(7)
Li···$C_{biphenyl}$	2.291(6)−2.786(6)		

The origin of MeLi, which was not used as the metalating agent, can be explained indirectly by the presence of the alkyl stannanes Me_2SnBu_2 and $SnMe_4$. This points to exchange reactions according to Equation (3) followed by the Sn−N cleavage reaction of **1a** according to Equation (4).

$$Me_3SnBu + LiBu \rightleftharpoons Me_2SnBu_2 + LiMe \quad (3)$$

$$R\text{-}N(SnMe_3)_2 + LiMe \longrightarrow R\text{-}N(SnMe_3)Li + SnMe_4 \quad (4)$$

However, it was not possible to detect MeLi in the cooled reaction mixture by means of ^{1}H and ^{13}C NMR spectroscopy, probably due to the Sn−N cleavage reactions proceeding very rapidly under these conditions. The equilibrium in Equation (3) was proved by reaction of Me_3SnBu with BuLi in a 1:1 molar ratio at −20 °C. The ^{1}H and ^{119}Sn NMR spectra showed that only ca. 30% of the products were formed under these conditions.[7]

The similarities in the lattices of **2a** and Li_2O may indicate that the Li−N bond is predominantly ionic in character despite a significant amount of covalent bonding as confirmed by our DFT studies. Additionally, Li−Li interactions may stabilize the cluster **2a**.

Astonishingly, the cluster compound **2a** is easily split into reactive cluster fragments, which makes it an ideal precursor for the formation of new element-nitrogen compounds. A convenient method of using the dilithium amide in solution even at low temperatures (−40 °C to −50 °C) is the reaction of **2a** with element halides according to Equation (5). A crucial condition for this procedure is the formation of the cluster compound in methyl *tert*-butyl ether (mtbe) as solvent and with methyllithium in ether as reagent.

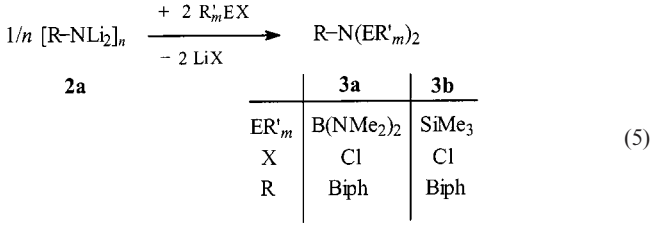

(5)

Using this technique diborylamines (**3a**) or disilylamines (**3b**) are accessible under mild conditions [Equation (5)]. These compounds are not easily synthesized by existing techniques and, to the best of our knowledge, routes including Si−N or Sn−N cleavage reactions do not yield satisfactory results.[7] The application of the synthetic potential of **2a** is not restricted to the examples described in this paper, it is also suitable for a variety of element halides as well as organyl groups R (e.g. R = *t*Bu, Me_3Si, Me_3Sn, C_6H_5, 2,6-*i*$Pr_2C_6H_3$, etc.). The extreme reactivity of the R-N^{2-} group is revealed by the existence of protonation reactions [Equation (6) and (7)] upon allowing the reaction mixture to warm to ambient temperature.[7]

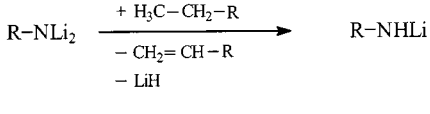

(6)

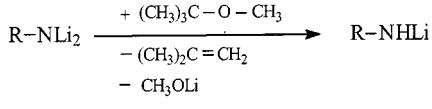

(7)

Experimental Section

General Remarks: Due to the moisture sensitivity of the compounds, some extremely so, all experiments and manipulations were carried out under argon purified by passage through a BTS catalyst. Reactions were performed by using standard Schlenk techniques and using dried, thoroughly deoxygenated solvents. The starting materials 2-aminobiphenyl, Me_3SiCl (all Aldrich) were used after redestillation. Me_3SnNMe_2[19] was prepared according to a literature procedure from Me_2NLi and Me_3SnCl. However, the yield could be improved by separation of surplus Me_2NLi before the addition of the exact stochiometric amount of Me_3SnCl. (2-Biphenyl)$N(SnMe_3)_2$[8c] and $(Me_2N)_2BCl$,[20] were prepared according to literature procedures. NMR spectra were recorded with Jeol GSX270 and Jeol EX400 spectrometers. A Perkin-Elmer Paragon 1000 PC spectrophotometer was used to record the IR spectra; solid substances were examined as Nujol mulls between KBr plates (vs: very strong, s: strong, m: medium, w: weak, vw: very weak, sh. shoulder).

(2-Biphenyl)dilithium amide (2a): A 1.1 mL portion of a solution of 2-biphenyl-$N(SnMe_3)_2$ (1.5 g, 3 mmol) dissolved in Et_2O (20 mL) was treated dropwise at −50 °C with *n*BuLi (3.75 mL, 1.6 M in hexane) diluted with 10 mL of hexane, resulting in a yellow solution. An orange solid precipitated from the solution, which redissolved (complete at −20 °C) upon allowing the reaction mixture to slowly warm to 0 °C. After removal of a sample for NMR investigations [$\delta^{7}Li$ = 3.5 (broad); $\delta^{119}Sn$ = 0.2 ($BuSnMe_3$), 2.6 ($SnMe_4$); signal ratio 100:12], the orange solution was cooled to −20 °C again, concentrated to a volume of ca 1.5 mL, diluted with 10 mL of Et_2O and stored at −78 °C for a fortnight. Some of the orange single crystals obtained by this procedure and suitable for X-ray structure analysis were isolated from the cooled solution. After separation of the solid from the solution, the crystalline material was dried in vacuo (10 °C/10^{-3} Torr). The residual yellow powder (0.31 g, 57%; m.p. > 280 °C, decomp.), which burns upon contact with air or moisture, changed color to dark brown when attempting to isolate a sample for elemental analysis, even under an argon atmosphere, hence the reported data are fairly inaccurate (ca. 12.5% too low). ^{1}H NMR (C_6D_6): δ = −1.31 [s, $(CH_3Li)_n$], 0.83 [t, $^{3}J_{H,H}$ = 7.0 Hz, $(CH_3CH_2)_2O$], 2.98 [q, $^{3}J_{H,H}$ = 7.0 Hz, $(CH_3CH_2)_2O$], 6.5−7.8 (unresolved m, aryl-*H*). ^{7}Li NMR (C_6D_6): δ = −4.9, −0.9 (very broad, signal ratio 11:100). ^{13}C NMR (C_6D_6): δ = −4.6 [s, $(CH_3Li)_n$], 14.9 [$(CH_3CH_2)_2O$], 65.2 [$(CH_3CH_2)_2O$], 120.7−155.8 (ca. 20 signals, aryl area, diphenyl groups). IR (nujol): $\tilde{\nu}$ = 3048 cm^{-1} w, 3034 w, 2972 m, 2929 m, 2871 m, 1573 s, 1443 s, 1411 vs, 1309 s, 1293 s, 1249 s, 1184 m, 1093 m, 987 m, 840 m, 762 m, 738 m, 600 m, 532 m, 497 m. $C_{12}H_9NLi_2$ (181.1): calcd. C 79.59, H 5.01, N 7.73; found C 69.57, H 4.34, N 6.66.

Bis[bis(dimethylamino)boryl](2-biphenyl)amine (3a): BuLi (3.1 mL, 1.6 M in hexane) was added dropwise at −55 °C to a stirred solution of 2-biphenyl-$N(SnMe_3)_2$ (**1a**; 1.1 g, 2.5 mmol) in mtbe (25 mL). The suspension turned to an orange solution at −30 °C. After stirring for 2 h at −30 °C, $(Me_2N)_2BCl$ (0.7 mL, 5 mmol), dissolved in hexane (12 mL), was added. After allowing the yellow suspension to warm to ambient temp. and stirring for a further 48 h the colorless solid was filtered off (G4-frit). [NMR spectroscopic data of the filtrate: $\delta^{11}B$ = 24.0, 28.6 (br, 2-Biph-$N[B(NMe_2)_2]_2$ **3a**); $\delta^{119}Sn$ = −3.6 (Bu_2SnMe_2), 0.2 ($BuSnMe_3$), 2.3 ($SnMe_4$), signal ratio: 24:100:24]. After removal of all volatile components in vacuo (40 °C/10^{-3} Torr), **3a** (0.66 g, 72%, bp. 87 °C/10^{-5} Torr) could be isolated as a yellow oil. ^{1}H NMR (C_6D_6): δ = 2.45 [broad, 24 H, $(Me_2N)_2$], 6.77 (m, 1 H, 3-H), 6.95 (m, 1 H, 5-H), 7.09−7.28 (m,

5 H, 2′- 6′-H), 7.49 (m, 2 H, 4-H/6-H). ^{11}B NMR (C_6D_6): δ = 29.1. ^{13}C NMR (C_6D_6): δ = 39.4 [broad, ($Me_2N)_2$], 121.2 (C3), 126.3 (C5), 127.2 (C1), 128.3 (C2′, C6′), 128.7 (C3′, C5′), 129.0 (C6), 132.2 (C4), 135.1 (C4′), 142.4 (C1′), 148.5 (C2). IR (nujol): $\tilde{\nu}$ = 3073 cm^{-1} w, 2992 m, 2896 s, 2791 m, 1580 w, 1510 s, 1388 s, 1349 s, 1246 m, 1224 s, 1136 m, 1122 m, 1064 m, 1028 m, 862 s, 744 m, 702 m. $C_{20}H_{32}B_2N_5$ (365.1): calcd. C 65.79, H 9.11, N 19.18; found C 63.69, H 8.94, N 18.18. MS: *m*/*z* = 365 [M$^+$].

Bis(trimethylsilyl)(2-biphenyl)amine (3b): BuLi (4.19 mL, 1.6 molar in hexane) was added dropwise at −55 °C to a stirred solution of the distannylamine **1a** (1.66 g, 3.35 mmol) dissolved in mtbe (25 mL) at the same temperature. After 1 h stirring at −10 °C the orange colored solution was cooled to −30 °C. Me_3SiCl (0.84 mL, 6.7 mmol) dissolved in hexane (12 mL) was then added dropwise and the solution was allowed to attain ambient temp. within 2 h. After additional stirring for 12 h the solid components were separated by filtration (0.35 g, 120% according to LiCl, G4-frit). The volatile compounds of the filtrate were removed in vacuo (30 °C/10^{-2} Torr) and **3b** (0.7 g, 67%, 80 °C/10^{-3} Torr, solidifying after 12 h) was obtained by distillation as a colorless liquid from the residual viscous, brown oil. ^{1}H NMR (400 MHz, C_6D_6): δ = 0.08 (s, 18 H, Me_3Si), 6.81 (m, 1 H, 3-H), 6.96 (m, 1 H, 5-H), 7.11−7.24 (m, 5 H, 2′-H/6′-H), 7.36−7.49 (m, 2 H, 4-H/6-H) ^{13}C NMR: δ = −0.01 (s, Me_3Si), 115.7 (C3), 118.3 (C5), 127.3 (C1), 128.0 (C2′, C6′), 128.8 (C3′, C5′), 129.2 (C6), 129.7 (C4), 130.6 (C4′), 131.1 (C1′), 144.8 (C2). ^{29}Si NMR: δ = 5.9. $C_{18}H_{27}N_1Si_2$ (313.6): calcd. C 68.94, H 8.68, N 4.47; found C 68.32, H 8.43, N 4.21. MS: *m*/*z* = 313 [M$^+$].

Computational Methods: The structural and vibrational data of several lithium-nitrogen clusters $(RNLi_2)_n$ (R = H, CH_3, Ph; *n* = 1−6; for CH_3 and Ph *n* = 1−4) were calculated by using the hybrid density functional theory (B3LYP) with the program package Gaussian 98.[9] For all elements a standard 6-31G(d,p) basis set was used. The computations were carried out at the DFT level using the hybrid method B3LYP which includes a mixture of Hartree−Fock exchange with hybrid DFT exchange correlations. Becke's three parameter functional where the non-local correlation is provided by the LYP expression (Lee, Yang, Parr correlation functional) was used as implemented in Gaussian 98. An NBO population analysis was carried out to investigate the bonding in these species.[10]

Acknowledgments

The support of this work by the Deutsche Forschungsgemeinschaft is gratefully acknowledged. We also thank the Chemetall GmbH, Frankfurt a. M. for the donation of lithium alkyls.

[1] [1a] M. F. Lappert, P. P. Power, A. R. Sanger, R. C. Srivastava, *Metal and Metalloid Amides*, Ellis Horwood-John Wiley: Chichester, **1980**, 689−691. [1b] P. G. Eller, D. C. Bradley, M. B. Hursthouse, D. W. Meek, *Coord. Chem. Rev.* **1977**, *24*, 1−95. [1c] M. Fieser, *Reagents for Organic Synthesis*, *Vol. 15*, Wiley-Interscience, New York **1990**, (and also volumes 1−14 of this series). [1d] J. L. Wardell, in *The Chemistry of the Metal-Carbon Bond, Vol 4 (The Use of Organometallic Compounds in Organic Synthesis)* (Ed.: F. R. Hartley), Wiley, Chichester **1987**. [1e] L. Brandsma, H. D. Verkruijsse, *Preparative Polar Organometallic Chemistry*, *Vol 1*, Springer, Berlin, **1987**.

[2] Solid state structures: [2a] R. E. Mulvey, *Chem. Soc. Rev.* **1998**, *27*, 339−346. [2b] A. M. Snapse, P. v. Ragué Schleyer, *Lithium Chemistry − A Theoretical and Experimental Overview, Chapter 5*, Wiley-Interscience, New York **1995**. [2c] K. Gregory, P. v. Ragué Schleyer, R. Snaith, *Adv. Organomet. Chem.* **1992**, *37*, 47−59. [2d] R. E. Mulvey, *Chem. Soc. Rev.* **1991**, *20*, 167−172. [2e] E.-U. Würthwein, K. D. Sen, J. A. Pople, P. v. Ragué Schleyer, *Inorg. Chem.* **1983**, *22*, 496−503. [2f] H. Jacobs, R. Juza, *Z. Anorg. Allg. Chem.* **1972**, *391*, 271−279; structures in solution: [2g] L. M. Jackman, L. M. Scarmoutzos, *J. Am. Chem. Soc.* **1987**, *109*, 5348−5361. [2h] L. M. Jackman, L. M. Scarmoutzos, L. M. Porter, *J. Am. Chem. Soc.* **1987**, *109*, 6524−6525. [2i] D. B. Collum, N. J. Kallman, *J. Am. Chem. Soc.* **1987**, *109*, 7466−7472. [2j] D. Barr, W. Clegg, R. E. Mulvey, R. J. Snaith, *J. Chem. Soc., Chem. Commun.* **1984**, 285−286; D. Barr, W. Clegg, R. E. Mulvey, R. J. Snaith, *J. Chem. Soc., Chem. Commun.* **1984**, 287−289.

[3] R. Juza, K. Opp, *Z. Anorg. Allg. Chem.* **1951**, *266*, 313−324.

[4] D. R. Armstrong, D. Barr, R. Snaith, *Angew. Chem.* **1991**, *103*, 1702−1704; *Angew. Chem. Int. Ed. Engl.* **1991**, *30*, 1707−1709.

[5] H. G. Richey, S. Cabre′, *J. Org. Chem.* **1983**, *48*, 3822−3825.

[6] W. Storch, T. Seifert, M. Vosteen, *Eur. J. Inorg. Chem.* **1998**, 1343−1349.

[7] M. Vosteen, PhD Thesis University of Munich, **1999**.

[8] [8a] K. Jones, M. F. Lappert, *Proc. Chem. Soc.* **1962**, 358−359. [8b] K. Jones, M. F. Lappert, *Organomet. Chem. Rev.* **1966**, 67−92. [8c] K. Jones, M. F. Lappert, *J. Chem. Soc.* **1965**, 1944−1951.

[9] Gaussian 98, Revision A. 6, M. J. Frisch, G. W. Trucks, H. B. Schlegel, G. E. Scuseria, M. A. Robb, J. R. Cheeseman, V. G. Zakrzewski, J. A. Montgomery, Jr., R. E. Stratmann, J. C. Burant, S. Dapprich, J. M. Millam, A. D. Daniels, K. N. Kudin, M. C. Strain, O. Farkas, J. Tomasi, V. Barone, M. Cossi, R. Cammi, B. Mennucci, C. Pomelli, C. Adamo, S. Clifford, J. Ochterski, G. A. Petersson, P. Y. Ayala, Q. Cui, K. Morokuma, D. K. Malick, A. D. Rabuck, K. Raghavachari, J. B. Foresman, J. Cioslowski, J. V. Ortiz, B. B. Stefanov, G. Liu, A. Liashenko, P. Piskorz, I. Komaromi, R. Gomperts, R. L. Martin, D. J. Fox, T. Keith, M. A. Al-Laham, C. Y. Peng, A. Nanayakkara, C. Gonzalez, M. Challacombe, P. M. W. Gill, B. Johnson, W. Chen, M. W. Wong, J. L. Andres, C. Gonzalez, M. Head-Gordon, E. S. Replogle, and J. A. Pople, Gaussian, Inc., Pittsburgh PA 15106 USA, **1998**.

[10] A. E. Reed, L. A. Curtiss, F. Weinhold, *Chem. Rev.* **1988**, *88*, 899−926 (NBO analysis); A. E. Reed, R. B. Weinstock, F. Weinhold, *J. Chem. Phys.* **1985**, *83*, 735−746.

[11] The calculated reaction enthalpies refer to the following reactions: monomer (**A**) + monomer (**A**) dimer (**B**), dimer (**B**) + monomer (**A**) trimer (**C**), trimer (**C**) + monomer (**A**) tetramer (**D**), tetramer (**D**) + monomer (**A**) pentamer **E**, etc.

[12] *X-ray structure determination:* Single crystals (0.10 × 0.10 × 0.10 mm), mounted on a glass fiber at −30 °C coated with oxygen-free perfluoropolyether oil. Crystal data were determined and intensity data recorded at −90 °C with a Siemens/Bruker P4 diffractometer (Mo-K_α radiation, λ = 0.71063 Å, graphite monochromator, $d_{detektor\text{-}crystal} \approx 50$ mm, CCD-area detector with Siemens LT2-device). Data reduction was performed with SAINT,[16] absorption correction with SADABS.[17] Structure solution was performed by direct methods (SHELXTL system)[18] and final refinement by using the SHELXL-97[16] program. The H-atoms of the methyl anions were localized by difference Fourier-synthesis. Crystal data: *a* = 14.332(4) Å, *b* = 46.98(2) Å, *c* = 13.387 Å, α = 90°, β = 96.05(1)°, γ = 90°, *V* = 8963(4) Å^3; monoclinic, space group $P2_1/c$, *Z* = 4, 2θ range for data collection: 13.62−50.06°, 14385 independent, 8710 observed reflections [$F > 4\sigma(F)$], R_{int} = 0.0730, *R*1 = 0.1016, wR^2 = 0.2290. CCDC-141383 contains the supplementary crystallographic data for this paper. These data can be obtained free of charge at www.ccdc.cam.ac.uk/conts/retrieving. html [or from the Cambridge Crystallographic Data Centre, 12, Union Road,

Cambridge CB2 1EZ, UK; Fax: (internat.) +44-1223/336-033; E-mail: deposit@ccdc.cam.ac.uk].

[13] Cluster compounds with such a composition of elements frequently show a drastic decrease in the number of reflections at larger decline angles Θ when small crystals (edge length < 0.1 mm) of low quality are measured. As a consequence the standard deviations of atom distances and bond angles increase, as do the conventional *R* value and the weighted *R* value, wR_2. Even exposures of 40 s/frame (ΔΦ and Δω = 0.3°) only result in a slight improvement of the data.

[14] A. Holleman, N. Wiberg, *Lehrbuch der anorganischen Chemie*, 101. edition, Walter de Gruyter, Berlin, New York, **1995**.

[15] Ch. Elschenbroich, A. Salzer, *Organometallchemie, 2. Edition*, B. G. Teubner, Stuttgart **1988**.

[16] Siemens Industrial Automation, **1995**.

[17] G. M. Sheldrick, SADABS, Universität Göttingen, **1998**.

[18] G. M. Sheldrick, SHELX-97 (SHELXS-97, SHELXL-97), Universität Göttingen, **1997.**

[19] C. M. Wright, E. L. Muetterties, *Inorg. Synth.* **1967**, *10*, 137−139.

[20] R. H. Cragg, A. F. Weston, *J. Organomet. Chem.* **1974**, *67*, 161−165.

Received September 3, 2001
[I01340]

The First Case of Local *cis* versus *trans* Coordination as the Controlling Factor for the Overall Structure in Dinuclear Assemblies

Guillem Aromí,[a] Patrick Gamez,[a] Olivier Roubeau,[a] Paula Carrero-Berzal,[a] Huub Kooijman,[b] Anthony L. Spek,[b] Willem L. Driessen,[a] and Jan Reedijk*[a]

Keywords: Stereochemistry / Self assembly / O ligands / Manganese / Nickel

The preparation and structure of two dinuclear assemblies $[M_2(HL)_2(py)_4]$ (M^{II} = Mn, Ni) with the phenol bis-β-diketone H_3L are presented. The octahedral N_2O_4 coordination environments around the metals are in *cis* and *trans* configuration for Mn and Ni, respectively, leading to structurally different assemblies. These results represent the first example where the overall structure of a complicated coordination architecture is controlled by the local stereochemistry imposed at the metal ions.

(© Wiley-VCH Verlag GmbH, 69451 Weinheim, Germany, 2002)

Introduction

In the creation of complicated coordination supramolecular assemblies, the information leading to the final architecture is contained in the structural and electronic properties of the ligands as well as in the specific requirements of the transition metals.[1] This is best illustrated by cases where very different structures are obtained when all but one of the parameters of the system are maintained constant.[2−7] For example, a ligand has been reported whose molecular information is expressed in form of either a circular or a cross-shaped dodecanuclear assembly depending on the set of metals that is allowed to react with it, and this is dictated by the coordination geometry imposed by them.[6] In a different example, small differences in the spacer between donor sites in polynucleating ligands determine whether a grid-like complex or a helicate is obtained from the same transition metal.[3,4] The understanding and control of the factors that lead to each particular architecture are paramount to bring about the ambitious potential technological applications of this field. We report here a unique example where the preferred *cis*/*trans* stereochemistry at the metal centers determines the overall architecture of the dinuclear complexes that they form with the same ligand.

[a] Leiden Institute of Chemistry, Gorlaeus Laboratories, Leiden University,
P. O. Box 9502, 2300 RA Leiden, The Netherlands
Fax: (internat.) + 31-71/527-4671
E-mail: reedijk@chem.leidenuniv.nl
[b] Bijvoet Center for Biomolecular Research, Crystal and Structural Chemistry, Utrecht University,
Padualaan 8, 3584 CH, Utrecht, The Netherlands
Fax: (internat.) + 31-30/253-3940
E-mail: a.l.spek@chem.uu.nl
Supporting information for this article is available on the WWW under http://www.eurjic.com or from the author.

Results and Discussion

The ligand H_3L[8] has been prepared recently[9] (Scheme 1) and its coordination properties with a variety of transition metals are just starting to be explored. The versatility provided by the presence of a phenol and two β-diketone units in this molecule has already afforded a diversity of supramolecular architectures.[10,11]

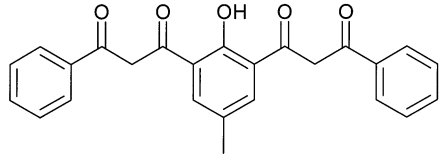

Scheme 1. H_3L in its ketonic form and *syn-syn* conformation

The X-ray structure of H_3L has been determined[12] using single crystals obtained from a solution in acetone and it is presented in this report (Figure 1). Consistent with the solution ^1H NMR spectroscopic data, the Fourier maps of this diffraction experiment also revealed the β-diketone groups to lie completely in their enolic form. In one of these units, the acidic H is found to be disordered between the oxygen atoms. One apparent and striking feature of this essentially flat molecular structure is the *anti-syn* conformation displayed by the β-diketone units with respect to the phenol group. No intermolecular hydrogen bonding or π-π contacts have been identified in the crystal lattice, suggesting this conformation to be the result of intramolecular

interactions, as supported by molecular modeling calculations performed on H_3L.[13] Presumably, this nuclear topology allows for the most favorable interactions between the numerous local electric dipoles present in this molecule.

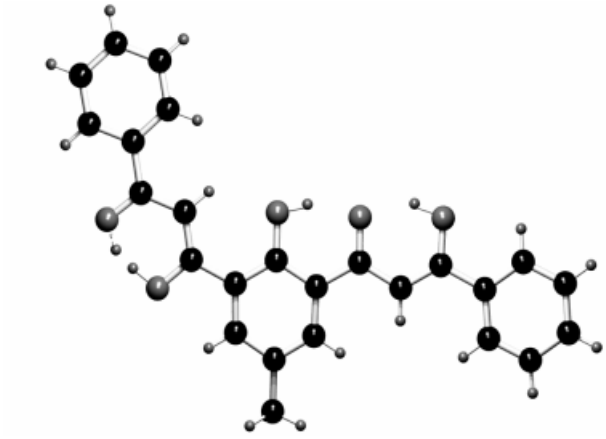

Figure 1. Pov-ray drawing of the X-ray structure of H_3L displaying its enolic form and *anti-syn* conformation

The reaction of equimolar amounts of H_3L and $Mn(OAc)_2$ or $Ni(OAc)_2$ in pyridine produced high yields of orange or green crystals of $[M_2(HL)_2(py)_4]$ (M = Mn, **1**; Ni, **2**) upon addition of Et_2O (**1**) or after layering the reaction mixture with toluene (**2**). Both types of crystals were suitable for X-ray crystallography and analyzed satisfactorily.[14]

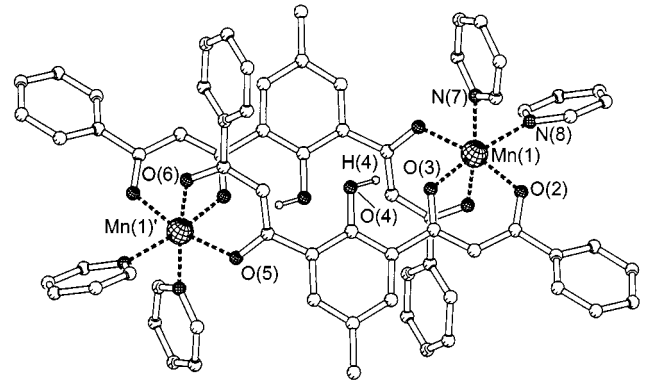

Figure 2. Platon drawing of $[Mn_2(HL)_2(py)_4]$ (**1**); selected bond lengths (Å): Mn(1)−O(2) 2.1522(15), Mn(1)−O(3) 2.1651(14), Mn(1)′−O(5) 2.1557(13), Mn(1)′−O(6) 2.1337(14), Mn(1)−N(7) 2.2415(17), Mn(1)−N(8) 2.2631(16), Mn(1)···Mn(1)′ 9.3018(13), O(3)···O(4) 2.4753(19)

The structure of **1**[12] (Figure 2) consists of a centrosymmetric complex of two Mn^{II} ions, chelated and bridged by two crystallographically equivalent HL^{2-} ligands. Interestingly, the ligands in this complex lie in the same conformation as that of the free ligand in the solid state, although much more removed from planarity [the angle between the idealized planes containing both β-diketonate groups is 40.74(9)° in **1** and 7.53(11)° in H_3L]. In addition, the presence of intramolecular hydrogen bonding between O(3) and O(4) is revealed in this structure [O(3)···O(4) = 2.4753(19) Å], where H(4) has been refined. The metals in this assembly are separated by a distance of 9.3018(13) Å, and are accommodated in a slightly distorted octahedral geometry. An oxidation state of 2+ has been assigned to Mn based on charge considerations, and is consistent with the magnetic properties of **1** (vide infra).

X-ray diffraction analysis performed on crystals of **2**[12] showed this compound to be an assembly of two Ni^{II} centers bridged by two HL^{2-} chelating ligands, with the coordination around each metal completed by two pyridine ligands (Figure 3). A crystallographic center of symmetry is also present in the middle of the molecule in this case. In contrast to **1**, however, the polynucleating ligands in this complex are found in the *syn-syn* conformation. This leads to an overall architecture that is completely different to that in **1** despite the fact that these two compounds share the same formulation, with the exception of the nature of the metals. A closer examination of the structure of **2** allows one to conclude that this major structural change is the consequence of the local stereochemistry at the metal centers. The coordination geometry around Ni is octahedral with a slight tetragonal elongation. Comparing **1** with **2**, it can be seen that the N_2O_4 coordination sphere around Ni^{II} is in a *trans* configuration, as opposed to the *cis* stereochemistry with Mn^{II}. The HL^{2-} ligand in **2** is not completely planar [the β-diketonate planes form an angle of 46.61(7)°] and also shows the same [O−H···O] interaction [O(3)···O(4) = 2.5047(15) Å] as in **1**. Furthermore, the conformational disparity between **1** and **2** leads to a markedly shorter metal-metal distance in the latter complex, the Ni···Ni distance being 7.9210(8) Å. The same arguments as for **1** are used for the assumption about the oxidation state of Ni in **2**. Crystals of the related complex $[Ni_2(HL)_2(py)_2(THF)_2]$ were also analyzed and show the same structural features as **2**. Details of this determination are included in the Supporting Information (see footnote on the first page of this article).

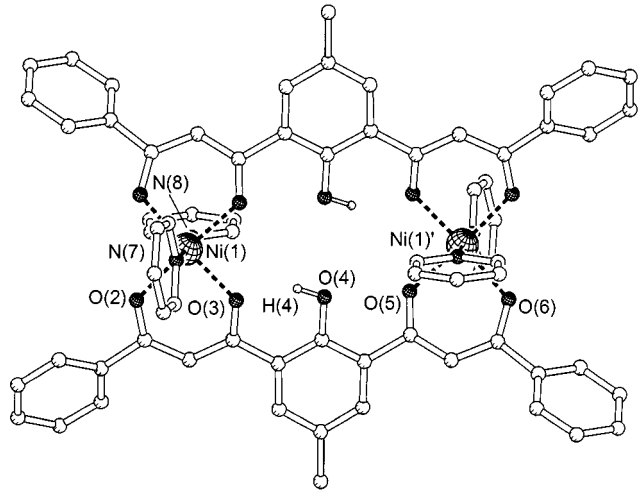

Figure 3. Platon drawing of $[Ni_2(HL)_2(py)_4]$ (**2**); selected bond lengths (Å): Ni(1)−O(2) 2.0297(10), Ni(1)−O(3) 2.0241(10), Ni(1)′−O(5) 2.0092(10), Ni(1)′−O(6) 2.0295(10), Ni(1)−N(7) 2.1067(13), Ni(1)−N(8) 2.1136(13), Ni(1)···Ni(1)′ 7.9210(8), O(3)−O(4) 2.5047(15)

The structural difference between **1** and **2** is not mirrored in their magnetic properties, as shown by bulk magnetization measurements in the 2−300 K temperature range at a constant field of 1 kG. In both cases, the magnetic susceptibility data could be fitted with a model that considers two noninteracting M^{II} centers, yielding ionic *g* values of 2.01 and 2.10 for Mn^{II} and Ni^{II}, respectively.

The local *trans* configuration preferred in complex **2** is ascribed to the larger crystal field stabilization energy that results from this donor distribution, one that is observed in the vast majority of Ni^{II} complexes with an equivalent set of ligands.[15] This thermodynamic argument does not apply to high-spin Mn^{II} (d^5). Therefore, the *cis* stereochemistry is observed at the metal ions in **1**, most probably because it is the one that allows for the most stable conformation of the polynucleating ligand. To the best of our knowledge, this is the first example where the overall structure of a polynuclear assembly is determined solely by the difference in the local *cis*/*trans* configuration of the metals. A related precedent exists where a dinucleating ligand delivers either a helicate or a mesocate, depending on the metal used, the structure of the assembly being dictated by the chirality at the coordination centers.[16] Additional examples of the simple principle manifested experimentally for the first time in the present work are currently under investigation with different metals. A thorough study will be published in due course.

Acknowledgments

Financial support by the European Union, under contract HPMF-CT99-00113 (Marie Curie Fellowship) to G. A. and TMR ERB-FMNRX-CT98-0199 to O.R., the NRSC (P. G.), the WFMO (J. R.) and the CW-NWO (A. L. S.) is gratefully acknowledged.

[1] J.-M. Lehn, *Supramolecular Chemistry − Concepts and Perspectives*; VCH: Weinheim, **1995**.
[2] B. Hasenknopf, J. M. Lehn, B. O. Kneisel, G. Baum, D. Fenske, *Angew. Chem. Int. Ed. Engl.* **1996**, *35*, 1838−1840.
[3] J. Rojo, F. J. Romero-Salguero, J. M. Lehn, G. Baum, D. Fenske, *Eur. J. Inorg. Chem.* **1999**, 1421−1428.
[4] E. C. Constable, R. Chotalia, *J. Chem. Soc., Chem. Commun.* **1992**, 64−66.
[5] P. N. W. Baxter, R. G. Khoury, J. M. Lehn, G. Baum, D. Fenske, *Chem. Eur. J.* **2000**, *6*, 4140−4148.
[6] D. P. Funeriu, J.-M. Lehn, K. M. Fromm, D. Fenske, *Chem. Eur. J.* **2000**, *6*, 2103−2111.
[7] D. W. Johnson, K. N. Raymond, *Inorg. Chem.* **2001**, *40*, 5157−5161.
[8] 1,3-Bis(3-oxo-3-phenylpropionyl)-2-hydroxy-5-methylbenzene.
[9] G. Aromí, P. Gamez, P. Carrero Berzal, W. L. Driessen, J. Reedijk, *Synth. Commun.* in press.
[10] G. Aromí, P. Carrero Berzal, P. Gamez, O. Roubeau, W. L. Driessen, H. Kooijman, A. L. Spek, J. Reedijk, *Angew. Chem. Int. Ed.* **2001**, *40*, 3444−3446.
[11] G. Aromí, P. Gamez, O. Roubeau, W. L. Driessen, H. Kooijman, A. L. Spek, J. Reedijk, *Angew. Chem. Int. Ed.* in press.
[12] Crystal structure determinations were carried out at 150 K. Data were measured on a Nonius KappaCCD diffractometer with a rotating anode (Mo-K_α radiation, graphite monochromator, $\lambda = 0.71073$ Å). Structures were solved by direct methods (SHELXS-86) and refined on F^2 with SHELXL-97. The coordinates of the hydroxyl hydrogen atoms were refined; other hydrogens were included in the refinement at calculated positions riding on their carrier atoms. No absorption correction was applied.
Data for $\mathbf{H_3L}$: $C_{25}H_{20}O_5$, $M_r = 400.41$, yellow, needle-shaped crystal (0.05 × 0.12 × 0.40 mm), orthorhombic, space group $Pna2_1$ (no. 33) with $a = 7.625(2)$, $b = 22.540(6)$, $c = 11.193(2)$, Å $V = 1923.7(8)$ Å^3, $Z = 4$, $D_c = 1.383$ g cm^{-3}, μ(Mo-K_α) = 0.096 mm^{-1}, 14561 reflections measured ($1.6° < \theta < 27.47°$), 2317 independent (Friedel pairs were averaged), $R_{int} = 0.0657$. A hydrogen atom was found to be disordered between O5 and O6; the coordinates of both positions were refined. The occupancy of the major component refined to 0.59(11). 285 parameters were refined, $wR2 = 0.0873$, $R1 = 0.0383$ [for 1796 reflections with $F_o > 4\sigma(F_o)$] $S = 1.020$, $-0.25 < \Delta\rho < 0.15$ e Å^{-3}.
Data for **1**: $C_{70}H_{56}Mn_2N_4O_{10}\cdot 5C_5H_5N$, $M_r = 1618.62$, orange, needle-shaped crystal (0.1 × 0.1 × 0.3 mm), monoclinic, space group $C2/c$ (no. 15) with $a = 25.215(3)$, $b = 15.166(2)$, $c = 21.295(2)$ Å, $\beta = 91.455(9)°$, $V = 8140.8(16)$ Å^3, $Z = 4$, $D_c = 1.321$ g cm^{-3}, μ(Mo-K_α) = 0.398 mm^{-1}, 72705 reflections measured ($1.6° < \theta < 25.21°$), 7323 independent, $R_{int} = 0.0761$. Electron density in a disordered solvent area containing 2.5 unique pyridine molecules was taken into account in the refinement via PLATON/SQUEEZE. Where relevant, the data cited above are given with the contribution of this disordered solvent. 393 parameters were refined, $wR2 = 0.1100$, $R1 = 0.0423$ [for 5551 reflections with $F_o > 4\sigma(F_o)$] $S = 1.066$, $-0.28 < \Delta\rho < 0.28$ e Å^{-3}.
Data for **2**: $C_{70}H_{56}N_4Ni_2O_{10}\cdot 2C_7H_8\cdot 2C_5H_5N$, $M_r = 1574.04$, light green, block-shaped crystal (0.15 × 0.20 × 0.30 mm), triclinic, space group $P\bar{1}$ (no. 2) with $a = 11.0980(10)$, $b = 12.0326(12)$, $c = 15.5168(15)$ Å, $\alpha = 88.854(10)°$, $\beta = 78.382(10)°$, $\gamma = 79.478(10)°$, $V = 1995.2(3)$ Å^3, $Z = 1$, $D_c = 1.309$ g cm^{-3}, μ(Mo-K_α) = 0.537 mm^{-1}, 58280 reflections measured ($1.6° < \theta < 27.49°$), 9138 independent, $R_{int} = 0.0414$, 510 parameters, $wR2 = 0.0840$, $R1 = 0.0321$ [for 7934 reflections with $F_o > 4\sigma(F_o)$] $S = 1.044$, $-0.49 < \Delta\rho < 0.53$ e Å^{-3}.
CCDC-174297−174300 contains the supplementary crystallographic data for this paper. These data can be obtained free of charge at www.ccdc.cam.ac.uk/conts/retrieving.html [or from the Cambridge Crystallographic Data Center, 12, Union Road, Cambridge CB2 1EZ, UK; Fax: (internat.) +44-1223/336-033; E-mail: deposit@ccdc.cam.ac.uk].
[13] This was done by molecular mechanics (MMF) and semi-empirical (PM3) methods as executed with the SPARTAN package (SPARTAN 5.1, Wavefunction, Inc., 18401 Von Karman Ave., Ste. 370, Irvine, CA 92612 U.S.A).
[14] **1**: $C_{70}H_{56}Mn_2N_4O_{10}$ (1223.1): calcd. C 68.74, H 4.61, N 4.58; found C 68.50, H 4.57, N 4.70. **2**·0.3py: $C_{71.5}H_{57.5}N_{4.3}Ni_2O_{10}$ (1254.33): calcd. C 68.58, H 4.47, N 4.81; found C 68.11, H 4.94, N 4.68.
[15] L. Sacconi, F. Mani, A. Bencini, *Comprehensive Coordination Chemistry*; Pergamon Press, **1987**.
[16] D. L. Caulder, K. N. Raymond, *J. Chem. Soc., Dalton Trans.* **1999**, 1185−1200.

Received December 4, 2001
[I01510]

Synthesis, Stereochemistry and Ligating Properties of Tetraalkyl-Substituted Ethanedithioamides − Evidence for the Lowering of High-Energy Rotation Barriers under the trans Influence of Pt-σ-Bonded Aryl Groups

Santo Lanza,*[a] Francesco Nicolò,[a] and Giuseppe Tresoldi[a]

Keywords: C−C hindered rotation / C−N hindered rotation / (*E*)/(*Z*) isomerisation / Tetraalkylethanedithioamides

The structural and coordinating properties of five tetrasubstituted tetraalkyldithioxamides (R_4DTO) have been studied: tetraethyldithioxamide (Et_4DTO, **1**), tetrabenzyldithioxamide (Bz_4DTO, **2**), (*E*,*E*)-*N*,*N*′-dibenzyl-*N*,*N*′-diethyldithioxamide [(*E*,*E*)-Bz_2Et_2DTO, **3**], (*E*,*Z*)-*N*,*N*′-dibenzyl-*N*,*N*′-diethyldithioxamide [(*E*,*Z*)-Bz_2Et_2DTO, **4**], (*Z*,*Z*)-*N*,*N*′-dibenzyl-*N*,*N*′-diethyldithioxamide [(*Z*,*Z*)-Bz_2Et_2DTO, **5**]. The solid structure of **4**, determined by single-crystal X-ray diffraction, is characterised by two planar thioamide groups positioned almost orthogonally to each other, connected by a C–C single bond. Each of these dithioxamides showed high-energy barriers to rotation around both the C–N and the central C–C bond. This latter is a chiral torsion, so that R_4DTO species exist as pairs of enantiomers. Compounds **3**, **4** and **5** slowly isomerised in solution to give equimolar mixtures of the three isomers; the activation enthalpy of the process was 30.0 kcal mol^{-1}. The ligands **1**–**5** reacted with [$Pt(Me_2SO)_2X_2$] (X = Cl, Br, Me, Ph) to give chiral chelate complexes [(R_4DTO-κ-*S*,*S*′)PtX_2], but **3** (and also **4** and **5**) provided a mixture of three isomeric platinum chelates in which the *S*,*S*′-coordinated ligands showed the (*E*,*E*), (*E*,*Z*) and (*Z*,*Z*) conformations. Furthermore, the presence of small amounts of the platinum complexes *cis*-[$Pt(Me_2SO)_2Ph_2$] or [(Et_4DTO-κ-*S*,*S*′)$PtPh_2$] caused the fast isomerisation of large quantities of a given isomerically pure ligand. We have explained the collapse of the R_4DTO rotational barriers by assuming that a release of electrons from the metal atom to incoming ligands in the transition state twists these into a partially reduced, dithiolenic form.

(© Wiley-VCH Verlag GmbH, 69451 Weinheim, Germany, 2002)

Introduction

We have previously found that the reactions (Scheme 1) between H_2R_2DTO (*N*,*N*′-dialkyldithioxamides) and *cis*-[PtL_2X_2]-type complexes (L = Me_2SO, Me_2S; X = Cl, Me, Ph) give rise to (i) rubeanate compounds or (ii) tight ion pairs in high yield, depending on starting material and/or reaction medium.

In fact, when X = Me or Ph, methane or benzene leaves the coordination sphere of platinum(II),[1] while when X = Cl and the reaction is carried out in low-polar, noncoordinating solvents, hydrochloric acid (HCl) remains as a guest in the ion pair.[2] HCl can be easily removed from this ion pair by means either of Lewis nitrogen bases or of Brønsted basic solvents (iii).

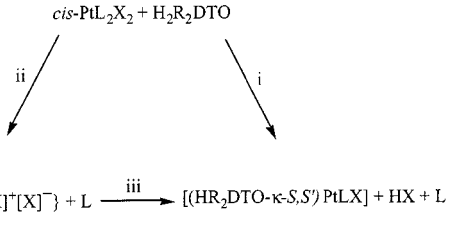

Scheme 1

Furthermore, we have previously observed that the tetraethyldithioxamides (Et_4DTO) react with *cis*-[$Pt(Me_2SO)_2X_2$] similarly to other common neutral chelating ligands to give rise to [(Et_4DTO-κ-*S*,*S*′)PtX_2] complexes.[3]

Clearly, the different reaction course of *N*,*N*′-dialkyldithioxamides with respect to the tetraalkyl-substituted ones is due to the two amide hydrogen atoms allowing loss of Cl^- in the Werner substrates *cis*-[PtL_2Cl_2], and cleavage of the Pt−C bond in the corresponding organometallic complexes *cis*-[PtL_2R_2].

Another, perhaps more relevant, difference between the *N*,*N*′-dialkyl- and tetraalkyldithioxamides arises from their conformations in solution: the energy barrier around the C(=S)−C(=S) axis in the H_2R_2DTO species is low, while the same barrier is of high energy in R_4DTO molecules. Thus, tetraalkyldithioxamides, because of the tilted array of the two NCS moieties, exist as pairs of enantiomers.

Both classes of compounds display high-energy achiral torsion barriers around the C−N bonds, and the secondary dithioxamides are locked in the more favourable (*Z*) forms.[4]

[a] Dipartimento di Chimica Inorganica, Chimica Analitica e Chimica Fisica, Università di Messina,
Vill. S. Agata, Salita Sperone 31, 98166 Messina, Italy
Fax: (internat.) + 39-090/393756
E-mail: Lanza@chem.unime.it

The conformational differences seen in the free ligands are still evident in their platinum complexes [(HR_2DTO-κ-*S*,*S*′)PtLX] (**I**), {[(H_2R_2DTO-κ-*S*,*S*′)PtLX]$^+$,[Cl^-]} (**II**) and [(Et_4DTO-κ-*S*,*S*′)PtX_2] (**III**). In the rubeanate complexes **I**, the S−C−C−S skeleton is planar, owing to the loss of one of the two amide hydrogen atoms. In the ion pairs **II**, dithioxamides act as neutral ligands, and this implies that the two NCS moieties are twisted relative to one another, because of repulsion of amide hydrogen atoms.[5] The torsion angle between amide planes (about 40°), measured by X-ray diffraction in several metal complexes, seems to be independent of the metal centre (Zn, Cu, Sn and Bi) and coordination geometry (square-planar, tetrahedral, octahedral, bipyramidal),[6] and it is therefore probably a structural characteristic of neutral chelating secondary dithioxamides. In solution, however, the amide planes flip rapidly (on the NMR timescale) because of the low-energy torsion barrier around the C(=S)−C(=S) axis.

In contrast, the compounds **III** display chiral torsion barriers as high in energy in solution as in the free ligand, and each of these complexes exists as a pair of potentially isolable enantiomers. We have already highlighted the significance of **III** as a new class of chiral chelate complexes,[3] in acknowledgment of the fact that this particular aspect in the chemistry of tetrasubstituted dithioxamide derivatives should be emphasised on account of the importance of metal complexes of chiral chelate ligands in asymmetric catalysis.[7]

Here we report a more extended series of R_4DTO platinum(II) coordination and organometallic complexes for achieving a better understanding of the chiral properties of such systems.

Results and Discussion

The synthetic route to the ligands started from dialkylamines and oxalyl chloride. The resulting oxamides were then treated with phosphorus pentasulfide to yield tetraalkyldithioxamides. Both oxamides and dithioxamides show barriers to rotation around both the amide bond and the central carbon−carbon (the pivot bond).[8] However, the barrier around the C−N bond is high in energy in both classes of compounds, while rotation around the pivot bond is hindered only in tetraalkyldithioxamides, the oxamide C(=O)−C(=O) barrier being of low energy (< 10 kcal/mol). As a consequence, the twisted dithioxamides are chiral molecules, as one can see from the resonances of the prochiral probes $-CH_2-C_6H_5$ and $-CH_2-CH_3$ in Table 1.

The barrier to rotation around the C−N bond means that both oxamides and dithioxamides with different substituents at each nitrogen atom display (*E*)/(*Z*) isomerism.

Actually, the synthesis of *N*,*N*′-dibenzyl-*N*,*N*′-diethyloxamide provides all possible geometrical isomers [(*E*,*E*), (*E*,*Z*), (*Z*,*Z*)] in equimolar ratio. The oxamide isomer mixture, on treatment with P_2S_5, is transformed into the corresponding isomers: (*E*,*E*)- (*E*,*Z*)- and (*Z*,*Z*)-*N*,*N*′-dibenzyl-*N*,*N*′-diethyldithioxamide. Each of these isomers exists as a pair of enantiomers, as a consequence of the twisting of the NCS fragments around the pivot bond.

Table 1. ^{1}H and ^{13}C NMR spectroscopic data (at 298 K, δ values relative to $SiMe_4$, *J* in Hz) for ligands **1**−**5**

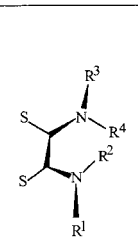

	R^1	R^2	R^3	R^4
1	Et	Et	Et	Et
2	Bz	Bz	Bz	Bz
3	Et	Bz	Et	Bz
4	Et	Bz	Bz	Et
5	Bz	Et	Bz	Et

	^{1}H NMR[a]	^{13}C NMR[b]
1[c,d]	3.20[e] (dq, $^2J_{H,H}$ = 13.9, $^3J_{H,H}$ = 7.1, 2 H, CH_2) 3.30[e] (dq, 2 H, CH_2) 3.77[f](dq, $^2J_{H,H}$ = 13.2, $^3J_{H,H}$ = 7.1, 2 H, CH_2) 3.41[f] (dq, 2 H, CH_2) 0.86 (t, 6 H, Me) 0.99 (t, 6 H, Me)	40.60 (s, 2 C, CH_2) 44.10 (s, 2 C, CH_2) 10.65 (s, 2 C, Me) 12.69 (s, 2 C, Me) 192.97 (s, 2 C, CS)
2[d,g]	4.40[e] (d, $^2J_{H,H}$ = 13.2, 2 H, CH_2) 4.96[e] (d, 2 H, CH_2) 4.90[f] (d, $^2J_{H,H}$ = 15.1, 2 H, CH_2) 5.52[f] (d, 2 H, CH_2) 7.27 (m, 20 H, *o*,*m*,*p*-Ph)	51.10 (s, 2 C, CH_2) 55.11 (s, 2 C, CH_2) 127.87, (s, 2 C, *p*-Ph) 128.41, (s, 2 C, *p*-Ph) 128.30, 128.46, 128.80, 128.83 (s, 8 C, *o*,*m*-Ph) 133.73 (s, 2 C, *q*-Ph) 134.84 (s, 2 C, *q*-Ph) 195.66, (s, 2 C, CS)
3[g]	3.80[e] (dq, $^2J_{H,H}$ = 15.1, $^3J_{H,H}$ = 7.1, 2 H, CH_2) 4.03[f] (dq, 2 H, CH_2) 4.36[f] (d, $^2J_{H,H}$ = 15.1, 2 H, CH_2) 5.00[f] (d, 2 H, CH_2) 1.16 (t, 6 H, Me) 7.35 (m, 10 H, *o*,*m*,*p*-Ph)	44.60(s, 2 C, CH_2-Me) 55.78 (s, 2 C, CH_2-Ph) 10.21 (s, 2 C, Me) 128.00 (s, 2 C, *p*-Ph) 128.37 (s, 2 C, *m*-Ph) 128.80 (s, 2 C, *o*-Ph) 134.18 (s, 2 C, *q*-Ph) 194.28 (s, 2 C, CS)
4[g]	3.47[e] (dq, $^2J_{H,H}$ = 14.3, $^3J_{H,H}$ = 7.1, 2 H, CH_2) 3.52[e] (dq, 2 H, CH_2) 3.82[f] (dq, $^2J_{H,H}$ = 14.3, $^3J_{H,H}$ = 7.1, 2 H, CH_2) 4.11[f] (dq, 2 H, CH_2) 5.01[e] (d, $^2J_{H,H}$ = 15.1, 2 H, CH_2) 5.06[e] (d, 2 H, CH_2) 5.40[f] (d, $^2J_{H,H}$ = 14.3, 2 H, CH_2) 5.45[f] (d, 2 H) 1.21 (t, 6 H, Me) 1.26 (t, 6 H, Me) 7.33 (m, 10 H, *o*,*m*,*p*-Ph)	44.27(s, 1 C, CH_2-Me) 47.03(s, 1 C, CH_2-Me) 51.18(s, 1 C, CH_2-Ph) 55.75 (s, 1 C, CH_2-Ph) 10.04 (s, 1 C, Me) 12.35 (s, 1 C, Me) 127.87 (s, 1 C, *p*-Ph) 128.41 (s, 1 C, *p*-Ph) 128.83, 128.30, 127.96 (3s, 8 C, *o*,*m*-Ph) 134.09 (s, 1 C, q-Ph) 135.12 (s, 1 C, q-Ph) 193.94 (s, 1 C, CS) 195.93 (s, 1 C, CS)
5[g]	3.55[e,h] (m, $^3J_{H,H}$ = 7.1, 4 H) 5.12[f] (d, $^2J_{H,H}$ = 14.3, 2 H) 5.45[f] (d, 2 H) 1.26 (t, 6 H, Me) 7.37 (m, 10 H, *o*,*m*,*p*-Ph)	44.92(s,2 C,CH_2-Me) 51.07 (s, 2 C, CH_2-Ph) 12.33 (s, 2 C, Me) 127.96 (s, 2 C, *p*-Ph) 128.03 (s, 2 C, *m*-Ph) 128.82 (s, 2 C, *o*-Ph) 135.83 (s, 2 C, q-Ph) 194.65 (s, 2 C, CS)

[a] At 300.13 MHz. [b] At 75.47 MHz. [c] C_6D_6. [d] The ligands **1** and **2** have already been published[22] but the NMR-spectroscopic data are completed for comparison. [e] Protons in *trans* position with respect to the sulfur atom. [f] Protons in *cis* position. [g] $CDCl_3$. [h] Overlapped signals, $^2J_{H,H}$ = not calculated.

By taking advantage of the different solubilities of the geometrical isomers in ethanol, we were able to obtain the pure (*E*,*E*) isomer **3** (insoluble in ethanol), as well as the (*E*,*Z*) isomer **4** (which crystallised from ethanol after ca. 1 h.) and the (*Z*,*Z*) isomer **5** (soluble in ethanol).

NMR spectroscopy provided useful information to establish the geometries of the isomers. Thus, compound **4**, the

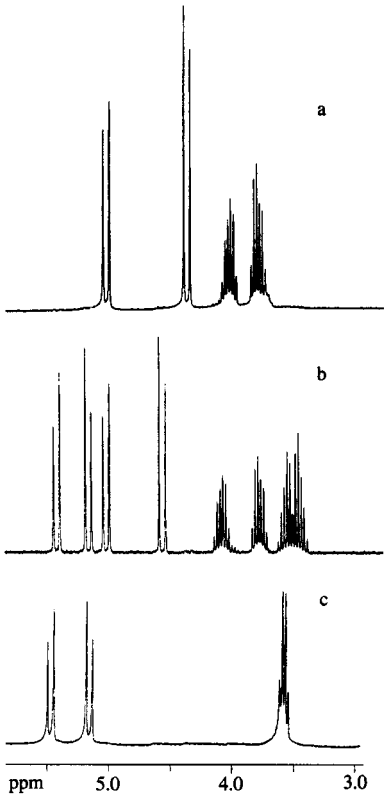

Figure 1. ^{1}H NMR spectra (methylene region) in $CDCl_3$ at 298 K of: a) (*E*,*E*)-Bz_2Et_2DTO (**3**), b) (*E*,*Z*)-Bz_2Et_2DTO (**4**) and c) (*Z*,*Z*)-Bz_2Et_2DTO (**5**)

enantiomeric couple in which the −CSNBzEt fragments have opposite (*E*,*Z*) geometries, showed in its ^{1}H NMR spectrum (Table 1 and Figure 1) two AB quadruplets, corresponding to the nonequivalent benzyl methylene protons, and two ABX_3 schemes featuring the ethyl hydrogen atoms as well.

Furthermore, studies of long-range coupling,[9] intramolecular nuclear Overhauser effects,[10] paramagnetic contact shifts[11] and benzene dilution[12] have shown that, in amides in which rotation about the N−CO bond is restricted, protons *cis* to the carbonyl groups are shielded more strongly than those in a "*trans*" arrangement, at least in the case of freely rotating alkyl substituents. In contrast, the corresponding thioamides display opposite magnetic anisotropies.[13] Thus, the (*E*,*E*) isomer **3**, insoluble in ethanol, showed the methylene proton signals of the ethyl group at lower fields in the ^{1}H NMR spectrum (and those of the benzyl group at higher field) than the corresponding resonances in **5**.

The preparative-scale separation of the above isomers offered an ideal opportunity to confirm the NMR assignment of their geometries by crystallographic analysis. For this reason, we grew a single crystal from a chloroform/ethanol (9:1, v/v) solution of **3**. Unfortunately, the crystal selected for the structural analysis was found to be (*E*,*Z*)-Bz_2Et_2DTO. This unexpected result indicated that spontaneous isomerisation of **3** had occurred in solution.

We observed afterwards that **3**, and also **4** and **5**, all became equimolar mixtures of the three enantiomeric couples within a few days when allowed to stand in chloroform at room temperature.

Kinetic monitoring of the above isomerisation process by ^{1}H NMR revealed a consecutive reversible process. This was a first-order reaction during the time in which the appearance of isomer **5** was negligible; we therefore measured the specific constants of the first-order process at 298, 310 and 323 K (Table 2). From these kinetic measurements, the activation enthalpy was estimated as 30.0 kcal mol^{-1}. This value agrees with the $\Delta H^{\ddagger}$ values for the (*Z*)/(*E*) isomerisation of several thioamides, determined by NMR spectroscopy, which have been found to be[14] in the range of 18−30 kcal mol^{-1}. Finally, the presence of **3**, **4** and **5** in equimolar quantities in the mixture indicated that the free-energy differences ΔG between the geometrical isomers were very small.

Table 2. First-order rate constants for uncatalysed and catalysed isomerisation process of **3**

T [K][a]	k_1 [s^{-1}]	Catalyst
323	1.89×10^{-3}	–
310	2.12×10^{-4}	–
298	3.24×10^{-5}	–
298	3.15×10^{-4}	$[Pt(Me_2SO)_2(C_6H_5)_2]$[b]
298	3.02×10^{-4}	$[Pt(Et_4DTO)(C_6H_5)_2]$[b]
298	3.58×10^{-5}	$[Pt(Et_4DTO)_2Cl_2]$[b]
298	2.73×10^{-5}	$[Pt(Et_4DTO)Br_2]$[b]
298	3.90×10^{-5}	$[Pt(Me_2SO)Cl_2]$[b]

[a] $CHCl_3$. [b] [(*E*,*E*)-Bz_2Et_2DTO]/[complex] = 30.

X-ray Structure of 4

The crystal structure of compound **4** consists of discrete molecules of the ligand $[(C_2H_5)(C_6H_5{-}CH_2)NCS{-}]_2$, packed together by van der Waals interactions. The crystallographic asymmetric unit is represented by one molecule, shown with the corresponding atom-labelling scheme in Figure 2. It was not possible to determine the absolute con-

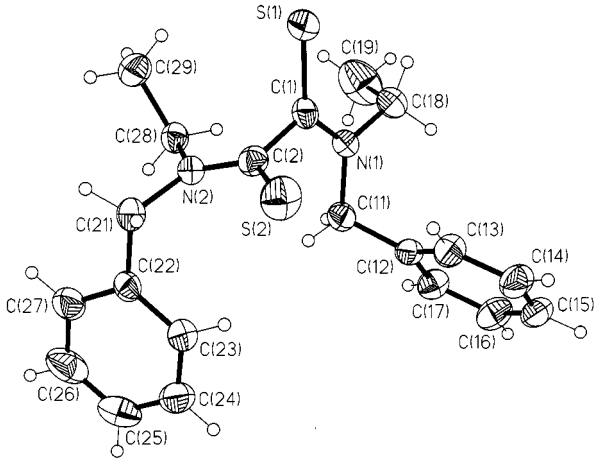

Figure 2. Molecular structure of **4** with the numbering scheme

figuration, expected from the crystallographic space group and spectroscopic evidence, despite the good quality of diffraction data and the structure model definition. In fact, the enantiomorph parameter of Flack,[15] included in the last cycle of the model refinement, converged stably to 0.55(9), a value in the middle of the theoretical extremes of 0.0 for the correct and 1.0 for the incorrect absolute configuration, respectively. This ambiguous situation has already been investigated[16] and the corresponding crystal sample was described as "inversion twin": a solid packing that is a perfect twin formed by the co-crystallisation of both enantiomers.

The ligand scheme comprises a central bulk made up of a dithionic fragment that carries an *N*-benzyl-*N*-ethylamine unit bonded to each carbon atom. On comparison of the geometric data of the two thioamides, the two $(C_2H_5)(C_6H_5{-}CH_2)NCS$ fragments appear to be very similar. The ethyl groups show some difference, which may be related to the disorder of the terminal methyl group [C(19)], as clearly evidenced by its significantly larger displacement parameters, when compared with the corresponding values for C(29). Electronic delocalisation inside each thioamide fragment is limited, as evidenced by the bond data for the almost flat geometry observed for each nitrogen atom. Both the C(1)C(2) bond length of 1.500(4) Å, denoting a single σ-bond, and the S=C−C=S torsion angle of 87.8(3)°, indicating the orthogonal disposition of the dithionic groups, point to the total absence of conjugation between the two thioamide fragments. This staggered arrangement is largely due both to steric and to electronic effects, as we have already pointed out in our previous work on an *N*,*N*,*N*′,*N*′-tetraethyl derivative,[3] in which the geometric parameters of the central N(=S)C−C(=S)N moiety are comparable. Hindrance effects play an important role in determining the disposition of substituents on both thioamide nitrogen atoms.

Metal Complexes of R_4DTO Ligands

S,*S*′−Pt chelation is postulated for all the complexes, since *N*,*N*′−Pt coordination is an unfavourable coordination mode both for steric and for electronic reasons. In fact, the nitrogen lone pairs are barely available for the coordination, because of their involvement in the CN partial double bond, especially since they are protected by bulky alkyl groups. Furthermore, *N*,*N*′−Pt coordination should be a disfavoured hard chelate ligand−soft metal interaction.

$(R^1_2R^2_2DTO)PtX_2$ compounds have been obtained as pure microcrystalline powders if $R^1 = R^2 =$ Et or Bz, X = Ph, Cl, Br.

In solution, all these complexes displayed well-resolved double ABX_3 (Et_4DTO derivatives) and AB (Bz_4DTO compounds) spectral schemes (Table 3). This means that the chiral torsion barriers around the pivot bonds, as well as the achiral torsion barriers around amide bonds, were of high energy even when tetraalkyldithioxamides were linked to platinum(II) fragments.

The Me derivative **11** was unstable and was characterised only in solution.

The three Bz_2Et_2DTO isomers displayed unexpected behaviour when they were treated with *cis*-$[Pt(Me_2SO)_2Ph_2]$ species; when one of the isomers (any one of the three) was treated with an equimolar quantity of the platinum complex, there was a mixture obtained containing the isomeric metal complexes [(*E*,*E*)-, (*E*,*Z*)-, (*Z*,*Z*)-Bz_2Et_2DTO)$PtPh_2$] in an equimolar ratio, together with the three isomers of the free ligand and the starting *cis*-$[Pt(Me_2SO)_2Ph_2]$. In other words, the equilibrium according to Scheme 2 took place and caused the isomerisation of the given pure isomer of Bz_2Et_2DTO.

Actually, the presence of catalytic amounts of *cis*-$[Pt(Me_2SO)_2Ph_2]$ complexes produced fast isomerisation of large amounts of a pure isomer (Table 2).

In turn, starting complex *cis*-$Pt(Me_2SO)_2Cl_2$, when treated with a stoichiometric amount of an isomerically pure ligand, quantitatively gave the three isomeric complexes [(*E*,*E*)-, (*E*,*Z*)-, (*Z*,*Z*)-Bz_2Et_2DTO)$PtCl_2$]. However, an excess of isomerically pure ligand, if present, isomerises at a similar rate of the spontaneous isomerisation process.

These findings supported the idea that chelation of a tertiary dithioxamide to a PtX_2 fragment lowered the energy of the barriers to rotation around CN and (S)C−C(S) bonds.

Table 3. ^{1}H and ^{13}C NMR spectroscopic data (at 300.13 and 75.47 MHz, δ values relative to $SiMe_4$, *J* in Hz) for complexes **6**−**13**

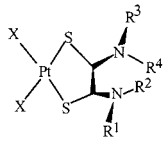

	R^1 R^2 R^3 R^4 X
6	Et Et Et Et Cl
7	Et Et Et Et Br
8	Et Et Et Et Ph
9	Bz Bz Bz Bz Cl
10	Bz Bz Bz Bz Ph
11	Bz Bz Bz Bz Me
12	Bz Et Bz Et Cl (*ZZ* isomer)
	Et Bz Et Bz Cl (*EE* isomer)
	Et Bz Bz Et Cl (*EZ* isomer)
13	Bz Et Bz Et Ph (*ZZ* isomer)
	Et Bz Et Bz Ph (*EE* isomer)
	Et Bz Bz Et Ph (*EZ* isomer)

	^{1}H NMR	^{13}C NMR
6[a,b]	3.80[c] (dq, $^2J_{H,H}$ = 13.8, $^3J_{H,H}$ = 7.2, 2 H, CH_2) 3.97[c] (dq, 2 H, CH_2) 4.10[d] (dq, $^2J_{H,H}$ = 13.4, $^3J_{H,H}$ = 7.2, 2 H, CH_2) 4.31[d] (dq, 2 H, CH_2) 1.43 (t, 6 H, Me) 1.46 (t, 6 H, Me)	16.72 (s, 4 C, Me) 54.12, 56.53 (2s, 4 C, CH_2) 195.94 (s, 2 C, CS)
7[a]	3.80[c] (dq, $^2J_{H,H}$ = 13.8, $^3J_{H,H}$ = 7.2, 2 H, CH_2) 3.97[c] (dq, 2 H, CH_2) 4.10[d] (dq, $^2J_{H,H}$ = 13.3, $^3J_{H,H}$ = 7.2, 2 H, CH_2) 4.31[d] (dq, 2 H, CH_2) 1.43 (t, 6 H, Me) 1.45 (t, 6 H, Me)	
8[b,e]	3.51[f] ($^3J_{H,H}$ = 7.2, m, 6 H, CH_2) 4.43[d] ($^2J_{H,H}$ = 13.5, $^3J_{H,H}$ = 7.2, dq, 2 H, CH_2) 1.38 (t, 6 H, Me) 1.48 (t, 6 H, Me) 6.94 (m, 6 H, *m*,*p*-Ph) 7.39 ($^3J_{PtH}$ = 83.5, *m*, 4 H, *o*-Ph)	11.49, 12.56 (2s, 4 C, Me); 46.31, 48.08 (2s, 4 C, CH_2); 121.00 ($^4J_{PtC}$ = 14.0, s, 2 C, *p*-Ph); 126.50 ($^2J_{PtC}$ = 86.8, s, 4 C, *o*-Ph); 138.10 ($^3J_{PtC}$ = 46.4, s, 4 C, *m*-Ph); 144.40 (s, 2 C, q-Ph); 186.91 (s, 2 C, CS)

Table 3. *(Continued)*

9[a]	5.06[c,d] (d, 4 H, CH_2) 5.20[c] (d, $^2J_{H,H}$ = 15.1, 2 H, CH_2) 5.42[d] (d, $^2J_{H,H}$ = 14.8, 2 H, CH_2) 7.30 (m, 20 H, *o,m,p*-bz)	57.73, 60.82 (2s, 4 C, CH_2); 128.88–129.71 (20C, *o,m,p*-bz); 131.99, 133.17 (2s, 4 C, q-bz); 196.15 (s, 2 C, CS)
10[g]	4.12[c,d] (m, 4 H, CH_2) 4.86[d] (d, $^2J_{H,H}$ = 14.3, 2 H, CH_2) 4.69[c] (d, $^2J_{H,H}$ = 14.3, 2 H, CH_2) 7.31 (m, 30 H, *o,m,p*-bz and *o,m,p*-Ph)	52.59, 54.40 (2s, 4 C, CH_2); 122.22 ($^4J_{PtC}$ = 14.0, s, 2 C, *p*-Ph); 126.77 ($^3J_{PtC}$ = 86.8, s, 2 C, *o*-Ph); 128.62–129.53 (m, 12 C, *m,p*-bz); 131.23, 133.08 (2s, 4 C, quat-bz); 137.95 ($^3J_{PtC}$ = 46.4, s, 2 C, *m*-Ph); 144.25 (s, 2 C, q-Ph); 183.72 (s, 2 C, CS)
11[g]	3.70[c] (d, $^2J_{H,H}$ = 14.1, 2 H, CH_2) 3.85[c] (d, 2 H, CH_2) 4.77[d] (m, 2 H, CH_2) 5.31[d] (d, $^2J_{H,H}$ = 14.1, 2 H, CH_2) 2.12 (s, $^2J_{PtH}$ = 93.4, 6 H, Pt-Me) 7.35 (m, 20 H, *o,m,p*-bz)	
12[g]	3.91[h] ($^3J_{H,H}$ = 7.14, m, 4 H, CH_2-Et) 4.88–5.64[h] (8d, $^2J_{H,H}$ = 14.3, 4 H, CH_2-bz) 1.23, 1.34, 1.46, (3t, 6 H, Me) 7.46 (m, 10 H, *o,m,p*-bz)	11.69, 13.00, 13.17 (4s, 6 C, Me); 50.02, 50.59, 52.98, 53.11 (2s, 2 C, CH_2-Et); 57.85, 58.09, 60.12, 60.73, (4s, 2 C, CH_2-bz); 129.13, 129.22 (2s, 2 C, *p*-bz); 129.54 – 129.89 (br, 8 C, *o,m*-bz); 130.59, 132.50, 132.73, 133.73 (4s, 2 C, q-bz); 93.21, 193.65, 194.03, 194.36 (4s, 2 C, CS)
13[g]	4.24, 3.46, 3.27 h (m, $^3J_{H,H}$ = 7.14, 4 H, CH_2-Et) 5.70–4.20 h (8d, $^2J_{H,H}$ = 14.3, 4 H, CH_2-bz) 1.23, 1.34, 1.47 (3t, 6 H, Me) 7.25 (m, 20 H, *o,m,p*-bz and *o,m,p*-Ph)	10.79, 10.91, 11.99, 12.11, (4s, 6 C, Me); 45.46, 45.55, 46.84 (3s, 2 C, CH_2-Et); 53.59, 55.63, 55.69 (3s, 2 C, CH_2-bz); 122.10 ($^4J_{PtC}$ = 14.1, s, 2 C, *p*-Ph); 122.44–128.57 (m, 10C, *o,m,p*-bz); 126.69 ($^3J_{PtC}$ = 88.6, s, 4 C, *o*-Ph); 131.37, 131.51, 133.17, 133.25 (4s, 2 C, q-bz);138.03, 138.06 ($^3J_{PtC}$ = 44.6, 2s, 4 C, *m*-Ph); 144.37, 144.40, 144.46, 144.53 (4s,2 C, q-Ph); 184.85, 185.01.185.57, 186.07 (4s, 2 C, CS).

[a] $[D_7]$DMF. [b] The complexes **6** and **8** have already been published,[3] but the NMR-spectroscopic data are included for comparison. [c] Protons *trans* to the sulfur atom. [d] Protons *cis* to the sulfur atom. [e] C_6D_6. [f] Three overlapped ABX_3 systems, $^2J_{H,H}$, for protons *trans* to sulfur, not calculated. [g] $CDCl_3$. [h] Overlapped signals.

$$bz_2Et_2DTO + cis\text{-}[Pt(Me_2SO)_2Ph_2] \rightleftharpoons (EE\text{-},EZ\text{-},ZZ\text{-}\ bz_2Et_2DTO)PtPh_2 + 2Me_2SO$$

Scheme 2

We assumed that, when the dithioxamide molecule approached the platinum atom in the transition state, a transfer of electron density from the metal centre to the ligand was able to occur, and the ligand was consequently able, in the transition state, to approach the planar dithiolenic form, this obviously bringing about the collapse of both CN and central C−C barriers. The subsequent evolution of the transition state toward the products, or also toward the reagents, restored the dithioxamides, free or coordinated, in all the possible isomeric forms.

The organometallic complexes *cis*-$[Pt(Me_2SO)_2Ph_2]$ and $[Pt(R_4DTO)Ph_2]$, but not the classical Werner compounds *cis*-$[Pt(Me_2SO)_2Cl_2]$ and $[Pt(R_4DTO)Cl_2]$, were able to catalyse the isomerisation of isomerically pure ligand (Table 2). The difference in the behaviour of the two classes of compound can be attributed to the great *trans* influence of the phenyl groups in **I** (Scheme 3), which favours the dissociation of one sulfoxide molecule and gives rise to an intermediate of reduced coordination number. The chemistry of such kinds of intermediate is well understood.[17]

In the absence of external sulfoxide, the proposed intermediate **II** can be saturated by one sulfur "tooth" of an isomerically pure dithioxamide molecule; the subsequent ring-closure process to give the chelate **IV** requires the collapse of both C−C and C−N rotational barriers, as evidenced by the spectral analysis of **IV** (Table 3). Further dissociation of **IV** produces **V** as a three-coordinated intermediate, which takes a new isomerically pure molecule and

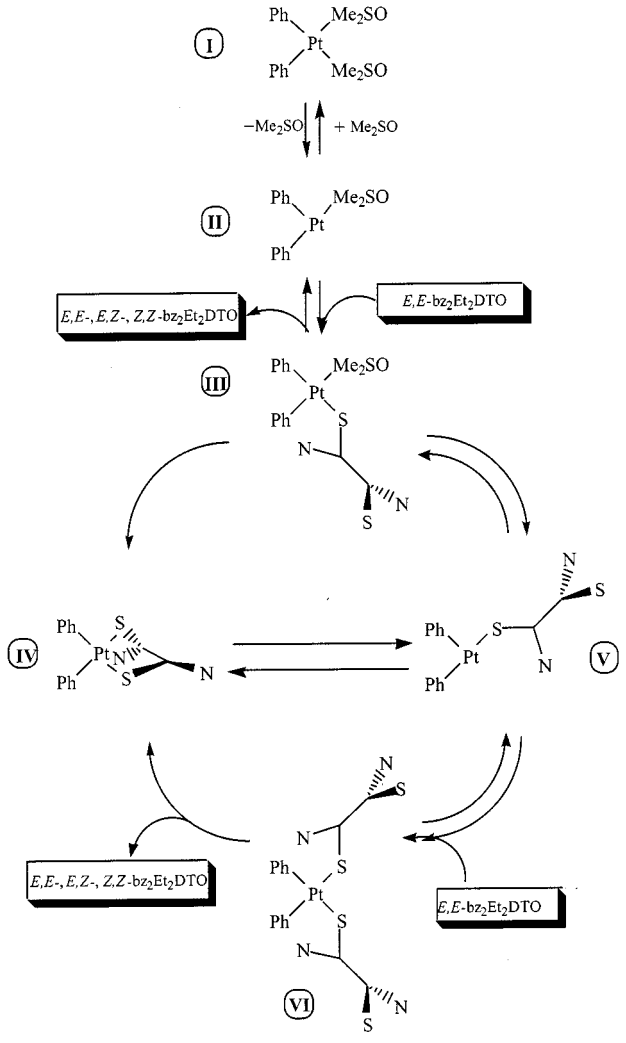

Scheme 3. Catalytic cycle for the isomerisation of (*E,E*)-Bz_2Et_2DTO ligand; the ligand input occurs in the steps II → III and V → VI, the output in the steps III → II and VI → IV

forms **VI** as a saturated intermediate. This, upon chelation, restores **IV** together with the equivalent quantity of (*E*,*E*)-, (*E*,*Z*)- and (*Z*,*Z*)-Bz_2Et_2DTO isomers. The alternative paths − **V** → **III** → **II** or **V** → **III** → **IV** − appear unlikely under the actual experimental conditions because of the exceedingly high [(*E*,*E*)-Bz_2Et_2DTO]/[Me_2SO] ratio. As evidence, the isomerisation rate of the (*E*,*E*) isomer when *cis*-[$Pt(Me_2SO)_2Ph_2$] was the catalyst ([DTO]/[Pt] = 30) was similar to that observed when [$Pt(Et_4DTO)Ph_2$] was used as catalyst ([DTO]/[Pt] = 30) and the sulfoxide path did not exist.

It is therefore possible to envisage a catalytic cycle in which the three-coordinate intermediates (**II** and **V** in Scheme 3) produce the input of isomerically pure dithioxamide, while the saturated intermediates (**VI** and **III**) produce the output of the isomerised mixture of ligands.

Studies on coordination of tetraalkyldithioxamides with various $Mo(CO)_{4-x}(PR_3)_x$ led tom Dieck to make the interesting assertion that dithioxamide links the metal atom as dithione−Mo^0 or dithiolene−Mo^{II}, depending on the electronic disposal at the metal centre.[18]

This proposal was supported by Wedd et al., who provided X-ray and NMR evidence for the dithiolenic coordination of Et_4DTO in *trans*-[$Mo(CO)_2(PR_3)_2$-(Et_4DTO)].[19]

These literature references support our hypothesis of a dithiolenic transition state as the key step in the isomerisation process of Bz_2Et_2DTO.

Unfortunately, the easy isomerisation of R_4DTO ligands as a consequence of their linkage with PtX_2 fragments indicates that the resolution of optically pure R_4DTO species through metal complexation is probably impracticable, in spite of the fact that the barrier around the pivot bond is of an energy high enough to allow, in principle, the separation of the two enantiomers.

Experimental Section

General Remarks: The precursors *cis*-$Pt(Me_2SO)_2Cl_2$,[20] *cis*-$Pt(Me_2SO)_2Br_2$,[20] *cis*-$Pt(Me_2SO)_2Ph_2$,[21] *cis*-$Pt(Me_2SO)_2Me_2$,[21] the ligands tetraethyldithioxamide (Et_4DTO) (**1**)[22] and tetrabenzyldithioxamide (Bz_4DTO) (**2**)[22] and the complexes [(Et_4DTO)$PtCl_2$] (**6**)[3] and [(Et_4DTO)$PtPh_2$] (**8**)[3] were prepared according to literature procedures. Solvents and other chemicals were of the highest purity grade commercially available and were used as purchased. ^1H and ^{13}C NMR spectra were recorded at 298 K unless stated otherwise, with a Bruker AMX-R 300 spectrometer at 300.13 and 75.47 MHz, respectively (δ in ppm relative to TMS, *J* in Hz). ^1H- and ^{13}C-NMR-spectroscopic data for the new ligands are given in Table 1 and for the complexes in Table 3. Compound **11** was not isolated in the solid state, and its characterisation was restricted to solution only.

Synthesis of (*E*,*E*)-*N*,*N*′-Dibenzyl-*N*,*N*′-diethyldithioxamide [(*E*,*E*)-Bz_2Et_2DTO, 3], (*E*,*Z*)-*N*,*N*′-Dibenzyl-*N*,*N*′-diethyldithioxamide [(*E*,*Z*)-Bz_2Et_2DTO, 4] and (*Z*,*Z*)-*N*,*N*′-Dibenzyl-*N*,*N*′-diethyldithioxamide [(*Z*,*Z*)-Bz_2Et_2DTO, 5]: Oxalyl chloride (6.346 g, 0.05 mol) and *N*-benzyl-*N*-ethylamine (27.042 g, 0.2 mol) were dissolved in benzene (120 mL). After the reaction mixture has stood overnight, diethylamine hydrochloride was filtered off, and benzene was distilled in vacuum from the filtrate to leave the crude *N*,*N*′-dibenzyl-*N*,*N*′-diethyloxamide as a mixture of (*E*,*E*), (*E*,*Z*) and (*Z*,*Z*) isomers. Phosphorus pentasulfide (3.825 g, 0.02 mmol) was added in small increments to a refluxing xylene solution (80 mL) of the crude oxamide. After the reaction mixture had been refluxed for 4 h, it was cooled and filtered from a black residue. Xylene was removed from the filtrate in vacuo, and a dithioxamide isomer mixture was obtained. This product was dissolved in ethanol (60 mL); the white, microcrystalline compound that remained undissolved provided the pure isomer **3**. The ethanolic filtrate, when allowed to stand, gave pure crystals of the isomer **4**. Finally, the pure isomer **5** was obtained when the solvent was removed from the ethanolic solution in vacuo.

Isomer 3: Yield 4.99 g (28%). $C_{20}H_{24}N_2S_2$ (356.55): calcd. C 67.37, H 6.78, N 7.86; found C 67.30, H 6.80, N 7.90.

Isomer 4: Yield 4.63 g (26%). $C_{20}H_{24}N_2S_2$ (356.55): calcd. C 67.37, H 6.78, N 7.86; found C 67.40, H 6.80, N 7.80.

Isomer 5: Yield 3.92 g (22%). $C_{20}H_{24}N_2S_2$ (356.55): calcd. C 67.37, H 6.78, N 7.86; found C 67.20, H 6.90, N 7.80.

Synthesis of [(Et_4DTO-κ-*S*,*S*′)$PtBr_2$] (7): Et_4DTO (0.232 g, 1 mmol) was added as solid to a stirred suspension of *cis*-$Pt(Me_2SO)_2Br_2$ (0.511 g, 1 mmol) in chloroform (60 mL) at ambient temperature. A deep red solution was obtained, and within a few minutes a red solid precipitated in high yield. The compound was washed with dichloromethane/diethyl ether (1:1) and dried in vacuo. Yield 0.499 g (85%). $C_{10}H_{20}Br_2N_2PtS_2$ (587.30): calcd. C 20.45, H 3.43, N 4.77; found C 20.40, H 3.50, N 4.70.

Synthesis of [(Bz_4DTO-κ-*S*,*S*′)$PtCl_2$] (9): The synthetic procedure was essentially the same as described above for **7**, from Bz_4DTO (0.481 g, 1 mmol), *cis*-$Pt(Me_2SO)_2Cl_2$ (0.422 g, 1 mmol) and chloroform (80 mL). The compound was obtained as red solid. Yield 0.597 g (80%). $C_{30}H_{28}Cl_2N_2PtS_2$ (746.69): calcd. C 48.26, H 3.78, N 3.75; found C 48.20, H 3.80, N 3.75.

Synthesis of [(Bz_4DTO-κ-*S*,*S*′)$Pt(C_6H_5)_2$] (10): Bz_4DTO (0.481 g, 1 mmol) and *cis*-[$Pt(Me_2SO)_2(C_6H_5)_2$] (505 mg, 1 mmol) were stirred in chloroform (60 mL). The resulting red solution was concentrated in vacuo (ca 20 mL), and hexane (40 mL) was then added. The compound precipitated as a red powder. Yield 0.564 g (68%). $C_{42}H_{38}N_2PtS_2$ (829.99): calcd. C 60.78, H 4.61, N 3.38; found C 60.40, H 6.70, N 3.30.

In situ Preparation of [(Bz_4DTO-κ-*S*,*S*′)$PtMe_2$] (11): Bz_4DTO (0.0252 g, 0.05 mmol) and *cis*-$Pt(Me_2SO)_2(CH_3)_2$ (0.0190 g, 0.05 mmol) were stirred in $CDCl_3$ (2 mL) for 1 h. The ^1H NMR spectrum of the solution was then recorded.

Synthesis of [Bz_2Et_2DTO-κ-*S*,*S*′)$PtCl_2$] (12) [Equimolar Mixture of the (*E*,*E*), (*E*,*Z*) and (*Z*,*Z*) Isomers]: The pure isomer (*E*,*E*)-Et_2Bz_2DTO (0.356 g, 1 mmol) and *cis*-$Pt(Me_2SO)_2Cl_2$ (0.422 g, 1 mmol) were stirred in chloroform (60 mL). The solution became red, and the compound, which was a mixture of three isomers, precipitated as deep red microcrystals. Yield 0.404 g (65%). $C_{20}H_{24}Cl_2N_2PtS_2$ (622.54): calcd. C 38.59, H 3.89, N 4.50; found C 38.40, H 3.90, N 4.40.

Synthesis of [(Bz_2Et_2DTO-κ-*S*.S′)$PtPh_2$] (13) [Equimolar Mixture of (*E*,*E*), (*E*,*Z*) and (*Z*,*Z*) Isomers]: *cis*-$Pt(Me_2SO)_2Ph_2$ (0.505 g,

1 mmol) and the pure isomer (*E*,*E*)-Bz_2Et_2DTO (1.068 g, 3 mmol) were stirred in chloroform (60 mL). The solution became red and the compound precipitated as red solid. Satisfactory analytical data were not obtained, due to the presence of the free ligand.

X-ray Data Collection and Structure Refinement of 4: Suitable crystals of compound **4** were obtained by slow concentration of a chloroform/ethanol (90:10, v/v) solution of **3**, which underwent spontaneous isomerisation during the crystallisation (see Discussion). Diffraction data were collected at room temperature with a Siemens P4 automatic four-circle diffractometer, by use of graphite-monochromated Mo-K_α radiation (λ = 0.71073 Å). Lattice parameters were obtained from least-squares refinement of the setting angles of 40 reflections with $11° \leq 2\theta \leq 30°$. No sign of crystal deterioration was found during the data collection up to $2\theta = 50°$ with variable-speed 2θ-ω scan type. The intensities of the 2340 measurements were evaluated by a 2θ profile procedure[23] and then corrected for Lorentz dispersion effects. An absorption correction was applied by fitting a pseudo-ellipsoid to the azimuthal scan data of 12 high c reflections[24] (R_{int} = 0.9%). The systematic absences unambiguously indicated the space group $P2_12_12_1$ of the orthorhombic system [a = 7.978(2), b = 12.777(2), c = 19.075(3) Å, Z = 4, D_c = 1.218 g/cm^3, μ = 22.77 cm^{-1}]. The structure was solved by Direct Methods with the SHELXTL-PLUS system[25] (also used to perform data reduction) and subsequently completed by a combination of least-squares techniques and Fourier syntheses. Whereas several hydrogen atoms were located on the final ΔF map, the H atoms were included in the refinement according to the "riding model" method with the X−H bond geometry depending on the parent atom X and with a unique common fixed isotropic displacement parameter (0.070 Å^2). The refinement, with all non-hydrogen atoms anisotropic and the function $w(F_o^2 - F_c^2)^2$ minimised for all the 2229 unique reflections, was carried out by the full-matrix, least-squares technique, based on F^2, with SHELXL93.[26] The model converged to the final residual $R(F_o) = [\Sigma||F_o| - |F_c||]/\Sigma|F_o| = 0.0279$, $wR(F_o^2) = [\Sigma w(F_o^2 - F_c^2)^2/\Sigma w(F_o^2)^2]^{1/2} = 0.0525$ and $GoF = [\Sigma w(|F_o| - |F_c|)^2/(N_{obsd.} - N_{var})]^{1/2} = 1.022$ with the final weighting scheme $w = \exp(\sin\theta/l)^2/[\sigma^2(F_o)^2 + \{0.0090 \times [\max(F_o^2,0) + 2F_c^2]\}^2]$ for 1546 reflections with $F \geq 4\sigma(F)$. A parameter for extinction correction was included in the last refinement cycles and assumed the final value $53(8)\cdot10^{-4}$. In the last difference Fourier map, the density residuals were not significant [range −0.11, 0.09 eÅ^{-3}]. The enantiomorph parameter[15] was included in the last refinement cycles of the structure model, and quickly converged to 0.55(9). Neutral atom scattering factors and anomalous dispersion correction were from ref.[27] Final geometrical calculations and drawings were carried out with the PARST program[28] and the XP utility of the Siemens package, respectively. CCDC-170711 contains the supplementary crystallographic data for this paper. These data can be obtained free of charge at www.ccdc.cam.ac.uk/conts/retrieving.html or from the Cambridge Crystallographic Data Centre, 12, Union Road, Cambridge CB2 1EZ, UK [Fax: (internat.) + 44-1223/336-033; E-mail: deposit@ccdc.cam.ac.uk].

[1] S. Lanza, L. Monsù Scolaro, G. Rosace, *Inorg. Chim. Acta* **1994**, *227*, 63−69.
[2] G. Rosace, G. Bruno, L. Monsù Scolaro, F. Nicolò, S. Sergi, S. Lanza, *Inorg. Chim. Acta* **1993**, *208*, 59−65.
[3] S. Lanza, G. Bruno, L. Monsù Scolaro, F. Nicolò, G. Rosace, *Tetrahedron: Asymmetry* **1993**, *11*, 2311−2314.
[4] V. Walter, E. Schaumann, K. J. Reubke, *Angew. Chem. Int. Ed. Engl.* **1968**, *7*, 467−469.
[5] O. Ermer, S. A. Mason, *J. Chem. Soc., Chem. Commun.* **1983**, 53−54.
[6] [6a] L. Antolini, A. C. Fabretti, G. Franchini, L. Menabue, G. C. Pellacani, H. Desseyn, R. Dommisse, H. C. J. Hoffmans, *J. Chem. Soc., Dalton. Trans.* **1987**, 1921−1928. [6b] M. G. B. Drew, J. M. Kisenyi, G. R. Willey, *J. Chem. Soc., Dalton Trans.* **1984**, 1723−1726.
[7] R. Noyori, H. Takaya, *Acc. Chem. Res.* **1990**, *23*, 345 −350.
[8] R. E. Carter, J. Sandström, *J. Chem. Phys.* **1972**, *76*, 642−647.
[9] [9a] M. T. Rogers, J. C. Woodbrey, *J. Phys. Chem.* **1962**, *66*, 540 −544. [9b] A. G. Whittaker, D. M. Moore, S. Siegel, *J. Phys. Chem.* **1964**, *68*, 3431−3433. [9c] R. C. Neuman, Jr., L. B. Young, *J. Phys. Chem.* **1965**, *69*, 1777−1780.
[10] F. A. L. Anet, A. J. R. Bourn, *J. Am. Chem. Soc.* **1965**, *87*, 5250−5251.
[11] B. B. Wayland, R. S. Drago, H. F. Henneike, *J. Am. Chem. Soc.* **1966**, *87*, 2455−2458.
[12] [12a] J. V. Hatton, R. E. Richards, *Mol. Phys.* **1960**, *3*, 253−263. [12b] D. L. Hooper, R. Kaiser, *Can. J. Chem.* **1965**, *43*, 2363−2367.
[13] H. Paulsen, K. Todt, *Angew. Chem. Int. Ed.* **1966**, *5*, 899−900.
[14] W. Walter, J. Voss, S. da Patai, *The Chemistry of Amides*, chapter 8 (Ed.: Jacob Zabicky), Interscience Publishers John Wiley & Sons, London, **1970**.
[15] [15a] D. Roger, *Acta Crystallogr., Sect. A* **1981**, *37*, 734−741. [15b] H. D. Flack, *Acta Crystallogr., Sect. A* **1983**, *39*, 876−881.
[16] G. Bernardinelli, H. D. Flack, *Acta Crystallogr., Sect. A* **1985**, *41*, 500−511.
[17] R. Romeo, *Comments Inorg. Chem.* **1990**, *11*, 21−57.
[18] H. tom Dieck, M. Form, *Angew. Chem. Int. Ed. Engl.* **1975**, *14*, 250−251.
[19] K. R. Barnard, A. G. Wedd, E. R. T. Tiekink, *Inorg. Chem.* **1990**, *29*, 891−892.
[20] Y. N. Kukushkin, Y. E. Viaz′menskii, L. I. Zorina, L. Yu Pazukina, *Russ. J. Inorg. Chem.* **1968**, 835−838.
[21] C. Eaborn, K. Kundu, A. J. Pidcock, *J. Chem. Soc., Dalton Trans.* **1981**, 933−938.
[22] R. N. Hurd, G. De La Mater, G. C. McElheny, R. J. Tuner, V. H. Wallingford, *J. Org. Chem.* **1961**, *26*, 3980−3987.
[23] R. Diamond, *Acta Crystallogr., Sect. A* **1969**, *25*, 43−55.
[24] G. Kopfmann, R. Huber, *Acta Crystallogr., Sect. A* **1968**, *24*, 348−351.
[25] G. M. Sheldrick, SHELXTL-PLUS, version 4.2, Siemens Analytical X-ray Instruments Inc., Madison, Wisconsin, **1991**.
[26] G. M. Sheldrick, SHELXL93, *Program for Crystal Structure Refinement*, Univ. of Göttingen, Germany, **1993**.
[27] *International Tables for X-ray Crystallography*, vol. IV, Kynoch Press, Birmingham, **1974**.
[28] M. Nardelli, *J. Appl. Crystallogr.* **1995**, *28*, 659, locally modified version.

Received September 17, 2001
[I01364]

Synthesis and Characterization of Derivatives of a Chelating Aluminum Dichloride Complex Containing a 3,5-Di-*tert*-butylpyrazolato Unit

Wenjun Zheng,[a] Herbert W. Roesky,*[a] Nadia C. Mösch-Zanetti,[a] Hans-Georg Schmidt,[a] and Mathias Noltemeyer[a]

Dedicated to Professor Richard L. Wells

Keywords: Aluminum / N ligands / Pyrazolato ligands / Structural elucidation

The chelating aluminum complex [{3,5-N-*t*Bu$_2$pz-N′–CH=C(SiMe$_3$)}AlR$_1$R$_2$] [R^1 = R^2 = Me (**2**); R^1 = R^2 = H (**3**); R^1 = R^2 = I (**4**)] was prepared in modest yield from an organoaluminum dichloride precursor [{3,5-N-*t*Bu$_2$pz-N′–CH=C(SiMe$_3$)}AlCl$_2$] (**1**). Compounds **2** and **3** were obtained from the reaction of **1** with MeLi in Et$_2$O or with LiAlH$_4$ in THF, respectively. Reaction of **2** or **3** with I$_2$ in toluene gave **4**. In addition, the reaction of **1** with two equivalents of water yielded the hydrolyzed product H[3,5-N-*t*Bu$_2$pz-N′–CH=C(SiMe$_3$)] (**5**). All compounds were characterized by elemental analysis, NMR spectroscopy, and mass spectrometry. The X-ray structure analysis shows that complex **2** exhibits one fused five-membered AlC$_2$N$_2$ ring and one pyrazolato ring system.

(© Wiley-VCH Verlag GmbH, 69451 Weinheim, Germany, 2002)

Introduction

Organoaluminum compounds have been explored widely owing to their importance in a variety of applications.[1] The chemistry of sterically hindered neutral derivatives of organoaluminum halides, hydrides and alkyls is especially important as they are key starting materials for a variety of compounds with unusual bonding and oxidation states, as well as unique structures.[2] Recent progress in aluminum chemistry has shown that aluminum halides with a bulky ligand may be used as precursors for synthesizing low-valent Al^{I} species.[3] Additionally, the reaction of aluminum alkyls with extremely strong Lewis acids such as B(C$_6$F$_5$)$_3$ leads to the formation of low-coordinate cationic compounds that are potential catalysts for olefin polymerization.[4] Furthermore, organoaluminum hydrides have been shown to be ideal starting materials for preparing various unusual compounds that were difficult to synthesize by other routes.[5,6] Obviously, the sterically demanding ligands play a crucial role during the formation of these compounds. In the course of the reaction of aluminum pyrazolato compounds and trimethylsilylacetylene, an unusual compound [{3,5-N-*t*Bu$_2$pz-N′−CH=C(SiMe$_3$)}AlCl$_2$] (**1**) was formed. It has been shown that the Al−Cl bonds in **1** are readily cleaved and can be substituted by other functional groups.[7] Apparently, the chelating [3,5-N-*t*Bu$_2$pz-N′−CH=C(SiMe$_3$)]$^-$ ligand in compound **1** is more sterically demanding than the simple 3,5-di-*tert*-butylpyrazole. Due to the interest in precursors of sterically demanding aluminum halides, alkyls and hydrides, reactions using **1** as a starting material have been examined.

Results and Discussion

A solution of **1** and two equivalents of MeLi in Et$_2$O was stirred at −78 °C for 3 h and then at ambient temperature for 15 h to give [{3,5-N-*t*Bu$_2$pz-N′−CH=C(SiMe$_3$)}AlMe$_2$] (**2**) in fair yield (ca. 70%; Scheme 1).[8] Compound **2** is extremely soluble in *n*-hexane and it can be purified in two steps. First, the resulting residue was sublimed at 0.01 mbar and 100 °C and then recrystallized from *n*-hexane at −26 °C to afford colorless crystals. The mass spectrum (EI) shows **2** to be monomeric {*m*/*z* (%) = 334 (10) [M$^+$], 319 (100) [M$^+$ − Me]}. The ^{1}H NMR spectrum shows a set of resonances for the chelating moiety {δ = 0.37 [Si(C*H*$_3$)$_3$], 1.00 [C(3)−C(C*H*$_3$)$_3$], 1.28 [C(1)−C(C*H*$_3$)$_3$], 5.86 [C(2)*H*], 7.63 [=C(4)*H*]} and one signal for the protons of the Al−Me groups at δ = −0.15, clearly indicating the formation of **2**. However, the ^{27}Al NMR resonance is too broad to be distinguished.

The crystallographic data of **2** are listed in Table 1. It crystallizes in the monoclinic crystal system, space group *C*2/*c* (Figure 1). The similar cell parameters of [{3,5-N-*t*Bu$_2$pz-N′−CH=C(SiMe$_3$)}AlMe$_2$] (**2**) and [{3,5-N-*t*Bu$_2$pz-N′−CH=C(SiMe$_3$)}AlCl$_2$] (**1**) indicate a structural relationship between these two compounds.[7] As in

[a] Institut für Anorganische Chemie der Universität Göttingen
Tammannstraße 4, 37077 Göttingen, Germany
Fax: (internat.) +49-(0)551/39-3373
E-mail: hroesky@gwdg.de

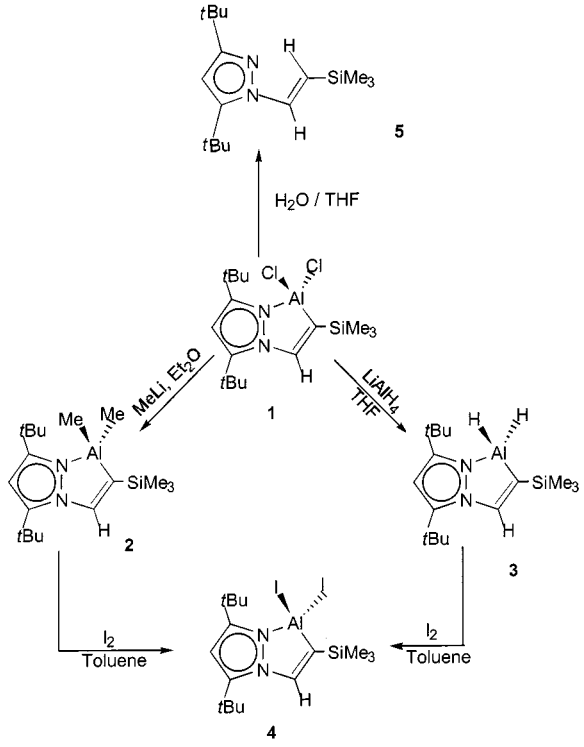

Scheme 1. Synthesis of compounds **2**–**5**

compound **1**, the geometry at the aluminum atom is a distorted tetrahedron [N1–Al1–C5 = 84.90(9)° and C21–Al1–C22 = 115.24(11)°] due to the strain imposed by the chelate ring. The fused five-membered AlC_2N_2 ring and the pyrazolato moiety are approximately coplanar. The C=C bond length of the inserted trimethylsilylacetylene molecule is significantly increased [C4–C5 = 1.328(3) Å] but is slightly shorter than the C=C double bonds of the σ complex of $AlCl_3$ with tetramethylcyclobutadiene [1.387(3) Å][9] and 1,4-dichloro-2,3,5,6-tetramethyl-1,4-dialumina-2,5-cyclohexadiene [1.367(3) Å].[10] The terminal Al(1)–C bond lengths [1.971(2) Å] are similar to those in [(η^1,η^1-3,5-*t*Bu_2pz)(μ-$AlMe_2$)]$_2$ [Al–C = 1.962(2) Å].[11]

Treatment of **1** with 2.1 equivalents of $LiAlH_4$ in THF at −30 °C yielded [{3,5-N-*t*Bu_2pz-N′–CH=C($SiMe_3$)}-AlH_2]·$(THF)_2$ [**3**·$(THF)_2$] as a white solid (Scheme 1) that is only slightly soluble in common organic solvents, except THF. Compound **3**·$(THF)_2$ is sensitive to oxygen and water. The mass spectrum (EI) suggests that **3**·$(THF)_2$ is a monomer {*m*/*z* (%) = 306 (100) [M^+]}, probably because of the sterically demanding chelating ligand [3,5-N-*t*Bu_2pz-N′–CH=C($SiMe_3$)]$^-$. The THF molecules of **3**·$(THF)_2$ can be removed by heating at 50 °C under high vacuum for 15 hours to give **3** {δ = 0.14, 1.410, 1.415, 3.80 (br.), 6.21 and 7.60 in [D_8]THF}. The ^{1}H NMR spectrum ([D_8]THF) reveals a set of resonances for the chelating moiety and a broad Al–H signal (δ = 3.80, $W_{1/2}$ = 85 Hz). The ^{27}Al NMR spectrum shows one signal at δ = 106.4, implying a coordination number of four at the Al atom. The two resonances of the protons of the nonequivalent *t*Bu groups are close to each other (δ = 1.410 and 1.415). The IR spectrum exhibits two strong bands in the expected range for Al–H stretching bands (1780 and 1812 cm^{-1}) implying terminal Al–H bonds in the solid state.[12] However, whether the THF molecules in **3**·$(THF)_2$ coordinate directly to the aluminum center or are incorporated in the crystal lattice is currently unknown.

Table 1. Crystallographic data for **2**

	2
Empirical formula	$C_{18}H_{35}AlN_2Si$
Molecular weight	334.55
Temperature (K)	200(2)
Wavelength	0.71073 Å
Crystal system	monoclinic
Space group	*C*2/*c*
Unit cell dimensions	*a* = 29.890(24) Å *b* = 9.478(10) Å *c* = 18.256(20) Å α = 90° β = 122.44(3)° γ = 90°
Volume	4364.7(75) Å^3
Z	8
Density (calculated)	1.018 Mg/m^3
Absorption coefficient	0.148 mm^{-1}
F(000)	1472
Crystal size	1.0 × 1.0 × 0.2 mm^3
θ range for data collection	3.77 to 25.02 °
Index ranges	$-35 \le h \le 35$ $-11 \le k \le 11$ $-21 \le l \le 21$
Reflections collected	7698
Independent reflections	3849 [*R*(int) = 0.0251]
Refinement method	full-matrix least-squares on F^2
Data/restraints/parameters	3845/0/210
Goodness-of-fit on F^2	1.032
Final *R* indices [$I > 2\sigma(I)$]	R_1 = 0.0457, wR_2 = 0.1241
R indices (all data)	R_1 = 0.0515, wR_2 = 0.1327
Largest different peak and hole [e·Å^{-3}]	0.532 and −0.376

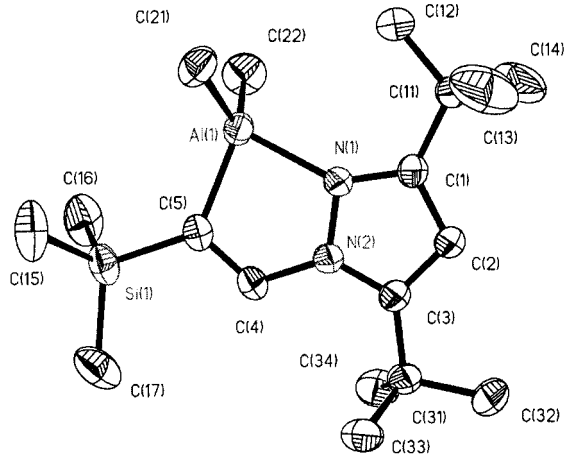

Figure 1. Perspective view of compound **2**, showing the numbering scheme and the thermal ellipsoids at the 50% probability level: Al(1)–C(5) 1.993(3), Al(1)–C(21) 1.971(2), Al(1)–C(22) 1.971(3), Al(1)–N(1) 2.016(3), C(4)–C(5) 1.328(3) Å; C(5)–Al(1)–N(1) 84.90(9)°, C(21)–Al(1)–C(22) 115.24(11)°

The reaction of **2** with two equivalents of I_2 in toluene afforded the compound [{3,5-N-*t*Bu$_2$pz-N′−CH=C(SiMe$_3$)}AlI$_2$] (**4**) after refluxing for 24 h (Scheme 1).[13] Compound **4** is readily soluble in toluene but only slightly soluble in *n*-hexane and can be readily purified by crystallization from toluene at −26 °C to give small pale crystals. The mass spectrum is in good agreement with the formulation of **4** as a monomer {*m*/*z* (%) = 558 (4) [M$^+$], 553 (15) [M$^+$ − Me], 431 (100) [M$^+$ − I]}. The ^{1}H NMR spectrum shows one set of resonances for the chelating moiety [3,5-N-*t*Bu$_2$pz-N′−CH=C(SiMe$_3$)]$^-$ (δ = 0.42, 082, 1.43, 5.81 and 7.36 in C_6D_6), indicating the formation of **4**. Alternatively, **4** can also be prepared by the reaction of **3** and two equivalents of I_2 under mild conditions (room temp.). The reaction of **3** with I_2 gives higher yields than that with **2**.[14] It is essential that the THF molecules in the precursor **3**·(THF)$_2$ are removed prior to the reaction of **3** with I_2 as otherwise the product is difficult to separate from the oily residue.

The reaction of [{3,5-N-*t*Bu$_2$pz-N′−CH=C(SiMe$_3$)}-AlCl$_2$] (**1**) with two equivalents of water in THF led to the formation of the free ligand [3,5-N-*t*Bu$_2$pz-N′−CH=CH(SiMe$_3$)] (**5**) (Scheme 1), which could be purified by sublimation at 90 °C under high vacuum (0.01 mbar). Compound **5** is soluble in both aliphatic and aromatic solvents at ambient temperature. The mass spectrum (EI) {*m*/*z* (%) = 278 (20) [M$^+$], 263 (100) [M$^+$ − Me]} and elemental analysis are in accordance with a monomeric formula for **5**. The ^{1}H NMR spectrum in C_6D_6 shows two doublets at δ = 6.77 and 7.48 (^2J = 16.3 Hz) for the two hydrogen atoms of the inserted TMS(H$_a$)C=(H$_b$) group. No proton resonance was observed in the range δ = 10−12 [the resonance of an N$_{(pyrazole)}$−H proton is usually found between δ = 10 and12 in C_6D_6],[15] confirming that the added H$_a$ atom is found in a terminal position at the TMS(H$_a$)C= group. Unfortunately, no lithium salt of **5** could be isolated from our attempts to deprotonate **5** with *t*BuLi at −78 °C or at ambient temperature. The reason why compound **5** is resistant to deprotonation is as yet unclear.

Conclusion

In summary, this paper reports the preparation of three aluminum complexes **2**−**4**, with an unusual chelating ligand containing a bulky 3,5-di-*tert*-butylpyrazolato unit, and the formation of ligand **5**, all from the readily accessible aluminum dichloride complex **1**. We have also shown that the Al−Cl bonds of **1** can be easily substituted partly[7] or completely by various basic substituents under different conditions, while the metallaheterocycle in these compounds seems to be rather stable. We are interested in a variety of aluminum complexes that have unique binding modes due to their potential applications as catalysts.[2] Compounds **1**−**4** are therefore ideal starting materials for further studies.

Experimental Section

General: All reactions were performed using standard Schlenk and dry box techniques. Solvents were appropriately dried and distilled under dinitrogen prior to use. All NMR spectra were obtained in 5-mm tubes with dry degassed [D$_6$]benzene as solvent (except for **3**, which was measured in [D$_8$]THF), referenced to external SiMe$_4$. Elemental analyses were performed by the Analytisch-Chemisches Laboratorium des Instituts für Anorganische Chemie, Göttingen.

Compound **1** was prepared according to the published method.[7]

Synthesis of [{3,5-N-*t*Bu$_2$pz-N′−CH=C(SiMe$_3$)}AlMe$_2$] (2): MeLi (4 mL, 4 mmol) in Et$_2$O (20 mL) was added slowly at −78 °C to a suspension of **1** (0.74 g, 2.0 mmol) in Et$_2$O (40 mL). The solution was allowed to warm to room temperature and then stirred for 15 h. The solvent was removed and the resulting residue sublimed at 100 °C under high vacuum (0.01 mbar) to give a white powder mainly consisting of **2**. Pure **2** was obtained by recrystallization from *n*-hexane at −26 °C (ca. 0.46 g, 70%). Crystals suitable for X-ray diffraction analysis were obtained from *n*-hexane at 4 °C. M.p. 157 °C. ^{1}H NMR (200.130 MHz, C_6D_6): δ = −0.15 (s, 6 H, Al−C*H*$_3$), 0.37 [s, 9 H, Si(C*H*$_3$)$_3$], 1.00 [s, 9 H, C(3)−C(C*H*$_3$)$_3$], 1.28 [s, 9 H, C(1)−C(C*H*$_3$)$_3$], 5.86 [s, 1 H, C(2)*H*], 7.63 [s, 1 H, =C(4)*H*]. ^{13}C NMR (125.758 MHz, C_6D_6): δ = −7.1 [br, Al-*C*(5)=], −0.9 (Al−*C*H$_3$), −0.01 [Si−*C*(16)], 29.7 [*C*(12,13,14)], 30.6 [*C*(11)], 31.4 [*C*(32,33,34)], 32.6 [*C*(31)], 103.2 [*C*(4)], 132.7 [*C*(2)], 150.7 [*C*(1)], 161.9 [*C*(3)]. MS (EI): *m*/*z* (%) = 334 (10) [M$^+$], 319 (100) [M$^+$ − Me]. $C_{18}H_{35}AlN_2Si$ (334.55): calcd. C 64.62, H 10.54, N 8.37; found C 64.3, H 10.1, N 8.2.

Synthesis of [{3,5-N-*t*Bu$_2$pz-N′−CH=C(SiMe$_3$)}AlH$_2$] (3): A solution of **1** (0.74 g, 2.0 mmol) in THF (20 mL) was added slowly at −30 °C to a suspension of LiAlH$_4$ (0.16 g, 4.2 mmol) in THF (30 mL). The suspension was stirred for an additional 15 h at room temperature and then filtered through celite. The solution was concentrated to ca. 8 mL and **3**·(THF)$_2$ crystallized as a white crystalline solid at −26 °C. After the removal of THF molecules of **3**·(THF)$_2$ at 50 °C under high vacuum for 15 h, **3** was obtained as a white powder (0.35 g, 57%). M.p.: 134 °C. ^{1}H NMR (200.130 MHz, [D$_8$]THF): δ = 0.14 [s, 9 H, Si−(C*H*$_3$)$_3$], 1.410 [s, 9 H, C(3)−C(C*H*$_3$)$_3$], 1.415 [s, 9 H, C(1)−C(C*H*$_3$)$_3$], 3.80 (br, s, 2 H, Al−*H*), 6.21 [s, 1 H, C(2)*H*], 7.60 [s, 1 H, =C(4)*H*]. ^{13}C NMR (125.758 MHz, [D$_8$]THF): δ = −0.01 [Si−*C*(16)], 29.9 [*C*(12,13,14)], 30.2 [*C*(11)], 32.4 [*C*(32,33,34)], 32.8 [*C*(31)], 104.2 [*C*(4)], 135.1 [*C*(2)], 143.6 (br, Al−*C*=), 152.0 [*C*(1)], 162.3 [*C*(3)]. ^{27}Al NMR (65.170 MHz, [D$_8$]THF): δ = 106.4. ^{29}Si NMR (99.362 MHz, [D$_8$]THF): δ = −6.2. MS (EI): *m*/*z* (%) = 306 (100) [M$^+$], 291 (70) [M$^+$ − Me]. IR (KBr, nujol mull): ν_{Al-H} = 1780 (ms), 1812 (ms) cm^{-1}. $C_{16}H_{31}AlN_2Si$ (306.50): calcd. C 62.70, H 10.19, N 9.14; found C 61.8, H 9.9, N 9.0

Synthesis of [{3,5-N-*t*Bu$_2$pz-N′−CH=C(SiMe$_3$)}AlI$_2$] (4). Method 1: A solution of I_2 (1.00 g, 4.0 mmol) in toluene (40 mL) was added slowly at room temperature to a solution of **2** (0.66 g, 2.0 mmol) in toluene (20 mL). The solution was stirred for 15 h at room temperature and then refluxed for 12 h. The solution was filtered through celite and then concentrated to ca. 10 mL to give small colorless crystals at −26 °C (0.82 g, 73%).

Method 2: A solution of I_2 (1.00 g, 4.0 mmol) in toluene (40 mL) was added slowly to a suspension of **3** (0.61 g, 2.0 mmol) in toluene (20 mL) and then stirred for 12 h at room temperature until the brown color disappeared. The solution was filtered through celite and the filtrate was concentrated to about 10 mL. Compound **4** crystallized as a pale solid at −26 °C (0.49 g, 43%). M.p.: 192 °C.

^{1}H NMR (200.130 MHz, C_6D_6): δ = 0.42 [s, 9 H, Si(CH_3)$_3$], 0.82 [s, 9 H, C(3)−C(CH_3)$_3$], 1.43 [s, 9 H, C(1)−C(CH_3)$_3$], 5.81 [s, 1 H, C(2)*H*], 7.36 [s, 1 H, =C(4)*H*]. ^{13}C NMR (125.758 MHz, C_6D_6): δ = 0.09 [Si−*C*(16)], 29.4 [*C*(12,13,14)], 31.39 [C(11)], 31.44 [*C*(32,33,34)], 33.3 [C(31)], 105.0 [*C*(4)], ca. 128 (br, Al−C=, overlapped by C_6D_6 signals), 134.7 [*C*(2)], 153.5 [*C*(1)], 165.3 [*C*(3)]. ^{29}Si NMR (99.362 MHz, C_6D_6): δ = −6.4. MS (EI): *m*/*z* (%) = 558 (4) [M^+], 543 (15) [M^+ − Me] , 431 (100) [M^+ − I]. $C_{16}H_{29}AlI_2N_2Si$ (558.29): calcd. C 34.42, H 5.24, N 5.02; found C 33.8, H 5.1, N 5.2.

Synthesis of [{3,5-N-*t*Bu$_2$pz-N′−CH=C(SiMe$_3$)}H] (5): 0.036 mL of a solution of water (2.0 mmol) in THF (10 mL) was added slowly to a solution of compound **1** (0.75 g, 2.0 mmol) in THF (30 mL) at room temperature. After stirring for 15 h at room temperature, the solvent was removed in vacuo. The resulting residue was sublimed at 90 °C under high vacuum (0.01 mbar) to afford the colorless solid **5** (0.39 g, 70%). M.p.: 173 °C. ^{1}H NMR (200.130 MHz, C_6D_6): δ = 0.12 [s, 9 H, Si(CH_3)$_3$], 1.17 [s, 9 H, C(3)−C(CH_3)$_3$], 1.44 [s, 9 H, C(1)−C(CH_3)$_3$], 6.01 [s, 1 H, C(2)*H*], 6.77 [d, $^2J_{H,H}$ = 16.3 Hz, 1 H, C(5)*H*], 7.48 [d, $^2J_{H,H}$ = 16.3 Hz, 1 H, =C(4)*H*]. ^{13}C NMR (125.758 MHz, C_6D_6): δ = −1.3 [Si−*C*(16)], 30.0 [*C*(12,13,14)], 30.3 [*C*(11)], 30.9 [*C*(32,33,34)], 33.1 [*C*(31)], 101.2 [*C*(4)], 111.2 [*C*(5)], 135.7 [*C*(2)], 150.8 [*C*(1)], 161.4 [*C*(3)]. MS (EI): *m*/*z* (%) = 278 (20) [M^+], 263 (100) [M^+ − Me]. $C_{16}H_{30}N_2Si$ (278.51): calcd. C 69.00, H 10.86, N 10.06; found C 70.4, H 11.0, N 10.3.

X-ray Crystallography: Crystals of **2** (*M* = 334.55) were grown from a concentrated *n*-hexane solution cooled to 4 °C. **2** crystallized in the monoclinic crystal system with space group *C*2/*c*. Relevant details and data are summarized in Table 1. The crystals were mounted on a glass fiber in a rapidly cooled perfluoropolyether.[16] Diffraction data were collected on a Stoe−Siemens four-circle diffractometer coupled to a Siemens CCD area detector at 200(2) K, with graphite-monochromated Mo-K_α radiation (λ = 0.71073 Å). The structure was solved by direct methods using SHELXS-96[17] and refined against F^2 on all data by full-matrix least-squares with SHELXS-97.[18] All non-hydrogen atoms were refined anisotropically. The hydrogen atoms were included in the model at their geometrically calculated positions and refined using a riding model. CCDC-170473 (**2**) contains the supplementary crystallographic data for this paper. These data can be obtained free of charge at www.ccdc.cam.ac.uk/conts/retrieving.html [or from the Cambridge Crystallographic Data Centre, 12, Union Road, Cambridge CB2 1EZ, UK; fax: (internat.) +44-1223/336-033; E-mail: deposit@ccdc.cam.ac.uk].

Acknowledgments

The financial support of the Deutsche Forschungsgemeinschaft and Göttinger Akademie der Wissenschaften is gratefully acknowledged.

[1] J. J. Eisch, in *Comprehensive Organometallic Chemistry* 2nd ed. (Ed.: C. E. Housecroft), Pergamon, Oxford, **1995**, vol. 1, p. 431−502.
[2] M. Witt, H. W. Roesky, *Curr. Sci.* **2000**, *78*, 410−430.
[3] [3a] G. Linti, H. Schnöckel, *Coord. Chem. Rev.* **2000**, *206*−*207*, 285−319, references therein. [3b] W. Uhl, *Rev. Inorg. Chem.* **1998**, *18*, 239−282, references therein. [3c] S. Schulz, H. W. Roesky, H.-J. Koch, G. M. Sheldrick, D. Stalke, A. Kuhn, *Angew. Chem. Int. Ed. Engl.* **1993**, *32*, 1729−1731. [3d] C. Cui, H. W. Roesky, H.-G. Schmidt, M. Noltemeyer, H. Hao, F. Cimpoesu, *Angew. Chem. Int. Ed.* **2000**, *39*, 4531−4533.
[4] C. E. Radzewich, I. A. Guzei, R. F. Jordan, *J. Am. Chem. Soc.* **1999**, *121*, 8673−8674.
[5] [5a] W. Zheng, H. W. Roesky, M. Noltemeyer, *Organometallics* **2001**, *20*, 1033−1035. [5b] W. Zheng, N. C. Mösch-Zanetti, H. W. Roesky, M. Noltemeyer, M. Hewitt, H.-G. Schmidt, T. R. Schneider, *Angew. Chem. Int. Ed.* **2000**, *39*, 4276−4278. [5c] W. Zheng, N. C. Mösch-Zanetti, H. W. Roesky, M. Hewitt, F. Cimpoesu, T. R. Schneider, A. Stasch, J. Prust, *Angew. Chem. Int. Ed.* **2000**, *39*, 3099−3101.
[6] R. J. Wehmschulte, P. P. Power, *Polyhedron* **2000**, *19*, 1649−1661 and references therein.
[7] W. Zheng, N. C. Mösch-Zanetti, T. Blunck, H. W. Roesky, M. Noltemeyer, H.-G. Schmidt, *Organometallics* **2001**, *20*, 3299−3303.
[8] Attempts to prepare compound **2** from [(η^1,η^1-3,5-*t*Bu$_2$pz)(μ-AlMe$_2$)]$_2$ [11] and HC≡CSiMe$_3$ were not successful, the reaction led to the formation of [{3,5-N-*t*Bu$_2$pz-N′−CH=C(SiMe$_3$)}Al(C≡CSiMe$_3$)$_2$].[5c]
[9] C. Krüger, P. J. Roberts, Y.-H. Tsay, J. B. Koster, *J. Organomet. Chem.* **1974**, *78*, 69−74.
[10] H. Schnöckel, M. Leimkühler, R. Lotz, R. Mattes, *Angew. Chem. Int. Ed. Engl.* **1986**, *25*, 921−922.
[11] W. Zheng, H. Hohmeister, N. C. Mösch-Zanetti, H. W. Roesky, M. Noltemeyer, H.-G. Schmidt, *Inorg. Chem.* **2001**, *40*, 2363−2367.
[12] J. F. Janik, E. N. Duesler, R. T. Paine, *J. Organomet. Chem.* **1997**, *539*, 19−25 and references therein.
[13] The formation of compound **4** was not observed when a solution of [(η^1,η^1-3,5-*t*Bu$_2$pz)(μ-AlI$_2$)]$_2$ [11] and HC≡CSiMe$_3$ in toluene was refluxed for 24 h.
[14] Ch. Elschenbroich, A. Salzer, *Organometallics: A Concise Introduction*, 2nd revised edition, VCH, Weinheim, **1992**, p. 75−86.
[15] C. Fernández-Castaño, C. Foces-Foces, N. Jagerovic, J. Elguero, *J. Mol. Struct.* **1995**, *355*, 265−271.
[16] T. Kottke, D. Stalke, *J. Appl. Crystallogr.* **1993**, *26*, 615−619.
[17] G. M. Sheldrick, SHELXS-90, Program for Structure Solution, *Acta Crystallogr., Sect. A* **1990**, *46*, 467−473.
[18] G. M. Sheldrick, SHELXL-97, *Program for Crystal Structure Refinement*, University of Göttingen, Germany, **1997**.

Received October 10, 2001
[I01402]

Pyrrolylaldiminato Complexes of Zn, Mg and Al

Haijun Hao,[a] Sonali Bhandari,[a] Yuqiang Ding,[a] Herbert W. Roesky,*[a] Jörg Magull,[a] Hans-Georg Schmidt,[a] Mathias Noltemeyer,[a] and Chunming Cui[a]

Dedicated to Professor Rüdiger Mews on the occasion of his 60th birthday

Keywords: Zinc / Magnesium / Aluminum / N ligands

The reaction of 2-(2,6-*i*$Pr_2C_6H_3N$=CH)-5-R-C_4H_2NH (R = H, L^1H; R = *t*Bu, L^2H) with one equivalent of $ZnMe_2$ or Mg*n*Bu_2 in toluene or *n*-hexane afforded the bis(pyrrolylaldiminato) complexes ZnL^1_2 (**1**), ZnL^2_2 (**2**) and MgL^2_2 (**3**). Crystalline MgL^1_2·THF (**4**·THF) was formed by treatment of LiL^1 with MeMgCl in THF followed by recrystallization from *n*-hexane. L^1AlMe_2 (**6**) and L^2AlMe_2 (**7**) were readily prepared by refluxing L^1H and L^2H with $AlMe_3$ in toluene or *n*-hexane for several hours. However, the reaction of LiL^1 with $AlCl_3$ in a 1:1 molar ratio provided L^1_2AlCl (**8**), while the reaction of KL^2 with $AlCl_3$ afforded L^2AlCl_2 (**9**). Compounds **2**, **3**, **5**, and **8** were characterized by a single-crystal X-ray structural analysis. Compounds **2**, **3**, and **5** all have a tetrahedral geometry around the metal atom, while the five-coordinate aluminum in **8** has a trigonal bipyramidal geometry.

(© Wiley-VCH Verlag GmbH, 69451 Weinheim, Germany, 2002)

Introduction

There are only a few reports on pyrrolylaldiminato complexes.[1,2] Bischelating pyrrolylaldiminato ligands with bulky substituents have not drawn as much attention as salicylaldiminato ligands, which have been shown to be excellent ligands for zirconium and nickel complexes that act as olefin polymerization catalysts.[3,4] Very recently, salicylaldiminato zinc compounds have been reported to be active for the copolymerization of CO_2 and epoxides.[5]

Both pyrrolylaldiminato and salicylaldiminato ligands are easily prepared and have similar steric demands; their steric and electronic properties may be varied by simply changing the substituents. The chelating pyrrolylaldiminato ligand forms five-membered ring systems with metal ions, whereas salicylaldiminato complexes tend to form six-membered rings (Scheme 1).

Here we present the synthesis and structures of divalent Zn, Mg and trivalent Al compounds ligated by the pyrrolylaldiminato ligands [2-(2,6-*i*$Pr_2C_6H_3N$=CH)-C_4H_3N]$^-$ (L^1) and [2-(2,6-*i*$Pr_2C_6H_3N$=CH)-5-*t*Bu-C_4H_2N]$^-$ (L^2).

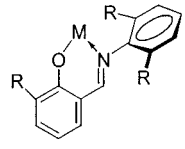

Salicylaldiminato complex

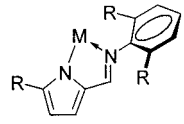

Pyrrolylaldiminato complex

Scheme 1

Results and Discussion

Synthesis and Spectroscopic Characterization of Compounds 1−9

Initially we attempted to prepare monoalkyl zinc and magnesium compounds, since there are plenty of monoalkyl zinc or magnesium compounds known that contain much less bulky amide groups,[6] and which are important precursors for various transformations.[5,7] However, the reaction of L^1H or L^2H with one equivalent of $ZnMe_2$ or Mg*n*Bu_2 in toluene or *n*-hexane resulted in the formation of the bis(pyrrolylaldiminato) compounds **1**−**3** (Scheme 2).

[a] Institut für Anorganische Chemie der Universität Göttingen, Tammannstrasse 4, 37077 Göttingen, Germany
Fax: (internat.) + 49-(0)551/393-373
E-mail: hroesky@gwdg.de

Darensbourg et al. have reported the preparation of mono(salicylaldiminato)methyl zinc compounds;[5] under similar conditions we were not able to isolate any mono(pyrrolylaldiminato) species. We attributed this failure to prepare methylzinc or -magnesium species to the stronger acidity of the pyrrole proton relative to that of the amine hydrogen, and the enhanced basicity of methyl in the monoalkyl intermediate relative to that in MR_2.[8–10] Attempts to prepare the methylmagnesium compounds from the reaction of LiL^1 with MeMgCl afforded the compound MgL^1_2·THF (**4**·THF), which is presumably derived from the dismutation of transient $[L^1MgMe]^‡$ to **4**·THF and $MgMe_2$ (Scheme 3), even though we were not able to isolate $MgMe_2$ from this reaction. Furthermore, compounds **1**–**4** do not react with $ZnMe_2$ or $MgMe_2$ in conventional solvents such as toluene or diethyl ether.

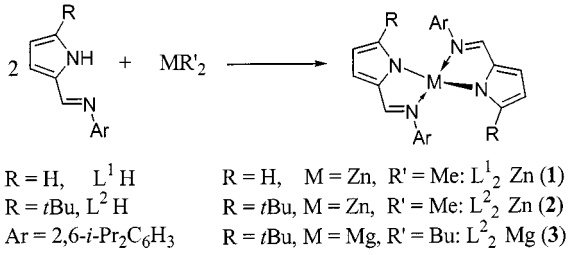

Scheme 2

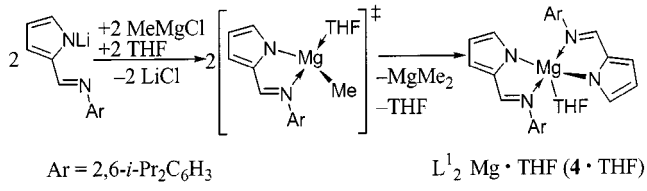

Scheme 3

The reaction of KL^2 with MeMgCl, after workup and keeping the solution at room temperature for 24 h, provided a small amount of fine colorless crystals. Although the amount of product isolated was too low to calculate the yield, it was sufficient for microanalysis. The EI-MS, ^1H NMR spectrum and X-ray structural analysis revealed that this compound is the methoxy-bridged dimer $(L^2Mg)_2(\mu\text{-}OMe)_2$ (**5**). The reaction was repeated twice. In the ^1H NMR spectrum, the hydrogen resonance of the methoxy group appears at $\delta = 3.58$ as a singlet. The elemental analysis is also in good agreement with this formula. Since we were not able to detect any mono(pyrrolylaldiminato)methylmagnesium in the products, we suppose that this compound is derived from the inadvertent presence of MeOMgCl in the Grignard reagent, or perhaps from small amounts of water present in the solvents. Exposure of **5** to air resulted in an unidentifiable amorphous powder. Due to the potential uses of mono(alkyloxy)magnesium species as catalysts for the ring-opening polymerization of lactides,[11] we tried to prepare **5** in high yield from the reaction of $MgMe_2$ with one equivalent of methanol, followed by reaction with L^2H. This led to a mixture containing L^2H, **3**, and **5** as indicated by EI-MS. Attempts to synthesize **5** from a one-pot reaction of MeMgCl with one equivalent of methanol followed by reaction with LiL^2, or from the metathesis reaction of **3** with $Mg(OMe)_2$, were also unsuccessful.

The reaction of L^1H and L^2H with $AlMe_3$ provided the corresponding dimethylaluminum complexes **6** and **7**, which apparently have a four-coordinate tetrahedral geometry around the Al atoms (Scheme 4), while the reaction of LiL^1 with one equivalent of $AlCl_3$ in THF provided the five-coordinate L^1_2AlCl (**8**) instead of the expected mono(pyrrolylaldiminato) aluminum dichloride L^1AlCl_2. However, treatment of KL^2 with $AlCl_3$ in diethyl ether followed by evaporation resulted in a brown-purple product. After extraction with toluene and recrystallization from diethyl ether, pale yellowish microcrystals were isolated in relatively low yield; they were subsequently characterized as L^2AlCl_2 (**9**). The reaction of **6** or **7** with bromine or iodine led to unidentifiable products.

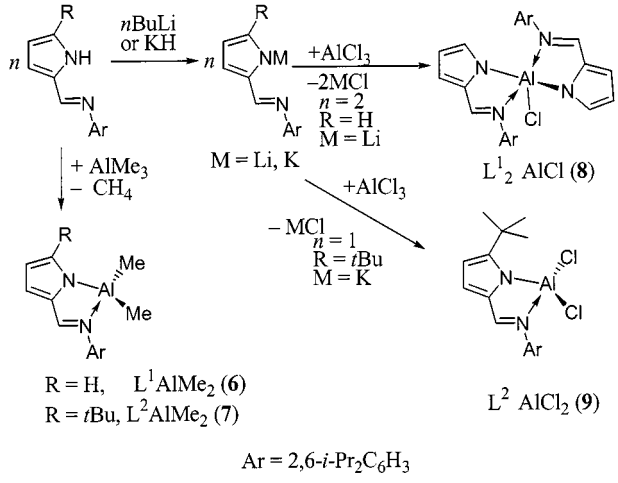

Scheme 4

Compounds **1**–**9** were fully characterized by EI-MS, ^1H NMR spectroscopy and elemental analysis. The EI-MS showed the molecular ion peaks in all cases. In the ^1H NMR spectra, the resonances for the methyl groups of the isopropyl substituents in **2**, **3**, and **8** appeared as four distinguishable doublets, while for the remaining compounds only two doublets were observed. These observations indicate that in **2**, **3**, and **8** the metals have more congested environments than the others in the series due to the *t*Bu substituents in **2** and **3** and the higher coordination number in **8**. Similar to the salicylaldiminato zinc complexes,[12] compounds **1**–**3** are chiral complexes with only C_2 symmetry; the other enantiomer is also formed in the product. Since the molecules have only C_2 symmetry, the isopropyl methyl groups of **1** display two sets of doublets even when rotation about the $N-C_{(phenyl)}$ bond is rapid at room temperature. In compounds **2** and **3**, the methyl groups of the isopropyl substituents display four sets of doublets due to the steric influence of the *t*Bu group causing a slow rotation about

the $N-C_{(phenyl)}$ bond on the NMR timescale. The ^1H NMR spectrum of the ligand in **4** resembles that of **1**, indicating that the coordinated THF has no observable influence on the rotation about the $N-C_{(phenyl)}$ bond at room temperature.

X-ray Single Crystal Analysis for 2, 3, 5, and 8

Compounds **2** and **3** crystallize in a triclinic system, space group $P\bar{1}$. Their structures exhibit a distorted tetrahedral geometry around the metal center with four nitrogen atoms arranged at the vertices (Figure 1 and 2, respectively). In compound **2** the $Zn-N_{(pyrrole)}$ (av. 2.00 Å) and $Zn-N_{(imine)}$ (av. 2.06 Å) bonds are shorter than the Mg−N bonds in **3** (av. 2.05 Å and 2.11 Å, respectively) leading to a slightly wider angle formed by the bischelating nitrogens and the metal atom (av. 85.56° in **2** vs. av. 84.72° in **3**). The $Zn-N_{(imine)}$ bond lengths are similar to those in bis(salicylaldiminato) zinc complexes (range 1.99−2.00 Å), while the $Zn-N_{(pyrrole)}$ bond lengths (av. 2.00 Å) are slightly longer than the Zn−O bond lengths (range 1.91−1.95 Å) in bis(salicylaldiminato) zinc complexes.[5]

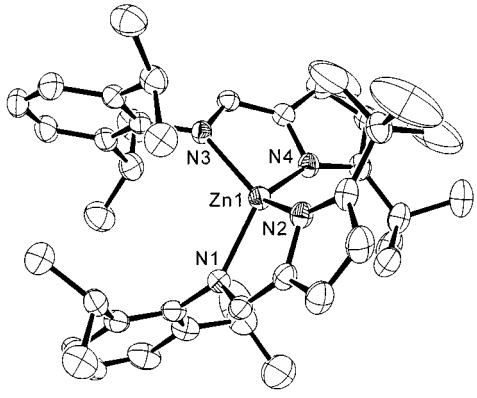

Figure 1. Molecular structure of **2** (hydrogen atoms are omitted for clarity)

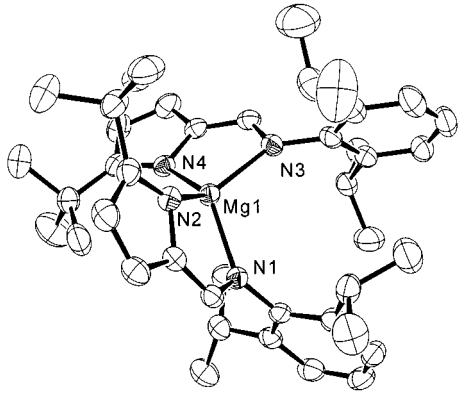

Figure 2. Molecular structure of **3** (hydrogen atoms are omitted for clarity)

Compound **5** is a centrosymmetric dimer with each magnesium atom having a tetrahedral geometry (Figure 3). The magnesium and oxygen atoms form a four-membered coplanar ring and there is a C_2 axis passing through the two Me−O bonds. The Mg−O−Mg−O ring is perpendicular to the Mg1−N1−N2 plane. The Mg−N bond lengths [Mg1−N2: 2.043(2) Å; Mg1−N1: 2.100(2) Å] are similar to those in **3**. The Mg−O bond lengths (av. 1.94 Å) are nearly the same as those in $[Mg(\mu\text{-}OMe)\{\eta^2\text{-}(i\text{Pr}_2)ATI\}]_2$ (av. 1.94 Å, ATI = *N*,*N*′-diisopropylaminotroponiminate).[13]

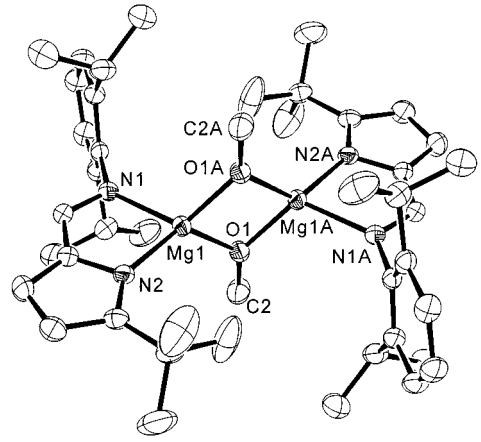

Figure 3. Molecular structure of **5** (hydrogen atoms are omitted for clarity)

The molecular structure of **8** (Figure 4) is best described as a distorted trigonal bipyramidal geometry around the aluminum atom with the N2 and N2A atoms located at the top of the vertex [N2−Al1−N2A: 165.16(8)°], and the chlorine atom, N1 and N1A atoms arranged at the equatorial positions (the Al1, Cl1, N1 and N1A atoms are essentially coplanar). There is a C_2 axis passing through the Al−Cl bond. The average $Al-N_{(imino)}$ bond length is 1.993 Å, slightly longer than those found in salicylaldiminato aluminum complexes (range 1.94−1.98 Å).[14,15] The $Al-N_{(pyrrole)}$ bond length (av. 1.96 Å) is slightly longer than that (av. 1.90 Å) in the recently reported compound $AlCl_2\{C_4H_3N(CH_2NMe_2)\text{-}2\}$ (**A**),[16] while the Al−Cl bond length [2.1582(8) Å] is slightly shorter than that in **A**. This can be attributed to a partial conjugation between the imine C and N atoms and the aromatic pyrrole ring.

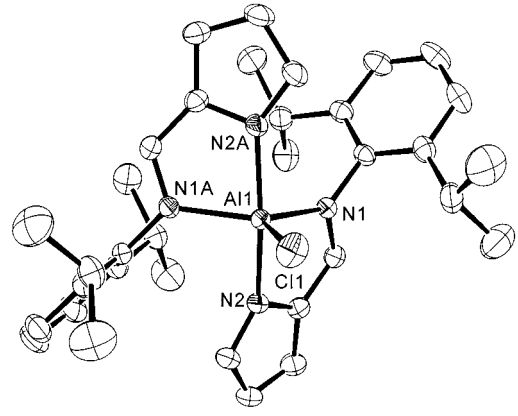

Figure 4. Molecular structure of **8** (hydrogen atoms are omitted for clarity)

The N−M−N angles associated with the bite of the pyrrolylaldiminato ligand in **2**, **5** and **8** (range 84−86° for Zn, 81.57(5)° for Al), are evidently more acute than the corresponding O−M−N angles in salicylaldiminato zinc[12] and aluminum[14,15] compounds (range 95−100° for Zn and 93−98° for Al). The M−N bond lengths (av. 2.00 Å for Zn in **2**, av. 1.96 Å for Al in **8**) are longer than the M−O distances (range 1.87−1.96 Å for Zn,[5,12] and 1.75−1.78 Å for Al[14,15] in salicylaldiminato complexes).

Conclusion

In summary, we have synthesized a series of pyrrolylaldiminato compounds of Zn, Mg, and Al. The structural investigations illustrate that the substituents at the 5-position of the pyrrole significantly enhance the steric demand. The variability of the steric properties of pyrrolylaldiminato ligands enhances the potential of these systems for catalytic processes.

Experimental Section

General Remarks: All experiments were carried out under an atmosphere of dry dinitrogen using standard Schlenk techniques. All solvents were dried by common methods and freshly distilled prior to use. Aluminum trichloride, trimethyl aluminum, di-*n*-butylmagnesium, methylmagnesium chloride and bromide, and dimethylzinc were purchased commercially. LiL^1 and LiL^2 were prepared according to the literature method.[1] KL^2 was prepared by the reaction of L^2H with KH in THF followed by filtration, evaporation in vacuo, and washing with *n*-hexane, and was used without further characterization. ^1H NMR spectra were recorded on Bruker AS-250 or Bruker AM-200 spectrometers. IR spectra were recorded on a Bio-Rad FTS-7 spectrometer as nujol mulls between KBr plates. EI-mass spectra were obtained on a Finnigan MAT8230 or a Varian MAT CH5 spectrometer.

ZnL^1_2 (1): A solution of L^1H (0.50 g, 2.0 mmol) in *n*-hexane (20 mL) was added to a solution of $ZnMe_2$ (1.0 mL of a 2.0 M solution in toluene, 2.0 mmol) diluted with *n*-hexane (20 mL) at −78 °C. After the addition the mixture was warmed slowly to ambient temperature and was then stirred at room temperature for 36 h. The volatiles were removed in vacuo and the residue was recrystallized from a mixed solvent of toluene and *n*-hexane (10:1) at −32 °C to afford a white solid. Yield: 0.45 g (20% based on L^1H). M.p. 221−224 °C. ^1H NMR (200.131 MHz, C_6D_6): δ = 0.6 (d, *J* = 6.8 Hz, 12 H, CH*Me*$_2$), 1.06 (d, *J* = 6.8 Hz, 12 H, CH*Me*$_2$), 3.13 (sept, *J* = 6.8 Hz, 4 H, C*H*Me$_2$), 6.54 (dd, *J* = 3.6, 1.7 Hz, 2 H, pyrrole), 6.83 (dd, *J* = 3.6, 1.0 Hz, 2 H, pyrrole), 6.85−7.10 (m, 8 H, aryl and pyrrole), 7.12 (d, *J* = 1.0 Hz, 2 H, pyrrole), 7.49 (d, *J* = 1.0 Hz, 2 H, N=C*H*). EI-MS: *m*/*z* (%) = 570 (100) [M^+]. $C_{34}H_{42}N_4Zn$ (572.11): calcd. C 71.38, H 7.44, N 9.79; found C 71.20, H 7.44, N 9.94.

ZnL^2_2 (2): A solution of L^2H (1.0 g, 3.2 mmol) in toluene (20 mL) was added to an excess of $ZnMe_2$ (2 mL of a 2.0 M solution in toluene, 4.0 mmol) diluted with toluene (20 mL) at −78 °C with stirring. The solution was warmed slowly to ambient temperature and stirred at room temperature for 16 h. After removal of all volatiles the residue was extracted with 10 mL of hot *n*-hexane. Colorless crystals formed while cooling the hot extract slowly to ambient temperature. Yield: 0.73 g (33% based on L^2H). M.p. 228−250 °C. ^1H NMR (200.13 MHz, C_6D_6): δ = 0.25 (d, *J* = 6.8 Hz, 6 H, CH*Me*$_2$), 0.97 (d, *J* = 6.8 Hz, 6 H, CH*Me*$_2$), 1.05 (d, *J* = 6.8 Hz, 6 H, CH*Me*$_2$), 1.12 (d, *J* = 6.8 Hz, 6 H, C*H*Me$_2$), 1.33 (s, 18 H, *t*Bu), 2.78 (sept, 2 H, *J* = 6.8 Hz, C*H*Me$_2$), 3.76 (sept, 2 H, *J* = 6.8 Hz, C*H*Me$_2$), 6.50 (d, *J* = 3.8 Hz, 2 H, pyrrole), 7.00−7.18 (m, 8 H, aryl, pyrrole), 7.47 (s, 2 H, N=C*H*). EI-MS: *m*/*z* (%) = 682 (100) [M^+]. $C_{42}H_{58}N_4Zn$ (684.29): calcd. C 73.72, H 8.54, N 8.19; found C 73.76, H 8.43, N 8.21.

MgL^2_2 (3): A solution of L^2H (0.93 g, 3.0 mmol) in *n*-hexane (30 mL) was added to an excess of Mg*n*Bu$_2$ (3.0 mL of a 1.0 M solution in toluene, 3.0 mmol) diluted with *n*-hexane (20 mL) at −78 °C whilst stirring. The solution was warmed slowly to ambient temperature and stirred at room temperature for 16 h. After filtration and washing the precipitate with *n*-hexane (20 mL), the combined filtrate was concentrated and stored at 0 °C in the refrigerator for 24 h to afford colorless crystals suitable for X-ray structural analysis. Yield: 0.58 g (30% based on L^2H). M.p. 240−242 °C. ^1H NMR (200.13 MHz, C_6D_6): δ = 0.28 (d, *J* = 6.8 Hz, 6 H, CH*Me*$_2$), 1.01 (d, *J* = 6.8 Hz, 6 H, CH*Me*$_2$), 1.08 (d, *J* = 6.9 Hz, 6 H, CH*Me*$_2$), 1.18 (d, *J* = 6.8 Hz, 6 H, C*H*Me$_2$), 1.33 (s, 18 H, *t*Bu), 2.81 (sept, 2 H, *J* = 6.8 Hz, C*H*Me$_2$), 3.57 (sept, 2 H, *J* = 6.9 Hz, C*H*Me$_2$), 6.45 (d, *J* = 3.6 Hz, 2 H, pyrrole), 6.88 (d, *J* = 3.6 Hz, 2 H, pyrrole), 6.90−7.00 (m, 8 H, aryl, pyrrole), 7.53 (s, 2 H, N=C*H*). EI-MS: *m*/*z* (%) = 642 (100) [M^+], 627 (50) [M^+ − Me]. $C_{42}H_{58}MgN_4$ (643.23): calcd. C 78.42, H 9.09, N 8.71; found C 78.34, H 9.11, N 8.69.

MgL^1_2·THF (4·THF): MeMgCl (0.67 mL of a 1.0 M solution in THF, 2.0 mmol) was added dropwise to a suspension of LiL^1 (0.50 g, 2.0 mmol) in THF (30 mL) at −78 °C. After the addition the mixture was warmed slowly to ambient temperature and stirred at room temperature for 16 h. The mixture was stripped of all volatiles and the residue was extracted with *n*-hexane (20 mL). The *n*-hexane extract was stored at 0 °C to afford colorless crystals. Yield: 0.35 g (29%). M.p. 208−210 °C. ^1H NMR (200.131 MHz, C_6D_6): δ = 1.03 (br, 4 H, THF), 1.15 (d, *J* = 6.9 H, CH*Me*$_2$), 1.18 (d, *J* = 6.9 Hz, 12 H, CH*Me*$_2$), 3.17 (sept, *J* = 6.9 Hz, 4 H, C*H*Me$_2$), 3.37 (br, 4 H, THF), 6.23 (d, *J* = 1.6 Hz, 2 H, pyrrole), 6.33 (dd, *J* = 3.4, 1.6 Hz, 2 H, pyrrole), 6.80 (dd, *J* = 3.4, 1.6 Hz, 2 H, pyrrole), 7.08−7.20 (m, 6 H, Aryl), 7.76 (d, *J* = 1.1 Hz, 2 H, C*H*=N). EI-MS: 530.2 (95) [M^+], 464.2 (100) [M^+ − 2Pr]. $C_{38}H_{50}MgN_4O$ (602.14, including one molecule of THF): calcd. C 75.67, H 8.66, N 9.29; found C 75.11, H 8.65, N 9.22.

$(L^2Mg)_2(\mu\text{-}OMe)_2$ (5): A solution of KL^2 (0.68 g, 2.0 mmol) in THF (20 mL) was added dropwise to a solution of MeMgCl (0.68 mL of a 3 M solution in THF, 2.0 mmol) in THF (20 mL) at −78 °C. After the addition it was warmed slowly to ambient temperature and stirred at room temperature for 16 h. After the removal of all volatiles, the residue was washed with *n*-hexane (20 mL) and extracted with toluene (40 mL). Colorless crystals of **5** formed on allowing the toluene solution to stand. The amount of **5** was small but sufficient for microanalysis. The reaction was repeated twice. M.p. 295−297 °C. ^1H NMR (200.131 MHz, C_6D_6): δ = 1.04 (d, *J* = 6.8 Hz, 12 H, CH*Me*$_2$), 1.18 (s, 18 H, *t*Bu), 1.20 (d, *J* = 6.8 Hz, 12 H, CH*Me*$_2$), 3.10 (sept, 4 H, C*H*Me$_2$), 3.58 (s, 6 H, OC*H*$_3$), 6.42 (d, *J* = 3.6 Hz, 2 H, pyrrole), 6.85 (d, *J* = 3.6 Hz, 2 H, pyrrole), 7.00−7.20 (m, 6 H, aryl), 7.63 (s, 2 H, N=C*H*). EI-MS: *m*/*z* (%) = 728 (100) [M^+]. $C_{44}H_{64}Mg_2N_4O_2$ (729.61): calcd. C 72.43, H 8.84, N 7.68; found C 71.97, H 8.79, N 7.53.

L^1AlMe_2 (6): A solution of L^1H (2.54 g, 10 mmol) and $AlMe_3$ (5.3 g of a 16% solution in *n*-hexane, 11 mmol) in toluene (40 mL)

was refluxed for 4 h. The solution was then cooled to ambient temperature. Subsequently, all volatiles were removed in vacuo. The residue was recrystallized from *n*-hexane at −32 °C to afford colorless crystals. Yield: 1.77 g (57%). M.p. 83−85 °C. ^{1}H NMR (200.13 MHz, C_6D_6): δ = −0.77 (s, 6 H, Al*Me*$_2$), 1.01 (d, *J* = 6.8 Hz, 6 H, CH*Me*$_2$), 1.11 (d, *J* = 6.8 Hz, 6 H, CH*Me*$_2$), 3.01 (sept, *J* = 6.8 Hz, 2 H, C*H*Me$_2$), 6.39 (d, *J* = 3.6 Hz, 1 H, pyrrole), 6.92 (dd, *J* = 3.6 Hz, 1 H, pyrrole), 7.05−7.20 (m, 4 H, Aryl), 7.26 (m, 1 H, pyrrole-*H*), 7.76 (d, *J* = 1.1 Hz, 1 H, N=C*H*). EI-MS: *m*/*z* (%) = 310 (0.1) [M$^+$], 295 (100) [M$^+$ − Me].

L^{2}AlMe$_2$ (7): A solution of L^{2}H (6.2 g, 20 mmol) in *n*-hexane (50 mL) was added dropwise to a solution of $AlMe_3$ (12 g of a 15% solution in *n*-hexane, 25 mmol) in *n*-hexane (50 mL). After the addition the resulting solution was warmed slowly to ambient temperature and stirred at room temperature for 16 h. After the removal of all volatiles the residue was extracted with *n*-hexane (20 mL). Cooling the extract to −32 °C for 16 h afforded colorless crystals. Yield: 6.3 g (86%). M.p. 117−119 °C. ^{1}H NMR (200.13 MHz, C_6D_6): δ = −0.23 (s, 6 H, Al*Me*$_2$), 0.92 (d, *J* = 6.8 Hz, 6 H, CH*Me*$_2$), 1.15 (d, *J* = 6.8 Hz, 6 H, CH*Me*$_2$), 1.35 (s, 9 H, *t*Bu), 3.20 (sept, *J* = 6.8 Hz, 2 H, C*H*Me$_2$), 6.34 (d, *J* = 3.8 Hz, 1 H, pyrrole), 6.78 (d, *J* = 3.8 Hz, 1 H, pyrrole), 7.00−7.18 (m, 4 H, aryl, pyrrole), 7.44 (s, 1 H, N=C*H*). EI-MS: *m*/*z* (%) = 366 (20) [M$^+$], 351 (100) [M$^+$ − Me]. $C_{23}H_{35}AlN_2$ (366.52): calcd. C 75.37, H 9.62, N 7.64; found C 75.38, H 9.67, N 7.56.

L$^1_2$AlCl (8): A solution of LiL^1 (1.3 g, 5.0 mmol) in THF (20 mL) was added dropwise to a solution of $AlCl_3$ (0.67 g, 5.0 mmol) in THF (20 mL) at −78 °C. After complete addition the resulting solution was warmed slowly to ambient temperature and stirred at room temperature for 16 h. After removal of all volatiles the residue was extracted with toluene (20 mL). Cooling the extract to −32 °C for 20 h afforded yellow crystals. Yield: 2.36 g (83% based on the ligand). M.p. 190−213 °C. ^{1}H NMR (200.13 MHz, C_6D_6): δ = 0.72 (d, *J* = 6.8 Hz, 6 H, CH*Me*$_2$), 0.96 (d, *J* = 6.8 Hz, 6 H, CH*Me*$_2$), 1.01 (d, *J* = 6.8 Hz, 6 H, CH*Me*$_2$), 1.42 (d, *J* = 6.8 Hz, 6 H, CH*Me*$_2$), 2.89 (sept, *J* = 6.8 Hz, 2 H, C*H*Me$_2$), 3.67 (sept, *J* = 6.8 Hz, 2 H, C*H*Me$_2$), 6.01 (dd, *J* = 3.7 Hz, 2 H, pyrrole), 6.16 (m, 2 H, pyrrole), 6.57 (dd, *J* = 3.7 Hz, 2 H, pyrrole), 6.85−7.10 (m, 12 H, Ar−*H*), 7.53 (d, *J* = 1.16 Hz, 2 H, N=C*H*). MS: *m*/*z* (%) = 568 (100) [M$^+$]. $C_{34}H_{42}AlClN_4$ (569.15): calcd. C 71.75, H 7.74, N 9.84; found C 72.05, H 7.63, N 9.90.

L^{2}AlCl$_2$ (9): A suspension of KL^2 (5.70 g, 16.0 mmol) in THF (20 mL) was added to a solution of $AlCl_3$ (2.13 g, 16.0 mmol) in THF (20 mL) at −90 °C whilst stirring. The resulting solution was warmed slowly to ambient temperature and was stirred at room temperature for 16 h. After the removal of all volatiles the residue was extracted with diethyl ether and the extract was stored at −32 °C to afford pale white microcrystals. Yield: 2.54 g (39%). M.p. 187−190 °C. ^{1}H NMR (200.13 MHz, C_6D_6): δ = 0.89 (d, *J* = 6.8 Hz, 6 H, CH*Me*$_2$), 1.27 (d, *J* = 6.8 Hz, 6 H, CH*Me*$_2$), 1.35 (s, 9 H, *t*Bu), 3.40 (sept, *J* = 6.8 Hz, 2 H, C*H*Me$_2$), 6.19 (d, *J* = 3.9 Hz, 1 H, pyrrole), 6.61 (d, *J* = 3.9 Hz, 1 H, pyrrole), 6.95−7.15 (m, 6 H, Ar−H), 7.27 (s, 1 H, N=C*H*). MS: *m*/*z* (%) = 406 (100) [M$^+$]. $C_{21}H_{29}AlCl_2N_2$ (407.36): calcd. C 61.92, H 7.18, N 6.88; found C 61.20, H 7.21, N 6.41.

X-ray Crystallographic Study: Single crystals of **2**, **3**, **5**, and **8** were taken from the flask under nitrogen gas and mounted on a glass fiber in a rapidly cooled perfluoropolyether.[17] Diffraction data for **2**, **3**, and **8** were collected on a Stoe−Siemens−Huber four-circle diffractometer coupled to a Siemens CCD area detector at 200(2) K while those for **5** were collected on a Stoe two-circle diffractometer at 133(2) K, with graphite-monochromated Mo-K_α radiation (λ = 0.71073 Å). The structures were solved by direct methods (SHELXS-96 for **2**, **3**, and **8**; SHELXS-97 for **5**)[18] and refined against F^2 using SHELXL-97.[19] All non-hydrogen atoms were refined anisotropically with similarity and rigid-bond restraints. All hydrogen atoms were included in the refinement in their geometrically ideal positions. Crystallographic data for **2**, **3**, **5**, and **8** are given in Table 1 and selected bond lengths and angles in Table 2. CCDC-171433 (**2**), CCDC-171434 (**3**), CCDC-171435 (**5**) and CCDC-171436 (**8**) contain the supplementary crystallographic data for this paper. These data can be obtained free of charge at www.ccdc.cam.ac.uk/conts/retrieving.html [or from the Cambridge Crystallographic Data Centre, 12, Union Road, Cambridge CB2 1EZ, UK; Fax: (internat.) +44-1223/336-033; E-mail: deposit@ccdc.cam.ac.uk].

Table 1. Crystallographic data for compounds **2**, **3**, **5,** and **8**

	2	**3**	**5**	**8**
Empirical formula	$C_{42}H_{58}N_4Zn$	$C_{42}H_{58}MgN_4$	$C_{44}H_{64}Mg_2N_4O_2$	$C_{34}H_{42}AlClN_4$
Molecular weight	684.29	643.23	729.61	569.15
Temperature	200(2) K	200(2) K	133(2) K	203(2) K
Wavelength	0.71073 Å	0.71073 Å	0.71073 Å	0.71073 Å
Crystal system	triclinic	triclinic	triclinic	monoclinic
Z	2	2	1	4
Space group	$P\bar{1}$	$P\bar{1}$	$P\bar{1}$	$P2_1/n$
Unit cell dimensions	*a* = 10.295(3) Å	*a* = 10.335(2) Å	*a* = 9.0932(10) Å	*a* = 20.284(4) Å
	b = 10.464(3) Å	*b* = 10.455(2) Å	*b* = 10.3835(10) Å	*b* = 9.8282(11) Å
	c = 19.861(6) Å	*c* = 20.080(4) Å	*c* = 12.9191(13) Å	*c* = 16.174(3) Å
	α= 75.56(3)°	α = 75.27(3)°	α = 109.864(8)°	
	β= 6.700(19)°	β = 86.82(3)°	β = 103.762(8)°	β = 99.89(2)°
	γ = 8.115(12)°	γ = 67.87(3)°	γ = 94.294(9)°	
Volume	1921.1(10) Å^3	1941.9(7) Å^3	1097.99(19) Å^3	3176.4(8) Å^3
Density (calculated)	1.183 Mg/m^3	1.100 Mg/m^3	1.103 Mg/m^3	1.190 Mg/m^3
Absorption coefficient	0.672 mm^{-1}	0.079 mm^{-1}	0.093 mm^{-1}	0.177 mm^{-1}
Final *R* indices	*R*1 = 0.0391	*R*1 = 0.0397	*R*1 = 0.0477	*R*1 = 0.0329
[$I > 2\sigma(I)$]	*wR*2 = 0.0895	*wR*2 = 0.1012	*wR*2 = 0.1365	*wR*2 = 0.0820
R indices	*R*1 = 0.0445	*R*1 = 0.0452	*R*1 = 0.0559	*R*1 = 0.0362
(all data)	*wR*2 = 0.0939	*wR*2 = 0.1059	*wR*2 = 0.1413	*wR*2 = 0.0870

Table 2. Selected bond lengths (Å) and bond angles (deg) for complexes **2**, **3**, **5**, and **8**

Compound **2**			
Zn1−N1	2.0683(18)	N1−Zn1−N4	132.73(7)
Zn1−N2	1.9956(19)	N2−Zn1−N3	129.19(7)
Zn1−N3	2.0548(19)	N2−Zn1−N4	116.62(7)
Zn1−N4	1.9985(19)	N3−Zn1−N1	134.62(14)
N1−Zn1−N2	85.75(8)	N3−Zn1−N4	85.26(7)
Compound **3**			
Mg1−N1	2.1005(13)	N4−Mg1−N1	131.06(5)
Mg1−N2	2.0525(12)	N2−Mg1−N1	84.49(6)
Mg1−N3	2.1154(13)	N4−Mg1−N3	84.95(5)
Mg1−N4	2.0476(13)	N4−Mg1−N2	134.00(5)
N4−Mg1−N2	116.87(5)	N4−Mg1−N3	112.14(5)
Compound **5**			
Mg1−O1A	1.938(1)	O1A−Mg1−N2	129.97(6)
Mg1−O1	1.940(1)	O1−Mg1−N2	125.69(6)
Mg1−N2	2.043(2)	O1A−Mg1−N1	118.15(6)
Mg1−N1	2.100(2)	O1−Mg1−N1	118.11(6)
O1−Mg1−O1A	84.95(5)	N2−Mg1−N1	83.99(6)
Compound **8**			
Al1−N1	1.9931(11)	N2−Al1−N1	81.57(5)
Al1−N2	1.9615(12)	N1A−Al1−N1	127.01(7)
Al1−Cl1	2.1582(8)	N2A−Al1−Cl1	97.42(4)
N2−Al1−N2A	165.16(8)	N2A−Al1−Cl1	97.42(4)
N2A−Al1−N1A	81.57(5)	N1A−Al1−Cl1	116.50(4)
N2−Al1−N1A	91.80(5)	N1−Al1−Cl1	116.50(4)
N2A−Al1−N1	91.80(5)		

Acknowledgments

This work was supported by the Deutsche Forschungsgemeinschaft and the Fonds der Chemischen Industrie. SB thanks the Alexander von Humboldt Foundation for a fellowship.

[1] D. M. Dawson, D. A. Walker, M. Thornton-Pett, M. Bochmann, *J. Chem. Soc., Dalton Trans.* **2000**, 459−466.
[2] V. C. Gibson, P. J. Maddox, C. Newton, C. Redshaw, G. A. Solan, A. J. P. White, D. J. Williams, *Chem. Commun.* **1998**, 1651−1652.
[3] S. Matsui, M. Mitani, J. Saito, Y. Tohi, H. Makio, N. Matsukawa, Y. Takagi, K. Tsuru, M. Nitabaru, T. Nakano, H. Tanaka, N. Kashiwa, T. Fujita, *J. Am. Chem. Soc.* **2001**, *123*, 6847−6856.
[4] T. R. Younkin, E. F. Connor, J. I. Henderson, S. K. Friedrich, R. H. Grubbs, D. A. Bansleben, *Science* **2000**, *287*, 460−462.
[5] D. J. Darensbourg, P. Rainey, J. Yarbrough, *Inorg. Chem.* **2001**, *40*, 986−993.
[6] M. Westerhausen, T. Bollwein, A. Pfizner, T. Nilges, H.-J. Deiseroth, *Inorg. Chim. Acta* **2001**, *312*, 239−244.
[7] M. Cheng, E. B. Lobkovsky, G. W. Coates, *J. Am. Chem. Soc.* **1998**, *120*, 11018−11019.
[8] M. Westerhausen, T. Bollwein, N. Makropoulos, T. M. Rotter, T. Habereder, M. Suter, H. Nöth, *Eur. J. Inorg. Chem.* **2001**, 851−857.
[9] M. M. Olmstead, W. J. Grigsby, D. R. Chacon, T. Hascall, P. P. Power, *Inorg. Chim. Acta* **1996**, *251*, 273−284.
[10] V. R. Magnuson, G. D. Stucky, *Inorg. Chem.* **1969**, *8*, 1427−1433.
[11] M. H. Chisholm, J. C. Huffman, K. Phomphrai, *J. Chem. Soc., Dalton Trans.* **2001**, 222−224.
[12] M. H. Chisholm, J. C. Gallucci, H. Zheng, J. C. Huffman, *Inorg. Chem.* **2001**, *40*, 5051−5054.
[13] P. J. Bailey, C. M. E. Dick, S. Fabre, S. Parsons, *J. Chem. Soc., Dalton Trans.* **2000**, 1655−1661.
[14] M. S. Hill, A. R. Hutchison, T. S. Keizer, S. Parkin, M. A. VanAelstyn, D. A. Atwood, *J. Organomet. Chem.* **2001**, *628*, 71−75.
[15] P. A. Cameron, V. C. Gibson, C. Redshaw, J. A. Segal, G. A. Solan, A. J. P. White, D. J. Williams, *J. Chem. Soc., Dalton Trans.* **2001**, 1472−1476.
[16] J.-H. Huang, H.-J. Chen, J.-C. Chang, C.-C. Zhou, G.-H. Lee, S.-M. Peng, *Organometallics* **2001**, *20*, 2647−2650.
[17] T. Kottke, D. Stalke, *J. Appl. Crystalogr.* **1993**, *26*, 615−619.
[18] G. M. Sheldrick, *Acta Crystallogr., Sect. A* **1990**, *46*, 467−473.
[19] G. M. Sheldrick, SHELXL 97; University of Göttingen, Göttingen, Germany, **1997**.

Received October 31, 2001
[I01408]

Synthesis, Structure and Dehalogenation of the Disilene RClSi=SiClR [R = (tBu$_3$Si)$_2$MeSi][‡]

Nils Wiberg,*[a] Wolfgang Niedermayer,[a] Gerd Fischer,[a][‡‡] Heinrich Nöth,[a][‡‡‡] and Max Suter[a][‡‡‡]

Dedicated to Professor Hans Bürger on the occasion of his 65th birthday

Keywords: Disilene / Disilyne / Silicon / Silylene / X-ray structure analysis

The reaction of R*$_2$MeSi–SiX$_2$X′ (X/X′ = Cl/Br, Br/Cl) with NaR* (R* = supersilyl SitBu$_3$) leads, probably via the silylenes R*$_2$MeSi–SiX, to the *trans*-configurated disilene (R*$_2$MeSi)ClSi=SiCl(SiMeR*$_2$), which could be isolated as orange-red crystals. According to an X-ray structure analysis, the central SiClSi=SiClSi framework of the disilene – the formation mechanisms of which are discussed – is planar. The Si=Si double bond is as short as 2.163(4) Å and shows a band in the Raman spectrum at 589 cm^{-1}. Due to its insolubility in organic solvents, no NMR spectra of the disilene in solution were obtained. The spatially overcrowded disilene is stable towards H_2O, MeOH, HF, and NaR*. It melts at 228 °C with decomposition. Reduction of the disilene occurs with $LiC_{10}H_8$ in THF with formation of a reaction mixture containing a chlorine-free product that gives a low field ^{29}Si NMR signal at δ = 91.5 (the region for unsaturated Si atoms). It transforms in solution with traces of oxygen into a substance which, according to mass spectrometry (chemical ionization), shows a mass for the disilyne R*$_2$MeSi–Si≡Si–SiMeR*$_2$ plus two oxygen atoms.
(© Wiley-VCH Verlag GmbH, 69451 Weinheim, Germany, 2002)

Introduction

Searching for a way to synthesize a disilyne RSi≡SiR, we recently tried to transform 1,2-bis[(disupersilyl)silyl]disilane R*$_2$HSi−SiH$_2$−SiH$_2$−SiHR*$_2$ into its tetrabromo derivative R*$_2$HSi−SiBr$_2$−SiBr$_2$−SiHR*$_2$ (R* = supersilyl SitBu$_3$),[1] as the latter might be a good starting point for the synthesis of the disilyne R*$_2$HSi−Si≡Si−SiHR*$_2$ (for a discussion of the disilyne problem see ref.[2]). Unfortunately, the spatially overcrowded 1,2-bis[(disupersilyl)silyl]disilane could only be dibrominated, probably for steric reasons (Scheme 1). The debromination of 1,2-dibromo-1,2-bis[(disupersilyl)silyl]disilane (**1**) with supersilylsodium, NaR*, leads to the disilene **2** as the main product, which was isolated as yellow, oxygen- and water-sensitive crystals [cf. Scheme 1; δ(^{29}Si) = 144.3 for the unsaturated silicon atoms].[3] Compound **2** slowly decomposes even at −20 °C with formation of the colorless product **3**.

Besides the above-mentioned yellow crystals, red crystals of the cyclotetrasilene **4** were also obtained (Scheme 1).[3] This compound may be formed by the elimination of two molecules of hydrogen bromide in the presence of NaR*, possibly via the desired disilyne R*$_2$HSi−Si≡Si−SiHR*$_2$ as a short-lived intermediate, although, of course, other pathways for the formation of **4** are also possible.

Obviously, the steric overcrowdedness of the (disupersilyl)silyl groups SiHR*$_2$ used as substituents is not sufficient to stabilize a disilyne against further reactions. Therefore, we turned to the sterically more overcrowded methyldi(supersilyl)silyl group SiMeR*$_2$ and first tried to prepare a disilene (R*$_2$MeSi)HalSi=SiHal(SiMeR*$_2$), the dehalogenation of which might lead to an isolable disilyne R*$_2$MeSi−Si≡SiMeR*$_2$. Here we report on the synthesis, structure and dehalogenation of the disilene (R*$_2$MeSi)ClSi=SiCl(SiMeR*$_2$).

(NB: We also make use of the sterically overloaded trimesitylsilyl group SiMes$_3$ and prepared a disilane Mes$_3$Si−SiH$_2$−SiH$_2$−SiMes$_3$.[4] Unfortunately, the extreme insolubility of this compound has prevented further experiments for the present.)

Results and Discussion

Synthesis of (R*$_2$MeSi)ClSi=SiCl(SiMeR*$_2$)

Whereas R*$_2$HSi−SiH$_2$−SiH$_2$−SiHR*$_2$ is easily prepared by dehalogenation of R*$_2$HSi−SiH$_2$Cl with so-

[‡] On the Way to a Disilyne RSi≡SiR, II. − Part I: Ref.[3] Compounds of Silicon and Homologues, 153. − Part 152: N. Wiberg, T. Blank, H. Nöth, M. Suter, M. Warchhold, *Eur. J. Inorg. Chem.* **2002**, 929−934. Unsaturated Silicon Compounds, 60. − Part 59: Ref.[3]
[‡‡] Mass spectra.
[‡‡‡] X-ray structure analysis.
[a] Department Chemie der Universität München, Butenandtstraße 5−13 (Haus D), 81377 München, Germany

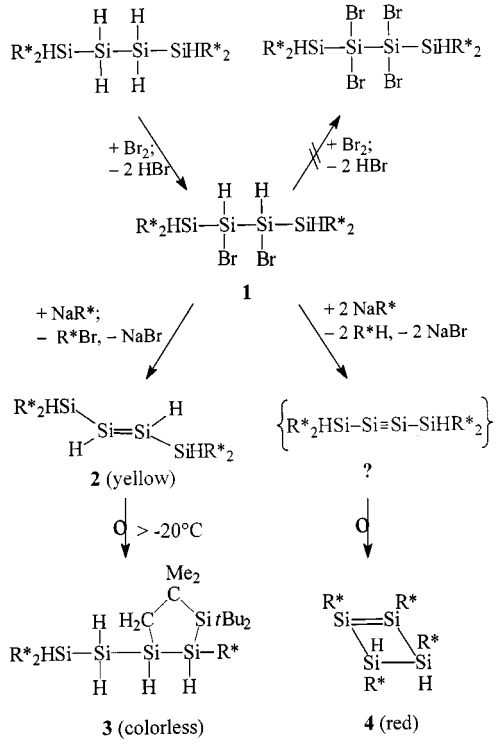

Scheme 1. Synthesis of the bis(silyl)disilane **1** and its reaction with supersilylsodium NaR* with formation of the disilene **2** (thermolysis under isomerization into product **3**) and the cyclotetrasilene **4** (R* = Si*t*Bu$_3$)

dium,[1] the same reaction is unsuitable for synthesizing R*$_2$MeSi−SiH$_2$−SiH$_2$−SiMeR*$_2$ (**5**) from R*$_2$MeSi−SiH$_2$Cl (**6**) and sodium (Scheme 2), probably for steric reasons. As a consequence, the reactions that lead to a disilene and, possibly, to a disilyne with SiHR*$_2$ substituents (Scheme 1) are not practicable to obtain the corresponding compounds with SiMeR*$_2$ substituents. However, we recently found that disilenes R*XSi=SiXR* (X = Cl, Br, I) are intermediates in the reactions of silanes R*SiX$_3$ with supersilylsodium NaR*.[5,6] We therefore tried to synthesize R*$_2$MeSi−SiX$_3$ compounds and then to transform these into disilenes (R*$_2$MeSi)XSi=SiX(SiMeR*$_2$). Indeed, the bromination of compound **6**, which was prepared by reaction of NaSiMeR*$_2$ and SiH$_2$Cl$_2$,[6] with bromine in CCl$_4$ at 0 °C leads to a mixture of R*$_2$MeSi−SiCl$_2$Br (**7a**) and R*$_2$MeSi−SiClBr$_2$ (**7b**) in a molar ratio of ca. 2:1 (Scheme 2), which we were not previously able to separate into its components by fractional crystallization.[1] Obviously, CCl$_4$ also acts as a halogenating agent for **6**. Heating a mixture of NaR* and **7** (mole ratio ca. 1.1:1) in tetrahydrofuran (THF) from −78 °C to room temperature causes the initial dark-red solution to become orange, and an orange residue precipitates slowly (in hours) leaving a nearly colorless solution. According to the mass spectrum, the amorphous residue is the disilene (R*$_2$MeSi)ClSi=SiCl(SiMeR*$_2$) (**10**). This disilene forms crystals suitable for X-ray structure analysis (see below) after warming the residue for several weeks in benzene at 50 °C.

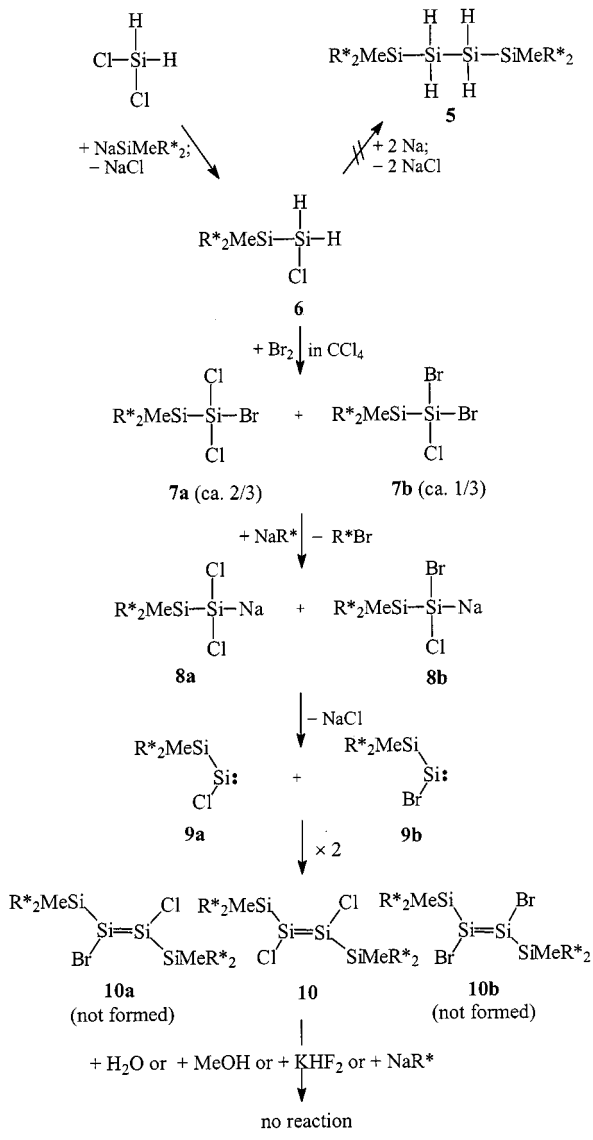

Scheme 2. Synthesis of the silylsilanes **7** and their reactions with NaR* with formation of the bis(silyl)disilene **10** (R = Si*t*Bu$_3$)

We have not studied in the mechanism of formation of **10** in detail. although we believe that the first step of the action of NaR* on **7** must involve an exchange of bromine for sodium with formation of the deep-red silanides **8**, which then eliminate NaCl with formation of the silylenes **9**. This proposal is supported by the extensively studied reaction of R*SiCl$_2$Br (the same is valid for R*SiBr$_3$, R*SiI$_3$) with NaR* in THF which leads, at −78 °C, to the deep-colored silanide NaSiCl$_2$R* (no exchange of chloride for sodium has been observed).[5,6] NaSiCl$_2$R* then eliminates NaCl at about −50 °C to give the silylene R*SiCl, which inserts into the Na−Si bond of its precursor with formation of the disilanide Na−R*SiCl−SiCl$_2$R*.[6] The latter finally eliminates NaCl above −20 °C to give R*ClSi=SiClR* as a short-lived intermediate.[7] An insertion of the silylenes **9** into the Na−Si bond of their precursors **8**, with formation

of disilanides possessing four-coordinate central Si atoms, is unlikely for steric reasons (see below), therefore it makes sense that the disilene **10** is the product of a silylene dimerization (Scheme 2).

Of the three disilenes **10**, **10a**, **10b** conceivable as products of the dehalogenation of **7** with NaR* (cf. Scheme 2), only one disilene (**10**) is obtained. Furthermore, compound **10** precipitates from the THF solution only after several hours, but then is basically insoluble. These facts point to the existence of relatively long-lived silylenes **9** in solution at room temperature, whereby **9a**, which is obviously stable in the presence of NaR* (see below), slowly dimerizes to give **10**. The reaction of **9b** with **9a** or another molecule of **9b** is excluded for steric reasons, although excess NaR* may debrominate **9b** (see below). These proposals are confirmed by recently published results,[8] which show that the silylene $[(Me_3Si)_3C]BrSi{\cdot}D$ [D = THF or, more probably, Br^-; prepared from $(Me_3Si)_3C-SiBr_3$ and $LiC_{10}H_8$; trapped by alcohols or dienes] is metastable in THF at room temperature.

Characterization of $(R^*_2MeSi)ClSi{=}SiCl(SiMeR^*_2)$

The disilene **10** is the first silicon compound with halogen atoms bound to unsaturated silicon atoms to be isolated as a pure substance. Its characterization (see below) improves our knowledge of disilenes, whose syntheses, reactivity and geometric and electronic structures have been thoroughly studied in the last 20 years. In fact, up to date ca. 40 disilenes have been isolated and many disilenes are proved as intermediates (cf. in this connection the reviews, summarized in refs.[9–14]).

The disilene **10** forms orange-red crystals that are practically insoluble in organic solvents such as alkanes, benzene and THF. As a consequence, we have not yet been able to obtain NMR spectra for **10** even at slightly raised temperatures (see below). The orange solution that is first obtained after warming a mixture of **7** and NaR* to room temperature shows three ^{29}Si NMR signals in regions expected for unsaturated silicon atoms: δ = 153.9 (less intense), 140.9 (more intense) and 91.5 (less intense). The signals at δ = 153.9 and 140.9 are probably not due to the disilene **10** or a mixture of disilenes **10**, **10a**, **10b** as one would expect only one low-field ^{29}Si signal for **10**, and four signals for **10**, **10a** and **10b** (the normal regions for >Si=Si< with four aryl substituents, two aryl and two silyl substituents or four silyl substituents are δ = 60–90, 90–130 and 140–160, respectively[14,15]). If, on the other hand, the reaction mixture contained the silylenes **9a** and **9b**, one would expect two low-fied ^{29}Si signals (the normal regions for >Si**:** with aminyl substituents or alkyl substituents are δ = 70–100 and >500, respectively[16]). For a discussion of the signal at δ = 91.5 see below.

In the Raman spectrum the Si=Si double bond vibration occurs at 589 cm^{-1} (for comparison:[14,15,17] $Mes_2Si{=}SiMes_2$: 539 cm^{-1}; Mes(*t*Bu)Si=Si(*t*Bu)Mes: 522 cm^{-1}; R*PhSi=SiPhR*: 592 cm^{-1}. See also ref.[18]).

The disilene **10** is unreactive towards water, methanol, or hydrogen fluoride and decolorizes very slowly (over several days) when exposed to air. A change of the disilene **10** with three-coordinate central Si atoms to disilanes with four-coordinate central Si atoms is not favorable for steric reasons. In addition, **10** does not react with NaR*. Moreover, it is much more thermally stable than the previously mentioned bis[(disupersilyl)silyl]disilene **2** and only melts at 228 °C with decomposition. Obviously, the methyl(disupersilyl)silyl groups $SiMeR^*_2$ are much better substituents for stabilizing the disilenes RXSi=SiXR than the (disupersilyl)silyl groups $SiHR^*_2$, and probably the same must be valid for disilynes. Although, there is only a small difference between $SiHR^*_2$ and $SiMeR^*_2$ its effect is much larger.

Dehalogenation of $(R^*_2MeSi)ClSi{=}SiCl(SiMeR^*_2)$

To dehalogenate the disilene **10** we combined a suspension of **10** in THF at −78 °C with lithium naphthalenide ($LiC_{10}H_8$) in THF. After heating the reaction mixture to room temperature, all volatile products were evaporated under an oil pump vacuum and the residue was treated with benzene to obtain an orange-red solution with insoluble components (among others LiCl and unchanged **10**). The question then arises: does this oxygen-sensitive solution contain the disilyne $R^*_2MeSi-Si{\equiv}Si-SiMeR^*_2$? We have so far been unable to grow crystals from the solution suitable for an X-ray structure analysis. However, the ^{29}Si NMR spectrum of the solution has a signal at δ = 91.5, along with various other signals. This signal appears in a region that might be reasonable for disilyne Si atoms. It is worth mentioning here that the orange solution that is first obtained after warming the mixture of **7** and NaR* to room temperature also shows a less-intense ^{29}Si NMR signal at δ = 91.5 (see above). This could indicate that the dehalogenation of **7** with NaR* might in part not stop at silylenes or disilenes.

The mass spectrum of the solution obtained in chemical ionization mode indicates the presence of chlorine-free molecules with the mass of the desired disilyne $R^*_2MeSi-Si{\equiv}Si-SiMeR_2$ plus two oxygen atoms. The dehalogenation of **10** in THF might, in fact, give a disilyne in solution, which, due to its extreme sensitivity towards air, might react with molecular oxygen when transferring it into the mass spectrometer. This result corresponds to the observation that the mass spectrum of a solution of tetrasupersilyl-*tetrahedro*-tetrasilane[19] shows a mass peak for the tetrahedrane dioxide $R^*_4Si_4O_2$, as well as for the expected tetrahedrane $R^*_4Si_4$.[7]

Structure of $(R^*_2MeSi)ClSi{=}SiCl(SiMeR^*_2)$

Figure 1 shows the structure of the disilene **10** (local symmetry C_i) in the crystal (orange-red prisms, triclinic, $P\bar{1}$) together with selected bond lengths and angles.

The central SiClSi=SiClSi framework of **10** is practically planar (torsion angles at >Si=Si< ca. 0°, angles sum at >Si= ca. 360°) with both the chlorine atoms and the $SiMeR^*_2$ groups in *trans*-positions. Only a few disilenes (*trans*-RR′Si=SiR′R with R/R′ = Mes/*t*Bu, 2,4,6-*i*$Pr_3C_6H_2$/*t*Bu or 2,4,6-*i*$Pr_3C_6H_2$/$SiMe_3$) have similar struc-

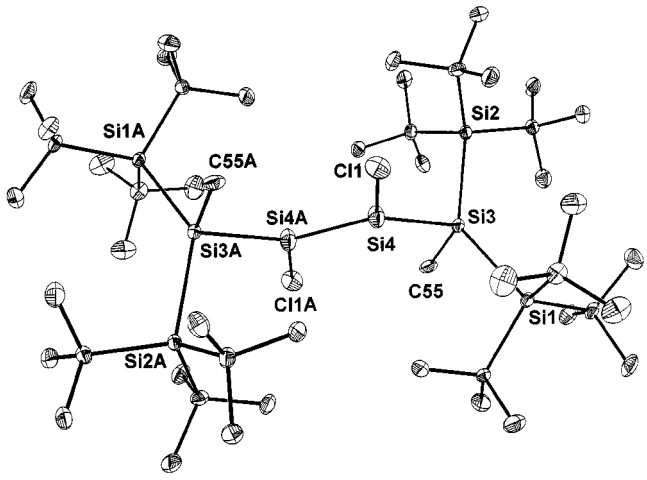

Figure 1. View of the molecule **10** (local symmetry C_i) in the crystal (ORTEP; H atoms excluded for clarity); selected bond lengths [Å] and angles [°]: Si1−Si2 2.553(3), Si2−Si3 2.531(3), Si3−Si4 2.401(3), Si4−Si4A 2.163(4) Si4−Cl1 2.091(3), Si3−C55 1.900(7), Si−C (mean value) 1.96; Si1−Si3−Si2 136.3(1), Si1−Si3−Si4 105.9(1), Si2−Si3−Si4 102.9(1), Si3−Si4−Si4A 132.0(2), Cl1−Si4−Si3 120.8(1), Cl1−Si4−Si4A 106.8(2), C55−Si3−Si1 101.3(2), C55−Si3−Si2 104.1(2), C55−Si3−Si4 102.0(3), C−Si−C (mean value) 109.7, C−Si−Si (mean value) 109.2; Si3−Si4−Si4A−Si3 180.0, Cl1−Si4−Si4A−Cl1A 180.0, Cl1−Si4−Si4A−Si3A 7.5, Cl1−Si4−Si3−C55 179.2, C55−Si3−Si3A−C55A 180.0, Cl1−Si4−Si3−Si1 73.6, Cl1−Si4−Si3−Si2 73.1, Si4A−Si4A−Si3−C55 9.2

tures, the other structurally studied disilenes show *trans*-bent angles between the >Si planes and the Si=Si vectors of up to 35° and/or twist angles of the >Si planes around the Si=Si bond of up to ca. 25°.[14,15] Obviously, the planar conformation of the central structural element of **10** is a consequence of a special three dimensional expansion of the SiMeR*$_2$ substituents at the Si=Si double bond. As mentioned previously, we believe that **10** is formed by dimerization of the silylene (R*$_2$MeSi)ClSi**:** (**9a**) which, as is normal for silylenes, should be in the singlet state (cf. Scheme 2 and ref.[6]). The approach of two such species must occur on the reaction coordinate with a *trans*-bent orientation of the silylene planes;[15] this requires a slowing down of the rate of dimerization.

The Si atom of one R* group of each SiMeR*$_2$ substituent is found above the Si atom of the other R* group below the central SiClSi=SiClSi plane, whereas the C atom of the Me group of each SiMeR*$_2$ substituent is located in the SiClSi=SiClSi plane. These Me groups are *trans* to each other (Me and Cl in *cis*-position). The same is true for the Si−Si−Si planes of both the SiMeR*$_2$ substituents, where the angle between the SiClSi=SiClSi and Si−Si−Si planes is 86.7°.

The Si=Si double bond in **10** is short (2.16 Å), despite the steric overcrowdedness of the SiMeR*$_2$ substituents. The Si=Si distances of acyclic tetraorganyl- or diorganyldisilyldisilenes lie typically in the range 2.14−2.16 Å, whereas the Si=Si distances in acyclic tetrasilyldisilenes can be as long as 2.25 Å.[9,14,15] Obviously, **10** possesses a comparatively strong double bond (see also the section describing the Raman spectrum above).

As a consequence of steric hindrance the R*$_2$MeSi−Si distances (2.40 Å) and especially the R*−Si (2.54 Å) and Si−Cl distances (2.09 Å) exceed the normal Si−Si and Si−Cl single bond lengths of 2.34 Å and 2.03 Å,[20] respectively. In addition, the Si−Si=Si and the Si−Si−Si angles (132.0° and 136.3°) are large. The central saturated Si atom of the =Si***Si***MeR*$_2$ moiety forms a flat pyramid (angles sum 345°) with its three Si neighbors, whereby the Me group at the top of the ***Si***Si$_3$ pyramid is nearly symmetrically placed with regard to the three other Si atoms (C−Si−Si angles 101−104°).

Experimental Section

All experiments were carried out in flame-dried glassware using standard Schlenk techniques under dry argon or nitrogen. Air and moisture were strictly excluded. The solvents (pentane, benzene, THF) were distilled from sodium/lead or sodium/benzophenone. Br_2, MeOH, KHF_2, C_6D_6 are available commercially and were used without further purification. The following compounds were synthesized according to literature procedures: **6**,[1] NaR*·2THF,[21] $LiC_{10}H_8$/THF.[22]

NMR Spectra: Jeol GX-270 (^{1}H/^{13}C/^{29}Si: 270.17/67.94/53.67 MHz) and a Jeol EX-400 (^{1}H/^{13}C/^{29}Si: 399.78/100.54/79.43 MHz). The NMR spectra were recorded conventionally or with the INEPT and DEPT pulse sequences using empirically optimized parameters for the mentioned groups. Mass Spectra: Jeol MStation JMS 700. The mass spectra were recorded by electron ionization (EI) or chemical ionization (CI; NH_3 and $Me_2C{=}CH_2$ as ionization agents). Raman Spectra: Perkin−Elmer, 2000 NIR FT-Raman with Na-YAG Laser (1064 nm).

Synthesis of 7a/7b: These compounds were synthesized as described elsewhere[1] by adding Br_2 (3.37 mmol) dropwise to a solution of **6** (1.69 mmol) in CCl_4 (15 mL) at 0 °C. After 5 min all volatile components were removed with an oil-pump vacuum. The remaining residue consisted of **7a**, **7b** and R*$_2$MeSiBr in the mol ratio ca. 6:3:2 (R*$_2$MeSiBr is possibly formed by Si−Si bond cleavage of **6**; identification of the products was by comparison with authentic samples[1]). The mixture could not be separated by recrystallization.

Synthesis and Characterization of the Disilene 10: A solution of NaR*·2THF (22 mmol) in THF (40 mL) was dropped slowly into a solution of **7a/7b** (ca. 20 mmol, 12.4 g; ca. 13.7 mmol **7a** and 5.9 mmol **7b** according to the NMR spectrum) in pentane (7 mL) at −78 °C (as stated above, the mixture of **7a/7b** also contains some R*$_2$MeSiBr) to give a dark-red reaction mixture (possibly due to the formation of silanides **8** and of NaSiMeR*$_2$). In the course of warming this mixture to room temperature, the color changed to orange-red (formation of silylenes **9**?). An insoluble precipitate was slowly formed from the solution over several hours and the color lightened. After removing all the volatile components under an oil-pump vacuum, the residue was extracted for 4 h with 10 mL of boiling benzene. The disilene *trans*-1,2-dichloro-1,2-bis[methyl(di-supersilyl)silyl]disilene (**10**) (1.20 g, 1.19 mmol; ca. 12%) precipitated from this benzene extract upon cooling, and was isolated at room temperature by filtration (m.p. 228 °C with decomposition). The disilene **10**: (i) is practically insoluble in benzene, alkanes or THF, (ii) does not react with either water or methanol, (iii) reacts very slowly with oxygen (decolorization in air only after eight

days), and (iv) is also unreactive towards HF (used as KHF_2) and NaR* (no reaction after 3 weeks at 60 °C in THF). Disilene **10** crystallizes after warming to 50 °C in benzene for several weeks. As a consequence of the insolubility of **10**, no NMR spectra of the disilene could be obtained. MS (EI): *m/z* (%) = 1012/1010/1008 (24) [M^+], 955/953/951 (33) [$M^+ - t$Bu], 869/867/865 (15) [$M^+ - t$Bu $- 2C_3H_7$], 813/811/809 (56) [M^+ − R*], 775/773 (32) [M^+ − R*H − Cl], 755/753/751 (15) [M^+ − R*H − *t*Bu], 613/611/609 (28) [M^+ − R*H − R*], 575/573 (100) [M^+ − R*Cl − R*]; all isotopic patterns agree well with the calculated spectrum. Raman (Nujol mull): $\tilde{\nu}$ = 123 cm^{-1} s, 277 w, 295 w, 559 m, 589 s (Si=Si), 647 w, 816 m, 1180 s, 1451 w, 1469 w, 2852 w. No analytic data were obtained. For the X-ray structure analysis see Figure 1.

Remarks: As mentioned previously, **10** precipitates only slowly from the reaction mixture of **7** and NaR* in pentane/THF at room temperature. The freshly prepared solution shows three ^{29}Si NMR signals in the low-field region (as well as other signals at higher field) at δ = 153.9, 140.9, 91.5 as discussed above.

Reaction of the Disilene 10 with $LiC_{10}H_8$: A solution of $LiC_{10}H_8$ (0.154 mmol) in THF (1.4 mL) was added dropwise to a suspension of **10** (0.079 g, 0.078 mmol) in THF (3 mL) at −78 °C to give a dark-red reaction mixture. The color of this mixture changed to light orange whilst warming to room temperature. After removal of all the volatile components under an oil-pump vacuum (including naphthalene), the remaining residue was combined with 1 mL of C_6D_6. After 4 weeks at 6 °C the obtained suspension contained no crystals suitable for X-ray structure analysis. The solution showed one ^{29}Si NMR signal in the low-field region (besides other signals at higher field): δ = 91.5 (see above). The MS of the solution after filtration indicated the presence of one type of chlorine-free molecule with the mass M = (**10** − Cl_2 + O_2) = 970.7: MS (CI with $Me_2C{=}CH_2$): *m/z* (%) = 971 (100) [M^+], 914 (38) [$M^+ - t$Bu], 772 (26) [M^+ − R*], 740 (40) [M^+ − R* − C_3H_6], 442 (25) [$R^*_2MeSi^+$]. MS (CI with NH_3): *m/z* (%) = 972 (20) [M^+ + H], 914 (2) [$M^+ - t$Bu], 459 (43) [$R^*_2MeSi^+ + NH_3$], 442 (92) [$R^*_2MeSi^+$], 217 (100) [$R^{*+} + NH_3$]. The MS of the components that are insoluble in benzene indicated the presence of **10** as well as **10** − Cl_2 + O_2.

X-ray Structure Determination of 10: Orange-red prisms, 0.1 × 0.1 × 0.1 mm, $C_{50}H_{114}Cl_2Si_4$, M_r = 1011.04, triclinic, space group $P\bar{1}$, *a* = 9.020(1), *b* = 12.150(1), *c* = 14.767(1) Å, α = 80.580(2)°, β = 89.118(2)°, γ = 71.221(2)°, *V* = 1510.4(3) $Å^3$, *Z* = 2, $\rho_{calcd.}$ = 1.112 Mg m^{-3}, μ = 0.297 mm^{-1}, *F*(000) = 560. Data collection: 2θ = 3.60−43.44°, $-9 \le h \le 9$, $-12 \le k \le 12$, $-15 \le l \le 15$, 5854 reflections of which 2997 were independent (R_{int} = 0.0496) and 2116 [$F > 4\sigma(F)$] refined. All non-hydrogen atoms were refined anisotropically and the H atoms were included in calculated positions. R_1 = 0.0681, wR_2 = 0.1648 [$F > 4\sigma(F)$], GOOF (F^2) = 1.031; max./min. residual electron density 1.377/−0.474 $Å^3$.

The intensities were measured with a Siemens SMART Area-detector (Mo-K_α, λ = 0.71073 Å). The crystals were mounted in perfluoropolyether oil at 193(2) K. The structure was solved by direct methods and refined against F^2 for all observed reflections. Structure solution with SHELXS-97 (Sheldrick, 1990), and refinement with SHELXL-97 (Sheldrick, 1997).

CCDC-171748 contains the supplementary crystallographic data for this paper. These data can be obtained free of charge at www.ccdc.cam.ac.uk/conts/retrieving.html [or from the Cambridge Crystallographic Data Centre, 12, Union Road, Cambridge CB2 1EZ, UK; Fax: (internat.) +44−1223/336−033; E-mail: deposit@ccdc.cam.ac.uk].

Acknowledgments

We thank the Deutsche Forschungsgemeinschaft and the Fonds der Chemischen Industrie for support of our research, T. Blank for helpful preparations and K. Karaghiosoff for the attempt to get NMR spectra of the disilene **10**.

[1] N. Wiberg, W. Niedermayer, H. Nöth, J. Knizek, W. Ponikwar, K. Polborn, D. Fenske, G. Baum, *Z. Anorg. Allg. Chem.* **2001**, *627*, 594−606.
[2] P. Jutzi, *Angew. Chem.* **2000**, *112*, 3953−3957; *Angew. Chem. Int. Ed.* **2000**, *39*, 3797−3800 and refs. cited therein.
[3] N. Wiberg, W. Niedermayer, H. Nöth, M. Warchhold, *Z. Anorg. Allg. Chem.* **2001**, *627*, 1−6.
[4] N. Wiberg, W. Niedermayer, unpublished results.
[5] N. Wiberg, W. Niedermayer, *Z. Naturforsch., Teil B* **2000**, *55*, 406−416.
[6] N. Wiberg, W. Niedermayer, *J. Organomet. Chem.* **2001**, *628*, 57−64; N. Wiberg, W. Niedermayer, H. Nöth, M. Warchhold, *J. Organomet. Chem.* **2001**, *628*, 46−56.
[7] N. Wiberg, H. Auer, S. Wagner, K. Polborn, G. Kramer, *J. Organomet. Chem.* **2001**, *69*, 110−131.
[8] M. E. Lee, H. M. Cho, M.-S. Ryu, C. H. Kim, W. Ando, *J. Am. Chem. Soc.* **2001**, *123*, 7732−7733.
[9] W. S. Sheldrick, in *The Chemistry of Organic Silicon Compounds* (Eds.: S. Patai, Z. Rappoport), Vol. 1, Wiley, Chichester, **1989**, 227−303.
[10] G. Raabe, J. Michl, in *The Chemistry of Organic Silicon Compounds* (Eds.: S. Patai, Z. Rappoport), Vol. 1, Wiley, Chichester, **1989**, 1015−1142.
[11] T. Tsumuraya, S. A. Batcheller, S. Masamune, *Angew. Chem.* **1991**, *103*, 916−944; *Angew. Chem. Int. Ed. Engl.* **1991**, *30*, 909−937.
[12] H. Sakurai, in *The Chemistry of Organic Silicon Compounds* (Eds.: Z. Rappoport, Y. Apeloig), Vol. 2, Wiley, Chichester, **1998**, 827−855.
[13] Y. Apeloig, M. Nakash, *Organometallics* **1998**, *17*, 1260−1265, 2307−2312.
[14] R. Okazaki, R. West, *Adv. Organomet. Chem.* **1996**, *39*, 231−273.
[15] M. Weidenbruch, in *The Chemistry of Organic Silicon Compounds* (Eds.: Z. Rappoport, Y. Apeloig), Vol. 3, Wiley, Chichester, **2001**, 391−428, and references cited therein.
[16] M. Kira, S. Ishida, T. Iwamoto, C. Kabuto, *J. Am. Chem. Soc.* **1999**, *121*, 9722−9723 and references cited therein.
[17] N. Wiberg, *Coord. Chem. Rev.* **1997**, *163*, 217−252.
[18] L. A. Leites, S. S. Bukalov, I. A. Garbuzova, R. West, J. Mangette, H. Spitzner, *J. Organomet. Chem.* **1997**, *536*, 425−432.
[19] N. Wiberg, Ch. M. M. Finger, K. Polborn, *Angew. Chem.* **1993**, *105*, 1140−1142; *Angew. Chem. Int. Ed. Engl.* **1993**, *32*, 1054−1056.
[20] W. S. Sheldrick, in *The Chemistry of Organic Silicon Compounds* (Eds.: S. Patai, Z. Rappoport), Vol. 1, Wiley, Chichester, **1989**, 287−303.
[21] N. Wiberg, K. Amelunxen, H.-W. Lerner, H. Schuster, H. Nöth, I. Krossing, M. Schmidt-Amelunxen, T. Seifert, *J. Organomet. Chem.* **1997**, *542*, 1−18.
[22] J. L. Wardell, in *Comprehensive Organometallic Chemistry* (Eds.: G. Wilkinson, F. G. A. Stone), Vol. 1, Pergamon, Oxford, **1982**, 109−111.

Received October 19, 2001
[I01412]

Magnetic Behaviour in the System $La_{1.33}Na_xMn_xTi_{2-x}O_6$

Ana Isabel Ruiz,*[a] Javier Campo,[b] María Luisa López,[a] José Luis Martínez Peña,[c] Carlos Pico,[a] and María Luisa Veiga[a]

Keywords: Perovskite phases / Neutron diffraction / Magnetic properties

A series of perovskite-type complex oxides of general formula $La_{1.33}Na_xMn_xTi_{2-x}O_6$ (x = 0.66, 0.55 and 0.44) have been obtained and characterised. Magnetic susceptibility measurements on these phases follow a Curie–Weiss-like dependence at high temperatures, although a more complex variation is observed at lower temperatures. The thermal variation of M/H from zero-field-cooled and field-cooled susceptibility measurements shows irreversible processes and magnetisation isotherms that differ from typical ferromagnetic behaviour. Neutron diffraction data collected at low temperature show no extra magnetic contribution in the nuclear peaks nor extra reflections. All the measurements carried out on this series, such as magnetic susceptibility (dc and ac), magnetisation and neutron diffraction can be interpreted as being due to a spin-glass behaviour.

(© Wiley-VCH Verlag GmbH, 69451 Weinheim, Germany, 2002)

Introduction

Perovskite-type oxides have the general formula ABO_3 and it is well-known that this structure allows a great number of cation substitutions at the A and/or B sites. In this way, both A and B sites can accommodate two different metal ions, with different oxidation states, that are expressed by the nominal compositions $AA'B_2O_6$,[1,2] $A_2BB'O_6$ [3,5] and $AA'BB'O_6$.[6–8] These systems have been the subject of intense research efforts due to the fact that they exhibit a wide variety of electrical and magnetic properties (high temperature superconductors, ferromagnetic and piezoelectric materials, magnetoresistors, etc.) that depend on variations in the chemical composition, stoichiometry and structure of the material.

In particular, hole-doped perovskite-type manganese oxides have attracted considerable interest in recent years motivated by the apparition of colossal magnetoresistance and the great variety of magnetic and transport properties in this class of materials.[9] Among the La-based systems, the ground state of the stoichiometric parent compound $LaMnO_3$ shows remarkable insulating A-type antiferromagnetic properties, which are attributed to a cooperative effect of orbital ordering and superexchange interactions.[10]

[a] Departamento de Química Inorgánica I, Facultad de Ciencias Químicas, Universidad Complutense,
28040 Madrid, Spain
E-mail: anairuiz@quim.ucm.es
[b] Institut Max Von Laue – Paul Langevin (ILL),
38042 Grenoble Cedex 9, France
[c] Departamento de Propiedades Ópticas, Magnéticas y de Transporte, Instituto Ciencia de Materiales, Consejo Superior de Investigaciones Científicas,
Cantoblanco 28049 Madrid, Spain

For these reasons, we have carried out previous research on the system $La_{1.33}Na_xMn_xTi_{2-x}O_6$ (x = 0.66, 0.55 and 0.44) oriented towards structural characterization by neutron diffraction[6] and electrical properties.[11] The aim of the present work was to analyse additional physical properties of these compounds by studying their magnetic behaviour.

Results and Discussion

Chemical Composition and Structural Results

Samples of the series $La_{1.33}Na_xMn_xTi_{2-x}O_6$ (x = 0.66, 0.55 and 0.44) were synthesised as polycrystalline powders. Table 1 gathers the Mn^{III} and Mn^{IV} concentrations present for the different compositions, which agree well with the respective nominal manganese content. From these results it is deduced that the amounts of Mn^{IV} are practically negligible in the x = 0.55 and 0.44 samples.

Table 1. Composition of manganese in the series $La_{1.33}Na_xMn_xTi_{2-x}O_6$

x	Mn^{III}	Mn^{IV}
0.66	0.55	0.11
0.55	0.50	0.05
0.44	0.39	0.05

All these compounds have characteristic diffraction patterns of the perovskite structure, in which some reflections are split indicating a noticeable distortion from the ideal cubic symmetry. It can be seen from neutron powder diffraction data[6] that an interesting structural transition be-

tween the orthorhombic (space group *Ibmm*) and rhombohedral (space group $R\bar{3}c$) symmetries takes place between 400 and 600 K in the $x = 0.66$ sample. In contrast, the phases $x = 0.55$ and 0.44 adopt a rhombohedral symmetry (space group $R\bar{3}c$) as is deduced from the X-ray diffraction results.[6]

These materials do not show any superlattice lines corresponding to an ordered distribution of the cations at the A and B sites. Taking into account the structural results, both lanthanum and sodium cations and vacancies are located at the A-sites, and manganese and titanium cations occupy, at random, the B-sites of the perovskite structure.

Magnetic Properties

Magnetic measurements were carried out on all the above compounds. Figure 1 shows the temperature dependence of magnetic susceptibility (a) and its reciprocal (b). Reciprocal susceptibility data can be fitted to a Curie−Weiss law [M/H = C/(T − θ)] over a relatively narrow temperature range that decreases as the x value increases, from which the experimental and theoretical magnetic moments and parameters C and θ were obtained (Table 2). The experimental magnetic moment should diminish in the same way as the Mn^{3+} concentration in the sample. However, a noticeable difference between the calculated (3.85 μ_B) and observed (3.43 μ_B) values is encountered for the $x = 0.66$ phase,

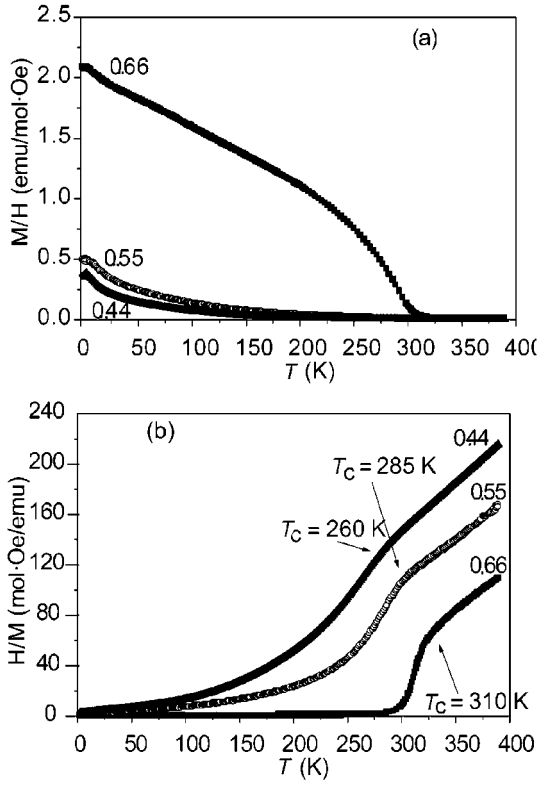

Figure 1. Susceptibility (a) and reciprocal susceptibility variations (b) for the system $La_{1.33}Na_xMn_xTi_{2-x}O_6$ ($x = 0.66$, 0.55 and 0.44)

Table 2. Magnetic data for $La_{1.33}Na_xMn_xTi_{2-x}O_6$

x	T range (K)	μ_{calc} (μ_B)	μ_{exp} (μ_B)	θ (K)
0.66	340−390	3.85	3.43	228
0.55	315−390	3.63	3.55	128
0.44	300−390	3.25	3.24	107

whereas both values are practically the same for the $x = 0.44$ composition. Thus, some magnetic interactions between the paramagnetic Mn^{3+} ions are to be expected in the first case and, possibly, in the intermediate composition $x = 0.55$. These assumptions seem to be supported by the fact that the respective Weiss constants are positive and decrease in good agreement with the Mn content in the sample. Figure 1b shows the increase in the value of the critical temperature, T_c, at which a magnetic phase-transition takes place; these increase as the manganese content increases (i.e., from 260 K for $x = 0.44$ to 310 K for $x = 0.66$). It is likely that this variation in T_c is due to magnetic dilution within the B sublattice.

In order to analyse the nature of the proposed cooperative interactions, field-cooled (FC) and zero-field-cooled (ZFC) susceptibility measurements are compared in Figure 2 for the $x = 0.66$ sample; they were obtained at an applied field (H_e) of 500 Oe. As the temperature is lowered from around 300 K, both FC and ZFC magnetisation curves increase and are basically identical in a wide region, $T_r \leq T \leq T_c$, implying a reversibility of the magnetisation. Below the temperature, T_r, at which the FC and ZFC graphs diverge, the ZFC magnetisation shows a broad maximum at 12.4 K that is taken as the spin freezing temperature, namely as T_{sg}, while the FC variation shows a bend and increases slightly. Thus the irreversibility appears far below T_c, a behaviour that is typical of reentrant spin-glass systems,[12] as in cluster-glass systems the irreversibility starts just below T_c and the difference between FC and ZFC magnetisation is usually much higher, reflecting the presence of ferromagnetic order within the clusters.[13]

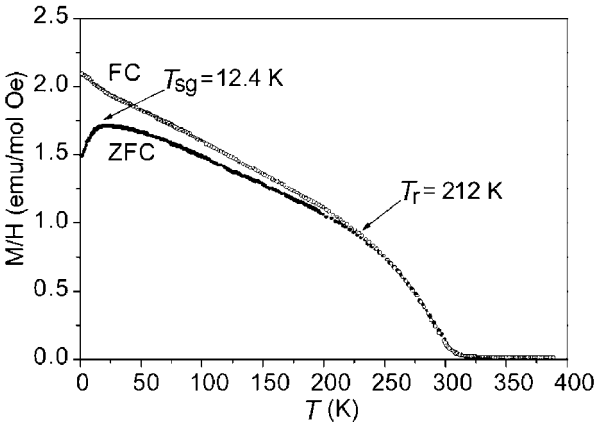

Figure 2. Temperature dependence of the magnetic susceptibility for $La_{1.33}Na_{0.66}Mn_{0.66}Ti_{1.34}O_6$ measured after zero-field cooling (ZFC) and field cooling (FC)

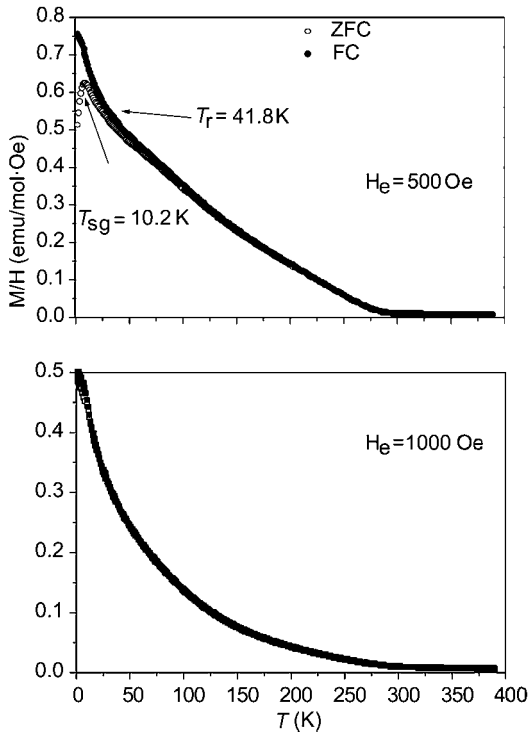

Figure 3. FC and ZFC M/H for $La_{1.33}Na_{0.55}Mn_{0.55}Ti_{1.45}O_6$ measured with an applied field (H_e) of 500 and 1000 Oe

With respect to the remaining compositions, Figure 3 shows the shape of the M_{FC} and M_{ZFC} curves for $x = 0.55$ at two different fields of 500 and 1000 Oe. Only a clear T_{sg} is detected for the lower field measurements; a similar behaviour was obtained for the sample $x = 0.44$ (not shown). However, when the manganese doping decreases in the sample, T_{sg} drops slightly and the respective cusp is less pronounced, suggesting that the magnetic interaction diminishes (12.4 K for $x = 0.66$ and 10.2 K for $x = 0.55$); the maximum is not observed for $x = 0.44$ at the same external field of 500 Oe. These changes suggest that the magnetic transitions below T_c in this system are very sensitive to the applied field and that they are completely suppressed by increasing H_e. Such a behaviour has also been reported for some other perovskite-type oxides[4,13,14] and was assumed to originate from the formation of a spin-glass.

Magnetisation measurements provide useful information about the magnetic behaviour of these systems and the isotherms obtained at different temperatures are depicted in Figure 4. Characteristic S-shaped curves were obtained in all cases and they do not saturate even in fields as high as 50 kOe. Curves below T_c show a clear ferromagnetic component with increasing importance when the temperature is lowered. Such a behaviour is evidence for a disordered spin-state (spin-glass-like state) induced by disorder and frustration due to competing ferro- and antiferromagnetic exchange interactions. The very narrow hysteresis loops indicate that these materials behave as weakly ferromagnetic. Finally, the low values of magnetisation could be explained

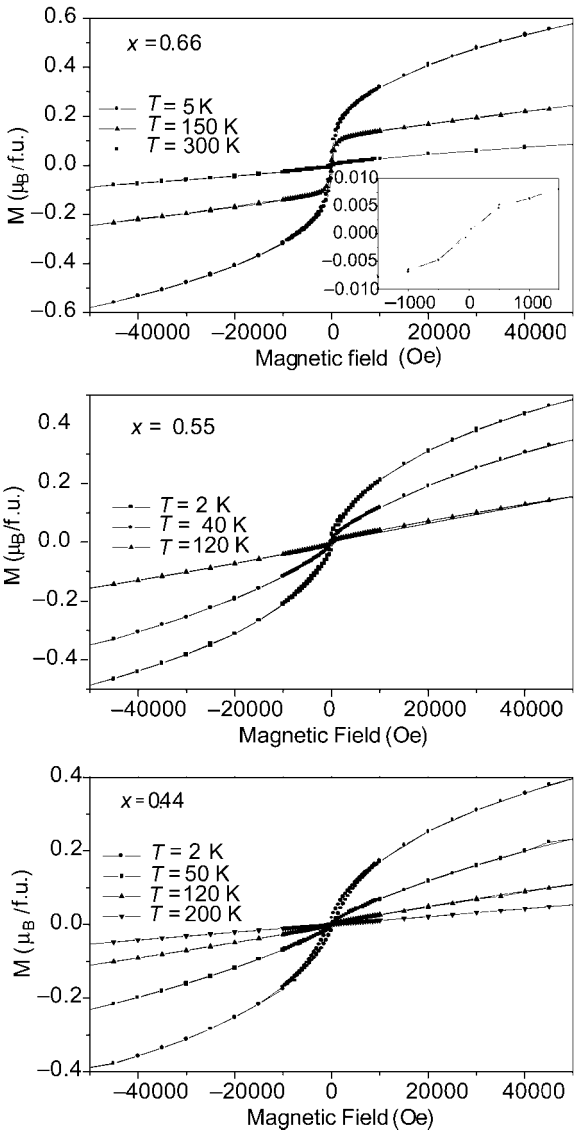

Figure 4. Magnetisation isotherms obtained at different temperatures for the system $La_{1.33}Na_xMn_xTi_{2-x}O_6$ ($x = 0.66$, 0.55 and 0.44)

by recalling that both paramagnetic Mn^{3+} and diamagnetic Ti^{4+} ions are randomly distributed over the B sites, thus preventing the establishment of a long-range ordering in these materials.[9]

In order to evaluate the importance of the above cooperative interactions, neutron diffraction experiments were carried out on these systems and Figure 5 shows thermal patterns for the sample $x = 0.66$ in the temperature range 1.6−262 K. Only a very weak ferromagnetic contribution could be observed near $2\theta = 70°$, whose intensity is practically negligible (see inset in Figure 5), so it was not possible to obtain a ferromagnetic component. Therefore it is more realistic to assume that no extra magnetic contributions (in the intensity of nuclear peaks nor extra peaks) are observed at low temperatures and, consequently, that there is no long range magnetic ordering in these materials.

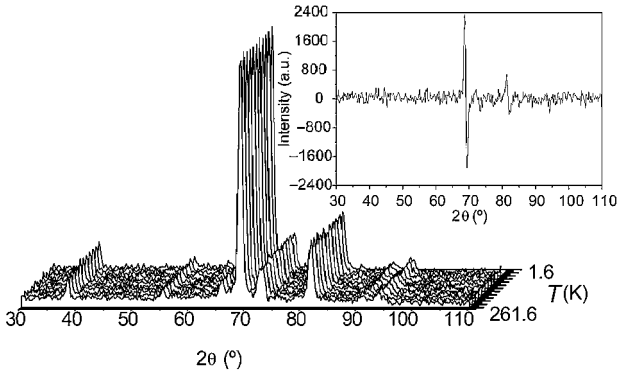

Figure 5. Neutron thermodiffractograms of $La_{1.33}Na_{0.66}Mn_{0.66}Ti_{1.34}O_6$ between 1.6 and 262 K and angular range 30−110°; the inset shows the difference diagram between 1.6 and 261.6 K (inset)

Finally, to gain a deeper insight into the spin-glass behaviour of this series, thermal variations of the ac susceptibility, χ_{ac}, at different frequencies were performed and they are depicted in Figure 6 for the sample $x = 0.66$. This demonstrates that the real part of χ_{ac} exhibits a broad maximum at about 67 K which decreases in intensity as the frequency increases (from 1 to 1000 Hz), as is expected for spin-glass systems,[15] thus confirming the above assumptions.

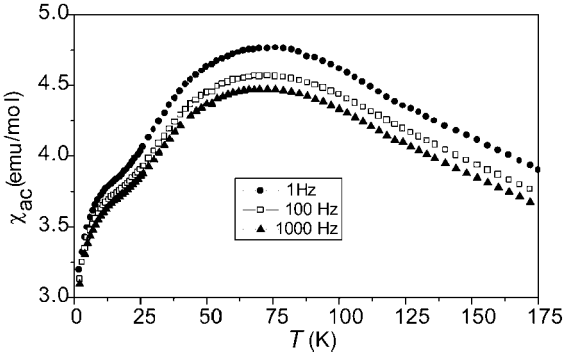

Figure 6. Thermal dependence of the ac susceptibility at different values of the excitation frequency

In summary, different magnetic and neutron diffraction measurements carried out on the series $La_{1.33}Na_xMn_xTi_{2-x}O_6$ ($x = 0.66$, 0.55, and 0.44) confirm a spin-glass behaviour that is attributed to cation disorder in the perovskite B sites. Such a disorder should contribute to the frustrated magnetic ground state and has also been found in related $AB_{1-x}B'_xO_3$ perovskite-type systems, in which the dilution of paramagnetic B cations seems to be crucial to the occurrence of spin-glass transitions at low temperatures. In the compounds under research the Ti^{4+}/Mn^{3+} ratio increases progressively from about 2 (for $x = 0.66$) to about 3.5 (for $x = 0.44$) and it becomes obvious that the effect of manganese dilution is crucial to the respective magnetic ordering. Similar features were previously observed in other related systems $LnMn_{1-x}B'_xO_3$, where lanthanum has been substituted by praseodymium or neodymium.[16,17]

Experimental Section

Polycrystalline samples of general composition $La_{1.33}Na_xMn_xTi_{2-x}O_6$ ($x = 0.66$, 0.55 and 0.44) were prepared by a classical ceramic method. Stoichiometric amounts of $La(NO_3)_3{\cdot}6H_2O$, $NaNO_3$, $C_{15}H_{21}MnO_6$ [manganese(III) acetylacetonate] and $C_{10}H_{14}O_5Ti$ [titanium(IV) acetylacetonate] were used as starting materials, and heated at 973 K for several days.

The Mn^{3+}/Mn^{4+} ratio was determined by redox titration with an excess of $FeSO_4$ solution and back titration with $KMnO_4$, with the samples being dissolved in H_2SO_4/H_2O (50:50). A known amount of $FeSO_4$ was introduced into the sample solution and the excess was determined with a standard $KMnO_4$ solution to give the total manganese ; the possible Mn^{4+} content was determined by the procedure described in ref.[10]

X-ray diffraction patterns were recorded with a Philips X'Pert-MPD diffractometer and a PW 3050/00 goniometer, using Ni-filtered Cu-K_α radiation and a 2θ step size of 0.05°, with a counting time of 12.5 s for each step. The goniometer was connected to a PC controlled by the commercial program PC-APD (Analytical Powder Diffraction Software, 4.0).

The neutron powder-diffraction data were recorded on the D1A high-resolution powder diffractometer (λ = 1.9110 Å) at the Institut Laue−Langevin (Grenoble, France). The neutron and X-ray diffraction patterns were analysed by the Rietveld method and the Fullprof program.[18] The multidetector D1B powder diffractometer with a wavelength of 2.52 Å was used for thermal patterns in the 1.6−300 K temperature range.

Magnetic measurements were obtained in a SQUID (Quantum Design, MPMS-XL model) with a sensitivity of 10^{-10} emu in the temperature range 2−400 K, applying a field of 500, 1000 Oe.

Acknowledgments

One of the authors (A.I.R.) is grateful to the C.A.M. for a fellowship. We are indebted to the CICYT (MAT 2000-1585-C03-02), Spain, for financial support. We also acknowledge the I.L.L. (CRG−D1B) for collecting the neutron diffraction data.

[1] A. I. Ruiz, M. L. López, M. L. Veiga, C. Pico, *J. Solid State Chem.* **1999**, *148*, 329−332.
[2] A. I. Ruiz, M. L. López, M. L. Veiga, C. Pico, *Intern. J. Inorg. Mat.* **1999**, *1*, 193−200.
[3] X. L. Wang, J. Horvat, H. K. Liu, A. H. Li, S. X. Dou, *Solid State Commun.* **2001**, *118*, 27−30.
[4] K. Yoshii, *J. Solid State Chem.* **2000**, *151*, 294−297.
[5] I. Julián, R. Sáez, J. Romero, J. L. Martínez, *J. Mater. Chem.* **1999**, *9*, 525−528.
[6] A. I. Ruiz, M. L. López, M. L. Veiga, C. Pico, *Eur. J. Inorg. Chem.* **2000**, 659−664.
[7] M. A. Arillo, J. Gómez, M. L. López, M. L. Veiga, C. Pico, *Solid State Ionics* **1997**, *95*, 241−248.
[8] M. L. López, I. Álvarez, M. Gaitán, A. Jerez, M. L. Veiga, C. Pico, *Solid State Ionics* **1993**, *63−65*, 599−602.

[9] C. N. R. Rao, B. Raveau, *Colossal Magnetoresistance, Change Ordering and Related Properties of Manganese Oxides*, World Scientific, Singapore, **1998**.
[10] E. O. Wollan, W. C. Koehler, *Phys. Rev.* **1955**, *100*, 545−563.
[11] A. I. Ruiz, M. L. López, C. Pico, M. L. Veiga, T. A. Ezquerra, *Intern. J. Inorg. Mat.* **2001**, *3*, 655−659.
[12] L. Guivelder, I. Abrego Castillo, M. A. Gusmao, J. A. Alonso, L. F. Cohen, *Phys. Rev. B* **1999**, *60*, 12184−12190.
[13] P. Goral, J. E. Greedan, *J. Solid State Chem.* **1982**, *43*, 204−212.
[14] K. Takase, Y. Kubota, Y. Takano, H. Negishi, M. Sasaki, M. Inoue, K. Sekizawa, *Phys. B* **2000**, *284*, 1517−1518.
[15] J. A. Mydosh, *Spin Glasses: An Experimental Introduction*, Taylor and Francis, London, **1993**.
[16] P. Martín, A. I. Ruiz, J. Campo, M. L. López, M. L. Veiga, C. Pico, *J. Solid State Chem.* **2001**, *161*, 294−299.
[17] P. Martín, A. I. Ruiz, M. L. López, M. L. Veiga, C. Pico, *J. Alloys Comp.* **2001**, *323*, 618−622.
[18] J. Rodriguez Carvajal, *Physica B* **1993**, *192*, 55−69.

Received November 12, 2001
[I01448]

Preparation of Trifluorophosphaneruthenium(II) Complexes from η^3:η^3-Cyclooctadienediylruthenium(IV) Compounds as Precursors

Helmut Werner,*[a] Wolfram Stüer,[a] Stefan Jung,[a] Birgit Weberndörfer,[a] and Justin Wolf[a]

Dedicated to Professor Gerhard E. Herberich on the occasion of his 65th birthday

Keywords: Allyl complexes / Carbene complexes / Hydrido complexes / P ligands / Ruthenium

The dinuclear cyclooctadienediylruthenium(IV) compound [{$RuCl_2(\eta^3:\eta^3\text{-}C_{10}H_{16})$}$_2$] (**1**) reacts with PCy_3 in 2-propanol under an H_2 atmosphere to give the hydrido(dihydrogen) complex [$RuHCl(H_2)(PCy_3)_2$] (**2**) in nearly quantitative yield. Treatment of **1** with PCy_3, P*i*Pr$_3$ or P*i*Pr$_2$Ph under argon affords the mononuclear products [$RuCl_2(\eta^3:\eta^3\text{-}C_{10}H_{16})(PR_3)$] (**3**–**5**) by chloride-bridge cleavage. The corresponding compound **6** with PF_3 as phosphane ligand reacts with PCy_3 by nucleophilic attack of PCy_3 at the carbon atom C3 of the dienediyl chain to give the zwitterionic η^2:η^3-alkene(allyl)-ruthenium(II) complex [$RuCl_2\{\eta^2:\eta^3\text{-}CH_2{=}C(Me){-}CH(PCy_3)(CH_2)_2CHC(Me)CH_2\}(PF_3)$] (**7**) the crystal and molecular structures of which have been determined. The reaction of **7** with excess PCy_3 in the presence of H_2 affords the five-coordinate hydrido compound [$RuHCl(PF_3)(PCy_3)_2$] (**8**), which upon treatment with acetylene gives the vinyl derivative [$RuCl(CH{=}CH_2)(PF_3)(PCy_3)_2$] (**9**). The related cationic carbene complex [$RuCl(=CHCH_3)(PF_3)(PCy_3)_2$]$BF_4$ (**10**) is obtained by protonation of **9** with HBF_4 in ether.

(© Wiley-VCH Verlag GmbH, 69451 Weinheim, Germany, 2002)

Introduction

In the search for coordinatively unsaturated vinylideneruthenium(II) complexes with [Ru(P*i*Pr$_3$)$_2$] and [Ru(PCy$_3$)$_2$] as building blocks, we recently discovered that the six-coordinate non-octahedral dihydridoruthenium(IV) compounds [$RuH_2Cl_2(PR_3)_2$] (R = *i*Pr, Cy) are excellent precursors for the preparation of the target molecules [$RuCl_2(=C=CHR')(PR_3)_2$].[1] If, however, instead of [$RuH_2Cl_2(PR_3)_2$] the corresponding hydrido(dihydrogen)ruthenium(II) complexes [$RuHCl(H_2)(PR_3)_2$] are used as starting materials, the reaction with HC≡CR′ in the presence of Brönsted acids and chloride ions leads to the formation of the Grubbs-type ruthenium carbenes [$RuCl_2(=CHCH_2R')(PR_3)_2$].[1,2] Since the reactivity of these species depends on the type of phosphane and since, to the best of our knowledge,[3] complexes of the general composition [$RuCl_2(=CHCH_2R')(PR_3)(PX_3)$] with two *different* phosphanes have not been reported in the literature, we were tempted to prepare the respective precursors [$RuHCl(H_2)(PR_3)(PX_3)$] in order to find out whether they are appropriate starting materials for the synthesis of the desired ruthenium carbenes. While we failed to prepare neutral carbenes [$RuCl_2(=CHCH_2R')(PR_3)(PX_3)$], we found in the course of these studies a stepwise synthetic route to ruthenium complexes with [Ru(PF$_3$)(PCy$_3$)$_2$] as a molecular unit. In the present paper we describe details of this route and report on the reactivity of the mixed trifluorophosphane(tricyclohexylphosphane)ruthenium(II) compounds.

[a] Institut für Anorganische Chemie der Universität Würzburg
Am Hubland, 97074 Würzburg, Germany
E-mail: anor097@rzbox.uni-wuerzburg.de
helmut.werner@mail.uni-wuerzburg.de

Results and Discussion

For the one-pot synthesis of the five-coordinate ruthenium carbenes [$RuCl_2(=CHCH_2R')(PR_3)_2$] (R = *i*Pr, Cy), recently developed in our laboratory, polymeric cyclooctadieneruthenium(II) dichloride [{$(\eta^4\text{-}C_8H_{12})RuCl_2$}$_n$] was used as the starting material.[4] By heating a suspension of this compound in 2-butanol for 6 h at 80 °C, in the presence of PCy_3 and H_2, the hydrido(dihydrogen) complex **2**[5] is formed. Since the conditions for the preparation of **2** with [{$(\eta^4\text{-}C_8H_{12})RuCl_2$}$_n$] as the precursor are rather severe, we decided to search for another starting material to generate **2**. The compound of choice was the dinuclear cyclooctadienediylruthenium(IV) complex **1**, which was first reported by Porri et al. in 1965[6] and in subsequent studies used as a catalyst for olefin metathesis.[7,8] Both Porri[6a] and others[9,10] have reported that the chloro bridges of **1** can easily be split by hard and soft Lewis bases to yield the mononuclear compounds [$RuCl_2(\eta^3:\eta^3\text{-}C_{10}H_{16})(L)$] (L = py, DMSO, CH_3CN, CN*t*Bu, CO, PPh_3, $P(OMe)_3$, PF_3 etc). It was also observed that the reaction of **1** with H_2 (1 bar,

25 °C) in dichloromethane leads quantitatively to the formation of 2,7-dimethylocta-2,6-diene.[6a]

Taking these results into consideration, we treated a suspension of **1** in 2-propanol with PCy_3 and replaced the argon atmosphere by dihydrogen. Upon stirring the suspension under these conditions at ca. 50 °C, an orange solid precipitated which was shown by comparison of the ^1H and ^{31}P NMR spectroscopic data to be **2**.[5] The isolated yield of **2** was 92%. If the reaction of **1** with PCy_3 was carried out in CH_2Cl_2 at −20 °C under argon (i.e., in the absence of H_2 and a hydrogen-transfer reagent such as 2-propanol), the cyclooctadienediylruthenium(IV) complex **3** was formed instead of **2** (Scheme 1). Other bulky tertiary phosphanes such as P*i*Pr$_3$ and P*i*Pr$_2$Ph behave analogously and afford the corresponding mononuclear compounds **4** and **5** in 89% and 91% yield, respectively. Compounds **3**−**5** are yellow to brownish solids that are only moderately air-sensitive but thermally quite labile and decompose both in solution and in the solid state at 40−50 °C. The ^1H NMR spectroscopic data of **3**−**5** and the ^{13}C NMR spectroscopic data of **4** and **5** are similar to those of the Ru(PF$_3$) complex **6**, the crystal and molecular structures of which have been determined crystallographically.[9b] The CH and CH_2 protons H1−H5 of **3**−**5** give rise to five resonances and the carbon atoms C1−C4 to four resonances in the NMR spectra (for assignment see Exp. Sect.), in agreement with the C_2 symmetry of the cyclooctadienediyl ligand.[6b][9b]

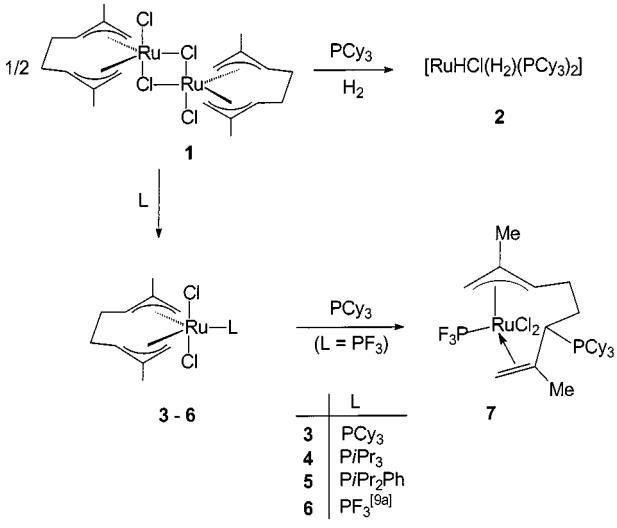

Scheme 1

The reactions of **4** and **5** with a slight excess of PCy_3 in the presence of H_2, undertaken with the aim to prepare the mixed-ligand compounds [RuHCl(H$_2$)(P*i*Pr$_2$R)(PCy$_3$)] (R = *i*Pr, Ph), led to a mixture of products that could not be separated by fractional crystallization or chromatographic techniques. When the reactions were monitored by ^1H or ^{31}P NMR spectroscopy, the formation of uncoordinated P*i*Pr$_3$ or P*i*Pr$_2$Ph was detected. Obviously, PCy_3 replaces the less bulky phosphanes and generates **3**, which upon treatment with PCy_3 and H_2 affords **2**.

In contrast to **4** and **5**, the related PF_3 derivative **6** reacts almost instantaneously with PCy_3, even in the absence of dihydrogen, to yield a single product **7**, the composition of which corresponds to a 1:1 adduct of the two starting materials. The pale-yellow, highly air-sensitive solid is soluble in chloroform and dichloromethane but decomposes in solution at room temperature quite rapidly. Whereas the ^1H and ^{13}C NMR spectra (measured at −50 °C in CD_2Cl_2) are rather complicated, the ^{31}P NMR spectrum displays a doublet at δ = 32.5 for the PCy_3 and a quadruplet of doublets at δ = 137.3 for the PF_3 phosphorus atoms. The rather small ^{31}P-^{31}P coupling constant of 19.3 Hz (for comparison see the data for **8**−**10**) indicate that only one phosphane molecule is coordinated to the metal center while the other is linked to the π-bonded chain-like ligand.

The result of the X-ray crystal structure analysis of **7** is shown in Figure 1. The coordination geometry around ruthenium can best be described as trigonal bipyramidal with the chlorine atoms occupying the apical positions of the bipyramid. The η^2:η^3-alkene(allyl) unit, formed by nucleophilic addition of PCy_3 at the allylic carbon atom C3 of the η^3:η^3-cyclooctadienediyl ligand, occupies two of the equatorial sites, while the third position is occupied by PF_3. In contrast to **6**,[9b] the PF_3 molecule of **7** is not disordered. The carbon atoms C1, C2, C7, C8, C10 and the phosphorus atom P1 lie in one plane, the largest deviation being found for C7 with 0.103(2) Å. Although **7** possesses two centers of chirality, the crystal contains only that pair of enantiomers in which the methyl group at C2 and the PCy_3 moiety are farthest apart. The bond angle between P1, Ru and the midpoint of the line between C7 and C10 is 122.5(2)° and thus deviates only slightly from the ideal value of 120°. The Ru−P1 bond length of 2.178(2) Å is somewhat shorter than in **6** [2.237(3) Å] but almost identical to the Ru−PF_3 distances in the octahedral compound [RuCl$_2$(PF$_3$)$_2$(PPh$_3$)$_2$] [2.160(2) and 2.180(2) Å].[9b] The olefinic fragment of the zwitterionic $C_{10}H_{16}$(PCy$_3$) ligand is unsymmetrically linked to the metal center, the bond lengths Ru−C1 and Ru−C2 pointing to a rather weak coordination compared to other alkeneruthenium complexes.[11] Similar Ru−C olefin distances are found in the compound [RuCl$_2$(η^3:η^2:η^3-C$_{12}$H$_{18}$)] which has been prepared from RuCl$_3$·3H$_2$O and butadiene.[12]

While we could not convert **7** to the desired hydrido(dihydrogen) complex [RuHCl(H$_2$)(PF$_3$)(PCy$_3$)], treatment of **7** in dichloromethane with excess PCy_3 under a hydrogen atmosphere leads to the formation of the five-coordinate hydridoruthenium(II) compound **8** in 63% isolated yield (Scheme 2). The presence of the hydrido ligand is clearly confirmed by the ^1H NMR spectrum, which displays a signal at high field (δ = −24.68). This signal is split into a doublet of triplets of quadruplets due to the coupling of the RuH proton with the ^{31}P and ^{19}F nuclei of the PCy_3 and PF_3 ligands.

The reactivity of the hydrido(trifluorphosphane)ruthenium(II) complex **8** is similar to that of the corresponding hydrido(carbonyl) derivatives [RuHCl(CO)(PR$_3$)$_2$]. By passing a slow stream of acetylene through a solution of **8** in

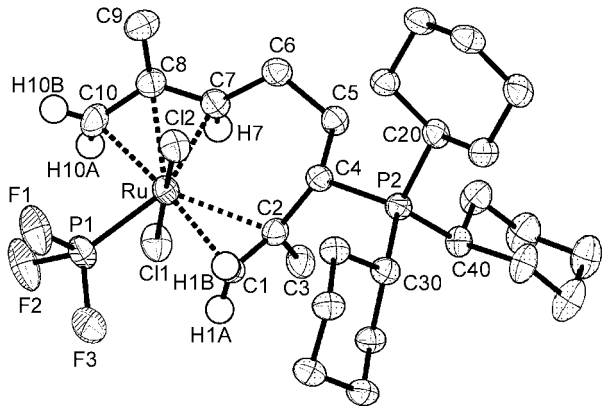

Figure 1. Molecular structure (SCHAKAL plot) of **7**; selected bond lengths [Å] and angles [°]: Ru−P1 2.178(2), Ru−Cl1 2.427(2), Ru−Cl2 2.433(2), Ru−C1 2.228(4), Ru−C2 2.360(4), Ru−C7 2.239(4), Ru−C8 2.246(4), Ru−C10 2.204(4), C1−C2 1.393(5), C2−C4 1.523(5), C7−C8 1.427(5), C8−C10 1.414(6), P2−C4 1.863(4); Cl1−Ru−Cl2 175.6(3), Cl1−Ru−P1 86.5(1), Cl1−Ru−C1 93.7(1), Cl1−Ru−C2 86.8(1), Cl1−Ru−C8 100.5(1), Cl1−Ru−C10 81.3(1), Cl2−Ru−P1 90.6(1), Cl2−Ru−C1 82.9(1), Cl2−Ru−C2 91.9(1), Cl2−Ru−C7 95.6(1), Cl2−Ru−C8 83.7(1), Cl2−Ru−C10 101.8(1), C1−C2−C3 117.5(3), C1−C2−C4 123.0(3), C2−C4−C5 113.1(3), C2−C4−P2 116.6(2), C5−C4−P2 108.7(2), C7−C8−C9 122.0(3), C7−C8−C10 119.6(3)

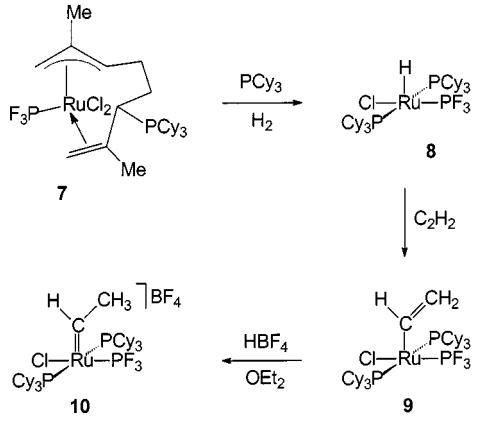

Scheme 2

hexane, a rapid change of color from yellow to bright-red occurs and, after removal of the solvent, the vinylruthenium(II) compound **9** is obtained in nearly quantitative yield. The ^{31}P NMR spectrum of **9** displays a doublet for the PCy_3 phosphorus atoms at δ = 24.3 and a quadruplet of triplets for the ^{31}P nuclei of coordinated PF_3 at δ = 119.2. Both the ^{31}P-^{31}P and ^{31}P-^{19}F coupling constants of 45.8 Hz and 1241 Hz, respectively, are of the same order of magnitude as for the hydrido complex **8**. The signals for the three vinyl protons of **9** appear in the ^1H NMR spectrum at δ = 8.51, 5.37 and 5.10 and are all shifted downfield relative to the related ruthenium carbonyl [RuCl(CH=CH_2)(CO)$(PCy_3)_2$].[13]

In analogy to the structurally related cationic vinylruthenium(II) derivative $[Ru(CH{=}CH_2)(CH_3CN)_2(PCy_3)_2]^+$, which reacts with HBF_4 in ether to generate the dicationic ruthenium carbene $[Ru(=CHCH_3)(CH_3CN)_2(PCy_3)_2](BF_4)_2$,[14] treatment of **9** with HBF_4 in CH_2Cl_2/OEt_2 gives the monocationic five-coordinate carbene compound **10** in moderate yield. The composition of **10** has been substantiated by elemental analysis and ^1H, ^{13}C, ^{19}F and ^{31}P NMR spectroscopy. Typical spectroscopic features of **10** are the signal for the RuCH proton at δ = 17.35 in the ^1H NMR spectrum and the multiplet for the carbene carbon atom at δ = 326.1 in the ^{13}C NMR spectrum. Similarly to **9**, the ^{31}P NMR spectrum of **10** exhibits two resonances at δ = 49.7 and 127.1, the splitting of which again corresponds to a doublet and a quadruplet of triplets. It should be noted that solutions of **10** (e.g., in dichloromethane or nitromethane) are stable only below −20 °C for a few hours; at room temperature decomposition occurs. While we failed to identify any Ru-containing decomposition products, the formation of the vinylphosphonium cation $[Cy_3PCH{=}CH_2]^+$ [with resonances for the vinyl protons at δ = 6.76 (dd), 6.35 (dd) and 6.15 (ddd) in the ^1H NMR spectrum] could be clearly confirmed.

In summary, the present work illustrates that with the dinuclear $\eta^3{:}\eta^3$-cyclooctadienediylruthenium(IV) compound **1** as the starting material and the unusual zwitterionic $\eta^3{:}\eta^3$-alkene(allyl)ruthenium(II) species **7** as an isolated intermediate five-coordinate hydrido-, vinyl- and carberuthenium complexes with PF_3 as a supporting ligand can be prepared. In contrast to the neutral ruthenium carbenes $[RuCl_2(=CHR)(PCy_3)_2]$,[3,15] the cation $[RuCl(=CHCH_3)(PF_3)(PCy_3)_2]^+$ is catalytically inactive in the ring-opening metathesis polymerization of cyclooctene, probably due to the ease of decomposition to give $[Cy_3PCH{=}CH_2]^+$. In this respect, the properties of the PF_3 derivative **10** are similar to those of the cationic carbene(carbonyl)ruthenium(II) complexes $[RuCl(=CHCH_2R)(CO)(P\mathit{i}Pr_3)_2]BF_4$ and $[RuCl(=CHCH_2R)(CO)(PCy_3)_2]BF_4$, the preparation and reactivity of which will be described in a forthcoming publication.

Experimental Section

All operations were carried out under argon using standard Schlenk techniques. The starting materials **1**[6b] and **6**[9a] were prepared as described in the literature. NMR spectra were recorded at room temperature on Bruker AC 200 and AMX 400 instruments, unless otherwise stated. Abbreviations used: s, singlet; d, doublet; t, triplet; q, quadruplet; m, multiplet; vt, virtual triplet; br, broadened signal; $N = {}^2J(PC) + {}^4J(PC)$. For assignment of protons and carbon atoms for the π-bonded ligands in compounds **3**−**5** and **7** see Figure 2. Melting and decomposition points were measured by differential thermal analysis (DTA).

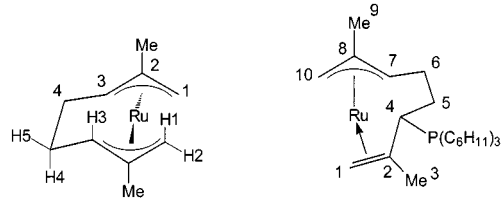

Figure 2. Assignment of proton and carbon atoms for the ligands in compounds **3**−**6** and **7**

Preparation of [RuHCl(H_2)(PCy_3)$_2$] (2) from 1: A suspension of **1** (510 mg, 0.827 mmol) in 2-propanol (40 mL) was treated with PCy_3 (1.86 g, 6.62 mmol) at room temperature. The Schlenk tube was evacuated and the argon atmosphere replaced by H_2. The suspension was warmed to ca. 50 °C and, after stirring for 40 min, an orange solid precipitated. This solid was separated from the mother liquor, washed twice with 20 mL portions of 2-propanol and dried. It was identified by comparing the ^{1}H and ^{31}P NMR spectra with those of an authentic sample;[5] yield 1.07 g (92%).

Preparation of [$RuCl_2$(η^3:η^3-$C_{10}H_{16}$)(PCy_3)] (3): A solution of PCy_3 (95 mg, 0.34 mmol) in CH_2Cl_2 (6 mL) was treated at −20 °C with **1** (104 mg, 0.17 mmol), leading to a change of color from violet to brown-yellow. After stirring the reaction mixture for 5 min, the solvent was evaporated in vacuo. The oily residue was treated with pentane (3 mL) and the suspension irradiated for 1 min in an ultrasound bath. A yellow solid precipitated which was separated from the mother liquor, washed twice with pentane (10 mL) and dried; yield 170 mg (85%); m.p. 46 °C (decomp). ^{1}H NMR (200 MHz, CD_2Cl_2): δ = 5.14 (m, 2 H, H3), 4.69 (d, $^3J_{P,H}$ = 7.6 Hz, 2 H, H1 or H2), 3.55 (d, $^3J_{P,H}$ = 3.2 Hz, 2 H, H2 or H1), 3.32 (m, 2 H, H4 or H5), 2.64−2.45 (m, 8 H, H5 or H4 and C_6H_{11}), 2.16 (s, 6 H, Me), 2.20−2.00, 1.83−1.67, 1.40−1.24 (all m, 27 H, C_6H_{11}). ^{31}P NMR (81.0 MHz, CD_2Cl_2): δ = 5.0 (s). $C_{28}H_{49}Cl_2PRu$ (588.7): calcd. C 57.13, H 8.39; found C 56.89, H 8.28.

Preparation of [$RuCl_2$(η^3:η^3-$C_{10}H_{16}$)(P*i*Pr_3)] (4): A solution of **1** (101 mg, 0.16 mmol) in CH_2Cl_2 (5 mL) was treated with P*i*Pr_3 (68 μL, 0.51 mmol) at room temperature, leading to a change of color from violet to red-brown. After stirring the reaction mixture for 30 min, the solvent was evaporated in vacuo. The oily residue was treated with pentane (5 mL) which after ca. 10 min led to the formation of a brownish solid. The solid was separated from the mother liquor, washed twice with 10 mL portions of pentane and dried; yield 137 mg (89%); m.p. 51 °C (decomp). ^{1}H NMR (400 MHz, CD_2Cl_2): δ = 5.12 (m, 2 H, H3), 4.81 (d, $^3J_{P,H}$ = 7.6 Hz, 2 H, H1 or H2), 3.52 (d, $^3J_{P,H}$ = 3.2 Hz, 2 H, H2 or H1), 3.33 (m, 2 H, H4 or H5), 2.82 (m, 3 H, PC*H*CH_3) 2.55 (m, 2 H, H5 or H4), 2.17 (s, 6 H, Me), 1.46 (dd, $^3J_{P,H}$ = 12.0, $^3J_{H,H}$ = 7.1 Hz, 9 H, PCHC*H*$_3$), 1.39 (dd, $^3J_{P,H}$ = 12.8, $^3J_{H,H}$ = 7.1 Hz, 9 H, PCHC*H*$_3$). ^{13}C NMR (100.6 MHz, CD_2Cl_2): δ = 124.9 (s, C2), 108.6 (d, $^2J_{P,C}$ = 9.1 Hz, C3), 62.6 (d, $^2J_{P,C}$ = 5.8 Hz, C1), 36.2 (s, C4), 28.8 (d, $^1J_{P,C}$ = 15.8 Hz, P*C*HCH$_3$), 20.7 (s, Me), 20.1 (d, $^2J_{P,C}$ = 3.0 Hz, PCH*C*H$_3$), 17.8 (br. s, PCH*C*H$_3$). ^{31}P NMR (162.0 MHz, CD_2Cl_2): δ = 17.7 (s). $C_{19}H_{37}Cl_2PRu$ (468.5): calcd. C 48.72, H 7.96; found C 48.23, H 7.59.

Preparation of [$RuCl_2$(η^3:η^3-$C_{10}H_{16}$)(P*i*Pr_2Ph)] (5): This compound was prepared as described for **4**, using **1** (523 mg, 0.85 mmol) and P*i*Pr_2Ph (306 mg, 1.80 mmol) as starting materials. Yellow solid; yield 781 mg (91%); m.p. 42 °C (decomp). ^{1}H NMR(400 MHz, CD_2Cl_2): δ = 8.05 (m, 2 H, Ph), 7.41 (m, 3 H, Ph), 5.14 (m, 2 H, H3), 4.45 (d, $^3J_{P,H}$ = 8.8 Hz, 2 H, H1 or H2), 3.46 (d, $^3J_{P,H}$ = 3.2 Hz, 2 H, H2 or H1), 3.32 (m, 2 H, H4 or H5), 3.08 (m, 3 H, PC*H*CH_3) 2.57 (m, 2 H, H5 or H4), 2.16 (s, 6 H, Me), 1.40 (dd, $^3J_{P,H}$ = 14.4, $^3J_{H,H}$ = 7.2 Hz, 3 H, PCHC*H*$_3$), 1.32 (dd, $^3J_{P,H}$ = 13.2, $^3J_{H,H}$ = 7.2 Hz, 3 H, PCHC*H*$_3$), 1.22 (dd, $^3J_{P,H}$ = 14.0, $^3J_{H,H}$ = 7.0 Hz, 3 H, PCHC*H*$_3$), 1.17 (dd, $^3J_{P,H}$ = 13.8, $^3J_{H,H}$ = 7.0 Hz, 3 H, PCHC*H*$_3$). ^{13}C NMR (100.6 MHz, CD_2Cl_2): δ = 134.2 (d, $J_{P,C}$ = 6 Hz, Ph), 132.9 (d, $J_{P,C}$ = 29.2 Hz, Ph), 129.6 (d, $J_{P,C}$ = 2 Hz, Ph), 127.8 (d, $J_{P,C}$ = 8 Hz, Ph), 126.0 (s, C2), 108.6 (d, $^2J_{P,C}$ = 9 Hz, C3), 63.8 (d, $^2J_{P,C}$ = 6 Hz, C1), 36.6 (s, C4), 27.6, 27.2 (both d, $^1J_{P,C}$ = 19.5 and 19.9 Hz, P*C*HCH$_3$), 21.0 (s, Me), 19.2, 18.5 (both s, PCH*C*H$_3$), 19.1, 18.5 [both d, $^2J_{P,C}$ = 2.6 and 2.7 Hz, PCH*C*H$_3$]. ^{31}P NMR (162.0 MHz, CD_2Cl_2): δ = 16.9 (s). $C_{22}H_{35}Cl_2PRu$ (502.5): calcd. C 52.59, H 7.02; found C 53.14, H 6.91.

Preparation of [$RuCl_2${η^2:η^3-CH_2=C(Me)CH(PCy_3)$(CH_2)_2$CHC(Me)CH_2}(PF_3)] (7): A solution of **6** (112 mg, 0.34 mmol) in toluene (5 mL) was treated dropwise with a solution of PCy_3 (106 mg, 0.38 mmol) in toluene (5 mL) at room temperature. A slow precipitation of an orange oil was observed. After stirring the reaction mixture vigorously for 10 min, the oil was partly converted into a yellow solid, the precipitation of which was facilitated by addition of pentane (5 mL) and by cooling the Schlenk tube to −78 °C. The solid was filtered, washed twice with 5 mL portions of pentane (−20 °C) and dried; yield 172 mg (83%); m.p. 62 °C (decomp). ^{1}H NMR (200 MHz, CD_2Cl_2, −50 °C): δ = 4.22−4.11 (m, 2 H, L), 3.54−3.50 (m, 1 H, L), 3.48−3.24 (m, 2 H, L), 2.95 (s, 1 H, L), 2.94−2.72 (m, 1 H, L), 2.60−2.39 (m, 6 H, C_6H_{11}), 2.19, 1.97−1.60, 1.46−1.30 (all m, 36 H, C_6H_{11} and Me of L); L is the abbreviation for the η^2:η^3-alkene(allyl) ligand. ^{13}C NMR (100.6 MHz, CD_2Cl_2, −50 °C): δ = 120.6 (s, C8), 73.2 (s, C2), 72.8 (dq, $^2J_{P,C}$ = 43.0, $^3J_{F,C}$ ca. 3 Hz, C7), 59.8 (d, $J_{P,C}$ = 4.7 Hz, C1 or C10), 55.5 (s, C10 or C1), 38.2 (d, $J_{P,C}$ = 21.0 Hz, C4), 31.5 (d, $^1J_{P,C}$ = 34.3 Hz, C_6H_{11}), 31.1, 24.5 (both d, $J_{P,C}$ = 9.6 and 11.5 Hz, C5 and C6), 28.5, 21.5 (both s, C3 and C9), 27.1 (br. s, C_6H_{11}), 26.7, 26.5 (both d, $J_{P,C}$ = 11.4 and 11.5 Hz, C_6H_{11}), 25.0 (s, C_6H_{11}). ^{19}F NMR (376.4 MHz, CD_2Cl_2): δ = −17.3 (d, $^1J_{P,F}$ = 1362 Hz, PF_3). ^{31}P NMR (162.0 MHz, CD_2Cl_2): δ = 137.3 (qd, $^1J_{P,F}$ = 1362 Hz, $J_{P,P}$ = 19.3 Hz, PF_3), 32.5 (d, $J_{P,P}$ = 19.3 Hz, PCy_3). $C_{28}H_{49}Cl_2F_3P_2Ru$ (676.6): calcd. C 49.70, H 7.30; found C 50.10, H 7.20.

Preparation of [RuHCl(PF_3)(PCy_3)$_2$] (8): A solution of **7** (125 mg, 0.19 mmol) in CH_2Cl_2 (4 mL) was treated with PCy_3 (312 mg, 1.11 mmol) and stirred for 2 h under an H_2 atmosphere (1 bar). A change of color from yellow to red occurred. After evaporation of the solvent in vacuo, the residue was suspended in acetone (4 mL) and the mixture stirred for 30 min. An orange-yellow solid precipitated, which was separated from the mother liquor, washed with acetone (4 mL) and dried in vacuo; yield 98 mg (63%); m.p. 40 °C (decomp). ^{1}H NMR (200 MHz, CD_2Cl_2): δ = 2.63−1.21 (m, 66 H, C_6H_{11}), −24.68 (dtq, $^2J_{P^2,H}$ = 57.8, $^2J_{P^1,H}$ = 16.9, $^3J_{F,H}$ = 4.4 Hz, 1 H, RuH); P^1 and P^2 assigned to the phosphorus atoms of PCy_3 and PF_3, respectively. ^{19}F NMR (188.3 MHz, CD_2Cl_2): δ = −98.1 (d, $^1J_{P,F}$ = 1225 Hz). ^{31}P NMR (81.0 MHz, CD_2Cl_2): δ = 128.7 (qm, $^1J_{F,P}$ = 1225 Hz, PF_3), 46.8 (d, $^2J_{P,P}$ = 45.8 Hz, PCy_3). $C_{36}H_{67}ClF_3P_3Ru$ (786.4): calcd. C 54.99, H 8.59; found C 54.99, H 8.73.

Preparation of [RuCl(CH=CH_2)(PF_3)(PCy_3)$_2$] (9): A slow stream of acetylene was passed for 10 s through a solution of **8** (88 mg, 0.11 mmol) in hexane (15 mL) at room temperature. A change of color from yellow to bright red occurred. The solvent was then evaporated in vacuo, and the remaining red solid washed with pentane (3 mL) and dried; yield 90 mg (99%); m.p. 88 °C (decomp). ^{1}H NMR (200 MHz, C_6D_6): δ = 8.51 (m, 1 H, C*H*=CH_2), 5.37 (m, 1 H, *cis*-H of CH=CH_2), 5.10 (dm, $^3J_{H,H}$ = 13.6 Hz, 1 H, *trans*-H of CH=CH_2), 2.85−1.11 (m, 66 H, C_6H_{11}). ^{13}C NMR (100.6 MHz, C_6D_6): δ = 153.9 (br. s, RuCH), 121.8 (br. s, =CH_2), 36.2 (vt, N = 17.4 Hz, C1 of C_6H_{11}), 30.8, 30.6 (both s, C3,5 of C_6H_{11}), 28.3, 28.1 (both s, C2,6 of C_6H_{11}), 27.0 (s, C4 of C_6H_{11}). ^{19}F NMR (188.3 MHz, C_6D_6): δ = −6.0 (d, $^1J_{P,F}$ = 1241 Hz). ^{31}P NMR (81.0 MHz, C_6D_6): δ = 119.2 (qt, $^1J_{F,P}$ = 1241, $^2J_{P,P}$ = 45.8 Hz, PF_3), 24.3 (d, $^2J_{P,P}$ = 45.8 Hz, PCy_3). $C_{38}H_{69}ClF_3P_3Ru$ (812.4): calcd. C 56.18, H 8.56; found C 56.59, H 8.06.

Preparation of $[RuCl(=CHCH_3)(PF_3)(PCy_3)_2]BF_4$ (10): A solution of **9** (80 mg, 0.10 mmol) in CH_2Cl_2 (2 mL) was treated with a 1.6 M solution of HBF_4 in ether (0.2 mL, 0.32 mmol) at room temperature. A change of color from red to yellow occurred. The solvent was evaporated in vacuo, the remaining yellow solid was washed twice with 3 mL portions of ether and dried; yield 45 mg (50%); m.p. 108 °C (decomp). ^{1}H NMR (200 MHz, CD_2Cl_2): δ = 17.35 (br. s, 1 H, Ru=CH), 2.95 (s, 3 H, CH_3), 2.70−1.13 (m, 66 H, C_6H_{11}). ^{13}C NMR (50.3 MHz, CD_2Cl_2, −20 °C): δ = 326.1 (m, Ru=CH), 51.0 (s, CH_3), 35.1 (br. m, C1 of C_6H_{11}). 29.5 (s, C3,5 of C_6H_{11}), 27.2 (m, C2,6 of C_6H_{11}), 25.5 (s, C4 of C_6H_{11}). ^{19}F NMR (188.3 MHz, CD_2Cl_2): δ = −11.6 (d, $^1J_{P,F}$ = 1282 Hz, PF_3), −153.5 (br. s, BF_4). ^{31}P NMR (81.0 MHz, CD_2Cl_2): δ = 127.1 (qt, $^1J_{F,P}$ = 1282, $^2J_{P,P}$ = 35.6 Hz, PF_3), 49.7 (d, $^2J_{P,P}$ = 35.6 Hz, PCy_3). $C_{38}H_{70}BClF_7P_3Ru$ (900.2): calcd. C 50.70, H 7.84; found C 50.25, H 7.31.

Determination of the X-ray Crystal Structure of 7: Single crystals were grown by cooling a saturated solution of **7** in acetone from 25 °C to −20 °C. Crystal data (from 5000 reflections, 2.49° < Θ < 28.23°): triclinic; space group $P\bar{1}$ (No. 2); a = 9.878(7), b = 13.93(1), c = 14.17(1) Å, α = 87.35(9)°, β = 84.80(9)°, γ = 74.22(9)°; V = 1868(2) Å^3, Z = 2; $d_{calcd.}$ = 1.410 g cm^{-3}; μ(Mo-K_α) = 0.686 mm^{-1}; crystal size 0.14 × 0.11 × 0.08 mm; IPDS (STOE), Mo-K_α radiation (0.71073 Å), graphite monochromator; T = 173(2) K; Θ-scan, max. 2Θ = 56.46°; 29465 reflections measured, 8456 independent ($R_{int.}$ = 0.0535), 6042 with $I > 2\sigma(I)$. Intensity data were corrected for Lorentz and polarization effects and an empirical absorption correction was applied. The structure was solved by direct methods (SHELX-97).[16] Atomic coordinates and anisotropic thermal parameters of the non-hydrogen atoms were refined by full-matrix least-squares methods using SHELXL-97.[17] The asymmetric unit of **7** includes two molecules of acetone which were refined anisotropically with restraints. The hydrogen atoms H1a, H1b, H6a, H6b, H7, H10a and H10b were found in a difference-Fourier synthesis and refined with fixed temperature factors $U_{eq.}$ The positions of all other hydrogen atoms were calculated according to an ideal geometry and refined by the riding method. Conventional R = 0.0455 [for 6042 reflections with $I > 2\sigma(I)$], and weighted wR_2 = 0.1234 for all 8456 located reflections; reflection/parameter ratio 19.90; residual electron density +0.806/−1.074 eÅ^{-3}.

CCDC-175166 contains the supplementary crystallographic data for this paper. These data can be obtained free of charge at www.ccdc.cam.ac.uk/conts/retrieving.html [or from the Cambridge Crystallographic Data Centre, 12, Union Road, Cambridge CB2 1EZ, UK; Fax: (internat.) +44-1223/336-033; E-mail: deposit@ccdc.cam.ac.uk].

Acknowledgments

This work was supported by the Deutsche Forschungsgemeinschaft (SFB 347), BASF AG, and the Fonds der Chemischen Industrie. We are grateful to the latter in particular for a Ph.D. grant (to W. S.). Moreover, we thank Mrs. R. Schedl and Mr. C. P. Kneis (DTA and elemental analysis), Mrs. M.-L. Schäfer and Dr. W. Buchner (NMR spectra), and Mr. S. Stellwag for valuable experimental assistance.

[1] [1a] C. Grünwald, O. Gevert, J. Wolf, P. González-Herrero, H. Werner, *Organometallics* **1996**, *15*, 1960−1962. [1b] J. Wolf, W. Stüer, C. Grünwald, O. Gevert, M. Laubender, H. Werner, *Eur. J. Inorg. Chem.* **1998**, 1827−1834.
[2] W. Stüer, Dissertation, Universität Würzburg, **1999**.
[3] Recent reviews on olefin metathesis with Ru-based catalysts: [3a] T. M. Trnka, R. H. Grubbs, *Acc. Chem. Res.* **2001**, *34*, 18−29. [3b] A. Fürstner, *Angew. Chem.* **2000**, *112*, 3140−3172; *Angew. Chem. Int. Ed.* **2000**, *39*, 3012−3043. [3c] R. H. Grubbs, S. Chang, *Tetrahedron* **1998**, *54*, 4413−4450.
[4] J. Wolf, W. Stüer, C. Grünwald, H. Werner, P. Schwab, M. Schulz, *Angew. Chem.* **1998**, *110*, 1165−1167; *Angew. Chem. Int. Ed.* **1998**, *37*, 1124−1126.
[5] Compound **2** was originally prepared from $[RuH_2(H_2)_2(PCy_3)_2]$ and CH_2Cl_2: M. L. Christ, S. Sabo-Etienne, B. Chaudret, *Organometallics* **1994**, *13*, 3800−3804. For the preparation of $[RuH_2(H_2)_2(PCy_3)_2]$ from $[Ru(\eta^3\text{-}2\text{-}MeC_3H_4)_2](\eta^4\text{-}C_8H_{12})]$ see: S. Busch, W. Leitner, *Chem. Commun.* **1999**, 2305−2306.
[6] [6a] L. Porri, R. Rossi, P. Deversi, G. Allegra, *Tetrahedron Lett.* **1965**, 4187−4189. An improved preparative procedure for **1** has been reported: [6b] D. N. Cox, R. Roulet, *Inorg. Chem.* **1990**, *29*, 1360−1365.
[7] [7a] L. Porri, R. Rossi, P. Deversi, A. Lucherini, *Makromol. Chem.* **1974**, *175*, 3097−3115. [7b] L. Porri, P. Deversi, A. Lucherini, R. Rossi, *Makromol. Chem.* **1975**, *176*, 3121−3125.
[8] W. A. Herrmann, W. C. Schattenmann, O. Nuyken, S. C. Glander, *Angew. Chem.* **1996**, *108*, 1169−1170; *Angew. Chem. Int. Ed. Engl.* **1996**, *35*, 1087−1088.
[9] [9a] R. A. Head, J. F. Nixon, J. R. Swain, C. M. Woodard, *J. Organomet. Chem.* **1974**, *76*, 393−400. [9b] P. B. Hitchcock, J. F. Nixon, J. Sinclair, *J. Organomet. Chem.* **1975**, *86*, C34−C36.
[10] [10a] D. N. Cox, R. Roulet, *J. Chem. Soc., Chem. Commun.* **1988**, 951−953. [10b] D. N. Cox, R. W. H. Small, R. Roulet, *J. Chem. Soc., Dalton Trans.* **1991**, 2013−2018. [10c] S. Wache, W. H. Herrmann, G. Artus, O. Nuyken, D. Wolf, *J. Organomet. Chem.* **1995**, *491*, 181−188.
[11] [11a] M. A. Bennett, T. W. Matheson, G. B. Robertson, A. K. Smith, P. A. Tucker, *Inorg. Chem.* **1981**, *20*, 2363−2365. [11b] U. Koelle, B.-S. Kang, T. P. Spaniol, U. Englert, *Organometallics* **1992**, *11*, 249−254. [11c] S. Hüffer, M. Wieser, K. Polborn, K. Sünkel, W. Beck, *Chem. Ber.* **1994**, *127*, 1369−1377. [11d] M. A. Bennett, A. C. Willis, L. Y. Goh, W. Chen, *Polyhedron* **1996**, *15*, 3559−3567.
[12] Preparation: [12a] J. K. Nicholson, B. L. Shaw, *J. Chem. Soc. (A)* **1966**, 807−808. Structure analysis: [12b] J. E. Lydon, M. R. Truter, *J. Chem. Soc. (A)* **1968**, 362−375.
[13] S. Jung, Dissertation, Universität Würzburg, **2001**.
[14] S. Jung, K. Ilg, J. Wolf, H. Werner, *Organometallics* **2001**, *20*, 2121−2123.
[15] [15a] P. Schwab, M. B. France, J. W. Ziller, R. H. Grubbs, *Angew. Chem.* **1995**, *107*, 2179−2181; *Angew. Chem. Int. Ed. Engl.* **1995**, *34*, 2039−2041. [15b] P. Schwab, R. H. Grubbs, J. W. Ziller, *J. Am. Chem. Soc.* **1996**, *118*, 100−110.
[16] G. M. Sheldrick, *Acta Crystallogr., Sect. A* **1990**, *46*, 467−473.
[17] G. M. Sheldrick, *SHELXL-97*, University of Göttingen, Göttingen, Germany, **1997**.

Received November 30, 3001
[I01492]

Anderson-Type Heteropolymolybdates Containing Tris(alkoxo) Ligands: Synthesis and Structural Characterization

Bernold Hasenknopf,[a] Renaud Delmont,[a] Patrick Herson,[a] and Pierre Gouzerh*[a]

Keywords: Coordination modes / Molybdenum / Polyoxometalates / Tridentate ligands

Anderson-type molybdopolyanions containing tris(alkoxo) ligands $[MMo_6O_{18}\{(OCH_2)_3CR\}_2]^{3-}$ (M = Mn^{III}, Fe^{III}) and $[H_2MMo_6O_{18}\{(OCH_2)_3CR\}_2]^{2-}$ (M = Ni^{II}, Zn^{II}), (R = CH_3, NO_2, CH_2OH), were prepared by treatment of $[N(C_4H_9)_4]_4[\alpha\text{-}Mo_8O_{26}]$ with tris(hydroxymethyl)methane derivatives in the presence of manganese(III) acetylacetonate, iron(III) acetylacetonate, nickel(II) acetate, or zinc(II) acetate. The complexes were structurally characterized in solution, and also by single-crystal X-ray diffraction in the cases of $[N(C_4H_9)_4]_3[MnMo_6O_{18}\{(OCH_2)_3CNO_2\}_2]$, $[N(C_4H_9)_4]_2[H_2NiMo_6O_{18}\{(OCH_2)_3CCH_2OH\}_2]$, and $[N(C_4H_9)_4]_2[H_2ZnMo_6O_{18}\{(OCH_2)_3CCH_3\}_2]$. Two tris(alkoxo) ligands replace the six hydroxo groups usually found in Anderson polyanions of formula $[H_6MMo_6O_{24}]^{n-}$. The complex structures may be divided into two groups: In the first one the tris(alkoxo) ligands are bound entirely to the central heteroatom, while in the second one they cap a tetrahedral cavity.

(© Wiley-VCH Verlag GmbH, 69451 Weinheim, Germany, 2002)

Introduction

Heteropolymolybdates of the general formula $[H_x(MO_6)Mo_6O_{18}]^{n-}$ ($x = 0-6$, $n = 2-6$) occur with metallic or nonmetallic heteroatoms M.[1,2] Two isomers, α and β, are known; both consist of edge-sharing octahedra.[3,4] The β isomer corresponds to a nonplanar, bent arrangement, as in the structures of $[Mo_7O_{24}]^{6-}$ [5] and $[W_7O_{24}]^{6-}$.[6,7] In the more common α isomer, the so-called Anderson structure, six molybdenum atoms form a planar hexagon around the central heteroatom. Two types of the Anderson structure may be distinguished: the nonprotonated A type, with heteroatoms in high oxidation states, and the hexaprotonated B type, with heteroatoms in low oxidation states.[8] The six nonacidic protons are usually located on the six oxygen atoms bound to the central heteroatom,[9] although a different protonation pattern has been reported in one case.[4]

Several B-type Anderson structures in which the six protons have formally been replaced by two $(As_3O_3)^{3+}$ groups have been reported.[10,11] Analogously, it should be possible to incorporate alkoxo groups in place of the hydroxo groups of the B-type structure, thus formally replacing protons by carbon atoms. The synthesis of Anderson polyanions in alcoholic solvents (methanol or ethanol) has been reported,[12] but no incorporation of the alcohol was found. We therefore decided to investigate the reaction in the presence of tris(hydroxymethyl)methane derivatives $RC(CH_2OH)_3$, because the three alkoxo groups should ideally replace all three hydroxo groups on each side of the Anderson structure. This capping effect should enhance the stability of the complex formed. The residue R could further serve for the introduction of a variety of functionalities.

Results and Discussion

Synthesis

On the basis of our own experience and that of others[12] in polyoxometalate synthesis in organic solvents, and also our previous preparation of $[H_2Mo_8O_{24}\{R(CH_2O)_3\}_2]^{4-}$,[13] we decided to use the same $[\alpha\text{-}Mo_8O_{26}]^{4-}$ precursor and to operate in acetonitrile. The heteroatom should be introduced with a labile ligand, and we chose the acetylacetonate (acac) or acetate (OAc) complexes of Mn^{III}, Fe^{III}, Ni^{II}, and Zn^{II}. Thus, we treated 1 equiv. of $[N(C_4H_9)_4]_4[\alpha\text{-}Mo_8O_{26}]$ with 1.5 equiv. of $M(acac)_3$ (M = Mn^{III}, Fe^{III}) or $M(OAc)_2$ (M = Zn^{II}, Ni^{II}) and 3 equiv. of tris(hydroxymethyl)methane derivatives $RC(CH_2OH)_3$ (R = CH_3, NO_2, CH_2OH) in refluxing acetonitrile. The complexes formed (Table 1) were isolated from the solution as their tetrabutylammonium salts by slow ether vapor diffusion and recrystallization from DMF/ether. While Anderson-type polyoxomolybdates with Mn^{II}, Fe^{III}, Ni^{II}, and Zn^{II} have been reported in the literature,[1,2,12,14,15] compounds **1** appear to be the first with Mn in oxidation state +III.

Crystal Structures

Compounds **1b**, **3c**, and **4a** were characterized by single-crystal X-ray diffraction; crystal structure data are summar-

[a] Laboratoire de Chimie Inorganique et Matériaux Moléculaires, UMR 7071, Université Pierre et Marie Curie,
Case Courrier 42, 4 place Jussieu, 75252 Paris cedex 05, France
E-mail: pg@ccr.jussieu.fr

Table 1. Compounds prepared

	a, R = CH_3	**b**, R = NO_2	**c**, R = CH_2OH
1, M = Mn^{III}	$[MnMo_6O_{18}\{(OCH_2)_3CCH_3\}_2]^{3-}$	$[MnMo_6O_{18}\{(OCH_2)_3CNO_2\}_2]^{3-}$	$[MnMo_6O_{18}\{(OCH_2)_3CCH_2OH\}_2]^{3-}$
2, M = Fe^{III}	$[FeMo_6O_{18}\{(OCH_2)_3CCH_3\}_2]^{3-}$	$[FeMo_6O_{18}\{(OCH_2)_3CNO_2\}_2]^{3-}$	$[FeMo_6O_{18}\{(OCH_2)_3CCH_2OH\}_2]^{3-}$
3, M = Ni^{II}	$[H_2NiMo_6O_{18}\{(OCH_2)_3CCH_3\}_2]^{2-}$	$[H_2NiMo_6O_{18}\{(OCH_2)_3CNO_2\}_2]^{2-}$	$[H_2NiMo_6O_{18}\{(OCH_2)_3CCH_2OH\}_2]^{2-}$
4, M = Zn^{II}	$[H_2ZnMo_6O_{18}\{(OCH_2)_3CCH_3\}_2]^{2-}$	$[ZnMo_6O_{18}\{(OCH_2)_3CNO_2\}_2]^{4-}$	$[H_2ZnMo_6O_{18}\{(OCH_2)_3CCH_2OH\}_2]^{2-}$

ized in Table 4. The molecular structures of these compounds belong to two groups, described below.

The structure of $[N(C_4H_9)_4]_3[MnMo_6O_{18}\{(OCH_2)_3CNO_2\}_2]\cdot 2DMF$ (**1b**·2DMF) is representative of the first group. It consists of three tetrabutylammonium cations, an $[MnMo_6O_{18}\{(OCH_2)_3CNO_2\}_2]^{3-}$ anion, and solvent molecules of crystallization. Two views of the anion are presented in Figure 1. The geometry of the polyanion is based on the common Anderson structure, with six MoO_6 octahedral edge-sharing units forming a hexagon around the central MnO_6 octahedron. All metal atoms essentially lie in a common plane, with a maximum deviation of 0.002 Å from the best least-squares plane. Selected bond lengths and angles are compiled in Table 2.

The six triply bridging oxygen atoms surrounding the Mn^{III} center belong to two $RC(CH_2O)_3$ residues. Thus, the organic alkoxide groups effectively replace the six hydroxide groups in B-type Anderson structures. They can be regarded as capping both sides of the planar metal arrangement. The coordination geometry of the central Mn^{III} ion is regular, with a mean Mn−O distance of 1.98(1) Å, and O−Mn−O bond angles of between 86° and 93°. The small distortions observed correspond to a slight compression of the octahedron, bringing the two faces capped by the organic ligands closer together. This distortion might arise from the expected Jahn−Teller effect for Mn^{III}. A similar small Jahn−Teller distortion, resulting in that case in the elongation of the central octahedron, has also been observed in the compound $[H_6CuMo_6O_{24}]^{4-}$.[16,17] The lack of flexibility of the Anderson polyoxometalate apparently prevents larger distortions. Thus, both chemical and crystallographic analysis are consistent with the presence of a Mn^{III} center. Preliminary EPR measurements are also in agreement with this conclusion. This series of compounds therefore represents the first Anderson molybdates with manganese in oxidation state +III. Only the analogous Mn^{II} molybdates have been reported previously.[14,15,18]

The MoO_6 octahedra are distorted, with Mo−O distances that fall into three ranges depending on the type of oxygen atoms bound. The longest distance is that towards the triply bridging alkoxide ligands (average 2.37 Å). The doubly bridging and the terminal oxygen atoms are at distances from the molybdenum atoms of 1.94 Å and 1.71 Å, respectively.

A single-crystal X-ray diffraction study of compound **1a** did not provide enough reflections to refine the structure satisfactorily. However, it was established without any doubt that the overall structure of the polyanion is identical

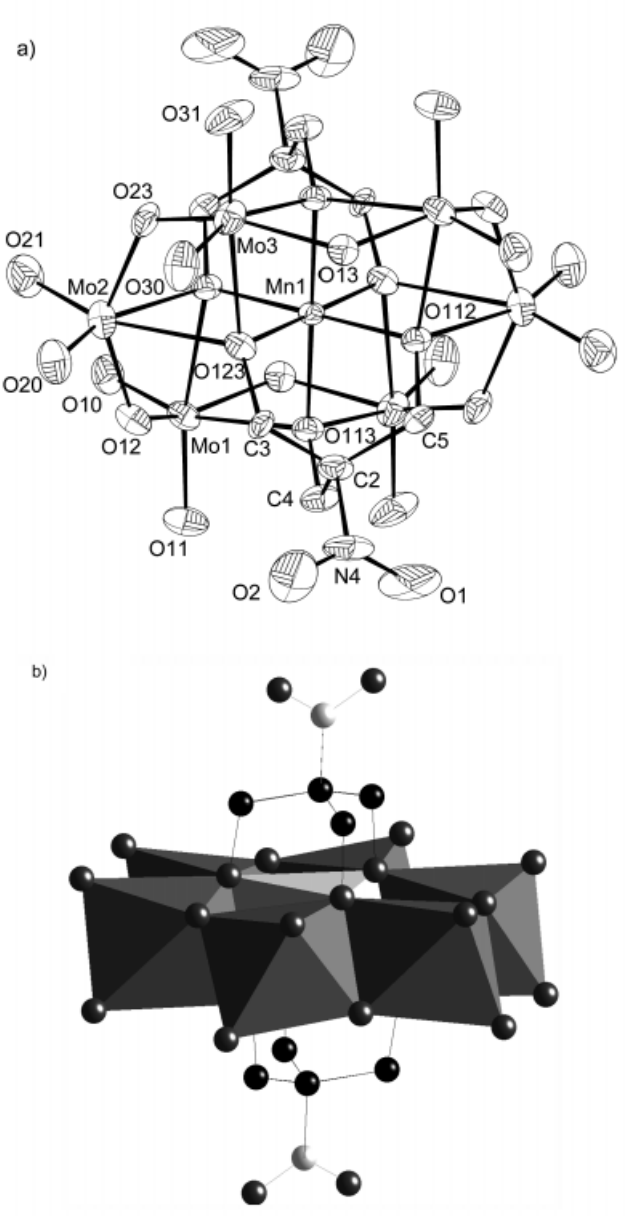

Figure 1. Structure and atom numbering of $[MnMo_6O_{18}\{(OCH_2)_3CNO_2\}_2]^{3-}$ (anion of **1b**); (a) thermal ellipsoids, (b) polyhedral representation

to that of **1b**; that is, the $CH_3C(CH_2O)_3$ residues cap the central Mn^{III} ion in the Anderson structure.

The structures of compounds **3c** and **4a** are representative of the second group. They both consist of a heteropolymolybdate − $[H_2MMo_6O_{18}\{(OCH_2)_3CR\}_2]^{2-}$ − that dif-

Table 2. Selected distances [Å] and angles [°] in **1b**, **3c**, and **4a**

1b		**3c**		**4a**	
Mn(1)−O(112)	2.024(7)	Ni(1)−O(112)	2.025(2)	Zn(1)−O(112)	2.030(3)
Mn(1)−O(113)	2.001(7)	Ni(1)−O(113)	2.085(2)	Zn(1)−O(113)	2.133(3)
Mn(1)−O(123)	1.940(7)	Ni(1)−O(123)	2.010(2)	Zn(1)−O(123)	2.041(3)
O(112)−Mn(1)−O(113)	92.1(3)	O(112)−Ni(1)−O(113)	98.5(1)	O(112)−Zn(1)−O(113)	98.7(1)
O(112)′ Mn(1)−O(113)	87.9(3)	O(112)−Ni(1)−O(113)′	81.5(1)	O(112)′ Zn(1)−O(113)	81.3(1)
O(112)−Mn(1)−O(123)	91.7(3)	O(112)−Ni(1)−O(123)	94.7(1)	O(112)−Zn(1)−O(123)	85.9(1)
O(112)′ Mn(1)−O(123)	88.3(3)	O(112)−Ni(1)−O(123)′	85.3(1)	O(112)′ Zn(1)−O(123)	94.1(1)
O(113)−Mn(1)−O(123)	91.8(3)	O(113)−Ni(1)−O(123)	98.2(1)	O(113)−Zn(1)−O(123)	81.8(1)
O(113)′ Mn(1)−O(123)	88.2(3)	O(113)−Ni(1)−O(123)′	81.8(1)	O(113)′ Zn(1)−O(123)	98.2(1)

fers remarkably from **1a** and **1b**. Yet again, the polyanion is based on the Anderson structure, with the heteroatom in the central cavity formed by six MoO_6 units. However, the organic ligands do not cap two faces of the central octahedron, but two tetrahedral cavities as shown in Figures 2 and 3. This causes the loss of the threefold symmetry as displayed in compounds **1a** and **1b**. The bond lengths (Table 2) are similar to those found in **1b**.

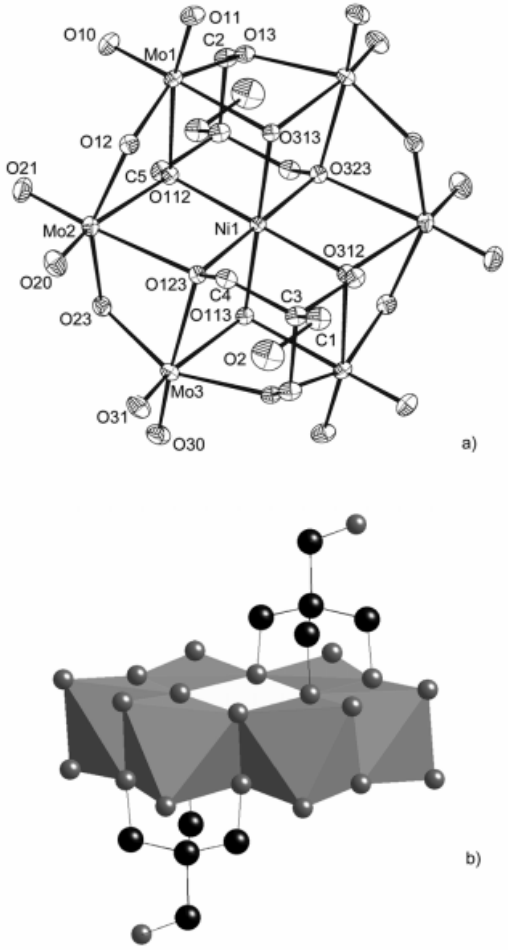

Figure 2. Structure and atom numbering of $[H_2NiMo_6O_{18}\{(OCH_2)_3CCH_2OH\}_2]^{2-}$ (anion of **3c**); (a) thermal ellipsoids, (b) polyhedral representation

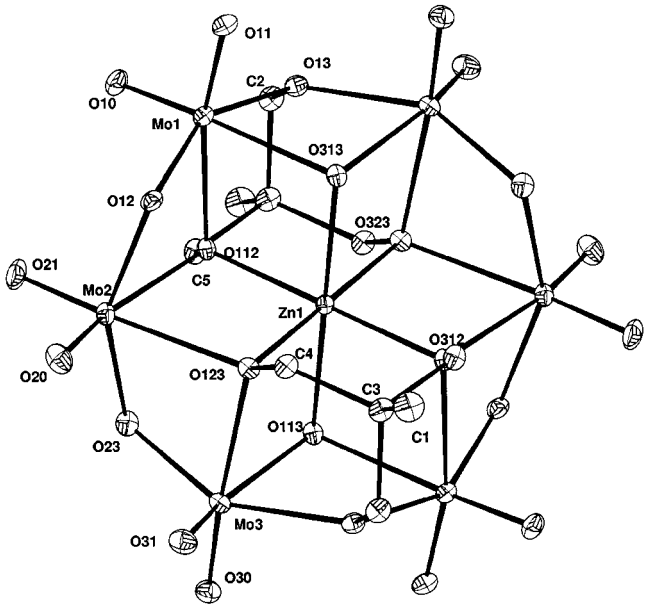

Figure 3. Structure and atom numbering of $[H_2ZnMo_6O_{18}\{(OCH_2)_3CCH_3\}_2]^{2-}$ (anion of **4a**), thermal ellipsoids

The crystals contain two $N(C_4H_9)_4$ cations per unit, thus indicating that the polyanions are doubly protonated. The quality of the X-ray diffraction data allowed the hydrogen atoms on the cations, anions, and the DMF molecules to be located. Furthermore, calculations of bond valence sums were performed in order to distinguish between O and OH ligands. It was clearly established that the remaining triply bridging oxygen atoms are protonated and form hydrogen bonds with the DMF oxygen atoms (distance 2.7 Å). The central metal is therefore coordinated to four μ_3-alkoxo and two μ_3-hydroxo ligands. The latter are at a slightly longer distance so that the coordination geometry of the central metal atom is an elongated octahedron.

It should be mentioned that the oxygen atoms bound to carbon atoms in **3c** and **4a** are protonated in the structure of $K_2[H_6\text{-}\alpha\text{-}PtMo_6O_{24}]\cdot 5H_2O$.[4] Thus, just as there are two different protonation patterns for B-type Anderson structures, there are two coordination modes for tris(hydroxymethyl)methane ligands. Below, we refer to the coordination mode in **1a** and **1b** as δ and in **3c** and **4a** as χ.

Table 3. Selected NMR-spectroscopic data

	1a R = CH_3	**1b** R = NO_2	**1c** R = CH_2OH	**4a** R = CH_3	**4b** R = NO_2	**4c** R = CH_2OH
^{1}H NMR CH_2O signals[a]	60.49	61.08	69.07	4.42 (d, 4 H), 4.51 (d, 4 H), 4.59 (s, 4 H)	4.93 (s, 12 H)	4.60 (d, 4 H), 4.65 (d, 4 H), 4.85 (s, 4 H)
^{13}C NMR CH_2O signals[a]				79.6, 89.4	77.6	76.8, 87.1
^{95}Mo NMR [b]				31.6 (2 Mo), 76.6 (4 Mo)	50.7 (6 Mo)	1.9 (2 Mo), 101.8 (4 Mo)

[a] Chemical shifts expressed in ppm relative to Me_4Si. [b] Chemical shifts expressed in ppm relative to aqueous alkaline Na_2MoO_4.

Spectroscopy

In order to assign the structures of the remaining compounds, and to determine their solution structures, we used NMR- and IR-spectroscopic methods.

The diamagnetic nature of compounds **4a**, **4b**, and **4c** allowed them to be investigated by multinuclear NMR. Selected NMR shifts are collected in Table 3; the complete description can be found in the Exp. Sect.

In order to interpret these results, one should discuss the expected pattern based on symmetry considerations [ignoring the atoms comprising R in the $RC(CH_2O)_3$ residues].

The δ form has an idealized D_{3d} symmetry. The methylene hydrogen and carbon atoms are chemically equivalent, as are the six molybdenum atoms. The oxygen atoms can be divided into three groups of terminal and doubly and triply bridging atoms.

The χ form, on the other hand, has a lower symmetry close to C_{2h}. The CH_2O hydrogen atoms can therefore be divided into three groups, and the carbon atoms into two. Furthermore, two types of molybdenum atoms and seven types of oxygen atoms are to be expected.

The ^{1}H and ^{13}C NMR spectra of compound **4b** in acetonitrile, which displayed only singlet signals (Table 3), clearly validated the δ form for the polyanion. Conversely, the spectra of **4a** and **4c** revealed the χ structure. In the latter, the CH_2O hydrogen atoms formed two ABX patterns, appearing as two doublets and one singlet of equal intensities. The corresponding carbon atoms gave rise to two signals of approximate 1:2 intensity. The molybdenum atoms were also observed, as expected, as two signals in a 2:4 ratio. The number of oxygen signals, however, was lower than expected. We found three signals of equal intensity (4 O) at $\delta \approx 900$, attributable to the three different terminal oxygen atoms by comparison with literature findings.[19] Four more signals should arise for the bridging oxygen atoms: four μ_3- and two μ_2-alkoxo, two μ_3-hydroxo and four μ_2-oxo ligands. Only two signals were observed, integrating as four and six oxygen atoms. There is no obvious assignment for these signals, but they are not incompatible with the proposed structure. Indeed, the chemical shifts fitted for bridging oxygen atoms, and hydroxy groups were not observed by ^{17}O NMR in other B-type heteropolymolybdates.[19]

Compound **4a** thus conclusively retains the χ form, as also found in the solid state, in solution. Compound **4c** has the same χ structure, but not compound **4b**, which adopts the δ form instead. This shows that the structure may vary with variation of the substituent R in the tris(hydroxymethyl)methane derivative. It should be mentioned that compound **4b** was obtained in significantly lower yield than **4a** and **4c**, and that it contained the $[\alpha\text{-}Mo_8O_{26}]^{4-}$ starting material as an impurity.

The paramagnetic compounds **1a**−**c**, **2a**−**c**, and **3a**−**c** were also investigated by ^{1}H NMR. In all cases, considerable line broadening was observed for the signals of the tetrabutylammonium cations. Signals for the organic ligand were observed only for compounds **1a**−**c**. They each displayed a broad singlet for the CH_2O groups at $\delta \approx 60$. This was suggestive of the δ structure, in which all CH_2O groups are at the same distance from the paramagnetic Mn^{III} center. In the χ structure, one CH_2O group of each ligand is not bound to the central Mn^{III}, and so these protons should be less deshielded.

In order to determine the structures of the remaining compounds in the series, we analyzed the IR spectra obtained in the solid state in detail. The two forms δ and χ are closely related, and their IR spectra were very similar; Figure 4 shows two representative examples (**1a** and **4a**) with the same tris(alkoxo) ligand. The spectra were typical of Anderson-type compounds,[12,15,20] with vibrational bands between 890 and 950 cm^{-1} for the terminal Mo=O units and between 660 and 710 cm^{-1} for the bridging Mo−O−Mo groups. The O−C bonds gave rise to bands between 1020 and 1120 cm^{-1}. The only difference detectable in the spectra of the compounds with known structures, established by the methods described above, concerned the bands around 700 cm^{-1}. The compounds with δ structure − **1a**, **1b**, and **4b** − each displayed a large and intensive band around 670 cm^{-1}, attributable to the vibration of the bridging Mo−O−Mo oxygen atoms. The reduction of the symmetry on passing to the χ form seemed to cause a splitting of this band. Indeed, **3c** and **4a** each displayed an additional signal of intermediate intensity, at 736 cm^{-1} and 732 cm^{-1}, respectively. On the assumption that an additional signal around 730 cm^{-1} exists in the spectra

of compounds with the χ arrangement, the structures containing the three-valent heteroatoms Mn^{III} and Fe^{III} are all identified as δ.

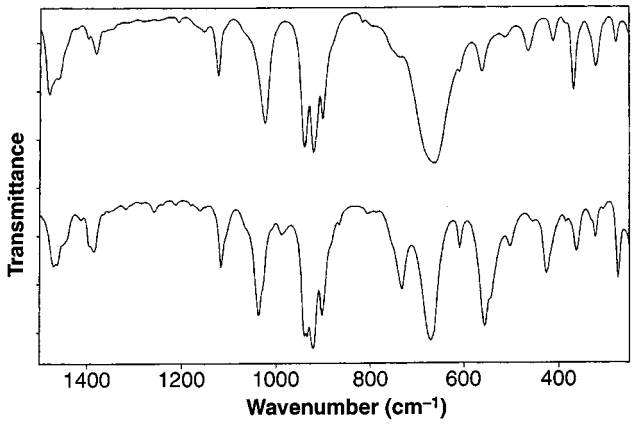

Figure 4. Infrared spectra of $[N(C_4H_9)_4]_3[MnMo_6O_{18}\{(OCH_2)_3CCH_3\}_2]$ (**1a**; top trace) and $[N(C_4H_9)_4]_2[H_2ZnMo_6O_{18}\{(OCH_2)_3CCH_3\}_2]$ (**4a**; bottom trace); note the splitting of the band around 700 cm^{-1} typical for the χ form

The Ni^{II}-containing compounds **3a** and **3b** each showed a very weak band in this region. This can be interpreted as resulting from a mixture of both form δ and form χ. This assumption was backed up by the elemental analyses of these compounds, which also correlated with mixtures of the two forms.

In summary, we have synthesized and structurally characterized a family of Anderson-type heteropolymolybdates containing tris(hydroxymethyl)methane derivatives. Two types of structures − δ and χ − differing in the site occupied by the alkoxide groups have been identified. In the presence of three-valent heteroatoms Mn^{III} and Fe^{III}, only the δ form occurred. The use of divalent heteroatoms Zn^{II} and Ni^{II} resulted in the formation of either δ or χ structures, or in mixtures of both. The reasons for preference for one or the other form are under investigation.

This work offers the potential to functionalize the heteropolymolybdates further by varying the R group on the $RC(CH_2OH)_3$ triol. If the R group were itself reactive, it should be possible to modify it while attached to the heteropolymolybdate. Thus, different functionalized polyoxometalates should be obtainable from a common precursor. Work in this area is in progress.

Experimental Section

Material: $[N(C_4H_9)_4]_4[\alpha\text{-}Mo_8O_{26}]$ was prepared by literature methods.[21] All other compounds, including solvents, were commercially available as reagent grade and used as received.

Spectroscopy: NMR spectra were recorded with Bruker AC 300 (^1H, ^{13}C) and Bruker AM 500 (^{95}Mo, ^{17}O) spectrometers. Deuterated solvent (CD_3CN unless otherwise stated) was used for ^1H and ^{13}C NMR. Chemical shifts (δ) are expressed in ppm relative to Me_4Si with residual solvent peak as standard. ^{13}C NMR spectra were recorded by use of an INEPT pulsing sequence. ^{17}O and ^{95}Mo NMR spectra were recorded at temperatures between 298 and 343 K at concentrations of 0.02 M in acetonitrile. Chemical shifts (δ) are expressed in ppm relative to water (^{17}O) and external aqueous alkaline Na_2MoO_4 (^{95}Mo). All compounds **4a**−**c** displayed the following signals for $N(C_4H_9)_4$ cations, integrating correctly for the number of cations required by the given formula. ^1H NMR: δ = 0.97 (t, $^3J_{H,H}$ = 7.3 Hz, 12 H, $NCH_2CH_2CH_2CH_3$), 1.38 (m, 8 H, $NCH_2CH_2CH_2CH_3$), 1.61 (m, 8 H, $NCH_2CH_2CH_2CH_3$), 3.10 (m, 8 H, $NCH_2CH_2CH_2CH_3$). ^{13}C NMR: δ = 13.8, 20.3, 24.3, 59.1. The signals were broadened in the case of paramagnetic compounds, without significant change in their chemical shifts. IR spectra were obtained on KBr pellets with a Bio-Rad FTS 165 spectrometer. All spectra contained the bands for tetrabutylammonium at 2960, 2874, 1472, and 1382 cm^{-1}. Relative intensities are given after the wavenumber as vs = very strong, s = strong, m = medium, w = weak, sh = shoulder, br = broad.

X-ray Crystal Structure Determination: A selected single crystal was set up on an automatic diffractometer. Unit-cell dimensions with estimated standard deviations were obtained from least-squares refinements of the setting angles of 25 well-centered reflections. Two standard reflections were monitored periodically; they showed no change during data collection. Crystallographic data and other pertinent information are summarized in Table 4. Corrections were made for Lorentz and polarization effects. Secondary extinction corrections were necessary. Computations were performed with the PC version of CRYSTALS.[22] Atomic form factors for neutral atoms were taken from tabulated values.[23] Real and imaginary parts of anomalous dispersion were taken into account. The structure was solved by direct methods[24] and successive Fourier maps. An absorption correction based on DIFABS[25] was applied. Non-hydrogen atoms were refined anisotropically. Least-squares refinements in full matrix were carried out by minimizing the function $\Sigma w(|F_o| - |F_c|)^2$, in which F_o and F_c are the observed and calculated structure factors. Models reached convergence with $R = \Sigma(||F_o| - |F_c||)/\Sigma wF_o$ and $Rw = [\Sigma w(|F_o| - |F_c|)^2/\Sigma w(F_o)^2]^{1/2}$ having the values listed in Table 4. In the last stages of the refinement, each reflection was assigned a weight $w = w'\{1 - [(||F_o| - |F_c||)/6\sigma|F_o|]^2\}^2$ with $w' = 1/\Sigma_r A_r T_r(X)$ with three coefficients for a Chebyshev series, for which $X = F_c/F_c(\text{max.})$. Criteria for a satisfactory complete analysis were the ratio of rms shift to standard deviations being less then 0.2 and no significant features in the difference map. The ellipsoid views of the molecules were obtained with Cameron,[26] polyhedral representations were produced with CrystalMaker.[27] Ellipsoids are shown at the 20% probability level. CCDC-167626 (**1b**), -167627 (**3c**), and -167625 (**4a**) contain the supplementary crystallographic data for this paper. These data can be obtained free of charge at www.ccdc.cam.ac.uk/conts/retrieving.html or from the Cambridge Crystallographic Data Center, 12, Union Road, Cambridge CB2 1EZ, UK [Fax: (internat.) + 44-1223/336-033; E-mail: deposit@ccdc.cam.ac.uk].

Synthesis

General Method for the Complexes 1−4 a-c: A solution of $[N(C_4H_9)_4]_4[\alpha\text{-}Mo_8O_{26}]$ (1.1 g, 0.5 mmol) and 0.75 mmol of $M(acac)_3$ (M = Mn^{III}, Fe^{III}) or $M(OAc)_2$ (M = Zn^{II}, Ni^{II}) in 20 mL of acetonitrile was heated to reflux overnight (approximately 17 h). On cooling, a very small quantity of an unidentified solid separated and was discarded. On vapor diffusion of ether into the solution over 2 d, a solid crystallized and was filtered off, washed with ether, and air-dried. Recrystallization from DMF/ether gave analytically pure samples.

Table 4. Crystal data and structure refinement for **1b**, **3c**, and **4a**

Compound	**1b**	**3c**	**4a**
Empirical formula	$C_{62}H_{134}N_7MnMo_6O_{30}$	$C_{48}H_{110}Mo_6N_4NiO_{30}$	$C_{48}H_{106}Mo_6N_4O_{26}Zn$
Formula mass	2088.37	1857.76	1796.41
a [Å]	22.550(11)	12.246(2)	12.348(4)
b [Å]	13.593(4)	12.503(5)	12.789(6)
c [Å]	28.776(16)	13.971(3)	13.457(5)
[°]	90	100.02(3)	107.17(3)
β [°]	95.90(1)	105.80(2)	101.80(3)
γ [°]	90	113.81(3)	113.10(3)
V [Å^3]	8774(20)	1782(1)	1739(1)
Z	4	1	1
Crystal system	monoclinic	triclinic	triclinic
Space group	*C*2/*c*	$P\bar{1}$	$P\bar{1}$
Crystal shape	parallelepiped	parallelepiped	parallelepiped
Crystal color	orange	colorless	colorless
Linear absorption coefficient μ [cm^{-1}]	10.17	13.35	14.42
Density ρ [g·cm^{-3}]	1.58	1.729	1.715
Diffractometer	Philips PW1100	MACH3 Enraf−Nonius	MACH3 Enraf−Nonius
Radiation	Mo-K_α (λ = 0.71069 Å)	Mo-K_α (λ = 0.71069 Å)	Mo-K_α (λ = 0.71069 Å)
Scan type	ω/2θ	ω/2θ	ω/2θ
Scan range [°]	0.8 + 0.345 tgθ	0.8 + 0.345 tgθ	0.8 + 0.345 tgθ
θ limits [°]	1−25	1−25	1−25
Temperature of measurement	room temperature	room temperature	−80 °C
Octants collected	−17, 17;0, 10;0, 17	0, 14;−14, 13; −16, 15	0, 14;−15, 13; −15, 15
No. of data collected	5782	6586	6418
No. of unique data collected	5196	6264	6108
No. of unique data used for refinement	3177 $(F_o)^2 > 3\sigma(F_o)^2$	4951 $(F_o)^2 > 3\sigma(F_o)^2$	4754 $(F_o)^2 > 3\sigma(F_o)^2$
Merging *R*	0.033	0.009	0.032
Decay of standard reflections (%)	< 1	3	7.2
R[a]	0.068	0.037	0.050
Rw[b]	0.070	0.045	0.060
Weighting coefficients[c]	4.34, −0.961, 3.28	6.94, −1.32, 4.85	8.58, −0.086, 6.39
Absorption correction	Difabs (min. 0.88, max. 1. 00)	Difabs (min. 0.74, max. 1. 00)	Difabs (min. 0.62, max. 1. 00)
Secondary extinction coefficient	291.1	97.9	9.64
Goodness of fit	1.093	1.008	1.073
Nb of variables	481	404	385
$\Delta\rho_{min}$ [e/Å^3]	−0.58	−0.55	−1.37
$\Delta\rho_{max}$ [e/Å^3]	0.76	1.44	1.38

[a] $R = \Sigma||F_o| - |F_c||/\Sigma|F_o|$. [b] $Rw = [\Sigma w(|F_o| - |F_c|)^2/\Sigma w(F_o)^2]^{1/2}$. [c] Weighting scheme of the form $w = w'\{1 - [(||F_o| - |F_c||)/6\sigma|F_o|]^2\}^2$ with $w' = 1/\Sigma_r A_r T_r(X)$ with coefficients for a Chebyshev series for which $X = F_c/F_c$(max.).

$[MnMo_6O_{18}\{(OCH_2)_3CR\}_2]^{3-}$ Anions of 1a−c: The reaction solutions were orange, with an unknown white solid. The complexes **1a**−**c** were isolated as orange crystals after recrystallization.

$[N(C_4H_9)_4]_3[MnMo_6O_{18}\{(OCH_2)_3CCH_3\}_2]$ (1a): Yield 0.91 g (72%). $C_{58}H_{126}MnMo_6N_3O_{24}$·2DMF (2026.42): calcd. C 37.93, H 6.96, Mn 2.71, Mo 28.41, N 3.46; found C 37.90, H 6.95, Mn 2.45, Mo 28.46, N 3.35. IR: $\tilde{\nu}_{max}$ = 1123 m, 1024 s, 939 vs, 919 vs, 900 s, 663 vs. ^{1}H NMR ([D$_6$]DMSO): δ =9.02 (br s, CH_3), 60.49 (br s, CH_2O).

$[N(C_4H_9)_4]_3[MnMo_6O_{18}\{(OCH_2)_3CNO_2\}_2]$ (1b): Yield 0.47 g (36%). $C_{56}H_{120}MnMo_6N_5O_{28}$·2DMF (2088.37): calcd. C 35.66, H 6.47, Mn 2.63, Mo 27.56, N 4.69; found C 35.78, H 6.40, Mn 2.48, Mo 26.57, N 4.60. IR: $\tilde{\nu}_{max}$ = 1539 m, 1337 m, 1153 w, 1083 vs, 1056 w, 946 vs, 926 vs, 909 s, 763 sh, 738 sh, 670 vs. ^{1}H NMR: δ = 69.07 (br s, CH_2O).

$[N(C_4H_9)_4]_3[MnMo_6O_{18}\{(OCH_2)_3CCH_2OH\}_2]$ (1c): Yield 0.70 g (55%). $C_{58}H_{126}MnMo_6N_3O_{26}$ (1912.23): calcd. C 36.43, H 6.64, Mn 2.87, Mo 30.1, N 2.2; found C 36.92, H 6.90, Mn 3.06, Mo 28.99, N 2.20. IR: $\tilde{\nu}_{max}$ = 3422 br, 1113 m, 1073 w, 1010 s, 938 vs, 918 vs, 900 s, 665 vs. ^{1}H NMR: δ = 10.01 (br s, CH_2OH), 61.08 (br s, CH_2O).

$[N(C_4H_9)_4]_3[FeMo_6O_{18}\{(OCH_2)_3CR\}_2]$ (2a−c): The reaction solutions were red orange and the unknown solid was orange. The complexes **2a**−**c** were isolated as yellow crystals after recrystallization.

$[N(C_4H_9)_4]_3[FeMo_6O_{18}\{(OCH_2)_3CCH_3\}_2]$ (2a): Yield 0.79 g (63%). $C_{58}H_{126}FeMo_6N_3O_{24}$ (1881.14): calcd. C 37.03, H 6.75, Fe 2.97, Mo 30.6, N 2.23; found C 37.24, H 6.81, Fe 2.93, Mo 30.39, N 2.20. IR: $\tilde{\nu}_{max}$ = 1121 m, 1037 s, 1018 s, 981 w, 938 vs, 919 vs, 902 s, 689 vs.

$[N(C_4H_9)_4]_3[FeMo_6O_{18}\{(OCH_2)_3CNO_2\}_2]$ (2b): Yield 0.45 g (35%). $C_{56}H_{120}FeMo_6N_5O_{28}$·$CH_3CN$ (1984.08): calcd. C 35.11, H 6.25, Fe 2.81, Mo 29.01, N 4.24; found C 35.12, H 6.29, Fe 2.86, Mo 29.31, N 4.33. IR: $\tilde{\nu}_{max}$ = 1538 m, 1337 m, 1169 w, 1083 vs, 946 vs, 927 vs, 909 vs, 812 m, 763 sh, 738 sh, 666 vs.

$[N(C_4H_9)_4]_3[FeMo_6O_{18}\{(OCH_2)_3CCH_2OH\}_2]$ (2c): Yield 0.86 g (68%). $C_{58}H_{126}FeMo_6N_3O_{26}$ (1913.14): calcd. C 36.41, H 6.64, Fe 2.92, Mo 30.09, N 2.20; found C 35.23, H 6.60, Fe 2.46, Mo 28.09,

N 2.20. IR: $\tilde{\nu}_{max}$ = 3354 br, 1152 w, 1111 m, 1071 w, 1013 m, 936 vs, 917 vs, 903 s, 757 sh, 692 vs.

$[N(C_4H_9)_4]_{4-x}[H_xNiMo_6O_{18}\{(OCH_2)_3CR\}_2]$ (3a−c): The reaction solutions were blue-green, with an unknown white solid. Compounds **3a−c** were isolated as green crystals after recrystallization.

$[N(C_4H_9)_4]_{4-x}[H_xNiMo_6O_{18}\{(OCH_2)_3CCH_3\}_2]$ (3a): Yield 0.84 g (60%). x = 0: $C_{74}H_{162}Mo_6O_{24}N_4Ni$ (2126.47): calcd. C 41.80, H 7.68, Mo 27.07, N 2.63, Ni 2.76; x = 2: $C_{42}H_{92}Mo_6O_{24}N_2Ni$ (1643.54): calcd. C 30.69, H 5.64, Mo 35.02, N 1.70, Ni 3.57; found C 36.63, H 6.91, Mo 27.91, N 3.18, Ni 3.20. IR: $\tilde{\nu}_{max}$ = 1116 m, 1043 s, 1024 m, 988 w, 933 vs, 915 vs, 895 s, 736 sh, 708 sh, 673 vs.

$[N(C_4H_9)_4]_{4-x}[H_xNiMo_6O_{18}\{(OCH_2)_3CCNO_2\}_2]$ (3b): Yield 0.62 g (43%). x = 0: $C_{72}H_{156}Mo_6O_{28}N_6Ni$ (2188.41): calcd. C 39.52, H 7.19, Mo 26.3, N 3.84, Ni 2.68; x = 2: $C_{40}H_{86}Mo_6O_{28}N_4Ni$ (1705.48): calcd. C 28.17, H 5.08, Mo 33.75, N 3.29, Ni 3.44; found C 38.92, H 6.95, Mo 26.81, N 4.01, Ni 2.70. IR: $\tilde{\nu}_{max}$ = 1520 m, 1334 m, 1154 w, 1101 vs, 1030 w, 922 vs, 911 vs, 891 s, 815 m, 744 m, 680 vs.

$[N(C_4H_9)_4]_{4-x}[H_xNiMo_6O_{18}\{(OCH_2)_3CCH_2OH\}_2]$ (3c): Yield 0.84 g (58%). x = 0: $C_{74}H_{162}Mo_6O_{26}N_4Ni$ (2158.47): calcd. C 41.18, H 7.57, Mo 26.67, N 2.60, Ni 2.72; x = 2: $C_{42}H_{92}Mo_6O_{26}N_2Ni$ (1675.54): calcd. C 30.11, H 5.53, Mo 34.36, N 1.67, Ni 3.50; x = 2: $C_{42}H_{92}Mo_6O_{26}N_2Ni{\cdot}2DMF{\cdot}2H_2O$ (1857.76): calcd. C 30.96, H 7.90, Mo 30.91, N 3.01, Ni 3.15; found C 34.53, H 6.37, Mo 27.93, N 1.97, Ni 3.43. IR: $\tilde{\nu}_{max}$ = 3433 br, 1104 m, 1069 w, 1022 m, 1014 m, 938 vs, 919 vs, 903 s, 736 s, 675 s, 650 m.

$[N(C_4H_9)_4]_{4-x}[H_xZnMo_6O_{18}\{(OCH_2)_3CR\}_2]$ (4a−c): The reaction solutions were colorless, with an unknown white solid. The compounds **4a−c** were isolated as colorless crystals after recrystallization.

$[N(C_4H_9)_4]_2[H_2ZnMo_6O_{18}\{(OCH_2)_3CCH_3\}_2]$ (4a): Yield 0.89 g (81%). $C_{42}H_{92}Mo_6O_{24}N_2Zn{\cdot}2DMF$ (1796.41): calcd. C 32.09, H 5.95, Mo 32.04, N 3.12, Zn 3.64; found C 32.21, H 6.05, Mo 32.06, N 3.32, Zn 3.60. IR: $\tilde{\nu}_{max}$ = 1115 m, 1037 s, 987 w, 939 vs, 933 vs, 921 vs, 904 s, 732 m, 671 vs. ^{1}H NMR: δ = 0.58 (s, 6 H, CH_3), 4.42 (d, 4 H, $^2J_{H,H}$ = 10.8 Hz, CH^aH^bO), 4.51 (d, 4 H, $^2J_{H,H}$ = 10.8 Hz, CH$^aH^b$O), 4.59 (s, 4 H, CH_2O). ^{13}C NMR: δ = 16.8 (CH_3), 79.6 (CH_2O), 89.4 (CH_2O). ^{95}Mo NMR (343 K): δ = 31.6 (2 Mo), 76.6 (4 Mo). ^{17}O NMR (343 K): δ = 322.5 (4 O), 422.5 (6 O), 907.8 (4 O), 914.4 (4 O), 926.2 (4 O).

$[N(C_4H_9)_4]_4[ZnMo_6O_{18}\{(OCH_2)_3CNO_2\}_2]$ (4b): Crude yield 0.50 g (34%, contaminated with $[N(C_4H_9)_4]_4[\alpha\text{-}Mo_8O_{26}]$). $C_{72}H_{156}Mo_6O_{28}N_6Zn$ (2195.09): calcd. C 39.40, H 7.16, Mo 26.22, N 3.83, Zn 2.98; found C 38.50, H 7.15, Mo 27.45, N 3.81, Zn 2.56. IR: $\tilde{\nu}_{max}$ = 1524 m, 1336 w, 1154 w, 1100 s, 1073 w, 931 vs 911 vs, 890 s, 814 m, 660 vs. ^{1}H NMR: δ = 4.93 (s, 12 H, CH_2O). ^{13}C NMR: δ = 77.6 (CH_2O). ^{95}Mo NMR (343 K): δ = 47.2; (298 K): δ = 50.7.

$[N(C_4H_9)_4]_2[H_2ZnMo_6O_{18}\{(OCH_2)_3CCH_2OH\}_2]$ (4c): Yield 0.56 g (70%). $C_{42}H_{92}Mo_6O_{26}N_2Zn{\cdot}2DMF$ (1828.41): calcd. C 31.53, H 5.84, Mo 31.48, N 3.06, Zn 3.58; found C 30.84, H 5.87, Mo 29.05, N 2.54, Zn 3.63. IR: $\tilde{\nu}_{max}$ = 3457 br, 1106 m, 1069 m, 1035 m, 1017 m, 1004 m, 937 vs, 918 vs, 898 vs, 728 m, 671 vs, 643 sh. ^{1}H NMR: δ = 3.26 (s, 4 H, CH_2OH), 4.60 (d, 4 H, $^2J_{H,H}$ = 10.8 Hz, CH^aH^{b}O), 4.65 (d, 4 H, $^2J_{H,H}$ = 10.6 Hz, CH$^aH^b$O), 4.85 (s, 4 H, CH_2O). ^{13}C NMR: δ = 63.4 (ca. 2 C, CH_2OH), 76.8 (ca. 4 C, CH_2O), 87.1 (ca. 4 C, CH_2O). ^{95}Mo NMR: (323 K): δ = 1.9 (2 Mo), 101.8 (4 Mo).

Acknowledgments

This research was supported by the Pierre and Marie Curie University and the CNRS. Furthermore, we would like to thank Dr. René Thouvenot for recording the NMR spectra.

[1] M. T. Pope, *Heteropoly and Isopoly Oxometalates*, Springer Verlag, Berlin, **1983**.
[2] M. T. Pope, in: *Comprehensive Coordination Chemistry*, vol. 3, 1st ed. (Eds.: S. G. Wilkinson, R. D. Gillard, J. A. McCleverty), Pergamon Press, Oxford, **1987**, pp. 1023−1056.
[3] C. H. Joo, K. M. Park, U. Lee, *Acta Crystallogr., Sect. C* **1994**, *50*, 1659−1661.
[4] U. Lee, *Acta Crystallogr., Sect. C* **1994**, *50*, 1657−1659.
[5] H. T. Evans Jr., B. M. Gatehouse, P. Leverett, *J. Chem. Soc., Dalton Trans.* **1975**, 505−514.
[6] K. G. Burtseva, T. S. Chernaya, M. I. Sirota, *Dokl. Akad. Nauk SSSR* **1978**, *243*, 104−107.
[7] J. Fuchs, E. P. Flindt, *Z. Naturforsch., Teil B: Anorg. Chem. Org. Chem.* **1979**, *34B*, 412−422.
[8] G. A. Tsigdinos, *Top. Curr. Chem.* **1978**, *76*, 1−59.
[9] A. Perloff, *Inorg. Chem.* **1970**, *9*, 2228−2239.
[10] J. Martin-Frère, Y. Jeannin, F. Robert, J. Vaissermann, *Inorg. Chem.* **1991**, *30*, 3635−3639.
[11] Q. He, E. Wang, *Inorg. Chem. Commun.* **1999**, *2*, 399−402.
[12] J. Fuchs, I. Brüdgam, *Z. Naturforsch., Teil B* **1977**, *32*, 403−407.
[13] R. Delmont, A. Proust, F. Robert, P. Herson, P. Gouzerh, *C. R. Acad. Sci. Paris, Sér. IIc* **2000**, *3*, 147−155.
[14] A. La Ginestra, F. Giannetta, P. Fiorucci, *Gazz. Chim. Ital.* **1968**, *98*, 1197−1212.
[15] K. Nomiya, T. Takahashi, T. Shirai, M. Miwa, *Polyhedron* **1987**, *6*, 213−218.
[16] F. Ito, T. Ozeki, H. Ichida, H. Miyamae, Y. Sasaki, *Acta Crystallogr., Sect. C* **1989**, *45*, 946−947.
[17] P. Gili, P. A. Lorenzo-Luis, P. Martin-Zarza, S. Dominguez, A. Sanchez, J. M. Arrieta, E. Rodriguez-Castellon, J. Jimenez-Jimenez, C. Ruiz-Pérez, M. Hernandez-Molina, *Transition Met. Chem.* **1999**, *24*, 141−151.
[18] P. Ray, A. Bhaduri, B. Sarma, *J. Indian Chem. Soc.* **1948**, *25*, 51−56.
[19] M. Filowitz, R. K. C. Ho, W. G. Klemperer, W. Shum, *Inorg. Chem.* **1979**, *18*, 93−103.
[20] I. L. Botto, A. C. Garcia, H. J. Thomas, *J. Phys. Chem. Solids* **1992**, *53*, 1075−1080.
[21] N. Hur, W. G. Klemperer, R.-C. Wang, in: *Inorg. Synth.*, vol. 27 (Ed.: A. P. Ginsberg), John Wiley & Sons, New York, **1990**.
[22] D. J. Watkin, C. K. Prout, J. R. Carruthers, P. W. Betteridge, *CRYSTALS*, An Advanced Crystallographic Computer Program, Chemical Crystallography Laboratory, Oxford **1989**.
[23] *International Tables for X-ray Crystallography*, vol. IV, Kynoch Press, Birmingham, **1974**.
[24] G. M. Sheldrick, *SHELXS86, Program for Crystal Structure Solution*, University of Göttingen,Göttingen, **1986**.
[25] N. Walker, D. Stuart, *Acta Crystallogr., Sect. A* **1983**, *39*, 158−166.
[26] D. J. Watkin, C. K. Prout, L. J. Pearce, *CAMERON*, Chemical Crystallography Laboratory, Oxford, **1996**.
[27] D. C. Palmer, *CrystalMaker 2.1.5*, Cambridge University Technical Services Ltd., Cambridge, **1997**.

Received August 20, 2001
[I01317]

Studies of Phosphonic Acids Containing a π-Conjugated Ferrocenyl Unit Grafted on Metal Oxides − Mössbauer and Electrochemical Behaviour

Richard Frantz,*[b] Jean-Olivier Durand,[b] Gérard F. Lanneau,[b] Jean-Claude Jumas,[a] Josette Olivier-Fourcade,[a] Marc Cretin,[c] and Michel Persin[c]

Keywords: Mössbauer spectroscopy / Electrochemistry / Phosphorus / Sandwich complexes

The modification of metal oxide surfaces by π-conjugated ferrocene units has been performed. A phosphonic acid functionality was used to covalently anchor the π-conjugated ferrocene moiety to SnO_2 and TiO_2 particles. The covalent attachment and the monolayer coverage at the surface of the particles were confirmed by solid-state MAS ^{31}P NMR spectroscopy, microanalysis and electronic microscopy (EDX). The properties of the ferrocene-modified oxides were analysed by cyclic voltammetry, which confirmed the electroactivity of the material, and ^{57}Fe Mössbauer spectrometry, which provided information about the oxidation state and environment of the iron atoms.
(© Wiley-VCH Verlag GmbH, 69451 Weinheim, Germany, 2002)

Introduction

The syntheses of materials with ferrocene units have attracted considerable interest in the last decades.[1] They have found increasing uses in many fields: molecular materials for non-linear optics,[1b] polymers for electrochemical applications,[1c] asymmetric catalysis,[1d] amperometric biosensors for glucose oxidase,[1e] and surfactant devices.[1f] The covalent coverage of surface oxides by organic molecules functionalised with ferrocene is particularly important for fundamental mechanistic studies,[2a] as well as for applications in the field of modified electrodes.[2b−2e] Great attention has been devoted to ferrocenes possessing a grafting function, such as a mercaptan[2c−2e] or a carboxylic acid,[2b] in order to achieve the preparation of new electrodes. Its application as electrochemical transducers for biosensors seems promising.[2f−2g] As the grafting of sophisticated molecules using a phosphonic acid functionality has been used for many purposes[3,2b] and is known to be very stable,[3c] we focused our attention to this functionality to covalently anchor ferrocene units to metal oxide particles. We have already described the preparation of phosphonic acids containing a π-conjugated ferrocenyl unit with a defined configuration of the conjugated backbone.[4] Analyses of their electrochemical properties in DMSO showed standard reversible redox waves assigned to the Fe^{II}/Fe^{III} couple.[4] Here, we present our studies on the grafting of these molecules on the surface of TiO_2 and SnO_2 particles. Electrochemistry is used as a powerful tool for detecting the electroactive species at the surface. ^{57}Fe Mössbauer spectroscopy informs us about the oxidation state of the iron atoms, the symmetry of its electronic environment and the nature of the chemical bonds involved. Additional information on the structural properties is obtained from the Mössbauer effect probability and its temperature dependence.

Results and Discussion

Two types of phosphonic acids with a π-conjugated ferrocenyl unit, **1** and **2**, have been synthesised (Scheme 1), and their electronic properties characterised in solution. We have shown that a better transmission of the electronic effects is obtained with the more conjugated phenylphosphonic acid **1** than the benzylphosphonic acid **2.**[4] The more conjugated phenylphosphonic acid **1** is a better electron-withdrawing group than the benzylphosphonic acid **2**. We then performed the grafting reaction of acids **1** and **2** (Scheme 1), in order to investigate the properties of the new hybrid organic-inorganic materials thus prepared, and particularly the modification of the electronic properties in the solid state. Three types of particle oxides were used. TiO_2 P25 Degussa (particle size of 21 nm) (**Ti**), SnO_2 synthesised by the sol-gel process[5] and pyrolysis at 700 °C (particle size 5−10 nm) (**Ss**), and SnO_2 Merck (particle size 20 nm) (**Sc**). The surface of the TiO_2 and SnO_2 particles were modi-

[a] Laboratoire des Agrégats Moléculaires et Matériaux Inorganiques (UMR 5072 CNRS), cc 015, Université Montpellier 2,
Place Eugène Bataillon, 34095 Montpellier, cedex 05, France
[b] Laboratoire de Chimie Moléculaire et Organisation du Solide (UMR 5637 CNRS), cc 007, Université Montpellier 2,
Place Eugène Bataillon, 34095 Montpellier, cedex 05, France
[c] Institut Européen des Membranes (UMR 5635 CNRS), cc047, Université Montpellier 2,
Place Eugène Bataillon, 34095 Montpellier cedex 05, France

fied by refluxing with the phosphonic acid **1** or **2** for 3 d in MeOH/H_2O (4:1) at 65 °C. This mixture of solvents was chosen because of the low solubility of the acids **1** and **2**. A large excess of acid was used to ensure the total coverage of the particle surfaces. The solids were first analysed using energy-dispersive X-ray techniques, microanalysis, and solid-state ^{31}P NMR spectroscopy. Elemental analyses (Table 1) showed the presence of P and Fe in all the samples, indicating the presence of the molecules **1** and **2** at the surface of the particles. The P/Fe ratios were between 0.7 and 0.85, which confirmed that cleavage of the P−C bond did not occur. The microanalyses were corroborated by energy-dispersive X-ray analyses. Variation of the P/MO_2 ratio was not observed from one experiment to another on the same sample, which showed that the solids were homogeneous on a micrometric scale. From the low P/MO_2 ratio we have concluded that a monolayer coverage resulted at the surface of the oxide.[3c] Note that the proportion of the organic part was higher for **Ss1** than **Sc1** because of the higher specific surface area for **Ss1** (particle size 5−10 nm for **Ss1** versus 20 nm for **Sc1**). Solid-state ^{31}P NMR spectra of compounds **1** and **2** and materials **Ti1** and **Ti2** are presented in Figure 1. Phosphonic acids **1** and **2** show sharp signals at δ = 28.8 and 20, respectively, which is characteristic of well-crystallised homogeneous compounds. Signals of **Ti1** and **Ti2** are shifted upfield at δ = 22.3 and 13.6, respectively, which is characteristic of the formation of P−O−metal bonds. The peak width at half maximum is close to δ = 10, which indicates that the phosphorus atom has different environments on the surface of the oxide because of the different coordination modes. One, two, or three P−O−metal bonds are likely to be involved in the anchoring on the surface. In the case of materials **Sc1** and **Ss1** (Figure 2), we observed the same type of behaviour with an upfield shift at δ = 14 for the two materials. The signal was less symmetrical than for **Ti1** and **Ti2**, thus the

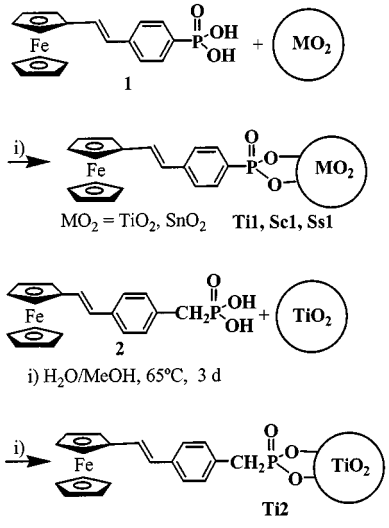

Scheme 1. Grafting of precursors **1** and **2** on TiO_2 and SnO_2

Table 1. Elemental analyses and EDX for **Ti1**, **Ti2**, **Sc1**, **Ss1**

Particles	Sample	Elemental analyses % P	% Fe	P/Fe	EDX % P	% Fe	P/Fe
TiO_2 P25	**Ti1**	1.50	2.20	0.7	3.99	4.14	0.96
TiO_2 P25	**Ti2**	1.75	2.20	0.8	4.07	3.5	1.16
SnO_2 Merck	**Sc1**	0.90	1.17	0.77	2.99	3.5	0.86
SnO_2 Synthesized	**Ss1**	1.40	1.65	0.85	3.5	2.8	1.25

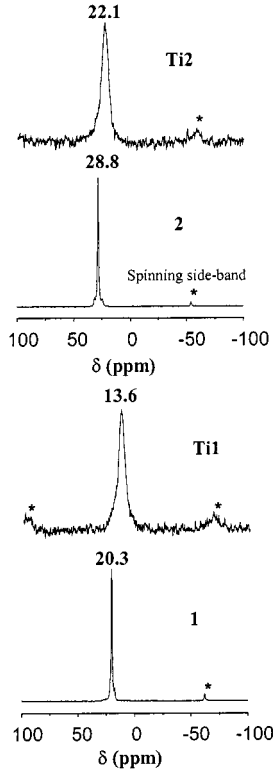

Figure 1. Solid-state hpdecmas ^{31}P NMR of compounds **1**, **2**, **Ti1**, **Ti2**

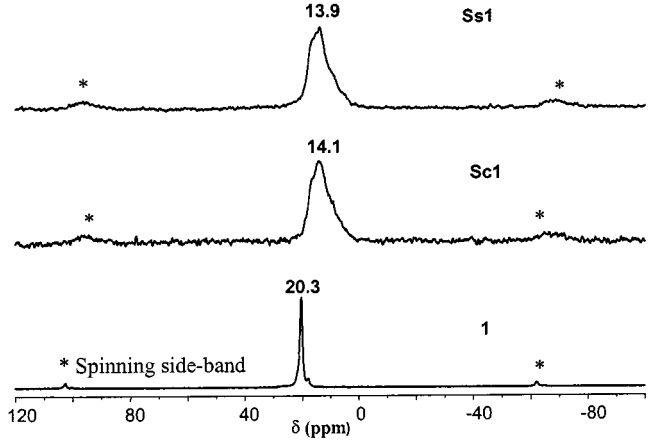

Figure 2. Solid-state hpdecmas ^{31}P NMR of compounds **1**, **Ss1**, **Sc1**

surface of SnO_2 is likely to be more carved than the surface of TiO_2.

Electrochemical Behaviour

After characterising the hybrid organic-inorganic materials, the electrochemical properties of the precursors and grafting materials were investigated by cyclic voltammetry by means of a potentiostat (E&GG model 273A). For the material powders, a modified electrode was prepared by pressing the particles on a flat pad made of stainless steel. A platinum electrode was used as the auxiliary electrode and a saturated calomel electrode was the reference, 0.1 M $LiClO_4$ was used as the electrolyte. The different voltammograms obtained are presented in Figures 3−5 and the half-wave potentials $E_{1/2}$ are gathered in Table 2. The electroactivity of the precursor **1** was first analysed in aqueous solution (Figure 3). We observed the quasi-reversible oxidation-reduction waves characteristic of the Fc^{II}/Fc^{III} couple. The oxidation and the reduction half-wave potentials were assigned at 150 mV/SCE and 200 mV/SCE, respectively. The electrochemical analyses, in the solid state, of the acid **1** and of the grafted TiO_2 powder (**Ti1**) are presented in Figure 4a. The non-reversibility of both systems is shown. In the solid state, the diffusion and the charge transfer processes do not obey the classical laws of electrochemistry in solution. The latter are, in many cases, slower than in solution, which explains the loss of the reversibility of the systems. The electrochemical behaviour of the acid **2** and of the grafted TiO_2 powder (**Ti2**) was studied after pressing the compounds on the stainless steel felt. The systems were non-reversible (Figure 4b), which confirmed the previous results. Moreover, comparison of the voltammograms of the grafted materials **Ti1** and **Ti2** shows that the oxidation and reduction potentials are close to those of the precursors **1** and **2**, respectively (Figure 4a,b). This confirms that the π-conjugated ferrocene unit was not damaged by the grafting on the oxide. The results obtained for the material **Ti2**, which differs from **Ti1** only by the presence of a CH_2 unit between the phenyl and phosphonic groups, confirms the ferrocene electroactivity. Furthermore, we observed the same behaviour as in a DMSO solution.[4] It is easier to oxidise acid **2** relative to acid **1** in the solid state (Table 2), due to the presence of the CH_2 group, which reduces the withdrawing effect of the phosphonic acid substituent. This effect is less visible on the grafted powders **Ti1** and **Ti2**. In Figure 5, the elec-

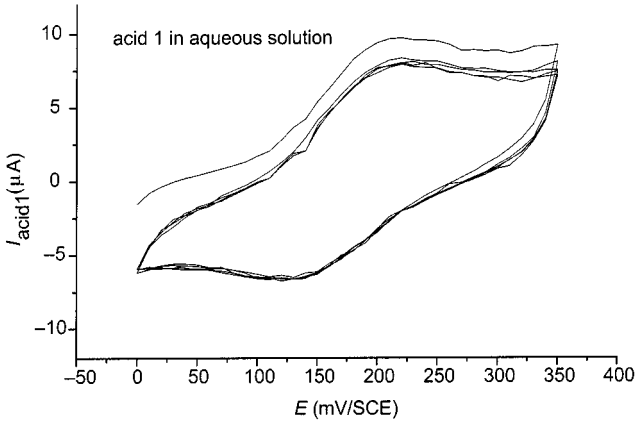

Figure 3. Cyclic voltammogram on stainless steel electrode, of acid **1** in aqueous solution (10^{-1} M $LiClO_4$) at 100 mVs^{-1}

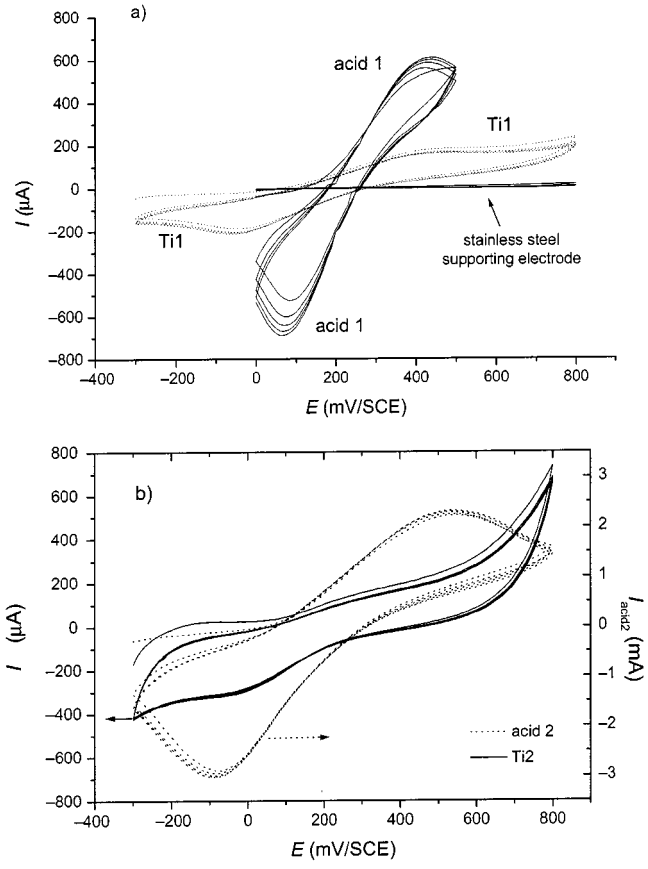

Figure 4. a) Cyclic voltammograms of **1** and **Ti1** in the solid state, stainless steel supporting electrode in aqueous solution (10^{-1} M $LiClO_4$) at 100 mVs^{-1}; b) cyclic voltammograms of **2** and **Ti2** in the solid state, stainless steel supporting electrode in aqueous solution (10^{-1} M $LiClO_4$) at 100 mVs^{-1}

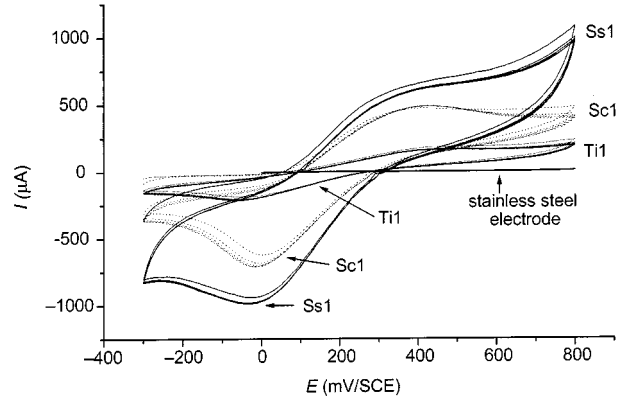

Figure 5. Cyclic voltammograms of **Ss1**, **Sc1** and **Ti1** in the solid state; stainless steel supporting electrode in aqueous solution (10^{-1} M $LiClO_4$) at 100 mVs^{-1}

Table 2. $E_{1/2}$ of **1**, **2**, **Ti1**, **Ti2**, **Sc1**, **Ss1**

	Acid **1** Solution	Solid state	Powder **Ti1**	Powder **Sc1**	Powder **Ss1**	Acid **2** Solid state	Powder **Ti2**
$E_{1/2}$ [mV] Oxidation	150	285	260	200	200	260	260
$E_{1/2}$ [mV] Reduction	200	175	110	160	160	100	100

troactivity of the ferrocene unit on both grafted SnO_2 powders **Sc1** and **Ss1** is conserved. The $E_{1/2}$ values and the intensity recorded in the cyclic voltammograms confirms that the electroactivity of the ferrocene group is to be better on the SnO_2 grafted powder than on the TiO_2 grafted powder. Note also that the SnO_2-based system seems to be more reversible than the TiO_2-based system ($\Delta E_{Ti1}^{peak} = 430$ mV, $\Delta E_{Sc1}^{peak} = 390$ mV).

Mössbauer Spectrometry

^{57}Fe Mössbauer experiments were performed with an EG&G constant acceleration spectrometer in transmission mode. The source of nominal activity was 10 mCi of ^{57}Co in an Rh matrix. The velocity scale was calibrated using the standard magnetic sextuplet of a high-purity iron foil absorber. The origin of the isomer shift scale was determined from the centre of the α-Fe spectrum recorded at room temperature. The absorbers were prepared from approximately 200 mg of the powders in a specific cell.

^{57}Fe Mössbauer spectroscopy has been widely used to explore the charge density and symmetry of the charge distribution around the metal atom of ferrocenyl derivatives.[6] The Mössbauer spectra of low-spin Fe^{II} in ferrocenyl derivatives show isomer shifts δ in the range $0.45 < \delta < 0.55$ mms^{-1} and quadrupolar splittings Δ in the range $2.2 < \Delta < 2.5$ mms^{-1}. Spectra of acids **1** and **2** are presented in Figure 6. The characteristic doublet of the ferrocene units are at $\delta = 0.443$ and 0.449 mms^{-1}, respectively, and the quadrupolar splitting is at $\Delta = 2.268$ and 2.270 mms^{-1}, respectively. A secondary signal was also observed in the two spectra. The contribution of the signal to the spectra was 3.2% and 8.1%, respectively (Table 3). Isomeric shifts were in the range of the ferrocene species (0.44 and 0.49 mms^{-1}, respectively), but the quadrupole splittings are much smaller (in the range 0 to 0.38 mms^{-1}), indicating the presence of a "ferrocenium-like" low-spin Fe^{III} compound. It seems that a small fraction of ferrocene Fe^{II} has been oxidised to the Fe^{III} species. For the low-spin Fe^{II} and low-spin Fe^{III} species, the isomer shift is not very sensitive to the formal oxidation state of iron because the effective electric charges on the iron are not very different. In contrast, the quadrupole splitting of the ferrocenium ion $(C_5H_5)_2Fe^+$ decreases remarkably. For the two acids **1** and **2**, the Mössbauer parameters remain unchanged compared with unsubstituted ferrocene. The σ-bonded substituents on the cyclopentadienyl ring do not affect the π-bonds of the ferrocene unit. After compounds **1** and **2** were grafted on TiO_2, the materials **Ti1** and **Ti2** were analysed at room temperature (Figure 6). Major changes in the Mössbauer signals are observed, with only one broadened doublet. Respective values of the isomer shift are 0.40 and 0.38, in the range of ferrocenyl compounds. Quadrupole splitting values of about 0.6−0.7 mms^{-1} suggest the presence of some kind of electronic effect. The line broadening and the weak absorption are consistent with an averaged valence state of iron. This is not surprising, as TiO_2 is known to be a photooxidant. Sato[6−7] has observed the same type of behaviour by adsorbing ferrocene on silica. After standing in air, the Mössbauer spectra at room temperature only showed ferrocenium. By performing the measurements at 78 K, the signal of the ferrocene Fe^{II} species appeared, together with the signal of ferrocenium Fe^{III}. Materials **Ti1** and **Ti2** were therefore analysed at low temperature. At 78 K (Figure 4c), the spectra consist of an inner- and outer-doublet which are assigned to a "ferrocenium-like" Fe^{III} and a "ferrocene-like" Fe^{II} doublet, with a ratio of about 3:1. The characteristic signal of the ferrocene unit in its Fe^{II} form is observed for both **Ti1** ($\delta = 0.51$, $\Delta = 2.26$ mms^{-1}) and **Ti2** ($\delta = 0.63$, $\Delta = 2.43$ mms^{-1}), together with the ferrocenium species for both **Ti1** ($\delta = 0.50$, $\Delta = 0.67$) and **Ti2** ($\delta = 0.49$, $\Delta = 0.65$ mms^{-1}). These last measurements show the temperature dependence of the mixed-valence state, where the valence-state changes from an averaged to a trapped valence state. This effect proves that there is an interaction between the π-electrons of the cyclopentadienyl ring of ferrocene and the metal oxides (MO_2).

Table 3. Mössbauer data for **1**, **2**, **Ti1**, **Ti2**

Compound	δ [mm s^{-1}]	Δ [mm s^{-1}]	Γ [mms^{-1}]	%
1	0.443 (2)	2.268 (8)	0.30 (1)	96.8
	0.44 (4)	0	0.30 (1)	3.2
2	0.449 (3)	2.270 (8)	0.30 (1)	91.9
	0.49 (3)	0.38 (4)	0.24 (5)	8.1
Ti1 (298 K)	0.40 (3)	0.63 (4)	0.42 (6)	100
Ti1 (78 K)	0.51 (1)	2.26 (2)	0.29 (3)	34.4
	0.50 (2)	0.67 (3)	0.56 (5)	65.6
Ti2 (298 K)	0.38 (2)	0.68 (3)	0.47 (4)	100
Ti2 (78 K)	0.60 (3)	2.43 (4)	0.44 (6)	36.0
	0.49 (2)	0.65 (3)	0.56 (6)	64.0

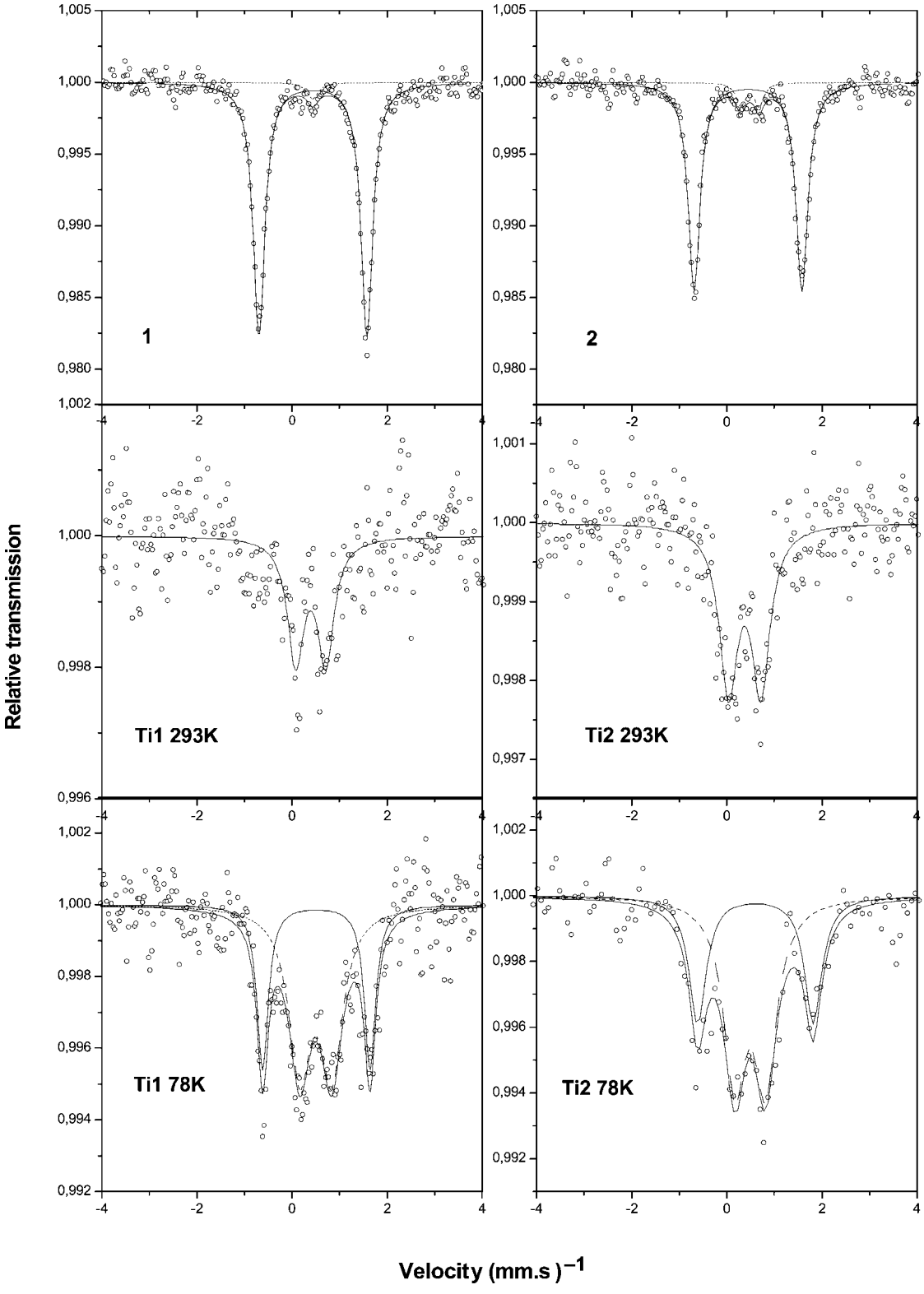

Figure 6. Mössbauer spectra of **1**, **2**, **Ti1**, **Ti2** at 293 K; **Ti1**, **Ti2**, at 78 K

Conclusion

The covalent attachment of ferrocenyl π-conjugated compounds **1** and **2** on metal oxides has been efficiently achieved by using the phosphonic acid functionality. In this way an organic monolayer at the surface of the oxide was formed. Solid-state electrochemistry has confirmed the electroactivity of the supported ferrocene units, the electrochemical system was irreversible. Electroactivity seemed to be better with the SnO_2 grafted powders than the TiO_2

grafted powders, although coverage is higher on TiO_2 then on SnO_2. The support is effective and could be of importance for the final materials made. Mössbauer spectroscopy has shown that the ferrocene moiety was partially oxidised, and that the π-electrons of the ferrocene interact with the metal oxide. Potential applications in the field of modified electrodes and sensors are in progress.

Experimental Section

General: All reactions were performed under argon. Energy-dispersive X-ray analyses (EDX) were performed with an electronic scanning microscope Cambridge Stereoscan 360 equipped with a Link AN 10000 probe. Microanalyses were performed by the central analysis service at CNRS (Vernaison). The syntheses of the ferrocene π-conjugated phosphonic acids **1** and **2** have been described elsewhere.[4] SnO_2 was synthesised from $SnCl_4$ as described.[5] Commercial SnO_2 was purchased from Merck and TiO_2 P25 was furnished by Degussa. These oxides were functionalised by the following general procedure: The metal oxide was suspended in a mixture of MeOH (40 mL), H_2O (10 mL). Phosphonic acid **1** or **2** was added and the mixture heated at 65 °C for 3 d whilst stirring. The suspension was then cooled, filtered through a millipore membrane (0.45 μm), washed successively with water, MeOH, EtOH, acetone, ether and dried at room temp.

Material Ti1: TiO_2 P25: 600 mg (7.51 mmol), acid **1**: 200 mg (0.524 mmol). Solid-state ^{31}P NMR (hpdec, δ value): 13.6. Microanalysis (%): Fe 2.20, P 1.50, Ti 48.20; EDX (%)**:** Fe 4.14, P 3.99**.**

Material Ti2: TiO_2 P25: 600 mg (7.51 mmol), acid **2**:200 mg (0.543 mmol). Solid-state ^{31}P NMR (hpdec, δ value): 22.1. Microanalysis (%): Fe 2.20, P 1.75, Ti 48.80. EDX (%): Fe 3.5, P 4.07.

Material Sc1: SnO_2 500 mg (3.32 mmol), acid **1**: 150 mg (0.41 mmol). Solid-state ^{31}P NMR (hpdec, δ value): 14.1. Microanalysis (%): Fe 1.17, P 0.90, Sn 65.45. EDX (%): Fe 3.5, P 2.99**.**

Material Ss1: SnO_2 500 mg (3.32 mmol), acid **1**: 150 mg (0.41 mmol). Solid-state ^{31}P NMR (hpdec, δ value):13.9. Microanalysis (%): Fe 1.65, P 1.40, Sn 65.55. EDX (%): Fe 2.8, P 3.5.

Acknowledgments

We thank the Degussa society for a gift of TiO_2 P25.

[1] [1a] A. Togni, T. Hayashi, *Ferrocenes*, VCH, Weinheim, Germany, **1995** and refs. cited therein. [1b] S. R. Marder, J. W. Perry, B. G. Tiemann, W. P. Schaefer, *Organometallics* **1991**, *10*, 1896. [1c] P. Nguyen, P. Gomez-Elipe, I. Manners, *Chem. Rev.* **1999**, *99*, 1515. [1d] B. Gotov, S. Toma, D. J. Macquarrie, *New J. Chem.* **2000**, *24*, 597. [1e] J. Losada, I. Cuadrado, M. Moran, C. M. Casado, B. Alonso, M. Barranco, *Anal. Chim. Acta* **1997**, *338*, 191. [1f] N. Aydogan, N. L. Abbott, *Langmuir* **2001**, *17*, 5703.

[2] [2a] P. Ferreira, I. S. Goncalves, F. Mosselmans, M. Pillinger, J. Rocha, A. Thursfield, *Eur. J. Inorg. Chem.* **2000**, 97. [2b] T. J. Gardner, C. D. Frisbie, M. S. Wrighton, *J. Am. Chem. Soc.* **1995**, *117*, 6927. [2c] A. S. Viana, A. H. Jones, L. M. Abrantes, M. Kalaji, *J. Electroanal. Chem.* **2001**, *500*, 290. [2d] P. S. Dudek, H. D. Sikes, C. E. D. Chidsey, *J. Am. Chem. Soc.* **2001**, *123*, 8033. [2e] M. Kazemekaite, A. Bulovas, V. Smirnovas, G. Niaura, E. Butkus, V. Razumas, *Tetrahedron Lett.*, in press. [2f]P. C. Pandey, S. Upadhyay, I. Tiwari, G. Singh, V. S. Tripathi, *Sensors Actuators B* **2001**, *72*, 224. [2g] H. Shinohara, T. Kusaka, E. Yokota, R. Monden, S. Masahiko, *Sensors Actuators B* **2000**, *65*, 144−146.

[3] [3a] J. Sotomayor, G. Will, D. Fitzmaurice, *J. Mater. Chem.* **2000**, *10*, 685. [3b] W. Gao, L. Dickinson, C. Grozinger, F. G. Morin, L. Reven, *Langmuir* **1996**, *12*, 6429. [3c] G. Guerrero, A. Vioux, H. Mutin, *Chem. Mater.*, in press. [3d]P. Bonhôte, J. E. Moser, R. Humphry-Backer, N. Vlachopoulos, S. M. Zakeeruddin, L. Walder, M. Grätzel, *J. Am. Chem. Soc.* **1999**, *121*, 1324. [3e] L. A. Vermeulen, J. L. Snover, L. S. Sapochak, M. E. Thomson, *J. Am. Chem. Soc.* **1993**, *115*, 11767.

[4] R. Frantz, F. Carré, J. O. Durand, G. F. Lanneau, *New J. Chem.* **2001**, *25*, 188.

[5] Y. Kobayashi, M. Okamoto, A. Tomita, *J. Mater. Sci.* **1996**, *31*, 6125.

[6] [6a] N. N. Greenwood, T. C. Gibbs, *Mössbauer Spectroscopy*, Chapman & Hall, U. K., London, **1971**. [6b] D. A. Durfey, R. U. Kirss, C. Frommen, W. Feighery, *Inorg. Chem.* **2000**, *39*, 3506. [6c] G. E. Southard, M. D. Curtis, *Organometallics* **2001**, *20*, 508. [6d] H. Sato, *Hyperfine Interact.* **1990**, *57*, 2089.

[7] [7a] H. Sato, H. Ikeura, N. Akutsu, *Hyperfine Interact.* **1991**, *69*, 783. [7b] H. Sato, I. Kusudo, M. Sugiyama, T. Hanasaki, N. Nakamura, *Hyperfine Interact.* **1994**, *93*, 1985.

Received October 19, 2001
[I01414]

A Polymer-Supported β-Ketoesterate Complex of Palladium as an Efficient, Phosphane-Free, Air-Stable, Recyclable Catalyst for the Heck Reaction

Maria M. Dell'Anna,[a] Piero Mastrorilli,[a] Francesco Muscio,[a] Cosimo F. Nobile,*[a] and Gian P. Suranna[a]

Keywords: Heck reaction / Supported catalysts / Palladium

The coupling between aryl iodides and bromides with olefins (Heck reaction) has been studied with a polymer-supported palladium catalyst in the presence of sodium or potassium acetate. The reactions can be performed in air without any activating phosphorus ligands and with non dried solvents. Under suitable conditions the catalyst, which exhibits high activity and selectivity, is recyclable several times with negligible leaching of metal.
(© Wiley-VCH Verlag GmbH, 69451 Weinheim, Germany, 2002)

Introduction

The Heck reaction[1] remains one of the most useful and versatile C−C bond forming reaction known. Although this vinylation of aryl halides has been widely studied in academia, there are not many industrial examples of its exploitation. The reasons for this are economic. Heck reactions are mostly catalysed by palladium complexes in homogeneous solution in the presence of phosphorus ligands, which are toxic and unrecoverable. In addition, these expensive catalysts give problems due to their instability at high reaction temperatures, and their separation and recovery after use. These problems can be overcome, however, by the use of heterogeneous systems,[2] made up of supported palladium complexes, which, moreover, are generally phosphane-free. Palladium metal colloids, in some cases stabilised by the presence of the support, appear to be the active species[3] for phosphane-free catalytic systems.

Polymer-supported palladium complexes have been used for the activation of aryl iodides by several research groups. An early report on a palladium catalyst based on triphenylphosphane-bonded polystyrene resin[4] describes the arylation of olefins by iodoarenes, although no studies on the activity of the recycled resin are reported. In a more recent paper, polymer-supported 1,2-bis(diisopropylphosphanyl)-benzene has been used for preparing a palladium catalyst for the reaction of iodobenzene with methyl acrylate.[5]

The reaction between Pd^{II} salts and a polypyrrole containing a phosphane-borane moiety resulted in another type of solid-supported palladium catalyst[6] that was moderately active in the coupling of iodobenzene with acrylic esters. The support could be recycled, though it needed to be recharged with $Pd(dba)_2$ in each subsequent run.

A palladium complex prepared from a triphenylphosphane amphiphilic resin and a palladium π-allyl chloride dimer has been used as an active catalyst for Suzuki cross-coupling and for the arylation of allylic acetates.[7]

All the heterogenised catalysts in which the support is a polymer with pendant phosphanes suffer from the same problem when used in Heck-type reactions: the irreversible loss of metal from the matrix due both to degradation of the phosphane moieties[2] and to the reaction mechanism itself.[8a] As an example, metal leaching was observed when palladium supported on glass beads was used as catalyst for Heck reactions, owing to the oxidation of phosphanes that bound the metal atoms onto the matrix.[9]

Various examples can be found in the literature concerning non-phosphinated organic polymers as supports for palladium-based catalysts. Among them, Pd^{II} coordinated to a pincer-type κ^3-S,C,S ligand attached to soluble organic polymers has been described as an active and recyclable catalyst for the olefination of iodoarenes at 95−110 °C under homogeneous[10] or liquid/liquid biphasic conditions.[11]

Polymer-supported carbene complexes of palladium have been used as recyclable catalysts for the Heck reaction of aryl bromides at 150 °C, although with significant loss of metal ($60\%_{wt}$) during the first run.[12]

Recently, a bis(pyrimidine)-based palladium polymer-supported catalyst for Heck-type reactions has been synthesised,[13] but no data on the activity of the recovered catalyst has been reported.

Another class of supports onto which catalytically active palladium is dispersed is represented by inorganic matrices. Pd on charcoal and Pd on different metal oxides have been found to be active catalysts for the Heck reaction of aryl

[a] Centro di studi C.N.R. M.I.S.O. and Dipartimento d'Ingegneria Civile ed Ambientale (Sezione Chimica) Politecnico di Bari,
Via Orabona, 4, 70125 Bari Italy
Fax: (internat.) + 39-080/596-3611
E-mail: nobile@poliba.it

iodides.[2] Arai et al.[14] have studied the coupling between iodobenzene and methyl acrylate at 160 °C in the presence of 0.28−1.4 mol % of Pd supported on carbon or silica. Unfortunately, these conventional supported palladium catalysts are unselective when the substrates are bromoarenes, with dehalogenation being the dominant reaction. Pd particles supported on mesoporous silica have also been employed for the coupling of aryl bromides,[15] although satisfactory yields were obtained only with activated substrates such as *p*-bromonitrobenzene.

Very recently, Djakovitch et al. have described Pd-modified zeolites that are very active and recyclable catalysts for the Heck reaction of aryl bromides with olefins.[16]

Herein we report our studies on Heck reactions using a β-ketoesterato polymeric palladium complex (referred to as Pd-pol) as catalyst that exhibits satisfactory activities towards activated and nonactivated iodo- and bromoarene substrates. The supported complex (1.98%$_w$ Pd) was obtained by co-polymerisation of Pd(AAEMA)$_2$ [AAEMA$^-$ is the deprotonated form of 2-(acetoacetoxy)ethylmethacrylate] with ethyl methacrylate and ethylene glycol dimethacrylate.[17]

In this work we have considered the influence of solvent, base, temperature and additives on the performance and the recyclability of the catalyst.

Results and Discussion

Scheme 1 illustrates the scope of the investigated Heck reactions catalysed by Pd-pol. The molar ratio between the limiting substrate (aryl halide) and palladium was optimised at 1000 for reactions with aryl iodide and 500 for reactions with aryl bromides. A general feature of all the Pd-pol catalysed reactions is the simplicity of the set-up and work-up. All manipulations could be performed in an air atmosphere and with non-dried solvents because of the oxygen and moisture stability of the supported catalyst.

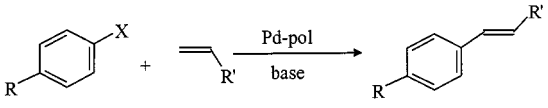

X = I, Br
R = H, CH_3, NO_2, $COCH_3$
R' = $COOCH_3$, CN, C_6H_5

Scheme 1

The effect of the base was examined first. In preliminary experiments triethylamine (the typical base for many homogeneous and heterogeneous catalytic Heck reactions[1,2]) was used, but this organic base caused significant metal leaching. This is probably due to the higher coordination ability of trialkylamines towards palladium[18] than inorganic bases such as alkaline acetates or carbonates. For this reason, all subsequent tests were performed using inorganic bases such as potassium or sodium acetate. As for the choice of solvent, among those tested [toluene, *N*-methylpyrrolidine, dioxane, dimethyl sulfoxide, *N*,*N*-dimethylformamide (DMF), diethylene glycol (DEG)] the best results in terms of catalyst activity were obtained using DMF (with aryl iodides) and DEG (with aryl bromides).

Table 1. Heck coupling reactions of aryl iodides catalysed by Pd-pol; reaction conditions: a molar ratio of 1:1.2:2.4 was used for the aryl iodide (5 mmol):alkene:base (AcOK) in 6 mL DMF; T = 90 °C; molar ratio Pd/ArI = 1:1000; for all reactions the conversion of the aryl iodide was quantitative

Entry	Aryl iodide	Alkene	Additive	*t* (h)	Yield (%)[a] *trans*	*cis*
1		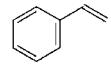	–	6	93	7
2	"		–	6	51	48
3	"	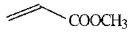	–	2	90	10
4	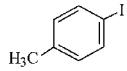	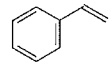	–	4	89	11
5	"		–	6	61	29
6	"	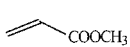	–	4	90	10
7		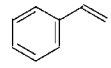	DMG[b]	5	90	10
8	"		DMG[b]	3	58	40
9	"	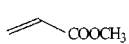	PPh_3[c]	2	95	5

[a] GLC yields. [b] Molar ratio Pd:DMG = 1:20. [c] Molar ratio Pd:PPh_3 = 1:5.

Table 1 summarises the results obtained in the reactions between activated and nonactivated aryl halides with different vinylic substrates. In all cases the conversions were quantitative.

The coupling between iodobenzene and styrene at 90 °C in the presence of 0.10 mol % of supported palladium gave, after 6 h, a 100% yield of stilbene (93% *trans*, 7% *cis*, entry 1). Under the same reaction conditions acrylonitrile afforded 99% cinnamonitrile with no selectivity between the *cis* and *trans* isomers (entry 2). The reaction between iodobenzene and methyl acrylate was faster, giving, at 90 °C, a 90% yield of *trans*-methyl cinnamate after 2 h (entry 3).

Reacting *p*-iodotoluene with styrene (entry 4), acrylonitrile (entry 5) or methyl acrylate (entry 6) resulted in quantitative yields of the desired coupling products.

The same reactions reported in entries 1, 2 and 3 of Table 1 were also carried out at 140 °C, in order to study the influence of the temperature. The reactions at 140 °C were slightly faster than those carried out at 90 °C. In particular, the reaction between iodobenzene and styrene was complete after 5 h, giving a 93% yield of *trans*-stilbene. The reaction between iodobenzene and methyl acrylate gave a quantitative conversion of the limiting substrate after 1 h with a 98% yield of *trans*-methyl cinnamate. The coupling

between iodobenzene and acrylonitrile was complete after 3 h giving a 76% yield of *trans*-cinnamonitrile and a 24% yield of *cis*-cinnamonitrile. In the two latter cases the selectivity was shifted towards the thermodynamically favoured *trans* adduct.

In order to study the influence of additives on the catalyst performance, the reactions of entries 1 and 2 were carried out in the presence of *N*,*N*-dimethylglycine (DMG), which is known to improve the activity and selectivity in the homogeneous phosphane-free Heck coupling of aryl bromides.[19] A slight improvement in the activity was observed. In fact, the TOFs for the reactions without DMG were 167 h^{-1} (entries 1, 2), whereas the TOFs for reactions carried out in the presence of a 20:1 DMG/Pd (mol/mol) ratio were 200 h^{-1} (styrene, entry 7) or 333 h^{-1} (acrylonitrile, entry 8).

The influence of a phosphorus additive, such as triphenylphosphane, was also investigated. The coupling between iodobenzene and methyl acrylate carried out in the presence of triphenylphosphane (5:1 P/Pd mol/mol) gave, after 2 h, a quantitative yield of methyl cinnamate (95% *trans* and 5% *cis*, entry 9), a result similar to that obtained in the phosphane-free reaction (entry 3). However, the presence of triphenylphosphane caused severe metal leaching from the supported catalyst.

In the case of the reaction of entry 9, the recovered catalyst became inactive after three cycles in the presence of PPh_3. On the contrary, the catalyst of the phosphane-free reaction described in entry 1 (Table 1) remained active for at least six cycles (Figure 1).

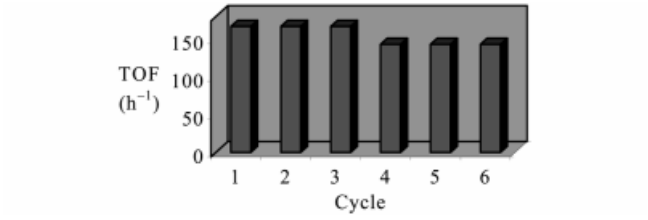

Figure 1. Recyclability of Pd-pol in Heck reactions between iodobenzene and styrene at 90 °C; in each reaction the conversion of iodobenzene was quantitative; TOF = [moles of coupling product (both isomers)]/[(moles of Pd) × (reaction time in hours)]

This behaviour was found to be general: the catalyst of all the phosphane-free reactions described in this work (including those in the presence of DMG) could be recycled at least three times with no loss of activity or selectivity.

The catalyst recycling was performed by filtration, washing with acetone and diethyl ether and with water (for removal of the excess base, its conjugate acid and the formed alkaline halides). This latter treatment did not affect the activity of the catalyst, as occurs in the case of palladium supported on zeolites and metal oxides.[20]

In addition, the mother liquor of all the described phosphane-free reactions (including those in the presence of DMG) showed negligible catalytic activity. On the other hand, the mother liquor of the reaction carried out in the presence of PPh_3 (entry 9) showed a moderate activity, giving a 50% conversion of fresh iodobenzene after 20 h reaction.

It is possible to explain the observed metal leaching in solutions containing PPh_3 as additive by referring to the commonly accepted mechanism.[1] Triphenylphosphane reduces palladium(II) to palladium(0) giving Ph_3PO and the coordinatively unsaturated $Pd(PPh_3)_2$, which can start the catalytic cycle through the oxidative addition of the aryl halide. Hence, the Pd^{II} centre must lose its counteranion (chloride, acetate, etc.) in order to enter the reaction cycle. Loss of the polymer-AAEMA$^-$ ligands, however, forms under-ligated palladium(0), which leaches irreversibly into solution.

Another mechanism, recently proposed by Amatore,[21] claims the intermediacy of anionic palladium complexes. In this case, the pre-activation step gives an anionic palladium(0) complex, which is able to start the catalytic cycle. This cycle is reported in Scheme 2 for the reaction promoted by Pd-pol in the presence of an *n*-fold excess PPh_3.

The anionic complex in our context should be $[Pd^0(PPh_3)_2(A\text{-}pol)]^-$ ([A-pol]$^-$ = polymer-bound β-ketoesterate). Following this type of mechanism the leaching should occur at the stage of the equilibrium (1) of Scheme 2.

In order to study the influence of equilibrium (1) on the metal leaching, one and two equivalents of base (respect to the olefin) were used in two parallel phosphane-assisted reactions. The reaction between iodobenzene and methyl acrylate carried out at 140 °C in the presence of one equivalent of base, 0.50 mol % of PPh_3 and 0.10 mol % of supported Pd, gave a 90% conversion and a 94% yield of *trans*-methyl cinnamate after 5 h. The same reaction carried out in the presence of two equivalents of base gave a quantitative conversion and a 98% yield of *trans*-methyl cinnamate after 1 h. In addition, the recovered resin of the former reaction (1 equiv. of base) was inactive for a second run, while the Pd-pol recovered after the second experiment (2 equiv. of base) was still active even after five further catalytic runs. However, contrary to what happens in phosphane-free reactions, the leaching is not completely inhibited even in the presence of 2 equiv. of base, since the mother liquor of the solution after each cycle revealed a high activity (80% of fresh iodobenzene converted after 3 h reaction).

The lower catalyst activity shown in the reaction carried out with 1 equiv. of base compared with that with 2 equiv. of base (the relevant TOF's are 200 h^{-1} and 1000 h^{-1}, respectively) can be ascribed to the formation of the less active[21a] cationic Pd complex $[ArPd(PPh_3)_2]^+$ generated through the equilibrium (1) of Scheme 2.

Although deeper mechanistic studies are required, these results seem to indicate that the reaction pathway proposed by Amatore is operative in our system.

The effect of the amount of base on metal leaching and on catalyst activity was observed by us also in the phosphane-free reactions. For example, the reaction between iodobenzene and styrene proceeded with TOFs of 83 h^{-1} or 167 h^{-1} when the molar ratio of olefin/base was 1 or 2, respectively. Furthermore, in the former case the copolymer leached out all its palladium loading after three cycles, whereas in the second case the metal content passed from

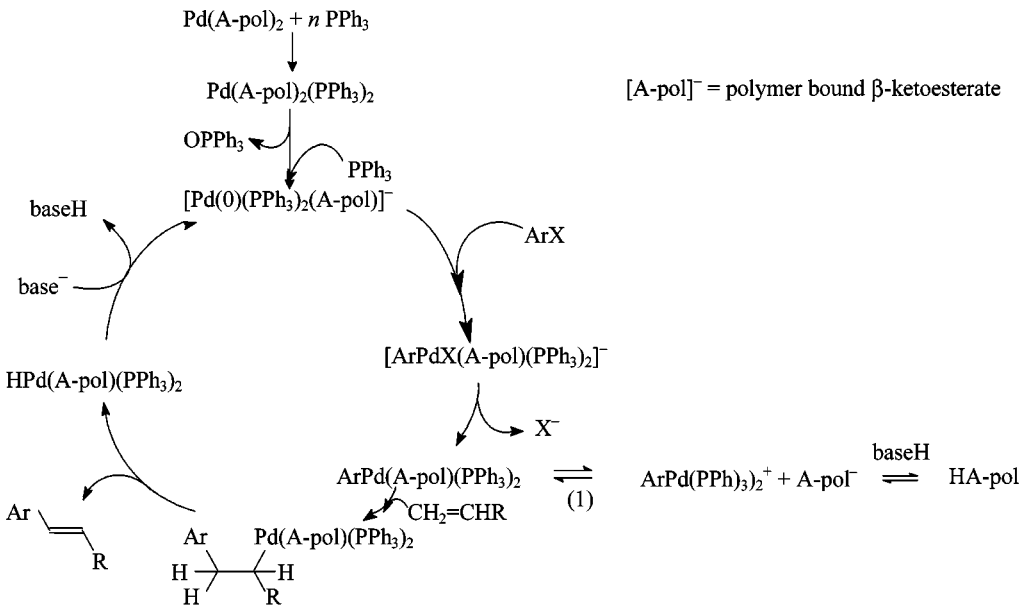

Scheme 2. Catalytic cycle via anionic palladium(0) complexes

1.98% before reaction to 1.67% after six cycles. It is possible to assume that the double amount of base inhibits the protonation of the polymer-supported β-ketoesterate ligand ($AAEMA^-$). Only if it remains anionic, in fact, is the polymeric ligand able to bind the palladium(II) and palladium(0) species involved in the different stages of the reaction cycle. The leaching of the metal could therefore be due to the protonation of the polymeric ligand by the acetic acid formed during the reaction.

In order to verify the influence of the presence of an acid in the reaction medium on metal leaching, the Suzuki reaction between aryl iodides and phenylboronic acid was carried out (Table 2). Quantitative yields of the corresponding coupling products were obtained starting from iodobenzene (entry 1) or *p*-iodotoluene (entry 2) with TOFs of 67 h^{-1} (iodobenzene) and 83 h^{-1} (*p*-iodotoluene). However, as expected, the initially yellow catalyst leached out all its palladium loading into solution and was inactive in subsequent runs.

Although in the case of the polymeric β-ketoesterato support the presence of a double amount of acetate results in increasing activity and recyclability of the supported catalyst, this effect is not generalizable.

The results reported in the literature seem to indicate that the amount of base and its nature can influence the metal leaching, *in function of the support used*. In fact, it has been recently claimed[22] that when Pd/alumina, Pd/C or sulfonated polystyrene-supported palladium are used to promote Heck reactions, the metal loss is enhanced by the presence of acetate ions (and of the aryl halide), presumably due to the formation of soluble $ArPdBr(OAc)_n$ or $ArPd(OAc)_n$ species.[8] Moreover, Arai et al.[14] reported that the Pd species leached out into the solvent during Heck reactions promoted by Pd/C or Pd/SiO_2 redeposited onto the surface of the supports at the end of the reaction only when 1 equiv. of Na_2CO_3 and 1 equiv. triethylamine were used at the same time.

Table 2. Suzuki and Sonogashira coupling reactions of aryl iodides catalysed by Pd-pol; typical reaction conditions: a molar ratio of 1:1.2:2.4 was used for ArI (5 mmol):phenyl boronic acid or phenylacetylene:base (AcOK) in 6 mL DMF; T = 90 °C; molar ratio Pd/aryl iodide = 1:1000; for all reactions the conversion of the aryl iodide was quantitative

Entry	Aryl iodide	Alkyl boron or Alkyne	Time (h)	Product	Yield(%) [a]
1	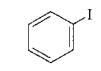	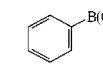	15	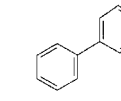	quantitative
2	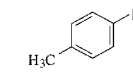	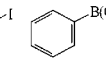	9	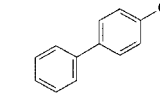	quantitative
3	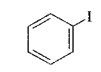	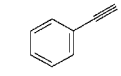	6	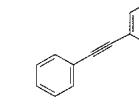	55
4	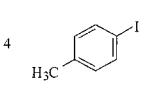	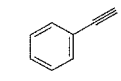	7	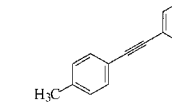	34

[a] GLC yields.

The possibility of activating economically more interesting aryl bromides was also examined (Table 3). Pd-pol was used as catalyst for the Heck reaction of bromobenzene with styrene at 160 °C using a 1:500 Pd/substrate molar ratio, in the presence of DMG. Under these reaction condi-

tions the conversion of the substrate was quantitative after 12 h affording a 95% yield of *trans*-stilbene (entry 1). In the absence of DMG the conversion was quantitative after 24 h and the yield of *trans*-stilbene was 91% (entry 2). After the initial catalytic run, the resin used in the reaction of entry 1 was recovered, washed and recycled five times with negligible loss of activity (Figure 2).

Table 3. Heck coupling reactions of aryl bromides catalysed by Pd-pol; typical reaction conditions: a molar ratio of 1:1.2:2.4 was used for ArBr (5 mmol):alkene:base (NaOAc) in 6 mL DEG; T = 160 °C; molar ratio Pd/ArBr = 1:500

Entry	Aryl bromide	Alkene	Additive	*t* (h)	Yield(%)[a] *trans*	*cis*
1		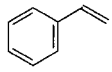	DMG [b]	12	95	5
2	"	"	–	24	91	9
3	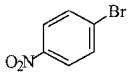	"	DMG [b]	10	90	10
4	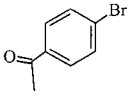	"	DMG [b]	10	92	8
			DMG [b]	12	95	5

[a] GLC yields. [b] Molar ratio Pd:DMG = 1:20.

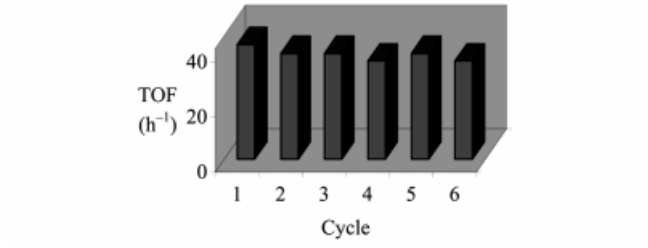

Figure 2. Recyclability of Pd-pol in Heck reactions between bromobenzene and styrene at 160 °C, in the presence of DMG; in each reaction the conversion of bromobenzene was quantitative; TOF = [moles of coupling product (both isomers)]/[(moles of Pd) × (reaction time in hours)]

The reactions of 4-bromonitrobenzene and 4-bromoacetophenone with styrene took 10 h to reach completion giving 90% (entry 3) and 92% yield (entry 4) of the *trans*-coupling adduct, respectively.

The possibility to use aryl chlorides as substrates in the Pd-pol catalytic system has also been examined. Unfortunately, the reactions between chlorobenzene and methyl acrylate or between *p*-chloronitrobenzene and styrene at 180 °C in the presence of DMG and Ph_4PCl[19b] were not effective, and only a small degree of dehalogenation occurred.

Finally, Pd-pol was used as catalyst for the coupling of aryl iodides with phenylacetylene at 90 °C (Sonogashira reaction), but the selectivities were poor (Table 2).

Experimental Section

All preparations, manipulations and reactions were carried out under air. All chemicals were purchased from Aldrich and used as received. The supported catalyst (Pd-pol) was prepared according to the procedure reported in ref.[17] The palladium content in the supported catalyst was determined by atomic absorption spectrometry using a Perkin−Elmer 3110 instrument. Chromatographic analyses were carried out on Hewlett Packard 6890 instruments using an HP-PLOT Molecular Sieve 5A (15.0m × 0.53 mm × 25.0 μm) column (injector temperature 280 °C, FID temperature 280 °C, carrier: nitrogen or helium). GCMS data (EI, 70 eV) were acquired on an HP 6890 instrument (injector temperature 280 °C, carrier: helium) using an HP-1 crosslinked methyl siloxane (60.0 m × 0.25 mm × 1.0 μm) capillary column coupled with a mass spectrometer HP 5973. The products were identified by comparison of their GC and GC-MS features with those of authentic samples. Conversions and yields were calculated by gas chromatography using *n*-dodecane as an internal standard calibrated to the corresponding pure compound. In the case of entry 1 of Table 1, the isolated yield was also assessed as described below.

General Procedure for the Heck, Suzuki and Sonogashira Reactions: A 50 mL pressure tube was charged with Pd-pol (1.98%$_w$ Pd), potassium or sodium acetate (12 mmol), aryl halide (5.0 mmol), olefin, alkyne or arylboronic acid (6.0 mmol), *n*-dodecane as internal standard, the additive (when present) and the solvent (DMF or DEG, 6 mL). The aryl iodide/Pd molar ratio was 1000, whereas the aryl bromide/Pd molar ratio was 500. The mixture was heated whilst stirring at the desired temperature until reaction completion as monitored by GLC and GCMS analyses. After reaction the catalyst was recovered by filtration, washed with acetone, water, acetone and diethyl ether, and dried under vacuum.

Isolation of *trans*-Stilbene: After separation of Pd-pol, the reaction mixture was diluted with CH_2Cl_2 (20 mL) and washed with H_2O (3 × 15 mL). After separation of the organic phase and drying over Na_2SO_4, the solution was concentrated under reduced pressure. Separation of the *cis*/*trans* isomers was carried out by silica gel chromatography with pentane/diethyl ether (1:1) solvent mixtures. The product was obtained in an analytically pure form after recrystallization from diethyl ether at −18 °C (0.808 g, isolated yield = 89.8%).

Catalytic Test for the Determination of the Activity of the Mother Liquor: The clear filtrate obtained from the catalyst was used as solvent for these experiments. This solution was obtained by filtration at 90 °C over celite, in order to remove the fine particles. Fresh reactants (5.0 mmol aryl halide, 6.0 mmol olefin, 12 mmol base) were added to the filtrate and the resulting mixture was heated at the desired temperature whilst stirring for 20 h. The reaction course (if any) was monitored by GLC as described above.

Acknowledgments

Mr. E. Pannacciulli is gratefully acknowledged for technical assistance. The Italian MIUR and CNR are gratefully acknowledged for financial support.

[1] [1a] R. F. Heck, *Palladium in Organic Synthesis*, Academic Press, London, **1985**. [1b] J. Tsuji, *Palladium Reagents and Catalysts*, Wiley Chichester, **1995**. [1c] S. Brase, A. de Meijere, in *Metal-Catalysed Cross-Coupling Reactions* (Eds.: F. Diederich, P. J. Stang), Wiley-VCH, Weinheim, **1997**.

[2] [2a] I. P. Beletskaya, A. V. Cheprakov, *Chem. Rev.* **2000**, *100*, 3009−3066 and references therein. [2b] H.-U. Blaser, A. Indolese, A. Schyner, H. Ser, M. Studer, *J. Mol. Catal. A* **2001**, *173*, 3−18 and references therein. [2c] A. Biffis, M. Zecca, M. Basato, *J. Mol. Catal. A* **2001**, *173*, 249−274 and references therein.
[3] [3a] J. Le Bars, U. Specht, J. S. Bradley, D. G. Blackmond, *Langmuir* **1999**, *15*, 7621−7625. [3b] M. T. Reetz, E. Westermann, *Angew. Chem. Int. Ed.* **2000**, *39*, 165−168. [3c] A. Biffis, *J. Mol. Catal. A* **2001**, *165*, 303−307.
[4] C. M. Andersson, K. Karabelas, H. Halberg, C. Andersson, *J. Org. Chem.* **1985**, *50* 3891−3895.
[5] P.-W. Wang, M. A. Fox, *J. Org. Chem.* **1994**, *59*, 5358−5364.
[6] N. Riegel, C. Darcel, O. Stephan, S. Juge, *J. Organomet. Chem.* **1998**, *567*, 219−233.
[7] Y. Uozumi, H. Danjo, T. Hayashi, *J. Org. Chem.* **1999**, *64*, 3384−3388.
[8] [8a] I. W. Davies, L. Matty, D. L. Hughes, P. J. Reider, *J. Am. Chem. Soc.* **2001**, *123*, 10139−10140, and references therein. [8b] It is worth noting that when carrying out the vinylation of iodobenzene with 4 equiv. of acetate, the resin Pd-pol suffered from severe metal leaching. After one cycle the Pd content was reduced to a half, probably due to the substitution of the polymer-supported β-keto esterate ligand with the acetate.
[9] M. S. Anson, M. P. Leese, L. Tonks, J. M. J. Williams, *J. Chem. Soc., Dalton Trans.* **1998**, 3529−3538.
[10] D. E. Bergbreiter, P. L. Osburn, Y.-S. Liu, *J. Am. Chem. Soc.* **1999**, *121*, 9531−9538.
[11] D. E. Bergbreiter, P. L. Osburn, A. Wilson, E. M. Sink, *J. Am. Chem. Soc.* **2000**, *122*, 9058−9064.
[12] J. Schwarz, V. P. M. Bohm, M. G. Gardiner, M. Grosche, W. A. Herrmann, W. Hieringer, G. Raudaschl-Sieber, *Chem. Eur. J.* **2000**, *6*, 1773−1780.
[13] M. R. Buchmeiser, T. Schareina, R. Kempe, K. Wurst, *J. Organomet. Chem.* **2001**, *634*, 39−46.
[14] F. Zhao, B. M. Bhanage, M. Shirai, M. Arai, *Chem. Eur. J.* **2000**, *6*, 843−848.
[15] C. P. Mehnert, D. W. Weaver, J. Y. Ying, *J. Am. Chem. Soc.* **1998**, *120*, 12289−12296.
[16] [16a] L. Djakovitch, K. Koehler, *J. Am. Chem. Soc.* **2001**, *123*, 5990−5999. [16b] L. Djakovitch, K. Koehler, *J. Mol. Catal. A: Chem.* **1999**, *142*, 275−284. [16c] L. Djakovitch, K. Koehler, H. Heise, *J. Organomet. Chem.* **1999**, *584*, 16−26.
[17] M. M. Dell'Anna, P. Mastrorilli, A. Rizzuti, G. P. Suranna, C. F. Nobile, *Inorg. Chim. Acta* **2000**, *304*, 21−25.
[18] M. Beller, T. M. Riermeir, *Tetrahedron Lett.* **1996**, *37*, 6535−6538.
[19] [19a] M. T. Reetz, E. Westermann, R. Lohmer, G. Lohmer, *Tetrahedron Lett.* **1998**, *39*, 8449−8452. [19b] M. T. Reetz, G. Lohmer, R. Schwickardi, *Angew. Chem. Int. Ed.* **1998**, *37*, 481−483.
[20] K. Koler, M. Wagner, L. Djakovitch, *Catal. Today* **2001**, *66*, 105−114.
[21] [21a] C. Amatore, A. Jutand, *J. Organomet. Chem.* **1999**, *576*, 254−278. [21b] C. Amatore, A. Jutand, *Acc. Chem. Res.* **2000**, *33*, 314−321.
[22] A. Biffis, M. Zecca, M. Basato, *Eur. J. Inorg. Chem.* **2001**, 1131−1133.

Received November 5, 2001
[I01436]

Synthesis and Characterization of Methyltrioxorhenium(VII) Immobilized in Bipyridyl-Functionalized Mesoporous Silica

Carla D. Nunes,[a] Martyn Pillinger,[a] Anabela A. Valente,[a] Isabel S. Gonçalves,*[a] João Rocha,[a] Paula Ferreira,[b] and Fritz E. Kühn*[b]

Keywords: Rhenium / Supported catalysts / Mesoporous materials / Lewis base adducts

Methyltrioxorhenium(VII) (MTO) has been immobilized in the mesoporous silica MCM-41 functionalized with pendant bipyridyl (bpy) groups of the type 4-[(–O)$_3$Si(CH$_2$)$_4$]-4′-CH$_3$-2,2′-bipyridine. Powder X-ray diffraction and N_2 adsorption-desorption studies confirm that the regular hexagonal symmetry of the host is retained during the grafting reaction and that the channels remain accessible. Solid-state magic angle spinning NMR spectroscopy (^{29}Si, ^{13}C) was also used to monitor the coupling reactions. The formation of a tethered Lewis base adduct of the type CH$_3$ReO$_3$·bpy is confirmed by IR, Raman, and X-ray absorption fine structure (XAFS) spectroscopy. The XAFS results do, however, indicate that not all rhenium ions are present in this form, and this agrees with elemental analysis which gives an Re/N ratio of 1:1.1 (0.55 mmol Re g^{-1}). It is likely that the excess rhenium atoms are present as uncoordinated MTO molecules assembled in the MCM channels. The model complexes (4-alkyl-4′-methyl-2,2′-bipyridine)(methyl)trioxorhenium (alkyl = methyl, *n*-butyl) were also prepared and characterized.

(© Wiley-VCH Verlag GmbH, 69451 Weinheim, Germany, 2002)

Introduction

Methyltrioxorhenium(VII) (MTO) has excellent catalytic properties in numerous oxy functionalizations,[1] some examples being the oxidation of olefins,[2] alcohols,[3] arenes,[4] and carbonylmetal compounds.[5] The epoxidation of olefins has received particular attention, using MTO to activate H_2O_2. Due to the Lewis acidity of the rhenium center, a major limitation of this system is the opening of the epoxide ring, leading to the formation of diols in the presence of water.[1,6] It was soon found, however, that amine additives, such as pyridine,[7] pyrazole,[8] and 3-cyanopyridine,[9] enhance the efficiency and selectivity of MTO-catalyzed oxidations. The aromatic N-base ligands work by coordinating to the metal center, thereby reducing the Lewis acidity of the catalyst and additionally accelerating the catalytic reactions. MTO forms trigonal-bipyramidal adducts with pyridines and related bases,[10a] and distorted octahedral adducts with bidentate Lewis bases, e.g. 4,4′-dimethyl-2,2′-bipyridine, 1,10-phenanthroline, and 2,2′-bipyrimidine.[10b] In the presence of H_2O_2 these complexes form very active and highly selective epoxidation catalysts.

Alternative strategies to improve MTO-catalyzed oxidations have involved host-guest inclusion chemistry. It was found that a urea/hydrogen peroxide complex is a very effective oxidant in heterogeneous olefin epoxidations and silane oxidations catalyzed by MTO.[11] With NaY-zeolite as host for these reactions also resulted in high yields and excellent product selectivities.[12] MTO has also been supported on silica functionalized with polyether tethers.[13] In the absence of an organic solvent, this catalytic assembly catalyzed the epoxidation of alkenes with 30% H_2O_2 with high selectivity compared to the ring-opened products observed in homogeneous media. In another example, MTO was heterogenized inside the porous system of a hybrid silica matrix by the sol-gel method using 4-[3-(triethoxysilyl)-propylamino]pyridine hydrochloride as a hydrolyzable ligand.[14] A supported catalyst of this type could, in principle, combine the advantages of a Lewis base adduct of MTO with the well-known benefits of a heterogeneous host-guest catalyst system.

Recently, we devised a stepwise procedure for the functionalization of the ordered mesoporous silica MCM-41 with pendant 4-alkyl-4′-methyl-2,2′-bipyridine groups.[15] Elemental analysis, powder X-ray diffraction (XRD), N_2 adsorption-desorption, solid-state magic angle spinning (MAS) NMR (^{13}C, ^{29}Si) and IR spectroscopy were used to monitor the different coupling reactions. The ligand−silica was subsequently examined as a support for the hetero-

[a] Department of Chemistry, University of Aveiro, Campus de Santiago,
3810-193 Aveiro, Portugal
Fax: (internat) + 351-234/370084
E-mail: igoncalves@dq.ua.pt
[b] Anorganisch-chemisches Institut der Technischen Universität München,
Lichtenbergstraße 4, 85747 Garching bei München, Germany
Fax: (internat) + 49-89/28913473
E-mail: fritz.kuehn@ch.tum.de

genization of the dioxomolybdenum(VI) complex $MoO_2Cl_2(THF)_2$. Instead of forming surface-bound monomeric complexes of the type $MoO_2Cl_2(bpy)$, weakly bound oxo-bridged dimers were formed with a metal−metal separation of 3.28 Å. In the present work, MTO is used as the oxometal species rather than the fragment MoO_2Cl_2, with the intention of forming surface-bound Lewis base adducts of the type **1**. The known MTO adduct **2**, containing the ligand 4,4′-dimethyl-2,2′-bipyridine, and also the novel complex **3**, containing the asymmetrical bipyridine ligand 4-(*n*-butyl)-4′-methyl-2,2′-bipyridine, have been prepared as model compounds. The hybrid material has been characterized by Raman spectroscopy and Re L-edge X-ray absorption fine structure (XAFS) spectroscopy, in addition to the techniques mentioned above.

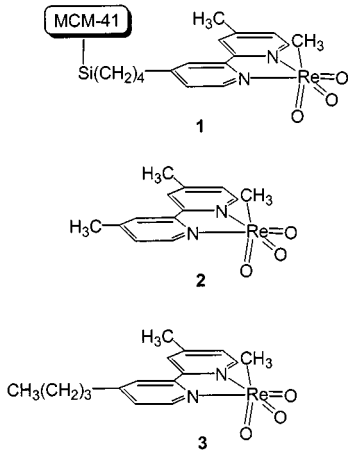

Results and Discussion

The preparation and characterization of MCM-41 functionalized with bipyridyl groups has been described in a previous paper.[15] In the first step, the pristine calcined hexagonally ordered mesoporous host (d_{100} = 36.3 Å, a = 41.9 Å) is covalently grafted with (3-chloropropyl)trimethoxysilane. The second step comprises substitution of about 21% of pendant chloro groups by the anion [4-CH_2-4′-CH_3-2,2′-bipyridine]$^-$ to give a material containing about 0.3 mmol bipyridyl groups per gram, designated as MCM-41-bpy. Powder XRD and N_2 adsorption-desorption analysis demonstrate that the textural characteristics of the support are preserved during the grafting experiments and that the channels remain accessible (BET specific surface area 720 $m^2\ g^{-1}$, total pore volume 0.37 $cm^3\ g^{-1}$).

The heterogenization of MTO was carried out by treating the ligand−silica MCM-41-bpy (0.5 g) with a dichloromethane solution of MTO (0.046 M, 0.92 mmol) at room temperature. The resulting material, designated as MCM-41-bpy/MTO, was recovered by filtration and washed repeatedly with dichloromethane. Drying the product under vacuum at room temperature did not liberate (sublime) MTO from the MCM channels (pure MTO sublimes at 25 °C when using an oil-pump vacuum). The material is moderately air- and light-sensitive. Elemental analysis indicated a metal loading of 10.24 mass-% Re (0.55 mmol g^{-1}), giving an Re/N molar ratio of 1:1.1. If it is assumed that all Re is present as MTO, and knowing the specific total pore volume before and after introduction of MTO (see below), the volume occupied by MTO molecules in MCM-41-bpy/MTO is calculated to be 0.04 $cm^3\ g^{-1}$. It follows that the mass of MTO molecules per unit volume occupied is 3.5 g cm^{-3} [= 0.1024×(249.2/186.2)/0.04]. This value is similar to the density of bulk MTO (4.1 g cm^{-3}).

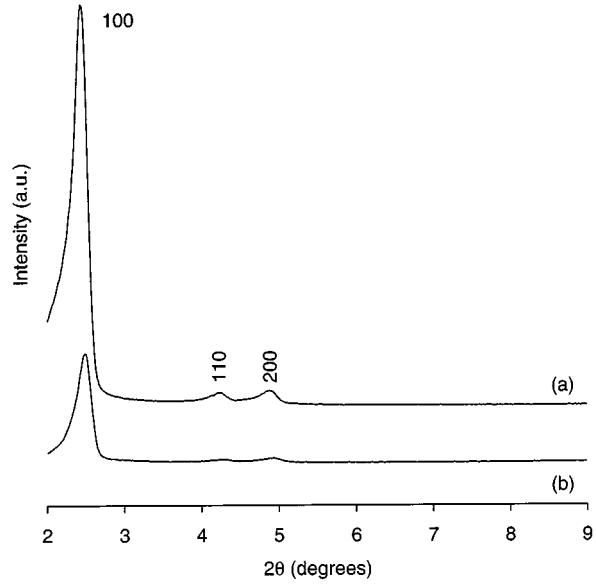

Figure 1. Powder XRD patterns of (a) MCM-41-bpy and (b) MCM-41-bpy/MTO

Figure 1 shows the powder XRD patterns of MCM-41-bpy and MCM-41-bpy/MTO. Three reflections are observed in the range 2θ = 2−8° for MCM-41-bpy, indexed assuming a hexagonal cell as (100), (110), and (200). The d value of the (100) reflection is 36.0 Å leading to a lattice constant of a = 41.6 Å. Three reflections are also observed for MCM-41-bpy/MTO, indicating retention of the long-range hexagonal symmetry. There is a slight contraction of the unit cell (d_{100} = 35.4 Å, a = 40.9 Å) and the intensities of the three reflections are considerably reduced compared to the starting ligand−silica. This is not interpreted as a severe loss of crystallinity. Instead, it is likely that there is a reduction in the X-ray scattering contrast between the silica wall and pore-filling material.[16] A similar phenomenon was observed for treatment of MCM-41-bpy with the complex $MoO_2Cl_2(THF)_2$,[15] and MCM-41 grafted with multiply bonded dimolybdenum complexes.[17]

Figure 2 shows the low-temperature N_2 adsorption-desorption isotherm for MCM-41-bpy/MTO. The corresponding isotherms for the pristine calcined MCM-41 host and the ligand−silica MCM-41-bpy are also shown for comparison. Each isotherm can be classified as type IV as defined by IUPAC,[18] characteristic of mesoporous solids (having pore widths between 2 and 50 nm). The isotherms show no evidence of hysteresis loops resulting from capillary condensation/evaporation, which has been attributed

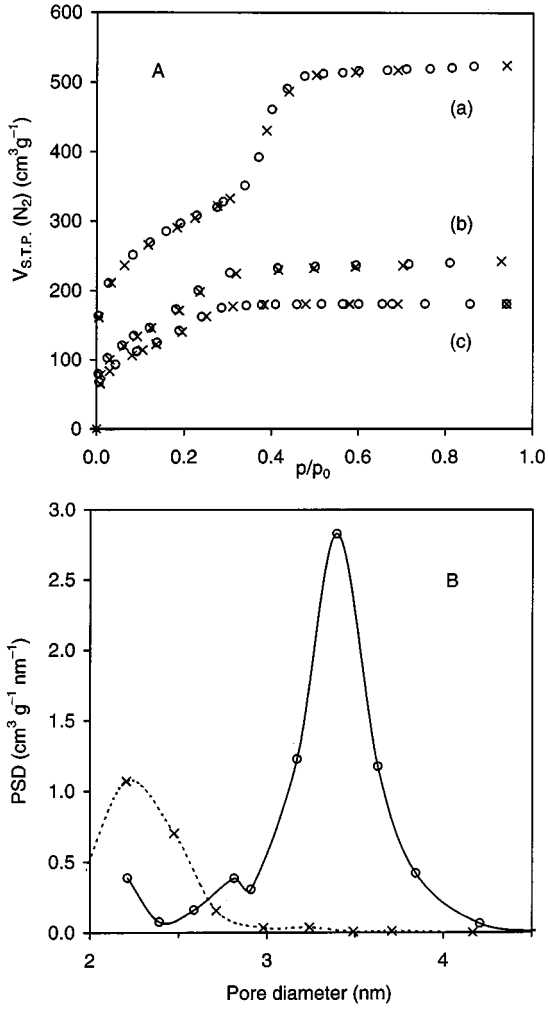

Figure 2. A: N_2 adsorption (×) and desorption (O) isotherms at 77 K of (a) pristine MCM-41, (b) MCM-41-bpy and (c) MCM-41-bpy/MTO; B: pore-size distribution profiles for pristine MCM-41 (——) and MCM-41-bpy/MTO (···)

to the instability of the liquid nitrogen meniscus.[18] Each of the modifications carried out to produce the two derivatized samples MCM-41-bpy and MCM-41-bpy/MTO leads to a decrease in the N_2 uptake at any given p/p_0, and both the BET specific surface area and pore volume decrease (Table 1). In the case of MCM-41, a pronounced step is observed between relative pressures of 0.32 and 0.42, arising from the condensation of nitrogen inside the primary mesopores. The sharpness of this step reflects the uniform pore size. A comparison of the pore size distribution (PSD) curves for MCM-41 and MCM-41-bpy/MTO reveals that the position of the maximum decreases from 34 to 23 Å (Figure 2). The decrease in the intensity of the maximum, together with an increase in the width at half height, indicates an increase in pore heterogeneity.

The material MCM-41-bpy/MTO was further characterized by thermogravimetric analysis (TGA), IR, Raman, MAS NMR, and XAFS spectroscopy. In order to assist the interpretation of these results, the known adduct **2** and the novel derivative **3** were prepared as model compounds. These complexes are readily obtained as yellow solids by

Table 1. Texture parameters of MCM-41 samples from N_2 isotherms at 77 K

Sample	S_{BET} [$m^2\ g^{-1}$]	ΔS_{BET} (%)[a]	V_P [$cm^3\ g^{-1}$]	ΔV_P (%)[b]
MCM-41	1029	–	0.81	–
MCM-41-bpy	718	−30	0.37	−54
MCM-41-bpy/MTO	574	−44	0.28	−66

[a] Variation of surface area in relation to parent MCM-41. [b] Variation of total pore volume in relation to parent MCM-41.

the reaction of MTO with 1 equiv. of bidentate N,N-ligand in tetrahydrofuran (THF) at room temperature (Scheme 1). Spectroscopic data (IR and ^1H NMR) for **2** are in agreement with that reported.[10b] The ^1H and ^{13}C NMR chemical shifts for the Re−CH_3 groups in **2** are located at δ = 1.20 and 25.9, respectively.[10b] The shifts in these resonances compared to those of uncoordinated MTO [δ(^{13}C) = 19.03; δ(^1H) = 2.67] are a consequence of electron donation to the Lewis-acidic metal center. In fact it has been shown that the weaker the donor ability of the Lewis base, the closer, in general, are the observed δ(^1H) and δ(^{13}C) values to those of uncoordinated MTO.[10] In the case of **3**, δ(^1H) and δ(^{13}C) of Re−CH_3 are located at δ = 1.09 and 26.0, respectively, and therefore the ligand in **3** can be considered as being a slightly stronger donor than that in **2**.

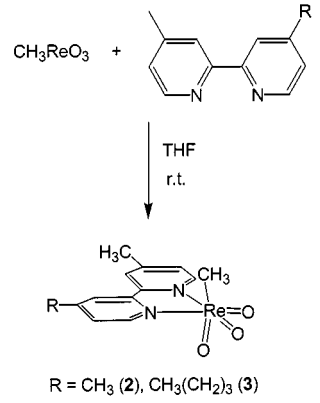

Scheme 1

TGA of MCM-41-bpy/MTO shows that the material decomposes in three steps up to 750 °C. It is stable under nitrogen up to about 50 °C, but then undergoes an abrupt mass loss, losing 6.0% up to 100 °C and a further 2.3% up to 200 °C. It is assumed that this is due to decomposition/sublimation of encapsulated MTO (MTO sublimes below 100 °C under TG conditions[19]). Further heating gives a residual mass of 81% at 750 °C. For comparison, the adduct CH_3ReO_3(4,4′-dimethyl-2,2′-bipyridine) (**2**) is stable under nitrogen up to 110 °C, then undergoes an abrupt mass loss of 24% up to 180 °C. This must correspond to rupture of the Re−N bond and sublimation of the now uncoordinated MTO. At 750 °C 42% remains as residual mass.

The IR spectrum of MCM-41-bpy/MTO contains one split band at 917 cm^{-1} (922 and 912 cm^{-1}) that is not observed in the spectrum of the ligand−silica MCM-41-bpy. This is attributed to an asymmetric Re=O stretching vibration. An associated symmetric stretching vibration should be present at higher frequency but is probably obscured by a broad band at 961 cm^{-1} arising from the silica host. The Raman spectrum shows more clearly the bands corresponding to the symmetric and asymmetric Re=O stretching vibrations (940 and 918 cm^{-1}, Figure 3). The model compound **3** displays very similar IR (940 and 919 cm^{-1}) and Raman (937 and 916 cm^{-1}) absorptions. From the IR data for **3** the force constant of the Re=O vibration can be calculated[20] to be 7.41 mdyn $Å^{-1}$. The corresponding bands for bulk MTO appear at 999 cm^{-1} (symmetric) and 957 cm^{-1} (asymmetric), yielding a force constant of 8.46 mdyn $Å^{-1}$.[10b] The decrease in the force constant indicates a weakening of the Re=O bonds, caused by electron donation from the coordinated bipyridyl groups to the Re^{VII} center.[10,21]

Further evidence for the formation of surface-bound adducts of the type $CH_3ReO_3(N-N)$ in MCM-41-bpy/MTO comes from the Raman bands of the tethered bipyridine groups. The precursor ligand−silica MCM-41-bpy displays bands at 1607 and 1559 cm^{-1} due to pyridyl ring stretching vibrations, and a band at 997 cm^{-1} due to an in-plane ring C−H deformation vibration (Figure 3). The corresponding ligand 4-(*n*-butyl)-4′-methyl-2,2′-bipyridine displays three identical bands. In complex **3** these bands shift to 1615, 1555 and 1030 cm^{-1}. Very similar results are obtained for the functionalized material MCM-41-bpy/MTO (bands at 1611, 1555 and 1031 cm^{-1}). The Raman spectrum of this material also contains a weak band at 997 cm^{-1}. This could be due to the ring C−H deformation vibration of uncoordinated bipyridyl groups, or alternatively to the Re=O symmetric stretching vibration of uncoordinated MTO molecules aggregated in the MCM channels. The Raman spectra of the complexes **2** and **3** contain a weak band at 555 cm^{-1} due to the Re−C stretching vibration (cf. 575 cm^{-1} for bulk MTO), and also a strong band at about 475 cm^{-1} that does not appear in the spectra of either the corresponding free ligand or bulk MTO. This latter band may be due to a C−Re=O deformation vibration.[22] While a band for the Re−C stretching vibration is not observed in the Raman spectrum of the material MCM-41-bpy/MTO, a band is clearly seen at 474 cm^{-1} that does not appear in the spectrum of MCM-41-bpy.

The ^{29}Si MAS and CP MAS NMR spectra of MCM-41-bpy/MTO are similar to those of the precursor MCM-41-bpy (Figure 4).[15] Two broad overlapping peaks at $\delta = -109.8$ and -102.0 are assigned to Q^4 and Q^3 units, respectively, of the silica framework, where $Q^n = Si(OSi)_n(OH)_{4-n}$. Two signals are also observed at $\delta = -58.7$ and -66.7, assigned to T^2 and T^3 organosilica species, respectively [$T^m = RSi(OSi)_m(OMe)_{3-m}$]. The ^{13}C CP MAS NMR spectrum of MCM-41-bpy/MTO is also largely unchanged compared to that of MCM-41-bpy (Figure 5).

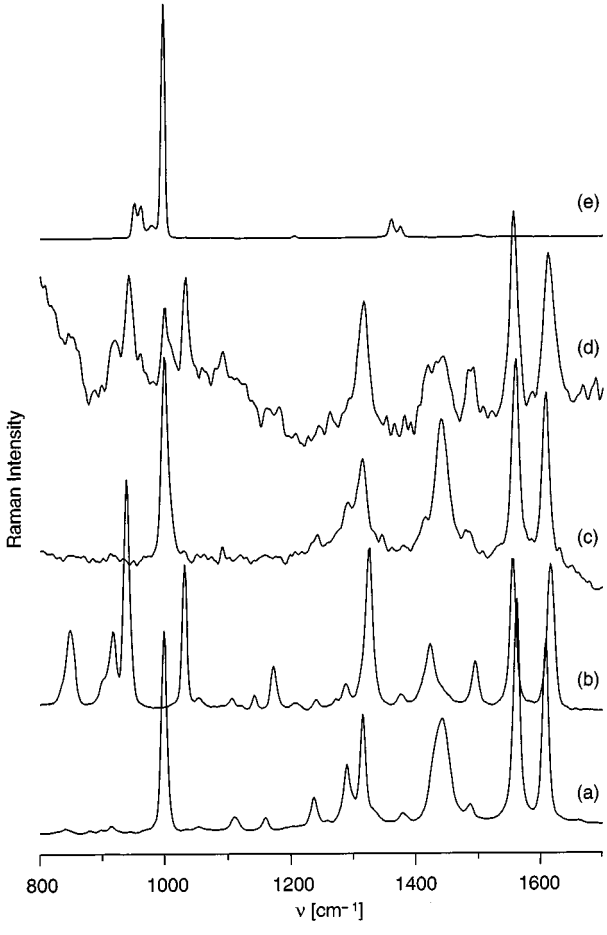

Figure 3. Raman spectra of (a) 4-(*n*-butyl)-4′-methyl-2,2′-bipyridine, (b) [4-(*n*-butyl)-4′-methyl-2,2′-bipyridine](methyl)trioxorhenium (**3**), (c) MCM-41-bpy, (d) MCM-41-bpy/MTO and (e) CH_3ReO_3

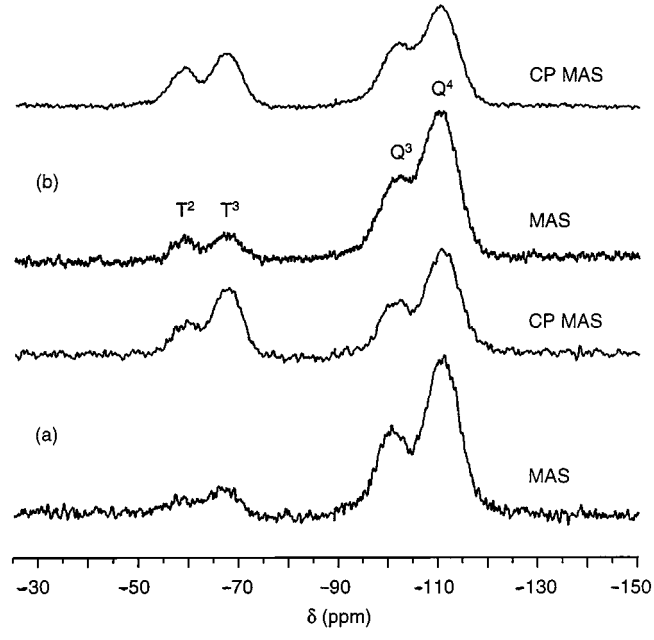

Figure 4. ^{29}Si MAS and CP MAS NMR spectra of (a) MCM-41-bpy and (b) MCM-41-bpy/MTO

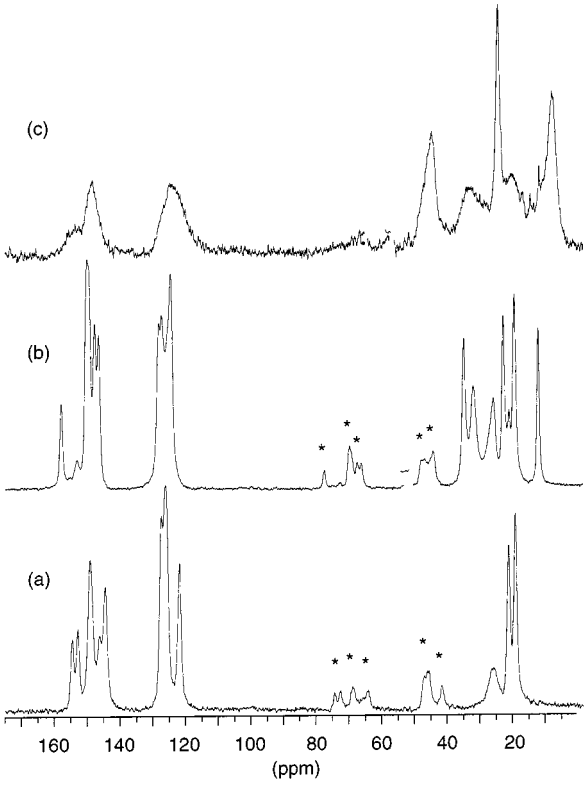

Figure 5. ^{13}C CP MAS NMR spectra of (a) (4,4′-dimethyl-2,2′-bipyridine)(methyl)trioxorhenium (**2**), (b) [4-(*n*-butyl)-4′-methyl-2,2′-bipyridine](methyl)trioxorhenium (**3**), and (c) MCM-41-bpy/MTO; asterisks denote spinning sidebands

Assignment of these spectra was supported by measuring the solution spectra of the ligand 4-(*n*-butyl)-4′-methyl-2,2′-bipyridine, and the MTO adduct of this ligand (**3**). Solid-state MAS NMR spectra were also recorded for **2** and **3** (Figure 5). In the ^{13}C CP MAS NMR spectrum of MCM-41-bpy/MTO, two broad peaks at δ = 149.3 and 125.7, and a shoulder at δ = 155.0, are assigned to the pyridyl ring carbon atoms. The other signals in the spectrum are attributed as follows: δ = 46.1 [Si(O*Me*)$_n$CH$_2$R and −*C*H$_2$Cl], 35.0 (−*C*H$_2$*C*H$_2$−bpy), 26.0 [Re−CH$_3$ and Si(OMe)$_n$CH$_2$*C*H$_2$−], 21.8 (*C*H$_3$−bpy), 9.6 [Si(OMe)$_n$-*C*H$_2$R]. Treatment of MCM-41-bpy with MTO produces only one measurable change in the ^{13}C NMR spectrum: the signal at δ = 123.3 shifts to δ = 125.7. A similar shift difference is observed for the corresponding resonances of the ligand 4-(*n*-butyl)-4′-methyl-2,2′-bipyridine and the MTO adduct of this ligand (**3**).

XAFS measurements at the Re L_I and L_{III} absorption edges were carried out at low temperature (20 K) for the Lewis base adduct **2** and MCM-41-bpy/MTO. The Re L_I X-ray absorption near edge structure (XANES) spectrum of **2** contains a weak pre-edge peak, caused by a 2s → 5d(Re) + 2p(O) electron transition (Figure 6).[23] With respect to the rhenium coordination, the intensity of this peak is usually strongest for systems with non-inversion symmetry, such as tetrahedral coordination. MTO, for example, exhibits an intense sharp pre-edge peak.[24] Any distortion of the regular tetrahedral symmetry leads to a decrease in the peak intensity. The XANES spectrum of **2** is therefore consistent with the expected rhenium coordination, i.e. distorted octahedral geometry. It is obvious that the XANES spectrum of MCM-41-bpy/MTO is quite different from that of **2**, in that the pre-edge peak is stronger and there are differences in the oscillations towards higher energy (Figure 6). In fact, the spectrum of MCM-41-bpy/MTO comes close to that reported for bulk MTO.[24]

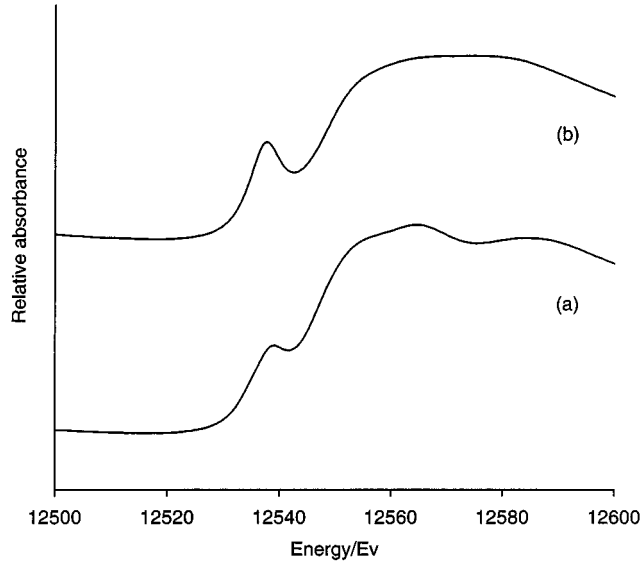

Figure 6. Re L_I-edge XANES spectra of (a) (4,4′-dimethyl-2,2′-bipyridine)(methyl)trioxorhenium (**2**), and (b) MCM-41-bpy/MTO

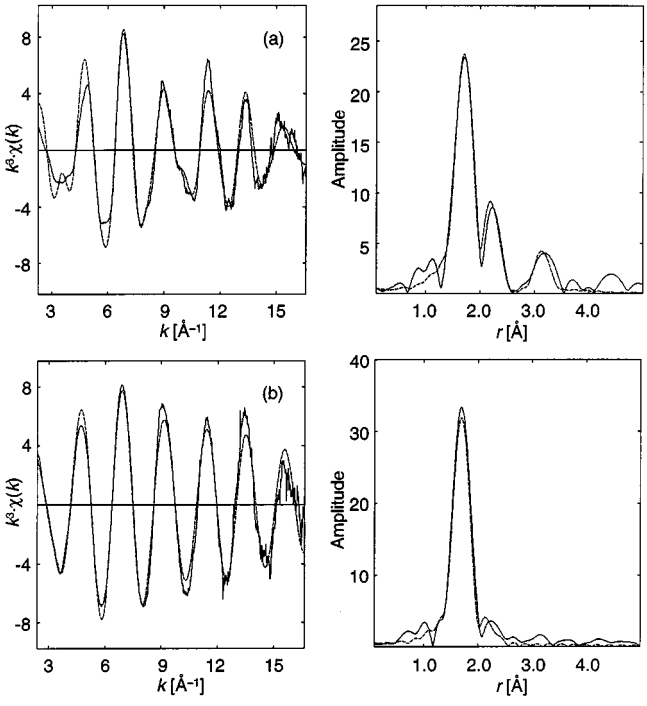

Figure 7. Re L_{III}-edge XAFS and Fourier transforms for (a) (4,4′-dimethyl-2,2′-bipyridine)(methyl)trioxorhenium (**2**), and (b) MCM-41-bpy/MTO; the solid line represents the experimental data and the dashed line shows the best fit using parameters given in Table 2

Table 2. Re L_{III}-edge XAFS-derived structural parameters for (4,4′-dimethyl-2,2′-bipyridine)(methyl)trioxorhenium (**2**) and MCM-41-bpy/MTO

Compound	Atom	CN[a]	r [Å]	$2\sigma^2$ [Å^2][b]	E_f [eV][c]	R (%)[d]
2[e]	O	3.0(1)	1.741(2)	0.0048(3)	−13.8(5)	27.2
	N	2.5(2)	2.246(5)	0.0052(8)		
	C	4.0(6)	3.192(11)	0.0078(19)		
MCM-41-bpy/MTO	O	3.3(1)	1.729(1)	0.0027(2)	−11.2(5)	19.0
	N	1.3(3)	2.216(11)	0.0091(24)		

[a] CN = Coordination number. Values in parentheses are statistical errors generated in EXCURVE. The true errors in coordination numbers are likely to be of the order of 20%; those for the interatomic distances ca. 1.5%.[25] [b] Debye−Waller factor; σ = root-mean-square internuclear separation. [c] E_f = edge position (Fermi energy), relative to calculated vacuum zero. [d] $R = (\int[\Sigma^{theory} - \Sigma^{exp.}]k^3 dk / [\Sigma^{exp.}]k^3 dk) \times 100\%$. [e] Compound **2** has been examined by single-crystal X-ray crystallography,[10b] but bond lengths and bond angles could not be determined reliably because the structure is disordered with respect to the position of the metal center.

Analysis of the Re L_{III} XAFS spectrum of **2** allowed three shells for O, N and C neighbors to be determined, in order of increasing distance from the absorbing atom (Figure 7, Table 2). The Re−O bond length of 1.74 Å is typical of all known (oxo)Re^{VII} complexes containing an Re=O double bond.[1f] Bidentate coordination of the bipyridyl ligand is confirmed by the presence of the other two shells for N (2.25 Å) and C (3.19 Å). The Re−N bond length is comparatively long, indicating a weak N→Re bonding interaction. Identical Re−N bond lengths were determined by single-crystal X-ray crystallography for the adducts $XReO_3$[4,4′-bis(*tert*-butyl)-2,2′-bipyridine] (X = Cl, Br).[26] The Re···N shell almost certainly includes a component for the carbon shell corresponding to Re−C, expected at about 2.1 Å. The similarity of the two elements as back-scatterers, together with the close proximity of the two shells, means that only one shell can be fitted. The Re L_{III} XAFS of MCM-41-bpy/MTO was initially fitted by a model comprising one shell of oxygen atoms. Both the refined distance (1.74 Å) and coordination number (3.3) are consistent with the presence of trioxorhenium species. Addition of a second shell for nitrogen atoms at 2.22 Å (coordination number = 1.3) reduced the R factor from 23.2 to 19.0% (Table 2, Figure 7). This shell was significant at the 99% level according to the statistical test of Joyner et al.[27] There was no evidence for a well-defined Re···Re outer coordination shell.

Conclusions

MCM-41 functionalized with bipyridyl groups has been successfully used as a support for the immobilization of methyltrioxorhenium(VII). Powder XRD and N_2 adsorption-desorption studies confirm that the regular hexagonal symmetry of the mesoporous host is retained during the grafting reaction and that the channels remain accessible. The formation of a tethered Lewis base adduct of the type CH_3ReO_3(bpy) is substantiated by IR, Raman, and XAFS spectroscopy. The latter technique does, however, indicate that not all rhenium atoms are present in this form and this is consistent with elemental analysis which gives an Re/N ratio of 1:1.1. It is likely that the excess rhenium atoms are present as uncoordinated MTO molecules assembled in the MCM channels. This phenomenon may be similar to that reported for MTO encapsulated in zeolite Y,[28] where it was proposed that each supercage contained a cluster of four MTO guest molecules aggregated by Re=O···Re intermolecular interactions.

Experimental Section

General: All manipulations were carried out using standard Schlenk techniques under nitrogen. Solvents were dried by standard procedures (THF, *n*-hexane and Et_2O with Na/benzophenone ketyl; CH_2Cl_2 with CaH_2), distilled under nitrogen and kept over 4 Å molecular sieves. Lithium diisopropylamide was prepared as described in the literature.[29] 4,4′-Dimethyl-2,2′-bipyridine was purchased from Aldrich and used as received. Microanalyses were performed at the Mikroanalytisches Laboratorium of the Technical University of Munich (M. Barth and co-workers). Powder XRD data were collected with a Phillips X'pert diffractometer using Cu-K_α radiation filtered by Ni. Nitrogen adsorption-desorption measurements were carried out at 77 K, using a gravimetric adsorption apparatus equipped with a CI electronic MK2-M5 microbalance and an Edwards Barocel pressure sensor. Before analysis, pristine calcined MCM-41 was degassed at 723 K overnight to a residual pressure of ca. 10^{-4} mbar. A lower degassing temperature of 413 K was used for the modified materials (to minimize destruction of the functionalities). The specific surface areas (S_{BET}) were determined by the BET method. The total pore volume (V_P) was estimated from the N_2 uptake at $p/p_0 \approx 0.95$, using the liquid nitrogen density of 0.8081 g cm^{-3}. The pore size distribution curves (PSD, the differential volume adsorbed with respect to the differential pore size per unit mass as a function of pore width) were computed from the desorption branch of the experimental isotherms, using a method based on the area of the pore walls.[18,30] Assuming open cylindrical pores of radius r_p, zero contact angle, and accounting for the statistical film thickness (t), r_p is given by the sum of the Kelvin radius and t.[18] The t values were derived from a standard nitrogen isotherm for nonporous hydroxylated silica (available from the literature[31]) using the Halsey equation.[18] Although it is known that such traditional methods based on the Kelvin equation underestimate the pore sizes in the range up to ca. 7.5 nm,[32] in this work these calculations are only intended to monitor changes in pore sizes after complexation, by comparing with the parent MCM-41. TGA studies were performed using a Perkin−Elmer TGA7 thermobalance system at a heating rate of 10 K min^{-1} under

nitrogen. IR spectra were measured with a Unican Mattson Mod 7000 FTIR spectrometer using KBr pellets. Raman spectra were recorded with a Bruker RFS 100/S FT Raman spectrometer using a 1064 nm excitation wavelength of the Nd/YAG laser. ^{1}H and ^{13}C solution NMR spectra were obtained with a Bruker AMX-300 spectrometer. ^{29}Si and ^{13}C solid-state NMR spectra were recorded at 79.49 and 100.62 MHz, respectively, with a (9.4 T) Bruker Avance 400P spectrometer. ^{29}Si MAS NMR spectra were recorded with 40° pulses, spinning rates 5.0−5.5 kHz and 60 s recycle delays. ^{29}Si CP MAS NMR spectra were recorded with 5.5 μs ^{1}H 90° pulses, 8 ms contact time, a spinning rate of 4.5 kHz, and 4 s recycle delays. ^{13}C CP MAS NMR spectra were recorded with a 4.5 μs ^{1}H 90° pulse, 2 ms contact time, a spinning rate of 8 kHz, and 4 s recycle delays. Chemical shifts are quoted in parts per million from tetramethylsilane (TMS). Re L_I- and L_{III}-edge X-ray absorption spectra were measured at 20 K in transmission mode on beamline BM29 at the ESRF (Grenoble), operating at 6 GeV in 2/3 filling mode with typical currents of 180−190 mA. One scan was performed for each sample and set up to record the pre-edge at 5 eV steps and the post-edge region in 0.025−0.05 Å^{-1} steps, giving a total acquisition time of ca. 40 min per scan. The order-sorting double Si(311) crystal monochromator was detuned to give 50% harmonic rejection. Solid samples were diluted with BN and pressed into 13 mm pellets. Air-sensitive samples were handled under an inert gas. Ionization chamber detectors were filled with Ar to give 30% absorbing I_o (incidence) and 70% absorbing I_t (transmission). The programs EXCALIB and EXBACK (SRS Daresbury Laboratory, UK) were used in the usual manner for calibration and background subtraction of the raw data. XAFS curve-fitting analyses, by least-squares refinement of the non-Fourier-filtered k^3-weighted XAFS data, were carried out using the program EXCURVE (version EXCURV98[33]) using fast curved-wave theory.[34] Theoretical phase shifts were obtained within this program using ab initio calculations based on the Hedin Lundqvist/von Barth scheme.

4-(*n*-Butyl)-4′-methyl-2,2′-bipyridine: Prepared by modification of a literature procedure.[29] A solution of 4,4′-dimethyl-2,2′-bipyridine (0.50 g, 2.71 mmol) in THF (15 mL) was added to a THF solution of lithium diisopropylamide (2.71 mmol). After 2 h, the orange-brown solution was cooled to −20 °C and $CH_3CH_2CH_2Br$ (0.25 mL) added. After 2 h, iced water was added to the green reaction mixture. The organic solution was dried with Na_2SO_4 and the solvent removed to give the crude product. The yellow residue was purified by recrystallization from diethyl ether to give a colorless solid. Yield: 0.55 g, 89%. $C_{15}H_{18}N_2$ (226.32): calcd. C 79.61, H 8.02, N 12.38; found C 79.48, H 7.98, N 12.18. IR (KBr): $\tilde{\nu}$ = 2957 m, 2925 s, 2870 m, 1596 s, 1553 m, 1460 s, 1376 m, 1104 m, 1023 m, 992 m, 824 s, 799 m, 670 m, 515 m cm^{-1}. Raman: $\tilde{\nu}$ = 3054 s, 2920 s, 2873 sh, 1607 s, 1561 s, 1487 w, 1442 m, 1379 w, 1315 m, 1290 m, 1237 m, 1159 w, 1110 w, 997 s, 737 m, 525 m, 344 w, 237 m cm^{-1}. ^{1}H NMR ($CDCl_3$, room temp., 300 MHz, TMS): δ = 0.86 (t, 3 H, CH_3), 1.29 (m, 2 H, CH_2), 1.60 (m, 2 H, CH_2), 2.36 (s, 3 H, py-CH_3), 2.62 (t, 2 H, py-CH_2), 7.05 (d, 2 H, py-H), 8.15 (s, 2 H, py-H), 8.47 (t, 2 H, py-H). ^{13}C {^{1}H} NMR ($CDCl_3$, room temp., 75.47 MHz, TMS): δ = 13.9 (CH_3CH_2), 21.2 (py-CH_3), 22.4 (CH_3CH_2), 32.5 (py-CH_2CH_2), 35.2 (py-CH_2), 121.3, 122.0, 123.9, 124.6, 148.9, 152.9, 156.0 (all py-C).

MCM-41 Functionalized with 4-[(−CH_2)$_4$]-4′-CH_3-2,2′-bipyridine (MCM-41-bpy): Prepared as described previously.[15] Raman: $\tilde{\nu}$ = 3057 m, 2899 s, 1607 s, 1559 s, 1440 s, 1314 s, 997 s, 732 w, 650 w, 238 m cm^{-1}.

MCM-41 Functionalized with Methyltrioxorhenium(VII) (MCM-41-bpy/MTO): To a suspension of MCM-41-bpy (0.50 g) in CH_2Cl_2 (5 mL) a solution of MTO (0.23 g, 0.92 mmol) in CH_2Cl_2 (10 mL) was added and the mixture stirred at room temperature for 24 h. The solution was filtered off and the pale yellow powder washed repeatedly with CH_2Cl_2 (4 × 20 mL), before drying under vacuum at room temperature for several hours; found C 11.80, H 2.40, Cl 3.34, N 0.83, Re 10.24, Si 27.70. IR (KBr): $\tilde{\nu}$ = 2938 w, 1559 w, 1438 w, 1384 w, 1233 sh, 1067 vs, 961 s, 921 vs, 913 vs, 801 s, 550 sh, 465 vs cm^{-1}. Raman: $\tilde{\nu}$ = 3069 w, 2913 m, 1611 m, 1556 m, 1484 w, 1442 w, 1317 m, 1031 m, 997 m, 941 m, 918 w, 733 w, 474 w, 237 w cm^{-1}. ^{29}Si MAS NMR: δ = −109.8, −102.0 (sh), −66.6, −58.5. ^{29}Si CP MAS NMR: δ = −109.8 (Q^4), −101.7 (Q^3), −66.7 (T^3), −58.7 (T^2). ^{13}C CP MAS NMR: δ = 9.6 [(−O)$_3$SiCH$_2$−], 21.8 (py-CH_3), 26.0 [(−O)$_3$SiCH$_2$*C*H$_2$− and Re−CH_3], 35.0 (py−CH_2CH_2−), 46.1 [Si(O*Me*)$_n$$CH_2$R and −$CH_2$Cl], 125.7, 149.3, 155.0 (all py-C).

(4,4′-Dimethyl-2,2′-bipyridine)(methyl)trioxorhenium (2): Prepared as described previously.[10b] Raman: $\tilde{\nu}$ = 3067 m, 2921 m, 1614 s, 1556 s, 1489 m, 1418 m, 1376 w, 1319 s, 1176 m, 1029 s, 937 vs, 912 s, 846 m, 833 m, 742 m, 668 w, 555 m, 474 s, 355 m, 343 m, 316 w, 271 m, 243 m, 196 m, 157 m cm^{-1}. ^{13}C CP MAS NMR: δ = 20.8 (py-CH_3), 22.8, 27.3 (Re−CH_3), 122.5, 126.8, 145.0, 149.4, 153.2, 154.7 (all py-C).

[4-(*n*-Butyl)-4′-methyl-2,2′-bipyridine](methyl)trioxorhenium (3): To a solution of MTO (0.56 g, 2.25 mmol) in CH_2Cl_2 (5 mL) 1 equiv. of 4-(*n*-butyl)-4′-methyl-2,2′-bipyridine was added. The resulting yellow solution was stirred for 1 h at room temperature. The solvent was evaporated, and the product washed with hexane and dried under vacuum. Yield: 1.02 g, 95%. $C_{16}H_{21}N_2O_3Re$ (475.56): calcd. C 40.41, H 4.45, N 5.89; found C 40.36, H 4.41, N 5.73. IR (KBr): $\tilde{\nu}$ = 3122 m, 3065 m, 3030 m, 2953 s, 2923 s, 2860 m, 1615 vs, 1555 s, 1492 s, 1466 m, 1419 s, 1375 m, 1310 s, 1243 m, 1030 s, 940 vs (Re=O), 918 vs (Re=O), 848 vs, 831 vs, 737 s, 555 m (Re−C), 540 m, 524 m, 480 m, 424 m, 358 s cm^{-1}. Raman: $\tilde{\nu}$ = 3070 m, 2921 s, 1615 s, 1555 s, 1495m, 1423 m, 1325 s, 1171 m, 1030 s, 937 vs, 916 m, 848 m, 743 m, 667 w, 555 w, 481 s, 352 m, 316 w, 265 m, 195 m cm^{-1}. ^{1}H NMR ($CDCl_3$, room temp., 300 MHz, TMS): δ = 0.98 (t, 3 H, CH_3), 1.09 (s, 3 H, Re−CH_3), 1.43 (m, 2 H, CH_2), 1.72 (m, 2 H, CH_2), 2.58 (s, 3 H, py-CH_3), 2.81 (t, 2 H, py-CH_2), 7.38 (d, 2 H, py-H), 8.09 (d, 2 H, py-H), 8.92 (m, 2 H, py-H). ^{13}C {^{1}H} NMR ($CDCl_3$, room temp., 75.47 MHz, TMS): δ = 13.8 (CH_3CH_2), 21.6 (py-CH_3), 22.3 (CH_3CH_2), 27.0 (Re−CH_3), 32.3 (py-CH_2CH_2), 35.4 (py-CH_2), 123.1, 123.8, 126.5, 127.2, 148.9, 150.2, 151.9, 156.7 (all py-C). ^{13}C CP MAS NMR: δ = 13.8 (CH_3CH_2), 21.1 (py-CH_3), 24.4 (CH_3CH_2), 27.4 (Re-CH_3), 33.5 (py-CH_2CH_2), 36.3 (py-CH_2), 125.2, 127.9, 128.7, 146.9, 148.0, 150.3, 153.3, 158.1 (all py-C).

Acknowledgments

This work was partly funded by FCT, POCTI and FEDER (Project PCTI/1999/QUI/32889). Financial support was also obtained from the Alexander von Humboldt foundation (to P. F.), Bayerische Forschungsstiftung (to I. S. G.), Deutsche Forschungsgemeinschaft and Fonds der Chemischen Industrie. A. A. V and M. P. thank FCT for post-doctoral grants, and C. N. thanks the University of Aveiro for a research grant. F. E. K. additionally thanks Prof. Dr. W. A. Herrmann for continuous and generous support. We are grateful to the director of the ESRF for the provision of facilities and to Stuart Ansell (local contact on BM29) for help in the XAFS

experiments. We also wish to thank Pedro Vaz for help with the Raman experiments and Marta Lopes for recording MAS spectra.

[1] [1a] G. S. Owens, J. Arias, M. M. Abu-Omar, *Catal. Today* **2000**, *55*, 317−363. [1b] F. E. Kühn, A. M. Santos, I. S. Gonçalves, C. C. Romão, A. D. Lopes, *Appl. Organomet. Chem.* **2001**, *15*, 43−50. [1c] F. E. Kühn, W. A. Herrmann, *Chemtracts: Org. Chem.* **2001**, *14*, 59. [1d] W. Adam, C. M. Mitchell, C. R. Saha-Möller, O. Weichold, *Struct. Bonding* **2000**, *97*, 237−286. [1e] J. H. Espenson, *Chem. Commun.* **1999**, 479−488. [1f] C. C. Romão, F. E. Kühn, W. A. Herrmann, *Chem. Rev.* **1997**, *97*, 3197−3246.

[2] [2a] W. A. Herrmann, R. W. Fischer, D. W. Marz, *Angew. Chem. Int. Ed. Engl.* **1991**, *30*, 1638−1641. [2b] W. A. Herrmann, R. W. Fischer, W. Scherer, M. U. Rauch, *Angew. Chem. Int. Ed. Engl.* **1993**, *32*, 1157−1160.

[3] [3a] W. A. Herrmann, J. P. Zoller, R. W. Fischer, *J. Organomet. Chem.* **1999**, *579*, 404−407. [3b] T. H. Zauche, J. H. Espenson, *Inorg. Chem.* **1998**, *37*, 6827−6831.

[4] W. Adam, W. A. Herrmann, J. Lin, C. R. Saha-Möller, R. W. Fischer, J. D. G. Correia, *Angew. Chem. Int. Ed. Engl.* **1994**, *33*, 2475−2476.

[5] [5a] W. R. Thiel, R. W. Fischer, W. A. Herrmann, *J. Organomet. Chem.* **1993**, *459*, C9−C11. [5b] W. A. Herrmann, J. D. G. Correia, F. E. Kühn, G. R. J. Artus, C. C. Romão, *Chem. Eur. J.* **1996**, *2*, 168−173.

[6] W. A. Herrmann, R. W. Fischer, M. U. Rauch, W. Scherer, *J. Mol. Catal.* **1994**, *86*, 243−266.

[7] [7a] J. Rudolph, K. L. Reddy, J. P. Chiang, K. B. Sharpless, *J. Am. Chem. Soc.* **1997**, *119*, 6189−6190. [7b] W. A. Herrmann, F. E. Kühn, M. R. Mattner, G. R. J. Artus, M. R. Geisberger, J. D. G. Correia, *J. Organomet. Chem.* **1997**, *538*, 203−209.

[8] W. A. Herrmann, R. M. Kratzer, H. Ding, W. R. Thiel, H. Glas, *J. Organomet. Chem.* **1998**, *555*, 293−295.

[9] [9a] C. Copéret, H. Adolfsson, K. B. Sharpless, *Chem. Commun.* **1997**, 1565−1566. [9b] H. Adolfsson, A. Converso, K. B. Sharpless, *Tetrahedron Lett.* **1999**, *40*, 3991−3994. [9c] H. Adolfsson, C. Copéret, J. P. Chiang, A. K. Yudin, *J. Org. Chem.* **2000**, *65*, 8651−8658.

[10] [10a] F. E. Kühn, A. M. Santos, P. W. Roesky, E. Herdtweck, W. Scherer, P. Gisdakis, I. V. Yudanov, C. D. Valentin, N. Rösch, *Chem. Eur. J.* **1999**, *5*, 3603−3615. [10b] P. Ferreira, W. -M. Xue, É. Bencze, E. Herdtweck, F. E. Kühn, *Inorg. Chem.* **2001**, *40*, 5834−5841.

[11] [11a] W. Adam, C. M. Mitchell, *Angew. Chem. Int. Ed. Engl.* **1996**, *35*, 533−534. [11b] W. Adam, C. M. Mitchell, C. R. Saha-Möller, O. Weichold, *J. Am. Chem. Soc.* **1999**, *121*, 2097−2103.

[12] W. Adam, C. R. Saha-Möller, O. Weichold, *J. Org. Chem.* **2000**, *65*, 2897−2899.

[13] R. Neumann, T. -J. Wang, *Chem. Commun.* **1997**, 1915−1916.

[14] K. Dallmann, R. Buffon, *Catal. Commun.* **2000**, *1*, 9−13.

[15] C. Nunes, A. A. Valente, M. Pillinger, A. C. Fernandes, C. C. Romão, J. Rocha, I. S. Gonçalves, *J. Mater. Chem.*, accepted for publication.

[16] [16a] B. Marler, U. Oberhagemann, S. Vortmann, H. Gies, *Micropor. Mater.* **1996**, *6*, 375−383. [16b] W. Hammond, E. Prouzet, S. D. Mahanti, T. J. Pinnavaia, *Micropor. Mesopor. Mater.* **1999**, *27*, 19−25.

[17] P. Ferreira, I. S. Gonçalves, F. E. Kühn, M. Pillinger, J. Rocha, A. Thursfield, W. M. Xue, G. Zhang, *J. Mater. Chem.* **2000**, *10*, 1395−1401.

[18] S. J. Gregg, K. S. W. Sing, *Adsorption, Surface Area and Porosity*, 2nd ed., Academic Press, London, **1982**.

[19] W. A. Herrmann, W. M. Wachter, F. E. Kühn, R. W. Fischer, *J. Organomet. Chem.* **1998**, *553*, 443−452.

[20] J. Mink, G. Keresztury, A. Stirling, W. A. Herrmann, *Spectrochim. Acta A* **1994**, *50*, 2039−2058.

[21] A. M. Santos, F. E. Kühn, W.-M. Xue, E. Herdtweck, *J. Chem. Soc., Dalton Trans.* **2000**, 3570−3574.

[22] S. Köstlmeier, G. Pacchioni, W. A. Herrmann, N. Rösch, *J. Organomet. Chem.* **1996**, *514*, 111−117.

[23] M. Fröba, K. Lochte, W. Metz, *J. Phys. Chem. Solids* **1996**, *57*, 635−641.

[24] M. Fröba, O. Muth, *Adv. Mater.* **1999**, *11*, 564−567.

[25] J. Evans, J. T. Gauntlett, J. F. W. Mosselmans, *Faraday Discuss. Chem. Soc.* **1990**, 107−118.

[26] F. E. Kühn, J. J. Haider, E. Herdtweck, W. A. Herrmann, A. D. Lopes, M. Pillinger, C. C. Romão, *Inorg. Chim. Acta* **1998**, *279*, 44−50.

[27] R. W. Joyner, K. J. Martin, P. Meehan, *J. Phys. C* **1987**, *20*, 4005−4012.

[28] A. Malek, G. Ozin, *Adv. Mater.* **1995**, *7*, 160−163.

[29] D. K. Ellison, R. T. Iwamoto, *Tetrahedron Lett.* **1983**, *24*, 31−32.

[30] J. M. Thomas, W. J. Thomas, *Principles and Practices of Heterogeneous Catalysis*, VCH, Weinheim, **1997**.

[31] M. R. Bhambhani, P. A. Cutting, K. S. W. Sing, D. H. Turk, *J. Colloid Interface Sci.* **1972**, *38*, 109.

[32] C. Lastoskie, K. E. Gubbins, N. Quirke, *J. Phys. Chem.* **1993**, *97*, 4786−4796.

[33] N. Binsted, *EXCURV98*, CCLRC Daresbury Laboratory computer program, **1998**.

[34] [34a] S. J. Gurman, N. Binsted, I. Ross, *J. Phys. C* **1984**, *17*, 143−151. [34b] S. J. Gurman, N. Binsted, I. Ross, *J. Phys. C* **1986**, *19*, 1845−1861.

Received November 8, 2001
[I01444]

A New MnO_x Cathode Material for Rechargeable Lithium Batteries

Arno Perner,*[a] K. Holl,[a] D. Ilic,[a] and M. Wohlfahrt-Mehrens[b]

Keywords: Lithium batteries / Manganese oxides / Cathode materials

Different manganese oxide phases have been synthesized. Rietveld analysis of XRD profiles and galvanostatic cycling in 2025 coin cells were performed for structural and electrochemical characterization. A new two-phase product, containing α-MnO_2 and β-MnO_2 components, was found to deliver better electrochemical results than single phase α-MnO_2, β-MnO_2 or α/ramsdellite-MnO_2. It is shown that the β-MnO_2 phase is responsible for the high discharge capacities and that the α-MnO_2 is responsible for a stable structure during lithium intercalation and extraction, as the hollandite structure shows a small unit-cell volume change. This new cathode material is therefore a β-MnO_2 phase stabilized with α-MnO_2. Furthermore, the reaction of the new α/β-MnO_2 with LiOH was examined. Some lithium atoms of LiOH are intercalated within the channels as Li_2O in order to stabilize the structure, so that no capacity loss after the first cycle appears, whilst others form a $Li_2O{\cdot}MnO_2$ phase that delivers an additional structure stabilization and therefore a better cycling performance.

(© Wiley-VCH Verlag GmbH, 69451 Weinheim, Germany, 2002)

Introduction

The development of secondary lithium batteries involves the use of high performance cathodic materials with numerous requirements such as high gravimetric and volume capacity, high density, high standard potential, fast electrode kinetics, reversible insertion reaction, satisfactory electronic conductivity, low solubility, a relatively low price for production, low toxicity, chemical compatibility with the electrolyte and good rechargeability. Therefore, intensive research has been carried out in the field of rechargeable positive electrodes.[1−9]

Manganese oxides are of interest as insertion electrodes for both primary and secondary lithium batteries.[10] The rechargeability of 3 V manganese oxide electrodes tends to be limited by the anisotropic expansion and contraction of the crystallographic unit cell when lithium is inserted into, and removed from, the manganese oxide. 3 V positive materials are used, for example, in button cells of different sizes for memory back-up (MBU) and bridging applications.[11]

The goal of this paper was to optimize 3 V cathode materials in order to improve the cycling stability and the discharge capacities. To fulfill these requirements we focused our efforts on stabilizing the α-MnO_2 structure with foreign phases. The structure of α-MnO_2 with the large [2 × 2] channels of the hollandite framework is not stable to lithium insertion/extraction. These [2 × 2] tunnels are usually occupied by cations (e.g. Ba^{2+}, K^+...) or water molecules (as OH^-) which hinder the lithium ion diffusion within the channels. As a consequence the α-MnO_2 framework must be stabilized by replacing these cations or water molecules with Li_2O[12,13] or by adding foreign phases[14] (e.g. ramsdellite-MnO_2, pyrolusite).

Thackeray proposed an α-MnO_2 (hollandite) structure stabilized with ramsdellite-MnO_2, which delivers higher discharge capacities than single-phase α-MnO_2 or ramsdellite-MnO_2.[14]

We report here a transformation of α/ramsdellite-MnO_2 when annealing at 350 °C. As a thermal transformation of ramsdellite to β-MnO_2 (pyrolusite) was observed by Ramsdell,[15] we assume a transformation of α/ramsdellite-MnO_2 to α/β-MnO_2. The structure and electrochemical properties of single-phase α-MnO_2, ramsdellite-MnO_2, β-MnO_2, α /ramsdellite-MnO_2 and the new α/β-MnO_2 are compared.

All these manganese oxides suffer from a large irreversible capacity loss after the first discharge (up to 30%) due to lithium trapped within the channels in order to stabilize the structure. The manganese oxides are chemically lithiated to reduce this irreversible capacity loss. We also observe that a reaction of the MnO_2 samples with LiOH results in a product consisting of lithium-stabilized MnO_2 with lithium intercalated within the channels [16] and an $Li_2O{\cdot}MnO_2$ phase.

[a] VARTA Gerätebatterie GmbH
Daimlerstrasse 1, 73479 Ellwangen, Germany
Fax: (internat.) + 49-(0)7961/83511
E-mail: arno.perner@varta.com
[b] Centre for Solar Energy and Hydrogen Research Baden-Wuerttemberg,
Helmholtzstr.8, 89081 Ulm, Germany

Results and Discussion

Structure

The new α/β-MnO_2 was synthesized by annealing α/ramsdellite-MnO_2 at 350 °C for several hours. Figure 1 shows the TG/DSC graph of α/ramsdellite-MnO_2 with endothermic peaks at 100−150 °C and 170−220 °C due to the loss of surface adsorbed water and structural water, respectively. There is an additional endothermic peak at around 300 °C due to the transformation of α/ramsdellite-MnO_2 to α/β-MnO_2.

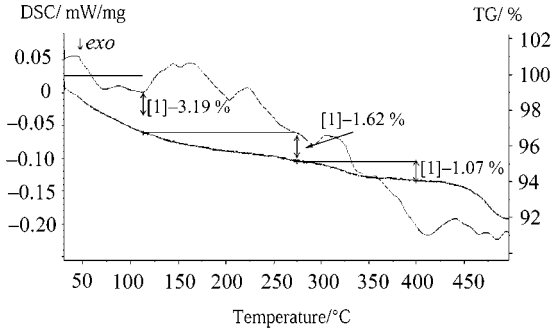

Figure 1. TG/DSC graph of α/Ramsdellite-MnO_2 with an endothermic peak at about 300 °C due to the transformation of α/Ramsdellite-MnO_2 to α/β-MnO_2

Figure 2 shows the different XRD patterns of single-phase α-MnO_2 with the hollandite structure, α/ramsdellite-MnO_2 [14] with the characteristic ramsdellite-MnO_2 Bragg line [110] at 22° and the new α/β-MnO_2. The pattern is characteristic of a two-phase product consisting of α-MnO_2 with a tetragonal unit cell (space group *I*4/*m*) and a β-MnO_2 phase with a pyrolusite structure (tetragonal symmetry).

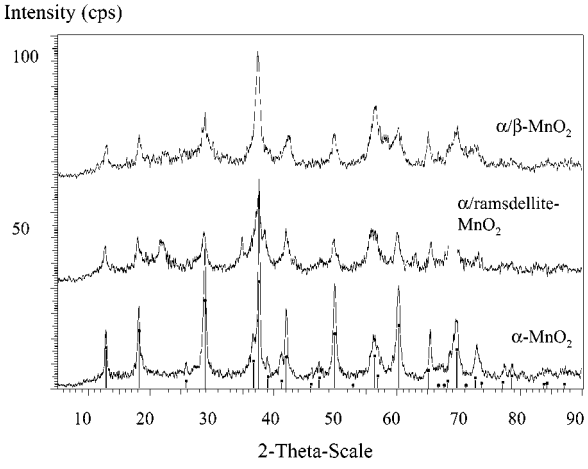

Figure 2. The different XRD patterns of single-phase α-MnO_2 with the hollandite structure, α/ramsdellite-MnO_2 with the characteristic Ramsdellite-MnO_2 reflex [110] at 22° and the new α/β-MnO_2

Table 1 compiles some characteristic reflexes of α-MnO_2 and β-MnO_2. The XRD lines at about 2θ = 28, 37, 42 and 56° of single phase α-MnO_2 coincide with the XRD lines of β-MnO_2. Figure 3 demonstrates that the [141], [600] and [521] lines recorded for α-MnO_2 are similar to the α/β-MnO_2 pattern, although there is an obvious difference in peak intensities. The XRD peak at about 56° of the synthesized α/β-MnO_2 shows a higher intensity than that of the single phase α-MnO_2 peak as the [211] line of β-MnO_2 coincides with the α-MnO_2 [600] line.

Table 1. Characteristic reflexes of α-MnO_2 and β-MnO_2

2θ (°)	Phase	*hkl*
12.781	α-MnO_2	[110]
18.112	α-MnO_2	[200]
28.882	α-MnO_2	[310]
28.670	β-MnO_2	[110]
37.488	α-MnO_2	[211]
37.342	β-MnO_2	[101]
41.993	α-MnO_2	[301]
42.800	β-MnO_2	[111]
49.847	α-MnO_2	[141]
56.356	α-MnO_2	[600]
56.645	β-MnO_2	[211]
60.253	α-MnO_2	[521]
59.363	β-MnO_2	[220]

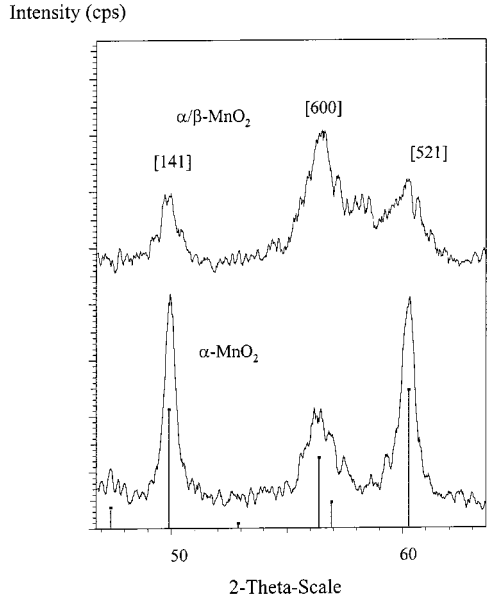

Figure 3. The [141], [600] and [521] reflexes of the measured XRD pattern of α-MnO_2 compared with the α/β-MnO_2 pattern

A [001] projection of the α-MnO_2 framework structure is given in Figure 4. The structure consists of [2×2] tunnels and of [1×1] tunnels with the pyrolusite structure. The structure of α/β-MnO_2 can be described by the model shown in Figure 5. It has an intergrown structure of layers of [2×2] channels and layers of [1×1] channels with disordered stacking. Layers with the hollandite structure alternate with several layers with the pyrolusite structure.

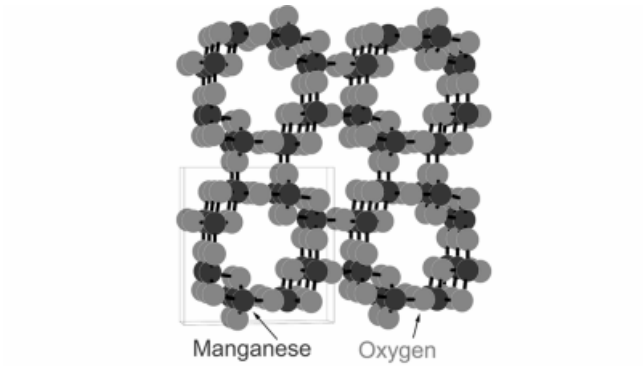

Figure 4. [001] projection of the α-MnO_2 framework structure

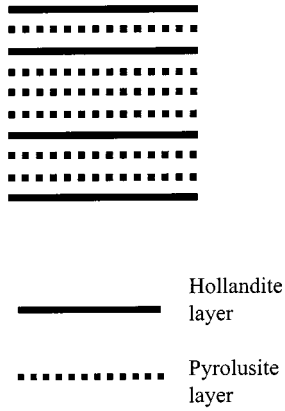

Figure 5. Proposed model of the α/β-MnO_2 structure

Figure 6 shows the Rietveld analysis (GOF: 1.35; *R*: 8.71) of the observed and calculated XRD pattern of α/β-MnO_2, assuming this structural model (α-MnO_2: PDF data 44−141; β-MnO_2: PDF data 24−735). There is quite a good agreement between the calculated pattern and the observed one. The cell parameters of a supposed tetragonal unit cell are: a = 9.791 Å and c = 2.862 Å. A peak can be observed at about 22° that doesn't belong either to the α-MnO_2 phase or to the β-MnO_2 phase. This peak can be assigned to ramsdellite-MnO_2 that has not completely transformed to β-MnO_2. As a consequence this new MnO_2 sample is a three-phase product consisting of α-MnO_2, β-MnO_2 and ramsdellite-MnO_2. The phase analysis yielded a composition of 56% α-MnO_2, 41% β-MnO_2 and 4% ramsdellite-MnO_2.

Electrochemistry

Figure 7 and 8 show the first discharge curves and the cycling behaviour, respectively, of single-phase α-MnO_2, β-MnO_2, ramsdellite-MnO_2 and the two-phase samples α/ramsdellite-MnO_2 and α/β-MnO_2. It is obvious that the stabilized α-MnO_2 delivers higher discharge capacities than single-phase α-MnO_2. Furthermore, β-MnO_2 and ramsdellite-MnO_2 show the highest discharge capacities. Single-phase α-MnO_2 shows an s-shaped discharge curve whereas β-MnO_2, ramsdellite-MnO_2 and the stabilized α-MnO_2 ex-

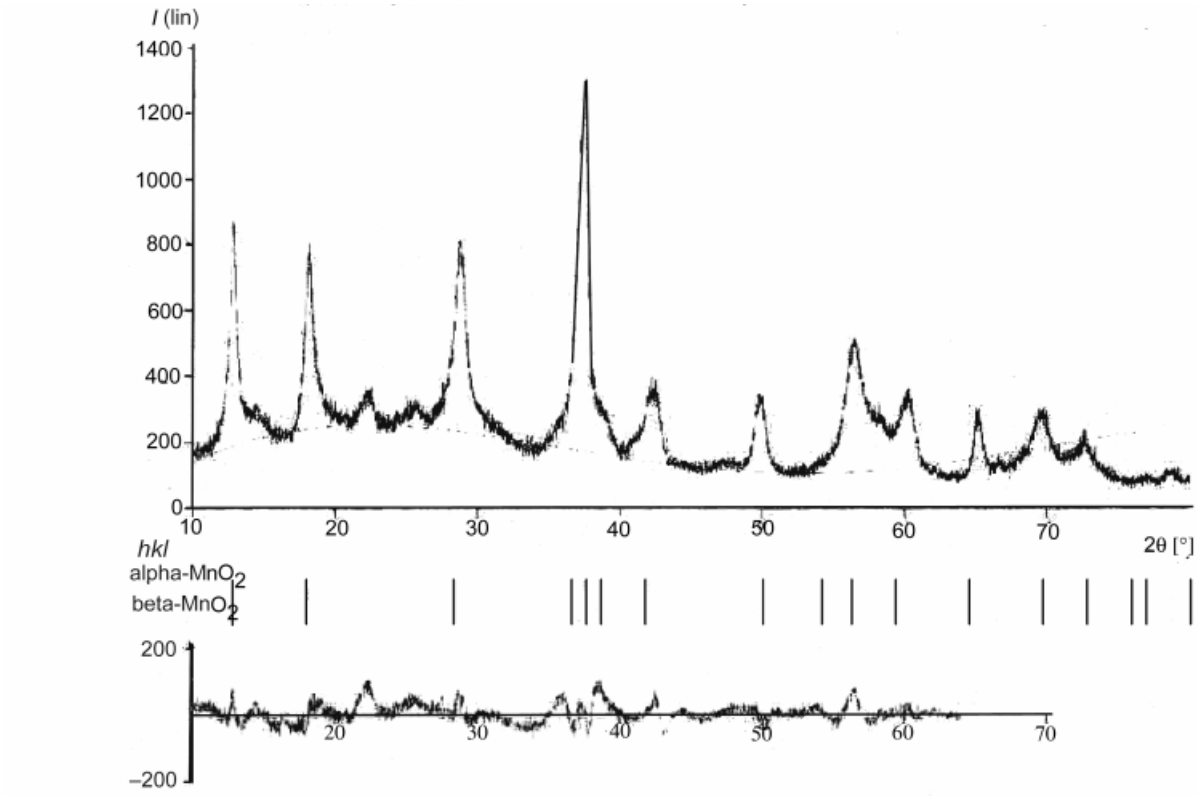

Figure 6. Observed and calculated (by Rietveld-method) XRD pattern of α/β-MnO_2 and the difference between these two patterns

hibit flat discharge curves with two voltage plateaux. The best cycling behaviour is obtained for single-phase α-MnO_2, due to small changes to the lattice parameters and unit cell volume,[18] single-phase ramsdellite-MnO_2 and the new α/β-MnO_2. The good cycling behaviour of ramsdellite-MnO_2 can be explained by a very small volume expansion and contraction during cycling, in contrast to other reports.[17] β-MnO_2 provides quite a good cycling performance even though it has always described as a cathode material for primary batteries.[19] Further work is underway to understand this feature in detail.

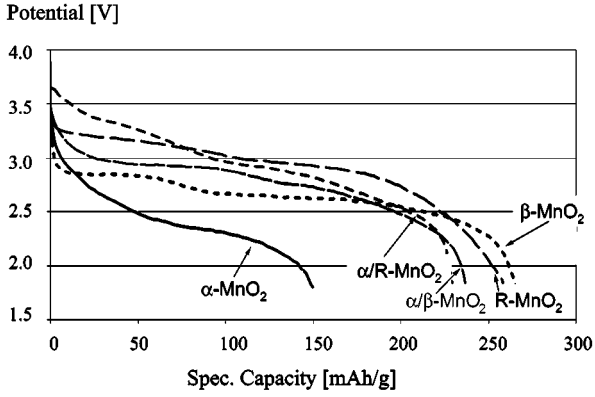

Figure 7. First discharge curves of single-phase α-MnO_2, β-MnO_2, ramsdellite-MnO_2 and the two-phase samples α/ramsdellite-MnO_2 and α/β-MnO_2

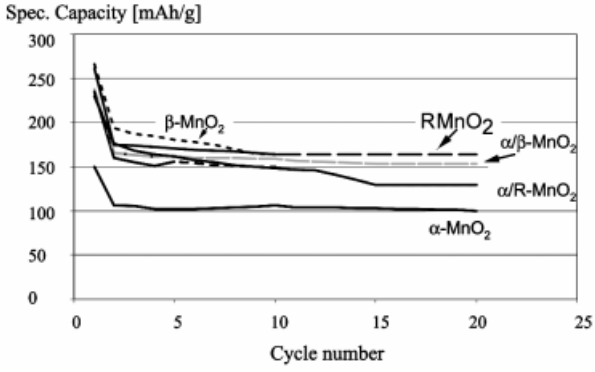

Figure 8. Cycling behaviour of single-phase α-MnO_2, β-MnO_2, ramsdellite-MnO_2 and the two-phase samples α/ramsdellite-MnO_2 and α/β-MnO_2

On the initial discharge the new α/β-MnO_2 electrode achieves a specific capacity of 237 mAh/g. After a decrease of the capacity to 168 mAh/g on the second discharge, the electrode shows good rechargeability, yielding 160 mAh/g after 10 cycles. The initial capacity loss of 30% suggests that about 0.3 mol of inserted lithium is used to provide the MnO_2 electrode with enhanced structural stability, and that this stabilizing lithium cannot easily be removed from the structure. Figure 9 shows the differential capacity plot of α/β-MnO_2 for the first and second cycle. The sharp intercalation peak at 2.9 V decreases in the second discharge due to partially irreversible intercalated lithium ions that stabilize the electrode structure during cycling. The extraction of the reversible ions from the [2×2] and [1×1] tunnel structure takes place at between 3.0 and 3.2 V, which is a higher deintercalation potential than the intercalation potential. This potential difference is mainly due to the slow kinetics of the lithium ions during extraction from the channels. The two voltage plateaux in the discharge profile of the two-phase α/β-MnO_2 are explained by the different intercalation sites.

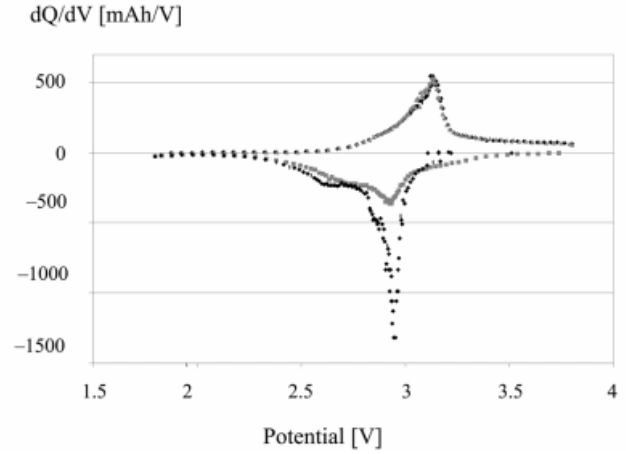

Figure 9. Differential capacity plot of α/β-MnO_2 (first and second cycle)

The high discharge capacities and the good cycling behaviour after the first cycle of this new two-phase product can be explained by the existence of interconnected α-MnO_2 and β-MnO_2 phase in the electrode structure. The β-MnO_2 is responsible for the high discharge capacities and flat discharge curve, whereas the α-MnO_2 is responsible for a stable structure during lithium intercalation and extraction, as the hollandite structure shows a small unit cell volume change. This new cathode material is therefore a β-MnO_2 stabilized with α-MnO_2.

Lithiated Manganese Oxides

In order to reduce the irreversible capacity loss after the first discharge the samples were lithiated with LiOH. Ohzuku et al. proposed a lithiation of EMD or heat-treated EMD with LiOH or other lithium salts.[21−23] This electrode material is a composite of γ-MnO_2 and β-MnO_2. Thackeray et al. described a lithiation of single-phase α-MnO_2 with LiOH.[18]

Figure 10 gives the XRD patterns of different lithiated α-MnO_2 samples. These patterns show two-phase products consisting of α-MnO_2 and a $Li_2O{\cdot}MnO_2$ (Li_2MnO_3) phase with the rock-salt structure ([002] peak at 18.7°). A different amount of $Li_2O{\cdot}MnO_2$ can be observed depending on the temperature and duration of the reaction with LiOH. There is only a small capacity loss of 5% observable after the first intercalation. The electrode structure is stabilized by Li_2O molecules introduced into the channels.[16] It appears that

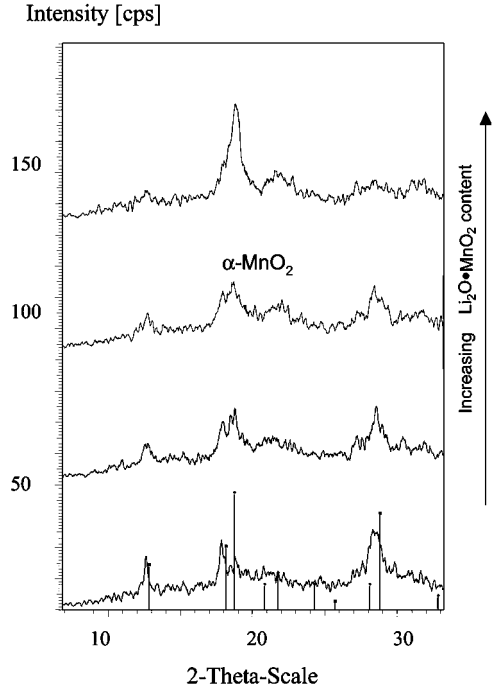

Figure 10. XRD patterns of α-MnO_2 with different Li_2MnO_3 content

no more lithium ions are trapped within the tunnels in order to stabilize the structure during electrochemical cycling. Our experiments proved that about 30% of the intercalation sites are necessary to stabilize the electrode structure. This stabilization can be done either electrochemically with lithium ions or chemically with Li_2O molecules (reaction with LiOH). It is therefore possible to insert/extract 0.7 mol of lithium reversibly.

The $Li_2O{\cdot}MnO_2$ phase provides an additional stabilization of the electrode that is responsible for a better cycling performance. The correlation between the amount of $Li_2O{\cdot}MnO_2$ and the cycling behaviour is shown in Figure 11. The capacity loss per cycle and the molar quantity of rechargeable lithium are plotted against the $Li_2O{\cdot}MnO_2$ content. The $Li_2O{\cdot}MnO_2$ phase stabilizes as a matrix (i.e. a stable rock salt structure) the large [2×2] channel structure of the α-MnO_2 framework. With increasing $Li_2O{\cdot}MnO_2$

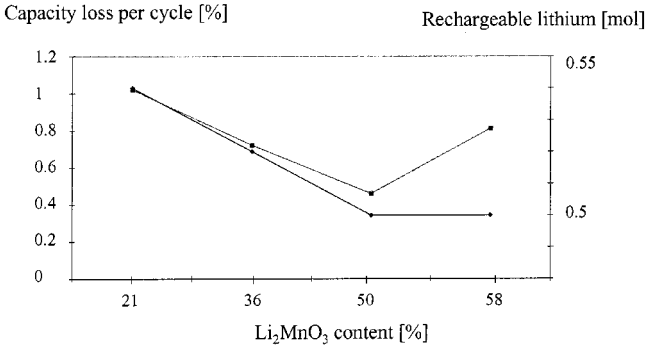

Figure 11. Correlation between Li_2MnO_3 content and cycling behaviour

content the rechargeable lithium decreases as $Li_2O{\cdot}MnO_2$ delivers only low discharge capacities.[20] We obtained the best electrochemical performance with about 30−40% $Li_2O{\cdot}MnO_2$.

The first discharge curves and the cycling behaviour of the lithiated α/β-MnO_2 in comparison to the other MnO_2 phases are shown in Figure 12 and 13, respectively. This lithiated α/β-MnO_2 is a MnO_2-based composite of α-MnO_2 and β-MnO_2 with Li_2MnO_3 as an additional phase. All the lithiated electrode materials show no, or only a small, capacity loss after the first cycle. The best electrochemical results were obtained with the lithiated α/β-MnO_2, which delivers a flat discharge curve and a good cycling stability with high discharge capacities (190 mAh/g after 10 cycles).

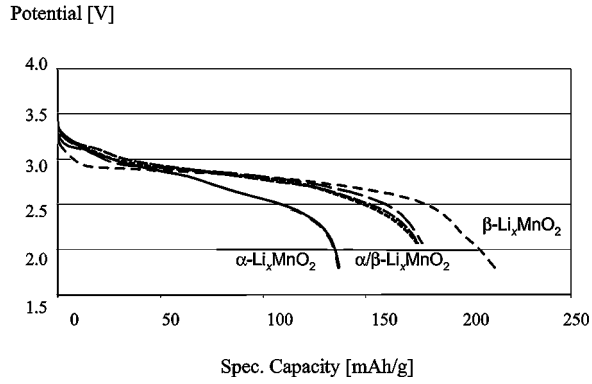

Figure 12. First discharge curves of lithiated manganese oxide phases

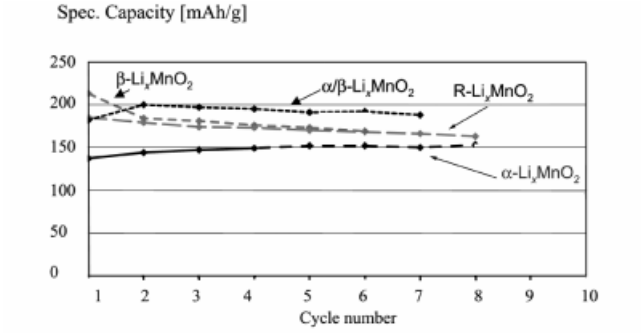

Figure 13. Cycling behaviour of the lithiated manganese oxide phases

The differential capacity plot of lithiated α/β-MnO_2 is displayed in Figure 14. There is no difference in peak intensities between the first and second cycles and there are two additional reduction/oxidation peaks in comparison to the non-lithiated α/β-MnO_2 phase. The peaks at 3.5 and 2.8 V are due to the presence of other lithium intercalation sites in the $Li_2O{\cdot}MnO_2$ framework.

Conclusion

We have demonstrated that a new synthesized α/β-MnO_2 electrode, containing α-MnO_2 and β-MnO_2 components,

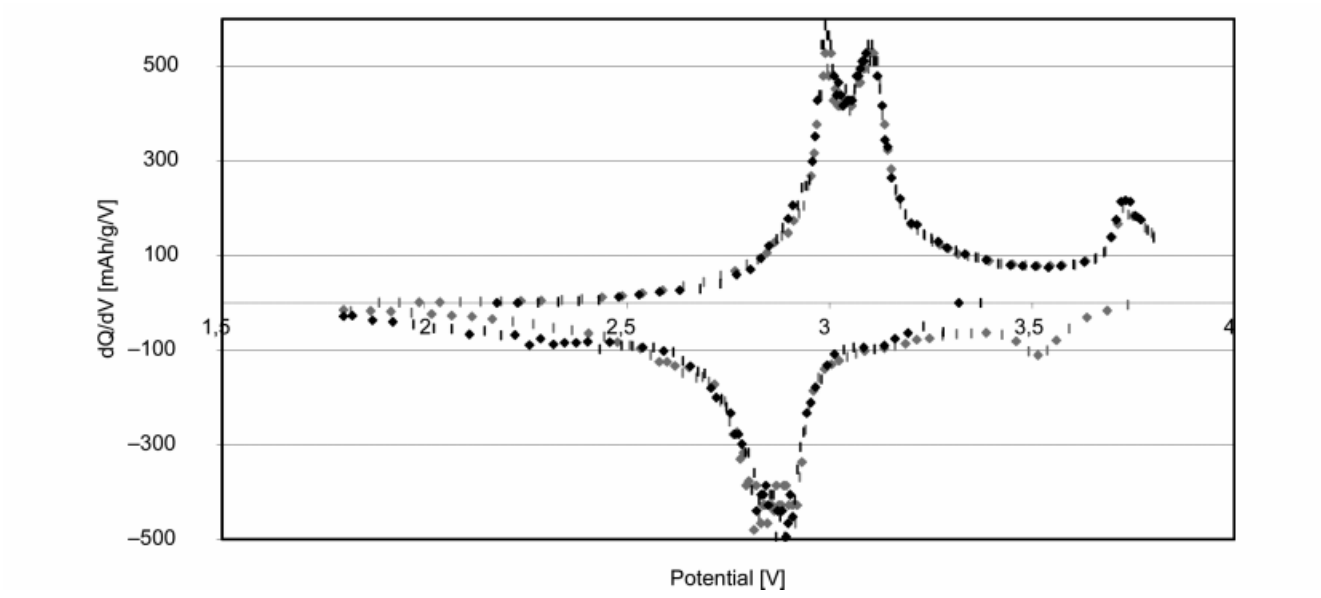

Figure 14. Differential capacity plot of lithiated α/β-MnO_2

exhibits better electrochemical features than either single phase α-MnO_2, β-MnO_2 or α/ramsdellite-MnO_2. Furthermore, it has been shown that a reaction of α-MnO_2 with LiOH forms a two-phase product consisting of a mixture of α-MnO_2 and a $Li_2O{\cdot}MnO_2$ phase. Some lithium ions of the LiOH are intercalated within the channels as Li_2O in order to stabilize the structure.[16] No capacity loss appears after the first cycle, and some lithium ions form a $Li_2O{\cdot}MnO_2$ phase that delivers an additional structure stabilization and therefore a better cycling performance. The electrochemical data indicate that lithiated α/β-MnO_2, which is a composite electrode of α-MnO_2, β-MnO_2 and Li_2MnO_3 as an additional phase, is an attractive 3 V electrode material that provides a betterr electrochemical performance than single-phase manganese oxides, with discharge capacities of 190 mAh/g after several cycles.

Experimental Section

Synthesis: The different α-MnO_2 samples were synthesized by treating α-Mn_2O_3 with sulfuric acid at different temperatures for several days with constant stirring. α-Mn_2O_3 (bixbyite-type structure) was obtained by heating EMD (Mitsui TAD 2) in air at 700 °C for 16 hours. Ramsdellite-MnO_2 was synthesized by treating a $LiMn_2O_4$ spinel with sulfuric acid. This ramsdellite-MnO_2 transforms to β-MnO_2 when heated to 350 °C for several hours. Lithiated samples were obtained by heat treatment of the different MnO_2 with LiOH between 300 and 400 °C for several hours.

Structural Characterization: X-ray diffraction profiles of the samples were determined with a Siemens D5000 diffractometer (Cu-K_α radiation). Scans were measured in the range from $2\theta = 5°$ up to 90° with a step size of 0.02°. Phase analysis was performed using the Bruker AXS software package Diffrac AT. Structural parameters were determined by Rietveld analysis of the diffraction profiles using the Bruker AXS program Win-Rietveld.

Electrochemical Characterization: Each electrode sample was prepared by grinding and mixing the active material with 4 wt.% carbon (Ketjenblack EC600) and 6 wt.% PTFE pressed into a tablet (diam 20 mm) under a pressure of 2 t/cm^2. The electrodes were dried for 16 h in vacuo at 120 °C. The separator was a polypropylene sheet (Celgard). The galvanostatic cycling took place in 2025 coin cells against metallic Li. As electrolyte a 1 M solution of $LiPF_6$ in ethylene carbonate (EC):ethylmethyl carbonate (EMC) (1:1) was used (Merck LP50). The cells were cycled galvanostatically between 3.8 and 1.8 V at a current density of 0.5 mA/cm^2 on a MACCOR test equipment. Cell assembly was performed in a glove box under argon atmosphere at room temperature.

TG/DSC measurements: The TG/DSC measurements were performed on a thermogravimetric analyser (TGA, Netsch STA 409, 5 K/min).

[1] A. Eichinger, J. O. Besenhard, *J. Electroanal. Chem.* **1976**, *72*, 1.
[2] M. S. Whittingham, *Science* **1976**, *192*, 1126.
[3] G. L. Holleck, J. P. Driscoll, *Electrochim. Acta* **1977**, *22*, 647.
[4] M. S. Whittingham, *Prog. Solid. State Chem.* **1978**, *12*, 41.
[5] D. W. Murphy, P. A. Christian, *Science* **1979**, *205*, 651.
[6] K. M. Abraham, *J. Power Sources* **1982**, *7*, 1.
[7] G. Pistoia, *J. Power Sources* **1983**, *9*, 307.
[8] J. P. Gabano, *Lithium Batteries*, Academic Press Ltd London, **1983**.
[9] J. Desilvestro, O. Haas, *J. Electrochem. Soc.* **1990**, *137*, 5C.
[10] M. M. Thackeray, M. H. Rossouw, A. de Kock, A. P. de la Harpe, R. J. Gummow, K. Pearce, D. C. Liles, *J. Power Sources* **1993**, *43−44*, 289−300.
[11] D. Ilic, M. Kilb, K. Holl, H. W. Praas, E. Pytlik, *J. Power Sources* **1999**, *80*, 112−115.
[12] C. S. Johnson, D. W. Dees, M. F. Mansuetto, M. M. Thackeray, D. R. Vissars, D. Argyriou, C.-K. Loong, L. Christensen, *J. Power Sources* **1997**, *68*, 570−577.

[13] M. A. Humbert, Ph. Biensan, M. Broussely, A. Lecref, A. Dolle′, H. Ladhily, *J. Power Sources* **1993**, *43−44*, 681−687.

[14] C. S. Johnson, M. F. Mansuetto, M. M. Thackeray, Y. Shao Horn, S. H. Hackney, *J. Electrochem. Soc.* **1997**, *144*, 2279−2283.

[15] L. S. Ramsdell, *Am. Mineral.* **1932**, *17*, 143−149.

[16] C. S. Johnson, D. W. Dees, M. F. Mansuetto, M. M. Thackeray, D. R. Vissers, D. Argyriou, C. K. Loong, L. Christensen, Abstract 874, p.1076, *The Electrochemical Society Meeting Abstracts*, Vol. 96−2, San Antonio, TX, Oct. 6−11, **1996**.

[17] M. M. Thackeray, M. H. Rossouw, R. J. Gummow, D. C. Liles, K. Pearce, A. de Kock, W. I. F. David, S. Hull, *Electrochim. Acta* **1993**, *38*, 1259.

[18] M. H. Rossouw, D. C. Liles, M. M. Thackeray, W. I. F. David, S. Hull, *Mat. Res. Bull.* **1992**, *27*, 221−230.

[19] M. M. Thackeray, *Prog. Batteries Battery Mater.* **1995**, *14*, 1−87.

[20] P. Kalyani, S. Chitra, T. Mohan, S. Gopukumar, *J. Power Sources* **1999**, *80*, 103−106.

[21] T. Ohzuku, K. Sawai, T. Hirai, *Chem. Express* **1989**, *4*, 777−780.

[22] T. Ohzuku, K. Sawai, T. Hirai, *Chem. Express* **1989**, *4*, 773−776.

[23] T. Ohzuku, K. Sawai, T. Hirai, *Proc. Electrochem. Soc.* **1991**, *91*, 318−325.

Received June 25, 2001
[I01226]

X-ray Crystal Structure of Triaquacopper(II) Dihydrogen 1,2,4,5- Benzenetetracarboxylate Trihydrate and Raman Spectra of Cu^{2+}, Co^{2+}, and Fe^{2+} Salts of 1,2,4,5-Benzenetetracarboxylic (Pyromellitic) Acid

Renata Diniz,[a] Heitor A. de Abreu,[a] Wagner B. de Almeida,[a] Maria T. C. Sansiviero,[a] and Nelson G. Fernandes*[a]

Keywords: Hydrogen bonds / X-ray diffraction / Raman spectroscopy / Transition metals

Some transition metal salts (Fe^{2+}, Co^{2+}, and Cu^{2+}) of 1,2,4,5-benzenetetracarboxylic acid (pyromellitic acid) have been synthesized: hexaaquairon(II) dihydrogen 1,2,4,5-benzenetetracarboxylate (**I**), hexaaquacobalt(II) dihydrogen 1,2,4,5-benzenetetracarboxylate (**II**), triaquacopper(II) dihydrogen 1,2,4,5-benzenetetracarboxylate trihydrate (**III**), and triaquacopper(II) 1,2,4,5-benzenetetracarboxylate tetrahydrate (**IV**). Single-crystal X-ray diffraction analysis of compound **III** has been performed. It crystallizes in the non-centrosymmetric space group *Pn* with two molecules per unit cell. Cu^{2+} and the ligand form an infinite linear chain. The metal atom is coordinated to five O atoms (three of the aqua ligand and two of the pyromellitate ligand) in a distorted trigonal-bipyramidal coordination. The carboxylic groups are involved in two medium intermolecular hydrogen bonds with water molecules. The O···O distances are 2.629(5) and 2.639(5) Å. The absolute structure parameter shows that the crystal and the atomic coordinate sets have the same polarity. Raman spectra of all the compounds and deuterated analogues of Fe^{2+} and Co^{2+} salts are reported. Spectral differences have been observed in the spectra of the compounds that present short hydrogen bonds (O···O distance less than 2.5 Å) in comparison to compounds that do not. In the crystal of compounds **I** and **II**, intramolecular short hydrogen bonds are present. Symmetric and asymmetric stretching vibrations of a short intramolecular hydrogen bond are observed at 307 and 874 cm^{-1} in salts **I** and **II**, respectively. The crystal structures of compounds **III** and **IV** do not show short hydrogen bonds, these bands are therefore not observed. These vibrational modes are tentative assignments by deuterium compounds and ab initio calculations of the dihydrogen pyromellitate ion.
(© Wiley-VCH Verlag GmbH, 69451 Weinheim, Germany, 2002)

Introduction

In general, a hydrogen bond, X−H···Y represents a relatively weak inter- or intramolecular interaction in which a positively charged hydrogen atom covalently bonded to X (the proton donor) is further attracted by a negative charge around Y (the proton acceptor). In most cases, the hydrogen atom in a hydrogen bond is more strongly bonded to one particular atom to form a clearly asymmetric hydrogen bond. Typically X and Y are electronegative elements such as N, O, F, Cl, etc. On the other hand, as the interaction H···Y becomes stronger, the X−H bond is successively elongated. Therefore, the H···Y distance becomes shorted and the hydrogen atom seems to be similarly attracted to both of them. In this situation, the donor−acceptor concept is not so clear. Anyhow, when a hydrogen bond is formed the contact between X···Y becomes closer than the sum of their van der Waals radii.[1] The hydrogen bond may be classified as: 1) strong, when the X···Y distance is short and the hydrogen atom is similarly attracted to X and Y atoms; 2) moderate, when the H atom is clearly bonded to X and electrostatically attracted to Y; 3) weak, when the H···Y interaction is weak, such that, the X···Y distance becomes long. For X = Y = oxygen atom, from the crystallographic point of view, the hydrogen bond is weak when the O···O distance is around 2.8−3.0 Å. The hydrogen bond is moderate when the O···O distance is somewhere between 2.5−2.8 Å and a hydrogen bond is short when the O···O distance is about 2.4−2.5 Å.

This work is part of a project involving crystallographic and spectroscopic studies of substances containing short hydrogen bonds (SHB). The 1,2,4,5-benzenetetracarboxylic acid, also known as pyromellitic acid [H_4Pm], is a very interesting system to study. At first, it can form different types of coordination compounds, due to the possibility of substitution of one to four hydrogen atoms. Therefore, it is possible to form intramolecular SHB, due to the proximity of the carboxylate and carboxylic groups. Some single-crystal structures of salts of this acid have been reported.[2−5] In most cases, there are SHB in these acid salt compounds. In Ni^{2+} and Co^{2+} acid salt compounds, two crystalline phases

[a] Departamento de Química, ICEx, Universidade Federal de Minas Gerais
Av. Antônio Carlos 6627, 31270-901, Belo Horizonte, MG, Brazil
Fax: (internat.) + 55-33/3499-5700
E-mail: nelsongf@apolo.qui.ufmg.br

have been identified. SHB have been observed in both phases. From the crystallographic point of view, in one phase (α) symmetric intramolecular SHB occur and in another phase (β) there are asymmetric intramolecular SHB. In the symmetric SHB, the H atom is located in a glide plane (*x*, 1/2, *z*). These complexes show potential practical interest such as detergent builders, catalysts, and heat stabilisers. The properties of these salts can be influenced by the presence of four carboxylic groups.[3] Multi-dentate complexing agents are able to form one-, two-, or three-dimensionally infinite connections between cations and anions. Due to the presence of four carboxylic groups in pyromellitic acid, its salts can coordinate in numerous ways and in different dimensionalities.

Various experimental and theoretical studies have reported on the nature of hydrogen-bonding systems.[6−8] Infrared spectroscopy has been very important in HB investigations. Spectra of a hydrogen-bonding system present broader, more intense and shifted bands than non-hydrogen-bonding systems.[6] However, hydrate compounds generally show some broad and intense envelope bands in the range of hydrogen-bond (HB) modes. In contrast, the water modes are very weak in Raman spectra. As a result of this, the Raman spectra of hydrate compounds are usually better than infrared spectra. Reid[9] interpreted the changes in the infrared spectra by making a semiempirical treatment of the hydrogen bond based on the Lippincott and Schroeder potential.[10] This treatment considers the coupling between the slow O···O stretching motion with the fast OH vibration. The O···O motion of two hydrogen-bonded oxygen atoms has been investigated much less than the O−H stretching mode, since it is in a range that is extremely difficult to separate from many other vibration modes. Reid used a harmonic oscillator approximation to calculate the O···O stretching frequency with respect to the O···O equilibrium distance. For a short O···O distance (< 2.5 Å), a frequency of ca. 850 cm^{-1} was found. Miller at al.[11] studied the O−H−O hydrogen bond in $CsH(CF_3CO_2)_2$ and $KH(CF_3CO_2)_2$. These compounds show very short O···O distances. They assigned the O···H···O mode at 798 and 792 cm^{-1} to Cs and K salts, respectively, by Raman spectroscopy. Hadzi, Orel, and Novak[12] also discussed the Raman and infrared spectra of the $MH(CX_3COO)_2$, where M = Na or K and X = H or F, and they assigned values of 720 and 320 cm^{-1} for the ν_{asym}(OHO) and ν_{sym}(OHO) bands, respectively. Luehrs et al.[13] investigated some salts of pyromellitic acid using infrared spectroscopy. They mentioned that an enlargement between 900 and 1800 cm^{-1} could be attributed to the presence of SHB.

In the present work, hydrogen bonds have been investigated in four salts: hexaaquairon(II) dihydrogen 1,2,4,5-benzenetetracarboxylate $\{[Fe^{2+}\cdot 6H_2O][C_{10}H_4O_8]^{2-}\}$ (FeH_2Pm) (**I**); hexaaquacobalt(II) dihydrogen 1,2,4,5 benzenetetracarboxylate $\{[Co^{2+}\cdot 6H_2O][C_{10}H_4O_8]^{2-}\}$ (CoH_2Pm) (**II**), triaquacopper(II) dihydrogen 1,2,4,5-benzenetetracarboxylate trihydrate $\{[Cu\cdot 3H_2O]C_{10}H_4O_8\cdot 3H_2O\}$ (CuH_2Pm) (**III**); triaquacopper(II) 1,2,4,5-benzenetetracarboxylate tetrahydrate $\{[Cu\cdot 3H_2O]_2C_{10}H_2O_8\cdot 4H_2O\}$ (Cu_2Pm) (**I**). From powder diffraction data, it can be concluded that FeH_2Pm and CoH_2Pm are isostructural. The crystal structure of CoH_2Pm was reported[3] earlier. These compounds show intramolecular SHB. The crystal structural investigation of CuH_2Pm is shown in this work and the crystal structure of Cu_2Pm was reported[2] elsewhere. These last two compounds show moderate intermolecular hydrogen bonds. All of these compounds are hydrated, with compounds **I**, **II**, and **III** having six water molecules in their structures, and compound **IV** showing ten water molecules. Due to this, Raman spectroscopy has been chosen to study spectral differences in short and long/medium HB modes. The SHB modes occur in a crowded region, thus Raman spectra of deuterated analogues of CoD_2Pm and FeD_2Pm have been obtained, and ab initio molecular orbital (MO) calculations have also been performed for the dihydrogen pyromellitate ion $[H_2Pm]^{2-}$ with the purpose of SHB mode assignment.

Results and Discussion

Description of Structures

Crystal Structure of CuH_2Pm

The crystal structure of CuH_2Pm is shown in Figure 1. Selected bond lengths and bond angles are listed in Table 1. The coordination number of Cu^{2+} is five, it is coordinated to three water molecules and two carboxyl groups of two ligand molecules $[H_2Pm]^{2-}$. The average of the Cu−O bonds is 1.944(2) Å to the ligand O atoms and 2.070(4) Å to the water molecules. The longest Cu−O bond length is Cu−O11 [2.235(4) Å]. At a first glance, Figure 1 could suggest a square-pyramidal oxygen atom arrangement around Cu^{2+}. The best least-squares plane through O1, Cu, $O5^i$, O9, and O10 shows that only the metal atom lies in this plane, however, O1, $O5^i$, O9, and O10 are on average 0.15(2) Å below and above that plane. The symmetry code of *i* is *x*, 1 + *y*, *z*. On the other hand, the best least-squares plane through the metal ion and the three oxygen atoms of the water molecules is the plane through Cu, O9, O10, and O11. All the atoms lie in this plane with an average distance of 0.005(3) Å. Therefore, it can be concluded that the oxygen arrangement around the metal ion is better described as a slightly distorted trigonal-bipyramidal structure. This geometry was observed in the Cu_2Pm crystal structure by Usubalieve et al.[2] The water molecules form the pyramid base and O−Cu−O angles are 165.4(2)° (O9,O10), 94.8(3)° (O9, O11), and 99.8(3)° (O10, O11). At the top and bottom of the coordination geometry O1 and O5 are attached to the ligand molecule. The average of O−Cu−O angles is 89.5(2)° and the O1−Cu−O5 angle is 176.3(2)°. Cu^{2+} atoms are bonded in a monodentate form to O1 and O5 atoms of different H_2Pm ligands. These O atoms are located on opposite sides of the benzene ring and the Cu^{2+}atoms are linked between ligand molecules. These bonds form an infinite linear chain, as can be seen from Figure 1.

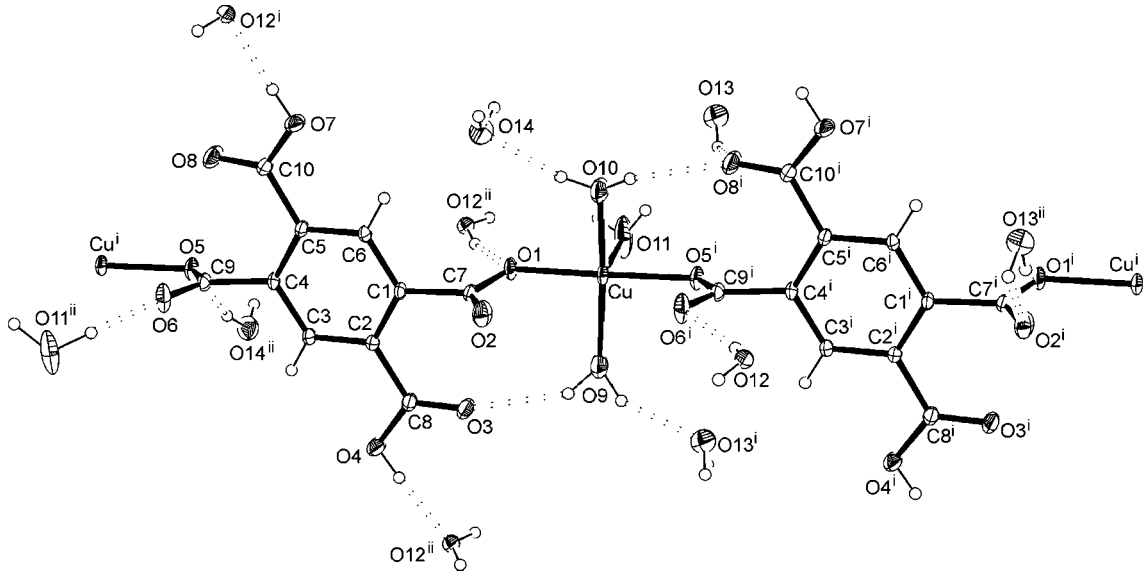

Figure 1. Atomic labelling scheme for CuH_2Pm and displacement ellipsoids with 30% probability level; symmetry codes: *i*: x, $1 + y$, z; *ii*: $0.5 + x$, $-y$, $0.5 + z$

Table 1. Selected bond lengths and bond angles for CuH_2Pm

Bond lengths [Å]					
Cu−O1	1.939(2)	O1−C7	1.284(5)	O5−C9	1.271(4)
Cu−O5^i	1.948(2)	O2−C7	1.227(5)	O6−C9	1.236(4)
Cu−O9	1.984(2)	O3−C8	1.213(4)	O7−C10	1.307(4)
Cu−O10	1.990(4)	O4−C8	1.314(4)	O8−C10	1.211(4)
Cu−O11	2.235(4)				
Bond angles [°]					
O1−Cu−O5^i	176.3(2)	O5−Cu−O9	91.4(2)	O9−Cu−O11	94.8(3)
O1−Cu−O9	88.7(2)	O5−Cu−O10	90.6(2)	O10−Cu−O11	99.8(3)
O1−Cu−O10	90.2(2)	O5−Cu−O11	84.8(1)	C7−O1−Cu	119.7(2)
O1−Cu−O11	91.4(2)	O9−Cu−O10	165.4(2)	C9−O5−Cu	114.3(2)
Hydrogen bonds					
D−H···A	Distance D−A [Å]	Bond angles [°]	D−H···A	Distance D−A [Å]	Bond angles [°]°
O4−H4A−O12^{ii}	2.639(5)	175.9(4)	O11−H11A−O6^{ii}	2.757(7)	170.4(4)
O7−H7A−O12^i	2.629(5)	172.6(4)	O12−H12A−O1^{ii}	2.694(5)	165.7(5)
O9−H9A−O3	2.927(6)	146.6(4)	O12−H12B−O6^i	2.685(5)	152.1(4)
O9−H9B−O13^i	2.701(7)	149.1(5)	O13−H13A−O8^i	3.000(6)	141.4(4)
O10−H10A−O8^i	2.905(5)	154.4(4)	O13−H13B−O2^{ii}	2.891(6)	171.9(5)
O10−H10B−O14	2.731(6)	168.3(6)	O14−H14A−O5^{ii}	2.975(5)	165.8(5)

In the carboxyl groups the averages of C−O and C=O bonds are 1.294(4) and 1.222(4) Å, respectively. In the carboxylate groups O1−C7−O2 and O5−C9−O6 the difference between C−O and C=O bonds is smaller than usually in carboxylic groups due to the delocalization of the electrons as can be seen in Table 1. The average of the C−C−C, O−C−O, and C−C−O angles is 120(3)°. The benzene ring is planar with a maximum deviation of 0.006 Å. The distances of the carboxyl group atoms to the benzene plane are 0.003(6), 0.009(6), −0.197(7), 0.039(6), 1.175(7), −1.055(6), 0.075(8), −0.058(7), 0.834(7), −1.348(6), 0.183(8), and −0.082(7) Å to C7, C8, C9, C10, O1, O2, O3, O4, O5, O6, O7, and O8, respectively. The COOH planes are rotated against the mean plane through the benzene ring by −7.1 and −3.2°, and the COO^- planes are rotated by −87.1 and +95.4°. This conformation is similar to that found in pyromellitic acid (H_4Pm) for which the torsion angles are 17.9 and 74.4°.[14] CuH_2Pm crystallizes in a non-centrosymmetric space group, so the absolute structure could be obtained. The absolute structure parameter x, Flack parameter, may be determined for any non-centrosymmetric crystal. This parameter is a variable in the least-squares refinement.[15] The Flack parameter was refined to 0.01(2). The refined value of x is independent of

the starting values. Therefore, this value indicates that the crystal and atomic coordinates have the same polarity.[15]

The carboxylic groups present are not involved in SHB. There are three water molecules of crystallization in this structure (O12, O13 and O14). These water molecules are also involved in medium and long hydrogen bonds. The ligand H_2Pm is an acceptor of two medium (O12) and three long (O13 and O14) hydrogen bonds from water molecules. The O12···O1^{ii}, O12···O6^{i}, O13···O2^{ii}, O13···O8^{i}, and O14···O5^{ii} distances are 2.694(5), 2.685(5), 2.891(6), 3.000(6), and 2.975(5) Å, respectively. The coordination water molecules are donors to one medium (O11) and two long (O9, O10) hydrogen bonds. The O6^{ii}···O11, O8^{i}···O10, and O3···O9 distances are 2.757(7), 2.905(5), and 2.927(6) Å, respectively. Two medium hydrogen bonds between the water molecules were observed. The O10···O14 and O9···O13 distances are 2.731(6) and 2.701(7) Å, respectively. The H_2Pm ligand is the donor of two medium hydrogen bonds to waters of crystallisation (O12). The O7−O12^{i} and O4−O12^{ii} distances are 2.629(5) and 2.639(5) Å, respectively. The symmetry code of *ii* is 0.5 + *x*, −*y*, 0.5 + *z*.

Powder Diffraction Data

As described in the Exp. Sect., there was not a suitable single crystal for X-ray analysis of FeH_2Pm. Therefore, powder diffraction methods were used to identify iron compounds. In order to make sure that in the absence of a single crystal, powder diffraction techniques can be useful for identification of a structure type, some X-ray powder patterns are shown in Figure 4. The program XPOW[16] was used to generate X-ray powder patterns.

CuH_2Pm and Cu_2Pm Structures

The calculated X-ray powder patterns of CuH_2Pm are based on the cell parameters, atomic position, and displacements obtained from single-crystal structure refinement described in this present work. The X-ray powder pattern of Cu_2Pm was obtained from a single-crystal structure by Usubalieve et al.[2] In Cu_2Pm the water molecules of crystallisation are involved in medium and long hydrogen bonds with the ligand. The average O···O distances in medium and long hydrogen bonds are 2.69(1) and 2.85(5) Å, respectively. Cu_2Pm forms two cross infinite chains, where the Cu^{2+} is the link between the ligand molecules (Figure 2). Cu^{2+} shows the same coordination geometry as CuH_2Pm. The powder patterns are shown in Figure 4 (a).

CoH_2Pm and FeH_2Pm

There are two crystal phases reported for the Co^{2+} salt.[3,5] In both of them there are intramolecular SHB, and Co^{2+} is coordinated by six water molecules in an octahedral geometry. The carboxyl groups are involved in a short intramolecular hydrogen bond with an O···O distance of about 2.4 Å. From a crystallographic point of view, one of these phases (α) shows symmetric intramolecular SHB[3] and the other (β) shows asymmetric SHB.[5] The α phase crystal

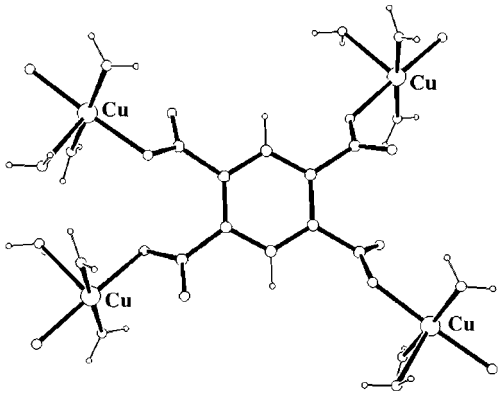

Figure 2. Crystal structure of Cu_2Pm

structure is shown in Figure 3. In the symmetric SHB, the H atom is located in a glide plane (*x*, 1/2, *z*). In the α phase the carboxyl groups are coplanar with the benzene ring while in the β phase the dihedral angles of the carboxyl group with the benzene ring are about 25°. In Figure 4 (b), experimental (Co^{2+} and Fe^{2+} salts) and calculated (α and β phase) X-ray powder patterns are shown. For the α phase the calculated pattern was obtained from single-crystal data by Ward and Luehrs.[3] For the β phase the calculated powder pattern has been performed from single-crystal data given by Rochon and Massarweh.[5]

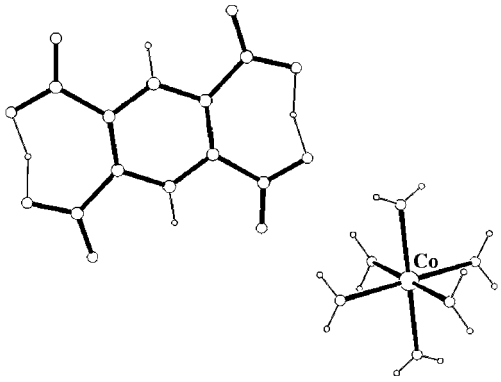

Figure 3. Crystal structure of the α phase of CoH_2Pm

Experimental FeH_2Pm and CoH_2Pm X-ray powder patterns are very similar, therefore, it can be concluded that they may be isostructural. This similarity shows that the Fe^{2+} and Co^{2+} salts obtained in this work have the same structure as the Co^{2+} salt published by Ward and Luehrs.[3]

Raman Spectroscopy and Vibrational Mode Assignment

Experimental Raman spectra of the compounds and a theoretical Raman spectrum of the H_2Pm^{-2} ion are displayed in Figures 5 and 6, and its deuterated counterpart for Fe^{2+} and Co^{2+} salts are shown in Figure 7. The Raman frequencies are shown in Tables 2 and 3.

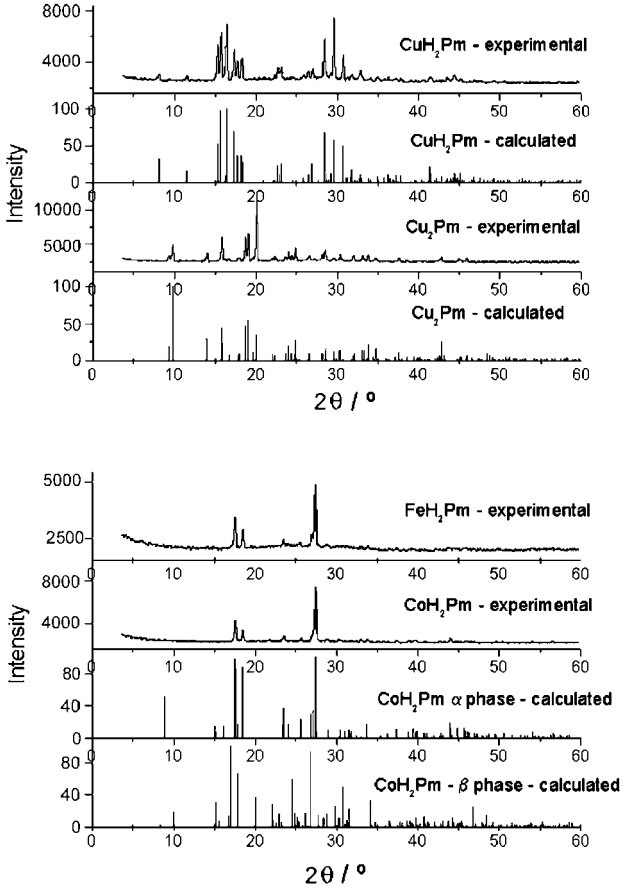

Figure 4. Experimental and calculated powder patterns of a) Cu_2Pm and CuH_2Pm and b) FeH_2Pm and CoH_2Pm

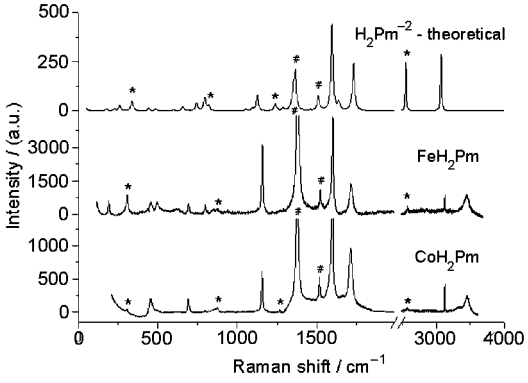

Figure 5. Raman spectra of Fe^{2+} and Co^{2+} salts of pyromellitic acid; the symbol * refers to bands relative to SHB vibrations; The symbol # refers to ν_{sym}(COO) and ν_{asym}(COO)

Carboxyl Modes

The stretching vibration of carboxyl groups is easily assigned as they are very intense and appear in a characteristic region. There are two stretching vibrations for the carboxylate group, one symmetric [ν_{sym}(COO)] and another asymmetric [ν_{asym}(COO)]. In CoH_2Pm and in FeH_2Pm the ν_{sym}(COO) and ν(C=O) are strongly coupled with δ(OH).

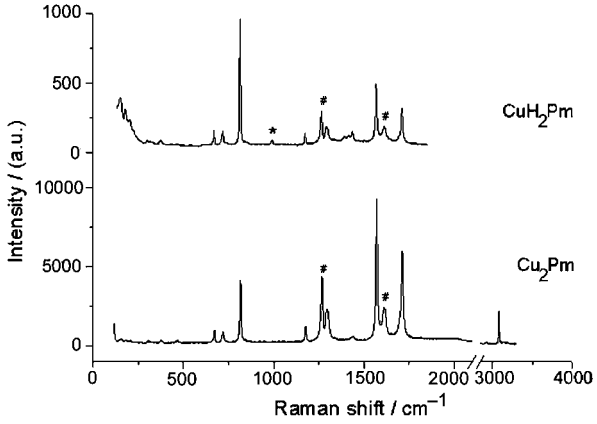

Figure 6. Raman spectra of copper salts of pyromellitic acid; the symbol * refers to γ(OH); the symbol # refers to ν_{sym}(COO) and ν_{asym}(COO)

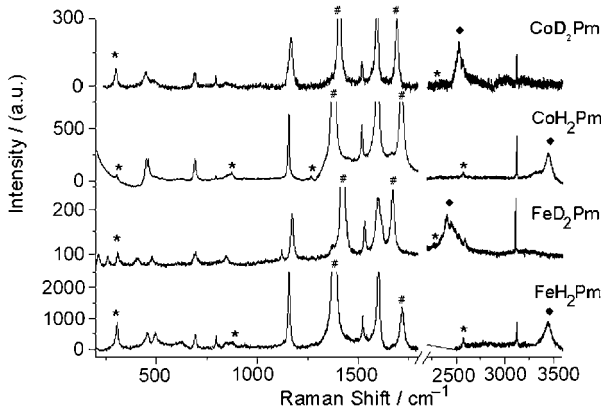

Figure 7. Raman spectra of the SHB region of FeH_2Pm, CoH_2Pm and deuterated analogues; the symbol * refers to bands relative to SHB vibrations; the symbol # refers to ν_{sym}(COO) and ν(C=O); the symbol ◆ refers to ν[OH(D)] from $H(D)_2O$

These couplings were confirmed by ab inito calculations and by the frequency shift of these bands in the Raman spectra of the deuterated analogues. In the CoH_2Pm salt the ν_{sym}(COO) and ν(C=O) were observed at 1378 and 1714 cm^{-1}, respectively, and they shift to 1406 and 1691 cm^{-1} after deuteration. Similar shifts were observed in the Fe^{2+} salt, ν_{sym}(COO) and ν(C=O) at 1381 and 1718 cm^{-1} respectively, and they shift to 1423 and 1670 cm^{-1}, respectively in the deuterated salt. These strong couplings and shifts were also observed in some hydrogen acetate salts.[12] The X-ray crystal data of CuH_2Pm show that Cu^{2+} is monodentately coordinated to the carboxylate groups of H_2Pm^{2-} and the carboxylic groups are involved in medium hydrogen bonds to water molecules, as seen in Figure 1. The ν_{sym}(COO) and ν_{asym}(COO) of the carboxylate groups were observed at 1260 and 1613 cm^{-1}. The ν(C−O) for carboxylic groups was assigned at 1318 cm^{-1} and ν(C=O) at 1694 and 1711 cm^{-1}. In Cu_2Pm, the ν_{sym}(COO) and ν_{asym}(COO) were observed at 1268 and 1611 cm^{-1} respectively, and the ν(C=O) at 1698 and 1713 cm^{-1}. In-plane bending [δ(COO)] occurs at 796, 798, 817, and 814 cm^{-1} for CoH_2Pm, FeH_2Pm, CuH_2Pm, and Cu_2Pm respectively, and

Table 2. Experimental Raman frequencies for FeH_2Pm and CoH_2Pm and theoretical Raman frequencies for the H_2Pm^{2-} ion

Frequency [cm^{-1}][a]			Tentative assignment
FeH_2Pm	CoH_2Pm	H_2Pm^{2-}	
298 m		258	δ(φ)
307 w (300)	307 w (309)	337	ν_{sym}(O···H···O)
		441	γ(C=C)
384 m	364 vw		ν(M−O)
495 w		485	γ(C=C)
694 w	692 m	684	δ(φ)
798 w	796 vw	743	δ(COO)
845 wb	854 wb	797	γ(COO)
874 wb	874 wb	822	ν_{asym}(O···H···O)
	1267 vw (993)	1240	γ(OH)
1381 vs (1423)	1378 vs (1406)	1366	ν_{sym}(COO) + δ(OH)
1522 m	1517 m	1510	ν_{asym}(COO)
1601 vs	1599 vs	1597	ν(C=C)
1718 m (1670)	1714 m (1691)	1733	ν(C=O) + δ(OH)
2575 vw	2577 vw	2551	$\nu(O-H)_{HB}$
3124 m	3121 m	3066	ν(C−H)
3192 m	3197 m	3072	ν(C−H)
3444 mb (2400)	3450 mb (2525)		$\nu(O-H)_F$

[a] ν_{asym} − asymmetric stretching, ν_{sym} − symmetric stretching, δ − deformation in plane, γ − deformation out of plane, φ − benzene ring deformation, HB − hydrogen bond, F − free hydrogen group, vw − very weak, w − weak, m − medium, ms − medium strong, s − strong, vs − very strong. Frequencies of deuterated salts are in parentheses.

Table 3. Raman frequencies for copper salts of pyromellitic acid

Frequency [cm^{-1}][a]		Tentative assignment
Cu_2Pm	CuH_2Pm	
377 vw	375 vw	ν(Cu−O)
672 w	670 w	δ(φ)
720 w	713 w	δ(φ)
817 ms	814 vs	δ(COO)
	991vw	γ(OH)
1177 w	1175 w	δ(C−H)
1268 m	1260 m	ν_{sym}(COO)
1296 m	1288 w	ν(C=C)
1297 m	1293 w	ν(C=C)
	1318 w	ν(C−O)
	1415 w	ν(C=C)
1437 vw	1437 w	ν(C−O)
1571 vs	1568 ms	ν(C=C)
1611 m	1613 m	ν_{asym}(COO)
1698 w	1694 w	ν(C=O)
1713 s	1711 m	ν(C=O)
3081 m		ν(C−H)
3143 m		$\nu(O-H)_F$

[a] ν_{asym} − asymmetric stretching, ν_{sym} − symmetric stretching, δ − deformation in plane, γ − deformation out of plane, φ − benzene ring deformation, HB − hydrogen bond, F − free hydrogen group, vw − very weak, w − weak, m − medium, ms − medium strong, s − strong, vs − very strong. Frequencies of deuterated salts are in parentheses.

out-of-plane bending [γ(COO)] was observed at 854 and 845 cm^{-1} for CoH_2Pm and FeH_2Pm. The difference (Δ) between symmetric and asymmetric carboxylate stretching vibrations can be used as a parameter to identify the coordination type. In FeH_2Pm and CoH_2Pm the Δ values are 141 and 139 cm^{-1}, respectively, and in Cu^{2+} salts Δ is about 343 cm^{-1}. The crystal data show that Cu^{2+} has monodentate coordination, while Fe^{2+} and Co^{2+} do not coordinate to the dihydrogen pyromellitate ion. These results are in agreement with those of acetate compounds,[17] for which the Δ value is larger in monodentate complexes than in the free ion.

Benzene Ring and M−O Modes

The assignments for the aromatic ring moiety were based on that for substituted benzene[18,19] and are listed in Tables 2 and 3. The M−O stretching modes were observed at about 375 and 377 cm^{-1} for CuH_2Pm and Cu_2Pm, and 384 and 364 cm^{-1} to FeH_2Pm and CoH_2Pm respectively.[20]

O−H Modes

Crystal data shows that in the crystal structure of the Cu^{2+} salts SHB are not present, while in both Fe^{2+}, and Co^{2+} salts there are intramolecular SHB. In FeH_2Pm and CoH_2Pm, the O−H stretching of the carboxylic group was observed at 2575 and 2577 cm^{-1}, respectively. For free OH this mode occurs at 3700 cm^{-1}. These shifts to lower frequencies of the O−H carboxylic stretching are due to the formation of SHB. In the deuterated analogues, the ν(O−D) of SHB may be tentatively assigned to a very weak band at 2300 cm^{-1} in the Co^{2+} salt and at 2359 cm^{-1} in the Fe^{2+} salt. The ν_{OH}/ν_{OD} ratios are 1.12 and 1.09, respectively, for Co^{2+} and Fe^{2+} salts. The O−H stretching of water molecules was observed at 3143 cm^{-1} for Cu_2Pm, at 3444 cm^{-1} for FeH_2Pm, and 3450 cm^{-1} for CoH_2Pm. The ν(O−D) of water molecules are assigned to a very broad band near 2525 and 2400 cm^{-1} for Co^{2+} and Fe^{2+} salts, respectively. The ν_{OH}/ν_{OD} ratios are 1.36 and 1.44 for Co^{2+} and Fe^{2+} salts, respectively. These ratios are in agreement with the isotopic substitution effect. The γOH mode is very weak in Raman spectra and was only observed in CoH_2Pm and CuH_2Pm at 1267 and 991 cm^{-1}, respectively. In deuterated salts, the γOD could not be assigned.

O···H···O Modes

The SHB stretching modes in the FeH_2Pm and CoH_2Pm were tentatively assigned to very broad and weak bands at 874 cm^{-1} for the asymmetric stretching mode [ν_{asym}(O···H···O)], and at 307 cm^{-1} for the symmetric mode [ν_{sym}(O···H···O)] in both salts. These tentative assignments are in accordance with the semiempirical treatment of the hydrogen bond.[9] As these regions have many modes, tentative assignments were made using deconvolution methods, isotopic substitution (OH/OD) and ab initio calculations for H_2Pm^{2-}. Although ab initio calculations have been done in the gaseous phase and without a metallic cation, their results are in agreement with solid-state data. The dihydrogen pyromellitate ion (H_2Pm) is not coordinated to metallic Fe^{2+} and Co^{2+}, thus the crystal packing is more important for geometric and vibrational changes than metal coordination. The starting point of the ab initio calcula-

tions was the X-ray crystal structure of the CoH_2Pm α phase,[3] which minimises differences between theoretical (gaseous phase) and experimental (solid phase) data due to crystal packing. In ab initio calculations the symmetric and asymmetric stretching modes were obtained at 337 and 822 cm^{-1}, respectively.

In Raman spectra, the ν_{sym}(O···H···O) mode is symmetric about the H atom. The hydrogen atom does not move and no frequency shift due to mass difference is expected upon deuteration.[11] In the deuterated analogues, the ν_{sym}(O···D···O) was observed at 309 and 300 cm^{-1} for Co^{2+} and Fe^{2+} salts, respectively. In CoH_2Pm and FeH_2Pm, the ν_{asym}(O···H···O) was tentatively assigned to 874 cm^{-1}. As this region is crowded and SHB modes become a little broader in deuterated analogues, the assignment becomes more difficult. On the other hand, it is known that deuteration causes little shift in asymmetric O−H−O stretching as was observed in the infrared spectra of potassium hydrogen maleate[21] and lithium hydrogen phthalate monohydrate.[22] In contrast, in Cu^{2+} salts, which do not show any SHB, similar bands were not observed in these regions.

The ν(O···H···O) of long and medium hydrogen bonds are expected at low frequencies (about 120 cm^{-1}). However, this region has lattice and hydrogen-bond water modes, which makes it difficult to assign the O···H···O mode.

Computations

Vibrational modes of the short hydrogen bond occur in regions where there are other Raman-active modes. In this work, quantum-mechanical calculations were used in an attempt to observe and assign those specific hydrogen-bond modes.

Geometry optimization and frequency calculations were made for H_2Pm^{2-} with intramolecular SHB. The starting point of the geometry calculations was the α phase of CoH_2Pm, as described by Ward and Luehrs.[3] In spite of the fact that the calculations have been performed in the gas phase, they are in good agreement with the experimental values of the Co^{2+} salt.[3] Table 4 contains both theoretical and experimental geometric parameters for H_2Pm^{2-}. This good agreement between experimental and theoretical data is due to the fact that in the crystal structure of the α-phase CoH_2Pm, Co^{2+} does not coordinate to H_2Pm^{2-}, therefore it is an ionic compound. Co^{2+} is coordinated to six water molecules in an octahedral geometry. There is a weak interaction between H_2Pm^{2-} and coordinated water molecules. H_2Pm^{2-} is the receptor of three long hydrogen bonds involving the water molecules. This is a weak interaction, therefore the greatest difference between the crystal and the gaseous phase is the crystal packing. However, the geometry optimization was performed using the coordinates of the crystal structure, which reduce crystal packing effects. As a result, theoretical and experimental data, geometry and frequency calculations and X-ray crystal data and the Raman spectrum of the ionic salt CoH_2Pm, could be compared and were similar.

Table 4. Bond lengths and bond angles of dihydrogen pyromellitate ion − experimental and calculation data

	Exp.[3]	Calcd.
Distances [Å]		
C1−C2	1.394(1)	1.392
C2−C2′	1.414(2)	1.408
C2−C3	1.522(1)	1.538
C3−O1	1.286(1)	1.211
C3−O2	1.299(1)	1.274
Angles [°]		
C2−C1−C2′	124.76(6)	124.36
C1−C2−C2′	117.64(7)	117.83
C1−C2−C3	113.66(10)	114.31
C2′−C2−C3	128.69(5)	127.87
C2−C3−O1	118.97(9)	118.22
C2−C3−O2	119.92(9)	117.77
O1−C3−O2	121.09(8)	123.97
C1−C2−C3−O1	2.01(15)	−15.79
C2′−C2−C3−O2	−176.56(10)	−18.4

The maximum deviations between theoretical and experimental data were 2 and 6%, respectively, for angles and bond lengths. The computed C−C bonds and C−C−C angles are in excellent agreement with experimental values. The computed O···O distance for a short symmetric intramolecular hydrogen bond (2.336 Å) is in good agreement with the experimental value (2.381 Å). The experimental C−Obond values are larger than the computed ones, and the carboxyl groups are more planar. This occurs due to the fact that in the crystal structure the water coordination molecules are involved in medium hydrogen bonds with carboxyl groups. The frequency calculations are listed in Tables 2 and 3. The simulated and experimental Raman spectra of the compounds are shown in Figure 4. Theoretical wavenumbers listed in Table 2 are multiplied by a scale factor of 0.8929. This scale factor is an average from the comparison of several computed and experimental data.[23]

The frequencies (ν_i) and the vibrational intensities (A_i), obtained in the ab initio calculation, were fitted to a Lorentzian-type function to describe the vibrational spectra. In this process, the concentration was considered equal to $c = 1\cdot10^{-3}$ in the Raman spectrum where $l = 1$ cm. To simplify the procedure, a constant value for the full width at half maximum (ω) was considered in all spectral regions, $\omega = 15$ cm^{-1}. Equation (1) represents the absorbance for a given frequency, ν.

$$A(\nu) = \left[\ln\left(\frac{I_0}{I}\right)\right]_\nu = cl\sum_{i=1}^{3N-6}\left[A_i\left(\frac{2\omega_i}{\pi}\right)\right]\cdot\left\{\frac{1}{\left[4(\nu-\nu_i)^2+\omega\right]}\right\} \quad (1)$$

The theoretical Raman spectrum of H_2Pm^{-2} is very similar to the spectra of Fe^{2+} and Co^{2+} salts. The short hydrogen-bond modes were obtained at 822 for ν_{asym}(O···H···O), and 337 for ν_{sym}(O···H···O). The relative deviations of experimental data were 5.9 and 9.8%, respectively. In the fre-

quency calculations, a shift to low frequencies was observed for the O−H stretching of the carboxylic group (2551 cm^{-1}). This stretching is very sensitive to hydrogen-bond interactions and is in good agreement with the experimental data (2575 cm^{-1}). The O−H deformation modes were obtained at 1054 and 1539 cm^{-1} for out-of-plane and in-plane, respectively. Theoretical benzene ring deformation modes are strongly coupled with C−H and COO deformation modes.

Conclusion

Although the vibrational modes of hydrogen bonds are weak in Raman spectroscopy, it was possible to carry out a study of these types of interactions. The O···H···O modes lie in a crowed region of the spectrum, but these modes were identified and tentatively attributed with the aid of deconvolution techniques, isotopic substitution and ab initio calculations. The optimized geometry in the gas phase is in good agreement with the experimental X-ray crystal data. Information about different types of hydrogen bonds (short or long) can be obtained using Raman spectroscopy.

FeH_2Pm and CoH_2Pm have a very short intramolecular hydrogen bond with an O···O distance of about 2.4 Å. The short hydrogen bond stretching observed in the Raman spectra was tentatively assigned to a broad band of weak intensity at 874 cm^{-1} for the asymmetric mode [ν_{asym}(O···H···O)] and at 307 cm^{-1} for the symmetric [ν_{sym}(O···H···O)] one. In deuterated analogues the ν_{sym}(O···H···O) band appears not to shift and the ν_{asym}(O···H···O) band is unfortunately not possible to assign. The evidence of deuteration was observed by the shift in the frequency of ν_{sym}(COO) and ν(C=O) modes, which are strongly coupled with the δOH(D) mode, and by the shift of the ν(OH) of water molecules, whose ν_{OH}/ν_{OD} is 1.36 for CoH_2Pm and 1.43 for FeH_2Pm.

CuH_2Pm crystallizes in the non-centrosymmetric space group *Pn*. The carboxyl groups of the H_2Pm^{-2} ions form a linear polymeric structure. In this compound, two medium intermolecular hydrogen bonds [2.639(5) Å and 2.629(5) Å] were observed and in Cu_2Pm, the pyromellitate ion is a receptor of medium hydrogen bonds with water molecules. The ν(O···H···O) of long and medium hydrogen bonds is expected at low frequencies (about 120 cm^{-1}).

Experimental Section

Synthesis: Powders and single crystals of the compounds were obtained by slow concentration of aqueous solutions at room temperature.

Fe^{2+} Salt: To a hot aqueous solution of pyromellitic acid (3.3 mmol; Aldrich B400-7, 96%), iron powder(3.2 mmol; Merck 3819, 99.5%) was added. The final solution was heated until the total oxidation of the iron powder had occurred, filtered, and stored at room temperature. A yellow powder was obtained and characterised as hexaaquairon(II) dihydrogen 1,2,4,5-benzenetetracarboxylate (FeH_2Pm). $C_{10}H_{16}FeO_{14}$ (416.08): calcd. C 28.87, H 3.85, Fe 13.42; found C 28.86, H 3.46, Fe 12.64. Its deuterated derivative was obtained by the reaction of metallic iron (powder) with pyromellitic acid and recrystallised from D_2O.

Co^{2+} Salt: To a hot aqueous solution of pyromellitic acid (3.3 mmol; Aldrich B400-7, 96%), an aqueous solution of cobalt(II) nitrate hexahydrate (2.9 mmol; Aldrich 23,037-5, 99%) was added. The final solution was filtered and stored at room temperature. Pink crystals were obtained and characterised as hexaaquacobalt(II) dihydrogen 1,2,4,5 benzenetetracarboxylate (CoH_2Pm). $C_{10}H_{16}CoO_{14}$ (412.22): calcd. C 28.65, H 3.82, Co 14.06; found C 28.67, H 3.83, Co 14.04. Its deuterated derivative was obtained by repeated recrystallization of CoH_2Pm in D_2O.

Cu^{2+} Salts: In a hot aqueous solution of pyromellitic acid (3.2 mmol; Aldrich B400-7 96%), basic copper(II) carbonate (1.6 mmol; Aldrich 20,789-6) was dissolved. The final solution was filtered and stored at room temperature. Two types of crystals were obtained, one dark blue and the other light blue. The dark blue crystals were characterised as triaquacopper(II) 1,2,4,5-benzenetetracarboxylate tetrahydrate (Cu_2Pm). $C_{10}H_{16}Cu_2O_{15}$ (503.32): calcd. C 21.55, H 3.95, Cu 22.80; found C 22.04, H 3.38, Cu 26.79. The light blue crystals were characterised as triaquacopper(II) dihydrogen 1,2,4,5-benzenetetracarboxylate trihydrate (CuH_2Pm). $C_{10}H_{16}CuO_{14}$ (423.78): calcd. C 28.34, H 3.78, Cu 15.00; found C 29.56, H 3.61, Cu 14.20.

Powder: X-ray powder patterns were obtained with a Rigaku diffractometer using Cu radiation (λ = 1.541838 Å) with 4 °·min^{-1} speed.

Raman Spectroscopy: Raman spectra were obtained with a micro-Raman instrument Dillor X-Y triple monochromator equipped with a CCD detector at room temperature. The 514.5 nm line of an argon ion laser was used as the exciting radiation.

Calculation Methods: Ab initio MO calculations were performed with the Gaussian 98 program package[24] using a Digital workstation. All calculations were carried out at the Hartee−Fock (HF) level. The 6-31++G** basis set with polarised and diffuse functions added to all the atoms was employed. The X-ray structure of the Co^{2+} salt of pyromellitic acid (CoH_2Pm)[3] was used as a starting point for geometry optimisation, followed by vibrational analysis. These salts are isostructural to FeH_2Pm. The theoretical vibrational spectra were calculated using the SIMULAT program.[25]

X-ray Crystallographic Study: $C_{10}H_{16}CuO_{14}$, M = 423.78, monoclinic, a = 6.763(1), b = 10.923(1), c = 9.646(1) Å, β = 91.925(3)°, V = 801.58(4) $Å^3$, T = 298 K, space group *Pn* (no. 07), Z = 2, μ(Mo-K_α) = 13.9 mm^{-1}, d = 1.756 g·cm^{-3}, 3220 reflections measured, 3085 unique (R_{int} = 0.009) which were used to refine 229 parameters. Final $R(F)$ and $wR(F^2)$ were 0.037 and 0.114, respectively (all data). The crystal was mounted on a four-circle P4 Siemens diffractometer. XSCANS program[26] was used to refine the unit-cell parameters and to manage the data collection. Analytical absorption, Lorentz and polarisation effects were corrected using JANA'98,[27] with maximum and minimum transmission of 0.984 and 0.881, respectively. The structure was solved by Patterson methods in a non-centrosymmetric space group with the XS program.[16] This space group is non-polar, therefore, Cu fractional coordinates were used as the origin. Hydrogen atoms were located from successive Fourier difference maps. Their atomic coordinates were optimised and fixed. Anisotropic displacement parameters were assigned to all non-hydrogen atoms, the structure was refined using SHELXL-93.[28] An empirical isotropic extinction parameter x was refined, according to the method describe by Larson.[29] The

structure was drawn by ORTEP-3 for windows.[30] CCDC-167303 contains the supplementary crystallographic data for this paper. These data can be obtained free of charge at www.ccdc.cam.ac.uk/conts/retrieving.html or from the Cambridge Crystallographic Data Centre, 12, Union Road, Cambridge CB2 1EZ, UK [Fax: (internat.) + 44-1223/336-033; E-mail: deposit@ccdc.cam.ac.uk].

Acknowledgments

We are grateful to Dr. Marcelo Augusto Silva de Oliveira and Dr. Marcos Assunção Pimenta for the Raman spectroscopy data obtained with a micro-Raman spectrometer at the Departamento de Física of the Universidade Federal de Minas Gerais, and to the Centro de Desenvolvimento de Tecnologia Nuclear (CDTN) for providing the D_2O. This work has been supported by the Fundação de Amparo à Pesquisa do Estado de Minas Gerais, FAPEMIG (Grant CEX 1123/90). R. D. and H. A. A. are grateful to the CNPq for providing the graduate fellowship.

[1] G. A. Jeffrey, *Topics in physical chemistry: An introduction to hydrogen bonding* (Ed.: D. G. Truhlar), New York, Oxford University Press, **1997**.
[2] B. T. Usubaliev, A. N. Shnulin, K. S. Mamedov, *Koord. Khim.* **1982**, *8*, 1532−1538.
[3] D. C. Ward, D. C. Luehrs, *Acta Crystallogr., Sect. C* **1983**, *39*, 1370−1372.
[4] S. M. Jessen, H. Küppers, *Z. Naturforsch., Teil B* **1992**, *47*, 1141−1153.
[5] F. D. Rochon, G. Massarweh, *Inorg. Chim. Acta* **2000**, *304*, 190−198.
[6] J. Emsley, *J. Chem. Soc. Rev.* **1980**, *9*, 91−124.
[7] W. Qian, S. Krimm, *J. Phys. Chem. A* **1997**, *101*, 5825−5827.
[8] S. M. Jessen, H. Küppers, *J. Mol. Struct.* **1991**, *263*, 247−265.
[9] C. Reid, *J. Chem. Phys.* **1959**, *30*, 182−190.
[10] E. R. Lippincott, R. Schroeder, *J. Chem. Phys.* **1955**, *23*, 1099−1106.
[11] P. J. Miller, R. A. Butler, E. R. Lippincott, *J. Chem. Phys.* **1978**, *57*, 5451−5456.
[12] D. Hadzi, B. Orel, A. Novak, *Spectrochim. Acta A* **1973**, *29*, 1745−1753.
[13] D. C. Luehrs, C. B. Cornilsen, C. B. Glover, T. L. Neils, *Inorg. Chim. Acta* **1998**, *145*, 81−84.
[14] F. Takusagawa, K. Hirotsu, A. Shimada, *Bull. Chem. Soc. Jpn.* **1971**, *44*, 1274−1278.
[15] H. D. Flack, *Acta Crystallogr., Sect. A* **1993**, *39*, 876−881.
[16] G. M. Sheldrick, *SHELXTL/PC*, Structure Determination Software Programs, Siemens Analytical X-ray Instruments Inc., Madison, Wisconsin, USA, **1990**.
[17] G. B. Deacon, R. J. Phillips, *J. Coord. Chem. Rev.* **1980**, *33*, 227−250.
[18] D. W. Scott, J. P. McCullough, W. N. Hubbard, J. F. Messerly, I. A. Hossenlopp, F. R. Frow, G. Waddington, *J. Am. Chem. Soc.* **1956**, *78*, 5463−5468.
[19] D. H. Whiffen, *J. Chem. Soc.* **1956**, 1350−1356.
[20] K. Nakamoto, *Infrared and Raman Spectra of Inorganic and Coordination Compounds*, 4th ed., John Wiley & Sons, New York, **1986**, pp. 229.
[21] M. M. Ilczyszyn, J. Baran, H. Ratajcak, A. J. Barnes, *J. Mol. Struct.* **1992**, *270*, 499−515.
[22] M. M. Ilczyszyn, A. J. Barnes, H. Ratajczak, *J. Mol. Struct.* **1993**, *291*, 135−143.
[23] A. P. Scott, L. Radom, *J. Phys. Chem.* **1996**, *100*, 16502−16513.
[24] M. J. Frisch, G. W. Trucks, H. B. Schlegel, G. E. Scuseria, M. A. Robb, J. R. Cheesman, V. G. Zakrzewski, J. A. Montgomery, R. E. Stratmann, J. C. Burant, S. Dapprich, J. M. Millam, A. D. Daniels, K. N. Kudin, M. C. Strain, O. Farkas, J. Tomasi, V. Barone, M. Cossi, R. Cammi, B. Mennucci, C. Pomelli, C. Adamo, J. Clifford, J. Ochterski, G. A. Peterson, P. Y. Ayala, Q. Cui, K. Morokuma, D. K. Malick, A. D. Rabuck, K. Raghavachari, B. Foresman, J. Cioslowski, J. V. Ortiz, B. B. Stefanov, G. Liu, A. Liashenki, P. Piskorz, I. Komaromi, R. Gomperts, R. L. Martin, D. J. Fox, T. Keith, M. A. Allaham, C. Y. Peng, A. Nanayakkara, C. Gonzalez, M. Challacombe, P. M. W. Gill, B. G. Johnson, W. Chen, M. W. Wong, J. L. Andres, M. Head-Gordon, E. S. Replogle, J. A. Pople, *Gaussian98* (Revision A.1), Gaussian Inc., Pittsburgh, PA, **1998**.
[25] H. F. Dos Santos, W. B. De Almeida, A. M. G. Do Val, C. Guimarães, *Quím. Nova* **1999**, *22*, 732−736.
[26] Siemens, *XSCANS*, Version 2.1, Siemens Analytical X-ray Instruments Inc., Madison, Wisconsin, USA, **1991**.
[27] V. Petrick, M. Dusek, *JANA-98*, Crystallographic Computing System, Institute of Physics, Academy of Sciences of Czech Republic, Praha, **1998**.
[28] G. M. Sheldrick, *SHELXL-93*, Program for Crystal Structure Solution, University of Göttingen, Germany, **1993**.
[29] A. C. Larson, *Crystallographic Computing* (Ed.: F. R. Ahmed), Munksgaard, Copenhagen, **1970**, pp. 291−294.
[30] C. K. Johnson, M. N. Burnett, L. J. Farrugia, *ORTEP-3 for Windows*, Version 1.0.2, University of Glasgow, Scotland, **1998**.

Received July 14, 2001
[I01262]

Coupling of Arylamines with Coordinated Arylazopyrimidines in Palladium(II) Complexes

Prasanta Kumar Santra,[a] Prithwiraj Byabartta,[a] Surajit Chattopadhyay,[b] Larry R. Falvello,[c] and Chittaranjan Sinha*[a]

Keywords: Nitrogen heterocycles / Palladium / N ligands / Aminations / X-ray structure / EHMO calculation

2-(Arylazo)pyrimidine (**1**) reacts with palladium chloride and gives Pd(aapm)Cl_2 (**2**) which undergoes a palladium(II)-mediated novel carbon–nitrogen bond formation reaction of the aromatic amines to the *ortho*-C–H function of the pendant aryl ring in the coordinated 2-(arylazo)pyrimidine. The reactant, Pd(papm)Cl_2 (**2a**) and the product, Pd(papm-N-C_6H_4-OCH_3-*p*)Cl (**5a**) have been characterised by X-ray crystal structure. The coupled products exhibit low energy transitions (NIR region) unlike the parent complex, Pd(aapm)Cl_2. The cyclic voltammogram shows an oxidation couple at positive potential to SCE. The EHMO calculation suggests that the spectral feature in Pd(aapm)Cl_2 (**2**) is due to the MLCT [d(Pd)→π*(azo)] whereas in Pd(aapm-N-C_6H_4-X-*p*)Cl (**3**–**6**) the transition at the NIR region is due to the intravalence charge transfer (IVCT) transition.

Introduction

Arylazoheterocycles are light-sensitive, redox-active, and efficient colorant materials.[1−9] Presence of an arylazo group at the *ortho* position of the N-heterocycles constitute an azoimine, −N=N−C=N−, function.[7−9] They have successfully been used to stabilise the low-valent metal redox state.[7−17] The coordination of arylazoheterocycles to a metal centre alter the electrophilic character of the ligand and provides a fascinating area in the metal-assisted organic synthesis. This has been observed in the metal complexes of 2-(arylazo)pyridines.[18−25] The complexes undergo different organic transformations at the pendant aryl ring such as hydroxylation,[18−20] thiolation,[21−23] and the C−N coupling[24,25] reaction with aromatic amines. This has encouraged us to design 2-(arylazo)pyrimidines [aapm (**1**)][13,14,19] that is more π-acidic than 2-(arylazo)pyridine due to the π-acidity order, pyrimidine > pyridine. Copper(I)[13] and isomers of ruthenium(II) complexes[14] of **1** have been reported from our group. Palladium(II) forms [2-(arylazo)pyrimidine]dichloropalladium(II) [Pd(aapm)Cl_2 (**2**)] and its reaction with OH^- in air or Tollen's reagent gives (azophenolatopyrimidine)palladium(II) complex.[19] This is believed to be formed by the hydroxylation of the C−H bond *ortho* to the azo group of 2-(arylazo)pyrimidine. Heterocyclic bases (e.g., pyridine and derivatives R-Py) react with Pd(aapm)Cl_2 and substitute the ligand followed by isomerisation to *trans*-Pd(R-Py)$_2Cl_2$.[26] In continuation of our work to explore the reactivity of palladium−aapm complexes, we discuss in this article the palladium(II)-mediated C−N coupling reaction of aromatic amines to the *ortho*-C−H function of the pendant aryl ring in the coordinated 2-(arylazo)pyrimidine. The reactant and product have been characterised by X-ray crystallography. The coupled products exhibit different electronic and redox behaviour from that of the reactants and have been accounted for by EHMO calculations.

[a] Department of Chemistry, The University of Burdwan, Burdwan 713 104, India
Fax: (internat.) + 91-0342/564452
E-mail: c_r_sinha@yahoo.com
[b] Department of Chemistry and Chemical Technology, Vidyasagar University, Midnapore 721102, India
[c] Departmento de Quimica Inorganica, Universidad de Zaragoza, Plaza San Fransisco S/N, 50009 Zaragoza, Spain
Supporting information for this article is available on the WWW under http://www.eurjic.com or from the author.

Results and Discussion

Synthesis of Parent Complexes

The general abbreviation of 2-(arylazo)pyrimidine is aapm (**1**). 2-(Phenylazo)pyrimidine [papm (**1a**)], 2-(*p*-tolylazo)pyrimidine [tapm (**1b**)], and 2-(*p*-chloro-phenylazo)pyrimidine [Clpapm (**1c**)] are three ligands used in this work. They act as *N*,*N*′-bidentate chelators with an azoimine function, −N=N−C=N−, where N refers to N(8)(azo) and *N*′ refers to N(3)(pyrimidine). The reaction of aapm with Pd(MeCN)$_2Cl_2$ in MeCN has yielded orange-red Pd(aapm)Cl_2 (**2**) in high yield.[19,27]

 © WILEY-VCH Verlag GmbH, 69451 Weinheim, Germany, 2002 1434−1948/02/0505−1124 $ 20.00+.50/0 *Eur. J. Inorg. Chem.* **2002**, 1124−1131

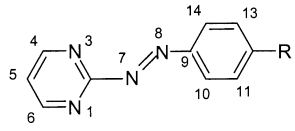

a: R = H, (papm)

b: R = H, 12-Me (*p*-tapm)

c: R = H, 12-Cl (*p*-Clpapm)

aapm, **1**

The C−N Coupling Reaction

Addition of $ArNH_2$ (in 1:1 stoichiometry) in an MeCN suspension of Pd(aapm)Cl_2 (**2**) under refluxing conditions, changes the intense orange-red colour to greenish-brown. Chromatographic purification of the reaction mixture separates an orange-brown band. The orange-brown band has been identified as an amine product coupled to Pd(aapm)Cl_2 and is abbreviated Pd(aapm-N-C_6H_4-X-*p*)Cl [where X= H (**3**), Me (**4**), OMe (**5**), Cl (**6**)]. The reaction is shown in Equation (1). The arylamination takes place at the *ortho* position of the aryl ring (B ring) of aapm to the azo function and forms a palladium(II) complex of tridentate *N*,*N*′,*N*′′-chelating ligand [where N is N(8)(azo); *N*′ is N(3)(pyrimidine); *N*′′ is N(15)(arylamine)]. Free ligands do not couple with arylamines even if forced but they react smoothly in the palladium(II) complex.

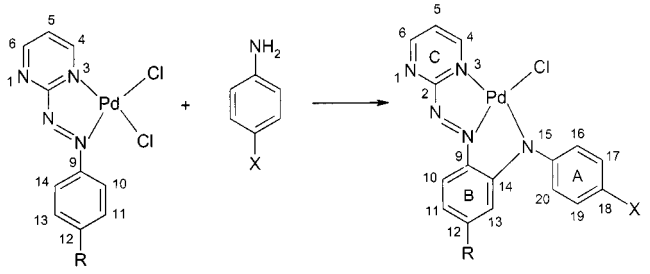

2 Pd(aapm-N–C_6H_4–X-*p*)Cl (**3** - **6**) (1)

Spectral Studies

Infrared spectra of Pd(aapm)Cl_2 (**2**) show two distinct Pd−Cl stretches [ν(Pd−Cl) = 340, 360 cm^{-1}] in agreement with *cis*-$PdCl_2$ configuration.[19,27] A sharp single band at 1400−1415 cm^{-1} corresponding to $\nu_{N=N}$ in the ligand is shifted to 1380−1385 cm^{-1} in Pd(aapm)Cl_2. This lowering of the frequency is due to N-coordination.[18] In the coupled products, Pd(aapm-N-C_6H_4-X-*p*)Cl (**3**−**6**), $\nu_{N=N}$ appears at 1290−1300 cm^{-1}; this significant reduction in azo stretching may be due to the intramolecular charge delocalisation from the fused N-C_6H_4-X-*p* fragment to the azo function (vide infra). A single stretch at 340−350 cm^{-1} in **3**−**6** supports the presence of a Pd−Cl bond. A chloroform solution of Pd(aapm)Cl_2 exhibits a strong absorption[19] at ca. 425 nm. On comparison with the free ligand solution spectra,[13] the transition has been assigned to the MLCT band which is also supported by an EHMO calculation (vide infra). The spectral structure changes abruptly in Pd(aapm-N-C_6H_4-X-*p*)Cl (**3**−**6**) and exhibits an intense band in the NIR region (750−1100 nm) with five/six well-defined transitions (Figure 1). The spectroscopic data are collected in Table 1. The transitions have been accounted from EHMO calculation and are assigned to HOMO→LUMO transitions where the HOMO has a major share from the arylamine group and the LUMO is dominated by the azo group (vide infra). The observed trend of the band maxima (λ_{max}) for the substituent in the aryl ring follows as *p*-chloroaniline (**6**) < aniline (**3**) < *p*-toluidine (**4**) < *p*-anisidine (**5**). The electron-donating substituent in the X-C_6H_4-N- fragment increased the energy of the HOMO[27,28] and in *p*-anisidine the energy was maximised. In *p*-choloroaniline the energy of the HOMO was reduced due to the electron-withdrawing effect of the Cl group. The substituent (R) in the arylazopyrimidine [R-C_6H_4-N=N-$C_4H_3N_2$ (**1**)] fragment also shifted the band maxima in the order Pd(Clpapm-N-C_6H_4-X-*p*)Cl (**c**) > Pd(papm-N-C_6H_4-X-*p*)Cl (**a**) > Pd(tapm-N-C_6H_4-X-*p*)Cl (**b**). This is due to the lowering of the energy of the LUMOs in **c** compared to **a** due to the electron-withdrawing power of Cl. The reverse case is seen in the complexes **b** due to the +I effect of the Me group that has a destabilising effect on the LUMOs.

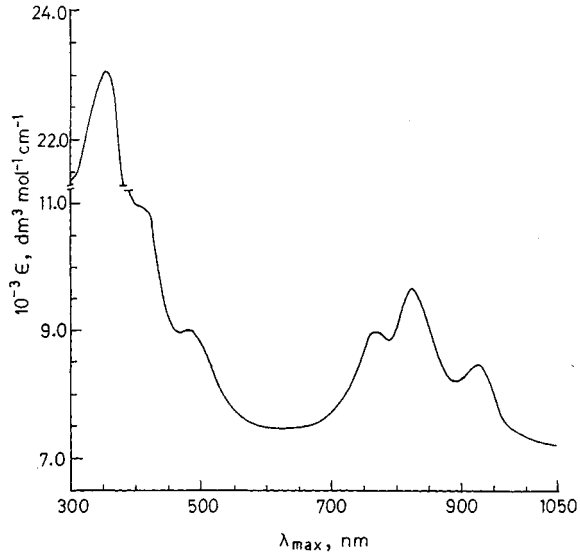

Figure 1. Electronic spectra of Pd(papm-N-OCH_3-*p*)Cl (**5a**) in $CHCl_3$

The ^{1}H NMR spectra of the complexes are compared in order to determine the bonding mode and stereochemistry. The ^{1}H NMR spectra of the ligands aapm (**1**) and Pd(aapm)Cl_2 (**2**) were reported from our group.[13,26] The signals were assigned on the basis of chemical shifts, spin-spin interaction and their effect on substitution. In Pd(aapm)Cl_2 the signals in general are downfield shifted compared to free ligand values.[26] Pd(aapm-N-C_6H_4-X-*p*)Cl show complex NMR spectra. The *N*-aryl (A-ring) and azoaryl (B-ring) proton signals appear on the upfield side. The effect of the substituent X (X-C_6H_4-N) on the signal movement of the arylamine protons (A-ring protons: 16-H to 20-H) is in accordance with the electronic property of X. It is observed that the electron-donating substituent (Me/OMe) moves the signals upfield while the electron-withdrawing group Cl moves them downfield with reference to

Table 1. Solution spectral and cyclic voltammetric data

Compound	Electronic spectroscopic data[a] λ_{max} [nm] (ε [$dm^3 \cdot mol^{-1} \cdot cm^{-1}$])	Cyclic voltammetric data[b] $E_{1/2}$ [V] (ΔE_p [mV]) Oxidation $E^1_{1/2}$	Reduction $-E^2_{1/2}$	$-E^3_{1/2}$	$-E^4_{1/2}$
Pd(papm-N-C_6H_5)Cl (**3a**)	914 (6289), 819 (7419), 760 (6353), 474 (5975)[c], 410 (10327), 340 (23019)	1.174 (107)	0.347 (88)	0.873 (140)	0.982 (167)
Pd(papm-N-C_6H_4-Me−*p*)Cl (**4a**)	921 (6518), 820 (7619), 761 (6925), 479 (6419)[c], 409 (8344), 345 (18295)	1.275 (105)	0.364 (90)	0.834 (160)	1.103 (100)
Pd(papm-N-C_6H_4-OCH_3−*p*)Cl (**5a**)	926 (8428), 821 (9648), 765 (8963), 473 (9046)[c], 416 (10919), 344 (23127)	1.021 (100)	0.627 (75)	0.958 (160)	1.109 (110)
Pd(papm-N-C_6H_4-Cl−*p*)Cl (**6a**)	901 (6531), 815 (7353), 755 (6689), 470 (6452)[c], 410 (8468), 343 (16846)	1.185 (91)	0.316 (90)	0.751 (110)	1.048[d]
Pd(tapm-N-C_6H_5)Cl (**3b**)	878 (6285), 792 (7532), 723 (6375), 470 (6014)[c], 409 (10469), 340 (22310)	1.042 (95)	0.382 (100)	0.943 (120)	1.192 (140)
Pd(tapm-N-C_6H_4-Me−*p*)Cl (**4b**)	882 (6687), 798 (7728), 733 (7081), 466 (7715)[c], 395 (11649), 340 (23337)	1.129 (100)	0.435 (110)	0.889 (90)	1.124 (120)
Pd(tapm-N-C_6H_4-OCH_3−*p*)Cl (**5b**)	894 (9323), 811 (11232), 756 (10426), 475 (11384)[c], 390 (15648), 340 (23254)	1.005 (98)	0.425 (92)	0.865 (120)	1.114 (110)
Pd(tapm-N-C_6H_4-Cl−*p*)Cl (**6b**)	865 (8736), 792 (10362), 722 (9840), 474 (10243)[c], 394 (1612 2), 341 (28015)	1.190 (105)	0.389 (94)	0.783 (100)	1.069[d]
Pd(Clpapm-N-C_6H_5)Cl (**3c**)	918 (6715), 825 (7830), 765 (7129), 476 (8117)[c], 411 (10925), 340 (22833)	1.000 (130)	0.422 (80)	0.825 (77)	1.107 (175)
Pd(Cllpapm-N-C_6H_4-Me−*p*)Cl (**4c**)	922 (8097), 828 (8995), 768 (8143), 481 (9660)[c], 405 (14475), 344 (26010)	1.115 (140)	0.436 (85)	0.832 (82)	1.120 (180)
Pd(Clpapm-N-C_6H_4-OCH_3−*p*)Cl (**5c**)	930 (1530)[c], 830 (1728), 772 (1590), 407 (3850), 309 (17822)	0.957 (160)	0.415 (75)	0.761 (70)	1.004 (200)
Pd(Clpapm-N-C_6H_4-Cl−*p*)Cl (**6c**)	905 (6792), 818 (7840), 760 (7145), 478 (7824)[c], 409 (11455), 336 (23121)	0.945 (150)	0.365 (83)	0.745 (70)	0.985 (170)

[a] Solvent $CHCl_3$. [b] Solvent MeCN, supporting electrolyte Bu_4NClO_4, Pt-disk milli working electrode, Pt-wire auxiliary electrode, reference electrode SCE, at 298 K. [c] Shoulder. [d] E_{pc}.

the unsubstituted system. A similar situation is also observed for the substituent R on the arylazopyrimidine (R-C_6H_4-N=N-$C_4H_3N_2$) protons of the B-ring (10-H to 13-H). The cross interactions i.e., the effect of substituent X at the *N*-aryl ring on the azoaryl protons or vice versa are not remarkable. Azoaryl signals (10-H to 13-H) are severely affected in Pd(aapm-N-C_6H_4-X-*p*)Cl relative to Pd(aapm)Cl_2 and are shifted upfield by 0.2−1.0 ppm. Pyrimidine protons (4-H to 6-H of C-ring) in **3**−**6** are shifted upfield by 0.1−0.5 ppm compared to the parent complex Pd(aapm)Cl_2 and are hardly affected by the substituents in the aryl rings (X or R). Coupling of arylamine with the aryl part of aapm (B-ring) has changed the electronic behaviour of the molecule. The azopyrimidine function is electron-deficient while the *N*-aryl (ring A) is a σ-donor and may cause an intramolecular charge-transfer transition. This may be the reason for the large upfield shifting of the arylazopyrimidine proton signals (4-H to 13-H). Solution electronic spectral properties also support this behaviour (vide supra).

X-ray Structure Studies

The X-ray structures of Pd(papm)Cl_2 (**2a**) and Pd(papm-N-C_6H_4-OCH_3-*p*)Cl (**5a**) have been determined. Perspective molecular views are shown in Figures 2 and 3 and the selected bond parameters are listed in Tables 2 and 3.

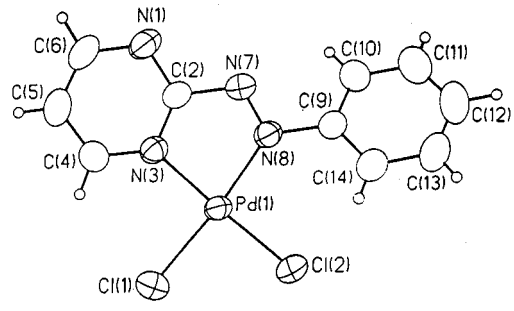

Figure 2. Drawing of Pd(papm)Cl_2 (**2a**), showing the atom numbering scheme; non-hydrogen atoms are represented by their 50% probability ellipsoids

a. Geometrical Features

The Pd(papm)Cl_2 has a *cis*-$PdCl_2$ configuration (Figure 2). The asymmetric unit of the crystal lattice consists of two molecules. These two molecules have parallel cores with a Pd···Pd separation of 3.4201(5) Å. The molecular packing diagram viewed down the *a* axis shows a Pd···Pd separation between asymmetric units of 3.9881(4) Å and the pendant phenyl rings are oriented in a parallel manner to ensure some sort of π-interaction. The packing also exhibits a benzene molecule at the special position and a weak Pd···Cl nonbonding intermolecular interaction (3.3−3.4 Å) where

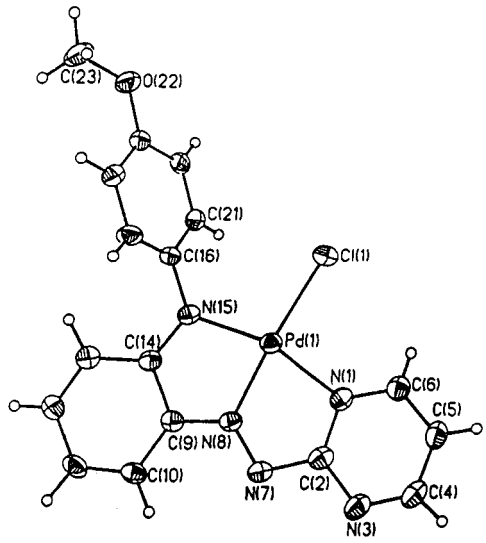

Figure 3. Drawing of Pd(papm-N-C_6H_4-OCH_3-*p*)Cl (**5a**), showing the atom numbering scheme; non-hydrogen atoms are represented by their 50% probability ellipsoids

Table 2. Selected bond lengths [Å] and angles [°] and their estimated standard deviations for **2a**

Distances			
Pd(1)−N(3)	2.014(3)	Pd(1A)−N(3A)	2.009(3)
Pd(1)−N(8)	2.041(3)	Pd(1A)−N(8a)	2.015(3)
Pd(1)−Cl(1)	2.2882(9)	Pd(1A)−Cl(1A)	2.2845(9)
Pd(1)−Cl(2)	2.2800(9)	Pd(1A)−Cl(2A)	2.2808(9)
N(7)−N(8)	1.260(3)	N(7A)−N(8a)	1.260(3)
C(2)−N(3)	1.344(4)	C(2)−N(7)	1.408(4)
C(2A)−N(3A)	1.346(4)	C(2A)−N(7A)	1.407(4)
Angles			
N(3)−Pd(1)−N(8)	77.74(10)	N(3A)−Pd(1A)−N(8A)	77.39(11)
Cl(1)−Pd(1)−Cl(2)	89.50(3)	Cl(1A)−Pd(1A)−Cl(2A)	90.93(4)
N(3)−Pd(1)−Cl(1)	93.98(8)	N(3A)−Pd(1A)−Cl(1A)	94.89(9)
N(3)−Pd(1)−Cl(2)	174.76(8)	N(3A)−Pd(1A)−Cl(2A)	171.90(8)
N(8)−Pd(1)−Cl(2)	98.82(8)	N(8A)−Pd(1A)−Cl(2A)	96.90(7)
N(8)−Pd(1)−Cl(1)	171.68(8)	N(8A)−Pd(1A)−Cl(1A)	172.15(8)

Table 3. Selected bond lengths [Å] and angles [°] and their estimated standard deviations for **5a**

Distances			
Pd(1)−N(3)	2.029(4)	C(2)−N(7)	1.379(5)
Pd(1)−N(8)	1.937(3)	Pd(1)−Cl(1)	2.302(1)
Pd(1)−N (15)	2.026(3)	C(9)−N(8)	1.336(5)
N(7)−N(8)	1.315(4)	C(14)−N(15)	1.333(5)
C(2)−N(3)	1.362(5)		
Angles			
N(3)−Pd(1)−N(8)	78.86(14)	N(8)−Pd(1)−Cl(1)	176.29(11)
N(8)−Pd(1)−N(15)	81.76(14)	N(1)−N(8)−N(7)	120.6(3)
N(3)−Pd(1)−Cl(1)	97.52(11)	Pd(1)−N(3)−C(2)	110.0(3)
N(15)−Pd(1)−Cl(1)	101.88(10)	Pd(1)−N(15)−C(14)	111.5(3)
N(3)−Pd(1)−N(15)	160.59(14)	Pd(1)−N(8)−C(9)	116.4(2)

Pd and Cl belong to two different molecules in the asymmetric unit. The two independent molecules are chemically similar. The PdN_2Cl_2 coordination sphere is planar with no atom deviating more than 0.06 Å from the mean plane. The chelate ring is planar (deviation < 0.04 Å) and the bond angle lies in the range 77.6±2°. This deviates from ideal square-planar angles. The Cl−Pd−Cl angle is ca. 90.2°. The pendant phenyl ring is no longer in plane with the chelated fragment and is twisted by ca. 42.5°.

The crystallographic asymmetry unit of Pd(papm-NC_6H_4-OCH_3-*p*)Cl contains 25 non-hydrogen atoms, of which 17 lie in a plane nearly perpendicular to the crystallographic *c* axis. These atoms comprise of two chelate rings, the aromatic groups fused to them, and the Pd and Cl atoms. The remaining atoms of the asymmetric unit comprise the methoxyphenyl group. The Pd atom lies in the square plane defined by the N_3Cl donor centres (deviation 0.02 Å). Two chelate planes Pd,N(3),C(2),N(7),N(8) (deviation < 0.01 Å) and Pd,N(15),C(14),C(9),N(8) (deviation < 0.01 Å) are coplanar and the chelate angles are 78.86(14) and 81.76(14)°, respectively. The pendant methoxyphenyl ring (A ring) is inclined at an angle of 54.99(15)° with the principal plane of 17 atoms.

b. Bond Parameters

In Pd(papm)Cl_2 the Pd−N(azo) bond length is slightly longer (ca. 2.03 Å) than that of the Pd−N(pyrimidine) (ca. 2.01 Å). This is the reverse in the case of other complexes. In copper(I) and ruthenium(II) complexes of papm, the M−N(azo) distance is significantly shorter than that of the M−N(pyrimidine) distance [Cu(papm)$_2$(ClO_4):[13] Cu−N(azo) 1.99 Å, Cu−N(pyrimidine) 2.03 Å; Ru(papm)$_2$$Cl_2$:[14] Ru−N(azo) 2.00 Å; Ru−N(pyrimidine) 2.06 Å]. This is due to π-back bonding involving metal t_2 and ligand π*(azo) orbitals.[7,13,14,29] The N=N bond length is 1.260(3) Å and is comparable with that of the copper(I)[13] complex but shorter than that of the ruthenium(II)[14] complexes. Efficient π-back bonding in (arylazopyrimidine)ruthenium(II) complexes enhances the N=N distance.[14] In Pd(papm-NC_6H_4-OMe-*p*)Cl the Pd−N(azo) [Pd−N(8)],

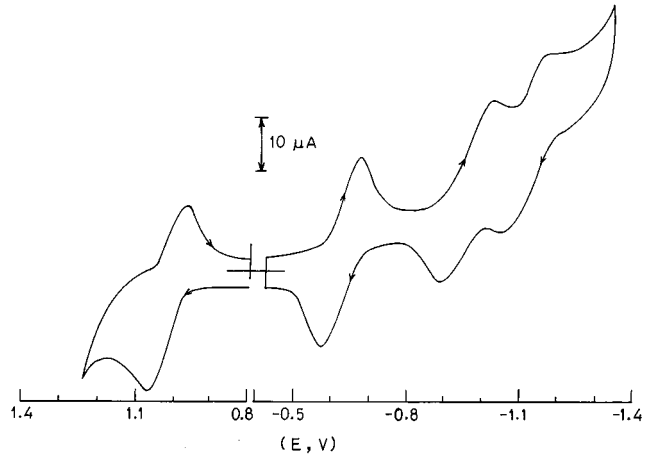

Figure 4. Cyclic voltammogram of Pd(papm-N-C_6H_4-OCH_3-*p*)Cl (**5a**) in MeCN (0.1 M Bu_4NClO_4) at 298 K

Pd−N(pyrimidine) [Pd−N(3)], and Pd−N(arylamine) [Pd−N(15)] distances are 2.028(4), 1.938(3), and 2.028(4) Å, respectively. The N=N length is 1.314(4) Å. The N=N distance is not available for the free ligand; however, the data available in some azo ligands[30−32] suggest that it is ca. 1.25 Å. In this case the N=N distance in **5a** is unusually long compared to the parent complex **2a**. This elongation may be due to intramolecular charge delocalisation from the arylamine fragment (vide supra) to the azopyrimidine.

Electrochemistry

The redox behaviour of **3**−**6** in acetonitrile solution was examined by cyclic voltammetry at a Pt-disk working electrode and the potentials are reported with reference to the SCE. The results are given in Table 1, and a representative voltammogram is shown in Figure 4. Pd(aapm)Cl_2 does not exhibit any redox response positive to the SCE and on the negative side a quasireversible redox couple ($\Delta E_P > 130$ mV) followed by an irreversible response at potential > -1.0 V is observed. Pd(aapm-N-C_6H_4-X-*p*)Cl (**3**−**6**) exhibited four successive redox couples: one of them at high positive potential (1.0−1.3 V) and three at the negative side of the SCE. Arylazopyrimidines are reduced at the negative potentials, −1.0 to −1.4 V.[13,14] The reduction is regarded as the electron accommodation in the LUMO characterised by the azoimine function. There are four successive redox-accessible levels in the azoimine function [Equations (2) to (5)]. In the present examples, three negative redox couples may correspond to three reductions [Equations (2) to (4)]. However, the couple at the positive potential is difficult to assign as Pd^{II} is redox-inactive. We suggest that this couple is due to oxidation of the ligand at the easily oxidisable azoarylamine chelated centre (chelate ring 2) [Equation (6)]. The first three redox couples [Equations (2), (3), and (6)] are quasireversible (ΔE_P = 70−100 mV) and the fourth response [Equation (4)] is irreversible in nature ($\Delta E_P > 130$ mV).

(2)

(3)

(4)

(5)

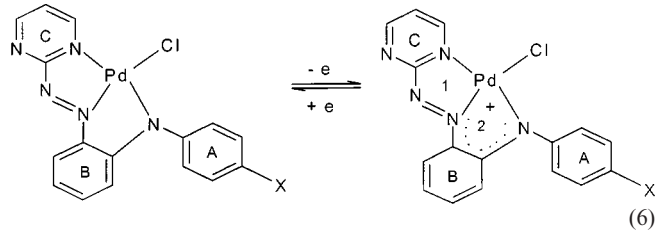

(6)

Table 4. Relative percentages of atomic contributions to the MOs of the complexes in **i** and **ii**

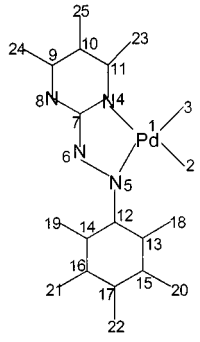

i

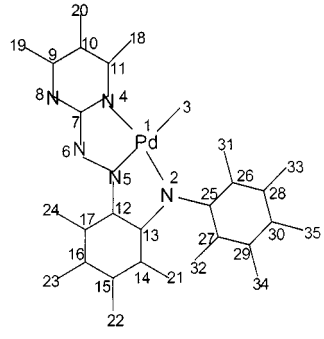

ii

% Contribution MO	Energy [eV]	Pd	N (pyrimidine)	N=N (azo)	azoaryl	arylamine
structure (**i**)						
45a (HOMO−1)	−11.781	93				
46a (HOMO)	−11.569	83	2	8		
47a (LUMO)	−10.714	9	1	67	7	
48a (LUMO+1)	−9.259		99			
structure (**ii**)						
57a (HOMO−2)	−11.623	84		6		
58a (HOMO−1)	−11.591	81	4	4		
59a (HOMO)	−11.457	37				53
60a (LUMO)	−10.724	9	9	68	13	
61a (LUMO+1)	−9.260		98			

The oxidation of coordinated *ortho*-phenylenediamine to semibenzoquinone diimine and benzoquinone diimine are known in the literature and support this observation.[34,35] The redox potential varies in the usual manner with the substituent at the *N*-aryl (A-ring) and azoaryl (B-ring) ring.[13,19]

Electronic Structure − EHMO Calculation

In order to have an insight into the difference in electronic behaviour of Pd(aapm)Cl_2 and Pd(aapm-N-C_6H_4-X-*p*)Cl towards their spectral and electrochemical properties, the MO calculations have been performed in the framework of extended Hückel formalism on a model complex as shown in structures **i** and **ii** (shown in Table 4). Crystallographic data were used as the parameters for bond lengths and bond angles. The relative percentages of the atomic contributions to the MOs are given in Table 4. In complex

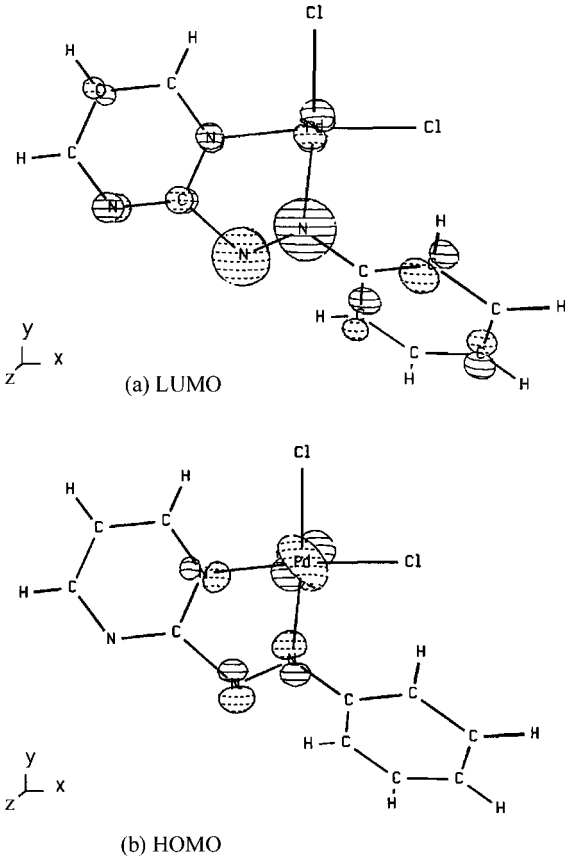

Figure 5. LUMO and HOMO of Pd(papm)Cl_2

Pd(aapm)Cl_2 the LUMO (47a) (Figure 5, a) is ligand-dominated with 67% character of azo (N=N), 5% of pyrimidine-N and a small contribution (9%) from the Pd d_{yz} orbital. The HOMO (46a) is mainly a metal orbital (83%) (Figure 5, b) and contributed from d orbitals (total 78%, of which d_z^2 41% and d_{xy} 37%) and a small part of the 4s orbital (5%). In complex Pd(aapm-N-Ar)Cl the LUMO

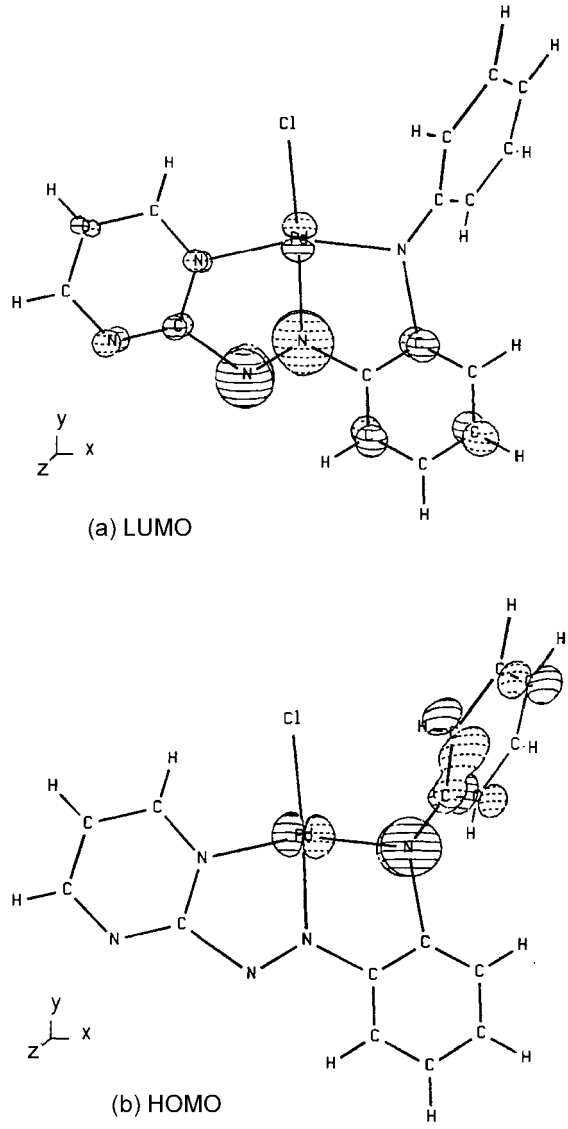

Figure 6. LUMO and HOMO of Pd(papm-N-C_6H_5)Cl

(60a) (Figure 6, a) is characterised by the azo group (68%), pyrimidine group (22%), and a small part of the metal orbital (d_{yz}, 9%). The HOMO (59a) (Figure 6, b) is computed from the admixture of the metal d_{xz} orbital (37%) and the *N*-aryl (ring A) (53%) and contributes to 90% of the character of the function.

Some experimental findings may be rationalised on the basis of EHMO results. The solution electronic spectra of complex **2** may exhibit a HOMO→LUMO (46a→47a) transition corresponding to the MLCT band. The first reduction will certainly be localised due to electron accommodation at the LUMO (47a) [π*(azo)] and the second electron will enter at the LUMO+1 (48a), which is purely pyrimidine in character (99%). Thus, the second reduction is irreversible in nature. The spectral and electrochemical behaviour of Pd(aapm-NAr)Cl is entirely different from the parent complex. The low-energy spectral band is associated with a HOMO→LUMO (59a→60a) charge transfer.[28,35,36] The HOMO is from a major portion (53%) of the N−Ar

group (ring A) and the LUMO shares 68% azo and 22% pyrimidine character. Thus, the transition is characterised as an intravalence charge-transfer transition (IVCT). Other spectral transitions may be characterised as HOMO−1 (58a)→LUMO (60a), HOMO−2 (57a)→LUMO (60a), HOMO (59a)→LUMO+1 (61a), etc. The redox behaviour at a positive potential to SCE may correspond to electron extraction from the HOMO (59a), which has a major share from the N−Ar group. The reductions correspond to sequential electron feeding at the LUMO (60a); LUMO+1 (61a) and LUMO+2 (62a).

Experimental Section

General Remarks: 2-(Arylazo)pyrimidines were prepared by the reported procedure.[13] $PdCl_2$ was purchased from Arora Matthey. Aniline, *p*-toluidine, *p*-anisidine, *p*-chloroaniline were received from the Sisco Research Lab. The purification of acetonitrile and preparation of tetrabutylammonium perchlorate (TBAP) for electrochemical work were done as before.[13] Dinitrogen was purified by bubbling through an alkaline pyrogallol solution. All other chemicals and solvents were of reagent grade and were used without further purification. Commercially available SRL silica gel (60−120 mesh) was used for column chromatography. Spectroscopic data were obtained using the following instruments: UV/Vis/NIR spectra: JASCO UV/Vis/NIR model V 570 and Hitachi U-3501. IR spectra (KBr disk, 4000−200 cm^{-1}): FTIR JASCO model 420. ^1H NMR spectra: Bruker (AC) 300 MHz FTNMR spectrometer. Electrochemical measurements were performed using a computer-controlled PAR model 270 VERSASTAT Electrochemical instruments with Pt-bead and GC-electrodes. All measurements were carried out under dinitrogen at 298 K with reference to a saturated calomel electrode (SCE) in acetonitrile. The reported potentials are uncorrected for junction potential.

Preparation of the Complexes: The dichloro[2-(arylazo)pyrimidine]-palladium(II) [Pd(aapm)Cl_2 (**2**)] complexes were prepared by a literature method[19] in the yield of 85−90%. A representative case is given in detail.

a. Dichloro[2-(phenylazo)pyrimidine]palladium(II) [Pd(papm)Cl_2 (2a)]: To an MeCN (10 mL) solution of $PdCl_2$ (0.18 g, 1.01 mmol), 2-(phenylazo)pyrimidine [papm (**1a**)] (0.2 g, 1.09 mmol) was added dropwise and the mixture was stirred for 1 h. The orange-red precipitate was filtered and washed with MeOH. The dried mass was dissolved in a minimum vol. of CH_2Cl_2 and purified by chromatography on a silica gel (60−120 mesh) column and the desired orange-red band was eluted with MeCN/benzene (30% v/v).Yield 85%. ***NOTE:*** Benzene is carcinogenic and precaution must be taken during its use!

b. Chloro[(2-(14-imidophenyl)phenylazo)pyrimidine-*N*,*N*′,*N*′′]palladium(II) [Pd(papm-N-C_6H_5)Cl (3a)]: To an acetonitrile solution (15 mL) of Pd(papm)Cl_2 (0.3 g, 0.83 mmol), an aniline (0.1 g, 1.08 mmol) solution in acetonitrile (10 mL) was slowly added. The reaction mixture was stirred and refluxed continuously for 4 h and the colour of the solution changed gradually from orange-red to greenish-brown. The solution was concentrated in air, and the residue was washed thoroughly first with water (2 × 5 mL) and then with 50% aqueous ethanol (3 × 5 mL). The residue was dissolved in dichloromethane (10 mL) and the solution was column-chromatographed on silica gel prepared in benzene. An orange-brown band was eluted with an acetonitrile/benzene (1:9) mixture. The eluted solution, on concentration in vacuo, gave a pure orange-brown compound, isolated in 45% yield. The orange-brown product is the desired coupled product, Pd(papm-N-C_6H_5)Cl. Pd(papm-N-C_6H_5)Cl (**3a**): $C_{16}H_{12}ClN_5Pd$ (416.2): calcd. C 46.16, H 2.89, N 16.83; found C 46.25, H 2.95, N 16.70. IR (cm^{-1}): $\nu_{Pd\text{-}Cl}$ 370, $\nu_{N=N}$ 1296, $\nu_{C=N}$ 1585. All the other compounds were prepared according to the same procedure, the yields varied between 40 and 65% for the orange-brown compound. Pd(papm-N-C_6H_4-Me-*p*)Cl (**4a**): $C_{17}H_{14}ClN_5Pd$ (430.2): calcd. C 47.45, H 3.26, N 16.28; found C 47.35, H 3.32, N 16.30. IR (cm^{-1}): $\nu_{Pd\text{-}Cl}$ 368, $\nu_{N=N}$ 1295, $\nu_{C=N}$ 1580. Pd(papm-N-C_6H_4-OCH_3-*p*)Cl (**5a**): $C_{17}H_{14}ClN_5OPd$ (446.2): calcd. C 45.75, H 3.14, N 15.69; found C 45.85, H 3.20, N 15.75. IR (cm^{-1}): $\nu_{Pd\text{-}Cl}$ 366, $\nu_{N=N}$ 1290, $\nu_{C=N}$ 1577. Pd(papm-N-C_6H_4-Cl-*p*)Cl (**6a**): $C_{16}H_{11}Cl_2N_5Pd$ (450.6): calcd. C 42.63, H 2.44, N 15.54; found C 42.50, H 2.51, N 15.63. IR (cm^{-1}): $\nu_{Pd\text{-}Cl}$ 365, $\nu_{N=N}$ 1298, $\nu_{C=N}$ 1580. Pd(tapm-N-C_6H_5)Cl (**3b**): $C_{17}H_{14}ClN_5Pd$ (430.2): calcd. C 47.45, H 3.26, N 16.28; found C 47.60, H 3.35, N 16.37. IR (cm^{-1}): $\nu_{Pd\text{-}Cl}$ 365, $\nu_{N=N}$ 1290, $\nu_{C=N}$ 1580. Pd(*p*-tapm-N-C_6H_4-Me-*p*)Cl (**4b**): $C_{18}H_{16}ClN_5Pd$ (444.2): calcd. C 48.66, H 3.60, N 15.77; found C 48.84, H 3.68, N 15.85. IR (cm^{-1}): $\nu_{Pd\text{-}Cl}$ 371, $\nu_{N=N}$ 1288, $\nu_{C=N}$ 1585. Pd(tapm-N-C_6H_4-OCH_3-*p*)Cl (**5b**): $C_{18}H_{16}ClN_5OPd$ (460.2): calcd. C 46.96, H 3.48, N 15.22; found C 46.89, H 3.56, N 15.30. IR (cm^{-1}): $\nu_{Pd\text{-}Cl}$ 370, $\nu_{N=N}$ 1285, $\nu_{C=N}$ 1578. Pd(tapm-N-C_6H_4-Cl-*p*)Cl (**6b**): $C_{17}H_{13}Cl_2N_5Pd$ (464.6): calcd. C 43.93, H 2.79, N 15.07; found C 43.75, H 2.85, N 15.15. IR (cm^{-1}): $\nu_{Pd\text{-}Cl}$ 367, $\nu_{N=N}$ 1280, $\nu_{C=N}$ 1585. Pd(Clpapm-N-C_6H_5)Cl (**3c**): $C_{16}H_{11}Cl_2N_5Pd$ (450.6): calcd. C 42.63, H 2.44, N 15.54; found C 42.40, H 2.50, N 15.62. IR (cm^{-1}): $\nu_{Pd\text{-}Cl}$ 365, $\nu_{N=N}$ 1295, $\nu_{C=N}$ 1580. Pd(Clpapm-N-C_6H_4-Me-*p*)Cl (**4c**): $C_{17}H_{13}Cl_2N_5Pd$ (464.6): calcd. C 43.93, H 2.79, N 15.07; found C 44.13, H 2.82, N 15.00. IR (cm^{-1}): $\nu_{Pd\text{-}Cl}$ 366, $\nu_{N=N}$ 1292, $\nu_{C=N}$ 1584. Pd(Clpapm-N-C_6H_4-OCH_3-*p*)Cl (**5c**): $C_{18}H_{15}Cl_2N_5OPd$ (494.7): calcd. C 44.96, H 3.12, N 14.57; found C 45.15, H 3.18, N 14.50. $\nu_{Pd\text{-}Cl}$ 365, $\nu_{N=N}$ 1290, $\nu_{C=N}$ 1585. Pd(Clpapm-N-C_6H_4-Cl-*p*)Cl (**6c**): $C_{16}H_{10}Cl_3N_5Pd$ (485.0): calcd. C 39.59, H 2.06, N 14.44; found C 39.40, H 2.10, N 14.38. IR (cm^{-1}): $\nu_{Pd\text{-}Cl}$ 368, $\nu_{N=N}$ 1300, $\nu_{C=N}$ 1588.

Molecular Orbital Calculations: Extended Hückel Molecular Orbital calculations[34,36] were performed using the ICON software package originally developed by Hoffmann. The orthogonal coordinate system chosen for the calculations are defined in Figures 5 and 6. The atomic parameters were taken from the crystallographic data (Table 5). For drawing figures and diagrams the graphic package CACAO was used.

X-ray Crystallography: Crystals of Pd(papm)Cl_2 suitable for X-ray work were grown by slow diffusion of benzene into a dichloromethane solution at 283 K. The crystal size was 0.26 × 0.25 × 0.23 mm. The crystals of Pd(papm-N-C_6H_4-OCH_3-*p*)Cl suitable for X-ray work were obtained from diffusion of hexane into a dichloromethane solution at 298 K. The crystal size was 0.22 × 0.19 × 0.10 mm. Crystal data and collection parameters are listed in Table 5. Data were gathered with a CAD4/PC V diffractometer with graphite monochrochromator (λ = 0.71073 Å) at 297(2) K. The crystals were mounted on glass fibres and covered with epoxy. Scan parameters were derived from ω-θ scans of 25 reflections. Three monitor reflections were measured after every 30 min of X-ray exposure as a check on experimental stability. The orientation of the crystal was checked after every 500 intensity measurements. Absorption corrections were based on ψ-scans of 12 reflections with bisecting-mode Eulerian χ values in the range of 0−86° for Pd(papm)Cl_2 and 2−83° for Pd(papm-N-C_6H_4-OCH_3-*p*)Cl. The structure was solved by direct methods and refined by full-matrix least squares. In Pd(papm)Cl_2 the asymmetric unit consists of two full molecules and a half molecule of benzene. Systematic absences are consistent

Table 5. Crystallographic data for **2a**·0.25C_6H_6 and **5a**

	2a·0.25C_6H_6	**5a**
Empirical formula	$C_{11.50}H_{9.50}Cl_2N_4Pd$	$C_{17}H_{14}ClN_5OPd$
Formula mass	381.03	446.18
Temperature [K]	299(2)	297(2)
Crystal system	monoclinic	orthorhombic
Space group	$P2_{1/n}$	$Pna2_1$
a [Å]	10.6455(7)	17.1717(19)
b [Å]	22.1264(16)	14.5001(14)
c [Å]	12.0316(10)	6.6869(5)
β [°]	109.216(6)	90
V [Å^3]	2676.1(3)	1665.0(3)
Z	8	4
$\rho_{calcd.}$ [g cm^{-3}]	1.891	1.780
2θ range [°]	4−55	5−55
Index range	$0 \le h \le 13$, $0 \le k \le 28$, $-15 \le l \le 14$	$0 \le h \le 22$, $-18 \le k \le 0$, $0 \le l \le 8$
R_1[a] [$I > 2\sigma(I)$] (%)	3.06	2.84
wR_2[b] (%)	6.57	6.17
GOF[c]	1.018	1.052
Transmission, max./min.	0.937/0.894	0.974/0.891
Largest diff. peak and hole [eÅ^{-3}]	0.416 and −0.429	0.331 and −0.383

[a] $R_1 = \Sigma||F_o| - |F_c||/\Sigma|F_o|$. [b] $wR_2 = [\Sigma w(F_o^2 - F_c^2)^2/\Sigma w(F_o^2)^{1/2}]$. [c] GOF is defined as $[w|F_o - F_c|/(n_o - n_v)]^{1/2}$, where n_o and n_v denote the numbers of data and variable, respectively.

with the space group of $Pna2_1$ or the centric group *Pnma* for Pd(papm-N-C_6H_4-OCH_3-*p*)Cl. The refinement in the centric group (*Pnma*) leads to residuals of $R_1 = 0.12$ and $wR2 = 0.44$. In space group $Pna2_1$ the values are $R_1 = 0.0287$ and $wR2 = 0.0630$ and thus chosen as the correct space group. All data were corrected for Lorentz polarisation and an empirical absorption correction was done on the basis of azimuthal scans. Of 6435 reflections in $Pd(papm)Cl_2$ 6117 [$I > 2\sigma(I)$] were used for the structure solution. In Pd(papm-N-C_6H_4-OCH_3)Cl the unique reflections (2068) were used for the structure solution. Data were processed with an Alpha Station 2004/166 (open VMS/Alpha V 6.2) using the program XCAD4B and the commercial package SHELXTL Rel. 505/VMS. All non-hydrogen atoms were located from subsequent difference Fourier maps. CCDC-135187 and -135188 contain the supplementary crystallographic data for [$Pd(papm)Cl_2$] (**2a**) and [Pd(papm-N-C_6H_4-OMe-*p*)Cl] (5a), respectively. These data can be obtained free of charge at www.ccdc.cam.ac.uk/conts/retrieving.html or from the Cambridge Crystallographic Data Centre, 12 Union Road, Cambridge CB2 1EZ, UK [Fax: (internat.) + 44-1223/336-033; E-mail: deposit@ccdc.cam.ac.uk].

Supporting Information: ^{1}H NMR spectroscopic data, a packing diagram, and Walsh diagrams are available (see footnote on the first page of this article).

Acknowledgments

We are thankful to the University Grants Commission, New Delhi for financial assistance. The Council of Scientific and Industrial Research, New Delhi provided a fellowship to P. B. Funding from the Directorate General of Higher Education and Scientific Research to the Departmento de Quimica Inorganica, Universidad de Zaragoza, Plaza San-Fransisco, S/NE-50009, Espana, for crystallographic work (grant PB 98-1593), is gratefully acknowledged.

[1] A. Hilton, T. Renouard, O. Maury, H. Le Bozec, I. Ledoux, J. Zyss, *Chem. Commun.* **1999**, 2521.
[2] J. Otsuki, K. Sato, M. Tsujino, N. Okuda, K. Araki, M. Seno, *Chem. Lett.* **1996**, 847.
[3] J. S. Kang, H. T. Wong, D. H. Choi, *Mol. Cryst. Liq. Cryst.* **1999**, *327A*, 1.
[4] T. G. Deligeorgiev, D. Simov, *Dyes Pigments* **1998**, *38*, 115.
[5] F. Hlel, L. Smiri, *J. Chem. Crystallogr.* **1999**, *29*, 667.
[6] O. Cakir, E. Bicer, *Electroanalysis* **1997**, *9*, 87.
[7] B. K. Ghosh, A. Chakravorty, *Coord. Chem. Rev.* **1989**, *95*, 239.
[8] S. Goswami, R. N. Mukherjee, A. Chakravorty, *Inorg. Chem.* **1983**, *22*, 2825.
[9] P. Majumdar, S.-M. Peng, S. Goswami, *J. Chem. Soc., Dalton Trans.* **1998**, 1569.
[10] D. Dutta, A. Chakravorty, *Inorg. Chem.* **1983**, *22*, 1085.
[11] T. K. Misra, D. Das, C. Sinha, *Polyhedron* **1997**, *16*, 4163.
[12] T. K. Misra, D. Das, C. Sinha, P. K Ghosh, C. K. Pal, *Inorg. Chem.* **1998**, *37*, 1672.
[13] P. K. Santra, D. Das, T. K. Misra, R. Roy, C. Sinha, S.-M. Peng, *Polyhedron* **1999**, *18*, 1909.
[14] P. K. Santra, T. K. Misra, D. Das, C. Sinha, A. M. Z. Slawin, J. D. Woollins, *Polyhedron* **1999**, *18*, 2869.
[15] W. Y. Wong, S. H. Cheung, S. M. Lee, S. Y. Leung, *J. Organomet. Chem.* **2000**, *596*, 36.
[16] K. Pramanik, M. Shivakumar, P. Ghosh, A. Chakravorty, *Inorg. Chem.* **2000**, *39*, 195.
[17] R. Samanta, P. Munshi, B. K. Santra, N. K. Loknath, M. A. Sridhar, J. S. Prasad, G. K. Lahiri, *J. Organomet. Chem.* **1999**, *579*, 311.
[18] C. K. Pal, S. Chattopadhyay, C. Sinha, D. Bandyopadhyay, A. Chakravorty, *Polyhedron* **1994**, *13*, 999.
[19] P. K. Santra, R. Roy, C. Sinha, *Proc. Indian Acad. Sci. (Chem. Sci.)* **2000**, *112*, 523.
[20] P. Bandyopadhyay, D. Bandyopadhyay, A. Chakravorty, F. A. Cotton, L. R. Falvello, S. Han, *J. Am. Chem. Soc.* **1983**, *105*, 6327.
[21] A. Bharath, B. K. Santra, P. Munshi, G. K. Lahiri, *J. Chem. Soc., Dalton Trans.* **1998**, 2643.
[22] B. K. Santra, G. K. Lahiri, *J. Chem. Soc., Dalton Trans.* **1997**, 129.
[23] B. K. Santra, P. Munshi, G. Das, P. Bharadwaj, G. K. Lahiri, *Polyhedron* **1999**, *18*, 617.
[24] A. K. Ghosh, P. Majumdar, L. R. Falvello, G. Mostafa, S. Goswami, *Organometallics* **1999**, *18*, 5086.
[25] A. Saha, A. K. Ghosh, P. Majumdar, K. N. Mitra, S. Mondal, K. Rajak, L. R. Falvello, S. Goswami, *Organometallics* **1999**, *18*, 3772.
[26] R. Roy, D. Das, M. Banerjee, C. Sinha, A. Mahapatra, *Transition Met. Chem.* **2001**, *26*, 205.
[27] R. Roy, P. K. Santra, D. Das, C. Sinha, *Synth. React. Inorg. Met.-Org. Chem.* **2000**, *30*, 1975.
[28] D. J. Gordon, R. F. Fenske, *Inorg. Chem.* **1982**, *21*, 2907.
[29] I. Chakraborty, S. Bhattacharyya, S. Banerjee, B. K. Dirghangi, A. Chakravorty, *J. Chem. Soc., Dalton Trans.* **1999**, 3747.
[30] D. Das, PhD Thesis, Burdwan University, India, **1998**.
[31] M. J. Alder, W. I. Cross, K. R. Flower, R. G. Pritchard, *J. Chem. Soc., Dalton Trans.* **1999**, 2563.
[32] K. S. Y. Leung, Y. Li, *Inorg. Chem. Commun.* **1999**, *2*, 599.
[33] H.-Y. Cheng, B.-C. Tzeng, S. -M. Peng, *Bull. Inst. Chem. Acad. Sin.* **1994**, 51 and references therein.
[34] C. K. Pal, S. Chattopadhyay, C. Sinha, A. Chakravorty, *Inorg. Chem.* **1996**, *35*, 2442.
[35] M. Haga, E. S. Dodsworth, A. B. P. Lever, *Inorg. Chem.* **1986**, *25*, 447.
[36] C. K. Pal, S. Chattopadhyay, C. Sinha, A. Chakravorty, *Inorg. Chem.* **1994**, *33*, 6140.

Received July 27, 2001
[I01280]

Triaminoboranes and Their Metallation to *N*-Lithiotriaminoboranes[‡]

Ulrike Braun,[a][‡‡] Tassilo Habereder,[a] Heinrich Nöth,*[a] Hans Piotrowski,[a] and Marcus Warchhold[a]

Keywords: Boranes / Deprotonation / Lithium / Nitrogen / X-ray diffraction

In order to study the competition between deprotonation, borate formation, and B–N bond cleavage, six triaminoboranes bearing 1–3 NH functions were treated with butyllithium. The 2-anilino-1,3,2-diazaborolidine **1** was cleanly deprotonated, but the resulting *N*-lithio compound could not be crystallized. However, as a result of slow hydrolysis, the lithium 2-oxido derivative **7** was isolated in low yield as a dimeric ether solvate. Double deprotonation of 2-(dimethylamino)-1,3,2-benzodiazaborolidine (**9**) was accompanied by B–N bond cleavage. The dilithio derivative reacted with Me_3SiCl to produce 2-dimethylamino-1,3-bis(trimethylsilyl)-1,3,2-benzodiazaborolidine (**11**). Similarly, dianilino(diphenylamino)borane (**2**) was readily deprotonated to the insoluble dilithium compound. B–N bond cleavage also occurred, however, and the solvates $Ph_2NLi{\cdot}dme$ (**13**) and $Ph_2NLi{\cdot}2py$ (**14**) were isolated. These are dimeric, the former with a planar Li_2N_2 ring, the latter possessing an N–Li–N–Li chain structure. Triply metallated trianilinoborane (**15**) crystallized as dimeric $B(NLiPh)_3{\cdot}LiCl{\cdot}(OEt_2)_3$ (**15A**). Treatment of trianilinoborane (**3**) with LiBu in 1:1 and 1:2 ratios showed that the deprotonation was accompanied by the formation of anilino(butyl)borates. Treatment of the dilithio derivative of **3** with Me_3SnCl afforded $B[N(SnMe_3)Ph]_3$ (**23**), a result of substituent exchange. Tris(2-pyridylamino)borane (**4**), with a planar skeleton, reacted with BuLi both by deprotonation and by B–N bond cleavage. The metallated triaminoborane crystallized as dimeric $Li_4B(NR^*)_3NHR^*(THF)_3$ (**18**; R^* = 2-pyridyl). Tris(8-quinolylamino)borane (**5**) can also be triply lithiated according to ^{11}B and ^7Li NMR spectroscopic data. X-ray determination of the structures of compounds **1**–**3** showed the absence of N–H···N hydrogen bonding, which seems to be responsible for the planar structures of compounds **4** and **5**. The planarity of the BN_3 units in **3** and **4** was retained in the trilithiated compounds **15A** and **18**, as ascertained by X-ray structure determination.

(© Wiley-VCH Verlag GmbH, 69451 Weinheim, Germany, 2002)

Introduction

The metallation of aminoboranes $R_{3-n}B(NHR')_n$ by organolithium reagents LiR to give (lithioamino)boranes acts in competition with the formation of aminoborates $Li[R_{4-n}B(NHR')_n]$ and/or B−N bond cleavage. This was demonstrated by us in 1980,[2] after the first successful lithiation of a cyclic aminoborane.[3] As expected, (lithioamino)boranes are useful reagents for the syntheses not only of other metallated aminoboranes[2,4,5−7] by transmetallation reactions, but also for syntheses of diborylamines[8−10] and BN heterocycles.[5,6,11] So far, only a few structures of (lithioamino)boranes have been determined: the ionic $[Li(OEt_2)_3][mes_2B{=}N{=}Bmes_2]$,[12] the dimeric $Li(OEt_2)_2$-$Nmes{-}Bmes_2$,[7] and the solvent-free trimeric (lithioamino)-9-borabicyclonane.[13] In the presence of chelating ligands, monomeric molecular (lithioamino)boranes, such as $t Bu_2B(t BuN)Li{\cdot}tmen$ or $(Me_3Sn)N{-}BC_8H_{14}Li{\cdot}$pmdeta (pmdeta = pentamethyldiethylenetriamine),[14,15] were obtained and their structures determined. In comparison with lithium organylamides[16,17] the tendency of the lithium (diorganylboryl)amides to associate through Li−N bridges did not seem to be significantly altered. Dimetallation of bis(*tert*-butylamino)organylboranes was reported by Meller et al.,[6] whilst it is only recently that a threefold lithiation of the borazine $(PhB{-}NH)_3$ was successfully achieved, resulting in the compound $(PhBNLi)_3{\cdot}(LiPh)_3{\cdot}(THF)_3$, characterized by X-ray diffraction analyses.[18]

N-Lithiation of triaminoboranes offers a unique chance to study the influence of electronic and steric effects. One might expect that the metallation of triaminoboranes of type $(R_2N)_2B{-}(NHR)$ would proceed more readily than that of R_2BNHR,[5] as the amino groups make the boron atom less prone to attack by a nucleophile, thereby promoting the deprotonation of the NH group. On the other hand, double and triple deprotonation of aminoboranes $B(NHR)_3$ would probably become more difficult as the number of deprotonation steps increased, because introduction of an increasing number of lithium atoms would be expected to result in highly associated molecular aggregates through Li−N coordination. For this reason we synthesized

[‡] Chemistry of Boron, 250. Part 249: Ref.[1]
[‡‡] Part of the PhD Thesis of U. Braun, University of Munich, **2000**.
[a] Department of Chemistry, University of Munich, Butenandtstraße 5−13, 81377 München, Germany

a number of new triaminoboranes possessing NHR groups, studied their metallation with BuLi, and characterized their *N*-lithio derivatives.

New Triaminoboranes

Synthesis

In order to study the competition between *N*-metallation, B−N bond cleavage, and borate formation, we first chose an aminoborane of type $(R_2N)_2BNHR$, with only one N−H bond. The molecule of choice was 2-anilino-1,3-diphenyl-1,3,2-diazaborolidine (**1**), obtained by treatment of 2-chloro-1,3-diphenyl-1,3,2-diazaborolidine with aniline in the presence of triethylamine as shown in Equation (1).

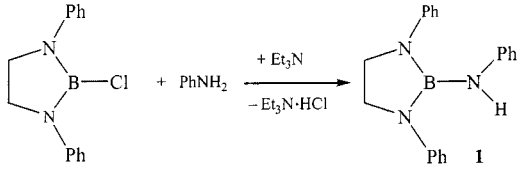

(1)

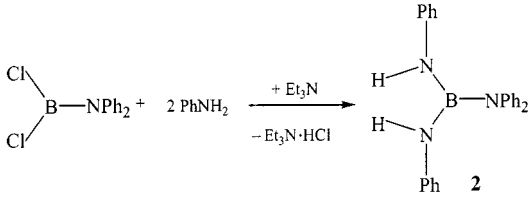

(2)

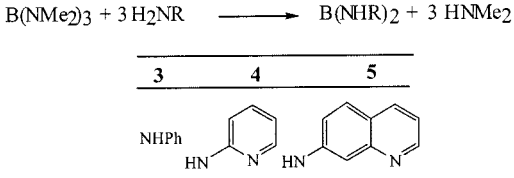

(3)

The preparation of dianilino(diphenylamino)borane (**2**) by aminolysis of $B(NMe_2)_3$ with diphenylamine (1:1 ratio), followed by aminolysis with aniline, was unsuccessful; we observed no reaction at reflux temperature between the tris(dimethylamino)borane and diphenylamine, although several successful syntheses of unsymmetrically substituted triaminoboranes by transamination reactions have been reported.[19,20] The low basicity of diphenylamine (pK_A = 0.9)[21,22] and steric effects may be responsible for the failure of this reaction, in spite of the fact that the resulting dimethylamine can readily be removed to drive the process towards the side of the transamination products. More surprising was the observation that $LiNPh_2$ did not react with $Cl-B(NMe_2)_2$ to produce $Ph_2N-B(NMe_2)_2$, either in THF or in toluene. However, dichloro(diphenylamino)borane reacted with aniline in the presence of triethylamine according to Equation (2) to give $Ph_2NB(NHPh)_2$ (**2**) in 71% yield.

Trianilinoborane (**3**) was readily obtained from aniline and $B(NMe_2)_2$,[19] whilst tris(2-pyridylamino)borane (**4**)[23] and tris(8-aminoquinolyl)borane (**5**) were prepared by the same procedure as shown in Equation (3).

Spectra

The NMR spectra (^1H, ^{11}B, ^{13}C, and ^{14}N) of compounds **1**−**5** were fully compatible with the suggested structures (e.g., chemically and magnetically equivalent anilino and amino heterocyclic groups). As was to be expected for triaminoboranes, the ^{11}B chemical shifts varied very little and were in the range typical of this class of compounds. The line widths, however, varied significantly. The sharpest signal was found for tris(2-pyridylamino)borane (**4**; $h_{1/2}$ = 220 Hz) and the broadest for the quinoline derivative **5** (450 Hz). Only a single broad ^{14}N resonance, at $\delta = -323$, was found for compound **2**, and one at $\delta = -292$ for compound **3**. On the other hand, the two types of N atoms in compounds **4** and **5** were readily recognizable. The resonances were at $\delta = -106$ and -79, respectively, for the heterocyclic N atoms, while those of the amino groups were observed at $\delta = -310$ and -327. This was consistent with ^{15}N NMR spectroscopic data of aminoboranes[24] and N-heterocycles.[25]

Interestingly, the ^1H resonances for the NH protons of the anilino groups were found as signals at $\delta = 4.65 \pm 0.14$, while those for **4** and **5** were observed at $\delta = 9.85$ and 8.15, respectively. We attribute this to intramolecular N−H···N interactions in the latter two compounds, and this was supported by the NH stretching vibrations found for these two aminoboranes at 3293 and 3340 cm^{-1}. In **1** to **3**, these vibrations were observed at higher wavenumbers (3384, 3387, and 3384 cm^{-1}). Obviously, the intramolecular N−H···N interaction was weaker in **5** than in **4**. This is consistent with the molecular structures of these compounds as determined by X-ray structure analysis.

Molecular Structures

The triaminoboranes **1**−**5** were characterized by X-ray structure analysis. Compound **1** crystallizes in the monoclinic system, space group *I*2/*a* and $Z = 8$. Figure 1 shows its molecular structure. The three B−N bonds are of equal lengths. Their common value (1.435 Å) corresponds very well with B−N bond lengths observed for other triaminoboranes.[26] All the N atoms and the B atom reside in planar environments, but because of the incorporation of the boron atom into a five-membered ring system a sharp N−B−N bond angle of 107.4(1)° results; this fits nicely for a five-membered ring system. Consequently, the other two N−B−N bond angles are wider than 120°. Typical for the structure of **1** is the propeller-like arrangement of the phenyl groups, with interplanar angles to the BN_3 plane of 31.6, 41.7, and 52.1°, the last being that made by the anilino group, which is more twisted than the other two phenyl groups. In the crystal there are neither intra- nor intermolecular N−H···N hydrogen bonds.

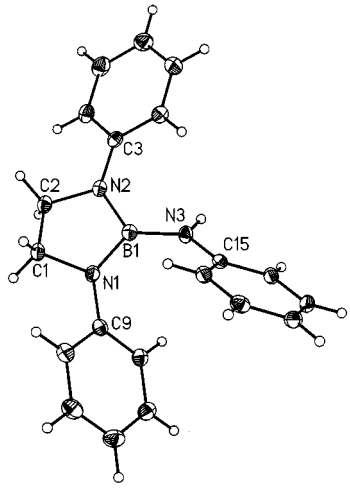

Figure 1. Molecular structure of **1** in ORTEP presentation; selected bond lengths and bond angles: B1−N1 1.436(2), B1−N2 1.437(2), B1−N3 1.433(2), N1−C9 1.409(2), N2−C3 1.402(2), N3−C15 1.400(2), N1−C1 1.473(2), N2−C2 1.471(2), C1−C2 1.523(2) Å; C1−N1−B1 109.0(1), C3−N2−B1 131.2(1), B1−N2−C2 108.9(1), C3−N2−C2 119.5(1), B1−N3−C15 127.5(1), N3−B1−N2 125.1(1), N1−B1−N2 107.4(1)°; torsion angle: N1−C1−C2−N2 −26.8°

Crystals of dianilino(diphenylamino)borane (**2**) are triclinic, space group $P\bar{1}$ with $Z = 2$. Figure 2 shows its molecular structure. In contrast to those in **1**, its B−N bond lengths differ significantly. The B−N bond of the diphenylamino group [1.470(3) Å] is longer than the B−N bonds to the anilino groups (average 1.425 Å). Since the angle between the BN_3 plane and the C1N1C2 unit of the diphenylamino group is at 26.6° only slightly larger than the interplanar angles to the anilino groups (24.5 and 23.5°), this longer B−N bond must be the result of the low basicity of the diphenylamine. Because of the steric requirement of the diphenylamino group, the phenyl groups of the anilino groups are pointing away from the Ph_2N substituent. This results in a *cisoidal* arrangement for the N−H units. The C−N−B bond angles of the anilino substituents are quite open (132.8° and 130.9°). This is not imposed by steric requirements of the diphenylamino group, as the same feature is also observed in compound **3**.

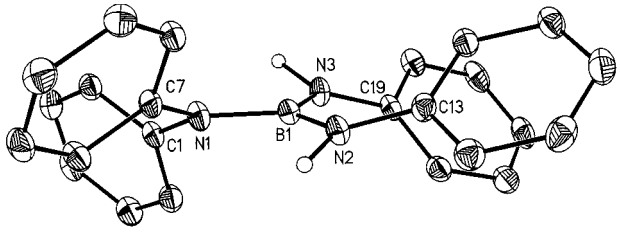

Figure 2. The molecular structure of **2** in the crystal; selected bond lengths and bond angles: B1−N1 1.470(3), B1−N2 1.422(3), B1−N3 1.427(3), N1−C1 1.330(3), N1−C7 1.423(3), N2−C13 1.415(3), N3−C19 1.414(3) Å; B1−N1−C1 120.7(2), B1−N1−C7 123.1(2), C1−N1−C7 116.2(2), B1−N2−C13 132.8(2), H2−N2−C13 113(1), H2−N2−B1 114(1), B1−N3−C19 130.9(2), H3−N3−C19 116(1), H3−N3−B1 113(1), N1−B1−N3 117.5(2), N2−B1−N3 125.9(2), N1−B1−N2 116.6(1)°

Trianilinoborane (**3**) crystallizes in the monoclinic system, space group $P2_1/c$, $Z = 4$. Its molecular structure is shown in Figure 3. Although one might expect that the three B−N bonds would be of equal lengths, one finds that this holds only for two of them (B1−N1 and B1−N2, average 1.430 Å), while the B1−N3 bond is slightly but significantly longer [1.442(2) Å]. As might be expected, the boron atom is sp^2-hybridized; the sum of its bond angles is 360°. As was also the case for the triaminoborane **2**, we observe B−N−C bond angles wider than the expected 120°. The three phenyl groups of **3** are arranged in a propeller-like fashion, and this has the effect that the N−H groups are *transoid* to each other. There are, however, no intermolecular N−H···N interactions.

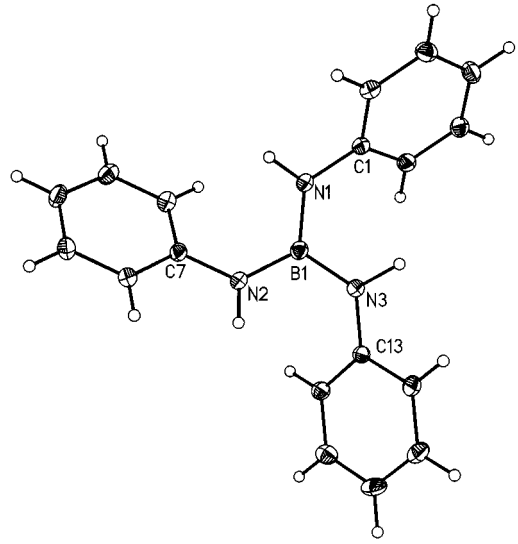

Figure 3. Structure representation of compound **3** in ORTEP description; selected bond lengths and bond angles: B1−N1 1.428(2), B1−N2 1.431(2), B1−N3 1.442(2), N1−C1 1.409(2), N2−C7 1.414(2), N3−C13 1.402(2) Å; N1−B1−N3 119.1(2), N2−B1−N3 119.5(2), N1−B1−N2 121.3(1), B1−N1−C1 127.8(1), B1−N2−C7 128.2(1), B1−N3−C13 129.0(1)°; angles between the planes of the phenyl groups: C1−C6/C7−C12 74.4, C1−C6/C13−C18 107.1, C7−C12/C13−C18 110.2°

The main difference between tris(2-pyridylamino)borane (**4**) and trianilinoborane (**3**) is that all atoms of the molecule of **4** lie in or close to a common plane (see Figure 4), the interplanar angles of the aminopyridine substituents to the BN_3 plane being less than 5.7°. All B−N bonds are of equal lengths (1.432 Å), and are typical of triaminoboranes.[26] Intramolecular N−H···N bridges are the most likely reason for the coplanarity of the molecule. On the other hand, the B−N−C bond angles lie between 130.5 and 132.0°. This certainly makes hydrogen bonds weaker, because a 120° B−N−C bond angle would allow a closer intramolecular N···N distance, which is actually 2.809 Å. The "hydrogen bond" bond angles range from 134 to 137°. This geometry therefore seems to be in better accord with a dipolar interaction N−H(δ+)···N(δ−). A similar structure has been observed for the hydrazinoborane $B(NH-NMe_2)_3$, which has a planar BN_6H_3 skeleton with the NC_2 group perpendicular

to the BN_6 plane. The N···N distance is 2.41(3) Å,[27] much shorter than in compound **4**.

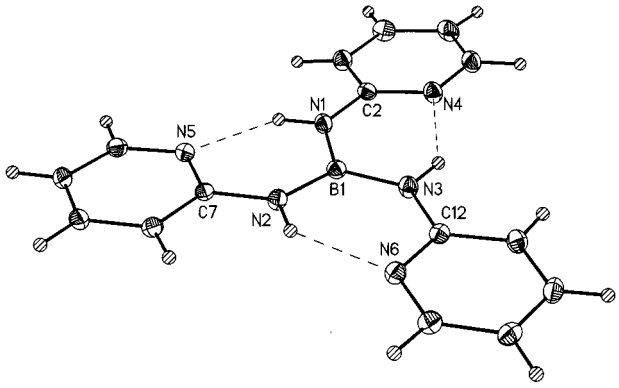

Figure 4. The molecular structure of **4** in the crystal; selected atom distances and bond angles: B1−N1 1.434(2), B1−N2 1.432(2), B1−N3 1.431(2), N1−C2 1.385(2), N2−C7 1.379(2), N3−C12 1.378(2), N5···H1 2.08, N4···H3 2.07, N6···H2 2.12 Å; B1−N1−C1 130.5(1), B1−N1−H1 114(1), B1−N2−C7 131.3(1), B1−N2−H2 115(1), H2−N2−C7 114(1), B1−N3−C12 132.0(1), B1−N3−H3 112(1), C12−N3−H3 116(1), N1−B1−N2 120.0(1), N1−B1−N3 119.9(1), N2−B1−N3 120.2(1)°

Tris(8-quinolylamino)borane (**5**) crystallizes in the triclinic system, space group $P\bar{1}$, $Z = 2$ (Figure 5). The molecular planes of the aminoquinoline substituents are not uniformly twisted relative to the BN_3 plane, but by 18.7° (N1), 33.9°(N3), and 24.4° (N5). Interactions between their N−H protons and the N atom of the heterocycle occur not between adjacent heterocycles as in compound **4**, but within its own heterocyclic system. The N···N distance is, at 2.720 Å, somewhat shorter than in **4**. As is to be expected for a five-membered "ring" (including a hydrogen bond), the angles at the bridging H atoms are sharp at ca. 100°.

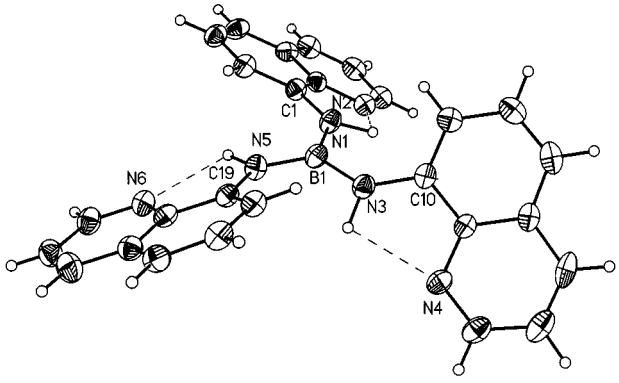

Figure 5. The molecular structure of **5** in the crystal; selected atom distances and bond angles: B1−N1 1.429(4), B1−N3 1.448(4), B1−N5 1.427(4), N1−C1 1.409(4), N3−C10 1.389(4), N5−C19 1.401(4), N2···H1−N 2.25, N4···H3−N 2.35, N6···H5−N 2.25 Å; B1−N1−C1 130.5(3), B1−N3−C10 131.2(3), B1−N5 C19 131.6(3), N1−B1−N3 119.3(3), N1−B1−N5 120.8(3), N3−B1−N5 119.6(3)°; torsion angle: C1−N1−C2−N2: −26.8

All B−N−C bond angles are wider than 130°, as found for all B(NHR) units in compounds **1**−**5**. However, it was surprising to find that one of the three B−N bonds of **5** is 0.02 Å longer than the other two. This indicates a somewhat weaker B−N bond with less π-bonding, and this longer bond is indeed associated with the substituent that shows the strongest twisting.

N-Lithiotriaminoboranes

Synthesis

The triaminoboranes mentioned above were metallated with *n*-butyllithium under various conditions. In the case of **1**, the metallation proceeded smoothly, according to Equation (4). Monitoring of the deprotonation by ^{11}B NMR was not advisable, because the shielding of the boron nucleus did not change significantly (from $\delta^{11}B = 23.8$ to 23.0 in this case). On the other hand, the ^{11}B NMR spectrum ruled out both the formation of a borate and B−N bond cleavage. In the first of these two cases, a highfield shift should be observed, in the second case a shift to lower field should be expected.[28] Attempts to crystallize compound **6** from toluene failed. Crystals were obtained after addition of pyridine, but these proved to be the hydrolysis product **7** [see Equation (5)]. Tetramethylethylenediamine seemed to be a better ligand than pyridine for crystal formation. However, the "crystals" of **8** proved to be amorphous.[29]

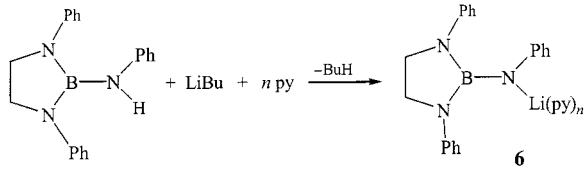

(4)

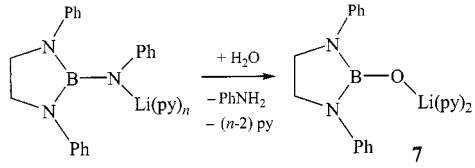

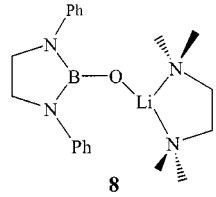

(5)

Double metallation of the benzodiazaborolidine **9** by 2 equiv. of LiBu at −78 °C occurred readily, only a single ^{11}B NMR signal being present after metallation ($\delta^{11}B = 29.3$). At −60 °C, however, a white solid separated from the gray-green suspension, and no ^{11}B NMR signals could any longer be observed in the solution. Obviously, the product **10** had become insoluble. For this reason it was impossible to grow single crystals, nor was it possible to obtain crystals from the solid dissolved in pyridine. On the other hand, the

elemental analysis of the precipitate was almost consistent with dimetallated **10** as far as the C/N ratio was concerned. In order to show that **10** had indeed been formed in the reaction described by Equation (6), the precipitate was treated with Me_3SiCl. As expected, the bis(trimethylsilyl) derivative **11** was obtained and characterized by NMR spectroscopy.

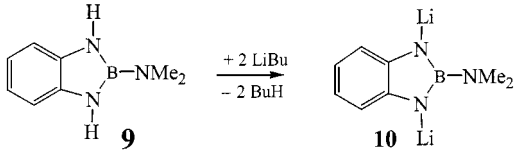

(6)

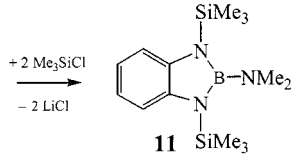

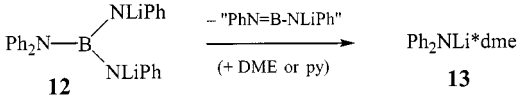

(7)

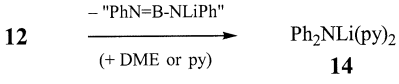

(8)

The lithiation of dianilino(diphenylamino)borane (**2**) by BuLi in the presence of dimethoxyethane (DME) produced a yellow orange solution, the ^{11}B NMR spectrum of which showed two signals at $\delta = 28.9$ and -10 in an intensity ratio of 85:15, provided that the spectrum was measured as rapidly as possible. We assigned the lowfield signal to the metallated product **12** and the highfield signal to a product containing tetracoordinated boron atoms. The orange solution turned brown within a few hours, with the formation of a white precipitate. No ^{11}B NMR signals could then be detected in the supernatant solution. Nevertheless, crystals separated slowly from the solution, and these were identified as $Ph_2NLi{\cdot}dme$ (**13**). Equation (7) describes a formal decomposition process for **12**.

When pyridine was used to stabilize **12**, a clear yellow solution resulted. Its ^{11}B NMR spectrum, with signals at $\delta = -17.6$, -15.4, 0.2, 1.9, 3.0, and 43.2, demonstrated a much more complex reaction than that observed in the presence of DME. Obviously, aminoborates such as $Li[(PhLiN)_2B(NPh_2)Bu]$ or aminoborane–pyridine adducts such as $(PhHN)_2(Ph_2N)B{\cdot}py$ may form besides $BuB(NPh_2)(NLiPh)$. Crystals separated from the solution, and these proved to be $LiNPh_2{\cdot}(py)_2$ [**14**; see Equation (8)]. The lithium diphenylamides **13** and **14** were dimeric in the solid state (vide infra) but had different structures.

So far, the stoichiometry of the reaction has not been determined, as $LiNPh_2$ was almost certainly not the main product. We assume that B–N bond cleavage of **2** occurred, most probably at a stage after dimetallation of **2**.

It followed from the previous observations that multimetallation required a polar solvent, in order to prevent the rapid formation of insoluble products. The triple lithiation of $B(NHPh)_3$ was therefore studied in the presence of ether. The reaction, as in Equation (9), proceeded readily at low temperature. Two ^{11}B NMR signals were found at $\delta = 35.4$ and -3.5, the latter representing a minor component. The signal at $\delta = 35.4$ was assigned to compound **15**. However, the formation of a precipitate could not be prevented. The solid, on dissolution in THF, showed the same signals as the ether solution. Moreover, the ^1H NMR spectrum showed the absence of NH protons, a good indication of successful triple metallation. The minor component was, most probably, due to the formation of $LiBuB(NHPh)_3$ or $LiB(NHPh)_4$.[30] From the solution, compound **15** was isolated as $B(NLiPh)_3{\cdot}LiCl{\cdot}3OEt_2$ (**15A**) in 86% yield.[31]

The triple metallation of **4** was performed in THF as a solvent, as the solubility of the aminoborane in ether was rather low. The solution obtained after metallation showed a single but rather broad ^{11}B NMR signal at $\delta \approx 40$. This lowfield shift ($\delta = 15.8$) indicated a reaction according to Equation (10), since there was also a lowfield shift of $\delta = 11.2$ found for the triple lithiation of compound **4**. However, the product proved to be not **16**, but rather its adduct with LiNHR. Therefore, B–N cleavage as in Equation (11) must also have occurred, to produce $Li_4B(NR^*)_3(NHR^*)(THF)_3$ (**18**; R* = 2-pyridyl). Equations (10) to (13) summarize the results. The formation of borate **19** was indicated by an ^{11}B NMR signal at $\delta^{11}B = -9$.[5,28]

Although the composition of **18** might suggest the formation of a tetraaminoborate, this was not the case, as verified by the ^{11}B NMR spectrum and the determination of its molecular structure (vide infra).

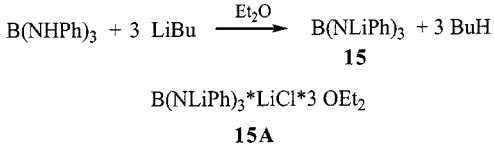

(9)

(10)

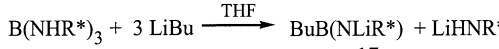

(11)

(12)

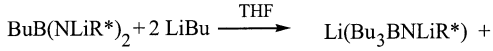

(13)

R*NH = 2-pyridylamino group

In order to provide more insight into the metallation of **4**, reactions in a 1:1 and a 1:2 ratio were studied in addition to the 1:3 ratio. The observed ^{11}B NMR signals are summarized in Table 1. In all cases, two main products were formed. The signal at $\delta^{11}B = 23.3$ indicated that the environment about the tris(2-pyridylamino)borane was not greatly changed by the *N*-metallation. It may well be that the signals represented a mono- and a dilithiated **4**. On trimetallation, however, a noticeable deshielding indicated significant changes in triply metallated **4**. Since ^{11}B NMR signals at $\delta = -9.5$ were absent in the 1:1 and 1:2 reactions but one was observed in the 1:3 reaction, it appeared that this signal resulted from the anion $[Bu_3BNHR^*]^-$, as there was a sufficient supply of Bu^- anions under these conditions, and the observed chemical shift observed was similar to the value for $Na(Et_3BNH_2)$ ($\delta^{11}B = -9.8$).[28] The boron resonances at $\delta = -1.5$ and -3.3 (see Table 1) were consistent with the formation of $Li[BuB(NHR^*)_3]$ or/and $Li[BuB(NHR^*)_2(NLiR^*)]$.[28]

Table 1. ^{11}B NMR signals observed in reactions of tris(2-pyridylamino)borane with various ratios of BuLi; the resonances in italics represent the main species

Reagent ratio						Solvent
1:1	−3.3	−0.9	*−1.5*	1.4	*23.3*	THF
1:2	*−3.3*	*−0.9*	*1.2*	*1.4*	*23.5*	THF
1:3	*−9.5*			1.3	*39.6*	THF
1.3	*−9.3*	0	0.6	1.5	36, br.[a]	diethyl ether
	−24.6, *−28.6*					

[a] The only signal obtained on dissolving the precipitate in THF.

$$B(NHR^*)_3 + LiBu \longrightarrow \underset{\mathbf{20}}{(R^*NH)_2B(NLiR^*)} + BuH \quad (14)$$

$$(R^*HN)_2B(NLiR^*) + Me_3SnCl \xrightarrow[-LiCl]{} \underset{\mathbf{21}}{(R^*HN)_2B(NSnMe_3R^*)} \quad (15)$$

$$(R^*HN)B(NLiR^*)_2 + 2\,Me_3SnCl \xrightarrow[-\,2\,LiCl]{} \underset{\mathbf{22}}{(R^*HN)B(NSnMe_3R^*)_2} \quad (16)$$

To provide experimental evidence for the existence of monolithio compound **20**, stannylation by Me_3SnCl as in Equation (14) was attempted. The mono(trimethylstannyl) compound **21** was obtained, but could be characterized only by ^{119}Sn NMR spectroscopy.[32] However, the reaction of $R^*NH-B(NLiR^*)_2$ as shown in Equation (15) did not generate compound **22**. The solution showed ^{119}Sn and ^{11}B NMR signals, as observed in the stannylation of **20**, but there were additional signals in both NMR spectra. Amongst these were ^{119}Sn ($\delta = 9.2$) and ^{11}B resonances ($\delta = 30.2$) that we assigned to tris[2-pyridyl(trimethylstannyl)amino]borane (**23**), a compound that could be isolated and structurally characterized by X-ray crystallography. Obviously, the distannylated molecule **22** had exchanged Me_3Sn groups to give **23** and **21** as represented in Equation (17).

$$2\,(R^*NH)B(NSnMe_3R^*)_2 \longrightarrow \begin{matrix}(R^*NH)_2B(NSnMe_3R^* & \mathbf{21}\\ + & \\ B(NSnMe_3R^*)_3 & \mathbf{23}\end{matrix} \quad (17)$$

In contrast to the triple metallation of **4**, attempts to achieve the triple metallation of tris(8-quinolylamino)borane (**5**) in THF were futile. No single crystals separated from the violet-red solution, although a single broad ^{11}B NMR signal at $\delta = 32.9$ might have been indicative of the triple metallation. This assumption was supported by a single ^7Li resonance. However, the ^1H and ^{13}C NMR spectra were inconclusive.

Structures

The pyridine adduct of lithium 1,3-diphenyl-2-oxido-1,3,2-diazaborolidine (**7**) crystallizes in the triclinic space group $P\bar{1}$ with two independent dimeric molecules (Figure 6 depicts only one of the two molecules). Each molecule has a crystallographic center of inversion, generating four-membered planar Li_2O_2 rings. The Li−O bonds of the rings are significantly different, with bond lengths of 1.926(4) and 1.894(3) Å in molecule 1 and 1.912(4) and 1.966(3) Å in molecule 2. Moreover, the O−Li−O and Li−O−Li bond angles are different for the two molecules (97.8° and 82.2°, and 118.8° and 84.0°, respectively). Two pyridine molecules per Li ion complete the coordination shell around the Li centers, with N−Li−N bond angles of 96.0° (molecule 1) and 93.9° (molecule 2). Surprisingly, these angles are more acute than the O−Li−O bond angles, in spite of the fact

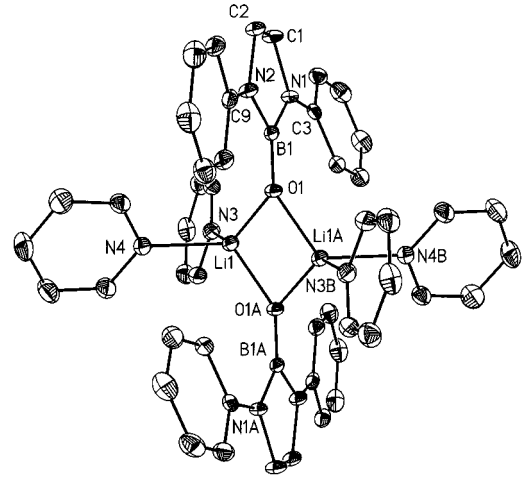

Figure 6. One of the two dimeric molecules of **7**; hydrogen atoms are omitted for clarity; selected bond lengths and bond angles: B1−O1 1.320(2), Li1−O1 1.926(4), Li1A−O1 1.894(3), B1−N2 1.467(3), B1−N1 1.478(3), N1−C3 1.391(3), N1−C1 1.466(2), C2−N2 1.455(2), N2−C9 1.386(3), Li1−N3 2.152(4), Li1−N4 2.128(4) Å; B1−O1−Li1 127.9(2), B1−O1−Li1A 146.4(2), Li1−O1−Li1A 82.2(2), O1−Li1−O1A 97.8(2), O1−Li1−N4 126.4(2), O1−Li1−N3 108.3(2),O1A−Li1−N3 117.1(2), N3−Li1−N4 95.0(2), O1−B1−O1A 128.0(2), O1−B1−N2 127.6(2), N1−B1−N2 104.4(2), C1−N1−C3 118.0(2), B1−N1−C3 129.9(2), B1−N1−C1 111.1(2), C2−N2−C9 118.5(2), B1−N2−C9 129.9(2), B1−N1−C2 111.4(2)°

that the N atoms are not part of a ring system. Consequently, the O−Li−N bond angles are more open, giving rise to Li ions with a rather distorted "tetrahedral" environment.

B−N bonds longer than those in compound **1** are found in **7**. The lengthening by ca. 0.04 Å is due to the negative charge at the oxygen atom. On the other hand, the B−O distance [1.320(3) Å] is shorter than those in $B(OMe)_3$, $(MeBO)_3$,[33] or $B_2(OMe)_4$,[34] and similar to the B−O distances of 1.317(6) Å found in $[thf{\cdot}LiOB(mes)_2]_2$ (mes = 2,4,6-trimethlphenyl)[35] and 1.345 Å in $[LiOB[CH(SiMe_3)_2]_2]_2$.[36] The B−O bond order in **7** is therefore higher than that in methylborates or trimethylboroxine, and this is also responsible for the longer B−N bonds.

The molecular structure of dimeric $Ph_2NLi{\cdot}dme$ (**13**) is shown in Figure 7. The centrosymmetric molecule has a four-membered, rhombic Li_2N_2 ring. Each Li ion is coordinated by two oxygen and two nitrogen atoms, with different Li−O and Li−N bond lengths, a sharp Li−N−Li bond angle (80(1)°], and a more open N−Li−N bond angle of 99(1)°.

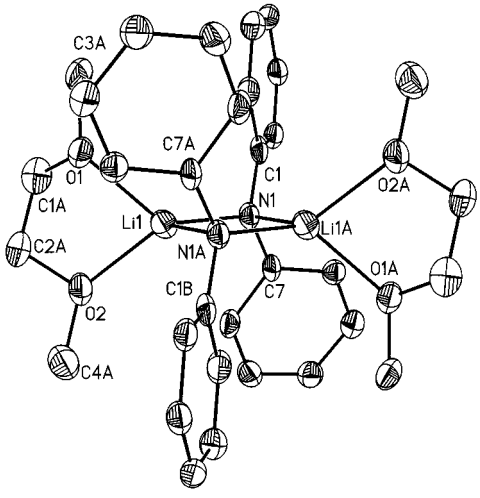

Figure 7. Molecular structure of the dimeric **13**; selected bond lengths and bond angles: Li1−N1 2.07(2), Li1A−N1 2.14(3), Li1−O1 2,07(2), Li1−O2 2.12(2), N1−C1 1.41(1), N1−C7 1.425(8) Å; Li1−N1−Li1A 80(1), N1−Li1−N1A 99(1), O1−Li1O2 79.7(7), O1−Li1−N1 125(1), Li1−N1−C7 124.2(5), C1−N1−C7 115.8(9)°

While the structure of **13** resembles the structures of dimeric $(smes)HNLi{\cdot}OEt_2$[37] [smes = 2,4,6-tris(*tert*-butyl)phenyl] or $(Me_3Si)[(Me_3Si)_3Si]NLi$[38] as far as the association through Li−N bonds is concerned, lithium amides with tetracoordinated Li centers are more common.[16] However, a much more interesting structure was found for dimeric $Ph_2NLi{\cdot}(py)_2$ (**14**), the molecular structure of which is shown in Figure 8. There are two kinds of Li ions. Li1 is surrounded by a plane of three nitrogen atoms in which the N1−Li1−N2 bond angle is quite open, at 139.8°. The longest Li−N bond is that formed with the pyridine nitrogen atom, followed by those with the nitrogen atom of the tetracoordinated Ph_2N group (2.042 Å), while the bond to the tricoordinated N2 atom is, as might be expected, even shorter (1.950 Å). While the Li1−N1−Li2 bond angle is almost tetrahedral, the C14−N1−C2 bond angle is more open, at 119.0(3)°. The tetracoordinated Li2 atom bears three pyridine molecules, with an average Li−N bond length of 2.111 Å. The phenyl rings at N2 form interplanar angles with the N_3Li plane of 17.6−0.7°, and the interplanar angle between $N2C_2$ and $Li1N_3$ at 95.6° shows an almost orthogonal orientation. This allows the pyridine ring N3 to adopt a staggered conformation not only with the phenyl groups at N2, but also with the plane around atom N1.

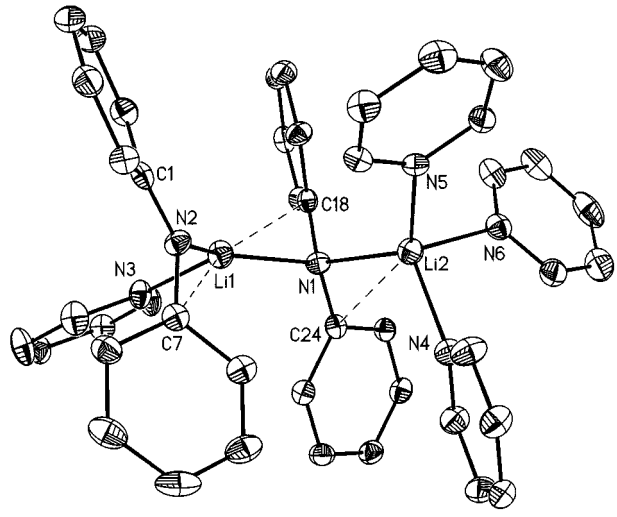

Figure 8. Molecular structure of dimeric **14**; selected bond lengths and bond angles: Li1−N1 2.042(6), Li1−N2 1.950(7), Li1−N3 2.054(7), Li2−N1 2.132(7), Li2−N4 2.137(7), Li2−N5 2.077(7), Li2−N6 2.119(6), C1−N2 1.368(4), C7−N2 1.393(4), C18−N1 1.405(4), C24−N1 1.410(4) Å; Li1−N1−Li2 108.1(3), Li1−N1−C18 95.3(3), Li1−N1−C24 121.0(3), Li2−N1−C18 111.7(3), Li2−N1−C24 101.8(2), C1−N2−C7 119.4(3), C1−N2−Li1 128.9(3), Li1−N2−C7 111.3(3), N1−Li1−N2 139.8(3), N1−Li1−N3 108.8(3), N2−Li1−N3 109.1(3), N5−Li2−N6 105.2(3), N1−Li2−N5 122.0(3), N1−Li2−N6 105.3(3), N4−Li2−N5 100.3(3), N4−Li2−N6 104.3(3), N1−Li2−N4 118.0(3)°

The triply lithiated trianilinoborane **15**, which crystallized as $B(NLiPh)_3{\cdot}LiCl{\cdot}3OEt_2$ (**15A**), once again proved to be dimeric in the solid state, its core structure containing eight Li atoms. Figure 9 shows the molecular structure. The dimeric molecule is centrosymmetric. Four Li atoms (Li1, Li1A, Li3, Li3A) are three-coordinated by one O, N, and Cl atom each, while the other four Li centers are tetracoordinated, atoms Li2 and Li2A by two N atoms, one O atom, and one Cl atom, and atoms Li4 and Li4A by three N atoms and one Cl atom. In order to describe the structure of **15A** it is best to start from the $B(NLiPh)_3$ unit. The core atoms of this molecule are shown in Figure 10.

The most important feature of compound **15A** is the planar BN_3 unit, which shows different B−N bond lengths of 1.429(9), 1.459(9), and 1.509(9) Å to atoms N1, N3, and N2, respectively. While B1−N1 is practically of the same length as in the parent compound **3**, the other two B−N

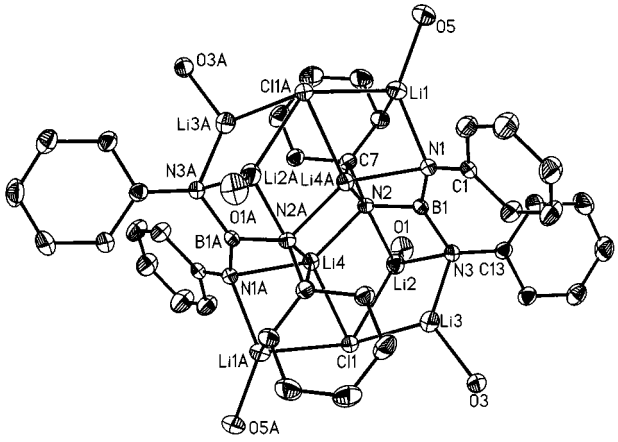

Figure 9. Molecular structure of compound dimeric **15A**; hydrogen atoms and C atoms of the ether molecules omitted for clarity

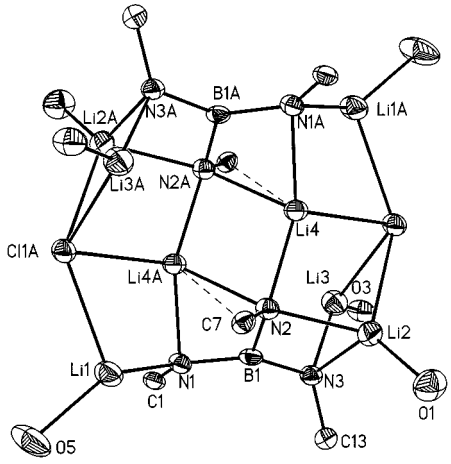

Figure 10. The core structure of $[B(NLiPh)_3{\cdot}LiCl{\cdot}3\ OEt_2]_2$ (**15A**)$_2$; only the *ipso*-C atoms of the phenyl rings are shown; the Et groups of the ether molecules have also been removed; selected bond lengths and bond angles: B1−N1 1.429(4), B1−N2 1.509(4), B1−N3 1.459(4), Li1 N1 2.021(6), N1−Li4A 2.029(5), Li3−N3 1.083(7), Li2−N3 1.983(7), Li4−N2 2.006(5), Li4A−N2 2.154(5), N1−C1 1.400(3), N2−C7 1.364(4), N3−C13 1.373(3). Cl1−Li2 2.564(5), Cl1−Li3 2.377(5), Cl1−Li4 2.362(5), Cl1A Li1 2.451(5), Li1−O1 1.901(6), Li2−O2 1.910(6), Li3−O3 1.925(6) Å; N1−B1−N3 132.9(3), N1−B1−N2 113.9(2), N3−B1−N2 112.1(2), Li1A−Cl1−Li3 121.1(2), Li1A−Cl1−Li2 130.2(2), Li4−Cl1−Li1A 64.7(2), Li4−Cl1−Li2 67.5(2), Li4−Cl1−Li3 88.7(2), Li2−Cl1−Li3 69.8(2)°

bonds are significantly elongated. Actually, the long B1−N2 bond corresponds to a single bond between sp^2-type B and N atoms. The reasons for these differences are the different N−B−N−C torsion angles and the number of coordinated Li atoms at the N atoms. Thus, the B1N1N2N3/B1N1C1 interplanar angle is 21.5°, which still allows for BN-π-bonding. While atom Li1 is part of the planar environment around atom N1 (sum of bond angles 357.8°), one may note that the atom Li4A has an N1−Li4A distance of 2.209(5) Å and lies 1.934 Å above the B1N1C1Li1 plane. However, the N1−Li1 distance is 2.961(6) Å, the same distance as found for N1−Li4A. The situation at atom N3 is similar to that at N1, but there is greater torsion, as demonstrated by the angle of 50.8° between the B1N1N3 and B1N3C13 planes. This has the consequence of weaker BN-π-bonding, as revealed by the longer B1−N3 bond. The distance from N3 to Li3 [1.983(7) Å] is shorter than that to Li2 [2.005(5) Å], but the B1N3C13Li3 atom system lies almost in a plane (B1 being −0.192 Å distant). Finally, the interplanar angle B1N1N2N3/B1N2C7 is 57.6°, and this seems to be a reason for the long B1−N2 bond to which the pentacoordinated atom N2 contributes. The coordination of Li2 and Li4A by two N atoms of the trianilidoborane unit is what most probably gives rise to an N1−B1−N3 bond angle as wide as 132.9(3)°.

As shown in Figure 10, the Cl anion is coordinated to the Li atoms of the $B(NLiPh)_3$ unit, with distances of 2.564, 2.377, and 2.362 Å to atoms Li2, Li3, and Li4, respectively. The presence of the chloride results in the formation of a distorted cubane unit in which one corner of the cube is missing. The Cl ion is surrounded by four Li ions. An unusually open coordination at Cl results, and this is best described as a strongly distorted trigonal bipyramid with a coordination partner missing in the equatorial plane. Atoms Li1, Li1A, Li3, and Li3A coordinate with three ligand atoms (O, N, Cl) in a nonplanar fashion.

The triply lithiated **4** crystallizes with one molecule of LiHNR* as $[Li_4B(NR^*)_3HNR^*(THF)_3]_2$ (**18**)$_2$. Its molecular structure is shown in Figure 11 and the monomeric unit is displayed in Figure 12. As may be noted, the metallation of compound **5** leaves the boron atom in a planar environment, the extra LiHNR* group not being bonded to atom B1 to generate a tetraamidoborate. One B−N bond of the $B(NLiR^*)_3$ unit is short, at 1.440(3) Å (B1−N1), while the other two are of almost equal lengths [1.476(3) for N2 and 1.467(3) Å for N3]. Thus, all B−N bonds are longer than those in the parent compound **4**. Each N atom of the BN_3 unit is coordinated to two Li atoms, but there is only one Li atom (Li3) that bridges two N atoms of the BN_3 unit. This gives rise to a small N1−B1−N3 bond angle of 111.8(2)°. The twisting of the CNB planes relative to the BN_3 plane is 24.4, 50.7, and 88.2° (at N1, N3, N2), respectively.

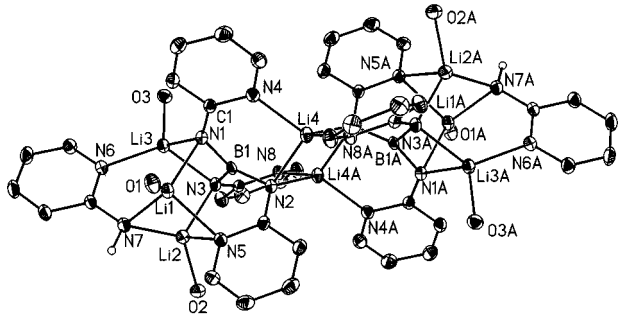

Figure 11. The molecular structure of $[B(NLiR^*)_3{\cdot}LiHNR^*(THF)_3]_2$ (**18**)$_2$; hydrogen atoms removed, as well as the C atoms of the coordinated THF molecules

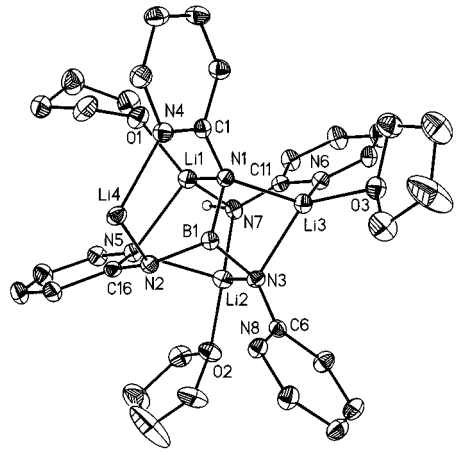

Figure 12. The asymmetric (monomeric) unit of **18**; bond lengths and bond angles: B1−N1 1.440(3), B1−N2 1.476(3), B1−N3 1.467(3), N1−C1 1.353(3), N2−C16 1.332(3), N3−C6 1.338(3), Li1−N1 2.114(5), Li3−N1 2.046(4), Li4−N2 2.065(4), Li2−N3 2.067(4) Å; N1−B1−N2 125.1(2), N1−B1 N3 111.8(2), N2−B1−N3 122.4(2), C1−N1−B1 123.9(2), C1−N1−Li3 138.3(2), C1−N1−Li1 106.8(2), B1−N2−C16 113.8(2), B1−N2−Li4 108.6(2), B1−N2−Li4A 104.7(2), Li4−N2−Li4A 78.4(2), Li4−N2−C16 117.7(2), Li4A−N2−C16 128.5(2), B1−N3−C6 122.9(2), B1−N3−Li2 96.5(2), B1−N3−Li3 87.6(2), C6−N3−Li2 123.3(2), C6−N3−Li3 125.4(2), Li2−N3−Li3 91.8(2)°

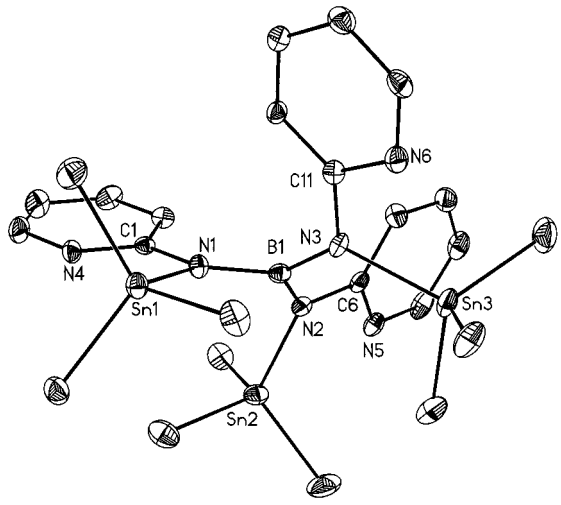

Figure 13. ORTEP plot of compound **23**; H atoms have been omitted for clarity; selected bond lengths and bond angles: B1−N1 1.443(7), B1−N2 1.435(6), B1−N3 1.457(6), N1−Sn1 2.109(4), N2−Sn2 2.119(4), N3−Sn3 2.110(3), Sn1···N4 2.717, Sn2···N5 2.703, Sn3···N6 2.672, N1−C1 1.396(5), N2−C6 1.383(6), N3−C11 1.385(5) Å; N1−B1−N2 121.2(4), N1−B1−N3 118.5(4), N2−B1−N3 120.3(4), B1−N1−C1 123.6(4), C1−N1−Sn1 108.2(3), B1−N1−Sn1 128.2(3), B1−N2−C6 123.7(4), C6−N2−Sn2 107.9(3), B1−N2−Sn2 128.4(3), B1−N3 C11 124.0(4), C11−N3−Sn3 107.8(3), B1−N3−Sn3 128.1(39, N1−Sn1−C16 104.6(2), N1−Sn1−C17 111.5(2), N1−Sn1−C18 113.0(2)°

The Li−N atom distances in $(\mathbf{18})_2$ span a range from 2.036(5) to 2.114(5) Å for the amino nitrogen atoms, and 2.038(4) to 2.155(4) Å for the pyridine nitrogen atoms, with the exception of the Li2−N5 distance of 2.286(4) Å. The reason for the long distance is most probably the specific situation at atom N5, since this atom in the only pyridine nitrogen atom that coordinates to two Li centers.

The (stannylamino)borane **23** crystallizes in the monoclinic system, its molecular structure being shown in Figure 13. The B−N bond lengths range from 1.435(6) to 1.457(6) Å. These are slightly longer than those in the parent compound **5**. All Sn−N bonds to the amino nitrogen atoms are of equal length. The pyridine nitrogen atoms are oriented towards the tin atoms of each Me_3SnNR^* unit. This may indicate the presence of Sn−N interactions. If there are any, then these must be quite weak, as the C−Sn−C bond angles deviate only slightly from the tetrahedral angle.

All amino nitrogen atoms reside in a planar environment, but the SnNC planes at N1, N2, and N3 are twisted relative to the BN_3 plane by 40.6, 38.1, and 46.1°, respectively. These torsion angles explain the lengths of the B−N bonds. The twisting results from the steric requirement of the trimethylstannyl groups and is the most striking difference on comparison of this structure with the parent compound **4**. As would be expected, the Sn−C bond lengths are in the typical range (2.12−2.15 Å).[39,40]

Discussion

The deprotonation of aminoboranes bearing RHN groups by butyllithium depends on the steric and electronic shielding of the boron atom, the structure of the aminoborane, and the solvent used. In almost all so far known cases, including the results presented here, there is competition between deprotonation and borate formation, as well as B−N bond cleavage. The last can be impeded if the boron atoms are part of a ring system, as shown for the triazaboradecalin system[3] or for borazines $(RB{=}NH)_3$.[18] However, an exocyclic B−N bond is comparatively easily cleaved, as demonstrated by compound **2**, while borate formation can be fully or at least partly suppressed by the use of *t*BuLi.[41] In the case of the double deprotonation of the aminoborane **2**, one observed the formation of a borate, most probably $Li[BuB(NPh_2)(NLiPh)_2]$, in solution besides $Ph_2NB(NLiPh)_2$. Both compounds might be the source of $LiNPh_2$, which was formed slowly. Isolated Ph_2NLi solvates form dimers, as is well known for various lithium diorganylamides. However, chain-like dimers of lithium diorganylamides are rare.[16,17]

Neither borate formation nor B−N bond cleavage was observed in the triple lithiation of trianilinoborane (**3**) in the presence of ether, unlike in the case of tris(2-pyridylamino)borane, in which B−N cleavage to give LiNHR* occurred. This amide cocrystallized with $B(NLiR^*)_3$ in a 1:1 ratio to give $(\mathbf{18})_2$, a cluster with an Li_8N_8 core. In addition, (2-aminopyridyl)butylborates were also formed. Nevertheless, deprotonation was the dominant reaction both for **3** and for **4**.

However, as we have seen for compound **18**, the metallated triaminoboranes did not add amide ions to form tetraaminoborates. These latter are scarce anyhow, and form readily only when the amido group is derived from a

heterocyclic system, such as the anions of pyrrole,[42] indole,[43] pyrazole,[44,45] or dihydropyridine.[46] In these cases, the parent triaminoborane is comparatively Lewis-acidic. This is obviously not the case for the tris(lithioamino)boranes; the negative charge at the nitrogen atoms reduces the Lewis acidity of the boron center. Therefore, an amide does not attack at the boron center, but rather forms coordinative Li−N bonds. The lithium atoms adopt coordination numbers ranging from 3 to 5. Therefore, in comparison with lithium amides,[16,17] the borylated lithium amides offer a much more versatile structural chemistry similar to that of lithiated silylamides[16] and aminophosphanes.[47] In addition, they are very useful reagents. This has been shown previously,[5−10,48] and we will report on this point in a forthcoming paper describing the synthesis and reactions of (*t*BuLiN)B(R)tmp (tmp = 2,2,6,6-tetramethylpiperidino) (see ref.[4]).

Experimental Section

General: All experiments required anhydrous conditions. Schlenk techniques were employed, with dinitrogen as a protecting gas. The amines are commercially available; the liquids were dried with either KOH or CaH_2 and distilled, and the solids were recrystallized before use. BuLi was obtained from Chemetall GmbH. NMR: Bruker ACP 200 (^{7}Li, ^{11}B, ^{119}Sn), JEOL GSX 270, and JEOL EX 400 (^{1}H, ^{13}C, ^{119}Sn) with Me_4Si, C_6D_6, $BF_3{\cdot}OEt_2$, and $SnMe_4$ as standards. Elemental analyses were performed in the microanalytical laboratory of this department. X-ray: Siemens P4 diffractometer equipped with a CCD area detector, graphite monochromator, and Mo-K_α source or a STOE IPS diffractometer (compounds **7** and **23**). Data sets were collected at −80 °C (Siemens LT2 device).

2-Anilino-1,3-diphenyl-1,3,2-diazaborolidine (1): Aniline (0.87 mL, 9.5 mmol) and triethylamine (1.32 mL) were added to a stirred solution of 2-chloro-1,3-diphenyl-1,3,2-diazaborolidine[48] (2.43 g, 9.50 mmol) in toluene (80 mL). A precipitate formed. The mixture was heated under reflux overnight, the solid was removed by filtration (glass frit), and the orange-yellow solution was concentrated to approximately 50 mL in vacuo. Needles of **1** separated from the solution. Yield: 2.7 g, 71%; m.p. 153 °C. NMR (in C_6D_6): δ^1H = 3.20 (s, 4 H, NCH_2), 4.49 (s br., 1 H, NH), 6.47 (d, $^3J_{H,H}$ = 7.3 Hz, 2 H, *o*-CH aniline), 6.66 (t, $^3J_{H,H}$ = 7.6 Hz, 1 H, *p*-CH aniline), 6.80 (t, ^3JH,H = 7.2 Hz, 2 H, *p*-H Ph), 6.90 (t, $^3J_{H,H}$ = 7.5 Hz, 2 H, *m*-CH aniline), 6.93 (d, $^3J_{H,H}$ = 7.6 Hz, 4 H, *o*-CH, Ph), 7.07 (t, $^3J_{H,H}$ = 8.8 Hz, 4 H, *m*-CH,Ph); δ^{13}C = 48.04 (CH_2), 119.5 (*o*-C, Ph), 119.6 (*o*-C, aniline), 120.2 (*p*-C, aniline), 120.9 (*p*-C, Ph), 128.8 (*m*-C, aniline), 129.0 (*m*-C, Ph), 143.1 (*i*-C, aniline), 146.6 (*i*-C, Ph); δ^{11}B = 23.0 ($h_{1/2}$ = 300 Hz). $C_{20}H_{20}BN_3$ (313.20): calcd. C 76.62, H 6.38, N 13.41; found C 76.31, H 6.67, N 13.31.

Dianilino(diphenylamino)borane (2): A solution of diphenylamine (4.23 g, 25.0 mmol) in toluene (150 mL) was cooled to −78 °C. A solution of BuLi in hexane (1.56 M, 16 mL) was added with stirring. A voluminous, white precipitate formed immediately, with some gas evolution. The suspension was allowed to attain ambient temperature. Stirring was continued for additional 3 h. After the mixture had again been cooled to −78 °C, a solution of BCl_3 in toluene (1.1 M, 22.7 mL, 25.0 mmol) was slowly added. Stirring was continued at ambient temperature overnight. The ^{11}B NMR spectrum taken after that time showed a signal at δ = 32.1 (**2**) and a tiny signal at δ = 41.1, corresponding to 2-butyl-1,3-diphenyl-1,3,2-diazaborolidine (ratio approximately 97:3). The solid was removed from the suspension by filtration. A mixture of aniline (4.6 mL, 50 mmol) and triethylamine (7.0 mL) was added at −78 °C to the slightly yellow filtrate. After the reaction mixture had been heated at reflux overnight and after removal of the solid, the filtrate was concentrated in volume to approximately 50 mL. Crystals separated from the solution within a few days. Crystallization from toluene yielded **2** (6.44 g, 71.0%), m.p. 185 °C. $C_{24}H_{22}BN_3$ (362.81): calcd. C 79.83, H 6.06, N 11.58; found C 78.09, H 6.21, N 11.08.

Trianilinoborane (3):[49] Aniline (5.5 mL, 60 mmol) was added to a solution of $B(NMe_2)_3$ (3.45 mL, 20 mmol) in toluene (70 mL). Gas evolution started, and became rapid on heating of the solution at reflux for 5 h. A single ^{11}B NMR signal at δ = 23.7 indicated a quantitative reaction. Crystals separated within a few hours. Half of the solvent was removed from the suspension in vacuo, and 6.6 g of **3** was isolated. Yield: 87%; m.p. 174 °C. NMR in C_6D_6: δ^1H = 4.83 (br. s, 3 H, NH), 6.75 (dd, $^3J_{H,H}$ =8.5, $^4J_{H,H}$ = 1.1 Hz,6 H, *o*-H), 6.80 (tt, $^3J_{H,H}$ = 7.6, $^4J_{H,H}$ = 1.2 Hz, 3 H, *p*-H), 7.06 (t, $^3J_{H,H}$ = 7.5 Hz, 6 H, *m*-H); δ^{13}C = 119.9, (*o*-C), 120.8 (*p*-C), 129.4 (*m*-C), 145.4 (*i*-C); δ^{11}B = 23.7 ($h_{1/2}$ = 214 Hz); δ^{14}N = −292.3.

Tris(2-pyridylamino)borane (4): 2-Aminopyridine (5.65 g, 59.4 mmol) and $B(NMe_2)_3$ (20.0 mmol) were heated under reflux in toluene (150 mL). Gas evolution (dimethylamine) rapidly started, and the amine was trapped at −78 °C. On cooling of the solution to ambient temperature, a white precipitate of **4** formed. After filtration, the filtrate was cooled to 0 °C. Colorless needles separated; these were suitable for X-ray structure determination. Yield: 5.2 g (90%), m.p. 121 °C. NMR in C_6D_6: δ^1H = 6.36 (ddd, $^3J_{H,H}$ = 8.5, $^3J_{H,H}$ = 5.4, $^4J_{H,H}$ = 0.8 Hz, 3 H, C5-H), 6.46 (dt, $^3J_{H,H}$ = 8.3, $^4J_{H,H}$ = 0.7 Hz, 3 H, C3-H), 6.99 (ddd, $^3J_{H,H}$ = 7.3, $^3J_{H,H}$ = 7.4, $^4J_{H,H}$ = 1.6 Hz, 3 H, C4r-H), 8.14 (ddm, $^3J_{H,H}$ = 5.3, $^4J_{H,H}$ = 1.8 Hz, 3 H, C6-H), 9.85(s, 3 H, NH); δ^{13}C = 113.6 (C3), 114.6 (C5), 137.4 (C4), 147.2 (C6), 159.6 (C2); δ^{11}B = 24.2 ($h_{1/2}$ = 218 Hz); δ^{14}N = −105.7 (pyN), −310.0 (NH). IR (Hostaflon, cm^{-1}): $\tilde{\nu}$ = 3293 (NH_2), 3090, 3059, 3043, 3022 (CH). $C_{16}H_{15}BN_5$ (290.13): calcd. C 57.14, H 5.71, N 26.62; found C 58.19, H 5.25, N 27.11.

Tris(8-quinolylamino)borane (5): Tris(dimethylamino)borane (1.8 mL, 19 mmol) was added to a suspension of 8-aminoquinoline (4.32 g, 30.0 mmol) in toluene (150 mL). The mixture was heated under reflux for 30 h. The red solution showed a broad ^{11}B NMR signal at δ = 24.7. After cooling of the solution to 0 °C, red needles separated within a few days. Yield: 3.75 g (85.3%), m.p. > 200 °C. NMR in C_6D_6: δ^1H = 6.74 (dd, $^3J_{H,H}$ = 3.7 Hz, 3 H, C3-H), 6.97 (d, br., $^3J_{H,H}$ = 7.8 Hz, 3 H, C5-H), 7.21 (dd, $^3J_{H,H}$ = 7.9, $^3J_{H,H}$ = 7.9 Hz, 3 H, C6-H), 7.54 (dd, $^3J_{H,H}$ = 8.4, $^4J_{H,H}$ = 1.8 Hz, 3 H, C4-H), 7.72 (d, $^3J_{H,H}$ = 7.5 Hz, 3 H, C7-H), 8.15 (s 3 H, NH), 8.48 (dd, $^3J_{H,H}$ = 4.0, $^4J_{H,H}$ = 1.5 Hz, 3 H, C2-H); δ^{13}C = 112.7 (C7), 116.6 (C5), 121.4 (C3), 129.2 (C10), 135.7(C9), 136.1, C6), 140.2 (C4), 143.4 (C8), 146.9(C2); δ^{11}B (in toluene) = 24.7 ($h_{1/2}$ = 450 Hz); δ^{14}N = −74.8 (ring N), −326.9 (NH). IR (Nujol, cm^{-1}): $\tilde{\nu}$ = 3340 (νNH). $C_{27}H_{21}BN_6$ (439.81): calcd. C 73.58, H 4.77, N 19.07; found C 73.33, H 482, N 18.61.

2-[Lithio(phenyl)amino]-1,3-diphenyl-1,3,2-diazaborolidine (6) and Formation of Lithium 2-Oxido-1,3-diphenyl-1,3,2-diazaborolidine (7): A solution of compound **1** (0.490 g, 1.56 mmol) in toluene (40 mL) was diluted with ether (10 mL), and the mixture was cooled to −78 °C. A solution of BuLi in hexane (1.0 mL, 1.56 mmol) was added by syringe, with stirring. The solution turned orange. At room temperature the solution showed only a single ^{11}B NMR sig-

nal at δ = 23.8 (**6**). The solid that was left on concentration of the solution also showed an ^{11}B NMR signal at δ = 23.8 in deuteriobenzene, which was assigned to **6**. Attempts to grow crystals from this solution failed. However, after addition of pyridine (3 mL) a few large crystals grew slowly at 0 °C over two weeks. These proved to be compound **7**, as also characterized by X-ray crystallography. **7:** NMR in C_6D_6: δ^1H = 3.47 (s, 4 H, NCH_2), 6.82 (d, $^3J_{H,H}$ = 8.5 Hz, 2 H, *p*-CH), 6.98 (t, $^3J_{H,H}$ = 7.6 Hz, 4 H, *o*-CH), 7.28 (t, $^3J_{H,H}$ = 7.8 Hz, 4 H, *m*-CH), 7.42 (t, $^3J_{H,H}$ = 8.6 Hz, 4 H, *p*-CH, py), 7.68 (t, $^3J_{H,H}$ = 7.6 Hz, 2 H, *p*-CH, py), 8.63 (d, $^3J_{H,H}$ = 4.5 Hz, 4 H, *o*-H, py); $\delta^{13}C$ = 43.0 (CH_2), 113.0 (*o*-C), 117.8 (*p*-C), 123.5 (*m*-C, py), 129.3 (*p*-C, py), 148.1 (ipso-C), 149.6 (*o*-C, py); $\delta^{11}B$ = 22.7 ($h_{1/2}$ = 350 Hz); δ^7Li = 1.59. $C_{24}H_{24}BLiN_4O$ (402.2): calcd. C 71.66, H 6.01, N 13.93; found C 68.37, H 6.35, N 12.07.

Double Metallation of 2-(Dimethylamino)-1,3,2-benzodiazaborolidine (9): The diazaborolidine **9**[50] (0.26 g, 1.6 mmol) was added to a solution of tetramethylethylenediamine (0.46 mL, 3.2 mmol) in tetrahydrofuran (80 mL). After this had been cooled to −78 °C, a hexane solution of BuLi (2.1 mL, 1.56 M) was added to the vigorously stirred solution. The color of the solution turned from yellow to gray-green. An ^{11}B NMR spectrum at −78 °C showed only one signal at δ = 29.3. On warming, a precipitate formed at about −60 °C, and no ^{11}B NMR signal was then observed in the supernatant solution at room temperature. When the solution was kept at −78 °C and the solvent was removed stepwise in vacuo, no crystals separated. The solid that was formed at −60 °C was dried in vacuo. Elemental analysis: C 48.12, H 5.88, N 17.92, corresponding to $C_8H_{11.6}N_{2.54}$ instead of $C_8H_{10}N_3(BLi_2)$ for **10**.

2-(Dimethylamino)-1,3-bis(trimethylsilyl)-1,3,2-benzodiazaborolidine (11): Me_3SiCl (0.34 mL) was added at −78 °C to **10** (1.35 mmol) in THF (80 mL). The stirred suspension was allowed to attain ambient temperature. All volatiles were removed from the gray-green solution in vacuo, and hexane (30 mL) was added to the oily residue. This resulted in a brown solution and a white insoluble product (LiCl). The solid was separated by filtration. From the filtrate all volatile material was removed. The liquid residue was dissolved in $CDCl_3$ and characterized as **11** by NMR spectroscopy. NMR: δ^1H = 0.55 (s, 18 H, SiMe), 2.67, (s, 6 H, NMe), 6.91 (m, 2 H, C3 H, C6-H), 7.25 (m, C4-H, C5-H); $\delta^{13}C$ = 1.9 SiMe, 41.4 (CMe=, 114.3, C3, C6), 118.9 (C4, C5), 142.0 (C1,C2); $\delta^{11}B$ = 32.0 (h_{12} = 227 Hz); $\delta^{27}Si$ = 4.7.

Double Metallation of Dianilino(diphenylamino)borane and Formation of $LiNPh_2$: Dimethoxyethane (0.41 g, 4.5 mmol) was added to compound **2** (1.63 g, 4.50 mmol) in toluene (80 mL). The solution was cooled to −78 °C. A hexane solution of LiBu (5.7 mL, 9.0 mmol) was added dropwise with stirring. After the yellow/orange solution had been allowed to attain ambient temperature, it showed two ^{11}B NMR signals at δ = 28.9 (**12**) and −10.0, in an intensity ration of 85:15. Solvent was removed in vacuo, to leave 10 mL of a solution. At 0 °C, colorless crystals separated within several days and proved to be $LiNPh_2$·dme (**13**). The supernatant liquid showed ^{11}B NMR signals at δ = −0.3 (weak), 30.8 (main signal), and 42.0

Table 2. Crystallographic parameters, information about data collection, and structure solution of compounds **1**−**5**

Compound	**1**	**2**	**3**	**4**	**5**
Empirical formula	$C_{20}H_{20}BN_3$	$C_{24}H_{22}BN_3$	$C_{18}H_{18}BN_3$	$C_{27}H_{21}BN_6$	$C_{15}H_{15}BN_6$
Formula mass	313.20	363.26	287.16	440.31	290.14
Crystal size [mm]	0.10 × 0.20 × 0.20	0.10 × 0.10 × 0.30	0.20 × 0.30 × 0.30	0.10 × 0.10 × 0.20	0.1 × 0.2 × 0.7
Crystal system	monoclinic	triclinic	monoclinic	triclinic	monoclinic
Space group	*I*2/*a*	$P\bar{1}$	$P2_1/c$	$P\bar{1}$	$P2_1/c$
a [Å]	19.015(1)	9.413(1)	10.0512(8)	7.2478(8)	16.249(1)
b [Å]	7.5388(5)	9.776(1)	19.902(2)	11.622(1)	5.4326(4)
c [Å]	23.557(2)	11.435(1)	8.3524(7)	13.531(2)	16.331(1)
α [°]	90	93.178(2)	90	89.536(2)	90
β [°]	90.446(1)	107.399(2)	113.114(1)	78.233(2)	96.031(9)
γ [°]	90	93.886(2)	90	86.265(2)	90
V [Å^3]	3376.8(4)	998.5(2)	1536.6(2)	1113.4(2)	1433.6(2)
Z	8	2	4	2	4
ρ(calcd.) [Mg/m^3]	1.232	1.208	1.241	1.313	1.344
μ [mm^{-1}]	0.073	0.071	0.074	0.080	0.085
F(000)	1328	384	608	460	608
Index range	$-24 \le h \le 24$ $-10 \le k \le 8$ $-29 \le l \le 29$	$-11 \le h \le 11$ $-12 \le k \le 12$ $-14 \le l \le 14$	$-13 \le h \le 6$ $-24 \le k \le 24$ $-10 \le l \le 10$	$-9 \le h \le 9$ $-14 \le k \le 15$ $-17 \le l \le 17$	$-19 \le h \le 19$ $-6 \le k \le 6$ $-19 \le l \le 19$
2θ [°]	57.74	57.88	58.30	58.00	51.70
Temp. [K]	188(2)	191(2)	193(2)	193(2)	200(2)
Refl. collected	9133	5816	9024	6528	7902
Refl. unique	3221	3045	2546	3420	2740
Refl. observed (4σ)	2630	2049	2060	1593	1873
R (int.)	0.0206	0.0288	0.0252	0.0301	0.0393
No. of variables	221	256	202	311	259
Weighting scheme[a] *x*/*y*	0.6340/1.2204	0.1100/0.0000	0.0640/0.3750	0.0480/0.000	0.1496/0.000
GOOF	1.032	0.980	1.026	0.843	0.684
Final *R* (4σ)	0.0410	0.0564	0.0420	0.0659	0.0355
Final *wR*2	0.1021	0.1456	0.1067	0.1751	0.0928
Larg. res. peak [e/Å^3]	0.143	0.219	0.147	0.291	0.157

[a] $w^{-1} = \sigma^2F_o^2 + (xP)^2 + yP$; $P = (F_o^2 + 2F_c^2)/3$.

(weak, Bu_2BNPh_2). In a similar experiment, pyridine was added as an auxiliary base to the metallated solution of **2**. A yellow solution resulted. At 0 °C crystals separated, and proved on X-ray crystallography to be $LiNPh_2 \cdot 2$ py (**14**). The supernatant solution showed ^{11}B NMR signals at δ = −17.6, −16.4, 0.2, 1.9, 3.0, and 43.2. The last signal is most probably due to Bu_2BNPh_2 (compounds of type Bu_2B-NR_2 show resonances in the range of δ = 51−45).[18]

Triple Metallation of Trianilinoborane: Compound **3** (0.97 g, the compound contained chloride!) was dissolved in ether (80 mL) and cooled to −78 °C, and BuLi in hexane (1.56 M, 10.2 mmol, 6.5 mL) was added with stirring. After the solution had attained ambient temperature, a white precipitate appeared. The yellow solution showed an ^{11}B NMR signal at δ = 35.4 ($h_{1/2}$ = 640 Hz). Solvent was removed until 30 mL of a solution remained, from which crystals separated within a few hours at 0°. The crystals readily lost coordinated ether in vacuo; if drying was carried out carefully, however, the composition of the crystals was $B(NLiPh)_3 \cdot LiCl \cdot 3OEt_2$ (**15A**). The ^{11}B NMR spectrum of the solid, dissolved in THF, was the same as that of the solution. The NMR spectroscopic data were consistent with the formation of $B(NLiPh)_3 \cdot n OEt_2$. NMR in C_6D_6: δ^1H = 0.92 (t, $^3J_{H,H}$ = 7.0 Hz, 18 H, Me), 3.14 (q, $^3J_{H,H}$ = 6.9 Hz, 12 H, OCH_2), 6.85 (t, $^3J_{H,H}$ = 7.0 Hz, 3 H, *p*-H), 6.96 (d, $^3J_{H,H}$ = 7.5 Hz, 6 H, *o*-H), 7.23 (t, $^3J_{H,H}$ = 7.0 Hz), 6 H, *m*-H); $\delta^{13}C$ = 14.6 (Me), 64.9 (OCH_2), 117.7 (*p*-C), 125.8 (*o*-C), 128.8 (*m*-C), 160.0 (CNLi); $\delta^{11}B$ = 35.4 ($h_{1/2}$ = 640 Hz); δ^7Li = 1.24. $C_{30}H_{45}BClLi_4N_3O_3$(569.71): calcd. C 63.19, H 7.90, N 7.37; found C 62.09, H 7.78, N 7.89.

Triple Metallation of Tris(2-pyridylamino)borane and Formation of 18: Compound **4** (0.490 g, 1.69 mmol) was dissolved in THF (40 mL). The solution was cooled to −78 °C, stirred, and allowed to react with a hexane solution of BuLi (1.56 M, 3.3 mL). After the solution had attained ambient temperature, the slightly turbid, yellow solution showed ^{11}B NMR signals at δ = 1.3 and −9.5. Solvents were evaporated from the clear filtrate in vacuo to leave 30 mL of a solution, which was layered with hexane (20 mL) and kept at −20 °C. Within 1 d colorless crystals had separated. These rapidly became turbid on standing at ambient temperature, and did so more rapidly in vacuo; no elemental analysis was therefore performed. The identity of **18** was ascertained by X-ray structure determination. The same reaction was performed in ether instead of THF. In this case, more solid material separated. The solid, dissolved in THF, showed only a single ^{11}B NMR signal at δ = 35.0 ($h_{1/2}$ = 1330) corresponding to **18** was observed. The filtrate gave ^{11}B resonances at δ = 1.5, 0.6, −24.6, and −28.6.

Triple Metallation of Tris(8-quinolylamino)borane: In analogy to the lithiation of compound **4**, compound **5** (0.97 g, 2.2 mmol), dissolved in THF (90 mL), was metallated at −78 °C with BuLi in hexane (1.56 M, 4.2 mL). An intensively violet solution formed. At ambient temperature, one ^{11}B NMR signal at δ = 32.8 ($h_{1/2}$ = 1240 Hz) and a single ^7Li signal at δ = 2.46 were found. All attempts to induce crystallization by cooling or dissolving the residue (after removal of THF and hexane) in ether, toluene, ether/pyridine, or pyridine failed, only violet oils being observed. A solution of the oil in [D_8]THF revealed more ^1H NMR signals than expected.

Double Metallation of 4 and Formation of Tris(trimethylstannyl-2-pyridylamino)borane (23): A solution of **4** (0.40 g, 1.4 mmol) in THF (80 mL) was metallated at −78 °C with a hexane solution of LiBu (1.77 mL, 2.80 mmol). The solution at ambient temperature

Table 3. Crystallographic parameters, information about data collection, and structure solution of compounds **7**, **13**, **14**, **15A**, **18**, and **23**

	7	**13**	**14**	**15A**	**18**	**23**
Empirical formula	$C_{48}H_{48}B_2Li_2N_8O_2$	$C_{32}H_{40}Li_2N_2O_4$	$C_{44}H_{40}Li_2N_6$	$C_{30}H_{45}BClLi_4N_3O_3$	$C_{36}H_{49}BLi_4N_8O_4$	$C_{24}H_{39}BN_6Sn_3$
Formula mass	804.451	530.54	666.70	569.71	696.40	778.548
Crystal size [mm]	0.50 × 0.50 × 0.65	0.02 × 0.20 × 0.30	0.10 × 0.30 × 0.30	0.10 × 0.20 × 0.20	0.3 × 0.3 × 0.4	0.05 × 0.08 × 0.20
Crystal system	triclinic	triclinic	monoclinic	monoclinic	triclinic	monoclinic
Space group	$P\bar{1}$	$P\bar{1}$	$P2_1/c$	$C2/c$	$P\bar{1}$	$P2_1/n$
a [Å]	13.354(2)	10.122(4)	20.986(2)	13.487(1)	11.9799(9)	12.692(1)
b [Å]	13.719(2)	10.876(4)	9.259(1)	20.448(2)	12.954(1)	15.230(1)
c [Å]	13.812(2)	14.756(5)	20.893(3)	24.929(2)	14.859(1)	15.878(2)
α [°]	88.87(2)	82.67(1)	90	90	80.759(1)	90
β [°]	79.41(2)	74.055(7)	113.670(2)	100.162(1)	67.421(1)	93.987(12)
γ [°]	60.43(2)	89.148(8)	90	90	66.129(1)	90
V [Å^3]	2155.6(5)	1548.8(9)	3718.3(7)	6767.0(9)	1947.0(3)	3061.8(5)
Z	2	2	4	8	2	4
ρ(calcd.) [Mg/m^3]	1.2394(3)	1.138	1.191	1.118	1.188	1.6890(3)
μ [mm^{-1}]	0.076	0.073	0.070	0.145	0.077	2.450
F(000)	848	568	1408	2432	740	1520
Index range	$-17 \le h \le 17$ $-18 \le k \le 17$ $-18 \le l \le 15$	$-12 \le h \le 7$ $-7 \le k \le 11$ $-10 \le l \le 18$	$-26 \le h \le 23$ $-11 \le k \le 11$ $-26 \le l \le 25$	$-18 \le h \le 13$ $-26 \le k \le 26$ $-30 \le l \le 30$	$-14 \le h \le 14$ $-16 \le k \le 16$ $-20 \le l \le 13$	$-15 \le h \le 13$ $-18 \le k \le 18$ $-19 \le l \le 19$
2θ [°]	56.08	57.92	58.26	58.56	57.34	51.84
Temp. [K]	200(3)	193(2)	193(2)	193(2)	193	200(3)
Refl. collected	15632	1792	20944	19239	11340	17655
Refl. unique	9511	1738	6024	6222	5919	5898
Refl. observed (4σ)	4756	554	2782	3164	4242	3695
R (int.)	0.0712	0.0087	0.1314	0.0692	0.0237	0.0705
No. of variables	554	361	469	405	479	316
Weighting scheme[a] *x*/*y*	0.0510/0	0.0472/0	0.05580/0	0.07440/0.8627	0.1022/0.3850	0.01320/0
GOOF	0.827	0.769	0.970	1.011	1.061	0.785
Final *R* (4σ)	0.0506	0.0566	0.0711	0.0613	0.0559	0.0309
Final *wR*2	0.1060	0.1296	0.1189	0.1338	0.1586	0.0498
Larg. res. peak [e/Å^3]		0.118	0.206	0.287	0.340	

[a] $w^{-1} = \sigma^2 F_o^2 + (xP)^2 + yP$; $P = (F_o^2 + 2F_c^2)/3$.

showed ^{11}B NMR signals at δ = 1.4, 1.2, −0.9, and −3.3, in addition to a dominant signal at δ = 23.5. While stirring, a solution of Me_3SnCl (0.28 g, 1.4 mmol) in THF was added. A ^{119}Sn NMR spectrum taken after 2 h showed signals at δ = 30.8, 26.2, and 9.2, the last signal resulting from **23**. The resonance at δ = 26.2 most probably corresponds to the monostannylation product **21**. Two signals were observed in the ^{11}B NMR spectrum, at δ = 30.9 and 22.9. THF was removed in vacuo. A waxy material was left behind, and was treated with toluene (20 mL). Crystals of **23** separated on cooling of the solution to −20 °C. Yield: 0.33 g (31%), m.p. 87 °C. NMR in C_6D_6: δ^1H = 0.39 (br., 27 H, Me), 6.18 [br., 3 H, C(5)H], 6.24 [m, 3 H, C(3)H], 7.84 [br., 3 H, C(6)H]; $\delta^{13}C$ = −0.87 (Me), 113.3 (C3), 137.3 (C4), 146.5 (C6); $\delta^{11}B$ = 30.9 ($h_{1/2}$ = 370 Hz); $\delta^{119}Sn$ = 9.2. $C_{24}H_{39}BN_6Sn_3$ (777.88): calcd. C 37.02, H 5.01, N 10.80; found C 37.16, H 5.16, B 10.62.

X-ray Structure Determinations: Crystals were covered with perfluoroether oil − those that readily lost coordinated solvent in precooled oil (approximately −40 °C). The selected crystal was placed on a glass fiber and mounted on the goniometer head. The reflections on five sets of frames were used for a preliminary determination of the unit cell, by use of the program implemented in SMART.[51] Data were collected in the hemisphere mode, and reduced with the SAINT program.[51] For absorption correction the SADABS[51] program was employed. The structures were solved by direct methods implemented in the SHELX97 program package.[52] Non-hydrogen atoms were refined in an isotropic description. Hydrogen atoms were placed in calculated positions and included in the final cycles of refinement by application of a riding model. One disordered ether molecule was found in the structure of compound **15A**, while compound **18** contains one uncoordinated THF molecule for each molecule of **18**. Tables 2 and 3 summarize data relevant to crystallography, data collection and refinement. CCDC-168322 to -168332 contain the supplementary crystallographic data for this paper. These data can be obtained free of charge at www.ccdc.cam.ac.uk/conts/retrieving.html or from the Cambridge Crystallographic Data Centre, 12, Union Road, Cambridge CB2 1EZ, UK [Fax: (internat.) + 44-1223/336-033; E-mail: deposit@ccdc.cam.ac.uk].

Acknowledgments

We thank the Fonds der Chemischen Industrie for support of this work, as well as Chemetall GmbH for support and generous gifts of butyllithium.

[1] B. Böck, H. Nöth, U. Wietelmann, *Z. Naturforsch., Teil B* **2001**, *56*, 659−670.
[2] H. Fußstetter, G. Kopietz, H. Nöth, *Chem. Ber.* **1980**, *113*, 728−738.
[3] I. Geisler, H. Nöth, *Chem. Ber.* **1973**, *106*, 1943−1951.
[4] U. Braun, Ph.D. thesis, University of Munich, **2000**.
[5] H. Fußstetter, R. Kroll, H. Nöth, *Chem. Ber.* **1977**, *110*, 3829−3842.
[6] D. Fest, C. D. Habben, A. Meller, G. M. Sheldrick, D. Stalke, F. Pauer, *Chem. Ber.* **1990**, *123*, 703−706.
[7] H. Chen, R. A. Bartlett, M. M. Olmstead, P. P. Power, S. C. Shoner, *J. Am. Chem. Soc.* **1990**, *112*, 1048−1055.
[8] H. Nöth, H. Vahrenkamp, *J. Organomet. Chem.* **1969**, *16*, 357−369.
[9] W. Beck, W. Becker, H. Nöth, B. Wrackmeyer, *Chem. Ber.* **1972**, *105*, 2823 −2837.
[10] H. Nöth, H. Vahrenkamp, *J. Organomet. Chem.* **1968**, *12*, 23−36.
[11] C. D. Habben, A. Heine, G. M. Sheldrick, D. Stalke, *Z. Naturforsch., Teil B* **1992**, *47,* 1367−1369.
[12] R. A. Bartlett, H. Chen, H. V. R. Dias, M. M. Olmstead, P. P. Power, *J. Am. Chem. Soc.* **1988**, *110*, 446−449.
[13] B. Wrackmeyer, B. Schwarze, J. Weidinger, M. Milius, *Z. Naturforsch., Teil B* **1997**, *52*, 431−434.
[14] P. Paetzold, C. Pelzer, R. Boese, *Chem. Ber.* **1988**, *121*, 51−59.
[15] T. Seifert, W. Storch, M. Vosteen, *Eur. J. Inorg. Chem.* **1998**, 1343−1349.
[16] A. Sapse, P. von Ragué-Schleyer, *Lithium Chemistry − A Theoretical and Experimental Overview*, Wiley Interscience Publ., New York, London, Sydney, **1995**.
[17] R. E. Mulvey, *Chem. Soc. Rev.* **1991**, *20*, 167−209.
[18] A. Troll, Ph.D. Thesis, University of Munich, **1999**.
[19] W. D. English, A. L. McCloskey, H. Steinberg, *J. Am. Chem. Soc.* **1960**, *82*, 2122−2124.
[20] R. J. Brotherton, T. Buckman, *Inorg. Chem.* **1963**, *2*, 424−425.
[21] *Handbook of Chemistry and Physics*, 66th ed., CRC Press, Inc., Boca Raton, FL, USA, **1986**, D-159.
[22] A. Streitwiese, Jr., C. H. Heathcock, *Organische Chemie*, Verlag Chemie, Weinheim, Deerfield Beach, Basel, **1980**, p. 1392.
[23] This compound has also been investigated by R. Contreras, M. J. Grevy, private communication, **1999**.
[24] H. Nöth, B. Wrackmeyer, *Chem. Ber.* **1974**, *107*, 3070−3103.
[25] G. J. Martin, M. L. Martin, J.-P. Gousenard, *^{15}N NMR Spectroscopy*, in: *Basic Principles and Progress* (Eds.: P. Diehl, E. Fluck, R. Kosfeld), Springer Verlag, Berlin, Heidelberg, New York, **1981**.
[26] H. Nöth, *Z. Naturforsch., Teil B* **1983**, *38*, 692−695.
[27] H. Nöth, R. Ullmann, H. Vahrenkamp, *Chem. Ber.* **1973**, *106*, 1165−1171.
[28] H. Nöth, B. Wrackmeyer, *Nuclear Magnetic Resonance of Boron Compounds*, in: *NMR Basic Principles and Progress* (Eds.: P. Diehl, E. Fluck, R. Kosfeld), Springer Publ., Berlin, Heidelberg, New York, **1978**.
[29] None of the crystals showed reflections at 2θ > 20°, and all reflections were weak and blurred even when fairly large crystals were investigated.
[30] Only a very few ^{11}B NMR spectroscopic data for triaminoborates or tetraaminoborates are known, e.g. $Me_3SiNHB[NH(CN_2C_3H_6)]_3^-$ ($\delta^{11}B$ = −4.8) (R. Contreras, private communication), $[BuB(NPhMe)_3]^-$ ($\delta^{11}B$ = −4.2) (M. Warchhold, private communication, **2001**). See also ref.[27]
[31] The origin of LiCl in the compound could be traced back to impure trianilinoborane obtained in the transamination of $(Me_2N)_2BCl$ containing tris(dimethylamino)borane. From solutions of triply metallated pure $B(NHPh)_3$ crystallization was unsuccessful.
[32] B. Wrackmeyer, *Ann. Rep. NMR Spectrosc.* **1985**, *16*, 73−186.
[33] S. H. Bauer, J. Y. Beach, *J. Am. Chem. Soc.* **1941**, 63,1394−1399.
[34] P. T. Brain, A. J. Downs, P. Maccallum, D. W. H. Rankin, H. E. Robertson, G. A. Forsyth, *J. Chem. Soc., Dalton Trans.* **1991**, 1195−1199.
[35] K. J. Weese, R. A. Bartlett, B. D. Murray, M. M. Olmstead, P. P. Power, *Inorg. Chem.* **1987**, *26*, 2409−2413.
[36] G. Beck, P. B. Hitchcock, M. F. Lappert, I. A. MacKinneon, *J. Chem. Soc., Chem. Commun.* **1989**, 1312−1314.
[37] M. Westerhausen, W. Schwarz, *Z. Anorg. Allg. Chem.* **1993**, *619*, 1053−1063.
[38] W. Lippert, Ph.D. Thesis, University of Munich, **1999**.
[39] T. Seifert, W. Storch, M. Vosteen, *Eur. J. Inorg. Chem.* **1998**, 1343−1349.
[40] A. Appel, C. Kober, C. Neumann, H. Nöth, M. Schmidt, W. Storch, *Chem. Ber.* **1996**, *129*, 175−190, and ref. cited therein.
[41] U. Höbel, H. Nöth, H. Prigge, *Chem. Ber.* **1986**, *119*, 325−337.
[42] V. A. Sazanova, L. P. Sorokina, *Dokl. Akad. Nauk SSSR* **1955**, *105*, 993−996.

[43] V. A. Sazanova, V. I. Karpov, *J. Gen. Chem. USSR* **1963**, *33*, 3241−3243.
[44] K. Niedenzu, P. M. Niedenzu, K. R. Warner, *Inorg. Chem.* **1985**, *24*, 1604−1606.
[45] K. Niedenzu, S. Trofimenko, *Top. Curr. Chem.* **1986**, *131*, 1−37.
[46] M. Warchhold, Ph.D. Thesis, University of Munich, **2001**.
[47] B. Eichhorn, H. Nöth, T. Seifert, *Eur. J. Inorg. Chem.* **1999**, 2355−2368.
[48] T. T. Wang, K. Niedenzu, J. W. Dawson, *Inorg. Chem.* **1970**, *9*, 2150−2152.
[49] D. J. English, A. L. McCloskey, H. Steinberg, *J. Am. Chem. Soc.* **1961**, *83*, 2122−2124.
[50] H. Beyer, K. Niedenzu, J. W. Dawson, *J. Organomet. Chem.* **1962**, *27*, 4701−4702.
[51] *SMART, SADABS, SAINT*, Siemens Analytical Instruments Madison, Vers. 5.1.
[52] G. W. Sheldrick, *SHELXL97*, University of Göttingen.

Received August 1, 2001
[I01283]

Interaction of Uranyl Ions with Daunorubicin and Adriamycin

Athanasios Papakyriakou,[a] Angeliki Anagnostopoulou,[a] Arlette Garnier-Suillerot,[b] and Nikos Katsaros*[a]

Keywords: Antibiotics / Antitumor agents / Anthracyclines / O ligands / Uranium

The interaction of the uranyl(VI) ion (UO_2^{2+}) with two anthracyclines, adriamycin (Adr) and daunorubicin (Dnr), has been studied by absorption, circular dichroism, fluorescence and NMR spectroscopy. We have shown that both drugs can form two complexes with UO_2^{2+}, a process strongly dependent on the dielectric constant of the solvent, the metal-to-ligand ratio (R), and the pH. The first complex (**I**) involves coordination of the metal ion to the [C(11)–O$^-$, C(12)=O] chelating site, while the second complex (**II**) involves coordination to the [C(6)–O$^-$, C(5)=O] site. In aqueous solutions at pH 6.5, the formation of complex **I** takes place with two drug molecules per UO_2^{2+} ion. At higher pH or R values, complex **II** forms, and probably has a polymeric structure with one uranyl ion bridging two drug chromophores through both the keto-phenolate sites. In methanolic solutions the simultaneous formation of both complexes **I** and **II** is demonstrated by both CD and NMR spectroscopy. Dissociation of the complexes occurs upon interaction of the drug complexes with native DNA, with the free anthracyclines intercalating between the base pairs of the nucleotide.

Introduction

Adriamycin (Adr, or doxorubicin) and daunorubicin (Dnr, or daunomycin) are two representative members of the anthracycline antibiotic family. These antibiotics contain an anthraquinone chromophore and an amino glycoside sugar (Scheme 1).[1] Despite their severe cardiotoxicity and other side effects, they are both used clinically as chemotherapeutic agents, especially Adr, which exhibits a rather broad spectrum of activity.[2,3] Their antineoplastic activity has been attributed mainly to their strong interaction with DNA, either via an intercalation process of their chromophore into the base pairs of the minor groove, or via free-radical damage of the ribose through the redox cycle of the anthraquinone moiety.[4]

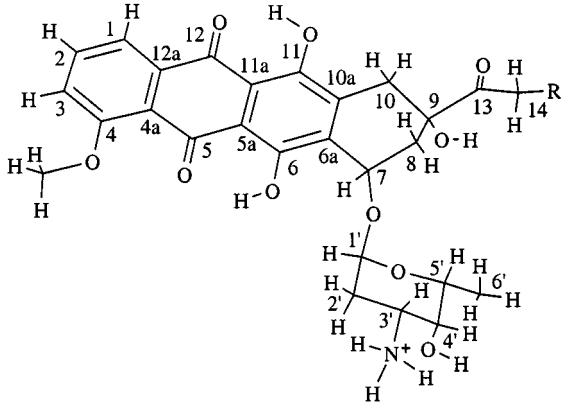

Scheme 1. Structures of daunorubicin (R = H) and adriamycin (R = OH) based on the crystal structure of Dnr[1]

Complexation of anthracyclines by metal ions has been suggested to provide less cardiotoxic compounds,[5,6] while their toxicity has also been related to the formation of reactive oxygen species generated by redox cycling of anthracycline metal complexes.[7,8] The uranyl ion has been used as a staining agent in electron microscopy,[9,10] mainly due to its high affinity for the phosphates of the DNA backbone.[11,12] In an effort to gain more information on the biological mechanisms of the action of anthracyclines we examined the interaction of UO_2^{2+} ion with both Adr and Dnr.

Results

The behavior of both daunorubicin (Dnr) and adriamycin (Adr) in the presence of uranyl (UO_2^{2+}) ions is almost identical. Therefore, we depict only the most characteristic results for either Dnr or Adr, indicating the potential differences for each case. We have also used the same symbols when referring to the corresponding complexes formed with the two drugs.

Formation of the Complexes in Aqueous Solution

Addition of uranyl nitrate to buffered solutions of the drugs at pH 6.5 resulted in a change of color from orange

[a] NCSR "Demokritos", Institute of Physical Chemistry, 15310 Agia Paraskevi Attikis, Athens, Greece
Fax: (internat.) + 30-1/651-1766
E-mail: katsaros@mail.demokritos.gr
[b] Chimie Bioinorganique LPBC CNRS ESA 7033, Univeristè Paris Nord, 74 rue Marcel Cachin, 93017 Bobigny Cedex, France
E-mail: garnier@lpbc.jussieu.fr

 © WILEY-VCH Verlag GmbH, 69451 Weinheim, Germany, 2002 1434–1948/02/0505–1146 $ 20.00+.50/0 *Eur. J. Inorg. Chem.* **2002**, 1146–1154

to purple. Further addition of the metal ion gradually changed the color of the solutions to deep violet and then to blue, while a precipitate was formed. In order to characterize the species formed at this pH, titration of the drugs with increasing quantities of the metal was monitored by both absorption and CD spectroscopy. In the visible region of the absorption spectra, two new bands appeared at around 560 and 605 nm, while the main band of the free drug at 480 nm decreased in intensity. Two clear isosbestic points were observed at 408 and 529 nm (Figure 1) for solutions with a metal-to-ligand molar ratio (R) of up to 0.5. Upon further addition of metal, the two new bands were further shifted to 575 and 625 nm, and the isosbestic points were replaced by two other points at 426 and 572 nm, which were present up to R = 1.5 (Figure 2).

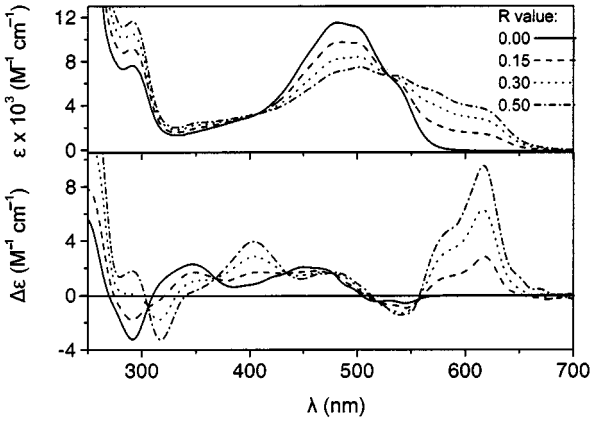

Figure 1. UV/Vis absorption (upper) and CD (lower) spectra of Adr and UO_2^{2+} in aqueous solutions at R < 0.5; [Adr] = 0.1 mM, Hepes buffer 0.01 M, pH = 6.5, NaCl = 0.01 M; the spectra were recorded 10 min after the addition of the metal ion at room temperature

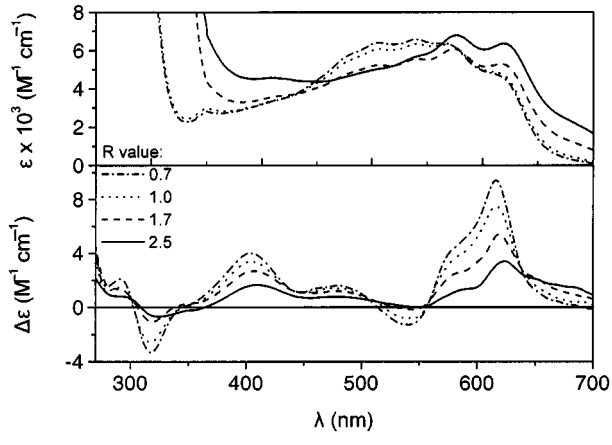

Figure 2. UV/Vis absorption (upper) and CD (lower) spectra of Adr and UO_2^{2+} in aqueous solutions at R > 0.5; [Adr] = 0.1 mM, Hepes buffer 0.01 M, pH = 6.5, NaCl = 0.01 M; the spectra were recorded 10 min after the addition of the metal ion at room temperature

The CD spectra of both drugs exhibited very characteristic changes upon addition of UO_2^{2+} at pH 6.5. The negative band at 290 nm decreased in intensity and moved to 317 nm. The positive band at 330 nm exhibited a red shift to 405 nm, and increased in intensity, while the 350 nm band also decreased in intensity and appeared as a shoulder at the same wavelength. In the visible region the band centered at 480 nm shifted by about 10 nm to higher wavelength, while the negative band at 540 nm increased in intensity (in the case of Adr, Δε increased in intensity almost threefold). Additionally, a band around 625 nm appeared with quite a high hyperchromic effect (Δε = 9.1 for Dnr at 626 nm and 9.5 for Adr at 618 nm) and a shoulder at about 585 nm. These changes occur with isodichroic points at 305, 368, 434, and 477 nm up to R = 0.5 (Figure 1). Further addition of UO_2^{2+} resulted in the hypochromicity of all the above bands, with isodichroic points at 343, 559, and 637 nm up to R = 1.5. At R > 2 a new band became visible at around 685 nm, while the bands at 350 and 317 nm gradually shifted by about 10 nm to higher wavelengths. At R = 3.0 the negative band at 535 nm had almost become positive (Figure 2).

In the solutions with R higher than two, a precipitate began to form after a couple of hours. This blue-violet precipitate was insoluble in either polar or nonpolar solvents. It readily dissolved in dilute HCl, accompanied by a color change to orange (probably due to dissociation to the free drug). Similar observations with such precipitates have been made previously with the Cu^{2+} [13] and Yb^{3+} [14] anthracycline complexes. In these cases, the authors suggested the formation of polymeric chain structure complexes, with the metal ion bound at both the keto-phenolate sites (C5/C6 and C11/C12) of two (or more) drug molecules.

The plots of ε and Δε versus R (molar ratio method, Figure 3) indicate the formation a 1:2 (metal:drug) complex at R ≈ 0.5 (**I**). This conclusion is supported mainly by the plot of ε at 575 nm, which is parallel to the *x*-axis up to R = 1.5. The plot at 625 nm exhibits a break point at R = 0.5 and continues to increase up to R = 1.5. The dependence of the CD bands upon the R value is also shown clearly in Figure 3b: the characteristics of the 1:2 complex fade out upon increasing R to above 0.5 (see Discussion). The 1:2 stoichiometry for complex **I** is also supported by the continuous variation method[15] (Job's method) applied to solutions with a total concentration of 50 μM. As shown in Figure 4a there is a clear maximum at a molar fraction of Dnr equal to 0.65 that corresponds to this stoichiometry.

The CD band at 625 nm has been used to monitor the pH dependence of the 1:2 species formed. As shown in Figure 4b, the complexation begins at pH > 4.5 and is completed at pH 6.5, a point above which the intensity of the band decreases. Furthermore, in solutions at pH higher than 7.5, a colored precipitate was formed. From this plot we can estimate that the pK_a for the complex formation is about 5.6, a value that is the same for both drugs.

The kinetics of the formation of the 1:2 species (complex **I**) is quite fast, whereas the intensity of the absorption band takes around 10 minutes to reach the maximum value. Both complexes are relatively stable, especially that of Dnr, which only dissociated by about 5% after four days at room temperature in the dark. Under the same conditions, the complex with Adr dissociated significantly more (about 35% as

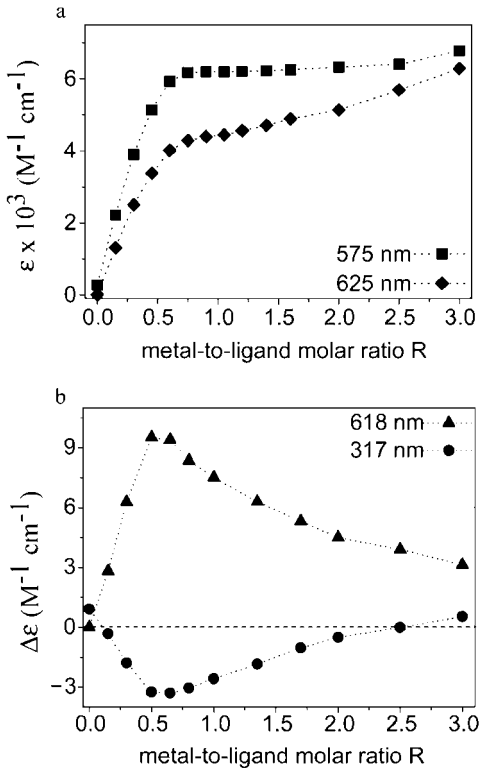

Figure 3. (a) Plots of ε at 625 and 575 nm and (b) Δε at 618 and 317 nm versus R (molar ratio method), of Adr titrated with UO_2^{2+}; experimental conditions as in Figure 1 and 2

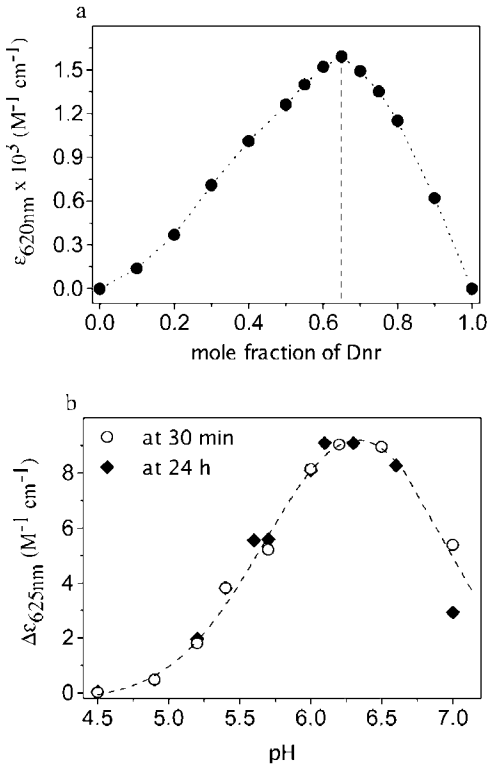

Figure 4. (a) Job's plot for Dnr 50 μM in Hepes buffer 0.01 M, NaCl 0.01 M, pH = 6.5 and (b) the pH dependence of the 1:2 UO_2^{2+}:Dnr complex monitored by the Δε at 625 nm; the pH of the solutions was measured just prior to the spectra acquisition, 30 min and 24 h after the addition of aliquots of NaOH (0.025 M) to solutions of Dnr 0.1 mM, with UO_2^{2+} 0.05 mM and NaCl 0.01 M; the dashed line is an empirical fit of the former data set

measured by the decrease in the intensities of the visible absorption bands).

The complexation with uranyl ions quenched the fluorescence of Dnr and Adr (Figure 5), as has been reported for most of the metal ions studied[16] (except the complex of Al^{3+} and Adr[17]).

From the decrease in the fluorescence intensity at λ_{max} = 555 nm (excitation at 480 nm) we have estimated the association constants K_s for the formation of the 1:1 species. Using Equation (1),[18] where F_o is the fluorescence intensity before the addition of the quencher, and F is the fluorescence intensity at concentration [Q] of uranyl ions, we obtained the linear plots shown in Figure 5. Their slope corresponds to the K_s values, calculated to be 25 mM^{-1} for Dnr and 14 mM^{-1} for Adr. At this anthracycline concentration (5μM) and up to an added [UO_2^{2+}] with R = 10, the linearity of these plots (> 0.997) indicates the formation of a species with a stoichiometry equal to 1:1.

$$F_o/F = 1 + K_s[Q] \quad (1)$$

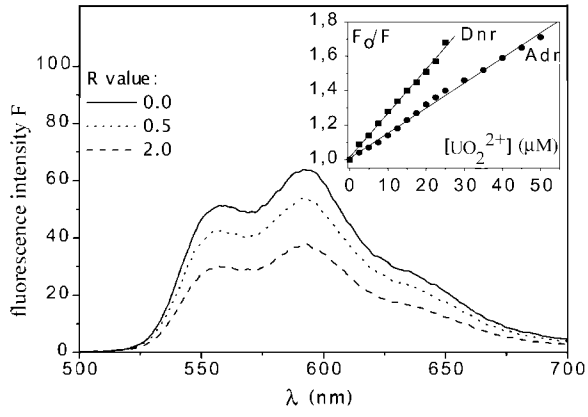

Figure 5. Uncorrected fluorescence spectra of Dnr and UO_2^{2+} at different R values recorded after 24 h (excitation wavelength at 480 nm); [Dnr] = 5 μM in Hepes buffer 0.01 M, pH = 6.5, NaCl 0.01 M; insert: plots of Fo/F at 555 nm versus the uranyl concentration added to solutions of the drugs made as above; the measurements were taken 1 min after the addition of the metal from a solution of [UO_2^{2+}] = 0.5 mM

Formation of the Complexes in 50% Methanolic Solutions

The complexation of UO_2^{2+} with Dnr and Adr was also studied in 50% (v/v) methanol/water solutions in order to examine the dependence of this process upon the aggregation state of the drugs. As has already been reported,[19] under such experimental conditions these compounds exist fully in the monomeric form, a fact that is reflected by the disappearance of the doublet centered at 480 nm in the CD spectra of the free anthracyclines, exhibiting only a positive band. The absorption spectral changes in the visible region of both drugs upon addition of uranyl (Figure 6) are very similar to those in pure water, with the main band at 480 nm decreasing in intensity and giving rise to the appearance of two new bands at 565 and 610 nm. These two

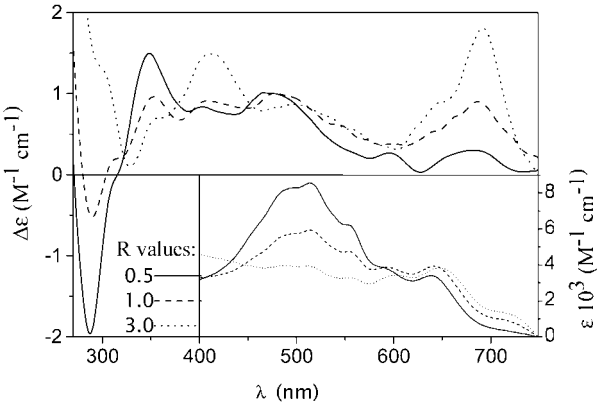

Figure 6. CD (upper) and visible absorption (lower) spectra of Adr and UO_2^{2+} in 50% MeOH solutions at different R values; [Adr] = 0.1 mM, Hepes buffer 0.01 M, pH = 6.5, NaCl 0.01 M

bands gradually shift by about 10 nm to lower energy when more metal is added (R > 2).

In contrast, the CD spectra exhibit much more informative changes following the addition of the metal ion. The negative peak at 290 nm readily decreased in intensity, and above R = 2 shifted to 330 nm. The positive band around 320 nm moved to 410 nm from an early stage of the titration (R ≈ 0.5) increasing in intensity, whereas the band at 350 nm gradually decreased in intensity and energy, shifting to 360 nm for R > 2. An intense red shift of the main band at 480 nm was also observed, yielding a broad band ranging from 600 to 700 nm. At low R values this band consists of a sharper band at 600 nm and a broader band centered at 660 nm, while at R > 2 the low energy band is formed at 675 nm and the high at 625 nm. At these high R values, a precipitate also formed with the same characteristics as those of the respective precipitates in pure aqueous media. There is no evidence for stacking of the drug molecules throughout the titration, at least as far as the spectra are concerned, which do not exhibit any negative band in the 530 nm region.

These changes indicate the formation of the same species as those in aqueous solutions, but with no clear step-points. Complex **I** (through the C11/C12 site) formation probably occurs along with complex **II** (through both the C11/C12 and C5/C6 sites), a possibility that is attested to by the appearance of a broad band at 600 to 700 nm from an early stage of the titration with the metal ion. Thus, the stoichiometry of both species could not be determined, since neither the molar ratio method nor the Jobs plot exhibited any clear break point. The intensity and the position of these CD bands can only support the conclusion that at low R values, complex **I** seems to be present in a higher concentration, while at higher R values (> 1) complex **II** begins to prevail, forming oligomers and polymers like those in pure water.

NMR Experiments in Methanol

Addition of UO_2^{2+} to aqueous solutions of Dnr and Adr in D_2O at pD > 5 resulted in an extensive line broadening of the acquired NMR spectra, therefore making the assignment of the peaks impossible. In order to examine the complexation process we performed NMR experiments in [D_4]methanol. Up to R = 10 one major complex was being formed (complex **I**), while increasing the R value above 20 resulted in the formation of another complex (complex **II**), which appears at lower fields. These two species are both present in the solution along with the free anthracycline, even at a hundredfold excess of UO_2^{2+} (Figure 7). The signals from the free anthracycline are still well resolved, suggesting that the drug is in slow exchange with its metal-bound form on the NMR time scale. The assignment has been successfully accomplished from the 800 MHz ^{1}H NMR spectra of the drugs at 10 mM concentration with UO_2^{2+} in excess (1 M). We have also performed 2D ^{1}H-^{13}C HMQC and HMBC experiments in order to assign the carbons of the anthracyclines and their complexes with UO_2^{2+}.

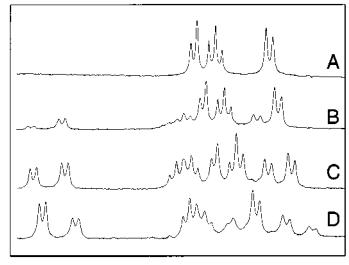

Figure 7. Expanded aromatic region of the 250 MHz ^{1}H NMR spectra of Dnr 10 mM titrated with UO_2^{2+} at R = 0 (A), 20 (B), 50 (C), and 100 (D)

Table 1 contains the ^{1}H NMR chemical shifts of free Dnr along with the chemical shifts of the two complexes formed and the uncomplexed Dnr present in the solution. From the peak intensities at R = 100 we can calculate the presence of the three species in the molar ratios of 2:3:5 (Dnr/complex **I**/complex **II**). The uncomplexed drug's protons present in these solutions exhibit a general upfield shift (0.1−0.2 ppm) upon addition of UO_2^{2+}. Complex **I** exhibits characteristic downfield shifts for H-1 (Δδ = 0.77 ppm) and for both H-10 protons (0.67 and 0.47 ppm for the equatorial and the axial proton, respectively). All other protons are also shifted downfield by 0.1−0.2 ppm. These observations indicate the complexation of Dnr to UO_2^{2+} through the [C(11)−O$^-$, C(12)=O] chelating site, given that the closest protons to C(11)−O$^-$ and C(12)=O are H-10 and H-1, respectively. Proton signals from complex **II** protons are shifted further downfield than those of complex **I** by 0.1−0.2 ppm, except H-1′, H-7, and 4-OCH$_3$, which exhibit rather large downfield shifts (0.84, 0.94, and 0.37 ppm, respectively, compared to free Dnr). These changes indicate the presence of a second UO_2^{2+} ion bound at the [C(6)−O$^-$, C(5)=O] donor site, since H-7, which shows the greatest downfield shift in complex **II** is the proton closest to C(6)−OH, while the 4-OCH$_3$ protons are less influenced by C(5)=O. As far as H-1′ is concerned, its rather large downfield shift in complex **II** reflects the change in the chemical environment around the sugar moiety upon

Table 1. ^{1}H chemical shift values (ppm) of Dnr and UO_2^{2+} in [D_4]methanol measured at 800 MHz and 25 °C; [Dnr] = 10 mM, [UO_2^{2+}] = 1 M; values in parenthesis are the calculated differences between the chemical shift values of the complexes and the respective uncomplexed drug present in the solutions; due to their signal overlapping, H-8 and H-2′ chemical shift values are given with lower accuracy

Protons	Free Dnr	Uncomplexed	Complex I	Complex II
H1	7.92	7.74	8.51 **(+0.77)**	8.67 **(+0.93)**
H2	7.83	7.65	7.88 (+0.24)	7.96 (+0.31)
H3	7.56	7.35	7.48 (+0.13)	7.63 (+0.28)
H1'	5.45	5.37	5.45 (+0.08)	6.21 **(+0.84)**
H7	5.06	4.96	5.10 (+0.14)	5.90 **(+0.94)**
H5′	4.31	4.21	4.26 (+0.05)	4.41 (+0.20)
4OCH$_3$	4.03	3.88	3.95 (+0.07)	4.25 **(+0.37)**
H4′	3.67	3.69	3.71 (+0.02)	3.74 (+0.05)
H3′	3.59	3.60	3.64 (+0.04)	3.68 (+0.08)
H10$_{eq}$	3.01	2.93	3.60 **(+0.67)**	3.66 **(+0.73)**
H10$_{ax}$	2.93	2.80	3.27 **(+0.47)**	3.47 **(+0.67)**
H14	2.36	2.26	2.38 (+0.12)	2.46 (+0.20)
H8$_{eq}$	2.32	~2.1	~2.3 (+0.2)	~2.5 (+0.4)
H8$_{ax}$	2.16			
H2′$_{ax}$	2.04	~1.8	~1.9 (+0.1)	~2.0 (+0.2)
H2′$_{eq}$	1.88			
5′CH$_3$	1.29	1.21	1.23 (+0.02)	1.33 (+0.12)

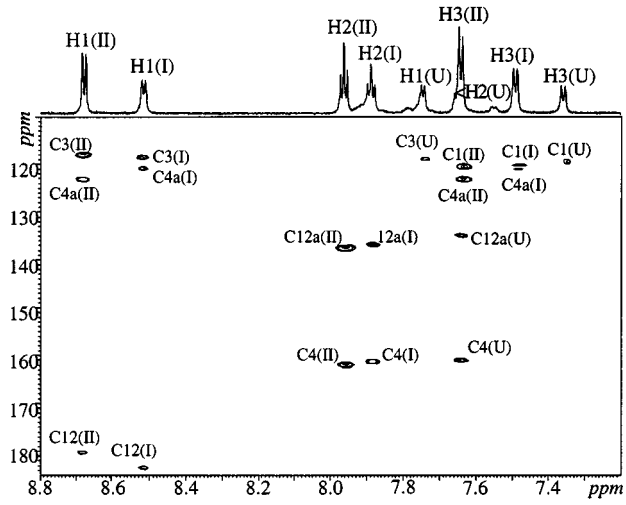

Figure 8. 800 MHz 2D HMBC ^{13}C-^{1}H NMR spectra of Dnr in the presence of a hundredfold excess of UO_2^{2+}; [Dnr] = 10 mM and [UO_2^{2+}] = 1 M; (U): uncomplexed, (I): complex **I**, (II): complex **II**

Table 2. ^{13}C chemical shift values (ppm) of Dnr and UO_2^{2+} in [D_4]methanol measured at 800 MHz and 25 °C; [Dnr] = 10 mM, [UO_2^{2+}] = 1 M; (–): signal not detected

Carbon	Free Dnr	Uncomplexed	Complex I	Complex II
C13	212.4	–	–	–
C5	187.3	187.0	184.7	181.7
C12	186.9	186.6	183.6	180.3
C4	161.5	161.3	161.5	162.2
C6	156.5	156.3	141.2	141.0
C11	155.2	155.0	143.9	143.8
C9	152.5	–	–	–
C2	136.3	–	–	–
C12a	135.4	135.2	137.1	137.9
C4a	134.9	134.6	121.2	123.5
C6a	134.8	134.5	–	–
C1	119.5	119.6	120.9	120.6
C3	119.3	119.3	118.9	118.5
C5a	111.4	–	–	–
C11a	111.2	–	–	–
C1′	100.1	–	–	–
C10a	76.2	–	–	–
C7	70.8	70.4	71.0	71.3
C5′	66.9	66.9	–	–
C4′	66.8	66.7	–	–
4OCH$_3$	56.1	56.0	56.3	56.6
C3′	48.0	47.7	–	–
C8	36.0	35.5	35.7	36.2
C10	32.1	32.1	33.6	34.0
C2′	28.5	28.1	28.2	28.3
C14	23.4	23.7	23.8	23.9
5′CH$_3$	15.9	15.6	15.9	16.1

binding the second UO_2^{2+} ion. We have no indications for participation of the amino group in the complexation process, since no other proton of daunosamine exhibits any significant chemical shift upon addition of the metal ion.

From the 2D ^{13}C-^{1}H NMR experiments (Figure 8) we have managed to assign all the carbons of the free anthracyclines and most of the carbons of the complexes formed (Table 2). Both complexes exhibit remarkable changes in the ^{13}C chemical shifts of the keto-phenolate sites (3−15 ppm upfield shifts), especially those of C(6) and C(11) due to delocalization of the negative charge of the phenolic oxygen atoms upon complexation. This effect was expected to be more striking for C(5a) and C(11a), but this was not the case. None of the other ^{13}C chemical shifts exhibit significant changes (< 2 ppm). Unlike the ^{1}H chemical shifts, the carbons of both keto-phenolate sites in complexes **I** and **II** are similarly influenced by the presence of the metal ion, probably due to ring-current effects.

In the UV/Vis and CD spectra of this system (R = 100) two new bands appear in the absorption spectra at 575 and 620 nm, while the CD spectra is characterized by a red shift of the main band from 480 nm to 610 and 650 nm. It is quite evident from the bands exhibited that the species formed in methanol must be the same as in semi-aqueous MeOH solutions, despite the fact that in the first case the formation constants of the complexes are quite low and a higher excess of UO_2^{2+} is required for the respective changes to take place.

Interaction of the Complexes with DNA

Two different sets of experiments were carried out with native DNA in aqueous solutions. In the first set, a uranyl ion solution was added to a mixture of anthracyclines-DNA in solution at different r values (r = drug-to-nucleotide molar ratio). At r < 0.1, where total binding of the drugs

has been reported,[20] the addition of uranyl to solutions containing the DNA-bound drugs did not cause any changes in the CD spectra, even when a tenfold excess of UO_2^{2+} was added. On the other hand, addition of uranyl to the DNA-bound Dnr and Adr at $r > 0.3$ resulted in almost the same CD spectral features as in the case of complex **I**, probably because of the complexation of uranyl with the free anthracycline molecules. This observation is in agreement with the data reported for the Cu^{II}-Dnr system at $r > 0.1$.[21]

In the second set of experiments a mixture of drug-UO_2^{2+} solution was added to DNA solutions at several r values. In this case the 1:2 complex **I** was formed with both Dnr and Adr. In the presence of DNA, the complexes dissociated in a time-dependent procedure as free Dnr and Adr intercalated between the nucleotide base pairs. This is evident from the CD spectra of a typical experiment at $r = 0.1$ (Figure 9) where the band at 625 nm, associated with the complex decreases in intensity with time, while the negative band at 320 nm red shifts by approximately 10 nm. The characteristic spectra of the intercalated anthracyclines were obtained after 24 h, with bands at around 310, 380, and 500 nm.[22] The half-life of this process was estimated from the plot of $\Delta\varepsilon$ at 626 nm versus time to be 15 min, while for the Fe^{III}-Dnr system it was reported to be 18 h.[23] In the case of Adr, when concentrations above 0.1 mM were used, precipitation occurred, with the precipitate probably containing DNA and the metal-Adr complex, as it indicated by the color of the precipitate, which is the same as the deep-violet solution's color when R is greater than 2 or the pH is greater than 7. This observation is in accordance with the results already reported for Adr complexes with other metal ions.[24]

We have also measured the melting temperature (*T*m) of calf thymus DNA in the presence of both anthracyclines and their 1:2 UO_2^{2+} complexes. The values measured were dependent on r, and were in agreement with those already reported for the Dnr-DNA system,[20] taking into account the variations of the ionic strength. The Tm values in the presence of the complexes were only about 1 °C lower than the respective values for the free drug. Additionally, when the absorbance at 620 nm was monitored while increasing the temperature from 25 to 95 °C for solutions of the complexes in the absence of the DNA, we observed that at 55 °C the complexes had dissociated by about 50%. It is known that UO_2^{2+} solutions are only stable at low pH and that polynuclear complexes and uranyl hydroxide precipitates are formed at higher pH.[25] Thus, under our experimental conditions the released metal ions were bound to hydrolyse. It is not impossible, however, that some may bind to the phosphates, since it has been shown that their affinity for nucleotides is high and it has been proposed that UO_2^{2+} may bind by bridging phosphate groups on opposite strands of the minor groove of DNA.[12]

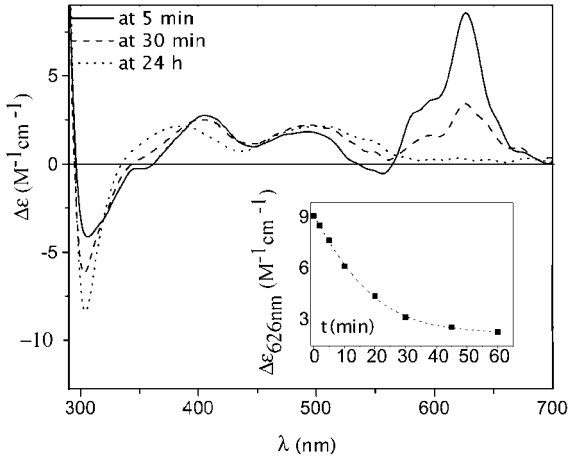

Figure 9. CD spectra of (UO_2^{2+}-Dnr_2)-DNA system as a function of time; [UO_2^{2+}-Dnr] = 50 μM, [DNA] = 0.5 mM, Hepes buffer 0.01 M, pH = 6.5, NaCl 0.01 M; insert: plot of $\Delta\varepsilon$ at 626 nm versus time elapsed after the addition of the nucleotide to the complex solution

Discussion

Our experience during the course of these studies with metal ion complexes of anthracyclines has shown the complexity of these systems.[26] Many conflicting reports have been published over the past 30 years, concerning either the stoichiometry of the complexes formed in solutions or their physicochemical characteristics. The formation of more than one species is evident for most of the metal ions examined, the predominance of which depends on the metal-to-ligand molar ratio, the pH, and the dielectric constant of the solvent. However, spectroscopic analysis, especially the CD spectra, can provide many detailed characteristics of the complexes formed,[27] while NMR spectroscopy has also proved to be a powerful tool for the study of these systems.[14,28]

In pure water and under our experimental conditions most anthracyclines exist in the fully protonated and dimeric state.[19,29] The formation of a major species with a stoichiometry of 1:2 (metal-to-drug) up to R = 0.5 is confirmed by both the clear isosbestic points in the absorption and CD spectra (Figure 1), as well as by the molar ratio and Job's method (Figure 3 and 4). The bathochromic shifts of the visible absorption and CD spectra bands show that complexation takes place to the drug's chromophore after deprotonation of either the C(11) or C(6) phenolic groups, in order of acidity.[19] The position of the absorption bands at 560−600 nm can account for the deprotonation of the first phenolic group[27] and coordination to UO_2^{2+} through the oxygens of the [C(11)−O^-, C(12)=O] donor site, forming a six-member chelate ring. In contrast, the red shift of the UV band from 290 to 320 nm in the CD spectra is characteristic of the deprotonation of the second phenolic group at C(6).[27]

A more detailed examination of these spectra reveal that this is not the case, however, since neither the red shift for the band at 350 nm nor the bathochromic shift of the main visible band from 450 to about 620 nm can account for this

deprotonation. Additionally, the intensity of the band at 317 nm is exactly the same as the original band at 290 nm, while C(6)−OH deprotonation is followed by a decrease in the intensity of this band.[27] Such a decrease in the energy of the $\pi\rightarrow\pi^*$ transitions along the sort axis of the chromophore has previously been observed in the case of Sn^{IV} with Adr.[30] The authors saw no evidence for participation of the phenolic groups, despite the fact that a shift of the band at 290 nm to higher wavelengths accompanied the complexation of Adr to Sn^{IV}. For this reason, it has been suggested that this occurs due to the aggregation of the drug molecules as in the case of Adr gels, for which the proposed structure is a supramolecular aggregate with Adr molecules stacked helically.[31,32] Additionally, when anthracyclines intercalate between the base pairs of DNA this band shifts to 305 nm. This observation can be attributed to a modification of the angle between the sugar moiety and the dihydroanthraquinone part, along with the influence of the hydrogen bonds between the C=O groups and their neighbors. This was confirmed by the crystal structure of Dnr complexed to d(CGTACG), in which the torsion angle around the O(7)−C(1′) bond was found to be 20° different from that of the free drug.[34] In our case the formation of the 1:2 species upon binding of UO_2^{2+} to Dnr and Adr at the [C(11)−O^-, C(12)=O] site probably promotes such a modification.

Upon increasing the metal-to-ligand ratio, the characteristic bands mentioned above decrease in intensity (Figure 2) and at $R > 2$ the appearance of a rather low-energy band at around 685 nm (shoulder), along with the continuous red shift of the band at 350 nm towards 360 nm, indicate further deprotonation of Dnr and Adr at C(6)−OH. As soon as UO_2^{2+} ions bind additionally at the [C(6)−O^-, C(5)=O] site, a precipitate was gradually formed from the blue solutions of the drugs. After 24 h Dnr and Adr have probably formed a polymeric complex, with UO_2^{2+} ions chelating two drug molecules through both the keto-phenolate sites of their chromophore. This has already been reported in the case of Cu^{2+} ions binding to Dnr and Adr,[13] and later in the case of Yb^{3+} binding to Adr,[14] both at high pH. Such a precipitation can occur with UO_2^{2+} at lower R values (< 2) when increasing the pH above 7, indicating that this process is strongly dependent on both the metal-to-ligand ratio and the proton concentration.

Decreasing the dielectric constant of water by adding 50% MeOH, at $R = 0.5$ at the same pH and ionic strength, resulted in significantly different CD features. First, no stacking interactions occur, as indicated by the absence of the negative band at 530 nm, while the UV band at 290 nm did not shift to higher wavelengths, but rather decreased in intensity. Although the absorption spectra exhibit the same characteristic bands at 565 and 610 nm as in the case of pure water, the CD spectra reveal the appearance of a band centered at 660 nm, which at $R = 3.0$ increased in intensity with a maximum at 675 nm (Figure 5). At this point, the band at 290 nm has red shifted to about 330 nm and the bands at 320 nm and 350 nm have shifted bathochromically to 410 nm and 360 nm, respectively. Therefore, the deprotonation of both the phenolic groups at C(11) and C(6) is demonstrated, a process that probably does not occur step-by-step, as is indicated by the appearance of a low energy band at around 660 nm even at low R values.

The parallel formation of more than one species is also supported by the NMR experiments in pure methanol. Up to $R = 10$ the formation of complex **I** took place with UO_2^{2+} binding to Dnr and Adr through the [C(11)−O^-, C(12)=O] chelating site, while at higher R ratios, complex **II** was also formed with participation of the [C(6)−O^-, C(5)=O] coordination site. The presence of both species is evident even under a very large excess of the metal ion, although complex **II** predominates at $R > 50$ (Figure 6). The participation of the amino group, as in the case of the Adr complexes of Pd^{II}, Pt^{II},[15,28] and Sn^{IV},[30] is excluded by the ^1H NMR chemical shifts of the daunosamine protons, which do not exhibit any significant change upon complexation to UO_2^{2+}, except the equatorial proton H-1′ in complex **II** (Table 1). This should also be true for the semi-aqueous MeOH solutions at $pH = 6.5$, where a gradual change of the CD spectra from the fully protonated to the fully deprotonated Dnr and Adr takes place as more UO_2^{2+} is added. No clear step-points were observed for this process, and as soon as both complexes (**I** and **II**) are present simultaneously in the solutions, the determination of their stoichiometry is very inaccurate.

Upon interaction of UO_2^{2+} with Dnr and Adr 1:2 complexes with calf thymus DNA ($r < 0.1$) at $pH = 6.5$, the complexes appeared to dissociate, with the free anthracyclines intercalating between the base pairs. This process is confirmed by the time-dependent change of their CD spectra (Figure 8) to the characteristic pattern of the intercalated drug. Additionally, no remarkable changes have been observed at the Tm values of the calf thymus DNA bound to the anthracyclines in the presence and absence of uranyl ions. This is probably due to the higher affinity of the drugs for DNA and that of uranyl ion for the phosphate groups of the DNA backbone.[12]

Conclusions

Uranyl ions form two complexes with Dnr and Adr, depending on the metal-to-ligand ratio, the pH, and the solvent. Complex **I** involves binding of UO_2^{2+} to the oxygen atoms of the drugs [C(11)−O^-, C(12)=O] donor site, while in complex **II** coordination also occurs through the [C(6)−O^-, C(5)=O] site. In aqueous solutions up to $R = 0.5$ and $pH = 6.5$ complex **I** is formed with the stoichiometry of 1:2 (metal-to-ligand), while at R above 0.5 or $pH > 7$ complex **II** formation takes place with drug molecules bridging two metal ions and forming oligomeric or polymeric structures (Scheme 2). In methanol these two complexes are formed at higher R values (> 10) and are both present in the solution as was shown by the NMR experiments.

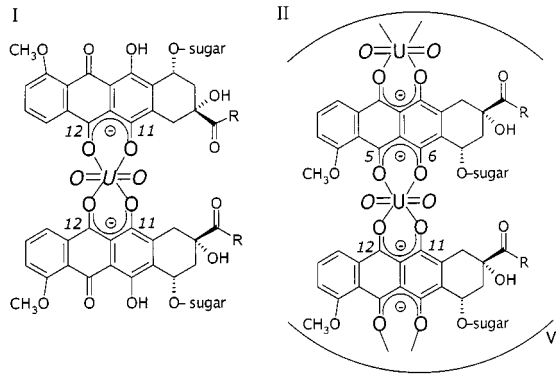

Scheme 2. The proposed structures of the complexes formed upon interaction of UO_2^{2+} ions with Dnr [R = $CH(OH)CH_3$] and Adr [R = $CH(OH)CH_2OH$]; for both drugs, *sugar* = daunosamine

Experimental Section

Daunorubicin and adriamycin hydrochloride 99% were a gift from Pharmacia & Upjohn, Greece. Uranyl nitrate hexahydrate [$UO_2(NO_3)_2{\cdot}6H_2O$] (99%) was purchased from Merck, Hepes buffer 99.5% from Aldrich, while [D_4]methanol (99.9%) and calf thymus DNA were purchased from Sigma and used without further purification. Deionized and doubly-distilled water was used throughout the experiments.

Anthracycline solutions were prepared just prior to use and their concentrations determined by their absorption at 480 nm using ε = 11500 $M^{-1}cm^{-1}$.[25] Uranyl stock solutions were prepared in slightly acidified water to avoid hydrolysis. DNA stock solutions were prepared as described previously[34] and kept at 4 °C for no longer than a week. After dilution to the buffer, the nucleotide concentrations were determined by their absorption at 260 nm using ε = 6600 $M^{-1}cm^{-1}$ (expressed as phosphate).

Absorption spectra were recorded on a JASCO V-560 spectrophotometer. Circular dichroism (CD) measurements were made on a JASCO V-715 dichrograph. All spectra were recorded using a 1.0 cm cell and the following acquisition parameters: λ = 250−750 nm, step 0.5 nm, speed 200 nm min^{-1}, response 1.0 s, bandwidth 1.0 nm, accumulations 4−10. Methanol and aqueous buffer blanks were used as references, depending on the experimental conditions, while the temperature was kept constant at 25 °C. Results are expressed as ε (molar absorption coefficient) and $\Delta\varepsilon = \varepsilon_L - \varepsilon_R$ (differential molar absorption coefficient). Both ε and $\Delta\varepsilon$ values are expressed as molar concentration of anthracyclines.

All 1D ^1H NMR spectra were recorded either on a Bruker AC 250 MHz spectrometer or on a Bruker Avance 800 MHz spectrometer at 25 °C. The NMR spectroscopic data were transferred to a SGI O2 workstation (IRIX OS) and were processed using the XWIN NMR software (version 2.6, Bruker). A typical NMR sample contained 10 mM anthracycline in [D_4]methanol. ^1H and ^{13}C chemical shifts were referenced to the solvent peak at δ = 3.31 (25 °C).

The ^1H-1D experiments were recorded with presaturation of the H_2O/HDO signal during the recycling delay. Typical parameters used were: 64 K data domain size, 0.5 s recycling delay, 10 KHz spectral width and 64 transients. The 1D FIDs were multiplied by an exponential window function (0.3 Hz line broadening added) and zero filing was performed prior to Fourier transformation.

^1H-Detected heteronuclear multiple-quantum coherence HMQC [35] and ^1H-detected heteronuclear multiple bond correlation HMBC [36] (optimized for long range couplings with a low-pass J-filter to suppress one bond correlations) experiments were acquired at 800 MHz and at 25 °C. Data sets with 2048 × 512 complex points were acquired with a 9 KHz sweep width in the proton dimension and 40 KHz in the carbon dimension. $J_{C\text{-}H}$ was set to 140 Hz and the solvent signal was selectively irradiated for 1.0 s during the relaxation delay period. A total of 32 scans were collected per t_1 increment and the spectra were processed with an exponential weighting function.

Acknowledgments

The authors gratefully acknowledge Prof. Ivano Bertini and the EU Large Scale Facility at the Magnetic Resonance Center (CERM) of the University of Florence for the 800 MHz NMR experiments performed by Massimo Lucci and Dr. Georgios Spyroulias. We would also like to thank Pharmacia & Upjohn, Greece for the generous supply of the anthracyclines and Dr. Georgios Pistolis for the fluorescence measurements.

[1] C. Courseille, B. Busetta, S. Geoffre, M. Hospital, *Acta Crystallogr., Sect. B* **1979**, *35*, 764−767.
[2] F. Arcamone, *Doxorubicin Anticancer Antibiotics*, Academic: New York, **1981.**
[3] G. Mazué, M. Iatropoulos, A. Imondi, S. Castellino, M. Brughera, A. Podestà, P. Della Torre, D. Moneta, *Int. J. Oncol.* **1995**, *7*, 713.
[4] N. R. Bachur, S. L. Gordon, M. W. Gee, *Mol. Pharmacol.* **1977**, *13*, 901−910.
[5] M. Gosalvez, M. F. Blanco, C. Vivero, F. Valles, *Eur. J. Cancer* **1978**, *14*, 1185−1190.
[6] T. J. Lampidis, A. Garnier-Suillerot, H. Tapiero, 78th Annual Meeting of the American Association of Cancer Research, **1987**.
[7] H. Doroshow, *Cancer Res.* **1983**, *43*, 460−472.
[8] L. Gianni, J. L. Zweier, A. Levy, C. E. Myers, *J. Biol. Chem.* **1985**, *260*, 6820−6826.
[9] H. Huxley, G. Zubay, *J. Mol. Biol.* **1960**, *2*, 10.
[10] P. Testillano, M. Sanchez-Pina, A. Olmedilla, M. Ollacarizqueta, C. Tandler, M. Risueno, *J. Histochem. Cytochem.* **1991**, *39*, 1427−1438.
[11] C. Zobel, M. Beer, *J. Biophys. Biochem. Cyt.* **1961**, *10*, 335−346.
[12] P. E. Nielsen, C. Hiort, S. H. Sönnichsen, O. Buchardt, O. Dahl, B. Nordèn, *J. Am. Chem. Soc.* **1992**, *114*, 4967−4975.
[13] F. T. Greenaway, J. C. Dabrowiak, *J. Inorg. Biochem.* **1982**, *16*, 91−107.
[14] X. Wei, L. J. Ming, *Inorg. Chem.* **1998**, *37*, 2255−2262.
[15] P. Job, *Ann. Chim.* **1936**, *6*, 97.
[16] M. M. L. Fiallo, A. Garnier-Suillerot, *Biochemistry* **1986**, *25*, 924−930.
[17] E. Pereira, M. M. L. Fiallo, A. Garnier-Suillerot, T. Kiss, H. Kozlowski, *J. Chem. Soc., Dalton Trans.* **1993**, 455−459.
[18] J. R. Lakowicz, *Principles of Fluorescence Spectroscopy*, Plenum Press, NY **1983**, IX.3, 264−5.
[19] R. Kiraly, R. B. Martin, *Inorg. Chim. Acta* **1982**, *67*, 13−18.
[20] J. B. Chaires, N. Dattagupta, D. M. Crothers, *Biochemistry* **1982**, *21*, 3933−3940.
[21] M. Spinelli, J. C. Dabrowiak, *Biochemistry* **1982**, *21*, 5862−5870.

[22] E. J. Gabbay, D. Grier, R. E. Fingerle, R. Reimer, R. Levy, S. W. Pearce, W. D. Wilson, *Biochemistry* **1976**, *15*, 2062−2070.
[23] H. Beraldo, A. Garnier-Suillerot, L. Tosi, F. Lavelle, *Biochemistry* **1985**, *24*, 284−289.
[24] A. Garnier-Suillerot, *Bioactive Molecules*, Elsevier: Amsterdam **1988**, Vol. 6, Ch. IV, p. 145.
[25] N. N. Greenwood, A. Earnshaw, *Chemistry of the Elements*, Pergamon Press: Oxford **1986**, p. 1478.
[26] M. M. L. Fiallo, A. Garnier-Suillerot, B. Matzanke, H. Kozlowski, *J. Inorg. Biochem.* **1999**, *75*, 105−115.
[27] M. M. L. Fiallo, H. Tayeb, A. Suarato, A. Garnier-Suillerot, *J. Pharm. Sci.* **1998**, *87*, 967−975.
[28] T. Allman, R. E. Lenkinski, *J. Inorg. Biochem.* **1987**, *30*, 35−45.
[29] I. J. McLennan, R. E. Lenkinski, Y. A. Yanuka, *Can. J. Chem.* **1985**, *63*, 1233−1238.
[30] E. Balestrieri, L. Bellugi, A. Boicelli, M. Giomini, A. M. Giuliani, M. Giustini, L. Marciani, P. J. Sadler, *J. Chem. Soc., Dalton Trans.* **1997**, 4099−4105.
[31] M. Giomini, A. M. Giuliani, M. Giustini, E. Trotta, *Biophys. Chem.* **1991**, *39*, 119−128.
[32] M. Giomini, A. M. Giuliani, M. Giustini, E. Trotta, *Biophys. Chem.* **1992**, *45*, 31−40.
[33] A. H. Wang, G. Ughetto, G. J. Quigley, A. Rich, *Biochemistry* **1987**, *26*, 1152−1163.
[34] E. Tselepi-Kalouli, N. Katsaros, *J. Inorg. Biochem.* **1989**, *37*, 271−282.
[35] A. Bax, R. H. Griffey, B. L. Hawkins, *J. Magn. Reson.* **1983**, *55*, 301.
[36] A. Bax, M. F. Summers, *J. Am. Chem. Soc.* **1986**, *108*, 2093−2094.

Received August 8, 2001
[I01314]

Influence of an Additional Gas on the Hydroformylation and Related Reactions

Mario Bianchi,[a] Piero Frediani,*[a] Franco Piacenti,[a] Luca Rosi,[a] and Antonella Salvini[a]

Keywords: Hydroformylation / Carbonyl ligands / Cobalt / Carbonylation / Dinitrogen complexes / Argon / Xenon

The initial rate of the catalytic carbonylations reported in this paper [the hydroformylation of olefins in the presence of $Co_2(CO)_8$, the carbonylation of orthoesters catalyzed by $Co_2(CO)_8$], and the formation of tetracarbonylhydridocobalt(I) from octacarbonyldicobalt and dihydrogen] was reduced by the addition of dinitrogen, argon, or xenon. The influence of xenon on the rate of hydroformylation was greater than that of dinitrogen or argon. Helium and neon, on the other hand, did not show any influence, as expected, in view of their chemical-physical features. The experimental data may be explained assuming that the additional gas competes with one or more reactants for a coordinatively unsaturated site responsible for their activation, thus affecting the reaction rate.
(© Wiley-VCH Verlag GmbH, 69451 Weinheim, Germany, 2002)

Introduction

In the mechanism for the hydroformylation reaction, Heck and Breslow proposed (Scheme 1)[1] that molecular hydrogen was involved in two steps of the catalytic cycle. In a first step (Scheme 1, step A) dihydrogen reacts with $Co_2(CO)_8$ to give $CoH(CO)_4$, while in a subsequent step (Step F) hydrogenolysis of an acylcarbonylcobalt intermediate gives the aldehyde, thus restoring the carbonylhydridocobalt. In an intermediate step (C) the olefin is activated by reaction with $CoH(CO)_3$. In this paper we report the results of some experiments aimed to collect evidence on the intermediates connected with the activation step of dihydrogen in the hydroformylation reaction. Taking into account the literature data, a dihydrogen metal complex should precede the oxidative addition of dihydrogen to the cobalt(0) complex (step A in Scheme 1).

Dihydrogen[2] and dinitrogen complexes[3] are well documented in the literature, the first dihydrogen complex $[W(\eta^2\text{-}H_2)(CO)_3(P\mathit{i}Pr_3)_2]$ being reported by Kubas et al.[2a] Preliminary data on xenon containing transition metal complexes have also been reported in a solid matrix, in liquid xenon, in supercritical fluids, and in gas phase.[4] Very recently, the first stable xenon complex $[AuXe_2^{2+}][Sb_2F_{11}^-]_2$ was characterized by X-ray crystal structure analysis.[5] The interactions in these non-classical complexes are relatively weak (between 1 and 10 kcal mol^{-1}).[4a,4g,6] Nevertheless, coordination may be considered as the initial step of an activation process by a metal-containing catalyst. For instance, dihydrogen complexes may be intermediates in the oxidative addition leading to a metal dihydride (Scheme 2).

Other weak interactions such as those between a transition metal and an alkyl group (agostic interactions $[M^{\cdots}H-C]$)[7] play an important role in catalytic processes, such as the polymerization of olefins.[8]

The identification of a dihydrogen-cobalt interaction in the photolysis of $CoH(CO)_4$ and in a solid H_2/Ar matrix[9] supports the suggestion that a dihydrogen cobalt complex may be the precursor of dihydrogen activation in the hydroformylation reaction. Dinitrogen was found to displace dihydrogen from the coordination of a cobalt(I) complex, as reported by Sacco and Rossi[3a] in the $CoH(H_2)(PR_3)_3$/$CoH(N_2)(PR_3)_3$ system and analogous equilibria are reported for Ru^{II} and Fe^{II} complexes.[3c,10] Taking into account these results we have investigated the influence of an appropriate "additional" gas, dinitrogen and others, on the rate of hydroformylation (and related reactions) and this paper reports new data on this subject.

Results and Discussion

The first additional gas employed in our experiments was dinitrogen and the investigation was then extended to rare gases such as helium, neon, argon, and xenon.[11] The initial rate for the hydroformylation of cyclohexene in the presence of an "additional gas" was established by determining the conversion of the substrate in isochronous experiments. An analogous methodology has been employed to study the carbonylation of orthoesters and the formation of $CoH(CO)_4$ from $Co_2(CO)_8$ and H_2.

Cyclohexene Hydroformylation

The influence of an additional gas on the rate of hydroformylation was determined by converting cyclohexene to the corresponding aldehyde (Scheme 3) in a set of experi-

[a] Department of Organic Chemistry, Università di Firenze, Via della Lastruccia, 13, 50019 Sesto Fiorentino (Fi), Italy
Supporting information for this article is available on the WWW under http://www.eurjic.com or from the author.

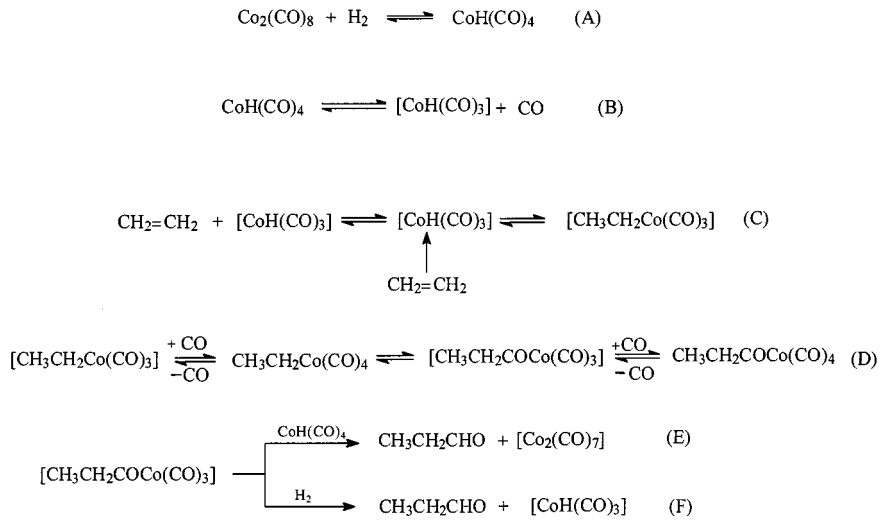

Scheme 1

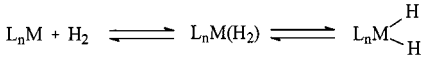

Scheme 2

ments carried out under the same reaction conditions [100 °C, p(CO) 85 bar, p(H_2) 85 bar, reaction time 3 h], but under different pressures of dinitrogen (0−1000 bar).

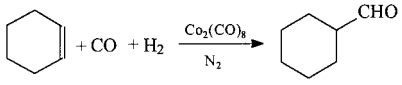

Scheme 3

Preliminary results on this reaction have been reported,[11] and the data obtained are summarized in Table 1. A relevant amount of dinitrogen in the reaction medium due to a dinitrogen pressure of 1000 bar, reduced the initial rate of the reaction from 627 to 250 μmol h^{-1}. A reduction of the rate might also be due to a decrease in concentration of the catalyst and substrate resulting from the volume increase of the solution caused by the dissolution of the additional gas. It has been experimentally determined that the amount of dinitrogen dissolved in 7 mL of toluene at 100 °C under 1000 bar produce a volume increase of 1.4 mL. If the volume additivity holds, the molar fraction of dinitrogen[12] is 0.381, the total volume of the solution becomes 8.4 mL. The effect of the dilution on the initial rate of the hydroformylation has been determined by a reference test using 8.5 mL of solvent. As shown in Table 2, the initial rate of the hydroformylation is almost unchanged (595 μmol h^{-1}) (Table 2). By doubling the volume of the solution to 14 mL, the initial rate was reduced to 474 μmol h^{-1}. These data clearly show that although dilution reduces the conversion at a given time, the rate reduction observed in the hydroformylation test carried out under the high pressure of dinitrogen adopted is significantly greater. The hydroformylation of cyclohexene carried out in the presence of argon as additional gas shows a behavior analogous to that observed in the presence of dinitrogen, see Table 1. A specific chemical effect must therefore operate. A purely physical effect due to the increase of dinitrogen pressure should also be excluded since the same reaction carried out in the presence of helium under the same pressure does not show any significant change in the initial rate.

Table 1. Influence of additional gases on the initial rate of cyclohexene hydroformylation[11a]; reaction conditions: toluene 7 mL; $Co_2(CO)_8$ 0.149 mmol (51 mg); cyclohexene 6.15 mmol (500 mg); p_{CO} 70 ± 1 bar at 100 °C; p_{H2} 85 ± 2 bar at 100 °C; reaction time 3 h; T = 100 °C

Gas	Additional gas pressure [bar]	Initial rate [μmol h^{-1}]	Initial rate reduction[a] [%]
N_2	0	627	0.0
	500	449	28.4
	800	353	43.7
	1000	250	60.1
He	0	627	0.0
	500	595	5.1
	800	554	11.6
Ne	0	627	0.0
	500	595	5.1
Ar	0	627	0.0
	500	373	40.5
	800	207	67.0
	1000	191	69.5

[a] Initial rate reduction: $[(\text{Initial rate})_{0\ bar} - (\text{Initial rate})_{observed}]/(\text{Initial rate})_{0\ bar}$.

The observed reduction of the rate of hydroformylation may be ascribed to the formation of a cobalt complex containing dinitrogen (or argon). The formation of a similar complex does in fact reduce the concentration of the catalytically-active cobalt complex and consequently the initial rate of the reaction, see Scheme 4.

Table 2. Hydroformylation of cyclohexene to $C_6H_{11}CHO$; influence of dilution on the rate; solvent: toluene; $Co_2(CO)_8$ 0.149 mmol (51 mg); cyclohexene 6.15 mmol (500 mg); p_{CO} = 70 ± 1 bar at 100 °C; p_{H2} = 85 ± 2 bar at 100 °C; reaction time 3 h; T = 100 °C

Solvent [mL]	Dilution [%]	Initial rate [μmol h^{-1}]	Initial rate reduction[a] [%]
7	0	627	0
8.5	20	595	5.1
14	100	472	24.7

[a] Initial rate reduction: [(Initial rate)$_{0\ bar}$ − (Initial rate)$_{observed}$]/(Initial rate)$_{0\ bar}$

$$RCo(CO)_3 + L \rightleftharpoons RCo(CO)_3L$$

R = H, $Co(CO)_4$; L = H_2, olefin, N_2, Ar

R = alkyl, acyl; L = H_2, N_2, Ar

Scheme 4

In other words, the reduced hydroformylation rate may be attributed to a lower concentration of the available active intermediate due to a competition between dinitrogen (or argon) and dihydrogen (or olefin) for the same vacant coordination site within the catalytically active species.

The ability of an electron-deficient cobalt complex to coordinate dinitrogen (or rare gases) may be related to the availability of outer shell electrons of this gas that is connected with the first ionization potential (IP).[13] Within rare gases, the IP decreases from helium to xenon. The large rare gases have been reported to coordinate a transition metal.[14,15]

The estimated bond dissociation enthalpy (BDE) for W−Xe in $W(CO)_5Xe$[16] is 35.1 ± 0.8 *k*J mol^{-1}. Furthermore, the estimated BDE's of the metal(0) pentacarbonyl derivatives[17] decrease from xenon (34.3 ± 4.2 *k*J mol^{-1}), to krypton (ca. 25 *k*J mol^{-1}), to argon (ca. 12 *k*J mol^{-1}).

In the hydroformylation of cyclohexene the initial rate was affected by the presence of xenon more than by argon or dinitrogen, while neon or helium had no effect, see Table 1, Table 3 and Table 4. The small difference in the observed rates when working in the presence of helium and neon may be attributed to their different solubility in toluene and therefore to the different volume increase. The concentration of N_2, Ar, Xe in toluene has been experimentally detected and the data are reported in the supplementary materials. The initial rate reduction evaluated for the same concentration of the additional gas in solution (Table 4), is 31.3 for Xe, 16.8 for N_2, and 8.2 [mM]$^{-1}$ for Ar.

Table 3. Influence of xenon on the initial rate of cyclohexene hydroformylation; toluene 7 mL; $Co_2(CO)_8$ 0.149 mmol (51 mg); cyclohexene 6.15 mmol (500 mg); reaction time 3 h; T = 100 °C

Xenon [g]	Initial rate [mmol h^{-1}]	Initial rate reduction[a] [%]
0	627	0.0
2.5[b][c]	513	18.2
3.8[b][d]	431	31.3

[a] Initial rate reduction: [(Initial rate)$_{0\ bar}$ − (Initial rate)$_{observed}$]/(Initial rate)$_{0\ bar}$. [b] Gases were introduced in the sequence: CO (1 bar), xenon, CO (53 bar a room temp., 70 ± 1 bar a 100 °C), p_{H2} 85 ± 2 bar at 100 °C. [c] Xenon pressure at 100 °C: 18.5 bar. [d] Xenon pressure at 100 °C: 23.5 bar.

Table 4. Hydroformylation of cyclohexene; initial rate reduction; data from Tables 1 and 3, solvent: toluene

	Ar	N_2	Xe
Additional gas [A. G.] (bar)	1000	1000	23.5[a]
A. G. in solution (mol/L)[b]	0.085	0.036	0.010
Initial rate reduction (%)	69.5	60.1	31.2
Initial rate reduction/ additional gas dissolved [mM]$^{-1}$	8.2	16.8	31.3

[a] Xenon 3.8 g. [b] The additional gas in solution was measured: see the supplementary materials.

The inhibiting effect of these additional gases (nitrogen, argon, or xenon) on the rate of hydroformylation may be considered as an indirect evidence of an interaction between these additional gases and a catalytically active cobalt complex. These interactions are presumably weak, and carrying out the hydroformylation of cyclohexene in heptane or toluene (Table 5) the initial rate is almost unaffected by the solvent although the solubilities of CO and H_2 differ significantly between heptane and toluene.[12]

Table 5. Hydroformylation of cyclohexene in different solvent; solvent 7 mL; $Co_2(CO)_8$ 0.149 mmol (51 mg); cyclohexene 6.15 mmol (500 mg); p_{CO} 70 bar at 100 °C; p_{H2} 85 bar at 100 °C; reaction time 3 h; T 100 °C

Solvent	Additional gas	Amount of additional gas	Initial rate [μmol h^{-1}]
Toluene	Argon	0	627
Heptane	Argon	650 bar	350
Toluene	Argon	500 bar	373
Toluene	Xenon	0	627
Heptane	Xenon	3.1 g	478
Toluene	Xenon	3.8 g	431

Carbonylation of Triethyl Orthoformate

The synthesis of aldehydes by carbonylation of orthoformic esters (Scheme 5) in the presence of $Co_2(CO)_8$ has the same kinetic dependence on CO and H_2 pressure, cata-

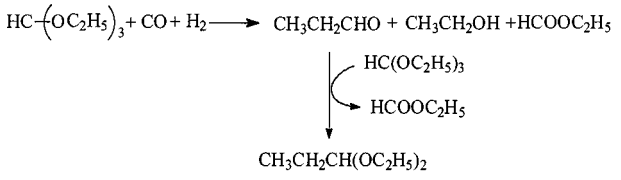

Scheme 5

lyst and substrate concentration as the hydroformylation of olefins.

The reaction proceeds through the protonation of one of the oxygen atoms of the ester,[18,19] followed by $RCo(CO)_4$ formation and collapse of the organic residue into ROH and HCOOR. Only one aldehyde is formed, due to the insertion of the formyl group onto the carbon atom of the alkyl group initially bound to the oxygen in the ester.

The aldehyde formed usually reacts through a fast reaction, with the orthoformic ester still present to provide the corresponding dialkyl acetal. The overall reaction is the formation of the acetal of the aldehyde (Scheme 5).

In this reaction no olefin is involved and there is no activation of the substrate by coordination to the metal atom of the catalyst. Coordination vacancies on the catalytically active intermediate should therefore be involved only for the activation of molecular hydrogen. The effect, if any, of the presence of the "additional gas" on the rate of this reaction, which uses the same catalyst as the hydroformylation, should therefore reveal the intervention of these gases on the specific activation steps of dihydrogen.

We have therefore tested the effect of the presence of "additional gases" on the carbonylation of orthoformic esters. The initial rate of the reaction was determined in isochronous (3 h) experiments carried out at 90 °C in the presence of an additional gas (pressure range: 0−1500 bar) through the conversion of triethyl orthoformate to 1,1-diethoxypropane, (see Scheme 5 and Table 6).

Table 6. Carbonylation of triethyl orthoformate: influence of additional gas on the initial rate; ethanol 8 mL; $Co_2(CO)_8$ 0.0789 mmol (27.0 mg); triethyl orthoformate 7.5 mmol (1.110 g); p_{CO} 50 ± 1 bar at 40 °C; p_{H2} 95 ± 2 bar at 90 °C; reaction time 3 h; T = 90 °C

Additional gas	Pressure [bar]	Initial rate [μmol h^{-1}]	Initial rate reduction[a] [%]
N_2	0	540	0.0
	1000	343	36.5
	1500	313	42.0
Ar	0	540	0.0
	500	400	25.9
	1000	233	56.9
	1500	100	81.5

[a] Initial rate reduction: $[(\text{Initial rate})_{0\ bar} - (\text{Initial rate})_{observed}]/(\text{Initial rate})_{0\ bar}$.

The additional gas remarkably affects the rate of carbonylation of orthoesters as in the case of cyclohexene hydroformylation. Argon apparently has an even higher influence than dinitrogen.

These data suggest that the steps responsible for the activation of dihydrogen (Scheme 1, steps A, F) are involved in the competition between dihydrogen and the additional gas for the coordinatively unsaturated site.

Formation of $CoH(CO)_4$ from $Co_2(CO)_8$ and Dihydrogen

During the carbonylation of organic substrates in the presence of $Co_2(CO)_8$ as a catalytic precursor, the first reaction is the formation of the catalytically active tetracarbonylhydridocobalt(I). Its kinetic[20] and general considerations, however, on the necessary activation of dihydrogen suggest the following steps (Scheme 6).

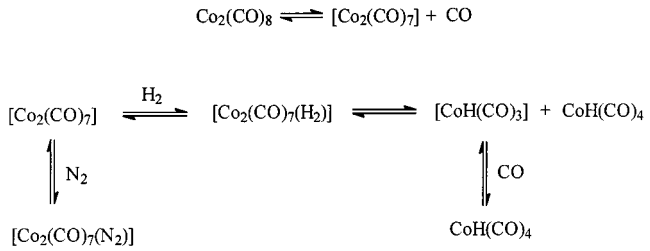

Scheme 6

In order to get further evidence, although indirect, on the presence of a coordinatively unsaturated intermediate responsible for the activation of dihydrogen, we tested the effect of the presence of an additional gas on the rate of formation of $CoH(CO)_4$.

A solution of $Co_2(CO)_8$ in hexadeuterobenzene was heated at 50 °C under carbon monoxide (1 bar) to stabilize the carbonyl complex which, even in the absence of O_2 would decompose to $Co_4(CO)_{12}$.[21] The CO was also used to reduce the reaction rate, which in its absence is fast.[22] Dihydrogen and the additional gas were then added. The results are reported in Table 7. Dinitrogen shows a marked influence on the initial rate of the reaction. The conversion of $Co_2(CO)_8$ was almost suppressed in the presence of 1000 bar of dinitrogen: only a trace of $CoH(CO)_4$ was found to be present in solution. The presence of helium (1070 bar) did not affect the rate of this reaction: a conversion of 14−15% was observed under the same conditions. We assume that dinitrogen and dihydrogen compete for a coordinatively unsaturated site of an intermediate, tentatively indicated as $Co_2(CO)_7$ in Scheme 6.

Table 7. Formation of $CoH(CO)_4$ from $Co_2(CO)_8$ and dihydrogen; influence of the additional gas on the initial rate; hexadeuteriobenzene 4 mL; $Co_2(CO)_8$ 0.2339 mmol (80.0 mg); T = 50 °C; p_{CO} = 1 bar at room temp.; p_{H2} = 50 bar at 50 °C; reaction time 3 h

Additional gas	Additional gas pressure at 50 °C [bar]	Initial rate [μmol h^{-1}]	Initial rate reduction[a] [%]
He	0	11.8	0.0
He	1070	5.6	52.6
N_2	0	11.8	0.0
N_2	1025	< 0.1	> 99.2

[a] Initial rate reduction: $[(\text{Initial rate})_{0\ bar} - (\text{Initial rate})_{observed}]/(\text{Initial rate})_{0\ bar}$

Conclusion

Several authors discussing the mechanism of the hydroformylation of olefins have indicated the reduction of an acylcarbonylcobalt intermediate as the rate determining step.[23,24] The negative influence of the pressure of carbon monoxide on the reaction rate[25] may be explained in terms of the shift of equilibrium D (Scheme 1) to the acyltricarbonylcobalt that was found to be more easily reducible than acyltetracarbonylcobalt.

The higher rate of hydroformylation under a low pressure of carbon monoxide may be attributed to the higher concentration in solution of the coordinatively unsaturated acyltricarbonylcobalt, necessary to activate dihydrogen, which is the predominant reducing agent in the system (Step F, Scheme 1).

Dihydrogen was suggested as the reducing agent[23,24] in consideration of its high concentration in solution when compared with that of the alternative reducing agent: tetracarbonylhydridocobalt(I).

Such an explanation is confirmed by the detected influence of the "additional gases" on the rate of hydroformylation. These gases do not take part in the formation of the product but compete with both dihydrogen and carbon monoxide for the coordinatively unsaturated site in the acyltricarbonylcobalt (Scheme 7). These interactions decrease the concentration of the intermediate available for the activation of dihydrogen and therefore retard its reaction with the acylcobalt complex that leads to the formation of the aldehyde.

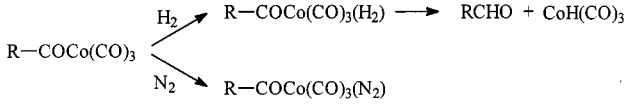

Scheme 7

Experimental Section

General Methods: Quantitative GC analyses were performed with a Shimadzu mod. GC-14A instrument equipped with a PPG column ("Polypropylenglicol" LB-550-X on Chromosorb W at 15%, 1/8" i.d., 2 m) and a Shimadzu mod. C-R4A integrator. Unless otherwise stated, no correction factors were introduced, in consideration of the analogy of the products examined. Products were identified by GC-MS using a Shimadzu apparatus having a GC14A chromatograph equipped with a CP-Sil8 (50 m) capillary column and a QP2000 mass detector. Elemental analyses were performed using a Perkin−Elmer mod. 2400 Series II elemental analyzer. IR spectra were recorded with a Perkin−Elmer mod. 1760-X FT-IR spectrophotometer. ^1H and $^{13}C\{^1H\}$ NMR spectra were recorded using a Varian VXR300 spectrometer operating at 299.987 MHz for ^1H, and at 75.429 MHz for ^{13}C, using $SiMe_4$ as external standard.

$Co_2(CO)_8$ (m.p. 56 °C) was prepared according to Natta and Ercoli,[26] and recrystallized from hexane; cyclohexene (Fluka) was purified (99.9% purity by GC) through elution on an Al_2O_3 column and then distilled (b.p. 83 °C) under dinitrogen; triethyl orthoformate: (Fluka) was distilled under dinitrogen (b.p. 146 °C); toluene was heated under reflux over sodium for 5 h, then distilled under dinitrogen (b.p. 110 °C).[27] Heptane was dried by heating under reflux over $LiAlH_4$. Dinitrogen (Sol Centro, 99.996% purity), argon (Sol Centro, 99.998% purity), neon, (Rivoira, 99.997% purity), xenon (Rivoira, 99.997% purity), and helium (Sol Centro, 99.998% purity) were used as received.

The experiments were carried out in a stainless-steel rocking reactor, inner volume 24.5 mL, tested to a total pressure of 4000 bar. The vessel was equipped with a high-pressure Nova Swiss valve used for the introduction of gases and liquids. The temperature was measured using a Pt100 indicator and regulated with an accuracy of ±1 °C. The pressure was measured through a transducer (Sensotec, model Z Absolute) with an accuracy of ±1 bar. The experimental conditions are reported in Table 1−3 and Table 5−7. The amount of reagents were chosen to avoid relevant pressure drops during each experiment.

Hydroformylation of Cyclohexene: The same procedure was adopted for the hydroformylation of cyclohexene in the presence of dinitrogen, argon, or helium. The catalyst was placed in the stainless-steel autoclave under dinitrogen the vessel was sealed and the gas evacuated. A solution of the olefin was prepared in a Schlenk tube and introduced into the autoclave by suction. CO of up to 5 bar was then added. The reactor was rocked and heated at 100 °C. When the solution reached the predetermined temperature, further CO up to 75 bar was added, followed by dihydrogen up to a total pressure of 160 bar (partial pressure of H_2, 85 ± 2 bar). The additional gas was then rapidly introduced up to the required pressure. Only a few minutes were necessary to perform these operations. The reactor was rocked for 3 h, then rapidly cooled to room temperature. The gases were vented and the pale yellow solution analyzed by GC to evaluate the conversion of cyclohexene to the aldehyde. GC conditions adopted when the experiments were carried out in toluene were the following: 50 °C for 5 min than up to 110 °C at a rate of 4 °C/min and kept at this temperature for 50 min. When heptane was the solvent, GC conditions were the following: 35 °C for 20 min then up to 110 °C at a rate of 4 °C/min and keeping this temperature for 60 min. Cyclohexane, cyclohexene, toluene or heptane, and cyclohexanecarboxyaldehyde were determined by gas-chromatography. The amount of cyclohexane present was less than 1% of the starting cyclohexene in all experiments.

The experiments with xenon were carried out using a different procedure. After the introduction of both catalyst and solvent, CO up to 1 bar was added. Liquid xenon was introduced at room temperature from a pressure cylinder, followed by CO up to 53 bar at room temperature. The amount of xenon introduced was evaluated by weight difference. The reactor was heated at 100 °C and then pressurized with hydrogen. The subsequent procedures were identical to those reported above. The data in the presence of xenon were compared with a reference test performed, with the same procedure, in the presence of helium.

The results of the hydroformylation tests on cyclohexene are reported in Table 1−5.

Carbonylation of Triethyl Orthoformate: All conditions employed are reported in Table 6. The catalyst was placed in the autoclave under dinitrogen. The vessel was sealed and the gas evacuated. A solution of triethyl orthoformate in anhydrous ethanol was prepared in a Schlenk tube and introduced into the autoclave by suction. CO up to 50 bar was then added and the vessel heated at 90 °C. When the selected temperature was reached, hydrogen up to a total pressure of 145 bar was introduced (hydrogen partial pressure 95 ± 2 bar) followed rapidly by the additional gas. The reactor was rocked for 3 h, and then rapidly cooled to room temperature. The

gases were vented and the pale yellow solution analyzed by GC using heptanol as internal standard, to evaluate the conversion of triethyl orthoformate into 1,1-diethoxypropane. The following GC conditions were adopted: 50 °C for 5 min, then heated up to 70 °C at a rate of 5 °C/min and kept at this temperature for 15 min, then heated up to 120 °C at a rate of 5 °C/min and kept at this temperature for 20 min. Ethanol, ethyl formate, 1,1-diethoxypropane, and heptanol were separated and quantified by GC. The results are reported in Table 6.

Synthesis of $CoH(CO)_4$ from $Co_2(CO)_8$ and Hydrogen: The experimental conditions used are listed in Table 7. Under CO, a solution of octacarbonyldicobalt in [D_6]benzene was introduced into the autoclave, which was then sealed and heated up to 50 °C. Dihydrogen and the additional gas (helium or dinitrogen) were then introduced and the autoclave rocked for 3 h. The vessel was cooled at 0 °C, the gases were slowly vented (about 20 min) and the autoclave opened under dihydrogen. An aliquot of the solution (1 mL, 0 °C) was examined by ^1H NMR after addition of 21.0 mg (0.0146 mmol) of $Ru_4H_4(CO)_8(PBu_3)_4$ as internal standard [$CoH(CO)_4$, $\delta = -11.6$; $Ru_4H_4(CO)_8(PBu_3)_4$, $\delta = -16.7$] and the conversion of $Co_2(CO)_8$ into $CoH(CO)_4$ was detected (Table 7).

The loss of $CoH(CO)_4$ was estimated by carrying out an experiment in the absence of an additional gas under the conditions reported in Table 7. At the end of the reaction, helium was introduced up to a pressure of 930 bar, the gases were vented and the amount of $CoH(CO)_4$ evaluated as previously described. The initial rate of the transformation of $Co_2(CO)_8$ into $CoH(CO)_4$ is 5.6 μmol h^{-1}: 50% of the hydride present in the solution was lost.

Supporting information available (see footnote on the first page of this article): Table with the data of the additional gas employed. Solubilities of dinitrogen in toluene, Method 1 and Method 2. Solubility of argon in toluene. Solubility of xenon in toluene. Relation between theoretical and effective pressure of dinitrogen at 10 °C. Relation between theoretical and effective pressure of dinitrogen at 100 °C. Fugacity coefficient of dinitrogen as a function of the pressure at 10 °C. Fugacity coefficient of dinitrogen as a function of the pressure at 100 °C.

Acknowledgments

The authors wish to thank the Università di Firenze and the Ministero della Università e della Ricerca Scientifica e Tecnologica (MURST), Programmi di Ricerca Scientifica di Notevole Interesse Nazionale, Cofinanziamento MURST 2000−2001, for financial support, and Professor Fausto Calderazzo, University of Pisa, for stimulating suggestions and discussions.

[1] [1a] R. F. Heck, D. S. Breslow, *Chem. Ind.* (London) **1960**, 467. [1b] R. F. Heck, D. S. Breslow, *J. Am. Chem. Soc.* **1961**, *83*, 4023.

[2] [2a] G. J. Kubas, *J. Acc. Chem. Res.* **1988**, *21*, 120. [2b] A. Gonzales, K. Zhang, S. P. Nolan, R. Lopez de la Vega, S. L. Mukerjiee, C. D. Hoff, G. J. Kubas, *Organometallics* **1988**, *7*, 2429. [2c] M. T. Haward, M. W. George, S. M. Howdle, M. Poliakoff, *J. Chem. Soc., Chem. Commun.* **1990**, 913. [2d] D. M. Heinekey, W. J. Oldham, *Chem. Rev.* **1993**, *93*, 913. [2e] S. Sabo-Etienne, B. Chaudret, H. A. el Makarim, J.-C. Barthelat, J.-P. Daudey, C. Mo'se, G. J. Leblanc, *J. Am. Chem. Soc.* **1994**, *116*, 9335. [2f] G. J. Kubas, J. E. Nelson, J. C. Bryan, J. Eckert, L. Wisniewski, K. Zilm, *Inorg. Chem.* **1994**, *33*, 2954. [2g] Z.-W. Li, H. Taube, *J. Am. Chem. Soc.* **1994**, *116*, 11584. [2h] J. Li, R. M. Dickson, T. Ziegler, *J. Am. Chem. Soc.* **1995**, *117*, 11482. [2i] B. Ma, C. L. Collins, H. F. Schaefer, III, *J. Am. Chem. Soc.* **1996**, *118*, 70. [2j] C. Bianchini, C. Mealli, M. Peruzzini, F. Zanobini, *J. Am. Chem. Soc.* **1992**, *114*, 5905. [2k] C. Bianchini, C. Mealli, M. Peruzzini, F. Zanobini, *J. Am. Chem. Soc.* **1987**, *109*, 5548. [2l] C. Bianchini, E. Farnetti, M. Graziani, J. Kaspar, F. Vizza, *J. Am. Chem. Soc.* **1993**, *115*, 1753. [2m] D. M. Heinekey, A. Liegeois, M. van Roon, *J. Am. Chem. Soc.* **1994**, *116*, 8388. [2n] D. G. Gusev, J. U. Notheis, J. R. Rambo, B. E. Hauger, O. Eisenstein, K. G. Caulton, *J. Am. Chem. Soc.* **1994**, *116*, 7409.

[3] [3a] A. Sacco, M. Rossi, *J. Chem. Soc., Chem. Commun.* **1967**, 316. [3b] P. W. Jolly, K. Jonas, *Angew. Chem. Int. Ed. Engl.* **1968**, *80*, 705. [3c] M. Aresta, P. Giannoccaro, M. Rossi, A. Sacco, *Inorg. Chim. Acta* **1971**, *5*, 203. [3d] J. A. Banister, M. W. George, S. Grubert, S. M. Howdle, M. Jobling, F. P. A. Johnson, S. L. Morrison, M. Poliakoff, U. Schubert, J. R. Westwell, *J. Organomet. Chem.* **1994**, *484*, 129. [3e] S. Gambarotta, *J. Organomet. Chem.* **1995**, *500*, 117. [3f] T. A. Bazhenova, A. V. Kulikov, A. F. Shestakov, A. E. Shilov, M. Yu. Antipin, K. A. Lyssenko, Yu. T. Struchkov, V. D. Makhaev, *J. Am. Chem. Soc.* **1995**, *117*, 12176. [3g] A. Sacco, M. Rossi, *Inorg. Chim. Acta* **1968**, *2*, 127. [3h] A. Yamamoto, S. Kitazume, L. S. Pu, S. Ikeda, *J. Am. Chem. Soc.* **1971**, *93*, 371. [3i] A. Misono, Y. Uchida, T. Saito, K. M. Song, *J. Chem. Soc., Chem. Commun.* **1967**, 419. [3l] J. H. Enemark, B. R. Davis, J. A. McGinnety, J. A. Ibers, *J. Chem. Soc., Chem. Commun.* **1967**, 96.

[4] [4a] M. B. Simpson, M. Poliakoff, J. J. Turner, W. B. Maier II, J. G. McLuaghlin, *J. Chem. Soc., Chem. Commun.* **1983**, 1355. [4b] J. R. Wells, E. Weitz, *J. Am. Chem. Soc.* **1992**, *114*, 2783. [4c] B. H. Weiller, *J. Am. Chem. Soc.* **1992**, *114*, 10910. [4d] A. A. Bengali, R. G. Bergman, C. B. Moore, *J. Am. Chem. Soc.* **1995**, *117*, 3879. [4e] C. E. Brown, Y. Ishikawa, P. A. Hackett, D. M. Rayner, *J. Am. Chem. Soc.* **1990**, *112*, 2530. [4f] R. N. Perutz, J. J. Turner, *J. Am. Chem. Soc.* **1975**, *97*, 4791. [4g] D. C. Grills, M. W. George, *Adv. Inorg. Chem.* **2001**, 52, 113 and references therein.

[5] S. Seidel, K. Seppelt, *Science* **2000**, *290*, 117.

[6] F. Calderazzo, "*Scientific Meeting, Consorzio Interuniversitario Reattività Chimica e Catalisi*", Bologna, Italy, February 14−15, **1997**.

[7] [7a] F. A. Cotton, T. LaCour, A. G. Stanislowski, *J. Am. Chem. Soc.* **1974**, *96*, 754. [7b] F. A. Cotton, A. G. Stanislowski, *J. Am. Chem. Soc.* **1974**, *96*, 5074. [7c] M. Brookhart, M. L. H. Green, *J. Organomet. Chem.* **1983**, *250*, 395. [7d] M. Brookhart, M. L. H. Green, L.-L. Wong, *Prog. Inorg. Chem.* **1988**, *36*, 1.

[8] [8a] D. T. Laverty, J. J. Rooney, *J. Chem. Soc., Faraday Trans.* I, **1983**, *79*, 869. [8b] H. Krauledat, H. H. Brintzinger, *Angew. Chem. Int. Ed. Engl.*, **1990**, *29*, 1412. [8c] L. Clawson, J. Soto, S. L. Buchwald, M. L. Steigerwald, R. H. Grubbs, *J. Am. Chem. Soc.* **1985**, *107*, 3377. [8d] M. Brookhart, A. F. Volpe, Jr., D. M. Lincoln, I. T. Horváth, J. M. Millar, *J. Am. Chem. Soc.* **1990**, *112*, 5634. [8e] C. Pellecchia, A. Grassi, A. Zambelli, *Organometallics* **1994**, *13*, 298. [8f] M. K. Leclerc, H. H. Brintzinger, *J. Am. Chem. Soc.* **1995**, *117*, 1651. [8g] J. A. Støvneng, E. Rytter, *J. Organomet. Chem.* **1996**, *519*, 277. [8h] L. Fan, A. Krzywicki, A. Somogyvari, T. Ziegler, *Inorg. Chem.* **1996**, *35*, 4003.

[9] [9a] R. L. Sweany, *J. Am. Chem. Soc.* **1982**, *104*, 3739. [9b] R. L. Sweany, F. N. Russell, *Organometallics* **1988**, *7*, 719.

[10] [10a] W. H. Knoth, *J. Am. Chem. Soc.* **1972**, *94*, 104. [10b] C. Bianchini, E. Farnetti, P. Frediani, M. Graziani, M. Peruzzini, A. Polo, *J. Chem. Soc., Chem. Commun.* **1991**, 1336. [10c] C. Bianchini, P. J. Perez, M. Peruzzini, F. Zanobini, A. Vacca, *Inorg. Chem.* **1991**, *30*, 135.

[11] [11a] F. Piacenti, F. Calderazzo, M. Bianchi, L. Rosi, P. Frediani, *Organometallics* **1997**, *16*, 4235. [11b] L. Rosi, F. Piacenti, M. Bianchi, P. Frediani, A. Salvini, *Eur. J. Inorg. Chem.* **1999**, 67.

[12] E. Wilhelm, R. Battino, *Chem. Rev.* **1973**, *73*, 1.

[13] *CRC Handbook of Chemistry and Physics*, (Eds.:D. R. Lide, H. P. R. Frederiske), Boca Raton-New York-London-Tokyo, 77th ed., **1994−5**, p.10.

[14] [14a] A. Bondi, *J. Phys. Chem.* **1964**, *68*, 441. [14b] R. Chauvin, *J. Phys. Chem.* **1992**, *96*, 9194. [14c] G. A. Cook, *Argon, Helium and the Rare Gases*, (Ed.: G. A. Cook), Vol. 1, J. Wiley, New York, **1961**. [14d] F. A. Cotton, G. Wilkinson, P. L. Gaus, *Basic Inorganic Chemistry*, 2 ed., CEA, **1991**, p. 59.

[15] J. B. Huheey, *J. Chem. Ed.* **1968**, *45*, 791.

[16] B. H. Weiller, *J. Am. Chem. Soc.* **1992**, *114*, 10910.

[17] J. R. Wells, E. Weitz, *J. Am. Chem. Soc.* **1992**, *114*, 2783.

[18] P. Pino, F. Piacenti, P. P. Neggiani, *Chim. Ind. (Milan)*, **1962**, *44*, 1367.

[19] F. Piacenti, M. Bianchi, P. Pino, *J. Org. Chem.* **1968**, *33*, 3653.

[20] [20a] R. D. V. Kemmitt, D. R. Russell, in *Comprehensive Organometallic Chemistry* (Eds.: G. Wilkinson, F. G. A. Stone, E. W. Abel, Pergamon, New York **1982**, Vol. 5, p. 10. [20b] N. H. Alemandaroglu, J. M. L. Penninger, E. Oltay, *Monatsh. Chem.* **1976**, *107*, 1043.

[21] [21a] R. D. V. Kemmitt, D. R. Russell, in *Comprehensive Organometallic Chemistry*, (Eds.: G. Wilkinson, F. G. A. Stone, E. W. Abel), Pergamon, New York, **1982**, Vol. 5, p. 7. [21b] L. Mond, H. Hirtz, M. D. Cowap, *J. Chem. Soc.* **1910**, 798. [21c] F. Ungvary, L. Markó, *J. Organomet. Chem.* **1974**, *71*, 283.

[22] [22a] R. Iwanaga, *Bull. Chem. Soc. Japan* **1962**, *35*, 774. [22b] P. Pino, R. Ercoli, F. Calderazzo, *Chim. Ind. (Milan)* **1955**, *37*, 782. [22c] J. W. Rathke, R. J. Klinger, T. R. Krause, *Organometallics* **1992**, *11*, 585.

[23] [23a] K. Istvan, F. Ungváry, L. Markó, *Organometallics* **1986**, *5*, 209. [23b] M. F. Mirbach, *J. Organomet. Chem.* **1984**, *265*, 205. [23c] P. Pino, F. Oldani, G. Consiglio, *J. Organomet. Chem.* **1983**, *250*, 481.

[24] [24a] F. Ungváry, A. Sisak, K. Istvan, L. Markó, *Kem. Kozl.* **1986**, *65*, 127. [24b] M. Borovikov, K. Istvan, F. Ungváry, A. Sisak, L. Markó, *J. Mol. Catal.* **1992**, *75*, L27.

[25] [25a] G. Natta, R. Ercoli, *Chim. Ind. (Milano)* **1952**, *34*, 503. [25b] A. R. Martin, *Chem. Ind. (London)* **1954**, 1636. [25c] G. Natta, R. Ercoli, S. Castellano, F. H. Barbieri, *J. Am. Chem. Soc.* **1954**, *37*, 6. [25d] H. Greenfield, S. Metlin, I. Wender, *Abstracts of Papers*, 126th ACS Meeting, New York, September 12−17, **1954**.

[26] G. Natta, R. Ercoli, *Chim. Ind. (Milan)* **1952**, *34*, 503.

[27] A. I. Vogel, *Vogel's Textbook of Practical Organic Chemistry,* IV ed., Longmans, **1978**, p. 268.

Received September 19, 2001
[I01370]

Complexation of Lanthanide(III) Ions with Polyhydroxy Carboxylic Acids in Aqueous Solutions

Sébastien Giroux,[a] Sabrina Aury,[a] Bernard Henry,[a] and Patrice Rubini*[a]

Keywords: Lanthanides / Cations / Acidity / Complexation / NMR spectroscopy

The complexation of lanthanum(III), europium(III), dysprosium(III), erbium(III), and lutetium(III) with D-gluconic acid (LH) was studied by pH potentiometry and NMR. The set of complexes formed in aqueous solutions and their stability constants β were determined, and the results were compared to those previously found for praseodymium(III) (S. Giroux et al., Polyhedron **2000**, *19*, 1567). A regular evolution of the β values was observed along the lanthanide series, particularly for the neutral complex MLH_{-2} (where two hydroxy functions were deprotonated) with a selectivity similar to that of EDTA. For the ML_2^+ complex, where the ligand was coordinated via the carboxylate groups, the analysis of the ^{13}C NMR pseudocontact shift showed that the carboxylate group was not bidentate and that there was a participation of the α-hydroxy group in the coordination. The study of the complexation of Pr^{III} with other hydroxy carboxylic acids: glyceric, threonic, 2-hydroxybutanoic, and 3-hydroxybutanoic acids confirms that in the complex MLH_{-2} the deprotonated hydroxy groups, that intervene in the coordination with the metal ion, are those in α and γ positions relative to the carboxylate group.
(© Wiley-VCH Verlag GmbH, 69451 Weinheim, Germany, 2002)

Introduction

Polyhydroxycarboxylic acids, particularly D-gluconic acid (**I**), have good complexing properties, and find more and more practical applications in the industrial domain.[1] The complexing ability of gluconic acid towards metallic ions is well known[2−11] even if the structure of the complexes formed in solution is not always well reported. The determination of the role and the nature of the alcohol groups concerned by the coordination to the metal ion is a difficult problem to solve. The combination of several techniques (potentiometry, NMR, circular dichroism) has proved to be efficient in obtaining such information.[7,11]

Lanthanide(III) ions are hard acids and their interaction with carboxylate groups or deprotonated hydroxy functions is strong.[2,10−12] The complexation of the praseodymium(III) ion with D-gluconic acid in aqueous solutions has been thoroughly studied[11] by potentiometry, UV/Vis spectrophotometry, NMR, and circular dichroism (CD) experiments. It was shown that six different complexes are formed in solution. Among them there are species where deprotonated OH groups participate in the coordination. It must also be noted that at neutral pH values, the formation of a neutral complex takes place that could, using a more hydrophobic ligand, allow for the extraction of this species into an organic phase.[13]

[a] Laboratoire de Chimie Physique Organique et Colloïdale, Université Henri Poincaré-Nancy I, Unité Mixte CNRS-UHP (SRSMC, UMR no. 7565)
B. P. 239, 54506 Vandoeuvre-Lès-Nancy Cédex, France
Fax: (internat.) + 33-3/83912532
E-mail: rubini@lesoc.uhp-nancy.fr

This work is devoted to a study of the complexation of the La^{III}, Eu^{III}, Dy^{III}, Er^{III}, and Lu^{III} ions with D-gluconic acid in order to know if there is an evolution of the complexing ability of this ligand along the lanthanide series, and whether this induces a possible selectivity. The complexes and their stability constants were determined by pH potentiometry. An NMR study allowed us to draw conclusions on the structure of the complexes.

In order to enhance our knowledge on the binding sites of gluconic acid in complexes where alcohol functions are deprotonated, we also studied the complexation of the praseodymium(III) ion with glyceric acid (**II**), threonic acid (**III**), 2-hydroxybutanoic acid (**IV**), and 3-hydroxybutanoic acid (**V**). Gluconic acid and threonic acid are polyhydroxylated carboxylic acids with three or four carbon atoms, and two or three OH functions, respectively. The presence of a primary alcohol function in the β or γ position relative to the carboxylic function, instead of a secondary alcohol one in gluconic acid, may generate variations in the complexing abilities. The two studied butanoic acids have only one OH function in α or β position relative to the carboxylic function. It was interesting to see if the presence of only one OH group in the ligand considerably lowered the complexation power of these molecules.

Results

Complexes of La^{III}, Pr^{III}, Eu^{III}, Dy^{III}, Er^{III}, and Lu^{III} with D-Gluconic Acid

Potentiometric measurements were made on mixtures of lanthanide(III) cations and D-gluconic acid as a function of

pH and for several ligand to metal ratios. For ligand/metal ratios smaller than 5:1 a precipitate was observed at pH < 11 (Table 1). For higher ratios no precipitation occurred. In the case of the Dy^{III} and Er^{III} cations, for small ligand/metal ratios, high concentrations, and for pH > 9, the viscosity of the solutions increased with time, and the formation of a gel was observed after a few minutes or a few tens of minutes.

Table 1. pH of precipitation for solutions of gluconic acid (L) and lanthanide(III) ions (M) for different [L]/[M] ratios; the metal ion concentration was varied from ca. 1×10^{-3} to ca. 5×10^{-3} mol·L^{-1} for a nearly constant gluconic acid concentration of ca. $6-8 \times 10^{-3}$ mol·L^{-1}

[L]/[M]	La^{III}	Pr^{III}	Eu^{III}	Dy^{III}	Er^{III}	Lu^{III}
1:1	9.0	8.5	7.4	8.2	7.4	7.4
1.5:1	9.9	8.5	8.2	8.3	7.5	[a]
3:1	10.1	8.9	9.5	[b]	[b]	7.8
5:1	[b]	[b]	[b]	[b]	[b]	[b]

[a] Not measured. [b] No precipitation observed up to pH = 11.3.

These experiments allowed us to determine that the same set of six complexes was formed for the La^{III}, Eu^{III}, Dy^{III}, Er^{III}, and Lu^{III} cations as for the Pr^{III} cation:[11] ML^{2+}, MLH_{-1}^{+}, MLH_{-2}, ML_2^{+}, ML_2H_{-1}, and $ML_2H_{-3}^{2-}$, and in addition, the complex $M_2L_2H_{-5}^{-}$. There were two exceptions: $ML_2H_{-3}^{2-}$ could not be found for Eu^{III} and MLH_{-1}^{+} for Lu^{III}. The formation constants of all these species are summarized in Table 2.

Distribution diagrams of these complexes as a function of pH are represented by Figure 1. At pH = 4, and for a gluconic acid concentration of 0.5 mol·L^{-1}, and for large ligand/metal ratios, the complex ML_2 was formed in 100% yield.

A ^{13}C NMR study of this complex was performed. For the diamagnetic cations, La^{3+} and Lu^{3+}, no shifts relative to the free ligand were observed, but for the paramagnetic ions the peaks were considerably shifted and broadened. To observe the signals, large ligand/metal ratios (10:1 to 250:1) were used. Only one mean signal for each carbon atom was detected because of a rapid exchange between free and bound gluconic acid. With an excess of free ligand the signals are reasonably shifted and broadened.

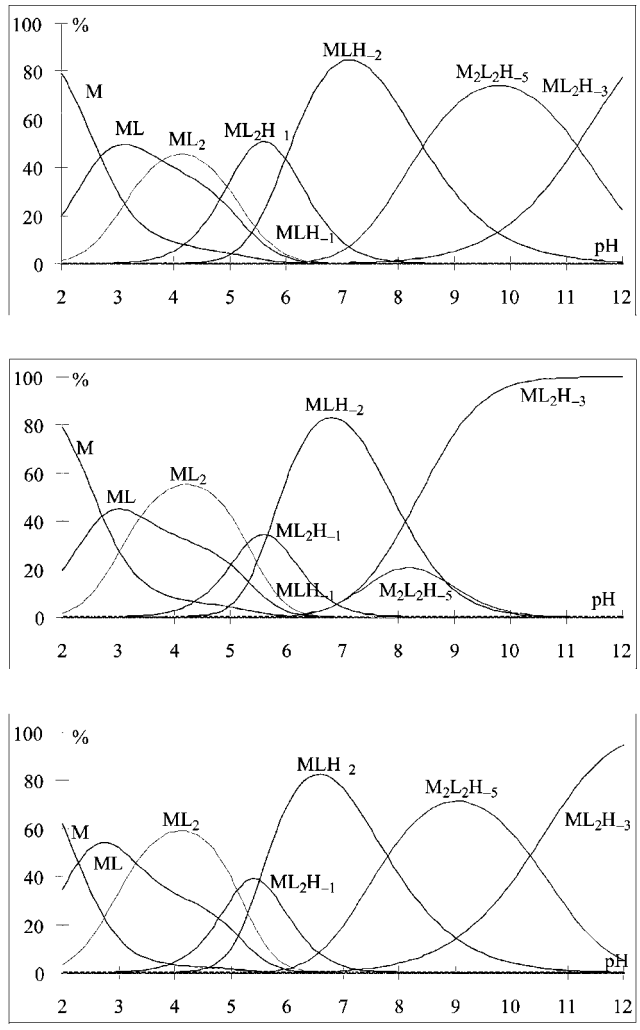

Figure 1. Distribution diagrams of the complexes formed at 25 °C between gluconic acid (5.10^{-3} mol·L^{-1}) and Dy^{III} (top), Er^{III} (center), and Lu^{III} (bottom) as a function of pH, for a ligand/metal ratio of 5:1

The chemical shift δ of the signals is related to the chemical shift of free (δ_f) and bound (δ_b) gluconic acid, as well as the molar fraction of free (p_f) and bound (p_b) ligand: $\delta = p_b\,\delta_b + p_f\,\delta_f$. As $p_f = 1 - p_b$, δ can be written as $\delta = \delta_f + p_b \cdot \Delta\delta$, where $\Delta\delta = \delta_b - \delta_f$.

Table 2. Formation constants (log β_{pqr}) for the different complexes formed in the system Ln^{III}/gluconic acid [T = 25 °C, I = 0.1 mol·L^{-1} ($NaClO_4$) determined from pH potentiometry measurements]

	La^{III}	Pr^{III} [a]	Eu^{III}	Dy^{III}	Er^{III}	Lu^{III}
ML	2.91 ± 0.02	2.78 ± 0.03	2.82 ± 0.05	3.21 ± 0.03	3.20 ± 0.02	3.58 ± 0.03
MLH_{-1}	−4.25 ± 0.03	−3.34 ± 0.02	−2.53 ± 0.03	−2.46 ± 0.10	−2.42 ± 0.04	X
MLH_{-2}	−11.65 ± 0.01	−10.09 ± 0.01	−8.65 ± 0.01	−7.58 ± 0.01	−7.45 ± 0.01	−6.69 ± 0.02
ML_2	4.85 ± 0.08	5.57 ± 0.03	5.74 ± 0.04	5.82 ± 0.04	5.97 ± 0.02	6.41 ± 0.03
ML_2H_{-1}	−2.29 ± 0.15	−0.67 ± 0.05	0.33 ± 0.05	0.87 ± 0.05	0.67 ± 0.04	1.28 ± 0.04
ML_2H_{-3}	−19.84 ± 0.05	−19.13 ± 0.08	X	−14.94 ± 0.09	−13.13 ± 0.07	−13.30 ± 0.06
$M_2L_2H_{-5}$	−31.44 ± 0.11	X	−26.21 ± 0.25	−20.59 ± 0.04	−20.21 ± 0.03	−18.16 ± 0.07
MH_{-1}	−9.33	−8.82	−8.58	−8.37	−8.26	−8.17

[a] From ref.[11]

The plot of δ as a function of p_b for each carbon atom for the Pr^{III}, Eu^{III}, and Dy^{III} complexes gives straight lines, the slope of which allows the determination of Δδ. An example of plot is given in Figure 2. The Δδ values are summarized in Table 3.

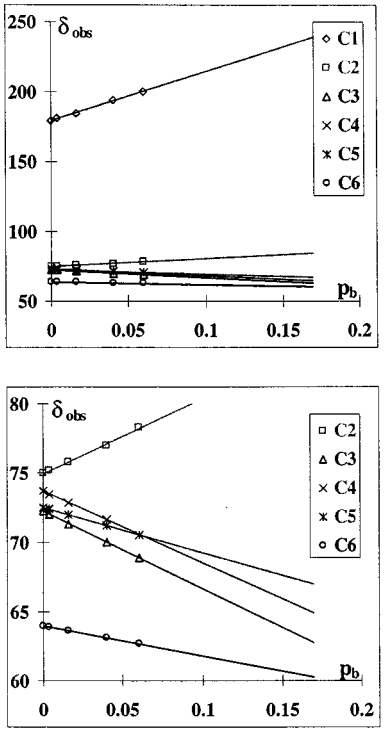

Figure 2. NMR chemical shifts of the different gluconic acid ^{13}C nuclei as a function of p_b, the molar fraction of gluconic acid bound to Dy^{III}

Table 3. ^{13}C NMR chemical shift difference Δδ (in ppm) between free gluconic acid and this ligand bound to various Ln^{III} ions in the ML_2 complexes

	Pr^{III}	Eu^{III}	Dy^{III}
C^1	32.7	−21.2	349.9
C^2	20.2	−7.8	54.0
C^3	2.5	−6.7	−55.4
C^4	−4.8	4.4	−51.8
C^5	−2.4	1.2	−32.4
C^6	−1.9	1.0	−22.0

Complexation of Pr^{III} with Glyceric, Threonic, 2-Hydroxybutanoic and 3-Hydroxybutanoic Acids

In order to determine the influence of the number and the position of hydroxy groups on the complexation behaviour of the polyhydroxy carboxylic acids, a potentiometric study of the complexation of Pr^{III} by D-glyceric acid (**II**), L-threonic acid (**III**), 2-hydroxybutanoic acid (**IV**), and (*R*)-3-hydroxybutanoic acid (**V**) was performed (Scheme 1).

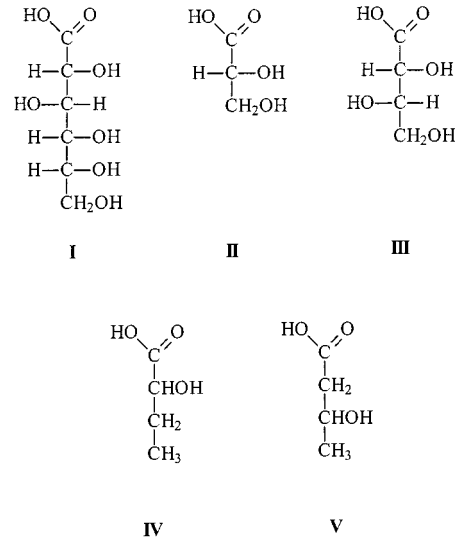

Scheme 1

The pK_a values of these acids are 3.52, 3.48, 3.64, and 4.34, respectively (gluconic acid: pK_a = 3.47). These values are in agreement with those reported in the literature. For glyceric acid, values of 3.32 (I = 0.1 mol·L^{-1}, KNO_3)[14] and 3.54 (I = 2 mol·L^{-1}, $NaClO_4$) are reported.[15] The pK_a value of 2-hydroxybutanoic acid from the literature data was found to be 3.70 or 3.80[16] at 25 °C and I = 0.1 mol·L^{-1}, that of 3-hydroxy-butanoic acid is reported to be 4.31 for an ionic strength of I = 0.5 mol L^{-1} in $NaClO_4$ at 25 °C[17] and 4.40 at 31 °C for I = 0.1 mol·L^{-1}.[18]

In the presence of Pr^{III}, the formation of a precipitate was observed at pH ≈ 8 for glyceric and threonic acids, and at pH ≈ 7 for the two butanoic acids. For **III**, **IV**, and **V** the complex ML was formed (the ligands, where the carboxylic function is not deprotonated, are noted LH) with log β_{110} = 2.76 ± 0.04, 2.56 ± 0.01, and 2.08 ± 0.02, respectively (2.78 ± 0.03 for gluconic acid[11]). It was the only complex that could be detected with **IV** and **V**. For **III**, the complexes MLH_{-1} and MLH_{-2} were also present (log β_{11-1} = −3.97 ± 0.03 and log β_{11-2} = −11.78 ± 0.02, compared to the corresponding values found for gluconic acid, −3.34 and −10.0[11]). Additionally the ML_2 species (log β_{120} = 5.19 ± 0.04) was also formed in the case of glyceric acid (log β_{120} = 5.11 ± 0.02; for gluconic acid, log β_{120} = 5.57). For **II**, in addition to ML_2, the complex ML_2H_{-2} and the binuclear species M_2L_2 and $M_2L_2H_{-2}$ were also detected (log β_{12-2} = −10.82 ± 0.06, log β_{220} = 7.79 ± 0.04, and log β_{22-2} = −6.61 ± 0.04, respectively). It should be noted that in this case, M_2L_2 and $M_2L_2H_{-2}$ could be replaced by ML and MLH_{-1}, but the fit is not as good, and the formation constant for ML is too low and not consistent with that of ML_2.

The ^1H and ^{13}C NMR study of these systems was made under conditions where the signals were not too broad nor significantly shifted, i.e. for large L/M ratios. For such L/M ratios, from the potentiometric results at pH < 7, the mean

species was ML_2 for glyceric acid, a mixture of ML and ML_2 (ML_2 predominant) for threonic acid, and ML for the butanoic acids (Figure 3). This study confirms the complexation by the carboxylate group. The most shifted ^{13}C NMR signals are those corresponding to the COO^- group and those corresponding to hydrogen atoms (^1H NMR) on the carbon atom adjacent to the carboxylate group.

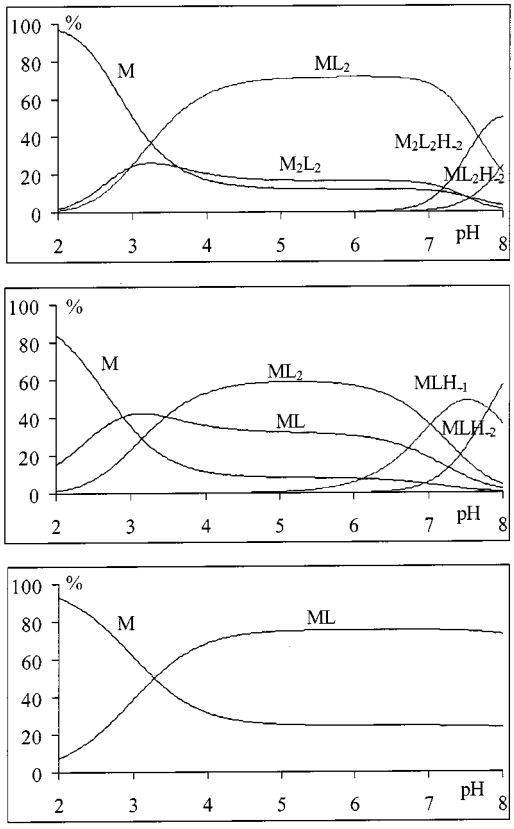

Figure 3. Distribution diagrams for the complexes formed at 25 °C between Pr^{III} and glyceric acid (top), threonic acid (center), and 2-hydroxybutanoic acid (bottom) as a function of pH; the concentration of the ligand was 0.01 mol·L^{-1} and the ligand/metal ratio was 5:1

Discussion

The systems of complexes formed between the six studied trivalent lanthanides and gluconic acid are very similar from one cation to another; only one species among seven is missing for Pr^{3+} ($M_2L_2H_{-5}$), Eu^{3+} (ML_2H_{-3}), and Lu^{3+} (MLH_{-1}). For an individual species, the formation constants are of the same order of magnitude, but show a regular increase along the lanthanide series with very few exceptions (Table 2). This can be put in relation with the increase in electrostatic interaction between the hard lanthanide ions, the radii of which decrease along the series, and the negatively charged oxygen atoms of the ligand that act as hard bases.

This continuous increase in the formation constants is shown for the complex MLH_{-2} in Figure 4. The amplitude in the variation from La^{3+} to Lu^{3+} is practically equal to five logarithmic units in this case, a value that can be compared to that obtained with the ethylenediamine tetraacetate ion (EDTA), 4.38.[19−20] The selectivity of gluconic acid towards lanthanide(III) ions through the formation of MLH_{-2} complexes is better than that of EDTA. This is important if one notes that MLH_{-2} is a non-charged species that can be extracted into an organic solvent. Gluconic acid, or a more hydrophobic form of this ligand, would be a good candidate for the liquid-liquid extraction of the trivalent lanthanide ions.[13]

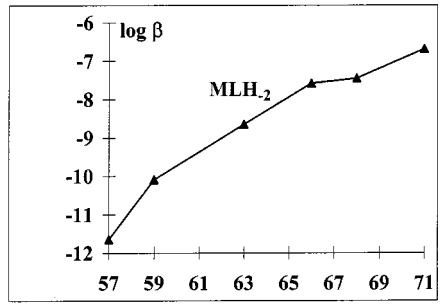

Figure 4. Variation of the log β_{11-2} value (MLH_{-2} complex) as a function of the lanthanide atomic number

The structure of the different Pr^{III} complexes has been largely discussed in a previous publication,[11] from potentiometric, NMR, UV/Vis, and CD experiments. For the ML_2 complex it is clear that the coordination takes place via the carboxylate group as demonstrated earlier,[11] but there is a presumption that the hydroxy group in α-position relative to the carboxylate group participates in the coordinating to the metal ion. Moreover, this OH function is that one that loses a proton, giving rise to the MLH_{-1} complex. The NMR study of systems with various paramagnetic cations may allow us to obtain more information on the structure of the ML_2 complex that can be formed at 100% without the presence of any other species at pH = 4.0. As was shown above, we could obtain the Δδ value for the different carbon atoms of gluconic acid ($\Delta\delta = \delta_b - \delta_f$). From these values it is possible to determine the part of the contact shift and that of the pseudo-contact shift in Δδ:[21−23]

$$\Delta\delta_i^j = f_i \langle S_z \rangle_j + D_j \cdot g_i.$$

The first term of the sum represents the contact shift, $\langle S_z \rangle_j$ is the projection of the total electron spin magnetization of the lanthanide j on the direction of the external magnetic field, and f_i is the product of the hyperfine coupling constant of carbon C_i and a coefficient. The second term is related to the dipolar (pseudo-contact) contribution. D_j is a constant for the lanthanide j, and g_i for a complex with an axial symmetry is defined as $g_i = k\,[3\cos^2(\theta - 1)]/r^3$, where k is a crystal field coefficient that is supposed to be constant along the lanthanide series; θ the angle between the principal axis of symmetry and the vector C_i-Ln^{3+} and r, the distance C_i-Ln^{3+}. The f and g coefficients can be determined from the plot $\Delta\delta_i^j/\langle S_z \rangle_j$ as a function of $D_i/\langle S_z \rangle_j$. In this case this plot must be a straight line, the slope of which is g_i. The structure of the complexes was not supposed to vary along the lanthanide series. The plot for the

C^1 (carboxylate) and C^2 carbon atoms are shown in Figure 5. The *f* and *g* values deduced from these plots and the corresponding contact and pseudo-contact contributions to the total shift are reported in Table 4. With the exception of the C^3 carbon atom, the pseudo-contact term is always larger than the contact term for the Pr^{3+} and Dy^{3+}ions. In the case of Eu^{3+}, the pseudo-contact part overcomes the contact term only for the C^1, C^4, and C^6 carbon atoms.

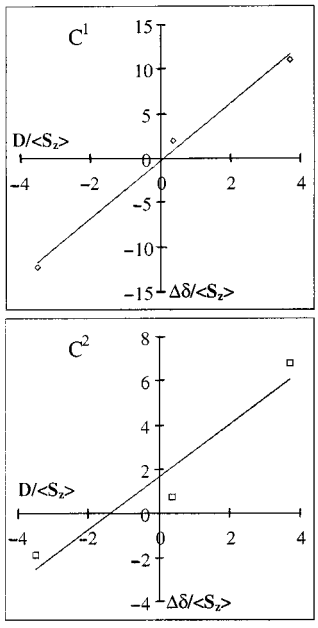

Figure 5. Plots $\Delta\delta/\langle S_z\rangle$ as a function of $D/\langle S_z\rangle$ for the C^1 (carboxylate) and C^2 carbon atoms of gluconic acid (L) in the complex PrL_2^+

Table 4. The *f* and *g* parameters for the ML_2 complex; contact and pseudo-contact contributions to the ^{13}C NMR chemical shift (M = Pr, Eu, and Dy)

	f	*g*	Pr^{III}		Eu^{III}		Dy^{III}	
			contact	pseudo	contact	pseudo	contact	pseudo
C^1	−0.3803	3.2406	−1.13	35.61	4.06	−13.12	10.86	324.1
C^2	1.6539	1.1935	4.91	13.11	−17.67	−4.83	47.21	119.4
C^3	1.1666	−0.1579	3.47	−1.73	−12.46	0.64	−33.30	−15.79
C^4	0.0245	−0.4783	0.07	−5.26	−0.26	1.94	−0.70	−47.83
C^5	0.1243	−0.2712	0.37	−2.98	−1.33	1.10	−3.55	−27.12
C^6	0.0542	−0.1952	0.16	−2.14	−0.58	0.79	−1.55	−19.52

From the *g* value, structural information can be obtained for the ML_2 complex. The question arises whether the gluconic acid carboxylate group acts as a bidentate ligand, as observed in the case of the acetate ion,[24] or if it can be envisaged that there is a participation of the hydroxy group borne by the C^2 carbon atom, leading to a monodentate coordination of the carboxylate head. The second type of coordination was observed in the solid state for manganese(II) D-gluconate dihydrate[25] and lead D-gluconate,[26] where there is a strong interaction of the hydroxy group with the metal ions leading to the formation of a five-membered chelate ring; in this case the metal−oxygen distances are of the same order of magnitude either for one of the oxygen atoms of the carboxylate group or the oxygen atom of the α-hydroxy group.

In the solid $Pr(acetate)_3{\cdot}H_2O$, two acetate ions are bidentate (one of the oxygen atoms is bonded to a second Pr^{3+} ion) and the Pr−O−C−O planes are planar to within 0.06 Å.[24] If the situation is the same for the Pr gluconate system, the ratio of the *g* values for the C^1 and C^2 carbon atoms can be easily calculated; the angles θ for these two carbon atoms are the same regardless of the position of the principal axis of the complex (since the C^2 carbon atom is also in the Pr−O−C−O plane because of the planar structure of the carboxylate group). The distances *r* may be evaluated from the data of ref.[24] The calculated ratio is ca. 3.6, to be compared to the experimental value of 2.7 (Table 4). Obviously, the calculated value is too high, indicating that the C^2 carbon atom is probably closer to the lanthanide(III) ion in the gluconate complex than in the acetate complex. This leads us to propose a structure in which the carboxylate ion is monodentate and the α-hydroxy group interacts with the Ln^{III} ions. Nevertheless, this interaction in probably weaker than that observed in the solid state for the manganese(II) and lead(II) species, probably due to a competition with the hydrogen bonding of the water molecules. Indeed, no CD effect was observed for this complex in the case of Pr^{III} ion, indicating that the α-hydroxy group is not tightly bound to the cation. The position of the C^2 carbon atom (and that of the O^2 oxygen atom of

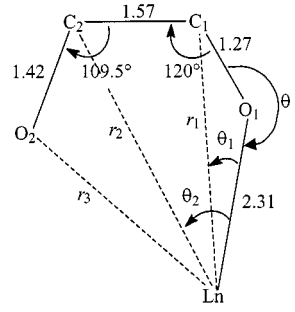

Scheme 2

the α-hydroxy group; see Scheme 2) may be evaluated from the g_1 and g_2 values ($g_1/g_2 \approx 2.7$). We made the assumption of an axial symmetry around the $Ln-O^1$ (acetate) bond, justified by fluxionality (rapid rotation) about this bond and by the fact that the coordination interaction with the carboxylate group is strong, compared to the other possible interactions.

The calculation of θ_1, θ_2, r_1, and r_2 was made by varying the angle θ, according to Scheme 2. The indicated angles and distances were estimated from the crystallographic structure discussed in ref.[26] for lead gluconate after correcting for the differences in the ionic radii of the Pb^{2+} and Pr^{3+} ions. There are two solutions for θ (130° and 210°), but only the second one gives rise to an interaction with the O^2 oxygen atom. The following values are consequently found: $\theta_1 = 10°$, $\theta_2 = 30°$; $r_1 = 3.46$ Å, $r_2 = 4.06$ Å, $r_3 = 3.39$ Å. It can be noted that the $Ln-O^2$ distance (ca. 3.4

Å) is much larger than the Ln−O^1 distance (2.3 Å), but that this weak interaction with the α-hydroxy group probably hinders the bidentate coordination of the carboxylate group and predisposes the OH group to be deprotonated in order to form the ML_2H_{-1} species.

The complexation of the lanthanide cations by hydroxy groups is important for the stability of the complex and it is probably a crucial stage before the deprotonation of these functions leading to an interaction with an alkoxide ion. We have just seen that in the complex ML_2 the complexation occurs via the carboxylate group, but that the cation also interacts with the α-hydroxy group. Previously, we concluded on the basis of CD results[11] that in the complex MLH_{-2} for the system Pr^{3+}/gluconic acid, the complexation occurred via a second deprotonated hydroxy function in addition to the deprotonated α-hydroxy group. Furthermore, this function was probably that in γ-position relative to the carboxylate group. If it is effectively the case, there is probably an interaction between the γ-hydroxy group and the cation, which occurs before the deprotonation of this function. If there is no tertiary alcohol function in γ-position, the complexation would undoubtedly occur via a β-hydroxy group, but it is probably energetically less favourable. In order to prove these assumptions, we studied some hydroxylated carboxylic acid ligands. The formation constants of the complexes ML and ML_2 for gluconic acid, threonic acid, and glyceric acid, which have nearly identical pK_a values, are very similar (practically identical for ML and slightly higher for ML_2 in the case of gluconic acid compared to the two other ligands with a difference of about 0.4 pK units).

It must be noted that all these ligands have a hydroxy function in α-position relative to the carboxylate group. For the two hydroxybutanoic acids the log β values are smaller than for the other ligands, contrary to what is generally observed: in the case of a hard base−hard acid interaction, log β(M + L → ML) usually increases when pK_a increases for ligands having comparable structures. The lower value observed for 2-hydroxybutanoic acid compared to **I**, **II** and **III**, seems to indicate that the OH groups other than those in the α-position also have a (weak) participation in complexation. The 3-hydroxybutanoic acid exhibits a significantly lower log β value because of the lack of an OH group in α-position relative to the carboxylate group. It must also be noted that the two hydroxybutanoic acids do not form MLH_{-1} and MLH_{-2} complexes.

The log β_{11-1} values ($M^{3+} + L^- \leftrightarrow MLH_{-1}^{+} + H^+$) for threonic acid is ca. 0.6 logarithm units lower than that for gluconic acid, indicating a small difference in the complexation strength of the two molecules. For gluconic acid, the γ-OH group plays a role in the complexation of Pr^{3+} in MLH_{-1} (this group deprotonates to form MLH_{-2}). For threonic acid the γ-OH group is not a secondary alcohol function, but a primary alcohol function with a higher acidity constant.

We can consider two possibilities: either the β-OH group intervenes in the complexation of the Pr^{3+} ion, inducing geometrical constraints due to the complexation of two consecutive OH functions (less favourable than those observed with the α- and γ-OH coordinations), or the γ-OH group interacts with the metal ion with a lower strength than in the case of gluconic acid. This second possibility would probably be due to the fact that there is a loss in hydrogen bonding with the solvent water molecules (there are no other OH groups in δ- and ε-positions unlike gluconic acid).

The difference in the complexation behaviour is amplified if we consider the formation of the MLH_{-2} complex: the β_{11-2} value for threonic acid is much lower than that for gluconic acid with a difference in the log β values of 1.8 logarithmic unit. All these remarks seem to prove that the hydroxy group in the γ-position is effectively the second deprotonated hydroxy function in gluconic acid.

Conclusion

This study confirms the view that gluconic acid is a good complexing agent towards the trivalent lanthanide ions. It also shows that the presence of five hydroxy functions in the chain is important for the stability of the complexes, either by their direct intervention in the complexation or by their interaction with solvent molecules in aqueous solutions. Polyhydroxy carboxylic acids with a smaller number of carbon atoms (and consequently of hydroxy functions) are less efficient.

The observation of a relative selectivity of complexation along the lanthanide series allows us to envisage using gluconic acid derivatives as extracting selective agents for lanthanides. For this purpose, hydrophobic derivatives must be synthesized − keeping the complexing ability of this molecule, but with a high solubility in organic solvents − for a use in liquid-liquid extraction. We already reported the preparation of hydrophobic derivatives of tartaric acid, HOOC−CHOH−CHOH−CONHR, where R is a long alkyl chain.[13] The preparation of hydrophobic ligands with a longer hydrophilic chain (with more OH functions) is in progress.

Experimental Section

Materials: Lanthanum, praseodymium, europium, dysprosium, and erbium nitrates (Strem Chem, 99.9%), lutetium perchlorate (Alfa Products, 99.9%), and sodium perchlorate (Fluka, 99%) were used without further purification. The concentration of the lanthanide(III) solutions was determined by a standard procedure using EDTA (Merck). pH-metric titrations were performed with NaOH (Merck or SDS) standard solutions. Potassium D-gluconate (99%), D-glyceric acid hemicalcium salt (≥ 98%), L-threonic acid hemicalcium salt (> 97%), and sodium 2-hydroxybutanoate (> 97%) were Fluka products. Sodium (*R*)-3-hydroxybutanoate (99%) was purchased from Aldrich.

pH-Metric Measurements: The acidity and complex formation constants were determined by pH-metric titrations at 298.0 ± 0.1 K and at an ionic strength I = 0.1 mol·L^{-1} ($NaClO_4$) under argon, using an automatic titration set, including a Metrohm Dosimat 665

autoburette and a Mettler Toledo Inlab 422 type combined glass electrode. The different equilibria were characterized by Equation (1), where M denotes the lanthanide(III) ion and L the ligand in the carboxylate form. Generally, charges were omitted, but they can be easily calculated.

$$pM + qL + rH \rightleftharpoons M_pL_qH_r$$

$$\beta_{pqr} = \frac{[M_p\ L_q\ H_r]}{[M]^p\,[L]^q\,[H]^r} \quad (1)$$

The description of the procedure for data evaluation using the PSEQUAD[27] computer program was described earlier.[28,29] The acidity and complex formation constants were determined, respectively, from four and six to eight independent titrations (about 100 data points per titration). The concentration of the ligands was about $5-8 \times 10^{-3}$ mol·L^{-1} and the ligand/metal (L/M) ratio was varied form 1:1 to 5:1. The pH-metric data between pH = 2 and 11.3 (or between pH = 2 and the pH of precipitation when precipitation occurred in the presence of a metal ion) were used for the evaluation of the acidity and complexation constants. The errors indicated for the complexation constants are those given by the PSEQUAD computer program. It was verified that the use of hemicalcium salts for glyceric and threonic acids had no consequence on the determination of the complexation constants. The acidity constants for compounds in the presence or absence of the calcium(II) ion are nearly identical. For the analysis of the titration curves, the formation of the hydroxo complex MOH^{2+} (MH_{-1}) was taken into consideration with the following values for the formation constant (log β_{10-1}): −9.33, −8.82, −8.58, −8.37, −8.26, and −8.17 for La^{III}, Pr^{III}, Eu^{III}, Dy^{III}, Er^{III}, and Lu^{III}, respectively.[30]

NMR Spectroscopy: ^{1}H and ^{13}C NMR spectra were recorded with a Bruker DRX400 apparatus at 400 and 100.6 MHz, respectively. The gluconic acid concentration, for the shift analysis, was 0.5 mol·L^{-1} and the L/M ratios varied from 10:1 to 250:1. The solvent was a mixture of H_2O/D_2O (80:20, v/v) and the pH was adjusted to 4.0 with NaOH or $HClO_4$. For the determination of the pseudocontact and contact contributions to the chemical shift, the parameters D and $\langle S_z \rangle$ are D = 2.972, −10.682, and −28.545, and $\langle S_z \rangle$ = 10.99, −4.05, and 100 for Pr ^{III}, Eu^{III}, and Dy^{III}, respectively.[22−23,31,32]

Acknowledgments

NMR spectra were recorded with the apparatus of the "Service Commun de RMN" of the University Henri Poincaré-Nancy 1. The authors are grateful to Stephane Parant for his technical assistance.

[1] S. Gosset, *Inf. Chim.* **1988**, *296*, 127.
[2] D. T. Sawyer, *Chem. Rev.* **1964**, *6*, 633 and references cited therein.
[3] K. Burger, L. Nagy in: K. Burger (Ed.), *Biocoordination chemistry*, Ellis Howard Series in Inorganic Chemistry (series Ed.: J. Burgess), Ellis Howard, Chichester, UK, **1990**, chapter III and references cited therein.
[4] W. R. Carper, D. B. Coffin, *Inorg. Chim. Acta* **1990**, *167*, 261.
[5] R. E. Sheperd, Y. Isaacson, L. Chensny, S. Zhang, R. Kortes, J. Kevin, *Inorg. Biochem.* **1993**, *49*, 23.
[6] M. L. Ramos, M. M. Caldeira, V. M. S. Gil, *Carbohydr. Res.* **1997**, *304*, 97.
[7] T. Gajda, B. Gyurcsik, T. Jakusch, K. Burger, B. Henry, J. J. Delpuech, *Inorg. Chim. Acta* **1998**, *130*, 275.
[8] G. D. Bailey, W. R. Carper, *J. Inorg. Nucl. Chem.* **1993**, *52*, 99.
[9] M. E. Escandar, L. F. Scala, M. G. Sierra, *Polyhedron* **1994**, *13*, 143.
[10] L. J. Katzin, *Inorg. Chem.* **1968**, *7*, 1183.
[11] S. Giroux, P. Rubini, B. Henry, S. Aury, *Polyhedron* **2000**, *19*, 1567.
[12] D. T. Sawyer, R. T. Ambroise, *Inorg. Chem.* **1962**, *1*, 296 from ref.[11].
[13] S. Giroux, P. Rubini, C. Gérardin, C. Selve, B. Henry, *New. J. Chem.* **2000**, *24*, 173.
[14] R. Motekaitis, A. Martell, *Inorg. Chem.* **1984**, *23*, 18.
[15] J. Krukak, I. Filipovic, *Croat. Chem. Acta* **1979**, *52*, 207.
[16] M. Hlaibi, S. Chapelle, M. Benaissa, *Inorg. Chem.* **1995**, *34*, 4434; S. Eberle, J. Schaefer, *J. Inorg. Nucl. Chem.* **1969**, *31*, 1523.
[17] G. Duc, G. Thomas-David, *Bull. Soc. Chim. Fr.* **1979**, *1*, 163.
[18] C. Crutchfield, W. NcNabb, J. Hazel, *J. Inorg. Nucl. Chem.* **1962**, *24*, 291.
[19] A. E. Martell, R. M. Smith, *Critical Stability Constants*, Plenum Press, New York, **1974−1977**, **1982**, vol. 1−5.
[20] T. Moeller, *J. Chem. Educ.* **1970**, *47*, 417.
[21] P. Rubini, C. Ben Nasr, L. Rodehüser, J.-J. Delpuech, *Magn. Reson. Chem.* **1987**, *27*, 609.
[22] M. Golding, M. P. Halton, *Aust. J. Chem.* **1972**, *27*, 2577.
[23] B. Bleaney, C. M. Dobson, B. A. Levine, R. B. Martin, R. J. Williams, A. V. Xavier, *J. Chem. Soc., Chem. Commun.* **1972**, 791.
[24] S. Ganapathy, V. P. Chacko, R. G. Bryant, M. C. Etter, *J. Am. Chem. Soc.* **1986**, *108*, 3159.
[25] T. Lis, *Acta Crystallogr., Sect. B* **1979**, *35*, 1699.
[26] T. Lis, *Acta Crystallogr., Sect. C* **1984**, *40*, 374.
[27] L. Zékány, L. Nagypal, *Computational Methods for the Determination of Stability Constants* (Ed.: D. Legget), Plenum, New York, **1995**, chapter 8.
[28] T. Gajda, B. Henry, A. Aubry, J.-J. Delpuech, *Inorg. Chem.* **1996**, *35*, 586.
[29] P. Surdy, P. Rubini, N. Buzas, B. Henry, L. Perrerito, T. Gajda, *Inorg. Chem.* **1999**, *38*, 346.
[30] U. K. Frolova, V. N. Kumok, V. V. Serebrennnikov, *Izvestiya Vysshikh Uchebnykh Zavedenii SSSR, Khimiya i Khimicheskaya Technologiya* **1966**, *9*, 176; *Chem. Abstr.* **1966**, *65*, 9816C.
[31] B. Bleaney, *J. Magn. Reson.* **1972**, *8*, 91.
[32] R. M. Golding, P. Pyykkö, *Mol. Phys.* **1973**, *26*, 1389.

Received October 1, 2001
[I01383]

Photochemical Studies of *cis*(CO),*trans*(Cl)-[Ru(bpy)(CO)$_2$Cl$_2$] (bpy = 2,2′-bipyridine): Ligand Exchange Reactions in Methanol

Esa Eskelinen,[a] Toni-J. J. Kinnunen,[a] Matti Haukka,*[a] and Tapani A. Pakkanen[a]

Keywords: Photochemistry / Ruthenium / Cyclic voltammetry / N ligands / O ligands

The complex *cis*(CO),*trans*(Cl)-[Ru(bpy)(CO)$_2$Cl$_2$] (**1**) (bpy = 2,2′-bipyridine) complex was photoirradiated with visible light in methanol. Light-induced ligand substitution and alcohol coordination was observed under these conditions. The replacement of a carbonyl ligand with methanol is proposed to be the initial reaction step. The reaction product was characterized by NMR spectroscopy and cyclic voltammetry. The substitution of weakly bound alcohol occurred readily in acetonitrile, leading to the formation of more stable [Ru(bpy)(CO)(CH$_3$CN)Cl$_2$]. Extended (24 h) irradiation of *cis*(CO),*trans*(Cl)-[Ru(bpy)(CO)$_2$Cl$_2$] in methanol resulted in the formation of the dinuclear, mixed-valence complex [{Ru(bpy)}$_2$(μ-OMe)$_2$(CO)Cl$_3$] (**2**). The structure of **2** consists of two Ru(bpy) moieties, which are linked by two methoxide bridges. These results showed that photoirradiation can be utilized in the synthesis of alkoxide-bridged ruthenium complexes.

(© Wiley-VCH Verlag GmbH, 69451 Weinheim, Germany, 2002)

Introduction

Alkoxides play an important role in organometallic chemistry owing to the increased need for the oxygenation of non-hydrocarbon ligands. The most straightforward way to synthesize metal alkoxides is the direct reaction of a main-group metal or metal complex with alcohols.[1,2] In the case of transition metals, the preparation of a metal−oxygen single bond is more complicated. The early transition metals tend to form more stable metal alkoxides than the late transition metals. The difference has been rationalized in terms of electronegativity: the more electropositive early transition metals form isolable alkoxo complexes.[2,3] Alkoxides are also hard, basic ligands while the late transition metals (groups 8−10) are seen as soft metals.[3]

In the course of the past ten years, the synthesis and reactions of (alkoxo)rhodium, -iridium, and -osmium complexes have been intensively studied.[4] However, much less attention has been paid to the ruthenium alkoxides, although complexes with the other related oxygen ligands such as aryloxo, or simple hydroxo, are well known.[4] Dinuclear, mixed-valence ruthenium complexes with bridging alkoxo ligands are even less common.[5−7] Mixed-valence complexes are of particular interest because they offer an opportunity to study electron transfer and electron delocalization in a dinuclear system.[8] Although alkoxy-bridged complexes are rare, there are several examples of other bridging ligand systems with mixed ruthenium valences. Probably the most familiar ones are the Creutz−Taube ion ($Ru^{II}Ru^{III}$) and dinuclear μ-oxo-ligated ruthenium complexes ($Ru^{III}Ru^{IV}$).[9]

Photoinduced reactions have been used as a synthetic route to the substituted (bipyridine)ruthenium(II) [Ru^{II}(bpy)] complexes. It is well known that in coordinating solvents such as CH_3CN, the photoirradiation of [Ru(bpy)(CO)$_2$Cl$_2$] leads to the replacement of monodentate ligands with a solvent molecule.[10−13] On the other hand, in weakly coordinating solvents such as CH_2Cl_2, the formation of the dimeric complex [Ru(bpy)(CO)Cl$_2$]$_2$ has been reported.[14] The solvent effects on Ru^{II}(bpy) complexes under UV/Vis irradiation have been studied and the coordination mode has been found to be associated with photoinduced oxidations and reductions.[15,16] It has also been shown that under steady-state irradiation the bipyridyl-based bridges in dinuclear Ru^{II} complexes are broken as a result of the photosolvation of acetonitrile or methanol.[17]

In the present paper we describe the photoirradiation of mono(bpy) complex *cis*(CO),*trans*(Cl)-[Ru(bpy)(CO)$_2$Cl$_2$] (**1**) in methanol. The stepwise reactions were monitored by means of cyclic voltammetry (CV) and spectroscopic methods.

Results and Discussion

Earlier studies[18,19] on the photochemical reactivity of the mono(bipyridine) complex [Ru(bpy)(CO)$_2$Cl$_2$] in a coordinating solvent (acetonitrile) showed that the initial photosubstitution takes place in two steps. In the first step, one

[a] Department of Chemistry, University of Joensuu,
P. O. Box 111, 80101 Joensuu, Finland
Fax: (internat.) + 358-13/251-3390
E-mail: Matti.Haukka@joensuu.fi

CO ligand is photosubstituted with CH_3CN, leading to the formation of $[Ru(bpy)(CO)(CH_3CN)Cl_2]$. When photoirradiation continues, further substitution occurs and the complex $[Ru(bpy)(CH_3CN)_3Cl]^+$ is formed.[18,19] On the other hand, photoirradiation in a noncoordinating solvent, CH_2Cl_2, is reported to lead to the dichloro-bridged dimer $[Ru(bpy)(CO)Cl_2]_2$ through a five-coordinate intermediate.[14]

Photoirradiation of *cis*(CO),*trans*(Cl)-[Ru(bpy)(CO)$_2$Cl$_2$] (1)

When the photoirradiation of complex **1** was performed in a closed, water-cooled vessel, a photoinduced loss of a carbonyl ligand was observed. During irradiation, the carbonyl ligand was probably replaced with methanol, forming $[Ru(bpy)(CO)(CH_3OH)Cl_2]$. The IR spectrum of the methanol solution of the initial complex **1** contained two strong carbonyl stretching bands at 2065 cm^{-1} and 2005 cm^{-1}. After 2 min of irradiation, a new peak at 1965 cm^{-1} was observed in the IR spectrum. The original CO peak pair disappeared completely after 30 min. The color of the methanol solution of **1** changed from pale yellow to dark orange during irradiation. Simultaneously, the absorption maximum in the visible-region spectra shifted from 340 nm to 492 nm, respectively. The similarities between the previously reported IR and absorption spectra of the *cis*(CO),*trans*(Cl)-$[Ru(bpy)(CO)_2Cl_2]$ irradiated in acetonitrile[19] and the current results in methanol, suggest the simple replacement of a carbonyl ligand by a neutral methanol ligand as the first reaction step.

The irradiation product was isolated as an orange-brown solid, which was dissolved in $[D_6]$DMSO and analyzed with ^{1}H NMR. The spectrum exhibited eight signals in the aromatic region, which are attributable to the two sets of aromatic protons. Such a pattern indicates that there are different ligands in *trans* positions to the bipyridine nitrogen atoms and that a structural rearrangement from *cis*(CO),*trans*(Cl)-$[Ru(bpy)(CO)_2Cl_2]$ to a less symmetrical product has occurred. Furthermore, the ^{1}H NMR spectrum also showed the characteristic peaks of methanol (see Exp. Sect.), indicating coordinated methanol and supporting $[Ru(bpy)(CO)(CH_3OH)Cl_2]$ as the first photoproduct.

The nature of the isolated photoproduct was further studied by dissolving it in strongly coordinating CH_3CN. The solution was then evaporated to dryness and the solid residue dried in a vacuum. The crystals obtained after this procedure were characterized by single-crystal X-ray crystallography. The X-ray analysis showed that the substitution of the MeOH ligand by CH_3CN had occurred, resulting in the formation of $[Ru(bpy)(CO)(CH_3CN)Cl_2]$. In this known structure,[19] the CH_3CN ligand is located in the *trans* position to the chloro ligand, which shows that a geometrical change takes place during the decarbonylation−acetonitrile coordination process.

The ligand replacement from CH_3OH to CH_3CN was also observed in CV studies. A clear, reversible-wave system ($E_{1/2}$ = 0.78 V, ΔE_p = 110 mV) was found with several weaker peak systems. It was found earlier that, after the irradiation of **1** in CH_3CN, a reversible-wave system appears at $E_{1/2}$ = 0.78 V, corresponding to the formation of $[Ru(bpy)(CO)(CH_3CN)Cl_2]$.[19] The ligand electrochemical parameter E_L (Lever parameter)[20] for $[Ru(bpy)(CO)(CH_3CN)Cl_2]$ was also calculated in order to find the most probable Ru^{II}/Ru^{III} potentials. The calculated value for $[Ru(bpy)(CO)(CH_3CN)Cl_2]$ is 0.70 V, which is reasonably close to the observed value. According to the CV data, no change in the oxidation state of the ruthenium metal was observed during the replacement of CH_3OH to CH_3CN. The preservation of the original oxidation state +II further supports the assumption of simple CO replacement by a neutral ligand, i.e., methanol, as the initial reaction step.

Prolonged Photoirradiation (24 h) of 1 and the Formation of [{Ru(bpy)}$_2$(μ-OMe)$_2$(CO)Cl$_3$] (2)

The infrared spectrum of the solution after long (24 h) irradiation in a closed, water-cooled reaction vessel showed the loss of the carbonyl peaks. The absorption spectrum of the final solution contained only one absorption maximum, in the visible-light region at 419 nm. The changes in the IR and UV/Vis spectra during the stepwise photoirradiation are shown in Figures 1 and 2.

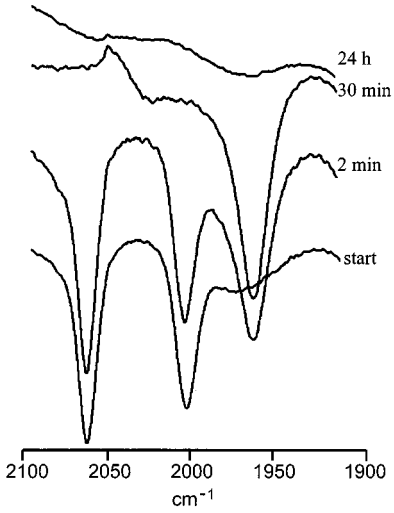

Figure 1. Changes in the ν(CO) region in methanol solution of *cis*(CO),*trans*(Cl)-Ru(bpy)(CO)$_2$Cl$_2$ (**1**) as a function of the photoirradiation time

The evaporation of solvent from the reaction mixture after 24 h of photoirradiation in a closed reaction vessel resulted in the formation of a brownish solid photoproduct, which shows a single carbonyl band at 1941 cm^{-1} in KBr. The same product was obtained in crystalline form by slow evaporation of the methanol in a refrigerator. The structure of this mixed-valence $Ru^{II}Ru^{III}$ dimer, $[\{Ru(bpy)\}_2(\mu\text{-}OMe)_2(CO)Cl_3]$ (**2**), is shown in Figure 3. In **2** the coordination environment surrounding the ruthenium center is octahedral. The Ru−O bond lengths of 2.040(2) Å and 2.087(2) Å are quite similar to the reported distances in the alkoxy-bridged Ru^{II} or Ru^{II}/Ru^{III} complexes in general.[5−8,21] The O−Me bond is slightly bent from the plane determined by Ru−Ru−O. In the closely related compound

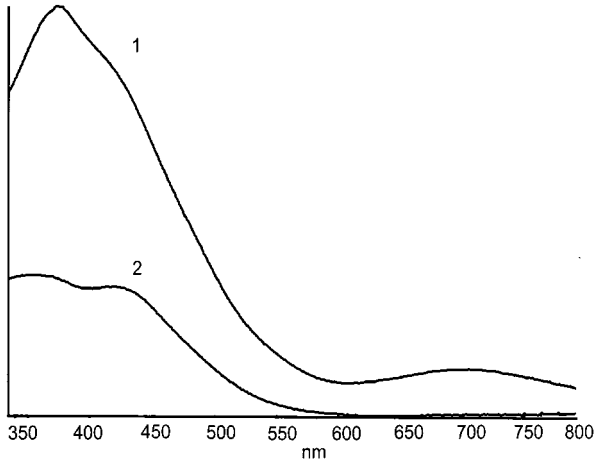

Figure 2. Absorption spectra of complex **1** after photoirradiation in open (1) and closed (2) reaction vessels measured directly from the methanol solutions

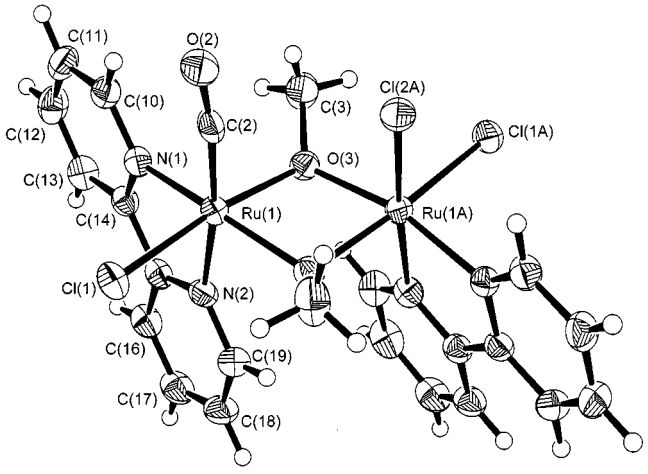

Figure 3. Structure of [{Ru(bpy)}$_2$(μ-OMe)$_2$(CO)Cl$_3$]

[{Ru(bpy)$_2$}$_2$(OMe)$_2$](PF$_6$)$_2$ the corresponding Ru−Ru−O−C torsion angles are 167.0° and 169.0°.[21] However, the torsion angles of 137.7° and 138.8° found in complex **2** are comparable with the values found in the Ru^{II} complexes.[8,21]

The photoinduced chloride ligand exchange reactions of [(mono)bipyridine]ruthenium compounds in strongly coordinating solvents with extended irradiation have been reported earlier.[19] The photoinduced ejection of chloride is also required in the case of [Ru(bpy)(CO)(CH$_3$OH)Cl$_2$] to obtain the bimetallic complex [{Ru(bpy)}$_2$(μ-OMe)$_2$-(CO)Cl$_3$]. Figure 3 shows that isomerization has taken place at some point during the photoirradiation. The *trans*(Cl) geometry of the starting complex, [Ru(bpy)(CO)$_2$Cl$_2$], has been converted into the *cis*(Cl) isomer. This change occurs during the initial coordination of methanol, as was concluded in the case of 30 min of irradiation. Moreover, the deprotonation of methanol is needed to build up the methoxy bridges. The origin of this deprotonation process may lie in the photochemical basis, where the reaction intermediate abstracts protons from nucleophilic methanol molecules.

During the formation of the mixed-valence complex **2**, one of the ruthenium centers is oxidized. However, the detailed reaction mechanism for this redox reaction is not clear. The first examples of alkoxy-bridged dinuclear ruthenium(II) complexes were reported by Ward et al. in the 1990s.[8,21] It should be noted that Ward et al. synthesized the [{Ru(bpy)$_2$}$_2$(μ-OMe)$_2$](PF$_6$)$_2$ complex in refluxing methanol using added KOH, while in our case the photoirradiation in MeOH resulted directly in [{Ru(bpy)}$_2$(μ-OMe)$_2$(CO)Cl$_3$] without any added hydroxide. The simple photoirradiation in alcohol is thus a convenient way to synthesize dinuclear alkoxy-bridged ruthenium complexes.

It is worth mentioning that the ν(CO) of [{Ru(bpy)}$_2$(μ-OMe)$_2$(CO)Cl$_3$] at 1941 cm^{-1} was observed only in the solid samples measured in KBr. In solution, no IR peaks were found after 24 h of irradiation. However, when, after a prolonged irradiation in a closed vessel, the solution was allowed to stand overnight in the dark, a partial recovery of the CO band at 1965 cm^{-1} was observed. This phenomenon must be due to the presence of a labile, completely decarbonylated reaction product in solution. In the dark, the liberated CO is then able to recoordinate and the formation of carbonyl-containing [Ru(bpy)(CO)(CH$_3$OH)Cl$_2$] occurs. Experiments in an open reaction vessel prevented the CO recovery completely, indicating the absence of a recoverable species in solution. When an open system was used during irradiation, the absorption spectrum also gave a different maximum at 711 nm, instead of the 419 nm found in the closed-vessel experiments (Figure 2). In this case, no recovery of CO bands was observed, even after the solution was extensively bubbled with CO for several hours.

Experimental Section

Materials: Methanol (Riedel−de Haën, p.a. grade) was used without further purification. Acetonitrile (J. T. Baker, analytical grade) and tetrabutylammonium perchlorate (TBAP) were used as received. Monomeric *trans*(Cl)-[Ru(bpy)(CO)$_2$Cl$_2$] complex (**1**) (bpy = 2,2′-bipyridine) was prepared by a literature method.[22]

Spectroscopic Studies: The FTIR spectra were measured with a Nicolet Magna 750 spectrometer, ^{1}H NMR spectra with a Bruker AMX 400 (400 MHz) spectrometer in [D$_6$]DMSO, and UV/Vis spectra with a Perkin−Elmer Lambda 900 UV/Vis/NIR spectrometer. The elemental analyses were performed with an EA1110 CHNS-O (Carlo Erba Instruments) analyzer.

Photochemical Instrumentation and Procedure: In the photolysis experiments all of the samples were irradiated using a 450-W Xe discharge lamp (Oriel model 8540, UV light blocked out at 320 nm with a glass filter). The photolysis cell was water-cooled to prevent heating and the vessel was closed with a septum. When necessary, the CO was removed through a needle. The path length of the cell was 3 cm and the distance from the lamp was approximately 20 cm. Irradiation of the sample solutions (30 mg of [Ru(bpy)(CO)$_2$Cl$_2$] in 30 mL of solvent) was performed under air and monitored by the IR and UV/Vis spectra. The total period of irradiation was 24 h.

Electrochemical Instrumentation and Procedure: The CV was performed under argon at room temperature in a three-electrode cell using an Autolab PGSTAT20 potentiostat-galvanostat. The solutions for measurements were prepared by concentrating the photoproduct sample to dryness and dissolving this residue in 0.1 M TBAP/CH_3CN. The sample solutions were purged with argon prior to use. The working electrode was a platinum disk (Metrohm, area 1.28 cm^2), and the counter electrode a glassy carbon disk (Metrohm, area 0.28 cm^2). Potentials were referred to an Ag^+/Ag electrode (0.01 mol/dm^3 $AgNO_3$ in CH_3CN). Under the experimental conditions, the Fc^+/Fc couple potential was 0.01 V. In all of the experiments the potential scan rate was 100 $mV \cdot s^{-1}$. The cyclic voltammograms were mainly recorded in a positive region because in [mono(bpy)]ruthenium complexes the Ru^{II}/Ru^{III} redox reactions typically take place at the positive potentials versus the Ag/Ag^+ reference electrode. At the negative potentials all of the redox peaks were assigned to the bipyridine-based reactions.

Characterization of Complex [Ru(bpy)(CO)(CH_3OH)Cl_2]: FT-IR (CH_3OH): $\tilde{\nu}$ = 1965 cm^{-1} (vs, ν_{CO}). UV/Vis (CH_3OH): λ_{max} = 492 nm. ^1H NMR ([D_6]DMSO): δ = 9.53 (d, 1 6-H), 8.96 (d, 1 6′-H), 8.76 (d, 1 3-H), 8.67 (d, 1 3′-H), 8.38 (t, 1 4-H), 8.16 (t, 1 4′-H), 7.94 (t, 1 5-H), 7.61 (t, 1 5′-H), 4.12 (q, 1 H, CH_3OH), 3.17 (d, 3 H, CH_3OH). Note: satisfactory elemental analysis was not obtained for this complex owing to the small amounts of impurities, which could be seen in the NMR spectra.

Characterization of Complex [{Ru(bpy)}$_2$(μ-OMe)$_2$(CO)Cl_3]: FT-IR (KBr): $\tilde{\nu}$ = 1941 cm^{-1} (vs, ν_{CO}). UV/Vis (CH_3OH): λ_{max} = 365 nm. [{Ru(bpy)}$_2$(μ-OMe)$_2$(CO)Cl_3]·(CH_3OH) (742.98): calcd. C 38.80, N 7.54, H 3.53; found C 35.68, N 7.18, H 3.47. Note 1: ^1H NMR spectra measured in [D_6]DMSO revealed the different nature of the two aromatic bipyridine ligands and the non-equivalency of four pyridine rings. Note 2: The difference between the calculated and found values in the elemental analyses is due to the varying amounts of solvent or water present in the bulk material even though the sample was carefully dried in a vacuum. The crystal structure was solved with one CH_3OH molecule per [{Ru(bpy)}$_2$(μ-OMe)$_2$(CO)Cl_3] unit.

Formation of [{Ru(bpy)}$_2$(μ-OMe)$_2$(CO)Cl_3] Crystals, X-ray Data Collection, and Structure Solution for [{Ru(bpy)}$_2$(μ-OMe)$_2$(CO)Cl_3]·(CH_3OH): Crystals of [{Ru(bpy)}$_2$(μ-OMe)$_2$(CO)Cl_3] suitable for structural characterization were formed from the photolyzed methanol solution of **1** after slow concentration in a refrigerator. The X-ray diffraction data were collected with a Nonius Kappa CCD diffractometer using Mo-K_α radiation (λ = 0.71073 Å) and the Collect[23] data collection program. The Denzo-Scalepack[24] program package was used for cell refinements and data reduction. The structure was solved by direct methods using the SHELXS97[25] program and the WinGX[26] graphical user interface. The structural refinement was carried out by means of the SHELXL97[27] program. The structure was solved in the orthorhombic space group *Pbcn* and the asymmetric unit consisted of one half-molecule. The carbonyl ligand C(2)−O(2) and chloride Cl(2) were disordered and mixed in two positions with the equal population parameter 0.5. The solvent methanol was disordered around a special position with equal population parameter and was only refined isotropically. As a result of the disorder, the OH hydrogen atom of the solvent molecule was omitted. All of the other hydrogen atoms were placed in idealized positions and constrained to ride on their parent atom. The crystallographic data are summarized in Table 1. Selected bond lengths and angles are shown in Table 2. The molecular structure of the complex is presented in Figure 3. CCDC-168110 contains the supplementary crystallographic data for this paper. These data can be obtained free of charge at www.ccdc.cam.ac.uk/conts/retrieving.html or from the Cambridge Crystallographic Data Centre, 12, Union Road, Cambridge CB2 1EZ, UK [Fax: (internat.) + 44-1223/336-033; E-mail: deposit@ccdc.cam.ac.uk].

Table 1. Crystallographic data for [{Ru(bpy)}$_2$(μ-OMe)$_2$-(CO)Cl_3]·(CH_3OH)

	1
Empirical formula	$C_{24}H_{26}Cl_3N_4O_4Ru_2$
Formula mass	742.98
Crystal system	orthorhombic
Space group	*Pbcn*
λ [Å]	0.71073
a [Å]	8.43100(10)
b [Å]	16.5539(3)
c [Å]	19.0094(2)
V [Å^3]	2653.06(6)
T [K]	150(2)
Z	4
$D_{calcd.}$ [g/cm^3]	1.860
μ [mm^{-1}]	1.480
Number of refl. collected	5056
Number of refl. observed	2306
Number of unique refl.	2710
R_{int}	0.0126
*R*1 ($I > 2$)	0.0327
*wR*2 ($I > 2$)	0.0788

Table 2. Selected bond lengths and angles for [{Ru(bpy)}$_2$(μ-OMe)$_2$(CO)Cl_3]·(CH_3OH)

Bond	Å
Ru(1)−Cl(1)	2.3880(9)
Ru(1)−Cl(2)	2.322(4)
Ru(1)−N(1)	2.047(3)
Ru(1)−N(2)	2.091(3)
Ru(1)−C(2)	1.868(16)
Ru(1)−O(3)	2.040(2)
Ru(1)−O(3A)	2.087(2)
C(2)−O(2)	1.152(18)
O(3)−C(3)	1.406(5)
Angle	**°**
N(1)−Ru(1)−N(2)	78.64(11)
Ru(1)−C(2)−O(2)	171(2)
Cl(1)−Ru(1)−Cl(2)	92.06(16)
Ru(1)−O(3)−C(3)	120.4(2)
Ru(1A)−O(3)−C(3)	122.5(2)
Ru(1)−O(3)−Ru(1A)	101.33(10)

Acknowledgments

The financial support provided by the Academy of Finland for this work is gratefully acknowledged.

[1] J. Mayer, *Polyhedron* **1995**, *14*, 3273−3292.
[2] D. C. Bradley, R. C. Mehrotra, D. P. Gaur, *Metal Alkoxides*; Academic Press, London, **1978**.
[3] H. E. Bryndza, W. Tam, *Chem. Rev.* **1988**, *88*, 1163−1188.
[4] R. G. Bergman, *Polyhedron* **1995**, *14*, 3227−3237.
[5] S. D. Loren, B. K. Campion, R. H. Heyn, T. D. Tilley, B. E. Bursten, K. W. Luth, *J. Am. Chem. Soc.* **1989**, *111*, 4712−4718.
[6] R. O. Gould, T. A. Stephenson, D. A. Tocher, *J. Organomet. Chem.* **1984**, *263*, 375−384.
[7] U. Kölle, J. Kossakowski, R. Boese, *J. Organomet. Chem.* **1989**, *378*, 449−455.
[8] D. Bardwell, J. C. Jeffery, L. Joulié, M. D. Ward, *J. Chem. Soc., Dalton Trans.* **1993**, 2255−2256.
[9] M. D. Ward, *Chem. Soc. Rev.* **1995**, 121−134.
[10] D. V. Pinnick, B. Durham, *Inorg. Chem.* **1984**, *23*, 1440−1445.
[11] B. Durham, J. L. Walsh, C. L. Carter, T. J. Meyer, *Inorg. Chem.* **1980**, *19*, 860−865.
[12] R. F. Jones, D. J. Cole-Hamilton, *Inorg. Chim. Acta* **1981**, *53*, L3−L5.
[13] S. Gould, T. O'Toole, T. J. Meyer, *J. Am. Chem. Soc.* **1990**, *112*, 9490−9496.
[14] G. B. Deacon, C. M. Kepert, N. Sahely, B. W. Skelton, L. Spiccia, N. C. Thomas, A. H. White, *J. Chem. Soc., Dalton Trans.* **1999**, 275−277.
[15] J. M. Kelly, C. M. O′Connell, J. G. Vos, *J. Chem. Soc., Dalton Trans.* **1986**, 253−258.
[16] C. C. Tong, M. Winkelman, A. Jain, S. P. Jensen, P. E. Hoggard, *Inorg. Chim. Acta* **1994**, *226*, 247−250.
[17] N. Veletsky, I. A. Dementiev, A. Yu. Ershov, A. B. Nikol'skii, *J. Photochem. Photobiol.* **1995**, *89*, 99−103.
[18] M.-N. Collomb-Dunand-Sauthier, A. Deronzier, R. Ziessel, *J. Organomet. Chem.* **1993**, *444*, 191−198.
[19] E. Eskelinen, M. Haukka, T. Venäläinen, T. A. Pakkanen, M. Wasberg, S. Chardon-Noblat, A. Deronzier, *Organometallics* **2000**, *19*, 163−169.
[20] A. B. P. Lever, *Inorg. Chem.* **1990**, *29*, 1271−1285.
[21] D. A. Bardwell, L. Horsburgh, J. C. Jeffery, L. F. Joulié, M. D. Ward, I. Webster, L. J. Yellowlees, *J. Chem. Soc., Dalton Trans.* **1996**, 2527−2531.
[22] M. Haukka, J. Kiviaho, M. Ahlgrén, T. A. Pakkanen, *Organometallics* **1995**, *14*, 825−833.
[23] *Collect, data collection software*, Nonius, **1999**.
[24] Z. Otwinowski, W. Minor, "DENZO-SCALEPACK, Processing of X-ray Diffraction Data Collected in Oscillation Mode", in: *Methods in Enzymology*, vol. 276 (Macromolecular Crystallography), part A (Eds.: C. W. Carter, Jr., R. M. Sweet), Academic Press, New York, **1997**, pp. 307−326.
[25] G. M. Sheldrick, *SHELXS97, Program for Crystal Structure Determination*, University of Göttingen, **1997**.
[26] L. J. Farrugia, *J. Appl. Crystallogr.* **1999**, *32*, 837−838.
[27] G. M. Sheldrick, *SHELXL97, Program for Crystal Structure Refinement*, University of Göttingen, **1997**.

Received October 1, 2001
[I01394]

Novel Ferrocene Derivatives with PH-Functionalized Phosphanylalkylcyclopentadienyl Ligands: Syntheses and Molecular Structures of *rac*-[Fe{(η^5-C_5H_4)CMe_2PHR}$_2$] (R = Ph, Mes) and *rac*-[Fe{(η^5-C_5H_4)$CMe_2PHPh(Cp^*TaCl_4)$}$_2$][‡]

Thomas Höcher,[a] Steffen Blaurock,[a] and Evamarie Hey-Hawkins*[a]

Dedicated to Professor Joachim Strähle on the occasion of his 65th birthday

Keywords: Metallocenes / P ligands / Bridging ligands / Secondary phosphanes / Tantalum

6,6-Dimethylfulvene reacts with LiPHMes (Mes = 2,4,6-$Me_3C_6H_2$) to give Li[(C_5H_4)CMe_2PHMes] (**1**). The ferrocene derivatives *rac*-[Fe{(η^5-C_5H_4)CMe_2PHR}$_2$] [R = Ph (**2**), Mes (**3**)] are obtained in high yield from the lithium reagents Li[(C_5H_4)CMe_2PHR] (R = Ph, Mes) and $FeCl_2$. Compound **2** reacts with [Cp^*TaCl_4] to give the heterotrinuclear complex *rac*-[Fe{(η^5-C_5H_4)$CMe_2PHPh(Cp^*TaCl_4)$}$_2$] (**4**). Compounds **1**–**4** were characterized spectroscopically, and crystal structure determinations were carried out on **2**–**4**.

(© Wiley-VCH Verlag GmbH, 69451 Weinheim, Germany, 2002)

Introduction

Since the first report of a cyclopentadienyl transition metal complex in which the cyclopentadienyl ligand bears a donor-functionalized side chain, by Mathey et al. in 1978,[1] this area has expanded rapidly.[2] While numerous *O*- and *N*-functionalized cyclopentadienyl ligands are known, the number of cyclopentadienes with a *P*-functionalized alkyl or silyl side chain is still small,[1,3] and only recently have we reported the first such compounds in which the P atom has a reactive P−H bond, namely, 1-$SiMe_2PHCy$-2,3,4,5-Me_4C_5H, Li_2[(C_5Me_4)$SiMe_2PR$] [R = Cy, 2,4,6-$Me_3C_6H_2$ (Mes)], Li[(C_5H_4)CMe_2PHR] (R = Ph, *t*Bu) and Li_2[(C_5H_4)CH_2CH_2PPh].[4,5] The molecular structures of [Li(tmeda)]$_2$[(C_5H_4)CMe_2PPh][6] and [Li(tmeda)]-[(C_5H_4)CMe_2PR_2][7] (R = Ph, Me) were also reported. Such compounds are useful precursors for mono- or dianionic bifunctional ligands in transition metal chemistry. Thus, the monoanionic phosphanylalkylcyclopentadienyl ligands can act as chelating ligands towards one metal center (**A**) or they can bridge two (different) metal centers (**B**) (M = metal, $M^1 = M^2$ or $M^1 \neq M^2$, L = ligands, X = spacer (alkylidene, arylidene), R = alkyl, aryl).

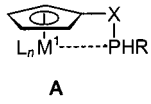

A

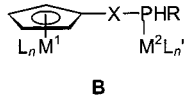

B

We have recently shown that Li_2[(C_5Me_4)$SiMe_2PR$] (R = Cy, Mes) reacts with $ZrCl_4$ to give [{(η^5-C_5Me_4)$_2SiMe_2$}$ZrCl_2$] and $(PCy)_4$ or $(PHMes)_2$, while Li[(C_5H_4)CMe_2PHR] reacts with $ZrCl_4$ or [$TiCl_3(THF)_3$] to yield [{(η^5-C_5H_4)CMe_2PHR}$_2ZrCl_2$] or [{(η^5-C_5H_4)CMe_2PHR}$_2$TiCl] (R = Ph, *t*Bu).[5] However, these complexes slowly decompose in solution with formation of [{(η^5-C_5H_4)$_2CMe_2$}MCl_2] (M = Zr, Ti).[5] Erker et al. reported that the complexes [{CyPCMe_2(η^5-C_5H_4)}$M(NR_2)_2$] (M = Ti, R = Me; M = Zr, R = Et) are active catalysts for the polymerization of α-olefins.[8]

We now report the synthesis of the novel stable PH-functionalized ferrocene derivatives *rac*-[Fe{(η^5-C_5H_4)-CMe_2PHR}$_2$] [R = Ph (**2**), Mes (**3**)] and the heterotrinuclear complex *rac*-[Fe{(η^5-C_5H_4)$CMe_2PHPh(Cp^*TaCl_4)$}$_2$] (**4**) of type **B**.

Ferrocene derivatives usually show enhanced stability and are generally nontoxic. Thus, their industrial applications range from additives for heating oil to reduce formation of soot, iron-containing fertilizers, UV absorbers and protective coatings for rockets and satellites.[9]

[‡] Parts of this work were presented as a poster at the 34th International Conference on Coordination Chemistry, Edinburgh, 9−14 July 2000 (abstract no. P0600) and at the XVth International Conference on Phosphorus Chemistry, Sendai, 29 July − 3 August 2001 (abstract no. PB065).

[a] Institut für Anorganische Chemie der Universität, Johannisallee 29, 04103 Leipzig, Germany
E-mail: hey@rz.uni-leipzig.de

Results and Discussion

Syntheses of Compounds 1−4.

As a general synthetic route to cyclopentadienes with *P*-functionalized side chains, the addition of alkali metal phosphanides to fulvenes has been employed.[3a−3c,4,5] Accordingly, 6,6-dimethylfulvene reacts with LiPHMes in Et_2O at room temperature to give the highly air and water sensitive compound Li[$(C_5H_4)CMe_2PHMes$] (**1**) [Equation (1)].

(1)

1

The ^1H NMR spectrum of **1** indicates that the methyl groups in P−C(Me_2) are prochiral and thus diastereotopic. Therefore, the two nonequivalent Me groups appear as two doublets due to P−H coupling [δ = 1.43 ($^3J_{P-H}$ = 8.8 Hz); δ = 1.41 ($^3J_{P-H}$ = 13.0 Hz)]. However, in the ^{31}P NMR spectrum, the two Me groups are equivalent, and a doublet of septets is observed. As was observed for Li[$(C_5H_4)CMe_2PHR$] (R = Ph,[4] Cy[5]), the signal is shifted to low field by ca. 110 ppm, and the P−H coupling constant increases by ca. 10−15 Hz relative to the primary phosphane [**1**: δ = −45.6 ($^1J_{P-H}$ = 216 Hz); PH_2Mes:[10] δ = −154.8 ($^1J_{P-H}$ = 203 Hz)]. Similarly, the signal of the PH group is shifted to low field in the ^1H NMR spectrum by ca. 0.2−0.9 ppm relative to the phosphane (**1**: δ = 4.36; PH_2Mes:[10] δ = 3.53). Compared with the signals of 6,6-dimethylfulvene (Me: δ = 2.19; C_5H_4: δ = 6.53−5.45),[11] the corresponding signals in **1** are shifted to high field (δ = 1.41, 1.43 and 5.56).

The ferrocene derivatives [Fe{(η^5-C_5H_4)CMe_2PHR}$_2$] [R = Ph (**2**), Mes (**3**)] are obtained in high yield from the lithium reagents Li[$(C_5H_4)CMe_2PHR$] (R = Ph, Mes (**1**)] and $FeCl_2$ in THF at room temperature [Equation (2)].

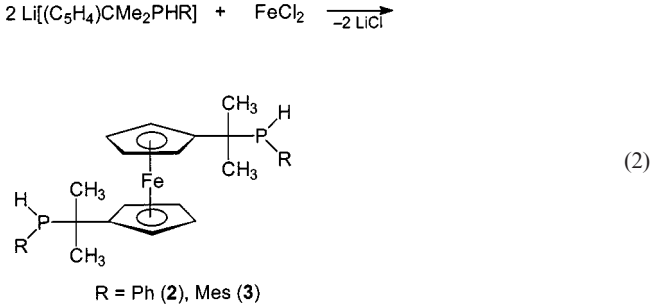

(2)

R = Ph (**2**), Mes (**3**)

After workup and repeated recrystallization from *n*-pentane (**2**) or toluene (**3**), the ferrocene derivatives are obtained as orange solids, which are air-stable, at least for a limited period of time. Due to the presence of two chiral phosphanyl groups, two diastereomers can be formed: the racemic form (*R*,*R* and *S*,*S* enantiomer) and the *meso* form (*S*,*R* enantiomer). As bulky substituents are present on the cyclopentadienyl rings, the antiperiplanar conformation is favored (see X-ray crystal structure determinations of **2**−**4** below).

No meaningful ^{31}P NMR spectra of the reaction mixture could be obtained due to the presence of small amounts of $FeCl_2$. However, the ^{31}P NMR spectra recorded for **2** at different stages of workup always indicated the presence of only one diastereomer. Thus, in the $^{31}P\{^1H\}$ NMR spectrum of crystalline **2**, only one signal is observed. However, in the ^{31}P NMR spectrum of **3**, obtained from *n*-hexane, two overlapping doublets of different intensity (ca. 4:1) are observed at δ = −33.4 and −33.9 with P−H coupling constants of 219 and 213 Hz, respectively, even at elevated temperature (340 K); this indicates the formation of both diastereomers, one of which is preferred. Recrystallization from toluene yields the preferred isomer (which was shown to be the *rac* isomer by crystal structure determination) as orange rod-like crystals. The *meso* isomer could not be obtained in pure form.

In the proton-coupled ^{31}P NMR spectrum of **2** and **3**, a doublet of multiplets is observed [**2**: δ = 8.8 ($^1J_{P-H}$ = 207 Hz); **3**: δ = −32.8 ($^1J_{P-H}$ = 214 Hz)], which are shifted to low field by ca. 10−13 ppm relative to Li[$(C_5H_4)CMe_2PHR$] (R = Ph, Mes). The complex coupling pattern in **2** arises from coupling of the protons of the Me and Ph groups. As was already observed for **1**, the ^1H NMR spectra of **2** and **3** indicate that the methyl groups in P−C(Me_2) are prochiral and thus diastereotopic. Thus, the two nonequivalent Me groups appear as two doublets due to P−H coupling [**2**: δ = 1.32 ($^3J_{P-H}$ = 12.0 Hz), 1.38 ($^3J_{P-H}$ = 12.4 Hz); **3**: δ = 1.39 ($^3J_{P-H}$ = 13.0 Hz), 1.45 ($^3J_{P-H}$ = 8.8 Hz)]. These signals and those of the P−H group are only slightly shifted relative to those of the lithium reagents, while a shift to high-field of ca. 1.8 ppm is observed for the C−H protons of the cyclopentadienyl rings.

At room temperature, the *ortho*-Me groups of the mesityl ring in **3** give a broad signal at δ = 2.27 in the ^1H NMR

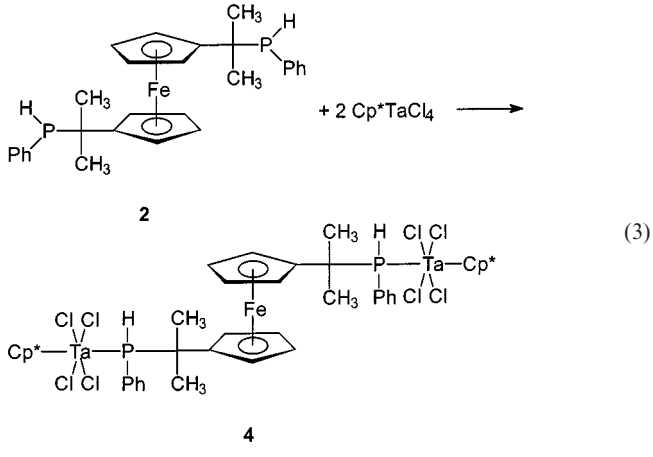

2

(3)

4

spectrum, indicating that rotation around the P−C(mesityl) bond is hindered. At 340 K, only one sharp signal is observed for the Me groups, while below 263 K two separate signals are observed. From the coalescence temperature [T_c = 291(2) K] the activation enthalpy ($\Delta G^{\#}$ = 56 ± 1 kJ/mol)[12] was determined by using the Eyring equa-

Table 1. Selected bond lengths [Å] and bond angles [°] for **2**−**4**

[Fe{(η^5-C_5H_4)CMe_2PHPh}$_2$] (**2**)			
Fe−C	2.045(5)−2.064(5)	P(1)−C(9)	1.823(3)
P(1)−C(6)	1.891(3)	P(1)−H(2P)	1.7(2)
P(1)−H(1P)	1.43(8)		
C(9)−P(1)−C(6)	103.3(1)	C(9)−P(1)−H(1P)	116(3)
C(6)−P(1)−H(1P)	101(3)	C(9)−P(1)−H(2P)	105(5)
C(6)−P(1)−H(2P)	119(5)	C(10)−C(9)−P(1)	120.8(3)
C(14)−C(9)−P(1)	120.7(3)	C(1)−C(6)−P(1)	103.4(2)
C(7)−C(6)−P(1)	109.4(3)	C(8)−C(6)−P(1)	110.8(3)
[Fe{(η^5-C_5H_4)CMe_2PHMes}$_2$] (**3**)			
Fe−C	2.042(2)−2.085(2)		
P(1)−C(14)	1.848(2)	P(1)−C(11)	1.903(2)
P(1)−H(1P)	1.25(3)	P(2)−C(26)	1.838(2)
P(2)−C(23)	1.901(2)	P(2)−H(2P)	1.0(1)
C(14)−P(1)−C(11)	107.55(9)	C(14)−P(1)−H(1P)	100(1)
C(11)−P(1)−H(1P)	98(1)	C(26)−P(2)−C(23)	106.87(9)
C(26)−P(2)−H(2P)	111(8)	C(23)−P(2)−H(2P)	99(8)
C(15)−C(14)−P(1)	117.7(2)	C(19)−C(14)−P(1)	123.2(2)
C(31)−C(26)−P(2)	122.7(2)	C(27)−C(26)−P(2)	118.8(2)
C(1)−C(11)−P(1)	110.7(1)	C(12)−C(11)−P(1)	108.8(2)
C(13)−C(11)−P(1)	103.3(2)	C(6)−C(23)−P(2)	110.3(1)
C(25)−C(23)−P(2)	109.4(1)	C(24)−C(23)−P(2)	103.8(1)
[Fe{(η^5-C_5H_4)CMe_2PHPh(Cp*$TaCl_4$)}$_2$] (**4**)			
Ta−C	2.446(5)−2.530(4)	Fe−C	2.040(5)−2.070(4)
Ta(1)−Cl(1)	2.400(1)	Ta(1)−Cl(2)	2.390(1)
Ta(1)−Cl(3)	2.404(1)	Ta(1)−Cl(4)	2.402(1)
Ta(2)−Cl(5)	2.393(1)	Ta(2)−Cl(6)	2.402(1)
Ta(2)−Cl(7)	2.388(1)	Ta(2)−Cl(8)	2.401(1)
Ta(1)−P(1)	2.758(1)	Ta(2)−P(2)	2.798(1)
P(1)−C(14)	1.829(4)	P(1)−C(11)	1.899(5)
P(1)−H(1P)	1.45(5)	P(2)−C(33)	1.821(4)
P(2)−C(30)	1.909(5)	P(2)−H(2P)	1.29(4)
Cl(2)−Ta(1)−Cl(1)	87.39(4)	Cl(2)−Ta(1)−Cl(4)	151.90(4)
Cl(1)−Ta(1)−Cl(4)	85.32(5)	Cl(2)−Ta(1)−Cl(3)	87.39(4)
Cl(1)−Ta(1)−Cl(3)	152.81(4)	Cl(4)−Ta(1)−Cl(3)	86.83(5)
Cl(2)−Ta(1)−P(1)	71.78(4)	Cl(1)−Ta(1)−P(1)	78.37(4)
Cl(4)−Ta(1)−P(1)	80.16(4)	Cl(3)−Ta(1)−P(1)	74.66(4)
C(14)−P(1)−Ta(1)	116.9(2)	C(11)−P(1)−Ta(1)	127.9(1)
C(14)−P(1)−C(11)	105.3(2)	C(14)−P(1)−H(1P)	99(2)
C(11)−P(1)−H(1P)	96(2)	Ta(1)−P(1)−H(1P)	106(2)
C(1)−C(11)−P(1)	104.7(3)	C(13)−C(11)−P(1)	112.6(4)
C(12)−C(11)−P(1)	106.8(3)	C(19)−C(14)−P(1)	118.8(4)
C(15)−C(14)−P(1)	123.1(4)	Cl(7)−Ta(2)−Cl(5)	152.66(4)
Cl(7)−Ta(2)−Cl(8)	86.34(5)	Cl(5)−Ta(2)−Cl(8)	88.10(5)
Cl(7)−Ta(2)−Cl(6)	86.91(4)	Cl(5)−Ta(2)−Cl(6)	85.19(5)
Cl(8)−Ta(2)−Cl(6)	151.24(4)	Cl(5)−Ta(2)−P(2)	74.66(4)
Cl(6)−Ta(2)−P(2)	72.44(4)	Cl(7)−Ta(2)−P(2)	78.01(4)
Cl(8)−Ta(2)−P(2)	78.80(4)	Ta(2)−P(2)−H(2P)	103(2)
C(33)−P(2)−Ta(2)	117.4(2)	C(30)−P(2)−Ta(2)	127.3(2)
C(30)−P(2)−H(2P)	100(2)	C(33)−P(2)−H(2P)	101(2)
C(6)−C(30)−P(2)	105.2(3)	C(31)−C(30)−P(2)	107.9(3)
C(32)−C(30)−P(2)	110.0(3)	C(38)−C(33)−P(2)	120.3(4)
C(34)−C(33)−P(2)	121.9(3)	C(33)−P(2)−C(30)	103.5(2)

tion.[13] Compound **2** reacts with [Cp*$TaCl_4$] in toluene at room temperature to give the heterotrinuclear complex *rac*-[Fe{(η^5-C_5H_4)CMe_2PHPh(Cp*$TaCl_4$)}$_2$] (**4**) [Equation (3)].

The trinuclear complex **4** is unstable in solution at room temperature. When brown crystals of **4** are dissolved in benzene or toluene at room temperature, a white precipitate forms after only a few minutes. Thus, for the NMR spectroscopic studies the crystals were cooled to −195 °C in an NMR tube and the solvent ([D_8]toluene or [D_6]benzene) was added at this temperature. The sample was warmed to ca. −50 °C prior to the NMR spectroscopic studies.

At −50 °C, two doublets are observed in the ^{31}P NMR spectrum at δ = 8.5 and 57.6 (ratio ca. 1:2), which collapse into one broad singlet at room temperature (δ = 33.7). Recrystallization from dichloromethane and toluene yielded small brown crystals suitable for crystal structure determination, which showed this to be the *rac* isomer.

Molecular Structures of 2−4

The ferrocene derivatives crystallize in the centrosymmetric monoclinic space group no. 14 [$P2_1/n$ (**2**, **3**) and $P2_1/c$ (**4**)]. For **2**, two molecules are present in the unit cell, while for **3** and **4**, four molecules are present.

In all three complexes, the substituted cyclopentadienyl rings adopt an antiperiplanar conformation, as expected for bulky substituents (see Table 1 for bond lengths and angles). An antiperiplanar conformation was also observed for [Fe{(η^5-C_5H_4)CH_2PPh_2}$_2$].[14]

In **2**, the Ph and cyclopentadienyl rings are almost coplanar [angle between plane of Ph ring and cyclopentadienyl ring 6.0(3)°]. The Fe atom is located on a crystallographic center of inversion. As the P−H proton is disordered over two positions (Figure 1), the configuration of the phosphanyl group could not be determined.

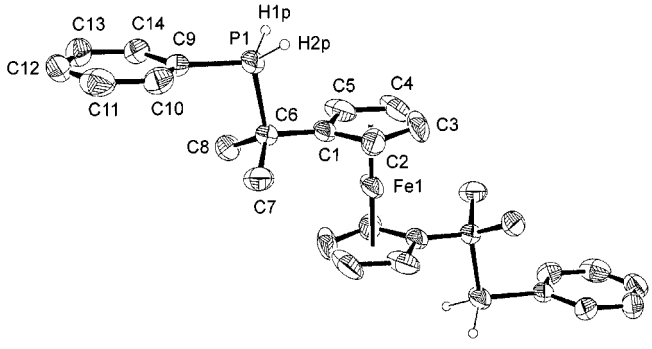

Figure 1. Molecular structure of *rac*-[Fe{(C_5H_4)CMe_2PHPh}$_2$] (**2**) showing the atom numbering scheme employed (ORTEP plot, 50% probability, SHELXTL PLUS; XP[23]); hydrogen atoms (other than P−H) are omitted for clarity; the P−H proton is disordered

In **3** (Figure 2) and **4** (Figure 3), the PH protons were located in the difference Fourier synthesis and refined isotropically. Only the *rac* isomer is present in the unit cell. As **4** is derived from **2**, in which the configuration could not be determined, the presence of the *rac* isomer can be deduced for **2**, too.

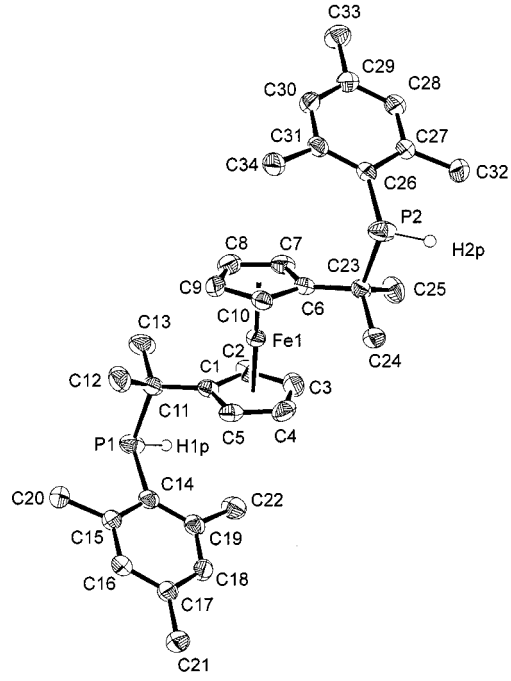

Figure 2. Molecular structure of *rac*-[Fe{(C_5H_4)CMe_2PHMes}$_2$] (**3**) showing the atom numbering scheme employed (ORTEP plot, 50% probability, SHELXTL PLUS; XP[23]); hydrogen atoms (other than P−H) are omitted for clarity; only the *R*,*R* isomer is shown.

In **3** and **4**, the aryl rings and the cyclopentadienyl rings adopt an angle of 31.2(1)° and 34.1(1)° (**3**) or 31.4(2)° and 33.3(2)° (**4**). In **4**, the Ta−P bond lengths of 2.758(1) and 2.798(1) Å are longer than those in the phosphane complex [Cp*$TaCl_4$(PH_2Ph)] [2.651(3) Å].[15] Apparently, replacement of the small H substituent by the bulky (C_5H_4)CMe_2 substituent at the P atom weakens the Ta−P bond. In **4**, the Ta atom is located 0.573(1) Å above the plane formed by the four Cl atoms. This distance is similar to that in [Cp*$TaCl_4$(PH_2Ph)] [0.602(2) Å] and smaller than that observed for [Cp*$TaCl_4$] [0.806(2) Å],[15] due to the higher steric demand of the phosphane ligands in [Cp*$TaCl_4$(PH_2Ph)] and **4**. Only one other trinuclear bis(phosphanylmethyl)ferrocene complex, namely [Fe{(η^5-C_5H_4)CH_2PPh_2[$RuCl_2$(η^6-1,2,3,4-Me_4C_6)]}$_2$], has been structurally characterized.[16,17]

The Fe−C bond lengths of 2.04−2.08 Å and the distance Fe−Cp^R_{center} of ca. 1.65−1.67 Å in **2**−**4** are in good agreement with those of related ferrocene derivatives.[14,16−19]

We are now extending these synthetic approaches to other cyclopentadienes with *P*-functionalized side chains and investigating their coordination properties towards other transition metals and main group metals.

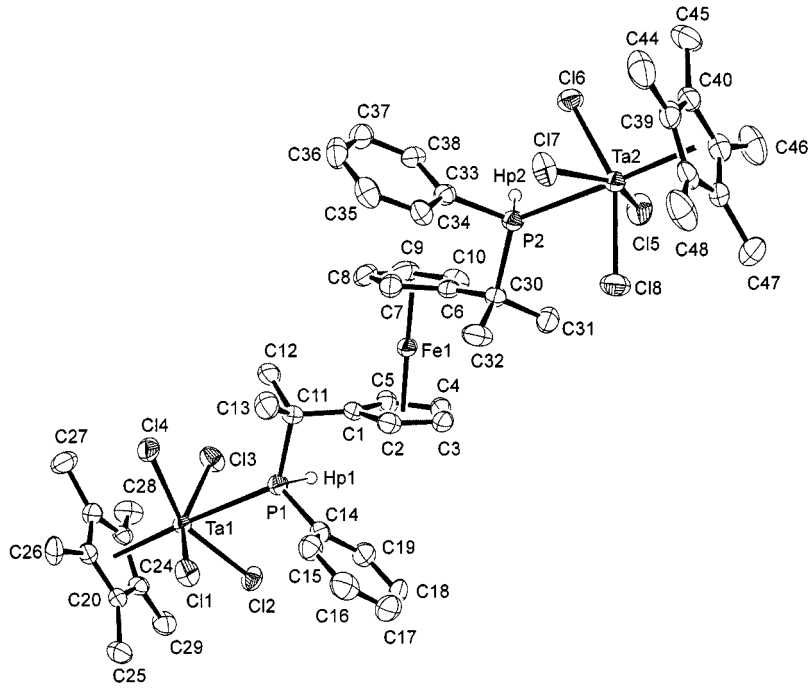

Figure 3. Molecular structure of *rac*-[Fe{(C_5H_4)CMe_2PHPh(Cp*$TaCl_4$)}$_2$] (**4**) showing the atom numbering scheme employed (ORTEP plot, 50% probability, SHELXTL PLUS; XP[23]); hydrogen atoms (other than P−H) are omitted for clarity; only the *S*,*S* isomer is shown

Experimental Section

General: All experiments were carried out under purified dry argon. Solvents were dried and freshly distilled under argon. The NMR spectra were recorded with an AVANCE DRX 400 spectrometer (Bruker), ^{1}H NMR (400 MHz): internal standard solvent, external standard TMS. ^{13}C NMR (100.6 MHz): external standard TMS, internal standard solvent. ^{31}P NMR (162 MHz): external standard 85% H_3PO_4. The IR spectra were recorded on an FT-IR spectrometer Perkin−Elmer System 2000 in the range 350−4000 cm^{-1}. MS: MAT 212 (Varian). The melting points were determined in sealed capillaries under argon and are uncorrected. 6,6-dimethylfulvene,[11] LiPHMes,[20] Li[(C_5H_4)CMe_2PHPh][4] and [Cp*$TaCl_4$][21] were prepared according to the literature procedures. $FeCl_2$ is commercially available (Aldrich).

Synthesis of Li[(C_5H_4)CMe_2PHMes] (1): 6,6-Dimethylfulvene (0.8 mL, 6.7 mmol) was added slowly in 0.1 mL portions to an orange suspension of LiPHMes (1.1 g, 6.7 mmol) in Et_2O (30 mL), and the resulting pale yellow reaction mixture stirred for 12 h. The resulting solid was isolated by filtration and washed twice with ca. 20 mL Et_2O, then twice with ca. 20 mL *n*-hexane and dried under vacuum to yield **1** as a white powder (1.4 g, 63%). M.p. 220 °C (dec.). ^{1}H NMR ([D$_8$]THF): δ = 1.41 (d, $^3J_{P-H}$ = 13.0 Hz, 3 H, CH_3 in CMe_2), 1.43 (d, $^3J_{P-H}$ = 8.8 Hz, 3 H, CH_3 in CMe_2), 2.19 (s, 3 H, *p*-CH_3 in Mes), 2.26 (s, 6 H, *o*-CH_3 in Mes), 4.36 (d, $^1J_{P-H}$ = 215.6 Hz, 1 H, PH), 5.56 (s, 4 H, CH in C_5H_4), 6.78 (s, 2 H, *m*-CH in Mes). ^{13}C NMR ([D$_8$]THF): δ = 21.0 (s, 1C, *p*-CH_3 in Mes), 23.9 (m, 2C, *o*-CH_3 in Mes), 30.4 (d, $^2J_{P-C}$ = 17.8 Hz, 1C, CH_3-C), 31.5 (d, $^2J_{P-C}$ = 9.7 Hz, 1C, CH_3−C), 37.2 (d, $^1J_{P-C}$ = 12.5 Hz, 1C, C−CH_3), 101.7 (d, $^3J_{P-C}$ = 3.5 Hz, 2C, C2, C5 in C_5H_4), 102.7 (s, 2C, C3, C4 in C_5H_4), 127.1 (d, $^2J_{P-C}$ = 9.6 Hz, 1C, C1 in C_5H_4), 129.1 (d, $^3J_{P-C}$ = 2.5 Hz, 2C, *m*-C in Mes), 132.6 (d, $^1J_{P-C}$ = 29.1 Hz, 1C, *ipso*-C in Mes), 137.3 (s, 1C, *p*-C in Mes), 143.8 (s, 2C, br, *o*-C in Mes). ^{31}P NMR ([D$_8$]THF): δ = −45.6 (d of m, $^1J_{P-H}$ = 216 Hz). IR (KBr): $\tilde{\nu}$ = 2337 (νPH, m), 1463 (νC=C m, br) cm^{-1}.

Synthesis of *rac*-[Fe{(η^5-C_5H_4)CMe_2PHPh}$_2$] (2): A solution of Li[(C_5H_4)CMe_2PHPh] (3.5 g, 15.6 mmol) in THF (30 mL) was slowly added to a suspension of $FeCl_2$ (1.0 g, 7.8 mmol) in THF. During the addition, $FeCl_2$ slowly dissolved, and the initially pale pink solution turned first yellow and finally red-brown. The solution was stirred for 16 h. The solvent was then evaporated under vacuum and the brown residue treated with Et_2O. The rust-brown powder was separated from the yellow solution by filtration and extracted repeatedly with Et_2O. The Et_2O fractions were combined and the solvent was evaporated under vacuum. The yellow residue was recrystallized repeatedly from *n*-hexane or *n*-pentane. At −20 °C orange needles of **2** were obtained. Yield: 2.2 g (59%), m.p. 97−100 °C (from *n*-pentane). ^{1}H NMR (C_6D_6): δ = 1.32 (d, $^3J_{P-H}$ = 12.0 Hz, 3 H, CH_3 in CMe_2), 1.38 (d, $^3J_{P-H}$ = 12.4 Hz, 3 H, CH_3 in CMe_2), 3.75−3.61 (m, 2 H, CH in C_5H_4), 3.95−3.91 (m, 2 H, CH in C_5H_4), 4.08 (d, $^1J_{P-H}$ = 206.7 Hz, 1 H, PH), 7.05 (m, 3 H, *o*- and *p*-CH in Ph), 7.16 (m, 2 H, *m*-CH in Ph). ^{13}C NMR (C_6D_6): δ = 28.4 (d, $^2J_{P-C}$ = 16.3 Hz, 1C, CH_3−C), 28.9 (d, $^2J_{P-C}$ = 16.0 Hz, 1C, CH_3−C), 33.6 (d, $^1J_{P-C}$ = 12.6 Hz, 1C, C−CH_3), 66.6 (s, 1C, C4 in C_5H_4), 67.1 (s, 1C, C3 in C_5H_4), 68.3 (d, $^3J_{P-C}$ = 21.0 Hz, 2C, C2, C5 in C_5H_4), 99.6 (d, $^2J_{P-C}$ = 7.2 Hz, 1C, C1 in C_5H_4), 126.6 (s, 1C, *p*-C in Ph), 129.3 (d, $^3J_{P-C}$ = 5.6 Hz, 2C, *m*-C in Ph), 135.5 (d, $^1J_{P-C}$ = 17.8 Hz, 1C, *ipso*-C in Ph), 137.0 (d, $^2J_{P-C}$ = 15.5 Hz, 2C, *p*-C in Ph). ^{31}P NMR (C_6D_6): δ = 8.8 (d of m, $^1J_{P-H}$ = 207 Hz). IR (KBr): $\tilde{\nu}$ = 2283 (νPH, m), 1463 and 1432 (νC=C, Ph, m), 741 and 697 (δC=C, Ph, st) cm^{-1}. EI MS: *m*/*z* (%) = 486 (15) [M$^+$], 377 (10) [M$^+$ − PHPh], 266 (100) [M$^+$ − 2 PHPh], 226 (5) [M$^+$ − 2 PHPh − CMe_2], and fragmentation products thereof. $C_{28}H_{32}FeP_2$ (486.3): calcd. C 69.1, H 6.6, P 12.7; found C 68.7, H 6.3, P 12.1.

Synthesis of *rac*-[Fe{(η^5-C_5H_4)CMe_2PHMes}$_2$] (3): A solution of Li[(C_5H_4)CMe_2PHMes] (1.6 g, 6.0 mmol) in THF (20 mL) was

Table 2. Crystal data and structure refinement for **2**, **3**, and **4**

	2	**3**	**4**
Empirical formula	$C_{28}H_{32}FeP_2$	$C_{34}H_{44}FeP_2$	$C_{48}H_{62}Cl_8FeP_2Ta_2$
M_r	486.33	570.48	1402.27
Temperature (K)	220(2)	220(2)	220(2)
Crystal system	monoclinic	monoclinic	monoclinic
Space group	$P2_1/n$ (no. 14)	$P2_1/n$ (no. 14)	$P2_1/c$ (no. 14)
a [Å]	6.1170(3)	8.0117(2)	15.2794(7)
b [Å]	21.2473(9)	17.7373(5)	14.8736(6)
c [Å]	9.6680(4)	20.7827(6)	22.925(1)
β [°]	102.292(1)	93.602(1)	95.607(1)
V [Å^3]	1227.74(9)	2947.5(1)	5184.9(4)
Z	2	4	4
$\rho_{calcd.}$ [Mg m^{-3}]	1.316	1.286	1.796
$F(000)$	512	1216	2752
Crystal size [mm]	0.50 × 0.40 × 0.20	0.40 × 0.40 × 0.40	0.20 × 0.10 × 0.05
Abs. coeff. [mm^{-1}]	0.758	0.642	4.993
Θ range [°]	1.92 to 28.85	1.51 to 28.81	1.34 to 28.29
Refl. collected	12421	29937	32451
Independent reflections	2994	7185	12325
R_{int}	0.0283	0.0440	0.0495
Parameters	192	510	780
R [$I > 2\sigma(I)$]	0.0673	0.0387	0.0339
$wR2$ (all data)	0.1641	0.1212	0.0618
$(\Delta/\rho)_{min.}$ [e Å^{-3}]	0.246	0.571	1.007
$(\Delta/\rho)_{max.}$ [e Å^{-3}]	−0.528	−0.379	−1.424

slowly added to a suspension of $FeCl_2$ (0.4 g, 3.0 mmol) in THF (30 mL). During the addition, $FeCl_2$ slowly dissolved, and the initially pale pink solution turned first yellow and finally red-brown. The solution was stirred for 16 h. Then the solvent was evaporated under vacuum, and the brown residue treated with Et_2O (20 mL). The insoluble rust-brown powder was separated from the orange solution by filtration and extracted repeatedly with Et_2O. The Et_2O fractions were combined and the solvent was evaporated under vacuum. The yellow residue was recrystallized repeatedly from *n*-hexane, *n*-pentane or toluene. At −20 °C yellow platelets (from hexane) or orange rod-like crystals (from toluene) of **3** were obtained. Yield: 0.9 g (55%), m.p. 162 °C (from toluene). ^{1}H NMR (C_6D_6): δ = 1.39 (d, $^3J_{P-H}$ = 13.0 Hz, 3 H, CH_3 in CMe_2), 1.45 (d, $^3J_{P-H}$ = 8.8 Hz, 3 H, CH_3 in CMe_2), 2.08 (s, 3 H, *p*-CH_3 in Mes), 2.27 (br. s, 6 H, *o*-CH_3 in Mes), 3.87−3.60 (m, 4 H, CH in C_5H_4), 4.4 (d, $^1J_{P-H}$ = 216.1 Hz, 1 H, PH), 6.76 (s, 2 H, *m*-H in Mes). ^{13}C NMR (C_6D_6): δ = 21.7 (s, 1C, *p*-CH_3 in Mes), 24.8 (br. s, 2C, *o*-CH_3 in Mes), 29.3 (br. s, 1C, *C*H_3−C), 29.6 (br, 1C, *C*H_3−C), 35.7 (d, $^1J_{P-C}$ = 15.2 Hz, 1C, *C*−CH_3), 66.8 (s, 1C, C3 in C_5H_4), 67.3 (s, 1C, C4 in C_5H_4), 68.5 (d, $^3J_{P-C}$ = 12.2 Hz, 2C, C2, C5 in C_5H_4), 127.1 (d, $^2J_{P-C}$ = 9.6 Hz, 1C, C1 in C_5H_4), 129.1 (d, $^3J_{P-C}$ = 2.5 Hz, 2C, *m*-C in Mes), 132.6 (d, $^1J_{P-C}$ = 29.1 Hz, 1C, *ipso*-C in Mes), 137.3 (s, 1C, *p*-C im Mes), 143.8 (s, 2C, br, *o*-C in Mes). ^{31}P NMR (C_6D_6): δ = −32.8 (d of m, $^1J_{P-H}$ = 214 Hz). IR (KBr): $\tilde{\nu}$ = 2345 and 2310 (νPH, m) cm^{-1}. EI MS: *m*/*z* (%) = 570 (10) [M$^+$], 418 (8) [M$^+$ − PHMes], 313 (5) [M$^+$ − $C_5H_4CMe_2PHMes$], 266 (100) [M$^+$ − 2 PHMes], and fragmentation products thereof. $C_{34}H_{44}FeP_2$ (570.5): calcd. C 71.6, H 7.8, P 10.9; found C 71.1, H 8.3, P 10.3.

Synthesis of *rac*-[Fe{(η^5-C_5H_4)CMe_2PHPh(Cp*$TaCl_4$)}$_2$] (4): A solution of **2** (0.7 g, 1.4 mmol) in toluene (15 mL) was added dropwise to a suspension of [Cp*$TaCl_4$] (1.3 g, 2.8 mmol) in toluene (30 mL). The color of the reaction mixture changed from orange to brown. The mixture was then heated to 70 °C for 2 h, allowed to cool, and stirred at room temperature overnight. The solid was separated from the solution by filtration. Cooling to −20 °C gave unconverted [Cp*$TaCl_4$], which was also separated by filtration. The solvent was evaporated under vacuum, and the resulting brown residue was extracted with CH_2Cl_2. The dichloromethane solution was concentrated. Cooling to −20 °C gave a fine brown solid, which was recrystallized repeatedly from toluene. Finally, small brown crystals were obtained together with a brown powder. Yield: 0.9 g (45%), m.p. 162−167 °C (from toluene). ^{1}H NMR ([D$_8$]toluene): δ = 1.65 (d, $^3J_{P-H}$ = 12.0 Hz, 6 H, CH_3 in CMe_2), 2.24 (s, 30 H, CH_3 in Cp*), 3.49 (m, 4 H, CH in C_5H_4), 3.75 (m, 2 H, CH in C_5H_4), 4.32 (m, 2 H, CH in C_5H_4), 6.97−7.01 (m, 10 H, C*H* in Ph). ^{13}C NMR ([D$_8$]toluene and C_6D_6): δ = 13.7 (s, CH_3 in Cp*), 27.4 [br. s, C(*C*H_3)], 27.6 (br. s, C(*C*H_3)], 37.8 [s, *C*(CH_3)], 54 (br. s, ?), 67.2 (s, C3 and C4 in C_5H_4), 68.6 (s, C2 and C5 in C_5H_4), 100.4 (br., C1 in C_5H_4), 128.9 (s, *C*−CH_3 in Cp*), 129.7 (s, *m*-C in Ph), 133.9 (s, *ipso*-C in Ph), 137.3 (s, *o*-C in Ph); *p*-C in phenyl obscured by solvent. ^{31}P NMR ([D$_8$]toluene): T = 230 K: δ = 57.6 (d, $^1J_{P-H}$ = 364 Hz), 8.5 (d, $^1J_{P-H}$ = 204 Hz); T = 300 K: δ = 33.6 (br). IR (KBr): $\tilde{\nu}$ = 2965 (CH_3, m), 2286 (PH, m), 1463 and 1435 (C=C Ph, m), 742 and 697 (C=C Ph, st) cm^{-1}.

Data Collection and Structural Refinement of 2, 3, and 4: Data (Mo-K_α = 0.71073 Å) were collected with a Siemens CCD (SMART) diffractometer. All observed reflections were used for refinement (SAINT) of the unit cell parameters. Empirical absorption correction with SADABS.[22] The structures were solved by direct methods (SHELXTL PLUS).[23] Fe, Ta, P, Cl, and C atoms were refined anisotropically; H atoms were located by difference maps and refined isotropically. Table 2 lists crystallographic details.

CCDC-173678 (**2**), -173679 (**3**) and -173680 (**4**) contain the supplementary crystallographic data for this paper. These data can be obtained free of charge at www.ccdc.cam.ac.uk/conts/retrieving.html [or from the Cambridge Crystallographic Data Centre, 12, Union Road, Cambridge CB2 1EZ, UK; Fax: (internat.) +44-1223/336-033; E-mail: deposit@ccdc.cam.ac.uk].

Acknowledgments

We gratefully acknowledge financial support from the Deutsche Forschungsgemeinschaft.

[1] C. Charrier, F. Mathey, *Tetrahedron Lett.* **1978**, *27*, 2407−2410.
[2] Review: P. Jutzi, T. Redeker, *Eur. J. Inorg. Chem.* **1998**, 663−674.
[3] [3a] D. M. Bensley Jr., E. A. Mintz, *J. Organomet. Chem.* **1988**, *353*, 93−102 (and ref. therein). [3b] R. T. Kettenbach, W. Bonrath, H. Butenschön, *Chem. Ber.* **1993**, *126*, 1657−1663. [3c] B. E. Bosch, G. Erker, R. Fröhlich, O. Meyer, *Organometallics* **1997**, *16*, 5449−5456. [3d] C. Charrier, F. Mathey, *J. Organomet. Chem.* **1979**, *170*, C41−C43. [3e] T. Kauffmann, J. Ennen, H. Lhotak, A. Rensing, F. Steinseifer, A. Woltermann, *Angew. Chem.* **1980**, *92*, 321−323; *Angew. Chem. Int. Ed. Engl.* **1980**, *19*, 328−330. [3f] T.-F. Wang, J.-P. Juang, Y.-S. Wen, *J. Organomet. Chem.* **1995**, *503*, 117−128. [3g] J. Szymoniak, J. Besançon, A. Dormond, C. Moïse, *J. Org. Chem.* **1990**, *55*, 1429−1432. [3h] N. E. Schore, *J. Am. Chem. Soc.* **1979**, *101*, 7410−7412. [3i] N. E. Schore, L. S. Benner, B. E. LaBelle, *Inorg. Chem.* **1981**, *20*, 3200−3208. [3j] N. E. Schore, S. Sundar, *J. Organomet. Chem.* **1980**, *184*, C44−C48. [3k] S. R. Iyer, D. R. Tueting, N. E. Schore, *J. Organomet. Chem.* **1987**, *320*, 339−348. [3l] N. E. Schore, B. E. LaBelle, *J. Org. Chem.* **1981**, *46*, 2306−2301. [3m] T. A. Mobley, R. G. Bergman, *J. Am. Chem. Soc.* **1998**, *120*, 3253−3254. [3n] D. M. Bensley Jr., E. A. Mintz, S. J. Sussangkarn, *J. Org. Chem.* **1988**, *53*, 4417−4419. [3o] Y. Kataoka, Y. Saito, K. Nagata, K. Kitamura, A. Shibahara, K. Tani, *Chem. Lett.* **1995**, 833−834. [3p] M. D. Fryzuk, S. S. H. Mao, M. J. Zaworotko, L. R. MacGillivray, *J. Am. Chem. Soc.* **1993**, *115*, 5336−5337. [3q] T. Kauffmann, J. Olbrich, *Tetrahedron Lett.* **1984**, *25*, 1967−1970. [3r] B. Antelmann, U. Winterhalter, G. Huttner, B. C. Janssen, J. Vogelgesang, *J. Organomet. Chem.* **1997**, *545−546*, 407−420. [3s] O. J. Curnow, G. Huttner, S. J. Smail, M. M. Turnbull, *J. Organomet. Chem.* **1996**, *524*, 267−270. [3t] Review: T. Cuenca, P. Royo, *Coord. Chem. Rev.* **1999**, *193−195*, 447−498. [3u] Review: C. S. Slone, D. A. Weinberger, C. A. Mirkin, *Prog. Inorg. Chem.* **1999**, *48*, 233−350.
[4] T. Koch, E. Hey-Hawkins, *Polyhedron* **1999**, *18*, 2113−2116.
[5] T. Koch, S. Blaurock, F. B. Somoza Jr., A. Voigt, R. Kirmse, E. Hey-Hawkins, *Organometallics* **2000**, *19*, 2556−2563.
[6] U. J. Bildmann, G. Müller, *Z. Naturforsch., Teil B* **2000**, *55*, 895−900.
[7] U. J. Bildmann, M. Winkler, G. Müller, *Z. Naturforsch., Teil B* **2000**, *55*, 1005−1010.
[8] K. Kunz, G. Erker, S. Döring, R. Fröhlich, G. Kehr, *J. Am. Chem. Soc.* **2001**, *123*, 6181−6182.
[9] A. Togni, T. Hayashi, *Ferrocenes*, VCH Verlagsgesellschaft mbH, Weinheim, **1995**.
[10] T. Oshikawa, M. Yamashita, *Chem. Ind. (London)* **1985**, 126−127.
[11] J. Thiele, H. Balhorn, *Justus Liebigs Ann. Chem.* **1906**, *348*, 1−15. J. Thiele, *Chem. Ber.* **1900**, *33*, 666−673.
[12] A similar value ($\Delta G^{\#}$ = 56.9 KJ/mol) was observed for the hindered rotation around the P−C(aryl) bond of (aryl)P=C=As(aryl) (aryl = 2,4,6-tBu$_3$C$_6$H$_4$): H. Ranaivonjatovo, H. Ramdane, H. Gornitzka, J. Escudié, J. Satgé, *Organometallics* **1998**, *17*, 1631−1633.
[13] M. Hesse, H. Meier, B. Zeeh, *Spektroskopische Methoden in der organischen Chemie*, Georg Thieme Verlag, Stuttgart New York **1995**.
[14] Y. Yamamoto, T. Tanase, I. Mori, Y. Nakamura, *J. Chem. Soc., Dalton Trans.* **1994**, 3191−3192.
[15] S. Blaurock, *Dissertation*, Universität Leipzig **2000**.
[16] J.-F. Mai, Y. Yamamoto, *J. Organomet. Chem.* **1998**, *560*, 223−232.
[17] J.-F. Mai, Y. Yamamoto, *J. Organomet. Chem.* **1997**, *545*, 577−579.
[18] N. J. Goodwin, W. Henderson, B. K. Nicholson, *Chem. Commun.* **1997**, 31−32.
[19] N. J. Goowin, W. Henderson, J. K. Sarfo, *Chem. Commun.* **1996**, 1551−1552.
[20] E. Hey, F. Weller, *J. Chem. Soc., Chem. Commun.* **1988**, 782−783.
[21] R. D. Sanner, T. S. Carter, W. J. Bruton Jr., *J. Organomet. Chem.* **1982**, *240*, 157−162.
[22] G. M. Sheldrick, *SADABS − a Program for Empirical Absorption Correction*, Göttingen, **1998**.
[23] *SHELXTL PLUS, Siemens Analyt. X-ray Inst. Inc.* **1990**, XS: *Program for Crystal Structure Solution*, XL: Program for Crystal Structure Determination, XP: Interactiv Molecular Graphics.

Received October 25, 2001
[I01420]

Titanium Complexes Containing Bulky η^2-1,2,4-Triazolato Ligands

Nadia C. Mösch-Zanetti,*[a] Manuel Hewitt,[a] Thomas R. Schneider,[a] and Jörg Magull[a]

Keywords: N ligands / Titanium / Structure elucidation

The unusual η^2-coordination of a 1,2,4-triazolato ligand to a transition metal is described. The synthesized compounds $[Ti(\eta^2\text{-tz})_4]$ (**1**), $[(C_5Me_4CH_2Ph)Ti(\eta^2\text{-tz})Cl_2]$ (**2**), $[Cp^*Ti(\eta^2\text{-tz})Cl_2]$ (**3**) and $[Cp^*Ti(\eta^2\text{-tz})_3]$ (**4**) (tzH = 3,5-diisopropyl-1,2,4-triazole) were characterized by ^1H and ^{13}C NMR spectroscopy and, in the case of **1** and **2**, by X-ray crystallography. Both structures confirm the η^2-coordination of the ligand. In compound **1** all four ligands coordinate in an η^2 fashion leading to a metal center surrounded by eight nitrogen atoms. The core of the fragment formed by the central atom and the triazolato planes exhibits a distorted D_{2d} symmetry. A variable temperature NMR spectroscopy experiment performed on **1** confirms the occurrence of two different isopropyl groups at low temperature. The structure of compound **2** shows the geometry of the molecule in a distorted C_s symmetry, with the mirror plane perpendicular to the cyclopentadienyl and triazolato rings. The tz ligand is oriented in a *transoid* position relative to the benzyl substituent of the $C_5Me_4CH_2Ph$ group.

(© Wiley-VCH Verlag GmbH, 69451 Weinheim, Germany, 2002)

Introduction

Pyrazoles and triazoles represent a class of molecules with ideal ligand properties that allow a wide variety of structures and bonding options.[1−4] The preparation of the parent heterocycle is in most cases achieved by straightforward organic reactions, enabling easy tuning of the substituents attached to the five-membered ring.[5,6] In addition, they may act as neutral or monoanionic ligands. All these factors explain their extensive use in coordination chemistry. The most common bonding modes in these complexes are η^1, bridging between two metal atoms in a μ_2-η^1:η^1 fashion, or a μ_3-η^1:η^1:η^1 fashion for triazolato ligands. However, many different bonding modes have been found in recent years.[4,7−9] With pyrazolato ligands, an η^2-coordination has been found in complexes of f-block[10−15] and, quite unexpectedly, d-block metals[16−22] as well as with main group elements.[23−27] However, with triazolato ligands only one crystallographically established η^2-coordination has been reported, namely in a benzo-1,2,3-triazolato potassium salt, where an η^2-interaction was found in the solid-state structure.[28] No example of an η^2-1,2,4-triazolato ligand has been described as yet.[29]

Herein, we present a series of compounds that contain the unusual η^2-coordination of a 1,2,4-triazolato ligand. The complexes $[Ti(\eta^2\text{-tz})_4]$ (**1**), $[(C_5Me_4CH_2Ph)Ti(\eta^2\text{-tz})Cl_2]$ (**2**), $[Cp^*Ti(\eta^2\text{-tz})Cl_2]$ (**3**) and $[Cp^*Ti(\eta^2\text{-tz})_3]$ (**4**) (tz = 3,5-diisopropyl-1,2,4-triazolato) have been synthesized by the appropriate metathesis reaction and characterized by NMR spectroscopy, mass spectrometry and elemental analysis. In addition, the solid state structures of **1** and **2** were determined by X-ray crystallography.

[a] Institut für Anorganische Chemie der Georg-August-Universität Göttingen,
Tammannstr. 4, 37077 Göttingen, Germany
Fax: (internat.) + 49-(0)551/393373
E-mail: nmoesch@gwdg.de

Results and Discussion

Preparation of Titanium Compounds

The requirements for an ideal ligand system for high oxidation state early transition metals are steric bulk, to avoid oligomerization, and/or electron donating properties to stabilize the electrophilic metal center. Sterically demanding alkyl groups seem to meet those premises. We recently described the synthesis of a triazole ligand bearing bulky isopropyl groups in the 3,5-positions.[30]

The reaction of tetrakis(dimethylamido)titanium(IV) with four equivalents of tzH in toluene at room temperature gave $[Ti(\eta^2\text{-tz})_4]$ (**1**), isolated as yellow crystals from hexane in good yield [Equation (1)].

$$[Ti(NMe_2)_4] + 4\ tzH \xrightarrow[-\,4\ NHMe_2]{toluene} [Ti(\eta^2\text{-tz})_4] \quad \mathbf{1}\ (68\ \%) \qquad (1)$$

The reaction is fast, as the formation of $HNMe_2$ was immediately apparent. The compound is highly soluble in hydrocarbon solvents, and thus had to be crystallized from concentrated solutions at low temperatures. The highest peak in the mass spectrum was assignable to the monomeric molecular ion. This is consistent with the solid-state structure determined by X-ray crystallography (vide infra).

The ^1H and ^{13}C NMR spectra at room temperature each exhibit one set of signals, indicating a highly symmetric coordination of the ligands. However, a variable temperature ^1H NMR spectroscopy experiment shows the signals to split into two sets with a coalescence temperature of approx. 200 K, pointing to an asymmetric coordination of the ligands at low temperature (Figure 1).

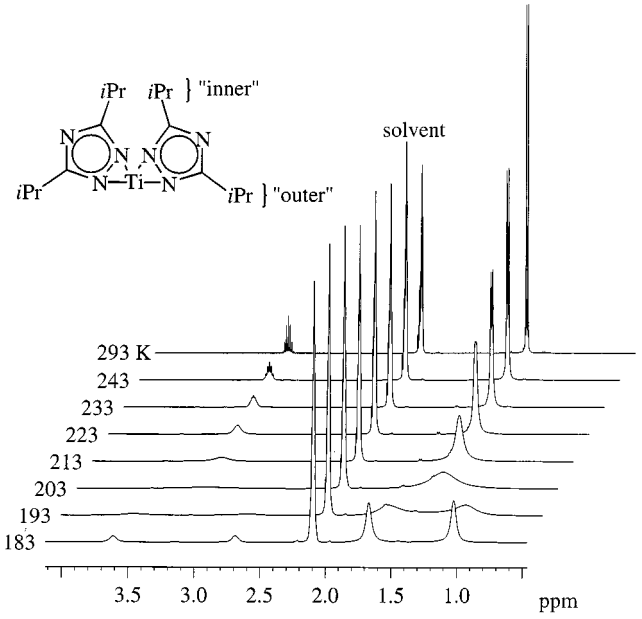

Figure 1. VT NMR spectra of **1** in [D_8]toluene; a fragment of **1** consisting of two coplanar triazolato ligands shows the two types of isopropyl groups

The spectrum at 183 K shows two relatively broad signals for six protons each (δ = 1.02 and 1.67) and two signals for one proton each (δ = 2.69 and 3.61) for two different isopropyl groups. A COSY NMR spectrum at 183 K reveals cross-peaks between the methyl signal at δ = 1.02 and the CH signal at δ = 2.69, while the resonance at δ = 1.67 has a cross-peak with that at δ = 3.61. The temperature could not be decreased further due to freezing of the solvent (toluene) thereby presumably preventing sharper signals that show the expected doublets and septuplets. With increasing temperature the structure apparently becomes more dynamic so that the room temperature spectrum shows only one averaged set of signals. The low-temperature spectrum is consistent with the solid-state structure determined by X-ray crystallography at 133 K, which shows two triazolato rings almost coplanar to each other, with the other two perpendicular to them. Two of the four nitrogen atoms coordinated to Ti in one plane form a large N−Ti−N angle [e.g. 169.25(6)° for N1−Ti1−N7], whereas the other two form a small one [e.g. 92.77(6)° N2−Ti1−N8]. This coordination leads to magnetically nonequivalent "inner" and "outer" isopropyl groups, which give rise to the two sets of signals.

The reaction of [($C_5Me_4CH_2Ph$)$TiCl_3$] and [Cp*$TiCl_3$], respectively, with one equivalent of tzK in toluene at room temperature afforded the complexes [($C_5Me_4CH_2Ph$)Ti(η^2-tz)Cl_2] (**2**) and [Cp*Ti(η^2-tz)Cl_2] (**3**) as red crystalline materials in medium to good yields (Scheme 1). The ^1H and ^{13}C NMR spectra show the coordination of one triazolato ligand in a symmetric fashion. The occurrence of an η^2-coordinated ligand was confirmed by the X-ray crystal structure analysis of **2** (vide infra). In the mass spectrum, the molecular ion could be detected indicating a thermal stability of the species.

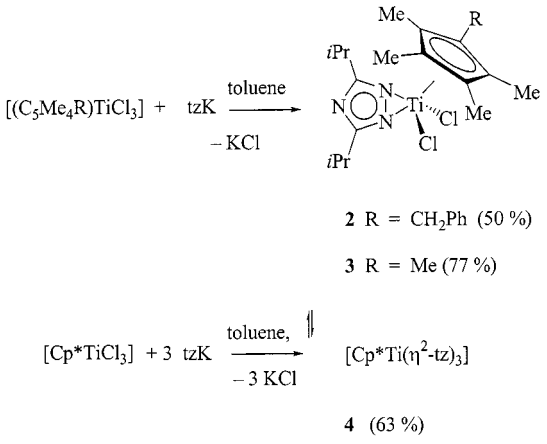

Scheme 1

The analogous Cp derivative [CpTi(η^2-tz)Cl_2] can be formed by the same reaction procedure as above, producing orange crystals. The X-ray crystal structure determination confirms the connectivity as well as the η^2-coordination of the triazolato ligand, although the insufficient quality of the structural analysis due to disorder and twinning problems prevents the discussion of bond lengths and angles. These are general problems in these mixed Cp/tz as well as Cp*/tz systems, as several attempts with different crystals did not improve the structures. The combination of the steric properties of the two ligands seems to lead to disordered and twinned structures that can only be avoided by the substitution of a methyl by a benzyl group at the Cp* ring. The behavior of [CpTi(η^2-tz)Cl_2] in solution is unclear. NMR spectra of crystalline material in C_6D_6 show several signals in the Cp and isopropyl group region pointing to an instability in solution. Presumably the steric protection provided by the Cp group and the isopropyl groups is not large enough, giving rise to oligomeric structures in solution.

The treatment of [Cp*$TiCl_3$] with three equivalents of tzK in refluxing toluene for 2 h afforded the orange compound [Cp*Ti(η^2-tz)$_3$] (**4**) in high yield as shown in Scheme 1. NMR spectroscopic data as well as an attempted X-ray crystal structure analysis are consistent with the formation of a compound that contains three η^2-coordinated triazolato ligands. The addition of only two equivalents of tzK to [Cp*$TiCl_3$] gave mixtures of **3** and **4**, but no evidence was found for the formation of the monochloride species [Cp*Ti(η^2-tz)$_2$Cl] either by NMR spectroscopy or mass spectrometry.

Structural Studies

X-ray crystallography on a single crystal of **1** confirms a monomeric species with a titanium atom in a distorted

tetrahedral environment, assuming the triazolato ligands occupy only one coordination site. All four ligands coordinate in an η^2 fashion, leading to a metal center surrounded by eight nitrogen atoms. Figure 2 shows an ORTEP view of **1**; crystallographic data are given in Table 1 and selected bond lengths and angles in Table 2.

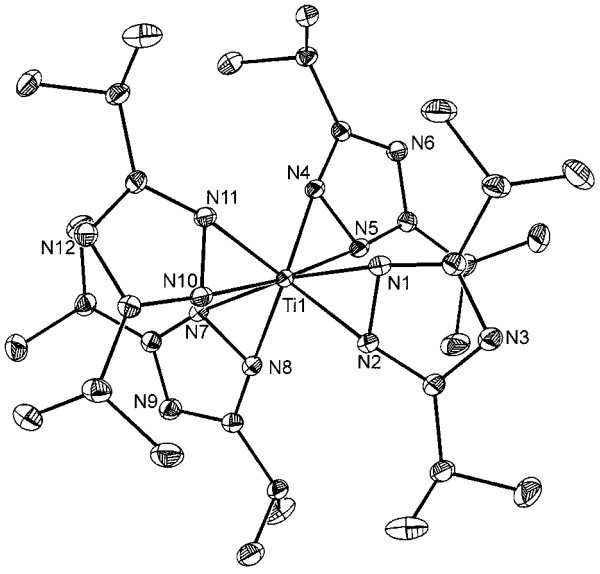

Figure 2. ORTEP view of **1** (thermal ellipsoids at the 50% probability level)

Table 1. Experimental crystallographic data for **1** and **2**

	1	**2**
Empirical formula	$C_{32}H_{56}N_{12}Ti$	$C_{24}H_{33}C_{12}N_3Ti$
Fw	656.79	482.33
Crystal system	monoclinic	triclinic
Space group	$P2_1/n$	$P\bar{1}$
a (Å)	10.826(2)	6.8029(14)
b (Å)	15.741(3)	12.361(3)
c (Å)	22.287(5)	14.845(3)
α (deg)		96.86(3)
β (deg)	90.89(3)	97.93(3)
γ (deg)		96.93(3)
V (Å^3)	3797.5(13)	1215.5(4)
Z	4	2
T (K)	133(2) K	133(2)
λ (Å)	0.71073	0.71073
$\rho_{calcd.}$ (mg/cm^3)	1.149	1.318
μ (mm^{-1})	0.263	0.588
Reflections measured	40821	10917
Reflections unique	6707 (R_{int} = 0.0527)	2830 (R_{int} = 0.0908)
$R1$ (%)	5.54	6.50
$wR2$ (%)	9.90	12.73

Table 2. Selected bond lengths (Å) and angles (°) for **1**

Ti1−N1	2.1289(16)	Ti1−N2	2.0338(15)
Ti1−N4	2.0284(15)	Ti1−N5	2.0816(16)
Ti1−N7	2.1285(16)	Ti1−N8	2.0151(16)
Ti1−N10	2.1019(16)	Ti1−N11	2.0591(16)
N1−Ti1−N2	38.73(6)	N1−Ti1−N7	169.25(6)
N2−Ti1−N8	92.77(6)	N1−Ti−N5	86.41(6)
N1−Ti−N10	91.87(6)	N4−Ti1−N5	39.43(6)

The triazolato rings can be grouped approximately into two, almost orthogonal planes. The average planarity in each group is satisfied within a few degrees, as evidenced by, for example, the torsion angles of 174.07(1)° (N1−N2−Ti1−N8) and 175.79(1)° (N5−N4−Ti1−N10). Whereas the core of the fragment formed by the central atom and the triazolato planes exhibits a symmetry close to D_{2d}, the steric hindrance between adjacent isopropyl groups leads to a deviation from the perfect arrangement. The eight coordinated nitrogen atoms may be considered as forming two tetrahedra, a very flattened, almost planar one, [N5−Ti1−N10 = 172.56(6)° and N1−Ti1−N7 = 169.25(6)] and another elongated one [N2−Ti1−N8 = 92.77(6) and N4−Ti1−N11 = 94.83(6)]. The bond lengths in the former tetrahedron are longer than in the latter by approx. 0.1 Å. The most interesting features of the structure are the three-membered TiN_2 metallacycles, with Ti−N bond lengths between 2.0151(16) and 2.1289(16) Å and N−Ti−N angles between 38.73(6)° and 39.43(6)°. Comparison of the structure of **1** with that of the η^2-pyrazolato species [Ti(η^2-3,5-Me_2pz)$_4$] employing a less bulky ligand, recently described by Winter and co-workers, reveals a similar geometry.[17] Apparently, steric hindrance seems not to be a prerequisite for the formation of the homoleptic species, whereas bulky substituents are important for the stability of the compounds **2**−**4**. Other titanium complexes with three-membered TiN_2 rings contain η^2-diazenido,[31] -diazo[32] or -hydrazido[33,34] ligands. Whereas the η^2-diazenido and -diazo ligands show similar structural features to those of **1**, the latter ones are slightly different in that the Ti−N bond lengths in η^2-hydrazido complexes differ by approx. 0.3 Å leading to a distinct tilting of the ligand.

The X-ray diffraction study of **2** confirms the η^2-coordination of the triazolato ligand. An ORTEP diagram is shown in Figure 3 and selected bond lengths and angles in

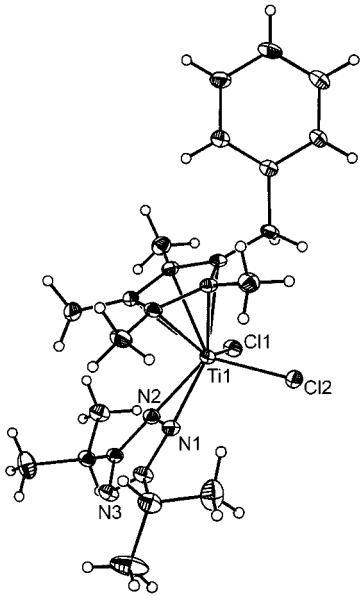

Figure 3. ORTEP view of **2** (thermal ellipsoids at the 50% probability level)

Table 3. Selected bond lengths (Å) and angles (°) for **2**

Ti1−N1	2.055(3)	Ti1−N2	2.061(3)
Ti1−Cl1	2.295(1)	Ti1−Cl2	2.284(1)
Ti1−C9	2.352(3)	Ti1−C10	2.357(4)
Ti1−C11	2.370(4)	Ti1−C12	2.384(4)
Ti1−C13	2.381(4)	N1−N2	1.372(4)
N1−Ti1−N2	38.95(12)	N1−Ti1−Cl1	123.97(10)
N2−Ti1−Cl1	91.91(10)	N1−Ti−Cl2	93.42(10)
N2−Ti1−Cl2	121.52(10)	Cl1−Ti1−Cl2	96.09(5)

Table 3. The structure shows the geometry of the molecule in a distorted C_s symmetry, with the mirror plane perpendicular to the Cp and tz rings.

The titanium atom is coordinated in a distorted tetrahedral geometry assuming that the Cp and tz ligand occupy only one coordination site. The tz ligand is oriented in a *transoid* position relative to the benzyl substituent of the Cp group for steric reasons. The bond lengths and angles of the three-membered TiN_2 ring are virtually identical to those in **1**, although the formal coordination number at Ti is smaller.

Conclusion

In summary, the unusual η^2-coordination of a triazolato ligand in a transition metal complex has been established. The formation of the symmetric homoleptic complex **1** as well as the less-symmetric heteroleptic systems **2**−**4** proves the relative stability of the η^2-pattern. The use of the potassium salt of the triazole enables a convenient route towards Ti^{IV} complexes for HSAB reasons.

Further investigations will concern the role of d electrons[22] in the stability of the η^2 pattern and an analysis of the related spectroscopic consequences, and we are also continuing to explore the coordination behavior and structural features of triazolato complexes of d-block metal ions.

Experimental Section

All preparations were carried out under an atmosphere of dry nitrogen. All common reagents and solvents were purchased from commercial suppliers and used without further purification unless otherwise indicated. Melting points were determined on a Büchi B-540 melting point apparatus in sealed glass tubes and are uncorrected. NMR spectra were recorded on Bruker Avance 200 and Bruker Avance 500 spectrometers (for the VT NMR experiment). The chemical shifts are referenced to external $SiMe_4$. Mass spectra were recorded on a Finnigan MAT 8230 or Varian MAT CH5 spectrometer.

Preparation of [Ti(η^2-tz)$_4$] (1): A solution of [Ti(NMe_2)$_4$] (0.58 g, 2.6 mmol) in toluene (75 mL) was added at room temperature to a suspension of tzH (1.59 g, 10.4 mmol) in toluene (20 mL). Evolution of dimethylamine was immediately apparent. The resulting yellow-brown solution was stirred overnight and then evaporated to dryness. The brown residue was extracted with hexane (50 mL) and filtered through Celite. The solvent was reduced to 10 mL and the product crystallized at −25 °C as yellow cubes (1.15 g, 68%). Crystals suitable for X-ray crystallography were grown from hexane at −25 °C. M.p. 98 °C. ^{1}H NMR (C_6D_6): δ = 1.30 [d, $^3J_{H,H}$ = 7 Hz, CH(CH_3)$_2$, 12 H], 3.14 [sept, $^3J_{H,H}$ = 7 Hz, CH(CH_3)$_2$, 1 H]. ^{13}C NMR (C_6D_6): δ = 21.9 [CH(*C*H$_3$)$_2$], 28.5 [*C*H(CH$_3$)$_2$], 163.1 (C ring). MS(EI): *m*/*z* (%) = 656 (5) [M$^+$], 504 (100) [M$^+$ − tz]. $C_{32}H_{56}N_{12}Ti$ (656.8): calcd. C 58.52, H 8.59, N 25.59; found C 58.07, H 8.64, N 25.15.

Preparation of [($C_5Me_4CH_2Ph$)Ti(η^2-tz)Cl$_2$] (2): A suspension of tzK (0.18 g, 0.94 mmol) in toluene (15 mL) was added at room temperature to a solution of [($C_5Me_4CH_2Ph$)$TiCl_3$] (0.32 g, 0.88 mmol) in 20 mL of toluene and the resulting red suspension was stirred overnight. The solvent was then removed, the residual solid extracted with hexane and filtered through Celite. The volume was reduced to 20 mL and 0.21 g (50%) of the red compound crystallized at −25 °C. M.p. 82 °C. ^{1}H NMR (C_6D_6): δ = 1.38 [d, $^3J_{H,H}$ = 7 Hz, CH(CH_3)$_2$, 12 H], 1.83 (s, CpCH_3, 6 H), 2.01 (s, CpCH_3, 6 H), 3.10 [sept, $^3J_{H,H}$ = 7 Hz, CH(CH$_3$)$_2$, 2 H], 4.06 (s, CH_2, 2 H), 6.84 (m, Ph, 2 H), 7.0 (m, Ph, 2 H), 7.12 (m, Ph, 1 H). ^{13}C NMR (C_6D_6): δ = 13.5 (CpMe), 14.1 (CpMe), 21.8 [CH(*C*H$_3$)$_2$], 28.7 [*C*H(CH$_3$)$_2$], 34.6 (CH_2), 126.8 (C_{para} Ph), 128.4 (C_{meta} Ph), 128.9 (C_{ortho} Ph), 134.67 (Cp ring), 134.88 (Cp ring), 136.4 (Cp ring), 139.5 (C_{ipso} Ph), 165.6 (tz ring). MS(EI): *m*/*z* (%) = 481 (20) [M$^+$], 329 (100) [M$^+$ − tz]. $C_{24}H_{33}Cl_2N_3Ti$ (482.4): calcd. C 59.77, H 6.90, N 8.71; found C 59.42, H 6.92, N 8.44.

Preparation of [Cp*Ti(η^2-tz)Cl$_2$] (3): The synthetic procedure used was analogous to **2** employing [Cp*$TiCl_3$] (0.51 g, 1.76 mmol) and tzK (0.36 g, 1.88 mmol). Yield: 0.55 g (77%). M.p. 132 °C. ^{1}H NMR (C_6D_6): δ = 1.37 [d, $^3J_{H,H}$ = 7 Hz, CH(CH_3)$_2$, 12 H], 1.87 (s, Cp*, 15 H), 3.07 [sept, $^3J_{H,H}$ = 7 Hz, CH(CH$_3$)$_2$, 2 H]. ^{13}C NMR (C_6D_6): δ = 13.6 (Cp* CH_3), 21.8 [CH(*C*H$_3$)$_2$], 28.6 [*C*H(CH$_3$)$_2$], 134.6 (Cp* ring), 165.5 (tz ring). MS(EI): *m*/*z* (%) = 405 (20) [M$^+$], 253 (100) [M$^+$ − tz]. $C_{18}H_{29}Cl_2N_3Ti$ (406.3): calcd. C 53.22, H 7.20, N 10.34; found C 53.68, H 7.24, N 10.10.

Preparation of [Cp*Ti(η^2-tz)$_3$] (4): Toluene (30 mL) was added to a mixture of [Cp*$TiCl_3$] (0.47 g, 1.62 mmol) and tzK (0.96 g, 5.03 mmol). The mixture was stirred under reflux for 2 h, the solvent removed, the residual solid extracted with hexane and filtered through Celite. The volume was reduced to 20 mL and the compound crystallized as yellow needles at −25 °C. Yield: 0.65 g (63%). M.p. 151 °C. ^{1}H NMR (C_6D_6): δ = 1.22 [d, $^3J_{H,H}$ = 6 Hz, CH(CH_3)$_2$, 12 H], 1.77 (s, Cp*, 15 H), 3.05 [sept, $^3J_{H,H}$ = 6 Hz, CH(CH$_3$)$_2$, 6 H]. ^{13}C NMR (C_6D_6): δ = 12.5 (Cp* CH_3), 22.3 [CH(*C*H$_3$)$_2$], 28.6 [*C*H(CH$_3$)$_2$], 129.9 (Cp* ring), 162.8 (tz ring). MS(EI): *m*/*z* (%) = 639 (5) [M$^+$], 504 [M$^+$ − Cp*] 487 (40) [M$^+$ − tz]. $C_{34}H_{57}N_9Ti$ (639.8): calcd. C 63.83, H 8.98, N 19.70; found C 63.25, H 8.98, N 19.70.

X-ray Crystallographic Studies: The selected crystals were covered with oil and mounted on a glass fiber. The data for **1** were collected on a Stoe−Siemens−Huber four-circle-diffractometer coupled to a Siemens CCD area-detector and for **2** on a Stoe IPDS II-array detector system instrument, in both cases with graphite-monochromated Mo-K_α radiation (λ = 0.71073 Å). The structures were solved by direct methods using SHELXS-97[35] and refined against F^2 on all data by full-matrix least-squares with SHELXL-97.[36] All non-hydrogen atoms were refined anisotropically. All hydrogen atoms were included in the model at geometrically calculated positions and refined using a riding model.

CCDC-173074 (**1**) and CCDC-173075 (**2**) contain the supplementary crystallographic data for this paper. These data can be obtained free of charge at www.ccdc.cam.ac.uk/conts/retrieving.html [or

from the Cambridge Crystallographic Data Centre, 12, Union Road, Cambridge CB2 1EZ, UK; Fax: (internat.) + 44-1223/336-033; E-mail: deposit@ccdc.cam.ac.uk].

Acknowledgments

We thank the Swiss National Foundation and Prof. Dr. H. W. Roesky for generous support.

[1] S. Trofimenko, *Chem. Rev.* **1972**, *72*, 497−509.
[2] A. P. Sadimenko, S. S. Basson, *Coord. Chem. Rev.* **1996**, *147*, 247−297.
[3] G. LaMonica, G. A. Ardizzoia, *Prog. Inorg. Chem.* **1997**, *46*, 151−238.
[4] J. G. Haasnoot, *Coord. Chem. Rev.* **2000**, *200*, 131−185.
[5] J. Elguero, in *Comprehensive Heterocyclic Chemistry* (Eds.: A. R. Katritzky, C. W. Rees, K. T. Potts), Pergamon Press, Oxford, **1984**, vol. 5, p 167−303.
[6] J. B. Polya, in *Comprehensive Heterocyclic Chemistry* (Eds.: A. R. Katritzky, C. W. Rees), Pergamon Press, Oxford, **1984**, vol. 5, p 733−790.
[7] F. Nief, *Eur. J. Inorg. Chem.* **2001**, 891−904.
[8] J. E. Cosgriff, G. B. Deacon, *Angew. Chem.* **1998**, *110*, 298−299; *Angew. Chem. Int. Ed.* **1998**, *37*, 286−287.
[9] J. R. Perera, M. J. Heeg, B. H. Schlegel, C. H. Winter, *J. Am. Chem. Soc.* **1999**, *121*, 4536−4537.
[10] C. W. Eigenbrot, K. N. Raymond, *Inorg. Chem.* **1981**, *20*, 1553−1556.
[11] C. W. Eigenbrot, K. N. Raymond, *Inorg. Chem.* **1982**, *21*, 2653−2660.
[12] J. E. Cosgriff, G. B. Deacon, B. M. Gatehouse, H. Hemling, H. Schumann, *Angew. Chem.* **1993**, *105*, 906−907; *Angew. Chem. Int. Ed. Engl.* **1993**, *32*, 874−875.
[13] G. B. Deacon, E. E. Delbridge, B. W. Skelton, A. H. White, *Angew. Chem.* **1998**, *110*, 2372−2373; *Angew. Chem. Int. Ed.* **1998**, *37*, 2251−2252.
[14] G. B. Deacon, E. E. Delbridge, C. M. Forsyth, *Angew. Chem.* **1999**, *111*, 1880−1882; *Angew. Chem. Int. Ed.* **1999**, *38*, 1766−1767.
[15] G. B. Deacon, E. E. Delbridge, B. W. Skelton, A. H. White, *Eur. J. Inorg. Chem.* **1999**, *5*, 751−761.
[16] D. Röttger, G. Erker, M. Grehl, R. Fröhlich, *Organometallics* **1994**, *13*, 3897−3902.
[17] I. A. Guzei, A. G. Baboul, G. P. A. Yap, A. L. Rheingold, H. B. Schlegel, C. H. Winter, *J. Am. Chem. Soc.* **1997**, *119*, 3387−3388.
[18] I. A. Guzei, C. H. Winter, *Inorg. Chem.* **1997**, *36*, 4415−4420.
[19] I. A. Guzei, G. P. A. Yap, C. H. Winter, *Inorg. Chem.* **1997**, *36*, 1738−1739.
[20] C. Yélamos, M. J. Heeg, C. H. Winter, *Inorg. Chem.* **1999**, *38*, 1871−1778.
[21] C. Yélamos, M. J. Heeg, C. H. Winter, *Organometallics* **1999**, *18*, 1168−1176.
[22] N. C. Mösch-Zanetti, R. Krätzner, C. Lehmann, T. R. Schneider, I. Usón, *Eur. J. Inorg. Chem.* **2000**, 13−16.
[23] D. Pfeiffer, M. J. Heeg, C. H. Winter, *Angew. Chem.* **1998**, *110*, 2674−2676; *Angew. Chem. Int. Ed.* **1998**, *37*, 2517−2519.
[24] C. Yélamos, M. J. Heeg, C. H. Winter, *Inorg. Chem.* **1998**, *37*, 3892−3894.
[25] G. B. Deacon, E. E. Delbridge, C. M. Forsyth, P. C. Junk, B. W. Skelton, A. H. White, *Aust. J. Chem.* **1999**, *52*, 733−739.
[26] G. B. Deacon, E. E. Delbridge, C. M. Forsyth, B. W. Skelton, A. H. White, *J. Chem. Soc., Dalton Trans.* **2000**, 745−751.
[27] W. J. Zheng, N. C. Mösch-Zanetti, T. Blunck, H. W. Roesky, M. Noltemeyer, H. G. Schmidt, *Organometallics* **2001**, *20*, 3299−3303.
[28] P. C. Andrews, W. Clegg, R. E. Mulvey, P. A. O'Neil, H. M. M. Wilson, *J. Chem. Soc., Chem. Commun.* **1993**, 1142−1144.
[29] A study by Winter and co-workers (C. Yélamos, K. R. Gust, A. G. Baboul, M. J. Heeg, H. B. Schlegel, C. H. Winter, *Inorg. Chem.* **2001**, *40*, 6451−6462), which was published after submission of this report, describes further examples of η^2-triazolato complexes.
[30] N. C. Mösch-Zanetti, M. Ferbinteanu, J. Magull, *Eur. J. Inorg. Chem.* **2002**, accepted for publication.
[31] I. A. Latham, G. J. Leigh, G. Huttner, I. Jibril, *J. Chem. Soc., Dalton Trans.* **1986**, 377−383.
[32] J. L. Polse, R. A. Andersen, R. G. Bergman, *J. Am. Chem. Soc.* **1996**, *118*, 8737−8738.
[33] I. A. Latham, G. J. Leigh, G. Huttner, I. Jibril, *J. Chem. Soc., Dalton Trans.* **1986**, 385−391.
[34] B. Goetze, J. Knizek, H. Nöth, W. Schnick, *Eur. J. Inorg. Chem.* **2000**, 1849−1854.
[35] G. M. Sheldrick, *Acta Crystallogr., Sect. A* **1990**, *46*, 467−473.
[36] G. M. Sheldrick, University of Göttingen, 1997.

Received October 31, 2001
[I01426]

A Mössbauer Study of $[Fe(edta)(O_2)]^{3-}$ Agrees with a High-Spin Fe^{III} Peroxo Complex

Olivier Horner,*[a] Claudine Jeandey,[a] Jean-Louis Oddou,[a] Pierre Bonville,[b] and Jean-Marc Latour[a]

Keywords: Iron / Peroxo ligands / Mössbauer spectroscopy / N ligands

An isotopically enriched $[^{57}Fe(edta)(O_2)]^{3-}$ complex, formed by the addition of H_2O_2 to a $^{57}Fe^{III}$-edta (edta = ethylenediaminetetraacetic acid) complex at elevated pH (pH = 11.3), was studied by Mössbauer spectroscopy. All Mössbauer parameters were determined for this nonheme high-spin ferric peroxo complex with an η^2-FeO_2 (side-on) arrangement by a numerical treatment of applied field Mössbauer data. The peroxo complex exhibits an isomer shift $\delta_{/Fe}$ = 0.65(1) mm s^{-1} and a quadrupole splitting ΔE_Q = +0.72(2) mm s^{-1} (T = 4.2 K). The isomer-shift value is very similar to the value of $\delta_{/Fe}$ = 0.61 mm s^{-1} published for the side-on peroxo complex $[Fe^{III}(N_4Py)(\eta^2\text{-}OO)]^+$ (Py = pyridine) [V. Vrajmasu, E. Münck, R. Ho, L. Que, Jr., G. Roefles, B. L. Feringa, *J. Inorg. Biochem.* **2001**, *86*, 472]. The set of Mössbauer parameters obtained herein is expected to aid the characterization of analogous species that may appear during dioxygen activation by nonheme mononuclear iron enzymes.

(© Wiley-VCH Verlag GmbH, 69451 Weinheim, Germany, 2002)

Introduction

The mechanism of dioxygen activation by nonheme iron systems has received much attention recently, and it has become clear that peroxo iron intermediates form a central part of these processes.[1] This has been thoroughly documented for diiron enzymes such as ribonucleotide reductase and methane monooxygenase, for which detailed spectroscopic characterizations of peroxo forms have been reported.[1b] Peroxo iron intermediates are also postulated for mononuclear nonheme iron enzymes, although their occurrence has been shown only in the antitumor drug bleomycin whose "activated" form was demonstrated to contain an Fe^{III}-OOH unit.[2] Similar species are likely to be involved in other mononuclear iron enzymes such as Fe-based superoxide dismutase,[3] and superoxide reductase.[4]

Great efforts are currently being made to obtain biologically relevant mononuclear nonheme iron(III) peroxide complexes. Some iron(III) hydrogenperoxo and peroxo complexes, which were proposed or demonstrated to contain a side-on peroxo group, have been identified in solution.[5] In some cases, these two forms can be interchanged by a protonation-deprotonation sequence (Scheme 1):[5a,5c,5d,5f]

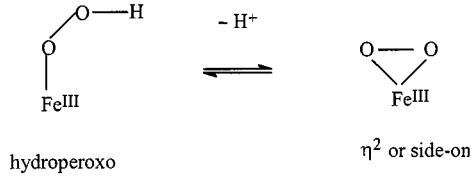

Scheme 1

The reactivity of the enzymatic systems will be dictated by the decomposition mode of the peroxide, which obviously depends on its protonation state and coordination geometry. Therefore a detailed investigation of the electronic structure of peroxo-iron species is a prerequisite to understanding their chemistry.

The only nonheme Fe^{III}-peroxo complex studied in any detail is the $[Fe(edta)(O_2)]^{3-}$ complex, a side-on peroxo species.[5g] $[Fe(edta)(O_2)]^{3-}$ was recently characterized by a wide range of spectroscopic techniques, including electron paramagnetic resonance (EPR), low-temperature absorption, variable temperature variable field magnetic circular dichroism (VTVH MCD) and resonance Raman spectroscopy; all the spectroscopic results, together with theoretical calculations, gave insight into the electronic structure of the complex.[6]

Mössbauer spectroscopy has proven invaluable to characterize biological iron sites[7] and it has been instrumental in probing the mechanism of action of the iron-containing

[a] Laboratoire de Physicochimie des Métaux en Biologie, FRE CEA/CNRS/UJF 2427, Département de Biologie Moléculaire et Structurale,
CEA/Grenoble, 38054 Grenoble Cedex 9, France
Fax: (internat.) + 33-4/3878-5090
E-mail: horner@cea.fr
[b] Service de Physique de l'Etat Condensé, Département de Recherche sur l'Etat Condensé, les Atomes et les Molécules, CEA/Saclay, 911991 Gif-sur-Yvette Cedex, France

component of ribonucleotide diphosphate reductase RNR R2,[8] and the hydroxylase component of methane monooxygenase MMOH[9] and stearoyl-ACP Δ^9-desaturase Δ9D.[10] Partial Mössbauer data have recently been published for the side-on peroxo complex $[Fe^{III}(N_4Py)(\eta^2\text{-}OO)]^+$ (Py = pyridine).[11] This prompted us to use Mössbauer spectroscopy to investigate the electronic structure of such complexes and their chemistry with respect to proton exchange. In this paper we report the Mössbauer characterization of the $[Fe(edta)(O_2)]^{3-}$ complex. Our study is a follow up from the work of Solomon et al.,[6] where Mössbauer spectroscopy was not used; we made use of their spectroscopic data [zero-field splitting (ZFS) parameters D and E]. The set of Mössbauer parameters obtained herein is expected to aid the characterization of analogous species that may appear during dioxygen activation by nonheme mononuclear iron enzymes.

Results and Discussion

The complex $[^{57}Fe(edta)(O_2)]^{3-}$ was synthesized following the procedure used by Solomon,[6] by adding H_2O_2 to a $^{57}Fe^{III}$-edta complex at elevated pH (a pH value of 11.3 was used) in buffered solution. It exhibits two weak EPR resonances at $g = 9.9$ and $g = 9.2$, and an intense derivation-type signal in the $g = 3-6$ region. Those resonances were shown to belong to an $S = 5/2$ system with rhombicity $E/D = 0.21$ and $D = -1.0 \pm 0.25$ cm^{-1}.[6,12]

The peroxo complex was studied by Mössbauer spectroscopy at low temperature in a low and a high magnetic field applied parallel to the propagation direction of the Mössbauer γ-rays. Figure 1 shows the Mössbauer spectra of $[Fe(edta)(O_2)]^{3-}$ in a 50 mT magnetic field (T = 4.2 K and 10 K), as well as the contribution of each Kramers doublet.

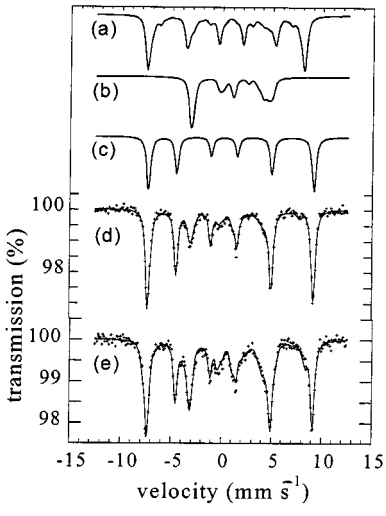

Figure 1. Mössbauer spectra of the $[Fe(edta)(O_2)]^{3-}$ complex; the experimental spectra shown in (d) and (e), taken at T = 4.2 K and T = 10 K, respectively in an applied parallel field of 50 mT, were fitted (solid curves) with the parameter set of Table 1; the solid curves in (a) – (c) show the contribution of each Kramers doublet

The peroxide complex Mössbauer spectrum was also recorded in a 7.0 T magnetic field (T = 4.2 K) and this is shown in Figure 2.

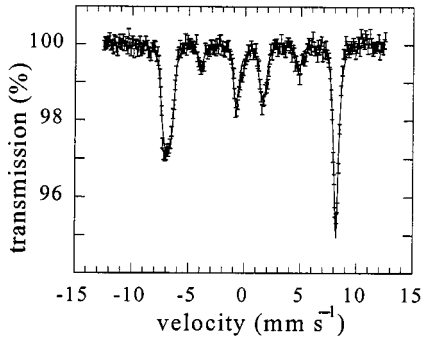

Figure 2. Mössbauer spectrum of the $[Fe(edta)(O_2)]^{3-}$ complex taken at 4.2 K in an applied parallel field of 7.0 T; the solid line corresponds to the fit of the spectrum with the set of Mössbauer parameters from Table 1

These spectra can be simulated within the spin-Hamiltonian formalism (see Exp. Sect. for details). All spectra were simultaneously fitted at the slow-relaxation limit using a unique set of parameters. The ZFS parameters were fixed to the values $D = -1.0$ cm^{-1} and $E/D = 0.21$.[6] The parameters obtained from the fits are shown in Table 1.

Table 1. Spin Hamiltonian parameters for the $[Fe(edta)(O_2)]^{3-}$ complex at T = 4.2 K; the electric field gradient (EFG) tensor, the hyperfine coupling tensor and the zero-field splitting tensor are colinear

	$[Fe(edta)(O_2)]^{3-}$
D (cm^{-1})	-1.0 cm^{-1} [6]
DE/D	0.21[6]
$g_x = g_y = g_z$	2.0
$A_x/g_n\beta_n$ (T)	$-23.1(3)$
$A_y/g_n\beta_n$ (T)	$-21.4(9)$
$A_z/g_n\beta_n$ (T)	$-20.8(1)$
η	0.4(2)
ΔE_Q (mm s^{-1})	+0.72(2)
$\delta_{/Fe}$ (mm s^{-1})	0.65(1)

Varying the ZFS parameter D from -1.25 cm^{-1} to -0.75 cm^{-1} changed the values of the set of parameters in Table 1 very slightly (except E/D, which was fixed at 0.21);[6] however, the best fit was obtained for $D = -1.0$ cm^{-1}.

For $E/D = 0.21$ ($D = -1.0$ cm^{-1}), the lower ("$M_S = \pm 5/2$") Kramers doublet of the $S = 5/2$ species is almost uniaxial and yields a sextuplet spectrum [Figure 1(c)]; the upper Kramers doublet ("$M_S = \pm 1/2$") is not uniaxial but also yields a sextuplet spectrum [Figure 1(a)]. The middle Kramers doublet ("$M_S = \pm 3/2$") is much more magnetically isotropic and yields a more complex-looking spectrum localized between -3.5 and $+6$ mm s^{-1} [Figure 1(b)].[13] At T = 4.2 K, the population of the upper doublet is significally less than that of the ground doublet. Therefore, the

contribution of the upper doublet to the experimental Mössbauer spectrum [Figure 1(d)] is negligible relative to the contribution from the lower and middle doublets. At T = 10 K, the populations of the upper and middle doublets and their contributions to the experimental spectrum increase [Figure 1(e)]. The intensity ratio of the spectral components is related to the Boltzmann factor and thus to the energy differences between the Kramers doublets, which, in turn, are related to the ZFS parameters D and E of the peroxo complex. At 77 K, the Mössbauer spectrum of the peroxo complex (50 mT applied magnetic field, data not shown) was poorly fitted at the slow relaxation limit, and at 200 K a broad unresolved spectrum was obtained (data not shown). This indicates that the fast relaxation limit is still not reached at this temperature.[14]

The $[Fe(edta)(O_2)]^{3-}$ complex exhibits an isomer shift $\delta_{/Fe}$ of 0.65 mm s^{-1} at 4.2 K and a quadrupole splitting $\Delta E_Q = +0.72$ mm s^{-1}. The former value is very similar to the value of 0.61 mm s^{-1} reported for the side-on peroxo complex $[Fe^{III}(N_4Py)(\eta^2\text{-}OO)]^+$.[11] Unfortunately, no quadrupole splitting value is available. Both parameters are also similar to those obtained by Mössbauer spectroscopy for the high-spin Fe^{III}-peroxo porphyrin $[Me_4N][Fe(OEP)O_2$ complex (OEP = octaethylporphyrin dianion);[15] this complex was suggested to contain a side-on peroxo group.[16] The porphyrin peroxo complex exhibits isomer shift and quadrupole splitting values (0.67 mm s^{-1} and + 0.62 mm s^{-1}, respectively, at 4.2 K) similar to those obtained for the $[Fe(edta)(O_2)]^{3-}$ complex, despite different iron environments. In addition, μ-1,2-peroxodiferric complexes exhibit isomer shifts in the range 0.60−0.66 mm s^{-1};[10] the isomer shift of the $[Fe(edta)(O_2)]^{3-}$ complex corresponds to the upper limit of this scale. The hyperfine coupling tensor of the peroxo complex is negative ($A_{av}/g_n\beta_n = -21.8$ T) because of the main contribution from the Fermi contact term (high-spin ferric iron case), and is also slightly anisotropic. For the $[Fe^{III}(N_4Py)(\eta^2\text{-}OO)]^+$ complex, a slighty anisotropic hyperfine tensor was also used with a similar average value ($A_{av}/g_n\beta_n = -21.1$ T).[11] For the $[Me_4N][Fe(OEP)O_2]$ complex, the hyperfine tensor was assumed to be isotropic ($A/g_n\beta_n = -23.3$ T).[14]

The absorbance of the peroxo complex at 520 nm (peroxo-to-iron ligand-to-metal charge transfer transition, LMCT band)[6] was recorded in solution at room temperature as a function of pH; it has been shown that this LMCT band reaches a plateau around pH = 10 (peroxide complex fully formed) and then collapses continuously to vanish at pH = 7.0.[17] In addition, no new bands appear between 400 and 800 nm (data not shown). It is thus not possible to generate, under those conditions, a hydrogenperoxo species by protonation of the peroxo complex, as discussed by Mc Kenzie et al,[5a] Girerd et al,[5c,5d] and Que et al.[5f] with nitrogen ligands.

In conclusion, we have fully characterized a mononuclear nonheme Fe^{III}-peroxo complex, where the peroxo group is coordinated to the iron center in a side-on way, by ^{57}Fe Mössbauer spectroscopy. The set of Mössbauer parameters obtained for the $[Fe(edta)(O_2)]^{3-}$ complex are close to those published for the high-spin ferric porphyrin complex $[Me_4N][Fe(OEP)O_2]$, which was suggested to contain a side-on peroxo group. The isomer shift value for the $[Fe(edta)(O_2)]^{3-}$ complex is also very close to the one reported by Münck et al. for the complex $[Fe^{III}(N_4Py)(\eta^2\text{-}OO)]^+$.[11] Therefore, our Mössbauer study of $[Fe(edta)(O_2)]^{3-}$ agrees with a high-spin Fe^{III} side-on peroxo complex. We are currently characterizing new mononuclear nonheme peroxo complexes by Mössbauer spectroscopy in our laboratory.

Experimental Section

All Mössbauer measurements were performed with a constant acceleration spectrometer calibrated with hematite, and isomeric shifts are reported relative to an Fe metal standard at room temperature. Variable temperature experiments were carried out with the sample placed in the tail section of a variable temperature cryostat. Temperatures of the sample were regulated to within ±0.2 K by a conventional PID system. The sample for Mössbauer spectroscopy contains about 4 mM ^{57}Fe. The Mössbauer spectra were analyzed, in a least-square fit procedure, by using the Hamiltonian **H** describing the system:

$$\mathbf{H} = D[\mathbf{S}_z^2 - (1/3)S(S+1) + (E/D)(\mathbf{S}_x^2 - \mathbf{S}_y^2)] + \beta_e\mathbf{.S.}[g]\mathbf{.B} + <\mathbf{S}>\mathbf{.}[A]\mathbf{.I} - g_n\beta_n\mathbf{B.I} + \mathbf{H_Q}$$

where D and E are the axial and rhombic zero field splitting parameters, respectively, β_e the electronic Bohr magneton, [g] the electronic tensor (considered here to be isotropic with a value fixed to 2), <**S**> the appropriately taken spin expectation value, [A] the magnetic hyperfine tensor, g_n the nuclear factor, β_n the nuclear Bohr magneton and $\mathbf{H_Q}$ the quadrupolar interaction Hamiltonian.[18] Each spectrum was then fitted with the set of parameters obtained when all the spectra were simultaneously fitted; the discrepancies found from this initial set allowed us to estimate the errors in each parameter.

Synthesis of the complex $[^{57}Fe(edta)(O_2)]^{3-}$

The $[^{57}Fe(edta)(O_2)]^{3-}$ complex was synthesized as reported recently.[8] Basically, a CHES (Sigma) buffered solution of fivefold excess ethylenediaminetetraacetic acid, tetrasodium salt (edta, Sigma) at pH = 11.3 was allowed to react with solid $^{57}FeCl_3{\cdot}6H_2O$. This mixture was heated until total dissolution of the solid material. The Fe^{III}-edta complex concentration was about 4 mM. The pH of the solution was then readjusted to 11.3 with sodium hydroxide and then filtered. The purple peroxo complex $[^{57}Fe(edta)(O_2)]^{3-}$ was formed by addition of a 10-fold excess of 30% H_2O_2 (Aldrich) to the former solution. For isotopic enrichment, the $^{57}FeCl_3{\cdot}6H_2O$ starting compound was obtained by dissolving $^{57}Fe_2O_3$ (AMT Ltd.) in 20 equivalents of concentrated HCl (Carlo Erba) under reflux and then by evaporating to dryness.

Acknowledgments

R. Vacher (CEA/Grenoble) is thanked for his help in the design and the building of the Mössbauer sample cells. J.-M. Mouesca (CEA/Grenoble) is thanked for useful discussions.

[1] [1a] L. Que, R. Y. N. Ho, *Chem. Rev.* **1996**, *96*, 2607−2624. [1b] E. I. Solomon, T. C. Brunold, M. I. Davis, J. N. Kemsley, S.-K. Lee, N. Lehnert, F. Neese, A. J. Skulan, Y.-S. Yang, J. Zhou,

Chem. Rev. **2000**, *100*, 235−349. [1c] M. Costas, K. Chen, L. Que, Jr., *Coord. Chem. Rev.* **2000**, *200−202*, 517−544.

[2] [2a] J. W. Sam, X.-J. Tang, J. Peisach, *J. Am. Chem. Soc.* **1994**, *116*, 5250−5256. [2b] R. J. Guajardo, J. D. Tan, P. K. Mascharak, *Inorg. Chem.* **1994**, *33*, 2838−2840.

[3] [3a] C. Bull, J. A. Fee, *J. Am. Chem. Soc.* **1985**, *107*, 3295−3304. [3b] D. M. Dooley, J. L. Karas, T. F. Jones, C. E. Coté, S. B. Smith, *Inorg. Chem.* **1986**, *25*, 4761−4766.

[4] M. Lombard, C. Houée-Levin, D. Touati, M. Fontecave, V. Nivière, *Biochemistry* **2001**, *16*, 5032−5040.

[5] [5a] K. B. Jensen, C. J. McKenzie, L. P. Nielsen, J. Z. Pedersen, H. M. Svendsen, *Chem. Commun.* **1999**, 1313−1314. [5b] P. Mialane, A. Novorojkine, G. Pratviel, L. Azéma, M. Slany, F. Godde, A. J. Simaan, F. Banse, T. Kargar-Grisel, G. Bouchoux, J. Sainton, O. Horner, J. Guilhem, L. Tcheranova, B. Meunier, J.-J. Girerd, *Inorg. Chem.* **1999**, *38*, 1085−1092. [5c] A. J. Simaan, F. Banse, P. Mialane, A. Boussac, S. Un, T. Kargar-Grisel, G. Bouchoux, J.-J. Girerd, *Eur. J. Inorg. Chem.* **1999**, 993−996. [5d] A. J. Simaan, S. Döpner, F. Banse, S. Bourcier, G. Bouchoux, A. Boussac, P. Hildebrandt, J.-J. Girerd, *Eur. J. Inorg. Chem.* **2000**, 1627−1633. [5e] C. Kim, K. Chen, J. Kim, L. Que, Jr., *J. Am. Chem. Soc.* **1997**, *119*, 5964−5965. [5f] R. Y. N. Ho, G. Roelfes, R. Hermant, R. Hage, B. L. Feringa, L. Que, Jr., *Chem. Commun.* **1999**, 2161−2162. [5g] S. Ahmad, J. D. McCallum, A. K. Shiemke, E. H. Appelman, T. M. Loehr, J. Sanders-Loehr, *Inorg. Chem.* **1988**, *27*, 2230−2233.

[6] F. Neese, E. I. Solomon, *J. Am. Chem. Soc.* **1998**, *120*, 12829−12848.

[7] [7a] P. Gütlich, R. Link, A. Trautwein, *Mössbauer Spectroscopy and Transition Metal Chemistry*, Springer-Verlag, Berlin, **1979**. [7b] V. Schünemann, H. Winkler, *Rep. Prog. Phys.* **2000**, *63*, 263−353.

[8] [8a] N. Ravi, J. M. Bollinger, Jr., B. H. Huynh, D. E. Edmondson, J. Stubbe, *J. Am. Chem. Soc.* **1994**, *116*, 8007−8014. [8b] J. M. Bollinger, Jr., W. H. Tong, N. Ravi, B. H. Huynh, D. E. Edmondson, J. Stubbe, *J. Am. Chem. Soc.* **1994**, *116*, 8015−8023. [8c] J. M. Bollinger, Jr., W. H. Tong, N. Ravi, B. H. Huynh, D. E. Edmondson, J. Stubbe, *J. Am. Chem. Soc.* **1994**, *116*, 8024−8032.

[9] [9a] K. E. Liu, A. M. Valentine, D. Wang, B. H. Huynh, D. E. Edmondson, A. Salifoglou, S. J. Lippard, *J. Am. Chem. Soc.* **1995**, *117*, 10174−10185. [9b] L. Shu, J. C. Nesheim, K. Kauffmann, E. Münck, J. D. Lipscomb, L. Que, Jr., *Science* **1997**, *275*, 515−518.

[10] J. A. Broadwater, C. Achim, E. Münck, B. G. Fox, *Biochemistry* **1999**, *38*, 12198−12204.

[11] V. Vrajmasu, E. Münck, R. Ho, L. Que, Jr., G. Roefles, B. L. Feringa, *J. Inorg. Biochem.* **2001**, *86*, 472.

[12] S. Fujii, H. Ohya-Nishiguchi, N. Hirota, *Inorg. Chim. Acta* **1990**, *175*, 27−30.

[13] E. Münck, in *Physical Methods in Bioinorganic Chemistry − Spectroscopy and Magnetism* (Ed.: L. Que, Jr.), University Science Books, **2000**, chapter 6.

[14] H. H. Wickman, M. P. Klein, D. A. Shirley, *Phys. Rev.* **1966**, *152*, 345−357.

[15] J. N. Burstyn, J. A. Roe, A. R. Miksztal, B. A. Shaevitz, G. Lang, J. S. Valentine, *J. Am. Chem. Soc.* **1988**, *110*, 1382−1388.

[16] P. Friand, J. Goulon, J. Fischer, L. Ricard, M. Schappacher, R. Weiss, M. Momenteau, *Nouv. J. Chim.* **1985**, *9*, 33−40.

[17] K. C. Francis, D. Cummins, J. Oakes, *J. Chem. Soc., Dalton Trans.* **1985**, 493−501.

[18] An extension of the program already published was used: F. Varret, *Phys. Chem. Solids* **1976**, *37*, 265−271.

Received October 10, 2001
[I01405]

Synthetic, Structural, Magnetic, and Mössbauer Spectral Study of $\{Fe[HC(3,5\text{-}Me_2pz)_3]_2\}I_2$ and Its Spin-State Crossover Behavior

Daniel L. Reger,*[a] Christine A. Little,[a] Mark D. Smith,[a] Arnold L. Rheingold,[b] Kin-Chung Lam,[b] Thomas L. Concolino,[b] Gary J. Long,*[c] Raphaël P. Hermann,[d] and Fernande Grandjean[d]

Keywords: Iron / N ligands / Spin crossover / Magnetic properties / Mössbauer spectroscopy

The complex $\{Fe[HC(3,5\text{-}Me_2pz)_3]_2\}I_2$ (**1**) has been prepared from the reaction of FeI_2 and $HC(3,5\text{-}Me_2pz)_3$ (pz = pyrazolyl ring) in a 1:2 ratio. The complex is high-spin in both the solid state and in solution at ambient temperature. In the solid state, magnetic susceptibility and Mössbauer spectral studies indicate that samples of the complex that have been crystallized and dried change completely from high-spin to low-spin upon cooling below 195 K, with a substantial two-step thermal hysteresis in the transition. The spin-crossover properties of **1** are sample dependent: powder samples do not change to low-spin at low temperatures. Two crystalline forms of **1** have been identified by X-ray crystallography, one form containing no solvent of crystallization and the other containing solvent. In both, there is only one iron site, with average Fe–N bond lengths of 2.18 and 2.17 Å, values that confirm that the complex is high-spin. Single crystals of the nonsolvated form shatter at low temperatures whereas single crystals of the solvated form can be cooled to 110 K with no loss of crystallinity and remain fully high spin at this temperature. Crystallographic information: nonsolvated form is triclinic, $P\bar{1}$, a = 8.8062(2) Å, b = 10.3549(2) Å, c = 11.3549(2) Å, α = 104.0768(10)°, β = 110.2473(10)°, γ = 92.6385(11)°, Z = 1; solvated form is monoclinic $P2_1/c$, a = 10.3214(5) Å, b = 12.7753(7) Å, c = 20.1995(11) Å, α = 90°, β = 97.5380(10)°, γ = 90°, Z =2.

(© Wiley-VCH Verlag GmbH, 69451 Weinheim, Germany, 2002)

Introduction

The properties of octahedral iron(II) complexes, especially those with an FeN_6 coordination environment, that undergo thermal spin-state crossovers between the high-spin (HS, S = 2) and low-spin (LS, S = 0) states have been widely investigated.[1] In general, iron(II) complexes that are HS in the solid state at room temperature may show a spin-state crossover to the LS electronic state upon cooling, whereas, complexes that are LS at room temperature may show a spin-state transition to the HS electronic state upon heating.[1,2]

We have recently reported, by using a combination of NMR, X-ray structural, magnetic, and Mössbauer spectral results, that $\{Fe[HC(3,5\text{-}Me_2pz)_3]_2\}(BF_4)_2$ (pz = pyrazolyl ring) shows unusual spin-crossover behavior in the solid state.[3] Even though only one iron site is observed by X-ray crystallography at ambient temperature, the solid abruptly changes from all-HS above 206 K to a 50:50 mixture of HS and LS (in this form the Fe−N bond lengths are reduced by ca. 0.2 Å, as expected[1]) below 200 K, the composition of the lower temperature mixed spin-state does not change as the temperature is lowered to 4.2 K. This spin-state crossover is reversible and shows no thermal hysteresis. Herein we report the synthesis, NMR, X-ray structural, magnetic, and Mössbauer spectral studies of $\{Fe[HC(3,5\text{-}Me_2pz)_3]_2\}I_2$ (**1**), a complex with the same dication as $\{Fe[HC(3,5\text{-}Me_2pz)_3]_2\}(BF_4)_2$, but paired with a different anion, a change that dramatically effects its properties.

[a] Department of Chemistry and Biochemistry, University of South Carolina,
Columbia, South Carolina 29208, USA
[b] Department of Chemistry and Biochemistry, University of Delaware,
Newark, Delaware 19716, USA
[c] Department of Chemistry, University of Missouri-Rolla,
Rolla, MO 65409-0010, USA
[d] Institut de Physique, B5, Université de Liège,
4000 Sart-Tilman, Belgium

Results and Discussion

Synthesis and Characterization

The reaction of FeI_2 and $HC(3,5\text{-}Me_2pz)_3$ in a 1:2 ratio yields $\{Fe[HC(3,5\text{-}Me_2pz)_3]_2\}I_2$ (**1**; Scheme 1). FeI_2 is black in solution. Upon addition of the ligand the homogeneous solution immediately becomes yellow and the desired product precipitates as a powder after several minutes. The solid is white as a powder and colorless as single crystals, indicat-

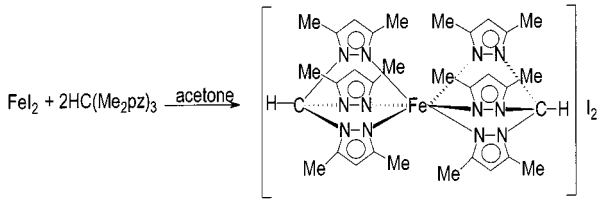

1

Scheme 1

ing that the iron(II) is HS at room temperature.[1] The solution ^{1}H NMR spectrum shows broad resonances shifted over the range from δ = 51.1 to −42.6, analogous to that previously reported for {Fe[HC(3,5-Me$_2$pz)$_3$]$_2$}(BF$_4$)$_2$ (**2**), indicating that the complex is also HS in solution.

The HS configuration of the iron(II) in **1** at ambient temperature was verified by the X-ray crystal structures (see Figure 1 and Table 1). Complex **1** crystallizes in two different forms under seemingly identical crystallization procedures. One form of these crystals contains no solvent molecules while the other form contains four molecules of CH_2Cl_2, the crystallization solvent, for every iron(II). In both cases, the crystals were found to fragment to microcrystals when taken out of solution. The crystals used for the X-ray structural studies were taken from a container that contained solvent and were immediately coated with an inert liquid.

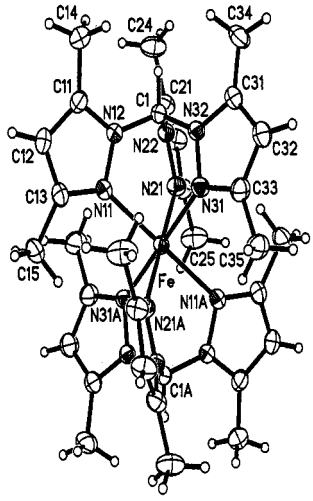

Figure 1. An ORTEP diagram of the cation of the solvated form of {Fe[HC(3,5-Me$_2$pz)$_3$]$_2$}I$_2$

The structures of the cations in both forms of **1** are similar (Figure 1) and similar to the cation in **2**, which has been reported previously.[3] Table 1 gives selected bond lengths and angles for all of the structures. The average Fe−N bond lengths are 2.18 Å in the nonsolvated form of **1** and 2.17 Å in the solvated form of **1** and in **2**, clearly indicating that iron(II) is in the high-spin configuration at 295 K; average bond lengths of ca. 1.97 Å are typically observed in LS octahedral FeN$_6$ complexes.[1] In all of the structures the iron(II) is located on a center of symmetry and has an N$_6$ coordination environment. The chelate rings restrict the intraligand N−Fe−N angles to an average of 84.5° in both forms of **1** and 84.3° in **2**, restrictions that lead to trigonally distorted octahedral structures.

There are important differences in the behavior of crystals of the two forms of **1** and of **2** upon cooling. Crystals of **2** change from colorless above 206 K to purple below this temperature; they also undergo a phase change from monoclinic to triclinic. These crystals, when reheated above 206 K, again become colorless, returning to the monoclinic space group, with no apparent degradation of crystal quality. Crystals of **2** that have been cooled are still suitable for X-ray structural studies at ambient temperature.[3] In contrast, crystals of **1** in the nonsolvated form shatter when cooled below 195 K, a temperature below which the solid turns purple. After being cooled, the crystals are no longer suitable for single crystal X-ray studies at either low temperature or after reheating to ambient temperature, at which temperature the sample is again white. Crystals of **1** in the solvated form *do not undergo the spin-state transition* down to 110 K. The quality of the crystals does not change, they remain colorless at 110 K, and there is no phase change at lower temperatures.

There is an interesting and important difference between the structures of the two forms of **1** relating to the degree of tilting of the pyrazolyl rings away from an ideal C_{3v} type arrangement. In the absence of tilting, the FeN(n1)−N(n2)−C(n1) torsion angles, where n denotes the ring number, would be 180° and the metal atom would reside in the planes defined by the pyrazolyl rings. We have previously commented on the fact that in octahedral {M[HC(3,5-Me$_2$pz)$_3$]$_2$}$^{n+}$ and M[HB(3,5-Me$_2$pz)$_3$]$_2$ complexes this ring tilting increases with increasing size of the metal.[4] The tilting also changes when the same cation is paired with different anions.[4] We have solved the structure of {Fe[HC(3,5-Me$_2$pz)$_3$]$_2$}(BF$_4$)$_2$ (**2**) at 220 K, where all of the cations are HS, and at 173 K, where half of the cations are HS and half LS. In the 220 K structure the torsion angle averages 169°, whereas for the HS form in the 173 K structure this torsion angle averages 162°. For the LS form of the 173 K structure this torsion angle averages 179°, reflecting the smaller size of LS iron(II). For the nonsolvated form of **1**, which changes to LS at low temperatures, this torsion angle averages 171°. In contrast, in the solvated form of **1**, the form that does not change to LS at low temperatures, it is 10° less at 161°.

Magnetic Susceptibility Studies

Both crystalline forms of {Fe[HC(3,5-Me$_2$pz)$_3$]$_2$}I$_2$ (**1**) discussed in the X-ray section above fragment to microcrystals when dried or if even briefly removed from the crystallization solvents. This process makes it impossible to directly measure the magnetic properties of the single crystals used in the X-ray structural studies.

The effective magnetic moment of a sample originating from the nonsolvated, crystalline form of **1** as a function of temperature between 5 and 325 K is shown in Figure 2. A sample originating from the solvated, crystalline form of **1**,

Table 1. Selected bond lengths and angles for the cation in nonsolvated $\{Fe[HC(3,5\text{-}Me_2pz)_3]_2\}I_2$, solvated $\{Fe[HC(3,5\text{-}Me_2pz)_3]_2\}I_2{\cdot}4CH_2Cl_2$ and $\{Fe[HC(3,5\text{-}Me_2pz)_3]_2\}(BF_4)_2$ (**2**)

Complex	Bond lengths (Å) Nonsolvated Form	Solvated Form	**2**
Fe−N(11)	2.156(3)	2.157(2)	2.155(3)
Fe−N(21)	2.200(4)	2.174(2)	2.179(2)
Fe−N(31)	2.176(3)	2.171(3)	2.177(2)
C(1)−N(12)	1.443(5)	1.451(4)	1.444(4)
C(1)−N(22)	1.446(6)	1.446(4)	1.451(3)
C(1)−N(32)	1.448(5)	1.447(4)	1.448(4)
Intraligand donor N···N average distance	2.93	2.916(2)	2.91
Distance Fe out of N_3 donor plane	1.371(2)	1.3562	1.373(2)
Bond Angles (deg)			
N(11)−Fe−N(21)	84.49(14)	84.75(9)	84.41(11)
N(11)−Fe−N(31)	83.57(13)	84.11(9)	83.70(10)
N(21)−Fe−N(31)	85.59(14)	84.77(9)	84.67(10)
N(11)−Fe−N(21A)	95.51(14)	95.25(9)	95.59(11)
N(11)−Fe−N(31A)	96.43(14)	95.89(9)	96.30(10)
N(21)−Fe−N(31A)	94.41(14)	95.23(9)	95.33(10)
N(11)−N(12)−C(1)	120.1(3)	119.5(2)	119.2(2)
N(21)−N(22)−C(1)	119.9(3)	119.1(2)	119.6(2)
N(31)−N(32)−C(1)	119.6(3)	120.1(2)	119.8(2)
N(12)−C(1)−N(22)	111.3(3)	111.0(2)	111.4(2)
N(12)−C(1)−N(32)	113.0(3)	111.3(2)	111.9(2)
N(22)−C(1)−N(32)	110.8(3)	111.1(2)	111.1(3)
FeN(11)−N(12)C(11) torsion	168.0(3)	164.2(2)	166.1(2)
FeN(21)−N(22)C(21) torsion	165.9(3)	164.1(2)	168.5(2)
FeN(31)−N(32)C(31) torsion	179.8(3)	157.9(2)	171.4(2)

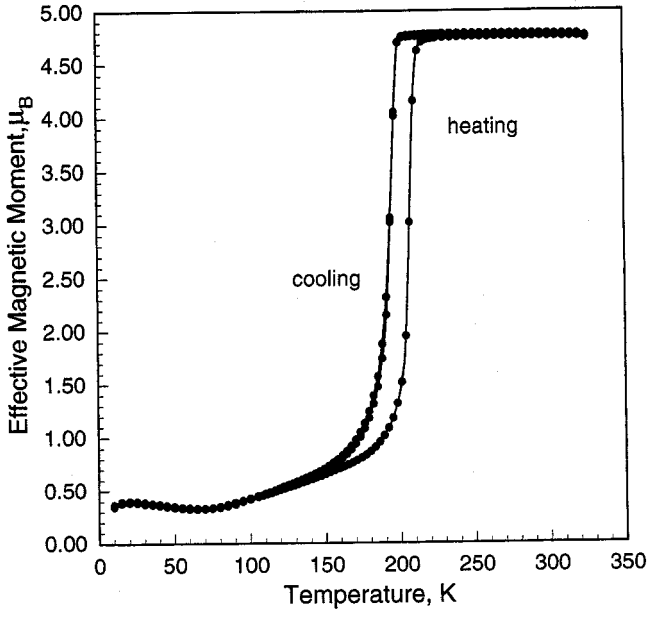

Figure 2. The effective magnetic moment as a function of temperature, measured by cooling, heating and recooling between 325 and 5 K, of crystallized $\{Fe[HC(3,5\text{-}Me_2pz)_3]_2\}I_2$ (**1**)

that had been dried and shown by elemental analysis to lose the CH_2Cl_2 of crystallization, has essentially the same magnetic properties as shown in Figure 2. At higher temperatures **1** is clearly HS with an effective moment of ca. 4.8 μ_B, a value that is very close to the iron(II) spin-only value of 4.9 μ_B. Upon cooling below 195 K there is a dramatic drop in the moment as would be expected for a spin-state crossover to a LS iron(II) complex. Continued cooling to 5 K yields a very small moment, except at the lowest temperatures where a trace of paramagnetic iron(III) impurity leads to a very small increase in the magnetic susceptibility. The low-temperature moment of ca. 0.4 μ_B is typical of the temperature-independent paramagnetism observed in low-spin iron(II) complexes. Subsequent warming of the sample above 5 K reveals very similar behavior but with the presence of a reproducible hysteresis of ca. 15 degrees in the spin-crossover such that at ca. 210 K, the sample has completely returned to the HS state.

The magnetic properties of complex **1** are dependent on the history of the sample. Figure 3 shows the magnetic behavior of the solid that precipitated from acetone in the original reaction, a sample that is a white powder and is pure as indicated by elemental analysis and NMR spectroscopy. This solid was subsequently used to prepare the crystalline samples, which once dried were used to obtain the

magnetic results shown in Figure 2. For the solid that precipitated from acetone, only a small change in the magnetic moment was observed as the temperature was lowered. The high temperature moment of this sample is the same as observed for both crystallized samples. In contrast, for the sample of **1** that precipitated from acetone, there is only a small decrease in the magnetic moment from μ_{eff} = 4.85 μ_B at higher temperatures to μ_{eff} = 4.5 μ_B below 185 K. As with the results presented in Figure 2, a hysteresis of ca. 15 degrees is observed upon cooling and heating for the small changeover. Presumably, the decrease of ca. 0.4 μ_B is due to the presence of a small amount of microcrystalline **1** that is present in the sample.

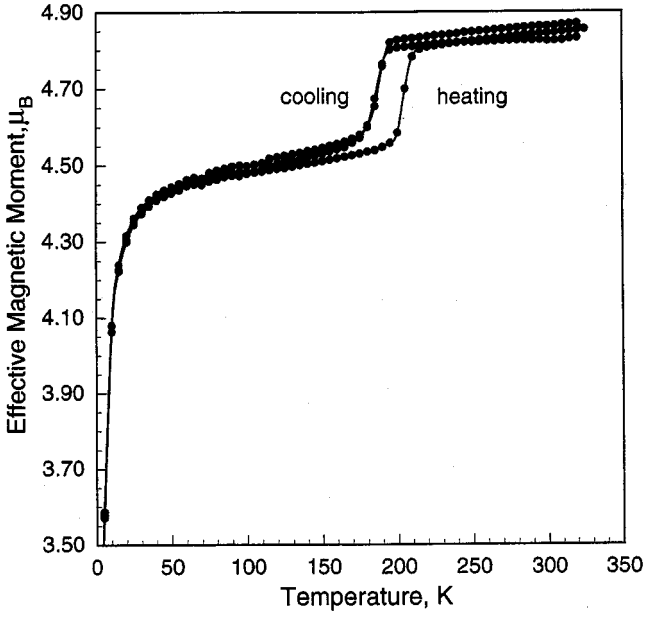

Figure 3. The effective magnetic moment as a function of temperature, measured by cooling, heating and recooling between 325 and 5 K, of a sample of {Fe[HC(3,5-Me$_2$pz)$_3$]$_2$}I$_2$ that precipitated from the reaction mixture

There is a sharp drop in the effective moment below ca. 30 K (see Figure 3). This drop is not unexpected for a distorted octahedral iron(II) complex in which the low-symmetry component of the crystal field, in conjunction with electron delocalization and spin-orbit coupling, are known[5] to lead to a decrease in the observed moments at very low temperatures.

Mössbauer Spectral Analysis

The Mössbauer spectra of {Fe[HC(3,5-Me$_2$pz)$_3$]$_2$}I$_2$ (**1**), measured on a sample that was crystallized from CH_2Cl_2/hexanes and dried, were obtained upon cooling from 295 to 4.2 K and upon warming from 175 to 215 K (Figures 4 and 5, respectively). Selected hyperfine parameters for this complex are given in Table 2. The complete temperature dependence of the isomer shift and quadrupole splittings for the HS and LS states are shown in Figures 6 and 7. As the sample is cooled, a dramatic change occurs in the spectra starting at ca. 190 K indicating a spin-state crossover from the HS to the LS state.[1] This change is clearly indicated by the appearance of a second doublet at ca. 0.5 mm/s. The change in population of the HS state, as reflected by the Mössbauer spectral absorption area of the HS component, is shown in Figure 8, and matches an analogous plot using data from the magnetic studies.

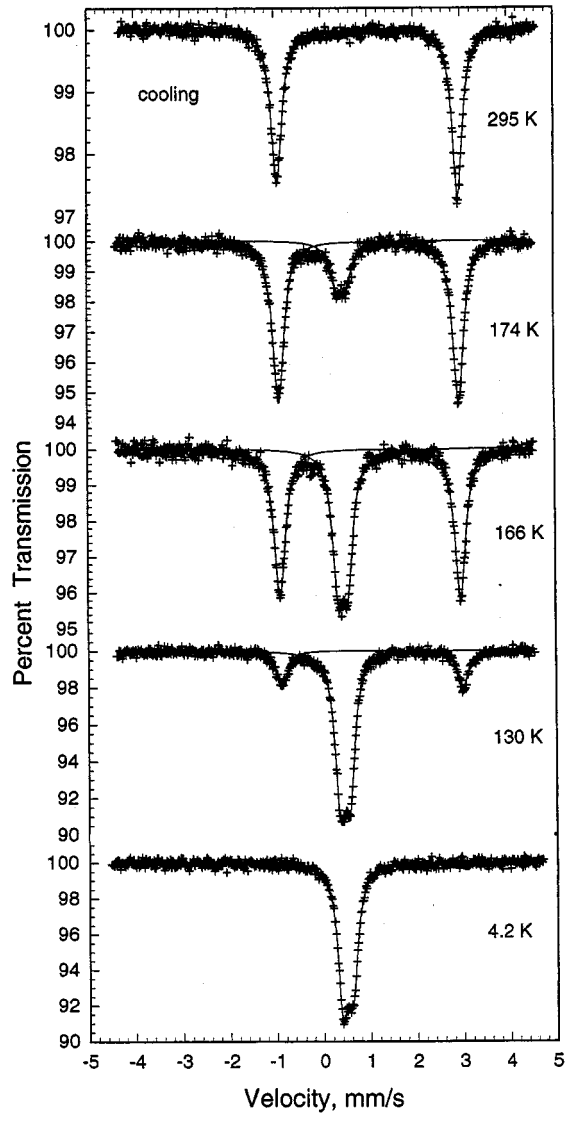

Figure 4. The Mössbauer spectra of crystallized {Fe[HC(3,5-Me$_2$pz)$_3$]$_2$}I$_2$ (**1**) obtained at the indicated temperatures upon cooling from 295 to 4.2 K

The hyperfine parameters reported in Table 2 are those expected for HS and LS iron(II) complexes with a distorted pseudooctahedral coordination geometry. The isomer shifts and quadrupole splittings for both the HS and LS states of **1** are virtually identical to those of the analogous complex {Fe[HC(3,5-Me$_2$pz)$_3$]$_2$}(BF$_4$)$_2$ (**2**), although the nature of the spin-crossover is different. In **1** the transition to the low-spin state is complete below 70 K but the transition occurs only to 75% in the temperature range from 70 to 150 K on cooling and 70 to 200 K on heating. The presence of a small amount of the HS complex in this temperature range is also

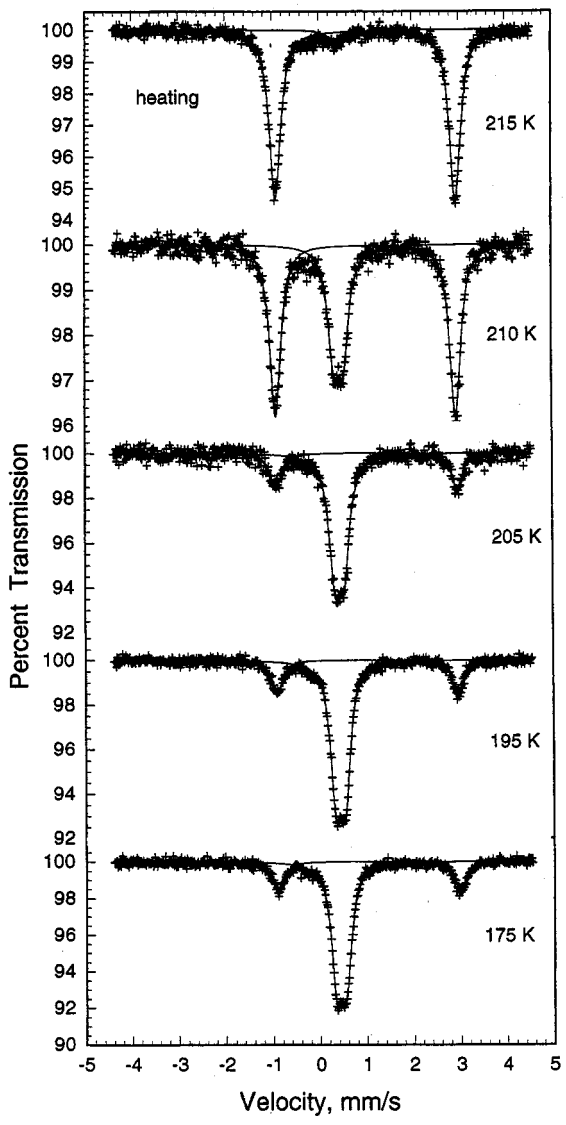

Figure 5. The Mössbauer spectra of crystallized {Fe[HC(3,5-$Me_2pz)_3]_2$}I_2 (**1**) obtained at the indicated temperatures upon heating from 4.2 K

Table 2. Selected Mössbauer spectral parameters for {Fe[HC(3,5-$Me_2pz)_3]_2$}I_2 (**1**)

T(K)	δ (mm/s)[a]	ΔE_Q (mm/s)	Γ (mm/s)	Relative area (%)	Assignment
295[b]	0.969	3.86	0.28	100	high-spin
190[b]	1.022	3.86	0.30	100	high-spin
180[b]	1.023	3.86	0.27	92	high-spin
	0.432	0.20	0.27	8	low-spin
174[b]	1.029	3.86	0.29	70	high-spin
	0.430	0.19	0.30	30	low-spin
166[b]	1.033	3.87	0.28	57	high-spin
	0.443	0.21	0.27	43	low-spin
130[b]	1.064	3.89	0.28	23	high-spin
	0.459	0.21	0.26	77	low-spin
70[b]	1.095	3.91	0.26	13	high-spin
	0.463	0.21	0.25	87	low-spin
4.2	0.463	0.21	0.26	100	low-spin
175[c]	1.039	3.88	0.28	23	high-spin
	0.440	0.20	0.26	77	low-spin
195[c]	1.012	3.88	0.27	22	high-spin
	0.435	0.20	0.26	78	low-spin
205[c]	1.017	3.87	0.28	25	high-spin
	0.429	0.20	0.27	75	low-spin
210[c]	1.007	3.84	0.28	89	high-spin
	0.418	0.21	0.28	11	low-spin
215[c]	1.010	3.85	0.29	95	high-spin
	0.419	0.20	0.34	5	low-spin
295[d]	1.009	3.90	0.29	100	high-spin
90[d]	1.118	3.92	0.28	85	high-spin
	0.500	0.22	0.25	15	low-spin

[a] The isomer shifts are given relative to room temperature α-iron foil. [b] Data obtained on the nonsolvated crystallized sample during the initial cooling from 295 to 4.2 K. [c] Data obtained on the nonsolvated crystallized sample after cooling to 4.2 K. [d] Data obtained on a powder sample.

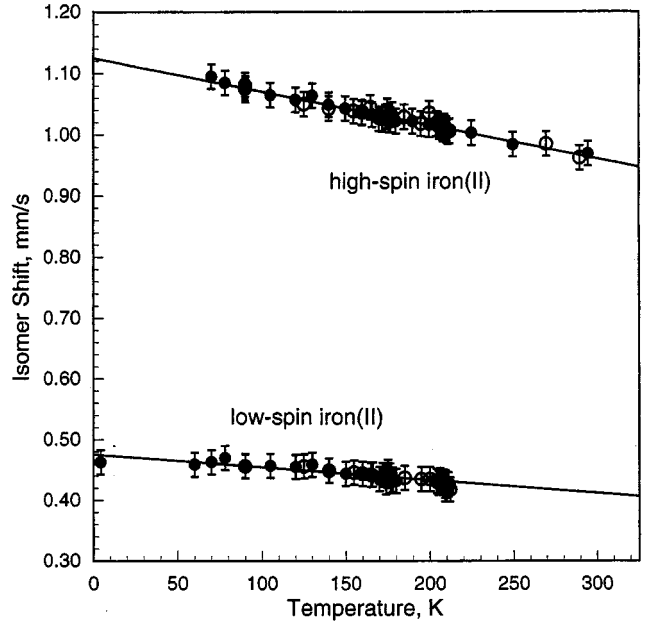

Figure 6. The temperature dependence of the Mössbauer spectral isomer shifts for {Fe[HC(3,5-$Me_2pz)_3]_2$}I_2 (**1**); the data obtained upon the initial cooling from 295 to 4.2 K are indicated by ● and the data obtained upon the subsequent heating from 4.2 K are indicated by ○

apparent in Figure 2 as a shoulder in the effective moment.

A comparison of Figure 2 with Figure 8 indicates that the temperature hysteresis observed in the magnetic measurements is approximately half that observed in the Mössbauer spectral studies. The exact reason for this difference is not apparent at this time, but is probably related to differences in sample preparation. We have shown that thermal equilibrium was achieved in the magnetic studies by stopping the change in temperature at a number of points in both the heating and cooling cycles around 200 K and observing no change of the magnetic moment with time.

Mössbauer spectra were obtained at 90 K and 295 K on the same sample that was used for the magnetic data shown in Figure 3, a sample that precipitated from acetone in the

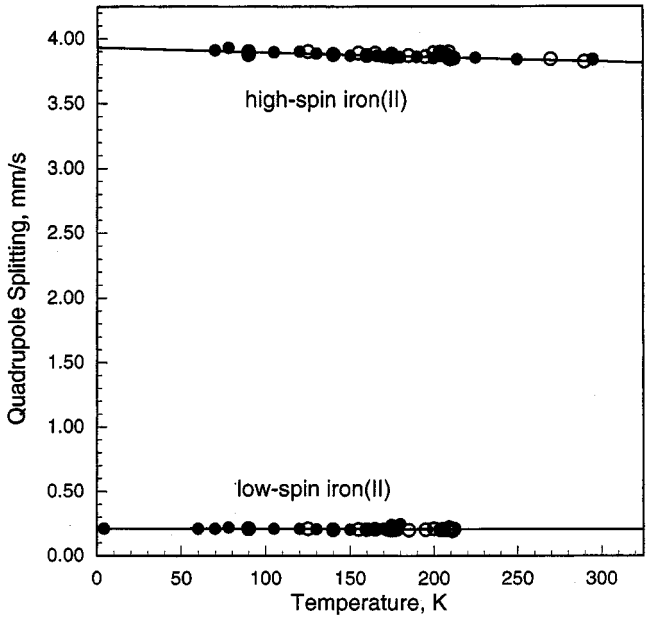

Figure 7. The temperature dependence of the Mössbauer spectral quadrupole splittings for {Fe[HC(3,5-Me$_2$pz)$_3$]$_2$}I$_2$ (**1**); the data obtained upon initial cooling from 295 to 4.2 K are indicated by ● and the data obtained upon the subsequent heating from 4.2 K are indicated by ○

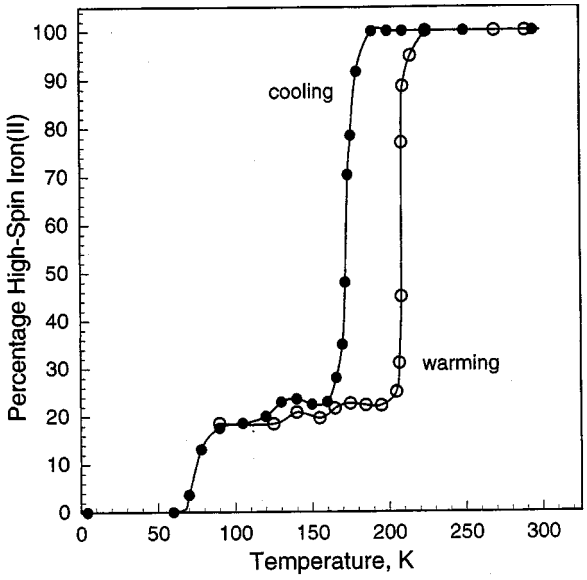

Figure 8. The temperature dependence of the percentage of high-spin iron(II) in {Fe[HC(3,5-Me$_2$pz)$_3$]$_2$}I$_2$ (**1**); the data obtained upon initial cooling from 295 to 4.2 K are indicated by ● and the data obtained upon the subsequent heating from 4.2 K are indicated by ○

original reaction. At 295 K the sample is fully HS with hyperfine parameters that match those observed with the crystallized samples. At 90 K, only 15% of the sample is LS, approximately the same amount that changes in the magnetic study.

Conclusions

The most interesting property of {Fe[HC(3,5-Me$_2$pz)$_3$]$_2$}I$_2$ (**1**) is the temperature-dependent changes in spin-state behavior, changes which are a function of the history of the sample. These changes are observed both in the X-ray diffraction studies carried out on single crystals and in the magnetic and Mössbauer spectral studies carried out on the fragmented microcrystals that form when the single crystals are taken out of solution. Two crystalline forms of **1** have been identified by X-ray crystallography. Although the average Fe−N bond lengths and angles of the FeN$_6$ cores in the two structures are the same, there are substantial differences in the FeN(n1)−N(n2)−C(n1) torsion angles. In the structure of the nonsolvated form of **1**, measured at 298 K, this torsion angle averages 171°. These crystals shatter when cooled below 195 K, a temperature below which the solid turns purple, indicating a change to the LS form. In the structure of the solvated form of **1**, this torsion angle is 10° less, at 161°. As shown by X-ray crystallography, this crystalline form does not change to LS upon cooling to 110 K. It should be noted that in the low spin form of {Fe[HC(3,5-Me$_2$pz)$_3$]$_2$}(BF$_4$)$_2$ (**2**) observed at 173 K, the structure has a torsion angle of 179°, the angle expected for the LS form of iron(II) in this dication. Thus the failure of the solvated crystalline form of **1**, which has a much smaller average torsion angle, to undergo a spin-state change may well result from the unfavorable energetics required to dramatically change the torsion angle as well as the bond lengths. These energetic changes may well be large enough to prevent the spin-state crossover.

Both magnetic and Mössbauer spectral studies of the fragmented microcrystals that form when the single crystals of either crystalline form are taken out of solution, show that both samples are HS at ambient temperatures but change over to the LS form at low temperatures. These samples of complex **1** behave similarly to many other iron(II) complexes with an FeN$_6$ coordination environment[1] in changing completely to the LS state at low temperatures. Surprisingly, a pure sample of **1** that precipitates from the original reaction mixture changes only partially over to the LS form at low temperatures. As with the solvated, crystalline form of **1**, the energetics of the changeover are clearly different for different samples.

The behavior of complex **2** is different from that of **1** in that only half of the iron(II) sites change to LS at low temperatures, although all crystalline samples studied behave the same way. Another difference is that for **1** there is an ca. 15 degree hysteresis in the temperature dependence of the spin-state crossover, whereas no hysteresis is observed for **2**. Clearly the environment of the {Fe[HC(3,5-Me$_2$pz)$_3$]$_2$}$^{2+}$ dication within the ionic lattice and the crystalline form influence its spin-crossover behavior.

Experimental Section

General Procedure: All operations were carried out under a nitrogen atmosphere using either standard Schlenk techniques or in a

Vacuum Atmospheres HE-493 inert atmosphere dry box. All solvents were dried and distilled prior to use. Anhydrous FeI_2 (99.99%) was purchased from Aldrich Chemicals. Proton NMR chemical shifts are reported in ppm versus TMS. $HC(3,5\text{-}Me_2pz)_3$ was prepared according to our recently reported procedures.[6] Elemental analyses were performed by Robertson Microlit Laboratories, Inc.

Magnetic susceptibilities were measured at 5 kG using a Quantum Design MPMS XL SQUID magnetometer. Gelatin capsules were used as sample containers for measurements taken in the temperature range 5−400 K. The very small diamagnetic contribution of the gelatin capsule had a negligible contribution to the overall magnetization, which was dominated by the sample. The molar magnetic susceptibilities were corrected for the diamagnetism of the complexes, which were calculated from tables of Pascal's constants to be -445×10^{-6} emu/mol for $\{Fe[HC(3,5\text{-}Me_2pz)_3]_2\}I_2$.

$\{Fe[HC(3,5\text{-}Me_2pz)_3]_2\}I_2$ (1): FeI_2 (0.19 g, 0.62 mmol) was dissolved in acetone (10 mL) and treated dropwise by cannula transfer with an acetone solution (10 mL) of $HC(3,5\text{-}Me_2pz)_3$ (0.370 g, 1.24 mmol). The solution turned yellow and after stirring for several minutes the desired product precipitated from solution as a white powder (0.47 g, 84%), dec. 333−339 °C. The crystals used for X-ray crystallographic studies were grown by layering a saturated dichloromethane solution with hexanes and allowing the two layers to slowly combine. Two forms of the crystals, a nonsolvated form and a solvated form of the formula $\{Fe[HC(3,5\text{-}Me_2pz)_3]_2\}I_2{\cdot}4CH_2Cl_2$ (as shown by X-ray crystallography, vide infra), are produced when this crystallization procedure is repeated under seemingly identical conditions. Both forms of these crystals fragment when dried, with the solvated form losing the CH_2Cl_2 of crystallization. Unless otherwise noted, these fragmented crystals were used in the magnetic and Mössbauer spectral studies. ^1H NMR (CD_2Cl_2): δ = −42.6 (v br, 2 H, *H*C), 41.1, 19.6 (v br, v br, 18 H, 18 H, Me_2), 51.1 (v br, 6 H, 4-*H* pz). $C_{32}H_{44}FeI_2N_{12}$ (906.4): calcd. C 42.40, H 4.89; found for the powder sample that precipitates from the reaction mixture: C 42.09, H 4.72; found for the nonsolvated crystalline form after drying: C 42.77, H 4.71; found for the solvated crystalline form after drying: C 42.47, H 4.78.

X-ray Structural Data

Nonsolvated Form of $\{Fe[HC(3,5\text{-}Me_2pz)_3]_2\}I_2$: Colorless crystals were taken from solution and immediately coated with epoxy resin. Crystal, data collection, and refinement parameters are given in Table 3. There is no evidence of symmetry higher than triclinic, and *E*-statistics and the presence of an inversion center for the iron(II) cation suggest the centrosymmetric space group $P\bar{1}$ for **1**, a space group that yields a chemically reasonable and computationally stable refinement. The structure was solved using direct methods, completed by subsequent difference Fourier syntheses, and refined by full-matrix least-squares procedures. *SADABS* absorption corrections were applied to all data sets. The asymmetric unit contains half of the cationic iron(II) complex, which lies on an inversion center, and one of the iodide anions. All non-hydrogen atoms were refined with anisotropic thermal displacement coefficients. The hydrogen atom of C(1) was located from the difference map and allowed to refine, all other hydrogen atoms were treated as idealized contributions. All software and sources of the scattering factors are contained in the SHELXTL (5.10) program library (G. Sheldrick, Siemens XRD, Madison, WI).

Table 3. Crystallographic data for the structural analyses of nonsolvated $\{Fe[HC(3,5\text{-}Me_2pz)_3]_2\}I_2$ and Solvated $\{Fe[HC(3,5\text{-}Me_2pz)_3]_2\}I_2{\cdot}4CH_2Cl_2$

	Nonsolvated Form	Solvated Form
Formula	$C_{32}H_{44}FeI_2N_{12}$	$C_{36}H_{52}Cl_8FeI_2N_{12}$
Molecular weight	906.44	1246.15
Space group	$P\bar{1}$	$P2_1/c$
a, Å	8.8062(2)	10.3214(5)
b, Å	10.3549(2)	12.7753(7)
c, Å	11.3549(2)	20.1995(11)
α, deg	104.0768(10)	90
β, deg	110.2473(10)	97.5380(10)
γ, deg	92.6385(11)	90
V, Å^3	949.44(4)	2640.5(2)
Z	1	2
Color	colorless	colorless
ρ(calcd), g cm^{-3}	1.585	1.567
μ(Mo-K_α), cm^{-1}	20.62	18.98
Temp, K	298	190
$R(F)$,[a] (wR^2)[a]	0.0454, 0.1186	0.0379, 0.0930

[a] Quantity minimized = $R(wF^2) = \Sigma[w(F_0^2 - F_c^2)^2/\Sigma w(F_0^2)^2]^{1/2}$; $R = \Sigma\Delta/\Sigma(F_o)$, $\Delta = |F_o - F_c|$

Solvated Form of $\{Fe[HC(3,5\text{-}Me_2pz)_3]_2\}I_2{\cdot}4CH_2Cl_2$: A colorless needle was coated with inert oil, mounted on the end of a thin glass fiber and transferred to the cold stream of a Bruker SMART APEX CCD-based diffractometer system. The X-ray intensity data were measured at 190(2) K. Crystal quality and initial unit cell parameters were determined based on reflections taken from a set of three scans measured in orthogonal regions of reciprocal space. Subsequently a hemisphere of frame data was collected with a scan width of 0.3° in ω and an exposure time of 10 s per frame. The first 50 frames were re-collected at the end of the data set to monitor crystal decay. The raw data frames were integrated into reflection intensity files with the Bruker SAINT+ program,[7] which also applied corrections for Lorentz and polarization effects. The final unit cell parameters are based on the least-squares refinement of 9412 reflections with $I > 5\sigma(I)$ from the data set. Analysis of the data showed negligible crystal decay during data collection. An empirical absorption correction based on the multiple measurements of equivalent reflections was applied with the program SADABS.[8]

$\{Fe[HC(3,5\text{-}Me_2pz)_3]_2\}I_2{\cdot}4CH_2Cl_2$ crystallizes in the space group $P2_1/c$ as determined by the systematic absences in the intensity data. The structure was solved by a combination of direct methods and difference Fourier syntheses, and refined by full-matrix least-squares against F^2, using the SHELXTL software package.[8] The iron(II) ion is located on a special position, a center of symmetry; all other atoms are on general positions. The asymmetric unit consists of the iron(II), one $HC(3,5\text{-}Me_2pz)_3$ ligand, one iodide anion and two dichloromethane molecules. All non-hydrogen atoms were refined with anisotropic thermal displacement parameters; hydrogen atoms were placed in idealized positions and refined using a riding model.

CCDC-171226 (nonsolvated form) and CCDC-171227 (solvated form) contain the supplementary crystallographic data for this paper. These data can be obtained free of charge at www.ccdc.cam.ac.uk/conts/retrieving.html [or from the Cambridge Crystallographic Data Center, 12, Union Road, Cambridge CB2 1EZ, UK; Fax: (internat.) +44-1223/336-033; E-mail: deposit@ccdc.cam.ac.uk].

Mössbauer Spectroscopic Data: The Mössbauer spectral absorber contained 47 mg/cm^2 of powder and the spectra were measured between 4.2 and 295 K on a constant-acceleration spectrometer which utilized a room temperature rhodium matrix cobalt-57 source and was calibrated at room temperature with an α-iron foil. The estimated absolute errors are ± 0.01 mm/s for the isomer shifts, ± 0.02 mm/s for the quadrupole splittings, and ± 0.5 percent for the relative areas of the high-spin and low-spin spectral components. The relative errors are estimated to be smaller by a factor of 2 to 5.

Acknowledgments

The authors acknowledge, with thanks, the help of Professor Hanno zur Loye and Katharine Stitzer for assistance in obtaining the magnetic data. The authors also thank the US National Science Foundation for grants CHE-0110493 to D. L. R. and DMR-9521739 to G. J. L. and the Petroleum Research Fund for grant 36368-AC3 to D. L. R. The Bruker CCD Single Crystal Diffractometer (at the University of South Carolina) was purchased with funds provided by the NSF Instrumentation for Materials Research Program through Grant DMR:9975623. F. G. thanks the "Fonds National de la Recherche Scientifique," Brussels, Belgium for grant 9.456595 and G. J. L. thanks them for support during a sabbatical leave in Belgium.

[1] [1a] P. Gütlich, in *Mössbauer Spectroscopy Applied to Inorganic Chemistry* (Ed.: G. J. Long), Plenum: New York, **1984**; Vol. 1: p 287. [1b] P. Gütlich, A. Hauser, H. Spiering, *Angew. Chem. Int. Ed. Engl.* **1994**, *33*, 2024−2044. [1c] O. Kahn, J. Martinez, *Science* **1998**, *279*, 44−68.

[2] [2a] F. Grandjean, G. J. Long, B. B. Hutchinson, L. Ohlhausen, P. Neill, J. D. Holcomb, *Inorg. Chem.* **1989**, *28*, 4406−4414. [2b] G. J. Long, B. B. Hutchinson, *Inorg. Chem.* **1987**, *26*, 608−613. [2c] J. P. Jesson, S. Trofimenko, D. R. Eaton, *J. Am. Chem. Soc.* **1967**, *89*, 3158−3164. [2d] J. P. Jesson, J. F. Weiher, S. J. Trofimenko, *Chem. Phys.* **1968**, *48*, 2058−2066. [2e] C. Cartier dit Moulin, P. Rudolf, A.-M. Flank, C.-T. Chen, *J. Phys. Chem.* **1992**, *96*, 6196−6200. [2f] C. Cartier dit Moulin, A. M. Flack, C.-T. Chen, *Jpn. J. Appl. Phys.* **1993**, *32*, Suppl. 32−2, 308−310. [2g] V. Briois, C. Cartier dit Moulin, M. Momenteau, P. Maillard, J. Zarembowitch, E. Dartyge, A. Fontaine, G. Tourillon, P. Thuéry, M. J. Verdaguer, *Chim. Phys.* **1989**, *86*, 1623−1634. [2h] N. A. Young, *J. Chem. Soc., Dalton Trans.* **1996**, 1275−1281. [2i] J.-A. Real, B. Gallois, T. Granier, F. Suez-Panama, J. Zarembowitch, *Inorg. Chem.* **1992**, *31*, 4972−4979. [2j] C. Janiak, T. G. Scharmann, T. Bräuniger, J. Holubová, M. Nádvorník, *Z. Anorg. Allg. Chem.* **1998**, *624*, 769−774.

[3] [3a] D. L. Reger, C. A. Little, A. L. Rheingold, M. Lam, T. Concolino, A. Mohan, G. J. Long, *Inorg. Chem.* **2000**, *39*, 4674−4675. [3b] D. L. Reger, C. A. Little, A. L. Rheingold, M. Lam, L. M. Liable-Sands, B. Rhagitan, T. Concolino, A. Mohan, G. J. Long, V. Briois, F. Grandjean, *Inorg. Chem.* **2001**, *40*, 1508−1520. [3c] D. L. Reger, C. A. Little, V. Young, M. Pink, *Inorg. Chem.* **2001**, *40*, 2870−2874.

[4] D. L. Reger, T. D. Wright, C. A. Little, J. J. S. Lamba, M. D. Smith, *Inorg. Chem.* **2001**, *40*, 3810−3814 and references therein.

[5] [5a] B. N. Figgis, J. Lewis, F. E. Mabbs, G. A. Webb, *J. Chem. Soc. (A)* **1967**, 442−447. [5b] G. J. Long, W. A. Baker, Jr., *J. Chem. Soc. (A)* **1971**, 2956−2959.

[6] D. L. Reger, T. C. Grattan, K. J. Brown, C. A. Little, J. J. S. Lamba, A. L. Rheingold, R. D. Sommer, *J. Organomet. Chem.* **2000**, *607*, 120−128.

[7] SMART Version 5.624, SAINT+ Version 6.02a and SADABS. Bruker Analytical X-ray Systems, Inc., Madison, Wisconsin, USA, **1998**.

[8] G. M. Sheldrick, SHELXTL Version 5.1; Bruker Analytical X-ray Systems, Inc., Madison, Wisconsin, USA, **1997**.

Received October 22, 2001
[I01417]

Two Molecular-Type Complexes of the Octahedral Rhenium(III) Cyanocluster Anion $[Re_6Se_8(CN)_6]^{4-}$ with M^{2+} (Mn^{2+}, Ni^{2+})

Sofia B. Artemkina,[a] Nikolai G. Naumov,*[a] Alexander V. Virovets,[a] Oliver Oeckler,[b] Arndt Simon,[b] Simon B. Erenburg,[a] Nikolai V. Bausk,[a] and Vladimir E. Fedorov[a]

Keywords: Rhenium / Cluster compounds / Structure elucidation / Cyanide ligands / XANES

Two novel octahedral rhenium(III) selenocyanide cluster complexes $[(n\text{Bu})_4\text{N}]_2\text{Ni}(\text{H}_2\text{O})_5[\text{Re}_6\text{Se}_8(\text{CN})_6]\cdot 2\text{H}_2\text{O}$ (**1**) and $[(n\text{Bu})_4\text{N}]_2\text{Mn}(\text{H}_2\text{O})_4[\text{Re}_6\text{Se}_8(\text{CN})_6]\cdot 2\text{H}_2\text{O}$ (**2**) have been prepared by the reaction of $K_4[Re_6Se_8(CN)_6]\cdot 3.5H_2O$, $(n\text{Bu})_4\text{NBr}$ and $Ni(OAc)_2$ (or $MnSO_4$) in aqueous solution. The complexes have been structurally solved in the orthorhombic unit cell *Pbca* with parameters: $a = 19.393(2)$, $b = 17.292(2)$, $c = 37.255(4)$ Å for **1**, and $a = 19.518(4)$, $b = 17.488(3)$, $c = 37.997(5)$ Å for **2**. The cluster anions and M^{2+} form ionic pairs $\{M(H_2O)_n[Re_6Se_8(CN)_6]\}^{2-}$ that are packed in the solid state with *n*-tetrabutylammonium cations. Coordinated and solvate water molecules as well as the nitrogen atoms of the anions form a network of hydrogen bonds in the structures. These compounds are isomorphous, although the coordination environments of the metal cations differ.

(© Wiley-VCH Verlag GmbH, 69451 Weinheim, Germany, 2002)

Introduction

The ability of CN ligands to form strong covalent bonds to *3d* transition metals is well-known and the coordination chemistry of mononuclear cyanometallates is well developed.[1] Complex cluster anions $[Re_6(\mu_3\text{-}Se)_8(CN)_6]^{4-}$ with terminal CN groups[2] can also interact with transition metals to form new polymeric cluster solids based on -Re−C≡N−M−N≡C−Re- bridges.[3,4] The type of polymeric compound formed and the coordination environment of the metal cation are influenced enormously by the nature of the additional cations present in the reaction mixture. We have found that an increase of cation size in the series $Cs^+ < Me_4N^+ < Et_4N^+ < n\text{Pr}_4N^+$ results in a reduction of the dimensionality of the formed solids. In the case of Cs^+,[3a] Me_4N^+ and Et_4N^+,[3b] a three-dimensional polymeric framework $\{M_3[Re_6Se_8(CN)_6]_2\}^{2-}$ is formed which includes these cations and water molecules in its cavities. In the case of $n\text{Pr}_4N^+$,[3c] polymeric chains or molecular-type structures built from complex anions and M^{2+} are obtained.

Here we report the synthesis and structures of two novel isomorphic complexes $(n\text{Bu}_4\text{N})_2\text{Ni}(\text{H}_2\text{O})_5[\text{Re}_6\text{Se}_8(\text{CN})_6]\cdot 2\text{H}_2\text{O}$ (**1**) and $(n\text{Bu}_4\text{N})_2\text{Mn}(\text{H}_2\text{O})_4[\text{Re}_6\text{Se}_8(\text{CN})_6]\cdot 2\text{H}_2\text{O}$ (**2**) obtained from the reaction of aqueous solutions of $K_4Re_6Se_8(CN)_6$ and M^{2+} (Mn^{2+} and Ni^{2+}) in the presence of Bu_4NBr. Although the space group, cell parameters and packing motifs in these structures are similar, the coordination spheres of Mn^{2+} and Ni^{2+} are quite different.

[a] Institute of Inorganic Chemistry SB RAS, 3,
Ak. Lavrentiev Ave., 630090 Novosibirsk, Russia
Fax: (internat.) + 7-3832/344-489
E-mail: naumov@che.nsk.su
[b] Max-Planck-Institut für Festkörperforschung,
Heisenbergstraβe 1, 70569 Stuttgart, Germany

Results and Discussion

Structures of Compounds 1 and 2

The anion $[Re_6Se_8(CN)_6]^{4-}$ has the usual $Re_6X_8L_6$ environment (Figure 1). Six rhenium atoms form an Re_6 octahedron with the faces μ_3-capped by eight selenium atoms. The CN ligands are coordinated to rhenium atoms through the carbon atom. The bond lengths and angles in the anion (see Table 1) do not differ from those found in other salts with an Re_6Se_8 cluster core [$K_4Re_6Se_8(CN)_6\cdot 3.5H_2O$:[2] Re−Re = 2.633 Å; Re−Se = 2.526 Å; Re−C = 2.11 Å; C−N = 1.15 Å; $NaCs_3Re_6Se_8(CN)_6$:[4] Re−Re = 2.634 Å; Re−Se = 2.52 Å; Re−C = 2.10 Å; C−N = 1.17 Å; $Cs_4Re_6Se_8I_6$:[5] Re−Re = 2.625; Re−Se = 2.519 Å].

The cluster anion forms bridging Re−CN−M contacts at one nitrogen atom, with the other five CN groups remaining terminal, therefore we have an ionic pair containing an M^{2+} cation. The structures of the ionic pairs $\{M(H_2O)_n[Re_6Se_8(CN)_6]\}^{2-}$ for **1** and **2** are shown in Figure 2, with water molecules completing the coordination sphere of M^{2+}.

In compound **1** the coordination environment of Ni^{2+} is a slightly distorted octahedron (N + 5O), with Ni−N distances of 2.032(7) Å and Ni−O distances ranging from 2.033(6) to 2.118(7) Å. The hydrogen bond system can be

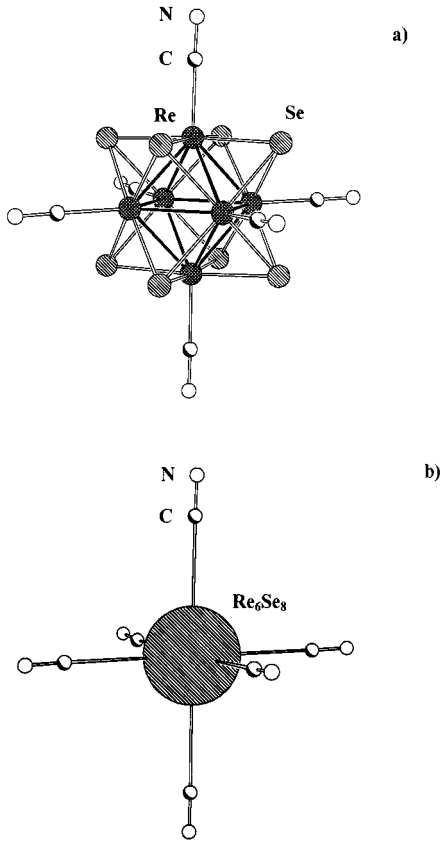

Figure 1. Structure of cluster anion $[Re_6(\mu_3\text{-}Se)_8(CN)_6]^{4-}$ (a) and its simplified presentation (b)

described as a superposition of two chains running along the *c* and *a* axes. The first of them consists of water molecules, O1 and O1w, and the terminal nitrogen atom N2 from the nickel-cluster ionic pair. The second includes O5, O2w and N6. The O···N and O···O distances are about 2.6−2.7 Å (Figure 3a).

In **2** the Mn^{2+} ion is coordinated by the nitrogen atom of the cluster anion and by four (rather than five) water molecules, with Mn−O distances ranging between 2.13(2) and 2.15(2) Å. Thus the coordination environment of Mn^{2+} is N + 4O and the coordination polyhedron is a distorted square pyramid (reversed umbrella) with an apex at the nitrogen atom. The manganese atom lies 0.55 Å out of the plane formed by the atoms O1, O2, O3, and O4. The next nearest water molecule, O1w, lies 3.65 Å from Mn1 (Figure 3b), forming a hydrogen bond with O3 (O···O distance of 2.70 Å). As in **1**, there are hydrogen bonded chains running roughly along *c* axis.

In the related compound $[(n\text{Pr})_4N]_2Mn(H_2O)_5[Re_6Se_8(CN)_6]\cdot H_2O$ (**3**), the environment of Mn^{2+} is different.[3c] An $\{Mn(H_2O)_5[Re_6Se_8(CN)_6]\}$ fragment of **3** is shown in Figure 2c and some bond lengths and angles are presented in Table 2 for comparison. In contrast to compounds **1** and **2**, the manganese(II) cation in **3** has a distorted octahedral coordination environment [1N + 5O(H_2O)] with an Mn−N−C angle of 158(5)° The reason for such a deviation from linearity is the different arrangement of the ionic pairs in the solid state. In **1** and **2** the ionic pairs are oriented along the *c* axis of the unit cell (Figure 3a and 3b) and have an arrangement similar to that in compound **3**.[3c] As in **3**, the cluster anions form a pseudo face-centred motif. In **1**

Table 1. Crystallographic data for compounds $(Bu_4N)_2Ni(H_2O)_5[Re_6Se_8(CN)_6]\cdot 2H_2O$ (**1**) and $(Bu_4N)_2Mn(H_2O)_4[Re_6Se_8(CN)_6]\cdot 2H_2O$ (**2**)

	1	**2**
Empirical formula	$C_{38}H_{86}N_8NiO_7Re_6Se_8$	$C_{38}H_{84}MnN_8O_6Re_6Se_8$
Molecular weight	2574.74	2552.95
Colour, habit	yellow, irregular polyhedron	red, octahedral
Crystal system	Orthorhombic	Orthorhombic
Space group	*Pbca*	*Pbca*
a (Å)	19.393(2)	19.518(4)
b (Å)	17.292(2)	17.488(3)
c (Å)	37.255(4)	37.997(5)
Z	8	8
Cell volume (Å^3)	12493(2)	12970(4)
Exp. *hkl* limits	$-25 \le h \le 25$	$0 \le h \le 23$
	$-22 \le k \le 22$	$0 \le k \le 20$
	$-48 \le l \le 48$	$0 \le l \le 45$
Calcd. density (g·cm^{-3})	2.738	2.615
Absorption correction	multi-scan	4 azimuthal scan curves
Absorption coefficient (mm^{-1})	16.580	15.87
Diffractometer type	Stoe IPDS	Enraf−Nonius CAD4 with graphite monochromator
Crystal size (mm)	0.214 × 0.243 × 0.257	0.6 × 0.4 × 0.2
$2\theta_{max}$ (°)	55	50
Reflections collected/unique	14338/11216 [*R*(int) = 0.0672]	7439/7118 [all unique]
Final *R* indices for all $F_o > 4\sigma(F_o)$	*R*1 = 0.0372; *wR*2 = 0.0819	*R*1 = 0.033; *wR*2 = 0.068
Weighting scheme	$w^{-1} = \sigma^2(F_0^2) + (0.0457P)^2 + 25.00P$ where $P = (F_0^2 + 2F_c^2)/3$	$w^{-1} = \sigma^2(F_0^2) + (0.0128P)^2$ where $P = (\text{Max}\ (F_0^2,0) + 2F_c^2)]/3$
Max., min. peak in final diff. map (e·Å^{-3})	2.537, −2.180	−1.00, 0.88

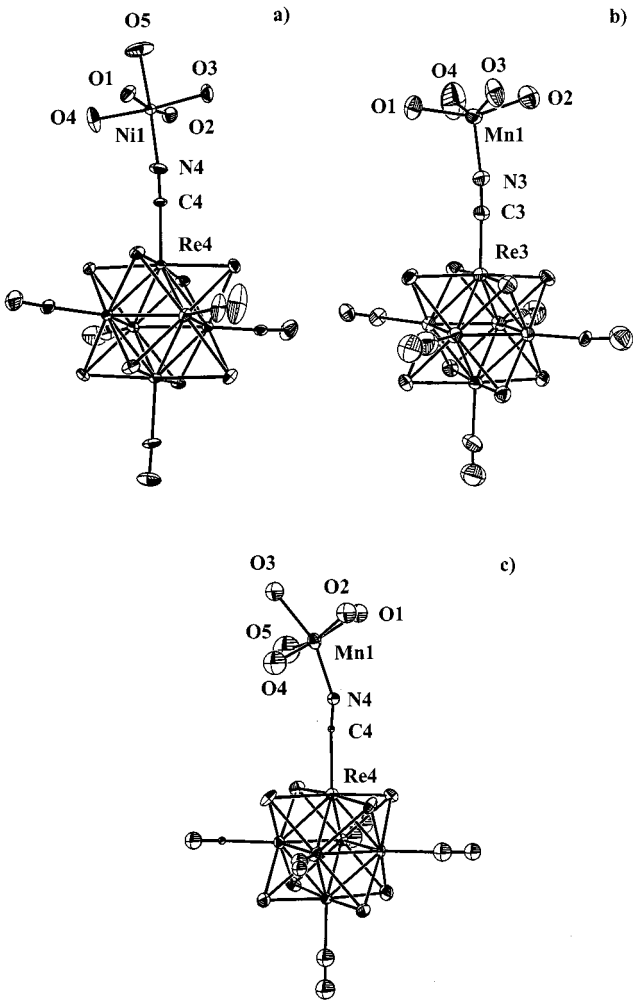

Figure 2. Structures of anionic pairs in compounds **1** (a), **2** (b) and **3** (c); thermal ellipsoids are drawn at a 50% probability level

the ionic pairs are connected by hydrogen bonds to the solvent water molecule O2w. The nickel atom has an almost regular octahedral environment and both the O5 and O2w water molecules form hydrogen bonds with normal distances (O5···O2w: 2.65 Å; O2w···N6: 2.76 Å) and angles (N6···O2w···O5: 131°). In **3** the ionic pairs interact directly through the O3···N2 hydrogen bond. This interaction forces a deviation of the C4−N4−Mn1 (158°) and N4−Mn1−O3 (159°) angles from linearity, thus allowing the O3 atom to form a normal hydrogen bond to N2 with an O−N distance of 2.77 Å and an Mn1−O3−N2 angle of 116°.

The space between the ionic pairs is occupied by Bu_4N^+ cations. Two crystallographically independent Bu_4N^+ cations have different conformations in the structure.

Although the coordination number of five for Mn^{2+} is known in the literature this environment is not usual for manganese and is mainly caused by steric factors, namely the volume of the organic ligands. Stelzig et al.[6] have reported the complexes $[Mn_2^{II}L^3(\mu_3\text{-OMe})(MeOH)]_2$ and $Na[Mn_3^{II}(L^3)_2(\mu_2\text{-OAc})]\cdot H_2O\cdot 0.25THF$, where L^3 = 1,5-bis(3-Cl, 5-NO_2-salicylideneamino)pentan-3-ol, a voluminous pentadentate ligand. The Mn^{2+} coordination arrangement here is 4O + N. It is also worthwhile to note the complex $[Mn_3(L^1O)_4(MeCN)][ClO_4]_2\cdot H_2O$, where L^1O is a deprotonated tridentate ligand (2-hydroxyphenyl)bis(pyrazolyl)methane.[7]

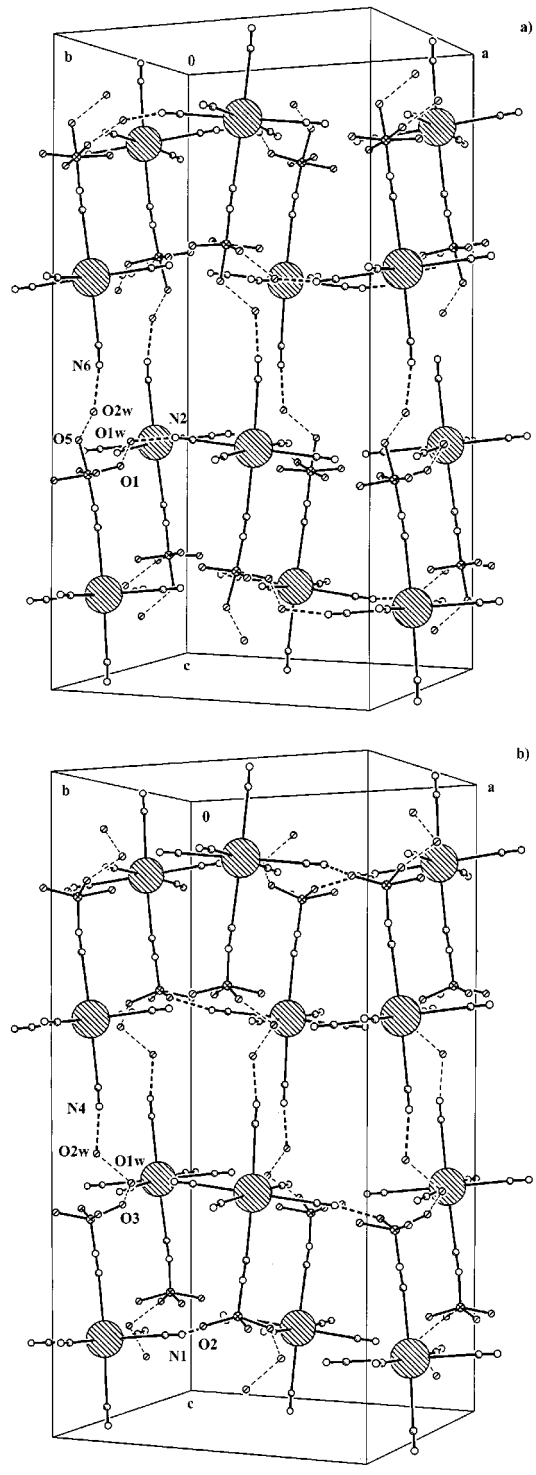

Figure 3. Packing motifs of ionic pairs for compounds **1** (a) and **2** (b); $n Bu_4N^+$ cations are omitted for clarity; large hatched circles represent the $\{Re_6Se_8\}$ cores of the cluster anions

To confirm the difference in the manganese environments in **2** and **3** we have recorded the MnK XANES (*X*-ray *A*bsorption *N*ear *E*dge *S*tructure) spectra for these com-

Table 2. Selected bond lengths and angles for compounds $(Bu_4N)_2Ni(H_2O)_5[Re_6Se_8(CN)_6]\cdot 2H_2O$ (**1**), $(Bu_4N)_2Mn(H_2O)_4[Re_6Se_8(CN)_6]\cdot 2H_2O$ (**2**), and $(Pr_4N)_2Mn(H_2O)_5[Re_6Se_8(CN)_6]\cdot H_2O$ (**3**) (Min. Max.; Mean)

	1	**2**	**3**
Bond lengths (Å)			
Re−Re	2.6182(4)−2.6372(4); 2.6262	2.6171(17)−2.6371(16); 2.630	2.609(5)−2.647(5); 2.629
Re−Se	2.4937(7)−2.5180(8); 2.5095	2.498(4)−2.528(4); 2.517	2.49(1)−2.54(1); 2.51
Re−C	2.070(7)−2.109(7); 2.093	2.05(3)−2.23(3); 2.11	2.14(6)−2.31(3); 2.20
M−N	2.032(7)	2.099(19)	2.08(4)
M−O	2.033(6)−2.118(7); 2.065	2.13(2)−2.15(2); 2.14	2.14(6)−2.24(4); 2.19
C−N	1.144(11)−1.157(10); 1.149	1.11(3)−1.22(3); 1.17	1.03(4)−1.24(8); 1.11
Bond angles (°)			
N−M−O	92.6(3)−95.0(3); 93.4	102.4(8)−110.9(10); 105.1	83(2)−106(2); 95
N−M−O (trans)	176.0(3)	−	159(2)
O−M−O	83.0(3)−91.0(3); 88.2	84.7(7)−87.9(7); 86.4	79(2)−109(2); 88
O−M−O (trans)	171.6(2), 174.9(3); 173.3	144.8(9), 154.7(7); 149.8	161(2)−168(2); 165
Re−C−N (terminal)	176.6(7)−179.2(8); 177.9	171.2(3)−178.7(3); 174.6	142.4(7)−177.9(6); 165.6
Re−C−N (*bridging*)	177.2(7)	176(3)	174(5)
M−N−C	174.9(6)	174(2)	158(5)

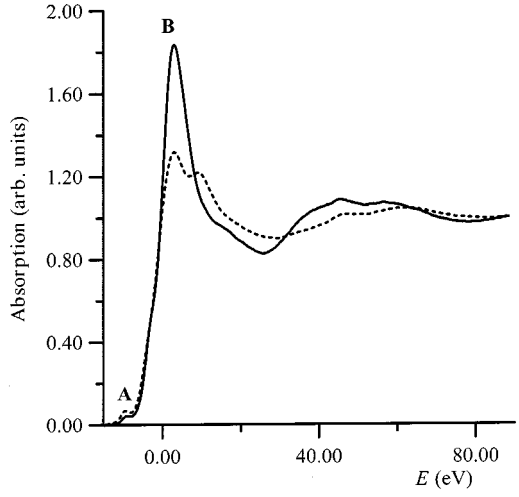

Figure 4. Mn-*K* XANES spectra of compounds **2** (dashed line) and **3** (solid line)

pounds (Figure 4). The maximum B in the spectra of **2** and **3** (Figure 4) corresponds to an electron transition from the Mn1s to the Mn4p level. The decrease of intensity of this maximum by a factor of two for compound **2** relative to compound **3** can clearly be seen. This decrease indicates a splitting of the 4p electronic levels due to substantially reduced symmetry for the first sphere of the Mn environment in **2**.[12] The pre-edge resonance (maximum A) corresponding to the quadrupole Mn1s−Mn3d transition (Figure 4) is sensible to symmetry distortion at the manganese atom. A noticeable increase of the intensity in **2** relative to **3** also indicates a symmetry lowering of the Mn environment in the former compound. These results are in accordance with the X-ray structural data for compounds **2** and **3**.

Experimental Section

Physical Measurements: Elemental analyses for C, H N, S (Carlo Erba 1106) were performed in the Laboratory of Microanalysis of the Institute of Organic Chemistry, Novosibirsk. Infrared spectra were measured on KBr disks with a Bruker IFS-85 Fourier spectrometer. For determination of water the curves of mass losses and TGD curves of the compounds were recorded at a heating rate of 3 °C/min (temperature range 20−300 °C) under an atmosphere of argon with a TGD-7000 RH thermal analysis controller (Sinku-Riku, Japan). Measurement of Mn-*K* XANES spectra were performed using synchrotron radiation of the VEPP-3 storage ring at the Budker Institute of Nuclear Physics at Novosibirsk. A channel-cut Si (111) single crystal was used as the two-crystal monochromator. The spectra were obtained using the transmission mode.

X-ray Structural Measurements: The structures of **1** and **2** were determined by X-ray structural analysis. Crystallographic data and details of diffraction measurements are given in Table 1. Both structures were solved by direct methods and refined by full-matrix least-squares methods on F^2.

Structural Studies of $[(n\text{Bu})_4N]_2Ni(H_2O)_5[Re_6Se_8(CN)_6]\cdot 2H_2O$ (1): The diffraction data were collected with a Stoe IPDS diffractometer with graphite-monochromated Mo-K_α radiation at T = 93(2) K using the φ-oscillation method. Absorption correction were applied using information from multiple scans. Anisotropic displacement parameters were refined for all non-H atoms. The final difference electron density map features were with no chemical meaning. Experimental crystal data are listed in Table 1. The calculations were performed with SHELX-97[8] and standard Stoe IPDS software.[9]

Structural Studies of $[(n\text{Bu})_4N]_2Mn(H_2O)_4[Re_6Se_8(CN)_6]\cdot 2H_2O$ (2): The diffraction data were collected with an Enraf−Nonius CAD4 diffractometer with graphite-monochromated Mo-K_α radiation at ambient conditions (T = 291 K). Reflection intensities were collected by standard techniques [θ/2θ scans with variable speed, ω range (deg.) = 0.9 + 0.35tg(θ)] and absorption corrections were applied by measuring azimuthal scan curves. Anisotropic displacement parameters were refined for all non-H atoms. The final difference electron density map features were with no chemical meaning. The calculations were performed with the standard Enraf−Nonius CAD4 programs (CD4CA0, CADDAT) and SHELX-93 (structure solution and refinement).[10]

Syntheses: The starting cluster compound $K_4[Re_6Se_8(CN)_6]\cdot 3.5H_2O$ was prepared from polymeric $Re_6Se_8Br_2$ [11] as described in refs.[2] All other reagents were employed as purchased.

$[(n\text{Bu})_4\text{N}]_2\text{Ni}(\text{H}_2\text{O})_5[\text{Re}_6\text{Se}_8(\text{CN})_6]\cdot 2\text{H}_2\text{O}$ (1): A mixture of $(n\text{Bu})_4\text{NBr}$ (160 mg, 0.48 mmol) and $\text{Ni(OAc)}_2\cdot 4\text{H}_2\text{O}$ (60 mg, 0.24 mmol) in 20 mL of water was gradually added to a hot solution of $\text{K}_4\text{Re}_6\text{Se}_8(\text{CN})_6\cdot 3.5\text{H}_2\text{O}$ (500 mg, 0.24 mmol) in 10 mL of water. The resulting mixture was stirred and heated for two hours. The fine orange precipitate was then washed with water (3 × 15 mL) and dried. Yield: quantitative (605 mg, 98%); $\text{C}_{38}\text{H}_{86}\text{N}_8\text{NiO}_7\text{Re}_6\text{Se}_8$ (2574.74): calcd. C 17.85, H 3.31, N 4.38; found C 18.10, H 3.46, N 4.49. Mass loss 4.4% at 105 °C (calcd 4.2% for six water molecules). IR: $\tilde{\nu}$ = 2109 (intense), 2142 (shoulder) (CN); 1620 cm^{-1} (weak) (H_2O).

$[(n\text{Bu})_4\text{N}]_2\text{Mn}(\text{H}_2\text{O})_4[\text{Re}_6\text{Se}_8(\text{CN})_6]\cdot 2\text{H}_2\text{O}$ (2): A mixture of $(n\text{Bu})_4\text{NBr}$ (160 mg, 0.48 mmol) and $\text{MnSO}_4\cdot 5\text{H}_2\text{O}$ (240 mg, 1 mmol) in 20 mL of water was gradually added to a hot solution of $\text{K}_4\text{Re}_6\text{Se}_8(\text{CN})_6\cdot 3.5\text{H}_2\text{O}$ (500 mg, 0.24 mmol) in 10 mL of water. The resulting mixture was stirred and heating for two hours. The fine orange precipitate was then washed with water (3 × 15 mL) and dried. Yield: quantitative (582 mg, 95%); $\text{C}_{38}\text{H}_{84}\text{MnN}_8\text{O}_6\text{Re}_6\text{Se}_8$ (2552.95): calcd. C 17.88, H 3.32, N 4.39; found C 18.00, H 3.49, N 4.45. IR: $\tilde{\nu}$ = 2108 (intense), 2130 (shoulder) (CN); 1649 cm^{-1} (weak) (H_2O).

Single Crystal Growth: Both compounds have low solubility and therefore crystals suitable for X-ray single crystal analysis were grown in a U-tube filled with silica gel as described in ref.[3a] The crystals were located near the middle part of the U-tube. The following reagents were used: $\text{K}_4\text{Re}_6\text{Se}_8(\text{CN})_6\cdot 3.5\text{H}_2\text{O}$, $n\text{Bu}_4\text{NBr}$, $\text{Ni(OAc)}_2\cdot 4\text{H}_2\text{O}$ for **1**, $\text{Mn(OAc)}_2\cdot 4\text{H}_2\text{O}$ for **2**. Octahedral red crystals can be easily separated from the silica gel manually. X-ray powder diffraction and IR spectroscopy confirmed the identity of these crystals.

CCDC-167585 (**1**) and CCDC-167586 (**2**) contain the supplementary crystallographic data for this paper. These data can be obtained free of charge at www.ccdc.cam.ac.uk/conts/retrieving.html [or from the Cambridge Crystallographic Data Centre, 12, Union Road, Cambridge CB2 1EZ, UK; Fax: (internat.) +44-1223/336-033; E-mail: deposit@ccdc.cam.ac.uk].

Acknowledgments

This work was supported by Russian Foundation for Basic Research, grant nos. 99-03-32789 and 99-03-33301. Authors thank the Program for Support of Young Scientists of the Siberian Branch of the Russian Academy of Sciences for financial support.

[1] K. R. Dunbar, R. A. Heintz, in *Progress in Inorg. Chem.* (Ed.: K. D.Karlin) **1997**, *45*, 283−391. T. Iwamoto, in *Comprehensive Supramolecular Chemistry* (Eds.: J. L. Atwood, J. E. D. Davies, D. D. Macnicol, F. Vögtle), Pergamon **1996**, *6*, 643−690. B. H. Chadwick, A. G. Sharpe, *Advances in Inorganic and Radiochemistry* (Eds.: H. J. Emeleus, A. G. Sharpe), Academic Press, New York **1996**, *8*, 83−177.

[2] N. G. Naumov, A. V. Virovets, N. V. Podberezskaya, V. E. Fedorov, *Russ. J. Struct. Chem.* **1997**, *38*, 857−862. H. Imoto, N. G. Naumov, A. V. Virovets, T. Saito, V. E. Fedorov, *Russ. J. Struct. Chem.* **1997**, *39*, 720−727. Yu. V. Mironov, J. A. Cody, T. E. Albrecht-Schmitt, J. A. Ibers, *J. Am. Chem. Soc.* **1997**, *119*, 493−498.

[3] [3a] N. G. Naumov, A. V. Virovets, M. N. Sokolov, S. B. Artemkina, V. E. Fedorov, *Angew. Chem. Int. Ed.* **1998**, *37*, 1943−1945. [3b] N. G. Naumov, A. V. Virovets, V. E. Fedorov, *Russ. J. Struct. Chem.* **2000**, *41*, 499−520. [3c] N. G. Naumov, S. B. Artemkina, A. V. Virovets, V. E. Fedorov, *J. Solid State Chem.* **2000**, *153*, 195−204. [3d] N. G. Naumov, A. V. Virovets, Yu. V. Mironov, S. B. Artemkina, V. E. Fedorov, *Ukr. Khim. Zh.* **1999**, *65*, 21−27.

[4] L. G. Beauvais, M. P. Shores, J. R. Long, *Chem. Mater.* **1998**, *10*, 3783−3786. M. P. Shores, L. G. Beauvais, J. R. Long, *Inorg. Chem.* **1999**, *38*, 1648−1649. L. G. Beauvais, M. P. Shores, J. R. Long, *J. Am. Chem. Soc.* **2000**, *122*, 2763−2772.

[5] J. R. Long, L. S. McCarty, R. H. Holm, *J. Am. Chem. Soc.* **1996**, *118*, 4603−4616.

[6] L. Stelzig, A. Steiner, B. Chansou, J. P. Tuchagues, *Chem. Commun.* **1998**, *7*, 771−772.

[7] T. C. Higgs, K. Spartalian, C. J. O'Connor, B. F. Matzanke, C. J. Carrano, *Inorg. Chem.* **1998**, *37*, 2263−2272.

[8] G. M. Sheldrick, SHELX-97, Release 97-2, University of Goettingen, Germany, **1998**.

[9] Stoe IPDS software, Darmstadt **1998**.

[10] G. M. Sheldrick, **1993**, *Acta Crystallogr. A49 (Suppl.)*, p. C53.

[11] A. Perrin, L. Leduc, M. Sergent, *Eur. J. Solid State Chem.* **1991**, *28*, 919−931.

[12] [12a] F. W. Lytle, R. B. Greegor, A. J. Panson, *Phys. Rev. B* **1988**, *37*, 1550−1562. [12b] H. T. Tsang, J. E. Penner-Hahn, C. J. Batie, *Physica B* **1989**, *158*, 115−116. [12c] R. A. Scott, *Physica B* **1989**, *158*, 84−86.

Received September 9, 2001
[I01349]

On the Intra- and Intermolecular Bonding in Polyiodides

Lars Kloo,*[a] Jan Rosdahl,[a] and Per H. Svensson[a]

Keywords: Iodine / Polyhalides / Bond theory

The nature of intra- and intermolecular interactions of polyiodides has been investigated by means of quantum chemical methods and structural statistical data. In the region of "secondary bonds" the interaction is adequately described in terms of covalent bonding accompanied by dispersion. At greater distances the interaction is dominated by ion-quadrupole interactions between ionic and neutral iodine building blocks of the polyiodide structures.
(© Wiley-VCH Verlag GmbH, 69451 Weinheim, Germany, 2002)

Introduction

Polyiodides have been extensively studied in the solid and liquid state and are characterized by a strong tendency to concatenation.[1] The solid structures may contain small, discrete polyiodides or large, extended anionic networks of interconnected units. Typically, polyiodides are described according to the stoichiometry of the discrete anions or the repeating units of the extended structures, such as triiodides **1**, pentaiodides **2**, heptaiodides **3** etc. Today, repeating units in complex networks have been claimed to contain up to almost 30 iodine atoms, for instance I_{29}^{3-} in $(Fc)_3I_{29}$ and I_{26}^{3-} in $(Me_3S)_3I_{26}$.[2,3] Almost all these structures can be described as consisting of only three fundamental building blocks: I^-, I_2 and I_3^-.

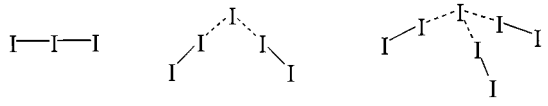

1 **2** **3**

In this context it is also worth noting that the triiodides occupy a special position in the sense that they typically contain discrete I_3^- ions with intermolecular I−I contacts near the van der Waals (vdW) distances, forming linear, zigzag or T-shaped packing patterns. Higher polyiodides can be regarded as constructed from the ions I^- or I_3^-, solvated by the neutral solvent molecules I_2, often into low-dimensional extended networks.

Depending on the extent of intermolecular bonding, I_2 displays I−I bond lengths between 2.69 and 2.80 Å. The triiodide ion is either centrosymmetric with an I−I bond length of about 2.91 Å or belongs to an asymmetric configuration with I−I distances between 2.85 and 3.00 Å. Thus, the intramolecular bond-length range for the fundamental building blocks can be defined as 2.69−3.00 Å. The sum of vdW radii for iodine is 4.3 Å and the I_2−I_2 vdW distance is normally set to 3.9−4.0 Å. With this in mind it is interesting to note the large number of intermolecular I−I contacts in the range between 3 and 4 Å. This was made clear by a structural statistical study of pentaiodides by Bittner.[4] I−I contacts in the intermediate range between typical intramolecular and vdW distances are normally referred to as "secondary bonds".

The assignment of an I−I contact as a secondary bond seems purely pragmatic. An arbitrary cut-off set to around 3.5 Å often allows a complicated network structure to be described in simpler terms (interconnected iodine molecules, pentaiodides etc.). However, polyiodide chemistry seems to have been focused on the search for larger and larger repeating units (i.e. higher I_2 contents) in recent years, and one can observe a progressive increase in the assigned distance cut-off. Is the secondary bond a completely artificial concept? Which type of interaction predominates at the typical intermolecular I−I distances between 3 and 4 Å? These questions were the motivation for this study.

For instance, pentaiodides (I_5^-) are found in three different forms irrespectively of whether they are discrete or part of an extended network: V-shaped $[(I^-)\cdot 2I_2]$, L-shaped $[(I_3^-)\cdot I_2]$ and linear $[(I^-)\cdot 2I_2]$. The bonding in these pentaiodides can be described in two principally different ways, in terms of either covalent interactions between mainly valence 5p orbitals or of closed-shell interactions (vdW interactions, charge-transfer interaction or dative bonds) between the building blocks.

The present study relies on statistical data for two archetypal structural fragments in polyiodide chemistry, employing the CSD database, and quantum chemical calculations providing potential energy surfaces (PES), bond order surfaces (BOS) and electron density maps of the same or similar fragments. The PES values obtained for

[a] Department of Inorganic Chemistry, Royal Institute of Technology,
10044 Stockholm, Sweden

Hartree−Fock (HF) and correlated levels are used to study the influence of correlation. The difference in energy between HF and correlated methods is axiomatically regarded as a measure of the correlation energy, thus providing information about the dispersion interaction. As pointed out in recent reviews, the interpretation of the PES is far from straightforward.[5,6] Although the explicit inclusion of the dynamic electron correlation provides insight into the intermolecular dispersion interaction, it also affects the intramolecular interactions. Therefore, difference PES values contain both intra- and intermolecular effects of correlation. The BOS values used in this work are based on a natural bond population analysis (NPA), although the very same information can be extracted from other types of population analyses, including the democratic method of Mulliken.[7]

Statistics

Figure 1 shows the histogram of the configuration in **4**. The histogram thus represents the "view" from an I_2 molecule with respect to both intra- and intermolecular contacts to another iodine atom. This representation is focused on "I_3^-" units in polyiodide structures and consequently is heavily dominated by the intramolecular contacts from 2.7−3.0 Å; the polyiodide structures are mainly triiodides (vide infra). The distribution of I−I contacts is largely uniform over the entire region of "secondary bonds", i.e. between 3 and 4 Å, whereas an increase is observed at distances greater than 4 Å. The latter effect can probably be attributed to purely statistical/sterical reasons, allowing more neighbours at greater distances. Ideally, an initial parabolic increase would be expected.

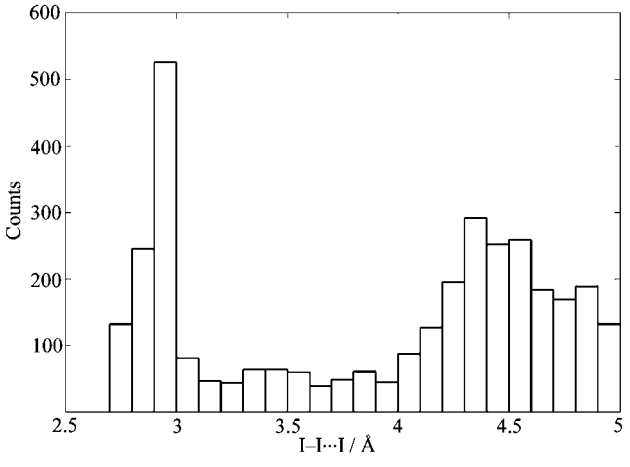

Figure 1. Histogram of the I−I distances from an I_2 fragment

4 **5**

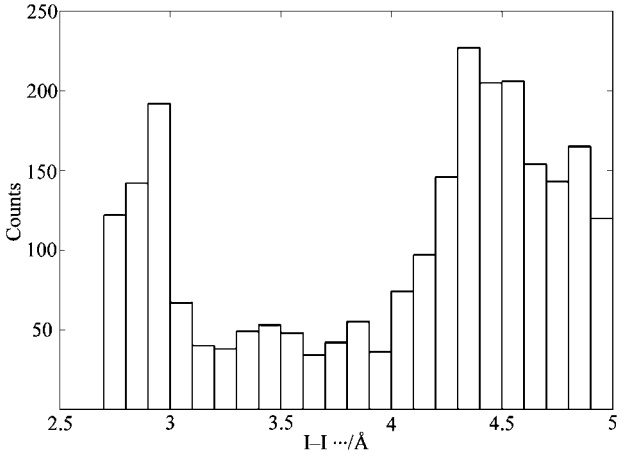

Figure 2. Histogram of the I−I distances from an I_3 fragment

Figure 2 shows the corresponding histogram for configuration **5**. Here, the diagram is completely dominated by intermolecular contacts from the "view" of a triiodide unit. Unfortunately, in the database there are quite a number of structures, in which the intramolecular I−I contacts have not been properly defined. As a result, these will also appear at short distances in this figure, making the overall distribution of I−I contacts very similar to that in Figure 1. Again, a very uniform distribution is observed between 3 and 4 Å.

The Triiodide System

The PES for I_3^- at the HF level is shown in Figure 3, corresponding to the configuration in **6**. Here, the distance *r1* and angle α are changed and the distance *r2* optimized at each point of the PES. It is clear that the preferred structure is centrosymmetrical (D_{ih}) with an I−I distance just below 3.0 Å. The intramolecular bonding in trihalide systems was extensively studied and the present results are in good agreement with previous work.[1,8] In order to estimate the influence of dynamic correlation, calculations at the MP2 and CCSD levels were also performed. The difference PES at MP2 level is given in Figure 4. Correlation at both levels gives an overall stabilization of the triiodide structure. A minimum valley (corresponding to a maximum in the

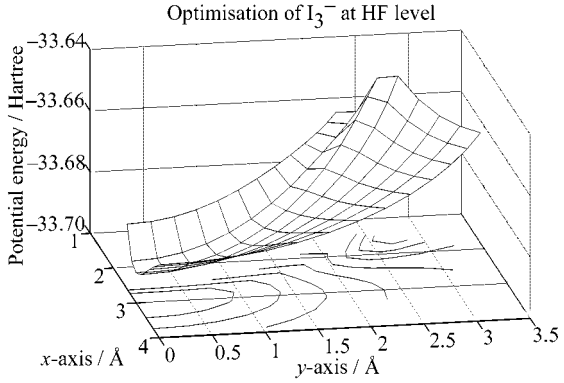

Figure 3. PES at HF level for the I_3^- ion

correlation stabilization) is observed near the optimum I−I distance (2.965, 2.943 and 2.964 Å for the HF, MP2 and CCSD levels, respectively). Remarkably enough, a minimum in the correlation energy seems to exist at a conformation corresponding to D_{3h} symmetry. However, this geometry is Jahn−Teller-unstable and not attainable by single-configuration methods. Nevertheless, this permits the conclusion that no obvious extra stabilization results from correlation at distances greater than the equilibrium intramolecular distance in I_3^-.

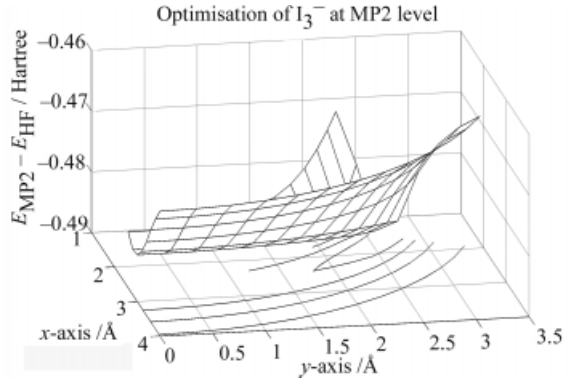

Figure 4. Difference PES between HF and MP2

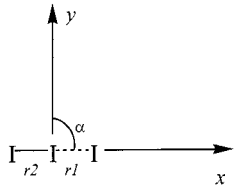

6

A plot of the NLMO/NPA BOS at the HF level is given in Figure 5. As expected, the bond order is close to 0.5 at the equilibrium distance and then progressively decreases as the I−I distance is increased. It is also notable that the decrease is less steep for the linear conformation, thus reflecting the behaviour of the corresponding PES. The BOS at the MP2 level is very similar, and the bond order at 4 Å is 0.046 and 0.087 at the HF and MP2 levels, respectively. A naive interpretation of these data suggests the postulation

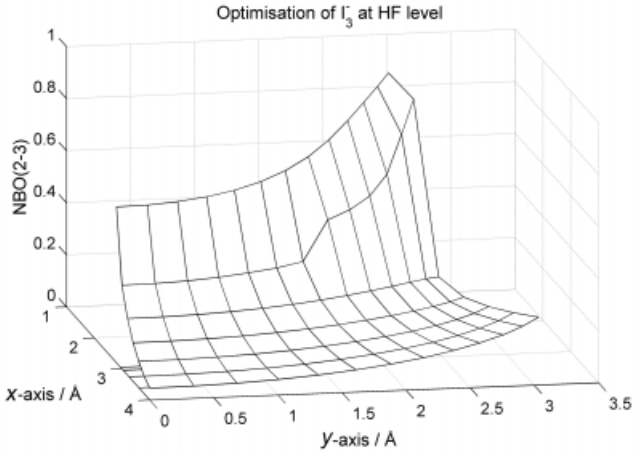

Figure 5. NLMO/NPA BOS for the I_3^- ion at HF level

of a weak covalent interaction between the I_2 and I^- fragments extending to the region of the so-called "secondary bonds". The interaction amounts to at least 15% − based on the overlap population data − of a "normal" I−I bond in I_3^-. This interpretation is also supported by the total electron density maps of $I_2\cdots I^-$ contacts at 5.0, 4.0 and 3.5 Å shown in Figure 6a−c. Below 4 Å there is a substantial electron density between the I_2 and I^- fragments. The difference electron density map in Figure 7 gives more detailed information about the bonding scheme. When brought into contact with an I_2 molecule (gradually from just above 4 Å), the I^- ion loses electron density from essentially a 5p orbital, and this electron density is transferred to the anti-

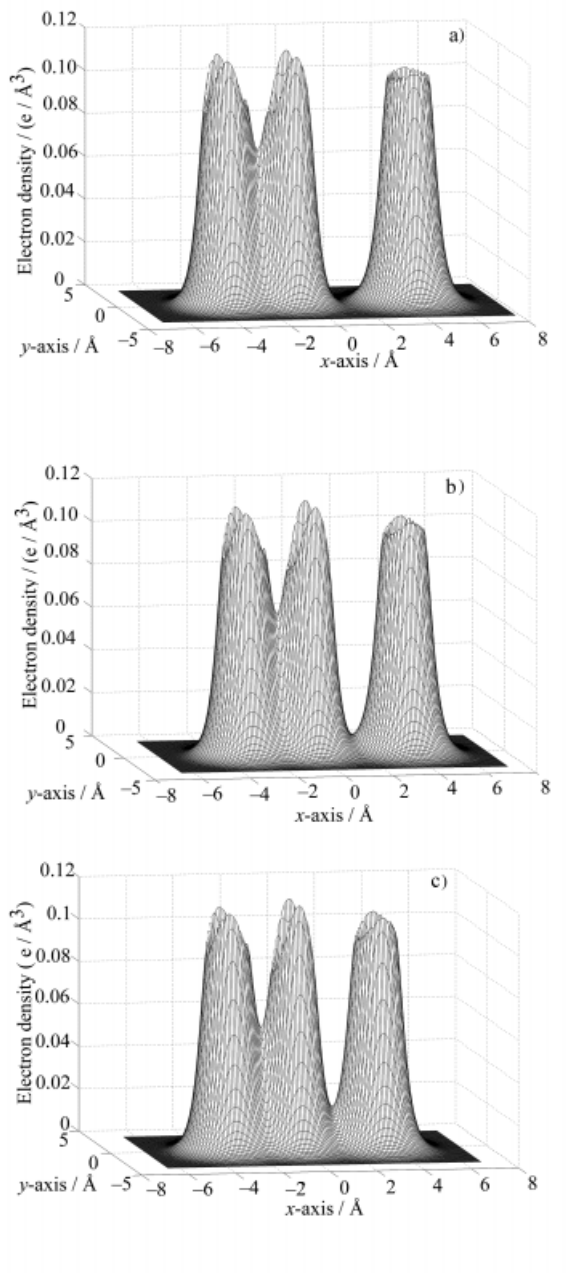

Figure 6. Total electron density of the $I^-\cdots I_2$ interaction in I_3^- at a) 5.0 Å, b) 4.0 Å and c) 3.5 Å

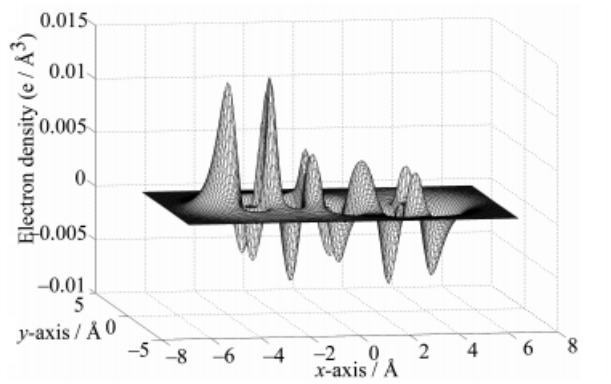

Figure 7. Difference electron density map of the $I^-\cdots I_2$ interaction in I_3^- at 3.5 Å (I^- on the right-hand side)

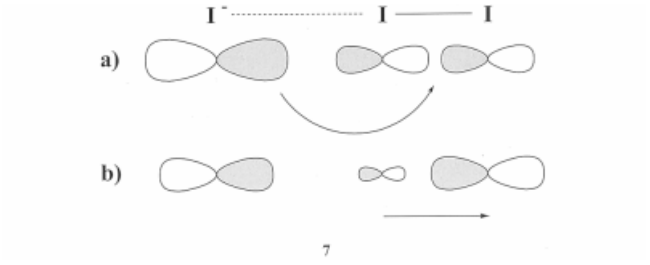

bonding LUMO of 5p−5p character in the I_2 fragment (a). As a secondary effect, the transferred electron density is polarized by the remaining negative charge on the I^- fragment (b), thus approaching the (−1/2)−(0)−(−1/2) charge distribution in the centrosymmetric I_3^- ion.

In order to further investigate the character of the bonding in I_3^-, the basis set superposition errors (BSSE) corrected interaction energy at the MP2 level was studied as a function of the distance between the centres of mass of the two fragments I_2 and I^- up to 20 Å separation. The BSSE at 4 Å is estimated to account for 2% of the total interaction energy, which gives an indication of the corrections involved in the present analysis. At greater distances the interaction is dominated by ion−quadrupole interactions because of the strong quadrupole moment of I_2 ($-1.17\ 10^{-38}$ Cm^2; MP2). The total interaction energy curve (IEC) is shown in Figure 8. The IEC is adequately described by ion−quadrupole, induction and dispersion interactions at distances greater than 7 Å. At shorter distances, the situation is of course complicated by the intramolecular interactions and charge-transfer effects. Here, a very simplistic approach is adopted: The long-range interactions are extrapolated down to the equilibrium I−I distance in I_3^- (about 3 Å). Although the induction and ion−quadrupole interactions were corrected for charges on the fragments, this is an oversimplification neglecting the damping of intermolecular interactions at shorter distances, especially concerning the dispersion interaction. Nevertheless, a maximum contribution to the total interaction energy in the "secondary bond" region may be estimated.

The remaining bonding interaction is assumed to arise mainly from intramolecular covalent and electrostatic interactions, which were modelled by a simple (exponential)

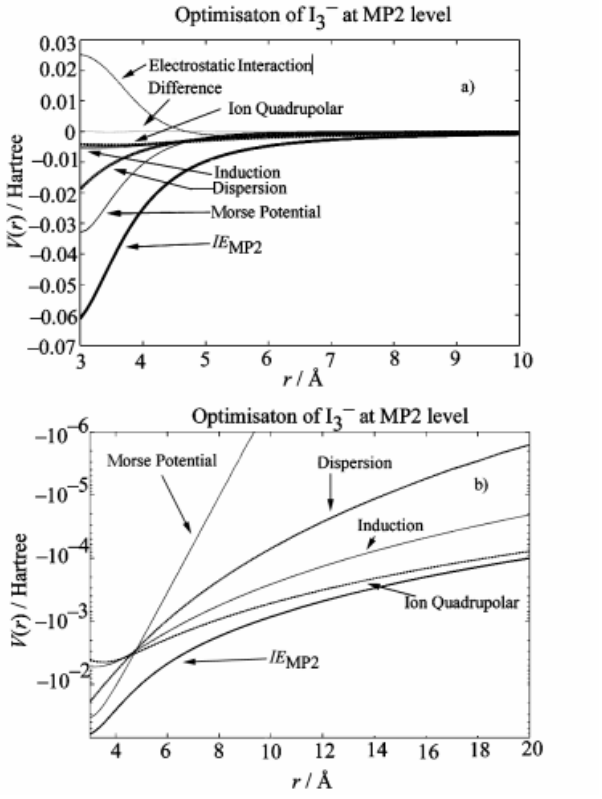

Figure 8. Interaction energy for the MP2 level and models as functions of the shortest distance between the fragments plotted in a) normal scale and b) logarithmic scale; the distance r refers to the distance between the centres of the iodide ion and the closest iodine atom in the I_2 molecule

Morse potential. The overall fit is excellent. Several fundamental conclusions can be drawn from the results.

Firstly, based on the Morse potential obtained the covalent interaction is significant up to distances of at least 5 Å. In Figure 8 the electrostatic interaction based on the NBO charges of the I^- and I_2 fragments is also included, although this was not used in the modelling of the total IEC. At greater distances the iodide ion induces a dipole on the iodine molecule, where polarization gives the closest iodine atom a partial positive charge and the most distant iodine atom a partial negative charge, resulting in a net attractive interaction. This situation prevails down to about 5 Å, where charge-transfer, inferring the beginning of orbital overlap, causes the repulsive factor to dominate. At shorter distances a strongly repulsive interaction is observed. The changeover from attractive to repulsive electrostatic interaction is at about 4.7 Å, thus giving an independent estimate of the extension of covalent interaction.

Secondly, in the region of "secondary bonds" (3−4 Å) the interaction energy is dominated by intramolecular and dispersion interactions. However, the dispersion contribution at these short distances is likely to be greatly overestimated. In addition, it is obvious from the repulsive electrostatic interaction that the covalent interaction compensates for extensive intramolecular ion−ion (or ion−dipole) repulsion. The results are very clear in one respect: There

is no specific justification based on bonding arguments for using a cut-off between intra- and intermolecular bonding somewhere in the region of "secondary bonds".

We are of course aware of the classical controversy regarding the bonding description of the X_2-X_2 interaction in condensed halogens, in particular that of Cl_2-Cl_2 (see for instance ref.[9]). The extensive literature on this subject, in many cases reduced to semantics rather than chemistry, clearly shows that different bonding models can be used to rationalize the interhalogen bonding. It is not our intention to revive this controversy with the present work. There are obvious similarities and differences between the bonding situation in "pure" halogens and the polyiodides, where the higher charge-transfer capability of the ionic fragments in polyiodides is the most important difference. This is emphasized by adopting a frontier orbital view: the HOMO energy of I^- (the 5p orbitals) is −3.33 eV, which should be compared with the HOMO (π_g) and LUMO (σ_u) energies of I_2 at −9.78 and −0.61 eV, respectively; here all values are taken from the results of the MP2 calculations. For the interactions in the region from primary to "secondary bonds" between the ionic and neutral building blocks of the polyiodides, the collective data from correlation effects, bond-order calculations, intermolecular interaction modelling and electron-density distributions thus lead us to propose that the bonding between 3 and 4 Å is dominated by covalent interactions, with additional dispersion interactions. Recently, a similar approach was used by Boese and co-workers in the rationalization of the crystal structure of ClF.[10]

The Pentaiodide System

The BSSE-corrected PES for a V-shaped I_5^- ion at the HF level is shown in Figure 9, corresponding to the configuration in **8** (*r2* optimized for each α and *r1*). As previously noted, the PES is very flat with respect to angular deformation. The optimum intermolecular ($I^-\cdots I_2$) distances and angles (*r1*/α) are 3.267 Å/110° and 3.048 Å/102° at HF and MP2 levels, respectively. This geometry and the structural data correspond well with those found experimentally. The difference PES at the MP2 level is shown in Figure 10. The

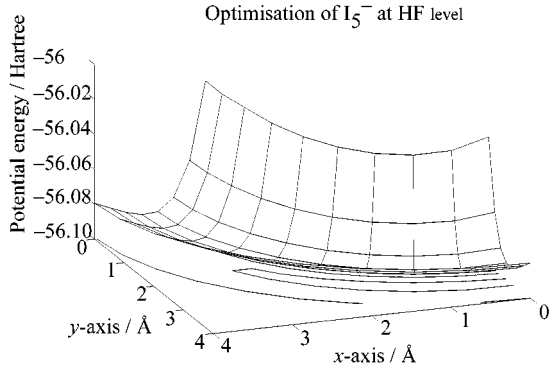

Figure 9. PES at the HF level for the V-shaped I_5^- ion (C_{2v} symmetry)

results of the theoretical study by Lin and Hall, where a decrease in intermolecular bond length is observed when dynamic correlation is taken into account, was taken as an indication of a substantial dispersion interaction.[11]

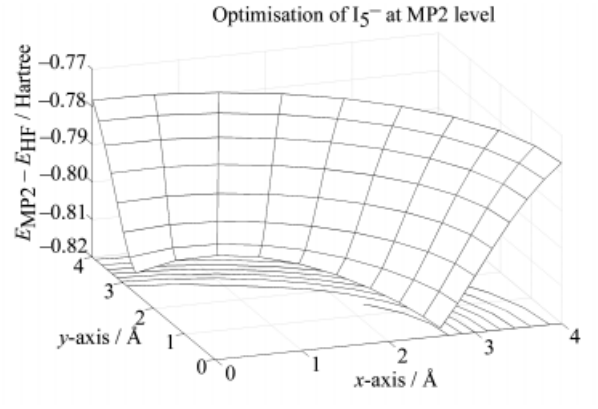

Figure 10. The difference PES between HF and MP2 levels for the V-shaped I_5^- ion

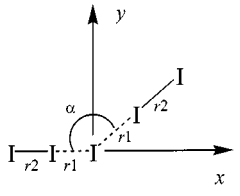

8

The same effect is seen in our results, where *r1* decreases for the MP2 level calculation. However, the difference PES values are similar to those for the I_3^- ion in being less informative on the intermolecular stabilization caused by the dispersion interaction. Again, both the NLMO/NPA BOS in Figure 11 and the total electron density map of an I_5^- ion at the optimized parameters in Figure 12 instead indicate a substantial charge transfer or covalent interaction in the range of "secondary bonding". Also, the difference electron density map shows a charge transfer from two independent 5p orbitals of the I^- fragment to the 5p−5p orbital-based LUMOs of the two I_2 fragments, thus mimicking the bonding situation in I_3^- (Figure 13). The V-shaped I_5^- ion can essentially be visualized as consisting of two I_3 legs with a common central iodine atom.

Conclusions

The present structural, statistical and computational data give no justification for the postulation of a "secondary bond" region other than for purely pragmatic reasons with respect to structural description and rationalization. The chemical bonding in the "secondary bond" region (between 3 and 4 Å) can be very adequately described in terms of intramolecular bonding with an additional dispersion interaction between the I^- and I_2 fragments in polyiodide compounds. The intramolecular interaction is comprised of attractive orbital overlap extending to almost 5 Å, compensating for a repulsive electrostatic interaction.

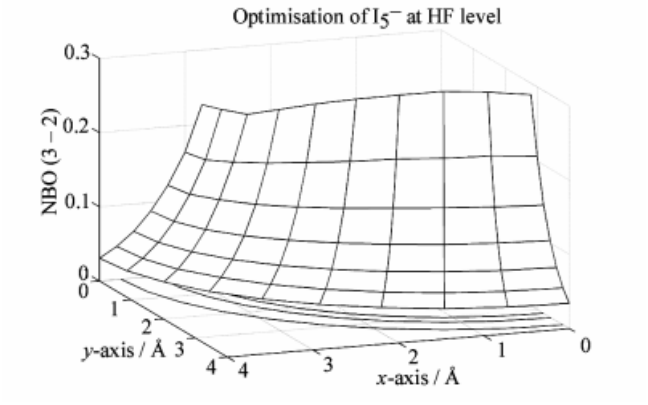

Figure 11. The NLMO/NPA BOS for the V-shaped I_5^- ion at HF level

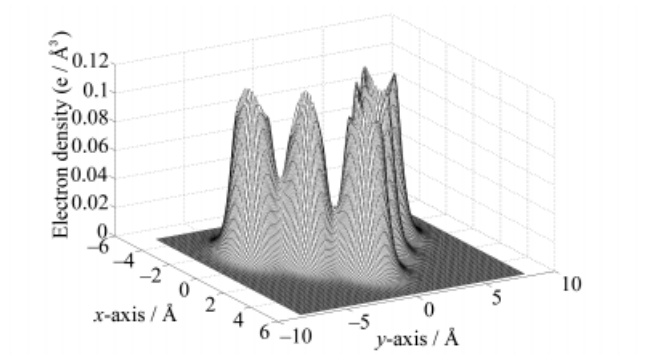

Figure 12. The total electron density of the $I^-\cdots I_2$ interaction in I_3^-

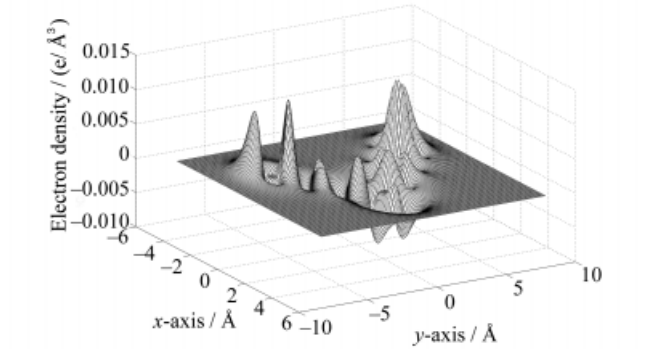

Figure 13. The difference electron density of the $I^-\cdots I_2$ interaction in I_5^-

Databases and Calculational Details

The structural statistical data were retrieved from the Cambridge Structural Database system (CSD).[12] Only structures with I···I interactions within polyiodides were included (thus, for example, I···I−S and I···I−P interactions were excluded). Structures with disorder, errors and $R \geq 10\%$ were excluded from the statistics. The database contains approximately 300 triiodides and 40 higher polyiodides. All quantum chemical calculations were performed using Gaussian 98 (revision A.7).[13] An ECP-based basis set was used for iodine, employing the Stuttgart group *quasi*-relativistic ECP and an uncontracted valence space (7s6p3d2f), see Table 1.[14] Calculations were performed at Hartree−Fock (HF), 2nd-order Møller−Plesset perturbation theory (MP2) and, where possible, coupled cluster levels including single and double excitations (CCSD). The PES values obtained were corrected for basis set superposition errors (BSSE). However, previous results for the $I_3^-\cdots I_2$ and $AuI_2^-\cdots I_2$ interactions suggest that the main features of these weak interactions are obtained without correction for BSSE.[15] In an attempt to describe the $I^-\cdots I_2$ interaction, the interaction energy curve (IEC) at MP2 level out to 20 Å was determined, allowing the I−I distance of the iodine unit to relax at each step. The model interactions were fitted to the calculated IEC by least-squares methods. At greater distances the IEC was adequately described by ion−quadrupole ($1/r^3$), induction ($1/r^4$), and dispersion ($1/r^6$) interactions.[16] The long-range interactions were fitted in the region 7−20 Å, while a Morse potential, used to model intramolecular interaction, was fitted in the region 3−20 Å. The induction and ion−quadrupole interactions were compensated for the charge on I^- by means of calculated NBO charges.

Table 1. Basis set for I (7s6p3d2f) optimized at the HF level

	Exponent
s	7.021141D+00
	6.344809D+00
	5.576563D+00
	1.437146D+00
	3.252227D−01
	1.568314D−01
	7.549193D−02
p	5.672424D+00
	3.655570D+00
	1.742992D+00
	3.736331D−01
	1.599806D−01
	6.578836D−02
d	1.325395D+00
	3.591044D−01
	1.425310D−01
f	5.212644D−01
	1.896558D−01

[1] P. H. Svensson, L. Kloo, *J. Chem. Soc., Dalton Trans.* **2000**, 2449.
[2] K.-F. Tebbe, R. Buchem, *Angew. Chem. Int. Ed. Engl.* **1997**, *36*, 1345.
[3] P. H. Svensson, G. Raud, L. Kloo, *Eur. J. Inorg. Chem.* **2000**, 1275.
[4] M. Bittner, PhD Thesis, Universität zu Köln, **1994**.
[5] P. Pyykkö, *Chem. Rev.* **1997**, *97*, 597.
[6] A. D. Buckingham, P. W. Fowler, J. M. Hutson, *Chem. Rev.* **1988**, *88*, 963.
[7] A. E. Reed, F. Weinhold, *J. Chem. Phys.* **1985**, *83*, 1736; A. E. Reed, P. von Rague Schleyer, *J. Am. Chem. Phys.* **1990**, *112*, 1434; E. D. Glenning, A. E. Reed, J. E. Carpenter, *Gaussian94 NBO*, version 3.1.

[8] G. A. Landrum, N. Goldberg, R. Hoffmann, *J. Chem. Soc., Dalton Trans.* **1997**, 3605.
[9] D. E. Williams, D. Gao, *Inorg. Chem.* **1997**, *36*, 782.
[10] R. Boese, A. D. Boese, D. Bläser, M. Y. Antipin, A. Ellern, K. Seppelt, *Angew. Chem. Int. Ed. Engl.* **1997**, *36*, 1489.
[11] Z. Lin, M. B. Hall, *Polyhedron* **1993**, *12*, 1499.
[12] Cambridge Structural Database System, Database V. 5.22, **2001**.
[13] M. J. Frisch, G. W. Trucks, H. B. Schlegel, G. E. Scuseria, M. A. Robb, J. R. Cheeseman, V. G. Zakrzewski, J. A. Montgomery, R. E. Stratmann, J. C. Burant, S. Dapprich, J. M. Millam, A. D. Daniels, K. N. Kudin, M. C. Strain, O. Farkas, J. Tomasi, V. Barone, M. Cossi, R. Cammi, B. Mennucci, C. Pomelli, C. Adamo, S. Clifford, J. Ochterski, G. A. Petersson, P. Y. Ayala, Q. Cui, K. Morokuma, D. K. Malick, A. D. Rabuck, K. Raghavachari, J. B. Foresman, J. Cioslowski, J. V. Ortiz, B. B. Stefanov, G. Liu, A. Liashenko, P. Piskorz, I. Komaromi, R. Gomperts, R. L. Martin, D. J. Fox, T. Keith, M. A. Al-Laham, C. Y. Peng, A. Nanayakkara, C. Gonzalez, M. Challacombe, P. M. W. Gill, B. G. Johnson, W. Chen, M. W. Wong, J. L. Andres, M. Head-Gordon, E. S. Replogle, J. A. Pople, *Gaussian 98*, Revision A.7, Gaussian, Inc., Pittsburgh, PA, **1998**.
[14] A. Bergner, M. Dolg, W. Küchle, H. Stoll, H. Preuss, *Molec. Phys.* **1993**, *80*, 1431.
[15] P. H. Svensson, J. Rosdahl, L. Kloo, *Chem. Eur. J.* **1999**, *5*, 305; J. Rosdahl, Diploma thesis, Lund University, **1997**.
[16] A. J. Stone, *The Theory of Intermolecular Forces*, Clarendon Press, Oxford, **1996**.

Received November 6, 2000
[I00437]

(Phosphido)platinum Complexes by Sodium-Promoted Reaction of *cis*-$PtCl_2(PHCy_2)_2$ − Synthesis and Crystal Structure of [*trans*-$Pt(PCy_2H)_2(PCy_2)Cl$], a Rare Example of a Terminal (Phosphido)platinum(II) Complex

Piero Mastrorilli,*[a] Cosimo F. Nobile,[a] Francesco P. Fanizzi,[b] Mario Latronico,[c] Chunhua Hu,[d] and Ulli Englert[d]

Keywords: Platinum / P ligands / Terminal phosphides / Hydrides / Small ring systems

cis-$PtCl_2(PHCy_2)_2$ (**1**) reacts at 0 °C in toluene with sodium metal to give the dinuclear Pt^I complexes *cis*-[$(PHCy_2)$-$(H)Pt(\mu\text{-}PCy_2)]_2$ (**2**) and [$(PHCy_2)(Cl)Pt(\mu\text{-}PCy_2)Pt(PHCy_2)_2$]-(*Pt–Pt*) (**3**). On standing in solution, complex **3** isomerizes to *trans*-[$(PHCy_2)(Cl)Pt(\mu\text{-}PCy_2)_2Pt(PHCy_2)(H)$] (**4**). When treated with sodium at room temperature, complex **3** transforms into [$Pt(\mu\text{-}PCy_2)(PHCy_2)]_2$(*Pt–Pt*) (**5**). The sodium reduction of **1** carried out at room temperature leads to the direct formation of the phosphido bridged dinuclear complex [$Pt(\mu\text{-}PCy_2)(PHCy_2)]_2$(*Pt–Pt*) (**5**) along with the mononuclear platinum(II) complex [*trans*-$Pt(PCy_2H)_2(PCy_2)Cl$] (**6**). Complex **6**, which has also been obtained by reaction of **1** with $LiPCy_2$, unambiguously shows by single-crystal X-ray diffraction the presence of a pyramidal terminal phosphido ligand.

(© Wiley-VCH Verlag GmbH, 69451 Weinheim, Germany, 2002)

Introduction

The reaction of sodium metal with phosphanyl divalent group-10 halide complexes has been widely used to access molecules in which a transition metal atom exhibits a low-valent and somehow unusual oxidation state. In particular, NiP_2X_2 (P = PEt_3, P*n*Bu_3, PEt_2Ph; X = Cl, Br) was reduced under argon to the zero-valent tetracoordinated species NiP_4, whereas $Ni(PCy_3)_2X_2$ (X = Cl, Br) gave $Ni(PCy_3)_3$ or $[NiX(PCy_3)_2]_2$.[1] The chelating diphosphane complexes $Ni(dp)Cl_2$ [dp = 1,2-bis(diphenylphosphanyl)ethane (dppe), 1,2-bis(diethylphosphanyl)ethane (depe), 1,2-bis(dicyclohexylphosphanyl)ethane (dcpe), 1,3-bis(dicyclohexylphosphanyl)propane (dcpp), 1,4-bis(dicyclohexylphosphanyl)butane (dcpb)] afforded the 14- (dp = dcpe, dcpp, dcpb), 16- (dp = dcpe, dcpb), or 18-electron (dp = dppe, depe, dcpe) complexes Ni(dp), $Ni_2(dp)_3$, and $Ni(dp)_2$, respectively, depending on the diphosphane and on the reaction conditions.[2] Phosphido-bridged dinuclear metal(I) complexes have been accessed by sodium reduction of $Ni(PCy_2Ph)_2Cl_2$,[3] $Pt(PH\textit{t}Bu_2)_2Cl_2$,[4] and $M(PHCy_2)_2Cl_2$ (M = Ni, Pd).[5] Moreover, when the sodium reaction of $Pd(PHCy_2)_2Cl_2$ was carried out at 0 °C, the isolation of [$(PHCy_2)(Cl)Pd(\mu\text{-}PCy_2)Pd(PHCy_2)_2$](*Pd−Pd*) (**7**) was achieved (Scheme 1).

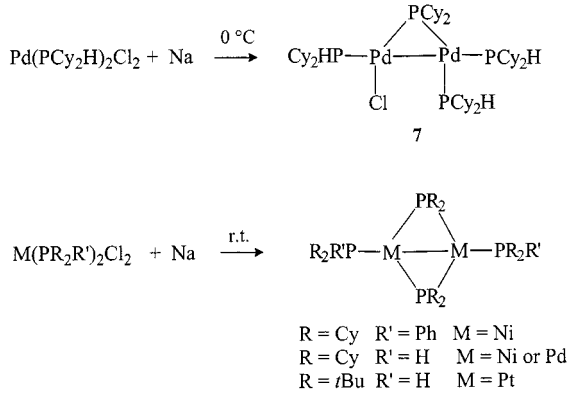

Scheme 1

In this paper we describe the reactivity of *cis*-$Pt(PHCy_2)_2Cl_2$ (**1**) towards sodium metal which was found to depend on the reaction temperature. At 0 °C the phosphido-bridged dinuclear platinum species *cis*-[$(PHCy_2)(H)Pt(\mu\text{-}PCy_2)]_2$ (**2**) and [$(PHCy_2)(Cl)Pt(\mu$-

[a] Centro di Studi C.N.R. M.I.S.O. and Dipartimento di Ingegneria Civile e Ambientale del Politecnico di Bari,
Via Orabona 4, 70125 Bari, Italy
Fax: (internat.) + 39-080/596-3611
E-mail: p.mastrorilli@poliba.it
[b] Dipartimento di Scienze e Tecnologie Biologiche ed Ambientali, Università degli Studi di Lecce,
Via Monteroni, 73100 Lecce, and
Consortium C.A.R.S.O., Cancer Research Centre,
70010 Valenzano, Italy
[c] Dipartimento di Ingegneria e Fisica dell'Ambiente, Università della Basilicata,
C. da Macchia Romana, 85100 Potenza, Italy
[d] Institut für Anorganische Chemie der RWTH,
Prof.-Pirlet-Str. 1, 52074 Aachen, Germany

$PCy_2)Pt(PHCy_2)_2](Pt-Pt)$ (**3**) were formed, whereas a mixture of $[Pt(\mu\text{-}PCy_2)(PHCy_2)]_2(Pt-Pt)$ (**5**) and the mononuclear (phosphido)platinum(II) complex [*trans*-$Pt(PHCy_2)_2(PCy_2)Cl]$ (**6**) was obtained when the reaction was carried out at room temperature.

Results and Discussion

The reaction of *cis*-$PtCl_2(PHCy_2)_2$ (**1**) with sodium metal carried out in toluene at 0 °C resulted in the formation of two dinuclear complexes **2** and **3** in an approximately 4:1 ratio. Complex **2** is fairly stable in the air but air-sensitive in aromatic solvents, where it easily dissolves. Taking advantage of insolubility in alcohols it was isolated as a white powder from the reaction mixture by treatment with methanol.

Complex **2** exhibits in the IR spectrum two characteristic bands at 2299 and 1940 cm^{-1} due to P−H and Pt−H stretching, respectively. The $^{31}P\{^1H\}$ NMR spectrum of **2** recorded at room temperature consists of three signals, all flanked by ^{195}Pt satellites: two doublets (δ = 24.8 and δ = −170.6) and a triplet of doublets (δ = −123.0). The high-field signals at δ = −123.0 and δ = −170.6, which are mutually coupled [^2J(P-P) = 104 Hz], are typical for bridging phosphides involved in four-membered rings,[6] and strongly support a dinuclear structure for **2**, with two inequivalent phosphide groups bound to two platinum atoms without *Pt−Pt* linkage. Moreover, the pattern of the phosphide ^{31}P signals (triplet of doublets and doublet) and the value of the coupling constant between the phosphorus signal at δ = −123.0 and that at δ = 24.8 [J(P-P) = 308 Hz] both suggest a symmetrical dimeric structure in which two platinum atoms, each bearing a dicyclohexylphosphane ligand are bridged by two dicyclohexylphosphide groups. In the dimer the dicyclohexylphosphane ligands are *cis* with respect to each other and *trans* with respect to the bridging phosphide group resonating at δ = −123.0. ^1H and proton-coupled ^{31}P NMR spectroscopy experiments together with IR data indicate that, on each platinum atom, the *cis* positions with respect to the terminal dicyclohexylphosphane ligands are occupied by terminal hydride ligands. In addition to the resonances of aliphatic protons and a broad doublet which can be attributed to the hydrogen atom directly bound to P in the coordinated dicyclohexylphosphane [δ = 4.50; ^1J(P-H) = 317 Hz], the ^1H NMR spectrum shows a doublet of doublet of doublets [J(P-H) = 143, 20, and 9 Hz] with ^{195}Pt satellites centred at δ = −3.84 [^1J(Pt-H) = 905 Hz]. This latter signal could be attributed to two equivalent terminal hydride ligands, *cis* with respect to each other and *trans* with respect to the bridging phosphide group resonating at δ = −170.6 as suggested by the high value of ^2J(P-H) (143 Hz).

In the proton-coupled ^{31}P NMR spectrum the signal at δ = −123.0 (phosphide P^3Cy_2, see Table 1 for numbering) remains substantially unchanged while the signal at δ = 24.8 (phosphanes P^2Cy_2H) splits into a pseudo-triplet due to the additional direct coupling ^1J(P-H) = 317 Hz, and the signal at δ = −170.6 (phosphide P^1Cy_2) splits into a triplet of doublets due to the additional coupling with the *trans* hydride ligands [^2J(P-H) = 143 Hz].

Table 1. NMR parameters for complex **2** ([D_6]benzene, 295 K); chemical shifts (bold) are in ppm; coupling constants (normal) are in Hz

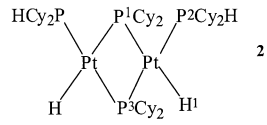

2

	P^1	P^2	P^3	H^1	Pt
P^1	**−170.6**	ca. 0	104	143	1322
P^2	ca. 0	**24.8**	308	20	1968
P^3	104	308	**−123.0**	9	2118
H^1	143	20	9	−3.84	905
Pt	1322	1968	2118	905	−4441

Finally, the value of ^1J(Pt-H) (905 Hz) and the position of the Pt−H stretching band in the IR spectrum both indicate terminal coordination for the hydride ligands. The dimeric structure of **2** formulated as *cis*-$[(PHCy_2)(H)Pt(\mu\text{-}PCy_2)]_2$ was also confirmed by the $^{195}Pt\{^1H\}$ NMR spectrum which consists of a doublet of doublets of doublets centred at δ = −4441 [^1J(Pt-P^1) = 1322, ^1J(Pt-P^2) = 1968 Hz, and ^1J(Pt-P^3) = 2118 Hz].

The minor product obtained in the sodium reduction of **1** at 0 °C, is a yellow-orange solid, the spectroscopic features and elemental analysis of which indicate the phosphido-bridged platinum(I) complex $[(PHCy_2)(Cl)Pt(\mu\text{-}PCy_2)Pt(PHCy_2)_2](Pt-Pt)$ (**3**), and represents the Pt analogue of the palladium complex **7**. In the region of the P−H stretching the IR spectrum of **3** shows the convolution of two bands of relative intensities 2:1 centred at 2295 cm^{-1} and 2255 cm^{-1}. The Pt−Cl band was found at 301 cm^{-1}. The $^{31}P\{^1H\}$ NMR spectrum of **3** recorded at room temp. shows signals centred at δ = 185.5, 37, and 16 and is reminiscent of that of **7**.

Among these signals, the only well-resolved one is that centred at δ = 185.5 (Figure 1) which does not significantly split in the proton coupled spectrum. This signal can be attributed to a bridging phosphide group involved in a three-membered Pt_2P ring[7] in which the two platinum atoms are inequivalent. The spectrum consists of a central doublet of triplets due to isotopomer **A**, which does not contain ^{195}Pt (43.8%) flanked by three different sets of satellites, two arising from isotopomers **B** and **C** (22.4% each), which contain only one ^{195}Pt nucleus and one due to isotopomer **D** (11.4%) which contains two ^{195}Pt nuclei. The coupling constants ^2J(P-P) = 231 and 26 Hz, which are clearly seen in the signal of isotopomer **A**, indicate that the phosphorus atom of the bridging phosphide group is coupled with a pseudo-*trans*- and two pseudo-*cis*-oriented phosphorus nuclei. The sets of satellites arising from both

isotopomers **B** and **C** appear as doublets of doublets of doublets. The couplings of P^1 with the two inequivalent platinum atoms gives the constants $^1J(Pt^2\text{-}P^1)$ = 3072 Hz and $^1J(Pt^1\text{-}P^1)$ = 3911 Hz whereas the coupling with P^2 and P^4 gives $^2J(P^1\text{-}P^2)$ = 34 Hz and $^2J(P^1\text{-}P^4)$ = 22 Hz (see Table 2 for P and Pt numbering). The third subset of signals due to the isotopomer **D** consists of a doublet of doublets of doublets of multiplets. The relevant coupling constants are $^1J(Pt^2\text{-}P^1)$ = 3080 Hz and $^1J(Pt^1\text{-}P^1)$ = 3916 Hz. Interestingly, the central signal appears as a doublet of triplets (instead of the expected ddd). This can be explained in terms of the isotopomer **A** having either coincident $^2J_{P,P}$ or a greater linewidth of the signal with respect to **B**, **C**, and **D**, due to difference in relaxation efficiency in different isotopomers. The latter explanation is in agreement with high-temperature spectra (82 °C) that also show the expected ddd for isotopomer **A**.[8]

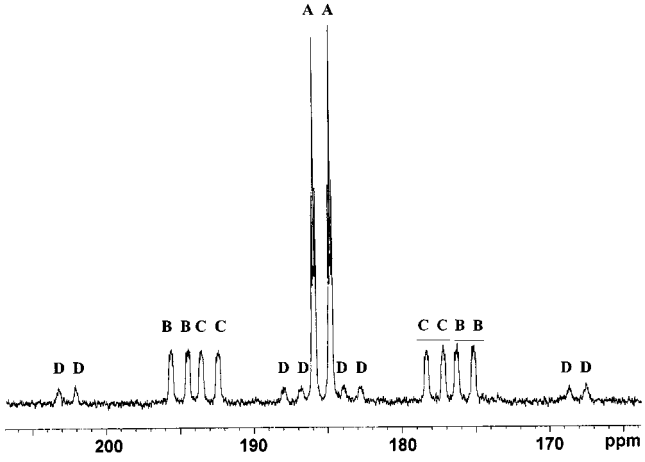

Figure 1. Phosphide region of the $^{31}P\{^1H\}$ NMR spectrum of **3** ([D_8]toluene, 202 MHz, 295 K); **A**: isotopomer with no ^{195}Pt atoms; **B**: isotopomer with NMR-active Pt^1; **C**: isotopomer with NMR-active Pt^2; **D**: isotopomer with NMR-active Pt^1 and Pt^2

Table 2. NMR parameters for complex **3** ([D_8]toluene, 295 K); chemical shifts (bold) are in ppm; coupling constants (normal) are in Hz

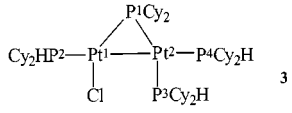

3

	P^1	P^2	P^3	P^4
P^1	**185.5**	34	231	22
P^2	34	**16.3**	16	154
P^3	231	16	**37**	12
P^4	22	154	12	**15.8**

The other $^{31}P\{^1H\}$ NMR resonances of **3** are a very broad signal centred at δ = 37 and a broad multiplet centred at δ = 16. The signal at δ = 37 can be attributed to P^3 of the dicyclohexylphosphane pseudo-*trans* to the phosphide group. Dynamic $^{31}P\{^1H\}$ NMR spectroscopic experiments showed that the signal at δ = 37, which does not change significantly by lowering the temperature down to −38°C, splits into a broad doublet [$^2J(P^1\text{-}P^3)$ = 231 Hz] at high temperatures (> 50 °C) due to the coupling with the bridging phosphide group. The broadness of this signal at or below room temperature, can therefore be explained in terms of hindered rotation around the P^3−Pt bond originating in a set of slowly interconverting rotamers.

For the related palladium complex **7** the signal of the $PHCy_2$ ligand *trans* to the bridging phosphide group is already a broad doublet at room temperature[5] and becomes a very broad singlet by lowering the temperature down to −38 °C (Figure 2). This is in agreement with a more pronounced fluxionality of palladium with respect to platinum complexes.

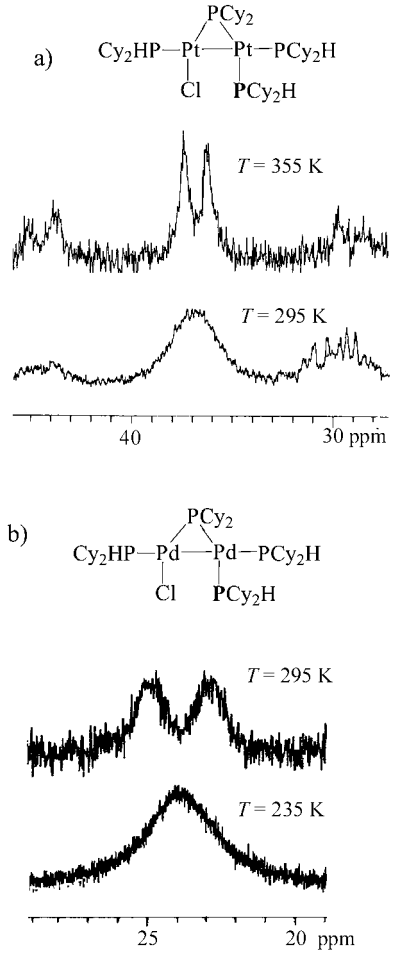

Figure 2. VT $^{31}P\{^1H\}$ NMR spectra of **3** and **7** in [D_8]toluene; (a) 202 MHz; (b) 81 MHz

In the case of complex **3**, P^2 and P^4 (the two phosphorus atoms of the phosphane ligands *cis* to the bridging phosphide group) belong to a second-order spin system and a direct analysis of the spectrum was not obtained. The $^{31}P\{^1H\}$ NMR spectrum simulation for the isotopomer containing no ^{195}Pt (ABMX spin system, A and B being P^2 and P^4) agrees well with the experimental data for the fol-

lowing parameters: $\delta(P^2) = 16.3$, $\delta(P^4) = 15.8$, $^3J(P^2\text{-}P^4) = 154$, $^3J(P^2\text{-}P^3) = 16$, $^2J(P^3\text{-}P^4) = 12$ Hz (Table 2).

Complex **3** is different from its Pd analogue **7** in that it is not stable in solution and, with the rate depending on the temperature, undergoes an intramolecular oxidative addition of a P−H bond with the rupture of the Pt−Pt bond affording the new hydrido phosphido dinuclear platinum(II) complex *trans*-[(PHCy$_2$)(Cl)Pt(μ-PCy$_2$)$_2$Pt(PHCy$_2$)(H)] (**4**).

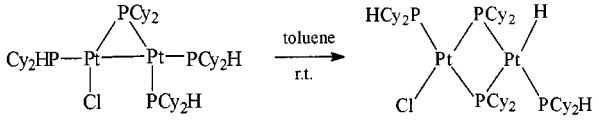

3 **4**

This complex shows one band at 281 cm^{-1} in the IR spectrum that is due to the Pt−Cl stretching, one broad band at 2301 cm^{-1} attributable to the P−H stretching, and one intense band at 1929 cm^{-1} due to the Pt−H stretching.

The $^{31}P\{^1H\}$ NMR spectrum of **4** consists of four signals, all flanked by ^{195}Pt satellites, centred at $\delta = 21.3$, $\delta = 12.5$, $\delta = -126.9$ and $\delta = -156.2$ (Table 3). The high-field signals at $\delta = -126.9$ and $\delta = -156.21$ indicate for **4**, as in the case of **2**, a dinuclear structure in which two phosphide groups are bound to two platinum atoms without Pt−Pt linkage.

Table 3. NMR parameters for complex **4** ([D$_6$]benzene, 295 K); chemical shifts (bold) are in ppm; coupling constants (normal) are in Hz

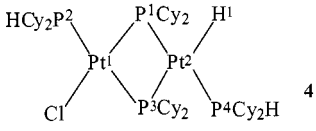

4

	P^1	P^2	P^3	P^4	H^1
P^1	**−126.9**	12	146	328	9
P^2	12	**12.5**	318		
P^3	146	318	**−156.2**	[a]	138
P^4	328		[a]	**21.3**	24
H^1	9		138	24	−3.19

[a] $^2J(P^3-P^4)$ not assessed because less than signal linewidth.

Moreover, proton-coupled ^{31}P NMR spectra show that, of the two phosphide groups, the phosphorus atom at $\delta = -156.2$ is strongly hydrogen-coupled [^2J(P-H) = 138 Hz]. The signals at $\delta = 21.3$ and $\delta = 12.5$ belong to two inequivalent terminally bound secondary phosphane ligands [^1J(P-H) = 320 and 314 Hz, respectively] with the first appearing as a doublet [^2J(P-P) = 328 Hz], and the second as a doublet of doublets [^2J(P-P) = 318 and 12 Hz]. These findings indicate that both of the terminal phosphane ligands are *trans* to a bridging phosphide group. From the ^{195}Pt satellites the coupling constants [^1J(Pt-P) = 2070 Hz, ^3J(Pt-P) = 124 Hz (phosphorus signal at $\delta = 21.3$), and ^1J(Pt-P) = 1760 Hz, ^3J(Pt-P) = 68 Hz (phosphorus signal at $\delta = 12.5$)] could be extracted.

The signals of the bridging phosphide groups at $\delta = -126.9$ and $\delta = -156.2$ are both doublets of doublets due to the mutual coupling [^2J(P-P) = 146 Hz] and also to the additional coupling of each of them with the *trans*-phosphane ligand. 2D COSY $^{31}P\{^1H\}$ NMR spectroscopic experiments enable one to clearly distinguish the satellites due to different couplings with Pt^1 and Pt^2 (such satellites, sixteen lines in total, are not unambiguously assigned in the monodimensional ^{31}P NMR spectrum) and the following values for the relevant coupling constants can be extracted: $^1J(P^1\text{-}Pt^1) = 2497$, $^1J(P^1\text{-}Pt^2) = 2239$, $^1J(P^2\text{-}Pt^1) = 1729$, $^1J(P^3\text{-}Pt^1) = 1766$, $^1J(P^3\text{-}Pt^2) = 1332$, $^1J(P^4\text{-}Pt^2) = 2070$ Hz.

The ^{1}H NMR spectrum shows, beside resonances due to aliphatic protons, two doublets centred at $\delta = 4.79$ and $\delta = 4.35$ as well as a doublet of doublets of doublets centred at $\delta = -3.19$ [J(H-P) = 138, 24, and 9 Hz]. The latter signal, which is flanked by ^{195}Pt satellites [^1J(Pt-H) = 912 Hz] is due to a terminal hydride ligand *cis* to P^4 (see Table 3 for P, H, and Pt numbering for **4**). Among the coupling constants shown by the hydride signal the largest one [^2J(H-P) = 138 Hz] is attributed to the coupling with *trans*-P^3, whereas the two smaller ones [^2J(H-P) = 24 and 9 Hz] are due to the couplings with *cis*-P^4 and *cis*-P^1, respectively.

When the Na reduction of **1** was carried out at room temperature (instead of at 0 °C), the reaction solution showed signals attributed to [Pt(μ-PCy$_2$)(PHCy$_2$)]$_2$(*Pt−Pt*) (**5**) and [*trans*-Pt(PHCy$_2$)$_2$(PCy$_2$)Cl] (**6**) in the $^{31}P\{^1H\}$ NMR spectrum. $^{31}P\{^1H\}$ NMR of **5** consists of two triplets centred at $\delta = 242.0$ and $\delta = 19.6$ [^2J(P-P) = 51 Hz] both with ^{195}Pt satellites.

The signal at $\delta = 242.0$ (Figure 3) which is flanked by two sets of satellites due to the isotopomers containing one or both NMR-active platinum atoms, does not change substantially in the proton-coupled spectrum, and belongs to the bridging phosphide groups that couple with the Pt nuclei [^1J(Pt-P) = 2598 Hz]. The low-field resonance of this bridging phosphide group indicates the presence of a three-membered Pt$_2$P ring[7a,7b] and, therefore, of a Pt−Pt bond in complex **5**. The triplet at $\delta = 19.6$ can be attributed to the terminal dicyclohexylphosphane ligands. The signal splits into a doublet of badly resolved triplets in the proton-coupled spectrum [^1J(P-H) = 318 Hz] and is flanked by satellites due to ^{195}Pt couplings [^1J(Pt-P) = 4811 Hz]. Neglecting signals due to the isotopomer containing two ^{195}Pt atoms, the main satellites each appear as a doublet of triplets due to the coupling with the phosphide groups [^2J(P-P) = 51 Hz] and with the other terminal phosphane ligand [^3J(P-P) = 70 Hz]. The relevant coupling constants found for the related complex [Pt{μ-P(SiMe$_3$)$_2$}(PEt$_3$)]$_2$(*Pt−Pt*) are: ^1J(Pt-P) = 4957, ^2J(P-P) = 63, and ^3J(P-P) = 66 Hz.[9]

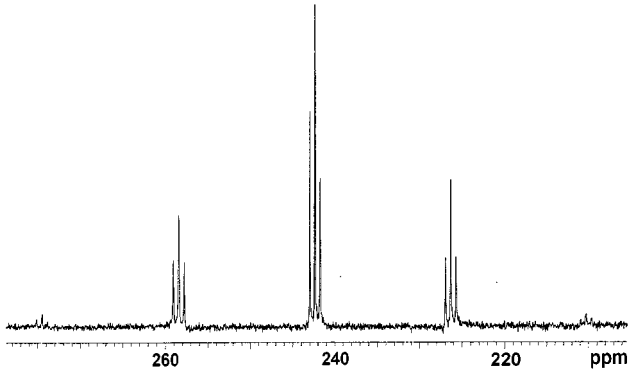

Figure 3. Phosphide region of the $^{31}P\{^{1}H\}$ NMR spectrum for **5** ([D_6]benzene, 81 MHz, 295 K)

The ^{1}H NMR spectrum of **5** shows the resonance of the hydrogen atoms directly bound to phosphorus atoms for the coordinated PCy_2H at low field. This resonance appears as a doublet of triplets [^{1}J(P-H) = 318 Hz and ^{3}J(μP-H) = 13 Hz] each broadened at the base due to H−Pt coupling (Figure 4). Moreover, each of the triplet components appears split into three peaks, due to the additional coupling with the cyclohexyl methyne protons, but the value of such coupling constants (< 4 Hz) could not exactly be assessed.

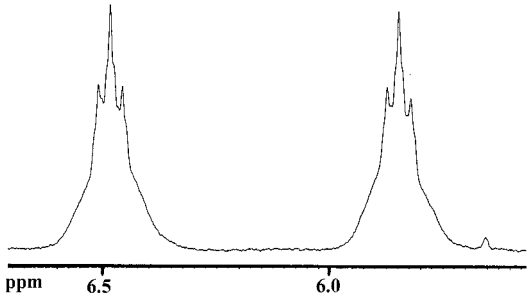

Figure 4. ^{1}H NMR spectrum in the low-field region for **5** ([D_6]benzene, 500 MHz, 295 K)

The IR spectrum of **5** shows a strong band at 2238 cm^{-1} attributed to the P−H stretching of the coordinated dicyclohexylphosphane ligand. Spectroscopically pure **5** was directly obtained in an NMR tube by treating **3** in [D_6]benzene with sodium at room temperature.

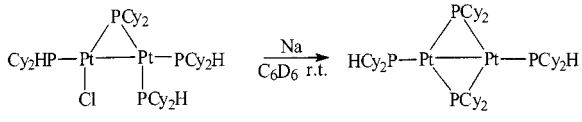

3 5

In the $^{31}P\{^{1}H\}$ NMR spectrum, complex **6** shows a doublet at δ = 27.6 and a triplet at δ = 20.6, in a 2:1 ratio (as assessed by the integrals in the proton coupled spectrum) with the same coupling constant of 41 Hz. The triplet at δ = 20.6, which does not substantially change in the proton-coupled spectrum, is flanked by satellites from which a coupling constant ^{1}J(P-Pt) = 931 Hz could be extracted. Therefore such a triplet can be ascribed to a terminal dicyclohexylphosphide group, coupled with two equivalent phosphorus atoms, directly bound to the platinum atom.

The doublet at δ = 27.6 is flanked by two satellites characterised by ^{1}J(P-Pt) = 3006 Hz. The pattern of the central signal (isotopomer without ^{195}Pt) in the proton-coupled spectrum is typical for the *A* part of a second-order spin system $(AXY_2)_2$[10] which is further coupled with a phosphorus atom [^{2}J(P-P) = 41 Hz]. In the present case *A* is ^{31}P, *X* is the proton bound to ^{31}P, and *Y* are the methyne protons of the cyclohexyl rings. In Figure 5 the experimental and simulated *A* part of the spectrum are reported. The spectroscopic features obtained through the analysis developed by Palmer and Whitcomb[10] are collected in Table 4. A similar pattern has been observed for the phosphorus atom of the coordinated secondary phosphane ligands in the palladium complexes [*trans*-$Pd(SPh)_2(PCy_2H)_2$][11] and [*trans*-$PdCl(CHCl_2)(PtBu_2H)_2$].[12]

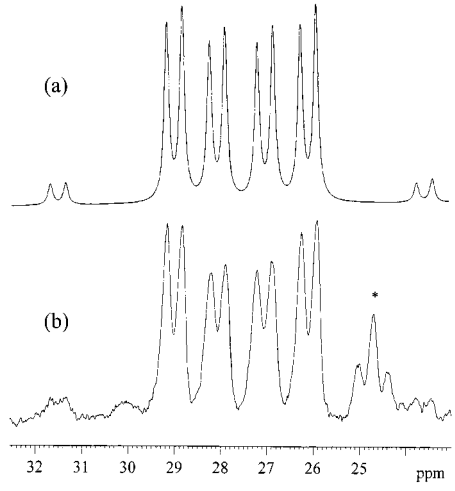

Figure 5. Proton-coupled ^{31}P NMR spectrum of complex **6** in the P^1 region ([D_6]benzene, 121 MHz, 295 K): (a) simulated, (b) experimental; the asterisked triplet belongs to P^2 satellites

The IR spectrum of **6** shows a strong band at 2324 cm^{-1} attributed to the P−H stretching of the coordinated dicyclohexylphosphane ligands and a medium 259 cm^{-1} band attributed to the Pt−Cl stretching. According to the above reported spectroscopic data, **6** can be formulated as [*trans*-$Pt(PHCy_2)_2(PCy_2)Cl$], a neutral terminal phosphido complex of platinum(II).

Due to the exceedingly high *trans*-effect of phosphido ligands, terminal (phosphido)platinum(II) complexes are quite rare, so that the pioneering work of Chatt and Davidson concluded that, at least in the case of diphenylphosphide, it seemed unlikely that such a ligand, terminally bound to platinum(II), could even exist.[13] Nevertheless, starting from the late 1980s, a number of terminal phosphido complexes of platinum(II) have been prepared. The first molecule of this type to be synthesised was the dichloro-

Table 4. Spectroscopic features for complexes **5** and **6** ([D_6]benzene, 295 K); chemical shifts are in ppm; coupling constants are in Hz

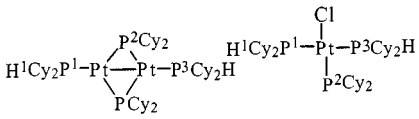

	5[a]	**6**[b]
δ (P^1)	19.6	27.6
δ (P^2)	242.0	20.6
δ (H^1)	6.17	4.09
δ (Pt)	–5514	–4825
$^2J(P^1–P^2)$	51	41
$^{2/3}J(P^1–P^3)$	70	420
$^1J(P^1–H^1)$	318	352
$^3J(P^2–H^1)$	13	6
$^2J(Pt–H^1)$	ca. 50	108
$^1J(P^2–Pt)$	2598	931
$^1J(P^1–Pt)$	4811	3006
ν(Pt–Cl)		259 cm^{-1}
ν(P–H)	2238 cm^{-1}	2324 cm^{-1}

[a] $|^2J(P^1\text{-Pt})| = 50$ Hz. [b] $^3J(P^3\text{-}H^1) = 1$ Hz.

phosphide complex $[PtCl(PEt_3)(PCl_2)]$.[14] Other examples are the cations $[Pt\{PPh(CH_2CH_2PPh_2)_2\}(PR_2)]^+$ (R = Cy, Ph)[15] and $[(xp_3)Pt(PEt_2)]^+$ [xp_3 = $N(CH_2CH_2PPh_2)_3$, $P(CH_2CH_2PPh_2)_3$][16] and the neutral $[Pt(NCN)PPh_2)]$ [NCN = $C_6H_3(CH_2NMe_2)_2$-2,6] complex.[17] More recently, Glueck et al. have described a series of terminal (phosphido)platinum(II) complexes of the type $[Pt(dppe)Me(X)]^{n+}$ (X = primary or secondary phosphide, $n = 0$ or 1).[18]

In all of these terminal (phosphido)platinum complexes, the chemical shifts of the phosphido phosphorus atom fall in the range δ = −88.4 to δ = 56.7 and give scarce information about the character of the phosphorus ligand. On the other hand, the relatively small ^1J(Pt-P) coupling constant expected between platinum and a terminal phosphido ligand, rationalised in terms of low *s* character of the Pt−P bond,[18b] can be taken as diagnostic of the presence of such a ligand. The value of the relevant $^1J_{Pt,P}$ for the aforementioned complexes ranges from 767 Hz to 1305 Hz. The ^1J(Pt-P) = 931 Hz found for **6** supports our assignment as [*trans*-$Pt(PCy_2H)_2(PCy_2)Cl$].[19]

In order to gain insight into the structure of complex **6**, a crystallographic analysis was undertaken. The X-ray diffraction study revealed that **6** crystallises in the space group $P\bar{1}$ and contains a distorted square-planar platinum(II) centre (Figure 6 and Table 5), the largest angle between ligands being 99.87(11)° [P(3)−Pt−P(2)]. A tetrahedral distortion from planarity is also evident from the 172.46(12)° [P(3)−Pt−P(1) and 171.98(12)° [P(2)−Pt−Cl] angles, significantly differing from the ideal 180°.

The phosphide P atom is pyramidal as indicated by the sum of the angles at P(2) of 320.5° (compared to 328.5° for a tetrahedral and 360° for a planar atom). The hydrogen atoms bonded to the phosphorus atom were located in a Fourier difference synthesis. The two P−H bonds of the dicyclohexylphosphane ligands are both oriented toward the phosphido ligand; such orientation minimises the repulsions between the six cyclohexyl groups around the Pt atom. The relatively long[20] Pt−Cl bond [2.421(3) Å] indicates a pronounced *trans* effect of the terminal phosphide group. The P(2)−Pt bond length [2.326(3) Å] is slightly shorter than those reported for related terminal phosphido platinum(II) complexes. The Pt−P(phosphido) bond lengths of Pt(dppe)(Me)(PHMes*),[18b] Pt(dppe)(Me)(P-Mes_2),[18b] and Pt(*S*,*S*-Chiraphos)(Me)(PPhIs)[18d] [Mes* = 2,4,6-(tBu)$_3C_6H_2$, Mes = 2,4,6-$Me_3C_6H_2$, Chiraphos = 2,3-bis(diphenylphosphanyl)butane, Is = 2,4,6-(iPr)$_3C_6H_2$] are, in fact, 2.378(5), 2.351(2), and 2.3622(15) Å, respectively.

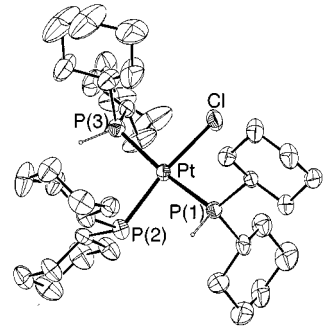

Figure 6. Displacement ellipsoid plot[29] of **6**; ellipsoids are scaled to 30% probability, H atoms are shown with arbitrary radii

Table 5. Selected bond lengths [Å] and angles [°] for **6**

Pt−P(3)	2.272(3)
Pt−P(1)	2.293(3)
Pt−P(2)	2.326(3)
Pt−Cl	2.421(3)
P(3)−Pt−P(1)	172.46(12)
P(3)−Pt−P(2)	99.87(11)
P(1)−Pt−P(2)	85.63(11)
P(3)−Pt−Cl(1)	86.03(11)
P(1)−Pt−Cl(1)	89.01(11)
P(2)−Pt−Cl(1)	171.98(12)

A possible pathway for the reaction of **1** with sodium at room temp. could start with the abstraction of two subsequent chloride ions giving the dicoordinated Pt^0 complex $[Pt(PHCy_2)_2]$ (Scheme 2). This intermediate could lead to intramolecular electrophilic attack of one coordinated $PHCy_2$ yielding $[Pt(H)(PCy_2)(PHCy_2)]$ which, in turn, can dimerise to **5** via reductive elimination of hydrogen.[21]

On the other hand, at room temperature, **1** could also react with sodium dicyclohexylphosphide (one of the products formed when **1** decomposes in the presence of sodium metal) giving **6** by substitution of the chloride ion with the dicyclohexylphosphide group (Scheme 2). A confirmation of this proposed mechanism came from the reaction between **1** and $LiPCy_2$ which gave pure **6**.[22]

The lack of formation of both **5** and **6** when the reaction of **1** with sodium metal is carried out at 0 °C can be explained by admitting that both chloride ion abstraction and intramolecular attack of a dicyclohexylphosphane ligand in $[Pt(PHCy_2)_2]$ leading to $[Pt(H)(PCy_2)(PHCy_2)]$ (Step *a* in Scheme 2) are temperature-sensitive and slow in the reac-

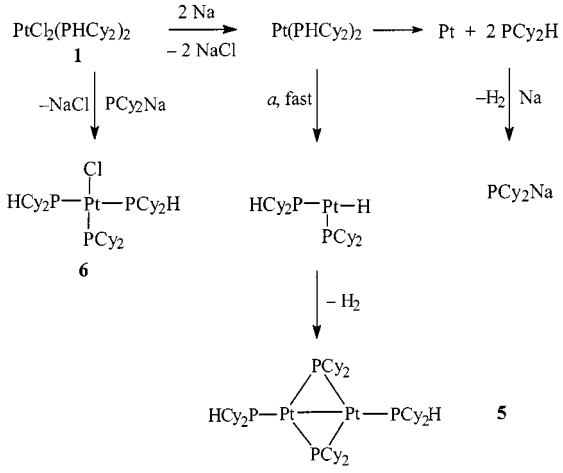

Scheme 2. Proposed mechanism for the sodium reduction of **1** at room temperature

tion at 0 °C. Under these conditions both intermediate $[PtCl(PHCy_2)_2]$ and $[Pt(PHCy_2)_2]$ could accumulate in the reaction medium (Scheme 3). Therefore $[Pt(PHCy_2)_2]$ may become the preferential target for the attack of $[Pt(H)(PCy_2)(PHCy_2)]$ which results in the formation of **2** (effectively found in the reaction solution at 0 °C as the major product). On the other hand, dimerization of $[PtCl(PHCy_2)_2]$ by HCl evolution (revealed as H_2 and NaCl formation in the presence of Na) could also account for the formation of compound **3** as the minor product.

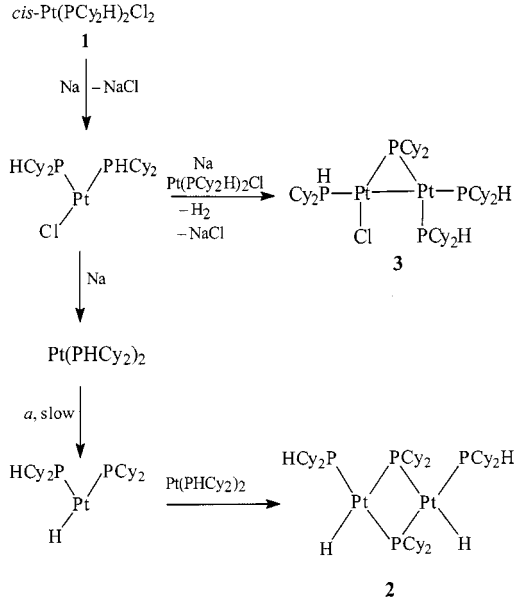

Scheme 3. Proposed mechanism for the sodium reduction of **1** at 0 °C

Experimental Section

General Remarks: All manipulations were carried out under pure dinitrogen, using freshly distilled and oxygen-free solvents. All aromatic deuterated solvents were carefully dehydrated (Na) and deoxygenated (freeze and pump). Dicyclohexylphosphane was purchased from Strem and used as received. PCy_2Li[23] and $PtCl_2(PhCN)_2$[24] were prepared by literature methods. Infrared spectra were recorded with a Bruker Vector 22 spectrometer. Elemental analyses (C, H) were carried out using a Carlo Erba model EA 1108 instrument. The Cl and P contents (where reported) were determined by potentiometric titration with AgCl (716DMS Metrohm) and by spectrophotometric methods (Uvikon 942 Kontron, λ = 460 nm), respectively. NMR spectra were recorded with BRUKER Avance DRX500 (CARSO), BRUKER Avance DPX300, and VARIAN XL200 spectrometers; frequencies are referenced to Me_4Si (^1H and ^{13}C), 85% H_3PO_4 (^{31}P), and H_2PtCl_6 (^{195}Pt).

***cis*-Dichlorobis(dicyclohexylphosphane)platinum(II) (1):**[25] 1.45 g of dicyclohexylphosphane, dissolved in 10 mL of toluene, was added dropwise to a toluene solution of *trans*-$PtCl_2(PhCN)_2$ (1.7 g in 30 mL) kept at 60 °C. After 1.5 h, the resulting white suspension was cooled at room temp. and the solid filtered off, washed with toluene (5 mL), and dried under vacuum affording pure **1** as a colourless microcrystalline powder (2.03 g, 85% yield). IR (nujol mull): $\tilde{\nu}_{max}$ = 2351 w (P−H), 285 m (Pt−Cl) cm^{-1}. ^1H NMR ($CDCl_3$, 500 MHz): δ = 3.60 [m, ^1J(P-H) = 362, ^2J(Pt-H) = 96, ^2J(*H*P-C*H*) = 6 Hz, PH]. ^{31}P NMR ($CDCl_3$, 202 MHz): δ = 18.6 [s, ^1J(P-Pt) = 3402, ^1J(P-H) = 362, ^2J(P-P′) = 19, ^3J(P-H′) = 8 Hz]. $^{195}Pt\{^1H\}$ NMR ($CDCl_3$, 64 MHz): δ = −4540 [t, ^1J(P-Pt) = 3402 Hz]. $C_{24}H_{46}Cl_2P_2Pt$ (662.58): calcd. C 43.51, H 7.00, Cl 10.70, P 9.35; found C 43.48, H 7.10, Cl 10.75, P 9.27.

Reduction of 1 with Sodium at 0 °C: A suspension of *cis*-$PtCl_2(PHCy_2)_2$ (**1**) (0.98 g, 1.48 mmol) and sodium metal (0.067 g, 2.91 mmol) in toluene (40 mL) was vigorously stirred at 0 °C (ice bath) for 9 h. In the course of the reaction dihydrogen evolved, as revealed by gas chromatographic analysis. The resulting suspension was filtered (to remove 0.243 g of unchanged **1** and 0.104 g of platinum metal) and the solvent was removed at low temperature (0 °C). Treatment of the obtained solid with cold methanol afforded pure **2** (0.12 g, 13.7% yield) as a white powder and a yellow solution from which, after solvent removal and crystallisation of the residue from THF/*n*-hexane (1:1) at −30 °C, pure **3** precipitated as a yellow solid (28 mg, 3.1% yield). ^1H NMR spectroscopic features of **2** other than those reported in Table 1 ([D_8]toluene, 295 K): δ = 4.50 [br. d, ^1J(P-H) = 317 Hz, *H*-P^2). IR (nujol mull): $\tilde{\nu}_{max}$ = 2299 w (P−H), 1940 s (Pt−H) cm^{-1}. $C_{48}H_{92}P_4Pt_2$ (1183.34): C 48.72, H 7.84, P 10.47; found C 47.86, H 7.95, P 10.13. ^1H NMR spectroscopic features of **3** other than those reported in Table 2 ([D_8]toluene, 295 K): δ = 4.31 [d, ^1J(P-H) = 319 Hz, *H*-P^4], δ = 4.45 [d, ^1J(P-H) = 312 Hz, *H*-P^2], δ = 5.3 [br. d ^1J(P-H) = 320 Hz, *H*-P^3]. IR (nujol mull): $\tilde{\nu}_{max}$ = 2295 w and 2255 w (P−H), 301 w (Pt−Cl) cm^{-1}. $C_{48}H_{91}ClP_4Pt_2$ (1217.78): calcd. C 47.34, H 7.53, Cl 2.91; found C 46.87, H 7.27, Cl 2.85.

Isomerisation of 3 To Give 4: A toluene solution of **3** was stirred at 50 °C for 5 h causing the colour to lighten from yellow-orange to pale yellow. Evaporation of the solvent afforded a solid, which was washed with cold methanol and after crystallisation from toluene/*n*-hexane (2:1), **4** was obtained as white needles. IR (nujol mull): $\tilde{\nu}_{max}$ = 2301 w (P−H), 1929 w (Pt−H), 281 w (Pt−Cl) cm^{-1}. ^1H NMR spectroscopic features of **4** other than those reported in Table 3 ([D_6]benzene, 295 K): δ = 4.35 [d, ^1J(P-H) = 314, ^2J(Pt-H) = 98 Hz, *H*-P^2], δ = 4.79 [d, ^1J(P-H) = 320 Hz, *H*-P^4]. $C_{48}H_{91}ClP_4Pt_2$ (1217.78): calcd. C 47.34, H 7.53, Cl 2.91, P 10.17; found C 46.38, H 7.68, Cl 2.85, P 10.12.

Reduction of 1 with Sodium at Room Temperature: A suspension of *cis*-$PtCl_2(PHCy_2)_2$ (0.30 g, 0.45 mmol) and sodium metal (0.10 g, 4.3 mmol) in toluene (30 mL) was vigorously stirred at room temperature (25 °C) for 70 min. In the course of the reaction dihydrogen was evolved, as revealed by gas chromatographic analysis. The resulting suspension was filtered and the solvent was removed in vacuo from the yellow-orange filtrate. The residue was redissolved in deuterated benzene and used for NMR spectroscopic analysis, revealing the formation of **5** and **6** in an approximately 1:3 ratio.

Reduction of 3 with Sodium: A light yellow solution of complex **3** in [D_6]benzene was treated with sodium sand in an NMR tube at room temperature until the hydrogen evolution stopped (about 0.5 h). The resulting dark yellow solution was analysed by NMR spectroscopy giving signals due to **5** alone.

***trans*-Chloro(dicyclohexylphosphido)bis(dicyclohexylphosphane)-platinum(II) [$Pt(PHCy_2)_2(PCy_2)Cl$] (6):** A suspension of *cis*-[$Pt(PHCy_2)_2Cl_2$] (0.54 g, 0.82 mmol) and PCy_2Li (0.166 g, 0.82 mmol) in toluene (20 mL) was vigorously stirred at 0 °C until a yellow solution was obtained (about 8 h). LiCl was filtered and the solution concentrated in vacuo to ca. 5 mL. By cooling at −20 °C pale yellow crystals of **6** precipitated which were isolated by filtration (0.435 g, 65%). IR (nujol mull): $\tilde{\nu}_{max}$ = 2324 s (P−H), 259 m (Pt−Cl) cm^{-1}. $C_{36}H_{68}ClP_3Pt$ (824.40): calcd. C 52.45, H 8.31, Cl 4.30, P 11.27; found C 51.93, H 8.45, Cl 4.37, P 11.32.

X-ray Data Collection, Structure Solution, and Refinement of 6:[26] Crystal data and parameters for intensity data collection and structure refinement are compiled in Table 6. A pale yellow rod with the approximate dimensions of 0.15 × 0.11 × 0.03 mm was studied at room temperature with a BRUKER-AXS SMART Apex diffractometer. An empirical absorption correction[27] was applied (max. trans. 1.000, min. trans. 0.797). The structure was solved by direct methods and refined on F^2 with the SHELXTL[28] suite of programs.

Table 6. Crystal data and structure refinement for **6**

Empirical formula	$C_{36}H_{68}ClP_3Pt$
Formula mass	824.35
Temperature [K]	293(2)
Wavelength [Å]	0.71073
Crystal system	triclinic
Space group	$P\bar{1}$ (no. 2)
Unit cell dimensions	
a [Å]	9.9460(10)
b [Å]	10.7743(11)
c [Å]	18.772(2)
α [°]	80.872(2)
β [°]	79.098(2)
γ [°]	82.054(3)
V [Å^3]	1938.1(3)
Z	2
$D_{calcd.}$ [Mg m^{-3}]	1.413
Absorption coeff. [mm^{-1}]	3.835
θ range for data coll. [°]	1.12−28.26
Independent reflections	9509
Observed reflections	3665
Refinement method	full-matrix least squares on F^2
Data/parameters	9509/370
Goodness-of-fit on F^2	0.840
Final R[a] [$I > 2\sigma(I)$][a]	0.0747
$wR2$[b] (all data)	0.1279
Largest diff. peak/hole [eÅ^{-3}]	1.657, −0.881 (close to Pt)

[a] $R = \Sigma||F_o| - |F_c||/\Sigma|F_o|$. [b] $R_w = [\Sigma w(|F_o| - |F_c|)^2/\Sigma w|F_o|^2]^{1/2}$.

Acknowledgments

We thank Dr. R. Giannandrea and Dr. M. Palma for invaluable help. Mr. E. Pannacciulli is gratefully acknowledged for technical assistance. Italian CNR and MURST are gratefully acknowledged for financial support.

[1] M. Aresta, C. F. Nobile, A. Sacco, *Inorg. Chim. Acta* **1975**, *12*, 167−178.
[2] P. Mastrorilli, G. Moro, C. F. Nobile, M. Latronico, *Inorg. Chim. Acta* **1992**, *192*, 183−187.
[3] C. F. Nobile, G. Vasapollo, P. Giannoccaro, A. Sacco, *Inorg. Chim. Acta* **1981**, *48*, 261−263.
[4] R. Giannandrea, P. Mastrorilli, M. Palma, C. F. Nobile, F. P. Fanizzi, U. Englert, *Eur. J. Inorg. Chem.* **2000**, 2573−2576.
[5] R. Giannandrea, P. Mastrorilli, C. F. Nobile, U. Englert, *J. Chem. Soc., Dalton Trans.* **1997**, 1355−1358.
[6] K. R. Dixon, A. D. Rattray, *Inorg. Chem.* **1978**, *17*, 1099−1103.
[7] [7a] P. E. Garrou, *Chem. Rev.* **1981**, *81*, 229. [7b] A. J. Carty, S. A. Maclaughlin, D. Nucciarone, in: *Phosphorus-31 NMR Spectroscopy in Stereochemical Analysis* (Eds.: J. G. Verkade, L. D. Quin), VCH, New York, **1987**, p. 559. Examples of Pt_2P three-membered rings can be found in: [7c]P. Leoni, S. Manetti, M. Pasquali, *Inorg. Chem.* **1995**, *34*, 749−752. [7d] P. Leoni, G. Chiaradonna, M. Pasquali, F. Marchetti, *Inorg. Chem.* **1999**, *38*, 253−259. [7e] J. Jans, R. Naegeli, L. M. Venanzi, A. Albinati, *J. Organomet. Chem.* **1983**, *247*, C37−C41. [7f] P. W. N. M. van Leeuwen, C. F. Roobeek, J. H. G. Frijns, A. Guy Orpen, *Organometallics* **1990**, *9*, 1211−1222. [7g] P. Leoni, M. Pasquali, V. Cittadini, A. Fortunelli, M. Selmi, *Inorg. Chem.* **1999**, *38*, 5257−5265. [7h] P. Leoni, S. Manetti, M. Pasquali, A. Albinati, *Inorg. Chem.* **1996**, *35*, 6045−6052. [7i] R. Bender, P. Braunstein, A. Dedieu, P. D. Ellis, B. Huggins, P. D. Harvey, E. Sappa, A. Tiripicchio, *Inorg. Chem.* **1996**, *35*, 1223−1234. [7j] P. Leoni, M. Pasquali, A. Fortunelli, G. Germano, A. Albinati, *J. Am. Chem. Soc.* **1998**, *120*, 9564−9573. [7k] S. Cristofani, P. Leoni, M. Pasquali, F. Eisentraeger, A. Albinati, *Organometallics* **2000**, *19*, 4589−4595. [7l] L. R. Falvello, J. Forniés, C. Fortuño, F. Martinez, *Inorg. Chem.* **1994**, *33*, 6242−6246. [7m] R. Bender, P. Braunstein, A. Tiripicchio, M. Tiripicchio Camellini, *Angew. Chem. Int. Ed. Engl.* **1985**, *24*, 861−862. [7n] H. Wachtler, W. Schuh, K. H. Ongania, K. Wurst, P. Peringer, *Organometallics* **1998**, *17*, 5640−5646. [7o] A. R. Siedle, R. A. Newmark, W. B. Gleason, *J. Am. Chem. Soc.* **1986**, *108*, 767−773. [7p] N. Hadj-Bagheri, J. Browning, K. Dehghan, K. R. Dixon, N. J. Meanwell, R. Vefghi, *J. Organomet. Chem.* **1990**, *396*, C47−C52. [7q] L. R. Falvello, J. Forniés, C. Fortuño, A. Martìn, A. P. Martìnez-Sariñena, *Organometallics* **1997**, *16*, 5849−5856. [7r] A. L. Bandini, G. Banditelli, G. Minghetti, *J. Organomet. Chem.* **2000**, *595*, 224−231. [7s] E. Alonso, J. Forniés, C. Fortuño, A. Martìn, A. G. Orpen, *Organometallics* **2001**, *20*, 850−859.
[8] For temperature dependence of relaxation time see: F. A. Bovey, *Nuclear Magnetic Resonance Spectroscopy*, Academic Press, New York, **1969**, pp. 6−16.
[9] H. Schaefer, D. Binder, *Z. Anorg. Allg. Chem.* **1988**, *560*, 65−79.
[10] R. A. Palmer, D. R. Whitcomb, *J. Magn. Res.* **1980**, *39*, 371−379.
[11] M. Pasquali, F. Marchetti, P. Leoni, T. Beringhelli, G. D'Alfonso, *Gazz. Chim. Ital.* **1993**, *123*, 659−664.
[12] P. Leoni, *Organometallics* **1993**, *12*, 2432−2434.
[13] J. Chatt, J. M. Davidson, *J. Chem. Soc.* **1964**, 2433−2445.
[14] A. J. Blake, R. W. Cockman, E. A. V. Ebsworth, S. G. D. Henderson, J. H. Holloway, N. J. Pilkington, D. W. H. Rankin, *Phosphorus Sulfur* **1987**, *30*, 143.

[15] A. Handler, P. Peringer, E. P. Muller, *J. Chem. Soc., Dalton Trans.* **1990**, 3725.
[16] F. Cecconi, C. A. Ghilardi, S. Midollini, S. Moneti, A. Orlandini, G. Scapacci, *Inorg. Chim. Acta* **1991**, *189*, 105−110.
[17] F. Maassarani, M. F. Davidson, I. C. M. Wehman-Ooyevaar, D. M. Grove, M. A. van Koten, W. J. J. Smeets, A. L. Spek, G. van Koten, *Inorg. Chim. Acta* **1995**, *235*, 327−338.
[18] [18a] D. K. Wicht, I. V. Kourkine, B. M. Lew, J. M. Nthenge, D. S. Glueck, *J. Am. Chem. Soc.* **1997**, *119*, 5039−5040. [18b] D. K. Wicht, S. N. Paisner, B. M. Lew, D. S. Glueck, G. P. A. Yap, L. M. Liable-Sands, A. L. Rheingold, C. M. Haar, S. P. Nolan, *Organometallics* **1998**, *17*, 652−660. [18c] D. K. Wicht, D. S. Glueck, L. M. Liable-Sands, A. L. Rheingold, *Organometallics* **1999**, *18*, 5130−5140. [18d] D. K. Wicht, I. Kovacik, D. S. Glueck, L. M. Liable-Sands, C. D. Incarvito, A. L. Rheingold, *Organometallics* **1999**, *18*, 5141−5151.
[19] In this regard it should be noted that the related complex *trans*-$Pt(PEt_3)(PPhH)Cl$ proposed as intermediate in the reaction between $(PPh)_5$ and $PtCl_2(PEt_3)_2$ on the basis of its spectroscopic features (I. P. Parkin, A. M. Z. Slawin, D. J. Williams, D. Woollins, *Inorg. Chim. Acta* **1990**, *172*, 159−163) exhibits a coupling constant ^1J(P-Pt) of 3460 Hz which seems to be very unusual for a terminal phosphide group.
[20] A. G. Orpen, L. Brammer, F. H. Allen, O. Kennard, D. G. Watson, R. Taylor, *Typical interatomic distances: organometallic compounds and coordination complexes of the d- and f-block metals, International Tables for Crystallography*, vol. C (Ed.: A. J. C. Wilson), Kluwer Academic Publishers, Dordrecht, The Netherlands, **1995**, pp. 707−791.
[21] A symilar mechanism has been suggested for the related Ni and Pd complexes $[Ni(PHCy_2)(\mu\text{-}PCy_2)]_2$ (see ref.[5]) and $[Pd(PHCy_2)(\mu\text{-}PCy_2)]_2$ (see: P. Leoni, M. Sommovigo, M. Pasquali, P. Sabatino, D. Braga, *J. Organomet. Chem.* **1992**, *423*, 263−270).
[22] Such a type of reaction is unprecedented for Pt species, except in the case of $(Et_3P)_2PtCl_2$ with $LiP(SiMe_3)_2$ reported in ref.[9] where unstable compounds such as $(Et_3P)_2Pt[P(SiMe_3)_2]Cl$ and $(Et_3P)_2Pt[P(SiMe_3)_2]_2$ form, the latter of which, in turn, affords, by splitting off of the phosphane ligands, a mixture of a (diphosphene)Pt^0 complex and a phosphido-bridged Pt^I complex.
[23] K. Issleib, W. Tschach, *Chem. Ber.* **1959**, *92*, 1118−1126.
[24] P. Braunstein, R. Bender, J. Jud, *Inorg. Synth.* **1992**, *29*, 341.
[25] T. Blum, P. Braunstein, A. Tiripicchio, M. Tiripicchio Camellini, *Organometallics* **1989**, *8*, 2504−2513.
[26] CCDC-172800 contains the supplementary crystallographic data for this paper. These data can be obtained free of charge at www.ccdc.cam.ac.uk/conts/retrieving.html or from the Cambridge Crystallographic Data Centre, 12, Union Road, Cambridge CB2 1EZ, UK [Fax: (internat.) + 44-1223/336-033; E-mail: deposit@ccdc.cam.ac.uk].
[27]]G. M. Sheldrick, *SADABS*, University of Göttingen, Germany, **1996**.
[28]]G. M. Sheldrick, *SHELXTL*, Version 5.1. Bruker AXS Inc., Madison, Wisconsin, USA, **1998**.
[29] A. L. Spek, *PLATON-94*, University of Utrecht, The Netherlands, **1994**.

Received October 30, 2001
[I01424]

Syntheses and First Crystal Structures of Rhenium Complexes Derived from ω-Functionalized Fatty Acids as Model Compounds of Technetium Tracers for Myocardial Metabolism Imaging

Christian M. Jung,[a] Werner Kraus,[b] Peter Leibnitz,[b] Hans-Jürgen Pietzsch,[a] Joachim Kropp,[c] and Hartmut Spies*[a]

Keywords: Rhenium / Technetium / Fatty acids / Drug research / Radiopharmaceuticals

In an attempt to develop new technetium-based radiopharmaceuticals for the noninvasive diagnosis of myocardial metabolism, we have synthesized three examples of novel metal-containing fatty acid derivatives according to the "3+1" mixed-ligand and the Schiff base/tricarbonyl design. The chelates contain the metal core in the oxidation states +5 and +1, respectively, and are attached to the end-position of a fatty acid chain. The complex formation was accomplished by ligand-exchange reactions with three different rhenium precursors, whereas the inactive rhenium metal was utilized as a surrogate of the technetium radionuclide. The molecular structures of the fatty acid complexes **7**, **10** and **14** were determined by single-crystal X-ray diffraction analyses and impressively show a general problem in technetium tracer research, namely the significant structural alterations of bioactive molecules by coordination even to small metal chelates. (© Wiley-VCH Verlag GmbH, 69451 Weinheim, Germany, 2002)

Introduction

Naturally occurring long-chain fatty acids serve as the main energy source of the normoxic myocardium. Regional alterations in the myocardial fatty acid oxidation may indicate ischemic heart diseases and cardiomyophaties at an early stage and therefore possess a remarkable diagnostic potential in nuclear medicine. Although radio-iodinated fatty acids such as 15-(*p*-[^{123}I]iodophenyl)pentadecanoic acid (IPPA) and its β-methyl-branched derivative BMIPP have proven their applicability for myocardial metabolism imaging in numerous clinical trials, fatty acid scintigraphy has not yet reached widespread application in nuclear medicine.[1] Compared to the technetium-99m-based perfusion tracers that are mainly applied at present, radiolabelled fatty acids allow more convincing scans of viable myocardium. However, logistical disadvantages and disproportionately high costs of the accelerator-produced radionuclide iodine-123 still conflict with a major acceptance of these tracers in routine cardiac diagnostics. On the other hand, the low-price availability from the ^{99}Mo/^{99m}Tc generator combined with its optimal radiophysical properties, and the commercial distribution of pre-prepared instant kits for various clinical examinations have made technetium-99m the preferred radiolabel in nuclear medicinal imaging.[2] The progress in ^{99m}Tc tracer design to monitor specific endogenic functions is nevertheless severely limited by the effect of the artificial radiometal and its coordination chemistry on the in vivo behaviour of labelled bioactive molecules.

The synthesis of technetium-containing long-chain fatty acids for accessing regional discrepancies in myocardial energy production has been a goal of many research groups since 1975.[3] Although a variety of different chelating moieties were used to attach the radiometal at the fatty acid skeleton, low myocardial extraction and poor recognition as a substrate for the β-oxidation in living cells has prevented an application of these ^{99m}Tc-labelled agents in nuclear medicine. A characteristic feature of almost all the technetium-99m fatty acid analogues described so far is the focus on polar tetradentate N_2S_2 chelates with a central oxometal(V) core. In our attempt to create new technetium-labelled fatty acids with an improved myocardial profile, we therefore concentrate on alternative coordination moieties according to the "*n*+1" mixed-ligand approach[4] and the Schiff base/tricarbonyl design.[5] Since working with radioactive compounds affords great care and is subjected to some restrictions, the third-row congener rhenium was used

[a] Forschungszentrum Rossendorf e.V., Institut für Bioanorganische und Radiopharmazeutische Chemie,
Postfach 510119, 01314 Dresden, Germany
Fax: (internat.) + 49-(0)351/260-3232
E-mail: H.Spies@fz-rossendorf.de
[b] Bundesanstalt für Materialforschung und -prüfung,
Richard-Willstätter-Straße 11, 12489 Berlin, Germany
E-mail: W.Kraus@bam.de
[c] Medizinische Fakultät Carl Gustav Carus an der Technischen Universität Dresden, Klinik und Poliklinik für Nuklearmedizin,
Fetscherstraße 74, 01307 Dresden, Germany
E-mail: jkmed@rcs.urz.tu-dresden.de

in our preliminary studies as a surrogate for the radioactive technetium.

Results and Discussion

In this paper we report the synthesis and crystal structure of three new classes of rhenium-containing fatty acid analogues. From our point of view, success in the development of bioactive metal-based fatty acid tracers is primarily dependent on the choice of a suitable chelating moiety, which allows a strong binding of the bioligand to the metal centre but preserves the physiological integrity of the fatty acid. Since the carboxylic group probably plays a fundamental role in the substrate cognition in vivo we decided to functionalize fatty acid ligands in their ω-position. For the head structures we used the skeleton of the IPPA tracer,[6] which has been well tested in clinical trials, and the metabolism-blocking sulfur-inserted fatty acid analogue 14-(*R*,*S*)-[^{18}F]fluoro-6-thiaheptadecanoic acid (FTHA),[7] as well as the naturally occurring lauric acid.

Suitable ω-sulfanyl fatty acid ligands required for the "3+1" mixed-ligand concept were synthesized starting from the corresponding ω-bromo derivatives. Whereas the pentadecanoic acid starting material was reasonably accessible by acidic ring opening of the corresponding ω-hydroxylactone by hydrobromic acid,[8] the thia-inserted heptadecanoic acid analogue **4** was prepared in three steps starting from the commercially available 5-bromovaleric acid **1**. After nucleophilic substitution of the halide at the end position by a sulfanyl unit, the fatty acid body was built up by coupling to 11-bromo-1-undecanol under basic conditions. Conversion of the hydroxy group into a bromide was accomplished by an adopted version of the Appel reaction.[9] Sulfonyl groups in the ω-position of the fatty acids **5** and **8** were finally introduced by nucleophilic attack of sodium thiophosphate and subsequent acidic hydrolysis[10] (Scheme 1).

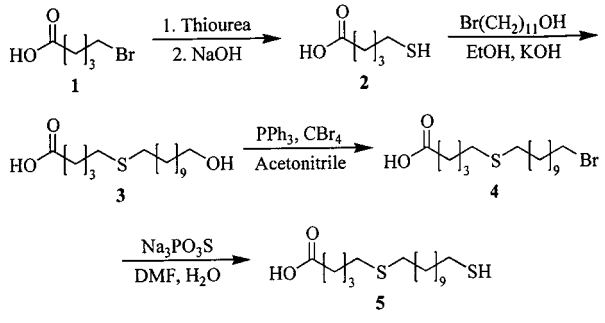

Scheme 1. Synthesis of ω-sulfanyl ε-thia fatty acid **5**

Coordination of the ω-sulfanyl fatty acid ligands **5** and **8** to the rhenium precursors **6**[11] and **9**[12] according the "3+1" approach offers access to the oxorhenium(V) complexes **7** and **10**, respectively. Preparation of **10** was accomplished in moderate yields by a one-pot synthesis of the tetrachlorooxorhenate **9**, the protected "SN(Me)S" tridentate and the ω-sulfanyl fatty acid **8** under basic conditions; complex **7** was obtained almost quantitatively by smooth chloride exchange of the thia fatty acid **5** at the preformed oxorhenium(V) precursor **6** (Scheme 2). The coordination sphere of these mixed-ligand complexes differs in the central donor atom of the tridentate chelator, being sulfur in the model compound **7** and nitrogen in complex **10**. Accompanied by the alteration of the tridentate ligand part is a change in colour from reddish-brown (for **7**) to dark green (for **10**). The infrared spectra of both complexes show a strong absorption band in the region of 955 cm^{-1}, which is distinctive of the central Re=O^{3+} moiety. In the ^{1}H NMR spectra of compound **7** the protons of the tridentate chelator give representative coupling patterns at δ_H = 4.27, 3.90, 3.09 and 1.95; the equivalent signals of the "SN(Me)S" ligand are partly widened and coincided and are observed between δ_H = 3.9−2.6.

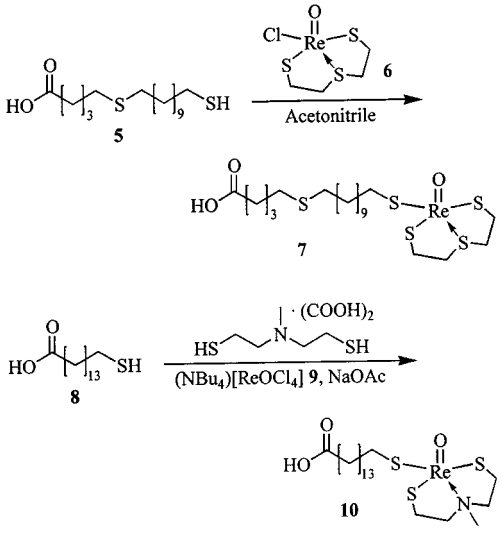

Scheme 2. Syntheses of "3+1" mixed-ligand complexes **7** and **10**

Both complexes **7** and **10** were obtained as crystalline solids by slow solvent evaporation at room temperature and were investigated by X-ray analysis. As characteristic of "SSS"-coordinated "3+1" mixed-ligand complexes, **7** possesses a square-pyramidal coordination sphere around the central metal core. The distorted basal surface, stretched by the four sulfur donor atoms, exhibits a twisted orientation with respect to the planar arrangement of the fatty acid chain (Figure 1). An alteration of the tridentate to the "SN(Me)S" chelator results in a transition of the coordination sphere to a distorted trigonal-bipyramidal geometry. In **10** (Figure 2) the axial positions are occupied by the nitrogen donor of the tridentate ligand and the sulfur atom of the monodentate fatty acid derivative, respectively; the corner sites of the triangular plane, however, are taken up by the oxygen atom of the Re=O^{3+} unit and the two sulfanyl groups of the "SN(Me)S" ligand. In structures **7** and **10**, bond lengths and angles within the chelate moieties are of the order of magnitude expected for these types of rhenium coordination compounds (Table 1). However, a special order/disorder phenomenon was detected in the crystal packing of **10**. As frequently observed in this type of complexes

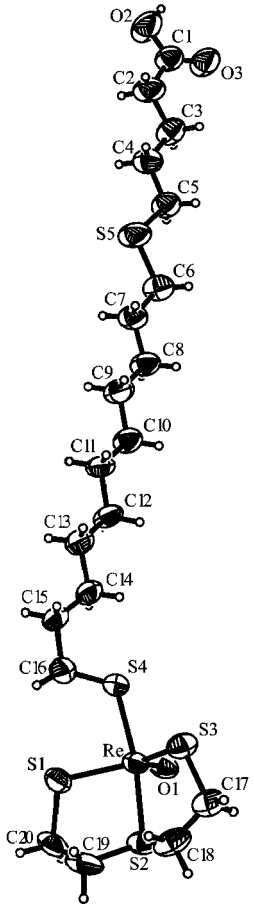

Figure 1. Molecular structure of "SSS"-coordinated "3+1" mixed-ligand complex **7**

Table 1. Selected bond lengths [Å] and angles [°] for "3+1" mixed-ligand complexes **7** and **10**

7		**10**	
Re−O(1)	1.684(8)	Re−O(1)	1.671(5)
Re−S(1)	2.303(3)	Re−N	2.208(7)
Re−S(2)	2.377(3)	Re−S(1)	2.273(4)
Re−S(3)	2.293(3)	Re−S(2)	2.265(3)
Re−S(4)	2.301(3)	Re−S(3)	2.295(3)
O(1)−Re−S(1)	114.2(3)	O(1)−Re−N	95.3(3)
O(1)−Re−S(2)	100.3(3)	O(1)−Re−S(1)	119.0(2)
O(1)−Re−S(3)	115.7(3)	O(1)−Re−S(2)	118.3(2)
O(1)−Re−S(4)	106.6(3)	O(1)−Re−S(3)	105.2(2)
S(1)−Re−S(2)	84.22(13)	N−Re−S(1)	82.72(16)
S(3)−Re−S(1)	129.88(14)	N−Re−S(2)	83.99(17)
S(3)−Re−S(2)	83.41(12)	N−Re−S(3)	159.44(18)
S(3)−Re−S(4)	81.05(11)	S(1)−Re−S(3)	88.54(8)
S(4)−Re−S(1)	88.76(11)	S(2)−Re−S(1)	121.99(11)
S(4)−Re−S(2)	152.78(12)	S(2)−Re−S(3)	84.96(10)

the "SN(Me)S" chelator can change its conformation by a flip-flop mechanism giving rise to a statistical distribution of two equal isomers within the crystal.[13]

Alberto et al. recently introduced the "*fac*-$[M(CO)_3]^+$" fragment as promising synthon for the labelling of biomolecules with technetium.[5] Due to the known tendency of the metal(I) core to interact strongly with soft donor compounds, bidentate aromatic Schiff base ligands are exceedingly suitable for coordinating the tricarbonylmetal(I) moiety. We therefore synthesized an appropriate fatty acid derivative; starting from commercially available ω-aminolauric acid (**11**), the corresponding Schiff base **12** was obtained by simple condensation of picolinaldehyde with the amino group of the analogous lauric acid salt. Since the resulting imines decompose even by neutralisation,[14] the protonation of the carboxyl function was carried out subsequent to the stabilizing attachment of the tricarbonylrhenium moiety. The two nitrogen donor atoms replace two bromide ions of the tricarbonylrhenium(I) precursor **13**.[15] The third halide substituent, however, is responsible for the compensation of the electrical charge and remains fixed in the coordination sphere of the metal(I) core (Scheme 3). Complex **14** was obtained as a deep orange compound and showed the characteristic carbonyl absorption bands at 2021 and 1902 cm^{-1} in the infrared spectrum. The imine proton of the fatty acid ligand was detected as a sharp singlet in the ^1H NMR spectrum at $\delta_H = 8.70$; the

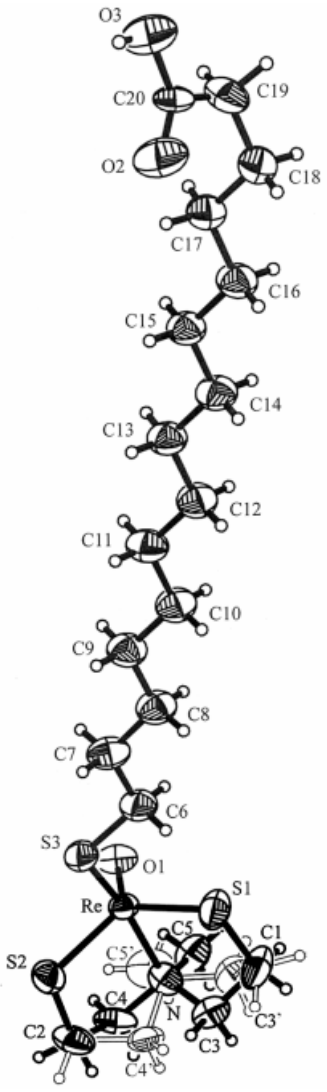

Figure 2. Molecular structure of "SN(Me)S"-coordinated "3+1" mixed-ligand complex **10**

^{13}C signals of the three carbonyl substituents were observed at δ_C = 196.6, 195.8 and 186.1.

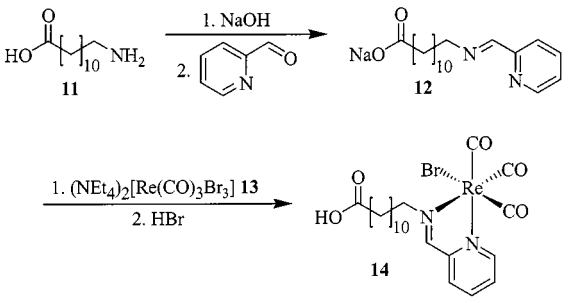

Scheme 3. Synthesis of tricarbonylrhenium(I) complex **14**

Compound **14** crystallized upon slow concentration of a saturated solution in acetonitrile. As expected for this type of complex, the molecular structure shows an octahedral coordination sphere around the central rhenium(I) core. The three carbonyl moieties are arranged facial to each other, and the remaining coordination sites are occupied by the bidentate Schiff base ligand and a bromine atom (Figure 3, Table 2).

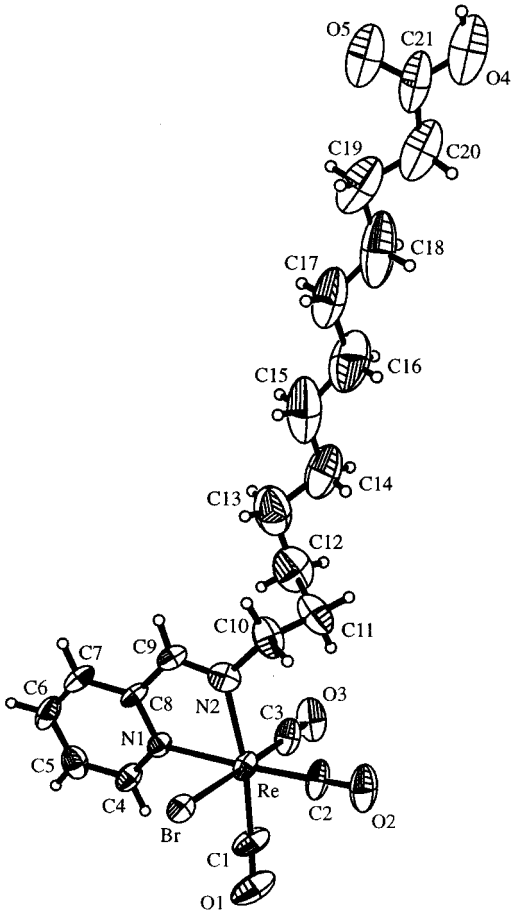

Figure 3. Molecular structure of tricarbonylrhenium(I) complex **14**

Table 2. Selected bond lengths [Å] and angles [°] for tricarbonylrhenium(I) complex **14**

14			
Re−C(1)	1.871(12)	C(1)−Re−C(2)	89.6(6)
Re−C(2)	1.883(12)	C(1)−Re−C(3)	88.6(6)
Re−C(3)	1.873(13)	C(3)−Re−C(2)	89.9(5)
Re−N(1)	2.159(7)	C(1)−Re−N(1)	97.2(5)
Re−N(2)	2.152(9)	C(1)−Re−N(2)	171.5(5)
Re−Br	2.6253(13)	C(2)−Re−N(1)	170.7(4)
O(1)−C(1)	1.158(14)	C(2)−Re−N(2)	98.6(5)
O(2)−C(2)	1.168(13)	C(3)−Re−N(1)	96.5(4)
O(3)−C(3)	1.137(14)	C(3)−Re−N(2)	93.9(5)
N(1)−C(8)	1.345(12)	C(1)−Re−Br(1)	92.6(4)
N(2)−C(9)	1.272(14)	C(2)−Re−Br(1)	89.2(4)
C(8)−C(9)	1.452(15)	C(3)−Re−Br(1)	178.5(4)
		N(1)−Re−Br(1)	84.3(2)
		N(2)−Re−Br(1)	85.0(2)
		N(2)−Re−N(1)	74.4(3)

Particularly conspicuous in the molecular structure of all three complexes, **7**, **10**, and **14**, are the proportions between the chelate moieties and the fatty acid ligands. The drastic structural alteration of the biomolecules, even by coordination to small-sized metal chelates, is certainly a main reason for the laborious progress in the development of new technetium-based radiotracers with the objective of assessment of specific endogenous processes and physiological functions. Nevertheless, structural integrity is only one of several parameters, besides others such as lipophilicity and polarity, that influence the in vivo behaviour of potential ^{99m}Tc radiotracers. Therefore further investigations concerning the biological profile of the technetium-99m analogues of **7**, **10** and **14** will be done to estimate the value of these compounds as potential radiotracers for myocardial metabolism imaging.

Experimental Section

General Remarks: All chemicals and solvents were of reagent grade and utilized without further purification, with the exception of picolinaldehyde, which was freshly distilled prior to use. 11-Bromo-1-undecanol and 12-aminolauric acid were purchased from Fluka. Sodium thiophosphate[16] and *N*-methyl-3-azapentane-1,5-dithiol−oxalic acid[17] were prepared according to the literature. The syntheses involving air-sensitive compounds were carried out under argon using the standard Schlenk technique. The standard workup procedure for product isolation was quenching the reaction mixture in an aqueous solution, followed by extracting thoroughly with $CHCl_3$, washing the extracts with saturated saline, drying owith $MgSO_4$ and evaporating the solvent under reduced pressure. Column chromatography was performed according to Still[18] by using Merck silica gel (0.040−0.063 mm). IR: Perkin−Elmer Specord 2000. NMR: Varian Inova-400. For ^1H NMR $CDCl_3$ (δ_H = 7.26) and CD_3OD (δ_H = 3.31) were used as solvents, for ^{13}C NMR $CDCl_3$ (δ_C = 77.0). Elemental analyses: LECO CHNS 932.

15-Sulfanylpentadecanoic Acid (8): 1.96 g (10.9 mmol) of sodium thiophosphate in 20 mL of H_2O was added to a solution of 1.75 g (5.45 mmol) of 15-bromopentadecanoic acid[8] in 50 mL of di-

methylformamide. The resulting slurry was stirred for 72 h while increasing the temperature from 25 to 50 °C. Afterwards, the mixture was quenched with 3.5% HCl (pH = 2) and stirred overnight. Dilution with additional 30 mL of H_2O and subsequent standard workup yielded a light yellow solid, which was purified by column chromatography (*n*-hexane/Et_2O/HOAc, 70:30:1). Yield: 1.22 g (82%). IR (KBr): $\tilde{\nu}$ = 1714 (C=O) cm^{-1}. ^1H NMR ($CDCl_3$): δ = 1.21−1.41 (m, 20 H, 10 × CH_2), 1.33 (t, ^3J = 7.7 Hz, 1 H, CH_2SH), 1.55−1.67 (m, 4 H, CH_2CH_2SH, CH_2CH_2COOH), 2.34 (t, ^3J = 7.5, 2 H, CH_2COOH), 2.52 (dt, ^3J = 7.4, CH_2SH, 2 H). $C_{15}H_{30}O_2S$ (274.47): calcd. C 65.46, H 11.02, S 11.68; found C 65.50, H 10.98, S 11.72.

5-Sulfanylvaleric Acid (2): A mixture of 5.00 g (27.6 mmol) of 5-bromovaleric acid (**1**) and 3.15 g (41.4 mmol) of thiourea in 50 mL of ethanol was heated under reflux for 16 h. After cooling off to room temperature, the solvent was evaporated under reduced pressure and the residue heated with 50 mL of 7.5 M NaOH for another 6 h. The mixture was carefully acidified with 2.5 M H_2SO_4, the organic layer separated and the aqueous phase extracted as usual. Purification of the remaining raw material was accomplished by distillation under vacuum. Yield: 3.04 g (82%). b.p. 102−104 °C/0.7 Torr. ^1H NMR ($CDCl_3$): δ = 1.35 (t, ^3J = 7.9, 1 H, CH_2SH), 1.59−1.80 (m, 4 H, $CH_2CH_2CH_2SH$), 2.37 (t, ^3J = 7.1, 2 H, CH_2COOH), 2.54 (dt, ^3J = 7.2, 2 H, CH_2SH), 10.2−11.3 (br, 1 H, COO*H*). ^{13}C NMR: δ = 23.3, 24.1 (CH_2S, CH_2CH_2COOH), 33.2, 33.4 (CH_2CH_2S, CH_2COOH), 179.8 (*C*OOH). $C_5H_{10}O_2S$ (134.20): calcd. C 44.75, H 7.51, S 23.89; found C 44.43, H 7.74, S 23.50.

17-Hydroxy-6-thiaheptadecanoic Acid (3): To a solution of 2.50 g (43.7 mmol) of KOH in 85 mL of ethanol was added, whilst stirring, 2.9 g (21.6 mmol) of **2** and subsequently 5.40 g (21.5 mmol) of 11-bromo-1-undecanol. After heating under reflux for 12 h, the mixture was acidified with 2.5 M H_2SO_4 and the solvent evaporated under reduced pressure. The residue was partitioned between 75 mL of H_2O and $CHCl_3$ and worked up by standard procedures. Crystallisation from MeOH at −15 °C yielded the pure fatty acid **3** as a colourless solid. Yield: 5.66 g (86%). IR (KBr): $\tilde{\nu}$ = 1690 (C=O) cm^{-1}. ^1H NMR ($CDCl_3$): δ = 1.19−1.39 (m, 14 H, 7 × CH_2), 1.47−1.76 (m, 8 H, CH_2CH_2OH, $CH_2CH_2SCH_2CH_2$, CH_2CH_2COOH), 2.33 (t, ^3J = 7.2, 2 H, CH_2COOH), 2.46 (t, ^3J = 7.4, 2 H), 2.48 (t, ^3J = 7.2, 2 H, CH_2SCH_2), 3.59 (t, ^3J = 6.7, 2 H, CH_2OH), 6.77 (br, 2 H, CH_2OH, COO*H*). $C_{16}H_{32}O_3S$ (304.49): calcd. C 63.11, H 10.59, S 10.53; found C 63.04, H 10.50, S 10.47.

17-Bromo-6-thiaheptadecanoic Acid (4): 646 mg (2.46 mmol) of PPh_3 was added, whilst stirring, to a solution of 817 mg (2.46 mmol) of CBr_4 and 250 mg (821 μmol) of **3** in 25 mL of acetonitrile at 0 °C. The mixture was allowed to reach ambient temperature and was stirred overnight. The solvent was evaporated under reduced pressure and the residue partitioned between 50 mL of H_2O and $CHCl_3$ followed by standard workup and column chromatography (*n*-hexane/Et_2O/HOAc, 75:25:1). Yield: 238 mg (79%). IR (KBr): $\tilde{\nu}$ = 1693 (C=O), 647 (C−Br) cm^{-1}. ^1H NMR ($CDCl_3$): δ = 1.22−1.48 (m, 14 H, 7 × CH_2), 1.50−1.80 (m, 6 H, $CH_2CH_2SCH_2CH_2$, CH_2CH_2COOH), 1.85 (quint, ^3J = 7.1, 2 H, CH_2CH_2Br), 2.38 (t, ^3J = 7.2, 2 H, CH_2COOH), 2.49 (t, ^3J = 7.5, 2 H,), 2.52 (t, ^3J = 7.4, 2 H, CH_2SCH_2), 3.40 (t, ^3J = 6.9, 2 H, CH_2Br). $C_{16}H_{31}BrO_2S$ (267.39): calcd. C 52.31, H 8.50, S 8.73; found C 52.28, H 8.38, S 8.53.

17-Sulfanyl-6-thiaheptadecanoic Acid (5): ω-Sulfanyl ligand **5** was prepared from 200 mg (544 μmol) of **4** by the procedure described for **8**. Yield: 122 mg (70%). IR (KBr): $\tilde{\nu}$ = 1694 (C=O) cm^{-1}. ^1H NMR ($CDCl_3$): δ = 1.20−1.41 (m, 14 H, 7 × CH_2), 1.32 (t, ^3J = 7.8, 1 H, CH_2SH), 1.49−1.79 (m, 8 H, CH_2CH_2SH, $CH_2CH_2SCH_2CH_2$, CH_2CH_2COOH), 2.37 (t, ^3J = 7.2, 2 H, CH_2COOH), 2.44−2.55 (m, 6 H, CH_2SCH_2, CH_2SH). $C_{16}H_{32}O_2S_2$ (320.56): calcd. C 59.95, H 10.06, S 20.01; found C 59.97, H 10.08, S 20.12.

Oxorhenium(V) Complex 7: 50 mg (128 μmol) of chloro(3-thiapentane-1,5-dithiolato)oxorhenium(V) (**6**)[11] was dissolved in 6 mL of hot acetonitrile while stirring. To this mixture 45 mg (140 μmol) of the fatty acid **5** was added. The mixture was refluxed for 30 min and then concentrated to dryness. The residue was purified by flash chromatography ($CHCl_3$/EtOAc/HOAc, 60:40:1). Crystals suitable for single crystal analysis were obtained by slow evaporation of a saturated $CHCl_3$/acetonitrile solution of **7** at room temperature. Yield: 81 mg (94%). IR (KBr): $\tilde{\nu}$ = 1703 (C=O), 958 (Re=O) cm^{-1}. ^1H NMR ($CDCl_3$): δ = 1.23−1.41 (m, 12 H, 6 × CH_2), 1.46−1.60 (m, 4 H), 1.64 (quint, ^3J = 7.3, 2 H), 1.74 (quint, ^3J = 7.4, 2 H, $CH_2CH_2SCH_2CH_2$, CH_2CH_2COOH, $CH_2CH_2CH_2SRe$), 1.88 (quint, ^3J = 7.6, 2 H, CH_2CH_2SReO"SSS"), 1.95 (ddd, J_1 = 4.9, J_2 = 9.9, J_3 = 14.6, 2 H, A-part ABCD system "SSS"), 2.38 (t, ^3J = 7.3, 2 H, CH_2COOH), 2.49 (t, ^3J = 7.3, 2 H), 2.52 (t, ^3J = 7.1, 2 H, $CH_2SCH_2CH_2CH_2$), 3.09 (dt, J_1 = 4.0, J_2 = 13.8, 2 H, B-part ABCD system "SSS"), 3.83 (t, ^3J = 7.5, 2 H, CH_2SReO"SSS"), 3.90 (dd, J_1 = 3.8, J_2 = 10.2, 2 H, C-part ABCD system "SSS"), 4.27 (dd, J_1 = 4.7, J_2 = 13.1, 2 H, D-part ABCD system "SSS"). $C_{20}H_{39}O_3ReS_4$ (674.06): calcd. C 35.64, H 5.83, S 23.79; found C 35.46, H 5.81, 23.86.

Oxorhenium(V) Complex 10: A mixture of 140 mg (510 μmol) of **8**, 109 mg (452 μmol) of *N*-methyl-3-azapentane-1,5-dithiol−oxalic acid, 265 mg (452 μmol) of tetrachlorooxorhenate **9**[12] and 4 mL of 1 M methanolic NaOAc in 25 mL of MeOH was stirred at 40 °C for 24 h. The solvent was removed under reduced pressure and the remaining brown solid partitioned between 25 mL of H_2O and $CHCl_3$. After standard workup, the pure complex was isolated by column chromatography ($CHCl_3$/EtOAc/HOAc, 50:50:1) and subsequent crystallisation from ethanol. Yield: 191 mg (68%). IR (KBr): $\tilde{\nu}$ = 1705 (C=O), 950 (Re=O) cm^{-1}. ^1H NMR ($CDCl_3$): δ = 1.20−1.38 (m, 18 H, 9 × CH_2), 1.47 (quint, ^3J = 7.4, 2 H, $CH_2CH_2CH_2SRe$), 1.63 (quint, ^3J = 7.4, 2 H, CH_2CH_2COOH), 1.85 (quint, ^3J = 7.4, 2 H, CH_2CH_2SRe"SNS"), 2.35 (t, ^3J = 7.6, 2 H, CH_2COOH), 2.63 (m, 2 H, "SNS"), 3.16−3.22 (m, 4 H, "SNS", CH_2SReO"SNS"), 3.35 (s, 3 H, NCH_3), 3.54 (m, 2 H, "SNS"), 3.5−3.9 (br, 2 H, "SNS"). $C_{20}H_{40}NO_3ReS_3$ (624.95): calcd. C 38.44, H 6.45, N 2.24, S 15.39; found C 38.52, H 6.65, N 2.21, S 15.47.

Sodium 12-{[(Pyridin-2-yl)methylene]amino}undecanoate (12): 200 mg (777 μmol) of amino fatty acid **11** was dissolved in 5 mL of MeOH, containing 31 mg (775 μmol) of NaOH. The solution was filtered and then concentrated to dryness. The residue was redissolved in 5 mL of MeOH and 125 mg (1.15 mmol) of freshly distilled picolinaldehyde was added whilst stirring at 0 °C. The mixture was stirred for additional 12 h at room temperature before removing the solvent and washing the residue carefully with several portions of acetone and Et_2O. Schiff base sodium salt **12** was obtained as a light brown powder without any further purification steps. Yield: 248 mg (87%). IR (KBr): $\tilde{\nu}$ = 1648 (CH=N), 1561 (C=O) cm^{-1}. ^1H NMR (CD_3OD): δ = 1.23−1.42 (m, 14 H, 7 × CH_2), 1.59 (m, 2 H), 1.73 (m, 2 H CH_2CH_2N, CH_2CH_2COONa), 2.14 (t, ^3J = 7.6, CH_2COONa, 2 H), 3.68 (t, ^3J = 7.0, 2 H, CH_2N), 7.48 (m, 1 H, $H_{5\text{-Ar}}$), 7.91 (m, 1 H, $H_{4\text{-Ar}}$), 7.99 (m, 1 H, $H_{3\text{-Ar}}$), 8.37 (s, 1 H, CH=N), 8.61 (m, 1 H, $H_{6\text{-Ar}}$). $C_{18}H_{27}N_2NaO_2$ (326.41): calcd. C 66.23, H 8.34, N 8.58; found C 65.94, H 8.53, N 8.87.

Table 3. Crystallographic data and structure refinement for complexes **7**, **10** and **14**

	7	**10**	**14**
Empirical formula	$C_{20}H_{39}O_3ReS_5$	$C_{20}H_{40}NO_3ReS_3$	$C_{21}H_{28}BrN_2O_5Re$
Formula mass	674.01	624.91	654.56
Crystal system	orthorhombic	monoclinic	triclinic
Space group	*Pbca*	$P2_1/c$	$P\bar{1}$
a [Å]	9.0585(3)	16.17(2)	6.6516(14)
b [Å]	13.1617(4)	11.082(16)	8.1605(16)
c [Å]	45.3602(15)	14.18(2)	23.325(5)
α [°]	90	90	89.678(4)
β [°]	90	92.15(3)	86.915(4)
γ [°]	90	90	74.811(4)
V [Å^3]	5408.1(3)	2538(6)	1220.0(4)
Z	8	4	2
$D_{calcd.}$ [g cm^{-3}]	1.656	1.635	1.782
Absorption coefficient [mm^{-1}]	4.898	5.054	6.649
F(000)	2704	1256	636
Crystal size [mm^{-1}]	0.450 × 0.360 × 0.054	0.21 × 0.11 × 0.05	0.4 × 0.28 × 0.1
θ range [°]	1.80−29.03	2.23−23.43	0.87−20.00
Index ranges	$-11 \le h \le 12$	$-17 \le h \le 17$	$-6 \le h \le 6$
	$-17 \le k \le 17$	$-12 \le k \le 10$	$-6 \le k \le 7$
	$-61 \le l \le 48$	$-15 \le l \le 15$	$-20 \le l \le 22$
Reflections collected	30609	10503	3785
Independent reflections	6759 [R_{int} = 0.0704]	3639 [R_{int} = 0.0608]	2282 [R_{int} = 0.0705]
Absorption correction	Ψ scan	Ψ scan	Ψ scan
Max. and min. transmission	0.350, 0.173	0.31671, 0.20085	0.409, 0.253
Refinement method	full-matrix least squares on F^2	full-matrix least squares on F^2	full-matrix least squares on F^2
Data/restraints/parameters	6654/0/263	3639/14/280	2282/11/271
Goodness-of-fit on F^2	1.161	0.666	0.866
Final *R* indices [$I > 2\sigma(I)$]	*R*1 = 0.0841, *wR*2 = 0.2088	*R*1 = 0.0345, *wR*2 = 0.0910	*R*1 = 0.0416, *wR*2 = 0.1147
R indices (all data)	*R*1 = 0.0928, *wR*2 = 0.2136	*R*1 = 0.0454, *wR*2 = 0.0983	*R*1 = 0.0454, *wR*2 = 0.1238
Largest diff. peak and hole [eÅ^{-3}]	2.170, −2.066	0.948, −1.670	0.898, −1.825

(Tricarbonyl)rhenium(I) Complex 14: 45 mg (130 μmol) of fatty acid ligand **12** was dissolved in 2 mL of MeOH and added to a solution of 100 mg (130 μmol) of tricarbonylrhenium(I) precursor **13**[15] in 1 mL of MeOH. The mixture immediately turned to a deep orange colour and became cloudy within 15 min. After stirring overnight at room temperature, the solvent was removed in a nitrogen stream. Then 1 mL of $CHCl_3$ and 1 mL of 4 M aqueous HBr were added and the mixture was vigorously stirred for another 24 h. Afterwards, the organic layer was separated and the aqueous phase thoroughly extracted in the usual manner. Purification of the obtained residue was accomplished by column chromatography ($CHCl_3$/EtOAc/HOAc, 100:25:4). Crystals of complex **14** suitable for single-crystal X-ray analysis were obtained by slow crystallization of **14** from an acetonitrile solution at room temperature. Yield: (74%). IR (KBr): $\tilde{\nu}$ = 2021, 1902 (C≡O), 1713 (C=O) cm^{-1}. ^{1}H NMR ($CDCl_3$): δ = 1.22−1.43 (m, 14 H, 7 × CH_2), 1.62 (quint, ^3J = 7.2, 2 H, CH_2CH$_2$COOH), 1.94−2.35 (m, 2 H, CH_2CH$_2$N), 2.34 (t, ^3J = 7.4, 2 H, CH_2COOH), 4.03 (m, 1 H), 4.26 (m, 1 H, CH_2N), 7.56 (m, 1 H, $H_{5\text{-Ar}}$), 7.90 (m, 1 H, $H_{4\text{-Ar}}$), 8.05 (m, 1 H, $H_{3\text{-Ar}}$), 8.70 (s, 1 H, CH=N), 9.04 (m, 1 H, $H_{6\text{-Ar}}$). $C_{21}H_{28}BrN_2O_5Re$ (654.57): calcd. C 38.53, H 4.31, N 4.28, Br 12.21; found C 38.40, H 4.35, N 4.24, Br 12.31.

X-ray Crystallographic Studies: Crystal data and details of structure determinations for complexes **7**, **10,** and **14** are listed in Table 3. Using Mo-K_α radiation, reflection intensities were collected at room temperature (293 K) with a Siemens SMART diffractometer, equipped with a CCD area detector. The structures were solved by direct methods using SHELXS-90 and refined with SHELXL-97.[19] An empirical absorption correction (Ψ-scan) was applied. All non-hydrogen atoms were refined anisotropically. The positions of hydrogen atoms were calculated corresponding to their geometrical conditions and refined using the riding model. Atomic numbering schemes are shown in Figure 1 (for **7**), Figure 2 (for **10**) and Figure 3 (for **14**). Selected bond lengths and angles are listed in Tables 1 and 2. For complex **7** only crystals of poor quality were available, reflected in a relatively high *R* value for this compound. CCDC-156312 (**7**), -172606 (**10**) and -172605 (**14**) contain the supplementary crystallographic data for this paper. These data can be obtained free of charge at www.ccdc.cam.ac.uk/conts/retrieving.html or from the Cambridge Crystallographic Data Centre, 12, Union Road, Cambridge CB2 1EZ, UK [Fax: (internat.) + 44-1223/336-033; E-mail: deposit@ccdc.cam.ac.uk].

Acknowledgments

This work was funded by grants from the Deutsche Forschungsgemeinschaft and Fonds der Chemischen Industrie.

[1] [1a] N. Tamaki, K. Morita, Y. Kuge, E. Tsukamoto, *J. Nucl. Med.* **2000**, *41*, 1525−1534. [1b] F. F. Knapp Jr., J. Kropp, *Eur. J. Nucl. Med.* **1995**, *22*, 361−381.
[2] J. R. Dilworth, S. J. Parrott, *Chem. Soc. Rev.* **1998**, *27*, 43−55.
[3] [3a] W. C. Eckelman, S. M. Karesh, R. C. Reba, *J. Pharm. Sci.* **1975**, *64*, 704−706. [3b] F. H. Liang, F. Virzi, D. J. Hnatovich, *Int. J. Radiat. Appl. Instrum. Part B, Nucl. Med. Biol.* **1987**, *14*, 63−67. [3c] R. H. Mach, H. F. Kung, P. Jungwiwattanaporn, Y.-Z. Guo, *Int. J. Radiat. Appl. Instrum. Part B, Nucl. Med. Biol.* **1991**, *18*, 215−226. [3d] H. Alagui, M. Vidal, F. Riché, A. du Moulinet d'Hardemare, J. P. Mathieu, R. Pasqualini, *Technetium and Rhenium in Chemistry and Nuclear Medicine*,

SGEditoriale, Padova, **1995**, vol. 4, p. 325−327. [3e] G. S. Jones Jr., D. R. Elmaleh, H. W. Strauss, A. J. Fischman, *Nucl. Med. Biol.* **1994**, *21*, 117−123. [3f] G. S. Jones Jr., D. R. Elmaleh, H. W. Strauss, A. J. Fischman, *Bioorg. Med. Chem. Lett.* **1996**, *6*, 2399−2404. [3g] W. Chun-Ying, J. Shu-Ren, F. Ping, Z. Xiang, C. Zheng-Ping, C. Guo-Xian, *Nucl. Sci. Tech.* **1998**, *9*, 29−32.

[4] H. Spies, H.-J. Pietzsch, B. Johannsen, *Technetium, Rhenium and other Metals in Chemistry and Nuclear Medicine*, SGEditoriali, Padova, **1999**, vol. 5, p. 101−108.

[5] [5a] R. Alberto, R. Schibli, A. P. Schubiger, U. Abram, H.-J. Pietzsch, B. Johannsen, *J. Am. Chem. Soc.* **1999**, *121*, 6076−6077. [5b] R. Waibel, R. Alberto, J. Willuda, R. Finnern, R. Schibli, A. Stichelberger, A. Egli, U. Abram, J.-P. Mach, A. Plückthun, P. A. Schubiger, *Nature Biotechnol.* **1999**, *17*, 897−901. [5c] N. Metzler-Nolte, *Angew. Chem.* **2001**, *113*, 1072−1076; *Angew. Chem. Int. Ed.* **2001**, *40*, 1040−1043.

[6] H.-J. Machulla, K. Dutschka, D. van Beuningen, T. Chen, *J. Radioanal. Chem.* **1981**, *65*, 279−286.

[7] T. R. DeGrado, *J. Labelled Compd. Radiopharm.* **1991**, *29*, 989−995.

[8] C. Galli, L. Mandolini, *Gazz. Chim. Ital.* **1975**, *105*, 367−376.

[9] R. Appel, *Angew. Chem.* **1975**, *87*, 863−874; *Angew. Chem. Int. Ed. Engl.* **1975**, *14*, 801−811.

[10] C. Bieniarz, M. J. Cornwell, *Tetrahedron Lett.* **1993**, *34*, 939−942.

[11] T. Fietz, H. Spies, H.-J. Pietzsch, P. Leibnitz, *Inorg. Chim. Acta* **1995**, *231*, 233−236.

[12] R. Alberto, R. Schibli, A. Egli, P. A. Schubiger, W. A. Herrmann, G. Artus, U. Abram, T. A. Kaden, *J. Organomet. Chem.* **1995**, *493*, 119−127.

[13] P. Leibnitz, G. Reck, H.-J. Pietzsch, H. Spies, *Structures of Technetium and Rhenium Complexes* (Ed.: Forschungszentrum Rossendorf), Wissenschaftlich-Technische Berichte FZR-311, Dresden, **2001**, p. 21.

[14] S. Ohta, M. Okamoto, *Chem. Pharm. Bull.* **1980**, *28*, 1917−1919.

[15] R. Alberto, A. Egli, U. Abram, K. Hegetschweiler, V. Gramlich, P. A. Schubiger, *J. Chem. Soc., Dalton Trans.* **1994**, 2815−2820.

[16] S. K. Yasuda, J. L. Lambert, *J. Am. Chem. Soc.* **1954**, *76*, 5356.

[17] M. Friebe, Dissertation, Technische Universität Dresden, **1999**.

[18] W. C. Still, M. Kahn, A. Mitra, *J. Org. Chem.* **1978**, *43*, 2923−2925.

[19] G. M. Sheldrick, *SHELXL-97*, Universität Göttingen, **1997**.

Received November 13, 2001
[I01455]

Copper(I) as a Homogeneous Catalyst for the Ullmann Reaction in Aqueous Solutions − The Transformation of 2-Bromobenzoate into Salicylate

Magal Saphier,*[a,b] Alexandra Masarwa,[a] Haim Cohen,[a,b] and Dan Meyerstein[a,c]

Keywords: Copper(I) / Aromatic compounds / Catalysis / Ullmann reaction

The Cu^I-catalyzed transformation of 2-bromobenzoic acid (2-Br-BA) into salicylic acid (main product), benzoic acid, and diphenoic acid was studied. The reaction was monitored by UV/Vis spectroscopy, HPLC, and ESR. Up to 25 turnovers were achieved for low Cu^I concentrations. An intermediate was observed that was assigned to a complex between copper and a follow-up product of the aromatic acid, probably a complex with a copper–carbon σ-bond. The process is probably initiated by the formation of a d-π* complex of Cu^I with the aromatic ring of 2-Br-BA followed by the reaction with a second Cu^I ion. The effect of the addition of CH_3CN or NH_3 on the catalytic process is reported. Both were found to accelerate the process when present at relatively low concentrations and slow it down at higher concentrations. A side product, 2-aminobenzoate was observed in the presence of NH_3.

Introduction

Copper(I) complexes are key intermediates in a variety of catalytic processes in aqueous solutions, e.g. the catalytic substitution of halogens at the aromatic ring by nucleophiles in the presence of copper(I) (Ullmann reaction).[1] The expected steady-state concentration of Cu^+_{aq} is extremely low due to the disproportionation of Cu^+_{aq} [Equation (1)[2]] and the low solubility of cuprous oxide/hydroxide[2] and halides.[2] Moreover, atmospheric dioxygen, dissolved in water, reacts rapidly with copper(I) oxidizing it to copper(II). The addition of stabilizing ligands can increase the concentration of copper(I) in aqueous solutions and thus improve the efficiency of the catalytic process. However, these ligands are also expected to affect the reactivity of Cu^I, i.e. stabilizing ligands are in principle expected to decrease the Cu^I reactivity and therefore to slow down the catalytic process. A well-known method for the preparation of Cu^I solutions is the addition of CH_3CN.[2] Recently, it was reported that a series of aromatic compounds, such as 2-chlorobenzoic acid, form relatively stable d-π* complexes with Cu^I and thus increase Cu^I concentration in solution.[3]

$$Cu^{2+} + Cu^0 \leftrightarrows 2\,Cu^+_{aq} \quad K_{aq} = 1.00\cdot10^{-6}\ \text{M}^{-1} \qquad (1)$$

$$Cu^+_{aq} + L \leftrightarrows CuL^+_{aq} \qquad (2)$$

[a] Chemistry Department Ben-Gurion University of the Negev, Beer-Sheva, Israel
E-mail: massarwa@bgumail.bgu.ac.il
[b] Nuclear Research Centre Negev
Beer-Sheva, Israel
[c] The College of Judea and Samaria,
Ariel, Israel

It was therefore of interest to study the implications, in terms of the mechanism of the catalytic process, of the addition of ligands in general and of Cu^I d-π* complex formation with aromatic compounds. In this study, the copper(I)-catalyzed substitution of halogen atoms at an aromatic ring was studied. As a model reaction, the transformation of 2-bromobenzoic acid into salicylic acid, benzoic acid, and diphenoic acid was chosen (Scheme 1).

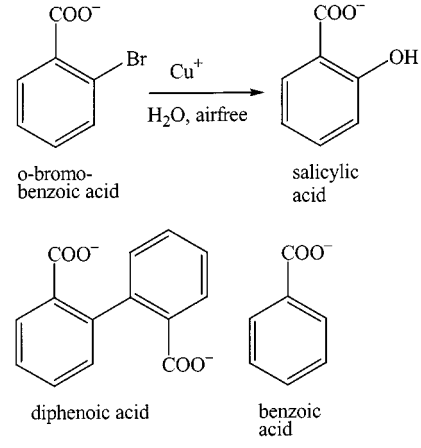

Scheme 1

Results

On addition of Cu^I to deoxygenated aqueous solutions of 2-bromobenzoic acid (2-Br-BA) a relatively slow reaction takes place yielding salicylic, diphenoic, and benzoic acid. The kinetics of this process can be monitored by UV/Vis spectrophotometry. A peak at 296 nm grows in intensity,

 © WILEY-VCH Verlag GmbH, 69451 Weinheim, Germany, 2002 1434−1948/02/0505−1226 $ 20.00+.50/0 *Eur. J. Inorg. Chem.* **2002**, 1226−1234

which is attributed to salicylate. The spectra of possible products of the reaction are shown in Figure 1. Moreover, organic products and the starting material can be identified and quantified by HPLC.

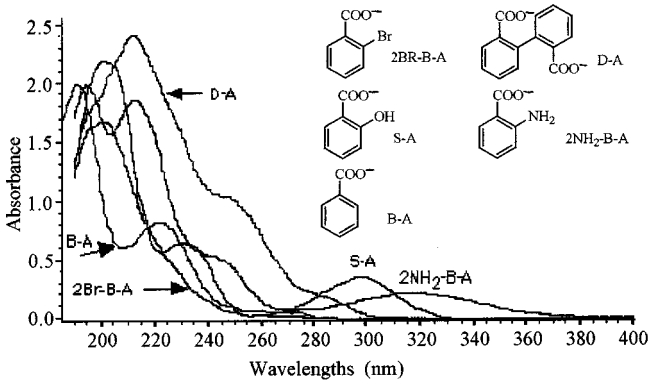

Figure 1. UV/Vis spectra of possible organic products and starting material (all 0.1 mM in aqueous solution)

The following sources of Cu^{I} were used in the course of this study:

1. Commercially available $Cu(CH_3CN)_4PF_6$ salt was added to deaerated aqueous solutions of *o*-bromobenzoic acid after addition of CH_3CN. Under these conditions, Cu(OH) precipitated (yellowish) only at pH > 9, whereas it precipitated already at pH = 7 without the addition of stabilizing ligands.

2. $[Cu(CH_3CN)_4]^{+}$ was prepared by the comproportionation of Cu^{II}_{aq} (source $CuSO_4$) and Cu^0 metal in deaerated aqueous solutions containing CH_3CN. Complete comproportionation was achieved when the concentration of acetonitrile was above 4%, in accordance with literature data.[4] This method can also be performed with different stabilizing ligands, e.g. higher concentrations of ammonia at basic pH.[2] The resulting Cu^{I} solution was subsequently injected into deaeraeted aqueous solutions of 2-bromobenzoic acid.

3. During the course of this study it emerged that Cu^{I} could also be prepared in situ by comproportionation of $CuSO_4$ and Cu metal in deaerated aqueous solutions containing 2-bromobenzoic acid. The bromobenzoic acid is expected to lead to comproportionation according to the measured stability constants.[3] Note that these stability constants increase with the increase in pH.[3] The comproportionation in this system was complete, as verified by the fact that the detected amounts of Cu^{I} were more than twofold the initial $CuSO_4$ concentration (as the catalytic cycle already starts with the addition of the 2-bromobenzoic acid).

Kinetics of Formation of Salicylic Acid Monitored by UV/Vis Spectrophotometry

Figure 2 shows typical spectral changes occurring during the initial phase of the reaction of 2-Br-BA and Cu^{I}. The absorbance at 296 nm increased, due to the formation of salicylic acid (SA), while the absorbance in the 310−430 nm region decreased during the course of about 1 h under the specific conditions used. It should be noted that time "zero" in these experiments is ca. 10 min after the solution was prepared. The spectral changes in the 310−430 nm region are attributed to the decomposition of an initially formed intermediate. The slow reaction can best be monitored when Cu^{I} is prepared in situ by comproportionation of $CuSO_4$ (0.001−0.01 M) and Cu^0 in 2-Br-BA solution. Figure 3 shows typical kinetic traces at 296 and 350 nm implying several overlying reactions.

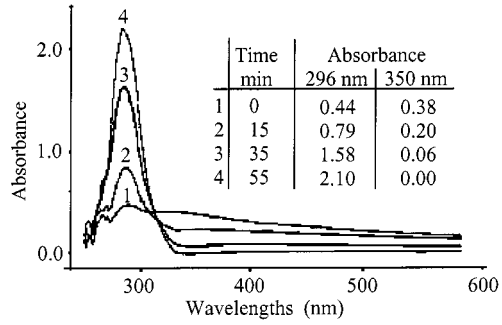

Figure 2. UV/Vis spectral changes during the reaction of 2-Br-BA with Cu^{+} [2-Br-BA (0.05 M), $CuSO_4$ (0.01 M), Cu^0, no air, pH_{init} = 7.0] (* 0-time is 10 min after mixing of the reactants, due to degassing time)

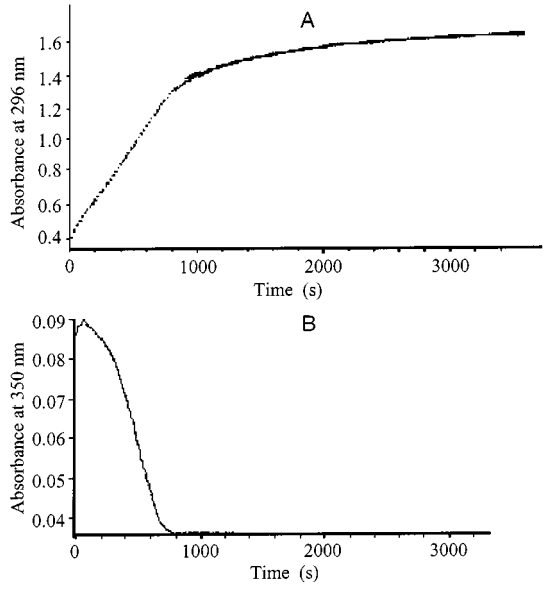

Figure 3. Kinetic traces monitored A) at 296 (SA) and B) at 350 nm (intermediate) during the reaction of 2-Br-BA with Cu^{+} [2-Br-BA (12.5 mM), $CuSO_4$ (0.1 mM), Cu^0, 4% MeCN, no air, pH_{init} = 6.7)] (* 0-time is 10 min after mixing of the reactants, due to degassing time)

During the disappearance of the intermediate, the formation of salicylic acid is fastest, but it continues after that time. The amount of salicylic acid formed within 2 h [calculated according to its absorption at 296 nm (ε = 3400 $M^{-1}cm^{-1}$), if necessary after dilution] was found to be proportional to the initial concentration of 2-Br-BA (Figure 4) under conditions of excess 2-Br-BA and a given Cu^{I} concentration. This Cu^{I} concentration was supplied by $Cu(CH_3CN)_4PF_6$ (without any addition of CH_3CN in this

case). The amount of salicylic acid formed was higher than the initial Cu^{I} concentration, implying a catalytic role of Cu^{I}. Moreover, varying the Cu^{I} salt concentration (employing ammonia as a stabilizing ligand) shows that the final amount of salicylic acid formed is independent of the initial Cu^{I} concentration (Figure 5), pointing again to its catalytic role. Up to 25 turnovers were achieved for the lowest Cu^{I} concentration and ca. 35% of the organic acid was converted under these specific conditions. The initial changes in salicylic acid (SA) concentration (d[SA]/dt calculated from the changes during the first 40 min of the reaction) are proportional to the square of the initial Cu^{I} concentration (Figure 6).

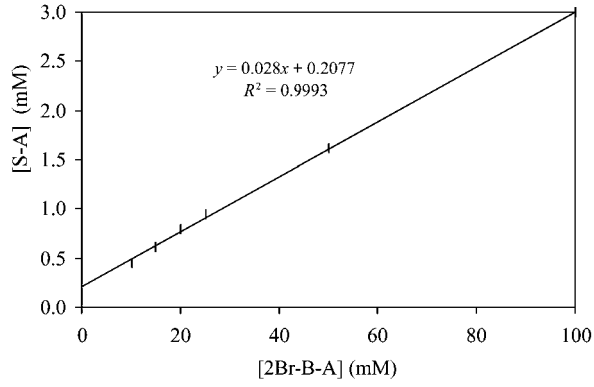

Figure 4. Dependence of SA production (after 120 min) on initial 2-Br-BA concentration {$Cu[MeCN]_4PF_6$ (0.33 mM), pH_{init} = 7.0}

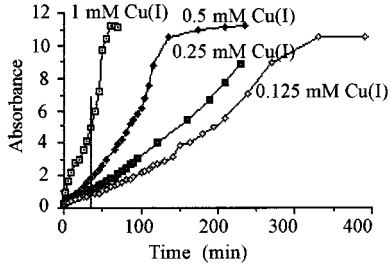

Figure 5. Kinetic traces monitored at 296 nm (SA) during the reaction of 2-Br-BA with Cu^{+} for different initial Cu^{+} concentrations {2-Br-BA (10 mM), $Cu[MeCN]_4PF_6$, NH_3 (0.0175 M), pH_{init} = 9.0} (* 0-time is 10 min after mixing of the reactants, due to degassing time)

Kinetics of the Formation of the Organic Products Monitored by HPLC

As the reaction is relatively slow, it is possible to monitor the formation of the organic products and decomposition of 2-Br-BA by HPLC. Figure 7 shows a typical kinetic run, with salicylic acid indeed being the main product of the process. Diphenoic acid formed with a similar kinetic profile, rate decreasing with the progress of the process, but with a significantly smaller yield. The formation of benzoic acid on the other hand was a slow but steady process, the final yield being similar to that of diphenoic acid, i.e. the relative yield of benzoic acid to that of salicylic, or diphenoic, acid increased with the progress of the reaction.

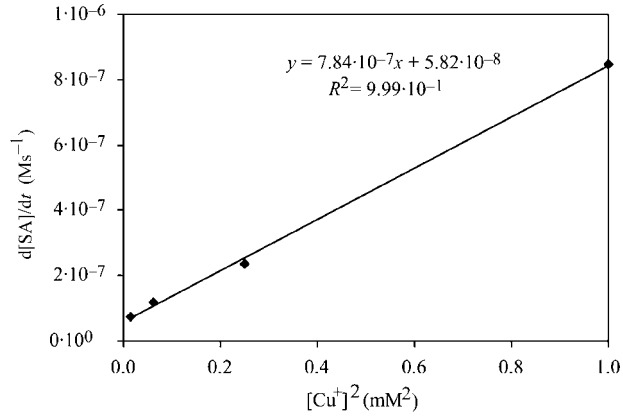

Figure 6. Dependence of SA production on the square of the initial Cu^{I} concentration {2-Br-BA (10 mM), $Cu[MeCN]_4PF_6$, NH_3 (0.0175 M), pH_{init} = 9.0}

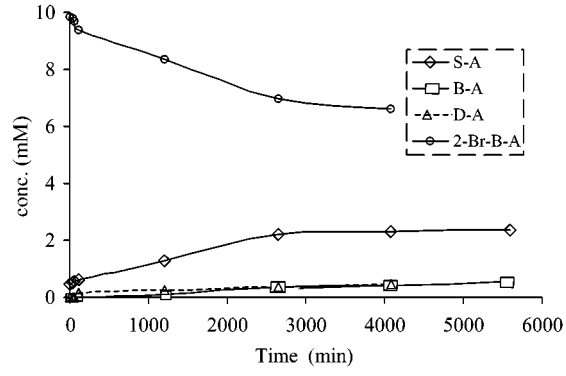

Figure 7. Kinetic traces of products and 2-Br-BA during the reaction of 2-Br-BA with Cu^{+} monitored using HPLC [2-Br-BA (10 mM), $CuSO_4$ (1 mM) + Cu^{0}, pH_{init} = 6.0]

pH Changes During the Process

Short-Term pH Changes

In recording the pH changes after the addition of Cu^{I} (salt or solution with acetonitrile as stabilizing ligand) to an acidic solution of 2-Br-BA (pH = 3−5) we observed an initial increase in pH over several 100 s (Figure 8) followed

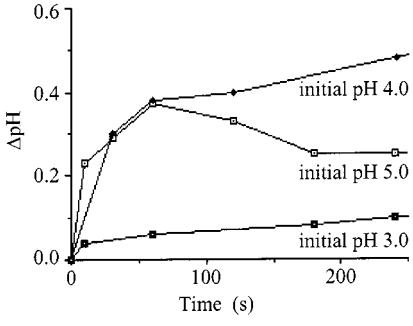

Figure 8. pH changes during the fast time scale of the reaction of 2-Br-BA with Cu^{+} {2-Br-BA (10 mM), $Cu[MeCN]_4PF_6$ (1 mM)}

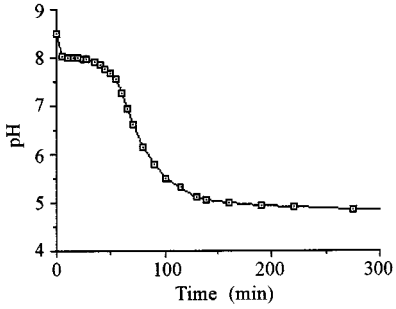

Figure 9. pH changes during the longer time scale of the reaction of 2-Br-BA with Cu^+ [2-Br-BA (10 mM), $CuSO_4$ (1 mM) + Cu^0]

by a slow decrease (Figure 9). The initial effect at pH = 3 was smaller than that for higher initial pH values, probably due to the buffer effect of 2-Br-BA (pK_a = 2.8).[5] Cu^I did not cause similar initial pH changes in the absence of 2-Br-BA, and we would rather expect an increase in acidity due to the addition of a metal salt to an aqueous solution. Furthermore, protons are released during the reaction of 2-Br-BA to form salicylic acid, see Equation (3), as was observed for longer reaction times.

$$\text{2-Br-BA} + H_2O\,[+\,Cu^+] \rightarrow \text{SA} + H^+ + \text{Br} \quad (3)$$

The initial increase in pH occurred over the same time span as the formation of the intermediate with the absorption around 350 nm, which was verified by simultaneous pH and UV/Vis measurements (employing fiber optics).

The increase in pH might in principle be due to an increase in the pK_a of the aromatic acid. Bonding of Cu^I to the aromatic ring (σ-donation from the HOMO of the π-system to Cu^I and π-back donation from Cu^I to the LUMO of the π-system) could cause such a change in pK_a. Indeed, excitation of aromatic acids induces a similar pK_a shift.[6] Assigning the intermediate with the absorption around 350 nm to a π-complex between Cu^I and 2-Br-BA poses several problems; no analogous complexes and no pH changes were detected when 2-Br-BA was replaced with benzoic acid. Furthermore, one expects that a complex formation of this kind should occur within a much shorter time. Alternatively, the formation of an intermediate with a σ-bond between the copper ion and a carbon atom of the aromatic ring (vide infra), might decrease the Cu^I–hydroxide interaction ($K_{sp} = 1 \cdot 10^{-14}$ M^2),[5] see Equation (4) where R$^\cdot$ is an aryl radical.

$$L_nCu^IOH + R^\cdot \rightarrow Cu^{II}\text{–}R + n\,L + OH^- \quad (4)$$

We investigated the effect of pH on the life time of the intermediate and found that the decay of the absorption at 350 nm was faster at lower pH values. Whereas the intermediate had a life time of a couple of 100 s at pH = 5–7 it seemed to be stable for more than 1 h at pH = 9.

Long-Term pH Changes

Over longer time scales (several 100 min) the pH of the Cu^I/2-Br-BA system dropped from the initial value (5–9) to 4.6. An example is shown in Figure 9. A titration pointed out that the yield of H_3O^+ equaled the yield of salicylic acid, as expected according to Equation (3).

Experiments were performed where the pH was kept constant by dropwise addition of 0.10 N NaOH or NH_3 during the reaction under argon (the reaction was monitored spectrophotometrically by using fiber optics). In both those experiments, more salicylic acid was produced than in parallel experiments without the addition of extra base. The yields were highest for the system with NH_3 addition.

When the system reached pH ≤ 4.7 a black precipitate formed on the Cu metal. The precipitate could be dissolved in a basic solution. According to the resulting spectrum and elemental analysis, this precipitate consisted of Br^- and Cu ions. No Cu ions remained in the reaction mixture after extraction of the covered Cu metal plate. Taking into account the fact that the relative yield of Cu/bromine was 1:1, by titrating the amount of dissolved Br (Vollhardt) and weighing the Cu plate before and after the reaction, we could conclude that nearly complete comproportionation took place. For example, 0.18 mM of Br^- was precipitated from an initial reaction solution containing 0.10 mM of Cu^{2+} (0.20 mM would have been expected for full comproportionation). A similar precipitate was also formed in experiments with 2-Cl-BA. According to the literature, such precipitates consist of mixed-valence Cu^I and Cu^{II} halides, e.g. $(CuBr)_n(CuBr_2)_m$.[7a,7b]

Influence of the Cu^{2+} Concentration on the Product Distribution

Figure 10 shows the dependence of the product distribution (measured after 24 h) on the initial Cu^{2+} concentration. Increasing the Cu^{2+} concentration favored the formation of salicylic acid on account of the dimer concentration. The effect on the yield of benzoic acid is negligible.

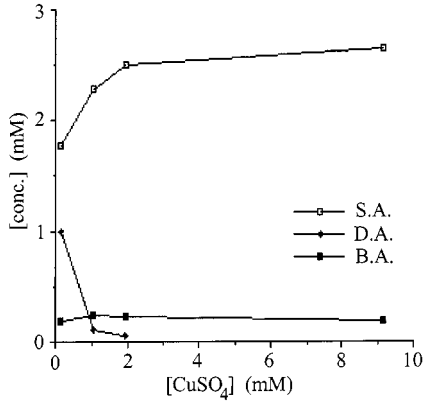

Figure 10. Dependence of the product distribution of the reaction of 2-Br-BA with Cu^+ (measured after 24 h) on the initial Cu^{2+} concentration [2-Br-BA (9 mM), Cu^I (2 mM) 5% MeCN, pH_{init} = 6.0]

ESR Measurements

In order to monitor the Cu^{2+} concentration during the reaction ESR spectroscopy was employed. Cu^{2+} (d^9) has an unpaired electron that makes it optimal for ESR studies, whereas Cu^{I} is ESR-silent (d^{10} system). A system containing Cu^{I} derived from comproportionation of Cu^{II} and Cu^0 metal in 4% CH_3CN did not produce an ESR signal, whereas a signal developed on addition of 2-Br-BA (g_{iso} = 2.16, see A and B in Figure 11). The final spectrum differs from that of Cu^{2+} with acetonitrile in aqueous solution and also from that of Cu^{2+} with 2-Br-BA (see A in Figure 12), but is very similar to that of Cu^{2+} with salicylic acid (see B in Figure 12).

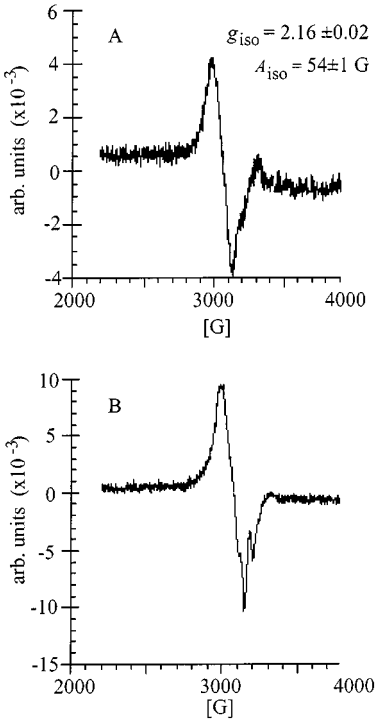

Figure 11. ESR spectra measured during the reaction of 2-Br-BA with Cu^{+}; A: after 120 s; B: after 24 h [2-Br-BA (10 mM), Cu^{I} (10 mM), 4% MeCN]

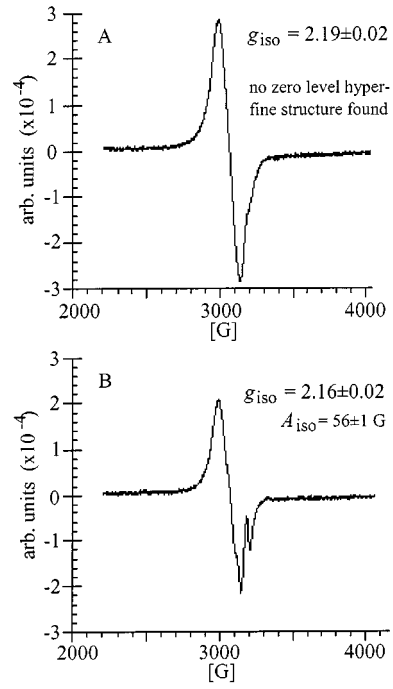

Figure 12. ESR spectra; A: 2-Br-BA (10 mM) with $CuSO_4$ (10 mM); B: SA (10 mM) with $CuSO_4$ (10 mM)

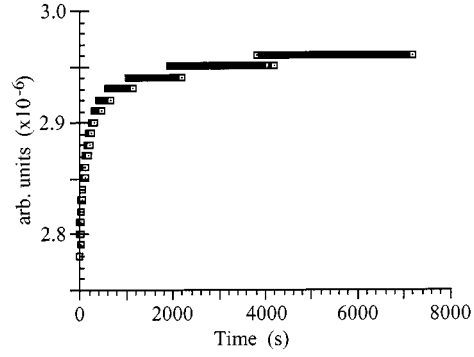

Figure 13. Time trace of ESR signal production due to Cu^{II} during the reaction of 2-Br-BA with Cu^{+} [2-Br-BA (10 mM), Cu^{I} (10 mM), 2% MeCN (* 0-time is 8 min after mixing of the reactants, due to technical reasons)]

Figure 13 shows a typical kinetic trace of the formation of the ESR signal in the Cu^{I}/2-Br-BA system. Under the experimental conditions necessary for the ESR measurements (relatively high concentrations of the reactants) most of the Cu^{2+} would have formed during the 8−10 min needed before the first measurement could be performed. Comparing the kinetics and form of the ESR signal with that of the Cu^{2+}/salicylic acid system it becomes obvious that the produced Cu^{2+} forms a complex with salicylic acid created during the reaction. The initial ESR spectrum (see A in Figure 11) differs slightly from the final spectrum, raising the possibility that initially Cu^{II} forms a complex with the intermediate. Unfortunately, ESR spectra taken at low temperatures could not assist in clarifying this assumption.

Influence of Different Ligands

The influence of different Cu^{I}-stabilizing ligands on the kinetics of the reaction was investigated.

Acetonitrile

A series of experiments in which Cu^{I} was formed by comproportionation under exclusion of dioxygen were performed for different concentrations of acetonitrile. The resulting Cu^{I} solutions were injected into solutions containing 2-Br-BA (under He). Figure 14 shows the change in absorbance due to SA formation at 296 nm (the absorbances were calculated from measurements in diluted solutions) after 2000 s as a plot of the CH_3CN percentage. For CH_3CN concentrations smaller than 4% the compropor-

tionation was incomplete, causing an increase in the formation of salicylic acid until about 4% CH_3CN. For concentrations > 4% CH_3CN there was a definite decrease in SA formation.

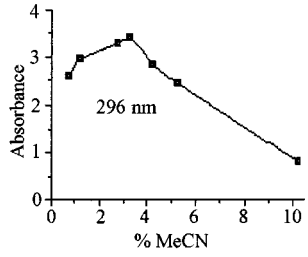

Figure 14. Change in absorbance due to SA formation at 296 nm after 2000 s as a plot of the CH_3CN percentage (the absorbances were calculated from measurements in diluted solutions) [2-Br-BA (25 mM), $CuSO_4$ (0.5 mM), Cu^0, MeCN, pH_{init} = 9]

In a similar experiment the formation of all organic products was investigated by HPLC (Figure 15). A decrease in the yield of all products with increasing CH_3CN concentration was observed. The influence on all the products is similar, therefore it is conceivable that CH_3CN plays a role in the first step of the reaction sequence.

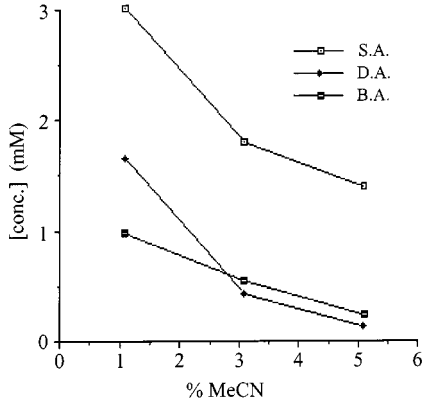

Figure 15. Changes in product distribution as a function of the CH_3CN percentage (the concentrations were determined after 24 h by HPLC) [2-Br-BA (10 mM), $CuSO_4$ (1 mM), Cu^0, MeCN, pH_{init} = 6]

Ammonia

NH_3 plays a major role in the formation of products. Its role cannot be explained solely by its stabilizing effect, as the reaction was also influenced at pH < 7, where NH_3 does not stabilize Cu^I anymore. A plot of the resulting absorbance at 296 nm vs. the concentration of NH_3 shows a similar pattern of increase and decrease of SA as for acetonitrile. At concentrations > 175 mM of NH_3 the formation of *o*-aminobenzoic acid was observed (verified by its absorbance at 318 nm, see Figure 1) in addition to the main product, SA.

Reaction with *o*-Chlorobenzoic Acid (2-Cl-BA)

In order to understand the influence of bromine, several parallel reactions with 2-Cl-BA instead of 2-Br-BA were studied. These reactions are considerably slower, but they seemed to follow a similar pathway.

Discussion

The above results for the Cu^I-catalyzed reaction of 2-Br-BA can be summarized by the following empirical observations:

1. As a first step an intermediate was formed with an absorbance in the 290−400 nm region. Transient complexes with copper−carbon σ-bonds[8a−8e] as well as d-π complexes of Cu^I [8d,9] with aromatic compounds are known to absorb in this wavelength region. For acidic starting pH values the pH initially rose during the formation of this intermediate. At acidic pH values (pH = 5) the intermediate was less stable than at basic pH values (pH = 9).

2. Several overlying reactions were observed at 296 nm, the absorption maximum of salicylic acid. The process can be divided into two time ranges so that the initial fast reaction covers the time when the concentration of the intermediate is relatively high.

3. During the fast time range the rate of reaction is linearly dependent on the 2-Br-BA concentration and quadratically dependent on the Cu^I concentration, implying the involvement of two Cu^I ions in the catalytic cycle.

4. During the reaction, Cu^{II} was formed, and most of it, according to the ESR measurements, during the initial phase. The ESR spectra of the final products indicate that most of the Cu^{II} is bound to salicylic acid.

5. pH dependence: The yield of the main product, salicylic acid, is considerably higher at basic pH than at acidic pH. The pH shifts during the reaction towards acidic pH and levels at pH ≈ 4.5. The proton yield stoichiometrically (1:1) equals the amount of salicylic acid formed. At pH = 4.5 a black precipitate, identified as $(CuBr)_n(CuBr_2)_m$,[7a,7b] forms and terminated the reaction. At pH values > 5 Cu^I apparently forms stronger complexes with the aromatic compounds.[3]

6. Excess Cu^{II} caused a relative decrease in the yield of the dimer and scarcely influenced the relative yields of salicylic and benzoic acids.

7. Influence of acetonitrile: Concentrations of more than 4% acetonitrile reduce the rate of formation of salicylic acid. For concentrations smaller than 3% the comproportionation was not yet complete, and therefore an increase in product formation was observed. Acetonitrile formed a complex with Cu^I and consequently was found to compete with 2-Br-BA for the Cu^I. At high acetonitrile concentrations the 2-Br-BA thus did not form the π-complex with 2-Br-BA. Alternatively, the formation of $Cu(CH_3CN)_n^+$ ($1 \leq n \leq 4$) shifted the redox potential of Cu^I anodically, leading to diminished reactivity.

8. Influence of ammonia: Similar to acetonitrile, ammonia also led to an increase in product formation at lower ammonia concentration, but to a decrease in rate at higher concentrations. Ammonia acted as a basic buffer and prevented the Cu^I ions from precipitating. Moreover, it formed

a σ-complex with Cu^{I} and thus changed its redox potential favorably, but a reaction of $Cu(NH_3)_2^+$ with a substrate requires a hybridization change probably from sp to sp^3. Such a hybridization change is endothermic and was recently shown to decrease the rate of reaction of Cu^{I} with $CCl_3CO_2^-$.[10]

9. The aromatic substrate, 2-Br-BA, induced comproportionation and catalyzed the formation of Cu^{I} by formation of a π-complex of Cu^{I} with the aromatic compound, thus shifting the equilibrium of the reaction according to Equation (1) to the Cu^{I} side.[3]

10. The isomers 3- and 4-Br-BA are considerably less reactive[1c,11,12] under the conditions used for the reaction of 2-Br-BA, implying that the interaction of Cu^{I} with Br as well as with the carboxylic substituent (chelate effect) is of importance.

11. A radical mechanism involving the $Ar^{\cdot}$ radical can be ruled out, as pulse radiolysis experiments (data not shown) point out that aryl radicals, produced in the presence of 2-Br-BA and Cu^{I}, reacted with the aromatic acid and not with Cu^{I}. The product of this reaction was the dimer bromodiphenoic acid, which is not a major product of the investigated catalytic process.

12. 2-Cl-BA reacted slower than 2-Br-BA, but otherwise followed the same pattern as discussed in the previous points, thus suggesting that the detachment of the halogen is the rate-determining step.

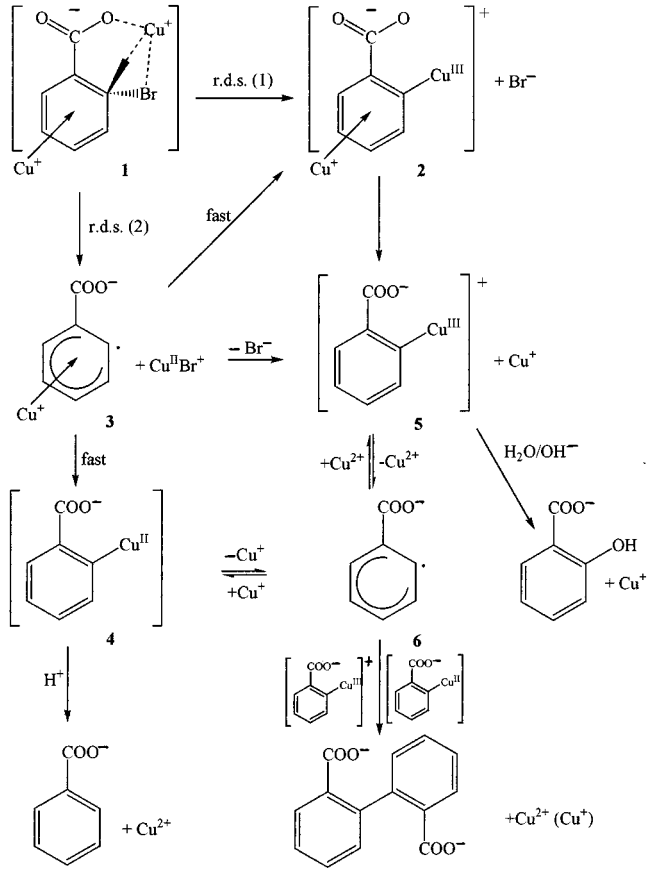

Scheme 3

The Proposed Mechanism

The results are consistent with the following mechanism for the formation of the reactive intermediate (Scheme 2). First a Cu^{I} ion forms a d-π* complex with the aromatic ring of 2-Br-BA followed by the interaction of a second Cu^{I} ion with the Br and carboxylate substituents.

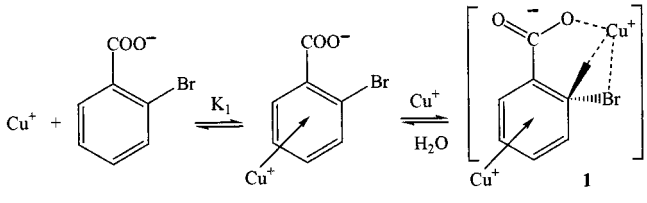

Scheme 2

The aromatic ring of the intermediate is probably distorted as the carbon atom, bearing the Br substituent, attains tetrahedral character, in agreement with previous proposals from the literature.[12a–12c] The coordination of the Cu^{I} ion to the aromatic ring probably distorts it and also lengthens the C–Br bond,[13a–13f] thus facilitating the abstraction of Br. The proposed follow-up reactions, which fit all the observed results are summed up in Scheme 3.

The rate-determining step is obviously the bond breakage of the C–Br bond, as this step involves two Cu^{I} ions and therefore fits the second-order dependence on Cu^{I}, as was found experimentally. Moreover, this hypothesis is corroborated by the fact that 2-Cl-BA reacted in a similar manner to 2-Br-BA, only much slower.

The bond breakage of C–Br might follow two possible routes. In one a formal oxidation takes place to obtain intermediate **2** or **5**. In a second possibility, intermediate **3** is formed, which either reacts with the $Cu^{II}Br$ formed in a cage to yield intermediates **2** or **5**, or transforms immediately into intermediate **4**. Intermediates **2** and **5** can decompose by two different pathways. In the first the Cu–C bond breaks heterolytically to produce the main products of the reaction, salicylic acid, Cu^{I}, and a proton. On the other hand, intermediate **5** can decompose homolytically in a side reaction to form Cu^{II} and the radical **6**, which might dimerize to produce diphenoic acid. The radical **6** can also react with the intermediate **5** to produce the dimer and Cu^{II}, a termination step leading to loss of Cu^{I}. This reaction is more plausible as $[Cu^{III}C_6H_4CO_2^-] >> [C_6H_4CO_2^{\cdot -}]$. For high concentrations of Cu^{II} the equilibrium of the homolytic decomposition of intermediate **5** is shifted towards its formation and therefore less dimer is formed at high concentrations of Cu^{II}.

Intermediate **4** might decompose heterolytically, in an acid-catalyzed reaction, to form benzoic acid and Cu^{II}. This is a side reaction, in which Cu^{I} is removed from the reaction system stoichiometrically, and therefore the rate of the overall reaction (formation of salicylic acid) will slow down with time. Intermediate **4** can also react with the radical to form Cu^{I} and the dimer, in this pathway Cu^{I} is restored to the catalytic cycle. In addition, intermediate **4** can decompose homolytically and can thus be restored to the salicylic acid producing cycle.

According to the experimental observations, the reaction can be divided into at least two time scales. During the short time scale, seconds to minutes (depending on the relative concentrations of Cu^{I}, 2-Br-BA, initial pH, and initial Cu^{II} concentration), the intermediate is observed, as well as the increase in pH, second-order dependence on Cu^{I} and the yield of salicylic acid and the dimer are relatively high. At the same time, a rapid increase in Cu^{II} concentration is observed. During the slower phase, hours to days, a slow further increase in salicylic acid and a considerably slower increase in the dimer yield are observed; it seems that the rate of formation of benzoic acid is pH-dependent and thus its relative yield increases with time. The yield of Cu^{II} is especially low compared to the first phase. The absorption at 350 nm is nearly non-existent, and therefore the intermediate concentration as well as the Cu^{I} concentration are presumably low.

The origin of the two time scales is probably the fast formation of Cu^{II} on account of Cu^{I}. Cu^{II} is produced during the formation of the dimer and the benzoic acid. The dimer, which is formed mainly during the first time frame, when the steady-state concentrations of the intermediates **5**, **6**, and **4** are relatively high, is responsible for the majority of the Cu^{II} formed, later its formation is hindered by high Cu^{II} concentration. The decrease in Cu^{I} concentration, which also stems from the formation of insoluble CuBr, causes a decrease in the concentration of the intermediate and slows down the reaction. Moreover, the pH, that decreases during the reaction slows down the process, and finally at pH = 4.7 and relatively high Cu^{II} concentrations the formation and precipitation of a mixed-valence compound stops the catalytic reaction as a result of removing the rest of Cu^{I} from the reaction system.

Concluding Remarks

This study proves that Cu^{I} species are the catalysts in the Ullmann reaction. Furthermore, the results clearly point out that the addition of ligands that stabilize Cu^{I} in aqueous solutions, beyond a given optional concentration, slow down the catalytic process. This observation is attributed to the effect of the ligands on the Cu^{II}/Cu^{I} redox potential and thus on the Cu^{I} reactivity. (The latter might also be affected by the binding mode of the Cu^{I} ion to the ligand.[10]) Therefore, the use of CH_3CN or alkenes as solvents for Cu^{I}-catalyzed reactions is not recommended.

Experimental Section

Materials: All solutions were prepared from reagent grade chemicals or better. Distilled water was further purified by passing through a Milli Q Millipore setup, final resistivity > 10 MΩ/cm. All experiments were carried out at room temperature (22±2 °C). Cu^{I} solutions were prepared by comproportionation of Cu^{II} solutions (usually $CuSO_4$) with Cu^0 metal (activated by concentrated HNO_3). The solution was stirred for at least 24 h. All experiments involving Cu^{I} were carried out in strictly de-aerated solutions using the syringe technique and helium or argon gas. Aqueous solutions of the aromatic acids were prepared by completely dissolving the solids in basic solutions (NaOH) and acidifying to the desired pH by titration with $HClO_4$.

Techniques: The pH was measured with a Corning 220 or a Hanna (HI 9017) pH meter and adjusted with $HClO_4$ and/or NaOH.

UV/Vis: Spectra were recorded with a Hewlett Packard 8452A diode array spectrophotometer. Special cells for anaerobic studies were used. The concentration of Cu^{2+}(aq) and indirectly Cu^{+} (after oxidation to Cu^{2+} with atmospheric dioxygen) was determined spectrophotometrically by the addition of ammonia to form the complex $Cu(NH_3)_4^{2+}$, which has a molar absorption coefficient of 60 $M^{-1}cm^{-1}$ at 604 nm. Fast reactions were monitored by employing an SFA-11 Rapid Kinetics Accessory (Hi-Tech). In some cases, where pH and spectral measurements were performed simultaneously, fiber-optical connections by Phonetics were employed.

HPLC: Organic starting materials and products were separated and identified with the help of a Spectraphysics Analytic Inc. HPLC (SP Thermo Separation, A 0099-510) in conjunction with a Spectrophotometer, Spectra Series (p200) which operates in the 200−400 or 400−800 nm region (5 nm resolution). A Merck 50942 LiChroCart 125-4, LiChrospher 100 RP-8 (5 μm) column was utilized. A mixture of 35% MeCN (HPLC grade) and 65% 0.05 M phosphate buffer at pH = 3.5 was used as the eluent at a rate of 0.3 mL/min; chromatograms were thus collected within 10 min. Calibrations for starting materials and possible products were performed at 220, 260, and 295 nm (area of peaks) if applicable.

ESR: Spectra were recorded with a Bruker EMX 220 X-band ESR spectrometer. The different complexes of Cu^{II} with the aromatic compounds could be identified at 120 K. In some instances kinetics were measured at room temp. by using air-tight ESR tubes.

NMR: Spectra were recorded with a Bruker DPX 200 MHz. $Cu(CH_3CN)_4PF_6$ was used as a source of Cu^{I}, dissolved in 3% CH_3CN/D_2O.

Acknowledgments

This study was supported in part by a grant from the Budgeting and Planning Committee of The Council of Higher Education and the Israel Atomic Energy Commission. D. M. wishes to express his thanks to Mrs. Irene Evens for her ongoing interest and support.

[1] [1a] F. Ullmann, *Ber. Dtsch. Chem. Ges.* **1904**, *37*, 853. [1b] A. A. Moroz, M. S. Shvartsberg, *Russ. Chem. Rev.* **1974**, *8*, 43. [1c] Kirk-Othmer, *Encyclopedia of Chemical Technology* (Th. 3), Wiley, New York, **1978**, vol. 8, p. 276.

[2] F. A. Cotton, G. Wilkinson, *Advanced Inorganic Chemistry*, 5th ed., Wiley Interscience, New York, **1988**, pp. 757−758.

[3] M. Saphier, A. Burg, S. Sheps, H. Cohen, D. Meyerstein, *J. Chem. Soc., Dalton Trans.* **1999**, 1845.
[4] A. J. Parker, *Search* **1973**, *4*, 426.
[5] J. A. Dean, *Lange's Handbook of Chemistry*, 14th ed. McGraw-Hill, Inc., New York, **1992**, Table 8.6.
[6] P. Day, *Endeavour* **1970**, *29*, 45.
[7] [7a] F. A. Hart, J. Newbery, P. Thornton, *Annu. Rep. Prog. Chem. Sect. A* **1980**, *77*, 232. [7b] C. J. Brown, P. J. McCarthy, I. D. Salter, *J. Organomet. Chem.* **1990**, *394*, 711.
[8] [8a] H. Cohen, D. Meyerstein, *Inorg. Chem.* **1987**, *26*, 2342. [8b] H. Cohen, D. Meyerstein, *Inorg. Chem.* **1986**, *25*, 1506. [8c] M. Masarwa, H. Cohen, D. Meyerstein, *Inorg. Chem.* **1991**, *30*, 1849. [8d] S. Goldstein, G. Czapski, H. Cohen, D. Meyerstein, *Inorg. Chim. Acta* **1992**, *192*, 87. [8e] D. Meyerstein, *Inorg. Chem.* **1975**, *14*, 1716.
[9] H. Cohen, D. Meyerstein, *Inorg. Chem.* **1986**, *25*, 1505.
[10] N. Navon, H. Cohen, D. Meyerstein, *Inorg. Chem.* **1997**, *36*, 3781.
[11] A. Bruggink, A. McKillop, *Tetrahedron* **1975**, *31*, 2607.
[12] [12a] B. Liedholm, *Acta Chem. Scand.* **1969**, *23*, 3175. [12b] B. Liedholm, *Acta Chem. Scand.* **1971**, *25*, 106. [12c] B. Liedholm, *Acta Chem. Scand.* **1976**, *30*, 141.
[13] [13a] R. W. Turner, E. L. Amma, *J. Am. Chem. Soc.* **1963**, *85*, 4046. [13b] R. W. Turner, E. L. Amma, *J. Am. Chem. Soc.* **1966**, *88*, 1877. [13c] H. Schmidbaur, W. Bublak, B. Huber, G. Reber, G. Muller, *Angew. Chem. Int. Ed. Engl.* **1986**, *25*, 1089. [13d] C. J. Brown, *J. Organomet. Chem.* **1990**, *394*, 711. [13e] P. J. McCarthy, *J. Chem. Soc., Chem. Commun.* **1989**, 395. [13f] G. B. Ansell, *Acta Crystallogr., Sect. C* **1984**, *40*, 365.

Received October 24, 2001
[I01419]

The Preparation and Structures of Group 12 (Zn, Cd, Hg) Complexes of the Soft Tripodal Ligand Hydrotris(methimazolyl)borate (Tm)

Iain Cassidy,[a] Mark Garner,[a] Alan R. Kennedy,[a] Graeme B. S. Potts,[a] John Reglinski,*[a] Paul A. Slavin,[a] and Mark D. Spicer*[a]

Keywords: Tripodal ligands / N ligands / S ligands / Group 12 complexes

Complexes of the hydrotris(methimazolyl)borate ligand (Tm) have been prepared with zinc, cadmium and mercury halides. Complexes of type [M(Tm)X] were obtained and characterised by NMR and mass spectrometry. X-ray crystallographic analysis of [Zn(Tm)X] (X = Cl, Br, I) reveals a symmetrical coordination mode of the ligand, but no significant change with different halides, which sit on the approximate C_3 axes of the complexes. The structures of [M(Tm)Br] (M = Cd, Hg) are isomorphous with one another. Again, the ligand is symmetrically coordinated to the metal, but the halide is now significantly displaced from the approximate C_3 axis of the M(Tm) unit, resulting in what approximates to a trigonal pyramidal geometry. Unlike in most distorted mercury structures, little bond length expansion (towards two- or three-coordinate geometries) occurs. This is ascribed to the strong affinity of the thione donors for Hg.
(© Wiley-VCH Verlag GmbH, 69451 Weinheim, Germany, 2002)

Introduction

The tripodal, anionic ligand hydrotris(pyrazolyl)borate (Tp) has been extensively studied since its preparation over 30 years ago.[1,2] Despite the relative ease of preparation of substituted analogues, and thus manipulation of the steric properties of the ligand, it is not possible to substantially alter the donor characteristics. To this end we have recently reported[3,4] the preparation of the novel, soft, anionic tripodal ligand hydrotris(methimazolyl)borate (Tm) (**1**) by adaptation of the method used by Trofimenko to prepare the Tp anion (Scheme 1).

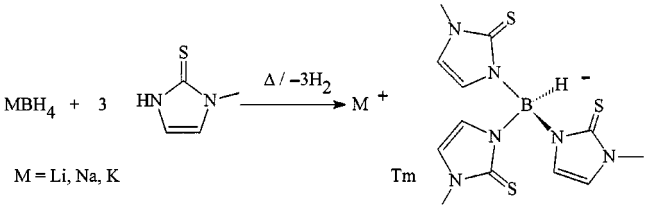

Scheme 1

Tm is broadly analogous to Tp in that it also presents a face-capping donor set, but differs in that: i) the donor set is much softer in character (3 S donor atoms compared to 3 N donor atoms), and ii) the chelate ring size formed on complexation is eight (rather than six in Tp complexes). Tm can be considered to be the softest in a series of $6e^-$ donor, face-capping anionic ligands *viz* Tp, Cp and Tm.

[a] Department of Pure and Applied Chemistry, University of Strathclyde,
295 Cathedral Street, Glasgow, G1 1XL, UK

Our initial studies of the complexation of Tm with late transition metals and with lower main group metals have shown that although the analogy holds with respect to the tripodal bonding mode adopted by the ligand, the chemistry is modulated considerably on going from the hard Tp to the soft Tm ligand. This is manifested particularly in the stability and reactivity of the complexes obtained. For instance, with bismuth(III) we have obtained[5] both the octahedral $[Bi(Tm)_2]^+$ cation and a chloro-bridged dimer $[Bi(Tm)Cl(\mu\text{-}Cl)]_2$, while no examples of Tp complexes of bismuth have been reported. Indeed, in our hands, reaction of NaTp with $BiCl_3$ under identical conditions results in the reduction of the bismuth to its elemental state.[6] Likewise, iodine oxidation of $[Tl^I(Tm)]$ results in the formation of the $[Tl^{III}(Tm)_2]^+$ cation, while [Tl(Tp)] is not oxidised by iodine, but undergoes ligand decomposition.[7] A further difference in reactivity has been noted by Hill,[8] who in an attempt to prepare the Tm analogue of [Ru(R)-(CO)(PPh_3)(Tp)] observed intramolecular activation of the bridgehead B−H bond with formation of a metalloboratrane. In the latter example the reactivity apparently arises from the greater flexibility afforded by the eight-membered chelate rings formed by Tm in its metal complexes.

In an effort to further understand the bonding of Tm to metals we decided to investigate the zinc triad of metals. These elements only have a single accessible oxidation state, which should lessen the likelihood of side reactions (which in our experience are mostly redox driven). Furthermore, there has been extensive use of Tp in attempts to model the zinc coordination sphere in metalloenzymes such as carbonic anhydrase and liver alcohol dehydrogenase.[9,10] Recently, to this end, Parkin and Vahrenkamp have prepared

analogues of the Tm ligand either containing an NS_2 donor set[11,12] or with modified steric bulk,[13,14] have reported their zinc complexes and highlighted aspects of their mimicry of the biological system.

We have previously reported in brief the formation and crystal structure of [Zn(Tm)Br],[3] and the preparation of [Zn(Tm)X] (X = Cl, I).[4] The relatively simple tetrahedral structure seems to give an ideal system in which to investigate the effects of metal ion size and counterions on the structures adopted in the absence of problems arising from redox activity. Here we describe the preparation of the full series of group 12 metal halide complexes and analyses of their solid-state structures.

Results and Discussion

The complexes [M(Tm)X] (M = Zn, Cd) are readily prepared by reaction of the metal(II) halide with TlTm in dichloromethane [Equation (1)]; the resulting thallium halide precipitates and reasonably pure materials are obtained after filtration and evaporation of the solvent.

$$MX_2 \cdot n\,H_2O \;+\; Tl(Tm) \xrightarrow{CH_2Cl_2} [M(Tm)X] \;+\; TlX\,(+\,nH_2O) \qquad (1)$$

The mercury(II) complexes were less amenable to this method of preparation and so a route using NaTm in acetone was utilised instead. Apparently, the formation of the thallium halide is inhibited in the presence of Hg^{II}. The complexes thus obtained are white to pale yellow powders. The ^1H NMR spectra all show a singlet at about $\delta = 3.5$ (CH_3) and a pair of either singlets or doublets at about $\delta = 6.9$ and $\delta = 7.2$, as would be expected. These resonances are slightly shifted to high field from the free ligand and are generally broadened, suggesting some chemical exchange is taking place. Relatively low solubilities in solvents other than DMSO have ruled out variable temperature NMR studies to investigate this phenomenon. Their formulations are further confirmed by low resolution mass spectrometry. The complexes generally show rather weak parent ion peaks corresponding to [M(Tm)X], indeed in one case the parent is not observed at all. However in all complexes very strong peaks due to $[M(Tm)]^+$ are observed, which suggests relatively facile halide loss but significant stability of the $[M(Tm)]^+$ fragment under these conditions.

The X-ray crystal structures of a series of complexes [M(Tm)X] (where M = Zn and X= Cl, Br, I; M = Cd, Hg and X= Br) have been obtained giving data which allows assessment of the effects of both changing anion and changing metal cation. For the zinc complexes X-ray crystallography reveals the expected pseudo-tetrahedral geometry (Figure 1) with the zinc, halide and B−H all lying on an approximate (or in the case of [Zn(Tm)Br], crystallographic) threefold axis (Figure 2). The S−Zn−S angles are a little less than expected (105−108°) while the S−Zn−X angles are commensurately larger (110−115°). The Zn−S distances are in the narrow range 2.35−2.38 Å, a little longer than the values in Parkin's [$Zn(Tm^{Mes})$(HOMe)] (2.32−2.34 Å)[13] — possibly reflecting the relative donor abilities of halide and methanol ligands — and show no discernible alteration with changing halide. There are no other structurally characterised monomeric zinc complexes with S_3X (X = halide) donor sets. The only examples of such donor sets are in the zinc thiolate clusters [$Zn_4(\mu$-$SPh)_6X_4$],[15] which have Zn−S distances in the range 2.33−2.38 Å. The Zn−X distances, as expected, closely mirror the change in halide-ion radius. We conclude that there is little influence of the halide on the overall structure. However, changing the metal cation to cadmium or mercury has a profound effect.

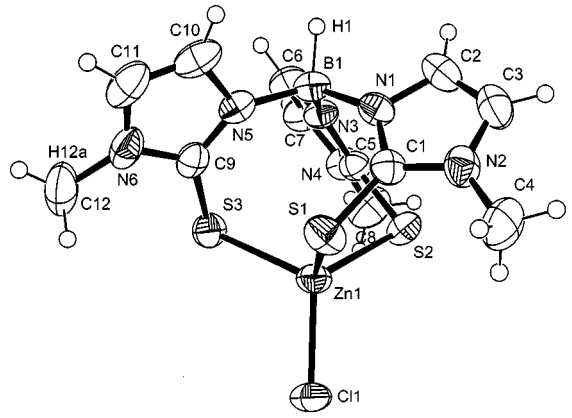

Figure 1. The X-ray Structure of [Zn(Tm)Cl]

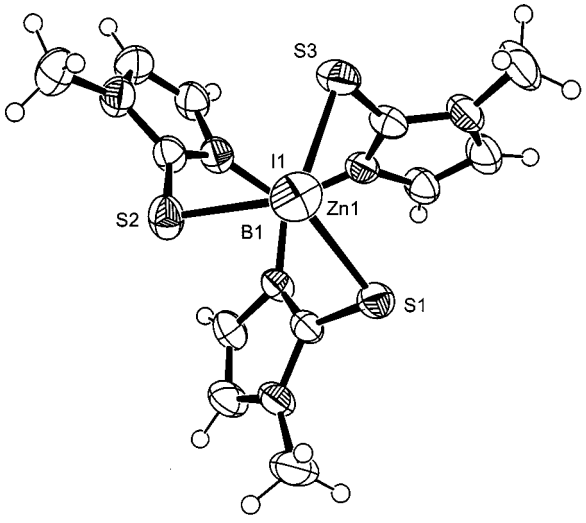

Figure 2. The X-ray Structure of [Zn(Tm)I], viewed down the approximate C_3 axis

The cadmium and mercury structures have remarkably similar structural parameters to one another, indeed it would appear that the compounds are crystallographically isomorphous. While the geometry is best described as

highly distorted tetrahedral (Figure 3), the Tm ligand remains symmetrically bound to the metal, with the S−M−S angles lying in the range 100−102°. This is somewhat less than in the corresponding zinc structures (vide supra) suggesting that the metal is displaced further from the ligand pocket. This is borne out by the increased B···M distances. The ligand further accommodates the larger cation by increasing the twist of the methimazole ring from the vertical (C_{3v}) arrangement as measured by the H−B−N−C torsion angles, with values of 36.7, 32.9 and 31.8° for the Zn structures and 40.1 and 40.3° for the Cd and Hg structures, respectively. This is further evidenced by the increase in the mean S···S nonbonded distances resulting from this twist, from 3.74, 3.76 and 3.77 Å in the Zn complexes to 3.97 and 3.98 Å in the Cd and Hg complexes, respectively. The metal and B−H unit are colinear, as in the zinc complexes. However, the halide no longer resides on this axis, but is markedly displaced. This results in a structure that tends towards a trigonal pyramid (Figure 4), with Br, S(1) and S(3) in the basal plane and S(2) in the apical position. The Br−M−S(1) and Br−M−S(3) angles are 120 and 125°, respectively. All the remaining angles are close to 100°.

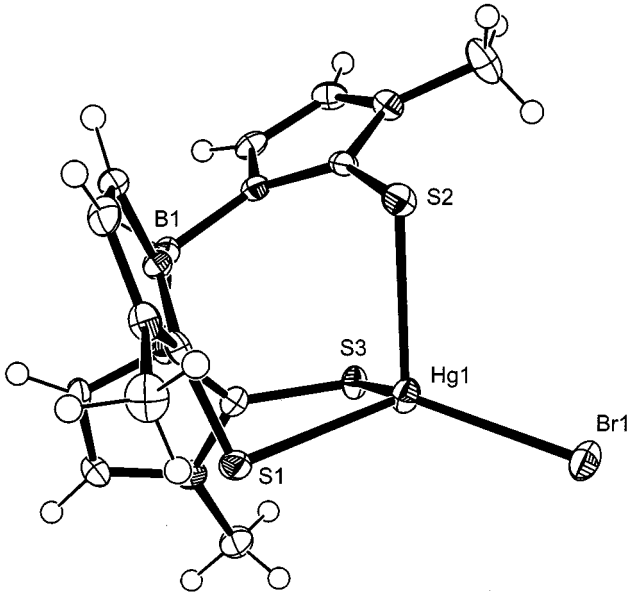

Figure 4. The X-ray Structure of [Hg(Tm)Br], emphasising the flattened trigonal pyramidal coordination geometry

Distorted structures are not uncommon in mercury chemistry, but are observed less frequently in cadmium chemistry. They are usually accompanied by significant lengthening of one or two metal-ligand bonds, tending towards either trigonal planar (e.g. [($Tp^{Me,Me}$)HgCN][16]) or linear (e.g. [{HOC(py)$_2$(*N*-MeIm)}HgMe][17]) coordination geometries. In this case, however, despite the distorted geometry, the variation of the metal-sulfur bond lengths (2.53−2.63 Å) is somewhat less than in other examples. We suppose that the strong affinity of mercury for sulfur donors (relative to the N-donors cited above) may in part explain this observation, although even in a complex with

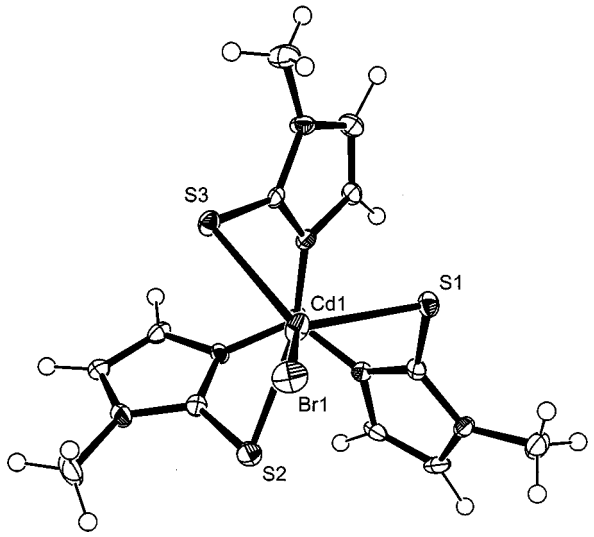

Figure 3. The X-ray Structure of [Cd(Tm)Br], showing the displacement of bromine from the H−B···M axis

an S_3X donor set, namely [{C(PSMe$_2$)$_2$(PSPh$_2$)}HgCl], the variation in bond lengths is 2.52−2.72 Å.[18]

Out of curiosity, the reaction of Hg_2Cl_2 with NaTm was also attempted. It was clear that disproportionation of the Hg_2^{2+} core had taken place by the immediate formation of a grey colouration and ultimately by the presence of small drops of metallic mercury. Analysis and NMR spectroscopy suggested that the product was not [Hg(Tm)Cl], and subsequently X-ray crystallography revealed the formation of the previously reported[19] dimer, [Hg(mt)(Hmt)(μ-mt)]$_2$ (Hmt = methimazole). We believe that the destruction of the Tm ligand is driven by the reducing nature of the B−H fragment, and its interaction with the redox active Hg_2^{2+} core.

What is clear from the crystallographic studies is that the Tm ligand binds strongly as a tridentate ligand to the metal centres, even towards metals that commonly exhibit lower coordination numbers. Because of the formation of eight-membered chelates in its metal complexes the ligand is able to show flexibility, adapting to the environment, with S−M−S angles able to vary from less than 90° in octahedral complexes such as [Tl(Tm)$_2$]$^+$ [7] and [Bi(Tm)$_2$]$^+$ [5] through to normal tetrahedral angles in the complexes reported here. While this results in versatility in terms of their ability to coordinate a range of metals, it also renders the ligands susceptible to interaction of the borohydride moiety with the metal and opens a potential route of decomposition, as observed in the reaction with Hg_2Cl_2.

Experimental Section

General: All reagents were obtained commercially and were used as received. NaTm and [Tl(Tm)] were prepared as described previously.[4] NMR spectra were recorded on a Bruker AMX400 spectrometer or a Jeol EX270 spectrometer. Electron Impact Mass Spectra were recorded on a JEOL JMS-AX505HA instrument.

Table 1. Analytical and spectroscopic data

Compound	Microanalysis[a] %C	%H	%N	LRMS[b]	^{1}H NMR	IR ν(B−H)/cm^{-1}
[Zn(Tm)Cl	31.33 (31.88)	3.13 (3.57)	18.49 (18.59)	−,[c] 415	3.54 (s, 3 H) 6.98 (s, 1 H) 7.30 (s, 1 H)	2407
[Zn(Tm)Br]	28.97 (29.03)	3.00 (3.25)	16.40 (16.92)	496, 415	3.55 (s, 3 H) 6.99 (s, 1 H) 7.30 (s, 1 H)	2403
[Zn(Tm)I]·0.5dcm	25.86 (25.69)	2.77 (2.93)	13.70 (14.39)	540, 415	3.55 (s, 3 H) 6.99 (s, 1 H) 7.31 (s, 1 H)	2441
[Cd(Tm)Cl]	30.24 (28.87)	3.85 (3.23)	15.60 (16.84)	500, 464	3.54 (s, 3 H) 6.89 (s, 1 H) 7.23 (s, 1 H)	2453
[Cd(Tm)Br]	26.94 (26.51)	2.48 (2.97)	14.80 (15.46)	543, 463	3.54 (s, 3 H) 6.91 (s, 1 H) 7.25 (s, 1 H)	2403
[Cd(Tm)I]	24.03 (24.40)	2.23 (2.73)	13.25 (14.23)	588,464	3.54 (s, 3 H) 6.96 (s, 1 H) 7.28 (s, 1 H)	−[c]
[Hg(Tm)Cl]·0.25Et_2O	26.06 (25.76)	2.81 (3.07)	13.37 (13.87)	−,[c] 552	3.55 (s, 3 H) 7.06 (s, 1 H) 7.32 (s, 1 H)	2394
[Hg(Tm)Br]	22.86 (22.81)	2.03 (2.55)	12.89 (13.30)	631, 551	3.55 (s, 3 H) 7.08 (s, 1 H) 7.32 (s, 1 H)	−[c]
[Hg(Tm)I]	20.77 (21.23)	2.50 (2.38)	12.12 (12.38)	677, 552	3.55 (s, 3 H) 7.09 (s, 1 H) 7.32 (s, 1 H)	−[c]

[a] Found (calcd.). [b] Electron impact MS; M^+ (calcd.) [c] Not observed.

[M(Tm)X] (M = Zn, Cd; X = Cl, Br, I). General Method: [Tl(Tm)] (0.200 g, 0.4 mmol) was suspended in acetone (30 mL) and a solution of the metal halide (0.4 mmol) dissolved in the minimum amount of acetone was slowly added. The mixture was stirred overnight at room temperature and the solid formed (TlX) was filtered off. The filtrate was taken to dryness and the resulting solid dried in vacuo. The crude product could be further purified by dissolving in the minimum amount of CH_2Cl_2 and cooling to −18 °C, whereupon colourless crystals were obtained. Crude yields were essentially quantitative, while yields of the recrystallised products were in the range 40−70%.

[Hg(Tm)X] (X = Cl, Br, I). General Method: The mercury(II) halide (2 mmol) and NaTm (2 mmol) were placed in a flask and acetone (25 cm^3) added. The mixture was stirred at room temperature for 20 h. The precipitate formed (NaX) was removed by filtration and the solvent removed in vacuo to yield crude product, which was recrystallised by slow diffusion of n-hexane into a saturated CH_2Cl_2 solution.

Reaction of Hg_2Cl_2 with NaTm: Hg_2Cl_2 (0.314 g, mmol) and NaTm (0.500 g, mmol) were placed in a flask with acetone (50 cm^3). The mixture was refluxed for 4 h and cooled. The solvent was removed on the rotary evaporator and the solid residue extracted with CH_2Cl_2 (3 × 20 cm^3). The solution was concentrated and the product precipitated as a white solid by addition of excess diethyl ether. Yield 0.5 g. Crystals for X-ray diffraction were obtained by slow evaporation of a CH_2Cl_2 solution.

Analytical and spectroscopic data for all the complexes are collected in Table 1.

X-ray Crystallography: Crystals of [Zn(Tm)Cl], [Zn(Tm)Br], [Zn(Tm)I], [Cd(Tm)Br] and [Hg(mt)(Hmt)(μ-mt)]$_2$ were obtained by slow evaporation of CH_2Cl_2 solutions at −18 °C, while crystals of the complex [Hg(Tm)Br] were obtained by diffusion of hexane into a solution of the complex in CH_2Cl_2. X-ray data were collected at 123 K on Rigaku AFC7S ([M(Tm)X], M = Zn; X= Cl, Br, I, M = Cd, X = Br) and Nonius Kappa-CCD ([Hg(Tm)Br]) diffractometers using graphite monochromated Mo-K_α radiation. The structures were solved by Patterson methods (SHELXS-86),[20] expanded by Fourier synthesis and refined by full-matrix least-squares refinement on F^2 with the exception of the Cd complex which was refined on F (SHELXL-97).[21] All calculations used the WinGX graphical interface.[22] Crystallographic data are collected in Table 2, selected bond lengths and angles in Table 3 and the structures shown in Figure 1−4.

Table 2. Crystallographic details

	[Zn(Tm)Cl]	[Zn(Tm)I]	[Cd(Tm)Br]	[Hg(Tm)Br]
Formula	$C_{12}H_{16}BClN_6S_3Zn$	$C_{12}H_{16}BIN_6S_3Zn.CH_2Cl_2$	$C_{12}H_{16}BBrCdN_6S_3$	$C_{12}H_{16}BBrHgN_6S_3$
M_r	452.12	628.49	543.60	505.44
Crystal System	Monoclinic	Monoclinic	Monoclinic	Monoclinic
Space Group	$P2_1/n$	$P2_1/n$	$P2_1/c$	$P2_1/c$
a/Å	12.722(2)	11.166(2)	10.103(2)	10.0799(2)
b/Å	12.626(5)	15.255(4)	10.042(1)	10.0528(2)
c/Å	11.967(2)	13.749(3)	18.957(2)	18.8840(4)
α/°	90	90	90	90
β/°	95.93(11)	99.32(2)	101.39(1)	101.2261(3)
γ/°	90	90	90	90
V/Å^3	1911.9(9)	2311.1(9)	1885.3(5)	1876.70(7)
Z	4	4	4	4
μ (Mo-K_α)/mm^{-1}	1.759	2.912	3.625	8.537
T/K	123	123	123	123
Reflns Measd	5028	6745	4164	15668
Unique Reflns	4613 (R_{int} = 0.016)	5580 (R_{int} = 0.090)	3940 (R_{int} = 0.023)	3825 (R_{int} = 0.061)
Obs Reflns	3375 [I >2σ(I)]	4161 [I > 2σ(I)]	2932 [I > 2σ(I)]	3490 [I > 2σ(I)]
R1	0.027	0.058	0.026	0.023
wR2	0.071	0.151	-	0.050
GOF	1.011	1.071	1.090	1.109

Table 3. Selected structural parameters [interatomic distances (Å), angles and torsion angles (°)]

	Zn(Tm)Cl	Zn(Tm)Br[a]	Zn(Tm)I	Cd(Tm)Br	Hg(Tm)Br
M−X	2.2409(7)	2.364(2)	2.5797(9)	2.5674(4)	2.5639(4)
M−S(1)	2.3503(8)	2.355(3)	2.3759(16)	2.544(1)	2.5659(9)
M−S(2)	2.3563(9)		2.3476(16)	2.616(1)	2.6377(10)
M−S(3)	2.3644(7)		2.3498(17)	2.5413(9)	2.5344(10)
M···B	3.626	3.674	3.697	3.820	3.820
S(1)−M−S(2)	106.65(3)	105.35(8)	106.10(6)	100.30(3)	100.52(3)
S(1)−M−S(3)	104.77(2)		106.36(6)	102.30(3)	100.11(3)
S(2)−M−S(3)	107.67(2)		104.37(6)	100.78(3)	102.05(3)
X−M−S(1)	113.20(3)	113.33(7)	114.89(4)	121.62(3)	120.49(2)
X−M−S(2)	113.57(3)		109.53(5)	101.94(2)	103.72(2)
X−M−S(3)	110.45(3)		114.75(5)	124.99(3)	125.84(2)
S···S(av)	3.77	3.74	3.76	3.97	3.98
H−B−N−C(av)	36.7	32.9	31.8	40.1	40.3

[a] See ref.[3] The complex lies on a crystallographic C_3 axis.

CCDC-171635 ([Zn(Tm)Cl]), -171636 ([Zn(Tm)I]), -171637 ([Hg(Tm)Br]) and -171638 ([Cd(Tm)Br]) contain the supplementary crystallographic data for this paper. These data can be obtained free of charge at www.ccdc.cam.ac.uk/conts/retrieving.html [or from the Cambridge Crystallographic Data Centre, 12, Union Road, Cambridge CB2 1EZ, UK; Fax: (internat.) +44-1223/336-033; E-mail: deposit@ccdc.cam.ac.uk].

[1] S. Trofimenko, *Scorpionates: The Coordination Chemistry of Polypyrazolylborate Ligands*, Imperial College Press, London, **1999**.
[2] S. Trofimenko, *Chem. Rev.* **1993**, *93*, 943−980.
[3] M. Garner, J. Reglinski, I. Cassidy, M. D. Spicer, A. R. Kennedy, *Chem. Commun.* **1996**, 1975−1976.
[4] J. Reglinski, M. Garner, I. Cassidy, P. A. Slavin, M. D. Spicer, D. R. Armstrong, *J. Chem. Soc., Dalton Trans.* **1999**, 2119−2126.
[5] J. Reglinski, M. D. Spicer, M. Garner, A. R. Kennedy, *J. Am. Chem. Soc.* **1999**, *121*, 2317−2318.
[6] J. Regliski, M. D. Spicer, Unpublished results.
[7] P. A. Slavin, J. Reglinski, M. D. Spicer, A. R. Kennedy, *J. Chem. Soc., Dalton Trans.* **2000**, 239−240.
[8] A. F. Hill, G. R. Owen, A. J. P. White, D. J. Williams, *Angew. Chem. Int. Ed.* **1999**, *38*, 2759−2761.
[9] G. Parkin, *Chem. Commun.* **2000**, 1971−1985.
[10] H. Vahrenkamp, *Acc. Chem. Res.* **1999**, *32*, 589−596.
[11] C. Kimblin, T. Hascall, G. Parkin, *Inorg. Chem.* **1997**, *36*, 5680−5681.
[12] J. Seebacher, M. Shu, H. Vahrenkamp, *Chem. Commun.* **2001**, 1026−1027.
[13] C. Kimblin, B. M. Bridgewater, D. G. Churchill, G. Parkin, *Chem. Commun.* **1999**, 2301−2302.
[14] M. Tesmer, M. Shu, H. Vahrenkamp, *Inorg. Chem.* **2001**, *40*, 4022−4029.
[15] P. A. W. Dean, N. C. Payne, J. Wranich, J. J. Vittal, *Polyhedron* **1998**, *17*, 2411−2416.
[16] G. G. Lobbia, P. Cecchi, R. Gobetto, G. Digilio, R. Spagna, M. Camalli, *J. Organomet. Chem.* **1997**, *539*, 9−17.
[17] A. J. Canty, N. Chaichit, B. M. Gatehouse, E. E. George, *Inorg. Chem.* **1981**, *20*, 4293−4300.
[18] S. O. Grim, P. H. Smith, S. Nittolo, H. L. Ammon, L. C. Satek, S. A. Sangokoya, R. K. Khanna, I. J. Colquhoun, W. McFarlane, J. R. Holden, *Inorg. Chem.* **1985**, *24*, 2889−2895.
[19] N. A. Bell, W. Clegg, J. R. Creighton, E. S. Raper, *Inorg. Chim. Acta* **2000**, *303*, 12−16.
[20] G. M. Sheldrick, SHELXS-86, *Program for Crystal Structure Solution*, University of Göttingen, **1986**.
[21] G. M. Sheldrick, SHELXL-97, *Program for Crystal Structure Refinement*, University of Göttingen, **1997**.
[22] L. J. Farrugia, *J. Appl. Crystallogr.* **1999**, *32*, 837−838.

Received November 27, 2001
[I01477]

EurJIC
European Journal of Inorganic Chemistry

June 2002
Issue 6
Pages 1241–1540

COVER PICTURE

The cover picture shows the molecular structure of the first crystallographically characterized complex containing a silver–tin bond. The stabilization of divalent tin by the tripodal amido ligands allows the coordination of stannates(II) to highly oxidizing metal centres making them versatile "ligands" for a broad range of transition metals. Details are discussed in the Microreview by L. H. Gade on p. 1257 ff. We thank Prof. R. Welter (Strasbourg) for his help in producing the colour picture.

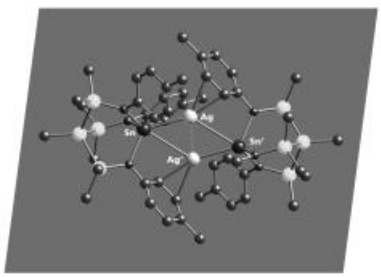

MICROREVIEWS

Contents

1257 **L. H. Gade**

Tripodal Triamidometallates of the Heavy Group 14 Elements: Inorganic Cages with Remarkable "Ligand Properties"

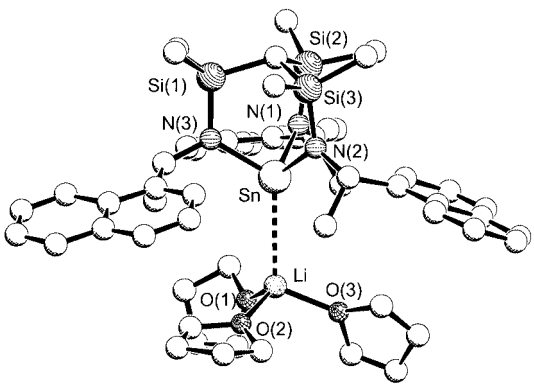

Keywords: Group 14 metals / Molecular cages / N ligands / Triamido metallates

 © WILEY-VCH Verlag GmbH, 69451 Weinheim, Germany, 2002 1434–1948/02/0606–1245 $ 20.00+.50/0

1269 **F. Rose-Munch,* E. Rose***

cine and *tele* Nucleophilic Substitutions in (η^6-Arene)tricarbonylchromium and Tricarbonyl(η^5-cyclohexadienyl)manganese Complexes

Keywords: Arene ligands / Carbonyl ligands / Chromium / Manganese / Nucleophilic substitution

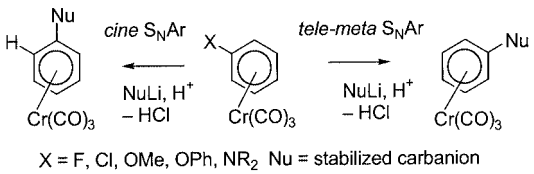

SHORT COMMUNICATIONS

1285 **P. Klüfers,* T. Kunte**

Copper(II) and Palladium(II) Complexes of the Reducing Sugar Lyxose

Keywords: Lyxose / Copper / Palladium / Aldose–metal complexes

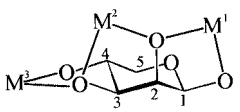

1290 **N. Segebarth,* J. Reisse**

Pressure Variations in Closed Sonochemical Reactors

Keywords: Sonochemistry / Pressure / Gas effect / Water chemistry / Radicals

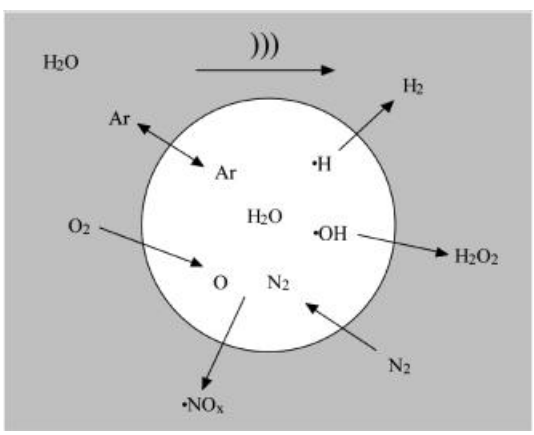

FULL PAPERS

1293 **M. J. Bayer, H. Pritzkow, W. Siebert***

1,1,1-Trisborylalkanes as Precursors for Dicarbapentaboranes(5) – Synthesis, Reactivity, and Structures of *closo*-1,5-Bis(neopentyl)-2,3,4-trichloro-1,5-dicarbapentaborane and Its Derivatives

Keywords: Alkynes / Boranes / Boron / Catechol / Hydroboration

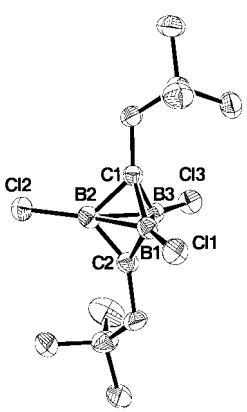

1301 M. Albrecht,* M. Schneider

Dinuclear Triple-Stranded Helicates from Rigid Oligo-*p*-phenylene Ligands: Self-Assembly and Ligand Self-Recognition

Keywords: Catechol / Titanium / Self-assembly / Helical structures / Molecular recognition

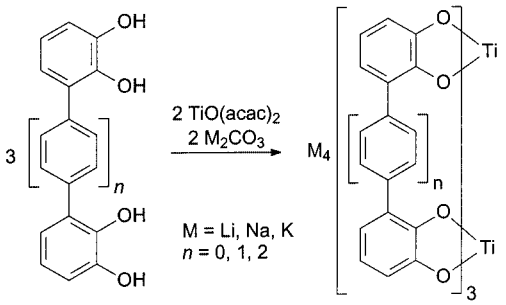

1307 G. Ma,* A. Fischer, J. Glaser*

Synthesis and Structure of Monomeric and Platinum-Bonded (1,10-Phenanthroline)thallium Complexes

Keywords: Metal−metal interactions / Platinum / Thallium / N ligands / NMR spectroscopy

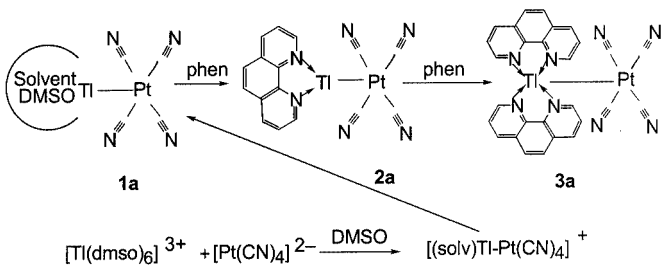

1315 H. Brunner, H. Cattey, D. Evrard, M. M. Kubicki, Y. Mugnier, E. Vigier, J. Wachter,* R. Wanninger, M. Zabel

Bis(η-*tert*-butylcyclopentadienyl)hydridoniobium Ditelluride, a Convenient Reagent for the Synthesis of Polynuclear Metal Telluride Complexes

Keywords: Niobium / Tellurium / Polynuclear complexes / Cyclopentadienyl complexes / Electrochemistry

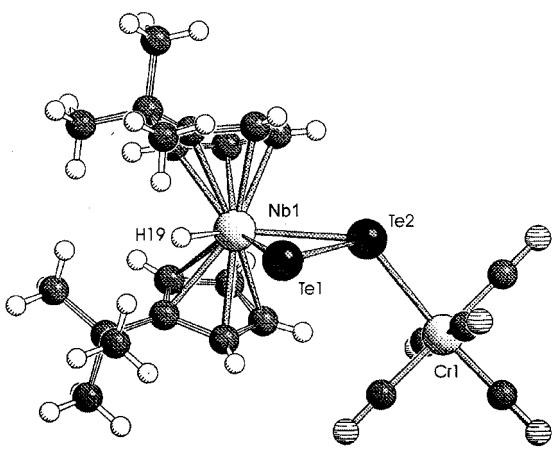

1326 A. Galindo, M. Gómez,* D. del Río, F. Sánchez

Synthesis and Reactivity of Ene-Diamido and Ene-Diolato [(Trimethylsilyl)cyclopentadienyl]-niobium(V) Complexes and a Comparative DFT Study of the Bonding Capabilities of Diazabutadiene and Butadiene Ligands

Keywords: Niobium / Alkene ligands / N ligands / Cyclopentadienyl complexes / Density functional calculations

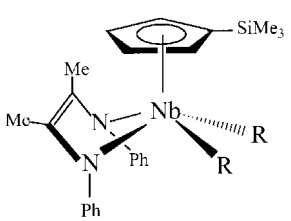

1336 **A. Castro, M. V. Galakhov, M. Gómez,* P. Gómez-Sal, A. Martín**

Synthesis of Hydride Tantalabenzocyclopentene and μ-Alkylidene Complexes by Direct Alkylation Reactions of $[TaCp^*Cp'Cl_2]$ − NMR Spectroscopic Study and X-ray Crystal Structure of $[TaCp^*Cp'(H)(\eta^2\text{-}CH_2\text{-}CMe_2\text{-}o\text{-}C_6H_4)]$, ($Cp^* = \eta^5\text{-}C_5Me_5$; $Cp' = \eta^5\text{-}C_5H_4SiMe_3$)

Keywords: Tantalum / Cyclopentadienyl complexes / Hydride complexes / Alkylidene complexes

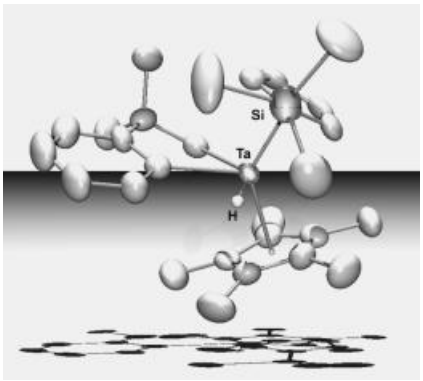

1343 **S.-G. Shyu,* R. Singh, C.-J. Su, K.-J. Lin**

Regiospecific Reaction between Dimetallic Phosphido-Bridged W−W Complexes and Phosphane Imide − Electrophilic Site Switching by Metal−Metal Bond Formation

Keywords: Tungsten / P ligands / Bridging ligands / Electrophilic site switching

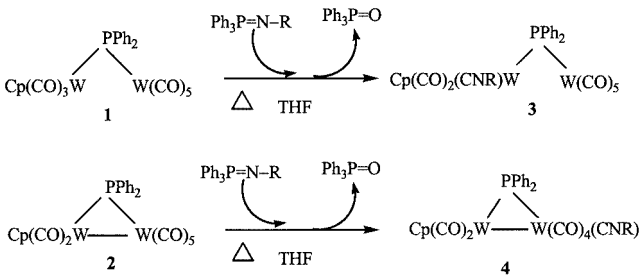

1349 **J. Kukral, P. Lehmus, M. Klinga, M. Leskelä, B. Rieger***

Oxygen-Containing, Asymmetric "Dual-Side" Zirconocenes: Investigations on a Reversible Chain Transfer to Aluminum

Keywords: Metallocenes / Propene polymerization / O ligands / Cyclopentadienyl ligands / Zirconium catalysts

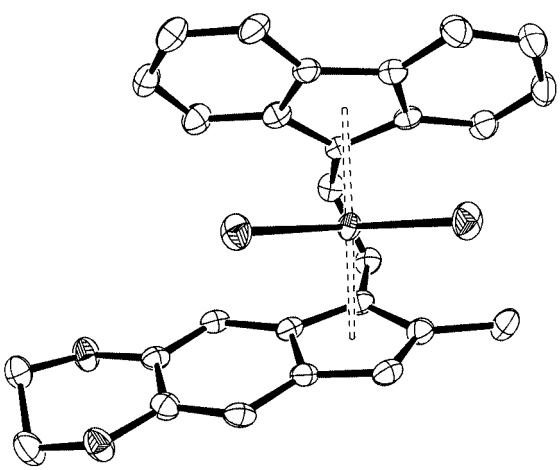

1357 **A. Ion, M. Buda, J.-C. Moutet,* E. Saint-Aman, G. Royal, I. Gautier-Luneau, M. Bonin, R. Ziessel**

Coordination of Ferrocenyl Ligands Bearing bipy Subunits: Electrochemical, Structural and Spectroscopic Studies

Keywords: N ligands / Sandwich complexes / Iron / Receptors / Cyclic voltammetry

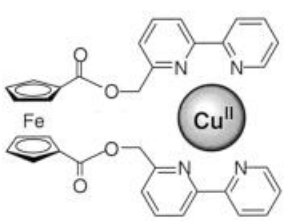

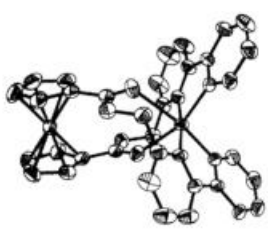

1367 **K. N. Gavrilov, O. G. Bondarev, R. V. Lebedev, A. A. Shiryaev, S. E. Lyubimov, A. I. Polosukhin, G. V. Grintselev-Knyazev, K. A. Lyssenko, S. K. Moiseev, N. S. Ikonnikov, V. N. Kalinin, V. A. Davankov, A. V. Korostylev,* H.-J. Gais**

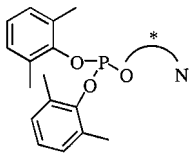

Easily Accessible Chiral *P,N*-Bidentate Aryl Phosphites, Their Complexation and Application in Enantioselective Allylic Alkylation, Sulfonylation and Hydrosilylation

82% e.e. in the Pd-catalyzed allylic alkylation
80% e.e. in the Pd-catalyzed allylic sulfonylation
50% e.e. in the Rh-catalyzed hydrosilylation of acetophenone

Keywords: Aryl phosphites / N,P ligands / Palladium / Allylation / Rhodium / Hydrosilylation

1377 **H. Werner,* F. Kukla, P. Steinert**

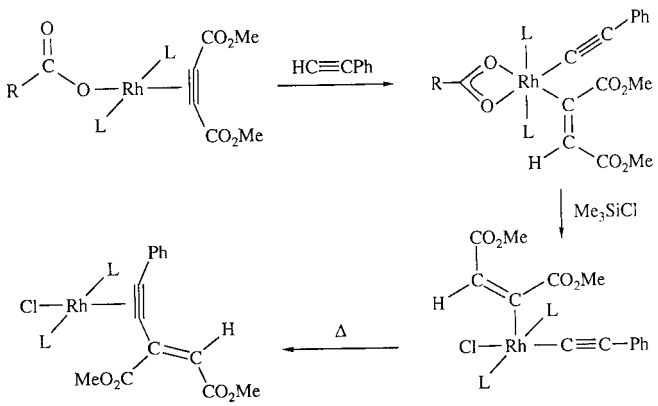

A New Family of Organometallic Rhodium Complexes with $[Rh(PiPr_2Ph)_2]$ and $[Rh(PiPrPh_2)_2]$ as Molecular Units

Keywords: Allyl ligands / Alkyne ligands / Vinylidene complexes / Rhodium / Phosphanes

1390 **C. Seward, J. Pang, S. Wang***

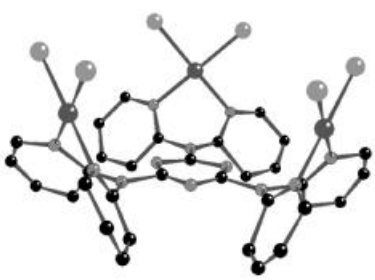

Luminescent Star-Shaped Zinc(II) and Platinum(II) Complexes Based on Star-Shaped 2,2′-Dipyridylamino-Derived Ligands

Keywords: Starburst molecules / Zinc / Platinum / N ligands / Luminescence

1400 **S. Albedyhl, D. Schnieders, A. Jancsó, T. Gajda,* B. Krebs***

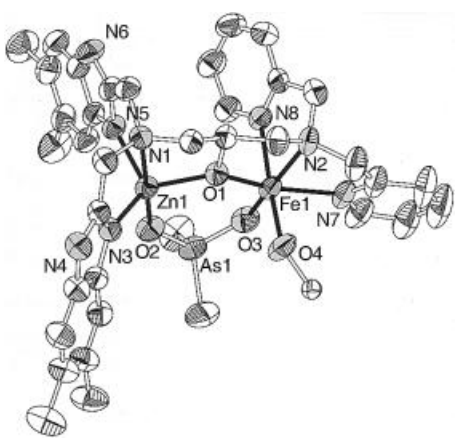

Heterodinuclear Zinc(II)−Iron(III) Complexes and Dinuclear Zinc Complexes as Models for Zinc-Containing Phosphatases

Keywords: Heterometallic complexes / Asymmetric ligands / Phosphates / Dinucleating ligands / Enzyme models

1410 **R. Belghiche, R. Contant, Y. Wei Lu, B. Keita, M. Abbessi, L. Nadjo,* J. Mahuteau**

Synthesis and Characterization of Fe- or Cu-Substituted Molybdenum-Enriched Tungstodiphosphates

Keywords: Heteropolyanions / Dawson-type structures / Molybdenum / Transition metal cations / Electrocatalysis

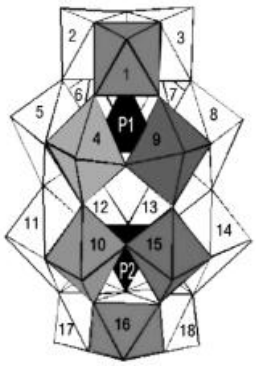

1415 **D. Saurenz, F. Demirhan, P. Richard, R. Poli,* H. Sitzmann**

Cyclopentadienylmolybdenum(VI) and Molybdenum(V) Oxo Chemistry: New Synthetic and Structural Features

Keywords: Cyclopentadienyl ligands / Molybdenum / Oxo ligands / X-ray crystallography

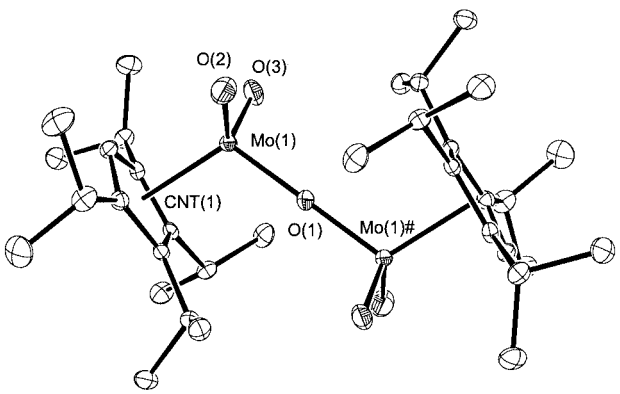

1425 **G. B. Deacon,* C. M. Forsyth, N. M. Scott**

Solvent-Free Lanthanoid Complexes Derived From Chelation-Supported Organoamide Ligands

Keywords: N,O ligands / Lanthanides / Halides / Metathesis / Structure elucidation

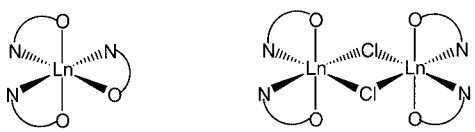

1439 **J.-C. Berthet,* C. Rivière, Y. Miquel, M. Nierlich, C. Madic, M. Ephritikhine***

Selective Complexation of Uranium(III) over Cerium(III) and Neodymium(III) by 2,2′:6′,2′′-Terpyridine − X-ray Crystallographic Evidence for Uranium-to-Ligand π Back-Bonding

Keywords: Actinides / Uranium / Cerium / Neodymium / Lanthanides / N ligands / Cations

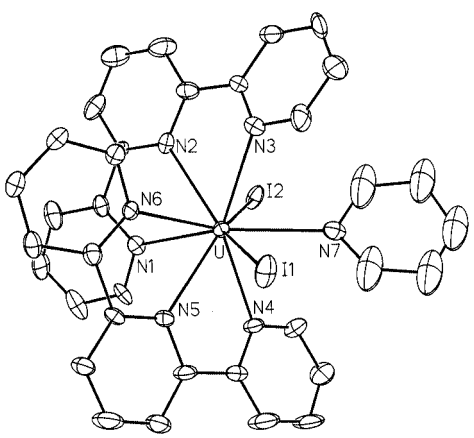

1447 **C. Pettinari,* F. Marchetti, R. Pettinari, A. Gindulyte, L. Massa, M. Rossi, F. Caruso***

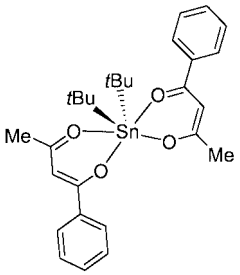

A Novel Configuration of a Benzoylacetonato-Diorganotin Species is Modified by an Electron-Withdrawing Substituent on Tin − Synthesis, IR and NMR Spectroscopy, Structure, and ab initio Studies

Keywords: Tin / O ligands / NMR spectroscopy / Crystal structure / Ab initio calculations

1456 **C.-M. Che,* H.-L. Kwong,* W.-C. Chu, K.-F. Cheng, W.-S. Lee, H.-S. Yu, C.-T. Yeung, K.-K. Cheung**

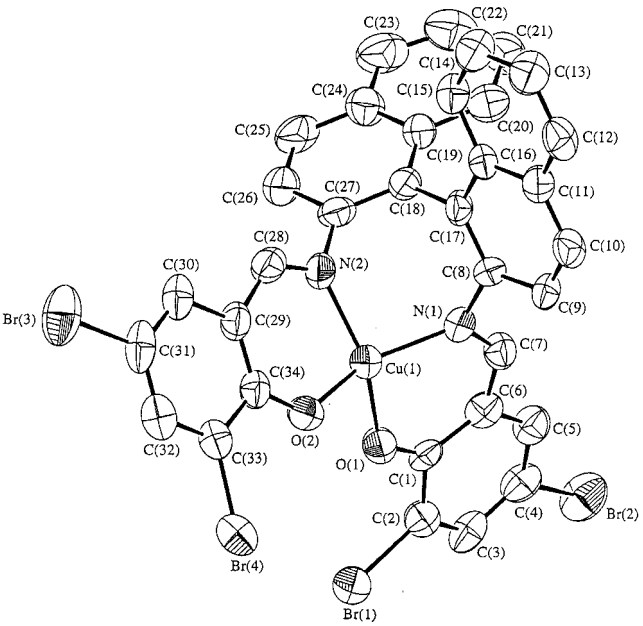

Copper Complexes of Chiral Tetradentate Binaphthyl Schiff-Base Ligands: Syntheses, X-ray Crystal Structures and Activity in Catalytic Asymmetric Cyclopropanation of Alkenes

Keywords: Asymmetric catalysis / Copper / Cyclopropanation / Schiff bases / Structure elucidation

1464 **P. Comba,* Y. D. Lampeka,* A. Y. Nazarenko, A. I. Prikhod'ko, H. Pritzkow**

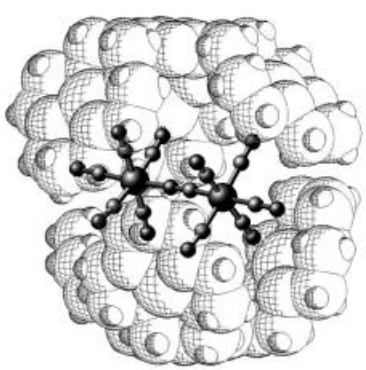

Interactions between Copper(II) Complexes of Mono-, Bis-, and Tris(macrocyclic) Ligands and Inorganic or Organic Guests

Keywords: Copper / Host-guest complexes / Macrocycles / Molecular recognition Template synthesis

1475 A. Bagno,* M. Bonchio

DFT Calculations of ^{99}Ru Chemical Shifts with All-Electron and Effective Core Potential Basis Sets

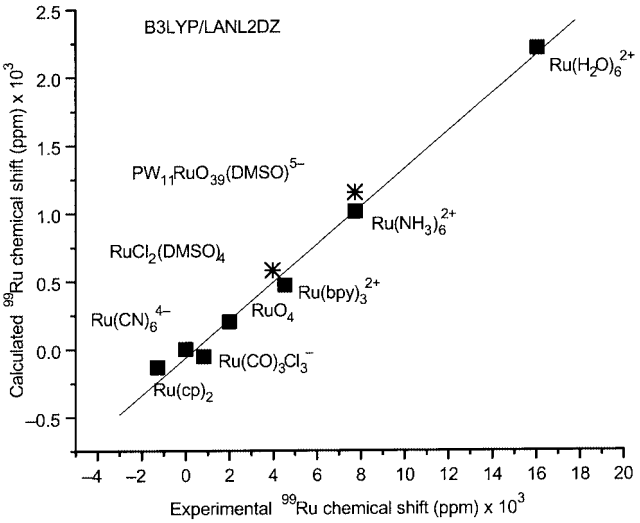

Keywords: Density functional calculations / Effective core potentials / NMR spectroscopy / Ruthenium

1484 J. Beckmann, D. Dakternieks,* J. O'Connell, K. Jurkschat, M. Schürmann

The First Well-Defined Tellurastannoxanes: the X-ray Structure of *trans*-[$(Bu_3SnO)_2\{CH_2$-$(Ph_2SnO)_2\}_2Te$]

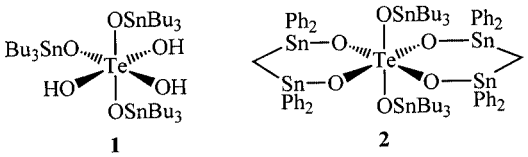

Keywords: Tin / Tellurium / Cluster compounds / NMR spectroscopy / X-ray diffraction

1488 J. Kramer, A. Scholten, W. L. Driessen,* J. Reedijk

The Recovery of a Rhodium-Containing Catalyst by Various New Silica-Based Amine Ion Exchangers

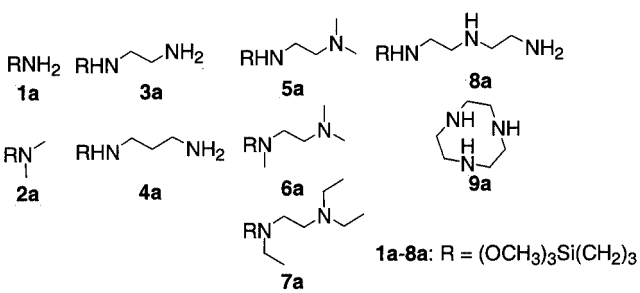

Keywords: Amine ligands / Complex stability / Ion exchange / Rhodium / Homogeneous catalysis

1495 H. Sachdev,* C. Preis

A New Type of Anionic Rearrangement in Metalated Benzylhydrazines

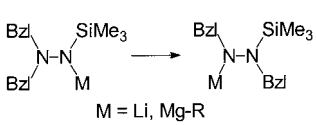

Keywords: Lithium / Magnesium / Hydrazides / Rearrangements / Structural characterisation

1502

G. A. Carriedo,* J. I. Fidalgo Martínez, F. J. García Alonso, E. Rodicio González, A. Presa Soto

The Reaction of Poly(chlorophosphazene)s with *p*-Aminophenol − Specific Formation of Aminophosphazenes with Terminal OH Groups and Aryloxyphosphazenes with Terminal NH_2 Groups

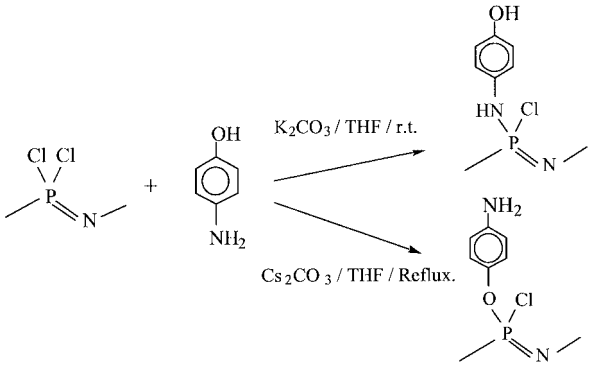

Keywords: Polymers / Inorganic polymers / Polyphosphazenes / *p*-Aminophenol

1511

M. Zehnder,* M. Neuburger, S. Schaffner, M. Jufer, D. A. Plattner*

Synthesis, X-ray Structures, NMR Studies and Density Functional Calculations of (η^2-Fumarodinitrile)palladium(0) Complexes Containing Dihydro(phosphanylphenyl)oxazole Ligands

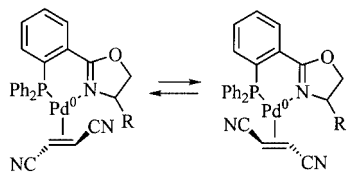

Keywords: Palladium / N,P ligands / Oxazolines / Alkene ligands / Density functional calculations

1518

D. R. van Staveren, E. Bothe, T. Weyhermüller, N. Metzler-Nolte*

Spectroscopic Properties, Electrochemistry, and Reactivity of Mo^0, Mo^I, and Mo^{II} Complexes with the [Mo(bpa)$(CO)_3$] Unit [bpa = bis(2-picolyl)amine] and Their Application for the Labelling of Peptides

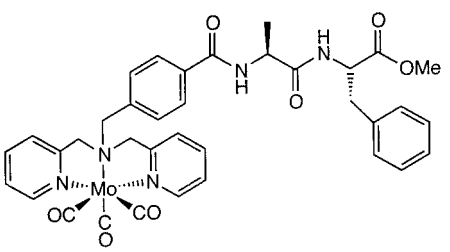

Keywords: Amino acids / Bioinorganic chemistry / Carbonyl ligands / Molybdenum / Spectroelectrochemistry

1530

A. Albinati, V. I. Bakhmutov,* N. V. Belkova, C. Bianchini,* I. de los Rios, L. Epstein,* E. I. Gutsul, L. Marvelli, M. Peruzzini,* R. Rossi,* E. Shubina, E. V. Vorontsov, F. Zanobini

Synthesis, Characterization, and Interconversion of the Rhenium Polyhydrides [$ReH_3(\eta^4$-$NP_3)$] and [$ReH_4(\eta^4$-$NP_3)]^+$ {NP_3 = tris[2-(diphenylphosphanyl)ethyl]amine}

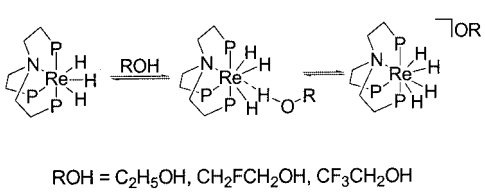

ROH = C_2H_5OH, CH_2FCH_2OH, CF_3CH_2OH

Keywords: Rhenium / Tripodal ligands / Phosphanes / Hydride ligands

Tripodal Triamidometallates of the Heavy Group 14 Elements: Inorganic Cages with Remarkable "Ligand Properties"

Lutz H. Gade[a]

Keywords: Group 14 metals / Molecular cages / N ligands / Triamido metallates

Anionic main group metal donors with potentially interesting ligand properties are obtained if ate complexes of the heavy p-block metals are formed by coordination between tripodal amides and divalent group 14 metal centres. The limitations of this approach, due to the potential oxidation by the central transition metal atom, may in part be suppressed by the presence of electronegative substituents at the M^{II} centre, which makes the metallates less reducing. The considerable stability of the triamidostannates(II) towards Ag^{I} or $Au^{I–III}$ is testimony to the practical significance of this. The most characteristic structural consequence of the rigid amido cages is the well-defined orientation of the peripheral N-substituents, which gives rise to very large cone angles for the monodentate ligands in their transition metal complex derivatives. These angles considerably exceed those of "ordinary" metallate groups or of the isolobal neutral group 15 ligands, and so would be expected to favour low coordination numbers in transition metal complexes.
(© Wiley-VCH Verlag GmbH, 69451 Weinheim, Germany, 2002)

Introduction

Molecular cages made up of main group metals, and also non-metals, have emerged as a basic structural principle in inorganic chemistry. They range from aggregates representing simple geometric bodies, such as the ubiquitous $\{M_4X_4\}$ cubes,[1] to very large, multi-shell "cluster" structures.[2]

Molecular fragments containing nitrogen and oxygen atoms, the components of amide, imide and alkoxide cages, have been studied in great detail. The field was comprehensively reviewed by Veith a decade ago,[3] and has reappeared in several more specialized overviews since.[4] In recent years, mixed-metal cage structures have attracted increased attention. Their rational synthesis (or at least an a posteriori rationalization of their assembly) remains a challenge and a current focus of research. In a perceptive analysis of the results of their work in this field, Wright et al. suggested that the p-block metals play the dominating role in dictating the structures of the mixed s-/p-block cage compounds.[5] This is thought to be the case since greater metal−ligand covalency of the metal−ligand interaction, and thus greater directionality of the bonding, results in more rigid metal coordination.

Several years ago, Veith and co-workers demonstrated that mixed metal alkoxide cages may be employed as (neutral) ligands in transition metal complexes.[6] Anionic main group metal donors with potentially interesting ligand properties are obtained if ate complexes of the heavy p-block metals are incorporated into such an array without "intra-cage" charge compensation. A conceptually simple

[a] Laboratoire de Chimie Organométallique et de Catalyse (CNRS UMR 7513), Institut Le Bel, Université Louis Pasteur Strasbourg,
4, rue Blaise Pascal, 67070 Strasbourg, France

Lutz H. Gade is a full professor of chemistry at the Université Louis Pasteur, Strasbourg and the Head of the Laboratory of Organometallic Chemistry and Catalysis. After completing his undergraduate studies at the University of Bonn and the Technical University of Munich, he went to Cambridge to work for his Ph.D. with Jack Lewis. Having returned to Germany after completing his thesis in 1991, he joined the Chemistry Department at the University of Würzburg, where he finished his habilitation in 1996 and where he subsequently worked as a lecturer. In 1998 he moved to Strasbourg to take up his present position, and in summer 2000 he was elected a member of the Institut Universitaire de France. His research interests are in the fields of coordination chemistry, organometallic chemistry and catalysis.

MICROREVIEWS: This feature introduces the readers to the authors' research through a concise overview of the selected topic. Reference to important work from others in the field is included.

approach that employs this strategy is based on a polydentate ligand with podand topology coordinating to a low-valent p-block metal and thus forming the anionic keystone of a ligand cage. The tripodal amides, which we introduced to the coordination chemistry of the early transition metals in the early 1990s,[7] have proved to be ideally suited for the pursuit of this goal and offer straightforward means of ligand design based on the metal cages. The recent progress in this field is the topic of this overview.

Metallates of the Divalent Group 14 Metals

The structural chemistry of anionic trisubstituted metallate(II) compounds of group 14 elements has received considerable attention. It began to develop in the 1980s, thanks to significant improvements in crystal preparation techniques and low-temperature crystal data collection. Veith and co-workers characterized a whole series of lithium trialkoxygermanates(II), -stannates(II) and -plumbates(II) that displayed characteristic cage structures, such as [Li(μ-$C_4H_3O)_3Sn$] (**1**) and [{$Sn(OtBu)_3M$}$_2$] (**2**), shown in Figure 1.[8]

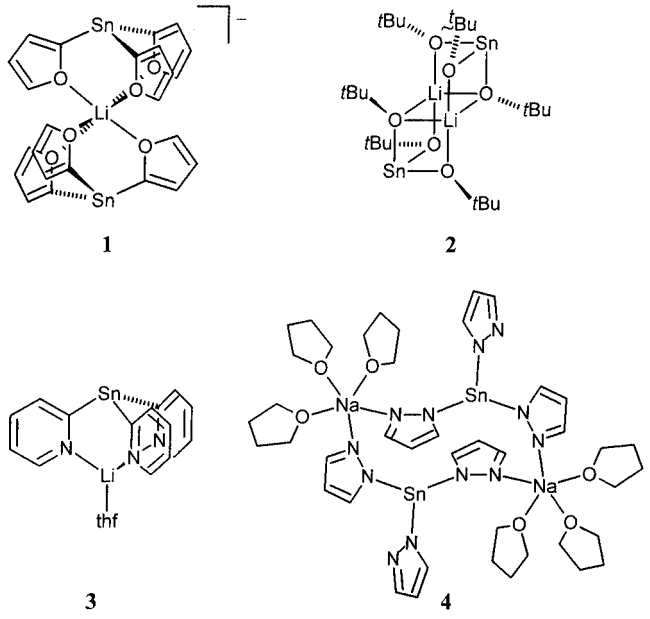

Figure 1. Four representative examples of cation−anion aggregation in stannates(II)

More recently, Wright et al. reported the structure of [Pb(2-py)$_3$Li(THF)] (**3**),[9] and Stalke and co-workers published the synthesis and X-ray diffraction study of several tris(pyrazolyl)germanates(II) and -stannates(II), such as [{$(Pz)_3SnNa(THF)_3(PzH)$}$_2$] (**4**), in which the heteroatom donor ligands at the p-block atom also serve as bridging units between the cations and metallate anions.[10]

A particularly interesting class of alkali metal group 14 and group 15 metallates are those containing a direct metal−metal contact between the cationic and the anionic metal centres, as found in the crystal structures of [$Ph_3Si-Li(THF)_3$] (**5**),[11] [Ph_3Sn-Li(pmdeta)] (**6**)[12] and [Ph_3Pb-Li(pmdeta)] (**7**)[13] (Figure 2).

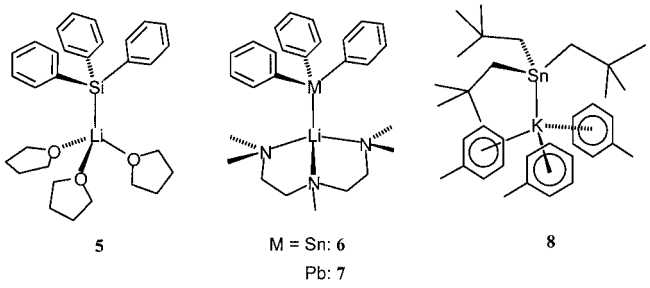

Figure 2. Metal−metal bonds between alkali metals and group 14 metals in trialkyl/aryl metallates(II)

The presence of a direct K−Sn bond was established both by NMR spectroscopy (^{119}Sn-^{39}K coupling) and by X-ray diffraction for the complex [$(Me_3CCH_2)_3Sn-K(toluene)_3$] (**8**), isolated by Lappert and co-workers from the reaction between the distannane [$(Me_3CCH_2)_3Sn]_2$ and potassium metal.[14] The systematic synthesis and structural investigation of these heterodimetallic compounds has also been extended to the heavier group 15 elements.[15]

The Tripodal Triamido Metallate Cages as *Ligands*: Some Basic Conceptual Considerations

An important consequence of the integration of divalent group 14 metal centres into the rigid cage structures of the tripodal triamidometallates is the reinforced pyramidality of the M^{II} centre. Thus, structural relaxation and concomitant stabilization of the $M(NR_2)_3$ fragment upon homolytic cleavage of M−M′ (M′ = transition metal) bonds in derivatives of these compounds is inhibited (Scheme 1). As for the stabilization of the triamido transition metal fragment in the early−late heterodimetallic complexes previously studied by us, destabilization of the amido complex fragment therefore contributes to the thermodynamic stability

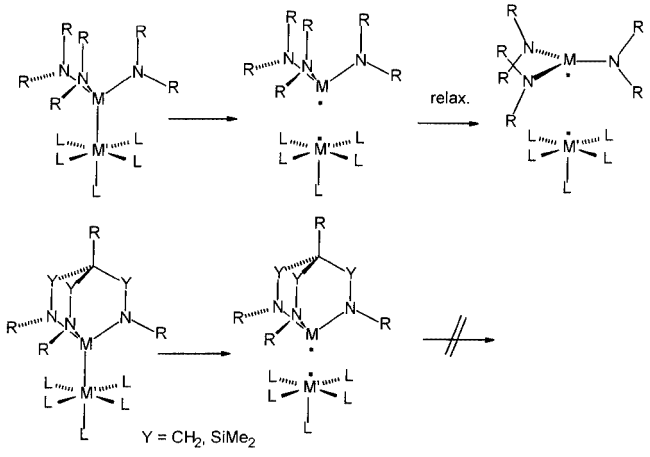

Scheme 1. Suppression of the structural relaxation of a triamido metal fragment upon homolytic cleavage of the M−M′ bond (M = group 14 metal, M′ = transition metal)

of the M−M′ complexes (or, viewed alternatively, to the stability of the complexation of M′ by the triamidometallate).[16]

The use of a divalent group 14 metallate as a ligand may in principle be limited by potential oxidation by the central transition metal atom. This may in part be suppressed by the presence of electronegative substituents at the M^{II} centre, which makes the metallates less reducing. Electronegative amido nitrogen atoms at the metal centre are therefore well suited for this purpose, and would be expected to match the established robustness of the halides and alkoxides. The considerable stability, discussed below, of the triamidostannates(II) studied in our group towards Ag^{I} or Au^{I-III} is testimony to the practical significance of this consideration.

The most characteristic structural consequence of the rigid amido cages is the well-defined orientation of the peripheral N-substituents, which gives rise to very large cone angles for the monodentate ligands in their transition metal complex derivatives. These angles considerably exceed those of "ordinary" metallate groups or of the isolobal neutral group 15 ligands, and thus should be expected to favour low coordination numbers in transition metal complexes. An illustrative example is the reaction product of $[Me\{SiMe_2N(p\text{Tol})\}_3SnLi(THF)_3]$ and the rhodium complex $[Rh_2Cl_2(P\textit{i}Pr_3)_4]$ (Scheme 2).[17]

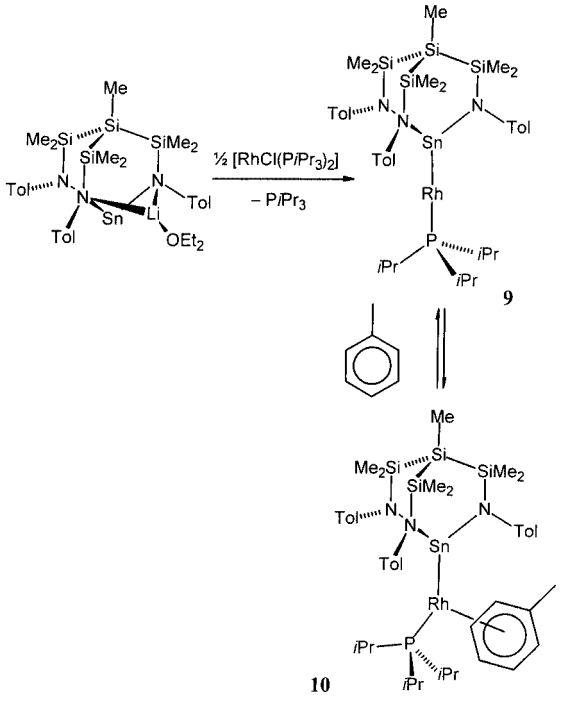

Scheme 2. Synthesis of the Sn−Rh complex **10**, which is in equilibrium in solution with the 12-electron complex **9**

A low-temperature ^{31}P, ^{13}C and ^{1}H NMR study in $[D_8]$toluene indicated the existence of a free 12-electron dicoordinate species **9**, which appeared to be in rapid equilibrium with the 18-electron complex **10** bearing an η^6-toluene ligand. The molecular structure of the isolated, crystalline solid **10** was determined by an X-ray diffraction study (Figure 3).[17]

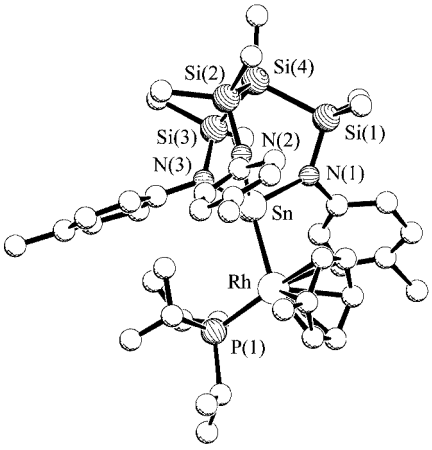

Figure 3. Molecular structure of $[Me\{SiMe_2N(p\text{Tol})\}_3Sn-Rh(P\textit{i}Pr_3)(\eta^6\text{-toluene})]$ (**10**)

The Structural Diversity of Lithium Triamidometallates Containing Tripodal Amido Ligands

As discussed above in more general terms, an interesting aspect of the structural chemistry of the lithium triamidometallates in solution and in the solid state is the type of interaction between the anionic cage and the counter-cation (in most cases solvated Li^+). Both solvent-separated salts and contact ions have been found. In the latter, the alkali metal ion is either directly bound to the group 14 metal (**I**) (Figure 4), in what is thought to be a primarily ionic metal−metal bonding interaction, or attached to the amido nitrogen atoms in a bridging coordination mode (**II**), thus breaking the overall threefold symmetry of the system.

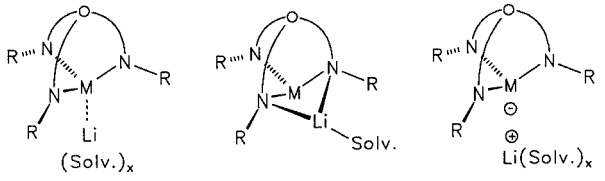

Figure 4. Three types of anion−cation association in lithium triamidometallates(II) of the group 14 elements

Treatment of the isolated lithium amides $[HC\{SiMe_2N(Li)(p\text{Tol})\}_3]$ and $[HC\{SiMe_2N(Li)[(S)\text{-1-(1-naphthyl)ethyl}]\}_3]$ with 1 mol-equiv. of $SnCl_2$ at 0 °C in diethyl ether/THF gave the lithium triamidostannates $[HC\{SiMe_2N(p\text{Tol})\}_3Sn-Li(THF)_3]$ (**11**)[18] and $[HC\{SiMe_2N[(S)\text{-1-(1-naphthyl)ethyl}]\}_3Sn-Li(THF)_3]$ (**12**), respectively.[12] Both compounds were characterized by single-

crystal X-ray structure analyses and found to possess direct Sn−Li bonds (**11**: 2.93 Å; **12**: 3.06 Å) (Figure 5).

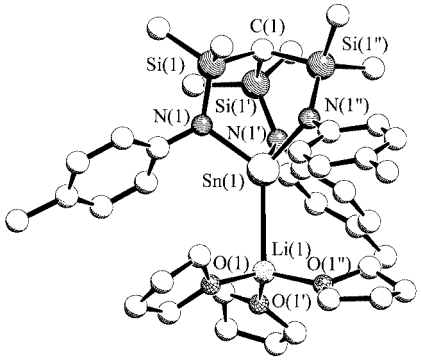

Figure 5. Molecular structure of $[HC\{SiMe_2N(p\text{Tol})\}_3SnLi(THF)_3]$ (**11**)

In the molecular structure of **11**, the Sn atom is displaced by 1.16(1) Å from the plane defined by the three amido nitrogen atoms, which have trigonal-planar geometry [$\Sigma\{<_N\} = 359.9(8)°$].[18] The average <(N−Sn−N′) of 93.3(4)° in the trigonal-monopyramidal SnN_3 unit indicates that Sn−N σ-bonding primarily involves the 4p orbitals of the tin atom, with the lone pair residing in a molecular orbital of essentially 4s character. However, it should be pointed out that the partially ionic nature of the Sn−N bonds may render orbital overlap and hybridization less important than in alkyl or aryl stannates. The absence of ionic conductivity of solutions of **11** in THF or diethyl ether indicates that the situation of a contact ion pair pertains even in a polar environment.

In view of the structure determined for **11**, it was of interest whether the presence of an additional stronger donor ligand would effect the disruption of the Sn−Li contact and produce an ion pair. The synthesis of compound **11** from the lithium amide and $SnCl_2$ in the presence of 2 mol-equiv. of pentamethyldiethylenetriamine (pmdeta) gave an anion−cation complex that was formulated as $[\{MeN(CH_2CH_2NMe_2)_2Li\}_2Cl][HC\{SiMe_2N(4\text{-}CH_3C_6H_4)\}_3Sn]$ (**13**).[18,20] A single-crystal X-ray structure analysis of **13** revealed that the Li^+ counterion is indeed separated from the stannate anion $[HC(SiMe_2Np\text{Tol})_3Sn]^-$ through coordination by a pmdeta ligand and a ClLi(pmdeta) unit to generate the complex cation $[\{MeN(CH_2CH_2NMe_2)_2Li\}_2Cl]^+$ (Figure 6).

In the crystal, the cation rides in a "piggyback" fashion on the trisilylmethane side of the stannate anion, and there is no significant interaction with the tin atom.[20]

A molecular structure in which a contact ion pair adopts a type **II** arrangement, with the lithium ions attached to the amido nitrogen atoms in a bridging coordination mode, was found in the triamidoplumbate $[MeSi\{SiMe_2N(t\text{Bu})\}_3PbLi(THF)]$ (**14**).[18] In general, triamidoplumbates containing tripod-amido ligands were most conveniently synthesized by treatment of the lithium amides with plumbocene, which avoided the competing redox reactions found with use of $PbCl_2$ (Scheme 3).[21] An X-ray diffraction study of **14** revealed that the (tripod-amido)plumbate cage comprising the four silicon atoms of the trisilylsilane unit and the PbN_3 unit is significantly distorted, due to the coordination of the $(THF)Li^+$ "counterion" to two of the amido nitrogen atoms (Figure 7).

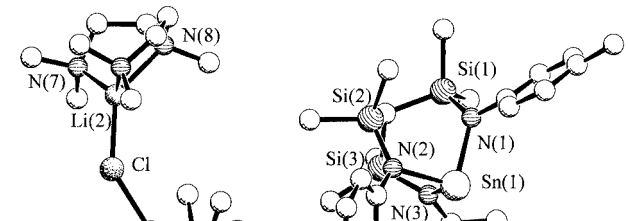

Figure 6. Representation of the molecular structure of $[\{MeN(CH_2CH_2NMe_2)_2Li\}_2Cl]$ $[HC\{SiMe_2N(4\text{-}CH_3C_6H_4)\}_3Sn]$ (**13**), showing the relative cation−anion arrangement in the crystal

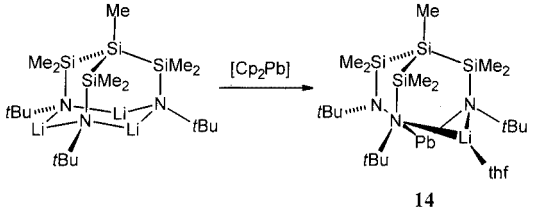

14

Scheme 3. Synthesis of the triamidoplumbate **14** by treatment of the lithium amide with plumbocene

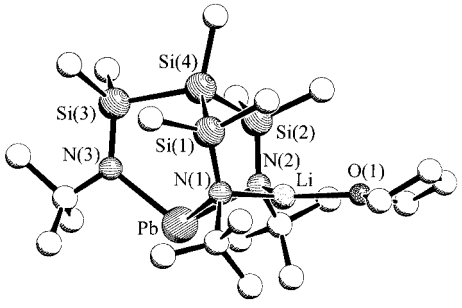

Figure 7. Molecular structure of the lithium triamidoplumbate $[MeSi\{SiMe_2N(t\text{Bu})\}_3PbLi(THF)]$ (**14**)

The molecule has idealized C_s symmetry, the virtual mirror plane being spanned by Si(4), Si(3), N(3), Pb(1), Li(1) and O(1). As a consequence of the binding of the (THF)Li group to the amido framework, the geometry of the two N-functions involved deviates from the trigonal planarity observed for the N(3) atom [$\Sigma\{<_{N(1)}\} = 346(2)°$, $\Sigma\{<_{N(2)}\} = 350(3)°$; however, $\Sigma\{<_{N(3)}\} = 359(3)°$]. Moreover, steric repulsion between the THF ligand and the N(1)- and N(2)-bonded *t*Bu groups forces the latter apart. On the other hand, the Li atom "ties" the two amido nitrogen atoms together to generate an N-donor atom arrangement that deviates from the otherwise more or less undistorted trigonal-monopyramidal arrangement of the N_3Pb unit

[<N(1)−Pb(1)−N(2) = 82.5(9)°, but <N(1)−Pb(1)−N(3) = 103(1)° and <N(2)−Pb(1)−N(3) = 109(1)°].

In the structure of **14**, the THF molecule coordinated to Li^+ is located between two of the peripheral N-substituents. This arrangement blocks potential cation mobility, which appears to require the absence of Li-bound co-ligands. We have been able to synthesize both the solvated (**15**) and the THF-free (**16**) lithium stannates of the C_3-chiral triamido cage $[HC\{SiMe_2N[(S)\text{-1-phenylethyl}]\}_3Sn]^-$ (Scheme 4), of which **15** was characterized by X-ray crystallography.[22]

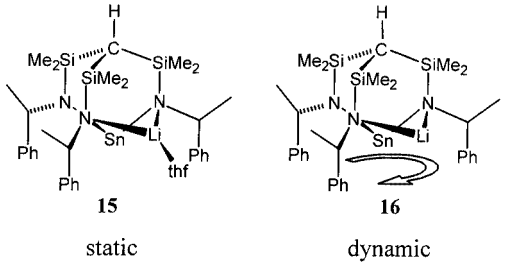

Scheme 4. "Locking" the cation mobility in a lithium triamidostannate by coordination of a co-ligand (THF)

While the signal patterns in the NMR spectra of **15** and **16** indicate closely related structures and are consistent with a retention in solution of the structural arrangement established for crystalline **15**, both compounds differ significantly with respect to dynamic behaviour in solution.[22] The coordinated THF ligand appears to "lock" the Li cation in the position between the two N atoms, thus conferring structural rigidity upon the molecules of **15** on the NMR timescale. On the other hand, the unsolvated compound **16** displays remarkable dynamic behaviour. As ^{1}H-EXSY studies have revealed, the Li atom appears to "rotate" around the N_3Sn unit, generating an effective threefold molecular symmetry at the fast exchange limit.[22,23] This intramolecular motion is reminiscent of the dynamic behaviour reported by Veith and co-workers for a tetraamidoindate, although it appears to take place much more rapidly in the latter case.[24]

The matter of which of the structural alternatives discussed above is observed in a given case was found to be largely unpredictable. It was therefore thought that the design of an amido tripod containing a specific binding site for the metal cation in the ligand periphery would yield "ion pairs" of predefined arrangement.

In an extension of our concept of the "active ligand periphery" in polydentate amides[25,26] containing additional donor functions for cation binding, we synthesised a tripod with peripheral 2-anisyl groups. The synthesis of the lithium stannate cage containing this ligand system (Scheme 5) did indeed give the expected aggregation pattern with intramolecular Li^+ solvation by two of the three *ortho*-anisyl groups, as confirmed by X-ray crystallography (Figure 8).[27]

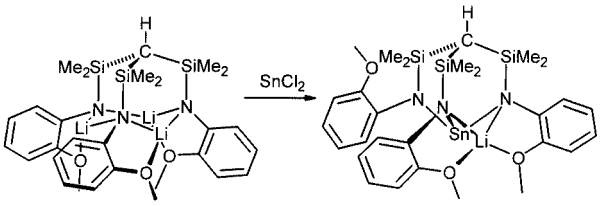

Scheme 5. Synthesis of a triamidostannate possessing secondary donor function for intramolecular cation solvation

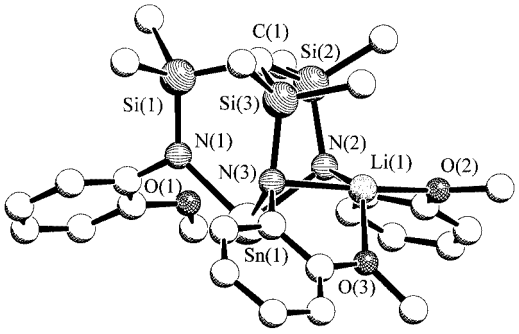

Figure 8. Intramolecular Li^+ solvation in the *ortho*-anisyl-substituted stannate $[HC\{SiMe_2N(2\text{-}MeOC_6H_4)\}_3SnLi]$

Triamidometallates Coordinated to Early Transition Metals

On going from the late to the early transition metals, the polarity and, concomitantly, the reactivity of the metal−metal bonds increase significantly.[28] Whereas group 4 M−Si compounds have found wide-ranging applications, such as in a variety of metal-mediated catalytic processes and in semiconductor growth,[29] their tin analogues remain extremely rare and thus poorly studied, despite numerous efforts to develop their chemistry.[30] A principal problem appears to be that many of the synthetic strategies employed for M−Sn bond formation do not work well when M is titanium, zirconium or hafnium.

A fundamental difficulty in group 4/group 14 metal−metal bond formation is the existence of energetically low-lying electron-transfer reaction pathways from the group 14 metal to the early transition metal. This problem is not unlike the situation in early−late heterodinuclear transition metal complexes, referred to above, in which metals from the two ends of the d-block are directly bonded to each other.[16]

With the aim of obtaining heterodinuclear complexes of greater stability than previously observed, the triamidostannate complex $[MeSi\{SiMe_2N(4\text{-}CH_3C_6H_4)\}_3SnLi(OEt_2)]$ was treated with the metallocene dichlorides $[Cp_2MCl_2]$ of all three titanium group metals.[31] Nucleophilic substitution of one of the chloro ligands in the metallocene dichlorides occurred cleanly in all three cases, yielding the corresponding dinuclear complexes as thermally stable solids (Scheme 6).

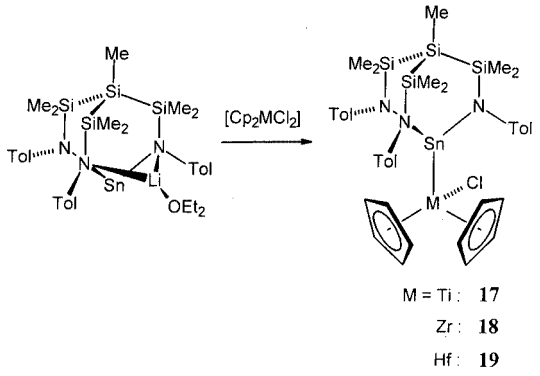

Scheme 6. Synthesis of the stable group 4/group 14 heterodimetallic complexes **17**–**19**

Single-crystal X-ray structure analyses of both **18** and **19** confirmed the molecular structures and established the presence of the group 4/group 14 metal–metal bonds (Figure 9).[31] The Zr–Sn bond length in compound **18** is, at 3.0231(2) Å, significantly longer than the sum of the covalent radii of the two metals as given by Pauling[32] (ca. 2.85 Å). However, it is in the same range as the Zr–Sn distances in $[Zr(CO)_5(SnMe_3)_2]^{2-}$ [3.011(3) Å] and $[Zr(CO)_4(dppe)SnMe_3]^-$ [3.061(2) Å] reported by Ellis and co-workers.[33] This observation is remarkable, since the latter compounds are low oxidation state zirconium complexes with high coordination numbers, and so should be expected to possess Zr–Sn bonds longer than those in **18**. It is quite likely that the length of the metal–metal bond in **18** is largely dictated by the repulsion of the ligand spheres of the two metal atoms.

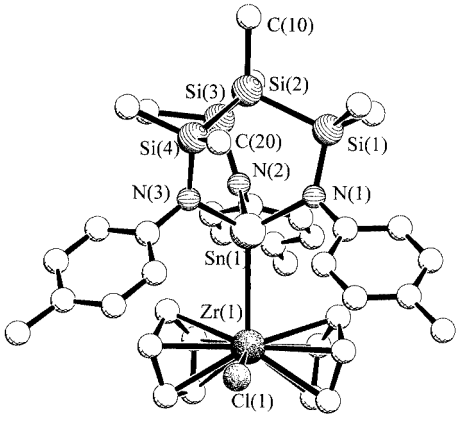

Figure 9. Molecular structure of the Zr–Sn heterodimetallic complex $[MeSi\{SiMe_2N(4\text{-}CH_3C_6H_4)\}_3Sn–Zr(Cp)_2Cl]$ (**18**)

On comparing the molecular structure of complex **19** with that of **18**, it was interesting to note that all bonds to hafnium in **19** are significantly shorter than those to the zirconium centre in **18**. In particular, the Hf–Sn distance of 2.9956(3) Å is shortened by almost 0.03 Å relative to the analogous Zr–Sn bond and is very similar to the Hf–Sn bond lengths determined in $[(\eta^6\text{-}C_6H_5CH_3)_2Hf(SnMe_3)_2]$, reported by Green and co-workers.[34] There had been one previous study in which two analogous Zr–Sn and Hf–Sn complexes were structurally characterized by X-ray diffraction, and this revealed a very similar relationship between the metal–metal bond lengths in both complexes.[35]

In spite of the long Zr–Sn and Hf–Sn bonds, both compounds **18** and **19** are remarkably stable. No appreciable decomposition was observed when they were heated at reflux in toluene, and as solids they may be briefly handled in air, very probably due to the effective shielding of the highly polar metal–metal bond by the surrounding bulky ligand periphery.

Triamidometallates Coordinated to Late Transition Metals

The triamidostannate cages discussed in this review may readily be coupled with carbonyl halide complexes of the late transition elements, by the same approach as described for the group 4 derivatives in the previous section.[36] Several examples of such late transition metal tin complexes, all obtained by salt metathesis of a stannate with the respective chloro or bromo complexes, are summarized in Scheme 7.[37]

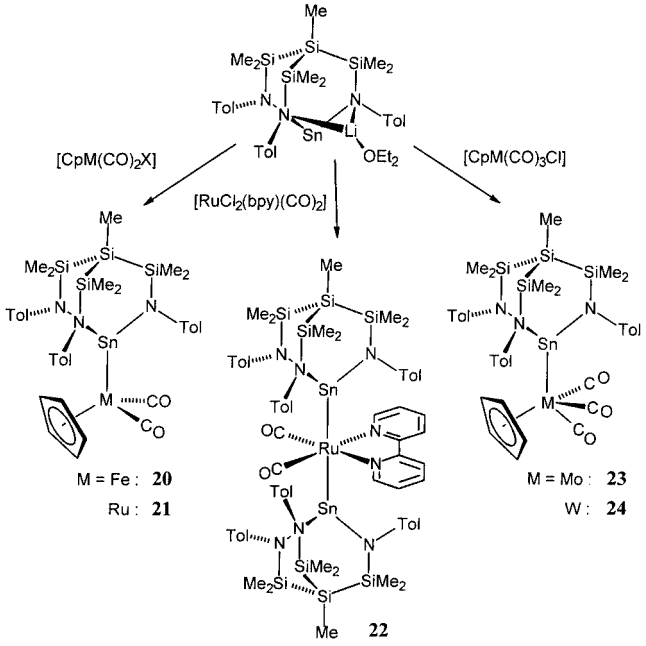

Scheme 7. Coordination of a tripodal triamidostannate to late transition metal complex fragments

In the molecular structure of **22**, depicted in Figure 10, the two $[MeSi\{SiMe_2N(4\text{-}CH_3C_6H_4)\}_3Sn]^-$ ligands are bonded to the Ru centre in a nearly linear fashion [Sn(1)–Ru–Sn(2) 174.26(2)°] and are staggered with respect to their tolyl groups. The Ru–Sn bond lengths of 2.7085(5) and 2.7324(5) Å are slightly longer than the typical value for Ru–Sn bonds (2.55–2.69 Å)

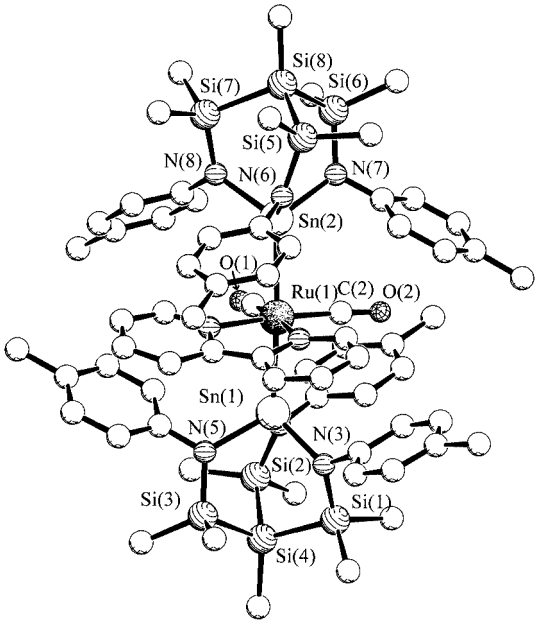

Figure 10. Molecular structure of the Sn−Ru−Sn complex **22**

.

Although the anionic complex $[(Ph_3Sn)Ni(CO)_3]^-$ was first reported by Kruck et al. in 1969, there had been no report of a crystal structure of an $[(R_3Sn)Ni(CO)_3]^-$ anion in the literature. Treatment of the chiral lithium stannate $[HC\{SiMe_2N[(S)\text{-1-phenylethyl}]\}_3Sn-Li(THF)]$ (**15**) with $[Ni(CO)_4]$ cleanly gave the Ni−Sn complex $[Li(THF)_4][HC\{SiMe_2N[(S)\text{-1-phenylethyl}]\}_3Sn-Ni(CO)_3]$ (**25**).[22] Crystals of **25** were found to be extremely air- and moisture-sensitive, and therefore had to be selected and mounted at ca. −80 °C. In the [2.2.2]bicyclooctane-derived cage, one of the bridgehead positions is occupied by the $Sn-Ni(CO)_3$ fragment (Figure 11).

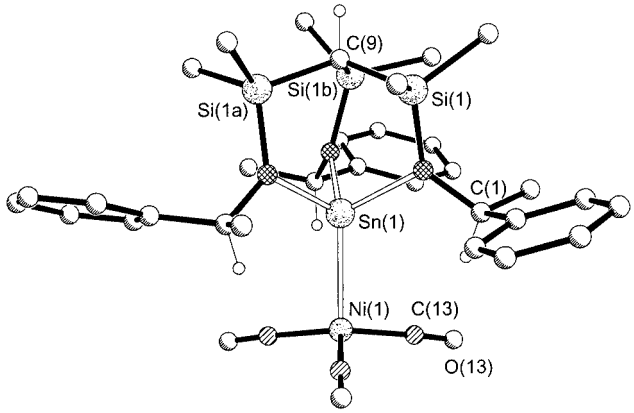

Figure 11. Molecular structure of the Ni−Sn complex $[HC\{SiMe_2N[(S)\text{-1-phenylethyl}]\}_3Sn-Ni(CO)_3]$ (**25**), containing a C_3-chiral triamidostannate

The Sn(1)−Ni(1) vector is aligned along the threefold crystallographic axis, imposing exact C_3 symmetry upon the anion. The Sn−Ni bond length of 2.492(2) Å is unexceptional; however, we note that the coordination of the Lewis acidic $Ni(CO)_3$ fragment to the Lewis basic stannate effects a significant shortening of the Sn−N distances [Sn(1)−N(1) 2.086(6) Å] in comparison to those in the lithium stannate **15** [average Sn−N 2.174(6) Å]. The stannate ligand is readily displaced from the nickel by better donors such as phosphanes and isocyanides.[22]

Triamidometallates Coordinated to the Coinage Metals: Copper, Silver and Gold(I, II and III) Complexes

In contrast to the extensive investigations into the chemistry of organometallic complexes of the coinage metals, there have, until recently, been comparatively few compounds containing direct metal−metal bonds between copper, silver or gold and the heavier group 14 elements.[38]

We were able to provide the first crystallographically characterized example of a digermanylaurate (**26**) by treatment of the triamidogermanate(II) $[MeC(CH_2NSiMe_3)_3Ge-Li(THF)_2]$ with $[Ph_4P][AuBr_2]$, the corresponding Sn−Au−Sn analogue also being accessible by the same route (Scheme 8).[39]

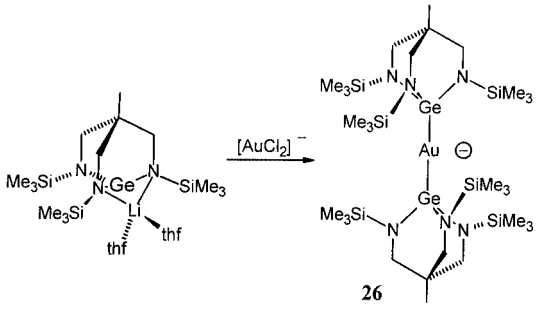

Scheme 8. Synthesis of the first digermanylaurate **26**

Treatment of the stannate $[MeSi\{SiMe_2N(4-CH_3C_6H_4)\}_3SnLi(OEt_2)]$ (**27**) with 0.25 mol-equiv. of $[CuCl(PPh_3)]_4$ or 1 equiv. of $[AuCl(PPh_3)]$ in toluene at room temperature gave the corresponding Sn−Cu and Sn−Au complexes $[MeSi\{SiMe_2N(4-CH_3C_6H_4)\}_3Sn-Cu-$

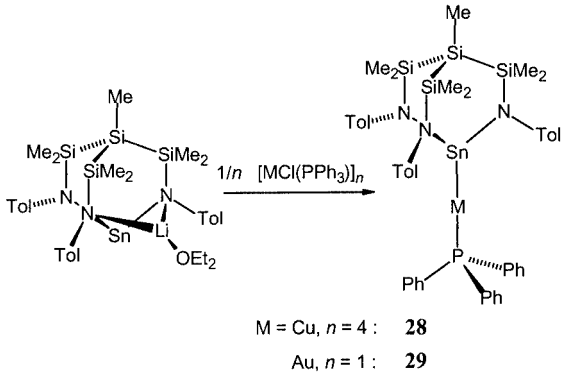

Scheme 9. Synthesis of the coinage metal/tin compounds **28** and **29**

$(PPh_3)]$ (**28**)[37] and $[MeSi\{SiMe_2N(4\text{-}CH_3C_6H_4)\}_3Sn-Au(PPh_3)]$ (**29**) (Scheme 9).[40] The formation of Sn−Cu and Sn−Au bonds in these complexes is supported by the observation of $^{117/119}Sn$ satellites in their ^{31}P NMR spectra. Neither compound apparently undergoes detectable redistribution reactions in solution.

The crystal structure of **29** confirms the conclusions drawn from the spectroscopic data. In its molecular structure (Figure 12), the triamidostannate cage is directly bonded to the Ph_3PAu unit [d(Au−Sn) = 2.5651(13) Å], the gold atom adopting an essentially linear geometry [<(Sn−Au−P(1) = 179.9(1)°], as expected for monovalent gold. This Sn−Au distance is slightly shorter than that found for $[Au_8(PPh_3)_7(SnCl_3)][SnCl_6]$ [2.625(3) Å],[41] and considerably shorter than those in the tricoordinate Au^I complex $[(PMe_2Ph)_2AuSnCl_3]$ [2.881(1) Å][42] and in the polynuclear compound $[Au_4(PPh_3)_4(\mu_2\text{-}SnCl_3)_2]$ [2.8150(7), 2.9725(8) Å], for which a weak Sn−Au interaction was proposed.[43]

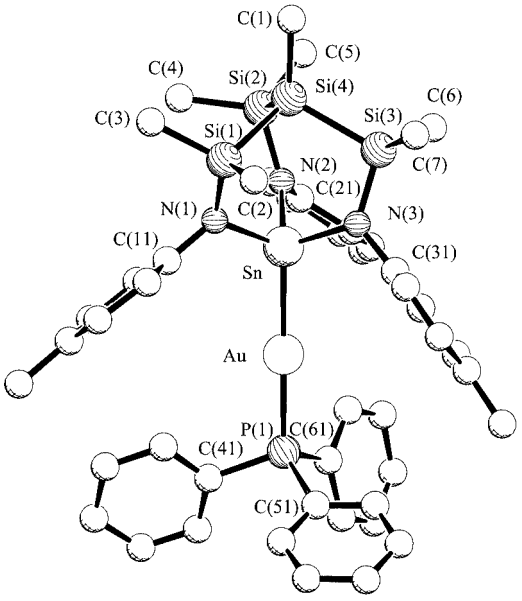

Figure 12. Molecular structure of $[MeSi\{SiMe_2N(4\text{-}CH_3C_6H_4)\}_3Sn-Au(PPh_3)]$ (**29**)

The stannate **27** reacts with various other gold halide complexes by salt metathesis and formation of the metal−metal bond to afford the respective tin−gold heteronuclear compounds. By this approach, gold(I−III) complexes **30**−**34** have been obtained upon treatment of the stannate with $[PPN][AuCl_2]$, $[PPN][AuCl(R)]$ (R = C_6F_5, mesityl), $[Au_2(CH_2PPh_2CH_2)_2Cl_2]$ and $[PPN][AuCl(C_6F_5)_3]$, respectively (Scheme 10).[40]

An X-ray diffraction study of the first example of an $Sn-Au^{II}$ complex **30** established the details of its molecular structure (Figure 13). The Sn−Au bond length is 2.6804(13) Å, and thus significantly longer than the Sn−Au distance in the gold(I) derivative $[MeSi\{Me_2SiN(p\text{Tol})\}_3SnAu(PPh_3)]$ (**29**) discussed above [2.5651(13) Å]. This may be a consequence of the steric repulsion between the periphery of the tripodal amido ligand and the bis(ylide) ligands coordinated to the Au_2 unit. The coordination geometry of the gold(II) centres is square-planar, as usually exhibited in gold(II) derivatives with gold−gold bonds. The $Au^{II}-Au^{II}$ distance is 2.7492(13) Å, one of the longest found in these type of gold(II) complexes, the only species with a longer Au−Au bond being $[\{(C_6F_5)Au(CH_2PPh_2CH_2)_2Au\}Au(C_6F_5)_2][Au(C_6F_5)_4]$ [2.755(1) Å].[44]

Ag−Sn heterobimetallic compounds are particularly rare, the only known molecular species containing an Ag−Sn bond prior to our studies being $[(Ph_3P)_3AgSnCl_3]$.[44] While this compound has been the object of several spectroscopic studies, there was no direct structural proof for an Sn−Ag bond. Since stannous chloride finds applications in photography as a reduction sensitizer for silver halide emulsions,[46] a more detailed investigation of such Ag^ISn^{II} systems was of general interest.

Upon treatment of **27** with 0.25 mol-equiv. of $[(Ph_3P)AgCl]_4$, the two Ag−Sn-bonded phosphane-containing products together with $[MeSi\{SiMe_2N(4\text{-}CH_3C_6H_4)\}_3Sn-Ag(PPh_3)]$ (**35**) and $[MeSi\{SiMe_2N(4\text{-}CH_3C_6H_4)\}_3Sn-Ag(PPh_3)_2]$ (**36**) were detected in solution, the latter being directly accessible by treatment of the stannate with $[Ag(PPh_3)_2][CF_3SO_3]$ (Scheme 11). The phosphane-free component **37** in this equilibrium mixture could be isolated by fractional crystallization. While the analytical data were consistent with a formulation of **37** as $[MeSi\{SiMe_2N(p\text{Tol})\}_3Sn-Ag]_n$, a single-crystal X-ray structure analysis established a dimeric structure corresponding to $[MeSi\{SiMe_2N(p\text{Tol})\}_3Sn-Ag]_2$ (Figure 14).[47]

The molecular structure of **37** is based on a centrosymmetric dimeric molecular unit featuring two Sn atoms, each coordinated by a tripod-triamido ligand. Each Sn atom links to an Ag atom through an Sn−Ag bond [d(Sn−Ag) = 2.6567(7) Å]. The two Ag centres in the complex are in close proximity; the d(Ag−Ag′) distance [= 2.6544(11) Å] is among the shortest ever observed in Ag^I aggregates and may indicate a significant $d^{10}-d^{10}$ attraction. In **37**, the ligand periphery plays an "active" role and facilitates the dimerization of the silver stannate units. These monomer units are linked by η^2-coordination of one tolyl group of each tripodal amido ligand to the silver atom of the opposite unit [d(Ag−C25′) = 2.604(5); d(Ag−C26′) = 2.374(4) Å], the asymmetry of the η^2-coordination in the complex being typical of arene−Ag^I interactions.[48]

The presence of a ligand redistribution equilibrium of the Ag−Sn complexes is a manifestation of the propensity of Ag^I species to attain coordination numbers higher than two. The displacement of the phosphane ligand may additionally be favoured by the possibility of "arene solvation" of the Ag centres. This study provided the first direct structural evidence for an Ag−Sn bond. More recently, however, Lappert and co-workers have reported another structurally characterized Ag−Sn heterodimetallic complex.[49]

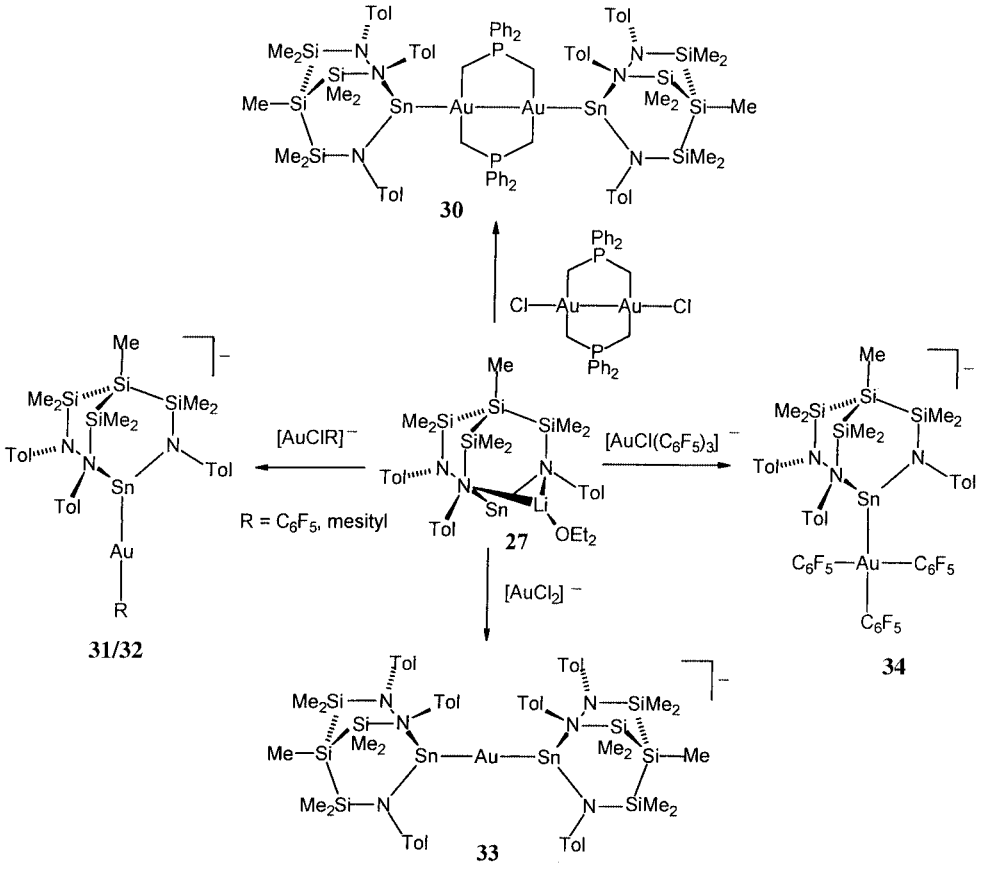

Scheme 10. Synthesis of $Au^{I}-Sn$, $Au^{II}-Sn$ and $Au^{III}-Sn$ complexes

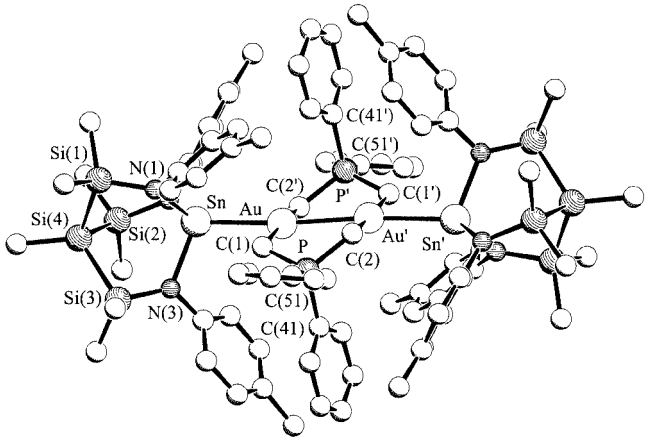

Figure 13. Molecular structure of the $Sn-Au^{II}-Au^{II}-Sn$ complex **30**

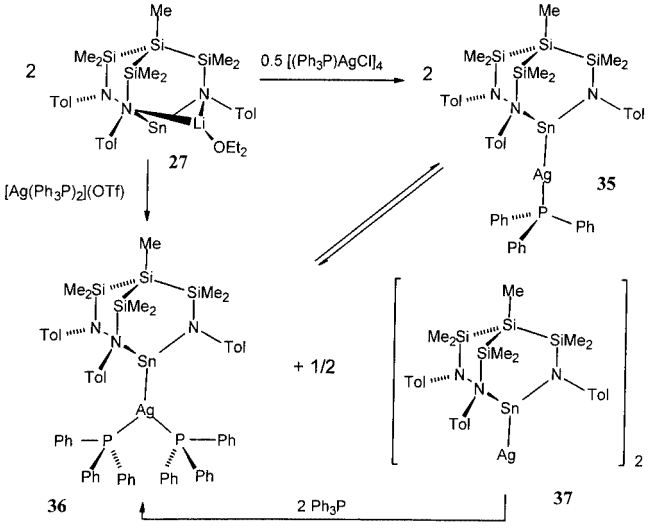

Scheme 11. Ag−Sn complexes **35−37**, which are in equilibrium in solution, upon treatment of the lithium stannate **27** with $[AgCl(PPh_3)]_4$

Group 12 Metal/Tin Complexes

Complexes containing bonds between group 12 metals and a group 14 element are versatile reagents in synthetic chemistry. The most prominent examples are cyclopropanation reactions with (α-halomethyl)mercury compounds,[50] the reductive replacement of mercury by hydrogen, the use of $Hg(SiMe_3)_2$ as a silylating reagent[51] and the photolytic cleavage of $Hg(SiMe_3)_2$ to yield silyl radicals.[52] Although a few examples of structurally characterized complexes with the lighter group 14 metals (Si, Ge)[53] have been reported, and compounds such as $R_3Sn-Hg-SnR_3$ have been spectroscopically studied in detail,[54] there was, at the time we began our studies, no direct structural characterization of

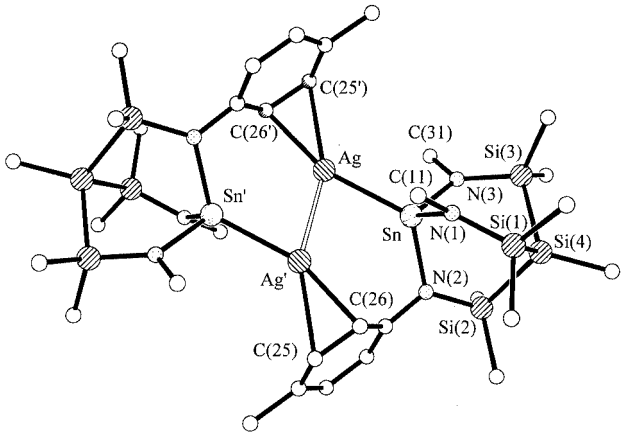

Figure 14. Molecular structure of the first crystallographically characterized Ag−Sn complex; the two molecular units are linked by attractive Ag−arene and Ag−Ag interactions; the peripheral tolyl groups not coordinated to Ag are omitted in this representation for clarity

either Sn−Hg or Sn−Cd bonds and only a single example of a crystallographically authenticated Sn−Zn complex[55] to be found in the literature.

Treatment of the lithium stannate **27** with MCl_2 (M = Zn, Cd, Hg) cleanly gave the corresponding Sn−M−Sn complexes **38**−**40** (Scheme 12).[56] Whereas the linear Sn−Hg−Sn complex is stable in solution, the cadmium compound **39** − while also linear in the crystal − is in equilibrium with a second, less symmetrical isomer, as became evident from NMR studies carried out in solution. This second structural arrangement is the most stable form of the Sn−Zn−Sn complex **38** and is also found in its crystal structure.[56] Here the tendency of the "dication" Zn^{2+} to adopt coordination numbers greater than two and ligands containing hard donor atoms becomes readily apparent.

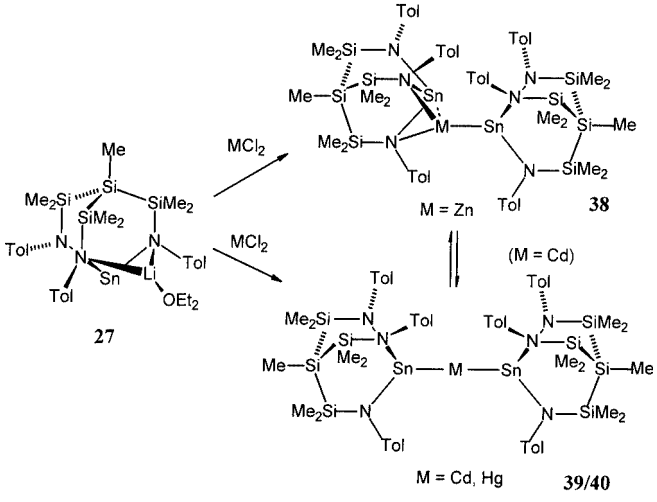

Scheme 12

Beyond the Rigid [2.2.2]Bicyclooctane Cage

Recent work from Veith's group indicates that the principles outlined in this overview might possibly be extendable to systems with less rigid structures. Those workers synthesized the tripodal amido ligand $[t\text{BuSi(OSiMe}_2\text{NPh)}_3]^{3-}$,[57] which was coordinated to divalent germanium, to give a lithium triamidogermanate with a direct Ge−Li bond $[t\text{BuSi(OSiMe}_2\text{NPh)}_3\text{Ge−Li(THF)}_3]$ (**41**). This compound was in turn hydrolysed to give the corresponding Ge−H germane **42** and oxidized to yield the lithium oxogermanate(IV) **43** (Scheme 13).[58]

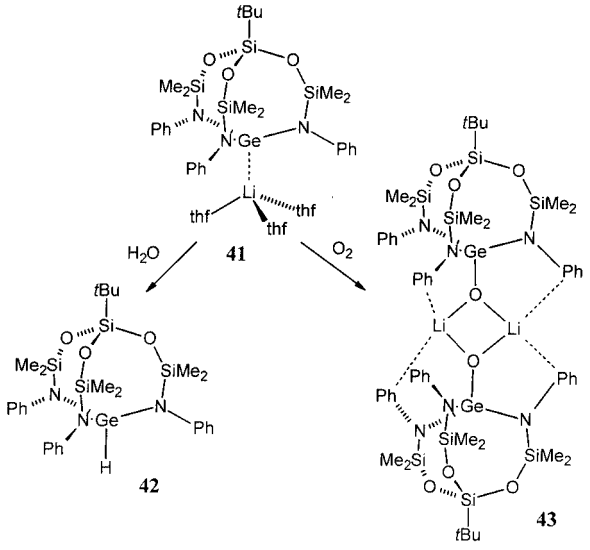

Scheme 13

The different orientation of the N-donor functions imposed by the expanded ligand framework allows for structural motifs somewhat different to those that we found for the systems discussed above. It will be interesting to learn more about the "ligand" properties of these systems.

Conclusions and Outlook

The combination of thermodynamic stabilization of the triamidometallates by their integration into a rigid molecular cage structure, along with the well-defined orientation and high variability of the peripheral N-substituents, has established tripodal triamidometallates as a versatile new class of ligands in the coordination chemistry of the transition metals. The electronegative N-substituents at the divalent metal atoms render them less oxidizable than would be expected for alkyl- or aryl-substituted derivatives.

The first results of our attempts to stabilize low-coordinate late transition metal complexes with catalytically relevant metals such as rhodium or palladium suggests that the monoanionic group 14 metallates, apart from being objects of study in their own right, may find applications in the development of novel homogeneous catalysts.

Acknowledgments

I thank my dedicated co-workers for their contributions to this chemistry. The field was opened up for us by Konrad Hellmann and then further developed by Bernd Findeis. Uta Kauper and Claudia Bott also provided significant input at this early stage.

Most recently, Matthias Lutz, who has been delocalized between our laboratory and the University of Joesuu in Finland, has made important advances. The fruitful collaboration with Tapani Pakkanen (Joensuu), Mary McPartlin (London), Dietmar Stalke (Würzburg) and Mariano Laguna (Zaragoza) has been a significant factor in developing the research programme. The author acknowledges funding by the Deutsche Forschungsgemeinschaft, the European Commission (TMR network MECATSYN) and the CNRS (France).

[1] Selected early examples of heterocubane cages. Alkali metal alkyl compounds: [1a] E. Weiss, E. A. Lucken, *J. Organomet. Chem.* **1964**, *2*, 197−205. [1b] M. Geissler, J. Kopf, B. Schubert, E. Weiss, *Angew. Chem.* **1987**, *99*, 569−570; *Angew. Chem. Int. Ed. Engl.* **1987**, *26*, 587−588. [1c] H. Hope, P. P. Power, *J. Am. Chem. Soc.* **1983**, *105*, 5320−5324. [1d] H. Schmidbaur, A. Schier, U. Schubert, *Chem. Ber.* **1983**, *116*, 1938−1046. Main group imido cubanes: [1e] G. Del Piero, M. Cesari, G. Dozzi, A. Mazzei, *J. Organomet. Chem.* **1977**, *129*, 281−288. [1f] M. Veith, O. Recktenwald, *Z. Naturforsch., Teil B* **1983**, *38*, 1054−1061. Main group alkoxy cubanes: [1g] L. F. Dahl, G. L; Davies, D. L. Wampler, K. J. West, *J. Inorg. Nucl. Chem.* **1962**, *24*, 357−363. Examples of fused Sn−N cubanes: [1h] F. Benevelli, E. L. Doyle, E. A. Harron, N. Feeder, E. A. Quadrelli, D. Saéz, D. S. Wright, *Angew. Chem.* **2000**, *112*, 1561−1563; *Angew. Chem. Int. Ed.* **2000**, *39*, 1501−1503. [1i] N. Feeder, E. A. Harron, M. E. G. Mosquera, A. D. Woods, D. S. Wright, *Chem. Commun.* **2001**, 1010−1011.

[2] See for example: [2a] M. Driess, *Acc. Chem. Res.* **1999**, *32*, 1017−1025. [2b] M. Driess, *Adv. Inorg. Chem.* **2000**, *50*, 235−284.

[3] M. Veith, *Chem. Rev.* **1990**, *90*, 3−16.

[4] See for example: [4a] R. Murugavel, V. Chandrasekhar, H. W. Roesky, *Acc. Chem. Res.* **1996**, *29*, 183−189. [4b] M. R. Mason, *J. Cluster Sci.* **1998**, *9*, 1−23. [4c] M. Unno, S. B. Alias, M. Arai, K. Takada, R. Tanaka, H. Matsumoto, *Appl. Organomet. Chem.* **1999**, *13*, 303−310. [4d] M. G. Walawalkar, H. W. Roesky, R. Murugavel, *Acc. Chem. Res.* **1999**, *32*, 117−126.

[5] M. A. Beswick, M. E. G. Mosquera, D. S. Wright, *J. Chem. Soc., Dalton Trans.* **1998**, 2437−2443.

[6] M. Veith, S. Weidner, K. Kunze, D. Käfer, J. Hans, V. Huch, *Coord. Chem. Rev.* **1994**, *137*, 297−322.

[7] [7a] L. H. Gade, N. Mahr, *J. Chem. Soc., Dalton Trans.* **1993**, 489−494. [7b] L. H. Gade, C. Becker, J. W. Lauher, *Inorg. Chem.* **1993**, *32*, 2308−2314. [7c] H. Memmler, L. H. Gade, J. W. Lauher, *Inorg. Chem.* **1994**, *33*, 3064−3071. [7d] M. Schubart, B. Findeis, L. H. Gade, W.-S. Li, M. McPartlin, *Chem. Ber.* **1995**, *128*, 329−334.

[8] [8a] M. Veith, R. Rösler, *Z. Naturforsch., Teil B* **1986**, *41*, 1071−1080. [8b] M. Veith, D. Käfer, V. Huch, *Angew. Chem.* **1986**, *98*, 367−368; *Angew. Chem. Int. Ed. Engl.* **1986**, *25*, 375−377. [8c] M. Veith, C. Ruloff, V. Huch, F. Töllner, *Angew. Chem.* **1988**, *100*, 1418−1419; *Angew. Chem. Int. Ed. Engl.* **1988**, *27*, 1381−1382.

[9] M. A. Beswick, M. K. Davies, P. R. Raithby, A. Steiner, D. S. Wright, *Organometallics* **1997**, *16*, 1109−1110.

[10] A. Steiner, D. Stalke, *J. Chem. Soc., Chem. Commun.* **1993**, 1702−1704.

[11] H. V. R. Dais, M. M. Olmstead, K. Ruhlandt-Senge, P. P. Power, *J. Organomet. Chem.* **1993**, *462*, 1−6.

[12] D. Reed, D. Stalke, D. S. Wright, *Angew. Chem.* **1991**, *103*, 1539−1540; *Angew. Chem. Int. Ed. Engl.* **1991**, *30*, 1459−1460.

[13] D. R. Armstrong, M. G. Davidson, D. Moncrieff, D. Stalke, D. S. Wright, *J. Chem. Soc., Chem. Commun.* **1992**, 1413−1414.

[14] P. B. Hitchcock, M. F. Lappert, G. A. Lawless, B. Royo, *J. Chem. Soc., Chem. Commun.* **1993**, 554−555.

[15] M. A. Paver, C. A. Russel, D. S. Wright, *Angew. Chem.* **1995**, *107*, 1677−1686; *Angew. Chem. Int. Ed. Engl.* **1995**, *34*, 1545−1554.

[16] L. H. Gade, *Angew. Chem.* **2000**, *112*, 2768−2789; *Angew. Chem. Int. Ed.* **2000**, *37*, 2658−2678.

[17] [17a] L. H. Gade, K. W. Hellmann, J. Wolf, H. Werner, I. J. Scowen, M. McPartlin, unpublished results. [17b] K. W. Hellmann, PhD Thesis, Universität Würzburg, **1997**.

[18] K. W. Hellmann, L. H. Gade, O. Gevert, P. Steinert, J. W. Lauher, *Inorg. Chem.* **1995**, *34*, 4069−4078.

[19] I. Haller, P. Renner, L. H. Gade, *Polyhedron (Symposia-in-Print)*, in press.

[20] K. W. Hellmann, P. Steinert, L. H. Gade, *Inorg. Chem.* **1994**, *33*, 3859−3960.

[21] A. J. Edwards, M. A. Paver, P. R. Raithby, C. A. Russell, D. S. Wright, *J. Chem. Soc., Chem. Commun.* **1993**, 1086−1088.

[22] H. Memmler, U. Kauper, L. H. Gade, D. Stalke, J. W. Lauher, *Organometallics* **1996**, *15*, 3637−3939.

[23] H. Memmler, PhD Thesis, Universität Würzburg, **1996**.

[24] M. Veith, M. Zimmer, S. Müller-Becker, *Angew. Chem.* **1993**, *105*, 1771−1773; *Angew. Chem. Int. Ed. Engl.* **1993**, *32*, 1731−1733.

[25] H. Memmler, K. Walsh, L. H. Gade, J. W. Lauher, *Inorg. Chem.* **1995**, *34*, 4062−4068.

[26] L. H. Gade, *Chem. Commun.* **2000**, 173−182.

[27] M. Lutz, C. Galka, M. Haukka, T. A. Pakkanen, L. H. Gade, to be submitted.

[28] M. S. Holt, W. L. Wilson, J. H. Nelson, *Chem. Rev.* **1989**, *89*, 11−49.

[29] K. M. Mackay, B. K. Nicholson in *Comprehensive Organometallic Chemistry* (Eds.: G. Wilkinson, F. G. A. Stone, E. W. Abel), Pergamon Press, New York, **1982**, vol. 6, p. 1043.

[30] [30a] R. S. P. Croutts, P. C. Wailes, *J. Chem. Soc., Chem. Commun.* **1968**, 260−261. [30b] B. M. Kingston, M. F. Lappert, *J. Chem. Soc., Dalton Trans.* **1972**, 69−73. [30c] H. M. Creemers, J. C. Verbeek, H. G. Noltes, *Organomet. Chem.* **1968**, *15*, 125−130. [30d] W. Zheng, D. W. Stephan, *Inorg. Chem.* **1988**, *27*, 2386−2388.

[31] M. Lutz, B. Findeis, M. Haukka, T. A. Pakkanen, L. H. Gade, *Organometallics* **2001**, *20*, 2505−2509.

[32] L. Pauling, *The Nature of the Chemical Bond*, 2nd ed., Cornell University Press, Ithaca, NY, **1960**.

[33] J. E. Ellis, P. Yuen, M. Jang, *J. Organomet. Chem.* **1996**, *507*, 283−286.

[34] F. G. N. Cloke, K. P. Cox, M. L. H. Green, J. Bashkin, K. Prout, *J. Chem. Soc., Chem. Commun.* **1981**, 117−118.

[35] J. E. Ellis, K.-M. Chi, A.-J. DiMaio, S. R. Frerichs, J. R. Stenzel, A. L. Rheingold, B. S. Haggerty, *Angew. Chem.* **1991**, *103*, 196−198; *Angew. Chem. Int. Ed. Engl.* **1991**, *30*, 194−196.

[36] K. W. Hellmann, S. Friedrich, L. H. Gade, W.-S. Li, M. McPartlin, *Chem. Ber.* **1995**, *128*, 29−34.

[37] M. Lutz, B. Findeis, M. Haukka, T. A. Pakkanen, L. H. Gade, *Eur. J. Inorg. Chem.* **2001**, 3155−3162.

[38] [38a] A. Bauer, A. Schier, H. Schmidbaur, *J. Chem. Soc., Dalton Trans.* **1995**, 2919−2920. [38b] A. Bauer, H. Schmidbaur, *J. Am. Chem. Soc.* **1996**, *118*, 5324−5325.

[39] M. Contel, K. W. Hellmann, L. H. Gade, I. Scowen, M. McPartlin, M. Laguna, *Inorg. Chem.* **1996**, *35*, 3713−3715.

[40] B. Findeis, M. Contel, L. H. Gade, M. Laguna, M. C. Gimeno, I. J. Scowen, M. McPartlin, *Inorg. Chem.* **1997**, *36*, 2386−2390.

[41] Z. Demidowicz, R. L. Johnston, J. C. Machell, D. M. P. Mingos, I. D. Williams, *J. Chem. Soc., Dalton Trans.* **1988**, 1751−1756.

[42] W. Clegg, *Acta Crystallogr., Sect. B* **1978**, *34*, 278−281.

[43] D. M. P. Mingos, H. R. Powell, T. L. Stolbert, *Trans. Met. Chem.* **1992**, *17*, 334−337.

[44] R. Usón, A. Laguna, M. Laguna, J. Jimenez, P. G. Jones, *Angew. Chem.* **1990**, *102*, 190−191; *Angew. Chem. Int. Ed. Eng.* **1991**, *30*, 198−199.

[45] [45a] J. A. Dilts, M. P. Johnson, *Inorg. Chem.* **1966**, *5*, 2079−2081. [45b] D. V. Sanghani, P. J. Smith, D. W. Allen, B. F. Taylor, *Inorg. Chim. Acta* **1982**, *59*, 203−206. [45c] R. V. Parish, P. J. Rowbotham, *J. Chem. Soc., Dalton Trans.* **1973**, 37−41.

[45d] M. J. Mays, P. L. Sears, *J. Chem. Soc., Dalton Trans.* **1974**, 2254−2256. [45e] P. A. Grutsch, M. V. Zeller, T. P. Fehlner, *Inorg. Chem.* **1973**, *12*, 1431−1433.
[46] [46a] S. S. Collier, *Photog. Sci. Eng.* **1979**, *23*, 113−117. [46b] J. M. Harbison, H. E. Spencer in *The Theory of the Photographic Process* (Ed.: T. H. James), McMillan, New York, **1977**, p. 149.
[47] B. Findeis, L. H. Gade, I. J. Scowen, M. McPartlin, *Inorg. Chem.* **1997**, *36*, 960−961.
[48] Early examples: [48a] H. G. Smith, R. E. Rundle, *J. Am. Chem. Soc.* **1958**, *80*, 5075−5080. [48b] R. W. Turner, E. L. Amma, *J. Am. Chem. Soc.* **1966**, *88*, 3243−3247. [48c] I. F. Taylor, E. A. Hall, E. L. Amma, *J. Am. Chem. Soc.* **1969**, *91*, 5745−5749. [48d] E. A. H. Griffith, E. L. Amma, *J. Am. Chem. Soc.* **1974**, *96*, 5407−5413. [48e] S. H. Strauss, M. D. Noirot, O. P. Anderson, *Inorg. Chem.* **1985**, *24*, 4307−4311. [48f] R. Uson, A. Laguna, M. Laguna, B. R. Manzano, P. G. Jones, G. M. Sheldrick, *J. Chem. Soc., Dalton Trans.* **1984**, 285−292.
[49] P. B. Hitchcock, M. F. Lappert, L. J. M. Pierssens, *Organometallics* **1998**, *17*, 2686−2688.
[50] [50a] D. Seyferth, *Acc. Chem. Res.* **1972**, *5*, 65−74. [50b] D. Seyferth, M. A. Eisert, L. J. Todd, *J. Am. Chem. Soc.* **1964**, *86*, 121−122.
[51] [51a] W. P. Neumann, K. Reuter, *J. Organomet. Chem. Libr.* **1979**, *7*, 229−255. [51b] F. Hoefler, *Top. Curr. Chem.* **1974**, *50*, 129−165.
[52] [52a] C. Eaborn, R. A. Jackson, R. Pearce, *J. Chem. Soc., Chem. Commun.* **1967**, 920−920. [52b] S. W. Bennett, C. Eaborn, R. A. Jackson, R. Pearce, *J. Organomet. Chem.* **1971**, *28*, 59−72.
[53] [53a] L. G. Kuz'mina, T. V. Timofeeva, Yu. T. Struchkov, M. N. Bochkarev, *Zh. Strukt. Khim.* **1981**, *22*, 60−67. [53b] D. Bravo-Zhivotovskii, M. Yuzefovich, M. Bendikov, K. W. Klinkhammer, Y. Apeloig, *Angew. Chem.* **1999**, *111*, 1169−1171; *Angew. Chem. Int. Ed.* **1999**, *38*, 1100−1102. [53c] M. J. Albright, T. F. Schaaf, W. M. Butler, A. K. Hovland, M. D. Glick, J. P. Oliver, *J. Am. Chem. Soc.* **1975**, *97*, 6261−265. [53d] W. H. Ilsley, M. J. Albright, T. J. Anderson, M. D. Glick, J. P. Oliver, *Inorg. Chem.* **1980**, *19*, 3577−3585. [53e] W. H. Ilsley, E. A. Sadurski, T. F. Schaaf, M. J. Albright, T. J. Anderson, M. D. Glick, J. P. Oliver, *J. Organomet. Chem.* **1980**, *190*, 257−265. [53f] N. Wiberg, K. Amelunxen, H.-W. Lerner, H. Nöth, A. Appel, J. Knizek, K. Polborn, *Z. Anorg. Allg. Chem.* **1997**, *623*, 1861−1870. [53g] S. N. Titova, V. T. Bychkov, G. A. Domrachev, G. A. Razuvaev, L. N. Zakharov, G. G. Aleksandrov, Yu. T. Struchkov, *Inorg. Chim. Acta* **1981**, *50*, 71−77. [53h] K. W. Klinkhammer, J. Weidlein, *Z. Anorg. Allg. Chem.* **1996**, *622*, 1209−1214. [53i] N. L. Pickett, O. Just, D. G. VanDerveer, W. S. Rees, *Acta Crystallogr., Sect. C* **2000**, *56*, 412−413.
[54] [54a] Yu. K. Grishin, V. A. Roznyatovskii, U. A. Ustynyuk, M. N. Bochkarev, G. S. Kalinina, G. A. Razuvaev, *Izv. Akad. Nauk. SSSR, Ser. Khim.* **1980**, 2190−2190. [54b] O. A. Kruglaya, G. S. Kalinina, B. I. Petrov, N. S. Vyazankin, *J. Organomet. Chem.* **1972**, *46*, 51−58. [54c] M. F. Larin, D. V. Gendin, V. A. Pestunovich, O. A. Kruglaya, N. S. Vyazankin, *Izv. Akad. Nauk. SSSR, Ser. Khim.* **1979**, 697−698. [54d] U. Blaukat, W. P. Neumann, *J. Organomet. Chem.* **1973**, *63*, 27−39. [54e] C. Eaborn, A. R. Thompson, D. R. M. Walton, *J. Chem. Soc., Chem. Commun.* **1968**, 1051−1052.
[55] J. T. B. H. Jastrzebski, H. A. J. Sypkens, F. J. A. de Tonbe, P. A. van der Schaaf, J. Boersma, G. van Koten, A. L. Spek, A. J. M. Duisenberg, *J. Organomet. Chem.* **1990**, *396*, 25−31.
[56] M. Lutz, B. Findeis, M. Haukka, T. A. Pakkanen, L. H. Gade, submitted for publication.
[57] M. Veith, O. Schütt, V. Huch, *Z. Anorg. Allg. Chem.* **1999**, *625*, 1155−1164.
[58] M. Veith, O. Schütt, V. Huch, *Angew. Chem.* **2000**, *112*, 614−617; *Angew. Chem. Int. Ed.* **2000**, *39*, 601−604.

Received November 5, 2001
[I01433]

cine and *tele* Nucleophilic Substitutions in (η^6-Arene)tricarbonylchromium and Tricarbonyl(η^5-cyclohexadienyl)manganese Complexes

Françoise Rose-Munch*[a] and Eric Rose*[a]

Keywords: Arene ligands / Carbonyl ligands / Chromium / Manganese / Nucleophilic substitution

Addition of a nucleophile to an (η^6-arene)tricarbonylchromium or a tricarbonyl(η^5-cyclohexadienyl)manganese complex substituted with a leaving group X (X = F, Cl, OMe, OPh, NR_2) affords (after treatment with acid) new complexes with the same η^6 or η^5 hapticity. The overall reaction involves addition of the nucleophile *ortho*, *meta*, or *para* with respect to the leaving group and HX elimination.

(© Wiley-VCH Verlag GmbH, 69451 Weinheim, Germany, 2002)

I. Introduction

Coordination of a transition metal atom to the π-system of an arene **1** and a cyclohexadienyl ring **3** activates the ring towards addition of nucleophiles to give (η^5-cyclohexadienyl)- and (η^4-cyclohexadiene)metal complexes **2** and **4**, respectively (Scheme 1). The (η^6-arene)tricarbonylchromium complexes **1** [M = $Cr(CO)_3$] undergo a number of very useful reactions, and have found significant applications in organic and organometallic syntheses.[1−4] Moreover, their preparation is very easy and they are usually air-stable, crystalline solids and, furthermore, the free arene may readily be released from complexation by mild oxidation of the metal atom. The neutral (η^5-cyclohexadienyl)manganese complexes **3** [M = $Mn(CO)_3$] are beginning to receive more and more attention because they are easily handled in nonpolar solvents and so may be purified very conveniently by silica gel chromatography. They are also easily obtained from the corresponding, highly electrophilic, cationic manganese complexes **1** [M = $Mn^+(CO)_3$] by addition of a wide range of nucleophiles. It has been shown that these neutral manganese complexes **3** display reactivity similar to some extent to that of the (η^6-arene)chromium complexes; thus *cine* and *tele* nucleophilic substitutions and − recently − Pd-mediated reactions[5] have been reported to occur under mild conditions.

[a] Laboratoire de Synthèse Organique et Organométallique, UMR CNRS 7611, Université Pierre et Marie Curie,
Tour 44, 1er étage, 4, Place Jussieu, 75252 Paris Cedex 05, France
Fax: (internat.) + 33-1/44275504
E-mail: rose@ccr.jussieu.fr
rosemun@ccr.jussieu.fr

Françoise Rose-Munch was born in Metz, France. She entered the CNRS in 1975 and received her "Doctorat d'Etat" in 1976 from the University Pierre et Marie Curie, Paris, working under the supervision of Prof. Jacques Levisalles. After a postdoctoral period in 1976 and 1977 at the University of Stanford, California, USA with Prof. Jim Collman, she returned to Paris and was promoted to "Directrice de Recherche" in 1992. Her research interests concern the organometallic chemistry of Pd, Fe, Cr, and Mn complexes, nucleophilic substitutions in (arene)metal complexes, and their application in nonlinear optics.

Eric Rose was born in Nancy, France. He entered the CNRS in 1970 and received his "Doctorat d'Etat" in 1975 from the University Pierre et Marie Curie, Paris, working under the supervision of Prof. Jacques Levisalles. After a postdoctoral period in 1976 and 1977 at the University of Stanford, California, USA, with Prof. Jim Collman, he then moved back to Paris and was promoted to "Directeur de Recherche" in 1985. His research interests focus on the preparation of models of hemoproteins (Mb, Hb, cyt P450) and of new chiral porphyrins as catalysts for the epoxidation of terminal olefins, as well as nucleophilic substitutions in (arene)metal complexes.

MICROREVIEWS: This feature introduces the readers to the authors' research through a concise overview of the selected topic. Reference to important work from others in the field is included.

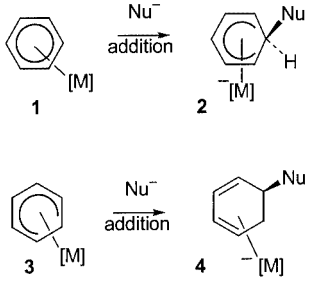

Scheme 1

In this review we focus on recent work investigating nucleophilic substitutions on (η^6-ligand)chromium complexes and (η^5-ligand)manganese complexes. After a brief description of the preparation of these complexes (Cr, Mn), some general reactivity patterns mostly related to the nucleophilic substitutions of (arene)$Cr(CO)_3$ are outlined. Later sections concern *cine* and *tele* nucleophilic substitution in chromium and manganese complexes, with up-to-date examples from current literature.

II. Complexation Methods

(Arene)tricarbonylchromium complexes[6] are usually prepared in good yields by heating the free arene with $Cr(CO)_6$ in a high-boiling solvent. The most popular method, described by Mahaffy and Pauson, uses a mixture of di-*n*-butyl ether and THF in a 9:1 ratio.[6c] These complexes are usually yellow, but can be orange or even dark red if the arene is conjugated to an aldehyde, a ketone, or a withdrawing group. They may also be prepared by use of $Cr(CO)_3L_3$,[6b,6e] where L is a two-electron ligand (L = NH_3, CH_3CN, pyridine) or L_3 = naphthalene.[6d] These complexes are decoordinated easily under mild conditions by treatment with I_2, CAN, CO, PPh_3, or Py,[6d] or simply by exposure to air or light.[1c−1e] (Arene)tricarbonylmanganese complexes can be prepared in good yield by treatment of the free arene with $BrMn(CO)_5$ [7a−7c] and $AgBF_4$ in CH_2Cl_2.[7d] Similarly, arene complexes are accessible by treatment of the arene with $Mn(CO)_5ClO_4$, $(acetone)_3Mn(CO)_3^+$ in CH_2Cl_2,[7e] $BrMn(CO)_5$ in the presence of $AlCl_3$,[7f] or $Mn_2(CO)_{10}$, or by transferring $Mn(CO)_3^+$ from cationic (polyarene)$Mn(CO)_3^+$ complexes.[7b,7c] A recent preparation involves a two-step methodology, starting from (η^5-1-halocyclohexadienyl)-$Mn(CO)_3^+$ and involving a Pd-catalyzed carbonylation followed by an easy η^5/η^6 rearomatization with Ph_3CBF_4. This gives a route to the previously unknown (η^6-RCO-arene)$Mn(CO)_3^+$ derivatives (RCO = ester, ketone, amide).[5a]

III. General Reactivity Patterns of (η^6-Arene)tricarbonylchromium Complexes

(Arene)tricarbonylchromium complexes are known to have unprecedented reactivities. It is now well established that η^6-coordinated arenes are susceptible to many manipulations thanks to the electron-withdrawing properties of the $Cr(CO)_3$ entity, which have been compared to the electron removal of a nitro group of nitrobenzene.[1c] It has been reported by Semmelhack et al.[8b] and by Card and Trahanowsky[8c] that carbanion addition occurs under very mild conditions.[8] It has been shown that benzylic and, in certain cases, homobenzylic carbanions are easily formed by deprotonation,[1,9] that benzylic carbocations are stabilized,[1d,9b,10a−10h] and recently that benzylic radicals are interesting intermediates.[11] The $Cr(CO)_3$ residue is also known to play a "stereodirecting" effect in reactions occurring at the periphery of the ring.[1c] The ring hydrogen atoms have increased acidity and are easily deprotonated with organolithium reagents.[1d,10a] In the context of this microreview, we focus, as mentioned, only on the nucleophilic addition reactions on the ring. Thus, before description of *cine* and *tele* S_N reactions, some general information on the reactivity of addition of a nucleophile to an (arene)$Cr(CO)_3$ complex is presented.

2-Lithio-1,3-dithiane reacts with (benzene)tricarbonylchromium [**1**, M = $Cr(CO)_3$] to give an anionic η^5-cyclohexadienyl complex **5a** (Scheme 2). This air-sensitive intermediate can be observed spectroscopically and has been characterized by X-ray diffraction analysis by Semmelhack et al.[8a] Another study of a similar η^5-structure (**5b**) has recently been reported.[8a] Oxidation of **5a** at −78 °C with at least 2.5 mol-equiv. of I_2 gives the substituted arene **6**, together with HI, Cr^{III} and CO.

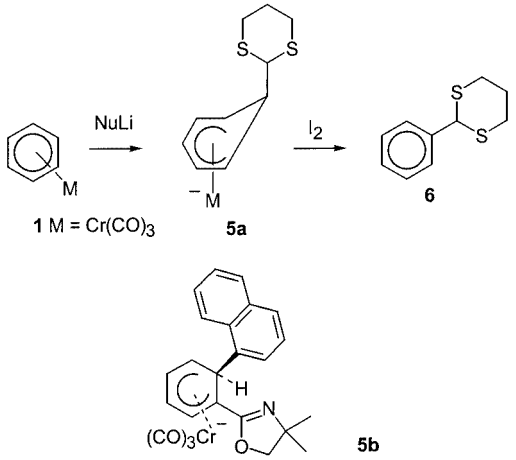

Scheme 2

This reaction has been generalized to other nucleophiles. Table 1 provides a representative sample of the carbanions tested.[8b,8c,12] The regioselectivity of carbon nucleophile addition to a substituted complex **7** is of interest because there are four possible ways to functionalize the ring. The nucleophile can react at the *ipso* carbon atom, bearing the X group, or at the positions *ortho*, *meta*, or *para* to the X group, to yield anionic intermediates **8a**, **8b**, **8c**, or **8d** (Scheme 3).

Table 1. Representative sample of carbanions tested with benzene tricarbonyl chromium

Unreactive carbanions	Successful carbanions	Other reaction[a]
	$LiCH_2CO_2tBu$[b]	
$LiCH_2CO_2tBu$	$LiCH_2CN$[b]	*n*BuLi
MeMgBr	$LiCH_2SPh$[b]	MeLi
Me_2CuLi	2-Li-1,3-dithiane[b]	*s*BuLi
	LiCH=CHR[b]	
	LiPh[b]	
	$LiCMe_3$ [c]	

[a] Metallation of the ring occurs. [b] Ref.[8b] [c] First addition of a carbanion to a (non-halogenated arene)$Cr(CO)_3$ unit.[8c]

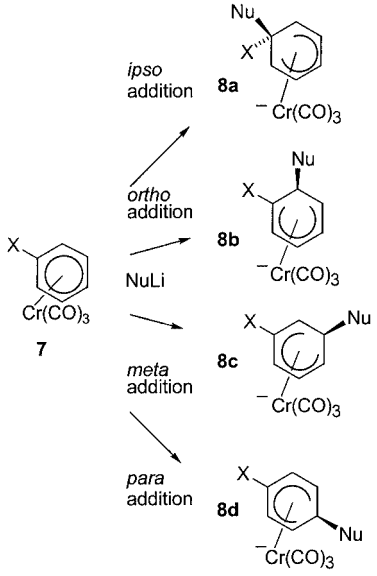

Scheme 3

Table 2. Regioselectivity of the addition of a carbon nucleophile to $C_6H_5XCr(CO)_3$, [8b]

Entry	X	LiNu	*m*/*p* ratio	Yield (%)
1	OMe	$LiCMe_2CN$	3:97:0	93
2	OMe	$LiCMe_2CO_2tBu$	0:100:0	76
3	NMe_2	$LiCMe_2CN$	1:99:0:	92
4	Me	$LiCMe_2CN$	1:97:2	95
5	Me	$LiCMe_2CO_2tBu$	3:97:0	96
6	Cl	$LiCMe_2CO_2tBu$	5:95:0	84
7	Cl	$LiCMe_2CN$	10:89:1	84
8	Me	$LiCH_2CN$	35:63:2	88
9	Cl	$LiCH_2CO_2tBu$	28:72:0	89

Addition of these carbanions can be reversible, but it is not so simple to know whether the addition occurs under kinetic or thermodynamic control.[12,13] In fact, the difference between the kinetic and thermodynamic selectivity is small in most cases, even if some exceptions are known. Thus, it is well precedented that arenes substituted with a donor substituent (**7**, X = OR, NR_2, Scheme 3) are attacked by the nucleophile at a *meta* position (Table 2, Entries 1, 3). The selectivity is also excellent with toluene or chlorobenzene complex in the case of tertiary stabilized carbanions (Table 2, Entries 4−7), but is not so high with primary carbanions (Table 2, Entries 8, 9).

Ullenius et al. presented an interesting example in which the kinetic and the thermodynamic products are not the same, in the particular case of tricarbonyl(*N*-methyltetrahydroquinoline)chromium (**9**, Scheme 4).[13c] Indeed, the ratio of **11/10** changes from 2:1 at −78 °C after 1 min reaction time to 96:4 after 8.6 h at −78 °C, changes being observed with time, temperature, and solvent (THF or THF and 4 equiv. HMPA).

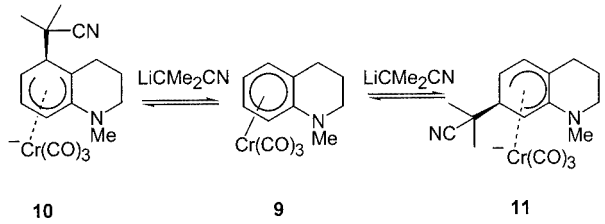

Scheme 4

Kündig et al. also reported interesting results in the case of the tricarbonyl(naphthalene)chromium complex **12**. On addition of $LiCMe_2CN$, a mixture of C_α and C_β complexes **14** and **13** was obtained in the ratio 42:58. Equilibration was avoided because a mixture of THF and HMPA was used. In THF, however, the only product was the α-substituted naphthalene **14** (Scheme 5).[13a] The same study has been undertaken with 1,4-dimethoxynaphthalene, the authors elegantly showing that the rate of equilibration could be slowed down by a factor of 50.000 by an appropriate choice of solvent mixture: THF, THF/HMPT (3:1).[13a] Replacement of lithium with the potassium counterion can slow the reaction down by a factor of 500.

The selectivity of the addition of a carbanion in polar solvents has been discussed in terms of charge control and orbital control. Thus, analysis of orbital control has been proposed by determination of the interaction of the frontier molecular orbitals [HOMO for the nucleophile and LUMO for the (arene)tricarbonylchromium complex].[12,13b] This picture does not explain the differences in selectivity between toluene and anisole complexes, because the LUMOs of these two arenes show the same pattern. Thus, charge control could be very important. This is the reason why the conformation of the complex should be considered. Indeed, in the case of the anisole complex, for example, it is well precedented that the methoxy group is eclipsed by a chromium−carbonyl bond. It is also well known that, in the case of the free anisole, the carbon atom bearing the OMe group is more electrophilic. There is therefore a synergic effect between the role of the methoxy group and that of the conformation of the $Cr(CO)_3$ entity. In solution, in fact, the percentage of the conformer eclipsing the methoxy group of (anisole)tricarbonylchromium should be higher than that of the conformer eclipsing the methyl group of (toluene)tricarbonylchromium. Thus, it might be predicted

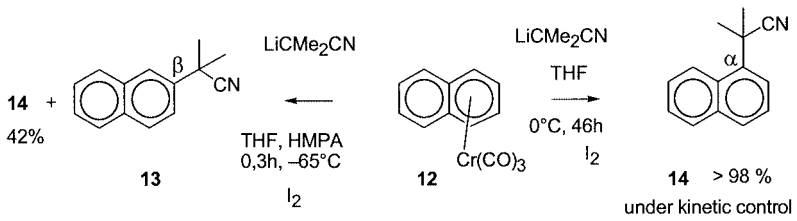

Scheme 5

that *meta* selectivity should be better with anisole than with toluene. The percentage of the major conformer takes into account the nature of the substituents attached to the arene ring. Indeed, it has been reported that in solution a substituted arene complex can be considered to be in equilibrium between two conformations: the *syn*-eclipsed conformation SE and the *anti*-eclipsed conformation AE (Figure 1).[3a,14] Thus, if D is an electron donor substituent, the major conformer is the SE one, and if X is an electron-withdrawing group, the major conformer is AE.

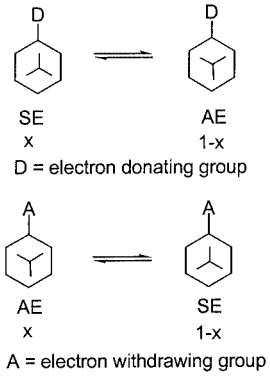

Figure 1. Conformation of the $Cr(CO)_3$ tripod

Addition of different nucleophiles to (benzene)tricarbonylchromium under carbon monoxide (the reaction medium being treated with CF_3CO_2H at −78 °C) has also been reported to give firstly the η^4 complexes **15a** and then the free substituted cyclohexadienes **16a** in 83% yield and $Cr(CO)_6$ in 75% yield [**16b** in 72% yield and $Cr(CO)_6$ in 78% yield] (Scheme 6). With the propionitrile carbanion, under CO, the cyclohexadiene **16c** is recovered and a 30 atm pressure of CO is necessary to obtain the decoordinated cyclohexadiene **16d** in 85% yield and $Cr(CO)_6$ in 85% yield.[15] Determination of the proportion of the cyclohexadienes **16e** (Nu = CMe_2CN) showed that the major isomer is the 1-substituted 1,3-cyclohexadiene (78%). The 2- and 5-sustituted 1,3-cyclohexadienes are obtained in 9 and 13% yields, respectively (Nu = CMe_2CN). A minor complex $[C_6H_5Cr(CO)_3(C_6H_7)]$ has been isolated as a single isomer; it is (1-η^6-phenyl)$Cr(CO)_3$(1,3-cyclohexadiene) (**18**), the formation of which can easily be interpreted in terms of addition of (phenyllithium)$Cr(CO)_3$ (**17**) to (benzene)$Cr(CO)_3$, followed by acid treatment and decoordination of the $Cr(CO)_3$ unit attached to the cyclohexadiene.

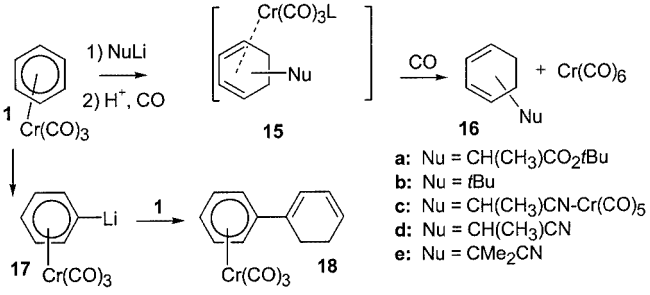

Scheme 6

Addition of the nucleophile to tricarbonyl(*meta*-diisopropylbenzene)chromium (**19**) occurs *meta* with respect to the isopropyl groups and, on treatment of the anionic complex **20** with acid under CO, the cyclohexadienes **21** are obtained in 83% yield, together with $Cr(CO)_6$ in 78% yield. The product can be aromatized by treatment with DDQ, giving the free 1,3,5-trisubstituted arene **22** (Scheme 7).[15]

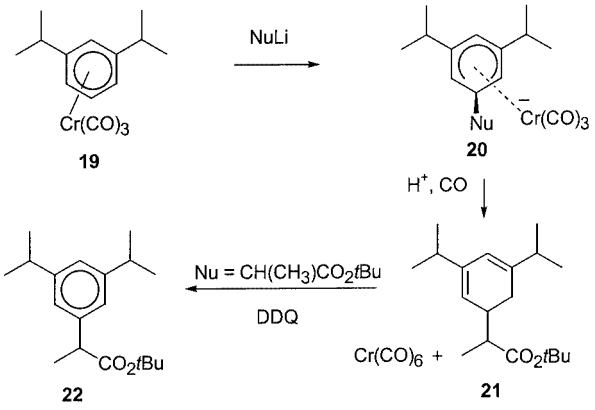

Scheme 7

An examination of the regioselectivity of the addition of a stabilized carbanion LiCHMeCN to a tricarbonyl(spiroindane)chromium complex **23**, giving complex **24** after I_2 oxidation, is interesting. We observed an 81% selectivity at the C-5 carbon atom (Scheme 8).[3c] In the solid state, the C-5 carbon atom is eclipsed by a chromium−carbon bond, and in solution the conformer with the major population (x = 72%) is the one eclipsing the C-5 carbon atom (Figure 2). Thus, the $Cr(CO)_3$ unit adopts a preferred conformation for steric reasons. The regioselectivity of the addition of $LiCH(CH_3)CN$ is the same at −78 °C and at 0

°C, both with THF and with a mixture of THF and HMPA, and involves the eclipsed C-5 carbon atom of the major conformer. This is the conclusion that we have reached in many examples using a stabilized carbanion at low temperature.

Scheme 8

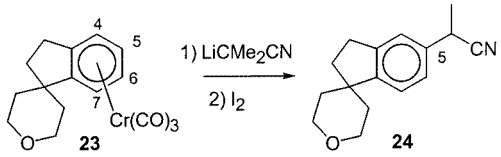

Figure 2. Population of the major conformer

In summary, the regioselectivity of the nucleophilic addition under kinetic control can be explained in terms of charge control and (or) orbital control. The substituents on the arene and the conformation of the $Cr(CO)_3$ tripod play important roles. Under thermodynamic control, the equilibrium can be interpreted in terms of steric and electronic interactions in the intermediate anions, such as **8b**−**d** (Scheme 3).

The anionic η^5-cyclohexadienyl intermediate **8**, obtained by addition of a carbon nucleophile to an arene complex, has been treated with electrophiles. Protonation, for example, occurs at low temperature, giving the η^4-coordinated cyclohexadienes **25** (Scheme 9), with L being (for example) a THF molecule in order to respect the 18-electron rule.[16b] In the case of anisole, the resulting η^4-methoxycyclohexadiene complex **25** has been hydrolyzed to give an enone **26**.[16]

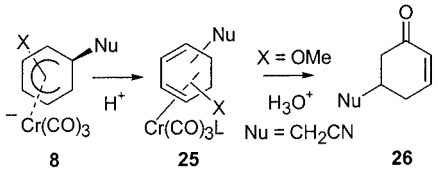

Scheme 9

The anionic intermediate **8** (Nu = 1,3-dithian-2-yl) has also been trapped with a limited set of electrophiles when the nucleophile addition is irreversible. It has been shown that addition of 2-lithio-1,3-dithiane to (η^6-benzene)tricarbonylchromium followed by addition of CH_3I yields a *trans*-disubstituted cyclohexadiene **30a** if the reaction medium is oxidized or treated with a two-electron ligand L (Scheme 10).[17b] CO inserted into the metal−alkyl bond of complex **27** to give the metal−acyl bond of complex **28a**. A reductive elimination can afford the η^4-cyclohexadiene complex **29a** and then the organic compound **30** and $Cr(CO)_2L_4$ through use of a ligand L (L = CO, PPh_3).[1b]

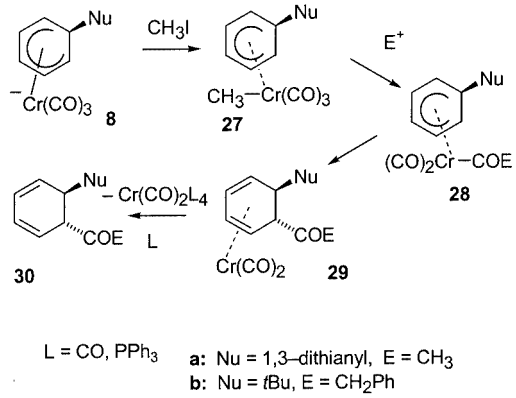

Scheme 10

If *t*BuLi is used as a nucleophile under CO pressure, the anionic intermediate can be trapped in order to recover $Cr(CO)_6$ necessary for the preparation of the starting complex. By addition of *t*BuLi to (benzene)$Cr(CO)_3$ and then benzyl iodide, for example, we obtain the *trans*-cyclohexadiene **30b** (Nu = *t*Bu, E = $CH_2C_6H_5$), but even under 100 atm CO, we recover only a small amount of $Cr(CO)_6$.[18]

IV. *cine* and *tele* Nucleophilic Aromatic Substitutions: (η^6-Arene)$Cr(CO)_3$ Complexes

IV. a. Organic Carbanions: C−O, C−Cl, C−F Cleavage

One of the first nucleophilic aromatic substitutions described in the literature concerns the addition of sodium methoxide to tricarbonyl(chlorobenzene)chromium (**7**, X = Cl), which gives (anisole)tricarbonylchromium complex (**7**, X = OMe) via the η^5-cyclohexadienyl intermediate **8a** (X = Cl, Nu = OMe). This is the classical *ipso* substitution of the methoxy group at the carbon atom bearing the chloro atom.[19] Usually, however, the kinetic site of addition is at a position bearing a hydrogen substituent, which yields anionic η^5-ligand complexes **8b**, **8c**, and **8d** (Scheme 3).[8b] If equilibration occurs, complexes **8b**−**d** give **8a** and then anisole complex with the irreversible departure of the leaving group X.[1g] It has been shown that the fluorobenzene complex **7** (X = F) is almost 2000 times more reactive than the chlorobenzene complex **7** (X = Cl), in good agreement with a rate-limiting addition of the methoxide anion on the arene ring followed by fast departure of halide. We will not describe these *ipso* reactions in detail − they have been well reported in different reviews[1g] − but will instead consider carbanion addition to carbon atoms *ortho*, *meta*, and *para* with respect to the carbon atom bearing the leaving group.

Whereas direct displacement of oxygen leaving group is not effective, we have shown that treatment of 2-lithio-2-methyl-1,3-dithiane with tricarbonyl(diphenyl ether)chro-

mium (**31a**) at room temperature gives the *ipso*-monosubstituted complex **32a** (Scheme 11).[20]

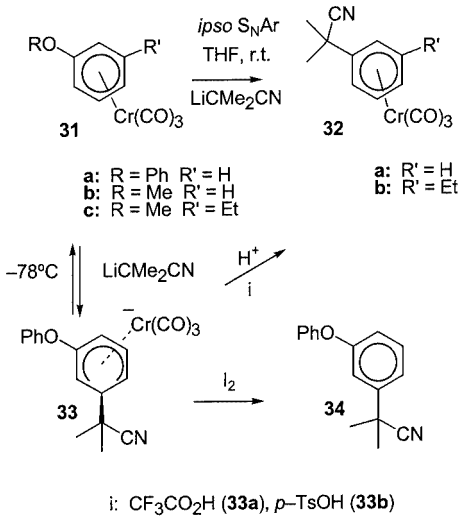

Scheme 11

More interestingly, addition of the same nucleophile at −78 °C affords the anionic intermediate **33**, which is quenched with I_2 at −78 °C to yield the *meta*-disubstituted arene **34** (Scheme 11). Addition occurs *meta* with respect to the PhO group, the overall reaction consisting of a *meta* substitution of a hydrogen atom by the nucleophile.[21]

If the anionic intermediate **33** is treated with CF_3CO_2H at −78 °C, complex **32** is again unexpectedly obtained (Scheme 11). The same study with (anisole)$Cr(CO)_3$ (**31b**) and isobutyronitrile carbanion and acid gives phenylisobutyronitrile complex **32a**, but the yield is very low. With *p*TsOH, elimination of MeOH is easier, and complex **32a** is formed in 62% yield. Similarly, treatment of (*meta*-ethylanisole)$Cr(CO)_3$ (**31c**) with $LiCMe_2CN$ and *p*-TsOH affords complex **32b** in 62% yield.[22b]

Taking into account that *ipso* reaction does not occur at −78 °C, we have to consider a new mechanism to explain these unusual results. Addition of $LiCMe_2CN$ to diphenyl ether complex **31a** (Scheme 12) gives (after CF_3CO_2H treatment) the chromium hydride **35**, which can undergo a reductive elimination on the C-4 and C-2 carbon atoms. The new η^4 intermediate **36**, for example, which is a dienol ether, cannot be hydrolyzed in the absence of water. An oxidative addition of the allylic hydrogen atom can give another η^5-cyclohexadienyl complex **37**. Again, a reductive elimination can give the η^4-cyclohexadiene **38**. By elimination of the *anti*-parallel hydrogen atom and the PhO group, a new η^6-arene **32a** is formed. The driving force of the reaction is the rearomatization of the ring, which corresponds to a 1,5-hydrogen shift of the proton located at the C-3 carbon atom (Scheme 12).[21] The nucleophiles that have been tested are the carbanions of CH_3CO_2Me (pK_a = 24.5), $CH_3CH_2CO_2Me$, $(CH_3)_2CHCO_2Me$, CH_3CN (pK_a = 25), CH_3CH_2CN, $(CH_3)_2CHCN$, and 2-phenyl-1,3-dithiane.

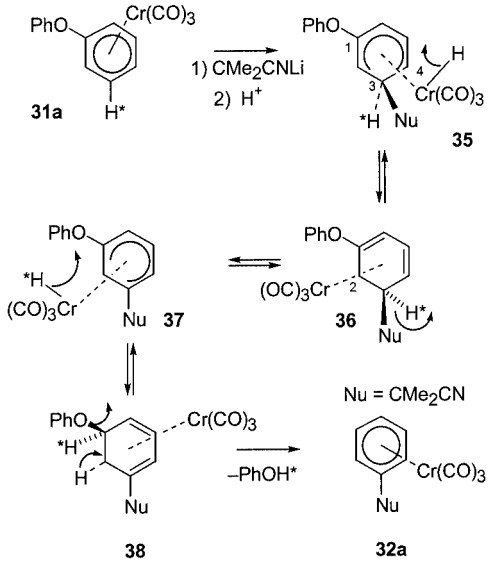

Scheme 12

In order to understand the mechanism of this reaction, we undertook the same experiment starting from the labeled tricarbonyl(5-deuterio-2,3-dimethylphenyl phenyl ether)chromium (**39**). We obtained the deuterated complex **40** after treatment with a nucleophile NuLi (Nu = CMe_2CN, CMe_2CO_2tBu, ...) and CF_3CO_2H or CF_3CO_2D (Scheme 13).[21a] This reaction involves a 1,5-deuteride migration from the C-5 carbon atom to the C-1 carbon atom.[21,22] With CF_3CO_2D, we recovered PhOD, showing that the deuterium of the acid is not incorporated into the arene ring. For precision, we called this reaction a *tele-meta* nucleophilic aromatic substitution, in accordance with IUPAC naming schemes. The term *tele* is used to denote reactions in which the entering group takes up a position further than one atom away from the atom to which the leaving group is attached.[23]

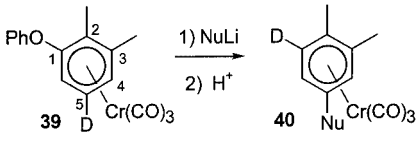

Scheme 13

Schmalz et al.[24] reported that addition of *n*BuLi to tetralin derivative complex **41** in THF/HMPA gives a high yield of complex **42**.[24f] This reaction is a *tele* substitution with methoxide as the leaving group. To be more precise, it is a *tele-meta* S_NAr reaction, detailed in Scheme 14. The mechanism should not involve incorporation of deuterium in the ring if the anionic species **43** is trapped with a deuterium source. It is worth noting the ease with which *n*BuLi adds to a carbon atom of the arene ring under conditions that should result in smooth benzylic deprotonation, which according to the authors is disfavored for stereoelectronic reasons. The selective formation of complex **42** is remark-

able because the methoxide expulsion is regioselective: no *tele-para* substitution is observed.

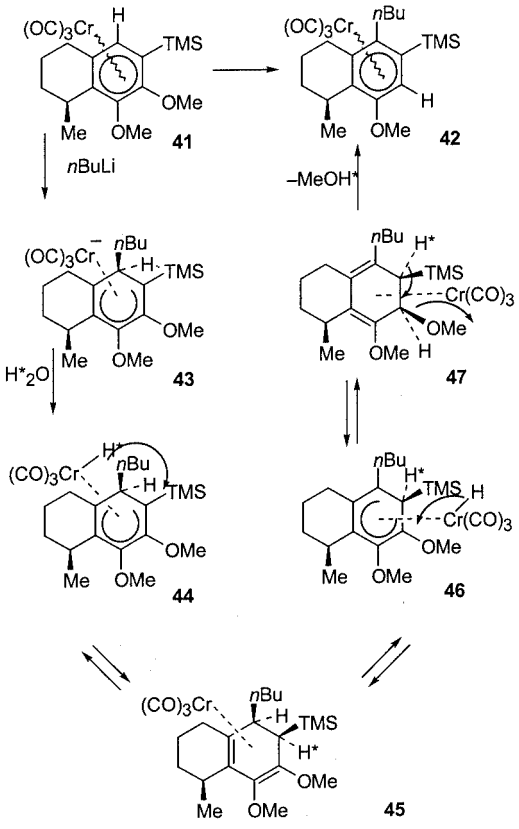

Scheme 14

The same group showed that *tele* substitution is the major pathway in S_NAr reactions of (*ortho*-alkylated η^6-anisole)$Cr(CO)_3$ derivatives such as **48** (Scheme 15).[24c,24e] Treatment of **48** with NuLi (Nu = 2-lithio-1,3-dithiane or *n*BuLi) followed by protonation with CF_3CO_2H does not give the expected enones **51** after hydrolysis of the dienol ethers **50** but, rather, complex **49** by way of a *tele-meta* S_NAr substitution of the MeO group by the nucleophile.

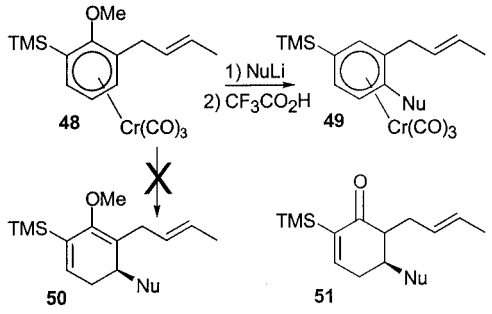

Scheme 15

In close analogy, desilylated complex **52**, when treated with 2-lithioisobutyronitrile and then with CF_3CO_2H, affords the *tele-meta* complex **53** as the major product (Scheme 16).[24e]

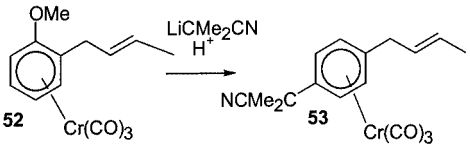

Scheme 16

The addition of stabilized carbanions to tricarbonyl(*para*-chlorotoluene)chromium complex **54** (NuLi and CF_3CO_2H) gives a *meta*-disubstituted complex **55**[25,26] (Nu = CMe_2CN, CMe_2CO_2tBu, p-$CH_3C_6H_4SO_2CHCH_3$. This is termed a *cine* nucleophilic aromatic substitution in accordance with IUPAC recommendations. Indeed a *cine* S_NAr is a reaction in which the incoming group (Nu) takes up a position at the carbon atom *ortho* to the leaving group.[23] With use of CF_3CO_2D, incorporation of deuterium takes place on the carbon atom that bore the leaving group (Scheme 17). If this reaction is performed with 2-lithio-2-methyl-1,3-dithiane, the η^4-cyclohexadiene **58** is obtained by a reductive elimination of the η^5-cyclohexadienyl complex **57**. It is likely that, the nucleophile being too bulky, the *endo*-hydrogen atom cannot be extracted from the carbon atom bearing this nucleophile and the isomerization process is therefore stopped. Instead, decoordination takes place, giving the cyclohexadiene **59**, X-ray analysis of which confirmed the proposed structure.[26b]

A *cine* S_NAr has been observed by Schmalz et al. in the case of an SmI_2-mediated radical cyclization of ketimines **62** (Scheme 18).[24a] The cyclization product is obtained from addition of azaketyl-type radical **63** to the complexed arene to form intermediate **64**, converted by a single electron transfer to the corresponding anionic complex **65**. Addition of acid affords a hydride, which gives rise to the formation of an η^4 intermediate **66**, which in turn yields complex **67** after a reductive elimination of MeOH. Another *cine* S_NAr with methoxide as a leaving group has been described for the synthesis of hydrophenalene complex **69**, starting from complex **68** (Scheme 19).[24d]

Another impressive example has been found in the case of tricarbonyl(1-chloro-2,6-dimethylbenzene)chromium complex **70** (Scheme 20).[27] In order to avoid addition *ortho* to the chloro atom, we protected the two positions *ortho* and *ortho'* of tricarbonyl(η^6-chlorobenzene)chromium. We thus forced the addition of the nucleophile *para* to the leaving chloride ion. By addition of $LiCMe_2CN$ and CF_3CO_2H, we observed the formation of the 1,3,5-trisubstituted complex **71** in 89% yield. This is a *tele-para* nucleophilic aromatic substitution.[28] Use of CF_3CO_2D results in complex **71** being labeled by a deuterium atom at the carbon atom that bore the leaving group. Thus, we completed the discovery of a trilogy: *cine*, *tele-meta*, and *tele-para* S_NAr.

We achieved an analogous reaction with tricarbonyl(η^6-1-fluoro-2,6-dimethylbenzene)chromium complex **72**, by using the reversible addition of $LiCMe_2CN$ in THF at −78 °C and CF_3CO_2H at −78 °C. A mixture of *tele-meta* and *tele-para* substitution products **73** and **74** was isolated in 26

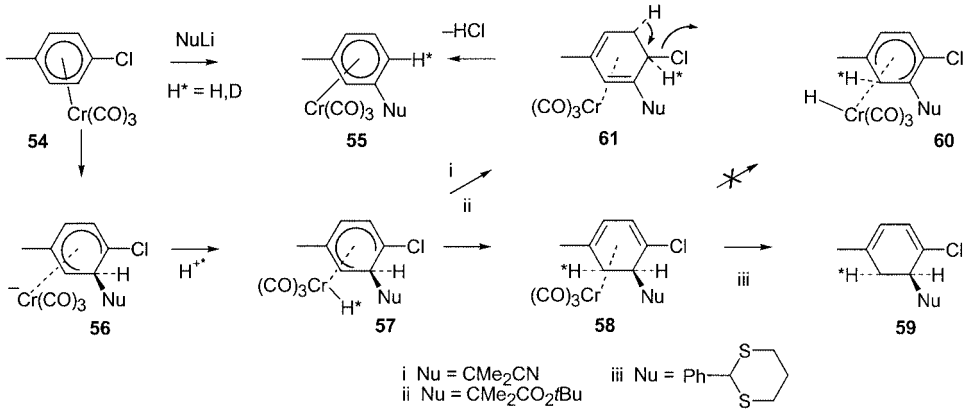

Scheme 17

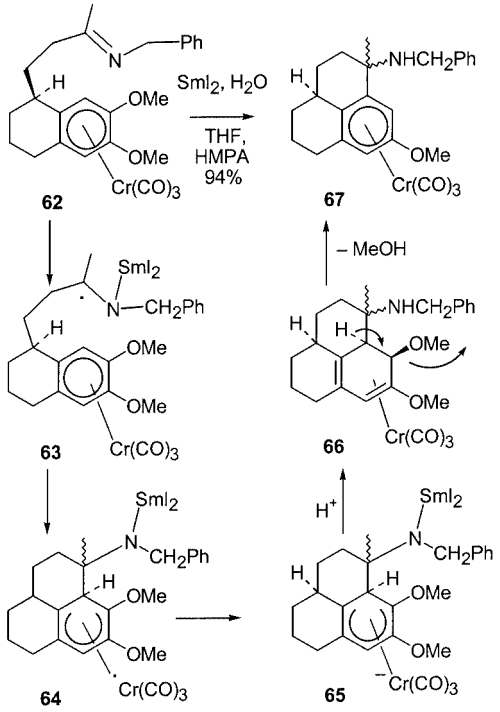

Scheme 18

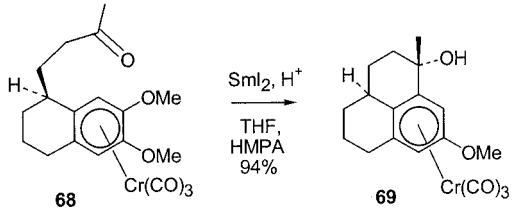

Scheme 19

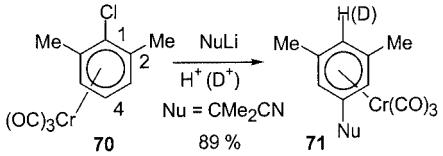

Scheme 20

and 16% yield, together with a mixture of isomeric cyclohexadienes **75** and **76** in low yield (Scheme 21).[29] In the presence of HMPA, the addition of the nucleophile was irreversible and regioselective, and we recovered mostly the 1,3,5-trisubstituted *tele-meta* complex **74**.

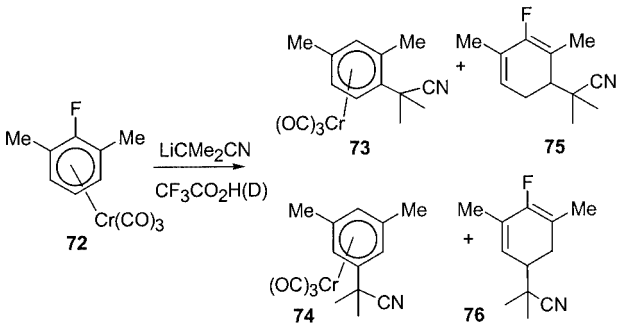

Scheme 21

It is worth noting the difference in the regioselectivities of addition of the nucleophile to the complexes **70** and **72**. In the first case, complex **70**, there is a weak effect from the chloro atom but an important effect from the methyl groups at the C-4 carbon atom. In the second case, that of complex **72**, the directing effect of the fluoro atom (strong *meta* effect) dominates over the effect of the two methyl groups. This study underlines the possibility of controlling the sites of *cine*, *tele-meta*, or *tele-para* substitutions: depending on the nature of the carbanion and on the nature of the leaving group, it is possible to obtain addition of the nucleophile *meta* or *para* to the halogenated atom.

If the *tele-meta* and *cine* substitution mechanisms are applied to the reaction studied by F. E. Hung et al. (Scheme 22), an easy explanation for the formation of the final products may be found. Tricarbonyl(*para*-fluoroanisole)chromium complex **77** was treated with lithium phenylacetylide in THF and HMPA at −78 °C for 1 h and then at −50 °C for 12 h to form two interesting compounds **81** and **82** in a 2:1 ratio and an overall yield of 41% after silica gel column chromatography.[30] We can predict competition between the addition of the nucleophile *meta* to the fluoro atom (strong *meta* effect) and *meta* to the methoxy group (strong mesomeric effect). The following mechanism, invol-

ving an irreversible addition of LiC≡CPh to give anionic intermediates **78a** and **78b**, can be suggested (Scheme 22), with these affording cyclohexadienes **80a** and **80b** on protic workup or on silica gel, via η^5-cyclohexadienyl complexes **79a** and **79b**. After isomerization (for **80a**) and elimination of HF, complexes **81** and **82** are obtained.

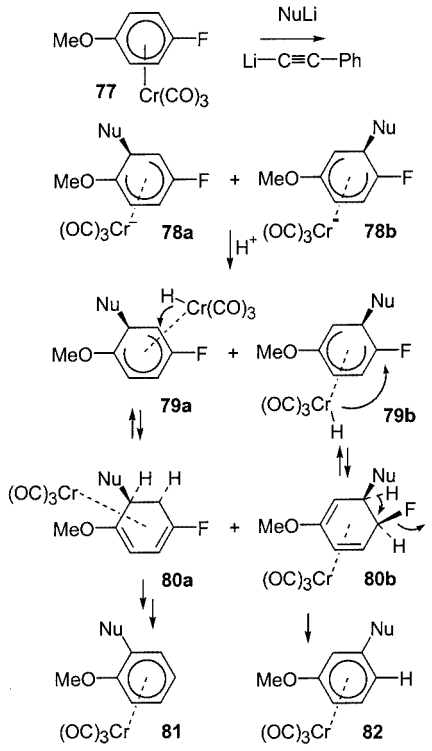

Scheme 22

IV. b. Organometallic Carbanions: C−O, C−F, C−Cl Cleavage

When performing the lithiation/silylation of tricarbonyl(-veratrole)chromium (**83**) with *n*BuLi and $ClSi(CHMe_2)_3$, we recovered not only the expected (3-triisopropylsilylveratrole)$Cr(CO)_3$ (**84**) in 17% yield and [3,6-bis(triisopropylsilyl)-veratrole]$Cr(CO)_3$ **85** in 14% yield, but also an unexpected dinuclear complex **91**.[31] Its formation is interpreted as a *cine* S_NAr substitution of one methoxy group of **84** by the lithiated derivative **86**, as depicted in Scheme 23. It is noteworthy that the formation of **91** does not require acid treatment. Thus, the irreversibly formed anionic complex **87** can deliver a chromium hydride **88** on protic workup. Migration of the hydride ion can afford the cyclohexadiene **89**, which is in equilibrium with another cyclohexadiene **90**. Elimination of MeOH finally yields complex **91** in 16% yield. The X-ray structure of this complex shows, as should be expected, the conformations of the two $Cr(CO)_3$ units *anti*-eclipsed with respect to the bulky triisopropylsilyl groups.

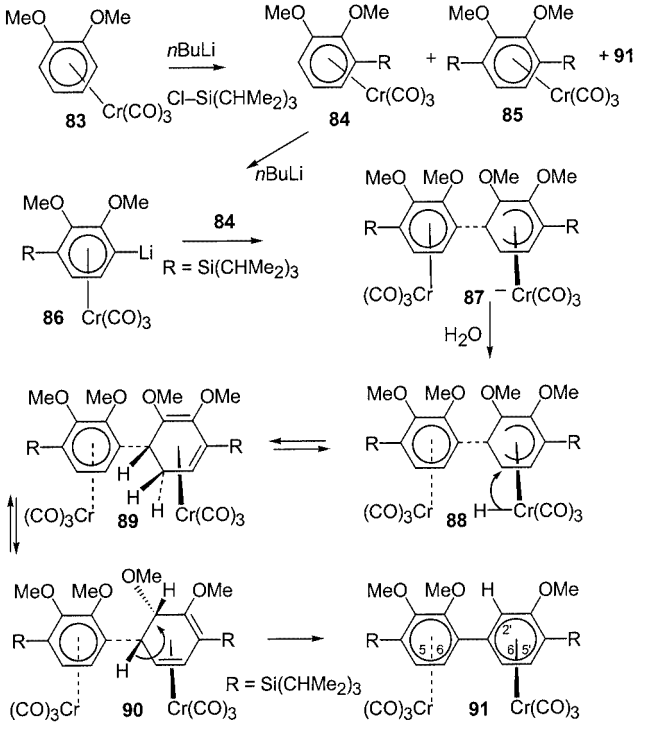

Scheme 23

We extended this reaction to (*para*-chlorotoluene)$Cr(CO)_3$ (**62**) (1 equiv.) and treatment with *n*BuLi (0.5 equiv.). Again, without any acid treatment, the dinuclear complex **94** is formed anyway, through a *cine* S_NAr reaction (Scheme 24). The mechanism of this reaction involves lithiation of *para*-chlorotoluene complex **62**, *ortho* to the chloro atom, and then addition of this aryllithium compound **92** *ortho* to the chloro atom of another molecule of **62**. After protonation and rearrangement of the hydride intermediate, elimination of HCl affords the dinuclear complex **94**.[32]

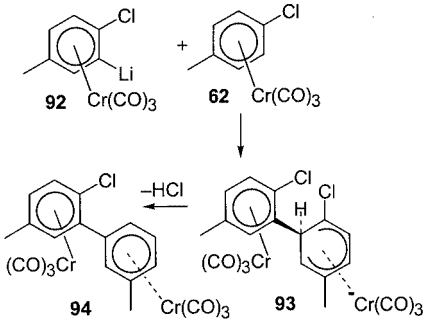

Scheme 24

Another dimetallic compound has been described to be formed by treatment of complex **95** with *n*BuLi and TMEDA at −20 °C followed by addition of TMSCl at 0 °C. The expected silylated complexes are not formed, but the dinuclear complex **96** is obtained instead in high yield

by a *tele-meta* substitution of one of the methoxy groups (Scheme 25).[24b]

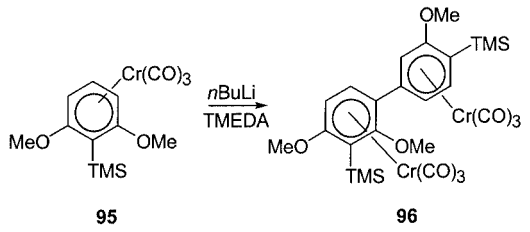

95 96

Scheme 25

IV. c. Hydrides as Nucleophiles: C−F, C−Cl, C−O, C−N Cleavage

We then investigated the regioselectivity and the reversibility of hydride addition such as that of $LiEt_3BH$ to dibenzofuran complex **97** (Scheme 26).[33,34a] If the reaction is performed at room temperature in a sealed NMR tube in $[D_8]$THF, an unstable anionic complex **98** is obtained. This is pyrophoric under air! If, however, the reaction is performed at 67 °C, complex **100** is isolated in 55% yield as a yellow powder. Many attempts to isolate the anionic intermediate failed, the starting dibenzofuran complex **97** being recovered. However, triphenyltin chloride reacts at the metal center to give the binuclear red complex **101**, the X-ray structure of which definitively corroborates not only the regioselectivity of the addition of the hydride ion but also the η^5-cyclohexadienyl structure, which looks more or less like an unprecedented η^4-cyclohexadiene complex. Indeed, the Cr−C-1a bond was unexpectedly longer (2.41 Å) than the other Cr−C_{ar} bonds: Cr−C-2 2.228 Å, Cr−C-3 2.19 Å, Cr−C-4 2.19 Å, Cr−C-4a 2.25 Å. Another structure **102** has been obtained treating triphenyltin chloride with the anionic adduct of the reaction between (benzene)tricarbonylchromium and 2-lithio-2-methyl-1,3-dithiane.[35] In this case, the bond lengths of the chromium atom to the η^5-cyclohexadienyl framework are not so different, at 2.28, 2.19, 2.18, 2.20, and 2.30 Å.

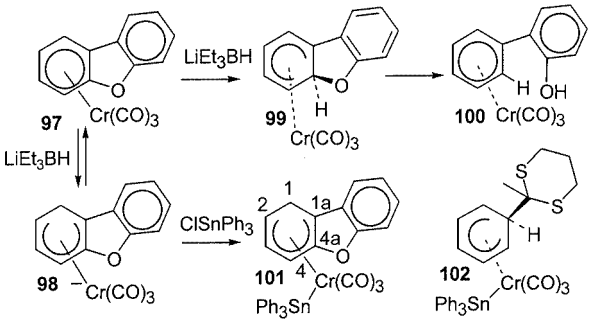

Scheme 26

We successfully performed an analogous reaction with (benzene)tricarbonylchromium (**1**) and obtained a new binuclear Sn−Cr complex **104** by addition of $LiEt_3BH$ and $ClSnPh_3$. The X-ray structure confirms the η^5 structure (Scheme 27).[34] In solution, the NMR spectra of these η^5 complexes are characteristic, and their data are listed in Table 3. The hydrogen atom 1-H_{exo} in all cases resonates at the highest field as a doublet resulting (for **98**) from a ^1J (11 Hz) geminal coupling with 1-H_{endo}. The latter appears as a doublet of triplets from combined ^1J (11 Hz) and ^3J (6 Hz) coupling of 1-H_{endo} with 1-H_{exo} and 2- ,6-H, respectively. It is noteworthy that treatment of the anionic complex **103** with CF_3CO_2H in $[D_8]$THF in a sealed NMR tube at −78 °C affords a deep red solution, which turns orange-yellow at room temp. The ^{1}H NMR spectrum indicates the formation of an unstable η^4-cyclohexadiene complex **105**, the ^{1}H NMR spectroscopic data of which show peaks at δ = 5.80, 3.80, and 2.10, in good agreement with the spectra of carbonyl(1,3-cyclohexadiene)chromium derivatives.[36]

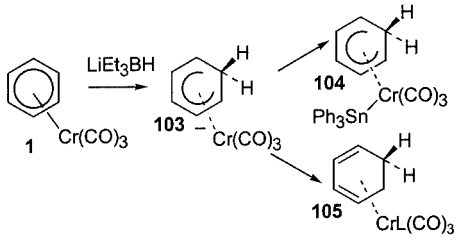

Scheme 27

Table 3. Selected ^{1}H and ^{13}C NMR spectroscopic data of (η^5-cyclohexadienyl)$Cr(CO)_3$

Complex	1-H_{exo}	1-H_{endo}	2-H	3-H	4-H
98[a]	2.76	3.59	2.63	4.57	5.63
101[a]	2.80	4.06	3.42	3.88	6.71
103[a]	2.58	2;85	2.53	4.74	5.43
104[a]	1.60	2.43	2.60	3.72	6.06
5a[a] [8b]	–	[b]	[b]	4.35	4.82
5b[c] [8a]	–	3.37	–	5.64	4.99[d]
102[e] [35]	–	3.57	3.80	4.32	6.00
Complex	C-1	C-2	C-3	C-4	
101[e]	28	61	90	67	
103[a]	27	46	98	76	
104[c]	26	60	95	85	

[a] $[D_8]$THF. [b] Under a multiplet at δ = 1.4−3.1. [c] C_6D_6. [d] Signal of 5-H at δ = 4.41, of 6-H at δ = 4.76.[e] $CDCl_3$.

We then investigated the cleavage of a carbon−nitrogen bond. Addition of $LiEt_3BH$ to *para*-methoxydimethylaniline complex **106** at room temp., followed by treatment with CF_3CO_2H, affords two complexes, the anisole and aniline complexes **107** and **108** in 34% and 24% yields, respectively, showing competition between carbon−oxygen cleavage and carbon−nitrogen cleavage (Scheme 28).[34,37] Addition of an excess of $LiEt_3BH$ to **108** is necessary to obtain (after CF_3CO_2H treatment at room temp.) a red solution (which

rapidly becomes yellow) of (benzene)$Cr(CO)_3$ and the starting material.

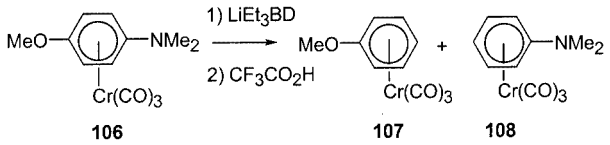

Scheme 28

We carried out a similar experiment with a complex possessing a well-defined $Cr(CO)_3$ conformation. We chose an [η^6-1-(dimethylamino)-2-(trimethylsilyl)benzene]$Cr(CO)_3$ (**109a**), which gave a mixture of 2- and 4-deuterio derivatives of [η^6-2-(trimethylsilyl)benzene]$Cr(CO)_3$ **110** and **111** in 56% yield in the ratio 84:16 (Scheme 29) after treatment with $LiEt_3BD$ and CF_3CO_2H. With *ortho*-chloro and *ortho*-fluoro(trimethylsilyl)benzene complexes **109b** and **109c**, however, we observed the almost quantitative formation of a single compound **111** through a *tele-meta* S_NAr.[34b]

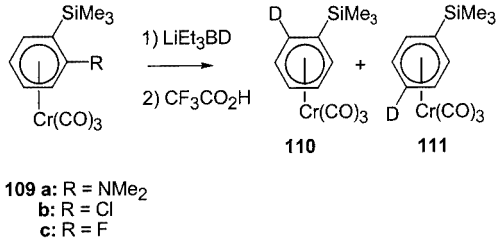

Scheme 29

Another example of C−O cleavage by a hydride ion is described by Hacksel et al., who obtained an interesting arene **113a**, with loss of an OMe group, after addition of $LiAlH_4$ to tetrahydronaphthalene complex **112**, and decoordination of $Cr(CO)_3$[38] (Scheme 30). Two kinds of substitution − a *tele-meta* S_NAr or an *ipso* substitution − seem likely at this stage and could explain the formation of the observed product. However, the authors, when performing the reaction with $LiAlD_4$, obtained the compound **113b**, deuterated at the carbon atom that bore the methoxy group, in good agreement with an *ipso* S_NAr. If a *tele-meta* S_NAr had occurred, a deuterio complex labeled at the position *meta* to the carbon atom that bore the methoxy group should have been obtained.

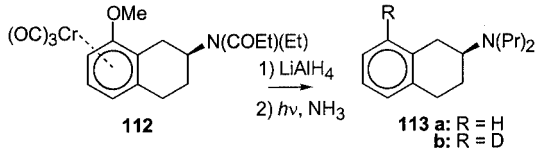

Scheme 30

V. *cine* and *tele* Nucleophilic Substitutions: (η^5-Cyclohexadienyl)$Mn(CO)_3$ Complexes

It is now well established that tricarbonyl[phenoxy-, methoxy-, chloro-, fluoro-, (dimethylamino)-substituted η^6-arene]chromium complexes undergo cleavage of aromatic C−O, C−Cl, C−F, C−NMe_2 bonds upon treatment first with a nucleophile or a hydride ion and then with acids. The first step of these reactions is the formation of anionic η^5 intermediates, which can undergo different isomerizations once protonated. We were interested in transposing this study to manganese complexes, encouraged by the convincing demonstration by Brookhart et al. of the facile isomerization of cyclohexenyl isomers **115** involving manganese−hydrogen−carbon agostic bonds (Scheme 31).[39] Indeed, these authors reported that treatment of the neutral complexes **3**, obtained by hydride addition to cationic tricarbonyl(X-substituted η^6-arene)manganese complexes **1**, resulted in the formation of anionic complexes **4** and, on addition of water, a stable complex **115**

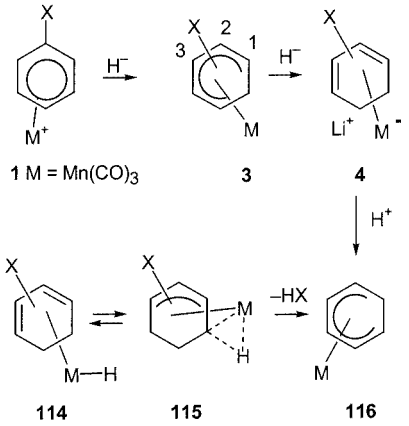

Scheme 31

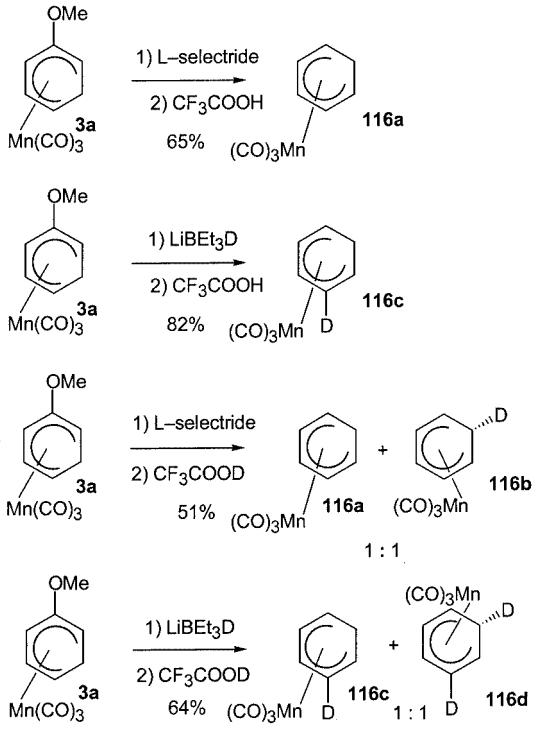

Scheme 32

with a three-center Mn−H−C agostic bond (X = OMe, for example) (Scheme 31). We therefore repeated this reaction, starting from various (η^5-cyclohexadienyl)manganese complexes substituted with a leaving group X, in order to eliminate HX after H^-, H^+ treatment. We obtained a new complex **116**, again with an η^5 structure.

V. a. C−O Cleavage

Addition of L-selectride to the η^5 complex **3a**, followed by protonation with MeOH or CF_3CO_2H, gives the known η^5-cyclohexadienyl complex **116a** in 65% yield if the reaction mixture is heated in THF for 3 h. With $LiEt_3BD$ and CF_3CO_2H, complex **116c** is recovered in 82% yield (Scheme 32). If $LiEt_3BH$ and CF_3CO_2D are used, a mixture of complexes **116a** and **116b**, deuterated at the *endo* position, is recovered in a ratio of 1:1 and in 51% yield. When complex **3a** is treated with $LiEt_3BD$ and MeOH, a single deuterated complex **116c** is obtained in 82% yield. Similarly, treatment of complex **3a** with $LiEt_3BD$ and CF_3CO_2D results in a mixture of complexes **116c** and **116d** being recovered in a 1:1 ratio and in 64% yield. These data are consistent with a four-step mechanism involving hydride addition, protonation, isomerization, and elimination. We will focus only on the last step. The formation of the various labeled products obtained has been explained in terms of the easy isomerization of different η^3-cyclohexenyl intermediates such as **115** in an acidic medium. We thus considered all the possible hydrogen migrations giving the mono- and the dideuterated complexes **116c** and **116d** in order to understand the elimination of MeOH(D) (Scheme 33).

The exact mechanism of this reaction is not yet known precisely, because the π-allyl complexes **115a**, **115b**, **115c**, and **115d**, which are in equilibrium, can be represented by two different agostic bonds in the cases of the symmetrical derivatives **115a** and **115d** and by four different agostic bonds in the cases of the unsymmetrical derivatives **115b** and **115c**. Thus, in the last elimination step, complex **115d**

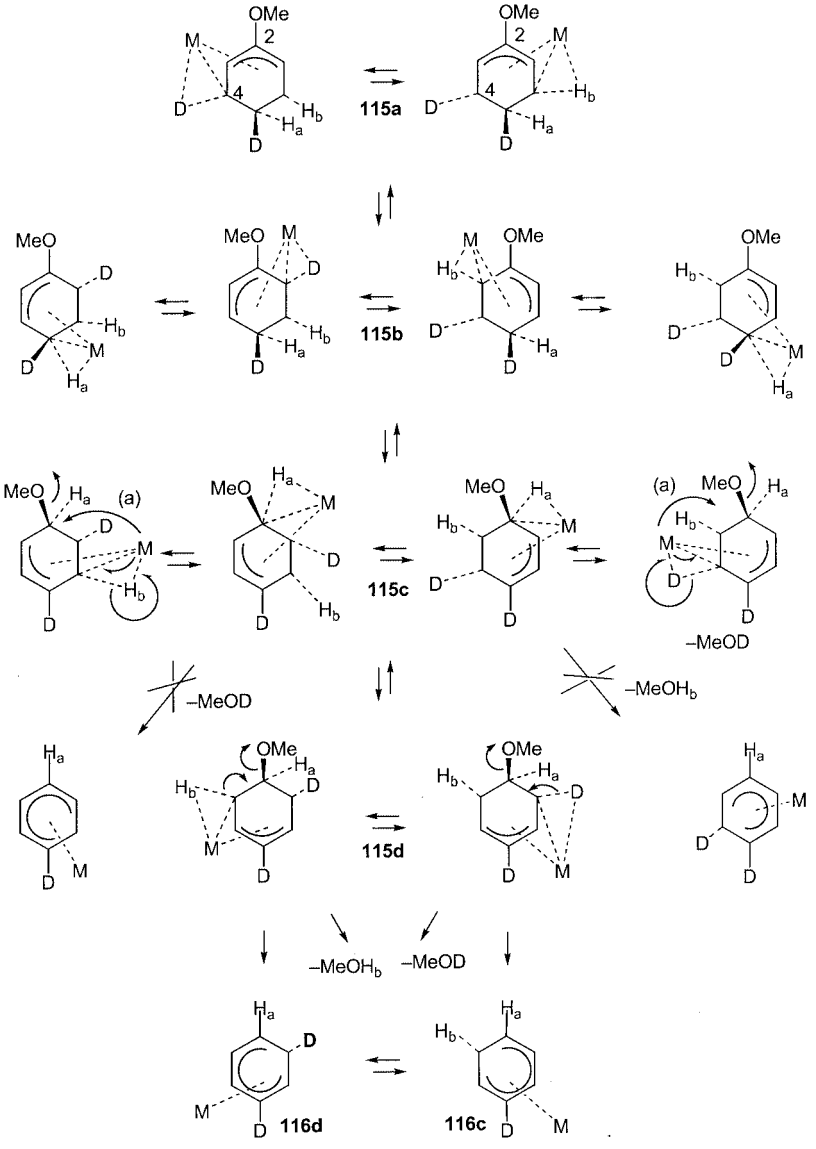

Scheme 33

could eliminate either $MeOH_b$ or MeOD, giving complexes **116c** and **116d**. In fact, we arrived at the conclusion that 1,5-elimination could occur between the OMe group and an agostic hydrogen atom, and we never observed a 1,2-elimination of OMe and a non-agostic hydrogen atom. Thus, the hydrido-demethoxylation of complex **3a** occurred by hydride ion addition at the C-5 carbon atom and elimination of the methoxy group at the C-2 carbon atom (Figure 3). By analogy with the chromium complexes, this is a *tele-para* nucleophilic substitution.[40]

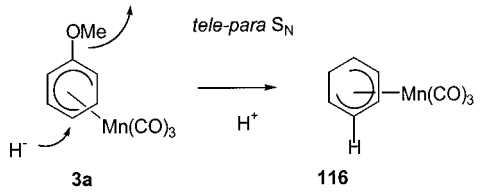

Figure 3. *tele-para* S_N

In the case of the tricarbonyl(*para*-dimethoxybenzene)manganese complex **117**, addition of $LiAlH_4$ in THF at −78 °C affords complex **118** in 46% yield (Scheme 34).

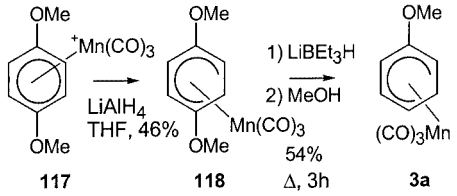

Scheme 34

The addition of L-selectride (4 equiv.) to complex **118**, followed by protonation with MeOH (6 equiv.) and heating of the solution for 3 h, resulted in the formation of a single isomer tricarbonyl(η^5-2-methoxycyclohexadienyl)manganese complex **3a** in 54% yield. The formation of this can be interpreted in terms of a *cine* or a *tele-meta* nucleophilic substitution (Figure 4). We extended these reactions to other examples showing the possibility of C−N, C−Cl and C−S bond cleavage.

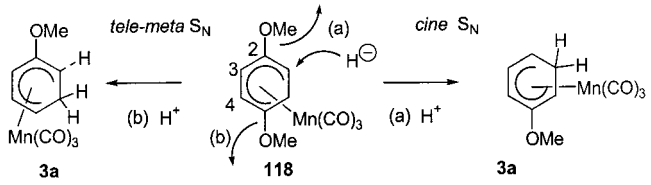

Figure 4. *cine* or *tele-meta* S_N

V.b. C−N Cleavage

Addition of $LiAlH_4$ to [(diethylamino)benzene]-$Mn^+(CO)_3$ (**119**) exclusively yields the expected *meta*-addition product **120** in 92% yield. Addition of L-selectride followed by protonation with CF_3CO_2H at −78 °C gives, after warming to room temp., the η^5-cyclohexadienyl complex **116a** in 54% yield (Scheme 35).[40]

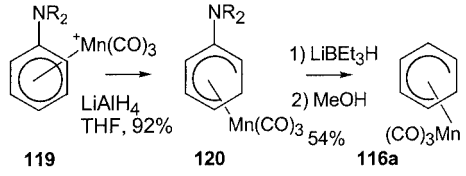

Scheme 35

V. c. C−X Cleavage (X = F,Cl)

Complex **122** (obtained in 57% yield from addition of $LiAlH_4$ to (*ortho*-chloroanisole)$Mn^+(CO)_3$ complex **121** behaves similarly, reacting with L-selectride and then CF_3CO_2H to afford the 2- and 3-methoxycyclohexadienyl complexes **3a** and **123** in a 45:55 ratio (Scheme 36). Cleavage of the C−Cl bond occurs very quickly even at low temperature, contrary to the C−O bond cleavage, which requires higher temperature.

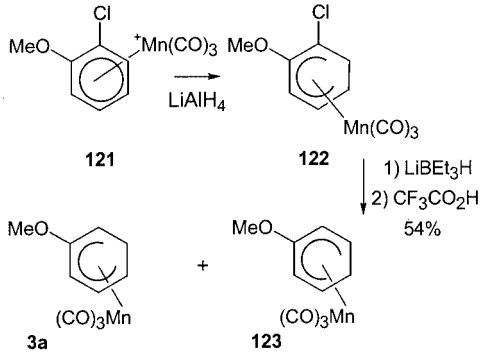

Scheme 36

V. d. C−S Cleavage

Addition of $LiAlH_4$ to (η^6-phenylthiobenzene)-$Mn^+(CO)_3$ complex **124** gives two neutral complexes **125** and **126** in 71% yield and in a 30:70 ratio. Complex **126**, if treated with L-selectride and water and heated in refluxing THF for 20 h, affords complex **116a** in 38% yield (Scheme 37). We have never succeeded in cleaving the C−S bond in the case of the corresponding (arene)$Cr(CO)_3$ complexes (Scheme 37).[40]

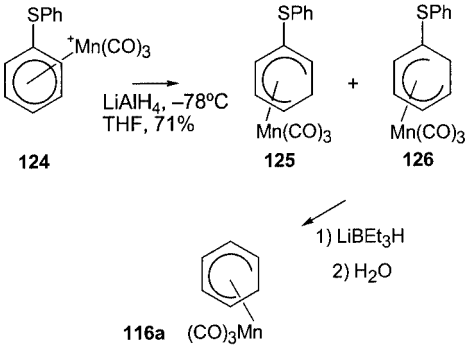

Scheme 37

VI. Concluding Remarks

The reactivity of (arene)tricarbonylchromium and -manganese complexes involved in *cine* and *tele* nucleophilic substitutions has been described. The use of chromium complexes provides rapid routes to compounds that are difficult to obtain in organic chemistry. Thus, addition at low temperature of a stabilized carbanion to an (arene)tricarbonylchromium complex substituted with a leaving group X, followed by addition of CF_3CO_2H, yields new arene complexes and HX through the cleavage of carbon−oxygen, carbon−halogen, and carbon−nitrogen bonds. The addition of the nucleophile occurs *ortho*, *meta*, or *para* to the leaving group, depending mainly on the nature and on the relative positions of the substituents on the arene ring. There is no doubt that development in this area will be extended in our laboratory and also elsewhere, not only in the cases of chromium or manganese complexes such as we have already discovered, but also in the case of other metals. These *cine* and *tele* S_N processes appear to be efficient organometallic reactions and represent a new tool for organic chemists. By taking advantage of the presence of the tripod $Cr(CO)_3$, which remains coordinated to the arene ring of the final product, a further functionalisation is possible and so broadens the scope of potential applications.[41]

Isomerization of η^4-cyclohexadiene intermediates occurs through 1,5-hydrogen shifts. The driving force of these reactions is the elimination of HX, with aromatization of the η^4 complexes into the η^6-arenes in the case of (η^6-ligand)Cr complexes.

In the case of Mn complexes, we extended these reactions and found that carbon−oxygen, carbon−halogen, carbon−nitrogen, and even carbon−sulfur bonds can be cleaved by *cine* and *tele* S_N processes if the starting neutral (substituted η^5-cyclohexadienyl)$Mn(CO)_3$ is treated with a hydride ion and a proton source, yielding (η^5-cyclohexadienyl)$Mn(CO)_3$ complex and HX. The driving force of these reactions is again the elimination of HX, transforming an η^3 complex into an η^5-cyclohexadienyl complex.

VII. Abbreviations

CAN: ceric ammonium nitrate; DDQ: 2,3-dichloro-5,6-dicyanobenzoquinone; HMPA: hexamethylphosphoramide; L: $2e^-$ ligand; LDA: lithium diisopropylamide; S_N: nucleophilic substitution; S_NAr: nucleophilic aromatic substitution; THF: tetrahydrofuran; TMEDA: tetramethylethylenediamine; TMSCl: trimethylsilyl chloride.

Acknowledgments

We thank the CNRS (Scientific National Research Center) for the support of our laboratory research for the published and unpublished work from our group. Grateful acknowledgment is given to an enthusiastic group of Ph.D. students − A. Auffrant, R. Chavignon, and S. Schouteeten − and to our collaborators B. Andrioletti (CNRS researcher) and J. P. Tranchier (Assistant Professor).

[1] For reviews see: [1a] D. Astruc in *Chimie Organométallique*, EDP Sciences; Les Ulis, France, **2000**, chapters 3−6, p. 87. [1b]A. R. Page, K. P. Kaliappan, E. P. Kündig, *Chem. Rev.* **2000**, *100*, 2917. [1c] F. Rose-Munch, E. Rose, J. P. Djukic, J. Vaissermann, *Eur. J. Inorg. Chem.* **2000**, 1295. [1d] F. Rose-Munch, E. Rose, *Curr. Org. Chem.* **1999**, *3*, 445. [1e] F. Rose-Munch, V. Gagliardini, C. Renard, E. Rose, *Coord. Chem. Rev.* **1998**, *178*, 249. [1f] S. G. Davies, T. D. McCarthy, in *Comprehensive Organometallic Chemistry II*, vol. 12 (Eds.: E. W. Abel, F. G. A. Stone, G. Wilkinson), Elsevier, Oxford, **1995**, p. 1039. [1g] M. F. Semmelhack,, *Comprehensive Organometallic Chemistry II*, vol. 12 (Eds.: E. W. Abel, F. G. A. Stone, G. Wilkinson), Pergamon Press, Oxford, **1995**, p. 979. [1h] F. J. McQuillin, D. G. N. Parker, G. R. Stephenson, *Transition Metals in Organic Synthesis*, Cambridge University Press, Cambridge, **1991**. [1i]L. Balas, D. Jhurry, L. Latxague, S. Grelier, Y. Morel, M. Hamdani, D. Astruc, *Bull. Soc. Chim. Fr.* **1990**, *127*, 401.

[2] [2a] A. J. Pearson, A. V. Gontcharov, P. D. Woodgate, *Tetrahedron Lett.* **1996**, *37*, 3087. [2b] M. F. Semmelhack, H.-G. Schmalz, *Tetrahedron Lett.* **1996**, *37*, 3089. [2c] P. J. Beswick, D. A. Widdowson, *Synthesis* **1985**, 492. [2d] P. J. Beswick, S. J. Leach, N. F. Masters, D. A. Widdowson, *J. Chem. Soc., Chem. Commun.* **1984**, 46. [2e] N. F. Masters, A. Widdowson, *J. Chem. Soc., Chem. Commun.* **1983**, 955. [2f] M. Uemura, N. Nishikawa, K. Take, M. Ohnishi, K. Hirotsu, T. Higuchi, Y. Hayashi, *J. Org. Chem.* **1983**, *48*, 2349. [2g] M. F. Semmelhack, W. Wulff, J. L. Garcia, *J. Organomet. Chem.* **1982**, *240*, C5. [2h] M. F. Semmelhack, J. Bisaha, M. Czarny, *J. Am. Chem. Soc.* **1979**, *101*, 768. [2i] M. F. Semmelhack, G. Clark, *J. Am. Chem. Soc.* **1977**, *99*, 1675.

[3] [3a] L. Besson, M. Le Bail, D. J. Aitken, J. P. Husson, F. Rose-Munch, E. Rose, *Tetrahedron Lett.* **1996**, *37*, 3307. [3b] F. Rose-Munch, K. Aniss, E. Rose, *J. Organomet. Chem.* **1990**, *385*, C1. [3c] J. C. Boutonnet, L. Mordenti, E. Rose, O. Le Martret, G. Precigoux, *J. Organomet. Chem.* **1981**, *221*, 147.

[4] [4a] D. Prim, J.-P. Tranchier, R. Chavignon, F. Rose-Munch, E. Rose, *Organometallics* **2001**, *20*, 1279. [4b] J. Giner Planas, D. Prim, F. Rose-Munch, E. Rose, D. Monchaud, J. Lacour, *Organometallics* **2001**, *20*, 4107. [4c] D. Prim, A. Auffrant, Z. Plyta, J. P. Tranchier, F. Rose-Munch, E. Rose, *J. Organomet. Chem.* **2001**, *624*, 124. [4d] F. Rose-Munch, R. Chavignon, J.-P. Tranchier, V. Gagliardini, E. Rose, *Inorg. Chim. Acta* **2000**, *300*, 693. [4e] E. Rose, C. Le Corre-Susanne, F. Rose-Munch, C. Renard, V. Gagliardini, F. Teldji, J. Vaisserman, *Eur. J. Inorg. Chem.* **1999**, 421. [4f] Z. Plyta, D. Prim, J.-P. Tranchier, F. Rose-Munch, E. Rose, *Tetrahedron Lett.* **1999**, *40*, 6769. [4g] C. Renard, R. Valentic, F. Rose-Munch, E. Rose, *Organometallics* **1998**, *17*, 1587.

[5] [5a] A. Auffrant, D. Prim, F. Rose-Munch, E. Rose, *C. R. Acad. Sci.,* in press. [5b]A. Auffrant, D. Prim, F. Rose-Munch, E. Rose, J. Vaissermann, *Organometallics* **2001**, *20*, 3214. [5c] D. Prim, A. Auffrant, F. Rose-Munch, E. Rose, J. Vaissermann, *Organometallics* **2001**, *20*, 1901. [5d] J.-P. Tranchier, R. Chavignon, D. Prim, A. Auffrant, J. G. Planas, F. Rose-Munch, E. Rose, R. Stephenson, *Tetrahedron Lett.* **2001**, *42*, 3311. [5e] D. Prim, J.-P. Tranchier, F. Rose-Munch, E. Rose, *Eur. J. Inorg. Chem.* **2000**, *5*, 901. [5f] J.-P. Tranchier, R. Chavignon, D. Prim, A. Auffrant, Z. Plyta, F. Rose-Munch, E. Rose, *Tetrahedron Lett.* **2000**, *41*, 3607.

[6] [6a] E. P. Kündig, C. Perret, S. Spichiger, G. Bernardinelli, *J. Organomet. Chem.* **1985**, *286*, 183. [6b] J. Vebrel, R. Mercier, J. Belleney, *J. Organomet. Chem.* **1982**, *235*, 197. [6c] C. A. L. Mahaffy, P. L. Pauson, *Inorg. Synth.* **1979**, *19*, 154 − [6d] G. Carganico, P. Del Buttero, S. Maiorana, G. Riccardi, *J. Chem. Soc., Chem. Commun.* **1978**, 989. [6e] M. D. Rausch, *Pure Appl. Chem.* **1972**, *30*, 523.

[7] [7a] S. S. Lee, T.-Y. Lee, J. E. Lee, I.-S. Lee, Y. K. Chung, M. S. Lah, *Organometallics* **1996**, *15*, 3664. [7b] S. Sun, L. K. Yeung, D. A. Sweigart, T. Y. Lee, S. S. Lee, Y. K. Chung, S. R. Switzer, R. D. Pike, *Organometallics* **1995**, *14*, 2613.[7c] J. D. Jackson, S.

J. Villa, D. S. Bacon, R. D. Pike, G. B. Carpenter, *Organometallics* **1994**, *13*, 3972. [7d] R. D. Pike, D. A. Sweigart, *Synlett* **1990**, 565. [7e] K. K. Bhasin, W. G. Balkeeen, P. L. Pauson, *J. Organomet. Chem.* **1981**, *204*, C25. [7f] T. H. Coffield, V. Sandel, R. D. Closson, *J. Am. Chem. Soc.* **1957**, *79*, 5826.

[8] [8a] A. Fretzen, A. Ripa, R. Liu, G. Bernardinelli, E. P. Kündig, *Chem. Eur. J.* **1998**, *4*, 251. [8b] M. F. Semmelhack, H. T. Hall Jr, R. Farina, M. Yoshifuji, G. Clark, T. Bargar, K. Hirotsu, J. Clardy, *J. Am. Chem. Soc.* **1979**, *101*, 3535. [8c] R. J. Card, W. S. Trahanovsky, *Tetrahedron Lett.* **1973**, *39*, 3823.

[9] [9a] H.-G. Schmalz, J. Hollander, M. Arnold, G. Dürner, *Tetrahedron Lett.* **1993**, *34*, 6259. [9b] G. Jaouen, *Pure Appl. Chem.* **1986**, *58*, 597. [9c] W. S. Trahanovsky, R. J. Card, *J. Am. Chem. Soc.* **1972**, *94*, 2897.

[10] [10a] R. A. Ewin, A. M. McLeod, D. A. Price, N. S. Simpkins, A. P. Watt, *J. Chem. Soc., Perkin Trans. 1* **1997**, 401. [10b] S. G. Davies, T. J. Donohoe, *Synlett* **1993**, 323. [10c] S. G. Davies, T. J. Donohoe, M. A. Lister, *Tetrahedron: Asymmetry* **1991**, *2*, 1085. [10d] S. Top, G. Jaouen, *J. Organomet. Chem.* **1987**, *336*, 143. [10e] M. Uemura, T. Kobayashi, T. Minami, Y. Hayashi, *Tetrahedron Lett.* **1986**, *27*, 2479.[10f] M. Uemura, K. Take, K. Isobe, T. Minami, Y. Hayashi, *Tetrahedron* **1985**, *41*, 5771. [10g] S. Top, G. Jaouen, *J. Org. Chem.* **1981**, *46*, 78. [10h] S. Top, G. Jaouen, J. McGlinchey, *J. Chem. Soc., Chem. Commun.* **1980**, 1110.[10i] M. Acampora, A. Ceccon, M. Dal Farra, G. Giacometti, G. Rigatti, *J. Chem. Soc., Perkin Trans. 2* **1977**, 483.

[11] [11a] C. A. Merlic, M. M. Miller, B. N. Hietbrink, K. N. Houk, *J. Am. Chem. Soc.* **2001**, *123*, 4904. [11b] A. Pfletschinger, T. K. Dargel, J. W. Bats, H.-G. Schmalz, W. Koch, *Chem. Eur. J.* **1999**, *5*, 537. [11c] C. A. Merlic, J. C. Walsh, D. J. Tantillo, K. N. Houk, *J. Am. Chem. Soc.* **1999**, *121*, 3596. [11d] N. Tarriguchi, T. Hata, M. Uemura, *Angew. Chem. Int. Ed.* **1999**, *38*, 1232. [11e] H.-G. Schmalz, C. B. de Koning, D. Bernicke, S. Siegel, A. Pfletschinger, *Angew. Chem. Int. Ed. Eng.* **1999**, *38*, 1620. [11f] H.-G. Schmalz, S. Siegel, J. W. Bats, *Angew. Chem. Int. Ed. Engl.* **1995**, *34*, 2383.

[12] [12a] M. F. Semmelhack, J. L. Garcia, D. Cortes, R. Farina, R. Hong, B. K. Carpenter, *Organometallics* **1983**, *2*, 467. [12b] M. F. Semmelhack, G. Clark, R. Farina, M. Saeman, *J. Am. Chem. Soc.* **1979**, *101*, 217.

[13] [13a] E. P. Kündig, V. Desobry, D. P. Simmons, E. Wenger, *J. Am. Chem. Soc.* **1989**, *111*, 1804. [13b] B. Ohlsson, C. Ullenius, S. Jagner, C. Grivet, E. Wenger, E. P. Kündig, *J. Organomet. Chem.* **1989**, *365*, 243. [13c] B. Ohlsson, C. Ullenius, *J. Organomet. Chem.* **1988**, *350*, 35. [13d] E. P. Kündig, *Pure Appl. Chem.* **1985**, *57*, 1855. [13e] B. Ohlsson, C. Ullenius, *J. Organomet. Chem.* **1984**, *267*, C34.

[14] [14a] J. Brocard, A. Laconi, D. Couturier, *Org. Magn. Reson.* **1984**, *22*, 369. [14b] A. Solladie-Cavallo, J. Suffert, *Org. Magn. Reson.* **1980**, *14*, 426. [14c] W. R. Jackson, W. B. Jennings, S. C. Renninson, R. Spratt, *J. Chem. Soc. B* **1969**, 1214.

[15] J. C. Boutonnet, J. Levisalles, J. M. Normant, E. Rose, *J. Organomet. Chem.* **1983**, *255*, C21.

[16] [16a] A. Pfletschinger, W. Koch, H.-G. Schmalz, *New J. Chem.* **2001**, *25*, 446. [16b] M. F. Semmelhack, J. J. Harrison, Y. Thebtaranonth, *J. Org. Chem.* **1979**, *44*, 3275.

[17] [17a] R. C. Cambie, G. R. Clark, S. R. Gallagher, P. S. Rutledge, M. J. Stone, P. D. Woodgate, *J. Organomet. Chem.* **1988**, *342*, 315. [17b] E. P. Kündig, D. P. Simmons, *J. Chem. Soc., Chem. Commun.* **1983**, 1320.

[18] D. Caillol, E. Rose, F. Rose-Munch, unpublished results.

[19] B. Nicholls, M. C. Whiting, *J. Chem. Soc.* **1959**, 551.

[20] J. C. Boutonnet, F. Rose-Munch, E. Rose, A. Semra, *Bull. Soc. Chim. Fr.* **1987**, 640.

[21] [21a] F. Rose-Munch, E. Rose, A. Semra, *J. Chem. Soc., Chem. Commun.* **1986**, 1108. [21b] J. C. Boutonnet, F. Rose-Munch, E. Rose, *Tetrahedron Lett.* **1985**, *26*, 3989.

[22] [22a] V. Gagliardini, V. Onnikian, F. Rose-Munch, E. Rose, *Inorg. Chim. Acta* **1997**, *259*, 265. [22b] J. C. Boutonnet, F. Rose-Munch, E. Rose, A. Semra, *Bull. Soc. Chim. Fr.* **1987**, 640.

[23] "Glossary of Terms used in Physical Organic Chemistry" (Ed.: V. Gold), *Pure Appl. Chem.* **1979**, *51*, 1725.

[24] [24a] O. Hoffmann, H.-G. Schmalz, *Synlett* **1998**, 1426. [24b] H. Schmalz, T. Volk, D. Bernicke, S. Huneck, *Tetrahedron* **1997**, *53*, 9219. [24c] H. G. Schmalz, K. Schellhaas, *Angew. Chem. Int. Ed. Engl.* **1996**, *35*, 2146. [24d] H.-G. Schmalz, S. Siegel, A. Schwartz, *Tetrahedron Lett.* **1996**, *37*, 2947. [24e] H. G. Schmalz, K. Schellhaas, *Tetrahedron Lett.* **1995**, *36*, 5511. [24f] H. G. Schmalz, M. Arnold, J. Hollande, J. W. Bats, *Angew. Chem. Int. Ed. Engl.* **1994**, *33*, 109.

[25] [25a] F. Rose-Munch, R. Khourzom, J.-P. Djukic, A. Perrotey, E. Rose, J. Brocard, *J. Organomet. Chem.* **1994**, *467*, 195. [25b] F. Rose-Munch, E. Rose, A. Semra, *J. Chem. Soc., Chem. Commun.* **1986**, 1551.

[26] [26a] F. Rose-Munch, E. Rose, A. Semra, C. Bois, *J. Organomet. Chem.* **1989**, *363*, 103. [26b] F. Rose-Munch, E. Rose, A. Semra, Y. Jeannin, F. Rose-Munch, *J. Organomet. Chem.* **1988**, *353*, 53.

[27] F. Rose-Munch, E. Rose, A. Semra, M. Philoche-Levisalles, *J. Organomet. Chem.* **1989**, *363*, 123.

[28] F. Rose-Munch, E. Rose, A. Semra, *J. Chem. Soc., Chem. Commun.* **1987**, 942.

[29] F. Rose-Munch, E. Rose, A. Semra, L. Mignon, J. Garcia-Oricain, C. Knobler, *J. Organomet. Chem.* **1989**, *363*, 297.

[30] F.-E. Hong, S.-C. Lo, M-W. Liou, Y.-T. Chang, C.-C. Lin, *J. Organomet. Chem.* **1996**, *506*, 101.

[31] F. Rose-Munch, E. Rose, A. Semra, *J. Organomet. Chem.* **1989**, *377*, C9.

[32] F. Rose-Munch, O. Bellot, L. Mignon, A. Semra, F. Robert, Y. Jeannin, *J. Organomet. Chem.* **1991**, *402*, 1.

[33] J. P. Djukic, F. Rose-Munch, E. Rose, Y. Dromzee, *J. Am. Chem. Soc.* **1993**, *115*, 6434.

[34] [34a] J. P. Djukic, F. Rose-Munch, E. Rose, *Organometallics* **1995**, *14*, 2027. [34b] J. P. Djukic, P. Geysermans, F. Rose-Munch, E. Rose, *Tetrahedron Lett.* **1991**, *32*, 6703.

[35] E. P. Kündig, J. A. F. Cunningham, P. Paglia, D. Simmons, G. Bernardinelli, *Helv. Chim. Acta* **1990**, *73*, 386.

[36] K. Kotzian, C. G. Kreiter, S. Özkar, *J. Organomet. Chem.* **1982**, *229*, 29.

[37] J. P. Djukic, F. Rose-Munch, E. Rose, *J. Chem. Soc., Chem. Commun.* **1991**, *22*, 1634.

[38] M. Persson, U. Hacksell, I. Csoregh, *J. Chem. Soc., Perkin Trans. 1* **1991**, 1453.

[39] M. Brookhart, A. Lukacs, *J. Am. Chem. Soc.* **1984**, *106*, 4161.

[40] F. Balssa, V. Gagliardini, F. Rose-Munch, E. Rose, *Organometallics* **1996**, *15*, 4373.

[41] This double nucleophilic substitution has been used in the case of an *ipso* S_NAr: F. Rose-Munch, L. Mignon, J. P. Sanchez, *Tetrahedron Lett.* **1991**, *32*, 6323.

Received October 12, 2001
[I01410]

Copper(II) and Palladium(II) Complexes of the Reducing Sugar Lyxose[‡]

Peter Klüfers*[a] and Thomas Kunte[a]

Keywords: Lyxose / Copper / Palladium / Aldose−metal complexes

The reaction of the reducing aldopentose lyxose towards the metal centres in the copper-based cellulose solvents Schweizer's reagent (cupric hydroxide in aqueous ammonia) and Cu-en (cupric hydroxide in aqueous ethylenediamine) was investigated. Crystals of the trinuclear complexes $[(NH_3)_4Cu^{II}_3(\beta\text{-D-Lyx}p1,2,3H_{-3})_2(H_2O)_2]\cdot 4H_2O$ (**1**) and $[(en)_2Cu^{II}_3(\beta\text{-D-Lyx}p1,2,3H_{-3})_2(H_2O)_2]\cdot 4H_2O$ (**2**) (Lyx*p* = lyxopyranose) were grown upon preventing Fehling-type aldose oxidation. One of the three cupric centres is coordinated by two chelating diolato ligands only, hence both ammonia and ethylenediamine are displaced from Cu^{II} by a carbohydrate ligand. A binuclear lyxose-palladium(II) complex is formed on reaction of lyxose with Pd-en ($[(en)Pd(OH)_2]$ in water), which is another cellulose solvent of the coordinating type. From racemic mixtures of the lyxose enantiomers, crystals of $[(en)_2Pd^{II}_2(\beta\text{-}rac\text{-Lyx}pH_{-4})]\cdot 7H_2O$ (**3**) were obtained. ^{13}C NMR spectra reveal the bimetallated lyxose tetraanions to be the main species in palladium-rich solutions.
(© Wiley-VCH Verlag GmbH, 69451 Weinheim, Germany, 2002)

Introduction

Reducing Sugars as Ligands

Metal complexation of reducing sugars is a particularly challenging field of carbohydrate-metal complexation because of the characteristic reactivity of aldoses and ketoses. While nonreducing sugars and sugar derivatives such as sugar alcohols, on- and ar-acids or glycosides have fixed configurations and hence a limited capability to match their oxygen-atom pattern with the binding sites of a metal ion, reducing sugars can isomerize to the various furanose and pyranose anomers. For the aldopentose D-lyxose, for example, Scheme 1 depicts the O-atom patterns of the anomeric α- and β-forms of D-lyxofuranose and -pyranose, the latter as the $^4C_1$ conformers. Structural information concerning how a reducing sugar is bound to a particular transition metal in a specified oxidation state is rare. The few structural analyses available are due to the pioneering work of Taylor and Waters on a binuclear molybdenum(VI) complex of D-lyxose in its β-furanose form,[1] a series of binuclear β-D-mannofuranose complexes of trivalent metals (V, Cr, Fe, Mn),[2a,2b] and a palladium(II) complex of the most important aldose, D-glucose, in its α-pyranose form.[3] Despite its significance as a metal for catalysis, there is no structural information on any copper complex of a reducing sugar. The main experimental difficulty when investigating

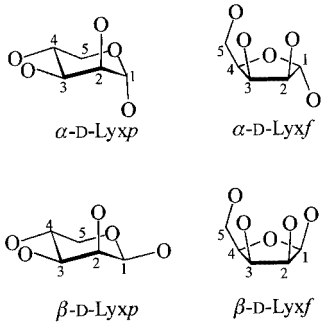

Scheme 1. Oxygen-atom patterns of the anomeric D-lyxofuranoses (right) and -pyranoses (left), the IUPAC-recommended abbreviations, and the atom numbering used throughout the text; NB the β anomers (bottom) provide two diol moieties of suitable torsion angle for metal complexation each, but not the α forms (top)

complexes of this kind is the ease of the Fehling reaction. However, the oxidation of a carbohydrate may be suppressed for prolonged periods of time by cooling to about 5 °C and avoidance of local or short-term temperature increases when preparing the solutions. We report here the first structural analyses of crystals obtained from lyxose solutions in the well-known cellulose solvents Schweizer's reagent (ammonia as a co-ligand) and Cu-en (ethylenediamine as the additional ligand).

Results and Discussion

Lyxose Complexes in Schweizer's Reagent and Cu-en

Blue, monoclinic crystals of $[(NH_3)_4Cu^{II}_3(\beta\text{-D-Lyx}p1,2,3H_{-3})_2(H_2O)_2]\cdot 4H_2O$ (**1**) were obtained from D-lyxose solutions in ice-cold Schweizer's reagent (cupric hy-

[‡] Polyol−Metal Complexes, 39. Part 38: X. Kästele, P. Klüfers, T. Kunte, *Z. Anorg. Allg. Chem.* **2001**, *627*, 2042−2044.

[a] Department Chemie der Ludwig-Maximilians-Universität München,
Butenandtstraße 5−13, 81377 München, Germany
Fax: (internat.) + 49-89/2180-7407
E-mail: kluef@cup.uni-muenchen.de

droxide dissolved in aqueous ammonia) in a large range of molar ratios of the components (Cu:Lyx from 0.5:1 to 2:1). To inhibit progress of the autocatalytic sugar oxidation in the course of crystallization, the solutions were filtered after preparation to remove small amounts of cuprous oxide. In the crystals of **1**, two bridging lyxose ligands adopt the β-pyranose form in C_2 symmetrical, trinuclear molecules; they are each threefold deprotonated along the *cis-cis* sequence of the hydroxy groups with C1, C2, and C3 (Figure 1). The coordination chemistry of the cupric centres is normal i.e. the bis-diolato-bonded Cu1 atom is square-planar coordinated with no further ligands, whereas Cu2, which is coordinated by a diolato ligand derived from the anomeric and the epimeric hydroxy groups, is surrounded by a square pyramid consisting of the two alkoxy oxygens, two ammine ligands and a water ligand at a longer distance. Intramolecular hydrogen bonds are established from N2−H donors and O3 acceptors. Also as usual in polyolato-metal compounds, the alkoxo atoms O1 and O3 are acceptors of two hydrogen bonds each; the acceptor capability of the bridging O2 atoms is weakened by an almost planar arrangement of its substituents (angle sum: 359.2°).

The capability of a polyolato ligand to replace ammine ligands is a prerequisite for the formation of **1**. To gain more insight into whether the molecular arrangement in **1** is unique to Schweizer's reagent, attempts were made to crystallize an analogous lyxose-copper complex in the related $Cu(OH)_2$/en/D-lyxose system with ethylenediamine instead of ammonia. Again, the stoichiometry was varied between half- and bimetallation of the saccharide. Blue, monoclinic crystals of $[(en)_2Cu^{II}_3(\beta\text{-D-Lyx}p1,2,3H_{-3})_2(H_2O)_2]\cdot 4H_2O$ (**2**) were obtained by the same procedure as with **1**, and also in all the Cu:Lyx ratios chosen. The molecular structure (Figure 2) resembles that in the ammine complex, including the detail of intramolecular hydrogen bonding from amine donors to alkoxide acceptors. The structure determination demonstrates that the stronger ethylenediamine ligand is also replaced by the lyxose anions. Both **1** and **2** crystallize in space group *C*2; however, despite the similarities in the lattice constants, the packing of the molecules is different. The lattice constants are therefore related according to $a_1 = 2c_2$, $b_1 = -b_2$, $2c_1 = a_2$, $\beta_1 = \beta_2$.

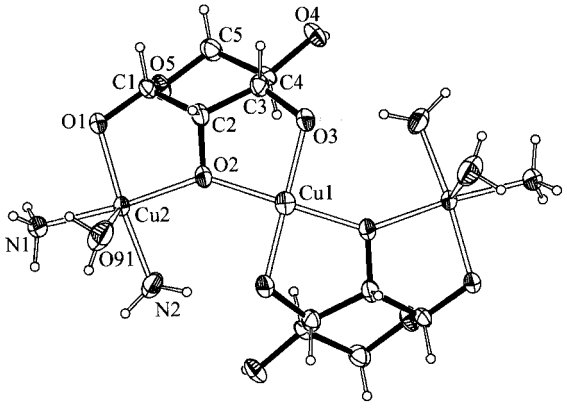

Figure 1. The structure of the $[(NH_3)_4Cu_3(\beta\text{-D-Lyx}p1,2,3H_{-3})_2(H_2O)_2]$ molecules in **1** projected down the twofold axis of space group *C*2; thermal ellipsoids are drawn at 60% probability; distances (Å) from Cu1 to: O3 1.932(3), O2 1.970(3); from Cu2 to: O1 1.930(2), N2 1.972(4), O2 1.983(3), N1 2.002(3), O91 2.427(4); O1−C1 1.372(5), O2−C2 1.417(5), O3−C3 1.410(5), O4−C4 1.430(5), O5−C5 1.429(5), O5−C1 1.459(6), C1−C2 1.526(6), C2−C3 1.523(6), C3−C4 1.521(6), C4−C5 1.527(6); torsion angles (°): O1−C1−C2−O2 48.2(5), O2−C2−C3−O3 −47.3(4), O3−C3−C4−O4 −71.9(4); puckering parameters of the lyxopyranose ring: Q = 0.555(4) Å, θ = 11.9(4)°, φ = 349(2)°

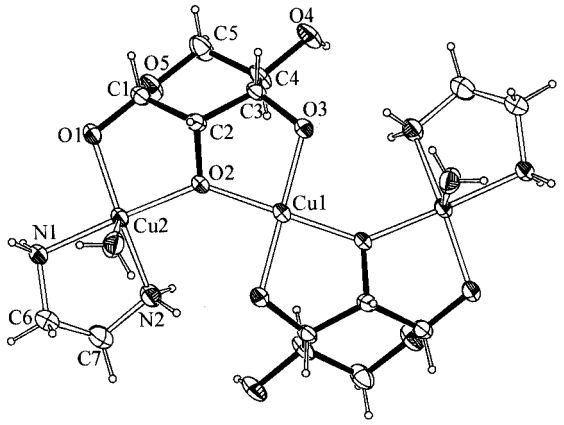

Figure 2. The structure of the $[(en)_2Cu_3(\beta\text{-D-Lyx}p1,2,3H_{-3})_2(H_2O)_2]$ molecules in **2** projected down the twofold axis of space group *C*2; thermal ellipsoids are drawn at 40% probability; distances (Å) from Cu1 to: O3 1.936(2), O2 1.940(2); from Cu2 to: O2 1.943(2), O1 1.946(2), N2 1.998(3), N1 2.004(3), O91 2.350(3); C1−O1 1.378(4), C1−O5 1.437(5), C2−O2 1.430(4), C3−O3 1.412(4), C4−O4 1.436(4), C5−O5 1.425(5), C1−C2 1.523(5), C2−C3 1.527(4), C3−C4 1.522(5), C4−C5 1.522(6); bond angles (°): O3−Cu1−O2 86.53(9), O2−Cu2−O1 86.07(9); torsion angles (°): O1−C1−C2−O2 47.5(4), O5−C1−C2−O2 −71.6(3), O2−C2−C3−O3 −47.1(4), O3−C3−C4−O4 −71.0(4), C2−C3−C4−O4 167.4(3), O4−C4−C5−O5 179.1(3); puckering parameters of the lyxopyranose ring: Q = 0.546(4) Å, θ = 11.7(4)°, φ = 327(2)°

The structures of the copper-lyxose complexes show that the retardation of Fehling-type reactions is not caused by a lack of contacts between the central copper atoms and the hemiacetal function of the monosaccharide. As should be expected from the acidities of the lyxose hydroxy groups, the OH group at C1 (as the most acidic one) is deprotonated and bonded to a copper ion. The high tendency of formation of **1** and **2** shows the difficulty in deriving rules for copper complexation in these ternary systems. Neither simple monometallated species of the kind $[(\text{N-ligand})_m\text{Cu(D-LyxH}_{-2})]$ nor bimetallated complexes of the type $[(\text{N-ligand})_n\text{Cu}_2\text{(D-LyxH}_{-4})]$ have been isolated despite the use of suitable molar ratios. One of the reasons for the formation of the more complicated structures of **1** and **2** is the higher stability of polyolato over am(m)ine complexes in solutions of sufficiently high pH, as has been shown for simple diolates,[4] possibly together with a particular stability of Cu_2-μ-triolate(3−) assemblies, which are known for glycerol complexes.[5]

Lyxose Complexes of Palladium(II)

The experiments with the copper-based cellulose solvents suggest that monosaccharide complexation should follow simpler rules if the spectator ligand is chosen such that the stabilities of the competing complexes are not in the same order of magnitude. Maintaining lyxose as the sugar component, this may be demonstrated by replacing Cu-en with Pd-en {as an aqueous solution of $[(en)Pd^{II}(OH)_2]$}, which is also a cellulose solvent.[6] The ethylenediamine ligand at the central palladium atoms is not prone to substitution by polyolato ligands. Thus Pd-en can only act as a diol-coordinating agent (the typical reactions following hydroxide addition to cellulose solutions in Schweizer's reagent — in particular cross-linking of polysaccharide strands due to bis-diolato-cuprate formation — are therefore missing with Pd-en.) On reaction with lyxose, the lowest number of species was found for Pd/lyxose molar ratios of 2:1 and higher. ^{13}C NMR spectra of the diamagnetic complexes reveal bimetallated lyxopyranose ligands by the typical "coordination induced shift" (CIS) of the carbon atoms 1−4. Crystals of the complex formed from D-lyxose and Pd-en could not be isolated, although yellow, centrosymmetric, triclinic crystals of $[(en)_2Pd^{II}_2(\beta\text{-}rac\text{-}Lyxp\mathrm{H}_{-4})]\cdot 7H_2O$ (**3**) were obtained from *rac*-lyxose solutions, which can be prepared easily due to the availability of both D- and L-lyxose. The structure of the complex molecules agrees well with the expectation that: (1) only diol moieties are bound to palladium, and (2) due to the high thermodynamic stability of the complexes, the maximum number of palladium atoms should be bonded to the monosaccharide. Scheme 1 shows that only two isomers are able to bind two palladium atoms for steric reasons: the β-pyranose form in its $^4C_1$ conformation, and the β-furanose form when 1,3-diolato complex formation is taken into consideration as well as 1,2-bonding. Figure 3 shows the actual structure with the lyxose ligands in the β-pyranose form. In agreement with the NMR spectra, O1−4 are deprotonated and bonded to the central palladium atoms. Hydrogen bonding is as usual with polyolato-metallates: each alkoxide O atom accepts two hydrogen bonds, mostly from water donors (2 N−H···O- and 14 O−H···O- contacts are established by the 16 lone pairs of the eight alkoxo ligands of the asymmetric unit). The water donors are incorporated in cooperative hydrogen bond sequences, which often start with an N−H donor.

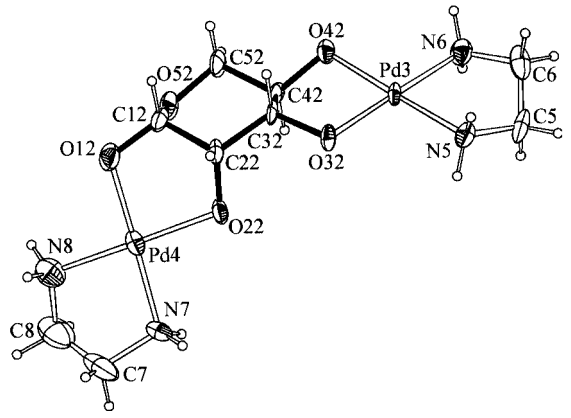

Figure 3. The structure of the $[(en)_2Pd_2(\beta\text{-D-}Lyxp\mathrm{H}_{-4})]$ isomer from the racemic mixture in **3** projected with almost the same view of the carbohydrate ligand as in the copper complexes; thermal ellipsoids are drawn at 60% probability; distances (Å) and angles (°) (the first entry is the specified distance, the second entry is the corresponding distance in the L-configured isomer): Pd3−O42 2.004(4), 2.006(4), Pd3−O32 2.024(4), 2.027(4), Pd4−O22 2.011(4), 1.990(4), Pd4−O12 1.993(5), 2.004(4), C12−O12 1.374(8), 1.372(7), C12−O52 1.434(9), 1.432(8), C22−O22 1.418(8), 1.414(8), C32−O32 1.421(7), 1.427(6), C42−O42 1.424(7), 1.414(8), C52−O52 1.424(8), 1.425(8), C12−C22 1.542(8), 1.551(8), C22−C32 1.529(8), 1.527(9), C32−C42 1.514(9), 1.509(9), C42−C52 1.517(8), 1.525(8); mean of eight Pd−N distances: 2.034 Å, standard deviation of the mean: 0.007 Å, mean standard deviation: 0.006 Å; torsion angles: O12−C12−C22−O22 49.8(7), −47.2(7), O22−C22−C32−O32 −55.6(8), 52.8(8), O32−C32−C42−O42 −55.9(6), 58.0(6); puckering parameters of the lyxopyranose ring: Q = 0.574(7), 0.579(7) Å, θ = 6.2(7), 173.0(7)° (the conformation is close to an ideal chair, hence no φ value is given)

In the ^{13}C NMR spectra, the aforementioned CIS is a maximum for C2. Though data on aldoses are scarce, this seems to be biased towards the axial substitution of the epimeric carbon atom to some extent.[7] At the concentrations given in Table 1, the binuclear $[(en)_2Pd^{II}_2(\beta\text{-D-}Lyxp\mathrm{H}_{-4})]$ complex is the main species at high palladium:lyxose ratios. Monometallated species occur in only small amounts, although they become the main species at a

Table 1. Signal positions in the ^{13}C NMR spectrum of solutions of D-lyxose in 1 M Pd-en; in addition to the chemical shift the "coordination induced shift" ("CIS", defined as $\delta_{complex} - \delta_{reference}$) is tabulated; the reference is an approx. 0.6 M solution of D-lyxose in D_2O;[a] signals of the en ligand are omitted; Δδ values that indicate a CIS are printed in **boldface**; in the last two columns, a rough estimate of the species distribution as derived from ^{13}C signal heights is given for different molar ratios: a "+" sign represents about one fifth of the tetraol, whereas a "−" sign accounts for less than about 10%; an unidentified form of lyxose (abundance: "−" at 2:1, "+" at 1:1 molar ratio) exhibits signals at δ = 90.6, 71.3, 68.7, 66.8, 56.6; from the fact that signal height closely corresponds to that of the monometallated form on Pd/Lyx ratio variation, the unidentified species may be another monometallated derivative, possibly with a lyxofuranose ligand

		C1	C2	C3	C4	C5	2:1	1:1
$[(en)_2Pd_2(\beta\text{-D-}Lyxp1,2,3,4H_{-4})]$	δ	108.6	85.6	84.1	74.5	65.0	++++	−
	Δδ	**12.7**	**14.1**	**9.9**	**6.5**	−0.7		
$[(en)_2Pd(\beta\text{-D-}Lyxp1,2H_{-2})]$	δ	107.2	82.8	72.9	70.4	64.8	−	++
	Δδ	**11.3**	**11.3**	−1.3	2.4	−0.9		
$[(en)_2Pd(\beta\text{-D-}Lyxp2,3H_{-2})]$	δ	96.4	81.5	80.1	66.9	64.7	−	++
	Δδ	0.5	**10.0**	**5.9**	−1.1	−1.0		

[a] M. J. King-Morris, A. S. Serianni, *J. Am. Chem. Soc.* **1987**, *109*, 3501−3508.

molar ratio of 1:1. Their concentration is governed by the relative acidities of the hydroxy groups of lyxose. The main species is the mononuclear [(en)Pd^{II}(β-D-Lyx*p*1,2H_{-2})] complex with the most acidic hydroxy group at O1 being deprotonated, although almost the same concentration is reached by the [(en)Pd^{II}(β-D-Lyx*p*2,3H_{-2})] species. A minor species in the 1:1 solutions has not been identified (cf. Table 1).

Attempts to synthesize a heteronuclear Pd_2Cu complex by reacting the [(en)Pd^{II}(β-D-Lyx*p*H_{-2})] complexes with $Cu(OH)_2$ failed according to NMR spectroscopy. Instead of increasing signal widths at the suggested copper-binding site (C2, C3), the signals of the binuclear [$(en)_2Pd^{II}_2$(β-D-Lyx*p*H_{-4})] complex emerge. Obviously, the dissolved cupric hydroxide forms homonuclear species of unknown composition that do not give rise to observable NMR signals and also consume lyxose.

Conclusion

Prior to undergoing redox chemistry, the aldose lyxose forms coordination compounds with copper atoms in alkaline aqueous solution. The compounds are prevented from Fehling-type reactions by cooling to 5 °C and removal of autocatalytically acting seeds of cuprous oxide. The most acidic hydroxy group at the anomeric carbon atom is involved in copper chelation. However, the prediction of a particular structure is complicated by the ability of diolato ligands to substitute nitrogen ligands at the cupric centres.

Table 2. Crystallographic data

	1	**2**	**3**
Empirical formula	$C_{10}H_{38}Cu_3N_4O_{16}$	$C_{14}H_{42}Cu_3N_4O_{16}$	$C_9H_{36}N_4O_{12}Pd_2$
M_r/g mol^{-1}	661.064	713.139	605.22
Crystal size/mm	0.30 × 0.16 × 0.08	0.27 × 0.06 × 0.02	0.52 × 0.35 × 0.10
T/K	200(2)	200(2)	200(2)
Radiation	Mo-K_α rotating anode	Mo-K_α rotating anode	Mo-K_α sealed anode
Diffractometer	Nonius Kappa CCD	Nonius Kappa CCD	Stoe IPDS
φ increment/°	1	1	1.2
Irradiation time	70 s deg^{-1}	60 s deg^{-1}	120 s plate^{-1}
Crystal system	monoclinic	monoclinic	triclinic
Space group	*C*2	*C*2	$P\bar{1}$
a/Å	21.1164(4)	19.7731(3)	9.6538(10)
b/Å	6.4130(2)	6.41900(10)	14.5600(15)
c/Å	9.4660(2)	12.3972(2)	15.6269(19)
α/°	90	90	77.008(13)
β/°	115.0241(12)	125.3170(10)	75.928(13)
γ/°	90	90	77.725(12)
V/Å^3	1161.55(5)	1283.92(3)	2046.9(4)
Z	2	2	4
Calcd. density/g cm^{-3}	1.89013(8)	1.84468(4)	1.9640(4)
μ/mm^{-1}	2.803	2.543	1.820
Absorption correction	numerical (9 faces)	numerical (8 faces)	numerical (10 faces)
Transmission factor range	0.6823−0.8207	0.6322−0.9675	0.5613−0.8490
Refls. measured	7104	11089	16223
R_{int}	0.025	0.038	0.059
Mean σ(*I*)/*I*	0.028	0.043	0.057
θ range/°	2.3−23.3	3.3−27.5	2.1−25.7
Observed refls.	1639	2695	5839
x, *y* (weighting scheme)	0.0340, 3.2527	0.0405, 1.2634	0.0648, 6.3502
Water-H refinement	[a]	[a]	[b]
Flack parameter	−0.03(2)	−0.02(2)	−
Refls. in refinement	1671	2887	7272
Parameters	183	191	573
Restraints	20	13	42
$R(F_{obs})$	0.025	0.031	0.047
$R_w(F^2)$	0.068	0.080	0.123
S	1.135	1.098	1.057
Shift/error$_{max}$	0.001	0.001	0.001
Max. diff. density/eÅ^{-3}	0.410	0.755	2.818
Min. diff. density/eÅ^{-3}	−0.765	−0.862	−1.352

[a] C- and N-bonded H atoms fixed; O−H and H−H distance fixed for water-H atoms at 0.83 and 1.31, respectively; one common *U* for all H atoms. [b] C- and N-bonded H atoms fixed; one common O−H distance refined for water-H atoms (0.94), H−H distance fixed to the 1.57-times that of O−H thus forcing a 105° bonding angle; one common *U* for all H atoms.

The latter characteristic does not hold for palladium(II) centres, to which nitrogen ligation is clearly favoured over alkoxide bonding. (en)Pd fragments thus bind to diol groups without loss of the ethylenediamine ligand. Hence the rules of carbohydrate-metal coordination appear to be less complicated in the palladium(II) case. For this metal, the maximum number of palladium atoms is bonded to as many diol groups as are needed for chelation in terms of the torsion angle (i.e. no axial-axial diols in pyranoses and no *trans*-diols in furanoses).

Experimental Section

D- and L-lyxose were purchased from the Institute of Chemistry, Bratislava. Ethylenediamine, ammonia and sodium hydroxide were purchased from Fluka. Cupric hydroxide was synthesized from cupric sulfate pentahydrate (Merck). Pd-en was stored under nitrogen at 4 °C before use. All experiments with Pd-en were carried out under nitrogen. NMR measurements were performed either with a Jeol EX 400 or a Jeol GSX 270 NMR spectrometer.

1: D-Lyxose (450 mg, 3.00 mmol) and cupric hydroxide (195 mg, 2.00 mmol) were stirred in 5 mL aqueous ammonia (25%) at 4 °C for 2 h. The dark blue solution was filtered off from excess cupric hydroxide. Blue platelets of **1** formed during the course of one week upon diffusing acetone vapours into the solution. Solutions kept at room temperature had decomposed after two days.

2: The entire procedure was conducted at a temperature of 4 °C: D-lyxose (300 mg, 2.00 mmol) and cupric hydroxide (195 mg, 2.00 mmol) were stirred in 5 mL water for 5 min. Sodium hydroxide (8 mg, 0.2 mmol) was then added and stirring was continued for a further 5 min, after which time ethylenediamine (120 mg, 2.00 mmol) was added. After stirring for 1 h, the dark blue solution was filtered. Blue platelets of **1** formed during the course of one week upon diffusing acetone vapours into the solution. Decomposition of the solutions at room temperature proceeds in the same way as with **1**.

3: Pd-en was prepared as described earlier.[6] *rac*-Lyxose (74 mg, 0.50 mmol) was dissolved in 5 mL of an aqueous 0.2 M Pd-en solution (1.0 mmol) and stirred for 24 h at 0 °C. Diffusion of acetone−water vapours (4:1) caused the formation of yellow platelets within one week.

X-ray Structure Determinations: Details of the structure analyses are summarized in Table 2. Disordered positions for hydrogen attached to two (**1**) or one (**2**) water-oxygen atoms were allowed for to account for hydrogen bonding between symmetry-related oxygen atoms.

CCDC-170697 (**1**), -170696 (**2**) and -170960 (**3**) contain the supplementary crystallographic data for this paper. These data can be obtained free of charge at www.ccdc.cam.ac.uk/conts/retrieving.html [or from the Cambridge Crystallographic Data Centre, 12, Union Road, Cambridge CB2 1EZ, UK; Fax: (internat.) +44-1223/336-033; E-mail: deposit@ccdc.cam.ac.uk].

Acknowledgments

This work was supported by the Deutsche Forschungsgemeinschaft, grant Kl624/5−1. Palladium was provided by dmc^2, Hanau.

[1] G. E. Taylor, J. M. Waters, *Tetrahedron Lett.* **1981**, *22*, 1277−1278.
[2] [2a] J. Burger, C. Gack, P. Klüfers, *Angew. Chem.* **1995**, *107*, 2950−2951; *Angew. Chem. Int. Ed. Engl.* **1995**, *34*, 2647−2649. [2b] A. Geißelmann, P. Klüfers, B. Pilawa, *Angew. Chem.* **1998**, *110*, 1181−1184; *Angew. Chem. Int. Ed.* **1998**, *37*, 1119−1121.
[3] P. Klüfers, T. Kunte, *Angew. Chem.* **2001**, *113*, 4356−4358; *Angew. Chem. Int. Ed.* **2001**, *40*, 4210−4212.
[4] W. Burchard, N. Habermann, P. Klüfers, B. Seger, U. Wilhelm, *Angew. Chem.* **1994**, *106*, 936−939; *Angew. Chem. Int. Ed. Engl.* **1994**, *33*, 884−887.
[5] P. Klüfers, H. Piotrowski, J. Schuhmacher, *Z. Anorg. Allg. Chem.* **1997**, *623*, 191−199, and references therein.
[6] R. Ahlrichs, M. Ballauff, K. Eichkorn, O. Hanemann, G. Kettenbach, P. Klüfers, *Chem. Eur. J.* **1998**, *4*, 835−844.
[7] P. Klüfers, T. Kunte, unpublished results.

Received November 9, 2001
[I01445]

Pressure Variations in Closed Sonochemical Reactors

Nicolas Segebarth*[a] and Jacques Reisse[a]

Keywords: Sonochemistry / Pressure / Gas effect / Water chemistry / Radicals

The pressure inside a closed sonochemical reactor evolves during sonication of a gas-saturated solution. The pressure evolution is dependent on the nature of the dissolved gas: after a common increase during the first 30 minutes, the pressure keeps increasing under argon, stays constant under dinitrogen and decreases under dioxygen and air. The reasons for these observed pressure variations and their implications on physico-sonochemical experiments are discussed in terms of gas solubility and gas reactivity of solutions submitted to intense pressure waves.
(© Wiley-VCH Verlag GmbH, 69451 Weinheim, Germany, 2002)

Introduction

Acoustic cavitation is the phenomenon by which intense ultrasonic waves induce the formation, oscillation, and implosion of gas bubbles in liquids. Chemical reactions (sonochemistry) and the emission of light (sonoluminescence) often accompany this process.[1] The light emission mechanism is due to the bubble interior achieving high temperatures and pressures during its quasi-adiabatic collapse.[2] These conditions also cause chemical reactions. For instance, in water, the bubble collapse leads to the homolysis of the water molecules into OH and H radicals and to the re-formation of water but also of H_2O_2 and H_2 after recombination of these radicals.[3]

Several studies on the influence of the hydrostatic pressure on sonochemistry and/or sonoluminescence have been published[3−7] and have shown the importance of this parameter. On the one hand, an increase of the pressure affects the bubble's dynamics, increasing, for instance, the cavitation threshold and the velocity of the bubble wall during the implosion.[6,7] On the other hand, a pressure increase affects indirectly the cavitation through a change of the acoustic impedance of the liquid, which itself induces changes in the transducer characteristics, including its resonance frequency.[4] Obviously, the concentration of the dissolved gas, which is known to have an effect on the chemical yields[8−10] of sonochemical reactions (whether they involve the dissolved gas or not) and which differs under sonication[11] from that predicted by Henry's law, is also a function of the gas partial pressure. Considering the broad range of parameters that depends on variations of the hydrostatic pressure above the sonicated solution, it was of interest to investigate the pressure evolution in a closed sonochemical reactor under sonication.

Results and Discussion

The typical evolution of the pressure in the closed sonochemical reactor during sonication of water saturated with air, argon, dinitrogen and dioxygen is represented in Figure 1. For each saturating gas, at least three experiments have been conducted and all show qualitatively the same evolution, although small differences of less than 5 mbar can be observed between two sets of data. Starting with an initial pressure equal to the atmospheric pressure, the same evolution is observed for the four gases during the first 30 minutes: a pressure increase of 10 to 15 mbar is observed. After this first phase (phase 1), and depending upon the gas, three different kinds of evolution are observed (phase

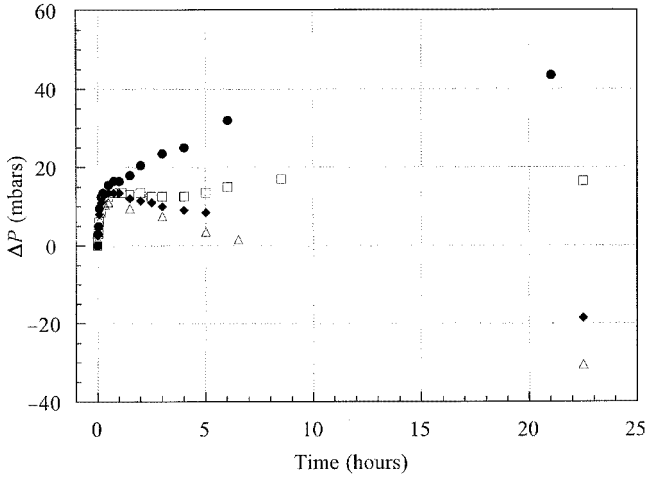

Figure 1. Evolution of the pressure in a closed reactor during sonication of water saturated with (●) argon, (□) N_2, (◆) O_2 and (△) air

[a] Service de Chimie Organique Physique − CP 160/08, Université Libre de Bruxelles,
50 av. F.D. Roosevelt, 1050 Brussels, Belgium
Fax: (internat.) +32-2/650-3606
E-mail: nsegebar@ulb.ac.be

2). Under argon, the pressure increases slowly during phase 2 (<1 mbar/hour) and experiments conducted over very long sonication times (> 70 hours) have not shown any plateau. When the experiment is conducted under dinitrogen, the pressure remains constant during phase 2. The evolution of the pressure under air is similar to that observed under dioxygen: phase 2 is characterized by a linear pressure decrease, at a rate of about 2 mbar/hour, leading to a reduction in pressure in the reactor.

Fluctuations in the temperature are insufficient to explain the observed pressure evolutions. Indeed, the experimental set-up (see Exp. Sect.) allows for a control of the temperature to within ±1 °C, in the liquid phase as well as in the gas phase, leading to pressure fluctuations in the reactor of a maximum of ±3.5 mbar, i.e. much smaller than the observed variations. Furthermore, the consistency observed between repeated experiments is incompatible with random temperature fluctuations.

The pressure increase during phase 1 is likely to be due to the well-known degassing effect of ultrasound: cavitation bubbles grow by rectified diffusion, pumping gas out of the liquid, and are pushed out of the liquid by buoyancy, leading to a lowering of the gas concentration in the solution.[11−15] In the case of open reactors, the resulting stationary gas concentration in the liquid is lower than that predicted by Henry's law. In our case, with a closed reactor, the decrease of the gas concentration in the solution will inevitably lead to an increase of the pressure in the gas phase.

In order to explain the differences that are observed during phase 2, it is necessary to resort to the chemical effects of ultrasound on water solutions of argon, dioxygen, dinitrogen and air. As the experimental set-up does not allow a continuous monitoring of the concentration of the different reaction products in the reactor, and as it is not possible to withdraw samples from it either, the discussion of the experimental results is based on the analysis of the final reaction products and also on what is known concerning the reactivity of water and water solutions when they are insonified.

In the case of dioxygen, the pressure decreases linearly during phase 2. This is due to the reactivity of dioxygen.[16] In addition to the sonochemical reactions that occur in cavitation bubbles filled with water vapour and an inert gas like argon (reactions 1−7), dioxygen-consuming reactions also take place (reaction 8−9).[3] This explains the linear pressure decrease that is observed as soon as a stationary concentration of dissolved dioxygen is reached, i.e. at the end of phase 1.

$$H_2O \rightarrow OH^{\cdot} + H^{\cdot} \quad (1)$$

$$H_2O \rightarrow H_2 + O \quad (2)$$

$$O + H_2O \rightarrow OH^{\cdot} + OH^{\cdot} \quad (3)$$

$$H^{\cdot} + H_2O \rightarrow H_2 + OH^{\cdot} \quad (4)$$

$$OH^{\cdot} + H^{\cdot} \rightarrow H_2O \quad (5)$$

$$OH^{\cdot} + OH^{\cdot} \rightarrow H_2O_2 \quad (6)$$

$$H^{\cdot} + H^{\cdot} \rightarrow H_2 \quad (7)$$

$$O_2 \rightarrow O + O \quad (8)$$

$$H^{\cdot} + O_2 \rightarrow OH^{\cdot} + O \quad (9)$$

In the case of argon, phase 2 is characterized by a weak pressure increase. As argon is inert, this increase probably reflects the production of H_2 (reactions 2 and 7) and, perhaps, the production of a small amount of dioxygen (reactions 10−12, or via another mechanism involving the dissociation of $HO_2^{\cdot}$ but leading to the same net result).[3]

$$OH^{\cdot} + H_2O_2 \rightarrow H_2O + HO_2^{\cdot} \quad (10)$$

$$OH^{\cdot} + HO_2^{\cdot} \rightarrow H_2O + O_2 \quad (11)$$

$$HO_2^{\cdot} + HO_2^{\cdot} \rightarrow H_2O_2 + O_2 \quad (12)$$

Dinitrogen is also usually considered as an inert gas, although this is usually not true in sonochemical reactions. As the dissociation energy of N_2 ($\Delta H_{D,N_2}$ = 944 kJ/mol) is much higher than that of O_2 ($\Delta H_{D,O_2}$ = 496 kJ/mol), thermal dissociation in the cavitation bubbles is not expected to be important. However, N_2 is reactive towards the products of the sonolysis of water, O and $OH^{\cdot}$. Indeed, dinitrogen is oxidised through a series of reactions to form eventually NO_2^- and NO_3^-.[17−19] The presence of nitrogen oxides in the solution at the end of the sonication was confirmed by the observation of strong absorption bands in the UV spectrum. The reactivity of N_2 towards O also explains why the pressure evolution under air, although composed of 80% N_2, is similar to the evolution under O_2. The increase of the concentration of the oxygen atoms, from thermal dissociation of the dioxygen present in air, will strongly favour the consumption of N_2, compared to a situation where the only oxygen atoms come from water sonolysis.

As pointed out earlier, the degassing effect of ultrasound leads to a gas stationary concentration lower than that predicted by Henry's law. The value of this stationary concentration is gas- and solvent-dependant and is generally situated between 60% and 90% of the saturation concentration.[11−15] Using Henry's law ($k_{H,Ar}$ = 714 atm/M) and the perfect gas law, it is easy to calculate the total amount of argon in the reactor and then to estimate its stationary concentration in the solution under sonication. The result of this calculation shows that the concentration of argon decreases to about 30% of the concentration predicted by Henry's law. In the case of air, the measure of [O_2] in water has shown that the concentration drops from 8.5 mg/L to 3.5 mg/L while the pressure drops from 1015 to 987 mbar (corresponding to an O_2 consumption of approximately 1 μmol/h, which is typical for a sonochemical reaction rate). Similar calculations, with the hypothesis that the ratio N_2/O_2 remains constant throughout sonication, lead to the conclusion that the stationary concentration of O_2 in sonicated water is only 40% of the equilibrium concentration, in the absence of sonication. In both cases, the stationary concentration under sonication is therefore significantly lower than what has been measured previously.

Conclusion

We have shown that the pressure inside a closed sonochemical reactor evolves during sonication and that the evolution is gas dependant. The differences that have been observed result from phenomena already described in the literature, namely the degassing effect of ultrasound and the reactivity of any gas other than the rare gases inside the cavitation bubbles.

These pressure variations, although relatively weak, might have a non-negligible impact on some sonochemical studies performed in closed reactors. For instance, in the case of studies in the literature concerning gas effects, it is common to find differences which are fairly small and which, generally, are never explained by pressure effects.[20,21] In this work we have shown that, starting from the same initial pressure, differences of 70 mbar can exist between a sonochemical experiment conducted under argon and the same sonochemical experiment conducted under air. In a similar manner, von Sonntag has shown that a pressure change above a water solution can modify the sonochemical yields of H_2O_2 production by up to 20%.[3] Under these conditions, if the pressure inside the reactor has not been carefully measured as a function of time, how can one assess what are, and in which proportions, the real causes for a gas effect: the gas itself, the hydrostatic pressure or, for instance, the gas concentration?

Experimental Section

General Remarks: The experiments were conducted in an Undatim Ultrasonics D-Reactor operating at 518 kHz, at a power, estimated by calorimetry, of 17 Watts. The hermetically closed reactor had a gas inlet and a gas outlet (equipped with a precision valve) and was connected to an Eirelec manometer (model MP 340A), allowing precise measurement (±1 mbar) of the reactor's internal pressure. The reactor was also equipped with a cooling jacket in order to keep the temperature constant at 23 ± 1 °C. All experiments were performed in a thermostatted room at 23 ± 1 °C, assuring the control of the gas phase temperature above the solution. The hermeticity of the reactor was tested by checking that a pressure of 1200 mbar could be maintained for 48 hours.

The experiments were conducted under air, argon (Air Liquide, N57), dinitrogen (Messer, 4.0) and dioxygen (Air Liquide, N48). The "Milli-Q" water was saturated with gas by bubbling the gas through it for 2 hours. It was then transferred into the reactor (under gas flux) and a second bubbling of 30 minutes was performed. Closing the reactor resulted in an overpressure that was adjusted, with the precision valve, to 1015 mbar. The water volume was 100 mL while the gas-phase volume was 165 mL. The concentration of dioxygen was measured with an Oxi 323-A/Set WTW Oxymeter.

Acknowledgments

The authors would like to thank the Belgian "*Fonds National de la Recherche Scientifique"* for financial support. This work has been done under the auspices of the COST D-10 program from the EC.

[1] K. S. Suslick, Y. T. Didenko, M. M. Fang, T. Hyeon, K. J. Kolbeck, W. B. McNamara III, M. M. Mdleleni, M. Wong, *Philos. Trans. R. Soc. London, Ser. A* **1999**, *357*, 335−353.
[2] Y. T. Didenko, W. B. McNamara III, K. S. Suslick, *J. Phys. Chem. A* **1999**, *103*, 10783−10788.
[3] C. von Sonntag, G. Mark, A. Tauber, H. P. Schuchmann, *Adv. Sonochem.* **1999**, *5*, 109−145.
[4] R. D. Finch, *Brit. J. Appl. Phys.* **1965**, *16*, 1543−1553.
[5] B. T. Balica, E. Whalley, *Can. J. Chem.* **1970**, *48*, 528−536.
[6] A. Henglein, M. Gutierrez, *J. Phys. Chem.* **1993**, *97*, 158−162.
[7] L. Kondic, C. Yuan, C. K. Chan, *Phys. Rev. E* **1998**, *57*, R32−R35.
[8] M. H. Entezari, P. Kruus, R. Otson, *Ultrason. Sonochemistry* **1997**, *4*, 49−54.
[9] N. Segebarth, O. Eulaerts, Y. Kegelaers, J. Vandercammen, J. Reisse, *Ultrason. Sonochemistry* **2002**, *9*, 113−119.
[10] Y. Nagata, H. Okuno, Y. Mizukoshi, Y. Maeda, *Chem. Lett.* **2001**, *2*, 142−143.
[11] O. A. Kapustina, *Sov. Phys. -Acoust.* **1969**, *15*, 54−59.
[12] O. A. Kapustina, *Sov. Phys. -Acoust.* **1970**, *15*, 328−331.
[13] A. N. Kotyusov, *Sov. Phys. -Acoust.* **1992**, *38*, 94−96.
[14] L. Broeckaert, T. Caulier, O. Fabre, C. Maerschalk, J. Reisse, J. Vandercammen, D. H. Yang, T. Lepoint, F. Mullie, in *Current Trends in Sonochemistry* (Ed.: G. J. Price), Royal Soc. *Chem.* Cambridge, **1992**, p. 8−25.
[15] T. G. Leighton, *The Acoustic Bubble*, Academic Press INC, London, **1994**.
[16] C.-H. Fischer, E. J. Hart, A. Henglein, *J. Phys. Chem.* **1986**, *90*, 1954−1956.
[17] E. J. Hart, C.-H. Fischer, A. Henglein, *J. Phys. Chem.* **1986**, *90*, 5989−5991.
[18] E. J. Hart, C.-H. Fischer, A. Henglein, *J. Phys. Chem.* **1986**, *90*, 5992−5995.
[19] C. A. Wakeford, R. Blackburn, P. D. Lickiss, *Ultrason. Sonochemistry* **1999**, *6*, 141−148.
[20] M. E. Fitzgerald, V. Griffing, J. Sullivan, *J. Phys. Chem.* **1956**, *25*, 926−933.
[21] E. L. Mead, R. G. Sutherland, R. E. Verrall, *Can. J. Chem.* **1976**, *54*, 1114−1120.

Received January 17, 2002
[I02031]

1,1,1-Trisborylalkanes as Precursors for Dicarbapentaboranes(5) − Synthesis, Reactivity, and Structures of *closo*-1,5-Bis(neopentyl)-2,3,4-trichloro-1,5-dicarbapentaborane and Its Derivatives

Michael J. Bayer,[a] Hans Pritzkow,[a] and Walter Siebert*[a]

Dedicated to Prof. Armin Berndt on the occasion of his 65th birthday

Keywords: Alkynes / Boranes / Boron / Catechol / Hydroboration

The treatment of 3,3-dimethyl-1-butynyllithium with boron trichloride followed by double hydroboration with $HBCl_2$ afforded 1,1,1-tris(dichloroboryl)-3,3-dimethylbutane (**1a**), characterized as its catechol derivative **1b**. Analogously, three isomers (**3a**, **4a**, and **5a**) were obtained with trimethylsilylacetylide and identified as catechol derivatives **3b**, **4b**, and **5b**. On heating, **1a** formed 2,3,4-trichloro-1,5-dicarba-*closo*-pentaborane(5) (**6a**) with elimination of boron trichloride. Compound **6a** reacted with methyllithium and trimethylaluminium, and also with pentamethylsilazane and acetylides, to give the corresponding carborane derivatives **6c**, **6d**, **6e**, and **6f**. The compositions of the products followed from analytical data and X-ray structure analyses of **1b**, **4b**, **5b**, **6a**, and **6f**.
(© Wiley-VCH Verlag GmbH, 69451 Weinheim, Germany, 2002)

Introduction

The first synthesis of triborylmethane derivatives was reported in 1968, by Matteson and Castle,[1,2] who obtained methanetriboronic esters by treatment of dimethoxychloroborane and carbon tetrachloride with lithium in tetrahydrofuran. Subsequently, tris(dichloroboryl)methane was synthesized.[3] Köster et al.[4] described the preparation of pentaalkyl-1,5-dicarba-*closo*-pentaboranes(5) by hydroboration of dialkyl(1-alkynyl)boranes $R_2BC{\equiv}CR^1$ with tetraalkyldiboranes $(R_2BH)_2$. They obtained 1,1-bis(dialkylboryl)-1-alkenes, although detection of 1,1,1-tris(dialkylboryl)alkanes as precursors for the carboranes was unsuccessful.[4] In 1995 a new route to pentaethyl-1,5-dicarba-*closo*-pentaborane(5) was established, through the use of a large excess of $(Et_2BH)_2$ as a "hydride bath" to give a 1-carba-*arachno*-pentaborane(10) derivative[5] as precursor.[6] Its formation most probably occurred through [BH]-catalyzed condensation of two molecules of undetectable 1,1,1-tris(diethylboryl)propane.[6]

The *closo*-C_2B_3-carboranes warrant particular interest because their structure and bonding may be described as midway between classical and nonclassical. In the last decade, the structures of these smallest *closo*-carboranes have been elucidated by X-ray diffraction analyses of amino-substituted derivatives[7,8] and pentaethyl-1,5-dicarba-*closo*-pentaborane(5),[6,9] by electron density distribution,[9] and by ab initio computations.[10]

We report here on the synthesis and the characterization of 1,1,1-tris(dichloroboryl)-3,3-dimethylbutane and its transformation into 2,3,4-trichloro-1,5-dicarba-*closo*-pentaborane(5) (**6a**). Substitution reactions of **6a** and the syntheses of other tris(dichloroboryl)alkanes are also described.

Results and Discussion

1,1,1-Tris(dichloroboryl)-3,3-dimethylbutane (1a)

The synthesis of **1a** started with lithiation of 3,3-dimethyl-1-butyne by *n*-butyllithium, followed by boron/metal exchange with BCl_3 and a double hydroboration of the boryl alkyne with dichloroborane prepared in situ[11] (Scheme 1). This reaction sequence afforded a 42% yield of **1a**, a colorless and extremely air- and moisture-sensitive liquid. Its ^{11}B NMR spectrum showed a signal at $\delta = 58.7$,

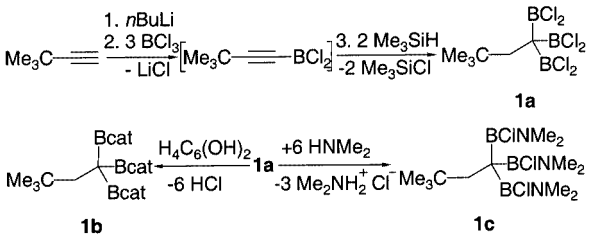

Scheme 1

[a] Anorganisch-Chemisches Institut der Universität Heidelberg, Im Neuenheimer Feld 270, 69120 Heidelberg, Germany
Fax: (internat.) +49-(0)6221-545-609
E-mail: ci5@ix.urz.uni-heidelberg.de

and in the ^{1}H NMR spectrum signals for the *tert*-butyl group (δ = 0.94) and the methylene group (δ = 2.77) were observed. The ^{13}C NMR spectrum exhibited four resonances: at δ = 31.9 (CH_3), 33.8 (CMe_3), 55.2 (CH_2), and 59 (broad, CB_3). A NICI mass spectrum showed the molecular ion peak [M^+] at *m*/*z* = 328 as the base peak.

On treatment of **1a** with three equivalents of catechol in dichloromethane at −78 °C, compound **1b** was synthesized in 95% yield (Scheme 1). Compound **1b** is a colorless solid, soluble in dichloromethane, toluene, and THF. Its composition was determined by NMR spectroscopy, MS spectrometry, and an X-ray structure analysis, single crystals of **1b** being grown from a solution in dichloromethane at room temperature. The molecular structure of **1b** in the crystal is shown in Figure 1. The heterocycles are planar and the boron-bound carbon atom C1 is almost tetrahedral. For all distances and bonding angles, no significant differences from those in similar compounds[12] are observed.

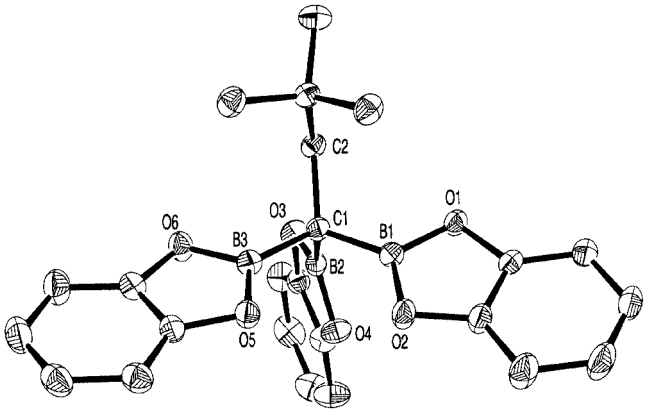

Figure 1. Molecular structure of **1b** in the crystal; selected bond lengths [Å] and angles [°]: B1-C1 1.569(2), B2−C1 1.573(2), B3−C1 1.575(2), B1−O1 1.395(1), B1−O2 1.383(1), B2−O3 1.386(1), B2−O4 1.388 (1), B3−O5 1.388(1), B3−O6 1.391(1), C1−C2 1.570(1), B1−C1−B2 103.51(8), B2−C1−B3 102.44(9), B1−C1−B3 114.79(9), B1−C1−C2 113.27(9), B2−C1−C2 108.72(8), B3−C1−C2 112.86(9)

To obtain information on its reactivity, **1a** was treated with six equivalents of dimethylamine to form **1c** as a colorless, viscous liquid in 88% yield (Scheme 1). Its ^{11}B NMR spectrum showed a signal at δ = 38.5, confirming that each boryl group had one dimethylamino and one chlorine substituent. In the ^{1}H and ^{13}C NMR spectra, the signals of the *tert*-butyl group, the dimethylamino groups, and the methylene group were found in the expected regions. As in **1a** and **1b**, the resonance of the quaternary CB_3 carbon atom was broad (δ = 42). The EI mass spectrum of **1c** exhibited the molecular ion peak [M^+] at *m*/*z* = 353.

1,1-Bis(dichloroboryl)-2-trimethylsilylethene (2a), 1,1,1-Tris(dichloroboryl)-2-trimethylsilylethane (3a), 1,1,2-Tris(dichloroboryl)-2-trimethylsilylethane (4a), and 1,1,2-Tris(dichloroboryl)-1-trimethylsilylethane (5a)

Treatment of trimethylsilylacetylene with *n*-butyllithium, BCl_3, and two equivalents of $HBCl_2$ in the same manner as described above provided isomeric products (Scheme 2). On distillation of the reaction mixture, two fractions were obtained, these containing 1,1-bis(dichloroboryl)-2-trimethylsilylethene (**2a**), and a mixture of **3a**, **4a**, and **5a**.

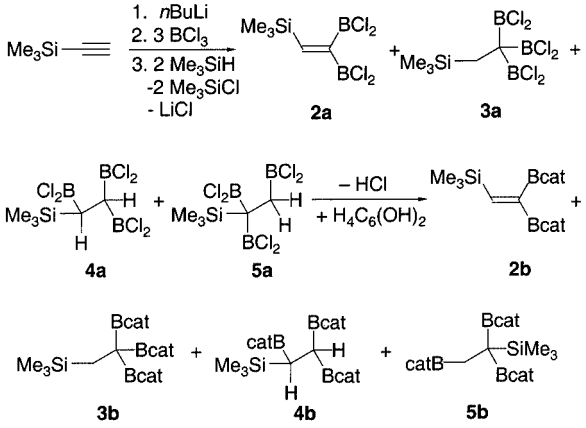

Scheme 2

The ^{11}B NMR spectrum of **2a** showed signals at δ = 57.4 and 60.5, indicating two inequivalent boron atoms, while the ^{29}Si NMR spectrum exhibited a signal at δ = −3.2, in the range for trimethylalkenylsilanes.[13] In the ^{1}H NMR spectrum, the signals for the $SiMe_3$ group and the olefinic proton were detectable at δ = 0.22 and 7.12, respectively. The EI mass spectrum of **2a** showed the molecular ion peak [M^+] at *m*/*z* = 260. Treatment of **2a** with catechol gave the corresponding catechol derivative **2b** in 85% yield, and this was characterized by ^{1}H and ^{11}B NMR spectroscopy and EI mass spectrometry. The NMR spectroscopic data of the second fraction could not be interpreted; its ^{29}Si NMR spectrum indicated the presence of three saturated compounds. However, the NICI mass spectrum showed only one molecular ion peak [M^+] at *m*/*z* = 342, indicating the presence of constitutional isomers. In order to obtain evidence regarding the product mixture and to characterize the components, the mixture was treated with an excess of catechol. The NMR spectroscopic data of the catechol derivatives indicated the presence of **3b**, **4b**, and **5b** in the ratio 15:8.5:1. In the EI mass spectrum, the molecular ion peak [M^+] of the isomers **3b**, **4b**, and **5b** was found at *m*/*z* = 456.

Crystals of compounds **4b** and **5b** suitable for X-ray structure analysis were obtained from solutions of the catecholboryl isomers in dichloromethane at 4 °C. The structures are shown in Figure 2 and 3, respectively. All bond lengths and angles are normal, and the coordination of the boron atoms is almost trigonal planar.

For the formation of three isomeric compounds **3a**, **4a**, and **5a**, we propose the following mechanism. In the first step, hydroboration of [$Me_3Si-C\equiv C-BCl_2$] occurs regioselectively to give product **2a**. $HBCl_2$ then hydroborates **2a** in both directions, giving rise to the compounds **3a** and **4a**, with the former being favored. Moreover, the trimethylsilyl group has the tendency to migrate,[14] and the trimethylsilyl and one dichloroboryl group in **3a** change their positions, with formation of **5a** (Scheme 3).

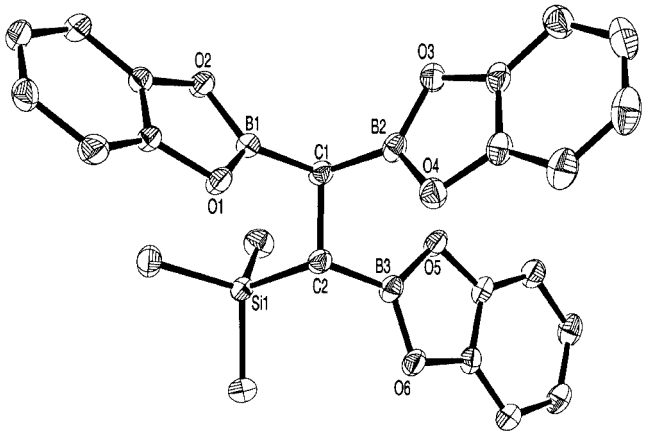

Figure 2. Molecular structure of **4b** in the crystal; selected bond lengths [Å] and angles [°]: B1−C1 1.564(3), B2−C1 1.560(3), B3−C2 1.548(3), B1−O1 1.388(3), B1−O2 1.392(2), B2−O3 1.391(3), B2−O4 1.393(3), B3−O5 1.395(3), B3−O6 1.393(3), C1−C2 1.579(3), C2−Si1 1.913(2), B1−C1−B2 109.5(2), B3−C2−C1 113.1(2), B1−C1−C2 111.8(2), B2−C1−C2 111.1(2), C1−C2−Si1 112.37(13), B3−C2−Si1 106.10(14)

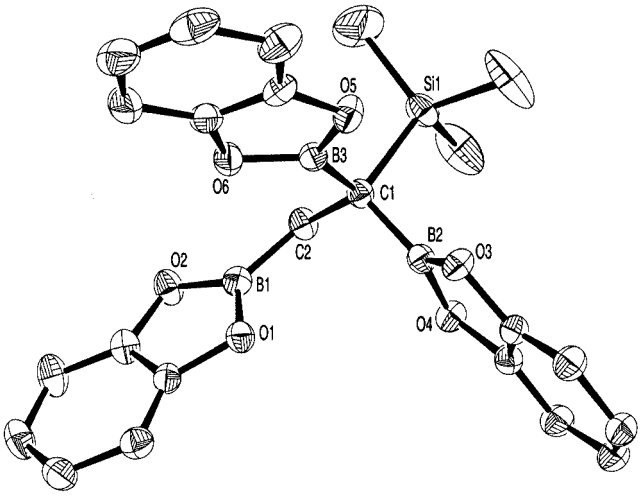

Figure 3. Molecular structure of **5b** in the crystal; selected bond lengths [Å] and angles [°]: B1−C2 1.555(3), B2−C1 1.556(3), B3−C1 1.551(3), B1−O1 1.388(3), B1−O2 1.383(2), B2−O3 1.392(2), B2−O4 1.395(2), B3−O5 1.391(2), B3−O6 1.389(2), C1−C2 1.566(2), C1−Si1 1.925(2), B2−C1−B3 110.98(15), B2−C1−C2 112.88(15), B3−C1−C2 111.30(15), B1−C2−C1 115.75(15), B2−C1−Si1 105.89(12), B3−C1−Si1 108.18(12)

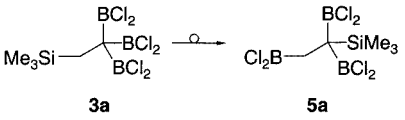

Scheme 3

2,3,4-Trichloro-1,5-dicarba-*closo*-pentaborane(5) (6a) and Its Substitution

On heating neat **1a** at 170 °C for two hours, elimination of BCl_3 occurred with formation of the *closo*-C_2B_3 carborane **6a**, which was obtained by distillation as a colorless, air-sensitive solid in 25% yield (Scheme 4). A signal at δ = 22.1 in its ^{11}B NMR spectrum supported the carborane structure. The ^1H NMR spectrum showed two singlets for the methyl and the methylene protons, at δ = 1.02 and 2.09, respectively, and the ^{13}C NMR spectrum exhibited four signals for CH_3 (δ = 29.7), the quaternary carbon atom (δ = 31.6), CH_2 (δ = 38.5), and the apical carbon atoms of the cluster (δ = 94, br.). The highest peak observed in an EI mass spectrum of **6a** was found at *m*/*z* = 289 [$M^+ - CH_3$], but the PICI mass spectrum showed [M^+] at *m*/*z* = 303 as the base peak. The composition of **6a** was confirmed by an X-ray structure analysis. The trimethyl derivative **6d** may be obtained by two routes (Scheme 4). Firstly, methylation of **1a** gave **1d**, which on heating was transformed into **6d** with elimination of trimethylborane. Compound **1d** was characterized by ^1H, ^{11}B and ^{13}C NMR spectroscopy and by PICI mass spectrometry.

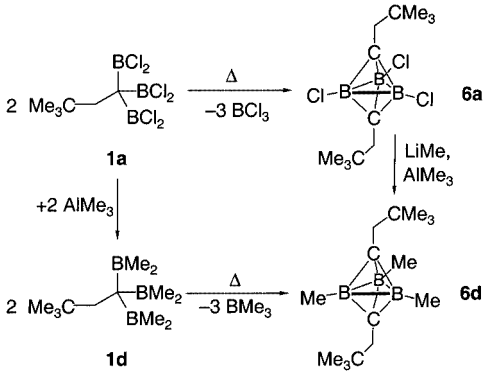

Scheme 4

The second route is of general interest, because **6d** was formed by direct methylation of **6a** with MeLi or $AlMe_3$ at low temperature. Substitution reactions of *closo*-C_2B_3 carboranes have not previously been investigated. In general, substitution reactions at boron atoms in carboranes are difficult[15] and not as developed as those at carbon atoms. The first successes were achieved with *closo*-C_2B_{10} carboranes.[15,16] The ^{11}B NMR signal for **6d** was shifted to higher field (δ = 17.3) relative to that of **6a**. In the ^1H NMR spectrum, the expected signals for *tert*-butyl (δ = 0.99) and the methylene group (δ = 2.17) were observed, whilst the signal of the methyl group at boron was located at δ = 1.23. The ^{13}C NMR spectrum exhibited the resonances of the *tert*-butyl substituent at δ = 29.7 for the methyl groups and at δ = 31.6 for the quaternary carbon atom. The signal of the methylene carbon atom appeared at δ = 39.6, while the signal for the methylboron group was broad at δ = 14. No signal was found for the apical carbon atoms. An EI mass spectrum of **6d** showed the molecular ion peak [M^+] at *m*/*z* = 244. When **6a** was treated with pentamethylsilazane at −30 °C (Scheme 5), colorless **6c** was formed as a solid in good yields. Its ^{11}B NMR spectrum showed a signal at δ = 21.3, in agreement with the reported[7,8] amino-substituted *closo*-$(RC)_2(BN\mathit{i}Pr_2)_3$. In the ^1H and ^{13}C NMR spectra, the expected signals for the *tert*-butyl, dimethylamino, and methylene groups were found, although no resonance was detected for the quaternary CB_3 carbon atom. The EI mass

spectrum of **6c** showed the molecular ion peak [M^+] at *m*/*z* = 331.

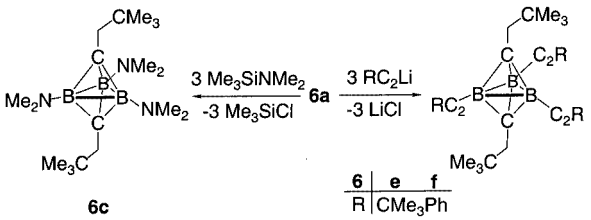

Scheme 5

Treatment of **6a** with 3,3-dimethyl-1-butynyllithium and 2-phenylethynyllithium afforded **6e** and **6f**, respectively (Scheme 5). Compound **6e** is a colorless solid and **6f** a yellow solid. Their compositions were determined by NMR spectroscopy, MS spectrometry, and X-ray structure analysis.

With sterically demanding lithium reagents (*t*BuLi, LiN*i*Pr$_2$, *n*BuLi, PhLi), only product mixtures were obtained. NMR spectroscopic and MS spectrometric data indicated the presence of the expected products; isolation of them failed, however. Attempts to substitute the chloro atoms with OH, OMe, O*t*Bu, and catechol were unsuccessful. In all cases the ^{11}B NMR spectra showed low-field signals at about δ = 32, indicating the decomposition of the carborane framework and the formation of dialkoxyboranes.

Discussion of the Structure of 6

The structure of **6a** was obtained by performing a single-crystal X-ray analysis. Colorless crystals of **6a** were grown from a solution in pentane at 4 °C; its molecular structure is shown in Figure 4. In the C_2B_3 framework, the B−B [1.842(3)−1.855(3) Å] and B−C distances [1.541(3)−1.586(3) Å] are in the range of the corresponding values for the parent *closo*-$C_2B_3H_5$, determined by electron diffraction.[17] The B−B bond lengths are substantially shorter than the structure data [1.965(8) Å] published by Meller et al.,[7,8] who classified their molecules as bicycles. The B−B distances in **6a** are somewhat shorter than those in the carborane $C_2B_3Et_5$ reported by Köster et al.[6] [1.876(4) Å]. Nevertheless, the B−B bond in **6a** is long and the B−C bond short in comparison with data relating to octahedral carboranes [B−B: 1.72 Å, C−B: 1.62 Å in 1,6-$C_2B_4H_6$].[17] The C_2B_3 carborane may be described as a classically bonded structure in which the trigonal bipyramid is bonded through 2c,2e C−B bonds, but involves no strong B−B overlap.[17,18] This was confirmed by measurements of the electron density distribution of the *closo*-cluster $C_2B_3Et_5$, which gave no electron density in the B−B−B plane of the molecule;[9] electron density was, however, found above each triangular CB_2 face. This indicates that the contribution of nonclassical multicenter bonds is as important as that of the conventional 2c,2e bonds.[9]

As far as the X-ray data are concerned, the classification of the C_2B_3 framework is ambiguous. In the light of ^{11}B NMR spectra of several dialkylchloroboranes in cyclic or

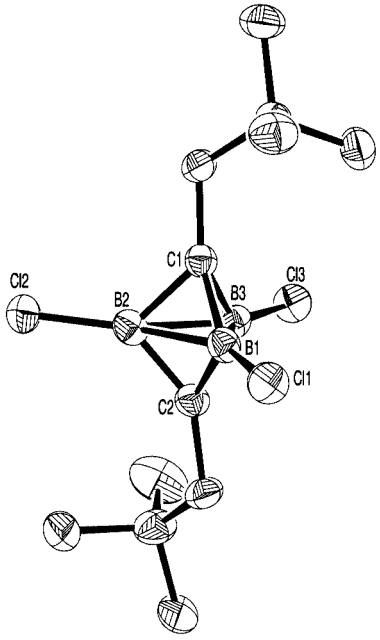

Figure 4. Molecular structure of **6a** in the crystal; selected bond lengths [Å] and angles [°]: C1−B1 1.541(3), C1−B2 1.580(3), C1−B3 1.569(3), C2−B1 1.586(3), C2−B2 1.546(3), C2−B3 1.550(3), B1−B2 1.842(3), B1−B3 1.853(3), B2−B3 1.855(4), B1−Cl1 1.746(2), B2−Cl2 1.742(2), B3−Cl3 1.742(3), C1−B1−C2 93.6(2), C1−B2−C2 93.6(2), C1−B3−C2 93.9(2), B2−B1−B3 60.28(12), B1−B2−B3 60.15(12), B1−B3−B2 59.57(13), B1−C1−B2 72.3(2), B1−C1−B3 73.1(2), B2−C1−B3 72.2(2), B1−C2−B2 72.1(2), B1−C2−B3 72.4(2), B2−C2−B3 73.7(2)

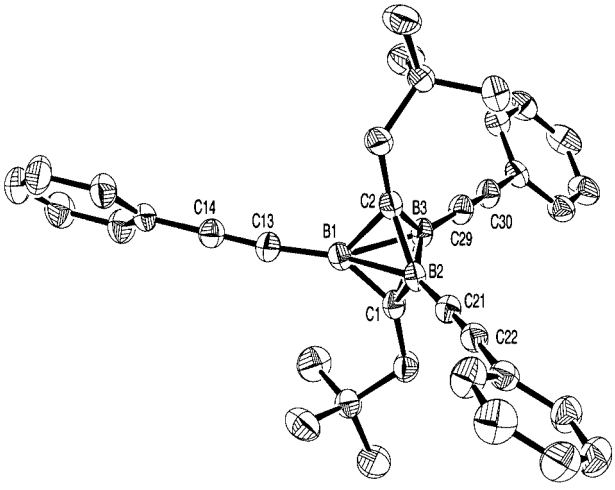

Figure 5. Molecular structure of **6f** in the crystal; selected bond lengths [Å] and angles [°]: C1−B1 1.536(3), C1−B2 1.567(3), C1−B3 1.594(3), C2−B1 1.596(3), C2−B2 1.557(3), C2−B3 1.539(3), B1−B2 1.855(3), B1−B3 1.852(3), B2−B3 1.849(3), B1−C13 1.511(3), B2−C21 1.508(3), B3−C29 1.509(3), C13−C14 1.208(3), C21−C22 1.206(3), C29−C30 1.206(3), C1−B1−C2 93.7(2), C1−B2−C2 94.1(2), C1−B3−C2 93.7(2), B2−B1−B3 59.83(12), B1−B2−B3 59.99(13), B1−B3−B2 60.19(13), B1−C1−B2 73.4(2), B1−C1−B3 72.5(2), B2−C1−B3 71.6(2), B1−C2−B2 72.1(2), B1−C2−B3 72.4(2), B2−C2−B3 73.3(2)

acyclic organoboranes, one would expect a signal at about δ = 74 for **6a** as a bicycle.[19] In fact, the resonance for **6a** is at higher field (δ = 22.1), which is compatible with a nonclassical description of the bonding situation and supports the carborane character of **6a**.

Crystals of compounds **6e** and **6f** suitable for X-ray structure analyses were obtained from toluene at 4 °C. As **6e** is disordered in the crystal, only the structure of **6f** is discussed here, because of its better crystallographic data. The molecular structure is shown in Figure 5. The B−B [1.848(3)−1.855(3) Å] and B−C [1.536(3)−1.596(3) Å] distances are in the same range as those in the chloro-substituted compound **6a**. As no elongations of the B−B bond lengths relative to those in **6a** are observed and the ^{11}B NMR spectra of **6e** and **6f** showed signals at δ = 11.4 (expected resonances for dialkylalkynylboranes lie at about δ = 72[20]) both compounds are regarded as carboranes.

Conclusion

In this paper we report on the treatment of alkynyllithium with boron trichloride, followed by double hydroboration with $HBCl_2$. 3,3-Dimethyl-1-butynyllithium as starting material afforded 1,1,1-tris(dichloroboryl)-3,3-dimethylbutane (**1a**), which was transformed into the chloro-substituted 1,5-dicarba-*closo*-pentaborane(5) **6a**. Furthermore, it was shown that substitution reactions at **6a** occurred in good yields. Substitution of **6a** with small groups (methyl in **6d**, dimethylamino in **6c**, or rod-like acetylides in **6e** and **6f**) was successful, while bulky substituents produced inseparable product mixtures of unknown composition. Treatment with oxygen-containing reagents decomposed the carborane framework. In the case of lithium trimethylsilylacetylide as starting material, a mixture of three constitutional isomers was formed.

Experimental Section

General: Reactions were carried out under dry argon or nitrogen, by standard Schlenk techniques. Solvents were dried, distilled, and saturated with nitrogen. Glassware was dried with a heat gun under high vacuum. ^1H, ^{11}B, and ^{13}C NMR: Bruker DRX 200 spectrometer, $Et_2O{\cdot}BF_3$ was used as the external standard for ^{11}B NMR. The signals of the deuterated solvents were used as internal references for ^1H and ^{13}C NMR spectra, and calculated relative to TMS. The mass spectra were measured on a ZAB-2F VH Micromass CTD spectrometer (EI and HR-EI techniques) and on a Jeol MS station JMS 700 (NICI, PICI, EI, and HR-EI techniques). Melting points (uncorrected) were measured with a Büchi apparatus in capillaries that were filled under argon or nitrogen, and sealed.

1,1,1-Tris(dichloroboryl)-3,3-dimethylbutane (1a): 3,3-Dimethyl-1-butyne (8.22 g, 0.1 mol) was added at −15 °C to a solution of *n*BuLi (0.1 mol) in 230 mL of pentane. The mixture was allowed to warm to room temp. and stirred for 2 h. The suspension was then cooled to −78 °C and added at −78 °C to a solution of BCl_3 (37.5 g, 0.32 mol) in 50 mL of pentane. After the mixture had stirred for 1 h, a solution of Me_3SiH (14.9 g, 0.2 mol) in 20 mL of pentane was added over 30 min from a dropping funnel cooled to − 30 °C. The reaction mixture was allowed to warm slowly to room temp. and was stirred for 10 h. After separation of the solution from the precipitate, the solvent was evaporated and the residue was distilled at 63 °C/0.057 mbar to yield **1a** (13.67 g, 41.6% yield) as a colorless and extremely air-sensitive liquid. ^1H NMR ($CDCl_3$, 200 MHz): δ = 0.94 [s, 9 H, $C(CH_3)_3$], 2.77 (s, 2 H, CH_2). ^{11}B NMR ($CDCl_3$, 64 MHz): δ = 58.7. ^{13}C NMR ($CDCl_3$, 50 MHz): δ = 31.9 [$C(CH_3)_3$], 33.8 [$C(CH_3)_3$], 55.2 (CH_2), 59 [br., $C(BCl_2)_3$]. EI-MS: *m*/*z* (%) = 313 (1) [$M^+ - CH_3$], 246 (1) [$M^+ - BCl_2$], 231 (4) [$M^+ - CH_3 - BCl_2$], 195 (1) [$M^+ - CH_3 - BCl_2 - HCl$], 128 (15) [$M^+ - 2BCl_2 - HCl$], 115 (51) [$M^+ - 2BCl_2 - HCl - CH_3$], 81 (63) [$BCl_2^+$], 57 (100) [$C_4H_9^+$], 41 (62) [$C_3H_5^+$]. NICI-MS: *m*/*z* (%) = 328 (100) [M^+].

1,1,1-Tris(catecholboryl)-3,3-dimethylbutane (1b): Catechol (660 mg, 6 mmol) was dissolved in CH_2Cl_2 (40 mL), and the solution was cooled to −60 °C. Compound **1a** (660 mg, 2 mmol) was then added dropwise to the reaction mixture, and the solution was allowed to warm to room temp. The CH_2Cl_2 was removed under vacuum to give colorless **1b** (840 mg, 95.0%, m.p. 163 °C). ^1H NMR ($CDCl_3$, 200 MHz): δ = 0.83 [s, 9 H, $C(CH_3)_3$], 2.62 (s, 2 H, CH_2), 7.03−7.27 (m, 12 H, C_6H_4). ^{11}B NMR ($CDCl_3$, 64 MHz): δ = 34.7. ^{13}C NMR ($CDCl_3$, 50 MHz): δ = 30.0 [$C(CH_3)_3$], 32.6 [$C(CH_3)_3$], 43.3 (CH_2), 112.7, 122.7, 148.2 (C_6H_4). EI-MS: *m*/*z* (%) = 440 (21) [M^+], 425 (5) [$M^+ - CH_3$], 383 (42) [$M^+ - C_4H_9$], 320 (4) [$M^+ - C_6H_4O_2BH$], 305 (1) [$M^+ - CH_3 - C_6H_4O_2BH$], 120 (4) [$C_6H_4O_2BH^+$], 57 (100) [$C_4H_9^+$]. HR-MS (EI): *m*/*z* = 440.1797 [M^+]; calcd. for $^{12}C_{24}{}^1H_{23}{}^{11}B_3{}^{16}O_6$: 440.1820 (Δ = 2.3 mmu).

1,1,1-Tris[chloro(dimethylamino)boryl]-3,3-dimethylbutane (1c): Compound **1a** (2.38 g, 7.25 mmol) was added to a solution of dimethylamine (1.96 g, 43.5 mmol) in 40 mL of hexane at −60 °C. The mixture was allowed to warm to room temp., the solution was separated from the precipitate, the solvent was evaporated, and the colorless oil **1c** was dried under vacuum. Yield: 2.27 g (88.4%). ^1H NMR ($CDCl_3$, 200 MHz): δ = 0.93 [s, 9 H, $C(CH_3)_3$], 2.20 (s, 2 H, CH_2), 2.86 [s, 9 H, $N(CH_3)_2$], 2.87 [s, 9 H, $N(CH_3)_2$]. ^{11}B NMR ($CDCl_3$, 64 MHz): δ = 38.5. ^{13}C NMR ($CDCl_3$, 50 MHz): δ = 31.0 [$C(CH_3)_3$], 33.0 [$C(CH_3)_3$], 40.0, 40.6 [$N(CH_3)_2$], 42 (br., CB_3), 48.3 (CH_2). EI-MS: *m*/*z* (%) = 353 (2) [M^+], 296 (10) [$M^+ - C_4H_9$], 262 (2) [$M^+ - HBClN(CH_3)_2$], 251 (4) [$M^+ - C_4H_9 - HN(CH_3)_2$], 228 (11) [$M^+ - BClN(CH_3)_2 - Cl$], 207 (9) [$M^+ - C_4H_8 - BClN(CH_3)_2$], 171 (100) [$M^+ - 2HBClN(CH_3)_2$], 90 (61) [$BClN(CH_3)_2^+$], 57 (48) [$C_4H_9^+$]. HR-MS (EI): *m*/*z* = 296.1006 [$M^+ - C_4H_9$]; calcd. for $^{12}C_8{}^1H_{20}{}^{11}B_3{}^{35}Cl_3{}^{14}N_3$: 296.1002 (Δ = 0.4 mmu).

1,1,1-Tris(dimethylboryl)-3,3-dimethylbutane (1d): Compound **1a** (1.00 g, 3.1 mmol) was dissolved in hexane (20 mL), and a solution of $AlMe_3$ (2 mL, 20.8 mmol) in 10 mL of hexane was added at −78 °C. The mixture was allowed to warm to room temp., the solution was separated from the precipitate, and all volatile components were removed under vacuum to give **1d** (520 mg, 83.0%) as a pale yellow oil. ^1H NMR ($CDCl_3$, 200 MHz): δ = 0.78 [s, 18 H, $B(CH_3)_2$], 0.82 [s, 9 H, $C(CH_3)_3$], 2.54 (s, 2 H, CH_2). ^{11}B NMR ($CDCl_3$, 64 MHz): δ = 82.6. ^{13}C NMR ($CDCl_3$, 50 MHz): δ = 16.5 [$B(CH_3)_2$], 30.9 [$C(CH_3)_3$], 32.6 [$C(CH_3)_3$], 46 (br.,CB_3), 50.7 (CH_2). EI-MS: *m*/*z* (%) = 150 (25) [$M^+ - B(CH_3)_3$], 149 (12) [$M^+ - C_4H_9$], 93 (64) [$M^+ - B(CH_3)_3 - C_4H_9$], 57 (100) [$C_4H_9^+$], 41 (97) [$C_3H_5^+$]. PICI-MS: *m*/*z* (%) = 207 (30) [$M^+ + H$], 57 (100) [$C_4H_9^+$]. HR-MS (EI): *m*/*z* = 150.1742 [$M^+ - B(CH_3)_3$]; calcd. for $^{12}C_9{}^1H_{20}{}^{11}B_2$: 150.1733 (Δ = 0.9 mmu): *m*/*z* = 149.1786 [$M^+ - C_4H_9$]; calcd. for $^{12}C_8{}^1H_{20}{}^{11}B_3$: 149.1727 (Δ = 5.9 mmu): *m*/*z* =

93.1045 [$M^+ - B(CH_3)_3 - C_4H_9$]; calcd. for $^{12}C_5{}^1H_{11}{}^{11}B_2$: 93.1044 ($\Delta$ = 0.1 mmu).

1,1-Bis(dichloroboryl)-2-trimethylsilylethene (2a), 1,1,1-Tris(dichloroboryl)-2-trimethylsilylethane (3a), 1,1,2-Tris(dichloroboryl)-2-trimethylsilylethane (4a), and 1,1,2-Tris(dichloroboryl)-1-trimethylsilylethane (5a): Trimethylsilylacetylene (9.82 g, 0.1 mol) was added at −15 °C to a solution of *n*BuLi (0.1 mol) in 230 mL of pentane. The mixture was allowed to warm to room temp. and stirred for 2 h. The suspension was then cooled to −78 °C and added at −78 °C to a solution of BCl_3 (37.5 g, 0.32 mol) in 50 mL of pentane. After the mixture had stirred for 1 h, a solution of Me_3SiH (14.9 g, 0.2 mol) in 20 mL of pentane was added over 30 min from a dropping funnel cooled to −30 °C. The reaction mixture was allowed to warm slowly to room temp. and stirred for 10 h. The solution was separated from the precipitate, the solvent was evaporated, and the residue was distilled to yield two fractions of colorless, extremely air-sensitive liquids: **2a** (43 °C/0.065 mbar, 6.00 g, 22.9%), and a mixture of **3a**, **4a**, and **5a** (65 °C/0.065 mbar, 5.23 g, 15.2%).

Compound 2a: ^{1}H NMR ($CDCl_3$, 200 MHz): δ = 0.22 [s, 9 H, $Si(CH_3)_3$], 7.12 (s, 1 H, CH). ^{11}B NMR ($CDCl_3$, 64 MHz): δ = 60.5 (s, 1B), 57.4 (s, 1B). ^{29}Si NMR ($CDCl_3$, 40 MHz): δ = −3.3. EI-MS: *m*/*z* (%) = 260 (6) [M^+], 245 (58) [$M^+ - CH_3$], 225 (10) [$M^+ - Cl$], 163 (34) [$M^+ - H - CH_3 - BCl_2$], 73 (100) [$Si(CH_3)_3{}^+$].

Mixture 3a, 4a, 5a: ^{11}B NMR ($CDCl_3$, 64 MHz): δ = 63.4 (s, 1B), 61.0 (s, 1B). ^{29}Si NMR ($CDCl_3$, 40 MHz): δ = 4.2, 4.3, 4.7. EI-MS: *m*/*z* (%) = 327 (12) [$M^+ - CH_3$], 272 (1) [$M^+ - HCl - Cl$], 245 (2) [$M^+ - H - BCl_2 - CH_3$], 73 (100) [$Si(CH_3)_3{}^+$], 36 (82) [HCl^+]. NICI-MS: *m*/*z* (%) = 342 (29) [M^+].

1,1-Bis(catecholboryl)-2-trimethylsilylethene (2b): Catechol (440 mg, 4 mmol) was dissolved in CH_2Cl_2 (40 mL) and cooled to −60 °C. Compound **2a** (520 mg, 2 mmol) was then added dropwise to the reaction mixture, and the solution was allowed to warm to room temp. The CH_2Cl_2 was removed under vacuum to give **2b** (750 mg, 84.6% yield) as a pale beige solid. ^{1}H NMR ($CDCl_3$, 200 MHz): δ = 0.31 [s, 9 H, $Si(CH_3)_3$], 6.99−7.36 (m, 8 H, C_6H_4), 7.95 (s, 1 H, CH). ^{11}B NMR ($CDCl_3$, 64 MHz): δ = 32.1. EI-MS: *m*/*z* (%) = 336 (25) [M^+], 321 (82) [$M^+ - CH_3$], 262 (4) [$M^+ - H - Si(CH_3)_3$], 229 (3) [$M^+ + H -$ Bcat], 203 (12) [$M^+ + H - CH_3 -$ Bcat], 92 (16) [$C_6H_4O^+$], 73 (100) [$Si(CH_3)_3{}^+$]. HR-MS (EI): *m*/*z* = 336.1187 [M^+]; calcd. for $^{12}C_{17}{}^1H_{18}{}^{11}B_2{}^{16}O_4{}^{28}Si$: 336.1161 ($\Delta$ = 2.6 mmu).

1,1,1-Tris(catecholboryl)-2-trimethylsilylethane (3b), 1,1,2-Tris(catecholboryl)-2-trimethylsilylethane (4b), and 1,1,2-Tris(catecholboryl)-1-trimethylsilylethane (5b): Catechol (660 mg, 6 mmol) was dissolved in CH_2Cl_2 (40 mL) and cooled to −60 °C. The mixture of **3a**, **4a**, and **5a** (690 mg, 2 mmol) was then added dropwise to the catechol, and the solution was allowed to warm to room temp. The CH_2Cl_2 was removed under vacuum to give a beige solid. Yield: 810 mg **3b**, **4b**, **5b** (88.7%), product ratio **3**:**4**:**5** = 15:8.5:1 (determined by ^{1}H NMR). ^{1}H NMR ($CDCl_3$, 200 MHz): **3b:** δ = 0.20 [s, 9 H, $Si(CH_3)_3$], 1.99 (s, 2 H, CH_2), 6.93−7.30 (m, 12 H, C_6H_4); **4b:** δ = 0.09 [s, 9 H, $Si(CH_3)_3$], 1.82 [d, $^3J_{H,H}$ = 9.5 Hz, 1 H, $(CH_3)_3SiCH$Bcat], 2.18 [d, $^3J_{H,H}$ = 9.5 Hz, 1 H, $CH(Bcat)_2$], 6.93−7.30 (m, 12 H, C_6H_4); **5b:** δ = 0.01 [s, 9 H, $Si(CH_3)_3$], 1.75 (s, 2 H, CH_2), 6.93−7.30 (m, 12 H, C_6H_4). ^{11}B NMR ($CDCl_3$, 64 MHz): δ = 35.8. ^{29}Si NMR ($CDCl_3$): δ = 4.0, 5.6, 8.1. EI-MS: *m*/*z* (%) = 456 (9) [M^+], 441 (7) [$M^+ - CH_3$], 383 (1) [$M^+ - Si(CH_3)_3$], 322 (7) [$M^+ - CH_3 -$ Bcat], 203 (1) [$M^+ - CH_3 -$ 2Bcat], 92 (7) [$C_6H_4O^+$], 73 (100) [$Si(CH_3)_3{}^+$]. HR-MS (EI): *m*/*z* = 456.1551 [M^+]; calcd. for $^{12}C_{23}{}^1H_{23}{}^{11}B_3{}^{16}O_6{}^{28}Si_1$: 456.1543 ($\Delta$ = 0.8 mmu).

2,3,4-Trichloro-1,5-dicarba-*closo*-pentaborane(5) (6a): Neat **1a** (5.30 g, 11.8 mmol) was heated for 2 h at 170 °C and elimination of BCl_3 was observed. The brown product mixture was distilled at 54 °C/0.02 mbar to give colorless, air-sensitive **6a** (606 mg, 24.6%), m.p. 61 °C. ^{1}H NMR ($CDCl_3$, 200 MHz): δ = 1.02 [s, 9 H, $C(CH_3)_3$], 2.09 (s, 2 H, CH_2). ^{11}B NMR ($CDCl_3$, 64 MHz): δ = 22.1. ^{13}C NMR ($CDCl_3$, 50 MHz): δ = 29.7 [$C(CH_3)_3$], 31.6 [$C(CH_3)_3$], 38.5 (CH_2), 94 (br., CB_3). EI-MS: *m*/*z* (%) = 289 (87) [$M^+ - CH_3$], 247 (21) [$M^+ - C_4H_9$], 57 (100) [$C_4H_9{}^+$]. PICI-MS: *m*/*z* (%) = 303 (100) [$M^+ - H$], 289 (11) [$M^+ - CH_3$], 261 (5) [$M^+ - C_3H_7{}^+$]. HR-MS (EI): *m*/*z* = 304.1034 [M^+]; calcd. for $^{12}C_{12}{}^1H_{22}{}^{11}B_3{}^{35}Cl_3$: 304.1001 ($\Delta$ = 3.3 mmu).

2,3,4-Tris(dimethylamino)-1,5-dicarba-*closo*-pentaborane(5) (6c): Pentamethylsilazane (310 mg, 2.20 mmol) was added at −30 °C to a solution of **6a** (224 mg, 0.73 mmol) in 15 mL of pentane. The solution was allowed to warm to room temp. and after 4 h stirring all volatile components were removed. Compound **6c** was obtained as a colorless oil. Yield: 193 mg (79.4%). ^{1}H NMR ($CDCl_3$, 200 MHz): δ = 1.00 [s, 18 H, $C(CH_3)_3$], 2.16 (s, 4 H, CH_2), 2.77 [s, 18 H, $N(CH_3)_2$]. ^{11}B NMR ($CDCl_3$, 64 MHz): δ = 21.3. ^{13}C NMR ($CDCl_3$, 50 MHz): δ = 32.1 [$C(CH_3)_3$], 34.9 [$C(CH_3)_3$], 38.9 (CH_2), 42.5 [$N(CH_3)_2$]. EI-MS: *m*/*z* (%) = 331 (45) [M^+], 316 (1) [$M^+ - CH_3$], 260 (1) [$M^+ - C_5H_{11}$], 57 (100) [$C_4H_9{}^+$], 44 (73) [$N(CH_3)_2{}^+$]. HR-MS (EI): *m*/*z* = 331.3499 [M^+]; calcd. for $^{12}C_{18}{}^1H_{40}{}^{11}B_3{}^{14}N_3$: 331.3497 ($\Delta$ = 0.2 mmu).

2,3,4-Trimethyl-1,5-dicarba-*closo*-pentaborane(5) (6d):
a) Compound **1d** (500 mg, 2.43 mmol) was dissolved in 5 mL of toluene, and this was heated under reflux for 2 h. The solvent and volatile compounds were removed under vacuum to yield a brown, viscous residue, consisting of **6d** and some by-products.
b) Compound **6a** (124 mg, 0.4 mmol) was dissolved in 10 mL of hexane and treated at −78 °C with a solution of $AlMe_3$ (0.4 mL, 4 mmol) in 5 mL of hexane. The reaction mixture was allowed to warm slowly to room temp. After filtration of a solid, the solvent was removed and **6d** was dried under vacuum to afford a pale yellow, viscous oil. Yield: 71 mg (71.6%).

c) Compound **6a** (170 mg, 0.56 mmol) was dissolved in 15 mL of diethyl ether and treated at −70 °C with a solution of methyllithium in diethyl ether (1.6 M, 1.1 mL, 1.7 mmol). The reaction mixture was allowed to warm slowly to room temp. After the solution had been separated from the precipitate, the solvent was removed and the pale yellow, viscous oil **6d** was dried under vacuum. Yield: 101 mg (74.3%). ^{1}H NMR ($CDCl_3$, 200 MHz): δ = 0.99 [s, 18 H, $C(CH_3)_3$], 1.23 (s, 9 H, BCH_3), 2.17 (s, 4 H, CH_2). ^{11}B NMR ($CDCl_3$, 64 MHz): δ = 17.3. ^{13}C NMR ($CDCl_3$, 50 MHz): δ = 14.1 (BCH_3), 29.7 [$C(CH_3)_3$], 31.6 [$C(CH_3)_3$], 39.6 (CH_2). EI-MS: *m*/*z* (%) = 244 (7) [M^+], 229 (7) [$M^+ - CH_3$], 187 (17) [$M^+ - C_4H_9$], 173 (8) [$M^+ - C_5H_{11}$], 131 (23) [$M^+ - C_4H_9 - C_4H_8$], 57 (100) [$C_4H_9{}^+$], 41 (80) [$C_3H_5{}^+$]. HR-MS (EI): *m*/*z* = 244.2715 [M^+]; calcd. for $^{12}C_{15}{}^1H_{31}{}^{11}B_3$: 244.2725 ($\Delta$ = 1.0 mmu).

2,3,4-Tris(3,3-dimethyl-1-butynyl)-1,5-dicarba-*closo*-pentaborane(5) (6e): 3,3-Dimethyl-1-butyne (172 mg, 2 mmol) was added at −15 °C to a solution of *n*BuLi (2 mmol) in 20 mL of hexane. The mixture was allowed to warm to room temp. and stirred for 30 min. The suspension was then cooled to −78 °C and added to a solution of **6a** (212 mg, 0.69 mmol) in 5 mL of hexane. The reaction mixture was allowed to warm slowly to room temp. After the solution had been separated from the precipitate, the solvent was removed, and the yellow, solid **6e** was dried under vacuum. Yield: 236 mg

Table 1. Crystal data and details of the structure determinations

	1b	**5b**	**5b**	**6a**	**6f**
Formula	$C_{24}H_{23}B_3O_6$	$C_{23}H_{23}B_3O_6Si$	$C_{23.5}H_{24}B_3ClO_6Si$	$C_{12}H_{22}B_3Cl_3$	$C_{36}H_{37}B_3$
M	439.85	455.93	498.40	305.08	502.09
Temperature [K]	173(2)	173(2)	173(2)	190(2)	190(2)
Crystal system	Triclinic	Triclinic	Triclinic	Monoclinic	Triclinic
Space group	$P\bar{1}$	$P\bar{1}$	$P\bar{1}$	$P2_1/c$	$P\bar{1}$
a [Å]	9.3558(2)	6.3424(1)	10.0111(3)	13.0672(13)	11.5657(12)
b [Å]	9.5761(2)	10.6553(2)	10.1299(3)	11.0691(11)	12.2601(13)
c [Å]	14.2103(2)	17.5659(4)	14.8106(4)	11.7038(11)	12.3944(13)
α [°]	96.423(1)	104.320(2)	74.219(2)	90	76.116(2)
β [°]	104.096(1)	97.559(2)	74.551(2)	100.488(2)	89.685(2)
γ [°]	113.380(1)	99.214(2)	60.980(2)	90	65.234(2)
V [Å^3]	1101.88(4)	1117.05(4)	1247.65(6)	1664.6(3)	1540.2(3)
Z	2	2	2	4	2
d_{calc} [g cm^{-3}]	1.326	1.356	1.327	1.217	1.083
μ (Mo-K_α) [mm]	0.092	0.144	0.239	0.530	0.059
F_{000}	460	476	518	640	536
Crystal size [mm]	0.42 × 0.28 × 0.26	0.27 × 0.25 × 0.16	0.42 × 0.35 × 0.08	0.40 × 0.19 × 0.19	0.60 × 0.12 × 0.07
Θ_{max} [°]	28.34	27.88	28.35	28.30	25.00
Measured reflections	14849	14501	16805	10523	17345
Independent (R_{int})	5381 (0.033)	5279 (0.036)	6100 (0.036)	3853 (0.035)	5423 (0.087)
No. of parameters	390	390	386	252	500
GooF	1.048	1.071	1.076	1.023	1.057
*R*1 ($I > 2\sigma I$)	0.0419	0.0481	0.0552	0.0398	0.0512
*wR*2	0.1196	0.1336	0.1614	0.1109	0.1429
Resid. electron dens. [e Å^{-3}]	0.363/−0.227	0.830/−0.335	0.899/−0.555	0.316/−0.213	0.224/−0.197

(76.8%), m.p. 83 °C. ^{1}H NMR ($CDCl_3$, 200 MHz): 1.04 [s, 18 H, $C(CH_3)_3$], 1.20 [s, 27 H, $C(CH_3)_3$], 2.27 (s, 4 H, CH_2). ^{11}B NMR ($CDCl_3$, 64 MHz): δ = 11.4. ^{13}C NMR ($CDCl_3$, 50 MHz): δ = 29.9 [$C(CH_3)_3$], 30.8 [$C(CH_3)_3$], 32.0 [$C(CH_3)_3$], 32.3 [$C(CH_3)_3$], 39.6 (CH_2). EI-MS: *m*/*z* (%) = 442 (100) [M^+], 427 (10) [$M^+ - CH_3$], 385 (43) [$M^+ - C_4H_9$], 329 (37) [$M^+ + H - 2C_4H_9$], 57 (49) [$C_4H_9^+$]. HR-MS (EI): *m*/*z* = 442.4151 [M^+]; calcd. for $^{12}C_{30}{}^1H_{49}{}^{11}B_3$: 442.4188 (Δ = 3.7 mmu).

2,3,4-Tris(2-phenyl-1-ethynyl)-1,5-dicarba-*closo*-pentaborane(5) (6f): Phenylacetylene (124 mg, 1.21 mmol) was added at −15 °C to a solution of *n*BuLi (1.21 mmol) in 15 mL of hexane. The mixture was allowed to warm to room temp. and stirred for 30 min. The suspension was then cooled to −78 °C and added to a solution of **6a** (123 mg, 0.4 mmol) in 5 mL of hexane. The reaction mixture was allowed to warm slowly to room temp. After the solution had been separated from the precipitate, the solvent was removed and the brown, viscous oil **6f** was dried under vacuum. Yield: 127 mg (62.7%), m.p. 94 °C. ^{1}H NMR ($CDCl_3$, 200 MHz): 1.19 [s, 18 H, $C(CH_3)_3$], 2.53 (s, 4 H, CH_2), 7.30−7.51 (m, 15 H, C_6H_5). ^{11}B NMR ($CDCl_3$, 64 MHz): δ = 11.4. ^{13}C NMR ($CDCl_3$, 50 MHz): δ = 29.9 [$C(CH_3)_3$], 32.4 [$C(CH_3)_3$], 39.9 (CH_2), 108.1 (CB_3) 122.9 (*ipso*-C_{Ph}), 128.3 (*m*-C_{Ph}), 129.1 (*p*-C_{Ph}), 132.1 (*o*-C_{Ph}). EI-MS: *m*/*z* (%) = 502 (55) [M^+], 446 (13) [$M^+ + H - C_4H_9$], 402 (9) [$M^+ + H - C_8H_5$], 389 (16) [$M^+ + H - 2C_4H_9$], 57(100) [$C_4H_9^+$]. HR-MS (EI): *m*/*z* = 502.3191 [M^+]; calcd. for $^{12}C_{36}{}^1H_{37}{}^{11}B_3$: 502.3207 (Δ = 1.6 mmu).

Crystal Structure Determinations of 1b, 4b, 5b, 6a, and 6f: A summary of the crystal data and details of the structure determinations is given in Table 1. Data were collected on a Bruker AXS Smart 1000 area detector (Mo-K_α radiation, λ = 0.71073 Å, ω-scans) at low temperature. Data were corrected for Lorentz polarisation and absorption effects (semiempirical, SADABS[21]). The structures were solved by direct methods and refined by full-matrix, least-squares methods based on F^2 (SHELXTL).[22] Non-hydrogen atoms were refined with anisotropic displacement parameters. Hydrogen atoms were located in difference Fourier syntheses and refined with isotropic displacement parameters [with the exception of the methyl groups in **5b** and those at the disordered $CH_2C(CH_3)_3$ group in **6a**, which were inserted in calculated positions and refined using a riding model].

CCDC-175653 (**1b**), -175654 (**4b**), -175655 (**5b**), -175656 (**6a**) and -175656 (**6f**) contain the supplementary crystallographic data for this paper. These data can be obtained free of charge at www.ccdc.cam.ac.uk/conts/retrieving.html [or from the Cambridge Crystallographic Data Centre, 12, Union Road, Cambridge CB2 1EZ, UK; Fax: (internat.) +44-1223/336-033; E-mail: deposit@ccdc.cam.ac.uk].

Acknowledgments

This work was supported by the Deutsche Forschungsgemeinschaft (SFB 247 and Schwerpunktprogramm Polyeder) and the Fonds der Chemischen Industrie.

[1] R. B. Castle, D. S. Matteson, *J. Am. Chem. Soc.* **1968**, *90*, 2194.
[2] R. B. Castle, D. S. Matteson, *J. Organomet. Chem.* **1969**, *20*, 19−28.
[3] D. S. Matteson, P. K. Mattschei, *Inorg. Chem.* **1973**, *12*, 2472−2475.
[4] R. Köster, H.-J. Horstschäfer, P. Binger, P. K. Mattschei, *Justus Liebigs Ann. Chem.* **1975**, 1339−1356.
[5] R. Köster, G. Seidel, B. Wrackmeyer, H.-J. Schanz, *Angew. Chem.* **1994**, *106*, 2380−2382, *Angew. Chem. Int. Ed. Engl.* **1994**, *33*, 2294−2296.
[6] R. Köster, R. Boese, B. Wrackmeyer, H.-J. Schanz, *J. Chem. Soc., Chem. Commun.* **1995**, 1691−1692.
[7] D. Bromm, U. Seebold, M. Noltemeyer, A. Meller, *Chem. Ber.* **1991**, *124*, 2645−2649.

[8] W. Maringgele, H. Knop, D. Bromm, A. Meller, S. Dielkus, R. Herbst-Irmer, G. M. Sheldrick, *Chem. Ber.* **1992**, *125*, 1807−1813.
[9] M. Antipin, R. Boese, D. Bläser, A. Maulitz, *J. Am. Chem. Soc.* **1997**, *119*, 326−333.
[10] P. v. R. Schleyer, G. Subramanian, A. Dransfeld, *J. Am. Chem. Soc.* **1996**, *118*, 9988−9989.
[11] R. Soundararajan, D. S. Matteson, *J. Org. Chem.* **1990**, *55*, 2274−2275.
[12] Y. Gu, H. Pritzkow, W. Siebert, *Eur. J. Inorg. Chem.* **2001**, 373−379.
[13] J.-P. Kintzinger, H. Marsmann, *Oxygen-17 and Silicon-29* (Eds.: P. Diehl, E. Fluck, R. Kosfeld), Springer-Verlag, **1981**.
[14] [14a] H. Klusik, C. Pues, A. Berndt, *Z. Naturforsch., Teil B* **1984**, *39*, 1042−1045. [14b] W. Siebert, M. Hildenbrand, P. Hornbach, G. Karger, H. Pritzkow, *Z. Naturforsch., Teil B* **1989**, *44*, 1179−1186.
[15] V. I. Bregadze, *Chem. Rev.* **1992**, *92*, 209−223.
[16] [16a] W. Jiang, C. B. Knobler, M. D. Mortimer, M. F. Hawthorne, *Angew. Chem.* **1995**, *107*, 1470−1473; *Angew. Chem. Int. Ed. Engl.* **1995**, *34*, 1332−1334. [16b] A. Herzog, A. Maderna, G. N. Harakas, C. B. Knobler, M. F. Hawthorne, *Eur. J. Inorg. Chem.* **1999**, *5*, 1212−1217. [16c] T. Peymann, A. Herzog, C. B. Knobler, M. F. Hawthorne, *Angew. Chem.* **1999**, *111*, 1130−1132; *Angew. Chem. Int. Ed.* **1999**, *38*, 1062−1064.
[17] F. A. McNeill, K. L. Gallaher, F. R. Scholer, S. H. Bauer, *Inorg. Chem.* **1973**, *12*, 2108−2111.
[18] C. S. Cheung, R. A. Beaudet, G. A. Segal, *J. Am. Chem. Soc.* **1970**, *92*, 4158−4164.
[19] T. Deforth, M. Kaschke, H. Stock, H. Pritzkow, W. Siebert, *Z. Naturforsch., Teil B* **1997**, *52*, 823−830.
[20] H. Nöth, B. Wrackmeyer, *NMR Spectroscopy of Boron Compounds* (Eds.: P. Diehl, E. Fluck, R. Kosfeld), Springer-Verlag, **1978**.
[21] G. M. Sheldrick, SADABS, Univ. Göttingen, **1999**.
[22] G. M. Sheldrick, SHELXTL 5.1, Bruker AXS, Madison, WI, **1998**.

Received December 11, 2001
[I01504]

Dinuclear Triple-Stranded Helicates from Rigid Oligo-*p*-phenylene Ligands: Self-Assembly and Ligand Self-Recognition

Markus Albrecht*[a] and Matthias Schneider[a]

Keywords: Catechol / Titanium / Self-assembly / Helical structures / Molecular recognition

The rigid rod oligo-*p*-phenylene type dicatechol ligands **1-3**-H_4 form dinuclear triple-stranded helicates $M_4[(\mathbf{1}–\mathbf{3})_3Ti_2]$ in the presence of appropriate counterions (M = Li, Na, K, or NH_4). Studies on the self-recognition ability of the ligands show that self-recognition takes place if mixtures of ligands with significantly different sizes (**1/2**) are used in coordination studies, or if ligands are used which do not match for geometric reasons (**1/4**). Mixtures of ligands with a similar geometric preference (**2/5**) do not lead to self-recognition, but instead give mixtures of hetero- and homoleptic complexes.

(© Wiley-VCH Verlag GmbH, 69451 Weinheim, Germany, 2002)

Introduction

Supramolecular aggregates are formed from molecular components by non-covalent interactions. The geometrical and electronic information contained in the single building blocks controls the success of the formation of a supermolecule. For a rational design of non-covalently linked structures it is important to understand the factors that control self-assembly processes such as, for example, supramolecular stereochemistry, regiochemistry or templating effects.[1,2]

We are interested in the chemistry of helicates[3–7] and of related complexes[8–12] because those simple supramolecular coordination compounds allow the study of a variety of mechanistic aspects of self-assembly processes. In this context, we have found a way to control the diastereoselectivity[13] and the regioselectivity of complex formation.[14] In addition we have investigated the ligand self-recognition during helicate or meso-helicate formation and found a template control of this process.[15] This is an option for "ligand self-recognition" in addition to the examples described by Lehn,[16] Raymond[17] or Stack,[18,19] where different numbers of metal binding sites, preferred coordination geometry at the metal centers, different ligand length, or chirality is used to control the self-recognition.

The formation of the titanium(IV) complex $K_4[(\mathbf{2})_3Ti_2]$ has already been discussed and its X-ray structural analysis communicated.[20] In this paper, we report the titanium(IV) coordination chemistry of the rigid oligo-*p*-phenylene derivatives **1-3**-H_4, with two catechol binding sites, in the presence of different cations (Li^+, Na^+, K^+) and we introduce them into ligand self-recognition experiments.

[a] Institut für Organische Chemie, Universität Karlsruhe, Richard-Willstätter-Allee, 76131, Germany
Fax: (internat.) + 49-(0)721/698-529
E-mail: albrecht@ochhades.chemie.uni-karlsruhe.de

Results and Discussion

Coordination Studies

The rigid ligands **1**-H_4, **2**-H_4, and **3**-H_4 (Figure 1) were prepared by use of a Suzuki coupling as a key step in the synthetic procedure. The linear oligo-*p*-phenylene derivatives **1-3**-H_4 have different lengths [9.2 (**1**-H_4), 13.5 (**2**-H_4), and 17.8 Å (**3**-H_4)] and the metal binding sites (catechol units) are fixed at defined distances to each other.[21] However, there is some flexibility at the C(aryl)–C(aryl) single bonds.

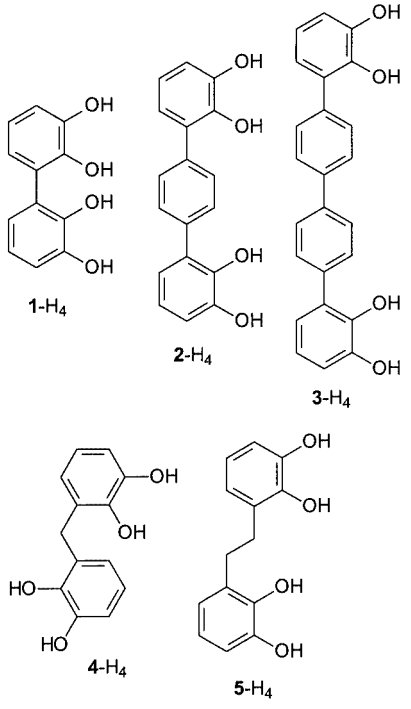

Figure 1. Ligands discussed in this study

Dinuclear titanium(IV) complexes $M_4[(\mathbf{1}-\mathbf{3})_3Ti_2]$ (M = Li, Na, K) of the ligands **1**-H_4, **2**-H_4, and **3**-H_4 were obtained upon stirring a mixture of the ligand (3 equiv.), $TiO(acac)_2$ (2 equiv.) and the corresponding alkali metal carbonate (2 equiv.) in methanol (Scheme 1). After removal of the solvent a red solid material was obtained, which was purified by filtration through Sephadex LH 20.

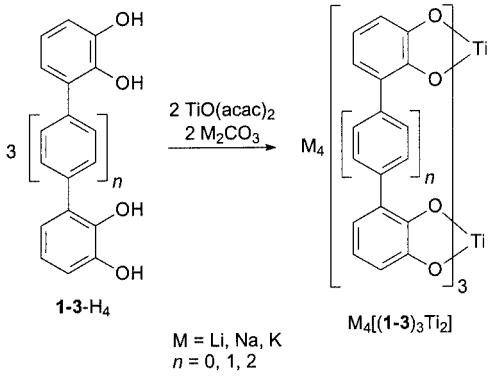

Scheme 1. Formation of triple-stranded helicates $M_4[(\mathbf{1}-\mathbf{3})_3Ti_2]$

The smallest ligand **1**-H_4, with a direct connection of the two catechol moieties, affords dinuclear triple-stranded helicates $M_4[(\mathbf{1})_3Ti_2]$ (M = Li, Na, K) in 61% to quantitative yield. The positive FAB MS spectra show peaks at *m/z* = 766 $[Li_4\{(\mathbf{1})_3Ti_2\}]^+$ and 760 $[Li_3\{(\mathbf{1})_3Ti_2\}H]^+$, *m/z* = 809 $[Na_3\{(\mathbf{1})_3Ti_2\}H_2]^+$ and 787 $[Na_2\{(\mathbf{1})_3Ti_2\}H_3]^+$, and *m/z* = 895 $[K_4(\{(\mathbf{1})_3Ti_2\}H]^+$, 857 $[K_3\{(\mathbf{1})_3Ti_2\}H_2]^+$ and 818 $[K_2\{(\mathbf{1})_3Ti_2\}H_3]^+$ revealing that the helicates are made up from three ligands and two titanium(IV) ions. To our surprise the ^1H NMR spectra of all three compounds were significantly different. The lithium and sodium compounds show a pattern of two doublets of doublets and one (pseudo)triplet at δ = 6.57 (dd), 6.47 (pt), and 6.28 (dd) ($Li_4[(\mathbf{1})_3Ti_2]$) and at δ = 6.62 (dd), 6.56 (pt), and 6.35 (dd) ($Na_4[(\mathbf{1})_3Ti_2]$). For the potassium salt $K_4[(\mathbf{1})_3Ti_2]$ two multiplets are observed at δ = 6.53 (12 H) and 6.34 (6 H).

The different ^1H NMR spectra indicate that the different countercations bind to the triple-stranded dinuclear titanium complex anion $[(\mathbf{1})_3Ti_2]^{4-}$ and thus lead to different anisotropic effects at the ligand protons. However, in contrast to earlier observations, this binding cannot proceed by encapsulation of the cation. The interior of the anion $[(\mathbf{1})_3Ti_2]^{4-}$, which is formed from three ligands **1**, is too small for the binding of an alkali metal cation. Binding has to occur from the outside of the cavity as was observed for the titanium(IV) complexes of ligand **4**. However, in the case of the titanium complex of ligand **4** a dinuclear species $[(\mathbf{4})_3Ti_2]^{4-}$ can only be stabilized by sodium and lithium cations; potassium destabilizes this complex and leads to a mixture of oligomeric coordination compounds.[22,23] In contrast to the flexible methylene-bridged ligand **4** the rigid derivative **1** seems to be more preorganized for the formation of dinuclear helicate-type complexes $[(\mathbf{1})_3Ti_2]^{4-}$, and therefore the formation of the dinuclear species does not depend on the countercation which is present. Due to the fixed geometry of the ligand the dinuclear complexes seem to be favored over oligonuclear complexes. $[(\mathbf{1})_3Ti_2]^{4-}$ can even be formed in the presence of ammonium cations, although this cation does not seem to be able to stabilize the dinuclear complex very well and therefore no pure compound which shows a correct elemental analysis could be isolated. Characteristic ^1H NMR signals can be observed at δ = 6.83 (dd), 6.69 (pt), and 6.40 (dd).

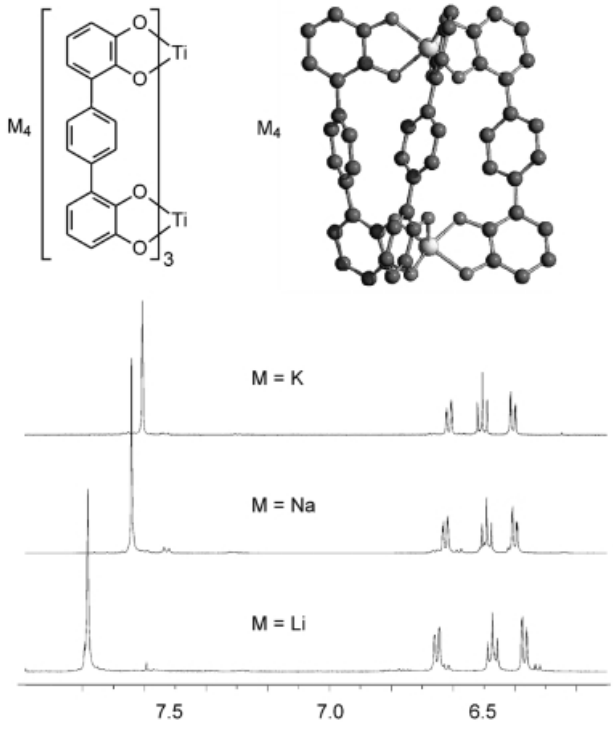

Figure 2. Dinuclear helicates $M_4[(\mathbf{2})_3Ti_2]$, a representation of the X-ray structure of $K_4[(\mathbf{2})_3Ti_2]$[20] and ^1H NMR spectra in [D_4]methanol

The formation and the X-ray structure (Figure 2, top) of the potassium salt $K_4[(\mathbf{2})_3Ti_2]$ of the *p*-phenylene bridged ligand **2**-H_4 was already been communicated by us.[20] A triple-stranded helicate structure $[(\mathbf{2})_3Ti_2]^{4-}$ was found which encapsulates two of the potassium counterions and which forms a dimer by DMF bridges between two potassium cations in the solid state. The two triple-stranded helicates of this dimer possess opposite helicity resulting in a *meso* configuration.[20]

The sodium and lithium salts $M_4[(\mathbf{2})_3Ti_2]$ can also be obtained. Figure 2 (bottom) shows a comparison of the ^1H NMR spectra of the three salts $M_4[(\mathbf{2})_3Ti_2]$ (M = Li, Na, K) in [D_4]methanol. At relatively high field two doublets of doublets [δ = 6.37 (Li), 6.40 (Na), 6.41 (K) and δ = 6.65 (Li), 6.63 (Na), 6.61 (K)] and a pseudo triplet [δ = 6.47 (Li), 6.49 (Na), and 6.50 (K)] are observed which show no significant shift differences for the three different alkali metal salts. However, the shift of the protons at the bridging *p*-phenylene moiety depends highly on the countercation which is present. Singlets are observed at δ = 7.78 (Li), 7.64 (Na), and 7.60 (K) for this proton. The observed NMR spectroscopic features indicate that one (or maybe two) of the cations of $M_4[(\mathbf{2})_3Ti_2]$ are bound in the interior of the

cavity formed by the three ligand strands **2** and the two titanium(IV) ions. Thus, they are located close to the protons of the spacer and lead to different shifts for the corresponding ^{1}H NMR resonances. The aromatic catechol hydrogen atoms are far away and experience the presence of the cations only in a very moderate way.

Due to the low solubility of the complexes $M_4[(\mathbf{2})_3Ti_2]$ (as well as $M_4[(\mathbf{3})_3Ti_2]$) in the FAB MS matrix (e.g., glycerine, 3-NBA) only poorly resolved positive FAB MS spectra could be obtained. Signals of the dinuclear complexes can be detected but show an extremely low intensity.

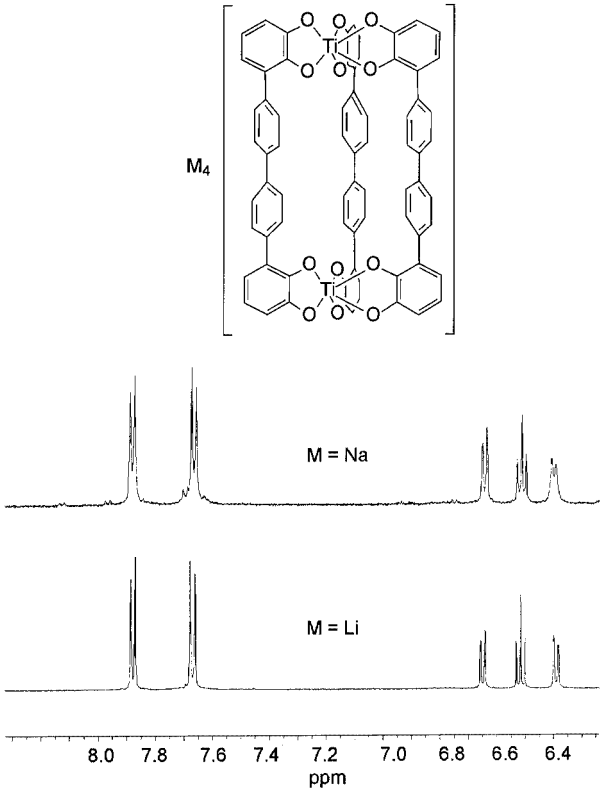

Figure 3. ^{1}H NMR spectra of $M_4[(\mathbf{3})_3Ti_2]$ in [D$_4$]methanol

Dinuclear complexes $M_4[(\mathbf{3})_3Ti_2]$ of ligand **3** (Figure 3) are formed only with sodium or lithium as countercations. With potassium as a cation we rather surprisingly could not obtain a well-defined titanium(IV) complex. The ^{1}H NMR spectra of the two salts $Li_4[(\mathbf{3})_3Ti_2]$ and $Na_4[(\mathbf{3})_3Ti_2]$ in [D$_4$]methanol (Figure 3) are very similar with signals at δ = 7.88 (d), 7.67/7.66 (d, Li/Na), 6.65/6.64 (dd), 6.52/6.51 (pt), and 6.39 (dd). The tetraanion $[(\mathbf{3})_3Ti_2]^{4-}$ possesses a huge internal cavity where it is supposed that lithium or sodium cations can be weakly bound in the interior but can be exchanged very fast.

Self-Recognition Studies

Raymond showed in 1997 that amide-bridged rigid linear dicatechol ligands with significantly different distances between metal binding sites can be introduced into self-recognition experiments and that, upon complex formation with gallium(III) ions, self-sorting of the ligands takes place and only homoleptic complexes (every metal complex contains only one kind of ligand) could be observed.[17] We showed that with alkyl-bridged dicatechol ligands (**4**-H$_4$, **5**-H$_4$) the formation of specific dinuclear titanium(IV) complexes is highly dependent on the templating alkali metal countercation.[15]

In a first investigation we mixed the two ligands **1**-H$_4$ and **2**-H$_4$ (ratio 1:1) and performed coordination studies with titanium(IV) ions in the presence of lithium carbonate (Na_2CO_3 and K_2CO_3 as base lead to essentially the same results).

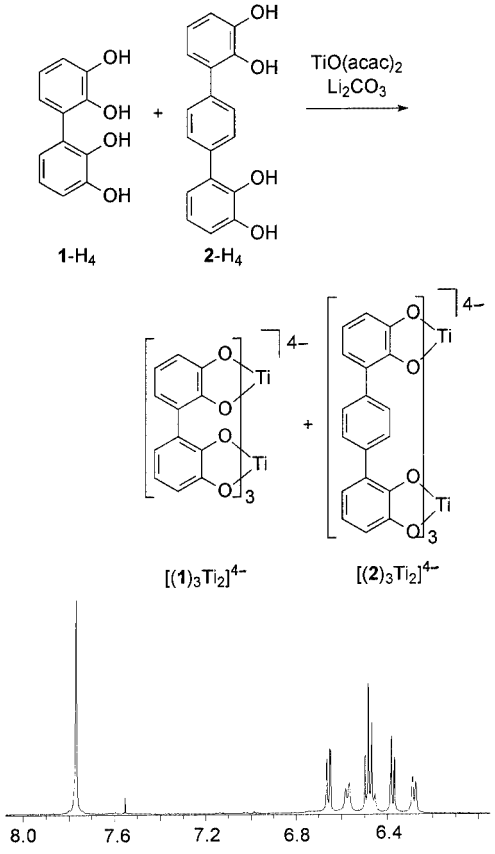

Scheme 2. Self-recognition experiment with a mixture of ligands **1**-H$_4$ and **2**-H$_4$ leading to homoleptic complexes by self-sorting

In Scheme 2 (bottom) the ^{1}H NMR spectrum of the self-recognition experiment with ligands **1** and **2** is presented, showing that only the two homoleptic complexes $Li_4[(\mathbf{1})_3Ti_2]$ and $Li_4[(\mathbf{2})_3Ti_2]$ are present. The signals of $Li_4[(\mathbf{1})_3Ti_2]$ appear at δ = 6.57 (d), 6.47 (pt), and 6.28 (d) while those of $Li_4[(\mathbf{2})_3Ti_2]$ are observed at δ = 7.77 (s), 6.66 (dd), 6.48 (pt), and 6.37 (dd). The ^{13}C NMR spectra also show only the signals of the two homoleptic coordination compounds. In this experiment we observed the same control mechanism as was described earlier by Raymond:[17] rigid linear ligands self-sort in self-recognition experiments due to the match (or mismatch) of the separation of the metal coordination sites.

In an additional experiment we mixed the rigid derivative **2**-H$_4$ with the more flexible ligands **4**-H$_4$ or **5**-H$_4$. The result of the coordination studies with a **2**-H$_4$/**4**-H$_4$ mixture (1:1)

depends strongly on the templating cation which is present. It was shown earlier that the dinuclear complex $[(\mathbf{4})_3Ti_2]^{4-}$ only assembles in the presence of lithium or sodium cations, while the larger potassium cation leads to the formation of a mixture of oligomeric complexes. This has to be taken into account when the self-recognition studies are performed.

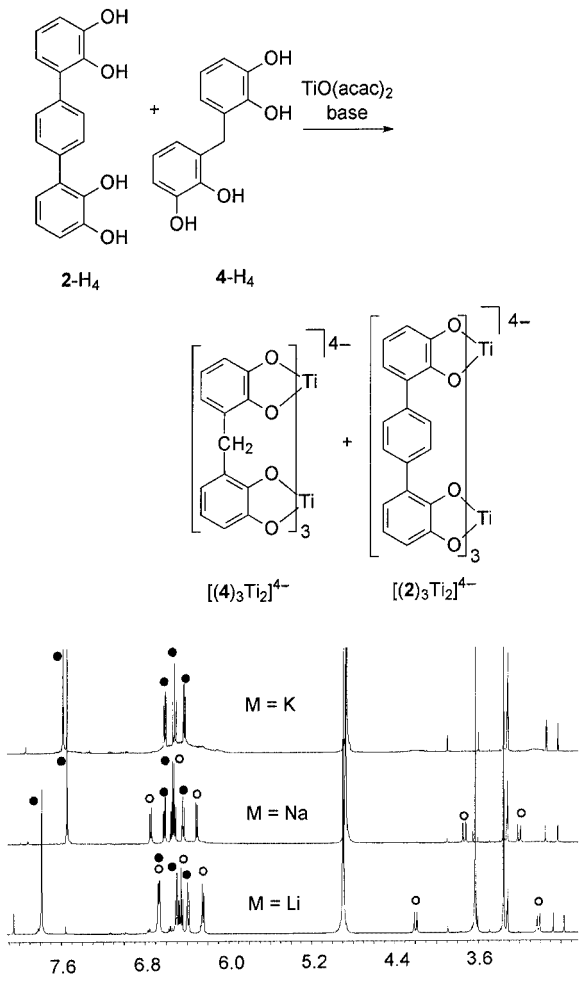

Scheme 3. Alkali metal cation dependant self-recognition of the ligands **2**-H_4 and **4**-H_4. ($[(\mathbf{2})_3Ti_2]^{4-}$: •; $[(\mathbf{4})_3Ti_2]^{4-}$: ○)

Scheme 3 shows the NMR spectra of the crude product of the reaction of a mixture of **2**- and **4**-H_4 (1:1) with titanium(IV) ions in the presence of alkali metal carbonates. If the experiment is performed with potassium carbonate the dinuclear helicate complex $K_4[(\mathbf{2})_3Ti_2]$ can be observed in the ^1H NMR spectrum ([D_4]methanol) at $\delta = 7.58$, 6.61, 6.52, and 6.42. (The shifts differ slightly from those observed for the pure complex due to the presence of several different species in solution.) No resolved resonances can be assigned to a titanium complex of ligand **4**. However, according to our earlier results,[22] broad signals of oligomeric material $\{K_4[(\mathbf{4})_3Ti_2]\}_n$ are detected at $\delta = 4.20$, 3.03 and in the region of aromatic signals. With lithium or sodium carbonate, however, nicely resolved NMR spectra are obtained showing the formation of only homoleptic complexes $M_4[(\mathbf{2})_3Ti_2]$ and $M_4[(\mathbf{4})_3Ti_2]$ by self-recognition of the dicatecholates. In Scheme 3 the signals of the dinuclear complex $[(\mathbf{2})_3Ti_2]^{4-}$ are marked with a•• and those of $[(\mathbf{4})_3Ti_2]^{4-}$ with a ○. No significant amounts of additional metal complexes were observed.

If a similar self-recognition experiment is performed with a mixture of ligands **2**-H_4 and **5**-H_4, no specific titanium(IV) complexes could be observed by NMR spectroscopy. An unspecific complex formation takes place.

The discrepancy in the results obtained in the self-recognition experiments of ligand **2** and **4** or **2** and **5** shows that subtle changes in the system can be important for observing selectivity in self-assembly processes. The ligand **5**-H_4 possesses only one methylene unit more in the spacer than **4**-H_4. This results in a somewhat larger separation of the binding sites and, maybe even more importantly, also results in a dramatic difference in the geometry of the compound.

Due to the rigidity of ligand **2**-H_4 only helical structures can be obtained in the dinuclear coordination compounds $[(\mathbf{2})_3Ti_2]^{4-}$ (for a non-helical complex the ligand has to adopt a very strained "C" type conformation). The ligand **4**-H_4, on the other hand, is predisposed to form the *meso*-helicate $[(\mathbf{4})_3Ti_2]^{4-}$ with two oppositely configured complex units. Therefore the geometries of the two ligands **2** and **4** do not match and only homoleptic complexes can be formed. Ligand **5**, like **2**, is predisposed for the formation of dinuclear helicates, so that for geometric reasons a matched situation results between those two ligands. No specificity is found in the coordination study.

Here the self-recognition in the formation of $[(\mathbf{2})_3Ti_2]^{4-}$ and $[(\mathbf{4})_3Ti_2]^{4-}$ from a mixture of the two ligands seems to be due to a geometric mismatch of the ligand strands. Thus, molecular recognition of the matching strands during complex formation leads to self-sorting and formation of the homoleptic complexes.

Conclusion

In this paper we have described the formation of dinuclear triple-stranded titanium(IV) helicates from rigid rod-type dicatechol ligands **1-3**-H_4 with two binding sites for metals. The formation of these coordination compounds seems not to be templated by the countercation, although interaction of the cations with the tetraanionic complexes $[(\mathbf{1/2})_3Ti_2]^{4-}$ can be deduced from the ^1H NMR spectra. Obviously the linear rigid ligand systems are suitably preorganized for the formation of dinuclear helicates.

In self-recognition studies with titanium(IV) ions a mixture of the derivatives **1**-H_4 and **2**-H_4 leads to the formation of only homoleptic complexes $[(\mathbf{1})_3Ti_2]^{4-}$ and $[(\mathbf{2})_3Ti_2]^{4-}$. This complex formation is controlled by the different length of the ligands.

Self recognition also takes place if a mixture of derivatives **2**-H_4 and **4**-H_4 is used, although not with a mixture of **2**-H_4 and **5**-H_4. Here a mismatch of the ligand geometries of **2** and **4** is supposed which leads to the formation of dinuclear complexes with only one kind of ligand. In the

case of **2** and **5**, however, both ligands possess a geometry that is ideal for the formation of helical complexes and therefore the geometric match of the derivatives prevents self-recognition.

Experimental Section

General Remarks: ^{1}H and ^{13}C NMR spectra were recorded on a Bruker DRX 500 spectrometer using DEPT techniques for the assignment of the multiplicity of carbon atoms. FT-IR spectra were recorded by diffuse reflection (KBr) on a Bruker IFS spectrometer. UV/Vis spectra were recorded on a Perkin−Elmer Lambda 2 spectrometer. Mass spectra (EI, 70 eV) were recorded on a Finnigan MAT 90 mass spectrometer. Elemental analyses were obtained with a Heraeus CHN-O-Rapid analyzer. All commercial reagents were purchased from Aldrich or Fluka. The ligands **1-3**-H_4 and **4/5**-H_4 were prepared as described previously.[21,24,25]

General Procedure for the Preparation of Dinuclear Titanium(IV) Complexes: A mixture of ligand (3 equiv.), $TiO(acac)_2$ (2 equiv.) and alkali metal carbonate (2 equiv.) in methanol was stirred overnight until a clear red solution had formed. The solvent was then removed under vacuum and the residue purified by filtration through Sephadex LH 20.

$Li_4[(1)_3Ti_2]$: Yield: 56 mg (100%), orange solid. ^{1}H NMR ([D$_4$]methanol): δ = 6.28 (dd, *J* = 7.7, 1.4 Hz, 6 H), 6.47 (pt, *J* = 7.7 Hz, 6 H), 6.57 (dd, *J* = 7.7, 1.4 Hz, 6 H). ^{13}C NMR ([D$_4$]methanol): δ = 111.0 (CH), 118.8 (CH), 122.1 (CH), 126.1 (C), 157.3 (C), 157.5 (C). IR (KBr): $\tilde{\nu}$ = 3371, 3057, 1602, 1519, 1420, 1250, 1181, 1135, 1059, 996, 871, 777, 742, 711 cm^{-1}. Positive FAB MS (3-NBA): *m*/*z* = 766 $[Li_4\{(\mathbf{1})_3Ti_2\}]^+$, 760 $[Li_3\{(\mathbf{1})_3Ti_2H\}]^+$. UV/Vis (methanol): λ = 214, 352 nm. $C_{36}H_{18}Li_4O_{12}Ti_2{\cdot}12H_2O$ (982.28): calcd. C 44.02, H 4.31; found C 43.74, H 4.13.

$Na_4[(1)_3Ti_2]$: Yield: 31 mg (61%), red solid. ^{1}H NMR ([D$_4$]methanol): δ = 6.35 (dd, *J* = 7.7, 1.4 Hz, 6 H), 6.56 (pt, *J* = 7.7 Hz, 6 H), 6.62 (dd, *J* = 7.7, 1.4 Hz, 6 H). ^{13}C NMR ([D$_4$]methanol): δ = 111.9 (CH), 120.4 (CH), 121.0 (CH), 123.8 (C), 155.4 (C), 157.7 (C). IR (KBr): $\tilde{\nu}$ = 3421, 3053, 1700, 1420, 1251, 1056, 998, 871, 778, 698, 647, 617 cm^{-1}. Positive FAB MS (3-NBA): *m*/*z* = 809 $[Na_3\{(\mathbf{1})_3Ti_2\}H_2]^+$, 787 $[Na_2\{(\mathbf{1})_3Ti_2\}H_3]^+$. UV/Vis (methanol): λ = 215, 354 nm. $C_{36}H_{18}Na_4O_{12}Ti_2{\cdot}8H_2O$ (974.41): calcd. C 44.37, H 3.52; found C 44.54, H 3.97.

$K_4[(1)_3Ti_2]$: Yield: 42 mg (84%), red solid. ^{1}H NMR ([D$_4$]methanol): δ = 6.34 (m, 6 H), 6.53 (m, 12 H). ^{13}C NMR ([D$_4$]methanol): δ = 111.9 (CH), 119.6 (CH), 119.9 (CH), 123.7 (C), 156.8 (C), 157.5 (C). IR (KBr): $\tilde{\nu}$ = 3403, 3051, 1421, 1251, 1055, 999, 871, 774, 646, 615 cm^{-1}. Positive FAB MS (3-NBA): *m*/*z* = 895 $[K_4\{(\mathbf{1})_3Ti_2\}H]^+$, 857 $[K_3\{(\mathbf{1})_3Ti_2\}H_2]^+$, 818 $[K_2\{(\mathbf{1})_3Ti_2\}H_3]^+$. UV/Vis (methanol): λ = 214, 360 nm. $C_{36}H_{18}K_4O_{12}Ti_2{\cdot}9H_2O$ (1056.86): calcd. C 40.91, H 3.43; found C 41.25, H 3.50.

$(NH_4)_4[(1)_3Ti_2]$: A red solid is obtained by use of ammonium acetate as base. ^{1}H NMR ([D$_4$]methanol): δ = 6.40 (dd, *J* = 7.8, 1.1 Hz, 6 H), 6.69 (pt, *J* = 7.8 Hz, 6 H), 6.83 (dd, *J* = 7.8, 1.1 Hz, 6 H). IR (KBr): $\tilde{\nu}$ = 3237, 3061, 1558, 1420, 1251, 1114, 1057, 993, 871, 773, 713 cm^{-1}. UV/Vis (methanol): λ = 214, 355 nm.

$Li_4[(2)_3Ti_2]$: Yield: 28 mg (100%), red solid. ^{1}H NMR ([D$_4$]methanol): δ = 6.37 (dd, *J* = 7.7, 1.2 Hz, 6 H), 6.47 (pt, *J* = 7.7 Hz, 6 H), 6.65 (dd, *J* = 7.7, 1.2 Hz, 6 H),7.78 (s, 12 H). ^{13}C NMR ([D$_4$]methanol): δ = 111.2 (CH), 117.3 (CH), 118.3 (CH), 125.8 (C), 129.4 (CH, double intensity), 138.6 (C), 158.4 (C), 160.6 (C). IR (KBr): $\tilde{\nu}$ = 3528, 3056, 1617, 1520, 1448, 1392, 1329, 1255, 1218, 1170, 1093, 1058, 918, 893, 782, 737, 688, 640 cm^{-1}. UV/Vis: λ = 206, 278 nm. $C_{54}H_{30}Li_4O_{12}Ti_2{\cdot}8H_2O$ (1138.51): calcd. C 56.97, H 4.07; found C 57.27, H 4.53.

$Na_4[(2)_3Ti_2]$: Yield: 84 mg (100%), orange solid. ^{1}H NMR ([D$_4$]methanol): δ = 6.40 (dd, *J* = 7.7, 1.4 Hz, 6 H), 6.49 (pt, *J* = 7.7 Hz, 6 H), 6.63 (dd, *J* = 7.7, 1.4 Hz, 6 H), 7.64 (s, 12 H). ^{13}C NMR ([D$_4$]methanol): δ = 111.5 (CH), 118.1 (CH), 118.3 (CH), 125.8 (C), 129.5 (CH, double intensity), 138.9 (C), 158.4 (C), 160.6 (C). IR (KBr): $\tilde{\nu}$ = 3567, 3422, 3054, 1635, 1559, 1517, 1447, 1390, 1330, 1252, 1220, 1092, 1058, 917, 839, 783, 735, 683, 636 cm^{-1}. UV/Vis (methanol): λ = 205, 273 nm. $C_{54}H_{30}Na_4O_{12}Ti_2{\cdot}10H_2O$ (1238.74): calcd. C 52.36, H 4.07; found C 52.39, H 4.03.

$K_4[(2)_3Ti_2]$: Yield: 50 mg (100%), red solid. ^{1}H NMR ([D$_4$]methanol): δ = 6.41 (dd, *J* = 7.7, 1.4 Hz, 6 H), 6.50 (pt, *J* = 7.7 Hz, 6 H), 6.61 (dd, *J* = 7.7, 1.4 Hz, 6 H), 7.60 (s, 12 H). ^{13}C NMR ([D$_4$]methanol): δ = 111.6 (CH), 118.1 (CH), 118.5 (CH), 125.5 (C), 129.7 (CH, double intensity), 139.3 (C), 158.3 (C), 160.7 (C). IR (KBr): $\tilde{\nu}$ = 3404, 3052, 1630, 1517, 1446, 1390, 1333, 1252, 1093, 1057, 917, 838, 783, 735, 635 cm^{-1}. UV/Vis (methanol): λ = 205, 270 nm. $C_{54}H_{30}K_4O_{12}Ti_2{\cdot}8H_2O$ (1267.14): calcd. C 51.19, H 3.66; found C 51.10, H 3.58.

$Li_4[(3)_3Ti_2]$: Yield: 26 mg (48%), orange solid. ^{1}H NMR ([D$_4$]methanol): δ = 6.39 (dd, *J* = 7.7, 1.2 Hz, 6 H), 6.52 (pt, *J* = 7.7 Hz, 6 H), 6.65 (dd, *J* = 7.7, 1.2 Hz, 6 H), 7.67 (d, *J* = 8.3 Hz, 12 H), 7.88 (d, *J* = 8.3 Hz, 12 H). ^{13}C NMR ([D$_4$]methanol): δ = 111.5 (CH), 118.5 (CH), 118.7 (CH), 125.4 (C), 127.0 (CH, double intensity), 130.7 (CH, double intensity), 139.5 (C), 140.1 (C), 158.1 (C), 160.8 (C). IR (KBr): $\tilde{\nu}$ = 3617, 3055, 3026, 1609, 1444, 1391, 1333, 1252, 1219, 1102, 1059, 1005, 916, 849, 828, 782, 765, 738, 678, 628 cm^{-1}. UV/Vis (methanol): λ = 210, 304 nm. $C_{72}H_{42}Li_4O_{12}Ti_2{\cdot}7H_2O$ (1348.79): calcd. C 64.12, H 4.18; found C 64.06, H 4.51.

$Na_4[(3)_3Ti_2]$: Yield: 18 mg (34%), orange solid. ^{1}H NMR ([D$_4$]methanol): δ = 6.39 (d, *J* = 7.4 Hz, 6 H), 6.51 (pt, *J* = 7.4 Hz, 6 H), 6.64 (d, *J* = 7.4 Hz, 6 H), 7.66 (d, *J* = 8.1 Hz, 12 H), 7.88 (d, *J* = 8.1 Hz, 12 H). ^{13}C NMR ([D$_4$]methanol): δ = 111.6 (CH), 118.1 (CH), 118.7 (CH), 125.1 (C), 127.2 (CH, double intensity), 130.7 (CH, double intensity), 139.5 (C), 140.4 (C), 158.2 (C), 161.2 (C). IR (KBr): $\tilde{\nu}$ = 3454, 3052, 1606, 1502, 1443, 1251, 1222, 1102, 1058, 916, 846, 828, 783, 765, 738, 673, 627 cm^{-1}. UV/Vis (methanol): λ = 209, 303 nm. $C_{72}H_{42}Na_4O_{12}Ti_2{\cdot}7H_2O$ (1412.99): calcd. C 60.43, H 4.09; found C 60.26, H: 4.44.

General Procedure for the Self-Recognition Studies: Ligand **A** (1.5 equiv.), ligand **B** (1.5 equiv.) $TiO(acac)_2$ (2 equiv.) and alkali metal carbonate (2 equiv.) were stirred overnight in methano until a clear red solution had formed. The solvent was removed under vacuum and the residue analyzed by ^{1}H and ^{13}C NMR spectroscopy.

Self-Recognition Studies with a 1:1 Mixture of Ligands 1-H_4 and 2-H_4 in the Presence of Lithium Carbonate: ^{1}H NMR ([D$_4$]methanol): δ = 6.28 (br. d, *J* = 7.1 Hz, 6 H), 6.37 (dd, *J* = 7.8, 1.4 Hz, 6 H), 6.47 (pt, *J* = 7.1 Hz, 6 H), 6.48 (t, *J* = 7.8 Hz, 6 H), 6.57 (br. d, *J* = 7.1 Hz, 6 H), 6.66 (dd, *J* = 7.8, 1.4 Hz, 6 H), 7.77 (s, 12 H). ^{13}C NMR ([D$_4$]methanol): δ = 111.0 (CH), 111.2 (CH), 117.3 (CH), 118.3 (CH), 118.8 (CH), 122.1 (CH), 125.8 (C), 126.1 (C), 129.4 (CH), 138.6 (C), 157.3 (C), 157.5 (C), 158.4 (C), 160.6 (C).

Self-Recognition Studies with a 1:1 Mixture of Ligands 2-H_4 and 4-H_4

Lithium Carbonate as Base: ^{1}H NMR ([D_4]methanol): δ = 3.01 (d, *J* = 12.9 Hz, 3 H), 4.19 (d, *J* = 12.9 Hz, 3 H), 6.28 (dd, *J* = 7.2, 1.1 Hz, 6 H), 6.39 (dd, *J* = 7.8, 1.4 Hz, 6 H), 6.47 (pt, *J* = 7.2 Hz, 6 H), 6.49 (pt, *J* = 7.8 Hz, 6 H), 6.66 (dd, *J* = 7.8, 1.4 Hz, 6 H), 6.67 (dd, *J* = 7.2, 1.1 Hz, 6 H), 7.78 (s, 12 H). ^{13}C NMR ([D_4]methanol): δ = 31.9 (CH_2), 111.0 (CH), 111.2 (CH), 117.9 (CH), 118.3 (CH), 119.0 (CH), 122.0 (CH), 125.9 (C), 127.6 (C), 129.4 (CH), 138.6 (C), 156.9 (C), 158.1 (C), 158.3 (C), 160.6 (C).

Sodium Carbonate as Base: ^{1}H NMR ([D_4]methanol): δ = 3.20 (d, *J* = 13.4 Hz, 3 H), 3.72 (d, *J* = 13.4 Hz, 3 H), 6.30 (dd, *J* = 7.8, 1.1 Hz, 6 H), 6.43 (dd, *J* = 7.8, 1.4 Hz, 6 H), 6.52 (pt, *J* = 7.8 Hz, 6 H), 6.54 (pt, *J* = 7.8 Hz, 6 H), 6.61 (dd, *J* = 7.8, 1.4 Hz, 6 H), 6.74 (dd, *J* = 7.8, 1.1 Hz, 6 H), 7.54 (s, 12 H). ^{13}C NMR ([D_4]methanol): δ = 31.5 (CH_2), 111.7 (CH), 111.7 (CH), 118.4 (CH), 118.4 (CH), 120.2 (CH), 122.8 (CH), 126.1 (CH), 126.8 (C), 129.6 (CH), 139.0 (C), 155.7 (C), 157.9 (C), 158.4 (C), 160.3 (C).

Potassium Carbonate as Base: ^{1}H NMR ([D_4]methanol): δ = 6.42 (dd, *J* = 7.7, 1.4 Hz, 6 H), 6.52 (pt, *J* = 7.7 Hz, 6 H), 6.61 (dd, *J* = 7.7, 1.4 Hz, 6 H), 7.58 (s, 12 H); additional broad signals were detected at δ = 4.20 and 3.03 as well as in the aromatic region. ^{13}C NMR ([D_4]methanol): δ = 111.7 (CH), 118.3 (CH), 118.5 (CH), 125.6 (C), 129.8 (CH), 139.4 (C), 158.3 (C), 160.6 (C).

Acknowledgments

This work was supported by the Fonds der Chemischen Industrie and the Deutsche Forschungsgemeinschaft.

[1] J.-M. Lehn, *Supramolecular Chemistry*, VCH, Weinheim, **1995**.
[2] F. Vögtle, *Supramolekulare Chemie*, Teubner Verlag, Stuttgart, **1992**.
[3] E. C. Constable, *Angew. Chem.* **1991**, *103*, 1482−1483; *Angew. Chem. Int. Ed. Engl.* **1991**, *30*, 1450−1451.
[4] M. Albrecht, *Chem. Soc. Rev.* **1998**, *27*, 281−288.
[5] J.-M. Lehn, *Chem. & Biol. (Introductory issue)* **1994**, xviii.
[6] C. Piguet, G. Bernardinelli, G. Hopfgartner, *Chem. Rev.* **1997**, *97*, 2005−2062.
[7] M. Albrecht, *Chem. Rev.* **2001**, *101*, 3457−3498.
[8] D. Caulder, K. N. Raymond, *J. Chem. Soc., Dalton Trans.* **1999**, 1185−1200.
[9] M. Fujita, *Chem. Soc. Rev.* **1998**, *27*, 417−425.
[10] A. Von Zelewsky, O. Mamula, *J. Chem. Soc., Dalton Trans.* **2000**, 219−231.
[11] R. W. Saalfrank, B. Demleitner, in *Transition Metals in Supramolecular Chemistry, Vol. 5* (Ed.: J.-P. Sauvage), John Wiley & Sons, New York, **1999**, pp. 1.
[12] B. J. Holliday, C. A. Mirkin, *Angew. Chem.* **2001**, *113*, 2076−2097; *Angew. Chem. Int. Ed.* **2001**, *40*, 2022−2042.
[13] M. Albrecht, *Chem. Eur. J.* **2000**, *6*, 3485−3489.
[14] M. Albrecht, R. Fröhlich, *J. Am. Chem. Soc.* **1997**, *119*, 1656−1661.
[15] M. Albrecht, M. Schneider, H. Röttele, *Angew. Chem.* **1999**, *111*, 512−515; *Angew. Chem. Int. Ed.* **1999**, *38*, 557−559.
[16] R. Krämer, J.-M. Lehn, A. Marquis-Rigault, *Proc. Natl. Acad. Sci. U. S. A.* **1993**, *90*, 5394−5398.
[17] D. Caulder, K. N. Raymond, *Angew. Chem.* **1997**, *109*, 1508−1510; *Angew. Chem. Int. Ed. Engl.* **1997**, *36*, 1440−1442.
[18] E. J. Enemark, T. D. P. Stack, *Angew. Chem.* **1998**, *110*, 977−981; *Angew. Chem. Int. Ed.* **1998**, *37*, 932−935.
[19] M. A. Masood, E. J. Enemark, T. D. P. Stack, *Angew. Chem.* **1998**, *110*, 973−977; *Angew. Chem. Int. Ed.* **1998**, *37*, 928−932.
[20] M. Albrecht, M. Schneider, R. Fröhlich, *New. J. Chem.* **1998**, 753−754.
[21] M. Albrecht, M. Schneider, *Synthesis* **2000**, 1557−1560.
[22] M. Albrecht, S. Kotila, *Chem. Commun.* **1996**, 2309−2310.
[23] M. Albrecht, *Chem. Eur. J.* **1997**, *3*, 1466−1471.
[24] M. Albrecht, *Synthesis* **1996**, 230−237.
[25] M. Albrecht, *Tetrahedron* **1996**, *52*, 2385−2394.

Received January 8, 2001
[I02009]

Synthesis and Structure of Monomeric and Platinum-Bonded (1,10-Phenanthroline)thallium Complexes

Guibin Ma,*[b] Andreas Fischer,[a] and Julius Glaser*[a]

Keywords: Metal−metal interactions / Platinum / Thallium / N ligands / NMR spectroscopy

Oxidative addition of (1,10-phenanthroline)thallium(III) complexes $[Tl(phen)_n(solv)]^{3+}$ (n = 1–2) (phen = 1,10-phenanthroline) to $[Pt(CN)_4]^{2-}$ in DMSO, in the presence of cyanide ions and in the absence of cyanide ions yielded heterodinuclear metal–metal-bonded complexes, $[(NC)_5Pt–Tl(phen)_n(solv)]$ and $[(NC)_4Pt–Tl(phen)_n(solv)]^+$ (n = 0, 1, and 2), respectively. The presence of a direct Pt–Tl bond in the complex is evident by a very strong one-bond $^{195}Pt–^{205}Tl$ spin-spin coupling detected by ^{205}Tl NMR: ^1J = 94.0 kHz (**1a**), 84.2 kHz (**2a**), and 77.1 kHz (**3a**) corresponding to n = 0, 1, and 2 in $[(NC)_4Pt–Tl(phen)_n(solv)]^+$, and ^1J = 65.4 kHz (**2b**) and 62.5 kHz (**3b**) for n = 1 and 2, respectively, in $[(NC)_5Pt–Tl(phen)_n(solv)]$. The crystal structures of $[(NC)_5Pt–Tl(phen)(DMSO)_3]\cdot(DMSO)$ (**2b**), $[(NC)_5Pt–Tl(phen)_2]\cdot(DMSO)_3$ (**3b**), and $[Tl(phen)_2Cl_2](ClO_4)$ (**4**) complexes were determined. Very short Pt–Tl bonds, 2.6296(3) and 2.6375(5) Å, are present in structures **2b** and **3b**, respectively. The corresponding force constants in the molecules in the solid state, 1.84 and 1.74 N/cm for **2b** and **3b**, respectively, were calculated using Raman stretching frequencies of the Pt–Tl vibrations, and are characteristic for a single, strong metal–metal bond. Electronic absorption spectra were recorded for selected compounds and the optical transition attributed to the metal–metal bond was assigned.
(© Wiley-VCH Verlag GmbH, 69451 Weinheim, Germany, 2002)

Introduction

Square-planar complexes of d^8 transition metal ions comply with the 16-electron rule, the occupied d_{z^2} orbital can act as a potential donor to another metal ion (M), resulting in a dative $M(d^8)\rightarrow M$ bond. Many $Pt^{II}-M$ dative-bond complexes have been reported.[1a] A direct metal−metal bond between platinum(II) and thallium(I) in the solid state was first described by Nagle et al.[1b] Recently, several compounds containing a Pt−Tl bond have been prepared.[2] In this laboratory, a family of four dinuclear platinum−thallium cyano compounds with the formula $[(NC)_5Pt-Tl(CN)_{n-1}(aq)]^{(1-n)}$ (n = 1−4 for compound **I**, **II**, **III** and **IV**, respectively), which contain a direct metal−metal bond unsupported by ligands, have been synthesized and characterized in aqueous solutions.[3] Due to the light sensitivity of the Pt−Tl metal−metal bond in these compounds, they are of principal interest. A study was initiated of the effects of modifications of these compounds with nitrogen donor and chromophore organic ligands, e.g. 2,2′-bipyridine and porphyrin (tpp, thpp).[4] When the compounds were exposed to daylight, two-electron transfer was induced between the metal ions. Thus, possible applications in photovoltaic devices, for example in a "wet" solar cell of Grätzel-type,[5] can be envisaged. In the search for suitable compounds for future applications, we report here the synthesis and structural characteristics of new complexes containing a direct metal−metal bond, $[(NC)_4Pt-Tl(phen)_n(solv)]^+$ with n = 0 (**1a**), 1 (**2a**), 2 (**3a**) and $[(NC)_5Pt-Tl(phen)_n(solv)]$ with n = 1 (**2b**), 2 (**3b**). For the first time, a naked Pt−Tl bond with the formal oxidation states Pt^{II} and Tl^{III} and the composition $[(NC)_4Pt-TlX]^+$ was synthesised and structurally characterised [X = $(phen)_n(solv)$, n = 0,1,2; solv = DMSO].

Results and Discussion

Characterization in Solution by ^{205}Tl NMR Spectroscopy

The preparation of Pt−Tl complexes with the N-donor ligand ethylenediamine was described in our previous paper.[4a] In a similar way, two new Pt−Tl complexes $[(NC)_4Pt-Tl(solv)]^+$ (**1a**) and $[(NC)_5Pt-Tl(solv)]$ (**1b**) could be prepared; these two species were then treated with 1,10-phenanthroline, whereby the complexes $[(NC)_4Pt-Tl(phen)(solv)]^+$ (**2a**), $[(NC)_5Pt-Tl(phen)(solv)]$ (**2b**), $[(NC)_4Pt-Tl(phen)_2(solv)]$ (**3a**), and $[(NC)_5Pt-Tl(phen)_2]$ (**3b**) in DMSO solution (Scheme 1) were prepared.

In the reaction between the solid compound $[Tl(DMSO)_6](ClO_4)_3$ and $[Pt(CN)_4{}^{2-}]$ in DMSO (cf. Scheme 1, lower part), it is clear from the ^{205}Tl NMR spectrum that only

[a] Department of Chemistry, Royal Institute of Technology (KTH)
10044 Stockholm, Sweden
E-mail: julius@inorg.kth.se
[b] Department of Chemistry, Shanxi University,
030006 Taiyuan, Shanxi Province, P. R. China
Supporting information for this article is available on the WWW under http://www.eurjic.com or from the author.

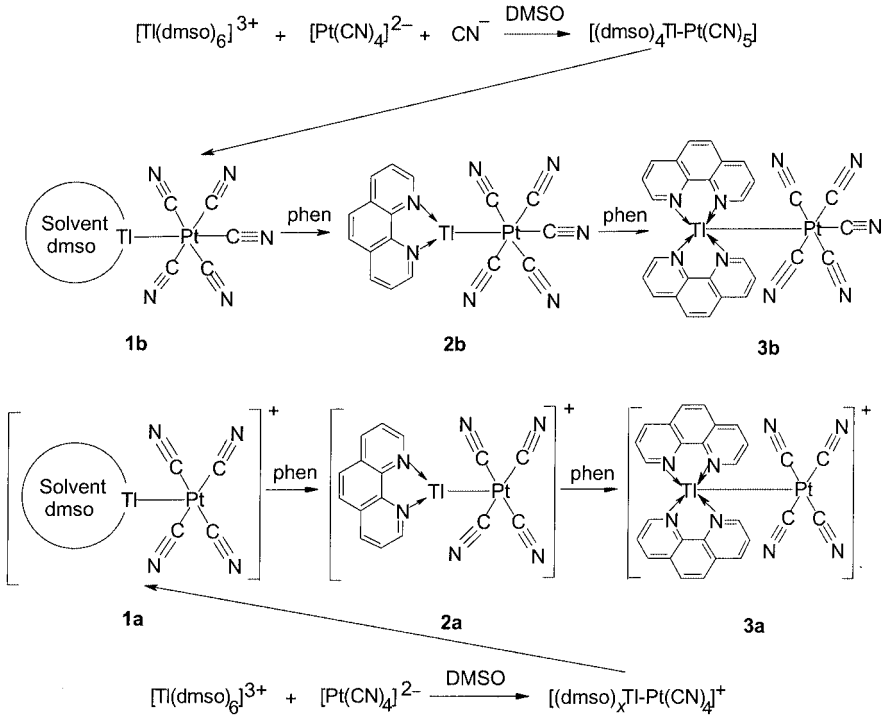

Scheme 1

one Pt−Tl dinuclear complex forms (**1a**); a 1:3.9:1 triplet peak appears centred at δ = 82 with a large spin-spin coupling constant (94000 Hz), this is characteristic for a non-buttressed Pt−Tl bond.[3] The ^{205}Tl NMR signal splits into a doublet by nuclear spin-spin coupling to the NMR-active isotope ^{195}Pt (natural abundance 33.8%, I = 1/2) and, together with the NMR-inactive Pt isotopes (natural abundance 66.2%), it shows a triplet pattern with the expected intensity ratio 1:3.9:1 (cf. Figure 1). Then, upon stepwise addition of 1,10-phenanthroline, two Pt−Tl species showed up in the spectra as typical triplet signals at δ = 472 (**2a**) and δ = 775 (**3a**) with the spin-spin coupling constants 84200 Hz and 77120 Hz, respectively.

The preparation and characterization of [(NC)$_5$Pt−Tl(solv)] (**1b**) was studied earlier[4a] and crystalline [(NC)$_5$Pt−Tl(DMSO)$_4$] was obtained. When the solid [(NC)$_5$Pt−Tl(DMSO)$_4$] was treated with 1,10-phenanthroline at different molar ratios (cf. Scheme 1, top part), it dissolved completely, and the complexes [(NC)$_5$Pt−Tl(phen)$_n$] (n = 1−2 for compounds **2b** and **3b**, respectively) formed in solution. The ^{205}Tl NMR chemical shifts for the two new phenanthroline species are δ = 992 and 1162, and spin-spin coupling constants ^1J(^{195}Pt-^{205}Tl) are 65440 and 62490 Hz for **2b** and **3b** in DMSO, respectively. Similar to the ^{205}Tl NMR spectrum discussed above, the signals are triplets with the expected intensity ratio 1:3.9:1 (Figure 2).

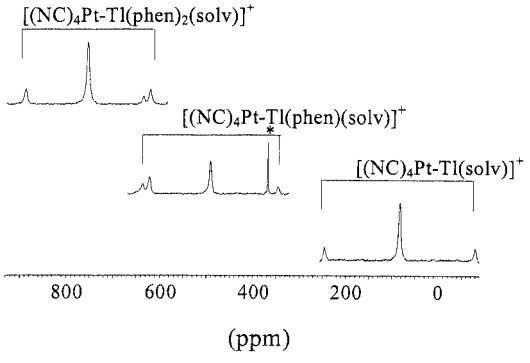

Figure 1. 288 MHz ^{205}Tl NMR spectra of Pt−Tl compounds in DMSO: [(NC)$_4$Pt−Tl(solv)]$^+$ (**1a**), [(NC)$_4$Pt−Tl(phen)(solv)]$^+$ (**2a**), and [(NC)$_4$Pt−Tl(phen)$_2$(solv)]$^+$ (**3a**); * represents Tl^I signal at δ = 363

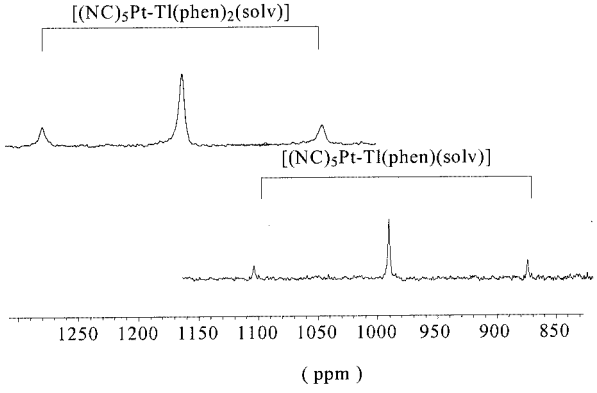

Figure 2. 288 MHz ^{205}Tl NMR spectra of the Pt−Tl compounds [(NC)$_5$Pt−Tl(phen)(DMSO)$_y$] (**2b**) and [(NC)$_5$Pt−Tl(phen)$_2$] (**3b**) in DMSO

The large spin-spin coupling constants show that a Pt−Tl bond is formed; the appearance of peaks with different and hitherto unreported chemical shifts and coupling constants suggests that new complexes $[(NC)_4Pt-Tl(phen)_n]^+$ (n = 1 and 2 for **2a** and **3a**, respectively) and $[(NC)_5Pt-Tl(phen)_n]$ (n = 1 and 2 for **2b** and **3b**, respectively) formed in solution (Scheme 1). Upon coordination of the second phen molecule to the thallium atom in all the studied Pt−Tl dinuclear complexes in DMSO, the spin-spin coupling constant $^1J(^{195}Pt\text{-}^{205}Tl)$ decreased. This strong coupling is a characteristic feature of the bonding between the two metal ions with the formal oxidation states $Pt^{II}-Tl^{III}$, and is an indication of a significant contribution of thallium 6s orbitals to the metal−metal bonding.[3b] Owing to the relativistic effects, the thallium 6s orbital is stabilized and contracted; this results in an increased electron density at the nucleus, which contributes to the Fermi contact term for spin-spin coupling.[2j,23] It was found that there is a correlation between the spin-spin coupling constant and the metal−metal separation/bond strength in the series of complexes $[(NC)_5Pt-Tl(CN)_n]^{n-}$ (n = 1−3). The stronger Pt−Tl bonding, the shorter Pt−Tl bond length and the larger spin-spin coupling constant.[6]

NMR chemical shifts for heavy metals with large chemical shift ranges are very sensitive to the oxidation state of the metal ion.[7] Thus, ^{205}Tl NMR chemical shifts of Tl^I species are in the range δ = −200 to +200 and those of Tl^{III} complexes are usually at δ = 2000 to 3000.[3d] In DMSO, ^{205}Tl NMR chemical shifts of $[Tl(DMSO)_6]^{3+}$ and Tl^+ are δ = 1886 and 361, respectively.[11] For the currently studied compounds, $[(NC)_4Pt-Tl(solv)]^+$, $[(NC)_4Pt-Tl(phen)_n]^+$ (n = 1−2), and $[(NC)_5Pt-Tl(phen)_n]$ (n = 1−2), ^{205}Tl NMR chemical shifts are in the Tl^+ region for $[(NC)_4Pt-Tl(solv)]^+$ and between Tl^I and Tl^{III} for all the others. Consequently, the thallium oxidation state in these compounds is between Tl^I and Tl^{III}.[6a] It could be of interest to compare the differences between the spin-spin coupling constants $^1J(^{195}Pt\text{-}^{205}Tl)$ for the two types of complexes prepared in this work in which the only difference between the compounds **a** and **b** is one extra cyanide ligand bound to the platinum atom. Still, the differences in coupling constants are very large: 28100 Hz [between ^1J(**1a**) and ^1J(**1b**)], 18800 Hz [between ^1J(**2a**) and ^1J(**2b**)], and 15600 Hz [between ^1J(**3a**) and ^1J(**3b**)].

Crystal Structures of Pt-Bonded and Monomeric Tl(phen) Compounds

$[(NC)_5Pt-Tl(phen)(DMSO)_3]$ (DMSO) (2b)

Single crystals of the dinuclear compound **2b** were obtained from the studied solution and the structure determined by X-ray diffraction method. The ORTEP perspective view of the molecular structure and the selected bond lengths of **2b** are shown in Figure 3. The Pt−Tl bond length is short, 2.6296(3) Å, significantly shorter than for other reported Pt−Tl bond lengths.[2] In the $Pt(CN)_5$ moiety the Pt−C bonds range between 2.005 and 2.053 Å; the axial cyanide has a slightly longer Pt−C distance than the equatorial ones. The Tl atom coordinates one phen ligand and three DMSO molecules forming a distorted octahedral geometry around the thallium atom. Atoms O1, O4, O5, and N2 define an equatorial plane, from which the Tl atom is displaced 0.57(1) Å towards the Pt atom. The four equatorial ligand atoms around Tl are in a staggered conformation to the adjacent square-planar $Pt(CN)_4$ unit. The angle between the Tl1−N1 bond and the plane formed by the atoms O1, O4, and O5 is 91.6°, close to perpendicular, whereas the angle N1−Tl1−Pt1 is 176.1°, close to 180°. In this compound, two kinds of DMSO molecules are present in the structure; three molecules coordinated to the thallium atom and one remains uncoordinated. The bond lengths of the coordinated DMSO molecules are altered compared to the uncoordinated one. The strong coordination gives a short Tl−O and a long S−O bond length [for coordinated DMSO: Tl1−O1 = 2.448(4) Å, S2−O1 = 1.527(5) Å; Tl1−O4 = 2.471(4) Å, S1−O4 = 1.511(5) Å; Tl1−O5 = 2.495(5) Å, S4−O5 = 1.499(6) Å; for free DMSO: S3−O6 = 1.483(8) Å]. The S−O bond order is diminished by coordination, and it is due to electrons of the oxygen atom moving toward the thallium atom upon coordination. Comparing these data to our previous structural data of $[Tl(DMSO)_6]^{3+}$ [Tl−O = 2.224(3) Å, S−O = 1.544(4) Å],[11] the Tl−DMSO coordination is much weaker in compound **2b**. It is probably due to the decreased positive charge of thallium in the dinuclear complex.

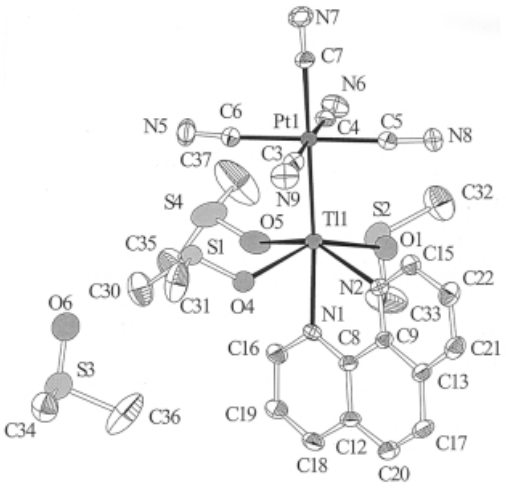

Figure 3. ORTEP view of the species $[(NC)_5Pt-Tl(phen)(DMSO)_3]$ found in the crystal structure of $[(NC)_5Pt-Tl(phen)(DMSO)_3]\cdot(DMSO)$ (**2b**), thermal ellipsoids are drawn at 30% probability level; selected bond lengths [Å] and angles [°]: Pt(1)−Tl(1) 2.6296(3), Pt(1)−C(3) 2.030(6), Pt(1)−C(4) 2.007(6), Pt(1)−C(5) 2.011(6), Pt(1)−C(6) 2.005(6), Pt(1)−C(7) 2.053(6), Tl(1)−N(1) 2.322(4), Tl(1)−N(2) 2.434(4), Tl(1)−O(1) 2.448(4), Tl(1)−O(4) 2.471(4), Tl(1)−O(5) 2.495(5), S(1)−O(4) 1.511(5), S(2)−O(1) 1.527(5), S(4)−O(5) 1.499(6); C(6)−Pt(1)−C(5) 177.4(2), C(3)−Pt(1)−C(4) 177.4(2), C(7)−Pt(1)−Tl(1) 177.58(18), N(1)−Tl(1)−Pt(1) 176.21(12)

$[(NC)_5Pt-Tl(phen)_2]$ 3(DMSO) (3b)

The ORTEP perspective view of the molecular structure and the selected bond lengths of **3b** are shown in Figure 4. Similar to compound **2b**, the main structural feature of **3b**

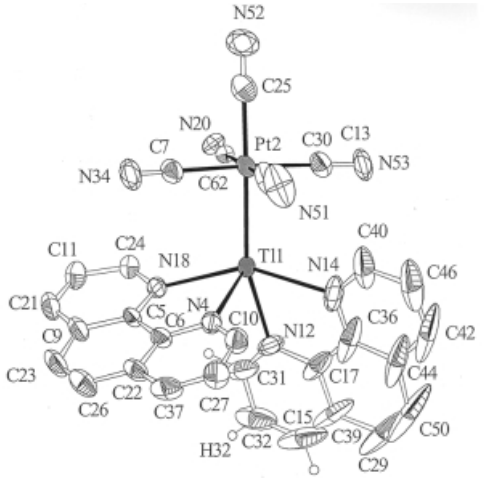

Figure 4. ORTEP view of the species $[(NC)_5Pt-Tl(phen)_2]$ found in the crystal structure of $[(NC)_5Pt-Tl(phen)_2]\cdot(3dmso)$ (**3b**); thermal ellipsoids are drawn at 30% probability level; selected bond lengths [Å] and angles [°]: Pt(1)−Tl(1) 2.6375(5), Pt(2)−C(7) 2.029(10), Pt(2)−C(13) 2.022(11), Pt(2)−C(25) 2.025(14), Pt(2)−C(30) 2.002(14), Pt(2)−C(62) 1.990(9), Tl(1)−N(4) 2.428(7), Tl(1)−N(12) 2.291(10), Tl(1)−N(14) 2.524(10), Tl(1)−N(18) 2.445(7); C(25)−Pt(2)−Tl(1) 178.3(4), N(4)−Tl(1)−Pt(2) 118.2(2), N(14)−Tl(1)−Pt(2) 103.1(4), N(18)−Tl(1)−Pt(2) 103.55(17), N(12)−Tl(1)−Pt(2) 158.6(2), C(30)−Pt(2)−C(13) 90.8(5), C(13)−Pt(2)−C(7) 177.6(4)

is the short and non-buttressed Pt−Tl bond [Pt−Tl = 2.6375(5) Å]. In addition to the Pt−Tl linkage, the platinum atom of **3b** is bonded to five carbon atoms of the cyanide ligands. Four carbon atoms constitute an almost square plane around the platinum atom, while the fifth carbon atom occupies an axial position in the pseudo-octahedron. The Tl atom is linked to four N atoms (two phen molecules), which together with the bond to Pt form irregular five-coordinated surroundings (Figure 4). The two coordination planes of the phenanthroline ligands around Tl are skewed relative to each other (torsion angle 60.8°), reminding one of butterfly wings. All carbon atoms located in the phenanthroline planes including N12 and N14 exhibit very large atomic displacement parameters; this is probably due to the relatively large free space around them.

The main structural feature of these dimetallic compounds is the short and unsupported Pt−Tl bond with the bond lengths 2.6296(3) and 2.6375(5) Å in **2b** and **3b**, respectively. These Pt−Tl distances fall into the range of values obtained previously in this laboratory for the family of related compounds: $[(NC)_5Pt-Tl(CN)_n(H_2O)_m]^{3-n}$ (n = 0−3; 2.598−2.638 Å),[6] $[(NC)_5Pt-Tl(DMSO)_4]$ (2.6131 Å),[4] $[(NC)_5Pt-Tl(en)_2]$ (2.6348 Å),[4] and $[(NC)_5Pt-Tl(bipy)_n]$ [n = 1−2; 2.6186(8) Å and 2.6117(5) Å, respectively]. The bond lengths of the hitherto characterized Pt−Tl compounds are related to the formal oxidation states of the metal ions $[Pt^0-Tl^I]$ (2.860−3.047 Å);[2a,2b] $Pt^{II}-Tl^I$ (2.876−3.152 Å);[1,2f−2i] $Pt^{II}-Tl^{II}$ (2.698−2.708);[2c,2d] and $Pt^{II}-Tl^{III}$ (2.598−2.638 Å) (refs.[3,4] and present work) Considering only the compounds of divalent platinum, it appears that the Pt−Tl bond becomes shorter when the formal oxidation state of thallium increases from Tl^I to Tl^{III}. This is consistent with both the decreasing size of the thallium cation and with the strengthening of the metal−metal interaction due to participation of the thallium 6s orbitals in the bonding.[3]

Raman vibration bands for the crystalline compounds $[(NC)_5Pt-Tl(phen)(DMSO)_3]$ and $[(NC)_5Pt-Tl(phen)_2]\cdot(DMSO)_3$ were detected at 177 and 172 cm^{-1}, respectively. The Pt−Tl force constants in the title molecules, 1.84 and 1.74 N/cm for **2b** and **3b**, were estimated using the diatomic oscillator approximation model.[8,9] These values are larger than those of the previously studied Pt−Tl cyano complexes (about 1.6 N/cm for the diatomic approximation).[3b,6] It shows that the phenanthroline ligand coordination stabilizes the Pt−Tl metal−metal bonding. The relation between the force constant and the Pt−Tl bond length was observed in the previously studied compounds $[(NC)_5Pt-Tl(CN)_n]^{n-}$ (n = 1−3) [the bond lengths are 2.598(3), 2.618(4), and 2.638(4) Å, which corresponds to force constants of 1.736, 1.693, and 1.563 N/cm, respectively).[6] A correlation seems to exist between the force constant and the Pt−Tl bond length within this series of compounds. In the present case, the ligand coordinated to the thallium atom is different, so the results are not expected to fit into the series of cyano compounds. A similar trend is, however, observed in **2b** and **3b**; the bond lengths are 2.6296(3) and 2.6375(5) Å, and the corresponding force constants are 1.85 and 1.74 N/cm, respectively. Even if the force constants increase when the cyano ligands are replaced by phenanthroline in the Tl sphere of the dinuclear Pt−Tl complex, the constants are still compatible with a single metal−metal bond.[10] The C≡N stretching region of the dinuclear species is also informative and can provide an additional support for the structure of the compounds. We assigned the two sharp bands at $\tilde{\nu}$ = 2174 and 2161 cm^{-1} for **2b** and at 2178 and 2160 cm^{-1} for **3b** to the symmetric (A_{1g}) and antisymmetric (B_{1g}) stretching vibrations of the four equivalent cyanide ligands of the $Pt(CN)_4$ unit in D_{4h} symmetry.[18] These bands shift to high frequency and are very close to the stretching bands at 2153 cm^{-1} (s) and 2137 cm^{-1}(m) for $[Pt(CN)_4]^{2-}$ in the solid state. The higher frequency bands at 2184 cm^{-1} and 2189 cm^{-1} were assigned to the axial cyanide in compounds **2b** and **3b**, respectively.

$[Tl(phen)_2Cl_2](ClO_4)$ (4)

The molecular structure of the cation $[Tl(phen)_2Cl_2]^+$ is shown in Figure 5. The thallium atom is six-coordinated and is bonded to four nitrogen atoms of two 1,10-phenanthroline ligands and to two chloride ions. Interestingly, the two phen planes are almost perpendicular to each other (torsion angle = 90.1°). The atoms within the phenanthroline ligands are almost within its molecular plane. The thallium complex can be viewed as consisting of two equivalent Tl(phen)Cl units, each located in its own hemisphere of the coordination shell of Tl. In **4**, thallium is *cis*-coordinated by two Cl ligands similarly to the *cis*-dichlorobis(2,2′-bipyridyl)gallium(III) cation.[24] Four N atoms and two chloride ions form a distorted octahedral geometry around Tl. The

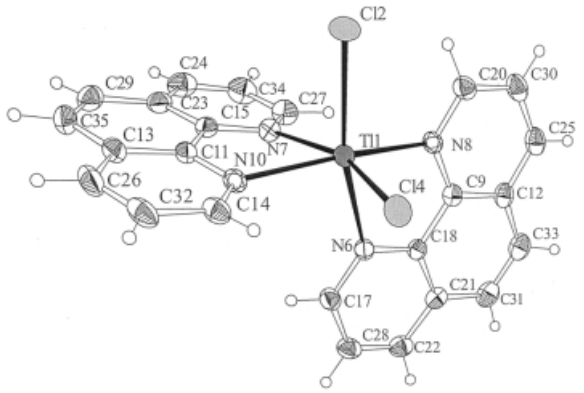

Figure 5. ORTEP view of the $[Tl(phen)_2Cl_2]^+$ cation found in the crystal structure of $[Tl(phen)_2Cl_2](ClO_4)$ (**4**); thermal ellipsoids are drawn at the 30% probability level; selected bond lengths [Å] and angles [°]: Tl(1)−N(8) 2.357(3), Tl(1)−N(7) 2.362(3), Tl(1)−N(10) 2.372(3), Tl(1)−N(6) 2.384(3), Tl(1)−Cl(4) 2.4655(9), Tl(1)−Cl(2) 2.4789(9); N(8)−Tl(1)−N(7) 96.81(10), N(7)−Tl(1)−N(10) 70.64(19), N(10)−Tl(1)−N(6) 98.95(10), N(8)−Tl(1)−Cl(4) 100.05(7), N(7)−Tl(1)−Cl(4) 160.29(8), N(10)−Tl(1)−Cl(2) 98.15(8), N(6)−Tl(1)−Cl(2) 159.35(7), Cl(4)−Tl(1)−Cl(2) 100.02(4)

mean Tl−N distance, 2.369(3) Å (2.357−2.384 Å), is similar to that in $[Tl(bipy)_3(DMSO)]^{3+}$ (2.356−2.372 Å), and the atomic arrangement is almost exactly the same as in the complex $[Tl(phen)Cl_3]$.[12] The mean Tl−Cl distance, 2.4722(9) Å (2.4655−2.4789 Å), is similar to the previously studied complex {$[Tl(phen)Cl_3]$: 2.467(3) Å}, but they are longer than those in tetrahedral $[TlCl_4]^-$ and shorter than those in $[TlCl_5(DMSO)]^{2-}$ [2.506(6)−2.636(6) Å][13] and $[TlCl_6]^{3-}$ (2.59 Å).[14]

Comparison of the Structures and Optical Properties

Apart from the previously discussed ^{205}Tl NMR chemical shift, the change in the actual oxidation state of the metal ions in the heterodinuclear compounds is also reflected by the bond lengths Tl−O and Tl−N. The bonds Tl−O [average 2.471(5) Å in **1**] and Tl−N [average 2.422(8) Å in **2**] are significantly longer than the corresponding distances in the mononuclear Tl^{III} complexes $[Tl(DMSO)_6]^{3+}$ [2.224(3) Å][11] and $[Tl(phen)_2Cl_2]^+$ [average 2.369(3) Å] (**4**). The increase in the Tl−O and Tl−N bond lengths in the studied Pt−Tl compounds is compatible with the decrease of the thallium oxidation state upon formation of the Pt−Tl bond. It confirms that the reaction of $[Tl^{III}(phen)_n]^{3+}$ (n = 1−2) with $[Pt^{II}(CN)_4]^{2-}$ to form heterodinuclear Pt−Tl metal−metal-bonded compounds $[(NC)_4Pt-Tl(phen)_n(solv)]^+$ and $[(NC)_5Pt-Tl(phen)_n(solv)]$ (n = 1,2) can be considered as an oxidative addition.

The optical properties of the dinuclear complexes $[(NC)_5Pt-Tl(CN)_n(aq)]^{n-}$ (n = 0−3) in aqueous solution are dominated by the metal−metal interaction. A very intensive electronic absorption band appears in the UV region, with the maximum in the range 238−259 nm (ε = $2.9-6.9\cdot10^4$ $L\cdot mol^{-1}\cdot cm^{-1}$) depending on the number of cyanide ligands in the compound.[3] The metal-to-metal charge-transfer band (MMCT) of the dinuclear complex $[(NC)_5Pt-Tl(solv)]$ in DMSO is found at 294 nm (ε = $2.1\cdot10^4$ $L\cdot mol^{-1}\cdot cm^{-1}$). Interestingly, the maximum MMCT band of $[(NC)_4Pt-Tl(solv)]^+$ in DMSO is found at 350 nm, which is a dramatic shift to the red compared to $[(NC)_5Pt-Tl(solv)]$. For all the dinuclear complexes studied, it seems that the maximum of the MMCT band is approximately proportional to the corresponding Pt−Tl spin-spin coupling constant. This phenomenon was also found for the dinuclear Pt−Tl cyano complexes. By comparing the electronic absorption spectra of $[(NC)_5Pt-Tl(phen)_2]$ and the parent complex $[Tl(phen)_3]^{3+}$, both in DMSO, the maximum for the former compound, at 274 nm (ε = $4.41\cdot10^4$ $L\cdot mol^{-1}\cdot cm^{-1}$), was assigned to the metal-to-metal charge transfer transition (MMCT). This corresponds to a shift by 15 nm to longer wavelength relative to the M−M transition in the complex $[(NC)_5Pt-Tl(H_2O)_5]$ in water. This shift is attributed to the change of thallium coordination (two phen ligands replace five water molecules). It can be concluded that there is no dramatic effect of the coordinated phenanthroline ligand on the MMCT transition.

^{195}Pt-^{205}Tl Spin-Spin Coupling Constants and ^{205}Tl NMR Chemical Shifts

Until now, ^{205}Tl NMR chemical shifts and Pt−Tl spin-spin coupling constants have been recorded for fifteen Pt−Tl heterodinuclear complexes in DMSO (cf. Supporting Information). Interestingly, the values of δ_{Tl} and $^1J(^{195}Pt-^{205}Tl)$ for all these complexes fall onto a straight line (Figure 6). This cannot be accidental, considering the very large intervals for both parameters, about 57000 Hz and 2140 ppm, respectively. As has been discussed previously,[20,21] the very large chemical shift variation is related to the oxidation state (large variation of the electron density) of the ^{205}Tl nucleus via the paramagnetic term of the Ramsey equation.[22] Also, the spin-spin coupling is related to the electron density: in the present case, the Pt−Tl coupling is transmitted via the s-electrons participating in the Pt−Tl bond.[23] The relation can be explained as follows: The Tl-coordinated ligands induce transfer of electrons from the Tl nucleus towards Pt. In this way, Tl becomes more deshielded, which leads to larger values of the Tl NMR chemical shift.

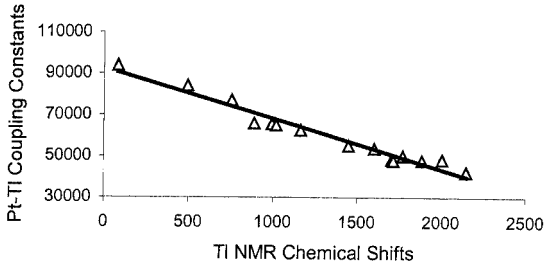

Figure 6. A correlation between the ^{205}Tl NMR chemical shifts (in ppm) and spin-spin coupling constants (in Hz) for all measured Pt−Tl bonded compounds in DMSO; the straight line follows the equation ^1J [Hz] = $-24.6\cdot\delta_{Tl}$ [ppm] + 92740

At the same time, the total electron density (and the density of the s electrons that contribute to the Fermi contact term)[23] of the Pt−Tl bond decreases, which leads to a decrease in the spin-spin coupling constant $^1J(^{195}Pt-^{205}Tl)$ and to a weakening of the Pt−Tl bond.

It would be interesting to compare the spin-spin coupling and chemical shifts of the two studied types of complexes $[(NC)_4Pt-Tl(phen)_n(solv)]^+$ and $[(NC)_5Pt-Tl(phen)_n(solv)]$ (n = 0, 1, and 2). A single cyanide ligand coordinated to the platinum atom in the axial position decreases the Pt−Tl coupling and increases the Tl chemical shifts dramatically. What could be the reason? It is probable that after the axial cyanide ligand has been coordinated, the electron-donating ability of the orbital d_{z^2} towards the Tl 6s orbital decreases, the electron density around Tl decreases and the Fermi contact term becomes small, so the real oxidation state increases. Meanwhile, the spin-spin coupling becomes small and the chemical shift increases.

It is also interesting to compare the Pt−Tl spin-spin coupling of the complex $[(NC)_5Pt-Tl]$ in two different solvents, water and DMSO. It is reasonable to consider that five molecules of H_2O or DMSO are coordinated to the thallium atom in the Pt−Tl dinuclear complex, in the same way as in the solid state.[6] In agreement with the stronger ability of DMSO to donate electron density to Tl^{III}, ^{205}Tl NMR chemical shift in solution of $[Tl(DMSO)_6]^{3+}$ (δ = 1886)[11] is smaller than that of $[Tl(H_2O)_6]^{3+}$ (δ = 2093).[19] Accordingly, the ^{205}Tl NMR chemical shift of the $[(NC)_5Pt-Tl]$ complex in DMSO should be smaller than for the same complex in aqueous solution. Also, the Pt−Tl coupling constant of $[(NC)_5Pt-Tl(DMSO)_5]$ should be larger than that of $[(NC)_5Pt-Tl(H_2O)_5]$. Surprisingly, both the ^{205}Tl NMR shifts and the coupling constants of the two complexes follow just the opposite trend, $[(NC)_5Pt-Tl(DMSO)_5]$ (δ = 887 and 65.9 kHz) and $[(NC)_5Pt-Tl(H_2O)_5]$ (δ = 786 and 71.1 kHz).

What could be the reason for this behaviour? One explanation is that the stronger electron donation from DMSO to the thallium atom would induce a partial transfer of electrons from Tl towards Pt, thus causing the observed trend for the chemical shifts and the spin-spin coupling constant Pt−Tl. An alternative explanation goes as follows: Very recently, theoretical calculations (DFT calculation considering relativistic effects)[23] led to a suggestion that short C≡N···H hydrogen bonds (N···H approximately 2.2 Å, see Scheme 2) are formed between the thallium-coordinated water molecules and the platinum-bonded cyanide ligands. This would lead to a strengthening of the Pt−Tl bond; indeed, the Pt−Tl distance would become quite short (Pt−Tl approximately 2.600 Å).[23] This type of hydrogen bond cannot form in DMSO solution; hence, it would be compatible with the (opposite to the expected) trend of the chemical shifts and the coupling constant.

Conclusions

Five novel Pt−Tl(phen) complexes in DMSO, $[(NC)_4Pt-Tl(solv)]^+$ (**1a**), $[(NC)_4Pt-Tl(phen)(solv)]^+$ (**2a**),

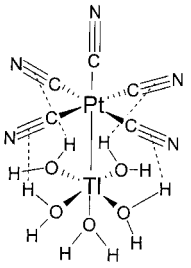

Scheme 2

$[(NC)_4Pt-Tl(phen)_2(solv)]^+$ (**3a**), $[(NC)_5Pt-Tl(phen)(solv)]$ (**2b**), and $[(NC)_5Pt-Tl(phen)_2(solv)]$ (**3b**) have been prepared and their formation shown by means of ^{205}Tl NMR. The very large ^{195}Pt-^{205}Tl spin-spin coupling constants, 94.0, 84.2, and 77.1 kHz for complex **1a**, **2a**, and **3a**, and 65.4 and 62.5 kHz for complex **2b** and **3b**, respectively, unambiguously demonstrate the presence of a direct metal−metal bond in the complexes. For the first time in Pt−Tl-bonded complexes, the species $[(NC)_4Pt-TlX]$ [where X = $(phen)_n(solv)$, n = 1 and 2] comply with the 16-electron rule, with respect to platinum. The results show that the complexes with 16 electrons are stable in solution, long enough for the study on the ^{205}Tl NMR time scale. Three solid compounds, $[(NC)_5Pt-Tl(phen)(DMSO)_3]$ (**2b**), $[(NC)_5Pt-Tl(phen)_2]$ (**3b**), and $[Tl(phen)_2Cl_2](ClO_4)$ (**4**), were crystallised from solution and their structures determined by X-ray diffraction. In compounds **2b** and **3b** unsupported metal−metal bonds are present. The Pt−Tl distances, 2.6296(3) and 2.6375(5) Å for **2b** and **3b**, respectively, are among the shortest reported separations between these two metals. The Pt−Tl force constants in the molecules **2b** and **3b**, 1.84 and 1.74 N/cm, respectively, calculated from Raman frequencies of the metal−metal stretching vibrations, are compatible with the intermetallic Pt−Tl separations; the values of the force constants are characteristic for a strong, single metal−metal bond. Attachment of phenanthroline to the thallium part of the dimetallic platinum−thallium(cyano) compounds resulted in a red shift of the metal-to-metal charge transfer band.

Experimental Section

Synthesis: The solid $[Tl(DMSO)_6](ClO_4)_3$ was prepared as described in a recent paper.[11] The complex $[(NC)_4Pt-Tl(solv)]^+$ (**1a**) was obtained by the reaction between solid compounds $[Tl(DMSO)_6](ClO_4)_3$ (49 mg, 0.05 mmol) and $K_2Pt(CN)_4$ (19 mg, 0.05 mmol), concentration 50 mM in 1 mL of DMSO. Upon addition of 1,10-phenanthroline to the solution of complex **1a**, the complexes **2a** and **3a** were prepared in solution. The reactions were monitored by ^{205}Tl NMR spectroscopy. The solid compound $[(NC)_5Pt-Tl(DMSO)_4](DMSO)$ was obtained as described previously.[4a] Two different routes were used to prepare compounds **2b** and **3b**: i) 49 mg of $[Tl(DMSO)_6](ClO_4)_3$ (0.05 mmol), 19 mg of $K_2Pt(CN)_4$ (0.05 mmol), and 9 mg or 18 mg of 1,10-phenanthroline (0.05 mmol or 0.1 mmol) for **2b** and **3b**, respectively, were added to 1 mL of DMSO in the presence of 50 mM NaCN. After stirring the

solutions for 5 h, compounds **2b** and **3b** formed in solution (see Scheme 1). ii) 46 mg (0.05 mmol) of solid $[(NC)_5Pt-Tl(DMSO)_4](DMSO)$ was dissolved in 1 mL of DMSO, then 11 mg (0.06 mmol) of 1,10-phenanthroline was added for compound **2b** and 20 mg (0.1 mmol) for compound **3b**. After stirring for half an hour, compounds **2b** and **3b** formed in solution. Crystals containing **2b** and **3b** suitable for X-ray analysis were crystallised by putting the resulting solutions inside a dark vacuum desiccator and slowly evaporating the solvent by degassing. Small round transparent white crystals formed at the bottom of the flask after several days. Raman spectra of the solid compounds **2b** and **3b** were recorded with a Renishaw System 1000 spectrometer equipped with a microscope (Leica DMLM). The abbreviations are: vs = very strong, s = strong, m = medium, w = weak. The band positions and assignments are as follows. **2b:** $\tilde{\nu}$ = 2995 m, 2915 s (CH_3 str.), 2184 s (axial C≡N str.), 2174 m, 2161 m (equatorial C≡N str.), 1206 w, 1102 m, 1002 m, 952 m (CH_3 bend), 712 s, 672 vs (CS str.), 452 s (TlO str.), 378 m, 308 m (CSC or OSC bend), 177 vs (Pt−Tl str.). $\tilde{\nu}$ (of coordinated phen) = 1621 w, 1603 w, 1588 w, 1516 m, 1446 m, 1412 vs, 1341 w, 1311 m, 1255 w, 1206 w, 1052 m, 862 w, 727 m, 552 s, 452 s 422 s, 402 m, 332 s 282 m, 257 w.

3b: $\tilde{\nu}$ = 2189 s (axial C≡N str.), 2178 m, 2160 m (equatorial C≡N str.), 172 vs (Pt−Tl str.). $\tilde{\nu}$ (of coordinated phen) = 1626 w, 1604 w, 1590 w, 1521 w, 1455 s, 1417 vs, 1344 w, 1306 s, 1252 w, 1207 w, 1139 w, 1103 m, 1060 m, 867 m, 728 s, 558 s, 463 s, 423 vs, 408 m, 332 s, 288 s, 261 m (for free phen: 1585 m, 1499 m, 1444 s, 1402 vs, 1341 m, 1291 s, 1094 m, 1032 s, 707 vs, 407 s, 242 m).

4: Colourless cubic crystals of compound **4** were obtained from a DMSO solution with the following composition: 50 mM $Tl(ClO_4)_3$, 100 mM 1,10-phenanthroline, and 200 mM Cl^- by slowly evaporating the solvent. Raman vibration bands of solid compound **4:** $\tilde{\nu}$ (of coordinated phen) = 1623 w, 1601 w, 1581 w, 1514 w, 1448 s, 1418 vs, 1336 w, 1306 s, 1248 w, 1198 w, 1144 w, 1102 m, 1052 m, 857 w, 726 s, 554 s, 437 s, 420 vs, 402 m, 280 m, 268 s. $\tilde{\nu}$ (of ClO_4^-) = 929 s.

^{205}Tl NMR Measurements: All ^{205}Tl NMR measurements were performed with a Bruker DMX500 spectrometer at a probe temperature of 25 (±0.5) °C. DMSO was used as solvent. The spectra were recorded at SF = 288.5 MHz; typical NMR parameters: flip angle about 30°; spectral window 86 kHz; pulse repetition time 0.5 s. The chemical shifts are reported in ppm toward higher frequency with respect to an external aqueous solution of $TlClO_4$ extrapolated to infinite dilution.

X-ray Crystal Structure Analysis: Suitable crystals of **2b**, **3b**, and **4** were selected under a polarizing microscope and mounted on a glass fibre. The data were collected with a Nonius Kappa CCD area detector, λ(Mo-K_α) = 0.71073 Å, using a graphite monochromator. Numerical absorption correction was applied.[15] The structures were solved by direct methods[16] and refined using full-matrix least squares on F^2 (SHELXL-97).[17] All the non-hydrogen atoms in compounds **2b**, **3b**, and **4** were refined with anisotropic displacement parameters. Hydrogen atoms were located at calculated positions and refined riding on their carrier atoms. In **3b**, one of the three non-coordinated DMSO molecules is disordered. Selected crystal data for compounds **2b**, **3b**, and **4** are listed in Table 1. CCDC-157362 (**2b**), -157363 (**3b**) and -157364 (**4**) contain the supplementary crystallographic data for this paper. These data can be obtained free of charge at www.ccdc.cam.ac.uk/conts/retrieving.html or from the Cambridge Crystallographic Data Centre, 12, Union Road, Cambridge CB2 1EZ, UK [Fax: (internat.) + 44-1223/336-033; E-mail: deposit@ccdc.cam.ac.uk].

Table 1. Selected crystal data for $[(NC)_5Pt-Tl(phen)(DMSO)_3]\cdot(DMSO)$ (**2b**), $[(NC)_5Pt-Tl(phen)_2]\cdot(DMSO)_3$ (**3b**), and $[Tl(phen)_2Cl_2](ClO_4)$ (**4**)

	2b	**3b**	**4**
Empirical formula	$C_{25}H_{32}N_7O_4S_4PtTl$	$C_{35}H_{34}N_9O_3S_3PtTl$	$C_{24}H_{16}Cl_3O_4N_4Tl$
Formula mass	1022.30	1124.38	735.16
Crystal system	monoclinic	monoclinic	triclinic
Space group	$P2_1/n$	$P2_1/c$	$P\bar{1}$
a [Å]	10.9206(2)	14.66400(10)	7.17280(10)
b [Å]	17.1743(3)	24.7240(3)	12.7524(2)
c [Å]	18.4541(3)	11.6700(2)	13.9575(16)
α [°]			107.1145(7)
β [°]	98.8160(6)	106.6090(4)	99.9867(7)
γ [°]			91.3280(19)
V [Å^3]	3420.20(10)	4054.46(9)	1197.94(3)
Z	4	4	2
Crystal size [mm]	0.12 × 0.25 × 0.29	0.13 × 0.12 × 0.26	0.13 × 0.13 × 0.25
$\rho_{calcd.}$ [g cm^{-3}]	1.728(1)	2.226(5)	2.936(5)
Temperature [K]	298(2)	298(2)	298(2)
μ (Mo-K_α) [mm^{-1}]	8.945	11.189	8.67
F(000)	1776	2520	981
θ range [°]	0.985−27.47	0.991−28.29	0.990−30.04
Limiting indices	$0 \le h \le 14$	$0 \le h \le 19$	$-8 \le h \le 10$
	$0 \le k \le 22$	$-32 \le k \le 32$	$-15 \le k \le 17$
	$-23 \le l \le 23$	$-15 \le l \le 14$	$-19 \le l \le 18$
N_{obs}, N_{par}	6849, 379	9992, 424	6938, 326
S (goodness of fit)	1.107	1.032	1.063
R_1,wR_2 [$I > 2\sigma(I)$][a]	0.0341, 0.0826	0.0569, 0.1311	0.0272, 0.0705
$\Delta\rho_{max}$, $\Delta\rho_{min.}$ [e/Å^3]	1.236, −1.489	1.192, −1.631	1.559, −1.468

[a] R values are defined as: $R(\text{int}) = \Sigma|F_o^2 - F_o^2(\text{mean})|/\Sigma[F_o^2]$, $S = \{\Sigma[w(F_o^2 - F_c^2)^2]/(n-p)\}^{1/2}$. $R_1 = \Sigma||F_o| - |F_c||/\Sigma|F_o|$, $wR_2 = \{\Sigma[w(F_o^2 - F_c^2)^2]/\Sigma[w(F_o^2)^2]\}^{1/2}$, $w = 1/[\sigma^2 F_o^2 + (ap)^2 + bp]$, $p = (1/3)\max(0,F_o^2) + (2/3)F_o^2$.

Supporting Information: See footnote on the first page of this article. Table of NMR parameters for Pt−Tl compounds and related platinum and thallium species in solution.

Acknowledgments

The authors are grateful to The Swedish Natural Science Research Council (NFR) for providing funds for purchasing the diffractometer and for the continuous financial support for the project. The Swedish Institute fellowship for the stay of G.-B. M. in Stockholm is gratefully acknowledged.

[1] [1a] T. Yamaguchi, F. Yamazaki, T. Ito, *J. Am. Chem. Soc.* **1999**, *121*, 7405−7406. (and references therein). [1b] J. K. Nagle, A. L. Balch, M. M. Olmstead, *J. Am. Chem. Soc.* **1988**, *110*, 319−321.

[2] [2a] O. Ezomo, M. P. Mingos, I. D. Williams, *J. Chem. Soc., Chem. Commun.* **1987**, 924−925. [2b] L.-J. Hao, J. J. Vittal, R. J. Puddephatt, *Inorg. Chem.* **1996**, *35*, 269−270. [2c] L.-J. Hao, J. Xiao, J. J. Vittal, R. J. Puddephatt, L. Manojlovic-Muir, K. W. Muir, A. A. Torabi, *Inorg. Chem.* **1996**, *35*, 658−666. [2d] L.-J. Hao, J. J. Vittal, R. J. Puddephatt, *Organometallics* **1996**, *15*, 3115. [2e] R. Uson, J. Fornies, M. Tomas, R. Garde, P. Alonso, *J. Am. Chem. Soc.* **1995**, *117*, 1837−1838. [2f] A. Balch, S. Rowley, *J. Am. Chem. Soc.* **1990**, *112*, 6139−6140. [2g] O. Renn, B. Lippert, *Inorg. Chim. Acta* **1993**, *208*, 219−223. [2h] I. Ara, J. R. Berenguer, J. Fornies, J. Gomez, E. Lalinde, R. I. Merino, *Inorg. Chem.* **1997**, *36*, 6461−6464. [2i] R. Uson, J. Fornius, M. Tomas, R. Garde, *Inorg. Chem.* **1997**, *36*, 1383−1387. [2j] V. J. Catalano, B. L. Bennett, S. Muratidis, B. C. Noll, *J. Am. Chem. Soc.* **2001**, *123*, 173, and references therein.

[3] [3a] K. E. Berg, J. Glaser, M. C. Read, I. Tóth, *J. Am. Chem. Soc.* **1995**, *117*, 7550. [3b] M. Maliarik, K. Berg, J. Glaser, M. Sandström, I. Tóth, *Inorg. Chem.* **1998**, *37*, 2910. [3c] M. Maliarik, J. Glaser, I. Tóth, M. W. da Silva, L. Zekany, *Eur. J. Inorg. Chem.* **1998**, 565. [3d] J. Glaser, *Advances in Inorganic Chemistry*, Academic Press, Inc., London, **1995**, vol. 43.

[4] [4a] G.-B. Ma, M. Kritikos, J. Glaser, *Eur. J. Inorg. Chem.* **2001**, 1311. [4b] G.-B. Ma, M. Kritikos, M. Maliarik, J. Glaser, *Inorg. Chem*, submitted. [4c] Unpublished results from this laboratory.

[5] Md. K. Nazeeruddin, P. Liska, J. Moser, N. Vlachopoulos, M. Grätzel, *Helv. Chim. Acta* **1990**, *73*, 1788.

[6] [6a] F. Jalilehvand, J. Glaser, M. Maliarik, J. Mink, I. Persson, P. Persson, M. Sandström, I. Tóth, *Inorg. Chem.*, **2001**, *40*, 3889−3899. [6b] F. Jalilehvand, PhD Thesis, Royal Institute of Technology (KTH), Stockholm, Sweden, **2000**.

[7] [7a] P. Laszlo, *NMR of Newly Accessible Nuclei*, Academic Press, New York, **1983**, vol. 2. [7b] J. Mason, *Multinuclear NMR*, Plenum Press, New York, **1987**.

[8] Force constants in N/cm were calculated from $k = (5.889 \cdot 10^{-7}) \cdot \tilde{\nu}^2 \cdot \mu$, where $\tilde{\nu}$ is wavenumber in cm^{-1} and $\mu = M_{Pt} \cdot M_{Tl}/(M_{Pt} + M_{Tl})$, with atomic masses of the metals in Daltons.

[9] Recently completed calculations of the metal−metal stretching force constants in the complexes $[(NC)_5Pt-Tl(CN)_n]^{n-}$ (n = 0−3) show that in a full model, taking into account all vibrational modes (both metal−metal and metal−ligands), about 92% is attributed to purely diatomic Pt−Tl stretch (see ref.[6a]).

[10] [10a] F. A. Cotton, R. A. Walton, *Multiple Bonds Between Metal Atoms*, 2nd ed., Clarendon Press, Oxford, **1993**. [10b] D. F. Shriver, C. B. Cooper, *Vibrational Spectroscopy of Metal-Metal Bonded Transition Metal Compouunds*, Heyden, London, **1980**, vol. 6, pp. 127−157.

[11] G.-B. Ma, A. Molla-Abbassi, M. Kritikos, A. Ilyukhin, F. Jalilehvand, V. Kessler, M. Skripkin, M. Sandström, J. Glaser, J. Näslund, I. Persson, *Inorg. Chem.* **2001**, *40*, 6432−6438.

[12] W. J. Baxter, G. Gafner, *Inorg. Chem.* **1972**, *11*, 176−178.

[13] B. D. James, M. B. Millikan, M. F. Mackay, *Inorg. Chim. Acta* **1983**, *77*, L251.

[14] [14a] J. Blixt, J. Glaser, I. Persson, P. Mink, M. Sandström, *J. Am. Chem. Soc.* **1995**, *117*, 5089−5104. [14b] J. Glaser, *Acta Chem. Scand., Ser. A* **1982**, *36*, 451.

[15] W. Herrendorf, H. Bärnighausen, *HABITUS, A program for numerical absorption correction*, University of Karlsruhe, **1993**.

[16] G. M. Sheldrick, *Acta Crystallogr., Sect. A* **1990**, *46*, 467−473.

[17] G. M. Sheldrick, *SHELXL97 Program for the Refinement of Crystal Structures*, University of Göttingen, Germany, **1997**.

[18] M. N. Memering, L. H. Jones, J. C. Bailar, *Inorg. Chem.* **1973**, *12*, 2793.

[19] I. Bányai, J. Glaser, *J. Am. Chem. Soc.* **1989**, *111*, 3186.

[20] M. Buhl, M. HÅkansson, A. H. Mahmoudkhani, L. Öhrström, *Organometallics.* **2000**, *19*, 5589.

[21] M. C. Read, J. Glaser, M. Sandström, *J. Chem. Soc., Dalton Trans.* **1992**, 233.

[22] [22a] N. F. Ramsey, *Phys. Rev.* **1950**, *78*, 699. [22b] J. Mason, *Chem. Rev.* **1987**, *87*, 1299.

[23] [23a] J. Autschbach, T. J. Ziegler, *J. Am. Chem. Soc.* **2001**, *123*, 5320. [23b] N. Kaltsoyannis, *J. Chem. Soc., Dalton Trans.* **1997**, 1. [23c] M. R. Russo, N. Kaltsoyannis, *Inorg. Chim. Acta* **2001**, *312*, 221−225.

[24] R. Restivo, G. J. Palenik, *J. Chem. Soc., Chem. Commun.* **1969**, 867.

Received July 2, 2001
[I01245]

Bis(η-*tert*-butylcyclopentadienyl)hydridoniobium Ditelluride, a Convenient Reagent for the Synthesis of Polynuclear Metal Telluride Complexes

Henri Brunner,[a] Helene Cattey,[b] David Evrard,[b] Marek M. Kubicki,[b] Yves Mugnier,[b] Estelle Vigier,[b] Joachim Wachter,*[a] Robert Wanninger,[a] and Manfred Zabel[a]

Keywords: Niobium / Tellurium / Polynuclear complexes / Cyclopentadienyl complexes / Electrochemistry

Reaction of $[Cp'_2NbH_3]$ ($Cp' = tBuC_5H_4$) with Te powder in THF gives $[Cp'_2Nb(Te_2)H]$ (**1**) and $[Cp'_6Nb_4Te_4O]$ (**2**). The yield of **1** varies between 10 and 81% depending on the degree of oxygen contamination of the reagents. Complexes **1** and **2** react with $[Cr(CO)_5THF]$ to give $[Cp'_2Nb(Te_2)H{\cdot}Cr(CO)_5]$ (**3**) and $[Cp'_6Nb_4Te_4O{\cdot}2Cr(CO)_5]$ (**4**), respectively. The crystal structures of **2**–**4** have been determined. In **3** a Te_2 unit and an H ligand are coordinated to a bent niobocene moiety; the $Cr(CO)_5$ group is attached to the lateral Te atom. The molecular cores of **2** and **4** are practically identical in that they contain two planar Nb_2Te_2 rings connected by a nearly linear oxygen bridge. Each of the "outer" Nb atoms bears two Cp′ ligands, whereas the "inner" Nb atom only has one such ligand. An additional structural feature in **4** is two $Cr(CO)_5$ groups, attached to one Te bridge of each Nb_2Te_2 ring. Thermolysis of **3** leads to the formation of diamagnetic $[Cp'_4Nb_2Te_2]$ (**5**), which also contains a planar Nb_2Te_2 core. The relatively long transannular Nb–Nb distance (3.647 Å) is consistent, according to DFT calculations, with a through-space Nb–Nb coupling. Complex **5** reacts with CH_3I with successive methylation of both Te bridges to give $[Cp'_4Nb_2Te(CH_3Te)]I$ (**[6]I**) and $[Cp'_4Nb_2(CH_3Te)_2]I_2$ (**[7]I_2**). The crystal structure of **[7]I_2** may be derived from that of **5**, the incoming CH_3 groups being fixed at the Te bridges in a *trans* position. ^1H NMR spectroscopic investigations reveal a restricted rotation around the Cp′–Nb bonds in **2** and **5** at –90 °C and in **4** and **[7]I_2** at ambient temperature. Electrochemical studies have been carried out on **5**, **[6]I**, and **[7]I_2**, showing that all compounds undergo two reversible one-electron reduction steps. The reduction potential decreases by ca. 1.6 V when going from **5** to **[7]I_2**. There is also a clear linear correlation between the reduction potentials measured for **5** to **[7]I_2** and the energies of the corresponding LUMO's calculated at the DFT/B3LYP level. These LUMO's bear some 70% contribution from both Nb atoms and, consequently, the reduction processes mainly operate at both metallic centers.

(© Wiley-VCH Verlag GmbH, 69451 Weinheim, Germany, 2002)

Introduction

Group 4 and 5 metallocene derivatives of the heavier chalcogens Se and Te are an attractive target for reactivity studies.[1−3] Recent examples include ligand rearrangements[4−6] and the stabilization of labile seleno- and telluroorganic ligands.[3,4] Niobocene or tantalocene dichalcogenides exist in the isomeric forms **A**−**C**, and depending on the nature of the cyclopentadienyl ligand (Cp) and the chalcogen X (X = Se or Te) the additional hydrogen is found in different bonding modes.[6] The only known example of isomer **A** is $[Cp^*_2Nb(\eta^2\text{-}Te_2H)]$ in which the Nb center bears electron-rich peralkylated C_5Me_5 (Cp^*) ligands along with a hydrogenditelluride ligand.[7] Its reactivity is characterized by an easy loss of Te^0 [7] or Te^{2-} [8−11] in the presence of reactive transition metal fragments, which finally leads to a series of homo- and heterometallic telluride clusters.

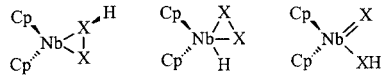

A **B** **C**

It has already been established that the formation of related niobocene sulfides strongly depends on the substituents at the Cp ligand.[12] Therefore, we decided to investigate the reaction of $[Cp'_2NbH_3]$ ($Cp' = tBuC_5H_4$) with tellurium. Our investigations show that the replacement of the electron-rich C_5Me_5 ligand by Cp′ exerts considerable influence on the electronic and steric parameters as well as on the subsequent formation of polynuclear metal telluride complexes.

Results and Discussion

Preparation and Characterization of Complexes 1−4

Reaction of $[Cp'_2NbH_3]$ with 2.5 equivalents of carefully degassed tellurium powder in freshly distilled THF at 40 °C

[a] Institut für Anorganische Chemie, Universität Regensburg, 93040 Regensburg, Germany
[b] Laboratoire de Synthèse et d'Electrosynthèse Organométalliques (UMR 5632), Université de Bourgogne, 21100 Dijon, France

gave dark orange $[Cp'_2Nb(Te_2)H]$ (**1**) in 81% yield. However, in the presence of traces of air complex **1** was obtained in yields of between 10 and 32% and red-violet $[Cp'_6Nb_4Te_4O]$ (**2**) formed in yields from 9−53% as an additional product (Scheme 1). Similar results were obtained in toluene at 80 °C. Solutions of **1** are very sensitive towards air and even the solid decomposes slowly when stored at −20 °C. In boiling toluene **1** slowly converts into **2**. In a typical example 18% of **2** was formed after 24 h. This behavior is in contrast with that of the structurally related $[Cp^*_2Ta(Te_2)H]$, which transforms into $[Cp^*_2Ta(=Te)H]$ under similar conditions.[4]

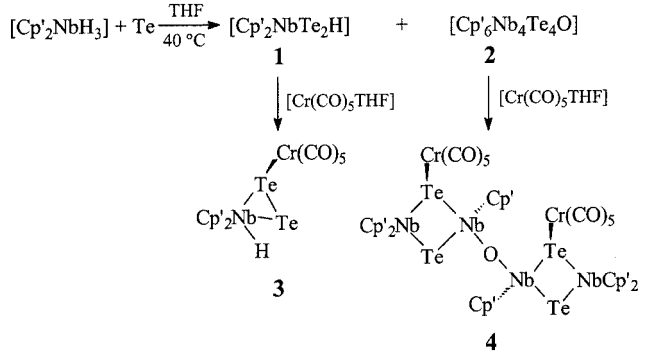

Scheme 1

The composition of complexes **1** and **2** was determined from FD mass spectra and confirmed by elemental analyses. The latter, however, gives good results only for **2** as the values obtained for **1** are always a little bit too low. Correct analytical data have been obtained for the $Cr(CO)_5$ adduct **3** (see below), which has successfully been subjected to an X-ray crystallographic investigation.

The ^1H NMR spectrum of **1** at room temperature as well as at −90 °C shows four multiplets of equal intensities for the aromatic protons and one singlet at $\delta = 1.39$ for the *t*Bu groups. An additional signal at $\delta = -3.50$ is observed with $^2J(H\text{-}^{125}Te) = 86.7$ Hz. One Te resonance was found by means of $^1H\text{-}^{125}Te$ polarization transfer techniques and this was confirmed in the ^{125}Te NMR spectrum, which revealed only one broad resonance ($h_{1/2} \approx 300$ Hz) at $\delta = -749.4$. The second resonance cannot be detected, probably due to partially relaxed scalar $^{125}Te\text{-}^{93}Nb$ interactions. Unfortunately, similar problems prevented the observation of ^{125}Te NMR spectra for the other compounds. An X-ray diffraction analysis carried out on $[Cp'_2Nb(Te_2)H{\cdot}Cr(CO)_5]$ (**3**) (see below) provides evidence for the presence of a $\mu,\eta^{1:2}\text{-}Te_2$ ligand. Localization of a hydride directly bonded to the Nb center and lying in the $NbTe_2$ plane allows for the determination of **3**, and very likely **1**, from the structural form **B**. Structural analogs of **1** are $[Cp^*_2Ta(Te_2)H]$,[4] $[Cp'_2Ta(S_2)H]$,[13] and $[Cp^*_2Nb(S_2)H]$.[12a] There is no evidence for the existence of any other isomeric form.

An X-ray diffraction analysis of a single crystal of **2** shows two planar Nb_2Te_2 rings (Figure 1) connected by an oxygen bridge. Each of the "outer" Nb atoms [Nb(1), Nb(4)] bears two Cp′ ligands, whereas the coordination sphere of the "inner" Nb atoms [Nb(2), Nb(3)] is completed by only one Cp′ ligand, thus forming two $Cp'_3Nb_2Te_2$ units. The linearity of the Nb−O−Nb bridge [angle (Nb−O−Nb) = 177.1(1)°] evokes a contribution of p_π oxygen orbitals as has been suggested for other linearly O-bridged bimetallic complexes.[14] The fact that the observed Nb−O distances [mean 1.909(2) Å] are longer than Nb=O bonds in oxoniobocene complexes (1.63−1.741 Å)[15] is not in contradiction with the above argument.[14] Within the Nb_2Te_2 rings there are two different Nb−Te distances. The Nb−Te bonds around Nb(2) and Nb(3) are shorter than the bonds around Nb(1) and Nb(4), by 0.18 Å (Table 1). They are also slightly shorter than typical Nb−Te single bonds.[16] Striking differences are found for the Te−Nb−Te angles, they range from 96.4(1)° [Te(3)−Nb(4)−Te(4)] to 107.1(1)° [Te(1)−Nb(2)−Te(2)], thus reflecting the different coordination spheres around both niobium centers. A similar structure has been found in $[Cp'_6V_4S_4O]$.[17]

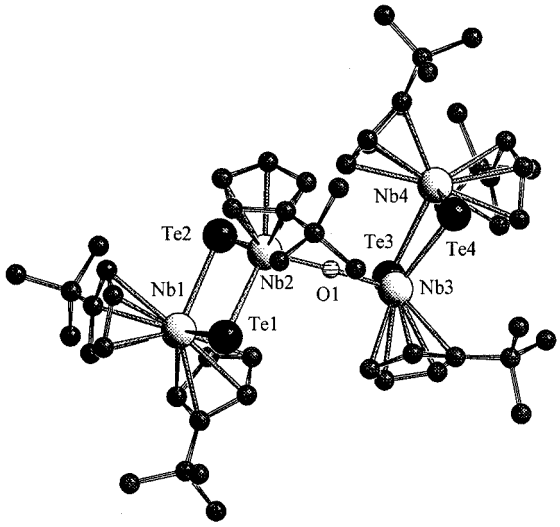

Figure 1. Molecular structure of $[Cp'_6Nb_4Te_4O]$ (**2**) (Schakal)

The diamagnetic nature of the molecule is deduced from its ^1H NMR spectrum (see below) and it may be explained by the presence of direct Nb−Nb interactions: Whereas the Te−Te distances (4.236 Å) approximately correspond to the sum of the van der Waals radii[18] the Nb−Nb distances (3.43 Å) are only slightly longer than those in $[(C_5H_5)_2Nb(\mu\text{-}S)]_2$ [*d*(Nb−Nb) 3.2340(8) Å][19] or in $[C_5H_5(C_5H_4)NbH]_2$ (3.105 Å),[20] for which Nb−Nb bonds have been postulated. The possibility of through-space Nb−Nb coupling in complexes containing Nb_2Te_2 rings has been investigated for compounds **5**, **[6]I**, and **[7]I_2** (see below).

The crystal structure of **2** also reveals that the bulky *t*Bu groups in the niobocene units "Nb(1)" and "Nb(4)" are oriented in a staggered conformation. The concerned $t\text{Bu}-Cp_{center}/t\text{Bu}-Cp'_{center}$ torsional angles are about 122°. Recently it has been shown that for bent group 4 metallocenes like $[(t\text{Bu}C_5H_4)_2ZrX_2]$ (X = halogen, alkyl, aryl), chiral ground-state geometries are able to epimerize upon rotation around the Cp′−metal bond.[21] The activation barrier for this rotation depends on the interaction of

Table 1. Selected distances [Å] and angles [°] for $[Cp'_6Nb_4Te_4O]$ (**2**) and $[Cp'_6Nb_4Te_4O{\cdot}2Cr(CO)_5]$ (**4**)

	2	**4**
Nb(1)−Te(1)	2.829(1)	2.809(1)
Nb(1)−Te(2)	2.809(1)	2.836(1)
Nb(2)−Te(1)	2.648(1)	2.632(1)
Nb(2)−Te(2)	2.641(1)	2.678(1)
Nb(2)−O(1)	1.914(2)	1.896(4)
Nb(3)−O(1)	1.904(2)	1.923(4)
Nb(3)−Te(3)	2.644(1)	2.633(1)
Nb(3)−Te(4)	2.642(1)	2.660(1)
Nb(4)−Te(3)	2.832(1)	2.821(1)
Nb(4)−Te(4)	2.829(1)	2.827(1)
Te(2)−Cr(1)		2.760(1)
Te(4)−Cr(2)		2.737(1)
Te(1)−Nb(1)−Te(2)	97.9(1)	98.7(1)
Te(1)−Nb(2)−Te(2)	107.1(1)	107.4(1)
Te(3)−Nb(3)−Te(4)	105.9(1)	105.9(1)
Te(3)−Nb(4)−Te(4)	96.4(1)	96.8(1)
Te(1)−Nb(2)−O(1)	106.4(1)	104.5(1)
Te(2)−Nb(2)−O(1)	100.7(1)	99.6(1)
Te(3)−Nb(3)−O(1)	104.0(1)	102.4(1)
Te(4)−Nb(3)−O(1)	102.4(1)	99.4(1)
Nb(2)−O(1)−Nb(3)	177.2(1)	175.9(2)
Cr(1)−Te(2)−Nb(2)		131.6(1)
Cr(1)−Te(2)−Nb(1)		128.8(1)
Cr(2)−Te(4)−Nb(3)		132.8(1)
Cr(2)−Te(4)−Nb(4)		130.3(1)
$C(1-5)_{center}$−Nb(1)−$C(10-14)_{center}$	134.2(1)	134.0(1)
$C(37-41)_{center}$−Nb(4)−$C(46-50)_{center}$	133.0(1)	133.1(1)

the Cp′-bonded substituent with the ligands X. In our case the ^{1}H NMR spectrum of **2** shows five signals of intensity 4:4:4:8:4 between δ = 4.18 and 5.75 for the C_5H_4 protons, at room temperature. Three singlets of equal intensities are observed for the six *t*Bu groups. Upon cooling to −90 °C the diastereotopic cyclopentadienyl protons split into several broad multiplets, while the *t*Bu groups give a set of not very well resolved signals (Figure 2). A much better resolution into distinct resonances is achieved in the sterically crowded $Cr(CO)_5$ adduct **4** (see below, Figure 2) even at room temperature.

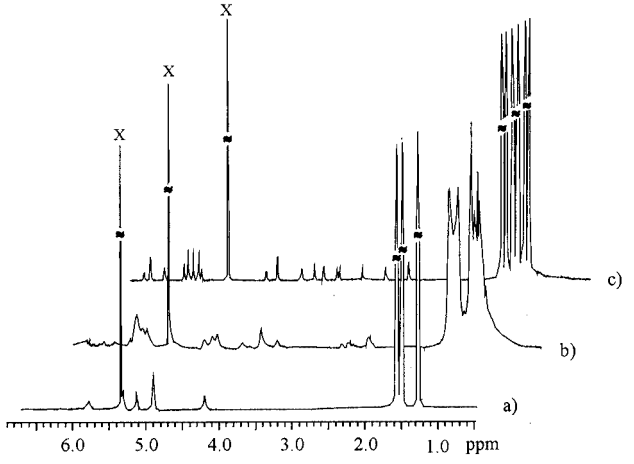

Figure 2. ^{1}H NMR spectra (*t*BuC_5H_4 signals) of **2** at 24 °C (a) and −90 °C (b), and of **4** at 24 °C (c) (X: CH_2Cl_2)

Reaction of $[Cp'_2NbTe_2H]$ with an excess of $[Cr(CO)_5THF]$ gave $[Cp'_2NbTe_2H{\cdot}Cr(CO)_5]$ (**3**) in 90% yield. An FD mass spectrum, elemental analysis and X-ray diffraction studies confirmed the composition of **3**. The IR spectrum of **3** contains absorptions at 2050, 1945, and 1895 cm^{-1} typical of the $Cr(CO)_5$ fragment, while the ν(Nb−H) frequency is too weak to be detected. The ^{1}H NMR spectrum in CD_2Cl_2 solution exhibits eight broad multiplets of equal intensity between δ = 4.64 and 6.58 at room temperature, which then sharpen at −20 °C. The observed pattern agrees with the presence of nonequivalent Cp′ rings. However, the singlet at δ = 1.31, which is characteristic for the *t*Bu groups, does not split even at low temperatures. The Nb−H resonance at δ = −2.95 is only slightly affected by coordination of the $Cr(CO)_5$ fragment compared to that of **1** (δ = −3.50). The ^2J(H-Te) coupling has disappeared. As **3** is thermally labile in solution (see below) heating of the solution in order to simplify the spectrum was not tried.

A single crystal of **3** was obtained from toluene/pentane (1:1) and studied by X-ray diffraction analysis. A bent metallocene structure with nearly eclipsed *t*Bu substituents is observed as the main structural feature (Figure 3). The Nb atom bears a Te_2 unit and an H atom both located in the plane bisecting the niobocene moiety. The Nb-coordinated hydride follows directly from the difference Fourier synthesis after refinement of all the other atoms. Thus, complex **3** is one of the few structurally characterized complexes containing a $\mu,\eta^{1:2}$-Te_2 ligand. Consequently, the structural type **B** may be assumed for precursor **1**. The Te−Te distance of 2.695(1) Å is similar to those in complexes containing side-on coordinated η^2-Te_2.[22] The coordination of the $Cr(CO)_5$ fragment at Te(2) may be responsible for two slightly different Nb−Te bonds, which are in turn in the

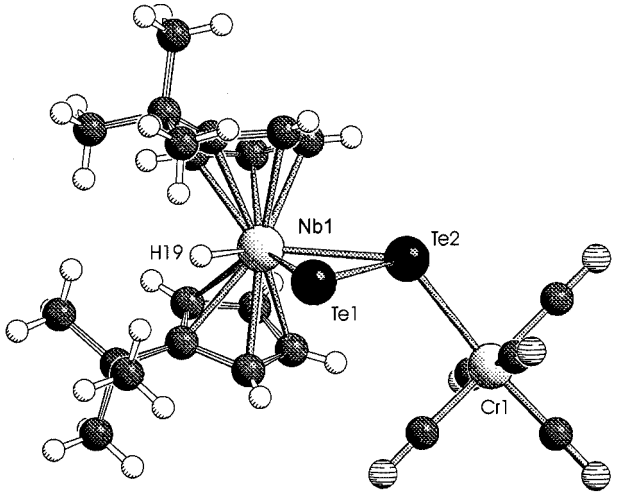

Figure 3. Molecular structure of $[Cp'_2NbTe_2H{\cdot}Cr(CO)_5]$ (**3**) (Schakal); selected distances [Å] and angles [°]: Te(1)−Te(2) 2.695(1), Te(1)−Nb(1) 2.846(1), Te(2)−Nb(1) 2.950(1), Te(2)−Cr(1) 2.712(1), Nb(1)−H(19) 1.60(5); Te(1)−Te(2)−Nb(1) 60.3(1), Te(2)−Te(1)−Nb(1) 64.3(1), Te(1)−Te(2)−Cr(1) 113.3(1), Nb(1)−Te(2)−Cr(1) 128.1(1), Te(1)−Nb(1)−H(19) 68.2(2), $C(1-5)_{center}$−Nb−$C(10-14)_{center}$ 134.1(1)

same range as Nb−Te single bonds (see complex **2**). The Te(2)−Cr distance is similar to those in other molecular chromium tellurides.[23]

The solid state structure of **2** has shown the niobocene components to be rather space filling. Therefore it was of interest to see whether the Te bridges were still sufficiently accessible for the addition of bulky Lewis acid complex fragments such as $[Cr(CO)_5]$. Indeed, reaction of THF solutions of **2** with excess $[Cr(CO)_5THF]$ gave $[Cp'_6Nb_4Te_4O{\cdot}2Cr(CO)_5]$ (**4**). Its composition follows from elemental analyses and X-ray crystallography, whereas FD mass spectra only showed the mass peak of the precursor complex **2**. The IR spectrum of **4** exhibits a CO absorption pattern typical for coordinated $Cr(CO)_5$ fragments. The ^1H NMR spectrum of **4** (Figure 2) shows six singlets for the *t*Bu groups between $\delta = 1.24$ and 1.59 and 18 multiplets for the C_5H_4 hydrogens between $\delta = 2.89$ and 6.50 at room temperature, as would be expected from the solid state structure. This result indicates that coordination of the $Cr(CO)_5$ groups gives rise to restricted rotation around the Cp′−Nb bonds in **4** at room temperature, whereas in the precursor complex **2** cooling to −90 °C is required in order to distinguish between the diastereotopic ring protons.

A crystallographic study shows **4** to possess the same structural framework as its precursor **2**. In addition, one Te bridge of each of the two four-membered Nb_2Te_2 rings bears a $Cr(CO)_5$ group (Figure 4). Upon comparing the bonding parameters of **2** and **4** (Table 1) it is evident that coordination of the $Cr(CO)_5$ fragments does not cause significant differences within the inorganic core of both molecules. Differences may only be noted for the conformations of the *t*Bu groups of the niobocene units "Nb(2)" and "Nb(4)" with respect to those of the Cp′ ligands attached at Nb(1) and Nb(3). Steric reasons may be responsible for the coordination of only two $Cr(CO)_5$ fragments at **2**. The Cr−Te−Nb angles in the range of 130° along with the acute dihedral angles (34.4°) formed by the Cr−Te bonds and the Nb_2Te_2 planes are indicative of strong steric interactions in **4** between the $Cr(CO)_5$ groups and the Cp′ ligands.

Preparation, Characterization, and Methylation of $[Cp'_4Nb_2Te_2]$ (5)

In contrast to $[Cp^*_2Nb(Te_2H)]$, which easily eliminates Te^0 units upon reaction with $[Cr(CO)_5THF]$ affording *cyclo*-$Te_4[Cr(CO)_5]_4$,[7] **1** gives the $Cr(CO)_5$ adduct **3**, whose solutions are surprisingly stable at room temperature. However, one may expect a thermal lability of **3** similar to that observed for the isostructural sulfur homologues $[Cp'_2Ta(S_2)H{\cdot}Cr(CO)_5]$[24] and $[Cp^*_2Nb(S_2)H{\cdot}Cr(CO)_5]$.[25] Solutions of these compounds readily lose CO upon heating, forming the heterotrimetallic complexes $[(Cp'_2TaS_2)_2Cr]$ and $[(Cp^*_2NbS_2)_2Cr]$, respectively.[8,9]

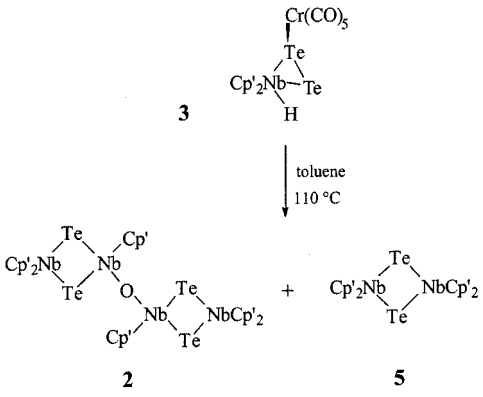

(1)

A solution of $[Cp'_2Nb(Te_2)H{\cdot}Cr(CO)_5]$ (**3**) in toluene gave green-black $[Cp'_4Nb_2Te_2]$ (**5**) upon heating, along with small amounts of **2** [Equation (1)]. Complex **5** has been obtained in still better yield from the reaction of **1** with $[Cr(CO)_6]$ in refluxing toluene.[25] The analytical and spectroscopic data of **5** are in agreement with the independently synthesized compound, the solid state structure of which has been described briefly. In this study direct bonding interactions between opposite atoms of the Nb_2Te_2 core were excluded.[25] The central feature of the structure is two niobocene units held together by two Te bridges, thus forming a planar Nb_2Te_2 core (Figure 5). As in compounds **2** and **4** the niobocene units are chiral, but the conformation found in the crystal structure of **5** corresponds to the achiral *meso* form. Although C_{2h} symmetry has been found in

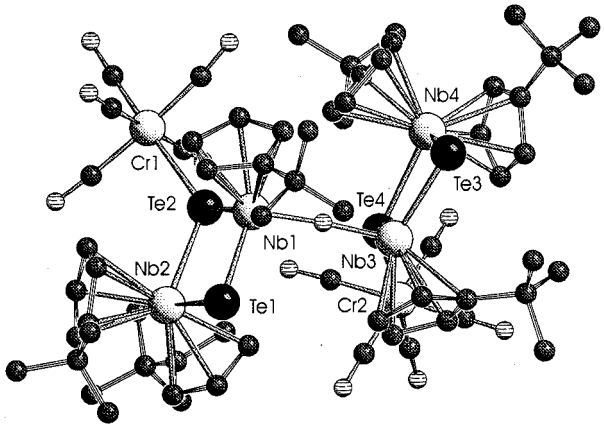

Figure 4. Molecular structure of $[Cp'_6Nb_4Te_4O{\cdot}2Cr(CO)_5]$ (**4**)

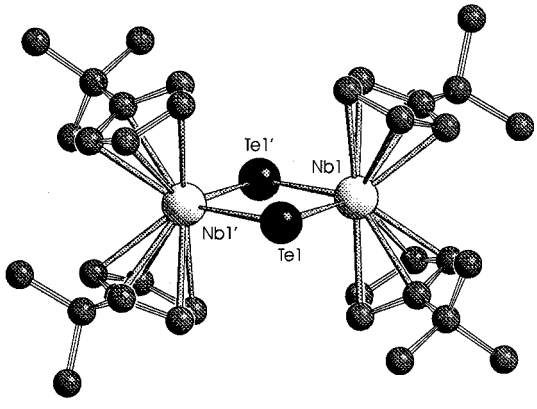

Figure 5. Molecular structure of $[Cp'_4Nb_2Te_2]$ (**5**)[25]

the related complex $[Cp'_4Zr_2Te_2]$ as well, in this complex the ^1H NMR spectra could not provide evidence for a restricted rotation around the Cp′−Zr axis.[21] In our case, examination of CD_2Cl_2 solutions reveals two signals for the C_5H_4 protons and one resonance for the *t*Bu group at ambient temperature, with splitting of the aromatic resonances into four multiplets at δ = 3.24, 4.79, 5.47, and 5.61 upon cooling to −90 °C. As expected the *t*Bu resonance remains unaffected.

Of particular interest is an analysis of the bonding system within the four-membered Nb_2Te_2 ring. In complex **5** each Nb center is surrounded by two Cp′ anions and two Te^{2-} bridges. A bonding interaction between opposite atoms Te(1) and Te(1′) [*d* = 4.262(1) Å] was excluded[25] in agreement with literature values given for planar M_2Te_2 rings: Whereas in the Ni_2Te_2 cycle of $[(iPr_4C_5H)_2Ni_2(\mu\text{-}Te)_2]$ the observed Te···Te distance of 3.052(5) Å has been ascribed to a bond order of nearly one,[26] a clearly nonbonding situation has been found in $[Cp'_4Zr_2Te_2]$ [*d*(Te···Te) = 4.006(1) Å].[21] Less evident is the interpretation of the Nb(1)···Nb(1′) distance in **5**. The found value of 3.647(1) Å is about 0.22 Å longer than that in compounds **2** and **4**. As a possibility to explain the observed diamagnetism of the molecule a through-space metal−metal coupling of both $Nb(d^1)$ centers was suggested[25] as has been recently established in the isoelectronic $[(C_5H_5)_4Zr_2(\mu\text{-}I)_2]$.[27] This direct Nb−Nb interaction has now been confirmed by DFT calculations (see below).

In order to get a better insight into the bonding system and the reactivity of **5** we decided to study methylation reactions and to carry out electrochemical studies on **5** and the reaction products. The methylation of μ_2-Te bridges in organometallic complexes has been reported recently.[28]

Green-black solutions of **5** in THF reacted with CH_3I with the formation of violet precipitates. These contain $[Cp'_4Nb_2Te(CH_3Te)]I$ ([**6**]**I**) or $[Cp'_4Nb_2(CH_3Te)_2]I_2$ ([**7**]$\mathbf{I_2}$) in quantitative yields depending on the employed stoichiometry (one or two equivalents of CH_3I). The composition of both compounds was confirmed by positive FAB mass spectra, which exhibit the peaks for the corresponding cations $[Cp'_4Nb_2Te(CH_3Te)]^+$ ([**6**]$^+$) and $[Cp'_4Nb_2(CH_3Te)_2]^{2+}$ ([**7**]$^{2+}$). The elemental analysis was close to the calculated value for [**6**]**I** and correct for [**7**]$\mathbf{I_2}$. The violet solution of [**7**]$\mathbf{I_2}$ in methanol was transformed into a dark blue precipitate in nearly quantitative yield upon addition of an aqueous solution containing two equivalents of NH_4PF_6. The composition $[Cp'_4Nb_2(CH_3Te)_2][PF_6]_2$ (**8**) roughly follows from the elemental analysis. The IR spectrum of **8** exhibits the typical absorption of the PF_6^- anion at 835 cm^{-1}. Complex **8** is poorly soluble in common solvents, thus preventing further spectroscopic investigations or recrystallization.

The ^1H NMR spectrum of [**6**]**I** (in CD_2Cl_2) shows one sharp singlet for the *t*Bu groups at δ = 1.53 and six multiplets between δ = 4.32 and 5.53 for the aromatic hydrogens. A singlet at δ = 2.45 was assigned to the μ-CH_3Te ligand. The ^1H NMR spectrum of [**7**]$\mathbf{I_2}$ (in CD_3OD) exhibits one slightly broadened singlet and two sharp singlets (intensity ratio 2:1:1) for the *t*Bu groups and eleven multiplets of different intensities between δ = 3.38 and 6.60 for the aromatic hydrogens. One sharp and one slightly broadened singlet at δ = 2.88 and 2.71, respectively, were tentatively assigned to the μ-CH_3Te ligands. From the solid state structure, which exhibits C_{2h} symmetry (see below), one might expect four equivalent Cp′ rings, i.e. one *t*Bu signal and four multiplets for the aromatic protons, provided the conformative flexibility of the Cp′ rings is blocked in solution.

The crystal structure of [**7**]$\mathbf{I_2}$ may be derived from its precursor $[Cp'_4Nb_2Te_2]$ (**5**). It contains a planar four-membered Nb_2Te_2 ring with four attached Cp′ ligands and two methyl groups, which are fixed at the Te bridges in a *trans* position (Figure 6). This arrangement, along with that of the *t*Bu groups in both niobocene units, gives rise to C_{2h} symmetry. The nonbonding Te(1)···Te(1′) distance (4.35 Å) and the angles at the Te bridges indicate that addition of electrophiles like CH_3^+ to **5** does not enhance attractive intraannular forces between the chalcogen atoms. Consequently, the positive charges may be localized at the Nb centers.

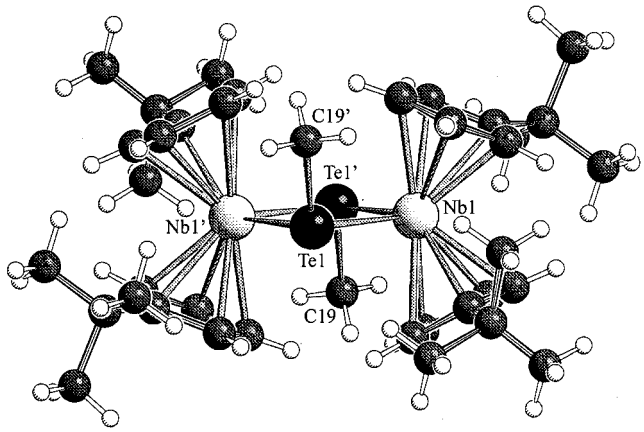

Figure 6. Molecular structure of $[Cp'_4Nb_2(CH_3Te)_2]^{2+}$ in [**7**]$\mathbf{I_2}$; selected distances [Å] and angles [°]: Nb(1)−Te(1) 2.838(3), Nb(1′)−Te(1) 2.876(4), Te(1)···Te(1′) 4.349(13), Nb(1)···Nb(1′) 3.707(9), Te(1)−C(19) 2.17(3); Nb(1)−Te(1)−Nb(1′) 80.9(1), Te(1)−Nb(1)−Te(1′) 99.1(1), Nb(1)−Te(1)−C(19′) 113.4(8), Nb(1′)−Te(1)−C(19′) 115.4(11), $C(1-5)_{center}$−Nb(1)−$C(10-14)_{center}$ 132.0(1)

The conformation found in the solid state may be caused by steric constraints, since the contacts between the $tBuC_5H_4$ hydrogens and the CH_3Te groups [*d*(H···H) ≥ 1.87 Å] are rather close. However, from the ^1H NMR spectra the presence of a further stereoisomer in solution with two nonequivalent Cp′ rings is evident. A further possibility would be an isomer with a *cis* arrangement of the CH_3Te ligands, the niobocene units being arranged as in the achiral *meso* form. Unfortunately, it was not possible to check this by dissolving separated crystals at low temperatures in order to carry out low temperature NMR investigations. However, there are some arguments supporting our hypotheses: a) Replacement of both CH_3 groups by the much bulkier $Cr(CO)_5$ groups leads to $[Cp'_4Nb_2Te_2{\cdot}2Cr(CO)_5]$ exclusively with C_{2h} symmetry. This follows from the room

temperature ^{1}H NMR spectrum, which exhibits only one singlet for the *t*Bu groups and four multiplets for the *t*BuC$_5$H$_4$ protons;[29] (b) electrochemical experiments carried out on **[7]I$_2$** (see below) confirm the homogeneity of the compound, so that a mixture of different compounds can be excluded.

Electrochemical Behavior of 5, [6]I, and [7]I$_2$

The electrochemical behavior of **5**, **[6]I**, and **[7]I$_2$** has been studied by cyclic voltammetry, rotating disk electrode (RDE) voltammetry, and electrolysis techniques. The voltammetric half-wave potentials are given in Table 2. For each compound, in the anodic area, reversible systems at +0.05 V (**5**) and +0.35 V (**[6]I**, **[7]I$_2$**) are observed, while the second oxidation steps at +0.59 V (**5**) and +0.80 V (**[6]I**, **[7]I$_2$**) are irreversible. The peaks at +0.35 and +0.80 V correspond to the oxidation of I^-.[30] The same oxidation peak potentials were obtained when Bu$_4$NI was used. In the cathodic part each complex exhibits two reversible one-electron systems in the potential range between −0.40 and −2.20 V (Figure 7). For these two reduction processes, the current ratio $i_{p,c}/i_{p,a}$ is equal to unity (or very close to it) for sweep rates v between 20 and 200 mV·s^{-1} and the peak current increases linearly with $v^{1/2}$. The half-wave potentials are independent of the potential scan rate and the peak shapes are characterized by $|E_{p,c} - E_{p,a}| \approx 60$ mV in agreement with a one-electron transfer controlled by diffusion.[31,32]

Table 2. $E_{1/2}$ values and HOMO and LUMO energies (eV) for complexes **5**, **[6]I** and **[7]I$_2$** (E values were determined with a carbon electrode vs. SCE; THF, 0.2 mol·L^{-1} Bu$_4$NPF$_6$)

	$E_{1/2\ ox2}$ [V]	$E_{1/2\ ox1}$ [V]	$E_{1/2\ red1}$ [V]	$E_{1/2\ red2}$ [V]	E_{HOMO}	E_{LUMO}
5	+0.59	+0.05	−1.83	−2.19	−4.427	−1.787
[6]I	+0.80	+0.35	−1.00	−1.34	−7.781	−5.615
[7]I$_2$	+0.80	+0.36	−0.39	−0.59	−11.414	−8.679

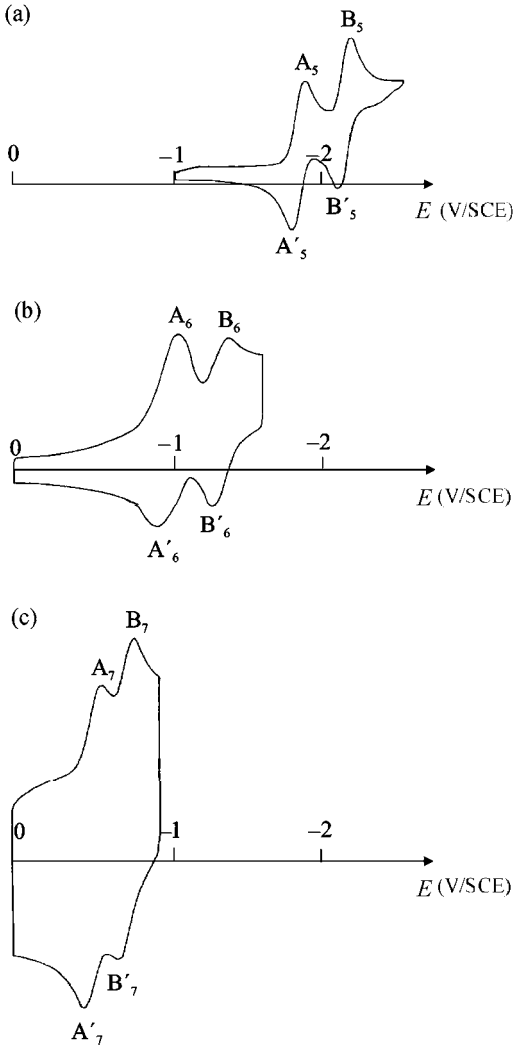

Figure 7. Cyclic voltammograms of complexes **5** (a), **[6]I** (b), and **[7]I$_2$** (c) in THF (0.2 mol·L^{-1} Bu$_4$NPF$_6$; initial potential 0 V, sweep rate 0.1 V·s^{-1})

The processes that take place during reduction of complex **5** are represented in Scheme 2a. The anionic species **[5]**$^-$ and **[5]**$^{2-}$ are relatively unstable on the electrolysis time scale and it was not possible to characterize them. In complex **[6]I**, two reversible waves are observed at −1.0 and −1.34 V, respectively. The corresponding reduction processes concern the cation **[6]**$^+$ as shown in Scheme 2b. It is interesting to note that after quantitative reduction of **[6]**$^+$ at the first reduction potential the two systems A_5/A_5' and B_5/B_5' are observed. This means that complex **5** has been reformed via quantitative CH_3 elimination. The two-electron reduction of **[6]**$^+$ leads to the very unstable monoanion **[6]**$^-$.

For complex **[7]I$_2$**, each reduction step is found by means of coulometry to correspond to a one-electron process [see (a) in Figure 8]. After reduction at −0.80 V (plateau of wave B_7), 2 F·mol^{-1} have been consumed and the color of the solution turns from opaque purple to translucent brown. The resulting species **7** (Scheme 2c) is stable even on the electrolysis time scale since no evolution of the RDE voltammogram waves (B'_7/A'_7) occurs [see (b) in Figure 8]. In order to get an ^{1}H NMR spectrum the solvent was evaporated from the electrolyzed solution and the residue extracted with toluene. Unfortunately, upon concentration the solution changed to violet. The slow evolution of **7** may also be observed in the UV spectrum.

By oxidation of solutions of **7** at −0.5 V (plateau of wave B'_7) the cation **[7]**$^+$ is obtained, which exhibits the reduction wave B_7 and the oxidation wave A'_7 [see (c) in Figure 8] as well as a ten-line ESR signal characteristic of a complex containing a paramagnetic niobium(IV) center ($a_{iso(Nb)}$ = 65 G; g_{iso} = 2.0400). The electrogenerated species **[7]**$^+$ is relatively unstable with respect to **7**, probably due to a slow partial evolution with release of CH_3, which would result in the formation of **[6]**$^+$.

We have also studied the reduction behavior of **5** in the presence of CH_3I. We have verified that **5** spontaneously

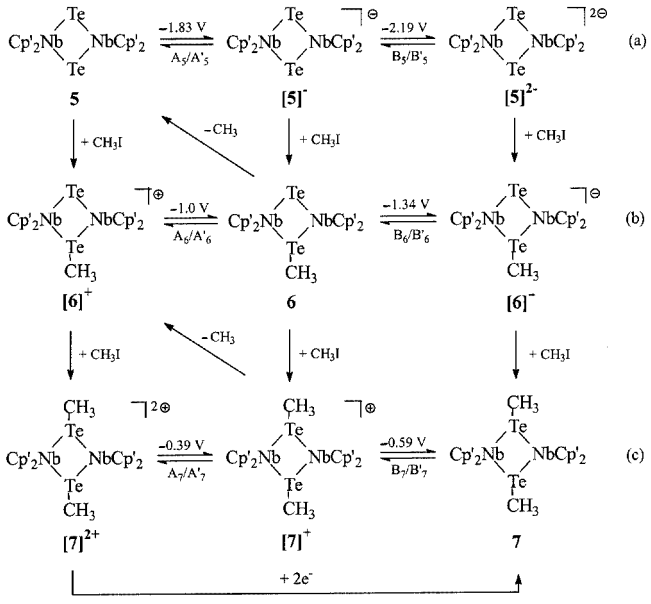

Scheme 2

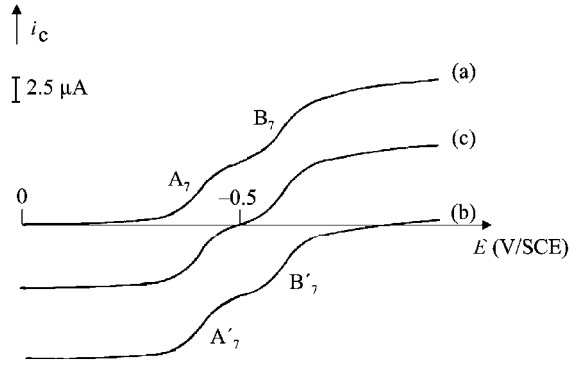

Figure 8. RDE voltammogram of [7]I_2 on carbon electrode in THF (0.2 mol·L^{-1} Bu_4NPF_6): (a) before electrolysis; (b) after 2 e^- reduction at −0.8 V; (c) after 1 e^- oxidation at −0.5 V

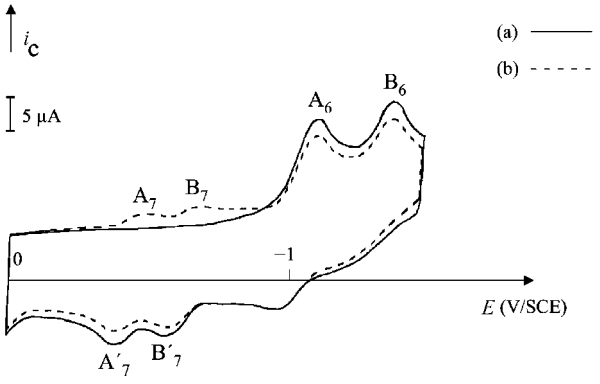

Figure 9. Cyclic voltammogram of **5** with CH_3I in THF (0.2 mol·L^{-1} Bu_4NPF_6): (a) first and (b) second sweeps. Initial potential 0 V, sweep rate 0.1 V·s^{-1}

gives $[6]^+$, for instead of the reduction peaks A_5/B_5 the peaks A_6/B_6 appear (Figure 9). When the potential sweep is reversed after B_6, two oxidation peaks A'_7 and B'_7 appear. This means that $[6]^-$ reacts quickly with CH_3I to give **7**. During the reverse sweep, peaks A_7 and B_7, characteristic of the dication $[7]^{2+}$, are observed.

The electrochemical results can be rationalized on the basis of a square scheme involving nine species. From one to the next species, one electron is exchanged horizontally (Scheme 2).

Theoretical Calculations

The bonding features of complexes **5**, $[6]^+$, and $[7]^{2+}$ have been investigated by DFT calculations. We have carried out geometry optimizations at the B3LYP/LANL2DZ level on models of these three complexes by introducing the unsubstituted C_5H_5 (Cp) ring instead of $tBuC_5H_4$ (Cp′). A full optimization yields a satisfactory agreement of calculated parameters with the experimental values for **5** and $[7]^{2+}$.[33] The most striking discrepancy has been found for the Nb−Nb distance in **5** [3.782 Å (Cp) vs. 3.647 Å (Cp′)]. The compositions and shapes of the HOMO and LUMO frontier orbitals are essentially the same for the three molecules studied. They are built of roughly a 35% contribution of 'd' atomic orbitals of each Nb atom and a 15% contribution of 'p' orbitals of each Te atom. The HOMO's exhibit a favorable Nb−Nb overlap and may be considered as metal−metal bonding orbitals while the LUMO's are the metal−metal antibonding ones. Their energies are included in Table 2. As an example, the shape of the LUMO for **5** is depicted in Figure 10.

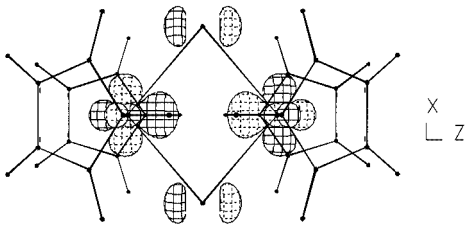

Figure 10. LUMO of **5**

The HOMO is concerned with the oxidation process, whereas the LUMO is used for reduction. As mentioned above, the oxidation waves for $[6]^+$ and $[7]^{2+}$ are probably covered by those of the I^-/I_2 system. However, the reduction potentials could be properly measured. There is a linear correlation between these reduction potentials for **5**, $[6]^+$, $[7]^{2+}$ and the calculated energies of the LUMO's of the corresponding model compounds (Table 2). Thus, the weak potential of −0.39 V is needed for reduction of $[7]^{2+}$, the LUMO of which is easily accessible for the incoming electron because of its low energy. Stronger potentials are necessary for reduction of $[6]^+$ and **5** because the energies of their LUMO's are higher. Assuming that a similar correlation (same slope) also holds for E_{HOMO} versus oxidation potential, the expected values for the first oxidation potentials should be close to 0.8 V for $[6]^+$ and 1.5 V for $[7]^{2+}$,with reference to 0.05 V, measured for **5**.

Conclusions

The reaction of $[Cp'_2NbH_3]$ with elemental tellurium gives $[Cp'_2Nb(Te_2)H]$ (**1**) in good yields. Complex **1** is a missing member of the class of group 5 dichalcogenido metallocene hydrides $[Cp_2M(X_2)H]$ (Cp = any cyclopentadienyl; M = Nb, Ta; X = S, Se, Te). In spite of some difficulties in obtaining complete analytical and spectroscopic data for **1** its structure may be deduced from the $Cr(CO)_5$ adduct **3**. Further support for the stabilization of the Nb(η^2-Te_2) moiety in the *t*Bu-niobocene part is also provided by the insertion of an $Fe_2(CO)_6$ unit into the Te−Te bond of **1**.[34] The fact that the bimetallic complex **3** gives the dinuclear, homometallic compound $[Cp'_4Nb_2Te_2]$ (**5**) under thermolytic conditions demonstrates the ability of **1** to eliminate Te. We have already shown that in the presence of suitable transition metal carbonyls **1** is a convenient Te transfer reagent for the synthesis of polymetallic metal telluride clusters.[25,35]

Experimental Section

General and Methods: All manipulations were performed with Schlenk techniques under N_2 or argon using dry solvents. Tellurium and SiO_2 (activity II-III, 63−200 μm) were degassed by several vacuum/N_2 cycles. Elemental analyses were performed at the Mikroanalytisches Laboratorium, Universität Regensburg. IR spectra were obtained with a Beckman 4240 instrument. ^{1}H NMR spectra were recorded with a Bruker ARX 400 instrument. FD and FAB mass spectra were obtained on a Finnigan MAT spectrometer. $[Cp'_2NbH_3]$ was prepared according to literature methods.[36] Electrochemistry: Cyclic voltammetry was carried out in a standard three-electrode cell with a Tacussel UAP4 unit cell. The reference electrode was a saturated calomel electrode (SCE) separated from the solution by a sintered glass disk. The auxiliary electrode was a platinum wire. For all voltammetric measurements, the working electrode was a vitreous carbon electrode. The controlled potential electrolysis was performed with an Amel 552 potentiostat coupled to an Amel 721 electronic integrator. Electrolyses were performed in a cell with three compartments separated with fritted glass of medium porosity. A carbon gauze was used as the cathode, a platinum plate as the anode and a saturated calomel electrode as the reference electrode. Computational details: All calculations on the closed shell complexes **5**, $[\mathbf{6}]^+$, and $[\mathbf{7}]^{2+}$ were performed using the GAUSSIAN 98 series of programs.[37] Density functional theory (DFT)[38] was applied with the B3LYP functional[39] and with the standard LANL2DZ basis set.[40] The input geometries for optimizations of **5** and $[\mathbf{7}]^{2+}$ were those from available X-ray data (C_5H_5 instead of $tBuC_5H_4$), while the averaged metric parameters from **5** and $[\mathbf{7}]^{2+}$ were used for the starting geometry of $[\mathbf{6}]^+$. The final wave functions and energy levels for **5**, $[\mathbf{6}]^+$, and $[\mathbf{7}]^{2+}$ were obtained from single point calculations carried out on optimized geometries at the same level of theory.

Synthesis of $[Cp'_2Nb(Te_2)H]$ (1): A mixture of $[Cp'_2NbH_3]$ (900 mg, 2.66 mmol), degassed tellurium powder (850 mg, 6.66 mmol), and freshly distilled THF (100 mL) was stirred for 48 h at 40 °C. During this time the color changed from bright brown to dark orange. After evaporation of the solvent the residue was suspended in toluene (12 mL) and transferred to the top of a chromatography column (SiO_2, column 15 × 3 cm). A dark orange band containing 1.27 g (2.15 mmol, 81%) of **1** was eluted with toluene. Red crystals were obtained from toluene/pentane (1:1). $C_{18}H_{27}NbTe_2$ (591.52): calcd. C 36.55, H 4.60; found C 35.36, H 4.25. Mol. mass 591.1 (FD-MS, toluene). ^{1}H NMR (400 MHz, CD_2Cl_2, 24 °C): δ = 6.56 (m, 2 H, C_5H_4R), 4.98 (m, 2 H, C_5H_4R), 4.74 (m, 2 H, C_5H_4R), 4.44 (m, 2 H, C_5H_4R), 1.39 (s, 18 H, CH_3), −3.50 (s, $^2J_{H,Te}$ = 86.7 Hz, 1 H, NbH). ^{125}Te{^{1}H} NMR (157 MHz, CD_2Cl_2): δ = −749.4.

Synthesis of $[Cp'_6Nb_4Te_4O]$ (2): A mixture of $[Cp'_2NbH_3]$ (900 mg, 2.66 mmol), untreated tellurium powder (850 mg, 6.66 mmol) and THF (100 mL) was stirred for 48 h at 40 °C, during which time the color changed to dark violet. After evaporation of the solvent the residue was suspended in toluene (12 mL) and chromatographed on SiO_2 (column 15 × 3 cm). A red-violet band containing $[Cp'_6Nb_4Te_4O]$ (**2**) in yields between 110 and 350 mg (0.07−0.22 mmol, 10−32%) was eluted with toluene. Then a dark orange band was eluted containing between 140 and 830 mg (0.24−1.40 mmol, 9−53%) of $[Cp'_2NbTe_2H]$ (**1**). Complex **2** was recrystallized from THF/Et_2O (4:1) $C_{54}H_{78}Nb_4OTe_4$ (1625.22): calcd. C 39.91, H 4.84; found C 40.13, H 5.01. Mol. mass 1625.7 (FD-MS, toluene). ^{1}H NMR (400 MHz, CD_2Cl_2): δ = 5.75 (m, 4 H, C_5H_4R), 5.30 (m, 4 H, C_5H_4R), 5.11 (m, 4 H, C_5H_4R), 4.88 (m, 8 H, C_5H_4R), 4.18 (m, 4 H, C_5H_4R), 1.54 (s, 18 H, CH_3), 1.47 (s, 18 H, CH_3), 1.26 (s, 18 H, CH_3).

Synthesis of $[Cp'_2Nb(Te_2)H{\cdot}Cr(CO)_5]$ (3): A solution of **1** (520 mg, 0.88 mmol) in THF (50 mL) was added to a solution of $[Cr(CO)_5THF]$ (4.40 mmol) in THF (150 mL). The mixture was stirred for 15 h at room temperature in the dark. After evaporation of the solvent the brown residue was dried under high vacuum in order to remove reformed or excess $[Cr(CO)_6]$. Then the residue was dissolved in a mixture of toluene (12 mL) and acetone (2 mL). Chromatography on SiO_2 (column 20 × 5 cm) gave a golden brown band, containing $[Cp'_2Nb(Te_2)H{\cdot}Cr(CO)_5]$ (**3**) (620 mg, 0.79 mmol, 90%), which was recrystallized from toluene/pentane (1:1). $C_{23}H_{27}CrNbO_5Te_2$ (783.56): calcd. C 35.26, H 3.47; found C 35.12, H 3.61. Mol. mass 783.7 (FD-MS, toluene). IR (KBr): $\tilde{\nu}$ = 2050 s, 1945 vs, 1895 vs cm^{-1} [ν(CO)]. ^{1}H NMR (400 MHz, CD_2Cl_2): δ = 6.58 (m, 1 H, C_5H_4R), 6.27 (m, 1 H, C_5H_4R), 5.20 (m, 1 H, C_5H_4R), 5.14 (m, 1 H, C_5H_4R), 4.87 (m, 1 H, C_5H_4R), 4.73 (m, 1 H, C_5H_4R), 4.69 (m, 1 H, C_5H_4R), 4.64 (m, 1 H, C_5H_4R), 1.31 (s, 18 H, CH_3), −2.95 (s, $^2J_{H,Te}$ = 93.0 Hz, 1 H, NbH).

Synthesis of $[Cp'_6Nb_4Te_4O{\cdot}2Cr(CO)_5]$ (4): A solution of **2** (330 mg, 0.203 mmol) in THF (50 mL) was added to a solution of $[Cr(CO)_5THF]$ (0.908 mmol) in THF (150 mL). The mixture was stirred for 15 h at room temperature in the dark. After evaporation of the solvent the residue was dissolved in toluene (15 mL). Chromatography on SiO_2 (column 15 × 3 cm) gave a broad dark red band upon elution with toluene, containing $[Cp'_6Nb_4Te_4O{\cdot}2Cr(CO)_5]$ (**4**) (310 mg, 0.154 mmol, 76%). Crystals of **4** containing 1.5 molecules of toluene were obtained from toluene. $C_{64}H_{78}Cr_2Nb_4O_{11}Te_4$ (2009.32): calcd. for **4**·1.5C_7H_8 C 41.66, H 4.22; found C 41.61, H 4.23. Mol. mass 1625.3 ($[Cp'_6Nb_4Te_4O]$ (**2**); FD-MS, toluene). IR (KBr): $\tilde{\nu}$ = 2050 s, 1975 vs, 1920 vs cm^{-1} [ν(CO)]. ^{1}H NMR (400 MHz, CD_2Cl_2): δ = 6.50 (m, 1 H, C_5H_4R), 6.42 (m, 2 H, C_5H_4R), 6.22 (m, 1 H, C_5H_4R), 5.98 (m, 1 H, C_5H_4R), 5.91 (m, 2 H, C_5H_4R), 5.85 (m, 2 H, C_5H_4R), 5.76 (m, 2 H, C_5H_4R), 5.72 (m, 1 H, C_5H_4R), 4.85 (m, 1 H, C_5H_4R), 4.70 (m, 2 H, C_5H_4R), 4.35 (m, 1 H, C_5H_4R), 4.19 (m, 1 H, C_5H_4R), 4.05 (m, 1 H, C_5H_4R), 3.87 (m, 1 H, C_5H_4R), 3.83 (m, 1 H, C_5H_4R), 3.51 (m, 1 H, C_5H_4R), 3.20 (m, 1 H, C_5H_4R), 2.89 (m, 2 H,

C_5H_4R), 1.59 (s, 9 H, CH_3), 1.55 (s, 9 H, CH_3), 1.45 (s, 9 H, CH_3), 1.40 (s, 9 H, CH_3), 1.28 (s, 9 H, CH_3), 1.24 (s, 9 H, CH_3).

Thermolysis of $[Cp'_2NbTe_2H{\cdot}Cr(CO)_5]$ (3): A solution of **3** (350 mg, 0.447 mmol) in toluene (120 mL) was stirred for 15 h at 110 °C in the dark. Then the solvent was removed in vacuo and the residue was purified by chromatography on SiO_2 (column 15 × 3 cm). Elution with toluene first gave a red-violet band containing $[Cp'_6Nb_4Te_4O]$ (**2**) (25 mg, 0.015 mmol, 14%) and then a black-green band was eluted containing $[Cp'_4Nb_2Te_2]$ (**5**) (130 mg, 0.140 mmol, 63%). $C_{36}H_{52}Nb_2Te_2$ (925.81): calcd. C 46.70, H 5.66; found C 45.78, H 5.69. Mol. mass 925.6 (FD-MS, toluene). ^{1}H NMR (400 MHz, CD_2Cl_2, 24 °C): δ = 5.05 (m, 8 H, C_5H_4R), 4.46 (m, 8 H, C_5H_4R), 1.44 (s, 36 H, *t*Bu).

Synthesis of $[Cp'_4Nb_2Te(CH_3Te)]I$ ([6]I): A black-green solution of **5** (130 mg, 0.140 mmol) in THF (50 mL) was treated with CH_3I (19.9 mg, 0.140 mmol). While stirring the mixture at room temperature it turned slightly violet and a fine precipitate formed. After 30 min the solvent was evaporated in vacuo and the residue was washed twice with pentane. The resulting powder was dried under high vacuum to give **[6]I** in quantitative yield. **[6]I** was recrystallized from CH_2Cl_2/pentane (3:1). **[6]I:** $C_{37}H_{55}INb_2Te_2$ (1067.75): calcd. C 41.62, H 5.19; found C 41.58, H 4.67. Mol. mass 941.1 $\{[Cp'_4Nb_2Te(TeCH_3)]^+$ ($[\mathbf{6}]^+$); PI-LSIMS, NBA/MeOH$\}$. ^{1}H NMR (400 MHz, CD_2Cl_2, 24 °C): δ = 5.53 (m, 4 H, C_5H_4R), 5.21 (m, 2 H, C_5H_4R), 5.01 (m, 2 H, C_5H_4R), 4.67 (m, 2 H, C_5H_4R), 4.62 (m, 2 H, C_5H_4R), 4.32 (m, 4 H, C_5H_4R), 1.53 (s, 36 H, CH_3), 2.45 (s, 3 H, $TeCH_3$). UV/Vis **[6]I**: λ_{max} = 553 nm (ε = 3460 $L{\cdot}mol^{-1}{\cdot}cm^{-1}$ in CH_3OH).

Synthesis of $[Cp'_4Nb_2(CH_3Te)_2]I_2$ ([7]I_2): The procedure is analogous to that described for the synthesis of **[6]I** with the exception that two equivalents of CH_3I were employed. Recrystallization of $[Cp'_4Nb_2(CH_3Te)_2]I_2$ ([7]I_2) from CH_3OH gave violet needles. $C_{38}H_{58}I_2Nb_2Te_2$ (1209.65): calcd. C 37.72, H 5.03; found C 37.50, H 5.08. Mol. mass 956.3 $\{[Cp'_4Nb_2(CH_3Te)_2]^+$ ($[\mathbf{7}]^+$); PI-LSIMS, NBA/MeOH$\}$. ^{1}H NMR (400 MHz, CD_3OD, 24 °C): δ = 6.61 (m, 1 H, C_5H_4R), 6.55 (m, 2 H, C_5H_4R), 6.43 (m, 1 H, C_5H_4R), 5.89 (m, 1 H, C_5H_4R), 5.62 (m, 2 H, C_5H_4R), 5.53 (m, 1 H, C_5H_4R), 5.10 (m, 2 H, C_5H_4R), 4.60 (m, 2 H, C_5H_4R), 4.21 (m, 1 H, C_5H_4R), 4.11 (m, 2 H, C_5H_4R), 3.38 (m, 1 H, C_5H_4R), 2.88 (s, 3 H, $TeCH_3$), 2.71 (s, 3 H, $TeCH_3$), 1.53 (s, 18 H, CH_3), 1.51 (s, 9 H, CH_3), 1.50 (s, 9 H, CH_3). UV/Vis [7]I_2: λ_{max} = 550 nm (ε = 9120 $L{\cdot}mol^{-1}{\cdot}cm^{-1}$ in CH_3OH).

Synthesis of $[Cp'_4Nb_2(CH_3Te)_2][PF_6]_2$ (8): A solution of NH_4PF_6 (22 mg, 0.135 mmol) in H_2O (3 mL) was added to a solution of [7]I_2 (80 mg, 0.07 mmol) in MeOH (10 mL). While stirring the violet mixture for 30 min at room temperature a dark blue precipitate formed. This precipitate was separated by filtration and washed three times with small amounts of H_2O and Et_2O. The crude product was dissolved in hot acetonitrile (20 mL) and filtered. Evaporation of the solvent and drying under high vacuum gave $[Cp'_4Nb_2(CH_3Te)_2][PF_6]_2$ (**8**) (75 mg, 0.060 mmol, 91%). $C_{38}H_{58}F_{12}Nb_2P_2Te_2$ (1245.80): calcd. C 36.63, H 4.69; found C 37.72, H 4.80. IR (KBr): $\tilde{\nu}$ = 835 vs cm^{-1} [$\nu(PF_6)$].

X-ray Structure Determination: The structures of **2**, **3**, **4**, and [7]I_2 were solved by direct methods (Table 3). Subsequent difference Fourier syntheses revealed the position of the non-hydrogen atoms

Table 3. Summary of crystallographic data

	2	**3**	**4·1.5C_7H_8**	**[7]$I_2{\cdot}CH_3OH$**
Formula	$C_{54}H_{78}Nb_4OTe_4$	$C_{23}H_{27}CrNbO_5Te_2$	$C_{74.5}H_{90}Cr_2Nb_4O_{11}Te_4$	$C_{39}H_{62}I_2Nb_2OTe_2$
MW	1625.22	783.56	2147.52	1241.69
Cryst syst	Triclinic	Monoclinic	Monoclinic	Triclinic
Space group	$P\bar{1}$	$P2_1/a$	$P2_1/n$	$P\bar{1}$
a [Å]	12.0353(11)	14.9510(8)	18.6414(9)	10.512(4)
b [Å]	15.4884(15)	10.1946(8)	20.3497(10)	10.803(5)
c [Å]	17.1097(15)	17.3753(10)	21.6608(10)	11.348(4)
α [deg]	82.831(11)	90	90	72.260(4)
β [deg]	84.058(11)	98.006(7)	103.986(6)	69.100(4)
γ [deg]	68.136(10)	90	90	87.740(5)
V [Å^3]	2931.2(5)	2622.5(3)	7973.4	1143.2
Z	2	4	4	1
$d_{calcd.}$ [g/cm^3]	1.841	1.985	1.793	1.804
F(000)	1564	1496	4188	596
Cryst size [mm^3]	0.40 × 0.10 × 0.09	0.40 × 0.28 × 0.11	0.38 × 0.27 × 0.19	0.16 × 0.06 × 0.03
Diffractometer	STOE-IPDS	STOE-IPDS	STOE-IPDS	STOE-IPDS
Temp [K]	297	173	173	297
θ [deg]	2.08−25.96	2.32−25.83	1.64−25.83	2.73−26.33
No. of reflns collected	26993	29053	46068	16022
No. of indep reflns	10649	4995	14273	4117
R_{int}	0.0180	0.0387	0.0720	0.1970
No. obsd. reflections [$I > 2\sigma(I)$]	8388	4618	8396	1557
μ [mm^{-1}]	2.75	3.06	2.31	3.13
No. of data/restraints/params	10649/0/568	4995/0/325	14273/0/805	4177/0/200
GOF on F^2	0.877	1.115	0.785	0.946
Absorption correction	numerical	numerical	numerical	none
T_{max}, T_{min}	0.8216, 0.6197	0.7403, 0.3852	0.9581, 0.8758	
*R*1, *wR*2 [$I > 2\sigma(I)$]	0.0228, 0.0584	0.0267, 0.0713	0.0361, 0.0640	0.1269, 0.3169
*R*1, *wR*2 (all data)	0.0311, 0.0633	0.0292, 0.0723	0.0818, 0.0714	0.2105, 0.3660

and all these atoms were refined with anisotropic thermal parameters with the exception of **[7]I_2**. Hydrogen atoms were introduced on idealized positions and refined using a riding model. The H atom H(19) fixed at the Nb atom in the structure of **3** was formed in the difference Fourier synthesis as the third peak (0.7 electrons). After refinement the *R* values decreased significantly. The residual electron density of 2.868 e·Å^{-3} that was found after all refinement cycles is in the proximity (0.91 Å) of Te(1). The structure solution of **[7]I_2** was handicapped by a poor crystal quality. In this case refinement with anisotropic temperature factors was only possible for the heavy atoms. A void at *x*, *y*, *z* = 0, 0.5, 0.5 was localized with the program SQUEEZE.[41] It has a volume of 161 Å^3 and contains 11 electrons. This roughly corresponds to one molecule of methanol.

Crystallographic data (excluding structure factors) for the structures reported in this paper have been deposited with the Cambridge Crystallographic Data Centre as supplementary publication nos. CCDC-172951 (**2**), CCDC-172952 (**3**), CCDC-172953 (**4**), and CCDC-172954 (**[7]I_2**). These data can be obtained free of charge at www.ccdc.cam.ac.uk/conts/retrieving.html [or from the Cambridge Crystallographic Data Centre, 12, Union Road, Cambridge CB2 1EZ, UK; Fax: (internat.) +44−1223/336-033; E-mail: deposit@ccdc.cam.ac.uk].

Acknowledgments

We thank Prof. Dr. B. Wrackmeyer for recording the ^{125}Te NMR spectrum of **1**. We are grateful to the Deutsche Forschungsgemeinschaft for support of this work (Wa 485/6-2). Parts of this work were supported by the Deutscher Akademischer Auslandsdienst and the jyMinistère des Affaires Etrangères (program PROCOPE).

[1] J. M. Fischer, W. E. Piers, L. R. MacGillivray, M. J. Zaworotko, *Inorg. Chem.* **1994**, *34*, 2499−2500.
[2] [2a] G. Tainturier, M. Fahim, B. Gautheron, *J. Organomet. Chem.* **1989**, *373*, 193−202. [2b] G. Tainturier, M. Fahim, G. Trouvé-Bellan, B. Gautheron, *J. Organomet. Chem.* **1989**, *376*, 321−332.
[3] [3a] W. A. Howard, G. Parkin, A. L. Rheingold, *Polyhedron* **1994**, *14*, 25−44. [3b] J. H. Shin, T. Hascall, G. Parkin, *Organometallics* **1999**, *18*, 6−9.
[4] J. H. Shin, G. Parkin, *Organometallics* **1995**, *13*, 2147−2149.
[5] J. H. Shin, G. Parkin, *Organometallics* **1994**, *14*, 1104−1106.
[6] H. Brunner, M. Kubicki, J.-C. Leblanc, W. Meier, C. Moise, A. Sadorge, B. Stubenhofer, J. Wachter, R. Wanninger, *Eur. J. Inorg. Chem.* **1999**, 843−848.
[7] O. Blacque, H. Brunner, M. M. Kubicki, B. Nuber, B. Stubenhofer, J. Wachter, B. Wrackmeyer, *Angew. Chem. Int. Ed. Engl.* **1997**, *36*, 352−353.
[8] H. Brunner, G. Gehart, M. M. Kubicki, E. Lehrl, D. Lucas, W. Meier, Y. Mugnier, B. Nuber, B. Stubenhofer, J. Wachter, *J. Organomet. Chem.* **1996**, *510*, 291−295.
[9] O. Blacque, H. Brunner, M. M. Kubicki, D. Lucas, W. Meier, Y. Mugnier, B. Nuber, B. Stubenhofer, J. Wachter, *J. Organomet. Chem.* **1998**, *564*, 71−79.
[10] H. Brunner, D. Lucas, T. Monzon, Y. Mugnier, B. Nuber, B. Stubenhofer, A. C. Stückl, J. Wachter, R. Wanninger, M. Zabel, *Chem. Eur. J.* **2000**, *6*, 493−503.
[11] H. Brunner, J. Wachter, R. Wanninger, M. Zabel, *J. Organomet. Chem.* **2000**, *603*, 135−137.
[12] [12a] H. Brunner, G. Gehart, W. Meier, B. Nuber, J. Wachter, *J. Organomet. Chem.* **1993**, *454*, 117−122. [12b] J.-C. Leblanc, C. Moise, F. Volpato, H. Brunner, G. Gehart, J. Wachter, B. Nuber, *J. Organomet. Chem.* **1995**, *485*, 237−242.
[13] H.-J. Bach, H. Brunner, J. Wachter, M. M. Kubicki, J.-C. Leblanc, C. Moise, F. Volpato, B. Nuber, M. L. Ziegler, *Organometallics* **1992**, *11*, 1403−1407.
[14] An analysis of the linear M−O−M bridging moiety is given in: J. W. Faller, Y. Ma, *J. Organomet. Chem.* **1988**, *340*, 59−69.
[15] H. Brunner, J.-C. Leblanc, D. Lucas, W. Meier, C. Moise, Y. Mugnier, B. Nuber, S. Rigny, A. Sadorge, J. Wachter, *J. Organomet. Chem.* **1998**, *566*, 203−210.
[16] [16a] W. Tremel, *J. Chem. Soc., Chem. Commun.* **1992**, 126−128. [16b] H. Kleinke, W. Tremel, *Chem. Commun.* **1999**, 1175−1176.
[17] O. M. Kekia, A. L. Rheingold, *J. Organomet. Chem.* **1997**, *545*, 277−280.
[18] J. Emsley, *The Elements*, Clarendon Press, Oxford **1989**, 186.
[19] Yu. V. Skripkin, I. L. Eremenko, A. A. Pasynskii, Yu. T. Struchkov, V. E. Shklover, *J. Organomet. Chem.* **1985**, *267*, 285−292.
[20] L. G. Guggenberger, *Inorg. Chem.* **1973**, *12*, 294−301.
[21] G. Erker, R. Nolte, G. Tainturier, A. Rheingold, *Organometallics* **1989**, *8*, 454−460.
[22] Te−Te bonds in other monomeric η^2-Te$_2$ complexes: [22a] [Cp*$_2$Ti(Te$_2$)] [2.703(2) Å].[1] [22b] [Cp*$_2$Zr(Te$_2$)CO] [2.688(1) Å].[3] [22c] [W(PMe$_3$)(CN*t*Bu)$_4$(Te$_2$)] [2.680(2) Å]: D. Rabinovich, G. Parkin, *J. Am. Chem. Soc.* **1993**, *115*, 9822−9823. [22d] [triphosNi(Te$_2$)] [2.668(1) Å]: M. Di Vaira, M. Peruzzini, P. Stoppioni, *Angew. Chem. Int. Ed. Engl.* **1987**, *26*, 916−918.
[23] [23a] W. A. Flomer, S. C. O′ Neal, J. W. Kolis, D. Jeter, A. W. Cordes, *Inorg. Chem.* **1988**, *27*, 969−971. [23b] L. C. Roof, W. T. Pennington, J. W. Kolis, *Inorg. Chem.* **1992**, *31*, 2056−2064. [23c] S. Stauf, C. Reisner, W. Tremel, *Chem. Commun.* **1996**, 1749−1750.
[24] H. Brunner, G. Gehart, J.-C. Leblanc, C. Moise, B. Nuber, B. Stubenhofer, F. Volpato, J. Wachter, *J. Organomet. Chem.* **1996**, *517*, 47−51.
[25] H. Brunner, J. Wachter, R. Wanninger, M. Zabel, *Eur. J. Inorg. Chem.* **2001**, 1151−1154.
[26] H. Sitzmann, D. Saurenz, G. Wolmershäuser, A. Klein, R. Boese, *Organometallics* **2001**, *20*, 700−705.
[27] [27a] M. M. Rohmer, M. Bénard, *Organometallics* **1991**, *10*, 157−163. [27b] R. L. DeKock, M. A. Peterson, L. E. L. Reynolds, L.-H. Chen, E. J. Baerends, P. Vernooijs, *Organometallics* **1993**, *12*, 2794−2805.
[28] W. A. Herrmann, J. Rohrmann, C. Hecht, *J. Organomet. Chem.* **1985**, *290*, 53−61.
[29] R. Wanninger, PhD thesis, Universität Regensburg **2000**.
[30] E. Samuel, D. Guery, J. Vedel, *J. Organomet. Chem.* **1984**, *263*, C43.
[31] R. W. Murray, C. N. Reitley, *Electroanalytical principles*, Interscience, New-York, **1963**.
[32] R. S. Nicholson, *Anal. Chem.* **1965**, *35*, 1351.
[33] Calculated parameters are given in the order **5**, [**6**]$^+$, [**7**]$^{2+}$: *d*(Nb−Nb): 3.7817, 3.6625, 3.6863 Å; *d*(Te−Te): 4.228, 4.377, 4.493 Å; *d*(Nb−Te): 2.834, 2.823(Te) and 2.884(TeMe), 2.890 Å.
[34] M. Brandl, H. Brunner, J. Wachter, M. Zabel, *Organometallics*, accepted.
[35] H. Brunner, A. C. Stückl, J. Wachter, R. Wanninger, M. Zabel, *Angew. Chem. Int. Ed.* **2001**, *40*, 2463−2465.
[36] J. A. Labinger, *Adv. Chem. Ser.* **1978**, *167*, 149.
[37] M. J. Frisch, G. W. Trucs, H. B. Schlegel, G. E. Scuseria, M. A. Robb, J. R. Cheeseman, V. G. Zakrzewski, J. A. Montgomery, R. E. Stratman, J. C. Burant, S. Dapprich, J. M. Millam, A. D. Daniels, K. N. Kudin, M. C. Strain, O. Farkas, J. Tomasi, V. Barone, M. Cossi, R. Cammi, B. Mennucci, C. Pomelli, C. Adamo, S. Clifford, J. Ochterski, G. A. Petersson, P. Y. Ayala, Q. Cui, K. Morokuma, D. K. Malick, A. D. Rabuck, K. Raghavachari, J. B. Foresman, J. Cioslowski, J. V. Ortiz, B. B. Stefanov, G. Liu, A. Liashenko, P. Piskorz, I. Komaromi, R. Gomperts, R. T. Martin, D. J. Fox, T. Keith, M. A. Al-Laham,

C. Y. Peng, A. Nanayakkara, C. Gonzalez, M. Challacombe, P. M. W. Gill, B. G. Johnson, W. Chen, M. W. Wong, J. L. Andres, M. Head-Gordon, E. S. Replogle, J. A. Pople, *GAUSSIAN98* (Rev. A.6), Gaussian, Inc., Pittsburgh PA, **1998**.
[38] R. G. Parr, W. Yang, *Density Functional Theory of Atoms and Molecules*, Oxford University Press, Oxford, UK, 1989.
[39] A. D. Becke, *J. Chem. Phys.* **1993**, *98*, 5648.
[40] T. H. Dunning, Jr., P. J. Hay, in *Modern Theoretical Chemistry* (Ed.: H. F. Schaefer, III), Plenum Press, New York, **1976**, p. 1; P. J. Hay, W. R. Wadt, *J. Chem. Phys.* **1985**, *82*, 270; P. J. Hay, W. R. Wadt, *J. Chem. Phys.* **1985**, *82*, 284; P. J. Hay, W. R. Wadt, *J. Chem. Phys.* **1985**, *82*, 299.
[41] P. v. d. Sluis, A. L. Spek, *Acta Crystallogr., Sect. A* **1990**, *46*, 194.

Received October 30, 2001
[I01423]

Synthesis and Reactivity of Ene-Diamido and Ene-Diolato [(Trimethylsilyl)-cyclopentadienyl]niobium(V) Complexes and a Comparative DFT Study of the Bonding Capabilities of Diazabutadiene and Butadiene Ligands

Agustín Galindo,[a] Manuel Gómez,*[b] Diego del Río,[a] and Fernando Sánchez[b]

Keywords: Niobium / Alkene ligands / N ligands / Cyclopentadienyl complexes / Density functional calculations

The reactions of [$NbCp'Cl_2(Me_3SiCCSiMe_3)$] ($Cp' = \eta^5$-$C_5H_4SiMe_3$) with 2,3-dimethyl-1,4-diphenyl-1,4-diaza-buta-1,3-diene (Me,Ph-DAD) and diketones R–CO–CO–R (R = Me, Ph) gave ene-diamido complexes [$NbCp'Cl_2$(Me,Ph-DAD)] (**1**) and ene-diolato complexes [$NbCp'Cl_2${O(R)CC(R)O}] (R = Me, **2**; Ph, **3**), respectively, with simultaneous elimination of bis(trimethylsilyl)acetylene. The NMR spectroscopic data of these compounds are in agreement with a *supine* conformation, with respect to the Cp′ ring, of the ene-diamido and ene-diolato ligands. In order to gain further information concerning the bonding capabilities of the ene-diamido ligand, a DFT study of the model complex [$NbCpCl_2$(HNCHCHNH)] (**I**) was performed. For comparison, a DFT analysis of the model compound [$NbCpCl_2(\eta^4$-$CH_2CHCHCH_2)$] (**II**) was also carried out. Differences in the bonding description of the diazabutadiene and butadiene ligands bonded to a common [$NbCpCl_2$] moiety are discussed. A detailed analysis of the fragment orbital interactions in **I** provides no evidence for any positive overlap between the Nb centre and the inner carbon atoms of the DAD ligand. Dialkylation of the dichloro complex **1** gave dialkyl derivatives [$NbCp'R_2$(Me,Ph-DAD)] (R = Me, **4**; CH_2SiMe_3, **5**; $CH_2C_6H_5$, **6**), for which the NMR spectroscopic data suggests a *prone* conformation of the DAD ligand. Treatment of the dimethyl derivative **4** with carbon monoxide and 2,6-dimethylphenyl isocyanide led to the formation of the oxa- and azaniobacyclopropane complexes [$NbCp'\{\eta^2$-$(E)CMe_2\}$(Me,Ph-DAD)] [E = O, **7**; $N(2,6\text{-}Me_2C_6H_3)$, **8**], respectively. Subsequent insertion of isocyanide into the Nb–C bond of **7** proceeds with formation of derivatives [$NbCp'\{\eta^2$-$(O)CMe_2$-$(CNAr)_x\}$(Me,Ph-DAD)], ($Ar = 2,6\text{-}Me_2C_6H_3$; x = 1, **9**; 2, **10**). All the complexes isolated were characterized by IR and NMR (^1H, $^{13}C\{^1H\}$) spectroscopy.

(© Wiley-VCH Verlag GmbH, 69451 Weinheim, Germany, 2002)

Introduction

Recent developments in the organometallic chemistry of early transition metals is due to the participation of metallocene systems as catalysts in important inorganic and organic reactions.[1] Modification of the cyclopentadienyl ligand by introduction of specific substituents, including an ansa-type bis(cyclopentadienyl) ligand, was the first strategy[2] in order to respond to each problem created in such processes. Another, more flexible approach, may be a half-metallocene system, in which one Cp ligand of the metallocene is replaced by different ancillary ligands. In any case, mono- and bis(cyclopentadienyl) complexes of early transition metals are now well established as important types of olefin polymerisation catalysts.[3] Although many systems are highly active and widely studied, precise reasons why certain ligands or ligand combinations produce effective catalysts remains obscure. In this context, nitrogen donor ligands have been incorporated into the cyclopentadienyl ring, such as the "constrained geometry" complexes,[4] and also mono- and polydentate amido complexes[5] without cyclopentadienyl ligands have been reported. In addition, dienes have been integrated as ligands, because [$M(\eta^5$-$C_5R_5)$(1,3-diene)] (M = Nb, Ta) fragments are isoelectronic and isolobal[6] to Group-4 metallocene fragments [$M(\eta^5$-$C_5R_5)_2$]. This relationship is extremely useful, since the metallocene species involved in synthetic and catalytic processes can potentially be replaced by monocyclopentadienyl(diene) complexes. In fact, these metallocene-like fragments stabilize reactive benzyne[7] species and their *cis*-dialkyl derivatives are catalyst precursors for the living polymerization of ethylene[8] and the stereoselective ROMP of norbornene.[9]

Several coordination modes have been reported[10] for transition metal complexes containing substituted 1,4-diaza-1,3-butadiene ligands (R,R′-DAD[11]). Scheme 1 shows a representation of the bonding modes found in mononuclear complexes in which the DAD ligand is bonded to the

[a] Departamento de Química Inorgánica, Universidad de Sevilla, Aptdo. 553, 41701 Sevilla, Spain
[b] Departamento de Química Inorgánica, Universidad de Alcalá de Henares, Campus Universitario, 28871 Alcalá de Henares, Spain
Fax: (internat.) + 34-91/885-4683
E-mail: manuel.gomez@uah.es
Supporting information for this article is available on the WWW under http://www.eurjic.com or from the author.

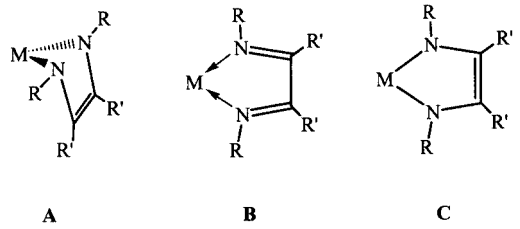

Scheme 1. Coordination bonding modes of 1,4-diaza-1,3-butadiene ligand (R,R′-DAD) found in mononuclear complexes in which the ligand is bonded to the metal centre through the two N atoms

metal centre through both N atoms. In the majority of early transition metals the diazabutadiene ligand acts as a dianionic ene-diamido chelate (mode **A**) and the metal-DAD moiety is characterized by a nonplanar disposition (folded envelope). The coordination mode **B**, α-diimine ligand, is well represented for many late transition metal complexes; meanwhile, bonding type **C**, a planar 2,5-diaza-1-metallacyclopent-3-ene, is less common in early transition metals.[12] In the last few years, the synthesis and characterization of a series of niobium and tantalum complexes containing 1,4-diaza-1,3-diene R,R′-DAD ligands[12a,13] (or closely related *o*-phenylenediamido ligands[14]) have been reported, in which the diazabutadiene behaves as a dianionic ene-diamido ligand (mode **A**) and shows a folded envelope geometry. When the compound has a cyclopentadienyl co-ligand, the DAD can adopt two conformations − *supine* and *prone* − relative to the Cp ring, depending on the coordination environment of the metal centre.[15]

In this paper, we report a synthetic study of half-sandwich niobium complexes containing ene-diamido and ene-diolato ligands and their chemical behaviour in alkylation and insertion reactions. Also, we present a comparative DFT study of the 1,4-diaza-1,3-butadiene and 1,3-butadiene ligands coordinated to the common $[NbCpCl_2]$ moiety, in order to look into the bonding capabilities of the diazabutadiene and butadiene ligands on high-valent complexes of early transition metals.

Results and Discussion

The treatment of $[NbCp'Cl_2(Me_3SiCCSiMe_3)]$[16] (Cp′ = η^5-$C_5H_4SiMe_3$) with 2,3-dimethyl-1,4-diphenyl-1,4-diazabuta-1,3-diene (Me,Ph-DAD) or diketones R−CO−CO−R (R = Me, Ph) in hexane leads to the precipitation of the corresponding half-sandwich complexes $[NbCp'Cl_2(Me,Ph\text{-}DAD)]$ (**1**) and $[NbCp'Cl_2\{O(R)CC(R)O\}]$ (R = Me, **2**; Ph, **3**), respectively, with elimination of bis(trimethylsilyl)acetylene (Scheme 2). The closely related half-sandwich 1,4-diaza-1,3-butadiene complexes with the general formula $[Nb(\eta^5\text{-}C_5R_5)Cl_2(DAD)]$[13d,13f,14a,14b] were previously known and they were essentially isolated by treatment of the tetrachloro compounds $[Nb(\eta^5\text{-}C_5R_5)Cl_4]$ (R = H, Me) with a dilithium salt of different DAD ligands. However, there is an example in which the experimental procedure is related to the synthesis of **1** and the DAD derivative was formed by a photochemical ligand-exchange reaction between $[NbCpCl_2(PMe_3)_3]$ and the *t*Bu,H-DAD ligand.[13a]

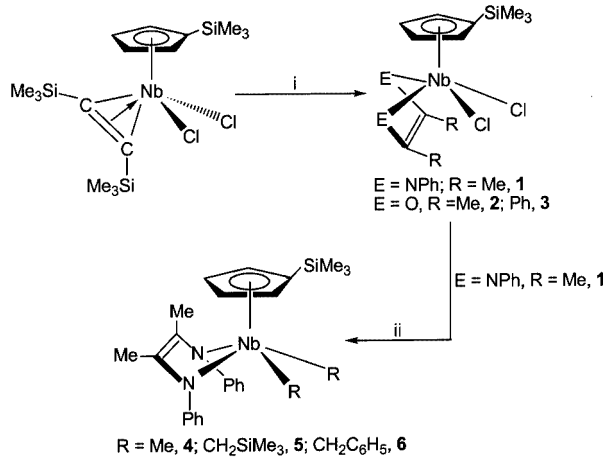

Scheme 2. Reagents and conditions: i: 1 equiv. E(R)C-C(R)E (E = NPh, R = Me, **1**; E = O, R = Me, **2**; Ph, **3**), hexane, 12 h, room temp.; ii: 2 equiv. MgClR (R = Me, **4**; CH_2SiMe_3, **5**; $CH_2C_6H_5$, **6**), diethyl ether, 12 h, room temp. (except for R = $CH_2C_6H_5$, −78 °C)

The IR spectra (Table 1) of **1**−**3** (and those of the other complexes of this work) show the characteristic absorptions for the (trimethylsilyl)cyclopentadienyl ring ($\nu_{C-H} \approx 841$ cm^{-1})[17] and the trimethylsilyl substituent [$\nu\delta_{as}(CH_3) \approx 1255$ cm^{-1}].[18] Absorptions due to the C=N, C=C, C−O, Nb−O, Nb−C and Nb−Cl stretching vibrations are observed at $\tilde{\nu} \approx$ 1630,[19] 1594,[20] 1173,[20e,21] 734,[22] 482[20e,21b] and 320[17,22,23] cm^{-1}, respectively. The ^1H and $^{13}C\{^1H\}$ NMR spectroscopic data (Table 2) are consistent with the stoichiometries and expected geometries of these complexes. The inner carbon atoms of the ene-diamido and ene-diolato ligands were observed as a singlet in the olefinic region between δ = 96 and 120. By contrast, the corresponding resonances of the uncoordinated DAD ligands are usually found in the region at δ ≈ 160 and those for 1,4-diazabuta-1,3-dienes coordinated in mode **B** the diene ^{13}C resonance occurs at an even lower field.[10a,24] This NMR spectroscopic data suggest an ene-diamido structure (mode **A**) for **1** and an ene-diolato one for the complexes **2** and **3**. Mashima et al. have recently highlighted[15] the geometric preferences of 1,4-diazadiene ligands on half-sandwich metallocene complexes of early transition metals. The ene-diamido ligand can adopt two conformations, *supine* and *prone*, relative to the η^5-C_5R_5 moiety. The adoption of a particular conformation depends on the coordination environment on the metal centre and the steric properties of the substituents of the DAD ligand. In most of the dichloro compounds this ligand adopts a *supine* conformation, except for a bulky substituted *t*Bu,H-DAD derivative $[TaCp^*Cl_2(t\text{Bu,H-DAD})]$[13e] and for the bis(trialkylsilyl)-*o*-phenylenediamido complexes, $[TaCp^*Cl_2\{(i\text{Pr}_3SiN)_2\text{-}o\text{-}C_6H_4\}]$[14a]

Table 1. IR data (Nujol mull, $\tilde{\nu}$, cm^{-1}) of the new complexes

	C=C	$SiMe_3$	C−H (Cp′)	Nb−Cl	Others
1	1588 (m)	1258 (vs)	841 (s)	313 (m)	1172 (w), 1078 (w), 1050 (m), 901 (w), 700 (w), 637 (m), 506 (m, ν_{Nb-N})
2	1653 (w)	1250 (m)	841 (m)	319 (w)	1172 (w), 1134 (m, ν_{C-O}), 1048 (w), 900 (w), 722 (w, ν_{Nb-O}), 651 (w),629 (w)
3	1569 (w)	1259 (s)	851 (s)	328 (w)	1174 (m), 1154 (m, ν_{C-O}), 1046 (m), 901 (w), 724 (w, ν_{Nb-O}), 662 (w), 616 (w)
4	1588 (m)	1249 (s)	839 (s)		1169 (w), 1074 (w), 1049 (m), 909 (w), 697 (m), 635 (w), 488 (w, ν_{Nb-C})
5	1590 (vs)	1253 (vs)	845 (vs)		1175 (m), 1075 (w), 1050 (w), 905 (w), 699 (m), 638 (w), 492 (w, ν_{Nb-C})
6	1592 (m)	1250 (m)	840 (s)		1172 (w), 1080 (w), 1045 (m), 904 (w), 697 (w)
7	1591 (s)	1257 (s)	834 (s)		1205 (m, ν_{C-O}), 1170 (m), 1087 (m), 1049 (w), 906 (m), 745 (s, ν_{Nb-O}), 697 (m), 632 (m), 473 (w, ν_{Nb-C})
8	1592 (m)	1257 (s)	836 (m)		1169 (w), 1072 (m), 1047 (w), 905 (w), 692 (m, ν_{Nb-N}), 499 (w)
9	1591 (m)	1259 (m)	839 (m)		1615 (m, $\nu_{C=N}$), 1197 (m, ν_{C-O}), 1169 (w), 1090 (w), 1047 (w), 904 (w), 740 (m, ν_{Nb-O}), 698 (w), 631 (w), 504 (m, ν_{Nb-C})
10	1590 (s)	1255 (vs)	834 (s)		1645 (m, $\nu_{C=N}$), 1197 (m, ν_{C-O}), 1169 (w), 1091 (w), 1049 (w), 907 (w), 741 (m, ν_{Nb-O}), 698 (m), 638 (w), 456 (m, ν_{Nb-C})

and $[M\{\eta^5\text{-}C_5H_3(SiMe_3)_2\}Cl_2\{(Me_3SiN)_2\text{-}o\text{-}C_6H_4\}]$[14b] (M = Nb, Ta). On the basis of the steric properties of the ligands and the NMR spectroscopic data of complexes **1**−**3** we conclude that both ene-diamido and ene-diolato ligands adopt the *supine* conformation (see Scheme 2).

Mealli, Ienco and Galindo have recently communicated a re-interpretation of the bonding scheme of the ene-diamido ligand in d^0-metal complexes.[25] Essentially, the folding of the DAD ligand (folded envelope geometry, mode **A**) in such complexes cannot be explained by using the standard description of σ^2,π adopted for the η^4 bonding of butadiene ligands to early transition metals. The experimentally observed folding cannot be attributed to the π donation from the central C=C linkage to the unsaturated metal centre, because this interaction is negligible, according to calculations.

In order to confirm this analysis we have performed DFT studies on the model complex $[NbCpCl_2(HNCHCHNH)]$ (**I**) analogous to derivative **1**. Also for comparison we have extended our calculations to the model complex $[NbCpCl_2(\eta^4\text{-}CH_2CHCHCH_2)]$ (**II**). Therefore, in this paper, we compare the ligands 1,4-diaza-1,3-butadiene (in its ene-diamido form) and 1,3-butadiene (in its 2-butene-1,4-diyl form) coordinated to the common moiety $[NbCpCl_2]$ (with a formal d^0 configuration). Full geometry optimisations were performed for the model compounds **I** and **II**. According to the remarks of Mashima et al.,[15] in dichloro-(cyclopentadienyl) Group-5 compounds the DAD ligand adopts a *supine* conformation, except for bulky substituted DAD derivatives. No steric crowding can be expected in model **I**, because it contains the simplest DAD ligand and, subsequently, only the *supine* orientation of the DAD ligand was calculated.[26] Analogously, for **II**, just the *supine* orientation of butadiene ligand was considered.[27] The use of BP86 or B3LYP functionals did not produce significant changes in the structural parameters and only data calculated at the B3LYP level of theory are discussed, while those at the BP86 level of theory are given as Supporting Information. The resulting final optimised geometries at the B3LYP level of theory are shown in Figure 1 and their coordinates are included as Supporting Information. Selected calculated parameters of complexes **I** and **II** and, for comparison, selected experimental data from X-ray crystallography have been collected in Tables 3 and 4, respectively.

In Table 3 we contrasted selected experimental data for several complexes containing the 1,4-diaza-1,3-butadiene fragment coordinated to the NbCp moiety with calculated parameters. Similarly, in Table 4 we made an analogous comparison for complexes containing the butadiene ligand coordinated to the same NbCp moiety. A general satisfactory agreement between the calculated and experimental values of geometrical parameters was found. In both cases (see Figure 1) the ligand was folded towards the metal centre and computed torsion angles of 120.7 (Nb−N1−N2−C2) and 92.8° (Nb−C1−C4−C3) for **I** and **II**, respectively, gave Nb−C contacts within the range of bonding distances (2.532 Å for **I** and 2.431 Å for **II**). The C1−C2 and C2−C3 bond lengths (1.407 Å in **I** and 1.395 Å in **II**, respectively) were shorter than that expected for a single C−C bond. In addition, the N1−C1 and N2−C2 bond lengths in **I** (1.366 Å) were longer than expected for a double N=C bond. The principal difference found in the common $[NbCpCl_2]$ fragment was the Cl−Nb−Cl bond angle, which opened up from 82.1° in **I** to 96.1° in **II**.

A qualitative FMO analysis helped to elucidate the major bonding components between 1,4-diaza-1,3-butadiene and 1,3-butadiene ligands and the common $[NbCpCl_2]$ fragment. When considering the substitution of 1,3-butadiene by the 1,4-diaza-1,3-butadiene ligand, we are replacing a ligand, capable of donating two pairs of electrons (two π pairs in the neutral form) by a ligand which is able to donate up to a maximum of four electron pairs (the equivalent two π pairs plus two in-plane σ pairs in the neutral form). A representation of the FMOs corresponding to the 1,4-diaza-1,3-butadiene ligand is shown in Scheme 3, in conjunction with the energy disposition of such orbitals and those well known for butadiene. Taking into account the

Table 2. ^1H and $^{13}C\{^1H\}$ NMR spectroscopic data ([D$_6$]benzene) of the new complexes; chemical shifts in δ

	^1H	$^{13}C\{^1H\}$
1	7.30 (m), 7.20 (m), 7.01 [m, 10 H, 2,3-$Me_2C_2N_2(C_6H_5)_2$], 6.71 (m, 2 H), 5.71 (m, 2 H, $H_4C_5SiMe_3$), 1.84 (s, 6 H, 2,3-$Me_2C_2N_2Ph_2$), 0.28 (s, 9 H, $Me_3SiC_5H_4$)	150.22 [C_i, 2,3-$Me_2C_2N_2(C_6H_5)_2$], 129.11, 126.13, 125.13 [C_o, C_p, C_m, 2,3-$Me_2C_2N_2(C_6H_5)_2$], 126.87 (C_i, $C_5H_4SiMe_3$), 119.34 (2,3-$Me_2C_2N_2Ph_2$), 115.81, 115.43 ($C_5H_4SiMe_3$), 14.34 (2,3-$Me_2C_2N_2Ph_2$), −0.52 ($Me_3SiC_5H_4$)
2	6.68 (m, 2 H), 6.37 (m, 2 H, $H_4C_5SiMe_3$), 1.94 (s, 6 H, 2,3-$Me_2C_2O_2$), 0.22 (s, 9 H, $Me_3SiC_5H_4$)	138.21 (C_i, $C_5H_4SiMe_3$), 123.20, 123.09 ($C_5H_4SiMe_3$), 96.26 (2,3-$Me_2C_2O_2$), 13.67 (2,3-$Me_2C_2O_2$), −0.90 ($Me_3SiC_5H_4$)
3	7.68 (m), 6.90 [m, 10 H, 2,3-$(H_5C_6)_2C_2O_2$], 6.71 (m, 2 H), 6.47 (m, 2 H, $H_4C_5SiMe_3$), 0.28 (s, 9 H, $Me_3SiC_5H_4$)	136.23 [C_i, 2,3-$(C_6H_5)_2C_2O_2$], 131.95, 131.02, 130.39 [C_o, C_p, C_m, 2,3-$(C_6H_5)_2C_2O_2$], 125.64 (C_i, $C_5H_4SiMe_3$), 123.89, 123.24 ($C_5H_4SiMe_3$), 101.51 (2,3-$Ph_2C_2O_2$), −0.79 ($Me_3SiC_5H_4$)
4	7.16 (m), 6.99 [m, 10 H, 2,3-$Me_2C_2N_2(C_6H_5)_2$], 6.40 (m, 2 H), 6.25 (m, 2 H, $H_4C_5SiMe_3$), 1.71 (s, 6 H, 2,3-$Me_2C_2N_2Ph_2$), 0.15 (s, 6 H, Nb-Me_2), −0.41 (s, 9 H, $Me_3SiC_5H_4$)	151.26 [C_i, 2,3-$Me_2C_2N_2(C_6H_5)_2$], 128.91, 123.90, 123.25 [C_o, C_p, C_m, 2,3-$Me_2C_2N_2(C_6H_5)_2$], 116.47 (C_i, $C_5H_4SiMe_3$), 114.94, 114.71 ($C_5H_4SiMe_3$), 108.29 (2,3-$Me_2C_2N_2Ph_2$), 24.51 (Nb-Me_2), 14.62 (2,3-$Me_2C_2N_2Ph_2$), −0.58 ($Me_3SiC_5H_4$)
5	7.18 (m), 7.00 (m), 6.92 [m, 10 H, 2,3-$Me_2C_2N_2(C_6H_5)_2$], 6.77 (m, 2 H), 5.55 (m, 2 H, $H_4C_5SiMe_3$), 1.77 (s, 6 H, 2,3-$Me_2C_2N_2Ph_2$), 0.31 [s, 18 H, Nb-$(CH_2SiMe_3)_2$], 0.12, −0.07 [AB, 4 H, $^2J_{H-H}$ = 11.7 Hz, Nb-$(CH_2SiMe_3)_2$], −0.54 (s, 9 H, $Me_3SiC_5H_4$)	150.93 [C_i, 2,3-$Me_2C_2N_2(C_6H_5)_2$], 128.70, 124.49, 123.84 [C_o, C_p, C_m, 2,3-$Me_2C_2N_2(C_6H_5)_2$], 118.52 (C_i, $C_5H_4SiMe_3$), 116.80, 113.14 ($C_5H_4SiMe_3$), 108.89 (2,3-$Me_2C_2N_2Ph_2$), 31.95 [Nb-$(CH_2SiMe_3)_2$], 15.49 (2,3-$Me_2C_2N_2Ph_2$), 4.18 [Nb-$(CH_2SiMe_3)_2$], −0.70 ($Me_3SiC_5H_4$)
6	7.61, 6.95, 6.87, 6.66 [Nb-$(CH_2C_6H_5)_2$; 2,3-$Me_2C_2N_2(C_6H_5)_2$], 6.38 (m, 2 H), 6.27 (m, 2 H, $H_4C_5SiMe_3$), 2.31, 2.05 [AB, 4 H, $^2J_{H-H}$ = 10 Hz, Nb-$(CH_2C_6H_5)_2$], 1.77 (s, 6 H, 2,3-$Me_2C_2N_2Ph_2$), −0.62 (s, 9 H, $Me_3SiC_5H_4$)	154.66, 150.43 [C_i, Nb-$(CH_2C_6H_5)_2$; 2,3-$Me_2C_2N_2(C_6H_5)_2$], 128.71, 127.53, 124.20, 123.55 [C_i, Nb-$(CH_2C_6H_5)_2$; 2,3-$Me_2C_2N_2(C_6H_5)_2$], 121.81, 120.13 ($C_5H_4SiMe_3$), 116.39 (C_i, $C_5H_4SiMe_3$), 110.06 (2,3-$Me_2C_2N_2Ph_2$), 52.82 [Nb-$(CH_2C_6H_5)_2$], 14.99 (2,3-$Me_2C_2N_2Ph_2$), −0.59 ($Me_3SiC_5H_4$)
7	7.20 (m), 6.90 [m, 10 H, 2,3-$Me_2C_2N_2(C_6H_5)_2$], 5.65 (m, 2 H), 5.29 (m, 2 H, $H_4C_5SiMe_3$), 1.65 (s, 6 H, 2,3-$Me_2C_2N_2Ph_2$), 1.58 (s, 6 H, Nb−CMe_2−O), 0.28 (s, 9 H, $Me_3SiC_5H_4$)	148.55 [C_i, 2,3-$Me_2C_2N_2(C_6H_5)_2$], 122.80, 122.48 [2,3-$Me_2C_2N_2(C_6H_5)_2$], 119.13 (C_i, $C_5H_4SiMe_3$), 113.57, 110.96 ($C_5H_4SiMe_3$), 108.24 (2,3-$Me_2C_2N_2Ph_2$), 92.57 (Nb−CMe_2−O−), 30.15 (Nb−CMe_2−O−), 15.21 (2,3-$Me_2C_2N_2Ph_2$), 0.20 ($Me_3SiC_5H_4$)
8	7.02 (m), 6.77 [m, 13 H, 2,3-$Me_2C_2N_2(C_6H_5)_2$; Nb−N(2,6-$Me_2C_6H_3$)], 6.11 (m, 2 H), 5.42 (m, 2 H, $H_4C_5SiMe_3$), 1.85 [s, 6 H, Nb−N(2,6-$Me_2C_6H_3$)], 1.64 (s, 6 H, 2,3-$Me_2C_2N_2Ph_2$), 1.46 (s, 6 H, Nb−CMe_2−), 0.14 (s, 9 H, $Me_3SiC_5H_4$)	153.83, 148.02 [C_i, 2,3-$Me_2C_2N_2(C_6H_5)_2$; Nb−N(2,6-$Me_2C_6H_3$)], 134.13, 127.80, 123.08 [2,3-$Me_2C_2N_2(C_6H_5)_2$; Nb−N(2,6-$Me_2C_6H_3$)], 123.81, 109.45 ($C_5H_4SiMe_3$), 110.18 (C_i, $C_5H_4SiMe_3$), 109.00 (2,3-$Me_2C_2N_2Ph_2$), 65.70 (Nb−CMe_2−), 30.70 (Nb−CMe_2−), 20.39 [Nb−N(2,6-$Me_2C_6H_3$)], 16.07 (2,3-$Me_2C_2N_2Ph_2$), 0.64 ($Me_3SiC_5H_4$)
9	7.30 (m), 6.90 [m, 13 H, 2,3-$Me_2C_2N_2(C_6H_5)_2$; Nb−C=N(2,6-$Me_2C_6H_3$)], 6.74 (m, 1 H), 6.56 (m, 1 H), 6.45 (m, 1 H), 5.89 (m, 1 H, $H_4C_5SiMe_3$), 2.54 (s, 3 H), 2.00 (s, 3 H, 2,3-$Me_2C_2N_2Ph_2$), 1.92 (s, 3 H), 1.88 [s, 3 H, Nb−C=N(2,6-$Me_2C_6H_3$)], 1.47 (s, 3 H), 1.03 (s, 3 H, Nb−OCMe_2−), −0.51 (s, 9 H, $Me_3SiC_5H_4$)	216.56 [Nb−C=N(2,6-$Me_2C_6H_3$)], 153.20, 151.13, 150.15 [C_i, 2,3-$Me_2C_2N_2(C_6H_5)_2$; Nb−C=N(2,6-$Me_2C_6H_3$)], 129.26, 127.65, 126.18, 125.24 [2,3-$Me_2C_2N_2(C_6H_5)_2$; Nb−C=N(2,6-$Me_2C_6H_3$)], 124.45, 121.55, 113.82, 110.05 ($C_5H_4SiMe_3$), not observed (C_i, $C_5H_4SiMe_3$), 108.22 (2,3-$Me_2C_2N_2Ph_2$), 98.80 (Nb−O−CMe_2−), 27.44, 26.86 (Nb−O−CMe_2−), 19.59, 19.30 [Nb−C=N(2,6-$Me_2C_6H_3$)], 16.98, 14.77 (2,3-$Me_2C_2N_2Ph_2$), −0.97 ($Me_3SiC_5H_4$)
10	7.20 (m), 6.80 [m, 16 H, 2,3-$Me_2C_2N_2(C_6H_5)_2$; Nb−C=N(2,6-$Me_2C_6H_3$)−; Nb−C=NAr−C=N(2,6-$Me_2C_6H_3$)], 6.59 (m, 2 H), 6.50 (m, 2 H, $H_4C_5SiMe_3$), 2.58 (s, 3 H), 2.04 (s, 3 H, 2,3-$Me_2C_2N_2Ph_2$), 2.02 (s, 3 H), 1.89 [s, 3 H, Nb−C=N(2,6-$Me_2C_6H_3$)−], 1.88 (s, 3 H), 1.74 [s, 3 H, Nb−C=NAr−C=N(2,6-$Me_2C_6H_3$)], 1.06 (s, 3 H), 0.76 (s, 3 H, Nb−O−CMe_2−), −0.41 (s, 9 H, $Me_3SiC_5H_4$)	not observed (Nb−C=NAr), 176.73 (Nb−C=NAr−C=NAr), 155.11, 151.39, 151.08, 148.17 [C_i, 2,3-$Me_2C_2N_2(C_6H_5)_2$; Nb−C=N(2,6-$Me_2C_6H_3$); Nb−C=NAr−C=N(2,6-$Me_2C_6H_3$)], 128.80, 127.67, 127.62, 127.59, 125.98, 125.81 [2,3-$Me_2C_2N_2(C_6H_5)_2$; Nb−C=N(2,6-$Me_2C_6H_3$); Nb−C=NAr−C=N(2,6-$Me_2C_6H_3$)], 118.41, 115.04, 112.52, 111.96 ($C_5H_4SiMe_3$), not observed (C_i, $C_5H_4SiMe_3$), 109.87 (2,3-$Me_2C_2N_2Ph_2$), 81.90 (Nb−O−CMe_2−), 29.24, 28.33 (Nb−O−CMe_2−), 20.55, 20.10, 19.12, 18.73 [Nb−C=N(2,6-$Me_2C_6H_3$); Nb−C=NAr−C=N(2,6-$Me_2C_6H_3$)], 16.64, 14.83 (2,3-$Me_2C_2N_2Ph_2$), −0.87 ($Me_3SiC_5H_4$)

known structural parameters of related complexes and the computed data, the best description would be to consider a formal d^0 configuration at the metal centre and dianionic ene-diamido (**I**) or 2-butene-1,4-diyl (**II**) ligands. The $MCpX_2$ metal fragment orbitals have been discussed[28] and they are a subset of three low-lying frontier orbitals, two

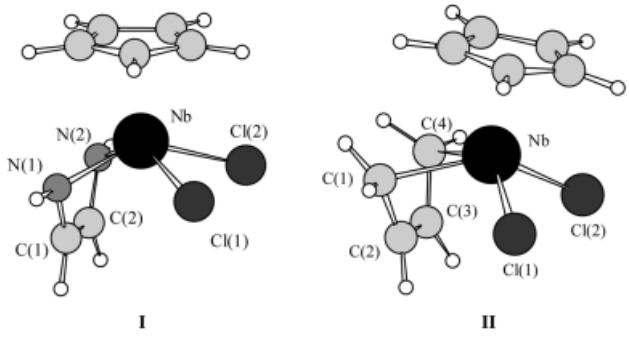

Figure 1. Optimised structures of the [$NbCpCl_2(HNCHCHNH)$] (**I**) and [$NbCpCl_2(CH_2CHCHCH_2)$] (**II**) model complexes

Table 3. Selected bond lengths [Å], angles and torsion angles [°] for calculated [$NbCpCl_2(HNCHCHNH)$] model complex **I** and, for comparison, selected experimental data for compounds [$NbCp^*Cl_2$(*p*-MeO−C_6H_4,H-DAD)], CSD refcode = LIWVES,[13f] and [$NbCpCl_2$(*t*Bu,H-DAD)], CSD refcode = WASHON[13a]

Complex or CSD refcode:[a]	**I**	LIWVES	WASHON
Nb−Cl(1)	2.487	2.483(1)	2.505(1)
Nb−Cl(2)	2.487	2.494(1)	2.527(1)
Nb−N1	2.051	2.049(3)	2.015(4)
Nb−C1	2.532	2.480(4)	2.409
Nb−C2	2.532	2.474(4)	2.402
Nb−N2	2.051	2.038(3)	2.021(4)
C1−C2	1.407	1.379(5)	1.402
N1−C1	1.366	1.367(5)	1.354
C2−N2	1.366	1.371(5)	1.364
Cl1−Nb−Cl2	82.1	79.39(4)	78.78(5)
Cl1−Nb−N1	85.3	83.76(9)	85.5(1)
Cl1−Nb−N2	139.7	138.4	140.4(1)
Cl2−Nb−N1	139.7	138.6	138.2(1)
Cl2−Nb−N2	85.3	85.25(9)	83.5(1)
N1−Nb−N2	80.0	82.8(1)	84.7(2)
Nb−N1−C1	93.5	90.9(2)	89.1
Nb−N2−C2	93.5	90.9(2)	88.2
N1−C1−C2	116.8	118.7(4)	118.7
C1−C2−N2	116.8	119.0(4)	119.2
Nb−N1−N2−C2	120.7	120.62(3)	118

[a] Cambridge Structural Database System, Cambridge Crystallographic Data Centre, 12 Union Road, Cambridge CB2 1EZ, UK [Fax: (internat.) + 44-1223/336-033; E-mail: deposit@ccdc.cam.ac.uk].

of *a′* (1*a′*, $d_{x^2-y^2}$, and 2*a′*, d_{z^2}) and one of *a″* (1*a″*, d_{xy}) symmetries, and a second subset, higher in energy, of two frontier orbitals (3*a′*, d_{xz} and 2*a″*, d_{yz}).

The interpretation of the bonding scheme of the η^4-butadiene ligand bound to early transition metals is well established.[29] In particular, a detailed early EHMO analysis was reported[30] for (cyclopentadienyl)tantalum complexes containing the bent 1-metallacyclopent-3-ene structure. The bonding description in **II** is similar and can be briefly summarized as follows: The strongest interactions are the donation of the π_2 orbital to 1*a″* and the donation of π_3* to 1*a′*, and also in minor proportion to the 2*a′* FMOs. Other minor details require no further discussion. The computed bond lengths in the butadiene fragment show the expected

Table 4. Selected bond lengths [Å], angles and torsion angles [°] for calculated [$NbCpCl_2(CH_2CHCHCH_2)$] model complex **II** and, for comparison, selected experimental data for compounds [$NbCp^*$\{*o*-$(CH_2)_2C_6H_4$\}Cl_2], CSD refcode = JABTIP,[44] [$NbCp^*$(butadiene)(η^3-cot)], CSD refcode = JABYEQ[44] and [$NbCp^*$(butadiene)\{$CH_2CH(C_{10}H_6)CH$\}], CSD refcode = ROMSIV01[9c]

Complex or CSD refcode:	**II**	JABTIP	JABYEQ	ROMSIV01
Nb−Cl(1)	2.445	2.409(1)	–	–
Nb−Cl(2)	2.445	2.419(1)	–	–
Nb−C1	2.302	2.240(5)	2.307(4)	2.18(3)
Nb−C2	2.431	2.544(4)	2.424(4)	2.34(2)
Nb−C3	2.430	2.556(4)	2.393(4)	2.33(2)
Nb−C4	2.302	2.236(5)	2.270(4)	2.28(2)
C2−C3	1.395	1.415(6)	1.382(6)	1.38(3)
C1−C2	1.449	1.457(7)	1.415(6)	1.38(3)
C3−C4	1.449	1.455(7)	1.423(6)	1.40(3)
Cl1−Nb−Cl2	96.1	92.58(5)		
Cl1−Nb−C1	83.4	83.8(2)		
Cl1−Nb−C4	138.8	138.9(2)		
Cl2−Nb−C1	138.8	137.9(1)		
Cl2−Nb−C4	83.4	84.2(2)		
C1−Nb−C4	71.3	72.2(2)	72.2(2)	71(1)
Nb−C1−C2	77.1	84.1(3)	84.1(3)	78(2)
Nb−C4−C3	77.1	84.9(3)	84.9(3)	74(1)
C1−C2−C3	116.4	115.4(5)	115.4(5)	116(3)
C2−C3−C4	116.4	114.2(5)	114.2(5)	115(2)
Nb−C1−C4−C3	92.8	101.8	101.8	93.6

long-short-long bond alternation, indicating the involvement of the σ^2,π bonding contribution, and compare well with other bond lengths reported in recent related DFT studies.[31]

With reference to **I**, the FMO analysis shows that the strongest interaction is also the donation of the π_2 orbital (that is now substantially lower in energy in comparison with the similar π_2 orbital in the butadiene ligand, see Scheme 3) to 1*a″*. This donation is now completed by the participation of the *out-of-phase* σ_{op} contribution. The donation of the π_3* orbital is also active but is now directed preferentially to the 2*a′* FMO and only in a small percentage to 1*a′*. The latter metal orbital is substantially saturated by the donation of *in-phase* σ_{ip} FMO. These subtle dissimilarities in the bonding analysis in **I** with respect to **II** are responsible for the important differences found in the HOMO of the two model complexes (see Figure 2).

In the HOMO of **I** the nitrogen π lobes overlap significantly with the lobes of the 2*a′* ($d_{x^2-y^2}$) orbital while the carbon π orbitals (part of the ligand's HOMO π_3*) do not overlap with the metal lobes and are only involved in the C−C bonding interaction. Moreover, a detailed analysis of the fragment orbital interactions provides no evidence for carbon π electron donation toward the metal centre. Contrarily, the HOMO of **II** shows the overlap of all carbon π lobes of π_3* with both the 1*a′* and 2*a′* FMOs. In conclusion, the bonding of the ene-diamido (or diazabutadiene) ligand is different with respect to the conventional σ^2,π-description of the butadiene ligand. The donation through the π component is contributed by the nitrogen atoms, con-

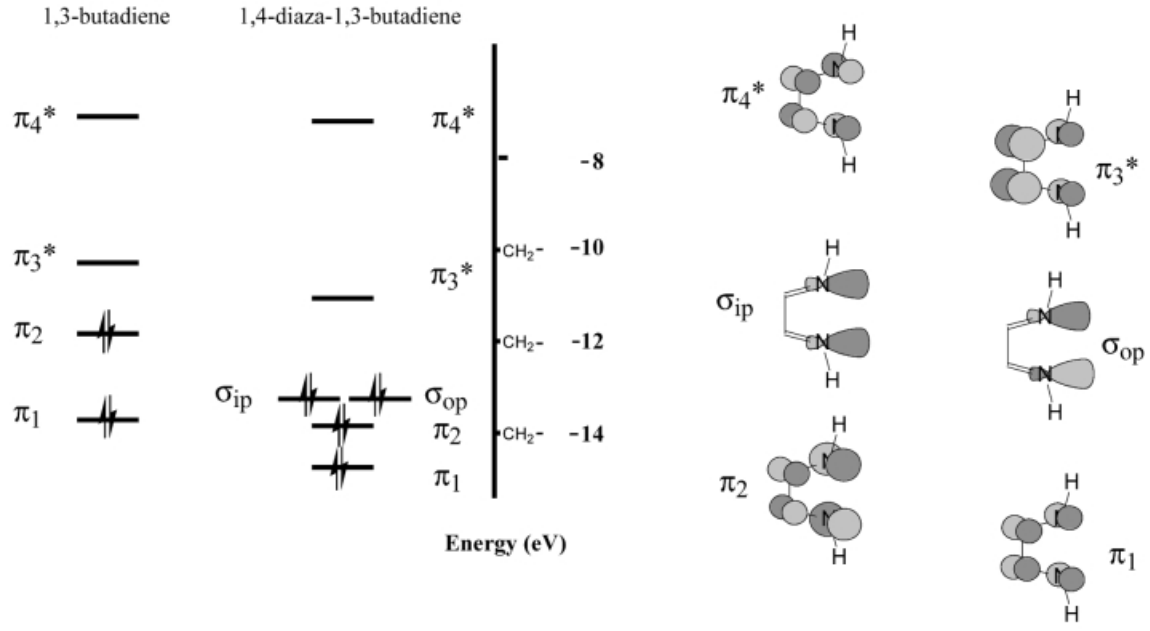

Scheme 3. Representation of the FMOs corrresponding to the 1,4-diaza-1,3-butadiene ligand and energy distribution of such orbitals in comparison with those of 1,3-butadiene ligand

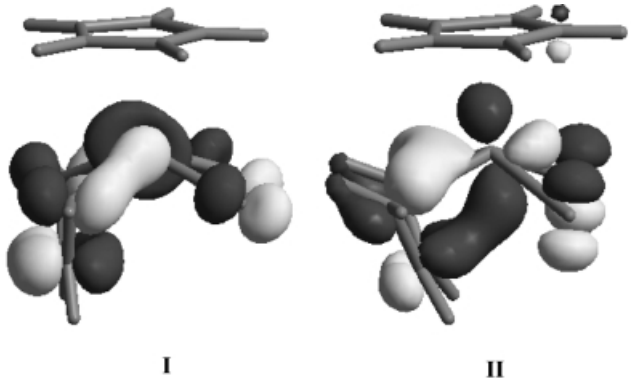

Figure 2. 3D isosurfaces corresponding to the HOMO of the [$NbCpCl_2(HNCHCHNH)$] (**I**) and [$NbCpCl_2(CH_2CHCHCH_2)$] (**II**) model complexes

sequently, the interaction between the Nb and carbon atoms is not significant.

Alkylation of **1** with Grignard reagents, in a 1:2 molar ratio, yields the dialkyl complexes [$NbCp'R_2$(Me,Ph-DAD)] (R = Me, **4**; CH_2SiMe_3, **5**; $CH_2C_6H_5$, **6**) as red-brown microcrystalline solids (Scheme 2). The ^1H NMR spectrum of **4** displays a singlet at $\delta = 0.15$ due to Nb−Me and show an AB spin system for diastereotopic α-CH_2 protons of alkyl groups in the complexes **5** and **6**. A singlet due to the methyl substituents of the ene-diamido ligand emerges at $\delta \approx 1.75$, this being at higher field compared with that ($\delta = 1.84$) of the starting dichloro complex **1**. Additionally, the ^{13}C resonances of the inner carbon atoms show a high field displacement. The data, along with the preferential orientation discussed by Mashima et al.[15] in related complexes, suggest that the alkylation reactions of the dichloro complex involves an orientation change in the ene-diamido ligand from the *supine* conformation in **1** to the *prone* form in the dialkyl derivatives **4**−**6**.[32]

Dimethyl complex **4** reacts with carbon monoxide (1 atm) at room temperature in toluene to give the oxaniobacyclopropane complex [$NbCp'\{\eta^2$-$(O)CMe_2\}$(Me,Ph-DAD)] (**7**), in good yield (Scheme 4), as a result of a double migration of two methyl groups, first to the electrophilic carbon atom of the coordinated CO and then to the related η^2-acyl intermediate, which cannot be detected. The oxaniobacyclopropane moiety which is not further transformed, is analogous to that reported for (acetone)tantalum complexes [TaCp*

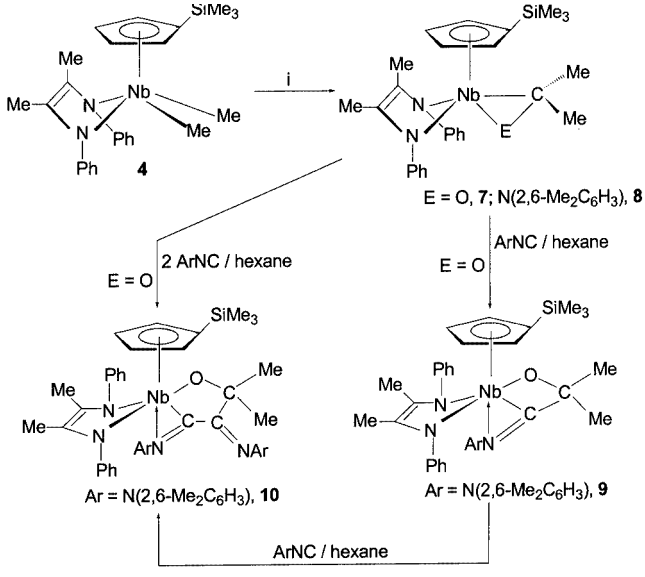

Scheme 4. Reagents and conditions: i: E = O, CO (1 atm), toluene, 5 d, room temp.; E = N(2,6-$Me_2C_6H_3$), 1 equiv. 2,6-$Me_2C_6H_3NC$, hexane, 12 h, room temp.

$X_2\{\eta^2\text{-}(O)CMe_2\}$] (X = Cl,[20e] Me[33]). When 1 equiv. of isocyanide 2,6-$Me_2C_6H_3NC$ is added to a hexane solution of **4** under rigorously anhydrous conditions, an orange solution is obtained, which after evaporation of the solvent produces the azaniobacyclopropane complex [NbCp′$\{\eta^2$-(ArN)$CMe_2\}$(Me,Ph-DAD)] (Ar = 2,6-$Me_2C_6H_3$, **8**). Formation of this compound can be explained as the result of two consecutive steps. The first step involves migration of one methyl group to the electrophilic isocyanide carbon atom, giving an η^2-iminoacyl intermediate,[19,34] which cannot be detected during monitoring of the entire reaction by ^{1}H NMR spectroscopy. Subsequent migration of the second methyl group to the iminoacyl carbon centre yields an azaniobacyclopropane system.[20a,20b,35] Dialkyl complexes **5**, **6** do not react with isocyanide at room temperature and when the solution is heated the reaction probably takes place simultaneously with the decomposition of the organometallic complex formed, leading to an unidentified product mixture.

On the other hand, azaniobacyclopropane complex **8** is obtained upon reaction of 2 equiv. of isocyanide with the dimethyl derivative **4**, in contrast to that observed in the case of the azatantalacyclopropane species [TaCp*$\{\eta^2$-(ArN)$CMe_2\}$][35b] (Ar = 2,6-$Me_2C_6H_3$; 2,4,6-$Me_3C_6H_2$), which in the presence of isocyanides gives the corresponding dichloro(imido) complexes [TaCp*Cl_2(NAr)] with elimination of the arylimine ketene Ar−N=C=CMe_2. However, the oxaniobacyclopropane complex **7** reacts with 1 or 2 equiv. of 2,6-$Me_2C_6H_3NC$ leading to the expected insertion products [NbCp′$\{\eta^2$-(O)CMe_2-$(CNAr)_x\}$(Me,Ph-DAD)] (Ar = 2,6-$Me_2C_6H_3$; x = 1, **9**; 2, **10**). Compound **9** can be transformed into **10** by a simple isocyanide insertion reaction.

The ^{1}H NMR spectra of complexes **7** and **8** show an AA′BB′ spin system for the proton atoms of the $C_5H_4SiMe_3$ ring, whereas the $^{13}C\{^1H\}$ NMR spectra show three carbon resonances for the same group, in agreement with the existence of a symmetry plane perpendicular to such a ring. At room temperature, the equivalence of both methyl groups of the oxa- and azaniobacyclopropane moiety (**7** and **8**), as evidenced by the ^{1}H and $^{13}C\{^1H\}$ NMR spectra, argue a metallacyclic structure whose plane defined by the niobium, oxygen (**7**) or nitrogen (**8**) and carbon atoms is perpendicular to the cyclopentadienyl ring plane. Unfortunately, we were not able to obtain crystals adequate for X-ray diffraction, but the structure must be reasonably similar to that presented for related azametallacyclopropane complexes [MCp*$X_2\{\eta^2$-(ArN)$CMe_2\}$] (Ar = 2,6-$Me_2C_6H_3$; X = Cl, Me; M = Nb,[35c] Ta[35b]). The chemical shifts of their DAD resonances are similar to that of **4**, indicating a *prone* conformation of the DAD ligand. Thus, the resonance at δ = 109.0 is assigned to the equivalent olefinic carbon atoms of the DAD ligand, while the signals corresponding to the C^α atom of the oxa- and azaniobacyclopropane systems appear at δ = 92.57 (**7**) and 75.7 (**8**); these signals shift to higher fields as compared with the acyl and iminoacyl carbon atom.[36]

In complexes **9** and **10**, the ^{1}H and $^{13}C\{^1H\}$ NMR spectra show four protons (ABCD spin system, although for **10** only two multiplets are observable as a result of the proton overlapped signals) and five carbon resonances for the $C_5H_4SiMe_3$ ring. The data are consistent with a metal centre chiral character and therefore there is not a symmetry plane perpendicular to the (trimethylsilyl)cyclopentadienyl ring. The ^{1}H NMR spectrum of both complexes **9** and **10** show six singlets corresponding to three protons each between δ = 2.54−1.03 and 2.58−0.76, respectively. The lower field resonances in both the interval δ = 2.54, 2.00 (**9**) and 2.58, 2.04 (**10**) can be assigned to the methyl substituents of the DAD ligand. These data suggest a 2,5-diazaniobacyclopent-3-ene mode for the DAD ligand. A similar behaviour has been found by Mashima et al.[13f] in the synthesis of mixed DAD-butadiene complexes of general formulation [M(η^5-C_5R_5)(η^2-Ar,H-DAD)(η^4-butadiene)] (M = Nb, R = Me, H Ar = 4-$MeOC_6H_4$; M = Ta, R = Me, H Ar = 4-$MeOC_6H_4$, 2-MeC_6H_4, Cy). The signals corresponding to the nonequivalent *o*-methylphenyl groups of the inserted isocyanide are observed as singlets at δ = 1.92 and 1.88 (**9**) and 2.02, 1.89, 1.88 and 1.74 (**10**), the two lower field resonances being assigned to the isocyanide directly bonded to the niobium atom. In addition, the rest of the signals, observed in its NMR spectra, are those expected for the proposed structures.

Conclusion

In this work, we synthesized several [(trimethylsilyl)cyclopentadienyl]niobium complexes with ene-diamido and ene-diolato ligands, through the reaction of [NbCp′Cl_2-($Me_3SiCCSiMe_3$)] with 2,3-dimethyl-1,4-diphenyl-1,4-diazabuta-1,3-diene (Me,Ph-DAD) and diketones. The spectroscopic data showed that the coordination mode of the chelating ligand depends, sensitively, on the ligand environment at the metal centre. Dichloro complexes **1**−**3** adopt a *supine* ene-diamido (**1**) or ene-diolato (**2**, **3**) structure. DFT studies have shown that the experimentally observed folding in DAD complexes (mode **A**) cannot be attributed to the π donation from the central C=C linkage because this interaction is negligible. The bonding of the ene-diamido ligand is different with respect to the conventional σ^2,π description of butadiene. The nitrogen atoms contribute to the donation through the π component and, consequently, the interaction between the niobium and carbon atoms is not significant. Reactions of dichloro complex **1** with alkylating reagents gave dialkyl complexes **4**−**6** and during the reaction course, the *supine* orientation of the ene-diamido ligand, bound to the metal centre, was flipped to the *prone* one. Dimethyl complex **4** reacts with carbon monoxide and isocyanide to give oxa- and azaniobacyclopropane derivatives **7** and **8** as a result of the migration of both methyl groups and via η^2-acyl and η^2-iminoacyl intermediates, respectively, which could not be observed. Successive isocyanide insertion reactions into the Nb−C bond take place in the

oxaniobacyclopropane complex **7** leading to the expected insertion products **9**, **10**.

Experimental Section

General: All reactions and manipulations were carried out under argon using standard Schlenk-tube and cannula techniques or in a conventional argon-filled glove-box. Solvents were refluxed in the presence of an appropriate drying agent and distilled and degassed prior to use: [D_6]benzene and hexane (Na/K alloy), diethyl ether (Na/benzophenone) and toluene (Na). Literature methods were employed for the synthesis of starting materials [Nb(η^5-$C_5H_4SiMe_3$)Cl_2($Me_3SiCCSiMe_3$)][16] and 2,3-dimethyl-1,4-diphenyl-1,4-diazabuta-1,3-diene (Me,Ph-DAD).[37] Reagent grades were purchased from commercial sources and used without further purification as follows: R−CO−CO−R (R = Me, Aldrich; R = Ph, Avocado), MgClR (Aldrich; R = Me 3 M in diethyl ether; R = CH_2SiMe_3, 1 M in diethyl ether; R = $CH_2C_6H_5$, 2 M in tetrahydrofuran), CO (Air Liquide) and 2,6-$Me_2C_6H_3NC$ (Fluka). Infrared spectra were recorded with Perkin−Elmer 883 and Spectrum 2000 spectrophotometers (4000−200 cm^{-1}) with samples as Nujol mulls between CsI plates or polyethylene pellets. ^1H and $^{13}C\{^1H\}$ NMR spectra were recorded with Varian Unity 300 and Varian Unity 500 Plus spectrometers; chemical shifts were referenced to the ^{13}C (δ = 128) and ^1H (δ = 7.15) residual resonances of the [D_6]benzene solvent. C, H and N analyses were carried out with a Perkin−Elmer 2400 microanalyser.

[NbCp′Cl_2(Me,Ph-DAD)] [Cp′ = η^5-$C_5H_4SiMe_3$; Me,Ph-DAD = PhNC(Me)C(Me)NPh] (1): A sample of [NbCp′Cl_2($Me_3SiCCSiMe_3$)] (0.70 g, 1.49 mmol) was dissolved in hexane (20 mL) in a Schlenk tube. After addition of a hexane (15 mL) solution of 2,3-dimethyl-1,4-diphenyl-1,4-diazabuta-1,3-diene (0.35 g, 1.49 mmol), the colour of the mixture changed to brown. The reaction mixture was stirred for 12 h at room temperature and then the resulting suspension was decanted and filtered. The residual solid was washed with cold hexane (2 × 5 mL), dried in vacuum and identified as complex **1**. Yield 0.71 g (89%). $C_{24}H_{29}Cl_2N_2NbSi$ (537.407): calcd. C 53.64, H 5.44, N 5.21; found C 53.52, H 5.53, N 5.11.

[NbCp′Cl_2{O(R)CC(R)O}] (R = Me, 2; Ph, 3): A solution of R−CO−CO−R (2.98 mmol; R = Me, 0.28 ml; Ph, 0.62 g) in hexane (20 mL) was added to a solution of [NbCp′Cl_2($Me_3SiCCSiMe_3$)] (1.40 g, 2.98 mmol) in hexane (25 mL) at room temperature. The mixture was stirred for 12 h. The resulting garnet suspension was filtered, the microcrystalline solid washed with cold hexane (2 × 5 mL), dried in vacuum and identified as **2** and **3**. **2:** Yield: 1.14 g (80%). $C_{12}H_{19}Cl_2NbO_2Si$ (387.179): calcd. C 37.23, H 4.95; found C 37.27, H 5.01. **3:** Yield: 1.26 g (85%). $C_{22}H_{23}Cl_2NbO_2Si$ (511.321): calcd. C 51.68, H 4.53; found C 51.58, H 4.66.

[NbCp′R_2(Me,Ph-DAD)] (R = Me, 4; CH_2SiMe_3, 5; $CH_2C_6H_5$, 6): A solution of MgClR (2.60 mmol; R = Me, 0.87 mL of a 3 M solution in diethyl ether; CH_2SiMe_3, 2.60 mL of a 1 M solution in diethyl ether; $CH_2C_6H_5$, 1.30 mL of a 2 M solution in THF) was added to a solution of **1** (0.70 g, 1.30 mmol) in diethyl ether (30 mL) at room temperature − except for R = $CH_2C_6H_5$ at −78 °C − and the mixture was stirred for 12 h. The $MgCl_2$ formed was removed by filtration and the resulting filtrate was concentrated to a volume of ca. 10 mL. On cooling to −40 °C, red-brown microcrystalline solids (**4**−**6**) were deposited. **4:** Yield: 0.41 g (64%). $C_{26}H_{35}N_2NbSi$ (496.571): calcd. C 62.89, H 7.10, N 5.74: found C 62.85, H 7.14, N 5.64. **5:** Yield: 0.50 g (60%). $C_{32}H_{51}N_2NbSi$ (584.765): calcd. C 65.73, H 8.79, N 4.79: found C 65.67, H 8.69, N 4.75. **6:** Yield: 0.51 g (60%). Repeated attempts to obtain a satisfactory microanalysis on this material were unsuccessful.

[NbCp′{η^2-(O)CMe_2}(Me,Ph-DAD)] (7): A toluene (20 mL) solution of **4** (0.70 g, 1.40 mmol) was placed into an ampoule under CO (1 atm) and then sealed. The reaction mixture was stirred at room temperature for 5 d. Then the ampoule was opened, the solution filtered, concentrated to ca. 5 mL and cooled to −40 °C to give **7** as red microcrystalline solid. Yield 0.55 g (75%). $C_{27}H_{35}N_2NbOSi$ (524.581): calcd. C 61.82, H 6.72, N 5.34; found C 61.72, H 6.68, N 5.27.

[NbCp′{η^2-(ArN)CMe_2}(Me,Ph-DAD)] (Ar = 2,6-$Me_2C_6H_3$) (8): A solution of isocyanide 2,6-$Me_2C_6H_3NC$ (0.18 g, 1.40 mmol) in hexane (10 mL) was added at room temperature to a reddish solution of **4** (0.70 g, 1.40 mmol) in hexane (30 mL) and stirred for 12 h. The resulting orange solution was filtered, concentrated to ca. 10 mL and cooled to −40 °C to give **8** as orange microcrystalline solid. Yield 0.62 g (70%). $C_{35}H_{44}N_3NbSi$ (627.749): calcd. C 66.97, H 7.06, N 6.69; found C 67.02, H 7.16, N 6.58.

[NbCp′{η^2-(O)CMe_2−$(CNAr)_x$}(Me,Ph-DAD)] [Ar = 2,6-$Me_2C_6H_3$; *x* = 1 (9); 2 (10)]. 9: A stirred solution of **7** (0.70 g, 1.33 mmol) in hexane (25 mL) was treated with 2,6-$Me_2C_6H_3NC$ (0.17 g, 1.33 mmol) in a 1:1 molar ratio and under rigorously anhydrous conditions for 48 h. The resulting solution was concentrated to ca. 10 mL and cooled to −40 °C to give **9** as dark brown microcrystalline solid. Yield 0.52 g (60%). $C_{36}H_{44}N_3NbOSi$ (655.759): calcd. C 65.94, H 6.76, N 6.41; found C 65.90, H 6.67, N 6.39. **10. Method A:** A dark-brown solution of **9** (0.70 g, 1.06 mmol) in hexane (30 mL) under rigorously anhydrous conditions in a Schlenk tube. After addition of a hexane (10 mL) solution of isocyanide 2,6-$Me_2C_6H_3NC$ (0.14 g, 1.06 mmol) the colour of the mixture changed to pale-brown. The reaction mixture was stirred for 48 h at room temperature and then the resulting suspension was decanted and filtered. The residual pale-brown solid was washed with cold hexane (2 × 5 mL), dried in vacuum and identified as **10**. **Method B:** The oxaniobacyclopropane complex **7** (0.70 g, 1.33 mmol) was dissolved in 30 mL of hexane and isocyanide 2,6-$Me_2C_6H_3NC$ (0.34 g, 2.66 mmol) in a 1:2 molar ratio. The solution was stirred and the brown solid formed after 4 d, it was collected by decanting the solvent, washed with 5 mL of cold hexane and identified as **10**. Yield 0.54 g (65%). Repeated attempts to obtain a satisfactory microanalysis on this material were unsuccessful.

Computational Details: The electronic structures and geometries of the model complexes were computed within the density functional theory at the BP86[38] and B3LYP[39] levels using the LANL2DZ[40] basis set. A set of *d* polarisation functions was added to Cl, C and N atoms. Only the results at the B3LYP level of theory have been discussed in the paper. BP86 results are completely equivalent and they have not been discussed but included as Supporting Information. All the optimised geometries were characterized as local energy minima by diagonalisation of the analytically computed Hessian (vibrational frequencies calculations). All the DFT calculations were performed using the Gaussian 98 suite of programs.[41] Molecular orbitals were visualised using the Chem3D Pro program.[42] The FMO analyses were performed with CACAO[43] using the coordinates, at the B3LYP level, of the optimised model complexes.

Acknowledgments

We are grateful to DGICYT (Projects PB 97-0761 and PB 97-0740) for financial support of this research. We thank the Spanish Ministerio de Educación, Cultura y Deporte for a student research grant (D. R.).

[1] [1a] G. Wilkinson, F. G. A. Stone, E. W. Abel (Eds.), *Comprehensive Organometallic Chemistry II*, Pergamon Press, Oxford, **1995**, vol. 4. [1b] K. Mashima, Y. Nakayama, A. Nakamura, *Adv. Polym. Sci.* **1997**, *133*, 1−51.

[2] [2a] P.-J. Sinnema, L. Van der Veen, A. L. Spek, N. Veldman, J. H. Teuben, *Organometallics* **1997**, *16*, 4245−4247. [2b] R. Kravchenko, A. Massood, R. M. Waymouth, C. L. Myers, *J. Am. Chem. Soc.* **1998**, *120*, 2039−2046. [2c] J. B. Jaquith, C. J. Levy, G. V. Bondar, S. Wang, S. Collins, *Organometallics* **1998**, *17*, 914−925. [2d] A. F. Kiely, C. M. Nelson, A. Pastor, L. M. Henling, M. W. Day, J. E. Bercaw, *Organometallics* **1998**, *17*, 1324−1332.

[3] [3a] H. H. Brintzinger, D. Fischer, R. Mülhaupt, B. Rieger, R. M. Waymouth, *Angew. Chem. Int. Ed. Engl.* **1995**, *34*, 1143−1170. [3b] M. Bochmann, *J. Chem. Soc., Dalton Trans.* **1996**, 255−270. [3c] J. A. Gladyzs, *Chem. Rev.* **2000**, *100*, 1167−1168 and the articles that appeared in this monographic issue devoted to metal-catalysed polymerisation.

[4] [4a] J. C. Stevens, F. J. Timmers, D. R. Wilson, G. F. Schmidt, P. N. Nickias, R. K. Rosen, G. W. Knight, S. Lai (to Dow), *Eur. Pat. Appl.* 416815, **1990**. [4b] J. A. M. Canich (to Exxon), *Eur. Pat. Appl.* 420436, **1990**. [4c] T. K. Woo, L. Fan, T. Ziegler, *Organometallics* **1994**, *13*, 432−433; T. K. Woo, L. Fan, T. Ziegler, *Organometallics* **1994**, *13*, 2252−2261. [4d] L. Fan, D. Harrison, T. K. Woo, T. Ziegler, *Organometallics* **1995**, *14*, 2018−2026. [4e] T. K. Woo, P. M. Margl, J. C. W. Lohrenz, P. E. Blöchl, T. Ziegler, *J. Am. Chem. Soc.* **1996**, *118*, 13021−13030.

[5] [5a] J. D. Scollard, D. H. McConville, *J. Am. Chem. Soc.* **1996**, *118*, 10008−10009. [5b] A. D. Horton, J. de With, *Chem. Commun.* **1996**, 1375−1376. [5c] S. Tinkler, R. J. Deeth, D. J. Duncalf, A. McCamley, *Chem. Commun.* **1996**, 2623−2624. [5d] A. D. Horton, J. de With, A. J. Van der Linden, H. Van de Weg, *Organometallics* **1996**, *15*, 2672−2674. [5e] F. G. N. Cloke, T. J. Geldbach, P. B. Hitchcock, J. B. Love, *J. Organomet. Chem.* **1996**, *506*, 343−345. [5f] J. D. Scollard, D. H. McConville, N. C. Payne, J. J. Vittal, *Macromolecules* **1996**, *29*, 5421−5243. [5g] S. A. A. Shan, H. Dorn, A. Voight, H. W. Roesky, E. Parisini, H. G. Schmidt, M. Noltemeyer, *Organometallics* **1996**, *15*, 3176−3181. [5h] R. Baumann, W. M. Davis, R. R. Schrock, *J. Am. Chem. Soc.* **1997**, *119*, 3830−3831. [5i] N. A. H. Male, M. Thornton-Pett, M. Bochmann, *J. Chem. Soc., Dalton Trans.* **1997**, 2487−2494.

[6] [6a] R. Hoffman, *Angew. Chem. Int. Ed. Engl.* **1982**, *21*, 711−724. [6b] D. N. Williams, J. P. Mitchell, A. D. Poole, U. Siemeling, W. Clegg, D. C. R. Hockless, P. N. O'Neil, V. C. Gibson, *J. Chem. Soc., Dalton Trans.* **1992**, 739−751.

[7] K. Mashima, Y. Tanaka, A. Nakamura, *Organometallics* **1995**, *14*, 5642−5651.

[8] [8a] K. Mashima, S. Fujikawa, A. Nakamura, *J. Am. Chem. Soc.* **1993**, *115*, 10990−10991. [8b] K. Mashima, S. Fujikawa, H. Urata, E. Tanaka, A. Nakamura, *J. Chem. Soc., Chem. Commun.* **1994**, 1623−1624. [8c] K. Mashima, S. Fujikawa, Y. Tanaka, Y. Urata, T. Oshiki, E. Tanaka, A. Nakamura, *Organometallics* **1995**, *14*, 2633−2640.

[9] [9a] K. Mashima, Y. Tanaka, M. Kaidzu, A. Nakamura, *Organometallics* **1996**, *15*, 2431−2433. [9b] K. Mashima, M. Kaidzu, Y. Nakayama, A. Nakamura, *Organometallics* **1997**, *16*, 1345−1348. [9c] K. Mashima, M. Kaidzu, Y. Tanaka, Y. Nakayama, A. Nakamura, J. G. Hamilton, J. J. Rooney, *Organometallics* **1998**, *17*, 4183−4195.

[10] [10a] G. van Koten, K. Vrieze, *Adv. Organomet. Chem.* **1982**, *21*, 151−239. [10b] K. Vrieze, *J. Organomet. Chem.* **1986**, *300*, 307−326.

[11] The notation R,R′-DAD represents the 1,4-diaza-1,3-butadiene RN=CR′CR′=NR. See for example the recent paper: J. Scholz, G. A. Hadi, K.-H. Thiele, H. Görls, R. Weimann, H. Schumann, J. Sieler, *J. Organomet. Chem.* **2001**, *626*, 243−259.

[12] [12a] L. R. Chamberlain, L. D. Durfee, P. E. Fanwick, L. M. Kobriger, S. L. Latesky, A. K. McMullen, B. D. Steffey, I. P. Rothwell, K. Folting, J. C. Huffman, *J. Am. Chem. Soc.* **1987**, *109*, 6068−6076. [12b] M. J. Scott, S. J. Lippard, *Organometallics* **1997**, *16*, 5857−5868. [12c] T. Spaniel, H. Görls, J. Scholz, *Angew. Chem. Int. Ed.* **1998**, *37*, 1862−1865.

[13] [13a] L. G. Hubert-Pfalzgraf, A. Zaki, *Acta Crystallogr., Sect. C* **1993**, *49*, 1609−1611. [13b] B. Richter, J. Scholz, J. Sieler, K.-H. Thiele, *Angew. Chem. Int. Ed. Engl.* **1995**, *34*, 2649−2651. [13c] J. Wunderle, J. Scholz, U. Baumeister, H. Hartung, *Z. Kristallogr.* **1996**, *211*, 423−424. [13d] K. Mashima, Y. Matsuo, K. Tani, *Chem. Lett.* **1997**, 767−768. [13e] H. Kawaguchi, Y. Yamamoto, K. Asaoka, K. Tatsumi, *Organometallics* **1998**, *17*, 4380−4386. [13f] K. Mashima, Y. Matsuo, K. Tani, *Organometallics* **1999**, *18*, 1471−1481. [13g] J. Sánchez-Nieves, P. Royo, M. A. Pellinghelli, A. Tiripicchio, *Organometallics* **2000**, *19*, 3161−3169.

[14] [14a] K. Aoyagi, P. K. Gantzel, T. D. Tilley, *Polyhedron* **1996**, *15*, 4299−4302. [14b] G. Jimenez Pindado, M. Thornton-Pett, M. Bochmann, *J. Chem. Soc., Dalton Trans.* **1998**, 393−400. [14c] J. M. Decams, S. Daniele, L. G. Hubert-Pfalzgraf, J. Vaissermann, S. Lecocq, *Polyhedron* **2001**, *20*, 2405−2414.

[15] A. Nakamura, K. Mashima, *J. Organomet. Chem.* **2001**, *621*, 224−230.

[16] A. Galindo, M. Gómez, P. Gómez-Sal, A. Martín, D. del Río, F. Sánchez, *Organometallics* **2002**, *21*, 293−304.

[17] A. Castro, M. Gómez, P. Gómez-Sal, A. Manzanero, P. Royo, *J. Organomet. Chem.* **1996**, *518*, 37−46.

[18] [18a] M. Gómez, G. Jimenez, P. Royo, J. M. Selas, P. R. Raithby, *J. Organomet. Chem.* **1992**, *439*, 147−154. [18b] I. de Castro, J. de la Mata, M. Gómez, P. Gómez-Sal, P. Royo, J. M. Selas, *Polyhedron* **1992**, *11*, 1023−1027.

[19] [19a] L. R. Chamberlain, L. D. Durfee, P. E. Fanwick, L. Kobriger, S. L. Latesky, A. K. McMullen, I. P. Rothwell, K. Folting, J. C. Huffman, W. E. Streib, R. Wang, *J. Am. Chem. Soc.* **1987**, *109*, 390−402. [19b] L. D. Durfee, I. P. Rothwell, *Chem. Rev.* **1988**, *88*, 1059−1079.

[20] [20a] W. K. Chiu, R. A. Jones, G. Wilkinson, A. M. R. Galas, M. B. Hursthouse, *J. Am. Chem. Soc.* **1980**, *102*, 7979−7980. [20b] W. K. Chiu, R. A. Jones, G. Wilkinson, A. M. R. Galas, M. B. Hursthouse, *J. Chem. Soc., Dalton Trans.* **1981**, 2088−2097. [20c] M. D. Curtis, S. Thanedar, W. M. Butler, *Organometallics* **1984**, *3*, 1855−1859. [20d] T. Y. Meyer, L. R. Garner, N. C. Baenzinger, L. W. Messerle, *Inorg. Chem.* **1990**, *29*, 4045−4050. [20e] M. Gómez, P. Gómez-Sal, G. Jimenez, A. Martín, P. Royo, J. Sánchez-Nieves, *Organometallics* **1996**, *15*, 3579−3587.

[21] [21a] C. D. Wood, R. R. Schrock, *J. Am. Chem. Soc.* **1979**, *101*, 5421−5422. [21b] A. Castro, M.V. Galakhov, M. Gómez, P. Gómez-Sal, A. Martín, F. Sánchez, *J. Organomet. Chem.* **2000**, *595*, 36−53.

[22] K. Nakamoto in *Characterization of Organometallics Compounds* (Ed.: M. Tsutsui), Interscience, New York, **1969**.

[23] [23a] A. Antiñolo, M. Fajardo, A. Otero, P. Royo, *J. Organomet. Chem.* **1982**, *234*, 309−314. [23b] A. Antiñolo, M. Fajardo, A. Otero, P. Royo, *J. Organomet. Chem.* **1983**, *246*, 269−278. [23c] A. Antiñolo, M. Fajardo, A. Otero, P. Royo, *J. Organomet. Chem.* **1984**, *265*, 35−43.

[24] J. Scholz, B. Richter, R. Goddard, C. Krüger, *Chem. Ber.* **1993**, *126*, 57−61.

[25] A. Galindo, A. Ienco, C. Mealli, *New J. Chem.* **2000**, *24*, 73−75.

[26] The optimisation of **I** with a *prone* conformation was unsuccessful. The attempts of optimisation of this isomer show a tendency of the metal−DAD moiety to attain a 2,5-diaza-1-metallacyclopent-3-ene structure with a five-membered ring ap-

proximately planar. This state is characterized by one imaginary frequency: D. del Río, A. Galindo, unpublished results.
[27] The *prone* configuration of butadiene ligand in **II** is 13.6 kcal mol^{-1} less stable than the *supine* isomer: D. del Río, A. Galindo, unpublished results.
[28] See for example: T. R. Ward, O. Schafer, C. Daul, P. Hofmann, *Organometallics* **1997**, *16*, 3207−3215.
[29] H. Yasuda, K. Tatsumi, A. Nakamura, *Acc. Chem. Res.* **1985**, *18*, 120−126.
[30] H. Yasuda, K. Tatsumi, T. Okamoto, K. Mashima, K. Lee, A. Nakamura, Y. Kai, N. Kanehisa, N. Kasai, *J. Am. Chem. Soc.* **1985**, *107*, 2410−2422.
[31] [31a] J. C. Green, M. L. H. Green, G. T. Taylor, J. Saunders, *J. Chem. Soc., Dalton Trans.* **2000**, 317−327. [31b] A. J. Sillanpää, K. E. Laasonen, *Organometallics* **2001**, *20*, 1334−1344. [31c] E. Le Grognec, R. Poli, *Chem. Eur. J.* **2001**, *7*, 4572−4583.
[32] Following the suggestion of one referee, we performed calculations on complex $NbCpMe_2(HNCHCHNH)$, as the simplest model of complexes **4**−**6**. The *prone* configuration of the DAD ligand in this model is a local minimum. However, the optimisation of the *supine* conformation was unsuccessful. Efforts to optimise this isomer yielded a planar five-membered ring where the metal−DAD moiety has a 2,5-diaza-1-metallacyclopent-3-ene structure, that is characterized by two imaginary frequencies. A complete report of this analysis will be published separately: D. del Río, A. Galindo, unpublished results.
[33] [33a] C. D. Wood, R. R. Schrock, *J. Am. Chem. Soc.* **1979**, *101*, 6450. [33b] J. M. Mayer, C. J. Curtis, J. E. Bercaw, *J. Am. Chem. Soc.* **1983**, *105*, 2651−2660.
[34] [34a] P. T. Wolczanski, J. E. Bercaw, *J. Am. Chem. Soc.* **1979**, *101*, 6450−6452. [34b] L. R. Chamberlain, I. P. Rothwell, J. C. Huffman, *J. Chem. Soc., Chem. Commun.* **1986**, 1203−1205. [34c] H. Brunner, J. Wachter, J. Schmidbauer, *Organometallics* **1986**, *5*, 2212−2219. [34d] L. D. Durfee, P. E. Fanwick, I. P. Rothwell, *J. Am. Chem. Soc.* **1987**, *109*, 4720−4722. [34e] L. R. Chamberlain, B. D. Steffey, I. P. Rothwell, J. C. Huffman, *Polyhedron* **1989**, *8*, 341−349. [34f] L. D. Durfee, J. E. Hill, P. E. Fanwick, I. P. Rothwell, *Organometallics* **1990**, *9*, 75−80.
[35] [35a] A. S. Guram, D. C. Swenson, R. F. Jordan, *J. Am. Chem. Soc.* **1992**, *114*, 8991−8996. [35b] M. V. Galakhov, M. Gómez, G. Jimenez, P. Royo, M. A. Pellinghelli, A. Tiripicchio, *Organometallics* **1995**, *14*, 1901−1910. [35c] A. Castro, M. V. Galakhov, M. Gómez, P. Gómez-Sal, A. Martín, F. Sánchez, P. Velasco, *Eur. J. Inorg. Chem.* **2000**, 2047−2054.
[36] T. V. Lubben, K. Plössl, J. R. Norton, M. H. Miller, O. P. Anderson, *Organometallics* **1992**, *11*, 122−127.
[37] H. Bock, H. T. Dick, *Chem. Ber.* **1967**, *100*, 228−246.
[38] [38a] A. D. Becke, *Phys. Rev. A.* **1988**, *38*, 3098−3100. [38b] J. P. Perdew, *Phys. Rev. B* **1986**, *33*, 8822−8824.
[39] [39a] A. D. Becke, *J. Chem. Phys.* **1993**, *98*, 5648−5652. [39b] C. Lee, W. Yang, R. G. Parr, *Phys. Rev. B* **1988**, *37*, 785−789.
[40] [40a] T. H. Dunning, Jr., P. J. Hay, *Modern Theoretical Chemistry*, Plenum, New York, **1976**, p. 1. [40b] P. J. Hay, W. R. Wadt, *J. Chem. Phys.* **1985**, *82*, 299−310.
[41] M. J. Frisch, G. W. Trucks, H. B. Schlegel, G. E. Scuseria, M. A. Robb, J. R. Cheeseman, V. G. Zakrzewski, J. A. Montgomery, Jr., R. E. Stratmann, J. C. Burant, S. Dapprich, J. M. Millam, A. D. Daniels, K. N. Kudin, M. C. Strain, O. Farkas, J. Tomasi, V. Barone, M. Cossi, R. Cammi, B. Mennucci, C. Pomelli, C. Adamo, S. Clifford, J. Ochterski, G. A. Petersson, P. Y. Ayala, Q. Cui, K. Morokuma, D. K. Malick, A. D. Rabuck, K. Raghavachari, J. B. Foresman, J. Cioslowski, J. V. Ortiz, A. G. Baboul, B. B. Stefanov, G. Liu, A. Liashenko, P. Piskorz, I. Komaromi, R. Gomperts, R. L. Martin, D. J. Fox, T. Keith, M. A. Al-Laham, C. Y. Peng, A. Nanayakkara, C. Gonzalez, M. Challacombe, P. M. W. Gill, B. Johnson, W. Chen, M. W. Wong, J. L. Andres, C. Gonzalez, M. Head-Gordon, E. S. Replogle, J. A. Pople, *Gaussian 98, Revision A.7*, Gaussian, Inc., Pittsburgh PA, **1998**.
[42] *Chem3D Pro 5.0*, CambridgeSoft Inc., Cambridge, MA.
[43] C. Mealli, D. M. Proserpio, *J. Chem. Educ.* **1990**, *67*, 399−402.
[44] K. Mashima, Y. Nakayama, M. Kaidzu, N. Ikushima, A. Nakamura, *J. Organomet. Chem.* **1998**, *557*, 3−12.

Received November 5, 2001
[I01435]

Synthesis of Hydride Tantalabenzocyclopentene and μ-Alkylidene Complexes by Direct Alkylation Reactions of [TaCp*Cp′Cl$_2$] − NMR Spectroscopic Study and X-ray Crystal Structure of [TaCp*Cp′(H)(η^2-CH$_2$-CMe$_2$-*o*-C$_6$H$_4$)], (Cp* = η^5-C$_5$Me$_5$; Cp′ = η^5-C$_5$H$_4$SiMe$_3$)

Aurora Castro,[a] Mikhail V. Galakhov,[b] Manuel Gómez,*[a] Pilar Gómez-Sal,[a] and Avelino Martín[a]

Keywords: Tantalum / Cyclopentadienyl complexes / Hydride complexes / Alkylidene complexes

The reaction of [TaCp*Cp′Cl$_2$] with 1 equiv. of [Mg(CH$_2$C$_6$H$_5$)$_2$(THF)$_2$] or 2 equiv. of LiCH$_2$R (R = SiMe$_3$, CMe$_3$) leads to the formation of bis(μ-alkylidene) complexes [(TaCp*Cp′)$_2$(μ-CHR)$_2$], (R = C$_6$H$_5$, **1**; SiMe$_3$, **2**; CMe$_3$, **3**), whereas the alkylation of [TaCp*Cp′Cl$_2$] with 2 equiv. of LiCH$_2$CMe$_2$Ph gives the hydride tantalabenzocyclopentene complex [TaCp*Cp′(H)(η^2-CH$_2$–CMe$_2$-*o*-C$_6$H$_4$)] (**4**). All the complexes were characterized by IR and NMR spectroscopy. The molecular structure of complex **4** has been determined by X-ray diffraction methods. Complex **4** crystallizes in the monoclinic space group $P2_1/c$, with unit cell dimensions of a = 8.976(1) Å, b = 16.596(1) Å, c = 17.929(1) Å, β = 99.26(1)°, V = 2636(1) Å^3, Z = 4, $\rho_{calcd.}$ = 1.478 g·cm^{-3}, $R1$ = 0.0481 and $wR2$ = 0.133.
(© Wiley-VCH Verlag GmbH, 69451 Weinheim, Germany, 2002)

Introduction

Early transition metal alkylidene complexes are versatile organometallic compounds due to their participation as intermediates in a number of important stoichiometric and catalytic processes.[1] Likewise, the importance of such complexes is quite clear in the studies of olefin metathesis reactions[2] having shown to catalyze the polymerization of strained ring systems in ring opening metathesis polymerization (ROMP) and polymerization of acyclic dienes (ADMET).[1d,11,4] μ-Alkylidene complexes with the ligand bridging two metal centers have been investigated in more recent times and postulated as intermediates in Fischer−Tropsch, olefin metathesis and Ziegler−Natta catalysis processes.[1] Alkylidene compounds can be made, among other methods,[1] by an α-H abstraction from transition metal alkyls[5] in an intramolecular or intermolecular process, as has been demonstrated both for early[5] and late[6] transition metal complexes.

Transition metal metallacycles are the subject of considerable current interest[7,8] and sufficient evidence has been gained to demonstrate conclusively their participation in a number of catalytic reactions such as alkene metathesis[9] and oligomerizations,[10] C−H bond activation[11] and hydrocarbon isomerization.[12] Metallacyclic complexes have been obtained by intramolecular activation of a distal C−H bond of a coordinated ligand,[8e,8k,8o,13] although harder conditions are required for their activation by γ-[8a,8f,14] or δ-[4g,15]hydrogen abstraction. If the coordinated ligand is an alkyl group with distal aromatic C−H bonds, a metallacyclic compound containing both a M−C(alkyl) and a M−C(aryl) bond may be formed.[4g,8e,8k,13b,13c,16]

We report herein the results obtained in the study of the reactivity of the mixed-ring dicyclopentadienyltantalum complex [TaCp*Cp′Cl$_2$] (Cp* = η^5-C$_5$Me$_5$; Cp′ = η^5-C$_5$H$_4$SiMe$_3$) towards alkylating reagents and an NMR spectroscopy study and the X-ray molecular structure of the complex [TaCp*Cp′(H)(η^2-CH$_2$-CMe$_2$-*o*-C$_6$H$_4$)].

Results and Discussion

Toluene solutions of [TaCp*Cp′Cl$_2$] react with 1 equiv. of [Mg(CH$_2$C$_6$H$_5$)$_2$(THF)$_2$] or 2 equiv. of LiCH$_2$R (R = SiMe$_3$, CMe$_3$, CMe$_2$Ph) under ambient conditions to give the bis-μ-alkylidene complex [(TaCp*Cp′)$_2$(μ-CHR)$_2$], (R = C$_6$H$_5$, **1**; SiMe$_3$, **2**; CMe$_3$, **3**) and the hydride tantalabenzocyclopent-2-ene [TaCp*Cp′(H)(η^2-CH$_2$-CMe$_2$-*o*-C$_6$H$_4$)] (**4**), with simultaneous elimination of R−CH$_3$ (R = C$_6$H$_5$, SiMe$_3$, CMe$_3$) and PhMe$_2$C−CH$_2$−CH$_2$−CMe$_2$Ph, respectively (Scheme 1). All of the eliminated organic products were identified by ^{1}H NMR spectroscopy when the re-

[a] Departamento de Química Inorgánica, Universidad de Alcalá de Henares, Campus Universitario, 28871 Alcalá de Henares, Spain
[b] NMR Spectroscopy Center, Universidad de Alcalá de Henares, Campus Universitario, 28871 Alcalá de Henares, Spain
Fax: (internat.) +34-91/885-4683
E-mail: manuel.gomez@uah.es

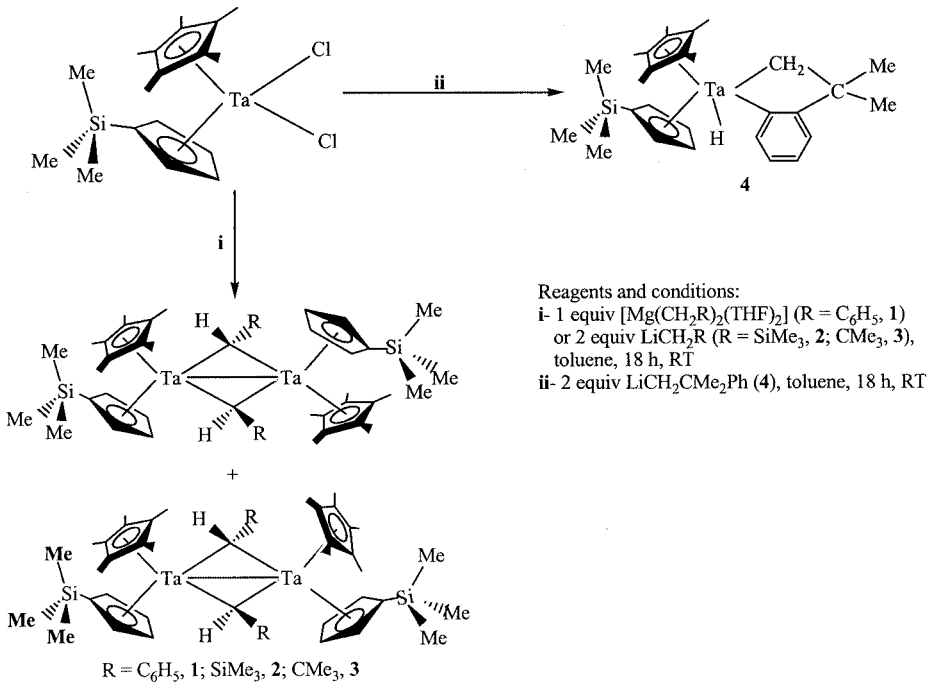

Scheme 1

actions were carried out in a sealed NMR tube with [D_6]benzene as solvent.

As a plausible reaction pathway we suggest the formation of the intermediate paramagnetic dialkyl complexes **I1**−**I4** in the first step (Scheme 2). These compounds can then evolve differently depending on the nature of the substituents: the intermediates **I1**−**I3**, undergo an α-H abstraction process[1d,1i,4g,5,7j,9d,17,18] to generate a transient tantalum(IV) alkylidene complex (step **i**), which then rearranges to form the bis-μ-alkylidene complexes **1**−**3**. It should be noted, however, that there are several examples where dialkyl [MCp_2R_2] complexes (M = Nb, Cp = η^5-C_5H_5, R = Me;[19a,19b] M = Ta, Cp = η^5-C_5H_4Me, R = Me;[19b] M = Nb, Ta, Cp = η^5-C_5H_5, R = CH_2SiMe_3;[19c] M = Ta, Cp = η^5-C_5H_5, R = Me[19d]) are thermally stable towards loss of alkane and undergo an α-elimination process.

The presence of the neophyl group in the intermediate complex **I4** leads to a different reactivity with respect to that of the intermediates **I1**−**I3**. Thus, the reduction of two **I4** molecules produces the organic elimination product 2,5-dimethyl-2,5-diphenylhexane,[20] detected when the reaction is followed by ^{1}H NMR spectroscopy, and the corresponding neophyl tantalum(III) derivative (see Scheme 2, **ii**). Subsequent orthometalation of the phenyl ring produces the hydride tantalabenzocyclopent-2-ene complex **4** through the oxidative addition of a δ_{C-H} bond[8a,8e,8f,8k,8o,13−15] to the metal center.

All the complexes are soluble in aromatic and saturated hydrocarbons, diethyl ether and tetrahydrofuran. They are air- and moisture-sensitive, and rigorously dried solvents and handling under a dry inert atmosphere were found to be imperative for successful preparations. The compounds decompose rapidly upon exposure to air, both as solids and in solution.

The spectroscopic data (see Exp. Sect.) are in agreement with the proposed structures. The IR spectra show the characteristic absorptions for both cyclopentadienyl rings (Cp* = C_5Me_5:[21,22] ν_{C-C} =1030 cm^{-1}; $C_5H_4SiMe_3$:[23] ν_{C-H} = 839 cm^{-1}), as well as other internal vibrations of the different substituents [$\nu_{\delta s}(CH_3)$[24] = 1243 cm^{-1}]. The ν_{Ta-H} stretching vibration in the complex **4** appears as a broad band at 1804 cm^{-1}, in agreement with the data reported for other hydride complexes.[25]

The NMR spectroscopic data of **1**−**3** indicate the presence of two isomers for each complex in different ratios, depending on the steric bulk of the substituents [R = C_6H_5 (**1**) 9:1], (R = $SiMe_3$ (**2**) 2:1] and [R = CMe_3 (**3**) approx. 6:1] (see Exp. Sect). The trimethylsilylcyclopentadienyl ring appears as an ABCD spin system in the ^{1}H NMR spectra and five carbon resonances in the $^{13}C\{^1H\}$ NMR spectra. This pattern can be explained by the *anti*-disposition of the R (or H) group in the μ-CHR moiety with respect to the central core, which has two chiral tantalum atoms, as shown in Scheme 1, since a *syn*-disposition should show an AA′BB′ spin system in the ^{1}H NMR and three signals in the $^{13}C\{^1H\}$ NMR spectrum. We propose that the formation of two isomeric structures for **1**−**3** is related to the mutual disposition of the two different cyclopentadienyl rings: the more populated isomers are those with an *anti*-disposition of the bulkier η^5-C_5Me_5 groups.

Formulation of **4** as a hydride tantalabenzocyclopent-2-ene complex has been confirmed by a single-crystal X-ray diffraction study. The molecular structure of compound **4** is shown in Figure 1 and selected bond lengths and angles are given in Table 1. The molecule has the typical bent-

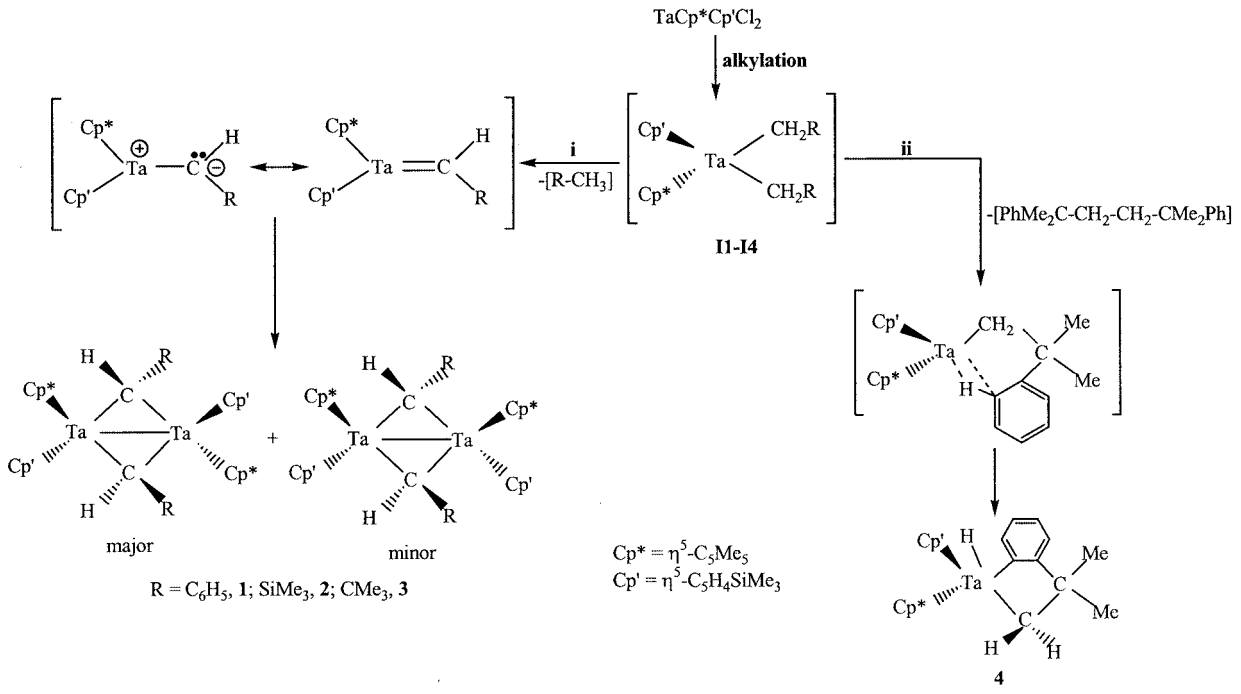

Scheme 2

metallocene structure with the tantalum atom bonded to two different cyclopentadienyl rings, and with a metallacycle system and a hydride atom located in the equatorial positions.

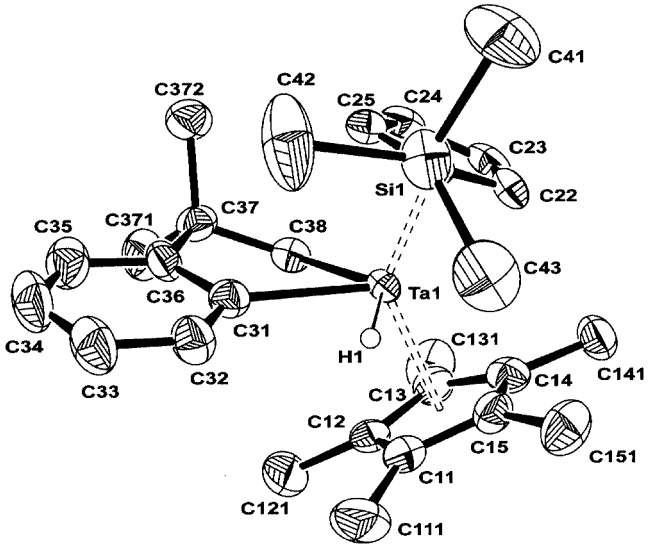

Figure 1. ORTEP view of the molecular structure of complex **4** with ellipsoids drawn at a 50% level

If Cp* and Cp′ are the centroids of the C_5Me_5 and the $C_5H_4SiMe_3$ rings, respectively, the angle Cp*−Ta−Cp′ is 133.96° and that between the planes of both cyclopentadienyl rings is 133.5°, implying that the η^5 coordination is maintained in both cases. These data are confirmed by the small range of C(Cp)−Ta distances [2.436(8) to

Table 1. Selected bond lengths (Å) and angles (°) for **4** [Cp* and Cp′ are the centroids of the C_5Me_5 and $C_5H_4(SiMe_3)$ rings, respectively]

Ta(1)−C(38)	2.306(8)	C(13)−C(131)	1.518(12)
Ta(1)−C(31)	2.309(8)	C(14)−C(15)	1.393(11)
Ta(1)−C(25)	2.406(8)	C(14)−C(141)	1.536(12)
Ta(1)−C(22)	2.406(8)	C(15)−C(151)	1.514(12)
Ta(1)−C(23)	2.414(8)	C(21)−C(25)	1.387(11)
Ta(1)−C(13)	2.440(8)	C(21)−C(22)	1.426(11)
Ta(1)−C(15)	2.437(8)	C(22)−C(23)	1.384(12)
Ta(1)−C(21)	2.438(8)	C(23)−C(24)	1.397(13)
Ta(1)−C(24)	2.450(8)	C(24)−C(25)	1.389(11)
Ta(1)−C(12)	2.457(8)	C(31)−C(36)	1.397(12)
Ta(1)−C(11)	2.464(8)	C(31)−C(32)	1.403(11)
Ta(1)−C(14)	2.466(8)	C(32)−C(33)	1.391(13)
Si(1)−C(43)	1.838(14)	C(33)−C(34)	1.385(15)
Si(1)−C(42)	1.860(11)	C(34)−C(35)	1.363(15)
Si(1)−C(41)	1.885(11)	C(35)−C(36)	1.423(12)
Si(1)−C(21)	1.884(8)	C(36)−C(37)	1.505(12)
C(11)−C(12)	1.387(13)	C(37)−C(38)	1.522(12)
C(11)−C(15)	1.408(12)	C(37)−C(371)	1.546(12)
C(11)−C(111)	1.506(12)	C(37)−C(372)	1.560(12)
C(12)−C(13)	1.428(12)	Cp*−Ta(1)	2.143
C(12)−C(121)	1.521(12)	Cp′−Ta(1)	2.112
C(13)−C(14)	1.398(12)		

C(38)−Ta(1)−C(31)	69.3(3)	C(31)−C(36)−C(37)	118.9(7)
C(43)−Si(1)−C(42)	111.4(7)	C(35)−C(36)−C(37)	121.2(8)
C(43)−Si(1)−C(41)	109.9(7)	C(36)−C(37)−C(38)	105.8(7)
C(42)−Si(1)−C(41)	108.7(7)	C(37)−C(38)−Ta(1)	119.8(5)
C(43)−Si(1)−C(21)	111.8(5)	Cp*−Ta(1)−Cp′	133.96
C(42)−Si(1)−C(21)	110.0(5)	C(38)−Ta(1)−Cp′	103.26
C(41)−Si(1)−C(21)	104.8(5)	C(38)−Ta(1)−Cp*	102.47
C(36)−C(31)−C(32)	116.2(8)	C(31)−Ta(1)−Cp′	111.30
C(36)−C(31)−Ta(1)	119.5(6)	C(31)−Ta(1)−Cp*	113.30
C(32)−C(31)−Ta(1)	124.3(7)		

2.466(8) Å for the Cp* ring and 2.406(8) to 2.449(8) Å for the Cp′ ring]. The Ta−Cp(centroid) distances are 2.143 Å for Cp* and 2.112 Å for Cp′. It is interesting to note that the value of the Cp*−Ta−Cp′ angle (133.96°) is smaller than that found in [TaCp*Cp′′H_3][21] (142.6°) or in [TaCp*$_2H_3$][23b] (148.3°), probably due to the bigger size of the equatorial ligand and the smaller size of the Cp′ ligand with respect to Cp′′, and it is even smaller than the angle found in *ansa*-bridged tantalum(III) hydride complexes such as [Ta{$Me_2Si(C_5Me_4)_2$}H(CO)][26] where the value is 139.7°.

The metallacycle moiety is located in the equatorial positions. If we define the equatorial plane with the Ta, C31 and C38 atoms, the distances to this plane of Cp*(1.96 Å) and Cp′(1.95 Å) are essentially the same, and the phenyl ring plane makes an angle of only 13.9(2)° with it. If we consider the Cp*−Ta−Cp′ plane, the metallacycle is located unsymmetrically with respect to it. The distances of C31, C36, C37 and C38 to this plane are 0.558, −0.418, −1.895 and −1.839 Å, respectively, with the more sterically demanding moiety of the ligand located in a lateral position leaving space for the hydride on the other side, near to the phenyl ring, as we can be seen in Figure 2. Compound **4** is the first hydrido tantalabenzocyclopent-2-ene complex reported until now, except for the telluro-formaldehyde complex [TaCp*$_2$(η^2-$TeCH_2$)H],[27] where a Ta−Te bond is described. The distances Ta−C31 [2.309(8) Å] and Ta−C38 [2.306(8) Å] are in the normal range for Ta−C single bonds. All the other parameters of the ligand are normal. No similar niobium(V) hydride metallacycle has been published either.

The ^{1}H NMR spectra of complex **4** in [D_6]benzene shows 13 signals with different multiplicities and one AB system (see Exp. Sect.), whereas in the carbon spectrum only 13 signals for the $C-H_n$ and five resonances for the quaternary carbon atoms are observed. Moreover, in the 2D ^{1}H-^{13}C heteronuclear correlation spectrum the cross peak for the ^{1}H doublet at δ = 2.60, which we assign to a classical Ta−*H* hydride resonance (T_1= 0.36 s at 233 K), was not observed. The observation of four protons and five resonances for the trimethylsilylcyclopentadienyl ring in the ^{1}H and the ^{13}C{^{1}H} NMR spectra, respectively, is due to the chiral nature of the tantalum atom.

The disposition of the hydride and the assignment of the H_α and H_β proton resonances of the Cp′ ring was realized with a differential NOE experiment by irradiating the $SiMe_3$ signal: NOE = 0.6% (δ = 3.52, H_α), 0.9% (δ = 4.55, H_β), 0.3% Ta−*H* and 0.6% *ortho*-H of phenyl ring. These data are in agreement with the location of the hydride atom close to the phenyl and trimethylsilyl groups as shown in Figure 2. The hydride is coupled (^3J = 4.4 Hz) with H38a (δ = 0.95) of the α-CH_2 group, which is in an *anti*-conformation (torsion angle ≈160°), and with H25 (δ = 4.34) of the η^5-$C_5H_4SiMe_3$ ring. Furthermore, in this spectrum we could also measure the spin-spin coupling constant (^4J = 0.85 Hz) between C_α-H38b (δ = 1.35) and the more deshielded H23 (δ = 6.14) of the Cp′ ring. This value must correspond to the "W" disposition of these protons, as shown in Figure 2c.

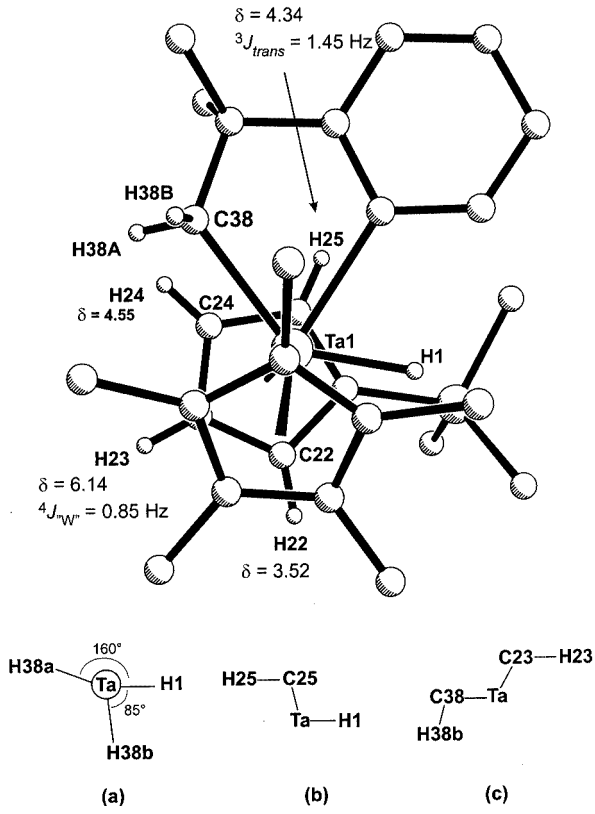

Figure 2. Top view of **4** with some relevant ^{1}H NMR spectroscopic data

Both the ^{1}H and ^{13}C spectra show a very large difference for the chemical shifts of the η^5-$C_5H_4SiMe_3$ ring (Δδ = 2.6 and 22.2 ppm, respectively) due to the cooperative electronic properties of the alkyl, phenyl and hydride groups bonded to the tantalum center.

Conclusions

The results discussed here demonstrate that μ-alkylidene tantalum and hydrido tantalabenzocyclopent-2-ene complexes can be obtained by treating the mixed dichlorodicyclopentadienyltantalum(IV) derivative [TaCp*Cp′Cl_2] with different alkylating reagents. In both cases the reaction takes place with the initial formation of dialkyl mixed tantalocene derivatives. When the alkylation is carried out with 1 equiv. of [$Mg(CH_2C_6H_5)_2(THF)_2$] or 2 equiv. of LiR (R = CH_2SiMe_3, CH_2CMe_3) the bis-μ-alkylidene complexes **1−3** are formed with simultaneous elimination of R−CH_3 (R = C_6H_5, $SiMe_3$, CMe_3). This transformation involves an α-H abstraction process to generate an intermediate tantalum(IV) alkylidene complex, which then rearranges to give a bis(μ-alkylidene) complex. However, if the starting dichloro derivative is treated with 2 equiv. of $LiCH_2CMe_2Ph$ the hydride tantalabenzocyclopent-2-ene complex **4** is isolated. Its formation can be explained by the reduction of the dialkyl derivative to give a neophyl radical, which dimerizes, and the corresponding mixed dicyclo-

pentadienyl neophyltantalum(III) derivative. A subsequent intramolecular activation of a distal aromatic C−H bond leads to **4**.

Experimental Section

General: All reactions and manipulations were carried out by using standard Schlenk techniques or in an argon-filled vacuum atmosphere glove box.[28] Solvents were refluxed over appropriate drying agents and distilled and degassed prior to use: [D_6]benzene and *n*-hexane (Na/K alloy), toluene (Na). Literature methods were employed for the syntheses of the starting materials [TaCp*Cp′Cl_2],[21] alkyllithium LiR (R = CH_2CMe_2Ph, CH_2SiMe_3, CH_2CMe_3)[29] and dibenzylmagnesium [$Mg(CH_2Ph)_2(THF)_2$].[30]

Infrared spectra were recorded with a Perkin−Elmer 583 spectrophotometer (4000−200 cm^{-1}) with samples as Nujol mulls between CsI plates or polyethylene pellets. ^1H and $^{13}C\{^1H\}$ NMR spectra were recorded on Varian Unity-300 or Varian UnityPlus-500 spectrometers; chemical shifts are referenced to the ^{13}C (δ = 128) and residual ^1H (δ = 7.15) resonances of the [D_6]benzene solvent. C and H analyses were carried out on a Perkin−Elmer 240 C microanalyzer.

Synthesis of [(TaCp*Cp′)$_2$(μ-CHR)$_2$] (R = C_6H_5, 1; $SiMe_3$, 2; CMe_3, 3) and [TaCp*Cp′(H)(η^2-CH_2−CMe_2-*o*-C_6H_4)] (4): A mixture of [TaCp*Cp′Cl_2] (0.70 g, 1.33 mmol) and [$Mg(CH_2C_6H_5)_2(THF)_2$] (0.47 g, 1.33 mmol) or $LiCH_2R$ (2.66 mmol; R = $SiMe_3$: 0.25 g; CMe_3: 0.21 g; CMe_2Ph: 0.37 g) was stirred in toluene (30 mL) at room temperature for 18 h. $MgCl_2$ or LiCl were filtered off and the resulting solution evaporated to dryness. The residue was extracted with *n*-hexane (2 × 10 mL) and cooled to −40 °C overnight to give **1**−**3** as somewhat brown (**1**) or red-brown (**2**,**3**) sticky solids and **4** as pale brown crystals.

When these experiments were carried out in a sealed NMR tube with [D_6]benzene as solvent, the elimination organic products R−CH_3 (R = C_6H_5, **1**; $SiMe_3$, **2**; CMe_3, **3**) and $PhMe_2C$−CH_2−CH_2−CMe_2Ph (**4**) were detected in the ^1H NMR spectrum.

1: Yield 0.43 g (60%). IR (Nujol): $\tilde{\nu}$ = 2950 cm^{-1} br., vs, 792 m, 1630 w, 1246 vs, 1190 w, 1169 s, 1087 s, 1025 m, 903 s, 840 br. s, 756 m, 695 m, 632 m, 479 m, 370 w. ^1H NMR (C_6D_6, 20 °C): **isomer A**, 90%, δ = 11.35 (s, *H*CC_6H_5), 7.10 (br. m), 7.05 (br. m, H_5C_6CH), 5.77 (m, 1 H), 5.04 (m, 1 H), 4.50 (m, 1 H), 4.10 (m, 1 H, $H_4C_5SiMe_3$), 1.92 (s, 15 H, C_5Me_5), 0.26 (s, 9 H, $Me_3SiC_5H_4$); **isomer B**, 10%, δ = 7.25 (br. m, H_5C_6CH), 6.58 (m, 1 H), 6.20 (m, 1 H), 6.05 (m, 1 H), 5.15 (m, 1 H, $H_4C_5SiMe_3$), 1.79 (s, 15 H, C_5Me_5), 0.30 (s, 9 H, $Me_3SiC_5H_4$). $^{13}C\{^1H\}$ NMR (C_6D_6, 20 °C): **isomer A**, δ = 254.4 (*C*HC_6H_5), 162.2, 141.9, 127.9, 125 (C_i, C_p, C_o, C_m, C_6H_5CH), 110.8(C_i, $C_5H_4SiMe_3$), 115.8, 114.8, 106.5, 99.7 ($C_5H_4SiMe_3$), 108.2 (C_5Me_5), 12.75(C_5Me_5), 0.47($Me_3SiC_5H_4$); **isomer B**, δ = 153, 126.2 (several phenyl, C_6H_5CH), 111 (C_i, $C_5H_4SiMe_3$), 116.8, 107.3, 101.6, 98.4 ($C_5H_4SiMe_3$), 104.2 (C_5Me_5), 11.4 (C_5Me_5), −0.69 (s, $Me_3SiC_5H_4$). $C_{25}H_{34}SiTa$ (543.56): calcd. C 55.24, H 6.30; found C 55.20, H 6.35.

2: Yield 0.57 g (75%). IR (Nujol): $\tilde{\nu}$ = 2951 cm^{-1} vs, 2905 vs, 1790 w, 1487 w, 1435 m, 1377 m, 1244 vs, 1175 m, 1047 s, 1010 m, 892 vs, 835 vs, 751 m, 674 w, 629 w, 464 w, 435 w, 347 w. ^1H NMR (C_6D_6, 20 °C): **isomer A**, 68%, δ = 10.50 (s, 1 H, *H*C$SiMe_3$), 6.26 (m, 1 H), 5.83 (m, 1 H), 4.48 (m, 1 H), 4.12 (m, 1 H, $H_4C_5SiMe_3$), 1.86 (s, 15 H, C_5Me_5), 0.33 (s, 9 H, Me_3SiCH), 0.30 (s, 9 H, $Me_3SiC_5H_4$); **isomer B**, 32%, δ = 10.42 (s, 1 H, *H*C$SiMe_3$), 6.79 (m, 1 H), 6.40 (m, 1 H), 5.03 (m, 1 H), 4.31 (m, 1 H, $H_4C_5SiMe_3$), 1.72 (s, 15 H, C_5Me_5), 0.37 (s, 9 H, Me_3SiCH), 0.35 (s, 9 H, $Me_3SiC_5H_4$). $^{13}C\{^1H\}$ NMR (C_6D_6, 20 °C): **isomer A**, δ = 249.4 (*C*H$SiMe_3$), 111.6(C_i, $C_5H_4SiMe_3$), 109.1(C_5Me_5), 107.2, 102.9, 102.4, 99.9 ($C_5H_4SiMe_3$), 12.5 (C_5Me_5), 4.1 (Me_3SiCH), 0.35 ($Me_3SiC_5H_4$); **isomer B**, δ = 243.2 (*C*H$SiMe_3$), 114.3(C_5Me_5), 111.3 (C_i, $C_5H_4SiMe_3$), 108.2, 106, 102, 96.75 ($C_5H_4SiMe_3$), 11.9 (C_5Me_5), 3.9 (Me_3SiCH), −0.17 ($Me_3SiC_5H_4$). $C_{22}H_{38}Si_2Ta$ (539.666): calcd. C 48.96, H 7.10; found C 48.76, H 7.19.

3: Yield 0.55 g (75%). IR (Nujol): $\tilde{\nu}$ = 2951 cm^{-1} br., s, 1780 s, 1586 m, 1455 br., s, 1377 s, 1353 m, 1245 vs, 1174 m, 1051 m, 1027 m, 957 m, 912 s, 838 br., vs, 755 m, 696 m, 633 m, 434 w, 335 m. ^1H NMR (C_6D_6, 20 °C): **isomer A**, 85%, δ = 9.85 (s, 1 H, *H*CCMe_3), 6.24 (m, 1 H), 5.68 (m, 1 H), 4.42 (m, 1 H), 4.04 (m, 1 H, $H_4C_5SiMe_3$), 1.92 (s, 15 H, C_5Me_5), 1.30 (s, 9 H, Me_3CCH), 0.29 (s, 9 H, $Me_3SiC_5H_4$); **isomer B**, 15%, δ = 10.22 (s, 1 H, *H*CCMe_3), 6.51 (m, 1 H), 5.36 (m, 1 H), 4.92 (m, 1 H), 4.68 (m, 1 H, $H_4C_5SiMe_3$), 1.62 (s, 15 H, C_5Me_5), 1.12 (s, 9 H, Me_3CCH), 0.23 (s, 9 H, $Me_3SiC_5H_4$). $^{13}C\{^1H\}$ NMR (C_6D_6, 20 °C): **isomer A**, δ = 249.6 (*C*HCMe_3), 111.5 (C_i, $C_5H_4SiMe_3$), 113.7, 110, 105.6, 98.5 ($C_5H_4SiMe_3$), 108.2(C_5Me_5), 49.1(Me_3*C*CH), 34.8(Me_3CCH), 13.1(C_5Me_5), 0.67($Me_3SiC_5H_4$); **isomer B**, δ = 243.8 (H*C*CMe_3), 111 (C_i, $C_5H_4SiMe_3$), 111.4, 102, 100.2, 93.9 ($C_5H_4SiMe_3$), 110.5 (C_5Me_5), 47.8 (Me_3*C*CH), 34 (Me_3CCH), 12.1 (C_5Me_5), 1.8 ($Me_3SiC_5H_4$). $C_{23}H_{38}SiTa$ (523.591): calcd. C 52.76, H 7.31; found C 52.68, H 7.27.

4: Yield 0.44 g (56%). IR (Nujol): $\tilde{\nu}$ = 1942 cm^{-1} w, 1804 w, 1596 m, 1322 w, 1293 w, 1243 vs, 1201 m, 1168 vs, 1081 m, 1063 m, 1046 m, 1030 vs, 953 w, 910 m, 870 vs, 839 vs, 814 s, 765 vs, 732 m, 702 s, 655 w, 633 m, 557 m, 430 m. ^1H NMR (C_6D_6, 20 °C): δ = 8.43, 7.25, 7.17, 7.10 (ABCD spin system, H1−H4, H_4C_6-*o*-CMe_2-CH_2-Ta), 6.14, 4.55, 4.33, 3.52 (ABCD spin system, $H_4C_5SiMe_3$), 2.60, 1.33, 0.95 (ABC, $^2J_{B-C}$ = 12.1, $^3J_{A-C}$ = 4.4 Hz, *H*-Ta-CH_2-CMe_2-*o*-C_6H_4), 1.63 (s, 3 H), 1.12 (s, 3 H, H_4C_6-*o*-CMe_2-CH_2-Ta), 1.55 (s, 15 H, C_5Me_5), 0.22 (s, 9 H, $Me_3SiC_5H_4$). $^{13}C\{^1H\}$ NMR (C_6D_6, 20 °C): δ = 155.1, 129.46, 127.76, 127.68, 125.06 (H_4C_6-*o*-CMe_2-CH_2-Ta, C_{ipso}-Ta not was detected), 116.7, 104.3, 99.4, 94.5 ($C_5H_4SiMe_3$), 107.2 (C_5Me_5), 107.1 (C_i, $C_5H_4SiMe_3$), 93.4 (H_4C_6-*o*-CMe_2-*C*H_2-Ta), 50 (H_4C_6-*o*-*C*Me_2-CH_2-Ta), 37.3, 34.4 (H_4C_6-*o*-CMe_2-CH_2-Ta), 11.53(C_5Me_5), 0.83($Me_3SiC_5H_4$). $C_{28}H_{41}SiTa$ (586.671): calcd. C 57.32, H 7.04; found C 57.28, H 6.96.

X-ray Structure Determination of 4: Crystals of compound **4** were obtained by crystallization from hexane. A suitably sized crystal sealed in a Lindemann tube was mounted on an Enraf−Nonius CAD 4 automatic four-circle diffractometer equipped with graphite monochromated Mo-K_α radiation (λ = 0.71073 Å). Crystallographic and experimental details of the structure are summarized in Table 2. Data were collected at room temperature. Intensities were corrected for Lorentz and polarization effects in the usual manner. No absorption or extinction corrections were made. The structure was solved, using the WINGX package,[31a] by direct methods (SHELXS-97)[31b] and refined by least-squares against F^2 (SHELXL-97).[31b] All non-hydrogen atoms were refined anisotropically, and the hydrogen atoms were introduced from geometrical calculations and refined using a riding model with thermal parameters equivalent to those of the carbon atoms to which they are attached, except for the hydride atom, which was found with the XHYDEX[31c] program, included and refined isotropically in the last cycles of refinement.

Table 2. Crystal data and structure refinement for **4**

Empirical formula	$C_{28}H_{41}SiTa$
Formula mass	586.65
Crystal habit	prismatic
Colour	pale brown
Crystal size	0.22 × 0.28 × 0.30 mm
Space group	monoclinic, $P2_1/c$
a (Å)	8.976(1)
b (Å)	16.596(1)
c (Å)	17.929(1)
β (°)	99.26(1)
V (Å^3)	2636.0(4)
Z	4
$D_{calcd.}$ (g cm^{-3})	1.478
F(000)	1184
μ (cm^{-1})	42.27
Scan mode	ω/2θ $2.30 < \theta < 24.98$
Number of reflections	
Measured	4628
Observed	3326 ($I < 2\sigma(I)$)
Range of *hkl*	$-10 < h < 10$, $0 < k < 19$, $0 < l < 21$
Standard reflections	3 every 200 reflections
Refinement method	full-matrix least-squares on F^2
Final R indices all data[a]	$R1 = 0.0481$, $wR2 = 0.1330$
Final R indices [$I > 2\sigma(I)$]	$R1 = 0.0699$, $wR2 = 0.1510$
Largest diff.peak and hole (e/Å^3)	1.929 and −2.990
Goodness of fit on F^2	1.108

[a] $R1 = \Sigma||F_o| - |F_c||/\Sigma|F_o|$; $wR2 = \{\Sigma[\omega((F_o^2 - F_c^2)^2]/\Sigma[\omega(F_o^2)^2]\}^{1/2}$.

CCDC-174670 contains the supplementary crystallographic data for this paper. These data can be obtained free of charge at www.ccdc.cam.ac.uk/conts/retrieving.html [or from the Cambridge Crystallographic Data Centre, 12, Union Road, Cambridge CB2 1EZ, UK; fax: (internat.) +44-1223/336-033; E-mail: deposit@ccdc.cam.ac.uk].

Acknowledgments

We are grateful to the DGICYT (Project PB-97−0761) and to the Universidad de Alcalá (Project E009/98) for financial support of this research.

[1] [1a] T. J. Katz, S. J. Lee, *J. Am. Chem. Soc.* **1980**, *102*, 422−424. [1b] S. H. Pine, R. Zahler, D. A. Evans, R. H. Grubbs, *J. Am. Chem. Soc.* **1980**, *102*, 3270− 3272. [1c] A. F. Dyke, S. A. R. Knox, P. J. Naish, G. E. Taylor, *J. Chem. Soc., Chem. Commun.* **1980**, 803−805. [1d] W. A. Herrmann, *Adv. Organomet. Chem.* **1982**, *20*, 159−263. [1e] R. H. Grubbs, *Comprehensive Organometallic Chemistry* (Ed.: G. Wilkinson), Pergamon Press: Oxford, **1982**; vol. 9, Chapter 54, 499−552. [1f]M. Brookhart, J. R. Tucker, G. R. Husk, *J. Am. Chem. Soc.* **1983**, *105*, 258−264. [1g] K. A. Brown-Wensley, S. L. Buchwald, L. F. Cannizzo, L. E. Clawson, S. H. Ho, J. D. Meinhart, J. R. Stille, D. A. Strauss, R. H. Grubbs, *Pure Appl. Chem.* **1983**, *55*, 1733−1744. [1h] K. H. Dötz, *Angew. Chem. Int. Ed. Engl.* **1984**, *23*, 587−608. [1i] J. E. Hahn, *Prog. Inorg. Chem.* **1984**, *31*, 205−264. [1j] L. E. Clawson, S. L. Buchwald, R. H. Grubbs, *Tetrahedron Lett.* **1984**, *25*, 5733−5736. [1k] L. F. Cannizzo, R. H. Grubbs, *J. Org. Chem.* **1985**, *50*, 2316−2323. [1l] M. A. Gallop, W. R. Roper, *Adv. Organomet. Chem.* **1986**, *25*, 121−198. [1m] L. R. Gilliom, R. H. Grubbs, *J. Am. Chem. Soc.* **1986**, *108*, 733−742. [1n] M. Brookhart, W. B. Studabaker, *Chem. Rev.* **1987**, *87*, 411−432.

[2] [2a] K. J. Ivin, *Olefin Metathesis*; Academic Press: London, **1983**. [2b]R. R. Schrock, *Acc. Chem. Res.* **1990**, *23*, 158−165. [2c] R. R. Schrock, R. T. De Pue, J. Feldman, K. B. Yap, D. C. Yang, W. M. Davis, L. Park, M. Di Mare, M. Schoenfield, J. Anhaus, E. Walborsky, E. Evitt, C. Krüger, P. Betz, *Organometallics* **1990**, *9*, 2262−2275. [2d] R. R. Schrock, J. S. Murdzek, G. C. Bazan, J. Robbins, M. Di Mare, M. O'Regan, *J. Am. Chem. Soc.* **1990**, *112*, 3875−3886. [2e] J. Feldman, W. M. Davis, J. K. Thomas, R. R. Schrock, *Organometallics* **1990**, *9*, 2535−2548. [2f] S. T. Nguyen, R. H. Grubbs, J. W. Ziller, *J. Am. Chem. Soc.* **1993**, *115*, 9858−9859. [2g] J. H. Oskam, R. R. Schrock, *J. Am. Chem. Soc.* **1993**, *115*, 11831−11845. [2h] H. H. Fox, J. K. Lee, L. Y. Park, R. R. Schrock, *Organometallics* **1993**, *12*, 759−768. [2i] R. O'Dell, D. H. McConville, G. E. Hofmeister, R. R. Schrock, *J. Am. Chem. Soc.* **1994**, *116*, 3414−3423. [2j] J. S. Moore, *Comprehensive Organometallic Chemistry* II; Pergamon: New York, **1995**; Vol. 12, Chapter 12.2. [2k]R. R. Schrock, *Polyhedron* **1995**, *14*, 3177−3195. [2l] R. R. Schrock, S. Luo, J. C. Lee Jr., N. C. Zanetti, W. M. Davis, *J. Am. Chem. Soc.* **1996**, *118*, 3883−3895.

[3] [3a] R. R. Schrock, J. Feldman, L. F. Cannizzo, R. H. Grubbs, *Macromolecules* **1987**, *20*, 1169−1172. [3b] K. C. Wallace, A. H. Liu, J. C. Dewan, R. R. Schrock, *J. Am. Chem. Soc.* **1988**, *110*, 4964−4977. [3c] K. B. Wagener, J. M. Boncella, J. G. Nel, R. P. Duttweiler, H. A. Hillmyer, *Makromol. Chem.* **1990**, *191*, 365−374.

[4] [4a] G. Minghetti, A. Albinati, A. L. Bandini, G. Banditelli, *Angew. Chem. Int. Ed. Engl.* **1985**, *24*, 120−121. [4b] M. L. H. Green, D. O'Hare, *J. Chem. Soc., Dalton Trans.* **1986**, 2469−2476. [4c] J. A. Bandy, M. L. H. Green, D. O'Hare, *J. Chem. Soc., Dalton Trans.* **1986**, 2477−2484. [4d] R. M. Bullock, M. T. Hembre, J. R. Norton, *J. Am. Chem. Soc.* **1988**, *110*, 7868−7870. [4e] B. Denise, D. Navarre, H. Rudler, *J. Organomet. Chem.* **1989**, *375*, 273−289. [4f] S. K. Noh, R. A. Heintz, C. Janiak, S. C. Sendlinger, K. H. Theopold, *Angew. Chem. Int. Ed. Engl.* **1990**, *29*, 775− 777. [4g] T. R. Belderraín, E. Gutierrez, A. Monge, M. C. Nicasio, M. Paneque, M. L. Poveda, E. Carmona, *Organometallics* **1993**, *12*, 4431−4442.

[5] [5a] R. R. Schrock, *Acc. Chem. Res.* **1979**, *12*, 98−104. [5b] N. J. Cooper, M. L. H. Green, *J. Chem. Soc., Dalton Trans.* **1979**, 1121−1127. [5c] C. McDade, J. C. Green, J. E. Bercaw, *Organometallics* **1982**, *1*, 1629−1634. [5d] H. W. Turner, R. R. Schrock, J. D. Fellmann, S. J. Holmes, *J. Am. Chem. Soc.* **1983**, *105*, 4942−4950. [5e] A. van Asselt, B. J. Burger, V. C. Gibson, J. E. Bercaw, *J. Am. Chem. Soc.* **1986**, *108*, 5347−5349. [5f] R. R. Schrock, *J. Organomet. Chem.* **1986**, *300*, 249−262. [5g] A. R. Bulls, W. E. Schaefer, M. Serfas, J. E. Bercaw, *Organometallics* **1987**, *6*, 1219−1226. [5h] H. van der Heijden, B. Hessen, *J. Chem. Soc., Chem. Commun.* **1995**, 145−146. [5i] R. Andrés, P. Gómez-Sal, E. de Jesús, A. Martín, M. Mena, C. Yélamos, *Angew. Chem. Int. Ed. Engl.* **1997**, *36*, 115− 117.

[6] [6a] M. J. Burk, M. P. McGrath, R. H. Crabtree, *J. Am. Chem. Soc.* **1988**, *110*, 620. [6b] M. D. Fryzuk, K. Joshi, *J. Am. Chem. Soc.* **1989**, *111*, 4498−4500.

[7] [7a] S. J. Simpson, R. A. Andersen, *J. Am. Chem. Soc.* **1981**, *103*, 4063−4066. [7b] R. P. Planalp, R. A. Andersen, *Organometallics* **1983**, *2*, 1675−1680. [7c] G. Erker, *Acc. Chem. Res.* **1984**, *17*, 103−109. [7d] D. J. Pasto, N.-Z. Huang, *Organometallics* **1985**, *4*, 1386−1395. [7e] E. Linder, *Adv. Heterocycl. Chem.* **1986**, *39*, 237−279. [7f] H. M. Büch, P. Binger, R. Benn, A. Rufinska, *Organometallics* **1987**, *6*, 1130−1133. [7g] G. M. Smith, M. Sabat, T. J. Marks, *J. Am. Chem. Soc.* **1987**, *109*, 1854−1856. [7h] G. Wilke, *Angew. Chem. Int. Ed. Engl.* **1988**, *27*, 185−206. [7i] R. R. Burch, J. C. Calabrese, S. D. Ittel, *Organometallics* **1988**, *7*, 1642−1648. [7j] A. D. Ryabov, *Chem. Rev.* **1990**, *90*, 403−424.

[8] [8a] P. Foley, R. DiCosimo, G. M. Whitesides, *J. Am. Chem. Soc.* **1980**, *102*, 6713−6725. [8b] J. P. Collman, L. S. Hegedeus, *Principles and Applications of Organotransition Metal Chemistry*, University Science Books, Mill Valley, CA, **1980**; pp.

211−228. [8c]S. J. Simpson, H. W. Turner, R. A. Andersen, *Inorg. Chem.* **1981**, *20*, 2991−2995. [8d] S. J. Simpson, R. A. Andersen, *Inorg. Chem.* **1981**, *20*, 3627−3629. [8e] T. H. Tulip, D. L. Thorn, *J. Am. Chem. Soc.* **1981**, *103*, 2448−2450. [8f] G. M. Whitesides, *Pure Appl. Chem.* **1981**, *53*, 287−292. [8g] R. DiCosimo, S. S. Moore, A. F. Sowinski, G. M. Whitesides, *J. Am. Chem. Soc.* **1982**, *104*, 124−133. [8h] J. A. Ibers, R. DiCosimo, G. M. Whitesides, *Organometallics* **1982**, *1*, 13−20. [8i] L. R. Chamberlain, J. Keddington, J. C. Huffman, I. P. Rothwell, *Organometallics* **1982**, *1*, 1538−1540. [8j] G. M. Whitesides, R. H. Reamey, R. L. Brainard, A. N. Izumi, F. J. McCarthy, *Ann. N. Y. Acad. Sci.* **1983**, *415*, 56−66. [8k] J. C. Calabrese, M. C. Colton, T. Herskovitz, U. Klabunde, G. W. Parshall, D. L. Thorn, T. H. Tulip, *Ann. N. Y. Acad. Sci.* **1983**, *415*, 302−313. [8l] H. Kletzin, H. Werner, *Angew. Chem. Int. Ed. Engl.* **1983**, *22*, 873−874. [8m] Y. Fuchita, H. Katsuma, T. Uchiyama, *J. Chem. Soc., Dalton Trans.* **1983**, 897−899. [8n] E. Constable, *Polyhedron* **1984**, *3*, 1037−1057. [8o] I. P. Rothwell, *Polyhedron* **1985**, *4*, 177−200.

[9] [9a] R. J. Puddephatt, *Coord. Chem. Rev.* **1980**, *33*, 149−183. [9b] J. H. Wengrovius, R. R. Schrock, M. R. Churchill, J. R. Missert, W. J. Youngs, *J. Am. Chem. Soc.* **1980**, *102*, 4515−4516. [9c] J. B. Lee, T. R. Howard, R. H. Grubbs, *J. Am. Chem. Soc.* **1980**, *102*, 6876−6878. [9d] S. M. Rocklage, J. D. Fellman, G. A. Rupprecht, L. W. Messerle, R. R. Schrock, *J. Am. Chem. Soc.* **1981**, *103*, 1440−1447. [9e] S. D. Chappell, D. J. Cole-Hamilton, *Polyhedron* **1982**, *1*, 739−777.

[10] K. J. Irvin, J. J. Rooney, C. D. Stewart, M. L. H. Green, R. Mantab, *J. Chem. Soc., Chem. Commun.* **1978**, 604−606.

[11] C. M. Fendrick, T. J. Marks, *J. Am. Chem. Soc.* **1984**, *106*, 2214−2216.

[12] [12a] R. Hugues, B. Besson, J. M. Basset, *J. Chem. Soc., Chem. Commun.* **1980**, 719−721. [12b] C. O'Donohoe, J. K. A. Clarke, J. J. Rooney, *J. Chem. Soc., Faraday Trans.* **1980**, *76*, 345−356.

[13] [13a] R. A. Andersen, R. A. Jones, G. Wilkinson, *J. Chem. Soc., Dalton Trans.* **1978**, 446−453. [13b] D. C. Griffiths, G. B. Young, *Polyhedron* **1983**, *2*, 1095−1100. [13c] J. W. Bruno, G. M. Smith, T. J. Marks, C. K. Fair, A. J. Schultz, J. M. Williams, *J. Am. Chem. Soc.* **1986**, *108*, 40−56. [13d] D. C. Griffiths, L. G. Joy, A. C. Skapski, D. J. Wilkes, G. B. Young, *Organometallics* **1986**, *5*, 1744−1745. [13e] Y.-D. Wu, Z.-H. Peng, K. W. K. Chan, X. Liu, A. A. Tuinman, Z. Xue, *Organometallics* **1999**, *18*, 2081−2090 and references therein.

[14] P. Foley, G. M. Whitesides, *J. Am. Chem. Soc.* **1979**, *101*, 2732−2733.

[15] S. D. Chappell, D. J. Cole-Hamilton, *J. Chem. Soc., Dalton Trans.* **1983**, 1051−1057.

[16] [16a] E. Carmona, F. Gonzalez, M. L. Poveda, J. L. Atwood, R. D. Rogers, *J. Chem. Soc., Dalton Trans.* **1980**, 2108−2116. [16b] E. Carmona, F. Gonzalez, M. L. Poveda, J. L. Atwood, R. D. Rogers, *J. Chem. Soc., Dalton Trans.* **1981**, 777−782. [16c] E. Carmona, M. Paneque, M. L. Poveda, R. D. Rogers, J. L. Atwood, *Polyhedron* **1984**, *3*, 317−323. [16d] M. A. Bennett, T. W. Hambley, N. K. Roberts, G. B. Robertson, *Organometallics* **1985**, *4*, 1992−2000. [16e] E. Carmona, J. M. Marín, M. Paneque, M. L. Poveda, *Organometallics* **1987**, *6*, 1757−1765. [16f] E. Carmona, E. Gutierrez-Puebla, J. M. Marín, A. Monge, M. Paneque, M. L. Poveda, C. Ruiz, *J. Am. Chem. Soc.* **1989**, *111*, 2883−2891.

[17] [17a] W. A. Herrmann, *Angew. Chem. Int. Ed. Engl.* **1978**, *17*, 800−812. [17b] R. A. Andersen, M. H. Chisholm, J. F. Gibson, W. W. Reichert, I. P. Rothwell, G. Wilkinson, *Inorg. Chem.* **1981**, *20*, 3934−3936. [17c] J. Müller, B. Passon, J. Pickardt, *J. Organomet. Chem.* **1982**, *228*, C51−C54. [17d] W. A. Herrmann, *J. Organomet. Chem.* **1983**, *250*, 319−343. [17e] K. Isobe, S. Okeya, N. J. Meanwell, A. J. Smith, H. Adams, P. M. Maitlis, *J. Chem. Soc., Dalton Trans.* **1984**, 1215−1221. [17f] E. A. Carter, W. A. Goddard III, *J. Am. Chem. Soc.* **1986**, *108*, 4746−4754. [17g] G. M. Smith, J. D. Carpenter, T. J. Marks, *J. Am. Chem. Soc.* **1986**, *108*, 6805−6807. [17h] Y.-D. Wu, K. W. K. Chan, Z. Xue, *J. Am. Chem. Soc.* **1995**, *117*, 9259−9264.

[18] [18a] F. W. Hartner Jr., J. Schwartz, S. M. Clift, *J. Am. Chem. Soc.* **1983**, *105*, 640−641. [18b] A. R. Bulls, W. P. Schaefer, M. Serfas, J. E. Bercaw, *Organometallics* **1987**, *6*, 1219−1226. [18c] L. Li, M. Hung, Z. Xue, *J. Am. Chem. Soc.* **1995**, *117*, 12746−12750. [18d] L. Li, Z. Xue, G. P. A. Yap, A. L. Rheingold, *Organometallics* **1995**, *14*, 4992−4993. [18e] J. B. Diminnie, H. D. Hall, Z. Xue, *Chem. Commun.* **1996**, 2383−2384. [18f] L. Liu, L. Li, J. B. Diminnie, G. P. A. Yap, A. L. Rheingold, Z. Xue, *Organometallics* **1998**, *17*, 4597−4606. [18g] M. D. Fryzuk, P. B. Duval, S. S. S. H. Mao, M. J. Zaworotko, L. R. MacGillivray, *J. Am. Chem. Soc.* **1999**, *121*, 2478−2487. [18h] C. G. Ortiz, K. A. Abboud, J. M. Boncella, *Organometallics* **1999**, *18*, 4253−4260.

[19] [19a] I. H. Elson, J. K. Kochi, U. Kablunde, L. E. Manzer, G. W. Parshall, F. N. Tebbe, *J. Am. Chem. Soc.* **1974**, *96*, 7374−7376. [19b] L. E. Manzer, *Inorg. Chem.* **1977**, *16*, 525−528. [19c] M. F. Lappert, C. R. C. Milne, *J. Chem. Soc., Chem. Commun.* **1978**, 925−926. [19d] G. Parkin, E. Bunel, B. J. Burger, M. S. Trimmer, A. van Asselt, J. E. Bercaw, *J. Mol. Catal.* **1987**, *41*, 21−39.

[20] [20a] ^{1}H NMR (C_7D_8, 20 °C): δ = 7.17 (m, 4 H), 7.05 (m, 2 H), 6.98 [m, 4 H, Me-C(Me)(C_6H_5)-$(CH_2)_2$-C(Me)(C_6H_5)-Me], 1.34 [s, 4 H, Me-C(Me)(C_6H_5)-$(CH_2)_2$-C(Me)(C_6H_5)-Me], 1.21 [s, 12 H, *Me*-C(*Me*)(C_6H_5)-$(CH_2)_2$-C(*Me*)(C_6H_5)-*Me*]. ^{13}C{^{1}H} NMR (C_7D_8, 20 °C): δ = phenyl region (overlapped with **4** and solvent resonances), 42.6 [Me−*C*(Me)(C_6H_5)-$(CH_2)_2$-*C*(Me)(C_6H_5)-Me], 39.9 [*Me*-C(*Me*)(C_6H_5)-$(CH_2)_2$-C(*Me*)(C_6H_5)-*Me*], 31.22 [Me−C(Me)(C_6H_5)-$(CH_2)_2$-C(Me)-(C_6H_5)-Me]. [20b] B. Åkermark, A. Ljungqvist, *J. Organomet. Chem.* **1979**, *182*, 47−58. [20c] D. Schomburg, M. Link, H. Linoh, R. Tacke, *J. Organomet. Chem.* **1988**, *339*, 69−80.

[21] A. Castro, M. Gómez, P. Gómez-Sal, A. Manzanero, P. Royo, *J. Organomet. Chem.* **1996**, *518*, 37−46.

[22] R. B. King, M. B. Bisnette, *J. Organomet. Chem.* **1967**, *8*, 287−297.

[23] [23a] H. P. Fritz, *Adv. Organomet. Chem.* **1964**, *1*, 239−316. [23b] F. A. Cotton, T. J. Marks, *J. Am. Chem. Soc.* **1969**, *91*, 7281−7285.

[24] [24a] M. Gómez, G. Jimenez, P. Royo, J. M. Selas, P. R. Raithby, *J. Organomet. Chem.* **1992**, *439*, 147−154. [24b] I. de Castro, J. de la Mata, M. Gómez, P. Gómez- Sal, P. Royo, J. M. Selas, *Polyhedron* **1992**, *11*, 1023−1027. [24c] A. Castro, M. V. Galakhov, M. Gómez, P. Gómez Sal, A. Martín, F. Sánchez, *J. Organomet. Chem.* **2000**, *595*, 36−53. [24d] A. Castro, M. V. Galakhov, M. Gómez, P. Gómez-Sal, A. Martín, F. Sánchez, P. Velasco, *Eur. J. Inorg. Chem.* **2000**, 2047−2054.

[25] [25a] R. A. Bell, S. A. Cohen, N. M. Doherty, R. S. Threlkel, J. E. Bercaw, *Organometallics* **1986**, *5*, 972−975. [25b] V. C. Gibson, J. E. Bercaw, W. J. Bruton Jr., R. D. Sanner, *Organometallics* **1986**, *5*, 976−979.

[26] J. H. Shin, G. Parkin, *Chem. Commun.* **1999**, 887−888.

[27] J. H. Shin, G. Parkin, *Organometallics* **1994**, *13*, 2147−2149.

[28] R. J. Errington, *Advanced Practical Inorganic and Metalorganic Chemistry*, Blackie Academic & Professional, An Imprint of Chapman & Hall, London, UK, **1997**.

[29] C. Tessiers-Youngs, O. T. Beachley Jr., *Inorg. Synth.* **1986**, *24*, 95−97.

[30] R. R. Schrock, *J. Organomet. Chem.* **1976**, *122*, 209−225.

[31] [31a] WinGX: L. J. Farrugia, *J. Appl. Cryst.* **1999**, *32*, 837−838. [31b] G. M. Sheldrick, SHELX-97, *Program for Crystal Structure Analysis* (Release 97-2), University of Göttingen, Göttingen, Germany, **1998**. [31c] XHYDEX: A. G. Orpen, *J. Chem. Soc., Dalton Trans.* **1980**, 2509−2516.

Received December 14, 2001
[I01511]

Regiospecific Reaction between Dimetallic Phosphido-Bridged W−W Complexes and Phosphane Imide − Electrophilic Site Switching by Metal−Metal Bond Formation

Shin-Guang Shyu,*[a] Ramsharan Singh,[a] Chi-Jung Su,[a] and Kuan-Jiuh Lin[a]

Keywords: Tungsten / P ligands / Bridging ligands / Electrophilic site switching

Reaction between $CpW(CO)_2(\mu\text{-}PPh_2)W(CO)_5$(*W–W*) (**2**) and $Ph_3P{=}NR$ (R = Pr, CH_2Ph, *i*Pr) in THF at refluxing temperature is regiospecific with the CNR ligand coordinated to the $W(CO)_4$ unit to produce $CpW(CO)_2(\mu\text{-}PPh_2)W(CO)_4$-(CNR)(*W–W*) (**4**). Spectroscopic data indicate that the complex exists in two stereoisomeric forms in solution. The structure of the *cis* isomer was determined by a single-crystal X-ray diffraction study which indicates that the CNR ligand is coordinated to the W atom of the $W(CO)_4$ unit and *cis* to the phosphido bridge. Reaction between $CpW(CO)_3(\mu\text{-}PPh_2)W(CO)_5$ (**1**) and $Ph_3P{=}NR$ (R = Pr, CH_2Ph, *i*Pr) in THF under similar condition is also regiospecific. However, the CNR ligand is coordinated to the CpW site to produce $CpW(CO)_2(CNR)(\mu\text{-}PPh_2)W(CO)_5$ (**3**). There are also two stereoisomers of the complex, which were separated by column chromatography. Structures of both isomers were determined by single-crystal X-ray diffraction studies.

(© Wiley-VCH Verlag GmbH, 69451 Weinheim, Germany, 2002)

Introduction

It is now evident that the formation of a metal−metal bond can influence the chemistry at adjacent metal centers in dinuclear complexes and clusters.[1] Recent studies of phosphido-bridged dimetallic complexes have revealed two interesting observations. First, one metal atom can promote substitution reactions at the adjacent metal carbonyl ligand upon the formation of the metal−metal bond.[2] Second, switching of the substitution site can occur when the metal−metal bond is formed.[2b] Apparently, the formation of the metal−metal bond can result in the donation of electron density from one metal atom to the other.[2a−2e] This electron density redistribution may alter the electrophilicity of the carbon atom of the carbonyl ligands attached to the metal atoms. Thus, the electrophilic site may switch from the carbonyl ligands on one metal atom to the carbonyl ligands on the other metal atom in heterodimetallic complexes upon the formation of the metal−metal bond.

Phosphane imides, deoxygenating reagents,[3] react with carbonylmetal compounds to produce (isocyanide)metal complexes.[4] Nucleophilic attack of a phosphane imide at the carbonyl carbon atom followed by the elimination of the triphenylphosphane oxides to generate the isocyanide ligand has been proposed as the reaction mechanism.[4a−4c] Here, we report a study of the regiospecific reactions between phosphane imides and phosphido-bridged dimetallic complexes $Cp(CO)_3W(\mu\text{-}PPh_2)W(CO)_5$ (**1**)[2d] and $Cp(CO)_2W(\mu\text{-}PPh_2)W(CO)_5$](*W−W*) (**2**)[2d] to produce $Cp(CO)_2(CNR)W(\mu\text{-}PPh_2)W(CO)_5$ (**3**) and $Cp(CO)_2W$-$(\mu\text{-}PPh_2)W(CO)_4(CNR)$(*W−W*) (**4**), respectively. Thus, there is electrophilic site switching in these phosphido-bridged dimetallic complexes upon metal−metal bond formation.

Results and Discussion

Regiospecific Reaction of 1 with Phosphane Imides and Molecular Structures of 3a and 3a′

Reaction of **1** with $Ph_3P{=}NR$ (R = Pr, CH_2Ph, *i*Pr) produced two yellow solids **3** and **3′** in good yields (41% and 55%, Scheme 1). The ν(CN) stretching frequencies in their IR spectra indicate the terminal involvement of CNR in the coordination.[5] Signals corresponding to the protons of one isocyanide ligand were observed in their ^1H NMR spectra. Both complexes exhibited $^{31}P\{^1H\}$ NMR signals with two sets of J_{P-W} satellites at δ = −62.26 (**3a**) and −61.55 (**3a′**), respectively, indicative of a bridging phosphido group and the absence of a metal−metal bond.[6] The structures of **3a** and **3a′** were determined by single-crystal X-ray diffraction studies. Their structures are shown in Figures 1 and 2.

In complex **3a**, the diphenylphosphido ligand bridges two tungsten atoms with a W−W distance of 4.454(5) Å. This indicates that there is no metal−metal bond between the tungsten atoms. This is consistent with the observed upfield position of the phosphido signal in its $^{31}P\{^1H\}$ NMR spectrum. The isocyanide ligand CNPr is terminally coordin-

[a] Institute of Chemistry, Academia Sinica, Taipei, Taiwan 11529, Republic of China

Supporting information for this article is available on the WWW under http://www.eurjic.com or from the author.

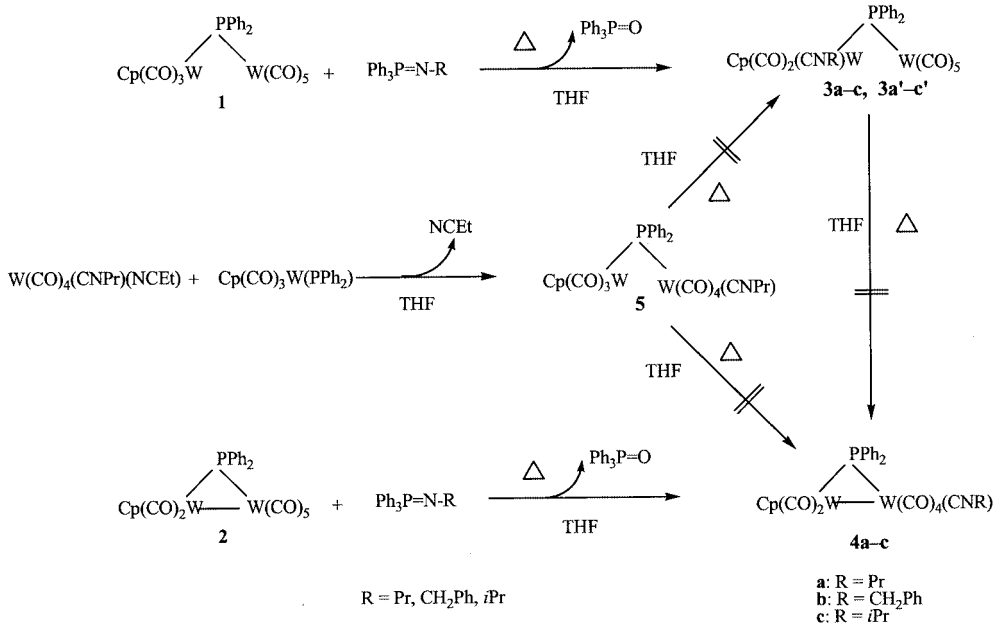

Scheme 1

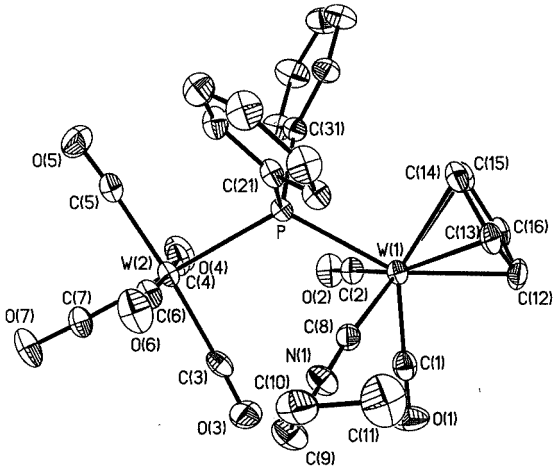

Figure 1. ORTEP drawing of **3a**, hydrogen atoms are omitted

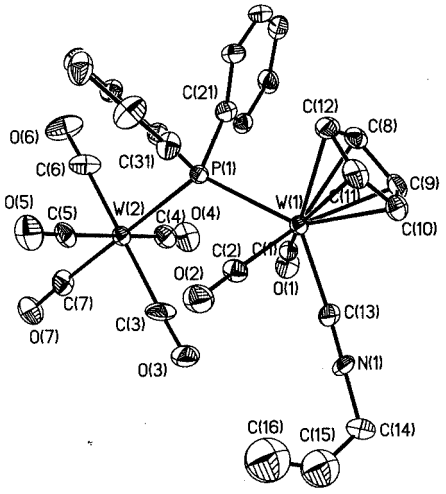

Figure 2. ORTEP drawing of **3a′**, hydrogen atoms are omitted

ated to W(1) of the CpW moiety. Thus, five CO ligands and $CpW(CO)_2(CNPr)PPh_2$ are coordinated to the W(2) atom to form a distorted octahedron around the W(2) atom. The doublet at δ = 200.44 (J_{P-C} =4.3 Hz, J_{C-W} = 123.8 Hz) in the $^{13}C\{^1H\}$ NMR spectrum is assigned to the four CO ligands on W(2) *cis* to the phosphido bridge. These four CO ligands are equivalent in the NMR spectrum because of the rotating of P−W(2) bond. Similar phenomena were observed in the $^{13}C\{^1H\}$ NMR spectra of complexes $CpFe(CO)_2(\mu\text{-}PPh_2)M(CO)_5$ (M = Cr, Mo, W).[10] The assignment is also based on the comparison of the resonance position of the *cis*-CO signal to the position of the *cis*-W(CO) signal [δ = 199.04 (d, J_{P-C} = 5.58 Hz, J_{W-C} = 121.29 Hz)] in $CpFe(CO)_2(\mu\text{-}PPh_2)W(CO)_5$.[7] The small doublet at δ = 201.62 (J_{P-C} = 18.12 Hz) is assigned to the *trans*-CO ligand based on a similar comparison with the resonance position [δ = 201.48 (d, J_{P-C} = 20.18 Hz)] of the *trans*-CO ligand of $CpFe(CO)_2(\mu\text{-}PPh_2)W(CO)_5$.[7] Also, the *trans*-CO ligand always has a lower field resonance than the resonance of the four *cis*-CO ligands as observed in $CpFe(CO)_2(\mu\text{-}PPh_2)M(CO)_5$ (M = Cr, Mo, W). The two carbonyl ligands on W(1) are non-equivalent and correspond to two broad humps (δ = 223 and 228) in the $^{13}C\{^1H\}$ NMR spectrum.

The structure of **3a′** is similar to the structure of complex **3a**. The isocyanide ligand is cordinated to the W(1) atom. The primary difference between them is that the two carbonyl ligands on W(1) are equivalent in **3a′** (cf. Figures 1 and 2). The doublet at δ = 223.40 (J_{P-C} = 15.10 Hz) in the ^{13}C NMR spectrum is assigned to the two equivalent carbonyl ligands based on the comparison of the resonance position of the CpW carbonyl ligands in $CpW(CO)_2(\mu\text{-}PPh_2)W(CO)_5(W\text{−}W)$ [δ = 226.56 (d, J_{P-C} = 17.19 Hz)][2d] and $CpW(CO)_2(\mu\text{-}PPh_2)Mo(CO)_5(W\text{−}W)$ [δ = 226.73 (d, J_{P-C} = 7.51 Hz)].[2e] Thus, the reaction between **1** and a

phosphane imide is regiospecific with the isocyanide ligand coordinated to the CpW moiety.

Regiospecific Reaction of $CpW(CO)_2(\mu\text{-}PPh_2)W(CO)_5$-(*W−W*) with $Ph_3P{=}NR$ (R= Pr, CH_2Ph, *i*Pr) and the Structure of *cis*-$CpW(CO)_2(\mu\text{-}PPh_2)W(CO)_4(CN\text{-}Pr)$-(*W−W*)

Interestingly, the reaction between **2** and a phosphane imide is also regiospecific. However, the attack is on a carbonyl ligand of the $W(CO)_5$ moiety (Scheme 1). Complex **2** reacted with a phosphane imide to produce a maroon red solid. Spectroscopic data (IR, variable-temperature ^1H and $^{31}P\{^1H\}$ NMR) and elemental analyses indicate that the product is a mixture of *cis* and *trans* isomers of **4**. We have based this conclusion on the comparison of these spectroscopic data to those of $Cp(CO)_2M(\mu\text{-}PPh_2)Mo(CO)_4(CNR)$(*M−Mo*) (M = Mo, W).[8] In addition the structure of *cis*-$CpW(CO)_2(\mu\text{-}PPh_2)W(CO)_4(CNPr)$(*W−W*) (**4a-*cis***) was determined by a single-crystal X-ray study (Figure 3).

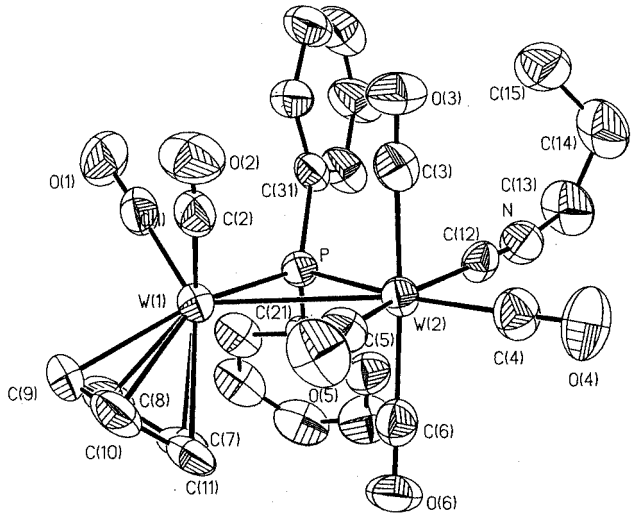

Figure 3. ORTEP drawing of **4a-*cis***, hydrogen atoms are omitted

The structure of **4a-*cis*** is similar to the structure of its W−Mo analogue $Cp(CO)_2W(\mu\text{-}PPh_2)Mo(CO)_4(CNPr)$-(*W−Mo*) where the isocyanide ligand coordinates to W in the *cis* position to the phosphido bridge.[8] A W−W distance of 3.1849(9) Å, which is similar to the W−Mo bond lengths of 3.1894(8) Å in $Cp(CO)_2W(\mu\text{-}PPh_2)Mo(CO)_4(CNPr)$(*W−Mo*) and 3.1942(12) Å in its parent compound **1**,[2d] indicates a metal−metal bond in the complex. This observation is consistent with the observed downfield resonance of the phosphorus signal in its $^{31}P\{^1H\}$ NMR spectrum.

Similar to $Cp(CO)_2Mo(\mu\text{-}PPh_2)M(CO)_4(CNR)$(*W−Mo*) (M = Mo, W), attempts to spectroscopically characterize the pure isomer failed.[8] When the crystals of the *cis* isomers were dissolved in solution, the ^1H and $^{31}P\{^1H\}$ NMR spectra of the solution were the same as that of the product mixture initially obtained. This indicates that isomerization occurs rapidly when the pure *cis* isomer is dissolved in the solvent.

Synthesis and Structure of $Cp(CO)_3W(\mu\text{-}PPh_2)W(CO)_4$-(CN*i*Pr) (5) − Possible Intramolecular Migration of the Isocyanide Ligand between W Atoms in Dimetallic Complex

In complex **1**, there are two sets of carbonyl ligands, one located on the $CpW(CO)_3$, and the other one on the $W(CO)_5$ unit. In principle, both sets of carbonyl ligands can be attacked by phosphane imides because there is no steric hindrance to protect the carbonyl ligands from the reaction. Intramolecular ligand exchanges have been observed in dimetallic complexes.[9] Thus, phosphane imides may attack the carbonyl ligand on the $W(CO)_5$ moiety followed by intramolecular ligand migration of the isocyanide ligand from W(2) to CpW(1). In order to evaluate the possibility of an intramolecular ligand exchange by an intermediate such as $Cp(CO)_3W(\mu\text{-}PPh_2)W(CO)_4(CNR)$, $Cp(CO)_3W(\mu\text{-}PPh_2)W(CO)_4(CN\textit{i}Pr)$ (**5**) was synthesized by the reaction between $CpW(CO)_3(PPh_2)$ and $W(CO)_4(CN\textit{i}Pr)(NCEt)$. In addition to spectroscopic characterizations, the structure of the complex was determined by a single-crystal X-ray study (Figure 4).

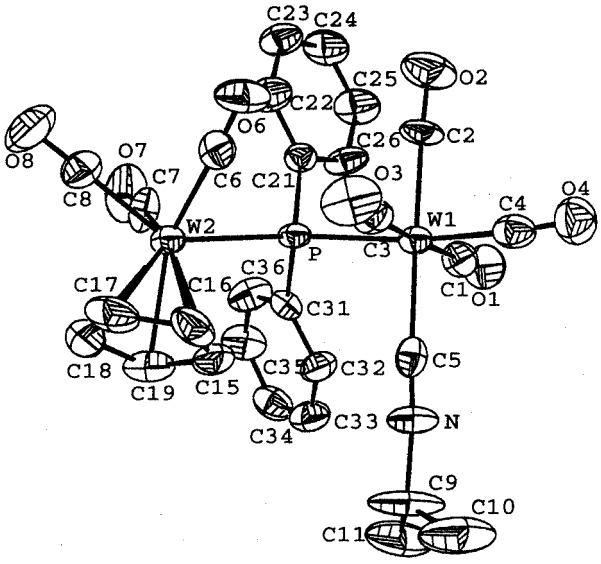

Figure 4. ORTEP drawing of **5**, hydrogen atoms are omitted

A W−W distance of 4.4548(7) Å indicates that there is no bonding between the two metal atoms in the complex. This observation is consistent with the observed upfield resonance of the phosphorus signal in its $^{31}P\{^1H\}$ NMR spectrum. The isocyanide ligand is coordinated to W(1) and is *cis* to the phosphido bridge ligand. The W−W distance of 4.4548(7) Å and the W(1)−P−W(2) angle of 116.71(9)° in **5** are similar to the W−W distance of 4.5096(11) Å and the W−P−W angle of 118.38(13)° in **1**.[2d] This indicates that the steric hindrance of the isocyanide ligand at the *cis* position in **5** is only slightly greater than the steric hindrance of the corresponding CO ligand in **1**.

Heating of **5** in THF to simulate the conditions of the reaction between **1** and phosphane imides does not produce **3** (Scheme 1). This observation excludes the possibility of an intramolecular exchange of the CNR ligand in an intermediate such as $Cp(CO)_3W(\mu\text{-}PPh_2)W(CO)_4(CNR)$ to form complex **3**. The regiospecific reaction between **1** and a phosphane imide is thus due to some electronic factor. The preferred attack on the carbonyl ligand of $CpW(CO)_3$ indicates that these carbonyl ligands must be more electrophilic than the carbonyl ligands of the $W(CO)_5$ unit.

Electrophilic Site Switching by Metal−Metal Bond Formation

The formation of a metal−metal bond may alter the regiospecificity of the reaction in two ways. First, it brings the two W atoms closer together, introducing steric crowding around the W(1) atom and rendering the attack of a phosphane imide at the CO ligands of the $CpW(CO)_2$ unit difficult. Second, the formation of the metal−metal bond can alter the electronic properties of the complex such that the CO ligands of the $W(CO)_5$ unit in **2** are more electrophilic than the CO ligands of the $CpW(CO)_2$ unit.

The CO ligands of the $CpW(CO)_2$ unit in **2** could still be attacked by a phosphane imide. Accordingly, one cannot exclude the steric hindrance argument completely. On the other hand, two considerations enable us to conclude that the electronic factor is dominant. First, in complex **1**, the carbonyl ligands of the $W(CO)_5$ unit are inert. Even under excess phosphane imide, no isocyanide ligand was observed to replace one of the CO ligands on the $W(CO)_5$ site. This observation indicates that the carbonyl ligand of the $W(CO)_5$ unit is not electrophilic enough to react with the nucleophilic phosphane imide under the reaction conditions. Second, one can consider the W−W bonding in **2** as a dative bond [donor−acceptor bond from W(2) to W(1)]. We may treat W(2) as a ligand of CpW(1) when one of the W(1) carbonyl ligands is removed from **1** by photolysis to form **2**.[2d,2e] Electron donation from the filled t_{2g} orbital of the W(2) atom to the W(1) atom upon formation of the metal−metal dative bond can reduce the electron density on W(2). The net result of this electron redistribution will be a decrease in $d_{xy}[W(2)] \rightarrow \pi^*(CO)$ bonding to the equatorial CO ligands.[2c−2e,2k] This will result in the reduction of the electron density on the carbon atoms of these equatorial CO ligands such that they become sufficiently electrophilic to react with the nucleophilic phosphane imides. In addition, when the electron-withdrawing CO ligand of the CpW(1) unit in **1** is replaced with the dative metal−metal bond to form **2**, electron back donation from W(1) to the two carbonyl ligands of W(1) becomes enhanced. The result is an increase in electron density of the carbon atoms of these CpW(1) carbonyl ligands. Thus, electronically, they are less reactive towards a nucleophile than the corresponding CpW(1) carbonyl ligands in **1**. We can consider that the formation of the metal−metal dative bond in **2** acts as a switch and triggers the nucleophilic attack on the $W(CO)_5$ carbonyl ligands by the activation of the equatorial CO ligands by W−W interactions. This switching of electrophilic site from the carbonyl ligands of the CpW unit in **1** to the carbonyl ligands of the $W(CO)_5$ unit in **2** in the heterodimetallic complexes by the formation of a metal−metal bond can be considered as a cooperative effect of the adjacent metal atom in dimetallic complexes.

Conclusions

Reaction between $CpW(CO)_2(\mu\text{-}PPh_2)W(CO)_5(W\text{−}W)$ and $Ph_3P{=}NR$ (R = Pr, CH_2Ph, *i*Pr) in THF is regiospecific with the CNR ligand coordinated to the $W(CO)_4$ unit to produce $CpW(CO)_2(\mu\text{-}PPh_2)W(CO)_4(CNR)$ $(W\text{−}W)$. Reaction between $CpW(CO)_3(\mu\text{-}PPh_2)W(CO)_5$ and $Ph_3P{=}NR$ (R = Pr, CH_2Ph, *i*Pr) under similar conditions is also regiospecific with the CNR ligand coordinated to the CpW site to produce $CpW(CO)_2(CNR)(\mu\text{-}PPh_2)W(CO)_5$. The switching of the electrophilic site from the carbonyl ligands of the CpW unit in **1** to the carbonyl ligands of the $W(CO)_5$ unit in **2** in the heterodimetallic complexes is considered as a cooperative effect of the adjacent metal atom in the dimetallic complexes. The redistribution of the electron density from W of the CpW moiety to the other W of the $W(CO)_5$ unit in **2** by the formation of a metal−metal bond is proposed as the reason for this switching.

Experimental Section

General Procedures: All reactions were carried out under purified nitrogen with standard Schlenk techniques. TLC and chromatographic work were performed in air. Infrared (IR) spectra were recorded with a Perkin−Elmer 882 infrared spectrophotometer. ^1H, ^{13}C and ^{31}P NMR spectra were recorded with Bruker AMX-500, AMX-400, AC-200 and AC-300 spectrometers. The ^{31}P NMR shifts are referenced to 85% H_3PO_4 with downfield chemical shifts as positive. Except as noted, NMR spectra were collected at room temperature. FAB mass spectra were recorded with a VG70-250S or a JEOL JMS-HX 110 mass spectrometer. Microanalyses were performed by the Microanalytical Laboratory at National Cheng Kung University, Tainan, Taiwan and Academia Sinica.

Materials: THF was distilled from potassium and benzophenone under purified nitrogen just before use. The complexes $CpW(CO)_3(\mu\text{-}PPh_2)W(CO)_5$ (**1**) and $CpW(CO)_2(\mu\text{-}PPh_2)W(CO)_5(W\text{−}W)$ (**2**) were prepared according to literature procedures.[2d] The compounds $Ph_3P{=}NR$ (R = Pr, CH_2Ph, *i*Pr) were prepared as described in the literature.[10]

$CpW(CO)_2(CNPr)(\mu\text{-}PPh_2)W(CO)_5$ (3a and 3a′): A mixture of **2** (0.120 g, 0.143 mmol) and $Ph_3P{=}NPr$ (0.094 g, 0.286 mmol) was dissolved in THF (20 mL) and the resulting solution was refluxed with stirring at 68 °C for about 70 h. The solvent was then removed under vacuum and the residue was chromatographed on grade III alumina and eluted with CH_2Cl_2/hexane to afford two fractions. The first yellow band was eluted with CH_2Cl_2/hexane (20:80) to obtain yellow solid compound **3a** after removing the solvent. Yield 0.052 g (41%). $C_{28}H_{22}NO_7PW_2$(883): calcd. C 38.08, H 2.51, N 1.59; found C 37.80, H 2.53, N 1.60. MS (FAB): m/z = 884 $[M + 1]^+$. The second band was eluted with CH_2Cl_2/hexane (25:75) to produce compound **3a′** as a yellow solid after removing the solvent. Yield 0.070 g (55%). $C_{28}H_{22}NO_7PW_2$(883): calcd. C 38.08, H 2.51,

N 1.59; found C 37.95, H 2.57, N 1.70. MS (FAB): *m*/*z* = 884 [M + 1]$^+$. Spectroscopic data of the complexes are presented in Table 1 of the Supporting Information (see also footnote on the first page of this article); for comparison, the spectroscopic data of the parent complexes **1** and **2** are also given there.

CpW(CO)$_2$(CNCH$_2$Ph)(μ-PPh$_2$)W(CO)$_5$ (3b and 3b′): Reaction and separation conditions similar to those for **3a** and **3a′** were applied to prepare **3b** and **3b′**. The reaction time was 70 h and 0.324 g (0.39 mmol) of **1** and 0.286 g (0.77 mmol) of Ph$_3$P=NCH$_2$Ph were used. **3b**: Yield: 0.168 g (46%). $C_{32}H_{22}NO_7PW_2$ (931): calcd. C 41.28, H 2.38, N 1.50; found C 41.13, H 2.45, N 1.43. MS (FAB): *m*/*z* = 932 [M + 1]$^+$. **3b′**: Yield: 0.166 g (46%). $C_{32}H_{22}NO_7PW_2$ (931): calcd. C 41.28, H 2.38, N 1.50; found C 41.34, H 2.47, N 1.47. MS (FAB): *m*/*z* = 932 [M + 1]$^+$. Spectroscopic data of the complexes are presented in Table 1 of the Supporting Information.

CpW(CO)$_2$(CN*i*Pr)(μ-PPh$_2$)W(CO)$_5$ (3c and 3c′): Reaction and separation conditions similar to those for **3a** and **3a′** were applied to prepare **3c** and **3c′**. The reaction time was 144 h and 0.380 g (0.45 mmol) of **1** and 0.288 g (0.90 mmol) of Ph$_3$P=N*i*Pr were used. 0.070 g of the parent complex **1** was recovered. **3c**: Yield: 0.036 g (11%). $C_{28}H_{22}NO_7PW_2$ (883): calcd. C 38.08, H 2.51, N 1.59; found C 37.87, H 2.55, N 1.56. MS (FAB): *m*/*z* = 884 [M + 1]$^+$. **3c′**: Yield: 0.070 g (22%). $C_{28}H_{22}NO_7PW_2$: (883) calcd. C 38.08, H 2.51, N 1.59; found C 37.70, H 2.55, N 1.61. MS (FAB): *m*/*z* = 856 [M − CO + 1]$^+$. Yields are based on the parent compound consumed in the reactions. Spectroscopic data of the complexes are presented in Table 1 in the Supporting Information.

CpW(CO)$_2$(μ-PPh$_2$)W(CO)$_4$(CNPr)(*W*−*W*) (4a-*cis* and 4a-*trans*): A mixture of **2** (0.306 g, 0.376 mmol) and Ph$_3$P=NPr (0.240 g, 0.752 mmol) was dissolved in THF (20 mL) and refluxed with stirring at 68 °C for about 12 h. The solvent was then removed under vacuum and the residue was chromatographed on grade III alumina and eluted with CH_2Cl_2/hexane to afford three fractions. A small amount of unchanged starting material was recovered from the first band on elution with 8% of dichloromethane in hexane. A small amount (0.011 g) of green compound was obtained from the second band on elution with 12% of dichloromethane in hexane and was not identified. A mixture of maroon red colored compounds CpW(CO)$_2$(μ-PPh$_2$)W(CO)$_4$(CNPr)(*W*−*W*) (**4a-*cis*** and **4a-*trans***) was obtained from the third band on elution with 16% of CH_2Cl_2/hexane. Combined yield of **4a-*cis*** and **4a-*trans***: 0.233 g (73%). $C_{27}H_{22}NO_6PW_2$ (855): calcd. C 37.92, H 2.59,N, 1.64; found C 38.02, H 2.74, N 1.65. Spectroscopic data indicate that the mixture consists of two isomers, which could not be separated by chromatography. Spectroscopic data are given in Table 1 of the Supporting Information.

CpW(CO)$_2$(μ-PPh$_2$)W(CO)$_4$(CNCH$_2$Ph)(*W*−*W*) (4b-*cis* and 4b-*trans*): Reaction and separation conditions similar to those for **4a-*cis*** and **4a-*trans*** were applied to prepare **4b-*cis*** and **4b-*trans***. The reaction time was 35 h and 0.354 g (0.440 mmol) of **2** and 0.324 g (0.870 mmol) of Ph$_3$P=NCH$_2$Ph were used. Combined yield of **4b-*cis*** and **4b-*trans***: 0.243 g (61%). $C_{31}H_{22}NO_6PW_2$ (903): calcd. C 41.23, H 2.46, N 1.55; found C 41.64, H 2.64, N 1.66. MS (FAB): *m*/*z* = 904 [M + 1]$^+$. Spectroscopic data indicate that the mixture consists of two isomers that could not be separated by chromatography. Spectroscopic data are given in Table 1 of the Supporting Information.

CpW(CO)$_2$(μ-PPh$_2$)W(CO)$_4$(CN*i*Pr)(*W*−*W*) (4c-*cis* and 4c-*trans*): Reaction and separation conditions similar to those for **4a-*cis*** and **4a-*trans*** were applied to prepare **4c-*cis*** and **4c-*trans***. The reaction time was 96 h and 0.407 g (0.500 mmol) of **2** and 0.319 g (1.000 mmol) of Ph$_3$P=N*i*Pr were used. Combined yield of **4c-*cis*** and **4c-*trans***: 0.180 g (42%). $C_{27}H_{22}NO_6PW_2$ (855): calcd. C 37.92, H 2.59,

Table 1. Crystal and intensity collection data for **3a**, **3a′**, **4a-*cis*** and **5**

	3a	**3a′**	**4a-*cis***	**5**
Empirical formula	$C_{28}H_{22}NO_7PW_2$	$C_{28}H_{22}NO_7PW_2$	$C_{27}H_{22}NO_6PW_2$	$C_{28}H_{22}NO_7PW_2$
Formula mass	883.14	883.14	855.13	883.16
Space group	$P\bar{1}$	*Cc*	$P\bar{1}$	$P2_1/c$
a [Å]	9.172(2)	12.759(3)	10.545(3)	16.2397(19)
b [Å]	10.414(2)	13.920(3)	10.588(3)	9.7464(17)
c [Å]	16.595(3)	16.038(3)	14.570(2)	18.132(3)
α [°]	82.40(3)	90	76.80(2)	90
β [°]	87.42(3)	91.70(3)	73.21(3)	102.165(12)
γ [°]	67.41(3)	90	62.42(2)	90
V [Å^3]	1450.6(5)	2847.2(11)	1371.5(6)	2805.5(8)
ρ(calcd.) [Mg m^{-3}]	2.022	2.060	2.070	2.091
Z	2	4	2	4
Cryst. size [mm]	0.2250.2450.34	0.2650.2850.32	0.2850.2450.18	0.1950.3850.38
Absorpt. coeff. μ(Mo-K_α) [mm^{-1}]	8.023	8.176	8.478	8.47
Temperature	room temp	room temp	room temp	room temp
Radiation	0.71069 Å	0.71069 Å	0.71069 Å	0.71069 Å
2θ range [°]	45	45	45	50
Scan type	2θ-ω	2θ-ω	2θ-ω	θ/2θ
No. of reflections	4072	1952	3817	4930
No. of observed reflections	3779	1897	3576	3447
Variables	352	342	335	353
R	0.0288	0.0271	0.0327	0.033
wR(F^2)	0.0787	0.0705	0.0849	0.034
S	1.091	1.067	1.050	1.45
$\Delta F_{max,min.}$ [e/Å^3]	1.727, −1.311	1.083, −1.226	2.354, −1.632	2.120, −1.020

N 1.64; found C 38.01, H 2.62, N 1.72. MS (FAB): m/z = 856 [M + 1]$^+$. Spectroscopic data indicate that the mixture consists of two isomers, which could not be separated by chromatography. Spectroscopic data are given in Table 1 of the Supporting Information.

$CpW(CO)_3(\mu\text{-}PPh_2)W(CO)_4(CN\textit{i}Pr)$ (5): A yellow solution of $Na[CpW(CO)_3]\cdot 2DME$[11] (0.350 g, 0.65 mmol) in THF (100 mL) was cooled to 0 °C. A solution of PPh_2Cl (0.132 mL, 0.71 mmol) in THF (50 mL) was then slowly added to the above solution. After 1 h, the color of the solution turned to orange red. A solution of $W(CO)_4(CN\textit{i}Pr)(NCEt)$[12] (0.250 g, 0.60 mmol) in THF (40 mL) was then added slowly to the above solution. After stirring overnight at room temperature, the solvent was removed and the residue was chromatographed on silica gel. Elution with CH_2Cl_2/hexanes (1:4) gave the yellow product. Yield: 0.10 g (18%). $C_{28}H_{22}NO_7PW_2$ (883): calcd. C 38.08, H 2.51; found C 38.05, H 2.23. MS (FAB): m/z = 884 [M + 1]$^+$. Spectroscopic data are given in Table 1 of the Supporting Information.

Structure Determinations of $CpW(CO)_2(CNPr)(\mu\text{-}PPh_2)W(CO)_5$ (3a and 3a′), $CpW(CO)_2(\mu\text{-}PPh_2)W(CO)_4(CNPr)$ (*W*−*W*) (4a-*cis*) and $CpW(CO)_3(\mu\text{-}PPh_2)W(CO)_4(CN\textit{i}Pr)$ (5): Crystals of complexes **3a**, **3a′**, **4a-*cis*** and **5** were grown by slow diffusion of hexanes into a saturated CH_2Cl_2 solution of the relevant complex at 0 °C in air. Diffraction measurements were made with an Enraf−Nonius CAD4 diffractometer with graphite-monochromated Mo-K_α radiation. Structures were solved by direct methods and refined by full-matrix least square using SHELXL-93 or NRCVAX programs. All non-hydrogen atoms were refined with anisotropic displacement parameters, and all hydrogen atoms were constrained to geometrically calculated positions. Crystal data and details of data collection and structure analysis are summarized in Table 1. Selected interatomic distances and bond angles are given in Table 2 of the Supporting Information (see also footnote on the first page of this article). CCDC-154007 (**3a**), -154008 (**3a′**), -173249 (**4a-cis**), and -172971 (**5**) contain the supplementary crystallographic data for this paper (excluding structure factors). These data can be obtained free of charge at www.ccdc.cam.ac.uk/conts/retrieving.html or from the Cambridge Crystallographic Data Centre, 12, Union Road, Cambridge CB2 1EZ, UK [Fax: (internat.) + 44-1223/336-033; E-mail: deposit@ccdc.cam.ac.uk].

Acknowledgments

We wish to thank the National Science Council, Republic of China and Academia Sinica for financial support of this work.

[1] [1a] R. D. Adams, T. S. Barnard, *Organometallics* **1998**, *17*, 2885−2890. [1b] P. Braunstein, J. Rose, in *Comprehensive Organometallic Chemistry II* (Eds.: E. W. Abel, F. G. A. Stone, G. Wilkinson), Pergamon, Oxford, New York, **1995**, vol. 10, chapter 7, p. 351−385. [1c] H. Vahrenkamp, *Angew. Chem. Int. Ed. Engl.* **1978**, *17*, 379−392.

[2] [2a] S.-G. Shyu, S. M. Hsiao, *Organometallics* **1998**, *17*, 1151−1154. [2b] S.-G. Shyu, P.-J. Lin, K.-J. Lin, Y.-S. Wen, M.-C. Chang, *Organometallics* **1995**, *14*, 2253−2264. [2c] S.-G. Shyu, S. M. Hsiao, K.-J. Lin, H.-M. Gau, *Organometallics* **1995**, *14*, 4300−4307. [2d] S.-G. Shyu, W. J. Wu, S.-M. Peng, G.-H. Lee, Y.-S. Wen, *J. Organomet. Chem.* **1995**, *489*, 113−122. [2e] S.-G. Shyu, J.-Y. Hsu, P.-J. Lin, W. J. Wu, S.-M. Peng, G.-H. Lee, Y.-S. Wen, K.-J. Lin, H.-M. Gau, *Organometallics* **1994**, *13*, 1699−1710. [2f] R. Rgragui, P. H. Dixneuf, N. J. Taylor, A. J Carty, *Organometallics* **1986**, *5*, 1−8. [2g] W. C. Mercer, R. R. Whittle, E. W. Burkhardt, G. L. Geoffroy, *Organometallics* **1985**, *4*, 68−74. [2h] J. Powell, M. R. Gregg, J. F. Sawyer, *Inorg. Chem.* **1989**, *28*, 4451−4460. [2i] J. Powell, J. F. Sawyer, M. V. R. Stainer, *Inorg. Chem.* **1989**, *28*, 4461−4470. [2j] J. Powell, C. Coutoure, M. R. Gregg, *J. Chem. Soc., Chem. Commun.* **1988**, 1208−1210. [2k] D. Miguel, J. A. Perez-Mertinez, V. Riera, *Organometallics* **1994**, *13*, 4667−4669. [2l] T. Adatia, K. Henrick, A. D. Horton, M. J. Mays, M. McPartlin, *J. Chem. Soc., Chem. Commun.* **1986**, 1206−1208.

[3] E. W. Abel, S. A. Mucklejoin, *Phosphorus Sulfur Relat. Elem.* **1981**, *9*, 235−266 and references therein.

[4] [4a] J. Kiji, A. Matsumura, T. Haishi, S. Okazaki, J. Furukawa, *Bull. Chem. Soc. Jpn.* **1977**, *50*, 2731−2733. [4b] H. Alper, R. A. Partis, *J. Organomet. Chem.* **1972**, *35*, C40−C42. [4c] C. A. Mirkin, K. L. Lu, G. L. Geoffroy, A. L. Rheingold, D. L. Staley, *J. Am. Chem. Soc.* **1989**, *111*, 7279−7281. [4d] L. C. Chen, M. Y. Chen, J. H. Chen, Y. S. Wen, K. L. Lu, *J. Organomet. Chem.* **1992**, *425*, 99−111. [4e] Y. W. Lin, H. M. Gau, Y. S. Wen, K. L. Lu,, *Organometallics* **1992**, *11*, 1445−1447. [4f] C. A. Mirkin, K. L. Lu, T. W. Snead, B. A. Young, G. L. Geoffroy, A. L. Rheingold, B. S. Haggerty, *J. Am. Chem. Soc.* **1991**, *113*, 3800−3810. [4g] K. L. Lu, C. C. Chen, Y. W. Lin, F. E. Hong, H. M. Gau, L. L. Gan, H. D. Luoh, *J. Organomet. Chem.* **1993**, *453*, 263−267.

[5] M. O. Albers, N. J. Coville, E. Singleton, *J. Organomet. Chem.* **1987**, *323*, 37−52.

[6] [6a] A. J. Carty, S. A. Maclaughlin, D. Nucciarone, in *Phosphrous-31 NMR Spectroscopy in Stereochemical Analysis: Organic Compounds and Metal Complexes* (Eds.: J. G. Verkade, L. P. Quin), VCH, New York, **1987**, chapter 16, and references cited therein. [6b]P. E. Garrou, *Chem. Rev.* **1981**, *81*, 229−266.

[7] S.-G. Shyu, P.-J. Lin, Y.-S. Wen, *J. Organomet. Chem.* **1993**, *443*, 115−121.

[8] S.-G. Shyu, R. Singh, K.-J. Lin, *Organometallics* **1998**, *17*, 4739−4743

[9] [9a] H. Langenbach, H. Vahrenkamp, *Chem. Ber.* **1979**, *112*, 3390−3412. [9b] P. Braunstein, M. Knoor, G. Reinhard, U. Schubert, T. Stahrfeldt, *Chem. Eur. J.* **2000**, *6*, 4265−4278.

[10] [10a] H. Zimmer, G. Singh, *J. Org. Chem.* **1963**, *28*, 483−486. [10b] H. Staudinger, J. Meyer, *Helv. Chim. Acta* **1919**, *2*, 635−646.

[11] R. Bender, P. Braunstein, J.-M. Jud, Y. Dusausoy, *Inorg. Chem.* **1983**, *22*, 3394−3407.

[12] [12a] M. O. Albers, E. Singleton, N. J. Coville,, *J. Chem. Educ.* **1986**, *63*, 444−447. [12b] C.-A. Dickson, A. W. Mcfarlane, N. J. Coville, *Inorg. Chim. Acta* **1989**, *158*, 205.

Received November 8, 2001
[I01446]

Oxygen-Containing, Asymmetric "Dual-Side" Zirconocenes: Investigations on a Reversible Chain Transfer to Aluminum

Jürgen Kukral,[a] Petri Lehmus,[a] Martti Klinga,[b][‡] Markku Leskelä,[b][‡] and Bernhard Rieger*[a]

Keywords: Metallocenes / Propene polymerization / O ligands / Cyclopentadienyl ligands / Zirconium catalysts

A series of new oxygen-substituted, asymmetric zirconocene dichlorides (*rac*-{1-[5,6-(ethylenedioxy)-2-methyl-1-η^5-indenyl]-2-(9-η^5-fluorenyl)ethane}zirconium dichloride (**3a**), *rac*-{1-[5,6-(ethylenedioxy)-2-methyl-1-η^5-indenyl]-2-(9-η^5-fluorenyl)ethane}dimethylzirconium (**3b**) and *rac*-{[5,6-ethylenedioxy)-2-methyl-1-η^5-indenyl](9-η^5-fluorenyl)dimethylsilane}zirconium dichloride (**3c**)} have been prepared and their polymerization behavior was investigated in dependence of monomer concentration, temperature and catalyst activation. The presence of oxygen substituents on the indenyl ring results in a strong increase of polymerization activities and also of polymer molecular weights with decreasing Al/Zr ratio. Significantly higher molecular masses and activities were found for the dimethyl complex **3b** after activation with $[(C_6H_5)_3C^+][(C_6F_5)_4B^-]$ deriving from the absence of chain transfer to aluminum and higher concentration of active catalyst species. The mechanism of stereoerror formation of the oxygen-containing C_1-symmetric catalyst was investigated by deuterium labeling studies on propene monomers. The results are discussed on the basis of a reversible chain transfer to aluminum.

Introduction

We reported recently on a new family of asymmetric Zr^{IV} complexes that allows to achieve and adjust elastic polymer properties by a controlled placement of isolated stereoerrors along isotactic polypropene chains.[1] A widely disregarded issue in the development of metallocene chemistry was the incorporation of heteroatoms into the ligand framework, but it found growing interest in the last years.[2,3] First investigations were mainly restricted to methoxy groups as π-donors substituents. A negative influence on the catalyst activity and the polymer molecular weights was observed and explained by the interaction between the donor substituents and methylalumoxane (MAO) resulting in electron withdrawal instead of electron donation.[4] The introduction of amino groups in 2-position of indenyl ligands[5,6] was found by Brintzinger et al.[5] to give modest activities after an induction time of several hours. On the other hand, the investigation of sterically shielded 2-siloxy-substituted bis-(indenyl) complexes by Leino et al.[2] and Lehmus et al.[3] evidenced these complexes not to suffer from induction periods and to give a considerable increase in ethene polymerization activities compared to their unsubstituted analogues. Recently, Ewen et al.[7] reported on heteroatom-containing aromatic ligands with a polymerization performance rivaling that of the corresponding unsubstituted complexes.

In the present work a matter of particular interest was to combine both, the unique polymerization properties of our C_1-symmetric metallocene catalysts and the high potential for extending the concept of ligand design by introducing heteroatoms into the ligand framework. Therefore, the oxygen-substituted complexes **3a**–**c** (Scheme 1) were synthesized and tested in propene polymerization experiments using MAO and $[(C_6H_5)_3C^+][(C_6F_5)_4B^-]$ as cocatalysts. By imbedding the heteroatoms into a dioxane ring, we aimed at a protection of the heterocycle against C–O splitting reactions with MAO and thus to improve the catalyst stability.[8] Polymerization studies using deuterated propene were performed to elucidate the role of the aluminum cocatalyst in the mechanism of stereoerror formation of **3a**/MAO.[1b]

Results and Discussion

Ligand and Complex Synthesis

The ethylene-bridged ligand **2a**H_2 (Scheme 2, top) was synthesized via the 1-bromo-2-(9-fluorenyl)ethane intermediate. Analogously, the dimethylsilane-bridged ligand **2b** was prepared by addition of excess $(CH_3)_2SiCl_2$ to a vigor-

[‡] X-ray structure analysis
[a] Department for Materials and Catalysis, University of Ulm, Albert-Einstein-Allee 11, 89069 Ulm, Germany
Fax: (internat.) + 49-731/502-3039
E-mail: bernhard.rieger@chemie.uni-ulm.de
[b] Laboratory of Inorganic Chemistry, Department of Chemistry, University of Helsinki, 00014 Helsinki, Finland

 © WILEY-VCH Verlag GmbH, 69451 Weinheim, Germany, 2002 1434–1948/02/0606–1349 $ 20.00+.50/0

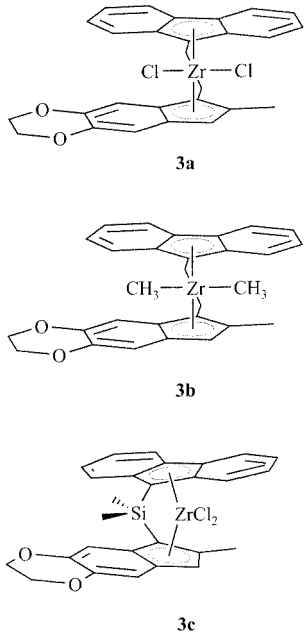

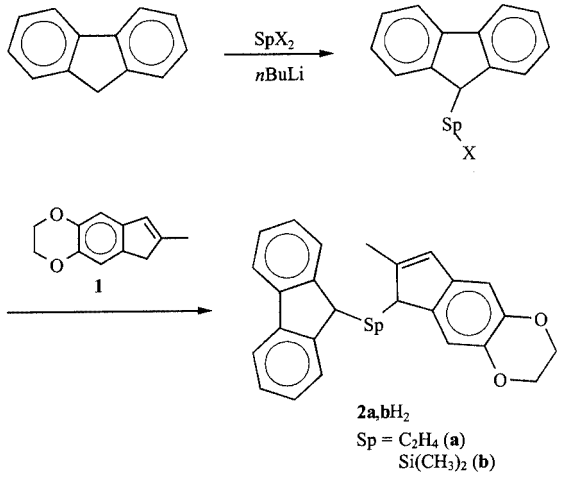

Scheme 1

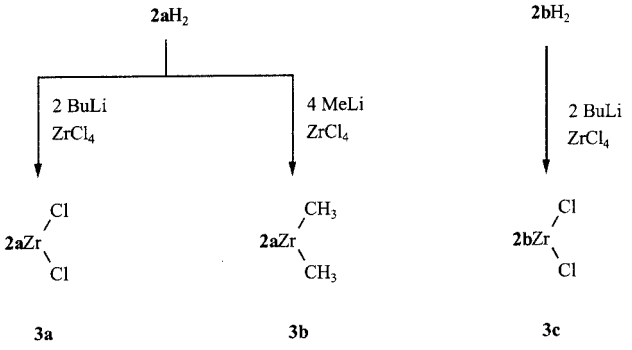

Scheme 2

ously stirred suspension of fluorenyllithium. Treatment of the ethylene- and silane-substituted fluorenyl intermediates with indenyllithium afforded the corresponding ligands **2a**,**b**H_2.[9] The zirconocene complexes **3a**−**c** (Scheme 2, bottom) were synthesized in moderate to high yields after reaction of the dilithium salt of the ligands **2a**,**b**H_2 with solid $ZrCl_4$ and purified by crystallization from toluene. Compounds **3a**,**b** are stable products and even the Si-bridged complex **3c** is, in contrast to related difluorenyl- or fluorenyl/indenylzirconium dichlorides,[1b,10] relatively stable in solution. The dimethyl derivative **3b** was obtained by a straightforward one-pot reaction of 4 equiv. of methyllithium with **2a**H_2, followed by the addition of $ZrCl_4$.[11] This simplified synthesis of the dimethylmetallocene evades separate preparation and isolation of the dichloro compounds and their subsequent reaction with methylmagnesium bromide or methyllithium.

Crystal and Molecular Structure

A single-crystal X-ray structure investigation was performed on complex **3a** (Figure 1, Table 4) which crystallizes in the monoclinic space group $P2_1/n$. The $Cp^{Flu}-Zr-Cp^{Ind}$ angle δ (Figure 2[12], Table 1, 128.1°) and φ (63.8°), the bite angle between the least-squares planes of the two Cp ligands, are in between those of the Zr complexes **EBI**[13] (δ = 126.9°[14], φ = 62.1°) and **EBF**[15] (δ = 129.0°[16], φ = 64.3°). In contrast, γ angles slightly larger than 180° (γ^{Flu} = 186.98°, γ^{Ind} = 182.82°) differ from results previously reported for other bridged indenyl and fluorenyl complexes for which typically values smaller than 180° were observed.[16] A genuine explanation of this effect cannot be given, yet. However, the resulting increased accessibility of the zirconium center is obviously one reason for the high activities of our asymmetric catalysts.[17]

The Zr−fluorenyl centroid bond of **3a** (2.59 Å) is distinctly longer than the distance between Zr^{IV} and the indenyl centroid (2.52 Å) leading to a nonsymmetric positioning of the Zr^{IV} center between the two Cp planes. A β^{Ind} value of 86.52° points toward a nearly ideal η^5-coordination of the indenyl ring to Zr^{IV}. This is different for the fluorenyl fragment. The value of β^{Flu} close to 80° (81.68°) and the corresponding Zr−C distances (ranging from 2.435 to 2.688 Å) clearly indicate a reduced hapticity of the fluorenyl fragment toward η^3-coordination.[18]

Propene Polymerization Experiments

Polymerization Activity

The experimental data (Table 2) indicate that all zirconocene compounds of the series **3a**−**c** are suitable catalysts for the polymerization of propene after MAO or $[(C_6H_5)_3C^+][(C_6F_5)_4B^-]$ activation.

The polymerization activities of the oxygen-containing complexes **3a**,**c**/MAO correlate tightly with the total amount of MAO. A distinct increase in catalyst activity could be observed with decreasing MAO concentration ($100 \leq Al/Zr \leq 2000$). The maximum activity is reached at Al/Zr ratios of around 300:1.[3] Seemingly, the polar oxygen substituents promote the approach of the Lewis acidic alu-

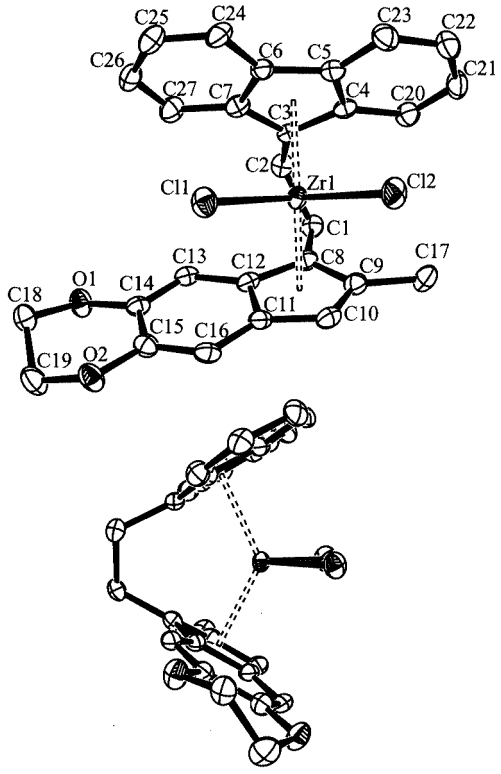

Figure 1. Two projections of the molecular structure and labeling scheme of complex **3a**

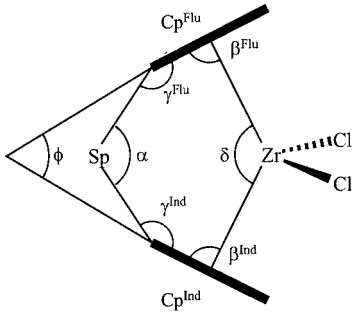

Figure 2. Schematic illustration of relevant band angles

minum cocatalyst to the zirconium center and accelerate the activation reaction in the apolar polymerization medium toluene. At higher cocatalyst concentrations excessive MAO operates as an polymerization-inhibiting agent. The incorporation of the heteroatoms into a ring system protects the oxygen groups sufficiently against MAO-induced C−O splitting and consequently inhibits catalyst decomposition.[19] A further significant activity increase up to a factor of 10 {at T_P = 30 °C up to 5100 kg PP (mol of Zr [C_3] h)$^{-1}$} could be observed for complex **3b/**[$(C_6H_5)_3C^+$][$(C_6F_5)_4B^-$] indicating that this cocatalyst provides a maximized concentration of active Zr^{IV} centers.[20]

The exchange of the ethylene bridge by a dimethylsilane unit results in slightly declined polymerization activities at T_P = 30 °C which, however, distinctly increases up to 3800 kg PP (mol of Zr [C_3] h)$^{-1}$ at 50 °C; **3c**/MAO is the first dimethylsilane-bridged system we investigated that shows not a rapid decomposition during the first minutes of the polymerization reaction,[1b] but rather leads to a constant propene consumption.

Table 1. Selected bonding parameters of complex **3a**

	3a[a]
α	–
β^{Flu}	81.7(5)
β^{Ind}	86.5(5)
γ^{Flu}	187.0(5)
γ^{Ind}	182.8(5)
φ	63.8(5)
δ	128.1(5)
Cl−Zr−Cl	98.00(4)
Zr−Cl(1)	2.4214(12)
Zr−Cl(2)	2.4264(13)
av. Zr−centroid(Cp^{Flu})[b]	2.588(4)
av. Zr−centroid(Cp^{Ind})[b]	2.519(4)
Zr−centroid(Cp^{Flu})	2.285(4)
Zr−centroid(Cp^{Ind})	2.211(4)
Zr1−C3 (Cp^{Flu})	2.435(4)
Zr1−C4 (Cp^{Flu})	2.554(4)
Zr1−C5 (Cp^{Flu})	2.676(4)
Zr1−C6 (Cp^{Flu})	2.688(4)
Zr1−C7 (Cp^{Flu})	2.589(4)
Zr1−C8 (Cp^{Ind})	2.459(4)
Zr1−C9 (Cp^{Ind})	2.496(4)
Zr1−C10 (Cp^{Ind})	2.512(4)
Zr1−C11 (Cp^{Ind})	2.603(4)
Zr1−C12 (Cp^{Ind})	2.526(4)

[a] Bond lengths are given in Å and angles in °. [b] av. Zr−centroid (Cp^{Flu},Cp^{Ind}) is the mean value of the 5 bonds of the carbon atom of the Cp plane to the Zr atom.

Molecular Weights

The molecular weights of the polypropenes obtained with **3a**−**c** decrease at higher Al/Zr ratios (Figure 3). The polydispersities of the polymer products are within the narrow range of 1.7 to 2.0 indicating homogeneous polymerization conditions. This decline shows again that chain transfer to aluminum plays a decisive role,[4,21] in line with the above discussion of catalyst activities. As a result of this facile chain termination reaction isopropyl end groups are observed after acidic workup (Figure 4)[5] instead of vinylic chain ends resulting from spontaneous β-H abstraction. After borate activation of **3b**, excluding the possibility of transfer to aluminum, the molecular weights improved from 3.0×10^4 up to 16.0×10^4 g mol^{-1} (Table 2, Entries 4, 8).

Stereoregularity

The [mmmm] pentad concentration of the polymers products resulting from **3a**−**c** varies over a broad range (34−65%, cf. Table 3) depending on temperature, monomer concentration and bridging unit. These results are in accordance with our recently published chain back-skip mechanism based on fluorenyl and indenyl units and with the slightly increased tacticity found for dimethylsilane-bridged zirconocenes.[1,22] Interestingly, the isotacticities of the polymers prepared with **3a**,**c**/MAO are independent of the Al/Zr

Table 2. Polymerization results of propene with the asymmetric complexes **3a**,**c**/MAO and **3b**/[$(C_6H_5)_3C^+$][$(C_6F_5)_4B^-$]

Run	Cat.	Amount [μmol]	T_p [°C]	[C_3] [mol L^{-1}]	Al/Zr	t_p [min]	Yield [g]	Activity[a]	M_w [b]	M_w/M_n	[mmmm] [%]
1	**3a**	25	30	3.0	100	7	8.5	1000	65	1.8	35.2
2	**3a**	10	30	3.0	300	15	9.0	1200	60	1.7	34.1
3	**3a**	10	30	3.0	1000	25	8.8	700	45	1.7	35.2
4	**3a**	20	30	3.0	2000	17	8.0	500	30	1.9	36.1
5	**3a**	5	30	5.1	300	24	15.0	1500	115	1.8	35.8
6	**3b**	6	30	1.2	–	13	8.0	5100	135	2.0	55.6
7	**3b**	3	30	3.0	–	20	8.7	2900	150	1.9	42.5
8	**3b**	2	30	5.1	–	16	8.3	3100	160	1.8	36.8
9	**3c**	10	30	3.0	100	–	–	–[c]	–	–	–
10	**3c**	10	30	3.0	200	28	8.2	600	90	1.9	54.1
11	**3c**	15	30	3.0	500	25	8.8	500	75	1.7	53.3
12	**3c**	30	30	3.0	1000	40	6.7	100	50	1.7	53.0
13	**3c**	20	30	3.0	2000	45	7.6	150	55	1.8	51.5
14	**3c**	10	50	3.0	500	5	9.4	3800	70	1.8	65.1

[a] [kg of PP (mol of Zr [C_3] h)$^{-1}$]. [b] [10^{-3} g mol^{-1}]. [c] No activity observed.

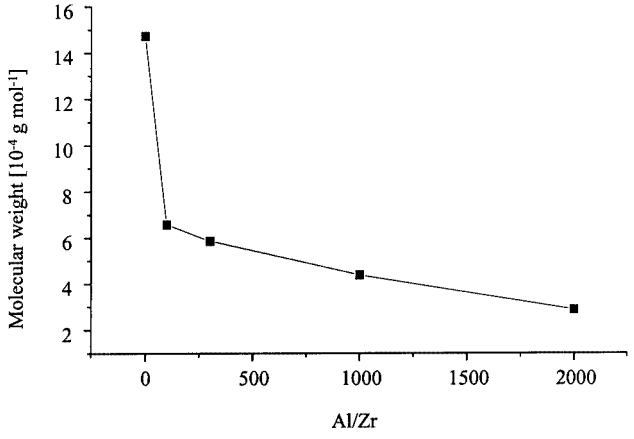

Figure 3. Plot of molecular weight versus Al/Zr ratio

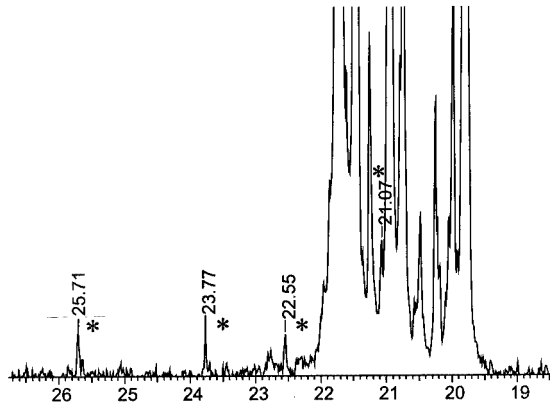

Figure 4. ^{13}C NMR spectra of the methyl region of a polypropene sample (**3a**/MAO; T_p = 30 °C; 1.2 mol L^{-1} 1-[D]-propene); the marked peaks denote signals arising from isobutyl end groups

ratio. This is a surprising finding because reduced activities and molecular weights indicate a direct interaction of MAO and Zr^{IV} centers which we expected to affect also the stereoselectivity of the insertion reaction. Moreover, borate activation (**3b**/[$(C_6H_5)_3C^+$][$(C_6F_5)_4B^-$]) leads to increased isotacticities (Table 3, Entries 1–4, 6, 7) proving that MAO does contribute to the overall stereoselectivity of the polymerization reaction. One possible explanation of this striking role of MAO in the error formation process might be a reversible chain transfer reaction. The reduced molecular weights of the polymer products at higher Al/Zr ratios proved the unidirectional transfer of polymer chains from Zr^{IV} to aluminum. Relocation from aluminum to the other enantiomer of the C_1-symmetric catalyst species would lead to the formation of a single stereoerror and could – at enhanced frequencies – account for the observed reduction of isotacticities in case of MAO-activated complexes.[23]

Besides electronics effects,[4,24] for which we assume that they are not relevant for our type of asymmetric catalysts and different side selectivity (back-skip), chain end epimerization[25] could be responsible for stereoerror formation. In order to rule out this mechanism, we performed deuterium labeling experiments on stereoerror distributions of the asymmetric zirconocene **3a** and referenced the results to **EBI**/MAO as a representative, C_2-symmetric catalyst typically undergoing chain end epimerization at low monomer concentrations.

For **3a**/MAO we could not detect isomerization-induced stereoerrors at any of the applied monomer concentrations,[26] while for **EBI**/MAO a decrease in the monomer concentration raised the amount of [D]-[mrrm] stereoerror pentads, as expected (Figure 5, Table 3). These findings reflect a significant difference in the mechanism of stereoerror formation for these two catalyst systems. For **EBI**/MAO [mrrm] stereoerrors result to a large extent from kinetically competitive chain end isomerization reactions. The decisive factor causing stereoerrors in **3a**/MAO at high monomer concentrations is the kinetic competition between chain back-skip and monomer coordination to the aspecific side of the catalyst structure. At low C_3 pressure, a significant fraction of stereoerrors can be most likely ascribed to the above discussed reversible transfer to aluminum.

Table 3. Polypropene pentad distribution for C_2-symmetric **EBI**/MAO and C_1-symmetric **3a**/MAO (T_p = 50 °C)

Entry	Cat.[a]	Mon.[b]	[Mon.] [mol L^{-1}]	Al/Zr	[mmmm] [%]	[mmrr]	[mrrm]	[D]-[mrrm]
1	**EBI**	C_3	0.4	3000	74	8.6	4.0	–
2	**EBI**	C_3	0.85	3000	80	5.6	2.9	–
3	**EBI**	C_3	1.9	3000	84	5.7	2.3	–
4	**EBI**	C_3	3.3	3000	85	4.7	1.9	–
5	**EBI**	[D]-C_3	0.4	1500	69	9.5	1.9	2.6
6	**EBI**	[D]-C_3	0.85	1500	79	6.4	2.0	1.3
7	**EBI**	[D]-C_3	1.3	1500	82	5.5	2.0	< 0.2
8	**3a**	C_3	1.9	1000	55	14.1	6.9	–
9	**3a**	C_3	1.9	2000	53	14.2	7.1	–
10	**3a**	C_3	1.9	5000	53	14.0	7.1	–
11	**3a**	C_3	0.4	1000	60	11.7	6.0	–
12	**3a**	[D]-C_3	1.9	300	57	14.1	6.5	n. o.
13	**3a**	[D]-C_3	0.4	300	65	12.6	5.1	n. o.

[a] [Zr] = $1-2 \times 10^{-5}$ mol L^{-1} for C_3 polymerizations, [Zr] = 3.3×10^{-4} mol L^{-1} for [D]-C_3 polymerizations. [b] Monomers: C_3 = propene, [D]-C_3 = 1-[D]-propene.

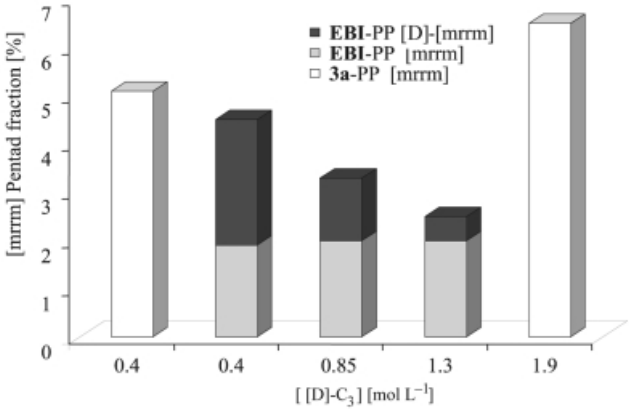

Figure 5. Amount of [mrrm] stereoerror pentads and fraction of isomerization induced [D]-[mrrm] stereoerrors as function of monomer concentration (**3a**,**EBI**/MAO; T_p = 50 °C)

Conclusion

The asymmetric, dual-side catalysts presented in the current study combine both, the excellent capability of C_1-symmeteric metallocenes to produce tailor-made polypropenes and the potential to incorporate functionalities into highly active metallocene catalysts. The introduction of the heteroatoms into a benzodioxane ring enhances the catalyst stability during the polymerization process. The oxygen substitution obviously promotes MAO approach to the catalyst center resulting in high rates of catalyst activation at low cocatalyst concentrations (high cocatalyst efficiency). On the other side, facile chain transfer to aluminum is already observed at lower Al/Zr ratios again pointing toward the close proximity of Zr^{IV} and Al^{MAO} ions. The observed catalyst stereoselectivities are discussed by chain back-skip and by a mechanism for which MAO operates as a transporting agent of polymer chains between zirconium centers. Thereby, relocation of a chain from one enantiomer to the other leads to stereoerrors which afford the formation of lower isotactic polypropenes.

Experimental Section

General Remarks: All reactions were performed under dry argon using standard Schlenk techniques. Hydrocarbon and ether solvents were dried by distillation from $LiAlH_4$, dichloromethane was distilled from CaH_2. Fluorene, 1,2-(ethylenedioxy)benzene, 1,2-dibromoethane, methacryloyl chloride, *n*BuLi, MeLi, $ZrCl_4$, $AlCl_3$ and (*Z*)/(*E*)-1-bromo-1-propene (98%) and [D_1]methanol (99.5%) were used as received from Merck and Aldrich. The complex **EBI**[1b] and the trityl borate $[(C_6H_5)_3C^+][(C_6F_5)_4B^-]$[27] were prepared according to literature procedures. Methylaluminoxane and triisobutylaluminum were purchased from Witco and toluene for the polymerization reactions from Merck. All compounds were analyzed by ^1H NMR with a Bruker AC 200 or AMX 500 at ambient temperatures and referenced to TMS. Mass spectra were acquired with Finnigan (SSQ 7000) and Varian (MAT-711) instruments. Elemental analyses were determined in the Microanalytical Laboratory of the University of Ulm.

1-[D]-Propene: A mixture of (*Z*)/(*E*)-1-bromo-1-propene (72 g, 0.6 mol) was added to freshly cut lithium (12.5 g, 1.8 mol) in 300 mL of ether at 0 °C. After stirring overnight, the mixture was filtered and the filtrate concentrated to dryness. The resulting white solid lithium compounds were suspended in 200 mL of toluene. At 0 °C [D_1]methanol (24 g, 0.73 mol) was added and the evolving gas was condensed through a cold trap at −50 °C into a steel vessel at −196 °C. The gas was further purified by passing it through molecular sieves and bubbling it through triisobutylaluminum, resulting in a yield of 20.5 g of 1-[D]-propene (80%). The ^1H NMR spectrum [$CDCl_3$ (δ = 7.24), 500 MHz] showed that the product contained 41% of (*E*)-1-[D]-propene (*H*DC=CHCH$_3$) [δ = 4.91 (dq, ^3J = 10.0, ^4J = 1.5 Hz, 1 H)] and 59% of (*E*)-1-[D]-propene [δ = 5.00 (dq, ^3J = 17.0, ^4J = 1.8 Hz, 1 H)].

Polymerization Reactions with 1-[D]-Propene: Polymerizations with deuterated propene were performed in a 50-mL steel autoclave. The solvent toluene, cocatalyst MAO and the catalyst were fed under argon and allowed to reach the desired polymerization temperature.

After 10 min of contact time, monomer was added, and temperature (±1 °C) and pressure (±100 mbar) were kept constant. The polymerization was stopped by pouring the reaction mixture into acidified methanol. The polymer product was washed with a methanol/HCl solution and with methanol. The product was filtered and dried in vacuo at 60 °C overnight. The yields of deuterated polypropene were between 0.2 and 0.8 g.

Propene Polymerization Reactions: The polymerization reactions were performed in a 0.5-L or a 1-L Büchi steel reactor at constant pressure and temperature. The autoclave was charged with 200 or 300 mL of toluene, respectively, and with the desired amount of MAO. Subsequently, the polymerization temperature was adjusted, the reactor was charged with propene up to the desired partial pressure, and the preactivated catalyst solution (Al/Zr = 100:1) was injected into the autoclave via a pressure burette. The monomer consumption was measured by the use of a calibrated gas flow meter (Bronkhorst F-111C-HA-33P), and the pressure was kept constant during the entire polymerization period (Bronkhorst pressure controller P-602C-EA-33P). Pressure, temperature and consumption of propene were monitored and recorded online. The polymerization reactions were stopped and treated as described above.

Polymer Analysis: ^{13}C NMR spectra were recorded with a Varian GEMINI 2000 spectrometer ($C_2D_2Cl_4$, 100 °C, 75 MHz, 10 mm probe) or a Bruker AMX 500 spectrometer ($C_2D_2Cl_4$, 80 °C, 125 MHz, 5 mm probe) in the inverse gated decoupling mode with a 3-s pulse delay and a 45° pulse to attain conditions close to the maximum signal-to-noise ratio. The number of transients accumulated was between 5 and 15 K. The spectra were analyzed by known methods.[28] Molecular weights and molecular weight distributions were determined by gel permeation chromatography (GPC, Waters 2000, 140 °C in 1,2,4-trichlorobenzene) relative to polystyrene and polypropene standards.

5,6-(Ethylenedioxy)-2-methylindene (1): 42.7 mL (367.2 mmol) of 1,2-(ethylenedioxy)benzene was added slowly at −78 °C to a stirred solution of 51.4 g of $AlCl_3$ (385.6 mmol) and 35.7 mL (367.2 mmol) of methacryloyl chloride in 300 mL of dichloromethane and allowed to attain room temperature overnight. The solution was carefully hydrolyzed with ice, and the organic phases were separated, washed with an aqueous solution of K_2CO_3 and dried with Na_2SO_4. After removing the solvent and crystallization in pentane, 5,6-(ethylenedioxy)-2-methylindan-1-one was obtained as a solid (62.7 g, 306.9 mmol, 84%). 40.0 g (195.9 mmol) of 5,6-(ethylenedioxy)-2-methylindan-1-one was diluted in 100 mL of Et_2O and added at −78 °C to a suspension of 5.0 g of $LiAlH_4$ (131.7 mmol) in 100 mL of Et_2O. The reaction mixture was stirred overnight and carefully hydrolyzed with ice and aqueous HCl. After separating the organic phases, the solution was neutralized with an aqueous solution of K_2CO_3 and dried with Na_2SO_4. After evaporation of the solvent and crystallization from toluene/hexane (ca. 3:2) the diastereomeric alcohols were obtained as a crystalline solid (27.3 g, 132.3 mmol, 68%). The alcohol (15.0 g, 72.73 mmol) was dissolved in 100 mL of toluene and 1.0 g of *p*-toluenesulfonic acid was added. The solution was heated under reflux using a water separation funnel until no further water was produced. The reaction mixture was neutralized by washing with aqueous KOH and was subsequently dried with Na_2SO_4. The solvent was evaporated, and the indene **1** was obtained as a crystalline solid (7.8 g, 41.46 mmol, 57%). Data of the ketone: ^1H NMR (200 MHz, $CDCl_3$): δ = 1.27 (d, 3 H, CH_3), 2.63 (m, 2 H, CH_2, indanone ring), 3.27 (m, 1 H, CH, indanone system), 4.29 (m, 4 H, CH_2, dioxane ring), 6.68, 7.25 (2 s, 2 H, aromatic). MS (GC-MS): *m*/*z* (%) = 204 (100) [M^+]. $C_{12}H_{12}O_3$ (204.2): calcd. C 70.58, H 5.92; found C 70.96, H 5.92. Data of the Alcohol: ^1H NMR (200 MHz, $CDCl_3$): δ = 1.11 (d, 3 H, CH_3), 1.79 (broad, 1 H, OH group), 2.33 (d, 2 H, CH_2, indanol ring), 2.95 (m, 1 H, CH, indanol ring), 4.13 (m, 4 H, CH_2, dioxane ring), 4.55 (d, 1 H, CH, indanol ring), 6.61, 6.80 (2 s, 2 H, aromatic). MS (GC-MS): *m*/*z* (%) = 206 (100) [M^+]. $C_{12}H_{14}O_3$ (206.2): calcd. C 69.88, H 6.84; found C 69.66, H 6.79. Data of **1**: ^1H NMR (200 MHz, $CDCl_3$): δ = 2.15 (s, 3 H, CH_3), 3.20 (s, 2 H, CH_2, indene ring), 4.21 (m, 4 H, CH_2 dioxane ring), 6.31 (s, 1 H, CH olefinic), 6.80, 7.30 (2 s, 2 H, aromatic). MS (GC-MS): *m*/*z* (%) = 188 (100) [M^+]. $C_{12}H_{12}O_2$ (188.2): calcd. C 76.57, H 6.43; found C 76.16, H 6.59.

1-[5,6-(Ethylenedioxy)-2-methylindenyl]-2-(9-η^5-fluorenyl)ethane (2aH_2): 4.35 g (26.16 mmol) of fluorene was dissolved in 100 mL of Et_2O and cooled to −78 °C. Addition of a 1.6 M solution of *n*BuLi in hexane (16.4 mL, 26.16 mmol) and stirring for additional 2 h afforded the formation of fluorenyllithium. Subsequent cooling to −78 °C and further treatment with an excess of 1,2-dibromoethane (13.6 mL, 160 mmol) formed the substituted fluorenyl compound. The remaining mixture was allowed to attain room temperature and stirred for additional 4 h. Removal of the solvent and excess of 1,2-dibromoethane yielded the fluorenyl intermediate as a beige solid. This solid was added after dilution with 100 mL of Et_2O at ambient temperature to the separately prepared lithium salt of the 5,6-(ethylenedioxy)-2-methylindene (**1**) (4.92 g, 26.16 mmol). The reaction mixture was stirred overnight and refluxed for 2 h. The crude product was treated with a saturated aqueous solution of NH_4Cl and washed several times with water. The organic phase was separated and dried with Na_2SO_4. Evaporation of the solvent and crystallization from *n*-hexane yielded **2a**H_2 as a white solid (4.45 g, 11.7 mmol, 45%). Data of **2a**H_2: ^1H NMR (200 MHz, $CDCl_3$): δ = 1.25−1.69 (m, 4 H, CH_2 bridge), 1.78 (s, 3 H, CH_3), 2.97 (t, 1 H, CH, indene), 3.8 (t, 1 H, CH, 9*H*-fluorene), 4.17 (m, 4 H, CH_2, dioxane ring), 6.23 (s, 1 H, olefinic indene), 6.60, 6.63 (2 s, 2 H, aromatic indene), 7.16−7.70 (m, 8H, aromatic fluorene). MS (EI): *m*/*z* (%) = 380 (100) [M^+]. $C_{27}H_{24}O_2$ (380.5): calcd. C 85.23, H 6.36; found C 85.15, H 6.48.

(5,6-Ethylenedioxy-2-methylindenyl)(9-η^5-fluorenyl)dimethylsilane (2bH_2): 4.09 g (24.62 mmol) of fluorene was dissolved in 150 mL of Et_2O and cooled to −78 °C. Addition of a 1.6 M solution of *n*BuLi in hexane (15.4 mL, 24.62 mmol) and stirring for additional 4 h resulted in the formation of fluorenyllithium. Subsequent cooling to −78 °C and further treatment with an excess of dichlorodimethylsilane (13.6 mL, 98.5 mmol) afforded the substituted fluorenyl compound. The remaining mixture was allowed to attain room temperature and stirred for additional 2 h. Removal of the solvent and excess of dichlorodimethylsilane in vacuo gave the fluorenyl intermediate as a beige powder. This solid was added after dilution with 100 mL of Et_2O at ambient temperature to the separately prepared lithium salt of 5,6-(ethylenedioxy)-2-methylindene (**1**) (4.63 g, 24.62 mmol). The reaction mixture was stirred overnight and refluxed for 2 h. The crude product was treated with a saturated aqueous solution of NH_4Cl and washed several times with water. The organic phase was separated and dried with Na_2SO_4. Evaporation of the solvent and recrystallization from *n*-hexane yielded **2b**H_2 as a white solid (7.2 g, 17.8 mmol, 72%). Data of **2b**H_2: ^1H NMR (200 MHz, $CDCl_3$): δ = −1.64, −1.57 − (2 s, 6 H, CH_3 bridge), 0.94 (s, 3 H, CH_3), 3.03 (m, 4 H, CH_2, dioxane ring), 5.26 (s, 1 H, CH, olefinic), 5.63, 5.77 (2 s, 2 H, aromatic indene), 6.02−6.74 (m, 8 H, aromatic fluorene). MS (EI): *m*/*z* (%) = 410 (100) [M^+]. $C_{27}H_{26}O_2Si$ (410.6): calcd. C 78.98, H 6.38; found C 78.65, H 6.41.

***rac*-{1-[5,6-(Ethylenedioxy)-2-methyl-1-η^5-indenyl]-2-(9-η^5-fluorenyl)-ethane}zirconium Dichloride (3a):** 1.7 g (4.47 mmol) of 1-[5,6-(ethylenedioxy)-2-methyl-1-η^5-indenyl]-2-(9-η^5-fluorenyl)-ethane (**2a**H_2) was dilssolved in 150 mL of Et_2O and cooled to −78 °C. After treatment of the ligand precursor with 5.6 mL of *n*BuLi at −78 °C, the reaction mixture was warmed to room temperature and stirred for 4 h. Subsequently, the solvent was removed in vacuo and the resulting lithium salt was diluted with 60 mL of toluene. Cooling to −78 °C and addition of solid $ZrCl_4$ (1.04 g, 4.47 mmol) afforded the formation of an orange suspension which was warmed to room temperature and stirred overnight. The mixture was filtered, and the remaining solid fraction was extracted with toluene until the organic phase remained colorless. Removal of the solvent gave an orange powder from which pure **3a** (2.05 g, 3.79 mmol, 91%) could be obtained by crystallization from toluene solution. Data of **3a**: ^{1}H NMR (500 MHz, $CDCl_3$): δ = 2.14 (s, 3 H, CH_3), 3.72−4.58 (m, 4 H, CH_2, bridge), 6.01, 6.75 (s, 1 H, aromatic indene), 7.14−7.95 (m, 9 H, aromatic indene, aromatic fluorene). MS (EI): *m*/*z* = 538 (peak distribution of isotopes according to expected contents). $C_{27}H_{22}Cl_2O_2Zr$ (540.6): calcd. C 59.99, H 4.10; found C 59.56, H 4.17.

***rac*-{1-[5,6-(Ethylenedioxy)-2-methyl-1-η^5-indenyl]-2-(9-η^5-fluorenyl)ethane}dimethylzirconium (3b):** 0.75 g (1.97 mmol) of 1-[5,6-(ethylenedioxy)-2-methyl-1-η^5-indenyl]-2-(9-η^5-fluorenyl)ethane (**2a**H_2) was dissolved in 50 mL of Et_2O and cooled to −78 °C. After treatment of the ligand precursor with 4.94 mL (7.90 mmol) of MeLi at −78 °C, the reaction mixture was warmed to room temperature and stirred for 4 h. Solid $ZrCl_4$ (0.46 g, 1.97 mmol) was added to the stirred suspension of the lithium salt of **2a**H_2 at room temperature and the reaction mixture was stirred for 24 h with a final formation of a light-brown suspension. The solvent was removed in vacuo and replaced with toluene. The suspension was filtered and the residual solid fraction was extracted with toluene until the organic phase remained colorless. Removal of the solvent gave a yellow powder from which pure **3b** (0.66 g, 1.32 mmol, 67%) could be obtained by crystallization from toluene. Data of **3b**: ^{1}H NMR (200 MHz, $CDCl_3$): δ = −2.34, −1.36, (2 s, 6 H, CH_3), 1.94 (s, 3 H, CH_3), 3.37−4.21 (m, 4 H, CH_2 bridge), 5.97 (s, 1 H, indene), 6.65, 6.89 (2 s, 2 H, aromatic indene), 6.99−7.94 (m, 8 H, aromatic fluorene). $C_{29}H_{28}O_2Zr$ (499.8): calcd. C 69.70, H 5.65; found C 69.43, H 5.88.

***rac*-{[5,6-(Ethylenedioxy)-2-methyl-1-η^5-indenyl](9-η^5-fluorenyl)dimethylsilane}zirconium Dichloride (3c):** 1-[5,6-(Ethylenedioxy)-2-methyl-1-η^5-indenyl]-2-(9-η^5-fluorenyl)dimethylsilane (**2b**H_2) (1.80 g, 4.38 mmol) was dissolved in 50 mL of Et_2O and cooled to −78 °C. After treatment of the ligand precursor with 5.5 mL of *n*BuLi at −78 °C, the reaction mixture was warmed to ambient temperature and stirred for 2 h. Subsequently, the solvent was removed in vacuo and the resulting lithium salt was diluted with 50 mL of toluene. Cooling to −78 °C and addition of solid $ZrCl_4$ (1.02 g, 4.38 mmol) afforded the formation of an orange suspension which was warmed to room temperature and stirred overnight. The mixture was filtered, and the remaining solid fraction was extracted with toluene until the organic phase remained colorless. Removal of the solvent gave an orange powder. The zirconocene **3c** (1.37 g, 2.41 mmol, 55%) could be purified by washing with Et_2O and pentane. Data of **3c**: ^{1}H NMR (200 MHz, $CDCl_3$): δ = −0.44, −0.37 (2 s, 6 H, CH_3, bridge), 2.13 (s, 3 H, CH_3), 4.22 (m, 4 H, CH_2, dioxane ring), 6.46 (s, 1 H, indene), 6.82, 6.96 (2 s, 2 H, aromatic indene), 7.14−7.88 (m, 8 H, aromatic fluorene). MS (EI): *m*/*z* = 568 (peak distribution of isotopes according to expected contents). $C_{27}H_{24}Cl_2O_2SiZr$ (570.7): calcd. C 56.82, H 4.24; found C 56.58, H 4.54.

X-ray Crystallography: The unit cell parameters were determined and the crystal data of **3a** was collected with a Rigaku AFC7S single-crystal diffractometer at 193(2) K using Mo-K_α radiation (graphite monochromator, 0.71073 Å); 2-θ/ω scans. Intensities were corrected for Lorentz and polarization effects; TEXSAN (Molecular Structure Corporation, **1993**).[29] A ψ-scan absorption correction was made, 0.89 < T < 1.00 (North et al., **1968**).[30] Solution and refinement: SHELX97 (Sheldrick, **1997**),[31] direct methods. All non-hydrogen atoms were refined anisotropically. Hydrogen atoms were refined on calculated positions. The displacement factors of the H atoms were 1.2× or 1.5× to that of the host atom. One disordered toluene molecule is occupying the centre of symmetry. Graphics: SHELXTL/PC (Sheldrick, **1990**).[32] Deatils are listed in Table 4. Crystallographic data (excluding structure factors) for the structure reported in this paper have been deposited with the Cambridge Crystallographic Data Centre as supplementary publication no. CCDC-164853. Copies of the data can be obtained free of charge on application to CCDC, 12 Union Road, Cambridge CB2 1EZ, UK [Fax: (internat.) + 44-1223/336-033; E-mail: deposit@ccdc.cam.ac.uk].

Table 4. Crystal data, data collection and structure refinement parameters of complex **3a**

Empirical formula	$C_{30.50}H_{26}Cl_2O_2Zr$
Formula mass	586.63
Crystal color and form	orange prism
Crystal system	monoclinic
Space group	$P2_1/n$
a [Å]	12.500(3)
b [Å]	15.671(3)
c [Å]	12.678(4)
β [°]	96.07(2)
V [Å^3]	2469.5(11)
Z	4
D_C [Mg/m^3]	1.578
μ [mm^{-1}]	0.690
F(000)	1196
Crystal size [mm]	0.38 × 0.25 × 0.16
Scan mode	2θ/ω
θ_{max} [°]	25.25
Index ranges	$0 \le h \le 15$ $0 \le k \le 18$ $-15 \le l \le 15$
No. of unique reflections	4446
No. of observed reflections [$I > 2\sigma(I)$]	3319
No. of parameters	352
Goodness of fit on $S(F^2)$[a]	1.039
Final *R* indices [$I > 2\sigma(I)$][b]	$R_1 = 0.0479$, $wR_2 = 0.1015$
R indices (all data)[b]	$R_1 = 0.0809$, $wR_2 = 0.1099$
Largest differential peak/hole [e/Å^3]	0.518/−0.399

$R(F) = \|\|F_o| - |F_c\|\|/|F_o|$; $wR(F^2) = [w(F_o^2 - F_c^2)^2/wF_o^4]^{1/2}$.

Acknowledgments

Generous financial assistance is gratefully acknowledged from Deutscher Akademischer Austauschdienst (DAAD). We also wish to thank Prof. Seppälä (Helsinki University of Technology) for the support in polymer characterization.

[1] [1a] U. Dietrich, M. Hackmann, B. Rieger, M. Klinga, M. Leskelä, *J. Am. Chem. Soc.* **1999**, *121*, 4348. [1b] J. Kukral, P. Lehmus, T. Feifel, C. Troll, B. Rieger, *Organometallics* **2000**, *19*, 3767.
[2] [2a] R. Leino, H. J. G. Luttikhedde, C.-E. Wilén, R. Sillanpää, J. H. Näsman, *Organometallics* **1996**, *15*, 2450. [2b] R. Leino, H. J. G. Luttikhedde, P. Lehmus, C.-E. Wilén, R. Sjöholm, A. Lehtonen, J. V. Seppälä, J. H. Näsman, *Macromolecules* **1997**, *30*, 3477.
[3] P. Lehmus, E. Kokko, O. Härrki, R. Leino, H. J. G. Luttikhedde, J. H. Näsman, J. V. Seppälä, *Macromolecules* **1999**, *32*, 3547.
[4] [4a] N. Piccolrovazzi, P. Pino, G. Consiglio, A. Sironi, M. Moret, *Organometallics* **1990**, *9*, 3098. [4b] I.-K. Lee, W. J. Gauthier, A. M. Ball, B. Iyengar, S. Collins, *Organometallics* **1992**, *11*, 2115. [4c] J. A. Ewen, *Macromol. Symp.* **1995**, *89*, 181. [4d] A. Winter, J. Rohrmann, M. Antberg, W. Spaleck, W. A. Herrmann, H. Riepl, Eur. Pat. Appl., EP 582195, **1994**.
[5] E. Barsties, S. Schaible, M.-H. Prosenc, U. Rief, W. Röll, O. Weyand, B. Dorer, H. H. Brintzinger, *J. Organomet. Chem.* **1996**, *520*, 63.
[6] H. J. G. Luttikhedde, R. P. Leino, C.-E. Wilén, J. H. Näsman, M. J. Ahlgrén, T. A. Pakkanen, *Organometallics* **1996**, *15*, 3092.
[7] [7a] J. A. Ewen, R. L. Jones, M. J. Elder, A. L. Rheingold, L. M. Liable-Sands, *J. Am. Chem. Soc.* **1998**, *120*, 10786. [7b] J. A. Ewen, J. M. Elder, R. L. Jones, A. L. Rheingold, L. M. Liable-Sands, D. Roger, R. D. Sommer, *J. Am. Chem. Soc.* **2001**, *123*, 4763.
[8] Collins, Consiglio et al. (refs.[4a,4b]) reported that MAO reacts with unshielded methoxy groups, which results in the formation of different active species and in the deactivation of the polymerization catalyst. Similar results were observed in our group in scouting polymerization experiments with alkoxy substituted catalysts.
[9] The detailed synthetic protocol for the formation of ethylene- and dimethylsilane-bridged ligands was already described elsewhere: [9a] J. Kukral, P. Lehmus, T. Feifel, C. Troll, B. Rieger, *Organometallics* **2000**, *19*, 3767. [9b] E. J. Thomas, J. C. W. Chien, M. D. Rausch, *Organometallics* **1999**, *18*, 1439.
[10] L. Resconi, R. L. Jones, A. L. Rheingold, G. P. A. Yap, *Organometallics* **1996**, *15*, 998.
[11] [11a] J. T. Park, B. W. Woo, S. C. Yoon, S. C. Shim, *J. Organomet. Chem.* **1997**, *535*, 29. [11b] L. Resconi, D. Balboni, G. Baruzzi, C. Fiori, S. Guidotti, *Organometallics* **2000**, *19*, 420.
[12] Definitions of the *ansa*-metallocene angles: α = dihedral angle formed by the bridge; β = deviation from perpendicularity of the Zr−centroid vector; γ = distortion of the bridge atom from the Cp plane; δ = angle formed by the metal center and the ring centroid vectors; φ = bite angle between the least square planes of the two Cp ligands.
[13] Ethylene(bisindenyl)zirconium dichloride.
[14] V. A. Dang, L.-C. Yu, D. Balboni, T. Dall'Occo, L. Resconi, P. Mercandelli, M. Moret, A. Sironi, *Organometallics* **1999**, *18*, 3781.
[15] Ethylene(bisfluorenyl)zirconium dichloride.
[16] [16a] H. Alt, W. Milius, S. Palackal, *J. Organomet. Chem.* **1994**, *472*, 113. [16b] L. Resconi, R. L. Jones, A. L. Rheingold, G. P. A. Yap, *Organometallics* **1996**, *15*, 998
[17] For the accessibility of Zr centers in C_2-symmetric complexes, cf.: [17a] K. Hortmann, H.-H. Brintzinger, *New J. Chem.* **1992**, *16*, 51. [17b] P. Burger, K. Hortmann, H.-H. Brintzinger, *Macromol. Chem. Macromol. Symp.* **1993**, *66*, 127.
[18] For other fluorenyl complexes with similar coordination properties, cf. ref.[10]; A. Razavi, D. Vereecke, L. Peters, K. Den Dauw, L. Nafpliotis, J. L. Atwood, in *Ziegler Catalysts* (Eds.: G. Fink, R. Mülhaupt, H.-H. Brintzinger), Springer-Verlag, Berlin, **1995**, p. 111 and references therein.
[19] Collins et al. found for the bis(5,6-dimethoxy-1-η^5-indenyl)zirconium dichloride polydispersities up to 3.1 and associated this observation with the formation of different active species generated by MAO coordination on unshielded methoxy groups, cf. ref.[4b]
[20] For the role of cocatalysts, cf.: [20a] E. Y.-X. Chen, T. J. Marks, *Chem. Rev.* **2000**, *100*, 1391. [20b] Z. Liu, E. Somsook, C. R. Landis, *J. Am. Chem. Soc.* **2001**, *123*, 2915. [20c] M. A. Giardello, M. S. Eisen, C. L. Stern, T. J. Marks, *J. Am. Chem. Soc.* **1995**, *117*, 12114. [20d] P. A. Deck, T. J. Marks, *J. Am. Chem. Soc.* **1995**, *117*, 6128. [20e] B. Rieger, C. Janiak, *Angew. Makromol. Chem.* **1994**, *215*, 35. [20f] X. Yang, C. L. Stern, T. J. Marks, *J. Am. Chem. Soc.* **1994**, *116*, 10015. [20g] J. C. W. Chien, W. Song, M. D. Rausch, *J. Polym. Sci. Part A* **1994**, *32*, 2387. [20h] J. C. W. Chien, W.-M. Tsai, M. D. Rausch, *J. Am. Chem. Soc.* **1991**, *113*, 8570.
[21] [21a] A. R. Siedle, R. A. Newmark, W. M. Lamana, J. N. Schroepfer, *Polyhedron* **1990**, *9*, 301. [21b] E. Barsties, S. Schaible, M.-H. Prosenc, U. Rief, W. Röll, O. Weyand, B. Dorer, H.-H. Brintzinger, *J. Organomet. Chem.* **1996**, *520*, 63.
[22] Cf. also: E. J. Thomas, J. C. W. Chien, M. D. Rausch, *Organometallics* **1999**, *18*, 1439.
[23] For similar suggestion on reversible transfer reactions, cf.: [23a] S. Lieber, H.-H. Brintzinger, *Macromolecules* **2000**, *33*, 9192. [23b] J. C. W. Chien, Y. Iwamoto, M. D. Rausch, W. Wedler, H. H. Winter, *Macromolecules* **1997**, *30*, 3447. [23c] J. C. W. Chien, Y. Iwamoto, M. D. Rausch, *J. Polym. Sci., Part A* **1999**, *37*, 2439. [23d] C. Przybyla, G. Fink, *Acta Polym.* **1999**, *50*, 77.
[24] [24a] J. J. Eisch, A. M. Peotrowski, S. K. Browstein, E. J. Gabe, F. L. Lee, *J. Am. Chem. Soc.* **1985**, *107*, 7219 and references given therein. [24b] M. Bochmann, L. M. Wilson, M. B. Hursthouse, M. Motevalli, *Organometallics* **1988**, *7*, 1148 and references given therein. [24c] G. Hlatky, H. W. Turner, R. R. Eckmann, *J. Am. Chem. Soc.* **1989**, *111*, 2728. [24d] R. F. Jordan, P. K. Bradley, N. C. Baenzinger, R. F. LaPointe, *J. Am. Chem. Soc.* **1990**, *112*, 1289. [24e] J. Lauther, R. Hoffmann, *J. Am. Chem. Soc.* **1976**, *98*, 1729.
[25] [25a] M. K. Leclerc, H. H. Brintzinger, *J. Am. Chem. Soc.* **1996**, *118*, 9024. [25b] M. K. Leclerc, H. H. Brintzinger, *J. Am. Chem. Soc.* **1995**, *117*, 1651. [25c] V. Busico, L. Caporaso, R. Cipullo, L. Landriani, G. Angelini, A. Margonelli, A. L. Segre, *J. Am. Chem. Soc.* **1996**, *118*, 2105. [25d] V. Busico, D. Brita, L. Caporaso, R. Cipullo, M. Vacatello, *Macromolecules* **1997**, *30*, 3971. [25e] V. Busico, R. Cipullo, L. Caporaso, G. Angelini, A. L. Segre, *J. Mol. Catal. A* **1998**, *128*, 53. [25f] L. Resconi, I. Camurati, O. Sudmeijer, *Top. Catal.* **1999**, *7*, 145. [25g] L. Resconi, *J. Mol. Catal. A* **1999**, *146*, 167.
[26] The same result was observed for the 5,6-cyclopenta-fused zirconocene "*rac*-[1-(9-η^5-fluorenyl)-2-(5,6-cyclopenta-2-methyl-1-η^5-indenyl)ethane]zirconium dichloride" (cf. ref.[1b]).
[27] J. C. W. Chien, W.-M. Tsai, M. D. Rausch, *J. Am. Chem. Soc.* **1991**, *113*, 8570.
[28] V. Busico, R. Cipullo, P. Corradini, L. Landriani, M. Vacatello, A. L. Segre, *Macromolecules* **1995**, *28*, 1887
[29] *Single Crystal Structure Analysis Software*, version 1.6, MSC, 3200 Research Forest Drive, The Woodlands, TX 77381, USA.
[30] A. C. T. North, D. C. Phillips, F. S. Mathews, *Acta Crystallogr., Sect. A* **1968**, *24*, 351.
[31] *SHELX-97, Program for the Solution and Refinement of Crystal Structures.*
[32] *SHELXTL/PC*, Siemens Analytical X-ray Instruments, Inc., Madison, Wisconsin, USA.

Received November 15, 2001
[I01458]

Coordination of Ferrocenyl Ligands Bearing bipy Subunits: Electrochemical, Structural and Spectroscopic Studies

Ana Ion,[a] Mihai Buda,[a] Jean-Claude Moutet,*[b] Eric Saint-Aman,[b] Guy Royal,[b] Isabelle Gautier-Luneau,[c] Michel Bonin,[d] and Raymond Ziessel[e]

Keywords: N ligands / Sandwich complexes / Iron / Receptors / Cyclic voltammetry

The coordinative properties of mono(bipy) and bis(bipy) (bipy refers to 6- or 6,6′-substituted 2,2′-bipyridine) carbonyloxy- and carboxamido-bridged derivatives of ferrocene $\mathbf{L^{1-5}}$ towards a number of metal cations (Cu^{I}, Cu^{II}, Ni^{II}, Fe^{II}, Co^{II}, Hg^{II}, Pb^{II}, Ag^{I}) have been investigated by the interplay of voltammetry, mass spectrometry and X-ray diffraction studies. Particular attention was paid to the electrochemical recognition properties of these redox-active ligands, as monitored by modulation of the ferrocene/ferricinium redox couple upon complexation. It was found that the bis(bipy)-bridged ligands exhibit a *sandwich effect* that gives rise to a well-behaved voltammetric wave for the ferrocene fragment as an elegant signature of complexation. The ferrocenyl ester-bridged bis(bipy) ligand $\mathbf{L^2}$ forms a 2:2 complex in the solid state with Cu^{I}, while the crystal structure of the Cu^{II} complex reveals 1:1 stoichiometry. Upon dissolution, the 2:2 species dissociate rapidly into the $[Cu\mathbf{L^2}]^{+}$ complex. Finally, electrochemical and FAB-MS data have been used to conclude that these ferrocenyl ligands bind to iron(II) to generate unusual $[Fe(bipy)_2]^{2+}$-type complexes.
(© Wiley-VCH Verlag GmbH, 69451 Weinheim, Germany, 2002)

Introduction

Molecular structures comprising two or more coordinated cations are of considerable interest as reversible electron reservoirs able to effect the successive release of electrons. Such polynuclear metal complexes are also useful models for studying the effect of electronic coupling between metal centres in different oxidation states and for the coupling of a remote redox-active metal centre to a putative catalytic site. In earlier work, it was demonstrated that polypyridine ligands functionalized with ferrocene[1−4] could be used for the electrochemical recognition of certain metal cations in both homogeneous solution[1,2] and polymeric films,[3] and that the resultant dinuclear complexes displayed significant levels of electronic coupling between the metal sites. In extending this work, we now report on the complexation of selected metal cations (Cu^{I}, Cu^{II}, Ni^{II}, Fe^{II}, Co^{II}, Hg^{II}, Pb^{II}, Ag^{I}) with 1-bipy (bipy = 2,2′-bipyridine) and carbonyloxy- or carboxamide-bridged 1,1′-bis(bipy) derivatives of ferrocene (ligands $\mathbf{L^{1-5}}$, Scheme 1). Special attention has been given to studying the effect of cation binding on the electrochemical properties of the ferrocene units.

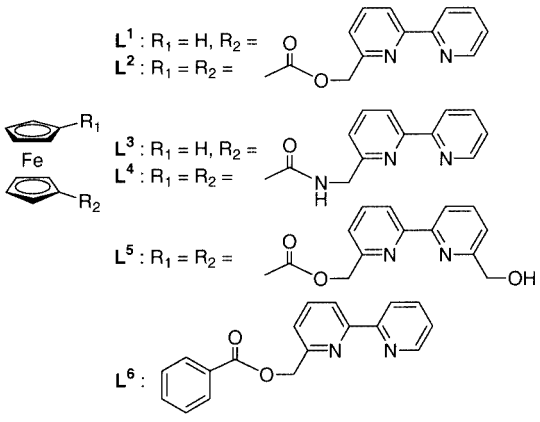

Scheme 1. Structures of ligands $\mathbf{L^{1-6}}$

In a preliminary study,[1] it was reported that the ester-bridged mono(bipy) and bis(bipy) derivatives of ferrocene ($\mathbf{L^1}$ and $\mathbf{L^2}$) are able to complex Cu^{I} and Cu^{II} by ensuring a bis(bipyridyl) environment around the bound cation. The crystal structure of the complex formed between $\mathbf{L^2}$ and Cu^{I} revealed the formation of a 2:2 (2 Cu^{I} + 2 $\mathbf{L^2}$) complex

[a] Department of Applied Physical Chemistry and Electrochemistry, Politehnica University, Bucharest, Romania
[b] Laboratoire d'Electrochimie Organique et de Photochimie Rédox, UMR CNRS 5630, Université Joseph Fourier Grenoble 1, BP 53, 38041 Grenoble Cédex 9, France
Fax: (internat.) + 33-4/76514267
E-mail: Jean-Claude.Moutet@ujf-grenoble.fr
[c] Laboratoire de Chimie Biomimétique, LEDSS, UMR CNRS 5616, Université Joseph Fourier Grenoble 1, BP 53, 38041 Grenoble Cédex 9, France
[d] University of Lausanne, Institute of Crystallography, BSP, 1015 Lausanne, Switzerland
[e] Laboratoire de Chimie, d'Electronique et de Photonique Moléculaires, Ecole de Chimie, Matériaux et Polymères, Université Louis Pasteur, 25 rue Becquerel, 67087 Strasbourg Cédex 02, France

having a *pseudo*-tetrahedral geometry around each cation. The molecular structure was best described as a double-stranded metallo-helicate, with each ligand wrapping around the two copper cations. X-ray structural determination of the $\mathbf{L^2}$ + Cu^{II} complex remains elusive at this time. However, the formation of a mononuclear Cu^{II} complex was evident from EPR experiments. It was further shown that redox ligands $\mathbf{L^1}$ and $\mathbf{L^2}$ recognize copper cations by way of a large shift in the ferrocene/ferricinium (Fc/Fc^+) redox couple. Recently,[2] the formation of bis(bipy)Fe^{II} species upon coordination of Fe^{II} with the carboxamide-bridged mono- and bis(bipy) derivatives $\mathbf{L^{3,4}}$ was deduced from voltammetry, ^1H NMR spectroscopy, FT-IR spectroscopy and mass spectrometry studies. Furthermore, X-ray structural determination of the 1:1 $\mathbf{L^4}$ + Fe^{II} complex showed that the Fe^{II} coordination environment is provided by four nitrogen atoms belonging to the bipy subunits and by two oxygen atoms of the carbonyl groups lying in a "*cis*" environment and describing a distorted octahedral arrangement.

In this paper, we describe the coordination chemistry of copper cations with these ligands, paying particular attention to the complexation process between $\mathbf{L^2}$ and Cu^I. Furthermore, the possibility of obtaining a complex involving an Fe^{II} cation in a bis(bipy) environment from the ester-bridged derivatives $\mathbf{L^{1,2}}$ is also examined, as well as the electrochemical recognition properties of ligands $\mathbf{L^{1-5}}$ towards Ni^{II}, Co^{II}, Hg^{II}, Pb^{II} and Ag^I metal cations.

Results and Discussion

The electrochemical behaviour of the free ligands $\mathbf{L^{1-5}}$ in CH_3CN or CH_2Cl_2 solution is characterized by a one-electron, reversible wave that can be attributed to the ferrocene/ferricinium (Fc/Fc^+) redox couple (Table 1). The main purpose of the current investigation is to examine how complexation of $\mathbf{L^{1-5}}$ by various metal cations (Cu^I, Cu^{II}, Ni^{II}, Fe^{II}, Co^{II}, Hg^{II}, Pb^{II}, Ag^I) affects the electrochemical properties of the ferrocene unit.

Table 1. Electrochemical data for free ligands

[a]	$\mathbf{L^1}$	$\mathbf{L^2}$	$\mathbf{L^3}$	$\mathbf{L^4}$	$\mathbf{L^5}$
CH_3CN	0.33[b]	0.56[b]	0.26[c]	0.53[c]	0.59
CH_2Cl_2	0.45[b]	0.69[b]	[d]	0.51[c]	[d]

[a] $E_{1/2}$ [V] vs. $Ag/AgNO_3$ (0.01 M) + CH_3CN + TBAP (0.01 M), measured by CV at 0.1 V s^{-1}. [b] From ref.[1] [c] From ref.[3] [d] Not determined.

In general, addition of increasing amounts of a given metal cation to a solution of ferrocenyl ligand might be expected to cause one of two effects on the electrochemical activity of the Fc centre. First, cation complexation might induce a gradual positive shift in the Fc/Fc^+ redox potential (one-wave behaviour) due to electrostatic repulsion between the bound cation and the electrogenerated positive charge on the oxidized ferrocenyl subunit. This leads to a decrease of the association constant K_+ with the oxidized ligand and to a destabilisation of the resulting complex.[5] Consequently, $\Delta E_{1/2}$ reflects the balance of interactions between the neutral and charged ligand in its oxidized form with the adventitious metal cation.

Second, we might observe the growth of a new redox wave (two-wave behaviour) at the expense of the original wave for the free ligand. The two-wave behaviour can be linked to a high binding constant K with the neutral ligand in association with a large K/K_+ ratio.[6] It may also, in part, be due to a structural effect i.e. complexation of the binding centre can lead to noncoplanarity of the Cp rings in the complex which is known to result in a marked positive potential shift in complexed[5,7] or strained[8] ferrocenophanes. It should be emphasized that a two-wave feature allows the amperometric recognition and titration of the guest cation, while a one-wave behaviour allows a potentiometric titration.

In general, mono(bipy) ligands $\mathbf{L^1}$ and $\mathbf{L^3}$ form 1:2 (metal/ligand) complexes and give rise to weak complexation and one-wave behaviour, while bis(bipy) ligands $\mathbf{L^2}$ and $\mathbf{L^4}$ form 1:1 complexes and give rise to two-wave behaviour. The bis(bipy) ligand $\mathbf{L^5}$ forms 1:1 complexes, but shows reduced bonding and one-wave behaviour.

In addition to the change in the electroactivity of the Fc centre, the rise of new redox peak systems due to the formation of an electroactive metal complex can be observed in the CV profile. When the emergent complex is fairly stable, all the electrochemical perturbations reach full development at a metal cation/ligand mol ratio corresponding to the stoichiometry of the resultant complex.

Complexation of $\mathbf{L^{1-5}}$ with Cu^I and Cu^{II} Cations

The electrochemical data for complexes formed between $\mathbf{L^{1-5}}$ and Cu^I are summarized in Table 2. The relatively high Cu^I/Cu^{II} redox potential found for these complexes are in good agreement with those reported previously for various copper polypyridyl compounds.[9] In comparative experiments, we found that the reversible $Cu^{I/II}$ oxidation for the $[Cu(bipy)_2]^+$ complex occurs at $E_{1/2} = -0.19$ V, and at 0.26 V for the $[Cu(\mathbf{L^6})_2]^+$ complex where $\mathbf{L^6}$ is a bipy ligand simply mono-substituted with an electron-withdrawing carbonyloxy group.

Table 2. Electrochemical data for $\mathbf{L^1}$, $\mathbf{L^2}$, $\mathbf{L^3}$, $\mathbf{L^4}$, $\mathbf{L^5}$ + Cu^I

[a]	2 $\mathbf{L^1}$ + Cu^I [b]		$\mathbf{L^2}$ + Cu^I [b]		2 $\mathbf{L^3}$ + Cu^I	
	Fc/Fc^+	Cu^I/Cu^{II}	Fc/Fc^+	Cu^I/Cu^{II}	Fc/Fc^+	Cu^I/Cu^{II}
CH_3CN	0.38	0.19	0.71	0.10	0.37	−0.04
CH_2Cl_2	ads.	0.33	0.84	0.23	[c]	[c]
	$\mathbf{L^4}$ + Cu^I		$\mathbf{L^5}$ + Cu^I			
	Fc/Fc^+	Cu^I/Cu^{II}	Fc/Fc^+	Cu^I/Cu^{II}		
CH_3CN	0.60	−0.20	0.64	0.08		
CH_2Cl_2	0.67	−0.15	[c]	[c]		

[a] $E_{1/2}$ [V] vs. $Ag/AgNO_3$ (0.01 M) (see Table 1). [b] From ref.[1] [c] Not determined.

Complexation of $\mathbf{L^1}$ and $\mathbf{L^5}$ with Cu^I in CH_3CN solution results in a one-wave behaviour for the electrochemical response of the Fc centre, along with the rise of a redox peak system attributable to the complexed Cu^I/Cu^{II} redox couple (Table 2). The positive potential shift in the Fc/Fc^+ wave is equal to 50 mV for both ligands. Similar features in the CV behaviour of $\mathbf{L^1}$ and $\mathbf{L^5}$ are evident upon addition of Cu^I or Cu^{II}. Maximal potential shift of the Fc/Fc^+ wave and maximal intensity of the complexed Cu^I/Cu^{II} peak system are obtained at a $Cu^I/\mathbf{L^1}$ and $Cu^I/\mathbf{L^5}$ molar ratio equal to 0.5 and 1, respectively. This result is in keeping with the formation of $[Cu(\mathbf{L^1})_2]^+$ and $[Cu\mathbf{L^5}]^+$ complexes that provide for a bis(bipyridyl) environment around the bound cation. The 1:2 stoichiometry for isolated $[Cu(\mathbf{L^1})_2]^+$ was previously established.[1]

The complexation of $\mathbf{L^{2-4}}$ with Cu^I cations causes the emergence of a new redox peak system (two-wave behaviour) corresponding to the complexed Fc/Fc^+ redox couple

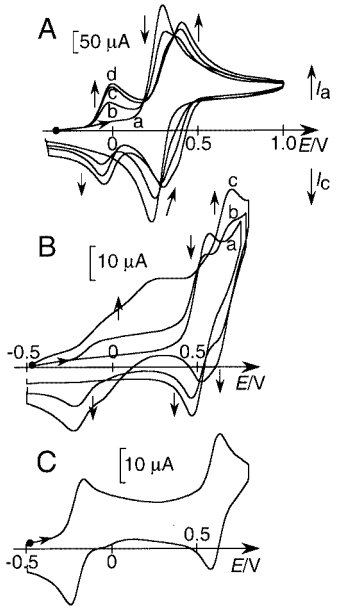

Figure 1. Cyclic voltammograms at a Pt disk (5 mm diameter) of (A) $\mathbf{L^3}$ (2.9 mM) in CH_3CN + TBAP 0.1 M: (a) free $\mathbf{L^3}$; (b) $\mathbf{L^3}$ + 0.2 Cu^+; (c) $\mathbf{L^3}$ + 0.4 Cu^+; (d) $\mathbf{L^3}$ + 0.5 Cu^+; (B) $\mathbf{L^4}$ (1.2 mM) in CH_2Cl_2 + TBAP 0.1 M: (a) free $\mathbf{L^4}$; (b) $\mathbf{L^4}$ + 0.5 Cu^+; (c) $\mathbf{L^4}$ + 1.0 Cu^+; (C) $[Cu\mathbf{L^4}](ClO_4)$ (0.5 mM) in CH_3CN + TBAP 0.1 M; scan rate 0.1 V s^{-1}

(see Figure 1, for example). Due to poor solubility of $\mathbf{L^4}$ in CH_3CN, complexation of this ligand with Cu^I was studied in CH_2Cl_2 (see B in Figure 1). The electrochemical data in CH_3CN solution were obtained, starting with the isolated $\mathbf{L^4}$ + Cu^I complex (see C in Figure 1).

A CV titration shows that the apparent stoichiometry of the complexes formed between $\mathbf{L^2}$, $\mathbf{L^3}$, or $\mathbf{L^4}$ and Cu^I or Cu^{II} is equal to 1:1, 1:2 and 1:1 (metal cation/ligand), respectively. The stoichiometry has been confirmed by MS data. The FAB-MS spectra of the isolated complexes exhibit peaks at m/z = 673 ($[Cu\mathbf{L^2}]^+$); 957 and 857 $\{[Cu(\mathbf{L^3})_2](ClO_4)^+$ and $[Cu(\mathbf{L^3})_2]^+$, respectively$\}$; 771 and 671 $\{[Cu\mathbf{L^4}](ClO_4)^+$ and $[Cu\mathbf{L^4}]^+$, respectively$\}$.

Complexation of Cu^I or Cu^{II} by $\mathbf{L^2}$ has been further studied. We reported previously that the crystal structure of the complex formed between $\mathbf{L^2}$ and Cu^I reveals the formation of a 2:2 (2 Cu^I + 2 $\mathbf{L^2}$) metallo-helicate complex, while the formation of a mononuclear Cu^{II} complex is evident from EPR experiments.[1] The latter result has been confirmed in this study where the X-ray structure of the isolated $[Cu\mathbf{L^2}](ClO_4)_2$ complex revealed the formation of a 1:1 complex (vide infra). The question of the conversion in solution between $[Cu_2(\mathbf{L^2})_2]^{2+}$ and $[Cu\mathbf{L^2}]^+$ thus remains to be addressed. In particular, identical electrochemical features, i.e. superimposable CV curves and same potentials for both complexed Cu^I/Cu^{II} and Fc/Fc^+ redox couples, were obtained following the addition of Cu^{II} instead of Cu^I. In addition, no change in the $E_{1/2}$ value and in the reversibility of the Cu^I/Cu^{II} and Fc/Fc^+ redox couples could be observed in the 5×10^{-2} M (saturated electrolytic solution, prepared from the isolated complex) to 10^{-5} M concentration range, demonstrating that no change occurs in the stoichiometry of the dissolved complex.[1]

Formation of 1:1 and 1:2 complexes from the dimer has been observed by high-resolution ES mass spectrometry upon dissolution of an authentic sample of $[Cu_2(\mathbf{L^2})_2](BF_4)_2$. ES mass spectra were recorded in the 5×10^{-5} to 5×10^{-3} M concentration range. Peaks at m/z (%) = 673.1 (100) and 1283.5 are observed from the ES mass spectra (Figure 2). The isotopic peaks are separated by 1.0 m/z unit, revealing a charge state of +1 for the corresponding ions. Therefore, the peaks at 673.3 and 1283.5 correspond to the $[Cu\mathbf{L^2}]^+$ and $[Cu(\mathbf{L^2})_2]^+$ species, respectively. In addition, the intensity of the peak at 1283.5 appears very weak and decreases with concentration from 1.1% at 5×10^{-3} M down to 0.5% at 5×10^{-5} M, while no peaks characteristic of the $[Cu_2(\mathbf{L^2})_2]^{2+}$ entity or additional peaks corresponding to other species could be detected in the ES-MS spectra. Interestingly, the formation of the 1:1 and 1:2 complexes from the genuine $[Cu_2(\mathbf{L^2})_2](BF_4)_2$ complex should be accompanied with the release of free Cu^I cations. Indeed, a weak peak at 186.7 (not shown in Figure 2) corresponding to $[Cu(CH_3CN)_3]^+$ is simultaneously observed during the ES-MS analyses.

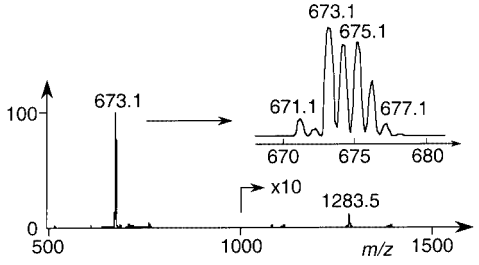

Figure 2. ES-MS spectrum of an acetonitrile solution of authentic $[Cu_2(\mathbf{L^2})_2](BF_4)_2$ (monocrystals) 5×10^{-3} M; Vc = 20 V; insert: isotopic pattern obtained for the peak at m/z = 673.1

On the basis of the electrochemical and electrospray mass spectrometry results, it can be clearly concluded that the 2:2 complex $[Cu_2(\mathbf{L^2})_2]^{2+}$ does not survive upon dissolution and dissociates rapidly to mainly form a 1:1 complex, along

with a minor 1:2 complex. The latter is not detected electrochemically and fully reversible CV behaviour is observed with Cu^{II} or Cu^{I} + $\mathbf{L^2}$ accounting for the reversible electroactivity of the 1:1 complex.

Comparing the electrochemical results obtained from $\mathbf{L^1}$−$\mathbf{L^5}$, we can highlight the benefit of a bis(bipyridyl)-bridged ferrocene ligand with respect to the electrochemical recognition of the metal cation. Complexation of $\mathbf{L^1}$ with copper leads to a one-wave feature for the Fc centre, while $\mathbf{L^2}$ allows amperometric titration of the copper through a two-wave behaviour for its Fc centre. However, complexation of the mono-substituted ligand $\mathbf{L^3}$ is responsible for an unexpected two-wave feature, although the wave corresponding to the complexed ferrocene centre partially overlaps that of the free ligand (see A in Figure 1). In contrast, the bis(bipyridyl)-bridged ligand $\mathbf{L^5}$ shows one-wave behaviour upon complexation of copper. As expected, the recognition properties of a given ligand are linked to its complexation ability. The presence of two additional electron-withdrawing groups in $\mathbf{L^5}$ and steric constraints imposed by the additional 6′-substitution in $\mathbf{L^5}$, as compared to $\mathbf{L^2}$, are responsible for weaker complexation and thus, for a decrease in its electrochemical recognition ability.

X-ray Molecular Structures of the Cu^{II} and Ni^{II} Complexes of Ligand L^2

The crystal structures of both complexes $\{Cu^{II}\mathbf{L^2}\}$ and $\{Ni^{II}\mathbf{L^2}\}$ reveal a 1:1 stoichiometry. The two compounds crystallize in the *C*2/*c* space group revealing 1.5 crystallographically independent dicationic molecular entities (Table 3). One entity is on the general position, and the second is lying on a twofold axis passing through the Fe and M^{II} (Cu2 or Ni2) atoms. The ORTEP view of the dicationic entities $[Cu\mathbf{L^2}]^{2+}$ is shown in Figure 3. The same atom labels are used in both complexes. Selected distances and bond angles of the two complexes are given in Table 4.

{$Cu^{II}L^2$}

The Cu^{II} environment is provided by four nitrogen atoms of the bipy subunits and two oxygen atoms of the carbonyl functions leading to a distorted octahedral coordination geometry. The square planes around Cu1 and Cu2 are defined by atoms O2, N1, N2, N3 and O6A, N5, N6, N5A, respectively (the mean-square deviations are 0.166 Å and 0.086 Å, respectively). The O4, N4 atoms and O6, N6 atoms occupy the axial positions, with the N4−Cu1−O4 and N6−Cu2−O6 angles equal to 168.7(1)° and 165.2(2)°, respectively. The Cu−N distances vary between 1.991(4) Å and 2.091(4) Å, and related Cu−O distances are significantly longer with Cu1−O2 = 2.226(4) Å and Cu1−O4 = 2.483(4) Å. The oxygen atoms adopt a *cis* position. The bipy units are slightly twisted (torsion angles between the cycles are equal to N1C5C6N2 = 4.7°; N3C25C26N4 = 12.1°; N5C45C46N6 = 10.1°). The cyclopentadienyl rings are almost parallel [the tilt angles are equal to 1.0(3)° for Fe1 and 0.35(20)° for Fe2] and the distances from the iron atom to the centroids of these planes are very similar [Fe1: 1.644(3) Å; Fe2: 1.639(3) Å]. An important observation is that the intermetallic distances [Fe1···Cu1 5.309(1) Å, Fe2···Cu2 5.153(2) Å] are far too long for any direct metal−metal interaction to be invoked.

{$Ni^{II}L^2$}

The Ni^{II} complex is isostructural with the Cu^{II} complex, the cation being surrounded by four nitrogen atoms provided by the bipyridine subunits and two oxygen atoms of

Table 3. Crystal data and structure refinement for $[Cu\mathbf{L^2}](ClO_4)_2$ and $[Ni\mathbf{L^2}](ClO_4)_2$

	$[Cu\mathbf{L^2}](ClO_4)_2$	$[Ni\mathbf{L^2}](ClO_4)_2$
Empirical formula	$C_{58}H_{51.5}Cl_3Cu_{1.5}Fe_{1.5}N_{8.5}O_{18.5}$	$C_{58}H_{53.5}Cl_3Ni_{1.5}Fe_{1.5}N_{7.5}O_{19}$
Formula mass	1449.01	1437.77
Crystal system	monoclinic	monoclinic
Space group	*C*2/*c*	*C*2/*c*
a [Å]	16.482(3)	16.161(3)
b [Å]	22.383(5)	22.441(5)
c [Å]	33.389(7)	34.264(7)
β [°]	98.47(3)	96.27(3)
V [Å^3]/Z	12348(4)/8	12352(8)/8
D_X [g cm^{-3}]	1.559	1.546
μ [cm^{-1}]	10.69	10.10
Crystal dim. [mm]	0.05 × 0.05 × 0.15	0.05 × 0.07 × 0.15
Shape/colour	needle/brown-dark	needle/green-dark
T [K]	200	170
$2\theta_{max}$ [°]	48	48.5
Number of reflections collected	27068	38058
Restraints/parameters	72/915	65/873
$R(F)$[a]	0.0561 for $I > 2\sigma(I)$	0.0525 for $I > 2\sigma(I)$
$R_w(F^2)$[b]	0.1739	0.1701
Goodness of fit *S*	1.02	0.83
$\Delta\rho_{min}/\Delta\rho_{max}$ [e Å^{-3}]	−0.57/0.96	−0.51/0.83

[a] $R = \Sigma||F_o| - |F_c||/\Sigma|F_o|$. [b] $R_w = [\Sigma w(|F_o| - |F_c|)^2/[\Sigma w F_o^2]^{1/2}$.

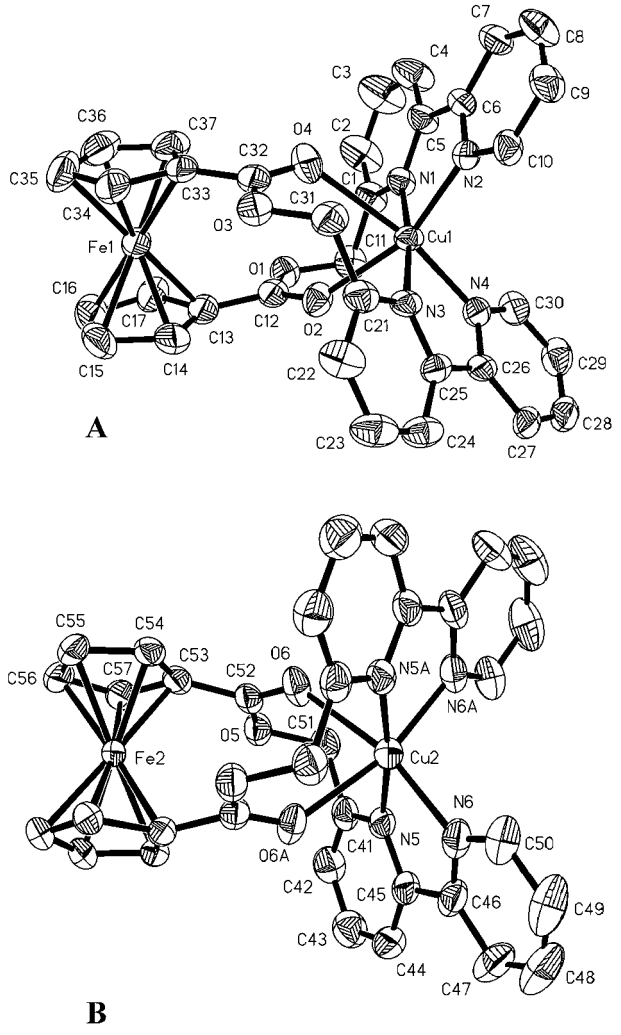

Figure 3. ORTEP plots of the two crystallographically independent units $[Cu\mathbf{L^2}]^{2+}$: (A) entity on general position; (B) entity on a 2-fold axis; hydrogen atoms are omitted for clarity; ellipsoids are drawn at a 30% probability level

Table 4. Selected bond lengths [Å] and bond angles [°] for $[Cu\mathbf{L^2}](ClO_4)_2$ and $[Ni\mathbf{L^2}](ClO_4)_2$ (symmetry equivalent position A = 1 − *x*, *y*, 0.5 − *z*)

$[Cu\mathbf{L^2}](ClO_4)_2$		$[Ni\mathbf{L^2}](ClO_4)_2$	
Cu(1)−Fe(1)	5.307(1)	Ni(1)−Fe(1)	5.072(1)
Cu(2)−Fe(2)	5.154(2)	Ni(2)−Fe(2)	4.963(1)
Cu(1)−N(1)	1.991(4)	Ni(1)−N(1)	2.074(4)
Cu(1)−N(2)	2.031(4)	Ni(1)−N(2)	2.033(4)
Cu(1)−N(3)	2.007(4)	Ni(1)−N(3)	2.060(3)
Cu(1)−N(4)	2.091(4)	Ni(1)−N(4)	2.019(4)
Cu(1)−O(2)	2.226(4)	Ni(1)−O(2)	2.152(3)
Cu(1)−O(4)	2.483(4)	Ni(1)−O(4)	2.145(3)
Cu(2)−N(5)	2.038(5)	Ni(2)−N(5)	2.093(4)
Cu(2)−N(6)	2.073(5)	Ni(2)N(6)	2.031(4)
Cu(2)−O(6)	2.263(4)	Ni(2)−O(6)	2.108(3)
N(1)−Cu(1)−N(2)	82.0(2)	N(1)−Ni(1)−N(2)	80.4(2)
N(1)−Cu(1)−N(3)	174.0(2)	N(1)−Ni(1)−N(3)	177.5(1)
N(2)−Cu(1)−N(3)	101.9(2)	N(2)−Ni(1)−N(3)	98.9(2)
N(1)−Cu(1)−N(4)	102.2(2)	N(1)−Ni(1)−N(4)	102.2(1)
N(2)−Cu(1)−N(4)	108.3(2)	N(2)−Ni(1)−N(4)	98.7(1)
N(3)−Cu(1)−N(4)	81.1(2)	N(3)−Ni(1)−N(4)	80.3(1)
N(1)−Cu(1)−O(2)	94.6(2)	N(1)−Ni(1)−O(2)	95.5(1)
N(2)−Cu(1)−O(2)	158.2(1)	N(2)−Ni(1)−O(2)	173.1(1)
N(3)−Cu(1)−O(2)	80.1(1)	N(3)−Ni(1)−O(2)	84.9(1)
N(4)−Cu(1)−O(2)	93.5(1)	N(4)−Ni(1)−O(2)	87.6(1)
N(1)−Cu(1)−O(4)	79.3(2)	N(1)−Ni(1)−O(4)	82.3(1)
N(3)−Cu(1)−O(4)	96.5(2)	N(3)−Ni(1)−O(4)	95.3(1)
N(2)−Cu(1)−O(4)	83.1(1)	N(2)−Ni(1)−O(4)	93.3(1)
N(4)−Cu(1)−O(4)	168.7(1)	N(4)−Ni(1)−O(4)	167.7(1)
O(2)−Cu(1)−O(4)	75.2(1)	O(2)−Ni(1)−O(4)	80.6(1)
N(5)−Cu(2)−N(6A)	104.2(2)	N(5)−Ni(2)−N(6A)	102.3(2)
N(5)−Cu(2)−N(6)	80.4(2)	N(5)−Ni(2)−N(6)	79.6(2)
N(5)−Cu(2)−N(5A)	172.3(2)	N(5)−Ni(2)−N(5A)	177.1(2)
N(5)−Cu(2)−O(6)	94.7(2)	N(5)−Ni(2)−O(6)	94.7(1)
N(5)−Cu(2)−O(6A)	79.3(2)	N(5)−Ni(2)−O(6A)	83.1(1)
N(6)−Cu(2)−O(6)	165.2(2)	N(6)−Ni(2)−O(6)	170.5(1)
N(6)−Cu(2)−N(5A)	104.2(2)	N(6)−Ni(2)−N(5A)	102.3(2)
N(6)−Cu(2)−N(6A)	107.8(3)	N(6)−Ni(2)−N(6A)	99.7(2)
N(6)−Cu(2)−O(6A)	87.0(2)	N(6)−Ni(2)−O(6A)	88.8(1)
O(6)−Cu(2)−O(6A)	78.4(2)	O(6)−Ni(2)−O(6A)	83.0(2)

the linkers describing a slightly distorted octahedral coordination sphere.

In both structures, the ester groups are almost coplanar with the Cp rings and coordination of the Cu^{II} or Ni^{II} cations by the carbonyl moieties involves a conjugated frame between the ferrocenyl subunit and the metal centres.

Complexation of $\mathbf{L^{1-5}}$ with Ni^{II} Cations

The electrochemical data for complexation of $\mathbf{L^{1-5}}$ with Ni^{II} in the CH_3CN or CH_2Cl_2 electrolyte are summarized in Table 5. In terms of electrochemical response, the recognition properties of these redox-active receptors towards Ni^{II} are similar to that observed with Cu^{I} and Cu^{II}.

Complexation of Ni^{II} with $\mathbf{L^1}$ and $\mathbf{L^5}$ results in a one-wave feature for the Fc centre (e.g. Figure 4A for $\mathbf{L^1}$ + Ni^{II}). Addition of Ni^{II} to a solution of $\mathbf{L^1}$ or $\mathbf{L^5}$ induces a progressive weak positive shift of up to 60 mV in the potential of the Fc/Fc^+ couple. The maximal value is reached when 0.5 and 1 mol-equiv. of Ni^{II} have been added to $\mathbf{L^1}$ and $\mathbf{L^5}$, respectively. This suggests the formation of $[Ni(\mathbf{L^1})_2]^{2+}$ and $[Ni\mathbf{L^5}]^{2+}$ complexes where a bis(bipy) environment is provided for the cation. In the negative potentials range, the $\mathbf{L^1}$ + Ni^{II} system is characterized by two new reversible waves at $E_{1/2} = -0.98$ and -1.45 V (Figure 4A). Their intensity increases linearly with the amount of Ni^{II}, then remains constant after the addition of more than a 0.5 mol equiv. Above 0.5 mol-equiv., the CV curve displays the electrochemical response of free Ni^{II} salts as an irreversible cathodic peak around −1.5 V with the corresponding anodic peak being located around 0.2 V on the reverse scan. As judged by coulometric titration, the two reduction waves correspond to one-electron transfer leading to $[Ni(\mathbf{L^1})_2]^+$ and $[Ni(\mathbf{L^1})_2]^0$, respectively. Unfortunately, the poor stability of the electroreduced species excluded the assignment from EPR studies of the redox orbitals involved in these reductions. In contrast, addition of Ni^{II} to a solution containing $\mathbf{L^5}$ gives rise to an ill-behaved irreversible cathodic wave around −1.2 V and to electrochemical features typical of free Ni^{II}, whatever the nickel concentration used. This indicates the formation of an unlocked complex $[Ni\mathbf{L^5}]^{2+}$, which liberates Ni^{II} cations.

Table 5. Electrochemical data for $\mathbf{L^1}$, $\mathbf{L^2}$, $\mathbf{L^3}$, $\mathbf{L^4}$, $\mathbf{L^5}$ + Ni^{II}

[a]	$2\mathbf{L^1}$ + Ni^{II} Fc/Fc^+	Ni^{II}/Ni^I	Ni^I/Ni^0	$\mathbf{L^2}$ + Ni^{II} Fc/Fc^+	Ni^{II}/Ni^I	Ni^I/Ni^0	$2\mathbf{L^3}$ + Ni^{II} Fc/Fc^+	Ni^{II}/Ni^I	Ni^I/Ni^0
CH_3CN	0.39	−0.98	−1.48	0.80	−1.16	−1.47	0.40	−1.33	−1.48
CH_2Cl_2	0.51	[b]	[b]	0.83	−1.04	−1.42	[c]	[c]	[c]
	$\mathbf{L^4}$ + Ni^{II} Fc/Fc^+	Ni^{II}/Ni^I	Ni^I/Ni^0	$\mathbf{L^5}$ + Ni^{II} Fc/Fc^+	Ni^{II}/Ni^I	Ni^I/Ni^0			
CH_3CN	0.74	[c]	[c]	0.65	[c]	[c]			
CH_2Cl_2	0.73	−1.43	[c]	[c]	[c]	[c]			

[a] $E_{1/2}$ [V] vs. $Ag/AgNO_3$ (0.01 M) (see Table 2). [b] Strong adsorption phenomena precluded determination of $E_{1/2}$. [c] Not determined.

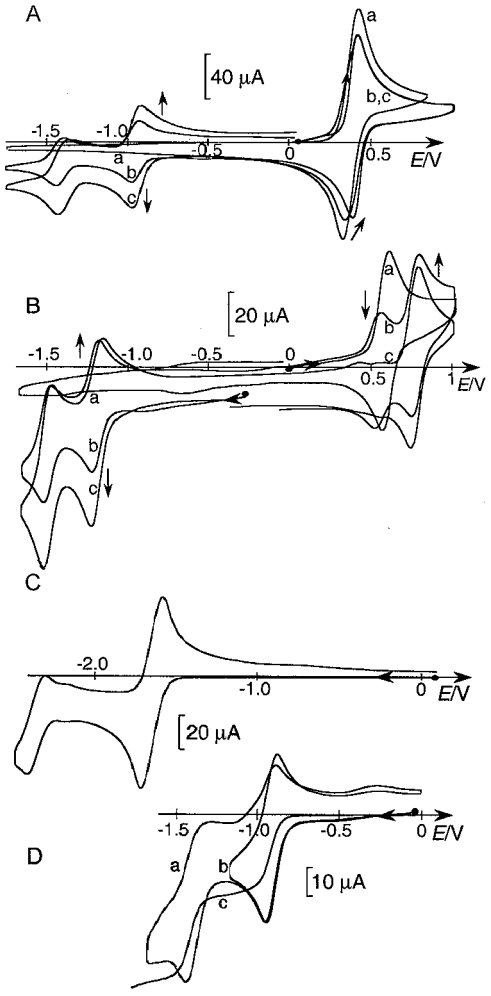

Figure 4. Cyclic voltammograms at $\nu = 0.1$ V s^{-1}, in CH_3CN + TBAP (0.1 M), at a Pt disk (5 mm diameter) of (A) $\mathbf{L^1}$ (2.5 mM): (a) free $\mathbf{L^1}$; (b) $\mathbf{L^1}$ + 0.25 Ni^{2+}; (c) $\mathbf{L^1}$ + 0.5 Ni^{2+}; (B) $\mathbf{L^2}$ (1.2 mM): (a) free $\mathbf{L^2}$; (b) $\mathbf{L^2}$ + 0.5 Ni^{2+}; (c) $\mathbf{L^2}$ + 1.0 Ni^{2+}; (C) $[Ni(bipy)_2](ClO_4)_2$ (0.5 mM); (D) $[Ni(\mathbf{L^6})_2](ClO_4)_2$ (0.5 mM): (a, b) CV curves; (c) RDE voltammetry curve (carbon disk, 3 mm diameter; 600 rev min^{-1}, $\nu = 0.01$ V s^{-1})

The $\mathbf{L^{2-4}}$ + Ni^{II} systems are best characterized by a two-wave behaviour for the Fc/Fc^+ redox couple in the presence of increasing amounts of Ni^{II} (see for example B in Figure 4; $\mathbf{L^2}$ + Ni^{II}). Upon progressive addition of Ni^{II} to $\mathbf{L^2}$, $\mathbf{L^3}$ or $\mathbf{L^4}$ in CH_3CN, a new redox wave corresponding to the complexed Fc/Fc^+ redox couple merges gradually at 0.80, 0.40 and 0.74 V, respectively. At the same time, the redox wave for the free Fc/Fc^+ couple vanishes. The cathodic electrochemical response of the complexes formed between Ni^{II} and $\mathbf{L^2}$ or $\mathbf{L^3}$ is revealed on the CV curves as two successive one-electron waves located at $E_{1/2} = -1.16$ and −1.47 V ($\mathbf{L^2}$; see B in Figure 4), and −1.33 and −1.48 V ($\mathbf{L^3}$). However, it must be noted that the electrochemical recognition properties of $\mathbf{L^3}$ are less marked than those of $\mathbf{L^2}$, for the following reasons: (*i*) the new signal corresponding to the complexed Fc/Fc^+ redox couple partially overlaps that of the free ligand, (*ii*) the two successive cathodic signals are ill-behaved and weakly separated, and (*iii*) a residual signal assigned to the free ligand remains observable in the presence of excess Ni^{II}.

Due to the poor solubility of $\mathbf{L^4}$ in CH_3CN solution, the cathodic features of the Ni^{II} + $\mathbf{L^4}$ system were determined in CH_2Cl_2 solution. In the accessible potential range only the first reduction of the $\mathbf{L^4}$ + Ni^{II} complex could be seen, at $E_{1/2} = -1.43$ V.

All perturbations due to the presence of Ni^{II} in solutions containing ligands $\mathbf{L^2}$, $\mathbf{L^3}$, or $\mathbf{L^4}$ reach their maximum intensity at a mol ratio Ni^{II}/ligand = 1, 0.5, and 1, respectively, suggesting the formation of complexes of the type $[Ni\mathbf{L^2}]^{2+}$, $[Ni(\mathbf{L^3})_2]^{2+}$, and $[Ni\mathbf{L^4}]^{2+}$. The stoichiometry of the $[Ni\mathbf{L^2}]^{2+}$ and $[Ni(\mathbf{L^3})_2]^{2+}$ species was confirmed by UV/Vis titration experiments. The titration curve (absorbance at λ_{max} = 460 nm of a CH_3CN solution of $\mathbf{L^2}$ as a function of increasing amounts of Ni^{II}) exhibits a sharp inflection point at an $Ni^{II}/\mathbf{L^2}$ mol ratio equal to 1 (ε_{max} = 140 M^{-1} cm^{-1}). The titration curve for the $\mathbf{L^3}$ + Ni^{II} complex (λ_{max} = 450 nm; ε_{max} = 500 M^{-1} cm^{-1}) displays an inflection point for $Ni^{II}/\mathbf{L^3} = 0.5$. In addition, FAB-MS spectra of the isolated $[Ni\mathbf{L^2}]^{2+}$ and $[Ni\mathbf{L^4}]^{2+}$ complexes display, exclusively, the *m/z* peaks corresponding to the 1:1 complex: *m/z* = 767 $\{[Ni\mathbf{L^2}](ClO_4)^+\}$ and 765 $\{[Ni\mathbf{L^4}](ClO_4)^+\}$.

The differences in the CV behaviour for these Ni^{II} complexes can be related to the nature of the $\mathbf{L^{1-5}}$ ligand. With $\mathbf{L^1}$ and $\mathbf{L^3}$ two ligands are involved in forming the complexes, while only one ligand is involved in the $\mathbf{L^2}$-, $\mathbf{L^4}$- and $\mathbf{L^5}$-based complexes, pointing to a bis(bipy) environment of the first coordination sphere of the metal centre. The *sand-*

wich effect provided by $\mathbf{L^2}$ or $\mathbf{L^4}$ causes a two-wave behaviour for the Fc/Fc^+ redox centre, while complexation of $\mathbf{L^1}$ or $\mathbf{L^3}$ leads to a simple anodic shift of the Fc oxidation ($\mathbf{L^1}$), or to a poorly resolved new signal ($\mathbf{L^3}$). As already discussed for its complexation with copper cations, the bis(bipy) ligand $\mathbf{L^5}$ shows reduced complexation ability and poor recognition properties.

The electrochemical reduction of nickel complexes proceeds by two successive one-electron transfers. This electrochemical behaviour is markedly different from that found for the complex formed between unsubstituted bipy and Ni^{II}. Under the same experimental conditions, the regular $[Ni(bipy)_2]^{2+}$ complex undergoes two successive, reversible electron transfers at $E_{1/2} = -1.55$ and -2.25 V in CH_3CN (see C in Figure 4). As reported previously,[10] reduction of $[Ni(bipy)_2]^{2+}$ is likely to occur following the $[Ni(bipy)_2]^{2+} \rightarrow [Ni(bipy)_2]^0 \rightarrow [Ni(bipy)_2]^-$ steps, the first step corresponding to a two-electron transfer. However, substitution of the bipy ligand with a simple electron-withdrawing group, as in $\mathbf{L^6}$, causes a dramatic change in this electrochemical mechanism. The CV curve recorded for Ni^{II} + 2 $\mathbf{L^6}$ in CH_3CN exhibits two reversible waves with comparable intensities at $E_{1/2} = -0.94$ and -1.43 V (see D in Figure 4). Further reduction is observed at a lower potential as an irreversible peak ($E_{1/2} = -2.02$ V, determined from RDE experiments). Coulometric titration has demonstrated that the three reductions are one-electron transfers, according to the following sequence: $[Ni(\mathbf{L^6})_2]^{2+} \rightarrow [Ni(\mathbf{L^6})_2]^{+} \rightarrow [Ni(\mathbf{L^6})_2]^0 \rightarrow [Ni(\mathbf{L^6})_2]^-$. Two additive effects could be responsible for such a change in the electrochemical behaviour of these complexes. It is obvious that substitution of the bipyridyl-binding site in $\mathbf{L^{1-6}}$ by electron-withdrawing groups leads to a stabilization of the reduced forms of the nickel complexes. Moreover, change in geometry between the unsubstituted bipy complex (likely to be square-planar) and the $\mathbf{L^{1-6}}$ complexes {likely to be octahedral as in $[Ni(\mathbf{L^2})]^{2+}$} might result in different redox properties.

Complexation of $\mathbf{L^{1-5}}$ with Fe^{II} Cations

Electrochemical data for complexation of $\mathbf{L^{1-5}}$ with Fe^{II} are summarized in Table 6. In a recent study,[2] we have shown that the complexation of $\mathbf{L^{3,4}}$ with Fe^{II} results in a two-wave behaviour for the Fc centre and in the formation of 1:2 $\{[Fe(\mathbf{L^3})_2]^{2+}\}$ and 1:1 $\{[Fe\mathbf{L^4}]^{2+}\}$ complexes. However, with $\mathbf{L^3}$ the intermediate formation at a low $Fe^{II}/\mathbf{L}$ ratio of the $[Fe(\mathbf{L^3})_3]^{2+}$ complex was evidenced from electrochemical experiments and UV/Vis titration.

Replacement of the amide linkage in $\mathbf{L^3}$ with the carbonyloxy linkage in $\mathbf{L^1}$ leads to strong modifications in the complexation pathway. Complexation of $\mathbf{L^1}$ with Fe^{II} in CH_3CN results in a one-wave behaviour of the electrochemical response for the Fc centre, which shifts from 0.33 V in free $\mathbf{L^1}$ to 0.37 V in the presence of excess Fe^{II}. The electrochemical response of the Fe^{II}/Fe^{III} redox couple in the $\mathbf{L^1}$-based complex is seen at $E_{1/2} = 0.95$ V, a value close to that found for $[Fe(\mathbf{L^3})_2]^{2+}$,[2] without any CV evidence for the intermediate formation of an "$Fe(bipy)_3$"-like species. The potentiometric titration curve displays a smooth inflection point around 0.5 mol-equiv. of Fe^{II}, which suggests the formation of an $[Fe(\mathbf{L^1})_2]^{2+}$ complex.

Table 6. Electrochemical data for $\mathbf{L^1}$, $\mathbf{L^2}$, $\mathbf{L^3}$, $\mathbf{L^4}$, $\mathbf{L^5}$ + Fe^{II}

[a]	$2\mathbf{L^1}$ + Fe^{II}		$\mathbf{L^2}$ + Fe^{II}		$2\mathbf{L^3}$ + Fe^{II}	
Fc/Fc^+	Fe^{II}/Fe^{III}		Fc/Fc^+	Fe^{II}/Fe^{III}	Fc/Fc^+	Fe^{II}/Fe^{III}
0.37	0.95		0.78[b]	0.98[b]	0.39[c]	0.97[c]
	$3\mathbf{L^3}$ + Fe^{II}		$\mathbf{L^4}$ + Fe^{II}		$\mathbf{L^5}$ + Fe^{II}	
Fc/Fc^+	Fe^{II}/Fe^{III}		Fc/Fc^+	Fe^{II}/Fe^{III}	Fc/Fc^+	Fe^{II}/Fe^{III}
0.39[c]	0.77[c]		0.64[c] [d]	0.99[c,d]	0.83[b]	0.98[b]

[a] $E_{1/2}$ [V] vs. $Ag/AgNO_3$ (0.01 M) (see Table 2), measured in CH_3CN electrolyte. [b] Irreversible oxidation. [c] From ref.[1] [d] $E_{1/2} = 0.73$ and 0.95 V in CH_2Cl_2.

In contrast, addition of Fe^{II} to a solution of $\mathbf{L^2}$ or $\mathbf{L^5}$ results in the appearance of a new Fc/Fc^+ oxidation wave at $E_{1/2} = 0.78$ and 0.83 V, respectively, at the expense of the free ligand (Figure 5). This wave reaches full development at an Fe^{II}/ligand mol ratio of 1 (Figure 5, curve b), suggesting the formation of 1:1 complexes in which the Fe^{II} centre is bound to two bipyridyl sites provided by the same metallo ligand, as established for bis(bipy)− and bis(phen)−ferrocene derivatives.[2] The stoichiometry of the complex $\mathbf{L^2}$ + Fe^{II} was confirmed from UV/Vis titration. Addition of Fe^{II} in a CH_3CN solution of $\mathbf{L^2}$ results in the appearance of an MLCT band ($\lambda_{max} = 450$ nm) of increasing intensity until 1 mol-equiv. of Fe^{II} has been added ($\varepsilon_{max} = 1.1 \times 10^3$ M^{-1} cm^{-1}). This result was further confirmed by the FAB mass spectrum of the isolated complex which displays peaks at $m/z = 765$ $\{[Fe\mathbf{L^2}](ClO_4)^+\}$ and 666 $\{[Fe\mathbf{L^2}]^{2+} - 1\}$.

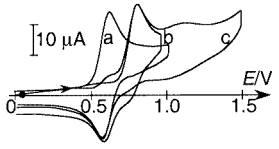

Figure 5. Cyclic voltammograms, in CH_3CN + TBAP (0.1 M), at a Pt disk (5 mm diameter) of 0.4 mM $\mathbf{L^2}$: (a) free $\mathbf{L^2}$; (b) $\mathbf{L^2}$ + 1.0 Fe^{2+} in the 0 to 0.95 V scan range; (c) $\mathbf{L^2}$ + 1.0 Fe^{2+} in the 0 to 1.45 V range; scan rate 0.1 V s^{-1}

However, oxidation of the complexed ligands $\mathbf{L^2}$ and $\mathbf{L^5}$ is irreversible in appearance. On the reverse scan, only the cathodic peak corresponding to the reduction of the ferrocene unit in the free ligand is observed (Figure 5, curve b). Thus, dissociation occurs upon oxidation of the $[Fe\mathbf{L^{2,5}}]^{2+}$ complexes, due to the establishment of repulsive electrostatic forces between the positively charged Fc^+ centre and the dicationic bound metal cation Fe^{II}. Moreover, in addition to the electrochemical signal due to the complexed Fc centre, the anodic response of the bound Fe^{II} cation is evident, on the CV curves, as a broad, ill-behaved irreversible wave at $E_{1/2} = 0.98$ V (determined from RDE experiments) for both complexes (Figure 5, curve c). It should be noted that a small wave corresponding to oxidation of free $\mathbf{L^2}$ re-

mains, even in the presence of a slight excess of Fe^{II}. As for the corresponding copper complexes, the $[FeL^5]^{2+}$ complex is less stable than its $[FeL^2]^{2+}$ analogue. Thus, the oxidation peak for free L^5 is apparent in the CV curves recorded even in the presence of a large excess of Fe^{II} (e.g. 2 mol-equiv.). These results are somewhat different from that found for the $[FeL^4]^{2+}$ complex, which shows reversible CV features. This is in keeping with a weaker binding of the Fe^{II} centre to the carbonyl oxygen atoms of the carbonyloxy group in L^1, compared to the amide donor group in L^3.

In addition, complexes formed from L^1, L^2, or L^5 with Fe^{II} display a broad, irreversible reduction wave at E_p = −1.38 V, −1.35 V, and −2.04 V, respectively. These features confirm that complexation affords species of the type $[Fe(bpy)_2]^{2+}$ rather than $[Fe(bpy)_3]^{2+}$-like complexes. The latter would be characterized by three reversible reduction waves in the negative potential region.

As has already been pointed out for the $[Fe(L^3)_2]^{2+}$ and $[FeL^4]^{2+}$ complexes,[2] ^1H NMR spectra of isolated $[Fe(L^1)_2](ClO_4)_2$ and $[FeL^2](ClO_4)_2$ complexes display resonances in a very large chemical shifts range (from δ = 83 to −10, and from δ = 81 to −9, respectively; see Exp. Sect.), attesting to a high spin configuration for these $\{Fe^{II}(bpy)_2\}$ species. This is confirmed by the rather low molar extinction coefficients of the visible transition in these complexes (600−1600 M^{-1} cm^{-1}; see Exp. Sect.), as compared to that found[11] with low-spin $[Fe(bipy)_2(CH_3CN)_2]^{2+}$ species (ε = 5600 M^{-1} cm^{-1} at 470 nm).

Complexation with Hg^{II}, Pb^{II}, Co^{II} and Ag^I Cations

Electrochemical data obtained in the course of complexation of L^2 with mercury(II), lead(II), cobalt(II) and silver(I) cations are summarized in Table 7. One-wave behaviour was found upon complexation of L^2 with Hg^{II}, with a maximum potential shift of 60 mV for the Fc/Fc^+ redox couple reached at an Hg^{II}/L^2 mol ratio of 1. The Hg^{II} + L^2 complex undergoes a reversible one-electron transfer at $E_{1/2}$ = 0.13 V. This indicates that Hg^I is stabilized upon complexation with L^2, since free Hg^{II} is reduced through a two-electron transfer to form Hg^0 at 0.22 V. Complexation of L^1 with Hg^{II} is also characterized by one-wave behaviour and leads to a lower positive potential shift (30 mV) in the Fc/Fc^+ redox potential, reached at an Hg^{II}/L^1 ratio close to 0.5. These results show the ability of L^1 and L^2 to provide a bipyridyl environment for the Hg^{II} metal cation. The stoichiometry has been further established by MS experiments. The FAB mass spectrum of the isolated L^2 + Hg^{II} complex, prepared as its triflate salt in the presence of an excess of ligand, displays only one peak at *m/z* = 961 $\{[HgL^2](CF_3SO_3)^+\}$ characteristic of a 1:1 complex. Analytical results are also in agreement with the formation of a 1:1 Hg^{II} + L^4 complex with the bis(carboxamide) ligand (see Exp. Sect.).

For Pb^{II}, the one-wave behaviour of the Fc/Fc^+ centre is characterized by a maximum potential shift of 80 mV that is reached at a Pb^{II}/L^2 mol ratio of 1. Reduction of the Pb^{II} + L^2 complex proceeds via several poorly defined steps. In contrast, two-wave behaviour is found upon addition of Co^{II} to L^2. The resultant Fc/Fc^+ redox couple appears at $E_{1/2}$ = 0.79 V, while the weakly reversible Co^{II} centred electron transfer is located at $E_{1/2}$ = 1.1 V. Maximum perturbation is reached at a Co^{II}/L^2 mol ratio of 1. However, the electrochemical signal for free L^2 remains visible on the CV curve even in the presence of excess Co^{II}. Finally, no complexation could be detected upon addition of Ag^I to L^2.

Conclusion

This study confirms the remarkable complexation and electrochemical recognition properties of bipyridyl−ferrocene metallo-synthons for adventitious metal cations. Complexation results in significant positive potential shifts of the ferrocene/ferricinium redox couple following a decrease in the electron density around the ferrocene centre. The bis(substitution) on the ferrocene centre improves the electrical connection between the bound metal cation and the ferrocenyl unit allowing effective electrochemical recognition of the metal cation through a two-wave behaviour for the ferrocene electrochemical response (*sandwich effect*). All the studied ligands afford a bis(bipyridyl) environment for the bound metal cations, which dictates the 1:1 stoichiometry with the bis(substituted) ligands and the 1:2 stoichiometry with the mono(substituted) ligands. In the solid state, Cu^I forms a 2:2 complex with L^2, which does not survive in solution, while Cu^{II} forms a 1:1 complex. The Cu^{II} and Ni^{II} complexes are isostructural with the cations being surrounded by four nitrogen atoms provided by the bipyridine subunits and two oxygen atoms of the linkers. Finally, formation of bis(bipy)-like complexes with Fe^{II} and other metal cations such as Hg^{II}, Pb^{II} and Co^{II} illustrates the wide versatility of the coordination features of these bipy−ferrocenyl ligands.

Experimental Section

Ligands: L^1, L^2, L^3, L^4 and L^5 were synthesized as reported previously.[1,3,4]

Table 7. Electrochemical data for L^2 + Hg^{II}, Pb^{II}, Ag^I and Co^{II}, and L^1 + Hg^{II}

[a] L^2 + Hg^{II}		L^2 + Ag^I	L^2 + Pb^{II}	L^2 + Co^{II}		$2L^1$ + Hg^{II}	
Fc/Fc^+	Hg^{II}/Hg^I	Fc/Fc^+	Fc/Fc^+	Fc/Fc^+	Co^{II}/Co^{III}	Fc/Fc^+	Hg^{II}/Hg^0
0.62	0.13	0.56[b]	0.64	0.79	1.10	0.59	−0.32

[a] $E_{1/2}$ [V] vs. $Ag/AgNO_3$ (0.01 M) (see Table 1), measured in CH_3CN electrolyte. [b] No electrochemical recognition.

L^6: L^6 was prepared according to a similar procedure based on the stoichiometric reaction of 6-(hydroxymethyl)-2,2′-bipyridine[12] with benzoyl chloride. Yield 85%. ^{1}H NMR (300 MHz, CD_3CN, 10 mM, 295 K): δ = 8.66 (1 H, *H*-6′-bipy), 8.41 (1 H, *H*-3-bipy), 8.32 (1 H, *H*-3′-bipy), 8.15 (2 H, *H*-*o*-bz), 7.77−7.87 (2 H, *H*-5-bipy and *H*-4-bipy), 7.44−7.59 (4 H, *H*-*m*-bz, *H*-*p*-bz, *H*-5′-bipy), 7.31 (1 H, *H*-4′-bipy), 5.60 (2 H, CH_2-bipy). FAB$^+$ MS: *m*/*z* = 291 [L^6 + 1]$^+$.

Complexes: All metal complexes were synthesized as their perchlorate or triflate salts, by reaction of stoichiometric amounts of the ligand (40 mg) and the salt of the selected metal cation [1 mol-equiv. in the case of the bis(bipy) derivatives and 0.5 mol-equiv. in the case of mono(bipy)] in a minimum volume of CH_3CN or CH_2Cl_2 at room temperature. The target complexes were precipitated on addition of diethyl oxide and isolated as orange solids by suction filtration (yields 80−90%). X-ray quality crystals were grown by vapour diffusion of diethyl oxide into an acetonitrile solution of the complexes {Cu^{II}L^2} or {Ni^{II}L^2}. [Cu(L^1)$_2$](ClO$_4$), [Cu$_2$(L^2)$_2$](ClO$_4$)$_2$, [Fe(L^3)$_2$](ClO$_4$)$_2$ and [FeL^4](ClO$_4$)$_2$ complexes have been previously described.[1,2] **Warning!** *Perchlorate salts are hazardous because of the possibility of explosion.*

[Cu(L^3)$_2$](ClO$_4$): UV/Vis (MLCT band; CH_3CN): λ_{max} (ε, M^{-1} cm^{-1}) = 442 nm (1718). FAB$^+$ MS: *m*/*z* = 857 [Cu(L^3)$_2$]$^+$. FT-IR: ν(CO) = 1602 cm^{-1}; due to hygroscopic properties, no reproducible elementary analysis could be obtained with this compound.

[CuL^4](ClO$_4$): UV/Vis (MLCT band; CH_3CN) λ_{max}, (ε, M^{-1} cm^{-1}) = 444 nm (3250). FAB$^+$ MS: *m*/*z* = 671 [CuL^4]$^+$. FT IR: ν(CO) = 1634 cm^{-1}. $C_{34}H_{28}ClCuFeN_6O_6\cdot 2H_2O$ (807.516): calcd. C 50.57, H 3.99, N 10.41; found C 50.28, H 3.62, N 10.55.

[Ni(L^1)$_2$](ClO$_4$)$_2$: UV/Vis (MLCT band; CH_3CN): λ_{max} (ε, M^{-1} cm^{-1}) = 458 nm (670). FAB$^+$ MS: *m*/*z* = 953 [Ni(L^1)$_2$](ClO$_4$)$^+$. FT IR: ν(CO) = 1603, 1645, 1714 cm^{-1}. $C_{44}H_{36}Cl_2Fe_2N_4NiO_{12}\cdot 2H_2O$ (1090.128): calcd. C 48.48, H 3.70, N 5.14; found C 47.93, H 3.63, N 5.17.

[NiL^2](ClO$_4$)$_2$: UV/Vis (MLCT band; CH_3CN): λ_{max} (ε, M^{-1} cm^{-1}) = 460 nm (140). FAB$^+$ MS: *m*/*z* = 767 [NiL^2](ClO$_4$)$^+$. FT IR: ν(CO) = 1603, 1631, 1668 cm^{-1}. $C_{34}H_{26}Cl_2FeN_4NiO_{12}\cdot 3H_2O$ (922.105): calcd. C 44.29, H 3.50, N 6.08; found C 44.49, H 3.05, N 6.20.

[Ni(L^3)$_2$](ClO$_4$)$_2$: UV/Vis (MLCT band; CH_3CN): λ_{max} (ε, M^{-1} cm^{-1}) = 445 nm (500). FAB$^+$ MS: *m*/*z* = 951 [Ni(L^3)$_2$](ClO$_4$)$^+$. FT IR: ν(CO) = 1601 cm^{-1}. $C_{44}H_{38}Cl_2Fe_2N_6NiO_{10}\cdot 2H_2O$ (1088.158): calcd. C 48.57, H 3.89, N 7.72; found C 48.97, H 3.82, N 7.74.

[NiL^4](ClO$_4$)$_2$: UV/Vis (MLCT band; CH_3CN): λ_{max} (ε, M^{-1} cm^{-1}) = 448 nm (360). FAB$^+$ MS: *m*/*z* = 765 [NiL^4](ClO$_4$)$^+$. FT IR: ν(CO) = 1605 cm^{-1}. $C_{34}H_{28}Cl_2FeN_6NiO_{10}\cdot 3H_2O$ (920.135): calcd. C 44.38, H 3.72, N 9.13; found C 44.44, H 3.53, N 9.04.

[Fe(L^1)$_2$](ClO$_4$)$_2$: UV/Vis (MLCT band; CH_3CN): λ_{max} (ε, M^{-1} cm^{-1}) = 448 nm (1610). FAB$^+$ MS: *m*/*z* = 951 [Fe(L^1)$_2$](ClO$_4$)$^+$. FT IR: ν(CO) = 1600, 1624, 1714 cm^{-1}. ^{1}H NMR (300 MHz, CD_3CN, 10 mM, 295 K): δ = 83.0 (2 H, *H*-*o*-bipy), 67.9, 56.4, 56.4 and 49.6 (2 H each, *H*-*m*-bipy), 13.8 (2 H, *H*-*p*-bipy), 7 to 0 (22 H, *H*-Cp, CH_2-bipy and *H*-*p*-bipy), −9.4 (4 H, CH_2-bipy). $C_{44}H_{36}Cl_2Fe_3N_4O_{12}\cdot 2H_2O$ (1087.275): calcd. C 48.61, H 3.71, N 5.15; found C 48.75, H 3.61, N 5.27.

[FeL^2](ClO$_4$)$_2$: UV/Vis (MLCT band; CH_3CN): λ_{max} (ε, M^{-1} cm^{-1}) = 450 nm (1100). FAB$^+$ MS: *m*/*z* = 765 [FeL^2](ClO$_4$)$^+$. FT IR: ν(CO) = 1661 cm^{-1}. ^{1}H NMR (300 MHz, CD_3CN, 10 mM, 295 K): δ = 80.5 (2 H, *H*-*o*-bipy), 62.0, 61.4, 56.6 and 17.8 (2 H each, *H*-*m*-bipy), 7.1 (2 H, *H*-*p*-bipy), 6.4 and 0.8 (4 H resp., *H*-Cp), −1.9 (2 H, *H*-*p*-bipy), −8.7 (4 H, CH_2-bipy). $C_{34}H_{26}Cl_2Fe_2N_4O_{12}\cdot H_2O$ (883.221): calcd. C 46.24, H 3.20, N 6.34; found C 45.97, H 3.10, N 6.37.

[HgL^2](CF$_3$SO$_3$)$_2$: UV/Vis (MLCT band; CH_3CN): λ_{max} (ε, M^{-1} cm^{-1}) = 432 nm (1720). FAB$^+$ MS: *m*/*z* = 961 [HgL^2](CF$_3$SO$_3$)$^+$. FT IR: ν(CO) = 1712 cm^{-1}. $C_{36}H_{26}F_6FeHgN_4O_{10}S_2$ (1109.177): calcd. C 38.98, H 2.36, N 5.05; found C 38.04, H 2.43, N 4.96.

[HgL^4](CF$_3$SO$_3$)$_2$: UV/Vis (MLCT band; CH_3CN): λ_{max} (ε, M^{-1} cm^{-1}) = 446 nm (450). FAB$^+$ MS: *m*/*z* = 959 [HgL^4](CF$_3$SO$_3$)$^+$. FT IR: ν(CO) = 1596, 1627 cm^{-1}. $C_{36}H_{28}F_6FeHgN_6O_8S_2\cdot 2H_2O$ (1143.238): calcd. C 37.82, H 2.82, N 7.35; found C 37.85, H 2.59, N 7.14.

Reagents, Instrumentation and Procedure: Acetonitrile (Rathburn, HPLC grade) was used as received. Dichloromethane was dried with neutral alumina (activity I) for at least 6 d before use. Tetra-*n*-butylammonium perchlorate (TBAP) was purchased from Fluka and dried under vacuum for 3 d at 80 °C. Electrochemical experiments were conducted in a conventional three-electrode cell under argon at 20 °C. The reference electrode was Ag/AgNO$_3$ (10 mM in CH_3CN containing 0.1 M TBAP). FAB (positive mode) mass spectra were recorded with an AEI Kratos MS 50 spectrometer fitted with an Ion Tech Ltd gun and using *m*-nitrobenzyl alcohol as matrix. ES-MS measurements were performed on a triple quadrupole mass spectrometer Quattro II (Micromass, Altrincham, UK). The ES source was heated to 80 °C. The sampling cone voltage (Vc) was 20 V to avoid any fragmentation processes. Sample solutions were introduced into the mass spectrometer source with a syringe pump (Harvard type 55 1111: Harvard Apparatus Inc., South Natick, MA, USA) with a flow rate of 4 μL min^{-1}. Calibration was performed using protonated horse myoglobin. Scanning was performed in the MCA (Multi Channel Analyser) mode, and several scans were summed to obtain the final spectrum. Elemental analyses were performed by the Service Central d'Analyses, CNRS, Lyon.

X-ray Structures: Crystals of the complexes between L^2 and M^{II} (where M^{II} is Cu^{II} or Ni^{II}) named {Cu^{II}L^2} and {Ni^{II}L^2}, respectively, were used for data collection with a STOE-IPDS diffractometer using Mo-K_α graphite-monochromated radiation (λ = 0.71073 Å). Intensity data were corrected for Lorentz and polarisation effects but not for absorption. Structure solution and refinement were performed with the SHELXTL package. A summary of the crystallographic data and structure refinement is given in Table 3. The two compounds {Cu^{II}L^2} and {Ni^{II}L^2} are isostructural. They crystallize in the *C*2/*c* space group with close cell parameters. Only the crystallization solvents are different. The crystallographically independent chemical formulae are [CuL^2]$_{1.5}$(ClO$_4$)$_3$ 0.5[(C_2H_5)$_2$O] 2.5(CH_3CN) and [NiL^2]$_{1.5}$(ClO$_4$)$_3$ [(C_2H_5)$_2$O] 1.5(CH_3CN) with a multiplicity of *Z* = 8; so there are 12 [ML^2]$^{2+}$ entities in the unit cell. All non-hydrogen atoms were refined with anisotropic thermal parameters, except for atoms of disordered solvents. Hydrogen atoms were generated in idealised positions (except for disordered solvents), riding on the carrier atoms with isotropic thermal parameters. CCDC-174044 {Cu^{II}L^2} and -174045 {Ni^{II}L^2} contain the supplementary crystallographic data for this paper. These data can be obtained free of charge at www.ccdc.cam.ac.uk/conts/retrieving.html or from the Cambridge Crystallographic Data Centre, 12, Union Road, Cambridge CB2 1EZ, UK [Fax: (internat.) + 44-1223/336-033; E-mail: deposit@ccdc.cam.ac.uk].

Acknowledgments

We warmly thank Drs. Hélène Nierengarten and Alain van Dorrselaer from the Laboratoire de Spectrométrie de Masse Bioorganique, at the ECPM in Strasbourg for their expertise in the ES-MS measurements.

[1] M. Buda, J.-C. Moutet, E. Saint-Aman, A. De Cian, J. Fischer, R. Ziessel, *Inorg. Chem.* **1998**, *37*, 4146.
[2] A. Ion, J.-C. Moutet, E. Saint-Aman, G. Royal, S. Tingry, J. Pecaut, S. Menage, R. Ziessel, *Inorg. Chem.* **2001**, *40*, 3632.
[3] M. Buda, J.-C. Moutet, A. Pailleret, E. Saint-Aman, R. Ziessel, *J. Electroanal. Chem.* **2000**, *484*, 164.
[4] M. Buda, A. Ion, J.-C. Moutet, E. Saint-Aman, R. Ziessel, *J. Electroanal. Chem.* **1999**, *469*, 132.
[5] J. C. Medina, T. T. Goodnow, M. T. Rojas, J. L. Atwood, A. E. Kaifer, G. K. Gokel, *J. Am. Chem. Soc.* **1992**, *114*, 10583.
[6] S. R. Miller, D. A. Gutowski, Z. H. Chen, G. K. Gokel, L. Echegoyen, A. E. Kaifer, *Anal. Chem.* **1988**, *60*, 2021.
[7] I. Ion, J.-C. Moutet, A. Popescu, L. Tomazeswki, I. Gauthier-Luneau, *J. Electroanal. Chem.* **1997**, *440*, 145.
[8] H. Scholl, K. Sochaj, *Electrochim. Acta* **1991**, *36*, 689.
[9] C. Dietrich-Bucheker, J.-P. Sauvage, J.-M. Kern, *J. Am. Chem. Soc.* **1989**, *111*, 7791 and refs. therein.
[10] B. J. Henne, D. E. Bartak, *Inorg. Chem.* **1994**, *23*, 369.
[11] M.-N. Collomb, A. Deronzier, C. Duboc Toia, M. Fontecave, K. Gorgy, J.-C. Leprêtre, S. Ménage, *J. Electroanal. Chem.* **1999**, *469*, 53.
[12] R. Ziessel, J.-M. Lehn, *Helv. Chim. Acta* **1990**, *73*, 1149.

Receiced November 21, 2001
[I01468]

Easily Accessible Chiral *P,N*-Bidentate Aryl Phosphites, Their Complexation and Application in Enantioselective Allylic Alkylation, Sulfonylation and Hydrosilylation

Konstantin N. Gavrilov,[a] Oleg G. Bondarev,[b] Roman V. Lebedev,[b] Alexei A. Shiryaev,[a] Sergey E. Lyubimov,[a] Alexei I. Polosukhin,[b] Gennady V. Grintselev-Knyazev,[b] Konstantin A. Lyssenko,[b] Sergey K. Moiseev,[b] Nikolay S. Ikonnikov,[b] Valery N. Kalinin,[b] Vladim A. Davankov,[b] Andrei V. Korostylev,*[c] and Hans-Joachim Gais[d]

Keywords: Aryl phosphites / N,P ligands / Palladium / Allylation / Rhodium / Hydrosilylation

New chiral *P,N*-hybrid aryl phosphites have been obtained by one-step phosphorylation of amino and imino alcohols. Complexation of the new ligands with $[Rh(CO)_2Cl]_2$, $[Pd(COD)Cl_2]$ and $[Pd(allyl)Cl]_2$ was found to give chelate complexes $[Rh(CO)Cl(\eta^2\text{-}P^{\frown}N)]$, $[PdCl_2(\eta^2\text{-}P^{\frown}N)]$ and $[Pd(allyl)(\eta^2\text{-}P^{\frown}N)]^+Cl^-$, respectively. With these new *P,N*-ligands, up to 82% *ee* enantioselectivity was achieved in the Pd-catalysed alkylation of ethyl 3-penten-2-yl carbonate with dimethyl malonate, up to 80% *ee* in the Pd-catalysed sulfonylation of methyl 3-penten-2-yl carbonate with sodium *p*-toluenesulfinate, and up to 50% *ee* in the Rh-catalysed hydrosilylation of acetophenone with diphenylsilane.
(© Wiley-VCH Verlag GmbH, 69451 Weinheim, Germany, 2002)

Introduction

Chiral *P,N*-bidentate compounds are one of the leading ligand groups in modern asymmetric catalysis.[1−3] Most such systems are phosphanes in nature, but phosphite-type *P,N*-hybrid ligands are acquiring progressively growing importance because of their synthetic availability, high π-acidity of the phosphorus atom and high resistance to oxidative destruction. In general, the presence of oxygen and/or nitrogen atoms in the first coordination sphere of the phosphorus atom offers the potential to tune the chemical stability of ligands, their donor/acceptor properties and steric demands. This has made it possible to achieve impressive results in catalytic enantioselective allylation, conjugate addition of organometallic compounds to enones, hydrosilylation and hydrogenation reactions.[1−9] Interestingly, each of the ligands mentioned has a phosphacyclic structure, normally constructed with the aid of effective chiral inductors such as BINOL, TADDOL, (1*R*,2*R*)-1,2-*N*,*N*′-bis(*p*-toluenesulfonylamino)-1,2-diphenylethane, (*S*)-2-(anilinomethyl)pyrrolidine etc.[1−9] Only one example[10] of the use of an achiral biphenol is known; the phosphitooxazoline derived from it is a phosphacyclic compound as well. We have recently reported syntheses of several chiral *P,N*-phosphites with acyclic phosphorus donor centres.[11,12]

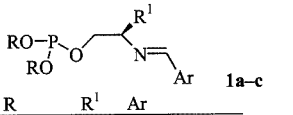

1a–c

R	R^1	Ar	
*i*Pr	Et	Ph	**(1a)**
Bornyl	Et	Ph	**(1b)**
*i*Pr	*i*Pr	4-$Me_2NC_6H_4$	**(1c)**

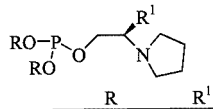

1d–f

R	R^1	
*i*Pr	Et	**(1d)**
*i*Pr	*i*Pr	**(1e)**
2,6-Me_2Ph	Et	**(1f)**

These gave up to 57% *ee* in the Pd-catalysed alkylation of 1,3-diphenylpropen-2-yl acetate with dimethyl malonate, and up to 61% *ee* when 3-phenylpropen-2-yl acetate was used as a substrate. In this article, we describe the synthesis, complexation with Rh^I and Pd^{II} precursors and catalytic applications of a new series of *P,N*-bidentate aryl phosphites bearing distant amino or imino groups.

[a] Department of Chemistry, Ryazan State Pedagogic University, 46 Svoboda Str., Ryazan 390000, Russia
[b] Institute of Organoelement Compounds, Russian Academy of Sciences, 28 Vavilova Str., Moscow 117813, Russia
[c] Institut für Organische Katalyseforschung an der Universität Rostock e.V., Buchbinderstraße 5−6, 18055 Rostock, Germany
[d] Institut für Organische Chemie der Rheinisch-Westfälischen Technischen Hochschule Aachen, Professor-Pirlet-Straße 1, 52056 Aachen, Germany
Supporting information for this article is available on the WWW under http://www.eurjic.com or from the author.

Results and Discussion

The new *P,N*-bidentate aryl phosphites were synthesized by one-step phosphorylation of the corresponding amino and imino alcohols with bis(2,6-dimethylphenyl) chlorophosphite.

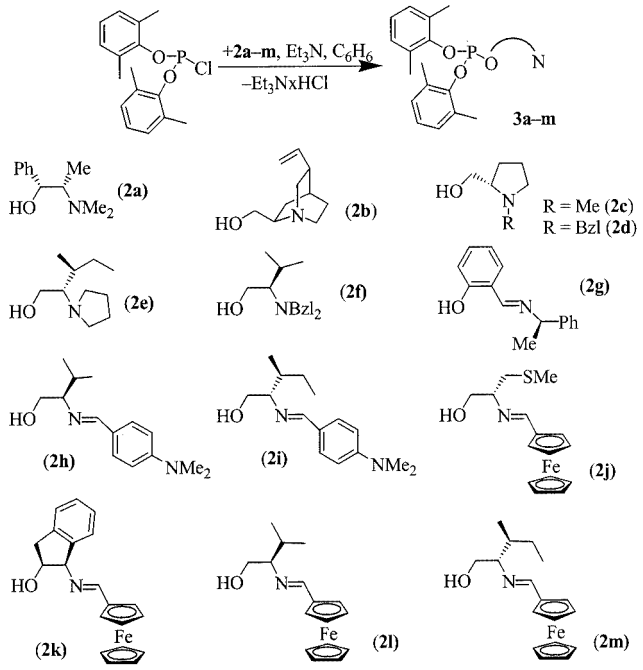

They divide into two groups: ligands **3a**−**3f**, possessing sp^3-hybridized nitrogen atoms, and ligands **3g**−**3m**, which have sp^2-hybridized nitrogen atoms. All the compounds **3a**−**m** are soluble in conventional organic solvents and stable under dry conditions for several months. On treatment with $[Rh(CO)_2Cl]_2$, their neutral carbonyl(chloro)Rh^I complexes were obtained.

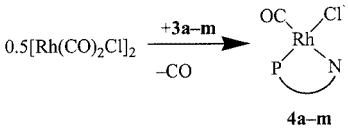

The ν(CO) and $^1J_{P,Rh}$ parameters in their IR and ^{31}P NMR spectra act as sensitive indicators, which characterise the mode of complexation of the *P,N*-ligands and allow the π-acceptor ability of the phosphorus centre and the degree of electronic non-symmetry of the ligands to be estimated.[13−15]

In general, ligands **3a**−**3m** give chelate complexes. Thus, the $^1J_{P,Rh}$, $^1J_{C,Rh}$, $^2J_{C,P}$, ν(CO) and ν(Rh−Cl) data for complexes **4a**−**4m** (Tables 1 and 2) are in good agreement with the suggested structures.[13,15] Significant (9−11 ppm) coordination shifts $\Delta\delta_C$ [= δ_C(complex) − δ_C(ligand)] for the azomethine carbon atoms in complexes **4i** and **4l** (Table 2) also attest to the coordination of distant imino groups with the rhodium atom. However, complexation of some ligands displays special features. Thus, compounds **4e**−**4g**, **4j** and **4k** exist as two or more conformers (Table 1) similarly to known cationic rhodium, iridium[16] and palladium[17] *P,N*-chelates. In addition, the reactions between $[Rh(CO)_2Cl]_2$ and the compounds bearing cyclic (**3b**−**3e**) or sterically hindered acyclic (**3f**) sp^3-nitrogen donor centres produced some quantities of *trans*-$[Rh(CO)Cl(\eta^1\text{-}P^{\frown}N)_2]$ complexes, in which the compounds function as *P*-monodentate ligands. This was shown by their characteristic[13,18] IR and ^{31}P NMR spectroscopic data (the percentage of *trans* complexes determined by ^{31}P NMR is given in parentheses) for **3b**: δ_P = 122.8, $^1J_{P,Rh}$ = 204.9 Hz (8%); for **3c**: δ_P = 121.4, $^1J_{P,Rh}$ = 207.6 Hz, ν(CO) = 1995 cm^{-1} (20%); for **3d**: δ_P = 122.1, $^1J_{P,Rh}$ = 203.5 Hz, ν(CO) = 2000 cm^{-1} (45%); for **3e**: δ_P = 124.6, $^1J_{P,Rh}$ = 205.6 Hz, ν(CO) = 1994 cm^{-1} (30%); for **3f**: δ_P = 122.6, $^1J_{P,Rh}$ = 195.4 Hz, ν(CO) = 1993 cm^{-1} (54%). It was notable that, the higher the steric demands of the aza centre, the larger the amount of $[Rh(CO)Cl(\eta^1\text{-}P^{\frown}N)_2]$ complex. The reason for this seems to be an increase in steric hindrance for coordination of nitrogen atoms and, as a result, a fall in the proportion of chelate $[Rh(CO)Cl(\eta^2\text{-}P^{\frown}N)]$ products. To overcome this effect, the synthesis of complex **4f** was performed in a different way, by the exchange reaction previously developed for *P*-monodentate ligands.[19]

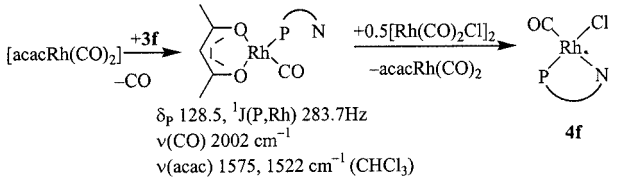

Imino phosphites **3g**−**3m**, independently of their steric demands, gave chelate products **4g**−**4m** only. They are therefore more typical chelate ligands than amino phosphites.

All the ligands **3a**−**3m** had highly π-acidic phosphorus centres. This was proved by the values of the ν(CO) and $^1J_{P,Rh}$ parameters for complexes **4a**−**4m**, which are significantly larger than those for the analogous amino phosphane based complexes (by 30−35 cm^{-1} and 80−100 Hz, respectively) and even their aminoalkyl phosphite counterparts (by 6−10 cm^{-1} and 10−15 Hz).[13−15] It is well known that increasing *P*-centre π-acidity in *P,N*-bidentate ligands favours high chemical and optical yields in such catalytic reactions as allylation, hydroboration/oxidation and hydrosilylation/oxidation of alkenes, and hydrosilylation of ketones.[1,2]

On the other hand, increasing σ-donor character in the *N*-centre results in higher optical yields in hydroboration/oxidation and hydrosilylation/oxidation of alkenes.[20,21] In this context, a concept of electronically non-symmetric ligands has been suggested (the higher the π-acceptor ability of the *P*-centre and the σ-donor ability of the *N*-centre, the more electronically non-symmetrical the compound).[14] This parameter can be estimated by the value of ν(CO) in the IR spectrum of the carbonyl(chloro) complex $[Rh(CO)Cl(P^{\frown}N)]$. In particular, for structurally similar complexes with identical phosphorus centres and different nitrogen centres, a compound with a lower value of ν(CO)

Table 1. IR and ^{31}P NMR spectroscopic data for complexes **4a−m** (in $CHCl_3$)

Compound	IR		^{31}P NMR	
	ν(CO) [cm^{-1}]	ν(Rh−Cl) [cm^{-1}]	δ_P	$^1J_{P,Rh}$ [Hz][a]
4a	2031	295	119.4	288.6
4b	2032	290	125.6	287.5
4c	2028	288	122.6	285.9
4d	2028	289	118.7	287.4
4e	2029	291	121.4, 122.6	290.0 (80%), 287.5 (20%)
4f	2024	280	120.1, 118.5	288.6 (70%), 288.1 (30%)
4g	2034	290	133.6, 129.7, 110.9	287.4 (83%), 273.2 (10%), 300.0 (7%)
4h	2024	288	125.8	273.4
4i	2024	287	125.3	275.5
4j	2028	287	122.8, 122.5	276.4 (85%), 278.0 (15%)
4k	2024	286	123.3, 116.4	278.4 (73%), 274.7 (27%)
4l	2026	290	121.8	279.8
4m	2025	291	121.9	279.4

[a] Percentage of each diastereomer of the complex

Table 2. ^{13}C NMR spectroscopic data for compounds **3i**, **4i**, **5i** and **3l**, **4l**, **5l** (in $CDCl_3$), δ_C ($J_{C,P}$ [Hz])

Compound	HC=	C_{Ar}	NCH	OCH_2	$N(CH_3)_2$	CH	CH_2	CH_3(Ar)	CH_3
3i	160.9	110.7−148.9	75.8	64.1	39.9	36.6	25.1	17.42, 17.46, 17.52, 17.58	11.0, 15.7
4i[a]	170.1	109.9−153.0	75.2	68.5	39.5	37.8	25.1	17.8, 18.2	10.2, 13.6
5i	170.8	110.4−153.6	73.7	69.2 (^2J = 2.6)	39.6	37.2	25.0	17.7, 18.1	10.2, 13.4

	HC=	C_{Ar}	NCH	Fc (*ipso*)	Fc	Fc (Cp)	OCH_2	CH	CH_3	CH_3(Ar)
3l	161.2	123.8−149.0	77.5 (^3J = 3.1)	80.6	68.3, 68.5, 69.97, 70.03	68.8	63.9	29.7	18.9, 19.9	17.59, 17.64
4l[b]	171.7	124.4−149.2	77.0	75.4	71.7, 71.8, 73.0, 75.6	69.8	67.5 (^2J = 5.0)	30.8	18.5, 20.8	18.1, 18.4
5l	173.7	125.0−148.4	76.2	74.0	70.7, 72.8, 73.9, 74.5	69.9	67.7 (^2J = 4.3)	30.0	17.6, 20.1	17.49, 17.53

[a] The resonance of the carbonyl-type carbon atom: δ_C = 187.62 ($^1J_{C,Rh}$ = 71.1, $^2J_{C,P}$ = 17.3 Hz). [b] The resonance of the carbonyl-type carbon atom: δ_C = 187.42 ($^1J_{C,Rh}$ = 71.4, $^2J_{C,P}$ = 18.1 Hz).

possesses a more active σ-donor nitrogen-containing centre and hence is more electronically non-symmetric.[14,15] From this point of view, imino phosphites are the most electronically non-symmetric ligands among compounds **3a−3m** (Table 1). The exceptions are amino phosphite **4f**, bearing an dibenzylamino group, and the imino phosphites **3g** and **3j**. However, compound **3g** has a slightly different phosphorus centre and is actually a triaryl phosphite (unlike the other ligands), while ligand **3j** has an additional sulfur atom in its structure. Analogously to complexation with Rh^I, the new *P,N*-hybrid aryl phosphites form metal chelates with Pd^{II}.

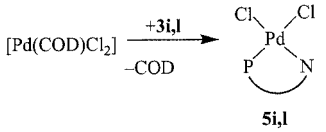

5i,l

The IR and NMR spectroscopic data for the obtained complexes, shown in Tables 2 and 3, strongly supported the suggested mode of coordination. In particular, the δ_P values for complexes **5i** and **5l** (Table 3) are typical for six-membered palladacycles based on *P,N*-bidentate phosphites with acyclic phosphorus centres.[11,22] Large coordination shifts $\Delta\delta_C$, similar to those seen in the rhodium complexes **4i** and **4l**, were observed for the azomethine carbon atoms in complexes **5i** and **5l** (Table 2). Two equally intense ν(Pd−Cl) bands in the far IR regions of **5i** and **5l** (Table 3) resulted from the *cis* configuration of chloro ligands and different *trans* influences of phosphorus and nitrogen atoms.

Table 3. IR and ^{31}P NMR spectroscopic data for palladium complexes **5i**, **5l** and **6**

Compound	ν(Pd−Cl) (nujol, CsI) [cm^{-1}]	δ_P ($CDCl_3$)
5i	342, 288	77.2
5l	336, 292	74.1
6	−	132.7

In order to investigate details of the complex geometry, complexes **4i**, **5i** and **5l** were studied by single-crystal X-ray diffraction (see Figures 1, 2 and 3, Table 4). Comparison of the crystal packings of **4i** and **5i** revealed that the two compounds were isostructural. The principal geometry of the complexes is therefore only very slightly dependent on the nature of the metal centre and the terminal ligands. In all the complexes, the metal atoms are characterized by square-planar coordination with slightly different degrees of planarity. The maximum deviations from the mean plane are 0.15, 0.12 and 0.08 Å for **4i**, **5i** and **5l**, respectively.

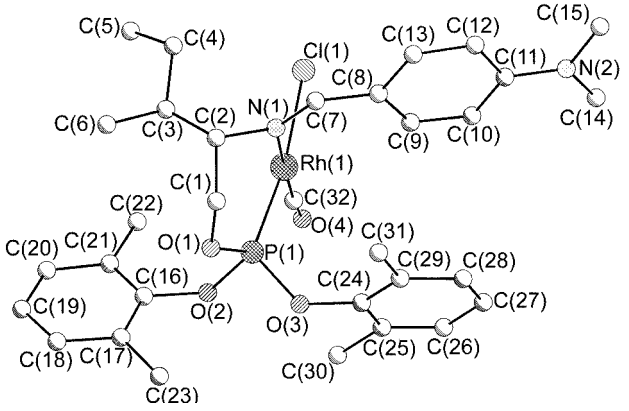

Figure 1. General view of complex **4i** and numbering scheme

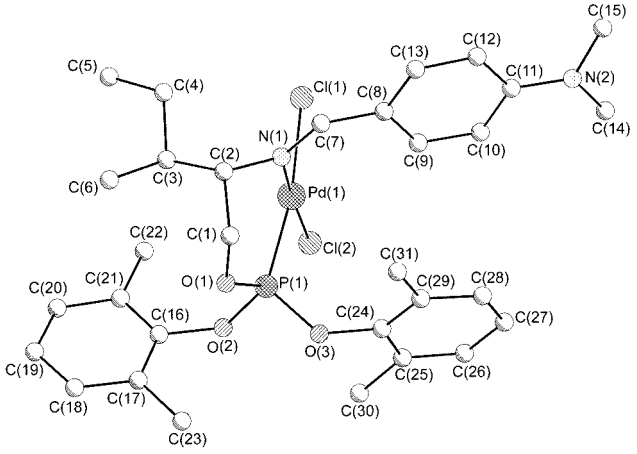

Figure 2. General view of complex **5i** and numbering scheme

The conformations of the six-membered metallacycles in the investigated compounds are far from regular, and can be described as distorted chairs in **4i** and **5i** and a distorted boat in **5l**. The difference in the conformation type seems to result from steric overcrowding due to introduction of the ferrocenyl moiety. In addition, the presence of the ferrocenyl substituent gives rise to significant changes in the mutual orientation of the 2,6-dimethylphenyl rings, with one of them approximately parallel to the Cp ring. Such an orientation of the C(8)−C(12) and C(26)−C(31) rings produces a decrease in the interplane separation to 3.32 Å, and could be regarded as an intramolecular stacking interaction. Despite this possible intramolecular stacking interaction, however, the geometry of the ferrocene moiety is actually unaffected. The ferrocene is characterized by the eclipsed conformation, with practically equal Fe(1)−centroid distances, 1.657 and 1.646 Å for the C(8)−C(12) and the C(13)−C(17) rings. In addition to the neutral dichloropalladium complexes, cationic complex **6** was obtained with ligand **3m**.

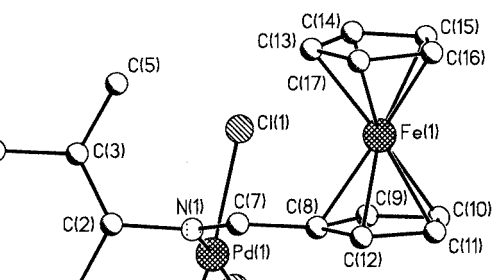

Figure 3. General view of complex **5l** and numbering scheme

Table 4. Selected bond lengths [Å] and angles [°] for **4i**, **5i** and **5l**

	4i	**5i**	**5l**
M(1)−C(32)	1.804(10)	−	−
M(1)−N(1)	2.111(7)	2.063(3)	2.027(4)
M(1)−P(1)	2.171(2)	2.1983(10)	2.2030(17)
M(1)−Cl(1)	2.3792(19)	2.3656(9)	2.3572(16)
M(1)−Cl(2)	−	2.2928(9)	2.2919(16)
P(1)−O(1)	1.580(5)	1.571(2)	1.579(4)
P(1)−O(2)	1.619(5)	1.588(2)	1.594(3)
P(1)−O(3)	1.605(4)	1.590(3)	1.576(4)
N(1)−C(7)	1.266(8)	1.282(4)	1.281(6)
C(7)−C(8)	1.426(9)	1.442(5)	1.440(7)
C(32)−M(1)−P(1)	91.3(2)	−	−
Cl(1)−M(1)−Cl(2)	−	91.15(3)	90.81(6)
N(1)−M(1)−P(1)	89.27(14)	90.60(7)	84.84(13)
N(1)−M(1)−Cl(1)	90.12(14)	90.79(7)	91.91(13)
P(1)−Pd(1)−Cl(2)	−	88.17(3)	92.49(6)
O(1)−P(1)−M(1)	116.2(2)	113.79(10)	107.35(15)
O(2)−P(1)−M(1)	117.71(17)	116.41(10)	114.59(15)
O(3)−P(1)−M(1)	120.02(16)	118.85(10)	124.67(15)
C(2)−N(1)−M(1)	115.3(5)	116.1(2)	114.7(3)
C(7)−N(1)−C(2)	115.4(7)	117.2(3)	116.0(4)
C(7)−N(1)−M(1)	129.0(4)	126.6(2)	129.0(4)

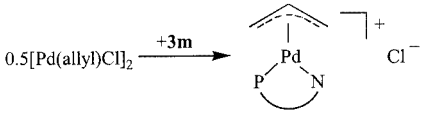

6

The ^{31}P and ^{13}C NMR spectra of complex **6** (see Exp. Sect. and Table 3) contained only one set of resonances, ex-

plicable either by the presence of only one of the possible *exo* and *endo* isomers or by their fast interconversion (see ref.[2], refs. cited therein and refs.[23,24]). It is noteworthy that the E_b(Cl2P) value of 198.4 eV in the XPS spectrum of compound **6** is close to the highest limit for chlorine anions.[25] Furthermore, the PD mass spectrum of complex **6** shows a rarely observable molecular ion peak (usually only the $[M - Cl]^+$ peak is observed). These facts allowed us to conclude that complex **6** exists as a contact ion pair.[26]

Some of the new *P,N*-(aryl phosphites) were tested in the palladium-catalysed allylic alkylation of ethyl 3-penten-2-yl carbonate with dimethyl malonate (Scheme 1, R = Et). The results are shown in Table 5. They allow the following conclusions to be made:

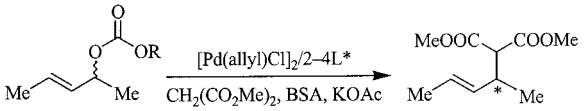

Scheme 1

Table 5. Enantioselective allylic alkylation of 3-penten-2-yl carbonate with dimethyl malonate according to Scheme 1 (L*/Pd = 2); DCM = dichloromethane

Entry	L*	Solvent	*T* [°C]	Yield (%)[a]	*ee* (%)[b]
1	**3b**	THF	room temp.	90	11 (*S*)
2	**3d**	THF	room temp.	35	2 (*R*)
3	**3f**	THF	room temp.	30	4 (*S*)
4	**3h**	THF	room temp.	60	24 (*S*)
5	**3i**	THF	room temp.	50	58 (*S*)
6	**3i**	DCM	room temp.	85	57 (*R*)
7	**3j**	DCM	room temp.	90	13 (*R*)
8	**3k**	THF	room temp.	65	52 (*S*)
9	**3l**	THF	room temp.	75	38 (*S*)
10	**3l**	THF	−18	40	21 (*S*)
11	**3m**	THF	65	65	49 (*R*)
12	**3m**	THF	room temp.	65	69 (*R*)
13	**3m**	THF	5	70	77 (*R*)
14	**3m**	THF	−18	25	52 (*R*)
15	**3m**	CH_3CN	room temp.	55	54 (*R*)
16	**3m**	DMF	room temp.	70	45 (*R*)
17	**3m**	$(CH_2OMe)_2$	room temp.	60	53 (*R*)
18	**3m**	toluene	room temp.	60	61 (*R*)
19	**3m**	DCM	room temp.	80	80 (*R*)
20	**3m**	DCM	5	75	81 (*R*)
21	**3m**	DCM	−18	30	76 (*R*)
22	**3m**[c]	DCM	room temp.	80	82 (*R*)

[a] Yield of analytically pure product after column chromatography. [b] The *ee* values were determined by chiral GC (fused silica capillary column DP-TFA-γ-CD, 90 °C, He, 1.8 bar). [c] L*/Pd = 1.

1. Systems with sp^3-hybridized nitrogen atoms were not effective (*ee* < 11%, Entries 1−3).

2. Among the imino phosphites, ligands **3i**, **3k** and **3m** (Entries 5, 8, 22) were the most effective (up to 82% *ee*).

3. Optical yields greatly depended on the substituent at the chiral centre, as clearly demonstrated by the homologous ligands **3h** (24% *ee*) and **3i** (58% *ee*), as well as **3l** (38% *ee*) and **3m** (82% *ee*).

4. Optical yields depended significantly on the solvent used and the temperature. Notably, for ligand **3m** the latter correlation was nonlinear in character (Entries 11−14).

5. The L*/Pd ratio did not influence the effectiveness of a catalytic system much (compare Entries 19 and 22).

What should be discussed separately are significant increases in *ee* values on going from ligand **3h** to **3e** (by 14%, Entries 4 and 9) and, especially, from **3i** to **3m** (by 23%, Entries 6 and 19). Since the ν(CO) and $^1J_{P,Rh}$ values for their rhodium complexes [Rh(CO)Cl(η^2-P$^\frown$N)] are practically identical (Table 1), the electronic characteristics of the ligands (including the degree of electronic non-symmetry) are very much the same. Therefore, the effect is steric in nature, and the steric parameters of the ligands are indeed responsible for the difference in the optical yields in the catalytic reaction. Ligands **3i** and **3l** have similar structures and only the −N=CHR fragments are different. To estimate the bulkiness of the substituents, the cone angles θ_R for the *p*-$C_6H_4NMe_2$ and Cp_2Fe fragments were calculated by constructing appropriate computer models and from the X-ray data. The calculated cone angle for the Cp_2Fe fragment [θ_R = 159° (AM1), 157° (X-ray, complex **5l**)] is significantly larger than the angle for the *p*-$C_6H_4NMe_2$ fragment [θ_R = 133° (AM1), 129° (X-ray, complex **5i**)]. Hence, bulky substituents attached to the imine group of the *P,N*-(imino phosphite) ligands are likely to afford higher optical yields in the catalytic reaction.

The catalytic effectiveness shown by the catalytic system with ligand **3m** was comparatively high, since 1,3-dimethyl-substituted allylic substrates belong to a group termed "unmanageable".[27] There are only two known *P,N*-ligands that also give more than 80% enantioselectivity, one of the new generation phosphanyloxazolines (70−90% *ee*)[28] and a 2-(phosphanylaryl)pyridine-derived ligand (Scheme 1, R = Me, *i*Pr, Ph, 78−93% *ee*).[27] It should be noted that the mentioned high enantioselectivities were achieved by thorough optimization of the reaction conditions at a low temperature (−25 to −40 °C) and sometimes by addition of crown ethers.[27,28]

Some of the new *P,N*-bidentate aryl phosphites were tested in the Pd-catalysed allylic substitution of methyl 3-penten-2-yl carbonate with $NaSO_2p$Tol (Scheme 2). The obtained results are shown in Table 6. It is easy to see that main tendencies in this catalytic process were similar to those in the reaction with the malonate nucleophile discussed above. In particular, the highest enantioselectivities were demonstrated by the ligands with distant imino groups. It is important to note that the optical yield produced by imino phosphite **3m** (80% *ee*) was the best so far achieved in the reaction using *P,N*-ligands. Helmchen's phosphanyloxazolines, the most effective previously described *P,N*-ligands,

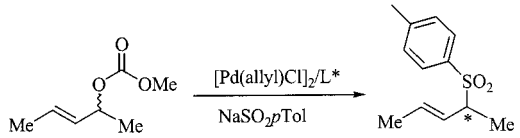

Scheme 2

gave up to 59% *ee*.[29] Moreover, unlike phosphanyloxazolines, our ligands did not give rise to the formation of a sulfinic acid ester as a side product. To the best of our knowledge, the only ligand giving higher results in this reaction [99% *ee*, with $Pd_2(dba)_3$ as a precatalyst] is one of Trost's *P*,*P*-bidentate ligands,[30] which form 13-membered chelate palladium complexes.[31]

Table 6. Enantioselective allylic sulfonylation of 3-penten-2-yl carbonate with $NaSO_2p$Tol according to Scheme 2

Entry	L*	L*/Pd	Solvent	*T* [°C]	Yield (%)[a]	*ee* (%)[b]
1	**3b**	2:1	THF	room temp.	47	12 (*S*)
2	**3c**	2:1	THF	room temp.	22	10 (*S*)
3	**3i**	2:1	THF	room temp.	63	44 (*R*)
4	**3i**	2:1[c]	THF	room temp.	53	46 (*R*)
5	**3i**	2:1	THF	0	48	56 (*R*)
6	**3i**	1:1	THF	room temp.	65	50 (*R*)
7	**3i**	1:1	DCM	room temp.	59	50 (*R*)
8	**3k**	2:1	THF	room temp.	69	45 (*S*)
9	**3k**	2:1	THF	0	42	54 (*S*)
10	**3k**	1:1	THF	−20	20	50 (*S*)
11	**3m**	2:1	THF	room temp.	74	63 (*R*)
12	**3m**	2:1	THF	0	51	78 (*R*)
13	**3m**	2:1[c]	THF	0	38	76 (*R*)
14	**3m**	1:1	DCM	room temp.	45	76 (*R*)
15	**3m**	1:1	DCM	0	21	80 (*R*)

[a] Yield of analytically pure product after column chromatography. [b] The *ee* values were determined by chiral GC (Lipodex-γ: 2,3-di-*O*-pentyl-6-*O*-methyl-γ-cyclodextrin (25m × 0.8 mm) column). [c] $Pd_2(dba)_3 \times CHCl_3$.

Ligands **3a**−**m** were also tested in the Rh-catalysed asymmetric hydrosilylation of acetophenone with diphenylsilane (Scheme 3). However, the achieved optical yields were rather low, with amino phosphites (up to 28% *ee*) once again being less effective than imino phosphites **3i** (45% *ee*) and **3m** (50% *ee*).

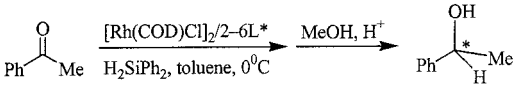

Scheme 3

Experimental Section

General Comments: All reactions were performed under argon in dehydrated solvents. IR spectra were recorded with a Specord M80 or Nicolet 750 instrument. ^{31}P, ^{13}C and ^{1}H NMR spectra were recorded with a Bruker AMX 400 instrument (162.0 MHz for ^{31}P, 100.6 MHz for ^{13}C and 400.13 MHz for ^{1}H). Complete assignment of all the resonances in ^{13}C NMR spectra was achieved by use of DEPT techniques. Chemical shifts (ppm) are given relative to Me_4Si (^{1}H and ^{13}C NMR) and 85% H_3PO_4 (^{31}P NMR). Mass spectra were recorded with a Kratos MS890 spectrometer (EI), an MSVKh TOF spectrometer with ionization by Cf-252 fission fragments (plasma desorption technique, PD), and a Micromass Platform 1 mass spectrometer through an "Openlynx" system (APCI technique). Electrospray (ES) ionisation mass spectra were measured with a Micromass BioQ II-ZS mass spectrometer. Organometallic compound solutions at 5−10 pmol/μL in THF or acetonitrile were infused by syringe pump (Harvard Apparatus Model 11) at 5 μL/min. Spectra were recorded over a mass range of 200−1200 Da and were calibrated relative to a mixed PEG standard. The X-ray photoelectron spectrum (XPS) was measured with a MAC-2 Riber spectrometer calibrated against Ag lines at 901.5 and 367.9 eV, correction for the sample charging was performed at C1s = 284.6 eV; the accuracy of the line maximum determination was ±0.1 eV. Cone angles θ_R of the substituents were determined from their conformations in the structures H-R obtained by computer calculations (AM1) and in the X-ray crystal structures of the corresponding complexes by the published approach.[32] Elemental analyses were performed at the Laboratory of Microanalysis (Institute of Organoelement Compounds, Moscow). Crystallographic data and refinement parameters for compounds **4i**, **5i** and **5l** are summarized in Table 7. The experimental data were collected at 110 K with a Bruker SMART 1000 CCD area detector by using graphite-monochromated Mo-K_α radiation (λ = 0.71072 Å, ω-scans with 0.3° steps in ω and 10 s per frame exposure). The absorption correction was applied semiempirically from equivalents. All the structures were solved by direct methods and refined by the full-matrix, least-squares technique against F^2 in the anisotropic (H atoms isotropic) approximation with the SHELXTL 5.1 package. Analysis of the Fourier density synthesis in **4i** showed that the isobutyl group [C(3)−C(6)] was disordered by two positions, which were included in the refinement with equal occupancies. The absolute configurations in **4i** and **5i** were determined by use of the Flack parameter. All hydrogen atoms with the exception of the disordered group were located from the Fourier synthesis and treated by a mixture of independent and constrained refinement. CCDC-173440 (**4i**), -173441 (**5i**) and -173442 (**5l**) contain the supplementary crystallographic data for this paper. These data can be obtained free of charge at www.ccdc.cam.ac.uk/conts/retrieving.html or from the Cambridge Crystallographic Data Centre, 12, Union Road, Cambridge CB2 1EZ, UK [Fax: (internat.) + 44-1223/336-033; E-mail: deposit@ccdc.cam.ac.uk]. $[Rh(CO)_2Cl]_2$,[33] $[Pd(COD)Cl_2]$,[34] $[Pd(allyl)Cl]_2$,[35] amino and imino alcohols **2d**,[36] **2f**,[37] **2g**,[38] **2h**,[11] **2l**[39] and bis(2,6-dimethylphenyl) chlorophosphite[12] were synthesized as published. The syntheses of compounds **2i**−**k** and **2m** were performed by techniques similar to that reported.[40] (*S*)-(+)-Isoleucinol, ferrocenecarboxaldehyde, 4-(dimethylamino)benzaldehyde and compounds **2a** and **2c** were purchased from Aldrich; (1*R*,2*S*)-(+)-*cis*-1-amino-2-indanol was purchased from Fluka. Amino and imino alcohols **2b** (quincoridine, Büchler GmbH), **2c**−**f**, **2h** and **2i** were azeotropically dried with benzene and distilled before use. Compounds **2a**, **2g** and **2j**−**2m** were dried under vacuum (2 Torr, 3 h) immediately before use.

Synthesis and Characterization

(2*S*,3*S*)-3-Methyl-2-(pyrrolidin-1-yl)pentan-1-ol (2e): A mixture of 1,4-dibromobutane (2.37 mL, 2×10^{-2} mol), (*S*)-(+)-isoleucinol (2.34 g, 2×10^{-2} mol) and K_2CO_3 (8.29 g, 6×10^{-2} mol) in acetonitrile (25 mL) was heated under reflux for 30 h. The mixture was then allowed to cool to room temp. and filtered, and the filter cake was washed with DCM (2×15 mL). The combined extracts were concentrated under vacuum (40 Torr) and the residue was distilled in high vacuum to give a yellow, paraffin-like product (2.297 g, 67% yield). B.p. 165−170 °C (0.8 Torr, kugelrohr distillation). ^{1}H NMR ($CDCl_3$): δ = 0.95 (t, ^{3}J = 7.4 Hz, 3 H, CH_2CH_3), 1.15 (d, ^{3}J = 6.8 Hz, 3 H, CH_3), 1.42 (m, 2 H, CH_2), 1.91 (m, 1 H, CH), 2.05 [m, 2 H, $(CH_2)_2$], 2.29[m, 2 H, $(CH_2)_2$], 3.00 (m, 1 H, CHN), 3.17 (m, 1 H, CH_2N), 3.22 (m, 1 H, CH_2N), 3.78 (m, 1 H, CH_2N), 3.94 (q, 1 H, CH_2N), 4.03 (m, 2 H, CH_2O), 4.27 (br. s, 1 H, OH). $C_{10}H_{21}NO$ (171.16): calcd. C 70.12, H 12.36, N 8.18; found C 69.86, H 12.12, N 7.98.

Table 7. Crystallographic data for **4i**, **5i** and **5l**

Compound	**4i**	**5i**	**5l**
Empirical formula	$C_{32}H_{41}ClN_2O_4PRh$	$C_{31}H_{41}Cl_2N_2O_3PPd$	$C_{32}H_{38}Cl_2FeNO_3PPd{\cdot}C_6H_6$
Formula mass	687.00	697.93	826.86
Crystal system, space group	orthorhombic, $P2_12_12_1$	orthorhombic, $P2_12_12_1$	orthorhombic, *Pbca*
a [Å]	12.883(8)	12.827(3)	13.826(6)
b [Å]	13.746(6)	14.333(3)	18.872(7)
c [Å]	18.178(11)	17.378(4)	27.296(9)
V [Å^3]	3219(3)	3194.9(11)	7122(5)
Z	4	4	8
D_x [Mg m^{-3}]	1.417	1.451	1.542
μ [cm^{-1}]	7.01	8.32	11.45
Crystal form, colour	prisms, yellow	prisms, yellow	needles, red
Crystal size [mm]	0.4×0.3×0.25	0.5×0.4×0.35	0.4×0.15×0.1
F(000)	1424	1440	3392
T_{min}, T_{max}	0.751, 0.839	0.653, 0.747	0.629, 0.892
θ_{max} [°]	29.00	29.06	27.00
Completeness to θ_{max}	98.1	100	99.0
No. of measured, independent and observed reflections	31319, 8280, 4952	20604, 8545, 7637	37362, 7719, 3187
R_{int}	0.0961	0.0366	0.0883
No. of parameters	417	389	430
Absolute structure parameter	0.00(4)	−0.03(2)	
wR_2 for all data	0.1321	0.0909	0.0788
R for observed data	0.0729	0.0405	0.0494
S	1.096	0.990	0.750
$\Delta\rho_{max}$, $\Delta\rho_{min}$ [e Å^{-3}]	1.191, −1.672	1.376, −1.198	0.686, −0.731

(2*S*,3*S*)-2-[4-(Dimethylamino)benzylideneamino]-3-methylpentan-1-ol (2i): (*S*)-(+)-Isoleucinol (1.17 g, 1×10^{-2} mol) was dissolved in 30 mL of dichloromethane. 4-(Dimethylamino)benzaldehyde (1.49 g, 1×10^{-2} mol), Na_2SO_4 (1 g) and 15 mL of dichloromethane were added to this solution with stirring, and the mixture was heated under reflux for 3 h. After the mixture had cooled to room temperature, the Na_2SO_4 was filtered off and washed with dichloromethane. The solvent was removed and the resulting residue was distilled under vacuum. Yellow viscous oil, 1.564 g (63% yield). n_D^{20} = 1.4411. B.p. 165−167 °C (0.8 Torr, kugelrohr distillation). ^{1}H NMR ($CDCl_3$): δ = 0.83 (t, ^3J = 7.6 Hz, 3 H, CH_2CH_3), 0.92 (d, ^3J = 6.8 Hz, 3 H, CH_3), 1.04 (m, 1 H, CH), 1.46 (m, 1 H, CH_2), 1.69 (m, 1 H, CH_2), 2.41 (br. s, 1 H, OH), 2.98 (m, 1 H, CHN), 3.00 [s, 6 H, $N(CH_3)_2$], 3.78 (m, 2 H, CH_2O), 6.67 (d, ^3J = 8.8 Hz, 2 H, H_{Ar}), 7.57 (d, ^3J = 8.8 Hz, 2 H, H_{Ar}), 8.08 (s, 1 H, CH=). ^{13}C NMR ($CDCl_3$): δ_C = 10.6 (s, CH_3), 15.2 (s, CH_3), 25.1 (s, CH_2), 36.2 (s, CH), 39.5 [s, $N(CH_3)_2$], 63.6 (s, CH_2O), 76.6 (s, CHN), 110.9−151.3 (s, C_{Ar}), 161.3 (s, CH=). $C_{15}H_{24}N_2O$ (248.19): calcd. C 72.54, H 9.74, N 11.28; found C 72.36, H 9.84, N 11.15.

(2*R*)-2-(Ferrocenylidineamino)-3-(methylthio)propan-1-ol (2j): This compound was synthesized analogously to **2i**, starting from (*R*)-2-amino-3-(methylthio)propan-1-ol (1.21 g, 1×10^{-2} mol) and ferrocenecarboxaldehyde (2.14 g, 1×10^{-2} mol). Orange-red solid, 2.636 g (83% yield). ^{1}H NMR(C_6D_6): δ = 1.87 (s, 3 H, CH_3), 2.62 (m, 2 H, CH_2S), 2.85 (s, 1 H, OH), 3.24 (m, 1 H, CHN), 3.69 (m, 2 H, CH_2O), 4.10 (m, 1 H, H_{Fc}), 4.12 (m, 1 H, H_{Fc}), 4.13 (s, 5 H, H_{Fc}), 4.46 (m, 1 H, H_{Fc}), 4.80 (m, 1 H, H_{Fc}), 8.02 (s, 1 H, CH=). $C_{15}H_{19}FeNOS$ (317.05): calcd. C 56.79, H 6.04, N 4.42; found C 56.50, H 3.87, N 4.13.

(1*R*,2*S*)-1-(Ferrocenylideneamino)indan-2-ol (2k): This compound was synthesized analogously to **2i**, starting from (1*R*,2*S*)-(+)-*cis*-1-amino-2-indanol (1.49 g, 1×10^{-2} mol) and ferrocenecarboxaldehyde (2.14 g, 1×10^{-2} mol). Dark yellow solid, 85% yield (2.933 g) after recrystallisation from toluene/heptane (1:1) mixture. ^{1}H NMR ($CDCl_3$): δ = 3.21 (m, 2 H, CH_2O), 3.99 (br. s, 1 H, OH), 4.21 (s, 5 H, H_{Fc}), 4.23 (t, ^1J = 1.9 Hz, 2 H, H_{Fc}), 4.42 (t, ^1J = 1.9 Hz, 2 H, H_{Fc}), 4.60 (m, 1 H, CHO), 4.67 (d, ^1J = 5.8 Hz, 1 H, CHN), 7.18 (m, 1 H, H_{Ar}), 7.28 (m, 1 H, H_{Ar}), 7.43 (m, 1 H, H_{Ar}), 7.49 (m, 1 H, H_{Ar}), 8.45 (s, 1 H, CH=). $C_{20}H_{19}FeNO$ (345.08): calcd. C 69.58, H 5.55, N 4.06; found C 69.31, H 5.29, N 4.00.

(2*S*,3*S*)-2-(Ferrocenylideneamino)-3-methylpentan-1-ol (2m): This compound was synthesized analogously to **2i**, starting from (*S*)-(+)-isoleucinol (1.17 g, 1×10^{-2} mol) and ferrocenecarboxaldehyde (2.14 g, 1×10^{-2} mol). Orange solid, 2.685 g (81% yield). ^{1}H NMR ($CDCl_3$): δ = 0.88 (t, ^3J = 7.2 Hz, 3 H, CH_2CH_3), 0.94 (d, ^3J = 6.8 Hz, 3 H, CH_3), 1.24 (m, 2 H, CH_2), 1.65 (m, 1 H, CH), 2.94 (m, 1 H, CHN), 3.82 (m, 2 H, CH_2O), 3.99 (1 H, *s, br*, OH), 4.10 (s, 5 H, H_{Cp}), 4.34 (m, 1 H, H_{Fc}), 4.37 (m, 1 H, H_{Fc}), 4.51 (m, 1 H, H_{Fc}), 4.72 (m, 1 H, H_{Fc}), 8.06 (s, 1 H, CH=). ^{13}C NMR ($CDCl_3$): δ = 10.8 (s, CH_3), 15.3 (s, CH_3), 25.7 (s, CH_2), 36.0 (s, CH), 63.8 (s, CH_2O), 66.9, 68.7, 69.9, 70.2, 70.3, 80.0 (all C_{Fc}), 77.9 (s, CHN), 161.9 (s, CH=). $C_{17}H_{23}FeNO$ (313.11): calcd. C 65.19, H 7.40, N 4.47; found C 65.47, H 7.23, N 4.09.

Preparation of Ligands; General Technique: A solution of bis(2,6-dimethylphenyl) chlorophosphite (0.832 g, 2.7×10^{-3} mol) in benzene (15 mL) was added dropwise to a stirred solution of the appropriate alcohol **2** (2.7×10^{-3} mol) and Et_3N (0.4 mL, 2.7×10^{-3} mol) in the same solvent (15 mL) at 0 °C. The reaction mixture was then heated to boiling point, allowed to cool down, stirred for 1 h at 50 °C, allowed to cool to room temp. and filtered. The solvent was removed under vacuum (40 Torr), and the residue was dissolved in hexane (20 mL), filtered, concentrated and dried under vacuum (1 Torr).

(1*R*,2*S*)-2-Dimethylamino-1-phenylpropyl Bis(2,6-dimethylphenyl) Phosphite (3a): Colourless oil, 0.913 g (75% yield). ^{31}P NMR ($CDCl_3$): δ = 146.7. ^{13}C NMR ($CDCl_3$): δ = 8.6 (s, CH_3), 17.53, 17.59, 17.72, 17.78 [CH_3(Ar)], 41.6 (s, NMe_2), 65.3 (d, ^3J = 3.8 Hz, CHN), 77.4 (d, ^2J = 13.3 Hz, CHO), 119.8−149.3 (C_{Ar}). MS (EI,

70 eV): *m/z* (%) = 451 (1) $[M]^+$, 380 (5), 273 (15), 162 (67), 122 (100). $C_{27}H_{34}NO_3P$ (415.22): calcd. C 71.82, H 7.59, N 3.10; found C 72.11, H 7.43, N 3.33.

Bis(2,6-dimethylphenyl) (2*R*,4*S*,5*R*)-(5-Vinylquinuclid-2-yl)methyl Phosphite (3b): Colourless oil, 0.841 g (71% yield). ^{31}P NMR (C_6D_6): δ = 138.4. ^{13}C NMR (C_6D_6): δ = 17.96, 18.00, 18.02, 18.05 [all *C*H_3(Ar)], 24.4 (s, CH*C*H_2CH), 26.9 (s, CH_2*C*H_2CH), 28.0 (s, CH_2*C*HCH_2), 40.2 (s, CH*C*HCH=), 48.0 (s, N*C*H_2CH), 49.2 (N*C*H_2CH_2), 56.2 (d, ^3J = 3.4 Hz, CHN), 64.1 (d, ^2J = 5.2 Hz, CH_2O), 114.3 (s, CH_2=), 140.8 (s, CH=), 119.9−149.5 (C_{Ar}). MS (EI, 70 eV): *m/z* (%) = 439 (4) $[M]^+$, 318 (95), 273 (9), 166 (42), 150 (100). $C_{26}H_{34}NO_3P$ (439.22): calcd. C 71.05, H 7.80, N 3.19; found C 69.85, H 7.52, N 3.40.

Bis(2,6-dimethylphenyl) [(2*S*)-1-Methylpyrrolidin-2-yl]methyl Phosphite (3c): Colourless oil, 0.724 g (69% yield). ^{31}P NMR (C_6D_6): δ = 137.3. ^{13}C NMR (C_6D_6): δ = 17.40 [s, *C*H_3(Ar)]. 17.44 [s, CH_3(Ar)], 22.6 [s, $(CH_2)_2$], 28.4 [s, $(CH_2)_2$], 41.2 (s, NCH_3), 57.2 (s, CH_2N), 64.0 (s, CHN), 65.1 (s, CH_2O), 119.4−149.2 (C_{Ar}). MS (EI, 70 eV): *m/z* (%): 387 (3) $[M]^+$, 289 (1), 273 (42), 122 (100). $C_{22}H_{30}NO_3P$ (387.19): calcd. C 68.20, H 7.80, N 3.62; found C 68.51, H 8.07, N 3.44.

[(2*S*)-1-Benzylpyrrolidin-2-yl]methyl Bis(2,6-dimethylphenyl) Phosphite (3d): Colourless oil, 0.962 g (77% yield). ^{31}P NMR (C_6D_6): δ = 136.6. ^{13}C NMR (C_6D_6): δ = 17.4 [s, *C*H_3(Ar)], 17.6 [s, *C*H_3(Ar)], 22.7 [s, $(CH_2)_2$], 28.4 [s, $(CH_2)_2$], 54.4 (s, CH_2Ph), 59.5 (s, CH_2N), 63.5 (d, ^3J = 4.2 Hz, CHN), 65.4 (d, ^2J = 3.4 Hz, CH_2O), 119.7− 149.3 (C_{Ar}). MS (EI, 70 eV): *m/z* (%) = 463 (1) $[M]^+$, 372 (3), 342 (47), 273 (3), 122 (85), 91 (100). $C_{28}H_{34}NO_3P$ (463.23): calcd. C 72.55, H 7.39, N 3.02; found C 72.81, H 7.01, N 3.36.

Bis(2,6-dimethylphenyl) (2*S*,3*S*)-3-Methyl-2-(pyrrolidin-1-yl)pentyl Phosphite (3e): Colourless oil, 0.813 g (68% yield). ^{31}P NMR ($CDCl_3$): δ = 136.1. ^{13}C NMR (C_6D_6): δ = 12.2 (s, CH_3). 14.6 (s, CH_3), 16.9, 17.3, 17.9, 18.1, [all *C*H_3(Ar)], 23.5 [s, $(CH_2)_2$], 27.4 (s, CH_2), 36.2 (s, CH), 51.5 (s, CH_2N), 65.3 (s, CH_2O), 76.1 (s, CHN), 119.6−149.5 (C_{Ar}). MS (EI, 70 eV): *m/z* (%) = 443 (1) $[M]^+$, 273 (38), 122 (100). $C_{26}H_{38}NO_3P$ (443.26): calcd. C 70.40, H 8.64, N 3.16; found C 72.66, H 8.94, N 3.38.

(2*R*)-2-(Dibenzylamino)-3-methylbutyl Bis(2,6-dimethylphenyl) Phosphite (3f): Colourless oil, 1.184 g (79% yield). ^{31}P NMR (C_6D_6): δ = 136.9. ^{13}C NMR (C_6D_6): δ = 18.0 [s, *C*H_3(Ar)], 18.1 [s, *C*H_3(Ar)], 20.5 (s, CH_3), 21.3 (s, CH_3), 27.9 (s, CH), 55.0 (s, CH_2Ph), 60.1 (s, CH_2O), 63.4 (d, ^3J = 4.0 Hz, CHN), 119.8−149.4 (C_{Ar}). MS (EI, 70 eV): *m/z* (%) = 555 (3) $[M]^+$, 464 (13), 273 (40), 122 (100). $C_{35}H_{42}NO_3P$ (555.29): calcd. C 75.65, H 7.62, N 2.52; found C 75.31, H 7.49, N 2.67.

Bis(2,6-dimethylphenyl) 2-({[(1*R*)-1-Phenylethyl]imino}methyl)-phenyl Phosphite (3g): Green oil, 1.099 g (82% yield). ^{31}P NMR (C_6D_6): δ = 139.9. ^{13}C NMR (C_6D_6): δ = 17.8 [s, CH_3(Ar)]. 17.9 [s, CH_3(Ar)], 25.4 (s, CH_3), 70.4 (s, CHN), 120.6−152.0 (s, C_{Ar}), 153.8 (s, CH=). MS (EI, 70 eV): *m/z* (%) = 498 (2) $[M + H]^+$, 376 (56), 408 (15), 273 (52), 105 (100). $C_{31}H_{32}NO_3P$ (497.21): calcd. C 74.83, H 6.48, N 2.82; found C 75.04, H 6.22, N 3.13.

(2*R*)-2-[4-(Dimethylamino)benzylideneamino]-3-methylbutyl Bis(2,6-dimethylphenyl) Phosphite (3h): Colourless oil, 1.093 g (80% yield). ^{31}P NMR (C_6D_6): δ = 136.8. ^{13}C NMR (C_6D_6): δ = 17.94 [s, *C*H_3(Ar)], 17.98 [s, *C*H_3(Ar)], 18.5 (s, CH_3), 20.1 (s, CH_3), 30.7 (s, CH), 40.0 [s, $N(CH_3)_2$], 65.1 (d, ^2J = 11.6 Hz, CH_2O), 77.1 (d, ^3J = 2.7 Hz, CHN), 111.8−152.1 (s, C_{Ar}), 161.2 (s, CH=). MS (EI, 70 eV): *m/z* (%) = 506 (2) $[M]^+$, 316 (52), 217 (66), 122 (100). $C_{30}H_{39}N_2O_3P$ (506.27): calcd. C 71.12, H 7.76, N 5.53; found C 71.41, H 8.05, N 5.77.

(2*S*,3*S*)-2-[4-(Dimethylamino)benzylideneamino]-3-methylpentyl Bis(2,6-dimethylphenyl) Phosphite (3i): Yellow oil, 1.165 g (83% yield). ^{31}P NMR ($CDCl_3$): δ = 136.4. MS (EI, 70 eV): *m/z* (%) = 520 (1) $[M]^+$, 400 (81), 316 (28), 122 (100). $C_{31}H_{41}N_2O_3P$ (520.29): calcd. C 71.51, H 7.94, N 5.38; found C 72.84, H 8.14, N 5.16.

Bis(2,6-dimethylphenyl) (2*R*)-2-(Ferrocenylideneamino)-3-(methylthio)propyl Phosphite (3j): Dark red oil, 1.193 g (75% yield). ^{31}P NMR (C_6D_6): δ = 135.9. ^{13}C NMR (C_6D_6): δ = 16.6 (s, SCH_3), 17.9 [s, *C*H_3(Ar)], 18.0 [s, *C*H_3(Ar)], 37.2 (s, CH_2S), 65.2 (s, CH_2O), 68.8, 69.3, 70.5, 70.6 (all C_{Fc}), 69.6 (s, C_{Cp}), 71.8 (d, ^3J = 3.4 Hz, CHN), 80.9 [s, C_{Fc}(*ipso*)], 124.4−149.5 (s, C_{Ar}), 162.3 (s, CH=). MS (EI, 70 eV): *m/z* (%) = 589 (3) $[M]^+$, 542 (36), 468 (98), 300 (34), 122 (100). $C_{31}H_{36}FeNO_3PS$ (589.15): calcd. C 63.16, H 6.16, N 2.38; found C 61.89, H 6.41, N 2.63.

Bis(2,6-dimethylphenyl) (1*R*,2*S*)-1-(Ferrocenylideneamino)indan-2-yl Phosphite (3k): Red oil, 1.197 g (72% yield). ^{31}P NMR (C_6D_6): δ = 138.2. ^{13}C NMR (C_6D_6): δ = 17.97, 18.02, 18.20, 18.26 [*C*H_3(Ar)], 38.9 (s, CH_2), 68.9, 69.6, 70.4, 70.5 (all C_{Fc}), 69.4 (s, C_{Cp}), 77.2 (d, ^2J = 3.4 Hz, CHO), 77.6 (s, CHN), 81.2 [s, C_{Fc}(*ipso*)], 120.2−153.3 (s, C_{Ar}), 160.9 (s, CH=). MS (EI, 70 eV): *m/z* (%) = 617 (2) $[M]^+$, 496 (2), 328 (24), 273 (7), 122 (100). $C_{36}H_{36}FeNO_3P$ (617.18): calcd. C 70.02, H 5.88, N 2.27; found C 69.79, H 6.14, N 2.55.

Bis(2,6-dimethylphenyl) (2*R*)-2-(Ferrocenylideneamino)-3-methylbutyl Phosphite (3l): Red oil, 1.233 g (80% yield). ^{31}P NMR ($CDCl_3$): δ = 135.1. MS (EI, 70 eV): *m/z* (%) = 571 (2) $[M]^+$, 450 (76), 282 (28), 122 (100). $C_{32}H_{38}FeNO_3P$ (571.19): calcd. C 67.26, H 6.70, N 2.45; found C 67.04, H 6.87, N 2.74.

Bis(2,6-dimethylphenyl) (2*S*,3*S*)-2-(Ferrocenylideneamino)-3-methylpentyl Phosphite (3m): Dark red oil, 1.343 g (85% yield). ^{31}P NMR (C_6D_6): δ = 135.9. ^{13}C NMR (C_6D_6): δ = 10.6 (s, CH_3). 15.3 (s, CH_3), 17.2 [s, *C*H_3(Ar)], 17.23 [s, *C*H_3(Ar)], 25.0 (s, CH_2), 36.3 (s, CH), 63.6 (s, CH_2O), 68.0, 68.2, 69.78, 69.80 (all C_{Fc}), 68.6 (s, C_{Cp}), 76.0 (s, CHN), 80.0 [s, C_{Fc}(*ipso*)], 123.5−148.7 (C_{Ar}), 160.6 (s, CH=). MS (APCI): *m/z* (%) = 586 (100) $[M + H]^+$, 464 (18), 314 (42), 122 (10). $C_{33}H_{40}FeNO_3P$ (585.21): C 67.70, H 6.89, N 2.39; found C 67.96, H 6.62, N 2.74.

Preparation of Complexes

Preparation of Rhodium Complexes 4b−4f and 4j: Rhodium complexes with ligands **3b−3h** and **3j** were synthesized for the NMR and IR experiments as follows. A solution of L* (3.6×10^{-4} mol) in $CHCl_3$ (1.5 mL) was added dropwise to a stirred solution of $[Rh(CO)_2Cl]_2$ (1.8×10^{-4} mol) in the same solvent (1.5 mL). A 1-mL sample of the resulting solution was then transferred to an NMR tube or IR cuvette and spectral experiments were carried out.

General Technique for Rhodium Complexes 4a, 4i and 4k−4m: A solution of the appropriate ligand (3.6×10^{-4} mol) in DCM (20 mL) was added dropwise to a stirred solution of $[Rh(CO)_2Cl]_2$ (0.070 g, 1.8×10^{-4} mol) in the same solvent (20 mL) at 20 °C. The reaction mixture was stirred at 20 °C for 30 min. The excess solvent was then removed under vacuum (40 Torr), and 10 mL of hexane was added to the residue. The obtained precipitate was separated by centrifugation, washed with hexane (2×10 mL) and dried under vacuum (2 Torr).

[Rh(CO)Cl(3a-P^N)] (4a): Yellow solid, 0.193 g (87% yield). IR (KBr): ν(CO) 2017 cm^{-1}. $C_{28}H_{34}ClNO_4PRh$ (617.10): calcd. C 54.43, H 5.55, N 2.27; found C 54.73, H 5.69, N 2.51.

[Rh(CO)Cl(3i-P^N)] (4i): Yellow solid, 0.221 g (89% yield). IR (KBr): ν(CO) 2008 cm^{-1}. $C_{32}H_{41}ClN_2O_4PRh$ (686.15): calcd. C 55.94, H 6.02, N 4.08; found C 56.28, H 5.74, N 4.39.

[Rh(CO)Cl(3k-P^N)] (4k): Yellow-brown solid, 0.260 g (92% yield). IR (KBr): ν(CO) 2010 cm^{-1}. $C_{37}H_{36}ClFeNO_4PRh$ (783.05): calcd. C 56.69, H 4.63, N 1.79; found C 56.93, H 4.31, N 2.10.

[Rh(CO)Cl(3l-P^N)] (4l): Yellow-brown solid, 0.239 g (90% yield). IR (KBr): ν(CO) 2008 cm^{-1}. MS (EI, 70 eV): *m/z* (%) = 702 (34) $[M - Cl]^+$, 674 (5) $[M - Cl - CO]^+$, 282 (52), 122 (100). MS (ES): *m/z* (%) = 702 (55) $[M - Cl]^+$, 300 (100). $C_{33}H_{38}ClFeNO_4PRh$ (737.06): calcd. C 53.72, H 5.19, N 1.90; found C 54.00, H 5.53, N 2.26.

[Rh(CO)Cl(3m-P^N)] (4m): Yellow-brown solid, 0.239 g (88% yield). IR (KBr): ν(CO) 2010 cm^{-1}. $C_{34}H_{40}ClFeNO_4PRh$ (751.08): calcd. C 54.31, H 5.36, N 1.86; found C 54.64, H 5.37, N 2.08.

[Rh(CO)Cl(3f-P^N)] (4f): A solution of ligand **3f** (0.200 g, 3.6×10^{-4} mol) in DCM (10 mL) was added dropwise to a stirred solution of [acacRh$(CO)_2$] (0.093 g, 1.8×10^{-4} mol) in the same solvent (10 mL) at 20 °C. The reaction solution was stirred for 30 min at room temp. to form [acacRh(CO)(η^1-P^N)] complex. A solution of [Rh$(CO)_2Cl]_2$ (0.070 g, 1.8×10^{-4} mol) in DCM (10 mL) was then added to this solution and, after the mixture had stirred for 1 h, all the volatiles were evaporated under vacuum (40 Torr). Regenerated [acacRh$(CO)_2$] was extracted from the residue with hexane (4×15 mL), and the final residue was dried under vacuum (2 Torr) to give the desired product. Yellow solid, 0.222 g (85% yield). IR (KBr): ν(CO) 2009 cm^{-1}. $C_{36}H_{42}ClNO_4PRh$ (721.16): calcd. C 59.88, H 5.86, N 1.94; found C 60.17, H 6.13, N 2.34.

General Technique for Palladium Complexes 5i and 5l: A solution of the appropriate ligand (**3i** or **3l**, 2×10^{-4} mol) in DCM (15 mL) was added dropwise to a stirred solution of [Pd(COD)Cl_2] (0.057 g, 2×10^{-4} mol) in the same solvent (15 mL) at room temp. After the mixture had been stirred for 1 h, the excess solvent was removed under vacuum (40 Torr) and 10 mL of ether was added to the residue. The obtained precipitate was separated by centrifugation, washed with ether (2×10 mL) and dried under vacuum (2 Torr).

***cis*-[PdCl$_2$(3i-P^N)] (5i):** Yellow solid, 0.126 g (91% yield). $C_{31}H_{41}Cl_2N_2O_3PPd$ (696.13): calcd. C 53.35, H 5.92, N 4.01; found C 53.62, H 6.22, N 3.87.

***cis*-[PdCl$_2$(3l-P^N)] (5l):** Yellow-brown solid, 0.135 g (90% yield). $C_{32}H_{38}FeCl_2NO_3PPd$ (747.04): calcd. C 51.33, H 5.12, N 1.87; found C 51.65, H 4.91, N 1.98.

[Pd(allyl)(3m-P^N)]$^+$Cl$^-$ (6): A solution of imino phosphite **3m** (0.234 g, 4×10^{-4} mol) in DCM (20 mL) was added dropwise to a stirred solution of [Pd(allyl)Cl]$_2$ (0.073 g, 2×10^{-4} mol) in the same solvent (20 mL) at room temp. After the mixture had been stirred for 1 h, the solvent was removed under vacuum, and the residue was washed with hexane (2×10 mL) and dried under vacuum (2 Torr). Yellow-brown solid, 0.288 g (94% yield). ^{13}C NMR (C_6D_6): δ = 11.6 (s, CH_3), 16.1 (s, CH_3), 18.7 [s, CH_3(Ar)], 18.8 [s, CH_3(Ar)], 25.1 (s, CH_2), 36.5 (s, CH), 55.0 (s, CH_2 [allyl, *trans*-N)], 67.0 (s, CH_2O), 68.2, 69.6, 70.2, 72.8 (all C_{Fc}), 69.4 (s, C_{Cp}), 75.3 (s, CHN), 80.2 [s, C_{Fc} (*ipso*)], 81.4 (d, ^2J = 42.8 Hz, CH_2 [allyl, *trans*-P)], 125.3 [d, ^2J = 8.2 Hz, CH(allyl)], 118.1−149.2 (s, C_{Ar}), 168.7 (s, CH=). MS (PD): *m/z* (%) = 767 (20) $[M]^+$, 732 (100) $[M - Cl]^+$, 690 (46), 585 (52), 121 (21). XPS: E_b [eV] = 338.2 (Pd $3d_{5/2}$), 134.0 (P 2p), 198.4 (Cl 2p), 399.6 (N 1s), 708.7 (Fe 2p). $C_{36}H_{45}FeClNO_3PPd$ (767.12): calcd. C 56.27, H 5.90, N 1.82; found C 56.58, H 6.11, N 2.02.

Catalytic Experiments

Palladium-Catalysed Alkylation of Ethyl 3-Penten-2-yl Carbonate with Dimethyl Malonate: [Pd(allyl)Cl]$_2$ (3.6 mg, 10^{-5} mol) and ligand **3** ($2-4 \times 10^{-5}$ mol) were dissolved in the appropriate solvent and the mixture was stirred at room temp. for 20 min. Ethyl 3-penten-2-yl carbonate (160 mg, 10^{-3} mol), dimethyl malonate (132 mg, 1.5×10^{-3} mol), BSA [*N,O*-bis(trimethylsilyl)acetamide] (305 mg, 1.5×10^{-3} mol) and KOAc (2.5 mg) were then added to the catalyst solution, and the mixture was stirred at room temp. for 24 h. The reaction mixture was then poured into saturated aqueous NH_4Cl solution and extracted with ether (2×50 mL). The combined organic extracts were washed with aqueous $NaHCO_3$ and water, dried (Na_2SO_4), filtered and concentrated under vacuum. Purification by flash chromatography (silica gel; petroleum ether/EtOAc, 8:1) gave the allylic alkylation product as a colourless oil. The (*S*) absolute configuration was ascribed to the product on the basis of the (−) sign of its optical rotation.[28]

Palladium-Catalysed Sulfonylation of Methyl 3-Penten-2-yl Carbonate with Sodium *p*-Toluenesulfinate: Ligand **3** ($1.1-2.2 \times 10^{-5}$ mol) was added to a solution of [Pd(allyl)Cl]$_2$ (2 mg, 5.5×10^{-6} mol) in the corresponding solvent at room temp. After the mixture had been stirred for 15 min, a solution of methyl 3-penten-2-yl carbonate (72.1 mg, 5×10^{-4} mol) in the appropriate solvent was added. Stirring was continued for 15 min and a suspension of $NaSO_2p$-Tol (178 mg, 10^{-3} mol) in the appropriate solvent was added. After the mixture had been stirred for 48 h, brine (10 mL) was added, and the mixture was extracted with THF. The organic phase was dried ($MgSO_4$) and concentrated under vacuum. Purification by flash chromatography (silica gel; hexane/EtOAc, 5:1) gave the product as a colourless oil. The (*R*) absolute configuration was ascribed to the product on the basis of the (−) sign of its optical rotation.[30]

Supporting Information: Experimental technique and catalytic results for the rhodium-catalysed hydrosilylation of acetophenone with diphenylsilane (see also footnote on the first page of this article).

Acknowledgments

The authors gratefully acknowledge receiving quincoridine from Büchler GmbH (Germany) and thank Dr. P. V. Petrovskii (Institute of Organoelement Compounds, Moscow) for assistance in characterising the products and Dr. V. Tsarev (Institute of Organoelement Compounds, Moscow) for a generous gift of (*R*)-2-amino-3-(methylthio)propan-1-ol. This work was partially supported by the Russian Foundation for Basic Research (Grants No. 00-15-99341, 00-15-97427 and 99-03-32899) and the Deutscher Akademischer Austauschdienst (Referat 325, PKZ A/01/20127).

[1] F. Fache, E. Schulz, M. L. Tommasino, M. Lemaire, *Chem. Rev.* **2000**, *100*, 2159−2231.
[2] K. N. Gavrilov, A. I. Polosukhin, *Russ. Chem. Rev.* **2000**, *65*, 661−682.
[3] M. McCarthy, P. J. Guiry, *Tetrahedron* **2001**, *57*, 3809−3844.
[4] R. Hilgraf, A. Pfaltz, *Synlett* **1999**, 1814−1816.
[5] I. H. Escher, A. Pfaltz, *Tetrahedron* **2000**, *56*, 2879−2888.
[6] J. M. Brunel, A. Tenaglia, G. Buono, *Tetrahedron: Asymmetry* **2000**, *11*, 3585−3590.

[7] G. Delapierre, J. M. Brunel, T. Constantieux, G. Buono, *Tetrathedron: Asymmetry* **2001**, *12*, 1345−1352.
[8] C. G. Arena, G. P. Calabro, G. Francio, F. Faraone, *Tetrahedron: Asymmetry* **2000**, *11*, 2387−2392.
[9] A. Alexakis, J. Burton, J. Vastra, C. Benhaim, X. Fournioux, A. Van der Heuvel, J.-M. Leveque, F. Maze, S. Rosset, *Eur. J. Org. Chem.* **2000**, 4011−4027.
[10] R. Pretot, A. Pfaltz, *Angew. Chem. Int. Ed.* **1998**, *37*, 323−325.
[11] K. N. Gavrilov, A. I. Polosukhin, O. G. Bondarev, A. V. Korostylev, S. E. Lyubimov, A. A. Shiryaev, Z. A. Starikova, V. A. Davankov, *Mendeleev Commun.* **2001**, 33−35.
[12] A. I. Polosukhin, O. G. Bondarev, A. V. Korostylev, R. Hilgraf, V. A. Davankov, K. N. Gavrilov, *Inorg. Chim. Acta* **2001**, 323/1−2, 55−61.
[13] K. N. Gavrilov, *Russ. J. Inorg. Chem.* **1997**, *42*, 368−384.
[14] A. Snyder, A. Togni, V. Weisli, *Organometallics* **1997**, *16*, 255−260.
[15] K. N. Gavrilov, A. I. Polosukhin, *Russ. J. Coord. Chem.* **2000**, *26*, 652−655.
[16] L. Dahlenburg, R. Götz, *J. Organomet. Chem.* **2001**, *619*, 88−98.
[17] C. G. Arena, D. Drommi, F. Faraone, *Tetrahedron: Asymmetry* **2000**, *11*, 2765−2779.
[18] E. Rotondo, G. Battaglia, G. Giordano, F. P. Cusmano, *J. Organomet. Chem.* **1993**, *450*, 245−252.
[19] E. E. Nifantyev, T. A. Shikovets, K. N. Gavrilov, A. T. Teleshev, *Russ. J. Coord. Chem.* **1986**, *12*, 854.
[20] A. Snyder, L. Hintermann, A. Togni, *Angew. Chem. Int. Ed. Engl.* **1995**, *34*, 931−933.
[21] A. Togni, R. Dorta, C. Kollner, G. Pioda, *Pure Appl. Chem.* **1998**, *70*, 1477−1485.
[22] A. V. Korostylev, O. G. Bondarev, A. Yu. Kovalevsky, P. V. Petrovskii, V. A. Davankov, K. N. Gavrilov, *Inorg. Chim. Acta* **2001**, *312*, 117−124.
[23] J. Park, Z. Quan, S. Lee, K. H. Ahn, C.-W. Cho, *J. Organomet. Chem.* **1999**, *584*, 140−146.
[24] Y. M. Malone, P. J. Guiry, *J. Organomet. Chem.* **2000**, *603*, 110−115.
[25] V. I. Nefedov, *Rentgenoelektronnaya spektroskopiya khimicheskih soedinenii (in Russian*), Khimiya, Moscow, **1984**, p. 100.
[26] H. A. Ankersmit, B. H. Loken, H. Kooijman, A. L. Spek, K. Vrieze, G. Van Koten, *Inorg. Chim. Acta* **1996**, *252*, 141−155.
[27] K. Ito, R. Kashiwagi, K. Iwasaki, T. Katsuki, *Synlett* **1999**, 1563−1566.
[28] B. Wiese, G. Helmchen, *Tetrahedron Lett.* **1998**, *39*, 5727−5730.
[29] H. Eichelmann, H.-J. Gais, *Tetrahedron: Asymmetry* **1995**, *6*, 643−646.
[30] B. Trost, R. Radinov, *J. Am. Chem. Soc.* **1997**, *119*, 5962−5965.
[31] B. M Trost, C. Lee, in *Catalytic Asymmetric Synthesis* (Ed.: I. Ojima), 2nd ed., Wiley-VCH, Inc., New York, **2000**, p. 604.
[32] D. Datta, D. Majumdar, *J. Phys. Chem.* **1991**, *4*, 611−617.
[33] J. A. McCleverty, G. Wilkinson, *Inorg. Synth.* **1966**, *8*, 211−214.
[34] D. Drew, J. R. Doyle, *Inorg. Synth.* **1972**, *13*, 52−53.
[35] P. R. Auburn, P. B. McKenzie, B. Bosnich, *J. Am. Chem. Soc.* **1985**, *107*, 2033−2046.
[36] T. Kobayashi, T. Inoue, S. Nishino, Y. Fujihara, K. Oizumi, T. Kimura, *Chem. Pharm. Bull.* **1995**, *43*, 797−817.
[37] M. Reetz, M. Drewes, A. Schmitz, *Angew. Chem.* **1987**, *99*, 1186−1188.
[38] H. Brunner, A. F. M. Rahman, *Z. Naturforsch., Teil B* **1983**, *38*, 1332−1338.
[39] G. Glorian, L. Maciejewski, J. Brocard, F. Agbossou, *Tetrahedron: Asymmetry* **1997**, *8*, 355−358.
[40] H. Brunner, I. Deml, W. Dirnberger, W. Reiber, *Eur. J. Inorg. Chem.* **1998**, 43−54.

Received November 27, 2001
[I01478]

A New Family of Organometallic Rhodium Complexes with [Rh(P*i*Pr$_2$Ph)$_2$] and [Rh(P*i*PrPh$_2$)$_2$] as Molecular Units

Helmut Werner,*[a] Frank Kukla,[a] and Paul Steinert[a]

Dedicated to Professor Walter Siebert on the occasion of his 65th birthday

Keywords: Allyl ligands / Alkyne ligands / Vinylidene complexes / Rhodium / Phosphanes

The π-allyl complexes [Rh(η^3-C_3H_5)(PR$_3$)$_2$] [PR$_3$ = P*i*Pr$_2$Ph (**4**), P*i*PrPh$_2$ (**5**)], prepared from [RhCl(C_8H_{14})$_2$]$_2$, PR$_3$ and the Grignard reagent C_3H_5MgBr, react with carboxylic acids and *p*-toluenesulfonic acid to give the chelate compounds [Rh(κ^2-O_2CR′)(PR$_3$)$_2$] (**8**–**10**) and [Rh{κ^2-O_2S(O)-*p*-Tol}(PR$_3$)$_2$] (**11**, **12**), respectively. While the reactions of **8**, **10** and **12** with CO afford the square-planar rhodium(I) complexes **13**–**15** with monodentate carboxylato and tosylato ligands, treatment of **8**–**10** and **11**, **12** with H_2 leads to the formation of the octahedral dihydridorhodium(III) derivatives [RhH$_2$(κ^2-O_2CR′)(PR$_3$)$_2$] (**16**–**18**) and [RhH$_2${κ^2-O_2S(O)-*p*-Tol}(PR$_3$)$_2$] (**19**, **20**). Similarly to CO, internal alkynes RC≡CCO_2Me (R = CO_2Me, Me) react with **8** and **9** by partial opening of the chelate bond to yield the π-alkyne complexes **21**–**23**, of which **23** with R = Me is quite labile and smoothly regenerates the starting material. In contrast, the reactions of **8** and **9** with terminal alkynes HC≡CR (R = Ph, CO_2Me) afford six-coordinate alkynyl(vinyl)rhodium(III) compounds **24**–**26** with a different stereochemistry at the C=C double bond depending on the substituent R. From **8** and HC≡CCH(Cl)Me the octahedral allenyl complex [RhCl(CH=C=CHMe)(κ^2-O_2CR′)(P*i*PrPh$_2$)$_2$] (**27**) is obtained, the molecular structure of which has been determined by X-ray crystallography. The reaction of [Rh(κ^1-O_2CR){η^2-C_2(CO_2Me)$_2$}(P*i*PrPh$_2$)$_2$] (**21**, **22**) with HC≡CPh also leads to the six-coordinate alkynyl(vinyl)rhodium(III) compounds **28**, **29**, which upon treatment with Me_3SiCl and thermolysis are stepwise converted into the four-coordinate π-enyne complex *trans*-[RhCl{η^2-Ph*C*≡*C*C(CO_2Me)=CHCO_2Me}(P*i*PrPh$_2$)$_2$] (**31**). The reaction of **31** with CO generates the uncoordinated substituted enyne. The rhodium(I) vinylidene complexes *trans*-[Rh(C≡CR′)(=C=CHR)(P*i*PrPh$_2$)$_2$] (**36**–**38**) were prepared in two steps from the tosylato complex **12** and terminal alkynes; they react with CO via migratory insertion to give the square-planar enynyl compounds *trans*-[Rh{η^1-C(C≡CR)=CHR′}(CO)(P*i*PrPh$_2$)$_2$] (**39**–**41**).

(© Wiley-VCH Verlag GmbH, 69451 Weinheim, Germany, 2002)

Introduction

In the context of our investigations on low-valent organorhodium compounds,[1] we recently reported a high-yield synthesis of the π-allyl complexes [Rh(η^3-2-C_3H_4R)(P*i*Pr$_3$)$_2$] (R = H, Me, Ph) which readily react with Brønsted acids by cleavage of the allyl-metal bond.[2] If terminal alkynes HC≡CR were used as acidic substrates, the alkynyl(vinylidene)rhodium(I) compounds *trans*-[Rh(C≡CR)(=C=CHR)(P*i*Pr$_3$)$_2$] were obtained which, in the presence of CO or isocyanides, undergo an intramolecular C−C coupling process.[3] Since we observed that the course of the reactions of rhodium(I) compounds [Rh(X)(P*i*Pr$_3$)$_2$] (where X could be a carboxylate or tosylate) with HC≡CR depends on both the anionic ligand X$^-$ and the substituent R of the alkyne, we became interested to find out whether the nature of the phosphane would also have an influence on the composition of the products. In a recent paper, some evidence for this assumption was already presented.[4] The present article describes preparative routes to four-coordinate carboxylato- and tosylatorhodium(I) complexes with P*i*PrPh$_2$ and P*i*Pr$_2$Ph as ligands and reports in detail on their reactivity toward internal and terminal alkynes.

Results and Discussion

The method recently used by us for the synthesis of [Rh(η^3-C_3H_5)(P*i*Pr$_3$)$_2$][2] could also be applied for the preparation of the related complexes **4** and **5** (Scheme 1). Treatment of a suspension of **1** in toluene with P*i*Pr$_2$Ph or P*i*PrPh$_2$ in 1:4 molar ratio, followed by the addition of a solution of the Grignard reagent C_3H_5MgBr in ether, results in the formation of the π-allylrhodium(I) compounds **4** and **5**, which were isolated as yellow solids in about 80% yield. If the violet solution, formed upon the addition of P*i*Pr$_2$Ph or P*i*PrPh$_2$ to the starting material **1** in toluene, is dried in vacuo, the bis(phosphane)rhodium(I) derivatives **2** and **3** were obtained. These dimeric complexes are some-

[a] Institut für Anorganische Chemie der Universität
Am Hubland, 97074 Würzburg, Germany
Fax: (internat.) + 49-(0)931/888-4623
E-mail: helmut.werner@mail.uni-wuerzburg.de

what less air-sensitive than the triisopropylphosphane counterpart $[RhCl(PiPr_3)_2]_2$ [5] and can be stored under argon at room temperature without decomposition. The ^{31}P NMR spectra of **2** and **3** show the expected doublet with a large ^{31}P-^{103}Rh coupling constant of ca. 198 Hz that is typical for rhodium(I) compounds with $[Rh(PR_3)_2]$ as a building block and *cis*-disposed phosphane ligands.[2,4,6]

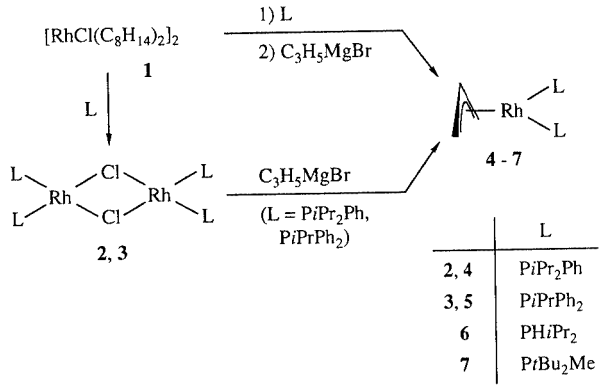

	L
2, 4	$PiPr_2Ph$
3, 5	$PiPrPh_2$
6	$PHiPr_2$
7	$PtBu_2Me$

Scheme 1

While the reactions of **2** and **3** with a twofold excess of the Grignard reagent C_3H_5MgBr also lead to the generation of **4** and **5**, the preparative route using **1** as the precursor is more convenient. It can also be applied for the synthesis of **6** and **7** with $PHiPr_2$ and $PtBu_2Me$ as the phosphane ligands. The ^1H NMR spectra of the π-allylrhodium(I) complexes **4** and **6** exhibit, besides the expected sets for the C_3H_5 protons, four resonances for the protons of the diastereotopic methyl groups of the $PiPr_2$ moieties, which are split into doublets of doublets due to ^{31}P-^1H and ^1H-^1H coupling. Moreover, the ^1H NMR spectrum of **6** shows a doublet of triplets at $\delta = 4.06$ with a large ^{31}P-^1H coupling constant of 256.5 Hz that is characteristic of a P-bonded hydrogen atom. The observation of two distinct signals for the nuclei of the *syn* and the *anti* protons of the terminal allylic CH_2 groups indicate that in solution at room temperature the $(\eta^3\text{-}C_3H_5)Rh$ unit is rigid and does not undergo an η^3-η^1-η^3 rearrangement.[7]

The π-allylic complexes **4** and **5** react smoothly with equimolar amounts of carboxylic acids or *p*-toluenesulfonic acid by cleavage of the allyl-metal bond (Scheme 2). The apparently more simple synthetic method, namely the reaction of **2** or **3** with RCO_2Na or RSO_3Na, led to mixtures of products which could not be separated by fractional crystallization or chromatographic techniques. Both the rhodium carboxylates **8**−**10** and the rhodium tosylates **11** and **12** are red air-sensitive solids which, with the exception of pentane, are readily soluble in common organic solvents. The IR spectra of the carboxylato compounds **8**−**10** display two bands in the region of 1425−1445 and 1480−1510 cm^{-1} assigned to the symmetric and asymmetric OCO stretching modes. According to various data from the literature,[8] there is no doubt that the RCO_2^- ligands of **8**−**10** are coordinated in a chelating and not in a bridging fashion as found for the bis(ethene)rhodium(I) and dicarbonylrhodium(I) derivatives $[\{Rh(\mu\text{-}O_2CR)(C_2H_4)_2\}_2]$ and $[\{Rh(\mu\text{-}O_2CR)(CO)_2\}_2]$, respectively.[9] We assume that a chelating bonding mode also results for the RSO_3^- unit in the complexes **11** and **12**, as has been confirmed for the bis(triisopropylphosphane) compound $[Rh\{\kappa^2\text{-}O_2S(O)R\}(PiPr_3)_2]$ (R = *p*-Tol; Tol = C_6H_4Me) by X-ray crystallography.[10]

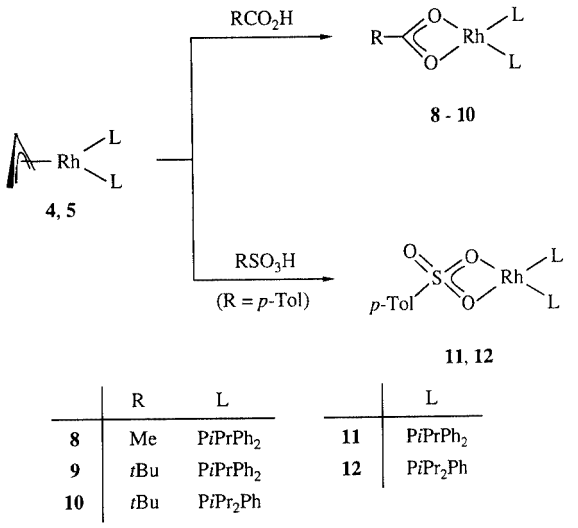

	R	L
8	Me	$PiPrPh_2$
9	*t*Bu	$PiPrPh_2$
10	*t*Bu	$PiPr_2Ph$

	L
11	$PiPrPh_2$
12	$PiPr_2Ph$

Scheme 2

With regard to the mechanism of formation of **8**−**10** and **11**, **12** from the π-allyl metal precursors **4** and **5**, we assume that the primary step consists of an oxidative addition of the acid HX to the rhodium(I) center to give the six-coordinate rhodium(III) intermediates $[RhH(\kappa^1\text{-}X)(\eta^3\text{-}C_3H_5)(PR_3)_2]$ (X = O_2CR, O_3SR), which upon reductive elimination of propene afford the products. We note that upon treatment of $[Rh(\eta^3\text{-}C_3H_5)(PiPr_3)_2]$ with an equimolar amount of CF_3CO_2H in pentane at −20 °C a stable compound $[RhH(\kappa^1\text{-}O_2CCF_3)(\eta^3\text{-}C_3H_5)(PiPr_3)_2]$ has been isolated which reacts at 40 °C to give $[Rh(\kappa^2\text{-}O_2CCF_3)(PiPr_3)_2]$ and C_3H_6.[2]

In the presence of CO, the carboxylato complexes as well as the tosylato derivatives are quite labile and react by partial opening of the chelate bond. This behavior has been exemplified by the preparation of the mononuclear compounds **13**−**15** (Scheme 3 and 4), which were isolated as pale-yellow, almost air-stable solids in 93−98% yield. In contrast to **8** and **10**, the IR spectra of **13** and **14** confirm that the RCO_2^- units are coordinated in a monodentate fashion. The two phosphane ligands of **13**−**15** are *trans*-disposed, which is illustrated by the appearance of one doublet in the ^{31}P NMR spectra, the respective ^{31}P-^{103}Rh coupling constant being significantly smaller than for the starting materials **8**, **10** and **12** with a *cis*-disposed $Rh(PR_3)_2$ moiety.

The carboxylato compounds **8**−**10** also react at room temperature with dihydrogen to give the octahedral dihydridorhodium(III) complexes **16**−**18** by oxidative addition. The white solids are much less sensitive towards air than the rhodium(I) precursors and can be stored under argon for weeks. The ^{31}P NMR spectra of **16**−**18** show only one

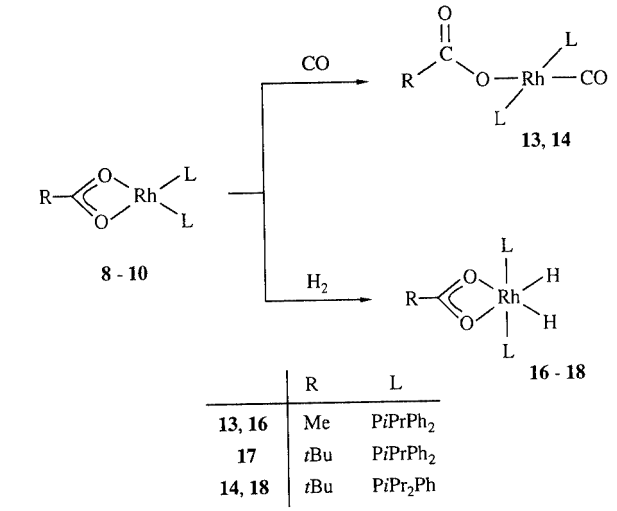

	R	L
13, 16	Me	P*i*PrPh$_2$
17	*t*Bu	P*i*PrPh$_2$
14, 18	*t*Bu	P*i*Pr$_2$Ph

Scheme 3

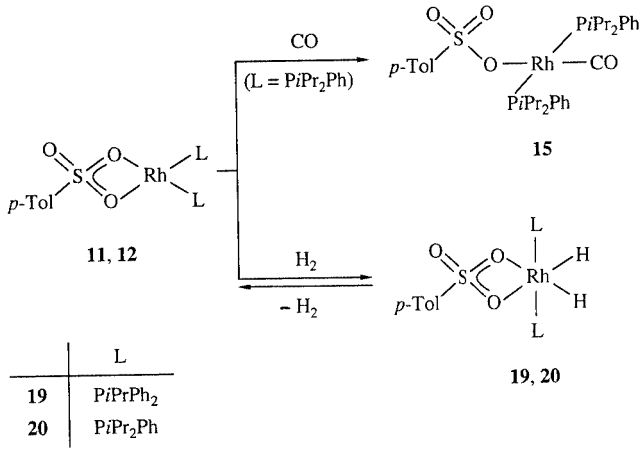

	L
19	P*i*PrPh$_2$
20	P*i*Pr$_2$Ph

Scheme 4

resonance, indicating that the two phosphanes remain in a *trans* disposition. In the ^{1}H NMR spectra, there is also only one set of signals at $\delta = -22.0$ to -22.7 for the hydride ligands, which is in agreement with the proposed structure shown in Scheme 3.

The tosylato derivatives **11** and **12** have the same reactivity towards H_2 as the carboxylato derivatives. However, the isolated dihydrido complexes **19** and **20** are less stable than **16**−**18** and in vacuo slowly lose dihydrogen to regenerate the starting materials **11** and **12**. Therefore, it is necessary that they are stored at low temperature under a H_2 atmosphere. Since the ^{1}H and ^{31}P NMR spectroscopic data of **19** and **20** are similar to those of **16**−**18**, we assume that at 25 °C the two possible stereoisomers rapidly interconvert on the NMR time scale. At −78 °C in [D$_8$]toluene, there is only a slight broadening of the single resonance in the ^{31}P NMR spectra, which indicates that even under these conditions the interconversion of the two isomers should be very fast.

The reactions of the carboxylato complexes **8** and **9** with $C_2(CO_2Me)_2$ proceed analogously to those with CO. Treatment of the starting materials in benzene with an equimolar amount of the alkyne at room temperature leads to an almost instantaneous change of color from dark red to yellow and finally affords the products **21** and **22** (see Scheme 5) in about 85% yield. The ^{1}H and ^{31}P NMR spectra of **21** and **22** are, with respect to the P*i*PrPh$_2$ ligands, quite similar to those of the carbonyl compound **13**, and thus there is no doubt that the coordination geometry around the metal center is square planar. The IR spectra of **21** and **22** show the ν(C≡C) stretching mode at 1810 cm^{-1} (for **21**) and 1785 cm^{-1} (for **22**), the decrease of about 450 cm^{-1} relative to free $C_2(CO_2Me)_2$ being in agreement with the strong π-acceptor character of the electron-poor alkyne.

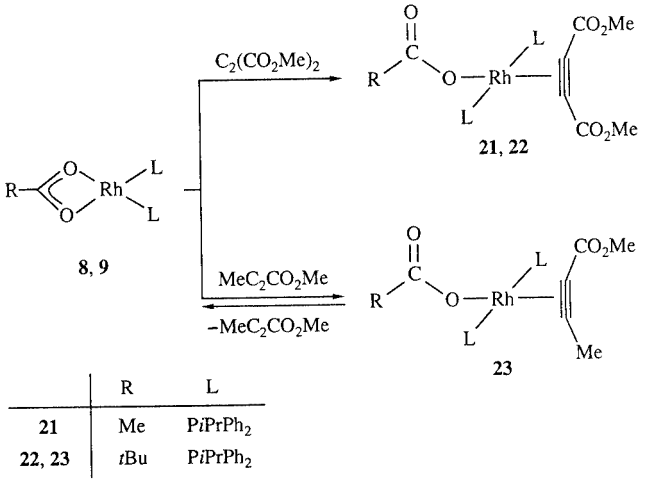

	R	L
21	Me	P*i*PrPh$_2$
22, 23	*t*Bu	P*i*PrPh$_2$

Scheme 5

While compound **8** does not react with MeC≡CCO$_2$Me in toluene at −20 °C, the corresponding reaction for **9** with MeC≡CCO$_2$Me under the same conditions takes place but is reversible. Only if the reaction mixture formed after stirring a solution of **9** and the alkyne in toluene at −20 °C for 2 h is worked-up rather quickly, and the crude product recrystallized from hexane at −78 °C, can a light yellow solid with the analytical composition corresponding to **23** be isolated. The ^{1}H and ^{31}P NMR spectra (measured in [D$_8$]toluene at −30 °C) differ only slightly from those of **22** and thus deserve no further comment.

The reactions of **8** and **9** with *terminal* alkynes take a different course to those of the same starting materials with $C_2(CO_2Me)_2$. Treatment of the carboxylato rhodium(I) complexes with two equiv. of phenylacetylene in toluene at −50 °C leads unexpectedly to the formation of the octahedral alkynyl(vinyl)rhodium(III) compounds **24** and **25** (Scheme 6), which were isolated as pale-yellow, only moderately air-sensitive solids in excellent yields. Although we attempted to detect the supposed intermediates [RhH(C≡CPh)(κ^2-O$_2$CR)(P*i*PrPh$_2$)$_2$] by monitoring the ^{1}H NMR spectra in [D$_8$]toluene at low temperature, we failed to observe the characteristic signals for such hydridometal species. Typical spectroscopic features of **24** and **25** are the two singlets for the stereochemically different protons of the C(Ph)=CH$_2$ ligand at about $\delta = 5.4$ to 6.0 in the ^{1}H NMR

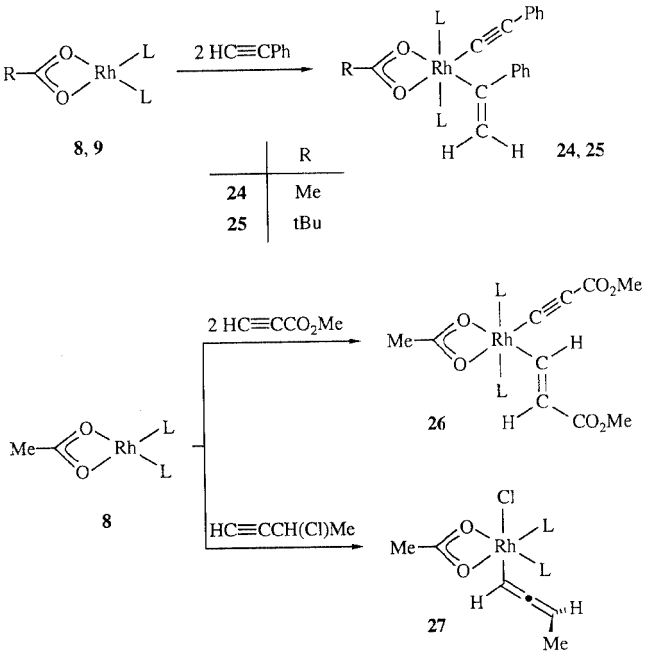

Scheme 6. (L = P*i*PrPh$_2$)

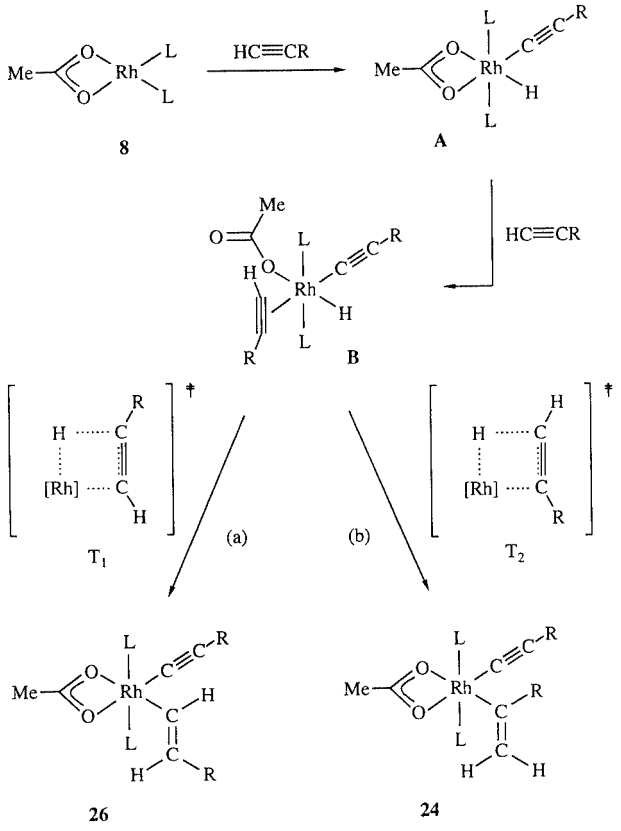

Scheme 7. (L = P*i*PrPh$_2$)

spectrum and the doublet of triplets resonances for the alkynyl and vinyl carbon atoms in the region of δ = 100 to 150 in the ^{13}C NMR spectra. The ^{31}P NMR spectra of **24** and **25** display a sharp doublet at about δ = 30 with a ^{31}P-^{103}Rh coupling constant of 105−106 Hz that is in agreement with a *trans*-disposed Rh(PR$_3$)$_2$ unit.

The reaction of the acetato compound **8** with methyl propiolate also affords an octahedral alkynyl(vinyl)rhodium(III) complex **26** but with a different stereochemistry at the C=C double bond than **24**. While the ^{1}H NMR spectrum of **24** displays the signals for the vinylic protons at δ = 5.87 and 5.42, the ^{1}H NMR spectrum of **26** exhibits the two resonances at δ = 9.18 and 6.33. Both are split into doublets of doublets of triplets due to ^{1}H-^{1}H, ^{1}H-^{31}P and ^{1}H-^{103}Rh coupling. There is no doubt, in particular owing to the size of the ^{1}H-^{1}H coupling constant of 14.6 Hz, that in **26** the two protons at the C=C double bond are *trans* to each other. The same configuration has been found for the bis(triisopropylphosphane) complex [Rh(κ^2-O$_2$CCH$_3$)(C≡CCO$_2$Me){(*E*)-CH=CHCO$_2$Me}(P*i*Pr$_3$)$_2$], which was prepared in a stepwise manner from [RhH$_2$(κ^2-O$_2$CCH$_3$)(P*i*Pr$_3$)$_2$] and three equiv. of HC≡CCO$_2$Me under similar conditions.[11,12]

A proposal for the mechanism of the reactions of **8** with alkynes HC≡CR is outlined in Scheme 7. Although we have no evidence for the formation of intermediate **A**, we assume, in analogy to the reaction of [Rh(κ^2-O$_2$CCH$_3$)(P*i*Pr$_3$)$_2$] with phenylacetylene,[11] that in the first step such an alkynyl(hydrido)rhodium(III) species is generated. The addition of a second molecule of HC≡CR should give intermediate **B**. With regard to the next step, it probably depends on steric as well as electronic effects whether pathway (a) or (b) with the four-center transition states T$_1$ and T$_2$, respectively, is preferred. The above-mentioned dihydridorhodium compound [RhH$_2$(κ^2-O$_2$CCH$_3$)(P*i*Pr$_3$)$_2$], containing two phosphane ligands that are more bulky than P*i*PrPh$_2$, reacts with both HC≡CPh and HC≡CCO$_2$Me to give insertion products with a Rh−CH=CHR stereochemistry.[11,12] Moreover, the reaction of the six-coordinate hydridoiridium(III) compound [IrHCl(C≡CCO$_2$Me){κ^1-*P*-*i*Pr$_2$P(CH$_2$)$_2$OMe}{κ^2-*P*,*O*-*i*Pr$_2$P(CH$_2$)$_2$OMe}] with HC≡CCO$_2$Me also leads to an alkynyl(vinyl) complex with an Ir−CH=CHR linkage.[13]

In contrast to HC≡CPh and HC≡CCO$_2$Me, the chloro-substituted alkyne HC≡CCH(Cl)Me reacts with one equiv. of **8** to give the allenylrhodium(III) compound **27** in 88% yield instead of an alkynyl complex (see Scheme 6). In this process a migration of the chloride from the γ-carbon atom of the alkyne to rhodium takes place, followed by the formation of a σ bond between the metal and the remaining C$_3$ unit. Although a variety of allenyl-transition metal complexes have been prepared with allenyl halides as substrates, there is ample evidence that propargylic chlorides or propargylic alcohols can also be used to generate an M−CH=C=CRR′ bond.[14,15] Characteristic spectroscopic data for the allenyl ligand in **27** are the signals for the =CH and =CCH$_3$ protons at δ = 4.96 and 1.53, respectively, which not only couple to each other but also exhibit a ^{1}H-^{1}H coupling with the proton at the α-carbon atom. The ^{13}C NMR spectrum of **27** displays the resonances for the allenyl carbons at δ = 198.1, 87.4 and 83.0, of which only that of the metal-bound C atom at δ = 87.4 shows a ^{13}C-^{31}P and ^{13}C-^{103}Rh coupling.

The result of the X-ray crystal structure analysis of **27** is shown in Figure 1. The coordination geometry around rhodium is distorted octahedral with the two phosphanes *cis* and the chloride and the allenyl ligand *trans* to each other. Both the O1−Rh−O2 and P1−Rh−P2 bond angles deviate significantly from 90°, which is due on one hand to the bite angle of the chelating acetate and on the other to steric hindrance between the substituents at the two phosphorus atoms. The Cl−Rh−C1 axis is somewhat bent, the bond angle of 171.0(2)° being nearly identical to that of the octahedral allenylosmium complex [OsCl$_2$(η^1-CH=C=CPh$_2$)(NO)(P*i*Pr$_3$)$_2$] [170.5(1)°].[15] The Rh−C1 distance [2.052(5) Å] is slightly shorter than in *trans*-[Rh{η^1-(*Z*)-C(CH=CH$_2$)=CHPh}(CO)(P*i*Pr$_3$)$_2$] [2.088(5) Å][16] and *trans*-[Rh{η^1-C(CN)=CAn$_2$}(CO)(P*i*Pr$_3$)$_2$] [2.106(4) Å; An = *p*-C$_6$H$_4$OMe][17] but significantly longer than in the vinylrhodium cation [Rh{η^1-(*E*)-CH=CHCy}(κ^2-acac)(P*i*Pr$_3$)$_2$]$^+$ [1.98(1) Å].[18] The Rh−C1−C2 bond angle is almost exactly 120° and thus in agreement with the sp^2-hybridisation at the α-carbon atom of the C$_3$ chain. In close analogy to uncoordinated allenes,[19] the two planes [Rh,C1,C2,H1] and [C2,C3,C4,H3] are nearly perpendicular to each other, with a dihedral angle of 88(2)°.

Whereas attempts to reductively eliminate the enyne CH$_2$=C(Ph)−C≡CPh by warming or irradiating solutions of **24** or **25** failed, treatment of **25** with excess phenylacetylene in benzene at room temperature leads to the dimerization of the alkyne. The catalytic C−C coupling process can also be initiated by the carboxylatorhodium(I) compound **9** (the starting material for the preparation of **25**) and gives, under the conditions described in the Exp. Sect., the branched enyne CH$_2$=C(Ph)−C≡CPh almost exclusively. According to the ^{1}H NMR spectrum of the solution, taken after 80% of phenylacetylene has been consumed, the isomers (*E*)- and (*Z*)-PhCH=CH−C≡CPh are formed in less than 1% yield. In this context we note that Vinogradov et al. previously reported that [RhCl(PMe$_3$)$_3$] catalyses the dimerization of terminal alkynes HC≡CR (R = C$_3$H$_7$, C$_4$H$_9$, C$_6$H$_{13}$) to afford a mixture of the enynes CH$_2$=C(R)−C≡CR and (*E*)-RCH=CH−C≡CR with a selectivity of 95−98%.[20] In this case the formation of alkynyl(vinyl)rhodium(III) compounds as intermediates has been postulated.

An enyne of the composition RCH=C(R)−C≡CPh with R = CO$_2$Me has been generated from the alkyne complexes **21** and **22** in a stepwise manner. Treatment of a solution of **21** or **22** in dichloromethane at −20 °C with phenylacetylene leads instantaneously to a change of color from pale-yellow to red, followed quickly by a reverse change of color from red to pale-yellow. After removal of the solvent and extraction of the residue with acetone, the pale-yellow air-sensitive solids **28** and **29**, with an analytical composition corresponding to 1:1 adducts of the starting materials and HC≡CPh, could be isolated (Scheme 8). Both the IR and NMR spectra of **28** and **29** indicate that the two alkynes have been converted to an alkynyl and a vinyl ligand in the coordination sphere of the metal, the latter being generated from the coordinated disubstituted alkyne and the acidic hydrogen atom of phenylacetylene. The supposed *cis*-position of H and Rh at the C=C double bond is supported by

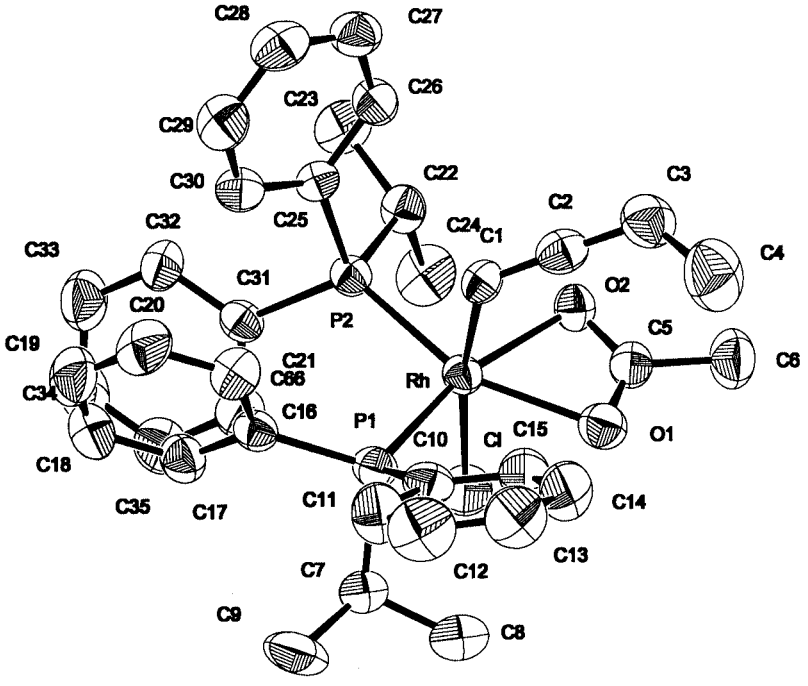

Figure 1. Molecular structure (ORTEP diagram) of **27**; selected bond lengths [Å] and angles [°]: Rh−P1 2.3050(17), Rh−P2 2.2910(19), Rh−O1 2.178(4), Rh−O2 2.135(3), Rh−Cl 2.4686(15), Rh−C1 2.051(5), C1−C2 1.263(7), C2−C3 1.336(8), C3−C4 1.475(9), O1−C5 1.255(6), O2−C5 1.264(6); P1−Rh−P2 100.61(6), P1−Rh−O1 103.41(11), P2−Rh−O1 155.78(10), P1−Rh−O2 163.94(12), P2−Rh−O2 95.11(12), P1−Rh−Cl 96.30(5), P2−Rh−Cl 98.12(5), P1−Rh−C1 87.73(15), P2−Rh−C1 89.08(15), Cl−Rh−C1 170.93(16), Cl−Rh−O1 82.35(11), Cl−Rh−O2 84.62(10), O1−Rh−C1 88.81(18), O2−Rh−C1 89.27(18), O1−Rh−O2 60.74(14), Rh−C1−C2 120.8(4), C1−C2−C3 177.0(6), C2−C3−C4 122.8(6)

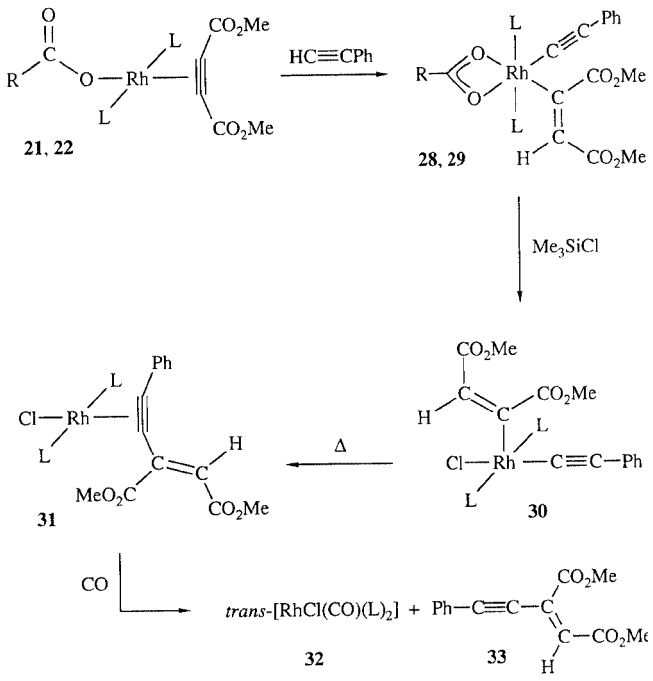

Scheme 8. (L = P*i*PrPh$_2$)

the chemical shift of the resonance of the vinylic proton in the ^{1}H NMR spectra, which is observed at δ = 6.00 (for **28**) and 6.04 (for **29**) and thus at higher field than in the case of a *trans*-position of H to rhodium.[3,16,21] The ^{13}C NMR spectroscopic data for the alkynyl and vinyl carbon atoms of **29** are quite similar to those of the structurally related compounds **24**−**26** and thus in agreement with the proposed structure. Regarding the course of the reaction of **21** and **22** with phenylacetylene, we assume that a similar mechanism is operative as suggested for the formation of **24** and **26**. Treatment of the square-planar starting materials **21** and **22** with HC≡CPh could lead via oxidative addition to a six-coordinate alkyne(alkynyl)hydridorhodium(III) species (see intermediate **B** in Scheme 7), which, after insertion of the alkyne RC≡CR into the Rh−H bond and concomitant closing of the chelate ring of the acetate, gives the products.

The alkynyl(vinyl) complexes **28** and **29** are thermally quite stable and even in the presence of CO do not react by intramolecular C−C coupling to yield *trans*-[Rh(κ^1-O$_2$CR)(CO)(P*i*PrPh$_2$)$_2$] and the enyne. Such a reductive elimination occurs if the related bis(triisopropylphosphane) compound [Rh(κ^2-O$_2$CCH$_3$)(C≡CCO$_2$Me){(*E*)-CH=CHCO$_2$Me}(P*i*Pr$_3$)$_2$] is stirred in benzene under a CO atmosphere at 80 °C.[12] However, if a solution of **28** or **29** in acetone is treated at −20 °C with an equimolar amount of Me$_3$SiCl, a fast reaction (illustrated by a quick change of color from pale-yellow to red) takes place and the five-coordinate chlororhodium(III) complex **30** is formed, along with the corresponding silyl ester RCO$_2$SiMe$_3$ (R = Me, *t*Bu; Scheme 8). While the signal for the vinylic proton in the ^{1}H NMR spectrum of **30** appears at practically the same position (δ = 6.04) as for the precursors **28** and **29**, the doublet resonance for the equivalent phosphorus atoms is observed in the ^{31}P NMR spectrum of **30** at δ = 18.9 and thus shifted upfield by 12−15 ppm from **28** and **29**. The change of the coordination number at rhodium could be responsible for this result. Although precise structural data for **30** (which is a red air-sensitive oil) are missing, we assume that the coordination geometry corresponds to a square pyramid with the vinyl group in the apical position, in analogy to [RhCl(C≡CPh){(*Z*)-CH=CHPh}(P*i*Pr$_3$)$_2$].[3]

The rearrangement of **30** to **31** by C−C coupling occurs smoothly and selectively in benzene at 60 °C and affords the enyne complex **31** as an orange, relatively air-stable solid in 75% isolated yield. The assumption that the enyne is coordinated through the triple bond is mainly supported by the IR spectrum, which shows the ν(C≡C) stretching mode at 1835 cm^{-1}, i.e. in a similar region as found for *trans*-[RhCl(η^2-PhC≡CPh)(P*i*Pr$_3$)$_2$].[22] Passing a slow stream of CO through a solution of **31** in CH$_2$Cl$_2$ at room temperature results in a displacement of the enyne by CO and leads to the carbonylrhodium(I) compound **32** and the free enyne **33**. The latter has been identified by comparison of its spectroscopic data with those from the literature.[23] As anticipated, **32** is also accessible from the dimer **3** and CO in virtually quantitative yield.

In contrast to the carboxylato derivatives **8** and **9**, the sulfonate **12** reacts with terminal alkynes HC≡CR (R = Ph, CMe$_2$OH) to give the four-coordinate rhodium(I) vinylidene complexes **34** and **35** instead of alkynyl(vinyl)- or allenylrhodium(III) complexes (Scheme 9). The reactions of **12** with HC≡CPh and HC≡CCMe$_2$OH in a molar ratio of 1:1 were carried out in toluene at room temperature and afford compounds **34** and **35** as violet air-sensitive solids almost quantitatively. Although it is safe to assume that in the initial step of the reaction an η^2-alkynerhodium(I) species is generated, which then rearranges, possibly via an alkynyl(hydrido)rhodium(III) intermediate, to the isolated product,[24] we failed to detect such a species by NMR spectroscopy. In analogy to the carboxylato complexes *trans*-

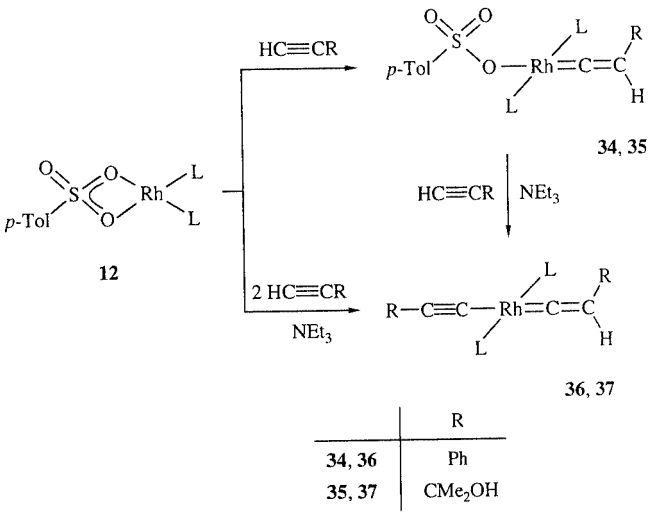

	R
34, 36	Ph
35, 37	CMe$_2$OH

Scheme 9. (L = P*i*Pr$_2$Ph)

[Rh(κ^1-O$_2$CR)(=C=CHPh)(P*i*Pr$_3$)$_2$] (R = CH$_3$, CF$_3$),[11] the ^{13}C NMR spectra of **34** and **35** display two low-field resonances at δ = 306.9 and 113.4 (for **34**) and δ = 308.2 and 115.7 (for **35**) assigned to the α- and β-carbon atoms of the vinylidene units.

The Rh−O bond in compounds **34** and **35** is quite labile and thus upon treatment of solutions of **34** or **35** in a 1:1 mixture of toluene and triethylamine with an equimolar amount of the corresponding alkyne HC≡CR at −50 °C a substitution of the tosylate by the alkynyl anion takes place. After warming to room temperature, removal of the solvent and extraction of the residue with ether the alkynyl(vinylidene) complexes **36** and **37** are isolated in 56−68% yield. These compounds, which are turquoise or dark-green solids, can also be obtained directly from **12** and a twofold excess of HC≡CR under similar conditions; in this case, however, the yield is only 34−45%. Compounds **36** and **37** are less stable in solution than the triisopropylphosphane derivatives *trans*-[Rh(C≡CR)(=C=CHR)(P*i*Pr$_3$)$_2$],[3] which could be due to a reduced shielding of the metal center by the smaller P*i*Pr$_2$Ph ligands. The alkynyl(vinylidene) compound **38**, with different substituents at the β-C atom of the carbon-bonded units, is accessible from **34** and the alkynol HC≡CCMe$_2$OH (see Scheme 10); it is significantly more air-sensitive than the counterparts **36** and **37**. Attempts to prepare the isomer of **38** with the composition *trans*-[Rh(C≡CPh)(=C=CHCMe$_2$OH)(P*i*Pr$_2$Ph)$_2$] failed. Treatment of a solution of **35** in toluene/NEt$_3$ with one equiv. of phenylacetylene affords a mixture of products which could not be separated by fractional crystallization or chromatographic techniques.

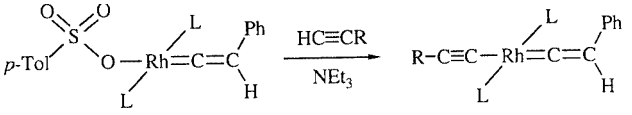

34 **38**

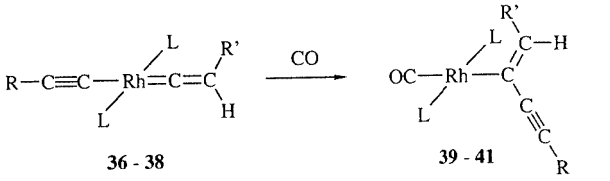

36 - 38 **39 - 41**

	R	R'
36, 39	Ph	Ph
37, 40	CMe$_2$OH	CMe$_2$OH
38, 41	CMe$_2$OH	Ph

Scheme 10. (L = P*i*Pr$_2$Ph)

The alkynyl(vinylidene) complexes **36**−**38** react quite rapidly with CO in dichloromethane at −20 °C to give exclusively the (*Z*) isomers of the enynylrhodium(I) compounds **39**−**41** in moderate to good yields (see Scheme 10). We assume that initially CO adds to the metal center, thus generating a five-coordinate 18-electron intermediate, which, after migration of the alkynyl ligand to the α-carbon atom of the vinylidene unit, transforms into the isolated product. The importance of steric factors probably explains why the attack of the alkynyl moiety occurs only at that side of the molecule that is opposite to the substituent R′. Compounds **39**−**41** are less air-sensitive than the precursors **36**−**38** both in the solid state and in solution. Typical spectroscopic data of **39**−**41** are the intense ν(CO) and ν(C≡C) stretching modes in the IR spectra at 1950−1955 cm^{-1} and 2070−2160 cm^{-1}, respectively, and the resonance for the vinylic =CH proton in the ^{1}H NMR spectra at δ = 8.07 (**39**), 7.18 (**40**) and 7.20 (**41**). The latter is split into a doublet of triplets due to ^{1}H-^{103}Rh and ^{1}H-^{31}P coupling. It should also be mentioned that the methyl groups of the P*i*Pr$_2$Ph ligands of **39**−**41** are diastereotopic and give rise to four doublets of virtual triplets in the ^{1}H NMR spectra. We interpret this observation by assuming a hindered rotation of the vinylic unit around the Rh−C σ-bond, probably caused by the steric requirements of the substituents at the phosphorus atoms and the C=C bond.

In conclusion, the work described in this paper illustrates that a series of rhodium(I) and rhodium(III) complexes with [Rh(P*i*Pr$_2$Ph)$_2$] and [Rh(P*i*PrPh$_2$)$_2$] as molecular building blocks is accessible starting from the π-allylrhodium(I) compounds **4** and **5**. Protolytic cleavage of the allyl-metal bond by carboxylic acids or *p*-toluenesulfonic acid leads to the formation of carboxylato- and tosylatorhodium(I) derivatives, which easily undergo both addition and oxidative addition reactions. With terminal alkynes as substrates, either alkynyl(vinyl)- or allenylrhodium(III) complexes were obtained. Provided that C≡CPh is the alkynyl and C(CO$_2$Me)=CH(CO$_2$Me) the vinyl ligand, the alkynyl(vinyl) complexes react with Me$_3$SiCl by intramolecular C−C coupling to give enynerhodium compounds from which the free enyne is generated upon treatment with CO. The alkynyl(vinylidene)rhodium(I) derivatives, which were prepared in a stepwise manner from rhodium tosylates and terminal alkynes, also react with CO by migratory insertion to afford stereoselectively four-coordinate enynylrhodium(I) complexes. Treatment of catalytic amounts of the pivalatorhodium compounds **9** or **25** with excess phenylacetylene leads to a dimerization of the alkyne and gives regioselectively the branched enyne CH$_2$=C(Ph)−C≡CPh.

Experimental Section

General: All operations were carried out under argon using Schlenk techniques. The starting materials **1**[25] and PH*i*Pr$_2$ [26] were prepared as described in the literature. NMR spectra were recorded at room temperature on Bruker AC 200, Bruker AMX 400 and JEOL FX 90 Q instruments, unless otherwise stated. Abbreviations used: s, singlet; d, doublet; t, triplet; m, multiplet; vt, virtual triplet; br, broadened signal; $N = {}^2J_{P,H} + {}^3J_{P,H}$ or ${}^2J_{P,C} + {}^4J_{P,C}$. The assignment of protons for the π-allyl ligand in compounds **4**−**7** is as follows: H$_m$ = proton at central carbon atom; H$_s$ = proton of terminal CH$_2$ groups in *syn* position to H$_m$; H$_a$ = proton of ter-

minal CH_2 groups in *anti* position to H_m. Melting and decomposition points were measured by differential thermal analysis (DTA).

Preparation of [RhCl(P*i*Pr$_2$Ph)$_2$]$_2$ (2): A suspension of **1** (250 mg, 0.35 mmol) in toluene (20 mL) was treated with P*i*Pr$_2$Ph (0.29 mL, 1.40 mmol) and stirred for 10 min at room temperature. The solvent was evaporated in vacuo, the remaining violet solid was washed three times with 5-mL portions of pentane and dried; yield 360 mg (98%); m.p. 105 °C (dec.). ^{1}H NMR (200 MHz, C_6D_6): δ = 7.37−6.79 (m, 20 H, C_6H_5), 2.28 (m, 8 H, PC*H*CH$_3$), 1.70, 1.11 (both m, 48 H, PCHC*H*$_3$). ^{31}P NMR (81.0 MHz, C_6D_6): δ = 58.9 (d, $^1J_{Rh,P}$ = 197.7 Hz). $C_{48}H_{76}Cl_2P_4Rh_2$ (1053.8): calcd. C 54.71, H 7.27; found C 54.49, H 7.79.

Preparation of [RhCl(P*i*PrPh$_2$)$_2$]$_2$ (3): This compound was prepared as described for **2**, with **1** (250 mg, 0.35 mmol) and P*i*PrPh$_2$ (0.32 mL, 1.40 mmol) as starting materials. Violet solid; yield 394 mg (95%); m.p. 98 °C (dec.). ^{1}H NMR (200 MHz, CD_2Cl_2): δ = 7.36−7.06 (m, 40 H, C_6H_5), 2.22 (m, 4 H, PC*H*CH$_3$), 0.92 (dd, $^3J_{P,H}$ = 14.4, $^3J_{H,H}$ = 6.9 Hz, 12 H, PCHC*H*$_3$). ^{31}P NMR (81.0 MHz, CD_2Cl_2): δ = 55.2 (d, $^1J_{Rh,P}$ = 197.6 Hz). $C_{60}H_{68}Cl_2P_4Rh_2$ (1189.8): calcd. C 60.57, H 5.76; found C 60.08, H 5.81.

Preparation of [Rh(η^3-C$_3$H$_5$)(P*i*Pr$_2$Ph)$_2$] (4): A suspension of **1** (574 mg, 0.80 mmol) in toluene (5 mL) was treated with P*i*Pr$_2$Ph (0.66 mL, 3.20 mmol) and stirred for 10 min at room temperature. After cooling the solution to 0 °C, a 0.5 M solution of C_3H_5MgBr in ether (3.2 mL, 1.60 mmol) was added dropwise. A change of color from brown-violet to yellow occurred. The solvent was evaporated in vacuo, the residue was extracted with pentane (30 mL) and the extract was dried in vacuo. A yellow air-sensitive solid was obtained which was washed three times with 2-mL portions of acetone (0 °C) and dried; yield 700 mg (82%); m.p. 77 °C (dec.). ^{1}H NMR (400 MHz, C_6D_6): δ = 7.41−6.83 (m, 10 H, C_6H_5), 5.02 (dtt, $^2J_{Rh,H}$ = 2.1, $^3J_{H,Ha}$ = 12.8, $^3J_{H,Hs}$ = 6.8 Hz, 1 H, H_m), 3.36 (d, $^3J_{H,Hm}$ = 6.8 Hz, 2 H, H_s), 2.49, 2.37 (both m, 4 H, PC*H*CH$_3$), 2.35 (dd, $^3J_{H,Hm}$ = 12.8, $^3J_{P,H}$ = 7.0 Hz, 2 H, H_a), 1.10 (dd, $^3J_{P,H}$ = 15.0, $^3J_{H,H}$ = 7.0 Hz, 6 H, PCHC*H*$_3$), 1.08 (dd, $^3J_{P,H}$ = 14.4, $^3J_{H,H}$ = 7.0 Hz, 6 H, PCHC*H*$_3$), 0.99 (dd, $^3J_{P,H}$ = 12.4, $^3J_{H,H}$ = 6.6 Hz, 6 H, PCHC*H*$_3$), 0.90 (dd, $^3J_{P,H}$ = 12.0, $^3J_{H,H}$ = 6.8 Hz, 6 H, PCHC*H*$_3$). ^{31}P NMR (81.0 MHz, C_6D_6): δ = 53.2 (d, $^1J_{Rh,P}$ = 196.2 Hz). $C_{27}H_{43}P_2Rh$ (532.5): calcd. C 60.90, H 8.14; found C 60.23; H. 8.01.

Preparation of [Rh(η^3-C$_3$H$_5$)(P*i*PrPh$_2$)$_2$] (5): This compound was prepared as described for **4**, with **1** (287 mg, 0.40 mmol), P*i*PrPh$_2$ (0.37 mL, 1.60 mmol) and a 0.5 M solution of C_3H_5MgBr in ether (1.6 mL, 0.80 mmol) as starting materials. Yellow air-sensitive solid; yield 384 mg (80%); m.p. 76 °C (dec.). ^{1}H NMR (400 MHz, C_6D_6): δ = 7.45−7.02 (m, 20 H, C_6H_5), 5.08 (dtt, $^2J_{Rh,H}$ = 2.1, $^3J_{H,Ha}$ = 12.2, $^3J_{H,Hs}$ = 6.8 Hz, 1 H, H_m), 3.31 (d, $^3J_{H,Hm}$ = 6.8 Hz, 2 H, H_s), 2.37 (dd, $^3J_{H,Hm}$ = 12.2, $^3J_{P,H}$ = 4.7 Hz, 2 H, H_a), 2.15 (m, 2 H, PC*H*CH$_3$), 0.99 (dd, $^3J_{P,H}$ = 14.7, $^3J_{H,H}$ = 6.9 Hz, 6 H, PCHC*H*$_3$), 0.91 (dd, $^3J_{P,H}$ = 14.4, $^3J_{H,H}$ = 7.0 Hz, 6 H, PCHC*H*$_3$). ^{31}P NMR (162.0 MHz, C_6D_6): δ = 49.9 (d, $^1J_{Rh,P}$ = 197.3 Hz). $C_{33}H_{39}P_2Rh$ (600.5): calcd. C 66.00, H 6.55; found C 65.90, H 6.56.

Preparation of [Rh(η^3-C$_3$H$_5$)(PH*i*Pr$_2$)$_2$] (6): This compound was prepared as described for **4**, with **1** (287 mg, 0.40 mmol), PH*i*Pr$_2$ (0.24 mL, 1.60 mmol) and a 0.5 M solution of C_3H_5MgBr in ether (1.6 mL, 0.80 mmol) as starting materials. Yellow air-sensitive solid; yield 253 mg (83%); m.p. 65 °C (dec.). ^{1}H NMR (400 MHz, C_6D_6): δ = 4.82 (dtt, $^2J_{Rh,H}$ = 1.9, $^3J_{H,Ha}$ = 12.7, $^3J_{H,Hs}$ = 7.2 Hz, 1 H, H_m), 4.06 (dt, $^1J_{P,H}$ = 256.5, $^3J_{H,H}$ = 4.8 Hz, 2 H, PH), 3.68 (d, $^3J_{H,Hm}$ = 7.2 Hz, 2 H, H_s), 2.22 (dd, $^3J_{H,Hm}$ = 12.7, $^3J_{P,H}$ = 5.9 Hz, 2 H, H_a), 2.01, 1.93 (both m, 4 H, PC*H*CH$_3$), 1.13 (dd, $^3J_{P,H}$ = 13.5, $^3J_{H,H}$ = 6.8 Hz, 6 H, PCHC*H*$_3$), 1.11 (dd, $^3J_{P,H}$ = 16.2, $^3J_{H,H}$ = 7.2 Hz, 6 H, PCHC*H*$_3$), 1.04 (dd, $^3J_{P,H}$ = 13.8, $^3J_{H,H}$ = 6.9 Hz, 6 H, PCHC*H*$_3$), 1.02 (dd, $^3J_{P,H}$ = 16.5, $^3J_{H,H}$ = 7.1 Hz, 6 H, PCHC*H*$_3$). ^{31}P NMR (36.2 MHz, C_6D_6): δ = 56.5 (d, $^1J_{Rh,P}$ = 187.6 Hz). $C_{15}H_{35}P_2Rh$ (380.3): calcd. C 47.38, H 9.28; found C 47.23; H 9.35.

Preparation of [Rh(η^3-C$_3$H$_5$)(P*t*Bu$_2$Me)$_2$] (7): This compound was prepared as described for **4**, with **1** (287 mg, 0.40 mmol), P*t*Bu$_2$Me (0.32 mL, 1.60 mmol) and a 0.5 M solution of C_3H_5MgBr in ether (1.6 mL, 0.80 mmol) as starting materials. Yellow air-sensitive solid; yield 320 mg (86%); m.p. 86 °C (dec.). ^{1}H NMR (400 MHz, C_6D_6): δ = 4.63 (dtt, $^2J_{Rh,H}$ = 2.1, $^3J_{H,Ha}$ = 11.7, $^3J_{H,Hs}$ = 6.7 Hz, 1 H, H_m), 3.74 (d, $^3J_{H,Hm}$ = 6.7 Hz, 2 H, H_s), 1.92 (dd, $^3J_{H,Hm}$ = 11.7, $^3J_{P,H}$ = 6.1 Hz, 2 H, H_a), 1.22 (d, $^3J_{P,H}$ = 12.0 Hz, 18 H, PCCH$_3$), 1.14 (d, $^2J_{P,H}$ = 4.3 Hz, 6 H, PCH$_3$), 1.11 (d, $^3J_{P,H}$ = 11.6 Hz, 18 H, PCCH$_3$). ^{31}P NMR (36.2 MHz, C_6D_6): δ = 53.3 (d, $^1J_{Rh,P}$ = 196.4 Hz). $C_{21}H_{47}P_2Rh$ (464.5): calcd. C 54.31, H 10.20; found C 54.82, H 10.32.

Preparation of [Rh(κ^2-O$_2$CCH$_3$)(P*i*PrPh$_2$)$_2$] (8): A solution of **5** (180 mg, 0.30 mmol) in benzene (2 mL) was treated with acetic acid (17 μL, 0.30 mmol) and stirred for 1 h at room temperature. A change of color from yellow to dark red occurred. The solvent was evaporated in vacuo, the residue was extracted with acetone (20 mL) and the extract was concentrated to ca. 3 mL in vacuo. A dark-red microcrystalline solid was obtained, which was filtered, washed twice with 2-mL portions of acetone (0 °C) and dried; yield 165 mg (89%); m.p. 108 °C. IR (C_6H_6): ν(OCO$_{as}$) = 1510, ν(OCO$_{sym}$) = 1445 cm^{-1}. ^{1}H NMR (400 MHz, C_6D_6): δ = 7.83−6.69 (m, 20 H, C_6H_5), 2.32 (m, 2 H, PC*H*CH$_3$), 1.95 (s, 3 H, O_2CCH_3), 1.10 (m, 12 H, PCHC*H*$_3$). ^{31}P NMR (162.0 MHz, C_6D_6): δ = 61.9 (d, $^1J_{Rh,P}$ = 199.7 Hz). $C_{32}H_{37}O_2P_2Rh$ (618.5): calcd. C 62.14, H 6.03; found C 61.75, H 5.98.

Preparation of [Rh{κ^2-O$_2$CC(CH$_3$)$_3$}(P*i*PrPh$_2$)$_2$] (9): This compound was prepared as described for **8**, with **5** (150 mg, 0.25 mmol) and $(CH_3)_3CCO_2H$ (26 μL, 0.25 mmol) as starting materials; reaction time: 6 h. Dark-red solid; yield 129 mg (78%); m.p. 93 °C (dec.). IR (KBr): ν(OCO$_{as}$) = 1485, ν(OCO$_{sym}$) = 1430 cm^{-1}. ^{1}H NMR (400 MHz, C_6D_6): δ = 7.52−6.81 (m, 20 H, C_6H_5), 2.37 (m, 2 H, PC*H*CH$_3$), 1.34 [s, 9 H, C(CH$_3$)$_3$], 1.02 (m, 12 H, PCHC*H*$_3$). ^{31}P NMR (162.0 MHz, C_6D_6): δ = 62.2 (d, $^1J_{Rh,P}$ = 226.0 Hz). $C_{35}H_{43}O_2P_2Rh$ (660.9): calcd. C 63.64, H 6.56; found C 64.03, H 6.81.

Preparation of [Rh{κ^2-O$_2$CC(CH$_3$)$_3$}(P*i*Pr$_2$Ph)$_2$] (10): This compound was prepared as described for **8**, with **4** (149 mg, 0.28 mmol) and $(CH_3)_3CCO_2H$ (29 μL, 0.28 mmol) as starting materials; reaction time: 6 h. Dark-red solid; yield 123 mg (74%); m.p. 97 °C (dec.). IR (C_6H_6): ν(OCO$_{as}$) = 1480, ν(OCO$_{sym}$) = 1425 cm^{-1}. ^{1}H NMR (200 MHz, C_6D_6): δ = 7.58−6.91 (m, 10 H, C_6H_5), 2.25 (m, 4 H, PC*H*CH$_3$), 1.53 (m, 12 H, PCHC*H*$_3$), 1.42 [s, 9 H, C(CH$_3$)$_3$], 1.15 (m, 12 H, PCHC*H*$_3$). ^{31}P NMR (81.0 MHz, C_6D_6): δ = 66.6 (d, $^1J_{Rh,P}$ = 202.1 Hz). $C_{29}H_{47}O_2P_2Rh$ (592.6): calcd. C 58.78, H 7.99; found C 58.51, H 8.02.

Preparation of [Rh{κ^2-O$_2$S(O)-*p*-Tol}(P*i*PrPh$_2$)$_2$] (11): A solution of **5** (180 mg, 0.30 mmol) in toluene (2 mL) was treated with 4-MeC$_6$H$_4$SO$_3$H (57 mg, 0.30 mmol) and stirred for 1 h at room temperature. A change of color from yellow to red occurred. The solvent was evaporated in vacuo, the residue was extracted with acetone (20 mL) and the extract was concentrated to ca. 2 mL in vacuo. Red crystals precipitated which were filtered, washed twice with 2-mL portions of acetone (0 °C) and dried; yield 185 mg (89%); m.p.

51 °C. ^{1}H NMR (200 MHz, C_6D_6): δ = 7.58−6.91 (m, 24 H, C_6H_4 and C_6H_5), 2.31 (m, 2 H, PC*H*CH$_3$), 1.95 (s, 3 H, $C_6H_4CH_3$), 0.96 (m, 12 H, PCHC*H*$_3$). ^{31}P NMR (81.0 MHz, C_6D_6): δ = 63.3 (d, $^1J_{Rh,P}$ = 212.2 Hz). $C_{37}H_{41}O_3P_2RhS$ (730.7): calcd. C 60.82, H 5.66, S 4.39; found C 60.82, H 5.89, S 4.33.

Preparation of [Rh{κ^2-O$_2$S(O)-*p*-Tol}(P*i*Pr$_2$Ph)$_2$] (12): This compound was prepared as described for **11**, with **4** (128 mg, 0.24 mmol) and 4-Me$C_6H_4SO_3H$ (46 mg, 0.24 mmol) as starting materials. Red air-sensitive crystals; yield 138 mg (87%); m.p. 85 °C (dec.). ^{1}H NMR (200 MHz, C_6D_6): δ = 8.46−6.79 (m, 14 H, C_6H_4 and C_6H_5), 2.10 (m, 4 H, PC*H*CH$_3$), 1.97 (s, 3 H, $C_6H_4CH_3$), 1.35, 1.03 (both m, 12 H each, PCHC*H*$_3$). ^{31}P NMR (81.0 MHz, C_6D_6): δ = 63.3 (d, $^1J_{Rh,P}$ = 212.2 Hz). $C_{31}H_{45}O_3P_2RhS$ (662.6): calcd. C 56.19, H 6.84, S 4.84; found C 55.82, H 6.53, S 4.71.

Preparation of *trans*-[Rh(κ^1-O$_2$CCH$_3$)(CO)(P*i*PrPh$_2$)$_2$] (13): A slow stream of CO was passed through a solution of **8** (62 mg, 0.10 mmol) in CH_2Cl_2 (10 mL) at room temperature for 10 s, leading to a rapid change of color from dark-red to light yellow. After removal of the solvent in vacuo, a light yellow solid was obtained, which was washed twice with 2-mL portions of acetone (0 °C) and dried; yield (98%); m.p. 135 °C. IR (KBr): ν(CO) = 1960, ν(OCO_{as}) = 1595, ν(OCO_{sym}) = 1370 cm^{-1}. ^{1}H NMR (400 MHz, C_6D_6): δ = 7.83−7.41 (m, 20 H, C_6H_5), 2.93 (m, 2 H, PC*H*CH$_3$), 1.36 (s, 3 H, O_2CCH_3), 1.21 (dvt, *N* = 15.8, $^3J_{H,H}$ = 7.4 Hz, 12 H, PCHC*H*$_3$). ^{31}P NMR (162.0 MHz, C_6D_6): δ = 40.7 (d, $^1J_{Rh,P}$ = 147.4 Hz). $C_{33}H_{37}O_3P_2Rh$ (646.5): calcd. C 61.31, H 5.77; found C 61.00, H 5.30.

Preparation of *trans*-[Rh{κ^1-O$_2$CC(CH$_3$)$_3$}(CO)(P*i*Pr$_2$Ph)$_2$] (14): This compound was prepared as described for **13**, with **10** (59 mg, 0.10 mmol) and CO as starting materials. Yellow solid; yield 59 mg (95%); m.p. 93 °C (dec.). IR (KBr): ν(CO) = 1955 cm^{-1}. ^{1}H NMR (200 MHz, C_6D_6): δ = 7.77−7.07 (m, 10 H, C_6H_5), 2.42 (m, 4 H, PC*H*CH$_3$), 1.37 (dvt, *N* = 16.1, $^3J_{H,H}$ = 7.3 Hz, 12 H, PCHC*H*$_3$), 1.14 [s, 9 H, C(CH$_3$)$_3$], 1.03 (dvt, *N* = 14.2, $^3J_{H,H}$ = 6.9 Hz, 12 H, PCHC*H*$_3$). ^{31}P NMR (81.0 MHz, C_6D_6): δ = 46.4 (d, $^1J_{Rh,P}$ = 133.7 Hz). $C_{30}H_{47}O_3P_2Rh$ (620.6): calcd. C 58.07, H 7.63; found C 57.60, H 7.46.

Preparation of [Rh{κ^1-O$_2$S(O)-*p*-Tol}(CO)(P*i*Pr$_2$Ph)$_2$] (15): This compound was prepared as described for **13**, with **12** (66 mg, 0.10 mmol) and CO as starting materials. Yellow solid; yield 64 mg (93%); m.p. 153 °C (dec.). IR (KBr): ν(CO) = 1950 cm^{-1}. ^{1}H NMR (200 MHz, C_6D_6): δ = 7.96−6.82 (m, 14 H, C_6H_5 and C_6H_4), 2.81 (m, 4 H, PC*H*CH$_3$), 1.95 (s, 3 H, $C_6H_4CH_3$) 1.44 (dvt, *N* = 16.9, $^3J_{H,H}$ = 7.5 Hz, 12 H, PCHC*H*$_3$), 0.96 (dvt, *N* = 14.5, $^3J_{H,H}$ = 7.0 Hz, 12 H, PCHC*H*$_3$). ^{31}P NMR (81.0 MHz, C_6D_6): δ = 47.7 (d, $^1J_{Rh,P}$ = 125.0 Hz). $C_{32}H_{45}O_4P_2RhS$ (690.6): calcd. C 55.65; H 6.57; found C 56.07, H 6.81.

Preparation of [RhH$_2$(κ^2-O$_2$CCH$_3$)(P*i*PrPh$_2$)$_2$] (16): A slow stream of H_2 was passed through a solution of **8** (62 mg, 0.10 mmol) in CH_2Cl_2 (5 mL) at room temperature for 5 min. After removal of the solvent in vacuo, a white solid was obtained which was washed twice with 1-mL portions of acetone (0 °C) and dried; yield 56 mg (90%); m.p. 84 °C (dec.). IR (KBr): ν(RhH) = 2100, ν(OCO_{as}) = 1540, ν(OCO_{sym}) =1430 cm^{-1}. ^{1}H NMR (400 MHz, C_6D_6): δ = 7.99−6.91 (m, 20 H, C_6H_5), 2.53 (m, 2 H, PC*H*CH$_3$), 1.52 (s, 3 H, O_2CCH_3), 1.21 (dvt, *N* = 15.9, $^3J_{H,H}$ = 8.0 Hz, 12 H, PCHC*H*$_3$), −22.01 (dt, $^1J_{Rh,H}$ = 22.4, $^2J_{P,H}$ = 18.0 Hz, 2 H, RhH). ^{31}P NMR (162.0 MHz, C_6D_6): δ = 49.7 (d, $^1J_{Rh,P}$ = 119.4 Hz). $C_{32}H_{39}O_2P_2Rh$ (620.5): calcd. C 61.94, H 6.33; found C 62.20, H 6.48.

Preparation of [RhH$_2${κ^2-O$_2$CC(CH$_3$)$_3$}(P*i*PrPh$_2$)$_2$] (17): This compound was prepared as described for **16**, with **9** (66 mg, 0.10 mmol) and H_2 as starting materials. White solid; yield 58 mg (88%); m.p. 76 °C (dec.). IR (KBr): ν(RhH) = 2115, ν(OCO_{as}) = 1525, ν(OCO_{sym}) = 1430 cm^{-1}. ^{1}H NMR (200 MHz, C_6D_6): δ = 6.99−6.71 (m, 20 H, C_6H_5), 2.33 (m, 2 H, PC*H*CH$_3$), 1.08 (dvt, *N* = 16.7, $^3J_{H,H}$ = 8.0 Hz, 12 H, PCHC*H*$_3$), 0.79 [s, 9 H, C(CH$_3$)$_3$], −21.13 (dt, $^1J_{Rh,H}$ = 21.8, $^2J_{P,H}$ = 17.4 Hz, 2 H, RhH). ^{31}P NMR (81.0 MHz, C_6D_6): δ = 49.8 (d, $^1J_{Rh,P}$ = 119.2 Hz). $C_{35}H_{45}O_2P_2Rh$ (662.6): calcd. C 63.45, H 6.85; found C 63.90, H 7.12.

Preparation of [RhH$_2${κ^2-O$_2$CC(CH$_3$)$_3$}(P*i*Pr$_2$Ph)$_2$] (18): This compound was prepared as described for **16**, with **10** (65 mg, 0.11 mmol) and H_2 as starting materials. Colorless oil; yield 65 mg (99%). IR (KBr): ν(RhH) = 2120, ν(OCO_{as}) = 1520, ν(OCO_{sym}) = 1420 cm^{-1}. ^{1}H NMR (200 MHz, C_6D_6): δ = 7.88−6.92 (m, 10 H, C_6H_5), 2.26 (m, 4 H, PC*H*CH$_3$), 1.28 (dvt, *N* = 14.5, $^3J_{H,H}$ = 7.3 Hz, 12 H, PCHC*H*$_3$), 1.14 [s, 9 H, C(CH$_3$)$_3$], 1.02 (dvt, *N* = 13.1, $^3J_{H,H}$ = 7.3 Hz, 12 H, PCHC*H*$_3$), −22.73 (dt, $^1J_{Rh,H}$ = 23.3, $^2J_{P,H}$ = 16.0 Hz, 2 H, RhH). ^{31}P NMR (81.0 MHz, C_6D_6): δ = 55.3 (d, $^1J_{Rh,P}$ = 119.1 Hz). $C_{29}H_{49}O_2P_2Rh$ (594.6): calcd. C 58.58, H 8.31; found C 58.45, H 8.28.

Preparation of [RhH$_2${κ^2-O$_2$S(O)-*p*-Tol}(P*i*PrPh$_2$)$_2$] (19): This compound was prepared as described for **16**, with **11** (73 mg, 0.10 mmol) and H_2 as starting materials. White solid which has to be stored under dihydrogen; yield 62 mg (85%); m.p. 86 °C (dec.). IR (KBr): ν(RhH) = 2100 cm^{-1}. ^{1}H NMR (200 MHz, C_6D_6): δ = 7.87−6.49 (m, 24 H, C_6H_5 and C_6H_4), 3.08 (m, 2 H, PC*H*CH$_3$), 1.80 (s, 3 H, $C_6H_4CH_3$), 1.12 (dvt, *N* = 15.8, $^3J_{H,H}$ = 7.9 Hz, 12 H, PCHC*H*$_3$), −21.51 (dt, $^1J_{Rh,H}$ = 27.6, $^2J_{P,H}$ = 15.8 Hz, 2 H, RhH). ^{31}P NMR (81.0 MHz, C_6D_6): δ = 50.2 (d, $^1J_{Rh,P}$ = 117.8 Hz). $C_{37}H_{43}O_3P_2RhS$ (732.7): calcd. C 60.66, H 5.92; found C 61.21, H 6.21.

Preparation of [RhH$_2${κ^2-O$_2$S(O)-*p*-Tol}(P*i*Pr$_2$Ph)$_2$] (20): This compound was prepared as described for **16**, with **12** (60 mg, 0.09 mmol) and H_2 as starting materials. Colorless oil which has to be stored under dihydrogen; yield 59 mg (98%). IR (KBr): ν(RhH) = 2130 cm^{-1}. ^{1}H NMR (200 MHz, C_6D_6): δ = 7.81−6.65 (m, 14 H, C_6H_5 and C_6H_4), 2.52 (m, 4 H, PC*H*CH$_3$), 1.87 (s, 3 H, $C_6H_4CH_3$), 1.28 (dvt, *N* = 14.5, $^3J_{H,H}$ = 7.3 Hz, 12 H, PCHC*H*$_3$), 0.98 (dvt, *N* = 14.5, $^3J_{H,H}$ = 7.3 Hz, 12 H, PCHC*H*$_3$), −24.04 (dt, $^1J_{Rh,H}$ = 27.6, $^2J_{P,H}$ = 16.0 Hz, 2 H, RhH). ^{31}P NMR (81.0 MHz, C_6D_6): δ = 51.8 (d, $^1J_{Rh,P}$ = 117.7 Hz). $C_{31}H_{47}O_3P_2RhS$ (664.6): calcd. C 56.02, H 7.13, S 4.82; found C 55.31, H 7.01, S 4.75.

Preparation of *trans*-[Rh(κ^1-O$_2$CCH$_3$){η^2-C$_2$(CO$_2$Me)$_2$}(P*i*PrPh$_2$)$_2$] (21): A solution of **8** (74 mg, 0.12 mmol) in benzene (5 mL) at room temperature was treated dropwise with $C_2(CO_2Me)_2$ (14 μL, 0.12 mmol) with continuous stirring. A quick change of color from dark-red to yellow occurred. The solvent was evaporated in vacuo and the oily residue dissolved in hexane (2 mL). After the solution was stored at −78 °C for 12 h, a pale-yellow solid precipitated, which was separated from the mother liquor, washed twice with 2-mL portions of pentane and dried in vacuo; yield: 78 mg (85%); m.p. 94 °C (dec.). IR (KBr): ν(C≡C) = 1810, ν(C=O) = 1680, ν(OCO) = 1610 cm^{-1}. ^{1}H NMR (200 MHz, C_6D_6): δ = 7.81−7.00 (m, 20 H, C_6H_5), 3.24 (s, 6 H, CO_2CH_3), 2.68 (m, 2 H, PC*H*CH$_3$), 1.55 (dvt, *N* = 14.0, $^3J_{H,H}$ = 7.0 Hz, 12 H, PCHC*H*$_3$), 1.34 (s, 3 H, O_2CCH_3). ^{31}P NMR (81.0 MHz, C_6D_6): δ = 34.6 (d, $^1J_{Rh,P}$ = 118.3 Hz). $C_{38}H_{43}O_6P_2Rh$ (760.6): calcd. C 60.01, H 5.70; found C 60.48, H 5.95.

Preparation of *trans*-[Rh{κ^1-O$_2$CC(CH$_3$)$_3$}{η^2-C$_2$(CO$_2$Me)$_2$}(P*i*PrPh$_2$)$_2$] (22): This compound was prepared as described for **21**,

with **9** (79 mg, 0.12 mmol) and $C_2(CO_2Me)_2$ (14 μL, 0.12 mmol). Pale-yellow solid; yield 79 mg (86%); m.p. 84 °C (dec.). IR (KBr): ν(C≡C) = 1785, ν(C=O) = 1685, ν(OCO_{as}) = 1610 cm^{-1}. ^1H NMR (200 MHz, C_6D_6): δ = 7.85−6.98 (m, 20 H, C_6H_5), 3.32 (s, 6 H, CO_2CH_3), 2.64 (m, 2 H, PC*H*CH_3), 1.03 (dvt, *N* = 12.8, $^3J_{H,H}$ = 5.7 Hz, 12 H, PCHC*H*$_3$), 0.75 [s, 9 H, C(CH_3)$_3$]. ^{31}P NMR (81.0 MHz, C_6D_6): δ = 35.9 (d, $^1J_{Rh,P}$ = 120.0 Hz). $C_{41}H_{49}O_6P_2Rh$ (802.7): calcd. C 61.35, H 6.15; found C 60.97, H 5.98.

Preparation of *trans*-[Rh{κ^1-$O_2CC(CH_3)_3$}(η^2-MeC≡CCO_2Me)(P*i*PrPh$_2$)$_2$] (23): A solution of **9** (92 mg, 0.14 mmol) in toluene (2 mL) was treated dropwise at −20 °C with MeC_2CO_2Me (14 μL, 0.14 mmol). After stirring the solution at −20 °C for 2 h and then warming to room temperature, the solvent was evaporated in vacuo. The oily residue was dissolved in hexane (2 mL) and the solution worked up as described for **21**. Pale-yellow solid; yield 67 mg (63%); m.p. 64 °C (dec.). IR (KBr): ν(C≡C) = 1900, ν(C=O) = 1705, ν(OCO_{as}) = 1670 cm^{-1}. ^1H NMR (200 MHz, [D_8]toluene, 243 K): δ = 7.92−6.84 (m, 20 H, C_6H_5), 3.33 (s, 3 H, CO_2CH_3), 2.38 (m, 2 H, PC*H*CH_3), 1.32 [s, 9 H, C(CH_3)$_3$], 1.30 (dvt, *N* = 17.3, $^3J_{H,H}$ = 8.6 Hz, 12 H, PCHC*H*$_3$), 1.10 (s, 3 H, ≡CCH_3). ^{31}P NMR (81.0 MHz, [D_8]toluene, 243 K): δ = 36.4 (d, $^1J_{Rh,P}$ = 123.5 Hz). $C_{40}H_{49}O_4P_2Rh$ (758.7):calcd. C 63.33, H 6.51; found C 63.45, H 6.55.

Preparation of [Rh(κ^2-O_2CCH_3)(C≡CPh){C(Ph)=CH_2}(P*i*PrPh$_2$)$_2$] (24): A solution of **8** (93 mg, 0.15 mmol) in toluene (5 mL) at −50 °C was treated dropwise with phenylacetylene (32 μL, 0.30 mmol). After stirring the solution for 5 min at −50 °C and then warming to room temperature, the solvent was evaporated in vacuo. The oily residue was dissolved in hexane (20 mL) and the solution stirred at 0 °C for 2 h. A pale-yellow solid slowly precipitated, which was filtered, washed twice with 2-mL portions of hexane and dried in vacuo; yield 106 mg (86%); m.p. 81 °C (dec.). IR (KBr): ν(C≡C) = 2060, ν(C=C) = 1580, ν(OCO_{as}) = 1520 cm^{-1}. ^1H NMR (400 MHz, C_6D_6): δ = 8.04−6.46 (m, 30 H, C_6H_5), 5.87, 5.42 (both s, 1 H each, =CH_2), 3.35 (m, 2 H, PC*H*CH_3), 1.45 (dvt, *N* = 14.8, $^3J_{H,H}$ = 7.4 Hz, 6 H, PCHC*H*$_3$), 1.22 (dvt, *N* = 14.6, $^3J_{H,H}$ = 7.2 Hz, 6 H, PCHC*H*$_3$), 1.20 (s, 3 H, O_2CCH_3). ^{13}C NMR (100.6 MHz, C_6D_6): δ = 182.2 (s, O_2C), 148.4 [dt, $^1J_{Rh,C}$ = 30.4, $^2J_{P,C}$ = 8.9 Hz, Rh*C*(=CH_2)Ph], 134.2−124.0 (m, C_6H_5), 128.6 [dt, $^2J_{Rh,C}$ = 1.2, $^3J_{P,C}$ = 0.8 Hz, =CH_2], 108.7 (dt, $^2J_{Rh,C}$ = 10.2, $^3J_{P,C}$ = 2.3 Hz, ≡*C*Ph], 98.5 [dt, $^1J_{Rh,C}$ = 50.7, $^2J_{P,C}$ = 18.5 Hz, Rh*C*≡CPh], 25.6 (vt, *N* = 25.3 Hz, P*C*HCH$_3$), 22.9 (s, O_2CCH_3), 18.2, 17.4 (both s, PCH*C*H$_3$). ^{31}P NMR (81.0 MHz, C_6D_6): δ = 31.0 (d, $^1J_{Rh,P}$ = 106.1 Hz). $C_{48}H_{49}O_2P_2Rh$ (822.8): calcd. C 70.07, H 6.00; found C 69.72, H 6.14.

Preparation of [Rh{κ^2-$O_2CC(CH_3)_3$}(C≡CPh){C(Ph)=CH_2}(P*i*PrPh$_2$)$_2$] (25): This compound was prepared as described for **24**, with **9** (99 mg, 0.15 mmol) and phenylacetylene (32 μL, 0.30 mmol) as starting materials. Pale-yellow solid; yield 109 mg (84%); m.p. 78 °C (dec.). IR (KBr): ν(C≡C) = 2050, ν(C=C) = 1580, ν(OCO_{as}) = 1485, ν(OCO_{sym}) = 1435 cm^{-1}. ^1H NMR (200 MHz, C_6D_6): δ = 8.02−6.83 (m, 30 H, C_6H_5), 5.96, 5.49 (both s, 1 H each, =CH_2), 3.54 (m, 2 H, PC*H*CH_3), 1.52 (dvt, *N* = 10.2, $^3J_{H,H}$ = 7.1 Hz, 6 H, PCHC*H*$_3$), 1.08 (dvt, *N* = 14.8, $^3J_{H,H}$ = 7.5 Hz, 6 H, PCHC*H*$_3$), 1.73 [s, 9 H, C(CH_3)$_3$]. ^{13}C NMR (100.6 MHz, C_6D_6): δ = 190.3 (s, O_2C), 150.5 [dt, $^1J_{Rh,C}$ = 28.7, $^2J_{P,C}$ = 18.5 Hz, Rh*C*(=CH_2)Ph], 135.5−125.4 (m, C_6H_5), 125.7 (dt, $^2J_{Rh,C}$ = 4.4, $^3J_{P,C}$ = 5.1 Hz, =CH_2), 109.3 (dt, $^2J_{Rh,C}$ = 8.7, $^3J_{P,C}$ = 4.7 Hz, ≡*C*Ph), 99.9 (dt, $^1J_{Rh,C}$ = 50.1, $^2J_{P,H}$ = 18.5 Hz, Rh*C*≡CPh), 39.4 [s, *C*(CH_3)$_3$], 27.1 [s, C(*C*H$_3$)$_3$], 26.4 (vt, *N* = 25.4 Hz, P*C*HCH$_3$), 19.3, 19.0 (both s, PCH*C*H$_3$). ^{31}P NMR (81.0 MHz, C_6D_6): δ = 29.5 (d, $^1J_{Rh,P}$ = 104.6 Hz). MS (70 eV, e-spray): *m/z* = 864 [M^+]. $C_{51}H_{55}O_2P_2Rh$ (864.9): calcd. C 70.83, H 6.41; found C 70.79, H 6.40.

Catalytic Dimerization of Phenylacetylene: A solution of either **9** (165 mg, 0.25 mmol) or **25** (260 mg, 0.25 mmol) in benzene (25 mL) was treated with phenylacetylene (2.7 mL, 25 mmol) and hexane (1 mL, as a reference for GC) and stirred whilst irradiating with an Osram 500 W lamp (λ = 300 nm) at room temperature. After 6 h, the GC plot (measured with a Shimadzu GC-8A gas chromatograph and a FFAP column) revealed that 80% of phenylacetylene had been consumed. The volatiles were removed in vacuo and the remaining red-brown oil investigated by ^1H NMR spectroscopy. The ^1H NMR spectrum showed that the major product was the enyne PhC≡CC(Ph)=CH_2, whereas the isomeric butenynes (*E*)- and (*Z*)-PhC≡CCH=CHPh were present in less than 1%. The red-brown oil was dissolved in benzene (2 mL) and the solution chromatographed on Al_2O_3 (neutral, activity grade I, height of column 15 cm). A yellow fraction was eluted with hexane, which was then dried in vacuo. The yellow oil (which slowly polymerizes at temperatures above −40 °C) was identified as PhC≡CC(Ph)=CH_2 by comparison of its NMR spectroscopic data with those of the literature.[27]

Preparation of [Rh(κ^2-O_2CCH_3)(C≡CCO_2Me){(*E*)-CH=$CHCO_2Me$}(P*i*PrPh$_2$)$_2$] (26): This compound was prepared as described for **24**, with **8** (74 mg, 0.12 mmol) and methyl propiolate (22 μL, 0.24 mmol) as starting materials. Pale-yellow solid; yield 83 mg (88%); m.p. 132 °C (dec.). IR (KBr): ν(C≡C) = 2090, ν(C=O) = 1675, ν(OCO_{as}) = 1570 cm^{-1}. ^1H NMR (200 MHz, C_6D_6): δ = 9.18 (ddt, $^3J_{H,H}$ = 14.6, $^3J_{P,H}$ = 2.9, $^2J_{Rh,H}$ = 0.9 Hz, 1 H, RhCH), 7.77−6.95 (m, 20 H, C_6H_5), 6.33 (ddt, $^3J_{H,H}$ = 14.6, $^4J_{P,H}$ = 1.5, $^3J_{Rh,H}$ = 1.5 Hz, 1 H, =C*H*CO_2CH_3), 3.38, 3.36 (both s, 6 H, CO_2CH_3), 3.06 (m, 2 H, PC*H*CH_3), 1.30 (dvt, *N* = 15.7, $^3J_{H,H}$ = 7.3 Hz, 6 H, PCHC*H*$_3$), 1.06 (dvt, *N* = 15.0, $^3J_{H,H}$ = 7.3 Hz, 6 H, PCHC*H*$_3$), 1.05 (s, 3 H, O_2CCH_3). ^{13}C NMR (100.6 MHz, C_6D_6): δ = 184.7 (s, RhO_2CCH_3), 168.0 (dt, $^1J_{Rh,C}$ = 29.3, $^2J_{P,C}$ = 9.8 Hz, RhCH), 162.7 (dt, $^3J_{Rh,C}$ = 2.7, $^4J_{P,C}$ = 1.3 Hz, CCO_2CH_3), 153.7 (dt, $^3J_{Rh,C}$ = 1.6, $^4J_{P,C}$ = 1.3 Hz, *C*O_2CH_3), 135.2, 134.7 (both vt, *N* = 9.8 Hz, *ortho*-C of C_6H_5), 130.3, 130.2 (both s, *para*-C of C_6H_5), 129.2, 129.2 (both vt, *N* = 41.8 Hz, *ipso*-C of C_6H_5), 128.0, 127.9 (both vt, *N* = 9.4 Hz, *meta*-C of C_6H_5), 127.5 (dt, $^2J_{Rh,C}$ = 9.3, $^3J_{P,C}$ = 4.5 Hz, =*C*HCO_2CH_3), 109.1 (dt, $^1J_{Rh,C}$ = 50.5, $^2J_{P,C}$ = 17.1 Hz, Rh*C*≡C), 103.6 (dt, $^2J_{Rh,C}$ = 11.0, $^3J_{P,C}$ = 2.4 Hz, RhC≡*C*), 50.4, 50.1 (both s, CO_2CH_3), 26.9 (vt, *N* = 26.5 Hz, P*C*HCH$_3$), 23.9 (s, O_2CCH_3), 18.9, 18.8 (both s, PCH*C*H$_3$). ^{31}P NMR (81.0 MHz, C_6D_6): δ = 33.6 (d, $^1J_{Rh,P}$ = 98.8 Hz). $C_{40}H_{45}O_6P_2Rh$ (786.7): calcd. C 61.07, H 5.77; found C 60.71, H 5.43.

Preparation of [RhCl(κ^2-O_2CCH_3)(CH=C=CHMe)(P*i*PrPh$_2$)$_2$] (27): A solution of **8** (93 mg, 0.15 mmol) in CH_2Cl_2 (5 mL) was treated at −20 °C with 3-chloro-1-butyne (13 μL, 0.15 mmol), leading to a rapid change of color from dark-red to yellow. After warming the solution to room temperature, the solvent was evaporated in vacuo. A yellow solid was obtained which was washed twice with 1-mL portions of acetone (0 °C) and dried; yield 93 mg (88%); m.p. 124 °C (dec.). IR (KBr): ν(OCO_{as}) = 1460 cm^{-1}. ^1H NMR (400 MHz, C_6D_6): δ = 7.88−6.75 (m, 20 H, C_6H_5), 4.96 (dq, $^3J_{H,H}$ = 6.8, $^4J_{H,H}$ = 6.4 Hz, 1 H, =C*H*CH_3), 4.71 (m, 1 H, RhCH), 3.42, 3.23 (both m, 2 H, PC*H*CH_3), 2.15 (s, 3 H, CO_2CH_3), 1.53 (dd, $^3J_{H,H}$ = 6.8, $^5J_{H,H}$ = 2.7 Hz, 3 H, =CHC*H*$_3$), 1.15 (dd, $^3J_{H,H}$ = 16.1, $^3J_{P,H}$ = 7.0 Hz, 3 H, PCHC*H*$_3$), 1.03 (dd, $^3J_{H,H}$ = 14.3, $^3J_{P,H}$ = 7.0 Hz, 3 H, PCHC*H*$_3$), 1.02 (dd, $^3J_{H,H}$ = 16.0, $^3J_{P,H}$ = 6.8 Hz, 3 H, PCHC*H*$_3$), 0.89 (dd, $^3J_{H,H}$ = 15.1, $^3J_{P,H}$ = 6.8 Hz, 3 H, PCHC*H*$_3$). ^{13}C NMR (100.6 MHz, C_6D_6): δ = 198.1

(s, RhCH=*C*), 189.4 (s, O_2CCH_3), 134.6 (d, $^3J_{P,C}$ = 7.5 Hz, *meta*-C of Ph), 134.3 (d, $^3J_{P,C}$ = 6.6 Hz, *meta*-C of Ph), 133.9 (d, $^3J_{P,C}$ = 7.4 Hz, *meta*-C of Ph), 133.7 (d, $^3J_{P,C}$ = 6.3 Hz, *meta*-C of Ph), 129.3, 129.0, 128.8, 128.5 (all s, *para*-C of Ph), 126.1 (d, $^2J_{P,C}$ = 8.7 Hz, *ortho*-C of Ph), 125.9 (d, $^2J_{P,C}$ = 9.0 Hz, *ortho*-C of Ph), 125.5 (d, $^2J_{P,C}$ = 10.0 Hz, *ortho*-C of Ph), 125.4 (d, $^1J_{P,C}$ = 50.0 Hz, *ipso*-C of Ph), 125.4 (d, $^1J_{P,C}$ = 52.1 Hz, *ipso*-C of Ph), 125.3 (d, $^2J_{P,C}$ = 10.2 Hz, *ortho*-C of Ph), 124.5 (d, $^1J_{P,C}$ = 46.0 Hz, *ipso*-C of Ph), 124.4 (d, $^1J_{P,C}$ = 48.2 Hz, *ipso*-C of Ph), 87.4 (dt, $^1J_{Rh,C}$ = 17.7, $^2J_{P,C}$ = 10.7 Hz, RhCH), 83.0 (s, =*C*HCH$_3$), 25.9 (d, $^1J_{P,C}$ = 25.9 Hz, P*C*HCH$_3$), 25.7(s, O_2CCH_3), 25.4 (d, $^1J_{P,C}$ = 26.5 Hz, P*C*HCH$_3$), 17.9, 17.7, 16.9, 16.7 (all s, PCH*C*H$_3$), 13.3 (s, = CH*C*H$_3$). ^{31}P NMR (81.0 MHz, C_6D_6): δ(A) = 51.8, δ(B) = 51.3 (ABX spin system, $J_{A,B}$ = 32.0 Hz, $J_{A,X}$ = $J_{B,X}$ = 139.4 Hz). MS (70 eV, e-spray): *m*/*z* = 671 [M$^+$ − Cl]. $C_{36}H_{42}ClO_2P_2Rh$ (707.0): calcd. C 61.16, H 5.99, Rh 14.55; found C 61.14, H 6.19, Rh 14.21.

Preparation of [Rh(κ^2-O_2CCH_3)(C≡CPh){(*E*)-C(CO$_2$Me)=CHCO$_2$Me}(P*i*PrPh$_2$)$_2$] (28): A solution of **21** (106 mg, 0.14 mmol) in CH_2Cl_2 (5 mL) was treated at −20 °C with phenylacetylene (16 μL, 0.14 mmol) and stirred for 5 min at −20 °C. After a few seconds a change of color from yellow to red occurred, followed by a subsequent change of color in the opposite direction. After warming the solution to room temperature, the solvent was evaporated in vacuo and the residue extracted with acetone (20 mL). The extract was dried in vacuo to give a pale-yellow solid which was washed twice with 1-mL portions of acetone (0 °C) and dried; yield 99 mg (82%); m.p. 140 °C (dec.). IR (KBr): ν(C≡C) = 2100, ν(C=O) = 1695, ν(OCO) = 1570 cm^{-1}. ^{1}H NMR (200 MHz, C_6D_6): δ = 8.11−6.99 (m, 25 H, C_6H_5), 6.00 (s, 1 H, =C*H*CO$_2$CH$_3$), 3.80 (s, 3 H, CO$_2$CH$_3$), 3.52 (m, 2 H, PC*H*CH$_3$), 3.37 (s, 3 H, CO$_2$CH$_3$), 1.40 (dvt, *N* = 15.4, $^3J_{H,H}$ = 7.7 Hz, 6 H, PCHC*H*$_3$), 0.99 (dvt, *N* = 14.6, $^3J_{H,H}$ = 7.3 Hz, 6 H, PCHC*H*$_3$), 0.98 (s, 3 H, O_2CCH_3). ^{31}P NMR (81.0 MHz, C_6D_6): δ = 34.3 (d, $^1J_{Rh,P}$ = 97.4 Hz). $C_{46}H_{49}O_6P_2Rh$ (862.7): calcd. C 64.04, H 5.72, Rh 11.93; found C 63.51, H 5.66, Rh 11.87.

Preparation of [Rh{κ^2-O$_2$CC(CH$_3$)$_3$}(C≡CPh){(*E*)-C(CO$_2$Me)=CHCO$_2$Me}(P*i*PrPh$_2$)$_2$] (29): This compound was prepared as described for **28**, with **22** (96 mg, 0.12 mmol) and phenylacetylene (14 μL, 0.12 mmol) as starting materials. Pale-yellow solid; yield 93 mg (86%); m.p. 116 °C (dec.). IR (KBr): ν(C≡C) = 2100, ν(C=O) = 1695, ν(OCO) = 1570 cm^{-1}. ^{1}H NMR (200 MHz, C_6D_6): δ = 7.98−7.03 (m, 25 H, C_6H_5), 6.04 (s, 1 H, =C*H*CO$_2$CH$_3$), 3.89 (s, 3 H, CO$_2$CH$_3$), 3.54 (m, 2 H, PC*H*CH$_3$), 3.40 (s, 3 H, CO$_2$CH$_3$), 1.33 (dvt, *N* = 15.0, $^3J_{H,H}$ = 7.5 Hz, 6 H, PCHC*H*$_3$), 1.04 (dvt, *N* = 14.4, $^3J_{H,H}$ = 7.5 Hz, 6 H, PCHC*H*$_3$), 0.70 [s, 9 H, C(*C*H$_3$)$_3$]. ^{13}C NMR (100.6 MHz, C_6D_6): δ = 192.1 [s, $O_2CC(CH_3)_3$], 173.1, 162.2 (both s, *C*O$_2$CH$_3$), 162.2 [dt, $^1J_{Rh,C}$ = 33.9, $^2J_{P,C}$ = 9.5 Hz, Rh*C*(CO$_2$CH$_3$)], 136.5−125.4 (m, C_6H_5), 120.5 (dt, $^2J_{Rh,C}$ = 4.3, $^3J_{P,C}$ = 4.3 Hz, =*C*HCO$_2$CH$_3$), 106.6 (dt, $^2J_{Rh,C}$ = 8.6, $^3J_{P,C}$ = 1.9 Hz, ≡*C*C$_6$H$_5$), 100.2 (dt, $^1J_{RhC}$ = 48.6, $^2J_{P,C}$ = 20.5 Hz, Rh*C*≡C), 51.0, 50.3 (both s, CO$_2$*C*H$_3$), 39.6 [s, *C*(CH$_3$)$_3$], 27.0 (vt, *N* = 25.3 Hz, P*C*HCH$_3$) 26.7 [s, C(*C*H$_3$)$_3$], 20.1, 19.1 (both s, PCH*C*H$_3$). ^{31}P NMR (81.0 MHz, C_6D_6): δ = 31.8 (d, $^1J_{Rh,P}$ = 97.2 Hz). $C_{49}H_{54}O_6P_2Rh$ (903.8): calcd. C 65.12, H 6.02; found C 65.44, H 6.18.

Preparation of [RhCl(C≡CPh){(*E*)-C(CO$_2$Me)=CHCO$_2$Me}(P*i*PrPh$_2$)$_2$] (30): A solution of either **28** (121 mg, 0.14 mmol) or **29** (127 mg, 0.14 mmol) in acetone (5 mL) was treated with freshly distilled Me$_3$SiCl (18 μL, 0.14 mmol) and stirred for 10 min at −20 °C. A rapid change of color from pale-yellow to red occurred. After warming the solution to room temperature and evaporating the solvent in vacuo, a red, thermally labile oil was obtained; yield 108 mg (92%) from **28** and 110 mg (94%) from **29**. IR (C_6H_6): ν(C≡C) = 2100, ν(C=O) = 1700 cm^{-1}. ^{1}H NMR (400 MHz, C_6D_6): δ = 8.16−6.66 (m, 25 H, C_6H_5), 6.04 (s, 1 H, = C*H*CO$_2$CH$_3$), 3.98 (m, 2 H, PC*H*CH$_3$), 3.12, 2.99 (both s, 3 H each, CO$_2$CH$_3$), 1.44 (dvt, *N* = 15.2, $^3J_{H,H}$ = 7.8 Hz, 6 H, PCHC*H*$_3$), 1.15 (dvt, *N* = 14.6, $^3J_{H,H}$ = 7.2 Hz, 6 H, PCHC*H*$_3$). ^{31}P NMR (162.0 MHz, C_6D_6): δ = 18.9 (d, $^1J_{Rh,P}$ = 94.3 Hz); $C_{44}ClH_{46}O_4P_2Rh$ (839.2): calcd. C 62.98, H 5.53; found C 63.04, H 6.00.

Preparation of *trans*-[RhCl{η^2-PhC≡CC(CO$_2$Me)=CHCO$_2$Me}(P*i*PrPh$_2$)$_2$] (31): A solution of **30** (109 mg, 0.13 mmol) was stirred for 1 h at 60 °C. A change of color from red to orange occurred. After cooling the solution to room temperature, the solvent was removed in vacuo, and the residue was extracted with acetone (20 mL). The extract was dried in vacuo to give an orange solid which was washed twice with 1-mL portions of acetone (0 °C) and dried; yield 82 mg (75%); m.p. 104 °C (dec.). IR (KBr): ν(C≡C) = 1835, ν(C=O) = 1704, ν(C=C) = 1565 cm^{-1}. ^{1}H NMR (200 MHz, C_6D_6): δ = 8.19−6.91 (m, 25 H, C_6H_5), 6.70 (s, 1 H, = C*H*CO$_2$CH$_3$), 3.48, 3.32 (both s, 3 H each, CO$_2$CH$_3$), 3.10 (m, 2 H, PC*H*CH$_3$), 1.35 (dvt, *N* = 15.0, $^3J_{H,H}$ = 7.3 Hz, 6 H, PCHC*H*$_3$), 1.19 (dvt, *N* = 15.4, $^3J_{H,H}$ = 7.3 Hz, 6 H, PCHC*H*$_3$). ^{13}C NMR (100.6 MHz, C_6D_6): δ = 166.5, 165.7 (both s, CO$_2$), 130.9 (s, = *C*CO$_2$CH$_3$), 173.0−124.9 (m, C_6H_5), 120.2 (s, =*C*HCO$_2$CH$_3$), 108.5 (dt, $^1J_{RhC}$ = 15.3, $^2J_{P,C}$ = 2.9 Hz, Ph*C*≡C), 81.7 (dt, $^1J_{RhC}$ = 16.2, $^2J_{P,C}$ = 2.0 Hz, PhC≡*C*), 51.9, 51.5 (both s, CO$_2$*C*H$_3$), 25.4 (vt, *N* = 23.5 Hz, P*C*HCH$_3$), 19.9, 19.3 (both s, PCH*C*H$_3$). ^{31}P NMR (81.0 MHz, C_6D_6): δ = 36.6 (d, $^1J_{RhP}$ = 117.7 Hz). MS (70 eV, e-spray): *m*/*z* = 803 [M$^+$ − Cl]. $C_{44}H_{46}ClO_4P_2Rh$ (839.2): calcd. C 62.98, H 5.53; found C 63.03, H 6.01.

Reaction of 31 with CO: A slow stream of CO was passed through a solution of **31** (84 mg, 0.10 mmol) in CH_2Cl_2 (10 mL) at room temperature for 10 s. An instantaneous change of color from orange to yellow occurred. The ^{1}H NMR spectrum of the solution indicated that the enyne **33** was formed along with **32**.[23] The solvent was evaporated in vacuo, the remaining yellow solid was washed twice with 1-mL portions of acetone (0 °C) and identified as **32**; yield 62 mg (98%).

Preparation of *trans*-[RhCl(CO)(P*i*PrPh$_2$)$_2$] (32): A slow stream of CO was passed through a suspension of **3** (48 mg, 0.04 mmol) in toluene (10 mL) at room temperature for 10 min. A change of color from violet to yellow occurred. After evaporation of the solvent in vacuo, the yellow solid was washed twice with 1-mL portions of acetone (0 °C) and dried; yield 50 mg (99%); m.p. 140 °C. IR (KBr): ν(CO) = 1960 cm^{-1}. ^{1}H NMR (200 MHz, C_6D_6): δ = 7.79−6.96 (m, 20 H, C_6H_5), 3.48 (m, 2 H, PC*H*CH$_3$), 1.10 (dvt, *N* = 15.5, $^3J_{H,H}$ = 7.5 Hz, 12 H, PCHC*H*$_3$). ^{31}P NMR (81.0 MHz, C_6D_6): δ = 41.0 (d, $^1J_{Rh,P}$ = 123.5 Hz). $C_{31}H_{34}ClOP_2Rh$ (622.9): calcd. C 59.77, H 5.50, Rh 16.52; found C 60.21, H 5.99, Rh 16.74.

Preparation of [Rh{κ^1-O$_2$S(O)-*p*-Tol}(=C=CHPh)(P*i*Pr$_2$Ph)$_2$] (34): A solution of **12** (106 mg, 0.16 mmol) in toluene (2 mL) was treated with phenylacetylene (19 μL, 0.16 mmol) and stirred for 3 h at room temperature. A change of color from red to violet occurred. The solvent was evaporated in vacuo and the residue extracted with ether (25 mL). After drying the extract in vacuo, the remaining violet solid was washed twice with 10-mL portions of pentane (0 °C) and dried; yield 120 mg (98%); m.p. 67 °C (dec.). IR (CH_2Cl_2): ν(C=C) = 1650 cm^{-1}. ^{1}H NMR (200 MHz, C_6D_6): δ = 7.75−6.56 (m, 19 H, C_6H_5 and C_6H_4), 2.82 (m, 4 H, PC*H*CH$_3$), 1.93 (s, 3 H, $C_6H_4CH_3$), 1.40 (dvt, *N* = 16.4, $^3J_{H,H}$ = 6.9 Hz, 12 H, PCHC*H*$_3$), 1.09 (dt, $^3J_{Rh,H}$ = 1.5, $^4J_{P,H}$ = 3.5 Hz, 1 H, =C*H*Ph), 0.93 (dvt,

N = 13.9, $^3J_{H,H}$ = 9.1 Hz, 12 H, PCHCH_3). ^{13}C NMR (100.6 MHz, C_6D_6): δ = 306.9 (dt, $^1J_{Rh,C}$ = 58.4, $^2J_{P,C}$ = 18.1 Hz, Rh=*C*=C), 143.7, 139.4, 134.9, 129.9, 128.6, 128.5, 127.9, 127.7, 126.8, 126.2, 125.3, 124.6 (all s, C_6H_5 and C_6H_4), 113.4 (dt, $^2J_{Rh,C}$ = 15.3, $^3J_{P,C}$ = 6.7 Hz, Rh=C=*C*), 30.4 (s, $C_6H_4CH_3$), 23.2 (vt, N = 22.3 Hz, P*C*HCH$_3$), 20.0, 18.5 (both s, PCH*C*H$_3$). ^{31}P NMR (81.0 MHz, C_6D_6): δ = 43.3 (d, $^1J_{Rh,P}$ = 143.9 Hz). $C_{39}H_{51}O_3RhS$ (764.8): calcd. C 61.25, H 6.72; found C 60.87, H 6.68.

Preparation of [Rh{κ^1-O$_2$S(O)-*p*-Tol}(=C=CHCMe$_2$OH)(P*i*Pr$_2$Ph)$_2$] (35): This compound was prepared as described for **34**, with **12** (106 mg, 0.16 mmol) and HC≡CCMe$_2$(OH) (16 μL, 0.16 mmol) as starting materials; reaction time 1 h. Violet solid; yield 113 mg (95%); m.p. 58 °C (dec.). IR (CH_2Cl_2): ν(C=C) = 1635 cm^{-1}. ^{1}H NMR (200 MHz, C_6D_6): δ = 7.59−6.81 (m, 14 H, C_6H_5 and C_6H_4), 2.87 (s, 3 H, $C_6H_4CH_3$), 2.57 (m, 4 H, PC*H*CH$_3$), 1.43 (dvt, N = 16.5, $^3J_{H,H}$ = 7.3 Hz, 12 H, PCHCH_3), 1.23 [s, 6 H, C(CH_3)$_2$OH], 1.05 (dvt, N = 13.9, $^3J_{H,H}$ = 6.9 Hz, 12 H, PCHCH_3), 1.00 (dt, $^3J_{Rh,H}$ = 0.6, $^4J_{P,H}$ = 3.1 Hz, 1 H, =C*H*R), signal of O*H* proton not found. ^{13}C NMR (100.6 MHz, C_6D_6): δ = 308.2 (dt, $^1J_{Rh,C}$ = 59.9, $^2J_{P,C}$ = 16.4 Hz, Rh=*C*=C), 143.9, 139.5, 135.2, 133.5, 130.1, 128.7, 128.1, 127.0 (all s, C_6H_5 and C_6H_4), 115.7 (dt, $^2J_{Rh,C}$ = 15.3, $^3J_{P,C}$ = 5.9 Hz, Rh=C=*C*), 43.0 [s, *C*(CH$_3$)$_2$OH], 31.8 (s, $C_6H_4CH_3$), 28.2 [s, C(*C*H$_3$)$_2$OH], 25.0 (vt, N = 25.9 Hz, P*C*HCH$_3$), 20.2, 18.7 (both s, PCH*C*H$_3$). ^{31}P NMR (81.0 MHz, C_6D_6): δ = 42.4 (d, $^1J_{Rh,P}$ = 143.9 Hz). $C_{36}H_{53}O_4P_2RhS$ (746.7): calcd. 57.90, H 7.15; found C 58.06, H 6.97.

Preparation of [Rh(C≡CPh)(=C=CHPh)(P*i*Pr$_2$Ph)$_2$] (36): a) A solution of **12** (100 mg, 0.15 mmol) in a 1:1 mixture of toluene and freshly distilled triethylamine (5 mL) was treated with phenylacetylene (34 μL, 0.30 mmol) and stirred for 5 min at −20 °C. A smooth change of color from red to dark green occurred. After warming the solution to room temperature, the solvent was evaporated in vacuo and the residue was extracted with 25 mL of ether (0° C). The extract was dried in vacuo, the remaining residue was dissolved in 5 mL of pentane (0° C) and the solution stored at this temperature. Turquoise crystals precipitated after 1 min, which were filtered, washed twice with 1-mL portions of pentane (0 °C) and dried; yield 35 mg (34%).

b) A solution of **34** (107 mg, 0.14 mmol) in a 1:1 mixture of toluene and freshly distilled triethylamine (5 mL) was treated at −50 °C with phenylacetylene (15 μL, 0.14 mmol). A quick change of color from violet to dark green occurred. After warming the solution to room temperature, it was worked up as described for a). Turquoise crystals were obtained; yield 54 mg (56%); m.p. 78 °C (dec.). IR (KBr): ν(C≡C) = 2060, ν(C=C) = 1635 cm^{-1}. ^{1}H NMR (200 MHz, C_6D_6): δ = 7.78−6.78 (m, 20 H, C_6H_5), 2.87 (m, 4 H, PC*H*CH$_3$), 1.42 (dvt, N = 17.9, $^3J_{H,H}$ = 6.9 Hz, 12 H, PCHCH_3), 1.28 (dt, $^3J_{Rh,H}$ = 0.7, $^4J_{P,H}$ = 3.7 Hz, 1 H, =C*H*Ph), 1.06 (dvt, N = 13.9, $^3J_{H,H}$ = 6.9 Hz, 12 H, PCHCH_3). ^{31}P NMR (81.0 MHz, C_6D_6): δ = 46.8 (d, $^1J_{Rh,P}$ = 141.0 Hz). $C_{40}H_{49}P_2Rh$ (694.7): calcd. C 69.16, H 7.11, Rh 14.81; found C 68.62, H 7.08, Rh 14.40.

Preparation of [Rh(C≡CCMe$_2$OH)(=C=CHCMe$_2$OH)(P*i*Pr$_2$Ph)$_2$] (37): This compound was prepared as described for **36**, either according to method a) from **12** (106 mg, 0.16 mmol) and HC≡CCMe$_2$(OH) (32 μL, 0.32 mmol) or according to method b) from **35** (106 mg, 0.14 mmol) and HC≡CCMe$_2$(OH) (14 μL, 0.14 mmol). Dark green solid; yield 47 mg (45%) for a) and 63 mg (68%) for b); m.p. 78 °C (dec.). IR (KBr): ν(OH) = 3555, 3540, ν(C≡C) = 2060, ν(C=C) = 1625 cm^{-1}. ^{1}H NMR (200 MHz, C_6D_6): δ = 7.44−7.04 (m, 10 H, C_6H_5), 2.88 (m, 4 H, PC*H*CH$_3$), 1.62 (s, 1 H, OH), 1.45 [s, 6 H, C(CH_3)$_2$OH], 1.36 (dvt, N = 16.1, $^3J_{H,H}$ = 7.3 Hz, 12 H, PCHCH_3), 1.06 (dvt, N = 13.5, $^3J_{H,H}$ = 6.2 Hz, 12 H, PCHCH_3), 0.92 [s, 6 H, C(CH_3)$_2$OH], 0.21 (dt, $^3J_{Rh,H}$ = 0.7, $^4J_{P,H}$ = 3.7 Hz, 1 H, =CHR), signal of the second OH proton not found. ^{31}P NMR (81.0 MHz, C_6D_6): δ = 45.7 (d, $^1J_{Rh,P}$ = 142.4 Hz). $C_{34}H_{53}O_2P_2Rh$ (658.7): calcd. C 62.00, H 8.11; found C 61.59, H 8.10.

Preparation of [Rh(C≡CCMe$_2$OH)(=C=CHPh)(P*i*Pr$_2$Ph)$_2$] (38): A solution of **34** (115 mg, 0.15 mmol) in a 1:1 mixture of toluene and freshly distilled triethylamine (5 mL) was treated at −50 °C with HC≡CCMe$_2$(OH) (15 μL, 0.15 mmol) and stirred for 5 min at this temperature. A change of color from violet to dark green occurred. After warming the solution to room temperature, the solvent was evaporated in vacuo. The residue was extracted with 25 mL of ether (0 °C) and the extract was dried in vacuo. The residue was dissolved in 3 mL of acetone (0 °C) and the solution stored for 3 min at this temperature. Dark green crystals precipitated, which were filtered, washed twice with 1-mL portions of acetone (0 °C) and dried; yield 40 mg (39%); m.p. 98 °C (dec.). IR (KBr): ν(OH) = 3350, ν(C≡C) = 2060, ν(C=C) = 1635 cm^{-1}. ^{1}H NMR (200 MHz, C_6D_6): δ = 7.44−7.04 (m, 15 H, C_6H_5), 3.12 (m, 4 H, PC*H*CH$_3$), 1.60 (dvt, N = 15.7, $^3J_{H,H}$ = 8.0 Hz, 12 H, PCHCH_3), 1.20 (dvt, N = 13.3, $^3J_{H,H}$ = 6.6 Hz, 12 H, PCHCH_3), 1.07 [s, 6 H, C(CH_3)$_2$OH], 0.96 (dt, $^3J_{Rh,H}$ = 0.8, $^4J_{P,H}$ = 3.6 Hz, 1 H, =CHR), signal of OH proton not found. ^{31}P NMR (162.0 MHz, C_6D_6): δ = 45.9 (d, $^1J_{Rh,P}$ = 141.0 Hz). $C_{37}H_{51}OP_2Rh$ (676.7): calcd. C 65.68, H 7.60; found C 65.33, H 7.48.

Preparation of *trans*-[Rh{(*Z*)-C(=CHPh)C≡CPh}(CO)(P*i*Pr$_2$Ph)$_2$] (39): A slow stream of CO was passed through a solution of **36** (97 mg, 0.14 mmol) in CH_2Cl_2 (5 mL) at −20 °C for 10 s. A change of color from dark green to yellow occurred. After warming the solution to room temperature, the solvent was evaporated in vacuo. The residue was extracted with 25 mL of acetone (10 °C) and the extract was dried in vacuo. The remaining yellow solid was washed twice with 1-mL portions of acetone (0 °C) and dried; yield 87 mg (86%); m.p. 144 °C (dec.). IR (KBr): ν(C≡C) = 2120, ν(CO) = 1955 cm^{-1}. ^{1}H NMR (200 MHz, C_6D_6): δ = 8.07 (dt, $^3J_{Rh,H}$ = 2.2, $^4J_{P,H}$ = 9.5 Hz, 1 H, =C*H*Ph), 7.81−6.94 (m, 20 H, C_6H_5), 2.78, 2.41 (both m, 2 H each, PC*H*CH$_3$), 2.26 (dvt, N = 15.9, $^3J_{H,H}$ = 7.0 Hz, 6 H, PCHCH_3), 1.13 (dvt, N = 15.0, $^3J_{H,H}$ = 7.3 Hz, 6 H, PCHCH_3), 0.87 (dvt, N = 15.2, $^3J_{H,H}$ = 6.6 Hz, 6 H, PCHCH_3), 0.65 (dvt, N = 16.1, $^3J_{H,H}$ = 7.3 Hz, 6 H, PCHCH_3). ^{31}P NMR (81.0 MHz, C_6D_6): δ = 41.4 (d, $^1J_{Rh,P}$ = 145.3 Hz). $C_{41}H_{49}OP_2Rh$ (722.7): calcd. C 68.14, H 6.83; found C 67.80, H 7.28.

Preparation of *trans*-[Rh{(*Z*)-C(=CHCMe$_2$OH)C≡CCMe$_2$OH}(CO)(P*i*Pr$_2$Ph)$_2$] (40): This compound was prepared as described for **39**, with **37** (86 mg, 0.13 mmol) and CO as starting materials. Yellow solid; yield 75 mg (84%); m.p. 80 °C (dec.). IR (KBr): ν(C≡C) = 2160, ν(CO) = 1955 cm^{-1}. ^{1}H NMR (200 MHz, C_6D_6): δ = 8.20−7.34 (m, 10 H, C_6H_5), 7.18 (dt, $^3J_{Rh,H}$ = 2.6, $^4J_{P,H}$ = 2.2 Hz, 1 H, =C*H*R), 4.64 (s, 1 H, OH), 3.00, 2.73 (both m, 2 H each, PC*H*CH$_3$), 2.00 (s, 1 H, OH), 1.97 [s, 6 H, C(CH_3)$_2$OH], 1.70 (dvt, N = 16.5, $^3J_{H,H}$ = 9.5 Hz, 6 H, PCHCH_3), 1.46 [s, 6 H, C(CH_3)$_2$OH], 1.42 (dvt, N = 13.9, $^3J_{H,H}$ = 8.4 Hz, 6 H, PCHCH_3), 1.35 (dvt, N = 12.1, $^3J_{H,H}$ = 6.6 Hz, 6 H, PCHCH_3), 1.25 (dvt, N = 13.9, $^3J_{H,H}$ = 7.3 Hz, 6 H, PCHCH_3). ^{31}P NMR (81.0 MHz, C_6D_6): δ = 39.1 (d, $^1J_{Rh,P}$ = 142.4 Hz). $C_{35}H_{53}O_3P_2Rh$ (686.7): calcd. C 61.22, H 7.78; found C 61.53, H 7.72.

Preparation of *trans*-[Rh{(*Z*)-C(=CHPh)C≡CCMe$_2$OH}(CO)(P*i*Pr$_2$Ph)$_2$] (41): This compound was prepared as described for **39**,

with **38** (101 mg, 0.15 mmol) and CO as starting materials. Yellow oil; yield 40 mg (38%). IR (KBr): ν(C≡C) = 2070, ν(CO) 1950 cm^{-1}. ^{1}H NMR (200 MHz, C_6D_6): δ = 7.93−7.25 (m, 15 H, C_6H_5), 7.20 (dt, $^3J_{Rh,H}$ = 2.4, $^4J_{P,H}$ = 2.2 Hz, 1 H, =C*H*R), 4.53 (s, 1 H, OH), 2.77, 2.51 (both m, 2 H each, PC*H*CH$_3$), 1.46 (dvt, *N* = 16.5, $^3J_{H,H}$ = 6.9 Hz, 6 H, PCHC*H*$_3$), 1.25 (dvt, *N* = 15.7, $^3J_{H,H}$ = 6.9 Hz, 6 H, PCHC*H*$_3$), 1.23 [s, 6 H, C(C*H*$_3$)$_2$OH], 1.12 (dvt, *N* = 13.5, $^3J_{H,H}$ = 6.9 Hz, 6 H, PCHC*H*$_3$), 1.00 (dvt, *N* = 14.3, $^3J_{H,H}$ = 6.6 Hz, 6 H, PCHC*H*$_3$). ^{31}P NMR (81.0 MHz, C_6D_6): δ = 39.1 (d, $^1J_{Rh,P}$ = 140.9 Hz). $C_{38}H_{51}O_2P_2Rh$ (704.7): calcd. C 64.77 H 7.29, Rh 14.60; found C 64.68 H 7.34, Rh 14.22.

Determination of the X-ray Crystal Structure of 27: Single crystals were grown upon diffusion of ether into a saturated solution of **27** in CH_2Cl_2/methylcyclohexane. Crystal data (from 23 reflections, 10° < Θ < 14°): monoclinic; space group $P2_1/c$ (No. 14); *a* = 10.496(5), *b* = 17.455(5), *c* = 18.629(7) Å, β = 97.33(2)°; *V* = 3385(2) Å^3, *Z* = 4; $d_{calcd.}$ = 1.387 g cm^{-3}; μ(Mo-K_α) = 7.0 cm^{-1}; crystal size 0.23 × 0.38 × 0.48 mm; Enraf−Nonius CAD4, Mo-K_α radiation (0.71073 Å), graphite monochromator; *T* = 293(2) K; Θ-scan, max. 2Θ = 47.94°; 5011 reflections measured, 4691 independent, 3135 with $I > 2\sigma(I)$. Intensity data were corrected for Lorentz and polarization effects and an empirical absorption correction was applied. The structure was solved by direct method (SHELXS-86).[28] Atomic coordinates and anisotropic thermal parameters of the non-hydrogen atoms were refined by full-matrix least-squares method using the program package SDP from Enraf−Nonius. The hydrogen atoms H1 and H3 were found in a difference-Fourier synthesis and refined isotropically. The positions of all other hydrogen atoms were calculated according to ideal geometry and refined with the riding method. Conventional R = 0.0421 and weighted wR_2 = 0.0857 [for data with $I > 2\sigma(I)$]; R = 0.1019 and weighted wR_2 = 0.0991 (for all data); reflection/parameter ratio 12.1; residual electron density +0.939/−0.323 eÅ^{-3}.

CCDC-175652 contains the supplementary crystallographic data for this paper. These data can be obtained free of charge at www.ccdc.cam.ac.uk/conts/retrieving.html [or from the Cambridge Crystallographic Data Centre, 12, Union Road, Cambridge CB2 1EZ, UK; Fax: (internat.) +44-1223/336-033; E-mail: deposit@ccdc.cam.ac.uk].

Acknowledgments

This work was supported by the Deutsche Forschungsgemeinschaft (SFB 347) and the Fonds der Chemischen Industrie. We thank Mrs. R. Schedl and Mr. C. P. Kneis for elemental analysis and DTA measurements, Mrs. M.-L. Schäfer and Dr. W. Buchner for NMR spectra, Dr. G. Lange and Mr. F. Dadrich for mass spectra, and Mr. C. D. Brandt for drawing the molecular diagram.

[1] Reviews: [1a] H. Werner, *Nachr. Chem. Tech. Lab.* **1992**, *40*, 435−444. [1b] H. Werner, *J. Organomet. Chem.* **1994**, *475*, 45−55. [1c] H. Werner, *Chem. Commun.* **1997**, 903−910.
[2] H. Werner, M. Schäfer, O. Nürnberg, J. Wolf, *Chem. Ber.* **1994**, *127*, 27−38.
[3] [3a] M. Schäfer, N. Mahr, J. Wolf, H. Werner, *Angew. Chem.* **1993**, *105*, 1377−1379; *Angew. Chem. Int. Ed. Engl.* **1993**, *32*, 1315−1318. [3b] M. Schäfer, Dissertation, Universität Würzburg, **1994**.
[4] F. Kukla, H. Werner, *Inorg. Chim. Acta* **1995**, *235*, 253−261.
[5] Preparation: [5a] H. Werner, J. Wolf, A. Höhn, *J. Organomet. Chem.* **1985**, *287*, 395−407. Molecular structure: [5b] P. Binger, J. Haas, G. Glaser, R. Goddard, C. Krüger, *Chem. Ber.* **1994**, *127*, 1927−1929.
[6] H. Werner, A. Hampp, K. Peters, E. M. Peters, L. Walz, H. G. von Schnering, *Z. Naturforsch., Teil B* **1990**, *45*, 1548−1558.
[7] K. Vrieze, H. C. Volger, P. W. N. M. van Leeuwen, *Inorg. Chim. Acta, Rev.* **1977**, *16*, 211−239.
[8] [8a] S. D. Robinson, M. F. Uttley, *J. Chem. Soc., Dalton Trans.* **1973**, 1912−1920. [8b] G. B. Deacon, R. J. Phillips, *Coord. Chem. Rev.* **1980**, *33*, 227−250. [8c] D. A. Tocher, R. O. Gould, T. A. Stephenson, M. A. Bennett, J. P. Ennett, T. W. Matheson, L. Sawyer, V. K. Shah, *J. Chem. Soc., Dalton Trans.* **1983**, 1571−1581.
[9] [9a] D. N. Lawson, G. Wilkinson, *J. Chem. Soc.* **1965**, 1900−1907. [9b] F. Bianchi, M. C. Gallazzi, L. Porri, P. Diversi, *J. Organomet. Chem.* **1980**, *202*, 99−105. [9c] M. A. Arthurs, S. M. Nelson, *J. Coord. Chem.* **1983**, *13*, 29−40. [9d] F. J. Lahoz, A. Martin, M. A. Esteruelas, E. Sola, J. L. Serrano, L. A. Oro, *Organometallics* **1991**, *10*, 1794−1799.
[10] H. Werner, M. Bosch, M. E. Schneider, C. Hahn, F. Kukla, M. Manger, B. Windmüller, B. Weberndörfer, M. Laubender, *J. Chem. Soc., Dalton Trans.* **1998**, 3549−3558.
[11] M. Schäfer, J. Wolf, H. Werner, *J. Organomet. Chem.* **1995**, *485*, 85−100.
[12] H. Werner, M. Schäfer, J. Wolf, K. Peters, H. G. von Schnering, *Angew. Chem.* **1995**, *107*, 213−215; *Angew. Chem. Int. Ed. Engl.* **1995**, *34*, 191−194.
[13] H. Werner, M. Schulz, B. Windmüller, *Organometallics* **1995**, *14*, 3659−3668.
[14] [14a] J. P. Collman, J. N. Cawse, J. W. Kang, *Inorg. Chem.* **1969**, *8*, 2574−2579. [14b] B. E. Mann, B. L. Shaw, N. I. Tucker, *J. Chem. Soc. A* **1971**, 2667−2673. [14c] C. J. Elsevier, H. Kleijn, J. Boersma, P. Vermeer, *Organometallics* **1986**, *5*, 716−720. [14d] R.-S. Keng, Y.-C. Lin, *Organometallics* **1990**, *9*, 289−291. [14e] A. Wojcicki, C. E. Shuchart, *Coord. Chem. Rev.* **1990**, *105*, 35−60. [14f] C. E. Shuchart, R. R. Willis, A. Wojcicki, *J. Organomet. Chem.* **1992**, *424*, 185−198. [14g] J. M. A. Wouters, R. A. Klein, C. J. Elsevier, L. Häming, C. H. Stam, *Organometallics* **1994**, *13*, 4586−4593.
[15] H. Werner, R. Flügel, B. Windmüller, A. Michenfelder, J. Wolf, *Organometallics* **1995**, *14*, 612−618.
[16] [16a] R. Wiedemann, P. Steinert, M. Schäfer, H. Werner, *J. Am. Chem. Soc.* **1993**, *115*, 9864−9865. [16b] H. Werner, R. Wiedemann, P. Steinert, J. Wolf, *Chem. Eur. J.* **1997**, *3*, 127−137.
[17] [17a] M. Laubender, H. Werner, *Angew. Chem.* **1998**, *110*, 158−160; *Angew. Chem. Int. Ed.* **1998**, *37*, 150−152. [17b] M. Laubender, H. Werner, *Chem. Eur. J.* **1999**, *5*, 2937−2946.
[18] M. A. Esteruelas, F. J. Lahoz, E. Oñate, L. A. Oro, L. Rodriguez, P. Steinert, H. Werner, *Organometallics* **1996**, *15*, 3436−3444.
[19] T. L. Jacobs, in *The Chemistry of the Allenes* (Ed.: S. R. Landor), Vol. 2, Academic Press, London, **1982**, p. 334.
[20] I. P. Kovalev, K. V. Yevdakow, Yu. A. Strelenko, M. G. Vinogradov, G. I. Nikishin, *J. Organomet. Chem.* **1990**, *386*, 139−146.
[21] D. L. Reger, D. G. Garza, *Organometallics* **1993**, *12*, 554−558.
[22] H. Werner, J. Wolf, U. Schubert, K. Ackermann, *J. Organomet. Chem.* **1986**, *317*, 327−356.
[23] J. B. Hendrickson, *J. Am. Chem. Soc.* **1961**, *83*, 2018−2019.
[24] [24a] H. Werner, F. J. Garcia Alonso, H. Otto, H. Wolf, *Z. Naturforsch., Teil B* **1988**, *43*, 722−726. [24b] Y. Wakatsuki, N. Koga, H. Werner, K. Morokuma, *J. Am. Chem. Soc.* **1997**, *119*, 360−366.
[25] A. van der Ent, A. L. Onderdelinden, *Inorg. Synth.* **1973**, *14*, 92−95.
[26] K. Timmer, D. H. M. W. Thewissen, J. W. Marsman, *Recl. Trav. Chim. Pays-Bas* **1988**, *107*, 249−255.
[27] J. Ohshita, K. Furumori, A. Matsuguchi, M. Ishikawa, *J. Org. Chem.* **1990**, *55*, 3277−3280.
[28] G. M. Sheldrick, *Acta Crystallogr., Sect. A* **1990**, *46*, 467−473.

Received December 20, 2001
[I01519]

Luminescent Star-Shaped Zinc(II) and Platinum(II) Complexes Based on Star-Shaped 2,2′-Dipyridylamino-Derived Ligands

Corey Seward,[a] Jun Pang,[a] and Suning Wang*[a]

Keywords: Starburst molecules / Zinc / Platinum / N ligands / Luminescence

New Zn^{II} and Pt^{II} complexes of the star-shaped ligands 2,4,6-tris(2,2′-dipyridylamino)-1,3,5-triazine (tdat), 1,3,5-tris(2,2′-dipyridylamino)benzene (tdab), 2,4,6-tris[*p*-(2,2′-dipyridylamino)phenyl]-1,3,5-triazine (tdapt) and 1,3,5-tris[*p*-(2,2′-dipyridylamino)phenyl]benzene (tdapb) have been synthesized and characterized. 1:1, 1:2 and 1:3 (ligand vs. the number of Zn atoms) Zn^{II} complexes of the tdat ligand have been identified. The 1:1 and 1:2 Zn^{II} complexes of tdat are dynamic in solution. For the tdab, tdapt and tdapb ligands, only 1:3 complexes of Pt^{II} and Zn^{II} have been isolated. Single-crystal X-ray diffraction analyses have been carried out for some of these new complexes, which revealed that there is a distinct difference in the arrangement of star-shaped ligands in the complexes of Zn^{II} and those of Pt^{II}. The Pt^{II} complexes of tdat and tdab adopt an unusual "bowl" shape and stack in a "head-to-tail" fashion in the crystal lattice. In contrast, the corresponding Zn^{II} complexes do not have a "bowl" shape. The difference between the Zn^{II} complexes and the Pt^{II} complexes can be attributed to the different coordination geometry preferred by the two metal ions. The Zn^{II} complex of tdapb displays several crystal motifs, two of which contain benzene molecules in the crystal lattices. All complexes are luminescent in the blue region, attributable to ligand-based $\pi \rightarrow \pi^*$ transitions.
(© Wiley-VCH Verlag GmbH, 69451 Weinheim, Germany, 2002)

Introduction

Luminescent metal complexes are a fascinating class of molecules that have found applications in many areas of chemistry and materials science. For example, it has been demonstrated recently that luminescent metal compounds can function as emitters in light emitting devices (LEDs).[1] Luminescent compounds have been used widely as sensors and probes for a variety of chemical and biological substances.[2] Luminescent transition metal compounds have also been demonstrated as models/centers for photochemical devices/reactions.[3] There is an increasing demand for new luminescent metal compounds that can perform one or two desired functions, such as emitting light in organic LEDs or detecting certain molecules of environmental concern. Toward that goal, recently we developed a class of blue luminescent star-shaped organic molecules of 2,2′-dipyridylamino derivatives based on 2,4,6-trisubstituted triazine and 1,3,5-trisubstituted benzene (Scheme 1) that have been found to be promising blue emitters in organic LEDs.[4] Star-shaped luminescent organic molecules have been explored extensively as either emitters or host materials in organic LEDs due to their good film-forming properties.[5] The corresponding luminescent star-shaped metal complexes may offer new properties that are not present in the organic molecules. For example, in a recent preliminary communication we reported that the star-shaped ligand tdapb {tdapb = 1,3,5-tris[*p*-(2,2′-dipyridylamino)phenyl]-benzene} forms a 1:3 complex with $ZnCl_2$ that is blue luminescent and has a highly selective fluorescent response toward benzene.[6] The highly selective fluorescent response of the zinc star-shaped complex was attributed to the extended molecular architecture in the crystal lattice. We have now extended our investigation to metal complexes of other members of our star-shaped ligands and Pt^{II} complexes. Unlike the Zn^{II} ion, which prefers a tetrahedral geometry, the Pt^{II} ion adopts a square-planar geometry. Consequently, it is anticipated that the molecular shape of Pt^{II} complexes will be quite different from those of the corresponding Zn^{II} complexes. Furthermore, Pt^{II} centers tend to enhance phosphorescence but quench fluorescence from the ligand, due to their d^8 electronic configuration. The replacement of Zn^{II} ions by Pt^{II} ions in the complex could therefore lead to a significant change of luminescent properties. Some interesting molecular and extended structural variations and dynamic behaviors in solution have been observed in the new complexes. In the present paper, we give a full account on the results of our comparative study on syntheses, structures and luminescent properties of Zn^{II} and Pt^{II} complexes with the four star-shaped ligands listed in Scheme 1.

[a] Department of Chemistry, Queen's University, Kingston, Ontario, K7L 3N6, Canada
wangs@chem.queensu.ca

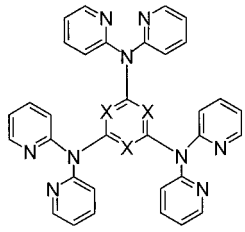

X = CH, tdab; X = N, tdat

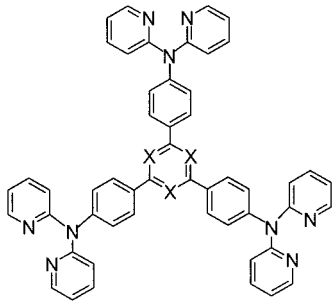

X = CH, tdapb; X = N, tdapt

Scheme 1

Results and Discussion

Syntheses and Structures

Zn^{II} Complexes of 2,4,6-Tris(2,2′-dipyridylamino)-1,3,5-triazine (tdat) and 1,3,5-Tris(2,2′-dipyridylamino)benzene (tdab)

The Zn^{II} complexes of tdat and tdab were obtained from the reactions of $ZnCl_2$ with the corresponding ligand in either CH_2Cl_2/THF solution or CH_2Cl_2/methanol solution. For the tdat ligand, by controlling the stoichiometry of the reaction, three Zn^{II} complexes, $(ZnCl_2)$(tdat) (**1a**), $(ZnCl_2)_2$(tdat) (**1b**), and $(ZnCl_2)_3$(tdat) (**1c**) with a tdat ligand/Zn^{II} ratio of 1:1, 1:2 and 1:3, respectively, were obtained and characterized. However, for the tdab ligand, only the 1:3 complex $(ZnCl_2)$(tdab) (**2**) was isolated, regardless of the ratio of the tdab ligand to $ZnCl_2$ employed in the reaction. The tdat and tdab Zn^{II} complexes are all stable under air in solution and in the solid state. Except for **1a**, these complexes are scarcely soluble in common organic solvents. Compounds **1a**−**1c** and **2** were characterized by ^{1}H NMR spectroscopy and elemental analyses. Single crystals of **1b** and **2**, suitable for X-ray diffraction analyses were obtained and their structures were determined by X-ray diffraction experiments. The crystal structures of **1b** and **2** are shown in Figures 1 and 2, respectively. Selected bond lengths and angles are given in Table 1.

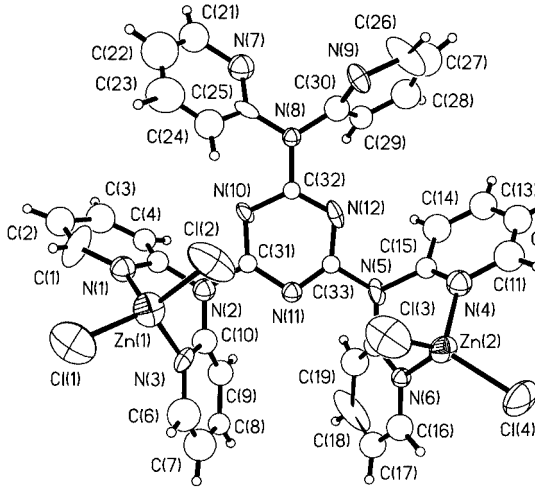

Figure 1. Molecular structure of **1b** with 50% thermal ellipsoids and labeling schemes

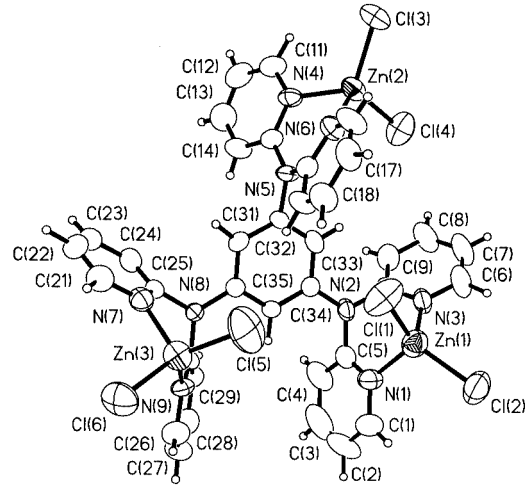

Figure 2. Molecular structure of **2** with 50% thermal ellipsoids and labeling schemes

As shown by Figure 1, the two $ZnCl_2$ units are chelated by two of the dipyridylamino groups in the tdat ligand in **1b** with a typical tetrahedral geometry and normal bond lengths.[7] The third dipyridylamino group does not coordinate. The two $ZnCl_2$ units are on the same side with respect to the triazine ring. The Zn(1)−Zn(2) distance is 7.302(2) Å. Based on the structure of **1b**, we can assume that in the 1:1 complex **1a** the $ZnCl_2$ unit is chelated by the dipyridylamino group in the same manner as observed in **1b**. Because of the existence of both coordinated and noncoordinated dipyridylamino groups in **1b**, one would expect that three sets of chemical shifts for the pyridyl groups (the two pyridyl groups bound to the Zn^{II} ion are not equivalent) should be observed in the ^{1}H NMR spectrum of **1b**. Similarly, three sets of chemical shifts for the pyridyl groups a, b and c (see Scheme 2) are expected for compound **1a**. However, at ambient temperature only one set of pyridyl chemical shifts was observed for both compounds **1a** and **1b**, which leads us to believe that there is a dynamic exchange for compounds **1a** and **1b** in solution. Compound **1b** does not have appreciable solubility in common organic solvents such as CH_2Cl_2, $CHCl_3$ or THF, precluding any low-temperature

Table 1. Range of selected bond lengths [Å] and angles [°] for **1b**, **2**−**4**, **6a** and **6b**

	M−Cl range	M−N range	C−N range	C−C range
1b	2.190(6)−2.221(5)	1.977(14)−2.067(13)	1.274(16)−1.447(19)	1.27(2)−1.46(2)
2	2.2820(17)−2.2209(16)	2.017(4)−2.075(4)	1.331(5)−1.438(5)	1.344(8)−1.411(9)
3	2.273(8)−2.331(8)	2.041(19)−2.07(2)	1.22(2)−1.48(3)	1.24(4)−1.55(4)
4	2.284(3)−2.286(3)	2.018(8)−2.025(8)	1.325(12)−1.464(17)	1.302(17)−1.393(12)
6a	2.190(3)−2.198(3)	2.017(8)−2.051(8)	1.315(11)−1.467(10)	1.321(16)−1.512(11)
6b	2.148(4)−2.212(3)	1.9696(11)−2.052(9)	1.326(12)−1.473(11)	1.336(15)−1.526(12)
	Cl−M−Cl range	Cl−M−N range	N−M−N range	
1b	120.0(2)−121.5(2)	105.2(5)−114.2(4)	88.4(6)−91.4(5)	
2	117.97(7)−123.05(7)	102.51(13)−118.16(13)	87.95(16)−89.00(17)	
3	89.3(3)−91.3(4)	89.6(6)−179.4(7)	89.0(8)−90.6(10)	
4	90.0(3)−91.29(12)	89.9(2)−178.4(2)	87.4(5)−87.8(3)	
6a	116.85(16)−117.24(14)	108.0(2)−116.4(2)	90.4(3)−90.6(3)	
6b	119.58(15)−122.80(14)	105.2(3)−116.0(3)	88.8(5)−90.1(4)	
	C−N−C range	C−C−N range	C−C−C range	
1b	111.7(15)−121.9(16)	116(2)−127.7(18)	111(2)−125(2)	
2	115.8(4)−126.5(4)	117.7(5)−124.6(6)	115.4(5)−121.5(5)	
3	112(3)−128(2)	116(3)−125(3)	115(3)−127(3)	
4	114.7(11)−122.8(7)	118.4(6)−123.5(8)	118.4(9)−123.2(12)	
6a	116.0(7)−127.8(7)	117.3(8)−125.6(10)	116.1(11)−124.3(11)	
6b	113.9(9)−129.5(9)	116.0(11)−128.2(12)	114.7(15)−123.6(12)	

NMR experiments. Compound **1a** has a sufficient solubility in CH_2Cl_2 and allows us to carry out variable-temperature ^{1}H NMR experiments. The ^{1}H NMR spectra of **1a** over the temperature range of 180−298 K recorded in CD_2Cl_2 are shown in Figure 3, which confirms the existence of dynamic exchange of **1a** in solution. If compound **1a** retains its structure as shown in Scheme 2, twelve chemical shifts corresponding to three sets of pyridyl groups should be observed in the ^{1}H NMR spectrum of **1a**. The 180 K spectrum of **1a** displays eleven reasonably resolved peaks with some overlaps, indicating that **1a** indeed retains the expected structure in solution at low temperature. However, at ambient temperature, it undergoes a rapid exchange process, which might be attributed to an intramolecular "merry-go-round" by the $ZnCl_2$ unit as shown by Scheme 2. Alternatively, an intermolecular process that involves the dissociation of $ZnCl_2$ from the ligand and the reattachment to the ligand is also possible. Given the fact that no intermolecular exchange was observed in our previously reported Zn^{II} complexes involving dipyridyl chelate ligands,[8] we believe that the intramolecular process is most likely responsible for the dynamic exchange of **1a**. A similar exchange process is also believed to be responsible for the observed dynamic behavior of **1b**.

As shown in Figure 2, the three $ZnCl_2$ units in compound **2** are all chelated by dipyridylamino groups in the same manner as observed for compound **1b**. Two of the $ZnCl_2$ units are on the same side with respect to the central phenyl ring. However, the third $ZnCl_2$ unit is nearly parallel to the central phenyl ring with the two attached pyridyl rings above and below, respectively. The Zn(1)−Zn(3) separation distance of 7.148(2) Å − the shortest Zn−Zn distance in **2** [Zn(1)−Zn(2) = 7.602(2) Å, Zn(2)−Zn(3) = 9.376(1) Å] − is considerably shorter than that of **1b**. The tdat 1:3 complex **1c** is believed to have a structure similar to **2**.

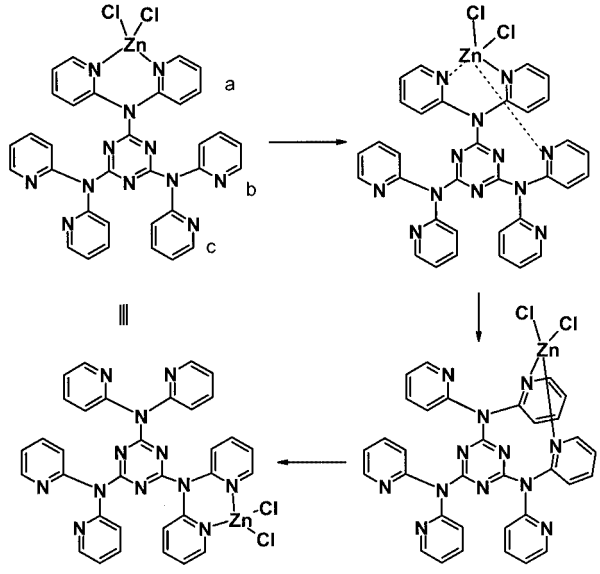

Scheme 2

Pt^{II} Complexes of tdat and tdab

The light yellow 1:3 Pt^{II} complexes of tdat and tdab, **3** and **4**, were obtained from the reactions of the corresponding ligands with K_2PtCl_4 in a 1:3 ratio by using a solvent-layering/slow diffusion method. This procedure is necessary to obtain sufficiently large single crystals of **3** and **4** for X-

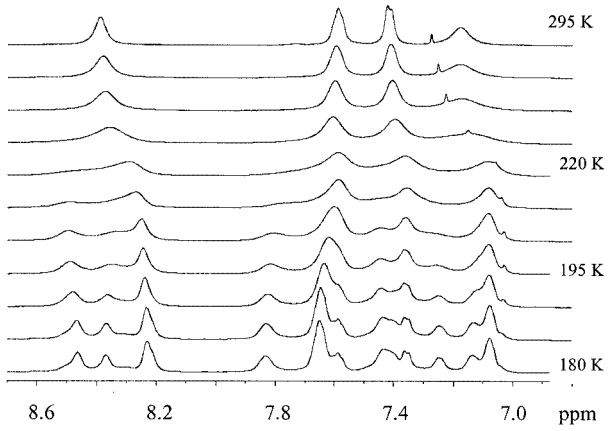

Figure 3. Variable-temperature ^{1}H NMR spectra of **1a** in CD_2Cl_2

ray diffraction analyses, due to the insolubility of the resulting complexes in organic solvents. Compounds **3** and **4** are stable in air. Because of the insolubility of **3** and **4** in organic solvents such as CH_2Cl_2 and DMSO, we were unable to obtain their ^{1}H NMR spectra. These two compounds were characterized by elemental analyses and single-crystal X-ray diffraction analyses. The structures of **3** and **4** are shown in Figures 4 and 6, respectively. Selected bond lengths and angles are listed in Table 1.

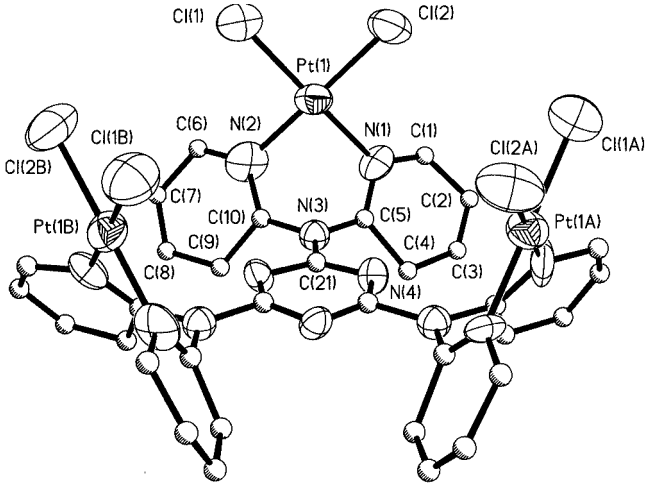

Figure 4. Molecular structure of one of the independent molecules of **3** with 50% thermal ellipsoids and labeling schemes; hydrogen atoms were omitted for clarity and carbon atoms are shown as ideal spheres

Compound **3** crystallizes in two different crystal lattices, hexagonal $R3c$ and monoclinic $P2_1/m$. The monoclinic form of **3** is isomorphous with that of **4**. Therefore, the discussion here focuses on the hexagonal form. There are two independent molecules of **3** in the asymmetric unit cells with similar structures. One of the independent molecules is shown in Figure 4. The three $PtCl_2$ groups in **3** are chelated by dipyridylamino units, resulting in a square-planar geometry for each of the Pt^{II} centers. The Pt−Cl and Pt−N bond lengths in **3** are normal.[3,9] Each molecule of **3** has a crystallographically imposed C_3 rotation symmetry. The intramolecular Pt−Pt separation distances of **3** are 7.710(2) Å and 7.570(2) Å, respectively, for the two independent molecules. The most remarkable feature of **3** is that all three $PtCl_2$ units are oriented on the same side of the triazine ring, thus forming a "bowl-shaped" structure. The absence of the "bowl" structure for compound **2** can be explained by the fact that this would bring the chloride ligands into close contact with each other because of the tetrahedral geometry of the Zn^{II} ion. The second remarkable feature of **3** is that the molecules of **3** stack in the crystal lattice along the C_3 axis, like a stack of bowls (Figure 5). The two neighboring molecules within the stack are rotated by about 40° with respect to each other, resulting in the formation of a polar column. Furthermore, these stacks of **3** are oriented to the same direction, thus resulting in the formation of the polar crystal lattice. The polar axial stacking of **3** could be attributed to intermolecular electrostatic interactions between the electronegative chloride ligands and the electropositive protons of the tdat ligand. The shortest intermolecular separation distance between the chlorine atom and the carbon atoms of the tdat ligand is 3.66 Å. The polar molecular stacking in the crystal lattice as displayed by compound **3** is quite uncommon and very interesting since it may lead to some unusual physical properties (i.e. nonlinear optical properties). We have not been able to

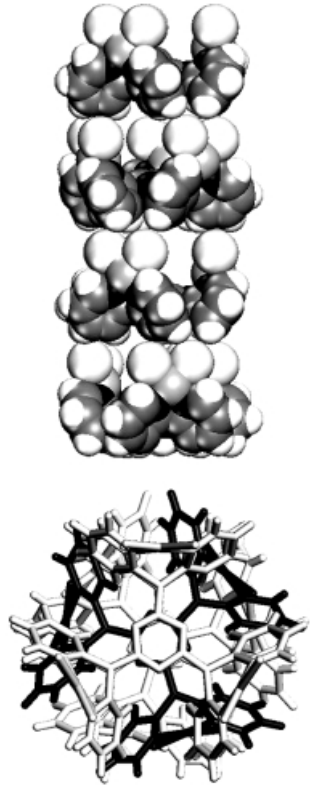

Figure 5. View of the stacking column of **3** projected along the C_3 axis (space-filling), and a view of the stacking column of **3** projected down the C_3 axis (stick)

study the optical/physical properties of the needle-like single-crystals of **3** because of their small sizes (< 0.1 mm in diameter).

The monoclinic form of compound **4** was identified and belongs to the centric monoclinic space group $P2_1/m$ with a crystallographically imposed mirror plane, upon which Pt(1), N(2), C(16) and C(19) lie. The structure of **4** is similar to that of **3**, except that the intramolecular Pt−Pt separation distances [8.271(2) Å, 8.279(2) Å] are much longer than those of **3** [the Pt−Pt separation distances of **3** in the $P2_1/m$ lattice are 7.829(2) Å and 8.069(2) Å], which could be attributed to the protons on the central phenyl ring in **4** that cause greater nonbonding interactions between the central phenyl ring and the pyridyl groups, compared to **3**. The major difference between the hexagonal form of **3** and the monoclinic form of **3** or **4** is the crystal lattice packing. In the crystal lattice of **4**, instead of stacking directly upon each other, the molecules are stacked in a "stair" fashion with a head-to-tail arrangement. In addition, the stacks of the molecules of **4** are oriented in two opposite directions as shown in Figure 6, thus resulting in a nonpolar crystal lattice. In the crystal lattices of **3** and **4** solvent molecules such as CH_2Cl_2 and H_2O were found, some of which were found to be trapped within the stacked column or inside the "bowl" of the Pt^{II} complex.

Zn^{II} Complexes of 2,4,6-Tris[p-(2,2′-dipyridylamino)-phenyl]-1,3,5-triazine (tdapt) and 1,3,5-Tris[p-(2,2′-dipyridylamino)phenyl]benzene (tdapb)

The colorless 1:3 zinc(II) complexes of tdapt and tdapb, namely $(ZnCl_2)_3$(tdapt) (**5**) and $(ZnCl_2)_3$(tdapb) (**6**) were obtained from the reactions of $ZnCl_2$ with the corresponding ligands in a 3:1 ratio in CH_2Cl_2/methanol solution. Both compounds are air-stable and have moderate solubility in organic solvents and have been characterized by elemental analyses and ^1H NMR spectroscopy. Attempts to obtain single crystals of **5** for X-ray diffraction analysis were unsuccessful. Compound **6** displays three different crystal motifs, depending on the solvent and the amount of each solvent used during crystallization. The first motif belongs to hexagonal space group $R\bar{3}$ with the formula $(ZnCl_2)_3$(tdapb)·$0.25C_6H_6$·$3CH_2Cl_2$ (**6a**), obtained from the solution of CH_2Cl_2 with a small amount of benzene. The second and third motifs belong to the triclinic space group $P\bar{1}$ with the formula $(ZnCl_2)_3$(tdapb)·$3C_6H_6$ (**6b**) and $(ZnCl_2)_3$(tdapb)·H_2O (**6c**), obtained from a solution of 1:1 CH_2Cl_2/benzene, and a methanol solution, respectively. Each of the crystal motifs was investigated by X-ray diffraction. The details of crystal structures of **6a** and **6b** are presented here. The molecular structure of the $(ZnCl_2)_3$(tdapb) molecule in all three motifs is similar, with an approximate C_3 symmetry. The C_3 symmetry for **6a** as shown in Figure 7 is rigorously imposed by the crystal symmetry. The molecular structure of compound **5** is believed to be similar to that of **6**. In the same manner as observed for compounds **1b** and **2**, the three $ZnCl_2$ units in compound **6** are chelated by the dipyridylamino groups with a typical tetrahedral geometry. The three $ZnCl_2$ units in **6a** are all on the same side with respect to the central phenyl ring. In the crystal lattice of **6a**, the two nearest molecules of **6** are paired and staggered in a *face-to-face* fashion with an intermolecular separation between the central phenyl rings of 3.85(1) Å. These pairs stack along the *c* axis to form a hexagonal column. As shown in Figure 8, a benzene molecule is situated directly above the central phenyl ring and sandwiched by two pairs of the Zn^{II} complex. The separation distance between the benzene molecule and the two central phenyl rings of **6** is 3.60(1) Å, indicative of the presence of π−π stacking interactions.

Figure 6. Stick diagram showing the stacking of **4** in the crystal lattice

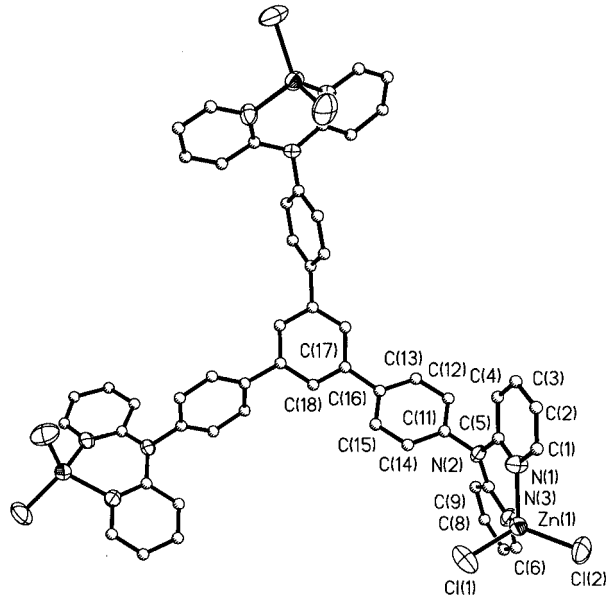

Figure 7. Molecular structure of one of the independent molecules of **6a** with 50% thermal ellipsoids and labeling schemes; hydrogen atoms are omitted for clarity; carbon atoms are shown as ideal spheres

There are three benzene solvent molecules per molecule of **6** in the crystal lattice of **6b**, which do not stack with the Zn^{II} complex in the *face-to-face* manner as observed in **6a**. Two of the benzene molecules are nearly perpendicular to the tdapb ligand while the remaining one is somewhat parallel to the tdapb ligand, but is perpendicular to a neighbor-

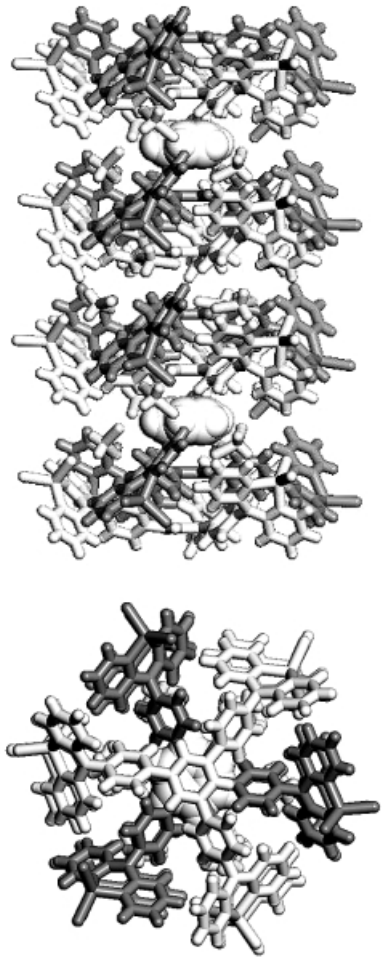

Figure 8. Diagram showing the pairing of **6a** (light gray and dark gray) and its stacking with benzene (space-filling) projected along the C_3 axis (left) and down the C_3 axis (right)

ing tdapb ligand of an adjacent molecule in the lattice. The π-π interactions in **6b** are therefore both *edge-to-face* and *face-to-face*.[10] The benzene solvent molecules are all located in the channels of the crystal lattice as shown by the unit cell packing diagram in Figure 9. The crystals of **6a** and **6b** indicate that compound **6** has a high affinity toward benzene in the solid state. In a recent report, we demonstrated that compound **6** is a highly selective fluorescent sensor for benzene vapor,[6] attributable to the high affinity of compound **6** in the solid state toward benzene. The free ligand tdapb is not effective as a fluorescent sensor for benzene, despite its bright blue luminescence. We believe that the coordination of the Zn^{II} ions to the tdapb ligand makes possible the formation of extended architectures in the solid state that attract benzene molecules and allow them to interact with the luminescent center effectively.

Pt^{II} Complexes of tdapt and tdapb

The 1:3 Pt^{II} complexes of tdapt and tdapb, namely $(PtCl_2)_3$(tdapt) (**7**) and $(PtCl_2)_3$(tdapb) (**8**) were obtained by using the same procedure as employed for **3** and **4**. Compounds **7** and **8** are insoluble in organic solvents, which precluded their study by solution NMR spectroscopy. Both

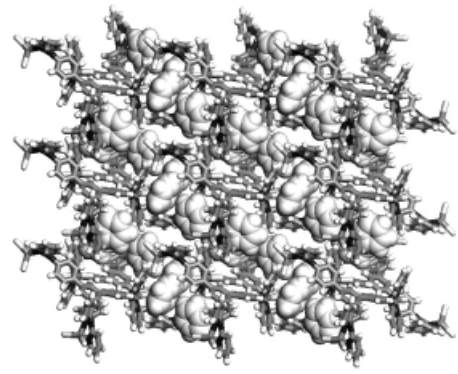

Figure 9. Unit cell packing diagram projected down the *b* axis; the benzene solvent molecules are highlighted as space-filling models

compounds form very thin, hair-like light yellow needles, too small for X-ray diffraction studies. Their compositions were confirmed by elemental analyses. We believe that the three $PtCl_2$ units in **7** and **8** are chelated by the dipyridylamino groups of the tdapt or tdapb ligand in the same manner as observed for compounds **3** and **4**.

Luminescent Properties

The free ligands tdat, tdab, tdapt and tdapb are blue-luminescent with a high quantum efficiency.[4] The nature of the emission of the free ligands is fluorescent, attributable to π→π* transitions. The Zn^{II} and Pt^{II} complexes of these ligands have also been found to be luminescent with broad emission bands that cover most of the blue region and resemble those of the free ligands. Therefore, we believe that the observed luminescence of the Zn^{II} and Pt^{II} complexes are ligand-based π→π* transitions localized mostly on the dipyridylamino chromophore. The luminescent intensity of the complexes is in general much weaker than that of the corresponding free ligand. For the Zn^{II} complexes, the decrease of luminescent intensity can be attributed to the chloride ligand, which is known to quench fluorescence through "heavy atom effects". The decrease of luminescent intensity of the Pt^{II} complexes can be attributed to the Pt^{II} center, which is an effective quencher of ligand fluorescence. No significant phosphorescence was observed for the Pt^{II} complexes. The luminescent data were obtained in solution and in the solid state for most of the Zn^{II} complexes. Because of their insolubility in organic solvents, only luminescent data in the solid state were obtained for the Pt^{II} complexes. For comparison purposes, the emission data of the free ligands (the details of luminescent data for the free ligands can be found in ref.[4]) are listed in Table 2, along with the luminescent data of the complexes. As a representative example, the emission spectra of tdapb and its Zn^{II} and Pt^{II} complexes **6** and **8** in the solid state are shown in Figure 10. The emission spectra of tdat and tdapt complexes are in general much broader than those of tdab and tdapb complexes. The contribution of the central triazine ring to the emission is likely to be responsible for the broad emission band. As shown in Table 2, the Zn^{II} complexes of tdab and tdapb show a significant red shift of

Table 2. Luminescence data

	Solution (CH_2Cl_2)			Solid	
	Excitation (λ_{max})	Emission (λ_{max})	Φ	Excitation (λ_{max})	Emission (λ_{max})
tdat	371	433	0.43	397	469
$(ZnCl_2)$(tdat) (**1a**)	295	418	0.011		
$(ZnCl_2)_2$(tdat) (**1b**)	292	399	0.08		
$(ZnCl_2)_3$(tdat) (**1c**)	292	318, 378	0.038	318	380
$(PtCl_2)_3$(tdat) (**3**)				346	414
tdab	385	412	0.53	387	412
$(ZnCl_2)_3$(tdab) (**2**)	316	426	0.097	385	447
$(PtCl_2)_3$(tdab) (**4**)				347	411
tdapt	420	440	0.78	423	461
$(ZnCl_2)_3$(tdapt) (**5**)	358	445	0.15	446	505
$(PtCl_2)_3$(tdapt) (**7**)				323	390
tdapb	367	384	0.16	380	409
$(ZnCl_2)_3$(tdapb) (**6**)	331	464	0.089	381	432
$(PtCl_2)_3$(tdapb) (**8**)				324	376

emission energy in solution, in comparison to the free ligands, which is consistent with our previously reported Zn^{II} complexes of tripyridylamines where two of the pyridyl groups are chelated to the Zn^{II} center and a similar red shift was observed.[7] The most dramatic red shift was displayed by the tdapt complex **5** which has an emission maximum at 505 nm in the solid state, even though it does not display a significant red shift in solution. This red shift is believed to be associated with intermolecular interactions of **5** in the solid state, but the details are not understood due to the lack of crystal data for **5**.

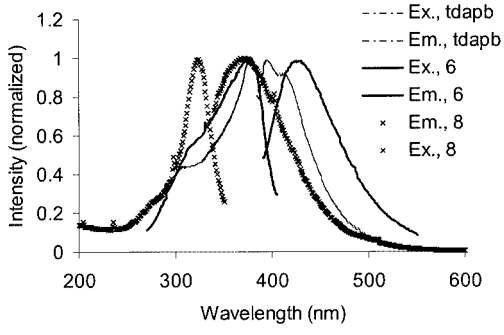

Figure 10. Excitation and emission spectra of tdapb, **6** and **8** in the solid state

For the Zn^{II} complex **6**, we examined the luminescent spectra of the three different crystal forms in the solid state, which revealed that there is no significant difference between their excitation or emission spectra. The exposure of complex **6** in the solid state or in a [poly(dimethylsiloxane)] (PDMS) matrix to a benzene vapor causes a decrease in emission intensity, attributable to fluorescent quenching via π−π interactions between benzene molecules and the complex (the details of the use of **6** as a fluorescent sensor for benzene can be found in ref.[4]). Blue-luminescent compounds are ideal for the detection of aromatic organic molecules because most aromatic organic molecules absorb strongly in the UV or near UV region. Therefore, in addition to the studies of **6**, systematic studies on the potential of the Zn^{II} complexes **1**, **2** and **5** as fluorescent sensors for aromatic organic solvent molecules are being carried out by our group and the results will be reported in due course.

The Pt^{II} complexes **3**, **4**, **7** and **8** have a broad emission band that is either similar to that of the free ligand or blue-shifted. The luminescent intensity of the Pt^{II} complexes in the solid state is clearly much weaker than those of the corresponding Zn^{II} compounds, attributable to fluorescent quenching by the Pt^{II} centers. Compounds **3** and **4** appear to have the tendency to attract small halogenated solvent molecules such as CH_2Cl_2 into their crystal lattices, as demonstrated by their crystal structural analyses. The effect of halogenated solvent molecules on the luminescence of compounds **3** and **4** in the solid state and the potential use of **3** and **4** as fluorescent sensors for halogenated molecules are being investigated.

In summary, we have demonstrated that the star-shaped ligands of tdat, tdab, tdapt and tdapb are capable of chelating to Zn^{II} and Pt^{II} centers to form a new class of luminescent star-shaped complexes. These complexes display interesting and unusual structural features and molecular arrangements in the solid state. Due to their low emission efficiency and poor volatility and solubility, these complexes are not suitable for electroluminescent applications. However, some of these complexes appear to have a high affinity toward certain organic solvent molecules and may find use as fluorescent sensors for these molecules.

Experimental Section

General: $ZnCl_2$ and K_2PtCl_4 were purchased from Strem Chemicals Co. Solvents were freshly distilled from appropriate drying reagents prior to use. ^1H NMR spectra were recorded by using Bruker Avance 300 MHz spectrometers. Elemental analyses were performed by Canadian Microanalytical Service, Ltd., Delta, British Columbia. Excitation and emission spectra were recorded with a Photon Technologies International QuantaMaster Model C-60 spectrometer. Melting points were determined with a Fisher−Johns melting point apparatus. The tdat, tdab, tdapt and tdapb ligands were synthesized based on the procedure reported recently.[4] All Pt^{II}

complexes reported herein are insoluble in common organic solvents. ^{1}H NMR spectra for these compounds are therefore not provided.

Synthesis of $(ZnCl_2)$(tdat) (1a): Zinc chloride (12 mg, 0.085 mmol) was dissolved in THF (10 mL); tdat (50 mg, 0.085 mmol) in 10 mL of CH_2Cl_2 was added to the zinc chloride solution at ambient temperature. The solution was stirred for 0.5 h. After the solution was allowed to stand for a few days, a colorless crystalline solid of $(ZnCl_2)$(tdat) was obtained (45 mg, yield 73%). ^{1}H NMR (CD_3OD, 298 K): δ = 8.28 (d, ^3J = 3.9 Hz, 6 H, py), 7.75 (dd, $^3J_1$ = 8.1, $^3J_2$ = 6.6 Hz, 6 H, py), 7.51 (d, ^3J = 8.4 Hz, 6 H, py), 7.21 (dd, $^3J_1$ = 7.2, $^3J_2$ = 4.8 Hz, 6 H, py). $C_{33}H_{24}Cl_2N_{12}Zn$ (724.29): calcd. C 54.67, H 3.34, N 23.19; found C 54.18, H 3.46, N 22.71.

Synthesis of $(ZnCl_2)_2$(tdat) (1b): Zinc chloride (23 mg, 0.17 mmol) was dissolved in THF (10 mL); tdat (50.0 mg, 0.085 mmol) in 10 mL of CH_2Cl_2 was added to the zinc chloride solution at ambient temperature. The solution was stirred for 0.5 h. After the solution was allowed to stand for a few days, a colorless crystalline solid of $(ZnCl_2)_2$(tdat) was obtained (37 mg, yield 50%). ^{1}H NMR ([D$_6$]DMSO, 298 K): δ = 8.24 (d, ^3J = 4.8 Hz, 6 H, py), 7.68 (dd, $^3J_1$ = 8.1, $^3J_2$ = 5.7 Hz, 6 H, py), 7.46 (d, ^3J = 8.1 Hz, 6 H, py), 7.12 (dd, $^3J_1$ = 5.7, $^3J_2$ = 4.8 Hz, 6 H, py). $C_{33}H_{24}Cl_4N_{12}Zn_2$ (860.58): calcd. C 46.02, H 2.81, N 19.52; found C 45.38, H 2.98, N 19.21.

Synthesis of $(ZnCl_2)_3$(tdat) (1c): Zinc chloride (35 mg, 0.255 mmol) was dissolved in THF (10 mL); tdat (50 mg, 0.085 mmol) in 10 mL of CH_2Cl_2 was added to the zinc chloride solution at ambient temperature. The solution was stirred for 0.5 h. After the solution was allowed to stand for a few days, a colorless crystalline solid of $(ZnCl_2)_3$(tdat) was obtained (62 mg, yield 74%). ^{1}H NMR ([D$_6$]DMSO, 298 K): δ = 8.24 (d, ^3J = 4.8 Hz, 6 H, py), 7.68 (dd, $^3J_1$ = 7.8, $^3J_2$ = 5.7 Hz, 6 H, py), 7.46 (d, ^3J = 8.1 Hz, 6 H, py), 7.12 (dd, $^3J_1$ = 5.7, $^3J_2$ = 4.8 Hz, 6 H, py). $C_{33}H_{24}Cl_6N_{12}Zn_3\cdot 1CH_2Cl_2\cdot 0.5THF$ (1117.77): calcd. C 38.64, H 2.68, N 15.02; found C 39.24, H 2.94, N 14.64.

Synthesis of $(ZnCl_2)_3$(tdab) (2): Zinc chloride (38 mg, 0.28 mmol) was dissolved in CH_3OH (10 mL); tdab (50 mg, 0.085 mmol) in 5 mL of CH_2Cl_2 was added to the zinc chloride solution at ambient temperature. The solution was stirred for 2 h. After the solution was allowed to stand for a few days at ambient temperature, a colorless crystalline solid of $(ZnCl_2)_3$(tdab) was obtained (64 mg, yield 75%). ^{1}H NMR ([D$_6$]acetone, 298 K): δ = 8.51 (d, ^3J = 5.4 Hz, 6 H, py), 8.08 (dd, $^3J_1$ = 9.0, $^3J_2$ = 6.9 Hz, 3 H, py), 7.63 (d, ^3J = 8.4 Hz, 6 H, py), 7.51 (dd, $^3J_1$ = 6.9, $^3J_2$ = 5.7 Hz, 6 H, py). 7.45 (s, 6 H, ph). $C_{36}H_{27}Cl_6N_9Zn_3\cdot 2CH_2Cl_2\cdot 3H_2O$ (1217.67): calcd. C 37.44, H 3.03, N 10.34; found C 37.20, H 2.46, N 10.66.

Synthesis of $[(PtCl_2)_3$(tdat)] (3): Benzene (4 mL) and a solution of K_2PtCl_4 (106 mg, 0.255 mmol) in a mixture of 3 mL of H_2O and 5 mL of DMSO were successively layered upon a solution of tdat (50 mg, 0.085 mmol) in 6 mL of CH_2Cl_2. The yellow K_2PtCl_4/H_2O/DMSO solution sank through the layer of benzene and settled upon the tdat/CH_2Cl_2 layer. The solvents were allowed to diffuse over several days at ambient temperature, yielding a yellow crystalline solid of $[(PtCl_2)_3$(tdat)] (52% yield). $C_{33}H_{24}Cl_6N_{12}Pt_3\cdot 1$DMSO (1466.68): calcd. C 28.65, H 2.04, N 11.46; found C 28.87, H 2.09, N 10.87.

Synthesis of $[(PtCl_2)_3$(tdab)] (4): Compound **4** was obtained in 38% yield by using the same procedure as for **3**. $C_{36}H_{27}Cl_6N_9Pt_3$ (1382.94): calcd. C 31.25, H 1.97, N 9.11; found C 31.25, H 2.25, N 8.95.

Synthesis of $(ZnCl_2)_3$(tdapt) (5): Zinc chloride (28 mg, 0.20 mmol) was dissolved in CH_3OH (10 mL); tdapt (50 mg, 0.061 mmol) in 5 mL of CH_2Cl_2 was added to the zinc chloride solution at ambient temperature. The solution was stirred for 2 h. After the solution was allowed to stand for a few days at ambient temperature, a colorless crystalline solid of $(ZnCl_2)_3$(tdapt) was obtained (39 mg, yield 42%). ^{1}H NMR ([D$_6$]DMSO, 298 k): δ = 8.67 (d, ^3J = 8.7 Hz, 6 H, py), 8.32 (d, ^3J = 8.7 Hz, 6 H, ph), 7.77 (dd, $^3J_1$ = 8.1, $^3J_2$ = 7.2 Hz, 6 H, py), 7.28 (d, ^3J = 8.7 Hz, 6 H, ph), 7.15 (dd, $^3J_1$ = 7.2, $^3J_2$ = 6.9 Hz, 6 H, py). 7.10 (d, ^3J = 8.1 Hz, 6 H, py). $C_{51}H_{36}Cl_6N_{12}Zn_3\cdot 0.5CH_2Cl_2$ (1267.32): calcd. C 48.76, H 2.91, N 13.25; found C 48.42, H 3.09, N 13.05.

Synthesis of $(ZnCl_2)_3$(tdapb) (6): A CH_2Cl_2 (5 mL) solution containing tdapb (50 mg, 0.061 mmol) was added to 10 mL of a CH_3OH solution containing $ZnCl_2$ (28 mg, 0.20 mmol) at ambient temperature; 10 mL of benzene was added to this solution. After stirring for 2 h, the mixture was allowed to stand for several days at ambient temperature. A colorless crystalline solid of $(ZnCl_2)_3$(tdapb) was obtained (58 mg, yield 76%). ^{1}H NMR ([D$_4$]methanol, 298 K): δ = 8.27 (d, ^3J = 5.1, 6 H, py), 7.90 (s, 3 H, Ph1), 7.86 (d, ^3J = 8.4 Hz, 6 H, Ph2), 7.77 (dd, $^3J_1$ = 6.3, $^3J_2$ = 2.1 Hz, 6 H, py), 7.31 (d, ^3J = 8.4 Hz, 6 H, Ph2), 7.14 (dd, $^3J_1$ = 5.1, $^3J_2$ = 2.1 Hz, 6 H, py), 7.11 (d, ^3J = 5.4 Hz, 6 H, py). $C_{54}H_{39}Cl_6N_9Zn_3\cdot 1/3C_6H_6$ (1247.87): calcd. C 53.85, H 3.20, N 10.10; found C 54.20, H 3.03, N 10.20. If the reaction was carried out in the absence of benzene and a small amount of benzene was added during the crystallization of **6**, the second crystal motif, $(ZnCl_2)_3$(tdapb)$\cdot 0.25C_6H_6\cdot 3CH_2Cl_2$, was obtained. $C_{54}H_{39}Cl_6N_9Zn_3\cdot 0.25C_6H_6\cdot 3CH_2Cl_2$ (1496.07): calcd. C 46.93, H 3.13, N 8.42; found C 46.61, H 2.94, N 8.80.)

Synthesis of $[(PtCl_2)_3$(tdapt)] (7) and $[(PtCl_2)_3$(tdapb)] (8): DMSO (2 mL), benzene (4 mL), and a solution of K_2PtCl_4 (76 mg, 0.184 mmol) in a mixture of 3 mL of H_2O and 5 mL of DMSO were successfully layered upon a solution of tdapt (50 mg, 0.061 mmol) or tdapb (50 mg, 0.061 mmol), respectively, in 6 mL of CH_2Cl_2. The Pt-containing solution sank through the benzene layer and into the DMSO layer and settled upon the tdapb or tdapt ligand layer in CH_2Cl_2. Solvents were allowed to diffuse over several days at ambient temperature, producing a yellow microcrystalline solid of $[(PtCl_2)_3$(tdapt)] (60% yield) and $[(PtCl_2)_3$(tdapb)] (95% yield), respectively. **7:** $C_{51}H_{36}Cl_6N_{12}Pt_3\cdot 1H_2O$ (1631.94): calcd. C 37.50, H 2.32, N 10.29; found C 37.19, H 2.39, N 10.09. **8:** $C_{54}H_{39}Cl_6N_9Pt_3\cdot 1CH_2Cl_2$ (1695.84): calcd. C 38.92, H 2.42, N 7.42; found C 38.52, H 2.61, N 7.48.

X-ray Crystallographic Analyses: Single crystals of **1b**, **2**−**4**, and **6** suitable for X-ray diffraction analyses were obtained. Attempts to obtain single crystals of the remaining compounds were unsuccessful. All crystals were mounted on glass fibers. Data were collected with a Bruker Smart CCD 1000 diffractometer with graphite-monochromated Mo-K_α radiation, operating at 50 kV and 35 mA at 23 °C, over a 2θ range of 3−57°. No significant decay was observed for any samples during the data collection. Data were processed with a Pentium III PC using the Bruker AXS SHELXTL NT software package. Neutral atomic scattering factors were taken from Cromer and Waber.[11] The crystals of **1b** were partially twinned and diffracted weakly. For compound **3**, two crystal motifs were observed, a hexagonal lattice and a monoclinic lattice. The monoclinic lattice of **3** is isostructural to that of **4** with unit cell dimensions of a = 9.9675(16), b = 21.356(4), c = 12.0891(19) Å, β = 98.532(4)°, V = 2544.9(7) Å^3. For compound **6**, three crystal motifs were observed, depending on the solvent used during crystallization. The unit cell parameters for two of the motifs **6a** and **6b** ob-

Table 3. Crystallographic data

	1b	**2**	**3**	**4**	**6a**	**6b**
	$(ZnCl_2)_2(tdat)\cdot H_2O$	$(ZnCl_2)_3(tdab)\cdot CH_3OH$	$(PtCl_2)_3(tdat)\cdot 1.5CH_2Cl_2\cdot H_2O$	$(PtCl_2)_3(tdab)\cdot 3CH_2Cl_2$	$(ZnCl_2)_3(tdapb)\cdot 0.25C_6H_6\cdot 3CH_2Cl_2$	$(ZnCl_2)_3(tdapb)\cdot 3C_6H_6$
Empirical formula	$C_{33}H_{24}Cl_4N_{12}Zn_2\cdot H_2O$	$C_{36}H_{27}Cl_6N_9Zn_3\cdot CH_3OH$	$C_{33}H_{24}Cl_6N_{12}Pt_3\cdot 1.5CH_2Cl_2\cdot H_2O$	$C_{36}H_{27}Cl_6N_9Pt_3\cdot 3CH_2Cl_2$	$C_{54}H_{39}Cl_6N_9Zn_3\cdot 0.25C_6H_6\cdot 3CH_2Cl_2$	$C_{54}H_{39}Cl_6N_9Zn_3\cdot 3C_6H_6$
Formula mass	879.20	1026.52	1532.01	1638.42	1497.06	1457.07
Space group	*Ia*	$P2_1/c$	*R*3*c*	$P2_1/m$	$R\bar{3}$	$P\bar{1}$
a [Å]	16.596(3)	8.2983(12)	22.471(4)	9.943(4)	33.517(4)	13.805(4)
b [Å]	14.208(3)	22.911(4)	22.471(4)	21.846(9)	$R\bar{3}$	14.848(5)
c [Å]	16.942(4)	21.869(3)	33.852(7)	12.163(5)	19.167(4)	17.384(5)
α [°]	90	90	90	90	90	87.208(6)
β [°]	107.473(4)	93.307(3)	90	97.575(8)	90	88.569(6)
γ [°]	90	90	120	90	120	77.828(8)
V [Å^3]	3810.5(14)	4150.9(11)	14803(5)	2618.8(19)	18647(4)	3478.7(18)
Z	4	4	12	2	12	2
μ [cm^{-1}]	15.85	21.49	90.13	86.44	8.8	13.04
$2\theta_{max.}$ [°]	56.7	56.6	56.6	56.7	56.6	57
Reflns. measured	13589	30012	33932	18966	46115	25315
Independent reflns.	7144 (R_{int} = 0.17)	9930(R_{int} = 0.086)	5717 (R_{int} = 0.132)	6391(R_{int} = 0.059)	10089 (R_{int} = 0.083)	16047 (R_{int} = 0.146)
Parameters	290	587	308	291	495	791
Final *R* [$I > 2\sigma(I)$]	R_1 = 0.1256[a], wR_2 = 0.1498[b]	R_1 = 0.0460[a], wR_2 = 0.0687[b]	R_1 = 0.0548[a], wR_2 = 0.1167[b]	R_1 = 0.0629[a], wR_2 = 0.1678[b]	R_1 = 0.1283[a], wR_2 = 0.3320[b]	R_1 = 0.0991[a], wR_2 = 0.1079[b]
Goodness of fit on F^2	0.772	0.740	0.922	1.065	1.136	1.136

[a] $R_1 = \Sigma\,||F_o|^2 - |F_c|^2|/\Sigma|F_o|^2$. [b] $wR_2 = \{\Sigma w[(F_o^2 - F_c^2)^2]/\Sigma[\,w(F_o^2)^2]\}^{1/2}$. $w = 1/[\sigma^2(F_o^2) + (0.075P)^2]$, where $P = [\max.(F_o^2,0) + 2F_c^2]/3$.

tained from benzene and CH_2Cl_2 solution are given in Table 3. The third motif **6c**, obtained from methanol solution, has the following unit cell parameters: triclinic, $P\bar{1}$, a = 13.134(9), b = 14.04(1), c = 16.67(1) Å, α = 73.01(1), β = 68.88(1), γ = 84.43(1)°, V = 2741(5) Å^3, Z = 2. The structure of **6c** is similar to that of **6b**, except that no benzene solvent molecules are present in the lattice. All structures were solved by direct methods. Almost all non-hydrogen atoms (except disordered solvent molecules) were refined anisotropically for all structures except compound **1b**. Due to the poor data quality of **1b**, only metal, chlorine and some nitrogen and carbon atoms could be refined anisotropically. Solvent molecules or H_2O were found in all crystals. Some of the solvent molecules are disordered. We invested considerable effort to model and refine the disordered solvent molecules. The positions for all hydrogen atoms except those of disordered solvent molecules or water molecules were either calculated or located directly from difference Fourier maps and their contributions to the structural factor calculation were included. The crystallographic data are given in Table 3. The ranges of selected bond lengths and angles are given in Table 1. CCDC-176676 (**1b**), -176678 (**2**), -176677 (**3**), -176675 (**4**), -163379 (**6a**), and -163380 (**6b**) contain the supplementary crystallographic data for this paper. These data can be obtained free of charge at www.ccdc.cam.ac.uk/conts/retrieving.html or from the Cambridge Crystallographic Data Centre, 12, Union Road, Cambridge CB2 1EZ, UK [Fax: (internat.) + 44-1223/336-033; E-mail: deposit@ccdc.cam.ac.uk].

Acknowledgments

We thank the Natural Sciences and Engineering Research Council of Canada and the Xerox Research Foundation for financial support.

[1] [1a] M. A Baldo, D. F. O'Brien, Y. You, A. Shoustikov, S. Sibley, M. E. Thompson, S. R. Forrest, *Nature* **1998**, *395*, 151. [1b] D. F. O'Brien, M. A. Baldo, M. E. Thompson, S. R. Forrest, *Appl. Phys. Lett.* **1999**, *74*, 442. [1c] R. C. Kwong, S. Sibley, T. Dubovoy, M. A. Baldo, S. R. Forrest, M. E. Thompson, *Chem. Mater.* **1999**, *11*, 3709. [1d] R. C. Kwong, S. Laman, M. E. Thompson, *Adv. Mater.* **2000**, *12*, 1134. [1e] C. J. Chen, J. Shi, *Coord. Chem. Rev.* **1998**, *171*, 161. [1f] N. X. Hu, M. Esteghamatian, S. Xie, Z. Popovic, A. M. Hor, B. Ong, S. Wang, *Adv. Mater.* **1999**, *11*, 17.

[2] [2a] M. A. Mansour, W. B. Connick, R. J. Lachicotte, H. J. Gysling, R. Eisenberg, *J. Am. Chem. Soc.* **1998**, *120*, 1329. [2b] Y. Kunugi, K. R. Mann, L. L. Miller, C. L. Exstrom, *J. Am. Chem. Soc.* **1998**, *120*, 589. [2c] E. Y. Fung, M. M. Olmstead, J. C. Vickery, A. L. Balch, *Coord. Chem. Rev.* **1998**, *171*, 151. [2d] J. C. Vickery, M. M. Olmstead, E. Y. Fung, A. L. Balch, *Angew. Chem. Int. Ed. Engl.* **1997**, *36*, 1179. [2e] G. De Santis, L. Fabbrizzi, M. Licchelli, A. Poggi, A. Taglietti, *Angew. Chem. Int. Ed. Engl.* **1996**, *35*, 202. [2f] A. P. de Silva, H. Q. N. Gunaratne, T. E. Rice, *Angew. Chem. Int. Ed. Engl.* **1996**, *35*, 2116. [2g] M. P. Houlne, T. S. Agent, G. F. Kiefer, K. McMillan, D. J. Bornhop, *Appl. Spectrosc.* **1996**, *10*, 225. [2h] K. H. Wong, M. C. W. Chan, C. M. Che, *Chem. Eur. J.* **1999**, *5*, 2845. [2i] W. Y. Wong, K. H. Choi, K. W. Cheah, *J. Chem. Soc., Dalton Trans.* **2000**, 113. [2j] H. Q. Liu, T. C. Cheung, C. M. Che, *Chem. Commun.* **1996**, 1039.

[3] [3a] W. Paw, S. D. Cummings, M. A. Mansour, W. B. Connick, D. K. Geiger, R. Eisenberg, *Coord. Chem. Rev.* **1998**, *171*, 125. [3b] S. D. Cummings, R. Eisenberg, *J. Am. Chem. Soc.* **1996**, *118*, 1949. [3c] S. Huertas, M. Hissler, J. E. McGarrah, R. J. Lachicotte, R. Eisenberg, *Inorg. Chem.* **2001**, *40*, 1183. [3d] M. Hissler, W. B. Connick, D. K. Geiger, J. E. McGarrah, D. Lipa, R. J. Lachicotte, R. Eisenberg, *Inorg. Chem.* **2000**, *39*, 447.

[4] J. Pang, Y. Tao, S. Freiberg, M. D'Iorio, S. Wang, *J. Mater. Chem.* **2002**, *12*, 206.

[5] [5a] N. Tamoto, C. Adachi, K. Nagai, *Chem. Mater.* **1997**, *9*, 1077. [5b] Z. Gao, C. S. Lee, L. Bello, S. T. Lee, R. M. Chen, T. Y. Luh, J. Shi, C. W. Tang, *Appl. Phys. Lett.* **1999**, *74*, 865. [5c] Y. Shirota, K. Okumoto, H. Inada, *Synth. Met.* **2000**, *111*, 387. [5d] S. Berleb, W. Brutting, M. Schwoerer, R. Wehrmann, A. Elschner, *J. Appl. Phys.* **1998**, *83*, 4403. [5e] K. Itano, T. Tsuzuki, H. Ogawa, S. Appleyard, M. R. Willis, Y. Shirota, *IEEE Trans. Electron. Devices* **1997**, *44*, 1218. [5f] Y. Kuwabara, H. Ogawa, H. Inada, N. Noma, Y. Shirota, *Adv. Mater.* **1994**, *6*, 677. [5g] I. Y. Wu, J. T. Lin, Y. T. Tao, E. Balasubramaniam, *Adv. Mater.* **2000**, *12*, 668.

[6] J. Pang, E. J. P. Marcotte, C. Seward, R. S. Brown, S. Wang, *Angew. Chem. Int. Ed.* **2001**, *40*, 4042.

[7] [7a] R. H. Prince, in *Comprehensive Coordination Chemistry* (Eds.: G. Wilkinson, R. D. Gillard, J. A. McCleverty), Pergamon Press, New York, **1987**, vol. 5, chapter 56.1. [7b] T. P. E. Auf der Heyde, *Acta Crystallogr., Sect. B* **1984**, *40*, 582. [7c] M. C. Kerr, H. S. Preston, H. L. Ammon, J. E. Huheey, J. M. Stewart, *J. Coord. Chem.* **1981**, *11*, 111. [7d] H. W. Smith, *Acta Crystallogr., Sect. B* **1975**, *31*, 2701. [7e] M. Mikami-Kido, Y. Saito, *Acta Crystallogr., Sect. B* **1982**, *38*, 452. [7f] Q. Wu, J. A. Lavigne, Y. Tao, M. D'Iorio, S. Wang, *Inorg. Chem.* **2000**, *39*, 5248;

[8] W. Yang, H. Schmider, Q. Wu, Y. Zhang, S. Wang, *Inorg. Chem.* **2000**, *39*, 2397.

[9] [9a] D. J. Cárdenas, A. M. Echavarren, *Organometallics* **1999**, *18*, 3337. [9b] G. W. V. Cave, N. W. Alcock, J. P. Rourke, *Organometallics* **1999**, *18*, 1801. [9c] M. J. Irwin, G. C. Jia, J. J. Vittal, R. J. Puddephatt, *Organometallics* **1996**, 5321.

[10] [10a] G. R. Desiraju, *Crystal Engineering: The Design of Organic Solids*, Elsevier, New York, **1989**. [10b] S. Tsuzuki, K. Honda, T. Uchimayu, M. Mikami, K. Tanabe, *J. Am. Chem. Soc.* **2002**, *124*, 104.

[11] D. T. Cromer, J. T. Waber, *International Tables for X-ray Crystallography*, Kynoch Press, Birmingham, AL, **1974**, vol. 4, Table 2.2A.

Received December 21, 2001
[I01528]

Heterodinuclear Zinc(II)−Iron(III) Complexes and Dinuclear Zinc Complexes as Models for Zinc-Containing Phosphatases

Sabine Albedyhl,[a] David Schnieders,[a] Attila Jancsó,[b] Tamás Gajda,*[b] and Bernt Krebs*[a]

Keywords: Heterometallic complexes / Asymmetric ligands / Phosphates / Dinucleating ligands / Enzyme models

Five new dinuclear model complexes for zinc-containing phosphatases with dinucleating ligands have been prepared and characterized by single-crystal X-ray crystallography. The heterodinuclear, μ-alkoxo-bridged zinc(II)–iron(III) complexes **1**–**3** contain the symmetric ligands *N*,*N*,*N*′,*N*′-tetrakis[2-(5,6-dimethyl)benzimidazolylmethyl]-1,3-diamino-2-propanol (Htdmbpo) and *N*,*N*,*N*′,*N*′-tetrakis{2-[*N*′′-(2-hydroxyethyl)]benzimidazolylmethyl}-1,3-diamino-2-propanol (Hthebpo), and the asymmetric ligand *N*,*N*-bis[2-(4,5-dimethyl)benzimidazolylmethyl]-*N*′,*N*′-bis(2-pyridylmethyl)-1,3-diamino-2-propanol (Hbdmbbppo), respectively. X-ray crystallography revealed that the zinc center exhibits a trigonal-bipyramidal coordination, while the octahedral coordination sphere of the iron center is completed by a solvent molecule. In contrast, the zinc complexes **4** and **5**, which also have (alkoxo)(cacodylato)dimetal cores with the dinucleating ligands used in **1** and **3**, exhibit both metal centers in a trigonal-bipyramidal environment. Additionally, the solution speciation of the zinc(II) complexes formed with Htdmbpo and Hbdmbbppo were determined and the activity of the in situ prepared zinc complexes towards the transesterification of the RNA model substrate 2-(hydroxypropyl)-4-nitrophenyl phosphate (hpnp) was investigated. The dinuclear $[Zn_2LH_{-1}(OH)]^{2+}$ complex of both ligands efficiently promotes the transesterification. The kinetic data indicated a higher activity for the complex of the asymmetric ligand Hbdmbbppo, as a result of its stronger substrate binding ability.

(© Wiley-VCH Verlag GmbH, 69451 Weinheim, Germany, 2002)

Introduction

Model compounds simulate the characteristic properties of the active sites in enzymes. The synthesis and characterization of structural and functional model complexes contribute to the structure clarification and the comprehension of the catalytic mechanism of metalloenzymes. Investigation of inhibitor complexes and product complexes gives insight into the coordination mode of the substrate.

In this work we focused on the preparation of dinuclear model complexes for zinc-containing phosphatases. The purple acid phosphatase isolated from plants, and the serine/threonine protein phosphatase 1 and 2B (calcineurine) contain a zinc(II)−iron(III) center in their active sites.[1−3] Purple acid phosphatases hydrolyze activated phosphate monoesters within a pH range of 4−7. The octahedrally coordinated metal centers are 3.26 Å apart, and a terminal hydroxide ion at the iron center, a water molecule at the zinc center and a bridging hydroxide ion, in addition to the bridging carboxylate group of aspartate were included into the X-ray structure analysis from spectroscopic data.[1] The coordination sphere of the metal ions, which are separated by 3.3 Å and 3.0 Å, in the serine/threonine protein phosphatases 1 and 2B, respectively, is square-pyramidal at the iron atom and trigonal-bipyramidal at the zinc atom.[2] A water molecule is coordinated to the iron center, while another water molecule bridges the two metal ions. The coordination number is increased to six due to the bidentate binding of the phosphate group to the metal centers.[3]

Alkaline phosphatase, phospholipase C, nuclease P1 and phosphotriesterase contain at least two zinc centers.[4−7] Alkaline phosphatase is a widely distributed nonspecific phosphomonoesterase, which catalyzes through a covalent phosphoseryl intermediate.[8] The active site contains two zinc ions at a distance of 4.0 Å, and one magnesium ion. According to recent publications, all three metal centers contribute to the mechanism.[4] The zinc centers with a N_2O_3 donor set in the dinuclear unit of phospholipase C and nuclease P1 are bridged by a hydroxide ion or a water molecule and the carboxylate group of aspartate, and exhibit a trigonal pyramidal coordination.[5,6] Their distance apart was shown to be 3.3 Å and 3.2 Å, respectively. The bridging

[a] Anorganisch-Chemisches Institut, Westfälische Wilhelms-Universität Münster,
Wilhelm-Klemm-Straße 8, 48149 Münster, Germany
Fax: (internat.) + 49-(0)251/83-38366
E-mail: krebs@uni-muenster.de
[b] Department of Inorganic and Analytical Chemistry, University of Szeged,
P. O. Box 440, 6701 Szeged, Hungary
Fax: (internat.) + 36-(0)62/420-505
E-mail: tamas.gajda@chem.u-szeged.hu

Supporting information for this article is available on the WWW under http://www.eurjic.com or from the author.

hydroxide ion is proposed to be the attacking nucleophile in the serine/threonine protein phosphatases 1 and 2B, nuclease P1 and phosphotriesterase.

In these enzymes the first coordination sphere of the metal centers is comprised of nitrogen and oxygen donor atoms that are in common with the ligands in our systems. Furthermore, the metal−metal distances in both the enzymes and the prepared complexes are in the range of 3.0 to 4.0 Å, which is important for the co-operative interaction.

There are some examples of crystallized model compounds with interesting features reported in the literature. The model complex $[Zn_2(bbap)(Bz)(H_2O)](ClO_4)_2 \cdot 4MeOH$ {Hbbap = 2,6-bis[bis(2-benzimidazolylmethyl)aminomethyl]-4-methylphenol} for phospholipase C contains two zinc ions with different coordination spheres.[9] A new structural and perhaps functional feature in the chemistry of oligozinc enzymes was detected in the X-ray structure of $[Zn_2L(H_2O)(OH)](BPh_4)_2 \cdot 2.5C_3H_6O$ {HL = 2,5-bis[*N*,*N*-(diethylaminoethyl)aminomethyl]pyrazol}, which includes an intramolecular $H_3O_2^-$ bridge.[10] The hydrolytic activity of the complex $[Zn_2(bpan)(\mu\text{-}OH)(\mu\text{-}O_2PPh_2](ClO_4)_2$ {bpan = 2,7-bis[2-(2-pyridylethyl)aminomethyl]-1,8-naphthyridin}, in which the naphthyridin simulates the *syn*,-*syn* coordination of a bridging carboxylate group, was investigated using different model substrates.[11,12]

Currently, there is interest in the development of new ligands, especially asymmetric ligands and their metal complexes, which may be used as enzymatic models.[13−20] In addition to complexes with dissimilar metal centers due to asymmetric coordination as found in enzymes, heterodinuclear complexes are important with respect to enzymes containing two different metal ions.[21] So far, only a few heterodinuclear zinc(II)−iron(III) complexes with symmetric dinucleating ligands are known. They include four pyridine groups and contain a μ-phenoxo bridge and two further bridging ligands like acetate, diphenyl phosphate or molybdate.[22−26] Suzuki and co-workers characterized mixed-valent (μ-alkoxo)diiron(II,III) complexes with the ligand *N*,*N*,*N*′,*N*′-tetrakis(2-pyridylmethyl)-1,4-diamino-2-butanol by X-ray crystallography.[27] The asymmetric bridging unit leads to five- and six-membered chelate rings.

Here, we report on the synthesis and characterization of three heterodinuclear zinc(II)−iron(III) complexes with distinct coordination spheres, μ-alkoxo-bridging symmetric and asymmetric dinucleating ligands, as well as two corresponding zinc complexes. Their structures were determined by X-ray crystallography and characterized by additional spectroscopic measurements.

In the complexes $[Zn^{II}Fe^{III}(tdmbpo)(O_2AsMe_2)(HOMe)](ClO_4)_3 \cdot 4MeOH \cdot 2H_2O$ (**1**), $[Zn^{II}Fe^{III}(thebpo)(O_2AsMe_2)(H_2O)](ClO_4)(NO_3)_2 \cdot 3H_2O$ (**2**) and $[Zn^{II}Fe^{III}(bdmbbppo)(O_2AsMe_2)(HOMe)](ClO_4)_3 \cdot 1.5MeOH$ (**3**) the zinc ion exhibits a trigonal-bipyramidal environment, and the octahedrally ligated iron center has a coordination site occupied by a solvent molecule. This terminal solvent molecule at the iron center may act as the attacking nucleophile. In contrast to the μ-phenoxo-bridged complexes,[22−26] which are doubly bridged by two further ligands, the complexes described here contain only one further μ-cacodylato bridge. These complexes are model compounds for the kidney bean purple acid phosphatase product complex with inorganic phosphate, and for the inhibitor complex with tungstate.[1]

The zinc ions in the complexes **4** and **5** formulated as $[Zn^{II}_2(tdmbpo)(O_2AsMe_2)](ClO_4)_2 \cdot 5MeOH$ and $[Zn^{II}_2(bdmbbppo)(O_2AsMe_2)](ClO_4)_2 \cdot H_2O$, respectively, have an N_3O_2 donor set. Both zinc centers in **4** and one zinc center in **5** is symmetrically coordinated by two 4,5-dimethylbenzimidazole groups, while the second zinc center in **5** is coordinated by two pyridine groups, resulting in an asymmetric complex.

The activity of the in situ prepared complexes of these ligands and zinc perchlorate was studied with respect to the transesterification of hpnp, in order to determine the influence of the different coordinating groups. Similar systems were used by Komiyama and co-workers who investigated the cleavage of ribonucleotide dimers and compared the activity between mono-, di- and trinuclear complexes. The latter is a model for trinuclear zinc-containing phosphodiesterases like phospholipase C and nuclease P1.[28,29] Very efficient di- and trinuclear zinc catalysts, which were also prepared in situ, were described by Engbersen, Reinhoudt and co-workers and are based on calix[4]arene.[30−33] Recently, zinc-containing complexes with dinucleating imidazole ligands have been studied.[34,35] As various types of mechanisms are discussed, particularly with regards to the reacting nucleophile and the coordination mode of the substrate, further information will be drawn from the study of model complexes. Important aspects are the determination of the crystal structure, the identification of the active species in solution and the mechanism of the reaction of model compounds with substrates.

Results and Discussion

X-ray Crystal Structures of 1, 2 and 3

In order to mimic the active site of kidney bean purple acid phosphatase we used the symmetric and asymmetric dinucleating ligands Htdmbpo, Hthebpo and Hbdmbbppo to form heterodinuclear μ-alkoxo-bridged zinc(II)−iron(III) complexes with two differently coordinated metal centers. The zinc ion has a trigonal-bipyramidal geometry with an N_3O_2 donor set, whereas the iron center resides in an octahedral environment that is completed by a solvent ligand. Structures of the cations in **1**, **2** and **3** are depicted in Figures 1, 2 and 3.

The zinc ions are facially coordinated by two benzimidazole nitrogen atoms (N3 and N5) and one tertiary aliphatic nitrogen atom (N1) of the ligand. The iron centers in **1** and **2** are also coordinated by two benzimidazole nitrogen atoms (N7 and N9) and one tertiary aliphatic nitrogen atom (N2) of the ligand. The iron center in **3** is facially ligated by two pyridine nitrogen atoms (N7 and N8) and one tertiary aliphatic nitrogen atom (N2) of the ligand bdmbbppo. The metal centers are connected by the deprotonated μ-alkoxo

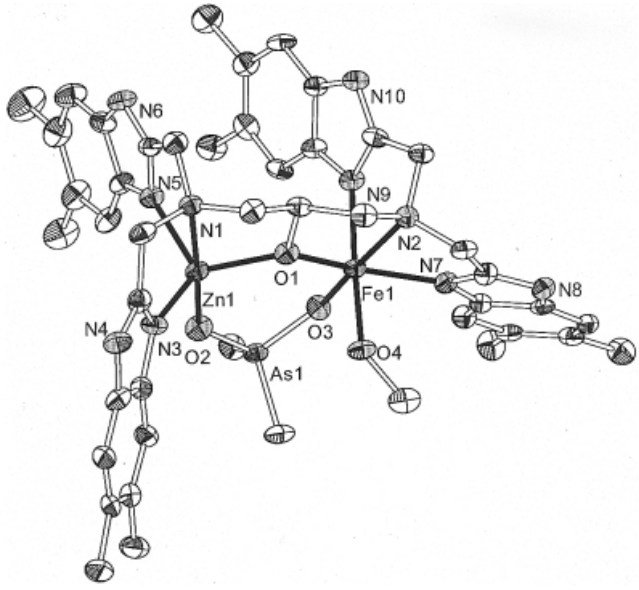

Figure 1. Structure of the cation in **1** showing 50% probability displacement ellipsoids; hydrogen atoms have been omitted for clarity

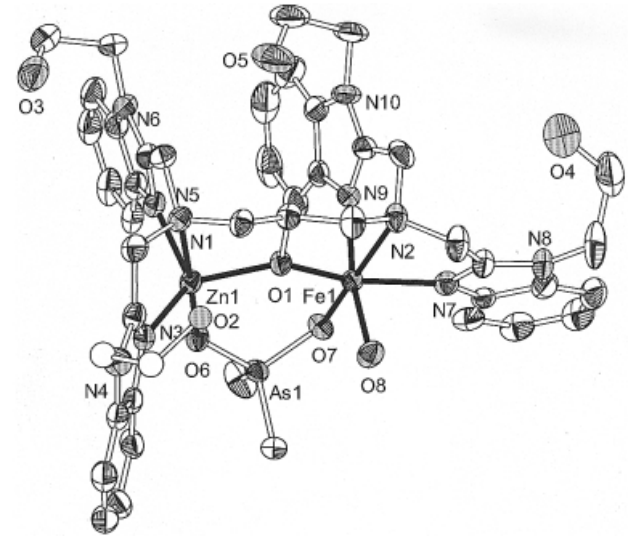

Figure 2. Structure of the cation in **2** showing 50% probability displacement ellipsoids; one hydroxyethyl group was refined isotropically; hydrogen atoms have been omitted for clarity

oxygen atom O1 of the ligand and the cacodylate bridge. An N_3O_3 donor set of the iron(III) center is formed by the additional coordination of a methanol molecule (O4−C46 and O4−C38) in **1** and **3**, respectively, and by a water molecule (O8) in **2**. The coordination polyhedra share one edge (O1). The cacodylate bridge in the inhibitor complexes shows the same bridging mode as in the enzyme. The inter-metal distances in **1**, **2** and **3** are 3.5635(12), 3.6053(13) and 3.5354(12) Å, respectively, and are slightly larger than in the enzyme. The Zn1−O1−Fe1 angles are 125.9(2)° in **1**, 127.7(2)° in **2** and 125.3(3)° in **3** and follow the same trend observed for the inter-metal distances (Table 1).

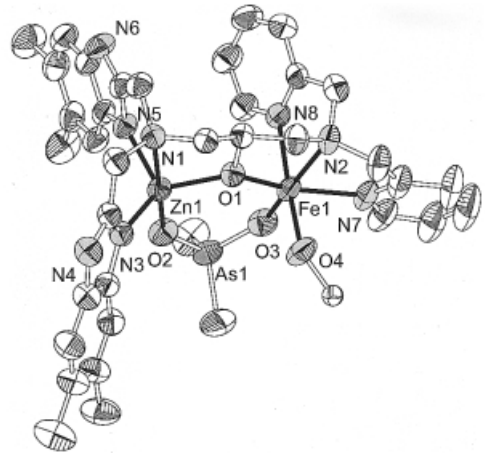

Figure 3. Structure of the cation in **3** showing 50% probability displacement ellipsoids

The axial positions of the trigonal-bipyramidal coordination polyhedra of the zinc ions are occupied by the tertiary nitrogen atom N1 and the oxygen atom of the cacodylate group, O2 in **1** and **3** and O6 in **2**. The distortion of the ideal coordination polyhedra towards the tertiary nitrogen atom results in angles smaller than 90° between N1 and the equatorially bound donor atoms. The geometrical distortion around the iron centers is demonstrated by the deviation of the three angles of the axial donor atoms by about 16° from the ideal 180° angle. The coordination polyhedra of the iron centers are distorted towards the tertiary nitrogen atom N2 in a similar manner as in the zinc centers. The angles between N2 and the atoms in *cis* position O1, N7 and N9 (N8 in **3**) are smaller than 90°, while the angles between N2 and the oxygen atoms O4 of the bound methanol molecules and the oxygen atom O8 of the water molecule are close to 90°.

The bond lengths between the tertiary nitrogen atoms (N1, N2) and the metal ions are much larger than the bond lengths between the aromatic nitrogen atoms of the ligands and the metal ions (Table 2). The bonds between Fe1 and the oxygen atoms O4 of the coordinating methanol molecules in **1** and **3** have lengths of 2.172(4) and 2.054(4) Å, respectively, as a result of the different properties of the benzimidazole and pyridine groups coordinated to the iron centers. The bond lengths between the oxygen atom O8 of the coordinating water molecule and Fe1 in **2** is 2.068(4) Å. The hydroxide ion coordinated to the iron(III) center has a much smaller distance of about 1.90 Å.[36]

To date, only the μ-cacodylato-bridged dinuclear complexes $[Fe^{III}_2(tbpo)(O_2AsMe_2)(OMe)(HOMe)](ClO_4)_3 \cdot 5MeOH \cdot 2H_2O$[37] [Htbpo = *N*,*N*,*N*′,*N*′-tetrakis(2-benzimidazolylmethyl)-1,3-diamino-2-propanol], $[Fe^{III}_2(tbpo)(O_2AsMe_2)(Cl)(H_2O)](ClO_4)_3 \cdot 5MeOH \cdot H_2O$[38] and $[Fe^{III}_2(mtbpo)(O_2AsMe_2)(Cl)_2(HOMe)](ClO_4)_2 \cdot 4MeOH$[39] [Hmtbpo = *N*,*N*,*N*′-tris(2-benzimidazolylmethyl)-*N*′-methyl-1,3-diamino-2-propanol] are known in which both iron centers have an octahedral coordination sphere. The distance between the oxygen atom of the water molecule and the iron(III) center in the second complex is 2.088(6)

Table 1. Selected angles [°] in **1**, **2** and **3**

1		**2**		**3**	
Zn(1)−O(1)−Fe(1)	125.9(2)	Zn(1)−O(1)−Fe(1)	127.7(2)	Zn(1)−O(1)−Fe(1)	125.3(3)
O(1)−Zn(1)−O(2)	104.0(2)	O(1)−Zn(1)−O(6)	101.9(2)	O(1)−Zn(1)−O(2)	102.6(2)
O(1)−Zn(1)−N(1)	78.4(2)	O(1)−Zn(1)−N(1)	79.6(2)	O(1)−Zn(1)−N(1)	78.3(1)
O(1)−Zn(1)−N(3)	116.0(2)	O(1)−Zn(1)−N(3)	117.4(2)	O(1)−Zn(1)−N(3)	118.0(2)
O(1)−Zn(1)−N(5)	112.6(2)	O(1)−Zn(1)−N(5)	106.9(2)	O(1)−Zn(1)−N(5)	109.8(2)
O(2)−Zn(1)−N(1)	177.0(2)	O(6)−Zn(1)−N(1)	176.4(2)	O(2)−Zn(1)−N(1)	178.9(2)
O(2)−Zn(1)−N(3)	99.6(2)	O(6)−Zn(1)−N(3)	99.8(2)	O(2)−Zn(1)−N(3)	102.1(2)
O(2)−Zn(1)−N(5)	104.9(2)	O(6)−Zn(1)−N(5)	105.8(2)	O(2)−Zn(1)−N(5)	105.2(2)
N(1)−Zn(1)−N(3)	77.7(2)	N(1)−Zn(1)−N(3)	76.7(2)	N(1)−Zn(1)−N(3)	76.9(2)
N(1)−Zn(1)−N(5)	75.5(2)	N(1)−Zn(1)−N(5)	76.7(2)	N(1)−Zn(1)−N(5)	75.1(2)
N(3)−Zn(1)−N(5)	117.1(2)	N(3)−Zn(1)−N(5)	122.1(2)	N(3)−Zn(1)−N(5)	116.9(2)
O(1)−Fe(1)−O(3)	104.5(2)	O(1)−Fe(1)−O(7)	104.2(2)	O(1)−Fe(1)−O(3)	107.6(2)
O(1)−Fe(1)−O(4)	80.8(2)	O(1)−Fe(1)−O(8)	88.0(2)	O(1)−Fe(1)−O(4)	86.5(2)
O(1)−Fe(1)−N(2)	81.2(2)	O(1)−Fe(1)−N(2)	80.2(2)	O(1)−Fe(1)−N(2)	81.7(2)
O(1)−Fe(1)−N(7)	152.7(2)	O(1)−Fe(1)−N(7)	154.1(2)	O(1)−Fe(1)−N(7)	155.8(2)
O(1)−Fe(1)−N(9)	92.1(2)	O(1)−Fe(1)−N(9)	93.1(2)	O(1)−Fe(1)−N(8)	87.8(2)
O(3)−Fe(1)−O(4)	96.2(2)	O(7)−Fe(1)−O(8)	96.8(2)	O(3)−Fe(1)−O(4)	97.9(2)
O(3)−Fe(1)−N(2)	173.4(2)	O(7)−Fe(1)−N(2)	173.5(2)	O(3)−Fe(1)−N(2)	167.1(2)
O(3)−Fe(1)−N(7)	100.3(2)	O(7)−Fe(1)−N(7)	101.3(2)	O(3)−Fe(1)−N(7)	96.1(2)
O(3)−Fe(1)−N(9)	97.4(2)	O(7)−Fe(1)−N(9)	96.3(2)	O(3)−Fe(1)−N(8)	93.2(2)
O(4)−Fe(1)−N(2)	87.8(2)	O(8)−Fe(1)−N(2)	88.1(2)	O(4)−Fe(1)−N(2)	91.5(2)
O(4)−Fe(1)−N(7)	85.5(2)	O(8)−Fe(1)−N(7)	84.2(2)	O(4)−Fe(1)−N(7)	85.5(2)
O(4)−Fe(1)−N(9)	165.9(2)	O(8)−Fe(1)−N(9)	166.2(2)	O(4)−Fe(1)−N(8)	168.6(3)
N(2)−Fe(1)−N(7)	74.8(2)	N(2)−Fe(1)−N(7)	74.9(2)	N(2)−Fe(1)−N(7)	75.8(2)
N(2)−Fe(1)−N(9)	79.0(2)	N(2)−Fe(1)−N(9)	78.6(2)	N(2)−Fe(1)−N(8)	77.9(2)
N(7)−Fe(1)−N(9)	95.8(2)	N(7)−Fe(1)−N(9)	89.0(2)	N(7)−Fe(1)−N(8)	95.7(2)

Table 2. Selected bond lengths [Å] in **1**, **2** and **3**

1		**2**		**3**	
Zn(1)···Fe(1)	3.5635(12)	Zn(1)···Fe(1)	3.6053(13)	Zn(1)···Fe(1)	3.5354(12)
Zn(1)−O(1)	2.035(4)	Zn(1)−O(1)	2.049(4)	Zn(1)−O(1)	2.024(3)
Zn(1)−O(2)	1.978(4)	Zn(1)−O(6)	1.955(4)	Zn(1)−O(2)	1.964(4)
Zn(1)−N(1)	2.406(4)	Zn(1)−N(1)	2.385(5)	Zn(1)−N(1)	2.448(4)
Zn(1)−N(3)	2.012(5)	Zn(1)−N(3)	2.034(5)	Zn(1)−N(3)	2.009(4)
Zn(1)−N(5)	2.017(4)	Zn(1)−N(5)	2.011(5)	Zn(1)−N(5)	2.002(4)
Fe(1)−O(1)	1.967(4)	Fe(1)−O(1)	1.967(4)	Fe(1)−O(1)	1.956(4)
Fe(1)−O(3)	1.880(4)	Fe(1)−O(7)	1.874(4)	Fe(1)−O(3)	1.871(4)
Fe(1)−O(4)	2.172(4)	Fe(1)−O(8)	2.068(4)	Fe(1)−O(4)	2.054(4)
Fe(1)−N(2)	2.283(4)	Fe(1)−N(2)	2.283(5)	Fe(1)−N(2)	2.203(5)
Fe(1)−N(7)	2.073(4)	Fe(1)−N(7)	2.103(5)	Fe(1)−N(7)	2.137(4)
Fe(1)−N(9)	2.075(4)	Fe(1)−N(9)	2.074(5)	Fe(1)−N(8)	2.147(4)

Å, and therefore is similar to the corresponding distance in **2**. The presence of only one iron(III) center in both complexes was confirmed by magnetic measurements, where a linear increase of $1/\chi$ with temperature and no coupling effects were observed. The experimental μ_{eff} values are in accordance with the theoretical value of 5.92 μ_B for a high-spin iron(III) ion.

X-ray Crystal Structures of 4 and 5

The structures of the cations in **4** and **5** are provided in the Supporting Information (Figures S1 and S2).

The metal centers in complexes **4** and **5** have a trigonal-bipyramidal coordination sphere, with an N_3O_2 donor set. Their inter-metal distances are 3.562(2) Å and 3.5147(16) Å, respectively. Each zinc ion is facially coordinated by two benzimidazole nitrogen atoms (N3, N5 and N7, N9) or two pyridine nitrogen atoms (N7 and N8) and one tertiary aliphatic nitrogen atom (N1 or N2) of the ligand. They are connected by the deprotonated μ-alkoxo oxygen atom O1 of the ligand and one cacodylate bridge. The coordination polyhedra share one edge (O1). The Zn1−O1−Zn2 angles are 128.0(4)° and 125.9(3)°, respectively (Table 3). The axial positions of the trigonal-bipyramidal coordination polyhedra of the zinc ions are occupied by the tertiary nitrogen atoms N1 or N2, and one oxygen atom O2 or O3 of the cacodylate bridge. The average deviation from 180° is 2.3° at one metal center and 8.7° at the other metal center. The coordination polyhedra are distorted towards the tertiary nitrogen atoms as observed at the zinc centers in the complexes **1**, **2** and **3**. The differences in the average values for

Table 3. Selected angles [°] in **4** and **5**

4		**5**	
Zn(1)−O(1)−Zn(2)	128.0(4)	Zn(1)−O(1)−Zn(2)	125.9(3)
O(1)−Zn(1)−O(2)	101.5(3)	O(1)−Zn(1)−O(2)	103.6(3)
O(1)−Zn(1)−N(1)	78.6(3)	O(1)−Zn(1)−N(1)	78.8(3)
O(1)−Zn(1)−N(3)	117.8(4)	O(1)−Zn(1)−N(3)	114.9(3)
O(1)−Zn(1)−N(5)	118.4(4)	O(1)−Zn(1)−N(5)	121.6(3)
O(2)−Zn(1)−N(1)	178.0(4)	O(2)−Zn(1)−N(1)	177.5(3)
O(2)−Zn(1)−N(3)	105.8(4)	O(2)−Zn(1)−N(3)	103.2(3)
O(2)−Zn(1)−N(5)	102.2(4)	O(2)−Zn(1)−N(5)	102.9(3)
N(1)−Zn(1)−N(3)	75.9(4)	N(1)−Zn(1)−N(3)	75.5(3)
N(1)−Zn(1)−N(5)	76.0(4)	N(1)−Zn(1)−N(5)	75.6(3)
N(3)−Zn(1)−N(5)	108.7(4)	N(3)−Zn(1)−N(5)	108.1(3)
O(1)−Zn(2)−O(3)	106.2(3)	O(1)−Zn(2)−O(3)	107.2(3)
O(1)−Zn(2)−N(2)	81.7(3)	O(1)−Zn(2)−N(2)	82.2(3)
O(1)−Zn(2)−N(7)	111.2(4)	O(1)−Zn(2)−N(7)	115.7(3)
O(1)−Zn(2)−N(9)	109.7(4)	O(1)−Zn(2)−N(8)	113.8(3)
O(3)−Zn(2)−N(2)	172.1(3)	O(3)−Zn(2)−N(2)	170.5(3)
O(3)−Zn(2)−N(7)	103.3(4)	O(3)−Zn(2)−N(7)	99.5(4)
O(3)−Zn(2)−N(9)	100.3(3)	O(3)−Zn(2)−N(8)	96.6(3)
N(2)−Zn(2)−N(7)	73.6(4)	N(2)−Zn(2)−N(7)	77.2(4)
N(2)−Zn(2)−N(9)	76.2(3)	N(2)−Zn(2)−N(8)	77.7(3)
N(7)−Zn(2)−N(9)	124.0(4)	N(7)−Zn(2)−N(8)	119.8(3)
O(2)−As(1)−O(3)	112.8(4)	O(2)−As(1)−O(3)	114.0(3)

the angles between the tertiary nitrogen atoms and the equatorially bound donor atoms of 76.8 and 77.2° in **4** and 76.6 and 79.0° in **5**, result from different coordinating groups at each metal center.

In addition, the bond lengths between the tertiary nitrogen atoms and the metal ions are longer than the bond lengths between the aromatic nitrogen atoms of the ligands and the metal ions (Table 4). The distances between the tertiary nitrogen atoms and the zinc ions are 2.375(9) Å and 2.387 (8) Å in **4**, and 2.467(7) Å and 2.255(8) Å in **5**. The greater difference (0.212 Å) between the distances observed in **5** is due to the asymmetry in complex **5**.

Table 4. Selected bond lengths [Å] in **4** and **5**

4		**5**	
Zn(1)···Zn(2)	3.562(2)	Zn(1)···Zn(2)	3.5147(16)
Zn(1)−O(1)	1.993(7)	Zn(1)−O(1)	1.980(7)
Zn(1)−O(2)	1.950(7)	Zn(1)−O(2)	1.953(6)
Zn(1)−N(1)	2.375(9)	Zn(1)−N(1)	2.467(7)
Zn(1)−N(3)	2.051(10)	Zn(1)−N(3)	2.015(8)
Zn(1)−N(5)	1.982(10)	Zn(1)−N(5)	2.024(10)
Zn(2)−O(1)	1.970(7)	Zn(2)−O(1)	1.966(7)
Zn(2)−O(3)	1.998(7)	Zn(2)−O(3)	1.955(6)
Zn(2)−N(2)	2.387(8)	Zn(2)−N(2)	2.255(8)
Zn(2)−N(7)	1.997(12)	Zn(2)−N(7)	2.094(10)
Zn(2)−N(9)	2.066(9)	Zn(2)−N(8)	2.068(8)

Solution Speciation

The solubility of the ligands and complexes in an ethanol/water mixed solvent allowed the solution study of the zinc(II) complexes of Htdmbpo (in 80 % ethanol/water, w/w) and Hbdmbbppo (in 35 % ethanol/water, w/w). These studies involved a series of pH-dependent measurements.

Table 5. Logarithmic formation constants for the proton and zinc(II) complexes of Htdmbpo (in 80 % ethanol/water, w/w, T = 298 K, I = 0.05 M $NaNO_3$) and of Hbdmbbppo (in 35 % ethanol/water, w/w , T = 298 K, I = 0.1 M $NaNO_3$); $\beta_{pqr} = [M_pL_qH_K]/[M]^p[L]^q[H]^r$, with estimated errors in parentheses (last digit)

pqr	β_{pqr} Htdmbpo	β_{pqr} Hbdmbbppo
011	5.91(2)	6.01(1)
012	10.54(2)	10.96(1)
013	14.35(2)	14.93(2)
014	16.71(2)	17.93(2)
112	−	16.37(4)
111	12.74(4)	12.47(8)
110	10.65(2)	9.80(3)
21−1	10.87(3)	9.56(4)
21−2	3.80(4)	2.43(5)
21−3	−4.00(5)	−6.90(5)
pK_{21-2}^{21-1}	7.07	7.13
pK_{21-3}^{21-2}	7.80	9.33
NP[a] (FP[b])	283 (0.012 cm^{-3})	300 (0.010 cm^{-3})

[a] NP: number of experimental points. [b] FP: fitting parameter.

The determined protonation and complex formation constants are listed in Table 5, together with some derived data (see pH-metric measurements in the Exp. Sect.). Four strongly overlapping deprotonation processes were observed at pH > 2 for both ligands. The fifth and sixth pK values are therefore much lower than 2, presumably due to the formation of a hydrogen bond between the two substituents of a given tertiary amino group.

In the presence of zinc(II) the same species were formed with both ligands. In an equimolar solution, the complex $[ZnL]^{2+}$ is dominant in the neutral pH range. Dinuclear $[Zn_2LH_{-x}]^{(4-x)+}$ complexes (x = 1−3) are also formed at pH > 7. The latter species already becomes dominant at pH = 4, in the presence of a twofold metal excess (Figure 4). The deprotonation during the formation of the first dinuclear complex ($[ZnL]^{2+} + Zn^{2+} = [Zn_2LH_{-1}]^{3+} + H^+$) takes place at surprisingly low pH (at pH ≈ 4), which suggests a concerted action of the two zinc(II) ions. The participation of the hydroxy group in this process should be particularly favorable, due to the preorganization of the metal ions by the ligand. In this way, the complex $[Zn_2LH_{-1}]^{3+}$ most likely has the same single μ-alkoxo-bridged structure as crystallographically determined for the complexes **4** and **5**. The succeeding two deprotonations, leading to the complexes $[Zn_2LH_{-2}]^{2+}$ and $[Zn_2LH_{-3}]^{+}$, involve the deprotonation of coordinated water molecules (the metal-induced deprotonation of the pyrrolic nitrogen atom of the benzimidazole moieties at pH ≈ 7−8, is very unlikely in the case of zinc(II)), thus they are better described as $[Zn_2LH_{-1}(OH)]^{2+}$ and $[Zn_2LH_{-1}(OH)_2]^{+}$. These two successive processes are rather well separated for the Hbdmbbppo complex ($pK_2 - pK_1 = \Delta pK$ = 2.2, see Table 5), which allows the formation of the species M_2LH_{-2} in relatively high concentrations, while ΔpK is only 0.73 for the Htdmbpo complex. The solution speciation of these systems is clearly different from that observed for a *N*,*N*′-dis-

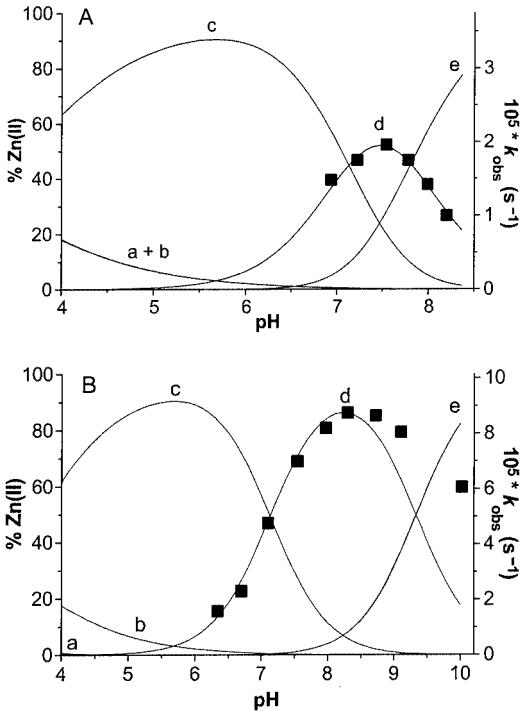

Figure 4. Species distribution curves (solid lines) and the effect of pH on the transesterification of hpnp (filled square) for the zinc(II)−Htdmbpo (A) and −Hbdmbbppo (B) systems (T = 298 K, [Htdmbpo] = 0.4 mM, [Hbdmbbppo] = 0.8 mM, $[Zn^{II}]/[L]$ = 2:1, [hpnp] = 1 mM); a: Zn^{II}, b: $[ZnL]^{2+}$, c: $[Zn_2LH_{-1}]^{3+}$, d: $[Zn_2LH_{-1}(OH)]^{2+}$, e: $[ZnLH_{-1}(OH)_2]^{+}$

ubstituted imidazole derivative of 1,3-diamino-2-propanol (in 65 % ethanol/water, w/w mixture)[34], where the process $[ZnL]^{2+} + Zn^{2+} = [Zn_2LH_{-1}(OH)]^{2+} + 2\ H^{+}$ takes place in a single step. This difference is probably the result of the higher stabilization of the 3*N*-coordinated zinc(II) ions in the present case. This can be demonstrated by the log K values of the above process, which are −7.06 for Htdmbpo, −7.37 for Hbdmbbppo and −11.34 for the *N*,*N*′-disubstituted imidazole derivative.[34]

Hydrolytic Studies

To screen the hydrolytic activity of the two systems described above, their ability to promote the transesterification of 2-(hydroxypropyl)-4-nitrophenyl phosphate (hpnp) was investigated. For these purposes pH-dependent measurements were carried out (see Exp. Sect.). In both the zinc(II)−Htdmbpo and −Hbdmbbppo ($[Zn^{II}]/[L]$ = 2:1) systems, notable transesterification activity was observed at pH > 6, parallel with the formation of the dinuclear species $Zn_2LH_{-1}(OH)$ (Figure 4). Based on the pH/rate constant profile, the successively formed $Zn_2LH_{-1}(OH)_2$ complex of Hbdmbbppo is also able to promote the transesterification, and its activity is almost half of the former $Zn_2LH_{-1}(OH)$ species. Such behavior was not observed with Htdmbpo. This difference may in part be due to the presence of the four bulky benzimidazole residues in Htdmbpo, which lower the binding ability of hpnp to the metal centers.

The rate of the transesterification shows first-order dependence on the concentration of the dinuclear complex

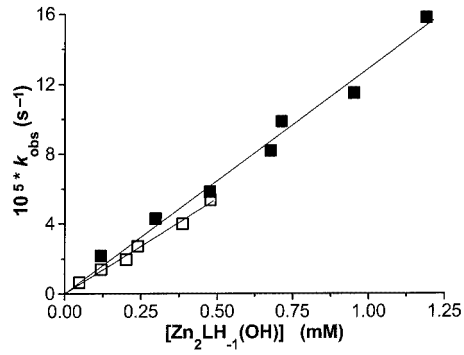

Figure 5. Dependence of k_{obs} on the concentration of $[Zn_2LH_{-1}(OH)]^{2+}$ complex of Htdmbpo (open square, pH = 7.50) and Hbdmbbppo (filled square, pH = 8.00); T = 298 K, $[Zn^{II}]/[L]$ = 2:1, [hpnp] = 1 mM

$[Zn_2LH_{-1}(OH)]^{2+}$ (Figure 5). The second-order rate constants determined from these plots are 0.109(3) $M^{-1}s^{-1}$ for Htdmbpo, and 0.129(4) $M^{-1}s^{-1}$ for Hbdmbbppo. These constants are somewhat higher than the second-order rate constant for the hydroxide ion catalyzed reaction (k_{OH} = 0.0745 $M^{-1}s^{-1}$).[34]

The initial rate of transesterification has also been determined as a function of the substrate concentration. The data depicted in Figure 6 show substrate saturation above 40−80-fold excess of hpnp. This indicates the validity of the Michaelis−Menten kinetics in our systems, i.e. the formation of a ternary $[Zn_2LH_{-1}(OH)(hpnp)]^{+}$ complex prior to the intramolecular transformation. The nonlinear least-squares fit of the data points, solid lines in Figure 6, gave the Michaelis constants (K_M) 12.9 mM and 5.2 mM, and catalytic rate constants (k_{cat}) 1.10×10^{-3} s^{-1} and 8.33×10^{-4} s^{-1} for the $[Zn_2LH_{-1}(OH)]^{2+}$ complexes of Htdmbpo and Hbdmbbppo, respectively. These k_{cat} values indicate ca. four orders of magnitude maximal rate acceleration for the hpnp transesterification by these complexes.[34] The dinuclear Htdmbpo zinc(II) complex possesses a somewhat higher catalytic rate constant, but its substrate binding ($1/K_M$) is two and a half times less effective than that of the corresponding Hbdmbbppo complex, which results in a higher overall activity of the latter complex.

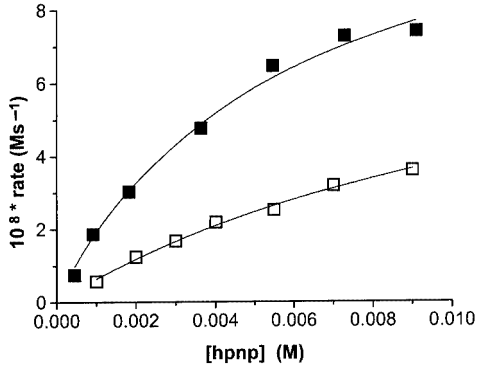

Figure 6. Saturation kinetic experiments for the transesterification of hpnp by the zinc(II)−Htdmpbo (open square, pH = 7.50, [L] = 1.6×10^{-4} M) and the zinc(II)−Hbdmbbppo (filled square, pH = 7.90, [L] = 1.8×10^{-4} M) systems; T = 298 K, $[Zn^{II}]/[L]$ = 2:1

By analogy with the crystal structure of complexes **4** and **5** (which contain the cacodylate bridging unit analogous to the phosphate), $\mu_{1,3}$-bridged coordination of the substrate hpnp can be envisaged for the dinuclear center. This would create a double Lewis acid activation for the transesterification reaction. However, the inactivity of the species $[Zn_2LH_{-1}]^{3+}$ (Figure 4), clearly demonstrates that this effect alone does not provide sufficient rate acceleration. This would need the concerted action of the double Lewis acid activation and the intramolecular general base catalysis by a metal-bound hydroxide ion, which becomes possible only in the successively formed $[Zn_2LH_{-1}(OH)]^{2+}$ complex (Scheme 1).

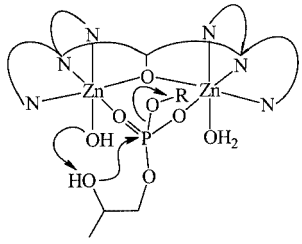

Scheme 1. The proposed mechanism for the transesterification of hpnp by the dinuclear zinc(II) complexes

Conclusion

With the syntheses of the complexes **1**, **2** and **3**, the first characterization of three structurally similar, heterodinuclear zinc(II)−iron(III) complexes with bridging μ-alkoxo units has been accomplished. According to their structural and spectroscopic properties they are excellent structural models of the active site of kidney bean purple acid phosphatase, serine/threonine protein phosphatase 1 and calcineurin. The use of an asymmetric ligand offers the possibility to prepare tailor-made heterodinuclear complexes. The trigonal-bipyramidally coordinated zinc ion and the octahedrally coordinated iron center are bridged by only one additional cacodylate ligand. The coordination of a water or a methanol molecule to the iron(III) center is very interesting with respect to the discussion of the nucleophilic species in the catalytic mechanism of kidney bean purple acid phosphatase.

The dinuclear zinc complexes **4** and **5** serve as models for alkaline phosphatase, phospholipase C, nuclease P1 and phosphotriesterase. The in situ prepared dinuclear $[Zn_2LH_{-1}(OH)]^{2+}$ complexes of Htdmbpo and Hbdmbbppo possess notable transesterification activity towards the RNA model hpnp, around the neutral pH range. The dinuclear complex formed with the asymmetric ligand Hbdmbbppo showed higher activity as compared with that of the symmetric ligand Htdmbpo, due to its higher substrate binding ability. The results suggest a bifunctional mechanism in the case of both ligands, i.e. the concerted action of the double Lewis acid activation provided by the dimetallic core and the intramolecular general base catalysis provided by a zinc(II)-bound hydroxide ion.

Experimental Section

General Remarks: All chemicals were obtained from commercial sources and used as received. ***CAUTION:*** Although no problems were encountered, suitable care and precautions should be taken when handling the perchlorate salts.

Physical Measurements: ^{1}H NMR spectra were recorded with a Bruker AC 200 instrument. The chemical shifts are reported relative to an internal standard of tetramethylsilane. Elemental analyses were performed with an elemental Vario El III instrument. IR spectra were recorded with a Bruker IFS 48 FT spectrometer. UV/Vis spectra were obtained using a UVIKON 933 spectrometer of Kontron Instruments equipped with 1.0-cm matched quartz cells and operating in the range 190−900 nm. Cyclic voltammetric measurements were carried out using a BAS CV-50 W potentiostat. All experiments were run at room temperature under argon. A standard three-electrode cell was used equipped with a platinum electrode, an Ag/AgCl/3 M NaCl reference electrode and a glassy carbon electrode. Tetra-*n*-butylammonium perchlorate (0.1 M) was used as the supporting electrolyte. Magnetic susceptibility measurements were carried out with a Quantum Design SQUID magnetometer at 3 T in a temperature range of 2−300 K. The mass spectra were recorded with an electrospray mass spectrometer Quattro LCZ with a nanospray inlet.

Synthesis: The barium salt of 2-(hydroxypropyl)-4-nitrophenyl phosphate (hpnp) was prepared according to a literature procedure.[40]

***N*,*N*,*N*′,*N*′-Tetrakis[2-(5,6-dimethyl)benzimidazolylmethyl]-1,3-diamino-2-propanol (Htdmbpo) and *N*,*N*,*N*′,*N*′-Tetrakis[2-(*N*′′-(2-hydroxyethyl)]benzimidazolylmethyl]-1,3-diamino-2-propanol (Hthebpo):** The symmetric ligands Htdmbpo and Hthebpo were synthesized as described previously.[41]

***N*,*N*-Bis[2-(4,5-dimethyl)benzimidazolylmethyl]-*N*′,*N*′-bis(2-pyridylmethyl)-1,3-diamino-2-propanol (Hbdmbbppo):** The asymmetric ligand Hbdmbbppo was prepared in a multi-step synthesis using *N*,*N*-bis(2-pyridylmethyl)-1,3-diamino-2-propanol. The preparation of the latter was carried out according to the procedure reported by Suzuki et al. with some modifications.[13] A mixture of phthalimidomethyloxirane and bis(2-pyridylmethyl)amine was heated for 3 d at 100−110 °C. The product was purified by silica gel column chromatography with a chloroform/methanol ratio of 9:1. The synthetic route of the final steps is depicted in Scheme 2.

Chloroacetic acid (2.58 g, 27 mmol) was dissolved in water (6 mL). An aqueous solution (8 mL) of sodium hydroxide (1.08 g, 35 mmol) was added under cooling in an ice bath. *N*,*N*-Bis(2-pyridylmethyl)-1,3-diamino-2-propanol (3.72 g, 14 mmol) was then added, and the mixture was heated to 65 °C. Once more an aqueous solution (8 mL) of sodium hydroxide (1.08 g, 35 mmol) was added over 1 h. After the solution had been stirred at 65 °C for 3 h, 6 M hydrochloric acid (13.6 mL, 90.9 mmol) was added. The solvent was removed in a rotary evaporator and the remaining solid was dissolved in ethanol. The precipitate was filtered off and the solvent was removed in a rotary evaporator to give *N*,*N*-bis(carboxyethyl)-*N*′,*N*′-bis(2-pyridylmethyl)-1,3-diamino-2-propanol. The product was used without further purification.

N,*N*-Bis(carboxyethyl)-*N*′,*N*′-bis(2-pyridylmethyl)-1,3-diamino-2-propanol (6.13 g, 16 mmol) and 4,5-dimethyl-1,2-phenylenediamine (4.49 g, 33 mmol) were dissolved in ethanol (5 mL) and thoroughly mixed, the solvent was subsequently removed. The mixture was heated for 3 h at 130 °C until no further water steam de-

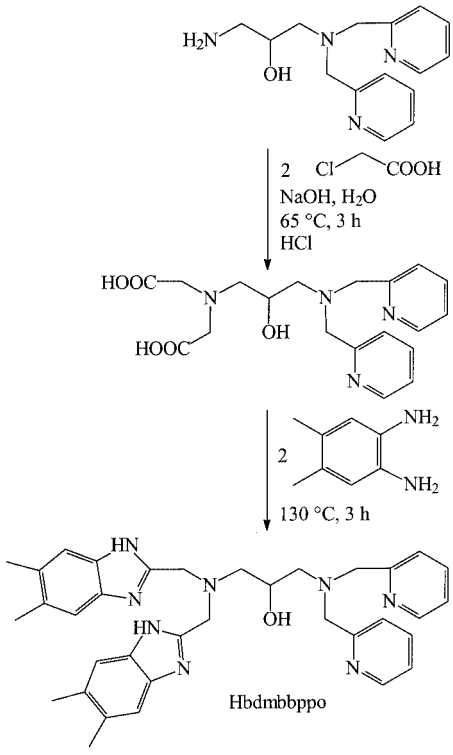

Scheme 2. Final synthetic steps in the preparation of Hbdmbbppo

veloped. The residue was dissolved in a minimum of ethanol in a sonic bath. This solution was added to a mixture of water (150 mL) and concentrated ammonia (7 mL). A brown oily product precipitated, which was purified by silica gel column chromatography with tetrahydrofuran/methanol, 3:1. Yield: 5.09 g (8 mmol, 50%). M.p. 168 °C. ^{1}H NMR (200 MHz, $CDCl_3$): δ = 2.08 (m, 4 H, CH−CH_2−N), 2.35 (s, 12 H, CH_3), 3.86 (m, 9 H, CH, N−CH_2), 7.26 (m, 10 H, Ar−H), 8.39 (d, 2 H, Ar−H). IR (KBr, 4000−400 cm^{-1}): $\tilde{\nu}$ [cm^{-1}] = 3391 (s), 3054 (w), 2922 (s), 1722 (w), 1634(w), 1593 (s), 1571 (w), 1538 (w), 1447 (s), 1364 (m), 1308 (m), 1262 (w), 1149 (w), 1121 (w), 1096 (w), 1048 (w), 1021 (w), 1001 (w), 980 (w), 858 (m), 799 (w), 764 (s), 666 (w), 630 (w), 461 (w), 436 (w). MS: *m*/*z* = 589 $[M + H]^+$.

[$Zn^{II}Fe^{III}$(tdmbpo)(O_2AsMe_2)(HOMe)](ClO_4)$_3$·4MeOH·2H_2O (1): A methanol solution (5 mL) containing $Zn(ClO_4)_2$·6H_2O (64 mg, 0.17 mmol) and $Fe(ClO_4)_3$·9H_2O (89 mg, 0.17 mmol) was added to a suspension of Htdmbpo (141 mg, 0.17 mmol) in methanol (5 mL). The sodium salt of cacodylic acid (37 mg, 0.17 mmol), dissolved in methanol (5 mL), was then added to the solution. After slow evaporation of the solvent, red orange crystals (132 mg, 0.09 mmol, 52%) were obtained after 2 d. UV/Vis (acetonitrile): λ_{max} = 402 nm (ε = 2458 $M^{-1}cm^{-1}$). $C_{50}H_{79}AsCl_3FeN_{10}O_{22}Zn$ (1474.7): calcd. C 40.72, H 5.40, N 9.50; found C 40.07, H 5.24, N 9.78. Cyclic voltammetry (250 mV/s) in acetonitrile (1 mM): $E_{1/2}$ = 99 mV (Zn^{II}−Fe^{II}/Zn^{II}−Fe^{III}). The cathodic peak at −760 mV is arsenic-centered, μ_{eff} = 5.92 μ_B.

[$Zn^{II}Fe^{III}$(thebpo) (O_2AsMe_2)(H_2O)](ClO_4)(NO_3)$_2$·3H_2O (2): An aqueous solution (2.3 mL) of $Zn(NO_3)_2$·6H_2O (45 mg, 0.15 mmol) was added to a solution of Hthebpo (137 mg, 0.15 mmol) in acetonitrile (7.5 mL). After a few minutes, an aqueous solution (2.5 mL) of $Fe(NO_3)_3$·9H_2O (61 mg, 0.15 mmol) was added dropwise. A solution of the sodium salt of cacodylic acid, dissolved in acetonitrile (2.5 mL), was added after a few minutes. The pH of the solution was determined to be 3. After a few days, orange crystals (45 mg, 0.04 mmol, 23%) suitable for X-ray crystallography were obtained by diffusion of diethyl ether into the solution. The perchlorate anion in the complex is taken from the perchlorate adduct of the ligand. $C_{45}H_{63}AsClFeN_{12}O_{21.5}Zn$ (1347.7): calcd. C 40.11, H 4.71, N 12.47; found C 40.27, H 4.67, N 12.38. Cyclic voltammetry (250 mV/s) in DMSO (1 mM): $E_{1/2}$ = −74 mV (Zn^{II}−Fe^{II}/Zn^{II}−Fe^{III}). The cathodic peak at −720 mV is assigned to arsenic, μ_{eff} = 6.06 μ_B.

[$Zn^{II}Fe^{III}$(bdmbbppo)(O_2AsMe_2)](ClO_4)$_2$·5MeOH (3): After the reaction of Hbdmbbppo (103 mg, 0.17 mmol) in methanol (3 mL) with a methanol solution (2.5 mL) of $Zn(ClO_4)_2$·6H_2O (64 mg, 0.17 mmol), a methanol solution (2.5 mL) of $Fe(ClO_4)_3$·H_2O (62 mg, 0.17 mmol) was added dropwise after a few minutes. Finally, the sodium salt of cacodylic acid (38 mg, 0.18 mmol) in methanol (2 mL) was added. Slow evaporation of the solvent yielded brown crystals (41 mg, 0.04 mmol, 24%) suitable for X-ray crystallography. UV/Vis (methanol): λ_{max} = 335 nm (sh) (ε = 2570 $M^{-1}cm^{-1}$). $C_{39.5}H_{55}AsCl_3FeN_8O_{27.5}Zn$ (1224.4): calcd. C 38.75, H 4.53, N 9.15; found C 37.60, H 4.67, N 9.12. Cyclic voltammetry (250 mV/s) in acetonitrile (1 mM): $E_{1/2}$ = 157 mV (Zn^{II}−Fe^{II}/Zn^{II}−Fe^{III}). The cathodic peak at −740 mV is arsenic-centered, μ_{eff} = 6.00 μ_B.

[Zn^{II}_2(tdmbpo)(O_2AsMe_2)(HOMe)](ClO_4)$_3$·4MeOH·2H_2O (4): A methanol solution (5 mL) of $Zn(ClO_4)_2$·6H_2O (128 mg, 0.34 mmol) was added to a suspension of Htdmbpo (141 mg, 0.17 mmol) in methanol (10 mL). Then the sodium salt of cacodylic acid (37 mg, 0.17 mmol), dissolved in methanol (5 mL), was added to the solution. Colorless crystals (74 mg, 0.06 mmol, 35%) were obtained after 2 d by slow evaporation of the solvent. $C_{50}H_{75}AsCl_2N_{10}O_{16}Zn_2$ (1348.8): calcd. C 44.52, H 5.61, N 10.39; found C 43.20, H 5.47, N 10.70.

[Zn^{II}_2(bdmbbppo)(O_2AsMe_2)](ClO_4)$_2$·H_2O (5): An aqueous solution (3 mL) of $Zn(ClO_4)_2$·6H_2O (128 mg, 0.34 mmol) and an aqueous solution (2 mL) of the sodium salt of cacodylic acid were added to a solution of Hbdmbbppo (101 mg, 0.17 mmol) in acetonitrile (5 mL). Diffusion of diethyl ether into the solution afforded colorless crystals (101 mg, 0.09 mmol, 55%) after 4 d. $C_{37}H_{47}AsCl_2N_8O_{12}Zn_2$ (1072.4): calcd. C 41.44, H 4.42, N 10.45; found C 40.27, H 4.55, N 10.14.

pH-Metric Measurements: The protonation and coordination equilibria were investigated by potentiometric titration in an ethanol/water solvent mixture (35 or 80 % ethanol, w/w) [*T* = 298 ± 0.1 K, *I* = 0.1 M and 0.05 M ($NaNO_3$) for 35 and 80 % ethanol/water, w/w mixture, respectively], using an automatic titration set including a Dosimat 665 (Metrohm) autoburette, an Orion 710A precision digital pH-meter and an IBM-compatible PC. 20-mL sample solutions were titrated with 0.1 M NaOH, prepared from solid NaOH (Fluka) in an ethanol/water mixture. The accurate concentration of the NaOH solution was determined by KH−phthalate. The sample solutions were prepared from stock solutions of $Zn(ClO_4)_2$ and the corresponding ligands. The Orion 8103BN semimicro pH glass electrode was calibrated using standard aqueous buffer solutions (pH = 4.0, 7.0 and 10, Sigma) and the actual pH in the mixed solvent was then determined by subtracting 0.10 or 0.11 units (for 35 and 80% ethanol/water, w/w mixture, respectively) from the pH-meter reading according to the method of Bates.[42] The ionization constants of water determined by us under the conditions used [pK_w = 14.53(2) and 15.31(2) for 35 and 80 % ethanol/water, w/w

mixture, respectively] are in good agreement with the literature data.[43] The species formed in the systems were characterized by the general equilibrium process of Equation (1), where M denotes the metal ion and L the nonprotonated (neutral) ligand molecule.

$$pM + qL + rH \xleftrightarrow{\beta_{M_pL_qH_r}} M_pL_qH_r \quad (1)$$

The corresponding formation constants ($\beta_{M_pL_qH_r} \equiv \beta_{pqr} = [M_pL_qH_r]/[M]^p[L]^q[H]^r$) were calculated using the computer program PSEQUAD,[44] as concentration constants. The protonation and complex formation constants were determined from 3 and 6 independent titrations (60−80 data points per titration), respectively. The metal/ligand ratios varied between 1:2 and 3:1, with the metal ion concentration between 1.0×10^{-3} and 2.5×10^{-3} mol·dm^{-3}.

Kinetic Measurements: The transesterification of 2-(hydroxypropyl)-4-nitrophenyl phosphate[40] (hpnp) was monitored in a buffered ethanol/water mixed solvent [I = 0.1 or 0.05 M ($NaNO_3$), T = 298 K] by detecting the increase in the absorbance maximum at 400 nm of the 4-nitrophenolate anion (ε = 18900) (Figure 6). In all cases 0.04 M buffer (HEPES and CHES) was used. The pK of 4-nitrophenol was determined independently for our conditions (pK = 7.50 ± 0.02 and 8.47 ± 0.02 for 35 and 80% ethanol/water mixture, respectively). The initial concentration of hpnp varied from 0.4 mM to 9 mM. The initial slope method (≤ 4% conversion) was used to determine the pseudo-first-order rate constants. The reported data are the average of triplicate measurements with a reproducibility better than 10%. In a typical experiment, the pH of the solution containing 0.4−0.8 mM ligand, 0.8−1.6 mM zinc(II), buffer and background electrolyte was adjusted to the desired value. 2 mL of this solution was equilibrated at 298 K in the spectrophotometer, 100 μL of 0.02 M hpnp was then injected into the solution with efficient mixing. The increase in the absorbance at 400 nm was immediately monitored. Second-order rate constants were obtained from plots of first-order rate constants against the concentration for the complex $Zn_2LH_{-1}(OH)$, calculated from the formation constants determined by pH-metry.

X-ray Data Collection and Crystal Structure Determinations: The unit cell parameters and basic information about data collection and structure refinement are given in Table 6. Structures were solved by heavy-atom methods (SHELXS-97) and refined by full-matrix least-squares methods based on F^2 (SHELXL-97).[45] The location of a half occupied nitrate anion in **2** was not possible due

Table 6. Crystallographic data for **1** to **5**

	1	**2**	**3**	**4**	**5**
Empirical ormula	$C_{50}H_{79}AsCl_3FeN_{10}O_{22}Zn$	$C_{45}H_{63}AsClFeN_{12}O_{21.5}Zn$	$C_{39.5}H_{55}AsCl_3FeN_8O_{17.5}Zn$	$C_{50}H_{75}AsCl_2N_{10}O_{16}Zn_2$	$C_{37}H_{47}AsCl_2N_8O_{12}Zn_2$
Formula mass	1474.72	1347.66	1224.41	1348.76	1072.39
a [Å]	35.239(7)	13.520(3)	11.088(2)	12.278(2)	11.148(2)
b [Å]	13.113(3)	15.172(3)	20.975(4)	14.079(3)	22.546(5)
c [Å]	28.375(6)	16.191(3)	22.636(5)	19.702(4)	18.854(4)
α [°]	90	84.76(3)	90	84.72(3)	90
β [°]	92.85(3)	74.67(3)	99.84(3)	81.41(3)	101.51(3)
γ [°]	90	68.61(3)	90	65.53(3)	90
V [Å^3]	13096(5)	2982.3(10)	5187.0(18)	3063.3(10)	4643.5(17)
Z	8	2	4	2	4
$d_{calcd.}$ [g/cm^3]	1.487	1.466	1.560	1.458	1.531
Crystal system	monoclinic	triclinic	monoclinic	triclinic	monoclinic
Space group	$C2/c$	$P\bar{1}$	$P2_1/c$	$P\bar{1}$	$P2_1/n$
Diffractometer	Smart CCD	Smart CCD	STOE IPDS	Siemens P3	STOE IPDS
Radiation, λ [Å]	Mo-K_α = 0.7107				
Monochromator	graphite plate				
Crystal size [mm]	0.32×0.21×0.17	0.30×0.20×0.19	1.16×0.16×0.16	0.35×0.28×0.23	0.40×0.32×0.10
T [K]	150(2)	150(2)	213(2)	153(2)	213(2)
Scan type, Θ range [°]	ω, 3.66−34.06	ω, 1.30−28.26	, 4.33−26.01	ω, 2.01−27.00	, 4.28−26.12
Index ranges	−48≤h≤42	−17≤h≤17	−12≤h≤13	−4≤h≤10	−13≤h≤13
	−14≤k≤17	−20≤k≤20	−25≤k≤25	−16≤k≤17	−27≤k≤27
	−37≤h≤42	−21≤h≤21	−27≤h≤26	−24≤h≤25	−22≤h≤22
Reflections measured	42187	25157	40449	11443	36688
Number of symmetry-independent reflections	15973	12082	9572	10822	8645
μ [mm^{-1}]	1.291	1.321	1.605	1.478	1.921
Solution	SHELXS-97, patterson method				
LS refinements	SHELXL-97, against F^2				
Refined reflections	15973	12082	9572	10822	8645
Parameters	849	703	719	761	570
GooF on F^2	0.990	1.052	1.051	1.341	1.017
Final $R1$ and $Rw2$ [$I > 2\sigma(I)$]	0.0752/0.1751	0.0821/0.2459	0.0651/0.1615	0.0989/0.2264	0.0977/0.2008
Final $R1$ and $Rw2$ (all data)	0.1519/ 0.2030	0.0896/0.2546	0.0937/0.1797	0.2115/0.2842	0.1699/0.2450
Largest diff. peak and hole	1.583/−0.739	4.338/−0.896	1.232/−0.652	1.649/−3.935	1.260/−0.747

to high remaining electron densities and severe disorder. The charge of the iron center was confirmed by magnetic susceptibility measurements. The nitrate anions, water molecules and one hydroxyethyl group of the ligand in **2** were refined with isotropic thermal parameters. All other non-hydrogen atoms were refined anisotropically, with the exception of the two water molecules in **1**, the disordered carbon atom of the methanol molecule that is coordinated to the iron center in **3**, one carbon atom of the ligand in **4** and a disordered oxygen atom of a perchlorate anion and a water molecule in **5**. Hydrogen atoms were placed in calculated positions and refined with a riding model with U_H(CH, CH_2, NH) = 1.2·U_{eq}(C) and U_H(CH_3, OH) = 1.5·U_{eq}(C) and 1.5·U_{eq}(O), respectively. High *R* values are caused by bad crystal quality. CCDC-169381−169385 contain the supplementary crystallographic data for this paper. These data can be obtained free of charge at www.ccdc.cam.ac.uk/conts/retrieving.html or from the Cambridge Crystallographic Data Centre, 12, Union Road, Cambridge CB2 1EZ, UK [Fax: (internat.) + 44-1223/336-033; E-mail: deposit@ccdc.cam.ac.uk].

Acknowledgments

The authors are grateful to Dr. F. Schweppe, Dr. K. Kirschbaum and Prof. Dr. A. A. Pinkerton for the X-ray crystallographic measurement of complex **1**. S. A., D. S. and B. K. thank the Deutsche Forschungsgemeinschaft and the Fonds der Chemischen Industrie for support. A. J. and T. G. thank the Foundation of Research Development at Universities (FKFP 0190/2000) for financial assistance.

[1] T. Klabunde, N. Sträter, R. Fröhlich, H. Witzel, B. Krebs, *J. Mol. Biol.* **1996**, *259*, 737−748.
[2] J. P. Griffith, J. L. Kim; E. E. Kim, M. D. Sintchak, J. A. Thompson, M. J. Fitzgibbon, M. A. Fleming, P. R. Caron, K. Hsiao, M. A. Navia, *Cell* **1995**, *82*, 507−522.
[3] J. Goldberg, H. Huang, Y. Kwon, P. Greengard, A. C. Nairn, I. Kurivan, *Nature* **1995**, *376*, 745−753.
[4] B. Stec, K. M. Holtz, E. R. Kantrowitz, *J. Mol. Biol.* **2000**, *299*, 1323−1331.
[5] E. Hough, L. K. Hansen, B. Birknes, K. Jynge, S. Hansen, A. Hordvik, C. Little, E. Dodson, Z. Derewenda, *Nature* **1989**, *338*, 357−360.
[6] A. Volbeda, A. Lahm, F. Sakiyama, D. Suck, *EMBO J.* **1991**, *10*, 1607−1618.
[7] J. L. Vanhooke, M. M. Benning, F. M. Raushel, H. M. Holden, *Biochemistry* **1996**, *35*, 6020−6025.
[8] E. E. Kim, H. W. Wyckoff, *J. Mol. Biol.* **1991**, *218*, 449−451.
[9] S. Uhlenbrock, B. Krebs, *Angew. Chem. Int. Ed. Engl.* **1992**, *31*, 1647−1648.
[10] F. Meyer, P. Rutsch, *Chem. Commun.* **1998**, 1037−1038.
[11] C. He, S. J. Lippard, *J. Am. Chem. Soc.* **2000**, *122*, 184−185.
[12] N. W. Kaminskaia, C. He, S. J. Lippard, *Inorg. Chem.* **2000**, *39*, 3365−3373.
[13] Y. Hayashi, T. Kayatani, H. Sugimoto, M. Suzuki, K. Inomata, A. Uehara, Y. Mizutani, T. Kitagawa, Y. Maeda, *J. Am. Chem. Soc.* **1995**, *117*, 11220−11229.
[14] C. Belle, G. Gellon, C. Scheer, J.-L. Pierre, *Tetrahedron Lett.* **1994**, *35*, 7019−7022.
[15] C. Belle, I. Gautier-Luneau, G. Gellon, J.-L. Pierre, I. Morgenstern-Badarau, E. Saint-Aman, *J. Chem. Soc., Dalton Trans.* **1997**, 3543−3546.
[16] C. Belle, J.-L. Pierre, E. Saint-Aman, *New J. Chem.* **1998**, 1399−1402.
[17] C. Belle, I. Gautier-Luneau, J.-L. Pierre, C. Scheer, E. Saint-Aman, *Inorg. Chem.* **1996**, *35*, 3706−3708.
[18] A. Neves, L. M. Rossi, A. Horn, Jr., I. Vencato, A. J. Bortoluzzi, C. Zucco, A. S. Mangrich, *Inorg. Chem. Commun.* **1999**, *2*, 334−337.
[19] E. Bernard, W. Moneta, J. Laugier, S. Chardon-Noblat, A. Deronzier, J.-P. Tuchagues, J.-M. Latour, *Angew. Chem. Int. Ed. Engl.* **1994**, *33*, 887−889.
[20] W. Kanda, W. Moneta, M. Bardet, E. Bernard, N. Debaecker, J. Laugier, A. Bousseksou, S. Chardon-Noblat, J.-M. Latour, *Angew. Chem. Int. Ed. Engl.* **1995**, *34*, 588−590.
[21] L.-H. Yin, P. Cheng, S.-P. Yan, X. Q. Fu, J. Li, D.-Z. Liao, Z.-H. Jiang, *J. Chem. Soc., Dalton Trans.* **2001**, *9*, 1398−1400.
[22] A. S. Borovik, L. Que, Jr., V. Papaefthymiou, E. Münck, L. F. Taylor, O. P. Anderson, *J. Am. Chem. Soc.* **1988**, *110*, 1986−1988.
[23] A. S. Borovik, V. Papaefthymiou, L. T. Taylor, O. P. Anderson, L. Que, Jr., *J. Am. Chem. Soc.* **1989**, *111*, 6183−6195.
[24] M. Ghiladi, C. J. McKenzie, A. Meier, A. K. Powell, J. Ulstrup, S. Wocadlo, *J. Chem. Soc., Dalton Trans.* **1997**, 4011−4018.
[25] K. Schepers, B. Bremer, B. Krebs, G. Henkel, E. Althaus, B. Mosel, W. Müller-Warmuth, *Angew. Chem. Int. Ed. Engl.* **1990**, *29*, 531−533.
[26] S. Albedyhl, M. T. Averbuch-Pouchot, C. Belle, B. Krebs, J.-L. Pierre, E. Saint-Aman, S. Torelli, *Eur. J. Inorg. Chem.* **2001**, 1457−1464.
[27] M. Suzuki, S. Fujinami, F. Hibino, H. Hori, Y. Maeda, A. Uehara, M. Suzuki, *Inorg. Chim. Acta* **1998**, *283*, 124−135.
[28] M. Yashiro, A. Ishikubo, M. Komiyama, *J. Chem. Soc., Chem. Commun.* **1995**, 1793−1794.
[29] M. Yashiro, A. Ishikubo, M. Komiyama, *Chem. Commun.* **1997**, 83−84.
[30] P. Molenveld, S. Kapsabelis, J. F. J. Engbersen, D. N. Reinhoudt, *J. Am. Chem. Soc.* **1997**, *119*, 2948−2949.
[31] P. Molenveld, J. F. J. Engbersen, H. Kooijman, A. L. Spek, D. N. Reinhoudt, *J. Am. Chem. Soc.* **1998**, *120*, 6726−6737.
[32] P. Molenveld, W. M. G. Stikvoort, H. Kooijman, A. L. Spek, J. F. J. Engbersen, D. N. Reinhoudt, *J. Org. Chem.* **1999**, *11*, 3896−3906.
[33] P. Molenveld, J. F. J. Engbersen, D. N. Reinhoudt, *Eur. J. Org. Chem.* **1999**, 3269−3275.
[34] T. Gajda, R. Krämer, A. Jancsó, *Eur. J. Inorg. Chem.* **2000**, 1635−1644.
[35] A. Jancsó, T. Gajda, E. Mulliez, L. Korecz, *J. Chem. Soc., Dalton Trans.* **2000**, 2679−2684.
[36] C. Duboc-Toia, S. Ménage, J.-M. Vincent, M. T. Averbuch-Pouchot, M. Fontecave, *Inorg. Chem.* **1997**, *27*, 6148−6149.
[37] R. Than, A. Schroft, L. Westerheide, R. van Eldik, B. Krebs, *Eur. J. Inorg. Chem.* **1999**, 1537−1543.
[38] B. Eulering, F. Ahlers, F. Zippel, M. Schmidt, H.-F. Nolting, B. Krebs, *J. Chem. Soc., Chem. Commun.* **1995**, 1305−1307.
[39] B. Eulering, M. Schmidt, U. Pinkernell, U. Karst, B. Krebs, *Angew. Chem. Int. Ed. Engl.* **1996**, *35*, 1973−1974.
[40] D. M. Brown, D. A. Usher, *J. Chem. Soc.* **1965**, 6558−6565.
[41] L. Westerheide, F. K. Müller, R. Than, B. Krebs, *Inorg. Chem.* **2001**, *8*, 1951−1961.
[42] R. G. Bates, *Determination of pH*, 2nd ed., John Wiley & Sons, New York, **1964**, p. 226−227.
[43] E. M. Wooley, D. G. Hurkot, L. G. Hepler, *J. Phys. Chem.* **1970**, *74*, 3908−3916.
[44] L. Zékány, I. Nagypál "PSEQUAD: A Comprehensive Program for the Evaluation of Potentiometric and/or Spectrophotometric Equilibrium Data Using Analytical Derivatives" in *Comptutational Methods for the Determination of Formation Constants* (Ed.: D. J. Leggett), Plenum Press, New York, **1991**.
[45] G. M. Sheldrick, *SHELXS-97, Program for the Solution and Refinement of Crystal Structures*, University of Göttingen, Germany, **1997**.

Received August 28, 2001
[I01334]

Synthesis and Characterization of Fe- or Cu-Substituted Molybdenum-Enriched Tungstodiphosphates

Robila Belghiche,[a,c] Roland Contant,[a] Yu Wei Lu,[a] Bineta Keita,[a] Mostefa Abbessi,[a,c] Louis Nadjo,*[a] and Jacqueline Mahuteau[b]

Keywords: Heteropolyanions / Dawson-type structures / Molybdenum / Transition metal cations / Electrocatalysis

Stereospecific routes were followed to synthesize five new Fe^{3+} and Cu^{2+}-substituted Mo-enriched Dawson-type heteropolyanions as aqueous soluble potassium salts: α_2-$K_7[Fe(OH_2)P_2W_{12}Mo_5O_{61}]$ and α_2-$K_7[Fe(OH_2)P_2W_{13}Mo_4O_{61}]$, α_1- and α_2-$K_8[Cu(OH_2)P_2W_{12}Mo_5O_{61}]$ and α_2-$K_8[Cu(OH_2)P_2W_{13}Mo_4O_{61}]$. The substituted species as well as their immediate lacunary precursors were characterized by IR, UV/Visible and ^{31}P NMR spectroscopy. In particular ^{31}P NMR spectroscopy indicates that isomerically pure compounds were obtained. The activity of these chemicals in electrocatalysis is illustrated by the reduction of nitrite for Fe^{3+} derivatives and the reduction of nitrate for Cu^{2+} compounds.
(© Wiley-VCH Verlag GmbH, 69451 Weinheim, Germany, 2002)

Introduction

Dawson-type tungstodiphosphates are interesting in their own right. More particularly, their ability to generate lacunary species and then metal cation substituted derivatives has aroused great attention.[1−10] The impetus was triggered by the pioneering remark of Baker[11] that monosubstituted heteropolyanions can be considered as the analogues of metalated porphyrins and used in catalytic processes with the advantage, relative to their organic counterparts, of thermal stability, robustness and inertness toward oxidizing environments. With regard to their electrochemistry and, correspondingly, their use in electrocatalysis, we are currently studying the parameters which eventually in conjunction with pH effects could induce the overlapping of the first waves of heteropolyanions (HPAs). The basic idea underlying this search is to trigger by reduced HPAs those energetically favourable cathodic processes that require several electrons to become effective.[6,8−10,12] Among several possibilities, the approach making use of substitution effects is considered in detail: in particular the location of the metal in the framework; the nature and number of substituents are expected to more or less influence the interactions between the electroactive centres within the HPA molecule. The two following examples can be cited in support of these anticipated results: i) A remarkably beneficial effect observed for the presence of molybdenum in the framework of Dawson-type HPAs used as electrocatalysts in the reduction of nitrite or nitric oxide aroused our interest.[5] For instance, the presence of a single Mo atom in the framework of $[P_2W_{17}MoO_{62}]^{6-}$ results in an improvement of 0.270 V in the potential at which the catalytic process is observed compared to the same process with $[P_2W_{18}O_{62}]^{6-}$. Such an improvement reaches 0.390 V with $[P_2Mo_{18}O_{62}]^{6-}$ instead of $[P_2W_{18}O_{62}]^{6-}$. At least two questions might result from this observation: they concern the influence of the number of Mo atoms in the molecule and the possible specificity of molybdenum in this particular process; ii) the presence of the Fe^{3+} cation in α_2-$[Fe(OH_2)P_2W_{15}Mo_2O_{61}]^{7-}$, abbreviated as α_2-$FeP_2W_{15}Mo_2$, substantially modifies the electrochemistry of this heteropolyanion compared with the behaviour of α_2-$[P_2Mo_3W_{15}O_{62}]^{6-}$ (α_2-$P_2Mo_3W_{15}$). In a pH 2 medium, the cyclic voltammogram of the latter compound begins with three diffusion-controlled one-electron waves. In contrast, the iron(III)-substituted complex displays a three-electron first wave at pH 2, as a result of the merging of the molybdenum and iron waves.[6,12] A study of this pattern as a function of pH allows the Fe^{3+} wave to be separated from the molybdenum reduction, thus confirming the mechanism leading to overlapping. Provisionally, it is also worth noting the use of Fe-substituted heteropolyanions in electrocatalytic processes.[4,13,14] The copper cation Cu^{2+} is another substituent known to be reducible in the close vicinity of the HPAs framework and therefore likely to result in a first wave in-

[a] Laboratoire de Chimie Physique, UMR 8000, CNRS, Electrochimie et Photoélectrochimie, Université Paris-Sud, Bâtiment 420,
91405 Orsay Cedex, France
Fax: (internat.) + 33-1/6915-4328
E-mail: louis.nadjo@lcp.u-psud.fr
[b] Service de RMN, UPRESA 8076, CNRS, Faculté de Pharmacie, Université Paris-Sud,
92296 Châtenay Malabry Cedex, France
[c] Departement de Chimie, Université de Annaba,
Algérie

volving several electrons.[9,10,15] Furthermore, copper and iron complexes exhibit useful behaviours in several catalytic processes.[16,17]

The purpose of the present paper is to give a detailed account of the synthesis and characterization of pure samples of several Mo-rich Dawson-type tungstodiphosphates monosubstituted by Fe^{3+} or Cu^{2+}. The electrocatalytic behaviours of these chemicals are also illustrated briefly.

Results and Discussion

Numbering of Atoms and Main Abbreviations

The new heteropolyanions (HPAs) are: α_2-K_7-$[Fe(OH_2)P_2W_{12}Mo_5O_{61}]$ (α_2-$P_2W_{12}Mo_5Fe$) and α_2-K_7-$[Fe(OH_2)P_2W_{13}Mo_4O_{61}]$ (α_2-$P_2W_{13}Mo_4Fe$); α_1 and α_2-$K_8[Cu(OH_2)P_2W_{12}Mo_5O_{61}]$ (α_1- and α_2-$P_2W_{12}Mo_5Cu$) and α_2-$K_8[Cu(OH_2)P_2W_{13}Mo_4O_{61}]$ (α_2-$P_2W_{13}Mo_4Cu$). Scheme 1 gives the numbering of atoms in the framework of $[P_2W_{18}O_{62}]^{6-}$ from which all the present compounds are derived. In conjunction with Table 1, it permits a precise localization of all the substituent atoms in the W skeleton.

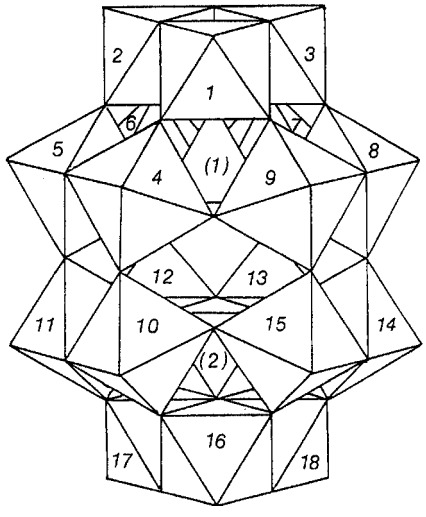

Scheme 1. Numbering scheme for $[P_2W_{18}O_{62}]^{6-}$ (Dawson structure)

Syntheses

Table 1 summarises the formulas of the main intermediate compounds and those of the final substituted products described in the following. Stereospecific routes to obtain the precursor lacunary species were established by one of the present authors.[18] The substituted compounds of interest here were then synthesized along the same lines as those followed for α_2-$P_2W_{15}Mo_2Cu$ and α_2-$P_2W_{15}Mo_2Fe$.[6,8] Specific details are given in the Exp. Sect. Table 1 also emphasizes the remarkably high yields obtained for all the syntheses in the present work. ^{31}P NMR spectra indicated that isomerically pure compounds were obtained. This observation is remarkable because several isomeric species could have been expected owing to possible migration of molybdenum atoms in all the compounds. The lack of heating might be one of the reasons for obtaining such pure samples.

UV/Vis and IR Characterization

As expected, no characteristic absorption band was observed in the UV/Vis spectra of the new HPAs except for some shift in the yellow direction due to the presence of Mo atoms in the molecules. However, in anticipation of subsequent work, the stability of these complexes in pH 3 and 5 media was checked by monitoring their UV/Vis spectra over a period of at least 24 hours. The species were found to be stable in these media. Figure 1 allows a comparison of the IR characteristics of the main new HPAs synthesized in this work. In tungstophosphates, the most characteristic IR band shifts correspond to P−O vibrations between 1200 and 1000 cm^{-1}, and these shifts characterize lacunary species. With an iron or a copper atom added in the vacancy, despite the presence of Mo atoms a greater symmetry is restored in the substituted molecule, at least as far as IR spectra are concerned. It is worth noting an important broadening of the bands, which become somewhat featureless roughly in the 850−700 cm^{-1} region. On the whole, in a first approximation, the IR spectra are close to those of the corresponding saturated compounds, even though a few new bands or slight differences could be detected on comparative scrutiny of the spectra. This situation prevents any sharp identification by IR spectra of a given anion.

^{31}P NMR Spectroscopy

The NMR study of paramagnetic element-containing HPAs was performed by Jorris et al.[19] on $[P_2W_{17}O_{61}]^{10-}$ derivatives. In agreement with their observations, work of this group[6,8] has confirmed that the chemical shift of the P atom furthest from the paramagnetic centre and noted P(2) is practically unaffected by the presence of this centre, while P(1) resonances are shifted radically and broadened. This shift and broadening might be important enough to make the corresponding signal hardly or not at all observable. Table 2 gives the chemical shifts measured for all the Fe^{3+} and Cu^{2+}-substituted compounds synthesized in this work. Values for the same metal complexes derived from $[(1),2,3\text{-}P_2Mo_2W_{15}O_{61}]^{10-}$ are included for comparison. The expected features were obtained throughout and do not call for further comments. Figure 2 illustrates specifically the ^{31}P NMR spectrum of α_1-$CuP_2Mo_5W_{12}$. For this compound, a single resonance peak was observed, corresponding to P(2). As shown in Table 2 and Figure 2, the two spectra for the α_1 and α_2 isomers are sufficiently different to

Table 1. Main characteristics of the HPAs synthesised in this work; the new HPAs are those substituted by Fe^{3+} and Cu^{2+}; abbreviated formulas are used, with the numbers of effectively determined water molecules; for further details, see text

Heteropolyanion	Position of Fe or Cu atom	Positions of Mo atoms	Molecular weight	Yield (%)	Colour
α_2-$K_{10}[P_2W_{12}Mo_5]\cdot 20H_2O$	–	4, 9, 10, 15, 16	4475	82	white
$K_6[P_2W_{12}Mo_6]\cdot 14H_2O$	–	1, 4, 9, 10, 15, 16	4322	98	yellow
$K_6[P_2W_{13}Mo_5]\cdot 14H_2O$	–	4, 9, 10, 15, 16	4411	89	orange
$K_6[P_2W_{14}Mo_4]\cdot 14H_2O$	–	4, 9, 10, 15	4499	96	orange
α_2-$K_{10}[P_2W_{13}Mo_4]\cdot 19H_2O$	–	4, 9, 10, 15	4545	88	white
α_1-$K_9Li[P_2W_{12}Mo_5]\cdot 20H_2O$	–	1, 9, 10, 15, 16	4443	95	white
α_2-$K_7[FeP_2W_{12}Mo_5]\cdot 14H_2O$	1	4, 9, 10, 15, 16	4306	73	dark yellow
α_2-$K_8[CuP_2W_{12}Mo_5]\cdot 16.5H_2O$	1	4, 9, 10, 15, 16	4398	74	yellow
α_1-$K_8[CuP_2W_{12}Mo_5]\cdot 15.5H_2O$	4	1, 9, 10, 15, 16	4380	66	yellow
α_2-$K_7[FeP_2W_{13}Mo_4]\cdot 15H_2O$	1	4, 9, 10, 15	4412	94	yellow
α_2-$K_8[CuP_2W_{13}Mo_4]\cdot 16.5H_2O$	1	4, 9, 10, 15	4485	89	yellow

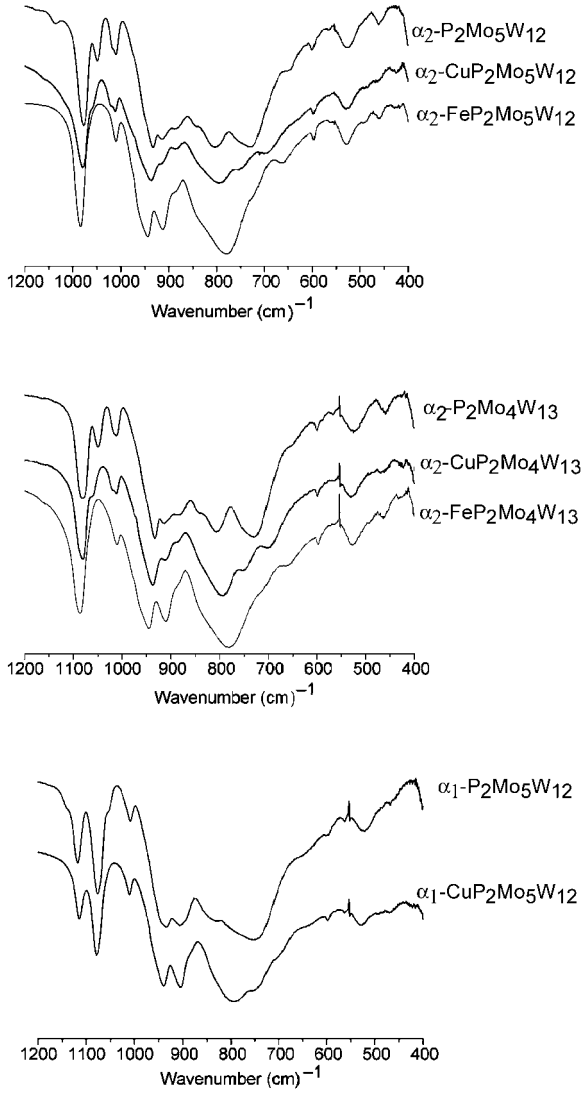

Figure 1. Selected IR spectra (KBr) for the hydrated heteropolyanions studied in this work

allow for the characterization of each isomer and the determination of their respective proportion in a mixture.

Electrocatalytic Behaviours of the (Fe or Cu)-Substituted Mo-Containing HPAs

The assessment of the behaviours of HPAs towards the reduction of NO_x constitutes one of our favourite electrocatalytic tests. Table 3 and 4 summarize several results selected to illustrate the combined influences of Mo and Fe or Cu in the HPA molecules. Our work establishes the beneficial effect of the presence of Mo atoms within the framework of HPAs on the electrocatalytic reduction of nitrites[5,17] and nitrates.[16] Cyclic voltammetry at a scan rate of 2 $mV\cdot s^{-1}$ was used throughout for these tables. Quantitatively, the activities of the HPAs were expressed through the catalytic efficiency, defined as $CAT = 100 \times [I_{(HPA + NO_x)} - I^d_{(HPA)}]/I^d_{(HPA)}$, where $I_{(HPA + NO_x)}$ is the peak current for the reduction of the heteropolyanion (HPA) in the presence of NO_x and $I^d_{(HPA)}$ is the corresponding diffusion peak current for the HPA alone. The quantity of NO_x is defined in terms of the excess parameter γ ($\gamma = C^\circ_{NO_x}/C^\circ_{HPA}$).

For the electrocatalytic reduction of nitrites, Table 3 illustrates the example of Fe-HPA derivatives: a pH 5 medium was selected to avoid competition between several NO_x species for the catalytic process; the increase of the catalytic efficiency with the number of Mo atoms is obvious. Typically, the catalytic efficiency showed a threefold increase when the number of Mo atoms increased from 2 to 5.

The catalytic efficiencies for the catalytic reduction of nitrate by reduced Cu-monosubstituted Mo-containing HPAs are given in Table 4. It is gratifying that the electrocatalytic reduction of nitrate by substituted HPAs could be observed for the first time. The process is efficient with all the compounds in Table 4 and also with compounds of the $P_2W_{17}Cu$ series (not shown). The comparison clearly indicates[16] the beneficial effect of the presence of Mo atoms for enhancing the catalytic current. In Table 4, the correlation between the number of Mo atoms and the catalytic efficiency is not straightforward, probably because the electrocatalysis is triggered at least partly by the electrodeposited

Table 2. ^{31}P NMR chemical shifts for $[M^x(H_2O)(P_2Mo_yW_{17-y}O_{61})]^{(10-x)-}$ with $M^x = Fe^{3+}$, Cu^{2+} or □, (□ designates a vacancy), y = 3, 4 or 5

HPA	δP(1) (ppm)	Δν P(1) (Hz)	δP(2) (ppm)	Δν P(2) (Hz)
α_2-$P_2Mo_2W_{15}$□ [a]	−4.93	5	−13.75	5
α_2-$P_2Mo_4W_{13}$□	−5.45	8	−11.31	7
α_2-$P_2Mo_5W_{12}$□	−5.53	5	−10.62	5
α_1-$P_2Mo_5W_{12}$□	−7.4	8	−9.94	110
α_2-$FeP_2Mo_2W_{15}$ [a]	≈ 900	> 30 000	−13.6	100
α_2-$CuP_2Mo_2W_{15}$ [a]	−27.2	1100	−13.0	60
α_2-$FeP_2Mo_4W_{13}$	not observed	not observed	−11.7	257
α_2-$CuP_2Mo_4W_{13}$	−39.5	2420	−10.2	80
α_2-$FeP_2Mo_5W_{12}$	not observed	not observed	−11.0	247
α_2-$CuP_2Mo_5W_{12}$	−38.4	2500	−9.64	22
α_1-$CuP_2Mo_5W_{12}$	not observed	not observed	−8.68	100

[a] See ref.[8]

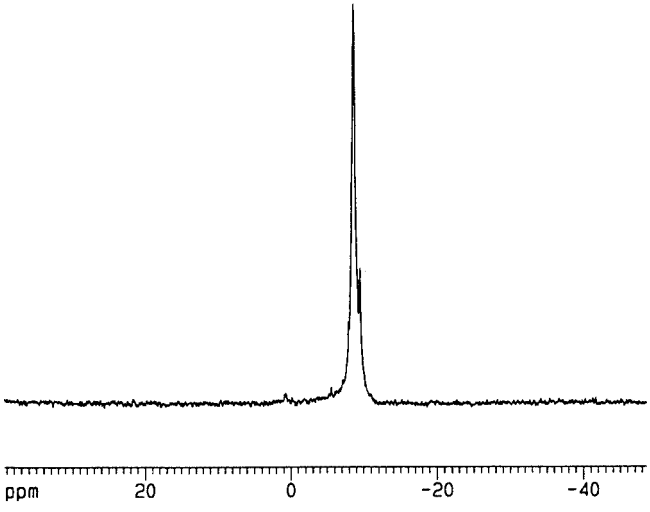

Figure 2. ^{31}P NMR spectrum of a mixture of α_1- (92%) and α_2-$Cu(OH_2)P_2Mo_5W_{12}$ (8%)

Table 3. Selected values of catalytic efficiencies in cyclic voltammetry for the electrocatalytic reduction of nitrite by Fe-substituted Mo-containing heteropolyanions; pH = 5; potential vs. SCE chosen for the evaluation: −0.700V; concentration of HPA: 2×10^{-4} M; γ = 100; scan rate: 2 mV·s^{-1}

Heteropolyanion	CAT%
α_2-$P_2W_{15}Mo_2Fe$	757
α_2-$P_2W_{13}Mo_4Fe$	1309
α_2-$P_2W_{12}Mo_5Fe$	2276

copper. Finally, a small isomeric effect between α_1- and α_2-$P_2W_{12}Mo_5Cu$ must be noted.

Conclusions

One of the basic ideas underlying this work originates in the observation that the presence of Mo atoms within the skeleton of tungsten-containing heteropolyanions results in a substantial improvement in the electrocatalytic behaviours of these compounds toward the reduction of nitrite or nitric oxide. Therefore, it was desirable to study the possibility of a correlation between the number and/or the location of these atoms in the framework with the catalytic efficiency. However, it soon appeared that an additional monosubstitution of the already Mo-substituted skeleton by Fe^{3+} or Cu^{2+} is also necessary in these catalysts. It was found that stereospecific synthesis routes available for obtaining several Mo-rich tungstodiphosphates allow direct access to the useful lacunary precursor species. It is gratifying that our procedures for the synthesis of the subsequent Fe^{3+} and Cu^{2+}-substituted derivatives result in pure compounds, as proved by several analytical techniques including IR spectroscopy and ^{31}P NMR spectroscopy. The usefulness of these new species in the electrocatalysis of nitrite and nitric oxide reduction was assessed. It is worth emphasizing particularly the activity of the present Cu-substituted derivatives toward the electrocatalytic reduction of nitrates. To the best of our knowledge, this process was observed for the first time with substituted heteropolyanions.

Table 4. Selected values of catalytic efficiencies in cyclic voltammetry for the electrocatalytic reduction of nitrate by Cu-substituted Mo-containing heteropolyanions; pH = 5; potential vs. SCE chosen for the evaluation: −0.800V; concentration of HPA: 2×10^{-4} M; γ = 500; scan rate: 2 mV·s^{-1}

Heteropolyanion	CAT%
α_2-$P_2W_{15}Mo_2Cu$	753
α_2-$P_2W_{13}Mo_4Cu$	882
α_2-$P_2W_{12}Mo_5Cu$	629
α_1-$P_2W_{12}Mo_5Cu$	780

Experimental Section

NMR, IR and UV/Visible Spectroscopy and Elemental Analysis: ^{31}P NMR spectra were recorded in 5 mm outer diameter tubes on a Bruker Avance 400 apparatus operating at 161.97 MHz, in the Fourier transform mode. The ^{31}P chemical shifts were measured

for 0.01 M solutions of the polyanions in 1 M LiCl/D_2O solutions and were referenced to H_3PO_4. IR spectra were recorded in 1% weight of HPA in a KBr pellet on a Bruker IFS 66 FT-IR spectrophotometer. UV/Visible spectra were recorded on a Perkin−Elmer Lambda 19 spectrophotometer. Elemental analyses were performed by CNRS Service Central d′Analyse at Vernaison (France). The crystal water content was determined by the following procedure: Two silica crucibles were thoroughly cleaned, dried at 250° C in an oven and finally left to cool to room temperature in a drying vessel containing P_2O_5 as a desiccant. Each crucible was loaded with 150 to 300 mg of the complex of interest and then heated at 250° C in the oven for one hour. After cooling in the drying vessel, the mass loss was measured and converted into mol of water per mol of complex.

Electrochemical Experiments: Pure water was used throughout. It was obtained by passing through a Milli-RO_4 unit and subsequently through a Millipore Q water purification set. All chemicals were of high-purity grade and were used as received. CH_3COONa and CH_3COOH were commercial products (Prolabo). The pH 5 solution was made up with 0.5 M CH_3COONa + CH_3COOH. The solutions were de-aerated thoroughly for at least 30 min with pure argon and kept under a positive pressure of this gas during the experiments. The source, mounting and polishing of the glassy carbon (GC, Tokai, Japan) electrodes has been described previously.[17] The glassy carbon samples had a diameter of 3 mm. The electrochemical setup was an EG & G 273 A driven by a PC with 270 software. Potentials are quoted relative to a saturated calomel electrode (SCE). The counter electrode was a platinum gauze of large surface area. All experiments were performed at room temperature.

Preparations: The potassium salts of α_2-$[P_2W_{12}Mo_5]^{10-}\cdot 20H_2O$, $[P_2W_{12}Mo_6]^{6-}\cdot 14H_2O$, $[P_2W_{13}Mo_5]^{6-}\cdot 14H_2O$, $[P_2W_{14}Mo_4]^{6-}\cdot 14H_2O$, α_2-$[P_2W_{13}Mo_4]^{10-}\cdot 19H_2O$ and the mixed potassium/lithium salt of α_1-$[P_2W_{12}Mo_5]^{10-}\cdot 20H_2O$ were prepared by the published stereospecific routes.[18]

α_2-$K_7[Fe(OH_2)P_2W_{12}Mo_5O_{61}]\cdot 14H_2O$: A sample of α_2-$K_{10}[P_2W_{12}Mo_5O_{61}]\cdot 20H_2O$ (9.40 g, 2.10 mmol) was dissolved in 20 mL of 0.12 M $Fe(NO_3)_3$ (2.4 mmol) and 60 mL of Millipore water and the mixture stirred for 30 min. After treatment with solid KCl (15 g) followed by a saturated KCl solution (60 mL), a dark yellow solid (6.57 g) was filtered off and dried in air. $K_7[Fe(OH_2)P_2W_{12}Mo_5O_{61}]\cdot 14H_2O$: calcd. H_2O 6.27, Fe 1.30, K 6.36, Mo 11.14, P 1.44, W 51.24; found H_2O, 5.85, Fe 1.27, K 7.50, Mo 10.70, P 1.67, W 48.90.

α_2-$K_8[Cu(OH_2)P_2W_{12}Mo_5O_{61}]\cdot 16.5H_2O$: A sample of α_2-$K_{10}[P_2W_{12}Mo_5O_{61}]\cdot 20H_2O$ (9.40 g, 2.10 mmol) was dissolved in 20 mL of 0.12 M $Cu(NO_3)_2$ (2.4 mmol) and 60 mL of Millipore water and the mixture stirred for 20 min. After treatment with a saturated KCl solution (60 mL), a yellow-green solid (6.84 g) was filtered off and dried in air. $K_8[Cu(OH_2)P_2W_{12}Mo_5O_{61}]\cdot 16.5H_2O$: calcd. H_2O 7.16, Cu 1.44, K 7.11, Mo 10.91, P 1.41, W 50.17; found H_2O 6.75, Cu 1.31, K 7.69, Mo 10.32, P 1.65, W 47.18.

α_1-$K_8[Cu(OH_2)P_2W_{12}Mo_5O_{61}]\cdot 15.5H_2O$: A sample of α_1-$K_{10}[P_2W_{12}Mo_5O_{61}]\cdot 20H_2O$ (9.40 g, 2.10 mmol) was dissolved in 20 mL of 0.14 M $Cu(NO_3)_2$ (2.8 mmol) and 60 mL of Millipore water and the mixture stirred for 20 min. After treatment with a saturated KCl solution (60 mL), a yellow solid (6.07 g) was filtered off and dried in air. $K_8[Cu(OH_2)P_2W_{12}Mo_5O_{61}]\cdot 15.5H_2O$: calcd. H_2O, 6.78, Cu 1.45, K 7.14, Mo 10.95, P 1.42, W 50.38; found H_2O, 6.37, Cu 1.45, K 7.23, Mo 9.89, P 1.53, W 48.89.

α_2-$K_7[Fe(OH_2)P_2W_{13}Mo_4O_{61}]\cdot 15H_2O$: A sample of α_2-$K_{10}[P_2W_{12}Mo_5O_{61}]\cdot 20H_2O$ (9.40 g, 2.10 mmol) was dissolved in 20 mL of 0.14 M $Fe(NO_3)_3$ (2.8 mmol) and 60 mL of Millipore water and the mixture stirred for 10 minutes. After treatment with solid KCl (15 g) followed by a saturated KCl solution (30 mL), a yellow orange solid (8.4 g) was filtered off and dried in air. $K_7[Fe(OH_2)P_2W_{12}Mo_5O_{61}]\cdot 15H_2O$: calcd. H_2O, 6.53, Fe 1.26, Mo 8.70, K 6.20, P 1.41, W 54.18; found H_2O 6.12, Fe 1.24, K 6.30, Mo 7.70, P 1.43, W 52.86.

α_2-$K_8[Cu(OH_2)P_2W_{13}Mo_4O_{61}]\cdot 16.5H_2O$: A sample of α_2-$K_{10}[P_2W_{12}Mo_5O_{61}]\cdot 20H_2O$ (9.40 g, 2.10 mmol) was dissolved in 20 mL of 0.14 M $Cu(NO_3)_2$ (2.8 mmol) and 60 mL of Millipore water and the mixture stirred for 15 min. After treatment with a saturated KCl solution (30 mL), a yellow solid (8.06 g) was filtered off and dried in air. $K_8[Cu(OH_2)P_2W_{13}Mo_4O_{61}]\cdot 16.5H_2O$: calcd. H_2O 7.02, Cu 1.42, K 7.2,, Mo 8.61 P 1.39, W 53.61; found H_2O 6.62, Cu 1.33, K 7.57, Mo 8.10, P 1.60, W 52.14.

Acknowledgments

This work was supported by the CNRS (UMR 8000) and the University Paris XI. The help of I. M. Mbomekalle, of our group, for the determination of the number of water molecules is gratefully acknowledged.

[1] C. L. Hill (Guest Ed.), *Chem. Rev.* **1998**, *98*, 1−389.
[2] M. T. Pope *Heteropoly and Isopoly Oxometalates*, Springer-Verlag, Berlin, **1983**.
[3] *Polyoxometalates: From Platonic Solids to Antiretroviral Activity* (Eds.: M. T. Pope, A. Muller), Kluwer Academic Publications, Dordrecht, **1994**.
[4] M. Sadakane, E. Steckhan, *Chem. Rev.* **1998**, *98*, 219−237.
[5] A. Belhouari, B. Keita, L. Nadjo, R. Contant, *New J. Chem.* **1998**, 83−86.
[6] R. Contant, M. Abbessi, J. Canny, A. Belhouari, B. Keita, L. Nadjo, *Inorg. Chem.* **1997**, *36*, 4961−4967.
[7] B. Keita, L. Nadjo, R. Contant, *J. Electroanal. Chem.* **1998**, *443*, 168−174.
[8] R. Contant, M. Abbessi, J. Canny, B. Keita, A. Belhouari, L. Nadjo, *Eur. J. Inorg. Chem.* **2000**, 567−574.
[9] B. Keita, Y. W. Lu, L. Nadjo, R. Contant, M. Abbessi, J. Canny, M. Richet, *J. Electroanal. Chem.* **1999**, *477*, 146−157.
[10] B. Keita, F. Girard, L. Nadjo, R. Contant, J. Canny, M. Richet, *J. Electroanal. Chem.* **1999**, *478*, 76−82.
[11] L. C. Baker, *Plenary Lecture. Proc. XV Int. Conf. Coord. Chem. 15th* 1973, Moscow
[12] B. Keita, A. Belhouari, L. Nadjo, R. Contant, *J. Electroanal. Chem.* **1998**, *442*, 49−57.
[13] B. Keita, A. Belhouari, L. Nadjo, R. Contant, *J. Electroanal. Chem.* **1995**, *381*, 243−250.
[14] J. E. Toth, F. C. Anson, *J. Am. Chem. Soc.* **1989**, *111*, 2444−2451.
[15] B. Keita, E. Abdeljalil, L. Nadjo, B. Avisse, R. Contant, J. Canny, M. Richet, *Electrochem. Commun.* **2000**, *2*, 145−149.
[16] B. Keita, E. Abdeljalil, L. Nadjo, R. Contant, R. Belghiche, *Electrochem. Commun.* **2001**, *3*, 56−62.
[17] B. Keita, F. Girard, L. Nadjo, R. Contant, R. Belghiche, M. Abbessi, *J. Electroanal. Chem.* **2001**, *508*, 70−80.
[18] R. Contant, J. P. Ciabrini, *J. Inorg. Nucl. Chem.* **1981**, *43*, 1525−1528.
[19] T. L. Jorris, M. Kozik, N. Casan-Pastor, P. J. Domaille, R. G. Finke, W. K. Miller, L. C. W. Baker, *J. Am. Chem. Soc.* **1987**, *109*, 7402−7408.

Received October 31, 2001
[I01429]

Cyclopentadienylmolybdenum(VI) and Molybdenum(V) Oxo Chemistry: New Synthetic and Structural Features

Dirk Saurenz,[a] Funda Demirhan,[a,b] Philippe Richard,[a] Rinaldo Poli,*[a] and Helmut Sitzmann[c]

Keywords: Cyclopentadienyl ligands / Molybdenum / Oxo ligands / X-ray crystallography

Convenient syntheses for Cp, Cp*, and related cyclopentadienyl derivatives (^{4}Cp = C_5H_iPr$_4$; Cp''' = C_5H_2tBu$_3$-1,2,4) of formula [(Ring)$_2$Mo$_2$O$_5$] are described. Compound [Cp$_2$Mo$_2$O$_5$] was produced in good yields by the rapid oxidation of red [CpMoO$_2$]$_4$ with PhIO in CH_2Cl_2. [Cp*$_2$Mo$_2$O$_5$] was obtained by CH_3COOH acidification of aqueous solutions of [Cp*MoO$_3$]$^-$Na$^+$, the latter being generated in a single step from [Cp*MoCl$_4$] and more than 5 equiv. of aqueous NaOH in air. Minor quantities of [Cp*MoO$_2$]$_2$ were also isolated from this reaction, although the formation of this by-product may be reduced by using a two-step basic hydrolysis procedure. Extension of the latter strategy also allowed the preparation of [^{4}Cp$_2$Mo$_2$O$_5$], [Cp'''$_2$Mo$_2$O$_5$], and [^{4}CpMoO$_2$Cl] in good yields, in addition to the by-product [Cp'''MoO$_2$]$_2$. X-ray structures are reported for compounds [^{4}Cp$_2$Mo$_2$O$_5$], [Cp'''$_2$Mo$_2$O$_5$], [Cp*MoO$_2$]$_2$, [Cp'''MoO$_2$]$_2$, and [^{4}CpMoO$_2$Cl].

(© Wiley-VCH Verlag GmbH, 69451 Weinheim, Germany, 2002)

Introduction

High oxidation state organometallic chemistry has experienced rapid development in the last 20 years, mostly justified by the search for efficient oxidation catalysts. Half-sandwich oxo derivatives of rhenium,[1–3] displaying a very rich chemical reactivity and catalytic activity, are an example of a well investigated class of compounds. Some of the earliest high oxidation state organometallics however, are the cyclopentadienyl oxo derivatives of molybdenum, first developed in the laboratory of M. L. H. Green.[4,5]

The stability of high oxidation state complexes requires the presence of electronegative and π-donating ligands such as halides or negatively charged oxygen- (oxo, alkoxo) or nitrogen-based (nitrido, imido, amido) ligands. The organic fragments most compatible with this ligand environment are odd-electron ones, such as alkyls (1-electron), allyls (3-electron), dienyls (5-electron), etc., while neutral organic fragments (olefins, arenes, etc.) need more electron-rich, low-valent metal centers to optimize bonding. These conditions confer a high degree of covalency on the resulting metal–carbon bonds, which consequently become quite resistant to hydrolytic conditions. It is therefore somewhat surprising that the physical behavior and chemical reactivity of high oxidation state organometallics has not been investigated systematically in water, although aqueous reagents are sometimes used for their syntheses. This contrasts with the well-developed aqueous chemistry of high oxidation state oxomolybdenum complexes.[6,7] On the other hand, the rich electrochemical behavior displayed by the metals involved, notably molybdenum, makes these molecules quite interesting for potential electrocatalytic applications. For these reasons, we initiated a research effort aimed at increasing our basic knowledge of the physical properties and chemical reactivity of organomolybdenum compounds in a variety of high oxidation states in water.

Although several investigations of cyclopentadienyl oxo complexes of molybdenum in high oxidation states have been reported,[8,9] routes to these materials cannot be considered to be completely satisfactory. In this first contribution, we focus on improvements in the synthetic procedures to produce compounds [Cp$_2$Mo$_2$O$_5$] and [Cp*$_2$Mo$_2$O$_5$], which we plan to use as starting materials for our studies. We also report an extension of the synthesis of analogues containing differently substituted cyclopentadienyl rings. We are interested in cyclopentadienyl rings with a high degree of substitution, as these are known to afford more inert metal-cyclopentadienyl bonds by restricting access to the

[a] Laboratoire de Synthèse et d'Electrosynthèse Organométalliques, Université de Bourgogne, Faculté de Science Gabriel,
6 boulevard Gabriel, 21000 Dijon, France
Fax: (internat.) + 33-03/8039-3720
E-mail: Rinaldo.Poli@u-bourgogne.fr
[b] Celal Bayar University, Faculty of Sciences & Liberal Arts, Department of Chemistry,
45030, Muradiye-Manisa, Turkey
[c] Fachbereich Chemie, Universität Kaiserslautern,
Erwin-Schrödinger-Straße 54, 67663 Kaiserslautern, Germany
Fax: (internat.) + 49-(0)631/205-2187
E-mail: sitzmann@chemie.uni-kl.de

metal center, while at the same time rendering the other ligands more labile. Interesting reactivity may thus be expected. Some basic aqueous chemistry related to the optimization of the syntheses reported in this paper is also discussed. Detailed studies of the behavior of these compounds in water as functions of pH[10] and of electrode potential[11] have also been completed, and are being reported separately.

Results

The Cyclopentadienyl Oxo Molybdenum(VI) System

Discussion of Previously Reported Routes

As mentioned in the introduction, $[Cp_2Mo_2O_5]$ has been known since 1964, but no reliably high-yielding and practical synthesis seems to be available yet. It was first obtained in 20% yield, together with several other products, from the photolytic degradation of $[CpMo(CO)_3]_2$ in chloroform.[4] It has also been formed in low yields by adventitious oxygenation of solutions of various CpMo derivatives.[4,5] A synthesis in higher yield (79%) by oxidation of the dinuclear Mo^V compound $[CpMoO_2]_2$ has been reported. This, however, required use of Ag_2O as the oxygen-transfer agent and warming in CH_2Cl_2 at 55 °C for 1.5 days.[12] The precursor complex could in turn be obtained by hydrolysis of $[CpMoX_4]$ (X = Cl, Br) with excess water. A red isomer, formulated as a tetranuclear compound, was obtained immediately, while longer exposure to water or dissolution of the red isomer in acetone or chloroform slowly afforded a dinuclear orange isomer.[5,12] A similar behavior has been described for analogous compounds with monosubstituted cyclopentadienyl ligands.[12] Since the reported behavior of the red tetrameric form suggested that it was a chemically more labile form, we wondered whether the oxidation of this red isomer by sufficiently rapid oxygen-transfer agents might provide an easier route to the desired Mo^{VI} product in high yield before its conversion into the less reactive orange isomer.

New Synthetic Strategy

Several effective reagents are commonly used for oxygen-transfer chemistry, the most easily accessible one being H_2O_2. We were hesitant to use this reagent, because the formation of peroxo compounds of Mo^{VI} or W^{VI}, such as $[Cp^*W(O_2)(O)R]$[13−15] or $[Cp^*M(O_2)(O)Cl]$ (M = Mo, W),[16,17] by treatment of suitable precursors with either H_2O_2 or hydroperoxides has been described previously. Indeed, oxidation tests with H_2O_2 gave unsatisfactory results. The use of PhIO,[18] on the other hand, provided a rapid and convenient synthesis in two steps (>50% overall yield) from $[CpMoCl_4]$, itself easily available from commercially available $[Mo(CO)_6]$ [Equations (1) and (2)].[19] The second step was complete within 15 min at room temperature, and the best results were obtained when the solution was worked up immediately. If the product was allowed to stand in the dichloromethane solution, darker, insoluble by-products began to form. The intermediate red Mo^V oxo complex had to be isolated and removed from water; an attempt to carry out the synthetic procedure without this isolation step gave unsatisfactory results. This procedure, however, constitutes a significant improvement over those previously available, especially in terms of time efficiency, as both steps can be carried out at room temperature and the overall procedure may be accomplished in half a day.

$$4\,[CpMoCl_4] + 8\,H_2O \rightarrow [CpMoO_2]_4 + 16\,HCl \quad (1)$$

$$[CpMoO_2]_4 + 2\,PhIO \rightarrow 2\,[Cp_2Mo_2O_5] + 2\,PhI \quad (2)$$

The procedure described below for the Cp* and related analogues, via the hitherto unknown $[CpMoO_3]^-$ anion,[20] does not give satisfactory results for the Cp system.

The Pentamethylcyclopentadienyl Oxo Molybdenum(VI) System

Discussion of Previously Reported Routes

The Cp* compound was first reported in 1985 by Herberhold et al. as the product of the aerial oxidation of $[Cp^*Mo(CO)_2(NO)]$,[21] and was subsequently shown to form in low yield as a by-product in a variety of other reactions.[22−25] A high-yielding synthesis by aerial oxidation of $[Cp^*Mo(CO)_2]_2$ in chloroform was reported by Faller and Ma, although the product was said to be contaminated by ca. 15% of the chloride complex $[Cp^*MoO_2Cl]$ and needed further exposure to acetone/water for purification,[26] while the synthesis of the starting compound from commercially available $[Mo(CO)_6]$ is itself not free from pitfalls.[27,28] This reaction was re-examined later by Bottomley and shown to yield a host of other incompletely oxidized products under a variety of conditions.[29,30] The preparation from $[Cp^*MoCl_4]$ in 70−75% yield reported by Umakoshi and Isobe[31] is related to the synthetic procedure reported by us here, but was not optimized for large-scale syntheses and uses the exotic sodium oxometallate salts Na_2MoO_4, Na_2WO_4, or $NaVO_3$ as oxidants. Another reported high-yielding synthesis was by protonolysis of the unusual starting compound $[Cp^*Mo(N\mathit{t}Bu)_2Cl]$ with aqueous HCl.[32]

Finally, work carried out in Geoffroy's laboratory showed that the hydrolysis of $[Cp^*MCl_4]$ (M = Mo, W) in the presence of an amine ($\mathit{t}BuNH_2$) yields $\mathit{t}BuNH_3^+[Cp^*MO_3]^-$ in good yields,[33] while Sundermeyer showed that the same anions also form on treatment of the oxo-bridged dimers $[Cp^*_2M_2O_5]$ with tetrabutylammonium hydroxide.[32] Acidification of the anion solution, examined in the Geoffroy study for the tungsten compound, gave back the dinuclear complex through the presumed condensation of initially formed $[Cp^*WO_2(OH)]$.[33]

A detailed discussion of this reversible anion/dimer transformation and the aqueous chemistry of the tetrachloride

compounds is essential, as it forms the basis of our improved synthetic strategy. Geoffroy et al. reported that treatment of [Cp*$MoCl_4$] with 2 equiv. of NaOH in acetone/water in an open flask for more than 30 min gave [Cp*MoO_2Cl], while use of an unspecified excess of NaOH afforded the dinuclear [Cp*$_2Mo_2O_5$].[34] The reaction between [Cp*MoO_2Cl] and excess (3 equivalents) NaOH was also reported to yield the dinuclear compound. These observations seemed odd to us in view of Sundermeyer's result mentioned above, which we have confirmed (see next section).[35] In contrast with the apparent lack of reactivity between [Cp*$_2Mo_2O_5$] and excess aqueous NaOH, excess aqueous *t*$BuNH_2$ (a weaker base than NaOH) under analogous conditions yielded *t*$BuNH_3^+$[Cp*MoO_3]$^-$ in good yields.[34] Furthermore, it was shown that acidification of dichloromethane solutions of the *t*$BuNH_3^+$[Cp*MoO_3]$^-$ salt with acetic acid afforded [Cp*$_2Mo_2O_5$], which was recovered in 58% yield. From these observations, it would seem logical to imagine a pH-dependent equilibrium between the anionic mononuclear and the neutral dinuclear forms [Equation (3)] in water.[36] The anion should therefore be the ultimate product when excess strong base (e.g. NaOH) is present, in contrast to Geoffroy's report. On the basis of this hypothesis, we have developed the new synthetic procedure reported in the following section. Preliminary investigations indeed showed that yellow [Cp*$_2Mo_2O_5$] solutions in MeOH/H_2O became nearly colorless upon treatment with NaOH, and the resulting basic solutions turned yellow once more when the pH was lowered by addition of strong acids.

$$[Cp^*_2Mo_2O_5] + 2\ OH^- \rightleftarrows 2\ [Cp^*MoO_3]^- + H_2O \quad (3)$$

New Synthetic Strategy

[Cp*$MoCl_4$] is conveniently prepared in high yields and purity[37] from commercially available [$Mo(CO)_6$] and was therefore the starting compound of choice for our synthetic work. As mentioned in the previous section, it seemed to us that excess NaOH under aerobic conditions should afford the cyclopentadienyltrioxomolybdate anion directly, according to the stoichiometry of Equation (4).

$$2\ [Cp^*MoCl_4] + 10\ OH^- + 1/2\ O_2 \rightarrow 2\ [Cp^*MoO_3]^- + 8\ Cl^- + 5\ H_2O \quad (4)$$

Treatment of acetone solutions of [Cp*$MoCl_4$] with a slight excess (ca. 6 equivalents) of aqueous NaOH in air for over a day at room temperature yielded a suspension of the pale yellow precipitate [Cp*MoO_3]$^-$$Na^+$, but also minor quantities of a soluble, colored by-product (identified as [Cp*MoO_2]$_2$, vide infra). Separation of this by-product was accomplished by complete evaporation of the solvent mixture and redissolution in pure water, which dissolved the sodium salt but not the by-product. Since the sodium organomolybdate salt might have been difficult to separate from NaCl and excess NaOH by fractional crystallization, we proceeded directly to its conversion into the neutral dimer, which is insoluble in pure water. Dropwise addition of acetic acid from a burette resulted, after neutralization of the excess base, in the instantaneous precipitation of the yellow product. Addition of acid was stopped when administration of one further drop of the acid solution did not cause any further precipitation. The synthetic procedure could therefore be handled as a simple titration reaction, allowing the use of close to the stoichiometric amount of acid. This was important because excess acetic acid is also partially extracted into the ether layer and large quantities of this compound may interfere with the crystallization procedure or even contaminate the organomolybdenum product. This procedure consistently gave a pure product with yields in excess of 60% on a 2 g scale. The synthesis could also be accomplished stepwise, by treatment of [Cp*$MoCl_4$] with three equivalents of NaOH for one day, followed by addition of three more equivalents of NaOH. In this fashion, the formation of the Mo^V by-product was avoided (see discussion). The isolated yield of the desired product, however, was not increased by this modified procedure.

Isolation and Structure of the [CpMoO_2]$_2$ By-Product*

The water-insoluble crop generated during the synthetic procedure described above contained orange-red crystalline [Cp*MoO_2]$_2$, which could be recovered in yields of up to 20% depending on the operating conditions. It seemed that not only the time of exposure to air but also the relative amount of water and acetone was important in determining the ratio between the Mo^V and Mo^{VI} products (see Discussion), smaller amounts of water seeming to favor a greater degree of oxidation. [Cp*MoO_2]$_2$ has been reported previously and shown to adopt two possible structures differing in the relative arrangement of the Cp* and terminal oxo ligands across the central Mo(μ-O)$_2$Mo plane: *syn* as in **I**[38] (like the analogous Cp system)[39] or *anti* as in **II**.[40] We have redetermined the structure of the *syn* form at lower temperature with a better precision. The results have been deposited with the CCDC but, since they do not differ significantly from those of the higher temperature structure, they are not explicitly reported here. The metal-metal distance in the *syn* polymorph [2.587(1) Å] is significantly shorter than that in the *anti* polymorph [2.647(3) Å],[40] undoubtedly because of the butterfly arrangement that allows the metals to approach each other, in contrast to the planar arrangement in the *anti* isomer. The same situation has been found for [(L)$_2Mo_2O_4$]$^{2+}$ (L = 1,5,9-triazacyclononane).[41,42]

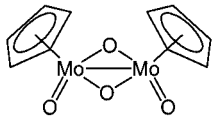

I

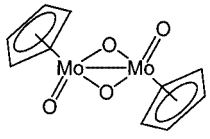

II

Oxo Molybdenum(VI) and Molybdenum(V) Systems with Sterically more Encumbering Cyclopentadienyl Rings

Syntheses

The procedure described above for the Cp* system was applied in a straightforward manner to the hydrolysis of [^{4}CpMoCl$_4$] and [Cp′′′MoCl$_4$]. Again, aerial hydrolysis in both cases afforded solutions containing the water-soluble $Na^+[(Ring)MoO_3]^-$ salt. This was not isolated, but its presence was indicated by its behavior upon acidification, identical to that seen in the corresponding Cp* system described above. [^{4}Cp$_2$Mo$_2$O$_5$] and [Cp′′′$_2$Mo$_2$O$_5$] were obtained as yellow or yellow-orange crystalline solids that were insoluble in water but soluble in ether. Both were crystallized, and their structures were confirmed by X-ray diffraction methods (see next section). Like their Cp and Cp* analogues,[4,22] they displayed two IR vibrations typical of the Mo=O functionalities (symmetric and asymmetric at ca. 885 and 920 cm^{-1}, respectively) and one due to the asymmetric Mo−O−Mo stretch (at ca. 760 cm^{-1}).

While the ^{4}Cp system afforded the expected dinuclear Mo^{VI} product with no indication of incomplete oxidation, the Cp′′′ system behaved like the Cp* system described above and also gave a water-insoluble fraction, from which the dinuclear Mo^V complex [Cp′′′MoO$_2$]$_2$ was recovered. This compound was also characterized by X-ray diffraction methods (see below).

X-ray Structures of the [(Ring)$_2$Mo$_2$O$_5$] Compounds

Several X-ray structural determinations of various polymorphs of [Cp*$_2$Mo$_2$O$_5$][23−26] have been reported over the years and a discussion of the similarities between them is already available.[25] It is interesting to see whether the steric bulk of the cyclopentadienyl ligand plays any role on the other structural parameters. The geometries of compounds [^{4}Cp$_2$Mo$_2$O$_5$] and [Cp′′′$_2$Mo$_2$O$_5$] are shown in Figures 1 and 2, respectively, and the relevant metric data are compared in Table 1. The ^{4}Cp compound has a symmetry-imposed inversion center on the bridging oxygen atom, and two independent half molecules are contained in the asymmetric unit. The Cp′′′ compound, on the other hand, has a single entire molecule in the asymmetric unit. While the Mo−O−Mo angle is forced to be linear in the first case, it deviates quite substantially from linearity in the second one. This deviation is larger than the largest one previously observed for the related Cp* polymorphs [172.7(3)°]. The Mo=O and Mo-(μ-O) distances for the Cp* structures were found to be in the 1.67−1.72 Å and 1.85−1.90 Å ranges, respectively. The same parameters are within these ranges for both ^{4}Cp and Cp′′′ structures, the Mo-(μ-O) distances being towards the long end of this range in both cases.

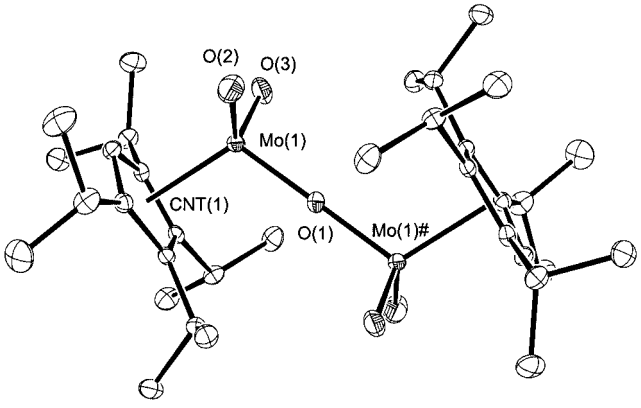

Figure 1. An ORTEP view of one of the two independent molecules of compound [^{4}Cp$_2$Mo$_2$O$_5$]; ellipsoids are drawn at the 50% probability level; the atom numbering scheme for the other molecule is as follows: Mo(2) for Mo(1), O(4) for O(1), O(5) for O(2), O(6) for O(3), and CNT(2) for CNT(1)

X-ray Structure of [Cp′′′MoO$_2$]$_2$

The geometry of [Cp′′′MoO$_2$]$_2$ is shown in Figure 3 and selected bonding parameters are reported in Table 2. The

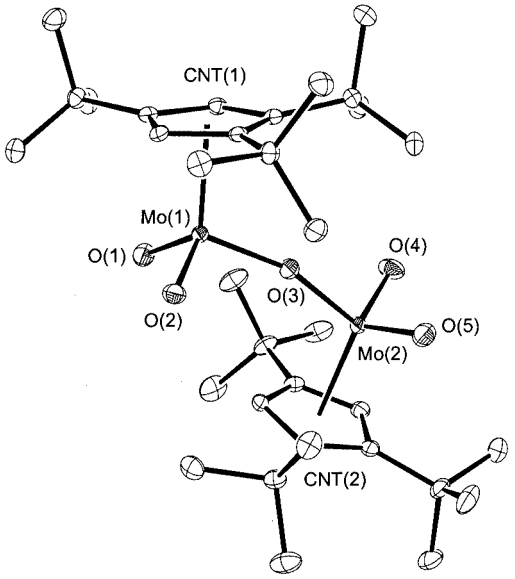

Figure 2. An ORTEP view of compound [Cp′′′$_2$Mo$_2$O$_5$]; ellipsoids are drawn at the 50% probability level

immediate striking feature is the relative *anti* arrangement of the two Cp′′′ groups: these are *syn* in the Cp analogue, while both arrangements are possible for the Cp* molecule. Although no unambiguous conclusion can be drawn, it seems reasonable to imagine that the steric bulk of the Cp′′′ ligand enforces the *anti* arrangement, while the compound might prefer the *syn* arrangement for electronic reasons. Therefore, the *syn* arrangement should be observed in the less crowded cases (such as Cp). It is easy to imagine how the placement of two Cp′′′ ligands into the *syn* structure (see drawing **I**) would introduce a severe strain in the molecule.

The Mo−Mo distance in [Cp′′′MoO$_2$]$_2$ compares quite well with that in the *anti* form of [Cp*MoO$_2$]$_2$ [2.647(3) Å].[40] This parameter is therefore much more sensitive to the geometry of the central Mo_2O_2 moiety (bent for the *syn* and planar for the *anti*) than to the type of cyclopentadienyl ring. The Mo=O and Mo-(μ-O) distances do not seem

Table 1. Selected bond lengths (Å) and angles (°) for compounds $[(Ring)_2Mo_2O_5]$ (Ring = ^{4}Cp, Cp′′′)

$[^4Cp_2Mo_2O_5]$ [a]			$[Cp'''_2Mo_2O_5]$	
Mo(1)−O(1)	1.89560(18)	1.89985(17)	Mo(1)−O(3)	1.8950(12)
			Mo(2)−O(3)	1.8978(11)
Mo(1)−O(2)	1.7092(15)	1.7071(15)	Mo(1)−O(1)	1.7088(12)
Mo(1)−O(3)	1.6969(15)	1.7034(14)	Mo(1)−O(2)	1.7125(12)
			Mo(2)−O(4)	1.7101(13)
			Mo(2)−O(5)	1.7050(13)
Mo(1)−CNT(1)	2.125(3)	2.123(3)	Mo(1)−CNT(1)	2.133(3)
			Mo(2)−CNT(2)	2.118(3)
O(1)−Mo(1)−O(2)	103.99(5)	103.46(5)	O(1)−Mo(1)−O(3)	103.43(5)
O(1)−Mo(1)−O(3)	102.93(5)	104.30(5)	O(2)−Mo(1)−O(3)	104.99(6)
			O(3)−Mo(2)−O(4)	103.23(6)
			O(3)−Mo(2)−O(5)	102.52(6)
O(2)−Mo(1)−O(3)	106.03(8)	105.89(8)	O(1)−Mo(1)−O(2)	104.49(6)
			O(4)−Mo(2)−O(5)	104.87(7)
CNT(1)−Mo(1)−O(1)	111.3(2)	112.3(2)	CNT1−Mo(1)−O(3)	111.1(2)
			CNT2−Mo(2)−O(3)	114.0(3)
CNT(1)−Mo(1)−O(2)	114.6(2)	116.1(2)	CNT1−Mo(1)−O(1)	116.9(3)
CNT(1)−Mo(1)−O(3)	116.6(2)	113.6(2)	CNT1−Mo(1)−O(2)	114.5(2)
			CNT2−Mo(2)−O(4)	114.7(3)
			CNT2−Mo(2)−O(5)	115.9(3)
Mo(1)−O(1)−Mo(1)#	180.0	180.0	Mo(1)−O(3)−Mo(2)	162.61(7)

[a] For the numbering scheme of the second independent molecule (second column), see caption of Figure 1.

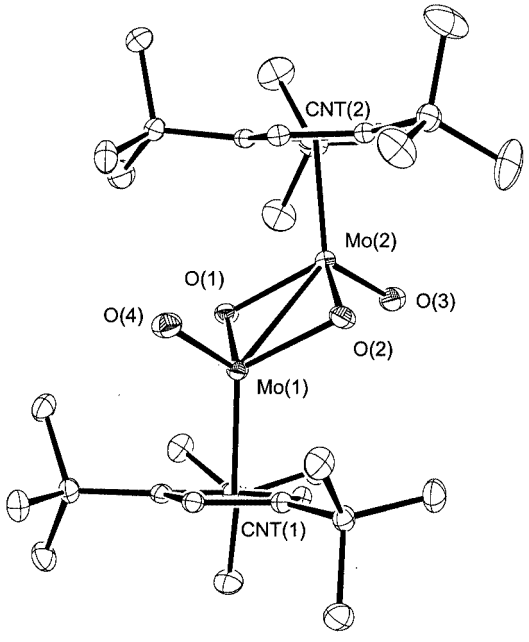

Figure 3. An ORTEP view of $[Cp'''MoO_2]_2$; ellipsoids are drawn at the 50% probability level

sensitive to either effect, and are essentially identical to those of all other previously described molecules with this stoichiometry, whether *syn* or *anti*.

The $[^4CpMoO_2Cl]$ System

According to previous Cp* literature,[34] the aerobic hydrolysis of the tetrachloro compound with two equivalents of aqueous NaOH directly afforded the corresponding dioxochloro derivative. For the less electron-rich Cp system, on the other hand, excess water quite rapidly yielded the dioxo system, as seen above, even in the absence of base.[5] The ^{4}Cp system behaved similarly to the Cp*, to which it is sterically and electronically more similar. Identical yields of $[^4CpMoO_2Cl]$ were obtained when $[^4CpMoCl_4]$ was hydrolyzed in the presence of either three or two equivalents of NaOH. In the IR spectrum, the compound showed, as expected, Mo=O stretching vibrations essentially identical to those in the related oxo-bridged dinuclear complex and no band in the Mo−O−Mo stretching region. The structure of this product has also been confirmed by X-ray crystallography (see Figure 4); the relevant bond lengths and angles are reported in Table 3. While no structure for a $[(Ring)MoO_2X]$ (X = Cl or other halogen) seems to have been reported previously, related structures are those of $[\{C_5Ph_4[C_6H_3(OMe)_2\text{-}2,5]\}MoO_2(OMe)]$[43] and $[Cp^*MoO_2\{(2,6\text{-}i\text{Pr}_2C_6H_3)N(SiMe_3)\}_2Si_2O_2(OH)_3]$.[44] The Mo=O distances are quite similar in all these compounds. The Mo−Cl distance compares with related Mo^V−Cl distances and appears to be affected mostly by the steric pressure of the cyclopentadienyl ring, as suggested by the following examples: $[Cp^*MoOCl]_2O$: 2.368(2) Å,[31] $[CpMoOCl_2]$: 2.301(4) Å (average),[45] $[Cp^*MoOCl_2]$: 2.245(9) and 2.330(5) Å (averages) in two independent reports.[30,46]

Discussion

From the previous literature reports and from our results, the following simplified picture emerges for the aerobic hydrolysis of $[(Ring)MoCl_4]$ compounds (see Scheme 1). Hydrolysis of the first two Mo−Cl bonds affords $[(Ring)MoOCl_2]$, which can either undergo further hydrolysis to

Table 2. Selected bond lengths (Å) and angles (°) for compound $[Cp'''MoO]_2$

Mo(1)−Mo(2)	2.65115(19)	CNT(2)−Mo(2)−Mo(1)	127.7(1)
Mo(1)−CNT(1)	2.082(2)	CNT(1)−Mo(1)−O(1)	114.5(1)
Mo(2)−CNT(2)	2.082(1)	CNT(2)−Mo(2)−O(1)	113.1(1)
Mo(1)−O(1)	1.9475(11)	CNT(1)−Mo(1)−O(2)	117.8(1)
Mo(2)−O(1)	1.9428(11)	CNT(2)−Mo(2)−O(2)	117.5(1)
Mo(1)−O(2)	1.9464(11)	CNT(1)−Mo(1)−O(4)	116.7(2)
Mo(2)−O(2)	1.9488(11)	CNT(2)−Mo(2)−O(3)	117.3(2)
Mo(1)−O(4)	1.7045(12)	O(2)−Mo(1)−O(1)	94.09(5)
Mo(2)−O(3)	1.7063(12)	O(1)−Mo(2)−O(2)	94.16(5)
Mo(2)−Mo(1)−O(1)	46.97(3)	O(1)−Mo(1)−O(4)	106.20(5)
Mo(1)−Mo(2)−O(1)	47.11(3)	O(1)−Mo(2)−O(3)	106.94(5)
Mo(2)−Mo(1)−O(2)	47.15(3)	O(2)−Mo(1)−O(4)	104.64(5)
Mo(1)−Mo(2)−O(2)	47.07(3)	O(2)−Mo(2)−O(3)	105.06(6)
Mo(2)−Mo(1)−O(4)	111.79(4)	Mo(1)−O(1)−Mo(2)	85.92(4)
Mo(1)−Mo(2)−O(3)	115.06(4)	Mo(1)−O(2)−Mo(2)	85.78(4)
CNT(1)−Mo(1)−Mo(2)	131.5(2)		

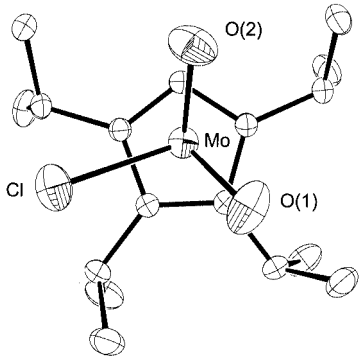

Figure 4. An ORTEP view of compound $[^4CpMoO_2Cl]$; ellipsoids are drawn at the 50% probability level

Table 3. Selected bond lengths (Å) and angles (°) for compound $[^4CpMoO_2Cl]$

Mo−Cl	2.3251(7)	Cl−Mo−O(2)	101.54(8)
Mo−O(1)	1.720(2)	Cl−Mo−CNT	108.8(2)
Mo−O(2)	1.700(2)	O(1)−Mo−O(2)	106.83(11)
Mo−CNT	2.113(3)	O(1)−Mo−CNT	118.1(2)
Cl−Mo−O(1)	102.15(8)	O(2)−Mo−CNT	117.2(3)

give $[(Ring)MoO_2]_2$ or may be oxidized to give $[(Ring)MoO_2Cl]$. Finally, the dioxo Mo^V dimer can be oxidized and the chlorodioxo Mo^{VI} complex can be hydrolyzed, to

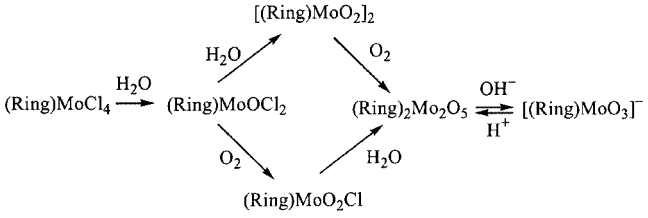

Scheme 1

yield $[(Ring)_2Mo_2O_5]$ in both cases. Under basic conditions, however, the final product converts to the $[(Ring)MoO_3]^-$ anion. Of course, other intermediates must also be formed during these transformations, notably hydroxo complexes, the relative stability of which is supported by some evidence.[12,31,34]

If hydrolysis prevails over oxidation at the level of the first dichlorooxo intermediate, resulting in the dinuclear, metal-metal bonded dioxo compound $[(Ring)MoO_2]_2$, further oxidization by dioxygen to the Mo^{VI} dimer is rather difficult. This is what happens for the simple Cp system. In fact, even oxygen-delivering agents such as Ag_2O react with it slowly.[12] However, the kinetic red form is more reactive, and a successful strategy for the formation of $[Cp_2Mo_2O_5]$ with PhIO by this route is presented in this paper.

The rate of hydrolysis seems to decrease as the steric bulk of the cyclopentadienyl ring increases. The greater donating power of the bulkier rings may also retard the complete hydrolysis for electronic reasons. Oxidation of the dichlorooxo Mo^V species, on the other hand, should be made more favorable by more electron-rich ligands. At any rate, the oxidation step may then prevail over hydrolysis, resulting in the chlorodioxo Mo^{VI} species provided there is dioxygen available. This is the situation encountered for the Cp* system, for which aerobic hydrolysis in the presence of two equivalents of NaOH was reported to give a good yield of $[Cp^*MoO_2Cl]$.[34] The same also occurs for the ^4Cp system reported here with either two or three equivalents of NaOH. The use of neutral aqueous conditions should produce three acid equivalents, as shown in Equation (5). Evidently, the last chloride ligand is not hydrolyzed under neutral conditions, whereas at high pH (excess NaOH) the only recovered product (after acidification) is $[^4Cp_2Mo_2O_5]$.

$$2\,[^4CpMoCl_4] + 3\,H_2O + 1/2\,O_2 \rightarrow 2\,[^4CpMoO_2Cl] + 6\,Cl^- + 6\,H^+ \quad (5)$$

The relative rates of hydrolysis and oxidation for $[(Ring)MoOCl_2]$ should also depend on other factors such as the concentration of water, the nature of the organic solvent, and the pH. Although we have not carried out a comprehensive study of these effects, we do have qualitative indications that more Mo^V dimer complex is obtained when a

larger amount of water is used for the Cp* and Cp′′′ systems. If Scheme 1 is valid, one would expect that a greater concentration of OH^- (larger NaOH excess) should favor the hydrolysis pathway, resulting in the $[(Ring)MoO_2]_2$ system. Indeed, we did obtain a significant amount of this compound as a by-product when the hydrolysis was carried out in the presence of more than five equivalents of NaOH, whereas a good yield of $[Cp^*MoO_2Cl]$ was obtained by Geoffroy et al. with only two equivalents, with no mention of formation of the Mo^V product.[34] Indeed, repetition of the synthesis of $[Cp^*_2Mo_2O_5]$ by stepwise addition of three equivalents of NaOH, followed by three more equivalents a day later (without isolation of the intermediate $[Cp^*MoO_2Cl]$ complex) completely avoided the formation of the $[Cp^*MoO_2]_2$ by-product.

Some subtleties, however, are not yet completely understood. For instance, the Mo^V dimer was obtained for the Cp′′′ system, as for the Cp* system, but no analogous product was obtained for the ^{4}Cp system, even when five equivalents of NaOH were used. The use of excess NaOH, however, allows access (provided that the oxidation route is followed) to the water-soluble sodium salts of $[(Ring)MoO_3]^-$. Although we have not isolated and characterized the new anions of this type for the ^{4}Cp and Cp′′′ systems, their formation is indicated by the protonation reactivity, which is identical to that of the Cp* system: acidification of the water solutions yields the yellow, water-insoluble $[(Ring)_2Mo_2O_5]$ products.[36]

Conclusion

High oxidation state monocyclopentadienyl oxo derivatives of molybdenum are often the end products of oxidative decompositions of lower valent derivatives and were previously available only in low yields or through the use of impractical starting materials and/or reagents. The hydrolytic route from the easily accessible cyclopentadienylmolybdenum(V) tetrachlorides has been optimized and extended to the preparation of new compounds with sterically more encumbered rings. The stability of these compounds in air and aqueous media makes the exploration of their aqueous chemistry and electrochemistry possible. Investigations in those directions are ongoing in our laboratory.

Experimental Section

General Remarks: All reactions were carried out in a Jacomex glove box or by use of standard Schlenk techniques under an argon atmosphere. The solvents were dried by conventional methods (THF, Et_2O, heptane, and pentane from sodium benzophenone ketyl and CH_2Cl_2 from P_4O_{10}) and distilled under argon prior to use. EPR measurements were carried out at the X-band microwave frequency on a Bruker ESP300 spectrometer. The spectrometer frequency was calibrated with DPPH (g = 2.0037). ^{1}H NMR spectra were recorded on a Bruker AC 200 and referenced to the residual solvent protons of the deuterated solvent. The elemental analyses were carried out by the analytical service of the Laboratoire de Synthèse et d′Electrosynthèse Organométallique with a Fisons EA 1108 apparatus. The compounds $[(Ring)MoCl_4]$ (Ring = Cp, Cp* and ^{4}Cp) were prepared as described in the literature.[19,37,47] The compound $[Cp'''MoCl_4]$ was prepared by a straightforward adaptation of those procedures as described below.

Tetrachloro(1,2,4-tri-*tert*-butylcyclopentadienyl)molybdenum(V), $[Cp'''MoCl_4]$: $Mo(CO)_6$ (2.64 g, 10.0 mmol) and $NaCp'''$ (2.66 g, 10.3 mmol) were mixed as solids and suspended in 40 mL THF. The suspension turned into an orange solution during a 10 min period. It was then heated under reflux for 18 h. IR monitoring indicated the formation of $[Cp'''Mo(CO)_3]^-Na^+$ (strong peaks at 1885, 1784 and 1736 cm^{-1}, similar to literature values for the Cp* analogue). After the mixture had cooled to room temperature, MeI (700 μL, 11.25 mmol) was added to the deep orange-red solution, causing darkening to brown. After additional heating under reflux for 3 h, the solvent was removed in vacuo to leave a yellow brown residue, which was extracted into 60 mL CH_2Cl_2. After filtration, the deep-orange solution was evaporated to dryness to yield 4.13 g (9.64 mmol; 96.4%) of yellow-brown $[Cp'''Mo(CO)_3Me]$.

A portion of this product, (3.11 g, 7.26 mmol) was dissolved in 40 mL CH_2Cl_2. A suspension of $PhICl_2$ (4.99 g, 18.2 mmol) in 50 mL CH_2Cl_2 was added in small portions, causing a darkening of the orange brown solution to brown and then to deep violet with vigorous CO evolution. After having been heated under reflux for 90 min, the mixture was allowed to cool to room temperature and the solvents were evaporated to dryness. The violet black residue was washed with 2 × 20 mL pentane to remove the iodobenzene by-product. The deep violet solid $[Cp'''MoCl_4]$ was dried in vacuo. Yield 3.21 g, (93.7%). $C_{17}H_{29}Cl_4Mo$ (471.2): calcd. C 43.34, H 6.20; found C 43.57, H 6.44. EPR (CH_2Cl_2): g = 1.99, a_{Mo} = 38.2 G.

Tetraoxo-μ-oxodicyclopentadienyldimolybdenum(VI), $[Cp_2Mo_2O_5]$: $[CpMoCl_4]$ (0.555 g, 1.83 mmol) was placed in a flask containing distilled water (10 mL). Shaking of the resulting suspension for a few minutes gave rise to the formation of fine, deep red microcrystals. The product $([CpMoO_2]_4)$[12] was separated by decantation of the mother liquor, washed with water (3 × 10 mL) and quickly with acetone (5 mL), and dried in vacuo for 2 h (yield 0.28 g, 79.5%). This material (1.45 mmol of Mo) was then dissolved in dichloromethane (ca. 100 mL), and solid PhIO (0.22 g, 1.0 mmol) was added to the resulting solution. The mixture was stirred at room temperature for 15 min, resulting in a color change from red to yellow. A longer reaction time should be avoided as it affords larger amounts of insoluble by-products. The solution was filtered and the filtrate was evaporated to give yellow microcrystals. The product was purified by recrystallization from CH_2Cl_2/pentane, and dried in vacuo. Yield 0.207 g, 71.1% (56.5% from $[CpMoCl_4]$). The analytical (IR, NMR) properties of the compound corresponded to those reported in the literature[4] and confirmed its purity.

Tetraoxo-μ-oxobis(pentamethylcyclopentadienyl)dimolybdenum(VI), $[Cp^*_2Mo_2O_5]$ and Dioxodi-μ-oxobis(pentamethylcyclopentadienyl)dimolybdenum(V), $[Cp^*MoO_2]_2$: Deep violet $[Cp^*MoCl_4]$ (3.48 g; 9.33 mmol) was added to a stirred solution of aqueous NaOH (19 mL; 3 M; 57 mmol) in acetone (200 mL) in an open beaker. The resulting dark brown suspension was stirred for 18 h, resulting in a lightening of the color to orange and the precipitation of a pale yellow solid. After evaporation to dryness the brownish residue was extracted into 75 mL of distilled water and filtered. The pale yellow filtrate was acidified with diluted glacial acetic acid, causing precipitation of a yellow solid at pH 3.8−4.0. The acetic acid addition was stopped when the addition of one further drop did not cause

any additional precipitation. The precipitate was extracted with 4 × 100 mL portions of ether, the last extract being colorless. The combined organic layers were washed with distilled water and dried over $MgSO_4$ overnight. Evaporation of the solvent yielded 1.55 g (2.86 mmol; 61.3%) of $[(Cp^*MoO_2)_2O]$ as a yellow solid. The ^1H NMR spectrum of this compound (singlet at δ = 2.01 in $CDCl_3$) corresponded to that described in the literature.[26]

In another experiment, starting from 2.03 g of $[Cp^*MoCl_4]$, the water-insoluble orange-red solid remaining from the water extraction was also worked up. It was washed with 20 mL ether and then with 20 mL pentane, and was dried in vacuo to afford the dinuclear Mo^V compound $[(Cp^*MoO_2)_2]$ as an orange, crystalline solid (192 mg, 0.37 mmol; 13.6%). $C_{10}H_{15}MoO_2$ (263.2): calcd. C 45.64, H 5.74; found C 45.36, H 5.71. The ^1H NMR spectrum (δ = 1.98 in $CDCl_3$) corresponded to that reported in the literature.[38] Suitable single crystals for X-ray diffraction could be grown by layering a saturated THF solution with heptane at room temperature. Normally up to ca. 20% of this by-product was recovered, depending on the reaction conditions.

Tetraoxo-μ-oxobis(tetraisopropylcyclopentadienyl)dimolybdenum(VI), $[^4Cp_2Mo_2O_5]$: Deep purple $[^4CpMoCl_4]$ (609 mg, 1.29 mmol) was quickly added, as a solid, to a stirred mixture of acetone (75 mL), THF (75 mL) and aqueous NaOH (2.6 mL, 3 M, 7.8 mmol) in an open beaker. A brown suspension formed immediately, which lightened to orange yellow over a period of 2 h. After the mixture had been stirred overnight, the solvents were evaporated and the resulting yellow residue was extracted with 100 mL of warm water (50 °C). After filtration, the aqueous phase was acidified with diluted glacial acetic acid as described in the previous section, causing the precipitation of a yellow solid at pH 4. Extraction of this solid with 3 × 100 mL portions of ether, followed by separation of the organic layer, washing with water, and drying over $MgSO_4$, yielded a yellow ether solution, which was allowed to stand overnight and then was evaporated to dryness to yield 222 mg (0.3 mmol; 46.6%) of yellow $[(^4CpMoO_2)_2O]$. $C_{34}H_{58}Mo_2O_5$ (738.7): calcd. C 55.28, H 7.91; found C 54.69, H 8.25. IR (Nujol mull): $\tilde{\nu}$ = 919 s, 889 s, 760 s cm^{-1}. ^1H NMR ($CDCl_3$): δ = 6.01 (s, 1 H, ring-H), 3.10 (m, 4 H, C*H*Me_2), 1.39 [d, $J_{H,H}$ = 7.3 Hz, 6 H, CH(CH_3)$_2$], 1.30 [d, $J_{H,H}$ = 7.3 Hz, 12 H, CH(CH_3)$_2$], 1.19 [d, $J_{H,H}$ = 6.7 Hz, 6 H, CH(CH_3)$_2$]. ^1H NMR (C_6D_6): δ = 6.14 (s, 1 H, ring-H), 3.14 (m, 4 H, C*H*Me_2), 1.47 [d, $J_{H,H}$ = 6.7 Hz, 6 H, CH(CH_3)$_2$], 1.44 [d, $J_{H,H}$ = 7.0 Hz, 6 H, CH(CH_3)$_2$], 1.23 [d, $J_{H,H}$ = 7.0 Hz, 6 H, CH(CH_3)$_2$], 1.02 [d, $J_{H,H}$ = 7.0 Hz, 6 H, CH(CH_3)$_2$]. The ^1H NMR spectrum did not show any detectable Mo^V by-product. Yellow-orange single crystals suitable for X-ray diffraction were grown by slowly cooling a hot saturated heptane solution to room temperature.

Attempted Synthesis of Dioxodi-μ-oxobis(tetraisopropylcyclopentadienyl)dimolybdenum(V), $[^4CpMoO_2]_2$: $[^4CpMoCl_4]$ (670 mg, 1.42 mmol) was added to 150 mL of a stirred 1:1 mixture of acetone and distilled water, immediately yielding a brown suspension. The mixture was stirred for 40 hours, during which aliquots were withdrawn and the solid was separated, washed with water, and investigated by ^1H NMR spectrosopcy, showing the spectrum of $[^4Cp_2Mo_2O_5]$ as the only NMR-active species. The final mixture was filtered and the solid was washed with water and redissolved in pentane. After evaporation of the solvent, the residue was dried in vacuo to leave 240 mg (0.33 mmol; 46.8%) of $[^4Cp_2Mo_2O_5]$ as a orange powder (confirmed by ^1H NMR spectroscopy). Orange-red crystals could be grown by slowly cooling a hot saturated heptane solution to room temperature or by cooling a pentane solution to −25 °C. A single crystal from this batch showed the same unit cell as that of the yellow-orange crystals obtained from the procedure in the previous section.

Tetraoxo-μ-oxobis(1,2,4-tri-*tert*-butylcyclopentadienyl)dimolybdenum(VI), $[Cp'''_2Mo_2O_5]$ and Dioxodi-μ-oxobis(pentamethylcyclopentadienyl)dimolybdenum(V), $[Cp'''MoO_2]_2$: Purple $[Cp'''MoCl_4]$ (1.36 g, 2.89 mmol) was added to a stirred mixture of THF (75 mL), acetone (75 mL), water (10 mL) and aqueous NaOH (5.7 mL, 3 M, 17.1 mmol) in an open beaker. Some foaming occurred, and a Bordeaux-red solution formed immediately. No precipitate was detected during the following 24 hours of stirring at room temperature. Subsequent gentle heating (40−50 °C) of the mixture for two hours caused the precipitation of a red-violet product, which was collected on a filter, washed with water, and redissolved in THF. The solvents were evaporated to dryness to leave the Mo^V dimer $[(Cp'''MoO_2)_2]$ as the main product. Yield: 380 mg (0.53 mmol, 36.7%). $C_{17}H_{29}MoO_2$ (361.4): calcd. C 56.51, H 8.09; found C 56.72, H 8.12. IR (Nujol mull): $\tilde{\nu}$ = 922 s, 885 s, 764 vs cm^{-1}. ^1H NMR (C_6D_6): δ = 6.43 (s, 2 H, ring-H), 1.46 (s, 18 H, CMe_3 1,2-positions), 1.37 (s, 9 H, CMe_3 4-position). Suitable single crystals were grown by slowly cooling a hot saturated heptane solution to room temperature.

The orange-yellow filtrate was collected and the solvents were evaporated to dryness. The resulting yellow residue was extracted with 70 mL of distilled water and the extract was acidified with diluted glacial acetic acid to pH 4, as described above for the Cp* analogue. The yellow solid that precipitated was extracted with several portions of ether, and the combined organic layers (300 mL) were washed with 200 mL of distilled water and dried over $MgSO_4$. The lustrous yellow ether phase was allowed to stand overnight and was then evaporated to dryness, yielding 120 mg (0.16 mmol. 11.2%) of yellow $[(Cp'''MoO_2)_2O]$. $C_{34}H_{58}Mo_2O_5$ (738.7): calcd. C 55.28, H 7.91; found C 55.04, H 7.94. ^1H NMR (C_6D_6): δ = 5.63 (s, 2 H, ring-H), 1.58 (s, 18 H, CMe_3 1,2-position), 1.48 (s, 9 H, CMe_3 4-position). Suitable single crystals were grown by slowly cooling a hot saturated heptane solution to room temperature.

Alternative Route to Pure $[Cp'''_2Mo_2O_5]$: Acetone (120 mL) was mixed with an aqueous NaOH solution (6.6 mL, 3 M, 19.8 mmol). Purple $[Cp'''MoCl_4]$ (1.55 g, 3.29 mmol) was added, producing a deep red solution, followed by the supernatant slowly turning orange with formation of a white yellow precipitate within a 3 h period. After the mixture had been stirred overnight, all solvents were evaporated under reduced pressure and the yellowish residue was extracted with 100 mL of water and layered with 100 mL of ether. The ether layer remained colorless until the aqueous one was acidified with diluted acetic acid, causing the formation of a lustrous yellow precipitate, which was extracted by the ether. After addition of the last traces of acid to give rise to further precipitation, the aqueous phase was clear and colorless. The ether phases was washed three times with distilled water and dried over $MgSO_4$ overnight. Evaporation to dryness gave 890 mg (1.20 mmol, 73.2%) of orange-yellow $[Cp'''_2Mo_2O_5]$ without any detectable Mo^V by-product.

Chlorodioxo(tetraisopropylcyclopentadienyl)molybdenum(VI), $[^4CpMoO_2Cl]$: Aqueous NaOH (2.89 mL, 3 M, 8.67 mmol) was added to 250 mL of acetone. After addition of solid $[^4CpMoCl_4]$ (1.362 g, 2.89 mmol) the solution turned red and a white precipitate was formed. Stirring overnight changed the color of the supernatant to a bright yellow-orange. All solvents were removed in vacuo, leaving a yellow residue that was extracted with 200 mL of pentane. This pentane solution was dried over Na_2SO_4 and filtered, and the solvents were evaporated to dryness to leave 1.0 g of a yellow-or-

ange solid (2.52 mmol, 87%), which was then recrystallized from a saturated heptane solution at −30 °C. $C_{17}H_{29}ClMoO_2$ (396.8): calcd. C 51.45, H 7.36; found C 51.04, H 7.87. IR (Nujol mull): $\tilde{\nu}$ = 920 s, 890 s cm^{-1}. ^1H NMR ($CDCl_3$): δ = 6.06 (s, 1 H, ring-H), 3.14 (m, 4 H, C*H*Me_2), 1.40 [d, $J_{H,H}$ = 7.4 Hz, 6 H, CH(CH_3)$_2$], 1.35 [d, $J_{H,H}$ = 7.3 Hz, 6 H, CH(CH_3)$_2$], 1.31 [d, $J_{H,H}$ = 6.7 Hz, 6 H, CH(CH_3)$_2$], 1.25 [d, $J_{H,H}$ = 7.0 Hz, 6 H, CH(CH_3)$_2$]. A single crystal suitable for X-ray analysis was grown by slowly cooling a hot saturated heptane solution to room temperature. The same reaction was found to take place with just two equivalents of NaOH used, yielding the same product in an identical overall yield.

X-ray Crystallographic Study: The crystal and refinement parameters for all structures are listed in Table 4. All sets of data were collected on an Enraf−Nonius KappaCCD diffractometer at 110 K, using Mo-K_α radiation. The structures were solved by means of a Patterson search program[48] and refined with full-matrix, least-squares methods[49] based on $|F^2|$ with the aid of the WINGX program.[50] All non-hydrogen atoms were refined with anisotropic thermal parameters. Hydrogen atoms were located on final Fourier difference maps and freely refined with isotropic temperature factors fixed to 1.2 or 1.5 (for CH_3) times those of the corresponding parent atoms. Selected bond lengths and angles are listed in Table 1 for both independent molecules of [$^4Cp_2Mo_2O_5$] and for [Cp′′′$_2$$Mo_2O_5$], in Table 2 for [Cp′′′$MoO_2$]$_2$, and in Table 3 for [^{4}CpMoO_2Cl]. CCDC-173139−173143 contain the supplementary crystallographic data for this paper. These data can be obtained free of charge at www.ccdc.cam.ac.uk/conts/retrieving.html [or from the Cambridge Crystallographic Data Center, 12, Union Road, Cambridge CB2 1EZ, UK; Fax: (internat.) +44-1223/336-033; E-mail: deposit@ccdc.cam.ac.uk].

Acknowledgments

We are grateful to the Ministère de la Recherche and the CNRS for support through UMR 5632 and the French and German Ministries of Foreign Affairs for a bilateral Procope grant. DS thanks the Conseil Régional de Bourgogne for a postdoctoral fellowship and FD thanks the Scientific and Technical Research Council of Turkey (TUBITAK) for a NATO Science Fellowship Programme scholarship, and Celal Bayar University for a leave of absence.

Table 4. Crystal data and structure refinement for all compounds

Compound	[$^4Cp_2Mo_2O_5$], **1**	[Cp″′$_2$$Mo_2O_5$], **2**	[Cp*$_2$$Mo_2O_4$], **3**	[Cp′′′MoO_2]$_2$, **4**	[^{4}CpMoO_2Cl], **5**
Empirical formula	$C_{34}H_{58}Mo_2O_5$	$C_{34}H_{58}Mo_2O_5$	$C_{20}H_{30}Mo_2O_4$	$C_{34}H_{58}Mo_2O_4$	$C_{17}H_{29}ClMoO_2$
Formula mass	738.68	738.68	526.32	722.68	396.79
T; K	110(2)	110(2)	110(2)	110(2)	110(2)
Crystal system	monoclinic	monoclinic	tetragonal	triclinic	monoclinic
Space group	$P2_1/c$	$P2_1/c$	$P4bar2_1c$	$P\bar{1}$	$P2_1/c$
a, Å	11.8993(2)	14.8025(2)	11.5418(9)	10.3976(1)	8.8290(2)
b, Å	20.0429(3)	10.3088(1)	11.5418(9)	11.9801(2)	12.3811(3)
c, Å	14.7150(2)	23.6064(3)	15.3875(3)	14.0109(2)	17.1372(6)
α, °	90	90	90	84.658(1)	90
β, °	95.597(1)	107.226(1)	90	88.904(1)	103.690(1)
γ, °	90	90	90	88.898(1)	90
V, Å^3	3492.74(9)	3440.66(7)	2049.8(2)	1737.09(4)	1820.09(9)
Z	4	4	4	2	4
F(000)	1544	1544	1064	756	824
$D_{calcd.}$, g/cm^3	1.405	1.426	1.705	1.382	1.448
Diffract., scan type	Kappa CCD, mixture of φ rotations and ω scans				
λ, Å	0.71073				
μ, mm^{-1}	0.755	0.766	1.245	0.755	0.870
Crystal size, mm^3	0.30 × 0.25 × 0.13	0.43 × 0.25 × 0.25	0.20 × 0.20 × 0.12	0.32 × 0.25 × 0.20	0.25 × 0.15 × 0.08
sin(θ)/λ max, Å^{-1}	0.65	0.65	0.65	0.65	0.69
Index ranges	*h*: −15; 15	*h*: −19; 19	*h*: −12; 14	*h*: −12; 13	*h*: −12; 6
	k: −25; 26	*k*: −13; 12	*k*: −14; 13	*k*: −15; 15	*k*: −16; 15
	l: −19; 19	*l*: −30; 30	*l*: −19; 18	*l*: −18; 18	*l*: −21; 23
RC = Refl. Collected	25939	22209	10012	13541	8953
IRC = unique RC/R(int)	7990/0.0403	7828/0.0243	2317/0.0284	7847/0.0141	4530/0.0190
IRCGT = IRC and [$I > 2\sigma(I)$]	5940	6728	2198	7073	3952
Refinement method	Full-matrix L.S. on F^2				
Data/restr./param.	7990/0/545	7828/0/545	2317/0/164	7847/0/535	4530/0/277
R for IRCGT	*R*1[a] = 0.0291	*R*1[a] = 0.0241	*R*1[a] = 0.0213	*R*1[a] = 0.0215	*R*1[a] = 0.0215
	*wR*2[b] = 0.0594	*wR*2[b] = 0.0520	*wR*2[b] = 0.0455	*wR*2[b] = 0.0519	*wR*2[b] = 0.0762
R for IRC	*R*1[a] = 0.0507	*R*1[a] = 0.0324	*R*1[a] = 0.0238	*R*1[a] = 0.0255	*R*1[a] = 0.0403
	*wR*2[b] = 0.0650	*wR*2[b] = 0.0548	*wR*2[b] = 0.0465	*wR*2[b] = 0.0539	*wR*2[b] = 0.0793
Flack param.	−	−	0.00(4)	−	−
Goodness-of-fit[c]	1.034	0.975	1.055	1.046	1.039
Δρ, max, min, e.Å^{-3}	0.571, −0.478	0.438, −0.499	0.324, −0.601	0.422, −0.620	1.090, −0.894

[a] $R1 = \Sigma(||F_0| - |F_c||)/\Sigma|F_0|$. [b] $wR2=[\Sigma w(F_0^2 - F_c^2)^2/\Sigma[w(F_0^2)^2]^{1/2}$ where $w = 1/[\sigma^2(F_0^2 + (aP)^2 + bP]$ and $P = (\max(F_0^2,0) + 2*F_c^2)/3$ where (a,b) = (0.028, 0.0) for **1**, (0.023, 1.69) for **2**, (0.26, 0.0) for **3**, (0.018, 0.79) for **4** and (0.024, 2.22) for **5**.

[1] W. A. Herrmann, *Comments Inorg. Chem.* **1988**, *7*, 73−107.
[2] W. A. Herrmann, *Angew. Chem. Int. Ed. Engl.* **1988**, *27*, 1297−1313.
[3] W. A. Herrmann, F. E. Kühn, *Acc. Chem. Res.* **1997**, *30*, 169−180.
[4] M. Cousins, M. L. H. Green, *J. Chem. Soc.* **1964**, 1567−1572.
[5] M. Cousins, M. L. H. Green, *J. Chem. Soc. (A)* **1969**, 16−19.
[6] R. H. Holm, *Chemical Reviews* **1987**, *87*, 1401−1449.
[7] D. T. Richens, in *The Chemistry of Aqua Ions*, J. Wiley & Sons, Chichester, **1997**, pp. 259−336.
[8] G. Wilkinson, F. G. A. Stone, E. W. Abel, *Comprehensive Organometallic Chemistry*, Pergamon, Oxford, **1982**.
[9] E. W. Abel, F. G. Stone, G. Wilkinson, *Comprehensive Organometallic Chemistry II, Vol. 8*, Pergamon, Oxford, **1995**.
[10] E. Collange, J. Garcia, R. Poli, submitted for publication.
[11] J. Gun, A. Modestov, O. Lev, D. Saurenz, M. Vorotyntsev, R. Poli, submitted for publication.
[12] M. J. Bunker, M. L. H. Green, *J. Chem. Soc., Dalton Trans.* **1981**, 847−851.
[13] P. Legzdins, E. C. Phillips, S. J. Rettig, L. Sánchez, J. Trotter, V. C. Yee, *Organometallics* **1988**, *7*, 1877−1878.
[14] J. W. Faller, Y. Ma, *Organometallics* **1988**, *7*, 559−561.
[15] J. W. Faller, Y. Ma, *J. Organomet. Chem.* **1989**, *368*, 45−56.
[16] M. B. Trost, R. G. Bergman, *Organometallics* **1991**, *10*, 1172−1178.
[17] D. Chakraborty, M. Bhattacharjee, R. Krätzner, R. Siefken, H. W. Roesky, I. Usón, H.-G. Schmidt, *Organometallics* **1999**, *18*, 106−108.
[18] H. J. Lucas, E. R. Kennedy, M. W. Formo, *Org. Synth.* **1942**, *22*, 483−485.
[19] J. C. Gordon, R. Poli, in *Synthetic Methods of Organometallic and Inorganic Chemistry (Herrmann/Brauer), Vol. 8* (Ed.: W. A. Herrmann), Georg Thieme Verlag, Stuttgart, **1997**, pp. 97−98.
[20] Studies aimed at the identification of this anion are currently underway in our laboratory.
[21] M. Herberhold, W. Kremnitz, A. Razavi, H. Schöllhorn, U. Thewalt, *Angew. Chem. Int. Ed. Engl.* **1985**, *24*, 601−602.
[22] K. Isobe, S. Kimura, Y. Nakamura, *J. Organomet. Chem.* **1987**, *331*, 221−228.
[23] P. Gomez-Sal, E. de Jesus, P. Royo, A. Vazquez de Miguel, S. Martinez−Carrera, S. Garcia-Blanco, *J. Organomet. Chem.* **1988**, *353*, 191−196.
[24] P. Leoni, M. Pasquali, L. Salsini, C. di Bugno, D. Braga, P. Sabatino, *J. Chem. Soc., Dalton Trans.* **1989**, 155−159.
[25] A. L. Rheingold, J. R. Harper, *J. Organomet. Chem.* **1991**, *403*, 335−344.
[26] J. W. Faller, Y. Ma, *J. Organomet. Chem.* **1988**, *340*, 59−69.
[27] R. B. King, M. B. Bisnette, *J. Organomet. Chem.* **1967**, *8*, 287−297.
[28] C. D. Abernethy, F. Bottomley, J. Chen, M. F. Kemp, T. C. Mallais, O. O. Womiloju, *Inorg. Synth.* **1998**, *32*, 207−214.
[29] F. Bottomley, J. Chen, *Organometallics* **1992**, *11*, 3404−3411.
[30] F. Bottomley, P. D. Boyle, J. H. Chen, *Organometallics* **1994**, *13*, 370−373.
[31] K. Umakoshi, K. Isobe, *J. Organomet. Chem.* **1990**, *395*, 47−53.
[32] J. Sundermeyer, U. Radius, C. Burschka, *Chem. Ber.* **1992**, *125*, 2379−2384.
[33] M. S. Rau, C. M. Kretz, L. A. Mercando, G. L. Geoffroy, A. L. Rheingold, *J. Am. Chem. Soc.* **1991**, *113*, 7420−7421.
[34] M. S. Rau, C. M. Kretz, G. L. Geoffroy, A. L. Rheingold, *Organometallics* **1993**, *12*, 3447−3460.
[35] On the other hand, it is interesting to note that the use of excess aqueous NaOH in the hydrolysis reaction of [Cp*WCl_4] does not induce displacement of the residual chloride ligand in [Cp*WO_2Cl].[34]
[36] In reality, the aqueous behavior is even more complex and interesting. A detailed study of the aqueous speciation of the Cp*Mo^{VI} system over the entire pH range will be the topic of a separate report.[10]
[37] D. W. Keogh, R. Poli, in *Synthetic Methods of Organometallic and Inorganic Chemistry (Herrmann/Brauer), Vol. 8* (Ed.: W. A. Herrmann), Georg Thieme Verlag, Stuttgart, **1997**, p. 98.
[38] H. Arzoumanian, A. Baldy, M. Pierrot, M. Petrignani, *J. Organomet. Chem.* **1985**, *294*, 327−331.
[39] C. Couldwell, K. Prout, *Acta Crystallographica* **1978**, *B34*, 933−934.
[40] E. de Jesus, A. Vazquez de Miguel, P. Royo, A. M. M. Lanfredi, A. Tiripicchio, *J. Chem. Soc., Dalton Trans.* **1990**, 2779−2784.
[41] M. Hahn, K. Wieghardt, *Inorganic Chemistry* **1984**, *23*, 3977−3982.
[42] K. Wieghardt, M. Guttmann, P. Chaudhuri, W. Gebert, M. Minelli, C. G. Young, J. H. Enemark, *Inorg. Chem.* **1985**, *24*, 3151−3155.
[43] W. M. Harrison, C. Saadeh, S. B. Colbran, D. C. Craig, *J. Chem. Soc., Dalton Trans.* **1997**, 3785−3792.
[44] R. Siefken, M. Teichert, D. Chakraborty, H. W. Roesky, *Organometallics* **1999**, *18*, 2321−2325.
[45] F. Bottomley, E. C. Ferris, P. S. White, *Organometallics* **1990**, *9*, 1166−1171.
[46] J. M. B. Blanchard, Q. Chen, Y.-D. Chang, M. B. Sponsler, *Inorg. Chim. Acta* **1994**, *221*, 147−150.
[47] M. Bastian, D. Morales, R. Poli, P. Richard, H. Sitzmann, submitted for publication.
[48] G. M. Sheldrick, *SHELXS-97. Program for Crystal Structure Solution*, University of Göttingen, Göttingen, Germany, **1997**.
[49] G. M. Sheldrick, *SHELXL-97. Program for Crystal Structure Refinement*, University of Göttingen, Göttingen, Germany, **1997**.
[50] L. J. Farrugia, *J. Appl. Crystallogr.* **1999**, *32*, 837−838.

Received November 5, 2001
[I01431]

Solvent-Free Lanthanoid Complexes Derived From Chelation-Supported Organoamide Ligands[‡]

Glen B. Deacon,*[a] Craig M. Forsyth,[a] and Natalie M. Scott[a]

Keywords: N,O ligands / Lanthanides / Halides / Metathesis / Structure elucidation

Treatment of $LnCl_3$ with three molar equivalents of LiL [(L = *N*-(2-methoxyphenyl)-*N*-(trimethylsilyl)amide (L^1) or *N*-(2-phenoxyphenyl)-*N*-(trimethylsilyl)amide (L^2)], generated in situ from LH and *n*BuLi, or with the isolated lithium complex $[Li(L^1)(OEt_2)]_2$ (for Ln = Yb) in THF afforded the solvent-free homoleptic complexes $[Ln(L)_3]$ [Ln = Yb (**1a**), Er (**1b**), Sm (**1c**), Pr (**1d**), Nd (**1e**), L = L^1; Ln = Yb (**2a**), Y (**2b**), Sm (**2c**), Nd (**2d**), La (**2e**), L = L^2). With a 2:1 LiL (generated in situ) to $LnCl_3$ molar ratio, the solvent-free heteroleptic complexes $[Ln(L)_2(\mu\text{-}Cl)]_2$ were obtained for L = *N*,*N*-dimethyl-*N*′-trimethylsilylethane-1,2-diaminate (en′) [Ln = Yb (**3a**), Er (**3b**), Sm (**3c**), Nd (**3d**), La (**3e**)], but not for L^1 or L^2, which gave $[Ln(L)_3]$ [Ln = Yb (**1a**), Nd (**1e**), L = L^1; Ln = Yb (**2a**), Nd (**2d**), La (**2e**), L = L^2]. However, treatment of $LnCl_3$ with two molar equivalents of the isolated crystalline lithium salt $[Li(L^1)(OEt_2)]_2$ in THF gave, for the heavier lanthanoids, the solvent-free heteroleptic complexes $[Ln(L^1)_2(\mu\text{-}Cl)]_2$ [Ln = Yb (**4a**), Er (**4b**), Tb (**4c**)], although the homoleptic complex $[Nd(L^1)_3]$ (**1e**) was obtained for Nd. In contrast, similar reactions of isolated $[Li(L^2)(DME)]$ with $LnCl_3$ yielded the heteroleptic species $[Ln(L^2)_2(\mu\text{-}Cl)]_2$ only for Ln = Nd [**5a**·$(PhMe)_2$]. At either end of the Ln series, the homoleptic $[Ln(L^2)_3]$ complexes [Ln = Yb(**2a**), La (**2e**)] were obtained. Single crystal X-ray analyses of **1e** or **2a**–**2e** (as their PhMe or C_5H_9Me solvates) showed these complexes to be monomeric and six-coordinate (*mer* isomer), whereas the heteroleptic complexes **4a**–**4c**, **5a** were found to be dimeric with bridging chloride atoms. Two chelating $[L^1]^-$ or $[L^2]^-$ units [*trans* O(Me/Ph) and *cis* amido groups] are bound to each lanthanoid centre completing a six-coordinate very distorted octahedral environment. The X-ray structure of $[Li(L^1)(OEt_2)]_2$ revealed a dimeric structure with each lithium four-coordinate and surrounded by one diethyl ether, two bridging amide nitrogens and a methoxy oxygen in a distorted tetrahedral array.
(© Wiley-VCH Verlag GmbH, 69451 Weinheim, Germany, 2002)

Introduction

The $6e^-$ donor cyclopentadienyl ligand (Cp) has been extensively used as a coligand with early transition metals for various types of catalytic transformations. Important applications include highly active group 4 and 5 metal and lanthanoid organometallic compounds in homogeneous Ziegler−Natta alkene polymerisation.[2−7] In the last decade an increasing number of investigators have turned their attention away from cyclopentadienyl ligands to find alternative systems to stabilise the metal-carbon bond for catalytic work.[7−9] Alternative systems using alkoxide and amide ligands in place of Cp have shown similar reaction chemistry with the stabilisation of early electron-deficient transition metals in medium to high oxidation states.[6,7,9−14] Of these two alternatives, greater opportunities for substituent variation exist for the amide ligand. There are numerous N-containing ligands that can stabilise heteroleptic lanthanoid complexes, such as bis(trimethylsilyl)amide,[15−18] benzamidinates,[19−21] aminotropiminates[22,23] and diazabutadienes.[24] These bulky ligands can block coordination sites around the metal centre leading to monomeric, hydrocarbon soluble, electron-poor species that display unique chemical properties. However, in comparison to the stability offered by the cyclopentadienyl ligand in $[Ln(Cp)_2(X)]$ (X = anion), the labile nature of organoamide ligands in such systems has often caused ligand redistribution, resulting in the isolation of homoleptic derivatives.[7,15,22,25,26] The incorporation of a supporting donor atom to give a bidentate amide ligand may improve the stability of the heteroleptic complexes. Encouragement for this idea came from the observation that *N*,*N*-dimethyl-*N*′-trimethylsilylethane-1,2-diaminate (en′) gave not only the homoleptic complexes $[Ln(en')_3]$ (Ln = Lu, Er, Eu, Sm, Nd, La) but also a single example of a heteroleptic derivative $[Er(en')_2Cl]$.[27] We now report a study of the use of the two new mixed N,O-donor bidentate amide ligands *N*-(2-methoxyphenyl)-*N*-(trimethylsilyl)amide (L^1)[28] and *N*-(2-phenoxyphenyl)-*N*-(trimethylsilyl)amide (L^2)[28,29] for preparing $[Ln(L)_3]$ and $[Ln(L)_2Cl]$ complexes, and extend the en′ heteroleptic series to lanthanoids other than Er. Previous studies on lanthanoid complexes containing the L^1 and L^2 ligands have shown them to be capable of supporting

[‡] Organoamido- and Aryloxo-Lanthanoids, 28. Part 27: see Ref.[1]

[a] School of Chemistry, Monash University, 3800 Victoria, Australia
E-mail: glen.deacon@sci.monash.edu.au

organo-oxo heteroleptic complexes viz. $[Yb(L^1)_2(\mu\text{-}OMe)]_2$ and $[Yb(L^2)_2(OPh)(THF)]$ (THF = tetrahydrofuran).[28]

Results and Discussion

A range of $[Ln(L)_3]$ complexes [L = L^1, Ln = Yb (**1a**), Er (**1b**), Sm (**1c**), Pr (**1d**), Nd (**1e**); L = L^2, Ln = Yb (**2a**), Y (**2b**), Sm (**2c**), Nd (**2d**), La (**2e**)] were prepared by treatment of $LnCl_3$ with three molar equivalents of LiL as the isolated $[Li(L^1)(OEt_2)]_2$ [Scheme 1 (i)] or generated in situ from the reaction of LH with *n*BuLi in THF [Scheme 1 (ii)]. The crystalline complexes $[Ln(L^1)_3]$ [Ln = Yb (**1a**), Er (**1b**), Sm (**1c**), Pr (**1d**), Nd (**1e**)] were isolated from hexane in good yield after removal of the precipitated LiCl. The $[Ln(L^2)_3]$ complexes [Ln = **2a**·(PhMe), **2a**·(C_5H_9Me) (from a 1:2 mol ratio synthesis − see below), **2b**·(C_5H_9Me), **2c**·(PhMe), **2d**·$(PhMe)_2$, **2e**·(PhMe)] were obtained by crystallisation of the bulk products from toluene. Whilst toluene solvates are not unusual, the isolation of methylcyclopentane solvates (as identified from X-ray crystallography) was unexpected. The latter are presumed to be derived from a trace impurity in one of the solvents (PhMe or hexane) used. Crystallisation of **2e**·(PhMe) from diethyl ether gave $[La(L^2)_3]$ (**2e**), which was used for an X-ray determination, whilst single crystals of solvent-free $[Nd(L^2)_3]$ (**2d**) were obtained by crystallisation of **2d**·$(PhMe)_2$ from hexane.

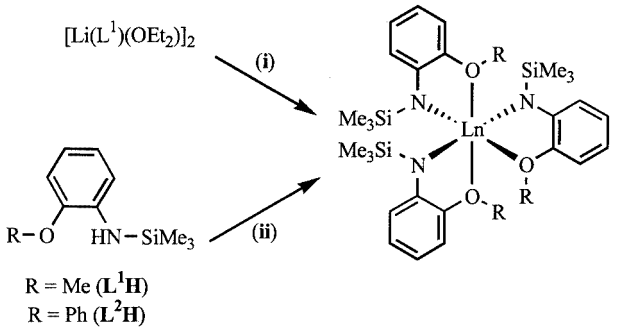

Scheme 1. Reagents and conditions: (i) THF, 0.33 equivalents of $YbCl_3$ followed by crystallisation from hexane (**1a**); (ii) *n*BuLi, THF, 0 °C, 0.33 equivalents of $LnCl_3$ followed by crystallisation from hexane (**1b**−**1e**) or toluene (**2a**·(PhMe), **2a**·(C_5H_9Me) (0.50 equivalents of $YbCl_3$), **2b**·(C_5H_9Me), **2c**·(PhMe), **2d**·$(PhMe)_2$, **2e**·(PhMe)]

Satisfactory elemental analyses (C, H N) were obtained for all of the homoleptic complexes although crystallographically characterised unsolvated **2e** was not examined as the corresponding toluene solvate was obtained analytically pure. In the case of **2a**·(C_5H_9Me) the analysis fitted for solvent-free $[Yb(L^2)_3]$ hence the methylcyclopentane was evidently removed from the lattice on drying the sample under vacuum. The corresponding undried yttrium complex analysed as the solvate. The infrared spectra of the complexes were virtually identical within each series and indicated the presence of coordinated L^1 or L^2 in accordance with the proposed compositions. For **2a**·(PhMe), **2c**·(PhMe), **2d**·$(PhMe)_2$ and **2e**·(PhMe) the presence of toluene could not be detected by infrared spectroscopy due to the large number of ligand bands. Asymmetric C−O−C stretching for $[Ln(L^1)_3]$ [Ln = Yb (**1a**), Er (**1b**), Sm (**1c**), Pr (**1d**), Nd (**1e**)] gives two sets of two bands while for L^1H only one set is observed.[28] For $[Ln(L^2)_3]$ [Ln = Yb {**2a**·(PhMe), **2a**·(C_5H_9Me)}, Y {**2b**·(C_5H_9Me)}, Sm {**2c**·(PhMe)}, Nd {**2d**·$(PhMe)_2$}, La {**2e**·(PhMe)}] this region displays three sets of two absorptions. This feature is different from the behaviour of L^2H, which displays only two sets of two absorptions in this region.[28] Generally, the ^1H NMR spectroscopic data for **1e**, **2b**·(C_5H_9Me), **2c**·(PhMe), **2d**·$(PhMe)_2$, **2e**·(PhMe) and **2e** indicate that one L environment is present in solution, in contrast to the two L environments observed in the solid state (see below). Presumably the ligands are rapidly exchanging under these conditions. Characteristic toluene resonances were observed for the **2c**−**2e**·$(PhMe)_n$ complexes and confirmed the number of toluene molecules of crystallisation per $[LnL_3]$ indicated by microanalysis. For **2b**·(C_5H_9Me) the ^1H NMR spectrum is consistent with the presence of methylcyclopentane,[30] although the integration indicated only half a methylcyclopentane molecule per $[Y(L^2)_3]$. However, the X-ray structure determination and elemental analyses indicated one C_5H_9Me per yttrium. Whilst the ^1H NMR spectrum of **1e** is similar to that of **2d**·$(PhMe)_2$ for structurally common protons, the paramagnetic behaviour of Nd^{3+} causes most backbone aromatic resonances on L^1 or L^2 to shift considerably from those of diamagnetic **2e** (see Exp. Sect.). In the mass spectra of **1c** and **1e**, the highest metal-containing fragment was attributable to the parent ion $[Ln(L^1)_3]^+$; loss of the groups $SiMe_3$ and OMe or OPh from the molecular ion was observed for **1b**, **2a**·(PhMe) or **2a**·(C_5H_9Me). The mass fragment $[Ln(L^1)_2]^+$ was observed in the spectra of all three complexes, as well as the metal-free fragment $[L^1H]^+$. The mass spectra of **2b**·(C_5H_9Me) and **2c**·(PhMe) showed a weak molecular ion $[Ln(L^2)_3]^+$ and associated fragment ions (notably $[Ln(L^2)_2]^+$ and $[Ln(L^2)]^+$) as well as an intense $[L^2H]^+$ ion. However for **2e**·(PhMe) the highest mass ion observed was $[La(L^2)_2]^+$. The UV/Vis/NIR spectrum of a solution of **1a** in DME exhibited absorptions characteristic of *f*←*f* transitions of the Yb^{3+} cation[31] near 1000 nm.

Single crystal X-ray diffraction data were collected for **1e** (Figure 1), **2a**·(PhMe) (Figure 2), **2d** and **2e**. Data were also obtained for **2a**·(C_5H_9Me) and **2b**·(C_5H_9Me) and have been deposited with the Cambridge Crystallographic Data Centre (CCDC-174206/7). Selected bond lengths and angles for **1e**, **2a**·(PhMe), **2b**·(C_5H_9Me), **2d** and **2e** are given in Table 1. Each of the molecules is monomeric with a six-coordinate metal centre surrounded by three bidentate L ligands (L = L^1 or L^2) with the bulky amido groups arranged in a *meridional* configuration. The geometry is best described as a distorted octahedron (best-fit polyhedron[32]) with the oxygen atoms [O(1) and O(3)], nitrogen atoms [N(1) and N(2)], and the other donor pair [O(2) and N(3)] occupying *transoid* sites. The *mer* arrangement of the L^1 or L^2 ligands differs from that of the closely related complex $[Ln(en')_3]$ (en′ = *N,N*-dimethyl-*N*′-trimethylsilylethane-1,2-diaminate)[27] which has a *fac* orientation of the bidentate

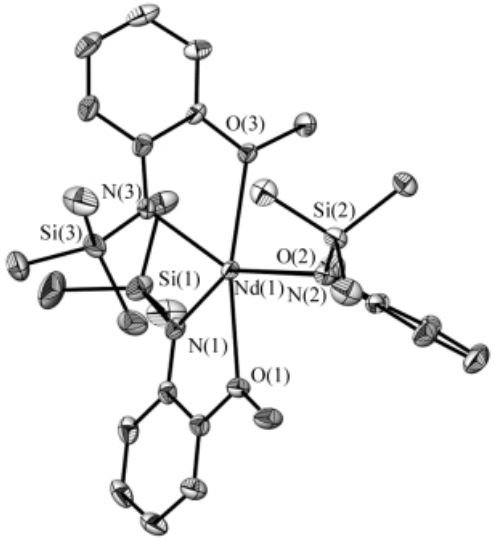

Figure 1. ORTEP view of $[Nd(L^1)_3]$ (**1e**) drawn with 50% ellipsoids; hydrogen atoms have been omitted for clarity

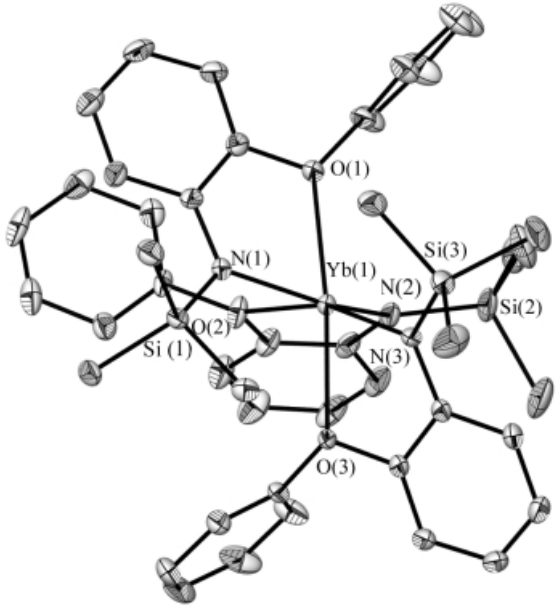

Figure 2. ORTEP view of $[Yb(L^2)_3]$.(PhMe) (**2a**·(PhMe)] drawn with 50% ellipsoids; hydrogen atoms and toluene of crystallisation have been omitted for clarity

en′ amide ligands. The latter was unexpected since the very bulky $NSiMe_3$ groups are all in a *cis* disposition. Thus the N−Ln−N angles lie in the range [104.8(5)−109.0(1)°] for $[Ln(en')_3]$ (Ln = Lu, Er, Eu)[27] whereas **1e**, **2a**·(PhMe), **2d** and **2e** have two similar angles but one larger *transoid* angle (Table 1). Even with the *mer* configuration, two of the $NSiMe_3$ groups are pushed above and below the equatorial plane presumably to reduce steric repulsion from the otherwise closely proximate bulky amides. The less sterically dominating O(Me/Ph) groups occupy the *trans* sites with O(1)−Ln(1)−O(3) angles verging on linear, although the angles between the remaining *transoid* donors N(1)−Ln−N(2) and N(3)−Ln−O(2) are significantly less than 180°. This is presumably due to a combination of the small bite angle of the chelated L^1 or L^2 ligands and the proximity of the *cis* amide groups.

The geometry of $[Nd(L^2)_3]$ is almost identical to that of $[Nd(L^1)_3]$ with the angles defining the coordinated atoms differing by less than 10° (Table 1). Whilst the general appearance of the $[Ln(L^2)_3]$ complexes is the same, significant differences are apparent between the solvated and solvent-free structures. The *trans* N−Ln−N angles for unsolvated **2d** and **2e** are approximately 12° smaller than those for **2a**·(PhMe) and **2b**·(C_5H_9Me), and a similar, but less marked, trend is also observed for the *cis* N−Ln−N angles (Table 1). Thus the solvates are closer to a regular octahedral structure. These differences are clearly not due to the gradual change in ionic radii from La (1.03 Å) to Yb (0.87 Å).[33] For example, the smaller elements would be expected to be more sterically crowded causing a widening of the *cis* N−Ln−N angles through greater repulsion between the bulky $SiMe_3$ groups. In fact the opposite is observed. However, the *cis* N−Ln−N angles are not unreasonably narrow and still compare well with those of *fac*-$[Ln(en')_3]$.[27] Therefore the variation in angles is possibly associated with differences in the crystal packing required to accommodate solvent molecules.

A comparison of the metal-nitrogen distances with those of other lanthanoid organoamides can be made by subtraction of the appropriate metal ionic radius (Table 2).[33] Selected examples from the literature are listed in Table 2 and the values derived for the current $[Ln(L)_3]$ complexes (L^1: 1.37−1.40 Å, L^2: 1.36−1.43 Å) lie near the middle of the observed range (1.34−1.49 Å) and are therefore not unusual. For **1e**, **2a**·(PhMe) and **2b**·(C_5H_9Me) there is some variation in the Ln−N distances with one shorter [Ln(1)−N(3)] and two longer bonds, whereas the three Ln(1)−N(amide) bond lengths of **2d** and **2e** are very similar (Table 1). Whilst bond lengthening of the mutually *trans* amides might be expected, this is not observed for any of the complexes. Perhaps the inconsistently shorter Ln−N(3) distance reflects extraneous factors, for example packing forces. Subtraction values derived from the Ln−O distances (1.48−1.60 Å) are significantly longer than those derived from organolanthanoid or halolanthanoid ether complexes [$LnR_3(ether)_n$: 1.34 ± 0.05 Å);[34] $LnX_3(THF)_n$: 1.39−1.44 Å][35] but the Nd−O distances are shorter than those [2.614(4)−2.740(4) Å] in the related neodymium bidentate amide complex $[Nd\{Me_2Si(OtBu)(NtBu)\}_3]$.[36] The ether fragments of $[Nd\{Me_2Si(OtBu)(NtBu)\}_3]$ and $[Ln(L)_3]$ are bulkier than a simple ether ligand such as THF, and this may account for the long Ln−O distances, although the bond lengthening may also be an indication of general steric crowding in these complexes. The contraction of the subtraction values for the Ln−OPh bonds from La to Yb in the $[Ln(L^2)_3]$/$[Ln(L^2)_3]\cdot S_n$ complexes (Table 2) is contrary to the expected trend since the increase in steric crowding associated with the smaller size of the metal centre may result in metal-oxygen bond lengthening. Since there are two distinct groups of data corresponding to the presence or absence of a solvent of crystallisation, these variations in

Table 1. Metal atom environments for $[Ln(L)_3]$ complexes

	$[Nd(L^1)_3]$ **1e**	$[Yb(L^2)_3]\cdot(PhMe)$ **2a**·(PhMe)	$[Y(L^2)_3]\cdot(C_5H_9Me)$ **2b**·(C_5H_9Me)[a]	$[Nd(L^2)_3]$ **2d**	$[La(L^2)_3]$ **2e**
Bond length (Å)					
Ln(1)–N(1)	2.385(3)	2.272(2)	2.306(3)	2.396(2)	2.454(2)
Ln(1)–N(2)	2.376(3)	2.289(3)	2.331(3)	2.387(2)	2.447(2)
Ln(1)–N(3)	2.349(3)	2.231(3)	2.270(3)	2.386(2)	2.446(2)
Average	2.37	2.26	2.30	2.39	2.45
Ln(1)–O(1)	2.534(2)	2.350(3)	2.381(2)	2.550(2)	2.609(1)
Ln(1)–O(2)	2.535(2)	2.359(3)	2.441(2)	2.543(2)	2.606(2)
Ln(1)–O(3)	2.536(2)	2.405(3)	2.386(2)	2.575(1)	2.633(1)
Average	2.54	2.37	2.40	2.56	2.62
Angles (°)					
N(1)–Ln(1)–N(2)	139.63(9)	150.10(10)	148.15(10)	136.05(6)	134.17(5)
N(1)–Ln(1)–N(3)	98.82(9)	104.40(10)	105.71(10)	107.77(6)	109.22(5)
N(2)–Ln(1)–N(3)	119.23(9)	105.298(10)	106.01(10)	115.47(6)	116.09(5)
N(1)–Ln(1)–O(1)	65.62(8)	71.37(8)	70.33(9)	66.32(5)	64.65(5)
N(2)–Ln(1)–O(2)	66.12(8)	69.39(9)	68.37(9)	65.95(5)	64.19(5)
N(3)–Ln(1)–O(3)	65.38(8)	72.16(8)	71.02(9)	65.51(5)	63.82(5)
O(1)–Ln(1)–O(2)	88.48(7)	86.56(8)	85.63(8)	86.02(5)	85.43(5)
O(1)–Ln(1)–O(3)	167.65(7)	174.55(7)	174.28(7)	168.08(5)	168.26(4)
O(2)–Ln(1)–O(3)	82.42(7)	90.06(8)	89.97(8)	83.28(5)	83.78(5)
O(1)–Ln(1)–N(2)	80.87(8)	94.39(9)	94.23(9)	82.08(6)	82.32(5)
O(1)–Ln(1)–N(3)	124.75(8)	111.47(9)	113.58(9)	125.49(6)	127.19(5)
O(2)–Ln(1)–N(1)	90.19(8)	83.30(9)	82.44(9)	81.51(5)	81.56(5)
O(2)–Ln(1)–N(3)	146.38(8)	161.78(8)	160.63(9)	148.44(5)	147.35(5)
O(3)–Ln(1)–N(1)	122.48(8)	104.00(8)	105.48(9)	116.96(5)	118.06(5)
O(3)–Ln(1)–N(2)	87.79(8)	88.41(9)	87.54(9)	88.75(5)	88.81(5)

[a] Crystallographic data for **2a**·(C_5H_9Me) in CCDC-174206.

Table 2. Subtraction values from Ln−N, O, Cl distances for a selection of organoamidolanthanoid complexes

Compound	Ref	Coordination number	Av. Ln–N length [d(N)] Å	Av. Ln–O length [d(O)] Å	Ionic Radii of Ln^{3+} (ir) Å[a]	d(N)–ir (Å)	d(O)–ir (Å)
$[Nd(L^1)_3]$ (**1e**)	This work	6	2.37	2.54	0.98	1.39	1.56
$[Yb(L^2)_3]\cdot(PhMe)$ [**2a**·(PhMe)]	This work	6	2.26	2.37	0.87	1.39	1.50
$[Nd(L^2)_3]$ (**2d**)	This work	6	2.39	2.56	0.98	1.41	1.58
$[La(L^2)_3]$ (**2e**)	This work	6	2.45	2.62	1.03	1.42	1.59
$[Y(L^2)_3\cdot(C_5H_9Me)$ [**2b**·(C_5H_9Me)]	This work	6	2.30	2.40	0.90	1.40	1.50
$[Nd\{N(SiMe_3)_2\}_3]$	[37]	3	2.29		0.82[b]	1.47	
$[Eu\{N(SiMe_3)_2\}_3]$	[38]	3	2.26		0.78[b]	1.48	
$[Yb\{N(SiMe_3)_2\}_3]$	[38]	3	2.16		0.71[b]	1.45	
$[Nd\{N(Ph)(SiMe_3)\}_3(THF)]$	[39]	4	2.31		0.88[b]	1.43	
$[Yb\{NH(2,6\text{-}(iPr)_2C_6H_3)_3\}(THF)_2]$	[11]	5	2.17		0.82[b]	1.35	
$[Sm\{N(Cy)_2\}_3(THF)]$[c]	[40]	4	2.28		0.90[b]	1.38	
$[Eu(en')_3]$	[27]	6	2.29		0.95	1.34	
$[Er(en')_3]$	[27]	6	2.24		0.89	1.35	
$[Lu(en')_3]$	[27]	6	2.19		0.86	1.33	
$[Nd\{Me_2Si(OtBu)(NtBu)\}_3]$	[36]	6	2.40	2.68	0.98	1.42	1.70
$[Pr\{4\text{-}MeOC_6H_4C(NSiMe_3)_2\}_3]$	[41]	6	2.48		0.99	1.49	
				Av. Ln–Cl length [d(Cl)] Å			d(Cl)–ir (Å)
$[Ln(L^1)_2(\mu\text{-}Cl)]_2$ [Ln = Yb(**4a**), Tb (**4b**), Er (**4c**)]	This work	6	2.19–2.26	2.68–2.74	0.92, 0.89, 0.87	1.32–1.34	1.79–1.83
$[Nd(L^2)_2(\mu\text{-}Cl)]_2.(PhMe)_2$ [**5a**·$(PhMe)_2$]	This work	6	2.32, 2.30	2.79, 2.86	0.98	1.32, 1.34	1.80, 1.87
$[Nd\{N(2,6\text{-}(iPr)_2C_6H_3)(SiMe_3)\}_2(THF)(\mu\text{-}Cl)_2Li(THF)_2]$	[39]	5	2.30	2.76	0.92[b]	1.38	1.84
$[Sm\{N(SiMe_3)_2\}_2(\mu\text{-}Cl)(THF)]_2$	[17]	5	2.27	2.78	0.90[b]	1.37	1.88
$[Gd\{N(SiMe_3)_2\}_2(\mu\text{-}Cl)(THF)]_2$	[15]	5	2.25	2.75	0.89[b]	1.36	1.86
$[Yb\{N(SiMe_3)_2\}_2(\mu\text{-}Cl)(THF)]_2$	[15]	5	2.19	2.68	0.82[b]	1.37	1.86
$[Sm\{N(Cy)_2\}_2(\mu\text{-}Cl)(THF)]_2$ [c]	[40]	5	2.21	2.80	0.90[b]	1.31	1.90
$[Nd\{(CF_3)_2C_6H_2C(NSiMe_3)\}_2(\mu\text{-}Cl)_2Li(THF)_2]$	[42]	6	2.53	2.71	0.98	1.55	1.73
$[Sm\{LitBuDAB)_2(THF)\}(\mu\text{-}Cl)_2Li(THF)_2]$[d]	[25]	8	2.45	2.88	1.08	1.37	1.80
$[Yb\{Me_2Si(OtBu)(NtBu)\}_2(\mu\text{-}Cl)_2Li(THF)_2]$	[36]	6	2.24	2.64	0.87	1.37	1.77
$[Er\{(iPr)TP\}(\mu\text{-}Cl)]_2$ [e]	[23]	6	2.32	2.73	0.89	1.44	1.84
$[Yb\{(iPr)TP\}(\mu\text{-}Cl)]_2$ [e]	[23]	6	2.30	2.71	0.87	1.43	1.84
$[Y(\eta^5,\eta^1\text{-}C_5Me_4SiMe_2NCMe_2Et)(THF)(\mu\text{-}Cl)]_2$	[43]	7	2.24	2.74	0.96	1.28	1.78
$[Yb(\eta^5\text{-}C_5H_5)_2(\mu\text{-}Cl)]_2$	[44]	8	–	2.64	0.98	–	1.66
$[Lu(\eta^5\text{-}C_5H_4SiMe_3)_2(\mu\text{-}Cl)]_2$	[45]	8	–	2.62	0.98	–	1.64
$[Sm(\eta^5\text{-}(C_5Me_5)_2(\mu\text{-}Cl)]_3$	[46]	8	–	2.88	1.08	–	1.80
$[Yb(Cl)_2(\mu\text{-}Cl)(THF)_2]_2$[f]	[47]	6	–	2.68	0.87	–	1.81

[a] Values derived from R. D. Shannon.[33] [b] Numbers extrapolated from values of higher coordination number from [a]. [c] Cy = cyclohexyl. [d] *t*BuDAB = di-*tert*-butyl-1,4-diazabutadiene. [e] $[(iPr)TP]^{2-}$ = 1,3-bis[2-(isopropylamino)troponiminato]propane. [f] Value of the Yb−μ-Cl distance only.

bond lengths and angles may be a result of a packing effect resulting from the presence or absence of the solvent.

With successful coordination of bidentate organoamide ligands [not only in the current examples, but also the previously reported [Ln(en′)$_3$] complexes (Ln = Lu, Er, Eu, Sm, Nd, La)],[27] the next challenge was to prepare heteroleptic chloride species of the type [Ln(L)$_2$Cl]. Such complexes are pivotal intermediates for the generation of catalytically active materials.[4,5,7] A one-pot reaction was initially reported[27] to be successful for the en′ ligand, yielding one example of the target molecules, [Er(en′)$_2$Cl]. This has now been shown to be general across the lanthanoid series with the preparation of the heteroleptic diorganoamidolanthanoid complexes [Ln(en′)$_2$(μ-Cl)]$_2$ [Ln = Yb (**3a**), Er(**3b**), Sm (**3c**), Nd (**3d**) and La (**3e**)] (Scheme 2). The lanthanoid products were very soluble in hydrocarbon solvents and were crystallised with difficulty from concentrated solutions at −20 °C. Furthermore, the removal of LiCl from the reaction mixture was tedious with numerous low temperature extractions required in order to obtain pure [Ln(en′)$_2$(μ-Cl)]$_2$ derivatives, which were subsequently isolated in only low to moderate yields.

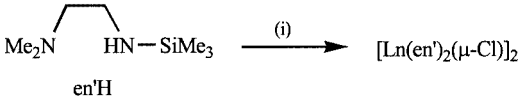

Scheme 2. Reagents and Conditions; (i) *n*BuLi, THF, 0 °C, then 0.5 equivalents of $LnCl_3$ (Ln = Yb, Er, Sm, Nd, La) followed by crystallisation from hexane

The addition of $LnCl_3$ to two molar equivalents of LiL (L = L^1, Ln = Yb, Nd; L = L^2, Ln = Yb, Nd, La), which was generated in situ in THF, resulted in complete dissolution of the starting materials. Extraction of the evaporated reaction mixtures with hexane gave the homoleptic complexes [Ln(L)$_3$] [L = L^1, Ln = Yb (**1a**), Nd (**1e**); L = L^2, Ln = Yb (**2a**·(C$_5$H$_9$Me) (from toluene/hexane), Nd (**2d**), La (**2e**)] instead of the target heteroleptic complexes [Ln(L)$_2$Cl] (Scheme 3). Subsequently, reactions using isolated crystalline lithium salts of L^1 and L^2, such as dimeric [Li(L^1)(-OEt$_2$)]$_2$ (below) or monomeric [Li(L^2)(DME)],[29] with a variety of $LnCl_3$ compounds in a 2:1 Li to $LnCl_3$ mol ratio, were found to give LnL_2Cl complexes [L = L^1, Ln = Yb (**4a**), Er (**4b**), Tb (**4c**); L = L^2, Ln = Nd {**5a**·(PhMe)$_2$}] (Scheme 3). Typically, hexane extraction was employed for the isolation of [Ln(L^1)$_2$(μ-Cl)]$_2$ (**4a**−**4c**) species whilst toluene was used for **5a**·(PhMe)$_2$ (Scheme 3). However, the isolation of the homoleptic products **2a** and **2e** from reactions of $LnCl_3$ with *two* equivalents of [Li(L^2)(DME)][29] was also observed. Thus these results show that for L^1 and L^2 there is only a narrow window of opportunity to prepare the heteroleptic chlorides. Access to complexes of the smaller lanthanoid elements Tb, Er and Yb is available with L^1, but the larger neodymium gives [Nd(L^1)$_3$] (**1e**) whilst L^2 yields the heteroleptic derivative for the larger Nd but not with the lighter (La) and heavier (Yb) extremes of the lanthanoid series. These results support the view of Lappert et al. that fully characterised isolated lithium complexes are more rewarding synthetically than reagents generated in situ.[48,49] The synthetic value of *pre-isolated* alkali metal alkyls has been demonstrated in routes to ytterbium(II) alkyls.[50]

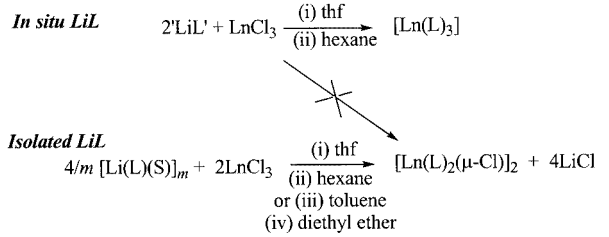

Scheme 3. Reagents and Conditions; In situ ′LiL′; (ii) L = L^1, Ln = Yb (**1a**), Nd (**1e**); L = L^2, Ln = Yb (**2a**) (crystallised from toluene/hexane), Nd (**2d**), La (**2e**). *Isolated* LiL; (ii) L = L^1, Ln = Yb, Er, Tb, target **4a**−**4c** obtained; Ln = Nd gives **1e**; (iii) L = L^2, Ln = Nd, **5a**·(PhMe)$_2$ obtained; Ln = Yb, La afforded **2a**, **2e**; iv) L = L^2, Ln = La, **2e** obtained

The direct formation of [Ln(L)$_3$] from a 2:1 (Li:Ln) reaction in THF would leave 0.33 equivalents of $LnCl_3$ unchanged, and lanthanoid halides have low solubility in this solvent. Since all the $LnCl_3$ dissolved, it suggests that the heteroleptic species is formed initially, possibly stabilised as an "ate" complex such as **A** in Scheme 4. The formation of "ate" complexes has previously been observed for other bulky organoamidolanthanoids, for example [Yb{Me$_2$Si(O*t*Bu)(N*t*Bu)}$_2$(μ-Cl)$_2$Li(THF)$_2$][36] and [Nd{(CF$_3$)$_3$C$_6$H$_2$C(NSiMe$_3$)$_2$}(μ-Cl)$_2$Li(THF)$_2$].[42] Therefore the rearrangement presumably occurs on addition of hexane [or for L^2, Ln = Yb, toluene (even with isolated LiL^2); for Ln = La, also diethyl ether; Scheme 4 (iii)] with precipitation of LiCl and $LnCl_3$ or even $LiLnCl_4$. This is contrary to the in situ [Ln(en′)$_2$(μ-Cl)]$_2$ preparations where the heteroleptic derivatives were obtained from hexane. Crystallisation of the "ate" complexes (**A** in Scheme 4) was unsuccessful due to the very high solubility of the reaction products. The reasons for the difference in outcome between the use of isolated and in situ formed LiL in two cases (L = L^1, Ln = Yb; L = L^2, Ln = Nd) are not clear but plausibly the in situ reagents are less pure.

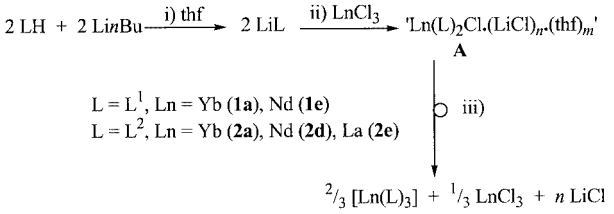

Scheme 4. Postulated rearrangement pathway

Elemental analyses (C, H, N and/or Ln) for the [Ln(L)$_2$(μ-Cl)]$_2$ complexes (except unanalysed **3b**, **3c**) were consistent with the proposed formulations and the absence of coordinated THF. For each ligand type the infrared spectra of the [Ln(L)$_2$(μ-Cl)]$_2$ complexes were almost identical, showing peaks attributable to the appropriate ligand and no evidence of THF. The spectra of **3a**−**3e** were very similar to those of the corresponding homoleptic species. In contrast

intense infrared absorptions of **4a**−**4c** attributable to C−O−C stretching of the MeOAr substituent were observed as two single bands at 1100−1000 cm^{-1}, whereas for *mer*-[Ln(L^1)$_3$] two bands were observed in each region. This may reflect the solely *trans* ether groups in **4a**−**4c** (below), whereas [Ln(L^1)$_3$] complexes have both *cis* and *trans* (Me)O−Ln−O(Me) arrays. Bands at 1266 and 859 cm^{-1} were observed for **5a**·(PhMe)$_2$ but not for **2d**·(PhMe)$_2$, and a band of the latter at 802 cm^{-1} was absent in the former, thereby distinguishing the spectra of the two complexes. Despite the paramagnetism of **5a**·(PhMe)$_2$, ^{1}H NMR resonances attributable to the L^2 ligand could be assigned (see Exp. Sect.), whilst those of toluene were in the usual diamagnetic region; integrations confirmed the proposed composition. Only a single L^2 environment was detected — consistent with the single type of L^2 coordination in the solid-state structure (below) — and the general spectral features were similar to those of **2d**·(PhMe)$_2$. The visible/near infrared spectrum of **5a**·(PhMe)$_2$ showed absorptions characteristic of Nd^{3+}.[31] Mass spectra identified a bimolecular species to be present for **3a**−**3e** with the highest-mass fragment, except for ytterbium, being the ion [Ln$_2$(en′)$_3$Cl$_2$]$^+$. (For the heavier ytterbium metal only the fragment [Yb$_2$(en′)$_2$Cl$_2$]$^+$ was detected due to limitations in the accessible mass spectrum range.) These data imply that the complexes have a dimeric structure of the type [Ln(en′)$_2$(μ-Cl)]$_2$ and contradict an earlier proposal of a monomeric structure for the Er complex also based on MS data.[27] Verification by X-ray diffraction studies has been unsuccessful owing to the difficulty in obtaining suitable crystals of the highly soluble complexes and an unsatisfactory data solution for the one set of apparently suitable crystals (**3d**).

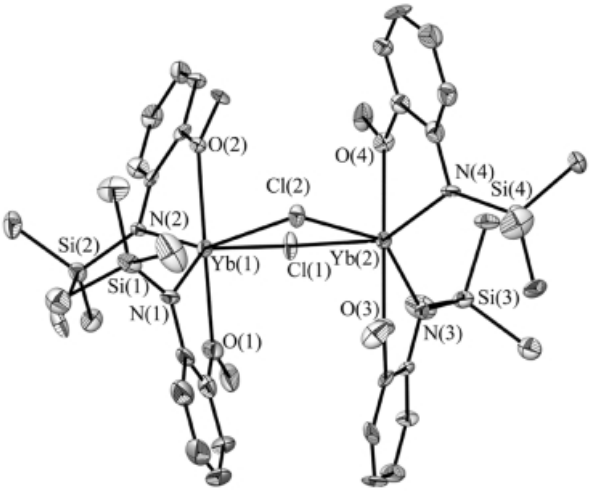

Figure 3. ORTEP view of one molecule of [Yb(L^1)$_2$(μ-Cl)]$_2$ (**4a**) drawn with 50% ellipsoids; hydrogen atoms have been omitted for clarity

The molecular structures of **4a** (Figure 3), **4b**, **4c** and **5a**·(PhMe)$_2$ (Figure 4) are dimeric with two lanthanoid atoms bridged by two chlorine atoms. The complexes **4a**−**4c** are isostructural and have the monoclinic centrosymmetric space group $P2_1/n$ with one dimer comprising the asymmetric unit. For **5a**·(PhMe)$_2$ a toluene of crystallisation is present in each asymmetric unit that comprises half the dimer with a crystallographic inversion centre located in the middle of the Nd_2Cl_2 plane. Selected bond lengths and angles for **4a**−**4c** and **5a**·(PhMe)$_2$ are given in Table 3. Two chelating [L]$^-$ (L = L^1 or L^2) units are bound to each lanthanoid centre in a similar fashion completing a six-coordination environment with a very distorted octahedral geometry. Clearly, the steric demand of two L ligands and one chloride is not sufficient to saturate all coordination sites on the lanthanoid metal since dimerisation takes place. Coordination of a molecule of THF generating monomeric [Ln(L)$_2$Cl(THF)] may occur in THF solution prior to workup in nonpolar solvents. The chloride-bridged dimer is presumably less crowded than [Ln(L)$_2$Cl(THF)] with the steric coordination number[51] for THF (1.2) larger than that for chloride (1.0). In addition, longer Ln−μ-Cl than Ln−Cl$_{ter}$ distances also reduce crowding. These factors favour elimination of any coordinated THF on isolation.

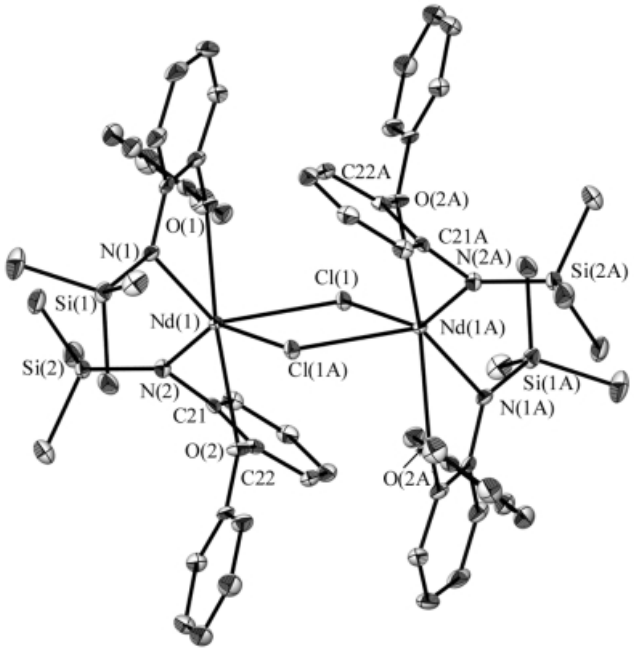

Figure 4. ORTEP view of [Nd(L^2)$_2$(μ-Cl)]$_2$.(PhMe)$_2$ (**5a**·(PhMe)$_2$] drawn with 50% ellipsoids; hydrogen atoms and toluene of crystallisation have been omitted for clarity

The coordination geometry in [Ln(L)$_2$(μ-Cl)]$_2$ is similar to that of the homoleptic derivatives [Ln(L)$_3$] (L = L^1, L^2). Two bridging chloride atoms in the former replace one equatorial L ligand of [Ln(L)$_3$]. The axial positions are occupied by the O(Me/Ph) group on L^1 or L^2 with O(1)−Ln(1)−O(2) angles close to the expected 180°. The remaining $NSiMe_3$ units and chloride atoms are located in mutually *cisoid* equatorial sites with the former lying above and below the equatorial plane. This arrangement presumably minimises steric repulsion between the *cis* $NSiMe_3$ groups as is also observed for the homoleptic complexes [Ln(L)$_3$] (see above). Generally the binding of the L^1 and L^2 ligands is similar to that in the corresponding homoleptic complexes, although there is a marginal shortening of the

Table 3. Metal environment in $[Ln(L)_2(\mu\text{-}Cl)_2]$ complexes

Complex	$[Yb(L^1)_2(\mu\text{-}Cl)]_2$ (**4a**)	$[Er(L^1)_2(\mu\text{-}Cl)]_2$ (**4b**)	$[Tb(L^1)_2(\mu\text{-}Cl)]_2$ (**4c**)		$[Nd(L^2)_2(\mu\text{-}Cl)]_2\cdot(PhMe)_2$ **5a**·$(PhMe)_2$
Bond length (Å)					
Ln(1)–N(1,2)	2.184(8), 2.190(7)	2.233(3), 2.221(3)	2.266(3), 2.265(3)	Nd(1)–N(1,2)	2.319(2), 2.299(2)
Ln(2)–N(3,4)	2.188(8), 2.202(8)	2.225(3), 2.223(3)	2.257(3), 2.257(3)	Nd(1)–O(1,2)	2.519(2), 2.567(2)
Ln(1)–O(1,2)	2.350(7), 2.370(6)	2.354(2), 2.383(2)	2.416(3), 2.437(3)	Nd(1)–Cl(1, 1A)[a]	2.785(1), 2.856(1)[a]
Ln(2)–O(3,4)	2.337(7), 2.354(6)	2.353(2), 2.363(2)	2.414(3) 2.414(3)	Nd(1)–C(21)	2.911(2)
Ln(1)–Cl(1,2)	2.680(2), 2.668(3)	2.713(1), 2.683(1)	2.748(1), 2.727(1)	Nd(1)–C(22)	3.035(2)
Ln(2)–Cl(1,2)	2.678(2), 2.675(2)	2.701(1), 2.703(1)	2.740(1), 2.734(1)		
Ln(1)–Ln(2)	4.066(1)	4.1048(8)	4.1545(9)	Nd(1)–Nd(2)	4.385(5)
Angles (°)					
N(1,3)–Ln(1)–N(2,4)	113.5(3), 112.7(3)	113.80(10), 113.21(10)	116.34(11), 117.06(11)	N(1)–Nd(1)–N(2)	114.69(7)
O(1,3)–Ln(1)–O(2,4)	162.2(3), 166.6(2)	162.54(8), 168.31(7)	161.28(9), 166.85(9)	O(1)–Nd(1)–O(2)	152.65(5)
Cl(1)–Ln(X)–Cl(2) (X = 1,2)	79.55(7), 79.47(7)	79.57(3), 79.42(3)	79.38(3), 79.38(3)	Cl(1)–Nd(1)–Cl(1A)	77.96(2)[a]
Ln(1)–Cl(X)–Ln(2) (X = 1,2)	98.72(8), 99.12(8)	98.62(3), 99.31(3)	98.41(3), 99.05(4)	Nd(1)–Cl(1)–Nd(1A)	102.04(2)[a]
N(1,2)–Ln(1)–O(1,2)	71.5(3), 71.1(2)	69.83(9), 70.84(9)	68.23(11), 69.45(10)	N(1,2)–Nd(1)–O(1,2)	67.53(6), 68.47(7)
N(3,4)–Ln(2)–O(3,4)	71.8(3), 72.0(3)	70.72(9), 71.47(9)	69.01(10), 69.82(10)		
N(1,3)–Ln(1,2)–O(2,4)	124.7(3), 120.0(3)	126.23(9), 119.63(9)	129.52(10), 123.66(10)	N(1)–Nd(1)–O(2)	137.36(6)
N(1,2)–Ln(1)–Cl(1,2)	88.5(2), 91.0(2)	88.85(7), 90.89(7)	88.71(9), 89.51(8)	N(1)–Nd(1)–Cl(1, 1A)	128.17(5), 87.21(6)[a]
N(1,2)–Ln(1)–Cl(2,1)	144.3(2), 151.2(2)	143.13(7), 150.89(7)	141.33(9), 149.43(8)	N(2)–Nd(1)–Cl(1, 1A)	104.20(5), 145.91(5)[a]
N(3,4)–Ln(2)–Cl(1,2)	143.3(2), 152.3(2)	142.32(7), 151.24(7)	140.26(8), 149.06(8)		
N(3,4)–Ln(2)–Cl(2,1)	86.7(2), 93.8(2)	86.64(7), 94.36(7)	86.33(9), 92.06(8)		
O(1,2)–Ln(1)–Cl(1,2)	108.49(19), 86.81(16)	108.02(7), 86.65(6)	107.56(7), 85.10(7)	O(1)–Nd(1)–Cl(1,1A)	78.61(5), 121.30(5)[a]
O(2,1)–Ln(1)–Cl(1,2)	81.17(16), 80.6(2)	81.12(6), 80.64(7)	81.19(7), 80.48(8),	O(2)–Nd(1)–Cl(1,1A)	87.60(5), 77.73(5)[a]
O(3,4)–Ln(2)–Cl(1,2)	79.92(18), 81.31(17)	79.89(6), 80.72(6)	79.30(7), 80.48(7)		
O(3,4)–Ln(2)–Cl(2,1)	106.82(18), 91.37(17)	106.38(6), 92.58(6)	105.33(7), 90.41(7)		
N(1,2)–Ln(1)–O(2,1)	124.7(3), 96.5(3)	126.23(9), 92.29(9)	129.52(10), 98.40(11)	N(2)–Nd(1)–O(1)	91.99(7)
N(3,4)–Ln(2)–O(4,3)	120.0(3), 98.2(3)	119.63(9), 100.00(9)	123.66(10), 102.11(10)		

[a] Symmetry transformations used to generate equivalent atoms: $-x + 2, -y + 2, -z + 1$.

Ln−N and Ln−O bond lengths consistent with the lower steric demand of two chlorides. The near planar (**4a**−**4c**) or planar [**5a**·$(PhMe)_2$] Ln_2Cl_2 cores exhibit symmetrical bridging of the chlorides in the L^1 complexes, although there is a difference of 0.07 Å between the two Nd−Cl distances of **5a**·$(PhMe)_2$. The distance between the lanthanoid centres is nonbonding (Table 3) and varies in line with the ionic radii of the respective metals (Table 2).

A notable feature of the coordination of the two L^2 ligands to neodymium in **5a**·$(PhMe)_2$ is the noticeable tilt in one of the aromatic backbones [C(21)−C(26)]. Thus the interplanar angle to the Nd−N−O plane is 61.41(7)° which is almost double that of the other L^2 ligand [31.49(6)°] and of the maximum observed for the homoleptic $[Ln(L^2)_3]$ derivatives. Associated with this tilt, two of the carbon atoms [C(21) and C(22)] approach the metal centre with distances of 2.911(2) and 3.035(2) Å, respectively, which are approximately 0.25 Å shorter than the corresponding distances for the other L^2 ligand. The former Nd−C distances are only marginally longer than π-arene lanthanoid interactions in, for example, $[Nd(\eta^6\text{-}PhH)(AlCl_4)_3]$[52] [Nd−C distances of 2.93(2) to 2.94(2) Å], and are similar to or shorter than intramolecular π-arene contacts [2.964(7)−3.158(9) Å] in neodymium aryloxide complexes such as $[Nd(Odpp)_3]$ ($Odpp^- = 2,6$-diphenylphenolate).[53] Thus, it appears that C(21) and C(22) form an intramolecular $\pi\text{-}\eta^2$ interaction with Nd and this bonding accounts for the tilt of the arene backbone.

For **3a**−**3e**, a similar dimeric structural type would be expected with *cis*-amide groups, *trans*-amine substituents and bridging chloride ions per six-coordinate lanthanoid centre (Figure 5), although other arrangements may also be possible.

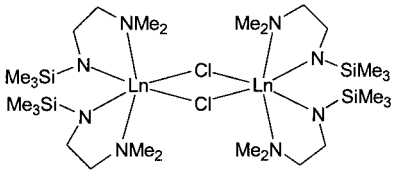

Figure 5. Postulated dimeric representation of $[Ln(en')_2(\mu\text{-}Cl)]_2$

Subtraction of the appropriate ionic radii from the Ln−Cl distances gives similar values to those of structurally characterised lanthanoid μ-chloride fragments supported by either amide or halide co-ligands (Table 2). For $[Nd(L^2)_2(\mu\text{-}Cl)]_2$ one value is slightly larger than in **4a**−**4c** complexes consistent with the greater steric crowding in the L^2 complex. Subtraction values for **4a**−**4c** and **5a**·$(PhMe)_2$ are similar to $[Yb(Cl)_2(\mu\text{-}Cl)(THF)_2]_2$ {which has an analogous donor array to $[Yb(L^1)_2(\mu\text{-}Cl)]_2$}[47] but are longer than those from the Yb−Cl distances of $[Yb(C_5H_5)_2(\mu\text{-}Cl)]_2$,[44] consistent with the greater steric coordination number[51] summation for $[Yb(Cl)_2(\mu\text{-}Cl)(THF)_2]_2$ (6.42) than $[Yb(C_5H_5)_2(\mu\text{-}Cl)]_2$ (6.08). The subtraction values for the Ln−Cl bonds in $[Ln(L^1)_2(\mu\text{-}Cl)]_2$ are similar to those of $[Sm(C_5Me_5)_2(\mu\text{-}Cl)]_3$ [46] (Table 2) suggesting a steric similarity between L^1 and C_5Me_5, even though the current structures are more like those of the unsubstituted cyclopentadienyl complex $[Yb(C_5H_5)_2(\mu\text{-}Cl)]_2$, as the $Sm(C_5Me_5)_2$ groups are rotated by 90°.[46] This may reflect both the more adaptable coordination environment of the

"edge-on" bound bidentate organoamide ligands compared with the "face-on" cyclopentadienyl ligand.

Synthesis and Crystal Structure of $[Li(L^1)(OEt_2)]_2$

The lithiation of L^1H with one equivalent of *n*BuLi in Et_2O afforded a white precipitate of $[Li(L^1)(OEt_2)]_2$. Satisfactory elemental analyses, despite numerous attempts, could not be obtained. The values are closer to those for LiL^1 and could suggest that loss of coordinated ether occurs during the lengthy journey to the analysis laboratories. However the ^1H NMR spectrum of $[Li(L^1)(OEt_2)]_2$ established the L^1 to Et_2O ratio, and showed a single methoxy ether peak and characteristic arene backbone signals (H-3−H-6). The room temperature ^7Li NMR spectrum of $[Li(L^1)(OEt_2)]_2$ shows a single lithium environment with a narrow ($\Delta\nu_{1/2}$ = 14 Hz) signal. The IR spectrum contained absorptions typical of a coordinated Et_2O molecule and of the L^1 ligand.

Crystals of $[Li(L^1)(OEt_2)]_2$ suitable for X-ray crystallography were obtained by recrystallisation of the crude material from diethyl ether. The structure of the complex $[Li(L^1)(OEt_2)]_2$ is dimeric (Figure 6). Selected geometric data are compiled in Table 4. Each four-coordinate lithium atom is surrounded by one diethyl ether, two bridging amide nitrogens [N(1) and N(1A)] and a methoxy oxygen atom in a distorted tetrahedral array. This distortion presumably arises from the restriction of the N−Li−O(Me) bite angle [83.6(2)°] as well as the ligation of the bridging amide nitrogens, N(1) and N(1A), to Li(1,1A). The N(1)−Li(1)−N(1A)−Li(1A) ring is essentially planar having the bidentate L^1 ligands parallel to each other, with the arene backbone approximately perpendicular to the central $(NLi)_2$ plane [74.9(1)°]. In comparison with L^1H,[28] binding of L^1 to lithium has little effect on the methoxy position in relation to the arene backbone plane [torsion angle: C(13)−C(12)−O(1)−C(10) 11.7(3)°]. The structure of $[Li(L^1)(OEt_2)]_2$ can be compared with those of other sterically-crowded $[\{Li(\mu\text{-}L)(OEt_2)\}_2]$ complexes [L = 8-quinolinyl(trimethylsilyl)amide (qsta)[54] or *N,N′*-di-*p*-tolylformamidinate (dtf)[55]]. However, the steric requirements for L^1 must be less than that of en′ which coordinates to lithium in an unsymmetrical dinuclear configuration in $[Li(en')_2Li(OEt_2)]$[27] with one four-coordinate and one three-coordinate Li. The Li−O(1) and Li−O(2) ether distances [2.000(4) Å, 1.991(4) Å respectively] in $[Li(L^1)(OEt_2)]_2$ are similar to those in related etherates (e.g. 1.94(3) Å in four-coordinate $[\{Li(qsta)(OEt_2)\}_2]$ and 1.943(6) Å in three-coordinate $[\{Li[N(SiMe_3)_2(OEt_2)\}_2]$[49]). The lithium bridging is not symmetrical as shown by the significant difference in the Li(1)−N(1) and Li(1)−N(1A) bond lengths of 0.129 Å. This unsymmetrical behaviour has been observed in the related $[\{Li(qsta)(OEt_2)\}_2]$ complex with bridging Li−N(amide) distances of 2.07(2) and 2.21(2) Å and is presumably due to the steric crowding by the chelating L^1 ligand. The sharp ^7Li and ^1H NMR spectra of $[Li(L^1)(OEt_2)]_2$ are consistent with observation of only one LiL^1 environment in the solid state.

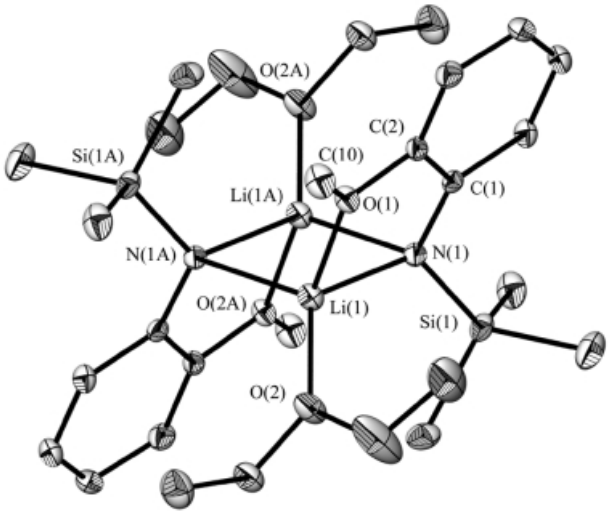

Figure 6. ORTEP view of $[Li(L^1)(OEt_2)]_2$ drawn with 50% ellipsoids; hydrogen atoms have been omitted for clarity

Table 4. Selected bond lengths (Å) and angles (°) with estimated standard deviations in parentheses for $[Li(L^1)(OEt_2)]_2$

Li(1)–N(1)	2.028(4)	O(2)–Li(1)–O(1)	107.2(2)
Li(1)–N(1A)[a]	2.157(4)	O(2)–Li(1)–N(1)	124.3(2)
Li(1)–O(1)	2.000(4)	O(1)–Li(1)–N(1)	83.6(2)
Li(1)–O(2)	1.991(4)	O(2)–Li(1)–N(1A)[a]	120.7(2)
		O(1)–Li(1)–N(1A)[a]	109.4(2)
		N(1)–Li(1)–N(1A)[a]	104.9(2)

[a] Symmetry transformations used to generate equivalent atoms: $-x, -y + 1, -z$.

Conclusions

The preparation of solvent-free lanthanoid organoamide complexes of the type $[LnL_3]$ or $[Ln(L)_2(\mu\text{-}Cl)]_2$ (L = L^1, L^2, en′) can be achieved through incorporation of a pendant donor on the amide ligand. For the ether-substituted L^1 and L^2 derivatives, isolation of $[Ln(L)_2(\mu\text{-}Cl)]_2$ is critically dependent upon the correct choice of, and size of, the ligand and the lanthanoid metal, since otherwise rearrangement to the homoleptic complex is observed. The $[Ln(L)_2(\mu\text{-}Cl)]_2$ (L = L^1, L^2, en′) complexes represent a new class of solvent-free heteroleptic lanthanoid(III) amides which should be capable of further functionalisation by replacement of the halide.

Experimental Section

All reactions were carried out under dry nitrogen using dry box and standard Schlenk techniques. Solvents were dried by distillation from sodium wire/benzophenone. IR data (4000−650 cm^{-1}) were recorded for Nujol mulls sandwiched between NaCl plates with a Perkin−Elmer 1600 Fourier transform infrared spectrometer. NMR spectra were obtained either on a Bruker AC200 MHz (^1H) or a Bruker AC 400 MHz spectrometer (^7Li and ^1H) as indicated. Deuterated solvents were degassed and distilled from Na/K

alloy prior to use. ^{1}H NMR spectra were referenced to the solvent (C_6D_6 and C_7D_8) signals; the chemical shift for the ^{7}Li spectrum is given relative to external 0.1 M LiCl in D_2O at room temperature. Mass spectra were recorded with a VG Trio-1 GC mass spectrometer. Each listed *m*/*z* value for metal-containing ions is the most intense peak of a cluster pattern in good agreement with the calculated pattern. Elemental analyses (C, H N) were determined by the Campbell Microanalytical Service, University of Otago, New Zealand. Lanthanoid analyses were by complexometric titration with $[Na_2EDTA]$.[53,56] $[LnCl_3(THF)_n]$,[35] $LnCl_3$,[57] L^1H,[28] L^2H,[28,29] en′H,[27] $[Li(L^2)(DME)]$[29] were each prepared according to a reported procedure. *n*BuLi (1.6 M) (Aldrich) was used unstandardised but transferred to and stored in a Schlenk flask under nitrogen immediately on opening a new batch.

$[Yb(L^1)_3]$ (1a). Method 1: $[Li(L^1)(OEt_2)]_2$ (0.62 g, 1.12 mmol) was added to a stirred suspension of $[YbCl_3(THF)_3]$ (0.37 g, 0.75 mmol) in THF (40 mL) and the resulting mixture was stirred for 12 h. The solvent was removed under vacuum and hexane added (30 mL) giving a white precipitate. The red solution was filtered and the filtrate concentrated to 15 mL. A red crystalline product was obtained on standing for 2 h (0.41 g, 72%). IR (Nujol): $\tilde{\nu}$ = 1593 vs, 1561 vs, 1485 s, 1465 m, 1321 vs, 1294 vs, 1283 s, 1245 vs, 1209 s, 1159 w, 1059 w, 1051 s, 1012 s, 1000 vs, 913 br. s, 843 br vs, 822 s, 787 m, 770 s, 743 s, 681 s, 629 s, 598 s cm^{-1}. Vis/near IR (DME): λ_{max} (ε) = 431 (185), 874 (9), 911 (14), 945 (6), 978 (35) nm (dm^3 mol^{-1}). $C_{30}H_{48}N_3O_3Si_3Yb$ (756.23): calcd. C 47.66, H 6.40, N 5.56; found C 47.88, H 6.44, N 5.63.

Method 2 [2:1 Li to Ln mol ratio (in situ)]: *n*BuLi was slowly added (2.31 mL, 3.70 mmol) to a stirred solution of L^1H (0.71 g, 3.60 mmol) in THF (40 mL) at 0 °C and the resulting solution was warmed to room temperature over ca. 1 h. $[YbCl_3(THF)_2]$ (0.76 g, 1.80 mmol) was added to the resulting solution and the reaction mixture rapidly stirred for 12 h. The solvent was removed in vacuo, and hexane (30 mL) was added affording a white precipitate. The red solution was filtered and the filtrate volume reduced to ca. 2 mL under vacuum . Red crystals of $[Yb(L^1)_3]$ (**1a**) were deposited on standing overnight. The infrared spectrum was identical to that of **1a** obtained from **Method 1**.

$[Er(L^1)_3]$ (1b): *n*BuLi (2.30 mL, 3.70 mmol) was added to a stirred solution of compound L^1H (0.72 g, 3.70 mmol) in THF (40 mL) at 0 °C, and the resulting solution was warmed to room temperature over ca. 1 h. $[ErCl_3(THF)_{3.5}]$ (0.63 g, 1.20 mmol) was then added and the reaction mixture stirred for 15 h. The solvent was then removed under vacuum and hexane (30 mL) was added giving a white precipitate. The light pink solution was filtered and the filtrate volume reduced to 10 mL under vacuum. The light pink crystals deposited on standing for 12 h (0.43 g, 48%). IR (Nujol): $\tilde{\nu}$ = 1593 vs, 1561 vs, 1485 s, 1464 m, 1321 vs, 1284 vs, 1240 s, 1209 s, 1156 vs, 1117 vs, 1058 w, 1051 s, 1011 s, 1000 vs, 911 br. s, 841 br vs, 784 s, 768 s, 735 s, 681 s, 627 s, 597 s cm^{-1}. MS: *m*/*z* (%) = 646 (<1) $[Er(L^1)_2NC_6H_4]^+$, 556 (<1) $[Er(L^1)_2]^+$, 480 (<1) $[Er(L^1)(C_6H_4NSi)]^+$, 195 (35) $[(L^1H)]^+$, 180 (20) $[(L^1H) - Me]^+$, 165 (100) $[(L^1H) - 2Me]^+$, 150 (35) $[(L^1H) - 3Me]^+$, 135 (20) $[C_6H_5ONSi]^+$, 73 (20) $[SiMe_3]^+$, 58 (10) $[SiMe_2]^+$. $C_{30}H_{48}ErN_3O_3Si_3$ (748.22): calcd. C 48.03, H 6.45, N 5.60; found C 48.16, H 6.70, N 5.73.

$[Sm(L^1)_3]$ (1c): A similar preparation method to that used for compound **1b** gave yellow crystals of **1c** (0.36 g, 41%). IR (Nujol): $\tilde{\nu}$ = 1585 vs, 1559 vs, 1481 s, 1307 vs, 1279 vs, 1237 s, 1211 s, 1173 vs, 1117 vs, 1076 vs, 1058 w, 1050 vs, 1030 vs, 937 s, 919 s, 842 s, 825 s, 772 vs, 741 vs, 735 s, 662 vs, 616 s, 597 s cm^{-1}. MS: *m*/*z* (%) = 734 (<1) $[Sm(L^1)_3]^+$, 630 (<1) $[Sm(L^1)_2NC_6H_4]^+$, 540 (<1) $[Sm(L^1)_2]^+$, 464 (<1) $[Sm(L^1)(C_6H_4NSi)]^+$, 195 (35) $[(L^1H)]^+$, 180 (20) $[(L^1H) - Me]^+$, 165 (100) $[(L^1H) - 2Me]^+$, 150 (35) $[(L^1H) - 3Me]^+$, 135 (20) $[C_6H_5ONSi]^+$, 73 (20) $[SiMe_3]^+$, 58 (10) $[SiMe_2]^+$. $C_{30}H_{48}N_3O_3Si_3Sm$ (734.21): calcd. C 49.13, H 6.60, N 5.73; found C 48.55, H 6.67, N 5.67.

$[Pr(L^1)_3]$ (1d): A similar preparation method to that used for compound **1b** gave green crystals of **1d** (0.49 g, 57%). IR (Nujol): $\tilde{\nu}$ = 1590 vs, 1561 vs, 1484 s, 1449 s, 1320 vs, 1285 vs, 1246 br. s, 1210 s, 1164 vs, 1117 vs, 1058 w, 1050 s, 1011 s, 1002 vs, 915 br. s, 841 br. s, 768 s, 743 s, 674 s, 625 s, 597 s cm^{-1}. $C_{30}H_{48}N_3O_3PrSi_3$ (723.21): calcd. C 49.78, H 6.68, N 5.80; found C 49.56, H 6.71, N 5.97.

$[Nd(L^1)_3]$ (1e). Method 1: A similar preparation method to that used for compound **1b** gave blue crystals of **1e** (0.57 g, 65%). IR (Nujol): $\tilde{\nu}$ = 1590 vs, 1560 m, 1484 s, 1319 vs, 1285 vs, 1246 m, 1209 s, 1163 s, 1117 vs, 1058 w, 1050 s, 1011 s, 1002 vs, 914 br. s, 841 br vs, 767 s, 743 vs, 675 m, 625 s, 597 s cm^{-1}. MS: *m*/*z* (%) = 726 (10) $[^{144}Nd(L^1)_3]^+$, 622 (5) $[^{144}Nd(L^1)_2C_6H_4N]^+$, 532 (30) $[^{144}Nd(L^1)_2]^+$, 305 (5) $[^{142}Nd(L^1) - OMe]^+$, 195 (40) $[(L^1H)]^+$, 180 (15) $[(L^1H) - Me]^+$, 165 (70) $[(L^1H) - 2Me]^+$, 150 (30) $[(L^1H) - 3Me]$, 135 (25) $[C_6H_5ONSi]^+$, 73 (100) $[SiMe_3]^+$, 58 (35) $[SiMe_2]^+$. ^{1}H NMR (300 MHz, C_6D_6, 298 K): δ = −16.98 (br. s, 9 H, OMe), −4.20 (br. s, 27 H, $SiMe_3$), 1.14 (s, 3 H, H-4 or H-5), 7.88 (s, 3 H, H-4 or H-5), 14.18 (s, 3 H, H-3 or H-6), 23.60 (s, 3 H, H-3 or H-6). $C_{30}H_{48}N_3NdO_3Si_3$ (724.21): calcd. C 49.55, H 6.65, N 5.78; found C 49.85, H 6.81, N 5.73.

Method 2 [using 1:2 Ln to L^1 mol ratio (in situ)]: *n*BuLi (2.31 mL, 3.70 mmol) was slowly added to a stirred solution of compound L^1H (0.71 g, 3.60 mmol) in THF (40 mL) at 0 °C and the resulting solution was warmed to room temperature over ca. 1 h. $[NdCl_3(THF)_2]$ (0.71 g, 1.80 mmol) was added to the resulting solution, and the reaction mixture was stirred rapidly for 12 h. The solvent was removed in vacuo, and hexane (30 mL) was added affording a white precipitate. The blue solution was filtered and the filtrate volume was reduced to ca. 2 mL under vacuum. Blue crystals deposited on standing overnight. The infrared spectrum was similar to that of **1e** (**Method 1**). Unit Cell data [$C_{30}H_{48}N_3NdO_3Si_3$, M = 724.2, monoclinic, a = 10.121(1), b = 18.876(1), c = 18.814(1) Å; α = 90°, β = 104.37(1)°, γ = 90°; V = 3500.2 Å^3, $T \approx$ 123 K] were in agreement with those of $[Nd(L^1)_3]$ from **Method 1** (Table 5).

Method 3 [using 1:2 Ln to Li (isolated) ratio)]: $[NdCl_3(THF)_2]$ (0.30 g, 0.75 mmol) and $[Li(L^1)(OEt_2)]_2$ (0.42 g, 0.75 mmol) were stirred together in THF (40 mL). After 12 h, the pale yellow solution was evaporated to dryness under reduced pressure and hexane added. The resulting white solid was filtered and the filtrate evaporated to dryness under vacuum affording a blue crystalline material (0.20 g, 55%). Infrared and ^{1}H NMR spectra were identical to those of **1e** (**Method 1**).

$[Yb(L^2)_3]$·(PhMe) [2a·(PhMe)]: *n*BuLi (1.88 mL, 3.00 mmol) was added to a stirred solution of L^2H (0.77 g, 3.00 mmol) in THF (40 mL) at 0 °C, and the resulting solution was warmed to room temperature over ca. 1 h. $[YbCl_3(THF)_2]$ (0.42 g, 1.0 mmol) was then added and the reaction mixture was stirred for 12 h. The solvent was then removed under vacuum and toluene (30 mL) was added giving a white precipitate. The red solution was filtered at −78 °C and the filtrate volume reduced to 25 mL under vacuum. Red crystals of good X-ray quality were deposited on standing overnight (0.70 g, 68%). IR (Nujol): $\tilde{\nu}$ = 1593 vs, 1558 m, 1480 s, 1278 vs, 1241 vs, 1186 vs, 1152 vs, 1097 s, 1072 w, 1051 s, 1020 m, 1005 w, 906 s, 858 sh w, 840 s, 824 s, 802 s, 778 m, 728 s, 692 vs, 626 w,

Table 5. Crystallographic and refinement parameters for $[Ln(L)_3]$ complexes

Compound	$[Nd(L^1)_3]$ **1e**	$[Yb(L^2)_3]\cdot(PhMe)$ **2a**·(PhMe)	$[Nd(L^2)_3]$ **2d**	$[La(L^2)_3]$ **2e**
Empirical formula	$C_{30}H_{48}N_3NdO_3Si_3$	$C_{52}H_{62}N_3O_3Si_3Yb$	$C_{45}H_{54}N_3NdO_3Si_3$	$C_{45}H_{54}LaN_3O_3Si_3$
Molecular Weight	727.22	1034.36	913.42	908.09
Crystal system	monoclinic	triclinic	monoclinic	monoclinic
Space Group	$P2_1/c$	$P\bar{1}$	$P2_1/n$	$P2_1/n$
Crystal size [mm]	0.25 × 0.20 × 0.13	0.25 × 0.18 × 0.10	0.35 × 0.28 × 0.27	0.30 × 0.25 × 0.20
a [Å]	10.1207(3)	13.4071(3)	16.1450(2)	16.2330(1)
b [Å]	18.9788(6)	13.4511(3)	15.4738(2)	15.4788(1)
c [Å]	18.8243(2)	14.7899(2)	18.0246(2)	18.0579(2)
α [deg]	90	100.240(1)	90	90
β [deg]	104.376(1)	92.274(1)	103.032(1)	103.313(1)
γ [deg]	90	110.243(1)	90	90
V [Å^3]	3502.5(12)	2447.8(9)	4387.0(15)	4415.4(15)
Z	4	2	4	4
d_{calcd}(g cm^{-3})	1.379	1.403	1.383	1.366
F(000)	1500	1062	1884	1872
μ(Mo-K_α) (mm^{-1})	1.617	2.028	1.307	1.090
$2\vartheta_{max}$(°)	56.6	61.0	56.6	56.6
N, N_o	8539, 5881	13093, 10634	10849, 9244	10885, 8914
Goof	1.033	1.038	1.025	1.021
R, R_w (observed data)	0.0343, 0.0612	0.0394, 0.0744	0.0271, 0.0588	0.0277, 0.0607
R, R_w (all data)	0.0673, 0.0693	0.0601, 0.0838	0.0378, 0.0629	0.0417, 0.0645

591 s, 568 w cm^{-1}. MS: *m/z* (%) = 942 (<1) $[Yb(L^2)_3]^+$, 849 (<1) $[Yb(L^2)_3(C_6H_4NSiMe_3)]^+$, 776 (16) $[Yb(L^2)_2(C_6H_4N)]^+$, 686 (35) $[Yb(L^2)_2]^+$, 671 (15) $[Yb(L^2)_2 - Me]^+$, 609 (18) $[Yb(L^2)(OC_6H_4NSiMe_3)]^+$, 593 (3) $[Yb(L^2)(C_6H_4NSiMe_3)]^+$, 523 (4) $[Yb(L^2)OC_6H_5]^+$, 430 (30) $[Yb(L^2)]^+$, 415 (35) $[Yb(L^2) - Me]^+$, 400 (7) $[Yb(L^2) - 2Me]^+$, 353 (3) $[Yb(OC_6H_4NSiMe_3)]^+$, 337 (5) $[Yb(C_6H_4NSiMe_3)]^+$, 257 (20) $[(L^2H)]^+$, 242 (16) $[(L^2H) - Me]^+$, 226 (10) $[(L^2) - 2Me]^+$, 165 (50) $[OC_6H_4NHSiMe_2]^+$, 150 (15) $[C_6H_4ONHSiMe]^+$, 73 (100) $[SiMe_3]^+$. $C_{52}H_{62}N_3O_3Si_3Yb$ (1034.36): calcd. C 60.38, H 6.04, N 4.06; found C 59.69, H 6.42, N 4.35.

$[Yb(L^2)_3]\cdot(C_5H_9Me)$ [2a·(C_5H_9Me)]. Method 1 (using a 1:2 Ln:Li ratio): THF (40 mL) was added to the solids $[Li(L^2)(DME)]$ (0.53 g, 1.50 mmol) and $[YbCl_3(THF)_2]$ (0.32 g, 0.75 mmol) and the resulting mixture was stirring for 12 h. The solvent was then removed under vacuum and toluene (25 mL) added giving a white precipitate. The red solution was filtered at −78 °C and the filtrate volume reduced to 20 mL under vacuum. Red crystals of $[Yb(L^2)_3]\cdot(C_5H_9Me)$ (suitable for X-ray analysis) deposited on standing overnight (0.15 g, 24% [based on L^2]). IR (Nujol): $\tilde{\nu}$ = 1593 vs, 1560 m, 1480 sh w, 1307 w, 1280 s, 1242 s, 1152 s, 1185 s, 1098 s, 1072 m, 1052 s, 1020 m, 1004 w, 908 s, 858 sh w, 840 s, 824 s, 802 s, 780 m, 726 s, 691 s, 618 s cm^{-1}. MS: *m/z* (%) = 776 (<1) $[Yb(L^2)_2(C_6H_4N)]^+$, 686 (4) $[Yb(L^2)_2]^+$, 507 (4) $[Yb(L^2)(OC_6H_5)]^+$, 430 (10) $[Yb(L^2)]^+$, 415 (10) $[Yb(L^2) - Me]^+$, 353 (10) $[Yb(OC_6H_4NSiMe_3)]^+$, 337 (10) $[Yb(C_6H_4NSiMe_3)]^+$, 257 (45) $[(L^2H)]^+$, 242 (40) $[(L^2) - Me]^+$, 226 (5) $[(L^2) - 2Me]^+$, 165 (100) $[OC_6H_4NSiMe_2]^+$, 150 (35) $[C_6H_4ONSiMe]^+$, 73 (50) $[SiMe_3]^+$. $C_{51}H_{66}N_3O_3Si_3Yb$ (solvate) (1026.37): calcd. C 59.68, H 6.48, N 4.09. $C_{45}H_{54}N_3O_3Si_3Yb$ ($[Yb(L^2)_3]$) (942.27): calcd. C 57.36, H 5.78, N 4.46; found C 57.47, H 6.01, N 4.22.

Method 2 [2:1 Li to Ln mol ratio (in situ)]: *n*BuLi (1.65 mL, 2.60 mmol) was slowly added to a stirred solution of compound L^2H (0.64 g, 2.50 mmol) in THF (40 mL) at 0 °C and the resulting solution was warmed to room temperature over ca. 1 h. $[YbCl_3(THF)_{3.5}]$ (0.66 g, 1.25 mmol) was added to the resulting solution, and the reaction mixture stirred rapidly for 12 h. The solvent was removed in vacuo, and toluene (20 mL) added affording a white precipitate. The red solution was filtered and the filtrate volume reduced to ca. 2 mL under vacuum. Hexane (15 mL) was added to the oily residue resulting in an immediate precipitation of LiCl and a red solution. Red crystals deposited on standing and were dried at room temperature under vacuum. The infrared spectrum was similar to that of **2a**·(C_5H_9Me) above.

$[Y(L^2)_3]\cdot(C_5H_9Me)$ [2b·(C_5H_9Me)]: A similar procedure to that used for compound **2a**·(PhMe) gave colourless crystals of the title complex (0.61 g, 71%). IR (Nujol): $\tilde{\nu}$ = 1592 vs, 1582 s, 1557 m, 1489 s, 1278 vs, 1239 vs, 1210 s, 1170 s, 1152 vs, 1099 vs, 1071 m, 1049 s, 1020 m, 1004 w, 911 br. s, 860 w, 824 s, 776 s, 735 vs, 692 vs, 675 w, 625 w, 592 s, 560 w cm^{-1}. MS: *m/z* (%) =857 (<1) $[Y(L^2)_3]^+$, 601 (20) $[Y(L^2)_2]^+$, 524 (5) $[Y(L^2)(OC_6H_4NSiMe_3)]^+$, 438 (5) $[Y(L^2)(OC_6H_5)]^+$, 330 (5) $[Y(L^2) - Me]^+$, 257 (40) $[(L^2H)]^+$, 242 (20) $[(L^2H) - Me]^+$, 164 (60) $[OC_6H_4NSiMe_2]^+$, 149 (25) $[C_6H_4ONSiMe]^+$, 73 (100) $[SiMe_3]^+$. ^{1}H NMR (300 MHz, C_6D_6, 298 K): δ = 0.43 (s, 27 H, $SiMe_3$), 0.89−1.45 (complex m, 6 H, C_5H_9Me), 5.97−6.15 (dd, ^3J = 7.1, ^4J = 1.2 Hz, 3 H, H-6), 6.20−6.30 (bd, ^3J = 6.9, ^4J = 1.5 Hz, 3 H, H-5), 6.40−6.97 (br. m, 21 H, H-3,H-4,H-2′-6′). $C_{51}H_{66}N_3O_3Si_3Y$ (solvate) (941.35): calcd. C 65.01, H 7.06, N 4.46. $C_{45}H_{54}N_3O_3Si_3Y$ ($[Y(L^2)_3]$) (857.25): calcd. C 62.99, H 6.34, N 4.90; found C 65.70, H 7.49, N 4.46.

$[Sm(L^2)_3]\cdot(PhMe)$ (2c): A similar preparation method to that used for compound **2a**·(PhMe) (**Method 1**) gave yellow crystals of the title complex (0.56 g, 56%). IR (Nujol): $\tilde{\nu}$ = 1591 vs, 1557 w, 1480 s, 1283 vs, 1248 vs, 1186 vs, 1155 vs, 1102 vs, 1071 w, 1053 s, 1021 w, 1005 w, 915 s, 826 s, 802 vs, 774 s, 727 vs, 694 vs, 676 w, 622 s, 593 s cm^{-1}. MS: *m/z* (%) = 922 (<1%) $[Sm(L^2)_3]^+$ 827 (<1), $[Sm(L^2)_2(C_6H_4NSiMe_3)]^+$, 757 (<1) $[Sm(L^2)_2(OC_6H_5)]^+$, 664 (10) $[Sm(L^2)_2]^+$, 587 (<1) $[Sm(L^2)(OC_6H_4NSiMe_3)]^+$, 408 (3) $[Sm(L^2)]^+$, 392 (3) $[Sm(L^2) - MeH]^+$, 331 (4) $[Sm(OC_6H_4NSiMe_3)]^+$, 315 (5) $[Sm(C_6H_4NSiMe_3)]^+$, 257 (100) $[(L^2H)]^+$, 242 (100) $[(L^2H) - Me]^+$, 226 (20) $[(L^2) - 2Me]^+$, 165 (100) $[OC_6H_4NHSiMe_2]^+$, 150 (40) $[C_6H_4ONHSiMe]^+$, 73 (70) $[SiMe_3]^+$. ^{1}H NMR (300 MHz, C_6D_6, 298 K): δ = −1.63 (s, 27 H,

$SiMe_3$), 2.10 (s, 3 H, Ph*Me*), 4.26 (br. s, 6 H, H-2′,H-6′), 5.31−5.45 (br. s, 6 H, H-3′, H-5′), 5.49−5.60 (br. s, 3 H, H-4′), 6.30−6.50 (d, ^3J = 7.5 Hz, 3 H, H-3 or H-6), 6.90−7.10 (m, 5 H, *Ph*Me), 7.40−7.46 (t, ^3J = 7.5 Hz, 3 H, H-4 or H-5), 8.28−8.31 (t, ^3J = 7.4 Hz, 3 H, H-4 or H-5), 10.67−10.70 (d, ^3J = 8.0 Hz, 3 H, H-3 or H-6). $C_{52}H_{62}N_3O_3Si_3Sm$ (1012.33): calcd. C 61.73, H 6.18, N 4.15; found C 62.83, H 6.74, N 4.22.

[Nd(L^2)$_3$]·(PhMe)$_2$ [2d·(PhMe)$_2$]. Method 1: A similar preparation method to that used for compound **2a**·(PhMe) gave blue crystals of the title complex (0.68 g, 62%). IR (Nujol): $\tilde{\nu}$ = 1591 vs, 1557 w, 1481 s, 1337 vs, 1285 vs, 1249 vs, 1187 vs, 1155 vs, 1103 vs, 1070 w, 1052 s, 1020 w, 1005 w, 916 vs, 826 s, 802 s, 773 s, 728 vs, 694 vs, 676 w cm^{-1}. ^{1}H NMR (300 MHz, C_6D_6, 298 K): δ = −8.05 (br. s, 6 H, H-2′,H-6′), −1.22 (br. s, 27 H, $SiMe_3$), 0.48 (br. s, 6 H, H-3′,H-5′), 0.90 (s, 3 H, H-4 or H-5), 1.20 (br. s, 3 H, H-4′), 2.11 (s, 6 H, Ph*Me*), 6.97−7.14 (m, 13 H, H-4 or H-5 and *Ph*Me), 13.90 (br. s, 3 H, H-3 or H-6), 23.28 (br. s, 3 H, H-3 or H-6). $C_{59}H_{70}N_3NdO_3Si_3$ (1094.38): calcd. C 64.56, H 6.43, N 3.83; found C 64.48, H 6.54, N 4.13. Recrystallisation of [Nd(L^2)$_3$]·(PhMe)$_2$ from hexane afforded crystals of solvent free [Nd(L^2)$_3$] (**2d**) used for X-ray crystallography.

Method 2 [2:1 Li to Ln mol ratio (in situ)]: *n*BuLi (1.65 mL, 2.60 mmol) was slowly added to a stirred solution of compound L^{2}H (0.64 g, 2.50 mmol) in THF (40 mL) at 0 °C and the resulting solution was warmed to room temperature over ca. 1 h. [$NdCl_3(THF)_2$] (0.49 g, 1.25 mmol) was added to the resulting solution, and the reaction mixture was rapidly stirred for 12 h. The solvent was removed in vacuo, and hexane (30 mL) added affording a white precipitate. The blue solution was filtered and the filtrate volume reduced to ca. 15 mL under vacuum. Blue crystals of [Nd(L^2)$_3$] (**2d**) deposited on standing. (Infrared identification) Unit Cell data [$C_{45}H_{54}N_3NdO_3Si_3$, M = 910.3, monoclinic, a = 16.154(1), b = 15.459(1), c = 17.992(1) Å; α = 90°, β = 103.0(1°), γ = 90°; V = 4378.1 Å^3, $T \approx$ 123 K] were in agreement with those obtained for crystals from **Method 1** (Table 5).

[La(L^2)$_3$]·(PhMe) (2e·(PhMe)]. Method 1: A similar preparation method to that used for compound **2a**·(PhMe) gave yellow crystals of the title complex (0.35 g, 35%). IR (Nujol): $\tilde{\nu}$ = 1589 vs, 1557 m, 1480 s, 1287vs, 1249 vs, 1188 vs, 1155 vs, 1103 vs, 1070 w, 1050 s, 1020 m, 1004 w, 919 s, 858 w, 824 m, 803 vs, 770 vs, 694 vs, 675 w, 618 s, 592 s, 562 w cm^{-1}. MS: *m*/*z* (%) = 651 (3) [La(L^2)$_2$]$^+$, 395 (<1) [La(L^2)]$^+$, 257 (70) [(L^{2}H)]$^+$, 242 (65) [(L^{2}H) − Me]$^+$, 226 (15) [(L^2) − 2Me]$^+$, 165 (100) [$OC_6H_4NHSiMe_2$]$^+$, 150 (40) [$C_6H_4ONHSiMe$]$^+$, 135 (30) [C_6H_4OSiNH]$^+$, 73 (50) [$SiMe_3$]$^+$. ^{1}H NMR (300 MHz, C_6D_6, 298 K): δ = 0.36 (s, 27 H, $SiMe_3$), 2.10 (s, 3 H, Ph*Me*), 6.11 (dd, ^3J = 8.1, ^4J = 1.4 Hz, 3 H, H-6), 6.28 (td, ^3J = 7.2, ^4J = 1.3 Hz, 3 H, H-5), 6.74−6.90 (m, 21 H, H-3, H-4, H-2′−6′), 6.97−7.13 (m, 5 H, *Ph*Me). $C_{52}H_{62}LaN_3O_3Si_3$ (999.32): calcd. C 62.44, H 6.25, N 4.20; found C 62.27, H 6.35, N 4.32. **Method 2 [La(L^2)$_3$] (2e) (using a 1:2 Ln to Li ratio):** $LaCl_3$ (0.18 g, 0.75 mmol) and [Li(L^2)(DME)] (0.53 g, 1.50 mmol) were stirred together in THF (40 mL). After 12 h, the pale yellow solution was evaporated to dryness under reduced pressure and toluene was added. The resulting white solid was filtered, the filtrate was evaporated to dryness and Et_2O was added (20 mL). The solution was concentrated to ca. 10 mL and on standing for two days colourless crystals of **2e** (suitable for an X-ray crystallographic study) were deposited (0.35 g, 77%). IR (Nujol): $\tilde{\nu}$ = 1590 vs, 1557 m, 1480 s, 1444 s, 1288 vs, 1251 vs, 1189 vs, 1155 vs, 1102 vs, 1072 w, 1052 s, 1020 m, 1004 w, 964 w, 917 s, 858 w, 826 m, 801 s, 771 s, 735 s, 722 s, 695 s, 674 w, 632 w, 622 s, 594 s, 559 w cm^{-1}. ^{1}H NMR (300 MHz, C_6D_6, 298 K): δ = 0.35 (s, 27 H, $SiMe_3$), 6.10 (dd, ^3J = 7.6, ^4J = 1.2 Hz, 3 H, H-6), 6.26 (td, ^3J = 7.5, ^4J = 1.6 Hz, 3 H, H-5), 6.72−6.90 (m, 21 H, H-3,H-4, H-2′-6′).

Method 3 [2:1 Li to Ln ratio (in situ)]: *n*BuLi (1.65 mL, 2.60 mmol) was slowly added to a stirred solution of compound L^{3}H (0.64 g, 2.50 mmol) in THF (40 mL) at 0 °C and the resulting solution was warmed to room temperature over ca. 1 h. [$LaCl_3(THF)_2$] (0.49 g, 1.25 mmol) was added to the resulting solution, and the reaction mixture stirred rapidly for 12 h. The solvent was removed in vacuo, and hexane (30 mL) added affording a white precipitate. The pale yellow solution was filtered and the filtrate volume reduced to ca. 15 mL under vacuum. Light yellow crystals were deposited on standing. The infrared spectrum was identical with that of [La(L^2)$_3$] [**2e** (**Method 2**)].

[Yb(en′)$_2$(μ-Cl)]$_2$ (3a): *n*BuLi (3.75 mL, 6.00 mmol) was slowly added to a stirred solution of en′H (0.88 g, 1.00 mL, 5.50 mmol) in THF (50 mL) at 0 °C and the resulting solution was warmed to room temperature over ca. 1 h. [$YbCl_3(THF)_3$] (1.36 g, 2.75 mmol) was added to this solution, and the reaction mixture was rapidly stirred for 12 h. The solvent was removed in vacuo, and hexane added affording a white precipitate. The orange solution was filtered and the filtrate volume reduced to ca. 2 mL under vacuum. Orange crystals deposited on standing overnight (0.79 g, 55%). IR (Nujol): $\tilde{\nu}$ = 1401 w, 1351 m, 1270 w, 1258 m, 1238 m, 1176 w, 1160 w, 1105 m, 1091 m, 1078 m, 1031 w, 1010 s, 952 s, 925 s, 858 s, 832 m, 778 w, 740 m, 679 w, 665 w cm^{-1}. MS: *m*/*z* (%) = 736 (<1) [M(dimer) − (2 L)]$^+$, 701 (<1) [$Yb_2(L)_2Cl]^+$, 527 (2) [$Yb(L)_2Cl]^+$, 333 (50) [Yb(L)]$^+$, 73 (45) [$SiMe_3]^+$, 58 (100) [$SiMe_2]^+$. $C_{28}H_{76}Cl_2N_8Si_4Yb_2$ (1054.32): calcd. C 31.90, H 7.27, N 10.66, Yb 32.83; found C 31.35, H 7.28, N 9.60, Yb 33.18.

[Er(en′)$_2$(μ-Cl)]$_2$ (3b): A similar preparation method to that used for compound **3a** gave pink crystals of **3b** (0.76 g, 53%). IR in satisfactory agreement with that reported for an analytically pure sample.[27] MS: *m*/*z* (%) = 883 (<1) [M(dimer) − (L)]$^+$, 724 (1) [M(dimer) − (2 L)]$^+$, 521 (1) [$Er(L)_2Cl]^+$, 325 (25) [Er(L)]$^+$, 73 (35) [$SiMe_3]^+$, 58 (100) [$SiMe_2]^+$.

[Sm(en′)$_2$(μ-Cl)]$_2$ (3c): A similar procedure to that used for compound **3a** gave yellow crystals of **3c** (0.58 g, 42%). IR (Nujol): $\tilde{\nu}$ = 1401 w, 1349 m, 1310 w, 1258 m, 1246 s, 1195 w, 1169 w, 1156 sh w, 1103m, 1087 m, 1079 m, 1035 w, 1020 s, 953 m, 924 s, 859 s, 828 br. s, 779 sh m, 735 m, 676 w, 662 m, 619 w, 554 w cm^{-1}. MS: *m*/*z* (%) = 689 (<1) [M(dimer) − (2 L)]$^+$, 507 (1) [$Sm(L)_2Cl]^+$, 348 (20) [Sm(L)Cl]$^+$, 311 (15) [Sm(L)]$^+$, 281 (25) [Sm(L) − 2Me]$^+$, 73 (50) [$SiMe_3]^+$, 58 (100) [$SiMe_2]^+$.

[Nd(en′)$_2$(μ-Cl)]$_2$ (3d): A similar procedure to that used for compound **3a** gave blue crystals of **3d** (0.70 g, 51%). IR (Nujol): $\tilde{\nu}$ = 1348 m, 1259 m, 1246 s, 1168 w, 1104 m, 1079 m, 1154 m, 1036 w, 1020 s, 952 w, 938 s, 924 s, 851 s, 827 br. s, 780 sh m, 734 m, 676 w, 662 m, 554 w cm^{-1}. MS: *m*/*z* (%) = 835 (<1) [{^{144}Nd(L)$_2$(μ-Cl)}$_2$ − (L)]$^+$, 676 (<1) [{^{144}Nd(L$_2$(μ-Cl)}$_2$ − (2 L)]$^+$, 482 (1) [$^{144}Nd_2(L)Cl]^+$, 338 (50) [^{144}Nd(L)Cl]$^+$, 73 (45) [$SiMe_3]^+$, 58 (100) [$SiMe_2]^+$. $C_{28}H_{76}Cl_2N_8Nd_2Si_4$ (990.28): calcd. Nd 28.94; found Nd 29.15.

[La(en′)$_2$(μ-Cl)]$_2$ (3e): A similar preparation to that for compound **3a** gave colourless crystals of **3e** (0.63 g, 46%). IR (Nujol): $\tilde{\nu}$ = 1439 w, 1348 w, 1314 w, 1239 br. s, 1160 s, 1121 s, 1092 s, 1077 w, 1037 w, 1021 w, 998 m, 962 m, 923 m, 848 s, 830 br. s, 748 w, 725 m, 694 m, 664 w, 541 w cm^{-1}. MS: *m*/*z* (%) = 825 (5) [M(dimer) − (L)]$^+$, 457 (30) [$La(L)_2]^+$, 333 (80) [La(L)Cl]$^+$, 73 (20) [$SiMe_3]^+$, 58 (100) [$SiMe_2]^+$. $C_{28}H_{76}Cl_2La_2N_8Si_4$ (984.28): calcd. La 28.17; found La 28.02.

[Yb(L^1)$_2$(μ-Cl)]$_2$ (4a): [Li(L^1)(OEt$_2$)]$_2$ (0.76 g, 1.37 mmol) was added to a stirred suspension of [YbCl$_3$(THF)$_3$] (0.68 g, 1.37 mmol) in THF (40 mL). The solution was stirred for 15 h, the solvent was removed under vacuum and hexane (30 mL) was added. After heating the stirred solution for 2 h, the warm mixture was filtered and on cooling to room temperature the filtrate afforded red crystals (suitable for X-ray analysis) of the title complex (0.51 g, 63%). IR (Nujol): $\tilde{\nu}$ = 1594 s, 1563 w, 1318 w, 1290 s, 1277 s, 1242 vs, 1210 m, 1158 s, 1117 vs, 1051 m, 1002 s, 917 s, 844 vs, 826 s, 792 w, 768 m, 730 vs, 679 m, 627 w, 597 w cm^{-1}. Vis/near IR (DME): λ_{max} (ε) = 457 (156), 935 (4), 982 (18), 985 (17) nm (dm^3 mol^{-1}). $C_{40}H_{64}Cl_2N_4O_4Si_4Yb_2$ (1194.30): calcd. C 40.23, H 5.40, N 4.69; found C 39.15, H 5.57, N 4.72.

[Er(L^1)$_2$(μ-Cl)]$_2$ (4b): Addition of [Li(L^1)(OEt$_2$)]$_2$ (0.55 g, 1.00 mmol) to a suspension of [ErCl$_3$(THF)$_2$] (0.42 g, 1.00 mmol) in THF (40 mL) resulted in precipitation of a white solid and formation of a pink solution. The solvent was removed under vacuum and hexane added (30 mL). The mixture was then warmed and filtered. The filtrate was concentrated to ca. 25 mL affording X-ray quality pink crystals of **4b** (0.36 g, 61%). IR (Nujol): $\tilde{\nu}$ = 1593 s, 1563 w, 1318 w, 1291 s, 1277 m, 1242 s, 1210 w, 1158 s, 1116 vs, 1051 m, 1001 s, 916 vs, 843 vs, 822 s, 788 m, 768 m, 729 vs, 679 m, 626 s, 597 s cm^{-1}. $C_{40}H_{64}Cl_2Er_2N_4O_4Si_4$ (1182.73): calcd. C 40.62, H 5.45, N 4.74; found C 39.79, H 5.54, N 4.96.

[Tb(L^1)$_2$(μ-Cl)]$_2$ (4c): A similar preparation method to that used for compound **4a** gave large pale yellow crystals of **4c** (0.40 g, 68%). IR (Nujol): $\tilde{\nu}$ = 1593 s, 1563 w, 1504 s, 1320 w, 1293 s, 1265 s, 1240 s, 1210 w, 1158 s, 1115 vs, 1051 m, 1001 s, 914 vs, 842 vs, 826 sh w, 783 m, 766 m, 727 vs, 669 m, 625 s, 596 s cm^{-1}. $C_{40}H_{64}Cl_2N_4O_4Si_4Tb_2$ (1166.06): calcd. C 41.20, H 5.53, N 4.80; found C 41.42, H 5.39, N 4.76.

[Nd(L^2)$_2$(μ-Cl)]$_2$·(PhMe)$_2$ [5a·(PhMe)$_2$]: [Li(L^2)(DME)] (0.72 g, 2.00 mmol) was added to a stirred solution of [NdCl$_3$(THF)$_2$] (0.40 g, 1.00 mmol) in THF (40 mL). The resulting blue solution was evaporated to dryness and toluene was added (30 mL). The reaction mixture was filtered and the filtrate volume was reduced under vacuum (ca.15 mL). Upon standing overnight single blue crystals suitable for X-ray crystallography formed (0.35 g, 72%). IR (Nujol): $\tilde{\nu}$ = 1585 s 1294 s, 1266 m, 1243 s, 1185 s, 1160 s, 1100 s, 1074 w, 1036 m, 1022 w, 936 vs, 859 m, 828 br. s, 774 m, 746 s, 727 s, 690 s, 679 w, 623 w cm^{-1}. Vis/near IR (DME): λ_{max} (ε) = 527 (55), 586 (75), 755 (25), 811 (28), 885 (22) nm (dm^3 mol^{-1}). ^{1}H NMR (300 MHz, C_6D_6, 298 K): δ = −8.73 (br. s, 8 H, H-2′,H-6′), −5.04 (br. s, 36 H, SiMe$_3$), 0.08 (s, 8 H, H-3′,H-5′), 1.18 (s, 4 H, H-4′), 1.49 (br. s, 8 H, H-4, H-5), 2.10 (s, 6 H, Ph*Me*), 7.02−7.20 (m, 10 H, *Ph*Me), 15.4 (br. s, 4 H, H-3 or H-6), 30.95 (br. s, 4 H, H-3 or H-6). $C_{74}H_{88}Cl_2N_4Nd_2O_4Si_4$ (1569.22): calcd. C 54.64, H 5.65, N 3.57; found C 54.47, H 5.53, N 3.63.

[Li(L^1)(OEt$_2$)]$_2$: *n*BuLi (32 mL, 0.05 mol) was added dropwise to a stirred solution of L^{1}H (0.05 mol, 10 g) in Et$_2$O (80 mL) at 0 °C, and the resulting solution was warmed to room temperature over ca. 1 h. The resulting white precipitate was cooled to −78 °C, washed with hexane (40 mL) and dried under vacuum (11.9 g, 86%). A small amount of [Li(L^1)(OEt$_2$)]$_2$ was redissolved in Et$_2$O whereupon light-sensitive colourless crystals of good X-ray quality formed. IR (Nujol): $\tilde{\nu}$ = 1585vs, 1558s, 1280s, 1239s, 1212s, 1171s, 1117vs, 1052s, 1029vs, 934s, 840s, 821s, 734vs, 660s, 594s cm^{-1}. MS: *m*/*z* (%) = 201 (100) [LiL^1]$^+$, 195 (25) [L^{1}H]$^+$, 165 (60) [L^{1}H − 2Me]$^+$, 150 (25) [L^{1}H − 3Me]$^+$, 135 (20) [C$_6$H$_5$ONSi]$^+$, 73 (40) [SiMe$_3$]$^+$, 58 (20) [SiMe$_2$]$^+$. ^{1}H NMR (300 MHz, C_7D_8, 298 K): δ = 0.11 (s, 18 H, SiMe$_3$), 1.04 [t, ^3J = 7.0 Hz, 12 H, Me (OEt$_2$)], 3.26 [q, ^3J = 7.0 Hz, 8 H, CH$_2$ (OEt$_2$)], 3.35 (s, 6 H, OMe), 6.50−6.57 (dd, ^3J = 7.2, ^4J = 1.6 Hz, 2 H, H-6), 6.62−6.68 (td, ^3J = 7.0, ^4J = 1.5 Hz, 2 H, H-5), 6.85−6.95 (td, ^3J = 7.0, ^4J = 1.6 Hz, 2 H, H-4), 6.96−7.04 (dd, ^3J = 7.2, ^4J = 1.7 Hz, 2 H, H-3). ^{7}Li NMR (155.51 MHz, C_7D_8, 298 K): δ = 1.85. $C_{28}H_{52}Li_2N_2O_4Si_2$ (550.79) (solvate): calcd. C 61.06, H 9.52, N 5.09. $C_{10}H_{16}LiNOSi$ (201.27) (LiL^2): calcd. C 59.68, H 8.01, N 6.96; found C 58.92, 59.08, H 8.84, 8.67, N 5.82, 6.01.

Structure Determinations: Data for the crystallographic structure determinations of compounds **1e**, **2a**·(PhMe), **2d** and **2e** are given in Table 5 while similar data for **4a**−**4c**, **5a**·(PhMe)$_2$ and [Li(L^1)-

Table 6. Crystallographic and refinement parameters for [Ln(L)$_2$(μ-Cl)]$_2$ and [Li(L^1)(OEt$_2$)]$_2$ complexes

Compound	[Yb(L^1)$_2$(μ-Cl)]$_2$ **4a**	[Er(L^1)$_2$(μ-Cl)]$_2$ **4b**	[Tb(L^1)$_2$(μ-Cl)]$_2$ **4c**	[Nd(L^2)$_2$(μ-Cl)]$_2$·(PhMe)$_2$ **5a**·(PhMe)$_2$	[Li(L^1)(OEt$_2$)]$_2$
Empirical formula	$C_{40}H_{64}Cl_2N_4O_4Si_4Yb_2$	$C_{40}H_{64}Er_2Cl_2N_4O_4Si_4$	$C_{40}H_{64}Cl_2N_4O_4Si_4Tb_2$	$C_{74}H_{88}Cl_2N_4Nd_2O_4Si_4$	$C_{28}H_{52}Li_2N_2O_4Si_2$
Molecular Weight	1194.3	1182.73	1166.06	1569.22	550.78
Crystal system	monoclinic	monoclinic	monoclinic	triclinic	triclinic
Space Group	$P2_1/n$	$P2_1/n$	$P2_1/n$	$P\bar{1}$	$P\bar{1}$
Crystal size [mm]	0.15 × 0.15 × 0.10	0.23 × 0.23 × 0.18	0.25 × 0.18 × 0.13	0.25 × 0.20 × 0.13	0.30 × 0.13 × 0.13
a [Å]	14.6143(3)	14.6389(1)	14.5575(1)	10.1897(1)	9.9320(5)
b [Å]	18.0518(4)	18.1148(1)	18.2621(2)	13.3375(2)	10.0400(5)
c [Å]	19.0058(5)	19.0169(2)	19.0461(2)	15.5566(2)	10.4465(4)
α [deg]	90	90	90	74.48(3)	117.651(3)
β [deg]	92.327(1)	92.875(1)	92.653(1)	77.36(3)	94.472(3)
γ [deg]	90	90	90	67.38(3)	111.482(2)
V [Å^3]	5009.9(17)	5036.6(17)	5058.0(18)	1848.0(6)	818.9(3)
Z	4	4	4	1	1
d_{calcd}(g cm^{-3})	1.583	1.560	1.531	1.410	1.117
F(000)	2376	2360	2336	802	300
μ(Mo-K_α) (mm^{-1})	3.953	3.550	3.013	1.575	0.140
$2\theta_{max}$(°)	56.6	56.6	56.6	56.6	56.5
N, N_o	12341, 6357	12025, 8910	12457, 9175	8040, 7457	3887, 2831
Goof	1.033	1.025	1.039	1.049	1.047
R, R_w (observed data)	0.0686, 0.1023	0.0308, 0.0667	0.0369, 0.0728	0.0250, 0.0552	0.0589, 0.1394
R, R_w (all data)	0.1795, 0.1272	0.0545, 0.0734	0.0639, 0.0803	0.0292, 0.0567	0.0912, 0.1541

$(OEt_2)]_2$ are listed in Table 6. Data for **2a**·(C_5H_9Me) and **2b**·(C_5H_9Me) are provided in CCDC-174206/174207. Crystals were mounted in an inert atmosphere under viscous oil onto a glass fibre. Low-temperature (≈123 K) data were collected on an Enraf−Nonius CCD area-detector diffractometer (Mo-K_α radiation, λ 0.7107_3 Å, frames comprised 1.0° increments in φ and ω yielding a sphere of data) with proprietary software (Nonius B.V., 1998). Each data set was merged (R_{int} as quoted) to N unique reflections; the structures were solved by conventional methods and refined with anisotropic thermal parameter forms for the non-hydrogen atoms by full-matrix least-squares on all F^2 data using SHELX 97 software package.[58] Hydrogen atoms were included in their calculated positions and allowed to ride on the parent carbon atom with isotropic thermal parameters. For **2a**·(C_5H_9Me) and **2b**·(C_5H_9Me), the lattice solvent was also modelled as PhMe, disordered PhMe, or THF, and in each case the refinement was unstable by contrast with C_5H_9Me, the presence of which was also indicated by the NMR spectrum of **2b**. CCDC-174197 to CCDC-174207 contain the supplementary crystallographic data for this paper. These data can be obtained free of charge at www.ccdc.cam.ac.uk/conts/retrieving.html [or from the Cambridge Crystallographic Data Centre, 12, Union Road, Cambridge CB2 1EZ, UK; Fax: (internat.) +44-1223/336-033; E-mail: deposit@ccdc.cam.ac.uk].

Acknowledgments

We gratefully acknowledge support of this work from the Australian Research Council and Australian Postgraduate and Monash Postgraduate Publication Awards to N. M. S.

[1] G. B. Deacon, C. M. Forsyth, N. M. Scott, B. W. Skelton, A. H. White, *Aust. J. Chem.* **2001**, *7*, 439−446.
[2] S. Gambarotta, J. Jubb, J. Song, D. Richeson, *Zirconium and Hafnium Complexes in Oxidation State +4, Chap. 11*, in *Comprehensive Organometallic Chemistry II* (Eds.: E. W. Abel, F. G. A. Stone, G. Wilkinson), Pergamon, Oxford, U. K., **1995**, *4*.
[3] A. N. Guram, R. F. Jordan, *Cationic Organozirconium and Organohafnium Complexes, Chap. 12*, in *Comprehensive Organometallic Chemistry II* (Eds.: E. W. Abel, F. G. A. Stone, G. Wilkinson), Pergamon, Oxford, U. K., **1995**, *4*.
[4] H. Schumann, J.-A. Meese-Markscheffel, L. Esser, *Chem. Rev.* **1995**, *95*, 865−986.
[5] F. T. Edelmann, *Scandium, Yttrium, Lanthanides and Actinides*, Chap. 2 in *Comprehensive Organometallic Chemistry II* (Eds.: E. W. Abel, F. G. A. Stone, G. Wilkinson), Pergamon, Oxford, U. K., **1995**, *4*, 11.
[6] M. N. Bochkarev, L. N. Zakharov, G. S. Kalinina, *Organoderivatives of Rare Earth Elements*, Kluwer Academic Publishers, Dordrecht/Boston/London, **1995**.
[7] R. Anwander, *Top. Organomet. Chem.* **1999**, *2*, 1−61.
[8] A. Togni, L. M. Venanzi, *Angew. Chem. Int. Ed. Engl.* **1994**, *33*, 497−526.
[9] R. Kempe, *Angew. Chem. Int. Ed.* **2000**, *39*, 468−493.
[10] F. T. Edelmann, *Coord. Chem. Rev.* **1995**, *137*, 403−481.
[11] W. J. Evans, M. A. Ansari, J. W. Ziller, S. I. Khan, *Inorg. Chem.* **1996**, *35*, 5435−5444.
[12] L. G. Hubert-Pfalzgraf, *Coord. Chem. Rev.* **1998**, *178−180*, 967−997.
[13] R. C. Mehrotra, A. Singh, U. M. Tripathi, *Chem. Rev.* **1991**, *91*, 1287−1303.
[14] D. C. Bradley, R. C. Mehrotra, I. P. Rothwell, A. Singh, *Alkoxo and Aryloxo Derivatives of Metals*, Academic Press, London, **2001**.
[15] D. C. Bradley, M. B. Hursthouse, H. C. Aspinall, K. D. Sales, N. P. C. Walker, B. Hussain, *J. Chem. Soc., Dalton Trans.* **1989**, 623−626.
[16] D. C. Bradley, M. B. Hursthouse, H. C. Aspinall, K. D. Sales, N. P. C. Walker, *J. Chem. Soc., Chem. Commun.* **1985**, 1585−1586.
[17] M. Karl, G. Seybert, W. Massa, S. Agarwal, A. Greiner, K. Dehnicke, *Z. Anorg. Allg. Chem.* **1999**, *625*, 1405−1407.
[18] J. Collin, N. Giuseppone, N. Jaber, A. Domingos, L. Maria, I. Santos, *J. Organomet. Chem.* **2001**, *628*, 271−274.
[19] F. T. Edelmann, *J. Alloys and Compounds* **1994**, *207/208*, 182−188.
[20] J. A. R. Schmidt, J. Arnold, *Chem. Commun.* **1999**, 2149−2150.
[21] R. Duchateau, C. T. van Wee, J. H. Teuben, *Organometallics* **1996**, *15*, 2291−2302.
[22] P. W. Roesky, *Chem. Ber./Recueil* **1997**, *130*, 859−862.
[23] P. W. Roesky, M. R. Bürgstein, *Inorg. Chem.* **1999**, *38*, 5629−5632.
[24] H. Görls, B. Neumüller, A. Scholz, J. Scholz, *Angew. Chem.* **1995**, *107*, 732−735; *Angew. Chem. Int. Ed. Engl.* **1995**, *34*, 673−676.
[25] R. Duchateau, T. Tumstra, E. A. C. Brussee, A. Meetsma, P. T. van Duijnen, J. H. Teuben, *Organometallics* **1997**, *16*, 3511−3522.
[26] R. Anwander, *Top. Curr. Chem.* **1996**, *179*, 33−112.
[27] G. B. Deacon, C. M. Forsyth, P. C. Junk, B. W. Skelton, A. H. White, *J. Chem. Soc., Dalton Trans.* **1998**, 1381−1387.
[28] G. B. Deacon, C. M. Forsyth, N. M. Scott, *Eur. J. Inorg. Chem.* **2000**, 2501−2506.
[29] G. B. Deacon, C. M. Forsyth, N. M. Scott, *J. Chem. Soc., Dalton Trans.* **2001**, 2494−2501.
[30] C. J. Pouchert, J. R. Campbell, *Aldrich Library of NMR Spectra*, Aldrich Chemical Company, Milwaukee, Wisconsin, **1974**, *1*, 32C.
[31] W. T. Carnall, *The Absorption and Fluorescence Spectra of Rare Earth Ions in Solution, in Handbook on the Physics and Chemistry of Rare Earths*, North-Holland, Amsterdam, **1979**, *3*, 171.
[32] M. Johnson, J. C. Taylor, G. W. Cox, *J. Appl. Crystallogr.* **1980**, *13*, 188−189.
[33] R. D. Shannon, *Acta Crystallogr., Sect. A* **1976**, *32*, 751−767.
[34] G. B. Deacon, P. I. MacKinnon, T. W. Hambley, J. C. Taylor, *J. Organomet. Chem.* **1983**, *259*, 91−97.
[35] G. B. Deacon, T. Feng, P. C. Junk, B. W. Skelton, A. N. Sobolev, A. H. White, *Aust. J. Chem.* **1998**, *51*, 75−89.
[36] A. Recknagel, A. Steiner, S. Brooker, D. Stalke, F. T. Edelmann, *J. Organomet. Chem.* **1991**, *415*, 315−326.
[37] R. A. Andersen, D. H. Templeton, A. Zalkin, *Inorg. Chem.* **1978**, *17*, 2317−2319.
[38] P. G. Eller, D. C. Bradley, M. B. Hursthouse, D. W. Meek, *Coord. Chem. Rev.* **1977**, *24*, 1−95.
[39] H. Schumann, J. Winterfeld, E. C. E. Rosenthal, H. Hemling, L. Esser, *Z. Anorg. Allg. Chem.* **1995**, *621*, 122−130.
[40] R. K. Minhas, Y. Ma, J.-I. Song, S. Gambarotta, *Inorg. Chem.* **1996**, *35*, 1866−1873.
[41] M. Wedler, F. Knösel, U. Pieper, S. Dietmar, F. T. Edelmann, H.-D. Amberger, *Chem. Ber.* **1992**, *125*, 2171−2181.
[42] A. Recknagel, F. Knösel, H. Gornitzka, M. Noltemeyer, F. T. Edelmann, U. Behrens, *J. Organomet. Chem.* **1991**, *417*, 363−375.
[43] S. Arndt, P. Voth, T. P. Spaniol, J. Okuda, *Organometallics* **2000**, *19*, 4690−4700.
[44] H. Lueken, J. Schmitz, W. Lamberts, P. Hannibal, K. Handrick, *Inorg. Chim. Acta* **1989**, *156*, 119−124.
[45] H. Schumann, M. R. Keitsch, J. Demtschuk, G. A. Molander, *J. Organomet. Chem.* **1999**, *582*, 70−82.
[46] W. J. Evans, D. K. Drummond, J. Grate, H. Zhang, J. L. Atwood, *J. Am. Chem. Soc.* **1987**, *109*, 3928−3936.
[47] G. B. Deacon, T. Feng, S. Nickel, B. W. Skelton, A. H. White, *J. Chem. Soc., Chem. Commun.* **1993**, 1328−1329.
[48] B. Cetinkaya, P. B. Hitchcock, M. F. Lappert, M. C. Misra, A. J. Thorne, *J. Chem. Soc., Chem. Commun.* **1984**, 148−149.

[49] M. F. Lappert, M. J. Slade, A. Singh, J. L. Atwood, R. D. Rogers, R. Shakir, *J. Am. Chem. Soc.* **1983**, *105*, 302−304.
[50] J. R. van den Hende, P. B. Hitchcock, S. A. Holmes, M. F. Lappert, S. Tian, *J. Chem. Soc., Dalton Trans.* **1995**, 3933−3939.
[51] J. Marcalo, A. P. De Matos, *Polyhedron* **1989**, *8*, 2431−2437.
[52] B. Fan, Q. Shen, Y. Lin, *J. Organomet. Chem.* **1989**, *377*, 51−58.
[53] G. B. Deacon, T. Feng, C. M. Forsyth, A. Gitlits, D. C. R. Hockless, Q. Shen, B. W. Skelton, A. H. White, *J. Chem. Soc., Dalton Trans.* **2000**, 961−966.
[54] L. M. Engelhardt, G. E. Jacobsen, P. C. Junk, C. L. Raston, B. W. Skelton, A. H. White, *J. Chem. Soc., Dalton Trans.* **1988**, 1011−1020.
[55] F. A. Cotton, S. C. Haefner, J. H. Matonic, X. Wang, C. A. Murillo, *Polyhedron* **1997**, *16*, 541−550.
[56] J. L. Atwood, W. E. Hunter, A. L. Wayda, W. J. Evans, *Inorg. Chem.* **1981**, *20*, 4115−4119.
[57] G. Meyer, *Binary Lanthanoid(III) Halides, MX_3 (X = Cl, Br, I)*, in *Syntheses of Lanthanoid and Actinide Compounds* (Eds.: G. Meyer, L. R. Morss), Kluwer, Dordrecht, **1991**.
[58] G. M. Sheldrick, *SHELX97, Program for Crystal Structure Determination*, Universität Göttingen, **1997**.

Received November 16, 2001
[I01461]

Selective Complexation of Uranium(III) over Cerium(III) and Neodymium(III) by 2,2′:6′,2′′-Terpyridine − X-ray Crystallographic Evidence for Uranium-to-Ligand π Back-Bonding

Jean-Claude Berthet,*[a] Christelle Rivière,[a] Yannick Miquel,[a] Martine Nierlich,[a] Charles Madic,[b] and Michel Ephritikhine*[a]

Keywords: Actinides / Uranium / Cerium / Neodymium / Lanthanides / N ligands / Cations

The addition of 2,2′:6′,2′′-terpyridine (terpy) to MI_3 (M = Ce, Nd, U) in anhydrous pyridine led to the quantitative formation of the bis-terpy complexes $[MI_2(terpy)_2]I$ [M = Ce (**1**) and Nd (**2**)] and $[MI_2(terpy)_2L]I$ [M = U and L = pyridine (**3**); M = Ce and L = H_2O (**4**)]. Conductometry measurements indicated that these complexes are 1:1 electrolytes in pyridine solution. ^1H NMR competition experiments showed that the terdentate ligand has a better affinity for U^{III} than for Ce^{III} or Nd^{III}. The X-ray crystal structures of solvates of **1**–**4** have been determined. The average U–N(terpy) bond lengths in **3** are 0.05 Å shorter than the mean Ce–N bond length in **4**; the U–N(central pyridine) distances are shorter than the U–N(distal pyridines) distances in **3**, while the reverse order is found in the early lanthanide compounds. These differences could reflect the presence of a π back-bonding interaction between the uranium atom and the terpy ligand.
(© Wiley-VCH Verlag GmbH, 69451 Weinheim, Germany, 2002)

Introduction

The separation of trivalent actinides (americium and curium) from trivalent lanthanides represents a challenging goal in the management of spent nuclear fuels. Such a separation process would permit the subsequent destruction of the long-lived americium and curium radionuclides by neutron bombardment, leading to their transmutation into short-lived isotopes; this scenario is called the partitioning and transmutation scenario (P & T).[1] Much attention has been paid to ligands that would favour the selective complexation of trivalent actinides (An^{III}) over trivalent lanthanides (Ln^{III}) in liquid/liquid solvent extraction processes. A generally accepted idea is that such a selectivity could be attainable by using soft nitrogen or sulfur ligands, since these would bind preferentially to the 5f ions as they are slightly less hard than the 4f ions.[2] These ligands should preferably be multidentate in order to compete with the water molecules in their coordination to the 4f and 5f ions. In fact, a number of nitrogen aromatic bases have been shown to selectively extract actinides rather than lanthanides from acidic aqueous effluents into an organic phase. In particular, it has been recently found that the terdentate ligand 2,2′:6′,2′′-terpyridine (terpy), in synergistic combination with 2-bromodecanoic acid, gave an Am^{III}/Eu^{III} separation factor $SF_{Am/Eu}$ of 7 at 0.01 M HNO_3, $SF_{Am/Eu}$ being defined as the ratio of the distribution ratios of Am^{III} and Eu^{III} in the organic and aqueous phases.[3] However, no actinide complex with terpy has been isolated and characterized so far, even though this ligand has been widely used in the coordination chemistry of the d transition metals[4] and 4f elements,[5−14] especially for the synthesis of complexes exhibiting unique luminescence and redox properties.

Following our comparative studies on the coordination of aromatic nitrogen bases to Ln^{III} and An^{III} ions, with the aim of investigating the factors that play a determining role in selectivity, the nature of the metal-ligand bond and the respective involvement of 4f and 5f electrons, we have examined the complexation of CeI_3, NdI_3 and UI_3 with terpy in anhydrous pyridine. As in our previous work on the complexation of these metal triiodides with 2,2′-bipyridine (bipy)[15] and 2,6-bis(5,6-dialkyl-1,2,4-triazin-3-yl)pyridines (btp),[16] U^{III} was used as an actinide analogue of the highly radiotoxic Am^{III} and Cm^{III}, and the similarly sized Ce^{III} and Nd^{III} were chosen as representatives of the lanthanides. The low complexing ability of the iodide counterion and the weaker solvation properties of pyridine relative to water are expected to favour the differentiation of the trivalent 4f and 5f ions. Here we report on the synthesis and characterization of the bis-terpy complexes $[MI_2(terpy)_2]I$ [M = Ce (**1**) and Nd (**2**)] and $[MI_2(terpy)_2L]I$ [M = U and L = pyridine (**3**); M = Ce and L = H_2O (**4**)]. The better affinity of the terdentate ligand for U^{III} vs. Ce^{III} and Nd^{III} was meas-

[a] Service de Chimie Moléculaire, DSM, DRECAM, CNRS URA 331, CEA/Saclay,
91191 Gif-sur-Yvette, France
Fax: (internat.) + 33-1/6908-6640
E-mail: ephri@drecam.cea.fr
berthet@drecam.cea.fr
[b] Direction de l'Energie Nucléaire, CEA/Saclay,
91191 Gif-sur-Yvette, France

ured by ^{1}H NMR competition experiments and the distinct coordination of terpy to the 5f ion was revealed by X-ray crystallography with a comparison of the metal-nitrogen bond lengths in solvates of compounds **1**−**4**.

Results and Discussion

Formation of the bis-Terpy Complexes

Addition of two equivalents of terpy to a pyridine solution of $[MI_3(py)_4]$ (M = Ce, Nd, U; py = pyridine) led to the formation of the bis-terpy complex $[MI_3(terpy)_2]$ [M = Ce (**1**) or Nd (**2**)] or $[UI_3(terpy)_2(py)]$ (**3**). After evaporation of the solvent, the compound was washed with tetrahydrofuran and isolated as an orange (Ce), yellow (Nd) or dark red powder (U) in good yield. Complexes **1**−**3** gave satisfactory elemental analyses (C, H, N).

The conductivity of a 10^{-2} M solution of **1** or **3** in anhydrous pyridine at 20 °C has a value of 120 μS cm^{-1} which corresponds to a 1:1 electrolyte. Complexes **1**−**3** are thus totally dissociated in solution into a cation/anion pair of $[MI_2(terpy)_2(py)_x]^+$ and I^-. This dissociation is also observed in the crystal structures (vide infra). It has previously been found that at the same concentration and temperature, the dissociation of $[MI_3(py)_4]$ (M = Ce, U) and $[CeI_3(bipy)_2(py)]$ is equal to 40 and 60%, respectively, corresponding to a conductivity of 45 and 75 μS cm^{-1}, whereas $[UI_3(bipy)_2(py)]$ is almost completely dissociated into $[UI_2(bipy)_2(py)_x]^+$ and I^-.[15]

The ^{1}H NMR spectra of **1**−**3** in [D$_5$]pyridine at 20 °C exhibit a set of resonances corresponding to equivalent and symmetrical terpy ligands, thus indicating that the complexes are fluxional in solution, as usually observed with f elements compounds that undergo facile intramolecular exchange of the ligands. Coalescence of the signals occurs at lower temperature, although the slow-limit spectra could not be obtained.

In order to observe a 1:1 complex as a possible intermediate in the formation of **1**−**3**, a 10^{-2} M solution of $[MI_3(py)_4]$ (M = Ce, Nd, U) in [D$_5$]pyridine was titrated at 20 °C with terpy in the presence of cyclohexane as internal standard. The ^{1}H NMR spectra showed that, whatever the number n of ligand equivalents ($0 \leq n \leq 2$), only the 1:2 complex **1**, **2** or **3** was formed in an immediate and quantitative manner. For $n > 2$, free terpy was observed in solution, with no exchange with coordinated ligands, and no 1:3 complex was detected. In agreement with the ^{1}H NMR titration, the conductivity of the solution at 20 °C was found to grow in a linear fashion, from 45 to 120 μS cm^{-1}, with increasing quantities of terpy ($0 \leq n \leq 2$) and was then constant for $n > 2$. Such a preference for the formation of the 1:2 or 1:3 complexes with respect to the 1:1 complex remains very rare in coordination chemistry; for lanthanides, it has been observed with bipy[15] and terdentate nitrogen ligands.[16,17]

The quantitative formation of **1**−**3** in pyridine contrasts with that of the 1:1 complexes $[LnCl(terpy)(H_2O)_x]Cl_2$ (Ln = Ce − Lu),[5] $[Ln(terpy)(H_2O)_x]Br_3$ (Ln = La, Er, Tm, Yb, Lu),[6] $[Ln(O_2CCCl_3)_3(terpy)(L)]$ (Ln = Yb and L = MeOH; Ln = Lu and L = H_2O),[7] $[Ln(NO_3)_3(terpy)(H_2O)_x]$ (Ln = Nd, Ho, Er, Tm, Yb),[8] $[Er(NO_3)_3(terpy)(EtOH)]$[9] and $[Ln(NO_3)_2(terpy)(H_2O)_x][NO_3]$ (Ln = La, Gd, Tb, Lu)[10] which were synthesized from the corresponding lanthanide salts and one equivalent of terpy in a mixture of water and alcohol or in acetonitrile. Addition of two equivalents of terpy to the halides LnX_3 (X = Cl, Br) in ethanol gave the 1:2 complexes $[LnCl_3(terpy)_2(H_2O)_x]$ in the case of the heavier lanthanides (Eu, Gd, Dy and Er), whereas attempts to prepare the analogues of the early lanthanides Nd and Sm failed.[11] The 1:1.5 complexes $[Ln(NO_3)_2(terpy)_2][Ln(NO_3)_4(terpy)]$ (Ln = La, Nd, Sm, Tb, Dy, Ho) were formed by addition of four equivalents of terpy to a solution of the hydrated lanthanide nitrate in acetonitrile.[8a,10] These results show the difficulty in forming the bis-terpy compounds of the lighter lanthanides by using counterions and/or solvents with strongly coordinating properties. It is only with the weakly coordinating perchlorate anion that the 1:3 species $[Ln(terpy)_3][ClO_4]_3$ (Ln = Ce, Eu, Lu) crystallized from acetonitrile or ethanol solutions.[13] In this context, the formation of the bis-terpy complexes **1**−**3** as the sole products of the reactions of $[MI_3(py)_4]$ (M = Ce, Nd, U) with terpy in anhydrous pyridine is remarkable.

Not surprisingly, terpy was found to have a better affinity for the trivalent f ions than bipy, since under the same conditions it was necessary to add more than 10 (M = Ce, U) or 20 (M = Nd) equivalents of the bidentate ligand to $[MI_3(py)_4]$ to observe the complete formation of the corresponding 1:2 complexes $[MI_3(bipy)_2(py)]$ or $[MI_2(bipy)_2(py)]I$.[15] By considering only the contribution of the chelate effect,[18] the apparent formation constants $\log\beta_2$ of complexes **1**−**3** would range between 3.1 and 3.7. However, terpy is a much weaker complexant than the btp molecules which readily give the 1:3 complexes $[M(btp)_3]I_3$ (M = Ce, U) in a quantitative manner.[16]

Selective Complexation of U^{III} over Ce^{III} or Nd^{III}

The competition reactions of Ce^{III} or Nd^{III} and U^{III} with terpy were monitored by ^{1}H NMR spectroscopy. Addition of two mol equivalents of terpy to one mol equivalent of both $[CeI_3(py)_4]$ and $[UI_3(py)_4]$ in [D$_5$]pyridine led to the formation of complexes **1** and **3** with a U^{III}/Ce^{III} separation factor of 3.0. Similar experiments with $[NdI_3(py)_4]$ gave compounds **2** and **3** with a U^{III}/Nd^{III} separation factor of 2.5 (here, the separation factor is expressed as the ratio of the concentrations of **3** and **1**, or **3** and **2**). These results demonstrate that the terdentate ligand has a much better affinity for the 5f ion than for its 4f analogues. The U^{III}/Ce^{III} separation factor of 3.0 observed with terpy is greater than that of 1.3 determined from competition reactions of $[CeI_3(py)_4]$ and $[UI_3(py)_4]$ with bipy in the molar ratio of 1:1:2.

Previous studies on the MI_3/bipy system revealed that the bidentate ligand bipy has a slightly better affinity for $[CeI_2(py)_x]^+$ than for $[CeI_3(py)_4]$ while it coordinates almost exclusively to the cationic species $[UI_2(py)_x]^+$.[15] It was then

difficult to determine if the weakly selective complexation of U^{III} over Ce^{III} or Nd^{III} in pyridine solution would result from the stronger complexation of the σ-donor ligand bipy to the hard cation $[UI_2(py)_x]^+$ and/or from the π back-donation of the 5f orbitals into the π* orbitals of the aromatic ring. A more clear-cut situation is encountered with terpy in the competition reactions between Ce^{III} or Nd^{III} and U^{III} since all the 1:2 complexes **1**−**3** are totally dissociated in solution. The preferred formation of the U^{III} derivative **3** should be related to a more important covalent contribution to the metal-nitrogen bonding.

Moreover, it is remarkable that even though complexes **1**−**3** have all been prepared and crystallized from pyridine, only the uranium compound **3** retains a solvent molecule in its coordination sphere; this ligand is not labile and could not be eliminated by heating under vacuum. This better affinity of U^{III} vs. Ce^{III} or Nd^{III} for the pyridyl moiety would be an additional indication of the relatively greater softness of the trivalent 5f ion. However, crystallization of the cerium derivative **1** in pyridine in the presence of traces of water gave the addition product $[CeI_2(terpy)_2(H_2O)]I$ (**4**) (vide infra), showing the capacity of the lanthanide ion to coordinate the hard oxygen ligand in preference to the softer aromatic nitrogen base. The synthesis of the uranium compound $[UI_2(terpy)_2(H_2O)]I$ was attempted in order to compare its crystal structure with that of **4**. However, in the presence of traces of water, **3** was oxidized into an U^{IV} oxo complex; this latter will be reported in a forthcoming paper.

The selectivity of terpy for trivalent actinides over trivalent lanthanides, although significant, is much less important than that observed with btp molecules, which is ca. ten times greater.[16,19] The high actinide(III)/lanthanide(III) separation factors obtained with these ligands have been attributed to their weaker basicity and the much softer nature of their nitrogen atoms, which result in the formation of stronger actinide-nitrogen bonds with increased covalent character.

The distinct affinities of bipy, terpy and btp ligands for 5f vs. 4f trivalent ions could also be assessed through the crystal structures of their analogous complexes.

X-ray Crystal Structures of $[MI_2(terpy)_2]I\cdot 2py$ (M = Ce, Nd), $[UI_2(terpy)_2(py)]I\cdot 2py$ and $[CeI_2(terpy)_2(H_2O)]I\cdot 1.5py\cdot 0.5Et_2O$

Pyridine solvates of **1**, **2** and **3** crystallized upon slow diffusion of diethyl ether into pyridine solutions of the complexes; crystallization of **1** from solvents containing traces of water gave yellow crystals of $[CeI_2(terpy)_2(H_2O)]I\cdot 1.5py\cdot 0.5Et_2O$. The crystals are composed of cation/anion pairs and solvent molecules; selected bond lengths and angles for the cations are listed in Table 1.

Compounds **1·2py** and **2·2py** are isostructural; the structure of the cation $[CeI_2(terpy)_2]^+$ is shown in Figure 1. The metal is eight-coordinate in a very distorted square antiprismatic configuration. The two iodide ligands and two distal nitrogen atoms (N_d) of the two terpy ligands [N(3) and N(4)] occupy the opposite corners of the first square base, respectively, whereas the second basis is defined by the two central nitrogen atoms (N_c) [N(2) and N(5)] and the other two distal nitrogen atoms of the terdentate molecule [N(1) and N(6)], which are mutually *trans*. The average Ln−I bond lengths of 3.182(3) Å (Ln = Ce) and 3.153(4) Å (Ln = Nd) are similar to those in $[CeI_3(i\text{PrOH})_3]$ [3.157(1) Å],[20] $[CeI_3(bipy)_2(py)]$ [3.23(3) Å][15] and $[NdI_2(C_5Me_5)(py)_3]$ [3.1603(5) Å].[21] The Ln−N bond lengths are also not exceptional, with mean values of 2.63(2) Å (Ln = Ce) and 2.60(2) Å (Ln = Nd), and are similar to those found in $[LnCl_2(terpy)(H_2O)_5]Cl_2\cdot 3H_2O$ [2.64(2) and

Table 1. Selected bond lengths [Å] and angles [°] for the cations $[MI_2(terpy)_2]^+$ (M = Ce and Nd) and $[MI_2(terpy)_2L]^+$ (M = U and L = py; M = Ce and L = H_2O)

	$[CeI_2(terpy)_2]^+$	$[NdI_2(terpy)_2]^+$	$[CeI_2(terpy)_2(H_2O]^+$	$[UI_2(terpy)_2(py)]^+$
M−I(1)	3.185(1)	3.1560(5)	3.253(1)	3.273(1)
M−I(2)	3.180(1)	3.1502(5)	3.345(1)	3.236(1)
M−N(1)	2.614(3)	2.577(4)	2.686(4)	2.624(9)
M−N(2)	2.641(3)	2.595(4)	2.692(4)	2.618(9)
M−N(3)	2.658(3)	2.626(4)	2.665(4)	2.657(10)
M−N(4)	2.662(3)	2.630(4)	2.652(4)	2.631(10)
M−N(5)	2.636(3)	2.594(4)	2.691(4)	2.602(10)
M−N(6)	2.597(3)	2.570(4)	2.673(4)	2.625(10)
U−N(7)				2.685(12)
Ce−O			2.468(3)	
<M−I>	3.182(3)	3.153(4)	3.30(6)	3.25(2)
<M−N(terpy)>	2.63(2)	2.60(2)	2.68(2)	2.63(2)
I(1)−M−I(2)	119.12(2)	119.07(1)	144.04(2)	147.22(3)
N(1)−M−N(2)	61.4(1)	62.0(1)	61.4(1)	62.1(3)
N(2)−M−N(3)	62.3(1)	63.1(1)	61.1(1)	62.0(3)
N(1)−M−N(3)	122.3(1)	123.7(1)	122.2(1)	124.0(3)
N(4)−M−N(5)	61.9(1)	62.8(1)	61.5(1)	62.4(3)
N(5)−M−N(6)	61.8(1)	62.6(1)	61.8(1)	62.6(3)
N(4)−M−N(6)	121.9(1)	123.6(1)	122.9(1)	125.0(3)
N(2)−M−N(5)	112.4(1)	113.1(1)	112.8(1)	118.7(3)

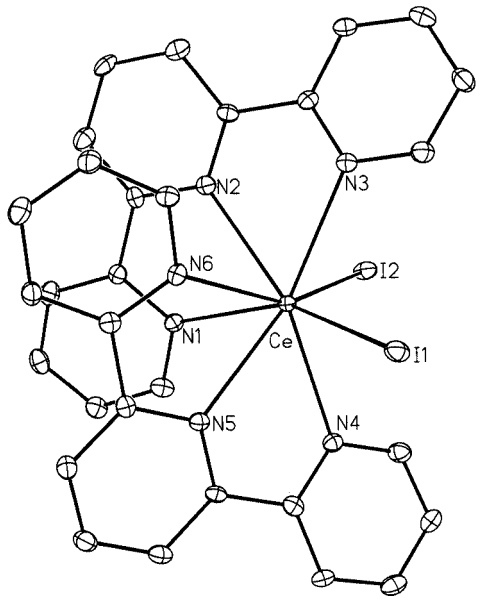

Figure 1. Crystal structure of the cation $[CeI_2(terpy)_2]^+$ in **1·2py** with displacement ellipsoids at the 30% probability level

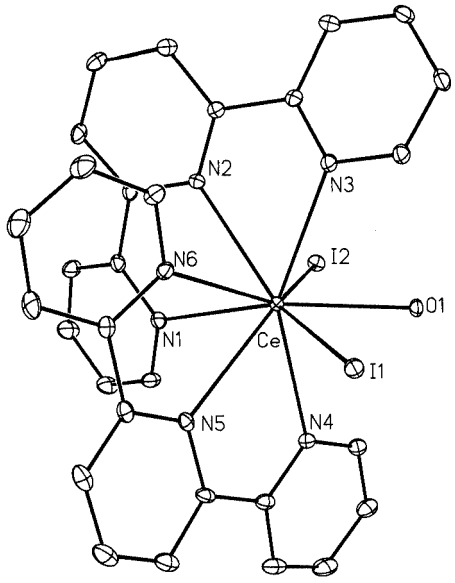

Figure 2. Crystal structure of the cation $[CeI_2(terpy)_2(H_2O)]^+$ in **4·1.5py·0.5Et$_2$O** with displacement ellipsoids at the 30% probability level

2.61(1) Å for Ln = Ce and Nd, respectively].[5] The Ce−I and Ce−N distances are systematically slightly longer than the Nd−I and Nd−N distances, in agreement with the 0.03 Å difference between the ionic radii of Ce^{III} and Nd^{III}.[22]

A comparison of the X-ray crystal structures of terpy complexes showed that the disparity that is usually observed between the $M-N_c$ and $M-N_d$ bond lengths (i.e. $M-N_c < M-N_d$) diminishes and is eventually reversed as the metal-ligand distance increases.[23] In the series of the lanthanide mono-terpy compounds, the experimental value of 2.58 Å has been found to be the limit for the $Ln-N_c$ distance at which this inversion would occur. Thus, the $Ln-N_c$ distances are generally longer than the $Ln-N_d$ distances for the early lanthanides, as observed in the cation $[Nd(NO_3)_2(terpy)_2]^+$.[8] However, the $Ln-N_c$ distances in **1** and **2** are intermediate between the $Ln-N_d$ distances in both terpy ligands. Such deviations from the general trend, which have also been observed in the other cations $[Ln(NO_3)_2(terpy)_2]^+$ (Ln = La, Sm, Tb),[8,12] have been explained by steric constraints in the coordination sphere.

The structures of the cations $[CeI_2(terpy)_2(H_2O)]^+$ and $[UI_2(terpy)_2(py)]^+$ are shown in Figure 2 and 3, respectively. The configuration of these nine-coordinate complexes can be described as a distorted square antiprism similar to that defined in compounds **1** and **2** which is capped on its I(1)N(3)I(2)N(4) base by a water or pyridine molecule. As a consequence of the coordination of this additional ligand, the I(1)−M−I(2) angles of 147.22(3)° (M = U) and 144.04(2)° (M = Ce) are larger than those found in **1** [119.12(2)°] and **2** [119.07(1)°], and the distortion from planarity of one of the two terdentate ligands [N(1)N(2)N(3)] is more pronounced, the standard deviations of the skeletal atoms from the median planes being ±0.21 Å in **3** and ±0.27 Å in **4**, almost 0.1 Å greater than those found in the other terpy ligands. A similar greater distortion of one of the terpy ligands has been observed in the cations $[Ln(NO_3)_2(terpy)_2]^+$ (Ln = Sm, Dy, Ho).[8] The average Ce−N bond length in **4** is 0.05 Å longer than that found in **1**, a difference which corresponds perfectly to that expected from the increase of the coordination number by one unit.[22] The $Ce-N_c$ distances of 2.691(4) and 2.692(4) Å are then longer than all the $Ce-N_d$ distances, which range between 2.652(4) and 2.686(4) Å. The Ce−I(1) bond length in **4** is 0.07 Å longer than the average Ce−I distance in **1**, although the Ce−I(2) bond length of 3.345(1) Å seems abnormally longer, perhaps reflecting the tendency for the iodide ion to dissociate. The $Ce-O(H_2O)$ bond length of 2.468(3) Å can be compared with the mean distance of 2.53(3) Å in the ten-coordinate complex $[CeCl_2(terpy)(H_2O)_5]Cl_2·3H_2O$.[5]

Because of the coordination of the extra pyridine molecule, the crystal structure of **3** cannot be compared directly with that of its cerium analogue, as was possible with the bipy and btp complexes $[UI_3(bipy)_2(py)]$[15] and $[U(btp)_3]I_3$.[16] However, careful examination of the terpy coordination in compounds **1**, **3** and **4** reveals quite distinct and interesting features. Firstly, the mean value of the U−N(terpy) bond lengths of 2.63(3) Å is exactly the same as the average Ce−N bond length in **1**, even though it would be expected to increase by about 0.05 Å in view of the coordination number of **3**, which is higher by one unit, and the ionic radius of U^{III}, which is about 0.01 Å longer than that of Ce^{III}.[22] It is noteworthy that the mean U−I bond length of 3.25(2) Å is 0.07 Å longer than the average Ce−I distance in **1** and corresponds effectively to the variation of the coordination number. On the other hand, the average U−N(terpy) bond length in **3** is 0.05 Å shorter than the mean Ce−N bond length in **4**, even though the two complexes have the same coordination number and exhibit quite similar geometrical parameters. These observations

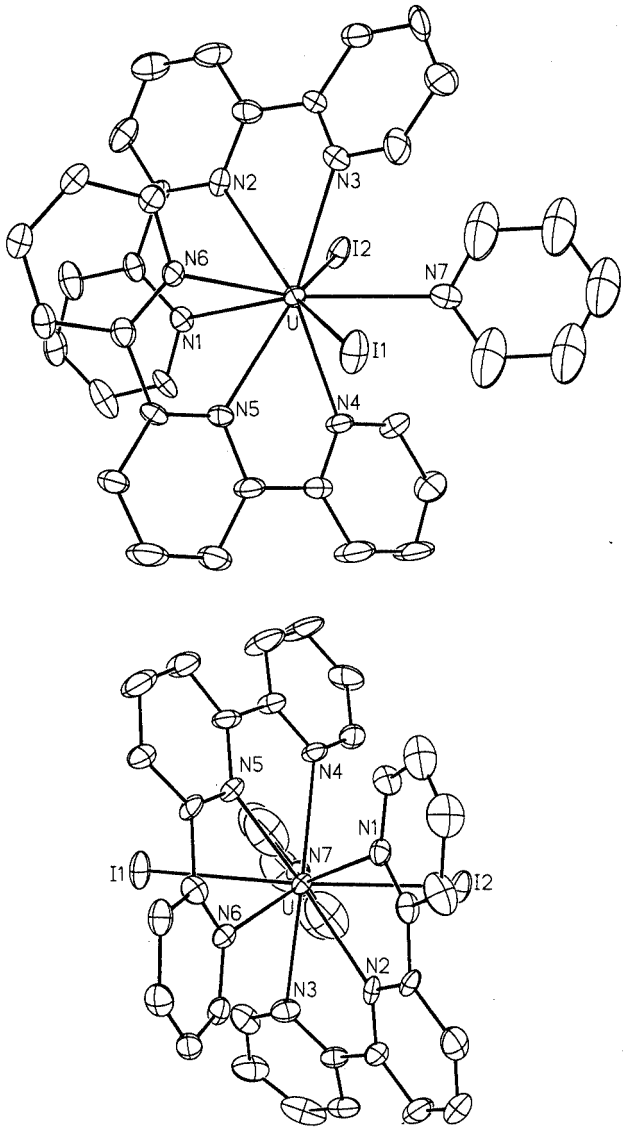

Figure 3. Crystal structure of the cation $[UI_2(terpy)_2(py)]^+$ in **3·2py** with displacement ellipsoids at the 30% probability level; views parallel (top) and perpendicular (bottom) to the bases of the distorted square antiprism

strongly suggest that the terpy ligand is more tightly bond to U^{III} in **3** than to Ce^{III} in **1** and **4**. If the U−N(terpy) bond lengths in **3** are considered to be ca. 0.05 Å shorter than those expected from a purely ionic bonding model, this variation is in the middle of the differences of 0.02 and 0.08 Å that have been measured between the U−N and Ce−N bond lengths in the analogous compounds $[MI_3(bipy)_2(py)]$[15] and $[M(btp)_3]I_3$ [16] (M = Ce, U), respectively. The shortening of the U−N bonds with respect to the Ce−N bonds follows the order bipy < terpy < btp which actually corresponds to the increasing preference of these molecules to bond $[UI_3(py)_4]$ vs. $[CeI_3(py)_4]$ in pyridine solutions. This trend in the interatomic distances indicates that the U−N bonds are stronger than the Ce−N bonds, probably due to a π back-bonding interaction between the uranium atom and the aromatic ligand that is much less likely in the lanthanide complex.[24]

The second striking feature in the structure of **3** concerns the U−N(2) and U−N(5) distances of 2.618(9) and 2.602(10) Å, which are shorter than all the other U−N(terpy) distances which vary from 2.624(9) to 2.657(10) Å. Complex **3** is a unique terpy compound in which the $M-N_c$ bond lengths, while being greater than 2.58 Å, are shorter than the $M-N_d$ bond lengths. As previously noted, the reverse order is generally observed in the terpy complexes of the early lanthanides, especially in **4**, and also in the bismuth compound $[Bi(S_2CNEt_2)I_2(terpy)]$ [$Bi-N_c$ = 2.63(2) Å; $Bi-N_d$ = 2.61(2) Å].[23] It is noteworthy that in these lanthanide and bismuth compounds, metal-to-ligand π back-bonding is unlikely. In the terpy complexes of the d transition metals, the $M-N_c$ distance is always shorter than the average $M-N_d$ bond length, a feature which has been attributed to a more efficient overlap of the metal t_{2g} orbitals with the π* orbitals of the central pyridyl moiety than with the distal pyridine rings.[25] Spectroscopic studies on terpy complexes of Cu^{II} have also shown that the central pyridine of the terpy ligand is a good π-acceptor.[26] That the $M-N_c$ bond length is the most sensitive to changes in the spin state of the metal ion was demonstrated by the structural studies of the cobalt complexes $[Co(terpy)_2]X_2$ (X = Cl, Br, I, SCN, ClO_4) in which the $Co-N_c$ distances contract by 0.21 Å on passing from a high-spin to low-spin electronic ground state, whereas the $Co-N_d$ distances contract by only 0.07 Å; this variation has been explained by a greater back-bonding from the cobalt to the central pyridine in the low-spin compound.[27] From these considerations, the fact that the $U-N_c$ distances are shorter than the $U-N_d$ distances in **3**, while the reverse situation is found in the aforementioned lanthanide and bismuth compounds, would be a further indication of the presence of a π back-bonding interaction between the metal centre and the terpy ligand in the uranium complex.

Conclusion

Addition of terpy to $[MI_3(py)_4]$ (M = Ce, Nd, U) in anhydrous pyridine gave the complexes $[MI_2(terpy)_2]I$ [M = Ce (**1**) and Nd (**2**)] and $[UI_2(terpy)_2(py)]I$ (**3**) which are unique examples of bis-terpy compounds of the early lanthanides and uranium. Competition experiments showed that terpy has a better affinity for UI_3 than for CeI_3 in pyridine solution, the separation factors being intermediate between those observed with the bipy and btp molecules. This order of selectivities, bipy < terpy < btp, corresponds to the order of the differences between the U−N and Ce−N bond lengths in the crystal structures of analogous U^{III} and Ce^{III} complexes. In the crystal structure of **3**, the first terpy complex of uranium, a further indication of the presence of a π back-bonding interaction between the trivalent 5f ion and the aromatic nitrogen ligand is given by the U−N(central pyridine) distances, which are shorter than

the U−N(distal pyridine) distances, while the reverse situation is observed in the early lanthanide terpy complexes.

Experimental Section

General: All experiments were carried out under argon (less than 2 ppm oxygen and water) using standard Schlenk and vacuum-line techniques or in a glove box. Solvents were thoroughly dried and deoxygenated by standard methods and distilled immediately before use. [D_5]pyridine was distilled over NaH and stored over 3 Å molecular sieves. The ^{1}H NMR spectra were recorded on a Bruker DPX 200 instrument and were referenced internally using the residual protio solvent resonances relative to tetramethylsilane ($\delta = 0$). Conductivity measurements were performed at 20 °C with a Consort C-832 conductometer; the cell constant was equal to 0.1 cm^{-1}. Elemental analyses were performed by Analytische Laboratorien at Lindlar (Germany). Terpyridine, CeI_3 and NdI_3 (Aldrich) were dried under vacuum, and [$UI_3(py)_4$] was synthesized as previously reported.[28]

Synthesis of [$CeI_2(terpy)_2$]I (1): A 25 mL round-bottomed flask was charged with CeI_3 (50 mg, 0.096 mmol) and terpy (45 mg, 0.19 mmol), and pyridine (20 mL) was condensed into it under vacuum at −78 °C. The suspension was heated at 100 °C until a clear solution was obtained. The solvent was evaporated off and the orange powder of **1** was washed with THF (15 mL) and dried under vacuum (90 mg, 94%). ^{1}H NMR (200 MHz, [D_5]pyridine): δ = 10.97 (d, J = 7.0 Hz, 2 H), 10.43 (s, 2 H), 10.36 (t, J = 7.0 Hz, 1 H), 8.47 (t, J = 7.0 Hz, 2 H), 6.51 (d, J = 7.0 Hz, 2 H), 3.88 (s, $w_{1/2}$ = 25 Hz, 2 H). $C_{30}H_{22}CeI_3N_6$ (987.4): calcd. C 36.49, H 2.24, N 8.51; found C 36.33, H 2.34, N 8.64.

Synthesis of [$NdI_2(terpy)_2$]I (2): An NMR tube was charged with NdI_3 (10.0 mg, 0.019 mmol), terpy (9.5 mg, 0.04 mmol) and freshly distilled pyridine (1.0 mL). The reaction mixture was heated at 110 °C for 30 min. After evaporation of the solvent, the yellow powder of **2** was washed with tetrahydrofuran (3 mL) and dried under vacuum (15 mg, 80%). ^{1}H NMR (200 MHz, [D_5]pyridine): δ = 11.85 (s,$w_{1/2}$ = 30 Hz, 4 H), 10.36 (s, $w_{1/2}$ = 20 Hz, 1 H), 9.18 (s, $w_{1/2}$ = 20 Hz, 2 H), 8.41 (s, $w_{1/2}$ = 25 Hz, 2 H), 7.7 (masked by the py resonance). $C_{30}H_{22}I_3N_6Nd$ (991.5): calcd. C 36.34, H 2.23, N 8.47; found C 36.57, H 2.34, N 8.53.

Synthesis of [$UI_2(terpy)_2(py)$]I (3): A 25 mL round-bottomed flask was charged with [$UI_3(py)_4$] (50 mg, 0.053 mmol) and terpy (25 mg, 0.20 mmol), and pyridine (20 mL) was condensed into it under vacuum at −78 °C. The dark solution was stirred for 30 min at 20 °C. The solvent was evaporated off and the dark red powder of **1** was washed with tetrahydrofuran (15 mL) and dried under vacuum (46 mg, 75%). ^{1}H NMR (200 MHz, [D_5]pyridine): δ = 24.61 (t, J = 7.0 Hz, 1 H), 18.20 (t, J = 7.0 Hz, 2 H), 10.49 (s, $w_{1/2}$ = 30 Hz, 4 H), 8.35 (s, $w_{1/2}$ = 20 Hz, 2 H), 7.02 (d, J = 6.0 Hz, 2 H). $C_{35}H_{27}I_3N_7U$ (1164.4): calcd. C 36.10, H 2.33, N 8.42; found C 36.39, H 2.93, N 8.17.

Conductometry Studies: A 10^{-2} M solution of Ce^{III} or U^{III} in anhydrous pyridine was prepared by dissolving CeI_3 (52.1 mg) or

Table 2. Crystal data and structure refinement for the complexes

	1·2py	**2·2py**	**3·2py**	**4·1.5py·0.5Et$_2$O**
Chemical formula	$C_{40}H_{32}CeI_3N_8$	$C_{40}H_{32}I_3N_8Nd$	$C_{45}H_{37}I_3N_9U$	$C_{39.5}H_{36.5}CeI_3N_{7.5}O_{1.5}$
M [g mol^{-1}]	1145.56	1149.68	1322.57	1161.08
Crystal system	triclinic	triclinic	monoclinic	triclinic
Space group	$P\bar{1}$	$P\bar{1}$	$C2/c$	$P\bar{1}$
a [Å]	11.081(2)	11.1008(7)	28.865(6)	11.717(2)
b [Å]	13.503(3)	13.4329(6)	12.889(3)	13.534(3)
c [Å]	14.360(3)	14.330(1)	23.840(5)	13.628(3)
α [°]	68.44(3)	68.529(4)	90.0	90.70(3)
β [°]	87.04(3)	87.109(3)	90.73(3)	106.17(3)
γ [°]	78.20(3)	78.252(3)	90.0	94.76(3)
V [Å^3]	1955.5(7)	1946.2(2)	8869(3)	2067.0(7)
Z	2	2	8	2
$\rho_{calcd.}$ [g cm^{-3}]	1.946	1.962	1.981	1.866
μ (Mo-K_α) [mm^{-1}]	3.572	3.754	5.792	3.383
Crystal size [mm]	0.60 × 0.20 × 0.20	0.25 × 0.20 × 0.15	0.20 × 0.15 × 0.15	0.20 × 0.15 × 0.10
T_{min}/T_{max}	0.469/0.489	0.380/0.410	0.262/0.369	0.511/0.535
F(000)	1090	1094	4968	1110
2θ range [°]	6−51	10−46	5−49	6−49
T [K]	123(2)	123(2)	123(2)	123(2)
No. of data collected	11717	7621	27690	12840
No. of unique data	6815	5237	7483	6464
Observed data [$I > 2\sigma(I)$]	5752	4191	4895	5690
R_{int}	0.034	0.047	0.088	0.028
No. of parameters	469	469	490	488
R_1 [a]	0.028	0.027	0.057	0.028
wR_2[b]	0.057	0.060	0.113	0.064
S	1.032	0.951	1.062	1.019
$\Delta\rho_{min}$ [e Å^{-3}]	-0.563	-1.457	-1.211	-0.997
$\Delta\rho_{max}$ [e Å^{-3}]	0.495	0.659	0.918	0.776

[a] $R_1 = \Sigma||F_o| - |F_c||/|F_o|$ (observed reflections). [b] $wR_2 = [\Sigma w(|F_o^2| - |F_c^2|)^2/\Sigma w|F_o^2|^2]^{1/2}$ (observed reflections).

$[UI_3(py)_4]$ (93.5 mg) in pyridine (10 mL). After 5 min at 20 °C, the electrode was immersed into the solution and the conductivity was equal to 45 μS cm^{-1}. The conductivity was found to grow linearly upon addition of n equivalents of terpy ($0 \leq n < 2$) to reach the maximum value of 120 μS cm^{-1} for $n \geq 2$. The conductivity of 10^{-2} M solutions of NaI or NR_4I (R = *n*-butyl or *n*-pentyl) in pyridine was also equal to 120 μS cm^{-1}.

Competition Experiments: An NMR tube was charged with CeI_3 (2.2 mg, 4.3 10^{-3} mmol) and $[UI_3(py)_4]$ (4.0 mg, 4.3 10^{-3} mmol) in $[D_5]$pyridine (1.0 mL), and cyclohexane (1.0 μL) was added with a microsyringe. Terpy (2.0 mg, 8.6 10^{-3} mmol) was added to the dark violet solution. After 10 min at 20 °C, the spectrum showed the complete complexation of terpy and the formation of **1** and **3** with a U^{III}/Ce^{III} molar ratio of 3.0. A similar experiment with NdI_3 in place of CeI_3 gave a mixture of **2** and **3** with a U^{III}/Ce^{III} molar ratio of 2.5.

An NMR tube was charged with CeI_3 (2.8 mg, 5.4 10^{-3} mmol) and $[UI_3(py)_4]$ (5.1 mg, 5.4 10^{-3} mmol) in $[D_5]$pyridine (1.0 mL), and cyclohexane (1.0 μL) was added with a microsyringe. Bipy (1.7 mg, 10.9 10^{-3} mmol) was added to the dark violet solution. After 10 min at 20 °C, the spectrum showed that 25% of the bipy was complexed, giving a mixture of the 1:1 and 1:2 complexes $[MI_3(bipy)(py)_x]$ and $[MI_3(bipy)_2(py)_x]$ (M = Ce, U)[12] with a U^{III}/Ce^{III} separation factor of 1.3.

X-ray Crystallography Studies: Crystal data and a summary of data collection and refinement parameters are given in Table 2. Diffraction collections were carried out on a Nonius diffractometer equipped with a CCD detector. The lattice parameters were determined from ten images recorded with 2° Φ scans and later refined on all data. A 180° Φ range was scanned with 2° steps with a crystal-to-detector distance fixed at 28 mm (**1**) or 30 mm (**2**, **3** and **4**). Data were corrected for Lorentz-polarization and absorption[29] effects. The structures were solved by the direct atom method and refined by full-matrix least-squares on F^2 with anisotropic thermal parameters for all non-hydrogen atoms. H atoms were introduced at calculated positions and constrained to ride on their parent C atom with an isotropic displacement parameter equal to 1.2 (CH, CH_2) or 1.5 (CH_3) times that of the parent atom. In compound **3**, all pyridine molecules were constrained to fit a regular hexagon with an equal anisotropic displacement parameter. In compound **4**, one pyridine and one diethyl ether solvent molecule were found on the same position and refined as disordered over two positions with an occupation factor of 0.5 each. All calculations were performed on an O2 Silicon Graphics Station with the SHELXTL package.[30]

CCDC-174669 (**1·2py**), -174667 (**2·2py**), -174668 (**3·2py**) and -174666 (**4·1.5py·0.5Et$_2$O**) contain the supplementary crystallographic data for this paper. These data can be obtained free of charge at www.ccdc.cam.ac.uk/conts/retrieving.html [or from the Cambridge Crystallographic Data Centre, 12, Union Road, Cambridge CB2 1EZ, UK; Fax: (internat.) +44-1223/336-033; E-mail: deposit@ccdc.cam.ac.uk].

[1] [1a] *Actinides and Fission Products Partitioning and Transmutation. Status and Assessment Report.* NEA/OECD Report; NEA/OECD: Paris, **1999**. [1b] *Actinides and Fission Products Partitioning and Transmutation.* Proceedings of the Fifth International Information Exchange Meeting, Mol, Belgium, 25−27 Nov 1998, NEA/OECD Report, Paris, **1999**.

[2] [2a] K. L. Nash, *Solv. Extr. and Ion Exch.* **1993**, *11*, 729−768. [2b] K. L. Nash, *Separation Chemistry for Lanthanides and Trivalent Actinides*, in *Handbook on the Physics and Chemistry of Rare Earths*, (Eds.: K. A. Gschneidner, L. Eyring, G. R. Choppin, G. H. Lander), North-Holland, Amsterdam, **1994**, vol. 18, 197. [2c] C. Madic, M. J. Hudson, J. O. Liljenzin, J. P. Glatz, R. Nannicini, A. Facchini, Z. Kolarik, R. Odoj, European Report EUR 19149 EN, **2000**.

[3] I. Hagström, L. Spjuth, Å. Enarsson, J. O. Liljenzin, M. Skälberg, M. J. Hudson, P. B. Iveson, C. Madic, P. Y. Cordier, C. Hill, N. François, *Solv. Extr. and Ion Exch.* **1999**, *17*, 221−242.

[4] [4a] E. C. Constable, *Adv. Inorg. Chem. Rad. Chem.* **1986**, *30*, 69−121. [4b] M. Maestri, N. Armaroli, V. Balzani, E. C. Constable, A. M. W. Cargill Thompson, *Inorg. Chem.* **1995**, *34*, 2759−2767. [4c] A. M. W. Cargill Thompson, *Coord. Chem. Rev.* **1997**, *160*, 1−152. [4d] E. C. Constable, A. J. Edwards, G. R. Haire, M. J. Hannon, P. R. Raithby, *Polyhedron* **1998**, *17*, 243−253. [4e] S. E. Hobert, J. T. Carney, S. D. Cummings, *Inorg. Chim. Acta* **2001**, *318*, 89−96.

[5] C. J. Kepert, L. Weimin, B. W. Skelton, A. H. White, *Aust. J. Chem.* **1994**, *47*, 365−384.

[6] L. I. Semenova, A. H. White, *Aust. J. Chem.* **1999**, *52*, 539−550.

[7] C. J. Kepert, L. Weimin, L. I. Semenova, B. W. Skelton, A. H. White, *Aust. J. Chem.* **1999**, *52*, 481−496.

[8] [8a] M. G. B. Drew, P. B. Iveson, M. J. Hudson, J. O. Liljenzin, L. Spjuth, P. Y. Cordier, Å. Enarsson, C. Hill, C. Madic, *J. Chem. Soc., Dalton Trans.* **2000**, 821−830.

[9] S. A. Cotton, P. R. Raithby, *Inorg. Chem. Commun.* **1999**, *2*, 86−88.

[10] L. I. Semenova, A. H. White, *Aust. J. Chem.* **1999**, *52*, 507−517.

[11] [11a] S. P. Sinha, *Z. Naturforsch., Teil A* **1965**, *20*, 552−560. [11b] L. J. Basile, D. L. Gronert, J. R. Ferraro, *Spectrochimica Acta* **1968**, *24A*, 707−716.

[12] M. Fréchette, C. Bensimon, *Inorg. Chem.* **1995**, *34*, 3520−3527.

[13] [13a] L. I. Semenova, A. N. Sobolev, B. W. Skelton, A. H. White, *Aust. J. Chem.* **1999**, *52*, 519−529. [13b] R. D. Chapman, R. T. Loda, J. P. Riehl, R. W. Schwartz, *Inorg. Chem.* **1984**, *23*, 1652−1657. [13c] D. A. Durham, G. H. Frost, F. A. Hart, *J. Inorg. Nucl. Chem.* **1969**, *31*, 833−838.

[14] H. R. Mürner, E. Chassat, R. P. Thummel, J. C. G. Bünzli, *J. Chem. Soc., Dalton Trans.* **2000**, 2809−2816.

[15] C. Rivière, M. Nierlich, M. Ephritikhine, C. Madic, *Inorg. Chem.* **2001**, *40*, 4428−4435.

[16] P. B. Iveson, C. Rivière, D. Guillaneux, M. Nierlich, P. Thuéry, M. Ephritikhine, C. Madic, *Chem. Commun.* **2001**, 1512−1513.

[17] [17a] C. Piguet, J. C. G. Bünzli, G. Bernardinelli, G. Hopfgartner, A. F. Williams, *J. Am. Chem. Soc.* **1993**, *115*, 8197−8206. [17b] P. Caravan, T. Hedlund, S. Liu, S. Sjöberg, C. Orvig, *J. Am. Chem. Soc.* **1995**, *117*, 11230−11238. [17c] S. Petoud, J. C. G. Bünzli, F. Renaud, C. Piguet, K. J. Schenk, G. Hopfgartner, *Inorg. Chem.* **1997**, *36*, 5750−5760. [17d] M. P. Lowe, P. Caravan, S. J. Rettig, C. Orvig, *Inorg. Chem.* **1998**, *37*, 1637−1647. [17e] R. Wietzke, M. Mazzanti, J. M. Latour, J. Pécaut, *Chem. Commun.* **1999**, 209−210. [17f] R. Wietzke, M. Mazzanti, J. M. Latour, J. Pécaut, *J. Chem. Soc., Dalton Trans.* **2000**, 4167−4173.

[18] R. D. Hancock, A. E. Martell, *Chem. Rev.* **1989**, *89*, 1875−1914.

[19] [19a] Z. Kolarik, U. Mullich, F. Gassner, *Solv. Extr. and Ion Exch.* **1999**, *17*, 23−32. [19b] Z. Kolarik, U. Mullich, F. Gassner, *Solv. Extr. and Ion Exch.* **1999**, *17*, 1155−1170.

[20] D. M. Barnhart, T. M. Frankcom, P. L. Gordon, N. N. Sauer, J. A. Thompson, J. G. Watkin, *Inorg. Chem.* **1995**, *34*, 4862−4867.

[21] D. L. Clark, J. C. Gordon, B. L. Scott, J. G. Watkin, *Polyhedron* **1999**, *18*, 1389−1396.

[22] R. D. Shannon, *Acta Crystallogr., Sect. A* **1976**, *32*, 751−767.

[23] C. L. Raston, G. L. Rowbottom, A. H. White, *J. Chem. Soc., Dalton Trans.* **1981**, 1383−1388.

[24] [24a] J. G. Brennan, S. D. Stults, R. A. Andersen, A. Zalkin, *Organometallics* **1988**, *7*, 1329−1334. [24b] J. Parry, E. Carmona, S. Coles, M. Hursthouse, *J. Am. Chem. Soc.* **1995**, *117*, 2649−2650. [24c] P. Roussel, W. Errington, N. Kaltsoyannis, P. Scott, *J. Organomet. Chem.* **2001**, *635*, 69−74.
[25] [25a] L. S. Erre, G. Micera, E. Garribba, A. C. Bényei, *New. J. Chem.* **2000**, *24*, 725− 728. [25b] P. E. Figgins, D. H. Busch, *J. Phys. Chem.* **1961**, *65*, 2236−2240.
[26] C. C. Su, C. B. Li, *Polyhedron* **1994**, *13*, 825−834.
[27] B. N. Figgis, E. S. Kucharski, A. H. White, *Aust. J. Chem.* **1983**, *36*, 1537−1561.
[28] L. R. Avens, S. G. Bott, D. L. Clark, A. P. Sattelberger, J. G. Watkin, B. D. Zwick, *Inorg. Chem.* **1994**, *33*, 2248−2256.
[29] A. L. Spek, MULABS, *PLATON*, University of Utrecht, The Netherlands, **1997**.
[30] *SHELXTL:* G. Sheldrick **1999**, Bruker-AXS, Madison, WI, USA.

Received December 3, 2001
[I01497]

A Novel Configuration of a Benzoylacetonato-Diorganotin Species is Modified by an Electron-Withdrawing Substituent on Tin − Synthesis, IR and NMR Spectroscopy, Structure, and ab initio Studies

Claudio Pettinari,*[a] Fabio Marchetti,[a] Riccardo Pettinari,[a] Asta Gindulyte,[a] Lou Massa,[a] Miriam Rossi,[d] and Francesco Caruso*[e]

Keywords: Tin / O ligands / NMR spectroscopy / Crystal structure / Ab initio calculations

Diorganotin(IV) complexes of the β-diketonato benzoylacetonato ligand were synthesized and characterized with IR and multinuclear (H, C, Sn) NMR spectroscopy. The X-ray diffraction study of bis(benzoylacetonato)di-*tert*-butyltin(IV) shows two independent molecules in the crystallographic unit cell. The metal polyhedron is a distorted octahedral (Skewed Trapezoidal Bipyramidal) with the *trans* angle C–Sn–C of 151.5(5)°. Each ligand chelates the metal with different donor abilities [Sn–O bond lengths of 2.423(8) Å and 2.135(8) Å in one ligand, and 2.107(9) Å and 2.357(8) Å in the other]; results for the 2nd molecule are similar. The coordination arrangement differs from those of related bis(β-diketonato)diorganotin derivatives containing asymmetric ligands, which are characterized by an approximate C_s symmetry, in that both benzoylacetonato ligands point their methyl (and phenyl) substituents across (*anti*) the metal atom. Chelate planarity and some phenyl-chelate coplanarity was observed. Hartree–Fock (HF) and Density Functional Theory (DFT) calculated structures are in good agreement with those obtained using X ray analysis. DFT and HF calculated structures of bis(benzoylacetonato)diphenyltin(IV), having a similar connectivity as bis(benzoylacetonato)di-*tert*-butyltin(IV), differ markedly: the phenyls subtend a C–Sn–C bond angle of 180°, all Sn–O bond lengths are equal and the tin coordination sphere is a regular octahedron with the ligand bzac being isobidentate. This arrangement is caused by the phenyl electronic withdrawal effect. However, IR data for this compound show several Sn–O bands inconsistent with this configuration and suggest a different connectivity. Additional DFT structural calculations for $(bzac)_2SnPh_2$, performed on the connectivity resembling the "normal" *syn* geometry, show a conformational energy slightly lower than that of the centrosymmetric arrangement. Low temperature NMR spectra illustrate the possible rearrangements in solution.

(© Wiley-VCH Verlag GmbH, 69451 Weinheim, Germany, 2002)

Introduction

The acetylacetonato-like donors represent one of the most important classes of chelating ligands in the field of coordination chemistry, not only because of their technological applications,[1−4] but also for theoretical structural studies performed on their metal complexes.[5,6] Several studies have appeared in the literature regarding structural and spectroscopic features of tin(II)[7−11] and tin(IV) acetylacetonates,[12−23] including their catalytic properties in the formation of polyurethane in foams,[24] their promising antineoplastic activity,[25−27] and more recently, their use as molecular precursors in LAD (laser ablation and subsequent deposition) technology.[28]

Diorganotin(IV) acetylacetonates adopt a *trans* regular octahedral geometry[12] (Figure 1), whereas dihalotin(IV) acetylacetonates prefer the *cis*-dihalo octahedral configuration.[18]

Subsequent studies on monothioacetylacetonatotin[29] derivatives revealed the possibility of large deviations from ideal geometries in accordance with the Zahrobsky[30] and Kepert models.[31] Other studies on asymmetric β-diketonates have appeared recently, including our own systematic

[a] Dipartimento di Scienze Chimiche, Università degli Studi di Camerino,
Via S. Agostino 1, 62032 Camerino (MC), Italy
E-mail: claudio.pettinari@unicam.it
[b] Hunter College, Department of Chemistry,
695 Park Avenue, New York, NY 10021 USA
[c] The Graduate School, City University of New York,
365 Fifth Avenue, New York, NY 10016, USA
[d] Vassar College, Department of Chemistry,
Poughkeepsie, NY, 12604−0484, USA
[e] Istituto di Strutturistica Chimica "G. Giacomello", CNR,
CP 10, 00016, Monterotondo Stazione, Rome, Italy
E-mail: francesco.caruso@mlib.cnr.it
Supporting information for this article is available on the WWW under http://www.eurjic.com or from the author.

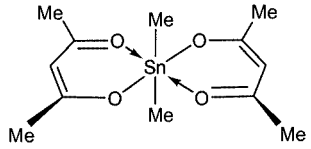

Figure 1. $(acac)_2Sn(CH_3)_2$

investigations on the structural aspects of tin(II)[32] and tin(IV)[33] derivatives containing 4-acyl-5-pyrazolonato ligands, which are β-diketonates fused to a pyrazole ring[34] containing three substituent groups. In these asymmetric ligands, the carbonyl nearest the heterocyclic ring is a better donor than the 4-acyl carbonyl group, and the diorganotin derivatives posses strongly deformed octahedral structures (Figure 2a) with both ligands pointing their equivalent arms in a *syn* configuration.

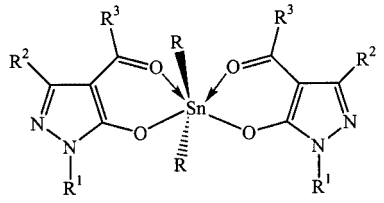

(a) *syn* configuration

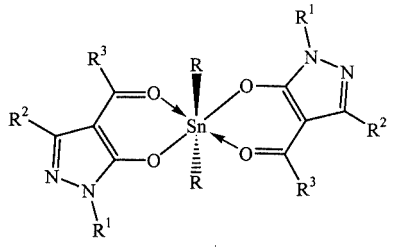

(b) *anti* configuration

Figure 2. (a) *syn* configuration (b) *anti* configuration

Our studies have revealed the following geometrical features of these tin complexes: i) the *trans* C−Sn−C bond angle can be as small as 150°, and ii) the R groups are folded towards the O(acyl) atoms. The O(pyrazolonato) atom (that is, the oxygen closest to the pyrazole ring) forms a short, covalent, Sn−O bond (range 2.09−2.14 Å), whereas the O(acyl) atom forms a long, coordinative, Sn−O bond (range 2.22−2.46 Å).[33b] The asymmetric binding of these ligands reflects the different electronic donating ability of the oxygen atoms and is responsible for the octahedral deformation described earlier. In contrast, the dimethyltin derivative of the symmetrical β-diketonato acac has maximum electronic delocalization in the chelate moiety and is a perfect octahedron[12] (Figure 1). We have also found, however, that an appropriate choice of peripheral substituents on N1 allows the synthesis of isomers with a centrosymmetrical (*anti*) configuration (see **b** in Figure 2).[35]

It seems that the features determining the *syn* and *anti* configurations are subtle and more factors than those first hypothesized are responsible. For example, in octahedral diphenyltin compounds, *cis*-diphenyl species are also known. Specifically, in the case of bis(4-acyl-5-pyrazolonato)diphenyltin compounds, the *cis* arrangement has been observed with Mössbauer spectroscopy.[33c] Subtle molecular changes can also induce the *trans* form in related compounds such as Ph_2SnCl_2(2,2′-bipyridine), which is a *trans*-diphenyl *cis*-dichloro species, whereas (*p*-tolyl)$_2SnCl_2$(2,2′-bipyridine) is a *cis*-ditolyl *trans*-dichloro isomer.[36] Therefore, we decided to reinvestigate the field of diorganotin(IV) classical β-diketonates giving special attention to the asymmetric donor 1-phenylbutane-1,3-dionato, also known as benzoylacetonato (bzac), to derive some fundamental principles from the stereochemistry of these compounds.

Results and Discussion

Synthesis of the Diorganotin(IV) Derivatives 1−6

Derivatives $(bzac)_2SnR_2$ **1−6** were synthesized by interaction of two mmoles of bzacH and one mmole of the appropriate diorganotin(IV) acceptor in methanol in the presence two mmoles of $NaOCH_3$ (Scheme 1).

$$2bzacH + 2NaOCH_3 + R_2SnX_2 \rightarrow (bzac)_2SnR_2 + 2NaX + 2CH_3OH$$

	R	X		R	X
1	Me	Cl	**4**	*t*Bu	Br
2	Et	Cl	**5**	Cy	Cl
3	*i*Bu	Cl	**6**	Ph	Cl

Scheme 1

The reactions were performed according to methods previously employed with 4-acyl-5-pyrazolonato donors,[33] since they avoid hydrolysis. The yields of the reactions were higher when a large excess of bzacH was employed.

Spectroscopic Characterization

The infrared spectra of derivatives **1−6** show the carbonyl ν(C=O) shifted to lower frequencies upon complex formation, as expected for coordination of the β-diketonato ligand through both the oxygen atoms.[37] In the far-IR region several strong Sn−O bands[37] can be seen in the range 390−460 cm^{-1}. In the spectra of derivatives **1−5**, some medium to weak absorptions between 450 and 600 cm^{-1} were assigned to the ν(Sn−C) on the basis of literature reports.[38] In the spectrum of **6**, three strong bands in the range 250−310 cm^{-1} are due to ν(Sn−C).[39] In the spectra of **1−6**, the presence of several ν(Sn−O) and ν(Sn−C) modes indicates either distortion from ideal *trans*-octahedral geometry in the solid state (confirmed for **4** by the diffraction study, see below) or the presence of *cis* isomers.

The ^1H NMR spectra of derivatives **1** and **2** show one set of resonances for each magnetically equivalent group of protons. On cooling the samples, each signal splits into sev-

eral signals, two of which are very intense with respect to the others. We have measured the $^2J_{Sn,H}$ coupling constants and related them to the C−Sn−C angle.[40] From the empirical relation derived by Lockhart[40a] a C−Sn−C angle for compound **1** of ca. 160°, typical of skewed *trans*-octahedral species,[40] was found. For this reason, the two main resonances observed at low temperature for the CH_{bzac} and Me_{bzac} protons can be attributed to *syn* and *anti* isomers. The less intense signals are likely due to either *cis* isomers or four- to five-coordinate species involved in the interconversion mechanism between *syn* and *anti* isomers.

The ^{119}Sn NMR spectra of **1** and **2** further support our hypothesis: at room temperature only one resonance was detected, which split into two at 218 K.

A similar situation was found for the derivatives **3**−**6** containing bulky or electron-withdrawing organic groups bonded to tin. In these compounds, the fluxionality is lost at higher temperature with respect to **1** and **2**. They show more than one set of resonances at room temperature, thus indicating that the energy required for the interconversion mechanism is a function of steric hindrance and electronegativity of the R groups coordinated to tin. At low temperatures, the ^{119}Sn NMR spectra of **5** and **6** show three resonances, two of which are dominant and are likely to be due to *syn* and *anti* isomers; the third is assigned to one *cis* $(bzac)_2SnR_2$ complex.[41]

Reports in the literature on possible mechanisms for configurational rearrangements of $(\beta\text{-diketonato})_2SnX_2$ complexes[39b,42] include: complete dissociation of one β-diketonato donor, to give a four coordinate intermediate; breaking of one M−O bond to give a five coordinate intermediate with a monodentate β-diketonato donor; and twisting mechanisms with subsequent rearrangement without any metal−ligand bond breaking.

To better understand the mechanism operating in solution for derivatives **1**−**6**, we carried out a ^{1}H NMR variable-temperature study of a mixture containing derivative **1** and the equivalent amount of free neutral bzacH proligand in $CDCl_3$. At room temperature, only one set of signals was observed, in accordance with ligand exchange in the complex, whereas at 218 K all resonances due to **1** and to the neutral bzacH in both enolic and ketonic forms were found. It seems that the twisting mechanism is excluded and the *syn-anti* conversion proceeds with breaking and re-formation of $Sn-O_{bzac}$ bonds through four- or five-coordinate intermediate species (Scheme 2). In the case of four coordinate intermediates the absence of conductivity in chlorohydrocarbon solvents could be attributed to ion pairing effects.

The variable-temperature ^{1}H NMR spectra indicate the following coalescence temperatures: 273 K (compounds **1** and **2**), 303 K (**3**), 323 K (**4** and **6**). These results further confirm the role of R groups on the configurational rearrangements.

The ^{119}Sn chemical shift is typical of six-coordinate SnC_2O_4 species, and is a function of steric and electronic features of R groups on tin. This is in agreement with previous studies on related $(4\text{-acyl-5-pyrazolonato})_2SnR_2$ derivatives.[33] The donating ability of $bzac^-$ is higher than that of 4-acyl-5-pyrazolonates, as the signals are generally high-field shifted with respect to that of 4-acyl-5-pyrazolonato complexes.

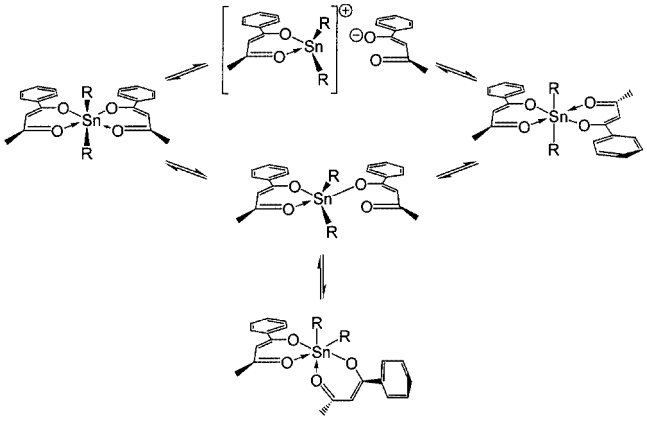

Scheme 2

The ^{13}C NMR spectra of **1**, **3**, and **4** show one broad set of resonances at room temperature. The magnitude of the $^1J(^{119}Sn-^{13}C)$ coupling constant of **1** (934 Hz) further supports the presence of *trans* isomers in solution.[40] The ^{13}C NMR spectrum of **6**, on the other hand, exhibits more than one set of resonances for each magnetically equivalent carbon atom, in accordance with the ^{1}H and ^{119}Sn NMR spectra.

X-ray Structural Discussion of Derivative $(bzac)_2Sn(tBu)_2$ (4)

The crystals of $(bzac)_2Sn(tBu)_2$ are formed by well separated molecules with no imposed crystallographic symmetry. Each asymmetric unit contains 2 molecules related by a local (non-crystallographic) inversion center at approximately [0.625, 0.0, 0.75] [see also Exp. Sect. and related Figure S1 (Supporting Information)]. Besides the inverted configuration only minor geometrical differences between these 2 molecules are observed, probably due to packing forces; one of these molecules is shown in Figure 3. The metal is six coordinate and surrounded by 4 O atoms from 2 bzac ligands, and 2 C atoms from the *tert*-butyl groups, which are almost eclipsed, as shown in Figure 4. Table 1 shows a selection of the structural data. The C−Sn−C bond angles [151.5(5)° for C11−Sn1−C15 in one molecule and 152.1(5)° for C51−Sn2−C55 in the other] are of the order found in bis(4-acyl-5-pyrazolonato)dialkyltin[33b] *syn* structures, as are the marked differences in Sn−O bonds in each ligand. The carbonyl closest to the methyl substituent in one ligand has the short Sn−O bond [Sn1−O2 = 2.135(8) Å], whereas in the other ligand the short bond is close to the phenyl substituent [Sn1−O21 = 2.107(9) Å]. This feature is uncommon for bzac compounds {but it does exist[43] in the anion $[(bzac)_4Eu]^-$} and contrasts with bis(4-acyl-5-pyrazolonato)diorganotin derivatives, where the short bond only appears in the carbonyl fused to the pyrazole ring, The ligand asymmetry differs from that of $(bzac)_2Sn^{II}$, which shows a short Sn−O bond for the

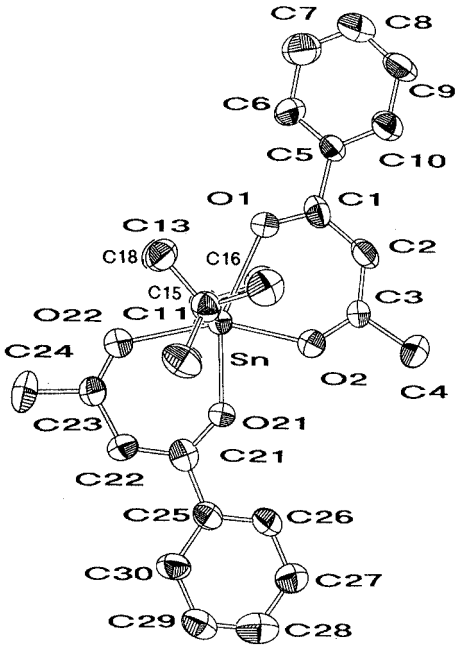

Figure 3. X-ray structure of $(bzac)_2Sn(tBu)_2$ (**4**). In this view, *tert*-butyl group C15−C18 (C15, C16, and C18 have small labels) is below the other *tert*-butyl C11−C14 (only C11 and C13 are labeled); H atoms are omitted.

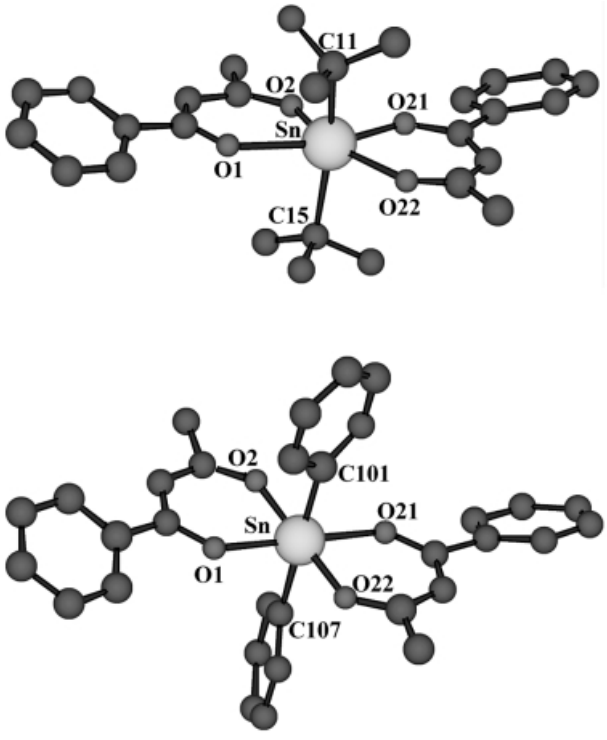

Figure 4. DFT structures of $(bzac)_2Sn(tBu)_2$ (**4**) and *anti* $(bzac)_2SnPh_2$ (**6**).

phenyl-carbonyl (2.13 Å) and a long Sn−O bond (2.29 Å) for the methyl-carbonyl, in both ligands.[10]

In analyzing the molecular arrangement, we see that the title compound has its bzac equivalent substituents (for instance both Ph groups) opposite each other. This is in contrast with *syn* bis(4-acyl-5-pyrazolonato)diorganotin derivatives that have the equivalent ligand substituents facing each other (see **a** in Figure 2). This opposite arrangement is reminiscent of the *anti* bis(4-acyl-5-pyrazolonato)diorganotin geometry[35] (see **b** Figure 2), although the latter also differs from the title compound and has a regular octahedral configuration with the C−Sn−C bond angle of 180°. Therefore, the structural form of the title compound is different from those so far observed.

X-ray data show planar chelate moieties. Thus, the least-square C1−C2−C3−O1−O2 plane has all atoms within 0.01 Å, and the C21−C22−C23−O21−O22 plane has all atoms within 0.04 Å; in the 2nd molecule these parameters are both 0.03 Å. The metals are contained in these chelate planes within 0.05 and −0.02 Å (for the 1st molecule) and −0.02 and 0.00 Å (for the 2nd molecule); therefore the molecule has a skewed trapezoidal bipyramidal (STB) configuration.[31] In addition, the dihedral angles between the two chelate planes are 2.4(2)°, in one molecule and 3.1(3)° in the other. Further, each phenyl substituent shows some co-planarity with its chelate moiety as seen by torsion angles O1−C1−C5−C6 [−19(2)°] and O21−C21−C25−C26 [−16(1)°].

There are two X-ray structures of di-*tert*-butyltin compounds containing four additional O atoms in the coordination sphere in the CSD database. These are di-*tert*-butyl-bis{[(*E*)-2-(2-hydroxy-5-methylphenyl)diazenyl]-benzoato-*O*,*O*′}tin(IV)[44] and di-*tert*-butyl-bis(1-phenyl-3-methylbenzoyl-pyrazolon-5-ato-*O*,*O*′)tin(IV).[45] In both complexes the oxygen ligands chelate the metal, as occurs in compound **4**. Comparison with compound **4** shows the former having a smaller C−Sn−C bond angle (141.0°) and a more deformed octahedron; the latter (containing a β-diketonato ligand) shows more similar features because its C−Sn−C bond angle is 150° and both *t*Bu groups are eclipsed as in compound **4** (see Figure 3).

Theoretical Study

The molecular structure of $(bzac)_2Sn(tBu)_2$ was also studied using theoretical methods. The starting coordinates were those obtained from the X-ray structure determination and were optimized by energy-minimization with the Hartree−Fock (HF) and Density-Functional Theory (DFT) methods. Structural data are included in Table 1. There is excellent agreement for the data obtained experimentally from the X-ray diffraction study for the deformed metal polyhedron including the sum of the *cis* O−Sn−O bond angles of 360°. The co-planarity in the chelate moieties resembles that observed with X-rays as shown by torsion angles in Table 1. The DFT structure is shown in Figure 4.

In previous studies on (4-acyl-5-pyrazolonato)organotin derivatives, we showed that an electron-withdrawing group on tin, such as Ph, behaves differently from alkyl groups.[33c] Due to the electron-withdrawing effect, phenyl groups pull electron density away from the metal and consequently induce more electron donation from the chelating ligands. Therefore, the normally weakly coordinated acyl carbonyl provides more electronic donation and this results in de-

Table 1. Selected structural data of $(bzac)_2Sn(tBu)_2$ (**4**)

Distances					
Method[a]	XR	HF	DFT	XR (2nd molecule)	
Sn−O1	2.423(8)	2.439	2.418	Sn2−O41	2.408(8)
Sn−O2	2.135(8)	2.137	2.092	Sn2−O42	2.138(8)
Sn−O21	2.107(9)	2.110	2.141	Sn2−O61	2.145(8)
Sn−O22	2.357(8)	2.360	2.390	Sn2−O62	2.367(7)
Sn−C11	2.19(1)	2.193	2.194	Sn2−C51	2.20(1)
Sn−C15	2.18(1)	2.177	2.194	Sn2−C55	2.18(1)
Angles					
Method	XR	HF	DFT	XR (2nd molecule)	
C11−Sn−C15	151.5(5)	151.3	155.3	C51−Sn2−C55	152.1(5)
O1−Sn−O2	78.6(3)	76.7	78.8	O41−Sn2−O42	78.9(3)
O21−Sn−O22	79.2(3)	76.7	78.8	O61−Sn2−O62	79.0(3)
O1−Sn−O22	126.2(3)	126.7	124.7	O41−Sn2−O62	127.4(3)
O21−Sn−O2	76.0(3)	79.9	77.7	O61−Sn2−O42	74.7(3)
Torsion angles					
Method	XR	HF	DFT		
O1−C1−C2−C3	3(2)	−3.5	−4.0		
O2−C3−C2−C1	0(2)	−1.3	−2.0		
C4−C1−C2−C3	−1(2)	−1.2	−2.6		
C5−C1−C2−C3	−173(1)	177.4	177.1		
O1−C1−C5−C6	−19(2)	−22.7	−20.0		
O21−C21−C22−C23	3(2)	−2.4	−1.1		
O22−C23−C22−C21	3(2)	−0.3	0.9		
C24−C21−C22−C23	1(2)	−0.1	1.6		
C25−C21−C22−C23	−178(1)	178.8	179.9		
O21−C21−C25−C26	−16(1)	−21.1	−18.1		

[a] Methods, X-ray diffraction (XR); Hartree−Fock (HF); Density Functional Theory (DFT).

creased octahedral deformation.[33c] For this reason, we wanted to see if replacing the *tert*-butyl groups with phenyl groups resulted in some structural change, and so we also studied $(bzac)_2SnPh_2$ (**6**) theoretically. Therefore, the *tert*-butyl groups from $(bzac)_2Sn(tBu)_2$ were replaced by phenyls and the energy minimized as above (Figure 4 also depicts this calculated DFT molecule and Table 2 includes selected geometric data). This resulted in a dramatic variation on the molecular structure: the C−Sn−C bond angle became 180° and a regular octahedron was found. In addition, increased involvement in binding to tin by O1 and O22 was observed and all Sn−O bonds were equal (about 2.14 Å for HF or 2.19 Å for DFT).

Therefore, replacing the *tert*-butyl groups on tin with phenyls while keeping the $(bzac)_2Sn(tBu)_2$ connectivity, modified the skewed trapezoidal bipyramidal arrangement to regular octahedral. Moreover, the phenyl groups on tin caused the asymmetric binding of the ligand bzac to disappear, e.g. the ligand bzac became isobidentate. Co-planarity between phenyl substituents and chelate moieties was less marked than in the *tert*-butyl derivative, as seen from the corresponding torsion angles in Table 1 and 2.

However, IR data for $(bzac)_2SnPh_2$ show several Sn−O bands that are inconsistent with the symmetrical tin environment found using ab initio methods. IR results could imply either a *cis*-diphenyl structure or a *syn* STB structure with equivalent ligand arms (methyls or phenyls) facing each other. In other words, the theoretical study shows that the $(bzac)_2Sn(tBu)_2$ connectivity is not possible for $(bzac)_2SnPh_2$.

Table 2. Selected ab initio structural data of *anti* $(bzac)_2SnPh_2$ (**6**)

Distances		
Method	HF	DFT
Sn−O1	2.149	2.189
Sn−O2	2.142	2.186
Sn−O21	2.147	2.191
Sn−O22	2.143	2.185
Sn−C101	2.138	2.146
Sn−C107	2.138	2.144
Angles		
C101−Sn−C107	179.8	179.1
O1−Sn−O2	84.9	85.5
O21−Sn−O22	85.0	85.6
O1−Sn−O22	95.3	94.1
O21−Sn−O2	94.8	94.9
Torsion angles		
O1−C1−C2−C3	−1.5	0.2
O2−C3−C2−C1	−1.0	0.3
C4−C1−C2−C3	−1.6	−0.3
C5−C1−C2−C3	179.9	−178.9
O1−C1−C5−C6	−26.9	−22.1
O21−C21−C22−C23	−1.5	0.1
O22−C23−C22−C21	−0.8	0.4
C24−C21−C22−C23	−1.2	−0.2
C25−C21−C22−C23	179.8	−178.9
O21−C21−C25−C26	−26.8	−22.4

We then performed an additional DFT structural calculation for $(bzac)_2SnPh_2$, with a connectivity resembling the common *syn* geometry (see Figure 5). From the coordinates of *anti* $(bzac)_2SnPh_2$, obtained above, the methyl and the Ph groups belonging to the O1···O2 chelate were exchanged

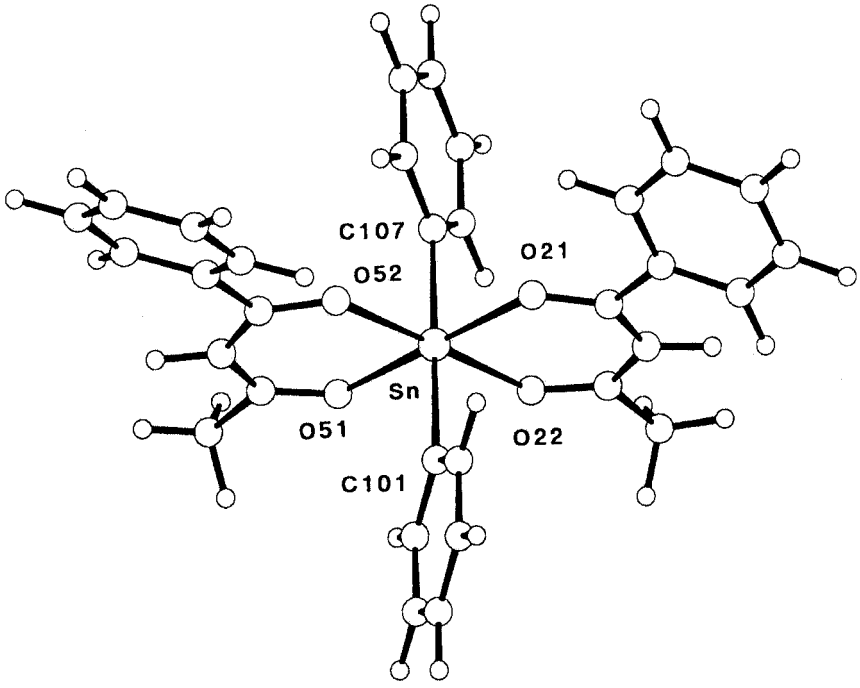

Figure 5. DFT structure of *syn* $(bzac)_2SnPh_2$ (**6**)

(this chelate is labeled O51···O52 in Figure 5), and a minimization process was performed as above. The resulting molecule posses a slight octahedral deformation characterized by a C−Sn−C bond angle of 178.3° and Sn−O bond lengths differ less in each ligand than in other *syn* (β-diketonato)SnR_2 compounds[33] (Sn−O21 = 2.198 Å and Sn−O22 = 2.176 Å in one ligand; Sn−O52 = 2.193 Å and Sn−O51 = 2.178 Å in the other ligand). From these results, the methyl carbonyl seems to be a slightly stronger donor that the phenyl carbonyl, which agrees with the phenyl electron-withdrawing and the methyl electron releasing effects. The Sn atom is included in the equatorial plane defined by the 4 oxygen atoms as expected for a STB geometry. Each chelate plane forms a similar dihedral angle with the corresponding attached phenyl ring (23.8 and 23.9°). The conformational energy of this *syn* structure is slightly lower than the one calculated with the *anti* geometry (0.03 kcal/mol). The experimental IR data seem consistent with the former option.

Conclusions

The already versatile stereochemistry of bis(β-diketonato)-diorganotin derivatives has been further enriched with the use of the ligand 1-phenylbutane-1,3-dionato (bzac). Derivative $(bzac)_2Sn(tBu)_2$ has a skewed trapezoidal bipyramidal (STB) configuration with methyl (and phenyl) ligand arms pointing opposite each other whereas in previously studied bis(β-diketonato)diorganotin derivatives,[33] the ligand arms were facing each other. The new structural form is ascribed to ligand asymmetry that induces different metal−O bond lengths.

The diffraction study shows that structural features of $(bzac)_2Sn(tBu)_2$ agree with HF and DFT calculated structures, including overall ligand planarity.

The molecular structure of $(bzac)_2Sn(tBu)_2$ contrasts with that of $(bzac)_2SnPh_2$ (calculated theoretically and *bearing the same connectivity*). The latter shows a regular octahedral configuration otherwise seen with the symmetric ligand acac. The phenyl groups on tin thus negate bzac ligand asymmetry, but since IR data for $(bzac)_2SnPh_2$ show several Sn−O bands indicating an asymmetrical Sn environment, the ab initio *anti* structure cannot be realistic. The *syn* structure, also calculated theoretically, agrees with IR results, though the energy difference between the *syn* and *anti* structures is small (0.03 kcal/mol) and comparison may be rather speculative. However, a *cis*-diphenyl structure is also an isomer that could explain the observed IR data. Further studies are planned to try to determine which is the actual isomer experimentally obtained.

It is concluded that a delicate balance of factors governs bis(β-diketonato)diorganotin stereochemistry. Several configurations are allowed dependent on a) tin's capacity for octahedral deformation; b) the interplay of electronic effects of the tin substituents; c) the intrinsic ligand asymmetry; and d) peripheral ligand modifications.

In closing, the NMR study shows that in the case of diorganotin(IV) complexes containing asymmetric β-diketonato ligands, a mixture of isomers is present in solution. Generally, the *trans* isomers are the most abundant and the conversions *cis-trans, syn-anti*, are strongly dependent on the temperature, and the bulkiness and electronegativity of the R groups. An asymmetric ligand demonstrates a completely different behavior in R_2Sn^{IV} species compared to symmetric

donors such as acac,[35] at least when electron-withdrawing substituents such as Ph are present.

Experimental Section

General Remarks: The organotin(IV) halides and benzoylacetone were purchased from Alfa (Karlsruhe) and Aldrich (Milwaukee) and used as received. The samples for microanalyses were dried under vacuum to constant weight (20 °C, about 0.1 Torr). Elemental analyses (C, H) were performed in house with Fisons Instruments 1108 CHNS-O Elemental Analyzer. IR spectra were recorded from 4000 to 100 cm^{-1} with a Perkin−Elmer System 2000 FT-IR instrument. ^1H, ^{13}C, and ^{119}Sn NMR spectra were recorded on a VXR-300 Varian spectrometer operating at 300 MHz for ^1H, 75 MHz for ^{13}C, and 111.9 MHz for ^{119}Sn, referred to TMS (^1H and ^{13}C) and $(CH_3)_4Sn$ (^{119}Sn). Relative intensities of signals are given in square brackets. The ^{119}Sn NMR experiments were carried with a spectral width of 900 ppm. Melting points were taken on an IA 8100 Electrothermal Instrument. The electrical conductances (reported as Ω^{-1} cm^2 mol^{-1}) of dichloromethane (M = mol/L) were measured with a Crison CDTM 522 conductimeter at room temperature.

Synthesis of the Complexes

Bis[1-phenylbutane-1,3-dionato]dimethyltin(IV) [(bzac)$_2$SnMe$_2$] (1): To a methanol solution (30 mL) of bzacH (2 mmol) was added $NaOCH_3$ (2 mmol) and $(t\text{Bu})_2SnCl_2$ (1 mmol). A precipitate slowly formed after stirring the mixture for 36 h. The precipitate was then filtered, washed with methanol (ca 10 mL), and dried under reduced pressure at room temperature. This was re-crystallized from chloroform/*n*-hexane. Yield 74%. m.p. 138−139 °C. $C_{22}H_{24}O_4Sn$: calcd. C 56.09, H 5.13; found C 56.34, H 5.04. IR (nujol, cm^{-1}): $\tilde{\nu}$ = 1587 s, 1555 vs, 1540 sh, 1507 vs, ν(C=O) + ν(C=C), 573 s, 521 s, 436 s, 408 s, 323 m, 280 m, ν(Sn−C) + ν(Sn−O) + δ(bzac). ^1H NMR ($CDCl_3$, 295 K): δ = 0.74 [s, $^2J(^{119}Sn\text{-}^1H)$ = 98.7, $^2J(^{117}Sn\text{-}^1H)$ = 94.8 Hz, 6 H, Sn−Me], 2.13 (s, 6 H, Me_{bzac}), 6.01 (s br, 2 H, CH_{bzac}), 7.4 (m), 7.88 (d, 10 H, Ph_{bzac}). ^1H NMR ($CDCl_3$, 273 K): δ = 0.75 [s, $^2J(Sn\text{-}^1H)$ = 97.5 Hz, 6 H, Sn−Me,), 2.14 (s, 6 H, Me_{bzac})], 6.01 [5], 6.2 [1] (s br, 2 H, CH_{bzac}), 7.4 (m), 7.9 (d, 10 H, Ph_{bzac}). ^1H NMR ($CDCl_3$, 248 K): δ = 0.76 [s, $^2J(Sn\text{-}^1H)$ = 97.8 Hz, 6 H, Sn−Me)], 2.15 [5], 2.21 [1] (s, 6 H, Me_{bzac}), 6.02 [5], 6.21 [1] (s, 2 H, CH_{bzac}), 7.4 (m), 7.88 (d, 10 H, Ph_{bzac}). ^1H NMR ($CDCl_3$, 218 K): δ = 0.76 [4], 0.77 [5] [s, 6 H, Sn−Me, $^2J(Sn\text{-}^1H)$ = 98 Hz], 2.17 [5], 2.22 [1] (s, 6 H, Me_{bzac}), 6.01 [5], 6.03 [4], 6.22 [2] (s, 2 H, CH_{bzac}), 7.4 (m), 7.88 (d, 10 H, Ph_{bzac}). ^1H NMR ($CDCl_3$, 326 K): δ = 0.75 [s, $^2J(Sn\text{-}^1H)$ = 97.5 Hz, 6 H, Sn−Me], 2.14 (s, 6 H, Me_{bzac}), 6.01 (s br, 2 H, CH_{bzac}), 7.4 (m), 7.88 (d, 10 H, Ph_{bzac}). ^1H NMR ($CDCl_3$+ equimolar quantity of bzac, 295 K): δ = 0.74 [s, $^2J(Sn\text{-}^1H)$ = 97.8 Hz, 6 H, Sn−Me], 2.15 [2], 2.19 [10], 2.23 [2] (s, 12 H, Me_{bzac}), 4.08 (s, 1 H, CH_{2bzac}), 6.00 [2], 6.20 [1], 6.20 [5], 6.24 [2] (s, 4 H, CH_{bzac}), 7.4 (m), 7.88 (d, 20 H, Ph_{bzac}), 16.4 (br, 3 H, OH_{bzac}). ^1H NMR ($CDCl_3$+ equimolar quantity of bzac, 223 K): δ = 0.75 [9], 0.79 [1] [s, $^2J(Sn\text{-}^1H)$ = 122 Hz, 6 H, Sn−Me], 2.16 (s, 12 H, Me_{bzac}), 6.11 (s br, 4 H, CH_{bzac}), 7.4 (m), 7.88 (d, 20 H, Ph_{bzac}). ^{13}C NMR ($CDCl_3$, 295 K): δ = 7.7 [s, $^1J(^{119}Sn\text{-}^{13}C)$ = 934, $^1J(^{117}Sn\text{-}^{13}C)$ = 886 Hz, Sn−Me] 28.9 (s, Me_{bzac}), 97.1 (s br, CH_{bzac}), 127.4, 128.3, 131.4, 138.8 (4s, Ph_{bzac}), 183.4 (s, CO_{bzac}), 193.0 (s, CO_{bzac}). ^{119}Sn ($CDCl_3$, 295 K): δ = −355. ^{119}Sn ($CDCl_3$, 273 K): δ = −356. ^{119}Sn ($CDCl_3$, 248 K): δ = −355 [4], 359 [5]. ^{119}Sn ($CDCl_3$, 218 K): δ = −356 [4], 361 [5]. Λм (10^{-3} м) = 0.05.

Derivatives **2**−**6** were synthesized in a similar way, **2** formed after stirring the solution for 36 h, **3** and **4** formed after 24 h, and **5** and **6** precipitated immediately upon mixing the reactants at 273 K.

Bis[1-phenylbutane-1,3-dionato]diethyltin(IV) [(bzac)$_2$SnEt$_2$] (2): Yield 80%. m.p. 157 °C dec. $C_{24}H_{28}O_4Sn$: calcd. C 57.75, H 5.65; found C 57.32, H 5.71. IR (nujol, cm^{-1}): $\tilde{\nu}$ = 1596 s, 1574 s, 1557 sh, 1519 m, ν(C=O) + ν(C=C); 568 m, 546 m, 531 m, 515 m, ν(Sn−C) + δ(bzac), 448 m, 413 m, ν(Sn−O). ^1H NMR ($CDCl_3$, 295 K): δ = 1.16 [t, $^3J(Sn\text{-}^1H)$ = 170 Hz, 6 H, Sn-Et], 1.47 [q, $^2J(Sn\text{-}^1H)$ = 98 Hz, 4 H, Sn−Et], 2.15 (s br, 6 H, Me_{bzac}), 6.0 (br, 2 H, CH_{bzac}), 7.4 (m), 7.87 (dd, 10 H, Ph_{bzac}). ^1H NMR ($CDCl_3$, 243 K): δ = 1.13 [t, $^3J(Sn\text{-}^1H)$ = 170 Hz, 6 H, Sn−Et], 1.47 [q, $^2J(Sn\text{-}^1H)$ = 98 Hz, 4 H, Sn−Et], 2.16 [5], 2.21 [4] (s, 6 H, Mebzac), 5.97 [5], 6.21 [4] (br, 2 H, CH_{bzac}), 7.78 (m), 7.87 (d, 10 H, Ph_{bzac}). ^{119}Sn ($CDCl_3$, 295 K): δ = −392, ^{119}Sn ($CDCl_3$, 243 K): δ = −390.5 [4], 392.5 [5]. Λм (10^{-3} м) = 0.1.

Bis[1-phenylbutane-1,3-dionato]diisobutyltin(IV) [(bzac)$_2$Sn(*i*Bu$_2$)] (3): Yield 55%. m.p. 209 °C (dec). $C_{28}H_{36}O_4Sn$ (555): calcd. C 60.57, H 6.53; found C 60.43, H 6.72. IR (nujol, cm^{-1}): $\tilde{\nu}$ = 1594 s, 1573 s, 1552 m, 1509 sh, ν(C=O) + ν(C=C); 599 br, 568 br, 550 m, 531 m, 517 m, 505 w, 493, 467 w, 440 br, ν(Sn−C) + ν(Sn−O). ^1H NMR ($CDCl_3$, 295 K): δ = 0.78 (t, 6 H, Sn-*i*Bu), 1.27 (m, 6 H, Sn-*i*Bu), 1.49 (m, 6 H, Sn-*i*Bu), 2.15 (s, 6 H, Me_{bzac}), 6.02 (br, 2 H, CH_{bzac}), 7.4 (m), 7.87 (dd, 10 H, Ph_{bzac}). ^{13}C NMR ($CDCl_3$, 295 K): δ = 13.78 (s, Sn-*i*Bu), 26.34 [s, $^1J(^{119}Sn\text{-}^{13}C)$ = 893, $^1J(^{117}Sn\text{-}^{13}C)$ = 810 Hz, Sn-*i*Bu], 27.14 (s, Sn-*i*Bu), 27.88 (s, Sn-*i*Bu), 28.0 (s, Me_{bzac}), 96.9 (s, CH_{bzac}), 127.25, 128.41, 131.81, 139.22 (s, Ph_{bzac}), 182.24 (s, CO_{bzac}), 193.31 (s, CO_{bzac}). ^{119}Sn NMR ($CDCl_3$, 295 K): Λ−389.8 [15], −392.4 [1]. Λм (10^{-3} м) = 0.1.

Bis[1-phenylbutane-1,3-dionato]di-*tert*-butyltin(IV) [(bzac)$_2$Sn(*t*Bu)$_2$] (4): Yield 71%. m.p. 151−153 °C. $C_{28}H_{36}O_4Sn$: calcd. C 60.57, H 6.53; found C 60.51, H 6.62. IR (nujol, cm^{-1}): 1592 s, 1558 s, ν(C=O) + ν(C=C); 575 s, 566 s, 528 s, 509 m, 447 m, 432 m, ν(Sn−C) + δ(bzac); 415 vs, 394 s, ν(Sn−O); 317 m, 305 m, 289 m, 261 s. ^1H NMR ($CDCl_3$, 295 K): δ = 1.20 [br, $^3J(^{119}Sn-^1H)$ = 131.7 Hz, $^3J(^{117}Sn-^1H)$ = 128.0 Hz, 18 H, Sn-*t*Bu], 2.13 [1], 2.16 [1] (s, 6 H, Me_{bzac}), 6.03 [1], 6.10 [1] (s, 2 H, CH_{bzac}), 7.38−7.52 (m, 6 H, Ph_{bzac}), 7.92 (d, 4 H, Ph_{bzac}). ^1H NMR($CDCl_3$, 218 K): δ = 1.16 [100], ($^3J(Sn-^1H)$ = 140.6 Hz), 1.24 [1], 1.28 [2], 1.40 [5] (br, 18 H, Sn-*t*Bu), 2.17 [7], 2.18 [7], 2.21 [3], 2.24 [1] (s, 6 H, Me_{bzac}), 6.03 [8], 6.07 [12], 6.14 [1], 6.17 [1], 6.21 [1], 6.23 [1] (s, 2 H, CH_{bzac}), 7.43−7.60 (m, 6 H, Ph_{bzac}), 7.84−8.02 (m, 4 H, Ph_{bzac}). ^{13}C NMR ($CDCl_3$, 295 K): δ = 29.4, 29.7, 29.9, 30.0 (4s, *t*Bu + Me_{bzac}), 49.4 (br, Sn−C), 97.7, 98.0, 98.1 (3s br, CH_{bzac}), 127.8, 128.8, 131.6, 132.2 (4s br, Ph_{bzac}), 183.8 (s, CO_{bzac}), 193.8 (s, CO_{bzac}). ^{119}Sn NMR ($CDCl_3$, 295 K): δ = −485.6. ^{119}Sn NMR ($CDCl_3$, 218 K): δ = −485.4 [1], −486.5 [2]. Λм (10^{-3} м) = 0.2.

Bis[1-phenylbutane-1,3-dionato]dicyclohexyltin(IV) [(bzac)$_2$SnCy$_2$] (5): Yield 56%. m.p. 150 °C (dec). $C_{32}H_{40}O_4Sn$: calcd. C 63.28, H 6.64; found C 63.36, H 6.71. IR (nujol, cm^{-1}): $\tilde{\nu}$ = 1593 s, 1575 m, 1560 m, 1558 vs, ν(C=O) + ν(C=C); 590 m, 580 m, 564 m, 546 m, 530 sh, 514 m, 500 m, 489 m, 474 m, 450 w, 440 m, 432 m, 419 m, 373 m, 328 m, ν(Sn−C) + ν(Sn−O) + δ(Ph). ^1H NMR ($CDCl_3$, 295 K): δ = 1.3 (br, 84 H, Sn-Cy), 1.6 (br, 10 H, Sn-Cy), 2.0 [2], 2.1 [1] (s br, 2 H, Sn-Cy), 6.0 [2], 6.11 [1], 6.13 [1], 6.20 [2] (s br, 2 H, CH_{bzac}), 7.5 (m, 6 H, Ph_{bzac}), 7.9 (d br, 4 H, Ph_{bzac}). ^{119}Sn NMR ($CDCl_3$, 295 K): δ = −466 [1], −467 [1] −468 [2]. Λм (10^{-3} м) = 0.3.

Bis[1-phenylbutane-1,3-dionato]diphenyltin(IV) [(bzac)$_2$SnPh$_2$] (6): Yield 74%. m.p. 130−132 °C. $C_{32}H_{28}O_4Sn$: calcd. C 64.57, H 4.74;

found C 64.34, H 4.66. IR (nujol, cm^{-1}): $\tilde{\nu}$ = 1592 s, 1564 vs, 1553 vs, ν(C=O) + ν(C=C); 580 s, 524 m, 455 s, 450 s, 430 m, 402 w, ν(Sn−O) + δ(bzac); 309 m, 267 vs, 253 s, ν(Sn−C); 237 m, 230, 223 m. ^{1}H NMR ($CDCl_3$, 295 K): δ = 2.12 [10], 2.16 [1], 2.19 [1] (s, 6 H, Me_{bzac}), 6.10 [5]. 6.17 [1] (s, 6 H, CH_{bzac}), 6.8−7.2 (m), 7.30−7.45 (m), 7.75 (dd), 7.90 (d, 20 H, Ph_{bzac} + Sn-Ph). ^{1}H NMR ($CDCl_3$, 325 K): δ = 2.12 (s br, 6 H, Me_{bzac}), 6.09 (s, 2 H, CH_{bzac}), 6.8−7.2 (m), 7.30−7.45 (m), 7.72 (d), 7.86 (d, 20 H, Ph_{bzac} + Sn-Ph). ^{1}H NMR ($CDCl_3$, 218 K): δ = 2.03 [10], 2.12 [10], 2.21 [1], 2.22 [10], 2.23 [12], 2.26 [2] (s, 6 H, Me_{bzac}), 6.14 [5]. 6.18 [4], 6.21 [4], 6.24 [4] (s, 6 H, CH_{bzac}), 6.9−8.0 (m, 20 H, Ph_{bzac} + Sn-Ph). ^{13}C NMR ($CDCl_3$, 295 K): δ = 26.4, 27.5, 28.6, 28.8 (4s, Me_{bzac}), 96.7, 97.8, 98.1 (3s br, CH_{bzac}), 127.0, 127.6, 127.9, 128.3, 128.5, 131.7, 132.3, 135.5, 135.9, 138.0, 148.5, 150.2 (s br, Ph_{bzac}), 184.0 (s, CO_{bzac}), 194.2, 194.6 (s, CO_{bzac}). ^{119}Sn NMR ($CDCl_3$, 296 K): δ = −509.9 [4], −510.5 [1]. ^{119}Sn NMR ($CDCl_3$, 218 K): δ = −503.8 [3], −504.3 [2], −504.7 [6]. ^{119}Sn NMR ($CDCl_3$, 325 K): δ = −511.2. Λм (10^{-3} м) = 0.4.

X-ray Crystallographic Studies

The structure was solved using direct methods with SIR.[46] Psi-scan showed no absorption anisotropy.

Crystals were obtained directly from the reaction mixture. Crystal data were collected with a Syntex P21 diffractometer. A diffraction quality crystal was selected and mounted on the diffractometer. The search subroutine showed orthorhombic axes and symmetry was the orthorhombic confirmed by taking rotation photograph about the 3 axes. Psi-scan showed no absorption anisotropy. Cell volume implies 8 molecules/cell and systematic extinctions indicated 2 possible space groups, *Pnma* and $Pna2_1$ (Table 3). Attempts to solve the structure in the centrosymmetric *Pnma* space group (which implies one molecule/asymmetric unit) failed, whereas using $Pna2_1$ space group (corresponding to 2 molecules in the asymmetric unit) allowed structure resolution with SIR.[46] The two independent molecules in the asymmetric unit show the [*x*,*y*,*z*] coordinates of corresponding atoms (for instance atoms named Sn and Sn2) add to [1.24, 0.02, 1.49]. Therefore an approximate local inversion point [0.625, 0.0, 0.75] relating the two independent molecules exists. Figure S1 depicts the cell packing approximately along axis *b*.

Table 3. Summary of crystal data

Empirical formula	$C_{28}H_{36}O_4Sn$
Formula mass	555.28
Cryst habit	hexagonal plate
Cryst size (mm)	0.40 × 0.25 × 0.10
Cryst system	orthorhombic
Space group	$Pna2_1$ (no. 33)
Crystal color	colorless
a (Å)	18.156(4)
b (Å)	10.012(2)
c (Å)	29.739(7)
V (Å^3)	5406(3)
Z	8
T (K)	298
$D_{calcd.}$ (Mg m^{-3})	1.365
$2\theta_{max}$ (°)	56
μ (mm^{-1})	0.983
Wavelength (Å) (graph monchr)	Mo-K_α
Scan speed (°min^{-1})	2
Transmission factors	0.99−1.00
Scan range (°)	1.2
Measured reflections	8713
Unique reflections	8039
Refined reflections $F>1.5\sigma(F)$	5773
Refined parameters	595
R,[a] R_w	0.043, 0.056
S[b]	0.82

[a] $R(F) = \Sigma|(Fo - Fc)|/\Sigma Fo$. [b] $S = [\Sigma\{w(F_0^2 - F_c^2)^2\}/(n - p)]^{0.5}$, *n* = no. of data and *p* = no. of refined parameters.

Each of the 4 pairs of molecules forming the cell is located approximately in each quarter of the picture and darker atoms are closest to the viewer. The four local inversion centers are evident. A further attempt to refine the structure in the *Pnma* space by shifting tin atom coordinates such that the inversion center found in $Pna2_1$ became the origin in *Pnma* was unsuccessful. This could be expected because there is no mirror plane evident (required for *Pnma*) in Figure S1; also the existence of only 4 inversion centers is coherent with 4 positions in $Pna2_1$ whereas a truly *Pnma* space group would require 8 inversion centers. The existence of local (non-crystallographic) centers of symmetry has been discussed by Marsh et al. who found that this feature accounts for at least 70% of all $Pna2_2$ structures explored in the CSD database.[47] Reflections collected: *h* [0−25], *k* [0−14], *l* [0−41]. H atoms riding on attached C atoms at 0.96 Å and hydrogen *B(iso)* fixed. Atomic scattering factors were taken from the literature.[48]

CCDC-171306 contains the supplementary crystallographic data for this paper. These data can be obtained free of charge at www.ccdc.cam.ac.uk/conts/retrieving.html [or from the Cambridge Crystallographic Data Centre, 12, Union Road, Cambridge CB2 1EZ, UK; Fax: (internat.) +44-1223/336-033; E-mail: deposit@ccdc.cam.ac.uk].

Theoretical Studies

All computations were carried out with the MULLIKEN program[49] package on an IBM/SP2 supercomputer. Hartree−Fock and MB3LYPDFT (Density-Functional Theory)[50] methods were used. The basis set used with both methods was 6−31G*. For the tin atom an ECP approximation[51−59] was applied, as implemented within MULLIKEN, using a double zeta basis. The MULLIKEN default convergence criteria were used in computations of energies and geometries.

Supporting Information (see also footnote on the first page of this article): HF and DFT Cartesian coordinates for $(bzac)_2Sn(tBu)_2$ and *anti* $(bzac)_2SnPh_2$, DFT Cartesian coordinates of *syn* $(bzac)_2SnPh_2$.

Acknowledgments

Financial support by Università di Camerino, Consiglio Nazionale delle Ricerche C.N.R.-Rome, The Camille and Henry Dreyfus Foundation (MR). This research was also supported by an IBM Shared University Research (SUR) grant, a CUNY Research Award, a CUNY Collaborative award, and a NASA JOVE grant.

[1] A. Maverick, G. L. Griffin, In *The Chemistry of Metal CVD*; (Eds.: T. T. Kodas, M. J. Hampden-Smith), VCH: Weinheim, **1994**, ch. 4, and references therein.
[2] P. Dobrzynski, J. Kasperczyk, M. Bero, *Macromolecules* **1999**, *32*, 4735.
[3] M. Bero, J. Kasperczyk, P. Dobrzynski, *Polymer Bulletin.* **1999**, *42*, 131.
[4] C. C. Chen, T. T. Huang, C. W. Lin, R. Cao, A. S. C. Chan, W. T. Wong, *Inorg. Chim. Acta* **1998**, *270*, 247.
[5] S. Dibella, G. Lanza, A. Gulino, I. Fragala, *Inorg. Chem.* **1996**, *35*, 3885.

[6] S. N. Slabzhennikov, V. I. Vovna, A. Y. Ustinov, *Koord. Khim.* **1995**, *21*, 451.
[7] K. D. Bos, H. A. Budding, E. J. Bulten, J. G. Noltes, *Inorg. Nucl. Chem. Lett.* **1973**, *9*, 961.
[8] I. Wakeshima, I. Kijima, *J. Organomet. Chem.* **1974**, *76*, 37.
[9] P. F. R. Ewings, P. G. Harrison, D. E. Fenton, *J. Chem. Soc., Dalton Trans.* **1975**, 821.
[10] P. F. R. Ewings, P. G. Harrison, T. J. King, *J. Chem. Soc., Dalton Trans.* **1975**, 1455.
[11] V. V. Bashilov, V. I. Sokolov, Y. L. Slovokhotov, Y. T. Struchkov, E. G. Mednikov, N. K. Eremenko, *J. Organomet. Chem.* **1987**, *327*, 285.
[12] G. A. Miller, E. O. Schlemper, *Inorg. Chem.* **1973**, *12*, 677.
[13] A. L. Allred, D. W. Thompson, *Inorg. Chem.* **1968**, *7*, 1196.
[14] C. Z. Moore, W. H. Nelson, *Inorg. Chem.* **1969**, *8*, 138,.
[15] D. W. Thompson, J. F. Lefelhocz, K. S. Wong, *Inorg. Chem.* **1972**, *11*, 1139.
[16] R. W. Jones, R. C. Fay, *Inorg. Chem.* **1973**, *12*, 2599.
[17] N. Serpone, K. A. Hersh, *Inorg. Chem.* **1974**, *13*, 2901.
[18] G. A. Miller, E. O. Schlemper, *Inorg. Chim. Acta* **1978**, *30*, 131.
[19] J. Otera, *J. Organomet. Chem.* **1981**, *221*, 57.
[20] G. Poli, C. J. Cheer, W. H. Nelson, *J. Organomet. Chem.* **1986**, *306*, 347.
[21] C. D. Chandler, G. D. Fallon, A. J. Koplick, *Aust. J. Chem.* **1987**, *40*, 1427.
[22] J. W. Faller, A. Davison, *Inorg. Chem.* **1967**, *6*, 182.
[23] W. H. Nelson, *Inorg. Chem.* **1967**, *6*, 1509.
[24] R. Merten, G. Loew, *U. S. No 3055845*, **1962**.
[25] H. J. Keller, B. Keppler, U. Krüger, R. Linder, *Eur. Pat. No* 49486, **1982**.
[26] D. Searle, P. J. Smith, N. A. Bell, L. A. March, I. W. Nowell, J. D. Donaldson, *Inorg. Chim. Acta* **1989**, *162*, 143.
[27] B. D. James, S. Gioskos, S. Chandra, R. J. Magee, *J. Organomet. Chem.* **1992**, *436*, 155.
[28] M. Vrnata, V. Myslik, F. Vyslouzil, M. Jelinek, *J. Electr. Eng.* **1998**, *49*, 200.
[29] C. Sreelatha, K. Srivastava, V. D. Gupta, *J. Chem. Soc., Dalton Trans.* **1988**, 407.
[30] R. F. Zahrobsky, *J. Am. Chem. Soc.* **1971**, *93*, 3313.
[31] D. L. Kepert, *Prog. Inorg. Chem.* **1977**, *23*, 1.
[32] C. Pettinari, F. Marchetti, A. Cingolani, C. Marciante, R. Spagna, M. Colapietro, *Polyhedron* **1994**, *13*, 939.
[33] [33a] F. Marchetti, C. Pettinari, A. Cingolani, L. Brocanelli, M. Rossi, F. Caruso, *J. Organomet. Chem.* **1999**, *580*, 344, and references therein. [33b] C. Pettinari, F. Marchetti, A. Cingolani, A. Lorenzotti, E. Mundorff, M. Rossi, F. Caruso, *Inorg. Chim. Acta* **1997**, *262*, 33. [33c] F. Caruso, D. Leonesi, F. Marchetti, E. Rivarola, M. Rossi, V. Tomov, C. Pettinari, *J. Organomet. Chem.* **1996**, *519*, 29. [33d] C. Pettinari, F. Marchetti, A. Cingolani, D. Leonesi, E. Mundorff, M. Rossi, F. Caruso, *J. Organomet. Chem.* **1998**, *557*, 187.
[34] [34a] B. S. Jensen, *Acta Chem. Scand.* **1959**, *13*, 1347, 1668, 1890. [34b] F. Bonati, L. A. Oro, M. T. Pinillos, *Polyhedron* **1985**, *4*, 357, and references therein. [34c] E. C. Okafor, B. A. Uzoukwu, *Radiochim. Acta.* **1990**, *51*, 167, and references therein. [34d] M. F. Mahon, K. C. Molloy, B. A. Omotowa, M. A. Mesubi, *J. Organomet. Chem.* **1996**, *525*, 239.
[35] F. Caruso, M. Rossi, F. Marchetti, C. Pettinari, *Organometallics* **1999**, *18*, 2398.
[36] [36a] L. Prasad, Y. Le Page, F. E. Smith, *Inorg. Chim. Acta* **1983**, *68*, 45. [36b] V. G. Kumar Das, C. Wei, Y. C. Keong, T. C. W. Mak, *J. Organomet. Chem.* **1986**, *299*, 41.
[37] K. Nakamoto, *Infrared and Raman Spectra of Inorganic and Coordination Compounds,* 4th ed., Wiley Interscience, New York, **1986**, chapter III, p. 259−257.
[38] [38a] M. McGrady, R. S. Tobias, *Inorg. Chem.* **1964**, *3*, 1157. [38b] R. W. Jones, R. C. Fay, *Inorg. Chem.* **1973**, *12*, 2599. [38c] I. Wharf, D. F. Shiver, *Inorg. Chem.* **1969**, *8*, 914. [38d] G. K. Sandhu, N. S. Boparoy, *J. Organomet. Chem.* **1991**, *411*, 89. [38e] F. Huber, M. Vornfield, G. Ruisi, R. Barbieri, *Appl. Organomet. Chem.* **1993**, *7*, 243. [38f] B. Y. K. Ho, J. J. Zuckerman, *Inorg. Chem.* **1973**, *12*, 1552.
[39] [39a] J. R. May, W. R. McWhinnie, R. C. Poller, *Spectrochim. Acta, Ser. A* **1971**, *27*, 969. [39b] A. L. Smith, *Spectrochim. Acta, Ser. A* **1967**, *24*, 695. [39c] M. S. Dance, W. R. McWhinnie, R. C. Poller, *J. Chem. Soc., Dalton Trans.* **1976**, 2349.
[40] [40a] T. P. Lockhart, W. F. Manders, *Inorg. Chem.* **1986**, *25*, 892. [40b] B. Wrackmeyer, *Ann. Rep. NMR Spectrosc.* **1985**, *16*, 73. [40c] W. F. Howard, Jr, R. W. Crecely, W. H. Nelson, *Inorg. Chem.* **1985**, *24*, 2204.
[41] [41a] D. G. Bickley, N. Serpone, *Inorg. Chem.* **1974**, *13*, 2908. [41b] D. G. Bickley, N. Serpone, *Inorg. Chim. Acta* **1978**, *28*, 169. [41c] D. G. Bickley, N. Serpone, *Inorg. Chem.* **1976**, *15*, 948. [41d] R. Willem, M. Gielen, H. Pepermans, K. Hallenga, A. Recca, P. Finocchiaro, *J. Am. Chem. Soc.* **1985**, *107*, 1153.
[42] [42a] J. A. S. Smith, E. J. Wilkins, *J. Chem. Soc. A* **1966**, 1749. [42b] R. Ueda, Y. Kawasaki, T. Tanaka, R. Okawara, *J. Organomet. Chem.* **1966**, *5*, 194. [42c] V. Doron, C. Fischer, *Inorg. Chem.* **1967**, *6*, 1917. [42d] J. W. Faller, A. Davison, *Inorg. Chem.* **1967**, *6*, 182. [42e] G. E. Glass, R. S. Tobias, *J. Organomet. Chem.* **1968**, *15*, 481.
[43] A. L. Rheingold, W. King, *Inorg. Chem.* **1989**, *28*, 1715.
[44] T. S. Basu Bau, E. R. T. Tiekink, *Z. Kristallogr.* **1999**, *214*, 566
[45] C. Pettinari, G. Rafaiani, F. Bonati, B. Bovio, *J. Organomet. Chem.* **1991**, *405*, 75.
[46] A. Altomare, M. C. Burla, M. Camalli, G. L. Cascarano, C. Giacovazzo, A. Guagliardi, A. G. G. Moliterni, G. Polidori, R. Spagna, *J. Appl. Cryst.* **1999**, *32*, 115.
[47] R. E. Marsh, V. Schomaker, F. H. Herbstein, *Acta Crystallogr., Sect. B* **1998**, *54*, 921.
[48] *International Tables for X-ray Crystallography*; Kinoch Press: Birmingham, UK, **1974**.
[49] MULLIKEN is IBM proprietary software.
[50] P. J. Stephens, F. J. Devlin, C. F. Chabalowski, M. J. Frisch, *J. Phys. Chem.* **1994**, *98*, 11623. MB3LYP is very similar to B3LYP defined in this paper, except it uses the local correlation functional of Perdew and Wang (J. P. Perdew, Y. Wang, *Phys Rev. B*, **1992**, *45*, 13244) instead of the Vosko, Wilk and Nusair functional.
[51] A. D. Becke, *J. Chem. Phys.* **1993**, *98*, 5648.
[52] W. Stevens, H. Basch, M. Krauss, *J. Chem. Phys.* **1984**, *81*, 6026.
[53] W. Stevens, P. G. Jasien, M. Krauss, H. Basch, *Can. J. Chem.* **1992**, *70*, 612.
[54] T. R. Cundari, W. J. Stevens, *J. Chem. Phys.* **1993**, *98*, 5555.
[55] L. F. Pacios, P. A. Christiansen, *J. Chem. Phys.* **1985**, *82*, 2664.
[56] M. M. Hurley, L. F. Pacios, P. A. Christiansen, R. B. Ross, W. C. Ermler, *J. Chem. Phys.* **1986**, *84*, 6840.
[57] L. A. LaJohn, P. A. Christiansen, R. B. Ross, T. Atashroo, W. C. Ermler, *J. Chem. Phys.* **1987**, *87*, 2812.
[58] R. B. Ross, J. M. Powers, T. Atashroo, W. C. Ermler, L. A. LaJohn, P. A. Christiansen, *J. Chem. Phys.* **1990**, *93*, 6654.
[59] W. C. Ermler, R. B. Ross, P. A. Christiansen, *Int. J. Quantum Chem.* **1991**, *40*, 829.

Received September 27, 2001
[I01380]

Copper Complexes of Chiral Tetradentate Binaphthyl Schiff-Base Ligands: Syntheses, X-ray Crystal Structures and Activity in Catalytic Asymmetric Cyclopropanation of Alkenes

Chi-Ming Che,*[a] Hoi-Lun Kwong,*[b] Wai-Cheung Chu,[a] Kin-Fai Cheng,[a] Wing-Sze Lee,[b] Hing-Sun Yu,[b] Chi-Tung Yeung,[b] and Keung-Kai Cheung[a]

Keywords: Asymmetric catalysis / Copper / Cyclopropanation / Schiff bases / Structure elucidation

A number of new chiral monomeric binaphthyl Schiff-base ligands H_2L [where H_2L = 2,2′-bis(3-R^1-5-R^2-2-hydroxybenzylideneamino)-1,1′-binaphthyl] and a series of chiral copper(II) complexes [CuL] were prepared in good or nearly quantitative yields. Some of the free ligands and the [CuL] complexes were structurally characterized by X-ray crystallography. Almost all the [CuL] complexes were found to be active catalysts for the asymmetric cyclopropanation of alkenes with ethyl or *tert*-butyl diazoacetate. Enantioselectivities of up to 77% *ee* were observed.
(© Wiley-VCH Verlag GmbH, 69451 Weinheim, Germany, 2002)

Introduction

Optically active cyclopropanes play an important role as intermediates in the syntheses of insecticides and drugs.[1] In this context, the search for effective catalysts for asymmetric cyclopropanation has continued to attract considerable interest.[2−3] Chiral ligands such as semicorrine,[4−7] bisoxazolines,[8−12] bipyridines[13−19] and Schiff bases[20−23] are the most efficient ligands for copper-catalyzed alkene cyclopropanation with diazoacetate.

Schiff-base ligands bearing a C_2-chiral auxiliary have been employed for a number of metal-catalyzed asymmetric reactions, such as Cu-catalyzed aziridination,[24−25] Mn-catalyzed epoxidation,[26] Co-catalyzed cyclopropanation,[27−29] Cr-catalyzed ring opening[30] and the hetero-Diels−Alder reaction.[31] In view of the excellent enantiofacial discriminating power exhibited by binaphthylic ligands in asymmetric metal catalysis,[32] we have previously studied the binaphthylic Schiff-base ligands 2,2′-bis(3-R^1-5-R^2-2-hydroxybenzylideneamino)-1,1′-binaphthyl (H_2L) and reported the use of their manganese and chromium complexes in the asymmetric oxidation of alkenes[33−35] and their titanium complexes in the asymmetric trimethylsilylcyanation of aldehydes.[36] Recently, great interest in the copper complexes of these binaphthylic Schiff-base ligands has arisen from a study of their derivatives as models for catalytic galactose oxidase.[37]

In the present work we describe the synthesis of a series of chiral copper(II)-binaphthyl Schiff-base complexes [CuL] together with several new chiral H_2L ligands. Some of the H_2L and [CuL] compounds were characterized by X-ray crystallography. The use of [CuL] complexes as catalysts for the asymmetric cyclopropanation of alkenes with an alkyl diazoacetate was explored, and this represents the first asymmetric alkene cyclopropanation catalyzed by metal complexes bearing a tetradentate binaphthyl Schiff-base ligand.

Results and Discussion

Synthesis of Chiral Schiff-base Ligands H_2L and Their Copper(II) Complexes [CuL]

Treatment of chiral 2,2′-diamino-1,1′-binaphthyl with various substituted salicylaldehydes afforded a series of chiral binaphthyl Schiff-base ligands H_2L^{1-13} in good yields. The preparation and characterization of $H_2L^{1,2,4-9}$ have been reported previously by us.[33,35] The new ligands $H_2L^{3,10-13}$ described in this work were obtained as orange crystalline solids and were characterized by IR, ^{1}H NMR and ^{13}C NMR spectroscopy (see Exp. Sect.). The key NMR spectral features of $H_2L^{3,10-13}$ include the imine proton resonances at δ = 8.53−8.73 (singlets), the aromatic proton resonances at δ = 6.62−8.15 (multiplets), the phenolic proton resonances at δ = 12.06−13.46 (broad singlets), and the

[a] Department of Chemistry and Open Laboratory of Chemical Biology of the Institute of Molecular Technology for drugs Discovery and Synthesis, The University of Hong Kong, Pokfulam Road, Hong Kong (China)
E-mail: cmche@hkucc.hku.hk
[b] Department of Biology and Chemistry and Open Laboratory of Chirotechnology of the Institute of Molecular Technology for drugs Discovery and Synthesis, City University of Hong Kong, Tat Chee Avenue, Kowloon, Hong Kong (China)
E-mail: bhhoik@cityu.edu.hk

^{13}C resonances of the CH=N groups at $\delta = 160.3-163.3$ (singlets), all of which are similar to those reported for $H_2L^{1,2,4-9}$.[33,35] The IR spectra of $H_2L^{3,10-13}$ each show a strong band in the 3075−3800 cm^{-1} region attributable to ν(OH) and a band at about 1613 cm^{-1} attributable to ν(C=N).

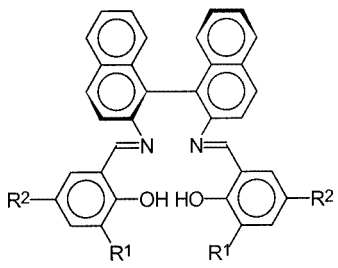

Ligand	R^1	R^2
H_2L^1	Cl	Cl
H_2L^2	Br	Br
H_2L^3	I	I
H_2L^4	*t*Bu	*t*Bu
H_2L^5	Cl	*t*Bu
H_2L^6	*t*Bu	Cl
H_2L^7	*t*Bu	NO_2
H_2L^8	Et	NO_2
H_2L^9	H	NO_2
H_2L^{10}	H	Cl
H_2L^{11}	Cl	H
H_2L^{12}	EtO	H
H_2L^{13}	H	Ph

The chiral copper complexes of H_2L^{1-13} were prepared from the reaction of optically active H_2L^{1-13} with $Cu(OAc)_2$ in dichloromethane/methanol at room temperature. These complexes are air stable both as solids and in solution, as revealed by visible or IR spectroscopy. Elemental analysis indicated that they have a Cu:L molar ratio of 1:1. A principal feature of the IR spectra of these complexes is the intense absorption band ranging from 1584 to 1619 cm^{-1} which is assigned to ν(C=N). These ν(C=N) bands are shifted by about 10−27 cm^{-1} from those of the corresponding H_2L^{1-13} ligands.

X-ray Structure Analyses

The structures of H_2L^{12} and $[CuL^2]$ were determined by X-ray crystallography (see Figure 1−2). The crystallographic data are summarized in Table 1. Selected bond lengths and bond angles are given in Table 2−3.

Previously we reported the X-ray crystal structure of the racemic form of complex $[CuL^1]$.[33] Like $[CuL^1]$, the complex $[CuL^2]$ features a distorted tetrahedral CuN_2O_2 core. The bond angles in the CuN_2O_2 core lie in the range 88.7°−154.0° ($[CuL^2]$). The Cu−N and Cu−O bond lengths are ≈1.97 and ≈1.90 Å, respectively. CuL^2 also possesses a twisted seven-membered CuN_2C_4 ring. The dihedral angle between the two naphthyl rings is 72.49°, which is similar to that in $[CuL^1]$ (≈75°) but is considerably smaller than that of the free H_2L^{12} ligand (85.54°). Comparison of the structures of $[CuL^{1,2}]$ with the reported X-ray structure of a copper complex of the chiral Schiff base with a cyclohexyl rather than a binaphthyl moiety clearly shows that the binaphthyl moieties of $[CuL^{1,2}]$ enforce a non-square planar coordination geometry, while the cyclohexyl moiety prefers a square planar environment.

Enantioselective Cyclopropanation of Alkenes Catalyzed by CuL

Having prepared the copper complexes $[CuL^{1-13}]$, we studied their catalytic activities towards the asymmetric cyclopropanation of styrene with alkyl diazoacetates N_2CHCO_2R (R = Et, *t*Bu). The results are compiled in Table 4. Note that all the reactions were carried out in styrene. To reduce the formation of side products such as fumarate and maleate, the alkyl diazoacetate was added slowly in each case.

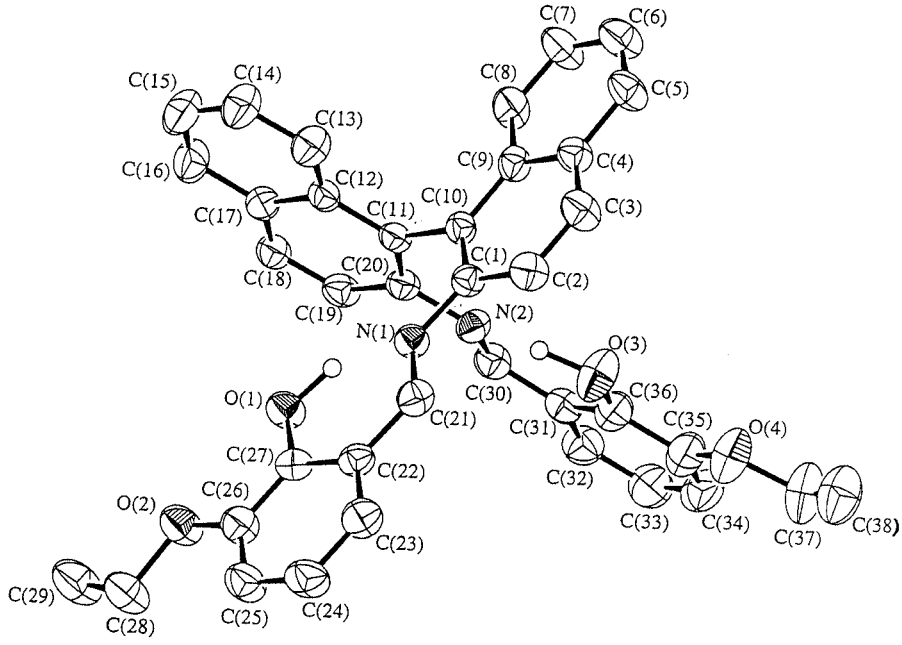

Figure 1. ORTEP drawing of H_2L^{12}

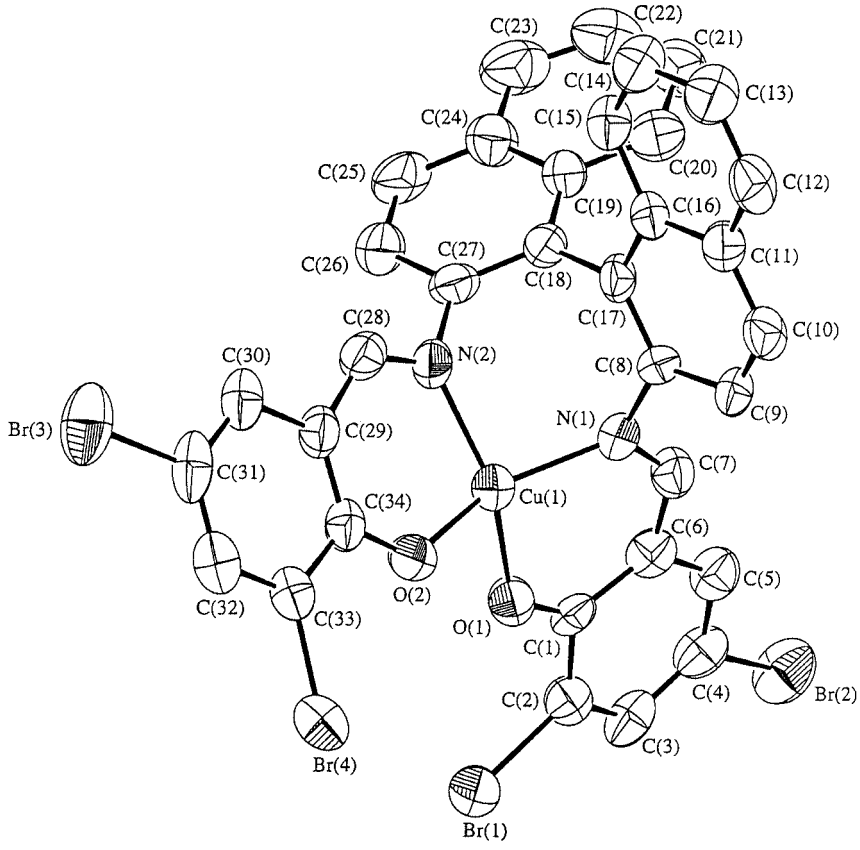

Figure 2. ORTEP drawing of [CuL^2]

Table 1. Crystallographic data for H_2L^{12} and [CuL^2]

	H_2L^{12}	[CuL^2]
Formula	$C_{38}H_{32}N_2O_4{\cdot}CH_2Cl_2$	$C_{34}H_{18}N_2O_2Br_4Cu{\cdot}2CH_2Cl_2$
F_w	665.61	1039.56
Color	orange	brown
Crystal system	triclinic	monoclinic
Space group	*P*1	*C*2/*c*
a [Å]	11.657(2)	36.453(3)
b [Å]	12.124(2)	12.581(2)
c [Å]	13.788(2)	17.039(3)
V [Å^3]	1652.3(6)	7600(1)
Z	2	8
Crystal dimensions [mm^3]	0.25 × 0.10 × 0.35	0.20 × 0.15 × 0.30
F(000)	696	4040
Radiation [Å]	0.7107	0.7107
hkl range *h*:	0 → 14	0 → 43
k	−12 → 14	0 → 14
l	−15 → 16	−19 → 14
Reflections collected (unique)	5164	6208
Obs. Reflections [$I > 3\sigma(I)$]	3295	3318
No. of variables	430	442
$2\theta_{max}$ [°]	51.1	51.0
(D-map) max. min. [e Å^{-3}]	0.48; 0.54	1.00; 0.89
R	0.070	0.055
R_w	0.108	0.066

Table 2. Selected bond lengths [Å] and angles [°] for H_2L^{12}

Bond lengths			
C(10)−C(l 1)	1.508(5)	O(1)−C(27)	1.347(5)
O(2)−C(26)	1.382(5)	O(2)−C(28)	1.447(5)
O(3)−C(36)	1.351(5)	O(4)−C(35)	1.371(6)
O(4)−C(37)	1.405(7)	N(1)−C(1)	1.411(5)
N(1)−C(21)	1.291(5)	N(2)−C(20)	1.414(5)
N(2)−C(30)	1.281(5)	C(21)−C(22)	1.437(6)
C(30)−C(31)	1.457(6)	C(28)−C(29)	1.517(7)
C(37)−C(38)	1.424(8)		
Bond angles			
C(26)−O(2)−C(28)	116.8(4)	C(35)−O(4)−C(37)	118.1(5)
C(1)−N(1)−C(21)	122.5(3)	C(20)−N(2)−C(30)	122.1(3)
N(l)−C(1)−C(2)	124.3(3)	N(1)−C(1)−C(10)	116.6(3)
N(2)−C(20)−C(11)	116.9(3)	N(2)−C(20)−C(19)	123.1(3)
N(l)−C(21)−C(22)	121.9(4)	N(2)−C(30)−C(31)	121.0(4)
O(2)−C(26)−C(25)	124.4(4)	O(2)−C(26)−C(27)	115.4(4)
O(1)−C(27)−C(22)	122.1(4)	O(1)−C(27)−C(26)	118.3(4)
O(2)−C(28)−C(29)	105.8(4)	O(4)−C(35)−C(34)	127.1(5)
O(4)−C(35)−C(36)	113.8(4)	O(3)−C(36)−C(31)	121.6(4)
O(3)−C(36)−C(35)	118.9(4)	O(4)−C(37)−C(38)	111.5(6)

Table 3. Selected bond lengths [Å] and angles [°] for $[CuL^2]$

Bond lengths			
Br(1)−C(2)	1.879(9)	Cu(1)−N(2)	1.912(7)
Br(2)−C(4)	1.906(9)	O(1)−C(1)	1.296(9)
Br(3)−C(31)	1.890(l)	O(2)−C(34)	1.306(9)
Br(4)−C(33)	1.881(l0)	N(1)−C(7)	1.290(l)
Cu(1)−O(1)	1.899(6)	N(1)−C(8)	1.440(l)
Cu(1)−O(2)	1.907(6)	N(2)−C(27)	1.430(l)
Cu(1)−N(1)	1.963(7)	N(2)−C(28)	1.290(l)
Bond angles			
O(1)−Cu(1)−O(2)	88.8(3)	Cu(1)−N(2)−C(27)	118.9(6)
O(1)−Cu(1)−N(1)	92.3(3)	Cu(1)−N(2)−C(28)	123.2(7)
O(1)−Cu(1)−N(2)	154.0(3)	C(27)−N(2)−C(28)	116.9(8)
O(2)−Cu(1)−N(1)	151.3(3)	Br(1)−C(2)−C(1)	117.6(7)
O(2)−Cu(1)−N(2)	94.2(3)	Br(1)−C(2)−C(3)	120.1(8)
N(1)−Cu(1)−N(2)	97.2(3)	Br(2)−C(4)−C(3)	120.3(8)
Cu(1)−O(1)−C(l)	127.0(6)	Br(2)−C(4)−C(5)	118.3(8)
Cu(1)−O(2)−C(34)	127.8(6)	Br(3)−C(31)−C(30)	118.0(10)
Cu(1)−N(1)−C(7)	124.3(7)	Br(3)−C(31)−C(32)	121.9(9)
Cu(1)−N(1)−C(8)	115.5(5)	Br(4)−C(33)−C(32)	119.3(8)
C(7)−N(1)−C(8)	119.2(8)	Br(4)−C(33)−C(34)	119.6(7)

The results in Table 4 reveal that complexes $[CuL^{1-3,5,8-13}]$ are active catalysts for the above styrene cyclopropanations. The yields of the isolated cyclopropyl esters were moderate to excellent (32−99%) and the enantioselectivities obtained range from 3 to 73% *ee*. GLC analysis of the reaction mixtures showed that the *trans*/*cis* ratios of the cyclopropyl esters fall in the range of 65:35 to 80:20. The absolute configurations of the cyclopropyl esters were determined to be (*1S,2S*) and (*1S,2R*) for the *trans*- and *cis*-isomers, respectively. Variation of the structure of the

Table 4. Catalytic asymmetric cyclopropanation of styrene with chiral [CuL] complexes

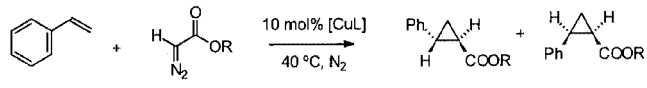

Entry[a]	Catalyst	R	*trans*:*cis*	% *ee* (*trans*)[b]	% *ee* (*cis*)[b]	% Yield[c]
1	$[CuL^1]$	Et	73:27	10 (1*S*,2*S*)	13 (1*S*,2*R*)	42
2		*t*Bu	75:25	35 (1*S*,2*S*)	48 (1*S*,2*R*)	48
3	$[CuL^2]$	Et	66:34	16 (1*S*,2*S*)	28 (1*S*,2*R*)	77
4		*t*Bu	73:27	47 (1*S*,2*S*)	66 (1*S*,2*R*)	80
5	$[CuL^3]$	Et	72:28	8 (1*S*,2*S*)	19 (1*S*,2*R*)	42
6		*t*Bu	71:29	33 (1*S*,2*S*)	56 (1*S*,2*R*)	73
7	$[CuL^4]$	Et	−	−	−	n.d.
8		*t*Bu	−	−	−	n.d.
9	$[CuL^5]$	Et	68:32	6 (1*S*,2*S*)	22 (1*S*,2*R*)	44
10		*t*Bu	75:25	10 (1*S*,2*S*)	40 (1*S*,2*R*)	39
11	$[CuL^6]$	Et	−	−	−	n.d.
12		*t*Bu	−	−	−	n.d.
13	$[CuL^7]$	Et	−	−	−	n.d.
14		*t*Bu	−	−	−	n.d.
15	$[CuL^8]$	Et	79:21	1 (1*S*,2*S*)	3 (1*S*,2*R*)	32
16		*t*Bu	80:20	22 (1*S*,2*S*)	43 (1*S*,2*R*)	57
17	$[CuL^9]$	Et	66:34	2 (1*S*,2*S*)	3 (1*S*,2*R*)	55
18		*t*Bu	69:31	15 (1*S*,2*S*)	38 (1*S*,2*R*)	44
19	$[CuL^{10}]$	Et	70:30	3 (1*S*,2*S*)	4 (1*S*,2*R*)	53
20		*t*Bu	74:26	14 (1*S*,2*S*)	35 (1*S*,2*R*)	82
21	$[CuL^{11}]$	Et	65:35	11 (1*S*,2*S*)	18 (1*S*,2*R*)	60
22		*t*Bu	77:23	74 (1*S*,2*S*)	73 (1*S*,2*R*)	83
23	$[CuL^{12}]$	Et	73:27	12 (1*S*,2*S*)	12 (1*S*,2*R*)	52
24		*t*Bu	76:24	26 (1*S*,2*S*)	31 (1*S*,2*R*)	66
25	$[CuL^{13}]$	Et	70:30	12 (1*S*,2*S*)	19 (1*S*,2*R*)	71
26		*t*Bu	74:26	14 (1*S*,2*S*)	35 (1*S*,2*R*)	99

[a] Styrene was used as solvent. [b] For R = Et, enantiomeric excesses were determined by HPLC with Daicel Chiralcel OJ column. For R = *t*Bu, enantiomeric excesses were determined by GC with a chiraldex β-PH column. Absolute configurations were determined by comparing the order of elution of samples with known configuration (ref.[4]). [c] Isolated yield after chromatography.

diazoacetates had a large effect on both *trans*/*cis* diastereoselectivity and enantioselectivity. As shown in Table 4, when the R group changes from ethyl to a bulkier *tert*-butyl group the reactions gave higher *trans*/*cis* ratios and *ee*'s. This is consistent with the trend previously observed for other copper catalysts.[4] To the best of our knowledge, complexes $[CuL^{1-3,5,8-13}]$ are the first examples of a well-defined tetrahedral copper complex that is active for alkene cyclopropanation.

We found that ligands with different substituents on the phenolic rings of the Schiff-base ligands gave different results in both reactivity and selectivity, similar to the observation reported by Jacobsen and co-workers in the Mn-catalyzed epoxidation of alkenes.[38] For example, $[CuL^2]$, with $R^1 = R^2 = Br$ (entries 3 and 4), gave a higher enantioselectivity than $[CuL^{1,3}]$, with $R^1 = R^2 = Cl$ (entries 1 and 2), or I (entries 5−6). The effect of R^1 groups on the catalyst activity can be evaluated by comparing the results obtained for $[CuL^{1,6,10}]$ ($R^2 = Cl$; $R^1 = Cl$, *t*Bu and H respectively; see entries 1, 2, 11, 12, 19, and 20), and for $[CuL^{7-9}]$ ($R^2 =$

NO_2; R^1 = *t*Bu, Et and H, respectively, see entries 13−18), which shows that ligands with either electron-withdrawing or electron-donating R^1 groups (such as Cl or Et) *increased* the enantioselectivity. However, the ligands with R^1 = *t*Bu form the complexes [$CuL^{4,6,7}$] that are inactive in cyclopropanation (entries 7, 8, 11−14). This might be due to the bulkiness of the *t*Bu groups, which prevents the copper centers from interacting effectively with the incoming diazoacetates or styrene. The effect of R^2 groups on the catalyst activity is different from that of the R^1 groups. Comparison of the results obtained for [$CuL^{1,5,11}$] (R^1 = Cl; R^2 = Cl, *t*Bu and H, respectively; see entries 1, 2, 9, 10, 21, and 22), and for [$CuL^{9,10,13}$] (R^1 = H; R^2 = NO_2, Cl and Ph, respectively; see entries 17−20, 25 and 26) reveals that ligands with either electron-withdrawing or electron-donating R^2 groups almost all *reduced* the enantioselectivity. Also, the catalyst with R^2 = *t*Bu groups is active in cyclopropanation (entries 9 and 10). These results demonstrate that the reactivity and selectivity of the [CuL^{1-13}]-catalyzed styrene cyclopropanations are greatly affected by both the steric and electronic properties of the R^1 groups and by the electronic properties of the R^2 groups in the catalysts.

Evidently, of the thirteen copper complexes [CuL^{1-13}], complexes [$CuL^{2,11}$] are the best catalysts for the styrene cyclopropanation in terms of the product yields and enantioselectivity (see Table 4). Therefore, we studied the cyclopropanation of other alkenes with these two catalysts. The reactions were carried out in dichloromethane instead of styrene in order to get a better comparison of the substrate effects. Table 5 shows the results obtained for the cyclopropanation of various alkenes with *tert*-butyl diazoacetate. The isolated yields of cyclopropyl esters were good to excellent (57−96%) and the *trans*/*cis* ratios ranged from 74:26 to 90:10. Comparison of entries 1 and 2 in Table 5 with entries 4 and 22 in Table 4 indicates that the *trans*/*cis* ratios obtained in dichloromethane are higher than in styrene, although lower enantioselectivities were attained in the former solvent. For the cyclopropanation of most of the al-

Table 5. Catalytic asymmetric cyclopropanation of alkenes with chiral [CuL] complexes

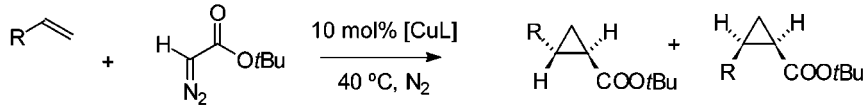

Entry	Catalyst	Substrate	Product	*trans*:*cis*	% ee (*trans*)[b]	% ee (*cis*)[b]	Yield %[c]
1	[CuL^2]		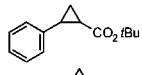	78:22	56 (*1S,2S*)	52 (*1S,2R*)	80
2	[CuL^{11}]			81:19	61 (*1S,2S*)	48 (*1S,2R*)	57
3	[CuL^2]	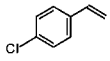	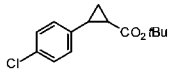	76:24	54	51	84
4	[CuL^{11}]			85:15	77	66	89
5	[CuL^{11}]	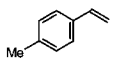	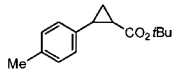	80:20	67	56	89
6	[CuL^{11}]	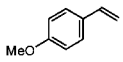	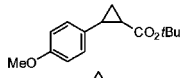	75:25	61	56	65
7	[CuL^{11}]	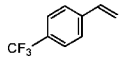	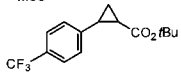	76:24	60	62	83
8	[CuL^2]		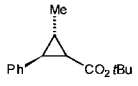	85:15	44	32	82
9	[CuL^{11}]			90:10	55	29	57
10	[CuL^2]		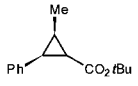	74:26	37	48	62
11	[CuL^{11}]			81:19	63	44	63
12	[CuL^2]		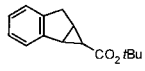	79:21	50	41	70
13	[CuL^{11}]			80:20	17	22	96
14	[CuL^2]	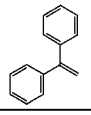	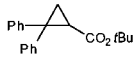	–	50		89
15	[CuL^{11}]			–	62		90

[a] Dichloromethane was used as solvent. [b] For entries 1−7 and 12−15, enantiomeric excesses were determined by GC with a chiraldex β-PH column. For entries 8−11, enantiomeric excesses were determined by literature procedure (ref.[4]). Absolute configurations were determined by comparing the order of elution of samples with known configuration (ref.[4]). [c] Isolated yield after chromatography.

kenes in Table 5, [CuL[11]] was a better catalyst than [CuL[2]]. The former catalyst gave 77 and 66% *ee* (*trans*- and *cis*-isomers, respectively) for the cyclopropanation of chlorostyrene (entry 4) and a 90:10 *trans*/*cis* ratio for the cyclopropanation of *trans*-β-methylstyrene (entry 9), which are the highest *ee* value or *trans*/*cis* ratio in Table 5.

To probe the nature of the active intermediates in the cyclopropanation reactions, we measured the relative rates of the [CuL[2]]-catalyzed cyclopropanation of substituted styrenes with EDA through competition experiments. The Hammett plot of $\log(K_X/K_H)$ versus σ^+ is shown in Figure 3, which indicates that substituted styrenes with electron-donating groups (such as 4-methoxy- and 4-methylstyrenes) gave larger cyclopropanation rates, whereas those with electron-withdrawing groups (such as 4-chloro- and 4-trifluoromethylstyrenes) gave smaller cyclopropanation rates. A good σ^+ correlation is obtained with $\rho = -0.72$. This value is similar to those of other copper catalysts such as copper-terpyridine ($\rho = -0.79$) and copper-di-pyridyl ketone ($\rho = -0.74$) recently reported by our group.[39,40] The small negative value of ρ obtained supports the formation of electrophilic metal−carbene intermediates and only a moderate positive charge build-up at the benzylic carbon in the transition state in both systems.

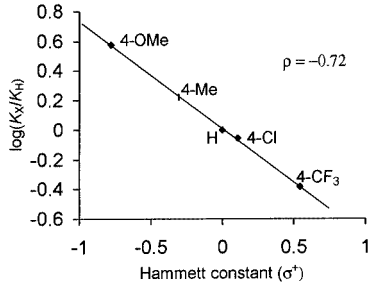

Figure 3. Hammett plot for the [CuL[2]]-catalyzed cyclopropanation of styrene with EDA

Conclusion

We have synthesizeds a series of tetrahedral copper(II) Schiff-base complexes [CuL] in nearly quantitative yield from the reaction of $Cu(OAc)_2$ with the chiral tetradentate binaphthyl Schiff-base ligands 2,2′-bis(3-R^1-5-R^2-2-hydroxybenzylideneamino)-1,1′-binaphthyl (H_2L). The structures of [CuL] feature distorted tetrahedral CuN_2O_2 cores, as revealed by X-ray crystallography. Almost all the chiral [CuL] complexes are good catalysts for the enantioselective cyclopropanation of alkenes with alkyl diazoacetate, affording the cyclopropyl esters in up to 77% *ee*. Both the steric and electronic properties of R^1 but only the electronic properties of R^2 have a large effect on the reactivity and enantioselectivity of the [CuL]-catalyzed cyclopropanation reactions. The highest enantioselectivity results from the catalyst bearing the new Schiff-base ligand L^{11} (R^1 = Cl, R^2 = H) prepared in this work.

Experimental Section

General: The chiral Schiff-base ligands $H_2L^{1,2}$ and H_2L^{4-9} were prepared as reported previously.[33,36] The substituted salicylaldehydes used in the syntheses were prepared by literature procedures.[41] Solvents for catalytic cyclopropanation were purified according to standard procedures.[42] *cis*-β-Methylstyrene was prepared by hydrogenation of 1-phenyl-1-propyne (Aldrich) using Lindlar catalysts.[43] All other alkene substrates used for catalytic cyclopropanation were purchased from Aldrich or Fluka and were purified either by vacuum distillation or by passing through activated alumina. IR spectra were recorded on a Shimadzu IR-470 or Nicolet 20sxc FTIR spectrometer, and NMR spectra were recorded on a Jeol GSX-270, Bruker 300 DPX or Bruker 500 DRX spectrometer in $CDCl_3$ unless otherwise stated, with TMS as internal standard at ambient temperature. Mass spectra were measured on a Finnigan MAT 95 high-resolution mass spectrometer and UV/Vis/NIR spectra on a Lambda 19 spectrometer. Analytical HPLC was performed on a Beckmann model 331 HPLC system with a model 163 variable UV/Vis detector or Hewlett Packard Model 1050 HPLC system. Chiral HPLC measurements were performed on a commercial column (Daicel Chemical Industries, Ltd., Chirlcel OJ). Analytical GC was performed on a Hewlett−Packard 5890 series II system equipped with an HP 5890A flame ionization detector and an HP 3395 integrator.

Preparation of the 1,1′-Binaphthyl Schiff-Base Ligands H_2L^3 and H_2L^{10-13}: A mixture of (*S*)-2,2′-diamino-l,l′-binaphthyl (0.5 mmol for H_2L^3, 1.0 mmol for the others) and the corresponding salicylaldehyde derivative (2.1 equiv.) in ethanol (10 mL for H_2L^3, 30 mL for the others) was stirred at room temperature for 3 h, resulting in precipitation of an orange solid. The precipitate was collected by filtration and washed with ethanol. Recrystallization from dichloromethane/ethanol afforded the desired product as an orange crystalline solid.

(*S*)-2,2′-Bis(2-hydroxy-3,5-diiodobenzylideneamino)-1,1′-binaphthyl [(*S*)-H_2L^3]: Yield: 79%, m.p. 196−198 °C, [α] = +302.1 (*c* = 0.968, $CHCl_3$). IR (Nujol): ṽ = 3290−3650 (OH), 1611 cm^{-1} (C=N). ^1H NMR (270 MHz, $CDCl_3$): δ = 7.08 (d, $J_{4'',6''}$ = 2.44 Hz, 1 H, 4"-H), 7.18 (d, *J* = 8.31 Hz, 1 H, 5-H or 8-H), 7.26 (d, $J_{4'',6''}$ = 2.44 Hz, 1 H, 6"-H), 7.28−7.31 (m, 1 H, 6-H or 7-H), 7.44−7.50 (m, 1 H, 6-H or 7-H), 7.59 (d, $J_{3,4}$ = 8.79 Hz, 1 H, 4-H), 7.97 (d, *J* = 8.06 Hz, 1 H, 5-H or 8-H), 8.11 (d, $J_{3,4}$ = 8.78 Hz, 1 H, 3-H), 8.55 (s, 1 H, ArC*H*=NAr), 12.76 (s, 1 H, 2"-OH). ^{13}C NMR (270 MHz, $CDCl_3$): δ = 116.8, 120.4, 122.4, 123.1, 126.4, 126.5, 127.3, 128.5, 129.7, 130.5, 132.5, 132.9, 133.1, 142.8, 155.4, 160.4.

(*S*)-2,2′-Bis(5-chloro-2-hydroxybenzylideneamino)-1,1′-binaphthyl [(*S*)-H_2L^{10}]: Yield: 84%, m.p. 144−146 °C, [α] = +425.6 (*c* = 0.972, $CHCl_3$). IR (Nujol): ṽ = 3290−3650 (OH), 1611 cm^{-1} (C=N). ^1H NMR (300 MHz, $CDCl_3$): δ = 6.62 (d, $J_{3'',4''}$ = 8.8 Hz, 1 H, 3"-H), 7.08 (d, *J* = 2.6 Hz, 1 H, 5-H or 8-H), 7.11 (d, *J* = 2.6 Hz, 1 H, 5-H or 8-H), 7.20−7.31 (m, 3 H, 6"-H, 6-H and 7-H), 7.44−7.49 (m, 1 H,), 7.63 (d, $J_{3,4}$ = 8.89 Hz, 1 H, 4-H), 7.97 (d, $J_{3'',4''}$ = 8.2 Hz, 1 H, 4"-H), 8.11 (d, $J_{3,4}$ = 8.8 Hz, 1 H, 3-H), 8.58 (s, 1 H, Ar′C*H*=NAr), 12.06 (s, 1 H, OH). ^{13}C NMR (300 MHz, $CDCl_3$): δ = 116.4, 120.0, 123.3, 124.6, 126.2, 126.4, 127.2, 128.3, 129.9, 130.2, 131.0, 132.6, 132.7, 133.1, 143.0, 159.3, 160.3.

(*S*)-2,2′-Bis(3-chloro-2-hydroxybenzylideneamino)-1,1′-binaphthyl [(*S*)-H_2L^{11}]: Yield: 82%, m.p. 213−215 °C, [α] = +175.0 (*c* = 0.508, $CHCl_3$). IR (Nujol): ṽ = 3290−3650 (OH), 1611 cm^{-1} (C=N). ^1H NMR (300 MHz, $CDCl_3$): δ = 7.25−7.31 (m, 1 H, 6-H or 7-H), 7.46−7.51 (m, 1 H, 6-H or 7-H), 7.58 (d, $J_{3,4}$ = 8.84 Hz, 1 H, 4-

H), 7.75−7.82 (m, 3 H, 4"-H, 5"-H and 6"-H), 8.00 (d, J = 8.17 Hz, 1 H, 5-H or 8-H), 8.08 (d, $J_{3,4}$ = 8.86 Hz, 1 H, 3-H), 8.59 (s, 1 H, Ar′CH=NAr), 12.79 (s, 1 H, OH). ^{13}C NMR (300 MHz, $CDCl_3$): δ = 117.3, 121.3, 122.4, 123.9, 126.1, 126.5, 126.8, 127.1, 128.4, 129.5, 130.3, 130.6, 132.9, 133.7, 142.7, 156.6, 161.9.

(*S*)-2,2′-Bis(3-ethoxy-2-hydroxybenzylideneamino)-1,1′-binaphthyl [(*S*)-H_2L^{12}]: Yield: 75%, m.p. 228−230 °C, [α] = +382.7 (c = 0.980, $CHCl_3$). IR (Nujol): $\tilde{\nu}$ = 3075−3800 (OH), 1615 cm^{-1} (C=N). ^{1}H NMR (300 MHz, $CDCl_3$): δ = 1.34 (t, J = 7.0 Hz, 3 H, CH_3CH$_2$O-), 3.62 (q, J = 7.0 Hz, 2 H, CH$_3$CH_2O-), 6.65−6.81 (m, 2 H, 4"-H and 5"-H), 6.83 (d, J = 7.96 Hz, 1 H, 5-H or 8-H), 7.15−7.26 (m, 2 H, 6-H and 7-H), 7.38−7.44 (m, 1 H, 6"-H), 7.50 (d, $J_{3'',4''}$ = 8.77 Hz, 1 H, 4-H), 7.91 (d, J = 8.16 Hz, 1 H, 5-H or 8-H), 8.00−(d, $J_{3,4}$ = 8.77 Hz, 1 H, 3-H), 8.53 (s, 1 H, ArCH=NAr), 12.30 (s, 1 H, OH). ^{13}C NMR (300 MHz, $CDCl_3$): δ = 14.75 (CH_3CH$_2$O), 64.6 (CH$_3$CH_2O), 116.4, 118.0, 118.1, 119.4, 124.1, 125.7, 126.5, 126.8, 128.3, 130.1, 132.4, 133.2, 144.7, 147.2, 151.2, 163.3.

(*S*)-2,2′-Bis(5-phenyl-2-hydroxybenzylideneamino)-1,1′-binaphthyl [(*S*)-H_2L^{13}]: Yield: 74%, m.p. 144−146 °C, [α] = +233.5 (c = 0.984, $CHCl_3$). IR (Nujol): $\tilde{\nu}$ = 3075−3800 (OH), 1619 cm^{-1} (C=N). ^{1}H NMR (300 MHz, $CDCl_3$): δ = 7.25−7.36 (m, 5 H, 3′-H, 4"-H, 6-H, 7-H and 5-H or 8-H), 7.39−7.47 (m, 5 H, Ar"′H), 7.49 (d, $J_{4'',6''}$ = 3.1 Hz, 1 H, 6"-H), 7.67 (d, $J_{3,4}$ = 8.87 Hz, 1 H, 4-H), 7.15−7.26 (m, 2 H, 6-H and 7-H), 7.38−7.44 (m, 1 H, 6"-H), 7.50 (d, $J_{3'',4''}$ = 8.77 Hz, 1 H, 4-H), 7.98 (d, J = 8.17 Hz, 1 H, 5-H or 8-H), 8.13 (d, $J_{3,4}$ = 8.83 Hz, 1 H, 3-H), 8.74 (s, 1 H, Ar′CH=NAr), 12.16 (s, 1 H, OH). ^{13}C NMR (300 MHz, $CDCl_3$): δ = 116.8, 117.5, 119.4, 126.0, 126.5, 126.8, 127.1, 128.3, 129.6, 130.1, 130.4, 131.6, 132.0, 132.6, 133.2, 140.1, 143.7, 160.3, 161.8.

General Procedure for the Synthesis of [CuL]: A solution of $Cu(OAc)_2$ (1.5 equiv.) in methanol was added to a solution of binaphthyl ligand H_2L in dichloromethane. The mixture was stirred at room temperature for 3 h, resulting in precipitation of crude [CuL] as a dark green solid. The crude product was collected by filtration, washed with methanol and recrystallized with dichloromethane/ethanol or dichloromethane/pentane. Yield: close to 100%.

[CuL^1]: $C_{34}H_{18}Cl_4CuN_2O_2$ (691.9): calcd. C 59.02, H 2.62, N 4.05; found C 59.02, H 2.60, N 4.10. IR (KBr): $\tilde{\nu}$ = 1607 cm^{-1} (C=N). Visible spectrum (CH_2Cl_2): λ_{max} (ε) = 414 (19500), 652 nm (336). FAB MS: m/z = 690 [M + H]$^+$.

[CuL^2]: $C_{34}H_{18}Br_4CuN_2O_2$ (869.7): calcd. C 46.96, H 2.09, N 3.22; found C 48.10, H 2.22, N 3.01. IR (KBr): $\tilde{\nu}$ = 1600 cm^{-1} (C=N). Visible spectrum (CH_2Cl_2): λ_{max} (ε) = 414 (20900), 649 nm (384). FAB MS: m/z = 866 [M + H]$^+$.

[CuL^3]: $C_{34}H_{18}CuI_4N_2O_2$ (1057.7): calcd. C 38.61, H 1.72, N 2.65; found C 40.20, H 2.10, N 2.41. IR (KBr): $\tilde{\nu}$ = 1584 cm^{-1} (C=N). Visible spectrum (CH_2Cl_2): λ_{max} (ε) = 418 (21300), 640 nm (465). FAB MS: m/z = 1058 [M + H]$^+$.

[CuL^4]: $C_{50}H_{54}CuN_2O_2$ (778.5): calcd. C 77.14, H 6.99, N 3.60; found C 76.69, H 6.90, N 3.50. IR (KBr): $\tilde{\nu}$ = 1586 cm^{-1} (C=N). Visible spectrum (CH_2Cl_2): λ_{max} (ε) = 419 nm (25900), 647 nm (626). FAB MS: m/z = 778 [M + H]$^+$.

[CuL^5]: $C_{42}H_{36}Cl_2CuN_2O_2$ (735.2): calcd. C 68.61, H 4.94, N 3.81; found C 69.42, H 4.85, N 3.47. IR (KBr): $\tilde{\nu}$ = 1611 cm^{-1} (C=N). Visible spectrum (CH_2Cl_2): λ_{max} (ε) = 418 (24000), 648 nm (546). FAB MS: m/z = 734 [M]$^+$.

[CuL^6]: $C_{42}H_{36}Cl_2CuN_2O_2$ (735.2): calcd. C 68.61, H 4.94, N 3.81; found C 69.91, H 5.09, N 3.50. IR (KBr): $\tilde{\nu}$ = 1595 cm^{-1} (C=N). Visible spectrum (CH_2Cl_2): λ_{max} (ε) = 414 (19500), 652 nm (336). FAB MS: m/z = 734 [M + H]$^+$.

[CuL^7]: $C_{42}H_{36}CuN_4O_6$ (756.3): calcd. C 66.70, H 4.80, N 7.41; found C 65.96, H 4.50, N 7.38. IR (KBr): $\tilde{\nu}$ = 1595 cm^{-1} (C=N). Visible spectrum (CH_2Cl_2): λ_{max} (ε) = 371 (46000), 654 nm (398). FAB MS: m/z = 756 [M + H]$^+$.

[CuL^8]: $C_{38}H_{28}CuN_4O_6$ (700.2): calcd. C 65.18, H 4.03, N 8.00; found C 63.6, H 3.83, N 7.62. IR (KBr): $\tilde{\nu}$ = 1608 cm^{-1} (C=N). Visible spectrum (CH_2Cl_2): λ_{max} (ε) = 368 (56000), 651 nm (500). FAB MS: m/z = 700 [M + H]$^+$.

[CuL^9]: $C_{34}H_{20}CuN_4O_6$ (644.1): calcd. C 63.40, H 3.13, N 8.70; found C 65.20, H 3.13, N 8.50. IR (KBr): $\tilde{\nu}$ = 1607 cm^{-1} (C=N). Visible spectrum (CH_2Cl_2): λ_{max} (ε) = 357 (56700), 652 nm (419). FAB MS: m/z = 644 [M + H]$^+$.

[CuL^{10}]: $C_{34}H_{20}Cl_2CuN_2O_2$ (623.0): calcd. C 65.55, H 3.24, N 4.50; found C 63.50, H 3.87, N 4.11. IR (KBr): $\tilde{\nu}$ = 1608 cm^{-1} (C=N). Visible spectrum (CH_2Cl_2): λ_{max} (ε) = 412 nm (2120). FAB MS: m/z = 622 [M + H]$^+$.

[CuL^{11}]: $C_{34}H_{20}Cl_2CuN_2O_2$ (623.0): calcd. C 65.55, H 3.24, N 4.50; found C 64.44, H 3.61, N 4.15. IR (KBr): $\tilde{\nu}$ = 1604 cm^{-1} (C=N). Visible spectrum (CH_2Cl_2): λ_{max} (ε) = 404 (19500), 653 nm (321). FAB MS: m/z = 622 [M + H]$^+$.

[CuL^{12}]: $C_{38}H_{30}CuN_2O_4$ (642.2): calcd. C 71.07, H 4.71, N 4.36; found C 71.46, H 4.55, N 4.04. IR (KBr): $\tilde{\nu}$ = 1605 cm^{-1} (C=N). Visible spectrum (CH_2Cl_2): λ_{max} (ε) = 410 (26800), 653 nm (428). FAB MS: m/z = 642 [M + H]$^+$.

[CuL^{13}]: $C_{46}H_{30}CuN_2O_2$ (706.3): calcd. C 78.22, H 4.25, N 3.96; found C 77.58, H 4.28, N 4.10. IR (KBr): $\tilde{\nu}$ = 1619 cm^{-1} (C=N). Visible spectrum (CH_2Cl_2): λ_{max} (ε) = 422 (23500), 640 nm (625). FAB MS: m/z = 706 [M + H]$^+$.

X-ray Crystallography: Suitable crystals of ligand H_2L^{12} and complex [CuL^2] were obtained by recrystallization of the compounds from dichloromethane/ethanol. Diffraction data were collected on a Rigaku AFC7R diffractometer at ambient temperature. Intensity data were corrected for Lorentz and polarization effects. Absorption corrections based on the χ scan technique were also applied. The structure was solved by direct methods (SIR 92) and refined on F by least-squares analysis. The absolute structure of the molecule was determined by analysis of both configurations including the anomalous scattering effect. Hydrogen atoms were placed in their ideal positions (C−H: 0.95 Å) and included in the structure factor calculations but were not refined. All calculations were performed on a silicon Graphic workstation with the teXsan package.[44]

CCDC-171639 and -171640 contain the supplementary crystallographic data for this paper (excluding structure factors). These data can be obtained free of charge at www.ccdc.cam.ac.uk/conts/retrieving.html [or from the Cambridge Crystallographic Data Centre, 12, Union Road, Cambridge CB2 1EZ, UK; Fax: (internat.) +44-1223/336-033; E-mail: deposit@ccdc.cam.ac.uk].

General Procedure for [CuL]-Catalyzed Diazoester Cyclopropanation of Styrene: A mixture of styrene (10 mmol) and [CuL] (0.5 mmol) was heated with stirring under nitrogen at 40 °C. To this mixture was added dropwise a solution of styrene (10 mmol) and ethyl or *tert*-butyl diazoacetate (5 mmol) over a period of 4 h. During this period, gas bubbles were evolved. The reaction was complete when no more bubbles were given off. The reaction products were isolated by column chromatography. The enantiomeric excess was measured by HPLC (Daicel Chemical Industries, Ltd., Chiral OJ column).

Relative Reactivity of Styrenes in the [CuL]-Catalyzed Cyclopropanation: In a typical competition reaction, equimolar amounts of styrene and substituted styrene (10 mmol each) and the copper

complex (0.5 mmol) were mixed in dichloromethane (5 mL) at 40 °C. To this mixture was added dropwise a solution of ethyl diazoacetate (1 mmol) over a period of 4 h. During this period, gas bubbles were evolved. The reaction was complete when no more bubbles were given off. The amounts of cyclopropyl esters formed were analyzed by GC and NMR spectroscopy.

Acknowledgments

We thank the Hong Kong Research Grants Council [PolyU 01/97C], Generic Drug Program of the University of Hong Kong, and City University of Hong Kong [CityU DAG 7100203] for financial support.

[1] T. Aratani, in *Comprehensive Asymmetric Catalysis* (Eds.: E. N. Jacobsen, A. Pfaltz, H. Yamamoto), Springer, Heidelberg, **1999**, p. 1451.
[2] M. P. Doyle, in *Catalytic Asymmetric Synthesis* (Ed.: I. Ojima), VCH, New York, **1993**, p. 63.
[3] M. P. Doyle, M. N. Protopopova, *Tetrahedron* **1998**, *54*, 7919
[4] H. Fritschi, U. Leutenegger, A. Pfaltz, *Helv. Chim. Acta* **1988**, *71*, 1553.
[5] H. Fritschi, U. Leutenegger, A. Pfaltz, *Angew. Chem. Int. Ed. Engl.* **1986**, *25*, 1005.
[6] H. Fritschi, U. Leuteneggar, K. Siegmann, A. Pfaltz, W. Keller, C. Kratky, *Helv. Chim. Acta* **1988**, *71*, 1541.
[7] D. Muller, G. Umbricht, B. Weber, A. Pfaltz, *Helv. Chim. Acta* **1991**, *74*, 232.
[8] D. A. Evans, K. A. Woerpel, M. M. Hinman, M. F. Faul, *J. Am. Chem. Soc.* **1991**, *113*, 726.
[9] R. E. Lowenthal, A. Abiko, S. Masamune, *Tetrahedron Lett.* **1990**, *31*, 6005.
[10] T. G. Gant, M. C. Noe, E. J. Corey, *Tetrahedron Lett.* **1995**, *36*, 8745.
[11] Y. Uozumi, H. Kyota, E. Kishi, K. Kitayama, T. Hayashi, *Tetrahedron: Asymmetry* **1996**, *7*, 1603.
[12] S. G. Kim, C. W. Cho, K. H. Ahn, *Tetrahedron: Asymmetry* **1997**, *8*, 1023.
[13] K. Ito, S. Tabuchi, T. Katsuki, *Synlett* **1992**, 575.
[14] K. Ito, T. Katsuki, *Tetrahedron Lett.* **1993**, *34*, 2661.
[15] K. Ito, T. Katsuki, *Synlett* **1993**, 638.
[16] H.-L. Kwong, W.-S. Lee, H.-F. Ng, W.-H. Chiu, W.-T. Wong, *J. Chem. Soc., Dalton Trans.* **1998**, 1043.
[17] R. Rios, J. Liang, M. M. C. Lo, G. C. Fu, *Chem. Commun.* **2000**, 377.
[18] D. Lötscher, S. Rupprecht, H. Stoeckli-Evans, A. von Zelewsky, *Tetrahedron: Asymmetry* **2000**, *11*, 4341.
[19] H. L. Wong, Y. Tian, K. S. Chan, *Tetrahedron Lett.* **2000**, *41*, 7723.
[20] T. Aratani, Y. Yoneyoshi, T. Nagase, *Tetrahedron Lett.* **1975**, 1707.
[21] T. Aratani, Y. Yoneyoshi, T. Nagase, *Tetrahedron Lett.* **1977**, 2599.
[22] T. Aratani, Y. Yoneyoshi, T. Nagase, *Tetrahedron Lett.* **1982**, *23*, 685.
[23] T. Aratani, *Pure Appl. Chem.* **1985**, *57*, 1839.
[24] Z. Li, K. R. Conser, E. N. Jacobsen, *J. Am. Chem. Soc.* **1993**, *115*, 5326.
[25] Z. Li, R. W. Quan, E. N. Jacobsen, *J. Am. Chem. Soc.* **1995**, *117*, 5889.
[26] W. Zhang, J. L. Loebach, S. R. Wilson, E. N. Jacobsen, *J. Am. Chem. Soc.* **1990**, *112*, 2801.
[27] T. Fukuda, T. Katsuki, *Synlett* **1995**, 825.
[28] T. Fukuda, T. Katsuki, *Tetrahedron* **1997**, *53*, 7201.
[29] T. Uchida, B. Saha, T. Katsuki, *Tetrahedron Lett.* **2001**, *42*, 2521.
[30] W. Zhang, E. N. Jacobsen, *J. Org. Chem.* **1991**, *56*, 2296.
[31] E. N. Jacobsen, W. Zhang, L. C. Muci, J. R. Ecker, L. Deng, *J. Am. Chem. Soc.* **1991**, *113*, 7063.
[32] R. Noyori, H. Takaya, *Acc. Chem. Res.* **1990**, *23*, 345 and refs. therein.
[33] C.-W. Ho, W.-C. Cheng, M.-C. Cheng, S.-M. Peng, K. F. Cheng, C.-M. Che, *J. Chem. Soc., Dalton Trans.* **1996**, 405.
[34] M.-C. Cheng, M. C.-W. Chen, S.-M. Peng, K.-K. Cheung, C.-M. Che, *J. Chem. Soc., Dalton Trans.* **1997**, 3479.
[35] X.-G. Zhou, X.-Q. Yu, J.-S. Huang, S.-G. Li, L.-S. Li, C.-M. Che, *Chem. Commun.* **1999**, 1789.
[36] X.-G. Zhou, J.-S. Huang, P.-H. Ko, K.-K. Cheung, C.-M. Che, *J. Chem. Soc., Dalton Trans.* **1999**, 3303.
[37] Y. Wang, J. L. Dubois, B. Hedman, K. O. Hodgson, T. D. P. Stack, *Science* **1998**, *279*, 537.
[38] E. N. Jacobsen, W. Zhang, M. L. Güler, *J. Am. Chem. Soc.* **1991**, *113*, 6703.
[39] H.-L. Kwong, L.-S. Cheng, W.-S. Lee, W.-L. Wong, W.-T. Wong, *Eur. J. Inorg. Chem.* **2000**, *9*, 1997.
[40] H.-L. Kwong, W.-S. Lee, *Tetrahedron: Asymmetry* **2000**, *11*, 2299.
[41] S. J. Angyal, P. J. Morris, J. R. Tetaz, J. G. Wilson, *J. Chem. Soc.* **1950**, 2141.
[42] D. D. Perrin, W. L. F. Armarego, D. R. Perrin, *Purification of Laboratory Chemicals*, 2nd ed., Pergamon, Oxford, **1980**.
[43] H. Lindler, R. Dubuis, *Org. Synth., Coll. Vol. V* **1973**, 880.
[44] *teXsan, Crystal Structure Analysis Package*, Molecular structure Corporation, Houston, Tx, USA, **1985**, **1992**.

Received October 5, 2001
[I01393]

Interactions between Copper(II) Complexes of Mono-, Bis-, and Tris(macrocyclic) Ligands and Inorganic or Organic Guests

Peter Comba,*[a] Yaroslaw D. Lampeka,*[b] Alexander Y. Nazarenko,[c] Alexander I. Prikhod'ko,[b] and Hans Pritzkow[a]

Keywords: Copper / Host-guest complexes / Macrocycles / Molecular recognition Template synthesis

The copper(II)-assisted condensation of $[Cu(2,3,2\text{-tet})]^{2+}$ [2,3,2-tet = bis-*N*,*N*′-(2-aminoethyl)propane-1,3-diamine] with formaldehyde and melamine (melamine = 2,4,6-triamino-1,3,5-triazine) afforded melamine-based mono-, bis-, and tris(macrocyclic) ligand/copper(II) complexes in approx. 30% overall yield. Three different monocopper(II), one dicopper(II), and one tricopper(II) complex structures are reported, as well as two structures of host-guest assemblies of the tricopper(II) complex with benzene-1,3,5-tricarboxylate and one resulting from a reaction with hexacyanoferrate(II) to afford an octanuclear Cu_6Fe_2 complex. These structures are discussed together with those of five previously reported similar compounds, and it is concluded that the two conformations of the tricopper(II) complex are similar in energy and that they are easily interconverted. The range of the structural flexibility of the tricopper(II) host is analyzed on the basis of the experimental structural data. The formation of the Cu_6Fe_2 assembly is assumed to be a stepwise procedure, the formation of the structurally previously unknown $[Fe_2(CN)_{11}]^{7-}$ anion is assisted by the Cu_3 host cation, and the host-guest assembly is stable in solution.

(© Wiley-VCH Verlag GmbH, 69451 Weinheim, Germany, 2002)

Introduction

Since the seminal work on the hexaamine cage ligands sepulchrate (sep)[1] and sarcophagine (sar) derivatives,[2,3] metal ion assisted Mannich-type condensations of primary amines with formaldehyde and amines or activated (acidic) alkanes have frequently been used to prepare open-chain, macrocyclic, and oligomacrocyclic ligands coordinated to various metal ions, primarily copper(II) and nickel(II).[4−14] Thanks to their rigidity, aromatic amines − and in particular the triamine melamine (melamine = 2,4,6-triamino-1,3,5-triazine) − are interesting candidates for "capping" groups in copper(II)-based template condensations. The poor acidity of the aniline-type amines in melamine is partially compensated by the presence of three azines, and we have established that the template reactions around copper(II) and nickel(II)[15] result in the desired products (see Scheme 1; similar results have also been published independently[16−18]).

Mono- and oligomacrocyclic ligands and their metal complexes have been used as hosts for organic and inorganic guest molecules.[19−24] Host-guest interactions range from π-stacking and van der Waals forces to hydrogen bonds and weak coordinative bonds. The last of these are interesting, specifically when labile sites such as the axial donors in Jahn−Teller active copper(II) complexes are involved, since the length and directionality of coordinative bonds allow the shape selectivity to be carefully tuned.[25] Examples of metal complex hosts include assemblies of tris[zinc(II)] compounds[26] and the stabilization of a reactive organic cation by a tetrahedral tetrakis[gallium(III)] complex host.[27] Here we present the syntheses of $[Cu(L^1)]^{2+}$, $[Cu_2(L^2)]^{4+}$, and $[Cu_3(L^3)]^{6+}$, together with structural studies of these complexes, as well as the structures of two host-guest complexes of $[Cu_3(L^3)]^{6+}$ with undecacyanodiferrate(II) and benzene-1,3,5-tricarboxylate.

[a] Universität Heidelberg, Anorganisch-Chemisches Institut,
Im Neuenheimer Feld 270, 69120 Heidelberg, Germany
Fax: (internat.) + 49-(0)6221/546617
E-mail: comba@akcomba.oci.uni-heidelberg.de
[b] L. V. Pisarzhevsky Institute of Physical Chemistry, National Academy of Science of Ukraine,
Prospekt Nauki 31, 03039 Kiev 39, Ukraine
Fax: (internat.) + 38-044/2656216
E-mail: ditop@iphch.kiev.ua
[c] Department of Chemistry, State University of New York, College at Buffalo,
1300 Elmwood Ave, Buffalo, NY 14222-1095, USA
Supporting information for this article is available on the WWW under http://www.eurjic.com or from the author.

Results and Discussion

Syntheses and Solution Properties of the Copper(II) Complexes

The reaction between $[Cu(2,3,2\text{-tet})]^{2+}$, formaldehyde, and melamine in the presence of base (triethylamine) resulted in the formation of a mixture of mono-, di-, and

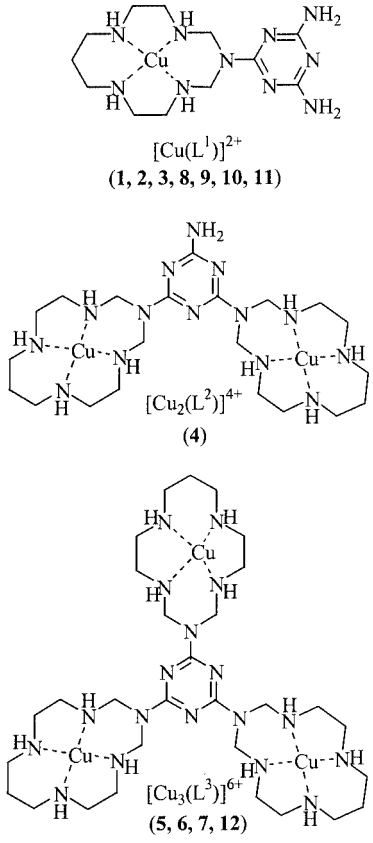

Scheme 1

trinuclear copper(II) compounds. Chromatographic separation yielded the pure copper(II) complexes of the mono-, bis- and tris(macrocyclic) melamine-based ligands: $[Cu(L^1)]^{2+}$, $[Cu_2(L^2)]^{4+}$ and $[Cu_3(L^3)]^{6+}$.

The infrared spectra of the three complexes were similar, and had features characteristic both of the melamine fragment and of the pentaazamacrocyclic ligand/copper(II) complexes. The number of bands corresponding to out-of-plane vibrations of the aromatic amino groups [$\delta(NH_2)$; 1660 cm^{-1} in crystalline melamine] were indicative of the nuclearity and the degree of protonation of the complexes: three bands (1690, 1640 and 1600 cm^{-1}) were observed in the protonated mono(macrocyclic) ligand complexes $[Cu(HL^1)](ClO_4)_3 \cdot H_2O$ and $[Cu(HL^1)](Cl)(ClO_4)_2 \cdot 0.5\ H_2O$, while two bands (1670 and 1600 cm^{-1}) were characteristic of the protonated bis(macrocyclic) ligand complex $[Cu_2(HL^2)](ClO_4)_5 \cdot 3H_2O$. Only one band was present in the spectra of the nonprotonated complexes $[Cu(L^1)](ClO_4)_2 \cdot H_2O$ (1600 cm^{-1}) and $[Cu_2(L^2)](ClO_4)_4 \cdot 2.5H_2O$ (1610 cm^{-1}). As expected, tris(macrocyclic) ligand complexes showed no strong band in this spectral region.

The electronic absorption spectra of the three complexes were also similar, and consisted of three transitions. The band in the visible region at 515 nm was typical of the four unresolved d-d transitions of the tetragonal copper(II) chromophore in complexes with 14-membered tetraazamacrocyclic ligands with weakly coordinated axial donors.[25,28] This transition did not depend on the nuclearity of the complex, and the molar absorptivity was proportional to the number of macrocyclic subunits in the molecule (see Exp. Sect.). This also applied for the LMCT transition at 253 nm. These two observations indicated that there was no significant direct electronic interaction between the copper chromophores in the oligomacrocyclic species. However, the high-energy electronic transition at approx. 210 nm, assigned to an intramolecular transition of the triazine residue [λ_{max} = 204 nm (ε = 52000 L mol^{-1} cm^{-1}) in melamine] showed a moderate bathochromic shift and a hyperchromic effect in the series $[Cu(L^1)]^{2+}$, $[Cu_2(L^2)]^{4+}$, $[Cu_3(L^3)]^{6+}$. This indicates increasing perturbation of the electronic structure of the aromatic ring by the attached macrocyclic ligand copper(II) complexes. The EPR spectrum of the mononuclear complex $[Cu(L^1)]^{2+}$ was typical for a tetragonal copper(II) tetraamine, with $g_{\|}$ = 2.190, $g_{\perp}$ = 2.041, and A_{II} = 205 10^{-4} cm^{-1}. Dipole-dipole interactions between the isolated chromophores were observed in EPR spectra of the oligonuclear complexes.[29]

Electrochemical oxidation of $[Cu(L^1)]^{2+}$, $[Cu_2(L^2)]^{4+}$, and $[Cu_3(L^3)]^{6+}$, measured by cyclic voltammetry with a glassy carbon electrode in neutral aqueous solution, was an irreversible process in each case. In highly acidic media (9.0 mol L^{-1} $HClO_4$) the copper(III) oxidation state can be stabilized,[30] and it is possible to obtain single, ill-resolved redox transformations with E_f at approx. 1.15 V vs. Ag/AgCl for all species {under similar conditions we have obtained the value E_f = 0.910 V for the $[Cu(cyclam)]^{3+/2+}$ couple (cyclam = 1,4,8,11-tetraazacyclotetradecane)}. The difference of approx. 200 mV reflected the electron-withdrawing effect of the melamine fragment, destabilizing the copper(III) state. Apparently, the destabilizing electrostatic effect due to the protonation of the triazine nucleus in highly acidic media is less important; this was also observed for the analogous nickel complexes.[15] Similarly to the behavior in the anodic region, all three copper compounds showed poorly resolved quasi-reversible $Cu^{II/I}$ cathodic waves at approx. −0.9 V vs. a saturated calomel electrode {acetonitrile solution, 0.1 mol L^{-1} [(nBu)$_4$N]ClO_4}.

Molecular and Crystal Structures of the Copper(II) Compounds

General Comments

Experimental solid-state structures of copper(II) complexes of mono-, di-, and trinucleating melamine-based ligands have been determined. They include the mono(macrocyclic) ligand complexes $[Cu(L^1)(OClO_3)_2] \cdot H_2O$ (**1**), $[Cu(HL^1)(OClO_3)_2](ClO_4) \cdot H_2O$ (**2**), and $\{[Cu(HL^1)(OH_2)(Cl)][Cu(HL^1)(OClO_3)(Cl)]\}(ClO_4)_3$ (**3**), the bis(macrocyclic) ligand complex $[Cu_2(L^2)(OClO_3)_4] \cdot H_2O \cdot CH_3OH$ (**4**), and the tris(macrocyclic) ligand complex $[Cu_3(L^3)(OH_2)_3](NO_3)_3(ClO_4)_3$ (**5**). The structures of two host-guest complexes with $[Cu_3(L^3)]^{6+}$ – $\{[Cu_3(L^3)]_2[Fe_2(CN)_{11}]\}(CN)(NO_3)_4 \cdot 34H_2O$ (**6**) and $[Cu_3(L^3)(OH_2)_6](C_9H_3O_6)_2 \cdot 40H_2O$ (**7**) ($C_9H_3O_6^{3-}$ = benzene-1,3,5-tri-

carboxylate) − have also been determined. These structures are discussed together with those recently reported for $[Cu(L^1)(OClO_3)_2]\cdot H_2O$ (**8**),[17] $[Cu(L^1)(CA\text{-}H)(OClO_3)]\cdot H_2O$ (**9**) (CA-H = cyanurate),[17] $[Cu(HL^1)(OClO_3)](ClO_4)_2\cdot 2H_2O$ (**10**),[16] $[Cu(HL^1)(OClO_3)_2](BA\text{-}H)\cdot 3H_2O$ (**11**) (BA-H = barbiturate),[17] and $[Cu_3(L^3)(OH_2)_2(OClO_3)_4](ClO_4)_2\cdot 3H_2O$ (**12**).[18]

The copper(II) ions in all structures reported here are coordinated to four nitrogen donors in the macrocycles, resulting in nearly planar CuN_4 chromophores (rms = 0.01−0.04 Å), with the copper(II) centers deviating from these planes only slightly (0.01−0.07 Å). The pentaaza macrocycles all have the expected *trans*-III (*RRSS*) configuration.[31] The metal−nitrogen distances (Table 1 and Supporting Information) fall in the range typical for copper(II) complexes with 14-membered tetraazamacrocyclic ligands.[32] Various coordination geometries are observed, including square-planar (4-coordinate, as in **10**), square-pyramidal (4 + 1, as in **6** and **9**), and square-bipyramidal [4 + 2, as in **4** and **7**; all interactions shorter than 3.0 Å are viewed as coordinative bonds, see Table 1].

The melamine rings in all complexes are nearly planar (rms = 0.00−0.02 Å). In view of the conjugation of the lone pairs of the melamine amino nitrogen atoms with the aromatic rings, the melamine residues were expected to be coplanar with the planes defined by the CNC fragments at the apexes of the substituted six-membered chelate rings (angle α: see Figure 1 and Table 1). However, this was only observed for one macrocyclic unit in the tris(macrocyclic) ligand complex **5** (α = 0.3°); in all other cases there were various degrees of deviation from coplanarity (2° ≤ α ≤ 27°). Also, the melamine-substituted CNC fragment is generally slightly tilted and this results in nonorthogonality of the mean plane of the triazine rings and the planes bisecting the macrocycles along the long axes (angle β, see Figure 1 and Table 1). Because of the *chair* conformation of the substituted six-membered chelate rings and the close to sp^2 hybridization of the bridgehead nitrogen atoms, the melamine rings are bent relative to the mean CuN_4 planes (angle γ in Figure 1 and Table 1). Therefore, the oligomacrocyclic ligand complexes each exist in two major conformations, depending on the orientation of the macrocyclic rings relative to the aromatic spacer group: *syn* (two macrocyclic units on the same side) or *anti* (two macrocyclic units on opposite sides) isomers for the bis(macrocyclic) compounds, and *syn*,*syn* or *syn*,*anti* isomers for the tris(macrocyclic) ligand complexes.

The conformational freedom (*syn* and *anti*) and the variability of the structural parameters α, β, and γ result in a variety of shapes of the oligonuclear copper(II) complexes. The largest variation is due to the tilt angle γ, which ranges from 11 to 62° (see Table 1). This gives rise to appreciable variation in the intramolecular copper−copper distances

Table 1. Structural parameters of the copper(II) complexes of the melamine-based oligomacrocyclic ligands L^1, L^2, and L^3

Complex	Intramolecular distances [Å]		Angles between the mean planes [°][a]				Orientation of the melamine rings	
	Cu−N (equatorial)	Cu−axial ligand(s)	Cu−Cu	α	β	γ	Angle [°]	Distance [Å]
1	2.015−2.025	2.458; 2.628 ($OClO_3$)	−	23.0	70.7	45.5	0	3.5
8[17]	2.009−2.026	2.511; 2.617 ($OClO_3$)	−	12.2	80.4	36.9	0	3.5
9[b] [17]	2.009−2.038	2.335[c]	−	16.4 18.7	80.0	51.3	−	−
	2.005−2.030	2.395;[c] 2.612 ($OClO_3$)			82.4	52.6		
2	2.013−2.029	2.585; 2.594 ($OClO_3$)	−	18.9	82.5	61.6	1.6	av.3.4
3[b]	2.011−2.028	2.718 (OH_2); 2.826 (Cl)	−	9.9	88.8	53.2	5.6	av. 3.6
	2.016−2.023	2.660 (Cl); 2.808 ($OClO_3$)		9.6	88.5	49.9		
10[b] [16]	2.008−2.019	2.521 (OH_2)	−	12.0	89.1	44.7	0	3.47
	2.006−2.052			12.4	86.4	46.7		
11[17]	1.999−2.041	2.457; 2.603 ($OClO_3$)	−	10.0	77.2	39.1	−	−
4	Cu(1) 2.009−2.035	2.461; 2.658 ($OClO_3$)	9.32	26.1	81.0	57.7	−	−
	Cu(2) 2.015−2.039	2.430; 2.614 ($OClO_3$)		19.3	79.1	43.5		
5	Cu(1) 1.996−2.017	2.405 (OH_2); 2.764 ($OClO_3$)	8.50 [Cu(1)−Cu(2)]	0.3	90.0	24.9	0	3.36
	Cu(2) 2.002−2.030	2.479 (OH_2)	7.99 [Cu(2)−Cu(2a)]	13.9	89.3	43.6		
6	Cu(1) 2.019−2.027	2.244 (NC)	7.72 [Cu(1)−Cu(2)]	4.0	86.9	25.4	5.0	av. 3.4
	Cu(2) 2.014−2.033	2.263 (NC)	8.22 [Cu(1)−Cu(3)]	16.8	80.8	53.2		
	Cu(3) 2.006−2.017	2.217 (NC)	7.66 [Cu(2)−Cu(3)]	12.0	90.0	49.7		
	Cu(4) 1.968−2.031	2.253 (NC)	7.99 [Cu(4)−Cu(5)]	6.8	87.5	27.7		
	Cu(5) 2.015−2.029	2.201 (NC)	7.51 [Cu(4)−Cu(6)]	10.4	84.8	50.6		
	Cu(6) 2.022−2.029	2.244 (NC)	7.77 [Cu(5)−Cu(6)]	11.6	88.9	52.5		
7	Cu(1) 2.005−2.024	2.454; 2.546 (OH_2)	10.05 [Cu(1)−Cu(2)]	15.4	84.6	10.7	2.5[d]	av. 3.4[d]
	Cu(2) 2.007−2.034	2.493; 2.512 (OH_2)	10.14 [Cu(1)−Cu(3)]	11.2	82.4	15.9	6.3[d]	av. 3.3[d]
	Cu(3) 2.007−2.032	2.416; 2.509 (OH_2)	9.66 [Cu(2)−Cu(3)]	4.2	81.5	21.3		
12[18]	1.982−2.023	2.654; 2.683 ($OClO_3$)	7.97; 9.36; 9.54	10.7	87.4	45.2	−	−
	2.002−2.034	2.425 (OH_2); 2.831 ($OClO_3$)		16.8	82.8	43.8		
	1.978−2.034	2.594 ($OClO_3$); 2.639 (OH_2)		2.3	88.9	34.0		

[a] For the definition of the angles see text and Figure 1. [b] Two independent molecules in the asymmetric unit. [c] Oxygen atom of cyanurate. [d] Melamine−carboxylate interactions.

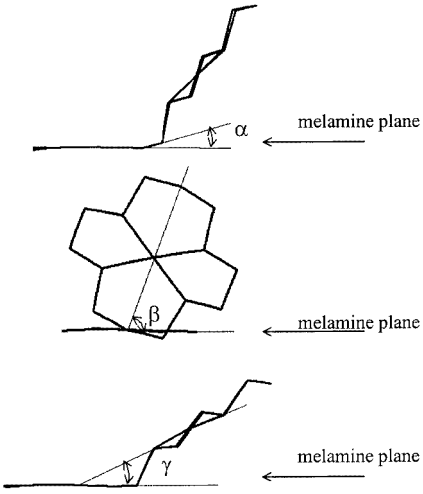

Figure 1. Definition of the geometric parameters of the melamine macrocycle fragments

and, for the trinuclear compounds, considerable plasticity of the cavities for anion binding.

Mono(macrocyclic) Ligand Complexes

Three new structures of copper(II) complexes of L^1 are reported here (for ORTEP plots[33] see Figure 2), while four have been published before;[16,17] structural parameters for these are also included in Table 1. In three of the structures (**1**, **8**, and **9**), copper(II) is coordinated to the parent ligand L^1, while in the other four (**2**, **3**, **10**, and **11**) the melamine fragment is protonated at the central nitrogen atom ([N(8) and N(18) in Figure 2b,c), and so copper(II) is coordinated to HL^1. In the published structures (**9** and **11**), specific supramolecular interactions of the melamine fragments with substrates (carboxylates) were discussed.[16,17]

The structural parameters of all complexes are very similar; the main variations are in the axial coordination and the angles α, β, and γ. The structures reported here are six-coordinate, with ClO_4^- (**1** and **2**) and H_2O, Cl^-, and ClO_4^- (**3**) as axial donors. The most pronounced variation of the angles describing the relative orientation of the macrocyclic and melamine planes is that of the angle γ (37−62°). There is no apparent correlation of these parameters with other features (e.g., the protonation of the ligand), as was also observed for the corresponding nickel(II) complexes.[15]

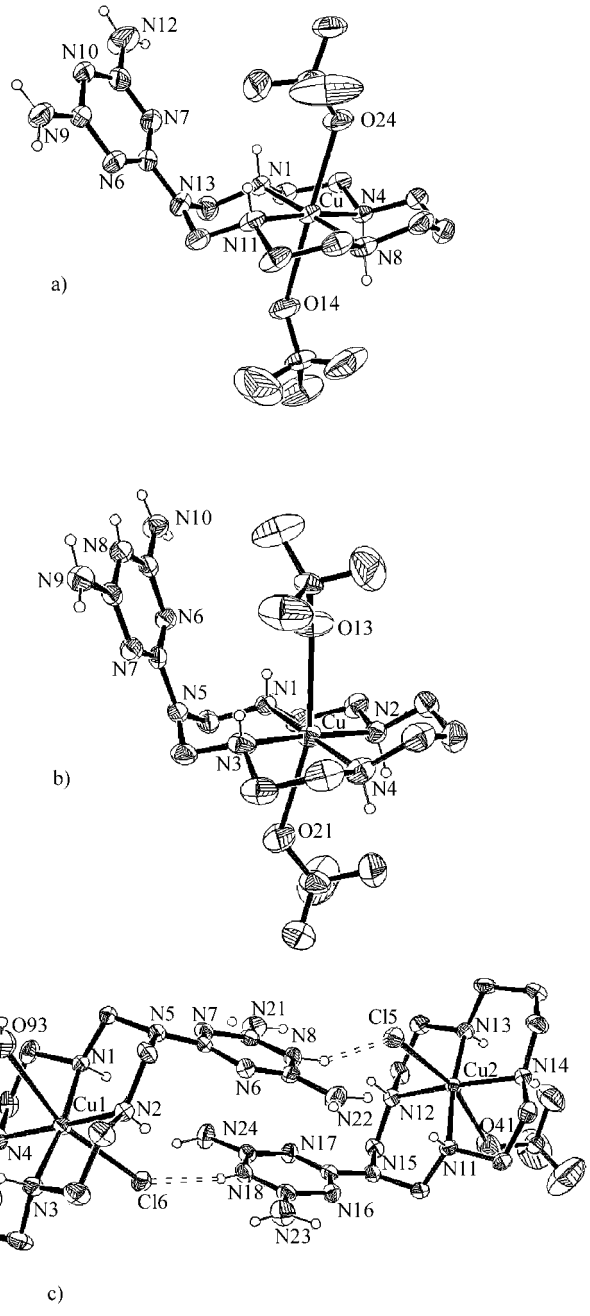

Figure 2. ORTEP[33] view (30% probability ellipsoids) of **1** (a), **2** (b), and **3** (c); C−H hydrogen atoms, lattice water molecules, and noncoordinated anions are omitted for clarity; selected distances and angles are shown in Table S1 (Supporting Information; see also footnote on the first page of this article)

Crystal Packing of the Mono(macrocyclic) Ligand Complexes

A major structural motif observed in the crystal lattices of the mononuclear melamine-based macrocyclic ligand/copper(II) complexes is the presence of infinite ribbons of copper(II) macrocycles, connected by hydrogen bonds, involving water molecules (**1**, **2**, **8**, **10**) or perchlorate anions (**3**). With the nonprotonated melamine groups (**1**, **8**) double-stranded tapes are formed between the self-complementary melamine rings [acceptor-donor-acceptor (ADA) pattern]. Protonation of the aromatic nitrogen atom of the triazine fragment breaks the self-complementarity (AAA pattern) and no double-stranded tapes are observed (**2**, **3**, **10**). Another common feature in the structures of the mono(macrocyclic) ligand complexes is an arrangement of the melamine rings that allows for π-stacking interactions; that is, the aromatic rings are nearly coplanar, with a distance of approx. 3.5.Å (Figure 3 and Table 1). An interesting variation in the structural motif of the π-stacked pairs within the hydrogen-bonded tapes is seen in **3** (see Figure 3, A- vs. B-type stacking for **1**, **2**, **8**, **10**, and **3**, respectively).

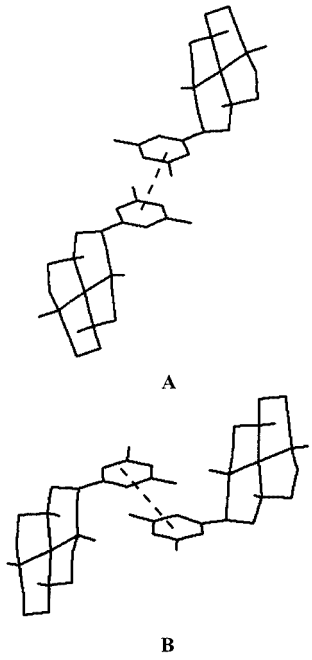

Figure 3. A- and B-type stacking in the lattices of the mono(macrocyclic) ligand complexes

Oligomacrocyclic Ligand Complexes

The bis(macrocyclic) ligand complex **4** crystallized as the *anti* isomer. Both copper(II) centers are six-coordinate (4 + 2, ClO_4^- donors, see Figure 4, Table 1 and Supporting Information) and the angle between the mean planes of the CuN_4 chromophores is 42.2°. Because of steric crowding there is no π-stacking of the melamine rings in the crystal lattice, but the aromatic rings of adjacent ligands are nearly coplanar.

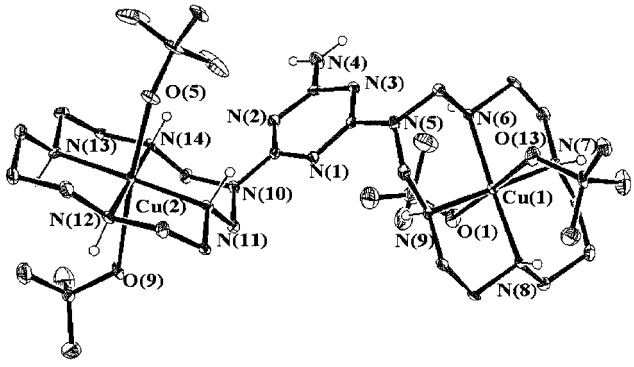

Figure 4. ORTEP[33] view (30% probability ellipsoids) of **4**; C−H hydrogen atoms and lattice solvent molecules are omitted for clarity; selected hydrogen bonds [Å]: Cl(5)···N(8) 3.072, Cl(6)···N(18) 3.099; selected distances and angles are shown in Table S2 (Supporting Information)

The three 14-membered rings of the tris(macrocyclic) ligand/copper(II) complex **5** are located on the same side of the melamine plane (*syn*,*syn* conformation), and the molecular cation looks like a flower with three petals (Figure 5a). This is a significant difference from the *syn*,*anti* conformation of the previously reported $[Cu_3(L^3)]^{6+}$ structure **12**.[18] There is a symmetry plane in **5**, bisecting the molecular cation through C(2)Cu(1)N(3)C(11)N(4). The angles between CuN_4 mean planes in **5** are 58.8° for the Cu(1)−Cu(2) and 74.6° for the Cu(2)−Cu(2a) chromophores, respectively, significantly larger than in **4**, and this is primarily due to differences in γ (see Table 1).

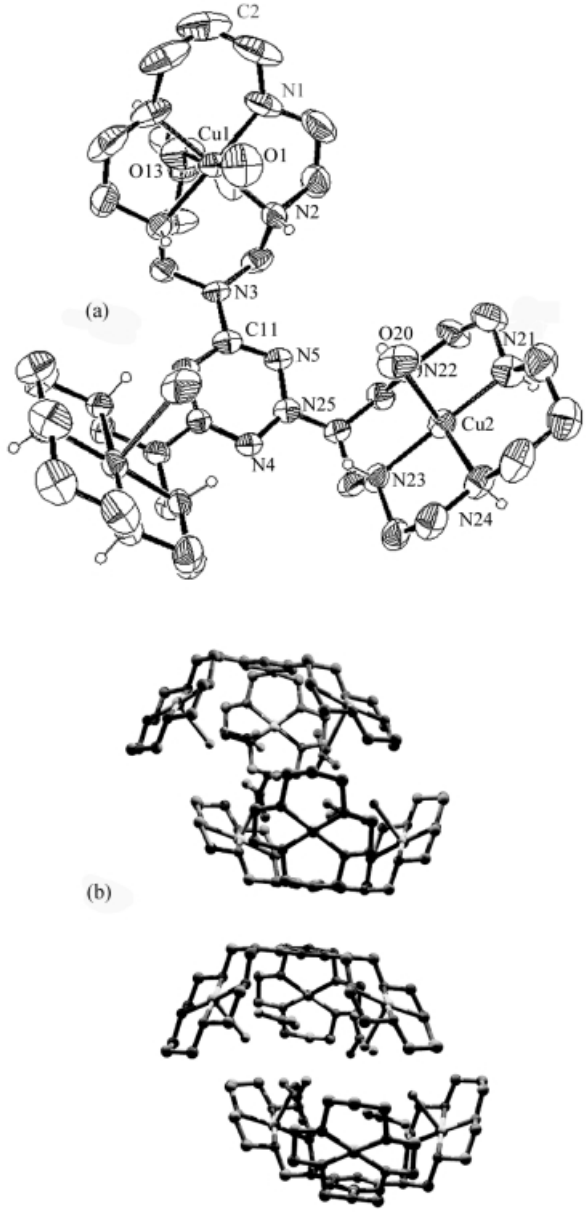

Figure 5. ORTEP[33] view (30% probability ellipsoids) of **5** (a) and its packing in the crystal lattice with the formation of the capsules (b); C−H hydrogen atoms, lattice water molecules, and anions are omitted for clarity; selected distances and angles are shown in Table S3 (Supporting Information)

In the crystal lattice, two concave "flowers" form an ellipsoidal "capsule", with the longest axis of approx. 15 Å (Figure 5b). The distance between parallel triazine rings in the capsule is 10.7 Å, and their centers are horizontally shifted by approx. 2.8 Å. Four disordered nitrate anions occupy the cavity of the capsule. Each of these forms hydro-

gen bonds to coordinated water molecules and to secondary nitrogen atoms of the macrocyclic ligands. Apparently, this bonding of NO_3^- is to some extent responsible for the stabilization of the *syn*,*syn* conformation of $[Cu_3(L^3)]^{6+}$ in **5**. The remaining anions and water molecules are located outside the capsules and form a network of hydrogen bonds. Interestingly, there are no obvious attractive interactions between the two symmetrically related halves of the capsule. In the crystal lattice the capsules are packed in order to allow for π-stacking interactions between coplanar and coaxial melamine rings (Figure 5b and Table 1).

Host-Guest Complexes Based on the $[Cu_3(L^3)]^{6+}$ Cation

The tricopper(II) compound **5**, based on the tris(macrocyclic) ligand, is a rare example of a rigid, hemispherical, positively charged transition metal complex host molecule (see Introduction and corresponding refs.). The interactions with the NO_3^- guest anions are nonspecific, but the charge, size, and shape of **5**, and in particular the fact that six axial sites of copper(II) centers are available for interactions in the hexanuclear capsules (see Introduction) indicated that − in terms of size, shape, and charge − carefully chosen guest molecules should give rise to interesting host-guest interactions. Evaluation of the geometry of the cavity indicated that corner-shared bis(octahedral) complexes have an ideal size and structure for selective interactions with the host **5**. Also, the structural plasticity of **5** (see above and Table 1) allows for some variation of the size of the guest molecules. To evaluate these ideas, the host complex **5** was treated with hexacyanoferrate(II).

Treatment of **5** with $K_4Fe(CN)_6$ in warm water resulted in the formation, in high yield, of a precipitate with the composition $[Cu_3(L^3)][Fe(CN)_6](NO_3)_2{\cdot}17H_2O$. Structural analysis revealed the unique and unprecedented structure $\{[Cu_3(L^3)]_2[Fe_2(CN)_{11}]\}(CN)(NO_3)_4{\cdot}34H_2O$ (**6**). Figure 6a is a structural plot of the molecular cation, and Figure 6b shows the arrangement of the $[Cu_3(L^3)]_2^{12+}$ capsules with the coordinated decacyano(μ-cyano)diiron(II)(7−) anion in the crystal lattice. The cationic halves of the capsule in **6** are, as to be expected, kept together by six Fe−CN−Cu bridges. Each $[Cu_3(L^3)]^{6+}$ cation is bound by two CN bridges to one iron center and by one CN bridge to the other iron center. This results in a rather symmetrical octanuclear Cu_6Fe_2 cluster with Cu−Fe distances of 5.16 ± 0.04 Å (crystallographically all six macrocyclic fragments of the capsule are nonequivalent).

The copper centers in **6** are five-coordinate, with one apical cyanide each (Cu−NC distances of 2.20−2.26 Å; see Table 1 and Supporting Information). These axial copper(II)−donor distances are in the expected range,[34] although both shorter[35−38] and longer[39,40] bonds have been found in complexes with $Fe^{II}-CN-Cu^{II}$ bridges. The relatively strong bonding of copper(II) to the axial ligands results in larger deviations of the atoms from the CuN_4 mean planes, as observed in the other copper(II) structures of L^1, L^2, and L^3 (rms = 0.08−0.09 Å), and in a significant shift of the copper centers towards the apical cyanide donors (0.15−0.21 Å). All CN bridges in **6** are bent (Cu−N−C in the range of 149−164°; see Supporting Information).

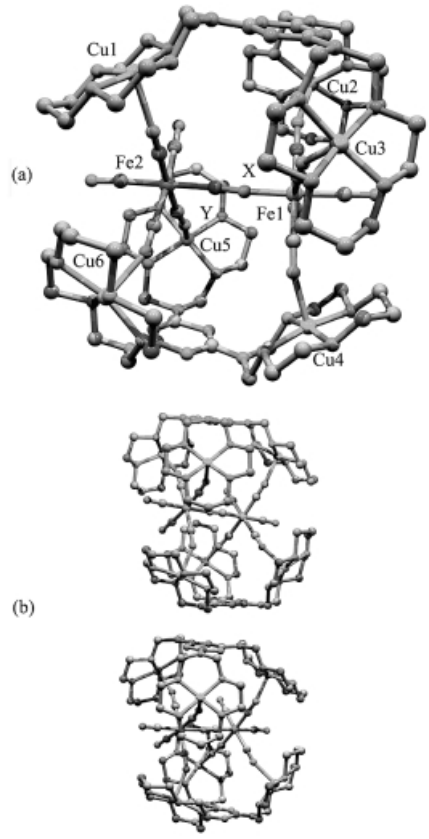

Figure 6. Structural plot of **6** (a) (X and Y = C or N) and its packing in the crystal lattice (b); hydrogen atoms, lattice water molecules, and anions are omitted for clarity; selected distances and angles are given as Supporting Information (Table S4)

The coordination of the dinuclear anion inside the cavity does not give rise to large distortions of the host complex, and no changes in the conformation of the trinuclear cations are observed (see angles and intermetallic distances for **5** and **6** in Table 1). However, the distance of approx. 12.8 Å between the melamine rings in a capsule and a tilt of approx. 5.0° in **6** are significant changes in the shape of the cavity with respect to that in **5** (10.7 Å and 0°, respectively). Also, the relative orientation of the cationic halves is slightly different (rotation around the melamine−melamine axis). Therefore, as would be expected, there is considerable plasticity of the capsules, and this involves the angles α, β, and γ, as well as the relative orientation of the $[Cu_3(L^3)]^{6+}$ subunits and subtle changes in the copper(II) chromophores.

In the structural analysis, the decacyano(μ-cyano)diiron(II) core in **6** is unprecedented. The only other discrete polycyanodiiron anion that has been structurally characterized is pentacyanoiron(III)(μ-cyano)amminetetracyanoiron(III).[41,42] The main difference between the two structures is the degree of rotation of the iron chromophores around the NC−Fe−CN−Fe−CN axis. While the chromophores in the published diiron(III) structure are

practically eclipsed, there is a torsion of approx. 25° in the diiron(II) structure reported here. This is probably due more to the stereochemical demand of the cationic host than to the preferences of the decacyano(μ-cyano)diiron(II) anion. The coordination geometries of the iron(II) centers in undecacyanodiferrate(II) are nearly octahedral, with *cis*-C−Fe−C (or N) angles varying between 86 and 94° (see Supporting Information). The Fe−C distances (1.88−1.93 Å) are slightly shorter than those in other complexes (average of approx. 1.94 Å[34]). The relatively poor quality of the structure prevents a more detailed analysis. The remaining nitrate and cyanide anions in **6**, as well as the water molecules, are located outside the capsules and form an extended network of hydrogen bonds. As in **5** and the mononuclear complexes discussed above, there is a π-stacking interaction between the melamine rings of different capsules (Figure 6b and Table 1).

The inertness of hexacyanoferrate(II) suggests that $[Fe_2(CN)_{11}]^{7-}$ is assembled with assistance by the $[Cu_3(L^3)]^{6+}$ host, and the relatively strong (Fe−CN)−Cu bonds, together with the size and shape of the cavity of $[Cu_3(L^3)]_2^{12+}$, are assumed to be the driving force for the formation of the μ-cyano-bridged diiron(II) species. The previous observation of the *syn*,*anti* isomer of $[Cu_3(L^3)]^{6+}$ [18] and the species resulting from the reaction between **5** and benzene-1,3,5-tricarboxylate (see below) indicate that the *syn*,*syn* and *syn*,*anti* conformations of $[Cu_3(L^3)]^{6+}$ have similar energies and a low activation barrier for interconversion. Therefore, we do not assume that $[Fe_2(CN)_{11}]^{7-}$ is assembled inside the cavity of the host; the formation of **6**, rather, is assumed to be a stepwise process. Scheme 2 shows possible intermediates and reaction pathways for the formation of the Cu_6Fe_2 cluster (the plots are based on the observed structural parameters). The formation of oligonuclear cyanoferrate(II) species usually involves the reduction of the corresponding iron(III) compounds,[43,44] the reaction of aqua- or aminopentacyanoferrate(II) with hexacyanoferrate(II), or the photochemical labilization of cyanide ligands in $[Fe(CN)_6]^{4-}$.[45] Therefore, the host-guest complex **6** was assumed to be stable in solution.

The solution electronic and MS spectra supported this assumption. The electronic spectrum of **6** had the expected d-d transition at 547 nm (ε = 565 L $mol^{-1}cm^{-1}$, 94 L $mol^{-1}cm^{-1}$ per Cu^{II}), and the bathochromic shift of the absorption band relative to that in **5** is assumed to be due to the interactions with the axial CN donors. The absorption of $[Fe_2(CN)_{11}]^{7-}$ (λ = 385 nm[45]) was too weak to be observed, and was covered by the low-energy tail of intense charge-transfer transitions of the hexakis[copper(II)] capsule. Although the signal corresponding to the octanuclear unit was not detected in the ESI+ MS spectrum, there were several other sets of peaks that corresponded, on the basis of their isotopic pattern, to different polynuclear particles (see Figure 7 for examples). They can be assigned as follows: peaks of monocations with *m*/*z* = 1264.5 to $\{[Cu_3L^3\ Fe_2(CN)_{11}]^{1-} - 2\ H\}^+$ (calcd. 1265.5), 1179.4 to $\{[Cu_3L^3\ Fe_2(CN)_7(H_2O)]^{3+} - 2\ H^+\}^+$ (calcd. 1179.4), 1152.0 to $\{[Cu_3L\ Fe_2(CN)_6(H_2O)]^{4+} - 3\ H^+\}^+$ (calcd. 1152.4), 1116.0 to $\{[Cu_3L\ Fe_2(CN)_4(H_2O)_2]^{6+} - 5\ H^+\}^+$ (calcd. 1116.4); peak of a dication with *m*/*z* = 527.3 to $\{[Cu_3L^3\ Fe(CN)_5]^{3+} - H^+\}^{2+}$ (calcd. 1054.6). These data unequivocally confirmed the persistence in solution of the capsules observed in the solid state and indicated that the main pathway of fragmentation was the rupture of metal−cyanide bonds in **6**.

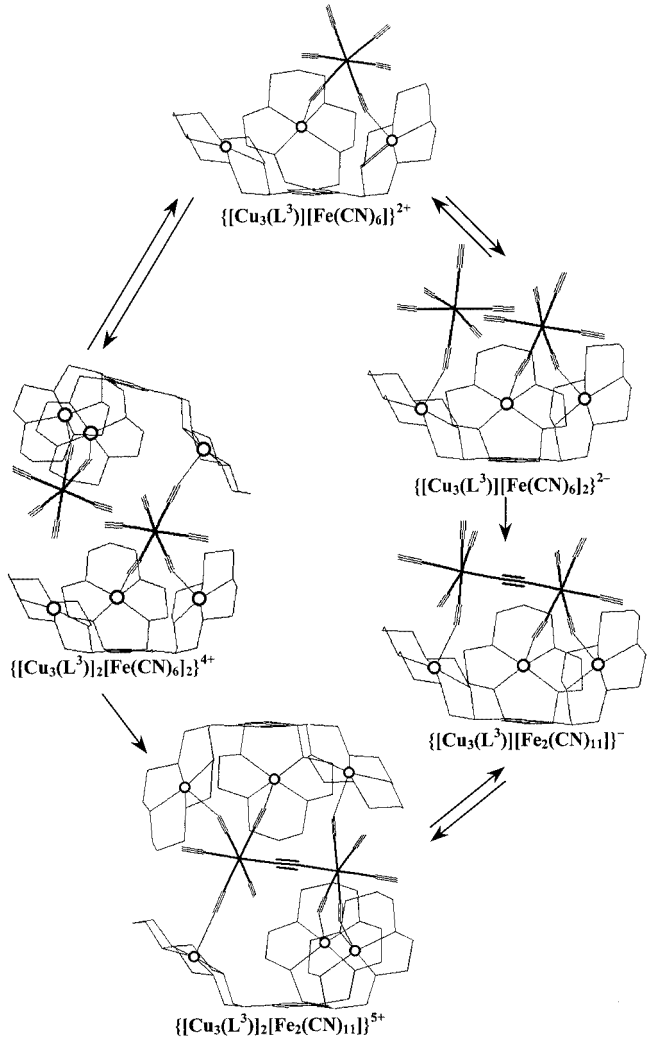

Scheme 2

Benzene-1,3,5-tricarboxylate was chosen as an example for an organic host molecular anion. Molecular models indicated that the tricarboxylate $C_9H_3O_6^{3-}$ might be included in the capsule. However, the crystallographic data of $[Cu_3(L^3)(OH_2)_6](C_9H_3O_6)_2{\cdot}40H_2O$ (**7**) (see Figure 8) reveal that $[Cu_3(L^3)]^{6+}$ now exists in the *syn*,*anti* conformation, with two tricarboxylate substrates bound by hydrogen bonds to the axial water donors and π-stacked to the melamine ring (see Table 1). We assume that this assembly is just one of the various local minimum structures, and this example shows how difficult it is to predict structures of supramolecular assemblies. Preliminary selectivity studies with tricarboxylates and with *m*- and *p*-phthalate indicated that **5** is a highly regioselective host,[46] and thorough select-

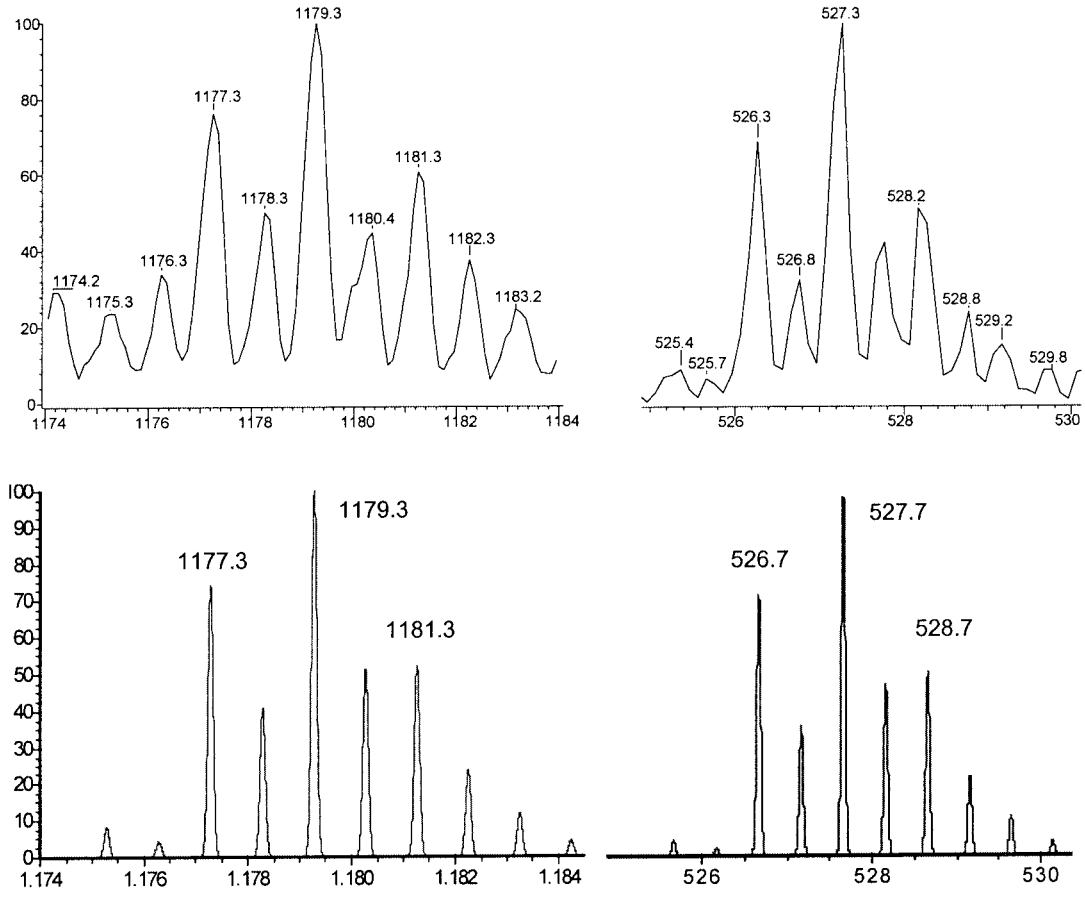

Figure 7. Fragments in the ESI MS of **6**: $\{[Cu_3L^3\ Fe_2(CN)_7(H_2O)]^{3+} - 2\ H^+\}^+$ (top left), $\{[Cu_3L^3\ Fe(CN)_5]^{3+} - H^+\}^{2+}$ (top right); bottom: calculated spectra

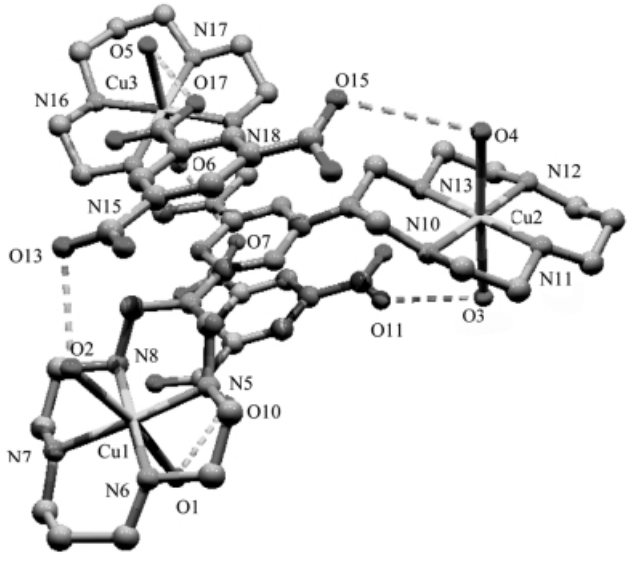

Figure 8. Structural plot of **7**; hydrogen atoms and lattice water molecules are omitted for clarity; selected H bonds [A]: O(6)···O(7) 2.858(3), O(1)···O(10) 2.703(3), O(3)···O(11) 2.736(3), O(2)···O(13) 2.805(3), O(4)···O(15) 2.714(3), O(5)···O(17) 2.804(3); selected distances and angles are shown in Table S5 (Supporting Information)

ivity studies and their interpretation might help in understanding of the structural preferences.

The structure of **7** is also of importance to illustrate the conformational flexibility and plasticity of **5**, and it supports the assumption that **5** acts as a flexible host that allows guest molecules to assemble in multi-step procedures with the assistance of the host, which in favorable circumstances might finally encapsulate (i.e., protect and shield) the guest molecules, as in the case of **6**. An interesting structural feature in this context is a significant flattening of the tricopper(II) host in **7**, especially in comparison with the structure of **12** (see Table 1). This is particularly apparent from the Cu−Cu distances and the angles γ, which are much smaller in **7** than in any other structure (see Table 1). This indicates a rather tight binding of benzene-1,3,5-tricarboxylates to the $[Cu_3(L^3)]^{6+}$ cation and is further evidence for the plasticity of the host molecule.

Conclusion

The copper(II)-assisted synthesis of melamine-based macrocyclic ligands coordinated to copper(II) produced the expected three products in moderate yield (approx. 30%).

The tris(macrocyclic) ligand complex (yield approx. 7%) exists in two major conformations, *syn*,*syn* and *syn*,*anti*, which are similar in stability. Structural studies indicated that the conformational equilibria may be influenced by host-guest interactions which may also influence the shape of each conformation of the tricopper(II) host through subtle structural changes. Preliminarily observed selectivities in host-guest complexation interactions, however, indicated that, although there is a certain structural plasticity of the melamine-based tricopper(II) host, deviation from the preferred geometry may result in a loss of steric energy. This also follows from the structural data of the entire set of copper(II) complexes.

The assembly of $[Fe_2(CN)_{11}]^{7-}$, assisted by the tricopper(II) host complex, and its full encapsulation is based on a combination of conformational flexibility of the host during the assembly procedure and a high degree of complementarity between the hexanuclear host and the dinuclear guest. The relatively strong and highly directional bonding of the guest to the axial copper(II) sites results an assembly that is stable in solution.

Experimental Section

Physical Methods: Infrared spectra (KBr pellets) were recorded with a Specord 75 IR (Carl Zeiss) spectrometer. Electronic absorption spectra were measured with a Specord M40 (Carl Zeiss) spectrophotometer. EPR spectra were recorded with a Bruker ESP300E spectrometer (9.4635 GHz) as approx. 1 10^{-3} mol dm^{-3} frozen (liquid nitrogen temperature) solutions in DMF/water (2:1). Triple-stage quadrupole mass spectra (ESI positive ion mode) were obtained with a Finnigan TSQ-700 mass spectrometer at 5.5 kV, 40 psi sheath gas and flow of liquid of 1.5 μL min^{-1}. Cyclic voltammograms were generated with a PI-50-1.1 potentiostat, equipped with a PR-8 function generator (Izmeritel, Gomel) and an N-307 X-Y recorder (ZIP, Krasnodar). A standard three-electrode scheme was used, consisting of a glassy carbon working electrode, a saturated calomel or Ag/AgCl reference electrode, and a Pt wire auxiliary electrode. All solutions for electrochemistry were purged with nitrogen before measurement. Analytical data were obtained from the microanalytical laboratory of the chemical institutes of the University of Heidelberg.

Structure Determinations: Reflections of representative crystals were measured with Siemens P4 (**1**, **2**, **3** and **5**) or Bruker AXS SMART 1000 (**4**, **6** and **7**) diffractometers with Mo-K_α radiation (λ = 0.71073 Å) and operating in the ω-scan mode. The absorption correction was applied in all cases. The structures were solved by direct methods (SHELXS86) and refined by full-matrix, least-squares methods based on F^2 (SHELXL97),[47] with use of anisotropic thermal parameters for all non-hydrogen atoms. Hydrogen atoms in **1**−**3** were placed in calculated positions; some disorder was observed for a water molecule and one of the perchlorate ions in **1**. Hydrogen atoms in **4** were also placed in calculated positions; only the hydrogen atoms at nitrogen atoms were located in a difference Fourier map and refined isotropically. Perchlorate anions are disordered. For **6**, one half of the capsule is disordered over two positions. Hydrogen atoms of the capsule were inserted in calculated positions. The anions and water molecules outside the capsule could not be located unambiguously and their hydrogen atoms were omitted. In **7**, only the hydrogen atoms of the molecular cation, the anions, and the coordinated water molecules were located and refined. The hydrogen atoms of the water clusters were located only partially, but not refined. Also, some water molecules in this part of the structure are probably disordered. The crystallographic data are given in Table 2. CCDC-171733 (**1**), -171702 (**2**), -171701 (**3**), -170075 (**4**), -134986 (**5**), -157762 (**6**), and -170076(**7**) contain the supplementary crystallographic data for this paper. These data can be obtained free of charge at www.ccdc.cam.ac.uk/conts/retrieving.html or from the Cambridge Crystallographic Data Centre, 12, Union Road, Cambridge CB2 1EZ, UK [Fax: (internat.) + 44-1223/336-033; E-mail: deposit@ccdc.cam.ac.uk].

Materials: AR grade chemicals and solvents were used as supplied for all reactions. $[Cu(2,3,2\text{-tet})](ClO_4)_2$ [2,3,2-tet = bis-*N*,*N*′-(2-aminoethyl)propane-1,3-diamine] and $[Cu(cyclam)](ClO_4)_2$ (cyclam = 1,4,8,11-tetraazacyclotetradecane) were prepared as described in the literature.[48]

Syntheses: ***Caution!*** Perchlorate salts of metal complexes are potentially explosive. Although we did not experience any problem, such complexes should be handled very carefully.

Template Synthesis: $[Cu(2,3,2\text{-tet})](ClO_4)_2$ (2.0 g, 4.7 mmol), melamine (1.0 g, 7.9 mmol), and triethylamine (5 mL) were dissolved under reflux in 120 mL of a water/ethanol (1:5) mixture. Aqueous formaldehyde (37%, 8.0 mL) was added dropwise over 1 h, and the mixture was refluxed for an additional 24 h and then cooled, filtered, and sorbed onto an SP-Sephadex C-25 cation exchange column (Na^+ form). The column was washed with water (1 L), and the macrocyclic products were eluted with aqueous solutions containing different concentrations of $NaClO_4$ or $NaNO_3$. The mono(-macrocyclic) ligand complex $[Cu(L^1)]^{2+}$ was eluted with 0.2 mol L^{-1} $NaClO_4$ as the second band, after unchanged $[Cu(2,3,2\text{-tet})]^{2+}$. For $[Cu(L^1)(OClO_3)_2]\cdot H_2O$ (**1**), the eluate was concentrated to 25 mL and cooled to room temperature. The purple precipitate of **1** was filtered off, washed with ethanol, and dried in air (yield 0.25 g, 9%). $C_{12}H_{28}Cl_2CuN_{10}O_9$ (590.87): calcd. C 24.39, H 4.78, N 23.71; found C 24.15, H 4.63, N 23.66. Electronic absorption spectrum (H_2O, 0.1 mol L^{-1} $NaNO_3$): λ_{max} (ε [L mol^{-1} cm^{-1}]) = 515 (87), 253 (8500), 209 nm (51000). Crystals of **1** suitable for X-ray analysis were grown by slow cooling of its basic (pH ≈ 10) aqueous solution, in the presence of $NaClO_4$. $[Cu(HL^1)(OClO_3)_2](ClO_4)\cdot H_2O$ **(2)** and $\{[Cu(HL^1)(OH_2)(Cl)]$-$[Cu(HL^1)(OClO_3)(Cl)]\}(ClO_4)_3$ **(3)** were obtained by recrystallization of **1** from 0.1 mol L^{-1} $HClO_4$ or HCl, respectively. The yields were nearly quantitative. **2:** $C_{12}H_{29}Cl_3CuN_{10}O_{13}$ (691.33): calcd. C 20.85, H 4.23, N 20.26; found C 20.86, H 4.42, N 20.00. **3:** $C_{12}H_{29}N_{10}Cl_3CuO_{8.5}$ (619.33): calcd. C 23.31, H 4.56, N 22.65; found C 23.35, H 4.94, N 22.75. The electronic spectra of both complexes in aqueous solution were identical to that of **1**. Crystals suitable for X-ray analysis were selected from precipitates formed after reaction. The bis(macrocyclic) ligand copper(II) complex $[Cu_2(L^2)]^{4+}$ was eluted with 0.4 mol L^{-1} $NaClO_4$. Cooling of concentrated (approx. 25 mL) eluate resulted in a purple precipitate with the stoichiometry $[Cu_2(L^2)](ClO_4)_4\cdot 2.5H_2O$. This was collected on a filter, washed with aqueous $NaClO_4$ (0.6 mol L^{-1}) and then ethanol, and dried in air (yield 0.34 g, 13%). $C_{21}H_{51}Cl_4Cu_2N_{14}O_{18.5}$ (1064.63): calcd. C 23.69, H 4.83, N 18.42; found C 23.91, H 4.74, N 18.24. An additional crop of $[Cu_2(L^2)]^{4+}$ in the form of the protonated ligand complex $[Cu_2(HL^2)](ClO_4)_5\cdot 3H_2O$ (up to 0.02 g) was obtained upon acidification of the filtrate with $HClO_4$ to pH ≈ 1. $C_{21}H_{53}Cl_5Cu_2N_{14}O_{23}$ (1174.09): calcd. C 21.48, H 4.55, N 16.70; found C 21.42, H 4.42, N 16.51. The electronic absorption spectra of the two complexes were identical (H_2O, 0.1 mol L^{-1} $NaNO_3$): λ_{max} (ε [L mol^{-1} cm^{-1}]) = 515 (176), 253 (16500), 213 nm (57600).

Table 2. Crystallographic data for the copper(II) complexes of the melamine-based ligands L^1, L^2 and L^3

	1	**2**	**3**	**4**	**5**	**6**	**7**
Empirical formula	$C_{12}H_{28}N_{10}$-Cl_2CuO_9	$C_{12}H_{29}$-$Cl_3CuN_{10}O_{13}$	$C_{24}H_{56}$-$Cl_6Cu_2N_{20}O_{17}$	$C_{22}H_{52}$-$Cl_4Cu_2N_{14}O_{18}$	$C_{30}H_{72}$-$Cl_3Cu_3N_{21}O_{24}$	$C_{70}H_{215}$-$Cu_6Fe_2N_{52}O_{46}$	$C_{48}H_{162}$-$Cu_3N_{18}O_{57}$
Formula mass	590.88	691.34	1236.64	1069.66	1408.02	3014.88	2094.58
Crystal system	triclinic	triclinic	monoclinic	monoclinic	monoclinic	triclinic	monoclinic
Space group	$P\bar{1}$	$P\bar{1}$	$P2_1/n$	$P2_1/c$	$C2/m$	$P\bar{1}$	$P2_1/n$
a [Å]	8.225(1)	8.5253(17)	9.674(4)	8.3734(9)	15.970(3)	16.262(3)	15.603(1)
b [Å]	8.726(1)	8.6380(14)	38.42(2)	16.376(2)	25.576(5)	17.534(3)	33.792(2)
c [Å]	17.851(2)	19.654(3)	12.748(4)	29.259(3)	14.599(2)	26.257(7)	19.671(1)
α [°]	78.99(1)	78.509(11)	90.00	90.00	90.00	80.17(2)	90.00
β [°]	77.92(1)	89.896(13)	91.44(3)	97.383(2)	101.65(1)	74.29(2)	100.865(1)
γ [°]	68.46(1)	67.841(12)	90.00	90.00	90.00	67.61(2)	90.00
V [Å^3]	1156.1(2)	1309.3(4)	4737(4)	3978.7(8)	5840.30(18)	6645(2)	10186
Z	2	2	4	4	4	2	4
T [°C]	293	293	293	−100	293	−83	−100
D [g cm^{-3}]	1.697	1.754	1.728	1.786	1.601	1.51	1.37
Refl., meas./ unique	4808/4487	4910/4576	11062/10552	31441/8106	5279/5084	45394/13836	67391/24571
$R1$ [$I > 2\sigma(I)$]	0.052	0.072	0.071	0.084	0.081	0.115	0.056
$wR2$ (all)	0.149	0.212	0.218	0.217	0.209	0.380	0.167
GOF	1.035	1.042	1.040	1.163	1.016	1.047	1.025

X-ray quality crystals of $[Cu_2(L^2)(OClO_3)_4]\cdot H_2O\cdot CH_3OH$ (**4**) were grown by vapor diffusion of diethyl ether in a methanol/water (2:1) solution of $[Cu_2(L^2)](ClO_4)_4\cdot 2.5H_2O$. The tris(macrocyclic) ligand complex $[Cu_3(L^3)]^{6+}$ was eluted with 0.8 mol L^{-1} $NaNO_3$. $[Cu_3(L^3)(OH_2)_3](NO_3)_3(ClO_4)_3$ (**5**) precipitated on concentration of the eluate to 25 mL, followed by the addition of 0.5 g of $NaClO_4$ (yield 0.15 g, 7%). **5:** $C_{30}H_{72}Cl_3Cu_3N_{21}O_{24}$ (1217.39): calcd. C 25.59, H 5.15, N 20.89; found C 25.82, H 5.20, N 21.11. Electronic absorption spectrum (H_2O, 0.1 mol L^{-1} $NaNO_3$): λ_{max} (ε [L mol^{-1} cm^{-1}]) = 515 (260), 253 (24400), 214 nm (87000). Purple crystals of **5** suitable for X-ray analysis were grown by slow cooling of an $NaNO_3$-saturated aqueous solution containing 10% of $NaClO_4$. Other salts of the tris(macrocyclic) ligand complex were also obtained. $[Cu_3(L^3)](ClO_4)_6\cdot 4H_2O$ was precipitated from an aqueous solution of **5** by addition of $NaClO_4$. The yield was nearly quantitative. $C_{30}H_{74}Cl_6Cu_3N_{18}O_{28}$ (1538.11): calcd. C 23.42, H 4.85, N 16.39; found C 23.28, H 4.98, N 16.68. Concentration of the initial eluate until the beginning of the precipitation of $NaNO_3$ yielded a purple compound, which was filtered, washed with small quantities of ice-cold water and ethanol, and dried in air (yield 0.03 g, 0.1%). According to its microanalytical data, the stoichiometry of the complex is $[Cu_3(L^3)](NO_3)_6\cdot 6H_2O$. $C_{30}H_{78}Cu_3N_{24}O_{24}$ (1349.47): calcd. C 26.70, H 5.82, N 24.91; found C 26.87, H 5.70, N 24.83. The absorption spectra of the two derivatives in aqueous solution were identical to that of **5**. The host-guest complex $\{[Cu_3(L^3)]_2[Fe_2(CN)_{11}]\}(CN)(NO_3)_4\cdot 34H_2O$ (**6**) was obtained by addition of an aqueous solution (5 mL) of $K_4[Fe(CN)_6]\cdot 3H_2O$ (0.0055 g, 0.013 mmol) to a hot aqueous solution (10 mL, 1 mol L^{-1} $NaNO_3$) of **5** (0.018 g, 0.013 mmol). The mixture was cooled very slowly. After several days, dark violet crystals were collected, washed with a small amount of ice-cold water and ethanol, and dried in air (yield 0.014 g, 72%). $C_{72}H_{200}Cu_6Fe_2N_{52}O_{46}$ (3023.13): calcd. C 28.60, H 6.67, N 24.09; found C 28.56, H 6.44, N 23.99. The CN stretching vibrations were observed as a single broad and intensive band, centered at 2032 cm^{-1}. Violet single crystals of **6** suitable for X-ray analysis were selected from the precipitate. The complex $[Cu_3(L^3)(OH_2)_6](C_9H_3O_6)_2\cdot 40H_2O$ (**7**) was prepared by addition of $C_6H_3(COONa)_3$ (0.01 g, 0.04 mmol) to a solution of $[Cu_3(L^3)](NO_3)_6\cdot 6H_2O$ (0.05 g, 0.04 mmol) in hot water (3 mL). The mixture was placed in a Dewar vessel filled with hot water and allowed to cool very slowly. Purple needles formed over a few days and were collected on a filter; single crystals suitable for X-ray analysis were then selected. The remaining crystals were washed with a small amount of ice-cold water, and dried in air, producing a purple powder (yield 0.026 g, 92% based on the carboxylate salt). According to its microanalytical data, the composition of the complex is $[Cu_3(L^3)](C_9H_3O_6)_2\cdot 15H_2O$: $C_{48}H_{99}Cu_3N_{18}O_{27}$ (1550.65): calcd. C 37.17, H 6.43, N 16.25; found C 37.10, 6.61, N 16.09.

Acknowledgments

Financial support by the German Science Foundation (DFG), the BMBF, and the Department of International Cooperation of the Ministry for Education and Science of Ukraine are gratefully acknowledged. We are also grateful to Dr. J. A. Gross for mass-spectrometric experiments and helpful discussion.

[1] I. I. Creaser, J. M. Harrowfield, A. J. Herlt, A. M. Sargeson, J. Springborg, R. J. Geue, M. R. Snow, *J. Am. Chem. Soc.* **1977**, *99*, 3181.
[2] R. J. Geue, T. W. Hambley, J. M. Harrowfield, A. M. Sargeson, M. R. Snow, *J. Am. Chem. Soc.* **1984**, *106*, 5478.
[3] A. M. Sargeson, *Coord. Chem. Rev.* **1996**, *151*, 89.
[4] N. V. Gerbeleu, V. B. Arion, J. Burgess, *Template Synthesis of Macrocyclic Compounds*, Wiley-VCH, Weinheim, New York, **1999**.
[5] O. Costisor, W. Linert, *Rev. Inorg. Chem.* **2000**, *20*, 63.
[6] M. P. Suh, *Adv. Inorg. Chem.* **1997**, *44*, 93.
[7] L. Fabbrizzi, A. M. M. Lanfredi, P. Pallavicini, A. Perotti, A. Taglietti, F. Ugozzoli, *J. Chem. Soc., Dalton Trans.* **1991**, 3263.
[8] S. V. Rosokha, V. D. Lampeka, I. M. Maloshtan, *J. Chem. Soc., Dalton Trans.* **1993**, 631.
[9] Y. D. Lampeka, A. I. Prikhod′ko, A. Y. Nazarenko, E. B. Rusanov, *J. Chem. Soc., Dalton Trans.* **1996**, 2017.
[10] P. Comba, T. W. Hambley, G. A. Lawrance, L. L. Martin, P. Renold, K. Várnagy, *J. Chem. Soc., Dalton Trans.* **1991**, 277.
[11] P. Comba, N. F. Curtis, G. A. Lawrance, A. M. Sargeson, B. W. Skelton, A. H. White, *Inorg. Chem.* **1986**, *25*, 4260.
[12] P. Comba, S. M. Luther, O. Maas, H. Pritzkow, A. Vielfort, *Inorg. Chem.* **2001**, *40*, 2335.

[13] M. Rossignoli, P. V. Bernhardt, G. A. Lawrance, M. Maeder, *J. Chem. Soc., Dalton Trans.* **1997**, 323.
[14] P. V. Bernhardt, G. A. Lawrance, S. Luther, M. Maeder, M. Rossignoli, *Inorg. Chim. Acta* **2000**, *306*, 1.
[15] P. Comba, Y. D. Lampeka, A. Y. Nazarenko, A. I. Prikhod'ko, H. Pritzkow, J. Taraszewska, submitted.
[16] P. V. Bernhardt, E. J. Hayes, *Inorg. Chem.* **1998**, *37*, 4214.
[17] P. V. Bernhardt, *Inorg. Chem.* **1999**, *38*, 3481.
[18] P. V. Bernhardt, E. J. Hayes, *J. Chem. Soc., Dalton Trans.* **1998**, 3539.
[19] J.-M. Lehn, *Supramolecular chemistry: Concepts and perspectives*, VCH Verlagsgesellschaft, New York, Weinheim, Basel, **1995**.
[20] D. J. Cram, J. M. Cram, *Container Molecules and Their Guests*, RSC, Cambridge, UK, **1994**.
[21] A. Müller, P. Kögerler, *Coord. Chem. Rev.* **1999**, *182*, 3.
[22] M. J. Hardie, C. L. Raston, *J. Chem. Soc., Dalton Trans.* **2000**, 2483.
[23] D. L. Caulder, K. N. Raymond, *Acc. Chem. Res.* **1999**, *32*, 975.
[24] L. F. Lindoy, I. M. Atkinson, *Self-Assembly in Supramolecular Systesm*, RSC, Cambridge, UK, **2000**.
[25] P. Comba, P. Jurisic, Y. D. Lampeka, A. Peters, A. I. l. Prikhod'ko, H. Pritzkow, *Inorg. Chim. Acta* **2001**, *324*, 99.
[26] S. Aoki, M. Shiro, T. Koike, E. Kimura, *J. Am. Chem. Soc.* **2000**, *122*, 576.
[27] M. Ziegler, J. L. Brumaghim, K. N. Raymond, *Angew. Chem. Int. Ed.* **2000**, *112*, 4285.
[28] A. B. P. Lever, *Inorganic Electronic Spectroscopy*, 2nd ed., Elsevier Science Publisher, Amsterdam − Oxford − New York − Tokyo, **1984**.
[29] P. Comba, Y. D. Lampeka, M. Kerscher, A. I. Prikhod'ko, manuscript in preparation.
[30] C. B. Castellani, L. Fabbrizzi, M. Licchelli, A. Perotti, A. Poggi, *J. Chem. Soc., Chem. Commun.* **1984**, 806.
[31] B. Bosnich, C. K. Poon, M. C. Tobe, *Inorg. Chem.* **1965**, *4*, 1102.
[32] J. C. A. Boeyens, S. M. Dobson, *Stereochemical and Stereophysical Behaviour of Macrocycles* (Ed.: I. Bernal), Elsevier, Amsterdam, New York, **1987**, p. 1.
[33] C. K. Johnson, *ORTEP, A Thermal Ellipsoid Plotting Program*, Oak National Laboratories, Oak Ridge, TN, **1965**.
[34] A. G. Orpen, L. Bramner, F. H. Allen, O. Kennard, D. G. Watson, R. Taylor, *J. Chem. Soc., Dalton Trans.* **1989**, S1.
[35] G. O. Morpurgo, V. Mosini, P. Porta, G. Dessy, V. Fares, *J. Chem. Soc., Dalton Trans.* **1981**, 111.
[36] H.-Z. Kou, D.-Z. Liao, P. Cheng, Z.-H. Jiang, S.-P. Yan, G.-L. Wang, X.-K. Yao, H.-G. Wang, *J. Chem. Soc., Dalton Trans.* **1997**, 1503.
[37] D. M. Corsi, N. N. Murthy, V. G. Young, D. D. Karlin, *Inorg. Chem.* **1999**, *38*, 848.
[38] R. J. Parker, L. Spiccia, S. R. Batten, J. D. Cashion, G. D. Fallon, *Inorg. Chem.* **2001**, *40*, 4696.
[39] H.-Z. Kou, H.-M. Wang, D.-Z. Liao, P. Cheng, Z.-H. Jiang, S.-P. Yan, X.-Y. Huang, G.-L. Wang, *Austr. J. Chem.* **1998**, *51*, 661.
[40] S.-W. Zhang, C.-Y. Duan, W.-Y. Sun, D.-G. Fu, W.-X. Tang, *Tans. Met. Chem.* **2001**, *26*, 127.
[41] P. Roder, A. Ludi, G. Chapuis, K. J. Schenk, D. Schwarzenbach, K. O. Hodgson, *Inorg. Chim. Acta* **1979**, *34*, 113.
[42] L. P. Michiels, G. Kolks, E. R. Nesbitt, P. T. Dimauro, R. M. Kirchner, J. V. Waszczak, *Inorg. Chim. Acta* **1985**, *100*, 211.
[43] R. Glauser, U. Hauser, F. Herren, A. Ludi, P. Roder, E. Schmidt, H. Siegenthaler, F. Wenk, *J. Am. Chem. Soc.* **1973**, *95*, 8457.
[44] A. D. James, R. S. Murray, *J. Chem. Soc., Dalton Trans.* **1976**, 1182.
[45] M. G. Emschwiller, *C. R. Acad. Sci., Ser. C.* **1969**, *268*, 692.
[46] P. Comba, Y. D. Lampeka, A. I. Prikhod'ko, H. Pritzkow, *Theor. Exp. Chem.* **2001**, *37*, 236.
[47] G. M. Sheldrick, *SHELXTL 5.1*, Bruker AXS, Madison, WI, **1998**.
[48] I. M. Maloshtan, Y. D. Lampeka, *Russ. J. Inorg. Chem.* **1996**, *41*, 1749.

Received October 10, 2001
[I01404]

DFT Calculations of ^{99}Ru Chemical Shifts with All-Electron and Effective Core Potential Basis Sets

Alessandro Bagno*[a] and Marcella Bonchio[a]

Keywords: Density functional calculations / Effective core potentials / NMR spectroscopy / Ruthenium

The nuclear shielding of ^{99}Ru in several complexes has been investigated computationally by DFT methods with effective core potential and all-electron basis sets. Shieldings calculated with ECP bases correlate very satisfactorily with available experimental data, although they are ca. one order of magnitude lower than the experimental values. The influence of molecular geometry (semiempirical vs. DFT) on the nuclear shielding is also examined and discussed, particularly in the case of species containing Ru–S bonds {[$RuCl_2(DMSO)_4$] and α-[$PW_{11}RuO_{39}(DMSO)$]$^{5-}$}. It is shown that such calculations may help the assignment of signals in ^{99}Ru NMR spectra of mono- and polynuclear complexes.
(© Wiley-VCH Verlag GmbH, 69451 Weinheim, Germany, 2002)

Introduction

NMR spectroscopy of transition metal nuclei is a very attractive tool for the elucidation of the structures of complexes of transition metals, and also for the determination of structure-activity relationships, since it directly probes the atomic centre most often responsible for reactivity, e.g. in catalysis.[1] However, general application of this experimental tool is often plagued by difficulties. Most transition metal nuclei span a very wide chemical shift range (10^3-10^4 ppm), and the dependence of this on the multiple coordination and binding modes of these metals is not easily predictable.[2,3] Furthermore, the majority of such nuclei have $I > 1/2$ and, as a result, NMR spectral lines tend to be broad, except where the local symmetry around the metal atom is relatively high. The practical difficulties associated with the detection of broad lines, together with the wide chemical shift range, sometimes renders signal assignment or even detection problematic. Therefore, it is highly desirable to be able to predict the major features of these NMR spectra.

Quantum chemical methods have proved very effective in predicting the nuclear shielding of many nuclei,[4] including transition metals.[5−7] Density-functional theory has proved to be especially effective in this regard.[5−8] However, such calculations with conventional all-electron basis sets on 2nd-row (and especially 3rd-row) transition metals are hampered by the rapid increase in the computational cost when many such heavy atoms are present (which is an important area of application; see below), and also by the onset of relativistic effects.[9] The obvious solution to this problem would be to employ a basis set with effective core potentials (ECPs), where the core electrons up to a given shell are treated in a simplified way by means of pseudopotentials (which also incorporate some relativistic corrections). The difficulty with regard to the calculation of NMR properties is that the functional form of ECPs leads, by construction, to incorrect behaviour (tending asymptotically to zero) at the nucleus. As a result, nuclear shieldings will be substantially underestimated.[10]

In relation to this issue, Moore and Healy[11] analysed the dependence of titanium shielding in titanium tetrahalides on all-electron and ECP basis sets. They found that the shielding contribution from inner shells is large but not very dependent on the basis set and the nature of the ligand, and that the contribution from the outermost core electrons (3s and 3p) is much smaller in magnitude, is paramagnetic and varies considerably. Therefore, these results suggest that the core contribution is essentially "transferable" among several species; however, the scope of such results is rather small, also considering the structural similarity of the species investigated.

Our own previous work on ^{183}W chemical shifts is consistent with the above results, which showed that the shieldings associated with a series of mono- and polynuclear tungsten complexes, calculated with ECP basis sets, are underestimated by ca. one order of magnitude. However, they correlate very well with experimental chemical shifts over a range of 8000 ppm.[12] We were then encouraged to expand the scope of these calculations to other transition metals of current interest.

Among the transition metals, ruthenium exhibits the widest range of oxidation states (eleven, from −II to +VIII) and several coordination geometries in each electronic configuration, as revealed by the large number of complexes

[a] Centro CNR Meccanismi Reazioni Organiche, Dipartimento di Chimica Organica, Università di Padova,
Via Marzolo 1, 35131 Padova, Italy
Fax: (internat.) + 39-049/827-5239
E-mail: alessandro.bagno@unipd.it
Supporting information for this article is available on the WWW under http://www.eurjic.com or from the author.

known that are of considerable interest in catalysis.[13] Ruthenium catalysts have indeed proved to be effective in a wide variety of organic transformations, generally featuring high efficiency and selectivity. These reactions include some fundamental processes, i.e. hydrogenation, carbon−carbon bond formation, and oxygenation by dioxygen activation.[13] In the latter field, two fairly diverse ruthenium-based catalysts, one carrying the tetramesitylporphyrinato ligand[14] and the more recent one using a totally inorganic polyoxotungstate framework,[15] have been claimed to be the most promising dioxygenase mimicking systems.

Ruthenium possesses two magnetically active isotopes (^{99}Ru and ^{101}Ru), both having $I > 1/2$, and hence are quadrupolar.[2,3] However, NMR spectroscopic investigations are usually restricted to ^{99}Ru ($I = 5/2$, $Q = 7.9$ fm^2),[16] since the other nuclide has a larger Q value. Even so, the NMR sensitivity of ^{99}Ru is rather low, which is often further complicated by the broad lines that are observed in species of low symmetry. It should also be mentioned that ruthenium NMR spectroscopy is practically feasible only on diamagnetic complexes, Ru^{II} (d^6) and Ru^{VIII} (d^0) species.

A relatively small data base of experimental NMR chemical shifts is available,[17−21] since the experimental difficulties mentioned above have prevented the detection of such signals in several low-symmetry environments.[2,3] However, the scope of ^{99}Ru NMR spectroscopy can indeed be broadened with modern spectrometers, as recently shown by Elsevier and co-workers;[22] further improvements regarding low-symmetry complexes are obtained by using supercritical fluids as solvents, where rotational correlation times can be decreased to a useful extent.[23] However, the available data extends over a few major types of compounds, notably various substituted bipyridyl, pyrazinyl, and mixed derivatives. ^{99}Ru shielding is extremely sensitive to its environment, spanning a known range of over 10^4 ppm from $\delta = -1363$ for $Ru(cp)_2$ to $\delta = 16050$ for $Ru(H_2O)_6^{2+}$.

Only one major computational study of ^{99}Ru NMR spectroscopic properties is available.[24] This work focussed on the quantitative prediction of such chemical shifts in a series of Ru complexes (mostly sharing a similar ligand pattern), which strictly mandates the use of all-electron basis sets. Thus, a comprehensive investigation of the performance of various basis sets and density functional methods was undertaken, which showed the high degree of accuracy that can be attained in such calculations. In particular, the better performance of hybrid functionals such as B3LYP was noted, both in terms of geometry and NMR spectroscopic properties.

However, as mentioned above, calculations with all-electron basis sets are intractable for large systems. Hence, in connection with the general interest in the catalytic properties of ruthenium-substituted polyoxometalates,[15,25,26] and based on our previous results[12] for ^{183}W, we have compared the performance of all-electron and ECP basis sets. We have carried out a computational investigation of the NMR spectroscopic properties of some ruthenium complexes for which experimental spectra, spanning most of the known shift range, are available. Our analysis includes a ruthenium-substituted polyoxotungstate anion, whose structural features and nuclear magnetic properties will be discussed in terms of the correlation with the ^{99}Ru NMR results.[26]

Computational Details

Few all-electron Gaussian basis sets are available for Ru;[27−30] in this study we employed the double-zeta polarised DZVP basis set.[29,31] No relativistic corrections were made, since very good results have also been obtained with non-relativistic calculations.[24] Since our earlier work on ^{183}W showed a similar performance of several ECPs,[12] notably those by Hay and Wadt (LANL2DZ),[32] Stevens−Basch−Krauss (CEP-121G)[33] and Dolg et al. (SDD),[34] this study will be limited to the first two.

In some cases (see Results) the LANL2DZ basis was augmented with one or two d functions from the 6-311G(d,p) or 6-311G(2d,2p) basis sets,[31] as follows. S: $\zeta = 0.650$ or $\zeta = 1.300$, 0.325; Cl: $\zeta = 1.500$, 0.375; C: $\zeta = 0.313$ or $\zeta = 1.252$, 0.313. Basis-set augmentation is denoted as LANL(*n*d,*n*d), where the first item refers to *n* d functions on S atoms, and the second (if present) to *n* d functions on Cl atoms. Thus, the basis augmented with 2 d functions both at S and at Cl will be denoted as LANL(2d,2d). The use of such augmented basis sets for the calculation of chemical shifts requires a corresponding augmentation of the basis set of the commonly accepted reference compound $Ru(CN)_6^{4-}$,[2,3] for which LANL(2d) and LANL(2d,2d) are identical since the augmentation always refers to carbon atoms. Hence, the LANL(2d) basis for $Ru(CN)_6^{4-}$ is equivalent to LANL(2d,2d) for S and Cl, since the basis of all ligands is augmented.[35] However, the augmentation of LANL(d) for $Ru(CN)_6^{4-}$ cannot be made in a consistent way, because this would actually imply one extra d function on just two equatorial carbon atoms, i.e. an inconsistent modelling of the cyano ligands. Hence, in this case only the shieldings calculated with this basis (but not the chemical shifts) will be compared.

^{99}Ru shieldings were calculated with the GIAO method by means of density functional theory (Becke's hybrid 3-parameter functional with Lee−Yang−Parr correlation, B3LYP[36])[24] and a (99,302) integration grid. Only the isotropic part of the shielding tensor [$\sigma = (\sigma_{11} + \sigma_{22} + \sigma_{33})/3$] is given. Calculated chemical shifts ($\delta = \sigma_{ref} - \sigma$) are referred to $Ru(CN)_6^{4-}$. All calculations were carried out with GAUSSIAN 98.[37]

Results and Discussion

For our analysis we chose a number of species of moderate size, evenly spanning the entire known chemical shift range (Table 1). In addition to these complexes, we also investigated a polyoxotungstoruthenate, α-$[PW_{11}RuO_{39}(DMSO)]^{5-}$, which can be obtained by metallation of the

Table 1. Calculated energies (au), calculated and experimental NMR chemical shifts (ppm) of ^{99}Ru in ruthenium complexes with the LANL2DZ and CEP-121G ECP basis sets

Species	LANL2DZ PM3(tm)[a]			LANL2DZ[b]			CEP-121G CEP-121G[c]			Exptl.
	E	σ	calcd. δ[d]	*E*	σ	calcd. δ[d]	*E*	σ	calcd. δ[d]	δ[e]
$Ru(cp)_2$[f]	−480.888559	−183.1	−88	−480.905987	−396.0	−133	−156.404137	−343.7	−235	−1270,[18] −1363[g]
$Ru(CN)_6^{4-}$	−650.513909	−271.3[h]	0	−650.538156	−529.0[i]	0	−186.758568	−579.2[j]	0	0[17,18]
$[Ru(CO)_3Cl_3]^-$ [k]	−478.920626	−317.8	46.5	−478.947778	−477.8	−51.3	−203.779083	−484.1	−95.1	816[24]
RuO_4	−394.634978	−671.0	400	−394.638460	−731.2	202	−157.681749	−763.7	184	2021[18]
$Ru(bpy)_3^{2+}$	−1579.493860	−838.1	567	−1579.514435	−998.0	469				4518,[18] 4609[19]
$Ru(NH_3)_6^{2+}$	−432.801885	−838.0	567	−432.837757	−1542	1013	−163.795650	−1688	1109	7680,[17] 7821[18]
$Ru(H_2O)_6^{2+}$	−551.890651	−2055	1784	−551.956823	−2741	2212	−196.478459	−3019	2440	16050[20]
$[RuCl_2(DMSO)_4]$[l]	−784.029546	−1039	768	−784.133356	−1650	1121	−287.549287	−1816	1237	3976[26]

[a] B3LYP/LANL2DZ//PM3(tm). [b] B3LYP/LANL2DZ//B3LYP/LANL2DZ. [c] B3LYP/CEP-121G//B3LYP/CEP-121G. [d] $\delta = \sigma_{ref} - \sigma$, relative to $Ru(CN)_6^{4-}$. [e] Literature reference given as superscript. [f] Eclipsed rings as in the experimental structure. The corresponding structure with staggered rings has the same energy, and $\sigma = -183.6$ [PM3(tm) geometry] or $\sigma = -405.6$ (LANL2DZ geometry). [g] Redetermined in this work (CH_2Cl_2 solution, 25 °C; see ref.[26] for experimental details). [h] Ru−C = 1.986 Å. [i] Ru−C = 2.105 Å. [j] Ru−C = 2.130 Å. [k] *fac* isomer. [l] *cis*,*fac* isomer (Scheme 1).

lacunary α-Keggin polyoxotungstate α-$[PW_{11}O_{39}]^{7-}$ with $[RuCl_2(DMSO)_4]$ under microwave irradiation.[26] The ^{99}Ru signal of α-$[PW_{11}RuO_{39}(DMSO)]^{5-}$ (observed at $\delta = 7737$), is quite removed from that of the ruthenium precursor ($\delta = 3976$), and provides the first NMR spectrum of ruthenium embedded in a polyoxotungstate cage.[26] Therefore, it is of interest to extend the scope of our study to Ru complexes in this new environment.

Geometrical features are discussed only in relevant cases (Scheme 1);[38−41] all calculated structures are given as Supporting Information as PDB files.

Shielding Calculations with ECP Basis Sets

The size of most complexes investigated in this work lies within the scope of current ab initio or DFT geometry optimisations. However, a comparison with shieldings obtained at geometries optimized with the PM3(tm) semiempirical level[43] was deemed necessary in order to establish whether shieldings calculated with the latter simpler method have some predictive value for ruthenium-containing polyoxometalates, whose size would be extremely demanding for higher-level methods.

Thus, ^{99}Ru shieldings were obtained for a series of Ru complexes, whose structures were optimised as reported in Table 1. The results calculated with ECP basis sets are presented in Table 1 and Figure 1.

Inspection of Table 1 firstly shows that with ECP basis sets the values of σ are smaller than the experimental values by one order of magnitude. However, calculated δ values correlate very well with the experimental data, as can be seen from the graphs in Figure 1. A linear fit is seen for δ_{calcd} vs. δ_{exptl} ($\delta_{calcd} = a\delta_{exptl} + b$). PM3(tm) geometry: $a = 0.10\pm0.04$, $b = 69\pm85$, $r^2 = 0.96$; LANL2DZ geometry: $a = 0.139\pm0.006$, $b = -59\pm42$, $r^2 = 0.995$; CEP-121G geometry: $a = 0.156\pm0.006$, $b = -90\pm45$, $r^2 = 0.997$. These correlation parameters can be used to estimate "experimental" chemical shifts from $\delta_{exptl} = (\delta_{calcd} - b)/a$. Based on the above standard deviations of *a* and *b*, error propagation formulas yield standard deviations on the estimated δ_{exptl} of about 300 ppm. This is of the same order as the typical spread of experimental values, which often differ by 200−300 ppm [up to 3000 ppm for $Ru(H_2O)_6^{2+}$].

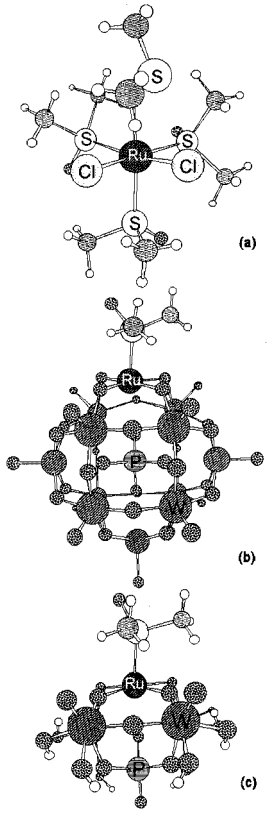

Scheme 1. Calculated structures of ruthenium complexes. (a) $[RuCl_2(DMSO)_4]$ (B3LYP/DZVP); (b) α-$[PW_{11}RuO_{39}(DMSO)]^{5-}$ [PM3(tm)]; (c) the model fragment $[PW_4RuO_{10}(OH)_8(DMSO)]^{5-}$ [B3LYP/LANL(d); see text]; O dotted, C solid grey, H white

Despite the low slope values observed (see below), the good correlations show that the calculation with ECP basis sets only introduces a systematic error, which is remarkably

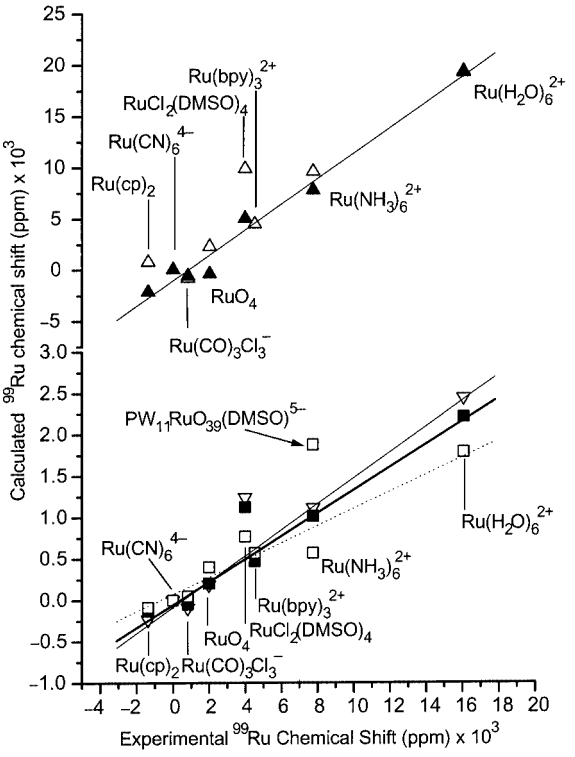

Figure 1. Correlation between experimental and calculated ^{99}Ru shieldings with ECP or all-electron basis sets; results of linear fittings are reported as $\delta_{calcd} = a\delta_{exptl} + b$; bottom panel: (a) empty squares, dotted line: B3LYP/LANL2DZ//PM3(tm); $a = 0.10\pm0.04$, $b = 69\pm85$, $r^2 = 0.96$; fit does not include the data for [RuCl$_2$(DMSO)$_4$] and α-[PW$_{11}$RuO$_{39}$(DMSO)]$^{5-}$; (b) solid squares, solid thick line: B3LYP/LANL2DZ//B3LYP/LANL2DZ; $a = 0.139\pm0.006$, $b = -59\pm42$, $r^2 = 0.995$; (c) down triangles, solid thin line: B3LYP/CEP-121G//B3LYP/CEP-121G; $a = 0.156\pm0.006$, $b = -90\pm45$, $r^2 = 0.997$); fits do not include the data points for [RuCl$_2$(DMSO)$_4$]; top panel: (d) empty triangles, no fit line: B3LYP/DZVP//B3LYP/LANL2DZ; (e) solid triangles, solid line: B3LYP/DZVP//B3LYP/DZVP; $a = 1.24\pm0.08$, $b = -1060\pm570$, $r^2 = 0.989$

constant for a wide array of species. The above correlations hold through the known chemical shift range of ca. 20000 ppm, thereby broadening the scope of such calculations beyond the range examined, e.g., in ref.[24]

Test calculations with pure functionals (BLYP, PW91PW91; data not reported) yielded very similar results in terms of absolute shieldings and more so in terms of the slope of the correlation lines.

We would like to point out that anionic, neutral and cationic species are equally well modelled, which implies a relatively minor solvent effect in determining the ^{99}Ru chemical shift. This may simply be a consequence of the very large range of chemical shifts investigated (i.e., solvent effects are smaller than our estimated accuracy of ±300 ppm), and should call for caution whenever smaller ranges are investigated, or when complexes with a labile coordination sphere are considered.

We also note that the performance of LANL2DZ and CEP-121G (at the respective geometries) is quite similar (Figure 1), but differ with the results of ref.[11] for Ti. The comparison of shifts calculated with a DFT geometry, rather than a semiempirical geometry shows that the fit quality is generally better even though the slope of the correlation line is not very different.

Hence, despite this large systematic error, ECP shielding calculations effectively model ^{99}Ru shifts to an accuracy that will enable the experimental NMR spectroscopist to close in on the spectral region where the signals may be expected, with obvious practical advantages. However, there are three major discrepancies emerging from the correlation in Figure 1.

(a) The calculated shielding of [Ru(NH$_3$)$_6^{2+}$], using the PM3(tm) geometry, fits rather badly in the correlation line, whereas if the geometry is optimized by an ECP method, the data fits very well; (b) the shielding of [RuCl$_2$(DMSO)$_4$] is only fairly well modelled with the PM3(tm) geometry, whereas both ECP geometries lead to an unacceptably deshielded chemical shift; (c) the shielding of α-[PW$_{11}$RuO$_{39}$(DMSO)]$^{5-}$ is grossly overestimated at the PM3(tm) geometry (the only practical approach for a molecule of this size), which yielded a Ru−S distance of 2.276 Å (Scheme 1). In the latter two cases, we are dealing with species possessing Ru−S bonds. The nature of the bonding of DMSO to ruthenium is a matter of current interest, justified by the recent discovery that haloruthenium (sulfoxide) complexes exhibit a remarkable anti-tumour activity, in addition to being versatile oxidation catalysts.[44] The effect of the Ru−S bond length on the ^{99}Ru shielding in [RuCl$_2$(DMSO)$_4$] and α-[PW$_{11}$RuO$_{39}$(DMSO)]$^{5-}$ has been studied in detail (see below).

Shielding Calculations with the All-Electron DZVP Basis Set

Although in practical terms ECP basis sets seem to perform remarkably well (except for the large systematic error), it is worthwhile to compare such results with the performance of an all-electron basis set, where the contribution of core electrons is explicitly taken into account. Thus, ^{99}Ru shieldings have been calculated for the same data set seen before, using both the previous LANL2DZ and newly optimized DZVP geometries (Table 2 and Figure 1).

The first major difference with respect to the previous results is, of course, that the order of magnitude of calculated shifts is now correct, as shown by the correlation parameters ($a = 1.24\pm0.08$, $b = -1060\pm570$, $r^2 = 0.989$), with a slope now close to unity. Shieldings calculated at this level of theory are, in fact, overestimated by 20%, which shows the need for a better basis set in order to arrive at the desired unit slope.[24] However, this is sufficient for the purposes of this work, since a well-behaved general trend is apparent.

The much better performance of the DZVP than the LANL2DZ geometries is also apparent. Since *valence* electrons are treated on a similar footing by both basis sets (e.g., no relativistic corrections are made, while scalar relativistic corrections are present only in the pseudopotentials pertaining to core electrons in LANL2DZ), the worse performance of the latter basis seems due to a deficiency in the valence region. In fact, the species giving the worst fitting (Figure 1d) is [RuCl$_2$(DMSO)$_4$], for which the LANL2DZ

Table 2. Calculated energies [au], calculated and experimental chemical shift [ppm] of ^{99}Ru in ruthenium complexes with the DZVP basis set

Species	LANL2DZ[a]			DZVP[b]			Exptl.
	E	σ	δ[c]	E	σ	δ[c]	δ[d]
$Ru(cp)_2$[e]	−4830.422148	−772.6	757	−4830.424271	−370.8	−2151	−1270, −1363
$Ru(CN)_6^{4-}$	−5000.087074	−15.70	0	−5000.124589	−2522[f]	0	0
$[Ru(CO)_3Cl_3]^-$	−6164.101958	−1682	−840	−6164.106358	−1920	−602	816
RuO_4	−4744.076322	−2299	2283	−4744.077196	−2111	−411	2021
$[RuCl_2(DMSO)_4]$[g]	−7576.467389	−9851	9835	−7576.547516	−7526	5004	3976
$Ru(bpy)_3^{2+}$	−4830.422148	−4463[h]	4447	[i]			4518, 4609
$Ru(NH_3)_6^{2+}$	−4782.293995	−9558	9542	−4782.298573	−10254	7731	7821, 7680
$Ru(H_2O)_6^{2+}$	−4901.402267	−19195	19179	−4901.405323	−21789	19267	16050

[a] B3LYP/DZVP//B3LYP/LANL2DZ, except where indicated. [b] B3LYP/DZVP//B3LYP/DZVP. [c] $\delta = \sigma_{ref} - \sigma$, relative to $Ru(CN)_6^{4-}$. [d] See Table 1 for sources. [e] See footnote [f] to Table 1. [f] Ru−C = 2.145 Å. [g] See footnote [l] to Table 1. [h] PM3(tm) geometry. [i] Not calculated, because the chemical shift lies well within the range encompassed by the other species and this compound is well behaved at the other theoretical levels, so that this large calculation is not expected to reveal new trends.

basis shown below is seen to be inadequate to model the Ru−S and Ru−Cl bonds.

Hence, in general terms the DZVP basis set has a performance similar to that of the ECP bases seen before. However, there is a considerable time penalty involved, DZVP calculations taking ca. 4 times longer than the corresponding LANL2DZ ones. The time issue may become crucial when planning to investigate systems containing a large number of heavy atoms, like polyoxometalates (see below).

Comparison of Shieldings Calculated with All-Electron and ECP Basis Sets

The large underestimation of the shieldings calculated with an ECP basis set is a known effect, previously observed by Ridard et al.[10] for ^{31}P, and by ourselves[12] for ^{183}W. This underestimation arises because molecular orbitals built from ECPs fall asymptotically to zero at distances smaller than the core radius, thereby losing all nodal features of orbitals replaced by the ECP. Since the shielding constant is calculated from integrals containing an r_N^{-3} term (r_N being an electron−nucleus distance), these integrals become too small in the vicinity of the nucleus.[10,12] The relationship between the data obtained by all-electron (AE, with DZVP) or ECP (with LANL2DZ) calculations is further investigated by dissecting the σ values into its diamagnetic (σ_d) and paramagnetic (σ_p) components, for a few representative complexes (Table 3).

Table 3. Diamagnetic and paramagnetic contributions to ^{99}Ru shielding with the DZVP and LANL2DZ basis sets

	DZVP[a]		LANL2DZ[a]	
	σ_d	σ_p	σ_d	σ_p
$Ru(cp)_2$	4281	−4652	252.4	−648.3
$Ru(CN)_6^{4-}$	4265	−6787	243.1	−772.2
$Ru(NH_3)_6^{2+}$	4263	−14520	234.6	−1776
$Ru(H_2O)_6^{2+}$	4261	−26050	234.2	−2975
RuO_4	4260	−6370	233.1	−964.4
av.	4266±10		239±10	

[a] At the respective geometries; see Tables 1−2.

Table 3 shows that σ_d is remarkably constant for all species investigated, with an average value of 4260±10 ppm (AE) or 240±10 ppm (ECP). The definition of core electrons in the LANL2DZ basis set includes all electrons up to the 3d shell. The hypothetical Ru^{16+} ion has only core electrons; accordingly, no shielding is calculated with the ECP basis, whereas σ_d = 3993 ppm is calculated with DZVP, which is in reasonably good agreement with the average value given above. On the other hand, the Ru^{8+} ion (with a [core] $4s^24p^6$ configuration) yields quite similar σ_d values with both AE and ECP methods (176 and 144 ppm, respectively). The further contribution to σ_d from 4d electrons is highlighted by the values for Ru^{2+} ([core] $4s^24p^64d^6$), which is again quite similar in both cases (80 ppm). Hence, although the valence region of the LANL2DZ basis is of somewhat lower quality than that of DZVP, the contribution of valence electrons to σ_d is calculated to be very similar; the small sensitivity of σ_d to the basis set is further confirmed. Indeed, the large difference of ca. 4000 ppm arising from the core electrons (being just an additive term) is irrelevant in the calculation of chemical shifts.

With regard to σ_p, we note that only a contribution from the 4d electrons can be expected, since all lower shells are closed. Thus, for Ru^{2+} we calculate σ_p = 362000 and 74000 ppm in the AE and ECP bases, respectively, with a ratio of 4.9. Table 3 shows that for Ru complexes a similar relationship also holds, $\sigma_p^{AE}/\sigma_p^{ECP}$ = 7−9. A linear fitting of σ_p^{AE} vs. σ_p^{ECP} yields a slope of 9.1, which corresponds to the relative slope (8.9) of the correlation lines in Figure 1b and e, and confirms that the large difference between experimental and ECP-calculated chemical shifts arises entirely from the paramagnetic term, in turn arising essentially from 4d electrons.

Ruthenium Shielding in $RuCl_2(DMSO)_4$

As noted above (see Figure 1), the calculated shifts for $RuCl_2(DMSO)_4$ fit reasonably well with the correlation line from the data obtained using the DZVP geometry, whereas all those with ECP or PM3(tm) geometries are too deshielded. We have investigated the origin of this discrepancy in

Table 4. Calculated and experimental Ru−S distances [Å] of the coordinated sulfur atoms in $[RuCl_2(DMSO)_4]$

Geometry[a]	Ru−S			Ru−Cl		Av. diff.[b]
	eq	eq	ax			
PM3(tm)	2.350	2.348	2.323	2.351	2.371	0.068
LANL2DZ	2.480	2.480	2.470	2.481	2.486	0.150
LANL(d)	2.376	2.369	2.346	2.515	2.521	0.096
LANL(2d)	2.345	2.336	2.310	2.530	2.539	0.082
LANL(2d,2d)	2.356	2.347	2.308	2.474	2.480	0.063
CEP-121G	2.490	2.492	2.478	2.486	2.490	0.158
DZVP	2.397	2.400	2.352	2.474	2.480	0.091
Experimental[c]	2.274	2.284	2.245	2.421	2.424	−

[a] B3LYP calculations, except PM3(tm). [b] Average of absolute deviations over all bonds for the specified level (see text). [c] Ref.[41]

detail by analysing the effect of augmenting the ECP basis on (a) the geometry (especially the Ru−S bonds) and, (b) the ^{99}Ru shielding. The experimental and calculated Ru−S distances are reported in Table 4, whereas basis set and geometry effects on the calculated shielding are collected in Table 5.

In the X-ray structure,[41] Ru−S distances of the three *S*-coordinated DMSO molecules are 2.274, 2.284 Å (equatorial) and 2.245 Å (axial). In the PM3(tm) structure, relative Ru−S distances (Table 4) agree with the experimental ones, but the PM3(tm) method overestimates the Ru−S distances by 0.07 Å on average. Geometry optimization with both the LANL2DZ and CEP-121G basis sets yield very similar Ru−S distances (Table 4). However, although the relative distances are once again correct, these basis sets overestimate experimental Ru−S distances by 0.21−0.22 Å, with a poor fit with either correlation already mentioned.

A possible cause for this poor performance may lie in an inadequate treatment of the valence region of the S or Cl atoms. To address this issue, the LANL2DZ basis was augmented at the sulfur and/or chlorine atoms [LANL(d), LANL(2d), and LANL(2d,2d); see Computational Details].

Table 4 shows that geometry optimisation with the LANL(d) and LANL(2d) basis sets leads to a marked shortening of the Ru−S distances. However, they remain longer than the experimental distances (by 0.10 and 0.06 Å, respectively), while the Ru−Cl bond lengths are substantially overestimated (by ca. 0.1 Å). Augmentation of the chlorine basis [LANL(2d,2d)] also results in a slight lengthening of the Ru−S bonds and a shortening of the Ru−Cl bonds, which deviate by 0.05−0.06 Å from the experimental values. The latter basis is the best, as indicated by the average deviation of 0.063 Å over the Ru−S and Ru−Cl bonds (Table 4).

Shielding calculations were performed with all variants of the LANL2DZ basis, in combination with geometries obtained at the various levels available, as detailed in Table 5. We would like to mention at this point that no calculation was carried out at the experimental geometry, to ensure consistency of treatment with the other species.

The effect of the geometry and basis set on the calculated shielding can be summarized as follows. Augmenting the LANL2DZ basis set with polarisation functions on the ligands, i.e. improving their valence region, has remarkable effects on the geometry, as seen before. Thus, σ values calculated with the augmented basis sets (between −1296 and −1059) are substantially more shielded than the reference value of −1650 (Table 1), which goes in the right direction. However, this effect is primarily a result of the mentioned geometry changes, rather than of the basis set per se. For example, shieldings of −1650, −1296, or −1211 are calculated with the same basis set (LANL2DZ) at the LANL2DZ, LANL(d), or LANL(2d) geometry, respectively. Conversely, the shielding calculated with the LANL(2d) basis at the LANL2DZ geometry (−1521) is only slightly better than the reference value.

Further improvement is achieved by adopting the augmented basis for the shielding calculation also, which brings the value down to −1089 with LANL(2d). Augmentation of the Cl basis, once again, has a noticeable effect on the shielding (−1059), only when the calculation is run on the optimized structure. The results of these calculations are

Table 5. Calculated and experimental NMR chemical shifts [ppm] of ^{99}Ru in $Ru(CN)_6^{4-}$ and $RuCl_2(DMSO)_4$ with the LANL2DZ ECP basis set, augmented variously

Level[a]	$Ru(CN)_6^{4-}$ σ_{ref}	$[RuCl_2(DMSO)_4]$ σ	calcd. δ[b]
LANL//LANL	−529.1	−1650	1121
LANL//LANL(d)	−565.3	−1296	[c]
LANL(d)//LANL(d)	−533.2	−1171	[c]
LANL//LANL(2d)[d]	−479.8	−1211	731.2
LANL(2d)//LANL	−509.7	−1521	1011
LANL(2d)//LANL(2d)	−479.8	−1089	609.2
LANL(2d,2d)//LANL(2d)	−479.8	−1087	607.2
LANL(2d,2d)//LANL(2d,2d)	−479.8	−1059	579.2
LANL(2d,2d)//PM3(tm)	−258.2	−930.7	672.5

[a] All calculation with the B3LYP functional; see Table 1 for general remarks and experimental values. The LANL2DZ basis is abbreviated as LANL. Basis-set augmentation is denoted as LANL(nd,nd), where the first item refers to *n* d-functions on sulfur atoms, and the second (if present) to *n* d-functions on chlorine atoms (see Computational Details). For $Ru(CN)_6^{4-}$, LANL(2d) and LANL(2d,2d) are identical since the augmentation always refers to carbon atoms. [b] $\delta = \sigma_{ref} - \sigma$; the calculation for $Ru(CN)_6^{4-}$ is carried out at the corresponding level. [c] σ_{ref} cannot be consistently calculated (see Computational Details). [d] Ru−C = 2.096 Å.

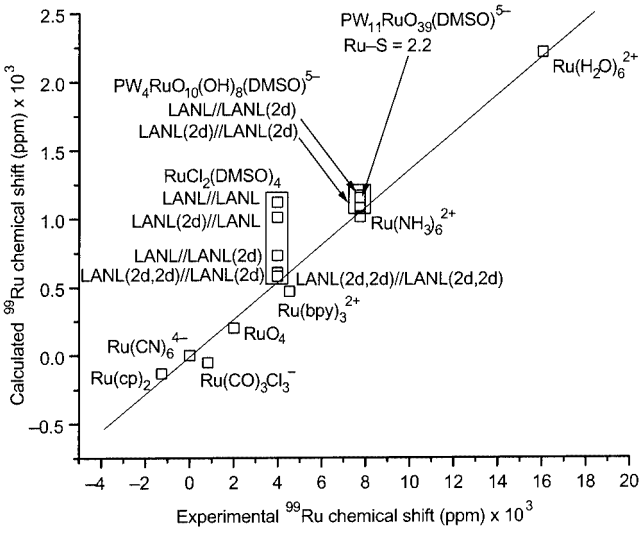

Figure 2. Basis-set and geometry effects on ^{99}Ru shieldings of $[RuCl_2(DMSO)_4]$, $[PW_4RuO_{10}(OH)_8(DMSO)]^{5-}$, and α-$[PW_{11}RuO_{39}(DMSO)]^{5-}$ (not included in the fit; see text for these data); the geometry is at the B3LYP/LANL2DZ level (cf. Figure 1), except where noted; the LANL2DZ basis is abbreviated as LANL

summarized in Figure 2, which highlights the progressive trend of the calculated values towards a good fit with the correlation line. The value δ = 4590 is obtained after the calculated δ value of 579 is corrected by the appropriate fitting parameters, and compares with the experimental value (δ = 3976).

At the PM3(tm) geometry, shieldings of −1039 (Table 1) and −931 (Table 5) are calculated with LANL2DZ and LANL(2d,2d), respectively. This point further illustrates the dependence of the shielding on geometry, and highlights the better performance of augmented LANL2DZ.

A similar effect was found in the case of $[Ru(CO)_3Cl_3]^-$. Again, a geometry optimisation with the LANL(2d,2d) basis leads to a better modelling of the experimental structure, with an average deviation of the Ru−C and Ru−Cl bond lengths from those of the experimental structure[24] of 0.04 Å (0.06 Å with LANL2DZ). Accordingly, a slight improvement is noted in the calculated chemical shift (δ = −17, rather than δ = −51 with the non-augmented basis) which has a better fit in the correlation line, with an experimental value of δ = 816.

These results allow us to draw the following conclusions. (a) Although augmenting the ECP basis set with polarisation functions on the ligands has remarkable effects on the molecular geometry, any effect on the ruthenium shielding is mostly due to such geometry changes, since calculations with augmented basis sets but with non-optimised geometries only lead to minor improvements. (b) Calculated chemical shifts correlate with experimental values over the whole chemical shift range, even though some deviations from experimental geometries may be present, at least in the case of $[RuCl_2(DMSO)_4]$. (c) Chemical shifts calculated with various augmented valence regions converge to a value falling within the correlation line previously found; this confirms that the large scaling factors do not depend much on the chemical nature of the complex. However, the adequacy of such scaling factors in obtaining very accurate estimates is, perhaps, yet to be assessed.

Ruthenium Shielding in α-$[PW_{11}RuO_{39}(DMSO)]^{5-}$

Although an experimental X-ray structure is not available, the general structural features are known from ^{183}W, ^{31}P, and ^{1}H NMR spectroscopic data.[26] The data point out that the complex (a) retains the basic α-Keggin structure, with one Ru atom replacing one W atom, and (b) one DMSO molecule is coordinated to the Ru atom, presumably through the S atom rather than the O atom. This indication is further strengthened by the fact that the PM3(tm) geometry optimisation of a structure with an *O*-coordinated DMSO molecule leads to the *S*-coordinated molecule.

The large size of this species renders a PM3(tm) geometry optimisation as the only feasible approach, which yields an Ru−S distance of 2.276 Å (structure b in Scheme 1). We note that this distance is shorter than the shortest distance in $RuCl_2(DMSO)_4$ (2.323 Å) computed at the same level. The calculated shielding at the B3LYP/LANL2DZ level is σ = −2146, corresponding to a calculated value of δ = 1875; after conversion into an estimated δ value through the pertinent correlation parameters, this corresponds to a very large overestimation (δ = 19000 vs. the experimental value of δ = 7737). The strategy adopted for improving the predictive power of such calculations is described as follows (see Table 6).

Table 6. Geometry effects on the ruthenium shielding in polyoxotungstoruthenates[a]

Geometry	*r*(Ru−S) [Å]	*E* [au]	σ
α-$[PW_{11}RuO_{39}(DMSO)]^{5-}$			
PM3(tm)	2.276[b]	−3947.416803	−2146[c]
PM3(tm)	2.245[d]	−3947.412974	−1916[c]
PM3(tm)	2.200[d]	−3947.410692	−1681[e]
$[PW_4RuO_{10}(OH)_8(DMSO)]^{5-}$			
LANL2DZ	2.849[b][f]	−2196.998676	−3187
LANL2DZ	1.990[d][g]	−2196.852029	−1651
LANL(2d)	2.196[b]	−2197.144188	−1620[h]
LANL(2d)	2.196[b]	−2197.015405	−1697[i]

[a] B3LYP/LANL2DZ, except where noted. [b] Optimised Ru−S distance. [c] SCF convergence criteria reduced to 10^{-7}. [d] Ru−S distance constrained as stated. [e] SCF convergence criteria reduced to 10^{-6}. [f] Partially optimised structure (expulsion of DMSO). [g] Rest of molecule as in the preceding item. [h] Shielding calculated with the LANL(2d) basis set. [i] Shielding calculated with the LANL2DZ basis set.

The Ru−S distance was firstly constrained to 2.245 Å, as in the experimental structure of $[RuCl_2(DMSO)_4]$ (Table 4) and reoptimised by PM3(tm) under this constraint. A smaller value of σ (−1916) was obtained (Table 6), which corresponds to δ = 15900; however, this is still too high. Nevertheless, this result provides a first indication that a relatively short Ru−S distance should be expected.

In view of the huge computational cost of calculations on the whole complex, test calculations were run on the model fragment $[PW_4RuO_{10}(OH)_8(DMSO)]^{5-}$, featuring only the upper lacunary sites and with some protonated WO_6 units, so as to have the same charge as the target compound (Scheme 1, structure c). A B3LYP/LANL2DZ geometry optimisation led to the expulsion of the DMSO molecule (Ru−S distance > 4 Å), and (quite predictably) to an even larger deshielding ($\sigma = -3187$).[45]

The better performance observed with the LANL(2d) basis in the case of $[RuCl_2(DMSO)_4]$ indeed suggests its use as a possible remedy. On the other hand, by constraining the Ru−S bond length to 1.990 Å, the resulting more shielded $\sigma = -1651$ value further indicates a short Ru−S bond in the species under examination.

A B3LYP/LANL(2d) geometry optimisation led to a Ru−S distance of 2.196 Å. The shielding calculated with the same basis (−1620) gives an excellent fit in the pertinent correlation line (Figure 2). The same calculation run with the non-augmented basis [i.e., LANL2DZ//LANL(2d)] yields a similar but slightly worse shielding ($\sigma = -1697$). Hence, all data point to a substantially shorter Ru−S distance in the polyoxometalate than in $RuCl_2(DMSO)_4$.

Based on these arguments, we ran a further calculation on α-$[PW_{11}RuO_{39}(DMSO)]^{5-}$ with the Ru−S distance fixed at 2.200 Å (close to the optimised value for the model, see above). The resulting shielding was $\sigma = -1681$ (Table 6). Thus, remarkably, shortening the Ru−S distance by 0.045 Å shields the ^{99}Ru nucleus by 235 ppm which, when converted into experimental data through the slope factor of 7.2, results in a value no less than 1700 ppm. This point illustrates the extreme sensitivity of ^{99}Ru chemical shifts to its coordination geometry.

Interpretation of these results should be based on the consideration that the geometry employed is derived partly (essentially all the polyoxometalate cage) from PM3(tm) and partly (the Ru−S distance) from DFT methods. However, since the Ru−S distance is apparently the most important parameter in determining the Ru shift, it is admissible to regard this data as belonging to the DFT correlation line (Figure 2), which shows an excellent fit. The calculated chemical shift would be (once corrected by the factor of 7.2) $\delta = 8700$, compared with the experimental value of $\delta = 7737$. We also note that, since the LANL(2d) basis overestimates the Ru−S distance by ca. 0.1 Å, we estimate that the distance in the polyoxometalate is 2.1 Å.

The general conclusion that can be drawn is that the valence region of the LANL2DZ basis set for sulfur is inadequate to model the Ru−S bond, leading to unacceptably long distances. However, this basis is acceptable for the calculation of the shielding, provided that the geometry is appropriate. We would also like to point out that despite the seemingly large error in this calculation (ca. 1000 ppm), this estimate would in fact be helpful in narrowing the spectral region to an extent which allows the reduction of the experimental problems associated with large spectral windows at low frequencies.[2]

Conclusion

ECP basis sets perform remarkably well in the calculation of ^{99}Ru chemical shifts, although such calculated shieldings are much smaller than those calculated by all-electron basis sets or experimental values. We should warn the reader that this approach is "semiempirical" in nature, since it assumes full transferability of the core contribution to the total shielding, and hence its cancellation when chemical shifts are calculated. We have provided a preliminary rationale for this assumption by analysing the relative contribution of the diamagnetic and paramagnetic terms; however, its scope must be independently tested, like in any other approach of this type. At this point, we have provided a set of data that should enable the NMR spectroscopist to obtain at least a rough estimate of the chemical shift of unknown complexes, even relatively large ones (after correction by an appropriate scaling factor). The all-electron DZVP basis set also performs well (albeit at an increased computational cost), particularly in the case of species containing Ru−S bonds. Such species are also successfully modelled by the LANL2DZ ECP basis set, provided that the valence region of the sulfur and chlorine atoms is augmented with d-type polarisation functions. The consistency of these data with those for ^{183}W[12] and ^{95}Mo[47] allows one to envision that the scope of such calculations can be expanded to other nuclei.

Acknowledgments

Part of this work was carried out on an SGI Origin 2000, with computer time granted by CINECA. The Authors thank Dr. A. Sartorel for his technical help.

[1] W. von Philipsborn, *Chem. Soc. Rev.* **1999**, *28*, 95.
[2] *Multinuclear NMR* (Ed.: J. Mason), Plenum, New York, **1987**.
[3] *Transition Metal Nuclear Magnetic Resonance* (Ed.: P. S. Pregosin), Elsevier, Amsterdam, **1991**.
[4] For a recent review, see: T. Helgaker, M. Jaszunski, K. Ruud, *Chem. Rev.* **1999**, *99*, 293.
[5] [5a] M. Bühl, O. L. Malkina, V. G. Malkin, *Helv. Chim. Acta* **1996**, *79*, 742. [5b] M. Kaupp, V. G. Malkin, O. L. Malkina, D. R. Salahub, *Chem. Eur. J.* **1996**, *2*, 24. [5c] M. Bühl, *Chem. Phys. Lett.* **1997**, *267*, 251. [5d] O. L. Malkina, B. Schimmelpfennig, M. Kaupp, B. A. Hess, P. Chandra, U. Wahlgren, V. G. Malkin, *Chem. Phys. Lett.* **1998**, *296*, 93.
[6] N. Godbout, E. Oldfield, *J. Am. Chem. Soc.* **1997**, *119*, 8065.
[7] P. J. Wilson, R. D. Amos, N. C. Handy, *Phys. Chem. Chem. Phys.* **2000**, *2*, 187.
[8] C. Adamo, V. Barone, *Chem. Phys. Lett.* **1998**, *298*, 113.
[9] See, for example: G. Schreckenbach, S. K. Wolff, T. Ziegler, *J. Phys. Chem. A* **2000**, *104*, 8244.
[10] J. Ridard, B. Levy, Ph. Millie, *Mol. Phys.* **1978**, *36*, 1025.
[11] E. A. Moore, A. Healy, *J. Chem. Soc., Faraday Trans.* **1995**, *91*, 1735.
[12] A. Bagno, M. Bonchio, *Chem. Phys. Lett.* **2000**, *317*, 123.
[13] T. Naota, H. Takaya, S. Murahashi, *Chem. Rev.* **1998**, *98*, 2599.
[14] J. T. Groves, R. Quinn, *J. Am. Chem. Soc.* **1985**, *107*, 5790.
[15] R. Neumann, M. Dahan, *J. Am. Chem. Soc.* **1998**, *120*, 11969, and references therein.
[16] *CRC Handbook of Chemistry and Physics*, 77th ed. (Ed.: D. R. Lide), CRC Press, Boca Raton, **1997**.
[17] R. W. Dykstra, A. M. Harrison, *J. Magn. Reson.* **1982**, *46*, 338.
[18] C. Brevard, P. Granger, *Inorg. Chem.* **1983**, *22*, 532.

[19] P. J. Steel, F. Lahousse, D. Lerner, C. Marzin, *Inorg. Chem.* **1983**, *22*, 1488.
[20] [20a] P. Bernhard, L. Helm, I. Rapaport, A. Ludi, A. E. Merbach, *J. Chem. Soc., Chem. Commun.* **1984**, 302. [20b] P. Bernhard, L. Helm, A. Ludi, A. E. Merbach, *J. Am. Chem. Soc.* **1985**, *107*, 312.
[21] C. Marzin, F. Budde, P. J. Steel, D. Lerner, *Nouv. J. Chim.* **1987**, *11*, 33.
[22] S. Gaemers, J. van Slageren, C. M. O'Connor, J. G. Vos, R. Hage, C. J. Elsevier, *Organometallics* **1999**, *18*, 5238.
[23] S. Gaemers, H. Luyten, J. M. Ernsting, C. J. Elsevier, *Magn. Reson. Chem.* **1999**, *37*, 25.
[24] M. Bühl, S. Gaemers, C. J. Elsevier, *Chem. Eur. J.* **2000**, *6*, 3272.
[25] C. Rong, M. T. Pope, *J. Am. Chem. Soc.* **1992**, *114*, 2932.
[26] A. Bagno, M. Bonchio, A. Sartorel, G. Scorrano, *Eur. J. Inorg. Chem.* **2000**, 17.
[27] K. D. Dobbs, W. J. Hehre, *J. Comput. Chem.* **1987**, *8*, 880.
[28] [28a] S. Huzinaga, B. Miguel, *Chem. Phys. Lett.* **1990**, *175*, 289. [28b] S. Huzinaga, M. Klobukowski, *Chem. Phys. Lett.* **1993**, *212*, 260.
[29] N. Godbout, D. R. Salahub, J. Andzelm, E. Wimmer, *Can. J. Chem.* **1992**, *70*, 560.
[30] R. Ahlrichs, K. May, *Phys. Chem. Chem. Phys.* **2000**, *2*, 943.
[31] Basis sets were obtained from the Extensible Computational Chemistry Environment Basis Set Database, as developed and distributed by the Molecular Science Computing Facility, Environmental and Molecular Sciences Laboratory which is part of the Pacific Northwest Laboratory, P. O. Box 999, Richland, Washington 99352, USA, and funded by the U. S. Department of Energy. The Pacific Northwest Laboratory is a multi-program laboratory operated by Battelle Memorial Institute for the U. S. Department of Energy under contract DE-AC06-76RLO1830. Contact David Feller or Karen Schuchardt for further information (see also http://www.emsl.pnl.gov:2080/forms/basisform.html).
[32] [32a] P. J. Hay, W. R. Wadt, *J. Chem. Phys.* **1985**, *82*, 270. [32b] W. R. Wadt, P. J. Hay, *J. Chem. Phys.* **1985**, *82*, 284. [32c] P. J. Hay, W. R. Wadt, *J. Chem. Phys.* **1985**, *82*, 299.
[33] W. Stevens, H. Basch, J. Krauss, *J. Chem. Phys.* **1984**, *81*, 6026.
[34] T. Leininger, A. Nicklass, H. Stoll, M. Dolg, P. Schwerdtfeger, *J. Chem. Phys.* **1996**, *105*, 1052, and previous papers by the same group.
[35] The Ru−C distance in $Ru(CN)_6^{4-}$ calculated with the LANL(2d) basis (2.096 Å) is the one that compares best with the experimental value of 2.039 Å[24] (see footnotes to Tables 1−2 for other data).
[36] A. D. Becke, *J. Chem. Phys.* **1993**, *98*, 5648.
[37] M. J. Frisch, G. W. Trucks, H. B. Schlegel, G. E. Scuseria, M. A. Robb, J. R. Cheeseman, V. G. Zakrzewski, J. A. Montgomery, Jr., R. E. Stratmann, J. C. Burant, S. Dapprich, J. M. Millam, A. D. Daniels, K. N. Kudin, M. C. Strain, O. Farkas, J. Tomasi, V. Barone, M. Cossi, R. Cammi, B. Mennucci, C. Pomelli, C. Adamo, S. Clifford, J. Ochterski, G. A. Petersson, P. Y. Ayala, Q. Cui, K. Morokuma, D. K. Malick, A. D. Rabuck, K. Raghavachari, J. B. Foresman, J. Cioslowski, J. V. Ortiz, B. B. Stefanov, G. Liu, A. Liashenko, P. Piskorz, I. Komaromi, R. Gomperts, R. L. Martin, D. J. Fox, T. Keith, M. A. Al-Laham, C. Y. Peng, A. Nanayakkara, C. Gonzalez, M. Challacombe, P. M. W. Gill, B. Johnson, W. Chen, M. W. Wong, J. L. Andres, C. Gonzalez, M. Head-Gordon, E. S. Replogle, J. A. Pople, *Gaussian 98, Revision A.7*, Gaussian, Inc., Pittsburgh PA, **1998**.
[38] The structure of $Ru(cp)_2$ may feature eclipsed or staggered cyclopentadiene rings, and both geometry optimizations successfully converge to the respective structures. Since the experimental structure[39] has eclipsed rings, all data presented herein will refer to structures with eclipsed rings; however, even though the calculated energy difference is negligible (< 1 kcal/mol), the chemical shift difference (< 100 ppm) is noticeable.
[39] [39a] G. L. Hardgrove, D. H. Templeton, *Acta Crystallogr.* **1959**, *12*, 28. [39b] P. Seiler, J. D. Dunitz, *Acta Crystallogr., Sect. B* **1980**, *36*, 2946.
[40] The X-ray structure of $[RuCl_2(DMSO)_4]$ features *cis*-equatorial Cl atoms, one axial DMSO molecule *O*-coordinated, the other three *S*-coordinated (Scheme 1).[41] Hence, this *cis*,*fac* isomer will be denoted as $RuCl_2(DMSO)_4$ hereafter. See also ref.[42] for other NMR solution studies.
[41] E. Alessio, G. Mestroni, G. Nardin, W. M. Attia, M. Calligaris, G. Sara, S. Zorzet, *Inorg. Chem.* **1998**, *27*, 4099.
[42] [42a] J. R. Barnes, R. J. Goodfellow, *J. Chem. Res. (S)* **1979**, 350. [42b] G. A. Heath, A. J. Lindsay, T. A. Stephenson, *J. Chem. Soc., Dalton Trans.* **1982**, 2429.
[43] *Spartan 5.1*, Wavefunction, Inc., 18401 Von Karman Ave., Ste. 370, Irvine, CA 92612, USA.
[44] J. J. Rack, H. B. Gray, *Inorg. Chem.* **1999**, *38*, 2, and references therein.
[45] An alternative modelling might employ the concept of locally dense basis sets,[46] i. e. featuring a high-quality basis set only on the atom whose properties are being calculated (Ru in this case). However, in the case of polyoxometalates like α-$[PW_{11}RuO_{39}(DMSO)]^{5-}$, this approach would not bring any substantial improvement in terms of computing time for such systems (containing a large number of heavy atoms), where a limiting factor is the size of the environment of the atom under study.
[46] A. C. De Dios, *Prog. Nucl. Magn. Reson. Spectr.* **1996**, *29*, 229.
[47] A. Bagno, M. Bonchio, A. Sartorel, G. Scorrano, manuscript in preparation.

Received October 11, 2001
[I01409]

The First Well-Defined Tellurastannoxanes: the X-ray Structure of *trans*-[$(Bu_3SnO)_2\{CH_2(Ph_2SnO)_2\}_2Te$]

Jens Beckmann,[a] Dainis Dakternieks,*[a] Jenny O'Connell,[a] Klaus Jurkschat,[b] and Markus Schürmann[b]

Keywords: Tin / Tellurium / Cluster compounds / NMR spectroscopy / X-ray diffraction

The syntheses of well-defined tellurastannoxanes, *mer*-$(Bu_3SnO)_3Te(OH)_3$ (**1**), and *trans*-$(Bu_3SnO)_2[CH_2(Ph_2SnO)_2]_2Te$ (**2**), are reported. The compounds were characterized by ^{119}Sn and ^{125}Te NMR spectroscopy and compound **2** also by single crystal X-ray diffraction.

(© Wiley-VCH Verlag GmbH, 69451 Weinheim, Germany, 2002)

Introduction

Currently there is great interest in molecular mixed-element oxides incorporating main group elemental oxide fragments such as $M(O^-)_3$ (M = B, Al, Ga), $MO(O^-)_3$ (M = P), or $M(O^-)_4$ (M = Si, Ge, Sn), mainly as a result of potential applications in material science and catalysis.[1,2] In most cases, the preferred valence numbers within these fragments preclude a degree of branching higher than four.

Although the synthesis of the first alkyl ester of orthotelluric acid, $Te(OH)_6$, was described early last century there have been only a few subsequent reports utilizing the acidic protons in $Te(OH)_6$ to build new organometallic complexes.[3] In one case molecular tellurasiloxanes, namely $[(Me_2SiO)_2]_3Te$ (**I**), and $(Me_3SiO)_8Te_2O_2$ (**II**)[4] were described and in another case a unique mixed-valence Te^{IV}-Te^{VI} species $\{OTe(C_8H_8)[(EtO)_2PS_2]\}_6Te$ (**III**) was reported.[5]

Here we present the syntheses of the first tellurastannoxanes *mer*-$[(Bu_3SnO)_3Te(OH)_3]$ and *trans*-$[(Bu_3SnO)_2\{CH_2(Ph_2SnO)_2\}_2Te]$. The former compound containing unsubstituted hydroxyl groups has potential as a building block for the preparation of ternary mixed-metal oxides, a class of compounds for which few examples are known.[6–8]

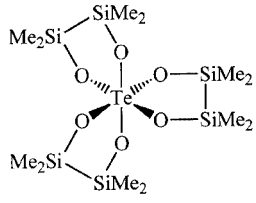

I

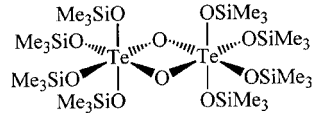

II

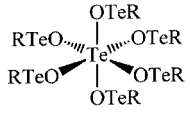

III

R = $(C_8H_8)(S_2P(OEt)_2)$

Results and Discussion

The reaction between $Te(OH)_6$ and three equivalents of Bu_3SnOMe quantitatively produced *mer*-$[(Bu_3SnO)_3Te(OH)_3]$ (**1**) [Equation (1)]:

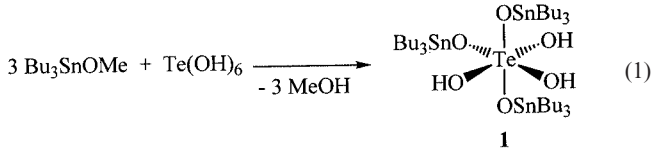

(1)

1

Compound **1** was obtained as a colorless, odorless low-melting waxy material that slowly crystallized over several weeks. The ^{119}Sn NMR spectrum ($CDCl_3$) of **1** reveals two signals at $\delta = 81.9$ [$^2J(^{119}Sn-O-^{125}Te) = 434$ Hz] and 93.6 [$^2J(^{119}Sn-O-^{125}Te) = 504$ Hz] with an integral ratio of 1:2. The number of signals confirms the exclusive formation of

[a] Centre for Chiral and Molecular Technologies, Deakin University,
Geelong, Victoria 3217, Australia
Fax: (internat.) +61-3/5227-1040
E-mail: dainis@deakin.edu.au
[b] Lehrstuhl für Anorganische Chemie II, Fachbereich Chemie der Universität Dortmund,
44221 Dortmund, Germany

the *mer*-isomer. The ^{125}Te NMR spectrum ($CDCl_3$) of **1** shows a signal at δ = 721.5 with two $^2J(^{125}Te-O-^{119}Sn)$ couplings of 501 and 432 Hz. Bearing in mind the natural abundance of the isotopes ^{117}Sn, ^{119}Sn, and ^{125}Te the integration of the satellites with respect to the main signal allows determination of the connectivity of the tin and tellurium atoms. This method has already been applied for the identification of other compounds showing heteronuclear couplings, such as ^{117}Sn/^{119}Sn,[9−11] ^{29}Si/^{119}Sn,[12] and ^{29}Si/^{125}Te.[4] The molecular weight determination of **1** ($CHCl_3$) unambiguously indicates that no condensation to higher aggregates had occurred and suggests that all three remaining hydroxyl groups are still present. The IR spectrum of **1** (KBr) further supports the presence of hydroxyl groups by revealing a very broad ν(OH) stretching vibration at 3372 cm^{-1}. The reason for selective formation of the *mer*-isomer under these reaction conditions is still not understood. Reactions of $Te(OH)_6$ with Bu_3SnOMe in stoichiometric ratios other than 1:3 provided mixtures of products with a varying degree of substitution, $[(Bu_3SnO)_nTe(OH)_{n-6}]$ $(n \geq 3)$.[13] The identity of these species was unambiguously proven by ^{119}Sn and ^{125}Te NMR spectroscopy, although all attempts to isolate pure compounds from the mixtures failed. Moreover, reactions between $Te(OH)_6$ and other triorganotin methoxides, R_3SnOMe (R = Me, *c*Hex, Ph), also provided mixtures of products that could not be purified.[14]

The reaction of *mer*-$[(Bu_3SnO)_3Te(OH)_3]$ (**1**) with two equivalents of $(Ph_2SnOH)_2CH_2$ [15] gave, with elimination of water and one equivalent of tributyltin hydroxide (Bu_3SnOH), the spirocyclic tellurastannoxane derivative *trans*-$[(Bu_3SnO)_2\{CH_2(Ph_2SnO)_2\}_2Te]$ (**2**) in good yields [Equation (2)].

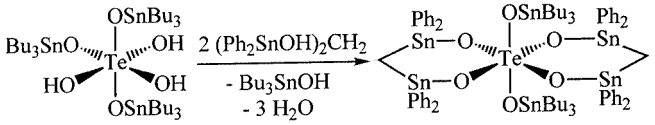

1 **2** (2)

Compound **2** is a colorless crystalline material. The ^{119}Sn NMR spectrum ($CDCl_3$) of **2** reveals two signals with an integral ratio of 2:1 belonging to the $(Ph_2SnO)_2CH_2$ moiety and the Bu_3SnO moiety, respectively, at δ = −40.2 $[^2J(^{119}Sn-O-^{117}Sn)$ = 632 Hz; $^2J(^{119}Sn-O-^{125}Te)$ = 353 Hz] and δ = 89.6 $[^2J(^{119}Sn-O-^{125}Te)$ = 393 Hz]. It is interesting to note that the chemical shift for the $(Ph_2SnO)_2CH_2$ moiety at δ = −40.2 is very close to that found for the *cyclo*-stannasiloxane $tBu_2Si(OSnPh_2)_2CH_2$ [$\delta(^{119}Sn)$ = −42.8], which also contains a $(Ph_2SnO)_2CH_2$ fragment incorporated into a six-membered ring.[16] The ^{125}Te NMR spectrum ($CDCl_3$) of compound **2** shows a signal at δ = 726.1 with two $^2J(^{125}Te-O-^{119}Sn)$ couplings of 397 and 355 Hz in the expected integral ratio. The number of signals in the ^{119}Sn NMR spectrum and the observed coupling patterns in both ^{119}Sn and ^{125}Te NMR spectroscopy confirms the coordination geometry of the tin atoms around the tellurium center.

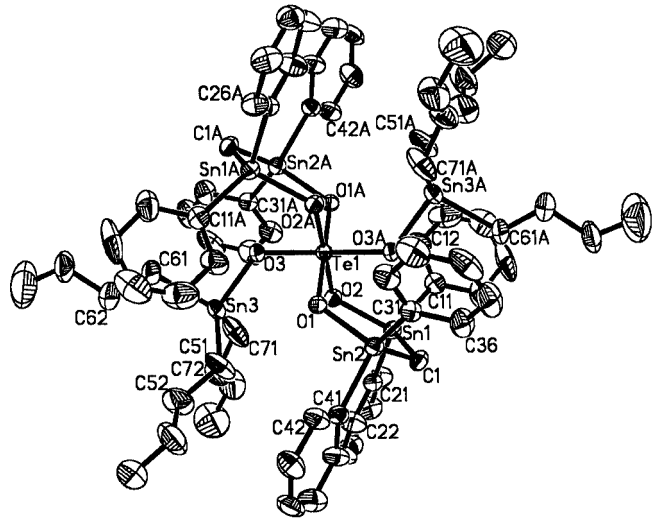

Figure 1. General view (SHELXTL-PLUS) of **2** showing 30% probability displacement ellipsoids and the atom numbering for **2** (symmetry transformations used to generate equivalent atoms: $a = -x + 0.5, -y - 0.5, -z + 1$)

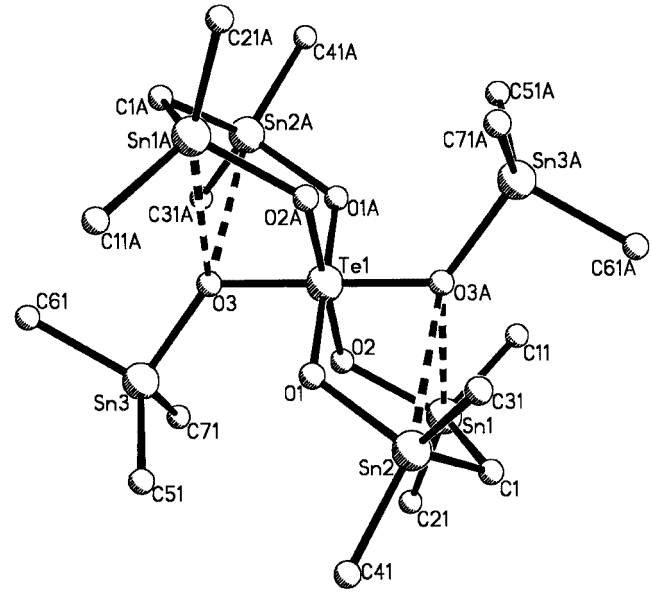

Figure 2. General view (SHELXTL-PLUS) of **2** demonstrating the [4+1] coordination of tin atoms Sn(1) and Sn(2); only primary carbon atoms are shown for clarity (symmetry transformations used to generate equivalent atoms: $a = -x + 0.5, -y - 0.5, -z + 1$)

The molecular structure of **2** is shown in Figure 1 and 2, and selected bond lengths, bond angles and torsion angles are listed in Table 1. The structure contains a crystallographic center of inversion across the tellurium atom Te(1), which coordinated in an octahedral fashion to six oxygen atoms. The mean Te−O bond length amounts to 1.912(3) Å, which is close to the bond length found in $[(Me_2SiO)_2]_3Te$.[4] The central mononuclear TeO_6 core is stannylated at O(3)/O(3a) by two tributylstannyl units and at O(1), O(2)/O(1a), O(2a) by two chelating bis(diphenylstannyl)methyl moieties, giving rise to the formation of a spiroundecane skeleton. The six-membered Te(1)−O(1)−Sn(2)−

Table 1. Selected bond lengths [Å], bond angles, and torsion angles [°] for **2** (symmetry transformations used to generate equivalent atoms: $a = -x + 1/2, -y - 1/2, -z + 1$)

Te(1)−O(1)	1.915(3)	Te(1)−O(2)	1.907(3)
Te(1)−O(3)	1.914(3)	Sn(1)−O(2)	1.986(3)
Sn(1)−O(3a)	2.944(3)	Sn(1)−C(1)	2.123(5)
Sn(1)−C(11)	2.137(6)	Sn(1)−C(21)	2.128(5)
Sn(2)−O(1)	1.982(3)	Sn(2)−O(3a)	3.003(3)
Sn(2)−C(1)	2.128(5)	Sn(2)−C(31)	2.117(5)
Sn(2)−C(41)	2.137(5)	Sn(3)−O(1)	3.518(3)
Sn(3)−O(2)	3.398(3)	Sn(3)−O(3)	2.015(3)
Sn(3)−C(51)	2.124(6)	Sn(3)−C(61)	2.124(6)
Sn(3)−C(71)	2.106(7)		
O(1)−Te(1)−O(2)	89.68(13)	O(1)−Te(1)−O(2a)	90.32(13)
O(1)−Te(1)−O(3)	90.78(13)	O(1)−Te(1)−O(3a)	89.22(13)
O(2)−Te(1)−O(3)	91.00(12)	O(2)−Te(1)−O(3a)	89.00(12)
O(1)−Te(1)−O(1a)	180.00(16)	O(2)−Te(1)−O(2a)	180.00(17)
O(3)−Te(1)−O(3a)	180.000(1)	O(2)−Sn(1)−O(3a)	62.28(10)
O(2)−Sn(1)−C(1)	110.01(15)	O(2)−Sn(1)−C(11)	108.1(2)
O(2)−Sn(1)−C(21)	101.58(16)	O(3a)−Sn(1)−C(1)	73.24(15)
O(3a)−Sn(1)−C(11)	83.08(16)	O(3a)−Sn(1)−C(21)	163.05(16)
C(1)−Sn(1)−C(11)	117.2(2)	C(1)−Sn(1)−C(21)	110.4(2)
C(11)−Sn(1)−C(21)	108.4(2)	O(1)−Sn(2)−O(3a)	61.32(10)
O(1)−Sn(2)−C(1)	112.33(15)	O(1)−Sn(2)−C(31)	108.01(18)
O(1)−Sn(2)−C(41)	101.32(16)	O(3a)−Sn(2)−C(1)	71.89(15)
O(3a)−Sn(2)−C(31)	86.24(10)	O(3a)−Sn(2)−C(41)	160.76(14)
C(1)−Sn(2)−C(31)	114.9(2)	C(1)−Sn(2)−C(41)	111.0(2)
C(31)−Sn(2)−C(41)	108.3(2)	O(3)−Sn(3)−C(61)	97.0(2)
O(3)−Sn(3)−C(51)	110.7(2)	C(51)−Sn(3)−C(61)	114.6(4)
O(3)−Sn(3)−C(71)	109.8(2)	C(61)−Sn(3)−C(71)	110.5(4)
C(51)−Sn(3)−C(71)	113.2(4)	Te(1)−O(1)−Sn(2)	122.17(16)
Te(1)−O(2)−Sn(1)	121.55(14)	Sn(1)−C(1)−Sn(2)	112.9(2)
Te(1)−O(3)−Sn(3)	127.55(15)		
C(1)−Sn(1)−O(2)−Te(1)	48.9(3)	C(1)−Sn(2)−O(1)−Te(1)	−40.1(3)
O(2)−Sn(1)−C(1)−Sn(2)	−1.8(3)	O(2)−Te(1)−O(1)−Sn(2)	71.65(19)
O(1)−Sn(2)−C(1)−Sn(1)	−1.5(3)	O(1)−Te(1)−O(2)−Sn(1)	−77.58(19)

C(1)−Sn(1)−O(2) ring exhibits an envelope conformation with Te(1) lying 1.133(3) Å above the plane of fitted atoms O(1), O(2), Sn(1), C(1), Sn(2). The maximal deviation of fitted atoms from the plane amounts to 0.027 Å. The Sn(1)−C(1)−Sn(2) angle of 112.9(2)° is close to the corresponding angle in the six-membered stannasiloxane ring *cyclo*-*t*$Bu_2Si(OSnPh_2)_2CH_2$ [113.9(4)°],[16] and related open-chain derivatives $H_2C(SnPh_2Cl)_2$ [113.4(10)°,[17] and $H_2C(SnPh_2Cl)_2$·HMPA (114.0°)].[18] A remarkable feature in the structure of compound **2** is the intramolecular Sn(1)−O(3a)/Sn(2)−O(3a) distances of 2.944(3)/3.003(3) Å, which are shorter than the sum of the van der Waals radii[19] of tin (2.20 Å) and oxygen (1.50 Å). As a consequence, the coordination geometry at Sn(1) and Sn(2) can best be described as a monocapped tetrahedron {[4+1]-coordination, geometrical goodness[20−22] Δ(Σ): 14.93° for Sn(1) and 14.62° for Sn(2)} with Sn(1) deviating 0.610(3) Å in the direction of C(21) from the plane defined by C(1), C(11), O(2), and Sn(2) deviating 0.609(3) Å in the direction of C(41) from the plane defined by C(1), C(31), O(1). Most interestingly, and caused by the ring constraint, the oxygen atom O(3a) approaches the Sn(1) and Sn(2) atoms through the faces defined by C(1), C(11), O(2) and C(1), C(31), O(1), and forces the phenyl rings containing C(21) and C(41), respectively, into the axial positions of the trigonal bipyramid, whereas O(2), C(1), C(11) and O(1), C(1), C(31) become equatorial. This is a rather unusual situation for pentacoordinated triorganotin compounds as the axial positions are usually occupied by the more electronegative substituents and the equatorial positions by the three organic substituents. Another consequence of the intramolecular Sn(1)−O(3a)/Sn(2)−O(3a) distances mentioned above is the increase of the O(3a)−Sn(3a) bond length [2.015(3) Å] with respect to the Sn(1)−O(2)/Sn(2)−O(1) bond lengths of 1.986(3)/1.982(3) Å, and the decrease of the Te(1)−O(3a)−Sn(3a) angle [127.55(15)°] in comparison with related Te−O−Si angles in $[(Me_3SiO)_8Te_2O_2]$ (**II**) (135.1−141.9°).[4] The intramolecular Sn(3)−O(1)/Sn(3)−O(2) distances of 3.518(3)/3.398(3) Å are also shorter than the sum of the van der Waals radii of the corresponding atoms but apparently they are not short enough to significantly disturb the tetrahedral geometry of Sn(3) (mean angle 109.3°).

Experimental Section

General Remarks: All manipulations were performed under an inert atmosphere of argon using standard Schlenk and vacuum line tech-

niques. Solvents were distilled from the appropriate desiccants prior to use. Literature procedures were used to prepare Bu_3SnOMe[23] and $(Ph_2SnOH)_2CH_2$.[15] The $Te(OH)_6$ was purchased from Fluka. NMR spectra were recorded in $CDCl_3$ using a Jeol GX 270 and a Varian 300 Unity Plus spectrometer at 85.39 (^{125}Te), 111.86 (^{119}Sn), 75.44 (^{13}C) and 299.98 (^{1}H) MHz. Chemical shifts (δ) are given in ppm and are referenced to Me_2Te (^{125}Te), Me_4Sn (^{119}Sn) and Me_4Si (^{13}C, ^{1}H). The elemental analyses were performed on an instrument from Carlo Erba Strumentazione (Modell 1106). The IR spectra were recorded on a Bruker FTIR IFS 113v spectrometer. The molecular weight measurement was carried out using a Knaur osmometer.

Synthesis of *mer*-[$(Bu_3SnO)_3Te(OH)_3$] (1): A mixture of Bu_3SnOMe (7.71 g, 24.0 mmol) and $Te(OH)_6$ (1.84 g, 8.0 mmol) was heated in toluene (10 mL) at 85 °C until the $Te(OH)_6$ was completely dissolved (approx. 4 h) and then for 2 h at 110 °C. Volatile components were removed in vacuum affording a colorless waxy residue of **1** (8.78 g, 8.0 mmol, 100%, m.p. 42 °C). ^{1}H NMR: δ = 0.92 (9 H), 1.24 (6 H), 1.34 (6 H), 1.61 (6 H). ^{13}C NMR δ = 13.8, 13.7 (β-*C*), 17.5 [$^1J(^1C-^{119}Sn)$ = 369 Hz; α-*C*], 17.8 [$^1J(^1C-^{119}Sn)$ = 366 Hz; α-*C*], 27.4, 27.5 (γ-*C*), 28.3 (δ-*C*). ^{119}Sn NMR: δ = 81.9 [1Sn, $^2J(^{119}Sn-O-^{125}Te)$ = 434 Hz], 93.6 [2 Sn, $^2J(^{119}Sn-O-^{125}Te)$ = 504 Hz]. ^{125}Te NMR: δ = 721.5 [$^2J(^{125}Te-O-^{119}Sn)$ = 501, $^2J(^{125}Te-O-^{119}Sn)$ = 432 Hz]. IR (KBr): $\tilde{\nu}$ = 3372 br. (ν_{OH}), 2956 vs, 2924 vs, 2871 vs, 2853.7 vs, 1463 s, 1377 m, 1074 m, 876 m, 734 s, 668 m, 621 s, 474 m cm^{-1}. $C_{36}H_{84}O_6Sn_3Te$ (1096.89): calcd. C 39.42, H 7.72; found C 40.25, H 8.20. MW ($CHCl_3$, 20 mg mL^{-1}): 1071.

Synthesis of *trans*-{$(Bu_3SnO)_2[CH_2(Ph_2SnO)_2]_2Te$]} (2): A mixture of **1** (1.10 g, 1 mmol) and $(Ph_2SnOH)_2CH_2$ (1.19 g, 2 mmol) in toluene (10 mL) was heated for 4 h at 80 °C. The precipitate formed (Bu_3SnOH) was separated by filtration and the volatile components were removed under vacuum. The solid residue was recrystallised from hexane/dichloromethane (3:1) affording **2** (1.57 g, 0.82 mmol, 82%, m.p. 173 °C). ^{1}H NMR: δ = 0.90 (6 H), 1.22 [4 H, $^2J(^1H-^{119}Sn)$ = 120 Hz; SnCH_2Sn], 1.23 (4 H), 1.34 (4 H), 1.62 (4 H), 7.0−8.1 (40 H, *Ph*). ^{13}C NMR: δ = −2.1 [$^1J(^{13}C-^{119}Sn)$ = 378 Hz; SnCH_2Sn], 13.6 (β-*C*), 17.4 [$^1J(^{13}C-^{119}Sn)$ = 360 Hz; α-*C*], 27.1 (γ-*C*), 28.0 (δ-*C*), 128.1 (*p*-*C*), 145.3 [$^1J(^{13}C-^{119}Sn)$ = 526 Hz; *i*-*C*], 128.3 (*p*-*C*), 128.8 (*m*-*C*), 129.0 (*m*-*C*), 136.0 (*o*-*C*) 136.1 (*o*-*C*), 143.5 [$^1J(^{13}C-^{119}Sn)$ = 684 Hz; *i*-*C*]. ^{119}Sn NMR: δ = −40.2 [4 Sn, $^2J(^{119}Sn-O-^{117}Sn)$ = 632, $^2J(^{119}Sn-O-^{125}Te)$ = 353 Hz; *Sn*CH_2Sn], 89.6 [2 Sn, $^3J(^{119}Sn-O-^{125}Te)$ = 393 Hz; *Sn*Bu_3]. ^{125}Te NMR: δ = 726.1 [$^2J(^{125}Te-O-^{119}Sn)$ = 397, $^2J(^{125}Te-O-^{119}Sn)$ = 355 Hz]. IR (KBr): $\tilde{\nu}$ = 3062 s, 3009 s, 2953 vs, 2918 vs, 2868 s, 1480 s, 1462 s, 1428 vs, 1374 m, 1345 m, 1297 m, 1188 m, 1076 vs, 1022 m, 997 m, 958 m, 867 m, 711 vs, 608 vs, 527 vs, 466 vs, 447 s, 343 s, 319s cm^{-1}. $C_{74}H_{98}O_6Sn_6Te$ (1923.6): calcd. C 46.21, H 5.14; found C 45.99, H 5.20.

X-ray Crystallographic Study. Crystal Data and Structure Solution of 2: $C_{74}H_{98}O_6Sn_6Te$, M_r = 1923.26, *monoclinic*, *C*2/*c*, *a* = 20.571(1), *b* = 14.150(1), *c* = 27.974(1) Å, β = 101.239(1)°, *V* = 7986.5(7) Å^3, *Z* = 4, $D_{calcd.}$ = 1.600 g·cm^{-3}, λ(Mo-K_α) = 0.71069 Å, *F*(000) = 3768, μ = 2.250 mm^{-1}, *T* = 291(1) K. The data collection covered almost the whole sphere of reciprocal space with 360 frames via ω-rotation (Δ/ω = 1°) at 2 × 10 s per frame on a Nonius KappaCCD diffractometer with a completeness of 93.2% in the θ range of 4.07 to 24.99°. The structure was solved by direct methods SHELXS-97[24] and refined by full-matrix least-squares calculations using SHELXL-97.[25] All non-H atoms were refined anisotropically. The H-atoms were placed in geometrically calculated positions using a riding model (including free rotation around C−C). The aromatic H atoms were refined with a common isotropic temperature factor [C−H_{aryl} 0.93 Å, U_{iso} 0.143(6) Å^2], while for the aliphatic H atoms the atomic displacement parameters were fixed to 1.5 times those of the C atoms. R_1 = 0.0317 for 3961 reflections with $I > 2\sigma(I)$ and wR_2 = 0.0698 for 6551 independent reflections with 395 refined parameters. The max./min. residual electron densities were 0.362 and −0.369 e Å^{-3}.

CCDC-173037 contains the supplementary crystallographic data for this paper (excluding structure factors). These data can be obtained free of charge at www.ccdc.cam.ac.uk/conts/retrieving.html [or from the Cambridge Crystallographic Data Centre, 12, Union Road, Cambridge CB2 1EZ, UK; Fax: (internat.) +44-1223/336-033; E-mail: deposit@ccdc.cam.ac.uk].

Acknowledgments

We thank the Australian Research Council, the Deutsche Forschungsgemeinschaft and the Freundegesellschaft der Universität Dortmund for financial support.

[1] M. G. Walawalkar, H. W. Roesky, R. Murugavel, *Acc. Chem. Res.* **1999**, *32*, 117−126.
[2] R. Murugavel, A. Voigt, M. G. Walawalkar, H. W. Roesky, *Chem. Rev.* **1996**, *96*, 2205−2236.
[3] G. Pellini, *Gazz. Chim. Ital.* **1916**, *46*, 247−250.
[4] M. Driess, C. Von Haenisch, K. Merz, *Z. Anorg. Allg. Chem.* **1999**, *625*, 493−496.
[5] D. Dakternieks, R. Di Giacomo, R. W. Gable, B. F. Hoskins, *J. Am. Chem. Soc.* **1988**, *110*, 6541−6546.
[6] J. Beckmann, K. Jurkschat, N. Pieper, M. Schürmann, *Chem. Commun.* **1999**, 1095−1096.
[7] M. Veith, S. Mathur, V. Huch, *J. Am. Chem. Soc.* **1996**, *118*, 903−904.
[8] M. Veith, S. Mathur, V. Huch, *Inorg. Chem.* **1996**, *35*, 7295−7303.
[9] H. Berwe, A. Haas, *Chem. Ber.* **1987**, *120*, 1175−1182.
[10] D. Dakternieks, K. Jurkschat, H. Wu, E. R. T. Tiekink, *Organometallics* **1993**, *12*, 2788−2793.
[11] J. Campbell, L. A. Devereux, M. Gerken, H. P. A. Mercier, A. M. Pirani, G. J. Schrobilgen, *Inorg. Chem.* **1996**, *35*, 2945−2962.
[12] J. Beckmann, B. Mahieu, W. Nigge, D. Schollmeyer, M. Schürmann, K. Jurkschat, *Organometallics* **1998**, *17*, 5697−5712.
[13] J. O′Connell, Honours thesis, Deakin University, **1994**.
[14] J. Beckmann, D. Dakternieks, K. Jurkschat, **1998**, unpublished results.
[15] M. Gielen, K. Jurkschat, *J. Organomet. Chem.* **1984**, *273*, 303−312.
[16] J. Beckmann, K. Jurkschat, S. Rabe, M. Schürmann, D. Dakternieks, A. Duthie, *Organometallics* **2000**, *19*, 3272−3279.
[17] J. Meunier-Piret, M. Van Meerssche, K. Jurkschat, M. Gielen, *J. Organomet. Chem.* **1985**, *288*, 139−143.
[18] M. Gielen, K. Jurkschat, J. Meunier-Piret, M. Van Meerssche, *Bull. Soc. Chim. Belg.* **1984**, *93*, 379−391.
[19] J. Huheey, E. A. Keiter, R. L. Keiter, *Anorganische Chemie. Prinzipien von Struktur und Reaktivität*, 2nd ed., de Gruyter, New York, Berlin, **1995**.
[20] M. Dräger, *Z. Anorg. Allg. Chem.* **1976**, *423*, 53−66.
[21] U. Kolb, M. Beuter, M. Dräger, *Inorg. Chem.* **1994**, *33*, 4522−4530.
[22] M. Beuter, U. Kolb, A. Zickgraf, E. Brau, M. Bletz, M. Dräger, *Polyhedron* **1997**, *16*, 4005− 4015.
[23] D. L. Alleston, A. G. Davies, *J. Chem. Soc.* **1962**, 2050−2054.
[24] G. M. Sheldrick, *Acta Crystallogr., Sect. A* **1990**, *46*, 467−473.
[25] G. M. Sheldrick, University of Göttingen, **1997**.

Received November 5, 2001
[I01434]

The Recovery of a Rhodium-Containing Catalyst by Various New Silica-Based Amine Ion Exchangers

Jurjen Kramer,[a] Arjen Scholten,[a] Willem L. Driessen,*[a] and Jan Reedijk[a]

Keywords: Amine ligands / Complex stability / Ion exchange / Rhodium / Homogeneous catalysis

Various mono-, di-, and triamine ligands have been successfully attached to an inert silica backbone. Their efficiency in the recovery of the model catalyst $RhCl_3$ has been thoroughly investigated. Correlation of the distribution coefficients for Rh^{3+} as a function of the pH with recovery experiments, shows a subtle balance between the stability of the ligand-to-metal complexes and the elution efficiency. Rhodium ion exchanger complexes with log *D* values above 2.5 appear to be too stable to ensure a high (> 70%) desorption. A very high desorption (> 90%) has been effected with 2 M HNO_3 with ion exchangers containing monoamine ligands or sterically hindered diamine ligands. The adsorption medium appeared to be of major influence, both on the extractability and on the elution possibility.

Introduction

Homogeneous catalysts, being very powerful agents for the improvement of many organic reactions, are widely used in industrial processes. The high selectivity and turnover numbers that can be attained for a specific reaction are major advantages. However, since all reagents (substrate, catalyst, products) are present in the same solvent phase, the separation of the catalyst after use can be troublesome. Catalyst recovery is of major importance, though, as contamination of the product should be reduced to a minimum, and also because very expensive transition metals often form part of the catalyst.[1]

Ion exchange has proven to be a very suitable technique for the recovery of low concentrations of metal ions, due to the ease of separation of the adsorbed metal ions from the product stream. Moreover, a high selectivity for certain metal ions can be obtained by immobilizing (chelating) ligands on an inert, chemically and thermodynamically stable backbone. Earlier findings on the selective recovery of Cu showed fast exchange kinetics when silica was used as a backbone.[2]

We have chosen to focus on the recovery of Rh-containing homogenous catalysts, since the scarcity of rhodium, linked to its wide application in industrial processes such as hydroformylation and hydrogenation reactions,[1,3,4] has resulted in very high prices for this metal.

[a] Leiden Institute of Chemistry, Gorlaeus Laboratories, Leiden University,
P. O. Box 9502, 2300 RA Leiden, The Netherlands
Fax: (internat.) + 31-71/527-4451
E-mail: driessen@chem.leidenuniv.nl

Previous investigations already pointed out the need to achieve optimal binding for efficient recovery.[5] This means that the affinity of the ligands for the Rh metal-ions should be sufficient for adsorption, but the affinity should not be too high, as this might prevent subsequent desorption. The elution process appears to be especially difficult, as shown by reports on incomplete desorption, unless very harsh, even damaging, conditions are applied.

Amine ligands are known to coordinate well to platinum group metals. Their special properties enable them to coordinate to transition metal ions,[7] as well as to interact with anionic complexes. In a previous report, our preliminary findings have been communicated on the recovery of Rh^{3+} with silica-based (poly)amine ion exchangers.[9] In the present paper a substantial extension of this study is given:

The ion exchangers **1b**−**9b** were prepared by immobilizing the corresponding ligands **1a**−**9a** onto silica, as depicted in Scheme 1. In order to gain insight into the factors that determine efficient recovery, the approach was manifold. Firstly, the effect of monodentate (ion exchangers **1b** and **2b**) versus bidentate (**3b**−**7b**) and possible tridentate (**8b** and **9b**) binding on the stability and recovery of rhodium metal ions was investigated. Secondly, the influence of *N*-alkylation was examined (**2b** and **5b**−**7b**), as protonation and deprotonation of amines are thought to play a prominent role in metal ion recovery. Thirdly, other features, such as the macrocyclic effect (**8b** vs. **9b**) and the size of the chelate ring (**3b** and **4b**) on the complex stability and Rh recovery, were considered. For this purpose, the stability of the various ligand-to-metal complexes was established by measuring the stability constants (log *D*) in dilute systems. Finally, the recovery was determined after initial adsorption in various media, with the additional aim to gain insight into the influence of the solvent on the recovery process.

 © WILEY-VCH Verlag GmbH, 69451 Weinheim, Germany, 2002 1434−1948/02/0606−1488 $ 20.00+.50/0 *Eur. J. Inorg. Chem.* **2002**, 1488−1494

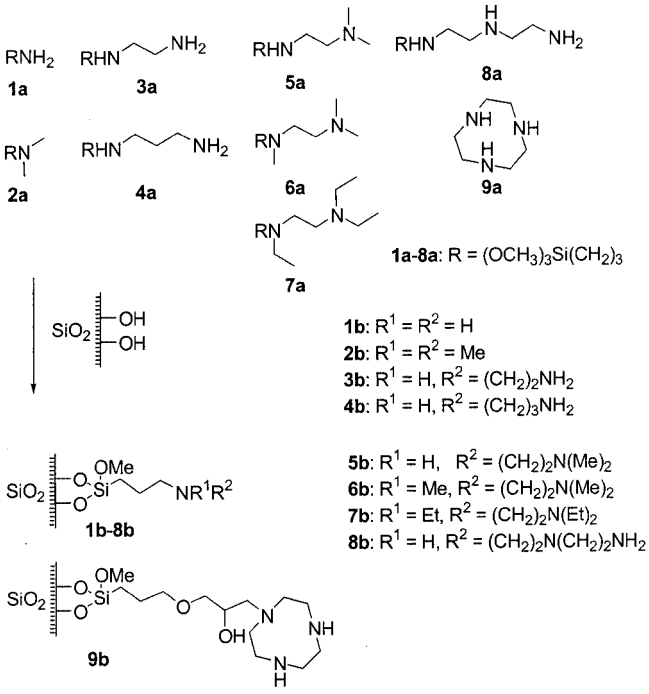

Scheme 1. Schematic representation of the synthesis of the (poly)-amine-containing ion exchangers **1b**−**9b**

Results and Discussion

Synthesis of the Ion Exchangers

The free trimethoxysilane ligands (**1a**−**8a**) were immobilized using a methanolysis reaction with the surface silanol groups of silica (see Scheme 1). To ensure monofunctionalization, the triazacyclononane (tacn, **9a**) ligand was coupled to a silica-anchored spacer (glymo, see Exp. Sect.). It is clear from the ligand concentration, based on the nitrogen and carbon contents, that the ligands are grafted, on average, through two OMe groups. Some of the remaining methoxy groups remain visible in the solid-state ^{13}C NMR spectrum (see Figure 1). The ligand concentrations of the functionalized silica were calculated from the weight percentage of nitrogen, as is generally done,[10] while the calculated C and H percentages, which are based on this ligand concentration, are given in parentheses (see Table 1). The ligand concentrations were found to increase with decreasing ligand size. This phenomenon is clearly demonstrated for the different diamine ligands (**3b**−**7b**), where the increasing bulkiness apparently hampers the grafting of the ligands. The relatively low ligand concentration of **9b** is the result of a different immobilization pathway (see Experimental Section). This sequence of grafting is less efficient, for steric reasons, and not all *tacn* ligands reacted with *glymo*-Si, clearly giving rise to a large difference in the observed and calculated values for carbon.

The solid-state CP MAS ^{13}C NMR spectra of the ion exchangers **1b**−**9b** are depicted in Figure 1−3. The characteristic ligand signals (see Table 1) of the solid-state spectrum correspond well to the ^{13}C NMR signals obtained in solution (see Experimental Section) for all the ion exchangers. However, as the resolution of solid-state NMR spectra is lower than that of solution NMR spectra, in some cases the close-lying peaks overlap, most notably for the alkylated diamine ion exchangers.

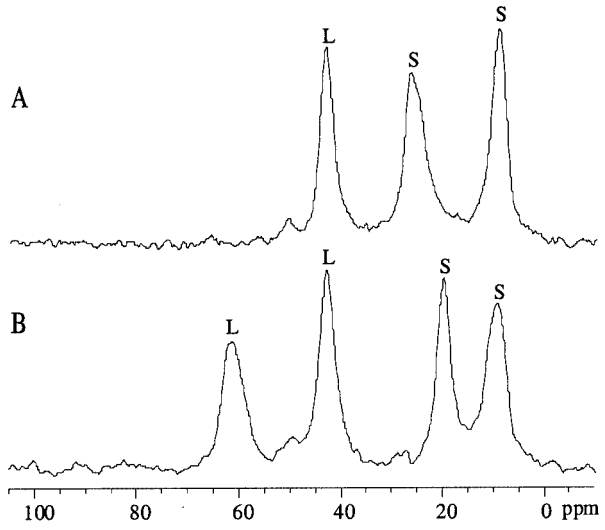

Figure 1. ^{13}C CP MAS NMR spectra of monoamine ion exchangers **1b** (A) and **2b** (B); peaks originating from $(R)_3SiCH_2CH_2$ are denoted **S**; all ligand signals, and signals originating from $(R)_3SiCH_2CH_2CH_2$, are marked **L**

pH-Dependent Complex Stability

The measurement of the distribution coefficient is a generally applied method for gaining insight into the stability of the metal-to-ligand binding,[11] and log *D* values of the different amine containing ligands with the rhodium metal-ions. These coefficients have been determined at different pH values. The stability results of the monoamine ion exchangers with Rh^{3+} are depicted in Figure 4, showing a similar pattern, although the log *D* values of the Rh-**2b** (NMe_2) complexes proved to be somewhat more pH dependent than those of the Rh-**1b** (NH_2) complexes. At pH < 2 the amines are predominantly protonated,[12,13] and binding is believed to occur via ion pairing, with positively charged amine groups binding to a negatively charged Rh complex of the type $[RhCl_{6-n}(H_2O)_n]^{(3-n)-}$ (with *n* generally 0−2).[14] Above pH 2, binding increasingly takes place through the lone pairs of the amine groups.

The lower stability, observed for both ion exchangers at pH 1−2, can be explained by the presence of high concentrations of chloride counterions, which compete for Rh binding with the ion exchangers. At higher pH, HOAc/NaOAc buffers were used, and the acetate ion clearly coordinated less strongly to the Rh metal-ions. The Rh binding of **2b** appears to be somewhat weaker than that of **1b**, as demonstrated by the lower log *D* values when large amounts of competing Cl^- ions are present.

The pH-dependent log *D* values of a series of different diamine ion exchangers are depicted in Figure 5. The highest stability was observed with the ethylenediamine (*en*) ion exchanger **3b**. The stability of the Rh complexes with **3b** proved to be some 3−10 times higher over the entire tested

Table 1. Characteristics of the ion exchangers **1b**−**9b**

Ion exchanger	^{13}C CP-MAS NMR (δ values)	% C (calcd.)	% H (calcd.)	% N[a]	Ligand conc.[a] (mmol/g)
1b	9, 27, 43	5.06 (5.52)	1.21 (1.27)	1.61	1.14
2b	10, 20, 43, 61	5.30 (5.30)	1.25 (1.11)	1.03	0.74
3b	10, 23, 41, 52	6.78 (7.18)	1.55 (1.61)	2.79	1.02
4b	10, 22, 32, 39, 47, 51	5.62 (5.75)	1.29 (1.24)	1.92	0.68
5b	10, 23, 44, 46, 52, 58	7.64 (7.98)	1.73 (1.67)	2.33	0.83
6b	10, 21, 41, 44, 56	7.37 (7.25)	1.72 (1.49)	1.88	0.67
7b	10, 20, 48, 57	8.85 (8.36)	1.86 (1.63)	1.62	0.58
8b	10, 23, 41, 49	6.30 (6.08)	1.45 (1.45)	2.66	0.63
9b	8, 23, 51, 73	9.34 (4.12)	1.75 (0.78)	1.20	0.29

[a] Ligand concentrations were calculated based on the nitrogen content.

pH range than the monoamine ion exchangers **1b** and **2b** (see Figure 4). Methylation of the amine groups [ion exchangers **5b** (*Me$_2$en*) and **6b** (*Me$_3$en*)] resulted in some lowering of the stability, especially at higher pH. However, the largest drop in the distribution coefficient was effected when the methyl groups were replaced by ethyl groups (**7b**, *Et$_3$en*). The complex stability is, on the average, 10 times lower than the non-alkylated **3b**. Finally, the complex stability of the propylenediamine-containing ion exchanger **4b** (*pren*) is significantly lower than **3b**.

The difference in Rh complex stability observed between the monoamine ion exchangers (see Figure 4) and *en* ion exchanger **3b** might be explained in terms of the capability of the latter to form highly stable five-membered chelate rings with the Rh metal ions, whereas the former can only bind in a monodentate fashion. The importance of the ring size appears to be demonstrated by comparison of **3b** and **4b**. The distribution coefficients of the *pren* ion exchanger are similar to **1b**, hence the advantage of bidentate binding seems to be nullified when the chelate ring size is not correct. This is in agreement with the findings of Comba[15] and Hancock[16] on metal ion selectivity, indicating the preference of chelating ligands that coordinate via five-membered chelate rings for relatively large metal ions such as those of the platinum group.

Alkylation of the amine functionalities affects the properties of the metal ion complexes in different, opposing ways. As alkyl substituents are electron donating groups, the nitrogen becomes a better σ donor upon replacement of the N−H group by a methyl or an ethyl moiety. On the other hand, the increased steric hindrance of the substituents negatively influences the complex stability. Furthermore, *N*-alkylation inhibits the formation of hydrogen bonds of the type M−N−H···O with the solvent, thus decreasing the outer-sphere solvation energy due to its greater hydrophobic nature. Consequently, the electron density on the nitrogen atom is decreased, resulting in weaker σ donating properties.[17,18] Which of these opposing factors contributes most is dependent on the metal ion.

A big drop in stability was observed when the methyl groups were replaced by ethyl moieties (**7b** vs. **6b**), presumably due to increased hydrophobicity and, to a lesser extent, steric hindrance. In the case of ion exchangers **5b** and **6b**, the loss of hydrogen bond formation seems to be compensated, to some extent, by the increased electron density on the nitrogen atoms; the steric influences of the smaller methyl groups appear to be less important.

The stability of the Rh-triamine complexes at varying pH is depicted in Figure 6. The stability at pH values where binding takes place via coordination, i.e. pH > 2, is similar for both **8b** (*dien*) and **9b** (*tacn*) and of the same order as the *en* ion exchanger **3b**. At low pH, the log *D* values of the *tacn*-Rh complexes dropped dramatically, a feature that was not observed for the linear equivalent.

A possible explanation may originate from the difference in protonation constants (log *K* values) of the two triamine ligands. The log K_2 and, even more pronounced, log K_3 values of *tacn* are much lower than those of *dien*, implying that protonation of the second and third amine atoms of tacn occurs at much lower pH than for dien.[7b,19] As the third amine in *tacn* is probably only starting to become protonated at pH 1, it is very likely that *tacn* has a 2^+ overall charge and hence this will not bind as strongly to the negatively charged Rh complexes as the *dien* ligands bearing a 3^+ charge. The retardation of the second and third protonation is predominantly caused by electrostatic repulsions in the small ring between the incoming protons and those already bound.[19] At high pH, this difference is absent, and both ion exchangers exhibit similar high log *D* values.

Recovery Experiments

Both the adsorption of Rh^{3+} in different solvents on the various different amine ion exchangers, and subsequent desorption were tested. Since the ligand concentrations of the ion exchangers vary significantly (see Table 1), it is more correct, in addition to the ligand capacity (*c*, in mmol/g), to look at the ligand occupation (*L*, in %) as well, which is defined as follows:

L = [uptake capacity for M^{n+} (in mmol/g ion exchanger)]/[ligand concentration (in mmol/g ion exchanger)].

As the solvent might influence the recovery of Rh metal ions, the adsorption was performed in three different media:

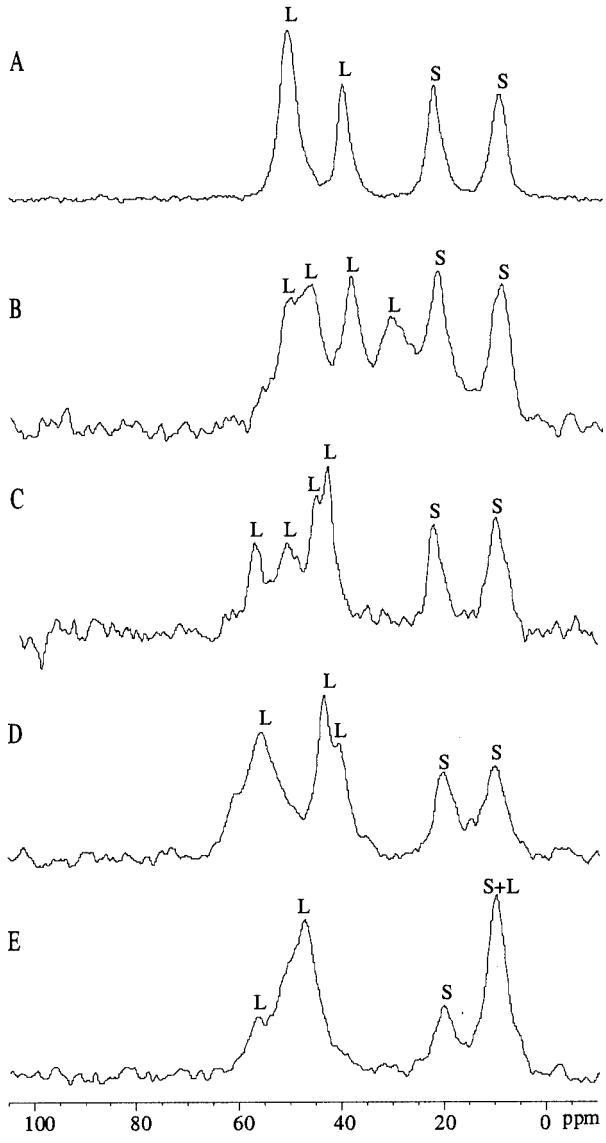

Figure 2. ^{13}C CP MAS NMR spectra of diamine ion exchangers **3B** (A), **4B** (B), **5B** (C), **6B** (D), and **7B** (E); peaks originating from $(R)_3SiCH_2CH_2$ are denoted **S**; all ligand signals, and signals originating from $(R)_3SiCH_2CH_2CH_2$, are marked **L**

distilled water, 1 M HCl, and absolute ethanol. Subsequent desorption was performed in 2 M HNO_3, as this eluent proved to be most efficient. The recovery results of amine ion exchangers are listed in Table 2. The most important recovery observations, for adsorption in water, are discussed below:

(1) Maximum ligand capacities of up to 0.5 mmol/g ($\approx$ 50 mg Rh/ g ion exchanger) were obtained, with ligand occupations not above 65%. For most ion exchangers, the ligand occupations lie around 50%, suggesting that the Rh metal-ions coordinate predominantly by an ML_2 fashion, in agreement with the observations of Zmievskaya[10b] and Tikhomirova.[7a]

(2) The desorption processes show the following trend: monoamines > diamines > triamines. Very high degrees of

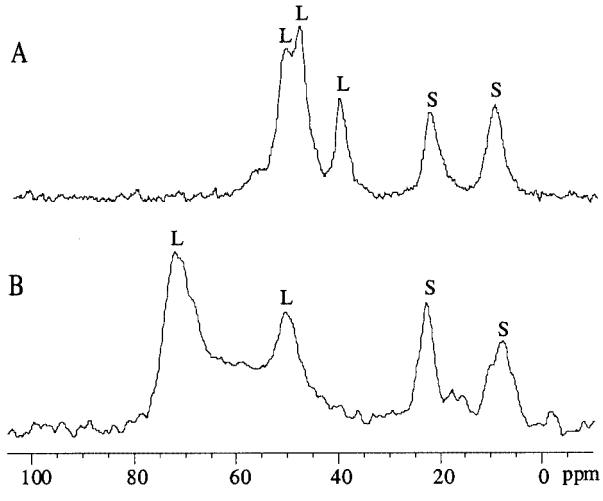

Figure 3. ^{13}C CP MAS NMR spectra of triamine ion exchangers **8b** (A) and **9b** (B); peaks originating from $(R)_3SiCH_2CH_2$ are denoted **S**; all ligand signals, and signals originating from $(R)_3SiCH_2CH_2CH_2$, are marked **L**

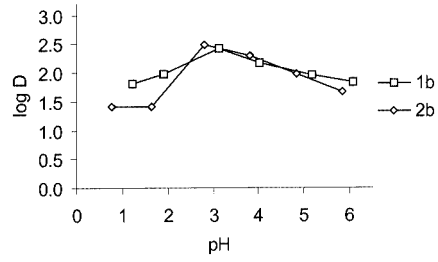

Figure 4. The distribution coefficients for Rh^{3+} as a function of the pH with the monoamine ion exchangers **1b** and **2b**

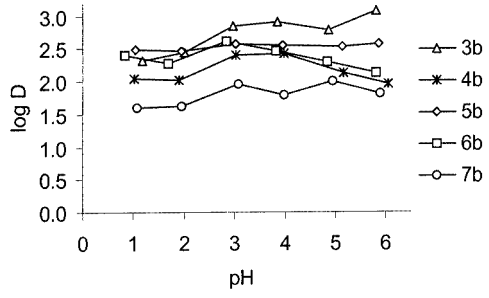

Figure 5. The distribution coefficients for Rh^{3+} as a function of the pH with the diamine ion exchangers **3b**–**7b**

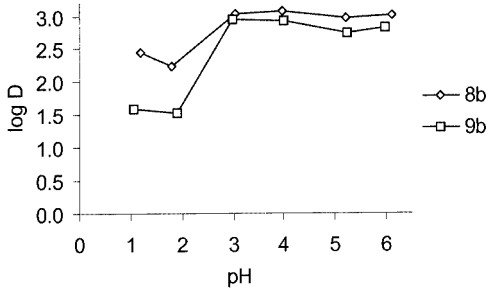

Figure 6. The distribution coefficients for Rh^{3+} as a function of the pH with the triamine ion exchangers **8b** and **9b**

Table 2. Recovery experiments of Rh^{3+}-loaded ion exchangers **1b**−**9b**; the adsorption of Rh^{3+} was done in H_2O, 1 M HCl, or EtOH absolute for 48 h; the desorption was performed in 2 M HNO_3 for 48 h

Ion exchanger	Adsorption in H_2O *c* in mmol/g, (*L* in%) desorption in%	Adsorption in HCl *c* in mmol/g, (*L* in%) desorption in%	Adsorption in EtOH *c* in mmol/g, (*L* in%) desorption in%
1b	0.48, (42.2) *93*	0.21, (18.0) *84*	0.51, (44.3) *61*
2b	0.22, (30.5) *99*	0.04, (5.9) *61*	0.31, (42.9) *83*
3b	0.50, (49.1) *71*	0.23, (20.6) *87*	0.63, (54.9) *49*
4b	0.44, (64.1) *91*	0.12, (17.0) *86*	0.44, (64.8) *28*
5b	0.38, (46.1) *60*	0.19, (22.9) *86*	0.47, (57.0) *39*
6b	0.32, (48.4) *72*	0.12, (18.6) *65*	0.51, (76.7) *54*
7b	0.22, (38.0) *95*	0.06, (10.0) *72*	0.34, (58.2) *69*
8b	0.35, (56.0) *46*	0.16, (24.9) *86*	0.45, (70.7) *17*
9b	0.14, (47.8) *51*	0.04, (13.0) *61*	0.18, (64.7) *38*

desorption, after adsorption in H_2O, were obtained for ion exchangers **1b**, **4b**, and **7b**, with an *almost quantitative desorption* for ion exchanger **2b**. This recovery trend clearly indicates that coordination via five-membered chelate rings has a positive effect on the complex stability (see previous section), but an inverse effect on the elution, as the desorption drops from 93% (**1b**) through 71% (**3b**) to only 46% (**8b**).

(3) The correlation of the recovery with the complex stability is even more striking, as the desorption pattern for the diamine ion exchangers is: *Et_3en* (**7b**) ≥ *pren* (**4b**) >> *Me_3en* (**6b**) ≥ *en* (**3b**) > *Me_2en* (**5b**). Methylation of the amine groups does not influence the adsorption or the desorption to a large extent, but replacement of the methyl groups with ethyl groups results in high elution percentages. Adversely, the ligand occupation is decreased, although not dramatically. Chelation via six-membered chelate rings (**4b**) appears to be strong enough for sufficient binding (64%) and weak enough to ensure a high desorption percentage (91%).

(4) The recovery pattern of the triamines is quite similar, as expected from the log *D* experiments (Figure 6).

For all the ion exchangers, the adsorption was found to increase with the different solvents in the following order: HCl << H_2O ≤ EtOH. The ligand occupations lie mainly between 40% and 75% for adsorption in water or ethanol, whereas the adsorption in HCl never exceeds 25%. The relatively low ligand occupation, when the adsorption is done in 1 M HCl, can be attributed to the different binding mode, as already mentioned above. At low pH, the amines are protonated and, as the complex stability is lower, the extraction is seriously hampered by the presence of large amounts of competing Cl^- ions. On the other hand, a reasonably good desorption was obtained with all the ion exchangers (> 80%), demonstrating the absence of binding in a chelate fashion under these conditions.

Finally, although the adsorption in EtOH was most successful in many cases, the desorption often proved to be problematic (Table 2, most right column). This problem has to do with partial reduction of the Rh metal ions in this solvent, as reported by Hernan[20] and Kriek.[21] This explanation has been confirmed by comparison of the potential for elution after adsorption in various alcohols and a non-reducing solvent, acetonitrile. The desorption, after adsorption in methanol or 1-propanol, proved equally problematic, and appeared to be greatly improved after adsorption in acetonitrile.

The possibility of re-using our ion exchangers was also investigated, and a constant recovery percentage over five cycles of adsorption and desorption was established. Hence, no leaching of amine ligands was taking place. The details of the results will be published in a separate manuscript.[22]

Conclusions

In summary, highly efficient recovery of Rh metal ions was effected with some of the presented amine-containing silica-based ion exchangers. Although the recovery of Rh is known to be troublesome, almost quantitative desorption was attained with a few of the tested materials under relatively mild conditions, using 2 M HNO_3. The desorption efficiency proved to be highly dependent on the ligand-to-metal stability of the complexes and the following conclusion can be drawn: To ensure optimal Rh recovery, the log *D* values of the ligand-to-metal complexes should lie between 2.0 and 2.5. Above log $D = 2.5$, the complex stability is too strong to ensure good desorption. Below log $D =$

2.0, the low complex stability prevents a high adsorption, even though the ligand occupation in water was never below 30%. Alkylation of the amine group(s) induced a reasonable complex destabilization.

The extractability and the subsequent elution were dependent on the chosen medium, which influenced the character of the Rh species.

In order to apply these materials in a continuous system, industrially important factors, such as ligand exchange kinetics and selectivity of extraction, are currently being investigated.

Experimental Section

Reagents and Analytical Methods: All reactions were performed under an argon atmosphere using standard Schlenk techniques. All reagents and solvents were purchased from commercial sources and were used without further purification unless stated otherwise. Toluene was distilled from Na under argon and stored over molecular sieves (3Å). Methanol was distilled from Mg under an argon atmosphere and stored over molecular sieves. Silica (Aldrich Silica gel Davisil™, particle size 4−20 μm, surface area 480 m^2/g, pore volume 0.75 cm^3/g) was activated before use by heating in vacuo (200 mbar) at 50 °C for at least 48 hours.

^{1}H NMR and ^{13}C NMR spectra were recorded on a Bruker DPX 300 spectrometer operating at 300.1 MHz and at 75.5 MHz for ^{1}H and ^{13}C NMR, respectively, and chemical shifts are quoted with respect to TMS and internal solvents, as internal reference for ^{1}H and ^{13}C NMR, respectively. Solid-state ^{13}C NMR CP-MAS NMR spectra were recorded on a Bruker MSL 400 spectrometer operating at 100.6 MHz with a rotational spin speed of 10.5 kHz. Metal analyses were performed on a Perkin−Elmer 3100 atomic absorption (AAS) and flame emission spectrometer using a linear calibration method. Elemental analyses (C, H, N) were carried out by the Microanalytical Laboratory of the University College in Dublin. Mass spectra were recorded on a Finnigan MAT 900 equipped with a custom-made electrospray interface (ESI).

$RhCl_3 \cdot 3H_2O$, 3-(trimethoxysilyl)propylamine (*NH*$_2$, **1a**), *N*-[3-(trimethoxysilyl)propyl] ethylenediamine (*en*, **3a**), and *N*-[3-(trimethoxysilyl)propyl] diethylenetriamine (*dien*, **8a**) were purchased from Acros. [3-(dimethylamino)propyl]trimethoxysilane (*Me*$_2$*N*, **2a**) was synthesized according to a literature procedure,[23] and *N*-[3-(trimethoxysilyl)propyl]propylenediamine (*pren*, **4a**) was synthesized as described previously.[9]

***N,N*-Dimethyl[3-(trimethoxysilyl)propyl]ethylenediamine (*Me*$_2$*en*, 5a):** A mixture of 3-chloropropyltrimethoxysilane (16.8 mL, 18.1 g, 91.1 mmol) and *N,N*-dimethylethylenediamine (20.0 mL, 16.1 g, 182.1 mmol) was heated at 150 °C for 6 h and then overnight at room temperature. The light-yellow, biphasic solution was purified by vacuum distillation (b.p. 105−107 °C/1 Torr). Yield **5a** (colourless liquid) 6.4 g (28%). ^{1}H NMR (300 MHz, $CDCl_3$): δ = 0.56 (t, 2 H, SiCH_2), 1.23 (br. s, 1 H, N*H*), 1.51 (dt, 2 H, $SiCH_2CH_2$), 2.14 (s, 6 H, N-CH_3), 2.30 (t, 2 H, $RNHCH_2CH_2NR_2$), 2.52 (t, 2 H, $SiCH_2CH_2CH_2$), 2.58 (t, 2 H, $RNHCH_2CH_2NR_2$), 3.45 (s, 9 H, OCH_3). ^{13}C NMR: δ = 6.5 (Si*C*H$_2$), 22.9 ($SiCH_2CH_2$), 45.4 [N(CH_3)$_2$], 47.1 ($SiCH_2CH_2CH_2$), 50.3 (O*C*H$_3$), 52.7 ($RNHCH_2CH_2NR_2$), 59.1 ($RNHCH_2CH_2NR_2$). ESI-MS *m*/*z* ($C_{10}H_{26}N_2O_3Si$, 250): 251 $[M + H]^+$.

***N,N,N′*-Trimethyl[3-(trimethoxysilyl)propyl]ethylenediamine (*Me*$_3$*en*, 6a):** A mixture of 3-chloropropyltrimethoxysilane (4.5 mL, 4.9 g, 24.5 mmol) and *N,N,N′*-trimethylethylenediamine (6.2 mL, 5.0 g, 48.9 mmol) was heated at 150 °C for 5 h. The clear, red, biphasic solution was purified by vacuum distillation (b.p. 140−143 °C/1 Torr). Yield **6a** (light yellow liquid) 2.15 g (33%). ^{1}H NMR (300 MHz, $CDCl_3$): δ = 0.51 (t, 2 H, SiCH_2), 1.47 (dt, 2 H, $SiCH_2CH_2$), 2.14 (s, 9 H, N-CH_3), 2.23−2.40 (m, 6 H, N-CH_2), 3.45 (s, 9 H, OCH_3). ^{13}C NMR: δ = 6.5 (Si*C*H$_2$), 19.9 ($SiCH_2CH_2$), 42.2 (N-*C*H$_3$), 45.6 [N(*C*H$_3$)$_2$], 50.3 (O*C*H$_3$), 55.3 ($SiCH_2CH_2CH_2$), 57.2 [$RN(CH_3)CH_2CH_2N(CH_3)_2$], 60.9 [$RN(CH_3)CH_2$-$CH_2N(CH_3)_2$]. ESI-MS *m*/*z* ($C_{11}H_{28}N_2O_3Si$, 264): 265 $[M + H]^+$.

***N,N,N′*-Triethyl[3-(trimethoxysilyl)propyl]ethylenediamine (*Et*$_3$*en*, 7a):** A mixture of 3-chloropropyltrimethoxysilane (5.1 mL, 5.5 g, 27.9 mmol) and *N,N,N′*-triethylethylenediamine (10.0 mL, 8.0 g, 55.8 mmol) was heated at 150 °C for 6 h. The product was purified by vacuum distillation, yielding 2.6 g (30%) of a turbid white liquid (b.p. 130−134 °C/1 Torr). ^{1}H NMR (300 MHz, $CDCl_3$): δ = 0.47 (t, 2 H, SiCH_2), 0.85−0.92 (m, 9 H, N-CH_2CH_3), 1.40 (dt, 2 H, $SiCH_2CH_2$), 2.14 (s, 9 H, N-CH_3), 2.30 (t, 2 H, $SiCH_2CH_2CH_2$), 2.36−2.43 (m, 10 H, N-CH_2), 3.42 (s, 9 H, OCH_3). ^{13}C NMR: δ = 6.5 (Si*C*H$_2$), 12.4, 12.5 (N-CH_2CH_3), 20.8 ($SiCH_2CH_2$), 48.2 [N(CH_2CH_3)$_2$], 48.8 ($SiCH_2CH_2CH_2NR_2$), 51.0 (O*C*H$_3$), 51.9 (N-*C*H$_2$CH$_3$), 52.5 ($R_2NCH_2CH_2NR_2$), 57.7 ($R_2NCH_2CH_2NR_2$). ESI-MS *m*/*z* ($C_{14}H_{34}N_2O_3Si$, 307): 308 $[M + H]^+$.

1,4,7-Triazacyclononane (*tacn*, 9a): *N,N′,N″*-Tris(*p*-toluenesulfonyl)-1,4,7-triazacyclononane (20.0 g, 33.8 mmol) was suspended in conc. H_2SO_4 (60 mL) in the presence of water (12 mL) and heated for 20 h at 140 °C. After cooling to room temp., the mixture was poured into EtOH (96%, 150 mL), cooled with a water bath. The suspension was filtered and dried with Et_2O, yielding the grey deprotected tacn-sulfuric acid salt (20.7 g). This salt was added to a mixture of NaOH (10 g, 0.25 mmol), water (15 mL), and toluene (70 mL) and heated under reflux for 2 h. The water was subsequently removed by a Dean−Stark separation in toluene for 3 h. Hot filtration of the suspension, followed by washing with hot toluene and chloroform (two times) and evaporation of the solvent, yielded 3.8 g (86%, 29.2 mmol) of **9a** as a light-yellow oil which slowly crystallized.

Synthesis of the Ion Exchangers: The free ligand (1.7 mmol **1a**−**8a**/g silica) was added to a suspension of silica in toluene (5−10 mL/g silica), and the mixture was stirred at room temperature for 48 h. After filtration, the residual reagents were removed by washing with toluene (3 ×). The ion exchangers **1b**−**8b** were further purified by heating under reflux in toluene in a Soxhlet apparatus for 24 hours, followed by drying at 50 °C in vacuo (200 mbar) until constant weight.

In the case of the *tacn* ligand **9a**, the following grafting procedure was followed: 3-glycidoxypropyltrimethoxysilane (glymo, 9.3 g, 41.9 mmol) was added to a suspension of silica (10.0 g) in toluene (75 mL) and the mixture heated for 24 h at 80 °C. The *glymo*-Si was washed, purified, and dried as indicated above. Ligand **9a** (3.1 g, 24.0 mmol) was added to a suspension of *glymo*-Si (9.5 g, ligand concentration: 0.88 mmol/g) in MeOH/toluene (both 50 mL) and the mixture was heated at 90 °C for 48 h. Purification was performed as discussed above.

log *D* Experiments: Distribution coefficients, with *D* = [mmol M^{n+}/g of dry ion exchanger]/[mmol M^{n+}/mL of solution], were determined as a function of the pH, employing 0.6 M NaCl/HCl buffer solutions (pH 1−2) and 0.6 M NaOAc/HOAc buffer solutions (pH 3−6). 25 mL of the appropriate buffer solution was added to a freshly[24] prepared solution of $RhCl_3 \cdot 3H_2O$, where the ligand-to-metal ratio was kept constant at 5 to 1, in 25 mL of demineralised

H_2O. Subsequently, 100 mg of ion exchanger was added and the suspension was agitated in polyethylene bottles mounted on a shaker for 48 hours at room temperature. After shaking, the samples were filtered and 25 mL of the filtrate was transferred into a 50 mL volumetric flask and the metal content subsequently analysed by AAS. The residue was washed with H_2O, EtOH, and Et_2O (3 ×), respectively, and dried in vacuo at 50 °C for 24 h. Samples for metal analysis were prepared by heating ca. 100 mg of loaded samples overnight in 5 mL of concentrated H_2SO_4. Subsequently, concentrated HNO_3 was added dropwise until the solutions became clear. After dilution in volumetric flasks the solution was filtered through a glass filter (P4) to remove residual, undigested silica. The filtrate was collected and analysed by AAS.

Blank uptake experiments with $RhCl_3$ using pure silica and *glymo*-Si were performed under various acidic conditions (up to 5 M HCl), neutral conditions, and using the above-mentioned buffer system. No significant uptake was detected. Hence, all uptake capacity can be attributed to the supported ligand system.

Recovery Experiments: For the adsorption experiments, 200 mg of ion exchanger was added to a fresh solution of $RhCl_3 \cdot 3H_2O$, where the ligand-to-metal molar ratio was kept constant at 1 to 1, in 50 mL of water, 1 M HCl, or EtOH (absolute). After agitation for 48 h, the suspension was filtered and the residue was washed with H_2O, EtOH, and Et_2O (3 ×), respectively. About 100 mg of the loaded ion exchanger was added to a 50 mL 2 M HNO_3 solution and the procedure was repeated. Both the loaded and eluted samples were subsequently dried and prepared for metal analysis as described above.

Acknowledgments

This research has been sponsored by IOP (Innovation Oriented research Programme, The Netherlands) Environmental Technology/Heavy Metals cluster Separation, project number IZW97411. Ing. F. ten Hoonte, Mrs. J. Erkelens, and Mr. J. J. M. van Brussel (Leiden Institute of Chemistry) are thanked for technical assistance. Mr. F. Lefeber, Mr. K. Erkelens, and Mr. J. G. Hollander are acknowledged for the collection of the solid-state ^{13}C CP MAS NMR spectra of the ion exchangers presented in this paper. *N,N′,N′′*-Tris(*p*-toluenesulfonyl)-1,4,7-triazacyclononane was kindly supplied to us by Dr. R. Hage (Unilever). Dr. W. Buijs (DSM Research) and Dr. R. Luckay (Stellenbosch University, South Africa) are acknowledged for stimulating discussions.

[1] B. Cornils, W. A. Herrmann, in *Applied Homogeneous Catalysis with Organometallic Compounds, Vol. 2* (Eds.: B. Cornils, W. A. Herrmann), VCH Publishers, NY, **1996**.
[2] H. J. Hoorn, P. deJoode, D. J. Dijkstra, W. L. Driessen, H. Kooijman, N. Veldman, A. L. Spek, J. Reedijk, *J. Mater. Chem.* **1997**, *7*, 1747.
[3] J. Blum, *Russ. Chem. Bull.* **1993**, *42*, 1619.
[4] M. M. Mdleleni, R. G. Rinker, P. C. Ford, *Inorg. Chim. Acta* **1998**, *270*, 345.
[5] J. Kramer, A. Scholten, W. L. Driessen, J. Reedijk, *Inorg. Chim. Acta* **2001**, *315*, 183.
[6] [6a] E. Benguerel, G. P. Demopoulos, G. B. Harris, *Hydrometallurgy* **1996**, *40*, 135, and references therein. [6b] M. S. Alam, K. Inoue, *Hydrometallurgy* **1997**, *46*, 373.
[7] [7a] T. I. Tikhomirova, V. I. Fadeeva, G. V. Kudryavtsev, P. N. Nesterenko, V. M. Ivanov, A. T. Savitchev, N. S. Smirnova, *Talanta* **1991**, *38*, 267. [7b] P. N. Nesterenko, A. V. Ivanov, N. A. Galeva, G. B. C. Seneveratne, *J. Anal. Chem.* **1997**, *52*, 736.
[8] [8a] J. Kramer, K. R. Koch, W. L. Driessen, J. Reedijk, *Hydrometallurgy* in press. [8b] B. R. Green, A. H. Potgieter, in *Ion Exchange Technology* (Eds.: D. Naden, M. Streat), Ellis Horwood, Chichester, **1984**, pp. 626. [8c] A. Warshawsky, in *Ion Exchange Technology* (Eds.: D. Naden, M. Streat), Ellis Horwood, Chichester, **1984**, pp. 604. [8d] E. Benguerel, G. P. Demopoulos, G. Cote, D. Bauer, *Solv. Extr. Ion Exc.* **1994**, *12*, 497. [8e] M. S. Alam, K. Inoue, K. Yoshizuka, *Hydrometallurgy* **1998**, *49*, 213. [8f] J. L. Cortina, E. Meinhardt, O. Roijals, V. Martí, *Reac. Funct. Polym.* **1998**, *36*, 149.
[9] J. Kramer, A. R. García, W. L. Driessen, J. Reedijk, *Chem. Commun.* **2001**, *23*, 2420.
[10] [10a] E. Kálalová, F. Radová, F. Švec, J. Kalál, *Collect. Czech. Chem. Commun.* **1978**, *43*, 604. [10b] I. R. Zmievskaya, A. T. Savitchev, V. I. Fadeeva, T. I. Tikhomirova, G. V. Kudryavtsev, *J. Anal. Chem. USSR* **1987**, *42*, 1168. [10c] X. Chang, Y. Li, X. Luo, G. Zhan, Z. Su, J. Gao, *Anal. Chim. Acta* **1991**, *245*, 13. [10d] W. Li, M. Coughlin, R. L. Albright, R. H. Fish, *React. Funct. Polym.* **1995**, *28*, 89.
[11] M. J. Hudson, in *Ion Exchange: Science and Technology* (Ed.: A. E. Rodrigues), Martinus Nijhoff, Dordrecht, **1986**, p. 35.
[12] B. K. Tait, D. P. Shillington, *S. Afr. J. Chem.* **1992**, *45*, 17.
[13] W. H. Höll, in *Ion Exchange Developments and Applications* (Ed.: J. A. Greig), RSC, Cambridge, **1996**, pp. 405.
[14] T. M. Buslaeva, S. A. Simanova, *Russ. J. Coord. Chem.* **1999**, *25*, 151.
[15] P. Comba, *Coord. Chem. Rev.* **1999**, *185−186*, 81.
[16] R. D. Hancock, A. E. Martell, *Chem. Rev.* **1989**, *89*, 1875.
[17] L. F. Lindoy, *Pure Appl. Chem.* **1997**, *69*, 2179.
[18] D. Meyerstein, *Coord. Chem. Rev.* **1999**, *185−186*, 141, and references therein.
[19] P. Chaudhuri, K. Wieghardt, in *Progress in Inorganic Chemistry, Vol. 35* (Ed.: S. J. Lippard), John Wiley & Sons, New York, **1987**, pp. 329.
[20] P. Hernan, C. del Pino, E. Ruiz-Hitzky, *Chem. Mater.* **1992**, *4*, 49.
[21] R. J. Kriek, W. J. Engelbrecht, J. J. Cruywagen, *J. S. Afr. I. Min. Metall.* **1995**, 75.
[22] J. Kramer, J. A. Erkelens, A. R. García, W. L. Driessen, J. Reedijk, *New J. Chem.* submitted for publication.
[23] R. Tacke, B. Pfrommer, M. Pülm, R. Bertermann, *Eur. J. Inorg. Chem.* **1999**, 807.
[24] As $RhCl_3$ shows extensive aquation (the formation of kinetically rather inert aquochloro complexes) with time, freshly prepared $RhCl_3$ solutions (< 10 minutes old) were always used.

Received January 10, 2002
[I02011]

A New Type of Anionic Rearrangement in Metalated Benzylhydrazines

Hermann Sachdev*[a] and Cordula Preis[a]

Keywords: Lithium / Magnesium / Hydrazides / Rearrangements / Structural characterisation

Metalation of *N*,*N*-dibenzyl-*N*′-(trimethylsilyl)hydrazine with organyllithium and -magnesium compounds led to the migration of the benzyl group, and the deprotonation of Si–Me groups was observed. The syntheses and crystal structures of $Bzl_2N–NH_2$, $[Bzl(Li)N–N(SiMe_3)Bzl]_2$, and $[Mg[BzlN–N(SiMe_2CH_2)Bzl]_2$ are presented.
(© Wiley-VCH Verlag GmbH, 69451 Weinheim, Germany, 2002)

Introduction

Precursors of lithium−, magnesium−, and aluminium−nitrogen compounds with low aggregation degrees are highly desired for their use in the synthesis of nitridic ceramic composite materials[1] by CVD techniques. Different ligand systems have been investigated in order to obtain low-coordinated, volatile precursors.[2] The structural chemistry of amides of group-1, -2, and -13 metals has already been widely explored and indicates the formation of oligomeric or polymeric ring and cage structures.[3−5]

Hydrazines are interesting ligands, and metalated hydrazines exhibit a different coordination chemistry due to an additional donor atom in the α-position. Some recent aspects of the coordination chemistry of alkali metal hydrazides have been reported in the past,[6−8] and the syntheses of aluminium and gallium hydrazides were also studied as possible precursors for AlN[9] and GaN.[10,11] The structural chemistry of group-2 metal hydrazides is rather unexplored, and therefore we studied the synthesis and reactivity of alkaline earth metal hydrazides in order to compare them with the corresponding hydrazides of group-1 and -13 elements.[6−8]

Results and Discussion

In this report, the properties of *N*,*N*-dibenzyl-*N*′-(trimethylsilyl)hydrazine (**2**), prepared by silylation of *N*,*N*-dibenzylhydrazine (**1**), were characterized with respect to the coordination to lithium and magnesium atoms. The aim was to achieve the corresponding lithium and magnesium hydrazides **2a** and **2b**, respectively, in a straightforward reaction involving hydrazine **2** and organolithium or -magnesium compounds according to Scheme 1. The reactions were carried out in hexane to avoid additional coordination of donor solvent molecules at the metal atoms.

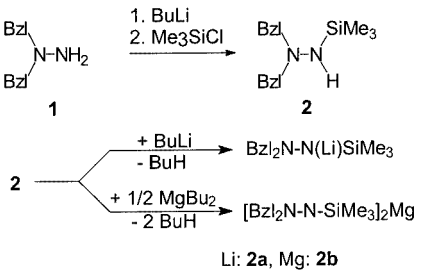

Scheme 1

Molecular Structures in the Solid State

In the course of this study, the solid-state structure of the starting material *N*,*N*-dibenzylhydrazine (**1**) was characterized. Single crystals suitable for X-ray structure determination could be obtained from freshly distilled *N*,*N*-dibenzylhydrazine by cooling at 4 °C.

The molecular structure is depicted in Figure 1. The crystals belong to the monoclinic system and the space group $P2_1/c$. The N−N bond length is 1.450(2) Å, the N−C distances are 1.467(2) Å [N(1)−C(7)] and 1.476(2) Å [N(1)−C(27)]. The nitrogen atom N(1) is threefold coordinated and shows sp^3-type bonding, as indicated by the sum of the bonding angles (330°).

The individual molecule is chiral in the solid state, but is linked to the corresponding enantiomer by hydrogen bonds via the $-NH_2$ groups. The N···H distance of the hydrogen bonds is 2.433 Å. This leads to a fourfold coordination of the nitrogen atom N(2), with N−N−H angles ranging from 103.4° to 108.9°, and a chain-like arrangement of the individual isomers in the crystal. It is interesting that the nitrogen atom N(2) of the hydrazide unit does not participate in the bonding via hydrogen bonds.

[a] Institute for Inorganic Chemistry FR 8.11, University of Saarland,
P. O. Box 1150, 66041 Saarbrücken, Germany

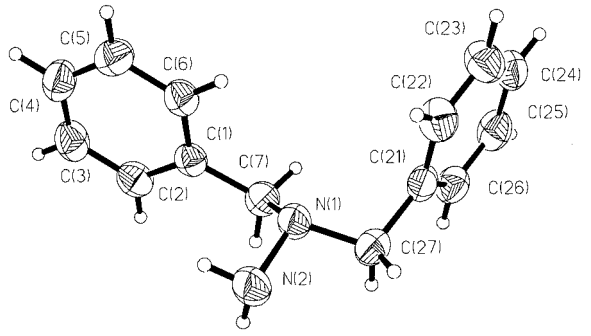

Figure 1. Molecular structure of *N*,*N*-dibenzylhydrazine (**1**); thermal ellipsoids are shown at a 50% probability level; selected bond lengths [Å] and bond angles [°]: N(1)−N(2) 1.4498(15), N(1)−C(7) 1.4672(18), N(1)−C(27) 1.4761(18), C(1)−C(7) 1.5184(19), C(21)−C(27) 1.5099(19); N(2)−N(1)−C(7) 111.37(10), N(2)−N(1)−C(27) 107.00(10), C(7)−N(1)−C(27) 111.42(11)

Light yellow crystals suitable for X-ray single-crystal structure determination could be obtained from the lithiation reaction in hexane (Scheme 1).[12] The molecular structure of the obtained product is depicted in Figure 2. It is a dimeric isomer of the anticipated product **2a**, *N*,*N*′-dibenzyl-*N*′-(trimethylsilyl)hydrazide (**3**), indicating the migration of a benzyl group.

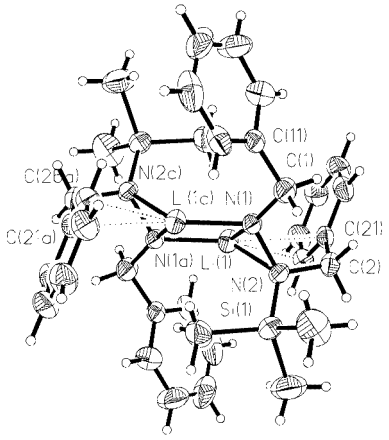

Figure 2. Molecular structure of dimeric lithium *N*,*N*′-dibenzyl-*N*′-(trimethylsilyl)hydrazide (**3**); thermal ellipsoids are shown at a 25% probability level and hydrogen atoms are omitted for clarity; selected atom distances [Å] and bond angles [°]: N(1)−N(2) 1.482(4), N(1)−C(1) 1.460(5), N(1)−Li(1) 1.924(8), N(1)−Li(1a) 1.954(7), C(1)−C(11) 1.483(6), Si(1)−N(2) 1.729(3), N(2)−C(2) 1.482(5), N(2)−Li(1) 2.091(8), C(2)−C(21) 1.489(6), C(21)−Li(1) 2.647(8),C(26)−Li(1) 2.678(8), Li(1)−Li(1a) 2.288(13); C(1)−N(1)−N(2) 111.4(3), C(1)−N(1)−Li(1) 150.6(4), N(2)−N(1)−Li(1) 74.5(3), C(1)−N(1)−Li(1a) 122.0(3), N(2)−N(1)−Li(1a) 120.0(3), Li(1)−N(1)−Li(1a) 72.3(3), N(1)−C(1)−C(11) 110.5(3), N(1)−N(2)−C(2) 113.9(3), N(1)−N(2)−Si(1) 115.5(2), C(2)−N(2)−Si(1) 119.2(3), N(1)−N(2)−Li(1) 62.4(2), C(2)−N(2)−Li(1) 103.9(3), Si(1)−N(2)−Li(1) 129.2(3), N(1)−Li(1)−N(1a) 107.7(3), N(1)−Li(1)−N(2) 43.08(19), N(1)a−Li(1)−N(2) 129.3(4)

The crystal belongs to the triclinic system and space group $P\bar{1}$ and contains two independent dimers of **3** per unit cell. The bonding parameters of the individual molecules are very similar.

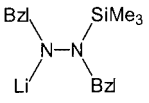

3

Figure 2 represents one centrosymmetric dimer with an Li_2N_4 core structure of two three-membered LiN_2 rings and a central four-membered Li_2N_2 ring. The observed Li_2N_4 core structure results from aggregation of two side-on-coordinated hydrazide units, a structural feature which has been observed for other dimeric lithiated silylhydrazides.[7,8]

In $(\mathbf{3})_2$, the nitrogen atoms of the hydrazide ligand show fourfold coordination, whereas the lithium atoms are threefold coordinated by two amide-type nitrogen atoms and one amine-type nitrogen atom.

The N−N bond length of the hydrazide unit is 1.482(4) Å. The Li−N distances of the four-membered Li_2N_2 ring [N(1)−Li(1) 1.924(8) Å, N(1)−Li(1a) 1.954(7) Å] are shorter than the distance between the coordinating α-nitrogen atom N(2) and the hydrazide ligand [N(2)−Li(1) 2.091(8) Å]. The distance between the lithium atoms Li(1)−Li(1a) is 2.288(13) Å; similar distances have been observed in other dimeric lithium silylhydrazides.[6−9]

Additional steric shielding of the lithium atoms results from interaction between the lithium atoms and the *ortho*-C−H position of the aromatic ring system of the benzyl groups of the hydrazide ligand [C(21)−Li(1) 2.647(8) Å, C(26)−Li(1) 2.678(8) Å]. Comparable Li−C distances were reported for lithiated hydrazides with aryl substituents.[7,8]

In a similar reaction of 2 equiv. of **2** with dibutylmagnesium according to Scheme 1, colourless single crystals suitable for X-ray structure determination were obtained from a hexane solution. The X-ray structure determination reveals the formation of a twofold deprotonated derivative **4** (1,2-dibenzyl-3,3-dimethyl-1,2-diaza-3-sila-5-magnesacyclopentane), instead of the anticipated hydrazide **2b**.

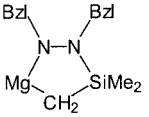

4

The crystal belongs to the triclinic system and space group $P\bar{1}$. The crystal structure of the hydrazide **4** is depicted in Figure 3.

The isolated product **4** is dimeric in the solid state. The magnesium atoms are coordinated by four nitrogen atoms and one carbon atom of the deprotonated trimethylsilyl group. This leads to an Mg_2N_4 core derived from side-on-coordinated MgN_2 rings. The Si−C bond length of the methylene group [Si(1)−C(15), 1.827 Å] is significantly shorter than the Si−C distances of the methyl groups (1.884 and 1.856 Å), due to the carbanionic nature of C(15).

Furthermore, there is a weak interaction between the magnesium atom and the π-electrons of the phenyl ring

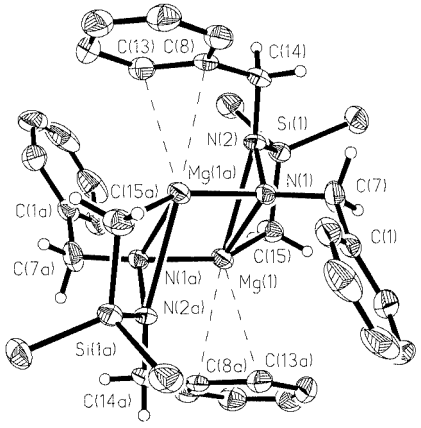

Figure 3. Molecular structure of **4**; thermal ellipsoids are shown at a 25% probability level and hydrogen atoms of aryl and methyl groups are omitted for clarity; selected bond lengths [Å] and bond angles [°]: N(1)−N(2) 1.491(4), Mg(1)−N(1) 2.121(3), Mg(1)−N(2) 2.596(3), Mg(1)−Mg(1a) 2.883(3), N(1)−Mg(1a) 2.044(3), N(2)−Mg(1a) 2.763(3), C(13)−Mg(1a) 2.789(4), C(8)−Mg(1a) 2.721(3), N(2)−C(14) 1.475(4), N(1)−C(7) 1.466(5), Si(1)−C(15) 1.827(4), Si(1)−C(16) 1.884(4), Si(1)−C(17) 1.856(4), Mg(1)−C(15) 2.129(4), Mg(1)−Mg(1a) 2.883(4); N(1a)−Mg(1)−N(1) 92.43(12), N(2)−Mg(1)−N(2a) 114.98(7), N(1)−Mg(1)−N(2) 35.05(10), N(2)−N(1)−Mg(1a) 101.65(19), N(2)−N(1)−Mg(1) 90.13(18), C(7)−N(1)−Mg(1a) 134.3(3), C(7)−N(1)−N(2) 110.1(2)

system. The C−Mg distances C(8)−Mg(1a) and C(13)−Mg(1a) range between 2.721 Å and 2.789 Å, and are shorter than the distance Mg(1a)−N(2) [2.763 Å]. When this interaction is considered as part of the coordination sphere, the magnesium atoms exhibit a sixfold coordination.

Both nitrogen atoms of the hydrazine ligand are involved in the coordination and the sum of the bond angles at the deprotonated nitrogen atom N(1) involving the surrounding atoms C(7), N(2), Mg(1) and Mg(1a) is 334.5° and 346.1°, respectively. Thus, the coordination geometry at the nitrogen centre N(1) is not planar, but resembles a distorted tetrahedral coordination. The C−N bond lengths (1.475 Å and 1.466 Å) are in the range of C−N single bonds (1.470 Å). The N−N bond length (1.491 Å) is slightly larger than that in *N*,*N*-dibenzylhydrazine (**1**) (1.450 Å).

The N−N bond lengths in the metalated species **3** and **4** are longer than that in **1**, due to the additional negative charge at the nitrogen atom. The C−N bond lengths of the benzylic groups are not significantly affected by the metalation. A comparable increase in the N−N bond length is reported for the structures of alkali metal organyl- and silylhydrazides.[6−9]

Discussion

The crystal structures of **3** and **4** both indicate the formation of an *N*,*N*′-dibenzylhydrazide isomer. Although *N*,*N*-dibenzyl-*N*′-(trimethylsilyl)hydrazine (**2**) was used as the starting material, migration of the benzyl group occurred during metalation with butyllithium and dibutylmagnesium according to Scheme 2, finally leading to compounds **3** and **4**. Thus, the rearrangement must have taken place during the reaction from the structural unit **A** to **B**, by migration of a benzyl group.

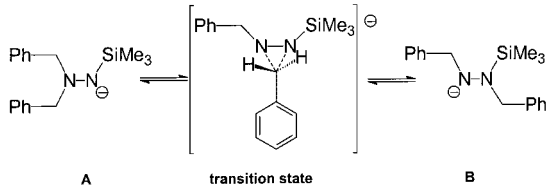

Scheme 2

The starting material consists of the pure isomer *N*,*N*-dibenzyl-*N*′-(trimethylsilyl)hydrazine (**2**), as indicated by the NMR spectroscopic data. The ^{29}Si NMR spectrum of **2** reveals a single resonance at δ = 2.23 and the ^{13}C NMR spectrum exhibits only one set of signals for the benzyl ligands (δ = 65.01, 126.96, 127.93, 129.85, and 138.01). The *N*,*N*′ isomer would have given rise to 10 resonances for the benzyl groups in the ^{13}C NMR spectrum, assuming free rotation of the ligands.

In the chemistry of silylated hydrazines, the migration of silyl groups is a common feature and has already been reported.[13,14] However, this is the first time that a similar rearrangement of benzyl groups is observed. Steric overcrowding cannot be considered to be responsible for this type of rearrangement, as indicated by the crystal structure of the unsubstituted hydrazine **1** (Figure 1), nor for the free rotation of the benzyl groups in solution of the hydrazines **1** and **2**, as indicated by the ^{13}C NMR spectroscopic data of these compounds. A stabilising effect of the negative charge by an aromatic system[7] is also not possible in this case. The migration of the benzyl group can be explained by an intramolecular S_N-type reaction caused by the increased nucleophilic character of the deprotonated hydrazide nitrogen atom in **A**, although stabilisation of the negative charge by the silyl group is possible (Scheme 2).

NMR Spectra

The ^{1}H and ^{13}C NMR spectra of the isolated crystals were recorded in C_6D_6 and indicate three different −CH_2− groups of the benzyl ligands and two different silyl groups. This is in accordance with the ^{29}Si and ^{7}Li NMR spectrum of the isolated crystal fraction. Two weak peaks (δ = 4.49 and 4.98) and two strong peaks (δ = −10.36 and 4.00) are present in the ^{29}Si NMR spectrum. Similar ^{29}Si NMR spectroscopic data were reported for other dimeric lithium silylhydrazides.[7,8] The ^{7}Li NMR spectrum exhibits two resonances at δ = −1.83 (major signal) and δ = −2.27. There is no change in the ^{29}Si and ^{1}H NMR spectra up to 60 °C. This indicates the presence of stable species in solution. According to the crystal symmetry of compound $(\mathbf{3})_2$, there are two different benzyl groups in the hydrazide unit, whereas the spectrum of compound $(\mathbf{2a})_2$ should exhibit only one set of signals for the benzylic groups in the case of free rotation of the substituents. The ^{1}H NMR spectroscopic data can be interpreted as a mixture of the dimer

isomers $(\mathbf{2a})_2$ and $(\mathbf{3})_2$ in solution, since there are three signals for the $N-CH_2-Ph$ groups, a resonance at $\delta = 3.74$ (25%, isomer **2a**) and two peaks at $\delta = 3.78$ and 4.07 (75%, isomer **3**).

The formation of the isomers **2a** and **3** can be explained by Scheme 3, which shows that during the lithiation of **2** the reaction proceeds in two different ways. In the first step, the monomer hydrazide **2a** is formed. In this monomer species, a rearrangement according to Scheme 2 is possible, leading to **3**.

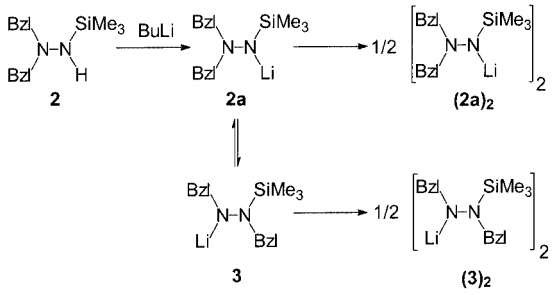

Scheme 3

The dimeric species $(\mathbf{2a})_2$ and $(\mathbf{3})_2$, once formed, are stable in solution and do not show any monomer−dimer equilibria or rearrangement equilibria, as indicated by measurement of high-temperature ^{29}Si NMR spectra in benzene up to 60 °C. The stability of the dimeric clusters is in agreement with rearrangement reactions observed in lithium silylhydrazides, which also show a high stability of the Li−N cluster once it is formed.[7,8]

Since the ^{7}Li and ^{29}Si NMR spectra of the solution and the crystals are similar, this indicates that the obtained crystal fraction is a mixture of the isomers $(\mathbf{2a})_2$ and $(\mathbf{3})_2$. It was not possible to isolate a suitable crystal of **2a** for a structure determination.[12] The rearrangement was not observed in hydrazines **1** and **2**, due to a weaker nucleophilic character of the deprotonated nitrogen atom.

An interesting feature of the synthesis of compound **2** from lithiated *N*,*N*-dibenzylhydrazine (**1a**) and chlorotrimethylsilane, is that the rearrangement was not observed during this reaction, although a hydrazide anion is formed as an intermediate according to Scheme 4.

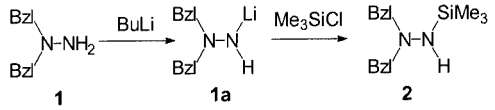

Scheme 4

The different reactivity of the hydrazides **2a** and **1a** can be attributed to their coordination chemistry. The retention of the *N*,*N*-dibenzyl isomer in the reaction involving **1a**, may be due to the different degree of aggregation of the lithiated intermediate **1a**, which is insoluble in donor-free solvents, in contrast to the silylated species **2a** and **3**. The aggregation might involve only the deprotonated nitrogen atom of the hydrazide ligand leading to highly aggregated oligomers of the type $(\mathbf{1a})_n$, which prevent the rearrangement under normal reaction conditions. Such a kind of aggregation was observed in other magnesium and zinc hydrazides.[15] If the deprotonated nitrogen atom is shielded by intermolecular coordination, the S_N2-type benzylic rearrangement becomes less likely.

Reaction of *N*,*N*-Dibenzyl-*N*′-(trimethylsilyl)hydrazine with Dibutylmagnesium

It was expected that the reaction of 2 equiv. of **2** with dibutylmagnesium would lead to the formation of a magnesium bis(hydrazide) **2b** according to Scheme 1. However, crystals of compound **4** were recovered in a 40% yield with respect to the magnesium content.

The solid-state structure of the isolated crystals of compound **4** reveals a magnesium hydrazide, where an additional deprotonation of a methyl group has taken place, leading to an $-N^{-}(Bzl)-SiMe_2-CH_2^{-}$ dianionic fragment. A mechanism explaining the formation of **4** is depicted in Scheme 5.

The first step of the reaction is the formation of organylmagnesium hydrazide **2c**. From this intermediate, migration of a benzyl group similar to that in lithium hydrazide **3** takes place, leading to the *N*,*N*′-dibenzyl isomer **2d**. From this intermediate **2d**, the reaction can proceed in two different directions. The butyl group acts as a base towards the proton of an Me_3Si- group in an intramolecular deprotonation reaction, leading to compound **4**, which was isolated and characterised by NMR spectroscopy and single-crystal diffractometry. The second reaction pathway leads to the formation of a magnesium bis(hydrazide) with unsymmetrically substituted ligands **2e**, by reaction of **2d** with the starting material **2**. Other types of deprotonation reactions involving $N-SiMe_3-$ groups were reported for solutions of heterobimetallic lithium and magnesium amides by elimination of an amine,[16] and by deprotonation of transition metal compounds with strong bases like butyllithium or lithium and sodium silylamides.[17] The formation of the five-membered $N-SiMe_2-CH_2-Mg$ ring structure in **4** may be attributed to the Lewis acidity of magnesium and the coordinating effects of the $Mg-N-N-$ unit, although a kinetic effect caused by the presence of *n*- and *sec*-butyl groups in commercially available dibutylmagnesium might be possible. However, the latter influence was not observed in the synthesis of other magnesium amides[16,18] and hydrazides[15] with sterically demanding silyl substituents, nor in the synthesis of organylmagnesium amides and hydrazides.[15]

The ^{29}Si NMR spectrum of the solution shows the starting material **2** ($\delta = 1.73$, highest intensity) to be present, as well as an additional signal at $\delta = 4.97$, of equal intensity, which is attributed to compound **4**. The resonance for the isolated compound **4** in C_6D_6 is at $\delta = 3.82$

Furthermore, weak resonances are present in the low-field region ($\delta = 3.65, 4.27, 4.92, 5.62, 11.24, 14.38$) and in the high-field region ($\delta = -8.76, -8.06, -7.33, -6.67$). The two resonances at lower field can be assigned to the

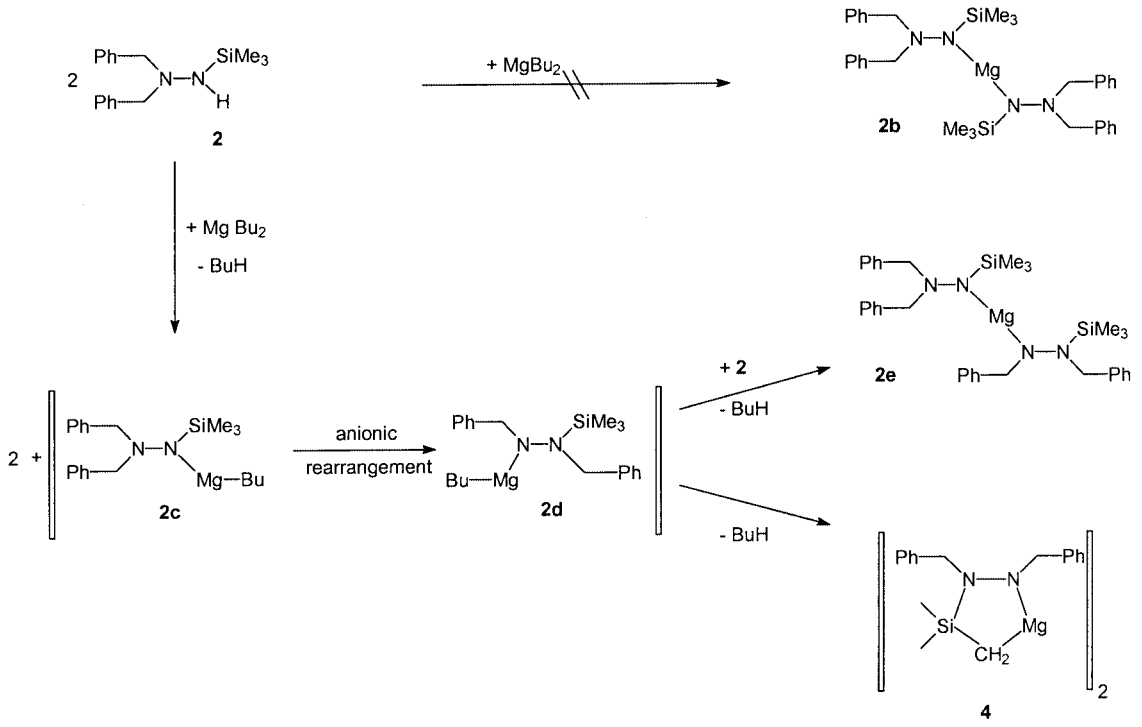

Scheme 5. Mechanism for the formation of the magnesium hydrazide **4**

rearranged dimeric organylmagnesium hydrazide **2d** (δ = 11.24, 14.38). The two sets of signals with four peaks each at δ = 3.65, 4.27, 4.92, 5.62 and δ = −8.76, −8.06, −7.33, −6.67 can be assigned to the dimeric magnesium hydrazide **2e**. At higher temperatures, no change in the intensity or peak shift was observed in the spectrum up to 60 °C.

An interesting feature to note is that there is no reaction when **4** is heated with the remaining starting material **2** up to 60 °C, although the basicity of the carbanion **4** should enable deprotonation of the hydrazide. This can be attributed to the high stability of the ionic core fragment and the steric shielding of **4**.

Conclusion

A new type of anionic rearrangement was observed in metalated benzylhydrazines, leading to the formation of *N*,*N*′-dibenzylhydrazides by migration of a benzyl group. With respect to the reaction of dibutylmagnesium with **2**, the rearrangement is the dominant reaction, instead of the formation of the corresponding magnesium hydrazide. The migration of the benzyl group is less dominant in the lithiation of the hydrazide **2**, which can be attributed to the different coordination and ionic nature of the metal−nitrogen bond. Furthermore, the influence of donor solvents on the coordination of the metal centres and the migration of the benzyl group has to be studied in more detail.

Experimental Section

General: All experiments were performed by using modified Schlenk techniques and anhydrous conditions under argon. Solvents were freshly distilled from Na/K alloy. Butyllithium (1.6 M in hexane), dibutylmagnesium (1 M in heptane, 1:1 isomer mixture of *n*- and *sec*-butyl groups), and *N*,*N*-dibenzylhydrazine were obtained commercially (Aldrich) and used as received. NMR spectra were recorded in C_6D_6 or $CDCl_3$ with a Bruker ACP 200 spectrometer (TMS as external standard; ^{1}H: 200 MHz, ^{13}C: 55.0 MHz, ^{29}Si: 39.7, ^{7}Li: 77.7 MHz). Attempts to prepare compound **3** and **4** in donor solvents like THF or ether failed and led to ether cleavage reactions, and deprotonation reactions of toluene were observed with compound **4** at higher temperatures. Compounds **3** and **4** may ignite if exposed to air. For the X-ray structure determination of the single crystals, a STOE IPDS diffractometer was used (Mo-K_α, λ= 0.71073 Å, graphite monochromator). The structures of the compounds **1** and **4** were solved by direct methods and for **2** the Patterson method was applied and refined by full-matrix least-squares methods (data are listed in Table 1). Anisotropic thermal parameters for all non-hydrogen atoms in the final cycles, isotropic refinement for hydrogen atoms positioned by geometry. SHELXS 97 and SHELXL 97 computer programs were used.[19] CCDC-168709 to -168711 contain the supplementary crystallographic data for this paper. These data can be obtained free of charge at www.ccdc.cam.ac.uk/conts/retrieving.html or from the Cambridge Crystallographic Data Centre, 12, Union Road, Cambridge CB2 1EZ, UK [Fax: (internat.) + 44-1223/336-033; E-mail: deposit@ccdc.cam.ac.uk].

Preparative Details

***N*,*N*-Dibenzylhydrazine (1):** Benzyl chloride (36 mL, 312 mmol) was added to a stirred solution of hydrazine (5.0 g, 156 mmol) and trie-

Table 1. Crystallographic data of compounds **1**, $(\mathbf{3})_2$ and $(\mathbf{4})_2$

	1	$(\mathbf{3})_2$	$(\mathbf{4})_2$
Empirical formula	$C_{14}H_{16}N2$	$C_{17}H_{23}LiN_2Si$	$C_{34}H_{44}Mg_2N_4Si_2$
Formula mass [gmol^{-1}]	212.29	290.40	613.54
Colour, habit	colourless plates	light yellow rhombs	colourless rhombs
Crystal system	monoclinic	triclinic	triclinic
Space group	$P2_1/c$	$P\bar{1}$	$P\bar{1}$
a [Å]	9.565(2)	10.723(2)	9.882(2)
b [Å]	5.6360(10)	10.878(2)	10.092(2)
c [Å]	22.886(5)	16.503(3)	10.394(2)
α [°]	90	83.38(3)	97.61(3)
β [°]	100.97(3)	78.02(3)	108.25(3)
γ [°]	90	69.89(3)	114.82(3)
V [Å^3]	1211.2(4)	1766.2(6)	850.6(3)
Z	4	4	1
d [g cm^{-3}]	1.164	1.092	1.154
crystal dimensions [mm]	0.3 × 0.3 × 0.5	0.5 × 0.5 × 0.5	0.5 × 0.5 × 0.5
μ, [mm^{-1}]	0.069	0.127	0.151
T [K]	293	293	293
2θ [°]	48.24	48.12	48.12
Index range	$-10 \le h \le 10$ $-5 \le k \le 5$ $-25 \le l \le 25$	$-12 \le h \le 11$ $-12 \le k \le 12$ $-18 \le l \le 18$	$-10 \le h \le 10$ $-11 \le k \le 11$ $-11 \le l \le 11$
R(int)	0.0619	0.0815	0.0791
No. of unique data	7070	11243	5378
No. of data [$I > 2\sigma(I)$]	1780	5228	2492
No. of parameters	153	385	200
$R1$ [$I > 2\sigma(I)$]	0.0365	0.0565	0.0691
$wR2$ (all data)	0.1030	0.1541	0.2132
max./min. e$^-$ density [eÅ^{-3}]	0.196/−0.114	0.518/−0.152	0.792/−0.387

thylamine (55 mL, 0.395 mmol) in 1 L of benzene, within 1 h. During the addition a white precipitate of the ammonium salt was formed. The mixture was heated for 2 h under reflux and the solid residue was then filtered off. The solvent was removed in vacuo and the remaining liquid was fractionally distilled. Bp. 110−112 °C/10^{-2} mbar. Yield: 13.2 g (40%). $C_{14}H_{16}N_2$ (212.29): calcd. C 79.21, H 7.59, N 13.20; found C 78.03, H 7.32, N 12.87. NMR ($CDCl_3$): δ^1H = 2.98 (br, 2 H, $-NH_2$), 3.73 (s, 4 H, $-CH_2-$), 7.18−7.36 (m, 10 H, Ph); δ^{13}C = 64.63 (Ph−*C*H$_2$−), 127.20 (*p*-Ph), 128.35 (*o*-Ph), 128.94 (*m*-Ph), 137.66 (*i*-Ph).

***N*,*N*-Dibenzyl-*N*′-(trimethylsilyl)hydrazine (2):** Butyllithium (12.7 mL of a 1.6 M solution) was added slowly to a solution of **1** (4.3 g, 20.2 mmol) in 250 mL of benzene, at room temperature. During the addition a white precipitate of the hydrazide was formed. The mixture was stirred for 1 h, after which chlorotrimethylsilane (2.6 mL, 20.2 mmol), dissolved in 10 mL of benzene, was added slowly over 1 h. The mixture was heated under reflux for 1 h, and after cooling, the solid residue was filtered off. The solvent was removed in vacuo and the remaining liquid was fractionally distilled. Bp. 104−106 °C/10^{-2} mbar. Yield: 4.20 g (73%). $C_{17}H_{24}N_2Si$ (284.48): calcd. C 71.78, H 8.50, N 9.85; found C 70.61, H 8.64, N 9.38. NMR ($CDCl_3$) δ^1H = −0.00 (s, 9 H, $SiMe_3$), 2.22 (s, N−H, 1 H), 3.75 [s, 4 H, (PhC*H*$_2$−)$_2$], 7.38−7.50 [m, 10 H, (PhC*H*$_2$−)$_2$]; δ^{13}C = −0.67 ($SiMe_3$), 65.10 [(Ph*C*H$_2$−)$_2$], 126.96 (*p*-Ph), 127.93 (*o*-Ph), 129.85 (*m*-Ph), 138.10 (*i*-Ph); δ^{29}Si = 2.22 ($SiMe_3$).

Lithium *N*,*N*′-Dibenzyl-*N*′-(trimethylsilyl)hydrazide (3): Butyllithium (2.9 mL of a 1.6 M solution) was added slowly to a solution of **2** (1.3 g, 4.6 mmol) in 25 mL of hexane, at room temperature. During the addition the solution became orange. After the evolution of butane was complete, the solution was stored at 4 °C. After one week, light yellow crystals were isolated. M.p. 131 °C (dec.). Yield: 0.20 g (15%). $C_{17}H_{24}LiN_2Si$ (290.41): calcd. C 70.31, H 7.98, N 9.65; found C 68.73, H 8.38, N 9.23. NMR (C_6D_6): δ^1H = −0.05−0.42 ($SiMe_3$, 9 H), 3.74 (25%) + 3.78/4.07 (75%) [s, 4 H, (PhC*H*$_2$−)$_2$]; 6.93−7.35 (m, 10 H, Ph); δ^{13}C = −0.14, 0.70, 1.46, 4.80, 5.79 ($SiMe_3$); 49.95, 53.21, 65.60, 66.28, 57.91, 60.18, (Ph*C*H$_2$−); 125.96, 126.17, 126.43, 127.30, 128.29, 128.80, 129.08, 129.32, 129.56, 129.72, 130.22, 138.63, 139.17, 140.06, 140.63 (Ph); δ^{29}Si = 4.49, 4.98 (weak); −10.36, 4.00 (strong); δ^7Li = −1.83 (br), −2.27.

Formation of 1,2-Dibenzyl-3,3-dimethyl-1,2-diaza-3-sila-5-magnesacyclopentane (4) from the Reaction of 2 with Dibutylmagnesium: Dibutylmagnesium (1.3 mmol, 1.3 mL of a 1 M solution) in heptane was added to **2** (0.73 g, 2.55 mmol), dissolved in 25 mL of hexane. The solution became light yellow and after the solution was stored for one week at room temperature, colourless crystals were isolated. M.p. 167 °C (dec.). Yield: 0.31 g (40%). $C_{34}H_{44}Mg_2N_4Si_2$ (613.54): calcd. C 66.56, H 7.23, N 9.13; found C 67.68, H 7.65, N 8.75. NMR (C_6D_6): δ^1H = −0.02, 0.25 [d, 2 H, Si(CH$_3$)$_2$C*H*$_2$−], 0.27 [s, 6 H, Si(C*H*$_3$)$_2$CH$_2$−], 3.78, 3.81 (d, 2 H, PhC*H*$_2$−N−Mg), 4.14 (s, 2 H, PhC*H*$_2$−N−SiMe$_2$), 7.14−7.31 [m, 10 H, (*Ph*CH$_2$−N−)$_2$]; δ^{13}C = −0.50 [Si(CH$_3$)$_2$*C*H$_2$−], −0.18 [Si(*C*H$_3$)$_2$CH$_2$−], 49.88 (Ph*C*H$_2$−N−Mg), 53.17 (Ph*C*H$_2$−N−SiMe$_2$), 127.24−129.32 (6 resonances), 139.14, 140.04 (*i*-Ph); δ^{29}Si = 3.82 ($SiMe_3$); $^1J(^{29}Si^{13}C)$ = 57.6 Hz.

Acknowledgments

H. S. gratefully acknowledges financial support from the Fonds der Chemischen Industrie, BMBF and the Deutsche Forschungsgemeinschaft, as well as Chemetall for the donation of alkyllithium compounds.

[1] M. Veith, A. Altherr, H. Wolfanger, *Chem. Vap. Deposition* **1999**, *5*, 87−90.
[2] M. Veith, *Mat. Sci. For.* **2000**, 343−346; M. Veith, *Mat. Sci. For.* **2000**, 531−538.
[3] R. E. Mulvey, *Chem. Soc. Rev.* **1991**, *20*, 167−209.
[4] C. Schade, P. v. Ragué Schleyer, *Adv. Organomet. Chem.* **1987**, *27*, 169−209.
[5] M. Veith, *Chem. Rev.* **1990**, *90*, 3−16.
[6] C. Drost, C. Jäger, S. Freitag, U. Klingebiel, M. Noltemeyer, G. M. Sheldrick, *Chem. Ber.* **1994**, *127*, 845−947.
[7] U. Klingebiel, S. Dielkus, C. Drost, R. Herbst-Irmer, *Angew. Chem.* **1993**, *105*, 1689−1690, *Angew. Chem. Int. Ed. Engl.* **1993**, *32*, 1625; H. Nöth, H. Sachdev, M. Schmidt, H. Schwenk, *Chem. Ber.* **1995**, *128*, 105−113; B. Gemünd, H. Nöth, H. Sachdev, M. Schmidt, *Chem. Ber.* **1996**, *129*, 1335−1344; J. Knizek, I. Krossing, H. Nöth, T. Seifert, *Chem. Ber/Recueil* **1977**, *130*, 1053−1062.
[8] N. Metzler, H. Nöth, H. Sachdev, *Angew. Chem.* **1994**, *106*, 1837−1839, *Angew. Chem. Int. Ed. Engl.* **1994**, *33*, 1746−1748. K. Bode, U. Klingebiel, M. Noltemeyer, H. Witte-Abel, *Z. Anorg. Allg. Chem.* **1995**, *621*, 500−505.
[9] W. Uhl, J. Moltar, R. Koch, *Eur. J. Inorg. Chem.* **2000**, 2255−2262. H. Nöth, T. Seifert, *Eur. J. Inorg. Chem.* **1998**, 1931−1938.
[10] D. Cho, J. E. Park, B. J. Bae, K. Lee, B. Kim, J. T. Park, *J. Organomet. Chem.* **1999**, *592*, 162−167.
[11] D. W. Peters, M. P. Power, E. D. Bourret, J. Arnold, *Chem. Commun.* **1998**, 753−754.
[12] The obtained crystal fraction is not homogeneous and consists of light yellow rhombs and small orange platelets. A structure determination of these platelets could not be performed.
[13] R. West, M. Ishikawa, R. E. Bailey, *J. Am. Chem. Soc.* **1966**, *88*, 4448−4454.
[14] K. Bode, U. Klingebiel, *Adv. Organomet. Chem.* **1996**, *40*, 1−43.
[15] H. Sachdev, to be published.
[16] L. Barr, A. Kennedy, J. MacLellan, J. Moir, R. E. Mulvey, P. Rodger, *Chem. Commun.* **2000**, 1757−1758.
[17] M. Putzer, B. Neumüller, K. Dehnicke, *Z. Anorg. Allg. Chem.* **1998**, *624*, 1087−91. S. Simpson, R. Andersen, *Inorg. Chem.* **1981**, *20*, 3627−31.
[18] R. A. Bartlett, M. M. Olmstead, P. P. Power, *Inorg. Chem.* **1994**, *33*, 4800−4803.
[19] G. M. Sheldrick, University of Göttingen, **1993**.

Received August 12, 2001
[I01306]

The Reaction of Poly(chlorophosphazene)s with *p*-Aminophenol − Specific Formation of Aminophosphazenes with Terminal OH Groups and Aryloxyphosphazenes with Terminal NH_2 Groups

Gabino A. Carriedo,*[a] José. I. Fidalgo Martínez,[a] F. J. García Alonso,[a] E. Rodicio González,[a] and A. Presa Soto[a]

Keywords: Polymers / Inorganic polymers / Polyphosphazenes / *p*-Aminophenol

The outcome of the reaction of the bifunctional reagent *p*-aminophenol (HO-C_6H_4-NH_2) with the cyclic triphosphazene [$N_3P_3Cl_6$] is very dependent on the solvent, the temperature, and the proton abstractor. In THF at room temperature with K_2CO_3 the reaction is very slow and takes place only through the NH_2 group to give a mixture of aminophosphazenes, but in refluxing acetone with Cs_2CO_3 the reaction is fast and occurs through both the NH_2 and the OH groups leading to crosslinked products. The analogous reaction with the bis-spirocyclodichlorotriphosphazene [$N_3P_3Cl_2(O_2C_{12}H_8)_2$] ($O_2C_{12}H_8$ = 2,2′-dioxybiphenyl) is also dependent on the conditions, but is more selective. At room temperature in THF with K_2CO_3 the reaction gives mostly aminophosphazene derivatives, while in refluxing acetone with Cs_2CO_3 the known aryloxyphosphazene [$N_3P_3(OC_6H_4NH_2)_2(O_2C_{12}H_8)_2$] (**1**) is obtained exclusively. Accordingly, the reactions of *p*-aminophenol with high molecular weight poly(dichlorophosphazene) $[NPCl_2]_n$ in THF at room temperature in the presence of K_2CO_3, occur exclusively through the NH_2 groups without crosslinking, forming solutions of the aminophosphazene random copolymers $\{[NPCl_2]_{1-x}[NPCl(NHC_6H_4OH)]_x\}_n$ (**2a**) ($x < 1$) and $\{[NP(NHC_6H_4OH)_2]_{x-1}[NPCl(NHC_6H_4OH)]_{2-x}\}_n$ (**2b**) ($x > 1$) that carry terminal OH groups. The reaction of **2a** with NH_2Bu (Bu = *n*-butyl) gave the stable and soluble polymers $\{[NP(NHBu)_2]_{1-x}[NP(NHBu)(NHC_6H_4OH)]_x\}_n$ (**3**). Also, in agreement with the cyclic models, the reaction of *p*-aminophenol with the partially substituted copolymer $\{[NP(O_2C_{12}H_8)]_{0.8}[NPCl_2]_{0.2}\}_n$ occurs only at refluxing temperatures and in the presence of Cs_2CO_3, producing the poly(aryloxyphosphazene) derivative $\{[NP(O_2C_{12}H_8)]_{0.8}[NP(OC_6H_4NH_2)_2]_{0.2}\}_n$ (**4**) possessing terminal NH_2 groups, or, if the chlorine substitution is completed with phenol, the analogous polymer $\{[NP(O_2C_{12}H_8)]_{0.8}[NP(OC_6H_5)(OC_6H_4NH_2)]_{0.2}\}_n$ (**5**).

(© Wiley-VCH Verlag GmbH, 1 Weinheim, Germany, 2002)

Introduction

Poly(phosphazene)s,[1] which consist of chains of -N=PX_2- units, are usually prepared by chlorine substitution in the parent poly(dichlorophosphazene) $[NPCl_2]_n$. Many aryloxyphosphazenes of the type $[NP(OC_6H_4R)_2]_n$ can therefore be synthesized by reacting $[NPCl_2]_n$ with phenoxides of the type $NaOC_6H_4R$. However, this method may not be effective in some special cases, for example with bifunctional reagents,[2] or with phenoxides carrying R groups that can also react with the P−Cl bonds, as these reactions could result in crosslinking.[3] The introduction of R groups that could incorporate interesting chemical reactivity to the phosphazenes polymers therefore presents several challenges frequently requiring protection and deprotection synthetic steps.[3]

One of the reactive groups with potential interest is R = NH_2. Although there are reports describing the incorporation of -$OC_6H_4NH_2$ functions to cyclic triphosphazenes directly from $NaOC_6H_4NH_2$,[4] the method most widely used is based on the formation of an -NO_2 derivative, followed by its catalytic reduction to the amine.[3,5−9] Other methods include the hydrolysis of an acetamido precursor.[10]

Previously, we have shown[11] that chlorine substitution reactions in phosphazenes may be carried out using one equivalent of phenol HOC_6H_4R in the presence of M_2CO_3 (M = K or Cs), and that the poly(dichlorophosphazene) $[NPCl_2]_n$ reacts with the bifunctional reagent 2,2′-(HO)C_6H_4-C_6H_4(OH) and K_2CO_3 without crosslinking, affording the phosphazene polymer $[NP(O_2C_{12}H_8)]_n$.[12a] We used the same type of direct reaction with binaphthol and produced the chiral poly(binaphthoxyphosphazene)s.[12b]

The above observations led us to investigate the direct reaction of the bifunctional *p*-aminophenol ($HOC_6H_4NH_2$) with chlorophosphazenes and Cs_2CO_3, and try to activate the OH group selectively with the aim of obtaining uncrosslinked poly(phosphazene)s with terminal -NH_2 groups

[a] Departamento de Química Orgánica e Inorgánica, Facultad de Química, Universidad de Oviedo
33071 Oviedo, Spain
Fax: (internat.) +34-985/103-446
E-mail: gac@sauron.quimica.uniovi.es

in one step. However, we found that the aminophenol reacts either through the OH or the NH_2 depending on the nature of the chlorophosphazenes and on the reaction conditions.

Results and Discussion

In order to obtain information about the reactivity of *p*-aminophenol ($HOC_6H_4NH_2$) towards chlorophosphazenes under various conditions, we first studied its reactions with two cyclic models: the unsubstituted hexachlorocyclotriphosphazene [$N_3P_3Cl_6$] and the partially substituted spirocyclic derivative bis(2,2′-dioxybiphenyl)dichlorocyclotriphosphazene [$N_3P_3Cl_2(O_2C_{12}H_8)_2$].[12a]

The reaction of $HOC_6H_4NH_2$ (6.1 equiv.) with [$N_3P_3Cl_6$] at room temperature in THF and using K_2CO_3 as a proton abstractor proceeded very slowly and exclusively through the NH_2 group. After 11 days the ^{31}P NMR spectrum of the THF solution showed the presence of two main products (Table 1), which, by comparison with known substituted cyclic aminophosphazenes,[13] could be identified as the geminally tetrasubstituted [$N_3P_3Cl_2(HNC_6H_4OH)_4$] and the hexasubstituted [$N_3P_3(HNC_6H_4OH)_6$] derivatives (for the related species [$N_3P_3(NHC_6H_4OMe)_6$] the value is δ = 6.4). No signals attributable to aryloxyphosphazenes were detected (the well-known [$N_3P_3(OC_6H_4NH_2)_6$] derivative[1d] has a singlet near δ = 11 in THF[5]).

Table 1. ^{31}P NMR spectroscopic data (δ) for the cyclic phosphazenes in THF solution; the data given are the center of the multiplets of the A_2 (pseudo doublet) and M (pseudo triplet) part of the A_2M spin systems, or the singlet of the A_3 spin systems

Derivative	A_2	M	A_3
[$N_3P_3Cl_2(HNC_6H_4OH)_4$]	2.1	23.6	
[$N_3P_3(HNC_6H_4OH)_6$]			5.5
[$N_3P_3Cl_2(O_2C_{12}H_8)_2$]	20.0	28.9	
[$N_3P_3Cl(NHC_6H_4OH)(O_2C_{12}H_8)_2$]	26.5	8.0	
[$N_3P_3(NHC_6H_4OH)_2(O_2C_{12}H_8)_2$]	28.3	2.4	
[$N_3P_3Cl(OC_6H_4NH_2)(O_2C_{12}H_8)_2$]	23.9[a]		
[$N_3P_3(OC_6H_4NH_2)_2(O_2C_{12}H_8)_2$]	26.9	11.8[b]	

[a] This A_2B system shows a complex signal centered at δ = 23.9. In acetone it appears at δ = 24.8. [b] In acetone at δ = 27.5 and 12.6, and in [D_6]DMSO at δ = 26.7 and 12.0.

This conclusion was corroborated by the ^{13}C NMR spectrum (**a** in Figure 1) that showed the presence of free *p*-aminophenol and sharp peaks for the C_6H_4 group at δ = 152.5 (one carbon atom), 133.2 (one carbon atom), 121.1 (two carbon atoms), and 115.0 (two carbon atoms). As will be further discussed below, comparison of these data with those corresponding to various phenols and phosphazene derivatives (Table 2), unambiguously demonstrates that they correspond to aminophosphazenes and not to aryloxyphosphazenes.

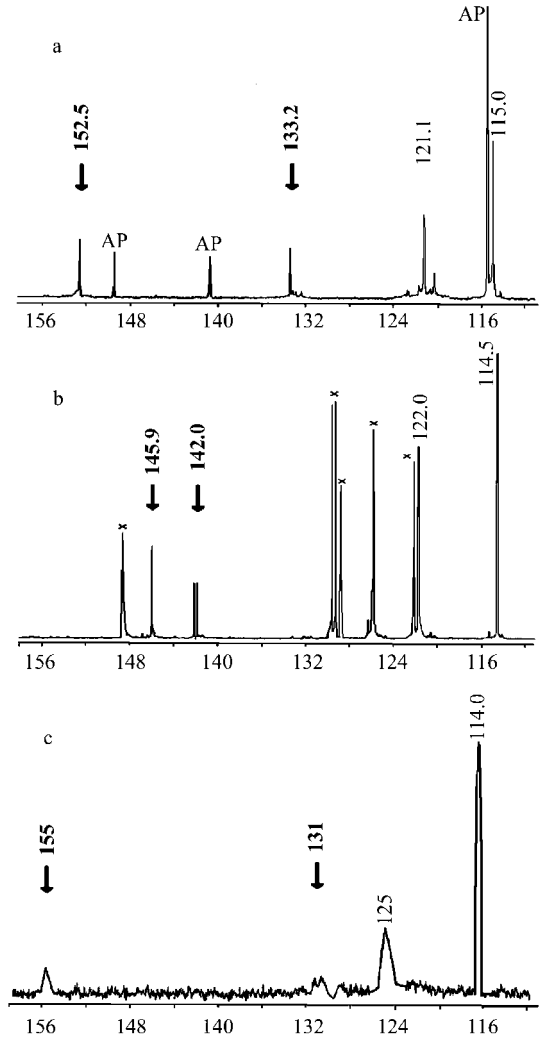

Figure 1. ^{13}C NMR spectra of: 1a) aminophosphazenes formed in the reaction between [$N_3P_3Cl_6$] and *p*-aminophenol in THF at room temperature with K_2CO_3 (AP = signals of the free *p*-aminophenol); 1b) [$NP(OC_6H_4NH_2)_2(O_2C_{12}H_8)_2$] (**1**) in THF (*x* = peaks corresponding to the carbon atoms of the $O_2C_{12}H_8$ group); 1c) THF solution of polymer **2a** (*x* = 0.4)

The data in Table 2 show that when a *para*-disubstituted benzene derivative of the type H-B-C_6H_4-R reacts with a phosphazene P−Cl bond to form -NP-B-C_6H_4-R units, the chemical shift of the carbon bonded to B decreases by ca. 5 ppm, while that of the carbon bonded to R increases by ca. 3 ppm (tendencies consistent with the data for the molecules H-B-C_6H_4-R and those of their E-B-C_6H_4-R derivatives, where E is an electron-withdrawing group[17]). Therefore, starting from *p*-aminophenol $H_2NC_6H_4OH$, for which the weak carbon atom peaks appear (in THF) at δ = 149.2 (C bonded to the OH) and 140.5 (C bonded to the NH_2), the formation of $NP(NHC_6H_4$-OH) units should give two well-separated peaks close to δ = 153 and 135, in complete agreement with the two secondary carbon signals of the products mentioned above, while for the formation of $NP(OC_6H_4$-$NH_2)$ units two very close peaks near δ = 143 would have been expected.

Table 2. ^{13}C NMR chemical shifts of the ring carbon atoms corresponding to the HB-C_6H_4-R molecules and to the A-C_6H_4-B groups bonded to poly(phosphazene); all the spectra were recorded in $CDCl_3$ unless otherwise stated

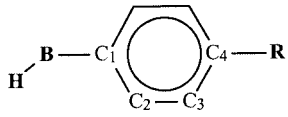

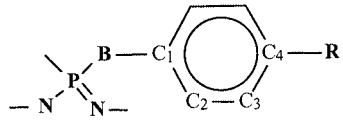

BH	R	C^1	C^2	C^3	C^4	ref.	C^1	C^2/C^3	C^4	ref.
OH	H	155	115.5	129.8	121.1	23, 24	151.6	121.2/128.8	123.6	25, 26
OH	Me	152.9	115.3	130.2	130.2	23, 24	149.6	121/129.1	132.1	25, 26, 16
OH	OMe	149.7	116.3	115.2	153.5	23, 24	146.1	122.8/114.4	156	27[a]
OH	CN	161.6	116.4	134.2	101.1	23[b]	155	122/134	108	28
OH	F	151.1	116.6	116.3	157.7	24	148	123.1/116.5	160.3[c]	29[a]
OH	Cl	153.8	116.8	129.6	126	23, 24	150.4	122.9/130.2	130.8	29[a]
OH	Br	154.3	117.3	132.6	113.1	23	149.8	122.1/132.2	118	30
OH	I	154.3	117.6	138.2	83.2	this work	150.8	120.2/138.6	89.1	30[d]
OH	C(O)OPr	161.1	115.5	132	122	23	154	120/130.8	126.8	26
OH	PPh_2	157.4	116.4	136.5	128.5	31	152	121.7/ 135.2	134.6 (hidden)	31
SH	Br	132.1	129.9	131.1	119.5	23	128.4	137.3/133	124.4	32
NH_2	H	146.5	115	129.3	118.4	23, 24	141.8	118.6/129.5	121.2	16

[a] Solvent not available. [b] [D_6]DMSO. as solvent. [c] J_{C-F} = 250 Hz. [d] 1-Methyl-2-pyrrolidinone (NMP) as solvent.

When carried out in refluxing acetone with Cs_2CO_3 as proton abstractor, the reaction of *p*-aminophenol with $[N_3P_3Cl_6]$ was much faster, although in this case both the NH_2 and the OH groups were activated. After one hour the ^{31}P NMR spectrum of the resulting solution showed very broad and complex signals, suggesting polymerized and crosslinked products, among which it was possible to detect some of the sharp peaks corresponding to the aminophosphazenes mentioned above, together with others closer to those expected for aryloxyphosphazenes.

The reaction of *p*-aminophenol (2.1 equivalents) with the dichlorophosphazene cyclic model $[N_3P_3Cl_2(O_2C_{12}H_8)_2]$ was also very dependent on the conditions but was much more selective. In THF at room temperature with K_2CO_3, therefore, the process was very slow and occurred selectively, but not exclusively, through the NH_2 group. After 20 days the ^{31}P NMR spectrum showed, in addition to the starting dichlorophosphazene (ca. 14 mol %), the presence of a mixture of $[N_3P_3Cl(NHC_6H_4OH)(O_2C_{12}H_8)_2]$ (65%), $[N_3P_3(NHC_6H_4OH)_2(O_2C_{12}H_8)_2]$ (12%), $[N_3P_3Cl(OC_6H_4NH_2)(O_2C_{12}H_8)_2]$ (5%), and another very weak A_2M spin system with the pseudo-triplet at δ = 13.1 and the pseudo-doublet at δ = 26.4, which could be attributed to the mixed species $[N_3P_3(NHC_6H_4OH)(OC_6H_4NH_2)(O_2C_{12}H_8)_2]$ (1%). The known compound[9] $[N_3P_3(OC_6H_4NH_2)_2(O_2C_{12}H_8)_2]$ (**1**) was not present (see below).

Again, this result was supported by the ^{13}C NMR spectrum of the THF solution, which, in addition to the signals of free aminophenol and those for the $O_2C_{12}H_8$ groups, showed the two expected sharp peaks at δ = 152.4 and 133.3 indicative of the $NP(NHC_6H_4OH)$ units, and two other much weaker signals at δ = 145.5 and 142.3 (doublet) corresponding to the aryloxyphosphazene derivatives.

In contrast, the reaction of *p*-aminophenol with $[N_3P_3Cl_2(O_2C_{12}H_8)_2]$ in refluxing acetone and using Cs_2CO_3 as proton abstractor gave first the aryloxyphosphazene intermediate $[N_3P_3Cl(OC_6H_4NH_2)(O_2C_{12}H_8)_2]$ (see Table 1), and finally the known bis(*p*-aminophenoxy)-containing compound $[N_3P_3(OC_6H_4NH_2)_2(O_2C_{12}H_8)_2]$ (**1**) (Scheme 1), which was isolated in good yield. This compound had been obtained previously by hydrogenation of the $-OC_6H_4NO_2$ derivative.[9] No products from the reac-

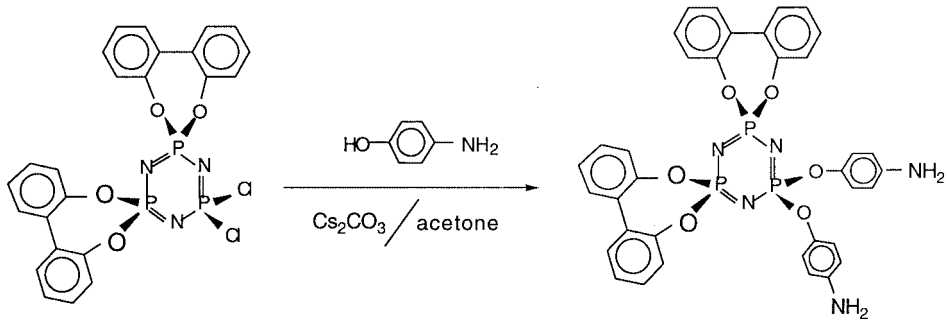

1

Scheme 1

tion between the P−Cl bonds and the NH_2 groups were observed.

As expected, the ^{13}C NMR spectrum of the *p*-hydroxyaminophosphazene[9](**1**) in THF (see **b** in Figure 1), showed signals for the weak carbon atoms of the C_6H_4 groups at $\delta = 145.9$ and 142.0 (doublet with $J_{P,C} = 7.3$ Hz) (see the Exp. Sect. for NMR spectroscopic data in [D$_6$]DMSO). These data confirmed all the conclusions outlined above and also showed that ^{13}C NMR spectroscopic data are very useful in distinguishing between NP-NHC_6H_4-OH and NP-OC_6H_4-NH_2 units.

The selectivity of the reactions of *p*-aminophenol with $[N_3P_3Cl_6]$ and $[N_3P_3Cl_2(O_2C_{12}H_8)_2]$ under the different conditions used in this work is totally consistent with the experimental knowledge accumulated from the substitution of chlorine atoms in chlorophosphazenes by phenols and amines.

We have established[11] that in refluxing acetone and in the presence of cesium carbonate the reactions of the phenols RC_6H_4OH with chlorocyclophosphazenes are very fast. With K_2CO_3 as proton abstractor they are slower, and in THF as solvent are much slower. Logically, at room temperature they are much slower than at reflux. Also, the phenols where R is an electron-donating group react more slowly. Therefore, in the case of *p*-aminophenol the reactions through the phenolic OH group should be extremely slow in THF at room temperature with K_2CO_3, but much faster in refluxing acetone and with Cs_2CO_3.

The reactions through the NH_2 group are also dependent on the temperature, although they are more affected by steric factors, less sensitive to the solvent and, as expected, they are almost independent of the alkaline carbonate used as proton abstractor. Consistently, the reaction with $[N_3P_3Cl_6]$ in THF at room temperature with K_2CO_3 occurs only through the NH_2 group, i.e., the aminophosphazenes are the expected kinetic products. In refluxing acetone with Cs_2CO_3 the OH becomes sufficiently activated and the *p*-aminophenol reacts through both groups leading to cyclomatrix products. The same effects operate in the case of the $[N_3P_3Cl_2(O_2C_{12}H_8)_2]$ derivative, although this compound is less reactive towards substitution than the $[N_3P_3Cl_6]$. Therefore, in THF at room temperature with K_2CO_3 a very slow reaction through the NH_2 group is the main process observed, whereas in refluxing acetone with Cs_2CO_3 the reaction through the OH group becomes sufficiently fast to give the aryloxyphosphazene derivatives exclusively (again under kinetic control).

The overall results from the reactivity of *p*-aminophenol with the cyclic models suggested to us the possibility of synthesizing high molecular weight poly(phosphazene)s with terminal *p*-hydroxyphenylamino or *p*-aminophenoxy groups in one step from *p*-aminophenol and poly(chlorophosphazene)s.

We observed that the reaction of $[NPCl_2]_n$ with x equivalents of $HOC_6H_4NH_2$ per $NPCl_2$ unit ($x < 1$), in THF at room temperature with $1.5x$ equivalents of K_2CO_3 (i in Scheme 2) occurred exclusively through the NH_2 groups, producing solutions of the random copolymers with composition $\{[NPCl_2]_{1-x}[NPCl(NHC_6H_4OH)]_x\}_n$ (**2a**) [$x = 0.1$, 0.2, 0.3, 0.4, 0.6]. Above $x = 1$ the copolymers had the formula $\{[NP(NHC_6H_4OH)_2]_{x-1}[NPCl(NHC_6H_4OH)]_{2-x}\}_n$ (**2b**) ($x > 1$), although, even when using a large excess of the *p*-aminophenol, it was not possible to reach substitution degrees higher than $x = 1.2$, as beyond that point the substitution process became very slow.

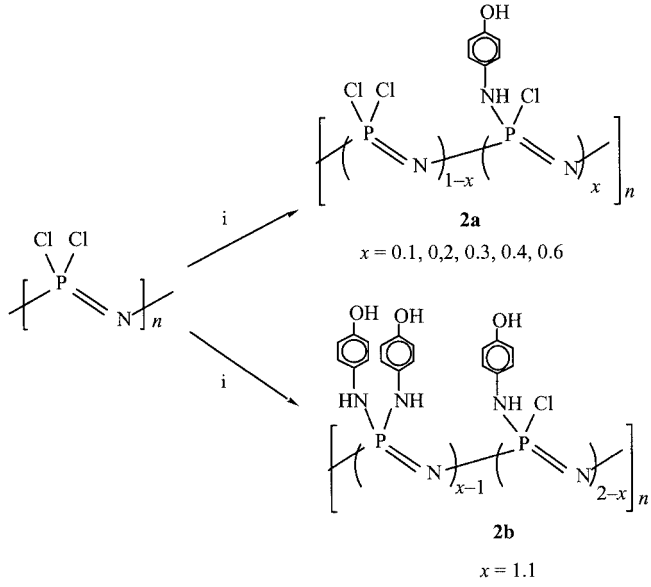

Scheme 2. i. nx $HOC_6H_4NH_2$ + K_2CO_3/THF, room temperature

The reaction was faster at reflux, but in this case gave insoluble materials, indicating the activation of the OH groups of the aminophenol and their concomitant crosslinking by reaction with the P−Cl bonds. Consistently, we observed that crosslinking could be favored by working with more concentrated solutions of the reactants, by using a large excess of the alkaline carbonate, or by using Cs_2CO_3 instead (as mentioned previously,[11] this reagent makes the reactions of phenols with chlorophosphazenes much faster). Moreover, solutions of the polymers **2a** are only moderately stable at room temperature, especially in the presence of carbonates, giving rise to gelatinous precipitates on standing for several days. We also checked that on carrying out the reaction in the absence of the K_2CO_3 only half the amount of *p*-aminophenol was incorporated into the polymers **2**, the other half reacting as a proton abstractor to give the ammonium salt.

The ^{31}P NMR spectra of THF solutions of the polymers **2** were consistent with their formulation. Thus, for example, for **2a** ($x = 0.4$) the spectrum (Figure 2) shows three signals: a sharp peak at $\delta = -17.4$, corresponding to the fraction of the $NPCl_2$ groups surrounded by two other $NPCl_2$ units and far from the $NPCl(NHC_6H_4OH)$ units, a very broad signal with a maximum at ca. $\delta = -25$, corresponding to the $NPCl_2$ groups surrounded by two $NPCl(NHC_6H_4OH)$ units; and a broad signal centered at ca. $\delta = -15$, due to the $NPCl(NHC_6H_4OH)$ units. For the other copolymers **2a** the spectra changed depending on the value of x. Thus, the

signal attributable to $NPCl(NHC_6H_4OH)$ varied from $\delta = -15$, when placed between two $NPCl_2$ groups, to $\delta = -7$ for those placed inside two other $[NPCl(NHC_6H_4OH)]$ units. Taking into account that the expected mechanism for the reaction of chlorophosphazenes with aromatic primary amines is non-geminal,[14,15] the fraction of $[NP(NHC_6H_4OH)_2]$ units can be considered negligibly small in **2a**. For **2b** ($x = 1.1$) the corresponding broad signal appeared at $\delta = -13$, in agreement with the reported value for similar bis-aminophosphazenes.[16]

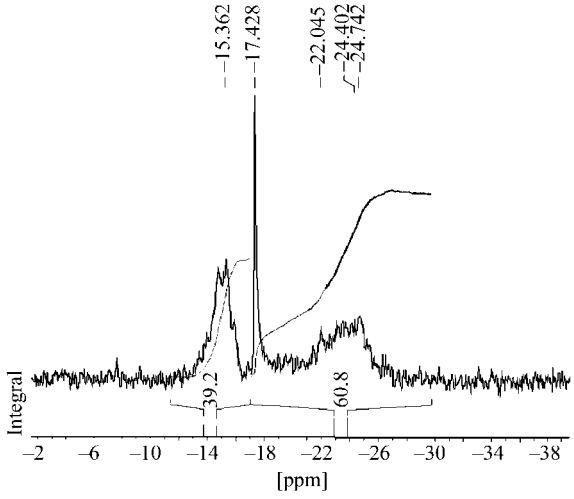

Figure 2. ^{31}P NMR spectrum of **2a** ($x = 0.4$) in THF (see text)

A very valuable proof of the nature of the polymers **2** came from the ^{13}C NMR spectra of the THF solutions (Figure 1c), which showed peaks at $\delta = 155$ (one carbon atom), 131 (one carbon atom), 125 (two carbon atoms) and 116 (two carbon atoms) for the C_6H_4 group, well in agreement with the expected values for NP-NHC_6H_4-OH units and not for NP-OC_6H_4-NH_2 units (see discussion above and Figure 1).

The formation of aminophosphazenes **2** instead of the aryloxyamino derivatives in the reactions of Scheme 2 was also supported by other chemical observations. We found that while the poly(dichlorophosphazene) reacts quickly at room temperature in THF with $NH_2C_6H_4OMe$ and K_2CO_3 to give very similar ^{31}P NMR spectra to those for **2** (the substitution was also incomplete), no reaction occurs with phenol HOC_6H_5 under the same conditions (only in the presence of cesium carbonate and refluxing for 40 hours is the totally substituted polymer obtained[11]). This demonstrates that under the conditions of Scheme 2, the *p*-aminophenol cannot react with $[NPCl_2]_n$ by the OH groups and, therefore, the products observed must be aminophosphazenes.

Attempts to use the polymers **2** as precursors for the synthesis of phosphazene copolymers possessing terminal OH groups by reacting them with *p*-substituted phenols (HOC_6H_4R) and cesium carbonate at room temperature were unsuccessful as the replacement of the chlorines by the corresponding phenoxy groups was far too slow to go to completion; heating at reflux led to insoluble products with residual chlorine contents close to 5% by weight.

As described in other cases,[18] however, the polymers **2a** could be stabilized by completing the chlorine substitution with *n*-butylamine (NH_2Bu) (see Scheme 3) to obtain the copolymers $\{[NP(NHBu)_2]_{1-x}[NP(NHBu)(NHC_6H_4OH)]_x\}_n$ (**3**) as stable solids. The chlorine content was very low (0.25%), confirming the complete substitution and ruling out the presence of quaternized ammoniun chlorides. The solubility decreased rapidly as x increased, and therefore polymers with $x > 0.3$ could not be prepared. Moreover, although soluble in THF when freshly prepared, their solubility decreases after some time in the solid state. Occasionally, the solid obtained after the first precipitation step in water (see Exp. Sect.) was sparingly soluble in THF. As the numbers of P−Cl bonds present in the substituted products is negligible, these effects may be attributed to the formation of a three-dimensional net of H-bonding interactions.

All the spectroscopic data for **3a** ($x = 0.3$; see Exp. Sect.) were in agreement with the proposed structure. Thus, the IR spectra showed, together with the expected phosphazene absorptions, a broad intense band centered at 3300 cm^{-1} due to all the -PNHR- units,[13,14,19] and two bands at 1515 and 827 cm^{-1} indicative of the *p*-disubstituted -C_6H_4- group. The latter are less intense in the polymers **3** with $x = 0.1$. The band of the terminal OH group was hidden under the broad absorption of the -PNH- group.

Significantly, as discussed above, the $^{13}CNMR$ spectrum showed, along with the peaks of the NPNHBu group,[18] signals at $\delta = 152.1$ and 136.5 as expected for the groups -$NPNHC_6H_4OH$, the intensity of which increased with x.

The molecular weight (M_w) of **3a** is of the order of 2×10^5, showing the expected degradation of the chains during reaction with the amine.[18] The thermogravimetric analysis

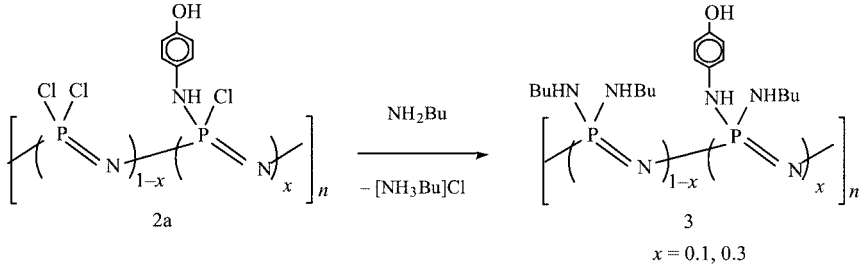

Scheme 3

(TGA) of **3** showed a decomposition beginning near 70 °C (see Exp. Sect.). This rather low thermal stability may be due, as in the case of other aminophosphazenes,[33] to the elimination of volatile amines. Surprisingly, no well-defined glass transition (T_g) was detected in the differential scanning calorimetry (DSC) curves from −100 °C to 150 °C.

In contrast to the case of $[NPCl_2]_n$, the partially substituted phosphazene copolymer $\{[NP(O_2C_{12}H_8)]_{0.8}[NPCl_2]_{0.2}\}_n$ [12] did not react with *p*-aminophenol at room temperature in the presence of K_2CO_3. Refluxing and the use of Cs_2CO_3 were necessary, although under those conditions, and in agreement with the cyclic models, the reaction occurred exclusively through the OH group to give the aryloxyphosphazene copolymer $\{[NP(O_2C_{12}H_8)]_{0.8}[NP(OC_6H_4NH_2)_2]_{0.2}\}_n$ (**4**) (Scheme 4). Long reflux times and various successive additions of aminophenol were, however, necessary to reach a product with chlorine contents below 0.1%. As a result, the M_w of **4** was only 2.5×10^5, and the yield was low (21%). Moreover, the polymers isolated from different experiments showed that the content of the $NP(OC_6H_4NH_2)_2$ units could be not be perfectly controlled, varying between 0.1 and 0.2, and that on reducing the reaction time with aminophenol the M_w of the products was higher, approaching 8×10^5.

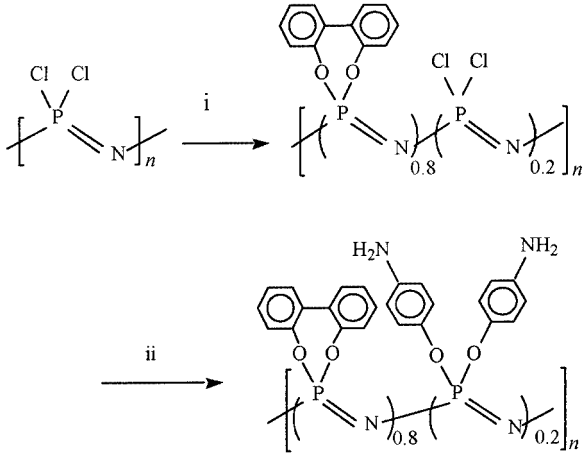

4

Scheme 4. i: HO-C_6H_4-C_6H_4-OH + K_2CO_3 in refluxing THF; ii: HO-C_6H_4-NH_2 + C_2CO_3 in refluxing THF

Clearly, prolonged refluxing in the presence of an excess of aminophenol caused extensive reduction of the chain length, which can be explained by taking into account that the aryloxides may be replaced by anilide ions in phosphazenes,[20] and that the poly(arylaminophosphazene)s are labile to nucleophilic cleavage.[21]

Our attempts to increase the $NP(OC_6H_4NH_2)_2$ units to 40% in the reaction of Scheme 4 resulted in the formation of brown insoluble materials with residual chlorine values of around 0.3% by weight. The known phosphazene polymers $\{[NP(OC_6H_5)_2]_{1-x}[NP(OC_6H_4NH_2)(OC_6H_5)]_x\}_n$ with $x = 0.3$ and 0.7, which have been prepared in high yields by reduction of a *p*-nitrophenoxy precursor,[5,6] are soluble.[5] Therefore, although the presence of the biphenoxy groups may reduce the solubility, it is likely that the insolubility of polymers of type **4** with more than 20% of $NP(OC_6H_4NH_2)_2$ units is due only to crosslinking side reactions during the second step of its synthesis.

These considerations led us to design the synthesis of the polymer $\{[NP(O_2C_{12}H_8)]_{0.8}[NP(OC_6H_5)(OC_6H_4NH_2)]_{0.2}\}_n$ (**5**), shown in Scheme 5, by first forming the intermediate $\{[NP(O_2C_{12}H_8)]_{0.8}[NPCl(OC_6H_4NH_2)]_{0.2}\}_n$ using the precise amount of aminophenol to avoid degradation, and then completing the substitution with HOC_6H_5. The product, isolated in 60% yield, contained only 0.14% residual chlorine and was a stable and soluble white polymer with an M_w of 9×10^5.

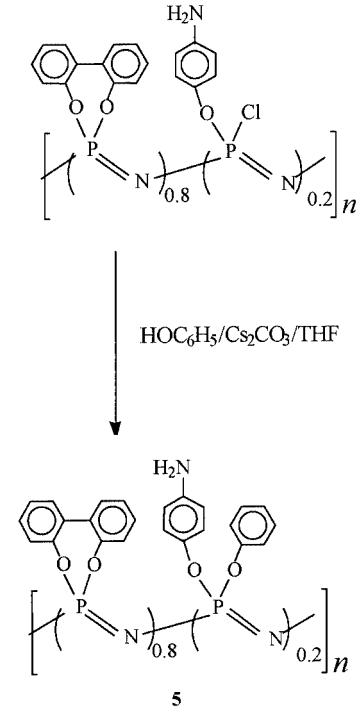

5

Scheme 5

All the analytical and spectroscopic properties of the polymers **4** and **5** were consistent with their proposed formulation (see Exp. Sect.). The IR spectra showed the two typical absorptions near 3450 and 3370 cm^{-1} (and another one at 1624 cm^{-1}) characteristic of the terminal NH_2 groups,[9] (also present in the cyclic model **1**) while no absorption for terminal OH was observed.

The ^{31}P NMR spectra showed a broad signal at around $\delta = -6$, characteristic of the skeletal phosphorus atoms of the $[NP(O_2C_{12}H_8)]$ units, which, as discussed elsewhere,[12] shows that the P atoms are part of a seven-membered ring, and a signal near $\delta = -19$ belonging to the $[NP(OC_6H_4NH_2)_2]$ or $[NP(OC_6H_5)(OC_6H_4NH_2)]$ units (for the known polymers $\{[NP(OC_6H_5)_2]_{1-x}[NP(OC_6H_4NH_2)_x]\}_n$, the chemical shift is $\delta = -19$[5,6]). The relative intensities of the two signals agreed well with the averaged formula of the copolymers, and no signals in the region of $\delta = -15$, corresponding to aminophosphazene units $[NP(NHC_6H_4OH)_2]$,[16] were observed.

The ^1H NMR spectra showed a broad signal near δ = 5, also present in the spectrum of **1**, that may be assigned to the NH_2 protons.[9] For the NH protons of the $[NP(NHC_6H_4R)_2]$ units the signal is expected at ca. δ = 3.[19]

The ^{13}C NMR spectrum showed broad peaks at δ = 145 and 142 (in $[D_6]$DMSO), which, as discussed above, correspond to aryloxyphosphazenes with pendant amino groups and not to aminophosphazenes with pendant OH groups. The weak broad signal at δ = 152 unambiguously corresponds to the phenoxy groups, and the intense one at δ = 148 to the abundant biphenoxy groups present in the chains.[12a]

The thermal stability of **4** and **5**, as measured by TGA, is only moderate. Thus, a slow decomposition begins at ca. 100 °C (**4**) or 50 °C (**5**); the residue left at 800 °C was of the order of 50% in both cases (see Exp. Sect.). As in the case of other aryloxyphosphazenes, the thermal decomposition occurs with elimination of volatile cyclic phosphazenes; other organic products also formed.

Because of the presence of dioxybiphenyl phosphazene units and polar NH_2 terminal groups it was expected that the polymers **4** and **5** should have high T_g values. In fact the DSC curves of both polymers showed very well-defined heat capacity steps with T_g = 155 °C for **4** and T_g = 140 °C for **5**.

Conclusion

Polymeric chlorophosphazenes may be selectively reacted in THF with substoichiometric amounts of *p*-aminophenol under kinetic control either at the OH or NH_2 groups, depending on the conditions. The reaction with poly(dichlorophosphazene) at room temperature and with K_2CO_3 occurs exclusively at the NH_2 group producing aminophosphazenes with terminal OH groups. However, if the available P−Cl bonds are not abundant, as is the case with partially substituted aryloxyphosphazene-chlorophosphazene copolymers, the process is very slow at room temperature, and on carrying out the reaction at reflux and in the presence of Cs_2CO_3 it occurs exclusively at the OH of the *p*-aminophenol, producing aryloxyphosphazenes with pendant NH_2 groups. These observations have led to the designed synthesis of phosphazene copolymers containing NHC_6H_4OH or $OC_6H_4NH_2$ groups directly from *p*-aminophenol.

Experimental Section

General Remarks: K_2CO_3 and Cs_2CO_3 were dried at 140 °C prior to use. Acetone was distilled from anhydrous $CaSO_4$. THF was treated with KOH and distilled twice from Na in the presence of benzophenone. Petroleum ether refers to that fraction with a boiling point in the range 60−65 °C. The diphenol $HOC_6H_4C_6H_4OH$ and *p*-aminophenol $NH_2C_6H_4OH$ were used as purchased (Aldrich). Butylamine was distilled from CaH_2. Hexachlorocyclotriphosphazene $[N_3P_3Cl_6]$ (Fluka) was purified from hot petroleum ether and dried under vacuum. The cyclic phosphazene $[N_3P_3Cl_2(O_2C_{12}H_8)_2]$ was prepared as described elsewhere.[12a] The starting polymer $[NPCl_2]_n$ was prepared as described by Magill et al.[22] All the reactions were carried out under dry nitrogen.

The IR spectra were recorded with a Perkin−Elmer Paragon 1000 spectrometer. NMR spectra were recorded on Bruker AC-200 and AC-300 instruments. ^1H and $^{13}C\{^1H\}$ NMR are given in δ relative to TMS. $^{31}P\{^1H\}$ NMR are given in δ relative to external 85% aqueous H_3PO_4. Coupling constants are in Hz. C, H and N analyses were performed with a Perkin−Elmer 240 microanalyzer. Cl analyses were performed by Galbraith laboratories. Unless stated otherwise, the analytical data given for the cyclic phosphazenes correspond to the isolated reaction products without purification. GPC were measured with a Perkin−Elmer apparatus equipped with a model LC 250 pump, a model LC 290 UV, and a model LC 30 refractive index detector. The samples were eluted with a 0.1wt.-% solution of tetra-*n*-butylammonium bromide in THF through Perkin−Elmer PLGel (Guard, 10^5, 10^4 and 10^3 Å) at 30 °C. Approximate molecular weight calibration was obtained using polystyrene standards having narrow molecular weight distributions. T_g values were measured with a Mettler DSC 300 equipped with a TA 1100 computer. TGA were performed on a Mettler TA 4000 instrument. The polymer samples were heated at a rate of 10 °C/min from ambient temperature to 800 °C under a constant flow of nitrogen.

$[N_3P_3(OC_6H_4NH_2)_2(O_2C_{12}H_8)_2]$ (1): $NH_2C_6H_4OH$ (0.33 g, 3.02 mmol) and Cs_2CO_3 (1.59 g, 4.88 mmol) were added to a solution of $[N_3P_3Cl_2(O_2C_{12}H_8)_2]$ (0.7 g, 1.22 mmol) in acetone (40 mL) and the mixture was refluxed with stirring for 19 hours to give a brown mixture. The volatile components were evaporated to dryness and the residue was washed successively with 0.5 M aqueous NaOH (3 × 50 mL) and water (2 × 50 mL). The residue was then dissolved in acetone, dried with solid anhydrous Na_2SO_4, filtered, and the solvents evaporated. The pale brown solid was washed with hexane (2 × 40 mL) and dried under vacuum. Yield: 0.78 g (88.9%). $C_{36}H_{28}N_5O_6P_3$ (719.56): calcd. C 60.1, H 3.92, N 9.73; found C 59.4, H 3.95, N 9.15. IR (KBr): $\tilde{\nu}$ = 3437 w, 3341 w (NH_2), 1625 (NH_2), 1230 s, 1173 vs (N=P), 1271 m, 1093 m (POC) cm^{-1}. $^{31}P\{^1H\}$ NMR ($[D_6]$DMSO): δ = 12.02 $[(POC_6H_4NH_2)_2]$, 26.7 [A_2M system, J_{AM} = 90 Hz, $P(O_2C_{12}H_8)$]. ^1H NMR ($[D_6]$DMSO): δ = 7.65 (d, *J* = 7.5, 4 H), 7.51 (dd, *J* = 7.4, 4 H), 7.42 (dd, *J* = 7.5, 4 H), 7.16 (d, *J* = 7.9, 4 H) ($O_2C_{12}H_8$), 6.96 (d, 4 H), 6.63 (d, *J* = 8, 4 H, OC_6H_4-N), 5.10 (br. s, NH_2). $^{13}C\{^1H\}$ NMR ($[D_6]$DMSO): δ = 147.2 (t), 130.1, 129.7, 127.9, 126.4, 121.6 ($O_2C_{12}H_8$), 146.4, 140.1 (d, $J_{P,C}$ = 7.3), 121.1 (d, $J_{P,C}$ = 4.1), 114.2 ($OC_6H_4NH_2$).

THF Solutions of $\{[NPCl_2]_{1-x}[NPCl(NHC_6H_4OH)]_x\}_n$ (2a) ($x < 1$), $\{[NP(NHC_6H_4OH)_2]_{x-1}[NPCl(NHC_6H_4OH)]_{2-x}\}_n$ (2b) ($x > 1$): $NH_2C_6H_4OH$ (0.94*x* g, 8.6*x* mmol) and K_2CO_3 (1.78*x* g, 12.9*x* mmol) were added to a solution of $[NPCl_2]_n$ (1 g, 8.6 mmol) in THF (200 mL) and the mixture was mechanically stirred for 10 hours ($x < 1$) or 40 hours ($x > 1$) at room temperature.

The ^{31}P NMR spectrum of the solutions of **2a** showed two groups of signals having maxima that depended on *x*, one in the region of δ = −25 to −17 ($NPCl_2$) and the other in the range δ = −15 to −7 [$NPCl(NHC_6H_4OH)$] with relative intensities (1 − *x*):*x*. For **2b** (x = 1.1) the ^{31}P NMR spectra showed a broad signal at δ = −13 attributable to $[NP(NHC_6H_4OH)_2]$ besides the [$NPCl(NHC_6H_4OH)$] signal at δ = −7.

The ^{13}C NMR of the solutions showed peaks at δ = 155, 131, 125 and 116.

The solutions were unstable on standing for several days, especially if heated, giving rise to a gelatinous precipitate.

$\{[NP(NHBu)_2]_{0.7}[NP(NHBu)(NHC_6H_4OH)]_{0.3}\}_n$ (3a): $NH_2C_6H_4OH$ (0.40 g, 3.66 mmol) and K_2CO_3 (0.60 g, 4.34 mmol) were added to a solution of $[NPCl_2]_n$ (1.40 g, 12.1 mmol) in THF (150 mL), and the mixture was stirred mechanically for 18 hours at room temperature. NH_2Bu (24.4 mL, 18.06 g, 246.9 mmol) was then added at 0 °C, the mixture stirred at this temperature for 30 minutes, and then for another 125 hours at room temperature. After adding 150 mL of THF, the mixture was filtered through celite, concentrated, and added to 1.5 L of water. The resulting fibrous, pink precipitate was washed with water (2 × 1.5 L) and the solid was dried overnight in a desiccator containing P_2O_5 at reduced pressure. The product was dissolved in THF (400 mL) and filtered through activated carbon to eliminate the pink color. The resulting solution was concentrated and added to hexane (1.5 L). The final solid was filtered and dried under vacuum at room temperature for two days. Yield: 1.42 g (59%). $C_{8.6}H_{18.8}N_3O_{0.3}P$ (200.03): calcd. C 51.6, H 9.47, N 21.0; found C 49.7, H 8.82, N 20.3. Chlorine content 0.25%. IR (KBr): $\tilde{\nu}$ = 3334 s, br., (NH), 1515 s, 827 s, (*p*-C6H4-), 1256 s, 1209 vs (N=P), 1118, 1093 m (PNC) cm^{-1}. $^{31}P\{^1H\}$ NMR ([D$_8$]THF): δ = 4.5 [NP(NHBu)$_2$], −3.7 [br. m, NP(NHC$_6$H$_4$OH)(NHBu)]. ^1H NMR ([D$_8$]THF): δ = 7.5 (OH), 7.16, 6.65 (br. m, C$_6$H$_4$), 3.01 (CH$_2$-NH), 2.67 (NH), 1.5 (br. m, -CH$_2$CH$_2$-), 1.05 (br. m, CH$_3$-). $^{13}C\{^1H\}$ NMR ([D$_8$]THF): δ = 152.1, 136.5, 120.0 (2 C), 116.1 (2 C), (C$_6$H$_4$), 41.5, 34.6, 20.8, 14.4 (NHBu). M_w (GPC): 230 000, M_w/M_n = 3.7. TGA: Continuous weight loss from 70 °C, with two fast stages at 220 °C (−32%) and 640 °C (−58%). Final residue at 800 °C: 2.2%.

Other polymers $\{[NP(NHBu)_2]_{1-x}[NP(NHBu)(NHC_6H_4OH)]_x\}_n$ with x between 0.1 and 0.3 were prepared similarly using $NH_2C_6H_4OH$ (1.32x g, 12.1x mmol), K_2CO_3 (2.0x g, 14.5x mmol) and NH_2Bu (273x mL, 202x g., x mmol). The yield was of the order of 50%. The compounds were sometimes slightly pink and lost their solubility on standing. On occasions the solid obtained from the first precipitation in water was only sparingly soluble. In all cases, the chlorine contents were of the order of 0.26% and the M_w (GPC) of ca. 500 000.

$[NP(O_2C_{12}H_8)]_{0.8}[NP(OC_6H_4NH_2)_2]_{0.2}\}_n$ (4): 2,2′-Biphenol (2.39 g, 12.84 mmol) and K_2CO_3 (7.1 g, 51.37 mmol) were added to a solution of $[NPCl_2]_n$ (1.86 g, 16.05 mmol) in THF (200 mL), and the mixture was refluxed with mechanical stirring for 24 hours. $NH_2C_6H_4OH$ (1.4 g, 12.83 mmol) and Cs_2CO_3 (4.18 g, 12.83 mmol) were then added and the refluxing was continued for 24 hours (t_1). More *p*-aminophenol (1.4 g, 12.83 mmol) was added to the resulting mixture and refluxing was further continued for 24 hours (t_2). Following the same procedure as above, the polymer **4** was isolated as a pale brown solid that was dried for three days under vacuum at 20 °C. Yield: 0.8 g (21%). $C_{12}H_{8.8}N_{1.4}O_2P$ (235.58): calcd. C 61.2, H 3.76, N 8.32; found C 61.1, H 3.45, N 7.71. Chlorine content 0.08%. IR (KBr): $\tilde{\nu}$ = 3440 w, 3372 w (NH_2), 1624 w (NH_2), 1247 s, 1194 vs (N=P), 1272 m, 1096 m (POC) cm^{-1}. $^{31}P\{^1H\}$ NMR ($CDCl_3$): δ = −5.9 [br. m, P(O$_2$C$_{12}$H$_8$)], −19.4 (br. m, P-OC$_6$H$_4$-). ^1H NMR ($CDCl_3$): δ = 7.4−6.6 (br. m, aromatic rings), 6.2 (NH_2). $^{13}C\{^1H\}$ NMR ([D$_6$]DMSO): δ = 148, 129, 128, 125, 122 (O$_2$C$_{12}$H$_8$), 145, 142, 121, 114 (OC$_6$H$_4$NH$_2$) (all broad). M_w (GPC): 250 000, M_w/M_n = 3.2. T_g (DSC) = 155 °C. ΔC_p = 0.30 J[gK]$^{-1}$. TGA: Decomposition begins at 100 °C (−3.5%). It is fast at 300 °C (−14%) and very fast at 400 °C. Final residue at 800 °C: 53%.

The same experimental procedure, but with t_1 = 48 h and t_2 = 30 h, gave a more soluble polymer in 43% yield as a pale brown solid having the formula $[NP(O_2C_{12}H_8)]_{0.9}[NP(OC_6H_4NH_2)_2]_{0.1}\}_n$. $C_{12}H_{8.4}N_{1.2}O_2P$ (232.37): calcd. C 62.0, H 3.64, N 7.2; found C 62.5, H 3.59, N 6.91. Chlorine content 0.05%. M_w (GPC): 800.000, M_w/M_n = 4.2. T_g (DSC) = 155 °C, ΔC_p = 0.26 J[gK]$^{-1}$.

$[NP(O_2C_{12}H_8)]_{0.8}[NP(OC_6H_5)(OC_6H_4NH_2)]_{0.2}\}_n$ (5): 2,2′-biphenol (1.95 g, 10.47 mmol) and K_2CO_3 (5.8 g, 42.0 mmol) were added to a solution of $[NPCl_2]_n$ (1.52 g, 13.1 mmol) in THF (200 mL), and the mixture was refluxed with mechanical stirring for 25 hours. $NH_2C_6H_4OH$ (0.81 g, 7.46 mmol) and Cs_2CO_3 (2.43 g, 7.46 mmol) were then added and the refluxing was continued for another 40 hours. HOC_6H_5 (0.5 g, 5.31 mmol) and more Cs_2CO_3 (1.73 g, 5.31 mmol) were added to the mixture, and refluxing was continued for a further 23 h. Following the same procedure as above, the polymer **5** was isolated as a white solid that was dried for three days under vacuum at 20 °C. Yield: 1.9 g (62%). $C_{12}H_{8.6}N_{1.2}O_2P$ (232.57): calcd. C 62.0, H 3.73, N 7.23; found C 61.8, H 3.92, N 7.43. Chlorine content 0.14%. IR (KBr): $\tilde{\nu}$ = 3451 w, 3374 w (NH_2), 1624 (NH_2), 1247 s, 1193 vs (N=P), 1272 m, 1096 m (POC) cm^{-1}. $^{31}P\{^1H\}$ NMR ($CDCl_3$): δ = −5.9 [br. m, P(O$_2$C$_{12}$H$_8$)], −20.0 (br. m, P-OC$_6$H$_4$-). ^1H NMR ($CDCl_3$): δ = 7.4−6.6 (br. m, aromatic rings), 6.2 (NH_2). $^{13}C\{^1H\}$ NMR ([D$_6$]DMSO): δ = 148, 129, 128, 125, 122 (O$_2$C$_{12}$H$_8$), 152, 120 (OC$_6$H$_5$), 145, 142, 121, 114 (OC$_6$H$_4$NH$_2$) (all broad). M_w (GPC): 900 000. M_w/M_n = 4.3. T_g (DSC) = 140 °C. ΔC_p = 0.28 J[gK]$^{-1}$. TGA: Decomposition begins at 40 °C and is continuous, gets faster at 125 °C and at 350 °C is very fast. Residue at 800 °C: 49%.

Acknowledgments

We are grateful to the Spanish FYCIT (Project PBMAT-98) and DGITYT (Project PB98) for financial support.

[1] [1a] J. E. Mark, H. R. Allcock, R. West, *Inorganic Polymers*, Prentice Hall, Engelwood Cliffs, N.J., USA, **1992**. [1b] I. Manners, *Angew. Chem. Int. Ed. Engl.* , **1996**, *35*, 1602−1621. [1c] C. W. Allen, *Coord. Chem. Rev.* **1994**, *130*, 137−173. [1d] R. de Jaeger, M. Gleria, *Prog. Polym. Sci.* **1998**, *23*, 179−276.
[2] H. R. Allcock, *Chem. Mater.* **1994**, *6*, 1476−1491.
[3] H. R. Allcock, *Appl. Organomet. Chem.* **1998**, *12*, 659−666.
[4] M. D. Bezoari. US Patent 4,864,047, 05 Sept. **1989**; **1990**, *113*, 24242h.
[5] H. R. Allcock, P. E. Austin, T. F. Rakowsky, *Macromolecules* **1981**, *14*, 1622−1625.
[6] H. R. Allcock, W. C. Hymer, P. E. Austin, *Macromolecules* **1983**, *16*, 1401−1406..
[7] R. Bertani, G. Facchin, M. Gleria, *Inorg. Chim. Acta* **1989**, *165*, 73−82.
[8] D. Kumar, T. L. ST Clair, *Polyhedron* **1992**, *11*, 1671−1678.
[9] D. Kumar, A. D. Gupta, *Macromolecules* **1995**, *28*, 6323−6329.
[10] S-K. Kwon, *Bull. Korean Chem. Soc.* **2000**, *21*, 969−972.
[11] G. A. Carriedo, F. J. García Alonso, P. A. González, *Macromol. Rapid Commun.* **1997**, *18*, 371−377.
[12] [12a] G. A. Carriedo, L. Fernández-Catuxo, F. J. García Alonso, P. Gómez Elipe, P. A. González, *Macromolecules* **1996**, *29*, 5320−5325. [12b] G. A. Carriedo, F. J. García Alonso, P. A. González, J. L. García Alvarez, *Macromolecules* **1998**, *31*, 3189−3196..
[13] S. Ganapathiappan, S. S. Krishnamurthy, *J. Chem. Soc., Dalton Trans.* **1987**, 579−584.
[14] S. Ganapathiappan, S. S. Krishnamurthy, *J. Chem. Soc., Dalton Trans.* **1987**, 585−590.
[15] C. W. Allen, *Chem. Rev.* **1991**, *91*, 119−135.
[16] H. R. Allcock, R. J. Fitzpatrick, L. Salvati, *Chem. Mater.* **1991**, *3*, 1120−1132.

[17] H.-O. Kalinowski, S. Berger, S. Braun, *Carbon-13 NMR Spectroscopy*, J. Wiley & Sons, New York, **1988**, p. 313 ff.
[18] M. N. Nobis, A. R. McWilliams, O. Nuyken, I. Manners, *Macromolecules* **2000**, *33*, 7707−7712.
[19] J. Y. Chang, S. B. Rhee, S. Cheong, M. Yoon, *Macromolecules* **1992**, *25*, 2666−2670.
[20] H. R. Allcock, L. A. Smeltz, *J. Am. Chem. Soc.* **1976**, *98*, 4143−4149.
[21] J. E. White, R. E. Singler, S. A. Leone, *J. Polym. Sci. Polym. Chem. Ed.* **1975**, *13*, 2531−2543.
[22] A. N. Mujumdar, S. G. Young, R. L. Merker, J. H. Magill, *Macromolecules* **1990**, *23*, 14−21.
[23] *Integrated Spectroscopic data Base System for Organic Compounds*, National Institute of Materials and Chemical Research, Tsukuba, Ibaraki 305−8565, Japan. (http://www.aist.go.jp/RIODB/SDBS/sdbs/owa/sdbs_sea.cre_frame_sea).
[24] W. Bremser, L. Ernst, B. Franke, R. Gerhards, A. Hardt, *Carbon-13 NMR Spectral data in Machine Readable Form*, Verlag Chemie, Weinheim, **1981**.
[25] H. R. Allcock, C. J. Nelson, W. D. Coggio, *Chem. Mater.* **1994**, *6*, 516−524.
[26] H. R. Allcock, C. T. Morrissey, W. K. Way, N. Winograd, *Chem. Mater.* **1996**, *8*, 2730−2738.
[27] A. Medici, G. Fantin, P. Pedrini, M. Gleria, F. Minto, *Macromolecules* **1992**, *25*, 2569−2574.
[28] M. A. Gómez, C. Marco, J. M. Gómez Fatou, G. A. Carriedo, F. J. García Alonso, P. Gómez Elipe, *Eur. Polym. J.* **1996**, *32*, 717−723.
[29] S. G. Young, M. Kojima, J. H. Magill, F. T. Lin, *Polymer* **1992**, *33*, 3215−3225.
[30] M. A. Olshavsky, H. R. Allcock, *Macromolecules* **1995**, *28*, 6188−6197.
[31] G. A. Carriedo, F. J. García Alonso, P. A. González, P. Gómez-Elipe, *Polyhedron* **1999**, *18*, 2853−2859.
[32] G. A. Carriedo, J. Jiménez, P. Gómez Elipe, F. J. García Alonso, *Macromol. Rapid. Commun.* **2001**, *22*, 444−447.
[33] H. R. Allcock, G. S. McDonnell, G. H. Riding, I. Manners, *Chem. Mater.* **1990**, *2*, 425−432.

Received August 10, 2001
[I01308]

Synthesis, X-ray Structures, NMR Studies and Density Functional Calculations of (η^2-Fumarodinitrile)palladium(0) Complexes Containing Dihydro(phosphanylphenyl)oxazole Ligands

Margareta Zehnder,*[a] Markus Neuburger,[a] Silvia Schaffner,[a] Martin Jufer,[b] and Dietmar A. Plattner*[b]

Keywords: Palladium / N,P ligands / Oxazolines / Alkene ligands / Density functional calculations

The (fumarodinitrile)palladium(0) complexes **4a**–**4d** with various 4-substituted 2-[2′-(diphenylphosphanyl)phenyl]-4,5-dihydrooxazole ligands **1a**–**1d** have been prepared and characterized. NMR spectroscopic investigations give evidence that the complexes exist in two forms in solution. The diastereomeric ratio is highly dependent on the 4-substituent at the oxazoline moiety. Substituents reaching into the fumarodinitrile area (**4a** and **4d**) favor one diastereoisomer. Less intrusive substituents (**4b** and **4c**) lead to a diastereomeric ratio of about 1:1. X-ray structures reveal that only one isomer is found in the crystalline solid state. For **4a** and **4d** it is the same as the major diastereoisomer in solution. The orientation of the fumarodinitrile ligand of **4b** is opposite to that of **4a** and **4d**. In all complexes, the fumarodinitrile ligand is not planar. The C–CN and C–H bonds are bent away from the palladium atom. The NC–C=C–CN torsion angle is about 150°. DFT/B3LYP calculations confirm the structural features found in the solid-state structures. For an accurate description of the coordination sphere, extended basis sets for the palladium and phosphorus atoms must be employed. The energetic difference computed for the two diastereoisomers of **4a** reflect the ratios in solution as observed by NMR spectroscopy.

(© Wiley-VCH Verlag GmbH, 69451 Weinheim, Germany, 2002)

Introduction

Pd-catalyzed enantioselective C−C and C−N bond-forming substitutions at allylic positions are an important and ever growing area of research.[1] In particular palladium complexes with chiral, bidentate mixed donor ligands have proven to be highly effective catalysts for this kind of reaction.[2] By applying chiral ligands of the dihydro(phosphanylaryl)oxazole type (**1**; Scheme 1), selectivities in the bond-forming reaction of up to 99% *ee* can be induced using allylic systems with bulky terminal substituents (R′ = Ph, *i*Pr).[3] However, selectivities are lowered when (*n*-alkyl)allyl substrates are used,[4] thus demanding a re-evaluation of the actual catalytic reaction mechanism.

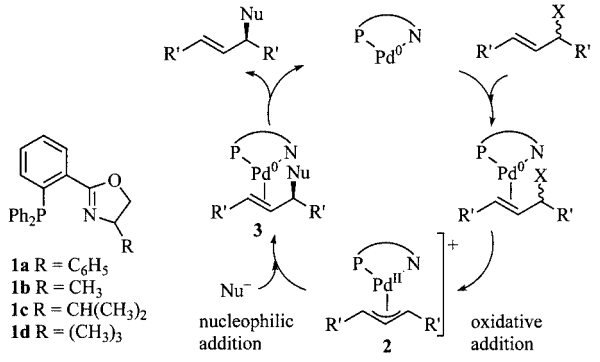

Scheme 1. Catalytic cycle of the allylic substitution reaction

The structural investigation of crucial reaction intermediates in the catalytic cycle is a prerequisite for mechanistic research. Cationic [Pd^{II}(η^3-allyl)(phosphanyloxazoline)] complexes **2** are generally assumed to be such reaction intermediates. Early studies were based on the assumption that the stereodetermining step in the allylic substitution would proceed by an early transition step, thus focusing mainly on the characterization of the cationic (η^3-allyl)palladium(II) species.[5−7] Later research, however, suggested a transition state occurring further along the reaction coordinate.[8] Therefore, the structure and reactivity of the Pd^0(olefin) complex formed by attack of the nucleophile at the allylic complex have to be addressed in order to establish a model that could account for the observed selectivities. Due to their instability, the actual (η^2-olefin)palladium(0) complexes **3** have not been accessible by X-ray analysis as yet.

[a] Institut für Anorganische Chemie der Universität Basel
Spitalstrasse 51, 4056 Basel Switzerland
Fax: (internat.) + 41-61/267-1018
E-mail: margareta.neuburger-zehnder@unibas.ch
[b] Laboratorium für Organische Chemie der Eidgenössischen, Technischen Hochschule Zürich, ETH-Zentrum,
Universitätstrasse 16, 8092 Zürich Switzerland
Fax: (internat.) + 41-1/632-1280
E-mail: plattner@org.chem.ethz.ch

Recently, structural information has been derived from extended NMR spectroscopic experiments.[9] X-ray structures of zero-valent palladium complexes with bidentate ligands and (*E*)-alkenes are restricted to those bearing electron-deficient olefins as dibenzylideneacetone (dba),[10] fumarodinitrile (fdn), and dimethylfumarate (dmfu).[11]

It is known that Pd^0(olefin) complexes can be involved in dynamic processes.[12] Asymmetric N,P ligands give rise to 2 isomers with symmetric substituted olefins and 4 isomers with asymmetric substituted olefinic groups. Interchanging processes by olefin rotation and a dissociation/reassociation process are assumed.[10–12] In this contribution, we report a combined NMR spectroscopic, X-ray crystallographic, and theoretical study of the structures of [Pd^0(η^2-fdn)(**1**)] complexes **4a**–**4d**, as models of the crucial intermediates in the Pd-catalyzed allylic substitution reaction (Scheme 2). To obtain more information about the characteristics of the [metal(phosphanyloxazoline)] moiety the crystal structures of [Pd^{II}(η^3-allyl)(**1a**)] cations **5** and of [Zn(**1a**)Cl_2] (**6**) were included for comparison.[7]

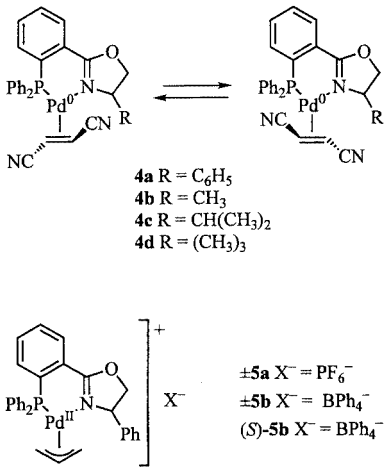

Scheme 2

Results and Discussion

Syntheses

The syntheses of the [Pd(fdn)(**1**)] complexes were performed by addition of the phosphanyloxazoline **1** to a $Pd_2(dba)_3$·$CHCl_3$ solution followed by addition of the fumarodinitrile (Scheme 3). Purification by column chromatography afforded **4** in moderate to good yield (60–90%). The compounds are of considerable stability. In solution they may be stored for several days without appreciable decomposition.

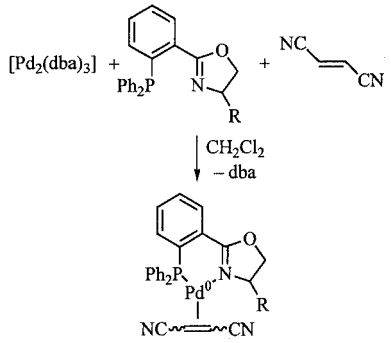

Scheme 3

NMR Spectroscopy

At room temperature, the complexes **4** exist in solution as a mixture of two diastereoisomers. The isomers differ in the orientation of the alkene with respect to the oxazoline substituent. The diastereomeric ratio is significantly dependent on the substituent at the 4-position of the oxazoline ring. In the phenyl (**4a**) and *tert*-butyl (**4d**) derivatives containing bulky oxazoline substituents reaching into the alkene area one isomer is favored. The diastereomeric ratio of the methyl and isopropyl derivatives **4b** and **4c** with less intrusive oxazoline substituents is about 1:1.

For an interconversion from isomer **M** to isomer **m**, a ligand dissociation/reassociation reaction is required. The equilibration process can be monitored by NMR spectroscopy: When the pure crystalline solid is dissolved in $CDCl_3$, only the signals of the solid-state isomer can be detected at first. Upon standing the second isomer arises until the equilibrium is reached within 2 h. As the crystal structures of **4a**, **4b**, and **4d** are known (see below), an unambiguous assignment of the signals to the two isomers was possible. In every case, the major diastereoisomer is found in the solid state.

The signals of the alkene protons demonstrate a high-field shift with respect to the free ligand (Table 1). They are assigned according to their $^3J_{H,P}$ coupling constants; $^3J_{H,P}$ is larger for a *trans* than for a *cis* coupling. The double doublet of the alkene proton *cis* to P ($J_{H,P} \approx 3$ Hz) appears at a lower field than the pseudotriplet of the alkene proton *trans* to P ($J_{H,H} \approx J_{H,P} \approx 10$ Hz) does.

Table 1. Selected NMR spectroscopic data: δ in ppm ($J_{H,H}$, $J_{H,P}$ in Hz)

		H–C_{cisP}	H–C_{transP}	P{H}
4a	80%	3.02 (9.4, 3.2)	1.89 (9.7)	18.93
	20%	3.00 ([a], 3.2)	2.43 (9.8)	19.36
4b	52%	3.22 (9.3, 3.0)	2.73 (9.7)	20.13
	48%	3.16 (9.3, 3.3)	2.81 (9.5)	19.56
4c	52%	3.15 (9.3, 3.3)	2.75 (9.5)	19.30
	48%	3.21 (9.6, 2.9)	2.71 (10.0)	19.48
4d	75%	3.20 (9.3, 3.3)	2.61 (9.3)	20.50
	25%	3.24 (9.8, 2.5)	2.72 (10.0)	19.73

[a] Signal overlap.

In **4a** the signal of the alkene proton *cis* to the oxazoline moiety of the major diastereoisomer is shifted to a higher field with respect to the corresponding signal of the minor isomer. The high-field shift is due to the aromatic shielding effect of the oxazoline substituent. This confirms the assignment of the major isomer to diastereoisomer **M**.

Crystal Structures

X-ray analyses of **4a**, ±**4b**, (*S*)-**4b**, and **4d** were carried out. Selected geometric parameters are reported in Table 2. Views are given in Figures 1, 2, 3, and 4. The methyl derivatives ±**4b** and (*S*)-**4b** differ solely in the chirality; in ±**4b** the racemic and in (*S*)-**4b** the enantiomerically pure phosphanyloxazoline was applied.

Table 2. Selected bond lengths [Å], bond angles [°] and torsion angles [°] for **4a**, ±**4b**, (*S*)-**4b**, and **4d**; comparison with the calculated structures **M4** and **m4**

	4a	±**4b**	(*S*)-**4b**	**4d**	**M4**	**m4**
Pd−N	2.118(2)	2.128(1)	2.133(3)	2.124(3)	2.15	2.16
Pd−P	2.278(1)	2.276(1)	2.275(1)	2.277(1)	2.33	2.36
Pd−C_{cis}P	2.052(2)	2.040(1)	2.035(4)	2.048(4)	2.11	2.11
Pd−C_{trans}P	2.099(2)	2.118(1)	2.105(4)	2.108(4)	2.15	2.15
C=C	1.450(3)	1.447(2)	1.438(6)	1.438(6)	1.46	1.47
N−Pd−P	89.19(5)	87.60(3)	85.4(1)	87.08(9)	89.9	85.2
C−Pd−C	40.86(9)	40.68(5)	40.6(2)	40.5(2)	40.2	40.2
NC−C=C−CN	−152.5	150.5	145.6	−149.2	−150.1	146.0
NPdP/CPdC	9.2	6.5	2.2	2.0	6.7	6.0
P−Pd−N−C(1)	−148.2	−153.4	−146.6	−153.3	−167.1	−147.5

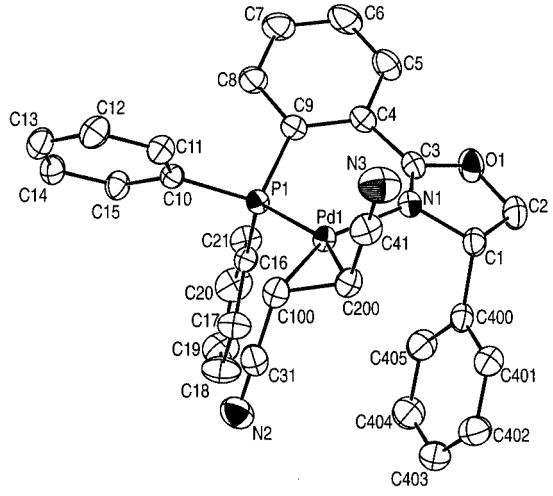

Figure 1. Molecular structure of **4a** with the atom numbering scheme

The alkene ligand of **4a** and **4d** adopts the orientation, which is considered to be sterically favored; the nitrile group *cis* to the dihydrooxazole moiety is on the opposite side of the coordination plane with respect to the oxazoline substituent. The alkene ligand in ±**4b** and (*S*)-**4b** is reversely orientated.

Except for the orientation of the fumarodinitrile the complexes demonstrate a close similarity. The coordination geometry is trigonal. The C=C bond of the fumarodinitrile

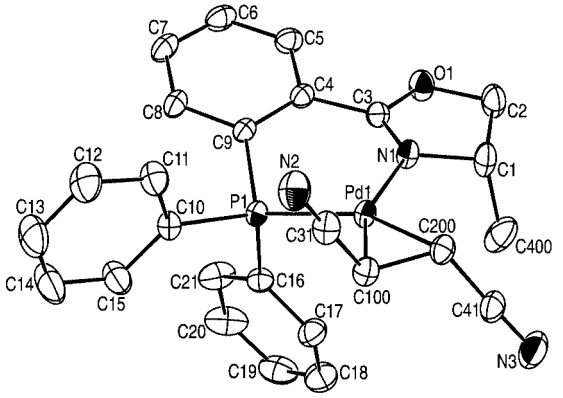

Figure 2. Molecular structure of ±**4b** with the atom numbering scheme

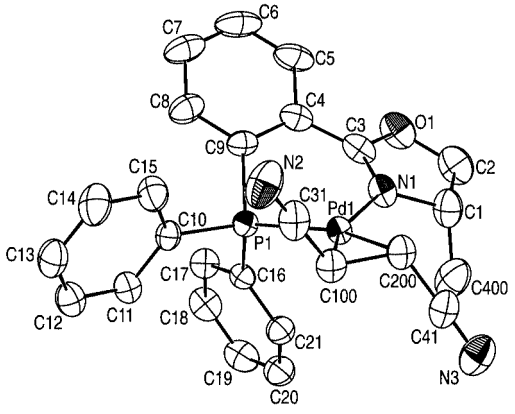

Figure 3. Molecular structure of (*S*)-**4b** with the atom numbering scheme

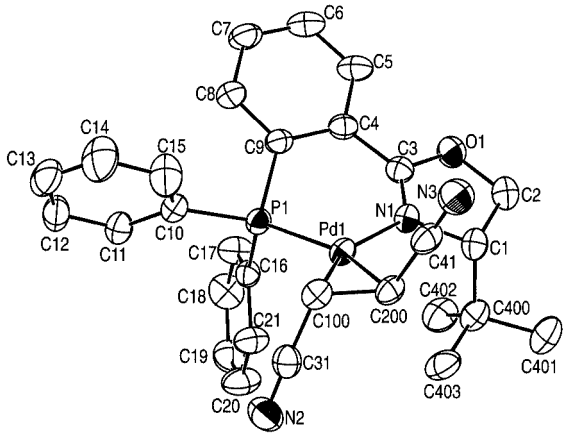

Figure 4. Molecular structure of **4d** with the atom numbering scheme

ligand is positioned approximately in the N/Pd/P coordination plane. Bond lengths and angles of the coordination sphere are in the same range for all compounds independent of the oxazoline substituent and the orientation of the alkene ligand. Due to the *trans* influence of the phosphorus atom the Pd−C distance *trans* to the phosphorus atom is longer than that *trans* to the nitrogen atom.

The fumarodinitrile ligand is not planar. The C−CN and C−H bonds are bent away from the palladium atom. The NC−C=C−CN torsion angle is about 150°. The average value of the C=C bond of 1.44 Å is significantly longer than that for the free olefin (1.36 Å). Both the deviation of the planarity and the elongation of the olefin bond provide evidence of a partial sp^3 hybridization of the olefinic carbon atoms.

The phosphanyloxazoline ligand adopts the characteristic conformation, which, so far, has been found in all coordinated phosphanyloxazolines of type **1**. Due to the nonplanarity of the chelate ring one *P*-phenyl group adopts a pseudoaxial and the other a pseudoequatorial position. The oxazoline substituent is axially positioned and lies on the same side of the coordination plane as the axial *P*-phenyl ring. Although the general features of the ligand conformation are similar, a superposition of the N/Pd/P coordination plane of the X-ray structures shows some variability of the puckering of the six-membered chelate ring (Figure 5). Independently of the conformation of the chelate ring the chiral center adopts a rather rigid position with respect to the N/Pd/P plane expressed in a nearly constant P−Pd−N−C(1) torsion angle of −150° for the ligand with (*S*) configuration.

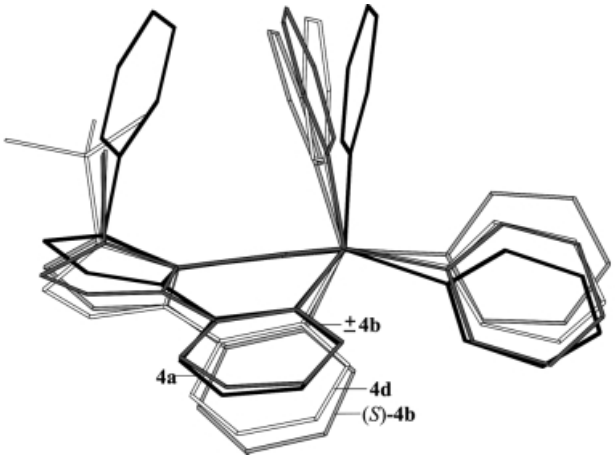

Figure 5. Superposition of the [Pd(**1**)] moiety of complexes **4a**, ±**4b**, (*S*)-**4b**, and **4d**; the N/Pd/P plane is perpendicular to the paper plane

DFT Calculations

Allylpalladium complexes have been the subject of numerous theoretical studies.[13] In contrast, much less computational effort has been directed at (olefin)palladium(0) complexes. Most (olefin)palladium(0) complexes computed so far are product complexes of nucleophilic attack at very simple allylpalladium model complexes and therefore lack any real-world counterpart.[14] Generally, systematic comparisons between computed geometries and experimental structural data of (olefin)palladium(0) complexes are missing, mainly due to the scarcity of available crystallographic data. For a meaningful description of the complete hypersurface of the reaction, starting from an allylpalladium complex and going to the olefin product complex via the transition state of a nucleophilic attack, a computational method should also be able to reproduce the geometrical features of the (olefin)palladium(0) species. With the X-ray crystallographic data at hand, we are now in a position to address this task.

In this work, the (fumarodinitrile)palladium(0) complex **4a** was computed as the complete chemical system (as **M4**) in order to account for all steric and electronic factors of the chiral ligand. The crystal structure of **4a** served as a starting point and reference for the geometry optimization. The electronic ground state of the complex was assumed to be a singlet, following theoretical work of Blomberg et al.[15] The LANL2DZ level was chosen as a starting point in our calculations in order to obtain a more or less accurate description of the geometry of the coordination sphere.[16] With regard to the overall conformation of the molecule, the LANL2DZ-optimized structure showed a qualitatively good agreement with the structure found in the solid state. The calculated distances between the olefinic carbon atoms and the metal center as well as the length of the olefinic carbon−carbon bond were in good agreement with the crystallographic data, as were all calculated bonds between C, H, N, and O atoms (differences < 3 pm). The LANL2DZ level failed mainly in the description of the Pd−P bond. The bond length exceeded the experimental one by more than 14 pm. This problem was addressed by augmenting the basis set with a different contraction scheme for palladium (3311/3111/211/1) and a fairly large full electron basis set (6-311G**) for phosphorus (basis set B). Using this augmented basis set, the calculated Pd−P bond length exceeded the experimental one by only 5 pm (see Tables 2 and 3).

Table 3. Selected bond lengths [Å], bond angles [°] and torsion angles [°] for **4a**, **5**, and **6**

	4a	**5a**	**±5b**	(*S*)-**5b**	**6**
M−N	2.118(1)	2.073(1)	2.071(6)	2.097(2)	2.066(3)
M−P	2.278(1)	2.257(1)	2.264(1)	2.262(1)	2.385(1)
N−M−P	89.2(1)	90.4(1)	88.0(2)	87.1(1)	87.2(1)
P−M−N−C(1)	−148.1	−152.1	−149.0	−149.1	−146.3

In a further step, the fumarodinitrile moiety was rotated 180° around the Pd−olefin bond, resulting in the diastereomeric complex **m4**. The geometry of **m4** was also optimized with basis set B. The difference in calculated energies between the diastereomeric complexes is very small, with the complex observed in solid state more stable by ca. 1 $kJ \cdot mol^{-1}$. This is in perfect agreement with our NMR spectroscopic studies which show that complex **4a** exists as a mixture of two diastereoisomers in solution, and the complex found to be energetically lower by the calculations, is favored.

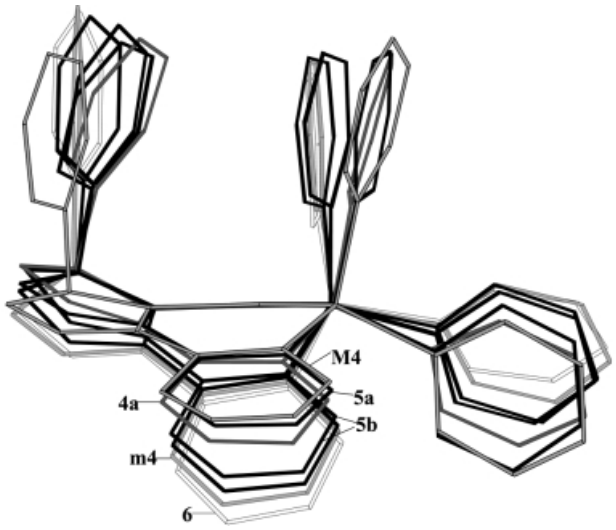

Figure 6. Superposition of the [M(**1a**)] moiety of complexes **4a**, **5**, **6**, and the calculated structures **M4** and **m4**; the N/Pd/P plane is perpendicular to the paper plane

A superposition (Figure 6) of the X-ray structures containing a [Pd(**1a**)] moiety and the calculated structures **M4** and **m4** (gray) demonstrates that the calculated structures almost represent the extremes of chelate ring puckering, **M4** with the flattest and **m4** with the most puckered chelate ring.

The conformation of **m4** is closer to zinc complex **6** (colorless) than to the palladium structures. However, the deviations are too small to be significant. **M4** demonstrates a flattening of the double ring system. The P−Pd−N−C(1) angle of −167° deviates from all other values lying in the range of 146−154°.

The good agreement between the calculated energy difference of the two diastereomeric complexes **M4** and **m4** with the NMR spectroscopic results, indicates that density functional methods in combination with selectively enlarged basis sets give a fairly accurate description of complexes such as **M4** or **m4**. Taking into account that employing the augmented basis set results in an almost negligible increase of computing time but drastically improves the quality of the calculation, we have now established a methodology which allows us to address further tasks such as computing the hypersurface for nucleophilic attack at an allylpalladium complex.

Conclusion

Due to their facile accessibility and their stability [(fumarodinnitrile)(phosphanyloxazoline)palladium(0)] complexes allow for the study of the interaction between the olefin and the chiral ligand. In solution the complexes demonstrate fluxional behavior. The diastereomeric ratio is dependent on the bulk of the oxazoline substituent. A comparison of the X-ray structures of Pd^0- and Pd^{II}(phosphanyloxazoline) complexes with various additional ligands shows that the phosphanyloxazoline backbone adopts a well-defined conformation independent of the oxidation state of the central atom and of additional ligands. DFT/B3LYP calculations with extended basis sets for the palladium and phosphorus atoms confirm the structural features found in the solid-state structures.

Experimental Section

General: $Pd_2(dba)_3{\cdot}CHCl_3$[17] and the phosphanyloxazoline ligands **1**[18] were prepared according to literature procedures. Commercially available material was recrystallized. Solvents for chromatography were distilled before use. The reactions were carried out under N_2 using dried glassware. Column chromatography (CC): SiO_2, C 560, 0.035−0.070 mm, F 254, Chemische Fabrik, Uetikon. NMR spectra were recorded at 25° C with a Varian-Gemini 300 spectrometer with $CDCl_3$ as solvent. ^{1}H NMR: 300 MHz, chemical shifts in ppm relative to $CHCl_3$ as internal reference (δ = 7.26), coupling constants J in Hz. ^{31}P{H} NMR: 121 MHz, triphenylphosphate as external reference (δ = −18.0).

(±)-{2-[2′-(Diphenylphosphanyl-κ*P*)phenyl]-4,5-dihydro-4-phenyloxazole-κ*N*]}(η^2-fumarodinitrile)palladium(0) (4a). General Procedure (GP): A solution of $Pd_2(dba)_3{\cdot}CHCl_3$ (206 mg, 0.20 mmol) and **1a** (163 mg, 0.40 mmol) in CH_2Cl_2 (7 mL) was stirred for 30 min at 20 °C until the dark purple solution turned dark brown. Subsequently, fumarodinitrile (31.2 mg, 0.4 mmol) was added. The solution was stirred for 2 h and turned yellow. The solution was concentrated and transferred onto a 10 × 2 cm SiO_2 column and eluted with hexane/EtOAc (2:1). Evaporation of the solvent yielded a yellow crystalline solid, stable to moisture and air (157 mg, 66.7%). Recrystallization in EtOH/CH_2Cl_2 (20:1) afforded yellow crystals suitable for X-ray analysis. Major isomer (80%): ^{1}H NMR: δ = 8.20−8.24 (m, 1 H, ArH), 6.93−7.62 (m, 18 H, ArH), 5.60 (dd, J = 10.4, 8.5 CH), 4.83 (dd, J = 10.4, 8.9, CH_2), 4.27 (dd, J = 8.9, 8.5, CH_2), 3.02 (dd, J = 9.4, $J_{H,P}$ = 3.2, H_{cisP}) 1.89 (t, J = 9.7, H_{transP}). ^{31}P{H} NMR: δ = 18.93. Minor isomer (20%): ^{1}H NMR: δ = 8.16−8.20 (m, 1 H, ArH), 6.93−7.62 (m, 18 H, ArH), 5.39 (dd, J = 10.4, 7.5 CH), 4.79 (dd, J = 10.4, 8.8, CH_2), 4.35 (dd, J = 8.8, 7.5, CH_2), 3.0 (dd, $J_{H,P}$ = 3.2, H_{cisP}) 2.43 (t, J = 9.8, H_{transP}). ^{31}P{H} NMR: δ = 19.36.

(±)-{2-[2′-(Diphenylphosphanyl-κ*P*)phenyl]-4,5-dihydro-4-methyloxazole-κ*N*]}(η^2-fumarodinitrile)palladium(0) (±4b): According to GP from $Pd(dba)_2$ (115 mg, 0.20 mmol) and ±**1b** (69 mg, 0.20 mmol) and fumarodinitrile (16.8 mg, 0.2 mmol). Yield 90 mg, 84.9%. Crystalline isomer (52%): ^{1}H NMR: δ = 8.01−8.05 (m, 1 H, ArH), 7.36−7.55 (m, 12 H, ArH), 6.94−7.00 (m, 1 H, ArH), 4.45−4.57 (m, 2 H), 3.99−4.03 (m, 1 H), 3.21 (dd, J = 9.5, $J_{H,P}$ = 3.1, H_{cisP}), 2.73 (t, J = 9.7, H_{transP}), 1.24 (d, J = 6.4, Me); ^{31}P{H}: δ = 20.13. Isomer II (48%): ^{1}H NMR: δ = 8.11−8.15 (m, 1 H, ArH), 7.34−7.56 (m, 12 H, ArH), 7.04−7.12 (m, 1 H, ArH), 4.45−4.55 (m, 2 H), 4.07−4.11 (m, 1 H), 3.16 (dd, J = 9.3, $J_{H,P}$ = 3.3, H_{cisP}), 2.81 (t, J = 9.4, H_{transP}), 1.34 (d, J = 6.2, Me); ^{31}P{H} NMR: δ = 19.57.

(*S*)-{2-[2′-(Diphenylphosphanyl-κ*P*)phenyl]-4,5-dihydro-4-methyloxazole-κ*N*]}(η^2-fumarodinitrile)palladium(0) [(*S*)-4b): According to GP from $Pd(dba)_2$ (115 mg, 0.20 mmol) and *S*-**1b** (69 mg, 0.20 mmol) and fumarodinitrile (16.8 mg, 0.2 mmol). Yield 87 mg, 82.1%.

(*S*)-{2-[2′-(Diphenylphosphanyl-κ*P*)phenyl]-4,5-dihydro-4-isopropyloxazole-κ*N*]}(η^2-fumarodinitrile)palladium(0) (4c): According to

GP from $Pd_2(dba)_3$·$CHCl_3$ (206 mg, 0.20 mmol) and **1c** (149 mg, 0.40 mmol) and fumarodinitrile (31.2 mg, 0.4 mmol). Yield 202 mg (90%). Crystalline isomer: ^{1}H NMR: δ = 8.08−8.12 (m, 1 H, ArH), 7.32−7.72 (m, 12 H, ArH), 7.06 (m, 1 H, ArH), 4.26−4.40 (m, 3 H), 3.15 (dd, J = 9.3, $J_{H,P}$ = 3.3, H_{cisP}) 2.75 (t, $J \approx 9.5$, H_{transP}), 2.26−2.38 (m, 1 H, $CH(Me)_2$], 0.88 (d, J = 7.0, Me) 0.42 (d, J = 7.1, Me); ^{31}P{H} NMR: δ = 19.30. Isomer II: ^{1}H NMR: δ = 8.08−8.12 (m, 1 H, ArH), 7.32−7.72 (m, 12 H, ArH), 6.97 (m, 1 H, ArH), 4.26−4.46 (m, 3 H), 3.21 (dd, J = 9.6, $J_{H,P}$ = 2.9, H_{cisP}), 2.71 (t, $J \approx 10$, H_{transP}), 2.25−2.37 [m, H−C$(Me)_2$], 0.91 (d, J = 7.1, Me), 0.15 (d, J = 6.8, Me); ^{31}P{H} NMR: δ = 19.48.

(*S*)-4-*tert*-Butyl-{2-[2′-(diphenylphosphanyl-κ*P*)phenyl]-4,5-dihydrooxazole-κ*N*]}(η^2-fumarodinitrile)palladium(0) (4d): According to GP from $Pd(dba)_2$ (115 mg, 0.20 mmol), **1d** (87.7 mg, 0.20 mmol) and fumarodinitrile (15.6 mg, 0.20 mmol). Yield 77 mg (67.3%). Major isomer (70%): ^{1}H NMR: δ = 8.15−8.19 (m, 1 H, ArH), 7.29−7.57 (m, 12 H, ArH), 7.00 (m, 1 H, ArH), 4.39−4.43 (m, 2 H), 4.14−4.18 (m, 1 H), 3.20 (dd, J = 9.3, $J_{H,P}$ = 3.3, H_{cisP}) 2.61 (t, J = 9.3, H_{transP}), 0.71 (s, 9 H, Me); ^{31}P{H} NMR: δ = 20.05. Minor isomer (30%): ^{1}H NMR: δ = 8.15−8.19 (m, 1 H, ArH), 7.29−7.57 (m, 12 H, ArH), 6.90 (m, 1 H, ArH), 4.38−4.43 (m, 2 H), 4.13−4.18 (m, 1 H), 3.24 (dd, J = 9.8, $J_{H,P}$ = 2.5, H_{cisP}) 2.72 (t, $J \approx 10$, H_{transP}), 0.67 (s, 9 H, Me); ^{31}P{H} NMR: δ = 19.73.

X-ray Crystallographic Studies: Crystal data and parameters of the data collections are compiled in Table 4. Data collection was performed at ambient temperature (293° K) with a KappaCCD diffractometer, Mo-K_α radiation (λ = 0.71069 Å, graphite monochromator). The data were indexed and scaled by using the programs DENZO and SCALEPACK.[20] The data were corrected for Lorenz and polarization effects. The structures were solved by direct methods.[21] Anisotropic least-squares refinement against F_o was carried out on all non-hydrogen atoms using the program CRYSTALS.[22] The hydrogen atoms of the alkene were located by Fourier difference synthesis and refined isotropically. All other hydrogen atoms were included in calculated positions. Scattering factors were taken from the International Tables of Crystallography, vol. IV. CCDC-165323 to -165326 contain the supplementary crystallographic data for this paper. These data can be obtained free of charge at www.ccdc.cam.ac.uk/conts/retrieving.html or from the Cambridge Crystallographic Data Centre, 12, Union Road, Cambridge CB2 1EZ, UK [Fax: (internat.) + 44-1223/336-033; E-mail: deposit@ccdc.cam.ac.uk].

Computational Methods: All calculations were performed with the Gaussian98 (Revision A9) suite of programs[23] using an HP PA8500 at the Swiss Center for Scientific Computing in Manno, Switzerland, with the hybrid Becke exchange functional[24] and the correlation functional of Lee, Yang, and Parr[25] (B3LYP). All structures were fully optimized without geometry constraints. The reported relative energies are not zero-point-corrected. Basis sets used for geometry optimizations and energy calculations were i) LANL2DZ (D95 on first row,[26] Los Alamos ECP plus DZ on Na-Bi[27]) which includes a 341/321/31 contraction scheme for palladium and ii) 3311/3111/211/1[14c] (3311/3111/211 contraction of the minimal basis set of Hay and Wadt,[27] augmented with one f-polarization function[28]) basis set with Los Alamos ECP for palladium and 6-311G**[29] for phosphorus and D95 for C, H N and O (referred to as basis set B).

Acknowledgments

The support of this project by the Swiss National Science Foundation (project No. 2000−05'8855.99.1) is gratefully acknowledged.

Table 4. Crystallographic data for **4a**, ±**4b**, (*S*)-**4b**, and **4d**

	4a	±**4b**	(*S*)-**4b**	**4d**
Empirical formula	$C_{31}H_{24}N_3OPPd$	$C_{26}H_{22}N_3OPPd$	$C_{26}H_{22}N_3OPPd·0·25H_2O$	$C_{29}H_{28}N_3OPPd$
Formula mass	591.93	529.85	533.85	571.94
Crystal size [mm]	0.05 × 0.15 × 0.20	0.11 × 0.21 × 0.29	0.09 × 0.18 × 0.48	0.08 × 0.12 × 0.32
a [Å]	8.6859(2)	10.2642(2)	9.3498(3)	9.7121(4)
b [Å]	17.0377(4)	11.2457(2)	10.8968(3)	10.6922(5)
c [Å]	18.0662(4)	12.7228(3)	23.4841(7)	13.1420(5)
α [°]	90	100.197(1)	90	90
β [°]	92.229(1)	108.013(1)	90	93.080(3)
γ [°]	90	113.867(1)	90	90
V [Å^3]	2671.55	1197.59	2392.63	1362.74
Crystal system	monoclinic	triclinic	orthorhombic	monoclinic
Space group	$P2_1/c$	$P\bar{1}$	$P2_12_12_1$	$P2_1$
Z	4	2	4	2
F(000)	1200	536	1082	584
$\rho_{calcd.}$ [g cm^{-3}]	1.47	1.47	1.48	1.39
Abs. coeff. [mm^{-1}]	0.77	0.85	0.85	0.75
θ_{max} [°]	30.03	34.97	27.88	27.48
No of meas. refl.	23859	41048	24687	32979
No. of indep. refl.	12612	16928	5108	5888
No. of refl. in refinement $I \geq 2\sigma(I)$	9118	14593	4524	5138
No. of parameters	343	298	307	325
Final R	0.035	0.032	0.033	0.034
Final R_w	0.043	0.044	0.043	0.044
$\Delta\rho_{max/min}$ [e·Å^{-3}]	0.64/−1.05	0.82/−0.88	0.56/−0.80	0.70/−1.08
Weighting scheme	Chebychev polynominal[19]	Chebychev polynominal[19]	Chebychev polynominal[19]	Chebychev polynominal[19]

We would also like to thank the Swiss Center for Scientific Computing at Manno for generous allocation of computational resources.

[1] [1a] Reviews: B. M. Trost, D. L. Van Vranken, *Chem. Rev.* **1996**, *96*, 395. [1b] M. A. Lautens, A. Pfaltz, *Allylic Substitution Reactions*, in: *Comprehensive Asymmetric Catalysis*, vol. 2 (Eds.: E. N. Jacobsen, A. Pfaltz, H. Yamamoto), Springer, Heidelberg, **1999**, pp. 833−884.

[2] [2a] N. W. Alcock, J. M. Brown, D. I. Hulmes, *Tetrahedron: Asymmetry* **1993**, *4*, 743. [2b] A. Togni, U. Burckhardt, V. Gramlich, P. S. Pregosin, R. Salzmann, *J. Am. Chem. Soc.* **1996**, *118*, 1031. [2c] G. Helmchen, A. Pfaltz, *Acc. Chem. Res.* **2000**, *33*, 336.

[3] [3a] P. von Matt, A. Pfaltz, *Angew. Chem.* **1993**, *105*, 614; *Angew. Chem. Int. Ed. Engl.* **1993**, *32*, 566. [3b] J. Sprinz, G. Helmchen, *Tetrahedron Lett.* **1993**, *34*, 1769. [3c] G. J. Dawson, C. G. Frost, J. M. J. Williams, S. J. Coote, *Tetrahedron Lett.* **1993**, *34*, 3149.

[4] [4a] J. V. Allen, S. J. Coote, G. J. Dawson, C. G. Frost, C. J. Martin, J. M. J. Williams, *J. Chem. Soc., Perkin Trans. 1* **1994**, 2065. [4b] P. von Matt, O. Loiseleur, G. Koch, A. Pfaltz, C. Lefeber, T. Feucht, G. Helmchen, *Tetrahedron: Asymmetry* **1994**, *5*, 573. [4c] G. Helmchen, S. Kudis, P. Sennhenn, H. Steinhagen, *Pure Appl. Chem.* **1997**, *69*, 513. It is notable that the phosphanebis(amide) ligands developed by Trost give excellent *ee*s with small allylic substrates but fail with the 1,3-diphenylallyl system: B. M. Trost, *Acc. Chem. Res.* **1996**, *29*, 355.

[5] M. Sjögren, S. Hansson, P.-O. Norrby, B. Åkermark, M. E. Cucciolito, A. Vitalgliano, *Organometallics* **1992**, *11*, 3954.

[6] J. Sprinz, M. Kiefer, G. Helmchen, M. Reggelin, G. Huttner, O. Walter, L. Zsolnai, *Tetrahedron Lett.* **1994**, *35*, 1523.

[7] [7a] N. Baltzer, L. Macko, S. Schaffner, M. Zehnder, *Helv. Chim. Acta* **1996**, *79*, 803. [7b] S. Schaffner, L. Macko, M. Neuburger, M. Zehnder, *Helv. Chim. Acta* **1997**, *80*, 463. [7c] S. Liu, J. F. K. Müller, M. Neuburger, S. Schaffner, M. Zehnder, *J. Organomet. Chem.* **1997**, *549*, 283. [7d] S. Schaffner, J. F. K. Müller, M. Neuburger, M. Zehnder, *Helv. Chim. Acta* **1998**, *81*, 1223.

[8] [8a] J. M. Brown, D. I. Hulmes, P. J. Guiry, *Tetrahedron* **1994**, *50*, 4493. [8b] A. Pfaltz, *Acta Chem. Scand.* **1996**, *50*, 189.

[9] [9a] H. Steinhagen, M. Reggelin, G. Helmchen, *Angew. Chem.* **1997**, *109*, 2199; *Angew. Chem. Int. Ed. Engl.* **1997**, *36*, 2108. [9b] J. Junker, B. Reif, H. Steinhagen, B. Junker, I. C. Felli, M. Reggelin, C. Griesinger, *Chem. Eur. J.* **2000**, *6*, 3281. The structure reported by Griesinger deviates substantially from the typical trigonal-planar coordination geometry of [Pd^0(olefin)] complexes; the olefinic bond lies outside of the Pd−P−N plane and the trigonal symmetry is distorted.

[10] [10a] C. G. Pierpont, R. M. Buchanan, H. H. Downs, *J. Organomet. Chem.* **1977**, *124*, 103. [10b] W. A. Herrmann, W. R. Thiel, C. Brossmer, K. Ofele, T. Priermeier, *J. Organomet. Chem.* **1993**, *461*, 51. [10c] J. Fawcett, R. D. W. Kemmitt, D. R. Russell, O. Serindac, *J. Organomet. Chem.* **1995**, *486*, 171.

[11] [11a] B. Jedlicka, R. E. Rülke, W. Weissensteiner, R. Fernández-Galán, F. A. Jalón, B. R. Manzano, J. Rodríguez-de la Fuente, N. Veldman, H. Kooijman, A. L. Spek, *J. Organomet. Chem.* **1996**, *516*, 97. [11b] R. Fernández-Galán, F. A. Jalón, B. R. Manzano, J. Rodríguez-de la Fuente, M. Vrahami, B. Jedlicka, W. Weissensteiner, G. Jogl, *Organometallics* **1997**, *16*, 3758. [11c] M. L. Ferrara, F. Giordano, I. Orabona, A. Panunzi, F. Ruffo, *Eur. J. Inorg. Chem.* **1999**, 1939.

[12] [12a] J. Krause, W. Bonrath, K. R. Pörschke, *Organometallics* **1992**, *11*, 1158. [12b] K. Selvakumar, M. Valentini, M. Wörle, P. S. Pregosin, A. Albinati, *Organometallics* **1999**, *18*, 1207.

[13] A. Dedieu, *Chem. Rev.* **2000**, *100*, 543, and references cited therein.

[14] See, for example: [14a] V. Branchadell, M. Moreno-Manãs, F. Pajuelo, R. Pleixats, *Organometallics* **1999**, *18*, 4934. [14b] F. Delbecq, C. Lapouge, *Organometallics* **2000**, *19*, 2716. [14c] H. Hagelin, B. Åkermark, P.-O. Norrby, *Chem. Eur. J.* **1999**, *5*, 902. [14d] P. E. Blöchl, A. Togni, *Organometallics* **1996**, *15*, 4125.

[15] M. R. A. Blomberg, P. E. M. Siegbahn, M. Svensson, *J. Phys. Chem.* **1992**, *96*, 9794.

[16] The bonding of the olefinic unit to the palladium center best fits the normal donation/back-donation picture, in contrast to the early transition metals, where the binding is best characterized as normal covalent bonding forming a metallacyclopropane. For a theoretical analysis of the binding of olefins to second-row transition-metal atoms see ref.[15] The same picture also applies to (alkyne)palladium(0) complexes, see for example: F. Schager, W. Bonrath, K. R. Pörschke, M. Kessler, C. Krüger, K. Seevogel, *Organometallics* **1997**, *16*, 4276.

[17] T. Ukai, H. Kawazura, Y. Ishii, J. J. Bonnet, J. A. Ibers, *J. Organomet. Chem.* **1974**, *65*, 253.

[18] G. Koch, G. C. Lloyd-Jones, O. Loiseleur, A. Pfaltz, R. Prétôt, S. Schaffner, P. Schnider, P. von Matt, *Recl. Trav. Chim. Pays-Bas* **1995**, *114*, 206.

[19] J. R. Carruthers, D. J. Watkin, *Acta Crystallogr., Sect. A* **1979**, *35*, 698.

[20] Z. Otwinowsky, W. Minor, *Processing of X-ray Diffraction Data in Oscillation Mode*, in: *Methods in Enzymology*, vol. 276 ("Macromolecular Crystallography, Part A") (Eds.: C. W. Carter, R. M. Sweet), Academic Press, London, **1997**, pp. 307−326.

[21] *SIR92*, A Program for Automatic Solution of Crystal Structures by Direct Methods: A. Altomare, G. Cascarano, C. Giacovazzo, A. Gualgliardi, M. C. Burla, G. Polidori, M. Camalli, *J. Appl. Crystallogr.* **1994**, *27*, 435.

[22] D. J. Watkin, *CRYSTALS*, Chemical Crystallography Laboratory, University of Oxford, **1990**, issue 9.

[23] M. J. Frisch, G. W. Trucks, H. B. Schlegel, G. E. Scuseria, M. A. Robb, J. R. Cheeseman, V. G. Zakrzewski, J. A. Montgomery, Jr., R. E. Stratmann, J. C. Burant, S. Dapprich, J. M. Millam, A. D. Daniels, K. N. Kudin, M. C. Strain, O. Farkas, J. Tomasi, V. Barone, M. Cossi, R. Cammi, B. Mennucci, C. Pomelli, C. Adamo, S. Clifford, J. Ochterski, G. A. Petersson, P. Y. Ayala, Q. Cui, K. Morokuma, D. K. Malick, A. D. Rabuck, K. Raghavachari, J. B. Foresman, J. Cioslowski, J. V. Ortiz, A. G. Baboul, B. B. Stefanov, G. Liu, A. Liashenko, P. Piskorz, I. Komaromi, R. Gomperts, R. L. Martin, D. J. Fox, T. Keith, M. A. Al-Laham, C. Y. Peng, A. Nanayakkara, M. Challacombe, P. M. W. Gill, B. Johnson, W. Chen, M. W. Wong, J. L. Andres, C. Gonzalez, M. Head-Gordon, E. S. Replogle, J. A. Pople, *Gaussian 98, Revision A.9*, Gaussian, Pittsburgh, PA, **1998**.

[24] A. D. Becke, *J. Chem. Phys.* **1993**, *98*, 1372.

[25] C. Lee, W. Yang, R. G. Parr, *Phys. Rev.* **1988**, *A37*, 785.

[26] T. H. Dunning, Jr., P. J. Hay, in: *Modern Theoretical Chemistry* (Ed.: H. F. Schaefer, III), Plenum, New York, **1976**, pp. 1−28.

[27] [27a] P. J. Hay, W. R. Wadt, *J. Chem. Phys.* **1985**, *82*, 270. [27b] W. R. Wadt, P. J. Hay, *J. Chem. Phys.* **1985**, *82*, 284. [27c] P. J. Hay, W. R. Wadt, *J. Chem. Phys.* **1985**, *82*, 299.

[28] A. W. Ehlers, M. Böhme, S. Dapprich, A. Gobbi, A. Höllwarth, V. Jonas, K. F. Köhler, R. Stegmann, A. Veldkamp, G. Frenking, *Chem. Phys. Lett.* **1993**, *208*, 111.

[29] [29a] A. D. McLean, G. S. Chandler, *J. Chem. Phys.* **1980**, *72*, 5639. [29b] R. Krishnan, J. S. Binkley, R. Seeger, J. A. Pople, *J. Chem. Phys.* **1980**, *72*, 650.

Received September 17, 2001
[I01363]

Spectroscopic Properties, Electrochemistry, and Reactivity of Mo^0, Mo^I, and Mo^{II} Complexes with the [Mo(bpa)$(CO)_3$] Unit [bpa = bis(2-picolyl)amine] and Their Application for the Labelling of Peptides

Dave R. van Staveren,[a][‡] Eberhard Bothe,[a] Thomas Weyhermüller,[a] and Nils Metzler-Nolte*[b]

Dedicated to Professor Karl Wieghardt on the occasion of his 60th birthday

Keywords: Amino acids / Bioinorganic chemistry / Carbonyl ligands / Molybdenum / Spectro-electrochemistry

The synthesis of the complexes [Mo(bpa)$(CO)_3$] (**1**) and [Mo(Bz-bpa)$(CO)_3$] (**2**) [bpa = bis(2-picolyl)amine; Bz-bpa = *N*-benzylbis(2-picolyl)amine] is described. These compounds have been characterized by spectroscopic techniques including multinuclear NMR spectroscopy (^{1}H, ^{13}C, and ^{95}Mo), and also by X-ray crystallography. Complexes **1** and **2** underwent reversible one-electron oxidations in acetonitrile and dichloromethane with Bu_4NPF_6 as supporting electrolyte to yield the 17-electron organometallic compounds $\mathbf{1}^+$ and $\mathbf{2}^+$. With Bu_4NBr as supporting electrolyte in dichloromethane, on the other hand, **1** and **2** underwent electrochemically irreversible two-electron oxidations, resulting in the formation of [Mo(bpa)$(CO)_3$Br]$^+$ and [Mo(Bz-bpa)$(CO)_3$Br]$^+$. Infrared spectra and electronic spectra of these oxidized species were recorded in spectro-electrochemical studies. The electrochemical behaviour and the infrared spectroscopic data of **1**, **2**, and their oxidized derivatives are compared in detail with those of analogous tricarbonylmolybdenum complexes with the ligands 1,4,7-triazacyclononane and hydridotris(pyrazolyl)borate. The complex [Mo(bpa)(CO)Br]Br_3 (**3**) could be prepared by oxidation of **1** with elemental bromine. Under aerobic aqueous conditions, **3** reacted further to yield the dinuclear diamagnetic Mo^V complex [Mo_2(bpa)$_2$(O)$_2$(μ-O)$_2$](Br,PF_6) (**4**). The identity of **4** was confirmed by a single-crystal X-ray crystallographic study. Finally, the syntheses of two bioconjugates of [Mo(bpa)$(CO)_3$], in which bpa ligands are covalently linked to the *N*-termini of an amino acid (Phe-OMe, **8a**) and of a dipeptide (Ala-Phe-OMe, **8b**), are described. These bioconjugates were comprehensively characterized (including elemental analysis, ^{1}H, ^{13}C, and ^{95}Mo NMR, IR, MS, and electrochemistry). All analytical data supported the proposed constitution and underscore the potential of the Mo(bpa)$(CO)_3$ group as a robust marker group in bioorganometallic chemistry.
(© Wiley-VCH Verlag GmbH, 69451 Weinheim, Germany, 2002)

Introduction

There is considerable interest in the labelling of biomolecules with organometallic fragments that possess carbonyl ligands.[1−3] The corresponding bioconjugates can be detected in picomolar quantities by infrared spectroscopy, as shown by Jaouen, Salmain, and co-workers.[4] Together with IR spectroscopy, electrochemistry of metal complexes is a very attractive detection method, offering good sensitivity and a high signal-to-background ratio.[5,6] We have recently introduced the versatile and robust Mo(allyl)$(CO)_2$ moiety as a marker group in bioorganometallic chemistry.[7−9] However, perhaps the most obvious low-valent Mo fragment is *fac*-Mo$(CO)_3$, in the form of octahedral [L_3Mo$(CO)_3$] complexes. For biological applications, the ligand L_3 must fulfil several requirements. It must be readily accessible, easily substituted with a handle for biomolecules, and furnish very stable Mo$(CO)_3$ complexes. Well-known examples of [L_3Mo$(CO)_3$] complexes include L_3 = 1,4,7-triazacyclononane (tacn; [9]aneN_3) and hydridotris(pyrazolyl)borate [HB$(pz)_3$] as tridentate ligands. We propose the bis(2-picolyl)amine ligand [*bis*(*picolyl*)*amine*, bpa] as an interesting alternative, because its Mo$(CO)_3$ complexes are readily accessible and very stable, as shown here. Moreover, in contrast to tacn and hydridotrispyrazolylborate, the bpa ligand can easily be derivatized with a (protected) acid functionality,[10,11] which makes binding to biomolecules possible.[11,12]

[a] Max-Planck-Institut für Strahlenchemie,
Stiftstrasse 34−36, 45470 Mülheim/Ruhr, Germany
[b] Pharmazeutisch-Chemisches Institut, Universität Heidelberg,
Im Neuenheimer Feld 364, 69210 Heidelberg, Germany
Fax: (internat.) + 49-(0)6221/546441
E-mail: Nils.Metzler-Nolte@urz.uni-heidelberg.de
[‡] Present address: Max-Planck-Institut für Kohlenforschung,
Kaiser-Wilhelm-Platz 1, 45470 Mülheim/Ruhr, Germany
Supporting information for this article is available on the WWW under http://www.eurjic.com or from the author.

The ligand bpa, first reported by Romary et al.,[13] is one of the classical tridentate nitrogen donor ligands in coordination chemistry, but (bpa)metal complexes containing *organometallic* fragments are relatively scarce. Only four organometallic bpa complexes have so far been structurally characterized by X-ray crystallography: namely, [Rh(bpa)(cod)]BPh_4 [cod = (*Z*,*Z*)-1,5-cyclooctadiene],[14] [Pt(bpa)CH_3]Cl,[15] [Pt(bpa)(η^1-allyl)$(CH_3)_2$]Br,[15] and [W(bpa)(η^3-allyl)$(CO)_2$]PF_6.[16] A significant number of *fac*-[L_3Mo$(CO)_3$] complexes, with L_3 being a tridentate nitrogen donor ligand, have been structurally characterized.[17–34] However, no Mo(bpa)$(CO)_3$ derivatives have yet been reported. Krüger and Helm reported the synthesis and X-ray crystal structure of a related compound, in which the potentially tetradentate ligand *N*,*N*′-dimethyl-2,11-diaza-[3.3](2,6)pyridinophane acts as a tridentate ligand structurally analogous to bpa.[17]

In this paper, we report the synthesis, structural characterisation, spectroscopic properties, electrochemical behaviour and chemical reactivity of Mo^0, Mo^I, and Mo^{II} complexes containing the Mo(R-bpa)$(CO)_3$ unit (R = H or Bz). Furthermore, the suitability of Mo(R-bpa)$(CO)_3$ complexes for the labelling of biomolecules is demonstrated by the synthesis of two derivatives, an amino acid (Phe) and a dipeptide (Ala-Phe), in which the Mo(R-bpa)$(CO)_3$ derivative is covalently linked to the *N*-termini.

Results and Discussion

Synthesis and Reactivity

The complexes [Mo(bpa)$(CO)_3$] (**1**) and [Mo(Bz-bpa)$(CO)_3$] (**2**) were synthesized by heating the ligand with $Mo(CO)_6$ in deoxygenated di-*n*-butyl ether (for **1**) or deoxygenated mesitylene (for **2**) at 150 °C for 1 h under argon, as shown in Scheme 1. Complex **1** was isolated as a deep yellow powder, whereas **2** was obtained as an orange solid. All the characterisation data for **1** and **2** were consistent with their proposed constitutions. These compounds were stable in air for days in the solid state. In solution, complex **1** was much more sensitive than **2** towards air, with decomposition of **1** taking place within 1–2 h.

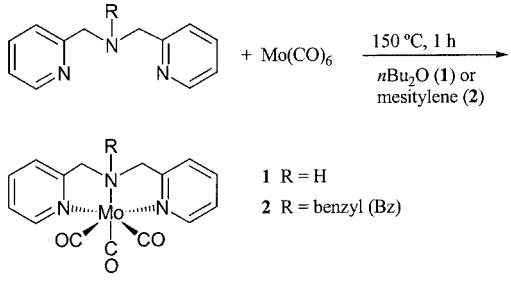

Scheme 1

When **1** was treated with elemental bromine in deoxygenated $CHCl_3$ under argon, the orange-brown complex [Mo(bpa)$(CO)_3$Br]Br_3 (**3**) was obtained (see Scheme 2), as concluded from the results of elemental analysis, infrared spectroscopy and ESI positive mass spectrometry. In the solid state, this compound was stable towards dioxygen for approximately 1 d, but in solution decarbonylation of complex **3** took place within 5–10 min when only traces of water were present. NMR spectroscopic data of compound **3** could not be obtained. When **3** was dissolved in MeOH under aerobic conditions and an aqueous solution of KPF_6 was added, the dinuclear complex [Mo_2(bpa)$_2(O)_2$(μ-$O)_2$](Br,PF_6) (**4**) invariably precipitated, and therefore appears to be the thermodynamic sink of the mixture (see Scheme 2). The reactivity of **3** differed from that of [Mo([9]aneN_3)$(CO)_3$Br]Br_3, as the latter compound can be crystallized from aerobic aqueous solutions.[35]

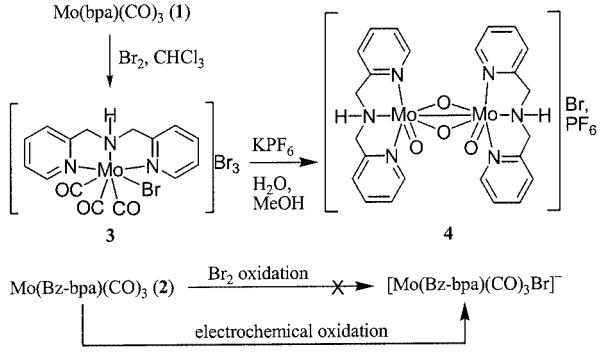

Scheme 2

When **2** was treated with Br_2 under conditions identical to those used for the synthesis of **3**, an oil formed initially, but an orange-brown solid was obtained upon removal of the solvent in vacuo. Although results from elemental analysis fitted well for [Mo(Bz-bpa)$(CO)_3$Br]Br_3, other characterisation data could not be obtained, due to the instability of this compound in solution. However, [Mo(Bz-bpa)$(CO)_3$Br]$^+$ could be generated by electrochemical methods (see Scheme 2), as concluded from spectro-electrochemical investigations (vide infra).

X-ray Crystal Structures of 1, 2, and 4

X-ray quality single crystals of complexes **1** and **2** were obtained by slow concentration of H_2O/CH_3CN solutions under streams of argon. The unit cell of each compound was found to consist of two crystallographically inequivalent molecules (named A and B), which display slightly different bond lengths and angles. ORTEP diagrams for one of the independent molecules of each of **1** and **2** are depicted in Figures 1 and 2, respectively. Geometrical information for both structures is summarized in Table 1. Molecules B of **1** and **2** are labelled consecutively: N(1) in A corresponds to N(4) in B, and C(35) in B corresponds to C(13) in A, etc. The two independent molecules in the two structures are fairly similar.

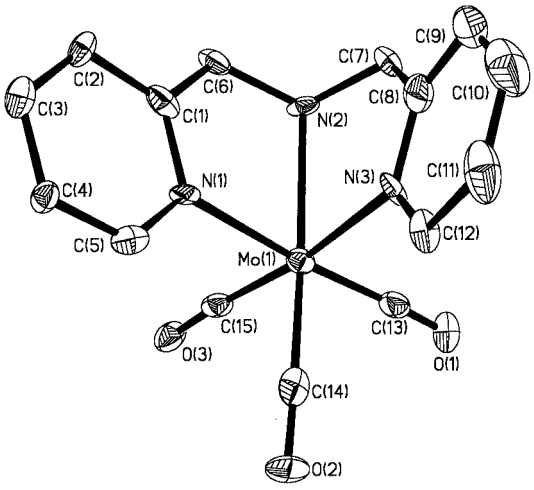

Figure 1. ORTEP projection for one of the two crystallographically independent molecules (A) of **1** with thermal ellipsoids at 50% probability level; hydrogen atoms have been omitted for clarity

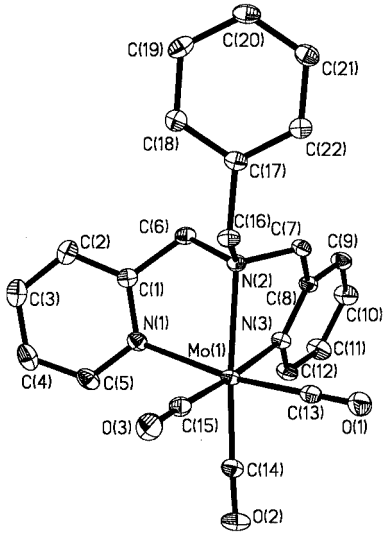

Figure 2. ORTEP plot for one of the two crystallographically independent molecules (A) of **2** with thermal ellipsoids at 50% probability level; hydrogen atoms have been omitted for clarity

The Mo atoms in both structures are in distorted octahedral $[N_3C_3]$ coordination environments, each with the three carbonyl groups and the (substituted) bis(2-picolyl)-amine ligand occupying a face of the octahedron. This facial arrangement of the carbonyl ligands has also been observed in analogous complexes with various tridentate N-donor ligands.[17−34] In both molecules of **1** and **2**, the Mo−N(amine) bond length is considerably longer than the Mo−N(pyridine) bond lengths. Unfortunately, the quality of the structure of **1** is not high enough to allow a detailed discussion of the other bond lengths in this structure. All of the differences between molecule A and molecule B of **2** are small and might be interpretable on the basis of packing effects. In both structures the deviation from idealized octahedral symmetry is evident from the C−Mo−C angles: values of less than 90° are observed for all of those. In fact,

Table 1. Selected bond lengths [Å] for $[Mo(bpa)(CO)_3]$ (**1**) and $[Mo(Bz\text{-}bpa)(CO)_3]$ (**2**)

	1	**2**
Molecule A:[a]		
Mo(1)−N(1)	2.229(10)	2.272(3)
Mo(1)−N(2)	2.301(10)	2.337(2)
Mo(1)−N(3)	2.234(11)	2.255(3)
Mo(1)−C(13)	1.92(2)	1.933(3)
Mo(1)−C(14)	1.91(2)	1.935(2)
Mo(1)−C(15)	1.91(2)	1.945(3)
Molecule B:[b]		
Mo(2)−N(4)	2.249(11)	2.250(3)
Mo(2)−N(5)	2.308(11)	2.331(2)
Mo(2)−N(6)	2.249(11)	2.252(3)
Mo(2)−C(35)	1.92(2)	1.938(3)
Mo(2)−C(36)	1.89(2)	1.932(3)
Mo(2)−C(37)	1.92(2)	1.953(3)

[a] The unit cells of both compounds contain two crystallographically independent molecules, named A and B. [b] Molecule B is labelled consecutively: i.e., N(4) in B corresponds to N(1) in A and C(35) in B corresponds to C(13) in A, etc.

all structures so far reported for *fac*-$Mo(CO)_3$ complexes with tridentate N-donor ligands display C−Mo−C angles smaller than 90°,[17−34] and this deviation thus appears to be a general feature for this type of compounds.

There is only one example in the literature of a structurally characterized *fac*-$Mo(CO)_3$ compound with the molybdenum atom coordinated by two pyridine nitrogen atoms and one amine nitrogen atom of the same ligand. The potentially tetradentate ligand *N*,*N*′-dimethyl-2,11-diaza[3.3]-(2,6)pyridinophane acts as a tridentate ligand in that compound.[17] The Mo−N(pyridine) bond lengths in the structure of that complex are approximately 0.04 Å longer than the Mo−N(amine) bond lengths. This is in sharp contrast with structures **1** and **2**, in which the Mo−N(pyridine) bond lengths are considerably shorter than the Mo−N(amine) bond lengths.

X-ray quality single crystals of $[Mo_2(bpa)_2(O)_2(\mu\text{-}O)_2](Br,PF_6)$ (**4**) were obtained by slow concentration of an $MeOH/H_2O$ solution. An ORTEP representation of the cationic part of **4** is shown in Figure 3, with selected bond length and bond angle information summarized in Table 2.

The cationic part of the structure consists of two Mo(bpa)(O) moieties bridged by two oxo ligands, with the terminal oxo ligands occupying *cis* positions relative to each other. The four-membered ring comprised of the two Mo atoms and the two bridging oxo ligands has the puckered conformation observed in all crystal structures containing a *syn*-$[Mo_2(O)_2(\mu\text{-}O)_2]$ core with additional multidentate ligands.[36−39] The short internuclear Mo−Mo distance of 2.5432(5) Å is indicative of an Mo−Mo single bond, consistent with the observed diamagnetism of the complex.

The bromide ion (not depicted in Figure 3) is involved in hydrogen bond interactions with the two NH groups, with Br···N contacts of 3.258(4) Å and 3.358(4) Å [Br···N(5) and Br···N(2), respectively]. Two very similar crystal structures

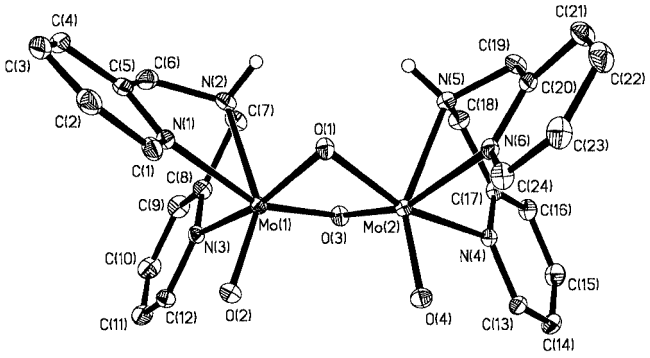

Figure 3. ORTEP representation for the cationic part in **4** with thermal ellipsoids at 50% probability level; hydrogen atoms, except amine hydrogen atoms, have been omitted for clarity

Table 2. Selected bond lengths [Å] and bond angles [°] for [Mo_2-$(bpa)_2(O)_2(\mu\text{-}O)_2$](Br,$PF_6$) (**4**)

Mo(1)−N(1)	2.219(2)	Mo(2)−N(6)	2.227(2)
Mo(1)−N(2)	2.313(2)	Mo(2)−N(5)	2.294(2)
Mo(1)−N(3)	2.263(2)	Mo(2)−N(4)	2.245(2)
Mo(1)−O(2)	1.687(2)	Mo(2)−O(4)	1.692(2)
Mo(1)−O(1)	1.934(2)	Mo(2)−O(1)	1.921(2)
Mo(1)−O(3)	1.935(2)	Mo(2)−O(3)	1.933(2)
Mo(1)−Mo(2)	2.5432(5)		
O(1)−Mo(1)−O(2)	110.10(7)	O(1)−Mo(2)−O(4)	110.70(7)
O(3)−Mo(1)−O(2)	111.83(7)	O(3)−Mo(2)−O(4)	112.29(7)
O(1)−Mo(1)−O(3)	91.43(6)	O(1)−Mo(2)−O(3)	91.88(6)
Mo(1)−O(1)−Mo(2)	82.55(6)	Mo(2)−O(3)−Mo(1)	82.22(6)

with ethyl or methylethyl linkers between the two bpa ligands have been reported,[37] and these display Mo-donor atom bond lengths nearly identical to those in **4**. Apparently, the hydrogen-bonded bromide ion forces the bpa ligands into the same conformation as the ethyl and methylethyl linkers do. It would be expected that this bromide ion would be bound very tightly because, apart from hydrogen bond interactions, it is also involved in an electrostatic interaction with the dinuclear molybdenum complex of charge 2+.

NMR Spectroscopy

In solution, the hydrogen atoms of the picolyl-CH_2 groups become magnetically inequivalent due to metal coordination of the three nitrogen atoms. Therefore, the ^1H NMR spectrum of **2** showed two doublets at $\delta = 4.67$ and $\delta = 3.72$ with intensity two and a ^2J coupling constant of 15.5 Hz (see Supporting Information, Figure S1). In the ^1H NMR spectrum of **1** on the other hand, the appearance of the picolyl-CH_2 hydrogen atom resonances was influenced by the amine NH group. This NH hydrogen atom resonated at $\delta = 6.14$, with a ^3J coupling constant of 6.6 Hz. One of the pairs of magnetically inequivalent picolyl-CH_2 hydrogen atoms resonated as a doublet at $\delta = 4.06$, with a ^2J coupling constant of 16.8 Hz, whereas the other pair appeared as a doublet of doublets at $\delta = 4.33$, with a ^2J coupling constant of 16.8 Hz and a ^3J coupling constant of 6.6 Hz. The size of these coupling constants in the ^1H NMR spectrum of **1** can be explained by the Karplus equation.[40] Analysis of the crystallographic data[41] shows that the absolute value of the HNCH torsion angles is close to 30° for one set of protons and close to 90° for the other (see Supporting Information, Figure S2 and Table S3). The calculated $^3J_{H,H}$ values of 5.9 Hz and 0.2 Hz, respectively, are in good agreement with the observed coupling constants in the ^1H NMR spectrum, indicating that the solid-state structure does not differ to any large extent from the structure of **1** in solution.

The ^{13}C NMR spectra of **1** and **2** each showed two signals corresponding to the CO ligands at $\delta \approx 230$ (see Exp. Sect.), with the signal at the higher chemical shift having approximately twice the intensity of the signal at lower frequency. The CO ligand *trans* to the amine nitrogen atom was more shielded due to increased π-backbonding, whereas the CO ligands in positions *trans* to the pyridine groups had to compete with the pyridine rings for π-backbonding.

Results from ^{95}Mo NMR measurements are summarized in Table 3, together with the chemical shifts for several other *fac*-$Mo(CO)_3$ compounds with N-donor ligands, for comparison. The chemical shifts of *fac*-[$Mo(N_3)(CO)_3$] complexes span a range of about 350 ppm, with compounds **1** and **2** showing resonances in the high frequency region of that range. The molybdenum nucleus in **2** was deshielded by 89 ppm compared to complex **1**. This downfield shift upon alkylation of the bis(picolyl)amine nitrogen atom is the reverse of the trend observed for the 1,4,7-triazacyclononane derivatives: [$Mo(Me_3[9]aneN_3)(CO)_3$] resonated 226 ppm upfield from [$Mo([9]aneN_3)(CO)_3$]. At first sight, an upfield shift should be expected, as the electron density at the Mo nucleus increases upon alkylation of the amine ligand. While this is true for the triazacyclononane series, the opposite trend holds for **1** and **2**. However, for heavier elements such as Mo, steric effects such as ligand bulkiness and chelate ring size, as well as local symmetry effects, have an important influence on the chemical shift of the element.[42,43] The downfield shift of **2** with respect to **1** may therefore be explained on the basis of steric effects. In fact, the Mo-donor atom bond lengths in the X-ray crystal struc-

Table 3. ^{95}Mo NMR spectroscopic data of **1**, **2**, and several other *fac*-[$Mo(N_3)(CO)_3$] compounds

Complex	Solvent	δ[a] [ppm]	$\Delta\nu_{1/2}$ [Hz]	Ref.
[$Mo(pyridine)_3(CO)_3$]	Pyridine	−800	7	[44]
[Mo(Bz-bpa)$(CO)_3$] (**2**)	MeCN	−849	47	this work
[$Mo([9]aneN_3)(CO)_3$]	CH_2Cl_2	−866	20	[45]
[Mo(bpa)$(CO)_3$] (**1**)	MeCN	−938	36	this work
[$Mo([12]aneN_3)(CO)_3$]	CH_2Cl_2	−1001	13	[45]
[Mo(dien)$(CO)_3$][b]	$HCONMe_2$	−1088	70	[46]
[$Mo(Me_3[9]aneN_3)(CO)_3$]	DMSO	−1092	160	[45]
[$Mo(MeCN)_3(CO)_3$]	MeCN	−1114	10	[47]
[$Mo\{HB(Me_2pz)_3\}(CO)_3$]$^-$	$HCONMe_2$	−1149	80	[45]

[a] Chemical shifts reported versus 2 M Na_2MoO_4 in D_2O at an apparent pH = 11. [b] dien = diethylenetriamine.

ture of **1** show a trend towards being somewhat shorter than their counterparts in **2**.

Electrochemistry

Both **1** and **2** underwent reversible one-electron oxidations in CH_3CN and CH_2Cl_2 with Bu_4NPF_6 as supporting electrolyte at potentials slightly more negative than the Fc/Fc^+ couple. The redox potentials for these complexes are listed in Table 4, together with those for the related 1,4,7-triazacyclonane (tacn) and hydridotris(3,5-dimethylpyrazolyl)borate [$HB(Me_2pz)_3$] complexes. The redox potentials for **1** and **2** appear to be solvent-dependent, with the lower oxidation potential measured in CH_2Cl_2. Table 4 shows that the oxidation potentials of **1** and **2** are very similar to those of the tacn and Me_3-tacn complexes. The hydridotris(3,5-dimethylpyrazolyl)borate anionic analogue $[Mo\{HB(Me_2pz)_3\}(CO)_3]^-$ undergoes a one-electron oxidation at slightly higher potential than the tacn, bpa and Bz-bpa complexes.

Table 4. Reversible one-electron oxidations of *fac*-$Mo(CO)_3$ compounds with tridentate N-donor ligands

Complex	$E_{1/2}$ (MeCN)[a]	$E_{1/2}$ (CH_2Cl_2)[a]
$[Mo(bpa)(CO)_3]$ (**1**)	−0.26[b]	−0.33[b]
$[Mo(Bz\text{-}bpa)(CO)_3]$ (**2**)	−0.22[b]	−0.28[b]
$[Mo([9]aneN_3)(CO)_3]$	−0.37[b]	−0.34[b]
$[Mo(Me_3[9]aneN_3)(CO)_3]$	−0.25[c]	−0.28[b]
$[Mo\{HB(Me_2pz)_3\}(CO)_3]^-$	0.08[d][e]	0.00[d][e]

[a] 0.1 M Bu_4NPF_6 as supporting electrolyte; vs. Fc/Fc^+; in Volt. [b] This work. [c] From ref.[48] [d] 0.1 M Bu_4NBF_4 as supporting electrolyte. [e] From ref.[49]

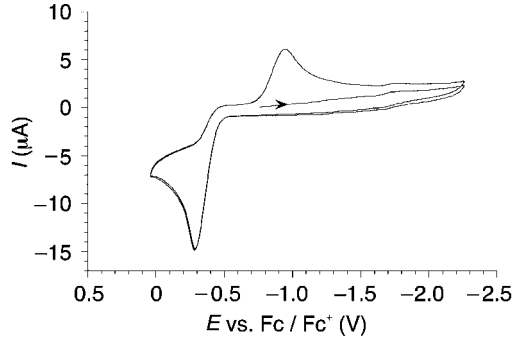

Figure 4. Cyclic voltammogram of **2** (10^{-3} M) in CH_2Cl_2 in the presence of Bu_4NBr (0.1 M); two consecutive cycles (scan rate 200 mV/s) starting from −0.8 V moving first to −2.3 V; note that the reduction peak at −0.95 V appears only in the second cycle

In CH_2Cl_2 and with Bu_4NBr as the supporting electrolyte, the electrochemical behaviour of **1** and **2** was completely different. Irreversible oxidations took place, with peak potentials of −0.37 V vs. Fc/Fc^+ (for **1**) and −0.28 V vs. Fc/Fc^+ (for **2**). Controlled potential coulometry on both compounds established these oxidations as two-electron processes, attributable to formation of the seven-coordinated complexes $[Mo(bpa)(CO)_3Br]^+$ and $[Mo(Bz\text{-}bpa)(CO)_3Br]^+$. Formation of seven-coordinated Mo^{II} species has also been reported for *fac*-$Mo(CO)_3$ complexes with two different tacn derivatives.[25,48] After generation of the seven-coordinated species $[Mo(bpa)(CO)_3Br]^+$ and $[Mo(Bz\text{-}bpa)(CO)_3Br]^+$, single reduction peaks were observed at more negative potentials, namely at −1.20 V vs. Fc/Fc^+ for $[Mo(bpa)(CO)_3Br]^+$ and −0.95 V vs. Fc/Fc^+ for $[Mo(Bz\text{-}bpa)(CO)_3]^+$, as shown in Figure 4 for complex **2**.

The reductive peaks only appeared during the second of two consecutive cyclic voltammograms. This demonstrates that the seven-coordinated complexes formed upon oxidation of the starting material in the first cycle are reduced at this potential. With the aid of controlled potential coulometry, the number of transferred electrons for this reduction process was shown to be two, again yielding the neutral compounds **1** and **2**. The bpa derivatives differ from the tacn analogues in this respect, because the corresponding reduction peak of the seven-coordinated species for the tacn complexes was not observed in the range from −2.0 V to +2.0 V.[25,48] Additional evidence for the chemical reversibility of the two-electron oxidation of **1** and **2** was also obtained from UV and IR spectroelectrochemical investigations (see below).

Electronic Spectroscopy

The electronic spectra of **1** and **2** in MeCN were very similar, each displaying two intense MLCT bands, with maxima at 327 nm ($\varepsilon = 6.1\cdot10^3$ $M^{-1}\cdot cm^{-1}$) and 416 nm ($\varepsilon = 6.9\cdot10^3$ $M^{-1}\cdot cm^{-1}$) for **1** and at 329 nm ($\varepsilon = 6.3\cdot10^3$ $M^{-1}\cdot cm^{-1}$) and 429 nm ($\varepsilon = 7.0\cdot10^3$ $M^{-1}\cdot cm^{-1}$) for **2**.

UV/Vis spectroelectrochemical investigations could only be performed on **2**, since $\mathbf{1}^+$ and $[Mo(bpa)(CO)_3Br]^+$ (the oxidation products of **1**) were both very reactive in solution and partially reacted further during the time required for coulometry (several minutes), probably to yield oxo species. The changes in the electronic spectrum during the electrochemical oxidation of complex **2** in CH_2Cl_2 were monitored with both Bu_4NPF_6 and Bu_4NBr as supporting electrolyte, as depicted in Figure 5. During oxidation, in the presence both of PF_6 and of bromide anions, the MLCT bands at 429 nm and 329 nm gradually disappeared, as a result of the decreased electron availability at the Mo ion in the Mo^I and Mo^{II} forms. With Bu_4NPF_6 as supporting electrolyte (formation of $\mathbf{2}^+$), a new shoulder appeared at around 350 nm, with a molar extinction coefficient of around $4.8\cdot10^3$ $M^{-1}\cdot cm^{-1}$, while an isosbestic point was present at 320 nm. In the presence of bromide anions [formation of $Mo(Bz\text{-}bpa)(CO)_3Br^+$], a new shoulder appeared at 370 nm, with a molar extinction coefficient of around $1.4\cdot10^3$ $M^{-1}\cdot cm^{-1}$, and an isosbestic point was present at 307 nm. After both oxidations, the formed complexes could be reduced at appropriate potentials, once again yielding the UV/Vis spectrum of **2**, without any significant loss in absorbance (i.e., within 99%). This finding is additional evidence for the chemical reversibility of the oxidations.

Infrared Spectroscopy

The infrared spectra of **1** and **2** in THF showed three ν_{CO} vibrations: at 1904, 1790, and 1779 cm^{-1} for **1**, and at 1906,

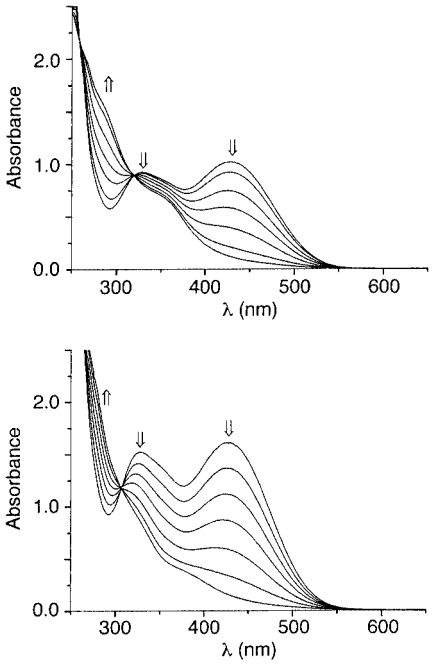

Figure 5. Changes in the electronic spectrum of **2** during coulometry in CH_2Cl_2 at 0° C; top: in the presence of 0.1 M Bu_4NPF_6, one-electron oxidation (formation of $\mathbf{2}^+$), $2.92\cdot10^{-4}$ M of **2**, path-length 0.5 cm; bottom: in the presence of 0.1 M Bu_4NBr, two-electron oxidation {formation of [Mo(Bz-bpa)$(CO)_3$Br]$^+$}, $4.61\cdot10^{-4}$ M of **2**, path length: 0.5 cm

1794, and 1782 cm^{-1} for **2**. This is consistent with C_s symmetry, for which three ν_{CO} vibrations are expected (A′ + 2 A′′). In the case of [Mo(Me_3[9]aneN_3)$(CO)_3$] the three nitrogen atoms are identical, resulting in a complex with C_{3v} symmetry, for which only two infrared-active vibrations should be expected (A_1 + E, at 1907 cm^{-1} and 1773 cm^{-1}, respectively).

The infrared spectrum of [Mo(bpa)(CO)Br]Br_3 (**3**) was measured conventionally between NaCl windows in THF solution, whereas infrared spectra of $\mathbf{1}^+$, $\mathbf{2}^+$, and [Mo(Bz-bpa)$(CO)_3$Br]$^+$ were recorded in situ during electrochemical oxidation of **1** and **2** in an OTTLE cell. As a representative example, the infrared spectral changes during the oxidation of **2** to $\mathbf{2}^+$ are depicted in Figure 6.

The carbonyl stretching vibrations in the infrared spectra of the compounds in this study are summarized in Table 5, together with values of analogous tacn and hydridotris(pyrazolyl)borate compounds. As can be observed, the ν_{CO} stretching vibrations of **1** and **2**, their 17-electron derivatives

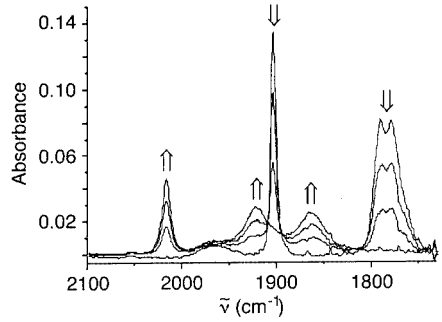

Figure 6. Infrared spectroscopic changes monitored during the one-electron oxidation of **2** to $\mathbf{2}^+$ (1.0 mM) in THF (0.1 M Bu_4NPF_6), performed in an OTTLE cell at 0° C

Table 5. Selected vibrational data for **1**, **2**, **8a**, **8b**, $\mathbf{1}^+$, $\mathbf{2}^+$, **3**, [Mo(Bz-bpa)$(CO)_3$Br]$^+$, and related compounds

Complex	Solvent	ν(CO) [cm^{-1}]	Ref.
Mo^0 compounds:			
[Mo(bpa)$(CO)_3$] (**1**)	THF	1904, 1790, 1779[a]	this work
[Mo(Bz-bpa)$(CO)_3$] (**2**)	THF	1906, 1794, 1782[a]	this work
[Mo(bpa-Phe-OMe)$(CO)_3$] (**8a**)	THF	1906, 1793, 1782[a]	this work
[Mo(bpa-Ala-Phe-OMe)$(CO)_3$] (**8b**)	THF	1906, 1793, 1782[a]	this work
[Mo([9]aneN_3)$(CO)_3$]	THF	1901, 1766[b]	this work
[Mo(Me_3[9]aneN_3)$(CO)_3$]	THF	1907, 1773[b]	this work
[Mo(benzyl$_3$[9]aneN_3)$(CO)_3$]	CH_2Cl_2	1907, 1768[b]	[50]
[Mo{HB(pz)$_3$}$(CO)_3$]$^-$	CH_3CN	1897, 1761[b]	[51]
[Mo{HB(Me_2pz)$_3$}$(CO)_3$]$^-$	CH_3CN	1891, 1751[b]	[51]
[Mo{HB(Me_2pz)$_3$}$(CO)_3$]$^-$	CH_2Cl_2	1884, 1742[b]	[33]
Mo^I compounds:			
[Mo(bpa)$(CO)_3$]$^+$ ($\mathbf{1}^+$)	THF	2015, 1910, 1859[c]	this work
[Mo(Bz-bpa)$(CO)_3$]$^+$ ($\mathbf{2}^+$)	THF	2018, 1922, 1864[c]	this work
[Mo(benzyl$_3$[9]aneN_3)$(CO)_3$]$^+$	CH_2Cl_2	2017, 1909, 1873	[50]
[Mo{HB(pz)$_3$}$(CO)_3$]	CH_2Cl_2	2010, 1885 (br)	[52]
[Mo{HB(Me_2pz)$_3$}$(CO)_3$]	CH_2Cl_2	1998, 1864 (br)	[53]
[Mo{HB(Me_2pz)$_3$}$(CO)_3$]	CH_2Cl_2	2001, 1860 (br)	[33]
Mo^{II} compounds:			
[Mo(bpa)$(CO)_3$Br]$^-$	THF	2055, 1989, 1935	this work
[Mo(Bz-bpa)$(CO)_3$Br]$^-$	CH_3CN	2055, 1980, 1957[c]	this work
[Mo([9]aneN_3)$(CO)_3$Br]$^-$	THF	2042, 1964, 1928	this work
[Mo{HB(pz)$_3$}$(CO)_3$Br]	CH_2Cl_2	2053, 1980, 1938	[54]

[a] Complex has C_s symmetry. [b] Complex has C_{3v} symmetry. [c] Complex generated electrochemically in an OTTLE cell.

$\mathbf{1}^+$ and $\mathbf{2}^+$, and the seven-coordinated complexes **3** and $[Mo(Bz\text{-}bpa)(CO)_3Br]^+$ showed trends similar to those seen with their tacn and hydridotris(pyrazolyl)borate analogues. The electron availability of the molybdenum ion in these species decreases upon increase of the metal ion's oxidation state, resulting in a shift of the ν_{CO} vibrations to higher wavenumbers.

EPR Spectroscopy

Because the electrochemical and spectro-electrochemical investigations on **2** indicated good stability of the one-electron oxidized complex $\mathbf{2}^+$, this latter compound was subjected to EPR spectroscopic investigation. The X-Band EPR spectrum of $\mathbf{2}^+$ (generated by coulometry) as a frozen CH_2Cl_2 solution is depicted in Figure 7, together with the resulting spectrum from the simulation procedure.

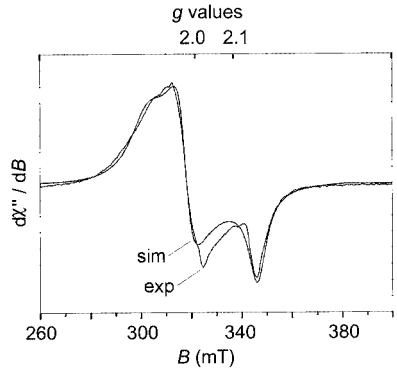

Figure 7. X-Band EPR spectrum of $\mathbf{2}^+$, generated by coulometry, in frozen CH_2Cl_2 solution (0.1 M Bu_4NPF_6) and its simulated spectrum; $T = 50$ K; power: 0.2 mW; frequency: 9.46494 GHz; modulation: 1.25 mT

Although the fit is not perfect, it clearly shows the rhombic nature of the $S = 1/2$ spectrum, with simulated g values $g_x = 2.238$, $g_y = 2.131$, and $g_z = 1.954$. These g values are slightly higher than those reported for $[Mo(benzyl_3[9]aneN_3)(CO)_3]^+$ in a frozen DMF solution, which were $g_x = 2.188$, $g_y = 2.040$, and $g_z = 1.992$.[50] The discrepancy between the simulated and the experimental spectrum of $\mathbf{2}^+$ might be due to the presence of small amounts of paramagnetic decomposition products. Indeed, no satisfactory EPR spectra of the related compound $\mathbf{1}^+$ could be obtained, because the EPR spectra contained several additional resonances. As mentioned above, the spectro-electrochemical investigations on **1** showed that $\mathbf{1}^+$ had partially decomposed during the time required for the coulometry (several minutes).

Labelling of Biomolecules

Complex **2** showed particularly good stability towards dioxygen and water. We have therefore set out to use this type of $(bpa)Mo(CO)_3$ derivative for the labelling of biomolecules, in particular amino acids and peptides. The synthetic strategy is outlined in Scheme 3. The ligand *N*-(*p*-carboxybenzyl)bis(2-picolyl)amine (**6**) was prepared in good yield from methyl *p*-(bromomethyl)benzoate and bis(2-picolyl)amine, followed by base hydrolysis of the methyl ester. With TBTU [*O*-(1*H*-benzotriazol-1-yl)-*N*,*N*,*N*′,*N*′-tetramethyluronium tetrafluoroborate] as the activating reagent, **6** was coupled to the amino groups of phenylalanine methyl ester and the dipeptide alanyl-phenylalanine methyl ester to yield **7a** and **7b**, respectively. With a view to future applications in the labelling of more sensitive biomolecules, **7** was not treated directly with $Mo(CO)_6$, because of the vigorous conditions required for quantitative labelling. Instead, the *fac*-$Mo(CO)_3$ fragment was introduced under very mild conditions, by treatment with $[Mo(CO)_3(EtCN)_3]$. After 5−10 min of stirring at room temperature, an orange precipitate formed. After filtration and drying in vacuo, compounds **8a** and **8b** were obtained in pure form in 80% yield.

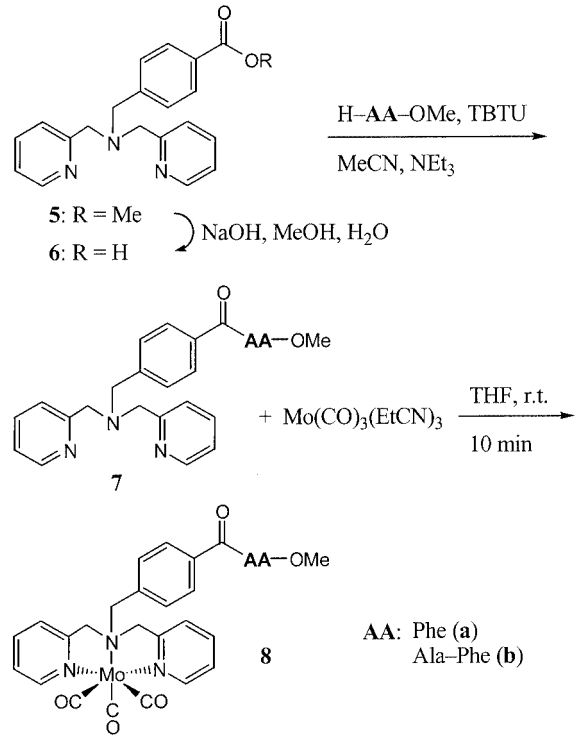

Scheme 3

The spectroscopic data of **8a** and **8b** confirmed the proposed constitution of the bioconjugates. First of all, the IR spectra showed three ν_{CO} vibrations at 1906, 1793, and 1782 cm^{-1} (Table 5). A ^{95}Mo NMR resonance was observed at $\delta = -849$ for both compounds, identical to the chemical shift of **2**. In addition, resonances for the metal carbonyl ligands at $\delta \approx 230$ were observed in the ^{13}C NMR spectra. Coordination of the *fac*-$Mo(CO)_3$ fragment to the nitrogen atoms of the substituted bpa ligand was also evident in the ^1H NMR spectra. The hydrogen atoms of the picolyl-CH_2 groups are magnetically inequivalent, forming an AB system with a coupling constant of about 15.5 Hz. Unlike in **2**, an additional small coupling of 1.5 Hz (**8a**) and 3.4 Hz (**8b**) was observed. All other NMR signals could be as-

signed unambiguously by analogy with **2** and with the help of 2D NMR spectroscopy. Finally, both compounds **8a** and **8b** were reversibly oxidized at −0.27 V vs. Fc/Fc^+ in CH_2Cl_2. All of these analytical properties demonstrated that neither the carbonyl group nor the attached biomolecule have a strong influence on the spectroscopic properties of the Mo(bpa)$(CO)_3$ group.

Discussion

The experimental and spectroscopic results described above show that the properties of **1** and **2** are similar to those of their 1,4,7-triazacyclonane and hydridotris(pyrazolyl)borate analogues. However, differences in reactivity and electrochemical behaviour between these three types of compounds were observed. Compounds **1** and **2** showed reversible one-electron oxidations with Bu_4NPF_6 as supporting electrolyte at potentials similar to those for the tacn derivatives, whereas the Mo^0/Mo^I transition for [Mo{HB$(Me_2pz)_3$}$(CO)_3]^-$ occurred at a slightly higher potential. With Bu_4NBr as supporting electrolyte, **1** and **2** each underwent electrochemically irreversible two-electron oxidation, to yield the seven-coordinated complexes [Mo(bpa)$(CO)_3Br]^+$ and [Mo(Bz-bpa)$(CO)_3Br]^+$, respectively. These Mo^{II} complexes could be reduced once more at a potential of around −1.0 V, again yielding complexes **1** and **2**. For the complexes [Mo(R_3-tacn)$(CO)_3$] (R = Me or benzyl), electrochemical formation of [Mo(R_3-tacn)$(CO)_3Br]^+$ was reported, but the corresponding re-reduction to yield the Mo^0 complexes was not observed between +2.0 V and −2.0 V.[25,48] One difference in reactivity between [Mo(bpa)$(CO)_3Br]^+$ and [Mo(tacn)$(CO)_3Br]^+$ is that the latter compound could be crystallized from aerobic aqueous solutions,[35] whereas the former reacted further to yield the dinuclear Mo^V complex [Mo_2(bpa)$_2(O)_2$(μ-$O)_2$](Br,PF_6).

Another difference from the analogous tacn and hydridotris(pyrazolyl)borate complexes was observed in the solution infrared spectra of **1** and **2**, since **1** and **2** have point-group symmetry C_s, whereas the tacn and hydridotris(pyrazolyl)borate complexes are of point-group symmetry C_{3v}. The degeneracy of the vibrations of *E* symmetry in the tacn and hydridotripyrazolylborate complexes is abolished in **1** and **2**.

A suitable organometallic labelling group for biomolecules must be readily introducible. For both the tacn and pyrazolylborate ligands, selective monosubstitution with a handle for labelling is difficult to achieve. The bpa ligand, on the other hand, is readily substituted with a carboxylic acid group. Reaction between (activated) organometallic acids and free amino groups in the biomolecule has long been known to be a successful strategy.[55−60] Secondly, the bioconjugate must be stable in water and air for quite some time. In addition, the property of the labelling group that is to be used for detection of the conjugate should not depend much on the attached biomolecule. Jaouen and coworkers have developed IR spectroscopy of bioorganometallic compounds into an immunoassay (*C*arbonyl *M*etallo *I*mmuno *A*ssay, CMIA) and thereby demonstrated the suitability of IR spectroscopy as a sensitive and reliable detection method.[2,4,61,62] We have recently reported amino acid and peptide derivatives of [CpMo(allyl)$(CO)_2$].[7] These compounds were readily isolated in the presence of water and showed promising spectroscopic properties. However, they could not be reversibly oxidized and did not show the required long-term stability in air. We were then able to show that isolobal replacement of the cyclopentadienyl ligand with histidinate resulted in complexes of the general type [Mo(His)(allyl)$(CO)_2$], with very favourable electrochemical properties and much increased stability towards air even in solution.[8,9]

In this work, we have demonstrated that *fac*-Mo$(CO)_3$ derivatives of the bpa ligand are well suited for the labelling of biomolecules. On comparing benzyl-substituted [Mo(Bz-bpa)$(CO)_3$] (**2**) to the bioconjugates **8** we note that there is very little influence of the attached biomolecule on the spectroscopic properties of the metal complex. Owing to this property, as well as its demonstrated stability in an aqueous, aerobic environment, this group is a well-suited marker for biomolecules. We are currently extending the chemistry described here to other biomolecules, as well as towards solid-phase synthesis of peptides.

Experimental Section

General: All syntheses and manipulations of the metal complexes were performed under argon by standard Schlenk techniques, unless otherwise noted. All solvents were deoxygenated before use unless otherwise noted. Elemental analyses were performed by H. Kolbe, Microanalytisches Laboratorium, Mülheim/Ruhr, Germany. Infrared spectra were recorded with a Perkin−Elmer FT-IR spectrophotometer 2000 as KBr disks and/or in THF solutions between NaCl windows (either a 0.5-mm or 1.0-mm spacer), with a spectral resolution of either 2.0 cm^{-1} or 4.0 cm^{-1}. For the IR spectroelectrochemical measurements, an OTTLE cell consisting of CaF_2 windows with a pathlength of 0.17 mm was used (2.0 cm^{-1} resolution). ^1H and ^{13}C NMR spectra were recorded with Bruker ARX 250 (^1H at 250.13 MHz), Bruker DRX 400 (^1H at 400.13 MHz) and Bruker DRX 500 (^1H at 500.35 MHz) spectrometers. The spectra were referenced to TMS, using the ^{13}C or residual protio signals of the deuterated solvents as internal standards. ^{95}Mo NMR spectra were recorded with a Bruker DRX 500 spectrometer (32.6 MHz for ^{95}Mo), with a 2 M Na_2MoO_4 solution in D_2O at an apparent pH = 11 as an external standard. Mass spectra in the electron impact mode (EI; 70 eV) were recorded with a Finnigan MAT 8200 mass spectrometer. Only characteristic fragments are given, with intensities in parentheses and possible composition between brackets. The spectra were normalized against the most intense peak, which therefore had intensity 100%. ElectroSpray Ionisation mass spectra (ESI-MS) in the positive ion mode were recorded with a Hewlett−Packard HP 5989 mass spectrometer. The solvent used is given in parentheses, and the possible composition of the peaks is between brackets. Electronic spectra were recorded with a Hewlett−Packard HP 8452A diode array spectrophotometer. Cyclic voltammograms and square-wave voltammograms in CH_2Cl_2 or MeCN solutions with Bu_4NPF_6 or Bu_4NBr as supporting electrolytes were recorded with an EG&G Potentiostat/Galvanostat 273A.

A three-electrode cell was employed, with a glassy-carbon working electrode, a platinum-wire auxiliary electrode and an $Ag/AgNO_3$ reference electrode (0.01 M $AgNO_3$ in MeCN). For determination of the redox potentials, ferrocene was added as an internal standard. Controlled potential coulometry measurements (both for preparative purposes and for UV/Vis spectroelectrochemical studies) were performed in CH_2Cl_2 solutions with the same supporting electrolytes by employing the potentiostat described above, but with a Pt-grid as working electrode, a Pt-brush auxiliary electrode separated from the working electrode compartment by a vycor frit and a $Ag/AgNO_3$ (0.01 M $AgNO_3$ in MeCN) reference electrode. Thin layer infrared spectro-electrochemical measurements were performed with an OTTLE cell of 0.17 mm optical pathlength consisting of a Pt-grid working electrode, a glassy-carbon counterelectrode and a Ag-wire as "quasi-reference electrode". The EPR spectrum was recorded as a frozen solution (generated by controlled potential coulometry) with a Bruker ESP 300E spectrometer, equipped with an ER 041 XK-D microwave bridge. The EPR spectrum was simulated with the program GFIT.[63] Bis(2-picolylamine) and $Mo(CO)_6$ were purchased from Aldrich. The compounds *N*-benzylbis(2-picolyl)amine,[64] $[Mo([9]aneN_3)(CO)_3]$,[35] $[Mo([9]aneN_3(CO)_3Br]Br_3$,[35] $[Mo(Me_3[9]aneN_3)(CO)_3]$,[48] and $[Mo(CO)_3(EtCN)_3]$[65] were synthesized according to literature procedures.

Compound 1: A suspension of bis(2-picolyl)amine (1.0 g, 5.0 mmol) and $Mo(CO)_6$ (1.3 g, 5.0 mmol) in degassed di-*n*-butyl ether (75 mL) was heated at 150 °C for 1 h, during which a deep yellow precipitate formed. After the mixture had been allowed to reach room temperature, the solid material was collected by filtration and dried in vacuo. Yield: 1.8 g (95%). Crystals suitable for X-ray analysis were grown by slow concentration of a CH_3CN/H_2O mixture (5:1, v/v) under a stream of argon. $C_{15}H_{13}MoN_3O_3$ (379.22): calcd. C 47.51, H 3.46, N 11.08; found C 47.15, H 3.40, N 11.03. IR (KBr): $\tilde{\nu}$ = 3323 (w) ν_{NH}, 1901 (s), 1891 (vs), 1784 (s), 1769 (s), 1742 (vs) ν_{CO}. IR (THF): $\tilde{\nu}$ = 1904 (vs), 1790 (s), 1779 (s) ν_{CO}. MS (EI): *m/z* (%) = 381 (14) $[M^+]$, 353 (2) $[M - CO]^+$, 325 (1) $[M - 2\,CO]^+$, 297 (31) $[M - 3\,CO]^+$, 93 (100). ^1H NMR ($[D_6]$DMSO, 400.13 MHz): δ = 8.73 (app. d, 2 H, H_{Pyr}), 7.65 (m, 2 H, H_{Pyr}), 7.27 (app. d, 2 H, H_{Pyr}), 7.14 (pseudo t, 2 H, H_{Pyr}), 6.14 (t, $^3J_{H,H}$ = 6.6 Hz, 1 H, NH), 4.33 (dd, $^2J_{H,H}$ = 16.8, $^3J_{H,H}$ = 6.6 Hz, 2 H, CH_2), 4.06 (d, $^2J_{H,H}$ = 16.8 Hz, 2 H, CH_2). ^{13}C NMR ($[D_6]$DMSO, 62.9 MHz): δ = 231.4, 229.3 (CO), 159.5, 150.1, 137.5, 123.0, 122.0 (C_{Pyr}), 59.6 (CH_2). ^{95}Mo NMR (CH_3CN, 32.6 MHz): δ = −938 ($\Delta_{1/2}$ = 36 Hz).

Compound 2: A suspension of *N*-benzylbis(2-picolyl)amine (0.96 g, 3.30 mmol) and $Mo(CO)_6$ (0.88 g, 3.30 mmol) in deoxygenated mesitylene (40 mL) was heated at 150° C for 1 h, during which an orange solid precipitated. After the mixture had been allowed to cool to ambient temperature, the precipitate was isolated by filtration, washed with *n*-hexane (10 mL) and dried in vacuo. Yield: 1.28 g (83%). Crystals suitable for X-ray structure determination were grown by slow concentration of a CH_3CN/H_2O (10:1, v/v) solution under a stream of argon. $C_{22}H_{19}MoN_3O_3$ (469.34): calcd. C 56.30, H 4.08, N 8.95; found C 56.18, H 4.02, N 9.05. IR (KBr): $\tilde{\nu}$ = 1898 (vs), 1776 (s), 1752 (vs) ν_{CO}. IR (THF): $\tilde{\nu}$ = 1906 (vs), 1794 (s), 1782 (s) ν_{CO}. MS (EI): *m/z* (%) = 471 (6) $[M^+]$, 443 (4) $[M - CO]^+$, 387 (13) $[M - 3\,CO]^+$, 197 (100). ^1H NMR ($[D_6]$DMSO, 400.13 MHz): δ = 8.68 (app. d, 2 H, H_{Pyr}), 7.68 (m, 2 H, H_{Ar}), 7.59 (m, 2 H, H_{Ar}), 7.46 (m, 3 H, H_{Ar}), 7.16 (pseudo d, 2 H, H_{Ar}), 7.08 (m, 2 H, H_{Ar}), 4.67 (d, $^2J_{H,H}$ = 15.5 Hz, 2 H, CH_2), 4.66 (s, 2 H, $CH_{2,Bz}$), 3.72 (d, $^2J_{H,H}$ = 15.5 Hz, 2 H, CH_2). ^{13}C NMR (CD_3CN, 125.8 MHz): δ = 232.3, 231.3 (CO), 159.9, 151.6, 138.4, 133.6, 132.5, 129.7, 129.4, 124.1, 123.3 (C_{Ar}), 71.0 ($CH_{2,Bz}$), 65.4 (CH_2). ^{95}Mo (CH_3CN, 32.6 MHz): δ = −849 ($\Delta_{1/2}$ = 47 Hz).

Compound 3: Br_2 (1.0 g, 0.3 mL, 6.3 mmol) was added dropwise to a suspension of **1** (0.5 g, 1.3 mmol) in degassed $CHCl_3$ (50 mL), resulting in a clear orange-red solution. The mixture was stirred for 45 min, during which an orange-brown powder precipitated. The solid was collected by filtration, washed with $CHCl_3$ (10 mL) and pentane (10 mL) and air-dried. Yield: 0.66 g (73%). $C_{15}H_{13}Br_4MoN_3O_3$ (698.84): calcd. C 25.78, H 1.88, N 6.01; found C 25.20, H 1.79, N 5.97. IR (KBr): $\tilde{\nu}$ = 3155 (w) ν_{NH}, 2037 (s), 1950 (br, vs) ν_{CO}. IR (THF): $\tilde{\nu}$ = 2055 (s), 1989 (s), 1935 (s) ν_{CO}. MS (ESI-pos., CH_2Cl_2): *m/z* = 460 $[Mo(bpa)(CO)_3Br]^+$, 432 $[Mo(bpa)(CO)_2Br]^+$, 404 $[Mo(bpa)(CO)Br]^+$, 376 $[Mo(bpa)Br]^+$.

Compound 4: $[Mo(bpa)(CO)_3Br]Br_3$ (**3**, 0.5 g, 0.7 mmol) was dissolved in MeOH (30 mL) under aerobic conditions, followed by addition of a KPF_6 (0.66 g, 3.60 mmol) solution in H_2O (10 mL). Upon standing overnight, an orange powder formed; this was isolated by filtration, washed with Et_2O (15 mL) and air-dried. Yield: 0.21 g (68%). Crystals suitable for X-ray diffraction were obtained by slow concentration of an MeOH solution. $C_{24}H_{26}BrF_6Mo_2N_6O_4P$ (879.25): calcd. C 32.78, H 2.98, N 9.56; found 32.67, H 2.91, N 9.47. IR (KBr): $\tilde{\nu}$ = 962 (m) $\nu_{Mo=O}$, 747 (m) $\nu_{as}[M - O]$. MS (ESI-pos., MeOH): *m/z* = 737 $[M - PF_6]^+$, 657 $[M - PF_6 - HBr]^+$, 327 $[M - PF_6 - Br]^{2+}$. ^{13}C NMR ($[D_6]$DMSO, 62.9 MHz): δ = 158.6, 151.7, 142.4, 125.7, 124.2 (C_{Pyr}), 55.3 (CH_2). ^1H NMR ($[D_6]$DMSO, 250.13 MHz) shows broadened signals at room temperature. This could be due to paramagnetic impurities or coalescence as found for a related compound.[37]

Compound 5: NEt_3 (0.69 mL, 5.00 mmol) was added to a solution of bis(2-picolyl)amine (1.0 g, 5.0 mmol) and methyl *p*-(bromomethyl)benzoate (1.15 g, 5.00 mmol) in THF (35 mL), and the mixture was refluxed for 1.5 h. The mixture was allowed to reach room temperature and subsequently filtered to remove a white precipitate. After removal of the solvent under reduced pressure, the oily residue was redissolved in Et_2O (40 mL) and filtered to remove a red solid. Evaporation of the solvent yielded 1.4 g (81%) of a light orange oil, which was used as such in the next step. $C_{21}H_{21}N_3O_2$ (347.4). MS (EI): *m/z* = 347 (2) $[M^+]$, 316 (2) $[M - OCH_3]^+$, 255 (100) $[M - C_6H_6N]^+$. ^1H NMR ($CDCl_3$, 250.1 MHz): δ = 8.49 (app. d, 2 H, H_{pyr}), 7.95 (d, $^3J_{H,H}$ = 8.3 Hz, 2 H, H_{Ar}), 7.62 (pseudo t, 2 H, H_{pyr}), 7.52 (pseudo d, 2 H, H_{pyr}), 7.46 (d, ^3J = 8.3 Hz, 2 H, H_{Ar}), 7.12 (pseudo t, 2 H, H_{pyr}), 3.87 (s, 3 H, OCH_3), 3.78 (s, 4 H, $CH_{2,picolyl}$), 3.71 (s, 2 H, CH_2). ^{13}C ($CDCl_3$, 100.6 MHz): δ = 166.9 (C=O), 159.3 (C_q, pyr), 148.9 (C_{Pyr}), 144.5 ($C_{Ar,q}$), 136.3 (C_{Pyr}), 129.5 (C_{Ar}), 128.9 ($C_{Ar,q}$), 128.6 (C_{Ar}), 122.7 (C_{Pyr}), 122.0 (C_{Pyr}), 60.0 (CH_2, picolyl), 58.1 (CH_2), 51.9 (OCH_3).

Compound 6: A solution of NaOH (0.8 g, 20 mmol) in 5 mL of H_2O was added to a solution of **5** (1.4 g, 4.0 mmol) in MeOH (20 mL), and the mixture was stirred for 2 h at ambient temperature. The pH was adjusted to 7 by dropwise addition of 2 M HCl, followed by removal of the solvent under reduced pressure. The sticky white residue was triturated with $CHCl_3$ (200 mL), followed by filtration to remove NaCl. The $CHCl_3$ solution was dried with $MgSO_4$. Removal of the solvent under reduced pressure afforded a yellow sticky oil, to which CH_3CN (30 mL) was added, followed by vigorous stirring. After approximately 15−30 min, a white precipitate formed. The solution was stored at 0 °C for 2 h, to effect further precipitation and the white solid was then isolated by filtration and dried in vacuo. Yield 0.7 g (53%). $C_{20}H_{19}N_3O_2$ (333.4). IR (KBr): $\tilde{\nu}$ = 1698 (m) $\nu_{C=O}$. MS (EI): *m/z* = 333 (1) $[M]^+$, 241 (100)

$[M - C_6H_6N]^+$. ^1H NMR ($CDCl_3$, 250.1 MHz): δ = 11.35 (br, 1 H, CO_2H), 8.59 (app. d, 2 H, H_{Pyr}), 8.01 (d, $^3J_{H,H}$ = 8.0 Hz, 2 H, H_{Ar}), 7.66 (pseudo t, 2 H, H_{Pyr}), 7.59 (app. d, 2 H, H_{Pyr}), 7.44 (d, $^3J_{H,H}$ = 7.7 Hz, 2 H, H_{Ar}), 7.80 (pseudo t, 2 H, H_{Pyr}), 3.85 (s, 4 H, CH_2), 3.73 (s, 2 H, $CH_{2,Bz}$). ^{13}C NMR ($CDCl_3$, 62.9 MHz): δ = 169.3 (C=O), 159.8, 148.4, 143.1, 137.2, 130.0, 128.8, 123.4, 122.4, 122.0 (all C_{Ar}), 59.3 (CH_2), 58.2 ($CH_{2,Bz}$).

Compound 7a: NEt_3 (1.0 mL, 0.7 g, 7.2 mmol), phenylalanine methyl ester hydrochloride (216 mg, 1.0 mmol), and TBTU (323 mg, 1.0 mmol) were added to a suspension of **6** (333 mg, 1.0 mmol) in CH_3CN (10 mL), and the mixture was stirred for 30 min at ambient temperature. After evaporation of the solvent in vacuo, CH_2Cl_2 (100 mL) was added to the sticky residue, followed by filtration to remove ammonium salts. The CH_2Cl_2 solution was washed with aqueous 2 M $NaHCO_3$ (75 mL) and the phases were separated. The aqueous phase was extracted with CH_2Cl_2 (2 × 75 mL) and the combined organic extracts were dried with $MgSO_4$. Most of the solvent was removed under reduced pressure, followed by further evaporation of the solvent in vacuo, affording a light yellow, glassy solid. Yield: 440 mg (89%). $C_{30}H_{30}N_4O_3$ (494.6). MS (EI): *m*/*z* = 494 (3) $[M]^+$, 463 (1) $[M - OCH_3]^+$, 435 (2) $[M - CO_2CH_3]^+$, 402 (100) $[M - C_6H_6N]^+$. ^1H NMR ($CDCl_3$, 250.13 MHz): δ = 8.49 (m, 2 H, H_{pyr}), 7.63 (m, 4 H, H_{Ar}), 7.50 (d, $^3J_{H,H}$ = 7.9 Hz, 2 H, H_{Ar}), 7.43 (d, $^3J_{H,H}$ = 7.9 Hz, 2 H, H_{Ar}), 7.24 (m, 3 H, H_{Ar}), 7.01 (m, 4 H, H_{Ar}), 6.57 (d, $^3J_{H,H}$ = 8.2 Hz, 1 H), 5.06 (m, 1 H, $C_\alpha H$), 3.76 (s, 4 H, CH_2), 3.72 (s, 3 H, OCH_3), 3.68 (s, 2 H, $CH_{2,Bz}$), 3.21 (m, 2 H, $C_\beta H_2$). ^{13}C NMR ($CDCl_3$, 62.9 MHz): δ = 172.1 ($C{=}O_{ester}$), 166.9 ($C{=}O_{amide}$), 159.0, 148.7, 142.9, 136.7, 136.0, 132.6, 129.1, 128.8, 128.5, 127.1, 127.0, 122.9, 122.2 (C_{Ar}), 59.7 (CH_2), 58.0 ($CH_{2,Bz}$), 53.6, 52.3 (C_α and OCH_3), 37.6 (C_β).

Compound 7b: The dipeptide Boc-Ala-Phe-OMe (350 mg, 1.0 mmol) was dissolved in CH_2Cl_2 (5 mL) and CF_3CO_2H (10 mL), and the mixture was stirred for 1 h at room temperature. After removal of the solvent in vacuo, Et_2O (15 mL) was added to the residue, followed by removal of the solvent in vacuo. This last step was performed three times in order to remove any traces of trifluoroacetic acid. The solid, white residue was suspended in CH_3CN (10 mL), followed by addition of NEt_3 (1.50 mL, 1.09 g, 10.8 mmol), compound **6** (333 mg, 1.0 mmol), and TBTU (323 mg, 1.0 mmol). After the mixture had been stirred at ambient temperature for 30 min, the solvent was removed in vacuo. To the sticky residue was added CH_2Cl_2 (100 mL), followed by filtration to remove ammonium salts. The CH_2Cl_2 solution was washed with aqueous $NaHCO_3$ (2 M, 75 mL), followed by separation of the phases. The aqueous phase was extracted with CH_2Cl_2 (2 × 75 mL), and the combined organic extracts were dried with $MgSO_4$. Most of the CH_2Cl_2 was removed under reduced pressure, followed by further evaporation of the solvent in vacuo, affording a white glassy solid. Yield: 520 mg (92%). $C_{33}H_{35}N_5O_4$ (565.7). MS (EI): *m*/*z* = 565 (6) $[M]^+$, 534 (3) $[M - OCH_3]^+$, 506 (1) $[M - CO_2CH_3]^+$, 473 (100) $[M - C_6H_6N]^+$. ^1H NMR ($CDCl_3$, 400.13 MHz): δ = 8.51 (app. d, 2 H, H_{Pyr}), 7.69 (m, 4 H, H_{Ar}), 7.53 (d, $^3J_{H,H}$ = 7.9 Hz, 2 H, H_{Ar}), 7.46 (d, $^3J_{H,H}$ = 7.9 Hz, 2 H, H_{Ar}), 7.18 (m, 2 H, H_{Ar}), 7.06 (m, 5 H, H_{Ar}), 6.92 (m, 2 H, both NH), 4.80 (m, 1 H, $C_\alpha H$), 4.66 (m, 1 H, $C_\alpha H$), 3.91 (s, 4 H, CH_2), 3.82 (s, 2 H, $CH_{2,Bz}$), 3.67 (s, 3 H, OCH_3), 3.09 (m, 1 H, $C_{\beta,Phe}H$), 3.00 (m, 1 H, $C_{\beta,Phe}H$), 1.40 (d, $^3J_{H,H}$ = 7.0 Hz, 3 H, CH_3). ^{13}C NMR ($CDCl_3$, 100.6 MHz): δ = 172.0, 171.7 ($C{=}O_{ester}$ and $C{=}O_{Ala\text{-}Phe}$), 166.7 (C=O), 157.7, 148.4, 137.3, 135.7, 132.9, 129.2, 129.1, 128.4, 127.3, 127.0, 123.5, 122.6 (C_{Ar}), 59.2 (CH_2), 58.1 ($CH_{2,Bz}$), 53.4, 52.3 (OCH_3 and $C_{\alpha,Phe}$), 49.0 ($C_{\alpha,Ala}$), 37.7 ($C_{\beta,Phe}$), 18.2 ($CH_{3,Ala}$).

Compound 8a: A solution of **7a** (0.40 g, 0.80 mmol) in THF (10 mL) was added dropwise to a stirred solution of $Mo(CO)_3(NCEt)_3$ (0.28 g, 0.80 mmol) in THF (15 mL). The mixture was stirred for 10 min at room temperature, during which an orange precipitate formed. The mixture was concentrated to about 15 mL in vacuo, and the orange solid was collected by filtration, washed with Et_2O (10 mL) and dried in vacuo. Yield: 0.44 g (82%). $C_{33}H_{30}MoN_4O_6$ (674.55): calcd. C 58.76, H 4.48, N 8.31; found C 53.13, H 4.67, N 8.92; (repeated attempts did not improve the C values). IR (KBr): $\tilde{\nu}$ = 1900 (vs) ν_{CO}, 1779 (s) ν_{CO}, 1759 (s) ν_{CO} + $\nu_{C=O}$. IR (THF): $\tilde{\nu}$ = 1906 (vs), 1793 (s), 1782 (s) ν_{CO}. MS (FAB-pos.; dimethoxybenzyl alcohol): *m*/*z* = 676 $[M]^+$, 648 $[M - CO]^+$. ^1H NMR (CD_3CN, 500.35 MHz): δ = 8.77 (m, 2 H, H_{Pyr}), 7.81 (d, $^3J_{H,H}$ = 8.1 Hz, 2 H, H_{Ar}), 7.62 (d, $^3J_{H,H}$ = 8.1 Hz, 2 H, H_{Ar}), 7.49 (m, 2 H, H_{Ar}), 7.31 (m, 5 H, NH and $H_{Ar,Phe}$), 7.24 (m, 1 H, $H_{Ar,Phe}$), 7.00 (m, 4 H, H_{Pyr}), 4.92 (m, 1 H, $C_\alpha H$), 4.76 (s, 2 H, $CH_{2,Bz}$), 4.51 (d, $^2J_{H,H}$ = 15.4 Hz, 2 H, CH_2), 3.73 (dd, $^2J_{H,H}$ = 15.4, $^4J_{H,H}$ = 1.6 Hz, 2 H, CH_2), 3.69 (s, 3 H, OCH_3), 3.32 (m, 1 H, $C_\beta H$), 3.17 (m, 1 H, $C_\beta H$). ^{13}C NMR (CD_3CN, 125.8 MHz): δ = 232.3, 231.3 (CO), 173.1 ($C{=}O_{ester}$), 167.4 ($C{=}O_{amide}$), 159.8, 151.7, 138.4, 138.3, 137.1, 135.0, 132.8, 130.2, 129.5, 128.2, 127.8, 124.1, 123.3 (C_{Ar}), 70.4 ($CH_{2,Bz}$), 65.5 (CH_2), 55.2, 52.9 (OCH_3 + C_α), 38.0 (C_β).

Compound 8b: A solution of **7b** (0.40 g, 0.80 mmol) in THF (10 mL) was added dropwise to a stirred solution of $Mo(CO)_3(NCEt)_3$ (0.28 g, 0.80 mmol) in THF (15 mL). Stirring was continued for 10 min at room temperature, during which an orange precipitate formed. The mixture was concentrated to about 15 mL in vacuo, and the orange solid was collected by filtration, washed with Et_2O (10 mL) and dried in vacuo. Yield: 0.47 g (79%). $C_{36}H_{35}MoN_5O_7$ (745.63): calcd. C 57.99, H 4.73, N 9.39; found C 58.09, H 4.82, N 9.26. IR (KBr): $\tilde{\nu}$ = 1900 (vs) ν_{CO}, 1778 (s) ν_{CO}, 1761 (s) ν_{CO} + $\nu_{C=O}$. IR (THF): $\tilde{\nu}$ = 1906 (vs), 1793 (s), 1782 (s) ν_{CO}. MS (FAB-pos.; dimethoxy benzyl alcohol): *m*/*z* = 747 $[M]^+$, 719 $[M - CO]^+$. ^1H NMR ([D$_6$]DMSO, 500.35 MHz): δ = 8.69 (app. d, 2 H, H_{Pyr}), 8.49 (d, $^3J_{H,H}$ = 7.6 Hz, 1 H, NH), 8.30 (d, $^3J_{H,H}$ = 7.6 Hz, 1 H, NH), 7.97 (d, $^3J_{H,H}$ = 8.1 Hz, 2 H, H_{Ar}), 7.80 (d, $^3J_{H,H}$ = 8.1 Hz, 2 H, H_{Ar}), 7.59 (pseudo t, 2 H, H_{Pyr}), 7.22 (m, 5 H, $H_{Ar,Phe}$), 7.15 (app. d, 2 H, H_{Pyr}), 7.09 (pseudo t, 2 H, H_{Ar}), 4.72 (s, 3 H, $CH_{2,Bz}$ and CH_2), 4.69 (d, $^4J_{H,H}$ = 3.4 Hz, 1 H, CH_2), 3.71 (dd, $^2J_{H,H}$ = 15.7, $^4J_{H,H}$ = 3.4 Hz, 2 H, CH_2), 4.56 (m, 1 H, $C_\alpha H$), 4.50 (m, 1 H, $C_\alpha H$), 3.59 (s, 3 H, OCH_3), 3.03 (m, 1 H, $C_\beta H_{Phe}$), 2.99 (m, 1 H, $C_\beta H_{Phe}$), 1.32 (d, $^3J_{H,H}$ = 7.2 Hz, 3 H, $CH_{3,Ala}$). ^{13}C NMR ([D$_6$]DMSO, 125.8 MHz): δ = 231.2, 230.3 (CO), 172.4, 171.8 ($C{=}O_{ester}$ + $C{=}O_{Ala}$), 165.6 (C=O), 158.8, 150.0, 137.5, 137.0, 135.4, 134.0, 131.4, 129.1, 128.2, 127.5, 126.5, 123.0, 122.3 (C_{Ar}), 68.9 ($CH_{2,Bz}$), 64.2 (CH_2), 53.6, 51.8 ($C_{\alpha,Phe}$ and OCH_3), 48.6 ($C_{\alpha,Ala}$), 36.6 ($C_{\beta,Phe}$), 17.7 ($CH_{3,Ala}$).

X-ray Crystallography: Transparent yellow single crystals of **1** and **2** were coated with perfluoropolyether, picked up with glass fibres and mounted on a Nonius Kappa-CCD diffractometer, equipped with a rotating Mo anode setup. An orange/yellow crystal of **4** was mounted on a Siemens SMART diffractometer with a sealed X-ray tube. Both diffractometers were equipped with graphite monochromators [λ(Mo-K_α) = 0.71073 Å] and a cryogenic nitrogen stream operating at 100(2) K. Crystallographic data of the compounds are listed in Table 6. Cell constants were obtained from a least-squares fit of the diffraction angles of several thousand strong reflections. Intensity data were corrected for Lorentz and polarisation effects. Crystal faces of **4** were determined and the face-indexed correction routine embedded in SHELXTL[41] was used to account for absorption, giving minimum and maximum transmission factors of 0.642 and 0.882. Intensity data of **2** were corrected by use of the

Table 6. Crystallographic data for **1**, **2**, and **4**

Compound	**1**	**2**	**4**
Empirical formula	$C_{15}H_{13}MoN_3O_3$	$C_{22}H_{19}MoN_3O_3$	$C_{24}H_{26}BrF_6Mo_2N_6O_4P$
Formula mass	379.22	469.34	879.27
Crystal size [mm]	0.27 × 0.18 × 0.10	0.22 × 0.06 × 0.03	0.50 × 0.30 × 0.06
Crystal system	orthorhombic	monoclinic	monoclinic
Space group	$Pna2_1$	Cc	$P2_1/n$
a [Å]	15.347(3)	7.1786(3)	13.0262(9)
b [Å]	8.449(2)	32.6222(5)	9.4274(7)
c [Å]	22.454(4)	17.2691(8)	24.258(2)
β [°]	90	96.09(2)	99.15(2)
V [Å^3]	2911.5(10)	4021.3(4)	2941.1(4)
Z	8	8	4
ρ (calcd.) [g/cm^3]	1.730	1.550	1.986
Absorption coefficient [mm^{-1}]	0.917	0.681	2.347
F(000)	1520	1904	1728
T [K]	100(2)	100(2)	100(2)
θ range for data collection [°]	2.58−23.99	2.37−32.50	1.67−32.50
Reflections collected	13280	32679	30836
Independent reflections/R(int)	3516/0.1324	12102/0.0738	10168/0.0354
Observed reflections [$I > 2\sigma(I)$]	2557	10853	8030
Data/restraints/parameters	3487/1/397	12077/2/523	10168/0/397
$R1$[a] /$wR2$[b](obsd. data)	0.0559/0.1269	0.0389/0.0913	0.0324/0.0732
$R1$[a] and $wR2$[b] (all data)	0.1024/0.2085	0.0522/0.1213	0.0493/0.0781
Goodness-of-fit on F^2 [c]	1.063	1.009	0.998
Largest diff. peak/hole [e/Å^3]	1.018/−1.038	0.764/−1.577	1.326/−0.843

[a] $R1 = \Sigma||F_o| - |F_c||/\Sigma|F_o|$. [b] $wR2 = [\Sigma[w(F_o^2 - F_c^2)^2]/\Sigma[w(F_o^2)_2]^{1/2}$, where $w = 1/\sigma^2(F_o^2) + (aP)^2 + bP$, $P = (F_o^2 + F_c^2)/3$. [c] GooF = $\{\Sigma[w(F_o^2 - F_c^2)^2]/(n - p)\}^{1/2}$, where n = no. of refl. and p = number of refined parameters.

semiempirical correction program MULSCANABS, part of the PLATON99[66] program suite, giving transmission factors of 0.757 and 0.944. Intensity data of **1** were left uncorrected. The Siemens SHELXTL[41] software package was used for solution, refinement, and depiction of the structures, and neutral atom scattering factors of the program were used. Non-hydrogen atoms were refined anisotropically, and hydrogen atoms were placed at calculated positions and refined as riding atoms with isotropic displacement parameters. CCDC-168208 (**1**), -168209 (**2**) and -168210 (**4**) contain the supplementary crystallographic data for this paper. These data can be obtained free of charge at www.ccdc.cam.ac.uk/conts/retrieving.html or from the Cambridge Crystallographic Data Centre, 12, Union Road, Cambridge CB2 1EZ, UK [Fax: (internat.) + 44-1223/336-033; E-mail: deposit@ccdc.cam.ac.uk].

Acknowledgments

The experimental work described in this article was carried out at the Max-Planck-Institut für Strahlenchemie. The authors are grateful to Professor K. Wieghardt for generous support of our work and to Professor P. Chaudhuri for many helpful discussions. Dr. E. Bill is thanked for his help with the EPR spectroscopic data acquisition and interpretation. Kerstin Sand and Jörg Bitter are kindly acknowledged for recording the NMR spectra. Heike Schucht and Petra Höfer are thanked for their technical assistance with the X-ray crystal structure determination and spectro-electrochemical measurements, respectively. This work was supported financially by the Fond der Chemischen Industrie and a Karl-Ziegler fellowship (N. M.-N.).

[1] G. Jaouen, A. Vessières, I. S. Butler, *Acc. Chem. Res.* **1993**, *26*, 361−369.
[2] M. Salmain, A. Vessières, P. Brossier, I. S. Butler, G. Jaouen, *J. Immun. Meth.* **1992**, *148*, 65−75.
[3] N. Metzler-Nolte, *Angew. Chem.* **2001**, *113*, 1072−1076; *Angew. Chem. Int. Ed.* **2001**, *40*, 1040−1043.
[4] A. Vessières, M. Salmain, P. Brossier, G. Jaouen, *J. Pharm. Biomed. Anal.* **1999**, *21*, 625−633.
[5] R. L. Cox, T. D. Schneider, M. D. Koppang, *Anal. Chim. Acta* **1992**, *262*, 145−159.
[6] H. Eckert, M. Koller, *J. Liq. Chromatogr.* **1990**, *13*, 3399−3414.
[7] D. R. van Staveren, T. Weyhermüller, N. Metzler-Nolte, *Organometallics* **2000**, *19*, 3730−3735.
[8] D. R. van Staveren, E. Bill, E. Bothe, T. Weyhermüller, M. Bühl, N. Metzler-Nolte, *Chem. Eur. J.*, in print.
[9] D. R. van Staveren, E. Bothe, T. Weyhermüller, N. Metzler-Nolte, *Chem. Commun.* **2001**, 131−132.
[10] D. D. Cox, S. J. Benkovic, L. M. Bloom, F. C. Bradley, M. J. Nelson, L. Que, Jr., D. E. Wallick, *J. Am. Chem. Soc.* **1988**, *110*, 2026−2032.
[11] N. Niklas, O. Walter, R. Alsfasser, *Eur. J. Inorg. Chem.* **2000**, 1723−1731.
[12] D. R. van Staveren, Ph.D. Thesis (Doktorarbeit), Ruhr-Universität, Bochum, **2001**.
[13] J. K. Romary, J. D. Barger, J. E. Bunds, *Inorg. Chem.* **1968**, *7*, 1142−1145.

[14] B. de Bruin, J. A. Brands, J. J. J. M. Donners, M. P. J. Donners, R. de Gelder, J. M. M. Smits, A. W. Gal, A. L. Spek, *Chem. Eur. J.* **1999**, *5*, 2921−2936.
[15] H. A. Jenkins, G. P. A. Yap, R. J. Puddephatt, *Organometallics* **1997**, *16*, 1946−1955.
[16] B. J. Brisdon, M. Cartwright, A. G. W. Hodson, M. F. Mahon, K. C. Molloy, *J. Organomet. Chem.* **1992**, *435*, 319−335.
[17] H. Kelm, H.-J. Krüger, *Eur. J. Inorg. Chem.* **1998**, 1381−1385.
[18] M. Rossignoli, P. V. Bernhardt, G. A. Lawrance, *J. Chem. Soc., Dalton Trans.* **1997**, 4247−4250.
[19] S. P. van Kouwenberg, E. H. Wong, G. R. Weisman, E. J. Gabe, F. L. Lee, P. Jackson, *Polyhedron* **1989**, *8*, 2333−2338.
[20] F. A. Cotton, G. A. Rusholme, A. Shaver, *J. Coord. Chem.* **1973**, *3*, 99−104.
[21] K.-B. Shiu, J. Y. Lee, Y. Wang, M.-C. Cheng, S.-L. Wang, F.-L. Liao, *J. Organomet. Chem.* **1993**, *453*, 211−219.
[22] C. P. Marabella, J. H. Enemark, *J. Organomet. Chem.* **1982**, *226*, 57−62.
[23] T. J. Desmond, F. J. Lalor, G. Ferguson, M. Parvez, *J. Organomet. Chem.* **1984**, *277*, 91−97.
[24] I. T. MacLeod, E. R. T. Tiekink, C. G. Young, *J. Organomet. Chem.* **1996**, *506*, 301−306.
[25] G. Haselhorst, S. Stoetzel, A. Strassburger, W. Walz, K. Wieghardt, B. Nuber, *J. Chem. Soc., Dalton Trans.* **1993**, 83−90.
[26] N. L. Armanasco, M. V. Baker, M. R. North, B. W. Skelton, A. H. White, *J. Chem. Soc., Dalton Trans.* **1998**, 1145−1149.
[27] A. Chandrasekeran, S. S. Krishnamurthy, M. Nethaji, *Curr. Sci.* **1991**, *60*, 700−701.
[28] A. Chandrasekeran, S. S. Krishnamurthy, M. Nethaji, *J. Chem. Soc., Dalton Trans.* **1994**, 63−68.
[29] G. G. Aleksandrov, V. N. Babin, A. P. Kharchenikov, Y. T. Struchkov, N. S. Kochetkova, *J. Organomet. Chem.* **1984**, *266*, 109−116.
[30] C.-Y. Kuo, Y.-S. Fuh, J.-Y. Shiue, S. J. Yu, G.-H. Lee, S.-M. Peng, *J. Organomet. Chem.* **1999**, *588*, 260−267.
[31] R. W. Hay, I. Fraser, G. Ferguson, *J. Chem. Soc., Chem. Commun.* **1987**, 1715−1716.
[32] R. W. Hay, I. Fraser, G. Ferguson, *J. Chem. Soc., Dalton Trans.* **1989**, 2183−2186.
[33] T. M. Bockman, J. K. Kochi, *New J. Chem.* **1992**, *16*, 39−49.
[34] F. A. Cotton, R. M. Wing, *Inorg. Chem.* **1965**, *4*, 314−317.
[35] P. Chaudhuri, K. Wieghardt, Y.-H. Tsai, C. Krüger, *Inorg. Chem.* **1984**, *23*, 427−432.
[36] K. Wieghardt, M. Hahn, W. Swiridoff, J. Weiss, *Angew. Chem.* **1983**, *95*, 499−500; *Angew. Chem. Int. Ed. Engl.* **1983**, *22*, 491−492.
[37] R. Hazama, K. Umakoshi, A. Ichimura, S. Ikari, Y. Sasaki, T. Ito, *Bull. Chem. Soc. Jpn.* **1995**, *68*, 456−468.
[38] A. Kojima, S. Ooi, Y. Sasaki, K. Z. Suzuki, K. Saito, H. Kuroya, *Bull. Chem. Soc. Jpn.* **1981**, *54*, 2457−2465.
[39] K. Z. Suzuki, Y. Sasaki, S. Ooi, K. Saito, *Bull. Chem. Soc. Jpn.* **1980**, *53*, 1288−1298.
[40] H. Günther, *NMR Spectroscopy*, John Wiley & Sons, New York, **1980**.
[41] *SHELXTL V. 5*, Siemens Analytical X-ray Instruments, Inc. **1994**.
[42] M. Minelli, J. H. Enemark, R. T. C. Brownlee, M. J. O'Connor, A. G. Wedd, *Coord. Chem. Rev.* **1985**, *68*, 169−278.
[43] D. Rehder, *Coord. Chem. Rev.* **1991**, *110*, 161−210.
[44] R. T. C. Brownlee, M. J. O'Connor, B. P. Shehan, A. G. Wedd, *J. Magn. Res.* **1985**, *64*, 142−144.
[45] K. Wieghardt, M. Gutmann, P. Chaudhuri, W. Gebert, M. Minelli, C. G. Young, J. H. Enemark, *Inorg. Chem.* **1985**, *24*, 3151−3155.
[46] A. F. Masters, R. T. C. Brownlee, M. J. O'Connor, A. G. Wedd, J. D. Cotton, *J. Organomet. Chem.* **1980**, *195*, C17−C20.
[47] E. C. Alyea, A. Somogyvari, in: H. F. Barry, P. C. H. Mitchell (Eds.), *Proceedings of the Climax Fourth International Conference on the Chemistry and Uses of Molybdenum*, Climax Molybdenum Company, Ann Arbor, MI, **1982**, p. 46.
[48] G. Backes-Dahmann, W. Herrmann, K. Wieghardt, J. Weiss, *Inorg. Chem.* **1985**, *24*, 485−491.
[49] J. H. MacNeil, A. W. Roszak, M. C. Baird, K. F. Preston, A. L. Rheingold, *Organometallics* **1993**, *12*, 4402−4412.
[50] T. Beissel, B. S. P. C. Della Vedova, K. Wieghardt, R. Boese, *Inorg. Chem.* **1990**, *29*, 1736−1741.
[51] S. Trofimenko, *J. Am. Chem. Soc.* **1969**, *91*, 588−595.
[52] M. D. Curtis, K.-B. Shiu, W. M. Butler, J. C. Huffman, *J. Am. Chem. Soc.* **1986**, *108*, 3335−3343.
[53] K.-B. Shiu, L.-Y. Lee, *J. Organomet. Chem.* **1988**, *348*, 357−360.
[54] M. D. Curtis, K.-B. Shiu, *Inorg. Chem.* **1985**, *24*, 1213.
[55] M. Savignac, A. Sasaki, P. Potier, G. Jaouen, *J. Chem. Soc., Chem. Commun.* **1991**, 615−617.
[56] B. El Mouatassim, H. Elamouri, J. Vaissermann, G. Jaouen, *Organometallics* **1995**, *14*, 3296−3302.
[57] D. Osella, M. Ravera, M. Vincenti, M. Salmain, G. Jaouen, *Organometallics* **1996**, *15*, 3037−3041.
[58] A. Gorfti, M. Salmain, G. Jaouen, *J. Chem. Soc., Chem. Commun.* **1994**, 433−434.
[59] A. Gorfti, M. Salmain, G. Jaouen, M. J. McGlinchey, A. Bennouna, A. Mousser, *Organometallics* **1996**, *15*, 142−151.
[60] M. Salmain, M. Gunn, A. Gorfti, S. Top, G. Jaouen, *Bioconjugate Chem.* **1993**, *4*, 425−433.
[61] A. Varenne, A. Vessières, S. M. S. Durand, P. Brossier, G. Jaouen, *Anal. Biochem.* **1996**, *242*, 172−179.
[62] M. Salmain, A. Vessières, A. Varenne, P. Brossier, G. Jaouen, *J. Organomet. Chem.* **1999**, *589*, 92−97.
[63] E. Bill, *GFIT*, unpublished.
[64] S. Dick, A. Weiss, *Z. Naturforsch., Teil B* **1997**, *52*, 188−192.
[65] G. J. Kubas, L. S. van der Sluys, *Inorg. Synth.* **1990**, *28*, 29−33.
[66] A. L. Spek, *PLATON, A Multipurpose Crystallographic Tool*, Utrecht University, Utrecht, The Netherlands, **1999**.

Received August 14, 2001
[I01310]

Synthesis, Characterization, and Interconversion of the Rhenium Polyhydrides $[ReH_3(\eta^4\text{-}NP_3)]$ and $[ReH_4(\eta^4\text{-}NP_3)]^+$ {NP_3 = tris[2-(diphenylphosphanyl)-ethyl]amine}

Alberto Albinati,[a] Vladimir I. Bakhmutov,*[b] Natalia V. Belkova,[c] Claudio Bianchini,*[d] Isaac de los Rios,[d] Lina Epstein,*[c] Evgenii I. Gutsul,[c] Lorenza Marvelli,[e] Maurizio Peruzzini,*[d] Roberto Rossi,*[e] Elena Shubina,[c] Evgeni V. Vorontsov,[c] and Fabrizio Zanobini[d]

Keywords: Rhenium / Tripodal ligands / Phosphanes / Hydride ligands

The rhenium(III) dichloride complex $[ReCl_2(\eta^4\text{-}NP_3)]Cl$ (**1**) was prepared from $[ReCl_3(CH_3CN)(PPh_3)_2]$ by treatment with the tripodal tetradentate ligand $N(CH_2CH_2PPh_2)_3$ (NP_3) in ethanol. The reaction of **1** with $LiAlH_4$ in THF gave the rhenium(III) trihydride $[ReH_3(\eta^4\text{-}NP_3)]$ (**2**), which was converted into the rhenium(V) tetrahydride $[ReH_4(\eta^4\text{-}NP_3)]BPh_4$ (**3**) by protonation in CH_2Cl_2 with $HBF_4{\cdot}OMe_2$, followed by a metathetical reaction with $NaBPh_4$. The classical polyhydride nature of **2** and **3**, as well as the overall molecular structures in solution, were determined by NMR spectroscopy, ^1H NMR relaxation, and IR spectroscopy. The polyhydride complexes **2** and **3** are stereochemically nonrigid in solution, and the thermodynamic parameters associated with the fluxional processes were determined by variable-temperature NMR studies. A single-crystal X-ray analysis of **3** has shown the complex cation $[ReH_4(\eta^4\text{-}NP_3)]^+$ to be eight-coordinated by the four donor atoms of NP_3 and by four terminal hydride ligands in a distorted dodecahedral geometry. An in situ IR study in CH_2Cl_2 has shown that the protonation of **3** occurs regioselectively at the metal center with no formation of a dihydrogen complex. Kinetic hydrogen bond products of the formula $[(\eta^4\text{-}NP_3)H_3Re{\cdots}HOR]$ (ROH = C_2H_5OH, CFH_2CH_2OH, CF_3CH_2OH) were intercepted by IR spectroscopy at low temperature. The thermodynamic parameters associated with the formation of the hydrogen bond adducts were determined by either IR spectroscopy applying the Iogansen equation or van't Hoff plots of the formation constant vs. temperature.

Introduction

In conjunction with phosphane ligands, rhenium can form stable polyhydride complexes in a variety of metal oxidation states, coordination numbers, and structures.[1] In particular, both classical ($Re-H_x$) and nonclassical $[Re-(H_2)_x]$ structures have been reported, which may contain as many as seven hydride ligands.[1] The ability to react with either dihydrogen or hydride ions from different sources makes phosphanerhenium systems effective hydrogen sponges. Unlike late transition metals, however, the coordinated hydrogen is not easily transferred to unsaturated substrates, which limits the application of rhenium-based catalysts in catalytic hydrogenations.[2] On the other hand, the capability to form homologous series of polyhydride complexes, often in equilibrium with each other by dihydrogen loss/uptake, confers to phosphanerhenium compounds a great potential both in hydrogen storage and transport, which will be a priority in chemistry in the next years,[3] and for model studies of hydride-containing enzymes such as nitrogenases and hydrogenases.[4] Moreover, the chemistry of rhenium is very similar to that of the germane element technetium-99, which is largely used in diagnostics and radio therapeutics.[5] Although we are not aware of any utilization of technetium-99 or rhenium-186/188 polyhydrides (polydeuterides), it cannon be excluded a priori that such compounds may have important applications in nuclear medicine.

Tripodal polyphosphane ligands are particularly amenable to forming stable polyhydride rhenium compounds due to the nucleophilicity of trivalent phosphorus as well as the ability to generate sterically congested pockets into which the metal atom is almost buried. These ligands may therefore react only with small molecules or ions.[6]

[a] Istituto Chimico, Farmaceutico e Tossicologico, Università di Milano,
Milano, Italy
[b] Centro de Investigación y de Estudios Avanzados del I. P. N., Apdo postal 14-740, 07000 México D.F., México
E-mail: vladimir@mail.cinvestav.mx
[c] A. N. Nesmeyanov Institute of Organoelement Compounds, Vavilov str. 28, V-334, Moscow, Russia, 117813
E-mail: epst@ineos.ac.ru
[d] Istituto di Chimica dei Composti Organo Metallici, ICCOM-CNR,
Via J. Nardi 39, 60132 Firenze, Italy
E-mail: bianchin@fi.cnr.it, peruz@fi.cnr.it
[e] Dipartimento di Chimica, Università di Ferrara,
Via Borsari 46, 44100 Ferrara, Italy
E-mail: mg1@dns.unife.it

 © WILEY-VCH Verlag GmbH, 69451 Weinheim, Germany, 2002 1434−1948/02/0606−1530 $ 20.00+.50/0 *Eur. J. Inorg. Chem.* **2002**, 1530−1539

The "hydride" chemistry of rhenium with the tripodal tridentate ligand $MeC(CH_2PPh_2)_3$ (triphos) has been intensely investigated in the last few years, leading to interesting results with regard to the formation of classical and nonclassical polyhydrides with the metal center in the oxidation states from +1 to +7.[7−9] In contrast, no rhenium complex with the potentially tetradentate aminophosphane $N(CH_2CH_2PPh_2)_3$ (NP_3) has been described in the literature, which is surprising as (NP_3)metal complexes are known for almost all middle and late-transition metals[6,10] including technetium.[11] A rhenium(III) tetrahydride with the tripodal phosphane ligand $P(CH_2CH_2PPh_2)_3$ has been described, but no X-ray structure was reported.[12]

The presence of the amine nitrogen donor and of two CH_2 spacers separating the phosphorus donors from the bridgehead atom makes NP_3 more flexible than triphos and also increases the overall basicity at the coordinated metal center.[13,14] Ultimately, this may result in increased stability of Re−H_x moieties as well as a richer diversity of coordination geometries since NP_3 may act as an η^4, η^3-*P*$_3$, η^3-*N*,*P*,*P*, and η^2-*P*,*P* ligand.[14]

In this article we describe the synthesis, structure, and spectroscopic characterization of the first rhenium(III) and rhenium(V) polyhydride complexes stabilized by NP_3, using $[ReCl_2(\eta^4\text{-}NP_3)]Cl$ (**1**) as a precursor. Particular attention was paid to the study of the solution structure of the complexes $[ReH_3(\eta^4\text{-}NP_3)]$ (**2**) and $[ReH_4(\eta^4\text{-}NP_3)]BPh_4$ (**3**), as well as the proton transfer that converts **2** into **3** via hydrogen bond adducts $[(\eta^4\text{-}NP_3)H_3Re\cdots HOR]$.

Results and Discussion

The preparations and the principal reactions described in this paper are reported in Scheme 1. Selected IR spectroscopic data for the new complexes are given in the Exp. Sect. together with analytical and physicochemical properties.

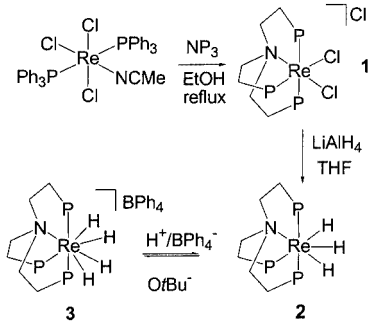

Scheme 1

Synthesis and Characterization of $[ReCl_2(\eta^4\text{-}NP_3)]Cl$ (1)

By reaction of NP_3 with the rhenium(III) complex $[ReCl_3(CH_3CN)(PPh_3)_2]$ in refluxing ethanol, the complex $[ReCl_2(\eta^4\text{-}NP_3)]Cl$ (**1**) was obtained in good yield as air-stable lemon-yellow microcrystals. The combined analytical, conductivity and spectroscopic characterization of **1** is unequivocally consistent with an octahedral geometry of the complex cation $[ReCl_2(\eta^4\text{-}NP_3)]^+$ with all the four donor atoms of NP_3 coordinated to the metal center. Complex **1** is paramagnetic (μ_{eff} = 2.0 μ_B) and thus the $^{31}P\{^1H\}$ NMR spectrum did not provide any useful information due to the rapid relaxation of the coordinated phosphorus nuclei. The ^1H NMR spectrum exhibit the typical Knight-shifted appearance[7] with relatively sharp resonances, some of which feature unusually large shifts (up to $\delta = -40.83$).

Synthesis and Characterization of the Classical Rhenium(III) and Rhenium(V) Polyhydrides $[ReH_3(\eta^4\text{-}NP_3)]$ (2) and $[ReH_4(\eta^4\text{-}NP_3)]BPh_4$ (3)

The dichloride **1** was quantitatively converted into the ivory-colored trihydride complex $[ReH_3(\eta^4\text{-}NP_3)]$ (**3**) by treatment with a large excess (ca. 20 equiv.) of $LiAlH_4$ in refluxing THF for 6 h. The reaction was conveniently monitored by $^{31}P\{^1H\}$ NMR spectroscopy, which showed no intermediate species along the conversion of **1** to **2**.

Complex **2** is air-stable in both the solid state and solutions of both CH_2Cl_2 and $CHCl_3$, in which no H/Cl exchange was observed within 24 h at room temperature. The IR spectrum contains two strong ν(Re−H) absorptions at 1949 and 1905 cm^{-1} that shifted to lower frequencies in the spectrum of the perdeuterated derivative $[ReD_3(\eta^4\text{-}NP_3)]$ (**2-D$_3$**) [ν(Re−D) = 1399 and 1371 cm^{-1}, $k_{H/D}$ = 1.39]. The perdeuterated derivative was prepared by treating **1** with $LiAlD_4$ in refluxing THF.

The trihydride **2** is fluxional on the NMR time scale. In CD_2Cl_2, the slow-exchange $^{31}P\{^1H\}$ NMR spectrum was attained at −63 °C in the form of two broad lines at δ = 52.9 (1 P) and 36.6 (2 P). On increasing the temperature, the two NMR signals coalesced between −30 and −35 °C and then transformed into a single resonance at δ = 41.9 at room temperature. The exchange process of the three phosphorus atoms matches the fluxionality of the hydride resonances. Indeed, the ^1H NMR spectrum of **2** at −63 °C showed two hydride signals at δ = −4.05 (1 H) and −9.50 (2 H) that transformed into a quadruplet at δ = −7.6 with *J*(HP) = 13.4 Hz on increasing the temperature to 22 °C. The coalescence of the hydride resonances was observed at −23 °C from which a free activation energy ($\Delta G^{\neq}_{250K}$) of 44.8 kJ mol^{-1} could be calculated by using the Shanan Atidi-Bar Eli approach that takes into account the different populations of the exchanging sites.[15] The low-temperature limiting spectrum of **2** points to a pentagonal-bipyramidal structure in solution (seven-coordination geometry) that has been already observed for rhenium polyhydrides.[1e,7,12]

Treatment of the trihydride **2** in THF or dichloromethane with protic acids such as $HOSO_2CF_3$, $HBF_4{\cdot}OMe_2$, or CF_3COOH, followed by a metathetical reaction with $NaBPh_4$ in EtOH, gave off-white crystals of the classical tetrahydride complex $[ReH_4(\eta^4\text{-}NP_3)]BPh_4$ (**3**). The protonation is reversible: the reaction with strong bases, such as KO*t*Bu, in THF regenerated the neutral trihydride **2** quantitatively.

Compound **3** was air-stable in both the solid state and solution and behaved as a typical 1:1 electrolyte in dichloro-

methane. The solid-state IR spectrum shows a strong and sharp absorption at 1996 cm^{-1} due to the ν(Re−H) vibration that shifted to 1435 cm^{-1} ($k_{H/D}$ = 1.39) in the perdeuterated derivative $[ReD_4(\eta^4\text{-}NP_3)]BPh_4$ (**3-D$_4$**). It is worth noting that no H/D exchange was observed when a solution of **3** in THF or CH_2Cl_2 was treated with either MeOD or D_2O even after prolonged heating to temperatures close to the boiling point (in situ NMR experiment). This behavior, which is not common for metal polyhydride complexes, is identical to that of the iron trihydride $[Fe(H)(\eta^2\text{-}H_2)(\eta^4\text{-}PP_3)]BPh_4$ containing the tripodal tetradentate ligand $P(CH_2CH_2PPh_2)_3$.[16] The addition of 1 equiv. of CF_3SO_3D to a CD_2Cl_2 solution of **3** at ambient temperature did not result in the incorporation of deuterium. At high temperature, extensive decomposition took place to give paramagnetic material, which was not characterized further.

In keeping with the behavior of the large majority of transition metal polyhydrides,[1e] the complex cation $[ReH_4(\eta^4\text{-}NP_3)]^+$ was stereochemically nonrigid in solution on the NMR time scale. At room temperature, the $^{31}P\{^1H\}$ NMR spectrum in CD_2Cl_2 showed a sharp ($\omega_{1/2} \approx 4$ Hz) singlet resonance at δ = 38.73 associated with a fast-exchange motion of the three phosphorus atoms of NP_3 (A_3 spin system). An off-resonance experiment, conserving a residual coupling between the hydride ions and the phosphorus atoms, transformed the singlet into a quintuplet [$J(PH)_{residual} \approx 7$ Hz], and confirmed the presence of four hydride ions coordinated to the rhenium atom. On decreasing the temperature, the ^{31}P NMR resonance broadened and then coalesced at ca. −70 °C to give a broad hump with $\omega_{1/2} \approx 185$ Hz. Decoalescence of the resonance occurred at a lower temperature, with formation of two distinct signals integrating 2:1. However, the decoalescence process was not complete as the resolution of the expected AM_2 splitting pattern was not observed even at −90 °C (δ = 41.85, $\omega_{1/2}$ = 90 Hz; δ = 33.69, $\omega_{1/2}$ = 89 Hz). Assuming the occurrence of an $A_3 \rightleftarrows A_2M$ exchange and applying the Gutowski−Holm equation corrected for the different population of the exchanging sites, a $\Delta G^{\neq}_{203K}$ value of 36.8 kJ mol^{-1} was estimated at the coalescence temperature.[15,17]

For a further decrease in the temperature down to −115 °C using a 1:1 (v/v) mixture of CD_2Cl_2 and $CFCl_3$ as solvent, the lower field resonance (2 P) significantly broadened and then transformed into a broad hump that was almost merged with the baseline ($\omega_{1/2}$ = 432 Hz). In contrast, the signal at higher field (1 P) became sharper (δ = 33.46, $\omega_{1/2}$ = 24 Hz) without showing any fine structure, however. This NMR behavior suggests the existence of a second dynamic process responsible for the magnetically nonequivalence of the three phosphorus nuclei of NP_3 and also points to an AMX splitting pattern in the slow motion regime.

Figure 1 shows the variable-temperature ^1H NMR spectra in the hydride region of **3**, dissolved in a 1:1 (v/v) mixture of CD_2Cl_2 and $CFCl_3$. At 20 °C, the spectrum showed a narrow quadruplet [$J(HP)$ = 13.1 Hz] centered at δ = −6.62, which is consistent with a complete and fast scrambling of the four hydride ions. A careful NMR integration of this signal, with respect to the aliphatic triphos resonances, confirmed the presence of four hydride ligands. As the temperature was lowered, the hydride resonance lost its multiplicity (−20 °C), transformed into a broad hump (−40 °C, $\omega_{1/2}$ = 64 Hz) before finally coalescing into the baseline (ca. −60 °C). Complete decoalescence of the signal occurred slightly below −90 °C to give two well-separated signals (integrating 1:3), which at −100 °C fell at δ = −3.00 ($\omega_{1/2}$ = 115 Hz) and δ = −7.74 δ ($\omega_{1/2}$ = 85 Hz), respectively. Below this temperature, broadening of both resonances occurred, but freezing out of the solvent did not allow us to obtain any information on the limiting spectrum.

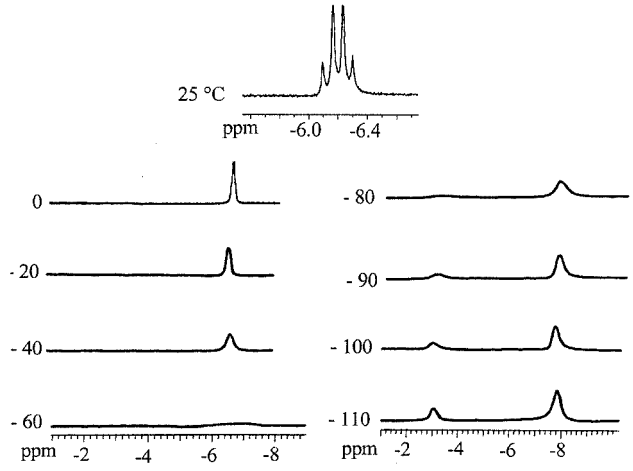

Figure 1. Variable-temperature ^1H NMR spectra in the hydride region of $[ReH_4(\eta^4\text{-}NP_3)]BPh_4$ (**3**) dissolved in a 1:1 (v/v) mixture of $CD_2Cl_2/CFCl_3$ (300 MHz, TMS reference)

The proton NMR spectroscopic data allowed us to calculate the free energy of activation for the process of exchanging the hydride ligands in **3**. A possible mechanism for this exchanged is proposed in Scheme 2.[1e] Introducing a Δν value of 1420 Hz, a $\Delta G^{\neq}_{213K}$ value of 38.1 *k*J mol^{-1} was calculated at the coalescence temperature. Remarkably, this value is in good agreement with the free activation energy obtained from the NMR coalescence analysis of the ^{31}P NMR spectra (vide supra). A line-shape analysis of the ^1H NMR spectra (Figure 1) with the DNMR-5 program in the temperature range from 253 to 183 K gave the following τ values for the less populated low-field signal: 0.0000067 s at 253 K, 0.000013 s at 233 K, 0.00027 s at 213 K, 0.0011 s at 193 K, and 0.0027 s at 183 K. From these values we calculated $\Delta H^{\neq}$ = 33.5 *k*J mol^{-1} and $\Delta S^{\neq}$ = −12.1 *k*J mol^{-1} K^{-1} (note that the slightly negative entropy is consistent with an intramolecular exchange) and hence $\Delta G^{\neq}_{203K}$ = 36.0 *k*J mol^{-1}, which is similar to the value obtained from the coalescence temperature.

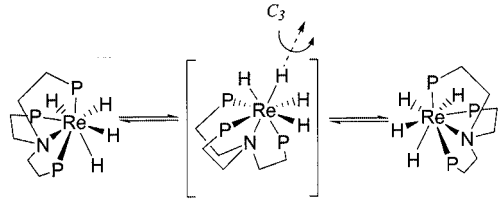

Scheme 2

Relaxation Study of the Rhenium Polyhydrides 2 and 3

The variable-temperature relaxation times T_1 for the hydride ligands in **2** and **3** were measured at different magnetic fields by using the standard inversion-recovery sequence (Table 1).

Table 1. Variable-temperature (T_1) NMR spectroscopic data for $[ReH_3(\eta^4\text{-}NP3)]$ (**2**) and $[ReH_4(\eta^4\text{-}NP_3)]^+$ (**3**)

Temp. [*K*]	T_1 [ms] A	B	C
	$[ReH_3(\eta^4\text{-}NP_3)]$ (400 MHz)[a][b]		
203		198	182
213		142	142
223		131	133
233		130	127
243		129	148
253	140−150		
	$[ReH_4(\eta^4\text{-}NP_3)]^+$ (400 MHz)[c] [b]		
203		125	133
213	96−98		
223	97		
233	98		
243	100		
253	109		
263	109		
	$[ReH_4(\eta^4\text{-}NP_3)]^+$ (300 MHz)[d] [b]		
173		111	106
183		97	94
193		81	86
213	[e]		
233	77		
253	83		
273	96		
293	106		

[a] The T_1 measurements on **2** were carried out at 400 MHz in CD_2Cl_2. [b] The letter A denotes the T_1 values of the hydride ligands in the fast motion regime. The letters B and C indicate the relaxation times of the two kinds of hydride resonances appearing below the coalescence temperature; B, low-field resonance; C, high-field resonance. [c] The T_1 measurements on **3**, prepared in situ from **2** by adding 4 equiv. of CF_3COOH, were carried out at 400 MHz in CD_2Cl_2. [d] The T_1 measurements on an isolated sample of **3** were carried out at 300 MHz in a 1:1 $CD_2Cl_2/CFCl_3$ mixture. [e] Due to broadness of the signal close to the coalescence temperature, no T_1 value is given.

At low temperature, when the hydride−hydride exchange is slow on the NMR time scale, the relaxation times of the two types of hydride ligands in **2** were found to be practically identical. A relatively long T_{1min} value was observed between −50 and −40 °C (129−127 ms) for both hydride resonances supporting the classical nature of the trihydride **2**.

The tetrahydride **3** was prepared in situ as trifluoroacetate salt by adding a fourfold excess of CF_3COOH to a CD_2Cl_2 solution of **2**, and the relaxation times T_1 were initially measured at 400 MHz. A rather small T_{1min} value of 97 ms was determined for the four exchanging hydride ions at ca. −50 °C. Spin-saturation transfer experiments showed the absence of any exchange between the hydride ligands of **3** and protons of the acid, even at −23 °C, which strongly supports the hypothesis that the observed T_{1min} value is undistorted. A comparison of $1/T_{1min}$ measured for both **2** and **3** allowed us to estimate the relaxation contribution to the overall relaxation rate provided by the additional hydride ligand in **3**. Using a contribution of 2.5 s^{-1}, a minimum hydride−hydride distance of 1.84 Å was obtained from Equation (1), in which ν is the spectrometer frequency.[18] The H−H separation estimated in this way nicely supports the classical tetrahydride formulation of **3** and is also consistent with the results of an X-ray structural analysis (see below).

$$r(H-H) = 5.815\,(T_{1min}/\nu)1/6 \quad (1)$$

The interpretation of T_{1min} data in terms of bond lengths in metal polyhydride complexes is affected by a rather high degree of ambiguity, particularly when the different hydride sites cannot be completely frozen out.[19] Additional uncertainty may come also from the contribution of dipolar interactions with the neighboring nuclei in the ancillary ligands that cannot be neglected, and from the presence of a quadrupolar nucleus (i.e. rhenium) which may affect remarkably the observed relaxation rate by a significant metal hydride dipole−dipole interaction.[20,21] In the case at hand, according to the protocol of Halpern and co-workers, a T_{1min} value of ca. 97 ms can be calculated by subtracting the contributions of the rhenium atom and of as many as 12 *ortho* protons of the tripodal ligands to the relaxation rate of **3**, scaled up to 500 MHz.[20] The calculated value is in line with that reported by Crabtree and co-workers for the classical polyhydride $[ReH_6\{PhN(CH_2CH_2PPh_2)_2\}]BF_4$ (T_{1min} = 93 ms),[22] and also matches well the T_{1min} value of 94 ms determined by Morris and co-workers for the cognate complex $[ReH_4(\eta^4\text{-}PP_3)]BF_4$, for which the absence of an intact dihydrogen ligand was suggested on the basis of similar T_1 arguments.[12]

In a second series of NMR experiments, the spin-lattice relaxation times for the hydride ligands in **3** were determined at 300 MHz in the temperature range from +20 to −110 °C in $CD_2Cl_2/CFCl_3$. The results were in line with those obtained using a higher magnetic field. A plot of T_1 [ms] vs. temperature ($1000/T$ [K^{-1}]) is presented in Figure 2, while T_1 data are collected in Table 1. At room temperature, when the four hydride ligands are rapidly exchanging, a relatively short T_1 of 106 ms was measured. As the temperature was lowered to the coalescence point, T_1 also decreased steadily, and at −40 °C, just above the coalescence point, a value of 77 ms was observed. Below the coalescence temperature, the two hydride sites showed longer and comparable relaxation times that increased with decreasing temperature. At −100 °C, when the dynamic process was still far from being completely frozen out, T_1 values as long as 111 and 106 ms were determined for the two distinct hydride resonances. Interpolation of the whole set of data al-

lowed us to find an average T_{1min} value of ca. 71 ms at −50 °C that agrees well, after scaling up to 400 MHz (94 ms), with the relaxation data obtained at higher magnetic field carried out in CD_2Cl_2 solution (97 ms).

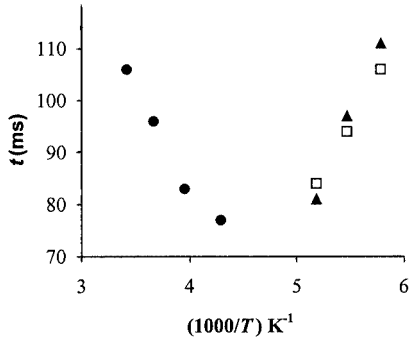

Figure 2. Plot of T_1 [ms; $CD_2Cl_2/CFCl_3$, 1:1 (v/v), 300 MHz] vs. temperature ($1000/T$ [K^{-1}]) for the polyhydride [$ReH_4(\eta^4$-$NP_3)]BPh_4$ (**3**); • T_1 values of the four hydride atoms in the fast-exchange motion ($\delta = -6.62$); □ T_1 values of the hydride signal ($\delta = -3.00$); T_1 values of the hydride signal ($\delta = -7.74$)

Further support for the classical nature of **3** was obtained from a comparison of its variable-temperature T_1 dependence with that exhibited by the authentic η^2-H_2 complex $[Ir(H)_2(H_2)(triphos)]^+$ [triphos = $CH_3C(CH_2PPh_2)_3$].[23] Below the coalescence point, the T_1 times for the two types of hydrides in **3** were found to lengthen considerably (Table 1), while the values for the two hydride ions in the iridium complex with triphos[23] showed a divergent behavior: the relaxation time of the classical hydrides increased, while that of the molecular hydrogen ligand continued to decrease with the temperature.

X-ray Crystal Structure of [$ReH_4(\eta^4$-$NP_3)]BPh_4$ (3)

An ORTEP view of the cation $[ReH_4(\eta^4$-$NP_3)]^+$ is given in Figure 3, while selected bond lengths and angles are listed in Table 2. The immediate coordination sphere of the rhenium atom consists of the nitrogen and phosphorus atoms of the NP_3 moiety and of four hydride ligands. As previously discussed (see Exp. Sect.), only three out of the four hydride ions (labeled as H1, H2, and H3 in Figure 3) were successfully refined. The fourth (H4) is also shown (in the position obtained from the Fourier difference map) to give a pictorial representation of the full coordination polyhedron.

As expected[24,25] for an eight-coordinated polyhydride, complex **3** adopts a distorted dodecahedral geometry in accordance with the ^1H NMR spectroscopic data. The Re−H distances [av. 1.67(7) Å] fall in the expected range, and are similar to those found by low-temperature neutron diffraction in $[ReH_5(PPh_3)_2(indole)]$[26] [av. 1.683(2) Å].

The expected low precision in the location of the hydride ions by X-ray diffraction, prevents a detailed discussion of their geometries. We note, however, that the H···H separations are consistent with both the NMR spectroscopic data and the classical nature of this complex.

Two types of Re−P distances have been found in the complex cation: two shorter [av. 2.376(7) Å] and one longer [2.402(2) Å] due to the influence of a pseudo-*trans*-hydride ion. All Re−P separations fall in the expected range and are comparable, for example, with those found in (triphos)-iridium complexes (2.30−2.40 Å)[27,28] All the other distances are unexceptional and do not deserve additional comment.

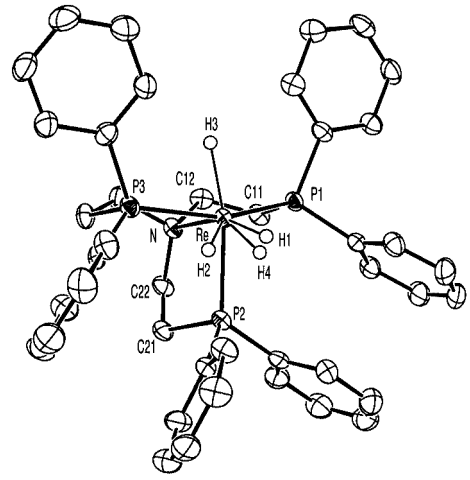

Figure 3. ORTEP view of the complex cation [$ReH_4(\eta^4$-$NP_3)]BPh_4$ (**2**) showing thermal ellipsoids at 30% probability; only H1, H2, and H3 have been refined (see text)

Table 2. Selected bond lengths [Å] and angles [°] for compound **3**, with e.s.d.s values in parentheses

Re−P(1)	2.381(2)	Re−Hy1	1.60(5)
Re−P(2)	2.402(2)	Re−Hy2	1.66(5)
Re−P(3)	2.371(2)	Re−Hy3	1.79(9)
Re−N	2.309(5)		
P(1)−Re−P(2)	98.48(6)	P(1)−Re−Hy1	96(2)
P(1)−Re−P(3)	154.98(6)	P(1)−Re−Hy2	144(2)
P(1)−Re−N	81.5(1)	P(1)−Re−Hy3	85(2)
P(2)−Re−N	81.1(1)	P(2)−Re−Hy3	166(2)
P(2)−Re−P(3)	96.11(6)		
P(3)−Re−N	80.8(1)		

In situ IR Study of the Interaction of 2 with Different Proton Donors

It has been recently demonstrated that proton-transfer reactions such as that occurring in the transformation of **2** into **3** may take place via intermediate species containing M−H···HOR hydrogen bonds.[29,30] A successful strategy to show the eventual formation of hydrogen bond adducts involves an in situ IR study of the interactions between the starting metal (poly)hydride and acids of different strength. We therefore decided to monitor the reactions of **2** with C_2H_5OH, CFH_2CH_2OH (MFE), CF_3CH_2OH (TFE), $CH_2ClCOOH$ (MClA), and CF_3COOH (TFA) by variable-temperature IR spectroscopy in CH_2Cl_2, taking into consideration the variation of the dielectric constant of the solvent with temperature.[30−32]

In the absence of added acid, the IR spectrum of **2** exhibits a complicated absorbance pattern in the ν(M−H) region, which is a common feature to many transition metal

polyhydrides.[33,34] After removing the contribution due to the overtones of the phenyl rings using the spectra of **1** and **2-D$_3$**, the spectrum showed the presence of three overlapped ν(Re−H) bands (1866, 1938, and 1977 cm^{-1}) whose intensities increased with decreasing temperature down to 200 K (see Figure 4a).

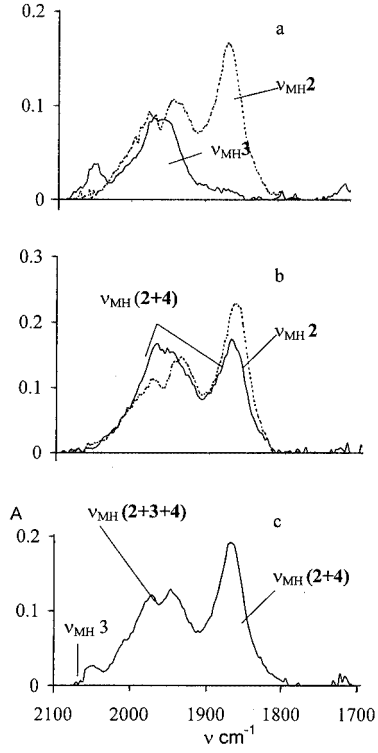

Figure 4. IR spectra in the ν(ReH) region (CH_2Cl_2 solution; −70 °C): a: spectra of **2** alone (0.0.1 M) (- - -) and in the presence of TFA (0.01 M) (———); b: spectra of **2** alone (0.015 M) (- - -) and in the presence of MFE (0.075 M) (———); c: spectrum of **2** (0.014 M) in the presence of TFE (0.014 M)

When a strong proton donor such as TFA or MClA was treated with **2** (metal hydride/acid, 1:1), a plain proton transfer occurred and the classical polyhydride **3** was generated with no detection of any intermediate species along the proton transfer process, i.e. the ν(ReH) stretching of **2** disappeared with concomitant formation of new bands due to **3** at higher energy [1960 (vs) cm^{-1} and 2050 (w) cm^{-1}] (see Figure 4a). The latter band was masked by the phenyl overtones of the tetraphenylborate anion in the solid-state spectrum. In addition, the typical ν(CO) bands of free MClA (1730−1720 cm^{-1}) and TFA (1810−1780 cm^{-1}) were replaced by new strong ν^{as}(OCO) bands due to the carboxylate anions at 1620 and 1685 cm^{-1}, respectively.

In an attempt to intercept a hydrogen bond adduct, weaker acids were used in the protonation of **2**. Indeed, irrespective of the hydrogen donor, the IR spectra in the ν(OH) region obtained at 290 K by addition of **2** (0.04 M) to CH_2Cl_2 solutions containing TFE, C_2H_5OH, or MFE (Table 3)[35] showed that the intensity of the band due to the stretching vibrations of the OH group in the free acid decreased, while a new broad and intense band, assigned to a hydrogen-bonded adduct, appeared at lower frequency. The frequency shifts [$\Delta\nu = \nu(OH)^{free} - \nu(OH)^{bonded}$] was found to increase with the proton-donor ability of the alcohol in the order C_2H_5OH < MFE < TFE.

Table 3. Spectral characteristics of the hydrogen bond adducts [$(NP_3)H_3Re\cdots HOR$] (**4a**−**c**), enthalpy values ($-\Delta H^0$) in CH_2Cl_2 at 290 K and E_j factors

[$(NP_3)H_3Re\cdots HOR$]	$\nu(OH)^{bonded}$ [cm^{-1}]	$\Delta\nu_{OH}$ [cm^{-1}]	$-\Delta H^0$ [kJ mol^{-1}]	E_j
C_2H_5OH (**4a**)	3375	212	18.8	1.45
MFE (**4b**)	3336	244	20.5	1.47
TFE (**4c**)	3220	385	26.4 (24.7)[a]	1.53 (1.45)

[a] The $-\Delta H^0$ value given in parentheses was obtained from the van't Hoff plot (Figure 5).

Once it had been established that the proton-transfer reaction involved in converting **2** to **3** was traversed by a detectable H-bonded intermediate, it only remained to discriminate between the two potential H bond acceptor sites in **2**, i.e. the hydride ligand or the metal center.[36] In reality, although the intermediacy of hydrogen bond adducts of the type ReH···HX, preceding the formation of nonclassical η^2-H_2 species, have been reported to occur in several cases,[29,30,37−40] the rhenium center in **2** possesses a lone electron pair that may be straightforwardly protonated to give the classical hydride **3**. Accordingly, we could not disregard a priori the preliminary formation of a metal-centered Re···HX adduct upon interaction of **2** with the alcohol.

The occurrence of a low frequency shift of the ν(M−H) band has been unequivocally established as a general spectroscopic criterion to assess the formation of hydrogen bonding involving the hydride ligand.[29,30] In the present case, the addition of a weak proton donor such as EtOH, MFE, or TFE to a CH_2Cl_2 solution of **2** did not result in the appearance of any new band or shoulder at *low frequency*. In contrast, either of these alcohols at −70 °C caused a little, but evident, *high frequency* shift (ca. 10 cm^{-1}) of the ν(Re−H) band at 1866 cm^{-1} as well as the envelop of the two other absorptions between 1945 and 1980 cm^{-1} (see Figure 4b). These spectral changes are therefore inconsistent with an interaction between an Re−H moiety and the proton donor, whereas they support the formation of hydrogen-bonded adducts of the type [$(NP_3)H_3Re\cdots HOR$] (**4a**−**c**) as shown in Scheme 3. The occurrence of a metal-centered hydrogen bonding preceding the protonation of the metal atom has been demonstrated for a few organometallic compounds.[41−44]

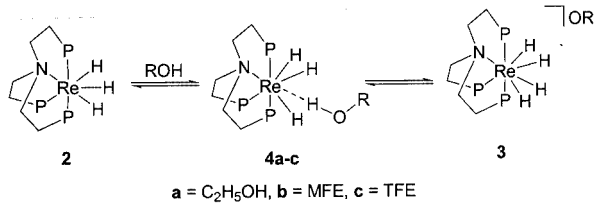

Scheme 3

The enthalpy associated with the hydrogen bond formation in the Re···HOR adducts (**4a**−**c**) was calculated from the experimental IR frequency shifts listed in Table 3 through the Iogansen correlation[45] reported in Equation (2).

$$-\Delta H^{\circ} = 18\,\Delta\nu/(720 + \Delta\nu) \quad (2)$$

In the case of **4c**, it was difficult to accurately determine the position of $\nu(OH)^{bond}$, because this band fell close to the ν(CH) bands of both **2** and the CH_2Cl_2 solvent. The thermodynamic parameters for **4c** were therefore independently calculated from the temperature dependence of the formation constant (K_f) using the van't Hoff Equation (3).

$$\ln K_f = -\Delta H^{\circ}/RT + \Delta S/R \quad (3)$$

The formation constant K_f for the equilibrium illustrated in Equation (4) was determined in the temperature range from +20 to −30 °C following the decrease in the optical density of the band assigned to the free OH group.

$$[ReH_3(NP_3)] + CF_3CH_2OH \rightleftharpoons [(NP_3)H_3Re\cdots HOCH_2CF_3] \quad (4)$$

The corresponding van't Hoff plot, shown in Figure 5, allowed us to figure out both the enthalpy and entropy changes [$-\Delta H^0 = 24.7 \pm 1.3$ kJ mol^{-1}, $-\Delta S^0 = 56.5 \pm 2.1$ kJ mol^{-1} K^{-1}]. Notably, the value of $-\Delta H^0$ calculated from the van't Hoff plot is close to that independently obtained by using Equation (2) (Table 3).

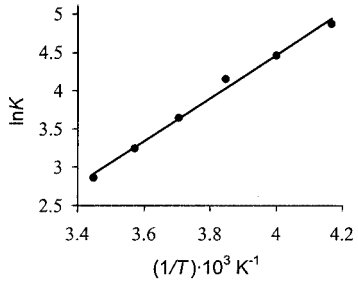

Figure 5. van't Hoff plot in the range +20 to −30 °C for the reaction of **2** with TFE

Table 3 also lists the basicity factors E_j relative to the different proton donors used in this study that were calculated by using the "rule of factors" [Equation (5)].[46]

$$E_j = \Delta H_{ij}/\Delta H_{11}\, P_i \quad (5)$$

The E_j values for **2** are practically constant (1.46 ± 0.01) for all the three proton donors listed in Table 3. Remarkably, the proton-accepting ability of the rhenium atom appeared to be higher than the E_j values previously determined for other metal-containing complexes.[29,30] Such a high E_j value for **2** might explain why the proton transfer was observed even in the presence of relatively weak proton donors such as TFE.

The study of the interaction of **2** with TFE at different temperatures and concentrations allowed us to observe the multiple equilibrium between the initial hydride **2**, the hydrogen bond adducts **4c**, and the final product **3** (Scheme 3). This equilibrium is significantly shifted to the right at either low temperature or high TFE concentrations. The solution IR spectrum of **2** in the presence of TFE at −70 °C is very complicated (see Figure 4c): the band at 1877 cm^{-1} was assigned to the ν(ReH) stretching of both the H-bonded complex **4c** and the starting hydride **2**, the band at 2050 cm^{-1} could be assigned to the ν(ReH) of **3**, while the broad absorbance between 1940 and 1970 cm^{-1} was attributed to the envelope of ν(ReH) bands due to the three rhenium species in equilibrium (Scheme 3). There is little doubt, however, that the spectral changes occurring in the ν(MH) region, following the addition of TFE to a solution of **2**, unequivocally point to the rhenium atom as the site where the hydrogen bond interaction with the proton donor primarily occurs.

A recently reported ab initio study of the protonation of [CpRe(PH$_3$)(NO)(H)] and [CpRe(CO)(NO)(H)] has shown that the substitution of CO by PH$_3$ increases the rhenium basicity and hence shifts the regioselectivity of proton attack from the terminal hydride ion to the metal center.[47] The remarkable nucleophilic character of the NP$_3$ ligand would analogously increase the basicity of the rhenium center in **2**, thus allowing for its regioselective protonation. As a matter of fact, the less electron-rich complex [ReH(CO)$_2$(triphos)] has been found to react with various proton donors forming selectively ReH···HOR adducts.[38,39]

Conclusions

We have described in this work the synthesis and characterization of the first rhenium polyhydride complexes stabilized by the tripodal polydentate ligand N(CH$_2$CH$_2$PPh$_2$)$_3$ (NP$_3$). In both [ReH$_3$(η^4-NP$_3$)] (**2**) and [ReH$_4$(η^4-NP$_3$)]BPh$_4$ (**3**) the polydentate ligand uses all its donor atoms for coordination. The classical polyhydride structure of **2** and **3** has been unambiguously determined by a variety of spectroscopic techniques in solution as well as a single-crystal X-ray analysis of the rhenium(V) derivative. Most importantly, an in situ IR study of the protonation of **2** by weak Brønsted acids has shown that the proton selectively attacks the metal atom to give kinetic hydrogen-bonded adducts of the formula [(η^4-NP$_3$)H$_4$Re···HOR] (ROH = C$_2$H$_5$OH, CFH$_2$CH$_2$OH, CF$_3$CH$_2$OH) that ultimately convert into the thermodynamically stable classical polyhydride **3** with no formation of transient η^2-H$_2$ species.

Experimental Section

General Procedures: Tetrahydrofuran (THF) and diethyl ether were purified by distillation from LiAlH$_4$ under nitrogen, dichlorome-

thane was heated under reflux overnight in the presence of P_2O_5 and distilled just prior of use. All other reagents and chemicals were reagent grade and, unless otherwise stated, were used as received from commercial suppliers. All reactions and manipulations were routinely performed under dry nitrogen by using standard Schlenk-tube techniques. The solid complexes were collected on sintered-glass frits and washed as indicated before being dried in a stream of nitrogen. The ligand $N(CH_2CH_2PPh_2)_3$ (NP_3)[48] and the complex $[ReCl_3(CH_3CN)(PPh_3)_2]$[49] were prepared as described in the literature. Deuterated solvents for NMR measurements (Merck and Aldrich) were dried with molecular sieves (4 Å). ^1H NMR spectra were recorded with Varian VXR 300 or Bruker AC200 spectrometers operating at 299.94 or 200.13 MHz (^1H), respectively. Peak positions are relative to tetramethylsilane and were calibrated against the residual solvent resonance. $^{31}P\{^1H\}$ NMR spectra were recorded with either the Varian VXR 300 or Bruker AC200 instruments operating at 121.42 and 81.01 MHz, respectively. Chemical shifts were measured relative to external 86% H_3PO_4 with downfield values taken as positive. The proton NMR spectra with broad-band phosphorus decoupling were recorded with the Bruker AC200 instrument equipped with a 5-mm inverse probe and a BFX-6 amplifier device using the wideband phosphorus decoupling sequence GARP. The variable-temperature spin-lattice relaxation times (T_1) in complexes **2** and **3** were measured in dichloromethane at 300 and 400 MHz by the inversion-recovery method using the standard $180°-\tau-90°$ pulse sequence. The calculations of the relaxation times were made using the fitting routines of the Varian VXR300 and Bruker AMX-400 spectrometers. The 90° pulse on the hydride samples was carefully measured at each temperature before running the T_1 measurements. The errors in T_1 determinations were less than 10%. Infrared spectra were recorded as Nujol mulls with a Perkin–Elmer 1600 series FT-IR spectrometer between KBr plates. The molar conductivity of **1** was measured with an AMEL model 134 conductance cell connected to a model 101 conductivity meter. The conductivity data were obtained at sample concentrations of 10^{-3} M in MeOH at room temperature (25 °C). Elemental analyses (C, H, N) were performed by using a Carlo Erba model 1106 elemental analyzer. IR measurements in CH_2Cl_2 were carried out with a Specord M82 spectrometer in CaF_2 cells. The cell width was 0.04–0.12 cm. The concentration range of the solutions for IR studies was between 10^{-1} and 10^{-3} M. For the low-temperature measurements a Carl Zeiss Jena cryostat was employed in the temperature range −80 to 30 °C using a stream of liquid nitrogen. The accuracy of temperature adjustment was ±0.5 °C. The position of ν(OH) bands corresponds to their barycenter. The formation constants at every temperature (−30 to +20 °C) were determined by the decrease of ν(OH) optical density of the absorption band assigned to the free OH group.

$[ReCl_2(\eta^4\text{-}NP_3)]Cl$ (1): A suspension of $[ReCl_3(CH_3CN)(PPh_3)_2]$ (0.30 g, 0.36 mmol) and NP_3 (0.30 g, 0.46 mmol) in ethanol (60 mL) was heated under reflux under nitrogen for ca. 4 h, during which time the orange solid dissolved to give a clear yellow solution. The solution was then reduced in volume to ca. 20 mL before adding diethyl ether (30 mL) whilst stirring to precipitate **1** as lemon-yellow microcrystals. Yield, based on Re 0.27 g, 0.29 mmol (80%). $C_{42}H_{42}Cl_3NP_3Re$ (875.38): calcd. C 53.3, H 4.5, N 1.5; found C 53.2, H 4.4, N 1.1. $\Lambda_{M(methanol)} = 146\ \Omega^{-1}\ cm^2\ mol^{-1}$.

$[ReH_3(\eta^4\text{-}NP_3)]$ (2): Solid $LiAlH_4$ (0.64 g, 16.86 mmol) was added portionwise to a stirred suspension of **1** (0.80 g, 0.85 mmol) in 100 mL of THF. The mixture was gently heated to reflux temperature and stirred for 6 h. After cooling to 0 °C, the excess $LiAlH_4$ was carefully hydrolyzed by addition of a mixture of THF/H_2O (30 mL, 10:1, v/v). The resulting slurry was filtered through a Hirsch funnel to remove the lithium and aluminum hydrolysis products. The volume of the filtrate was reduced to ca. 20 mL before adding 20 mL of a 1:2 (v/v) EtOH/*n*-hexane solution. Concentration of the solution under a stream of nitrogen gave ivory-colored microcrystals of **2**. Yield, 0.53 g, 0.63 mmol (74%). $C_{42}H_{45}NP_3Re$ (842.95): calcd. C 59.8, H 5.4, N 1.7; found C 60.1, H 5.5, N 1.6. IR (Nujol mull): $\tilde{\nu}$ = 1949 (ν_{ReH}), 1905 cm^{-1}. The perdeuterated derivative $[ReD_3(\eta^4\text{-}NP_3)]$ (**2-D_3**) was prepared with an isotopic purity higher than 90% (^1H NMR) by substituting $LiAlD_4$, D_2O, and C_2H_5OD for the protonated analogues in the above procedure.

$[ReH_4(\eta^4\text{-}NP_3)]BPh_4$ (3): A Schlenk tube was charged with 0.50 g of **2** (0.59 mmol) and 10 mL of degassed dichloromethane. To this solution, cooled to 195 K with a dry ice/acetone bath, was added via syringe an excess of $HBF_4{\cdot}OMe_2$ (0.2 mL, 1.6 mmol), and the temperature was raised to ca. 20 °C before adding a solution of $NaBPh_4$ (0.50 g, 1.46 mmol) in EtOH (5 mL) whilst stirring. Concentration under nitrogen gave off-white crystals of **3**. Colorless plates of **3** were obtained by slow crystallization from a diluted CH_2Cl_2/EtOH (2:1, v/v) solution. Yield 0.63 g, 0.54 mmol (92%). $C_{66}H_{66}BNP_3Re$ (1163.20): calcd. C 68.2, H 5.7, N 1.2; found C 68.6, H 5.9; N 1.2. IR (KBr): $\tilde{\nu}$ = 2030 w, br. (ν_{ReH}), 1996 m br.; ν_{BPh4} 1680, 610 cm^{-1}. The perdeuterated derivative $[ReD_4(\eta^4\text{-}NP_3)]BPh_4$ (**3-D_4**) was prepared with an isotopic purity higher than 95% (^1H NMR) from **2-D_3** by using CF_3OSO_2D and C_2H_5OD in place of HBF_4 and ethanol.

Reaction of 3 with KO*t*Bu: Addition of solid KO*t*Bu (0.20 g, 1.78 mmol) to a THF solution of **3** (0.20 g, 0.17 mmol) regenerated the neutral trihydride **2**. Yield 89%.

X-ray Crystallography: Single crystals of **3** suitable for an X-ray diffraction analysis were obtained as described above. A crystal was mounted on a glass fiber, on a CAD4 diffractometer, which was used for the space group determination and for the data collection, which was carried out at −80(2) °C. Unit cell dimensions were obtained by least-squares fit of the 2θ values of 25 high-order reflections. Crystallographic and other relevant data are listed in Table 4. Data were measured with variable scan speed to ensure constant statistical precision on the collected intensities. Three standard reflections were used to check the stability of the crystals and of the experimental conditions and measured every hour. The collected intensities were corrected for Lorentz and polarization factors and empirically (Ψ scans) for absorption.[50] The standard deviations on intensities were calculated in terms of statistics alone. The structure was solved by a combination of Patterson and Fourier methods and refined by full-matrix least squares[51] {the function minimized being $\Sigma[w(F_o - 1/kF_c)^2]$}. All non-hydrogen atoms were treated anisotropically. Towards the end of the refinement, four strong peaks were found, in a Fourier difference maps, at distances consistent with those expected for the hydrido ligands. Therefore these peaks were included in the refinement and treated isotropically. However, while three hydrogen atoms converged to give a reasonable geometry, maintaining also positive values for the displacement parameters, the fourth gave an Re–H separation that was considered too short, as well as a negative thermal factor, and thus was discarded. No other acceptable peak for the missing hydride ion was found in the Fourier difference maps. No extinction correction was deemed necessary. The scattering factors used, corrected for the real and imaginary parts of the anomalous dispersion, were taken from the literature.[52] The contribution of the hydrogen atoms in calculated positions [C–H = 0.95 Å, B(H) = 1.3

$\times$ B(C_{bonded}) Å^2] was taken into account but not refined. Upon convergence no significant features were found in the Fourier difference maps of both compounds. A selection of bond lengths and angles is given in Table 2 (vide infra). All calculations were performed using the MOLEN crystallographic package,[51] and the structures drawn using the program ORTEP.[53] The supplementary crystallographic data for this paper are contained in publication CCDC-179058. These data can be obtained free of charge at www.ccdc.cam.ac.uk/conts/retrieving.html or from the Cambridge Crystallographic Data Centre, 12, Union Road, Cambridge CB2 1EZ, UK [Fax: (internat.) + 44-1223/336-033; E-mail: deposit@ccdc.cam.ac.uk].

Table 4. Experimental data for the X-ray diffraction study of compound **3**

Empirical formula	$C_{67}H_{64}BCl_2NP_3Re$
Formula mass	1244.10
T [C°]	−80(2)
Crystal system	triclinic
Space group	$P\bar{1}$
a [Å]	12.358(2)
b [Å]	14.871(2)
c [Å]	16.545(6)
α [°]	107.04(3)
β [°]	91.98(3)
γ [°]	91.44(2)
V [Å^3]	2903(1)
Z	2
$\rho_{calcd.}$ [g cm^{-3}]	1.42
μ [cm^{-1}]	23.35
Radiation	Mo-K_α (graphite-monochromated, λ = 0.71069 Å)
No. independent data collected	8793
No. observed reflections	7762 [$\|I_o\| > 3.5\sigma(I)$]
Transmission coeff.	1.00−0.94
R[a]	0.033
R_w	0.066
GOF	1.55

[a] $R = \Sigma(|F_o - (1/k)F_c|)/\Sigma|F_o|$; $R_w = [\Sigma_w(F_o - (1/k)F_c)^2/\Sigma_w|F_o|^2]^{1/2}$, where $w = [\sigma^2(F_o)]^{-1}$; $\sigma(F_o) = [\sigma^2(F_o^2) + f^4(F_o^2)]^{1/2}/2F_o$.

Acknowledgments

Thanks are due to INTAS (contract 00-00179), NATO (contract HTECH-CRG 972135), CNR/RAS bilateral agreement and RFBR (project No 99-03-33270) for financial support. Support from the EC (RTN network HYDROCHEM) is also gratefully acknowledged. I. d. l. R. thanks the Ministerio de Ciencia y Tecnologia (Spain) for a post-doctoral grant.

[1] See for example: [1a] D. Gusev, A. Llamazares, G. Artus, H. Jacobsen, H. Berke, *Organometallics* **1999**, *18*, 75. [1b] G. Albertin, S. Antoniutti, S. Garcia-Fontán, R. Carballo, F. Padoan, *J. Chem. Soc., Dalton Trans.* **1998**, 2071. [1c] D. M. Heinekey, M. H. Voges, D. M. Barnhart, *J. Am. Chem. Soc.* **1996**, *118*, 10792. [1d] Y. Kim, H. Deng, J. C. Gallucci, A. Wojicicki, *Inorg. Chem.* **1996**, *35*, 7166. [1e] D. G. Gusev, H. Berke, *Chem. Ber.* **1996**, *129*, 1143 and references therein. [1f] X. L. R. Fontaine, T. P. Layzell, B. L. Shaw, *J. Chem. Soc., Dalton Trans.* **1994**, 917. [1g] X.-L. Luo, R. H. Crabtree, *J. Am. Chem. Soc.* **1990**, *112*, 6912.

[2] H. Brunner, in *Applied Homogeneous Catalysis with Organometallic Compounds* (Eds.: B. Cornils, W. A. Herrmann), Verlag Chemie, Weinheim, Germany, **1996**, vol. 1, chapter 2, p. 201.

[3] A. J. Maeland, in *Recent Advances in Hydride Chemistry* (Eds.: M. Peruzzini, R. Poli), Elsevier, Amsterdam, NL, **2001**, chapter 18.

[4] [4a] R. Cammack, P. van Vliet, in *Bioinorganic Catalysis* (Eds.: J. Reedijk, E. Bowman), Marcel Dekker, New York, NY, USA, **1998**, chapter 9. [4b] R. A. Henderson in *Recent Advances in Hydride Chemistry* (Eds.: M. Peruzzini R. Poli), Elsevier, Amsterdam, NL, **2001**, chapter 16.

[5] [5a] J. B. Arterburn, K. V. Rao, D. M. Goreham, M. V. Valenzuela, M. S. Holguin, K. A. Hall, K. C. Ott, J. C. Bryan, *Organometallics* **2000**, *19*, 1789. [5b] E. Deutsch, K. Libson, S. Jurisson, L. F. Lindoy, *Prog. Inorg. Chem.* **1983**, *30*, 75. [5c] S. S. Jurisson, J. D. Lydon, *Chem. Rev.* **1999**, *99*, 2205. [5d] W. A. Wolkert, T. J. Hoffman, *Chem. Rev.* **1999**, *99*, 2269. [5e] J. R. Dilworth, S. J. Parrott, *Chem. Soc. Rev.* **1998**, *27*, 43. [5f] F. Tisato, F. Refosco, G. Bandoli, *Coord. Chem. Rev.* **1994**, *135*, 235.

[6] [6a] L. Sacconi, F. Mani, *Transition Met. Chem. (NY)* **1982**, *8*, 214. [6b] F. Mani, L. Sacconi, *Comments Inorg. Chem.* **1983**, *2*, 157. [6c] H. Mayer, W. Kaska, *Chem. Rev.* **1994**, *94*, 1239. [6d] F. A. Cotton, B. Hong, *Prog. Inorg. Chem.* **1992**, *40*, 179.

[7] C. Bianchini, M. Peruzzini, F. Zanobini, L. Magon, L. Marvelli, R. Rossi, *J. Organomet. Chem.* **1993**, *451*, 97.

[8] S. C. Abrahams, A. P. Ginsberg, T. F. Koetzle, P. Marsh, C. R. Sprinkle, *Inorg. Chem.* **1986**, *25*, 2500.

[9] M. T. Costello, P. E. Fanwick, M. A. Green, R. A. Walton, *Inorg. Chem.* **1992**, *31*, 2369.

[10] [10a] L. Sacconi, I. Bertini, *J. Am. Chem. Soc.* **1967**, *89*, 2235. [10b] L. Sacconi, I. Bertini, *J. Am. Chem. Soc.* **1968**, *90*, 5443. [10c] L. Sacconi, *Coord. Chem. Rev.* **1972**, *8*, 351. [10d] R. Morassi, I. Bertini, L. Sacconi, *Coord. Chem. Rev.* **1973**, *11*, 343.

[11] J. R. Dilworth, D. V. Griffiths, J. M. Hughes, S. Morton, *Inorg. Chim. Acta* **1992**, *196*, 146.

[12] G. Jia, A. J. Lough, R. H. Morris, *J. Organomet. Chem.* **1993**, *461*, 147.

[13] C. Bianchini, A. Meli, M. Peruzzini, F. Vizza, F. Zanobini, *Coord. Chem. Rev.* **1992**, *120*, 193.

[14] C. Mealli, C. A. Ghilardi, A. Orlandini, *Coord. Chem. Rev.* **1992**, *120*, 361.

[15] [15a] M. Friebolin, *Basic One- and Two-Dimensional NMR Spectroscopy*, 2nd ed., Verlag Chemie, Weinheim, Germany, **1993**, chapter 11. [15b] H. Shanan-Atidi, K. H. Bar-Eli, *J. Phys. Chem.* **1970**, *74*, 961. [15c] K. Pihlaja, E. Kleinpeter, *Carbon-13 NMR Chemical Shifts and Stereochemical Analysis*, Verlag Chemie, Weinheim, Germany, **1994**, p. 299−302.

[16] C. Bianchini, M. Peruzzini, A. Polo, A. Vacca, F. Zanobini, *Gazz. Chim. Ital.* **1991**, *121*, 643.

[17] D. Fost, E. H. Carlson, M. Raban, *J. Chem. Soc., Chem. Commun.* **1971**, 656.

[18] V. I. Bakhmutov, E. V. Vorontsov, *Rev. Inorg. Chem.* **1998**, *18*, 183.

[19] R. H. Crabtree, *Acc. Chem. Res.* **1990**, *23*, 95.

[20] P. J. Desrosiers, L. Cai, Z. Lin, R. Richards, J. Halpern, *J. Am. Chem. Soc.* **1991**, *113*, 4173.

[21] D. G. Gusev, A. B. Vymenits, V. I. Bakhmutov, *Inorg. Chem.* **1991**, *30*, 3118.

[22] X.-L. Luo, R. H. Crabtree, *J. Chem. Soc., Dalton Trans.* **1991**, 587.

[23] C. Bianchini, S. Moneti, M. Peruzzini, F. Vizza, *Inorg. Chem.* **1997**, *36*, 5818.

[24] G. G. Hlatky, R. H. Crabtree, *Coord. Chem. Rev.* **1985**, *65*, 1.

[25] C. A. Bayse, M. B. Hall, *J. Am. Chem. Soc.* **1999**, *121*, 3992.

[26] B. A. Patel, J. Wessel, W. Yao, J. C. Lee, T. F. Koetzle, G. P. A. Yap, J. B. Fortin, J. S. Ricci, A. Albinati, O. Eisenstein, A. L. Rheingold, R. H. Crabtree, *New J. Chem.* **1996**, *21*, 413.

[27] R. Bau, M. H. Drabnis, *Inorg. Chim. Acta* **1997**, *259*, 27.

[28] A. Albinati, L. M. Venanzi, *Coord. Chem. Rev.* **2000**, *200*, 687.

[29] L. M. Epstein, N. V. Belkova, E. S. Shubina, in *Recent Advances in Hydride Chemistry* (Eds.: M. Peruzzini, R. Poli), Elsevier, Amsterdam, NL, **2001**, chapter 14.
[30] E. S. Shubina, N. V. Belkova, L. M. Epstein, *J. Organomet. Chem.* **1997**, *536–537*, 17.
[31] D. V. Yandulov, K. G. Caulton, N. V. Belkova, E. S. Shubina, L. M. Epstein, D. V. Khoroshum, D. G. Musaev, K. Morokuma, *J. Am. Chem. Soc.* **1998**, *120*, 12553 and references therein.
[32] E. T. Papish, M. P. Magee, J. R. Norton, in *Recent Advances in Hydride Chemistry* (Eds.: M. Peruzzini, R. Poli), Elsevier, Amsterdam, NL, **2001**, chapter 12.
[33] R. B. Girling, P. Grebenik, *Inorg. Chem.* **1986**, *25*, 31.
[34] D. V. Yandulov, D. Huang, J. C. Huffman, K. G. Caulton, *Inorg. Chem.* **2000**, *39*, 1919.
[35] In order to avoid self-association processes, the concentrations of the various proton-donor reagents were kept in the range 0.01–0.03 M.
[36] The problem of the metal vs. hydride preference in protonation reactions has been extensively discussed by Norton and coworkers in ref.[32]
[37] N. V. Belkova, E. S. Shubina, E. I. Gutsul, L. M. Epstein, S. E. Nefedov, I. L. Eremenko, *J. Organomet. Chem.* **2000**, *610*, 58.
[38] E. S. Shubina, N. V. Belkova, E. V. Bakhmutova, E. V. Vorontsov, V. I. Bakhmutov, A. V. Ionidis, C. Bianchini, L. Marvelli, M. Peruzzini, L. M. Epstein, *Inorg. Chim. Acta* **1998**, *280*, 302.
[39] N. V. Belkova, E. V. Bakhmutova, E. S. Shubina, C. Bianchini, M. Peruzzini, V. I. Bakhmutov, L. M. Epstein, *Eur. J. Inorg. Chem.* **2000**, 2163.
[40] V. I. Bakhmutov, E. V. Bakhmutova, N. V. Belkova, L. M. Epstein, E. S. Shubina, E. V. Vorontsov, C. Bianchini, D. Masi, M. Peruzzini, F. Zanobini, *Can. J. Chem.* **2001**, *79*, 479.
[41] E. Scharrer, S. Chang, M. Brookhart, *Organometallics* **1995**, *14*, 5686.
[42] E. S. Shubina, A. N. Krylov, N. V. Belkova, L. M. Epstein, A. P. Borisov, V. D. Mahaev, *J. Organomet. Chem.* **1995**, *439*, 275.
[43] E. S. Shubina, L. M. Epstein, *Ber. Bunsenges. Phys. Chem.* **1998**, *102*, 359.
[44] K. Abdur-Rashid, T. P. Fong, B. Greaves, D. G. Gusev, J. G. Hinman, S. E. Landau, A. J. Lough, R. H. Morris, *J. Am. Chem. Soc.* **2000**, *122*, 9155.
[45] The empirical rule of factors reported by Iogansen[46] demonstrates the invariability of the proton-donor (P_i) and proton-acceptor (E_j) properties of organic acids and bases in hydrogen bonding. In Equation (5), ΔH_{11} is the enthalpy of hydrogen bonding for a standard donor/acceptor couple (i.e. PhOH/Et_2O: $P_1 = E_1 = 1$). E_j depends on neither the nature of the proton donor nor the solvent and may therefore be assumed as an absolute measurement of the proton-accepting ability of each potential site of hydrogen bonding.[30]
[46] A. V. Iogansen, *Theor. Experim. Khim.* **1971**, *7*, 302.
[47] G. Orlova, S. Scheiner, *J. Phys. Chem. A* **1998**, *102*, 4813.
[48] R. Morassi, L. Sacconi, *Inorg. Synth.* **1976**, *16*, 174.
[49] J. Chatt, R. J. Dosser, F. King, G. J. Leigh, *J. Chem. Soc., Dalton. Trans.* **1976**, 2436.
[50] A. C. T. North, D. C. Philips, F. S. Mathews, *Acta Crystallogr., Sect. A* **1968**, *24*, 351.
[51] *MOLEN: Molecular Structure Solution Procedure*, Enraf–Nonius, Delft, The Netherlands, **1990**.
[52] *International Tables for X-ray Crystallography*, Kynoch Press, Birmingham, England, **1974**, vol. IV.
[53] C. K. Johnson, *ORTEP II*, Report ORNL-6138, Oak Ridge National Laboratory, Oak Ridge, TN, **1976**.

Received November 2, 2001
[I01470]

EurJIC
European Journal of Inorganic Chemistry

July 2002
Issue 7
Pages 1541–1884

COVER PICTURE

The cover picture shows the ability of a new unsymmetrical ligand to act as either monodentate or bidentate; controlling this behaviour is important in catalytic processes. Details are discussed in the article by J. D. Woollins et al. on p. 1635 ff.

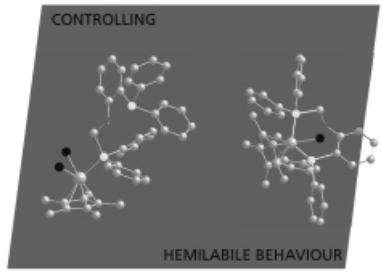

MICROREVIEWS

Contents

1559 **J. A. Cabeza**

The Important Role of Some Ancillary Ligands in the Chemistry of Carbonylmetal Cluster Complexes − Selected Reactivity of Triruthenium Clusters Containing Deprotonated 2-Aminopyridines

Keywords: Ruthenium / Cluster compounds / N ligands / Aminopyridines / Hemilabile ligands

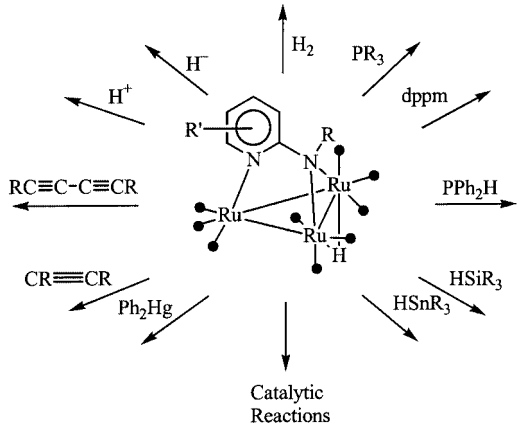

 © WILEY-VCH Verlag GmbH, 69451 Weinheim, Germany, 2002 1434–1948/02/0707–1545 $ 20.00+.50/0

1571 **A. Ceulemans,* E. Lijnen**

The Polyhedral State of Molecular Matter

Keywords: Group theory / Topological chemistry / Polyhedra / Fullerenes / Cubanes / Boranes

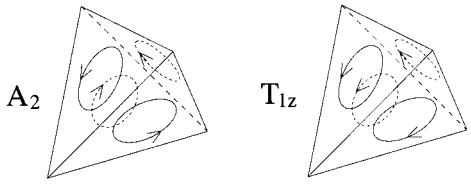

SHORT COMMUNICATIONS

1583 **P. C. Andrews,* S. M. Calleja, M. Maguire, P. J. Nichols**

A 1,3-Sigmatropic Rearrangement Revealed in the Solid and Solution State Structures of a Chiral Sodium 1-Azaallyl Complex Derived from (*S*)-*N*-(α-Methylbenzyl)allylamine

Keywords: Sodium / N ligands / Chirality / Amines / Sigmatropic rearrangement / Structure elucidation

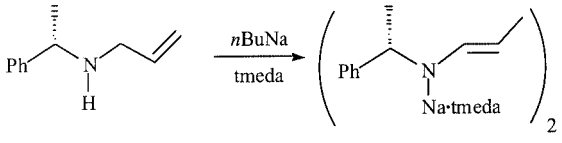

1588 **M. Isola,* V. Luizzo, F. Marchetti, A. Raffaelli**

A Self-Assembled Dinuclear Double-Stranded Helicate Based on a Square-Planar Coordination Geometry

Keywords: Nickel / Schiff-base ligands / Self-assembly / N,O ligands / Supramolecular chemistry

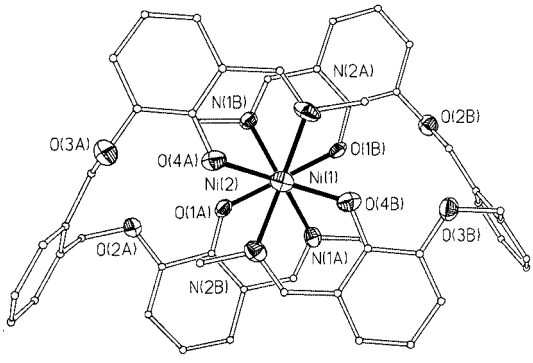

1591 **C.-M. Liu, D.-Q. Zhang,* Y.-L. Song, C.-L. Zhan, Y.-L. Li, D.-B. Zhu***

Synthesis, Crystal Structure and Third-Order Nonlinear Optical Behavior of a Novel Dimeric Mixed-Ligand Zinc(II) Complex of 1,3-Dithiole-2-thione-4,5-dithiolate

Keywords: Zinc / N ligands / S ligands / Crystal structure / Nonlinear optics

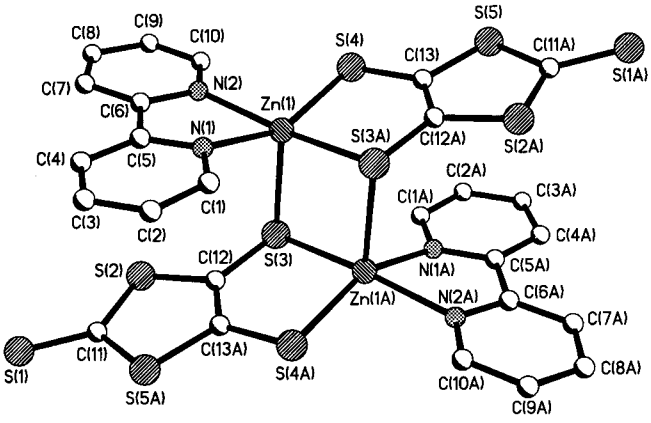

1595 **C.-M. Liu, D.-Q. Zhang,* A.-J. Qin, C. Ye, H.-M. Hu, D.-B. Zhu***

A Novel Nickel(II) Complex Adopting a *cis*-Configuration: Solvothermal Synthesis and Crystal Structure of $[NiL_2(H_2O)_4]$ (L = 1,4-Dihydropyrazine-2,3-dione-5,6-dicarboxylate)

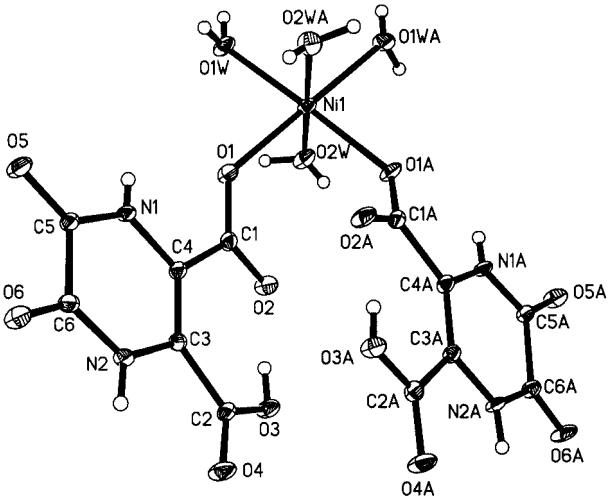

Keywords: Nickel / Solvothermal synthesis / Carboxylate ligands / Crystal structure

1599 **G. A. Bogdanovic, A. Spasojević-de Biré, S. D. Zarić***

Evidence Based on Crystal Structures and Calculations of a C−H···π Interaction Between an Organic Moiety and a Chelate Ring in Transition Metal Complexes

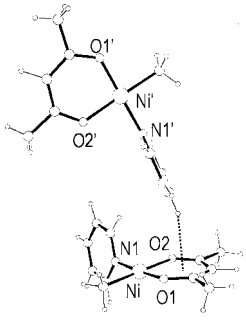

Keywords: C−H···π interactions / Chelates / Noncovalent interactions / Density functional calculations / Weak hydrogen bonds

1603 **F. Bellouard, M. Clemente-León, E. Coronado,* J. R. Galán-Mascarós, C. J. Gómez-García, F. Romero, K. R. Dunbar**

Unusual Magnetic Behavior in the Layered Ferromagnet $[Ni(C_6H_{14}N_2)_2]_3[Fe(CN)_6]_2 \cdot 2H_2O$

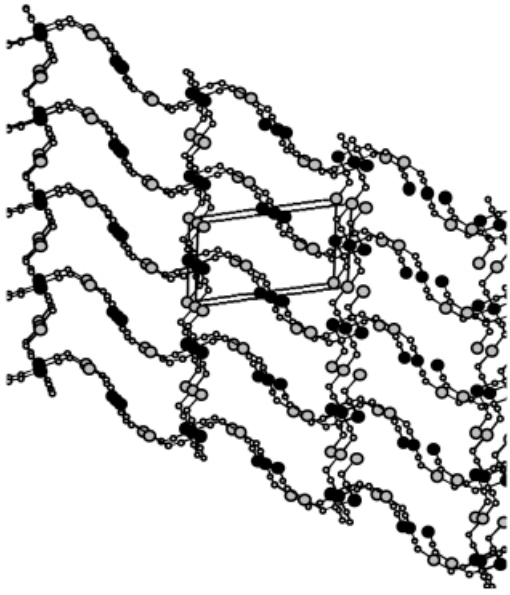

Keywords: Molecular magnets / Ferromagnetism / Cyanides / Nickel / Magnetic properties

FULL PAPERS

1607 **A. Weiss, H. Pritzkow, W. Siebert***

Synthesis, Structures and Reactivity of *N*-Borane-Protected 1,1′-Bisimidazoles with Different Bridging Functions

Keywords: Boranes / Carbenes / Carbene complexes / Nitrogen heterocycles / Macrocycles

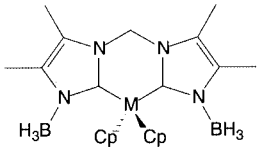

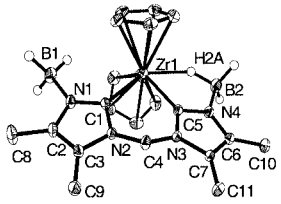

1615 **M. Döring,* M. Ciesielski, O. Walter, H. Görls**

Salicylaldimine Dizinc Complexes: Activation of Water Molecules and Fixation of CO_2 in the Coordination Sphere of Zinc

Keywords: Zinc / N ligands / N,O ligands / Carbon dioxide fixation / Enzyme models

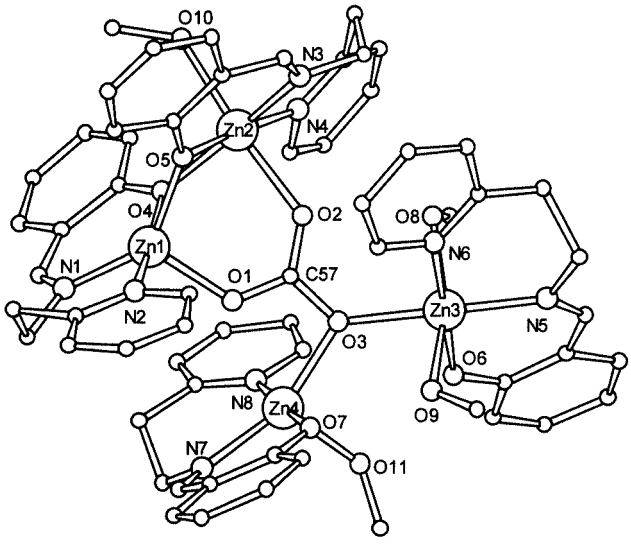

1622 **U. Mazurek, D. Schröder, H. Schwarz***

Gas-Phase Reactions of Chromium and Chromium Fluoride Cations CrF_n^+ (n = 0−4) with Water and Nitrous Oxide

Keywords: Chromium / Chromium fluorides / Hydrolysis / Gas-phase ion chemistry / Thermochemistry

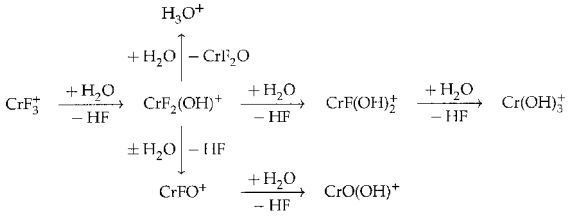

1635 **Q. Zhang, S. M. Aucott, A. M. Z. Slawin, J. D. Woollins***

Synthesis and Coordination Chemistry of the New Unsymmetrical Ligand $Ph_2PCH_2NHC_6H_4$-PPh_2

Keywords: Unsymmetrical ligands / Phosphanes / Chelates / Monodentate complexes / Heterometallic complexes

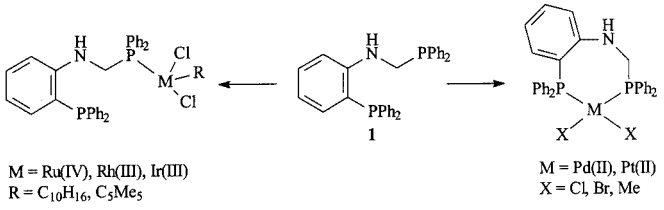

1647

K. Bieger, J. Díez, M. P. Gamasa,* J. Gimeno, M. Pavlišta, Y. Rodríguez-Álvarez, S. García-Granda, R. Santiago-García

(Alkenylalkylidene)(indenyl)ruthenium(II) Complexes: Synthesis by Protonation of Alkenyl Derivatives

Keywords: Ruthenium / Hydride ligands / Alkenyl complexes / Alkylidene complexes / P ligands

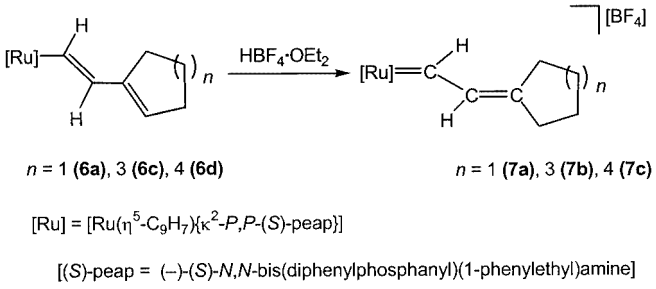

1657

X. Sava, A. Marinetti,* L. Ricard, F. Mathey

Optically Active Phospholes: Synthesis and Use as Chiral Precursors for Phosphinidene and Phosphaferrocene Complexes

Keywords: Phosphorus heterocycles / Asymmetric catalysis / P ligands / Phosphinidene complexes / Chiral phospholes / Phosphaferrocenes

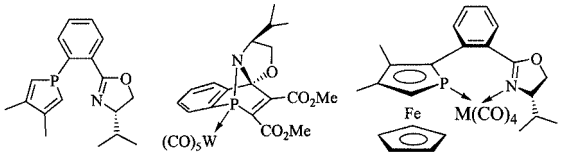

1666

B. Boitrel,* V. Baveux-Chambenoît, P. Richard

Investigation of the Enantioselectivity Observed in Epoxidation Reactions Catalysed by Bis-Strapped Chiral Porphyrins Derived from L-Proline

Keywords: L-Proline / Epoxidations / Porphyrins / Enantioselectivity / Iron

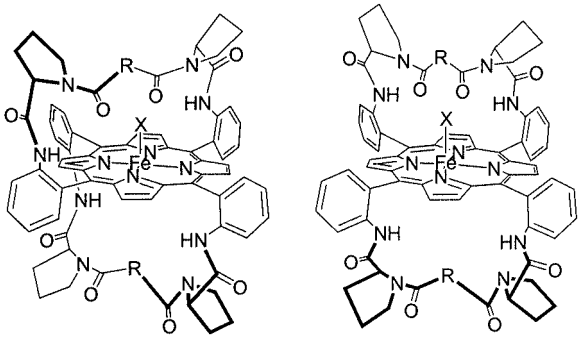

1673

F. Soetebier, W. Urland*

Structural Chemistry and Magnetism of Tb^{3+}-β′′-Alumina ($Tb_{0.46}Al_{10.62}Mg_{0.38}O_{17}$)

Keywords: Aluminum / Magnesium / Terbium / Ion exchange / Crystal structure / Magnetic properties

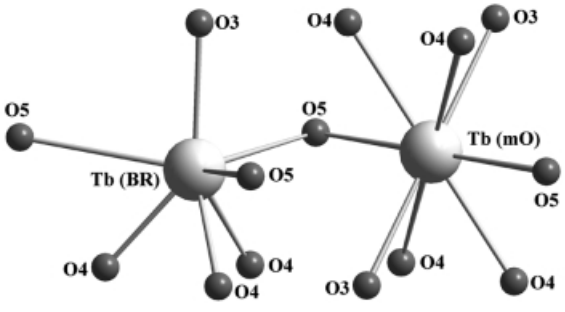

1677 **T. Farrell,* A. R. Manning,* G. Mitchell, J. Heck,* T. Meyer-Friedrichsen, M. Malessa, C. Wittenburg, M. H. Prosenc, D. Cunningham, P. McArdle**

Synthesis and Properties of a Novel Series of Organometallic Merocyanines Combining the Potent Electron-Donating [$(CpFeCO)_2$(μ-CO)-(μ-C=CH−)] Fragment with Tropylium-Type Acceptors

Keywords: Organometallic compounds / Merocyanines / Azulenes / Bond length alternation / Solvatochromism / Nonlinear optics (NLO) / Long-wavelength hyper-Rayleigh scattering (HRS)

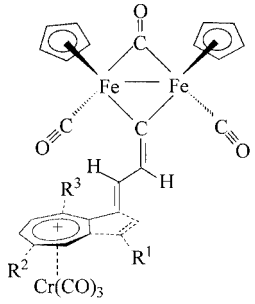

1687 **E. Balogh-Hergovich, Z. Gréczi, J. Kaizer, G. Speier,* M. Réglier, M. Giorgi, L. Párkányi**

Kinetics and Mechanism of the Copper-Catalysed Oxygenation of 2-Nitropropane

Keywords: 2-Nitropropane / Copper nitronates / Oxygenation / Copper / Kinetics / Dioxygenase

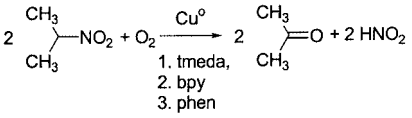

1697 **S. H. Liu, X. Huang, Z. Lin,* C. P. Lau,* G. Jia***

Synthesis and Characterization of Dihydrogen-(olefin)osmium Complexes with (E)-Ph_2P-$(CH_2)_2CH{=}CH(CH_2)_2PPh_2$

Keywords: Dihydrogen / Diphosphane / Hydride / Osmium

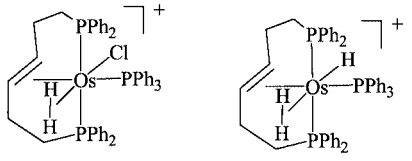

1703 **I. Cacelli, L. Carbonaro,* P. La Pegna**

Kinetics and Equilibria of Nickel(II)−Schiff Base Adducts Formation

Keywords: Kinetics / Nickel / Schiff base / Adducts / Substituent effects

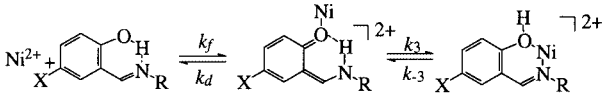

1711 **A. Jutand,* S. Négri, J. G. de Vries**

Rate and Mechanism of the Oxidative Addition of Benzoic Anhydride to Palladium(0) Complexes in DMF

Keywords: Palladium / Kinetics / Electrochemistry / Benzoic anhydride / Oxidative addition

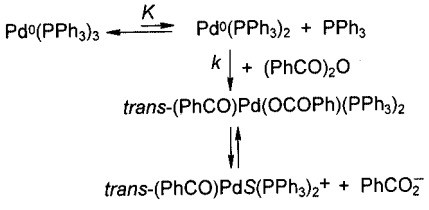

1718 V. Daga, S. K. Hadjikakou, N. Hadjiliadis,* M. Kubicki, J. H. Z. dos Santos, I. S. Butler

Synthesis, Spectroscopic and Structural Characterization of Novel Diiodine Adducts with the Heterocyclic Thioamides, Thiazolidine-2-thione (tzdtH), Benzothiazole-2-thione (bztzdtH) and Benzimidazole-2-thione (bzimtH)

Keywords: Bioinorganic chemistry / Charge-transfer complexes / Iodine / S ligands / Sulfur heterocycles

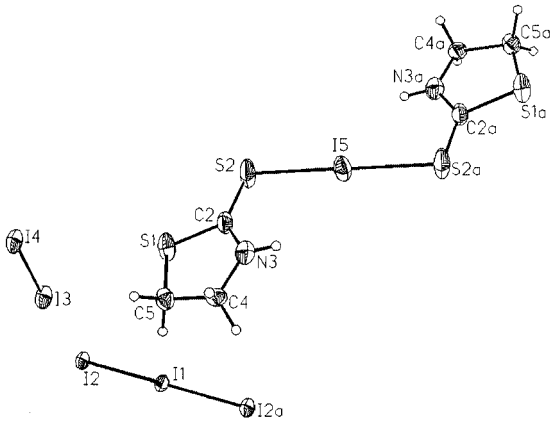

1729 J. Stroot, R. Beckhaus,* W. Saak, D. Haase, A. Lützen

Reactions of Pentafulvene Complexes of Titanium with Carbonyl Compounds − Diastereoselective Synthesis of σ,π-Chelate Complexes with Cp~O Ligands

Keywords: Titanium / Fulvene complexes / Reaction mechanism / Substituent effects / Stereoselectivity / O ligands / Cyclopentadienyl ligands

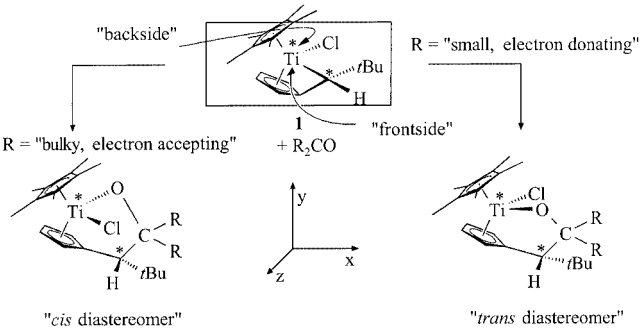

1738 M. Hollosi, Z. Majer, E. Vass, Z. Raza, V. Tomišić, T. Portada, I. Piantanida, M. Žinić, V. Šunjić

Structural and Chiroptical Properties of Acyclic and Macrocyclic 1,5-Bis(oxazoline) Ligands and Their Copper(I) and Silver(I) Complexes

Keywords: Circular dichroism / Conformation analysis / Copper / Silver / Bis(oxazoline) ligands / Macrocyclic ligands

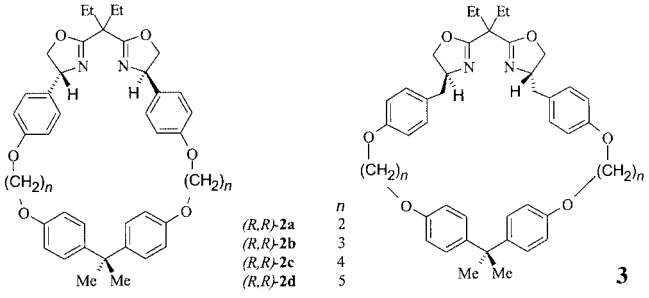

1749 M. R. Maurya,* S. Khurana, W. Zhang, D. Rehder

Vanadium(IV/V) Complexes Containing $[VO]^{2+}$, $[VO]^{3+}$, $[VO_2]^{+}$ and $[VO(O_2)]^{+}$ Cores with Ligands Derived from 2-Acetylpyridine and *S*-Benzyl- or *S*-Methyldithiocarbazate

Keywords: Malonate / Oxo transfer / Sulfur ligands / Hydrazones / Vanadium

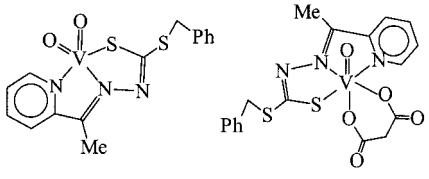

1761 **B. Wenzel, P. Lönnecke, E. Hey-Hawkins***

Gold(I) Thiolates as Metalloligands for the Synthesis of the First Zirconocene−Gold Complexes

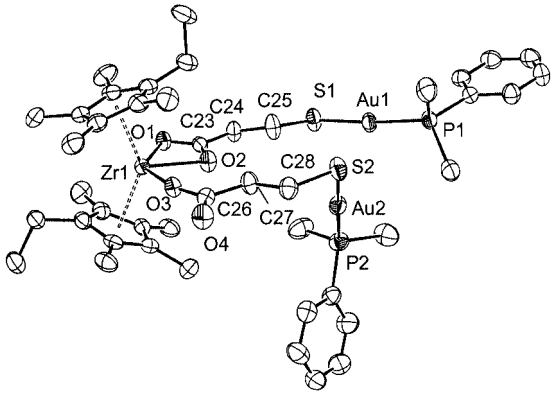

Keywords: Metallocenes / Zirconium / Gold / O,S ligands / Bridging ligands

1765 **B. Mehmetaj, J. G. Haasnoot,* L. De Cola, G. A. van Albada, I. Mutikainen, U. Turpeinen, J. Reedijk**

Syntheses, Characterization, X-ray Crystal Structure, Redox and Photophysical Properties of Polypyridylruthenium(II) Complexes Containing Carboxylate-Substituted Pyridyltriazoles

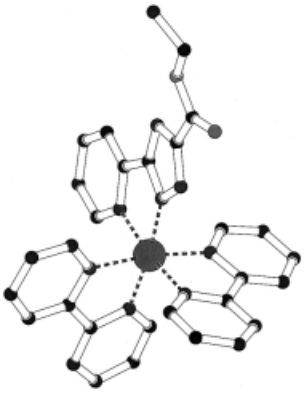

Keywords: Ruthenium / N ligands / Crystal structure / Photophysical properties / Redox potentials

1772 **H. Watanabe,* H. Suzuki, S. Takahashi, K. Ohyama, Y. Sekiguchi, H. Ohmori, M. Nishiyama, M. Sugo, M. Yoshikawa, N. Hirai, Y. Kanuma, T. Adachi, M. Makino, K. Sakata, K. Kobayashi, T. Kudo,* H. Matsuyama, N. Kamigata, M. Kobayashi, M. Kijima,* H. Shirakawa, K. Honda, M. Goto***

Peralkylated Four- and Five-Membered Cyclosilanes Containing a Heteroatom: Synthesis, Structure, and Properties

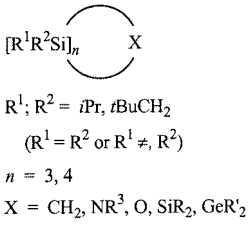

Keywords: HOMO−LUMO interactions / Photolysis / Small ring systems / Silicon / Strained molecules

1794 **M.-L. Martínez-Sarrión,* L. Mestres, M. Herráiz, O. Maqueda, A. Bakkali, N. Fernández**

Phase Diagram and Impedance Spectroscopy Study of the $La_{0.5+x-y}Bi_yLi_{0.5-3x}TiO_3$ System

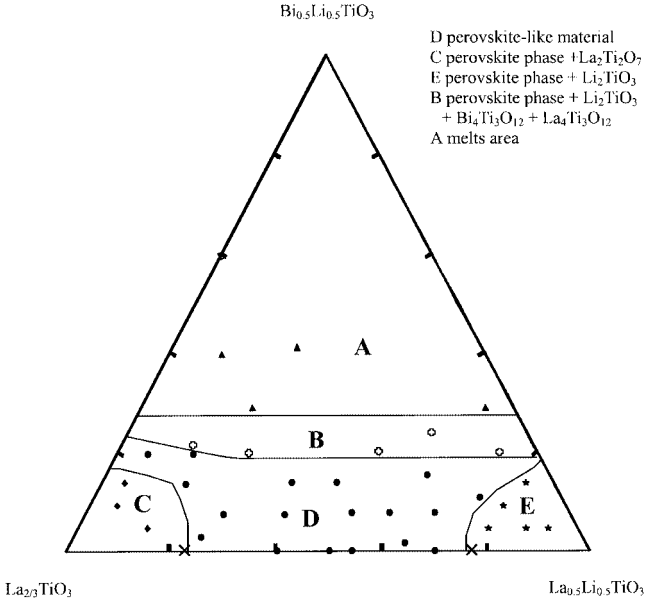

Keywords: Phase diagrams / Perovskite phases / Conducting materials / Lanthanides

1801 **M.-L. Martínez-Sarrión,* L. Mestres, M. Herraiz, A. M. Balagurov, A. I. Beskrovniy, S. G. Vasilovskij, L. S. Smirnov**

Synthesis and Characterization of a New Aurivillius Phase

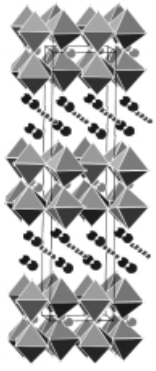

Keywords: Aurivillius phase / Neutron diffraction / Solid-state structures / Perovskite phases

1806 **J. Wojaczyński, M. Stępień, L. Latos-Grażyński***

Monomeric and Dimeric Iron(III) Complexes of 5-Hydroxy-10,15,20-triphenylporphyrin: Formation of Cyano and Pyridine Complexes of (5-Oxo-10,15,20-triphenylphlorin)iron

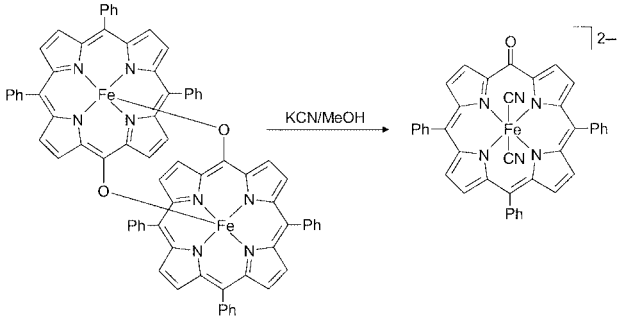

Keywords: Porphyrinoids / Oxophlorins / Iron / Electronic structure / NMR spectroscopy

1816 **A. J. Blake, M. H. M. Caçote, F. A. Devillanova, A. Garau, F. Isaia, V. Lippolis,* C. M. Pereira, F. Silva, L. Tei**

Coordination Chemistry of 2,5,8-Trithia[9],(2,9)-1,10-phenanthrolinophane (L) toward Rhodium(III) at the Polarised Water/1,2-Dichloroethane Interface − A Possible New Approach to the Problem of Separating Rh^{III} from Chloride Media

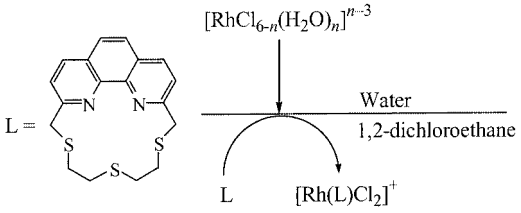

Keywords: Rhodium / Macrocyclic ligands / Interfaces / Cyclic voltammetry

1823 **S.-Q. Liu, J. Pécaut, J.-C. Marchon***

Control of Epoxidation Enantioselectivity by Axial Ligation in Manganese Chiroporphyrins with Diastereotopic Faces

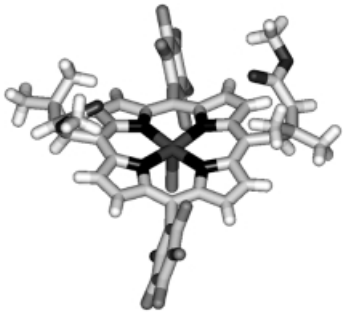

Keywords: Porphyrins / Enantioselectivity / Ligand effects / Manganese

1827 **R. Dorta, L. J. W. Shimon, H. Rozenberg, D. Milstein***

Facile Oxidative Addition of C−Cl Bonds to New Neutral and Cationic Rhodium(I)-Bipyridine Complexes

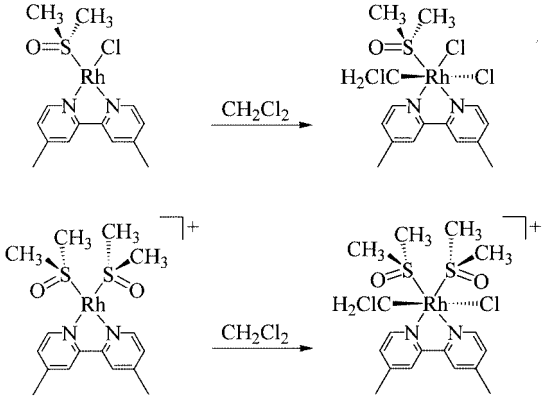

Keywords: Rhodium / N ligands / Oxidative addition / Peroxo complexes

1835 **P. Starynowicz,* K. Bukietyńska**

A Europium(II) Complex with Benzo-15-Crown-5

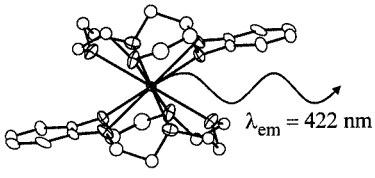

Keywords: Europium / Crown compounds / X-ray diffraction / Luminescence / Lanthanides

1839 **N. Niklas, F. Hampel, O. Walter, G. Liehr, R. Alsfasser***

Synthesis, Structures, and Redox Properties of Copper Complexes with Chiral and Achiral Amino Acid Derived Ligands

Keywords: Amino acids / Chirality / Copper / Redox chemistry

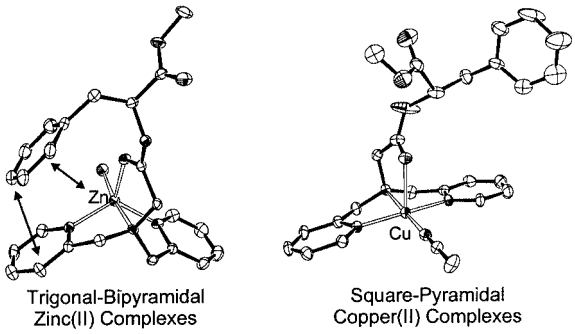

1848 **S. Top,* S. Masi, G. Jaouen***

The $[Re(CO)_6]^+$ Cation as a Ligand-Transfer Reagent with Ferrocene Derivatives

Keywords: Carbonyl(cyclopentadienyl)rhenium / Hexacarbonylrhenium / Ferrocene / Ligand transfer

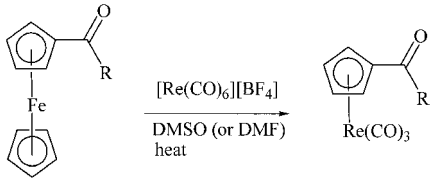

1854 **M. Reiher,* A. Sundermann**

Do Divalent [{HC(CR′NR′′)$_2$}E] Compounds Contain E(I) or E(III) (E = B, Al, Ga, In)? On the Correspondence of Formal Oxidation Numbers, Lewis Structures, and Reactivity

Keywords: Oxidation number analysis / Group-13 carbene analogs / Density functional calculations

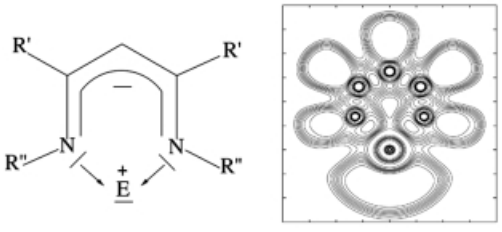

1864 **B. Badraoui, A. Bigi,* M. Debbabi, M. Gazzano, N. Roveri, R. Thouvenot**

Physicochemical Properties and Structural Refinement of Strontium-Lead Hydroxyapatites

Keywords: Hydroxyapatite / X-ray diffraction / IR spectroscopy / ^{31}P MAS NMR / Ionic substitution

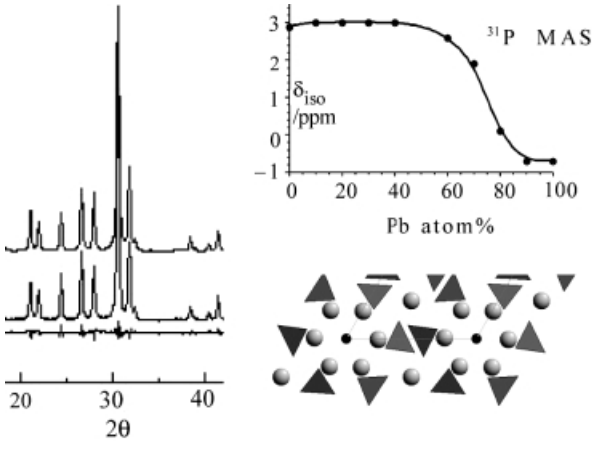

1871 **P. Comba,* Y. D. Lampeka,* A. Y. Nazarenko, A. I. Prikhod'ko, H. Pritzkow, J. Taraszewska**

Cooperative Effects in the Binding of Substrates to Nickel(II) and Nickel(III) Complexes with a Bis(macrocyclic) Ligand

Keywords: Template reaction / Spin equilibrium / Recognition / Cooperative effects / Nickel / N ligands

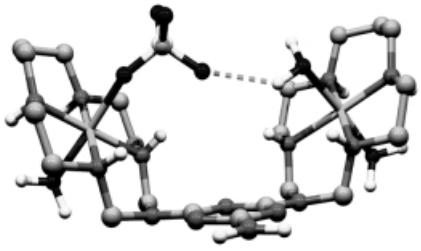

CORRECTION

1883 **T. Höcher, S. Blaurock, E. Hey-Hawkins***

Novel Ferrocene Derivatives with PH-Functionalized Phosphanylalkylcyclopentadienyl Ligands: Syntheses and Molecular Structures of *rac*-[Fe{(η^5-C_5H_4)CMe_2PHR}$_2$] (R = Ph, Mes) and *rac*-[Fe{(η^5-C_5H_4)$CMe_2PHPh(Cp^*TaCl_4)$}$_2$]

The Important Role of Some Ancillary Ligands in the Chemistry of Carbonylmetal Cluster Complexes − Selected Reactivity of Triruthenium Clusters Containing Deprotonated 2-Aminopyridines

Javier A. Cabeza[a]

Dedicated to my former mentors, Professors Luis A. Oro, Peter M. Maitlis and Víctor Riera

Keywords: Ruthenium / Cluster compounds / N ligands / Aminopyridines / Hemilabile ligands

The presence of deprotonated 2-aminopyridines (apy ligands) as face-capping ancillary ligands in carbonyltriruthenium cluster complexes facilitates their reactivity (mild reaction conditions) and increases the regioselectivity of their reactions. This is probably due to the hemilabile character of the apy ligands that help maintain the cluster nuclearity and also provides reaction pathways of low activation energy. Thus, the presence of apy ligands in triruthenium cluster complexes of the type $[Ru_3(\mu\text{-}H)(\mu_3\text{-}apy)(CO)_9]$ has allowed an extensive and regioselective derivative chemistry that is surveyed in this review. A comparative study of the reactivity of 2-amino-, 2-mercapto- and 2-hydroxypyridines with triruthenium clusters is followed by a survey of selective reactions of apy-bridged triruthenium cluster complexes that covers substitution processes, protonation reactions, oxidative addition of hydrogen, hydrosilanes and hydrostannanes, reactions with alkynes and diynes, reactions of coordinated alkenyl and ynenyl ligands, synthesis and reactivity of cationic non-hydridic clusters, preparation of higher-nuclearity clusters and some catalytic applications.
(© Wiley-VCH Verlag GmbH, 69451 Weinheim, Germany, 2002)

I. Introduction

Regioselectivity is a major concern in the derivative chemistry of carbonyl transition metal cluster complexes.[1] Mixtures containing mono- and/or dinuclear complexes are frequently formed as reaction products and, even when no cluster fragmentation occurs, single products are seldom observed.[2]

The above statement is particularly true for the derivative chemistry of the most common ruthenium and osmium cluster starting materials, such as $[Ru_3(CO)_{12}]$, $[Os_3(CO)_{12}]$ and many of their trinuclear derivatives. The low regioselectivity of many of their reactions is a consequence of some intrinsic characteristics of this type of compounds: (a) they are saturated species (48 valence electrons) with high kinetic stability, frequently requiring thermal or photochemical activation to undergo chemical transformations; (b) metal−metal bonds are rather weak and are easily cleaved under thermal or photochemical conditions; and (c) due to their polynuclear nature, cluster complexes may undergo transformations at more coordination sites than mononu-

[a] Departamento de Química Orgánica e Inorgánica, Instituto de Química Organometálica "Enrique Moles", Universidad de Oviedo,
33071 Oviedo, Spain
Fax: (internat.) + 34-985/103446
E-mail: jac@sauron.quimica.uniovi.es
http://www12.uniovi.es/investigacion/jac/

Javier A. Cabeza was born in Soria (Spain) in 1958. He obtained his Ph.D. from the University of Zaragoza in 1983, working on heteropolynuclear complexes of the platinum-group metals, under the supervision of Luis A. Oro. After two years of postdoctoral studies at the University of Sheffield, investigating arene complexes of osmium, with Peter M. Maitlis, he returned to Zaragoza as a postdoctoral researcher in October 1985. There he started his work on carbonylruthenium cluster complexes, in collaboration with Luis A. Oro. In 1987 he was appointed "Profesor Titular" of Inorganic Chemistry at the University of Oviedo, where he currently leads a research group interested in fundamental aspects of organometallic cluster chemistry.

MICROREVIEWS: This feature introduces the readers to the authors' research through a concise overview of the selected topic. Reference to important work from others in the field is included.

clear species and, consequently, once the corresponding activation energy has been reached (particularly if this is high), their reactions often lead to mixtures of products.

Ligand (generally CO) dissociation is usually a requisite for reactions of saturated carbonyl transition metal cluster complexes, since a vacant site is often necessary for the incoming reagent to enter the coordination shell of the cluster complex.[3,4] It is implicit that the lower the activation energy of this step, the more selective the reaction will be, since the risks of cluster fragmentation and reactions at different cluster coordination sites are diminished. To ensure selectivity, a low activation energy should be associated with an appropriate energy minimum. Several methods have been devised to reduce the activation energy of reactions of such cluster complexes, the following being the most important ones:

(a) To carry out the reactions in the presence of trimethylamine oxide.[5] This reagent can react with coordinated CO to give CO_2, in the presence of the appropriate ligand, even at very low temperatures (−78 °C).

(b) To start from "activated" cluster complexes containing weakly coordinating ligands.[6] Acetonitrile is easily displaced by many reagents from complexes such as $[M_3(CO)_{12-x}(MeCN)_x]$ (M = Ru,[6a] Os;[6b] x = 1, 2 or 3). These complexes are normally prepared by treating the parent carbonylmetal complexes with acetonitrile in the presence of the appropriate amount of trimethylamine oxide. Alkenes[6c] and dienes[6d] have also been used as weakly coordinating ligands.

(c) Redox catalysis.[7] The substitution of CO by other ligands can be carried out under mild conditions (room temperature) by performing the reactions in the presence of catalytic amounts of strong reducing reagents, such as the benzophenone ketyl radical anion.

(d) Chemical catalysis. The presence of catalytic amounts of hard anions, such as halides, pseudohalides, carboxylates (as PPN^+ salts, in the absence of ion pairing),[8] or methoxide[9] or hydride[10] sources can promote the substitution of CO ligands by other ligands.

As far as reactivity is concerned, cluster complexes containing bridging ligands with hard-donor atoms[11] are a particular case among carbonyl transition metal cluster complexes because they exhibit an *enhanced substitutional lability*,[12] undergoing reactions under mild conditions. Such ancillary ligands have been termed as *hemilabile* ligands.[12] Although a few examples of bridging monodentate hemilabile ligands are known (chloride,[13] isocyanate[14]), most hemilabile ligands are bidentate and contain both soft- and hard-donor atoms.[15,16] As carbonyl transition metal cluster complexes have soft metal atoms, the softer donor atom of the ligand binds strongly to the metal atom(s), while coordination of the harder donor atom should be labile enough to provide reaction pathways of low activation energy. In addition to helping prevent cluster breakup, these ligands direct the cluster reactivity to reaction sites close (usually *cis*) to the hard-donor atom, thus inducing regioselective reactions.

As long as it is not inconvenient to a particular research project to have a hemilabile ligand attached to the metal cluster, and provided the right hemilabile ligand is chosen, cluster compounds containing a hemilabile ligand have been shown to be the starting materials of choice for studying cluster−ligand interactions,[15,17] for exploring the reactivity of cluster-coordinated ligands,[15,17] and for preparing cluster catalysts.[18]

During the last ten years, Lavigne's and Cabeza's groups have shown that deprotonated 2-aminopyridines (apy) are superb hemilabile ligands in carbonyltriruthenium cluster complexes. This microreview comments on the synthesis and selected reactivity of apy-bridged carbonyltriruthenium cluster complexes. A comparative study of the reactivity of 2-amino-, 2-mercapto- and 2-hydroxypyridines with triruthenium clusters is followed by a survey of selective reactions of apy-bridged cluster complexes that comprises not only substitution processes, but also oxidative additions, protonation reactions, reactions of coordinated ligands, preparation of higher-nuclearity clusters and some catalytic applications. The review is concluded by describing the properties of apy ligands, highlighting the great influence that such ancillary ligands have on the reactivity of the cluster compounds they are coordinated to.

II. Comparative Reactivity of 2-Amino-, 2-Mercapto- and 2-Hydroxypyridines with Triruthenium Clusters

We reported the synthesis and X-ray structure of the first carbonyltriruthenium cluster containing an apy ligand in 1988.[19] It was prepared by treating $[Ru_3(CO)_{12}]$ with 7-azaindole in refluxing hexane (Scheme 1). This work was prompted by the finding that ethylene glycol and methanol could be prepared from synthesis gas using a combination of $[Ru_3(CO)_{12}]$ and 7-azaindole as catalyst precursors.[20]

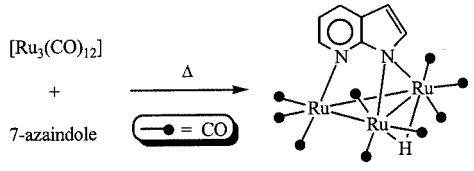

Scheme 1

These results led us to examine the reactivity of $[Ru_3(CO)_{12}]$ with a series of 2-amino-, 2-mercapto- and 2-hydroxypyridines. These ligand precursors are structurally very similar, but differ in their acid-base properties. All reactions need thermal activation (60−110 °C). 2-Aminopyridines (Hapy) afford only trinuclear hydrido derivatives containing face-capping ligands, regardless of the presence of substituents on the pyridine ring or on the exocyclic nitrogen atom, and regardless of the ratio of the reactants (Scheme 2).[21] However, 2-mercapto- and 2-hydroxypyridine (HSpy and HOpy, respectively) lead to several products depending on the ratio of the reactants. No evidence was obtained for the presence of an intermediate trinuclear

complex in the reactions of $[Ru_3(CO)_{12}]$ with 2-hydroxypyridine.[21] The complex $[Ru_3(\mu\text{-}H)(\mu_3\text{-}Spy)(CO)_9]$ was isolated in a low yield because it reacts readily with 2-mercaptopyridine to give polymeric $[\{Ru_2(\mu_3\text{-}Spy)(CO)_4\}_n]$ (analogous to the polymer derived from 2-hydroxypyridine) and/or monomeric $[Ru(Spy)_2(CO)_2]$ (Scheme 2).[22]

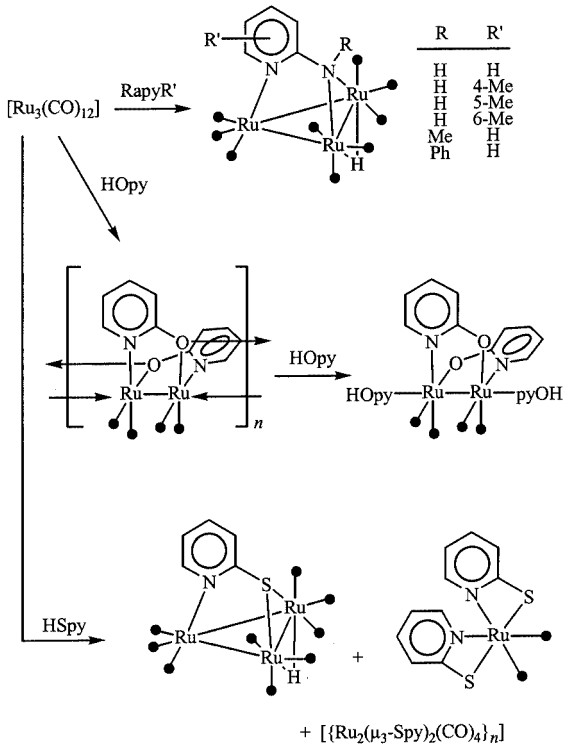

Scheme 2

In parallel to our work, Lavigne's group studied the reactions of $[Ru_3(CO)_{12}]$ with deprotonated 2-anilino-, 2-mercapto- and 2-hydroxypyridines (Phapy, Spy and Opy, respectively) and showed that the results were comparable with those of the reactions of $[Ru_3(\mu\text{-}H)(CO)_{11}]^-$ with the neutral ligands (Scheme 3).[23] While only a face-capping derivative was observed for the Spy ligand, both edge-bridging and face-capping derivatives were observed for the Phapy and Opy ligands. Interestingly, interconversion of the decacarbonyl and nonacarbonyl derivatives of the Phapy ligand is observed under milder conditions (25 °C, CO or inert gas purge), while interconversion of the corresponding Opy derivatives is not observed (the decacarbonyl Opy complex could only be partially decarbonylated after prolonged refluxing under a stream of inert gas).[23]

The very mild conditions under which the above-mentioned interconversion of the anionic Phapy derivatives takes place indicate that the reversible opening of the amido bridge in μ_3-apy ligands is a low activation energy process. Although such a bridge opening has been observed only in very few occasions in neutral cluster complexes containing μ_3-apy ligands (vide infra), it is believed that in their reactions such an opening may also be responsible for their high reactivity.[23] This, in addition to the higher stability of the trinuclear apy derivatives than that of the Opy and Spy

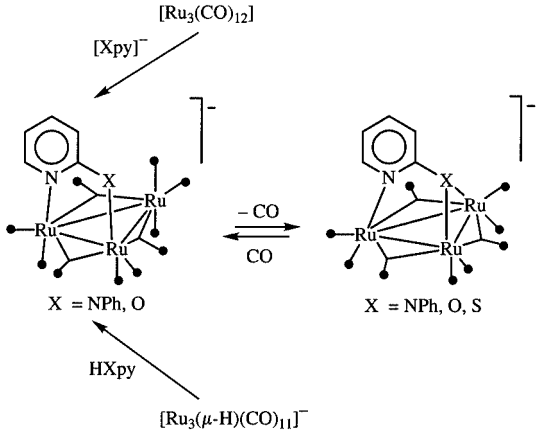

Scheme 3

complexes, makes the apy ligands excellent ancillary ligands for triruthenium cluster complexes. This statement is demonstrated by the rich, easy and regioselective derivative chemistry commented in the following section of this review.

III. Selected Reactivity of Triruthenium Clusters Containing Deprotonated 2-Aminopyridines

As starting material, we chose the complex $[Ru_3(\mu\text{-}H)(\mu_3\text{-}apyMe)(CO)_9]$ (**1**, HapyMe = 2-amino-6-methylpyridine, Scheme 4) because the presence of the methyl group on the pyridine ring facilitates the monitoring of the reactions by NMR spectroscopy, without sterically interacting with other ligands. In addition, the presence of the N−*H* hydrogen atom results in an appropriate solubility/insolubility of the complexes in polar/nonpolar solvents.

III.a. Reactions with Phosphanes

Simple carbonyl substitution reactions are frequently used to determine the position of reactive sites in cluster complexes. Schemes 4 and Scheme 5 show the reactivity of complex **1** and its protonated derivative $[Ru_3(\mu\text{-}H)_2(\mu_3\text{-}apyMe)(CO)_9]^+$ (**2**) with triphenylphosphane[24,25] and bis(diphenylphosphanyl)methane,[26] respectively. It is remarkable that all reactions are regioselective and that the successive substitutions take place stepwise. Moreover, the first substitutions occur instantaneously at room temperature, while further substitutions require gentle heating (60−70 °C). With triphenylphosphane, under kinetic conditions, the substitutions take place in positions *cis* to the bridging amido fragment and/or *cis* to the hydrido ligand, indicating a strong *cis*-labilizing effect of these ligands. The rigidity of the dppm ligand results in the coordination of the two P atoms at the equatorial sites on adjacent metal atoms. In the case of some cationic complexes, the kinetic products isomerize on heating resulting in the thermodynamic products by dissociative mechanisms (such isomerizations are inhibited by the presence of the free phosphanes in solution). Stable neutral methoxycarbonyl derivatives (not

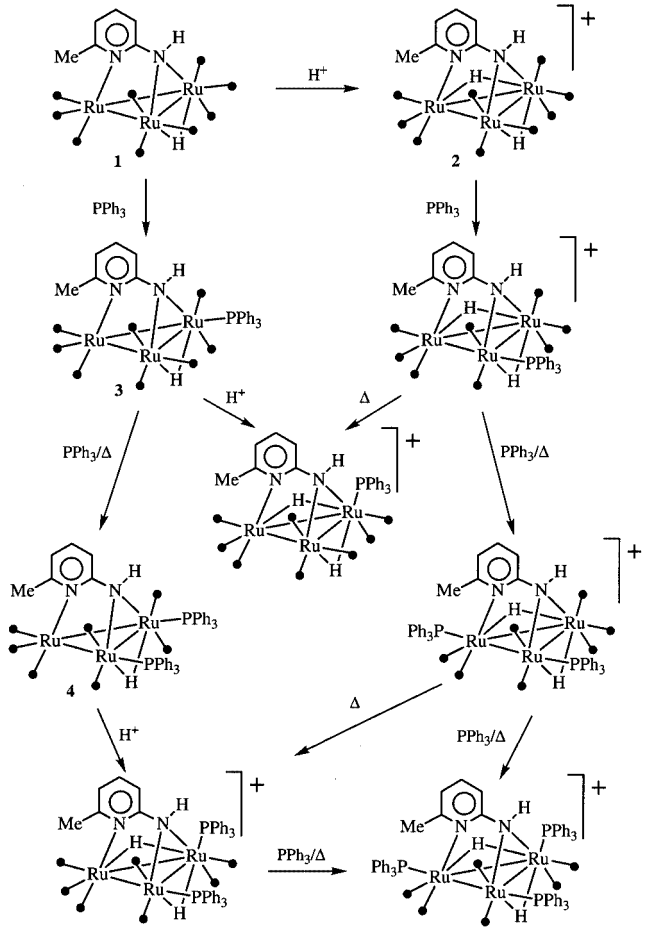

Scheme 4

represented in Schemes 4 and Scheme 5) are produced when the cationic complexes are treated with potassium methoxide.[24−26]

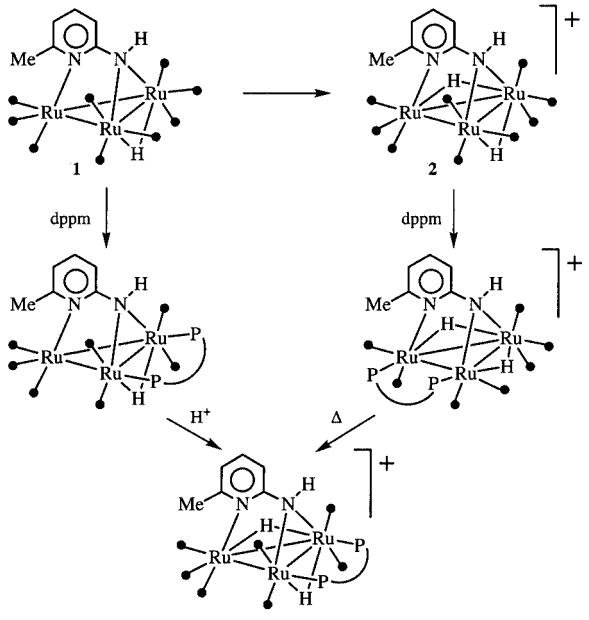

Scheme 5

Facile activation of the P−H bond of diphenylphosphane has been observed on heating diphenylphosphane derivatives of complex **1** (Scheme 6).[27]

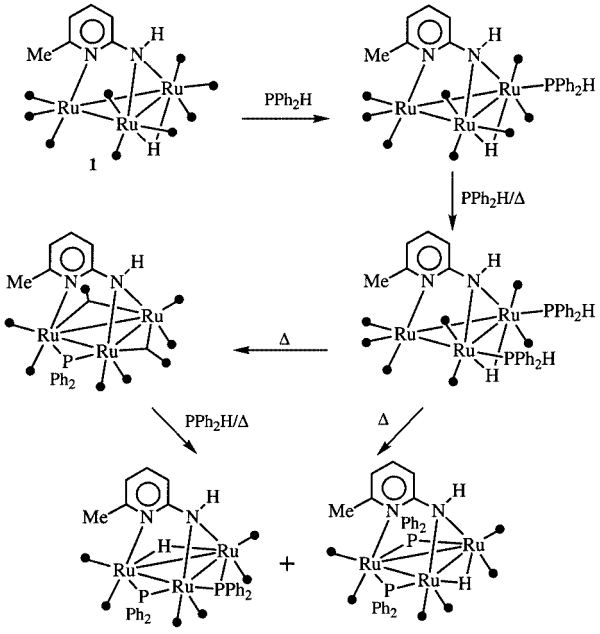

Scheme 6

Basolo and Lavigne studied the mechanism of exchange of CO by phosphane ligands in a series of anionic complexes $[Ru_3(\mu_3\text{-Rapy})(CO)_9]^-$, having different R substituents on the exocyclic N atom (Scheme 7).[28] Second-order kinetics were found (associative-type mechanism), which is consistent with a two-step process in which the first step is the coordination of the phosphane with the concomitant opening of an Ru−N arm. This adduct evolves into the final substituted product. The energy barrier for the second step depends on the nucleophilicity of the amido group. In fact, the initial adduct can be isolated when R = Ph, but it is too short-lived when R = Me. These results clearly demonstrate the hemilabile character of the apy ligands in these complexes.

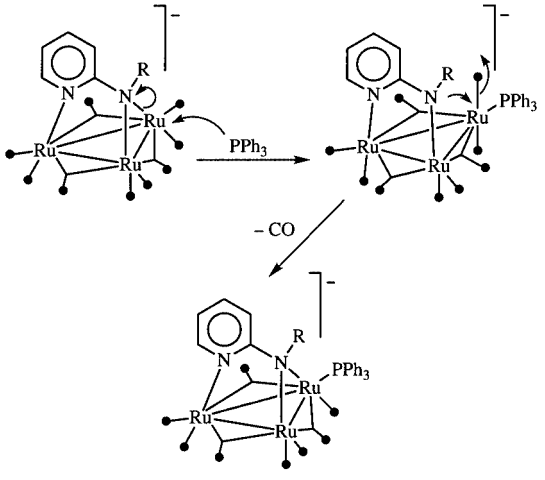

Scheme 7

III.b. Reactions with Hydrogen, Silanes and Stannanes

The reactions of these three reagents with unsaturated organic substrates are of great practical importance and need the intermediacy of metal catalysts. We wondered whether such reactions could be promoted by apy-bridged triruthenium clusters.

Prior to this study, the reactivity of carbonyltriruthenium cluster complexes with these three reagents had been relatively uninvestigated. This is probably because their reactions with $[Ru_3(CO)_{12}]$ frequently give products of different nuclearity, i.e. $[Ru_4(\mu\text{-}H)_4(CO)_{12}]$,[29] $[Ru_2(SiR_3)_2(CO)_8]$ and $[Ru(ER_3)_2(CO)_4]$ (E = Si, Sn).[30] Interestingly, a few trinuclear products containing ER_3 groups have been obtained using $[Ru_3(MeCN)(CO)_{11}]$,[31] $[Ru_3(\mu\text{-}H)(CO)_{11}]^-$,[32] or ligand-bridged clusters[33] as starting materials.

Complex **1** is an efficient catalyst precursor for the homogeneous hydrogenation of alkynes to alkenes and dienes to monoenes.[34] This catalytic activity prompted us to study the stoichiometric reactions that might be involved in the catalytic process. The reaction of complex **1** with hydrogen (1 atm, 110 °C) leads to the hexanuclear hexahydrido 92-electron derivative $[Ru_6(\mu_3\text{-}H)_2(\mu\text{-}H)_4(\mu_3\text{-}apyMe)_2(CO)_{14}]$ (**5**, Scheme 8),[35] erroneously formulated as $[Ru_3(\mu\text{-}H)_3(\mu_3\text{-}apyMe)(CO)_8]$ when it was first reported.[34] This remarkable complex consists of two unsaturated (46-electron) trinuclear units connected to each other through two bridging hydride ligands. The shortest Ru···Ru distance between the two trinuclear units is 3.292(3) Å, too long to be considered an Ru−Ru bond. It regenerates complex **1** when exposed to carbon monoxide (1 atm, 20 °C), but undergoes CO substitution instead of ligand addition when treated with P(*p*-tolyl)$_3$ at room temperature. Complex **5** is even more effective than **1** as a catalyst precursor for the homogeneous hydrogenation of diphenylacetylene under very mild conditions (1 atm, 50 °C).[36]

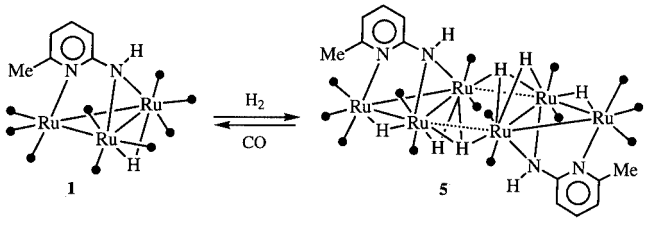

Scheme 8

As occurs with $[Os_3(\mu\text{-}H)_2(CO)_{10}]$,[29] the hydrogenation of **1** implies the oxidative addition of hydrogen to a trinuclear cluster complex and the elimination of two CO ligands to give an unsaturated 46-electron species. While the osmium species is stable, the ruthenium species dimerizes to give **5**. Unsaturated 46-electron clusters of ruthenium are very rare. To date, only one trinuclear derivative has been reported, i.e. $[Ru_3(\mu\text{-}H)(\mu\text{-}PPh_2)(CO)_9]$.[37] A hexanuclear complex related to **5**, but containing thioureate instead of apyMe ligands, has also been reported.[38]

While the substituted complex $[Ru_3(\mu\text{-}H)(\mu_3\text{-}apyMe)(PPh_3)(CO)_8]$ (**3**; Scheme 4) does not react with hydrogen, the disubstituted derivative $[Ru_3(\mu\text{-}H)(\mu_3\text{-}apyMe)(PPh_3)_2(CO)_7]$ (**4**) undergoes two P−C bond activation processes on reaction with hydrogen (1 atm, 110 °C), leading to a complex containing a bridging phenyl group and two bridging diphenylphosphido ligands, i.e. $[Ru_3(\mu\text{-}Ph)(\mu_3\text{-}apyMe)(\mu\text{-}PPh_2)_2(CO)_6]$ (Scheme 9).[39] A few more triruthenium clusters containing bridging phenyl groups derived from PPh_3 ligands have been reported in the last few years.[17,40−42] It appears that cluster complexes of this type have an unusual ability of stabilizing bridging phenyl groups.

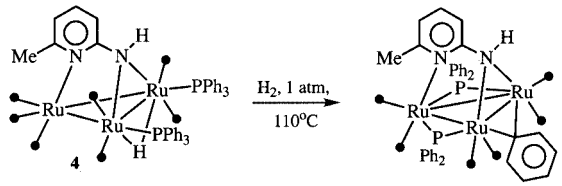

Scheme 9

The clusters $[Ru_3(\mu\text{-}H)(\mu_3\text{-}apyMe)(PPh_3)_x(CO)_{9-x}]$ [x = 0 (**1**), 1 (**3**), 2 (**4**)] react with $HSiEt_3$ to give the oxidative substitution products $[Ru_3(\mu\text{-}H)_2(\mu_3\text{-}apyMe)(SiEt_3)(PPh_3)_x(CO)_{8-x}]$ [x = 0 (**6a**), 1 (**7a**), 2 (**8a**)]. Similar reactions with $HSnBu_3$ afford $[Ru_3(\mu\text{-}H)_2(\mu_3\text{-}apyMe)(SnBu_3)(PPh_3)_x(CO)_{8-x}]$ [x = 0 (**6b**), 1 (**7b**), 2 (**8b**)], which are isostructural with the corresponding silyl derivatives (Scheme 10).[43] The reactions of **6a** and **7a** with PPh_3 results in the elimination of $HSiEt_3$, rendering the complexes **3** and **4**. However, similar reactions with the tin-containing compounds **6b** and **7b** afford the substitution products **7b** and **8b**, respectively. Further, while **6b** is stable under carbon monoxide, the silyl derivative **6a** regenerates complex **1** under the same conditions. These reactions, which represent the first systematic study of the reactivity of triruthenium clusters with silanes and stannanes, demonstrate

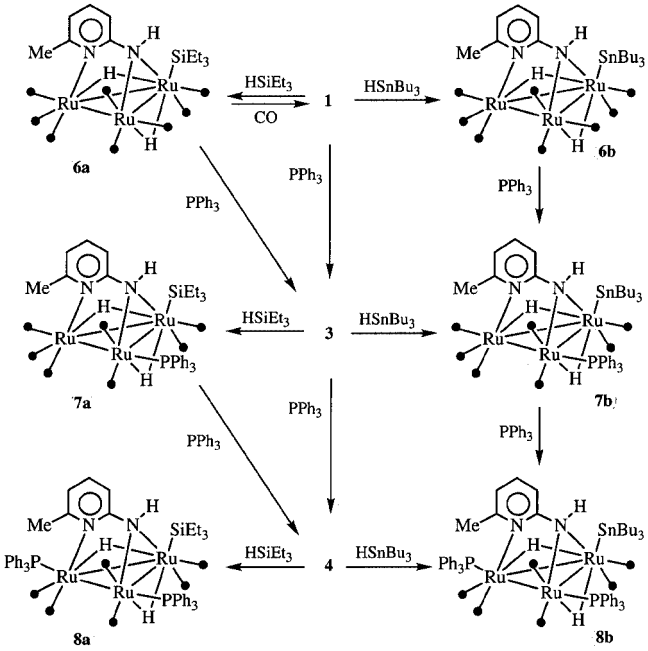

Scheme 10

that the hydrido(stannyl) complexes are much more stable than the hydrido(silyl) derivatives towards the elimination of the corresponding triorganostannanes or triorganosilanes.

III.c. Reactions with Alkynes

Alkynes have always attracted the attention of organometallic cluster chemists because of their versatile reactivity.[44] They are good ligands that bind strongly to the metal atoms, and are prone to undergo facile insertion processes and coupling reactions with other ligands.

Cluster complexes of the type $[Ru_3(\mu\text{-}H)(\mu_3\text{-}apy)(CO)_9]$ react easily (10−20 min, 40−60 °C) with alkynes to give derivatives that contain edge-bridged alkenyl ligands. For steric reasons, the position of the alkenyl group within the clusters depends on the presence or absence of substituents on the amidic N atom (Scheme 11).[23,45]

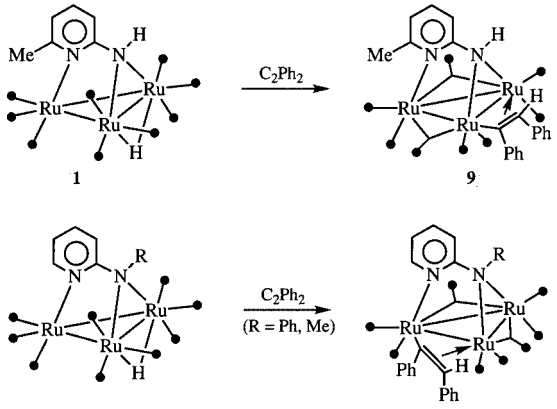

Scheme 11

The phosphane-substituted complexes **3** and **4** also react with diphenylacetylene to give alkenyl derivatives (Scheme 12).[46,47] The conditions needed for the reaction of the disubstituted complex **4** (110 °C, 75 min) induced the cleavage of a P−C bond giving a phenyl derivative that can be isolated.[47] The monosubstituted alkenyl derivative $[Ru_3(\mu_3\text{-}apyMe)(\mu\text{-}PhCH{=}CPh)(PPh_3)(CO)_7]$ promotes the catalytic hydrogenation of diphenylacetylene under mild conditions (1 atm, 80 °C). A kinetic analysis of this reaction indicated the presence of intermediate trinuclear clusters as catalytic species.[48]

The reaction of diphenylacetylene with the hydrido(silyl) compound $[Ru_3(\mu\text{-}H)_2(\mu_3\text{-}apyMe)(SiEt_3)(CO)_8]$ (**6a**) gives the alkenyl complex $[Ru_3(\mu_3\text{-}apyMe)(\mu\text{-}PhCH{=}CPh)(CO)_8]$ (**9**) and $HSiEt_3$.[46] Analogous reactions of hydrido(stannyl) compounds give a mixture of two isomeric hydrido(stannyl)-alkenyl derivatives (Scheme 13).[49] Interestingly, the reactions of the alkenyl complex **9** with tertiary silanes and stannanes give similar mixtures of compounds including (alkenyl)hydrido(silyl) and (alkenyl)hydrido(stannyl) derivatives.[46,49] It should be noted that in all the compounds having alkenyl and ER_3 ligands, these ligands are attached to different metal atoms. This may explain why no hydrosilylated or hydrostannated diphenylacetylene is observed when diphenylacetylene and triorganosilanes or triorganostannanes are allowed to react in the presence of complex **1**.

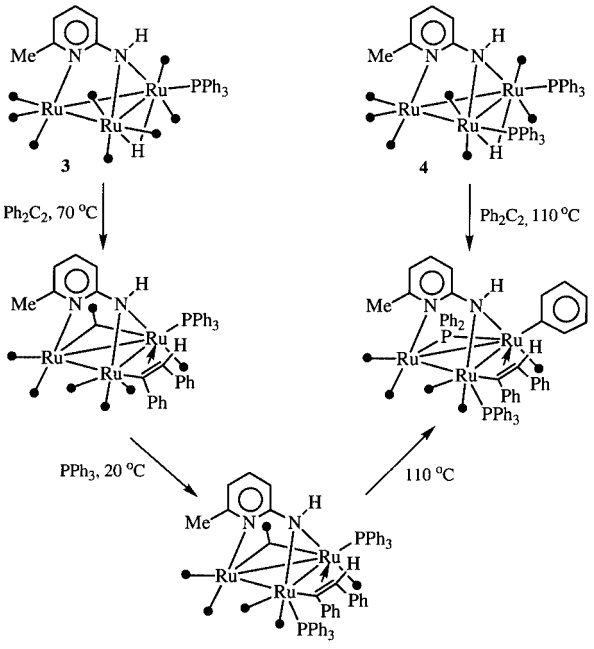

Scheme 12

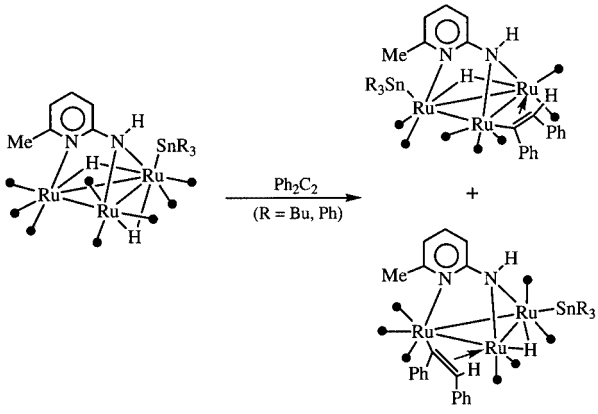

Scheme 13

It has been reported that $[Ru_3(\mu\text{-}H)(\mu_3\text{-}Phapy)(CO)_9]$ promotes the regioselective polymerization of phenylacetylene to *cis*-polyphenylacetylene, but only in the presence of a catalytic amount of $HSiEt_3$.[50] The role played by the silane remains unknown. In the absence of silane, 1,2,4-triphenylbenzene is obtained. When (triphenylsilyl)acetylene is used as the incoming substrate, a poor catalytic dimerization to (*E*)-1,4-bis(triphenylsilyl)but-1-yn-3-ene is observed.[50]

Compound **1** reacts with diphenylbutadiyne and 1,6-diphenoxyhexa-2,4-diyne in THF at refluxing temperature to give the ynenyl derivatives $[Ru_3(\mu_3\text{-}apyMe)(\mu\text{-}RC{\equiv}CC{=}CHR)(CO)_8]$ [R = Ph (**11**), CH_2OPh (**13**); Scheme 14]. These products contain a 1,4-disubstituted butynen-3-yl ligand η^3-coordinated to two ruthenium atoms. The remarkable compound $[Ru_3(\mu\text{-}apyMe)\{\mu_3\text{-}\eta^6\text{-}PhCC_5(C{\equiv}CPh)$-

$HPh_2\}(CO)_7$] (**12**), which contains an η^5-cyclopentadienyl ring and a bridging carbene fragment, has also been obtained from the reaction of **1** with diphenylbutadiyne.[51]

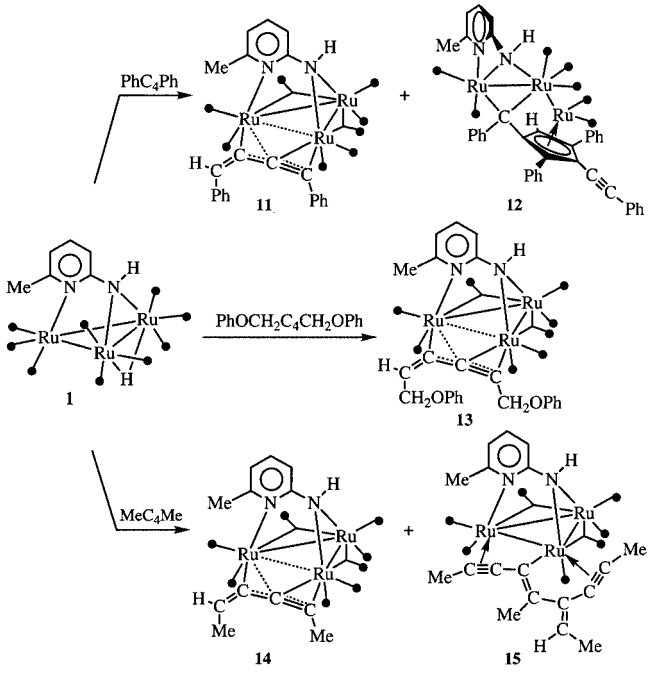

Scheme 14

As diynes contain asymmetric alkyne fragments, there are two possible products resulting from the insertion of one of their alkyne fragments into a metal−hydride bond.[51] While compounds **11** and **13** contain butynen-3-yl ligands that clearly result from one of the two possible insertion regioisomers, compound **12** arises from an unprecedented [3+2]-cycloaddition reaction of an unobserved 1,4-diphenylbutynen-4-yl ligand (of the other insertion regioisomer) with a triple bond of a second diphenylbutadiyne molecule. Both insertion regioisomers have been isolated from the reaction of [Ru_3(μ-H)(μ_3-Phapy)$(CO)_9$] with diphenylbutadiyne.[52]

The reaction of complex **1** with an excess of hexa-2,4-diyne in refluxing THF gives the trinuclear derivative [Ru_3-(μ_3-apyMe)$\{\mu$-η^5-MeC≡CC(=CHMe)CMe=CC≡CMe$\}$-$(CO)_7$] (**15**) as the final product (Scheme 14). This compound contains an unprecedented diynedienyl ligand that arises from the coupling of hexa-2,4-diyne with the hex-2-yn-4-en-4-yl ligand of the intermediate [Ru_3(μ_3-apyMe) μ-MeCH=CC≡CMe)$(CO)_8$] (**14**). This intermediate is the first compound observed in the reaction of **1** with hexa-2,4-diyne, but it could not be isolated free of **15**.[53]

From the results described above, it can be inferred that alkynes can easily be activated in the form of alkenyl (vinyl) ligands by carbonyl(hydrido)triruthenium clusters containing bridging apy ligands. It is worth noting that the presence of the face-capping ligand in the clusters is essential in maintaining the cluster nuclearity, since it is well known that the reactions of alkynes and alkenes with hydridotriruthenium clusters containing edge-bridging ligands provoke the loss of one metal center, rendering bridged dinuclear products.[54]

III.d. Reactivity of Alkenyl Derivatives

Many of the alkenyl complexes commented on above were considered to be ideal candidates for reactivity studies, including the chemical modification of the alkenyl ligand itself.

Both the neutral alkenyl complex [Ru_3(μ_3-apyMe)(μ-PhCH=CPh)$(CO)_8$] (**10**) and its protonated derivative [Ru_3(μ-H)(μ_3-apyMe)(μ-PhCH=CPh)$(CO)_8$][BF_4] (**16**) promote the catalytic hydrogenation of diphenylacetylene under very mild conditions. The neutral complex is more efficient (TOF = 38.8 h^{-1})[55] than the cationic complex (TOF = 29.2 h^{-1})[56] under comparable reaction conditions [333 K, $p(H_2)$ = 0.573 atm]. (*Z*)-Stilbene is the kinetic product, but it is progressively isomerized to (*E*)-stilbene. Hydrogenation of stilbenes to 1,2-diphenylethane was not detected. Detailed chemical and kinetic studies on these reactions indicated the presence of intermediate trinuclear clusters as catalytic species in both cases.

Lavigne's group has studied a number of very interesting C−C bond-forming reactions starting from [Ru_3(μ_3-Rapy)(μ-PhCH=CPh)$(CO)_8$] (R = Ph or Me), that are outlined in Scheme 15.

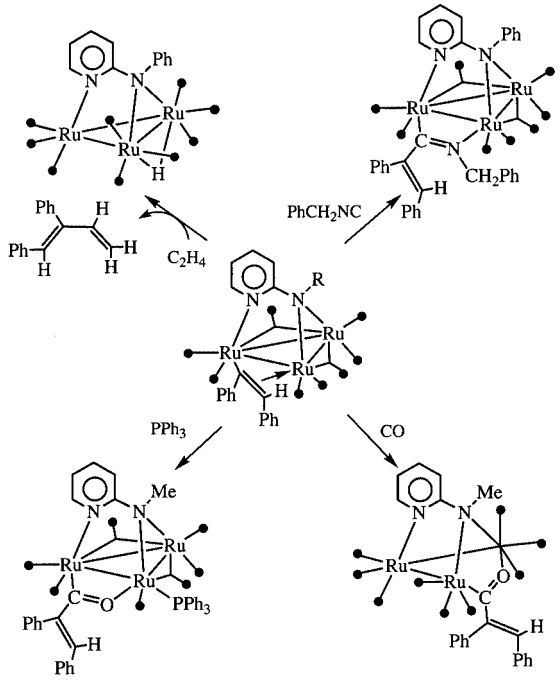

Scheme 15

Stoichiometric ethylene−diphenylacetylene codimerization has been observed on treating [Ru_3(μ_3-Phapy)(μ-PhCH=CPh)$(CO)_8$] with ethylene.[57] The mononuclear complex [Ru(PhCH=CPhCH=CH_2)$(CO)_3$] is a by-product of this reaction. It is proposed that the reaction proceeds by ethylene insertion into the metal−alkenyl group, followed by β-elimination. The elimination of free butadiene

competes with the elimination of the mononuclear butadiene complex.

The reaction of $[Ru_3(\mu_3\text{-Phapy})(\mu\text{-PhCH=CPh})(CO)_8]$ with benzyl isocyanide at room temperature leads to $[Ru_3(\mu_3\text{-Phapy})(\mu\text{-PhCH=CPhC=NCH}_2\text{Ph})(CO)_8]$, which contains an alkenylimino ligand (Scheme 15).[50] This insertion reaction is related to the rapid uptake of triphenylphosphane (room temperature), giving the acyl derivative $[Ru_3(\mu_3\text{-Meapy})(\mu\text{-PhCH=CPhC=O})(PPh_3)(CO)_7]$.[58] Second-order kinetics indicate that the initial step is an associative addition of the PPh_3 ligand to the metal cluster without CO loss.

In addition, a related 50-electron acyl derivative, i.e. $[Ru_3(\mu_3\text{-Meapy})(\mu\text{-PhCH=CPhC=O})(CO)_9]$, is formed when the alkenyl precursor is exposed to CO (Scheme 15).[58] Hydrogenation (25 °C, 5 atm) of this complex causes the elimination of α-phenylcinnamaldehyde and the recovery of the hydrido complex $[Ru_3(\mu\text{-H})(\mu_3\text{-Meapy})(CO)_9]$. The overall transformation constitutes a stepwise hydroformylation of diphenylacetylene. Attempts to achieve a catalytic process led to the isolation of the catalytically inactive dinuclear derivative $[Ru_2(MeCOapy)_2(CO)_6]$ as the major metal-containing product (Scheme 16).[58] This reaction represents the first (and so far unique) example of the degradation of an apy-bridged triruthenium cluster, probably due to the harsh reaction conditions.

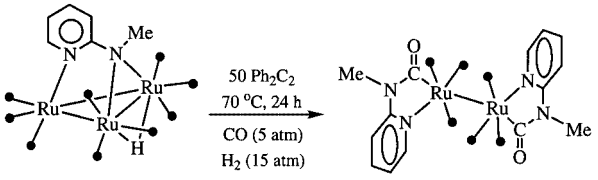

Scheme 16

The reactivity of the ynenyl derivatives $[Ru_3(\mu_3\text{-apyMe})(\mu\text{-RC}\equiv\text{CC=CHR})(CO)_8]$ [R = Ph (**11**), CH_2OPh (**13**)] with diynes and alkynes has been studied.[51] In all cases, the products contain a ruthenacyclopentadienyl fragment formed by the coupling of the coordinated ynenyl ligand of the starting material with a triple bond of the new reagent (Scheme 17). While all compounds derived from **11** have the alkenyl C=CHR (R = Ph) fragment with an (*E*) configuration (R *trans* to Ru, Scheme 17), most of the products derived from **13**, have the alkenyl C=CHR (R = CH_2OPh) fragment with an (*E*) configuration.

It is interesting to note that all these ruthenacyclopentadienyl derivatives, as well as complex **12** (Scheme 14), have a 5-electron donor apyMe ligand attached to only two metal atoms, a coordination mode previously unobserved for apy ligands in cluster chemistry that strongly supports the hemilabile character of these ligands.

III.e. Synthesis and Reactivity of Cationic Non-Hydridic Clusters

Simple protonation of neutral carbonyl cluster complexes frequently leads to cationic hydridic derivatives.[19,24,25]

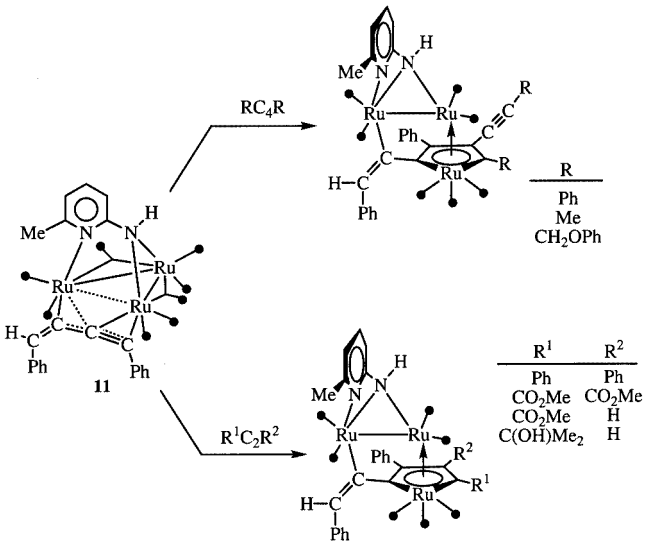

Scheme 17

However, very few non-hydridic cationic carbonyl clusters have been described. For ruthenium, prior to the cluster complexes commented on below, only a few examples of trinuclear 50-,[59] 47-[60] or 46-electron[60] species were known.

The presence of the alkenyl and hydride ligands in the cationic complex $[Ru_3(\mu\text{-H})(\mu_3\text{-apyMe})(\mu\text{-PhCH=CPh})(CO)_8][BF_4]$ (**16**) prompted us to study reactions that might induce the reductive elimination of (*Z*)-stilbene, and that would give cationic cluster compounds containing non-hydridic ligands. Although reactions with phosphane ligands only lead to CO-substitution products,[61] complex **16** reacts gently (1 atm, 20 °C) with carbon monoxide giving the cationic complex $[Ru_3(\mu_3\text{-apyMe})(CO)_{10}][BF_4]$ (**17**) in quantitative yield (Scheme 18). (*Z*)-Stilbene is a by-product of this reaction.[62] No other non-hydridic 48-electron cationic triruthenium cluster complexes were known prior to the publication of complex **17**.

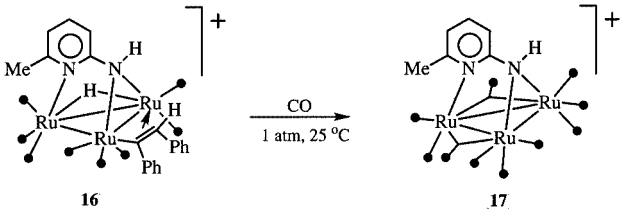

Scheme 18

The reactivity of complex **17** markedly reflects a very high electrophilicity. It easily undergoes CO-substitution reactions on treatment with a variety of nucleophiles, including phosphanes,[62] hydrides, halides and carboxylates (Scheme 19), and is unstable in donor solvents (acetone, THF).[63]

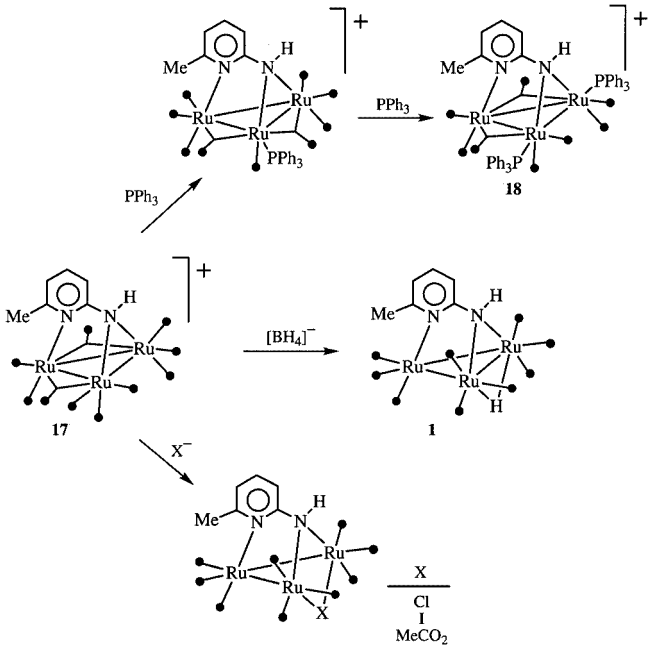

Scheme 19

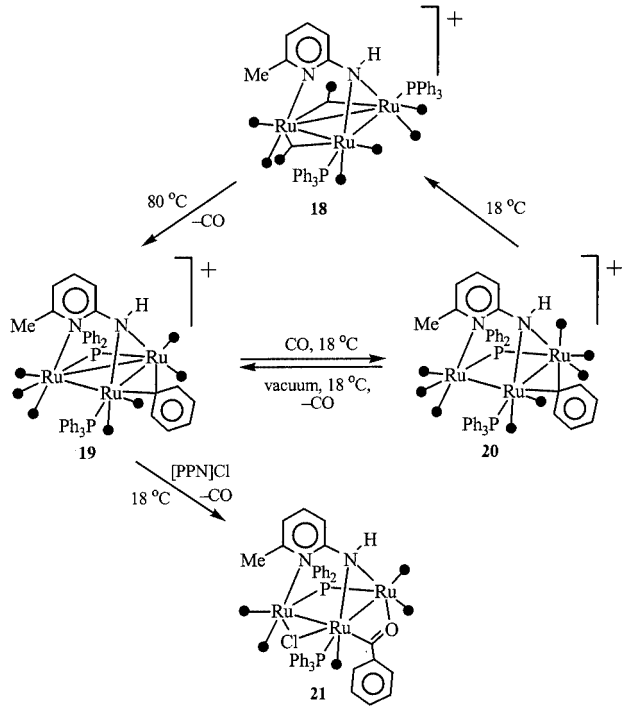

Scheme 20

It is worth noting that the thermal activation of a P−C bond of the disubstituted compound $[Ru_3(\mu_3\text{-apyMe})(PPh_3)(CO)_8][BF_4]$ (**18**) leads to the phenyl derivative $[Ru_3(\mu\text{-Ph})(\mu_3\text{-apyMe})(\mu\text{-}PPh_2)(PPh_3)(CO)_7][BF_4]$ (**19**). Treatment of **19** with carbon monoxide regenerates **18** via the 50-electron intermediate $[Ru_3(\mu\text{-Ph})(\mu_3\text{-apyMe})(\mu\text{-}PPh_2)(PPh_3)(CO)_8][BF_4]$ (**20**) (Scheme 20).[41] These reactions represent the only reversible triphenylphosphane P−C bond activation reaction reported in carbonyl cluster chemistry. The characterization of the neutral acyl derivative $[Ru_3(\mu\text{-PhCO})(\mu\text{-Cl})(\mu_3\text{-apyMe})(\mu\text{-}PPh_2)(PPh_3)(CO)_5]$ (**21**), which arises from the reaction of **19** with [PPN]Cl, supports the formulation assigned to **19**.[41]

III.f. Reactions Leading to Higher-Nuclearity Clusters

As part of the study of the reactivity of the cationic complex **17**, we treated it with aqueous NaOH. Two complexes were obtained, i.e. **1** and the hexanuclear derivative $[Ru_6(\mu_3\text{-apyMe})_2(CO)_{18}]$ (**22**) (Scheme 21).[64] The latter is the only example of a hexanuclear cluster consisting of two vertex-linked metal triangles in the chemistry of ruthenium.

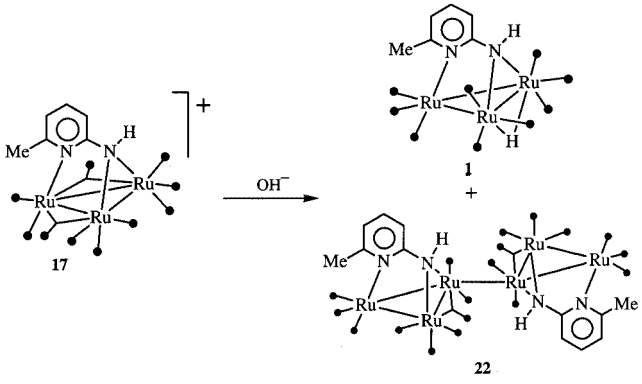

Scheme 21

A possible reaction pathway for this transformation is sketched in Scheme 22.[64] It involves the nucleophilic attack of the coordinated CO ligand of complex **17** by the hydroxide anion, to give an unstable hydroxycarbonyl species that rapidly releases CO_2, rendering the neutral hydride **1**. Before all of complex **17** has been consumed, complex **1** deprotonates with more OH^- giving the anionic derivative $[Ru_3(\mu_3\text{-apyMe})(CO)_9]^-$ (**23**). Finally, **23** reacts with the remaining complex **17** to give CO and the hexanuclear cluster **22**. This reaction sequence is supported by the facts that **17** does react with **23** to give **2**, and that **1** can be deprotonated with NaOH to afford **23**. Alternatively, compound **22** can also be prepared by zinc reduction of complex **17**.[64]

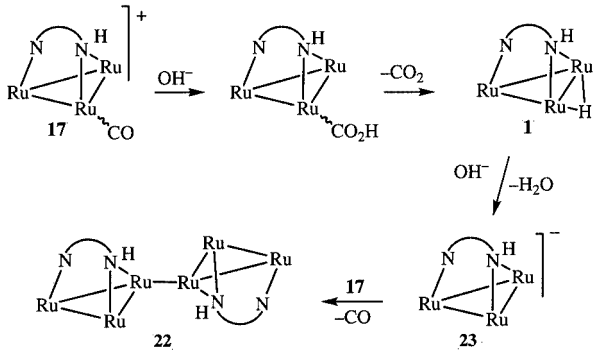

Scheme 22

The hexanuclear compound $[Ru_6(\mu\text{-H})(\mu_4\text{-S})(\mu_3\text{-apyMe})(CO)_{17}]$ (**24**), which consists of two closed trimetal units connected by two metal−metal bonds, has been prepared

by reaction of the cationic complex **17** with the anionic cluster $[Ru_3(\mu_3\text{-}S)(CO)_9]^{-2}$ (Scheme 23).[63] Although other related carbonylhexaruthenium cluster compounds containing μ_4-S ligands are known,[38][65] they are electron-rich derivatives since their electron count (94-electrons) has two electrons more than those required by electron-precise clusters containing eight metal−metal bonds (92 electrons). In contrast, compound **24** is electron-precise.

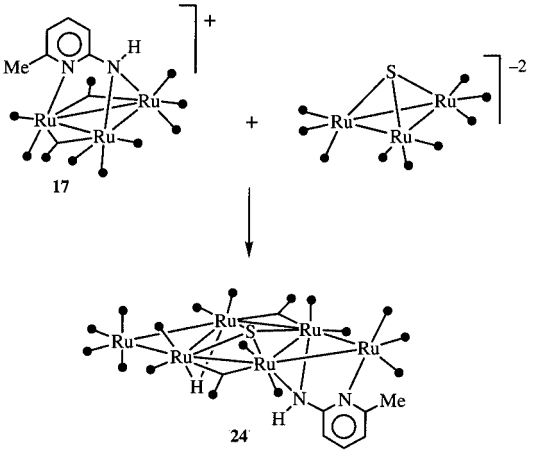

Scheme 23

The reactions of anionic carbonyl clusters with mononuclear cations have often been used to prepare higher-nuclearity cluster compounds.[66] However, no reactions of cationic carbonyl clusters with anionic complexes had been reported prior to the publication of compound **17**. This is probably because cationic non-hydridic clusters were not readily accessible and because a proton transfer from the cation to the anion occurs when cationic hydridic clusters are used. This results in a mixture of two neutral complexes rather than a cluster of higher nuclearity.

The mercury-containing hexaruthenium cluster $[Ru_6(\mu_4\text{-}Hg)(\mu_3\text{-}apyMe)_2(CO)_{18}]$ (**25**) has been prepared by treating complex **1** with diphenylmercury (Scheme 24).[67] This complex reacts with mercury(II) chloride to give $[Ru_3(\mu\text{-}HgCl)(\mu_3\text{-}apyMe)(CO)_9]$ (**26**). In both cases, the mercury atoms span the same Ru−Ru edge as the amido moiety.

Redistribution reactions of compound **26** with the metal−metal-bonded dimers $[M_2Cp_2(CO)_6]$ (M = Mo, W) and $[Co_2(CO)_8]$ give mixtures of the mixed-metal clusters $[\{Ru_3(\mu_3\text{-}apyMe)(CO)_9\}(\mu\text{-}Hg)ML_n]$ (ML_n = $MoCp(CO)_3$, $WCp(CO)_3$, $Co(CO)_4$] and the corresponding chloro complexes $[MClL_n]$ (Scheme 24).[68] These mixtures can be separated. Besides these reactions, the only additional example of a reaction of a metal cluster containing an HgX (X = halogen) moiety with a neutral complex containing metal−metal bonds is that of $[Ru_3(\mu\text{-}HgI)(\mu_3\text{-}C_2t\text{Bu})(CO)_9]$ with $[Ru_3(CO)_{12}]$, which gives $[\{Ru_3(\mu_3\text{-}C_2t\text{Bu})(CO)_9\}_2(\mu_3\text{-}Hg)_2Ru(CO)_4]$ as the major product.[69]

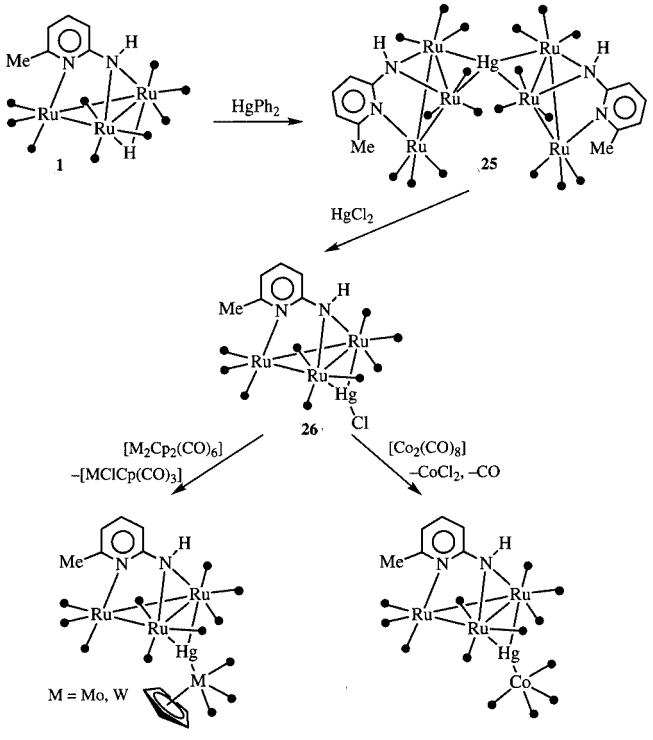

Scheme 24

IV. Concluding Remarks

The following are the principal features associated with apy ligands in carbonyltriruthenium clusters:

(a) The apy ligands remain unchanged under most reaction conditions, thus avoiding undesirable side reactions.

(b) The reactions take place under mild conditions (25−100 °C), probably induced by a hemilabile effect of the apy ligands.

(c) Reactivity (CO substitution) is directed to positions *cis* to the apy amido group, thus leading to regioselective reactions in most cases.

(d) The trinuclear cluster framework is preserved during the reactions because of the mild reaction conditions, and because of the anchor effect of the apy ligands, which maintains the metal atoms in adequate proximity.

(e) This type of cluster complexes show an unusual ability to stabilise bridging phenyl groups.

(f) The compounds have a convenient solubility in polar solvents (insoluble in nonpolar solvents), particularly if the exocyclic nitrogen atom is part of an N−H group.

(g) The basicity of the apy ligands can be tuned by introducing substituents on the exocyclic nitrogen atom.

(h) The reactions can easily be monitored by ^{1}H NMR spectroscopy, particularly if the pyridine ring contains a methyl substituent.

Up to date, over a hundred carbonyltriruthenium cluster complexes containing bridging apy ligands have been reported. This wide-ranging cluster chemistry includes quite a few outstanding reactions and products, which have been surveyed in this review. No doubt, this rich derivative chemistry has been facilitated by the presence of deprotonated 2-aminopyridines as ancillary ligands in the clusters.

Acknowledgments

The author wishes to thank the researchers cited in the references for their contribution to the chemistry surveyed in this review and, in particular, his colleagues and friends José M. Fernández-Colinas and Ignacio del Río. Continuous financial support from the Spanish Ministry of Education is also acknowledged (Projects PB92-1007, PB95-1042, and PB98-1555).

[1] Throughout this review, the term cluster complex refers to a complex containing at least three metal atoms supported by at least two metal−metal bonds.

[2] For a general overview of cluster reactivity, see: *Metal Clusters in Chemistry* (Eds.: P. Braunstein, L. A. Oro, P. R. Raithby), Wiley-VCH, Weinheim, **1999**.

[3] See, for example: D. J. Darensbourg, in *The Chemistry of Metal Cluster Complexes* (Eds.: D. F. Shriver, H. D. Kaesz, R. D. Adams), VCH Publishers, New York, **1990**, p.171.

[4] The activation parameters ($\Delta H^{\#}$, $\Delta S^{\#}$ [kJ/mol]) for dissociative ligand substitution reactions of $[Ru_3(CO)_{12}]$[4a] and $[Os_3(CO)_{12}]$[4b] are 133.1, 84.5 and 137.5, 31.8, respectively.[4a] A. J. Poë, M. W. Twigg, *J. Chem. Soc., Dalton Trans.* **1974**, 1860. [4b] A. J. Poë, V. Shekar, *Inorg. Chem.* **1985**, *24*, 4376.

[5] See, for example: J. K. Shen, Y. L. Shi, Y. C. Gao, Q. Z. Shi, F. Basolo, *J. Am. Chem. Soc.* **1988**, *110*, 2414.

[6] [6a] G. A. Foulds, B. F. G. Johnson, J. Lewis, *J. Organomet. Chem.* **1985**, *296*, 147. [6b] A. J. Deeming, *Adv. Organomet. Chem.* **1986**, *26*, 1. [6c] M. Tachikawa, J. R. Shapley, *J. Organomet. Chem.* **1977**, *124*, C19. [6d] E. G. Brian, B. F. G. Johnson, J. W. Kelland, J. Lewis, M. McPartlin, *J. Chem. Soc., Chem. Commun.* **1976**, 254.

[7] See, for example: M. I. Bruce, *Coord. Chem. Rev.* **1987**, *76*, 1.

[8] [8a] G. Lavigne, H. D. Kaesz, *J. Am. Chem. Soc.* **1984**, *106*, 4647. [8b] G. Lavigne, H. D. Kaesz, in *Metal Clusters in Catalysis* (Eds.: B. C. Gates, L. Guczi, H. Knözinger), Elsevier, Amsterdam, **1986**, p.43. [8c] G. Lavigne, B. de Bonneval, in *Catalysis by Di- and Polynuclear Metal Cluster Complexes* (Eds.: R. D. Adams, F. A. Cotton), Wiley-VCH, Weinheim, **1998**, p. 39.

[9] [9a] M. Anstock, D. Taube, D. C. Gross, P. C. Ford, *J. Am. Chem. Soc.* **1984**, *106*, 3696. [9b] D. J. Darensbourg, R. L. Gray, M. Pala, *Organometallics* **1984**, *3*, 1928.

[10] G. Lavigne, N. Lugan, J. J. Bonnet, *Inorg. Chem.* **1987**, *26*, 2347.

[11] R. G. Pearson, *Chemical Hardness*, Wiley-VCH, Weinheim, **1997**.

[12] G. Lavigne, *Eur. J. Inorg. Chem.* **1999**, 917.

[13] [13a] S. Rivomanana, G. Lavigne, N. Lugan, J. J. Bonnet, *Organometallics* **1991**, *10*, 2285. [13b] J. K. Shen, F. Basolo, *Gazz. Chim. Ital.* **1994**, *124*, 439.[13c] C. E. Kampe, N. M. Boag, H. D. Kaesz, *J. Am. Chem. Soc.* **1983**, *105*, 2896.

[14] [14a] J. L. Zuffa, M. L. Blohm, W. L. Gladfelter, *J. Am. Chem. Soc.* **1986**, *108*, 552. [14b] J. L. Zuffa, W. L. Gladfelter, *J. Am. Chem. Soc.* **1986**, *108*, 4669.

[15] G. Lavigne, in *The Chemistry of Metal Cluster Complexes* (Eds.: D. F. Shriver, H. D. Kaesz, R. D. Adams), VCH Publishers, New York, **1990**, p. 201.

[16] For additional examples of triruthenium clusters containing possible hemilabile ligands, prepared in our laboratory, see: [16a] M. A. Pellinghelli, A. Tiripicchio, J. A. Cabeza, L. A. Oro, *J. Chem. Soc., Dalton Trans.* **1990**, 1509. [16b] P. L. Andreu, J. A. Cabeza, V. Riera, C. Bois, Y. Jeannin, *J. Organomet. Chem.* **1990**, *384*, C25. [16c] J. A. Cabeza, J. M. Fernández-Colinas, A. Llamazares, V. Riera, *Organometallics* **1992**, *11*, 4355. [16d] J. A. Cabeza, M. A. Martínez-García, V. Riera, S. García-Granda, J. F. Van der Maelen, *J. Organomet. Chem.* **1996**, *514*, 197. [16e] J. A. Cabeza, M. A. Martínez-García, V. Riera, D. Ardura, S. García-Granda, *Eur. J. Inorg. Chem.* **2000**, 499.

[17] See, for example: J. A. Cabeza, I. del Río, V. Riera, S. García-Granda, S. B. Sanni, *Organometallics* **1997**, *16*, 3914.

[18] [18a] J. A. Cabeza, in *Metal Clusters in Chemistry* (Eds.: P. Braunstein, L. A. Oro, P. R. Raithby), Wiley-VCH, Weinheim, **1999**, chapter 2.5, p. 715. [18b]J. A. Cabeza, J. M. Fernández-Colinas, A. Llamazares, *Synlett* **1995**, 579.

[19] J. A. Cabeza, L. A. Oro, A. Tiripicchio, M. Tiripicchio-Camellini, *J. Chem. Soc., Dalton Trans.* **1988**, 1437.

[20] Y. Kiso, K. Saeki, *J. Organomet. Chem.* **1986**, *309*, C26.

[21] P. L. Andreu, J. A. Cabeza, V. Riera, Y. Jeannin, D. Miguel, *J. Chem. Soc., Dalton Trans.* **1990**, 2201.

[22] P. L. Andreu, J. A. Cabeza, J. M. Fernández-Colinas, V. Riera, *J. Chem. Soc., Dalton Trans.* **1990**, 2927.

[23] N. Lugan, F. Laurent, G. Lavigne, T. P. Newcomb, E. W. Liimatta, J. J. Bonnet, *Organometallics* **1992**, *11*, 1351.

[24] P. L. Andreu, J. A. Cabeza, V. Riera, C. Bois, Y. Jeannin, *J. Chem. Soc., Dalton Trans.* **1990**, 3347.

[25] P. L. Andreu, J. A. Cabeza, M. A. Pellinghelli, V. Riera, A. Tiripicchio, Y. Jeannin, *Inorg. Chem.* **1991**, *30*, 4611.

[26] P. L. Andreu, J. A. Cabeza, J. L. Cuyás, V. Riera, *J. Organomet. Chem.* **1992**, *427*, 363.

[27] P. L. Andreu, J. A. Cabeza, V. Riera, *Inorg. Chim. Acta* **1991**, *186*, 225.

[28] J. K. Shen, F. Basolo, P. Nombel, N. Lugan, G. Lavigne, *Inorg. Chem.* **1996**, *35*, 755.

[29] S. A. R. Knox, W. J. Koepke, M. A. Andrews, H. D. Kaesz, *J. Am. Chem. Soc.* **1975**, *97*, 3942.

[30] [30a] J. D. Cotton, S. A. R. Knox, F. G. A. Stone, *J. Chem. Soc., Chem. Commun.* **1967**, 965. [30b] J. D. Cotton, S. A. R. Knox, F. G. A. Stone, *J. Chem. Soc. A* **1968**, 2758. [30c] L. Vancea, W. A. G. Graham, *Inorg. Chem.* **1974**, *13*, 511. [30d] G. N. van Buuren, A. C. Willis, F. W. B. Einstein, L. K. Peterson, R. K. Pomeroy, D. Sutton, *Inorg. Chem.* **1981**, *20*, 4361.

[31] G. A. Foulds, B. F. G. Johnson, J. Lewis, *J. Organomet. Chem.* **1985**, *296*, 147.

[32] G. Süss-Fink, J. Ott, B. Schmidkonz, K. Guldner, *Chem. Ber.* **1982**, *115*, 2487.

[33] See, for example: [33a] J. A. Cabeza, R. J. Franco, A. Llamazares, V. Riera, C. Bois, Y. Jeannin, *Inorg. Chem.* **1993**, *32*, 4640. [33b] J. A. Cabeza, R. J. Franco, V. Riera, *Inorg. Chem.* **1994**, *33*, 5952. [33c] J. A. Cabeza, R. J. Franco, V. Riera, S. García-Granda, J. F. Van der Maelen, *Organometallics* **1995**, *14*, 3342.

[34] J. A. Cabeza, J. M. Fernández-Colinas, A. Llamazares, V. Riera, *J. Mol. Catal.* **1992**, *71*, L7.

[35] J. A. Cabeza, J. M. Fernández-Colinas, S. García-Granda, A. Llamazares, F. López-Ortiz, V. Riera, J. F. Van der Maelen, *Organometallics* **1994**, *13*, 426.

[36] J. A. Cabeza, I. del Río, J. M. Fernández-Colinas, A. Llamazares, V. Riera, *J. Organomet. Chem.* **1995**, *494*, 169.

[37] S. A. MacLaughlin, A. J. Carty, N. J. Taylor, *Can. J. Chem.* **1982**, *60*, 87.

[38] L. Hoferkamp, G. Rheinwald, H. Stoeckli-Evans, G. Süss-Fink, *Inorg. Chem.* **1995**, *34*, 5786.

[39] P. Briard, J. A. Cabeza, A. Llamazares, L. Ouahab, V. Riera, *Organometallics* **1993**, *12*, 1006.

[40] J. A. Cabeza, R. J. Franco, A. Llamazares, V. Riera, E. Pérez-Carreño, J. F. Van der Maelen, *Organometallics* **1994**, *13*, 55.

[41] J. A. Cabeza, I. del Río, V. Riera, S. García-Granda, S. B. Sanni, *Organometallics* **1997**, *16*, 1743.

[42] [42a] L. Hoferkamp, G. Rheinwald, H. Stoeckli-Evans, G. Süss-Fink, *Organometallics* **1996**, *15*, 704. [42b] J. A. Cabeza, M. A. Martínez-García, V. Riera, D. Ardura, S. García-Granda, *Eur. J. Inorg. Chem.* **2000**, 499.

[43] J. A. Cabeza, A. Llamazares, V. Riera, S. Triki, L. Ouahab, *Organometallics* **1992**, *11*, 3334.

[44] For a review on reactivity of alkynes with metal clusters, see: P. R. Raithby, M. J. Rosales, *Adv. Inorg. Chem. Radiochem.* **1985**, *29*, 169.

[45] The structure of $[Ru_3(\mu_3\text{-apyMe})(\mu\text{-PhCH=CPh})(CO)_9]$ (**9**) has not been determined by diffraction methods. A structure similar to that of $[Ru_3(\mu_3\text{-Phapy})(\mu\text{-PhCH=CPh})(CO)_9]$[23] was as-

signed to **9** in early publications.[34,46,49] However, subsequent reactivity studies demonstrated that both the alkenyl ligand and the amido fragment span the same Ru−Ru edge.[55]

[46] J. A. Cabeza, S. García-Granda, A. Llamazares, V. Riera, J. F. Van der Maelen, *Organometallics* **1993**, *12*, 2973.

[47] J. A. Cabeza, A. Llamazares, V. Riera, P. Briard, L. Ouahab, *J. Organomet. Chem.* **1994**, *480*, 205.

[48] J. A. Cabeza, J. M. Fernández-Colinas, A. Llamazares, V. Riera, *Organometallics* **1993**, *12*, 4141.

[49] J. A. Cabeza, S. García-Granda, A. Llamazares, V. Riera, J. F. Van der Maelen, *Organometallics* **1993**, *12*, 157.

[50] P. Nombel, N. Lugan, F. Mulla, G. Lavigne, *Organometallics* **1994**, *13*, 4673.

[51] J. A. Cabeza, I. del Río, S. García-Granda, G. Lavigne, N. Lugan, M. Moreno, P. Nombel, M. Pérez-Priede, V. Riera, A. Rodríguez, M. Suárez, J. F. Van der Maelen, *Chem. Eur. J.* **2001**, *7*, 2370.

[52] [52a] P. Nombel, PhD Thesis, Université Paul Sabatier, Toulouse, **1996**. [52b] P. Nombel, N. Lugan, G. Lavigne, unpublished results.

[53] J. A. Cabeza, I. del Río, S. García-Granda, M. Moreno, V. Riera, *Organometallics* **2001**, *20*, 4973.

[54] See, for example: [54a] J. A. Cabeza, J. M. Fernández-Colinas, A. Llamazares, V. Riera, *Organometallics* **1992**, *11*, 4355. [54b] C. E. Kampe, H. D. Kaesz, *Inorg. Chem.* **1984**, *23*, 4646. [54c] N. M. Boag, W. J. Sieber, C. E. Kampe, C. B. Knobler, H. D. Kaesz, *J. Organomet. Chem.* **1988**, *355*, 385. [54d] Z. Xue, W. J. Sieber, C. B. Knobler, H. D. Kaesz, *J. Am. Chem. Soc.* **1990**, *112*, 1825 and references therein.

[55] [55a] J. A. Cabeza, J. M. Fernández-Colinas, A. Llamazares, V. Riera, S. García-Granda, J. F. Van der Maelen, *Organometallics* **1994**, *13*, 4352. [55b] J. A. Cabeza, J. M. Fernández-Colinas, A. Llamazares, V. Riera, S. García-Granda, J. F. Van der Maelen, *Organometallics* **1995**, *14*, 3120.

[56] J. A. Cabeza, I. del Río, J. M. Fernández-Colinas, V. Riera, *Organometallics* **1996**, *15*, 449.

[57] N. Lugan, F. Laurent, G. Lavigne, T. P. Newcomb, E. W. Liimatta, J. J. Bonnet, *J. Am. Chem. Soc.* **1990**, *112*, 8607.

[58] P. Nombel, N. Lugan, B. Donnadieu, G. Lavigne, *Organometallics* **1999**, *18*, 187.

[59] [59a] J. A. Cabeza, F. J. Lahoz, A. Martín, *Organometallics* **1992**, *11*, 2754. [59b] J. S. Field, R. J. Haines, J. A. Jay, *J. Organomet. Chem.* **1990**, *395*, C16. [59c] H. K. Nagra, R. J. Batchelor, A. J. Bennet, *J. Am. Chem. Soc.* **1996**, *118*, 1207.

[60] N. G. Connely, N. J. Forrow, S. A. R. Knox, K. A. MacPherson, A. G. Orpen, *J. Chem. Soc., Chem. Commun.* **1985**, 16.

[61] J. A. Cabeza, I. del Río, A. Llamazares, V. Riera, *J. Organomet. Chem.* **1996**, *511*, 103.

[62] J. A. Cabeza, I. del Río, A. Llamazares, V. Riera, S. García-Granda, J. F. Van der Maelen, *Inorg. Chem.* **1995**, *34*, 1620.

[63] J. A. Cabeza, I. del Río, V. Riera, F. Grepioni, *Organometallics* **1997**, *16*, 812.

[64] J. A. Cabeza, I. del Río, V. Riera, F. Grepioni, *Organometallics* **1995**, *14*, 3124.

[65] [65a] R. D. Adams, J. E. Babin, M. Tasi, *Inorg. Chem.* **1987**, *26*, 2561. [65b] B. R. Cockerton, A. J. Deeming, *Polyhedron* **1994**, *13*, 2085. [65c] G. Süss-Fink, U. Bodensiek, L. Hoferkamp, G. Rheinwald, H. Stoeckli-Evans, *J. Cluster Sci.* **1992**, *3*, 469. [65d] G. Süss-Fink, U. Bodensiek, L. Hoferkamp, H. Stoeckli-Evans, *J. Chem. Soc., Dalton Trans.* **1993**, 127.

[66] See, for example: E. J. Voss, C. L. Stern, D. W. Shriver, *Inorg. Chem.* **1994**, *33*, 1087 and references therein.

[67] P. L. Andreu, J. A. Cabeza, A. Llamazares, V. Riera, C. Bois, Y. Jeannin, *J. Organomet. Chem.* **1991**, *420*, 431.

[68] P. L. Andreu, J. A. Cabeza, A. Llamazares, V. Riera, S. García-Granda, J. F. Van der Maelen, *J. Organomet. Chem.* **1992**, *434*, 123.

[69] E. Rosenberg, D. Rickman, I. N. Hsu, R. W. Gellert, *Inorg. Chem.* **1986**, *25*, 194.

Received November 13, 2001
[I01453]

The Polyhedral State of Molecular Matter

Arnout Ceulemans*[a] and Erwin Lijnen[a]

Keywords: Group theory / Topological chemistry / Polyhedra / Fullerenes / Cubanes / Boranes

The review introduces the mathematical concept of a complex, as an original way to describe the topology of a polyhedral molecule. It shows how this concept can be applied to electronic structures and magnetic and vibrational properties. Using symmetry it identifies topologically invariant orbitals and moments.
(© Wiley-VCH Verlag GmbH, 69451 Weinheim, Germany, 2002)

1. Introduction

A molecule is a set of atomic nuclei held together by a cloud of electrons. In its simplest representation this form of matter can be conceived as a collection of beads held together by strings. The mathematical concept, which corresponds to this representation, is the concept of a *graph*.[1] In the graph-like state only the connections between atoms count, and there is no information on their spatial arrangement. Nonetheless this representation is extremely useful, not only to retrieve molecules in a data-base, but also to rationalise many important molecular properties.[2]

The topic of this review will be a higher form of molecular organisation, which we describe as the *polyhedral* state. Inorganic chemists already have an intuitive knowledge of polyhedra, as structural units of many inorganic compounds. In its polyhedral state, molecular matter is not just a set of points and lines, but it is furthermore specified that certain closed loops of lines will form faces. In turn faces themselves may enclose a finite region of space which is a cell or a chamber. The mathematical concept, which corresponds to this polyhedral representation, is the concept of a *polyhedral complex*.[3]

Unlike its graph relative, the complex concept is not known outside mathematics. In section 2 we will thus first have to explain its proper meaning. For this no special mathematical background will be required, except for a general knowledge of group theory for chemists, as may be found in Cotton's book.[4] In section 3 we will then represent a fundamental result about the symmetries of polyhedral complexes, which opens up this concept for applications on molecular matter. In the subsequent sections, several applications related to electronic structure and elastic and magnetic properties of network molecules are reviewed.

2. Polyhedral Complexes

In the chemical literature a polyhedron refers to a surface which is wrapped around a finite region of space, and consists of many polygons or faces; in turn the faces are bor-

[a] Division of Quantum Chemistry, Katholieke Universiteit Leuven,
Celestijnenlaan 200F, 3001 Leuven, Belgium
Fax: (internat.) + 32-16/327992
E-mail: Arnout.Ceulemans@chem.kuleuven.ac.be

Arnout Ceulemans (left) is full Professor of Chemistry at the University of Leuven. He received his Ph. D. in Leuven while working in the group of Luc Vanquickenborne on theoretical models for ligand field photochemistry. He habilitated in 1986 in Leuven with a thesis on the Jahn−Teller effect in complexes and clusters. He teaches Group Theory, Chemical Physics, and Inorganic Chemistry. His main research interests are the application of group-theoretical and topological methods at the border between chemistry and physics.

Erwin Lijnen (right) graduated in chemistry at the University of Leuven in 2001. He is currently Aspirant of the Fund for Scientific Research − Flanders (Belgium) and prepares a doctoral thesis in the laboratory of Quantum Chemistry at the K. U. Leuven on topological representations of tridimensional molecular structures.

MICROREVIEWS: This feature introduces the readers to the authors' research through a concise overview of the selected topic. Reference to important work from others in the field is included.

dered by edges; finally the edges connect vertices. Chemists are also familiar with Euler's celebrated theorem that states that the numbers of vertices, edges, and faces, denoted as v, e, and f, respectively, obey the rule as given in Equation (1).

$$v - e + f = 2 \tag{1}$$

This theorem holds for any polyhedron that can be mapped on the surface of a sphere.[5] It can, however, be generalised to polyhedral nets on surfaces with other topologies as shown in Equation (2).

$$v - e + f = \chi \tag{2}$$

Here χ is a fixed integer, the Euler characteristic, which marks the particular topology of the surface on which the polyhedron is embedded. As an example for a sphere with g handles or holes, the Euler characteristic reads as given in Equation (3) with $g = 0$ for a sphere, $g = 1$ for a torus or doughnut, $g = 2$ for a pretzel etc.; g is also called the genus of the surface.

$$\chi = 2 - 2g \tag{3}$$

Turning from chemistry to mathematics we must now become acquainted with the ingredients of the polyhedral complex in the mathematical sense. Of course the same structural elements, vertices, edges, and faces, will appear, but there are some nontrivial amendments, and, above all, we must find out what happens to the Euler characteristic.

Vertices are zero-dimensional objects, and therefore are trivial. A given vertex will be denoted as v^i. At the next level, an edge is already not just a line connecting two vertices, but rather an arrow, pointing from one of these vertices to the other. Hence an edge between two vertices, say v^i and v^j will be denoted as the *ordered* pair $(v^i v^j)$, where we agree to identify the first vertex, v^i, as the tail of the arrow, and the second, v^j, as its head. The ordering itself is purely a matter of choice. We might as well denote the same edge by the inverted ordering, $(v^j v^i)$. Since the corresponding arrow points in the opposite direction, we can write Equation (4).

$$(v^i v^j) = -(v^j v^i) \tag{4}$$

The requirement that the edges be ordered is therefore not just a trivial feature: it transforms the edges to signed quantities, and therefore creates algebra on the surface of the polyhedron. At this point it is of course difficult to appreciate all its implications, but we hope this will gradually become clear in the forthcoming sections.

In a similar way a face is an ordered closed loop of vertices. Consider for instance three vertices, say v^i, v^j, and v^k, which form a triangular face, then we may denote this face as the ordered trio $(v^i v^j v^k)$. This notation defines the face as a closed loop, $v^i \rightarrow v^j \rightarrow v^k \rightarrow v^i$. For an external observer this circulation will have a definite sense, either clockwise or anticlockwise. Again if we invert the ordering, we invert this sense, and we can write Equation (5).

$$(v^i v^j v^k) = -(v^k v^j v^i) \tag{5}$$

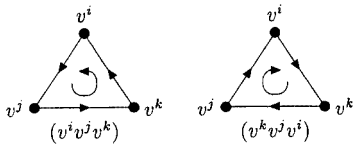

Vertices, edges, and faces are layers of organisation, involving objects of dimension zero (point), one (line), and two (plane), respectively. We could also include the next layer of 3D objects or cells, but will not further consider this here.

As in all organised structures consecutive layers are in touch. The topdown descent from higher to lower dimensional objects is called *bordering* or *taking the boundary.*

The boundary of a face is a sum of the arrows along the surrounding edges. We will avoid the rigorous mathematical definition of this operation and write it in a simple pictorial way as

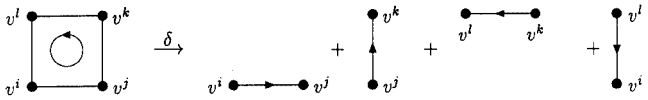

or as

$$\delta(v^i\ v^j\ v^k\ v^l) = (v^i\ v^j) + (v^j\ v^k) + (v^k\ v^l) + (v^l\ v^i)$$

where the Greek letter δ represents the boundary operation. Likewise the boundary of an edge is the difference between its head vertex and its tail

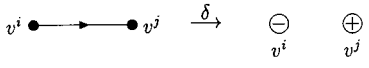

or

$$\delta(v^i\ v^j) = v^j - v^i.$$

Interestingly, not all combinations of a given level have boundaries. As an example, when the number of incoming and outgoing arrows on a given vertex is the same, this vertex is not a boundary, e.g.

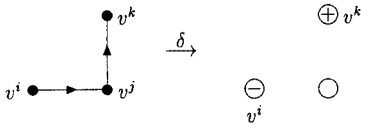

This part of the theory is the most interesting from our point of view: we must look for combinations that are not boundaries of some higher level, and have no boundaries on some lower level. Such combinations are *topological invariants* of the polyhedron, and are extremely important from the point of view of electronic structures. In mathematics they are called *homologies*.[6] These are the concepts behind the Euler characteristic. Our task will be to identify them properly, since they hold the key to the topology. To summarise, in Table 1 we list the ingredients of a tetrahedral complex. This complex can be embedded on a sphere and therefore has Euler characteristic $\chi = 2$. It indeed contains two homologies, which we will try to find in the next section with the help of group theory.

Table 1. Elements of a tetrahedral complex

Vertices or Atoms	Edges or Bonds	Faces
v^0	(v^0v^1)	$(v^0v^1v^2)$
v^1	(v^0v^2)	$(v^0v^1v^3)$
v^2	(v^0v^3)	$(v^0v^2v^3)$
v^3	(v^1v^2)	$(v^1v^2v^3)$
	(v^1v^3)	
	(v^2v^3)	

3. From Topology to Symmetry and Back

If the polyhedron exhibits a point-group symmetry, we can apply its symmetry elements to the set of vertices. The action of a symmetry element on a vertex is very simple: it just maps this vertex on some other vertex of the complex. It therefore can be described as a permutation of the elements in the set of vertices. Hence we can write Equation (6), where R_i is the image of i under this mapping.

$$Rv^i = v^{R_i} \tag{6}$$

This expression is all one needs to determine how the ordered objects, edges and faces, of the polyhedral complex behave under symmetry operations. Indeed one has for an ordered pair Equation (7).

$$R(v^iv^j) = (v^{R_i}v^{R_j}) \tag{7}$$

The resulting image $(v^{Ri}v^{Rj})$ is again an edge, which will also belong to the complex, although it might have been defined in opposite order as $(v^{Rj}v^{Ri})$ in which case we can always rewrite the equation as Equation (8).

$$R(v^iv^j) = -(v^{R_j}v^{R_i}) \tag{8}$$

Similarly, mapping of face circulations under symmetry elements may produce images that differ by a sign from the selected list of faces, but in any case a face will always be mapped by R on another face which will be symmetric to the former one.

In this way we can easily determine the transformation matrices describing the action of the symmetry elements on the components of the polyhedral complex. These matrices form representations of the symmetry group. In Table 2 we introduce appropriate symbols for the representations of vertices, edges and faces.

Table 2. Symmetry representation for the elements of a complex

Element	Symbol	Type
vertex	$\Gamma_\sigma(v)$	scalar
edge	$\Gamma_\parallel(e)$	vector
face	$\Gamma_\odot(f)$	rotor

Here Γ is the general symbol for induced symmetry representations.[7] The index σ for the vertex representations indicates that point vertices are symmetric objects with respect to the symmetry elements that pass through the vertex sites, in the same way as s or p_z orbitals in axially symmetric sites. For the edge representations the symbol $\parallel$ refers to the set of arrows along the edges, while the index $\odot$ in the face-representations refers to the circular arrows on the faces. All these representations are in principle *reducible*, which means that they can be decomposed into standard irreducible representations, which describe the basic symmetry patterns in the point group.

These so-called *irreps* can easily be found using the standard techniques of character theory.[4] As an example for the tetrahedral complex in Table 1, one immediately obtains these representations in the T_d symmetry group, see Equation (9).

$$\begin{aligned} \Gamma_\sigma(v) &= A_1 + T_2 \\ \Gamma_\parallel(e) &= T_1 + T_2 \\ \Gamma_\odot(f) &= A_2 + T_1 \end{aligned} \tag{9}$$

Of these combinations only the vertex terms are familiar to chemists. They simply represent the SALCs (symmetry-adapted linear combinations of atomic orbitals) of MO (molecular orbitals) theory, and look as follows.

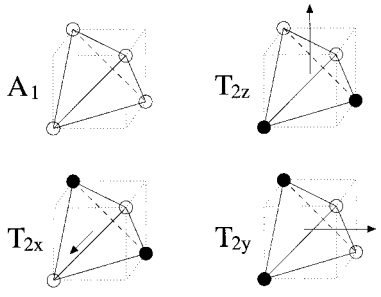

The representations on the edges can be constructed in an entirely similar way, only the constituent objects are not s-like orbitals on the atomic vertices, but with arrows along the edges. As an example we show the z components of T_1 and T_2. In the T_{2z} combination the tetrahedron is oriented in the upright z direction, and the arrows along the four lateral edges are pointing upwards. The same arrows are present in the T_{1z} combination but now their orientation alternates between pointing up and down. The x and y components are oriented in an analogous way along their respective directions.

Finally the face terms correspond to symmetry-adapted linear combinations of circular arrows on the face centres. Here we show the A_2 and T_{1z} components.

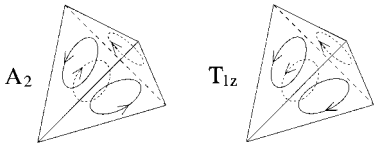

In Figure 1 we gather all these components in a schematic overview. We have also added the boundary relations that exist between the different layers, to this figure. It is very important to realise that taking the boundaries of faces or edges will *not* alter the symmetries. This operation indeed simply corresponds to the expansion of the circular face arrows to the bordering edges and the edge arrows to the head and tail vertices. As a result, the T_1 face terms will be bordered by the equisymmetric T_1 edge terms, while the T_2 edge modes indeed are bordered by the equisymmetric T_2 vertex combinations.

Two combinations stand on their own, not being bordered by a lower ranking component, nor being themselves borders of some higher component: the A_1 vertex combination and the A_2 face combination. Indeed by taking the boundary of the latter, we generate on all edges pairs of opposite arrows, which therefore cancel. Similarly, the former cannot be the boundary of an edge mode, since all vertices have the same weight, implying no net changes along edges.

Hence by using symmetry and elimination we have found combinations, which are very special topological invariants: they cannot be the origin or image of the boundary mapping.

These combinations can easily be filtered out by taking the alternating sum of all three representations, Equation (10).

$$\Gamma_\sigma(v) - \Gamma_\parallel(e) + \Gamma_\odot(f) = A_1 + T_2 - T_1 - T_2 + A_2 + T_1 = A_1 + A_2 \tag{10}$$

Indeed in this way all terms which are taking part in the boundary will cancel.

Obviously, the structure of Equation (10) involves the familiar Euler theorem for a surface of genus zero. Indeed if we ignore all symmetry elements, or equivalently suppose that the only symmetry element is the trivial unit element of the point group, all representations in Equation (10) would reduce to multiples of the trivial A representation of the C_1 point group, and the multiplication factor would simply

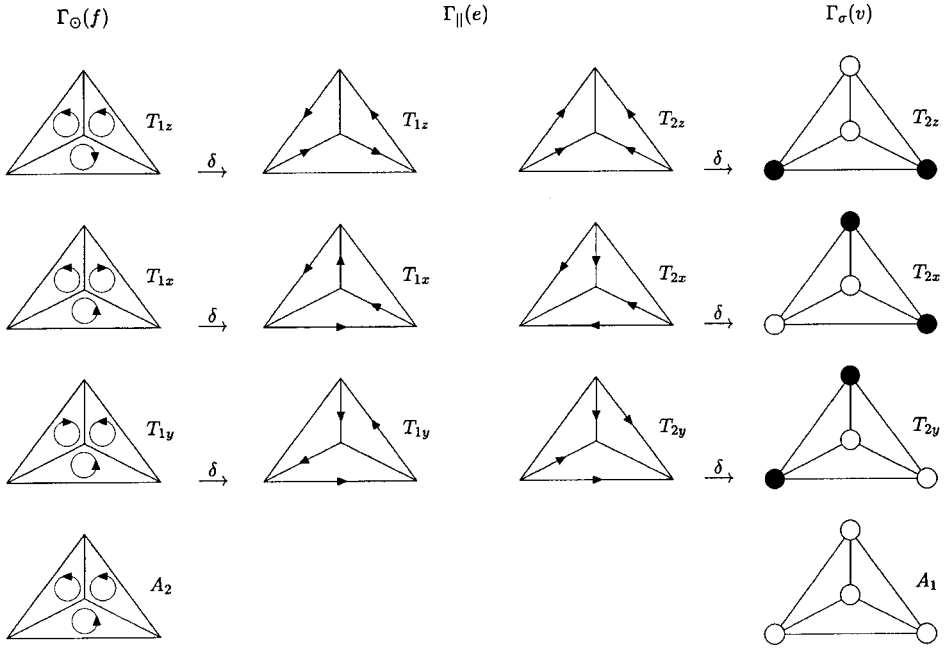

Figure 1. SALCs for the tetrahedral complex

equal the number of vertices, edges, or faces, see Equation (11).

$$\begin{aligned} \Gamma_\sigma(v) &= v.A \\ \Gamma_\parallel(e) &= e.A \\ \Gamma_\odot(f) &= f.A \end{aligned} \tag{11}$$

With $A_1 + A_2 \rightarrow 2\ A$, Equation (10) then reduces to a purely dimensional formula, $v - e + f = 2$, which is exactly Euler's result. Hence, by bringing together symmetry and topology, it is possible to reveal the topological aspects of Euler's rule:

1. We understand now that, not only are the numbers of the polyhedral structure elements related, but also their symmetries. In this respect the number rule is just the (dimensional) top of a symmetry iceberg.

2. The topological invariants, which appear as the remainders of the alternating sum over the structural layers, are characterised by irreducible symmetry representations. These symmetries are keys to relating the topological invariants to chemical and physical properties.

For polyhedra, which can be mapped on the surface of a sphere, the result in Equation (10) can be cast in the general form as given in Equation (12).

$$\Gamma_\sigma(v) - \Gamma_\parallel(e) + \Gamma_\odot(f) = \Gamma_0 + \Gamma_\epsilon \tag{12}$$

The representations Γ_0 and Γ_ε, which appear here on the right-hand side are, respectively, the totally symmetric and pseudo-scalar representation, which is symmetric under proper rotations and antisymmetric under improper rotations. In Mulliken's notation for the point groups, the Γ_0 representation receives labels such as: A_1, A_{1g}, or $A_1{}'$, while the corresponding Γ_ε representation is denoted as A_2, A_{2u}, or $A_2{}''$. A general proof of this result has been given,[8] and its connection to the abstract theory of homology groups has been explained.[9]

Similar results can be obtained for polyhedra with other Euler characteristics. In each case the alternating sum of representations will generate a characteristic set of homologies.

In Table 3 we give an overview of the different topologies we have examined so far. The final two items in the table concern polyhedra that are embedded on a 3D surface. In this case a further structural element must be added, which is the cell or chamber. In the same way as faces are defined as rings of edges, cells are closed regions of space surrounded by faces. In this case the Euler theorem must be extended to include the number of cells, c: Equation (13).

$$v - e + f - c = \chi \tag{13}$$

As an example in the case of a body-centred tetrahedron one has $v = 5$, $e = 10$, $f = 10$, $c = 4$, resulting in the Euler characteristic $\chi = 1$, as indicated in Table 3 for polyhedra with the topology of a solid sphere.

Table 3. Overview of topological structures for which symmetry relationships have been derived

Topology	χ	Polyhedron	Example	Ref.
hollow sphere (2D)	2	deltahedron	*closo*-boranes	[8]
		trivalent	fullerenes	[8]
torus (2D)	0	deltahedron	-	[11]
		trivalent	carbon toroid	[11]
double torus (2D)	-2	pretzel	-	[11]
		triple hoop	-	[11]
disk (2D)	1	polyhex	benzenoid	[11]
plane (2D)	0	2D periodic lattice	graphite sheet	[12]
negative curvature surfaces (2D)	-4	trivalent	schwarzites	[13]
solid sphere (3D)	1	centred	-	-
		concentric	multishell clusters	[10]
space (3D)	0	3D periodic lattice	diamond	[12]

4. Applications

In this section we review two typical cases of polyhedral electronic structures and identify the topologically determined properties.

4.1 The Antibonding Orbitals in Trivalent Clusters

Electron counting rules are an important tool for addressing the problem of cluster bonding, and new developments continue to appear.[14,15] Here we will examine a straightforward application of the general graph-theoretical result, which is encountered in the electronic structure of so called "electron-precise" trivalent clusters.[8]

In a trivalent polyhedral cage, each cluster atom has three neighbours. From each vertex radiate three edges, while in turn every edge is linked to two vertices, see Equation (14).

$$3v = 2e \tag{14}$$

The cluster will be completely edge-bonding if each cluster atom has three valence orbital hybrids, which point along the edges and are each occupied by one electron. This requires one inward pointing (radial) hybrid and a tangential $\{p_x, p_y\}$ pair.

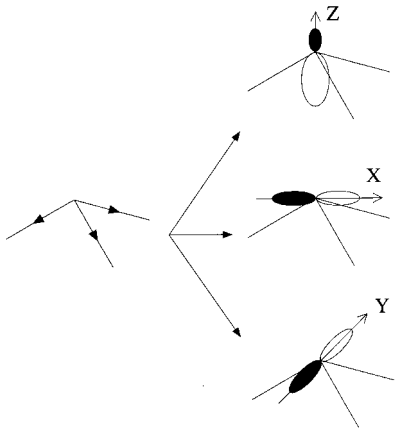

In this way one obtains a saturated or "electron-precise" electronic structure with precisely $3v/2$ valence electron pairs, forming an equal number of σ bonds along the edges. Examples are the polyhedranes C_vH_v such as tetrahedrane ($v = 4$), cubane ($v = 8$), or dodecahedrane ($v = 20$), or the equivalent transition-metal clusters, built on the isolobal $Co(CO)_3$ or $Ir(CO)_3$ fragments.[16]

The electronic levels of such compounds were investigated by Johnston and Mingos.[17,18] The $3v/2$ occupied bonding orbitals have precisely $3v/2$ antibonding counterparts. These empty orbitals on the edges can be grouped together in $[v/2] + 1$ strongly antibonding face-combinations and $v - 1$ less antibonding vertex-localised orbitals, Equation (15).

$$3v/2 = [v/2 + 1] + [v - 1] \tag{15}$$

Since in a trivalent cage one has $3v = 2e$ [Equation (14)] and $f = v/2 + 2$, Equation (15) is just a manifestation of Euler's rule, written as in Equation (16).

$$e = [f - 1] + [v - 1] \tag{16}$$

We can now extend this rule to the symmetries of these antibonds. Antibonds along edges with a positive head and a negative tail have precisely the same symmetry as arrows along edges, hence the symmetries of the antibonding shell correspond to $\Gamma_{\|}(e)$.

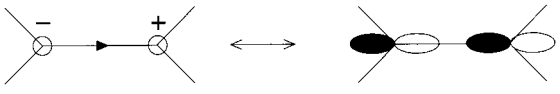

The symmetry result then predicts Equation (17).

$$\begin{array}{rcccc} e & = & [f-1] & + & [v-1] \\ \Gamma_{\|}(e) & = & [\Gamma_{\odot}(f) - \Gamma_{\epsilon}] & + & [\Gamma_{\sigma}(v) - \Gamma_0] \end{array} \tag{17}$$

The first term on the right-hand side of dimension $(f - 1)$ refers to symmetries of faces in the polyhedral complex. We have represented these earlier as circular arrows, which indeed precisely correspond to the face antibonds of Mingos and Johnston.

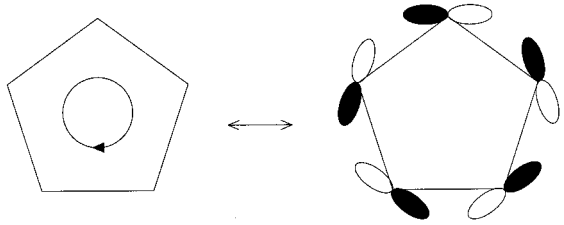

The topological basis of this result clearly explains why the number of these highly antibonding orbitals is one less than the number of faces. Indeed if we set up an antibonding combination in which all the face antibonds are rotating in the same direction, there will be two opposite arrows along every edge, which will therefore exactly cancel.

The second term of the equation contains the remaining $v - 1$ terms, which are vertex-localised and therefore less antibonding, as was found by the previous model calculations of Johnston and Mingos.[17] Again the topology of the polyhedron explains why the number of these is one less than the number of vertices. The combination that is lacking transforms as Γ_0, and simply corresponds to the sum of all vertex orbitals of σ-type. This combination is of course completely bonding, and cannot be contained in the edge-antibonding orbitals.

We thus have found important features of the electronic structure of trivalent clusters, which clearly belong to the polyhedral state of molecular matter. The repartitioning of the edge antibonds in face-related and vertex-related parts is entirely based on the polyhedral relationships, as expressed by the symmetry extension of Euler's rule. In electron-precise compounds both sets are empty, yielding an electron count of $3v/2$ skeletal pairs.

4.2 Electronic Properties of Toroidal Polyhedra

The invariants, which arise in the abstract topological treatment, can be understood very simply in terms of densities and currents on a polyhedral surface.

As a simple physical example we take a model of fluid flow on a polyhedral surface. One could think of a flooded polyhedron, with observers on the vertices, edge centres, and face centres. The observers on the vertices measure the net increase or decrease in density which is taking place at the vertices during a given time interval. They thus report a scalar quantity, which stands for the vertex term in the expression. The observers on the edges measure the fluid flow along the edges. The quantity that they report is a vectorial component of flow pointing along the direction of the edge; this is precisely the edge term in the expression. Finally, the observers on the faces measure net circular currents going around the face centres. This corresponds to a component of a rotor, perpendicular to the face, as is expressed by the face term. The theorem then makes a comparison of these three reports: it finds that the flow along the edges exactly accounts for the net changes of density on

the vertices and net circulation around the face centres, except for two modes, which leave no trace in the bookkeeping of the edge currents: the simultaneous increase of density on all vertices, the Γ_0 term, and the simultaneous rotatory currents on all faces in the same sense, as expressed by the Γ_ε term.

If the fluid consists of electrons, the first term represents changes of the total electrical charge of the polyhedron. This mode will be zero if charge is conserved. It cannot give rise to charge flows over the network.

The second mode is less trivial, but in fact equally fundamental. It represents the total magnetic charge of the polyhedral cluster. Electromagnetism requires this charge to be zero, in the absence of magnetic monopoles. Hence both modes refer to conserved quantities which cannot be generated or annihilated by external fields.

In this respect toroidal polyhedra, i.e. polyhedral networks that can be mapped on the surface of a torus or doughnut, offer far more interesting perspectives, since they have topological invariants that have the symmetry of electric and magnetic dipoles.

For a toroidal polyhedron, the Euler theorem reads as in Equation (18).

$$v - e + f = 0 \tag{18}$$

The zero on the right-hand side hides no less than four topological invariants, which make their appearance when the theorem is written in symmetry form, Equation (19).

$$\Gamma_\sigma(v) - \Gamma_\parallel(e) + \Gamma_\odot(f) = \Gamma_0 + \Gamma_\epsilon - \Gamma(T_z) - \Gamma(R_z) \tag{19}$$

The two negative terms on the right-hand side that were absent in the globular polyhedra, are the irreducible symmetry representations of the translation along the central symmetry axis of the torus (T_z), and of the rotation about the same axis (R_z). Both these terms refer to special combinations of edge arrows which have no boundaries at the vertices, and do not interfere with face circulations.[11] These modes are represented by circular motions going around the torus as shown in Figure 2. The $\Gamma(T_z)$ mode corresponds to a circulation linking the inside and outside of the toroidal ring. It is antisymmetric with respect to the inversion centre and horizontal symmetry plane, and symmetric under the principal rotational symmetry axis, exactly as a translation mode in the z direction. On the other hand the $\Gamma(R_z)$ mode constitutes a circulation about the principal axis. It is also symmetrical under this axis, as well as under the inversion centre and the horizontal symmetry plane.

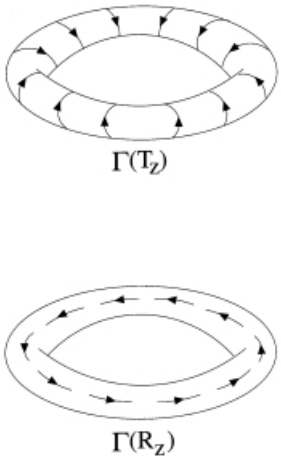

Figure 2. Topologically invariant edge currents on a torus, transforming as translation $\Gamma(T_z)$ and rotation $\Gamma(R_z)$

In ideal cylindrical symmetry, $D_{\infty h}$, these terms match the symmetry representations Σ_u^+ and Σ_g^- which are, respectively, the symmetries of the electric and magnetic dipole. Interestingly, both these invariants can be introduced by external fields. If one places a toroidal polyhedron in a homogeneous magnetic field, with its z axis parallel to the direction of the field, one will indeed induce circular bond currents on the torus, which correspond to the $\Gamma(R_z)$ mode. Open-shell molecules can furthermore sustain spontaneous currents that have precisely this topology.

In contrast, the second mode, $\Gamma(T_z)$, is much subtler. It introduces a moment that is known from nuclear physics[19] as an "anapole" moment. If one simply places the torus in a homogeneous magnetic field along the z direction it would not generate a permanent circulation of the type shown in Figure 2. What is required in order to induce such an anapole is a magnetic field that would run along the spine or internal loop of a torus. Such a field is necessarily inhomogeneous and requires specially designed magnet geometries.[20] However, if the toroid is chiral the two types of motion will belong to the same Σ representation and can therefore be coupled. A homogeneous magnetic field along the z axis is then sufficient to induce an anapole moment: physically this means that in chiral tubes the current which goes around the central hole of the torus follows a spiral pattern, which includes a whirling of the $\Gamma(T_z)$-type. These effects have indeed been demonstrated by model calculations on small toroidal carbon cages.[21]

Chemistry has made steady progress towards the development of toroidal polyhedra, formed by a molecular network that can be mapped on the surface of a torus or doughnut. First Liu et al.[22] reported the observation of closed tubular structures in a batch of multiwalled nanotubes. Later on it was shown by Martel et al.[23] that single-walled carbon nanotubes could be bent by treatment with ultrasonic waves. The STM images of these structures show nice toroidal shapes, but the authors warn that these are very likely coils rather than tori. Very recently Sano et al.[24]

have managed to induce chemical bonds between the functionalised edges of a nanotube.

5. Complexes and Bundles

So far we have defined a polyhedral complex as a set of vertices with edge and face relationships. We now come to the next step, which is to define functions, which are centred at the vertex positions. As an example we may be interested in the elastic properties of clusters. In that case we define on each cluster atom, three Cartesian displacement coordinates and solve the equation of motion in this space of $3v$ displacements.

The special mathematical structure which is created in this way has the following ingredients: i) the set of vertex points or nodes of the complex, referred to as the base space B, ii) a unitary model space of functions, W, representing the object which will be associated with the individual vertices, in our example W contains the three Cartesian displacements, $W = (\Delta x, \Delta y, \Delta z)$, and $W_i = (\Delta x_i, \Delta y_i, \Delta z_i)$ then corresponds to the Cartesian displacements of vertex v^i, iii) the total function space containing all $3v$ displacements of the complex, $E = \{W_i\}_{i=1,v}$ and finally iv) the projection p which connects a given object to its node, $pW_i = v^i$. This link constitutes a fibre, and the total structure (E, B, W, p) is a fibre bundle.[25] With this structure our next task is to find out what happens to the topological invariants, which we have detected in the base space. Hence, what will be the functional forms they connect to?

Again this question can be solved by group-theoretical means. We first derive the symmetry representations of the functional space, and then insert in these expressions the symmetry relations of section 3.

We will illustrate this for the case of the displacement space. To obtain the answer we need to look at a fundamental result of the theory of induced representations.[7,26] It states that the representation of the $3v$ displacements of a cluster with v vertices or atoms is simply given by the direct product of the vertex representation, $\Gamma_\sigma(v)$, with the symmetry of the three translations, $\Gamma(T)$; Equation (20).

$$\Gamma_{x,y,z}(v) = \Gamma_\sigma(v) \times \Gamma(T) \tag{20}$$

This product representation is usually called the mechanical representation, while the vertex representation is obviously the positional representation. The connection in this case is obviously very simple, since it takes the form of a direct product.

We can now substitute the vertex term to yield Equation (21).

$$\Gamma_{x,y,z}(v) = [\Gamma_\parallel(e) - \Gamma_\odot(f)] \times \Gamma(T) + [\Gamma_0 + \Gamma_\epsilon] \times \Gamma(T) \tag{21}$$

The invariants in this equation are both multiplied by $\Gamma(T)$. These products can easily be evaluated, since multiplication with the totally symmetric representation, Γ_0, is a unit operation, while multiplication with the pseudo-scalar representation, Γ_ε, changes the parity and thus turns translations into rotations, see Equation (22).

$$\begin{aligned} \Gamma_0 \times \Gamma(T) &= \Gamma(T) \\ \Gamma_\epsilon \times \Gamma(T) &= \Gamma(R) \end{aligned} \tag{22}$$

Hence the forms in the displacement space, which correspond to the topological invariants of the positional space, are found to transform as the translations and rotations. The topological invariants of the complex thus connect to the collective motions that form the six external degrees of freedom of the cluster. In view of this special topological connection, these are indeed separate solutions of the displacement problem that cannot mix with the internal elastic modes.

In the next section we will show how the mechanical representation can further be resolved in the case of deltahedral clusters. In a further application we will also meet these special functional forms in the Fermi region of fullerene clusters.

6. Applications

Here we review two applications where functions are defined on a complex. One concerns atomic displacements, and the other atomic orbitals.

6.1 The Complete Force Field of Deltahedral Clusters

A deltahedral cluster is made up of triangles. The prototype is the closoborane series, $B_nH_n^{2-}$. Through the isolobal analogy several carbonyl transition-metal clusters have been synthesised with similar structures.

Deltahedral polyhedra are the dual forms of the trivalent polyhedra, discussed in section 4.1. The Euler relationship for trivalent cages, $3v = 2e$ [Equation (14)], can thus be converted into its dual form, which is valid for deltahedral cages; Equation (23).

$$3f = 2e \tag{23}$$

By combining this expression with Euler's theorem, we obtain a relationship between numbers of vertices and edges; Equation (24).

$$3v - 6 = e \tag{24}$$

One immediately recognises in this equation the number of internal degrees of freedom $3v - 6$ of a molecule with v atoms. This number is equal to the number of edges, e. The necessary and sufficient condition that the set of all stretch-

ings of edges would form a nonredundant set of vibrational coordinates is that not only the number but also the symmetries coincide. This equivalence of the vibrational and edge representation is indeed a fact for all deltahedra that can be mapped on the surface of a sphere. The proof is contained in the following fibre equation,[8] that is valid for deltahedra; Equation (25).

$$\Gamma_\sigma(v) \times \Gamma(T) - \Gamma(T) - \Gamma(R) = \Gamma_\sigma(e) \tag{25}$$

On the left the first term of dimension $3v$ is the representation of all Cartesian displacements of all atoms. From this we subtract the six external modes, comprising the translations and rotations. On the right $\Gamma_\sigma(e)$ is the symmetry representation of the set of edge centres. The stretching of an edge is σ-symmetric with respect to all symmetry elements going through the edge, and therefore is also covered by $\Gamma_\sigma(e)$. This expression is highly relevant for the force field of deltahedral clusters. It states that the symmetries of the displacements of the cluster atoms span the symmetries of the edge stretchings plus the six external degrees of freedom. Hence the edge stretchings exactly match the internal degrees of freedom. By putting a spring on every edge of a deltahedral cluster we construct a complete force field. The potential energy of this cluster can thus be written as given in Equation (26), where $\langle ij \rangle$ is the edge between atoms i and j and the summation runs over all edge pairs.

$$2V = \sum_{\langle ij \rangle \langle mn \rangle} k_{\langle ij \rangle \langle mn \rangle} \Delta r_{\langle ij \rangle} \Delta r_{\langle mn \rangle} \tag{26}$$

This equation is a typical example of a polyhedral relationship: a property of the vertices, in this case a displacement, is related to a property of a higher structural component, here the stretching of an edge. A mechanical proof of this property was already known to the famous French engineer and geometrician, Cauchy.[27] Boyle and Parker,[28] in their study of force fields in dodecaborane, noted the peculiar identity of the symmetries of the internal modes and the edge stretchings, but did not realise it was a general result for all deltahedra, which derives directly from the symmetry extension of Euler's theorem.

Table 4. Force constants for B_{12} in N/m

constant		value
k_1	$\langle ij \rangle \langle ij \rangle$	221.48
k_2	$\langle ij \rangle \langle im \rangle$	-33.12
k_3	$\langle ij \rangle \langle ik \rangle$	41.46
k_4	$\langle ij \rangle \langle km \rangle$	-29.57
k_5	$\langle ij \rangle \langle lm \rangle$	-17.36
k_6	$\langle ij \rangle \langle kl \rangle$	17.56
k_7	$\langle ij \rangle \langle kn \rangle$	0.88
k_8	$\langle ij \rangle \langle ln \rangle$	-3.95
k_9	$\langle ij \rangle \langle no \rangle$	8.06

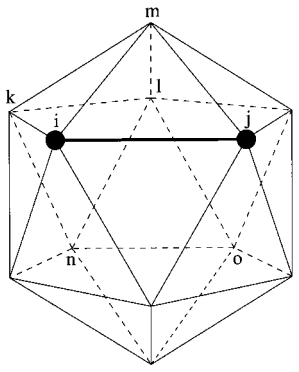

Figure 3. Vertex labelling for the boron skeleton in dodecaborane

In a recent study,[29] we have calculated the Hessian for $B_{12}H_{12}^{2-}$, using DFT techniques, and then derived the force constants. The results are listed in Table 4, following the bond labelling in Figure 3. It can be seen that the interactions between the bond stretchings decrease when the bonds are further apart, but quite remarkably, even bonds that do not have a common atom, still interact significantly. This confirms the delocalised nature of the bonding in these electron-deficient compounds.

6.2 The Frontier Orbitals of Fullerenes

In the innumerable fullerene family, Buckminsterfullerene, C_{60}, stands out in several ways. It is the smallest cage where all pentagons are isolated, and this contributes greatly to its stability, but in addition it is also a closed-shell molecule. In this respect it is the smallest member of the leapfrog class of closed-shell fullerenes.[30] A leapfrog fullerene, C_{3v}, is constructed from a smaller fullerene, C_v, by first capping all of its faces and then taking the dual of the resulting polyhedron. Since the smallest fullerene is the dodecahedron with twenty carbon atoms, the smallest leapfrog fullerene will indeed be C_{60}.[31]

The leapfrog construction (Figure 4) implies that the vertices in the parent will be transformed into hexagonal faces in the leapfrog. As a result all original faces will be surrounded by a ring of hexagons. This corresponds precisely to the "dilution" of the dodecahedron by hexagons to produce the familiar football shape.

The edges of the parent are also present in the leapfrog but are rotated by 90°. In C_{60} they correspond to the thirty edges separating the hexagons.

As a result the π-bonding in a leapfrog can be described by two extreme bonding schemes: either we put ethylenic bonds on all edges, that are derived from the edges of the parent cage, or we put aromatic sextets to all faces that are derived from the parent faces.

In Figure 5 these bonding extremes are connected in a Walsh-like correlation diagram, where we can move from the left to the right by gradually increasing the double-bond lengths and decreasing the single-bond lengths.[32]

On the left we have thirty isolated double bonds and thus thirty π-bonding orbitals and an equal number of π-anti-

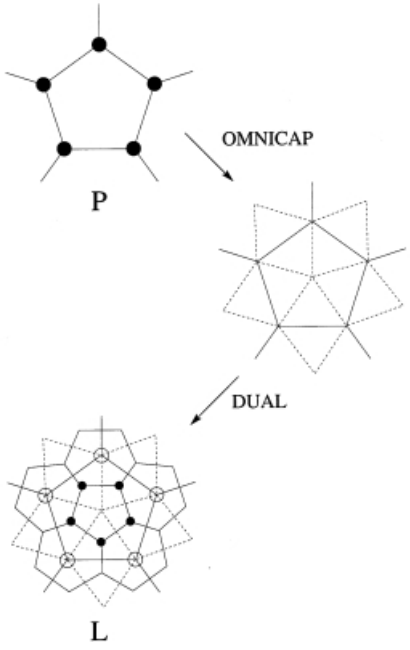

Figure 4. The leapfrog transformation; P is a piece of the parent, L is the leapfrog; vertices in P are hexagon centres in L; faces in P remain faces in L

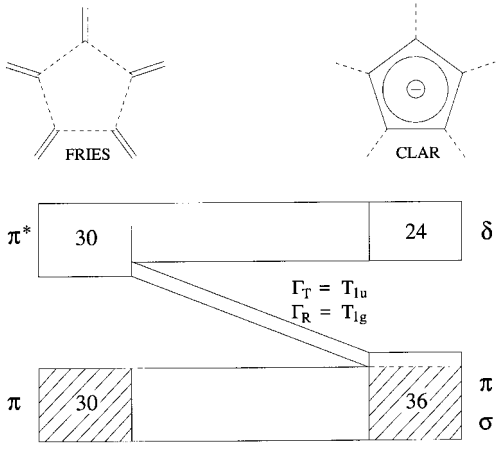

Figure 5. Walsh diagram for C_{60} with correlation between two bonding extremes: a "Fries" structure on the left with localised double bonds between pentagons, and a "Clar" structure on the right with aromatic sextets on the pentagon

bonding orbitals. On the right we recognise the bonding orbitals of twelve isolated pentagons, with the bonding σ and π shells that form the aromatic sextet, and antibonding δ-type orbitals. When we move away from the bonding extremes the localised levels broaden and become the molecular orbitals of C_{60}. Quite remarkably, the *symmetries* of all thirty bonding combinations on the left are present in the thirty-six bonding combinations on the right. The six remaining combinations will correlate with the π* orbitals on the left, and cross the nonbonding line almost halfway between the two extremes. As a result C_{60} has a closed shell of thirty bonding orbitals, followed by a set of low-lying almost nonbonding orbitals. These transform in icosahedral symmetry as T_{1u} and T_{1g} representations, which happen to be the representations of translation and rotation.

This pattern is characteristic for all leapfrog fullerenes. There is always a set of six low-lying frontier orbitals with the $\Gamma(T) + \Gamma(R)$ symmetry. For a general leapfrog fullerene the number of bonding orbitals on the left will be equal to the number of edges, *e*, in the parent. Similarly, the number of bonding orbitals on the right will be equal to three times the number of faces, 3*f*, in the parent. These numbers indeed differ by six, see Equation (27), which follows from Euler's rule, for trivalent cages.

$$e = 3f - 6 \tag{27}$$

As in the previous example, for the correlation in the Walsh diagram to hold, more is required than a simple dimensional agreement. The symmetries of the bonding orbitals on the left should match the symmetries on the right. This is indeed the case according to the following fibre rule for trivalent cages, which is of course the dual of the fibre rule for deltahedra in Equation (25), see Equation (28).

$$\Gamma_\sigma(e) = \Gamma_\sigma(f) \times \Gamma(T) - \Gamma(T) - \Gamma(R) \tag{28}$$

The $\Gamma_\sigma(e)$ term in this equation precisely corresponds to the symmetries of ethylenic bonding orbitals on the edges of the parent, since these are symmetric combinations of the p_z orbitals at either end of the edge. The left-hand side of the expression thus describes the symmetries of the bonding combinations on the left of the Walsh diagram. Similarly, the term $\Gamma_\sigma(f) \times \Gamma(T)$ spans the symmetries of the aromatic sextets on the right of the diagram: each aromatic sextet comprises three orbitals which transform as σ, π_x, and π_y with respect to the centre of the pentagon: i.e. a set which transforms as the three Cartesian components. The direct product $\Gamma_\sigma(f) \times \Gamma(T)$ then generates the bonding orbitals on all twelve pentagons. The group-theoretical results then state that for any fullerene which is a leapfrog, matching of the two bonding extremes will provide a closed-shell structure, with a set of low-lying orbitals transforming as $\Gamma(T) + \Gamma(R)$.

These special frontier orbitals are once again defined as the fibre, which connects to the topological invariances of the polyhedral complex.

A similar analysis can also be extended to other trivalent cages containing triangular or quadrilateral defects. It has also been performed for the graphene sheet.[12] In this case the topologically relevant orbitals are identified as the four semi-occupied nonbonding orbitals in the K-point of the honeycomb lattice.

Conclusion

In many respects molecules are graph-like objects. The Hückel model is essentially based on the molecular graph. Probably in the whole of quantum chemistry, there isn't a

single theory that can compete with this model in terms of minimal effort for maximum relevance.

In this review we point to the existence of equally general molecular relationships, which go beyond the vertex-edge picture, and imply face structures. Especially in the area of clusters and network molecules this leads to useful new insights, both for the description of electronic and elastic properties. In the polyhedral complex steric aspects of molecular structure are taken into account. Note that the elements of a complex are not spatial coordinates, but relationships between atomic nodes.

Further theoretical efforts are certainly needed to expand the theoretical framework. The fibre bundles that we have considered in section 6 are indeed trivial examples, where the connection is a straightforward product. More intricate problems are offered by the description of tunnelling between Jahn−Teller minima on a surface. These await further analysis.

We finally hope the present microreview will invite chemists to acquire a practical understanding of topological concepts. Our main ally in applying these concepts to molecular properties clearly is group theory. Group theory and topology are not rival mathematical disciplines but go admirably together, reinforcing each others results.

Acknowledgments

Financial support from the Flemish Government (Concerted Action Scheme) and the Fund for Scientific research − Flanders (Belgium) is gratefully acknowledged. A. C. is greatly indebted to Patrick Fowler (Exeter) and Marek Szopa (Katowice) for extensive collaborations on the topic of this review during the past ten years.

[1] A. T. Balaban, *Chemical Applications of Graph Theory*, Academic Press, London, **1976**.
[2] A. R. Leach, *Molecular Modelling: Principles and Applications*, Longman, Harlow, **1996**.
[3] P. J. Giblin, *Graphs, Surfaces and Homology*, Chapman and Hall, London, **1977**.
[4] F. A. Cotton, *Chemical Applications of Group Theory*, 3rd ed., Wiley, New York, **1990**.
[5] P. J. Federico, *Descartes on Polyhedra*, Springer, New York, **1982**. A collection of proofs of the Euler theorem is assembled on web page http://www.ics.uci.edu/~eppstein/junkyard/euler
[6] For a thorough mathematical treatise on homologies, consult: P. J. Hilton, S. Wylie, *Homology Theory*, Cambridge University Press, Cambridge, **1960**.
[7] S. L. Altmann, *Induced Representations in Crystals and Molecules*, Academic Press, London, **1971**.
[8] A. Ceulemans, P. W. Fowler, *Nature (London)* **1991**, *353*, 52−54.
[9] A. Ceulemans, M. Szopa, P. W. Fowler, *Europhys. Lett.* **1996**, *36*, 645−649.
[10] P. W. Fowler, A. Rassat, A. Ceulemans, *J. Chem. Soc., Faraday Trans.* **1996**, *92*, 4877−4884.
[11] A. Ceulemans, P. W. Fowler, *J. Chem. Soc., Faraday Trans.* **1995**, *91*, 3089−3093.
[12] A. Ceulemans, L. F. Chibotaru, P. W. Fowler, M. Szopa, *J. Chem. Phys.* **1999**, *110*, 6916−6926.
[13] A. Ceulemans, R. B. King, S. A. Bovin, K. M. Rogers, A. Troisi, P. W. Fowler, *J. Math. Chem.* **1999**, *26*, 101−123.
[14] E. D. Jemmis, M. M. Balakrishnarajan, P. D. Pancharatna, *J. Am. Chem. Soc.* **2001**, *123*, 4313−4323.
[15] R. L. Johnston, *Struct. Bonding (Berlin, Ger.)* **1997**, *87*, 1−34.
[16] R. Hoffmann, *Angew. Chem. Int. Ed. Engl.* **1982**, *21*, 711−724.
[17] R. L. Johnston, D. M. P. Mingos, *J. Organomet. Chem.* **1985**, *280*, 407−418.
[18] D. M. P. Mingos, D. J. Wales, *Introduction to Cluster Chemistry*, Prentice Hall, Englewood Cliffs, New York, **1990**.
[19] B. Y. Zel'dovich, *Zh. Eksp. Teor. Fiz.* **1957**, *33*, 1531.
[20] D. Loss, P. Goldbart, A. V. Balatsky, *Phys. Rev. Lett.* **1990**, *65*, 1655−1658.
[21] A. Ceulemans, L. F. Chibotaru, P. W. Fowler, *Phys. Rev. Lett.* **1998**, *80*, 1861−1864.
[22] J. Liu, H. J. Dai, J. H. Hafner, D. T. Colbert, R. E. Smalley, S. J. Tans, C. Dekker, *Nature (London)* **1997**, *385*, 780−781.
[23] R. Martel, H. R. Shea, P. Avouris, *J. Phys. Chem. B* **1999**, *103*, 7551−7556.
[24] M. Sano, A. Kamino, J. Okamuri, S. Shinkay, *Science* **2001**, *293*, 1299−1301.
[25] J. Biel, R. Chatterjee, T. Lulek, *J. Chem. Phys.* **1987**, *86*, 4531−4540.
[26] A. Ceulemans, *Mol. Phys.* **1985**, *54*, 161−181.
[27] A. L. Cauchy, *J. Ec. Imp. Polytech. (Paris)* **1813**, *19*, 87−98.
[28] L. L. Boyle, Y. M. Parker, *Mol. Phys.* **1980**, *39*, 95−109.
[29] A. Ceulemans, B. C. Titeca, L. F. Chibotaru, I. Vos, P. W. Fowler, *J. Phys. Chem. A* **2001**, *105*, 8284−8295.
[30] P. W. Fowler, J. I. Steer, *J. Chem. Soc., Chem. Commun.* **1987**, 1403−1405.
[31] D. E. Manolopoulos, P. W. Fowler, *An Atlas of Fullerenes*, Clarendon Press, Oxford, **1995**.
[32] P. W. Fowler, A. Ceulemans, *J. Phys. Chem.* **1995**, *99*, 508−510.

Received October 16, 2001
[I01411]

A 1,3-Sigmatropic Rearrangement Revealed in the Solid and Solution State Structures of a Chiral Sodium 1-Azaallyl Complex Derived from (*S*)-*N*-(α-Methylbenzyl)allylamine

Philip C. Andrews,*[a] Simone M. Calleja,[a] Melissa Maguire,[a] and Peter J. Nichols[a]

Keywords: Sodium / N ligands / Chirality / Amines / Sigmatropic rearrangement / Structure elucidation

The reaction of *n*BuNa with (*S*)-*N*-(α-methylbenzyl)allylamine, followed by the addition of tmeda, gives a chiral sodium 1-azaallyl complex, $\{[(S)\text{-}\alpha\text{-}[PhC(H)MeN^{\cdot\cdot}C(H)^{\cdot\cdot}CHCH_3)]Na\cdot tmeda\}_2$, as confirmed by single crystal X-ray diffraction and solution NMR spectroscopy, and is most likely the result of a 1,3-sigmatropic rearrangement and subsequent delocalisation within the resulting enamide.

(© Wiley-VCH Verlag GmbH, 69451 Weinheim, Germany, 2002)

Introduction

There is significant interest in the solution and solid state structures of alkali metal amides and in relating this structural knowledge to explanations of the degree of selectivity that can be achieved when used in enantioselective reactions.[1a−1k] In particular, the successful utilisation of chiral lithium amides in conjugate addition and selective deprotonation reactions with consequent high *ee* values has attracted considerable attention.[2a−2i] In contrast, there have been relatively few investigations into the synthetic utility of Na or K amides in such reactions,[3] not because of unexpected internal structural rearrangements but mainly because these reagents are expected to behave in a similar manner to their Li counterparts, although with greater reactivity and reduced selectivity.

Through recent investigations into the alkali metal complexes derived from commonly used chiral amines, such as α-(methylbenzyl)benzylamine[4a,4b] and α-bis(methylbenzyl)-amine,[5] we have discovered the surprising structural transformations that can occur in the amide moiety on changing the metal from lithium to sodium; α-(methylbenzyl)benzylamine was found to undergo transformation to a 2-azaallyl complex while α-bis(methylbenzyl)amine was cleaved to give a metallated primary enamide. In extending this work we have turned our attention to an analogous amine, (*S*)-*N*-(α-methylbenzyl)allylamine which, because of the ease with which the allyl group is cleaved, has been shown by Davies to be often superior to lithium α-(methylbenzyl)benzylamide in the formation of β-amino acids and β-lactams.[6a−6c] With the allyl group essentially being a less-constrained fragment of a benzyl group we were particularly interested in: (i) whether there would be any close interactions of the metal and the $C(H)=CH_2$ unit, and (ii) the possibility of any β-H elimination processes and the formation of 2-azaallyl species as observed for α-(methylbenzyl)benzylamide and dibenzylamide complexes.[7]

To-date, mono-lithiation reactions of the chiral allylamine in the presence of several typical Lewis donors has produced only a series of deep red and orange coloured oils. However, on moving to studying the heavier metal complexes we found that reaction with *n*BuNa, followed by addition of tmeda (*N*,*N*,*N*′,*N*′-tetramethylethylenediamine), is one of the few reactions which has, so-far, produced a crystalline product.

The large yellow crystals isolated from the reaction have been identified by single crystal X-ray diffraction to be the dimeric azaallyl complex $\{[(S)\text{-}\alpha\text{-}[PhC(H)MeN^{\cdot\cdot}C(H)^{\cdot\cdot}CHCH_3)]Na\cdot tmeda\}_2$ (**1**), with ^1H and ^{13}C NMR spectroscopy indicating that this configuration is retained in solution.

Results and Discussion

The two methods by which crystals of **1** were obtained are outlined in Scheme 1. The addition of the amine to *n*BuNa produces a pale brown suspension. Subsequent addition of tmeda causes dissolution to a red solution from which crystals are obtained over several days at 4 °C. Since we have not yet been able to obtain a crystalline product using the typical tridentate donor pmdta (*N*,*N*,*N*′,*N*′,*N*′′-pentamethyldiethylenetriamine), one equivalent of THF was added in an attempt to deaggregate the dimer in order to study possible 2-azaallyl formation. However, this again resulted in crystals of **1** as the exclusive product. We did note, though, that if more than one equivalent of THF is

[a] School of Chemistry, Monash University, Clayton, Melbourne, Vic. 3800, Australia
Fax: (internat.) +61-3/9905-4597
E-mail: p.andrews@sci.monash.edu.au

added it can be difficult to obtain a solid product. Over time this solution becomes very dark red and may indicate some further reaction including the base-catalysed ring opening of the THF.

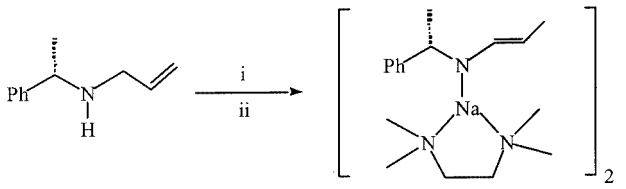

Scheme 1. Syntheses of [{(*S*)-α-[PhC(H)MeN⋯CH⋯CHCH$_3$]}Na·tmeda]$_2$ (**1**); i) *n*BuNa, hexane, tmeda, room temp; ii) *n*BuNa, hexane, tmeda/thf, room temp.

The crystal structure of **1**, shown in Figure 1, is a noncentrosymmetric dimer (monoclinic, $P2_1$) in which each of the two "monomers" adopts a different configuration. These are shown in Figure 2 and differ with respect to the positional exchange of the Ph and Me groups within the benzylmethyl moiety. An analysis of the bond lengths in the N1−C9−C10 [1.365(3), 1.345(3) Å] and N2−C20−C21 [1.370(3), 1.331(3) Å] fragments indicates that **1** is best described as an η^1-*N*-azaallyl complex, and most likely results from a 1,3-sigmatropic rearrangement to an enamide and subsequent delocalisation of the negative charge (Figure 3).

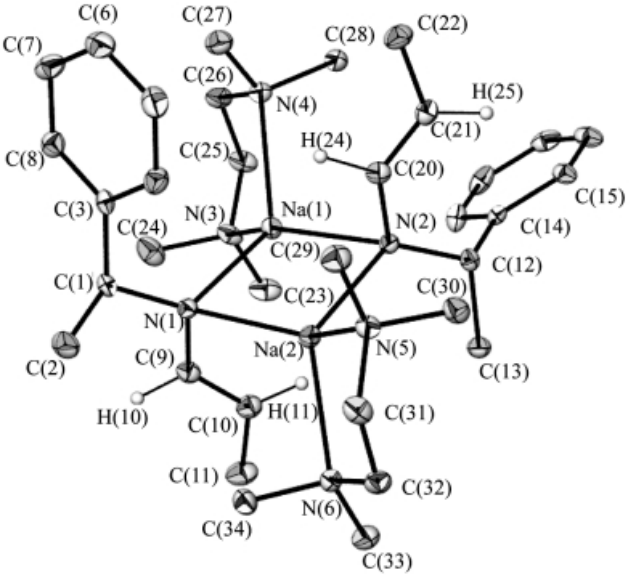

Figure 1. Molecular structure of [{(*S*)-α-[PhC(H)MeN⋯C(H)⋯CHCH$_3$]}Na·tmeda]$_2$ (**1**); thermal ellipsoids at 30% probability; selected bond lengths (Å) and angles (°); Na1−N1 2.410(2), Na1−N2 2.408(2), Na1−N3 2.480(2), Na1−N4 2.516(2), Na2−N1 2.411(2), Na2−N2 2.389(2), Na2−N5 2.500(2), Na2−N6 2.512(2), N1−C1 1.468(3), N1−C9 1.365(3), C9−C10, 1.345(3), C10−C11 1.510(4), N2−C12 1.451(3) N2−C20 1.370(3), C20−C21 1.331(3) C21−C22 1.519(3); N1−Na1−N2 96.78(7), N1−Na2−N2 97.27(7), Na1−N1−Na2 82.43(6), Na1−N2−Na2 82.94(6), C1−N1−C9 112.83(19), N1−C9−C10 128.8(2), C9−C10−C11 123.7(3), N2−C20−C21 134.1(2), C20−C21−C22 123.0(2)

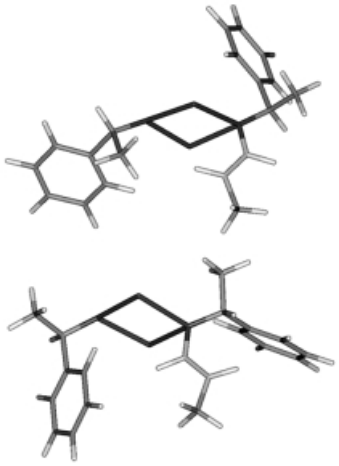

Figure 2. View relative to the $(NaN)_2$ ring of the relationship of the two different "monomers" found in dimeric **1**; tmeda has been omitted for clarity

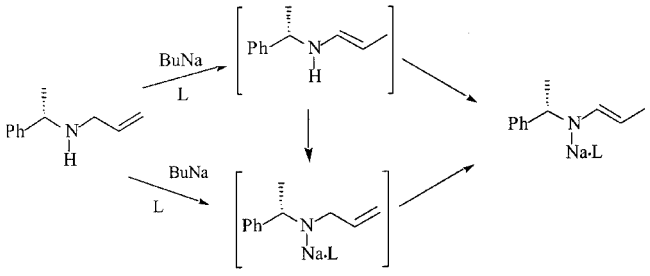

Figure 3. Possible routes of formation for **1**; 1,3 sigmatropic rearrangement and enamide and azaallyl configurations; L = tmeda

The core feature of **1** is the common structural motif of a central four-membered $(NaN)_2$ ring about which the amido moieties are in a *trans* arrangement.[8] However, on this occasion the four-membered ring is not planar but adopts a very shallow butterfly conformation, deviating from the plane by 5.7°. A more general analysis of the structure shows that one phenyl ring adopts an orientation almost co-planar with the $(NaN)_2$ ring and almost perpendicular to the other phenyl ring. This places C13 close to Na2 but, at about 3.4 Å, is beyond what would be considered a reasonable bonding distance (the sum of the van der Waals radii is 3.2 Å). The tetrahedral environment at each N is extremely distorted, most likely for steric reasons, with the azaallyl groups forming acute angles in relation to the $(NaN)_2$ ring. Thus, N2−N1−C9 and N1−N2−C20 are 103.7° and 96.6°, respectively, while the concomitant angles to the benzylic carbon are 142.9° for N2−N1−C1 and 149.0° for N1−N2−C12. So, while the formal coordination number of each Na centre is four, each is able to engage in very short compensatory agostic contacts with nearby C and H atoms of the azaallyl groups. The closest contacts for Na1 are 2.921(3) Å to C9 and 2.818(3) Å to C20, while the comparable distances for Na2 are 3.012(3) Å (C20), 2.923(3) Å (C9) and 3.022(3) Å (C10). Similar close con-

tacts have recently been observed in the uncomplexed sodium amide dimer $[(PhMe_2Si)(Me_3Si)NNa]_2$.[8] The orientation of the azaallyl groups, which deviate from an ideal C20−N2−N1−C1 plane by 14.8°, are nonsymmetrical in relation to the $(NaN)_2$ ring. The hydrogen (H24) on C20 overhangs the $(NaN)_2$ ring, dissecting the two metal centres at distances of 2.75 Å (Na1−H24) and 3.01 Å (Na2−H24), while hydrogen H10 on C9 points away from the ring leaving the hydrogen (H11) on C10 to sit between the two Na cations at distances of 2.74 Å (Na1) and 2.57 Å (Na2). Within the ring the Na−N bond lengths are shorter than those typically observed for dimeric sodium amides {c.f. $[(i\text{Pr})_2\text{NNa·tmeda})]_2$,[9] 2.441(2)-2.453Å; [Cy(*i*Pr)-NNa·tmeda]$_2$ [9] 2.438(2), 2.443(2) Å} but are similar to those observed for $[(PhCH_2)_2\text{NNa·tmeda})]_2$ [10] (2.397, 2.412 Å), which tends to be a reflection of the steric nature of the groups in the amide moiety.

Solution NMR spectra (^{1}H, ^{13}C, COSY and HMQC) were obtained in three solvents; [D$_6$]benzene, [D$_8$]toluene and [D$_8$]THF with variable temperature experiments conducted in [D$_8$]toluene (down to −80 °C) and in [D$_8$]THF (down to −90 °C). At 30 °C the same basic spectra were observed in all three cases, with each confirming that the complex had undergone a 1,3-sigmatropic rearrangement and that the azaallyl configuration, observed in the crystal structure, is retained in solution. In comparing the ^{1}H spectra in [D$_8$]THF of **1**, shown in Figure 4, and the starting allylamine the most telling features are the complete disappearance of the signals of the NCH_2 protons of the amine and the appearance of a doublet at δ = 1.57 ppm (CH_3), which, from 2D experiments, correlates with a doublet of quadruplets at δ = 3.25 ppm (1 H), which in turn correlates with a new doublet at δ = 6.59 ppm ($J_{H,H}$ = 13 Hz, 1 H), which we have assigned to the single H remaining from the transformed NCH_2 group. While this doublet is very sharp in [D$_8$]THF, in spectra obtained in [D$_8$]benzene and [D$_8$]toluene it is slightly broader and is partially obscured by the aromatic signals.

The retention of the azaallyl configuration in solution is supported by an analysis of the change in chemical shift for the central H in the former allyl group (now H25 and H11 in **1**). An upfield shift of 3 ppm is observed relative to its position in the free amine, while the associated C, which now appears at δ = 74.2 ppm, has shifted upfield by almost 60 ppm, both indicating a significant reduction in double bond character and charge distribution. All of the *C*H signals in the ^{13}C spectrum at 30 °C are weak and broad with a large downfield shift observed for the new N*C*H, which ^{1}H/^{13}C correlation and coupling experiments showed to be directly under the signal for the quaternary carbon at δ = 154.1 ppm.

Variable temperature experiments in [D$_8$]THF and [D$_8$]toluene did reveal slightly different solution behaviour for each complex, most likely resulting from deaggregation occurring in THF and retention of the dimer in toluene. As such the [D$_8$]THF spectra are slightly less complex. Looking first at the toluene spectra. At 30 °C the Ph(Me)C*H* protons appear at δ = 4.2 ppm and the C*H* protons (H11 and H25) in the azaallyl group at δ = 3.7 ppm. By −60°C 2D ^{1}H/^{1}H correlation indicates that these split into six distinct signals, four relating to Ph(Me)C*H* protons and two for the azaallyl protons. All the other protons also show substantially differing environments at low temperature. In THF at −60°C the corresponding central azaallylic proton, which is located at δ = 3.25 ppm at 30 °C, splits in two, shifting to δ = 2.86 ppm and δ = 3.57 ppm, with integrals indicating a 2:1 ratio. The Ph(Me)C*H* protons also split in two in a similar ratio, although the signals are not distinct but overlap. The azaallylic protons N⋯C(*H*)⋯C (H10 and H24), initially observed at δ = 6.59 ppm, are also split in two though one is very sharp and the other broad. The Me signals simply broaden.

In attempting to understand the low temperature spectra we undertook some basic molecular modelling experiments.[11] These indicated that the dimer is extremely crowded with very little opportunity for internal reorganisation of the molecule. The *trans* configuration observed within the azaallyl moiety in the crystal structure, and confirmed in solution, is retained due to a significantly restricted rotation around both the azaallyl C⋯N and C⋯C bonds, and the C_{chiral}−N bond, with the latter being a lower energy process. As such, the low temperature spectra in [D$_8$]toluene is consistent with the crystal structure and the two different "monomer" configurations highlighted in Figure 2. The complexity is a consequence of the two different azaallyl environments, with each of the four possible conformations of the benzylmethyl groups resulting from restricted 120° rotations.

In [D$_8$]THF the NMR spectra are consistent with deaggregation to a monomer containing coordinated THF. A model monomer with a single tmeda and a THF was only marginally less restricted than the dimer. However the lower energy barriers to rotation at each of the N−C bonds means that the various more simple possible configurations caused by rotation of the benzylmethyl group are not evident until lower temperatures. And, in fact, they do begin to appear in the spectrum obtained at −90 °C.

1-Azaallyl complexes of the alkali metals are almost exclusively formed by deprotonation of ketimines or aldimines, or by the 1,2-addition to nitriles. The variety of complexes and their bonding modes formed have been reviewed recently.[12] However, it is only in the last few years that an η^1 structural arrangement has been observed with characterisation of the complexes $[\{CH_3CH_2CH_2C(H)C⋯(t\text{Bu})⋯N(H)Li·(hmpa)\}]_n$ and $[\{CH_3CH_2CH_2C(H)C⋯(t\text{Bu})⋯N(H)Na·(hmpa)_2\}]_n$, formed in the reaction of either *n*BuLi or *n*BuNa with *t*BuCN followed by a 1,3-sigmatropic H shift.[13] The azaallyl arrangement in these complexes is calculated as the most stable configuration and is retained in solution, as we observed for **1**. In contrast, though, **1** is formed by deprotonation and metallation of a secondary allylamine leading to the formation of a metal enamide. Several studies have indicated that the base-catalysed isomerisation of *N*,*N*-allylamines in the presence of *t*BuOK, LDA or KH to give the corresponding enamine is energetically favourable.[14a−14e] Whether this isomerisation can oc-

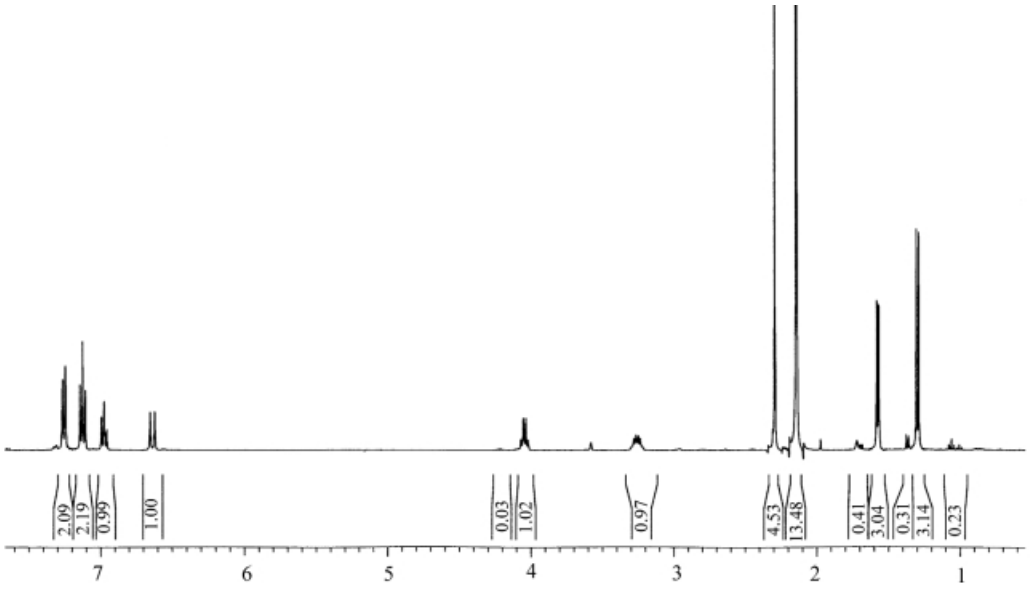

Figure 4. ^{1}H NMR of **1** in [D_8]THF showing the new CH_3 (δ = 1.57 ppm) and CH (δ = 6.59 ppm) signals from the rearrangement of the allyl group

cur with secondary allylamines prior to deprotonation taking place or occurs after metallation requires further study. We did not observe any isomerisation of the (*S*)-*N*-(α-methylbenzyl)allylamine prior to addition of the metallating reagent.

Evidence from the use of adducts of lithium *N*-(α-methylbenzyl)allylamide in conjugate addition reactions suggests that the amide moiety is in the allylic form prior to final deallylation, although cleavage of the allyl group requires ketimine formation prior to hydrolysis.[6,15] In light of this we are continuing our attempts to structurally characterise a lithium complex in the hope of discovering whether this rearrangement is general for the alkali metals and whether there are any important synthetic implications.

Experimetal Section

General Remarks: All compound manipulations were carried out under inert atmosphere and dry conditions using a vacuum/argon line, Schlenk techniques and a high purity argon gas recirculating dry box. Prior to use, solvents were dried by reflux over Na/K alloy and stored over 4 Å molecular sieves. (*S*)-*N*-(α-Methylbenzyl)allylamine was prepared by a literature procedure.[16] *n*BuNa was prepared from the metathesis reaction of *n*BuLi and NaO*t*Bu in hexane and stored as a solid. (Note: this solid is extremely pyrophoric). Tmeda was refluxed over CaH_2, distilled and stored over 4 Å molecular sieves. NMR spectra were obtained on a Bruker DRX-400 spectrometer with chemical shifts referenced to the appropriate deuterated solvent. Elemental analyses were carried out by CMAS, Australia.

Synthesis of 1: (*S*)-*N*-(α-Methylbenzyl)allylamine (0.81 g, 5.0 mmol) was added dropwise to a suspension of *n*BuNa (0.43 g 5 mmol) in hexane (20 mL) at room temperature resulting in a light brown coloured suspension. After 30 min tmeda (0.76 mL, 5.0 mmol) was added causing dissolution of the suspension and formation of a deep red solution. On filtration and cooling to 4 °C over several days pale yellow crystals of X-ray quality were produced. Yield 0.91 g, 61% (not maximised), m.p. 85−87 °C. ^{1}H NMR (400 MHz, 30 °C, [D_8]THF): δ = 7.25 (d, ^1J = 7.06 Hz, 2 H, *o*-H), 7.13 (t, ^1J = 7.45, 2 H, *m*-H), 6.97 (t, ^1J = 7.27, 1 H, *p*-H), 6.65 [d, ^1J = 12.54 Hz, 2 H, N-C(*H*)=C], 4.06 (q, ^1J = 6.56, 1 H, PhC(*H*)CH_3], 3.25 (dq, ^1J = 5.78, ^2J = 11.76, 2 H, C-C(*H*)=CH_3), 2.29 (s, 4 H, NCH_2), 2.14 (s, 12 H, NCH_3), 1.57 (d, ^1J = 5.86 Hz, 3 H, C=CH_3), 1.29 [d, ^1J = 6.62 Hz, 3 H, PhC(H)CH_3] ppm. ^{13}C NMR (100.6 MHz, 30 °C, [D_8]THF): δ = 17.2 (CH_3), 27.3 [PhC(H)CH_3], 46.1 (CH_3N), 58.8 (NCH_2), 62.7 [PhC(H)CH_3], 74.2 [C=C(H)-CH_3], 125.3 (*p*-*C*), 127.4 (*m*-*C*), 128.1 (*o*-*C*), 154.1 [*q*-*C*, N-*C*(H)=C] ppm. $C_{34}H_{60}N_6Na_2$ (598.9): calcd. C 68.2, H 10.1, N 14.0; found C 68.4, H 9.8, N 13.8.

Crystallographic Data for 1: $C_{34}H_{60}N_6Na_2$, M = 598.86, T = 123 K, monoclinic $P2_1$, a = 11.006(2), b = 12.009(2), c = 14.255(3) Å, β = 96.51(3)°, V = 1871.9(7) Å^3, D_c = 1.062 g·cm^{-3}, Z = 2; F(000) = 656, $\mu_{Mo\text{-}K_\alpha}$ = 0.83 cm^{-1}, $2\theta_{max}$ = 56.6°, final R, R_w = 0.052, 0.094. N_o = 5318 observed reflections [$I > 2\sigma$ (I)] out of N = 9213, R_{int} = 0.057. GooF = 0.955. The Flack parameter was indeterminate and the final stereochemistry was based on that of the starting amine. The crystal was coated in oil,[17] mounted on a fibre and data collected at 123 K on an Enraf Nonius Kappa CCD diffractometer equipped with Mo-K_α radiation (λ = 0.71073Å). The structure was solved by direct methods (SHELXS-97)[18] and refined by full-matrix least-squares on F^2. All H atoms were located in the difference map and refined isotropically. All other atoms were refined anisotropically.

CCDC-172280 contains the supplementary crystallographic data for this paper. These data can be obtained free of charge at www.ccdc.cam.ac.uk/conts/retrieving.html [or from the Cambridge Crystallographic Data Centre, 12, Union Road, Cambridge CB2 1EZ, UK; Fax: (internat.) +44-1223/336-033; E-mail: deposit@ccdc.cam.ac.uk].

Acknowledgments

We thank the Australian Research Council and Monash University for financial support.

[1] [1a] G. Hilmersson, B. Malmros, *Chem. Eur. J.* **2001**, *7*, 337−341. [1b] A. Johansson, A. Pettersson, Ö. Davidsson, *J. Organomet. Chem.* **2000**, *608*, 153−163. [1c] C. Sun, P. G. Williard, *J. Am. Chem. Soc.* **2000**, *122*, 7829−7830. [1d] P. I. Arvidsson, Ö. Davidsson, *Angew. Chem. Int. Ed.* **2000**, *39*, 1467−1469. [1e] R. I. Olsson, P. Ahlberg, *Tetrahedron: Asymmetry* **1999**, *10*, 3991−3998. [1f] D. R. Armstrong, K. W. Henderson, A. R. Kennedy, W. J. Kerr, F. S. Mair, J. H. Moir, P. H. Moran, R. Snaith, *J. Chem. Soc., Dalton Trans.* **1999**, *22*, 4063−4068. [1g] A. Corruble, J-Y. Valnot, J. Maddaluno, P. Duhamel, *J. Org. Chem.* **1998**, *63*, 8266−8275. [1h] D. Barr, D. J. Berrisford, R. V. H. Jones, A. M. Z. Slawin, R. Snaith, F. Stoddart, D. J. Williams, *Angew. Chem. Int. Ed.* **1998**, *28*, 1044−1046. [1i] G. Hilmersson, P. I. Arvidsson, Ö. Davidsson, M. Håkansson, *Organometallics* **1997**, *16*, 3352−3362. [1j] A. J. Edwards, S. Hockley, F. S. Mair, P. R. Raithby, R. Snaith, N. S. Simpkins, *J. Org. Chem.* **1993**, *58*, 6942−6943. [1k] D. Sato, H. Kawasaki, I. Shimada, Y. Arata, K. Okamura, T. Date, K. Koga, *J. Am. Chem. Soc.* **1992**, *114*, 761−763.

[2] [2a] J. Busch-Peterson, E. J. Corey, *Tetrahedron Lett.* **2000**, *41*, 6941−6944. [2b] S. G. Davies, O. Ichihara, *Tetrahedron Lett.* **1998**, *39*, 6045−6048. [2c] K. Koga, *Pure Appl. Chem.* **1994**, *66*, 1487−1492. [2d] T. Honda, N. Kimura, M. Tsubuki, *Tetrahedron: Asymmetry* **1993**, *4*, 21−24. [2e] T. Honda, N. Kimura, M. Tsubuki, *Tetrahedron: Asymmetry* **1993**, *4*, 1475−1478. [2f] K. Aoki, H. Naguchi, K. Koga, K. Tomioka, *Tetrahedron Lett.* **1993**, *34*, 5105−5108. [2g] B. J. Bunn, N. S. Simpkins, *J. Org. Chem.* **1993**, *58*, 533−534. [2h] P. J. Cox, A. Persad, N. S. Simpkins, *Synlett* **1992**, *3*, 194−196. [2i] P. J. Cox, N. S. Simpkins, *Tetrahedron: Asymmetry* **1991**, *2*, 1−26.

[3] A. Johansson, Ö. Davidsson, *Chem. Eur. J.* **2001**, *7*, 3461−3465.

[4] [4a] P. C. Andrews, P. J. Duggan, G. D. Fallon, T. D. McCarthy, A. C. Peatt, *J. Chem. Soc., Dalton Trans.* **2000**, 1937−1940. [4b] P. C. Andrews, P. J. Duggan, G. D. Fallon, T. D. McCarthy, A. C. Peatt, *J. Chem. Soc., Dalton Trans.* **2000**, 2505−2507.

[5] P. C. Andrews, P. J. Duggan, M. Maguire, P. J. Nichols, *Chem. Commun.* **2001**, 53−54.

[6] [6a] S. G. Davies, D. R. Fenwick, *Chem. Commun.* **1997**, 565−566. [6b] S. G. Davies, D. R. Fenwick, O. Ichicara, *Tetrahedron; Asymmetry* **1997**, *8*, 3387−3391. [6c] S. G. Davies, D. R. Fenwick, *J. Chem. Soc., Chem. Commun.* **1995**, 1109−1110.

[7] P. C. Andrews, D. R. Armstrong, D. R. Baker, R. E. Mulvey, W. Clegg, L. Horsburgh, P. A. O′Neill, D. Reed, *Organometallics* **1995**, *14*, 427−439.

[8] F. Antlolini, P. B. Hitchcock, M. F. Lappert, P. Merle, *Chem. Commun.* **2000**, 1301−1302.

[9] P. C. Andrews, N. D. R. Barnett, R. E. Mulvey, W. Clegg, P. A. O′Neil, D. Barr, L. Cowton, A. J. Dawson, B. J. Wakefield, *J. Organomet. Chem.* **1996**, *518*, 85−95 and references therein.

[10] P. C. Andrews, D. R. Armstrong, W. Clegg, M. MacGregor, R. E. Mulvey, *J. Chem. Soc., Chem. Commun.* **1991**, 497−498.

[11] Insight II Molecular Modelling Program (Discover minimisation module CVFF), Molecular Simulations Inc., San Diego, CA, USA.

[12] C. F. Caro, M. F. Lappert, P. G. Merle, *Coord. Chem. Rev.* **2001**, *219−221*, 605−663.

[13] D. R. Armstrong, W. Clegg, L. Dunbar, S. T. Liddle, M. MacGregor, R. E. Mulvey, D. Reed, S. Quinn, *J. Chem. Soc., Dalton Trans.* **1998**, 3431−3436.

[14] [14a] J. J. Eisch, J. H. Shah, *J. Org. Chem.* **1991**, *56*, 2955−2957. [14b] P. Beeken, F. Fowler, *J. Org. Chem.* **1980**, *45*, 1336−1368. [14c] J. Sauer, H. Prahl, *Tetrahedron Lett.* **1966**, 2863−2866. [14d] M. Riviere, M. Lattes, *Bull. Soc. Chim. Fr.* **1968**, 4430. [14e] J. Sauer, H. Prahl, *Chem. Ber.* **1969**, *102*, 1917−1927.

[15] S. Lemaire-Audoire, M. Savignac, C. Dupuis, J. P. Genêt, *Bull. Soc. Chim. Fr.* **1995**, *32*, 1156−1166.

[16] M. Yus, F. Foubelo, L. R. Falvello, *Tetrahedron: Asymmetry* **1995**, *6*, 2801−2092.

[17] D. Stalke, *Chem. Soc. Rev.* **1998**, *27*, 171−178.

[18] SHELXS-97, *Program for the Solution of Crystal Structures*, G. M. Sheldrick, **1997**, Göttingen, Germany.

Received January 9, 2002
[I02010]

A Self-Assembled Dinuclear Double-Stranded Helicate Based on a Square-Planar Coordination Geometry

Mauro Isola,*[a] Vincenzo Liuzzo,[a] Fabio Marchetti,[b] and Andrea Raffaelli[c]

Keywords: Nickel / Schiff-base ligands / Self-assembly / N,O ligands / Supramolecular chemistry

The nickel(II) complex of a new bis-*N,O*-bidentate Schiff base, in which two salicylaldiminate units are connected by an α,α′-dioxo-*ortho*-xylidene spacer via the 3-position of salicyl moieties, was structurally characterised in the solid state and in solution as a dinuclear double helicate based on a square-planar coordination geometry.
(© Wiley-VCH Verlag GmbH, 69451 Weinheim, Germany, 2002)

In the field of supramolecular chemistry, intense research activities have been focused on the helicates.[1] Almost all supramolecular structures of this type have been prepared by using neutral ligands containing nitrogen donor sets, so that the helical metal moieties have positive charges.[2]

Only in a few cases have anionic ligands been used, thus leading to neutral[3a−3f] or negatively charged helical structures.[3g,3h] Furthermore, in the four-coordinate helicates, the metal ions are invariably tetrahedral, suggesting that such a geometry is a requisite for generating a helicate with tetracoordinated metals.

Recently, we reported a facile preparation of nickel(II) complexes (Scheme 1) derived from a new class of bis-bidentate Schiff-base ligands capable of generating supramolecular architectures.[4] These new ligands contain two *N,O*-bidentate chelating moieties linked through a flexible polymethylene spacer (**H_2L^{1-3}**).

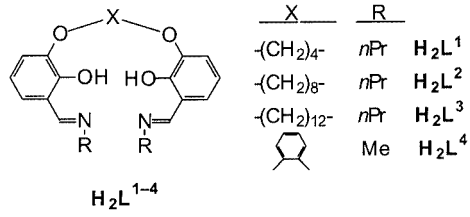

Scheme 1

In particular, by a self-assembly process the base with the octamethylene bridge yields the double-helical dinuclear complex $[Ni_2(L^2)_2]\cdot THF$, where each metal atom is linked in a *trans*-square-planar geometry by two *N,O*-coordination sites of different ligands. As far as we are aware, this is the first example of a structurally characterised helicate based on a square-planar geometry.[5] However, in $CHCl_3$ solution this supramolecular structure undergoes a disassembly process resulting in an equilibrium mixture in which the mononuclear species is largely predominant.

In light of these results, we started an investigation in order to explore the role of the spacers and the substituent on the imine nitrogen in determining the outcome of self-assembly reactions. To favour the formation of stable helicates, an ideal candidate for the replacement of the polymethylene bridging unit was envisaged to be the more rigid *ortho*-xylidene group, in which the flexibility is restricted to the methylene groups and the *ortho*-linkage is suitable for helication. On the basis of this premise, H_2L^4 was prepared following the general procedure previously described.[4] Reaction of H_2L^4 with $[Ni(OAc)_2]\cdot 4H_2O$ in a 1:1 molar ratio in ethanol at room temperature yielded olive green microcrystals after recrystallization from chloroform that analysed as $[Ni_2(L^4)_2]\cdot CHCl_3$.

Single crystals of the compound were obtained by slow evaporation of a chloroform solution. The X-ray structural analysis clearly shows that the compound has a dinuclear helical structure in the solid state. The molecular structure is sketched in the two projections of Figure 1. Each metal atom is linked in a *trans*-square-planar geometry by *N,O*-coordination sites from two different ligands, winding in a helical loop from Ni(1) to Ni(2). The nickel atoms and chelating groups lie approximately(± 0.25 Å) on two parallel planes, with a Ni(1)···Ni(2) distance of 3.554 Å. The two phenylene rings of the bridges are approximately perpendicular to the previous ones. The concurrence of ligand sizes with the distance between the coordination planes makes

[a] Dipartimento di Chimica e Chimica Industriale, Università di Pisa, Via Risorgimento 35, 56126 Pisa, Italy
Fax: (internat.) +39-050/918-210
E-mail: misola@dcci.unipi.it
[b] Dipartimento di Ingegneria Chimica, dei Materiali, delle Materie Prime e Metallurgia, Università degli Studi di Roma "La Sapienza",
Via del Castro Laurenziano 7, 00161 Roma, Italy
[c] Centro di Studio del CNR per le Macromolecole Stereordinate ed Otticamente Attive,
Via Risorgimento 35, 56100 Pisa, Italy

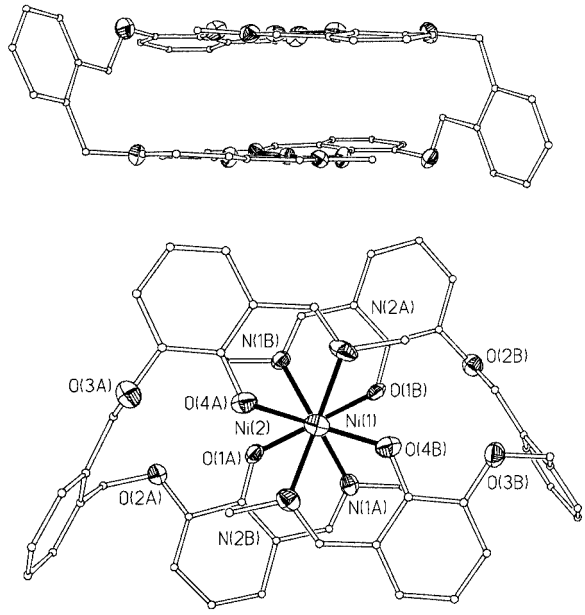

Figure 1. Two projections of the molecular structure of $[Ni_2(L^4)_2]$ along the pseudo-twofold axis (up) and down the coordination planes (down); Ni, O and N atoms are represented by 30% probability thermal ellipsoids; C atoms are represented by small spheres and H atoms are omitted for clarity; relevant bond lengths (Å) and angles (°): Ni(1)−O(1A) 1.82(1), Ni(1)−O(1B) 1.84(1), Ni(1)−N(1A) 1.89(2), Ni(1)−N(1B) 1.92(1), Ni(2)−O(4B) 1.82(1), Ni(2)−O(4A) 1.84(1), Ni(2)−N(2A) 1.90(2), Ni(2)−N(2B) 1.92(1); O(1A)−Ni(1)−O(1B) 177.2(5), O(1A)−Ni(1)−N(1A) 92.8(5), O(1B)−Ni(1)−N(1A) 87.7(5), O(1A)−Ni(1)−N(1B) 86.7(5), O(1B)−Ni(1)−N(1B) 92.8(5), N(1A)−Ni(1)−N(1B) 179.0(6), O(4B)−Ni(2)−O(4A) 176.2(5), O(4B)−Ni(2)−N(2A) 87.5(7), O(4A)−Ni(2)−N(2A) 92.4(7), O(4B)−Ni(2)−N(2B) 93.5(6), O(4A)−Ni(2)−N(2B) 86.8(6), N(2A)−Ni(2)−N(2B) 177.1(7)

the nickel coordination squares almost exactly staggered with an O(1A)−Ni(1)···Ni(2)−O(4A) dihedral angle of 43.7°. The molecule does not possess any crystallographic symmetry, but it shows nearly local symmetry 2(C_2), with the twofold axis parallel to the coordination planes and passing between the two metals. One chloroform molecule, not shown in Figure 1, is also present in the solid, with its hydrogen atom pointing towards a position between O(1B) and O(2B).

A mass spectrometry analysis using electrospray ionization suggests the presence of the dinuclear species as the only molecular species in solution. The main signal observed at m/z = 921 in the ESI-MS spectrum is indeed due to the protonated dinuclear complex, whereas the other important ions present in the spectrum at m/z = 405, 461 and 865 are attributable to the free ligand, to the mononuclear species and to the $[Ni_2(L^4)_2]-Ni^{II}$ species, respectively. MS-MS experiments suggest that these three ions are due to the fragmentation of the main peak at m/z = 921.

The ^{1}H NMR spectrum of the complex in $CDCl_3$ confirms the presence of a unique molecular species and the persistence in solution of the helical arrangement. In general, all the resonances of the complex are shifted upfield relative to the free ligand, and some resonances undergo significant changes upon coordination, giving important information regarding intramolecular interactions. The largest coordination shifts observed are the upfield shifts of the iminic protons (≈ 1.5 ppm) and of the methyl groups (≈ 1.2 ppm). In the crystal structure of the helicate, these protons lie above the salicyl moiety of the other ligand and are in the shielding region generated by the aromatic ring. The signal of the methylene groups of the bridge is a singlet at δ = 5.33 ppm in the free ligand, but upon complexation appears as doublets at δ = 5.21 and 5.01 ppm. On the whole, these spectral changes, particularly the manifestation of the diastereotropism, provide strong evidence for the persistence of the helical structure in solution.

Reaction of H_2L^4 with $[Cu(OAc)_2]\cdot 4H_2O$ in a 1:1 molar ratio, followed by usual treatment, yielded a light brownish-green compound, whose elemental analysis indicates a 1:1 metal:ligand ratio. Also in this case the ESI mass spectroscopic data are consistent with a dinuclear complex, i.e., $[Cu_2(L^4)_2]$. Despite several attempts, we could not isolate X-ray quality crystals, but the 2:2 metal:ligand stoichiometry suggests that, like the nickel(II) complex, the copper(II) complex is a double helicate. Efforts to elucidate the structure are in progress.

To summarise, we have shown that by careful selection of spacer sub-unit the behaviour of related ligands in the self-assembly process may be controlled. Applying this principle, we have tailored a new ligand to construct a dinuclear double-stranded helical nickel(II) complex, which is the second example of a helicate based on a square-planar geometry, but the first to be stable both in the solid state and in solution.

We are currently exploring the potential of this new class of ligands and investigating alternative linkage strategies for modelling supramolecular structures.

Experimental Section

IR spectra were collected on a Perkin−Elmer Paragon 500 FTIR spectrophotometer and electronic absorption spectra with a Perkin−Elmer Lambda 9 spectrophotometer in chloroform; λ_{max} in nm and ε in $M^{-1}\,cm^{-1}$. ESI mass spectra were recorded on a PE Sciex API III plus triple quadrupole mass spectrometer equipped with an Atmospheric Pressure Ionization source and an articulated Ionspray interface. The sample was dissolved in chloroform (1 mg/mL) and diluted 1:100 with acetonitrile.

NMR measurements were performed on a Varian VXR-300 spectrometer in $CDCl_3$ as solvent and were referred to TMS as external standard.

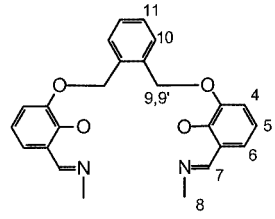

Preparation of Precursor Dialdehyde α,α′-Bis(3-formyl-2-hydroxy)-phenoxy-*o*-xylene: This compound was prepared in 74% yield from

2,3-dihydroxybenzaldehyde and α,α′-dibromo-*o*-xylene according to our previously reported procedure.[4] M.p. 176−180 °C. IR (Nujol): $\tilde{\nu}$ = 1646 cm^{-1} (C=O). ^1H NMR ($CDCl_3$): δ = 5.34 (s, 2 H), 6.84−7.51 (m, 5 H), 9.86 (s, 1 H), 11.03 (s, 1 H) ppm. $C_{22}H_{18}O_6$ (378.38): calcd. C 69.83, H 4.79; found C 69.62, H 4.61.

Preparation of the Ligand H_2L^4: This Schiff base was synthesised following standard procedures.[4] A mixture of dialdehyde (0.30 g, 0.79 mmol) and methylamine (40 wt.-% solution in water; 1 mL, 12.9 mmol) in ethanol (20 mL) was heated to reflux for 2 h. After cooling, a yellow solid precipitated out on addition of water. Recrystallisation from $CHCl_3$/hexane yielded a yellow crystalline material (0.26 g, 81%). M.p. 169−172 °C. IR (Nujol): $\tilde{\nu}$ = 1634 cm^{-1} (C=N). ^1H NMR ($CDCl_3$): δ = 3.47 (d, *J* = 1.6 Hz, 3 H, H8), 5.33 (s, 2 H, H9+H9′), 6.69 (dd, *J* = 7.6, 7.6 Hz, 1 H, H5), 6.84 (dd, *J* = 7.6, 1.6 Hz, 1 H, H6), 6.97 (dd, *J* = 7.6, 1.6 Hz, 1 H, H4), 7.28 (m, 1 H, H11), 7.51 (m, 1 H, H10), 8.29 (q, *J* = 1.6 Hz, 1 H, H7), 13.89 (s, 1 H, OH) ppm. $C_{24}H_{24}N_2O_4$ (404.46): calcd. C 71.27, H 5.98, N 6.93; found C 71.02, H 5.85, N 6.71. UV/Vis ($CHCl_3$): λ_{max} (10^{-3} ε) = 261 (24.6), 327 (6.53), 425 (0.85).

Preparation of the Complexes: A solution of H_2L^4 (0.74 mmol) in EtOH (20 mL) was added dropwise to a solution of $[Ni(CH_3COO)_2]\cdot 4H_2O$ or $[Cu(CH_3COO)_2]\cdot 4H_2O$ (0.74 mmol) in EtOH (20 mL). After stirring at room temperature for 2 h, solid complexes were collected by filtration, washed with diethyl ether and dried in vacuo. Yields ≥ 90%. Recrystallisation from $CHCl_3$ or $CHCl_3$/diethyl ether led to olive-green crystals of $[Ni_2(L^4)_2]\cdot CHCl_3$ or brownish-green crystals of $[CuL^4]$, respectively.

$[Ni_2(L^4)_2]\cdot CHCl_3$: M.p. 192−195 °C. IR (Nujol): $\tilde{\nu}$ = 1618 cm^{-1} (C=N). ESI-MS: *m*/*z* (%) = 405 (75) $[H_2L^4 + H]^+$, 461 (60) $[NiL^4 + H]^+$, 865 (40) $[Ni(L^4)_2 + 3H]^+$, 921 (100) $[Ni_2(L^4)_2 + H]^+$. ^1H NMR ($CDCl_3$): δ = 2.34 (s, 3 H, H8), 5.01 (d, *J* = 13.6 Hz, 1 H, H9), 5.21 (d, *J* = 13.6 Hz, 1 H, H9′), 6.36 (dd, *J* = 8.0, 7.6 Hz, 1 H, H5), 6.59 (dd, *J* = 8.0, 1.3 Hz, 1 H, H6), 6.78 (dd, *J* = 7.6, 1.3 Hz, 1 H, H4), 6.79 (br. s, 1 H, H7), 7.26 (m, 1 H, H11), 7.52 (m, 1 H, H10) ppm. $C_{48}H_{44}N_4Ni_2O_8\cdot CHCl_3$ (1041.65): calcd. C 56.50, H 4.35, N 5.38; found C 56.25, H 4.20, N 5.18. UV/Vis ($CHCl_3$): λ_{max} (10^{-3} ε) = 269 (88.1), 334 (15.9), 417 (7.05), 625 (0.10).

$[CuL^4]$: M.p. 210 °C (dec.). IR (Nujol): $\tilde{\nu}$ = 1628 cm^{-1} (C=N). ESI-MS *m*/*z* (%) = 405 (35) $[H_2L^4 + H]^+$, 466 (30) $[CuL^4 + H]^+$, 931 (60) $[Cu_2(L^4)_2 + H]^+$, 948 (50) $[Cu_2(L^4)_2 + NH_4]^+$, 953 (50) $[Cu_2(L^4)_2 + Na]^+$. $C_{24}H_{22}CuN_2O_4$ (465.99): calcd. C 61.86, H 4.76, N 6.01; found C 62.18, H 4.96, N 5.73. UV/Vis ($CHCl_3$): λ_{max} (10^{-3} ε) = 276 (42.8), 365 (14.7).

X-ray Crystallographic Study: X-ray diffraction measurements were carried out with a Bruker P4 diffractometer equipped with Mo-K_α radiation (λ = 0.71073 Å).

$[Ni_2(L^4)_2]\cdot CHCl_3$: olive green prismatic crystals, $C_{49}H_{45}Cl_3N_4Ni_2O_8$; *M* = 1041.66; *T* = 293(2) K, monoclinic, space group *C*2/*c* (No. 15); *a* = 50.056(15), *b* = 11.309(3), *c* = 16.340(5) Å, β = 95.92(2)°, *U* = 9201(5) $Å^3$; *Z* = 8; μ = 1.052 mm^{-1}; crystal size (mm) 0.22 × 0.18 × 0.15. 6604 reflections collected, 5631 independent, R_{int} = 0.1010. Such a high R_{int} value is probably due to the long *a* axis and the consequent difficulty in neatly resolving adjacent reflections and to the low diffraction power of the crystal characterised by a large fraction of weak intensities. The structure was solved by standard automatic direct methods and refined by full-matrix least-squares methods. Hydrogen atoms were located in calculated positions and in the final refinement cycles anisotropic thermal factors were used for all non hydrogen atoms.

The solution and refinement were performed by means of the SHELX-97 program.[6] The final reliability factors for 595 refined parameters were: R_1 = 0.0954 calculated for 2606 reflections with $I > 2\sigma(I)$, wR_2 = 0.2818 for all 5631 reflections in the refinement; *GOF* = 1.076.

CCDC-171594 contains the supplementary crystallographic data for this paper. These data can be obtained free of charge at www.ccdc.cam.ac.uk/conts/retrieving.html [or from the Cambridge Crystallographic Data Centre, 12, Union Road, Cambridge CB2 1EZ, UK; Fax: (internat.) +44-1223/336-033; E-mail: deposit@ccdc.cam.ac.uk].

Acknowledgments

Financial support from the Ministero dell'Università e della Ricerca Scientifica e Tecnologica, Progetti di Rilevante Interesse Nazionale 2000−2001 and the National Research Council (CNR) is acknowledged.

[1] J.-M. Lehn, *Supramolecular Chemistry, Concepts and Perspectives*, VCH Verlagsgesellschaft, Weinheim, **1995**; F. Vögtle, *Supramolecular Chemistry*, John Wiley & Sons, Chichester, **1991**.

[2] Reviews and very recent references: C. Piguet, G. Bernardinelli, G. Hopfgartner, *Chem. Rev.* **1997**, *97*, 2005−2062; E. C. Constable, *Prog. Inorg. Chem.* **1994**, *42*, 67−138; A. von Zelewsky, O. Mamula, *J. Chem. Soc., Dalton Trans.* **2000**, 219−231; G. Baum, E. C. Constable, D. Fenske, C. E. Housecroft, T. Kulke, M. Neuburger, M. Zehnder, *J. Chem. Soc., Dalton Trans.* **2000**, 945−959; M. Greenwald, D. Wessely, E. Katz, I. Willner, Y. Cohen, *J. Org. Chem.* **2000**, *65*, 1050−1058; Y. Zhang, L. Jianmin, M. Nishiura, H. Hou, W. Deng, T. Imamoto, *J. Chem. Soc., Dalton Trans.* **2000**, 293−297; J. J. Jodry, J. Lacour, *Chem. Eur. J.* **2000**, *6*, 4297−4304; H. Cheng, D. Chun-ying, F. Chenjie, M. Qing-jin, *J. Chem. Soc., Dalton Trans.* **2000**, 2419−2424; R. L. Paul, S. M. Couchman, J. C. Jeffery, J. A. McCleverty, Z. R. Reeves, M. D. Ward, *J. Chem. Soc., Dalton Trans.* **2000**, 845−851; C. R. Rice, S. Wörl, J. C. Jeffery, R. L. Paul, M. D. Ward, *J. Chem. Soc., Dalton Trans.* **2001**, 550−559; O. Mamula, F. J. Monlien, A. Porquet, G. Hopfgartner, A. E. Merbach, A. von Zelewsky, *Chem. Eur. J.* **2001**, *7*, 533−539; R. Annunziata, M. Benaglia, M. Cinquini, F. Cozzi, C. R. Woods, J. S. Siegel, *Eur. J. Org. Chem.* **2001**, 173−180; V. Amendola, L. Fabbrizzi, L. Gianelli, C. Maggi, C. Mangano, P. Pallavicini, M. Zema, *Inorg. Chem.* **2001**, *40*, 3579−3587.

[3] [3a] N. Yoshida, H. Oshio, T. Ito, *J. Chem. Soc., Perkin Trans. 2* **1999**, 975−983 and references therein. [3b] N. Yoshida, K. Ichikawa, M. Shiro, *J. Chem. Soc., Perkin Trans. 2* **2000**, 17−26. [3c] P. E. Kruger, N. Martin, M. Nieuwenhuyzen, *J. Chem. Soc., Dalton Trans.* **2001**, 1966−1970. [3d] M. Vázquez, M. R. Bermejo, M. Fondo, A. M. Gonzáles, J. Mahía, L. Sorace, D. Gatteschi, *Eur. J. Inorg. Chem.* **2001**, 1863−1868. [3e] E. J. Corey, C. L. Cywin, M. C. Noe, *Tetrahedron Lett.* **1994**, *35*, 69−72. [3f] G. Struckmeier, U. Thewalt, J. H. Fuhrhop, *J. Am. Chem. Soc.* **1976**, *98*, 278−279. [3g] M. Albrecht, *Chem. Eur. J.* **2000**, *6*, 3485−3489, and references therein. [3h] B. Kersting, M. Meyer, R. E. Powers, K. N. Raymond, *J. Am. Chem. Soc.* **1996**, *118*, 7221−7222.

[4] L. Carbonaro, M. Isola, V. Liuzzo, F. Marchetti, F. Balzano, C. S. Pomelli, A. Raffaelli, *Eur. J. Inorg. Chem.* **2001**, 353−357.

[5] A copper(II) double-stranded tetranuclear helicate has been described in which the Cu^{II} adopts both square-planar and distorted tetrahedral geometries; see ref.[3a]

[6] G. M. Sheldrick, SHELXL-97, *A FORTRAN program for the solution and refinement of X-ray structures*, University of Göttingen, Germany, **1997**.

Received September 28, 2001
[I01382]

Synthesis, Crystal Structure and Third-Order Nonlinear Optical Behavior of a Novel Dimeric Mixed-Ligand Zinc(II) Complex of 1,3-Dithiole-2-thione-4,5-dithiolate

Cai-Ming Liu,[a] De-Qing Zhang,*[a] Ying-Lin Song,[b] Chuan-Lang Zhan,[a] Yu-Liang Li,[a] and Dao-Ben Zhu*[a]

Keywords: Zinc / N ligands / S ligands / Crystal structure / Nonlinear optics

The first dimeric mixed-ligand zinc(II) complex of 1,3-dithiole-2-thione-4,5-dithiolate (dmit) $[Zn(dmit)(2,2'\text{-bpy})]_2$ (2,2′-bpy = 2,2′-bipyridine) (**1**), which exhibits a good third-order nonlinear refraction effect, was synthesized by a ligand exchange reaction between $[(Et_4N)_2Zn(dmit)_2]$ and $[Cu(2,2'\text{-bpy})(NO_3)_2]\cdot 2H_2O$. A Z-scanning measurement of complex **1** gives the third-order nonlinear refraction index $n_2 = 3.72 \times 10^{-18}$ m²/W and the real part $Re\chi^{(3)} = 1.01 \times 10^{-12}$ esu. Crystal data for **1**: monoclinic, $P2_1/c$ (No.14), a = 11.556(2) Å, b = 9.141(2) Å, c = 15.020(3) Å, β = 109.55(3)°, Z = 4.
(© Wiley-VCH Verlag GmbH, 69451 Weinheim, Germany, 2002)

Introduction

Metal bis-dithiolene complexes have aroused more and more interest over the past decades due to their potential applications as precursors for electrical conductors and superconductors;[1] the optical properties of these compounds are also very interesting. For example, in 1972 Drexhage and co-workers discovered that transition metal dithiolene complexes are very stable to intense irradiation in the near-infrared region and are particularly suitable for Q-switching lasers.[2,3] Recently, more and more symmetrical bis-dithiolene complexes with third-order optical nonlinearity or optical limiting effects have been explored.[4] Because of the large values of their third-order nonlinear susceptibility $\chi^{(3)}$ [1a,5] and negative molecular first hyperpolarizability(β),[1a,6] unsymmetrical dithiolene complexes have also become promising candidates for nonlinear optical materials. Herein we report the synthesis, crystal structure and third-order nonlinear optical behavior of a novel dimeric mixed-ligand zinc(II) complex of 1,3-dithiole-2-thione-4,5-dithiolate (dmit) $[Zn(dmit)(2,2'\text{-bpy})]_2$ (**1**). To the best of our knowledge, this is the first example of a dimeric mixed-ligand complex of dmit.

[a] Organic Solids Laboratory, Center for Molecular Science, Institute of Chemistry, Chinese Academy of Sciences
Beijing 100080, P. R. China
Fax: (internat.) +86-106/255-9373
E-mail: dqzhang@infoc3.icas.ac.cn
[b] Department of Applied Physics, Harbin Institute of Technology
Harbin 150001, P. R. China

Results and Discussion

$[(Et_4N)_2Zn(dmit)_2]$ and $[Cu(2,2'\text{-bpy})(NO_3)_2]\cdot 2H_2O$ were successfully employed for the preparation of complex **1**. This result illustrates that even complexes with different metal ions can be utilized for ligand-exchange reactions with transition metal dithiolene complexes.[1a,7] As we know, the metal ions are usually the same when a ligand exchange reaction, which takes place between symmetrical metal bischelate of dmit and that of the other ligand,[7c,7d] was used.

In the IR spectra of **1** the C=S and S−C−S stretching bands of the dmit ligand show no significant differences from the symmetrical dmit complexes.[1,8] The electronic spectrum of **1** in DMF exhibits two bands in the 270−700 nm region: the sharp band at 286 nm is assigned to a π-π* transition and the broad band at 497 nm to an n-π* transition of the dmit ligand. Both bands show blue shifts relative to those in $[Na_2(dmit)]$ (316, 514 nm in MeOH),[9] $[NBu_4]_2[Zn(dmit)_2]$ (300, 530 nm in MeCN)[9] and $[NMe_4]_2[Zn(dmit)(Sph)_2]$ (327, 512 nm).[1a]

The crystal structure of **1** consists of discrete neutral dmit complex dimers $[Zn(dmit)(2,2'\text{-bpy})]_2$. As shown in Figure 1, each zinc atom is coordinated in a distorted square-pyramidal geometry, with two nitrogen atoms from the 2,2′-bipyridine ligand and two sulfur atoms from one dmit ligand forming the base of the pyramid and one sulfur from the other dmit ligand occupying the apical site. One of the two sulfur atoms in each dmit ligand therefore acts as a μ_2-bridge to link two zinc atoms; a similar μ_2-S bridging mode of dmit was also observed in the symmetrical dmit complexes $[NnBu_4][Fe(C_3S_5)_2]$ and $[Fe(C_5Me_5)_2][Fe(C_3S_5)_2]$.[10]

The Zn−N and Zn−S bond lengths [average 2.136(2) and 2.4424(9) Å, respectively] are a little longer than those in another dimeric zinc complex $[Zn_2(i\text{-MNT})_2(4\text{-mpy})_4]\cdot CHCl_3$ (*i*-MNT = isomaleonitrile dithiolate) [average 2.056(4) and 2.319(1) Å, respectively].[11] The Zn−Zn distance (3.357 Å) is also a little longer than the Fe−Fe distances in $[NnBu_4][Fe(C_3S_5)_2]$ (3.17 Å) and $[Fe(C_5Me_5)_2]$-$[Fe(C_3S_5)_2]$ (3.169 and 3.164 Å).[10] It is noteworthy that complex **1** is, to the best of our knowledge, the first dimeric mixed-ligand complex with dmit, although dimers with metal-sulfur bonds in symmetrical bis-dithiolene complexes are common.[12]

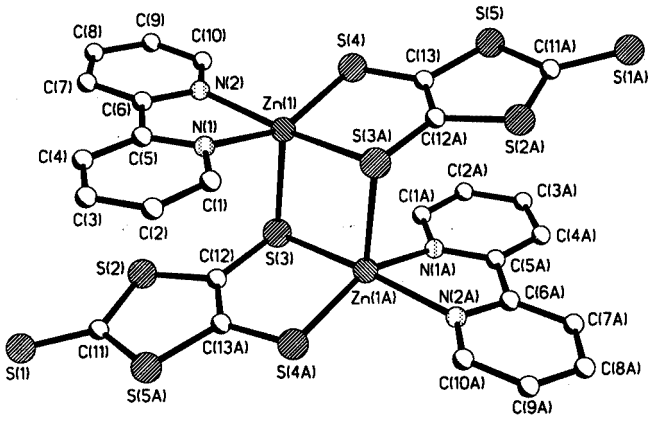

Figure 1. Molecular structure of complex **1**; selected bond lengths (Å) and angles (°): Zn(1)−N(1) 2.104(2), Zn(1)−N(2) 2.168(2), Zn(1)−S(4) 2.3374(8), Zn(1)−S(3) 2.4902(9), Zn(1)−S(3A) 2.4995(11); N(1)−Zn(1)−N(2) 76.06(8), S(3A)−Zn(1)−S(4) 91.18(3), N(2)−Zn(1)−S(4) 93.80(7), N(1)−Zn(1)−S(3A) 94.04(6), N(1)−Zn(1)−S(3) 97.26(6), N(2)−Zn(1)−S(3) 95.57(6), S(4)−Zn(1)−S(3) 106.94(3), S(3A) −Zn(1)−S(3) 95.42(3)

Another interesting structural feature is the molecular arrangement of the $[Zn(dmit)(2,2'\text{-bpy})]_2$ dimers (Figure 2). Unlike other metal bis-dithiolene dimers,[10,12] the $[Zn(dmit)(2,2'\text{-bpy})]_2$ dimers link each other through short S···Zn contacts rather than through short S···S contacts. These S···Zn contacts (3.676 Å) also suggest that there are π-π stacking interactions among dmit groups rather than 2,2′-bipyridine ligands from neighboring $[Zn(dmit)(2,2'\text{-bpy})]_2$ dimers. The center-to-center distance between the C_3S_2 five-membered rings of two adjacent dmit groups is 3.745 Å. Therefore, discrete $[Zn(dmit)(2,2'\text{-bpy})]_2$ dimers are further extended into an interesting one-dimensional supermolecular array by π-π stacking interactions between dmit groups.

Complex **1** crystallizes in the centrosymmetric space group $P2_1/c$, which cannot meet the essential requirement of electronic asymmetry for second-order nonlinear optical (NLO) effects.[13] However, complex **1** does possess third-order nonlinear optical behaviour. The third-order optical nonlinearity of complex **1** was determined by using the *Z*-scan technique.[14−16] These results are shown in Figure 3, where the filled and open circles were measured with and without the aperture, respectively. The valley/peak pattern of the normalized transmittance shows a characteristic self-focusing behavior of the propagating light in the sample.

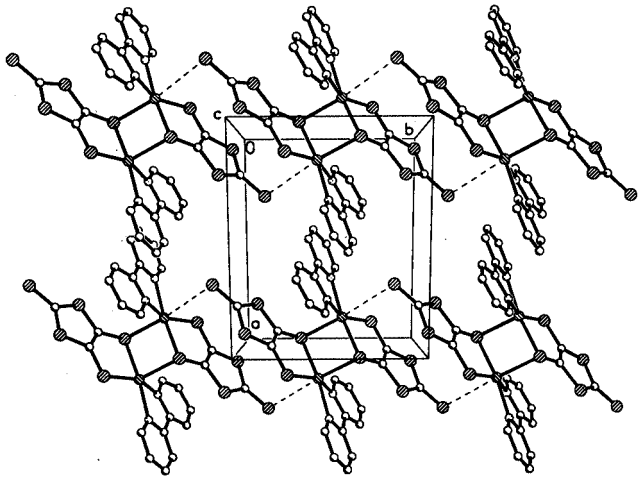

Figure 2. A packing diagram of the unit cell of complex **1** looking down the *c* axis showing how the discrete $[Zn(dmit)(2,2'\text{-bpy})]_2$ dimers are further extended into interesting one-dimensional supermolecular arrays through short S···Zn contacts or π-π stacking interactions between dmit groups

According to the method described in literature,[14−16] the value of the third-order nonlinear refraction index n_2 is calculated to be 3.72×10^{-18} m²/W and the real part of the third-order nonlinear susceptibility $Re\chi^{(3)}$ to be 1.01×10^{-12} esu. The value of $Re\chi^{(3)}$ of **1** is similar to other promising NLO media such as phthalocyanine, porphyrin and pentaazadentate and stilbazolium derivatives,[15] indicating that complex **1** is a good candidate for a nonlinear optical material.

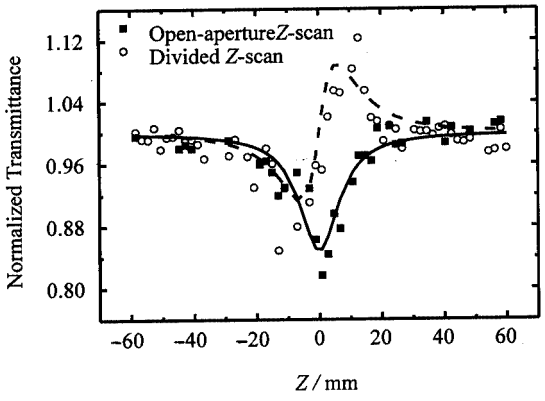

Figure 3. *Z*-scan measurement of complex **1** in a 4.05×10^{-5} mol·dm^{-3} solution of DMF at 532 nm with $I_0 = 0.6$ GW/cm²; the data collected under the closed-aperture configuration show the self-focusing effect

In conclusion, an interesting dimeric mixed-ligand zinc(II) complex of dmit $[Zn(dmit)(2,2'\text{-bpy})]_2$, which exhibits good third-order nonlinear refraction effect, was synthesized by a ligand-exchange reaction between $[Et_4N]_2[Zn(dmit)_2]$ and $[Cu(2,2'\text{-bpy})(NO_3)_2]\cdot 2H_2O$. This demonstrates that the ligand-exchange reaction method for preparing mixed-ligand complexes of dmit is also feasible when the metal ions of the two reactants are different.

Experimental Section

All reagents were obtained from commercial sources and used without further purification. The elemental analyses were performed on a Heraeus Chn-Rapid elemental analyzer. The infrared spectra were recorded on a Perkin−Elmer 2000 spectrophotometer with pressed KBr pellets. Bis(tetraethylammonium) bis(1,3-dithiole-2-thione-4,5-dimercapto)zincate {$[Et_4N]_2[Zn(dmit)_2]$} was prepared according to the literature method.[8]

Synthesis of 1: Single crystals were grown in a test tube. Solid $[Cu(2,2'\text{-bpy})(NO_3)_2]\cdot 2H_2O$ (0.2 mmol) was dissolved in 3 mL of water and 5 mL of MeOH, and to this solution was added carefully a solution of $[Et_4N]_2[Zn(dmit)_2]$ (0.2 mmol) in Me_2CO (10 mL). The test tube was then allowed to stand undisturbed at room temperature for three days, yielding a dark red block of **1** on the tube wall (8.4 mg, ca. 20% yield based on Zn) together with some unknown black amorphous materials at the bottom. $C_{26}H_{16}N_4S_{10}Zn_2$ (835.8): calcd. C 37.37, H 1.93, N 6.70; found C 37.29, H 1.98, N 6.62. IR (KBr): $\tilde{\nu}$ = 1595(m), 1566(w), 1489(w), 1472(m), 1440(s), 1429(s), 1315(m), 1249(w), 1171(w), 1158(w), 1059(s), 1031(vs), 891(m), 765(s), 733(m), 652(w), 629(w), 529(w), 465(m), 415(w) cm^{-1}. UV (1×10^{-4} M DMF): λ_{max} = 286 nm ($\varepsilon = 3.73 \times 10^4$ $M^{-1}cm^{-1}$), 497 nm ($\varepsilon = 1.49 \times 10^4$ $M^{-1}cm^{-1}$). ^1H NMR (300 MHz, $[D_6]$DMSO): δ = 8.73 (br, 1 H, Hpy), 8.43 (br, 1 H, Hpy), 8.02(br, 1 H, Hpy), 7.52 (br, 1 H, Hpy) ppm.

Crystallographic Analysis: A dark-red single crystal with dimensions of 0.2 × 0.1 × 0.1 mm was mounted on a Bruker SMART CCD diffractometer equipped with Mo-K_α radiation (λ = 0.71073 Å) at room temperature and data were collected with the ω-scan technique. Cell parameters were obtained by the global refinement of the positions of all collected reflections. A total of 13737 data of which 5504 independent reflections (R_{int} = 0.0417) were collected in the range of $5.30° \le 2\theta \le 66.92°$($-15 \le h \le 17$, $-13 \le k \le 12$, $-22 \le l \le 22$), and 3043 with $I > 2\sigma(I)$ were used in the refinement of the structure. The data were corrected for Lorentz-polarization effects during data reduction using XSCANS.[17a] Empirical absorption corrections based on Ψ-scan measurements were applied ($T_{min,max}$: 0.759012, 1.000000).

Table 1. Crystal data for complex **1**

	1
Chemical formula	$C_{13}H_8N_2S_5Zn$
Fw	417.88
Space group	$P2_1/c$ (No. 14)
a, Å	11.556(2)
b, Å	9.141(2)
c, Å	15.020(3)
α, deg	90
β, deg	109.55(3)
γ, deg	90
V, Å^3	1495.1(5)
Z	4
D_c, g cm^{-3}	1.856
μ (Mo-K_α), mm^{-1}	2.331
R_1, wR_2 [$I > 2\sigma(I)$][a]	0.0452, 0.0583

[a] $R_1 = ||F_o| - |F_c||/|F_o|$, $wR_2 = [w(F_o^2 - F_c^2)^2/w(F_o^2)^2]^{1/2}$.

The structure was solved by direct methods and refined by a full-matrix least-squares technique based on F^2 using the SHELXL-97 program.[17b] All non-hydrogen atoms were refined anisotropically and all hydrogen atoms were treated as riding atoms. Selected crystallographic data and structure determination parameters for complex **1** are given in Table 1.

CCDC-176197 contains the supplementary crystallographic data for this paper. These data can be obtained free of charge at www.ccdc.cam.ac.uk/conts/retrieving.html [or from the Cambridge Crystallographic Data Centre, 12, Union Road, Cambridge CB2 1EZ, UK; Fax: (internat.) +44-1223/336-033; E-mail: deposit@ccdc.cam.ac.uk].

Non-Linear Optical Measurements: The NLO properties of a solution of **1** in DMF were determined by using a standard *Z*-scan setup with a Q-switched, frequency-doubled Nd:YAG laser.[18] The pulse-repetition rate was 10 Hz. The transmittance of the aperture in front of the detector for a closed-aperture measurement was 0.1. The solution was contained in a 2 mm thick quartz cell.

Acknowledgments

This work was supported by Chinese Academy of Sciences and the Major State Basic Research Development Program (G2000077500) of P. R. China. The authors also thank the referees for their excellent suggestions for improving the manuscript.

[1] [1a] J. Dai, G. Q. Bian, X. Wang, Q.-F. Xu, M.-Y. Zhou, M. Munakata, M. Maekawa, M.-H. Tong, Z.-R. Sun, H.-P. Zeng, *J. Am. Chem. Soc.* **2000**, *122*, 11007−11008 and references therein.[1b] A. E. Pullen, R.-M. Olk, *Coord. Chem. Rev.* **1999**, *188*, 211−262. [1c] R.-M. Olk, B. Olk, W. Dietzsch, R. Kirmse, E. Hoyer, *Coord. Chem. Rev.* **1992**, *117*, 99−131. [1d] Q. Zhang, P. Wu, S. Sun, D. Zhu, M. Xong, Z. Ma, N. Shi, *Synth. Met.* **1998**, *98*, 103−106. [1e] S. Sun, P. Wu, D. Zhu, *Synth. Met.* **1998**, *96*, 199−204. [1f] S. Sun, P. Wu, D. Zhu, Z. Ma, N. Shi, *Inorg. Chim. Acta* **1998**, *26*, 103−107.

[2] K. H. Drenold, U. T. Muller-Westerhoff, *US Pat.* 3 743 964, **1973**.

[3] G. A. Reynolds, K. H. Drexhage, *J. Appl. Phys.* **1975**, *46*, 4852−4853.

[4] [4a] C. S. Winter, C. A. S. Hill, A. E. Underhill, *Appl. Phys. Lett.* **1991**, *58*, 107−109. [4b] J.-L. Zuo, T.-M. Yao, F. You, X.-Z. You, H. K. Fun, B. C. Yip, *J. Mater. Chem.* **1996**, *6*, 1633−1637. [4c] J.-F. Bai, J.-L. Zuo, W.-L. Tan, W. Ji, Z. Shen, H.-K. Fun, K. Chinnakali, I. A. Razak, X.-Z. You, C.-M. Che, *J. Mater. Chem.* **1999**, *9*, 2419−2423. [4d] H. Ushijima, T. Kawasaki, T. Kamata, T. Kodzasa, H. Matsuda, T. Fukaya, Y. Fujii, F. Mizukami, *Mol. Cryst. Liq. Cryst.* **1996**, *286*, 597−602.

[5] C. A. S. Hill, A. Charlton, A. E. Underhill, K. M. A. Malik, M. B. Hursthouse, A. I. Karaulov, S. N. Oliver, S. V. Kershaw, *J. Chem. Soc., Dalton Trans.* **1995**, 587−594.

[6] C.-T. Chen, S.-Y. Liao, K.-J. Lin, L.-L. Lai, *Adv. Mater.* **1998**, *3*, 334−338.

[7] [7a] R. Vicente, J. Ribas, C. Sourisseau, *Polyhedron* **1986**, *5*, 2033−2038. [7b] I. V. Jourdain, M. Fourmigué, F. Guyon, J. Amaudrut, *J. Chem. Soc., Dalton Trans.* **1998**, 483−488. [7c] W. Dietzsch, S. Rauer, R.-M. Olk, R. Kirmse, K. Köhler, L. Golič, B. Okl, *Inorg. Chim. Acta* **1990**, *169*, 55−62. [7d] R.-M. Olk, W. Dietzsch, J. Kahlmeier, P. Jörchel, R. Kirmse, J. Sieler, *Inorg. Chim. Acta* **1997**, *254*, 375−379.

[8] [8a] Y. Liu, Y. Xu, D. Zhu, *Thin Solid Films.* **1996**, *284/285*, 526−529. [8b] K. Kawabata, G. Saito, *Synth. Met.* **1987**, *19*, 663−668.

[9] [9a] G. Matsubayashi, M. Hirao, T. Tanaka, *Inorg. Chim. Acta* **1988**, *144*, 217−221. [9b] G. Matsubayashi, K. Takahashi, T. Tanaka, *J. Chem. Soc., Dalton Trans.* **1988**, 967−972.

[10] G. Matsubayashi, S. Tanaka, *J. Chem. Soc., Dalton Trans.* **1992**, 2837−2843.
[11] R.-G. Xiong, J.-L. Zuo, X.-Z. You, *Inorg. Chem.* **1997**, *36*, 2472−2474.
[12] S. Alvarez, R. Vicente, R. Hoffmann, *J. Am. Chem. Soc.* **1985**, *107*, 6253−6277.
[13] W. Lin, O. R. Evans, R.-G. Xiong, Z. Wang, *J. Am. Chem. Soc.* **1998**, *120*, 13272−13273.
[14] M. Sheik-Bahae, A. A. Said, T. H. Wei, D. J. Hagan, E. W. Wan Stryland, *IEEE J. Quantum Electron.* **1990**, *26*, 760−769.
[15] W. Sun, M. M. McKerns, C. M. Lawson, G. M. Gray, C. L. Zhan, D. Wang, *Proc. SPIE* **2000**, *4106*, 280−288 and references therein.
[16] M. Sheik-Bahae, A. A. Said, E. W. Van Stryland, *Opt. Lett.* **1989**, *14*, 955−957.
[17] [17a] XSCANS (version 2.1), Siemens Analytical X-ray Instruments, Madison, WI, 1994.[17b] G. M. Sheldrick, SHELX-97, PC Version, University of Göttingen, 1997.
[18] H. Hou, B. Liang, X. Xin, K. Yu, P. Ge, W. Ji, S. Shi, *J. Chem. Soc., Faraday Trans.* **1996**, 2343−2346.

Received December 13, 2001
[I01508]

A Novel Nickel(II) Complex Adopting a *cis*-Configuration: Solvothermal Synthesis and Crystal Structure of $[NiL_2(H_2O)_4]$ (L = 1,4-Dihydropyrazine-2,3-dione-5,6-dicarboxylate)

Cai-Ming Liu,[a] De-Qing Zhang,*[a] An-Jun Qin,[a] Chen Ye,[a] Huai-Ming Hu,[a] and Dao-Ben Zhu*[a]

Keywords: Nickel / Solvothermal synthesis / Carboxylate ligands / Crystal structure

Under solvothermal reaction conditions, the reaction of 5,6-dichloropyrazine-2,3-dicarbonitrile and $[Ni(ClO_4)_2]\cdot 6H_2O$ produces a novel *cis*-nickel(II) complex $[NiL_2(H_2O)_4]$ (**1**) (L = 1,4-dihydropyrazine-2,3-dione-5,6-dicarboxylate), whereas only hydrated 1,4-dihydropyrazine-2,3-dione-5,6-dicarboxylic acid (**2**) was obtained as a single phase when $[Cd(ClO_4)_2]\cdot 6H_2O$ was used instead of $[Ni(ClO_4)_2]\cdot 6H_2O$.

(© Wiley-VCH Verlag GmbH, 69451 Weinheim, Germany, 2002)

Introduction

Recently, the use of hydro(solvo)thermal techniques for synthesizing coordination compounds with interesting optical and/or magnetic properties has attracted increasing interest.[1,2] Most examples focus on high-dimensional coordination polymers, and the hydrolysis of substituted cyano, ester or aldehyde groups into a carboxylate group has often been used as the key step in designing such functionalized coordination polymers. However, rare examples have involved the hydrolysis of other substituted groups under hydro(solvo)thermal conditions. Here we present the hydro(solvo)thermal synthesis and crystal structure of a novel nickel(II) complex $[NiL_2(H_2O)_4]$ (**1**) (L = 1,4-dihydropyrazine-2,3-dione-5,6-dicarboxylate), which adopts an unusual *cis*-configuration. Interestingly, no cadmium complex could be isolated from the reaction when $[Cd(ClO_4)_2]\cdot 6H_2O$ was used instead of $[Ni(ClO_4)_2]\cdot 6H_2O$ under the same solvothermal conditions: only hydrated 1,4-dihydropyrazine-2,3-dione-5,6-dicarboxylic acid (**2**) was formed. The cyano groups of the reactant 5,6-dichloropyrazine-2,3-dicarbonitrile were found to have been hydrolyzed into carboxylate groups and the chloro groups into hydroxyl groups (there is an autoisomerization from the enol form into the ketone form) during the hydro(solvo)thermal reaction in both cases (Scheme 1).

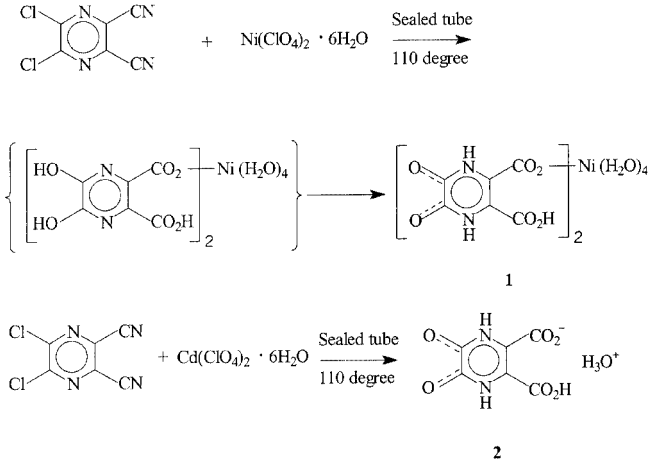

Scheme 1

Results and Discussion

Green crystals of **1** were obtained by treating 5,6-dichloropyrazine-2,3-dicarbonitrile and $[Ni(ClO_4)_2]\cdot 6H_2O$ under solvothermal conditions. Two strong peaks at $\tilde{\nu}$ = 1688 and 1555 cm^{-1} in the IR spectrum of complex **1** could be assigned to the antisymmetric C=O stretching vibrations of uncoordinated and coordinated carboxylate groups, respectively. The absence of characteristic peaks for cyano groups in the region of 2200 cm^{-1} indicates the formation of carboxylate groups by the hydrolysis of the precursor ligand.[1c] Two strong and sharp peaks around $\tilde{\nu}$ = 3551 and 3448 cm^{-1} indicate the presence of coordinated water

[a] Organic Solids Laboratory, Center for Molecular Science, Institute of Chemistry, Chinese Academy of Sciences
Beijing 100080, P. R. China
Fax: (internat.) +86-106/255-9373
E-mail: dqzhang@infoc3.icas.ac.cn

molecules.[3] The strong and sharp peak at $\tilde{\nu}$ = 3373 cm^{-1} is assigned to the N−H stretching mode of ammonium while the broad strong band around $\tilde{\nu}$ = 3116 cm^{-1} can be assigned to the O−H stretching mode of a protonated carboxylate group. A TGA study shows that **1** is thermally stable to about 155 °C and decomposes with the loss of four molecules of water and two molecules of CO_2 over the temperature range 155−290 °C; this also indicates that all four water molecules are coordinated to metal center.[4]

As shown in Figure 1, the crystal structure of **1** consists of isolated 1,4-dihydropyrazine-2,3-dione-5,6-dicarboxylatonickel(II) tetrahydrate molecules $[NiL_2(H_2O)_4]$, where the two 1,4-dihydropyrazine-2,3-dione-5,6-dicarboxylate ligands adopt an unusual *cis*-configuration. To the best of our knowledge, this is the first mononuclear *cis* complex of carboxylate-substituted pyrazine derivatives, although the *cis*-configuration is quite normal for molybdenum complexes of 3,6-di-*tert*-butylcatechol,[5] and the two-dimensional copper complex $[Cu_2(pzdc)_2(pyz)]_n$ (pzdc = pyrazine-2,3-dicarboxylate, pyz = pyrazine) also exhibits such a *cis*-coordination.[6a] This coordination mode is quite similar to that in $[Co^{II}\{OOC(CH_2)_{10}COO\}]\cdot 2H_2O$,[7] where each cobalt atom is coordinated by three carboxylate groups from three *n*-dodecane-α,ω-dioate ligands from one side and two water molecules, in a *cis*-orientation. Generally, there is a chelating interaction involving the nitrogen atom and the oxygen atom of adjacent deprotonated carboxylate ligands in complexes of singly and doubly deprotonated 2,3-pyrazinedicarboxylic acid ($pyzdcH_2$).[4,6] However, the hydrogen atoms bonded to the nitrogen atoms of the pyrazine rings in complex **1** prevent the formation of such a chelate.

The nickel atom has a distorted octahedral environment. It is coordinated by four water molecules and two oxygen atom from the carboxylate groups of two 1,4-dihydropyrazine-2,3-dione-5,6-dicarboxylate ligands, which are found in a *cis*-orientation. The uncoordinated carboxylate groups of the 1,4-dihydropyrazine-2,3-dione-5,6-dicarboxylate ligands are still protonated. The O2···O3 distance of 2.412 Å indicates that there is no intramolecular hydrogen bond involving the carboxylate hydrogen and O2. This is quite different from complexes of singly deprotonated 2,3-pyrazinedicarboxylic acid $[Co\{pz(COO)COOH\}_2(H_2O)_2]$[6b] and $[Ni(pyzdcH)_2(H_2O)_2]$,[4] both of which show a *trans*-configuration, a chelate interaction and a strong intramolecular hydrogen bond between the carboxylate hydrogen and the nearest oxygen atom of the deprotonated carboxylate group. The $Ni-O_{carboxylate}$ bond length [2.046(2) Å] is a little longer than that in $[Ni(pyzdcH)_2(H_2O)_2]$ [2.021(1) Å],[4] whereas the Ni−Ow bond lengths [average 2.050(3) Å] are a little shorter than those in $[Ni(pyzdcH)_2(H_2O)_2]$ [2.091(1) Å].[4] The C5−O5 and C6−O6 bond lengths [1.234(3) and 1.227(3) Å, respectively] are shorter than those of C−O single bonds, indicating that the 1,4-dihydropyrazine-2,3-dione-5,6-dicarboxylate ligands are present as their ketone tautomers.

The intermolecular hydrogen bonds play an important role in the stabilization of the structure of **1**. As shown in Figure 2, there are extensive hydrogen bonds between coordinated water molecules and uncoordinated carboxylate groups ($Ow\cdots O_{carboxylate}$ = 2.774 Å), coordinated water molecules and dione groups ($Ow\cdots O_{dione}$ = 2.885Å), uncoordinated carboxylate groups and dione groups ($O_{dione}\cdots O_{carboxylate}$ = 2.862 Å), and also between dione groups and the nitrogen atoms of the pyrazine rings ($O_{dione}\cdots N$ = 2.887 or 2.954 Å) from neighboring molecules. Consequently, a two-dimensional supramolecular structure is formed.

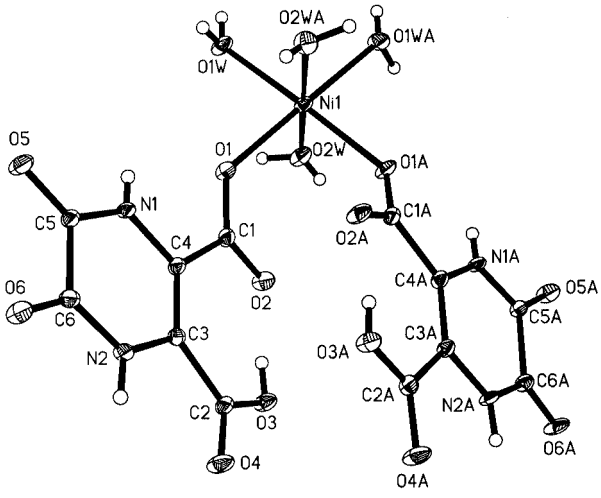

Figure 1. ORTEP drawing of complex **1** with labeling scheme and thermal ellipsoids at the 50% probability level for C, N and O atoms; the spheres of the hydrogen atoms have been arbitrarily reduced; selected bond lengths (Å) and angles (°): Ni(1)−O(1w) 2.041(3), Ni(1)−O(1) 2.046(2), Ni(1)−O(2w) 2.059(3); O(1)−Ni(1)−O(1w) 84.86(10), O(1)−Ni(1)−O(1a) 93.94(13)

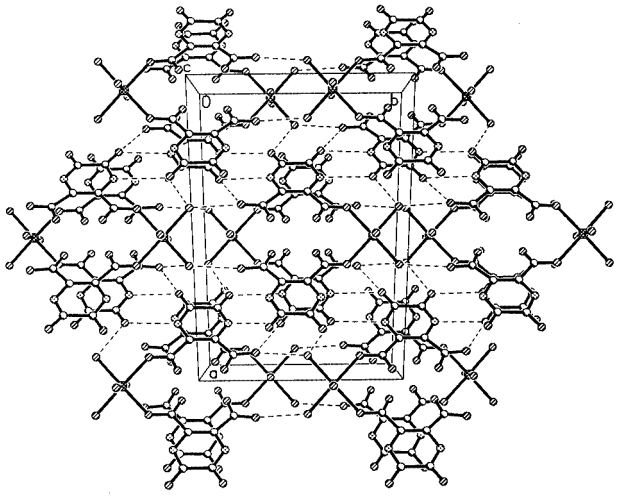

Figure 2. Projection down the *c*-axis of complex **1**

Only one carboxylate group of compound **2** is deprotonated. The hydrogen atom position indicates the two carboxylate groups in compound **2** share a single proton (Figure 3); a similar trend has also been observed in the complex $[Co\{pz(COO)COOH\}_2(H_2O)_2]$.[6b] The other proton is combined with a water molecule to form the cation H_3O^+. The crystal structure of **2** is therefore composed of discrete H_3O^+ cations and singly deprotonated 1,4-dihydropyrazine-2,3-dione-5,6-dicarboxylate anions. The C1−O3 bond length [1.214(2) Å] is a little smaller than the $C-O_{dione}$ bond lengths in the 1,4-dihydropyrazine-2,3-dione-5,6-dicarboxylate ligands of **1** [the C5−O5 and C6−O6 bond lengths are1.234(3) and 1.227(3) Å, respectively]. There are extensive hydrogen bonds between protonated water molecules and the oxygen atoms of the dione groups ($Ow\cdots O_{dione}$ = 2.879 Å) and also the carboxylate groups from neighboring singly deprotonated 1,4-dihydropyrazine-2,3-dione-5,6-dicarboxylate anions ($Ow\cdots O_{carboxylate}$ = 2.874 Å). These hydrogen bonding interactions force the structure into an interesting two-dimensional layered supramolecular array, as shown in Figure 4.

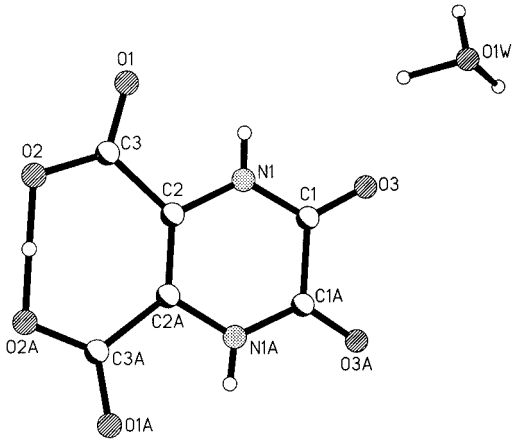

Figure 3. ORTEP drawing of complex **2** showing 50% probability displacement ellipsoids and the atom numbering scheme

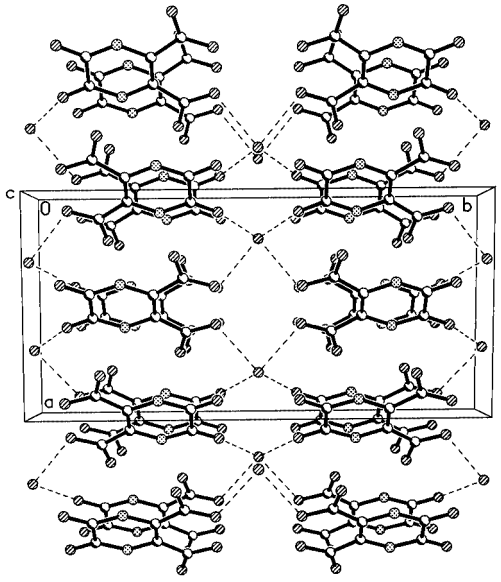

Figure 4. Projection down the *c*-axis of complex **2**

In conclusion, this study illustrates that chloro groups can also undergo a hydrolysis reaction under hydro(solvo)-thermal conditions. This new reaction could be useful for designing structures with a novel topology. Furthermore, such a reaction may also find potential applications in organic synthesis. More investigations are currently underway.

Experimental Section

Synthesis of 1: 5,6-Dichloropyrazine-2,3-dicarbonitrile (80 mg, 0.4 mmol) and $[Ni(ClO_4)_2]\cdot 6H_2O$ (73 mg, 0.2 mmol) were placed in a thick Pyrex tube (ca. 20 cm long). After addition of 0.2 mL of water and 0.8 mL of ethanol, the tube was frozen with liquid N_2, evacuated under vacuum and sealed with a torch. The tube was then heated at 110 °C for three days to give pure green rod-shaped crystals of **1** in 60% yield (63 mg) based on 5,6-dichloropyrazine-2,3-dicarbonitrile. Compound **1** is insoluble in common organic solvents. $C_{12}H_{14}N_4NiO_{16}$ (529.0): calcd. C 27.25, H 2.67, N 10.59; found C 27.12, H 2.81, N 10.47. IR (KBr): $\tilde{\nu}$ = 3551(s), 3448(s), 3373(s), 3116(s), 1688(vs), 1555(s), 1459(s), 1370(s), 1250(w), 1159(m), 1103(m), 889(m), 805(w), 767(m), 702(w), 500(w), 464(m) cm^{-1}.

Synthesis of 2: This compound was prepared as brown tablet-shaped crystals from 5,6-dichloropyrazine-2,3-dicarbonitrile and $[Cd(ClO_4)_2]\cdot 6H_2O$ by the procedure described above for **1**. Yield: 65 mg (75%). $C_{12}H_{12}N_4O_{14}$ (436.2): calcd. C 66.08, H 5.55, N 25.69; found C 65.94, H 5.62, N 25.39%. IR (KBr): $\tilde{\nu}$ = 3444(b, m), 3204(vs), 1718(vs), 1587(s), 1497(s), 1434(vs), 1367(s), 1233(m), 1150(w), 1095(w), 981(w), 857(m), 798(w), 771(w), 709(w), 669(m), 589(w), 461(w) cm^{-1}.

Caution: *$Ni(ClO_4)_2\cdot 6H_2O$ and $Cd(ClO_4)_2\cdot 6H_2O$ are potentially explosive and should be handled with care!*

X-ray Crystal Structure Determination: Crystal data collection was carried out using a Rigaku RAXIS RAPID IP imaging plate system with Mo-K_α radiation (λ = 0.71073Å). The data were corrected for Lorentz-polarization effects, and absorption corrections were applied. The structure was solved by direct methods and refined by a full-matrix least-squares technique based on F^2 using the SHELXL-97 program.[8] All non-hydrogen atoms were refined anisotropically and all hydrogen atoms were located in difference Fourier maps.

Crystal Data For 1: $C_{12}H_{14}N_4NiO_{16}$, monoclinic, space group *C*2/*c*, *Mr* = 528.98, *a* = 17.858(4), *b* = 11.098 (2), *c* = 9.869(2) Å, β = 119.87(3)°, *V* = 1696.1(6) $Å^3$, *Z* = 4, *Dc* = 2.072 g·cm^{-3}, *T* = 293(2)K, μ = 1.254 mm^{-1}, R_1 = 0.0441, wR_2 = 0.0875 for 1356 observed reflections [$I > 2\sigma(I)$] from 1927 independent reflections, GOF = 0.962.

Crystal Data For 2: $C_{12}H_{12}N_4O_{14}$, monoclinic, space group *C*2/*m*, *Mr* = 218.13, *a* = 8.8928(18), *b* = 18.176(4), *c* = 5.0350 (10) Å, β = 96.65(3)°, *V* = 808.4(3) $Å^3$, *Z* = 4, *Dc* = 1.792 g·cm^{-3}, *T* = 293(2)K, μ = 0.168 mm^{-1}, R_1 = 0.0510, wR_2 = 0.1587 for 848 observed reflections [$I > 2\sigma(I)$] from 954 independent reflections, GOF = 1.083.

CCDC-178134 (**1**) and CCDC-178135 (**2**) contain the supplementary crystallographic data for this paper. These data can be obtained free of charge at www.ccdc.cam.ac.uk/conts/retrieving.html [or from the Cambridge Crystallographic Data Centre, 12, Union

Road, Cambridge CB2 1EZ, UK; fax: (internat.) +44-1223/336-033; E-mail: deposit@ccdc.cam.ac.uk].

Acknowledgments

This work was supported by Chinese Academy of Sciences and the Major State Basic Research Development Program (G2000077500) of P. R. China. The authors also thank the anonymous reviewers for their excellent suggestions to improve our manuscript.

[1] [1a] W. Lin, O. R. Evans, R.-G. Xiong, Z. Wang, *J. Am. Chem. Soc.* **1998**, *120*, 13272−13273. [1b] O. R. Evans, R.-G. Xiong, Z. Wang, G. K. Wong, W. Lin, *Angew. Chem. Int. Ed.* **1999**, *38*, 536−538. [1c] W. Lin, Z. Wang, L. Ma, *J. Am. Chem. Soc.* **1999**, *121*, 11249−11250. [1d] W. Lin, L. Ma, O. R. Evans, *Chem. Commun.* **2000**, 2263−2264. [1e] O. Owen, W. Lin, *Chem. Mater.* **2001**, *13*, 2705−2712.

[2] [2a] R.-G. Xiong, J.-L. Zuo, X.-Z. You, B. F. Abrahams, Z.-P. Bai, C.-M. Che, H.-K. Fun, *Chem. Commun.* **2000**, 2061−2062. [2b] J. Zhang, R.-G. Xiong, J.-L. Zuo, X.-Z. You, *Chem. Commun.* **2000**, 1495−1496. [2c] J. Zhang, R.-G. Xiong, J.-L. Zuo, C.-M. Che, X.-Z. You, *J. Chem. Soc., Dalton Trans.* **2000**, 2898−2900. [2d] J. Tao, M.-L. Tong, J.-X. Shi, X.-M. Chen, S. W. Ng, *Chem. Commun.* **2000**, 2043−2044.

[3] [3a] C.-M. Liu, R.-G. Xiong, X.-Z. You, H.-K. Fun, K. Sivakumar, *Polyhedron* **1997**, *16*, 119−123. [3b] L. S. Gelfand, F. J. Iaconianni, L. L. Pytlewski, A. N. Speca, C. M. Mikulski, N. M. Karayannis, *J. Inorg. Nucl. Chem.* **1980**, *42*, 377−385.

[4] L. Mao, S. J. Rettig, R. C. Thompson, J. Trotter, S. Xia, *Can. J. Chem.* **1996**, *74*, 433−444.

[5] C.-M. Liu, P. Restorp, E. Nordlander, C. G. Pierpont, *Chem. Commun.* **2001**, 2686−2687.

[6] [6a] M. Kondo, T. Okubo, A. Asami, S. Noro, T. Yoshitomi, S. Kitagawa, T. Ishii, H. Matsuzaka, K. Seki, *Angew. Chem. Int. Ed.* **1999**, *38*, 140−143. [6b] C. J. O'Connor, E. Sinn, *Inorg. Chem.* **1981**, *20*, 545−551.

[7] J.-M. Rueff, N. Masciocchi, P. Rabu, A. Sironi, A. Skoulios, *Eur. J. Inorg. Chem.* **2001**, 2843−2848.

[8] G. M. Sheldrick, SHELX-97, PC Version, University of Göttingen, 1997.

Received January 15, 2002
[I02022]

Evidence Based on Crystal Structures and Calculations of a C−H···π Interaction Between an Organic Moiety and a Chelate Ring in Transition Metal Complexes

Goran A. Bogdanović,[a,b] Anne Spasojević-de Biré,[a] and Snežana D. Zarić*[c]

Keywords: C−H···π interactions / Chelates / Noncovalent interactions / Density functional calculations / Weak hydrogen bonds

Structural and computational evidence is given for a special type of C–H···π interaction where the C–H group interacts with the π-system of a six-membered chelate ring. An investigation of crystal structures shows that these interactions take place in quite a number of metal complexes, including organometallic compounds; in the CSD we found over 1200 structures with these interactions. These interactions exist in complexes of different metals and various chelate rings. DFT calculations on three model systems show that the energy of these interactions is about 1 kcal/mol.
(© Wiley-VCH Verlag GmbH, 69451 Weinheim, Germany, 2002)

Introduction

Noncovalent interactions involving π-systems have been extensively studied in the last few years and the importance of these interactions has been shown in different molecular systems from molecular biology to crystal engineering.[1−8]

Noncovalent interactions in metal complexes between π-systems and ligands with X−H groups (X = N, O, C) have been found and investigated by searching databases of crystal structures[9−11] and by quantum chemical calculations.[11−14] It has been shown that these interactions play a role in crystal engineering[7−9] and in the stability of metalloproteins, and it has been proposed that they can play a role in the mechanism of enzymatic reactions.[10] In metal complexes, the partial positive charge of the hydrogen atom belonging to the ligand, gained upon coordination to the metal cation, makes the interactions with the π-system stronger.[8−14] The stabilization energy of the metal ligand aromatic cation − π (MLAC-π) interactions in crystal structures, where ligands coordinated to a metal interact with aromatic groups, was evaluated by quantum chemical calculations to be between 4 and 10 kcal/mol.[10,11]

[a] Laboratoire de Structures, Propriétés et Modélisation des Solides, (SPMS), UMR 8580 du CNRS, École Centrale Paris, Grande Voie des Vignes 92295 Châtenay-Malabry Cedex, France
E-mail: goranb@vin.bg.ac.yu
spaso@spms.ecp.fr
[b] Vinča Institute of Nuclear Sciences, Laboratory of Theoretical Physics and Condensed Matter Physics, 11001 Belgrade, PO Box 522, Yugoslavia
[c] Department of Chemistry, University of Belgrade, Studentski trg 16, PO Box 158, 11001 Belgrade, Yugoslavia, Fax: (internat.) +381-11/638-785
E-mail: szaric@chem.bg.ac.yu

C−H···π interactions are the weakest among X−H···π interactions. C−H groups are very abundant in organic and biomolecules therefore these interactions appear very frequently and are very important for molecular recognition.[6,15,16] Theoretical calculations have shown the energy and the nature of these interactions,[6,15−18] leading to calculated values close to 1 kcal/mol. C−H···π interactions have also been found in metal complexes.[9,11,16,19−23] However, a C−H···π interaction, where a C−H group belonging to an organic moiety interacts with the π-system of a chelate ring containing a metal atom, have not been reported before. In this article we will give evidence for this type of interaction.

Results and Discussion

Searching crystal structures of transition metal complexes from the Cambridge Structural Database (CSD) shows that specific C−H···π interactions — interactions between C−H groups and the π-systems of chelate ring — can be observed in many crystal structures. It is supposed that the metal atom in these chelate rings is involved in π-delocalisation.[24] In the CSD, we found 5091 structures containing almost planar chelate rings, with delocalised π-bonds. Among these structures, there are 1265 structures[25] with a weak C−H···π interaction ($\alpha > 110°$, $\beta < 16°$, and H···Ω distance < 3.0 Å; α, β, and Ω are defined in Figure 1) and 151 structures with a very strong interaction ($\alpha > 145°$, $\beta < 12°$, and H···Ω distance < 2.6 Å). For many of these structures there is more than one interaction per molecule. The geometrical parameters for some examples are shown

in Table 1. All these examples have a very short H···Ω distance (H···Ω < 2.6 Å), the H atom is almost centered over the chelate ring center (β < 12.5°) and the X−H···Ω line is not too bent (α < 145°). From a geometrical point of view, interactions in these structures are similar to strong C−H···π interactions in organic molecules.[6,16] An example from Table 1 is shown in Figure 2.

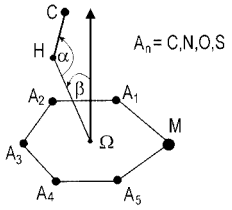

Figure 1. Geometric parameters used for the determination of the C−H···π interaction

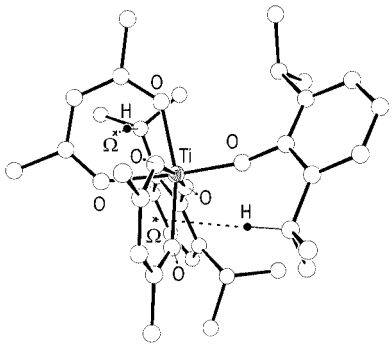

Figure 2. Perspective view of ACIPTI[26] as a selected example for a C−H···π interaction with the π-system of the chelate rings; the carbon atoms are unlabelled

From Table 1, it is clear that these interactions occur in metal complexes — including organometallic compounds — of different metals and various chelate rings. In the interactions shown in Table 1, some of the C donor atoms are sp^3 hybridized and some of them are sp^2. For all the $C_{sp}{}^3$ cases, the carbon atom is bonded to two or three other non-hydrogen atoms, therefore the position of the H atom which is directed toward the chelate ring is reliable. Most of these interactions are intermolecular, and only the ACIPTI compound presents an intramolecular interaction.

It is very interesting to notice that in all the examples shown in Table 1 the complexes are neutral and both the chelate ring and the C−H group are in the same molecule. In the case of intermolecular interactions, the interaction occurs between two identical molecules: the C−H group from one molecule interacting with the chelate ring from the other molecule. For this type of interaction, we assume that the neutrality of the complexes is important, as, on the one hand, the chelate ring should not have any partial positive charge, which would be the case if the complex were positively charged, and, on the other hand, the π-system from the chelate ring should not interact with a negatively charged complex. In the case of a neutral complex the interacting H atom has a partial positive charge, which is enough for a weak C−H···π interaction.

Table 1. Selected crystal structures of metal complexes where a C−H group interacts with the π-system of a chelate ring[a]

CSD refcode	α (°)[b]	β (°)[c]	H···Ω[d] (Å)	C···Ω (Å)	Chelate ring	D[e]	*R* (%)[f]	ref.
ACIPTI	165.3	2.0	2.43	3.51	TiOCCCO	$C_{sp}{}^3$	6.60	26
BEPZOL	175.6	3.8	2.48	3.56	CuNCNCN	$C_{sp}{}^3$	3.20	27
COTQAD	155.1	1.2	2.38	3.39	ZrNCCCN	$C_{sp}{}^2$	4.03	28
COTQEH	155.2	0.6	2.36	3.38	HfNCCCN	$C_{sp}{}^2$	2.63	28
FEBTAH	167.7	1.4	2.39	3.45	NiNCCCN	$C_{sp}{}^3$	3.00	29
GORYER	176.6	1.6	2.46	3.54	MnOCCCN	$C_{sp}{}^3$	5.23	30
GOXDAY	150.9	5.0	2.48	3.46	FeNCCCN	$C_{sp}{}^2$	5.80	31
HALWAS	146.8	3.9	2.40	3.36	ZnNCCCN	$C_{sp}{}^2$	4.10	32
HAMDAA	148.8	3.7	2.40	3.38	ZnNCCCN	$C_{sp}{}^2$	7.40	32
HAMGUX	148.9	4.7	2.46	3.43	ZnNCCCN	$C_{sp}{}^2$	5.20	32
JOXGIM	158.1	6.2	2.59	3.68	CuOCCCN	$C_{sp}{}^3$	5.80	33
LICSEV	154.2	4.7	2.31	3.32	CuNCCCN	$C_{sp}{}^3$	6.59	34
LOFZOV	150.5	3.4	2.36	3.35	NiOCCCN	$C_{sp}{}^2$	4.27	35
MAMTOJ	165.8	5.3	2.46	3.52	CoOCCCN	$C_{sp}{}^2$	3.54	36
MAMTUP	167.1	1.0	2.32	3.38	CuOCCCN	$C_{sp}{}^3$	5.09	36
PIQZUK	175.1	4.7	2.45	3.53	ReOCCCN	$C_{sp}{}^2$	3.71	37
SUMXIH	145.7	5.1	2.50	3.45	FeNCCCN	$C_{sp}{}^3$	3.61	38
VAFQIC	173.5	3.6	2.30	3.38	ZnNCCCN	$C_{sp}{}^2$	4.90	39
YINLUC	159.1	3.1	2.54	3.60	NiOCCCO	$C_{sp}{}^2$	3.70	40
ZAXDOR	155.9	5.3	2.30	3.31	ZnOCCCN	$C_{sp}{}^3$	3.57	41
ZONQOI	149.4	4.4	2.34	3.32	CoNCCCN	$C_{sp}{}^2$	7.20	42
ZOPYUY	157.4	12.4	2.34	3.37	CuOCCCN	$C_{sp}{}^3$	3.80	43

[a] Data for normalised H-atom positions. [b] α is the C−H···Ω angle (Figure 1). [c] β is the angle between the normal of the chelate ring and the Ω···H line (Figure 1). [d] H···Ω is the distance between the normalised H-atom position and the center of the ring (Figure 1). [e] $C_{sp}{}^2$ is bonded to two non-hydrogen atoms. $C_{sp}{}^3$ is bonded to two or three non-hydrogen atoms. [f] *R* is the reliability factor taken from CSD.

In order to evaluate the energy of this type of interaction, DFT calculations were performed on model systems made from the structures JOXGIM, YINLUC and ZOPYUY. Since the molecules in which these interactions occur are rather large, and there are at the same time other intermolecular interactions, we chose the structures where we were able to separate the C−H···π interaction from other interactions, and the calculations were performed on smaller model systems. These model systems were built from the crystal structures by substituting all groups that are not important for the interaction with hydrogen atoms. The model systems for YINLUC and ZOPYUY contain two complex molecules that interact with each other, whereas the model system for JOXGIM has one complex molecule interacting with a molecule of methane (Figure 3). In the JOXGIM model system we used a methane molecule instead of the second molecule of complex as other intermolecular interactions could exist between two complex molecules in the crystal structure, and therefore the calculated energy of interaction of these two molecules would not be only the energy of the C−H···π interaction. The geometries of the interactions were kept the same as they were in the crystal structures. The calculated energies of interactions are 0.89, 1.33, and 1.38 kcal/mol for model systems from JOXGIM, YINLUC and ZOPYUY, respectively. The calculated energies depend upon the H···Ω distance: the distance is the largest in JOXGIM and the shortest in ZOPYUY (Table 1). The calculated values for interacting energies are similar to calculated values of C−H···π interactions in organic molecules.[6]

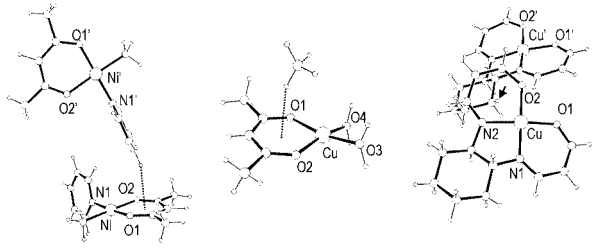

Figure 3. Model systems used for DFT calculations of the energy of C−H···π interactions with a chelate ring; YINLUC (left), JOXGIM (middle), ZOPYUY (right); the carbon atoms are unlabelled

Conclusion

The results presented here show that there is another noncovalent interaction that cannot exist in organic molecules but only in metal complexes. This interaction, where metal-containing chelate rings can be involved in C−H···π interactions, is widespread in metal complexes, including organometallic compounds. It has been estimated by DFT calculations that the energy of this interaction is about 1 kcal/mol. This kind of interaction, like other noncovalent interactions, can be used in nonorganic crystal engineering to design crystals with desired structures and properties. We are continuing our extensive investigations into this kind of interaction using a more detailed analysis of crystal structures from the CSD, enhanced by quantum chemical calculations.

Data Screening and Computational Methods

The Cambridge Structural Database (CSD)[44] was screened in order to find C−H···π interactions with a chelate ring. We searched for the crystal structures of metal complexes that have six-membered, almost-planar chelate rings with delocalized bonds and with N, S, or O atoms coordinated to a transition metal atom, and we found 5091 such structures. In these structures we demanded that there is an hydrogen atom at a distance shorter than 3.0 Å from Ω, the center of the six-membered ring, and presenting an X−H···Ω axis in a narrow cone perpendicular to the ring ($\alpha > 110°$, $\beta < 16°$) (Figure 1). These screening criteria are more restrictive than criteria used previously for similar screenings.[45,46] All C−H distances were normalized to 1.083 Å. In this way we obtained 1265 crystal structures.

Quantum chemical calculations were performed on model systems built from crystal structures using the B3LYP method and 6−31g** basis set on all atoms, except for the metal atoms, where the LANL2DZ basis set was used. The calculations were perfomred with Gaussian-98.[47]

Acknowledgments

The authors would like to thank Prof. E. W. Knapp for useful discussions. This work was supported by the Serbian Ministry of Science and Technology (grant no. 02E09). S. Z. was supported by an Alexander von Humboldt fellowship. The calculations were carried out at the computer centre of the Free University of Berlin.

[1] G. A. Jeffrey, W. Saenger, *Hydrogen Bonding in Biological Structures*, Springer, Berlin, **1991**.
[2] D. A. Dougherty, *Science* **1996**, *271*, 163.
[3] J. C. Ma, D. A. Dougherty, *Chem. Rev.* **1997**, *97*, 1303.
[4] J. P. Gallivan, D. A. Dougherty, *J. Am. Chem. Soc.* **2000**, *122*, 870.
[5] J. P. Gallivan, D. A. Dougherty, *Proc. Natl. Acad. Sci. USA* **1999**, *96*, 9459.
[6] G. R. Desiraju, T. Steiner, *The Weak Hydrogen Bonds in Structural Chemistry and Biology*, Oxford University Press, **1999**.
[7] D. Braga, F. Grepioni, *Acc. Chem. Res.* **2000**, *33*, 601.
[8] D. Braga, F. Grepioni, *Coord. Chem. Rev.* **1999**, *183*, 19.
[9] D. Braga, F. Grepioni, E. Tedesco, *Organometallics* **1998**, *17*, 2669.
[10] S. D. Zarić, D. Popović, E. W. Knapp, *Chem. Eur. J.* **2000**, *6*, 3935.
[11] M. Milčić, S. D. Zarić, *Eur. J. Inorg. Chem.* **2001**, 2143.
[12] S. D. Zarić, *Chem. Phys. Lett.* **1999**, *311*, 77.
[13] S. D. Zarić, *Chem. Phys.* **2000**, *256*, 213.
[14] J. Šponer, J. E. Šponer, J. Leszczynski, *J. Biomol. Struct. Dyn.* **2000**, *17*, 1087.
[15] J. F. Malone, C. M. Murray, M. H. Charlton, R. Docherty, A. J. Lavery, *J. Chem. Soc., Faraday Trans.* **1997**, *93*, 3429.
[16] M. Nishio, M. Hirota, Y. Umezawa, *The CH/π Interaction, Evidence, Nature and Consequences*, John Wiley & Sons, Inc., New York, **1998**.
[17] J. J. Novoa, F. Mota, *Chem. Phys. Lett.* **2000**, *318*, 345.
[18] U. Samanta, P. Chakrabarti, J. Chandrasekhar, *J. Phys. Chem. A* **1998**, *102*, 8964.
[19] L. Carlucci, G. Ciani, D. Proserpio, *Chem. Commun.* **1999**, 449.

[20] T. Steiner, M. Tamm, *J. Organomet. Chem.* **1998**, *570*, 235.
[21] K. S. B. Hancock, J. W. Steed, *Chem. Commun.* **1998**, 1409.
[22] C. B. C Colbert, J. Lewis, N. J. Long, P. R. Raithby, A. J. P. White, D. J. Williams, *J. Chem. Soc., Dalton Trans.* **1997**, 99.
[23] A. Cavaglioni, R. Cini, *J. Chem. Soc., Dalton Trans.* **1997**, 1149.
[24] H. Masui, *Coord. Chem. Rev.* **2001**, *957*, 219.
[25] G. A. Bogdanović, A. Spasojević-de Biré, S. Zarić, AFC 2001, Orsay, 3−6 juillet 2001, 112.
[26] P. H. Bird, A. R. Fraser, C. F. Lau, *Inorg. Chem.* **1973**, *12*, 1322.
[27] A. Pajunen, S. Pajunen, *Acta Crystallogr., Sect. B* **1982**, *38*, 1586.
[28] J. L. Thorman, I. A. Guzei, V. G. Young Junior, L. K. Woo, *Inorg. Chem.* **1999**, *38*, 3814.
[29] N. W. Alcock, W.-K. Lin, A. Jircitano, J. D. Mokren, P. W. R. Corfield, G. Johnson, G. Novotnak, C. Cairns, D. H. Busch, *Inorg. Chem.* **1987**, *26*, 440.
[30] N. Svenstrup, A. Bogevig, R. G. Hazell, K. A. Jorgensen, *J. Chem. Soc., Perkin Trans. 1* **1999**, 1559.
[31] N. Ueyama, N. Nishikawa, Y. Yamada, T. Okamura, A. Nakamura, *Inorg. Chim. Acta* **1998**, *283*, 91.
[32] M. P. Byrn, C. J. Curtis, Yu. Hsiou, S. I. Khan, P. A. Sawin, S. K. Tendick, A. Terzis, C. E. Strouse, *J. Am. Chem. Soc.* **1993**, *115*, 9480.
[33] W. S. Rees Junior, C. R. Caballero, W. Hesse, *Angew. Chem. Int. Ed. Engl.* **1992**, *31*, 735.
[34] P. A. Liddell, K. R. Gerzevske, J. J. Lin, M. M. Olmstead, K. M. Smith, *J. Org. Chem.* **1993**, *58*, 6681.
[35] G. Scherhag, M. D. Spicer, *J. Chem. Soc., Dalton Trans.* **2000**, 1237.
[36] J. T. Pulkkinen, R. Laatikainen, M. J. Ahlgren, M. Perakyla, J. J. Vepsalainen, *J. Chem. Soc., Perkin Trans. 2* **2000**, 777.
[37] K. J. C. van Bommel, W. Verboom, H. Kooijman, A. L. Spek, D. N. Reinhoudt, *Inorg. Chem.* **1998**, *37*, 4197.
[38] E. Vogel, S. Will, A. S. Tilling, L. Neumann, J. Lex, E. Bill, A. X. Trautwein, K. Wieghardt, *Angew. Chem. Int. Ed. Engl.* **1994**, *33*, 731.
[39] X.-Z. Song, L. Jaquinod, W. Jentzen, D. J. Nurco, S.-L. Jia, R. G. Khoury, J.-G. Ma, C. J. Medforth, K. M. Smith, J. A. Shelnutt, *Inorg. Chem.* **1998**, *37*, 2009.
[40] M. Maekawa, M. Munakata, T. Kuroda-Sowa, *Inorg. Chim. Acta* **1994**, *227*, 149.
[41] R. Knoch, H. Elias, H. Paulus, *Inorg. Chem.* **1995**, *34*, 4032.
[42] A. K. -S. Tse, R.-J. Wang, T. C. W. Mak, K.-S. Chan, *Chem. Commun.* **1996**, 173.
[43] K. Bernardo, S. Leppard, A. Robert, G. Commenges, F. Dahan, B. Meunier, *Inorg. Chem.* **1996**, *35*, 387.
[44] F. H. Allen, J. E. Davies, J. J. Galloy, O. Johnson, O. Kennard, C. F. Macrae, E. M. Mitchell, G. F. Mitchell, J. M. Smith, D. G. Watson, *J. Chem. Inf. Comput. Sci.* **1991**, *31*, 187−204.
[45] Z. Ciunik, G. R. Desiraju, *Chem. Commun.* **2001**, 703.
[46] T. Steiner, G. R. Desiraju, *Chem. Commun.* **1998**, 891.
[47] Gaussian 98, Revision A.6, M. J. Frisch, G. W. Trucks, H. B. Schlegel, G. E. Scuseria, M. A. Robb, J. R. Cheeseman, V. G. Zakrzewski, J. A. Montgomery, Jr., R. E. Stratmann, J. C. Burant, S. Dapprich, J. M. Millam, A. D. Daniels, K. N. Kudin, M. C. Strain, O. Farkas, J. Tomasi, V. Barone, M. Cossi, R. Cammi, B. Mennucci, C. Pomelli, C. Adamo, S. Clifford, J. Ochterski, G. A. Petersson, P. Y. Ayala, Cui, Q., K. Morokuma, D. K. Malick, A. D. Rabuck, K. Raghavachari, J. B. Foresman, J. Cioslowski, J. V. Ortiz, B. B. Stefanov, G. Liu, A. Liashenko, P. Piskorz, I. Komaromi, R. Gomperts, R. L. Martin, D. J. Fox, T. Keith, M. A. Al-Laham, C. Y. Peng, A. Nanayakkara, C. Gonzalez, M. Challacombe, P. M. W. Gill, B. Johnson, W. Chen, M. W. Wong, J. L. Andres, C. Gonzalez, M. Head-Gordon, E. S. Replogle, J. A. Pople, Gaussian, Inc., Pittsburgh PA **1998**.

Received November 19, 2001
[I01471]

Unusual Magnetic Behavior in the Layered Ferromagnet $[Ni(C_6H_{14}N_2)_2]_3[Fe(CN)_6]_2 \cdot 2H_2O$

Frederic Bellouard,[a] Miguel Clemente-León,[a] Eugenio Coronado,*[a] José R. Galán-Mascarós,[a] Carlos J. Gómez-García,[a] Francisco Romero,[a] and Kim R. Dunbar[b]

Keywords: Molecular magnets / Ferromagnetism / Cyanides / Nickel / Magnetic properties

The cyano-bridged molecular complex $[Ni(C_6H_{14}N_2)_2]_3[Fe(CN)_6]_2 \cdot 2H_2O$, with a rectangular 2D structure, displays long-range ferromagnetic ordering at 14 K, and exhibits unusual magnetic properties for this type of material, as confirmed by the appearance of two different peaks in the AC magnetic susceptibility plot, and a high coercive field (2.3 kOe) and remnant magnetization (6.8 μ_B).

(© Wiley-VCH Verlag GmbH, 69451 Weinheim, Germany, 2002)

Cyanide-bridged bimetallic assemblies based upon hexacyanometalate building blocks, $[M(CN)_6]^{n-}$, constitute an extensive family of molecular-based materials with interesting magnetic and magneto-optical properties.[1–9] Bimetallic Prussian blue solids behave as magnets with high critical temperatures;[1] however, the face-centered cubic structures adopted by these phases result in a low magnetic anisotropy, and, furthermore, it is very difficult to obtain single crystals. One approach to overcome these problems is to synthesize materials based on $[M(CN)_6]^{n-}$ building blocks condensed with coordinatively unsaturated transition metal complexes such as $[Ni(L)_2]^{2+}$ (L = ethylenediamine derivative) or $[NiL]^{2+}$ (L = polyaza macrocyclic ligand). The resulting Ni_3M_2 (M^{III} = Fe, Cr) based polymeric complexes exhibit a remarkably diverse structural chemistry and a variety of cooperative properties including ferro-, ferri-, and metamagnetism. In fact, a slight modification of the ligand is sufficient to alter the structure, and hence the magnetic properties, completely. For instance, when ethylenediamine is used, a 1D rope-ladder structure is obtained, while the use of *N*-methylethylenediamine affords a 2D honeycomb sheet structure.[10] Interestingly, in the layered materials, a tuning of the bulk magnetic properties can be achieved by changing the interlayer spacing: the behavior can be tuned from metamagnetic for a small spacing (less than 10 Å), to ferromagnetic for a larger spacing, due to the competition between intralayer ferromagnetic interactions with the interlayer antiferromagnetic dipolar interactions. This versatility encouraged us to explore the structure-directing role of diamine ligands exhibiting a larger spatial extension, for example 1,2-diaminocyclohexane, which should favor a larger interlayer spacing and thus a ferromagnetic ordering.

Slow interdiffusion of $K_3[Fe(CN)_6]$ and $[Ni(L)_2]Cl_2$ (L = *trans*-1,2-diaminocyclohexane) in water afforded large brown crystals of $[Ni(C_6H_{14}N_2)_2]_3[Fe(CN)_6]_2 \cdot 2H_2O$.[11] The structure consists of a neutral network of bimetallic cyanide layers that are decorated with organic cyclohexane groups projecting above and below into the interlamellar region.[12] This double layer of bulky diamine ligands imposes a large intersheet separation, with Ni–Ni or Fe–Fe interlayer distances equal to 12.639 Å and a shorter Ni–Fe interlayer distance of 10.889 Å (Figure 1, top). The layers are composed of deformed rectangular grids of twelve octahedral metal sites in which alternating *trans*-$[Ni(C_6H_{14}N_2)_2]^{2+}$ cations and $[Fe(CN)_6]^{3-}$ anions are linked by CN^- bridges (Figure 1, center). Water molecules occupy the free space within these rectangular grids. In contrast with the other 12-gon motifs reported recently,[13] in the present case there are two distinct $[Fe(CN)_6]^{3-}$ units, situated at the corners and at the center of the sides of the grid, which act as tetradentate and bidentate ligands connecting four and two *trans*-$[Ni(C_6H_{14}N_2)_2]^{2+}$ complexes, respectively. Another unusual feature is the extremely bent Ni–N–C bond angles. In related compounds reported so far, the lowest values have been found to be around 148°.[14] Only copper-containing compounds have shown a lower angle for bridging cyanides, near 120°.[15] However, values as low as 128.69° and 122.53° for Ni1–N2–C2 and Ni2–N3–C3, respectively, are observed in the title compound (Figure 1, bottom).

The magnetic susceptibility of the bimetallic compound, measured on polycrystalline samples in the temperature

[a] Instituto de Ciencia Molecular, Universidad de Valencia, Dr. Moliner 50, 46100 Burjasot, Spain
E-mail: eugenio.coronado@uv.es
[b] Department of Chemistry. Texas A&M University, College Station, TX, 77843, USA

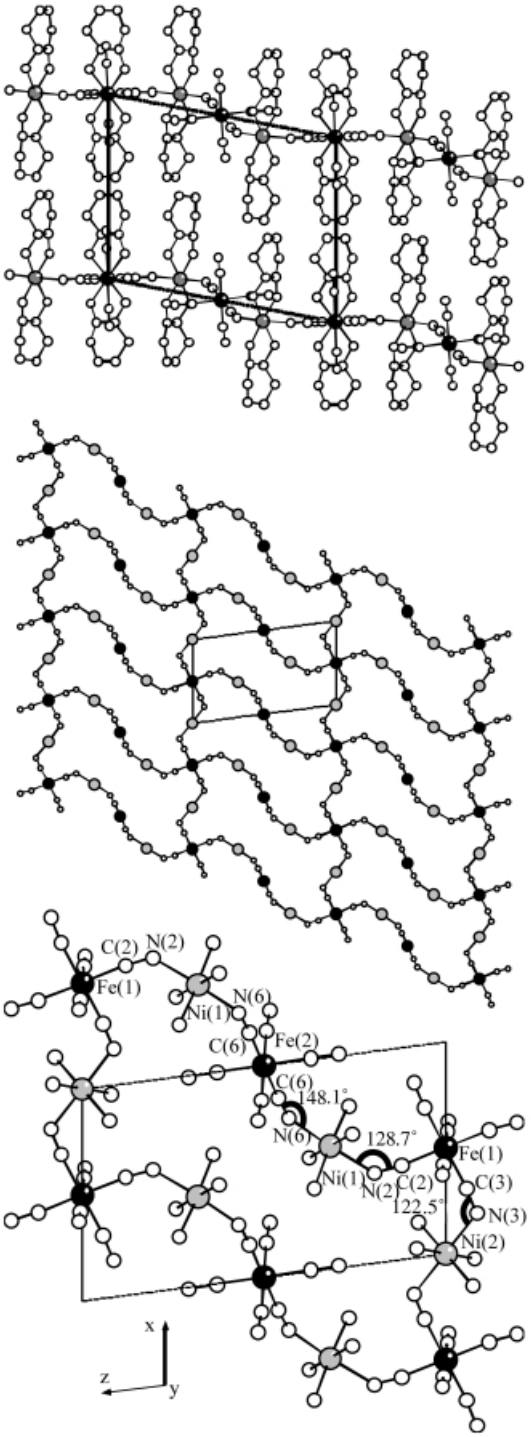

Figure 1. Top: View of the structure of the title compound showing the layers in the *ac* plane. Center: Schematic view of the layers in the *ab* plane. Bottom: View of the Fe_6Ni_6 ring showing the distortions in the bridging Ni−N−C bridges; the cyclohexane rings have been omitted for the sake of clarity (Fe atoms in black and Ni atoms in gray); selected distances in Å: Fe(1)−C(2) 2.088(3), Fe(1)−C(3) 1.916(4), Ni(1)−N(2) 2.168(3), Ni(1)−N(6) 2.088(3), Ni(2)−N(3) 2.154(3), Fe(2)−C(6) 1.931(4)

range 2−300 K under a field of 1000 Oe, follows a Curie−Weiss law above 50 K with a Weiss constant θ of 21.1 K. The positive sign of θ indicates the presence of dominant ferromagnetic interactions between neighboring Fe^{III} and Ni^{II} ions. Below 15 K, χ_m increases sharply and saturates at a lower temperature. In addition, the zero field cooled (ZFC) and field cooled (FC) measurements of the DC magnetic susceptibility deviate from each other at 14 K (Figure 2, inset), with the remnant magnetization disappearing below this temperature. This behavior suggests the onset of a long-range ferromagnetic transition.

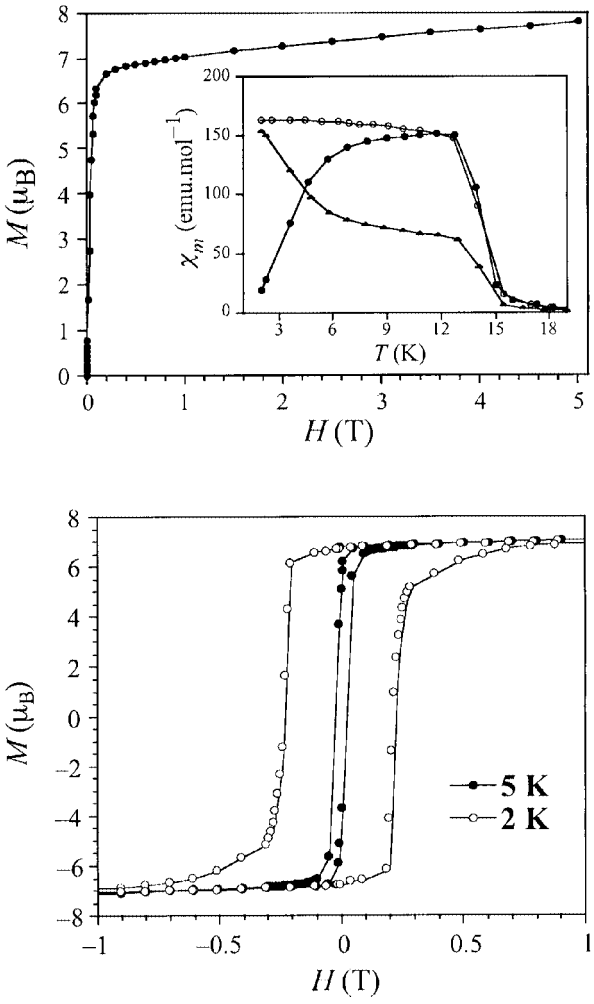

Figure 2. Top: Field dependence of the magnetization at 2 K for the title compound; inset: zero-field cooled (full circles) and field cooled (empty circles) plots of the DC magnetic susceptibility at 1 G, and remnant magnetization (triangles). Bottom: Hysteresis loop for the title compound at 2 and 5 K

The nature of the magnetic transition was confirmed by the field dependence of the isothermal magnetization performed at 2 K (Figure 2). In fact, a rapid increase of the magnetization to a value of ca. 6.5 μ_B is observed at 1 kOe, and increases to 7.7 μ_B at 50 kOe. This latter value is slightly smaller than, but very close to, 8 μ_B, which is the expected value for a ferromagnetic alignment of the interacting spins in the Ni_3Fe_2 unit ($S_{Ni} = 1$, $S_{Fe} = 1/2$; $S = 4$ per Ni_3Fe_2 unit). Hence, the compound behaves as a ferromagnet, although the lower than expected saturation value suggests the presence of some spin canting.

At 2 K this ferromagnet exhibits magnetic hysteresis with a coercive field as large as 2.3 kOe and a high remnant magnetization of 6.8 μ_B per Ni_3Fe_2 unit. This leads to an energy product of 7.3 $kJ\cdot m^{-3}$, which is similar to that obtained in very hard magnetic materials. To the best of our knowledge, the only precedent for a structurally characterized Ni_3Fe_2 ferromagnet is the recently reported layered compound $[NiL]_3[Fe(CN)_6]_2\cdot 12H_2O$ (L = 3,10-diethyl-1,3,5,8,10,12-hexaazacyclotetradecane),[13a] which orders ferromagnetically at 9.1 K. At T = 1.6 K, the material exhibits a coercive field of 1.5 kOe and a remnant magnetization of 1.36 μ_B. In our new layered magnet, the coercivity is larger and the energy product is about one order of magnitude bigger.

One main feature of note in this study is the observation that the Ni^{II} and Fe^{III} centers are ferromagnetically coupled, in spite of the fact that the Ni−N−C angles are much more acute than those reported for known cyanide compounds of these two metals.[14] Our findings underscore the fact that there is a wide range of angles that stabilize a ferromagnetic $Ni^{II}-Fe^{III}$ coupling through a CN^- bridge.

In order to determine precisely the critical temperature at which this transition occurs AC magnetic measurements were performed (Figure 3). We observed a sharp increase below ca. 15 K and a broad and asymmetric maximum in the real part of the susceptibility, χ_m', at about 13.5 K. This signal is accompanied by an out-of-phase signal, χ_m'', that becomes non-zero below a temperature of 14.0 K, which defines T_c. Interestingly, the χ_m'' signal displays a shoulder at ca. 12 K, which is frequency independent, and a maximum at ca. 4 K which is strongly frequency dependent (Figure 3). This result, together with the observation that the compound behaves as a hard magnet only below 5 K (at higher T the coercive field is very small), indicates that the movement of the domain walls is strongly hindered below this temperature. The very same features were observed when measurements were performed on a single crystal. This proves that the anomalous behavior is actually intrinsic for this compound, and not sample dependent.

A plausible explanation of this behavior would be that the magnetic transition at 14.0 K corresponds to a ferromagnetic ordering within the magnetic layer that it is triggered by the magnetic anisotropy of the metallic ions. At lower temperatures (below 5 K), the dipolar coupling between layers becomes relevant and induces an anchoring of the domain walls. If this is the case, the frequency dependence of χ'' can be related to the activation energy required to unblock these domain walls.[16] Fortunately, since this compound can be grown as well-shaped single crystals, a more detailed physical characterization, including neutron diffraction, can be performed that will provide detailed information on the anisotropy and magnetic phase diagram of this novel molecule-based ferromagnet. The unusual features observed in the AC magnetic susceptibility measurements are similar to those observed in other layered magnets with large interlayer separations,[17] suggesting that these effects should be related to the low dimensionality of these systems. Molecular layered magnets are ideal to study this novel behavior since the interlayer separation of a given system can easily be tuned simply by changing the spacers in each case.

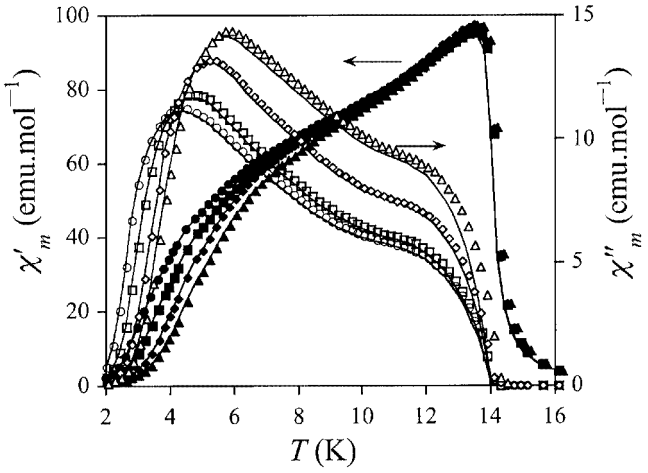

Figure 3. Thermal variation of the molar AC magnetic susceptibility for the title compound (χ': filled symbols, χ'': empty symbols) at frequencies of 1, 10, 110 and 332 Hz (circles, squares, diamonds and triangles, respectively) showing the frequency dependence of χ'' in the peak around 4 K and the appearance of a χ'' signal below 14.0 K

Finally, it is worth mentioning that a racemic mixture of the ligand *trans*-1,2-diaminocyclohexane was used for the synthesis of the title compound and therefore both stereoisomers are present, yielding a centrosymmetric solid state structure. The organic ligands are disordered in two different crystallographic positions corresponding to the two stereoisomers, due to statistical distribution. More work is in progress to obtain a pure enantiomeric structure that would be of interest to study possible magneto-chiral effects.[10] In this case the chirality appears only in the organic ligand and not in the metallic complexes, therefore more subtle effects could be expected.

Experimental Section

Synthesis: The precursor $[Ni(C_6H_{14}N_2)_2]Cl_2$ was prepared by the literature method developed for ethylenediamine complexes.[19] All reagents were of commercial grade and used without further purification.

$[Ni(C_6H_{14}N_2)_2]_3[Fe(CN)_6]_2\cdot 2H_2O$ (1): A solution containing 1,2-diaminocyclohexane (2 mmol, 245 mL) in 40 mL of methanol was added to an aqueous solution of $NiCl_2\cdot 6H_2O$ (2 mmol, 476 mg) in 60 mL of water. A solution of $K_3[Fe(CN)_6]$ (1.3 mmol, 439 mg) in 60 mL of water was then added dropwise to the resulting brown solution,. A brown precipitate was filtered off and the yellow filtrate was allowed to stand in the dark overnight. Brown plates were collected by suction filtration and washed with water and ethanol. Single crystals suitable for X-ray single crystal analysis were obtained after a week by slow diffusion of $[Ni(C_6H_{14}N_2)_2]Cl_2$ (102 mg, 0.28 mmol) and $K_3[Fe(CN)_6]$ (94 mg, 0.28 mmol) placed in the sides of an H-type diffusion tube. Water (55 mL) was used as solvent.

Physical Measurements: X-ray data sets were collected on a SMART 1K area detector diffractometer equipped with graphite monochromated Mo-K_α radiation (λ = 0.71073 Å). The frames were integrated in the Siemens SAINT[20] software package and the data were corrected for absorption using the SADABS program.[21] The structure was solved by direct methods followed by Fourier synthesis (SIR-97),[22] and refined on F^2 (SHELXL-97).[23] Variable temperature susceptibility measurements were carried out in the temperature range 2−300 K at a magnetic field of 0.1 T on polycrystalline samples with a magnetometer (Quantum Design MPMS-XL-5) equipped with a SQUID sensor. Susceptibility data were corrected from the diamagnetic contributions of the compound as deduced from Pascal's constant tables. Isothermal magnetization measurements at low temperatures were carried out up to 5 T on the same apparatus.

Acknowledgments

This work was supported by the European Union (TMR Network on Molecular Magnetism: from materials to the devices) and by the Spanish Ministerio de Ciencia y Tecnología (MAT2001-3507-C02-01). K. R. D. gratefully acknowledges the National Science Foundation for support of this work (NSH CHE-9906583) and for funding the CCD diffractometer (CHE-9807975).

[1] [1a] D. Babel, *Comments Inorg. Chem.* **1986**, *5*, 285. [1b] W. R. Entley, G. Girolami, *Science* **1995**, *268*, 397−400. [1c] T. Mallah, S. Thiebaut, M. Verdaguer, P. Veillet, *Science* **1993**, *262*, 1554−1557. [1d] S. Ferlay, T. Mallah, R. Ouahes, P. Veillet, M. Verdaguer, *Nature* **1995**, *378*, 701−703.

[2] [2a] M. Ohba, N. Fukita, H. Okawa, T. Enoki, J. M. Latour, *J. Am. Chem. Soc.* **1994**, *116*, 11566−11567. [2b] M. Ohba, N. Fukita, H. Okawa, *J. Chem. Soc., Dalton Trans.* **1997**, 1733−1738.

[3] M. Ohba, N. Usuki, N. Fukita, H. Okawa, *Inorg. Chem.* **1998**, *37*, 3349−3354.

[4] M. Ohba, H. Okawa, N. Fukita, Y. Hashimoto, *J. Am. Chem. Soc.* **1997**, *119*, 1011−1019.

[5] [5a] S. Ferlay, T. Mallah, J. Vaissermann, F. Bartolome, P. Veillet, M. Verdaguer, *Chem. Commun.* **1996**, 2481−2482. [5b] E. Colacio, J. M. Domínguez-Vera, M. Ghazi, R. Kikeväs, F. Lloret, J. M. Moreno, H. Stoeckli-Evans, *Chem. Commun.* **1999**, 987−988. [5c] E. Colacio, M. Ghazi, H. Stoeckli-Evans, F. Lloret, C. Perez, *Inorg. Chem.* **2001**, *40*, 4876−4883.

[6] M. Salah El Falah, E. Rentchler, A. Caneschi, R. Sessoli, D. Gatteschi, *Angew. Chem. Int. Ed. Engl.* **1996**, *35*, 1947−1749.

[7] [7a] R. J. Parker, D. C. R. Hockles, B. Moubaraki, K. J. S. Murray, L. Spiccia, *Chem. Commun.* **1996**, 2789−2790. [7b] T. Mallah, C. Auberger, M. Verdaguer, P. Veillet, *J. Chem. Soc., Chem. Commun.* **1995**, 61−62. [7c] A. Scuiller, T. Mallah, M. Verdaguer, A. Nivorozkhin, J. Tholence, P. Veillet, *New J. Chem.* **1996**, *20*, 1−3.

[8] K. Van Langenberg, S. R. Batten, K. J. Berry, C. R. Hockless, B. Moubaraki, K. S. Murray, *Inorg. Chem.* **1997**, *36*, 5006−5015.

[9] J. A. Smith, J. R. Galán-Mascarós, R. Clérac, K. R. Dunbar, *Chem. Commun.* **2000**, 1077−1078.

[10] M. Ohba, H. Okawa, *Coord. Chem. Rev.* **2000**, *198*, 313−328.

[11] Crystal data for $C_{48}H_{88}Fe_2N_{24}Ni_3O_2$, M_w = 1321.26, triclinic, space group $P\bar{1}$, a = 9.068(2), b = 12.639(3), c = 14.920(3) Å, α = 98.77(4), β = 93.95(3), γ = 109.62(3)°, V = 1578.6(6) Å^3, T = 110(2) K, Z = 1, D_c = 1.390 Mg·m^{-3}, graphite monochromated Mo-K_α radiation (λ_α = 0.71069 Å), Bruker CCD difractometer, $F(000)$ = 696, μ = 1.383 mm^{-1}, 0.35 × 0.26 × 0.03 mm, 10176 reflections measured, 7157 unique (R_{int} = 0.0343). All non-hydrogen atoms were refined anisotropically, except for the disordered carbon atoms from the cyclohexane rings. The final refinement led to $R(F)$ = 0.575 and $R_\omega(F^2)$ = 0.1488 for 5297 reflections [$I > 2\sigma(I)$]. H-atoms were placed in calculated positions. CCDC-162937 contains the supplementary crystallographic data for this paper. These data can be obtained free of charge at www.ccdc.cam.ac.uk/conts/retrieving.html [or from the Cambridge Crystallographic Data Centre, 12, Union Road, Cambridge CB2 1EZ, UK; Fax: (internat.) +44-1223/336-033; E-mail: deposit@ccdc.cam.ac.uk].

[12] A preliminary account on these structures was reported by: N. Fukita, M. Ohba, H. Okawa, *Mol. Cryst. Liq. Cryst.* **2000**, *342*, 217−224.

[13] [13a] H. Z. Kou, S. Gao, B. Q. Ma, D. Z. Liao, *Chem. Commun.* **2000**, 1309−1310. [13b] H. Z. Kou, S. Gao, W. M. Bu, D. Z. Liao, B. Q. Ma, Z. H. Jiang, S. P. Yan, Y. Fan, G. L. Wang, *J. Chem. Soc., Dalton Trans.* **1999**, 2477−2480. [13c] H. Z. Kou, W. M. Bu, S. Gao, D. Z. Liao, Z. H. Jiang, S. P. Yan, Y. G. Fan, G. L. Wang, *J. Chem. Soc., Dalton Trans.* **2000**, 2996−3000.

[14] H. Z. Kou, W. M. Bu, D. Z. Liao, Z. H. Jiang, S. P. Yan, Y. G. Fan, G. L. Wang, *J. Chem. Soc., Dalton Trans.* **1998**, 4161−4164.

[15] I. Escorihuela, L. R. Falvello, M. Tomás, *Inorg. Chem.* **2001**, *40*, 636−640.

[16] In fact, the frequency dependence of the maxima of χ'' follows an Arrhenius law, from which an activation energy of 77.6 cm^{-1} (111.6 K) can be estimated.

[17] E. Coronado, J. R. Galán-Mascarós, C. J. Gómez-García, V. Laukhin, *Nature* **2000**, *408*, 447−449.

[18] G. L. J. A. Rikken, E. Raupach, *Nature* **1997**, *390*, 493−494.

[19] H. M. State, *Inorg. Synth.* **1960**, *6*, 198−199.

[20] SAINT, Program for area detector absorption correction, Siemens Analytical X-ray Instruments Inc., Madison WI 53719, USA, **1994**−**1996**.

[21] Program in the SHELXTL software.

[22] SIR-97: A. Altomare, M. C. Burla, M. Camalli, G. L. Cascarano, C. Giacovazza, A. Guagliardi, A. G. G. Moliterni, G. Polidori, R. Spagna, *J. Appl. Crystallogr.* **1999**, *32*, 115−119.

[23] SHELXL-97: G. M. Sheldrick, SHELXL-97, Program for refining crystal structures, University of Göttingen, **1997**.

Received February 12, 2002
[I02072]

Synthesis, Structures and Reactivity of *N*-Borane-Protected 1,1′-Bisimidazoles with Different Bridging Functions

Andre Weiss,[a] Hans Pritzkow,[a] and Walter Siebert*[a]

Dedicated to Prof. Dr. Otto J. Scherer

Keywords: Boranes / Carbenes / Carbene complexes / Nitrogen heterocycles / Macrocycles

The bridging functions Me_2Si, $[(CH_2)_3(CMe_2)_2N]B$ and CH_2 have been used to connect two imidazoles in the 1,1′-position. The bisimidazolyl compounds were treated with BH_3 or BEt_3, and the resulting *N*,*N*′-bisborane-protected products **1**, **3b**, **4a**, and **5b** were characterized by X-ray structure analyses. Reaction of 1,1′-bis(4,5-dimethylimidazolyl)methane with BBr_3 yielded the macrocyclic dicationic tetraimidazolyl compound **6**. The behavior of the N-protected bisimidazoles **1** and **3**–**5** towards deprotonating agents was investigated and it was found that 1,1′-bis(3-borane-4,5-dimethylimidazolyl)methane (**5b**) is deprotonated to give a dianionic dicarbene compound. Its reaction with Cp_2MCl_2 allowed the formation of the corresponding titanocene and zirconocene complexes **8** and **9**, which were characterized by X-ray structure analyses. In **9** a 3c,2e B–H–Zr bond is present.

(© Wiley-VCH Verlag GmbH, 69451 Weinheim, Germany, 2002)

Introduction

The coordination behavior of *N*-heterocyclic carbenes has been studied very intensely since the isolation of 1,3-bis(adamantyl)imidazolin-2-ylidene **A** by Arduengo et al. in 1991.[1] Many *N*,*N*-methylene- and -ethylene-bridged bis(imidazolin-2-ylidene)metal complexes have since been prepared.[2] Recently the catalytic activity in Heck and Suzuki coupling reactions of the diiodopalladium(II) complex of 1,1′-methylenebis(3-methylimidazolin-2-ylidene) **B** has been investigated.[3]

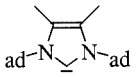

A

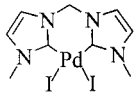

B

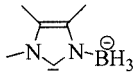

C (= L)

Addition of BH_3 to 1-alkylimidazoles leads to neutral *N*-borane adducts, which are deprotonated by butyllithium to give anionic 3-borane-1-alkylimidazol-2-ylidenes **C** (L). These anions were found to be excellent ligands to form transition metal complexes of manganese[4] (**D**), titanium[5] (**E**), iron[4−6] (**F**−**H**) and the distorted tetrahedral anionic complexes of vanadium[5,6] (**I**) and scandium[6] (**J**). In the latter case the formation of four 3c,2e B−H−Sc bonds was observed.

The dinuclear compound **K**[7] is the only structurally characterized imidazol-2-ylidene complex of titanium.

[a] Anorganisch-Chemisches Institut der Universität Heidelberg, Im Neuenheimer Feld 276, 69120 Heidelberg, Germany
E-mail: ci5@ix.urz.uni-heidelberg.de

In the following we report on new N,N-bridging functions in 1-borane-protected bisimidazolyl compounds and their behavior towards treatment with butyllithium to give chelating dianionic dicarbene ligands.

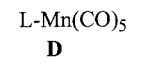

D

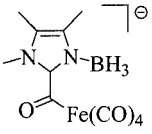

F

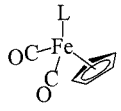

G

E

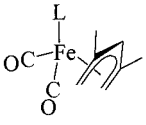

H

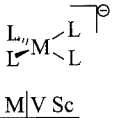

I J

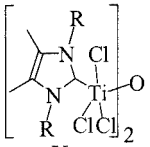

K

Results and Discussion

Formation and Reactivity of Bisimidazolyl Compounds 1, 2a−b, 3a−b, 4a, and 5a−b

The addition of two equivalents of BH_3·thf to a solution of 1,1′-bis(imidazolyl)dimethylsilane[8] yields the colorless *N*,*N*-bis-borane adduct **1**, which crystallizes from a saturated THF solution (Scheme 1).

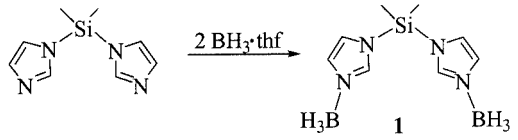

Scheme 1

The ^{11}B NMR spectrum shows a quadruplet at $\delta = -21.5$; three imidazole signals in the proton NMR spectrum and one singlet for the methyl groups prove the symmetry of the molecule. In the crystal, **1** has a twofold rotation axis (Figure 1). The N2−B1 distance [1.580(2) Å] is typical for borane adducts of nitrogen compounds. The coordination geometry at the silicon atom is distorted tetrahedral with N1−Si−N1A and C4−Si−C4A angles of 104.4(1)° and 117.7(1)°, respectively. Attempts to doubly deprotonate **1** in the 2,2′-positions with alkyllithium compounds (MeLi, *t*BuLi, *n*BuLi) to generate a dicarbene were unsuccessful due to decomposition.

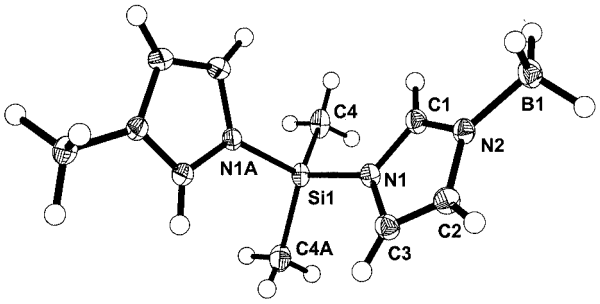

Figure 1. Structure of **1** in the crystal; selected bond lengths [Å] and angles [°]: Si−N1 1.776(1), N1−C3 1.392(1), C2−C3 1.350(2), C2−N2 1.381(1), N2−C1 1.315(1), C1−N1 1.356(1), N2−B1 1.580(2); N1−Si−N1A 104.4(1), C4−Si−C4A 117.7(1), Si−N1−C1 126.0(1), N1−C1−N2 111.2(1)

We have shown that attempts to synthesize imidazolylboranes by reaction of 1-trimethylsilylimidazoles with haloboranes lead to polymeric or (under certain conditions) oligomeric products.[9] This is caused by donor/acceptor interactions of the electron pair at the nitrogen in the 3-position with the empty p_z orbital at the boron atom. Formation of oligomeric adducts is avoided when the borane compound is substituted by a sterically demanding and electron-donating group such as 2,2′,6,6′-tetramethylpiperidide (TMP): reactions of (tmp)BCl_2 with two equivalents of 1-trimethylsilylimidazole or 4,5-dimethyl-1-trimethylsilylimidazole yielded the first monomeric bis(imidazolyl)boranes **2a** and **2b**, respectively (Scheme 2).

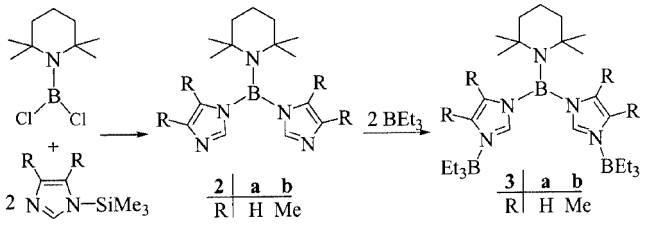

Scheme 2

The ^{11}B NMR chemical shifts [δ = 28.2 (**2a**), 28.5 (**2b**)] indicate a trigonal coordination at the boron atoms. Compound **2a** shows the expected set of signals in the proton NMR spectrum (three imidazolic protons, one singlet for methyl groups and a multiplet for methylene groups of TMP), whereas the methyl groups of the TMP substituent in **2b** appear as two singlets ($|\nu_a - \nu_b| = 14.8$ Hz), caused by restricted rotation at the N−B bond. Proton NMR spectra at different temperatures (Figure 2) provide a coalescence temperature of 26 °C. The resulting free activation enthalpy of rotation ($\Delta G^{\#}$) at the B−N bond is 64.6 kJ/mol, calculated by the Eyring equation.[10]

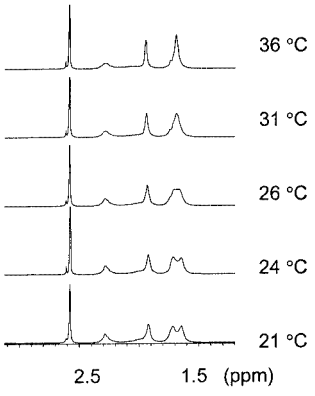

Figure 2. ^1H NMR spectra of **2b** at different temperatures

Attempts to alkylate **2a** in the 3,3′-positions (with CH_3I, 2-iodopropane, or Me_3OBF_4) led to decomposition products, and treatment with Me_3SiBr or BH_3·thf to quaternization of the boron atoms. The reaction of **2a** and **2b** with two equivalents of BEt_3 yields the 3,3′-bis(triethylborane) adducts **3a** and **3b** (Scheme 2), as indicated by an additional signal in the ^{11}B NMR spectra at $\delta \approx -1$. Restricted rotation at the B−N bond also exists in **3b**; there are two signals for the methyl groups.

The X-ray structure analysis of a single crystal of **3b** confirms the steric demand of the substituents coordinated at B1 (Figure 3). The angle of 55° between the C23−N5−C27 and N1−B1−N3 planes is a compromise between the mutual repulsion of the TMP and imidazolyl substituents and donation of the electron pair of N5 to the p_z orbital of B1. The planarity around N5 and the bond length of B1−N5 [1.405(2) Å] show that an effective overlap of the p_z orbitals is possible even at a torsion angle of 55°. Electron donation to the central boron atom from the imidazole rings is negligible because the B1−N1,3 distances (1.476 Å) are in a range typical of B−N single bonds. The N1−B1−N3 angle [115.1(1)°] is smaller than the two neighboring angles [N1−B1−N5: 121.9(2)°; N3−B1−N5: 123.0(1)°].

Treatment of **3a** and **3b** with *n*BuLi or *t*BuLi to yield bisimidazol-2-ylidenes always led to decomposition (quaternisation of the central boron atom is observed by ^{11}B NMR spectroscopy). Further reactions of **3a,b** with metal compounds such as $M(OAc)_2$ (M = Zn, Ni, Pd) and $Ti(NMe_2)_4$ to give metal carbene complexes were unsuccessful.

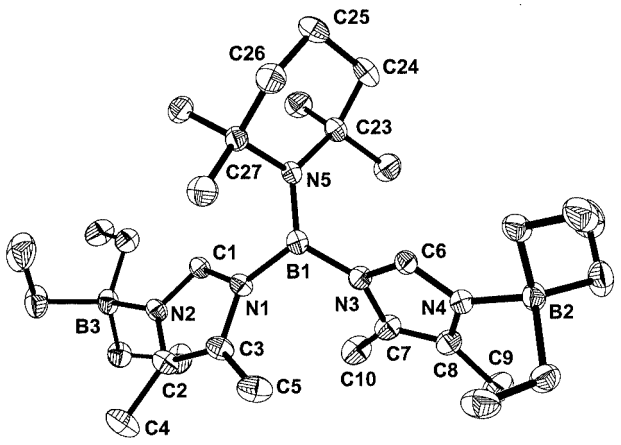

Figure 3. Structure of **3b** in the crystal; the hydrogen atoms have been omitted for clarity; selected bond lengths [Å] and angles [°]: N1−C1 1.352(2), N1−C3 1.401(2), N1−B1 1.475(2), N2−C1 1.307(2), N2−C2 1.406(2), N2−B3 1.645(2), N3−B1 1.477(2), N5−B1 1.405(2), C2−C3 1.364(3), C2−C4 1.486(3); C1−N1−C3 106.2(1), C1−N1−B1 122.1(1), N5−B1−N1 121.9(2), N5−B1−N3 123.0(1), N1−B1−N3 115.1(1), N2−C1−N1 112.4(1)

Addition of two equivalents of BEt_3 to 1,1′-bis(imidazolyl)methane yields the crystalline bis(triethylborane) adduct **4a** (80%; Scheme 3).

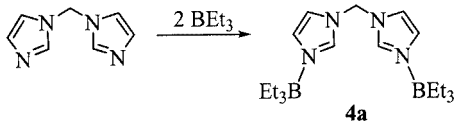

Scheme 3

The ^{11}B NMR signal of **4a** ($\delta = -1.6$) is in the same region as that of **3a,b**. In the ^1H NMR spectrum the signals of the ethyl groups appear at $\delta = 0.30$ (CH_2) and 0.58 (CH_3), the methylene signal is at $\delta = 6.09$ and the signals of imidazolic protons are at $\delta = 7.06$, 7.23 and 7.91. These shifts show that the imidazolic protons are not as strongly deshielded when forming a triethylborane adduct as when they are alkylated to form imidazolium cations.

The molecular structure of **4a** is shown in Figure 4. In the crystal, **4a** has a C_2 symmetry. The N1−C1−N1A angle [110.6(1)°] is smaller than the comparable angle of **3b** as a result of the tetrahedral bridging function. The coordination geometry at the boron atoms is distorted tetrahedral. While the average C−B1−C angle is 112.5°, the angles C−B1−N2 [av. 106.3(1)°] are smaller. The imidazole rings are nearly symmetric: the C2−N2 and N2−C3 distances barely deviate from those of C2−N1 and N1−C4.

Treatment of 1,1′-bis(imidazolyl)methane or 1,1′-bis(4,5-dimethylimidazolyl) methane with BH_3·thf gives the corresponding 3,3′-bisborane adducts **5a,b** as air- and moisture-sensitive solids in quantitative yields.

In the mass spectra, the molecular peak of **5a** could not be found as it easily loses a BH_3 ligand under EI-MS conditions to give $m/z = 161$ $[M - H - BH_3]^+$. The ^1H NMR spectrum of **5a** shows four signals of equal intensity. The methylene signal ($\delta = 6.32$) and the imidazole protons at

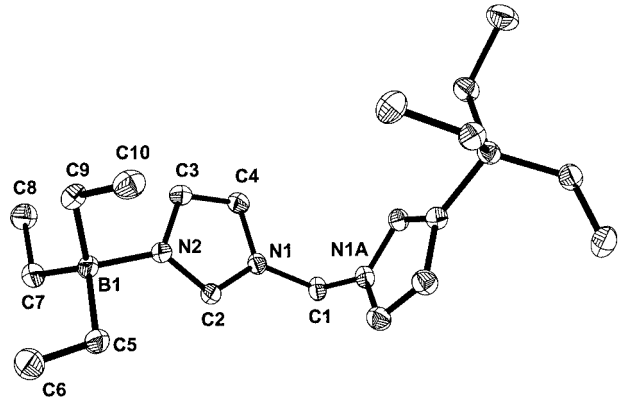

Figure 4. Structure of **4a** in the crystal; the hydrogen atoms have been omitted for clarity; selected bond lengths [Å] and angles [°]: C1−N1 1.454(1), N1−C2 1.349(1), C2−N2 1.322(1), N2−C3 1.384(1), C3−C41.349(2), C4−N11.380(1), N2−B11.649(1); N1−C1−N1A 110.6(1), C1−N1−C2125.6(1), C2−N2−B1127.1(1), N2−B1−C5106.1(1)

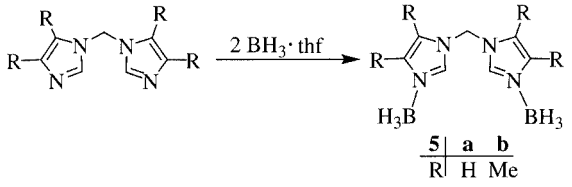

Scheme 4

C4,5 ($\delta = 7.10$, 7.67) have almost the same chemical shifts as in **4a**. In contrast, however, the signal for the proton at C2 is shifted toward lower field ($\delta = 8.64$). A very broad signal at $\delta = 2$ indicates the presence of boron-bonded hydrogen atoms. No proton coupling was observed to the ^{11}B NMR signal at $\delta = -18.4$. Similar spectroscopic results were obtained for **5b**: an ^{11}B NMR signal at $\delta = -20.3$ indicates addition of BH_3, and the ^1H NMR spectrum confirms the formation of **5b**. Its structure was determined by an X-ray diffraction analysis (Figure 5).

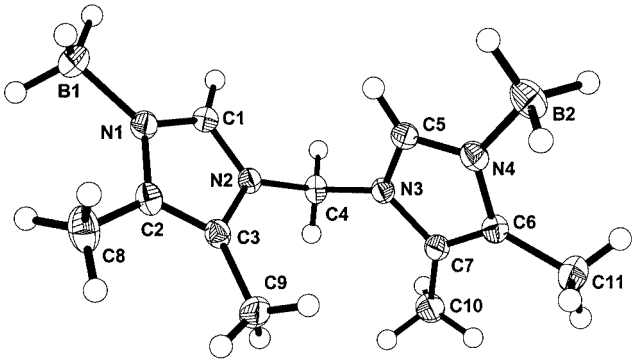

Figure 5. Structure of **5b** in the crystal; selected bond lengths [Å] and angles [°]: B1−N1 1.577(1), N1−C1 1.318(1), C1−N2 1.346(1), N2−C3 1.395(1), C2−C3 1.359(1), N1−C2 1.392(1), N2−C4 1.448(1), C2−C8 1.488(1); B1−N1−C1 125.9(1), N1−C1−N2 109.8(1), N2−C4−N3 110.9(1)

The bond lengths and angles in **5b** are similar to those of **4a**. The N1−C1−N3 angle is 110.9(1)°, and the tetrahedral coordination geometry at the boron atoms is not as strongly distorted as in **4a** [av. angle H−B−H: 111.4(1)°; N−B−H: 107.5(1)°]. The imidazole rings are not symmetric, the N2−C2 and N4−C5 bonds are 0.03(1) Å shorter than N1−C2 and N3−C5.

When 1,1′-bis(4,5-dimethylimidazolyl)methane is allowed to react with BBr_3 in a 1:1 ratio, a yellow solid is obtained that is soluble only in Me_2SO (Scheme 5). The ^{11}B NMR spectrum shows one signal at δ = −12.3, and the ^1H NMR spectrum indicates the formation of a highly symmetric product: two signals are observed for the methyl groups at δ = 2.21 and 2.23, a singlet for the methylene protons is at δ = 6.70 and a signal for the proton at the C2 position is detected at δ = 9.38. In comparison with the compounds **4** and **5** this signal is shifted significantly towards low-field, and is found in a region typical of imidazolium cations rather than borane adducts. This observation together with the very high polarity and symmetry of the product indicate the formation of the cyclic diboronium dibromide **6**.

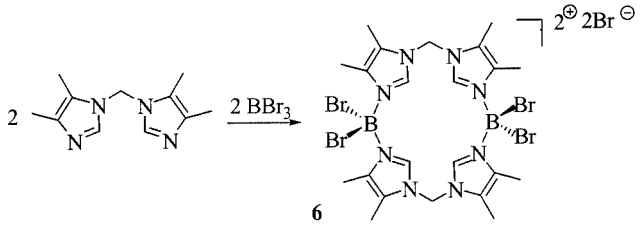

Scheme 5

The signals for the carbon atoms of the imidazole rings are observed at δ = 135.4, 126.4 and 126.1, the methylene bridging carbon atoms at δ = 55.7 and the methyl groups at δ = 9.1 and 8.0. The FAB mass spectrum exhibits peaks derived from the cation of **6** at *m*/*z* = 749 $[M - H]^+$ and *m*/*z* = 579 $[M - BBr_2]^+$.

Attempts to generate dianionic bis(imidazol-2-ylidene) species were unsuccessful starting either from borane adducts of bis(imidazolyl)silane **1** or from the bis(imidazolyl)-boranes **3**. However, the reaction of **5b** with two equivalents of butyllithium at −78 °C causes the ^1H NMR signal of the C2 bonded hydrogen atoms to disappear when the reaction is carried out in $[D_8]$thf and the solution is kept cold. After warming to 20 °C only decomposition products of the dianionic dicarbene **7** were detected, and these could not be characterized. In order to stabilize **7** the titanium complex **8** and the zirconium complex **9** were synthesized by adding a freshly prepared solution of **7** to a solution of the corresponding metallocene dichloride at −78 °C (Scheme 6). Bis(imidazol-2-ylidene)titanium complexes have been prepared previously.[1b]

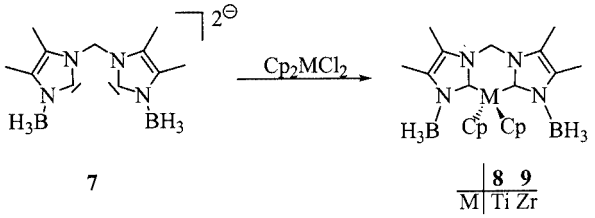

Scheme 6

Compound **8** is an extremely air- and moisture-sensitive red solid. On exposure to air the color changes to green immediately. Remarkably, in the proton NMR spectrum two signals for the Cp rings are observed at δ = 6.45 and 6.53 and two signals for the methylene bridge at δ = 6.08 and 6.31. In the ^{13}C NMR spectrum two signals for Cp rings are found at δ = 109.9 and 111.8, the signal of the methylene carbon is located at δ = 42.1, and the imidazole carbons (C4,4′ and C5,5′) are observed at δ = 132.9 and 134.1. No signal was found for the metal-bonded carbon atoms. In the EI-MS the molecular peak $[M - H]^+$ is detected at *m*/*z* = 407 as well as a peak for $[M - BH_2]^+$ at *m*/*z* = 395. A different fragmentation pattern was found for the colorless **9**: $[M]^+$ was not observed but rather $[M - Cp - H]^+$ at *m*/*z* = 384. More differences are seen in the NMR spectra: **8** exhibits one ^{11}B NMR signal at δ = −22.3, whereas **9** shows two signals at δ = −17.8 and −20.9, respectively. In the proton NMR spectrum of **9**, only one signal is observed for the methylene bridge (δ = 5.47) and for the Cp rings (δ = 6.27). The zirconium-bonded carbon atoms show a signal at δ = 173.6.

The differences in the NMR spectra of **8** and **9** can be explained on results of their X-ray structure analyses. Compound **8** crystallizes with two independent, and almost identical, molecules in the unit cell (Figure 6). The methylene bridge of **8** is turned out of the coordination plane formed by the imidazole rings and the titanium, and, subsequently, the methylene protons become different, one be-

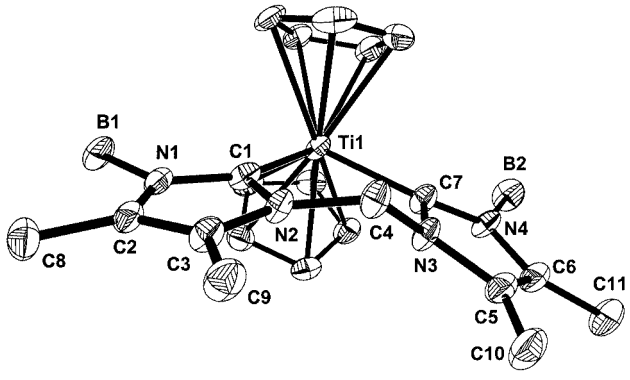

Figure 6. Structure of **8** in the crystal; the CH_2Cl_2 molecule and the carbon-bonded hydrogen atoms have been omitted for clarity; selected bond lengths [Å] and angles [°]: C1−Ti 2.210(5), C7−Ti 2.215(5), N1−B1 1.574(6), N1−C1 1.347(6), C1−N2 1.369(6), N2−C3 1.400(6), C2−C3 1.345(7), N1−C2 1.391(6); N2−C4 1.442(6); C1−Ti−C7 88.3(2), Ti−C1−N2 122.7(3), C1−N2−C4 124.9(4), N2−C4−N3 113.0(4), B1−N1−C1 127.3(4)

coming axial and the other equatorial. The ligand is folded along the C1−Ti axis. A similar behavior of bisimidazolyl ligands has been described by Herrmann et al.[2c] and of a palladium(II) carbene complex of a bistriazole ligand by Diez-Barra et al.[11] Flipping up and down of the methylene bridge does not occur in solution at 20 °C, and this rigid six-membered ring is obviously also the reason for the two different signals of the Cp rings. The C2−Ti−C5 angle is 88.3(2)°, and the N1−C1−N3 angle is a little larger than in **5b** [113.0(4)° vs. 110.9(1)°]. The carbene-carbon to titanium distances are between 2.202(5) and 2.215(5) Å (values for both independent molecules).

The methylene bridge of **9** in the crystal is weakly turned out of the coordination plane and there is no folding observed along the C1−Zr axis (Figure 7). That is the reason why only one signal is found for the methylene protons and for the Cp rings in the ^{1}H NMR spectrum. The C2−Zr−C5 angle is smaller than in **8** (75.4°), and the N1−C1−N3 angle is similar (114.2°), although the carbene-carbon to zirconium distances are quite different: 2.38 (C2−Zr) and 2.30 Å (C5−Zr). This difference is caused by a 3c,2e interaction between B2−H2A−Zr which is non-fluxional in solution at 20 °C according to the two signals in ^{11}B NMR spectrum. Because of this bond compound **9** is an 18-electron complex, while **8** has only 16 valence electrons, which may be the reason for its lower stability.

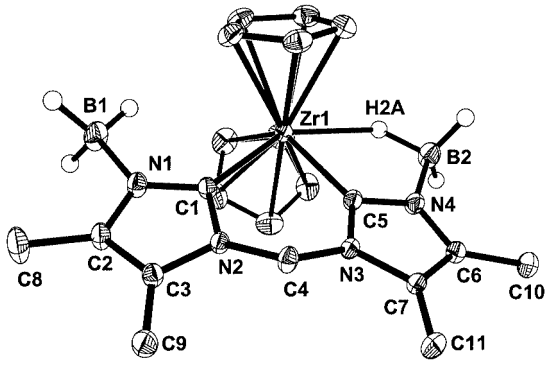

Figure 7. Structure of **9** in the crystal; the carbon-bonded hydrogen atoms have been omitted for clarity; selected bond lengths [Å] and angles [°]: C1−Zr 2.383(1), C5−Zr 2.299(1), N1−B1 1.577(2), N1−C1 1.357(2), C1−N2 1.379(2), N2−C3 1.396(1), C2−C3 1.353(2), N1−C2 1.394(2), N2−C4 1.455(1), B2−H2A 1.23(2), H2A−Zr 2.16(2); C1−Zr−C5 75.4(1), Zr−C1−N2 128.7(1), C1−N2−C4 128.7(1), N2−C4−N3 114.2(1), B1−N1−C1 129.9(1), B2−N4−C5 117.5(1)

Conclusion

It is possible to synthesize monomeric bis(imidazolyl)-boranes when a large, electron-donating substituent such as tetramethylpiperidide is used. Due to the steric requirements of TMP a restricted rotation at the B−N bond is observed for **2b** and **3b**. Treatment of *N*,*N*′-borane-protected bis(4,5-dimethylimidazolyl)methane (**5b**) with butyllithium yields a dianionic dicarbene which coordinates to titanocene and zirconocene complex fragments to form the neutral compounds **8** and **9**. Different coordination numbers at the titanium and the zirconium atom are observed in the X-ray structure analyses of the complexes **8** and **9**.

Experimental Section

General: All reactions were carried out under dry argon, using standard Schlenk techniques. Solvents were dried, distilled and saturated with nitrogen. Glassware was dried with a heat-gun under high vacuum. 1,1′-Bis(imidazolyl)dimethylsilane,[8] 2,2′,6,6′-tetramethylpiperidyldichloroborane,[12] 1,1′-bis(imidazolyl)methane,[13] 1,1′-bis(4,5-dimethylimidazolyl)methane,[13] and 4,5-dimethyl-1-trimethylsilylimidazole[14] were prepared according to literature procedures.

1,1′-Bis(3-borane-imidazolyl)dimethylsilane (1): A 1 M solution of BH_3·thf (20.5 mL) in THF was added dropwise at −78 °C to a solution of 1,1′-bis(imidazolyl)dimethylsilane (1.93 g, 10.0 mmol) in 60 mL of THF. After warming to 20 °C the solvent was removed and the residue washed with pentane, CH_2Cl_2 and recrystallized from a hot saturated solution in THF at −20 °C. The yield was increased by further concentration of the solution to give colorless cubes (1.77 g, 80%). ^{1}H NMR (200 MHz, [D$_8$]THF): δ = 1.11 (s, 6 H, CH_3), 2.2 (br., 6 H, BH_3), 7.15 (s, 2 H, CH=C*H*−N), 7.27 (s, 2 H, C*H*=CH−N), 8.19 (s, 2 H, N=CH−N). ^{11}B NMR (64.2 MHz, [D$_8$]THF): δ = −21.5 (q, $^1J_{B\text{-}H}$ = 91 Hz). ^{13}C NMR (50.3 MHz, [D$_8$]THF): δ = −5.9 (CH_3), 119.9 (*C*H=CH−N), 127.9 (CH=*C*H−N), 139.2 (N=CH−N).

1,1′-Bis(imidazolyl)-1-(2,2′,6,6′-tetramethylpiperidyl)borane (2a): 1-Trimethylsilylimidazole (5.25 g, 37.5 mmol) was added to a solution of 2,2′,6,6′-tetramethylpiperidyldichloroborane (4.10 g, 18.7 mmol) in 100 mL of CH_2Cl_2 at −30 °C. After stirring for 2 h the mixture was allowed to warm to 20 °C and the solvent was removed under vacuum. The product was washed with hexane and dried to give a colorless **2a**. Yield: 4.00 g (75%), m.p. 122 °C. ^{1}H NMR (200 MHz, CD_2Cl_2): δ = 1.15 (s, 12 H, CH_3), 1.60 (m, 4 H, CH_2), 1.85 (m, 2 H, CH_2), 7.04 (s, 2 H, CH=C*H*−N), 7.13 (s, 2 H, C*H*=CH−N), 7.79 (s, 2 H, N=CH−N). ^{11}B NMR (64.2 MHz, CD_2Cl_2): δ = 28.2. ^{13}C NMR (50.3 MHz, CD_2Cl_2): δ = 17.6 ($CH_2CH_2CH_2$), 32.2 (CH_3), 39.6 ($CH_2CH_2CH_2$), 56.5 [$C(CH_3)_2$], 121.9 (*C*H=CH−N), 131.4 (CH=*C*H−N), 142.8 (N=CH−N). EI-MS: *m*/*z* (%) = 285 (2) [M]$^+$, 270 (1) [M − CH_3]$^+$. HR EI-MS ($C_{15}H_{24}{}^{11}BN_5$): calcd. 285.2125; found 285.2111; Δ*m* = 1.4 mmu.

1,1′-Bis(4,5-dimethylimidazolyl)-1-(2,2′,6,6′-tetramethylpiperidyl)-borane (2b): The synthesis of this compound was carried out analogously to **2a** with 4,5-dimethyl-1-trimethylsilylimidazole. Yield: 74%. ^{1}H NMR (200 MHz, CD_2Cl_2): δ = 1.19 (s, 6 H, CH_3-TMP), 1.25 (s, 6 H, CH_3-TMP), 1.47 [s, 6 H, CH_3 (Im)], 1.55 (m, 2 H, CH_2), 1.83 (m, 4 H, CH_2), 2.08 [s, 6 H, CH_3 (Im)], 7.55 (s, 2 H, N=CH−N). ^{11}B NMR (64.2 MHz, CD_2Cl_2): δ = 28.5. ^{13}C NMR (50.3 MHz, CD_2Cl_2): δ = 9.0 [CH_3(Im)], 12.9 [CH_3(Im)], 17.0 ($CH_2CH_2CH_2$), 32.8 (CH_3-TMP), 35.3 (CH_3-TMP), 38.6 ($CH_2CH_2CH_2$), 56.3 [$C(CH_3)_2$], 125.2 (*C*Me=CMe−N), 138.2 (CMe=*C*Me−N), 140.3 (N=CH−N). EI-MS: *m*/*z* (%) = 341 (17) [M]$^+$, 326 (88) [M − CH_3]$^+$. HR EI-MS ($C_{19}H_{32}{}^{11}BN_5$): calcd. 341.2751; found 341.2738; Δ*m* = 1.4 mmu. $C_{19}H_{32}BN_5$ (341.3): calcd. C 66.86, H 9.45, N 20.52; found C 65.52, H 9.37, N 20.09.

1-(2,2′,6,6′-Tetramethylpiperidyl)-1,1′-bis(3-triethylborane-imidazolyl)borane (3a): Triethylborane (2.54 g, 25.9 mmol) was added dropwise to a solution of **2a** (3.71 g, 13.0 mmol) in 60 mL of CH_2Cl_2 at −60 °C. After warming to 20 °C the solution was stirred overnight. The solvent was removed under vacuum and the product

washed with hexane. Recrystallization from CH_2Cl_2 at −20 °C yielded 3.06 g (49%) of a pale-yellow solid, m.p. 114 °C. ^{1}H NMR (200 MHz, $CDCl_3$): δ = 0.34 (q, $^3J_{H-H}$ = 7 Hz, 12 H, CH_2CH$_3$), 0.61 (t, $^3J_{H-H}$ = 7 Hz, 18 H, CH$_2$CH_3), 1.19 (s, 12 H, CH$_3$), 1.65 (m, 4 H, CH$_2$), 1.88 (m, 2 H, CH$_2$), 6.91 (s, 2 H, CH=C*H*−N), 7.28 (s, 2 H, C*H*=CH−N), 7.89 (s, 2 H, N=CH−N). ^{11}B NMR (64.2 MHz, $CDCl_3$): δ = 28.2 (br.,BN$_3$), −0.8 (br., N-BEt$_3$). ^{13}C NMR (50.3 MHz, $CDCl_3$): δ = 9.6 (CH$_2$*C*H$_3$), 14.8 (br., *C*H$_2$CH$_3$), 16.9 (CH$_2$*C*H$_2$CH$_2$), 32.7 (CH$_3$), 39.2 (*C*H$_2$CH$_2$*C*H$_2$), 56.4 [*C*(CH$_3$)$_2$], 121.6 (*C*H=CH−N), 127.5 (CH=*C*H−N), 139.9 (N=CH−N).

1-(2,2′,6,6′-Tetramethylpiperidyl)-1,1′-bis(3-triethylborane-4,5-dimethylimidazolyl)borane (3b): Compound **3b** was prepared from **2b** analogously to **3a**. Yield: 57% colorless cubes. ^{1}H NMR (200 MHz, $CDCl_3$): δ = 0.41 (q, $^3J_{H-H}$ = 7 Hz, 12 H, CH_2CH$_3$), 0.56 (t, $^3J_{H-H}$ = 7 Hz, 18 H, CH$_2$CH_3), 1.15 (s, 6 H, CH$_3$), 1.35 (s, 6 H, CH$_3$), 1.48 (s, 6 H, CH$_3$), 1.56 (m, 2 H, CH$_2$), 1.89 (m, 4 H, CH$_2$), 2.22 (s, 6 H, CH$_3$), 7.73 (s, 2 H, N=CH−N). ^{11}B NMR (64.2 MHz, $CDCl_3$): δ = 29.7 (br., BN$_3$), − 0.9 (br., N-BEt$_3$). ^{13}C NMR (50.3 MHz, $CDCl_3$): δ = 8.5 [CH$_3$(Im)], 9.7 (CH$_2$*C*H$_3$), 10.9 [CH$_3$(Im)], 13.48 (br., *C*H$_2$CH$_3$), 15.4 (CH$_2$*C*H$_2$CH$_2$), 32.2 (CH$_3$-TMP), 35.1 (CH$_3$-TMP), 37.1 (*C*H$_2$CH$_2$*C*H$_2$), 60.0 [*C*(CH$_3$)$_2$], 126.1 (*C*Me=CMe−N), 135.0 (CMe=*C*Me−N), 138.6 (N=CH−N). EI-MS: *m*/*z* (%) = 341 (66) [M − 2BEt$_3$]$^+$, 326 (100) [M − 2BEt$_3$ − CH$_3$]$^+$.

1,1′-Bis(3-triethylboraneimidazolyl)methane (4a): Compound **4a** was prepared from 1,1′-bis(imidazolyl)methane in THF analogously to **3a**. Yield: 80% colorless crystals, m.p. 96 °C. ^{1}H NMR (200 MHz, CD_2Cl_2): δ = 0.30 (q, $^3J_{H-H}$ = 7 Hz, 12 H, CH_2CH$_3$), 0.58 (t, $^3J_{H-H}$ = 7 Hz, 18 H, CH$_2$CH_3), 6.09 (s, 2 H, CH$_2$), 7.06 (s, 2 H, CH=C*H*−N), 7.23 (s, 2 H, C*H*=CH−N), 7.91 (s, 2 H, N=CH−N). ^{11}B NMR (64.2 MHz, CD_2Cl_2): δ = −1.6 (br.). ^{13}C NMR (50.3 MHz, CD_2Cl_2): δ = 9.4 (CH$_2$*C*H$_3$), 14.4 (br., *C*H$_2$CH$_3$), 58.2 (CH$_2$), 118.6 (*C*H=CH−N), 126.9 (CH=*C*H−N), 134.6 (N=CH−N).

1,1′-Bis(3-boraneimidazolyl)methane (5a): A solution of 1,1′-bis-(imidazolyl)methane (1.42 g, 9.58 mmol) in 50 mL of THF was cooled to −78 °C. At this temperature 19.2 mL of BH$_3$·thf (as a 1 M solution in THF) was added through a dropping funnel. The reaction mixture was allowed to warm and stirred for 4 h at 20 °C. During this period a precipitate was formed, which was filtered and washed with pentane. Yield: 1.65 g (98%) white solid. ^{1}H NMR (200 MHz, [D$_6$]DMSO): δ = 2.10 (br., 6 H, BH$_3$), 6.32 (s, 2 H, CH$_2$), 7.10 (s, 2 H, CH=C*H*−N), 7.67 (s, 2 H, C*H*=CH−N), 8.64 (s, 2 H, N=CH−N). ^{11}B NMR (64.2 MHz, [D$_6$]DMSO): δ = −18.4 (br.). ^{13}C NMR (50.3 MHz, [D$_6$]DMSO): δ = 56.8 (CH$_2$), 120.9 (*C*H=CH−N), 127.5 (CH=*C*H−N), 137.9 (N=CH−N). EI-MS: *m*/*z* (%) = 161 (1) [M − BH$_3$ − H]$^+$, 148 (16) [M − 2BH$_3$ + 2H]$^+$.

1,1′-Bis(3-borane-4,5-dimethylimidazolyl)methane (5b): Compound **5b** was prepared from 1,1′-bis(4,5-dimethylimidazolyl)methane analogously to **5a**. Yield: 97%, white solid, m.p. 193 °C. ^{1}H NMR (200 MHz, [D$_6$]DMSO): δ = 2.03 (s, 6 H, CH$_3$), 2.10 (s, 6 H, CH$_3$), 6.25 (s, 2 H, CH$_2$), 8.49 (s, 2 H, N=CH−N). ^{13}C NMR (50.3 MHz, [D$_6$]DMSO): δ = 8.9 (CH$_3$), 9.9 (CH$_3$), 54.6 (CH$_2$), 125.1 (*C*Me=CMe−N), 131.4 (CMe=*CMe*−N), 137.2 (N=CH−N). ^{11}B NMR (64.2 MHz, [D$_6$]DMSO): δ = −20.3 (br.).

Cyclic Diboronium Dibromide 6: 1,1′-Bis(4,5-dimethylimidazolyl)-methane (186 mg, 0.91 mmol) and tribromoborane (228 mg, 0.91 mmol) were each dissolved in 20 mL of CH_2Cl_2. Both solutions were added simultaneously within 45 min to 100 mL of CH_2Cl_2 through dropping funnels. After addition the suspension was stirred for 1 h, the precipitate was filtered off, washed with pentane and dried to yield 133 mg (32%) of **6** as a colorless solid. ^{1}H NMR (200 MHz, [D$_6$]DMSO): δ = 2.21 (s, 12 H, CH$_3$), 2.23 (s, 12 H, CH$_3$), 6.70 (s, 4 H, CH$_2$), 9.38 (s, 4 H, N=CH−N). ^{11}B NMR (64.2 MHz, [D$_6$]DMSO): δ = −12.3. ^{13}C NMR (50.3 MHz, [D$_6$]DMSO): δ = 8.0 (CH$_3$), 9.1 (CH$_3$), 55.7 (CH$_2$), 126.1 (*C*Me=CMe−N), 126.4 (CMe=*C*Me−N), 135.4 (N=CH−N). FAB-MS: *m*/*z* (%) = 749 (1) [M − H]$^+$, 579 (11) [M − BBr$_2$]$^+$.

1,1′-Methylene-(3-borane-4,5-dimethylimidazolyl)-2-diylidene (7): In a Teflon sealed NMR tube, 0.08 mL (0.20 mmol) of *n*BuLi (as a 2.5 M solution in hexane) were evaporated to dryness. At −78 °C 20 mg of **5b** (0.09 mmol) was added, followed by 1 mL of cold [D$_8$]THF. The yellow reaction mixture was shaken and the NMR spectrum measured directly (without warming to 20 °C). ^{1}H NMR (200 MHz, [D$_8$]THF): δ = −1.14 (br.), −0.15 (br.), 0.89 (br.), 1.26 (br.) (signals from BuH and BuLi), 1.79 (s, 6 H, CH$_3$), 1.92 (s, 6 H, CH$_3$), 6.00 (s, 2 H, CH$_2$).

[1,1′-Methylene-(3-borane-4,5-dimethylimidazolyl)-2-diylidene]-dicyclopentadienyltitanium (8): Compound **5b** (220 mg, 0.95 mmol) in 30 mL of THF was treated with 0.8 mL (2.00 mmol) of *n*BuLi (2.5 M solution in hexane) at −78 °C to yield a solution of **7**. After 30 min this solution was added to a stirred mixture of Cp_2TiCl_2 (250 mg, 1.00 mmol) in 10 mL of THF at −78 °C with a transfer cannula. Within 4 h the reaction mixture was allowed to warm to 20 °C. Evaporation of the solvent, washing of the residue with hexane and drying yielded 291 mg (75%) of dark-red **8**. ^{1}H NMR (200 MHz, [D$_6$]DMSO): δ = 2.02 (s, 6 H, CH$_3$), 2.10 (s, 6 H, CH$_3$), 6.08 and 6.31 (br., 2 H, CH$_2$), 6.45 (s, 5 H, C$_5$H$_5$), 6.53 (s, 5 H, C$_5$H$_5$). ^{11}B NMR (64.2 MHz, [D$_6$]DMSO): δ = −22.3 (br.). ^{13}C NMR (50.3 MHz, [D$_6$]DMSO): δ = 8.9 (CH$_3$), 9.9 (CH$_3$), 42.1 (CH$_2$), 109.9 (C$_5$H$_5$), 111.8 (C$_5$H$_5$), 132.9 (*C*Me=CMe−N), 134.1 (CMe=*C*Me−N). EI-MS: *m*/*z* (%) = 407 (2) [M − H]$^+$, 395 (58) [M − BH$_2$]$^+$. HR EI-MS ($C_{21}H_{29}{}^{11}B_2N_4Ti$) [M − H]$^+$: calcd. 407.2058; found 407.2079; Δ*m* = 2.1 mmu.

[1,1′-Methylene-(3-borane-4,5-dimethylimidazol)-2-diylidene]-dicyclopentadienylzirconium (9): Compound **9** was prepared analogously to **8** with Cp_2ZrCl_2. Yield: 80%, white solid. ^{1}H NMR (200 MHz, CD_2Cl_2): δ = 2.08 (s, 6 H, CH$_3$), 2.20 (s, 6 H, CH$_3$), 5.47 (s, 2 H, CH$_2$), 6.27 (s, 10 H, C$_5$H$_5$). ^{11}B NMR (64.2 MHz, [D$_6$]DMSO): δ = −17.8, −20.9. ^{13}C NMR (50.3 MHz, CD_2Cl_2): δ = 9.2 (CH$_3$), 9.3 (CH$_3$), 57.4 (CH$_2$), 110.8 (C$_5$H$_5$), 124.7 (*C*Me=CMe−N), 131.9 (CMe=*C*Me−N), 173.6 (N−C−N). EI-MS: *m*/*z* (%) = 384 (100) [M − Cp − H]$^+$.

Crystal Structure Determinations of 1, 3b, 4a, 5b, 8 and 9: Crystal data and details of the structure determinations are listed in Table 1 and 2. Intensity data were collected at 173 K (**3b**, **4a**), at 190 K (**1**, **8** and **9**) or at 293 K (**5b**) with a Bruker AXS area detector (Mo-K_α radiation λ = 0.71073 Å, graphite monochromator, ω-scan). The structures were solved by direct methods (SHELXS-86)[15] and refined by least-squares methods based on F^2 with all measured reflections (SHELXL-97).[16] All non-hydrogen atoms were refined anisotropically. Hydrogen atoms were located in difference Fourier maps and refined.

CCDC-174038 (**1**), -174039 (**3b**), -174040 (**4a**), -174041 (**5b**), -174042 (**8**) and -174043 (**9**) contain the supplementary crystallographic data for this paper. These data can be obtained free of

Table 1. X-ray crystallographic data for compounds **1**, **3b** and **4a**

	1	**3b**	**4a**
Empirical formula	$C_8H_{18}B_2N_4Si$	$C_{31}H_{62}B_3N_5$	$C_{19}H_{38}B_2N_4$
Formula weight	219.97	537.29	344.15
Crystal system	Monoclinic	Monoclinic	Orthorhombic
Space group	*C*2/*c*	$P2_1/n$	*Pbcn*
a [Å]	16.370(2)	23.000(8)	11.0322(6)
b [Å]	6.3079(5)	11.363(6)	13.3381(8)
c [Å]	14.204(1)	26.98(1)	14.5648(8)
β [°]	117.210(2)	97.83(3)	90
Volume [Å^3]	1304.4(2)	6984(5)	2143.2(2)
Z	4	8	4
Density (calculated) [g/cm^3]	1.120	1.022	1.067
Absorption coefficient [mm^{-1}]	0.155	0.059	0.062
F(000)	472	2384	760
Crystal size [mm^3]	0.33 × 0.31 × 0.12	0.40 × 0.37 × 0.35	0.55 × 0.46 × 0.26
Theta range [°]	2.80 to 32.46	1.09 to 27.10	2.40 to 27.87
Index ranges	−24/+21, 0/+9, 0/+21	−29/+29, 0/+14, 0/+34	0/+14, 0/+17, 0/+18
Reflections collected	13086	58271	13498
Independent reflections	2209 [*R*(int) = 0.030]	15391 [*R*(int) = 0.040]	2462 [*R*(int) = 0.025]
Parameters	105	1196	190
Final *R* indices [$I > 2\sigma(I)$]	*R*1 = 0.0367	*R*1 = 0.0543	*R*1 = 0.0367
R indices (all data)	w*R*2 = 0.1073	w*R*2 = 0.1632	w*R*2 = 0.1031
Largest diff. peak and hole [e/Å^3]	0.428 and −0.191	0.760 and −0.313	0.314 and −0.172

Table 2. X-ray crystallographic data for compounds **5b**, **8** and **9**

	5b	**8**	**9**
Empirical formula	$C_{11}H_{22}B_2N_4$	$C_{21}H_{30}B_2N_4Ti{\cdot}0.5CH_2Cl_2$	$C_{21}H_{30}B_2N_4Zr$
Formula weight	231.95	450.47	451.33
Crystal system	Monoclinic	Triclinic	Orthorhombic
Space group	$P2_1/c$	$P\bar{1}$	$Pna2_1$
a [Å]	8.4793(9)	10.7849(12)	15.4843(8)
b [Å]	15.095(2)	14.693(2)	11.7675(6)
c [Å]	11.316(1)	14.753(2)	11.6797(6)
α [°]	90	90.661(2)	90
β [°]	107.601(2)	104.260(3)	90
γ [°]	90	93.631(2)	90
Volume [Å^3]	1380.5(3)	2260.4(4)	2128.2(2)
Z	4	4	4
Density (calculated) [g/cm^3]	1.116	1.324	1.409
Absorption coefficient [mm^{-1}]	0.067	0.513	0.530
F(000)	504	948	936
Crystal size [mm^3]	0.42 × 0.30 × 0.28	0.30 × 0.23 × 0.04	0.60 × 0.44 × 0.38
Theta range [°]	2.32 to 32.40	1.95 to 25.00	2.17 to 32.16
Index ranges	−12/+12, 0/+21, 0/+16	−12/+12, −17/+17, 0/+17	0/+23, 0/+17, −16/+16
Reflections collected	15064	25227	27203
Independent reflections	4572 [*R*(int) = 0.024]	7947 [*R*(int) = 0.091]	6995 [*R*(int) = 0.021]
Parameters	242	767	373
Final *R* indices [$I > 2\sigma(I)$]	*R*1 = 0.0450	*R*1 = 0.0754	*R*1 = 0.0205
R indices (all data)	w*R*2 = 0.1315	w*R*2 = 0.2396	w*R*2 = 0.0569
Largest diff. peak and hole [e/Å^3]	0.426 and −0.186	1.210 and −1.363	0.372 and −0.301

charge at www.ccdc.cam.ac.uk/conts/retrieving.html [or from the Cambridge Crystallographic Data Centre, 12, Union Road, Cambridge CB2 1EZ, UK; Fax: (internat.) +44-1223/336-033; E-mail: deposit@ccdc.ac.uk].

Acknowledgments

We thank the Deutsche Forschungsgemeinschaft (SFB 247) for financial support.

[1] [1a] A. J. Arduengo, R. L. Harlow, M. Kline, *J. Am. Chem. Soc.* **1991**, *113*, 361−363. [1b] A. J. Arduengo has presented bis(imidazol-2-ylidene)titanium complexes in many of his lectures, although the compounds are yet to be published. Details may be obtained from his web page (http://home.att.net/~ajarduengo/MOLSELDRIVER8.html)

[2] [2a] W. A. Herrmann, M. Elison, J. Fischer, C. Köcher, G. R. J. Artus, *Chem. Eur. J.* **1996**, *2*, 772−780. [2b] R. D. Douthwaite, M. L. H. Green, P. J. Cilcock, P. T. Gomes, *Organometallics*

2001, *20*, 2611−2615. [2c] K. Öfele, W. A. Herrmann, D. Mihalios, M. Elison, E. Herdtweck, T. Priermeier, P. Kiprof, *J. Organomet. Chem.* **1995**, *498*, 1−14. [2d] K. Öfele, W. A. Herrmann, D. Mihalios, M. Elison, E. Herdtweck, W. Scherer, J. Mink, *J. Organomet. Chem.* **1993**, *459*, 177−184.

[3] [3a] W. A. Herrmann, C.-P. Reisinger, M. Spiegler, *J. Organomet. Chem.* **1998**, *557*, 93−96. [3b] Z. Zhang, J. Huang, M. L. Trudell, S. P. Nolan, *J. Org. Chem.* **1999**, *64*, 3804−3805.

[4] A. Wacker, H. Pritzkow, W. Siebert, *Eur. J. Inorg. Chem.* **1998**, 843−849.

[5] A. Wacker, Dissertation, Universität Heidelberg **1999**.

[6] A. Wacker, C. G. Yan, G. Kaltenpoth, A. Ginsberg, A. M. Arif, R. D. Ernst, H. Pritzkow, W. Siebert, *J. Organomet. Chem.*, in print.

[7] N. Kuhn, T. Kratz, D. Bläser, R. Boese, *Inorg. Chim. Acta* **1995**, *238*, 179−181.

[8] A. Frenzel, M. Gluth, R. Herbst-Irmer, U. Klingenbiel, *J. Organomet. Chem.* **1996**, *514*, 281−286.

[9] A. Weiss, H. Pritzkow, W. Siebert, *Angew. Chem.* **2000**, *112*, 558−559; *Angew. Chem. Int. Ed.* **2000**, *39*, 547−549.

[10] M. Hesse, H. Meier, B. Zeeh, *Spektroskop. Meth. Organ. Chem.* 5. Aufl. **1995**, Georg Thieme Verlag, Stuttgart, New York.

[11] G. Bertrand, E. Diez-Barra, J. Fernandez-Baeza, H. Gornitzka, A. Moreno, A. Otero, R. I. Rodriguez-Curiel, J. Tejeda, *Eur. J. Inorg. Chem.* **1999**, 1965−1971.

[12] H. Nöth, S. Weber, *Z. Naturforsch., Teil B* **1983**, *38*, 1460−1465.

[13] R. M. Claramunt, J. Elguero, T. Meco, *J. Heterocycl. Chem.* **1983**, *20*, 1245−249.

[14] C. Bruynes, *J. Org. Chem.* **1982**, *20*, 3966.

[15] G. M. Sheldrick, *SHELXS-86*, Univ. Göttingen, **1986**.

[16] G. M. Sheldrick, *SHELXL-97*, Univ. Göttingen, **1997**.

Received November 27, 2001
[I01481]

Salicylaldimine Dizinc Complexes: Activation of Water Molecules and Fixation of CO_2 in the Coordination Sphere of Zinc

Manfred Döring,*[a] Michael Ciesielski,[a] Olaf Walter,[a] and Helmar Görls[b]

Dedicated to Prof. Ernst Anders on the occasion of his 60th birthday

Keywords: Zinc / N ligands / N,O ligands / Carbon dioxide fixation / Enzyme models

Bi- and tetranuclear zinc complexes of the tridentate N,N,O ligand [{[2-(2-pyridyl)ethyl]imino}methyl]phenol (HL) and their enzyme-like reactions are described. The coordinated water molecules in a dizinc complex of this ligand can be deprotonated reversibly similar to those in the resting states of zinc enzymes. The resulting tetranuclear complex bearing bridging hydroxide ions allows the reversible uptake of CO_2. Whereas the coordination of hydrogen carbonate has not been observed, a tetranuclear carbonate complex with a unique structure was isolated. Its carbonate ion is coordinated to all four zinc atoms. The X-ray structures of the reported complexes are discussed.
(© Wiley-VCH Verlag GmbH, 69451 Weinheim, Germany, 2002)

Introduction

Zinc-containing enzymes accelerate the reversible hydration of carbon dioxide, the cleavage of peptide bonds, the hydrolysis of phosphate monoesters, and many other hydrolytic processes in biological systems with a high efficiency. The catalytic function of the zinc enzymes is not only essential for organisms but also of great theoretical interest. The activation of carbon dioxide and cleavage of amide and ester bonds in the coordination sphere of a metal also represent important reactions in synthetic chemistry. It is not surprising, therefore, that many efforts have been made to synthesize zinc-containing complexes that mimic the structural and functional features of the active centres in zinc enzymes.

Recent investigations revealed a distorted tetrahedral ligand geometry around the zinc ions in many zinc enzymes. Three coordination sites at their metal centres are coordinated by various amino acid residues (imidazolyl, -COOH, -SH), depending on the specific functions of the enzymes.[1] In the resting states of the enzymes, the fourth coordination site is occupied by a water molecule, which can be easily deprotonated, thus providing the catalytically active hydroxide form of the enzyme.

[a] Institute for Technical Chemistry (ITC-CPV), Forschungszentrum Karlsruhe, P. O. Box 3640, 76021 Karlsruhe, Germany
Fax: (internat.) +49-7247/822-244
E-mail: manfred.doering@itc-cpv.fzk.de
[b] Institute for Inorganic and Analytical Chemistry, Friedrich-Schiller-Universität Jena, August-Bebel-Str. 2, 07743 Jena, Germany
E-mail: goerls@xa.nlwl.uni-jena.de

To synthesize zinc complexes by mimicking the active centres of mononuclear zinc enzymes, encapsulating tripodal hydrotris(pyrazolyl)borates (Tp ligands) and cyclen ligands are most frequently used. Vahrenkamp et al.[2–4] have developed the "Freiburg enzyme model" — zinc complexes with the aforementioned Tp ligands bearing sterically demanding substituents. Such complexes possess structural parameters similar to those of the active centre of the hydroxide and the water form of the zinc enzyme carbonic anhydrase (CA). The tetrahedral geometries around the zinc ions in these compounds are enforced by the pocket-like rigid Tp ligands. Parkin et al.[5] converted such a tetrahedral TpZnOH complex into the corresponding aqueous form by protonation and were even able to reverse this process. Tetrahedral zinc complexes with tripodal cyclen ligands like 1,5,9-triazacyclododecane have been reported to be some of the best functional models for CA.[6–10] Apart from the above examples, other more flexible unsymmetrical ligands with mixed N_xO_y donor environments have been established.[11–14] These ligands have been made to reproduce structural and functional properties of biologically relevant enzymes with more than one zinc ion in their active sites.

Zinc complexes with enzyme-analogous hydrolytic activities could be valuable in synthetic chemistry, too. However, the application of zinc complexes as catalysts for hydrolytic processes requires a deeper insight into their structure-reactivity relationship, and, especially, additional information about the reactivity of water molecules in the coordination sphere of zinc. In the present article, we describe bi- and tetranuclear zinc complexes of the Schiff base 2-[{[2-(2-pyridyl)ethyl]imino}methyl]phenol HL.

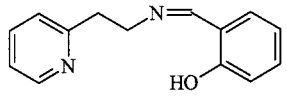

HL

Although the tridentate ligand chosen is not sufficiently rigid to enforce a tetrahedral geometry around the zinc centre, a zinc complex with coordinated and reactive water molecules is readily accessible. The Zn-OH_2 unit in this binuclear complex can be deprotonated by the addition of sodium hydroxide. Even the uptake of carbon dioxide is performed as a reversible pH-dependent process. However, attempts to isolate a complex with coordinated hydrogen carbonate were not successful. Only a carbonate-containing complex with an unusual structural motif was obtained. The above reactions were found to be very sensitive, and other products could be obtained under slightly different conditions. The complexes were characterized by X-ray structural determinations.

Results and Discussion

The binuclear complex **1** is formed by the reaction of equivalent amounts of HL, zinc perchlorate and sodium hydroxide in aqueous methanol. Compound **1** bears the deprotonated ligand L and a water molecule at both zinc ions. With less water in the solvent, the complexation yields the binuclear complex **2** with zinc-coordinated methanol molecules instead of the complexed water.

$[\mathbf{L}\ Zn(H_2O)]_2\,(ClO_4)_2$ **1**

$[\mathbf{L}\ Zn(CH_3OH]_2\,(ClO_4)_2$ **2**

Both complexes were subjected to X-ray structural determinations. The X-ray structural analysis of **1** and **2** revealed distorted square-pyramidal environments around the metal centres, which are linked by phenolate bridges (see Figure 1 and 2).

The coordinated water molecules in **1** are arranged in a *cis* configuration, whereas the methanol molecules in **2** are in a *trans* configuration. Both configurations are possible in dizinc complexes of L because of the flexibility of the ligand and the flexibility of the phenolate links. The water molecules in the coordination sphere of **1** are acidified in a similar manner to those in the Zn-OH_2 units of zinc enzymes. Therefore, this complex is accessible to a number of conversions.

In a methanolic solution of **1** with half an equivalent of sodium hydroxide at moderate temperatures (20−50 °C) under anaerobic conditions, one water molecule in **1** is deprotonated and the tetranuclear complex **3** is formed by dimerization.

$[(\mathbf{L}\ Zn)_2OH]_2\,(ClO_4)_2$ **3**

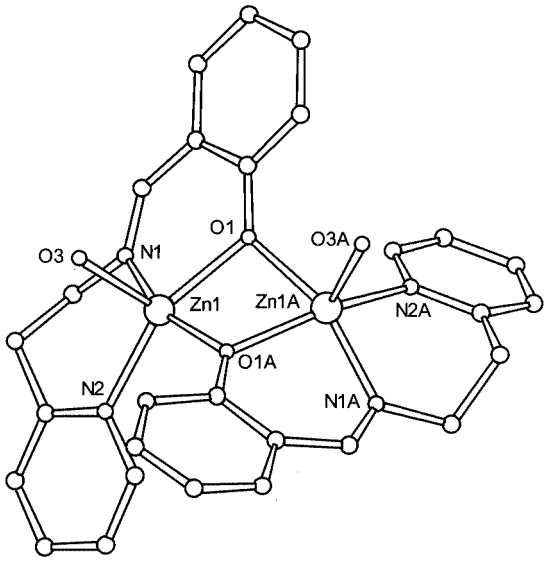

Figure 1. Molecular structure of **1** (cation only) with selected bond lengths [Å] and angles [°]: Zn1−O1 2.056(2), Zn1−O2 2.040(2), Zn1−N2 2.052(3), Zn1−N1 2.106(3), Zn1−O3 2.090(3), Zn2−O1 2.031(2), Zn2−O2 2.053(2), Zn2−O4 2.084(3), Zn1−Zn2 3.1035(6); O1−Zn1−N1 155.48(10), O1−Zn1−O3 102.62(10), O1−Zn2−O2 75.78(10), O1−Zn2−N4 160.93(10), O1−Zn2−O4 99.14(11), O1−Zn2−N3 98.15(10), O2−Zn1−O1 75.55(10), O2−Zn1−O3 98.55(12), O2−Zn1−N1 97.05(10), O2−Zn1−N2 160.43(11), O2−Zn2−N3 154.93(10), O2−Zn2−N4 87.09(11), O3−Zn1−N1 101.59(11), O4−Zn2−N3 102.11(11), N2−Zn1−O1 87.60(11), N2−Zn1−O3 94.73(13), N2−Zn1−N1 94.27(11), N4−Zn2−N3 93.86(11), N4−Zn2−O4 92.72(12), Zn1−O2−Zn2 98.62(10), Zn1−O1−Zn2 98.81(10)

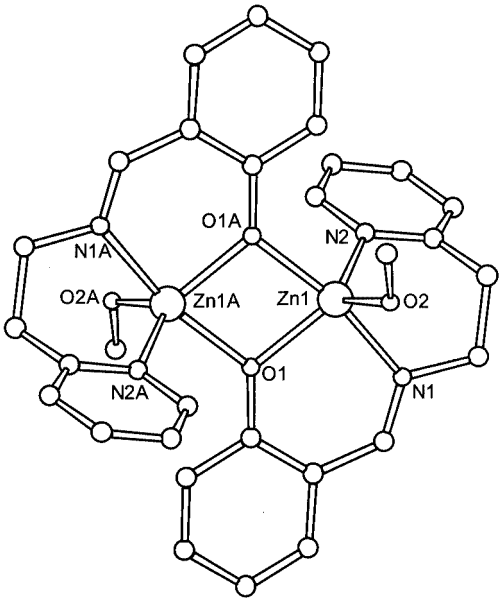

Figure 2. Molecular structure of **2** (cation only) with selected bond lengths [Å] and angles [°]: Zn1−O1 2.0154(10), Zn1−O2 2.0564(12), Zn1−O1A 2.0618(10), Zn1−N1 2.0697(12), Zn1−N2 2.0641(13), Zn1−Zn1A 3.1511(4); O1−Zn1−O2 114.96(5), O1−Zn1−O1A 78.78(4), O2−Zn1−O1A 95.63(5), O1−Zn1−N2 122.08(5), O2−Zn1−N2 122.92(5), O1A−Zn1−N2 96.88(5), O1−Zn1−N1 89.93(5), O2−Zn1−N1 89.62(5), O1A−Zn1−N1 168.70(5), N2−Zn1−N1 88.59(5)

Compound **3** has a dimeric structure with two identical binuclear halves linked via two Zn−OH−Zn bridges between the zinc ions. In **3**, all zinc ions are in distorted square-pyramidal coordination spheres and the metal centres in the halves are linked by phenolates as in complex **1**. The bond lengths and angles in the dizinc units of **3** are very similar to those in **1**. Therefore, **3** can be considered an OH-bridged dimer of **1**. Zinc complexes containing Zn−OH−Zn bridging moieties have been reported previously.[14−18]. The nonbonding distances between the zinc ions in the Zn−O−Zn moieties of **3** are 3.5 Å. Very similar Zn−Zn separations (3.55 Å, 3.61 Å) have been reported for other zinc complexes with only one hydroxide bridge between the zinc centres.[15,18] Compound **3** can be reprotonated to the water complex **1**. In the presence of a larger amount of sodium hydroxide the conversion of **1** becomes irreversible. Under these conditions, a ligand distribution reaction occurs. Zinc hydroxide is precipitated from the mixture and complex **4** is formed.

$$[L_2\,Zn]_2\,[Na\,(MeOH)\,ClO_4]$$

4

Its molecular structure is shown in Figure 3. Compound **4** can be considered as a dimer with two mononuclear complexes. The mononuclear halves of **4** are only linked by a fivefold coordinated sodium ion. In contrast to the other complexes reported here, two molecules of the deprotonated ligand are bound to each metal in **4**. The zinc ions in **4** are also fivefold coordinated and appear in a strongly distorted square-pyramidal geometry.

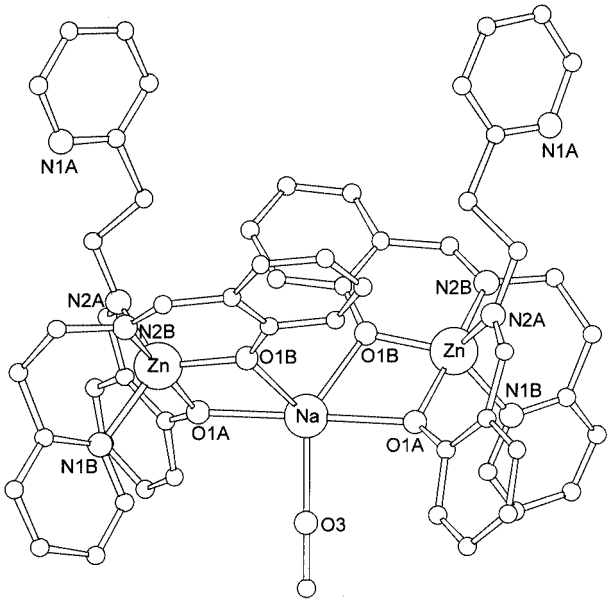

Figure 3. Molecular structure of **4** (cation only) with selected bond lengths [Å] and angles [°]: Zn−O1A 2.035(4), Zn−O1B 1.986(3), Zn−N1B 2.125(5), Zn−N2A 2.094(5), Zn−N2B 2.144(5), Na−O3 2.297(11), Na−O1A 2.385(3), Na−O1B 2.392(4); O1A−Zn−O1B 84.4(1), O1A−Zn−N1B 91.7(2), O1A−Zn−N2A 89.1(2), O1A−Zn−N2B 170.6(2), O1B−Zn−N1B 121.6(2), O1B−Zn−N2B 89.7(2), O1B−Zn−N2A 122.7(2), N2A−Zn−N1B 115.5(2), N1B−Zn−N2B 85.2(2)

The reactivity of **1** towards air and carbon dioxide has also been investigated. Carbon dioxide is taken up by deprotonated **1** in the presence of air. The gas is released again after the mixture has been acidified carefully. Similar to the hydration of CO_2 in the catalytic cycle of CA, this reaction is found to be reversible at moderate temperatures and is pH-dependent. The CA mechanism involves the formation of an intermediate with a Zn-CO_2H unit. It turned out to be impossible to isolate a complex with coordinated hydrogen carbonate. In the reaction of **1** with CO_2 from air and half an equivalent of NaOH, only the complex **3a** is obtained at moderate temperatures.

$$[(L\,Zn)]_2\,(OH)]_2\,(ClO_4)_{2-x}\,(CO_3H)_x \qquad (0 < x < 1)$$

3a

Its X-ray structure is presented in Figure 4. Compound **3a** contains the same coordination sphere as described for **3**. Only one perchlorate anion is partially replaced by hydrogen carbonate. The content of HCO_3^- in **3a** depends on the partial pressure of CO_2 in the atmosphere. The hydrogen carbonate is not formed by a simple absorption of carbon dioxide in an alkaline solution, because the reaction mixture does not contain any excess of hydroxide ions. The uptake of carbon dioxide can be explained by an intermediate interaction of CO_2 with the zinc centres in **3**.

At higher temperatures and in the presence of pure carbon dioxide, the CO_2 is incorporated into the coordination sphere of zinc, and the reaction provides the carbonate complex **5**.

$$[(L\,Zn)_4\,CO_3\,(MeOH)_4]\,(ClO_4)_2$$

5

Most revealing is the molecular structure of **5** (Figure 5), which was obtained by X-ray structural analysis. Complex **5** has a binuclear substructure, two mononuclear units, and a carbonate anion, which is encapsulated inside the molecule. Carbonate-containing zinc complexes of polydentate ligands are well known[9,13,19−21] and, usually, three identical metal centres are attached to the carbonate oxygen atoms. In **5** the carbonate is coordinated to four zinc ions. Furthermore, the carbonate acts as a bridging ligand linking both mononuclear units of the molecule with an oxygen atom. Two differently bound zinc ions are six-coordinated with slightly distorted octahedral geometries. One zinc ion is surrounded by the tridentate ligand L, two methanol molecules, and a carbonate oxygen. The other zinc ion is incorporated into the binuclear substructure of **5** and bears two molecules of the ligand, a methanol molecule, and a carbonate oxygen. One L acts as a bridging ligand, and only its phenolate oxygen is bound to this zinc. The remaining two zinc ions in **5** are fivefold coordinated with a different bonding. One of these zinc ions belongs to the binuclear substructure of **5**. It bears two molecules of L as well as a carbonate oxygen. It is the only zinc ion in **5** without any coordinated methanol. The geometry around this zinc can be described as highly distorted square pyramidal. Whereas

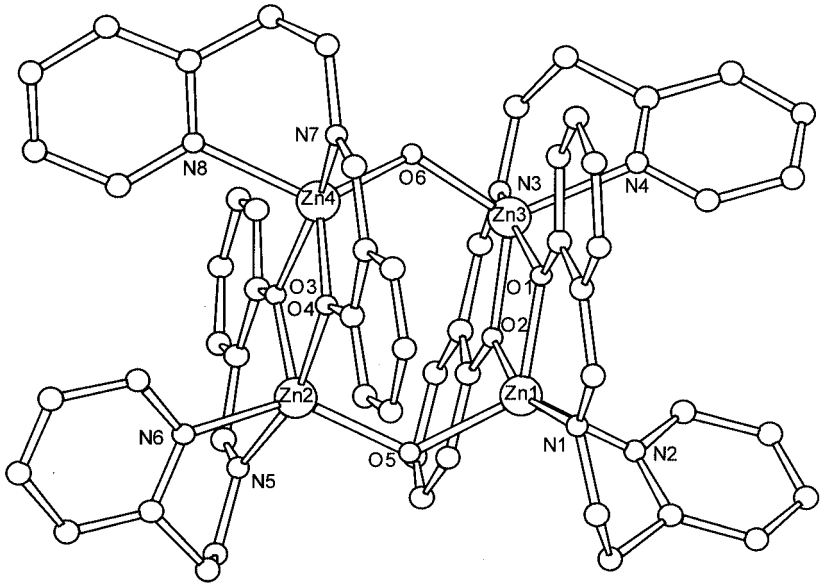

Figure 4. Coordination environments of the zinc ions in **3a** with selected bond lengths [Å] and angles [°]: Zn1−O1 2.013(5), Zn1−O2 2.109(5), Zn1−O5 1.952 (5), Zn1−N1 2.081(6), Zn1−N2 2.132(6), Zn2−O3 2.004(5), Zn2−O4 2.104(6), Zn2−O5 1.952(5), Zn2−N5 2.099(7), Zn2−N6 2.127(7), Zn3−O1 2.111(5), Zn3−O2 2.2.012(5), Zn3−O6 1.949(5), Zn3−N3 2.107(6), Zn3−N4 2.150(6), Zn4−O3 2.137(5), Zn4−O4 2.010(6), Zn4−O6 1.958(5), Zn4−N7 2.092(7), Zn4−N8 2.121(7); O1−Zn1−O2 77.4(2), O1−Zn1−O5 124.4(2), O1−Zn1−N1 89.0(2), O1−Zn1−N2 111.8(2), O2−Zn1−O5 97.4(2), O2−Zn1−N2 90.8(2), O5−Zn1−N1 98.5(2), N1−Zn1−N2 85.0(2), O3−Zn2−O5 123.1(2), O3−Zn2−O4 77.2(2), O3−Zn2−N5 90.0(2), O3−Zn2−N6 113.0(3), O4−Zn2−O5 95.7(2), O4−Zn2−N6 91.0(3), O5−Zn2−N5 99.2(2), O5−Zn2−N6 123.7(2), N5−Zn2−N6 85.3(3), O1−Zn3−O2 77.3(2), O1−Zn3−O6 96.1(2), O1−Zn3−N3 161.4(2), O1−Zn3−N4 91.4 (2), O2−Zn3−O6 120.1(2), O2−Zn3−N3 88.3(2), O2−Zn3−N4 85.5(2), O6−Zn3−N3 101.4(2), O6−Zn3−N4 119.7(2), O3−Zn4−O4 76.3(2), O3−Zn4−O6 98.1(2), O3−Zn4−N7 160.7(3), O3−Zn4−N8 91.8(2), O4−Zn4−O6 125.7(2), O4−Zn4−N7 88.0(3), O4−Zn4−N8 117.5(3), O6−Zn4−N7 100.3(3), N7−Zn4−N8 85.3(3), Zn1−O1−Zn3 102.6(2), Zn1−O2−Zn3 102.7(2), Zn1−O5−Zn2 123.6(2), Zn2−O3−Zn4 102.5(2), Zn2−O4−Zn4 103.5(2), Zn3−O6−Zn4 123.7(3)

one L molecule is bound to this zinc ion by its three donor atoms, the second one only occupies one coordination site with its phenolate oxygen. The phenolate oxygen acts as bridging atom and links the two metal centres in this substructure. The other fivefold coordinated zinc ion in **5** is the centre of a mononuclear unit and has a slightly distorted square-pyramidal geometry. The coordination sphere contains three donor atoms of L as well as a methanol oxygen and a carbonate oxygen.

Generally, the insertion of CO_2 into Zn−OH−Zn bridges does not occur. However, Karlin et al.[20] reported an exceptional case of a dinuclear zinc hydroxide complex that absorbed atmospheric carbon dioxide. Our experimental results indicate that complexes **3** and **3a** are not sufficiently reactive to bind the carbon dioxide in the coordination sphere of zinc, although it could be possible that the bonds in the Zn−OH−Zn bridges of **3** or **3a** are weakened at higher temperatures, leading to the insertion of water molecules. Complexes with the resulting Zn−OH···H_2O−Zn unit are reported to be more reactive towards CO_2 [18] and able to coordinate it as hydrogen carbonate. The last step of this reaction cascade would consist of the conversion of the hydrogen carbonate containing complex into **5**. Unfortunately we were not able to isolate any of the intermediates proposed.

Solutions of the zinc complexes of L show a remarkably intense blue fluorescence if irradiated with UV light.

Conclusion

The Schiff base L shows a great variety in its complex chemistry with zinc. The key to the successful exploitation of its synthetic potential is the smooth access to the binuclear water-containing complex **1**, which was found to be a suitable starting material for subsequent conversions. Our intention of performing enzyme-like biomimetic reactions with **1** was fulfilled in some respects. Like the resting states in zinc enzymes, **1** could be activated by deprotonation of its coordinated water molecules. The resulting hydroxide-containing complex was subjected to further conversions. Unfortunately, a complex with a highly reactive Zn-OH unit such as is found in the active form of the natural zinc enzymes has not been obtained. The OH ions in the isolated complexes of **3** and **3a** are involved in Zn−OH−Zn bridges and are significantly less reactive. Therefore, the hydroxide function in **3** was found to be unreactive towards carbon dioxide at moderate temperatures. The reaction of **3** was effected at higher temperatures but resulted in the carbonate-containing complex **5**. Thus, a complex with the Zn-OCO_2H motif has not been obtained. Nevertheless, the unique structural features of the carbonate complex **5** reveal the extraordinary synthetic capacity of L in zinc complex chemistry. One property of L is its capability to form multinuclear shell-like systems that encapsulate small molecules like carbonate.

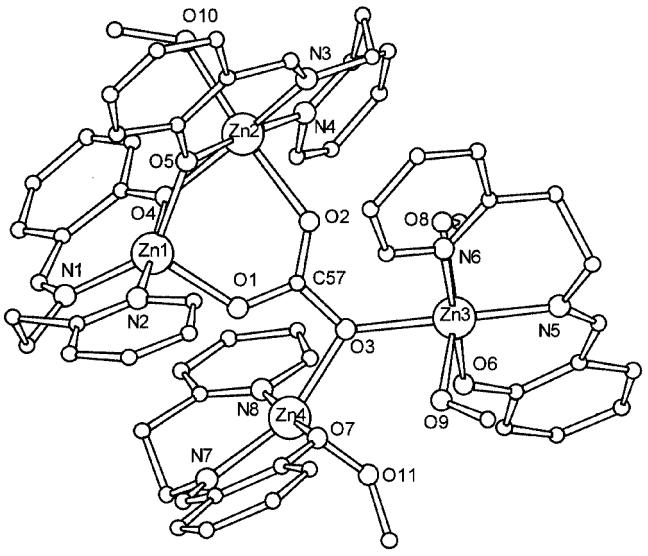

Figure 5. Molecular structure of **5** (cation only) with selected bond lengths [Å] and angles [°]: Zn1−O1 2.002(3), Zn1−O4 2.101(4), Zn1−O5 2.015(3), Zn1−N1 2.0023(4), Zn1−N2 2.146(5), Zn2−O2 2.150(3), Zn2−O4 2.114(3), Zn2−O5 2.077(4), Zn2−O10 2.166(4), Zn2−N3 2.068(4), Zn2−N4 2.133(4), Zn3−O3 2.151(3), Zn3−O6 2.040(4), Zn3−O8 2.226(4), Zn3−O9 2.111(4), Zn3−N5 2.078(4), Zn3−N6 2.172(4), Zn4−O3 2.076(3), Zn4−O7 2.034(4), Zn4−O11 2.081(4), Zn4−N7 2.010(5), Zn4−N8 2.205(5); O1−Zn1−O5 104.89(14), O1−Zn1−N1 115.36 (17), O5−Zn1−N1 138.71(17), O1−Zn1−O4 93.31(14), O5−Zn1−O4 89.88(16), O1−Zn1−N2 92.01(16), O5−Zn1−N2 94.84(16), N1−Zn1−N2 92.65(18), O4−Zn1−N2 172.47(16), O1−Zn1−Zn2 83.31(10), O5−Zn1−Zn2 42.28(10), N1−Zn1−Zn2 132.22(13), O4−Zn1−Zn2 43.53(9), N2−Zn1−Zn2 132.16(12), O5−Zn2−O4 76.99(14), N3−Zn2−O4 164.94(16), O5−Zn2−N4 175.22(15), N3−Zn2−N4 93.03(18), O4−Zn2−N4 101.92(16), O5−Zn2−O2 92.96(14), N3−Zn2−O2 89.78(15), O4−Zn2−O2 90.39(13), N4−Zn2−O2 82.37(15), O5−Zn2−O10 94.40(14), N3−Zn2−O10 89.01(16), O4−Zn2−O10 92.70(14), N4−Zn2−O10 90.30(15), O2−Zn2−O10 172.50(14), O5−Zn2−Zn1 40.75(10), N3−Zn2−Zn1 122.86(13), O4−Zn2−Zn1 43.19(10), N4−Zn2−Zn1 135.98(12), O2−Zn2−Zn1 74.01(9), O10−Zn2−Zn1 112.75(10), O6−Zn3−N5 88.50(16), O6−Zn3−O9 91.57(16), N5−Zn3−O9 101.59(16), O6−Zn3−O3 84.68(13), N5−Zn3−O3 170.44(16), O9−Zn3−O3 85.32(14), O6−Zn3−N6 178.24(17), N5−Zn3−N6 92.12(17), O9−Zn3−N6 86.69(17), O3−Zn3−N6 94.89(15), O6−Zn3−O8 98.89(15), N5−Zn3−O8 90.81(15), O9−Zn3−O8 164.01(14), O3−Zn3−O8 83.65(13), N6−Zn3−O8 82.76(15), N7−Zn4−O7 90.59(18), N7−Zn4−O3 156.59(16), O7−Zn4−O3 86.96(15), N7−Zn4−O11 109.08(17), O7−Zn4−O11 94.51(16), O3−Zn4−O11 94.33(14), N7−Zn4−N8 92.51(19), O7−Zn4−N8 175.95(17), O3−Zn4−N8 89.16(15), O11−Zn4−N8 86.92(16), N7−Zn4−O1 99.73(6), O7−Zn4−O1 95.34(15), O3−Zn4−O1 57.43(12), O11−Zn4−O1 149.39(14), N8−Zn4−O1 81.58(14)

A systematic variation of the ligand structure should enable the synthesis of hydroxide-containing zinc complexes with a higher hydrolytic reactivity than **3**.

If the Zn−OH−Zn bridges in **3** are sufficiently weakened, they might become more reactive towards CO_2 and other substrates even at ambient temperatures. With the flexibility of the ligand being maintained, a better reaction pathway of the substrate would be achieved, as for the carbonate ion in **5**. Furthermore, an additional activation of the coordinated substrate by an adjacent zinc centre in bi- or multinuclear complexes would also be advantageous. The challenge of designing zinc complexes with an enzyme-like hydrolytic activity towards carbon dioxide and amide bonds persists.

Experimental Section

Starting materials were obtained commercially and used without purification.

1: 2-(2-Aminoethyl)pyridine (1.83 g, 15 mmol) in 10 mL of methanol and salicylaldehyde (1.83 g, 15 mmol) in 15 mL of methanol were combined at ambient temperature to give a deep yellow solution. Then, zinc perchlorate hexahydrate (5.59 g, 15 mmol) in 25 mL of aqueous 90% methanol was added. The solution was warmed to 35 °C, and sodium hydroxide (0.6 g, 15 mmol) in 20 mL of methanol was added while stirring. After stirring at 35 °C, the mixture was filtered. A strong fluorescent pale-yellow solution and yellow crystals of the product were obtained. Yield 78%. $C_{28}H_{30}Cl_2N_4O_{12}Zn_2$ (816.24): calcd. C 41.20, H 3.70, Cl 8.69, N 6.86; found C 40.80, H 3.45, Cl 8.55, 7.05 N.

2: 2-(2-Aminoethyl)pyridine (1.83 g, 15 mmol) and salicylaldehyde (1.83 g, 15 mmol) were combined in 50 mL of dry methanol, and zinc perchlorate hexahydrate (5.59 g, 15 mmol) in 20 mL of dry methanol was added. After warming to 35 °C, a solution of sodium hydroxide (0.6 g, 15 mmol) in 20 mL of methanol was added while stirring. The mixture was then filtered. Yellow crystals of the product were formed from the pale-yellow fluorescent solution. Yield 75%. $C_{32}H_{42}Cl_2N_4O_{12}Zn_2$ (908.34): calcd. C 42.31, H 4.66, Cl 7.81, N 6.17; found C 41.88, H 4.87, Cl 7.69, N 5.99.

3: A solution of **1** in 100 mL of methanol freshly prepared from 2-(2-aminoethyl) pyridine (1.83 g, 15 mmol), salicylaldehyde (1.83 g, 15 mmol), zinc perchlorate hexahydrate (5.59 g, 15 mmol), and sodium hydroxide (0.6 g, 15 mmol) was heated to reflux, and sodium hydroxide (0.3 g, 7.5 mmol) was added. Whilst heating at reflux for 30 min under argon the NaOH dissolved and a product precipitated. The mixture was filtered hot, and the volume of the pale-yellow filtrate was reduced. The solution was then cooled slowly in a closed vessel. Compound **3** precipitated as large colourless crystals. Yield about 70%. $C_{56}H_{54}B_2F_8N_8O_6Zn_2$ [22] (1239.46): calcd. C 54.27, H 4.39, N 9.04; found C 54.19, H 4.35, N 9.11.

3a: A solution of **3** in 100 mL of methanol was freshly prepared from salicylaldehyde (1.83 g, 15 mmol), 2-(2-aminoethyl)pyridine (1.83 g, 15 mmol), zinc perchlorate hexahydrate (5.59 g, 15 mmol), and sodium hydroxide (0.9 g, 15 mmol). The mixture was then stirred at 60 °C for 45 min in the presence of air. The mixture was filtered hot and slowly cooled to 5 °C. Compound **3a** was obtained as large colourless crystals. Yield about 70%.[23]

Reaction of 3 with Perchloric Acid: Compound **3** (2.05 g, 1.5 mmol) was dissolved in 100 mL of methanol. 5% aqueous perchloric acid (6.03 mL, 3 mmol) was then added within a period of 10 min at room temperature. The mixture was stirred for 30 min. Crystals of **1** were obtained upon reducing the volume of the solution slowly.

Reaction of 3a with Perchloric Acid: In an analogous manner, **3a** was treated with 5% aqueous perchloric acid. Crystals of **1** were obtained upon reducing the volume of the solution slowly.

4: A solution of **1** in 100 mL of aqueous methanol freshly prepared from salicylaldehyde (1.83 g, 15 mmol), 2-(2-aminoethyl)pyridine (1.83 g, 15 mmol), zinc perchlorate hexahydrate (5.59 g, 15 mmol), and sodium hydroxide (0.6 g, 15 mmol) was heated to reflux. Then, sodium hydroxide (0.6 g, 15 mmol) was added, and the mixture was

Table 1. Crystallographic data of the complexes **1**, **2**, **3a**, **4**, and **5**

	1	**2**	**3a**	**4**	**5**
Empirical formula	$C_{28}H_{30}Cl_2N_4O_{12}Zn_2$	$C_{32}H_{42}Cl_2N_4O_{14}Zn_2$	$C_{57}H_{52}Cl_{1.5}N_8O_{14.4}Zn_4$ [a]	$C_{57}H_{55}ClN_8NaO_9Zn_2$	$C_{64.7}H_{79.1}Cl_2N_8O_{24.7}Zn_4$ [b]
Molecular weight	816.24	908.34	1394.12	1185.32	1696.44
Crystal system	monoclinic	monoclinic	triclinic	orthorhombic	triclinic
Space group	$P2_1/n$	$P2_1/c$	$P1$	$Iba2$	$P1$
a [Å]	12.3312(4)	10.4282(8)	12.0174(8)	19.0520(5)	11.9642(8)
b [Å]	15.9495(8)	10.7218(8)	12.6098(8)	15.1148(4)	18.1471(12)
c [Å]	16.0259(8)	16.8474(13)	22.4790(14)	18.7647(5)	18.9783(12)
α [°]	90.00	90.00	87.9000(10)	90.00	82.5670(10)
β [°]	98.318(3)	93.5250(10)	77.9940(10)	90.00	86.7630(10)
γ [°]	90.00	90.00	71.0640(10)	90.00	72.0110(10)
Volume [Å^3]	3118.8(2)	1880.1(2)	3149.8(3)	5403.6(2)	3885.5(4)
Z	4	4	2	4	2
Calcd. density [g/cm^{-3}]	1.738	1.604	1.470	1.418	1.450
Absorp. coeff. [mm^{-1}]	1.781	1.490	1.636	1.006	1.367
F(000)	1664	936	1421	2388	1750
Crystal size [mm]	0.35×0.32× 0.28	0.6×0.6×0.3	0.6×0.4×0.3	0.38×0.32× 0.28	0.4×0.3×0.2
Θ-range [°]	3.05−23.29	1.96−28.28	1.71−28.33	2.14−23.28	1.70−28.29
Index-ranges	0/13	−13/+13	−16/15	−21/+21	−15/+15
	−17/17	−14/+14	−16/16	0/16	−24/+23
	−17/17	−21/+22	−29/29	−20/20	−25/+24
No. of reflections					
unique	4331	4529	15058	3786	18524
observed [$I > 2\sigma(I)$]	8331	18.984	34327	7046	42264
Parameters	480	260	810	343	969
Final R indices $R1$ [$I > 2\sigma(I)$]	0.0400	0.0243	0.0826	0.0473	0.0570
$wR2$	0.1121	0.0659	0.2747	0.1354	0.1750
Largest diff. peak/hole[e/ Å]	0.557/−0.638	0.433/−0.391	1.770/−1.441	1.207/0.794	0.980/−0.750

[a] Compound **3a** crystallizes from a mixture of 0.5 equivalents of methanol and 0.5 equivalents of water; the anions were found: 1.5 equivalents of perchlorate and 0.5 equivalents of hydrogencarbonate. [b] Compound **5** crystallizes from a mixture of 3.7 equivalents of methanol and 2 equivalents of water (OH atoms are missing in the formula).

stirred under reflux for 30 min. As the sodium hydroxide dissolved a precipitate of zinc hydroxide separated from the mixture. The precipitate was then filtered off and the filtrate was cooled slowly. Compound **4** crystallised as a colourless solid. Yield 76%. $C_{57}H_{55}ClN_8NaO_9Zn_2$ (1185.32): calcd. C 57.76, H 4.68, Cl 2.99, N 9.45; found C 57.69, H 4.65, Cl 2.67, N 9.50.

5: Salicylaldehyde (1.83 g, 15 mmol) was dissolved in 50 mL of methanol and 2-(2-aminoethyl)pyridine (1.83 g, 15 mmol) in 20 mL of methanol was added at room temperature. After 10 min, zinc perchlorate hexahydrate (5.59 g, 15 mmol) in 50 mL of methanol was added, and the mixture was heated to 60 °C. A solution of sodium hydroxide (0.90 g, 22.5 mmol) in 50 mL of methanol was added and a cloudy mixture was obtained. Then, a stream of carbon dioxide was passed through the mixture for 45 min at 60 °C; most of the reaction products dissolved. The remaining undissolved solid was filtered off and the filtrate was cooled in a closed flask to 0 °C under a CO_2 atmosphere. After a few days, compound **5** crystallised as a colourless solid. Yield 55%. $C_{61}H_{68}Cl_2N_8O_{19}Zn_4 \cdot 3.7CH_3OH \cdot 2.5\,H_2O$ (1713.27): calcd. C 45.36, H 5.17, Cl 4.14, N 6.54; found C 45.77, H 4.76, Cl 4.32, N 6.88.

X-ray Crystallographic Study: Data for complexes **1** and **4** were collected on a NONIUS Kappa CCD diffractometer (Mo-K_α, λ = 0.71073 Å, and ω scans), at 183 K, up to Θ = 27.44°. The structures were solved by direct methods (refinement by least-squares against F^2, SHELX program[24]). Diffraction data for the complexes **2**, **3**, **3a**, and **5** were recorded at 200 K with a Siemens SMART 1000 CCD diffractometer fitted with a molybdenum tube (Mo-K_α, λ = 0.71073 Å) and a graphite monochromator. The structures were solved by direct methods and refined anisotropically with the SHELX program. The structural parameters were refined against F^2. Figures were produced with the winray program.[25] Table 1 lists the crystallographic data[26] of the complexes **1**, **2**, **3a**, **4**, and **5**.

Acknowledgments

We are grateful to the Deutsche Forschungsgemeinschaft (SFB 436) for financial support.

[1] G. Parkin, *Chem. Commun.* **2000**, 1971−1985.
[2] R. Alsfasser, M. Ruf, S. Trofimenko, H. Vahrenkamp, *Chem. Ber.* **1993**, *126*, 703−710.
[3] M. Ruf, H. Vahrenkamp, *Inorg. Chem.* **1996**, *35*, 6571−6578.
[4] H. Vahrenkamp, *Acc. Chem. Res.* **1999**, *32*, 589−596.
[5] C. Bergquist, G. Parkin, *J. Am. Chem. Soc.* **1999**, *121*, 6322−6323.
[6] X. Zhang, R. van Eldik, T. Koike, E. Kimura, *Inorg. Chem.* **1993**, *32*, 5149−5155.
[7] X. Zhang, R. van Eldik, *Inorg. Chem.* **1995**, *34*, 5606−5614.

[8] X. Zhang, R. van Eldik, T. Koike, E. Kimura, *Inorg. Chem.* **1993**, *32*, 5749−5755.
[9] A. Schrodt, A. Neubrand, R. van Eldik, *Inorg. Chem.* **1997**, *36*, 4579−4584.
[10] E. Kimura, T. Koike, *Chem. Soc. Rev.* **1998**, 179−184.
[11] S. S. Tandon, S. Chander, L. K. Thompson, J. N. Bridson, V. McKee, *Inorg. Chim. Acta* **1994**, *219*, 55−65.
[12] A. Trösch, H. Vahrenkamp, *Eur. J. Inorg. Chem.* **1998**, 827−832.
[13] A. Trösch, H. Vahrenkamp, *Inorg. Chem.* **2001**, *40*, 2305−2311.
[14] C. Flassbeck, K. Wieghardt, E. Bill, C. Butzlaff, A. X. Trautwein, B. Nuber, J. Weiss, *Inorg. Chem.* **1992**, *31*, 21−26.
[15] R. Alsfasser, H. Vahrenkamp, *Chem. Ber.* **1993**, *126*, 695−701.
[16] P. Chaudhuri, C. Stockheim, K. Wieghardt, W. Deck, R. Gregorzik, H. Vahrenkamp, B. Nuber, J. Weiss, *Inorg. Chem.* **1992**, *31*, 1451−1457.
[17] C. Bazzacapuli, A. Bencini, A. Bianchi, V. Fusi, L. Mazzanti, P. Paoletti, B. Valtancoli, *Inorg. Chem.* **1995**, *34*, 3003−3010.
[18] F. Meyer, P. Rutsch, *Chem. Commun.* **1998**, 1037−1038.
[19] T. Itoh, Y. Fujii, T. Tada, Y. Yoshikawa, H. Hisada, *Bull. Chem. Soc. Jpn.* **1996**, *69*, 1265−1274.
[20] N. N. Murthy, K. D. Karlin, *J. Chem. Soc., Chem. Commun.* **1993**, 1236−1238.
[21] C. Bazzicalupi, A. Benini, A. Bianchi, F. Corona, V. Fusi, C. Giorgi, P. Paoli, P. Paoletti, B. Valtancoli, C. Zanchini, *Inorg. Chem.* **1997**, *36*, 5540−5548.
[22] Because of experimental problems (ClO_4^- counterion), an elementary analysis of **3** could not be performed. The results of the elementary analysis of a complex with an identical cation, but with BF_4^- as counterion, are presented.
[23] The varying content of HCO_3^- in the crystals of **3a** prevented an accurate elementary analysis of this complex.
[24] G. M. Sheldrick, *SHELX-97*, Universität Heidelberg, **1997**.
[25] R. Soltek, *winray*, Universität Heidelberg, **1997**.
[26] CCDC-175934 (**1**), -175955 (**2**), -1785957 (**3a**), -175935 (**4**) and -175956 (**5**) contain the supplementary crystallographic data for this paper. These data can be obtained free of charge at www.ccdc.cam.ac.uk/conts/retrieving.html [or from the Cambridge Crystallographic Data Centre, 12, Union Road, Cambridge CB2 1EZ, UK; Fax: (internat.) +44-1223/336-033; E-mail: deposit@ccdc.cam.ac.uk].

Received December 14, 2001
[I01509]

Gas-Phase Reactions of Chromium and Chromium Fluoride Cations CrF_n^+ ($n = 0-4$) with Water and Nitrous Oxide

Ulf Mazurek,[a] Detlef Schröder,[a] and Helmut Schwarz*[a]

Dedicated, with admiration and in friendship, to Fulvio Cacace

Keywords: Chromium / Chromium fluorides / Hydrolysis / Gas-phase ion chemistry / Thermochemistry

The reactions of atomic chromium and chromium fluoride monocations CrF_n^+ (n = 0–4) with water and nitrous oxide were investigated by Fourier transform ion cyclotron resonance (FT-ICR) mass spectrometry. Besides slow condensation, Cr^+ is unreactive towards water, whereas all chromium fluoride cations undergo at least one Cr–F bond hydrolysis yielding the corresponding hydroxide concomitant with loss of neutral HF. While hydrolysis is complete for CrF^+ and CrF_2^+, proton transfer and HF losses compete with the hydrolysis of the second Cr–F bond in CrF_3^+ and CrF_4^+. Nevertheless, complete Cr–F bond hydrolysis is observed for the latter two cations as well. The results for the ion-molecule reactions with nitrous oxide are as follows: With the exception of CrF_3^+, which gives CrF_3O^+ in a good yield, all species investigated were found to be essentially unreactive towards N_2O. The ionisation energy of CrF_3O has been determined, IE = 11.3 ± 0.2 eV. In addition, limits for the standard heats of formation of several chromium-containing cations have been derived.
(© Wiley-VCH Verlag GmbH, 69451 Weinheim, Germany, 2002)

Introduction

In previous studies, we investigated the formation of chromium and chromium fluoride monocations CrF_n^+ (n = 0−4) and their reactions with alkanes C_1 through C_4,[1] and phosphane.[2] The appearance of the species $Cr(OH)^+$, $CrF(OH)^+$, $Cr(OH)_2^+$, $CrF_2(OH)^+$, $CrF(OH)_2^+$, $Cr(OH)_3^+$ and CrF_3O^+ was detected, and attributed to the reactions of the chromium fluoride cations with water from the background of the mass spectrometer's high-vacuum system. As the presence of water is a widespread nuisance in mass spectrometry, we wanted to establish sound kinetic models for the reactions of chromium and chromium fluoride monocations with this neutral species. When investigating reactions of chromium and chromium fluoride cations with neutral species other than water, the kinetic models established here would allow for a more accurate description of the reaction systems as the contributions of background water could then be accounted for quantitatively.

In addition, we wanted to establish a firm basis for the formation of CrF_3O^+ hitherto attributed to a reaction of CrF_4^+ with water,[1] but not fitting into the general Cr−F bond hydrolysis scheme:

$$CrF_n^+ \xrightarrow[-HF]{+H_2O} CrF_{n-1}(OH)^+$$

[a] Institut für Chemie, Technische Universität Berlin, Straße des 17. Juni 135, 10623 Berlin, Germany
Fax: (internat.) + 49-30/314-21102
E-mail: Helmut.Schwarz@www.chem.tu-berlin.de

Furthermore, we intended to expand our study to the generation of other chromium oxyfluoride cations and to investigate their gas-phase chemical properties.

Results and Discussion

Reactions with Water

The reactions of the CrF_n^+/H_2O systems are summarised in Figure 1. Species given in square brackets in this comprehensive reaction scheme were not observed experimentally but postulated, (i) as necessary intermediates in an observed reaction sequence [e.g., $CrF_2(OH)_2^+$] or, (ii) as products of reactions assumed to be reasonable by analogy to observed ones. A detailed discussion with regard to the parent ions CrF_n^+ (n = 0−4) follows below.

Cr^+

For argon-thermalised Cr^+ cations, only slow condensation yielding mono and di adducts was observed. However, for methane-thermalised Cr^+ cations, the di adduct $Cr(H_2O)_2^+$ was not detected. Consequently, this species is given in square brackets in Figure 1. Besides the water mono adduct $Cr(H_2O)^+$, a number of minor products that cannot be formed directly from Cr^+ and water [namely H_3O^+, CrO^+, $Cr(OH)^+$, CrO_2^+, and $Cr(OH)_2^+$] were observed. From these results, we draw the following conclusions: (i) Ground-state (^6S) bare chromium cations ($3d^5$) are essentially unreactive towards water. The only reaction ob-

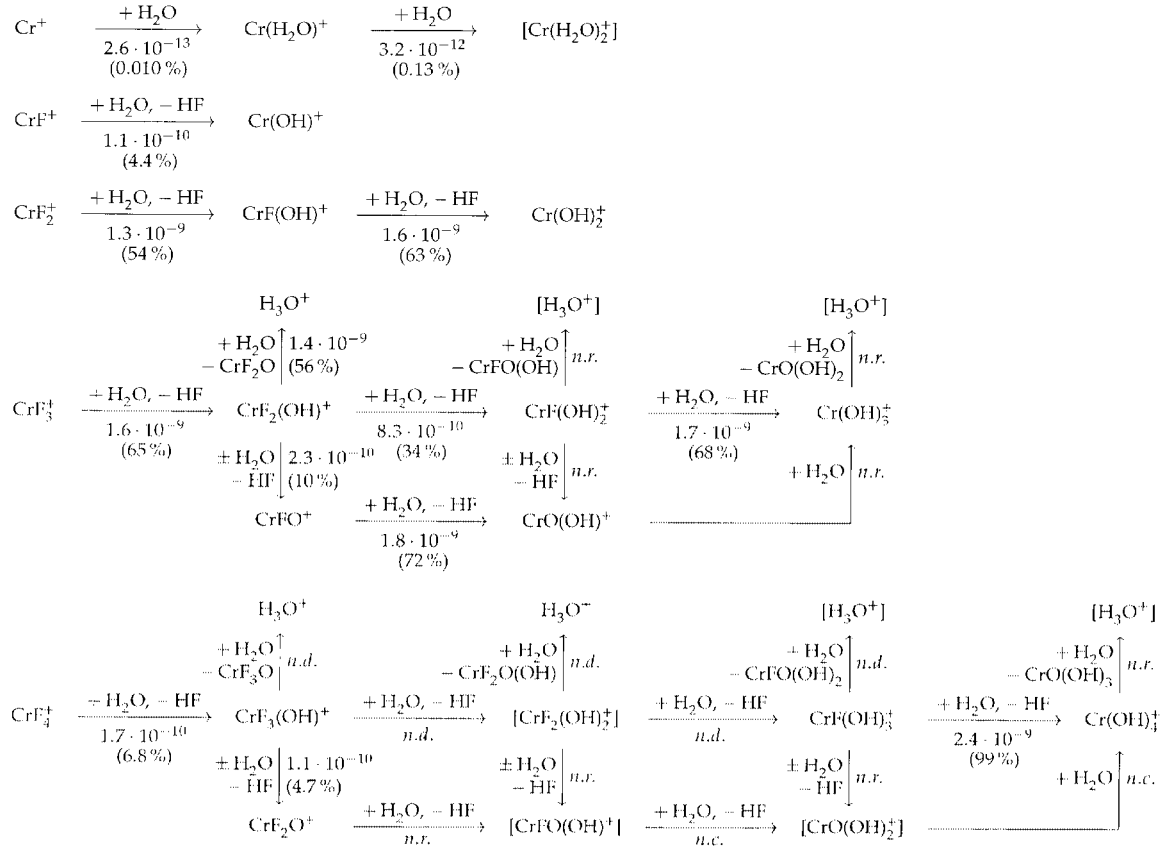

Figure 1. Reactions of CrF_n^+ ($n = 0-4$) with water; rate constants and reaction efficiencies φ (values in parentheses) are given as defined in the Exp. Sect.; for discussion, see text; abbreviations: *n.d.* = not determined (see text), *n.r.* = "no reactivity" indicating a reaction efficiency $\varphi < 0.05\%$, *n.c.* = not covered by this study because the reactant ion was not observed, see text

served is the slow mono adduct formation similar to that observed by Buckner et al. for the Cr^+/NH_3 system,[3] and by us for the CrF_n^+/PH_3 systems.[2] The failure of Cr^+ to activate O−H bonds parallels previous experimental findings for C−H[1,4] and N−H[3] bonds. (ii) Most probably, the condensation of ground-state Cr^+ by H_2O involves termolecular processes. In addition to water, prime candidates for third-body interactions are hydrocarbons and molecular oxygen present in the background of the mass spectrometer; the presence of the latter is supported by the formation of the cations CrO^+ and CrO_2^+. Interestingly, in a mass-spectrometric study of CrO_2^+ isomers, water was observed to catalyse the conversion of $Cr(O_2)^+$ to the chromyl cation.[5] Thus, the interplay between water and molecular oxygen is likely to exert a cooperative effect on the reactivity of Cr^+ cations. (iii) Based on this cooperative effect, we assume that the formation of $Cr(H_2O)_2^+$ from $Cr(H_2O)^+$ is outnumbered by reactions of the latter ion with O_2 rather than with H_2O. (v) The rate constants and reaction efficiencies, given in Figure 1, apply to argon-thermalised chromium cations. Due to the unknown influence of third-body interactions, they should be taken as upper limits of the effective bimolecular rate constants.

CrF^+

The only product of the reaction of CrF^+ with H_2O is $Cr(OH)^+$, corresponding to the loss of neutral HF, whose thermochemical stability may be considered as the driving force for the Cr−F bond hydrolysis. The reaction is rather inefficient compared with the corresponding reactions of CrF_2^+ and CrF_3^+ (see below).

CrF_2^+

In a reaction roughly twelve times as fast as that of CrF^+, CrF_2^+ reacts with water to form $CrF(OH)^+$ which, in turn, undergoes fast hydrolysis of the remaining Cr−F bond. Interestingly, the formal Cr^{III} species $CrF(OH)^+$ and $Cr(OH)_2^+$ do not undergo proton transfer to water, whereas several of their formal Cr^{IV} and Cr^V congeners (see below) do so.

CrF_3^+

CrF_3 reacts with water even faster than CrF_2^+, and undergoes facile hydrolysis of the first Cr−F bond. However, once $CrF_2(OH)^+$ has been formed, three different reaction channels exist as shown in Figure 1. First, $CrF_2(OH)^+$ may

undergo further Cr−F bond hydrolysis, thus following the reaction scheme already observed for $CrF(OH)^+$. In addition, proton transfer from $CrF_2(OH)^+$ to water is facile, and the loss of HF yielding $CrFO^+$ is also observed. The latter reaction shall be discussed in more detail. At a first glance, HF loss from $CrF_2(OH)^+$ can proceed as a unimolecular reaction, thus apparently indicating that $CrF_2(OH)^+$ is a metastable ion. Otherwise, the activation energy needed to form a weakly binding HF ligand would have to be acquired by collision with another molecule. The actual observation of $CrF_2(OH)^+$ on the time scale of an FT-ICR experiment, however, implies that this cannot hold true. Limited to both a maximum of 10^3-10^4 ions for all species detected and a lower detection limit of 10^2 ions for *one* species,[6] the population of an ionic species is too small to be detected by an FT-ICR mass spectrum if that species undergoes unimolecular decay with rate constants of typically some 100 s^{-1}. Furthermore, the intramolecular formation of HF from two ligands pointing away from each other seems to be rather unlikely. For geometrically comparable cations, e.g. $HO-Fe^+-OH$[7−9] and $HO-V^+-OH$,[10] considerable energy barriers were determined for the 1,3-H shifts, and it is fair to assume comparable barriers to be associated with an unimolecular HF formation. By reference to the results for the iron and vanadium systems, we conclude that the loss of HF from $CrF_2(OH)^+$ proceeds as a water-mediated reaction as indicated in Figure 2.

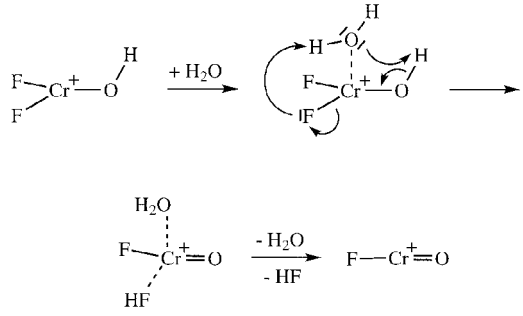

Figure 2. Conceptual illustration of water-mediated HF loss from $CrF_2(OH)^+$

It is suggested that water acts as a "proton shuttle" [11,12] in this reaction sequence, and that the intermediate is a metastable van-der-Waals complex of ionic $CrFO^+$, water, and HF, which looses both ligands easily. Notably, similar water-molecule participation has also been observed for the $Cr(O_2)^+$ cation,[5] the isomerisation of iron-coordinated cyclohexadienone to phenol,[13] and several metal-free systems.[14−16] While HF is known to be a weakly bound ligand and to "boil off" readily, the loss of H_2O from the intermediate complex can only be postulated from the observation of $CrFO^+$. The intermediate $CrFO^+\cdots H_2O$ cannot be distinguished from the long-lived cation $CrF(OH)_2^+$ by mass analysis only, because both cations have the same elemental composition.

At a first glance, the reaction mechanism depicted in Figure 2 may also explain the absence of the formal reaction $CrF(OH)^+ \rightarrow CrO^+ + HF$. If the O−Cr−F part of the $CrF(OH)^+$ cation was linear, the water molecule could no longer bridge the distance between the OH group and the fluoride ligand. However, based on its estimated endothermicity of at least 35 kcal mol^{-1}, this reaction can be ruled out a priori on thermochemical grounds.

In contrast to the variety of reactions observed for its predecessor $CrF_2(OH)^+$, ionic $CrF(OH)_2^+$ only undergoes hydrolysis of the remaining Cr−F bond. Both HF loss and proton transfer to water, as included in Figure 1, were ruled out on kinetic grounds. For an explanation of this different behaviour, we considered the electronic properties of $CrF(OH)_2^+$.

In a broader sense, the different effects of a fluorine atom and a hydroxy group on an adjacent atom shall be discussed with the help of Equation (1).

	CH_3OH		$CH_2F^\bullet$	→	$CH_2OH^\bullet$	+	CH_3F
$\Delta_f H°_{298}$ (kcal mol^{-1}):[17]	−48.2 ± 0.1		−8 ± 2		−6.2 ± 1.5		−59

(1)

The overall reaction enthalpy of $\Delta_r H°_{298} = -9 \pm 2.5$ kcal mol^{-1} indicates a comparable influence of the substituent X (X = F, OH) on a C−H bond. However, as the two corresponding cations require an ionisation energy of 9.1 eV and 7.6 eV, respectively, they are clearly distinct as far as thermochemistry is concerned. Delocalisation of the positive charge in CH_2OH^+ is a prime explanation for the lower *IE* of the corresponding neutral species. As a consequence, the corresponding reaction of cations, rather than radicals, [Equation (2)] strongly favours the formation of CH_2OH^+ as indicated by $\Delta_r H°_{298} = -41.8 \pm 0.1$ kcal mol^{-1}.

	CH_3OH	+	CH_2F^+	→	CH_2OH^+	+	CH_3F
$\Delta_f H°_{298}$ (kcal mol^{-1})[17]	−48.2 ± 0.1		199		168		−59

(2)

With respect to the chromium systems, we can conclude that the hydroxochromium cation can also be described as protonated chromium oxide, thus allowing for a considerable reduction of the formal charge on the metal centre compared with the chromium fluoride cation. From this explanation, it is evident that the stabilising effects of an OH group on a metal cation is much larger than the mere difference between the electronegativities of OH and F. Consequently, it is reasonable to assume that the metal centre in $CrF(OH)_2^+$ is less electron-deficient than in $CrF_2(OH)^+$. Thus, the tendency to increase the electron density at the metal centre in $CrF(OH)_2^+$ by the formation of a Cr−O double bond is less pronounced.

The oxyfluoride $CrFO^+$ undergoes facile hydrolysis of the remaining Cr−F bond, thus yielding $CrO(OH)^+$. This ion, in turn, could undergo addition of water similar to that investigated both experimentally and theoretically for various vanadium[10] and iron[9,18,19] oxides and oxohydroxide

monocations. However, the kinetic data suggest that addition of water to $CrO(OH)^+$ is slow, if it occurs at all, in the pressure region examined. Thus, for the reactions of CrF_3^+ with water, three terminal product ions are observed with decreasing abundances; H_3O^+, $Cr(OH)_3^+$, and $CrO(OH)^+$. Regardless of their actual way of formation, the cationic chromium fragments eventually underwent hydrolysis of all Cr−F bonds originally present in CrF_3^+.

CrF_4^+

On reaction with water, $CrF_3(OH)^+$ is formed as the initial product. One might expect a further increase in the reaction rate relative to CrF_3^+; however, this hydrolysis reaction is remarkably slow. This "passive" behaviour of *thermalised* CrF_4^+ has already been observed in the reactions of this ion with methane and NF_3;[1] any excited CrF_4^+ cations can safely be assumed to have been hydrolysed during the period necessary to isolate CrF_4^+ due to the fact that they are much more reactive. However, the overall behaviour of the CrF_4^+/H_2O system resembles that of its CrF_3^+/H_2O congener: (i) The terminal reaction product, H_3O^+ (obtained by proton transfer from hydrolysed CrF_4^+ to H_2O) dominates over $Cr(OH)_4^+$ (complete Cr−F bond hydrolysis) and CrF_2O^+ where the latter is, by analogy, assumed to be formed by water-mediated HF loss from $CrF_3(OH)^+$. While CrF_2O^+ might be expected to undergo at least one further Cr−F bond hydrolysis, the product $CrFO(OH)^+$ could not be detected in our study, and the kinetic data suggest that CrF_2O^+ is indeed a terminal reaction product. (ii) Three different reaction pathways can be accessed from the first intermediate, $CrF_3(OH)^+$: proton transfer to water, further Cr−F bond hydrolysis, and water-mediated HF loss. While the latter reaction has already been addressed, the other two reaction channels shall be discussed in more detail here. The generation of H_3O^+ from CrF_4^+ and H_2O may occur, in principle, by two different reaction pathways [Equations (3) and (4)].

$$CrF_4^+ \xrightarrow[-HF]{+H_2O} CrF_3(OH)^+ \xrightarrow[-CrF_3O]{+H_2O} H_3O^+ \quad (3)$$

$$CrF_4^+ \xrightarrow[-CrF_4]{+H_2O} H_2O^+ \xrightarrow[-OH]{+H_2O} H_3O^+ \quad (4)$$

However, both the ionisation energies of CrF_4 and water (see Table 1), the failure to observe cationic H_2O^+ during the decay of CrF_4^+ and the concurrent increase in H_3O^+ disfavour the second reaction channel [Equation (4)]. Furthermore, in a double-resonance experiment, ejection of $CrF_3(OH)^+$ from the reaction cell caused the signal of H_3O^+ to vanish completely. Thus, the generation of H_3O^+ is attributed to the first reaction channel [Equation (3)]. However, additional formation of H_3O^+ from further-hydrolysed ions $CrF_2(OH)_2^+$ and $CrF(OH)_3^+$, cannot be ruled out so far and will be discussed in more detail below.

Remarkably, the signal for putative intermediate $CrF_2(OH)_2^+$ did not surpass the noise level in the kinetic investigation, while the signals for its supposed Cr−F bond hydrolysis products $CrF(OH)_3^+$ and $Cr(OH)_4^+$ did so; the latter species is a terminal product of the reaction sequence. The failure to observe $CrF_2(OH)_2^+$ turns the kinetic analysis into a nontrivial problem as is discussed as follows: (i) There is no single source for the protons transferred to water. If proton transfer from both $CrF_3(OH)^+$ and the formal Cr^{IV} species $CrF_2(OH)^+$ (see the CrF_3^+ section above) to water was allowed, it would be rather arbitrary to rule out a similar reaction for the formal Cr^V species $CrF_2(OH)_2^+$ and $CrF(OH)_3^+$. Whilst an F/OH ligand exchange reduces the electron deficiency at the chromium centre, the influence of this exchange on the OH proton acidity is not necessarily large. In contrast, the mere existence of two or even three OH groups in $CrF_2(OH)_2^+$ or $CrF(OH)_3^+$, respectively, compared with one in $CrF_3(OH)^+$ may, on statistical grounds, even increase the rate of proton transfer to water. On the other hand, proton abstraction from $Cr(OH)_4^+$ could be ruled out because the latter ion was found to be a terminal product of the reaction sequences. Thus, a gradual decrease in proton transfer relative to further Cr−F bond hydrolysis is likely. The overall picture is that for $CrF_n(OH)_m^+$, the acidity of the OH protons increases with n but decreases with m. However, it is impossible to establish the particular step sizes of that decrease a priori. (ii) If $CrF_2(OH)_2^+$ could have been observed in the kinetic study, the distribution between proton abstraction and further Cr−F bond hydrolysis could be determined on the basis of the evolution of the ion concentrations over time. However, as $CrF_2(OH)_2^+$ had to be regarded as a reactive intermediate formed in very low steady-state concentrations, any distribution ratio could occur between the two reaction pathways. If proton abstraction from $CrF_3(OH)^+$ is favoured, then proton abstraction for $CrF_2(OH)_2^+$ is not favoured, and vice versa. Similarly, if proton abstraction from $CrF_2(OH)_2^+$ is favoured, then proton abstraction for $CrF(OH)_3^+$ is not favoured, and again, vice versa.

The kinetic analysis was made easier by the following: (i) CrF_2O^+ was found to be a terminal product of the reaction system. In addition, the cations $CrFO(OH)^+$ and $CrO(OH)_2^+$ were not observed. Consequently, the reaction sequence $CrF_4^+ \rightarrow CrF_2O^+ \rightarrow Cr(OH)_4^+$ can be ruled out. (ii) While the $CrF_2(OH)_2^+$ ion, which is not observed, is to be considered as a reactive intermediate, its consumption by one or more reactions with water cannot be faster than the collision rate. (iii) The very same argument applies to $CrF(OH)_3^+$; regardless of its actual rate of formation, the cation cannot be consumed at a reaction rate exceeding the collision limit. (iv) In turn, the temporal evolutions of $CrF(OH)_3^+$, and especially $Cr(OH)_4^+$, set upper limits to the reaction rates in question.

However, one cannot determine without additional experiments (namely exposing isolated intermediates to water or double-resonance experiments) the extent to which H_3O^+ is formed from $CrF_3(OH)^+$, $CrF_2(OH)_2^+$, and perhaps $CrF(OH)_3^+$. In parallel, the fraction of $CrF_3(OH)^+$ which yields $CrF_2(OH)_2^+$ remains unknown as do the fractions of $CrF_2(OH)_2^+$ and $CrF(OH)_3^+$, which yield

$CrF(OH)_3^+$ and $Cr(OH)_4^+$, respectively. However, these additional experiments would be adversely affected by the unfavourable signal-to-noise ratios already hampering the present investigations. As a consequence, isolation of intermediates was not attempted, and we ceased the investigation and determined only the rate constants reported in Figure 1.

Relative Reaction Rates of Hydrolysis

Remarkably, the reaction rate of the first Cr−F bond hydrolysis (see Figure 1) increases by about one order of magnitude from CrF^+ to CrF_2^+. While the rates of the first hydrolysis reactions are similar for CrF_2^+ and CrF_3^+, a subsequent decrease by about one order of magnitude is observed when going from CrF_3^+ to CrF_4^+. We think that the interplay of the effective charge on the chromium centre, the steric hindrance exerted by the increasing number of fluorine atoms attached to the metal centre, and the "surface charge" (originating from the high electron density on the fluorine atoms constituting the ligand sphere of the chromium cation) of the different CrF_n^+ cations provides an appropriate explanation for the observed differences in the rate constants.We will discuss this interplay in more detail: (i) The increased rate of hydrolysis of CrF_2^+ compared with CrF^+ can be explained by the threefold influence of the higher effective charge on the chromium centre on increasing fluorination. First, the formation of the collision complex between the ion and the polar water molecule should be much more facile. Secondly, the resulting collision complex should possess a longer life-time due to the larger ion-dipole interaction. Finally, assuming a four-centre transition state, the increased effective charge at the chromium centre can be assumed to favour the actual Cr−OH bond formation/HF abstraction from the collision complex. (ii) While all arguments mentioned above hold true for the change from CrF_2^+ to CrF_3^+ as well, the increase in the rate constant is much less pronounced. Steric hindrance exerted by the three fluorine atoms attached to the chromium cation can be assumed to slow down the formation of the initial collision complex, irrespective of whether CrF_3^+ keeps the trigonal-planar structure of neutral CrF_3 (Cr−F bond length 1.732 Å[20,21]) or not. (iii) We suppose that the formal Cr^V species CrF_4^+ more or less keeps the tetrahedral structure of neutral CrF_4 (Cr−F bond length 1.704 Å[21,22]), since the formal Cr^V species CrF_3O forms a trigonal-pyramidal structure, i.e. a slightly distorted tetrahedral structure.[21] Thus, the outer-sphere of the CrF_4^+ ion is assumed to be dominated by four electron-rich fluorine atoms, such that formation of the collision complex with water proceeds rather slowly while the actual hydrolysis reaction should proceed at a rate similar to that for CrF_2^+ and CrF_3^+. Accordingly, we conclude that the retardation of the hydrolysis of the "inert" CrF_4^+ cation is not due to the actual F/OH exchange but to the formation of the initial collision complex.

In the preceding discussion, the focus was placed on the structural properties of the chromium fluoride cations. However, spin restrictions[23] discussed in more detail in the Thermochemistry Section below may contribute to the hydrolysis rate differences as well. For example, hydrolysis of a Cr−F bond in CrF_n^+ allows for the above-mentioned delocalisation of the positive charge of the reaction product. This delocalisation, in turn, might allow for a spin inversion on the chromium centre, thus giving rise to a considerable reaction barrier. However, the results of quantum-chemical calculations would be needed to discuss this point in more detail.

Reactions with Nitrous Oxide

The observation of several oxochromium fluoride cations during the hydrolysis reactions reported above prompted our interest in looking for a more facile way of generating them. Our results are described below.

Initial Experiments

When a mixture of chromium and chromium fluoride monocations CrF_n^+ ($n = 0-4$) was subjected to an oxygen pressure of $1.0 \cdot 10^{-8}$ mbar for a period of 24 s, at least 95% of the total ion intensity was due to the cations CrF_n^+ ($n = 0-4$) and their hydrolysis and/or charge-transfer products. Oxochromium fluorides and ions originating from them included $CrFO^+$ (max. 1%), its supposed hydrolysis product $CrO(OH)^+$ (max. 2%), CrF_3O^+ (max. 1%), and the possible hydrolysis product of CrF_2O^+, $CrO(OH)_2^+$ (max. 1%). Therefore, O_2 deemed inappropriate and was replaced by N_2O as a putatively more suitable oxidant. From a thermochemical point of view, the latter should be a much better oxygen-atom donor, irrespective of the substrate present [see Equations (5) and (6)].

$$O_2 \rightarrow O + O \qquad \Delta_f H^\circ_{298} = 119.2 \text{ kcal mol}^{-1}\ [17] \qquad (5)$$

$$N_2O \rightarrow N_2 + O \qquad \Delta_f H^\circ_{298} = 40.0 \text{ kcal mol}^{-1}\ [17] \qquad (6)$$

In a second initial experiment, subjecting a mixture of chromium and chromium fluoride monocations to nitrous oxide pressures of $2.0 \cdot 10^{-8}$ mbar and $5.0 \cdot 10^{-7}$ mbar for 32 s allowed for the detection of substantial amounts of CrF_3O^+. In addition, both NO^+, NF_2O^+ [24] and small amounts of $CrO(OH)^+$ (probably from $CrFO^+$), $CrFN_2O_2^+$, and $CrF_2N_2O_2^+$ were detected.

Reactions of Mass-Selected Ions

(i) Based on the already observed inertness of ground-state (^6S) bare chromium cations towards nitrous oxide[25,26] and the outcome of the initial experiments, no further attempts were undertaken to generate CrO^+. (ii) In the reaction of isolated CrF^+ and N_2O, the desired species $CrFO^+$ could not be detected, whereas $Cr(OH)^+$ formed by hydrolysis with background water dominated the product ion spectrum. Traces of H_3O^+ and NO^+ (not surmounting 3% of the total ion concentration) were attributed to the presence of excited CrF^+ cations. (iii) When isolated CrF_2^+ was

exposed to N_2O, CrF_2O^+ was formed with a reaction efficiency of φ = 0.16%, and the abundance of the ion was not more than 2% of the total ion concentration. Besides hydrolysis products and NO^+ (not exceeding 1% of the total ion concentration), the intermediate N_2O^+ and the final product H_3O^+, accounting for 2% of the total ion concentration, were detected (see the Thermochemistry Section below for discussion). Due to the low abundance of CrF_2O^+, isolation of this cation was not attempted. (iv) When isolated CrF_3^+ was subjected to N_2O pressure of $1.0 \cdot 10^{-8}$ mbar for a period of 20 s, CrF_3O^+ was formed with a reaction rate of $(7 \pm 1)\ 10^{-11}$ cm^3 molecules^{-1} s^{-1} (φ = 9 ± 1%), regardless of whether CrF_3^+ was generated from Cr^+ by NF_3/Ar or pure NF_3 pulses. Note that the small error bars reported here are based on good agreement between two experiments, whereas the systematic error introduced by the pressure measurement (see the Exp. Sect.) has not yet been considered. The only other oxofluoride species observed was $CrFN_2O_2^+$, which accounted for 3% of the total ion concentration. One might suppose $CrFN_2O_2^+$ to be generated by addition of N_2O to $CrFO^+$, which, in turn, is generated from CrF_3^+ by a single Cr−F bond hydrolysis and subsequent HF abstraction (see above). However, double-resonance experiments revealed that $CrFN_2O_2^+$ is formed from $CrF_2(OH)^+$ exclusively, and not at all from $CrFO^+$. Consequently, the generation of $CrFN_2O_2^+$ from $CrF_2(OH)^+$ is attributed to the water-assisted rearrangement of $CrF_2(OH)^+$ into $(HF)CrFO^+$, and subsequent HF/N_2O ligand exchange to yield $(N_2O)CrFO^+$. Note that ligand-mediated H−F bond formation and subsequent ligand loss have already been referred to in the above discussion of the formal reactions $CrF_2(OH)^+ \rightarrow CrFO^+ + HF$ and $CrF_3(OH)^+ \rightarrow CrF_2O^+ + HF$. As N_2O is a weakly bound ligand,[27] subsequent ligand exchange with background water yields $(H_2O)CrFO^+$. Supposedly, the latter rearranges, probably assisted by a neutral water molecule in a reaction sequence similar to that in Figure 2, to its isomer $CrF(OH)_2^+$, which finally undergoes hydrolysis of the remaining Cr−F bond to yield $Cr(OH)_3^+$. Rate constants for both the formation and consumption of $CrFN_2O_2^+$ could not be determined due to the low signal-to-noise ratio of the ion. With regard to Cr−F bond hydrolysis of the observed species, CrF_3O^+ was found to be remarkably inert towards water, but the reaction of its predecessor ion CrF_3^+ with background water was found to be fast and hence limited the yield of CrF_3O^+ to a maximum of about 15% of the total ion concentration. (v) In order to achieve a good signal-to-noise ratio, CrF_4^+ was not mass-selected. When a mixture of CrF_4^+ (23%) and the noninterfering CrF_3O^+ (77%) was subjected to N_2O pressure of $1.0 \cdot 10^{-6}$ mbar for 8 s, CrF_4O^+ could not be detected. This result is in agreement with chemical intuition which suggests that it is unlikely that oxidation of the formal Cr^V species CrF_4^+ would be observed since the reaction product CrF_4O^+ would constitute a formal Cr^{VII} cation, i.e. a hypervalent cation.

The reactions of mass-selected chromium and chromium fluoride monocations with nitrous oxide are summarised in Figure 3. As in Figure 1, possible but experimentally not observed oxidation products are given in square brackets, and both reaction rate constants and reaction efficiencies φ (values in parentheses) are given as defined in the Exp. Sect.

$$Cr^+ \xrightarrow[n.r.]{+N_2O,\ -N_2} [CrO^+]$$

$$CrF^+ \xrightarrow[n.r.]{+N_2O,\ -N_2} [CrFO^+]$$

$$CrF_2^+ \xrightarrow[1.2 \cdot 10^{-12}\ (0.16\,\%)]{+N_2O,\ -N_2} CrF_2O^+$$

$$CrF_3^+ \xrightarrow[7.5 \cdot 10^{-11}\ (9.9\,\%)]{+N_2O,\ -N_2} CrF_3O^+$$

$$CrF_4^+ \xrightarrow[n.r.]{+N_2O,\ -N_2} [CrF_4O^+]$$

Figure 3. Reactions of CrF_n^+ (n = 0−4) with nitrous oxide; for discussion, see text; abbreviation: *n.r.* = "no reactivity" indicating a reaction efficiency φ < 0.05%

Gas-Phase Generation of CrF_3O^+

While the absence of efficient oxygen transfer to chromium and chromium fluoride monocations CrF_n^+ (n = 0−2, 4) limited the present study to CrF_3^+, it simplified the experiments to a great extent. In contrast to requiring the use of two pulse valves, isolating a hydrolysis-sensitive intermediate, and optimising gas pressures and pulse lengths for two pulse valves,[2] good CrF_3O^+ intensities could be achieved by optimising the generation of CrF_3^+ from bare Cr^+ and pulsed-in NF_3, and then adding N_2O to the pulse valve already filled with NF_3. Subsequent optimisation of the length of the combined NF_3/N_2O pulse was not necessary; furthermore, isolation of CrF_3O^+ did not impose any problems.

Ionisation Energy

Chromium fluorides show a strong correlation between the number of electron-withdrawing fluorine atoms connected to the metal centre and the respective ionisation energies (see Table 1). However, the presence of doubly bonded oxygen does not necessarily affect the *IE*. On one hand, an oxygen ligand will withdraw electron density from the metal centre, and on the other hand, it may even donate electron density when the metal centre is already highly electron-deficient. Consequently, we wanted to establish a sound value for the yet unknown ionisation energy of CrF_3O. Exposures of CrF_3O^+ to ethylene [*IE* = 10.5 eV, charge-transfer (CT) reaction efficiency φ = 170%] and to molecular oxygen (*IE* = 12.1 eV, CT reaction efficiency φ < 0.05%) provide lower and upper limits, respectively, for the ionisation energy in question. The reaction with ethylene appears to proceed faster than the rate at which the reactants collide according to the capture theory.[28,29] While the agreement between rate constant determined by experiment and by this theory is very good for electron-

transfer processes between species of similar *IE*s,[30] some pitfalls seem to exist when describing outer-sphere electron transfer between species with large *IE* differences. Most probably, the cross-section is underestimated in the latter case.

Unfortunately, a more precise determination of the ionisation energy of CrF_3O was adversely affected by the following facts: (i) For a large variety of readily available compounds, e.g. alkanes (C_2H_6, *IE* = 11.5 eV; C_3H_8, *IE* = 11.0 eV),[17] haloalkanes (CH_3Cl, *IE* = 11.2 eV; CH_2Cl_2, *IE* = 11.3 eV; CH_2ClF, *IE* = 11.7 eV),[17] and SiH_4 (*IE* = 11.6 eV),[17] dissociative ionisation is preferred and the yields of stable radical cations on removal of an electron are rather poor. (ii) The readily available cyano-substituted ethylenes, which yield stable radical cations (acrylonitrile, *IE* = 10.9 eV; both 1,2-dicyanoethylenes, *IE* = 11.2 eV; 1,1-dicyanoethylene, *IE* = 11.4 eV; tricyanoethylene, *IE* = 11.6 eV; tetracyanoethylene, *IE* = 11.7 eV),[31] are either difficult to handle or are insufficiently volatile to be employed in an FT-ICR experiment. (iii) Hexafluoroacetone (*IE* = 11.6 eV), which forms a stable radical cation and is sufficiently volatile undergoes α cleavage instead of charge-transfer when reacting with CrF_3O^+. Thus, for the determination of the *IE* of CrF_3O, the use of the "bracketing method", while relying largely on only one charge-transfer reaction [namely $CrF_3O^+ + COS$ (*IE* = 11.2 eV) → $CrF_3O + COS^+$; reaction efficiency φ = 80%], deemed not indicated. Consequently, we correlated the efficiency of the presumably barrier-free reaction to the ionisation energy difference, [32] thus estimating the ionisation energy of CrF_3O to be 11.3 eV ± 0.2 eV (rounded up, and the error bar was based on the reaction rate uncertainty mentioned in the Exp. Sect.). Interestingly, this value is considerably lower than the ionisation energies of CrF_2O_2, as well as of CrF_4, and even slightly lower than the ionisation energy of the oxygen-free species CrF_3 (though within the experimental error margins, Table 1). Two reasons can account for the similarity of the ionisation energies of CrF_3 and CrF_3O. (i) In the formal Cr^{III} species CrF_3, the central chromium atom is already highly electron-deficient which disfavours additional electron withdrawal. (ii) Oxygen is not as electronegative as fluorine, thus it does not necessarily withdraw electron density from the chromium atom; in contrast, doubly bound oxygen may even donate electron density to the electron-deficient metal centre. However, in order to account for the influence of a Cr=O double bond on the ionisation energy quantitatively, the ionisation energies of CrF_nO (n = 1, 2) are needed as well.

Table 1. Ionisation energies (*IE*) of CrF_3O and other species of interest[a]

Species	*IE* (eV)	Ref.
C_2H_4	10.5	[17]
COS	11.2	[17]
CF_3COCF_3	11.6 ± 0.1	[31]
O_2	12.1	[17]
H_2O	12.6	[17]
N_2O	12.9	[17]
Cr	6.8	[17]
CrF	8.4 ± 0.3	[17]
CrF_2	10.1 ± 0.3	[17]
CrF_3	11.5 ± 0.4	[1]
CrF_4	12.3 ± 0.3	[1]
CrO	7.9	[17]
CrO_2	10.3 ± 0.5	[17]
	9.7 ± 0.2	[66][b]
CrO_3	11.6 ± 0.5	[17]
CrF_2O_2	12.9	[31]
CrF_3O	11.3 ± 0.2	this work

[a] Values and error bars are rounded off to multiples of 0.1 eV; error bars are not given when they are less than 0.1 eV. [b] OCrO.

Reactions

As CrF_3^+ is relatively easily oxidised to CrF_3O^+, we wondered if that property of the system could be employed in a catalytic oxidation cycle. First, we were interested in the oxidation of small alkanes. Kang and Beauchamp[33] found CrO^+ to selectively oxidise alkanes except methane. While the higher valency of the metal in CrF_3O^+ may help to fulfil this task, no reactions with methane were observed. In contrast, replacing methane by ethane caused the formal transfer of a hydride anion from the hydrocarbon to CrF_3O^+; products indicative of the cleavage of the Cr−O bond were not observed. One might argue that unsaturated hydrocarbons like toluene or buta-1,3-diene could be suitable substrates for oxidation. While this might be perfectly true, it seems unlikely that CrF_3O^+ would transfer oxygen to them, rather than abstract hydride anions or capture electrons from the π-systems, simply because the *IE*s of these substrates are considerably lower than the *IE* of CrF_3O^+. The failure to transfer oxygen atoms to organic substrates has already been observed for other transition-metal complexes of higher oxidation states. For example, both MoO_3^+ and MoS_3^+ show exclusive electron capture and hydride abstraction from toluene,[34] and for the PtO_2^+/ethane system, electron and hydride anion transfer dominate the reactivity (40% and 15% of the reaction products, respectively).[35] Further, OsO_n^+ (n = 3, 4) exclusively abstracts one or two hydrogen atoms from methane, ethane, and propane.[36] From these previous and our present results, we inferred that CrF_3O^+ would also abstract hydride anions from higher alkanes, but is not suited for selectively oxidising them. Thus, we ceased this particular investigation and addressed the oxidation of carbon monoxide. Again, we were not successful: Carbon monoxide does not react with CrF_3O^+. A summary of the investigated reactions is given in Table 2.

Table 2. Reactions of CrF_3O^+ investigated in this study[a] [b] [c] [d]

IE determination							
CrF_3O^+	+	C_2H_4	(*IE* = 10.5 eV)	$\xrightarrow{170\,\%}$	$[Cr,F_3,O]$	+	$C_2H_4^+$
	+	COS	(*IE* = 11.2 eV)	$\xrightarrow{80\,\%}$	$[Cr,F_3,O]$	+	COS^+
	+	C_3F_6O[e]	(*IE* = 11.6 eV)	$\xrightarrow{n.d.}$	$[Cr,F_6,C,O]$	+	$C_2F_3O^+$
	+	O_2	(*IE* = 12.1 eV)	$\xrightarrow{n.r.}$			
Potential applications							
CrF_3O^+	+	CH_4		$\xrightarrow{n.r.}$			
	+	C_2H_6		$\xrightarrow{50\,\%}$	$[Cr,F_3,O,H]$	+	$C_2H_5^+$
				$\xrightarrow{3.4\,\%}$	$[Cr,F_3,O,H_2]$	+	$C_2H_4^+$
	+	CO		$\xrightarrow{n.r.}$			

[a] Reaction efficiencies φ are given as defined in the text. [b] For reaction efficiencies φ apparently greater than unity, see text. [c] *n.d.* = reaction efficiency φ not determined because the observed reaction is unsuited to determine the ionisation energy of CrF_3O. [d] *n.r.* = "no reactivity" indicating a reaction efficiency $\varphi < 0.05\%$. [e] Hexafluoroacetone.

Thermochemistry

Finally, we address the investigated reactions from a thermochemical point of view. Unless otherwise noted, two assumptions shall be made throughout this section: (i) The reactants are properly thermalised and (ii) severe kinetic barriers or spin restrictions[23] do not exist. Assumption (i) allows for the exclusion of endothermic reactions while assumption (ii) limits the reasons for a reaction's nonoccurrence to endothermicity (or the existence of at least one other, more exothermic reaction channel). As a consequence, the mere occurrence or absence of a reaction allows for establishing a $\Delta_fH°_T$ limit for one of the species involved, provided the standard heats of formation of all other species are known. To be more precise, the occurrence of a reaction at a temperature T allows for establishing a lower limit of a reactant's $\Delta_fH°_T$ value or an upper limit of a product's $\Delta_fH°_T$ value, whereas the absence of a reaction allows for establishing an upper limit of a reactant's $\Delta_fH°_T$ value or a lower limit of a product's $\Delta_fH°_T$ value. Maximum $\Delta_fH°_T$ values of reaction products can be utilised in follow-up reactions. Unfortunately, that does not hold true for minimum $\Delta_fH°_T$ values which makes an "inherited" bracketing impossible. However, the procedure is straightforward, and the limits are derived in Table 3 and presented together with those of their neutral counterparts in Table 4. From the heats of formation bond dissociation energies (*BDE*s) may be calculated in a straightforward manner. However, we do not report *BDE*s in this work because $\Delta_fH°_T$ *limits* allow for deriving bond-dissociation energy *limits* only, whereas other experimental techniques are available to determine the actual values.

Chromium Fluoride Hydrolysis Products

For $Cr(OH)^+$, a double upper limit of $\Delta_fH°_{298}$ can be derived (Table 3, Entries 1 and 2). While both results agree with each other and the literature value [(185.8 ± 3.0) kcal mol^{-1}[17,37]], their significance is low. Further, the smaller error bar of the higher value does not provide an advantage. A lower limit for $\Delta_fH°_{298}[Cr(OH)^+]$ cannot be derived on the basis of the reactions investigated here. Similar arguments apply to $\Delta_fH°_{298}[CrF(OH)^+]$ (Table 3, Entries 3 and 4) and to $\Delta_fH°_{298}[Cr(OH)_2{}^+]$ (Table 3, Entries 5 and 6). However, for $CrF(OH)^+$, the $\Delta_fH°_{298}$ limit obtained from the absence of proton transfer is more precise from the point of both its error bar and value, and for $Cr(OH)_2{}^+$, the difference between the two values is less pronounced and mostly due to the decrease in the size of the error bar.

For the hydrolysis of $CrF_3{}^+$ and its follow-up products, deriving the maximum $\Delta_fH°_{298}$ values for the hydrolysis products (Table 3, Entries 7, 9, and 10) is straightforward. Based on the *observed* proton transfer from $CrF_2(OH)^+$ to H_2O (Table 3, Entry 8), a *lower* limit for the heat of formation of the reactant ion can be determined for the first time in this study. In turn, the failure to observe proton transfer from both $CrF(OH)_2{}^+$ and $Cr(OH)_3{}^+$ (Table 3, Entry 11) to H_2O allows, in principle, for re-evaluating maximum $\Delta_fH°_{298}$ values for these cations but fails, in practice, for $CrF(OH)_2{}^+$ because the standard heat of formation of the

Table 3. Reactions investigated in this study and thermochemical data derived[a] [b]

Reaction[c]								Limit(s) Derived for **Boldface** Species	
(1)	CrF^+	+ H_2O	⟶	**$Cr(OH)^+$**	+ HF				$\Delta_f H^\circ_{298} < 205.6 \pm 7.3$[d]
(2)	**$Cr(OH)^+$**	+ H_2O	↛	CrO	+ H_3O^+				$\Delta_f H^\circ_{298} < 242.4 \pm 1.6$
(3)	CrF_2^+	+ H_2O	⟶	**$CrF(OH)^+$**	+ HF				$\Delta_f H^\circ_{298} < 137.0 \pm 7.5$
(4)	**$CrF(OH)^+$**	+ H_2O	↛	CrFO	+ H_3O^+				$\Delta_f H^\circ_{298} < 125.5 \pm 1.9$[d]
(5)	$CrF(OH)^+$	+ H_2O	⟶	**$Cr(OH)_2^+$**	+ HF				$\Delta_f H^\circ_{298} < 144.3 \pm 7.5$
(6)	**$Cr(OH)_2^+$**	+ H_2O	↛	CrO(OH)	+ H_3O^+				$\Delta_f H^\circ_{298} < 139.8 \pm 1.2$[d]
(7)	CrF_3^+	+ H_2O	⟶	**$CrF_2(OH)^+$**	+ HF				$\Delta_f H^\circ_{298} < 72.7 \pm 9.8$
(8)	**$CrF_2(OH)^+$**	+ H_2O	⟶	CrF_2O	+ H_3O^+	$45.5 \pm 3.4 <$			$\Delta_f H^\circ_{298}$
(9)	$CrF_2(OH)^+$	+ H_2O	⟶	**$CrF(OH)_2^+$**	+ HF				$\Delta_f H^\circ_{298} < 80.0 \pm 9.8$
(10)	$CrF(OH)_2^+$	+ H_2O	⟶	**$Cr(OH)_3^+$**	+ HF				$\Delta_f H^\circ_{298} < 87.3 \pm 9.8$
(11)	**$Cr(OH)_3^+$**	+ H_2O	↛	$CrO(OH)_2$	+ H_3O^+				$\Delta_f H^\circ_{298} < 66.8 \pm 4.8$[d]
(12)	$CrF_2(OH)^+$		⟶	**$CrFO^+$**	+ HF				$\Delta_f H^\circ_{298} < 137.8 \pm 9.8$
(13)	$CrFO^+$	+ H_2O	⟶	**$CrO(OH)^+$**	+ HF				$\Delta_f H^\circ_{298} < 145.1 \pm 9.8$[d]
(14)	**$CrO(OH)^+$**	+ H_2O	↛	CrO_2	+ H_3O^+				$\Delta_f H^\circ_{298} < 175.1 \pm 1.2$
(15)	CrF_4^+	+ H_2O	⟶	**$CrF_3(OH)^+$**	+ HF				$\Delta_f H^\circ_{298} < 20.9 \pm 7.2$
(16)	**$CrF_3(OH)^+$**	+ H_2O	⟶	CrF_3O	+ H_3O^+	$-18.2 \pm 12.4 <$			$\Delta_f H^\circ_{298}$
(17)	$CrF_3(OH)^+$	+ H_2O	⟶	**$CrF_2(OH)_2^+$**	+ HF				$\Delta_f H^\circ_{298} < 28.2 \pm 7.2$
(18)	$CrF_2(OH)_2^+$	+ H_2O	⟶	**$CrF(OH)_3^+$**	+ HF				$\Delta_f H^\circ_{298} < 35.5 \pm 7.2$
(19)	$CrF(OH)_3^+$	+ H_2O	⟶	**$Cr(OH)_4^+$**	+ HF				$\Delta_f H^\circ_{298} < 42.8 \pm 7.2$
(20)	**$Cr(OH)_4^+$**	+ H_2O	↛	$CrO(OH)_3$	+ H_3O^+				$\Delta_f H^\circ_{298} < 9.8 \pm 12$[d]
(21)	$CrF_3(OH)^+$		⟶	**CrF_2O^+**	+ HF				$\Delta_f H^\circ_{298} < 86.0 \pm 7.2$
(22)	CrF^+	+ N_2O	↛	**$CrFO^+$**	+ N_2	$217.9 \pm 7.3 <$			$\Delta_f H^\circ_{298}$
(23)	CrF_2^+	+ N_2O	↛	**CrF_2O^+**	+ N_2	$149.3 \pm 7.5 <$			$\Delta_f H^\circ_{298}$
(24)	CrF_3^+	+ N_2O	⟶	**CrF_3O^+**	+ N_2				$\Delta_f H^\circ_{298} < 85.0 \pm 9.8$

[a] Unless otherwise noted, data in kcal mol^{-1}. [b] For discussion, especially of multiple and/or seemingly contradicting entries, see text. [c] The table entries are numbered consecutively beginning with one. In order to avoid confusion with reactions given in the text, those given in this table will be referred to as, e.g., "Table 3, Entry 1". [d] Value considered to be more reliable. For discussion, see text.

corresponding neutral oxochromium hydroxide CrFO(OH) is unknown.

In addition, having established the upper limit for $\Delta_f H^\circ_{298}[CrF_2(OH)^+]$, the maximum standard heats of formation for both $CrFO^+$ and its hydrolysis product $CrO(OH)^+$ can be derived (Table 3, Entries 12 and 13, respectively). However, these two limits should be used with care: all reactions discussed so far involved the same number of reactants and products thus allowing, by and large, for the neglecting of entropic terms. With the number of molecules changing in the course of the HF abstraction reaction (Table 3, Entry 12), this does not apply any longer, and uncertainties in the range of several kcal mol^{-1} may be introduced by neglecting entropic factors. The absence of proton transfer from $CrO(OH)^+$ to water (Table 3, Entry 14) does not allow for deriving a more precise $\Delta_f H^\circ_{298}$ limit for that species.

The discussion of the CrF_4^+/H_2O system essentially parallels that of the CrF_3^+/H_2O system. The only remarkable difference is the occurrence of a second proton transfer reaction $CrF_2(OH)_2^+ + H_2O \rightarrow CrF_2O(OH) + H_3O^+$ which would have allowed for the determination of another minimum $\Delta_f H^\circ_{298}[CrF_2(OH)_2^+]$ value provided $\Delta_f H^\circ_{298}[CrF_2O(OH)]$ had been known.

Oxidation by Nitrous Oxide

As mentioned above, CrO^+ could not be generated from Cr^+ and N_2O, although the reaction is thermochemically favourable. We attribute this to a considerable twofold reaction (activation) barrier introduced by (i) the need to break the $3d^5$ configuration of the chromium cation and (ii) the missing electronic correlation between reactants and products of the reaction, N_2O ($^1\Sigma^+$) + Cr^+ (^6S) → N_2 ($1\Sigma_g^+$) + CrO^+ ($^4\Pi$[38]), already pointed out by Armentrout et al.[39]

We would like to discuss this absence of a thermochemically favourable reaction in more detail. From the point of the experimentalist, assuring proper thermalisation of the reactants is a mere question of careful experimental set-up. Thus, a "false positive" (a reaction occurring despite its endothermicity) can be prevented. In contrast, activation barriers and spin restrictions are *intrinsic* properties of the sys-

Table 4. Heats of formation of chromium fluoride cations and other species of interest[a] [b] [c]

Species	$\Delta_f H^\circ_{298}$ (Neutral)		$\Delta_f H^\circ_{298}$ (Mono-cation)	
Cr	94.8	[17]	250.8	[17]
CrF	4.6 ± 2.4	[21]	198.3 ± 7.3	[1,17,21][d]
CrF_2	−103.2 ± 3.0	[21]	129.7 ± 7.5	[1,17,21][d]
CrF_3	−199.8 ± 3.4	[21]	65.4 ± 9.8	[1,21][e]
CrF_4	−270.0 ± 2.1	[21]	13.6 ± 7.2	[1,21][e]
CrO	43.6 ± 1.6	[67]	225.8 ± 1.6	[17,21][f]
CrO_2	−23.7 ± 1.2	[67]	213.8 ± 11.6	[17,21][f]
			209 ± 12	[66][g]
CrO_3	−77.3 ± 1.0	[67]	190.2 ± 11.6	[17,21][f]
CrFO	−73.3 ± 1.9	[21]	< 137.8 ± 9.8	
CrF_2O	−153.3 ± 3.4	[21]	< 86.0 ± 7.2	
CrF_3O	−217.0 ± 12.4	[21]	43.6 ± 13.2	
CrF_4O	−262.5 ± 8.9	[21]		
Cr(OH)	18.9 ± 1.8	[67]	185.8 ± 3.0	[17,37][h]
			< 205.6 ± 7.3	
$Cr(OH)_2$	−76.9 ± 1.2	[67]	< 139.8 ± 1.2	
$Cr(OH)_3$	−150.9 ± 2.4	[67]	< 66.8 ± 4.8	
$Cr(OH)_4$	−207.6 ± 2.4	[67]	< 9.8 ± 12	
$Cr(OH)_5$	−259.9 ± 4.8	[67]		
$Cr(OH)_6$	−305 ± 12	[67]		
CrO(OH)	−59.0 ± 1.2	[67]	< 145.1 ± 9.8	
$CrO(OH)_2$	−132.0 ± 4.8	[67]		
$CrO(OH)_3$	−189 ± 12	[67]		
$CrO(OH)_4$	−242 ± 12	[67]		
CrF(OH)			< 125.5 ± 1.9	
$CrF(OH)_2$			< 80.0 ± 9.8	
$CrF(OH)_3$			< 35.5 ± 7.2	
$CrF_2(OH)$			see Table 3	
$CrF_2(OH)_2$			< 28.2 ± 7.2	
$CrF_3(OH)$			see Table 3	
N_2O	19.6	[17]		
O	59.6	[17]	373.6	[17]
OH	9.3 ± 0.3	[17]	309.1	[17]
H_2O	−57.8	[17,21]	233.0	[17]
H_3O			141	[17]
HF	−65.1 ± 0.2	[17,21]		

[a] All data in kcal mol^{-1}. [b] This work unless otherwise noted. [c] We report only "best values" here. For data evaluation, see the limits reported in Table 3 and the discussion in the text. [d] Calculated from the heat of formation[21] and the ionisation energy.[1,17] [e] Calculated from the heat of formation[21] and the ionisation energy.[1] [f] Calculated from the heat of formation[21] and the ionisation energy.[17] [g] OCrO. [h] Calculated from the heats of formation of Cr^+ and OH[17] and the bond dissociation energy (*BDE*) of Cr^+-OH.[37]

tem and cannot be circumvented by any experimental condition. Thus, a "false negative" (a reaction not occurring despite its exothermicity) cannot be detected without an independent determination of the thermochemical data.

Finally, one more point regarding oxidation by nitrous oxide shall be discussed here. Due to an orbital reorganisation,[40] linear N_2O needs to get bent in order to facilitate oxygen-atom transfer onto its reaction partner.[41,42]

The failure to generate $CrFO^+$ from CrF^+ and N_2O can be explained by the following. (i) The oxidation reaction is endothermic corresponding to $\Delta_f H^\circ_{298}(CrFO^+) > 217.9 \pm 7.3$ kcal mol^{-1} (Table 3, Entry 22). However, this limit contradicts that derived from the decomposition of $CrF_2(OH)^+$, $\Delta_f H^\circ_{298}(CrFO^+) < 137.8 \pm 9.8$ kcal mol^{-1} (Table 3, Entry 12), and this explanation cannot hold true. (ii) $CrFO^+$, once formed, is readily oxidised to yield $CrFO_2^+$. However, as the formal Cr^{VI} species $CrFO_2^+$ was not observed, it would have to be a fast-reacting intermediate, thus posing the question of its reaction partners and the resulting products. While traces of H_3O^+ and NO^+ were detected, the direct formation of H_3O^+ from $CrFO^+$ and background water is impossible, and the transfer of the nitride anion from N_2O appears rather unlikely. In parallel, hydride anion abstraction from H_2O would yield HO^+, which cannot be observed by our mass spectrometer (thus allowing for both facile formation and consumption of $CrFO_2^+$). However, the formation of HO^+ is highly unlikely on thermochemical grounds. Hence, this second explanation is excluded as well. (iii) The above-mentioned spin-inversion phenomena prevent the reaction from proceeding, i.e. assumption (ii) introduced in the first paragraph of this section does not apply. In this particular case, however, an upper limit for $\Delta_f H^\circ_{298}(CrFO^+)$ could be derived independently from a reaction that does take place (Table 3, Entry 12), thus allowing for the ruling out of an erroneous $\Delta_f H^\circ_{298}(CrFO^+)$ limit derivation (Table 3, Entry 22).

While CrF_2O^+ could be obtained in traces, it was impossible to isolate it from the mixture of hydrolysis products, which included traces of NO^+, the intermediate N_2O^+ and the final product H_3O^+. For a discussion, we apply the three-item scheme already utilised for $CrFO^+$: (i) Endothermicity of the reaction (Table 3, Entry 23) can be ruled out (Table 3, Entry 21). (ii) Facile oxidation of CrF_2O^+ by N_2O would yield $CrF_2O_2^+$, i.e., a formal Cr^{VII} species, which could explain the observation of N_2O^+ and H_3O^+ when CrF^+_2 is exposed to N_2O according to Equations (7)−(11). Furthermore, it should be noted that $CrF_2O_2^+$ has been generated and its *IE* value determined.[43]

$$CrF_2 + N_2O \rightarrow CrF_2O^+ + N_2 \quad (7)$$

$$CrF_2O^+ + N_2O \rightarrow CrF_2O_2^+ + N_2 \quad (8)$$

$$CrF_2O_2^+ + N_2O \rightarrow CrF_2O_2^+ + N_2O^+ \quad (9)$$

$$N_2O^+ + H_2O \rightarrow N_2O + H_2O^+ \quad (10)$$

$$H_2O^+ + H_2O \rightarrow H_3O^+ + OH \quad (11)$$

While the generation of H_3O^+ from N_2O^+ via H_2O^+ is consistent with established thermochemical data (Table 4), and its temporal evolution appeared to be properly modelled, the temporal evolution of N_2O^+ could not be reproduced on the basis of Equations (7)−(11). Furthermore, the value of k_{11} obtained by modelling was about two orders of magnitude smaller than the literature value.[44] Consequently, the generation of N_2O^+ was attributed to a par-

ent ion or ions activated during the mass selection of CrF_2^+, and the formation of the formal Cr^{VII} species $CrF_2O_2^+$ from properly thermalised precursors was ruled out. (iii) As in CrF^+, the spin-inversion problem is a prime candidate for preventing the oxidation reaction of CrF_2^+.

In contrast to the CrF_n^+ cations discussed so far, CrF_3^+ reacts with N_2O to give CrF_3O^+ in good yields. Hence, an upper limit of $\Delta_f H°_{298}(CrF_3O^+)$ can be derived (Table 3, Entry 24). On combination with the ionisation energy of the corresponding neutral species (see Table 1), an upper limit of $\Delta_f H°_{298}(CrF_3O) < -177.9$ kcal mol^{-1} is obtained. Basically, our value is in agreement with literature data;[21] however, it is about 40 kcal mol^{-1} too large. Thus, the inverted procedure, i.e. combining the literature value of $\Delta_f H°_{298}(CrF_3O)$ with the *IE* determined in this study, provides a reasonable value for $\Delta_f H°_{298}(CrF_3O^+)$ as given in Table 4.

Another conclusion is that the spin conservation requirement no longer hampers the transfer of the oxygen atom to the chromium fluoride cation. This could be explained by the fact that as the oxidation state of the chromium centre increases, the spin-orbit coupling increases, thus enabling a more facile intersystem crossing (spin inversion) and, consequently, a lower reaction barrier. This explanation may also account for the trend in the oxidation efficiencies from Cr^+ and CrF^+ (no reactivity observed) via CrF_2^+ (traces of CrF_2O^+ generated) to CrF_3^+ (facile reaction), which parallels, at least qualitatively, the increasing formal oxidation state of the chromium centre.

Conclusion

In this study, we have investigated the reactions of chromium and chromium fluoride monocations CrF_n^+ (n = 0−4) with water. Besides slow condensation, Cr^+ is unreactive, whereas progressive hydrolysis of the Cr−F bonds proceeds for CrF^+, CrF_2^+, CrF_3^+, and CrF_4^+. However, for the species $CrF_2(OH)^+$, efficient proton abstraction parallels the hydrolysis of the next Cr−F bond, and in the case of $CrF_3(OH)^+$, that proton transfer is even preferred over further Cr−F bond hydrolysis.

Furthermore, we have investigated the reactions of chromium and chromium fluoride monocations with the established oxygen-transferring agent nitrous oxide. Significant transfer of oxygen was observed for CrF_3^+ only. The ionisation energy of CrF_3O is 11.3 ± 0.2 eV. Attempts to transfer the oxygen atom from CrF_3O^+ to small alkanes or to carbon monoxide failed.

Experimental Section

Reactants: Nitrogen trifluoride (Praxair, 99.99%), nitrous oxide (Linde, 99.5%), argon (AGA Gas, 99.996%), and solid chromium (Balzers, > 99.9%) were used as purchased. Tap water was used without further purification. The water was put into a half-micro test tube directly connected to the gas-inlet system of the mass spectrometer and degassed by two freeze-evacuate-thaw cycles. Hexafluoroacetone, C_3F_6O, was liberated from its sesquihydrate (Merck-Schuchardt, > 97%) by reaction with phosphoric anhydride, P_4O_{10}, in analogy to literature procedures.[45−47] The dehydration reaction was carried out in a half-micro test tube directly connected to a leak valve of the mass spectrometer. Due to the differences between the boiling points of hexafluoroacetone (−28 °C/p_0)[46] and its water-containing hydrate (55−56 °C/107 mbar),[48] we assumed the dehydration process to be complete in the sense that no hexafluoroacetone hydrate was admitted into the reaction cell from the leak valve. However, the admission of water itself to the reaction cell could not be prevented in this "on-line" preparation of hexafluoroacetone. All reactant gases not mentioned so far were purchased from Linde and used without further purification.

Mass Spectrometer: All experiments were performed with a Bruker Spectrospin CMS-47X Fourier transform ion-cyclotron resonance (FT-ICR) mass spectrometer. The setup and operation have been described previously.[49,50] In brief, chromium monocations were generated from targets of pure chromium by laser desorption/laser ionisation[51,52] in the external ion source of the spectrometer using an Nd:YAG laser (Spectron Systems, λ_{max} = 1064 nm). The chromium ions were extracted from the source and transferred into the analyser cell via a system of electrostatic potentials. Next, the most abundant isotope ^{52}Cr (relative abundance 83.8%[53]) was mass-selected using FERETS,[54] a computer-controlled ion-ejection protocol that combines frequency sweeps and single-frequency pulses to optimise resonant excitation and ejection of all unwanted ions. After mass-selection, $^{52}Cr^+$ cations were allowed to react with pulsed-in reactant gas mixtures as described below.

Reactions with Water: After mass-selection, $^{52}Cr^+$ ions were exposed to pulsed-in nitrogen trifluoride/argon mixtures. Both the composition of the gas mixture and the length of the gas pulse were adjusted to maximise the yield of the desired chromium fluoride cation, CrF_n^+ (n = 1−4). Subsequently, the ion of interest was mass-selected using FERETS. Electronically excited Cr^+ ions, which are known to be efficiently thermalised by collision with methane[55] rather than argon,[1] were allowed to multiply collide with pulsed-in methane. In an additional series of experiments, however, Cr^+ cations were allowed to react with water after multiple collisions with argon rather than with methane. CrF^+ ions which are known to require thermalisation as well[1] were allowed to undergo multiple collisions with water and re-isolated using FERETS. Thermalisation deemed unnecessary for CrF_n^+ (n = 2−4) due to the purely exponential decays of their intensities during the reactions investigated. Water was admitted to the cell via a leak valve at a constant pressure measured by a calibrated[56] BALZERS IMG 070 ion gauge. The effective water pressures were $7.7\cdot10^{-9}$ mbar, $4.7\cdot10^{-9}$ mbar, $2.5\cdot10^{-9}$ mbar, and $7.7\cdot10^{-9}$ mbar for CrF^+, CrF_2^+, CrF_3^+, and CrF_4^+, respectively. For Cr^+, the pressure was in the range of $6.5\cdot10^{-9}$ to $1.0\cdot10^{-5}$ mbar.

Reactions with Nitrous Oxide: After mass selection, $^{52}Cr^+$ ions were exposed to pulsed-in nitrogen trifluoride/argon or nitrogen trifluoride/nitrous oxide mixtures, respectively. Both the composition of the gas mixtures and the length of the gas pulse were adjusted to maximise the yield of the desired chromium fluoride cation, CrF_n^+ (n = 1−4), or oxochromium fluoride cation, CrF_nO^+ (n = 1−4). The ion of interest was isolated using FERETS. Reactant gases were admitted to the cell via a leak valve at a constant pressure in the order of 10^{-8} to 10^{-7} mbar while the background pressure in the analyser cell of the spectrometer was in the range of $(2-4)\cdot10^{-9}$ mbar. To generate the ions of interest, we employed, in that order, (i) the established methodology of generating chromium fluoride monocations using nitrogen trifluoride, NF_3, as the fluorinating

agent[1,2] and (ii) the time-honoured use of nitrous oxide, N_2O, for the transfer of the oxygen atoms. The latter has been proven to transfer oxygen to a wide variety of metal cations like Ti^+,[25] V^+,[25] Fe^+,[18,25] Zr^+,[25] Nb^+,[25] Mo^+ [57] and U_2^+.[58] It was not indicated to use the alternative approach of first generating chromium oxide monocations, CrO^+, and subsequently transferring fluorine atoms to them, due to the inefficient oxygen transfer to bare chromium ions, Cr^+,[25] which requires CrO^+ to be generated from CrO_2Cl_2.[33] CrF^+ ions, which are known to need thermalisation,[1] were allowed to multiply collide with nitrous oxide and re-isolated using FERETS. All other ions CrF_n^+ ($n = 2-4$) did not require thermalisation as mentioned above.

Analysis of Experimental Results: Elemental compositions of ions were determined by high-resolution mass spectrometry. Reaction sequences were derived from the temporal evolution of ion intensities and complementary double-resonance experiments.[59] In a double-resonance experiment, a supposed intermediate [e.g., $^{52}CrF(OH)^+$, $m/z = 87.94165$] is continuously ejected from the reaction cell by employing a constant radio-frequency pulse for a certain period of time. The resulting spectrum is compared with a reference spectrum originating from the very same experimental conditions, except that ejecting the supposed intermediate is replaced by "ejecting" a nonexisting hypothetical ion (e.g., $m/z = 500$). The disappearance of the signal of a product ion indicates that this ion originates, directly or indirectly, from the ejected one. Reaction kinetics were analysed using a computer program that determines rate constants and distribution ratios based on the experimentally observed evolution of ion intensities over time, and a flexible kinetic model.[60] The reported rate constants are measured bimolecular rate constants given in units of cm^3 $molecules^{-1}$ s^{-1}, whereas reaction efficiencies φ are given as fractions of the measured bimolecular rate constants and the gas-kinetic collision rates according to the capture theory.[28,29] The parameters used for H_2O were: dipole moment 1.854 D,[61] polarisability $1.45 \cdot 10^{-24}$ cm^3,[61] relative ion gauge sensitivity 0.97.[62] The parameters used for N_2O were: dipole moment 0.161 D,[61] polarisability $3.03 \cdot 10^{-24}$ cm^3,[61] relative ion gauge sensitivity 1.20.[62] The absolute error of the experimentally determined rate constants is in the range of ± 30%, while the relative rates are more precise (± 10%).[56] However, for reactions of CrF_n^+ ($n = 2-4$) ions with H_2O, the error is estimated to be in the range of ± 40% for the rate constants and ± 15% for their ratios due to the lower signal intensities. Ionisation energies can be determined by the "charge-transfer bracketing" method described in the following: In a series of experiments, the ion of interest is allowed to react with neutral species of known ionisation energies. Then, a *synopsis* of the ionisation energies of the reaction partners and the experimentally observed presence or absence of charge-transfer (CT) between the ion and the reaction partners allows for an estimation of the ionisation energy. Alternatively, the reaction efficiency φ of a charge-transfer reaction is correlated to the ionisation energy difference between the ion and its reaction partner: $\Delta_r G = \Delta_r G° - RT \ln K$ with $K = k_{CT}/k_{reverse\ CT}$, $k_{CT} = \ln(\varphi/\varphi_{max})$, and $k_{reverse\ CT} = 1 - \ln(\varphi/\varphi_{max})$.[32] Both methods rely on the reasonable assumption that the activation barriers associated with the charge-transfer reactions are negligible. Heats of formation $\Delta_f H°$ given in this publication, are in thermochemical kilocalories ($kcal_{th}$) unless otherwise stated. When converting published values given in kilojoules, a conversion factor of 1 $cal_{th} = 4.184$ J[63] was applied. Ionisation energies (*IE*) are given in electron volts (eV), the conversion factors are 1 eV = 96.48534 kJ mol^{-1} = 23.06055 kcal mol^{-1}.[64] On calculating ion heats of formation from heats of formation and ionisation energies of the corresponding neutral species, the "stationary electron" or "ion" convention[65] was applied. To convert the data obtained at 298 K so that they are consistent with the "thermal electron" or "electron" convention, the amount of 1.481 kcal mol^{-1} needs to be added.[65]

Acknowledgments

This work was supported by the Deutsche Forschungsgemeinschaft, the Fonds der Chemischen Industrie, and the Volkswagen-Stiftung. The authors wish to thank Dr. Robert Berger and Prof. Dr. Christoph van Wüllen for helpful discussions.

[1] U. Mazurek, D. Schröder, H. Schwarz, *Collect. Czech. Chem. Commun.* **1998**, *63*, 1498−1512.
[2] U. Mazurek, H. Schwarz, *Inorg. Chem.* **2000**, *39*, 5586−5590.
[3] S. W. Buckner, J. R. Gord, B. S. Freiser, *J. Am. Chem. Soc.* **1988**, *110*, 6606−6612.
[4] J. B. Schilling, J. L. Beauchamp, *Organometallics* **1988**, *7*, 194−199.
[5] M. K. Beyer, C. B. Berg, U. Achatz, S. Joos, G. Niedner-Schatteburg, V. E. Bondybey, *Mol. Phys.* **2001**, *99*, 699−702.
[6] A. G. Marshall, *Acc. Chem. Res.* **1996**, *29*, 307−316.
[7] S. Bärsch, D. Schröder, H. Schwarz, *Helv. Chim. Acta* **2000**, *83*, 827−835.
[8] D. Schröder, S. Bärsch, H. Schwarz, *J. Phys. Chem. A* **2000**, *104*, 5101−5110.
[9] S. Bärsch, D. Schröder, H. Schwarz, *Chem. Eur. J.* **2000**, *6*, 1789−1796.
[10] G. K. Koyanagi, D. K. Bohme, I. Kretzschmar, D. Schröder, H. Schwarz, *J. Phys. Chem. A* **2001**, *105*, 4259−4271.
[11] D. K. Bohme, *Int. J. Mass Spectrom. Ion Processes* **1992**, *115*, 95−110.
[12] A. J. Chalk, L. Radom, *J. Am. Chem. Soc.* **1997**, *119*, 7573−7578.
[13] H. Becker, D. Schröder, W. Zummack, H. Schwarz, *J. Am. Chem. Soc.* **1994**, *116*, 1096−1100.
[14] H. E. Audier, D. Leblanc, P. Mourges, T. B. McMahon, S. Hammerum, *J. Chem. Soc., Chem. Commun.* **1994**, 2329−2330.
[15] T. D. Fridgen, J. M. Parnis, *Int. J. Mass Spectrom.* **1999**, *190/191*, 181−194.
[16] M. A. Trikoupis, P. C. Burgers, P. J. A. Ruttink, J. K. Terlouw, *Int. J. Mass Spectrom.* **2001**, *210/211*, 489−502.
[17] S. G. Lias, J. E. Bartmess, J. F. Liebman, J. L. Holmes, R. D. Levin, W. G. Mallard, *J. Phys. Chem. Ref. Data, Suppl. 1* **1988**, *17*, 1−861.
[18] M. Brönstrup, D. Schröder, H. Schwarz, *Chem. Eur. J.* **1999**, *5*, 1176−1185.
[19] P. Jackson, J. N. Harvey, D. Schröder, H. Schwarz, *Int. J. Mass Spectrom.* **2001**, *204*, 233−245.
[20] E. Z. Zasorin, A. A. Ivanov, L. I. Ermolaeva, V. P. Spiridonov, *Russ. J. Phys. Chem.* **1989**, *63*, 363−365.
[21] B. B. Ebbinghaus, *Combust. Flame* **1995**, *101*, 311−338.
[22] L. Hedberg, K. Hedberg, G. L. Gard, J. O. Udeaja, *Acta Chem. Scand., Ser. A* **1988**, *42*, 318−323.
[23] D. Schröder, S. Shaik, H. Schwarz, *Acc. Chem. Res.* **2000**, *33*, 139−145.
[24] F. Cacace, F. Pepi, F. Grandinetti, *J. Phys. Chem.* **1994**, *98*, 8009−8013.
[25] M. M. Kappes, R. H. Staley, *J. Phys. Chem.* **1981**, *85*, 942−944.
[26] M. F. Ryan, D. Stöckigt, H. Schwarz, *J. Am. Chem. Soc.* **1994**, *116*, 9565−9570.
[27] V. Baranov, D. K. Bohme, *Int. J. Mass Spectrom.* **2001**, *204*, 209−221.
[28] T. Su, W. J. Chesnavich, *J. Chem. Phys.* **1982**, *76*, 5183−5185.
[29] T. Su, *J. Chem. Phys.* **1988**, *89*, 5355.
[30] A. J. Midey, S. Williams, A. A. Viggiano, *J. Phys. Chem. A* **2001**, *105*, 1574−1578.
[31] S. G. Lias, in *NIST Chemistry WebBook, NIST Standard Reference Database Number* 69 (Eds.: W. G. Mallard, P J. Linstrom),

National Institute of Standards and Technology, Gaithersburg, MD 20899, February **2000** (http://webbook.nist.gov).
[32] G. Bouchoux, J. Y. Salpin, D. Leblanc, *Int. J. Mass Spectrom. Ion Processes* **1996**, *153*, 37−48.
[33] H. Kang, J. L. Beauchamp, *J. Am. Chem. Soc.* **1986**, *108*, 7502−7509.
[34] I. Kretzschmar, D. Schröder, H. Schwarz, *Int. J. Mass Spectrom. Ion Processes* **1997**, *167/168*, 103−115.
[35] M. Brönstrup, D. Schröder, I. Kretzschmar, H. Schwarz, J. N. Harvey, *J. Am. Chem. Soc.* **2001**, *123*, 142−147.
[36] K. K. Irikura, J. L. Beauchamp, *J. Am. Chem. Soc.* **1989**, *111*, 75−85.
[37] T. F. Magnera, D. E. David, J. Michl, *J. Am. Chem. Soc.* **1989**, *111*, 4100−4101.
[38] J. F. Harrison, *J. Phys. Chem.* **1986**, *90*, 3313−3319.
[39] P. B. Armentrout, L. F. Halle, J. L. Beauchamp, *J. Chem. Phys.* **1982**, *76*, 2449−2457.
[40] D. R. Yarkony, *J. Chem. Phys.* **1983**, *78*, 6763−6772.
[41] B. G. Wicke, *J. Chem. Phys.* **1983**, *78*, 6036−6044.
[42] C.-F. Nien, J. M. C. Plane, *J. Chem. Phys.* **1991**, *94*, 7193−7203.
[43] G. D. Flesch, R. M. White, H. J. Svec, *Int. J. Mass Spectrom. Ion Phys.* **1969**, *3*, 339−363.
[44] V. G. Anicich, *J. Phys. Chem. Ref. Data* **1993**, *22*, 1469−1569.
[45] A. L. Henne, J. W. Shepard, E. J. Young, *J. Am. Chem. Soc.* **1950**, *72*, 3577−3579.
[46] R. N. Haszeldine, *J. Chem. Soc.* **1953**, 3565−3573.
[47] R. N. Haszeldine, *J. Chem. Soc.* **1954**, 1273−1279.
[48] A. T. Morse, P. B. Ayscough, L. C. Leitch, *Can. J. Chem.* **1955**, *33*, 453−457.
[49] K. Eller, H. Schwarz, *Int. J. Mass Spectrom. Ion Processes* **1989**, *93*, 243−257.
[50] K. Eller, W. Zummack, H. Schwarz, *J. Am. Chem. Soc.* **1990**, *112*, 621−627.
[51] B. S. Freiser, *Talanta* **1985**, *32*, 697−708.
[52] B. S. Freiser, *Anal. Chim. Acta* **1985**, *178*, 137−158.
[53] K. J. R. Rosman, P. D. P. Taylor, *Pure Appl. Chem.* **1997**, *70*, 217−236.
[54] R. A. Forbes, F. H. Laukien, J. Wronka, *Int. J. Mass Spectrom. Ion Processes* **1988**, *83*, 23−44.
[55] W. D. Reents, Jr., F. Strobel, R. B. Freas, III, J. Wronka, D. P. Ridge, *J. Phys. Chem.* **1985**, *89*, 5666−5670.
[56] D. Schröder, H. Schwarz, D. E. Clemmer, Y. Chen, P. B. Armentrout, V. Baranov, D. K. Böhme, *Int. J. Mass Spectrom. Ion Processes* **1997**, *161*, 175−191.
[57] I. Kretzschmar, A. Fiedler, J. N. Harvey, D. Schröder, H. Schwarz, *J. Phys. Chem. A* **1997**, *101*, 6252−6264.
[58] H. H. Cornehl, C. Heinemann, J. Marçalo, A. Pires de Matos, H. Schwarz, *Angew. Chem.* **1996**, *108*, 950−952; *Angew. Chem. Int. Ed. Engl.* **1996**, *35*, 891−894.
[59] M. B. Comisarow, V. Grassi, G. Parisod, *Chem. Phys. Lett.* **1978**, *57*, 413−416.
[60] U. Mazurek, H. Schwarz, *ICR Kinetics, v. 3.0.1*, TU Berlin, Berlin, **1998**.
[61] D. R. Lide (Ed.), *CRC Handbook of Chemistry and Physics*, 79th ed., CRC Press, Boca Raton, FL, **1998**.
[62] J. E. Bartmess, R. M. Georgiadis, *Vacuum* **1983**, *33*, 149−153.
[63] I. Mills, T. Cvitas, K. Homann, N. Kallay, K. Kuchitsu (Eds.), *Quantities, Units and Symbols in Physical Chemistry*, Blackwell Scientific, Oxford, **1993**.
[64] B. N. Taylor, P. J. Mohr, *The NIST Reference on Constants, Units, and Uncertainty*, National Institute of Standards and Technology, Gaithersburg, MD 20899, **1998** (http://physics.nist.gov/cuu/Constants/index.html).
[65] S. G. Lias, J. E. Bartmess, J. F. Liebman, J. L. Holmes, R. D. Levin, W. G. Mallard, *J. Phys. Chem. Ref. Data, Suppl. 1* **1988**, *17*, 8−10.
[66] A. Fiedler, I. Kretzschmar, D. Schröder, H. Schwarz, *J. Am. Chem. Soc.* **1996**, *118*, 9941−9952.
[67] B. B. Ebbinghaus, *Combust. Flame* **1993**, *93*, 119−137.

Received January 23, 2002
[I02038]

Synthesis and Coordination Chemistry of the New Unsymmetrical Ligand $Ph_2PCH_2NHC_6H_4PPh_2$

Qingzhi Zhang,[a] Stephen M. Aucott,[a] Alexandra M. Z. Slawin,[a] and J. Derek Woollins*[a]

Keywords: Unsymmetrical ligands / Phosphanes / Chelates / Monodentate complexes / Heterometallic complexes

Condensation of Ph_2PCH_2OH with 2-(diphenylphosphanyl)-aniline in toluene gave the new unsymmetrical ligand $Ph_2PCH_2NHC_6H_4PPh_2$ (**1**) in good yield. Oxidation of **1** with H_2O_2 or elemental sulfur led to the oxidised products $Ph_2P(O)CH_2NHC_6H_4P(O)Ph_2$ (**2**) and $Ph_2P(S)CH_2NHC_6H_4P(S)Ph_2$ (**3**). The new ligand **1** demonstrates three distinct modes of coordination. Reaction of compound **1** with $[MX_2(cod)]$ (M = Pd, Pt; X = Cl, Br, Me) or $[Mo(CO)_4(pip)_2]$ gave the chelate complexes $[PdCl_2(Ph_2PCH_2NHC_6H_4PPh_2\text{-}P_X,P_A)]$ (**4**), $[PdBr_2(Ph_2PCH_2NHC_6H_4PPh_2\text{-}P_X,P_A)]$ (**5**), $[PtCl_2(Ph_2PCH_2NHC_6H_4PPh_2\text{-}P_X,P_A)]$ (**6**), $[PtMe_2(Ph_2PCH_2NHC_6H_4PPh_2\text{-}P_X,P_A)]$ (**7**) and $[Mo(CO)_4(Ph_2PCH_2NHC_6H_4PPh_2\text{-}P_X,P_A)]$ (**8**). Coordination of **1** with $[\{RuCl(\mu\text{-}Cl)(\eta^3\text{:}\eta^3\text{-}C_{10}H_{16})\}_2]$ or $[\{RhCl(\mu\text{-}Cl)(\eta^5\text{-}C_5Me_5)\}_2]$ gave the monodentate complexes $[RuCl_2(\eta^3\text{:}\eta^3\text{-}C_{10}H_{16})(Ph_2PCH_2NHC_6H_4PPh_2\text{-}P_X)]$ (**9**) and $[RhCl_2(\eta^5\text{-}C_5Me_5)(Ph_2PCH_2NHC_6H_4PPh_2\text{-}P_X)]$ (**10**). Reaction of **1** with $[\{IrCl(\mu\text{-}Cl)(\eta^5\text{-}C_5Me_5)\}_2]$ led to a mixture from which the monodentate complex $[IrCl_2(\eta^5\text{-}C_5Me_5)(Ph_2PCH_2NHC_6H_4PPh_2\text{-}P_X)]$ (**11**) and the chelate cationic complex $[IrCl(\eta^5\text{-}C_5Me_5)(Ph_2PCH_2NHC_6H_4PPh_2\text{-}P_X,P_A)][Cl]$ (**12**) were separated. Abstraction of the chloride ligands from complexes **9** and **10** with $AgClO_4$ gave the cationic chelate complexes $[RuCl(\eta^3\text{:}\eta^3\text{-}C_{10}H_{16})(Ph_2PCH_2NHC_6H_4PPh_2\text{-}P_X,P_A)][ClO_4]$ (**13**) and $[RhCl(\eta^5\text{-}C_5Me_5)(Ph_2PCH_2NHC_6H_4PPh_2\text{-}P_X,P_A][ClO_4]$ (**14**). Compound **1** also functions as a bridging ligand when reacted with two molar equivalents of [AuCl(tht)] or one molar equivalent of $[\{RhCl(\mu\text{-}Cl)(\eta^5\text{-}C_5Me_5)\}_2]$ to give the bimetallic complexes $[Ph_2P\{AuCl\}CH_2NHC_6H_4PPh_2\{AuCl\}]$ (**15**) and $[\{RhCl_2(\eta^5\text{-}C_5Me_5)\}_2(Ph_2PCH_2NHC_6H_4PPh_2)]$ (**16**). The dioxidised compounds **2** and **3** and several typical complexes **8**, **9**, **11** and **14** were structurally characterised by X-ray diffraction.

(© Wiley-VCH Verlag GmbH, 69451 Weinheim, Germany, 2002)

Introduction

Chemically symmetrical bisphosphane ligands have been intensively investigated in all aspects of inorganic and organometallic chemistry, and $Ph_2PCH_2PPh_2$ [bis(diphenylphosphanyl)methane (dppm)], $Ph_2PCH_2CH_2PPh_2$ [bis(diphenylphosphanyl)ethane (dppe)], and its $-(CH_2)_n-$ backboned homologues, the aromatic $Ph_2PC_6H_4PPh_2$ [1,2-phenylenebis(diphenylphosphane)] and the ferrocene backboned 1,1′-bis(diphenylphosphanyl)ferrocene are all well-known examples of this class of ligand.[1−9] Unsymmetric bisphosphanes, with the notable exception of chiral aminophosphane-phosphinites,[10] have received relatively little attention (for recent examples see refs.[11−15]). We recently described the synthesis of $Ph_2PC_6H_4NHPPh_2$ an unsymmetrical diphosphane derived from 2-(diphenylphosphanyl)-aniline[16] in which the two phosphorus atoms demonstrated different coordination activities.[17,18] Herein we report another unsymmetrical diphosphane $Ph_2PCH_2NHC_6H_4PPh_2$ which has an additional methylene spacer group between the NH and the PPh_2 moieties giving the ligand a flexible $PCNC_2P$ spine. Other rare literature examples of $PCNC_2P$ backboned ligand systems include diphenyl[3-(2-diphenylphosphanylphenylsydonyl)-phosphane[19] **A**, the substituted quinazolinone ligand **B**[20] and the bis(diphenylphosphanyl)- and bis(dicyclohexylphosphanyl)pyrrole-derived diphosphanes **C** and **D**[21] (Scheme 1). The synthesis of $Ph_2PCH_2NHC_6H_4PPh_2$ and its reactivity towards a variety of late transition metals are described. The products from these reactions have been characterised principally by multi-element NMR spectroscopy and X-ray crystallography.

[a] Department of Chemistry, University of St Andrews, Fife, Scotland KY16 9ST, UK
Fax: (internat.) + 44-1334/463-384
E-mail: jdw3@st-and.ac.uk

Results and Discussion

Preparation and Characterisation of the Ligand

The condensation of equimolar quantities of diphenylphosphanylmethanol and 2-(diphenylphosphanyl)aniline in toluene at 90−95 °C gave the unsymmetrical bisphosphane $Ph_2PC_6H_4NHCH_2PPh_2$ (**1**) in excellent yield (84.4%) (Scheme 2). The white solid product was stable to moisture and air. The $^{31}P\{^1H\}$ NMR spectrum of **1** in $CDCl_3$ shows two distinct singlets at $\delta_P = -18.77$ and $\delta_P = -22.30$. Although it is not easy to assign the signals in reference to

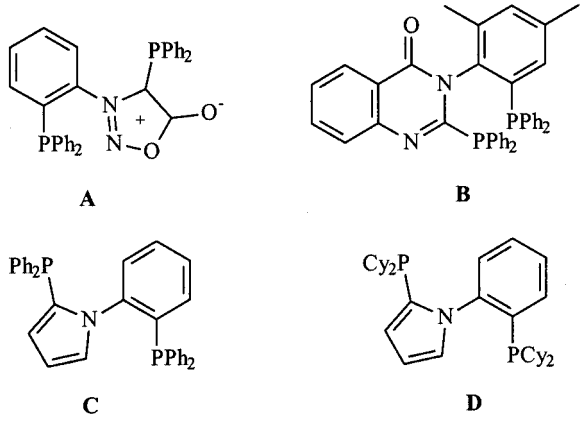

Scheme 1. Examples of $PCNC_2P$ backboned ligands

the starting reactant 2-(diphenylphosphanyl)aniline[16] (**17**) or the previously reported $Ph_2PNHC_6H_4PPh_2$ [17] (**18**) (Scheme 2, Table 1), the resonance at $\delta_P = -18.77$ was assigned to the phosphorus (P_X) of the $NHCH_2PPh_2$ group and the other signal at $\delta_P = -22.30$ to the triarylphosphane moiety (P_A) by comparing the $^{31}P\{^1H\}$ NMR spectra of its monodentate complexes **9**−**11**, which will be discussed below. These assignments are also in accordance with those in other reported molecules (**19**−**22**)[22−25] shown below (Scheme 3, Table 1).

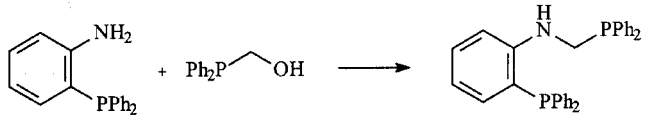

Scheme 2. Preparation of ligand **11**

Table 1. $^{31}P\{^1H\}$ NMR chemical shifts of **1**, and related compounds **17**−**22**

Compound	Chemical shifts $\delta(P_X)$[a]	$\delta(P_A)$[a]	Compound	Chemical shifts $\delta(P_X)$[a]	$\delta(P_A)$[a]
1	−18.77	−22.30	**20**[b]	−16.8	−
17[b]	−	−19.75	**21**[b]	−17.9	−
18[b]	29.6	−19.5	**22**[b]	−	−21.5
19[b]	−18.16	−			

[a] P_X is the phosphorus of either $NHCH_2PPh_2$ or $NHPPh_2$ groups and P_A is the phosphorus of triarylphosphane. [b] Literature compounds.

In the ^1H NMR spectrum, the resonances of the aromatic protons are found between $\delta_H = 7.40$ and 6.64. The NH proton appears as a broad singlet at $\delta_H = 4.97$. The triplet at $\delta_H = 3.83$ was assigned to the methylene group, with equal couplings ($^3J_{P,CH} = {}^3J_{CH,NH} = 5$ Hz). The infrared spectrum of **1** shows ν_{NH} at 3345 cm^{-1}. Attempts to grow crystals of **1** suitable for X-ray analysis were not successful. However, the structures of its oxidised counterparts **2** (Figure 1, Table 2) and **3** (Figure 2, Table 2) were obtained. Compound **2** was prepared by the oxidation of **1** with H_2O_2 and compound **3** by oxidation of **1** with elemental sulfur.

Compounds **2** and **3**, like their parent compound **1**, gave good microanalysis and the expected FAB-MS spectral patterns. The $^{31}P\{^1H\}$ NMR spectrum of **2** (in CD_2Cl_2) exhibits two singlets at higher frequency than those of **1**. The singlet at $\delta_P = 36.38$ was assigned to the triarylphosphane (P_A) and that at $\delta_P = 28.58$ to the phosphorus (P_X) of the $NHCH_2PPh_2$ moiety by comparison with the signals of compounds **23** and **24** (Scheme 4, Table 3). The two singlets of compound **3** at $\delta_P = 39.35$ and 38.46 in CD_2Cl_2 were too close to be assigned unambiguously, but we have assigned the singlet at $\delta_P = 39.35$ to the triarylthiophosphinoyl (P_A) and that at $\delta_P = 38.46$ to the $NHCH_2P(S)Ph_2$ moiety (P_X) by comparing the signals with those of compounds **25** and **26** (Scheme 4, Table 3). The synthesis and complex formation of compounds **23**−**26** in Scheme 4 will be reported elsewhere.

The ^1H NMR spectra of **2** and **3** show similar aromatic proton signals to that of **1**. However, the NH resonance in **2** was obscured by the aromatic proton resonances; the ^1H-^1H COSY spectrum reveals that the NH signal lies at ca. $\delta_H = 7.30$. In compound **3** the NH signal was confirmed by an H/D exchange reaction. In both cases, the NH resonances are shifted to higher frequency by ca. 2 ppm relative to **1**. In the IR spectra, the ν_{NH} absorption was also shifted to lower frequency by 30 cm^{-1} for **2** and 138 cm^{-1} for **3**. This is attributed to the intramolecular hydrogen bonding interactions that occur in compounds **2** and **3**, as seen in the crystal structures.

In the solid state, **2** and **3** (Figure 1a and 2, respectively) both form an envelope-like pseudo six-membered ring via intramolecular hydrogen bonding interactions between the H(13n) and the O(2) or S(2) at P(2). The O(2) atom in compound **2** is 0.60 Å out of the P(2)−C(15)−C(14)−H(13n)−N(13) mean plane (mean deviation of 0.07 Å) with a fold angle of 32°. In compound **3**, the deviation of S(2) from the P(2)−C(15)−C(14)−H(13n)−N(13) mean plane (mean deviation from each other 0.05 Å) of −1.27 Å is bigger than that in compound **2** due to the different bond lengths of P=O and P=S (Table 2), as well as the strength of the H bonding [H(13n)···O(2): 1.98 Å; O(2)···H(13n)−N(13): 144°; H(13n)···S(2): 2.47 Å; S(2)···H(13n)−N(13): 144°]. The hinge angle between the S(2)−P(2)−H(13) plane and the P(2)−C(15)−C(14)−H(13n)−N(13) mean plane along the P(2)−H(13n) axis is 46°. In addition to the intramolecular hydrogen bonding, compounds **2** and **3** share other common features: the two P=E (E = O, S) groups lie in an *anti*-position; the geometry around each phosphorus atom is approximately tetrahedral; the main skeleton of molecules **2** and **3** — P(2)−C(15)−C(14)−N(13)−C(13) — lies in a mean plane with a mean deviation of 0.04 Å and 0.02 Å, respectively. The planar skeleton can be explained from the sp^2 hybrid state of C(15) and C(14) as well as the conjugation of N(13) with the aromatic ring. The C(14)−N(13)−C(13) bond angle is 124.5(4)° and 126.0(2)° in **2** and **3**, respectively. There is one additional feature in

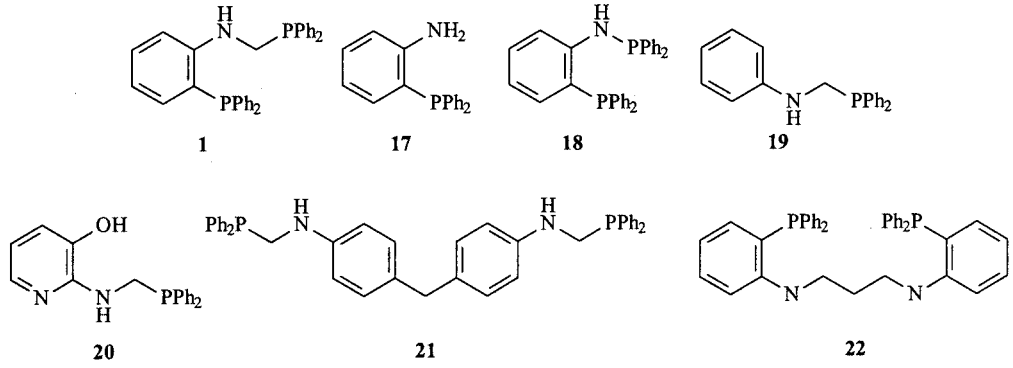

Scheme 3. Compound **1** and other related molecules

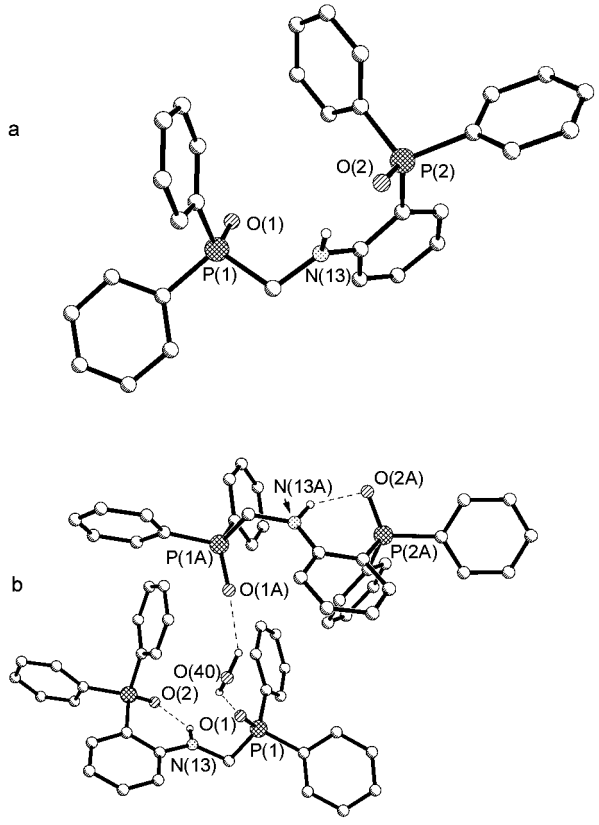

Figure 1. (a) Crystal structure of $Ph_2P(O)CH_2NHC_6H_4P(O)Ph_2$ (**2**): a single molecule; (b) crystal structure of $Ph_2P(O)CH_2NHC_6H_4P(O)Ph_2$ (**2**) showing the hydrogen bonded dimer pairs

compound **2** (Figure 1b) that is not observed in compound **3**: each molecule of **2** crystallises with 0.5 molecules of water. The water links two molecules of **2** through weak intermolecular hydrogen bonding interactions with the oxygen atom of the $NCH_2P(O)Ph_2$ moiety and O(1) and O(1A) [O(1)···H(40): 2.49 Å; O(1)···H(40)−O(40): 102°]. Therefore, it is not surprising to see that there is little difference between the two P=O bond lengths [P(1)−O(1): 1.487(3) Å; P(2)−O(2): 1.483(4) Å] in compound **2**, while, in contrast, P(2)−S(2) [1.9719(11) Å] is longer than P(1)−S(1) [1.9443(12) Å] in **3**.

Table 2. A comparison of the bond lengths (Å) and angles (°) in compounds **2** and **3**

	2	**3**
P(1)−E(1)	1.483(4)	1.9443(12)
P (1)−C(13)	1.812(5)	1.833(3)
N(13)−C(13)	1.450(6)	1.447(3)
N(13)−C(14)	1.383(6)	1.378(4)
C(14)−C(15)	1.414(6)	1.428(4)
C(15)−P(2)	1.808(5)	1.818(3)
P(2)−E(2)	1.487(3)	1.9717(11)
E(1)−P(1)−C(13)	112.6(2)	113.95(11)
N(13)−C(13)−P(1)	110.5(3)	112.0(2)
C(14)−N(13)−C(13)	124.5(4)	126.0(2)
N(13)−C(14)−C(15)	119.0(4)	119.7(2)
C(14)−C(15)−P(2)	120.5(4)	121.1(2)
E(2)−P(2)−C(15)	112.4(2)	114.34(10)

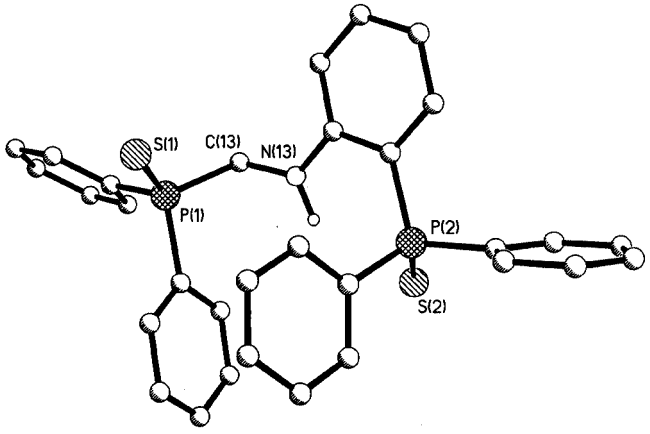

Figure 2. Crystal structure of $Ph_2P(S)CH_2NHC_6H_4P(S)Ph_2$ (**3**)

Coordination Chemistry of Compound 1

Both of the phosphorus atoms of **1** can coordinate with late transition metals. When reacted with Pd^{II}, Pt^{II} or Mo^0, **1** functions as a bidentate ligand to give the seven-membered chelate complexes **4**−**8** (Scheme 5). However, due to their different chemical environments the reactivity of the two phosphorus atoms is different. The less bulky and less

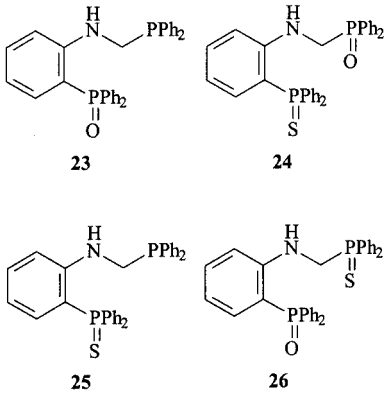

Scheme 4. Compounds related to **2** and **3**

Table 3. $^{31}P\{^1H\}$ NMR chemical shifts of **2**, **3** and related compounds

Compound	Chemical shifts $\delta(P_X)$[a]	$\delta(P_A)$[a]	Compound	Chemical shifts $\delta(P_X)$[a]	$\delta(P_A)$[a]
2	28.58	36.38	**24**[a]	27.82	39.98
3	38.46	39.35	**25**[a]	−20.46	39.67
23 [a]	−19.90	36.59	**26**[a]	38.32	36.60

[a] P_X is the phosphorus of $NHCH_2PPh_2$ groups and P_A is the phosphorus of triarylphosphane.

electron-delocalized phosphorus (P_X) of the $NHCH_2PPh_2$ group is more reactive than triarylphosphane (P_A). When **1** reacts with Rh^{III}/Ru^{IV} chloride-bridged dimers in a 2:1 molar ratio, the "dangling" monodentate complexes **9** and **10** were obtained (Scheme 5). However, reaction of **1** with $[\{IrCl(\mu\text{-}Cl)(\eta^5\text{-}C_5Me_5)\}_2]$ in a 2:1 molar ratio led to the cationic chelate complex **12** together with monodentate **11**. Abstraction of chloride from **9** and **10** with silver perchlorate gave the cationic chelate complexes **13** and **14**. When [AuCl(tht)] was employed, both (P_X) and (P_A) in **1** coordinate to the gold centre. We believe that steric effects control the reaction. Changing the reactants molar ratio also change the products: when two molar equivalents of [AuCl(tht)] or one molar equivalent of $[\{RhCl(\mu\text{-}Cl)(\eta^5\text{-}C_5Me_5)\}_2]$ was reacted with ligand **1**, the bidentate bridging complexes **15** and **16** were obtained (Scheme 5).

Bidentate Chelate Complexes

Reactions of equimolar quantities of ligand **1** and $[PdCl_2(cod)]$, $[PdBr_2(cod)]$, $[PtCl_2(cod)]$, $[PtMe_2(cod)]$ or $[Mo(CO)_4(pip)_2]$ gave the corresponding seven-membered ring chelate complexes $[PdCl_2(Ph_2PCH_2NHC_6H_4PPh_2\text{-}P_X,P_A)]$ (**4**), $[PdBr_2(Ph_2PCH_2NHC_6H_4PPh_2\text{-}P_X,P_A)]$ (**5**), $[PtCl_2(Ph_2PCH_2NHC_6H_4PPh_2\text{-}P_X,P_A)]$ (**6**), $[PdMe_2(Ph_2PCH_2NHC_6H_4PPh_2\text{-}P_X,P_A)]$ (**7**) and $[Mo(CO)_4(Ph_2PCH_2NHC_6H_4PPh_2\text{-}P_X,P_A)]$ (**8**), respectively. All of the

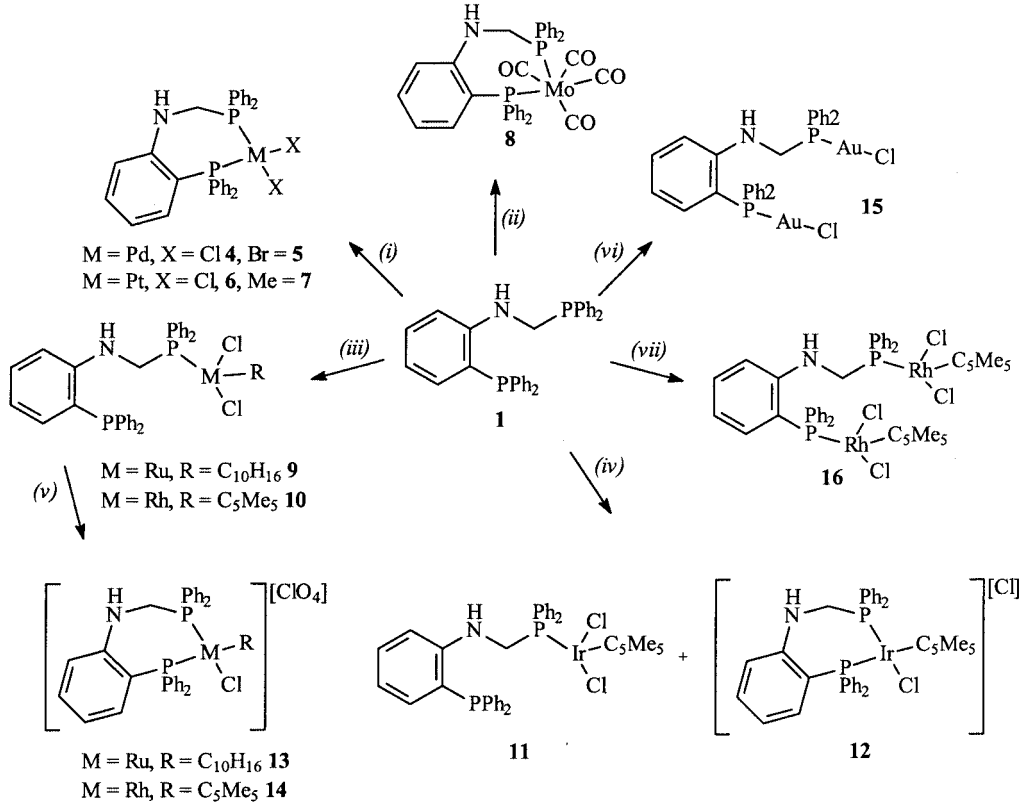

Scheme 5. (i) $[MX_2(cod)]$ (M = Pd, X = Cl or Br; M = Pt, X = Cl or Me); (ii) $[Mo(CO)_4(pip)_2]$; (iii) 0.5 equiv. of $[\{RuCl(\mu\text{-}Cl)(\eta^3\text{:}\eta^3\text{-}C_{10}H_{16})\}_2]$ or $[\{RhCl(\mu\text{-}Cl)(\eta^5\text{-}C_5Me_5)\}_2]$; (iv) 0.5 equiv. of $[\{IrCl(\mu\text{-}Cl)(\eta^5\text{-}C_5Me_5)\}_2]$; (v) $AgClO_4$; (vi) 2 equiv. of [AuCl(tht)]; (vii) $[\{RhCl(\mu\text{-}Cl)(\eta^5\text{-}C_5Me_5)\}_2]$

complexes gave satisfactory microanalysis and the expected fragmentation patterns in their positive ion FAB mass spectra. In the $^{31}P\{^1H\}$ NMR spectra of **4** and **5** no ^{31}P-^{31}P coupling was observed, both compounds displayed two singlets at around $\delta_P = 42$ and $\delta_P = 21$. The $^{31}P\{^1H\}$ NMR spectra of the platinum complex **6** exhibited a two-bond ^{31}P-^{31}P coupling and the expected platinum satellites at $\delta_P = 20.25$ (d, $^1J_{Pt,P} = 3647$ Hz, $^2J_{P,P} = 18$ Hz) and $\delta_P = 1.80$ (d, $^1J_{Pt,P} = 3573$, $^2J_{P,P} = 18$ Hz). The large one-bond ^{31}P-^{195}Pt coupling constants are in agreement with the proposed *cis*-geometry of **6**. In compound **7**, two doublets at $\delta_P = 30.73$ and 11.91 ($^2J_{P,P} = 12$ Hz) with platinum satellites are observed. The coupling constants $^1J_{Pt,P} = 1853$ Hz and $^1J_{Pt,P} = 1720$ Hz are in agreement with those coupling constants found in compounds in which phosphane ligands are *trans* to methyl groups. The molybdenum complex **8** also displays coupling of the two phosphorus atoms at $\delta_P = 41.43$ and $\delta_P = 28.31$ ($^2J_{P,P} = 25$ Hz) in the $^{31}P\{^1H\}$ NMR spectrum. The assignment of the phosphorus resonances in the above chelate complexes is not straightforward. However, by comparing them with the corresponding complexes of $PPh_2C_6H_4NHPPh_2$ [18] (Scheme 6, Table 4), we assigned the signal at higher frequency in the $^{31}P\{^1H\}$ NMR spectra of each chelate complex to the phosphorus of the $NHCH_2PPh_2$ group (P_X) and the lower frequency resonance to the triarylphosphane (P_A). The ^1H NMR spectra of **4**–**8** show similar patterns for the aromatic proton resonances, although the NH and CH_2 signals are slightly different depending upon the nature of the solvent and the complexes. The NH resonances of **4** and **5** appear as broad doublets of triplets in [D$_6$]DMSO at $\delta_H = 5.53$ ($^3J_{PN,CH} = 10$, $^3J_{NH,CH} = 3$ Hz) and $\delta_H = 5.44$ ($^3J_{PN,CH} = 25$, $^3J_{NH,CH} = 3$ Hz), respectively. Their CH_2 signals were found at ca. $\delta_H = 3.9$ as a triplet ($^2J_{P,CH} = {}^3J_{NH,CH} = 3$ Hz).

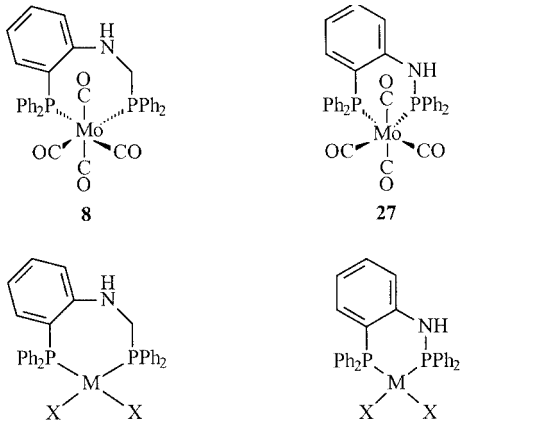

Scheme 6. Chelate complexes of **1** and $Ph_2NHC_6H_4PPh_2$

In the ^1H NMR spectrum of **6**, the doublet of triplets signal of NH was observed at $\delta_H = 3.55$ ($^3J_{NH,CP} = 16$ Hz). The doublet of doublets with two platinum satellites ($^3J_{Pt,CH} = 36$ Hz) at $\delta_H = 3.96$ was assigned to CH_2. The coupling constants $^2J_{P,CH} = 3$ Hz and $^3J_{NH,CH} = 6$ Hz were determined by an exchange reaction with D_2O.

Table 4. Chemical shifts of complexes **4**–**8** and those from $Ph_2PNHC_6H_4PPh_2$

Complex	Chemical shifts $\delta(P_X)$[a]	$\delta(P_A)$[a]	Complex	Chemical shifts $\delta(P_X)$[a]	$\delta(P_A)$[a]
8	41.43	28.31	**27**[b]	91.7	33.6
4	42.72	22.98	**28**[b]	77.8	18.1
5	41.93	20.55			
6	20.25	1.80	**29**[b]	53.8	−0.4
7	30.73	11.91	**30**[b]	70.6	10.7

[a] P_X is the phosphorus of either $NHCH_2PPh_2$ or $NHPPh_2$ groups and P_A is the phosphorus of triarylphosphane. [b] Literature complexes.[8]

In the ^1H NMR spectrum of complex **7**, the NH and CH_2 resonances overlap at $\delta_H = 3.99$. Addition of D_2O to the $CDCl_3$ solution of **7** gives a $^2J_{P,CH}$ coupling constant of 9 Hz. Other information obtained from this compound is the two doublets of doublets at $\delta_H = 0.60$ and 0.34 with platinum satellites for two CH_3 groups. Although the coupling constants are available ($^3J_{P,CH} = 7$, $^3J_{P',CH} = 9$, $^2J_{Pt,CH} = 70$, $^2J_{Pt,CH'} = 69$ Hz) the accurate assignment of the two doublets is impossible. The resonance for the NH proton in complex **8** was obscured by aromatic multiplets. The CH_2 group in **8** appears as a broad singlet at $\delta_H = 4.04$.

In the infrared spectra, compounds **4**, **5** and **6** show the ν_{NH} absorption at around 3250 cm^{-1}, shifted to lower frequency relative to **1**. Metal-halide stretches at ca. 320 cm^{-1} and 290 cm^{-1} are in agreement with the *cis*-geometry of the complexes. However, the ν_{NH} absorption at 3337 cm^{-1} in compound **7** and 3389 cm^{-1} in **8** occurs at a significantly higher frequency than in **4**–**6**. Obviously there is less opportunity for hydrogen bonding between the NH proton of the ligand and the methyl or carbonyl groups of **7** and **8**, respectively, than between the metal-bound chlorides and the amine protons of complexes **4**–**6**. The infrared spectrum of compound **8** also displayed $\nu_{C\equiv O}$ absorption bands at 2013 cm^{-1}, 1914 cm^{-1}, 1892 cm^{-1} and 1878 cm^{-1}.

Pale yellow crystals of **8** suitable for X-ray analysis (Figure 3, Table 5) were obtained by layering methanol onto a dichloromethane solution of **8** for four days. As shown in Figure 3, the coordination geometry around Mo(1) is approximately octahedral, with P(1) and P(2) occupying the *cis* positions. The bite angle of the ligand is 87.47(2)°, slightly less than the expected 90° for a regular octahedron. The *cis* bond angles at Mo(1) are 84.29(2)–91.51(11)°, while the *trans* angle are in the range 172.59(10)–176.66(8)°. The seven-membered chelate ring is twisted, with N(13)–C(14)–C(15)–P(1)–P(2) coplanar (mean deviation 0.01 Å) and C(13) lying 0.96 Å above, and Mo(1) 1.49 Å below, the mean plane. The fold angles between the N(13)–C(14)–C(15)–P(1)–P(2) mean plane and the N(13)–C(13)–P(1) and P(2)–Mo(1)–P(1) planes are 54° and 88° respectively. The N(13)–C(14)–C(15) [124.7(2)°] and C(14)–C(15)–P(2) [124.6(2)°] bond angles are slightly more open than those in compounds **2** and **3**.

Table 5. Selected bond lengths (Å) and angles (°) for compound **8**

Mo(1)−C(41)	2.041(3)	Mo(1)−C(42)	1.992(3)
Mo(1)−C(43)	2.021(3)	Mo(1)−C(44)	1.985(3)
Mo(1)−P(1)	2.5048(6)	Mo(1)−P(2)	2.5884(6)
P (1)−C(13)	1.847(2)	N(13)−C(13)	1.460(3)
N(13)−C(14)	1.401(3)	C(14)−C(15)	1.414(3)
C(15)−P(2)	1.856(2)		
C(41)−Mo(1)−C(42)	87.97(10)	C(41)−Mo(1)−C(43)	172.59(10)
C(41)−Mo(1)−C(44)	91.51(11)	C(42)−Mo(1)−C(43)	85.99(11)
C(42)−Mo(1)−C(44)	90.79(11)	C(43)−Mo(1)−C(44)	84.29(11)
C(41)−Mo(1)−P(1)	94.78(7)	C(42)−Mo(1)−P(1)	176.66(8)
C(43)−Mo(1)−P(1)	91.12(7)	C(44)−Mo(1)−P(1)	87.25(7)
C(41)−Mo(1)−P(2)	87.00(8)	C(42)−Mo(1)−P(2)	94.58(8)
C(43)−Mo(1)−P(2)	97.74(8)	C(44)−Mo(1)−P(2)	174.38(8)
P(1)−Mo(1)−P(2)	87.47(2)	C(13)−P(1)−Mo(1)	112.36(7)
N(13)−C(13)−P(1)	107.9(2)	C(14)−N(13)−C(13)	122.6(2)
N(13)−C(14)−C(15)	124.7(2)	C(14)−C(15)−P(2)	124.6(2)
C(15)−P(2)−Mo(1)	119.01(7)		

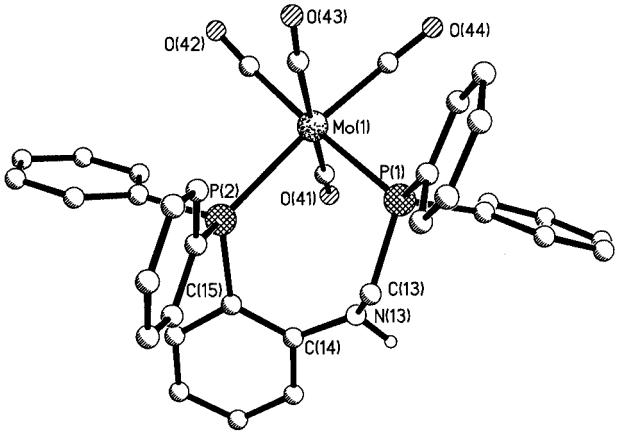

Figure 3. Crystal structure of $[Mo(CO)_4(Ph_2PCH_2NHC_6H_4PPh_2\text{-}P_X,P_A)]$ (**8**)

Monodentate Complexes

Monitoring of the reaction between **1** and either $[\{RuCl(\mu\text{-}Cl)(\eta^3\text{:}\eta^3\text{-}C_{10}H_{16})\}_2]$ or $[\{RhCl(\mu\text{-}Cl)(\eta^5\text{-}C_5Me_5)\}_2]$ by $^{31}P\{^1H\}$ NMR spectroscopy showed that the monodentate complexes $[RuCl(\eta^3\text{:}\eta^3\text{-}C_{10}H_{16})(Ph_2PCH_2NHC_6H_4PPh_2\text{-}P_X)]$ (**9**) and $[RhCl(\eta^5\text{-}C_5Me_5)(Ph_2PCH_2NHC_6H_4PPh_2\text{-}P_X)]$ (**10**) are readily formed. The reaction of $[\{IrCl(\mu\text{-}Cl)(\eta^5\text{-}C_5Me_5)\}_2]$ and **1**, however, is not so straightforward. Several singlets between $\delta_P = 0.0$ and $\delta_P = -22$ appear in the crude reaction mixtures. Longer reaction times do not affect the product distribution. After several attempts to separate this mixture a monodentate complex $[IrCl(\eta^5\text{-}C_5Me_5)(Ph_2PCH_2NHC_6H_4PPh_2\text{-}P_X)]$ (**11**) was isolated as well-formed crystals from dichloromethane/acetone in low yield. Also obtained was the chelate cationic complex $[Ir(\eta^5\text{-}C_5Me_5)(Ph_2PCH_2NHC_6H_4PPh_2\text{-}P_X,P_A)]$ (**12**), although in much lower purity.

All of the monodentate complexes gave satisfactory microanalysis and the expected fragmentation patterns and molecular ions in the positive ion FAB mass spectra. Compound **9**−**11** have similar $^{31}P\{^1H\}$ NMR spectra, with the coordinated phosphorus resonance shifted to higher frequency and that of the dangling phosphorus at ca. $\delta_P = -22.5$ unmoved. For the rhodium complex **10**, a typical $^1J_{Rh\text{-}P}$ coupling constant of 141 Hz was observed at $\delta_P = 32.74$. The higher-frequency signal was assigned to the phosphorus of the $NHCH_2PPh_2$ group (P_X) and the unshifted $\delta_P = -22.5$ to triarylphosphane (P_A). This assignment was confirmed by single-crystal X-ray diffraction studies of complexes **9** and **11** (see below).

The ^1H NMR spectra of **9**−**11** show aromatic proton resonances close to the values for the free ligand. The signals for the NH and methylene protons of the complexes are slightly different. Complexes **10** and **11** display a slightly broad quadruplet for NH at ca. $\delta_H = 4.9$ ($^3J_{NH,CH} = {}^3J_{NH,CP} = 7$ Hz) and a doublet at $\delta_H = 4.48-4.66$ for CH_2. No coupling between the CH_2 protons and the phosphorus was observed. In complex **9**, the NH proton signal is a well-resolved multiplet at $\delta_H = 4.95$. The CH_2 group was observed as a doublet of doublets at $\delta_H = 4.59$. The coupling constants were verified by H/D exchange with D_2O ($^2J_{P,CH} = 2$, $^3J_{NH,CH} = 6$ Hz). Complexes **10** and **11** show coupling between (P_X) and the methyl protons of the pentamethylcyclopentadienyl group, [$J_{P\cdots CH} = 3$ Hz]. The complicated signals of complex **9** were also assigned by a ^1H-^1H COSY spectrum. The IR spectra of **9**−**11** show the ν_{NH} absorption at about 3320 cm^{-1}, implying little hydrogen bonding.

Slow evaporation of a dichloromethane solution of **9** gave well-formed deep purple crystals suitable for X-ray analysis. The crystal structure of **9** (Figure 4, Table 6) reveals a monodentate complex coordinated by the $NHCH_2PPh_2$ phosphorus atom, whilst the triarylphosphane moiety remains unbound. The Ru(1) centre adopts an approximately trigonal bipyramidal geometry with Cl(1) and Cl(2) occupying the axial sites while P(1) and the two allylic groups occupy the equatorial positions. The arrangement of the allylic groups, which have local C_2 symmetry, is similar to that found in related complexes.[26] The ligand backbone

P(2)−C(15)−C(14)−N(13), as observed in **2**, **3**, and **8**, is coplanar (mean deviation 0.01 Å). The dangling phosphorus P(2) remains pyramidal as expected.

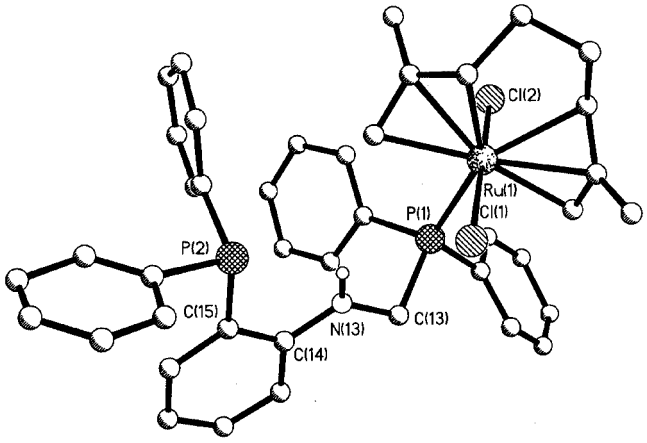

Figure 4. Crystal structure of $[RuCl_2(\eta^3{:}\eta^3\text{-}C_{10}H_{16})(Ph_2PCH_2NHC_6H_4PPh_2\text{-}P_X)]$ (**9**)

Table 6. A comparison of the bond lengths (Å) and angles (°) in compounds **9** and **11**

	9	**11**
M(1)−P(1)	2.393(4)	2.2986(13)
M(1)−Cl(1)	2.413(4)	2.4119(15)
M(1)−Cl(2)	2.387(4)	2.4035(16)
P(1)−C(13)	1.862(11)	1.833(6)
N(13)−C(13)	1.399(14)	1.457(7)
N(13)−C(14)	1.379(15)	1.384(7)
C(14)−C(15)	1.364(16)	1.415(8)
C(15)−P(2)	1.798(12)	1.825(6)
P(2)−C(20)	1.810(16)	1.831(6)
P(2)−C(26)	1.801(13)	1.830(6)
Cl(1)−M(1)−Cl(2)	172.84(15)	88.86(6)
Cl(1)−M(1)−P(1)	89.25(13)	88.27(5)
Cl(2)−M(1)−P(1)	84.01(13)	88.04(5)
M(1)−P(1)−C(13)	114.4(4)	112.50(19)
N(13)−C(13)−P(1)	111.0(8)	112.3(4)
C(14)−N(13)−C(13)	123.7(11)	123.9(5)
N(13)−C(14)−C(15)	120.2(12)	119.3(5)
C(14)−C(15)−P(2)	118.8(10)	117.8(4)
C(20)−P(2)−C(15)	102.4(6)	104.0(3)
C(20)−P(2)−C(26)	101.1(7)	102.2(3)
C(15)−P(2)−C(26)	103.4(6)	102.2(3)

The X-ray structure of **11** (Figure 5) shares many common features with **9**: the pendant triarylphosphane P(2) adopts a pyramidal geometry; the main backbone of the ligand extends in a mean plane P(2)−C(15)−C(14)−N(13) (mean deviation 0.06 Å); the bond lengths and angles (Table 6) are in the expected range; no hydrogen bonding is observed. The geometry around Ir(1) can be viewed as a three-legged "piano stool" with the two chlorides and the phosphorus P(1) supporting the pentamethylcyclopentadienyl top. The bond angles between the "legs" are approximately 90°.

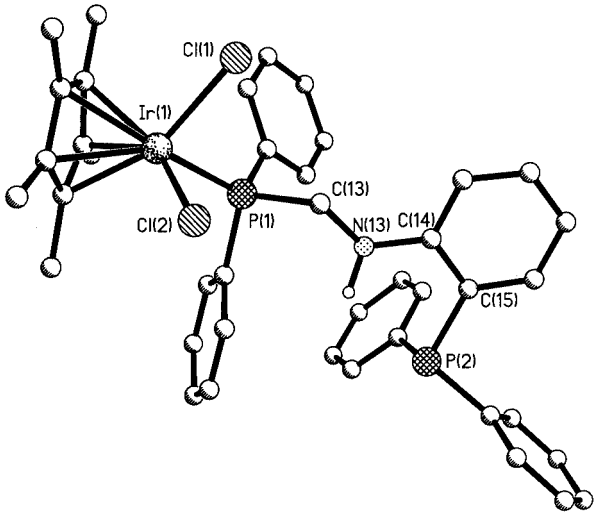

Figure 5. Crystal structure of $[IrCl_2(\eta^5\text{-}C_5Me_5)(Ph_2PCH_2NHC_6H_4PPh_2\text{-}P_X)]$ (**11**)

Cationic Chelate Complexes

As mentioned above, a cationic chelate complex of iridium(III) **12** formed together with the monodentate species **11**. Other cationic chelate complexes of ligand **1** can be obtained by abstraction of a chloride ligand from the monodentate complexes. For example, abstraction of one chloride from complexes **9** and **10** with $AgClO_4$ gave the chelate cationic complexes $[RuCl(\eta^3{:}\eta^3\text{-}C_{10}H_{16})(Ph_2PCH_2NHC_6H_4PPh_2\text{-}P_X,P_A)][ClO_4]$ (**13**) and $[RhCl(\eta^5\text{-}C_5Me_5)(Ph_2PCH_2NHC_6H_4PPh_2\text{-}P_X,P_A)][ClO_4]$ (**14**), respectively. Both complexes gave satisfactory microanalysis and positive FAB mass spectra. Their IR spectra displayed the ν_{NH} at 3272 cm^{-1} and 3332 cm^{-1}, respectively, and the strong band of ClO_4^- at ca. 1095 cm^{-1}. The $^{31}P\{^1H\}$ NMR spectrum of **13** showed two singlets at $\delta_P = 36.89$ and $\delta_P = 21.86$ in $CDCl_3$, which were assigned to the phosphorus atoms of the $NHCH_2PPh_2$ (P_X) and the triarylphosphane (P_A) groups, respectively, by reference to the other chelate complexes mentioned above. The ^1H NMR spectrum of **13** showed a broad singlet at $\delta_H = 5.02$ for NH and a doublet of doublet of doublets at $\delta_H = 4.67$ for the ligand methylene protons with $^3J_{NH,CH} = 6$, $^3J_{P,CH} = 15$ Hz and $^2J_{P,CH} = 52$ Hz. Characterisation of **14** by multinuclear NMR proved unsuccessful. The $^{31}P\{^1H\}$ NMR spectrum of **14** exhibited very broad peaks around $\delta_P = 31$ and $\delta_P = 37$, and the ^1H NMR spectrum of this compound also contains broad resonances. The low solubility of **14** in common organic solvents precludes a low temperature NMR study. In solution we believe that there may be an exchange process between several species taking place, possibly the cationic chelate, a monodentate species and perhaps even a cationic bidentate bridging species.

In spite of the uninformative NMR spectroscopic data we were able to obtain single crystals of compound **14** enab-

ling characterisation by X-ray crystallography (Figure 6, Table 7). The crystal structure of **14** reveals that the complex adopts a chair-like seven-membered chelate ring with a ligand bite angle P(1)−Rh(1)−P(2) of 95.12(4)°. The top mean plane of the "chair", C(14)−C(15)−P(2)−N(13) (mean deviation 0.02 Å), is 123° folded back from the "back of the chair", N(13)−P(2)−C(13)−Rh(13) mean plane (mean deviation 0.12 Å). The "bottom of the chair", P(1)−Rh(1)−C(13), is 144° folded forward from the N(13)−P(2)−C(13)−Rh(13) mean plane. Again, the coordination around the rhodium adopts a three-legged "piano stool" geometry. The crystal structure also displays two weak hydrogen bonding interactions between the NH and two of the oxygen atoms of the tetrahedral ClO_4^- anion [H(13n)···O(1): 2.42 Å; H(13n)···O(3): 2.44 Å; N(13)−H(13n)···O(1): 145°; N(13)−H(13n)···O(3): 157°]. The crystal structure also reveals that each molecule of complex **14** crystallises with 0.25 molecules of dichloromethane.

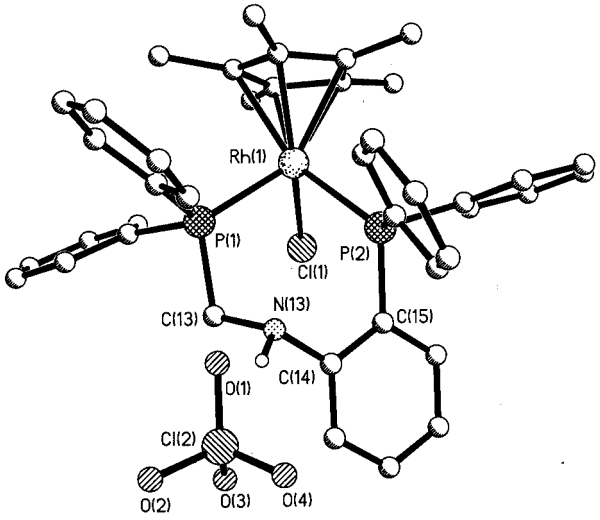

Figure 6. Crystal structure of [RhCl(η^5-C_5Me_5)($Ph_2PCH_2NHC_6H_4PPh_2$-P_X,P_A][ClO_4] (**14**); the solvent of crystallisation is omitted for the sake of clarity

Table 7. Selected bond lengths (Å) and angles (°) in compound **14**

Rh(1)−P(1)	2.3303(12)	Rh(1)−P(2)	2.3806(11)
Rh(1)−Cl(1)	2.4016(12)	P (1)−C(13)	1.854(4)
N(13)−C(13)	1.452(6)	N(13)−C(14)	1.414(6)
C(14)−C(15)	1.389(6)	C(15)−P(2)	1.836(4)
P(1)−Rh(1)−P(2)	95.12(4)	P(1)−Rh(1)−Cl(1)	89.50(4)
P(2)−Rh(1)−Cl(1)	84.76(4)	C(13)−P(1)−Rh(1)	115.8(2)
N(13)−C(13)−P(1)	113.4(3)	C(14)−N(13)−C(13)	114.4(4)
N(13)−C(14)−C(15)	118.7(4)	C(14)−C(15)−P(2)	117.7(4)
C(15)−P(2)−Rh(1)	120.5(2)		

Bimetallic Complexes

While the Ru^{IV} or Rh^{III} metal centres of the bulky dimers [{RuCl(μ-Cl)(η^3:η^3-$C_{10}H_{16}$)}$_2$] and [{RhCl(μ-Cl)(η^5-C_5Me_5)}$_2$] selectively coordinate through the (P_X) or $NHCH_2PPh_2$ moiety of ligand **1**, [AuCl(tht)] displays no such selectivity for either (P_A) or (P_X) of ligand **1**. The reaction between [AuCl(tht)] and **1** in a 1:1 ratio showed two broad peaks at δ_P = 33.4 and 25.0 in the $^{31}P\{^1H\}$ NMR spectrum, implying that both (P_X) and (P_A) were involved in some type of coordination. Workup of this mixture was not attempted. Addition of one more molar equivalent of [AuCl(tht)] to this mixture led to the same bidentate bridging complex **15** as in the one step reaction of [AuCl(tht)] with **1** in a 2:1 molar ratio. Complex **15** exhibits two sharp singlets at δ_P = 24.95 and δ_P = 18.64 which are assigned to (P_X) of the $NHCH_2PPh_2$ group and the (P_A) of the triarylphosphane according to the general trend of the complexes discussed in this paper. The ^1H NMR spectrum of **15** showed a well-resolved and well-shaped multiplet at δ_H = 4.94 for the NH proton and a doublet of doublets at δ_H = 4.34 for CH_2. A ^1H-^1H COSY spectrum of the compound in $CDCl_3$ showed no coupling between the NH and aromatic proton 6-H. Therefore it was concluded that both of the phosphorus atoms coupled with the NH group. The coupling constants were obtained through a D_2O exchange reaction in $CDCl_3$ solution ($^2J_{P,CH}$ = 3, $^3J_{NH,CH}$ = 6, $^3J_{PC,NH}$ = $^4J_{PCCNH}$ = 3 Hz).

The reaction of [{RhCl(μ-Cl)(η^5-C_5Me_5)}$_2$] with **1** in a 1:1 molar ratio gave another bimetallic complex [{$RhCl_2$(η^5-C_5Me_5)}$_2$($Ph_2PCH_2NHC_6H_4PPh_2$)] (**16**). The $^{31}P\{^1H\}$ NMR spectrum of **16** displays two doublets at δ_P = 32.44 ($^1J_{Rh,P}$ = 138 Hz) and δ_P = 27.79 ($^1J_{Rh,P}$ = 144 Hz). Upon comparison with the $^{31}P\{^1H\}$ NMR spectrum of **9**, the doublet at δ_P = 32.44 was assigned to the $NHCH_2PPh_2$ group (P_X), and the other at δ_P = 27.79 to the triarylphosphorus atom (P_A). The ^1H NMR spectrum of **16** displayed two doublets for the two pentamethylcyclopentadienyl groups. The NH resonance appears at δ_H = 5.33 as a broad triplet and that of the ligand methylene protons at δ_H = 4.90 as a broad doublet of doublets ($^3J_{NH,CH}$ = 5, $^2J_{P,CH}$ = 16 Hz). Both bridging complexes gave satisfactory microanalysis and the anticipated FAB mass spectral patterns. Their IR spectra show vibrations for ν_{NH} at 3309 and 3280 cm^{-1} and $\nu_{M\text{-}Cl}$ at 329 and 398 cm^{-1}, respectively.

Conclusion

We have shown that the unsymmetrical bisphosphane ligand $Ph_2PCH_2NHC_6H_4PPh_2$ is readily prepared by the condensation of diphenylphosphanylmethanol (Ph_2PCH_2-OH) and 2-(diphenylphosphanyl)aniline ($Ph_2PC_6H_4NH_2$), and that treatment of $Ph_2PCH_2NHC_6H_4PPh_2$ with H_2O_2 or elemental sulfur gives rise to the dioxide and disulfide. In addition, we have clearly demonstrated that $Ph_2PCH_2NHC_6H_4PPh_2$ has the potential to ligate in a variety of bonding modes. The different steric properties or ba-

sicities of the two phosphorus centres can be exploited to obtain mononuclear complexes where $Ph_2PCH_2NHC_6H_4PPh_2$ is monodentate (via the Ph_2PCH_2 moiety) or chelating, and this latter bonding mode can also be induced by the use of a halide abstracting agent such as Ag^I.

Binuclear complexes where $Ph_2PCH_2NHC_6H_4PPh_2$ adopts a bidentate bridging coordination mode are also readily accessible. The compounds described represent rare examples of either complexes containing $PCNC_2P$ pendant ligands or $MPCNC_2P$ metallacycles. Further studies are currently in progress into the synthesis of heterobimetallic complexes of late transition metals of $Ph_2PCH_2NHC_6H_4PPh_2$ and the coordination properties of its dichalcogen derivatives $Ph_2P(O)CH_2NHC_6H_4P(O)Ph_2$ and $Ph_2P(S)CH_2NHC_6H_4P(S)Ph_2$.

Experimental Section

General: All solvents and reagents were purchased from Aldrich and Lancaster. Dichloromethane was heated to reflux over powdered calcium hydride and distilled under nitrogen. Diethyl ether and tetrahydrofuran were purified by reflux over sodium/benzophenone and distillation under nitrogen. Ligand preparations were performed under an oxygen-free nitrogen atmosphere using standard Schlenk techniques. Coordination reactions and workup were performed in dry solvents. 2-(Diphenylphosphanyl)aniline,[16] diphenylphosphanylmethanol,[27] $[MX_2(cod)]$ (M = Pt, X = Cl or Me; M = Pd, X = Cl, Br; cod = cycloocta-1,5-diene),[28−30] $[Mo(CO)_4(pip)_2]$ (pip = piperidine),[31] [AuCl(tht)] (tht = tetrahydrothiophene),[32] $[\{MCl(\mu\text{-}Cl)(\eta^5\text{-}C_5Me_5)\}_2]$ (M = Rh, Ir),[33] and $[\{RuCl(\mu\text{-}Cl)(\eta^3\text{:}\eta^3\text{-}C_{10}H_{16})\}_2]$[34] were prepared using literature procedures.

Infrared spectra were recorded (KBr discs) on a Perkin−Elmer system 2000 spectrometer, and ^1H NMR spectra (300 MHz) on a Varian Gemini 2000 spectrometer, $^{31}P\{^1H\}$ NMR spectra at 101.3 MHz with δ referenced to external 85% H_3PO_4. Microanalysis were performed by the University Service within this Department and fast atom bombardment (FAB) or chemical ionization (CI) mass spectra by the Swansea Mass Spectrometer Service. Precious metal salts were provided on loan by Johnson Matthey plc.

2-$Ph_2PC_6H_4NHCH_2PPh_2$ (1): Ph_2PCH_2OH (3.00 g, 13.87 mmol) was added to a solution of 2-(diphenylphosphanyl)aniline (3.84 g, 13.85 mmol) in toluene (150 cm^3). The reaction mixture was stirred at 90−95 °C for 20 h. The solvent was removed in vacuo and the sticky residue was dissolved in 20 cm^3 of Et_2O. Degassed absolute ethanol (100 cm^3) was then added to the ether solution and the mixture was concentrated in vacuo until a white solid began to precipitate. Storage in the fridge overnight and filtration gave the product as a white solid. Yield: 5.46 g (84.4%). $C_{31}H_{27}NP_2$ (475.5): calcd. C 78.30, H 5.72, N 2.95; found C 77.17, H 5.48, N 2.75. $^{31}P\{^1H\}$ NMR ($CDCl_3$): δ = −22.30 (s, P_A), −18.77 (s, P_X). ^1H NMR ($CDCl_3$): δ = 3.83 (t, $^2J_{P,CH} = {}^3J_{CH,NH}$ = 5 Hz, 2 H, CH_2), 4.97 (br. s, 1 H, NH), 6.64 (t, 1 H, ArH), 6.80 (m, 2 H, ArH), 7.40−7.20 (m, 21 H, ArH). IR (KBr disc): ν_{NH} = 3345m cm^{-1}. CI-MS: *m*/*z* = 476 $[M + H]^+$.

$Ph_2P(O)CH_2NHC_6H_4P(O)Ph_2$ (2): Aqueous hydrogen peroxide (30% w/w, 0.17 cm^3, 1.5 mmol) was added dropwise to a solution of **1** (0.355 g, 0.75 mmol) in THF (20 cm^3) and the mixture was stirred for 1.5 hours at 0−5 °C. The solvent was then removed in vacuo to give a viscous oil which was taken up in dichloromethane (20 cm^3) and dried over magnesium sulfate. The drying agent was removed by filtration and the filtrate was evaporated to dryness. Addition of diethyl ether to the residue precipitated the product. The product was collected by suction filtration and dried in vacuo. Yield: 0.275 g (73%). $C_{31}H_{27}NO_2P_2$ (507.5): calcd. C 73.37, H 5.36, N 2.76; found C 71.01, H 5.29, N 2.74. $^{31}P\{^1H\}$ NMR ($CDCl_3$): δ = 28.58 (s, P_X), 36.38 (s, P_A). ^1H NMR ($CDCl_3$): δ = 4.04 (dd, $^3J_{NH,CH}$ = 6, $^2J_{P,CH}$ = 9 Hz, 2 H, CH_2), 6.59−6.53 (m, 1 H, ArH), 6.78−6.70 (m, 2 H, ArH), 7.68−7.26 (m, 22 H, NH + ArH). IR (KBr disc): ν_{NH} = 3315m cm^{-1}, $\nu_{P=O}$ = 1179vs, 1167vs, 1118vs cm^{-1}. FAB: *m*/*z* = 508 $[M + H]^+$, 530 $[M + Na]^+$.

$Ph_2P(S)CH_2NHC_6H_4P(S)Ph_2$ (3): Compound **1** (0.582 g, 1.224 mmol) and elemental sulfur (0.079 g, 2.47 mmol) were stirred in THF (20 cm^3). A white solid began to precipitate in 10 minutes. Stirring was continued overnight and the product was collected by suction filtration, washed with diethyl ether (3 × 1 cm^3) and dried in vacuo. Yield: 0.519 g (78.6%). $C_{31}H_{27}NS_2P_2$ (539.6): calcd. C 69.00, H 5.04, N 2.60; found C 69.09, H 4.94, N 2.68. $^{31}P\{^1H\}$ NMR (CD_2Cl_2): δ = 38.46 (s, P_X), 39.35(s, P_A). ^1H NMR (CD_2Cl_2): δ = 4.12 (dd, $^3J_{NH,CH}$ = 5, $^2J_{P,CH}$ = 7 Hz, 2 H, CH_2), 6.75−6.33 (m, 3 H, ArH), 7.03 (br. q, $^3J_{NH,CH} = {}^3J_{NH,CP}$ = 5 Hz, 1 H, NH), 7.67−7.27 (m, 21 H, ArH). IR (KBr disc): ν_{NH} = 3287m cm^{-1}. FAB: *m*/*z* = 540 $[M + H]^+$, 562 $[M + Na]^+$.

[$PdCl_2$($Ph_2PC_6H_4NHCH_2PPh_2$-P_X,P_A)] (4): $[PdCl_2(cod)]$ (109 mg, 383 μmol) was added to a solution of $Ph_2PC_6H_4NHCH_2PPh_2$ (**1**; 183 mg, 385 μmol) in CH_2Cl_2 (20 cm^3). The reaction mixture was stirred for 25 min and then concentrated in vacuo to about 1 cm^3 whereupon diethyl ether (10 cm^3) was added to precipitate the product as an orange powder. Yield: 244 mg (98.0%). $C_{31}H_{27}Cl_2NP_2Pd$: calcd. C 57.12, H 4.17, N 2.15; found C 56.51, H 3.77, N 2.18. $^{31}P\{H\}$ NMR ([D_6]DMSO): δ = 22.98 (s, P_A), 42.72 (s, P_X). ^1H NMR ([D_6]DMSO): δ = 3.96 (t, $^2J_{P,CH} = {}^3J_{NH,CH}$ = 3 Hz, 2 H, CH_2), 5.53 (br. dt, $^3J_{NH,PC}$ = 10 Hz, 1 H, NH), 6.12−6.07 (m, 1 H, ArH), 6.28 (m, 1 H, ArH), 6.85−6.80 (m, 1 H, ArH), 7.23−7.19 (m, 1 H, ArH), 7.56−7.35 (m, 20 H, ArH). IR (KBr disc): ν_{NH} = 3253s cm^{-1}, $\nu_{Pd\text{-}Cl}$ = 312m, 293w cm^{-1}. FAB: *m*/*z* = 616 $[M - Cl]^+$, 580 $[M - 2Cl]^+$, 674 $[M + Na]^+$.

[$PdBr_2$($Ph_2PC_6H_4NHCH_2PPh_2$-P_X,P_A)] (5): $[PdBr_2(cod)]$ (77 mg, 206 μmol) was added to a solution of $Ph_2PC_6H_4NHCH_2PPh_2$ (**1**; 100 mg, 210 μmol) in CH_2Cl_2 (5 cm^3) and the reaction mixture was stirred for 30 min. The orange suspension of $[PdBr_2(cod)]$ dissolved immediately and a yellow solid product precipitated gradually. This precipitate was collected by suction filtration, washed with petroleum ether (60−80, 3 × 1 cm^3) and diethyl ether (3 × 1 cm^3), yield: 196 mg (68%). $C_{31}H_{27}Br_2NP_2Pd$ (741.7): calcd. C 50.27, H 3.67, N 1.89; found C 50.11, H 3.89, N 1.86. $^{31}P\{^1H\}$ NMR ([D_6]DMSO): δ = 20.55 (s, P_A), 41.93 (s, P_X). ^1H NMR ([D_6]DMSO): δ = 3.92 (br. t, $^2J_{P,CH} = {}^3J_{NH,CH}$ = 3 Hz, 2 H, CH_2), 5.44 (br. d, $^3J_{P,NH}$ = 25 Hz, 1 H, NH), 6.08 (m, 1 H, ArH), 6.80 (m, 1 H, ArH), 7.16 (m, 1 H, ArH), 7.55−7.33 (m, 21 H, ArH). IR (KBr disc): ν_{NH} = 3246s cm^{-1}, $\nu_{Pd,Cl}$ = 332m, 302vw cm^{-1}. FAB: *m*/*z* = 663 $[M - Br]^+$.

[$PtCl_2$($Ph_2PC_6H_4NHCH_2PPh_2$-P_X,P_A)] (6): This colourless complex was prepared in the same manner as compound **4** using $Ph_2PC_6H_4NHCH_2PPh_2$ (**1**; 80 mg, 168 μmol) in CH_2Cl_2 (20 cm^3) and $[PtCl_2(cod)]$ (62 mg, 168 μmol). Yield: 120 mg (96.0%). $C_{31}H_{27}Cl_2NP_2Pt$ (741.5): calcd. C 50.21, H 3.67, N 1.89; found C 51.42, H 3.70, N 1.75. $^{31}P\{^1H\}$ NMR ($CDCl_3$): δ = 1.80 (d, $^1J_{Pt,P_A}$ = 3573 Hz, P_A), 20.25 (d, $^1J_{Pt,P_X}$ = 3647 Hz; $^2J_{P_A,P_X}$ = 18 Hz, P_X). ^1H NMR (CD_2Cl_2): δ = 3.55 (dt, $^3J_{NH,CP}$ = 16 Hz, 1 H, NH),

3.96 (dd, $^3J_{NH,CH}$ = 6, $^2J_{P,CH}$ = 3, $^3J_{Pt,CH}$ = 36 Hz, 2 H, CH_2), 6.29−6.25 (m, 1 H, ArH), 6.78−6.72 (m, 1 H, ArH), 7.09−7.06 (m, 1 H, ArH), 7.53−7.27 (m, 17 H, ArH), 7.74−7.66 (m, 4 H, ArH). IR (KBr disc): ν_{NH} = 3265m cm^{-1}, ν_{Pt-Cl} = 316m, 293m cm^{-1}. FAB: *m/z* = 741 $[M]^+$, 705 $[M - Cl]^+$, 764 $[M + Na]^+$.

[PtMe$_2$(Ph$_2$PC$_6$H$_4$NHCH$_2$PPh$_2$-*P*$_X$,*P*$_A$)] (7): [$PtMe_2$(cod)] (50 mg, 149 μmol) was added to a solution of $Ph_2PC_6H_4NHCH_2PPh_2$ (**1**; 71 mg, 149 μmol) in CH_2Cl_2 (5 cm^3). The reaction mixture was stirred for 30 min and then concentrated in vacuo to about 0.5 cm^3 and diethyl ether (1 cm^3) and petroleum ether (3 cm^3, 60−80) were added to precipitate the product as an off-white powder. Yield: 85 mg (82.0%). $C_{33}H_{33}NP_2Pt$ (700.7): calcd. C 56.57, H 4.75, N 2.00; found C 55.68, H 4.49, N 1.93. $^{31}P\{^1H\}$ NMR ($CDCl_3$): δ = 11.91 (d, $^1J_{Pt,P_A}$ = 1720 Hz, P_A), 30.73 (d, $^1J_{Pt,P_X}$ = 1853 Hz; $^3J_{P_A,P_X}$ = 12 Hz, P_X). ^1H NMR ($CDCl_3$): δ = 0.34 (dd, $^3J_{P',CH}$ = 7, $^3J_{P,CH}$ = 9, $^2J_{PtCH'}$ = 69 Hz, 3 H, CH_3), 0.60 (dd, $^3J_{P,CH}$ = 7, $^3J_{P'CH}$ = 9, $^2J_{Pt,CH}$ = 70 Hz, 3 H, CH_3), 3.99 (m, $^2J_{P,CH}$ = 9 Hz, 3 H, CH_2 + NH), 6.23 (m, 1 H, ArH), 6.55 (m, 1 H, ArH), 6.80 (m, 1 H, ArH), 6.93 (t, 1 H, ArH), 7.66−7.20 (m, 20 H, ArH). IR (KBr disc): ν_{NH} = 3337m cm^{-1}. FAB: *m/z* = 700 $[M]^+$, 685 $[M - CH_3]^+$, 670 $[M - 2CH_3]^+$.

[Mo(CO)$_4$(Ph$_2$PC$_6$H$_4$NHCH$_2$PPh$_2$-*P*$_X$,*P*$_A$)] (8): [$Mo(CO)_4(pip)_2$] (119 mg, 315 μmol) was added to a solution of $Ph_2PC_6H_4NHCH_2PPh_2$ (**1**; 150 mg, 315 μmol) in CH_2Cl_2 (25 cm^3). The reaction mixture was stirred at reflux for 3 h and then filtered through Celite. MeOH (10 cm^3) was added to the filtrate, which was then concentrated under vacuum until trace amounts of solid appeared. The solution was stored in a fridge overnight. Filtration, washing with cold MeOH (0.5 cm^3) and Et_2O (3 × 0.5 cm^3) gave the product as a grey solid. Yield: 105 mg (53%). $C_{35}H_{27}MoNO_4P_2$ (683.5): calcd. C 61.50, H 3.98, N 2.05; found C 61.15, H 3.86, N 2.14. $^{31}P\{^1H\}$ NMR (CD_2Cl_2): δ = 28.31 (d, P_A), 41.43 (d, $^3J_{P_A,P_B}$ = 25 Hz, P_X). ^1H NMR (CD_2Cl_2): δ = 4.04 (br. s, 2 H, CH_2), 6.63−6.56 (m, 1 H, ArH), 6.78−6.71 (m, 2 H, ArH), 7.55−7.26 (m, 22 H, ArH + NH). IR (KBr disc): ν_{NH} = 3389w cm^{-1}, $\nu_{C\equiv O}$ = 2013vs, 1914vs, 1878vs, 1892vs cm^{-1}. FAB: *m/z* = 684 $[M]^+$, 656 $[M - CO]^+$, 628 $[M - 2CO]^+$, 600 $[M - 3CO]^+$, 572 $[M - 4CO]^+$.

[RuCl$_2$(η^3:η^3-C$_{10}$H$_{16}$)(Ph$_2$PCH$_2$NHC$_6$H$_4$PPh$_2$-*P*$_X$)] (9): [{RuCl(μ-Cl)(η^3:η^3-$C_{10}H_{16}$)}$_2$] (80 mg, 130 μmol) was added to a solution of $Ph_2PC_6H_4NHCH_2PPh_2$ (**1**; 124 mg, 261 μmol) in THF (5 cm^3). The mixture was stirred for 1.5 h and then concentrated to ca. 0.5 cm^3. Addition of Et_2O (2 cm^3), filtration and washing with Et_2O (3 × 1 cm^3) gave the product as a pale brown solid. Yield: 179 mg (88%). $C_{41}H_{43}Cl_2NP_2Ru$ (783.7): calcd. C 62.84, H 5.53, N 1.79; found C 62.61, H 5.72, N 1.71. $^{31}P\{H\}$ NMR ($CDCl_3$): δ = −22.51(s, P_A), 16.80 (s, P_X). ^1H NMR (CD_2Cl_2): δ = 2.15 (s, 6 H, CH_3), 2.65 (m, 2 H, CH_2), 3.18 (m, 2 H, CH_2), 3.43 (d, 2 H, CH), 4.03 (d, 2 H,CH), 4.59 (dd, $^3J_{NH,CH}$ = 6, $^2J_{P,CH}$ = 2 Hz, 2 H, CH_2), 4.95 (m, 1 H, NH), 5.13 (br. m, 2 H, CH), 6.73−6.54 (m, 3 H, ArH), 7.38−6.99 (m, 17 H, ArH), 7.76−7.59 (m, 4 H, ArH). IR (KBr disc): ν_{NH} = 3314w cm^{-1}. FAB: *m/z* = 784 $[M]^+$, 748 $[M - Cl]^+$, 713 $[M - 2Cl]^+$.

[RhCl$_2$(η^5-C$_5$Me$_5$)(Ph$_2$PCH$_2$NHC$_6$H$_4$PPh$_2$-*P*$_X$)] (10): [{RhCl(μ-Cl)(η^5-C_5Me_5)}$_2$] (68 mg, 110 μmol) was suspended in THF (4 cm^3) and $Ph_2PC_6H_4NHCH_2PPh_2$ (**1**; 105 mg, 220 μmol) was added to the stirred suspension as a solid in one portion. The suspension dissolved and after 15 minutes stirring, an orange solid deposited from the deep red solution. After stirring for a total of 2 h the orange solid was collected by suction filtration, washed with diethyl ether (3 × 1 cm^3) and dried in vacuo. Yield: 145 mg (87%). $C_{41}H_{42}Cl_2NP_2Rh$ (784.5): calcd. C 62.77, H 5.40, N 1.79; found C 62.72, H 5.38, N 1.84. $^{31}P\{^1H\}$ NMR (CD_2Cl_2): δ = −22.84 (s, P_A), 32.74 (d, $^1J_{Rh,P_X}$ = 141 Hz, P_X). ^1H NMR (CD_2Cl_2): δ = 1.33 (d, $^4J_{P...CH}$ = 3 Hz, 15 H, CH_3), 4.66 (d, $^3J_{NH,CH}$ = 7 Hz, 2 H, CH_2), 4.97 (br. q, $^3J_{NH,CH}$ = $^3J_{PC,NH}$ = 7 Hz, 1 H, NH; no $^2J_{P,CH}$ observed), 6.30 (m, 1 H, ArH), 6.40 (m, 1 H, ArH), 6.60 (m, 1 H, ArH), 6.85 (m, 1 H, ArH), 7.77−7.04 (m, 20 H, ArH),. IR (KBr disc): ν_{NH} = 3326w cm^{-1}. FAB: *m/z* = 748 $[M - Cl]^+$, 713 $[M - 2Cl]^+$.

[IrCl$_2$(η^5-C$_5$Me$_5$)(Ph$_2$PCH$_2$NHC$_6$H$_4$PPh$_2$-*P*$_X$)] (11) and [IrCl(η^5-C$_5$Me$_5$)(Ph$_2$PCH$_2$NHC$_6$H$_4$PPh$_2$-*P*$_X$, *P*$_A$)]Cl (12): [{IrCl(μ-Cl)(η^5-C_5Me_5)}$_2$] (70 mg, 88 μmol) was added to a solution of $Ph_2PC_6H_4NHCH_2PPh_2$ (**1**; 84 mg, 176 μmol) in THF (5 cm^3). The mixture was stirred for 1.5 h and the solvent was removed in vacuo. The yellow solid residue was dissolved in CH_2Cl_2 (0.5 cm^3) followed by addition of acetone (0.5 cm^3). Storage of this solution at room temperature overnight led to the formation of well-shaped orange crystals of **11**. The crystals were collected by suction filtration and washed with acetone (0.5 cm^3). Addition of Et_2O (2.0 cm^3) to the filtrate caused the precipitation of **12** as an orange powder.
11: Yield: 30 mg (19.5%). $C_{41}H_{42}Cl_2IrNP_2$ (873.9): calcd. C 56.35, H 4.84, N 1.60; found C 56.52, H 4.78, N 1.54. $^{31}P\{^1H\}$ NMR (CD_2Cl_2): δ = −22.80 (s, P_A), 0.10 (s, P_X). ^1H NMR (CD_2Cl_2): δ = 1.33 (d, $^4J_{P...CH}$ = 3 Hz, 15 H, CH_3), 4.66 (d, 2 H, CH_2; no $^2J_{PCH}$ observed), 4.91 (q, $^3J_{NH,CH}$ = $^3J_{PCNH}$ = 7 Hz, 1 H, NH), 6.34 (m, 1 H, ArH), 6.42 (m, 1 H, ArH), 6.61 (m, 1 H, ArH), 7.71−6.91 (m, 21 H, ArH). IR (KBr disc): ν_{NH} = 3328w cm^{-1}. FAB: *m/z* = 838 $[M - Cl]^+$, 803 $[M - 2Cl]^+$.
12: Yield: 29 mg (19%). $C_{41}H_{42}Cl_2IrNP_2$ (873.9): calcd. C 56.35, H 4.84, N 1.60; found C 48.67, H 4.33, N 1.08. $^{31}P\{^1H\}$ NMR (CD_2Cl_2): δ = −0.32 (s), 0.48 (s). IR (KBr disc): ν_{NH} = 3283w cm^{-1}. FAB: *m/z* = 838 $[M - Cl]^+$, 803 $[M - 2Cl]^+$.

[RuCl(η^3:η^3-C$_{10}$H$_{16}$)(Ph$_2$PCH$_2$NHC$_6$H$_4$PPh$_2$-*P*$_X$,*P*$_A$)][ClO$_4$] (13): [{RuCl(μ-Cl)(η^3:η^3-$C_{10}H_{16}$)}$_2$] (64 mg, 103 μmol) was added to a solution of $Ph_2PC_6H_4NHCH_2PPh_2$ (**1**; 99 mg, 208 μmol) in THF (5 cm^3). The mixture was stirred for 1.5 h and then $AgClO_4$ (43 mg, 207 μmol) was added. Stirring was continued overnight and the precipitated AgCl was removed by filtration through Celite. The dark filtrate was concentrated in vacuo to ca. 0.5 cm^3. Addition of Et_2O (5 cm^3), filtration and washing with Et_2O (3 × 1 cm^3) gave the product as a black solid. Yield: 162 mg (92%). $C_{41}H_{43}Cl_2NO_4P_2Ru$ (847.7): calcd. C 58.09, H 5.11, N 1.65; found C 56.88, H 4.85, N 2.05. $^{31}P\{^1H\}$ NMR ($CDCl_3$): δ = 21.86 (s, P_A), 36.89 (s, P_X). ^1H NMR ($CDCl_3$): δ = 2.14 (s, 6 H, CH_3), 2.64 (br. m, 2 H, CH_2), 3.22 (d, 2 H, CH), 3.43 (m, 2 H, CH_2), 4.12 (d, 2 H, CH), 4.67 (ddd, $^2J_{P,CH}$ = 52, $^3J_{P,CH}$ = 15, $^3J_{CH,NH}$ = 6 Hz, 2 H, CH_2), 5.02 (br. s, 1 H, NH), 5.13 (br. m, 2 H, CH), 6.42 (m, 2 H, ArH), 6.63 (m, 1 H, ArH), 7.75−7.05 (m, 21 H, ArH). IR (KBr disc): ν_{NH} = 3272w cm^{-1}, $\nu_{ClO_4^-}$ = 1099 vs cm^{-1}. FAB: *m/z* = 748 $[M - ClO_4]^+$.

[RhCl(η^5-C$_5$Me$_5$)(Ph$_2$PCH$_2$NHC$_6$H$_4$PPh$_2$-*P*$_X$,*P*$_A$)][ClO$_4$] (14): This orange product was prepared in the same way as the ruthenium compound **13** from [{RhCl(μ-Cl)(η^5-C_5Me_5)}$_2$] (25 mg, 40 μmol), $Ph_2PC_6H_4NHCH_2PPh_2$ (**1**; 39 mg, 82 μmol) and $AgClO_4$ (17 mg, 82 μmol). Yield: 63 mg (93%). Red crystals suitable for X-ray analysis were obtained by layering THF and petroleum ether (60−80) on a dichloromethane solution of **14** for four days. $C_{41}H_{42}Cl_2NO_4P_2Rh$ (848.5): calcd. C 58.03, H 4.99, N 1.65; found C 57.49, H 4.87, N 1.52. IR (KBr disc): ν_{NH} = 3332m cm^{-1}, $\nu_{ClO_4^-}$ = 1095vs cm^{-1}. FAB: *m/z* = 748 $[M - ClO_4]^+$.

[Ph$_2$P{AuCl}CH$_2$NHC$_6$H$_4${AuCl}PPh$_2$] (15): [AuCl(tht)] (135 mg, 420 μmol) was added to a solution of $Ph_2PC_6H_4NHCH_2PPh_2$ (**1**;

Table 8. Details of the X-ray data collections and refinements for compounds **2, 3**, **8**, **9**, **11** and **14**

	2·0.5H$_2$O	**3**	**8**	**9**	**11**	**14**
Empirical formula	$C_{31}H_{27}NO_{2.50}P_2$	$C_{31}H_{27}NP_2S_2$	$C_{35}H_{27}MoNO_4P_2$	$C_{41}H_{43}Cl_2NP_2Ru$	$C_{41}H_{42}Cl_2IrNP_2$	$C_{41.25}H_{42.50}Cl_{2.50}NO_4P_2Rh$
Crystal colour, habit	clear, prism	clear, prism	clear, prism	purple, prism	Orange, block	Red, prism
Crystal dimensions/mm	0.21 × 0.1 × 0.1	0.1 × 0.1 × 0.08	0.16 × 0.13 × 0.13	0.12 × 0.1 × 0.06	0.15 × 0.1 × 0.1	0.18 × 0.12 × 0.1
Crystal system	Monoclinic	Triclinic	Monoclinic	Triclinic	Monoclinic	Triclinic
Space group	*C*2/*c*	$P\bar{1}$	$P2_1/c$	$P\bar{1}$	$P2_1/c$	$P\bar{1}$
a (Å)	26.754(2)	9.6227(3)	14.3816(3)	10.676(2)	18.5451 (2)	12.3348(5)
b (Å)	9.0619(6)	12.3446(4)	9.9445(2)	13.333(3)	9.1119(1)	12.3577(5)
c (Å)	25.046(2)	13.2192(3)	22.5402(4)	13.646(3)	22.3655(1)	14.1891(6)
α (°)	90	108.7150(10)	90	76.527(5)	90	77.3270(10)
β (°)	119.409(2)	110.4580(10)	103.5250(10)	74.373(4)	92.5500(10)	78.15
γ (°)	90	93.9340(10)	90	79.345(5)	90	81.8740(10)
U (Å^3)	5289.8(7)	1364.24 (7)	3134.25(11)	1803.6(6)	3775.60(6)	2054.6(2)
Z	8	2	4	2	4	2
M	516.48	539.60	683.46	783.67	873.80	724.43
D_c (g cm^{-3})	1.297	1.314	1.448	1.443	1.537	1.406
μ (mm^{-1})	0.196	0.334	0.560	0.702	3.792	0.697
F(000)	2168	564	1392	808	1744	893
Measured reflections	12820	6916	13208	9120	15695	14534
Independent reflections (R_{int})	3756 (0.0806)	3882 (0.0176)	4485 (0.0256)	5066 (0.1443)	5376 (0.0367)	5860 (0.0280)
Final *R*1, ω*R*2[$I > 2\sigma(I)$]	0.0566, 0.1316	0.0412, 0.0993	0.0236, 0.0558	0.0842, 0.1770	0.0293, 0.0650	0.0434, 0.1127
Largest difference peak hole (eÅ^{-3})	0.337, −0.448	0.250, −0.230	0.222, −0.171	0.670, −0.882	0.200, −0.254	0.731, −0.528

100 mg, 210 μmol) in CH_2Cl_2 (10 cm^3). The mixture was stirred for 30 minutes and then filtered through Celite. The filtrate was concentrated to ca. 0.5 cm^3. Addition of 60−80 petroleum ether (10 cm^3), filtration and washing with Et_2O (3 × 1 cm^3) gave the product as a white solid. Yield: 176 mg (90%). $C_{31}H_{27}Au_2Cl_2NP_2$ (940.3): calcd. C 39.60, H 2.89, N 1.49; found C 39.91, H 2.91, N 1.48. $^{31}P\{^1H\}$ NMR ($CDCl_3$): δ = 18.64 (s, P_A), 24.95 (s, P_X). ^1H NMR ($CDCl_3$): δ = 4.34 (dd, $^2J_{P,CH}$ = 3 Hz, 2 H, CH_2), 4.94 (m, $^3J_{NH,CH}$ = 6, $^3J_{PCNH}$ = $^4J_{PCCNH}$ = 3 Hz, 1 H, NH), 6.61 (m, 1 H, ArH), 6.79 (m, 1 H, ArH), 6.99 (m, 1 H, ArH), 7.58−7.40 (m, 21 H, ArH). IR (KBr disc): ν_{NH} = 3309m cm^{-1}, $\nu_{Au\text{-}Cl}$ = 329m cm^{-1}. FAB: *m*/*z* = 904 [M − Cl]$^+$.

[{RhCl$_2$(η^5-C$_5$Me$_5$)}$_2$(Ph$_2$PCH$_2$NHC$_6$H$_4$PPh$_2$)] (16): This compound was prepared in the same way as compound **10** from a 1:1 molar ratio of [{RhCl(μ-Cl)(η^5-C_5Me_5)}$_2$] (93 mg, 150 μmol) and $Ph_2PC_6H_4NHCH_2PPh_2$ (**1**; 73 mg, 151 μmol). Yield: 148 mg (90%). $C_{51}H_{57}Cl_4NP_2Rh$ (1093.6): calcd. C 54.33, H 5.25, N 1.28; found C 56.01, H 4.66, N 1.16. $^{31}P\{^1H\}$ NMR ($CDCl_3$): δ = 27.79 (d, $^1J_{Rh,P_A}$ = 144 Hz, P_A), 32.44 (d, $^1J_{Rh,P_X}$ = 138 Hz, P_X). ^1H NMR ($CDCl_3$): δ = 1.23 (d, $^4J_{P,CH}$ = 3 Hz, 15 H, CH_3), 1.27 (d, $^4J_{P,CH}$ = 3 Hz, 15 H, CH_3), 4.90 (dd, $^3J_{NH,CH}$ = 5, $^2J_{P,CH}$ = 16 Hz, 2 H, CH_2), 5.33 (br. s, 1 H, NH), 5.78 (m, 1 H, ArH), 6.28 (m, 1 H, ArH), 6.52 (m, 1 H, ArH), 6.70 (m, 1 H, ArH), 7.89−6.90 (m, 20 H, ArH). IR (KBr disc): ν_{NH} = 3280m cm^{-1}. FAB: *m*/*z* = 1056 [M − Cl]$^+$.

X-ray Crystallography: Table 8 lists details of data collections and refinements for **2**, **3**, **8**, **9**, **11** and **14**. Data were collected at room temperature using Mo-K_α radiation with a SMART system. Intensities were corrected for Lorentz polarisation and for absorption. The structures were solved by the heavy atom method or by direct methods. The positions of the hydrogen atoms were idealised. Refinements were by full-matrix least-squares based on F^2 using SHELXTL.[35] CCDC-172648−172653 (corresponding to compounds **2**, **3**, **8**, **9**, **11**, and **14**, respectively) contain the supplementary crystallographic data for this paper. These data can be obtained free of charge at www.ccdc.cam.ac.uk/conts/retrieving.html [or from the Cambridge Crystallographic Data Centre, 12, Union Road, Cambridge CB2 1EZ, UK; Fax: (internat.) +44-1223/336-033; E-mail: deposit@ccdc.cam.ac.uk].

Acknowledgments

We wish to thank the JREI for equipment grants and Johnson Matthey plc for the loan of precious metals. Qingzhi Zhang is indebted to St Andrews University for financial support.

[1] R. J. Puddephatt, *Chem. Soc. Rev.* **1983**, 99−127.
[2] I. Haiduc, I. S. Dumitrescu, *Coord. Chem. Rev.* **1986**, *69*, 127−258.
[3] B. Chaudret, B. Delavaus, R. Poilblanc, *Coord. Chem. Rev.* **1988**, *86*, 191−243.
[4] E. Drent, J. A. M. van-Broekhoven, M. J. Doyle, *J. Organomet. Chem.* **1991**, *417*, 235−251.
[5] C. P. C. M. Dekker, C. J. Elsevier, K. Vrieze, P. W. N. M. van Leeuwen, *Organometallics* **1992**, *11*, 1598−1603.
[6] E. M. Barranco, M. C. Gimeno, P. G. Jones, A. Laguna, M. D. Villacampa, *Inorg. Chem.* **1999**, *38*, 702−706.
[7] B. Buriez, I. D. Burns, A. F. Hill, A. J. P. White, D. J. Williams, J. D. E. T. Wilton-Ely, *Organometallics* **1999**, *18*, 1504−1516.
[8] B. S. Williams, K. I. Goldberg, *J. Am. Chem. Soc.* **2001**, *123*, 2576−2587.
[9] A. R. J. Genge, N. J. Hill, W. Levason, G. Reid, *J. Chem. Soc., Dalton Trans.* **2001**, 1007−1012.
[10] F. Agbossoll, J.-F. Carpentier, F. Hapiot, I. Suisse, A. Mortreux, *Coord. Chem. Rev.* **1998**, *178*, 1615−1645.
[11] B. C. Hamann, J. F. Hartwig, *J. Am. Chem. Soc.* **1998**, *120*, 7369−7370.
[12] M. E. G. Mosquera, J. Ruiz, V. Riera, *Organometallics* **2000**, *19*, 5533−5536.
[13] K. Pignat, J. Vallotto, F. Pinna, G. Strukul, *Organometallics* **2000**, *19*, 5160−5167.
[14] C. A. Carraz, E. J. Ditzel, A. G. Orpen, D. D. Ellis, P. G. Pringle, G. J. Sunley, *Chem. Commun.* **2000**, 1277−1278.
[15] G. Tsiavaliaris, S. Haubrich, C. Merckle, J. Blumel, *Synlett* **2001**, *3*, 391−393.
[16] M. K. Copper, J. M. Downes, P. A. Duckworth, E. R. T. Tiekink, *Aust. J. Chem.* **1992**, *45*, 595−609.

[17] S. M. Aucott, A. M. Z. Slawin, J. D. Woollins, *J. Organomet. Chem.* **1999**, *582*, 83−89.
[18] S. M. Aucott, A. M. Z. Slawin, J. D. Woollins, *J. Chem. Soc., Dalton Trans.* **2001**, 2279−2287.
[19] S. T. Lin, H. S. Choe, L. S. Liu, J. C. Wang, *J. Organomet. Chem.* **2000**, *610*, 1−7.
[20] X. Dai, S. Virgil, *Tetrahedron: Asymmetry* **1999**, *10*, 25−29.
[21] H. J. Drexler, W. Baumann, A. Spannenberg, C. Fischer, D. Heller, *J. Organomet. Chem.* **2001**, *621*, 89−102.
[22] K.-H. Wong, M. C.-W. Chan, C.-M. Che, *Chem. Eur. J.* **1999**, *5*, 2845−2849.
[23] S. E. Durran, M. B. Smith, A. M. Slawin, J. W. Steed, *J. Chem. Soc., Dalton Trans.* **2000**, 2771−2778.
[24] E. Linder, M. Mohr, F. Christiane, R. Fawzi, G. Henkel, *J. Organomet. Chem.* **2000**, *595*, 166−177.
[25] M. K. Cooper, P. A. Duckworth, T. W. Hambley, G. J. Organ, K. Henrick, M. Mcpartlin, A. Pardkh, *J. Chem. Soc., Dalton Trans.* **1989**, 1067−1073.
[26] J. G. Toerien, P. H. van Rooyen, *J. Chem. Soc., Dalton Trans.* **1991**, 1563−1568.
[27] H. Hellmann, J. Bader, H. Birkner, O. Schumacher, *Justus Liebigs Ann. Chem.* **1962**, 49−63.
[28] J. X. McDermott, J. F. White, G. M. Whitesides, *J. Am. Chem. Soc.* **1976**, *98*, 6521−6528.
[29] D. Drew, J. T. Doyle, *Inorg. Synth.* **1972**, *13*, 47−55.
[30] H. C. Clark, L. E. Manzer, *J. Organomet. Chem.* **1973**, *59*, 411−428.
[31] *Inorganic Experiments* (Ed.: J. D. Woollins), VCH, Weinheim, **1994**, 110−112.
[32] R. Uson, A. Laguna, M. Laguna, *Inorg. Synth.* **1989**, *26*, 85−91.
[33] C. White, A. Yates, P. M. Maitlis, *Inorg. Synth.* **1992**, *29*, 228−234.
[34] L. Porri, M. C. Ballazzi, A. Columbo, G. Allegra, *Tetrahedron Lett.* **1965**, *47*, 4187−4189.
[35] G. M. Sheldrick, SHELXTL, Bruker AXS, Madison, WI, **1999**.

Received October 31, 2001
[I01430]

(Alkenylalkylidene)(indenyl)ruthenium(II) Complexes: Synthesis by Protonation of Alkenyl Derivatives

Klaus Bieger,[a] Josefina Díez,[a] M. Pilar Gamasa,*[a] José Gimeno,[a] Martin Pavlišta,[a] Yolanda Rodríguez-Álvarez,[a] Santiago García-Granda,[b] and Rafael Santiago-García[b]

Keywords: Ruthenium / Hydride ligands / Alkenyl complexes / Alkylidene complexes / P ligands

The alkenyl complexes [Ru{(*E*)-C(CO_2Me)=C(H)R}(η^5-C_9H_7){κ^2-*P,P*-(*S*)-peap}] [R = CO_2Me (**3**), H (**4**)], [Ru{(*E*)-CH=C(H)Ph}(η^5-C_9H_7){κ^2-*P,P*-(*S*)-peap}] (**5**) have been prepared by reaction of the hydride complex [RuH(η^5-C_9H_7){κ^2-*P,P*-(*S*)-peap}] (**2**) [(*S*)-peap = (–)-(*S*)-*N,N*-bis(diphenylphosphanyl)(1-phenylethyl)amine] with an equimolar amount of dimethyl acetylenedicarboxylate, or with an excess of the terminal alkynes methyl propiolate or phenylacetylene. Similarly, vinylalkenyl complexes **6a**–**d** have been synthesized by the regio- and stereoselective reaction of the hydride complex **2** with 1-ethynylcycloalkynols. Protonation of the vinylalkenyl moiety of complexes **6a**,**c**,**d** with HBF_4·OEt_2 in diethyl ether afforded the cationic alkenylalkylidene complexes **7a**–**c**. The structures of complexes [RuH(η^5-C_9H_7){κ^2-*P,P*-(*S*)-peap}] (**2**) and [Ru{(*E*)-C(CO_2Me)=CH(CO_2Me)}(η^5-C_9H_7){κ^2-*P,P*-(*S*)-peap}] (**3**) have been determined by X-ray diffraction methods. The catalytic activity of (alkenylalkylidene)(indenyl)ruthenium(II) complexes **7a**–**c**, **8** and **9** in the ring-closing metathesis (RCM) of diethyl diallylmalonate has been examined.

(© Wiley-VCH Verlag GmbH, 69451 Weinheim, Germany, 2002)

Introduction

The discovery of (alkylidene)ruthenium(II) five-coordinate complexes [Ru{=C(H)R′}Cl_2(PR_3)$_2$] (R = Ph, Cy; R′ = Ph, CH=CPh_2) by Grubbs and co-workers[1] as efficient catalysts of olefin metathesis[2] has been the most important cornerstone in the remarkable development of the chemistry of (carbene)ruthenium complexes. A relevant feature of these catalysts is their tolerance towards most functional groups and protic media. The search for novel species, aiming at reproducing or increasing the performance of the Grubbs catalysts, has been an important goal during the last few years. Besides benzylidene,[3] benzyl or methylcarbene[4] complexes **A** and alkenylalkylidene complexes **B** (Scheme 1) are genuine examples of this type of catalysts. The parent complexes **A** and **B** (R = Ph) were originally obtained from the reaction of [$RuCl_2$(PPh_3)$_3$] with either phenyldiazomethane[1c] or 3,3-diphenylcyclopropene.[1a] A few derivatives of **B**, obtained through triphenylphosphane exchange processes or halide metathesis, are also known. These include [Ru(=CH−CH=CPh_2)X_2(PR_3)$_2$] (X = Cl, Br, I; PR_3 = PCy_3, PCy_2Ph, P*i*Pr_3, P*i*Pr_2Ph)[5] and [Ru(=CH−CH=CPh_2)X_2(PPh_3)$_2$] (X = CF_3CO_2).[6] However, other synthetic approaches, which have been designed as alternative procedures in order to avoid the relatively difficult access of the carbene source, are currently known: i) Reaction of *gem*-dichloride $PhCHCl_2$ with [Ru(cod)(cot)] in the presence of PCy_3 gives the complex **A** [Ru(=CHPh)Cl_2(PCy_3)$_2$].[7] A multi-step procedure starting from [$RuCl_2$(cod)], using phenylacetylene as the carbene source,[3a] and a new general synthetic method involving sulfur ylides[3b] have also been recently reported. ii) Reaction of the (hydrido)dihydrogen complex [Ru(Cl)(H)(H_2)(PCy_3)$_2$] with propargyl or vinyl halides gives vinylcarbene complexes [Ru(=CH−CH=CR_2)Cl_2(PCy_3)$_2$].[8] iii) Treatment of the dinuclear hydrido complex [Ru(H)(μ-Cl)(P−P)]$_2$ (P−P = *t*$Bu_2$$PCH_2$P*t*$Bu_2$) with dimethylpropargyl chloride gives [Ru{=CHCH=CMe_2}Cl_2(P−P)]. The related cationic derivative [Ru(=CHCH=CMe_2)Cl(solvent)(P−P)][OTf], which is formed by the treatment of the parent alkenylalkylidene complex with Me_3SiOTf, is also known.[9] iv) Reaction of [$RuCl_2$(PPh_2)$_3$] with diphenylpropargyl alcohol leads to the phenylindenylidene complex [Ru(3-phenylindenylid-1-ene)Cl_2(PPh_3)$_2$] (**C**, Scheme 1). The PPh_3 ligands can be substituted by better donor ligands such as PCy_3, and to the best of our knowledge only one mixed-phosphane-substituted derivative is known, namely the complex [Ru(3-phenylindenylid-1-ene)-Cl_2(PR_3)L] (R = Ph, Cy; L = 1,3-diarylimidazol-2-ylidene).[10]

We have reported a systematic route for the synthesis of a series of (alkenylalkylidene)ruthenium(II) complexes

[a] Departamento de Química Orgánica e Inorgánica, Instituto de Química Organometálica "Enrique Moles" (Unidad Asociada al C.S.I.C.), Facultad de Química, Universidad de Oviedo, Julián Clavería no. 8, 33071 Oviedo, Spain
E-mail: pgb@sauron.quimica.uniovi.es
[b] Departamento de Química Física y Analítica, Facultad de Química, Universidad de Oviedo
Julián Clavería no. 8, 33071 Oviedo, Spain
E-mail: sgg@sauron.quimica.uniovi.es

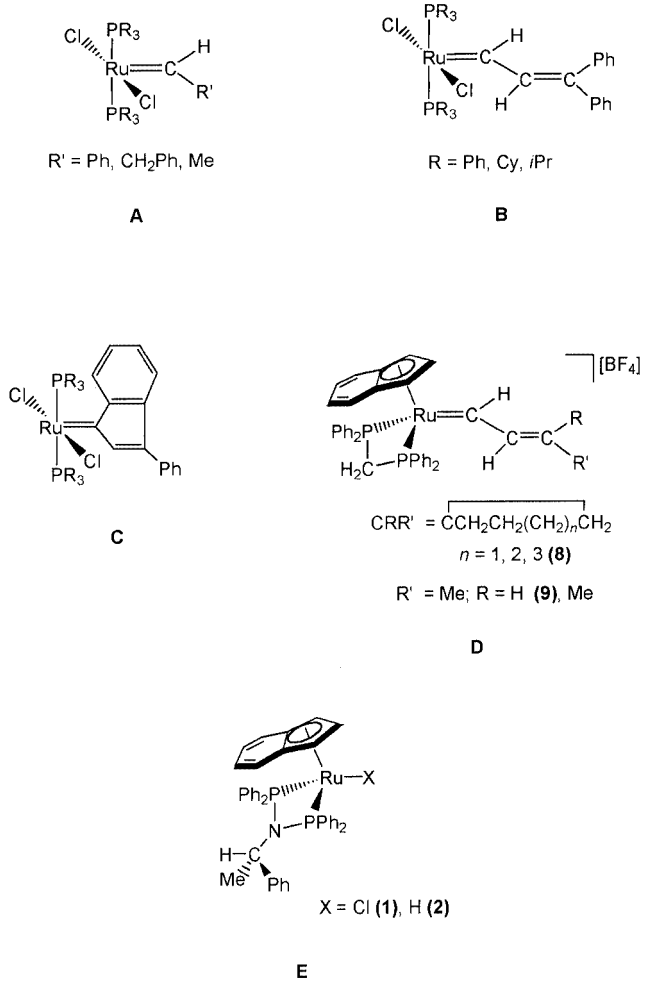

Scheme 1

[Ru(=CH−CH=CR_2)(η^5-C_9H_7)(dppm)][BF_4] [**D**, Scheme 1; dppm = bis(diphenylphosphanyl)methane] in which the unsaturated carbene group is bound to an (indenyl)(phosphane)ruthenium(II) fragment.[11] They have been obtained in high yields by protonation of the vinylalkenyl complexes [Ru{(*E*)-CH=CH−CHR_2)(η^5-C_9H_7)(dppm)]. More recently, this procedure has also been used as an alternative synthetic route for Grubbs catalyst **B** (Scheme 1).[12] Since access to these precursors {by reactions of the hydride complex [RuH(η^5-C_9H_7)(dppm)] with propargyl alcohols} is limited to the presence of the small bite chelate ligand dppm in the hydride precursor, we believed it would be of interest to investigate the applicability of this synthetic methodology using an analogous chelate ligand.

In this paper we report on the synthesis of novel ruthenium(II) precursors **E** (Scheme 1) in which the metal fragment bears the diphosphazane chelate ligand (*S*)-peap [(*S*)-peap = (−)-(*S*)-*N*,*N*-bis(diphenylphosphanyl)(1-phenylethyl)amine], which has a similar small bite angle as dppm. Further, their use as convenient starting materials for the synthesis of alkenylalkylidene complexes is investigated. The synthetic route involves two steps; the synthesis of alkenyl precursors, which are prepared by insertion reactions of the corresponding propargyl alcohol into the Ru−H bond of the hydride complex [RuH(η^5-C_9H_7){κ^2-*P*,*P*-(*S*)-peap}], followed by the protonation with HBF_4·OEt_2 to give the desired alkenylalkylidene complexes. Moreover, we have also investigated the ability of the starting hydride complex to undergo insertion at the terminal or internal alkynes, and the catalytic activity of some (alkenylalkylidene)(indenyl)ruthenium(II) in the RCM of olefins (diethyl diallylmalonate). The X-ray crystal structures of the complexes [RuH(η^5-C_9H_7){κ^2-*P*,*P*-(*S*)-peap}] and [Ru{(*E*)-(CO_2Me)C=CH(CO_2Me)}(η^5-C_9H_7){κ^2-*P*,*P*-(*S*)-peap}] are also reported.

Results and Discussion

Synthesis of the Precursor Complexes [RuX(η^5-C_9H_7){κ^2-*P*,*P*-(*S*)-peap}] [X = Cl (1), H (2); (*S*)-peap = (−)-(*S*)-*N*,*N*-bis(diphenylphosphanyl)(1-phenylethyl)amine]

The starting material is the complex [RuCl(η^5-C_9H_7){κ^2-*P*,*P*-(*S*)-peap}] (**1**), which has been synthesized (83%) by heating a mixture of [RuCl(η^5-C_9H_7)(PPh_3)$_2$] and the diphosphazane (*S*)-peap in toluene under reflux [Equation (1)]. Complex **1** was isolated as an air-stable red solid and characterized by means of spectroscopic methods and elemental analysis (see Exp. Sect. for details). In particular,

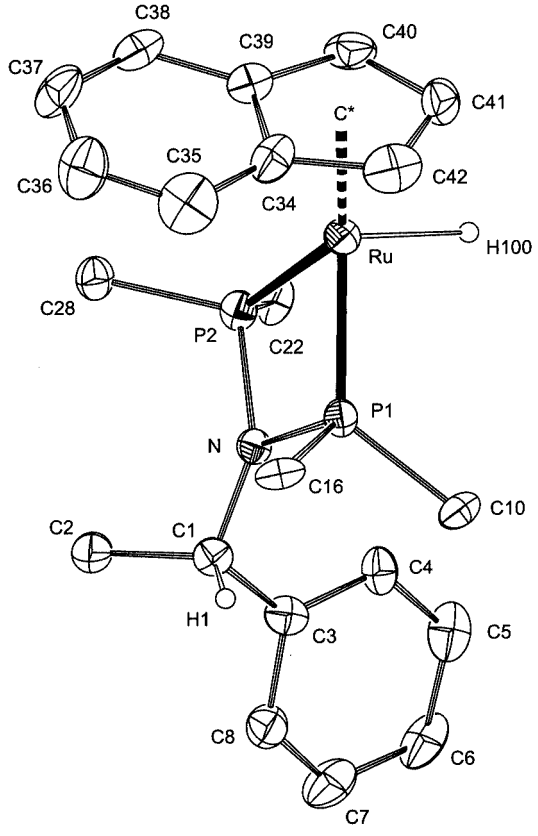

Figure 1. ORTEP-type diagram of [RuH(η^5-C_9H_7){κ^2-*P*,*P*-(*S*)-peap}] (**2**) with ellipsoids drawn at a 30% probability; phenyl rings of the Ph_2P groups in the diphosphazane have been omitted for clarity

Table 1. Selected bond lengths and slip parameter Δ [Å] and bond angles and dihedral angles HA, FA and CA [°] for complex **2**

Distances			
Ru−C*	1.97(2)	Ru−C(40)	2.266(12)
Ru−H	1.86(8)	Ru−C(41)	2.258(12)
Ru−P(1)	2.199(3)	Ru−C(42)	2.269(12)
Ru−P(2)	2.234(3)	P(1)−N	1.705(8)
Ru−C(34)	2.364(11)	P(2)−N	1.734(9)
Ru−C(39)	2.350(11)	N−C(1)	1.484(13)
Δ[a]	0.089(12)		
Angles			
P(1)−Ru−P(2)	70.44(12)	C*−Ru−P(1)	134.7(7)
P(1)−Ru−H	95(3)	C*−Ru−P(2)	139.4(8)
P(2)−Ru−H	93(3)	C*−Ru−H	109(4)
HA[b]	2.5(10)	CA[c]	20.8(24)
FA[d]	6.8(9)		

[a] Δ = *d*[Ru−C(34),C(39)] − *d*[Ru−C(40),C(42)]. [b] HA (hinge angle) = angle between normals to least-squares planes defined by [C(40), C(41), C(42)] and [C(34), C(39), C(40), C(42)]. [c] CA (conformational angle) = angle between normals to least-squares planes defined by [C**, C*, Ru] and [C*, Ru, H]. C* = centroid of C(34), C(39), C(40), C(41), C(42); C** = centroid of C(34), C(35), C(36), C(37), C(38), C(39). [d] FA (fold angle) = angle between normals to least-squares planes defined by [C(40), C(41), C(42)] and [C(34), C(35), C(36), C(37), C(38), C(39)].

its $^{31}P\{^1H\}$ NMR spectrum shows two doublet signals at δ = 83.2 and 91.4 ($^2J_{P,P'}$ = 112.7 Hz) of an AB system, which is in agreement with the presence of two diastereotopic phosphorus nuclei from the chiral chelate ligand. The ^1H and $^{31}C\{^1H\}$ NMR spectra also display resonances revealing the presence of the indenyl group and the diphosphazane ligand (see Exp. Sect.).

$$[RuCl(\eta^5\text{-}C_9H_7)(PPh_3)_2] + (S)\text{-peap} \rightarrow [RuCl(\eta^5\text{-}C_9H_7)\{\kappa^2\text{-}P,P\text{-}(S)\text{-peap}\}] + 2\ PPh_3 \quad (1)$$

According to the classical route for the synthesis of transition metal hydride derivatives based on the β-hydrogen elimination from a methoxide complex,[13] the hydride complex [RuH(η⁵-C_9H_7){κ²-*P*,*P*-(*S*)-peap}] (**2**) has been prepared (85% yield) by treatment of complex **1** with an excess of NaOMe in refluxing methanol, see Equation (2).

$$[RuCl(\eta^5\text{-}C_9H_7)\{\kappa^2\text{-}P,P\text{-}(S)\text{-peap}\}] + NaOMe \rightarrow [RuH(\eta^5\text{-}C_9H_7)\{\kappa^2\text{-}P,P\text{-}(S)\text{-peap}\}] + H_2C{=}O + NaCl \quad (2)$$

Complex **2** was isolated as an air-stable yellow solid and has been characterized by elemental analysis, IR and NMR (^1H,$^{13}C\{^1H\}$ and $^{31}P\{^1H\}$) spectroscopy, which support the proposed formulation. The most significant signals arise from the presence of the two nonequivalent phosphorus nuclei: a) the hydride resonance which appears in the ^1H NMR spectrum as a triplet at δ = −14.33 (t, $^2J_{H,P}$ = $^2J_{H,P'}$ = 29.8 Hz) and b) two doublet resonances in the $^{31}P\{^1H\}$ spectrum at δ = 101.22 and 101.73 ($^2J_{P,P'}$ = 87.6 Hz) typical of an AB system. The structure of complex **2** has also been determined by X-ray diffraction. An ORTEP-type view of the molecular structure is shown in Fig-

Table 2. $^{31}P\{^1H\}$ and ^1H NMR spectroscopic data for the alkenyl complexes **3**, **4**, **5** and vinylalkenyl complexes **6a−d**

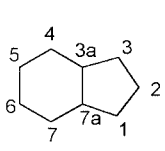

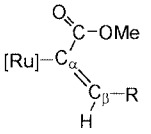

R = CO_2Me **(3)**
R = H **(4)**

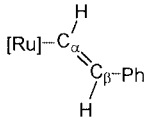

5

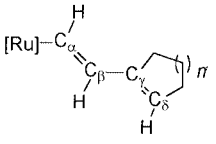

n = 1 **(6a)**, 2 **(6b)**, 3 **(6c)**, 4 **(6d)**

Complex	$^{31}P\{^1H\}$[a][d]	^1H[a][b] (*S*)-peap *CH[e]	Me	η⁵-C_9H_7[c] 1,2,3-H	$C_\alpha H$[c]	$C_\beta H$[c]	$C_\delta H$[c]	Others
3	97.26 d, 104.32 d (106.3)	4.80 m	1.11 d (7.2)	4.97 s, 4.98 s, 5.10 s	–	5.10 s	–	3.29, 3.67 (s, CO_2Me), 6.75−7.64 (m, PPh_2, *CPh, 4,5,6,7-H)
4	93.62 d, 95.57 d (118.0)	4.23 m	0.32 d (7.6)	4.91 s, 4.97 s, 5.30 s	–	4.46 d (2.3), 6.53 bs	–	2.99 (s, CO_2Me), 6.80−7.96 (m, PPh_2, *CPh, 4,5,6,7-H)
5	99.23 d, 107.33 d (106.3)	4.36 m	0.47 d (7.2)	5.27 s, 5.31 s, 5.33 s	[f]	5.65 d (15.9)	–	6.82−8.28 (m, $C_\alpha H$, PPh_2, *CPh, =CPh, 4,5,6,7-H)
6a[g]	98.81 d, 102.33 d (101.7)	4.42 m	0.52 d (7.3)	5.14 s, 5.15 s, 5.18 s	6.30 m	5.66 d (16.4)	4.50 bs	1.52−2.17 (m, CH_2), 6.77−7.80 (m, PPh_2, *CPh, 4,5,6,7-H)
6b	98.86 d, 102.50 d (104.2)	4.50 m	0.68 d (7.0)	5.28 s, 5.29 s, 5.36 s	6.62 m	5.82 d (16.1)	5.14 bs	1.54−2.22 (m, CH_2), 6.84−7.82 (m, PPh_2, *CPh, 4,5,6,7-H)
6c	98.84 d, 102.12 d (103.8)	4.46 m	0.64 d (7.0)	5.27 bs, 5.32 s	6.66 m	5.69 d (15.7)	5.22 t (6.5)	1.39−2.28 (m, CH_2), 6.83−7.88 (m, PPh_2, *CPh, 4,5,6,7-H)
6d[h]	97.53 d, 101.86 d (105.8)	4.54 m	0.72 d (7.4)	5.13 s, 5.15 s, 5.16 s	6.38 m	5.60 d (16.1)	4.73 t (8.7)	0.89−2.18 (m, CH_2), 6.77−7.68 (m, PPh_2, *CPh, 4,5,6,7-H)

[a] Spectra were recorded in C_6D_6. δ in ppm and *J* in Hz. Abbreviations: s, singlet; d, doublet; t, triplet; m, multiplet; bs, broad singlet. [b] $J_{H,H}$ in parentheses. [c] Legend for indenyl and alkenyl skeletons. [d] $^2J_{P,P'}$ in parentheses. [e] *C = asymmetric carbon atom of (*S*)-peap ligand. [f] Signal overlapped by aromatic signals. [g] ^1H NMR spectrum recorded in CD_2Cl_2. [h] Spectra recorded in $CDCl_3$.

ure 1 and selected bond lengths and angles are presented in Table 1. The complex shows the typical pseudo-octahedral three-legged piano-stool geometry of indenylruthenium(II) complexes,[14] in which the metal atom is bonded to the η^5-indenyl group, the two phosphorus atoms of the chelate diphosphazane and the hydrogen atom. Significantly, the bite angle P(1)−Ru−P(2) [70.44(12)°] of the chelate (*S*)-peap ligand shows a value that is quite similar to that seen in the complex [$PdCl_2\{\kappa^2$-*P,P*-(*S*)-peap}] [71.5(1)°][15] and by the analogous chelate dppm ligand in the complex [$RuH(\eta^5$-C_9H_7)(dppm)] [dppm = bis(diphenylphosphanyl)methane] [71.28(2)°].[16] The rest of the main structural parameters [i.e. Ru−P(1) = 2.199(3) Å, Ru−P(2) = 2.234(3) Å, Ru−C* = 1.97(2) Å (C* = centroid of the five-membered indenyl ring), hinge angle (HA) = 2.5(10)°, fold angle (FA) = 6.8(9)°, slippage parameter (Δ) = 0.089(12) Å) are rather similar to those found for analogous (indenyl)(phosphane)ruthenium(II) complexes reported by us,[14] and therefore do not merit further comments.

Synthesis of Alkenyl Complexes [Ru{(*E*)-C(CO_2Me)=C(H)R}(η^5-C_9H_7){κ^2-*P,P*-(*S*)-peap}] [R = CO_2Me (3), H (4)], [Ru{(*E*)-CH=C(H)Ph}(η^5-C_9H_7){κ^2-*P,P*-(*S*)-peap}] (5) and Vinylalkenyl Complexes 6a−d

The hydride complex **2** reacted with an equimolar amount of dimethyl acetylenedicarboxylate in refluxing diethyl ether to give the (*E*)-alkenyl complex **3** (71% yield). Similarly, complex **2** reacted with an excess of the terminal alkynes methyl propiolate or phenylacetylene in toluene at 60 and 110 °C, respectively, affording the alkenyl complexes **4** (66% yield) and **5** (73% yield), respectively (Scheme 2). They have been isolated as orange solids and their analyt-

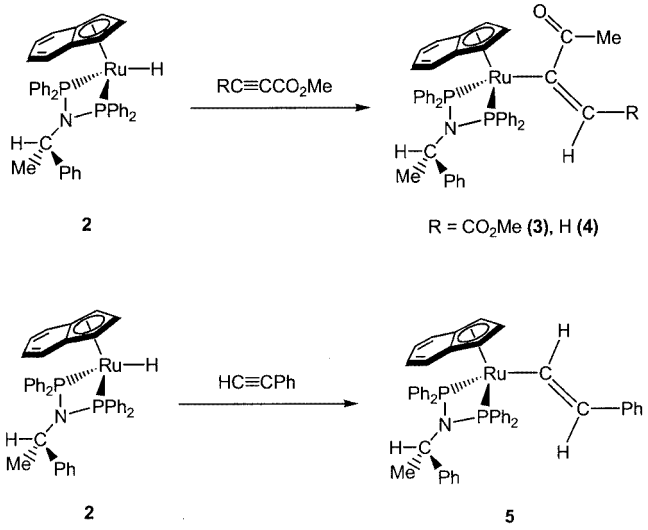

Scheme 2

Table 3. $^{13}C\{^1H\}$ NMR spectroscopic data [spectra recorded in C_6D_6; δ in ppm and $J_{C,P} = J_{C,P'}$ in Hz (in parentheses); abbreviations: s, singlet; d, doublet; t, triplet; m, multiplet] for the alkenyl complexes **3**, **4**, **5** and vinylalkenyl complexes **6a−d**

Complex	(*S*)-peap Me	*C	*CC_{ipso}	η^5-C_9H_7 C-1,3	C-2	C-3a,7a	C_α	C_β[a]	C_γ	C_δ	Others
3	24.94 s	64.80 t (6.9)	144.49 s	73.50 d (5.3), 76.32 d (3.1)	95.95 s	110.59 s, 112.60 d (3.1)	188.68 t (12.8)	[b]	–	–	51.87, 55.60 (s, CO_2*Me*), 126.08, 126.17, 126.72, 127.11 (s, C-4,5,6,7), 128.30−137.16 (m, PPh_2, *C*Ph*, C_β), 141.83−143.35 (m, PC_{ipso}), 163.75, 182.01 (s, *C*O_2Me)
4	21.09 s	62.91 t (7.0)	142.26 s	70.90 d (4.1), 71.99 d (6.4)	94.60 s	110.16 s	154.85 t (12.5)	135.57 s	–	–	50.75 (s, CO_2*Me*), 123.37, 123.68, 123.88, 124.86 (s, C-4,5,6,7), 127.30−133.66 (m, PPh_2, *C*Ph*), 138.61−140.30 (m, PC_{ipso}), 176.33 (s, *C*O_2Me)
5[c]	20.68 s	62.09 t (7.0)	[d]	69.40 d (4.1), 69.82 d (3.8)	92.98 s	107.68 t (2.3), 107.95 t (2.9)	154.21 t (14.3)	138.23 s	–	–	121.93, 122.10, 122.18 (s, 3C, C-4,5,6 or 7), 123.32−134.89 (m, PPh_2, *C*Ph*, =C*Ph*, 1 C, C-4,5,6 or 7), 139.59−140.30 (m, PC_{ipso}), 141.56, 141.64 (s, *CC_{ipso}, C_β*C*$_{ipso}$)
6a	23.82 s	64.19 t (7.2)	144.56 s	72.62 s, 73.12 s	97.71 s	110.43 s, 111.32 s	156.33 t (15.1)	149.27 s	139.59 s	117.58 s	25.92, 33.80, 35.04 (s, CH_2), 124.77, 125.08, 126.01, 126.11 (s, C-4,5,6,7), 127.85−136.48 (m, PPh_2, *C*Ph*), 136.88−142.05 (m, PC_{ipso})
6b[c]	21.56 s	62.07 t (6.1)	142.30 s	70.12 s, 70.72 s	94.62 s	108.35 s, 108.65 s	147.22 t (14.7)	141.81 s	139.01 s	116.45 s	23.63, 23.79, 24.65, 25.82 (s, CH_2), 122.37, 122.50, 123.63 (s, C-4,5,6,7), 126.73−135.77 (m, PPh_2, *C*Ph*, PC_{ipso}), 138.41−139.40 (m, PC_{ipso})
6c	21.60 s	62.12 t (6.1)	142.42 s	70.29 s, 70.71 s	95.06 s	108.47 s, 109.13 s	145.59 t (15.1)	142.97 s	146.64 s	121.39 s	26.97, 27.54, 28.59, 28.87, 33.72 (s, CH_2), 122.54, 122.75, 123.90, 123.96 (s, C-4,5,6,7), 126.73−134.35 (m, PPh_2, *C*Ph*), 138.92−139.85 (m, PC_{ipso})
6d	22.00 s	62.00 t (6.3)	142.82 s	70.71 s, 71.29 s	95.55 s	108.37 s, 109.46 s	146.51 t (14.9)	142.60 s	[b]	119.56 s	24.54, 26.99, 27.68, 27.88, 29.58, 31.94 (s, CH_2), 122.71, 123.05, 124.04, 124.12 (s, C-4,5,6,7), 127.17−134.31 (m, PPh_2, *C*Ph*, C_δ), 134.46−140.55 (m, PC_{ipso})

[a] Assigned by using DEPT 135 data. [b] Signal overlapped by aromatic signals. [c] Spectrum recorded in $CDCl_3$. [d] 141.56, 141.64 (s, *CC_{ipso}, C_β*C*$_{ipso}$). [e] Spectrum recorded in CD_2Cl_2.

ical and spectroscopic data (IR and ^1H, ^{13}C and $^{31}P\{^1H\}$ NMR) are in accordance with these formulations. The IR spectra of complexes **3** and **4** show ν(C=O) absorptions in the range of 1675−1699 cm^{-1}, which are typical of uncoordinated CO_2Me groups. The NMR spectroscopic data are shown in Table 2 (^1H and $^{31}P\{^1H\}$) and in Table 3 ($^{13}C\{^1H\}$), and are in agreement with the proposed structures. The $^{13}C\{^1H\}$ and ^1H NMR spectra show the expected resonances of the alkenyl groups which can be compared with those of the analogous (alkenyl)(dppm)ruthenium(II) complexes.[17] In particular, some resonances of the ^1H NMR spectra show coupling constants arising from a *cis* (geminal) arrangement for complex **4** (the relatively small $J_{H,H}$ = 2.3 Hz of the nonequivalent vinylic protons indicates α-metalation) and an (*E*) configuration for complex **5** (the large proton coupling constant $J_{H,H}$ = 15.9 Hz indicates the mutually *trans* arrangement). In order to confirm the stereochemistry of complex **3**, an X-ray crystal structure determination has been carried out. An ORTEP-type view of the molecular structure is shown in Figure 2; selected bond lengths and angles are presented in Table 4. The pseudo-octahedral geometry around the ruthenium atom is quite similar to that found for complex **2**, where the alkenyl group has occupied the hydride position of **2**. The bond lengths Ru−C* = 1.937(13) Å, Ru−P(1) = 2.248(3) Å, Ru−P(2) = 2.259(13) Å, the chelating bite angle P(1)−Ru−P(2) = 70.53(9)° and all the distortion parameters of the indenyl group (HA, FA and Δ) are similar to those shown by complex **2** (see Table 1). The most remarkable feature of the structure is the (*E*) configuration of the alkenyl group which exhibits an Ru−C(1) bond length of 2.030(12) Å that can be compared with the reported values in other alkenylruthenium(II) complexes with the two CO_2Me groups in a mutually *cis* configuration, e.g. 2.07(1) Å and 2.096(7) Å in the complexes [Ru{(*E*)-C(CO_2Me)=CH(CO_2Me)}(η^5-C_5H_5)(dppm)][18] and [Ru{(*E*)-C(CO_2Me)=CH(CO_2Me)}(η^5-Ph_4C_4COH)$(CO)_2$],[19] respectively. The C(1)−C(2) bond length of 1.373(17) Å (typical of a carbon−carbon double bond) and all the remaining values involving the ester functionalities of the alkenyl group are as expected.

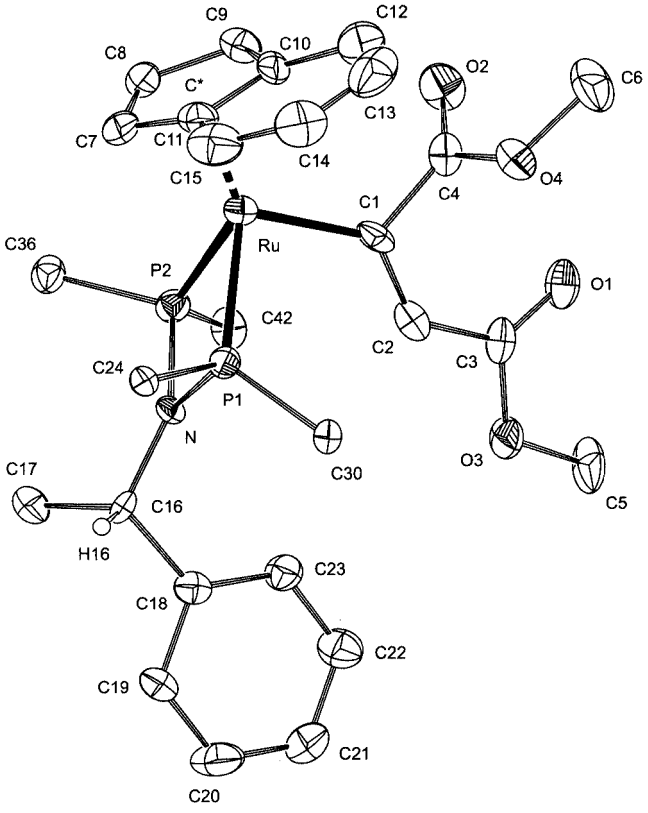

Figure 2. ORTEP-type diagram of [Ru{C(CO_2Me)=CH(CO_2Me)}(η^5-C_9H_7){κ^2-*P*,*P*-(*S*)-peap}] (**3**) with ellipsoids drawn at a 30% probability; phenyl rings of the Ph_2P groups in the diphosphazane have been omitted for clarity

Table 4. Selected bond lengths and slip parameter Δ [Å] and bond angles and dihedral angles HA, FA and CA [°] for complex **3**

Distances			
Ru−C*	1.937(13)	N−C(16)	1.499(12)
Ru−P(1)	2.248(13)	Ru−C(1)	2.030(12)
Ru−P(2)	2.259(13)	C(1)−C(2)	1.373(17)
Ru−C(7)	2.219(12)	C(1)−C(4)	1.488(15)
Ru−C(8)	2.254(12)	C(2)−C(3)	1.422(17)
Ru−C(9)	2.270(11)	C(3)−O(1)	1.191(14)
Ru−C(10)	2.324(14)	C(4)−O(2)	1.221(12)
Ru−C(11)	2.332(16)		
Δ[a]	0.083(14)		
Angles			
P(1)−Ru−P(2)	70.53(9)	C*−Ru−C(1)	126.0(5)
C(1)−Ru−P(1)	92.5(3)	Ru−C(1)−C(2)	129.3(9)
C(1)−Ru−P(2)	91.2(3)	Ru−C(1)−C(4)	118.6(8)
C*−Ru−P(1)	130.2(4)	P(1)−N−P(2)	97.7(4)
C*−Ru−P(2)	129.4(4)	HA[b]	5.4(9)
CA[c]	69.0(5)	FA[d]	6.7(9)

[a] Δ = *d*[Ru−C(10),C(11)] − *d*[Ru−C(7),C(9)]. [b] HA (hinge angle) = angle between normals to least-squares planes defined by [C(7), C(8), C(9)] and [C(7), C(9), C(10), C(11)]. [c] CA (conformational angle) = angle between normals to least-squares planes defined by [C**, C*, Ru] and [C*, Ru, C(1)]. C* = centroid of C(7), C(8), C(9), C(10), C(11); C** = centroid of C(10), C(12), C(13), C(14), C(15), C(11). [d] FA (fold angle) = angle between normals to least-squares planes defined by [C(7), C(8), C(9)] and [C(10), C(12), C(13), C(14), C(15), C(11)].

Complex **2** also reacted with 1-ethynylcycloalkynols in toluene at 100 °C affording the vinylalkenyl complexes **6a**−**d** (Scheme 3). Although no attempts to isolate the intermediate species have been made, the reactions proceed stereo- and regioselectively in a *cis*- (*syn*) and *anti*-Markovnikov fashion through the formation of the corresponding hydroxyalkenyl complexes,[11,20,21] that dehydrate spontaneously to give the desired complexes (69−74% yield). All the alkenyl complexes are isolated as air-stable red-orange solids and have been characterized by elemental analysis, mass spectra (FAB) and NMR spectroscopy (Tables 2 and 3). The $^{31}P\{^1H\}$ NMR spectra show, as for complexes **3**−**5**, doublet signals due to the nonequivalent nature of the two

phosphorus atoms of the chiral diphosphazane. The ^1H and $^{13}C\{^1H\}$ NMR spectroscopic data are consistent with those reported for similar α,β-unsaturated alkenylruthenium(II) complexes.[11,21,22] Significant features are the $^3J_{H,H}$ coupling constants (15.7−16.4 Hz) which support the *trans* stereochemistry for the RuC*H*=C*H*R double bond. The $^{13}C\{^1H\}$ NMR spectra exhibit all the resonances corresponding to the α,β-unsaturated alkenyl ligands. Significantly, the Ru*C*H=*C*HR carbon resonances appear as triplet ($^2J_{C,P} = {}^2J_{C,P'}$ = 14.3−15.1 Hz) and singlet signals at δ = 145.59−156.33 and 141.81−149.27, respectively. The spectra also exhibit resonances of the indenyl and (*S*)-peap ligand, along with the rest of the expected resonances for the alkenyl groups (see Tables 2 and 3).

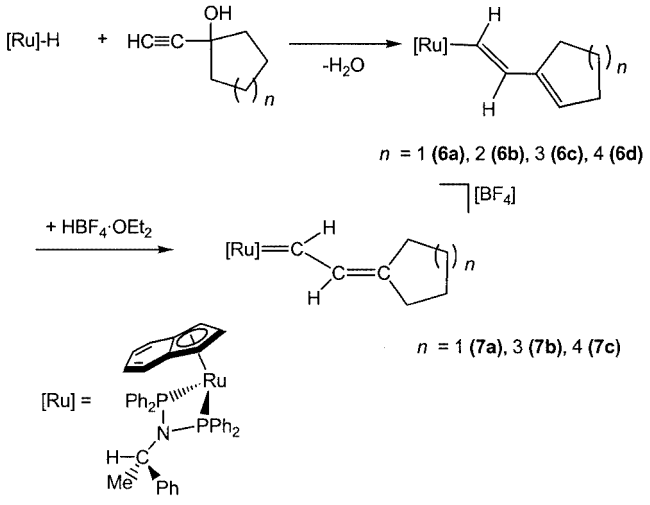

Scheme 3

Synthesis of Alkenylalkylidene Complexes 7a−c

In accordance with the well-established reactivity of alkenyl complexes towards electrophiles[11] which leads to the formation of carbene complexes (theoretical studies support the nucleophilic nature of the C_β atom of the alkenyl group),[23] the treatment of solutions of complexes **6a**, **c** and **d** in diethyl ether with $HBF_4{\cdot}Et_2O$ at −40 °C gave, by precipitation, the alkylidene complexes **7a−c**, respectively (Scheme 3). They were isolated as air-sensitive orange tetrafluoroborate salts (87−92%). They are soluble in chlorinated solvents and acetone. The conductivity data in acetone show values that are expected for 1:1 electrolytes and the IR spectra exhibit the typical ν(B−F) strong absorptions (see Exp. Sect.). All the complexes are characterized by mass spectra (FAB) which support the formulations, and by NMR spectroscopy (Tables 5 and 6). The ^1H and $^{13}C\{^1H\}$ NMR spectra reveal the presence of the alkenylalkylidene groups, which are formally generated from the protonation at the C_δ atoms of the alkenyl chain. The most relevant data arise from the $^{13}C\{^1H\}$ NMR spectra which show the typical low-field carbene resonance at δ = 290.99−294.60 ($^2J_{C,P} = {}^2J_{C,P'}$ = 10.1−12.6 Hz). Resonances that appear more upfield are assigned to the remaining carbon atoms of the hydrocarbon chain [e.g. 142.67−146.27 (C_β); 159.41−165.93 (C_γ)]. The ^1H NMR spectra also show downfield resonances at δ = 13.84−14.09, which are characteristic of the Ru=C*H* proton. The $^{31}P\{^1H\}$ NMR spectra display, as expected, two doublet resonances more upfield than those of the precursor complexes (δ = 91.26−92.20; 94.25−95.20). Similar spectroscopic data have been reported for analogous (alkenylalkylidene)(dppm)(indenyl)ruthenium(II) complexes.[11]

The catalytic activity of **7a−c** and the analogous dppm complexes **8** and **9**[11] (see Scheme 1, **D**) in the RCM of diethyl diallylmalonate was investigated (Scheme 4). The reactions were performed in a sealed tube containing a solution of 5 mol % of the catalyst precursor in CD_2Cl_2 and monitored by ^1H NMR spectroscopy. No transformation of the substrate was observed over 24 h at room or higher temperatures (limited by the thermal stability of the catalyst ca.

Table 5. $^{31}P\{^1H\}$ and ^1H NMR spectroscopic data [spectra recorded in CD_2Cl_2 (**7a**) or in $CDCl_3$ (**7b**, **c**); δ in ppm and *J* in Hz; abbreviations: s, singlet; d, doublet; t, triplet; m, multiplet] for the alkenylalkylidene complexes **7a−c**

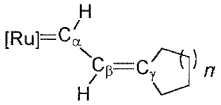

n = 1 (**7a**), 3 (**7b**), 4 (**7c**)

Complex	$^{31}P\{^1H\}$[a]	^1H[b] (*S*)-peap *CH	Me	η^5-C_9H_7 1,3-H	2-H	$C_\alpha H$	$C_\beta H$	Others
7a	91.26 d, 94.25 d (83.4)	5.17 m	1.32 d (6.4)	5.69 s, 5.94 s	5.54 t (2.7)	13.84 m	6.72 d (8.6)	1.44-2.12 (m, CH_2), 6.91-8.07 (m, PPh_2, *CPh, 4,5,6,7-H)
7b	91.71 d, 95.00 d (83.4)	5.19 m	1.34 d (7.1)	5.68 s, 5.97 s	5.46 s	14.09 m	6.79 d (8.2)	1.35-1.99 (m, CH_2), 6.87-7.73 (m, PPh_2, *CPh, 4,5,6,7-H)
7c	92.20 d, 95.20 d (81.4)	5.21 m	1.34 d (7.4)	5.67 s, 5.98 s	5.44 t (2.6)	14.08 m	6.80 d (8.1)	1.40-1.87 (m, CH_2), 6.85-7.90 (m, PPh_2, *CPh, 4,5,6,7-H)

[a] $^2J_{P,P'}$ in parentheses. [b] $J_{H,H}$ in parentheses.

Table 6. $^{13}C\{^1H\}$ NMR spectroscopic data (spectra recorded in $CDCl_3$; δ in ppm and J in Hz. $J_{C,P} = J_{C,P'}$ in parentheses; abbreviations: s, singlet; d, doublet; t, triplet; m, multiplet) for the alkenylalkylidene complexes **7a−c**

Complex	(*S*)-peap CH_3	*C	*CC_{ipso}	η^5-C_9H_7 C-1,3	C-2	C-3a,7a	C_α	C_β [a]	C_γ	Others
7a	22.71 s	62.22 t (5.9)	139.88 s	80.22 s, 80.44 s	98.53 s	110.42 s, 113.53 s	294.60 t (10.1)	142.67 s	165.93 s	25.09, 25.33, 31.45, 35.68 (s, CH_2), 122.68, 123.67, 126.31 (s, 3C, C-4,5,6 or 7), 127.47−132.91 (m, PPh_2, *C*Ph*, 1C, C-4,5,6 or 7), 133.24−134.67 (m, PC_{ipso})
7b	22.81 t (3.6)	62.21 t (6.3)	140.07 s	81.34 s, 81.42 s	97.85 s	110.57 s, 113.59 s	292.43 t (12.6)	145.92 s	159.41 s	25.56, 26.37, 28.35, 29.10, 31.60, 38.98 (s, CH_2), 122.98, 123.74 (s, C-4,7 or C-5,6), 126.48−135.01 (m, PPh_2, *C*Ph*, C-4,7 or C-5,6)
7c	22.89 s	62.15 t (5.4)	140.17 s	81.59 s	97.67 s	110.56 d (1.8), 113.55 s	290.99 t (10.8)	146.27 s	162.13 s	24.77, 25.19, 26.30, 27.53, 27.65, 30.71, 38.51 (s, CH_2), 123.05, 123.81 (s, C-4,7 or C-5,6), 126.54−133.35 (m, PPh_2, *C*Ph*, C-4,7 or C-5,6), 133.50−135.23 (m, PC_{ipso})

[a] Assigned by using DEPT 135 data.

90−100 °C). The substrate also remained unchanged when the reactions were performed in $[D_8]$THF, as well as in the presence of CuCl (10 equiv. with respect to the catalyst) under similar conditions. The addition of CuCl as a co-catalyst has proven to activate the ring-closing metathesis of the substrate with other ruthenium(II) catalysts.[24]

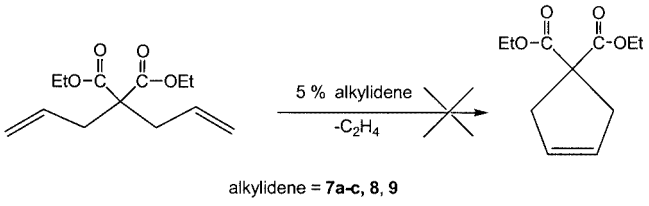

Scheme 4

Conclusions

A series of novel alkenyl- and (vinylalkenyl)ruthenium(II) complexes [Ru{(*E*)-CR=CHR′)(η^5-C_9H_7){κ^2-*P*,*P*-(*S*)-peap}] [R = CO_2Me; R′= CO_2Me (**3**); R = CO_2Me; R′= H (**4**); R = H; R = Ph (**5**)], **6a−d** containing the chelate diphosphazane ligand (−)-(*S*)-*N*,*N*-bis(diphenylphosphanyl)(1-phenylethyl)amine [(*S*)-peap], have been prepared in good yields. The latter complexes have proven to be good precursors for the synthesis of cationic alkenylakylidene complexes **7a−c** that are synthesized in good yields by protonation of the alkenyl derivatives. Disappointingly, these complexes (along with the dppm analogues **8** and **9**) are completely unreactive towards diethyl diallylmalonate under reaction conditions similar to those used for other ruthenium(II) complexes active in the ring-closing metathesis of olefins.[2,25] Analogous pseudo-octahedral cationic ruthenium complexes, namely [Ru(=CHPh)Tp(S)(PCy_3)]$^+$ [Tp = hydrotris(pyrazolyl)borate; S = H_2O, Py, Me_3CN],[24] have also shown no catalytic activity. Although substitution reactions have been reported in other indenylruthenium(II) complexes favored by a dissociative *indenyl effect*,[26] the cationic nature of the complexes leads to a substantial decrease of the lability of the ligand which is required to allow the coordination of the diolefin substrate.

Experimental Section

General Remarks: The reactions were carried out under dry nitrogen using standard Schlenk techniques. The solvents were dried by standard methods and distilled under nitrogen before use. The complexes [RuCl(η^5-C_9H_7)(PPh_3)$_2$],[27] **8** and **9**[11] and the diphosphazane ligand $(Ph_2P)_2N$[(*S*)-*CHMePh],[15] were prepared by published methods. Dimethyl acetylenedicarboxylate, methyl propiolate, phenylacetylene, propargylic alcohols, HBF_4·OEt_2 and dimethyl diallylmalonate were used as received. Infrared spectra were recorded with a Perkin−Elmer FT-1720-Y spectrometer. C, H and N analyses were carried out with a Perkin−Elmer 240-B microanalyzer (inconsistent analyses are found for complexes **7a−c** due to incomplete combustion). Mass spectra (FAB) were recorded using a VG-Autospec spectrometer, operating in the positive mode; 3-nitrobenzyl alcohol (NBA) was used as the matrix. The conductivities were measured at room temperature, in ca. 10^{-3}·mol·dm^{-3} acetone solutions, with a Jenway PCM3 conductimeter. NMR spectra were recorded with a Bruker DPX-300 or AC-300 instrument operating at 300 MHz (^1H), 121.5 MHz (^{31}P) and 75.4 MHz (^{13}C) or a Bruker AC-200 instrument operating at 200 MHz (^1H), 81.01 MHz (^{31}P) and 50.32 MHz (^{13}C), using $SiMe_4$ or 85% H_3PO_4 as the standard. ^1H, $^{31}P\{^1H\}$ and $^{13}C\{^1H\}$ NMR spectroscopic data for some complexes are presented in Tables 2, 3, 5 and 6.

[RuCl(η^5-C_9H_7){κ^2-*P*,*P*-(*S*)-peap}] (1): A mixture of [RuCl(η^5-C_9H_7)(PPh_3)$_2$] (1 g, 1.29 mmol) and a slight excess of the diphosphazane ligand $(Ph_2P)_2N$[(*S*)-*CHMePh] [(*S*)-peap)] (0.79 g, 1.61 mmol) in 20 mL of toluene was heated under reflux for 8 h. The removal of toluene gave a solid residue which was purified by flash chromatography on silica gel. The triphenylphosphane and the excess diphosphazane were eluted with a mixture of hexane and diethyl ether (10:1), and the red product **1** was eluted with a mixture of dichloromethane and methanol (10:1). The solvent was

evaporated and the dark red oil obtained was recrystallized from diethyl ether, yielding 0.793 g of the red solid **1** (83%). $^{31}P\{^1H\}$ NMR ($CDCl_3$): δ = 83.20 (d), 91.40 (d, $^2J_{P,P'}$ = 112.7 Hz). ^1H NMR ($CDCl_3$): δ = 0.77 (d, $J_{H,H}$ = 7.1 Hz, 3 H, Me), 4.24, 4.27 and 4.48 (s, 1 H each, 1,2,3-H), 4.59 (m, 1 H, *CH), 6.85−7.93 (m, 29 H, PPh_2, *CPh, 4,5,6,7-H). $^{13}C\{^1H\}$ NMR ($CDCl_3$): δ = 21.19 (t, $^3J_{C,P} = {}^3J_{C,P'}$ = 2.2 Hz, Me), 62.21 (t, $^2J_{C,P} = {}^2J_{C,P'}$ = 6.5 Hz, *C), 65.42 (m, C-1 and C-3), 92.56 (s, C-2), 110.07 (m) and 111.51 (d, $^2J_{C,P}$ = 3.6 Hz) (C-3a and C-7a), 123.47, 124.12, 125.29 and 126.11 (s, C-4,5,6,7), 127.00−134.69 (m, PPh_2, *C*Ph*, PC_{ipso}), 137.45−139.41 (m, PC_{ipso}), 141.07 (s, *CC_{ipso}). $C_{41}H_{36}ClNP_2Ru$ (741.22): calcd. C 66.44, H 4.90, N 1.89; found C 66.88, H 5.15, N 1.89.

[RuH(η^5-C_9H_7){κ^2-*P,P*-(*S*)-peap}] (2): An excess of NaOMe (ca. 5:1, prepared in situ from NaH and MeOH) was added to a suspension of **1** (0.74 g, 1 mmol) in MeOH (100 mL). The mixture was heated under reflux for 1 h and the color of the solution changed from red to yellow. The solution was cooled at ambient temperature, the liquid decanted and the yellow-orange solid obtained was washed with methanol (3 × 20 mL) and vacuum-dried to yield 0.60 g of **2** (85%). IR (KBr): $\tilde{\nu}$ = 1992 cm^{-1} [w, ν(Ru−H)]. $^{31}P\{^1H\}$ NMR ($CDCl_3$): δ = 101.22 (d), 101.73 (d, $^2J_{P,P'}$ = 87.6 Hz). ^1H NMR ($CDCl_3$): δ = −14.33 (t, $^2J_{H,P} = {}^2J_{H,P'}$ = 29.8 Hz, Ru−H), 0.58 (d, $J_{H,H}$ = 6.9 Hz, 3 H, Me), 4.24 (m, 1 H, *CH), 5.01, 5.06 and 5.36 (s, 1 H each, 1,2,3-H), 6.27−8.01 (m, 29 H, PPh_2, *CPh, 4,5,6,7-H). $^{13}C\{^1H\}$ NMR (C_6D_6): δ = 21.87 (s, Me), 61.05 (t, $^2J_{C,P} = {}^2J_{C,P'}$ = 6.9 Hz, *C), 66.89 (t, $^2J_{C,P} = {}^2J_{C,P'}$ = 4.6 Hz) and 68.56 (t, $^2J_{C,P} = {}^2J_{C,P'}$ = 4.6 Hz) (C-1 and C-3), 88.43 (s, C-2), 106.29 and 107.69 (s, C-3a and C-7a), 121.97, 122.58, 123.26 and 126.33 (s, C-4,5,6,7), 127.39−135.83 (m, PPh_2, *C*Ph*), 139.05−140.87 (m, PC_{ipso}), 143.11 (s, *CC_{ipso}). $C_{41}H_{37}NP_2Ru$ (706.78): calcd. C 69.67, H 5.28, N 1.98; found C 69.47, H 5.47, N 1.96.

[Ru{(*E*)-C(CO_2Me)=CH(CO_2Me)}(η^5-C_9H_7){κ^2-*P,P*-(*S*)-peap}] (3): A mixture of **2** (0.25 g, 0.35 mmol) and an equimolar amount of dimethyl acetylenedicarboxylate (43 μL, 0.35 mmol) in diethyl ether (40 mL) was heated under reflux for 3 h. The solvent was evaporated and the solid obtained was dried under vacuum, yielding 0.21 g (71%) of **3** as an orange solid. IR (KBr): $\tilde{\nu}$ = 1688 s, 1699 cm^{-1} (s, 2 CO_2Me). $^{31}P\{^1H\}$, ^1H and $^{13}C\{^1H\}$ NMR spectroscopic data are presented in Tables 2 and 3. $C_{47}H_{43}NO_4P_2Ru$ (848.89): C 66.50, H 5.11, N 1.65; found C 65.50, H 5.03, N 1.53.

[Ru{C(CO_2Me)=CH_2}(η^5-C_9H_7){κ^2-*P,P*-(*S*)-peap}] (4): A mixture of **2** (0.25 g, 0.35 mmol) and an excess of methyl propiolate (95 μL, 1.05 mmol) in toluene (40 mL) was heated at 60 °C for 6 h. The solvent was removed under vacuum and the solid obtained was washed with pentane (3 × 10 mL) and dried under reduced pressure to yield 0.183 g (66%) of **4** as an orange solid. MS (FAB): *m*/*z* = 791 [M$^+$], 760 [M$^+$ − OMe], 706 [M$^+$ − R], 629 [M$^+$ − R − Ph], 590 [M$^+$ − R − C_9H_7 − 1]; R: CH_2=C(CO_2Me) (correct isotope patterns observed for each fragment). IR (KBr): $\tilde{\nu}$ = 1675 cm^{-1} (s, CO_2Me). $^{31}P\{^1H\}$, ^1H and $^{13}C\{^1H\}$ NMR spectroscopic data are presented in Tables 2 and 3.

[Ru{(*E*)-CH=CHPh}(η^5-C_9H_7){κ^2-*P,P*-(*S*)-peap}] (5): A mixture of **2** (0.25 g, 0.35 mmol) and a large excess of phenylacetylene (385 μL, 3.5 mmol) in toluene (40 mL) was heated at 110° C for 4 h. The solvent was removed under vacuum and the solid obtained was washed with pentane (3 × 10 mL) and dried under reduced pressure to yield 0.207 g (73%) of **5** as an orange solid. $C_{49}H_{43}NP_2Ru$ (808.91): calcd. C 72.76, H 5.36, N 1.73; found C 72.52, H 5.44, N 1.46. $^{31}P\{^1H\}$, ^1H and $^{13}C\{^1H\}$ NMR spectroscopic data are presented in Tables 2 and 3.

Complexes 6a−d: A solution of **2** (0.25 g, 0.35 mmol) and an excess of the corresponding propargylic alcohol (3.5 mmol) in toluene (40 mL) was heated at 100 °C for 3 h. The solvent was evaporated to dryness and the resulting red-orange solid was washed with pentane (3 × 20 mL) and dried under vacuum to give **6a−d**. NMR spectroscopic data are presented in Tables 2 and 3. Yield, analytical data and mass spectrum (FAB, correct isotope patterns observed for each fragment) are as follows. **6a:** 71%. $C_{48}H_{45}NP_2Ru$ (798.92): calcd. C 72.16, H 5.68, N 1.75; found C 71.72, H 5.66, N 1.65. **6b:** 69%. $C_{49}H_{47}NP_2Ru$ (812.94): calcd. C 72.39, H 5.83, N 1.72; found C 70.66, H 6.10, N 1.33. *m*/*z* = 813 [M$^+$], 706 [M$^+$ − C_8H_{11}], 590 [M$^+$ − C_8H_{11} − C_9H_7 − 1], 401 [M$^+$ − C_8H_{11} − (*S*)-peap]. **6c:** 73%. $C_{50}H_{49}NP_2Ru$ (826.97): calcd. C 72.62, H 5.97, N 1.69; found C 71.29, H 6.33, N 1.31. *m*/*z* = 827 [M$^+$], 706 [M$^+$ − C_9H_{13}], 590 [M$^+$ − C_9H_{13} − C_9H_7 − 1], 401 [M$^+$ − C_9H_{13} − (*S*)-peap]. **6d:** 74%. $C_{51}H_{51}NP_2Ru$ (841.00): calcd. C 72.84, H 6.11, N 1.66; found C 71.81, H 6.08, N 1.46.

Complexes 7a−c: A dilute solution of HBF_4 in diethyl ether (0.13 mmol) was added dropwise to a stirred solution of the corresponding vinylalkenyl complex (**6a**, **c**, **d**; 0.12 mmol) in 20 mL of diethyl ether, cooled at − 40 °C. Immediately, an orange solid precipitated. The liquid was decanted and the solid washed with diethyl ether (3 × 20 mL) and vacuum-dried. NMR spectroscopic data are presented in Tables 5 and 6. Yield, IR (KBr), conductivity (acetone, 20 °C) and mass spectrum (FAB, correct isotope patterns observed for each fragment) are as follows: **7a:** 87%. $\tilde{\nu}$ = 1062 cm^{-1} [b, s, ν(BF_4^-)]. 134 Ω^{-1}cm^2 mol^{-1}. *m*/*z* = 800 [M$^+$], 706 [M$^+$ − C_7H_{10}]. **7b:** 90%. $\tilde{\nu}$ = 1063 cm^{-1} [b, s, ν(BF_4^-)]. 128 Ω^{-1}cm^2 mol^{-1}. *m*/*z* = 828 [M$^+$], 706 [M$^+$ − C_9H_{14}], 401 [M$^+$ −C_9H_{14} − (*S*)-peap]. **7c:** 92%. $\tilde{\nu}$ = 1060 cm^{-1} [b, s, ν(BF_4^-)]. 117 Ω^{-1}cm^2 mol^{-1}. *m*/*z* = 842 [M$^+$], 706 [M$^+$ − $C_{10}H_{16}$].

Procedure for Ring-Closing Metathesis of Diethyl Diallylmalonate: Solutions of the complexes **7a−c**, **8** or **9** (5 μmol) and diethyl diallylmalonate (0.1 mmol, 24 μL) in CD_2Cl_2 (0.4 mL) were combined in a sealed tube. The reaction mixtures were stirred at room temperature and under more drastic conditions (heating the solutions until 100 °C in an oil bath) for 24 h. The development of the reactions was monitored by ^1H NMR spectroscopy. The diene signals appeared intact in the spectra. In addition, CuCl (10 equiv. based on **7c**) was added to a solution of complex **7c** as a co-catalyst under similar reaction conditions, but we have found that the mixture of alkylidene/CuCl is inactive for olefin metathesis.

X-ray Crystallographic Study of 2 and 3: Data were collected with a Nonius CAD4 single-crystal diffractometer. The intensities were measured using the ω-2θ scan technique with a scan angle of 1.5° intensity of the primary and a variable scan rate with a maximum scan time of 60 s per reflection. The beam was checked throughout the collection by monitoring three standard reflections every 60 min. Profile analysis was performed on all reflections.[28] Some double measured reflections were averaged and Lorentz and polarization corrections were applied. The structures were solved by Patterson interpretation and phase expansion using DIRDIF.[29] Isotropic least-squares refinement on F^2 using SHELXL97.[30] During the final stages of the refinements, all positional parameters and the anisotropic temperature factors of all the non-H atoms were refined. The H atoms were geometrically located and riding with common isotropic thermal parameters, except the hydride H atom (H100) in complex **2** which was located by Fourier difference synthesis and isotropically refined. The function minimized was $([\Sigma w F_o^2 - F_c^2)/\Sigma w(F_o^2)]^{1/2}$ where $w = 1/[\sigma^2(F_o^2) + (nP)^2]$ (n = 0.0337 for **2** and n = 0.0467 for **3**) with $\sigma(F_o^2)$ from counting statistics and $P = [\mathrm{Max}(F_o^2,0) + 2F_c^2]/3$. Atomic scattering factors were taken

Table 7. Crystallographic data for complexes **2** and **3**

	2	**3**
Empirical formula	$C_{41}H_{37}NP_2Ru$	$C_{47}H_{43}NO_4P_2Ru$
a [Å]	12.595(5)	10.907(4)
b [Å]	13.576(3)	18.091(2)
c [Å]	19.319(5)	20.77(12)
Formula mass	706.73	848.83
Z	4	4
V [Å^3]	3303.5(17)	4098(23)
$D_{calcd.}$ [g cm^{-3}]	1.421	1.376
Wavelength [Å]	0.71073	0.71073
Temperature [K]	293(2)	293(2)
Radiation	Mo-K_α	Mo-K_α
Space group	$P2_12_12_1$	$P2_12_12_1$
Crystal system	orthorhombic	orthorhombic
Crystal size [mm]	0.46 × 0.23 × 0.13	0.36 × 0.26 × 0.1
μ [mm^{-1}]	0.602	0.505
F(000)	1456	1752
Diffraction geometry	ω-2θ	ω-2θ
θ range [°]	1.83−25.98	1.49−25.97
Index ranges for data collection	$0 \le h \le 15$	$0 \le h \le 13$
	$0 \le k \le 16$	$0 \le k \le 22$
	$0 \le l \le 23$	$0 \le l \le 25$
S	1.014	1.006
Reflections collected	3626	4435
Independent reflections	3626	4434 [*R*(int) = 0.0528]
Final *R* factors [$I > 2\sigma(I)$]	$R_1 = 0.0445$, $\omega R_2 = 0.0802$	$R_1 = 0.0461$, $\omega R_2 = 0.0934$
R indices (all data)	$R_1 = 0.1920$, $\omega R_2 = 0.1165$	$R_1 = 0.2048$, $\omega R_2 = 0.1318$

from International Tables for X-ray Crystallography.[31] Plots were made with the EUCLID package.[32] Geometrical calculations were made with PARST.[33] All calculations were made at the Scientific Computer Centre of the University of Oviedo and with the X-ray group computers. Selected crystal and refinement data are presented in Table 7. The unit-cell dimensions were determined from the angular settings of 25 reflections in the range $6° \le \theta \le 10°$ for **2**, and in the range $10° \le \theta \le 15°$ for **3**. CCDC-174083 (**2**) and -174084 (**3**) contain the supplementary crystallographic data for this paper. These data can be obtained free of charge at www.ccdc.cam.ac.uk/conts/retrieving.html or from the Cambridge Crystallographic Data Centre, 12 Union Road, Cambridge CB2 1EZ, UK [Fax: (internat.) + 44-1223/336-033; E-mail: deposit@ccdc.cam.ac.uk].

Acknowledgments

This work was supported by the Dirección General de Investigación Científica y Técnica of Spain (DGICYT, Project PB96−0558) and the EU (Human Capital Mobility Program, Project ERBCHRXCT 940501). K. B. and M. P. thank the EU and the "European Tempus Program" for a postdoctoral grant and a fellowship, respectively.

[1] [1a] S. T. Nguyen, L. K. Johnson, R. H. Grubbs, J. W. Ziller, *J. Am. Chem. Soc.* **1992**, *114*, 3974−3975. [1b] S. T. Nguyen, R. H. Grubbs, J. W. Ziller, *J. Am. Chem. Soc.* **1993**, *115*, 9858−9859. [1c] P. Schwab, R. H. Grubbs, J. W. Ziller, *J. Am. Chem. Soc.* **1996**, *118*, 100−110.

[2] For a recent review see: [2a] A. Fürstner, *Angew. Chem. Int. Ed.* **2000**, *39*, 3012−3043. [2b] T. M. Trnka, R. H. Grubbs, *Acc. Chem. Res.* **2001**, *34*, 18−29.

[3] [3a] P. A. van der Schaaf, R. Kolly, A. Hafner, *Chem. Commun.* **2000**, 1045−1046 and references therein. [3b] M. Gandelman, B. Rybtchinski, N. Ashkenazi, R. M. Gauvin, D. Milstein, *J. Am. Chem. Soc.* **2001**, *123*, 5372−5373.

[4] [4a] C. Grünwald, O. Gevert, J. Wolf, P. González-Herrero, H. Werner, *Organometallics* **1996**, *15*, 1960−1962. [4b] J. Wolf, W. Stüer, C. Grünwald, H. Werner, P. Schwab, M. Schulz, *Angew. Chem. Int. Ed.* **1998**, *37*, 1124−1126.

[5] E. L. Dias, S. T. Nguyen, R. H. Grubbs, *J. Am. Chem. Soc.* **1997**, *119*, 3887−3897.

[6] Z. Wu, S. T. Nguyen, R. H. Grubbs, J. W. Ziller, *J. Am. Chem. Soc.* **1995**, *117*, 5503−5511.

[7] T. R. Belderrain, R. H. Grubbs, *Organometallics* **1997**, *16*, 4001−4003.

[8] T. E. Wilhelm, T. R. Belderrain, S. N. Brown, R. H. Grubbs, *Organometallics* **1997**, *16*, 3867−3869.

[9] [9a] S. M. Hansen, M. O. Volland, F. Rominger, F. Eisenträger, P. Hofmann, *Angew. Chem. Int. Ed.* **1999**, *38*, 1273−1276. [9b] S. M. Hansen, F. Rominger, M. Metz, P. Hofmann, *Chem. Eur. J.* **1999**, *5*, 557−566.

[10] L. Jafarpour, H.-J. Schanz, E. D. Stevens, S. P. Nolan, *Organometallics* **1999**, *18*, 5416−5419.

[11] M. P. Gamasa, J. Gimeno, B. M. Martín-Vaca, *Organometallics* **1998**, *17*, 3707−3715.

[12] K. J. Harlow, A. F. Hill, T. Welton, *J. Chem. Soc., Dalton Trans.* **1999**, 1911−1912.

[13] M. I. Bruce, M. G. Humphrey, A. G. Swincer, R. C. Wallis, *Aust. J. Chem.* **1984**, *37*, 1747.

[14] V. Cadierno, J. Díez, M. P. Gamasa, J. Gimeno, E. Lastra, *Coord. Chem. Rev.* **1999**, *193−195*, 147−205.

[15] R. P. K. Babu, S. S. Krishnamurthy, M. Nethaji, *Tetrahedron: Asymmetry* **1995**, *6*, 427−438.
[16] M. Y. Hung, S. M. Ng, Z. Zhou; P. Lau, G. Jia, *Organometallics* **2000**, *19*, 3692−3699.
[17] M. Bassetti, P. Casellato, M. P. Gamasa, J. Gimeno, C. González-Bernardo, B. Martín-Vaca, *Organometallics* **1997**, *16*, 5470−5477.
[18] M. I. Bruce, A. Catlow, M. G. Humphrey, G. A. Koutsantonis, M. R. Snow, E. R. T. Tiekink, *J. Organomet. Chem.* **1988**, *338*, 59−80.
[19] Y. Shvo, I. Goldberg, D. Czerkie, D. Reshef, Z. Stein, *Organometallics* **1997**, *16*, 133−138.
[20] G. Jia, W. F. Wu, R. C. Y. Yeung, H. Xia, *J. Organomet. Chem.* **1997**, *538*, 31−40.
[21] M. A. Esteruelas, F. J. Lahoz, E. Oñate, L. A. Oro, B. Zeier, *Organometallics* **1994**, *13*, 4258−4265.
[22] M. A. Esteruelas, F. Liu, E. Oñate, E. Sola, B. Zeier, *Organometallics* **1997**, *16*, 2919−2928.
[23] N. M. Kostic, R. F. Fenske, *Organometallics* **1982**, *1*, 974−982.
[24] M. S. Sanford, H. Henling, R. H. Grubbs, *Organometallics* **1995**, *17*, 5384−5389.
[25] Complexes **7c** and **8** have also shown no catalytic activity in the polymerization of norbornene (reflux in CH_2Cl_2; 10 h).
[26] M. P. Gamasa, J. Gimeno, C. Gonzalez-Bernardo, B. M. Martín-Vaca, D. Monti, M. Bassetti, *Organometallics* **1996**, *15*, 302−308.
[27] L. A. Oro, M. A. Ciriano, M. Campo, C. Foces-Foces, F. H. J. Cano, *J. Organomet. Chem.* **1985**, *289*, 117−131.
[28] [28a] M. S. Lehman, F. K. Larsen, *Acta Crystallogr., Sect. A* **1974**, *30*, 580−584. [28b] D. F. Grant, E. J. Gabe, *J. Appl. Crystallogr.* **1978**, *11*, 114−120.
[29] P. T. Beurskens, G. Admiraal, G. Beurskens, W. P. Bosman, S. García-Granda, R. O. Gould, J. M. M. Smits, C. Smykalla, *The DIRDIF Program System; Techical Report of the Crystallographic Laboratory*; University of Nijimegen: Nijimegen, The Netherlands, **1992**.
[30] G. M. Sheldrick, *SHELXL-97, Program for the Refinement of Crystal Structures*, University of Göttingen, **1997**.
[31] *International Tables for X-ray Crystallography*, Kynoch Press, Birmingham, present distributor: Kluwer Academic Publishers, Dordrecht, **1974**, vol. IV.
[32] A. L. Spek, *PIATON, a multipurpose crystallographic tool*, Utrecht University, Utrecht, The Netherlands, **2000**.
[33] M. Nardelli, *Comput. Chem.* **1983**, *7*, 95−98.

Received November 23, 2001
[I01482]

Optically Active Phospholes: Synthesis and Use as Chiral Precursors for Phosphinidene and Phosphaferrocene Complexes

Xavier Sava,[a] Angela Marinetti,*[b] Louis Ricard,[a] and François Mathey*[a]

Keywords: Phosphorus heterocycles / Asymmetric catalysis / P ligands / Phosphinidene complexes / Chiral phospholes / Phosphaferrocenes

Phospholes bearing chiral menthyl, myrtanyl, and (4-isopropyloxazolino)phenyl groups at the phosphorus atom were prepared. They were used as precursors for 7-phosphanorbornadienes and phosphinidene complexes. Unexpectedly, the [(4-isopropyloxazolino)phenyl]phosphinidene gave an intramolecular adduct with the imine moiety, which behaved as a 1,3-dipole in cycloaddition reactions. This afforded a new, general approach to 7-aza-1-phosphanorbornadiene and norbornene derivatives. The (4-isopropyloxazolino)phenyl-substituted phosphole was also used for the synthesis of new chiral phosphaferrocene complexes bearing oxazoline moieties.
(© Wiley-VCH Verlag GmbH, 69451 Weinheim, Germany, 2002)

Introduction

The organic chemistry of phospholes is extremely rich and varied, as has been shown by the work of many groups during the last decades.[1] Besides simple modifications of the phosphole ring substituents, three main transformations giving access to other classes of phosphorus derivatives are known: these are [4+2] cycloaddition reactions at the dienic system, which afford 7-phosphanorbornenes[2,3] or 7-phosphanorbornadiene[4] derivatives; [1,5] sigmatropic shifts of the aryl, vinyl, or other labile phosphorus substituents around the phosphole nucleus, which lead to 1-phosphanorbornadienes;[5] and finally, the reactivity of either phospholes themselves or phospholyl anions towards suitable transition metal derivatives, which affords an easy access to phosphacyclopentadienyl complexes and phosphametallocenes.[6,7]

Despite the wide synthetic potential of phosphole chemistry, the use of chiral species as synthetic tools has barely been considered. A few optically active phospholes, mainly dibenzophosphole derivatives, have been applied as chiral auxiliaries in transition metal promoted reactions.[8] Recent reports from T. Hayashi disclose the synthesis of enantiomerically pure 2,5-dimenthyl-1-phenylphosphole and its use for the preparation of phosphaferrocene, phosphacymantrene, and diphosphole derivatives.[9]

[a] Laboratoire Hétéroéléments et Coordination, Ecole Polytechnique
91128 Palaiseau Cedex, France
[b] Laboratoire de Synthèse Sélective Organique et Produits Naturels, ENSCP
11, rue Pierre et Marie Curie, 75231 Paris Cedex, France
Fax: (internat.) + 33-1/44071062
E-mail: marinet@ext.jussieu.fr

According to an analogous strategy, i.e. taking advantage from the reactivity of nonracemic phospholes to prepare chiral phosphanes with nonconventional structures and potential interest in catalysis, we started the work presented herein. This includes the synthesis of some new chiral phospholes and their use as precursors for phosphirenes, phosphaferrocenes, and new azaphosphanorbornadiene derivatives.

Results and Discussion

Synthesis of Chiral Phospholes

Chirality in phospholes could be provided by optically pure substituents on either the carbon or the phosphorus atoms. The phosphole ring itself has a low phosphorus inversion barrier (ca. 16 kcal/mol), so it racemizes at room temperature. From a synthetic point of view, the most attractive compounds seem to be phospholes bearing a chiral group on the phosphorus atom, whose easy preparation from phospholyl anions and chiral electrophiles contrasts with the restricted availability of optically active diene moieties.

In this work, two kinds of chiral auxiliaries were considered as phosphorus substituents: alkyl groups derived from chiral pool terpene alcohols (menthol and myrtanol), and valine-derived phenyloxazoline moieties. Both terpene alcohols and amino acids can be conveniently used as stoichiometric chiral auxiliaries because of their large-scale availability.

Chiral phospholes are obtained from 3,4-dimethyl-1-phenylphosphole (**1**)[10] via the corresponding phospholyl anion by substitution on the phosphorus atom, as shown

in Scheme 1. After cleavage of the phosphorus−phenyl bond of **1** with lithium, the phospholyl anion **2** gives nucleophilic substitution reaction on the mesylate of (−)-menthol to afford the *P*-neomenthyl-substituted phosphole **3a**.

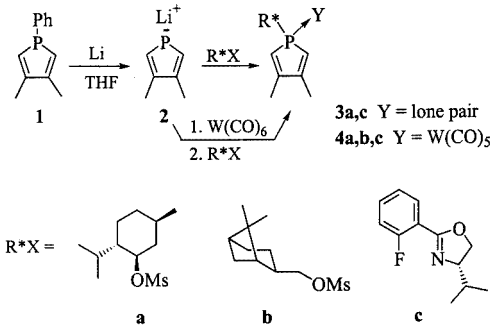

Scheme 1. Synthesis of chiral phospholes

The analogous reaction between the phospholyl anion and the mesylate of (1*S*)-myrtanol[11,12] afforded the corresponding, highly air-sensitive *P*-myrtanylphosphole compound. It was isolated only as its $W(CO)_5$ complex **4b**.

Reaction of **2** with the (−)-(*S*)-2-(2-fluorophenyl)-4-isopropyloxazoline gave the air-stable phosphole **3c** in good yield (61%). The (fluorophenyl)oxazoline has already been used as an electrophile in the analogous *P*-arylation of a dibenzophospholyl anion.[8e]

The optically active phospholes **3a** and **3c** provide new chiral ligands for transition metal promoted asymmetric catalysis. Their potential applications are likely to be those where other phospholes have already been used successfully: for example hydroformylation, hydrogenation, and carbonylation reactions. Moreover, phosphole **3c** should find applications in a number of catalytic reactions usually promoted by phosphanyloxazoline ligands.[13] As a very preliminary test, we checked the effectiveness of phosphole **3c** as chiral ligand in the palladium-catalyzed substitution of 1,3-diphenylpropenyl acetate with sodium malonate under standard conditions. As expected, the observed catalytic activity, as well as the enantioselectivity, is quite satisfactory (Scheme 2).

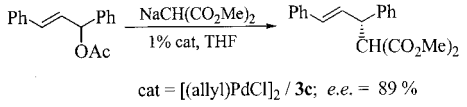

Scheme 2. Palladium-catalyzed allylic substitution

Exhaustive catalytic screening of phospholes **3** lies beyond the scope of this work and will be reported later. Indeed, the main purpose of this work was to check the use of phospholes **3** as chiral intermediates for the synthesis of new phosphorus derivatives through either Diels−Alder cycloaddition reactions on the dienic system or [1,5] sigmatropic shifts of the aryl moiety of **3c**. Results are given hereafter.

Synthesis of (7-Phosphanorbornadiene)$W(CO)_5$ Complexes − Generation of Chiral Phosphinidenes

(7-Phosphanorbornadiene)$W(CO)_5$ complexes are easily accessible from the corresponding phosphole complexes by Diels−Alder cycloadditions with activated alkynes.[4] These compounds were mainly used as synthetic precursors for terminal phosphinidene complexes, which are highly reactive intermediates with carbene-like behavior.[14,15] For instance, addition of (phosphinidene)$M(CO)_5$ complexes to olefins and alkynes leads to the corresponding phosphirane and phosphirene complexes, respectively. When the phosphinidene phosphorus atom bears an optically pure substituent, chiral induction can be expected in its addition to unsymmetrical olefins and acetylenes. To verify this theory, we examined the preparation of the 7-phosphanorbornadiene complexes **5**, as well as their thermolysis and the subsequent phosphinidene trapping reactions, as shown in Schemes 3 and 4.

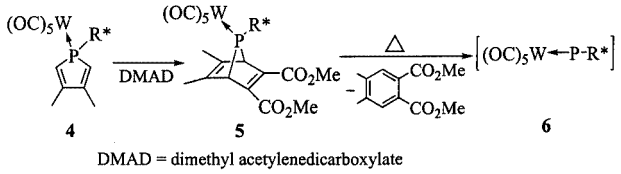

Scheme 3. Generation of phosphinidene complexes

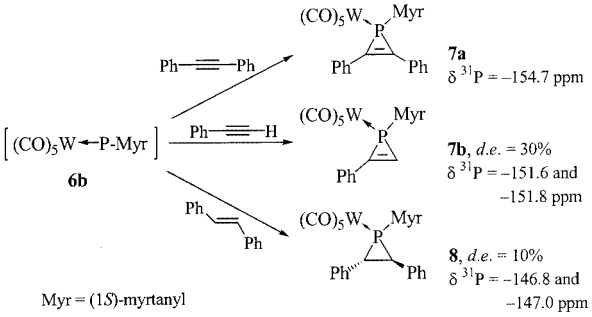

Scheme 4. Trapping reactions of transient phosphinidene complexes

The phosphole complexes **4a−c** could be obtained by treating the preformed phospholes **3** with the (THF)$W(CO)_5$ complex. For the air-sensitive phosphole **3b**, the most convenient procedure[16] included complexation of the phospholyl anion, followed by reaction of the phospholyltungsten complex with myrtanyl mesylate to give **4b** (see Exp. Sect.).

The course of the reaction between **4** and DMAD was largely dependent on the nature of the phosphorus substituent R*. When R* = neomenthyl, the Diels−Alder cycloaddition was prevented by the steric hindrance of the phosphorus substituent. When R* = myrtanyl, the steric hindrance around the phosphorus atom was greatly reduced and the Diels−Alder reaction with DMAD leads to the expected 7-phosphanorbornadiene **5b**, which was isolated and fully characterized.

The generation and trapping of the pentacarbonyl(*P*-myrtanylphosphinidene)tungsten complex from **5b** was checked in small-scale experiments by ^{31}P NMR spectroscopy on crude reaction mixtures (Scheme 4). Diphenylacetylene, phenylacetylene, and *trans*-stilbene were used as trapping reagents because, in such cases, the anticipated complexed phosphirene and phosphirane products should give very characteristic ^{31}P NMR signals at high-field shifts.[14,17]

These experiments show that thermolysis of **5b** under the usual experimental conditions,[14,17] affords the pentacarbonyl(*P*-myrtanylphosphinidene)tungsten complex **6b**, which displays the expected electrophilic behavior toward olefins and alkynes. Phosphirane and phosphirene complexes are obtained as the only reaction products, by [2+1] cycloaddition reactions.

In the case of unsymmetrical alkynes and olefins, chiral induction from the optically active myrtanyl substituent should give diastereoselective addition reactions. Unfortunately, mixtures of diastereomers, with rather poor diastereomeric excesses, are obtained upon cycloaddition of **6b** with phenylacetylene and *trans*-stilbene, leading to **7b** and **8**, respectively. To be stereoselective, the reaction with phenylacetylene requires diastereoselective formation of a chiral phosphorus center, while the diastereoselective addition of **6b** on *trans*-stilbene requires enantiofacial selectivity. The low efficiency of the myrtanyl group as chiral auxiliary in both these reactions is probably due to the presence of the flexible CH_2 spacer between the phosphorus atom and the chiral centers of the myrtanyl moiety. The diastereoselectivity is likely to be improved by using chiral auxiliaries bearing stereogenic centers closer to the phosphorus atom.[18]

Finally, trapping reactions of the *P*-myrtanylphosphinidene **6b** should give a convenient access to optically pure phosphirane[19] and phosphirene derivatives, but only when symmetrically substituted unsaturated substrates are used, as shown by the synthesis of **7a**. Otherwise, separation of the diastereomeric mixtures would be required.

Given that several procedures are known for removing phosphirenes and phosphiranes from their pentacarbonyltungsten or -molybdenum complexes,[20−22] reactions in Scheme 4 should represent new potential sources of chiral ligands for enantioselective catalysis.

In the reaction of the phosphole complex **4c** {R* = 2-[(*S*)-4-isopropyloxazolino]phenyl} with DMAD, the expected 7-phosphanorbornadiene derivative **5c** was not detected. Nevertheless, a clean reaction occurred to give a new phosphorus derivative as a mixture of two isomers. Spectroscopic data and NMR analysis of the crude reaction mixture showed formation of dimethyl phthalate. This suggests that the Diels−Alder reaction took place as expected, but that the 7-phosphanorbornadiene complex decomposed instantaneously to generate the corresponding phosphinidene **6c** (Scheme 3). The excess DMAD was suspected to be the trapping reagent for the intermediate phosphinidene.

This hypothesis is supported by spectroscopic analysis of the pure final product, which was in agreement with the bicyclic structure **9** shown in Scheme 5. Nevertheless, an unambiguous assignment was prevented by the presence of the two inseparable isomers **9a** and **9b**, in a 4:1 ratio.

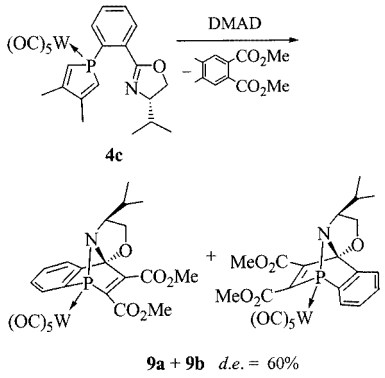

Scheme 5. Reaction of the {3,4-dimethyl-1-[2-(4-isopropyl-4,5-dihydro-1,3-oxazol-2-yl)phenyl]phosphole}$W(CO)_5$ complex **4c** with dimethyl acetylenedicarboxylate

To confirm the structural assignment, we decided to perform the same reaction starting from the achiral (oxazolylphenyl)phosphole complex **4d**, which should lead to a single isomer of the final product and thus facilitate its purification and characterization (Scheme 6).

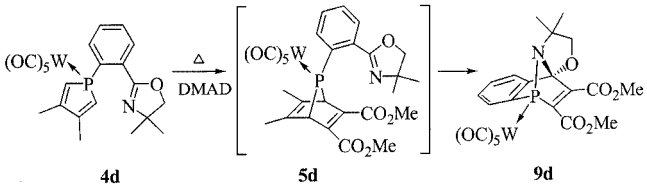

Scheme 6. Reaction of the {3,4-dimethyl-1-[2-(4,4-dimethyl-4,5-dihydro-1,3-oxazol-2-yl)phenyl]phosphole}$W(CO)_5$ complex **4d** with dimethyl acetylenedicarboxylate

The expected reaction between the phosphole complex **4d** and DMAD led to the 7-aza-1-phosphanorbornadiene **9d**, which was easily isolated and fully characterized. An X-ray diffraction study of **9d** confirmed the proposed structure (Figure 1).

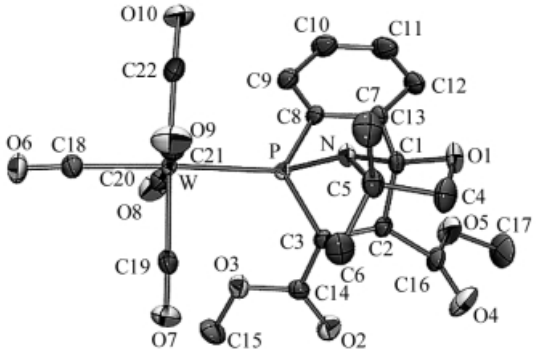

Figure 1. ORTEP diagram for complex **9d**; selected bond lengths [Å]: W−P 2.4495(7), P−N 1.707(2), P−C(8) 1.845(3), P−C(3) 1.890(3), N−C(1) 1.474(3); selected bond angles [°]: P−W−C(18) 172.13(9), C(3)−P−C(8) 94.4(1), P−N−C(1) 100.0(2), C(1)−N−C(5) 106.9(2), O(1)−C(1)−N 106.1(2)

To date, only one example of a 7-aza-1-phosphanorbornadiene has been reported,[23] which was obtained by trapping a (pentamethylcyclopentadienyl)phosphinidene complex with a nitrile. The first formed adduct rearranges through a [4+2] cycloaddition to give the norbornadiene.

In the reactions of Schemes 5 and 6, formation of the 7-aza-1-phosphanorbornadiene complexes **9** can be explained as follows. The [4+2] cycloaddition between **4c** (or **4d**) and excess DMAD gives the 7-phosphanorbornadiene complex **5c** (or **5d**), which instantaneously generates the corresponding phosphinidene complex. The easy decomposition of these 7-phosphanorbornadiene complexes can be explained by the intramolecular interaction between the phosphorus atom and the nitrogen lone pair of the oxazoline moiety, as it has already been shown that amines and strongly basic phosphanes catalyze such reactions.[24] The phosphinidene complex is thus generated as an adduct between the imine nitrogen atom and the electron-deficient phosphorus atom, which can be described by the two resonance structures **I** and **II** in Scheme 7.

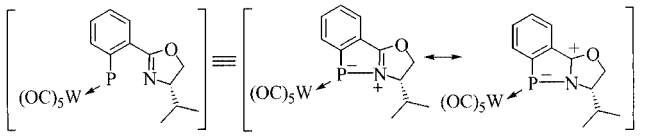

Scheme 7. {*P*-[2-(4-Isopropyl-4,5-dihydro-1,3-oxazol-2-yl)phenyl]-phosphinidene}$W(CO)_5$ complex **6c**

Structure **II** clearly emphasizes the 1,3-dipolar nature of the adduct and explains its [3+2] cycloaddition with DMAD leading to **9**. The reaction intermediate of Scheme 7, can be considered as a phosphaazomethine ylide.

As far as we know, phosphinidene−imine adducts have never been described before. However, other P/N adducts are known. A pyrazolyl−phosphinidene complex has been reported by Cowley. In this case, the coordination of the nitrogen lone pair substantially reduced the electrophilicity of the phosphinidene, thus permitting its isolation.[25] Phosphinidene−nitrile adducts have been generated as reactive intermediates and their reactivity in 1,3-dipolar cycloadditions has been studied by Streubel.[26−28]

Azomethine ylides,[29] as well as (iminomethylene)phosphoranes and analogs[30] were found to be useful as synthetic building blocks through [3+2] cycloadditions. Thus, the use of the phosphaazomethine ylides above as synthetic tools can be envisaged.

Results given in Schemes 5 and 6 point out the strongly nucleophilic behavior of the (2-oxazolylphenyl)phosphinidene complexes, which contrasts with that of simple alkyl- or aryl-substituted pentacarbonyl(phosphinidene)tungsten complexes. Further experiments showed that the [3+2] cycloaddition with DMAD took place preferentially even in the presence of excess diphenylacetylene, an usually efficient phosphinidene trapping reagent.

Preliminary tests (^{31}P NMR analysis of crude reaction mixtures) show that electron-deficient olefins and alkynes other than DMAD can be used as trapping reagents (Scheme 8). In the presence of methyl acrylate (or ethyl phenylpropionate), diastereomeric mixtures of the bicyclic derivatives **10a** (or **10b**) were obtained. However, complex **9** is still formed in some amount (**10/9** ≈ 80:20), even when a threefold excess of the trapping reagent was used, showing that DMAD competes well with the other reagents. The whole reaction sequence can be improved by using ethyl phenylpropionate as the only cycloaddition partner for both the Diels−Alder reaction on phosphole **4d** and the phosphinidene trapping. Under such conditions, the crude reaction mixture contains complex **10** as the major product.

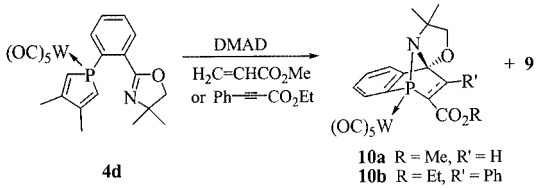

Scheme 8. Reactivity of the {3,4-dimethyl-1-[2-(4,4-dimethyl-4,5-dihydro-1,3-oxazol-2-yl)phenyl]phosphole}$W(CO)_5$ complex **4d**

To summarize, the cycloaddition reactions shown in Schemes 6 and 8 demonstrate the generation of new phosphinidene intermediates, which display an unprecedented 1,3-dipolar behavior. Their reactivity allows the synthesis of new tricyclic 7-aza-1-phosphanorbornadiene derivatives.

Application of such reactions to the preparation of new optically pure ligands for transition metal catalysis should be possible, provided that the separation of the diastereoisomers of **9** (or **10**) and the removal of the azaphosphanorbornadienes from their tungsten complexes could be performed. Although 7-aza-1-phosphanorbornadienes are new compounds whose catalytic properties are difficult to predict, the use of 1-phosphanorbornadienes as auxiliaries in transition metal catalysis, including asymmetric catalysis, is already well documented.[31]

Studies on the synthetic applications of the 1,3-dipolar cycloadditions above are in progress.

Synthesis of Chiral Phosphaferrocene Derivatives

Phosphaferrocenes[32] are usually obtained from phospholes by two different procedures: 1) lithium-induced cleavage of the phosphorus substituent and reaction of the phospholyl anion with either iron halides[33,34] or arene(cyclopentadienyl)iron derivatives;[35] and 2) thermal [1,5] sigmatropic shift of the phosphorus substituent and subsequent trapping of the intermediate 2*H*-phosphole by suitable iron complexes.[36,37] The second approach was selected for the synthesis of phosphaferrocenes starting from phosphole **4c** and $[CpFe(CO)_2]_2$ (Scheme 9).

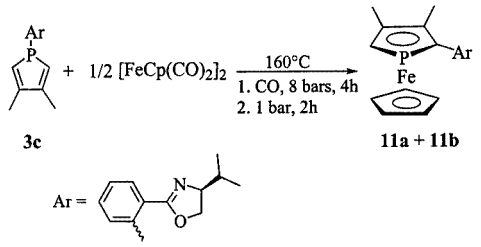

Scheme 9. Synthesis of the phosphaferrocene derivatives **11**

Under the usual reaction conditions, the aryl group of **4c** underwent a [1,5] sigmatropic shift, followed by deprotonation of the 2*H*-phosphole and complexation to the cyclopentadienyliron moiety to afford **11** as a mixture of two isomers in a 1:2 ratio and in a moderate yield. The α-substituted phosphaferrocenes display planar chirality, so the formation of two diastereoisomers was expected. Chiral induction from the oxazoline moiety favors one of them, but the diastereoselectivity level is not yet satisfactory.

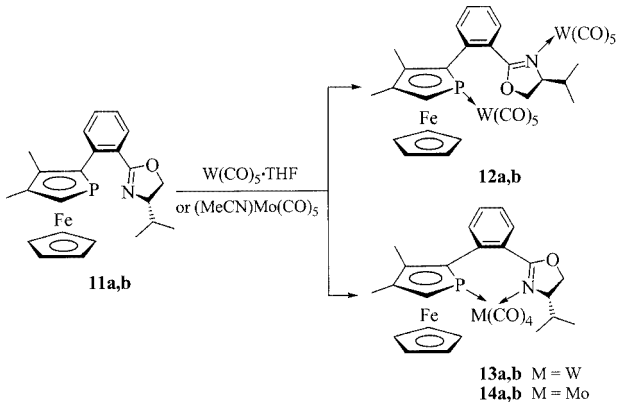

Scheme 10. Tungsten and molybdenum complexes of the phosphaferrocene **11**

Purification of the final products **11** and separation of isomers, proved to be difficult because of their air sensitivity. Thus, complexation of the phosphaferrocenes by pentacarbonyltungsten or -molybdenum was envisaged and furnished stable, easily isolable species (Scheme 10).

The main product obtained by reaction of **11** with an excess of the tungsten complex $(THF)W(CO)_5$, was the dimetallic complex **12**, where both the phosphorus and nitrogen atoms are complexed by a $W(CO)_5$ group. The major

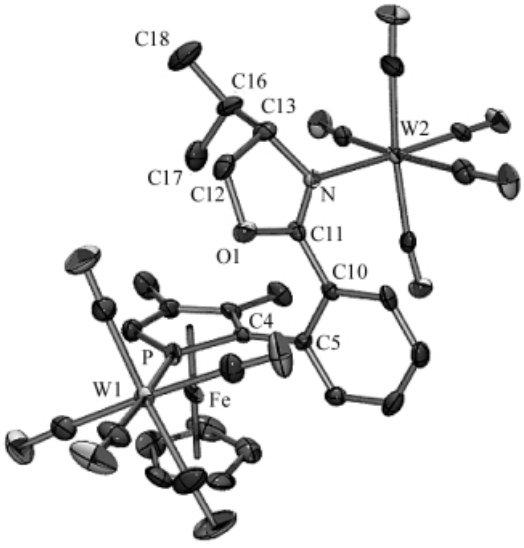

Figure 2. ORTEP diagram for the tungsten complex **12a**; selected bond lengths [Å]: W(1)−P 2.462(2), W(2)−N 2.284(5), Fe−P 2.253(2); selected bond angles [°]: C(1)−P−C(4) 91.8(3), C(11)−N−C(13) 107.7(5), W(2)−N−C(11) 130.0(4), W(2)−N−C(13) 122.2(4)

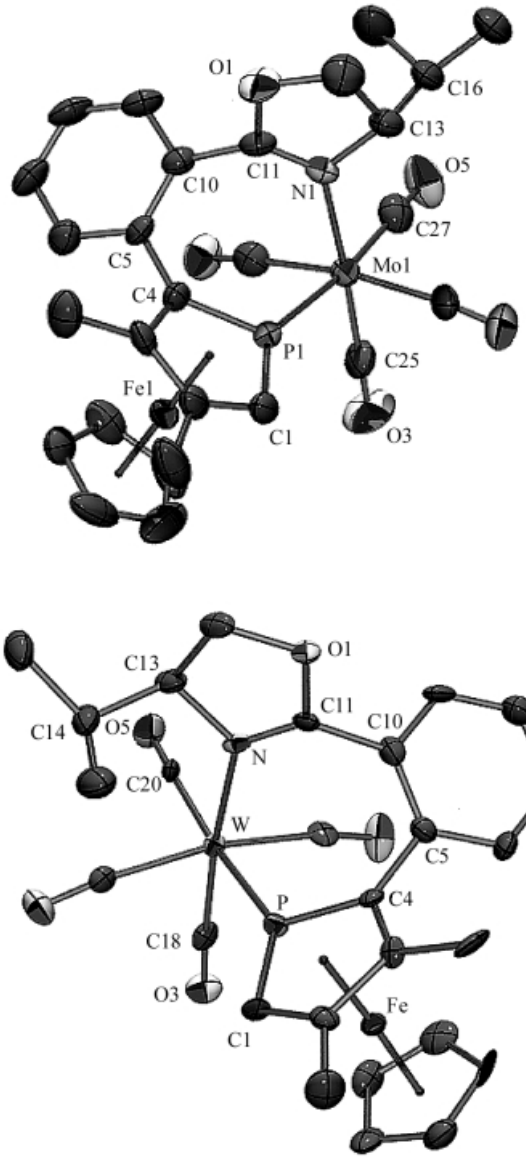

Figure 3. ORTEP diagrams for the molybdenum and tungsten complexes **14a** and **13b**; selected bond lengths [Å]: **14a**: Mo−P 2.475(1), Mo−N 2.277(4), Fe−P 2.240(2); **13b**: W−P 2.425(3), W−N 2.274(8), Fe−P 2.231(3); selected bond angles [°]: **14a**: P−Mo−N 79.4(1), C(1)−P−C(4) 90.6(3), C(11)−N−C(13) 106.9(4), Mo−N−C(11) 130.1(4), Mo−N−C(13) 122.6(3); **13b**: P−W−N 79.5(2), C(1)−P−C(4) 91.9(5), C(11)−N−C(13) 107.7(8), W−N−C(11) 128.4(7), W−N−C(13) 123.8(6)

diastereomer, (*S*,*S*)-**12a** (M = W), was obtained in pure form after crystallization. Its structure was confirmed by X-ray crystallography, as shown in Figure 2.

Minor amounts of the chelate derivative **13** (M = W) were also present in the reaction mixture. Crystals of one diastereomer (**13b**) were isolated and analyzed by X-ray crystallography (Figure 3, bottom). Its absolute configuration was determined as (*S*,*S*).

In the reaction with the molybdenum complex $(THF)Mo(CO)_5$, the P,N-bidentate phosphaferrocene **11** exclusively formed the chelate derivative **14** (M = Mo) as an isomeric mixture. The main isomer was obtained in pure form after crystallization and was characterized by X-ray diffraction studies. The ORTEP drawing for **14a** as well as selected bond angles and distances are given in Figure 3 (top). From the X-ray data, an (*R*,*S*) absolute configuration can be assigned to the isolated complex.

Isolation of complexes **13** and **14** shows that the geometry of the P,N-bidentate ligand **11** is suitable for chelate formation. This is a key feature of the ligand, as far as its use as a chiral auxiliary in catalysis is concerned. The high catalytic efficiency of oxazolines coupled with phosphanylferrocene moieties is well established to date,[38] and the use of phosphaferrocenes in catalysis is a field of growing interest.[39] Thus, ligands **11**, which associates the phosphaferrocene and the oxazoline moieties, should find interesting applications in organometallic asymmetric catalysis. Nevertheless, improvement of the synthetic approach and an efficient separation procedure for the two diastereomers **11a** and **11b** is required.

An alternative synthetic approach to the phosphaferrocenes **11** and other metallocene analogs could be the formation of the corresponding phospholylpotassium derivative after [1,5] shift of the aryl group.[40] The phospholyl anion could be treated with various metal halide complexes under milder conditions, and would hopefully be more diastereoselective in its outcome.

Conclusion

This work shows that phospholes bearing various optically pure substituents at the phosphorus atom are easily accessible species. They can either be applied as chiral auxiliaries in asymmetric transition metal catalysis or used as versatile synthons. As a very preliminary study, we have shown here that chiral phosphinidene complexes and phosphaferrocene derivatives can be obtained from these phospholes. The (oxazolylphenyl)phosphole **3c** seems to be a particularly promising starting material. On one hand, an unprecedented, [1,3]-dipole-like reactivity of the corresponding terminal phosphinidene complex has been demonstrated, and on the other hand, phosphole **3c** underwent a [1,5]-sigmatropic shift of the phosphorus substituent and should allow application of the well-known 2*H*-phosphole chemistry to the asymmetric synthesis of phosphorus derivatives.

Experimental Section

General: All reactions were routinely performed under nitrogen by using Schlenk technique and dry deoxygenated solvents. NMR spectra were obtained at 25 °C with a Bruker AC 200 SY spectrometer operating at 200.13 MHz for ^{1}H, 50.32 MHz for ^{13}C, and 81.01 MHz ^{31}P. Chemical shifts are expressed in ppm downfield from external TMS (^{1}H and ^{13}C) and 85% H_3PO_4 (^{31}P), and coupling constants are given in Hz. Mass spectra were obtained at 70 eV with an HP 5989 B spectrometer coupled with an HP 5890 chromatograph by the direct inlet method. IR spectra were obtained with a Perkin−Elmer 297. Elemental analyses were performed by the Service d'Analyse du CNRS at Gif sur Yvette, France.

1-(2-Isopropyl-5-methylcyclohexyl)-3,4-dimethylphosphole (3a): A solution of lithium 3,4-dimethylphospholide in 30 mL of THF was prepared by treating 3,4-dimethyl-1-phenylphosphole (3 g, 16 mmol) with excess lithium at room temperature. Menthyl mesylate (3.7 g, 16 mmol) was added, and the solution was allowed to reflux for 1 h. After hydrolysis, evaporation of THF, and extraction of the aqueous layer with diethyl ether, the organic phase was dried with $MgSO_4$. The product was purified by chromatography on silica gel with hexanes, affording **3a** as a colorless oil. Yield: 25% (1.0 g). ^{31}P NMR ($CDCl_3$): δ = −3.0. ^{1}H NMR ($CDCl_3$): δ = 0.85 (d, $^3J_{H,H}$ = 6.1 Hz, 3 H, Me), 0.94 (d, ^3J = 6.4 Hz, 3 H, Me), 0.95 (d, ^3J = 6.5 Hz, 3 H, Me), 1.04−1.99 (m, 9 H), 2.08 [s, 3 H, $C(CH_3)$], 2.09 [s, 3 H, $C(CH_3)$], 2.56 (m, 1 H), 6.41 (d, $^2J_{P,H}$ = 36.9 Hz, 2 H, 2-H and 5-H). ^{13}C NMR ($CDCl_3$): δ = 17.75 (Me), 17.81 (Me), 21.2 (Me), 21.5 (Me), 22.7 (Me), 26.5 (d, *J* = 8.7 Hz, CH_2), 28.7 (d, *J* = 6.1 Hz, CH), 31.2 (d, *J* = 7.8 Hz, CH), 36.1 (CH_2), 38.8 (d, *J* = 4.6 Hz, CH), 42.6 (CH_2), 48.8 (d, *J* = 11.6 Hz, CH), 129.1 (CH=), 146.5 (CH=), 146.7 (s, C).

(*S*)-2-[2-(3,4-Dimethyl-1*H*-phosphol-1-yl)phenyl]-4-isopropyl-4,5-dihydro-1,3-oxazole (3c): A mixture of lithium 3,4-dimethylphospholide (96 mmol), prepared from lithium metal and 3,4-dimethyl-1-phenylphosphole (18.0 g, 96 mmol), and (*S*)-2-(2-fluorophenyl)-4-isopropyl-4,5-dihydrooxazole (14.8 g, 72 mmol) in THF was heated at 45 °C for 48 h. After hydrolysis and extraction of the aqueous layer with diethyl ether, the organic phase was dried with $MgSO_4$. After evaporation of the solvent, the residue was purified by chromatography on silica gel with a hexane/ether (95:5) mixture, giving **3c** as a colorless oil. Yield: 61% (13.0 g). ^{31}P NMR ($CDCl_3$): δ = 0.9. ^{1}H NMR ($CDCl_3$): δ = 0.99 [d, *J* = 6.7 Hz, 3 H, $CH(CH_3)_2$], 1.10 [d, *J* = 6.7 Hz, 3 H, $CH(CH_3)_2$], 1.87 [m, *J* = 6.6 Hz, 1 H, $CH(CH_3)_2$], 2.10 (d, $^4J_{P,H}$ = 4.2 Hz, 6 H, CH_3), 4.29 (m, 3 H, CHN and OCH_2), 6.62 (d, $^2J_{P,H}$ = 34.3 Hz, 2 H, P−CH), 7.24−7.31 (m, 2 H, Ar-H), 7.35−7.41 (m, 1 H, Ar-H), 7.79−7.86 (m, 1 H, Ar-H). ^{13}C NMR ($CDCl_3$): δ = 17.8 (d, ^3J = 2.3 Hz, 2 CH_3), 18.7 [$CH(CH_3)_2$], 19.1 [$CH(CH_3)_2$], 33.1 [$CH(CH_3)_2$], 70.4 (OCH_2), 73.5 (CHN), 127.6 (CH), 128.9 (d, *J* = 13.8 Hz, CH), 129.1 (CH), 130.4 (CH), 130.7 (d, ^2J = 18.6 Hz, C), 133.5 (CH), 136.4 (d, ^1J = 21.4 Hz, C), 147.7 (d, ^2J = 9.5 Hz, C), 147.9 (d, ^2J = 10.5 Hz,), 162.8 (C=N). MS: *m*/*z* (%) = 299 (78) [M^+], 230 (100). $C_{18}H_{22}NOP$ (299.35): calcd. C 72.22, H 7.41, N 4.68; found C 71.88, H 7.54, N 4.51. $[\alpha]_D$ = +64 (*c* = 1, toluene).

2-[2-(3,4-Dimethyl-1*H*-phosphol-1-yl)phenyl]-4,4-dimethyl-4,5-dihydro-1,3-oxazole (3d): A mixture of lithium 3,4-dimethylphospholide (48 mmol), prepared from lithium metal and 3,4-dimethyl-1-phenylphosphole (9.0 g, 48 mmol), and 2-(2-fluorophenyl)-4,4-dimethyl-4,5-dihydrooxazole (8.9 g, 46 mmol) in 40 mL of THF was heated at 45 °C for 48 h. After hydrolysis, evaporation of THF, and extraction of the aqueous layer with diethyl ether, the solution was

dried with $MgSO_4$. After concentration, the residue was purified by chromatography on a silica gel column with hexane/ether (95:5) as the eluent. Yield: 70% (9.2 g). ^{31}P NMR ($CDCl_3$): δ = 0.2. ^1H NMR ($CDCl_3$): δ = 1.43 [s, 6 H, $C(CH_3)_2$], 2.09 (dd, $^4J_{P,H}$ = 4.0, ^4J = 0.5 Hz, 6 H, CH_3), 4.13 (s, 2 H, OCH_2), 6.59 (dd, $J_{P,H}$ = 34.6, ^4J = 0.5 Hz, 2 H, P−CH), 7.2−7.3 (m, 3 H, Ar-H), 7.7−7.8 (m, 1 H, Ar-H). ^{13}C NMR ($CDCl_3$): δ = 17.7 (d, ^3J = 2.8 Hz, CH_3), 28.5 [$C(CH_3)_2$], 68.4 [$C(CH_3)_2$], 79.0 (OCH_2), 127.7 (CH-Ar), 128.9 (P−CH), 129.1 (d, ^2J = 4.3 Hz, C), 130.3 (CH-Ar), 131.2 (d, ^2J = 19.6 Hz, C), 133.4 (CH-Ar), 135.1 (d, ^1J = 21.4 Hz, C), 147.9 (d, ^2J = 10.6 Hz), 161.8 (s, C=N).

{1-(2-Isopropyl-5-methylcyclohexyl)-3,4-dimethylphosphole}W-(CO)$_5$ (4a): A solution of hexacarbonyltungsten (1.55 g, 4.4 mmol) in 250 mL of THF was irradiated under UV light for 30 min. To this solution was added a solution of **3a** (1.0 g, 4 mmol) in 10 mL of THF. After 1 h of stirring, the solvent was evaporated. The product was then purified by chromatography on silica gel, with hexane as eluent (R_f = 0.25), affording **4a** as a yellow powder. Yield: 91% (2.1 g). ^{31}P NMR ($CDCl_3$): δ = 11.4 ($^1J_{P,W}$ = 203.2 Hz). ^1H NMR ($CDCl_3$): δ = 0.80 (d, ^3J = 6.0 Hz, 3 H, Me), 0.92 (d, ^3J = 6.0, Hz, 3 H, Me), 0.93 (d, ^3J = 6.1 Hz, 3 H, Me), 1.14−1.80 (m, 8 H), 2.15 (s, 6 H, CH_3), 2.32−2.45 (m, 1 H), 2.77 (s, 1 H), 6.43 (d, $^2J_{P,H}$ = 37.2 Hz, 1 H, PCH), 6.53 (d, $^2J_{P,H}$ = 36.7 Hz, 1 H, PCH). ^{13}C NMR ($CDCl_3$): δ = 17.8 (d, ^3J = 3.4 Hz, Me), 17.1 (d, ^3J = 4.4 Hz, Me), 21.6 (Me), 21.8 (Me), 22.24 (Me), 26.0 (d, J = 2.8 Hz, CH_2), 28.8 (CH), 30.13 (CH), 35.4 (CH_2), 39.8 (d, J = 5.9 Hz, CH_2), 42.1 (d, J = 14.6 Hz, CH), 50.9 (d, J = 6.0 Hz, CH), 131.3 (d, ^1J = 38.1 Hz, PCH), 131.8 (d, ^1J = 35.2 Hz, PCH), 146.3 (d, ^2J = 9.3 Hz, C), 146.5 (d, ^2J = 9.0 Hz, C), 197.0 (d, ^2J = 6.2 Hz, 4 CO_{cis}), 199.3 (d, ^2J = 16.8 Hz, CO_{trans}). MS (EI): m/z (%) = 574 (7) [M^+], 192 (100).

{1-[(6,6-Dimethylbicyclo[3.1.1]hept-2-yl)methyl]-3,4-dimethyl-1*H*-phosphole}W(CO)$_5$ (4b): A mixture of lithium 3,4-dimethylphospholide (56 mmol), prepared from lithium metal and 3,4-dimethyl-1-phenylphosphole (10.5 g, 56 mmol) in 60 mL of THF, and hexacarbonyltungsten (19.7 g, 56 mmol) was stirred for 24 h at room temperature. Then 13.0 g (56 mmol) of myrtanyl mesylate were added and the mixture was stirred again for 48 h. After hydrolysis, the THF was evaporated under vacuum. The residue was extracted with diethyl ether, and the organic layer dried with $MgSO_4$. The product was then purified by chromatography on silica gel with hexane as eluent. Yield: 42% (13.5 g). ^{31}P NMR ($CDCl_3$): δ = 5.8 ($J_{P,W}$ = 206.9 Hz). ^1H NMR ($CDCl_3$): δ = 0.85 (d, J = 12.3 Hz, 1 H), 0.94 [s, 3 H, $C(CH_3)_2$], 1.19 [s, 3 H, $C(CH_3)_2$], 1.2−1.4 (m, 1 H), 1.8−2.1 (m, 8 H), 2.16 (s, 6 H, CH_3), 2.2−2.3 (m, 1 H), 6.28 (d, $^2J_{P,H}$ = 36.7 Hz, 1 H, P-CH), 6.33 (d, $^2J_{P,H}$ = 36.7 Hz, 1 H, P−CH). ^{13}C NMR ($CDCl_3$): δ = 17.1 (Me), 17.3 (Me), 23.3 (CH_3), 23.9 (d, ^3J = 4.7 Hz, CH_2), 26.1 (CH_2), 27.8 (CH_3), 32.9 (CH_2), 38.4 (P−CH_2−*C*H), 38.5 [$C(CH_3)_2$], 38.7 (d, ^1J = 22.9 Hz, P−CH_2), 40.8 (CH), 48.1 (d, ^3J = 10.3 Hz, CH), 129.3 (d, ^1J = 17.0 Hz, P−CH), 130.1 (d, ^1J = 18.1 Hz, P−CH), 149.8 (d, ^2J = 7.8 Hz, C), 150.2 (d, ^2J = 7.8 Hz, C), 196.4 (d, ^2J = 7.2 Hz, 4 CO_{cis}), 199.3 (d, ^2J = 16.7 Hz, CO_{trans}). MS: m/z (%) = 572 (26) [M^+], 407 (100). $C_{21}H_{25}O_5PW$ (572.23): calcd. C 44.08, H 4.40; found C 43.69, H 4.41.

{(*S*)-2-[2-(3,4-Dimethyl-1*H*-phosphol-1-yl)phenyl]-4-isopropyl-4,5-dihydro-1,3-oxazole}W(CO)$_5$ (4c): A solution of hexacarbonyltungsten (0.89 g, 2.5 mmol) in 250 mL of THF was irradiated under UV for 30 min. To this solution was added a solution of **3c** (0.76 g, 2.5 mmol) in 10 mL of THF. After 30 min of stirring, the solvent was evaporated. The product was then purified by chromatography on silica gel with a hexane/diethyl ether gradient (from 24:1 to 9:1) affording **4c** as a yellow powder (R_f = 0.4 in hexane/diethyl ether, 3:2),. Yield: 85% (1.34 g). ^{31}P NMR ($CDCl_3$): δ = 9.2 ($^1J_{P,W}$ = 213 Hz). ^1H NMR ($CDCl_3$): δ = 1.00 [d, J = 6.7 Hz, 3 H, $CH(CH_3)_2$], 1.09 [d, J = 6.7 Hz, 3 H, $CH(CH_3)_2$], 2.08 [m, J = 5.3 Hz, 1 H, $CH(CH_3)_2$], 2.12 (s, 3 H, CH_3), 2.18 (s, 3 H, CH_3), 4.22−4.53 (m, 3 H, CHN and OCH_2), 6.64 (d, $J_{P,H}$ = 33.0 Hz, 1 H, P−CH), 6.90 (d, $J_{P,H}$ = 32.9 Hz, 1 H, P−CH), 7.39−7.45 (m, 2 H, Ar-H), 7.57−7.67 (m, 1 H, Ar-H), 8.0−8.1 (m, 1 H, Ar-H). ^{13}C NMR ($CDCl_3$): δ = 17.1 (d, ^3J = 10.1, Me), 17.3 (d, ^3J = 11.1 Hz, Me), 17.6 [$CH(CH_3)_2$], 19.0 [$CH(CH_3)_2$], 32.3 [$CH(CH_3)_2$], 69.6 (OCH_2), 72.7 (CHN), 129.1 (d, J = 10.5 Hz), 129.6, 129.7, 130.0 (d, J = 6.0 Hz), 130.6, 130.7, 131.8 (d, J = 7.0 Hz), 134.0 (d, ^1J = 35.1 Hz, PCH), 148.9 (d, ^2J = 9.8 Hz, C), 149.1 (d, ^2J = 10.2 Hz, C), 162.1 (C=N), 196.9 (d, ^2J = 7.1 Hz, 4 CO_{cis}), 200.0 (d, ^2J = 18.5 Hz, CO_{trans}). MS: m/z (%) = 623 (1) [M^+], 595 (33) [M − CO], 380 (100).

{2-[2-(3,4-Dimethyl-1*H*-phospholyl)phenyl]-4,4-dimethyl-4,5-dihydro-1,3-oxazole}W(CO)$_5$ (4d): A solution of hexacarbonyltungsten (1.85 g, 5.2 mmol) in 250 mL of THF was irradiated under UV light for 30 min. To this solution was added a solution of **3d** (1.5 g, 5.2 mmol) in 10 mL of THF. After 30 min of stirring, the solvent was evaporated. The product was then purified by chromatography on silica gel, with a hexane/diethyl ether gradient. Complex **4c** was obtained as a yellow powder (R_f = 0.35 in hexane/diethyl ether, 3:2). Yield: 80% (2.54 g). ^{31}P NMR ($CDCl_3$): δ = 11.8 ($^1J_{P,W}$ = 214 Hz). ^1H NMR ($CDCl_3$): δ = 1.50 [s, 6 H, $C(CH_3)_2$], 2.12 (s, 6 H, CH_3), 4.19 (s, 2 H, OCH_2), 6.72 (dd, $J_{P,H}$ = 33.2, ^4J = 0.8 Hz, 2 H, P−CH), 7.37−7.47 (m, 2 H, Ar-H), 7.53−7.63 (m, 1 H, Ar-H), 7.98−8.04 (m, 1 H, Ar-H). ^{13}C NMR ($CDCl_3$): δ = 17.3 (d, ^3J = 11.8 Hz, CH_3), 28.3 [$C(CH_3)_2$], 68.8 [$C(CH_3)_2$], 79.2 (OCH_2),129.3 (d, J = 5.1 Hz, C), 128.8, 129.4, 129.7, 130.5, 130.7, 130.8, 131.9, 132.0, 134.1 (d, ^1J = 35.1 Hz, PCH), 149.1 (d, ^2J = 10.7 Hz, C), 160.9 (C=N), 197.2 (d, ^2J = 7.2 Hz, CO_{cis}), 200.4 (d, ^2J = 19.6 Hz, CO_{trans}).

{Dimethyl 7-[(6,6-dimethylbicyclo[3.1.1]hept-2-yl)methyl]-5,6-dimethyl-7-phosphabicyclo[2.2.1]hepta-2,5-diene-2,3-dicarboxylate}W(CO)$_5$ (5b): To a solution of **4b** (11.4 g, 20 mmol) in 50 mL of toluene was added 15 mL (120 mmol) of dimethyl acetylenedicarboxylate. The solution was heated to 84 °C for 30 h. The solvent was evaporated under vacuum. The residue was purified by chromatography on silica gel with hexane/diethyl ether (95:5) as the eluent. Recrystallization afforded pure **5b** as yellow crystals. Yield: 74% (10.5 g). ^{31}P NMR ($CDCl_3$): δ = 217.5 ($^1J_{P,W}$ = 234.3 Hz). ^1H NMR ($CDCl_3$): δ = 0.90 (d, J = 9.9 Hz, 1 H) 0.97 [s, 3 H, $C(CH_3)_2$], 1.16 [s, 3 H, $C(CH_3)_2$], 1.40 (m, 1 H), 1.72−1.80 (m, 1 H), 1.83−1.90 (m, 3 H), 1.94 (s, 3 H, CH_3), 1.95 (s, 3 H, CH_3), 2.19−2.58 (m, 5 H), 3.56 (m, $^2J_{P,H}$ = 3.0, ^4J = 3.0 Hz, 2 H, P−CH), 3.82 (s, 3 H, OCH_3), 3.84 (s, 3 H, OCH_3). ^{13}C NMR ($CDCl_3$): δ = 15.9 (Me), 16.0 (Me), 22.6 (d, ^3J = 4.5 Hz, CH_2), 22.6 (CH_3), 26.2 (CH_2), 27.9 (CH_3), 33.8 (CH_2), 38.3 (d, ^1J = 17.9 Hz, P−CH_2), 38.5 [$C(CH_3)_2$], 41.0 (CH), 43.1 (P−CH_2*C*H), 47.3 (d, ^3J = 7.7 Hz, CH), 52.5 (OMe), 59.9 (d, ^1J = 19.6 Hz, P-CH), 60.3 (d, ^1J = 18.4 Hz, P-CH), 138.9 (d, ^2J = 2.6 Hz, C), 139.1 (d, ^2J = 14.6 Hz, C), 145.3 [d, ^2J = 5.1 Hz, *C*(CO_2Me)], 146.0 [d, ^2J = 4.8 Hz, *C*(CO_2Me)], 165.0 [d, ^3J = 3.0 Hz, C(*C*O_2Me)], 165.4 [d, ^3J = 2.7 Hz, C(*C*O_2Me)], 196.2 (d, ^2J = 6.6 Hz, 4 CO_{cis}), 197.8 (d, ^2J = 25.7 Hz, CO_{trans}). MS: m/z (%) = 714 (4) [M^+], 191 (100).

(7-Aza-1-phosphabicyclo[2.2.1]hept-2-ene)W(CO)$_5$ Complexes 9a and 9b: A solution of **4c** (0.66 g; 1.0 mmol) and dimethyl acetylenedicarboxylate (0.26 mL; 2.1 mmol) in 3 mL of toluene was heated under reflux for 15 h. The crude mixture was purified directly by chromatography on silica gel with toluene as eluent. Two diastereo-

mers were obtained in a 4:1 ratio. Yield: 63% (0.43 g). ^{31}P NMR (toluene): δ = 38.5 (minor diastereomer), 41.8 (major diastereomer). The mixture was dissolved in toluene and layered with hexane. Storage of the solution at 6 °C gave orange crystals of the main diastereomer. ^{31}P NMR ($CDCl_3$): δ = 42.1 ($^1J_{P,W}$ = 289 Hz). ^{1}H NMR ($CDCl_3$): δ = 0.68 [d, *J* = 7.0 Hz, 3 H, $CH(CH_3)_2$], 0.71 [d, *J* = 6.6 Hz, 3 H, $CH(CH_3)_2$], 2.00 [m, *J* = 3.5 Hz, 1 H, $CH(CH_3)_2$], 3.33 (m, *J* = 14.9 et 3.5 Hz, 1 H, CHN), 3.54 (s, 3 H, OMe), 3.59 (s, 3 H, OMe), 4.00 (AB, *J* = 7.7 Hz, 2 H, OCH_2), 6.91−7.14 (m, 2 H, Ar-H), 7.33−7.38 (m, 1 H, Ar-H), 7.41−7.53 (m, 1 H, Ar-H). ^{13}C NMR ($CDCl_3$): δ = 14.5 (Me), 19.8 (Me), 29.0 [$CH(CH_3)_2$], 52.6 (OMe), 52.7 (OMe), 58.6 (d, ^2J = 2.6 Hz, N−CH), 72.9 (d, ^3J = 7.6 Hz, OCH_2), 115.8 (N−C−O), 121.3 (d, *J* = 3.0 Hz, CH-Ar), 126.4 (d, *J* = 12.3 Hz, CH-Ar), 128.5 (d, *J* = 15.6 Hz, CH-Ar), 129.5 (CH-Ar), 142.6 (C-Ar), 146.4 [P−C=*C*(CO_2Me)], 148.8 [d, ^1J = 44.2 Hz, P−*C*(CO_2Me)], 160.4 (d, *J* = 6.8 Hz, P−C-Ar), 164.0 [d, ^2J = 14.3 Hz, P−C(*C*O_2Me)], 164.2 [d, *J* = 12.1 Hz, P−C=C(*C*O_2Me)], 194.2 (d, ^2J = 8.1 Hz, W−CO_{cis}), 195.9 (d, ^2J = 30.3 Hz, W−CO_{trans}).

(7-Aza-1-phosphabicyclo[2.2.1]hept-2-ene)W(CO)$_5$ (9d): A solution of **4d** (2.0 g; 3.3 mmol) and dimethyl acetylenedicarboxylate (0.9 mL; 7.3 mmol) in 8 mL of toluene was heated under reflux for 14 h. The crude mixture was purified directly by chromatography on silica gel with toluene as eluent. The product was dissolved in toluene and layered with hexane. Storage of the solution at 6 °C gave **9d** as orange crystals. Yield: 54% (1.2 g). ^{31}P NMR ($CDCl_3$): δ = 32.2 ($^1J_{P,W}$ = 286 Hz). ^{1}H NMR ($CDCl_3$): δ = 1.16 [s, 3 H, $C(CH_3)_2$], 1.24 [s, 3 H, $C(CH_3)_2$], 3.53 (s, 3 H, OMe), 3.60 (s, 3 H, OMe), 3.98 (AB, 2 H, OCH_2), 6.92−7.14 (m, 2 H, Ar-H), 7.34−7.44 (m, 2 H, Ar-H). ^{13}C NMR ($CDCl_3$): δ = 25.8 [d, *J* = 6.3 Hz, C(*C*H_3)$_2$], 28.3 [C(*C*H_3)$_2$], 52.4 (OMe), 52.7 (OMe), 60.1 [*C*(CH_3)$_2$], 85.9 (d, ^3J = 4.7 Hz, OCH_2), 115.0 (s, N−C), 121.0 (d, *J* = 3.8 Hz, CH-Ar), 126.1 (d, *J* = 12.2 Hz, CH-Ar), 127.7 (d, *J* = 15.6 Hz, CH-Ar), 128.95 (CH-Ar), 145.2 (C-Ar), 149.2 [d, *J* = 5.9 Hz, P−C=*C*(CO_2Me)], 149.3 [d, *J* = 43.8 Hz, P−*C*(CO_2Me)], 160.9 (d, *J* = 5.9 Hz, P−C(Ar)], 163.4 [d, *J* = 14.0 Hz, P−C(*C*O_2Me)], 164.1 [d, *J* = 11.2 Hz, P−C=C(*C*O_2Me)], 194.4 (d, *J* = 8.1 Hz, W−CO_{cis}), 195.9 (d, *J* = 30.2 Hz, W−CO_{trans}). $C_{22}H_{18}NO_{10}PW$ (671.19): calcd. C 39.37, H 2.70; found C 39.33, H 2.67.

2-{2-[(*S*)-4-Isopropyl-4,5-dihydro-1,3-oxazol-2-yl]phenyl}-3,4-dimethyl-1-phosphaferrocene (11a and 11b): A solution of **3c** (0.73 g, 2.4 mmol) and dicarbonyl(η^5-cyclopentadienyl)iron dimer (0.42 g, 1.2 mmol) in 40 mL of toluene was heated at 160 °C for 4 h under 8 bar of CO. The carbon monoxide pressure was then released and the solution heated for additional 3 h. The solution was then allowed to cool to room temperature. The final products **11a** and **11b** were characterized only by ^{31}P NMR as the crude mixture. Two diastereomers were present in a 2:1 ratio. ^{31}P NMR (toluene): δ = −67.1 (minor diastereomer), −68.0 (major diastereomer).

(μ-{2-{2-[(*S*)-4-Isopropyl-4,5-dihydro-1,3-oxazol-2-yl]phenyl}-3,4-dimethyl-1-phosphaferrocene})[W(CO)$_5$]$_2$ (12a and 12b): A solution of W(CO)$_5$(THF), prepared from 1.70 g (4.8 mmol) of hexacarbonyltungsten in 250 mL of THF, was poured into the crude mixture of **11a**,**b**. The solution was stirred at room temperature for 0.5 h. After evaporation of the solvent, the mixture was purified by chromatography on silica gel with toluene, affording **12a** and **12b** as an orange powder. The chelate compounds **13a** and **13b** were also isolated from the reaction mixture. Yield of **12a**,**b** from **3c** was 60% (1.53 g). The major diastereomer [(*S*,*S*)-**12a**] was obtained in pure form after crystallization from hexane. **12a**: ^{31}P NMR ($CDCl_3$): δ = −34.5 ($^1J_{P,W}$ = 263, $^2J_{P,H}$ = 32.4 Hz). ^{1}H NMR ($CDCl_3$): δ = 0.42 [d, *J* = 6.7 Hz, 3 H, $CH(CH_3)_2$], 0.88 [d, *J* = 7.0 Hz, 3 H, $CH(CH_3)_2$], 2.11 (s, 3 H, CH_3), 2.20 (s, 3 H, CH_3), 2.63 [m, 1 H, C*H*(CH_3)$_2$], 3.70 (d, $J_{P,H}$ = 32.4 Hz, P−CH), 3.93−4.34 (m, 3 H, CHN, OCH_2), 4.51 (s, 5 H, Cp), 7.49−7.61 (m, 4 H, Ar-H). ^{13}C NMR ($CDCl_3$): δ = 12.9 [$CH(CH_3)_2$], 15.4 (d, *J* = 3.0 Hz, Me), 16.2 (d, *J* = 4.5 Hz, Me), 19.0 [$CH(CH_3)_2$], 29.9 [*C*$H(CH_3)_2$], 67.8 (OCH_2), 69.9 (P−CH), 74.1 (Cp), 77.5 (CHN), 93.1 (C), 93.12 (C), 93.7 (d, *J* = 2.2 Hz, P−C), 127.7 (CH-Ar), 130.1 (CH-Ar), 130.9 (d, *J* = 3.2 Hz, C), 131.3 (CH-Ar), 133.9 (d, *J* = 3.5 Hz, CH-Ar), 134.4 (d, *J* = 13.8 Hz, C-2′), 171.6 (C=N), 194.5 (d, *J* = 8.0 Hz, CO_{cis}-P), 197.8 (CO_{cis}-N), 197.8 (d, *J* = 32.0 Hz, CO_{trans}-P), 200.8 (CO_{trans}-N). $C_{33}H_{26}FeNO_{11}PW_2$ (1067.06): calcd. C 37.14, H 2.46; found C 37.22, H 2.33. [α]$_D$ = −249 (*c* = 1, toluene). The structure of **12a** has been confirmed by X-ray diffraction studies. The minor diastereomer (*R*,*S*)-**12b** was characterized only by ^{31}P NMR ($CDCl_3$): δ = −31.4 ($^1J_{P,W}$ = 261.6, $^2J_{P,H}$ = 31.8 Hz).

(2-{2-[(*S*)-4-Isopropyl-4,5-dihydro-1,3-oxazol-2-yl]phenyl}-3,4-dimethyl-1-phosphaferrocene)W(CO)$_4$ (13a and 13b): These compounds were obtained as side products during the synthesis of **12a**,**b** and were isolated by chromatography on silica gel. Crystals of the major diastereomer (**13b**) were obtained from a hexane solution. Yield (**13a** and **13b**): 3% (50 mg). ^{31}P NMR (toluene): δ = −0.7 (main diastereomer), −9.6 (minor diastereomer). The structure of **13b** was established by X-ray diffraction studies.

(2-{2-[(*S*)-4-Isopropyl-4,5-dihydro-1,3-oxazol-2-yl]phenyl}-3,4-dimethyl-1-phosphaferrocene)Mo(CO)$_4$ (14a and 14b): To a crude solution of **11a**,**b**, prepared from 2 g (6.7 mmol) of **3c**, was added 1 equiv. of the (MeCN)Mo(CO)$_5$ complex [prepared from 1.76 g (6.7 mmol) of hexacarbonylmolybdenum and 0.74 g (6.7 mmol) of trimethylamine *N*-oxide in 30 mL of acetonitrile]. The solution was stirred at room temperature for 1 h. After evaporation of the solvent, the mixture was purified by chromatography on silica gel with hexane/toluene (4:1), affording an isomeric mixture of the chelate complexes **14a** and **14b** as an orange powder. Yield over two steps: 47% (1.96 g). The minor diastereomer was characterized by ^{31}P NMR ($CDCl_3$): δ = 8.6. The major diastereomer [(*R*,*S*)-**14a**] was obtained in pure form by crystallization in hexane. **(*R*,*S*)-14a:** ^{31}P NMR ($CDCl_3$): δ = 1.5. ^{1}H NMR ($CDCl_3$): δ = 0.86 [d, *J* = 6.7 Hz, 3 H, $CH(CH_3)_2$], 0.93 [d, *J* = 7.0 Hz, 3 H, $CH(CH_3)_2$], 2.27 (s, 6 H, CH_3), 2.80 [m, 1 H, C*H*(CH_3)$_2$], 3.71 (d, $J_{P,H}$ = 34.0 Hz, P−CH), 4.05−4.20 (m, 3 H, CHN, OCH_2), 4.34 (s, 5 H, Cp), 7.11−7.45 (m, 4 H, Ar-H). ^{13}C NMR ($CDCl_3$): δ = 13.5 [$CH(CH_3)_2$], 13.9 (Me), 16.9 (d, *J* = 2.8 Hz, Me), 18.9 [$CH(CH_3)_2$], 29.4 [*C*$H(CH_3)_2$], 67.4 (OCH_2), 68.8 (d, *J* = 17.5 Hz, P−CH), 74.5 (Cp), 76.4 (CHN), 90.0 (d, *J* = 13.1 Hz, P−C), 92.4 (C), 94.1 (d, *J* = 2.6 Hz, C), 126.4 (CH-Ar), 128.4 (CH-Ar), 129.9 (CH-Ar), 130.1 (d, *J* = 16.0 Hz), 133.1 (d, *J* = 5.4 Hz, CH-Ar), 136.9 (d, *J* = 13.4 Hz, C), 169.5 (C=N), 204.9 (d, *J* = 12.1 Hz, CO_{cis}-P), 208.4 (d, *J* = 10.5 Hz, CO_{cis}-P), 215.7 (d, *J* = 47.0 Hz, CO_{trans}-P), 219.8 (d, *J* = 9.2 Hz, CO_{cis}-P). IR (ν_{CO}): $\tilde{\nu}$ = 2017 (m), 1895 (s), 1846 cm^{-1} (s). $C_{27}H_{26}FeMoNO_5P$ (627.26): calcd. C 51.70, H 4.18; found C 51.87, H 4.05.

[1] F. Mathey, *Chem. Rev.* **1988**, *88*, 429−453.
[2] L. D. Quin, K. A. Mesch, *J. Chem. Soc., Chem. Commun.* **1980**, 959−961.
[3] F. Mathey, F. Mercier, *Tetrahedron Lett.* **1981**, *22*, 319−322.
[4] A. Marinetti, F. Mathey, J. Fischer, A. Mitschler, *J. Chem. Soc., Chem. Commun.* **1982**, 667−668.
[5] F. Mathey, F. Mercier, C. Charrier, J. Fischer, A. Mitschler, *J. Am. Chem. Soc.* **1981**, *103*, 4595−4597.

[6] F. Mathey, A. Mitschler, R. Weiss, *J. Am. Chem. Soc.* **1978**, *100*, 5748−5755.
[7] G. de Lauzon, B. Deschamps, J. Fischer, F. Mathey, A. Mitschler, *J. Am. Chem. Soc.* **1980**, *102*, 994−1000.
[8] [8a] T. P. Dang, J. C. Poulin, H. B. Kagan, *J. Organomet. Chem.* **1975**, *91*, 105−115. [8b] T. Hayashi, M. Tanaka, Y. Ikeda, I. Ogata, *Bull. Chem. Soc. Jpn.* **1979**, *52*, 2605. [8c] G. Consiglio, S. C. A. Nefkens, *Tetrahedron: Asymmetry* **1990**, *1*, 417−420. [8d] J. J. Brunet, M. Gomez, H. Hajouji, D. Neibecker, *Phosphorus Sulfur Silicon Relat. Elem.* **1993**, *85*, 207. [8e] M. Peer, J. C. de Jong, M. Kiefer, T. Langer, H. Rieck, H. Schell, P. Sennhenn, J. Sprinz, H. Steinhagen, B. Wiese, G. Helmchen, *Tetrahedron.* **1996**, *52*, 7547−7583. [8f] I. Toth, C. J. Elsevier, J. G. de Vries, J. Bakos, W. J. J. Smeets, A. L. Spek, *J. Organomet. Chem.* **1997**, *540*, 15−25. [8g] W. A. Schenk, M. Stubbe, M. Hagel, *J. Organomet. Chem.* **1998**, *560*, 257−263.
[9] [9a] M. Ogasawara, K. Yoshida, T. Hayashi, *Organometallics* **2001**, *20*, 1014−1019. [9b] M. Ogasawara, K. Yoshida, T. Hayashi, *Organometallics* **2001**, *20*, 3913−3917.
[10] A. Brèque, G. Muller, H. Bonnard, F. Mathey, P. Savignac, Eur. Pat. 41447, **1981**; *Chem. Abstr.* **1982**, *96*, 143076x.
[11] H. C. Brown, A. K. Mandal, *Synthesis* **1980**, 153−155.
[12] G. Giacomelli, L. Lardicci, F. Palla, *J. Org. Chem.* **1984**, *49*, 310−313.
[13] [13a] G. J. Dawson, C. G. Frost, J. M. J. Williams, S. J. Coote, *Tetrahedron Lett.* **1993**, *34*, 3149−3150. [13b] J. Sprinz, G. Helmchen, *Tetrahedron Lett.* **1993**, *34*, 1769−1772. [13c] P. von Matt, A. Pfaltz, *Angew. Chem. Int. Ed. Engl.* **1993**, *32*, 566−568. [13d] G. C. Lloyd-Jones, A. Pfaltz, *Angew. Chem. Int. Ed. Engl.* **1995**, *34*, 462−464. [13e] A. Pfaltz, *Acta Chim. Scand.* **1996**, *50*, 189. [13f] S. Kudis, G. Helmchen, *Angew. Chem. Int. Ed.* **1998**, *37*, 3047−3050. [13g] O. Loiseleur, P. Meier, A. Pfaltz, *Angew. Chem. Int. Ed. Engl.* **1996**, *35*, 200−202. [13h] O. Loiseleur, M. Hayashi, N. Schmees, A. Pfaltz, *Synthesis* **1997**, 1338−1345. [13i] L. N. Newman, J. M. J. Williams, R. McCague, G. A. Potter, *Tetrahedron: Asymmetry* **1996**, *7*, 1597−1598. [13j] T. Langer, J. Janssen, G. Helmchen, *Tetrahedron: Asymmetry* **1996**, *7*, 1599−1602. [13k] P. Schnider, G. Koch, R. Prétôt, G. Wang, F. M. Bohnen, C. Krüger, A. Pfaltz, *Chem. Eur. J.* **1997**, *3*, 887. [13l] D. Flubacher, G. Helmchen, *Tetrahedron Lett.* **1999**, *40*, 3867−4868. [13m] For a recent review on phosphanyloxazoline ligands see: G. Helmchen, A. Pfaltz, *Acc. Chem. Res.* **2000**, *33*, 336−345.
[14] A. Marinetti, F. Mathey, J. Fischer, A. Mitschler, *J. Am. Chem. Soc.* **1982**, *104*, 4484−4485.
[15] [15a] F. Mathey, *Angew. Chem. Int. Ed. Engl.* **1987**, *26*, 275−286. [15b] F. Mathey, N. H. Tran Huy, A. Marinetti, *Helv. Chim. Acta* **2001**, *84*, 2938−2957.
[16] S. Holand, F. Mathey, J. Fischer, *Polyhedron* **1986**, *5*, 1413−1421.
[17] A. Marinetti, F. Mathey, *Organometallics* **1982**, *1*, 1488−1492.
[18] Bringing stereogenic centers closer to the phosphorus atom could lower the reactivity of the corresponding phospholes with DMAD and thus preclude the generation of phosphinidene complexes by this method. In such cases the phosphinidene complexes bearing chiral phosphorus substituents could be better generated by thermolysis of the corresponding phosphirane complexes (see: A. Marinetti, C. Charrier, F. Mathey, J. Fischer, *Organometallics* **1985**, *4*, 2134−2138), which are easily accessible through cyclization reactions (see ref.[19b]).
[19] Previous syntheses of optically active phosphirane derivatives: [19a] A. Marinetti, L. Ricard, F. Mathey, *Synthesis* **1992**, 157−162. [19b] X. Li, K. D. Robinson, P. P. Gaspar, *J. Org. Chem.* **1996**, *61*, 7702−7710.
[20] A. Marinetti, F. Mathey, A. Mitschler, *J. Chem. Soc., Chem. Commun.* **1984**, 45−46.
[21] A. Marinetti, F. Mathey, L. Ricard, *Organometallics* **1993**, *12*, 1207−1212.
[22] N. Maigrot, L. Ricard, C. Charrier, P. Le Goff, F. Mathey, *Bull. Soc. Chim. Fr.* **1992**, *129*, 76−78.
[23] U. Rhode, F. Ruthe, P. G. Jones, R. Streubel, *Angew. Chem. Int. Ed.* **1999**, *38*, 215−217.
[24] P. Le Floch, A. Marinetti, L. Ricard, F. Mathey, *J. Am. Chem. Soc.* **1990**, *112*, 2407−2410.
[25] A. H. Cowley, R. L. Geerts, C. M. Nunn, *J. Am. Chem. Soc.* **1987**, *109*, 6523−6254.
[26] H. Wilkens, A. Ostrowski, J. Jeske, F. Ruthe, P. G. Jones, R. Streubel, *Organometallics* **1999**, *18*, 5627−5642.
[27] R. Streubel, U. Schiemann, N. Hoffmann, Y. Schiemann, P. G. Jones, D. Gudat, *Organometallics* **2000**, *19*, 475−481.
[28] R. Streubel, U. Schiemann, P. G. Jones, N. H. Tran Huy, F. Mathey, *Angew. Chem. Int. Ed.* **2000**, *39*, 3686−3688.
[29] For reviews see: [29a] M. L. Deem, *Synthesis* **1982**, 701−716. R. Huisgen, *1,3-Dipolar Cycloaddition Chemistry*, vol. 1 (Ed.: A. Padwa), John Wiley & Sons, New York, **1984**, p. 1. [29b] O. Tsuge, S. Kanemasa, *Adv. Heterocycl. Chem.* **1989**, *45*, 231.
[30] [30a] E. Niecke, A. Seyer, D-A. Wildbredt, *Angew. Chem. Int. Ed. Engl.* **1981**, *20*, 675−677. [30b] E. Niecke, D-A. Wildbredt, *Chem. Ber.* **1980**, *113*, 1549−1565. [30c] E. Niecke, J. Böske, B. Krebs, M. Dartmann, *Chem. Ber.* **1985**, *118*, 3227−3240. [30d] R. Streubel, A. Ostrowski, H. Wilkens, F. Ruthe, J. Jeske, P. G. Jones, *Angew. Chem. Int. Ed. Engl.* **1997**, *36*, 378−381.
[31] [31a] D. Niebecker, R. Réau, *Angew. Chem. Int. Ed. Engl.* **1989**, *28*, 500−501. [31b] W. A. Hermann, C. W. Kohlpaintner, R. B. Manetsberger, H. Bahrmann, H. Kottmann, *J. Mol. Catal. A* **1995**, *97*, 65−72. [31c] F. Robin, F. Mercier, L. Ricard, F. Mathey, M. Spagnol, *Chem. Eur. J.* **1997**, *3*, 1365. [31d] S. R. Gilbertson, D. G. Genov, A. L. Rheingold, *Org. Lett.* **2000**, *2*, 2885−2888.
[32] For a review on phosphaferrocene chemistry, see: F. Mathey, *Coord. Chem. Rev.* **1994**, *137*, 1−52.
[33] G. De Lauzon, F. Mathey, M. Simalty, *J. Organomet. Chem.* **1978**, *156*, C33−C36.
[34] E. W. Abel, N. Clark, C. Towers, *J. Chem. Soc., Dalton Trans.* **1979**, 1552−1556.
[35] R. M. G. Roberts, A. S. Wells, *Inorg. Chim. Acta* **1986**, *112*, 171−175.
[36] F. Mercier, F. Mathey, *J. Organomet. Chem.* **1984**, *263*, 55−66.
[37] B. Deschamps, L. Ricard, F. Mathey, *J. Organomet. Chem.* **1997**, *548*, 17−22.
[38] For a recent review see: C. J. Richards, A. J. Locke, *Tetrahedron: Asymmetry* **1998**, *9*, 2377−2407.
[39] [39a] C. Ganter, L. Brassat, C. Glinsböckel, B. Ganter, *Organometallics* **1997**, *16*, 2862−2867. [39b] C. Ganter, L. Brassat, B. Ganter, *Tetrahedron: Asymmetry* **1997**, *8*, 2607−2611. [39c] C. Ganter, L. Brassat, B. Ganter, *Chem. Ber./Recueil* **1997**, *130*, 1771−1776. [39d] C. E. Garrett, G. C. Fu, *J. Org. Chem.* **1997**, *62*, 4534−5435. [39e] S. Qiao, G. C. Fu, *J. Org. Chem.* **1998**, *63*, 4168−4169. [39f] C. Ganter, C. Kaulen, U. Englert, *Organometallics* **1999**, *18*, 5444−5446. [39g] R. Shintani, M. M-C. Lo, G. C. Fu, *Org. Lett.* **2000**, *2*, 3695−3697. [39h] K. Tanaka, S. Qiao, M. Tobisu, M. M-C. Lo, G. C. Fu, *J. Am. Chem. Soc.* **2000**, *122*, 9870−9871. [39i] S. Arai, S. Bellemin-Laponnaz, G. C. Fu, *Angew. Chem. Int. Ed.* **2001**, *40*, 234−236.
[40] S. Holand, M. Jeanjean, F. Mathey, *Angew. Chem. Int. Ed. Engl.* **1997**, *36*, 98−100.

Received December 7, 2001
[I01502]

Investigation of the Enantioselectivity Observed in Epoxidation Reactions Catalysed by Bis-Strapped Chiral Porphyrins Derived from L-Proline

Bernard Boitrel,*[a][‡] Valérie Baveux-Chambenoît,[a] and Philippe Richard[a]

Keywords: L-Proline / Epoxidations / Porphyrins / Enantioselectivity / Iron

The enantiomeric excesses obtained during the epoxidation reactions of *p*-chlorostyrene or 1,2-dihydronaphthalene catalysed by two different series of chiral porphyrins are reported. An attempt is made to correlate the enantioselectivity with the steric hindrance generated by the straps of these catalysts. It is shown that this steric hindrance is influenced by the nature of the strap and that it can be approximated. Additionally, the same strap is tethered in two different fashions on each side of the porphyrin, leading to either D_2- or C_2-symmetrical catalysts, for which the two sides are identically functionalised.

(© Wiley-VCH Verlag GmbH, 69451 Weinheim, Germany, 2002)

Introduction

Metalloporphyrins have been well known, for two decades, to be effective catalysts for unfunctionalised alkene epoxidation[1−3] or alkane hydroxylation.[4] More recently, they have also been investigated as effective catalysts for cyclopropanation[5] and aziridination[6] reactions. Indeed, when compared with metallosalens, porphyrinoid catalysts are expected to exhibit much higher turnover numbers.[7] This criterion is of course extremely important in any catalysis, but may be much more important in the case of "destructive" catalysis, such as oxidation. In the case of chiral molecules, although different encouraging results have been reported, the obtained enantioselectivities are generally lower than those described for metallosalens, and also much more difficult to rationalise. This observation can be partially explained by the fact that the complete series of these latter catalysts have been synthesised and extensively studied.[8−10] We believe that the study of a series of potential catalysts can help our understanding of how the enantioselectivity can be achieved.[11−13] Indeed, for oxidation reactions, although the use of aromatic structures such as BINAP-related straps lead to a robust catalyst, it is difficult to predict the effectiveness of the same catalyst in terms of selectivity.[7]

Recently, we have reported on the synthesis of a complete family of potential chiral catalysts for epoxidation reactions. We were able to obtain an X-ray structure of one of the catalysts metallated by zinc(II) and hence have a precise image of the chiral superstructure. Moreover, the ^{1}H NMR spectroscopic studies of the same molecule indicated that the solution structure was in agreement with the structure in the solid state.[14] In this paper, we now report on the catalytic activity of two different series of iron(III) chiral catalysts, related by the point of attachment of the chiral straps, in the asymmetric epoxidation of *p*-chlorostyrene and 1,2-dihydronaphthalene by iodosylbenzene.

Results and Discussion

In previous studies, excellent enantiomeric excesses (*ee*) and good turnover numbers have been reported on. The main goal of this study is to determine if the enantioselectivities observed for a given reaction, namely the epoxidation of an unfunctionalised olefin, can be directly correlated with the steric hindrance of the strap in a D_2-symmetrical environment, as in the first series of porphyrins **1**−**6** (Figure 1, left column). For that purpose, we needed to make use of several potential catalysts for which we have a precise representation of the catalyst in solution.

We have already published the crystal structure of the zinc counterpart of porphyrin **1**.[14] In Figure 2 we have represented two other views of the same molecule in order to describe a structural parameter that we have defined as *R*, the ratio of the steric hindrance of the chiral strap and the steric hindrance of the porphyrin core itself (R = S/P). This ratio gives an unbiased representation of the steric hindrance of the strap whilst taking into account the planarity of the porphyrin. It is graphically measured as indicated in Figure 2, with a spatial extent limited to the carbon atoms. Indeed, this ratio has been evaluated by molecular mechanics modelling for six different bis-strapped porphyrins,

[a] L.S.E.O. − UMR-CNRS 5632, Université de Bourgogne, 6, boulevard Gabriel, 21000 Dijon, France
[‡] New address: Institut de Chimie, UMR-CNRS 6509, Université de Rennes 1, Campus de Beaulieu, Av. du Général Leclerc, 35042 Rennes Cedex, France
Fax: (internat.) + 33-2/23235637
E-mail: Bernard.Boitrel@univ-rennes1.fr

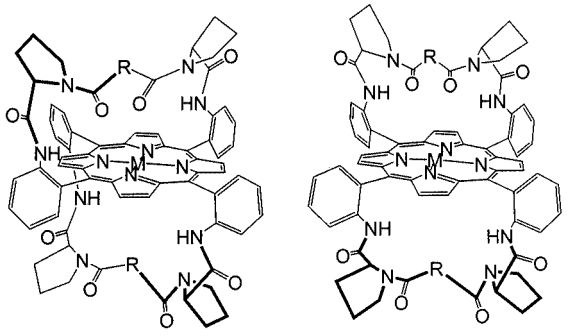

1 R = -$(CH_2)_2$- **4** R = -CH=CH- **7** R = -$(CH_2)_2$- **10** R = -*m*-phenyl-

2 R = -$(CH_2)_3$- **5** R = -*p*-phenyl- **8** R = -$(CH_2)_3$- **11** R = O*t*Bu, *t*BuO

3 R = -$(CH_2)_4$- **6** R = -*m*-phenyl- **9** R = -$(CH_2)_4$-

Figure 1. Chemical structure of the different catalysts (left column: synthesised from the αβαβ atropisomer of TAPP; right column: synthesised from the ααββ atropisomer of TAPP; M = H_2, Fe, or Zn)

and is found to range from 0.20 to 0.51 (Table 1).[15] For our study, we have assumed that the conformation observed for the zinc(II)−porphyrin is not very different from that in the iron(III) complex used in the epoxidation reaction. Furthermore, we have validated our results by modelling and comparing the *R* value calculated theoretically with the experimental value in the case of **1Zn**; the values of 0.49 and 0.51, respectively, are strikingly similar. This also proves that the intramolecular coordination of the zinc atom does not significantly influence this parameter.

The results of the modelling of the six chiral porphyrins synthesised in the first αβαβ series are depicted in Figure 3. They are represented according to the same point of view as in Figure 2.[16] It is obvious that the *R* value increases as we examine the catalysts from (a) to (f). This means that if the enantioselectivity is a function of the steric hindrance during the approach of the olefin, we should obtain increasing values of *ee* as we examine the catalysts through the series **6**, **4**, **5**, **1**, **2**, and **3**. Different results emerged from the observation of the first four lines of Table 1. First of all, the different *ee* values are extremely low, as long as the straps of the catalyst are composed of a non-aromatic linker, and independent of the olefin. Indeed, with linkers such as the succinyl, fumaryl, adipyl, or glutaryl moieties, the *ee* values range from 1 to 7% in the case of a terminal olefin. Obviously, these linkers are attached just above the iron−oxo species generated by the action of iodosylbenzene on the iron(III)−porphyrin, and are likely to be easily oxidised instead of the olefin. These low *ee* values are also to be compared with those reported by Rose and Collman[17] with their "blank picket" porphyrins, for which they reported that the *ee* values vary inversely to the number of chiral pickets. It seems that our catalysts, although not at all comparable, are as poor catalysts as these picket porphyrins. On the other hand, the explanation advanced by the authors for their picket catalysts could also be valid for our

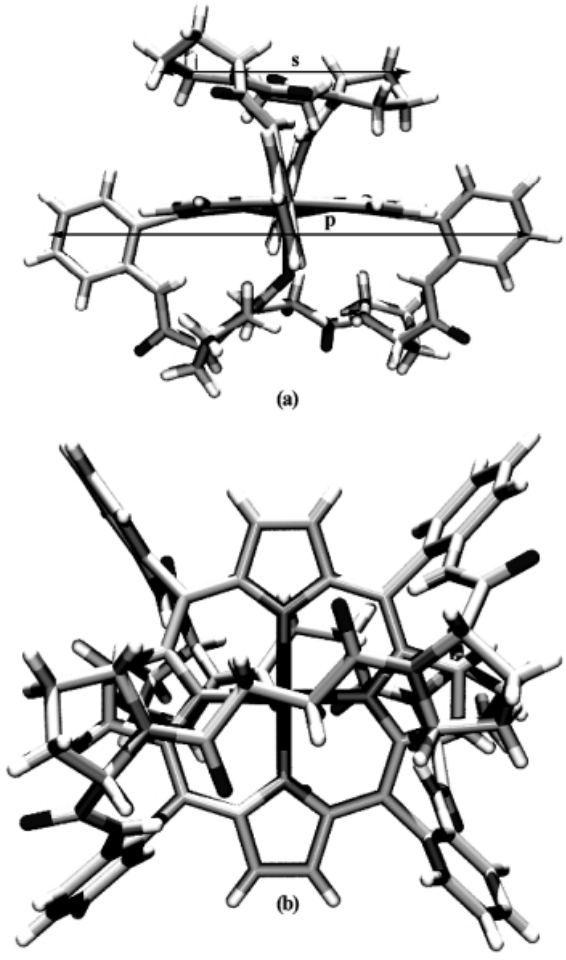

Figure 2. Stick representation (including hydrogen atoms) of the crystal structure of **1Zn**; (a) "*meso*-C_5-C_{15}" lateral view, (b) apical view

Table 1. Enantiomeric excesses obtained with the iron catalysts for two different olefins with the characteristic steric ratio *R* for catalysts **1**−**6**

Catalyst[a]	*p*-Chlorostyrene[b]	1,2-Dihydronaphthalene[b]	*R*[c]
Disucc-αβαβ (**1**)	1	0	0.49
Diglut-αβαβ (**2**)	7	4	0.50
Diadip-αβαβ (**3**)	3	1	0.54
Difum-αβαβ (**4**)	2	2	0.26
Ditere-αβαβ (**5**)	18	3	0.36
Diiso-αβαβ (**6**)	5	19	0.20
Disucc-ααββ (**7**)	26	3	−
Diglut-ααββ (**8**)	20	8	−
Diadip-ααββ (**9**)	31	26	−
Diiso-ααββ (**10**)	28	14	−

[a] Reaction conditions: catalyst (1 μmol), substrate (1000 μmol), and PhIO (100 μmol) react at room temperature in CH_2Cl_2 (2 mL).[b] Determined by GC with a Cyclodex-B chiral column. [c] In the case of **1Zn** (Figure 2), calculated equal to 0.51.

strap catalysts because the lowest *ee* value was obtained with the catalyst Disucc-αβαβ (**1**), for which the *R* value is almost the highest calculated and equal to 0.49. Now, if we

compare the side views (d) of Disucc-αβαβ (**1**) (R = 0.49) and (b) of Difum-αβαβ (**4**) (R = 0.26) (Figure 3), and if the *ee* value was to follow the lateral steric hindrance, the *ee* value should be found to be much lower in the case of Difum-αβαβ (**4**). Actually, they are almost the same. This means that either there is no relationship between this steric hindrance and the enantioselectivity or, this relation is not applicable in this case for other reasons. Indeed, the oxidative degradation of the catalyst could be consistent with this observation. The straps in catalysts such as **1**−**4** are so close to the metal centre and so sensitive to oxidation that they are oxidised immediately, and in fact, the measured *ee* value could reflect the enantioselectivity of the resulting mixture of degraded compounds. This explanation is consistent with previous results[17] for which it is believed that providing more access to the metal centre could increase the selectivity. The results obtained in the case of a (*Z*)-disubstituted olefin (1,2-dihydronaphthalene) follow the same trend and are as disappointing as in the case of the terminal olefin. Undeniably, the approach of such an encumbered olefin must be very limited and the *ee* values are even lower than for *p*-chlorostyrene.

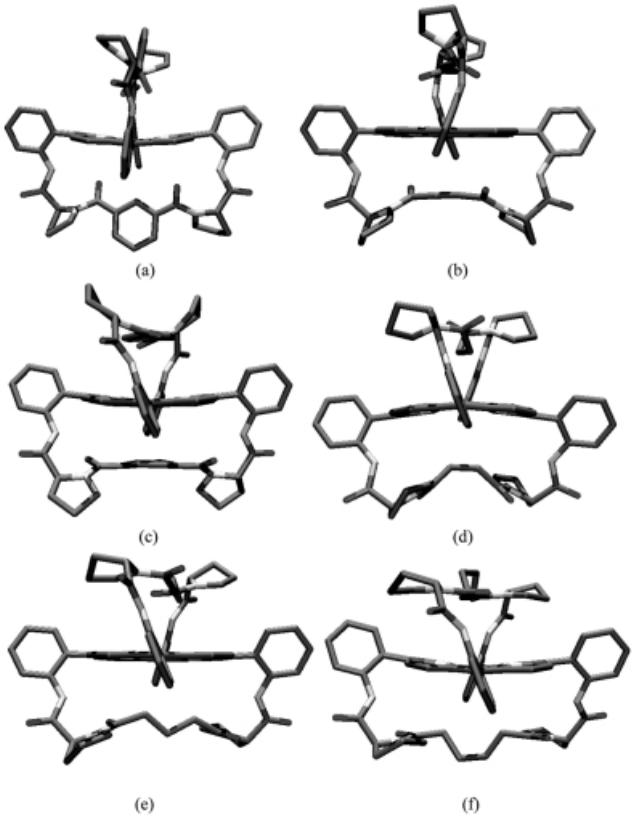

Figure 3. Stick representations of (a) **6**, (b) **4**, (c) **5**, (d) **1**, (e) **2**, and (f) **3** obtained by molecular mechanics modelling[15]

In a second study, we investigated a similar type of catalyst, but for which the linker is based on an aromatic diacyl dichloride, namely the porphyrins Ditere-αβαβ (**5**) and Diiso-αβαβ (**6**). The results of this comparison are much more informative, since the correlation between steric hindrance and enantioselectivity appears to be verified, but only for the terminal olefin. Actually, the results are contradictory when one compares the *ee* values obtained for the terminal olefin and the (*Z*)-disubstituted alkene. For porphyrin Ditere-αβαβ (**5**), which exhibits a greater R value than Diiso-αβαβ (**6**) (0.36 vs. 0.20), the observed *ee* value is 18% with *p*-chlorostyrene, but only 3% for 1,2-dihydronaphthalene. Conversely, for the catalyst Diiso-αβαβ (**6**), the *ee* value is 5% with *p*-chlorostyrene, but increases to 19% for 1,2-dihydronaphthalene. It clearly appears that with the terminal olefin, the steric hindrance is a pertinent parameter with a positive effect, whereas for a disubstituted olefin, the opposite effect is observed. This result, a priori difficult to anticipate, can be rationalised by considering two major facts. Firstly, the olefin cannot approach from the top of the catalyst,[18] but only from the side with its aromatic ring parallel to the mean plane of the porphyrin (side approach).[19] Secondly, it is striking that the aromatic rings of the straps in these two catalysts are in two extreme perpendicular positions. This observation is particularly visible in Figure 3 [views (a) and (c), bottom strap]. For catalyst Diiso-αβαβ (**6**) (a), the aromatic ring is perpendicular to the mean plane of the porphyrin whereas, for porphyrin Ditere-αβαβ (**5**) (c), it is parallel to the porphyrin plane. In the case of **5**, the enantioselectivity is much better for *p*-chlorostyrene because the olefin can introduce its double bond just above the iron−oxo species and perpendicular to the strap, with its aromatic ring avoiding the steric bulk of the L-proline ring. In the case of 1,2-dihydronaphthalene, this approach is not possible, and therefore its double bond remains parallel to the strap, resulting in no real discrimination by steric hindrance. Furthermore, in the case of **5**, the aromatic ring of the strap, parallel to the porphyrin plane, actually decreases the apparent hindrance of the five-membered ring of the L-proline. On the other hand, for catalyst **6** [Figure 3, view (a), top strap], there is a slight steric effect, mainly because the aromatic cycle remains in the plane of the strap (R = 0.20). Apparently, this subtle modification is sufficient to discriminate between the two different approaches of the disubstituted olefin, but not at all in the case of the terminal one. This explanation is in agreement with previous studies related to chiral picket porphyrins.[17] This particular comparison of two closely related catalysts with two different types of olefins is another example of how a fine difference in conformation can induce dramatic changes in the enantioselectivity, and also demonstrates that there should be a relation between the steric hindrance and the observed enantioselectivity, whether this relation is favourable or not. Furthermore, our catalyst Ditere-αβαβ (**5**), the L-prolinoyl analogue of Rose's L-alanine bis(handle) porphyrin,[20,21] must be compared with Mansuy's catalyst[22,23] that involves L-phenylalanine. In the L-phenylalanine series, an *ee* value of 50% was reported for the epoxidation of *p*-chlorostyrene, a value 2.5 times higher than the 18% *ee* obtained with **5**. This result, again, points out that a non-flexible structure such as the ring of L-proline is not a good structural feature for efficient enantioselectivity, and that L-phenylalanine, even with the possible rotation of the phenyl group around the methylene group of the lateral

chain, is a much better chiral inducer. This criterion has to be considered for further developments of chiral catalysts that involve L-proline.

In light of these instructive but relatively low enantioselectivities, we decided to extend our approach to another family of catalysts. Since 1995, we were aware of a study involving the four atropisomers of a chiral catalyst, synthesised by the condensation of a BINAP-type aldehyde with pyrrole,[24] leading to the aromatic analogues of the well-known "chiroporphyrins".[25] It was shown in this report that the iron−αααββ atropisomer was the most enantioselective catalyst among the four atropisomers for the epoxidation of styrene (59% *ee* vs. 7.5% *ee* for the αβαβ atropisomer). At a later stage this result was published,[13] and successfully generalised for a porphyrin bearing BINAP straps.[7] Thus, we have prepared the four new catalysts **7**−**10**, the analogues of **1**−**3** and **6**, respectively, with the αααββ geometry (Figure 1, right column). The lack of a crystal structure prevented us from evaluating the steric hindrance of the strap above the metal centre of the porphyrin as precisely as we did in the αβαβ series. However, we were able to estimate the steric hindrance in solution by examining the proton NMR spectra.

The ^{1}H NMR spectra of the two catalysts obtained by condensation of the glutaryl dichloride, **8** (top trace) and **2** (bottom trace) with the αααββ and αβαβ geometry, respectively, are represented in Figure 4. Clearly, in the case of **2**, the three multiplets that appear between δ = 0 and −3.5 can be assigned unambiguously to the three methylene groups of the glutaryl residues. However, an unexpected result can be seen for the chemical shifts of these three methylene groups with an αααββ geometry: their signals should be more downfield since the straps do not cross over the ring current of the porphyrin. The methylene protons with this geometry are as shielded as the methylene protons in the αβαβ geometry, and this seems to indicate that they are close to the porphyrin plane in both cases.

The results of the asymmetric epoxidation for the two olefins are interesting. The most obvious difference is represented by the *ee* values themselves. Indeed, for the epoxidation of the terminal olefin, they are much higher than for the first series. In addition, they seem to be almost the same (about 30% *ee*) for the three catalysts **7**, **9**, and **10**. Our preliminary modelling results seem to indicate that the bending of the straps over the porphyrin centre does not differ significantly when the length of the strap is varied from one methylene group to three groups. This could explain why the observed enantioselectivities are of the same order of magnitude in the case of *p*-chlorostyrene. For the disubstituted alkene, the *ee* value of one obtained for catalyst Diadip-αααββ (**9**) appears significantly different (26% *ee*) from that for the other catalysts, but is almost the same as that for the terminal olefin. This second observation can be explained by the fact that the structural feature that favours the discrimination between the two types of olefins for the catalysts in the αβαβ family, does not apply in the αααββ family. Indeed, during a side approach, the crevasse built by the bending of the straps over the porphyrin core can accommodate both types of olefins, with a slightly better selectivity for the terminal one. The two low *ee* values obtained by catalysts Disucc-αααββ (**7**) (3% *ee*) and Diglut-αααββ (**8**) (8% *ee*) for the disubstituted olefin can occur as

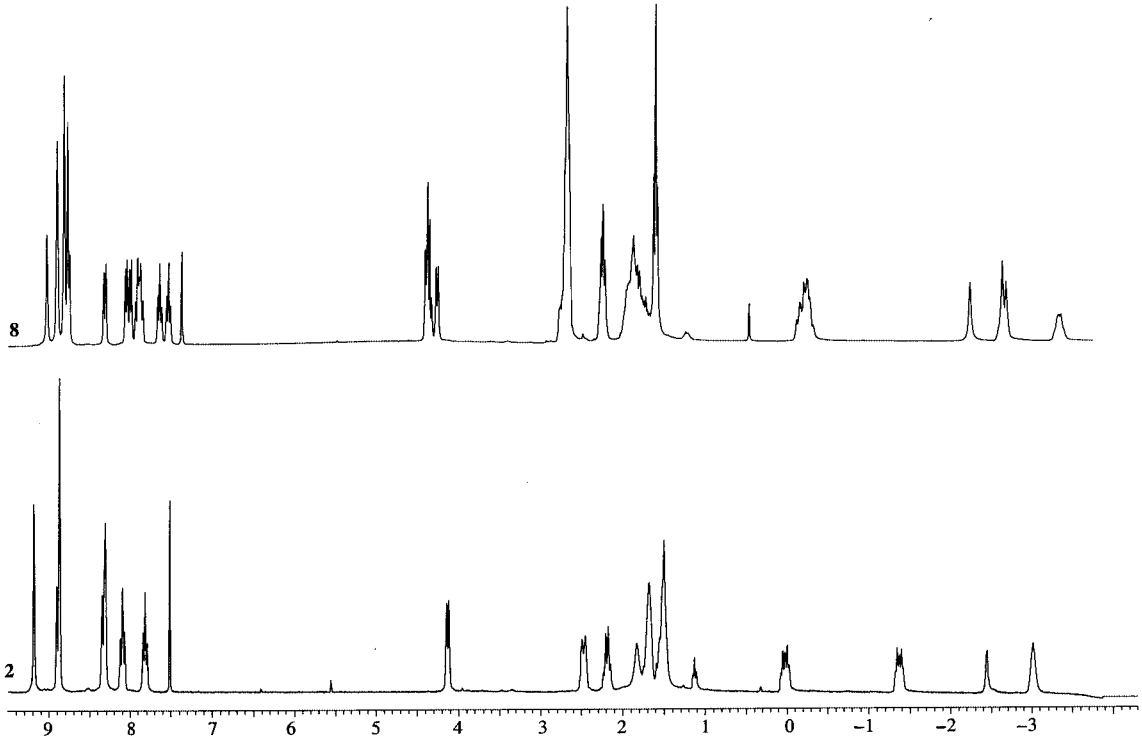

Figure 4. ^{1}H NMR spectra of porphyrins **8** and **2** ($CDCl_3$, 300 MHz, 300 K)

result of a less pronounced bending over the porphyrin, which is logical for catalysts with shorter straps than for the porphyrins Diiso-ααββ (**10**) or Diadip-ααββ (**9**). Globally, we can summarise this second part by the fact that if the linker (the diacyl dichloride employed in the last step of the synthesis) is long enough to allow the strap to bend over the metal centre, the enantioselectivity should not be decreased by switching from the αβαβ to the ααββ geometry. This phenomenon is observed only in the case of catalyst **9**, prepared with adipoyl dichloride.

Conclusion

We have reported and discussed the enantioselectivity of two closely related series of chiral bis(strapped) porphyrins, synthesised from L-prolinoyl residues. The first family, with an αβαβ geometry, with a strap crossing the porphyrin over the metal centre on each side, has been prepared to study the relationship between the steric hindrance of the strap and the observed enantiomeric excesses. For most of the catalysts under investigation, we found that congestion around the metal centre could not induce good enantioselectivities. In fact, these catalysts are poor in terms of reaction yield, and the measured enantiomeric excess does not reflect the activity of the initially designed molecule but rather of some degradation intermediates. It is important to underline that this hypothesis has already been reported for very different chiral catalysts and can now be generalised. For some well-defined catalysts, we have been able to establish that the enantioselectivity was correlated to the steric hindrance, but not always as expected. The molecules for which such a relationship exists are rather rare and deserve to be studied exhaustively. However, it must be underlined that this direct relationship between the steric hindrance and the *ee* value does not exist from a general point of view, the observed *ee* values may be influenced by many different factors. The comparison of the second series of catalysts with the first one confirms the previous explanation, namely that the enantioselectivity increases as the congestion around the metal centre decreases. Additionally, it also confirms that similar chiral inducers are more efficient with the ααββ geometry than with the αβαβ geometry. This was already known for picket structures, and is now applicable to strapped catalysts. Further studies are under investigation with these catalysts, both to evaluate them for asymmetric processes for which the catalyst is not destroyed, and to obtain a more accurate perception of their real structure in solution.

Experimental Section

General Remarks: Unless otherwise stated, the analytical facilities were provided by the Université de Bourgogne (C.S.M.) in Dijon. ^{1}H (500.13 MHz or 300.14 MHz) and ^{13}C (125.05 MHz or 75.47 MHz) NMR spectra were recorded with Bruker Avance DRX 500 or Avance 300 spectrometers and referenced to the residual protonated solvents. Mass spectra were performed with a MS/MS ZABSpec TOF spectrometer at the Université de Rennes I (C.R.M.P.O.). UV/Vis spectra were recorded with a Varian Cary 1E spectrometer. IR spectra were recorded with a Bruker IFS 66 spectrometer. All solvents (ACS for analysis) were purchased from Carlo Erba. THF was distilled from potassium metal. CH_2Cl_2 was used as received. Triethylamine and *N*-methylpiperidine were distilled from CaH_2. The starting materials were generally used as received (Acros, Aldrich) without any further purification. All reactions were performed under argon and monitored by TLC (silica, CH_2Cl_2/CH_3OH). Column flash chromatography was performed on silica gel (Merck TLC-Kieselgel 60 H, 15 μm). Enantiomeric excesses were determined by gas chromatography with a Chirasil-Dex CB as chiral capillary column (25 m × 0.25 mm, Chrompack). Compounds **1**, **4**, **5**, **6**, and **1Zn** have already been characterised. The two following porphyrins were prepared as previously reported, by reaction of a diacyl dichloride with the known α-5,15:β-10,20-tetrakis[2-(L-prolinoylamido)phenyl]porphyrin under high-dilution conditions.[14]

α-5,15:β-10,20-Bis{2,2′-[*N,N*′-bis(1,5-dioxo-1,5-pentanediyl)-L-prolinoyldiamido]diphenyl}porphyrin (2): This compound was prepared from glutaryl dichloride and obtained in 27% (37 mg) yield. ^{1}H NMR (300 MHz, $CDCl_3$, 300 K): δ = −3.24 (m, 4 H, glut), −2.67 (s, 2 H, NH_{pyr}), −1.60 (m, 4 H, glut), −0.21 (m, 4 H, glut), 1.29 (m, 8 H, Pro), 1.45 (m, 8 H, Pro), 1.95 (m, 4 H, Pro), 2.25 (m, 4 H, Pro), 3.90 (d, ^3J = 7.3 Hz, 4 H, Pro*), 7.58 (t, ^3J = 7.3 Hz, 4 H, aro), 7.86 (t, ^3J = 7.5 Hz, 4 H, aro), 8.09 (m, 8 H, aro + β-pyr), 8.64 (s, 4 H, NHCO), 8.66 (d, ^3J = 8.2 Hz, 4 H, aro), 8.95 (s, 4 H, β-pyr). ^{13}C NMR (75 MHz, $CDCl_3$, 300 K): δ = 15.0, 24.6, 27.3, 31.4, 46.4, 60.6, 115.4, 122.4, 123.6, 129.3, 130.3, 131.9, 134.4, 139.3, 169.6, 171.6. MS (MALDI-TOF): *m*/*z* = 1254.34 $[M]^+$. $C_{74}H_{70}N_{12}O_8{\cdot}CH_3OH{\cdot}CH_2Cl_2$ (1372.40): calcd. C 66.51, H 5.58, N 12.25; found C 66.52, H 6.05, N 11.88. UV/Vis (CH_2Cl_2): λ (10^{-3} ε [$M^{-1}{\cdot}cm^{-1}$]) = 421 (280.1), 516 (15.1), 549 (3.4), 588 (4.6), 643 nm (1.7). IR (KBr): ν̃ = 3477 (NH), 1691, 1631 cm^{-1} (CO).

α-5,15:β-10,20-Bis{2,2′-[*N,N*′-bis(1,6-dioxo-1,6-hexanediyl)-L-prolinoyldiamido]diphenyl}porphyrin (3): This compound was prepared from the adipoyl dichloride and obtained in 11% (15 mg) yield. ^{1}H NMR (300 MHz, $CDCl_3$, 300 K): δ = −3.95 (m, 4 H, adip), −2.52 (m, 6 H, adip + NH_{pyr}), −1.79 (m, 4 H, adip), −0.05 (m, 4 H, adip), 1.42 (m, 4 H, Pro), 1.70 (m, 4 H, Pro), 1.88 (m, 4 H, Pro), 2.29 (m, 8 H, Pro), 2.58 (m, 4 H, Pro), 4.33 (d, ^3J = 7.3 Hz, 4 H, Pro*), 7.42 (m, 8 H, aro), 7.82 (td, 4 H, ^3J = 7.7, ^4J = 2.1 Hz, aro), 8.47 (d, 4 H, ^3J = 8.1 Hz, aro), 8.67 (s, 4 H, β-pyr), 8.85 (s, 4 H, β-pyr), 9.69 (s, 4 H, NHCO). ^{13}C NMR (75 MHz, $CDCl_3$, 300 K): δ = 19.9, 24.9, 26.4, 31.2, 46.6, 60.4, 115.8, 124.2, 124.7, 129.5, 129.9, 133.4, 134.0, 135.5, 137.7, 169.9, 172.1. HR-MS (LSI-MS); *m*/*z*($C_{76}H_{75}N_{12}O_8$ [M + H]$^+$): calcd. 1283.5831; found 1283.5848. UV/Vis (CH_2Cl_2): λ (10^{-3} ε [$M^{-1}{\cdot}cm^{-1}$]) = 424 (288.5), 519 (15.2), 553 (3.9), 592 (4.7), 651 nm (2.2). IR (KBr): ν̃ = 3473 (NH), 1689, 1621 cm^{-1} (CO).

Typical Procedure for the Synthesis of Porphyrins 7−10: These porphyrins were synthesised according to the above-mentioned procedure, fully described for α-5,15:β-10,20-tetrakis[2-(L-prolinoylamido)-phenyl]porphyrin. Obviously, to obtain porphyrins **7**−**10**, the procedure was applied to the ααββ atropisomer, namely α-5,10:β-15,20-tetrakis[2-(L-prolinoylamido)phenyl]porphyrin. Thus, a solution of the former porphyrin, freshly prepared in 10 mL of THF, and a solution of the desired diacyl dichloride (0.264 mmol, 2.4 equiv.) in 10 mL of THF were added over 5 h with a syringe pump to a solution of NEt_3 (1.37 mL, 9.8 mmol, 90 equiv.) in 120 mL of THF placed under argon in an ice bath. The solution was stirred for 10 h. THF was removed under vacuum and the product was

chromatographed on silica gel. A CH_2Cl_2/CH_3OH mixture (98:2) was used for the elution.

α-5,10:β-15,20-Tetrakis[2-(*N*-*tert*-butoxycarbonyl-L-prolinoylamido)phenyl]porphyrin (11): *N*-Boc-L-proline (19.46 g, 90.4 mmol, 100 equiv.) was dissolved in dry THF (120 mL) under argon at −20 °C. *N*-Methylpiperidine (16.5 mL, 135 mmol, 150 equiv.) and then isobutyl chloroformate (11.15 mL, 85.9 mmol, 95 equiv.) were added. Immediately, a white precipitate appeared. A solution of TAPP ααββ (610 mg, 0.9 mmol) in 50 mL of THF, maintained at −20 °C, was then added. The reaction mixture was stirred for 3 h at this temperature and then warmed to room temperature. The mixture was filtered and the precipitate washed with diethyl ether. The solution was concentrated under vacuum and the residue was chromatographed on silica gel [elution with a CH_2Cl_2/CH_3OH (98:2)]. 1.18 g of pure product was obtained (89% yield). ^{1}H NMR (500 MHz, $CDCl_3$, 300 K): δ = −2.68 (s, 2 H, NH_{pyr}), −1.96 (s, 1 H, Pro), −1.63 (m, 1 H, Pro), −0.99 (m, 1 H, Pro), −0.44 (m, 2 H, Pro), −0.12 (m, 4 H, Pro), 0.63 (m, 4 H, Pro), 0.89 (m, 6 H, Pro), 1.17 (m, 36 H, Boc), 1.61 (s, 3 H, Pro), 2.66 (m, 2 H, Pro), 3.49 (m, 4 H, Pro*), 7.18 (s, 2 H), 7.64 (d, ^3J = 7.0 Hz, 2 H), 7.90 (m, 4 H), 8.00 (d, ^3J = 7.5 Hz, 4 H), 8.10 (s, 2 H), 8.16 (m, 4 H), 8.61 (d, ^3J = 6.5 Hz, 2 H), 8.71 (s, 2 H), 8.80 (s, 4 H, NHCO), 8.87 (s, 2 H). ^{13}C NMR (125 MHz, $CDCl_3$, 300 K): δ = 28.7, 28.9, 30.1, 43.9, 46.4, 59.5, 61.7, 114.5, 117.7, 120.6, 123.7, 124.6, 125.0, 127.3, 127.5, 130.2, 130.6, 131.8, 133.2, 134.0, 136.09, 139.1, 145.9, 152.9, 154.3, 170.5, 171.5. MS (FAB): *m*/*z* = 1463.0 $[M]^+$. HR-MS (LSI-MS); *m*/*z*($C_{84}H_{94}N_{12}NaO_{12}$ $[M + Na]^+$): calcd. 1485.7012; found 1485.6994. UV/Vis (CH_2Cl_2): λ (10^{-3} ε [$M^{-1}\cdot cm^{-1}$]) = 419 (308.2), 513 (16.8), 546 (3.9), 587 (4.9), 642 nm (1.7). IR (KBr): ṽ = 3383 (NH), 1698 cm^{-1} (CO). For the removal of the Boc group, **11** (0.16 g, 0.11 mmol) was dissolved in 10 mL of CH_2Cl_2 under argon. 1 mL of TFA was added. After 30 min, the solvent was removed under vacuum. The reaction was almost quantitative (0.11 g) and α-5,10:β-15,20-tetrakis[2-(L-prolinoylamido)phenyl]porphyrin used without any further purification.

α-5,10:β-15,20-Bis{2,2′-[*N,N*′-bis(1,4-dioxo-1,4-butanediyl)-L-prolinoyldiamido]diphenyl}porphyrin (7): This compound was prepared from succinyl dichloride and obtained in 45% (57 mg) yield. ^{1}H NMR (500 MHz, [D_5]pyridine, 383 K): δ = −1.78 (s, 2 H, NH), −1.52 (s, 2 H), −0.19 (s, 2 H), 0.12 (s, 2 H), 0.92 (s, 2 H), 1.08 (m, 8 H), 1.28 (m, 2 H), 1.43 (m, 2 H), 1.58 (m, 2 H), 1.79 (m, 2 H), 2.12 (m, 2 H), 2.46 (s, 2 H), 2.70 (m, 2 H), 2.85 (m, 2 H), 3.91 (m, 2 H, Pro*), 4.29 (m, 2 H, Pro*), 7.43 (t, ^3J = 7.5 Hz, 2 H, aro), 7.84 (m, 8 H), 8.04 (d, ^3J = 7.0 Hz, 2 H, aro), 8.34 (s, 2 H), 8.84 (d, ^3J = 4.5 Hz, 2 H, β-pyr), 8.89 (d, ^3J = 4.5 Hz, 2 H, β-pyr), 8.95 (s, 2 H), 9.04 (m, 4 H), 9.12 (s, 2 H), 9.63 (s, 2 H). ^{13}C NMR (500 MHz, $CDCl_3$, 300 K): δ = 24.2, 25.1, 25.7, 26.2, 27.6, 28.7, 45.2, 46.9, 60.1, 61.1, 114.2, 117.0, 119.7, 121.3, 122.4, 123.7, 130.1, 130.4, 131.5, 133.5, 135.1, 136.8, 138.1, 140.0, 169.7, 170.7. MS (FAB): *m*/*z* = 1227.50 $[M + H]^+$. $C_{72}H_{66}N_{12}O_8\cdot H_2O\cdot CH_2Cl_2$ (1330.32): calcd. C 65.91, H 5.30, N 12.63; found C 65.78, H 5.58, N 12.25. UV/Vis (CH_2Cl_2): λ (10^{-3} ε [$M^{-1}\cdot cm^{-1}$]) = 422 (265.2), 516 (14.4), 549 (3.5), 589 (4.9), 646 nm (1.2). IR (KBr): ṽ = 3449 (NH), 1681 cm^{-1} (CO).

α-5,10:β-15,20-Bis{2,2′-[*N,N*′-bis(1,5-dioxo-1,5-pentanediyl)-L-prolinoyldiamido]diphenyl}porphyrin (8): This compound was prepared from the glutaryl dichloride and obtained in 24% (33 mg) yield. ^{1}H NMR (300 MHz, $CDCl_3$, 300 K): δ = −3.88 (m, 2 H, glut), −3.16 (m, 4 H, glut), −2.72 (s, 2 H, NH_{pyr}), −0.63 (m, 6 H, glut), 1.55 (m, 10 H, Pro), 1.93 (m, 4 H, Pro), 2.90 (m, 10 H, Pro), 4.16 (m, 4 H, Pro*), 7.44 (t, ^3J = 7.3 Hz, 2 H, aro), 7.56 (t, ^3J = 7.3 Hz, 2 H, aro), 7.84 (m, 4 H, aro + β-pyr), 7.92 (d, ^3J = 7.6 Hz, 2 H, aro), 7.98 (d, ^3J = 7.6 Hz, 2 H, aro), 8.25 (d, ^3J = 8.2 Hz, 2 H, aro), 8.73 (d, ^3J = 7.3 Hz, 4 H, aro), 8.79 (s, 4 H, NHCO), 8.87 (m, 4 H, β-pyr), 9.01 (s, 2 H, β-pyr). ^{13}C NMR (75 MHz, $CDCl_3$, 300 K): δ = 14.6, 15.9, 20.2, 24.6, 24.7, 26.2, 26.4, 27.3, 28.8, 31.7, 33.3, 33.6, 46.1, 47.0, 60.2, 60.5, 60.9, 115.3, 116.0, 121.6, 123.0, 124.6, 125.8, 129.8, 129.9, 131.9, 134.5, 135.6, 136.6, 138.2, 138.6, 169.6, 170.2, 171.4, 172.1, 173.4, 177.6. UV/Vis (CH_2Cl_2): λ (10^{-3} ε [$M^{-1}\cdot cm^{-1}$]) = 424 (301.2), 518 (15.4), 551 (4.2), 591 (5.1), 646 nm (1.8). HR-MS (LSI-MS); *m*/*z*($C_{74}H_{71}N_{12}O_8$ $[M + H]^+$): calcd. 1255.5518; found 1255.5516. IR (KBr): ṽ = 3467 (NH), 1690, 1625 cm^{-1} (CO).

α-5,10:β-15,20-Bis{2,2′-[*N,N*′-bis(1,6-dioxo-1,6-hexanediyl)-L-prolinoyldiamido]diphenyl}porphyrin (9): This compound was prepared from the adipoyl dichloride and obtained in 15% (22 mg) yield. ^{1}H NMR (500 MHz, [D_6]DMSO, 423 K): δ = −2.49 (m, 6 H, adip), −2.32 (m, 2 H, NH_{pyr}), −1.34 (m, 2 H, adip), −0.55 (m, 4 H, adip), 0.89 (m, 4 H, adip), 1.21 (m, 4 H, Pro), 1.29 (m, 6 H, Pro), 1.59 (m, 6 H, Pro), 2.18 (m, 4 H, Pro), 2.29 (m, 4 H, Pro), 3.79 (m, 2 H, Pro*), 3.92 (m, 2 H, Pro*), 7.55 (t, 2 H, ^3J = 6.8 Hz, aro), 7.63 (t, ^3J = 7.3 Hz, 2 H, aro), 7.77 (s, 4 H), 7.85 (q, ^3J = 8.2 Hz, 4 H, aro), 8.05 (d, ^3J = 6.4 Hz, 2 H, aro), 8.32 (s, 4 H), 8.61 (s, 4 H), 8.69 (s, 2 H), 8.77 (s, 4 H). ^{13}C NMR (75 MHz, $CDCl_3$, 300 K): δ = 14.6, 20.5, 24.5, 24.7, 34.3, 46.5, 60.4, 60.7, 115.6, 123.5, 124.3, 124.5, 124.9, 130.1, 130.3, 130.8, 131.8, 132.4, 133.2, 133.9, 134.8, 135.0, 135.7, 136.1, 138.6, 138.8, 149.5, 172.5, 172.7. UV/Vis (CH_2Cl_2): λ (10^{-3} ε [$M^{-1}\cdot cm^{-1}$]) = 423 (170.3), 517 (9.6), 551 (2.8), 591 (2.9), 647 nm (0.9). HR-MS (LSI-MS); *m*/*z* ($C_{76}H_{75}N_{12}O_8$ $[M + H]^+$): calcd.1283.5831; found 1283.5835. IR (KBr): ṽ = 3477 (NH), 1694, 1636 cm^{-1} (CO).

α-5,10:β-15,20-Bis{2,2′-[*N,N*′-bis(isophthaloyl)-L-prolinoyldiamido]diphenyl}porphyrin (10): This compound was prepared from the isophthaloyl dichloride and obtained in 29% (48 mg) yield. ^{1}H NMR (500 MHz, [D_6]DMSO, 373 K): δ = −3.30 (s, 2 H, NH_{pyr}), 0.89 (m, 2 H), 1.30 (m, 4 H), 1.42 (m, 2 H), 1.62 (m, 2 H), 1.80 (m, 6 H), 1.93 (m, 4 H), 2.51 (m, 4 H), 3.90 (m, 2 H), 4.10 (m, 4 H), 5.04 (m, 4 H), 5.70 (m, 2 H), 7.58 (m, 4 H), 7.86 (m, 8 H), 8.15 (d, ^3J = 7.1 Hz, 4 H), 8.43 (m, 2 H), 8.51 (d, ^3J = 7.7 Hz, 2 H), 8.55 (s, 2 H), 8.62 (s, 2 H), 8.67 (s, 4 H). ^{13}C NMR (125 MHz, $CDCl_3$, 300 K): δ = 22.9, 23.1, 25.5, 25.6, 25.7, 26.0, 26.6, 28.9, 29.5, 30.2, 33.5, 40.3, 40.4, 40.6, 48.1, 49.5, 49.4, 50.5, 51.2, 51.4, 61.2, 62.5, 62.8, 117.7, 119.9, 120.6, 121.3, 123.3, 123.6, 123.8, 124.4, 124.8, 125.0, 126.5, 127.0, 127.2, 127.8, 128.3, 129.9, 130.2, 130.7, 135.8, 136.5, 136.7, 136.9, 138.0. 139.0, 152.8, 154.3, 157.9, 169.1, 170.4, 171.4. HR-MS (LSI-MS); *m*/*z*($C_{80}H_{66}N_{12}NaO_8$ $[M + Na]^+$): calcd. 1345.5024; found 1345.5079. UV/Vis (CH_2Cl_2): λ (10^{-3} ε [$M^{-1}\cdot cm^{-1}$]) = 419 (219.7), 513 (12.5), 546 (3.3), 588 (3.8), 644 nm (1.4). IR (KBr): ṽ = 3412 (NH), 1684, 1639 cm^{-1} (CO).

Typical Procedure for the Insertion of Iron Ions in Porphyrins: 50 mg of **2**−**3**, or **7**−**10** was dissolved in toluene (10 mL) inside a glove box maintained under 1 ppm of dioxygen. 2,6-Lutidine and an excess of $FeBr_2$ were added to the mixture. The solution was heated at reflux for 12 h until the reaction was complete as indicated by UV/Vis spectroscopy. The product was oxidised by air for 1 h. The solvent was removed under vacuum. The residue was dissolved in CH_2Cl_2, and washed with brine. The product was chromatographed on silica gel. A CH_2Cl_2/CH_3OH mixture (95:5) was used for the elution. The yield was almost quantitative (95%).

(α-5,15:β-10,20-Bis{2,2′-[*N,N*′-bis(1,5-dioxo-1,5-pentanediyl)-L-prolinoyldiamido]diphenyl}porphyrin)iron(III) Chloride (2Fe): This compound was prepared from **2**. MS (MALDI-TOF): *m*/*z* = 1308.07 $[M - Cl]^+$. $C_{74}H_{68}ClFeN_{12}O_8\cdot 3CH_3OH$ (1440.83): calcd.

C 64.19, H 5.60, N 11.67; found C 64.20, H 5.31, N 10.44. UV/Vis (CH_2Cl_2): λ (10^{-3} ε [$M^{-1}\cdot cm^{-1}$]) = 422 (58.2), 580 nm (4.4). IR (KBr): $\tilde{\nu}$ = 3471 (NH), 1691, 1655 cm^{-1} (CO).

(α-5,15:β-10,20-Bis{2,2′-[*N,N′*-bis(1,6-dioxo-1,6-hexanediyl)-L-prolinoyldiamido]diphenyl}porphyrin)iron(III) Chloride (3Fe): This compound was prepared from **3**. MS (MALDI-TOF): *m/z* = 1336.55 [M − Cl + H]$^+$. $C_{76}H_{72}ClFeN_{12}O_8\cdot CH_2Cl_2\cdot CHCl_3\cdot CH_3OH$ (1609.11): calcd. C 58.97, H 4.95, N 10.45; found C 58.98, H 5.53, N 10.38. UV/Vis (CH_2Cl_2): λ (10^{-3} ε [$M^{-1}\cdot cm^{-1}$]) = 422 (49.7), 580 nm (5.8). IR (KBr): $\tilde{\nu}$ = 3415 (NH), 1692, 1620 cm^{-1} (CO).

(α-5,10:β-15,20-Bis{2,2′-[*N,N′*-bis(1,4-dioxo-1,4-butanediyl)-L-prolinoyldiamido]diphenyl}porphyrin)iron(III) Chloride (7Fe): This compound was prepared from **7**. MS (FAB): *m/z* = 1281.70 [M − Cl + H]$^+$. UV/Vis (CH_2Cl_2): λ (10^{-3} ε [$M^{-1}\cdot cm^{-1}$]) = 420 (7.6), 504 nm (1.1). IR (KBr): $\tilde{\nu}$ = 3416 (NH), 1638 cm^{-1} (CO).

(α-5,10:β-15,20-Bis{2,2′-[*N,N′*-bis(1,5-dioxo-1,5-pentanediyl)-L-prolinoyldiamido]diphenyl}porphyrin)iron(III) Chloride (8Fe): This compound was prepared from **8**. MS (MALDI-TOF): *m/z* = 1307.54 [M − Cl]$^{+\cdot}$. UV/Vis (CH_2Cl_2): λ (10^{-3} ε [$M^{-1}\cdot cm^{-1}$]) = 421 (9.6), 513 nm (1.4). IR (KBr): $\tilde{\nu}$ = 3447 (NH), 1693, 1629 cm^{-1} (CO).

(α-5,10:β-15,20-Bis{2,2′-[*N,N′*-bis(1,6-dioxo-1,6-hexanediyl)-L-prolinoyldiamido]diphenyl}porphyrin)iron(III) Chloride (9Fe): This compound was prepared from **9**. MS (MALDI-TOF): *m/z* = 1336.44 [M − Cl]$^+$. $C_{76}H_{72}ClFeN_{12}O_8\cdot CH_2Cl_2\cdot CHCl_3$ (1577.07): calcd. C 59.40, H 4.79, N 10.66; found C 59.28, H 4.95, N 10.52. UV/Vis (CH_2Cl_2): λ (10^{-3} ε [$M^{-1}\cdot cm^{-1}$]) = 421 (67.1), 579 nm (6.2). IR (KBr): $\tilde{\nu}$ = 3415 (NH), 1695, 1636 cm^{-1} (CO).

(α-5,10:β-15,20-Bis{2,2′-[*N,N′*-bis(isophthaloyl)-L-prolinoyldiamido]diphenyl}porphyrin)iron(III) Chloride (10Fe): This compound was prepared from **10**. MS (FAB): *m/z* = 1377.60 [M − Cl + H]$^+$. UV/Vis (CH_2Cl_2): λ (10^{-3} ε [$M^{-1}\cdot cm^{-1}$]) = 420 (36.1), 578 nm (2.6). IR (KBr): $\tilde{\nu}$ = 3394 (γNH), 1698 cm^{-1} (CO).

General Procedure for Asymmetric Olefin Epoxidation: The catalyst (1 μmol) and the olefin (1000 μmol) were dissolved in degassed CH_2Cl_2 (2 mL) in a Schlenk tube. While stirring under N_2, PhIO (100 μmol) was added in one portion. The mixture was stirred at room temperature for 30 min and then quenched with 2% PPh_3 in CH_2Cl_2. The solvent was removed under reduced pressure. Pentane was added and the mixture was filtered. Dodecane (10 μL, GC standard) was added. Enantiomeric excesses were determined by GC on a Chirasil-Dex CB capillary column. The GC conditions were as follows (epoxide, oven temperature, retention time): *p*-chlorostyrene oxide, 120 °C, 22.5 and 24.3 min; 1,2-dihydronaphthalene oxide, 130 °C, 18.9 and 20.4 min.

Acknowledgments

The authors thank the CNRS and the Région de Bourgogne for financial support and analytical facilities. V. B.-C. gratefully acknowledges the MENRT for her grant.

[1] J. T. Groves, T. E. Nemo, R. S. Myers, *J. Am. Chem. Soc.* **1979**, *101*, 1032−1033.
[2] J. P. Collman, X. M. Zhang, V. J. Lee, E. S. Uffelman, J. I. Brauman, *Science* **1993**, *261*, 1404−1411 and references therein.
[3] E. Rose, M. Quelquejeu, R. P. Pandian, A. Lecas-Nawrocka, A. Vilar, G. Ricart, J. P. Collman, Z. Wang, A. Straumanis, *Polyhedron* **2000**, *19*, 581−586.
[4] B. Meunier, *Chem. Rev.* **1992**, *92*, 1411−1456.
[5] M. P. Doyle, in: *Catalytic Asymmetric Synthesis* (Ed.: I. Ojima), VCH Publishers, New York, **1993**, pp. 63−99.
[6] J. P. Simonato, J. Pécaut, W. R. Scheidt, J.-C. Marchon, *Chem. Commun.* **1999**, 989−990.
[7] J. P. Collman, Z. Wang, A. Straumanis, M. Quelquejeu, E. Rose, *J. Am. Chem. Soc.* **1999**, *121*, 460−461.
[8] W. Zhang, J. L. Loebach, S. R. Wilson, E. N. Jacobsen, *J. Am. Chem. Soc.* **1990**, *112*, 2801−2803.
[9] E. N. Jacobsen, in: *Catalytic Asymmetric Synthesis* (Ed.: I. Ojima), VCH Publishers, New York, **1993**, pp. 159−202.
[10] H. Jacobsen, L. Cavallo, *Chem. Eur. J.* **2001**, *7*, 800−807.
[11] Z. Gross, S. Ini, *J. Org. Chem.* **1997**, *62*, 5514−5521.
[12] C. Pérollier, J. Pécaut, R. Ramasseul, J.-C. Marchon, *Inorg. Chem.* **1999**, *38*, 3758−3759.
[13] G. Reginato, L. D. Bari, P. Salvadori, R. Guilard, *Eur. J. Org. Chem.* **2000**, 1165−1171.
[14] B. Boitrel, V. Baveux-Chambenoît, P. Richard, *Eur. J. Org. Chem.* **2001**, 4213−4221.
[15] All the geometry optimisations were performed by using the MM+ force field. This force field is an extension of MM2 developed by Allinger (N. L. Allinger, *J. Am. Chem. Soc.* **1977**, *99*, 8127−8134) and implemented in the HyperChem software.
[16] To synthesize the two different groups of molecules in Figure 1, two atropisomers of the *meso*-tetrakis(*o*-aminophenyl)porphyrin (TAPP) were used. The αβαβ atropisomer leads to the series of catalysts **1**−**6** with the two straps attached across the porphyrin macrocycle where the ααββ atropisomer yields the second series with the straps grafted on two adjacent *meso* positions.
[17] E. Rose, M. Soleilhavoup, L. Christ-Tommasino, G. Moreau, J. P. Collman, M. Quelquejeu, A. Straumanis, *J. Org. Chem.* **1998**, *63*, 2042−2044.
[18] J. T. Groves, R. S. Myers, *J. Am. Chem. Soc.* **1983**, *105*, 5791−5796.
[19] J. T. Groves, T. E. Nemo, *J. Am. Chem. Soc.* **1983**, *105*, 5786−5791.
[20] B. Boitrel, A. Lecas, Z. Renko, E. Rose, *New J. Chem.* **1989**, *13*, 73−99.
[21] E. Rose, A. Lecas, M. Quelquejeu, A. Kossanyi, B. Boitrel, *Coord. Chem. Rev.* **1998**, *178*−*180*, 1407−1431.
[22] D. Mansuy, P. Battioni, J.-P. Renaud, P. Guerin, *Chem. Commun.* **1985**, 155−156.
[23] J.-P. Renaud, P. Battioni, D. Mansuy, *Nouv. J. Chim.* **1987**, *11*, 279−290.
[24] G. Reginato, Thesi Di Laurea, Università Degli Studi Di Pisa, Italy, **1995**.
[25] C. Pérollier, M. Mazzanti, J.-P. Simonato, F. Launay, R. Ramasseul, J.-C. Marchon, *Eur. J. Org. Chem.* **2000**, 583−589.

Received December 19, 2001
[I01516]

Structural Chemistry and Magnetism of Tb^{3+}-β′′-Alumina ($Tb_{0.46}Al_{10.62}Mg_{0.38}O_{17}$)

Frank Soetebier[a] and Werner Urland*[a]

Keywords: Aluminum / Magnesium / Terbium / Ion exchange / Crystal structure / Magnetic properties

The structure of completely exchanged Tb^{3+}-β′′-Al_2O_3 ($Tb_{0.46}Al_{10.62}Mg_{0.38}O_{17}$) crystals has been investigated by single crystal X-ray diffraction methods at room temperature [trigonal, $R\bar{3}m$, $Z = 3$, $a = 560.91(8)$ pm, $c = 3330.3(8)$ pm]. The terbium ions are found to occupy BR (49.2%) and mO positions (50.8%) in nearly the same amount. The structural results are discussed in relation to magnetic measurements on crushed single crystals, where ligand field calculations applying the angular overlap model have been taken into account.
(© Wiley-VCH Verlag GmbH, 69451 Weinheim, Germany, 2002)

Introduction

The fast ion conductor Na^+-β′′-Al_2O_3, so-called β′′-alumina, is generally described by the formula given by Bettman and Peters as $Na_{1+x}Mg_xAl_{11-x}O_{17}$ ($x = 0.24-0.7$).[1] It crystallizes in the trigonal space group $R\bar{3}m$ and consists of close-packed spinel blocks separated by conduction planes containing the mobile Na^+ cations. Covalent Al−O−Al bonds and Coulomb attraction forces of the in-plane cations to the spinel bock anions connect the blocks. Due to the high mobility of the Na^+ ions they can be replaced by other mono-, di- and trivalent cations, especially by lanthanide ions (Ln^{3+}).[2,3] There are two possible crystallographic positions for the cations within the conduction plane: the sevenfold coordinated (smaller) Beevers−Ross (BR) site (C_{3v} symmetry, 6c Wyckoff notation in $R\bar{3}m$) and the eightfold coordinated (larger) mid-Oxygen (mO) site (C_{2h} symmetry, 9d Wyckoff notation in $R\bar{3}m$). The content of Na^+ cations affects the height of the conduction slabs and therefore the lattice constant c.[4]

Previous investigations on Ln^{3+}-exchanged compounds like La^{3+}-β′′-Al_2O_3,[5] Pr^{3+}-β′′-Al_2O_3,[6] Nd^{3+}-β′′-Al_2O_3, Eu^{3+}-β′′-Al_2O_3 and Gd^{3+}-β′′-Al_2O_3 [7] show a main occupation of the higher coordinated mO site. In this paper the structure and the magnetic behaviour of completely exchanged Tb^{3+}-β′′-Al_2O_3 single crystals are presented. The determination of the ionic distribution within the conduction plane is important to understand the mobility of trivalent cations.[8,9] The observed occupancy is correlated with susceptibility measurements on crushed Tb^{3+}-β′′-Al_2O_3 crystals where ligand-field calculations applying the angular overlap model (AOM) for f-electrons[10−12] have been taken into account.

Results and Discussion

The structure of the spinel blocks (Mg/Al distributions, vacancies, etc.) is similar to other β′′-aluminas studied before and will therefore not be discussed in further detail. The ion distribution within the conduction planes (*ab*-planes) is of main interest. The structural refinements lead to a distribution of 49.2% Tb^{3+} cations on the smaller BR site and 50.8% on the larger mO site. Due to the nearly equal atomic form factors, Mg^{2+} and Al^{3+} ions within the spinel blocks were not distinguishable. Because of charge neutrality the Mg^{2+} content could be estimated from the refined cationic/anionic occupancy ratio. This results in the formula $Tb_{0.46}Al_{10.62}Mg_{0.38}O_{17}$. The site multiplicities, fractional atomic coordinates, site occupation factors and equivalent displacement parameters are given in Table 1, some interatomic distances are shown in Table 2.

Table 1. Site multiplicities, fractional atomic coordinates, site occupation factors (s.o.f.) and equivalent displacement parameters [pm^2] for $Tb_{0.46}Al_{10.62}Mg_{0.38}O_{17}$

Atom	site	*x/a*	*y/b*	*z/c*	s.o.f	U_{eq}
Tb1	6c	0	0	0.1781(3)	0.091(4)	230(30)
Tb2	9d	5/6	1/6	1/6	0.094(4)	580(40)
Al1	3a	0	0	0	1	50(12)
Al2	6c	0	0	0.3506(1)	1	68(10)
Al3	18h	0.3350(4)	0.5 *x/a*	0.0721(2)	1	86(8)
Al4	6c	0	0	0.4516(1)	1	91(10)
O1	18h	0.1539(5)	2 *x/a*	0.0350(2)	1	116(13)
O2	6c	0	0	0.2950(2)	1	78(19)
O3	6c	0	0	0.0981(2)	1	100(20)
O4	18h	0.1632(5)	2 *x/a*	0.2346(1)	1	87(13)
O5	3b	1/3	2/3	1/6	1	2400(400)

[a] Institut für Anorganische Chemie der Universität Hannover, Callinstrasse 9, 30167 Hannover, Germany
Fax: (internat.) + 49-(0)511/762-19032
E-mail: urland@acc.uni-hannover.de

Table 2. Selected interatomic distances [pm] in $Tb_{0.46}Al_{10.62}Mg_{0.38}O_{17}$

Tb1−O3 (1x)	266.5(13)
Tb1−O4 (3x)	246.0(9)
Tb1−O5 (3x)	326.0(1)
Tb2−O3 (2x)	279.9(7)
Tb2−O4 (4x)	277.2(4)
Tb2−O5 (2x)	280.5(1)
Al1−O1 (6x)	189.6(4)
Al2−O1 (3x)	184.1(6)
Al2−O2 (1x)	185.2(9)
Al3−O1 (2x)	199.4(4)
Al3−O2 (1x)	196.4(5)
Al3−O3 (1x)	184.3(4)
Al3−O4 (2x)	182.9(3)
Al4−O4 (3x)	177.6(5)
Al4−O5 (1x)	161.0(4)

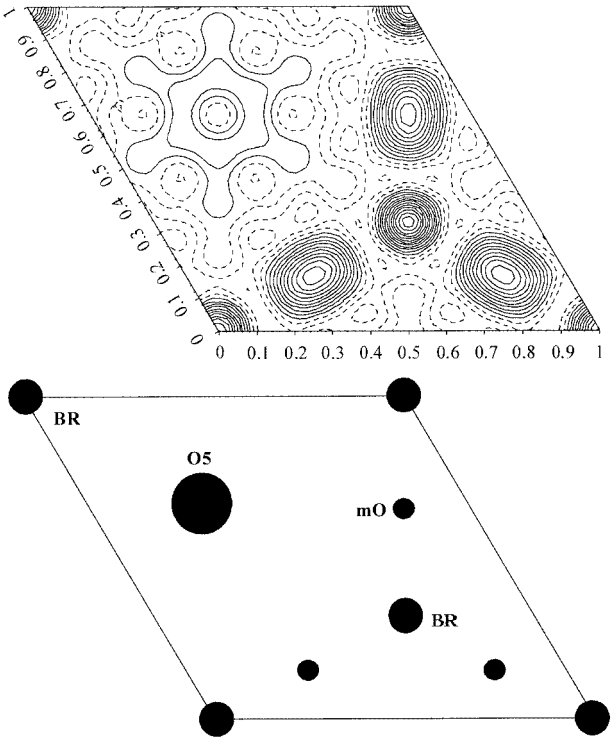

Figure 1. Electron density map (ρ_{obs}) of the conduction plane (z = 1/6); the contour intervals are 1 e·Å^{-3}; a schematic representation of the occupied sites is given beneath

As can be seen from Figure 1 the electron density is extended for all positions in the conduction plane, indicating large local disordering induced by Coulomb interactions between the ions. The Tb^{3+} ions in the mO sites are shifted towards neighbouring empty BR positions. The sites of the column oxygens O5 are influenced by the local cation environment, leading to large displacement parameters.

We observed that the size and the ionic distribution (BR/mO ratio) of the lanthanide ions are correlated with each other. The larger cations such as Nd^{3+} ions prefer the eightfold coordinated mO site (93%)[7] and the smaller ones (for example Ho^{3+} ions) the sevenfold coordinated BR site (84%).[13] Thus the BR/mO ratio of 49.2:50.8 found here for the terbium ion distribution is in line with previous findings.

From these results the ionic conductivity of La^{3+}-β′′-Al_2O_3,[5] Pr^{3+}-β′′-Al_2O_3 [14] and Ho^{3+}-β′′-Al_2O_3,[15,16] which differs in the temperature at which lanthanide ion mobility begins (574 K for La^{3+}, 564 K for Pr^{3+} and 496 K for Ho^{3+}), can be explained: the decrease of this temperature is due to an easier occupation of the BR site with smaller cations.

Magnetic susceptibility measurements on crushed single crystals were performed with a SQUID magnetometer in the 2.0−300.0 K temperature range at field strengths of 2 and 5 kOe. The magnetic susceptibilities are practically independent of the magnetic field (see Figure 2). In order to interpret the measured susceptibilities we carried out ligand-field calculations applying the angular overlap model within the basis set ^7F for Tb^{3+} and using the spin-orbit coupling constant of 1705 cm^{-1}.[17] The angular overlap parameters e_σ and e_π (Table 3) representing σ- and π-bonding between terbium ions and coordinated oxygen atoms were obtained by fitting procedures using the spiral algorithm.[18] The theoretical susceptibilities for both sites (BR and mO site) were calculated and fitted to the measured data. These were added up according to the occupancy ratio obtained from the structural investigation. The good agreement between the observed and calculated (fitted) inverse susceptibilities (R value:[19] 0.62%) of Tb^{3+}-β′′-Al_2O_3 is shown in Figure 2.

Table 3. Angular overlap parameters e_σ and e_π [cm^{-1}] for $Tb_{0.46}Al_{10.62}Mg_{0.38}O_{17}$

	e_σ	e_π
Tb1(BR)−O_S [a]	630	270
Tb1(BR)−O_C	536	142
Tb2(mO)−O_S	252	73
Tb2(mO)−O_C	341	79

[a] O_S: spinel block oxygen atoms (O3, O4), O_C: conduction plane oxygen atoms (O5).

The calculated e_σ/e_π ratios range between 2.3 and 4.3, in line with values for other lanthanide compounds (2.66 for $LaCl_3$:Tb^{3+},[20] 2.89 for $CaWO_4$:Tb^{3+},[21] 3.4 for $TbAl_3Cl_{12}$ [17]). Assuming a d^{-7} dependency of e_σ [21] (where d represents the distance between Tb^{3+} and coordinated oxygen atom) and taking d[Tb^{3+}(BR)−O_S] = 251 pm and d[Tb^{3+}(mO)−O_S] = 278 pm (averaged from Table 2) we obtain from Table 3 values for d[Tb^{3+}(BR)−O_C] = 257 pm and d[Tb^{3+}(mO)−O_C] = 266 pm. These calculated distances are smaller than the crystallographic ones (cf. Table 2). This is because the partial occupation of the BR and mO sites leads to a local coordination of the Tb^{3+} ions because of Coulomb attraction and this differs from the

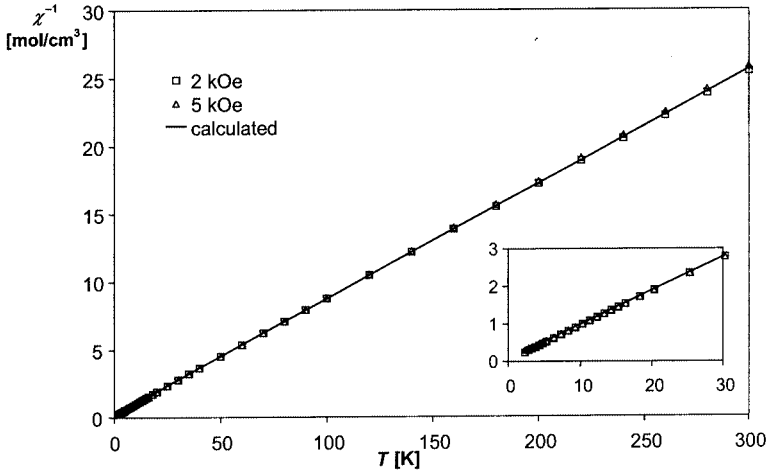

Figure 2. Observed inverse magnetic susceptibilities at different field strengths and calculated values for $Tb_{0.46}Al_{10.62}Mg_{0.38}O_{17}$ (−)

averaged coordination observed by X-ray investigation. This expresses itself in the low displacement parameters of O_S (see O3, O4 in Table 1) and the large ones of O_C (see O5 in Table 1).

Experimental Section

Na^+-β′′-Al_2O_3 (1): Na^+-β′′-alumina crystals were grown by flux evaporation from a mixture of 32.4 mol % Na_2O (from Na_2CO_3, Chempur, 99.99%), 8.0 mol % MgO (Chempur, 99.99%) and 59.6 mol % Al_2O_3 (Chempur, 99.99+%). The Na_2O-rich flux was heated for 19 days in a platinum foil coated crucible of corundum at 1680 °C according to an empirical temperature program.[22]

Tb^{3+}-β′′-Al_2O_3 (2): For the ion-exchange reaction a platinum net containing clear and colourless crystals of **1** was immersed under an argon atmosphere in an anhydrous $TbCl_3$ melt (Aldrich, 99.99%). To ensure a nearly complete exchange the crystals were exposed to the melt for 72 hours at 650 °C. No further heat treatments were applied after quenching the crystals to room temperature.

Magnetic Measurements: Measurements of the magnetic susceptibility were performed with a SQUID magnetometer (MPMS5, Quantum Design) in the 2.0 to 300 K temperature range at field strengths of 2 and 5 kOe. A polycrystalline sample of crushed single crystals was placed in a gelatine capsule and fixed with conventional cotton wool. The raw magnetic data were corrected for diamagnetism by measuring susceptibilities of Na^+-β′′-Al_2O_3.

X-ray Crystallographic Study: Crystallographic data were collected with a Stoe-IPDS diffractometer at room temperature. An optical clear single crystal was chosen for X-ray measurements. For details of the measurement see Table 4. The initial parameters used in the least-squares refinement of the spinel blocks and the bridging oxygen ions (O5) were taken from published parameters of Na^+-β′′-Al_2O_3.[1] BR and mO positions were occupied with Tb^{3+} ions (Tb1 and Tb2, respectively). The final refinement results in a distribution of 49.2% Tb^{3+} cations on the smaller BR site and 50.8% on the larger mO site. Due to the nearly equal atomic form factors, Mg^{2+} and Al^{3+} ions within the spinel blocks were not distinguishable. Because of charge neutrality the Mg^{2+} content could be estimated from the refined cationic/anionic occupancy ratio. The atomic sites, coordinates, site occupation factors, equivalent displacement parameters and selected interatomic distances are shown in Table 1 and 2.

Further details of the crystal-structure investigation may be obtained from the Fachinformationszentrum Karlsruhe, 76344 Eggenstein-Leopoldshafen, Germany, on quoting the depository number CSD-412282.

Table 4. Crystallographic data for $Tb_{0.46}Al_{10.62}Mg_{0.38}O_{17}$

Compound	$Tb_{0.46}Al_{10.62}Mg_{0.38}O_{17}$
Crystal system	trigonal
Space group	$R\bar{3}m$
Lattice constants [pm]	a = 560.91(8) c = 3330.3(8)
V [pm^3]	907.4(3)·10^6
Z	3
ρ (X-ray) [g/cm^3]	3.527
Absorption coefficient [μ/mm^{-1}]	3.681
F(000)	927
Crystal dimensions [mm^3]	0.241·0.518·0.047
Diffractometer	Stoe-IPDS
Temperature [K]	293(2)
Wavelength	Mo-K_α (λ = 71.073 pm)
θ range [°]	3.3 ≤ 2θ ≤ 52.1
Index range (h, k, l)	±6, ±6, ±40
R_{int}	0.1116
No. of collected reflections	4237
No. of independent reflections	261
Observed reflections with F>2σ	248
Absorption correction	numerical
Structure refinement	Full-matrix, least-squares
Programs used	SHELXS-97[23] and SHELXL-97[24]
No. of refined parameters	44
Goodness-of-fit	1.236
R_1, wR_2 [$I > 2\sigma(I)$]	R_1 = 0.0646; wR_2 = 0.1688
R_1, wR_2 (all data)	R_1 = 0.0666; wR_2 = 0.1703
Min., max Δ ρ [e·pm^{-3}·10^{-6}]	−1.115/1.748

[1] M. Bettmann, C. R. Peters, *J. Phys. Chem.* **1969**, *73*, 1774−1780.
[2] G. C. Farrington, B. Dunn, J. O. Thomas, *Appl. Phys. A* **1983**, *32*, 195−161.
[3] F. Tietz, W. Urland, *Solid State Ionics* **1991**, *46*, 331−335.
[4] F. Harbach, *J. Mater. Sci.* **1983**, *18*, 2437−2452.
[5] J. Köhler, W. Urland, *Z. Anorg. Allg. Chem.* **1997**, *623*, 231−238.
[6] J. Köhler, W. Urland, *Z. Anorg. Allg. Chem.* **1996**, *622*, 191−196.
[7] W. Carillo-Cabrera, J. O. Thomas, G. C. Farrington, *Solid State Ionics* **1988**, *28−30*, 317−323.
[8] J. Köhler, W. Urland, *Angew. Chem. Int. Ed. Engl.* **1997**, *36*, 85−87.
[9] J. Köhler, N. Imanaka, W. Urland, G. Adachi, *Angew. Chem. Int. Ed.* **2000**, *39*, 904−907.
[10] W. Urland, *Chem. Phys.* **1976**, *14*, 393−401.
[11] W. Urland, *Chem. Phys. Lett.* **1977**, *46*, 457−460.
[12] H. Lueken, *Magnetochemie*, Teubner-Verlag, Stuttgart, Leipzig, **1999**.
[13] F. Soetebier, W. Urland, *Z. Anorg. Allg. Chem.* **2002**, *628*, 711−714.
[14] J. Köhler, W. Urland, *Solid State Ionics* **1996**, *86−88*, 93−98.
[15] F. Tietz, W. Urland, *Solid State Ionics* **1995**, *78*, 35−40.
[16] J. Köhler, PhD Dissertation, Univ. of Hannover, **1996**.
[17] G. R. Patzke, R. Wartchow, W. Urland, *Z. Anorg. Allg. Chem.* **2000**, *626*, 789−792.
[18] A. Jones, *Comp. J.* **1970**, *13*, 301−308.
[19] J. Schmitz, H. Schilder, H. Lueken, *J. Alloys Comp.* **1994**, *209*, 49−58.
[20] W. Urland, *Chem. Phys. Lett.* **1978**, *53*, 296−299.
[21] W. Urland, *Chem. Phys.* **1979**, *38*, 407−412.
[22] F. Tietz, J. Koepke, W. Urland, *J. Cryst. Growth* **1992**, *118*, 314−318.
[23] G. M. Sheldrick, *SHELXS-97, Program for the solution of crystal structures*, Universität Göttingen, **1997**.
[24] G. M. Sheldrick, *SHELXL-97, Program for crystal structure refinement*, Universität Göttingen, **1997**.

Received January 10, 2002
[I02015]

Synthesis and Properties of a Novel Series of Organometallic Merocyanines Combining the Potent Electron-Donating [(CpFeCO)$_2$(μ-CO)(μ-C=CH−)] Fragment with Tropylium-Type Acceptors

Tony Farrell,*[a] Anthony R. Manning,*[a] Gemma Mitchell,[a] Jürgen Heck,*[b] Timo Meyer-Friedrichsen,[b] Maik Malessa,[b] Christian Wittenburg,[b] Marc H. Prosenc,[b] Des Cunningham,[c] and Pat McArdle[c]

Dedicated to Prof. Dr. Gottfried Huttner on the occasion of his 65th birthday

Keywords: Organometallic compounds / Merocyanines / Azulenes / Bond length alternation / Solvatochromism / Nonlinear optics (NLO) / Long-wavelength hyper-Rayleigh scattering (HRS)

The potent electron-donating group [(CpFeCO)$_2$(μ-CO)(μ-C=CH–)] was combined with different tropylium-based acceptors yielding the push-pull complexes [(CpFeCO)$_2$(μ-CO)(μ-C=CH–CH=A)][BF$_4$] where =A represents [=CH–(η^7-C$_7$H$_6$)Cr(CO)$_3$]$^+$ (**5**), [={C$_{10}$H$_7$}]$^+$ (azulenylium) (**7**) [={C$_{10}$H$_4$Me$_2$*i*Pr}]$^+$ (guaiazulenylium) (**8**). Crystal structures of the precursor complexes [(CpFeCO)$_2$(μ-CO)(μ-C=CH–CH=CH–C$_7$H$_7$)] (**3**), [(CpFeCO)$_2$(μ-CO){μ-C=CH–CH=CH–(η^6-C$_7$H$_7$)Cr(CO)$_3$}] (**4**) and the push-pull derivative **5** are presented. Whereas complexes **3** and **4** demonstrate localised carbon–carbon double and single bonds in the π-bridge between the diiron moiety and the seven-membered ring a small but distinct π-bond delocalisation can be observed in the π-linker of the cationic derivative **5**. From the NMR spectroscopic results a correlation between the ^{13}C NMR shift of the bridging carbon atom μ-C of the diiron unit and the coupling constant J(^{1}H-^{1}H) of the β- and γ-protons of the π-bridge was found. This correlation indicates an increased π-bond delocalisation throughout the conjugated bridge with respect to the electron-accepting capability in the order tricarbonyl(η^7-cycloheptatrienylium)chromium < guaiazulenylium < azulenylium implying a predominantly charge-delocalised form in the case of the azulenylium complex **7**. Considerably large first hyperpolarisabilities β were determined for **5** and **8** by means of hyper-Rayleigh scattering. Based on the two-level model β$_0$ values were calculated and related to the bond-length alternation in the π-linker.

(© Wiley-VCH Verlag GmbH, 69451 Weinheim, Germany, 2002)

Introduction

A major feature of the research into materials capable of doubling the frequency of incident light (second harmonic generation, SHG), a second-order nonlinear optical (NLO) property, is the determination of the first hyperpolarisability β.[1] Dipolar chromophores of the form D−π−A are the most important class of compounds capable of frequency doubling, where D represents an electron donor, A an electron acceptor and a π-bridge of unsaturated bonds providing the electronic communication between the termini. One of our approaches has been to synthesise organometallic merocyanine complexes which utilise the cationic diiron [(CpFeCO)$_2$(μ-CO)(μ-C−)]$^+$moiety as an electron acceptor[2] and the related μ-vinylidene [(CpFeCO)$_2$(μ-CO)(μ-C=CH−)] fragment as an electron donor[3] in candidates for SHG. The rationale being that theoretical[4] and experimental[5] research have demonstrated that electronic interaction between the Fe$_2$μ-C component and the conjugated system is maintained throughout rotation of the μ-C−vinyl bond.

Azulene displays many of the criteria essential for the exhibition of large first hyperpolarisabilities: it has an asymmetric charge distribution (azulene has a dipole moment of 0.8 D)[6] and it is noncentrosymmetric. Also unlike conventional organic donors such as *para*-(dialkylamino)-phenyl substituents which lose resonance stabilisation upon charge separation, azulene and their alkylated derivatives are quite unique in that the disruption of aromaticity on going from the neutral to the charged form is counterbal-

[a] University College Dublin,
Belfield, Dublin 4, Ireland
E-mail: farrell@rz.uni-potsdam.de
Anthony.Manning@ucd.ie
[b] Institut für Anorganische und Angewandte Chemie, Universität Hamburg,
Martin-Luther-King-Platz 6, 20146 Hamburg, Germany
E-mail: heck@chemie.uni-hamburg.de
[c] Chemistry Dept., National University of Ireland,
Galway, Ireland

anced by the gain of resonance energy upon formation of the azulenylium carbocation, a 6π-electron aromatic tropylium analogue (Figure 1).[7] Thus, azulene appears to be an extremely novel and versatile system and it is surprising that there are very few reports to date of azulenic NLO chromophores.[7–10] The present study focuses on the synthesis and charcterisation of a novel series of organometallic merocyanines linking the [(CpFeCO)$_2$(μ-CO)(μ-C=CH−)] fragment to tropylium-based electron acceptors.

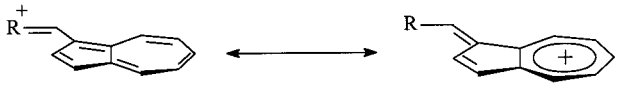

Figure 1. Resonance forms of a substituted azulenylium carbocation

Results and Discussion

Synthesis

Previous work revealed that the presence of the strong electron-donating dinuclear carbene reduces the reactivity of the formyl-substituted diiron complex [(CpFeCO)$_2$(μ-CO)(μ-C=CH−CHO)][11] (**1**) towards phosphorane nucleophiles but that extended μ-vinylidene complexes of the type [(CpFeCO)$_2$(μ-CO)(μ-C=CH−CH=CH−R)] are available using the more reactive Wittig−Horner−Wadsworth−Emmons (WHWE) reagents.[3] The diethyl (cycloheptatrienylmethyl)phosphonate (**2**) was prepared in a Michaelis−Arbuzov reaction from 1-chlormethyl-1,3,5-cycloheptatriene,[12] and treated with **1** in THF using *t*BuOK to yield the μ-vinylidene complex [(CpFeCO)$_2$(μ-CO)(μ-C=CH−CH=CH−C$_7$H$_7$)] (**3**) (Scheme 1). The

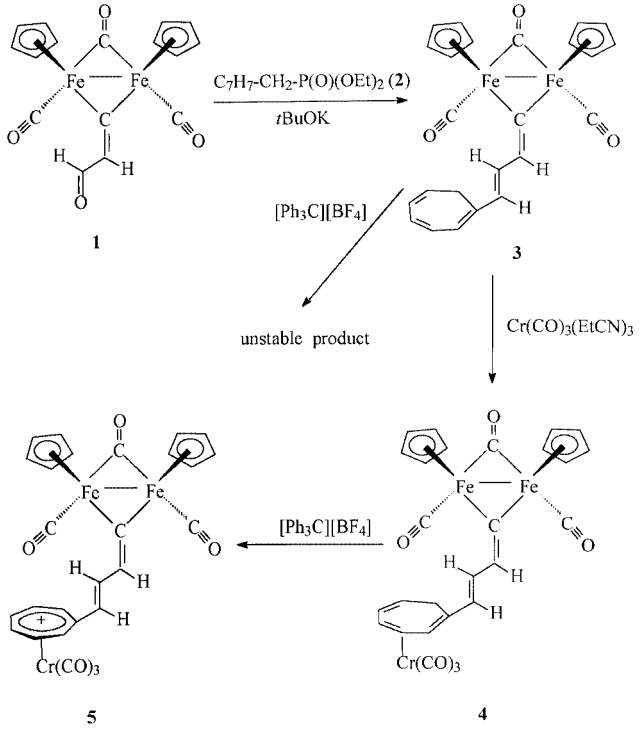

Scheme 1. Synthesis of the cationic dimetallic D−π−A complex **5**

trityl salt [Ph$_3$C][BF$_4$] was added to a solution of **3** in CH_2Cl_2 in order to abstract a hydride and to produce the tropylium derivative [(CpFeCO)$_2$(μ-CO)(μ-C=CH−CH=CH−C$_7$H$_6$)][BF$_4$]. A colour change from red-brown to blue was observed during the reaction and the IR spectrum of the reaction mixture showed the expected ν(CO) modes (2030, 1997, 1845 cm^{-1}), which are strongly shifted to higher energies compared to the corresponding ν(CO) modes of **3** (1996, 1960, 1795 cm^{-1}). However, the reaction mixture discoloured quickly and attempts to isolate the pure product were unsuccessful.

It was expected that coordination of the Cr(CO)$_3$ fragment to the seven-membered ring would greatly enhance the stability of the tropylium derivative and this was achieved by first treating **3** with Cr(CO)$_3$(EtCN)$_3$ (Scheme 1) to generate the neutral heterometallic complex [(CpFeCO)$_2$(μ-CO){μ-C=CH−CH=CH−(η^6-C$_7$H$_7$)Cr(CO)$_3$}] (**4**) as a mixture of the isomers **4a** and **4b** (Figure 2). As before, the addition of the trityl cation to a solution of the complex **4** in CH_2Cl_2 was accompanied by a dramatic colour change from red-brown to deep blue indicating a strong enhancement in the electronic communication between the diiron terminus and the cationic tricarbonyl(tropylium)chromium moiety. By layering the reaction mixture with diethyl ether a microcrystalline solid was obtained which was characterised as the cationic heterometallic merocyanine [(CpFeCO)$_2$(μ-CO){μ-C=CH−CH=CH-(η^7-C$_7$H$_6$)Cr(CO)$_3$}][BF$_4$] (**5**).

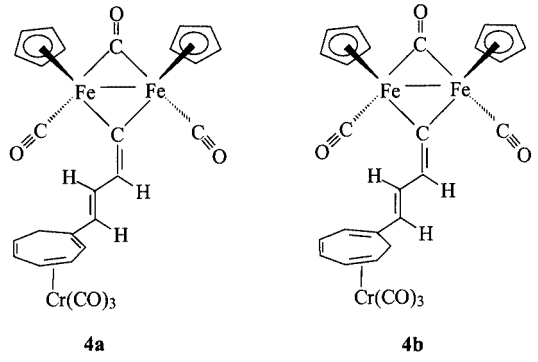

Figure 2. Different diastereoisomers of the neutral complex **4**

The reaction of the μ-ethylidyne complex [(CpFeCO)$_2$(μ-CO)(μ-C−CH$_3$)][BF$_4$][13] (**6**) with aldehydes has been found to be a facile methodology towards the preparation of cationic diiron chromophores.[2] Nonetheless, purification problems have been experienced when longer reaction periods were necessary due to the formation of [CpFe(CO)$_3$][BF$_4$] which was extremely difficult to remove.[2a] Consequently, two complimentary procedures were attempted in order to isolate the organometallic azulenylium [{C$_{10}$H$_7$}]$^+$ and guaiazulenylium [{C$_{10}$H$_4$Me$_2$*i*Pr}]$^+$ merocyanines [(CpFeCO)$_2$(μ-CO)(μ-C=CH−CH={C$_{10}$H$_7$})][BF$_4$] (**7**) and [(CpFeCO)$_2$(μ-CO)(μ-C=CH−CH={C$_{10}$H$_4$Me$_2$*i*Pr})][BF$_4$] (**8**), and also to provide versatile access to a wide range of other vinyl−carbene/carbyne complexes. Azulene- and guaiazulene-1-carboxaldehyde[14] are readily available by literature procedures and

these aldehydes were condensed with **6** in CH_2Cl_2 at 40 °C overnight giving intensely coloured reaction mixtures (Scheme 2). The air-stable merocyanine salts **7** and **8** were isolated upon filtering the reaction mixture and layering the filtrate with diethyl ether.

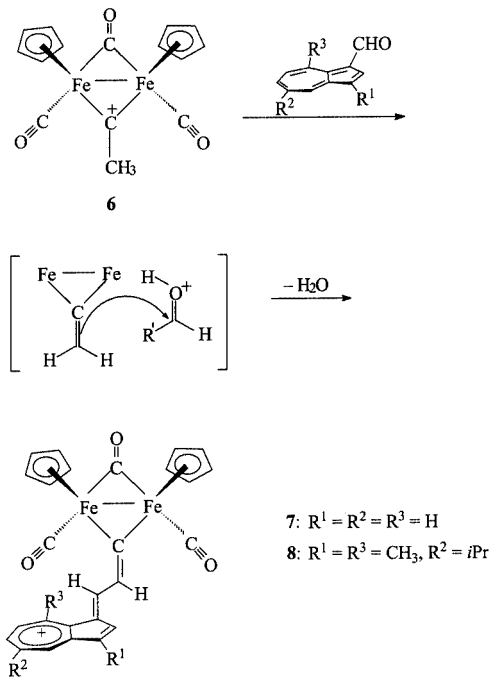

Scheme 2. Synthesis of the azulenylium and guaiazulenylium D−π−A complexes **7** and **8**

As organic[15] and organometallic[7] aldehydes have been found to react with azulenes under acidic conditions to form azulenylium based carbocationic complexes, an alternative synthetic route towards **7** and **8** was envisaged by the reaction of the formyl-substituted μ-vinylidene complex **1** with azulene and guaiazulene (Scheme 3). Condensation of **1** with an equimolar amount of azulene or guaiazulene in THF with a large excess of HBF_4 was indeed successful and again led to the isolation of **7** and **8** in high yields.

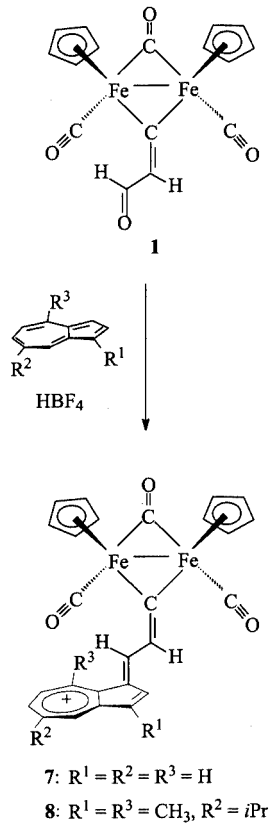

Scheme 3. Alternative synthetic route to **7** and **8**

Crystal Structures of 3, 4 and 5

Crystal and structure refinement data for the X-ray analyses are presented in Table 1 and selected bond lengths and angles are listed in Table 2. Views of the molecular structures are illustrated in Figures 3−5 along with atom labelling. The $Fe_2(\eta\text{-}C_5H_5)(CO)_2(\mu\text{-}CO)(\mu\text{-}C)$ moiety has a *cis* structure while the π-linker displays an all-*trans* geometry in all of the structures. Of note is the similarity between the bond lengths across the all-$C_{sp2}-C_{sp2}$ π-bridge (C14−C17) in **3** and **4**, whereas **5** displays slightly shorter carbon−carbon single and elongated double bonds. This suggests a predominantly μ-carbene structure in **3** and **4** with little interaction between the diiron and cycloheptatriene moiety as depicted by the olefinic mesomeric form **I** in Figure 6. In **5** the alternation in the bond lengths of the π-bridge indicates an increased electronic interaction between the termini in the solid state, which can be rationalised as a distinct contribution of the vinylcarbyne mesomeric form **II** to the electronic ground state (GS).

The extent of the bond length alternation (BLA), which is defined as the difference between the average lengths of carbon−carbon single and double bonds, has been established as a useful indicator of high first hyperpolarisabilities.[16] Several attempts to relate β to both the molecular electronic and structural parameters led to the prediction that optimal NLO activity is achieved when BLA = 0.03−0.05 Å. The BLA across the π-bridge of complexes **3** and **4** is 0.10 Å and ca. 0.11 Å, respectively, whereas for **5** the BLA is 0.07 Å, which implies a medium first hyperpolarisability value for **5**.

Another notable feature of the X-ray diffraction study, which fortifies the evidence for the strong π-communication between the termini, especially in the case of the push-pull chromophore **5**, are the calculated dihedral angles. The larger angle between the planes made by Fe_2μ-C and C14−C16 for **5** denotes a more flexible C14−C15 bond with a relatively lower bond order than for both **3** and **4**. Furthermore, the angle between the planes C14−C16 and C15−C17 increases in the order **5** < **4** < **3** (but are nonetheless quite low), attesting to the π-interaction of the entire conjugated linker.

Analysis of IR, ^{13}C and ^{1}H NMR spectra

One of the main considerations when characterising D−π−A-type compounds is the electronic configuration of

Table 1. Crystal data and structure refinement details for complexes **3**, **4** and **5**

	3	**4**	**5**
Formula	$C_{24}H_{20}Fe_2O_3$	$C_{27}H_{20}CrFe_2O_6$	$C_{28}H_{21}BCl_2CrF_4Fe_2O_6$
M_r	468.10	604.13	774.86
λ [pm]	7.1073	7.1073	7.1073
T [K]	153	153	293
Crystal system	triclinic	monoclinic	triclinic
Space group	$P\bar{1}$	$P2(1)/c$	$P\bar{1}$
a [Å]	8.7933(3)	7.305(4)	10.071(5)
b [Å]	9.5299(3)	27.261(16)	12.458(6)
c [Å]	12.7653(4)	12.163(7)	13.426(7)
α [°]	97.7220(10)	90	94.87(4)
β [°]	108.1740(10)	90.449	109.07(4)
γ [°]	90.500(10)	90	99.86(4)
V/ Å^3	1005.67(6)	2422(2)	1550.5(14)
Z	2	4	2
$\rho_{calcd.}$ [g cm^{-3}]	1.546	1.657	1.660
Abs. coeff. [mm^{-1}]	1.465	1.664	1.504
F(000)	480	1224	776
Crystal size [mm]	0.05 × 0.3 × 0.4	0.7 × 0.10 × 0.10	0.6 × 0.5 × 0.45
θ range [°]	2.44−30.00	1.49−25.03	2.46−27.5
Index range	$-12 \le h \le 12$	$-8 \le h \le 8$	$-1 \le h \le 13$
	$-13 \le k \le 13$	$-32 \le k \le 32$	$-16 \le k \le 15$
	$-17 \le l \le 17$	$-14 \le l \le 14$	$-17 \le l \le 16$
Total reflns.	25247	23460	7947
Unique reflns.	5789	4278	7112
Reflections [$I > 4\sigma(I)$]	5789	4278	7112
Parameters	244	326	407
GoF[a]	1.073	1.082	1.032
R_{int}	0.0372	0.1947	0.0326
*R*1/*wR*2 [$I > 2\sigma(I)$][b]	0.0384/0.1044	0.0857/0.1965	0.0524/0.1364
*R*1/*wR*2 (all data)[b]	0.0426/0.1069	0.1461/0.2314	0.0712/0.1531
Min./max. resd. [eA^{-3}]	−0.636/1.016	−1.010/0.853	−0.510/0.681

[a] GoF = $[\Sigma w(F_o^2 - F_c^2)^2/(n - p)]^{1/2}$; *n* = numbers of reflections, p = numbers of parameters. [b] *R*1 = $(\Sigma||Fo| - |Fc||)/\Sigma|Fo|$, *wR*2 = $[\Sigma w(F_o^2 - F_c^2)^2]/\Sigma w(F_o^2)^2]^{1/2}$.

Table 2. Selected bond lengths [Å] and angles [°] for **3**, **4** and **5**

Bond Lengths	**3**	**4**	**5**
C(1)−O(1)	1.173(2)	1.199(15)	1.137(5)
C(2)−O(2)	1.142(2)	1.142(17)	1.142(5)
C(3)−O(3)	1.136(2)	1.119(15)	1.181(5)
C(14)−C(15)	1.339(2)	1.332(18)	1.350(5)
C(15)−C(16)	1.449(2)	1.447(18)	1.423(5)
C(16)−C(17)	1.353(2)	1.341(17)	1.360(5)
C(17)−C(18)	1.452(2)	1.437(17)	1.439(5)
C(18)−C(19)	1.508(2)	1.520(17)	1.418(5)
C(18)−C(24)	1.363(2)	1.375(17)	1.431(5)
C(19)−C(20)	1.508(2)	1.486(17)	1.399(6)
C(20)−C(21)	1.331(3)	1.382(18)	1.406(7)
C(21)−C(22)	1.448(3)	1.416(19)	1.384(7)
C(22)−C(23)	1.345(3)	1.375(19)	1.413(6)
C(23)−C(24)	1.442(2)	1.408(19)	1.390(5)
Dihedral angles			
[Fe(1)−C(14)−Fe(2)][C(14)−C(16)][a]	3.7(3)	2.2(1)	−4.6(4)
[C(14)−C(16)][C(15)−C(17)][a]	12.3(4)	9.6(2)	2.4(5)
[C(15)−C(17)][C(16)−C(18)][a]	6.0(4)	0.8(2)	3.0(5)

[a] Angle between the two planes.

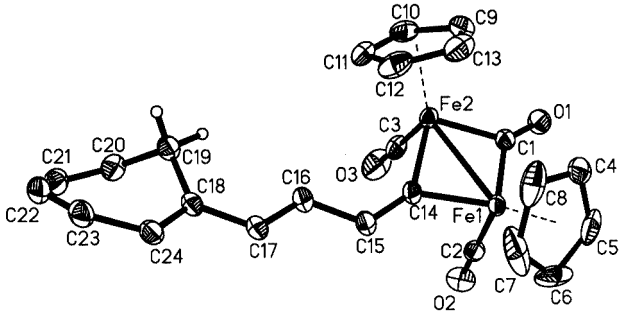

Figure 3. Molecular structure of **3** (30% ellipsoids; the hydrogen atoms are omitted for clarity except for C19, which is the C_7H_7 sp^3-carbon atom)

the molecules and how this affects the properties of the material. The systematic modification of a system coupled with the detailed analysis of the resulting changes may allow us to formulate a relationship between the molecular structure and the properties. This would greatly enhance our ability to tune a system structurally in order to maximise a particular output. In the case of these μ-vinylidene complexes the GS electronic constitution is easily evaluated by considering (i) the carbonyl stretching frequencies,

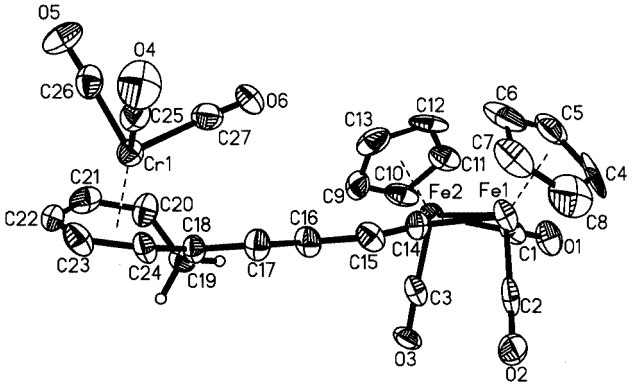

Figure 4. Molecular structure of **4** (30% ellipsoids; the hydrogen atoms are omitted for clarity except for C19, which is the C_7H_7 sp^3-carbon atom)

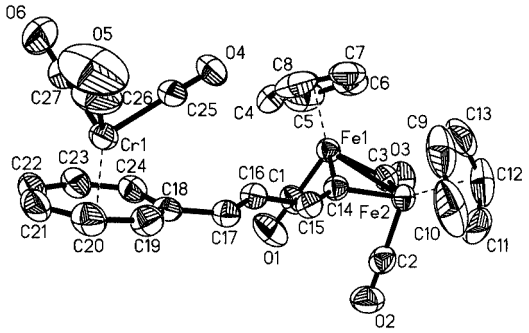

Figure 5. Molecular structure of **5** (30% ellipsoids; hydrogen atoms and the BF_4^- counterion are omitted for clarity)

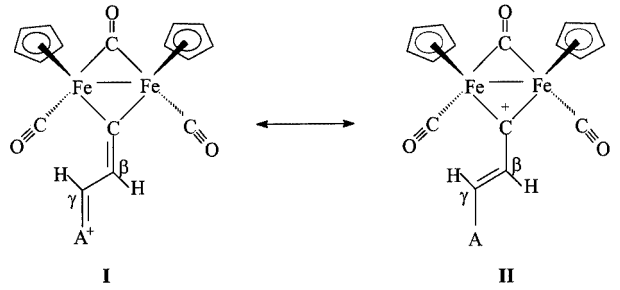

Figure 6. Mesomeric forms of the cationic donor−acceptor complexes $[(CpFeCO)_2(\mu\text{-}CO)(\mu\text{-}C{=}CH{-}CH{=}A^+)]$ where A^+ = $[CH{-}(\eta^7\text{-}C_7H_6)Cr(CO)_3]^+$ (**5**), $[C_{10}H_7]^+$ (azulenylium) (**7**), $[C_{10}H_4Me_2iPr]^+$ (guaiazulenylium) (**8**)

(ii) the number of Cp signals in both the ^1H and ^{13}C NMR spectra, (iii) the ^1H-^1H coupling constants across the unsaturated bridging ligand, and (iv) the chemical shift of the μ-carbon signal in the ^{13}C NMR spectra.

The solution IR spectra of all the complexes prepared reveal one bridging and two terminal carbonyl stretching modes, the relative intensities of which are consistent with a *cis* arrangement of these CO ligands. The wavenumbers of these ν(CO) bands are very informative in determining the extent of electronic coupling between the $Fe_2\mu$-C=CH- and the tropylium-based termini (Table 3). A predominant μ-vinylidene resonance contribution to the GS (**I**, Figure 6), can be concluded from ν(CO) bands at lower wavenumbers [ν(CO): ca. 1992, 1953 cm^{-1}].[3,17] On the other hand, charge delocalisation throughout the molecule due to increased contribution from the mesomeric form **II** to the GS (Figure 6), decreases the electron density at the $Fe_2\mu$-C core reducing the degree of M→CO back donation. The resulting ν(CO) shift to higher wavenumbers tends towards that of **6** [ν(CO): 2046, 2000 cm^{-1}][2,18] where the positive charge is fully localised on the diiron end group. As expected, the neutral fragment $[(\eta^6\text{-}C_7H_7)Cr(CO)_3]$ is the weakest electron acceptor with ν(CO) bands at 1997, 1961 cm^{-1}, followed by the corresponding cation $[(\eta^7\text{-}C_7H_6)Cr(CO)_3]^+$ with the CO stretching modes at 2007 and 1975 cm^{-1}. As expected, the azulenylium-type end groups are stronger electron acceptors due to the resonance stabilisation in both extreme mesomeric forms and display increased contribution from the μ-vinyl−carbyne resonance forms **II** to the overall GS structure. Alkylation of the azulenylium moiety results in a more stable carbocation and a weaker electron acceptor with the result that the azulenylium complex **7** exhibits the highest ν(CO) modes.

Table 3. IR, ^1H and ^{13}C NMR spectroscopic data for the complexes $[(CpFeCO)_2(\mu\text{-}CO)(\mu\text{-}C{=}CH{-}A)]$

Acceptor A		IR (cm^{-1})[a] ν(CO)		ν(μ-CO)	^1H NMR (Hz) $J(H_\beta\text{-}H_\gamma)$	^{13}C NMR (ppm) μ-C
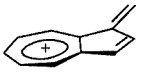	(**7**)	2024	1993	1832	13.5[b]	395[b]
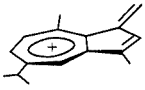	(**8**)	2017	1990	1829	12.6[b]	382[b]
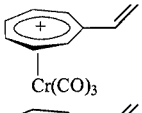	(**5**)	2007	1975(sh)	1812	11.0[b]	324[b]
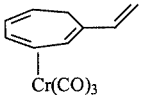	(**4**)	1997	1961	1796	10.3[c]	292[c]
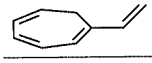	(**3**)	1996	1960	1795	10.1[c]	288[c]

[a] Solvent CH_2Cl_2. [b] Solvent $(CD_3)_2CO$. [c] Solvent $CDCl_3$.

An excellent diagnostic of the degree of charge delocalisation is the chemical shift of the μ_2-carbon atom of the π-bridge between the donor and acceptor in the ^{13}C NMR spectra (Table 3).[2,3] Increasing the potency of the electron acceptor augments the electronic interaction between the termini and the contribution from the (vinylcarbyne)diiron mesomeric form **II**. The reduction of electron density at the diiron framework results in the bridging carbon signal occurring at lower field strengths. From the position of these μ-C signals we can conclude that the azulenylium carbocations are by far the strongest electron acceptors within the presented series.

Comparing the ^1H-^1H coupling constants across the bridging $C_\beta{-}C_\gamma$ (Figure 6) bond should also aid in elucidating the GS electronic arrangement with $J(^1H_\beta\text{-}^1H_\gamma)$ increasing as the bond order increases (Table 3). Considering

the limiting mesomeric form **I** (Figure 6), which contains an sp^2-carbon−sp^2-carbon single bond between C_β and C_γ, $^1H_\beta$-$^1H_\gamma$ coupling constants of about 10 Hz are to be expected.[3,19] For **3** and **4** the structural data are in agreement with a $C_\beta-C_\gamma$ localised carbon−carbon single bond and the neutral "true" μ-vinylidene compound **3** exhibits the lowest coupling constant at $J = 10.1$ Hz. For compound **4** the $^1H_\beta$-$^1H_\gamma$ coupling value is slightly larger and the μ-^{13}C nucleus is deshielded to a smaller extent compared to **3**, demonstrating a small increase in the electron-withdrawing capability of the cycloheptatriene moiety due to the $Cr(CO)_3$ coordination. Consequently, the $C_\alpha-C_\beta$ bond remains predominantly a carbon−carbon double bond with a restricted rotation about the μ-C=CH bond. Hence, the Cp and terminal CO ligands are formally in different environments, and **3** as well as **4** exhibit two Cp and two CO signals in the ^1H and ^{13}C NMR spectra, respectively. When the bond order between C_β and C_γ displays increased C−C double bond character, as occurs in (μ-vinylcarbyne)diiron cations (mesomeric form **II** in Figure 6), the $^1H_\beta$-$^1H_\gamma$ coupling constants increase to 14.9 Hz and only one Cp and CO signal appear in the NMR spectra.[2]

The increase in $J(^1H_\beta$-$^1H_\gamma)$ agrees with the general downfield shift of the μ-C_α resonance signal of the diiron moiety and a graphic displays a linear correlation between $\delta(\mu$-$^{13}C)$ and $J(^1H_\beta$-$^1H_\gamma)$ (Figure 7). These results present strong indications that in solution there exists an increasing charge delocalisation in the order **3** < **4** << **5** << **8** < **7** for the electronic ground state, which concurs with the ordering of electron-accepting strength from the IR data. It is noteworthy that only one Cp and one CO signal are observed in the NMR spectra for all of the cationic chromophores. This is in accordance with the structural data of **5**, which displays a marked decrease of the μ-$C_\alpha-C_\beta$ double-bond character and increase of $C_\beta-C_\gamma$ bond order in the solid state. This effect may be augmented by the ion-pair separation in solution whereas in the solid state the inter ion-pair Coulomb interaction will diminish the D−A interaction within the entire cation. The correlation between $\delta(\mu$-$^{13}C)$ and $J(H_\beta$-$H_\gamma)$ indicates a considerable contribution of the μ-vinylcarbyne mesomeric form **II** to the electronic ground states for **7** and **8** in solution, which even dominates for **7**. Hence, the diiron derivatives under study represent a rare example of organometallic D−π−A complexes wherein the electronic ground state can be varied from an organometallic merocyanine-type species, in which the positive charge is mainly localised on the seven-membered ring moiety as in **5**, to a merocyanine wherein the positive charge is mainly localised on the diiron terminus as in **7**. A suitable selection of the cationic acceptor would enable the development of an organometallic polymethine with a complete delocalisation of the positive charge.

Electronic Absorption Spectra

A commonly used model called the two-level approximation relates β to the molecular optical properties and predicts that large first hyperpolarisabilities are favoured by molecules possessing intense, low-energy and highly solvatochromic charge transfer (CT) transitions.[20] These fundamental parameters cannot be optimised independently and may not be weighted equally for a particular system. For example, for the series of compounds $[(CpFeCO)_2(\mu$-$CO)(\mu$-$C-\{\pi$-bridge$\}-Fc)][BF_4]$[2b] (Fc = ferrocenyl) it was found that a large solvatochromic shift and extinction coefficient upon photoexcitation were more important to the enhancement of β than the energy of the transition.

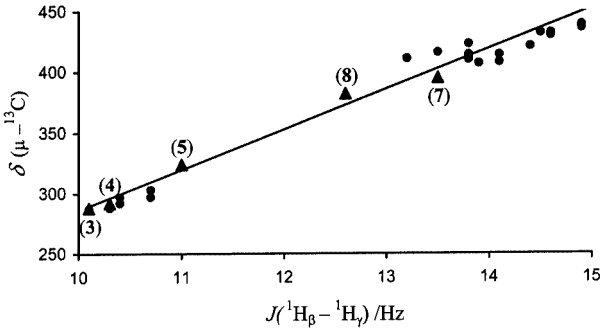

Figure 7. Correlation between $\delta(^{13}C)$ of the μ-C atom and the J coupling constants between H_β and H_γ of the π-bridge (•: data points from refs.[2,3])

The optical absorption data for the chromophores are presented in Table 4. The electronic spectra of the merocyanine salts display an intense asymmetric absorption in the visible region between 570 and 635 nm indicating a superimposition of different transitions. The two azulenylium chromophores also reveal a much weaker transition at lower energies (Figure 8). We assign the stronger absorption band to a donor−acceptor charge-transfer (DACT) transition and propose that the lower energy band is an azulene-localised π−π* transition. The strong electronic transitions are governed by medium negative solvatochromism which points towards a slightly more charge delocalised photoexcited state. However, the negative solvatochromism is much smaller than that observed for other cationic diiron NLO chromophores,[2a] confirming a certain degree of charge delocalisation in the electronic ground state as already concluded from the NMR results. This finding is also corroborated in that the solvatochromism and thus dipole change Δμ between the ground and the excited state decreases with increasing charge delocalisation: **5** > **8** > **7**. Also of note is that increasing the electron-accepting capabilities of the tropylium-based termini results in a blue shift to the CT bands (Figure 9). This is consistent with an energetically lower lying molecular orbital being involved in the CT transition as a consequence of higher GS charge delocalisation.

Hyperpolarisability Measurements

The complexes **5**, **7** and **8** were subjected to hyper-Rayleigh scattering (HRS) studies[21] but as they absorb substantially in the area of 532 nm [i.e. $I(2\omega)$ when the incident light has a wavelength of $I(\omega) = 1064$ nm], the stimulating laser light was shifted to a higher wavelength (1500 nm). Thus, the superposition of a strong absorption and the HRS signal is minimised, which makes the calculated static

Table 4. Linear and nonlinear optical data of the complexes for the complexes $[(CpFeCO)_2(\mu\text{-}CO)(\mu\text{-}C{=}CH{-}A)]$

Acceptor		λ_{max} (ε) [nm (M^{-1} cm^{-1})][a] CH_2Cl_2	CH_3CN	$\Delta\tilde{\nu}$[b] (cm^{-1})	β[a] (10^{-30} esu)	β_0 esu
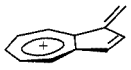	(**7**)	579 (55621)	571 (41437)	–242	nd[d]	–
		732 (1240)	721 (1651)	–208		
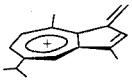	(**8**)	608 (62569)	599 (53877)	–247	274	79
		771 (2287)	756 (1412)	–257		
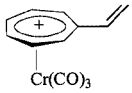	(**5**)	635 (67211)	625 (67389)	–252	451	117
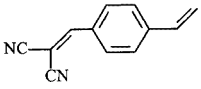	(**9**)[c]	523 (34450)	509 (29100)	–526	156	68
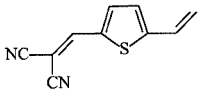	(**10**)[c]	565 (29590)	556 (33280)	–286	227	84

[a] Measured in CH_2Cl_2 solution at λ = 1500 nm, using DR1 as standard: β(DR1, CH_2Cl_2) = 70 × 10^{-30} esu. [b] $\Delta\tilde{\nu} = \tilde{\nu}_{max}(CH_2Cl_2) - \tilde{\nu}_{max}(CH_3CN)$. [c] Taken from ref.[3] [d] nd: not detected.

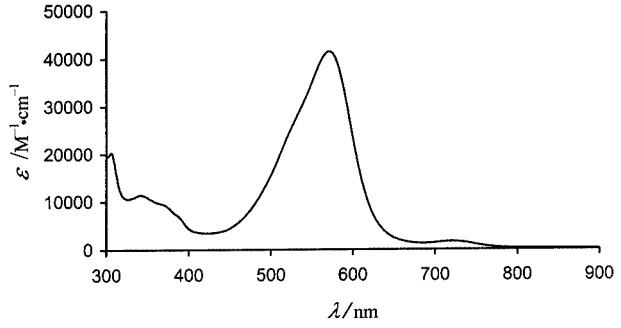

Figure 8. Electronic absorption spectra of **7** in CH_3CN

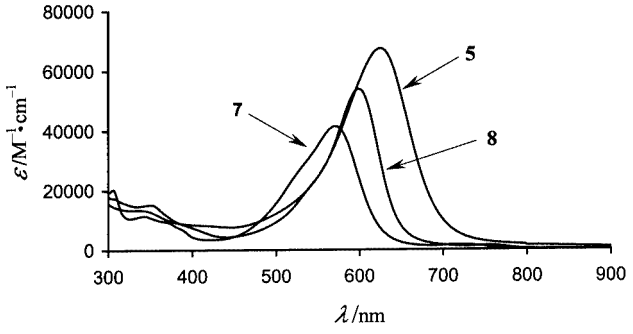

Figure 9. Electronic absorption spectra of **5**, **7** and **8** in CH_3CN

hyperpolarisability (β_0)[20] more reliable.[22,23] Another important reason for using the higher wavelength incident beam, is an attempt to discriminate between a true SHG signal and a two-photon absorption-induced fluorescence (TPAF) enhanced signal[24–26] The 1500-nm incident-beam HRS examinations were achieved using a tuneable optical parametric oscillator (OPO) based set-up.[23] All measurements were carried out using Desperse Red 1 (DR1) as an external standard. The reference hyperpolarisability β of DR1 in CH_2Cl_2 was calculated by comparing the slopes of the standard in CH_2Cl_2 and $CHCl_3$ to obtain the ratio of β_{solute}.[27] Using the value $\beta(CHCl_3) = 80 \times 10^{-30}$ esu[24] the hyperpolarisability of DR1 in CH_2Cl_2 is estimated to be 70×10^{-30} esu. The effect of the refractive indices of the solvents was corrected using the simple Lorentz local field.[28]

The first hyperpolarisability β could only be obtained for the cationic dimetallic complex **5** (451×10^{-30} esu) and the guaiazulenylium derivative **8** (274×10^{-30} esu) (Table 4), complex **7** did not show any intensity in the HRS experiment. The obtained β values are in the order of magnitude of β values found for the neutral diiron donor-based complexes containing dicyanovinyl-substituted arenes as electron acceptors ($\beta = 156 \times 10^{-30}$ esu and $\beta = 227 \times 10^{-30}$ esu, Table 4).[3] The very low extinction coefficients for the complexes **5** and **8** at λ = 750 nm allows a reliable calculation of the static hyperpolarizability β_0 using the two-level model[20b] [β_0(**5**) = 117×10^{-30} esu and β_0(**8**) = 79×10^{-30} esu]. It is noteworthy that the static hyperpolarisabilities of the four diiron donor-based NLO chromophores in Table 4 can be correlated with $J(H_\beta\text{-}H_\gamma)$, which is a measure of the carbon–carbon bond order between C_β and C_γ (vide supra) and thus, synonymous to the carbon–carbon bond length (Figure 10). The β_0 values improve with increasing $J(H_\beta\text{-}H_\gamma)$ values beyond 11 Hz and then decreases distinctly for $J(H_\beta\text{-}H_\gamma)$ = 12.6 Hz for **8**, and for complex **7** with $J(H_\beta\text{-}H_\gamma)$ = 13.5 Hz the first hyperpolarisability even vanishes. This behaviour very much resembles the correlation between the static hyperpolarizability β_0 and the bond-length alternation (BLA) in donor–acceptor-substituted polyenes found by Marder et al.[16] Therefore, the small β_0 value for **8** may be explained by the smaller BLA due to the large contribution of the μ-vinylcarbyne mesomeric form **II** to the ground state. Since the X-ray data demonstrate that in the solid state the BLA for **5** is still beyond the optimum value of 0.03–0.05, we suggest that a maximum of the β_0 values in the diiron-based NLO chromophores may be obtained, when the accepting capability of the seven-membered ring moiety is slightly enhanced compared to the $[(\eta^7\text{-}C_7H_6)Cr(CO)_3]^+$ acceptor but less potent than for the guaiazulenylium or even azulenylium electron acceptors.

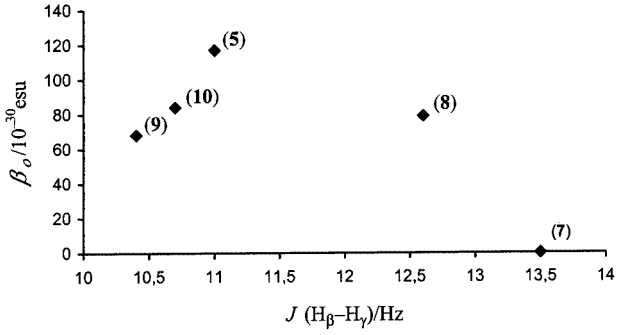

Figure 10. Correlation between the first static hyperpolarisability β_0 and the coupling constants $J(H_\beta\text{-}H_\gamma)$

The NLO properties of a series of organometallic merocyanines utilising the $[(CpFeCO)_2(\mu\text{-}CO)(\mu\text{-}C{=}CH{-})]$ fragment as an electron donor linked to thiobarbituric acid by olefinic units, demonstrated the effectiveness of the diiron unit.[27] The second-order optical nonlinearities were determined using electric-field-induced second harmonic generation (EFISH). However, as there exist problems in comparing results obtained from different techniques[25,26] no correlations will be attempted. Static hyperpolarisabilities from 1500-nm HRS experiments have been reported for organic 1D, 2D and 3D NLO chromophores.[27,28] An extremely large β_0 value was reported for the 2D NLO truxenone derivative ($\beta_0 = 169 \times 10^{-30}$ esu)[29] which is still larger than the value of β_0(**5**). However, in terms of their static hyperpolarisability to molecular mass ratio β_0/M, which is often used as a figure of merit, values of β_0/M(**5**) $= 0.153 \times 10^{-30}$ (esu·mol^{-1}·g^{-1}) and β_0/M(**8**) $= 0.149 \times 10^{-30}$ (esu·mol^{-1}·g^{-1}) were calculated for the present organometallic merocyanines, which compare well with the corresponding value of the truxenone chromophore $\beta_0/M = 0.124 \times 10^{-30}$ (esu·mol^{-1}·g^{-1}).

Conclusion

The facile synthesis is presented for a series organometallic merocyanines based on the diiron moiety $[(CpFeCO)_2(\mu\text{-}CO)(\mu\text{-}C{=}CH{-})]$ as the electron donor and the cationic tropylium derivatives $[-C{=}CH(\eta^7\text{-}C_7H_6)Cr(CO)_3]^+$ and azulenylium and guaiazulenylium as electron-accepting units, which tune the electronic properties of these D−A complexes. In ^{13}C NMR spectroscopic studies an increased deshielding of the μ-C atom of the π-bridge is observed in the order **5** < **8** < **7**, thus demonstrating the increased electron-accepting capability of the cationic seven-membered ring units in that order. Additionally, a correlation between $\delta(\mu\text{-}^{13}C)$ and $J(H_\beta\text{-}H_\gamma)$ is found which indicates a slightly stronger contribution of the μ-vinylcarbyne mesomeric form **II** to the ground state in solution for the azulenylium and guaiazulenylium congeners **7** and **8**, whereas for the tropylium derivative **5** the ground state displays extensive contribution from the μ-vinylidene mesomeric form **I**. The cationic complexes reveal a strong absorption band in UV/Vis spectra around 600 nm due to a DA−CT transition, which undergoes a medium negative solvatochromic shift. The analysis of the nonlinear optical properties by means of HRS measurements was successful for **5** and **8** and reveals that the combination of the diiron donor and the tricarbonyl(η^7-tropylium)chromium cation provides the larger experimental and static first hyperpolarisabilities β and β_0, respectively. A correlation between $J(H_\beta\text{-}H_\gamma)$ and the static hyperpolarisability β_0 very much resembles the dependence of β_0 on the bond length alternation (BLA). Hence, although the guaiazulenylium cation is a considerably stronger electron acceptor, the smaller β_0 value of **8** may be explained by a smaller bond length alternation due to the larger contribution of the μ-vinylcarbyne mesomeric form **II**.

Experimental Section

Solvent Purification and Instrumentation: Dichloromethane, diethyl ether and THF were dried by refluxing in the presence of calcium hydride and distillation prior to use. THF was further distilled from sodium/benzophenone. Infrared spectra were recorded with a Perkin−Elmer Paragon 1000 spectrometer. UV/Vis spectra were recorded with a Perkin−Elmer Lambda 6 spectrometer and a Perkin−Elmer model 554. NMR spectra were recorded with JEOL JNM-GX 270 FT and Varian Gemini 200 BB spectrometers using TMS as an internal standard. Elemental analyses were carried out by the Microanalytical Laboratory, University College, Dublin and the Institut für Anorganische und Angewandte Chemie, Universität Hamburg.

$[(CpFeCO)_2(\mu\text{-}CO)(\mu\text{-}C{=}CH{-}CH{=}CH{-}C_7H_7)]$ (3): *t*BuOK (0.13 g, 1.16 mmol) was added to a solution of $[(CpFeCO)_2(\mu\text{-}CO)(\mu\text{-}C{=}CH{-}CHO)]$[11] (**1**) (0.3 g, 0.79 mmol) and diethyl (cycloheptatrienylmethyl)phosphonate (**2**)[12] (1.1 equiv.) in dry THF (50 mL). Stirring was continued for 1 h under nitrogen, water (30 mL) was added and the mixture was extracted with dichloromethane. The organic layer was dried with $MgSO_4$ and the solvent was removed. The residue was taken up in dichloromethane and chromatographed on alumina. Product **3** eluted with dichloromethane and was recrystallised from CH_2Cl_2/hexane. Yield: 0.30 g (82%). ^1H NMR ($CDCl_3$): δ = 8.17 (d, *J* = 10.1 Hz, 1 H, μ-C=C*H*), 7.03 (dd, *J* = 10.1, 15.2 Hz, 1 H, μ-C=CH−C*H*), 6.62 (m, 1 H, C_7H_7), 6.46 (m, 1 H, C_7H_7), 6.20 (m, 3 H, μ-C=CH−CH=C*H*, C_7H_7), 5.44 (m, 1 H, C_7H_7), 4.90 (s, C_5H_5), 4.81 (s, C_5H_5), 2.74 (m, 2 H, C_7H_7) ppm. $^{13}C\{^1H\}$ NMR ($CDCl_3$): δ = 288.3 (μ-C), 270.8 (μ-CO), 210.7, 210.6 (CO), 144.3, 132.8 124.9 (μ-C=CH−CH=CH), 134.0 (C_q, C_7H_7), 131.6, 129.3, 128.1, 124.2, 122.1 (C_7H_7), 88.4, 87.8 (C_5H_5), 29.1 (C_7H_7) ppm. IR (CH_2Cl_2): $\tilde{\nu}$ = 1996 (vs), 1960 (m) [ν(CO)]; 1795 (s) [ν(μ-CO)]; 1607 (m), 1558 (w) [ν(C=C)] cm^{-1}. $C_{24}H_{20}Fe_2O_3$ (468.10): calcd. C 61.58, H 4.31; found C 61.04, H 4.68.

$[(CpFeCO)_2(\mu\text{-}CO)\{\mu\text{-}C{=}CH{-}CH{=}CH{-}(\eta^6\text{-}C_7H_7)Cr(CO)_3\}]$ (4): Compound **3** (0.3 g, 0.64 mmol) and $Cr(CO)_3(EtCN)_3$[29] (0.19 g, 0.63 mmol) were stirred in dry THF (40 mL) overnight under N_2. The solvent was removed and the residue taken up in the minimum volume of dichloromethane and chromatographed on alumina. The column was washed with toluene to remove traces of unreacted **3**. Product **4** eluted with dichloromethane and was recrystallised from CH_2Cl_2/hexane. Yield: 0.28 g (73%). ^1H NMR ($CDCl_3$, only one isomer given): δ = 8.21 (d, *J* = 10.3 Hz, 1 H, μ-C=C*H*), 6.86 (dd, *J* = 10.4, 15.0 Hz, 1 H, μ-C=CH−C*H*), 5.89 (m, 2 H, η^6-C_7H_7), 5.74 (d, *J* = 15.2 Hz, 1 H, μ-C=CH−CH=C*H*), 5.13 (m, 1 H, η^6-C_7H_7), 4.96 (s, C_5H_5), 4.86 (s, C_5H_5), 4.85 (hidden, 2 H, η^6-C_7H_7), 3.35 (m, 2 H, η^6-C_7H_7) ppm. $^{13}C\{^1H\}$ NMR ($CDCl_3$): δ = 292.1 (μ-C), 269.6 (μ-CO), 232.6 [$Cr(CO)_3$], 209.9, 209.8 (CO), 143.3, 134.1 123.3 (μ-C=CH−CH=CH), 100.7, 98.0, 97.6, 96.8, 96.3 (η^6-C_7H_7), 88.0, 87.5 (C_5H_5), 23.7 (η^6-C_7H_7) ppm. IR (CH_2Cl_2): $\tilde{\nu}$ = 1997 (vs), 1961 (m), 1898 (vs), 1869 (s) [ν(CO)]; 1796 (s) [ν(μ-CO)]; 1607 (m), 1558 (w) [ν(C=C)] cm^{-1}. $C_{27}H_{20}CrFe_2O_6$ (604.13): calcd. C 53.68, H 3.34; found C 53.09, H 3.60.

$[(CpFeCO)_2(\mu\text{-}CO)\{\mu\text{-}C{=}CH{-}CH{=}CH{-}(\eta^7\text{-}C_7H_6)Cr(CO)_3\}][BF_4]$ (5): $[Ph_3C][BF_4]$ (0.10 g, 0.30 mmol) was added to a solution of **4** (0.2 g, 0.33 mmol) in dry CH_2Cl_2 (50 mL) at −70 °C. The reaction mixture was allowed to warm to room temperature and then filtered. Product **5** was obtained by layering the filtrate with dry diethyl ether (50 mL) and cooling overnight. Yield: 0.16 g (70%). ^1H NMR [$(CD_3)_2CO$]: δ = 8.69 (d, *J* = 11.0 Hz, 1 H, μ-

C=C*H*), 8.04 (dd, *J* = 11.0, 14.6 Hz, 1 H, μ-C=CH−C*H*), 6.95 (m, 2 H, η^7-C_7H_6), 6.70 (m, 4 H, η^7-C_7H_6), 6.39 (d, 1 H, μ-C=CH−CH=C*H*), 5.22 (s, 10 H, C_5H_5). $^{13}C\{^1H\}$ NMR [$(CD_3)_2CO$]: δ = 323.7 (μ-C), 265.6 (μ-CO), 225.1, [$Cr(CO)_3$], 211.6 (CO), 146.9, 145.7 116.5 (μ-C=CH−CH=CH), 135.3 (C_q, η^7-C_7H_6), 106.0, 103.5, 98.4 (η^7-C_7H_6), 89.8 (C_5H_5) ppm. IR (CH_2Cl_2): ṽ = 2043 (s), 2007 (vs), 1970 (sh) [ν(CO)]; 1812 (m) [ν(μ-CO)]; 1606 (w), 1562 (m), 1468 (vs), 1456 (s) [ν(C=C)] cm^{-1}. $C_{27}H_{19}BCrF_4Fe_2O_6 \cdot CH_2Cl_2$ (774.86): calcd. C 43.36, H 2.71; found C 43.63, H 2.67.

General Procedure for the Condensation of Azulenic Aldehydes with [(CpFeCO)$_2$(μ-CO)(μ-C−CH$_3$)][BF$_4$] (6): Complex **6** (0.25 g, 0.57 mmol) and an excess of aldehyde (1.2 equiv.) were stirred in CH_2Cl_2 (50 mL) at 35 °C for 12 h. The reaction mixture was filtered and the product precipitated from the filtrate by carefully adding diethyl ether (25 mL) and cooling overnight.

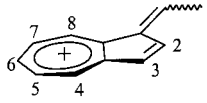

[(CpFeCO)$_2$(μ-CO)(μ-C=CH−CH={C$_{10}$H$_7$})][BF$_4$] (7): Yield: 0.23 g (70%). ^1H NMR ($CDCl_3$): δ = 9.88 (d, *J* = 13.5 Hz, 1 H, μ-C−C*H*=CH), 9.24 (d, *J* = 9.6 Hz, 1 H, 4-H), 8.74 (d, *J* = 9.9 Hz, 1 H, 8-H), 8.71 (d, *J* = 4.2 Hz, 1 H, 2-H), 8.38 (d, *J* = 13.5 Hz, 1 H, μ-C−CH=C*H*), 8.23 (t, *J* = 9.6 Hz, 1 H, 6-H) 8.02 (m, 2 H, 5-H, 7-H), 7.77 (d, 1 H, *J* = 4.22 Hz, 3-H), 5.34 (s, 10 H, C_5H_5) ppm. $^{13}C\{^1H\}$ NMR (CD_3CN): δ = 394.5 (μ-C), 258.9 (μ-CO), 209.5 (CO), 149.1, 146.2 (μ-C−CH=CH), 152.2, 148.7, 127.1 (C_q, $C_{10}H_7$), 143.9, 141.5, 138.5, 135.2, 134.0, 127.3 ($C_{10}H_7$), 91.1 (C_5H_5) ppm. IR (CH_2Cl_2): ṽ = 2024 (vs), 1993 (m) [ν(CO)]; 1832 (s) [ν(μ-CO)]; 1605 (m), 1546 (m), 1518 (vs), 1464 (m) [ν(C=C)] cm^{-1}. $C_{26}H_{19}BF_4Fe_2O_3$ (577.92): C 53.98, H 3.29; found C 54.19, H 3.62.

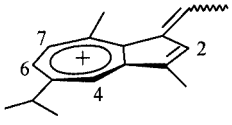

[(CpFeCO)$_2$(μ-CO)(μ-C=CH−CH={C$_{10}$H$_4$Me$_2$*i*Pr})][BF$_4$] (8): Yield: 0.29 g (80%). ^1H NMR ($CDCl_3$): δ = 9.66 (d, *J* = 12.6 Hz, 1 H, μ-C−C*H*=CH), 8.61 (d, *J* = 12.6 Hz, 1 H, μ-C−CH=C*H*), 8.50 (s, 1 H, 2-H), 8.44 (s, 1 H, 8-H), 8. (m, 2 H, 6-H, 7-H), 5.26 (s, 10 H, C_5H_5), 3.4 [m, 1 H, CH, *i*Pr], 3.34 (s, 3 H, CH_3), 2.65 (s, 3 H, CH_3), 1.42 [d, 1 H, *J* = 7.03 Hz, $(CH_3)_2$, *i*Pr]. $^{13}C\{^1H\}$ NMR (CD_3CN): δ = 382.0 (μ-C), 259.8 (μ-CO), 209.7 (CO), 152.7, 148.9 (μ-C−CH=CH), 153.6, 151.2, 150.4, 144.8, 142.2, 129.3 (C_q, $C_{10}H_4Me_2$*i*Pr), 140.6, 139.9, 136.7, 135.9 ($C_{10}H_4Me_2$*i*Pr), 90.4 (C_5H_5), 39.2, 13.8 (CH_3), 29.7 (CH, *i*Pr), 24.7 [$(CH_3)_2$, *i*Pr] ppm. IR (CH_2Cl_2): ṽ = 2017 (vs), 1990 (m) [ν(CO)]; 1829 (s) [ν(μ-CO)]; 1605 (m), 1552 (m), 1534 (s), 1501 (s) [ν(C=C)] cm^{-1}. $C_{31}H_{29}BF_4Fe_2O_3$ (648.05): C 57.45, H 4.51; found C 57.81, H 4.90.

Reaction of azulene and guaiazulene with [(CpFeCO)$_2$(μ-CO)(μ-C=CH−CHO)] (1): An excess of HBF_4 (54% solution in diethyl ether) was added to an equimolar solution of azulene or guaiazulene and **1** (0.25 g, 0.57 mmol) in dichloromethane (50 mL). The reaction mixture was concentrated until a colour change occurred and then stirred for 2 h. The products were precipitated from the solution by adding diethyl ether (75 mL) and cooling overnight. The resulting precipitates were filtered off and washed well with diethyl ether. The yields were 0.28 g (85%) of **7** and 0.30 g (83%) of **8**.

X-ray Structure Determination: Crystals suitable for an X-ray structure analysis were obtained by diffusion of Et_2O into a CH_2Cl_2 solution of **5** and by layering a CH_2Cl_2 solution of **3** and **4**, respectively with hexane. Complex **5** crystallises with three independent molecules of CH_2Cl_2. The data for structures **3** and **4** were obtained with a Bruker SMART-APEX diffractometer with an Mo-K_α X-ray tube as radiation source. The data for the structure of **5** was collected on a four-circle diffractometer Hilger & Watts, Mo-K_α, λ = 0.71073 Å. Complex **4** crystallises as a merohedral twin with two perpendicular monoclinic unit cells (with opposite oriented *z* axes) leading to a nearly orthorhombic cell. Symmetry-absence conditions did not give any suitable orthorhombic space group. The structure was solved and refined as a twin in the monoclinic space group $P2_{1/c}$ with β = 90.449°. Refinement in the same space group without the TWIN option leads to an R_1 value above 19% and worse standard deviations for geometric parameters. All structures were resolved by direct methods (SHELXL-86).[30] Refinement on F^2 was carried out by full-matrix least-squares techniques (SHELXL-93, SHELXL-97).[31,32] All non-hydrogen atoms were refined with anisotropic thermal parameters. The hydrogen atoms were refined by the riding-model method with a fixed isotropic thermal parameter related by a factor of 1.2 to the value of the equivalent isotropic thermal parameter of their carrier atoms. Weights were optimised in the final refinement cycles. CCDC-178112 (**3**), -178111 (**4**), -178113 (**5**) contain the supplementary crystallographic data for this paper. These data can be obtained free of charge at www.ccdc.cam.ac.uk/conts/retrieving.html or from the Cambridge Crystallographic Data Centre, 12, Union Road, Cambridge CB2 1EZ, UK; [Fax: (internat.) + 44-1223/336-033; E-mail: deposit@ccdc.cam.ac.uk].

HRS Measurements of the First Hyperpolarisabilities: The measurements at a wavelength of 1500 nm were carried out as described in ref.[23] Instead of the third harmonic (355 nm) generated from an Nd:YAG laser with a wavelength of 1064 nm the optical parametric oscillator (OPO)[33] in use was pumped with the second harmonic (532 nm). The signal intensity at 824 nm and the fundamental at 532 nm were removed from the Idler using dichroic mirrors (HR 650−850 and HR 532), a green light and a silicon filter (transparent > 1000 nm). An additional Glan-Taylor polarizer ensured the vertical polarisation of the beam into the measurement cell. Measurements were performed with ca. 10^{-4} to 10^{-6} M solutions of **5**, **7** and **8** in CH_2Cl_2. The validity of Beer's law was proven by UV/Vis measurements of samples with corresponding concentration. Disperse Red 1 (DR1) was used as an external standard with a value of β_{1500}(DR1) = 70 × 10^{-30} esu. This value was obtained by comparing the slopes of the reference in CH_2Cl_2 and $CHCl_3$ to obtain the ratio of β_{solute}.[27] Using the value β($CHCl_3$) = 80 × 10^{-30} esu[24] the hyperpolarisibility of DR1 in CH_2Cl_2 is estimated to be 70 × 10^{-30} esu. The effect of the refractive indices of the solvents was corrected using the simple Lorentz local field.[28]

Acknowledgments

This work was supported by the European Union through TMR Network Contract No. ERBFMRX-CT98-0166 and COST D14/0008/99, the Deutsche Forschungsgemeinschaft HE 1309/3-4 and the Fonds der Chemischen Industrie.

[1] [1a] D. J. Williams, *Angew. Chem.* **1984**, *96*, 637−651; *Angew. Chem. Int. Ed. Engl.* **1984**, *23*, 690−703. [1b] R. W. Boyd in:

Nonlinear Optics, Academic Press, Inc., **1992**; G. H. Wagnière in: *Linear and Nonlinear Optical Properties of Molecules*, VCH, Weinheim, **1993**. [1c] P. N. Prasad, D. J. Williams in: *Nonlinear Optical Effects In Molecules & Polymers*, Wiley & Sons, New York, **1991**. [1d] H. S. Nalwa, S. Miyata (Eds.) in: *Nonlinear Optics of Organic Molecules and Polymers*, CRC Press, New York, **1997**. [1e] J. C. Calabrese, L.-T. Cheng, J. C. Green, S. R. Marder, W. Tam, *J. Am. Chem. Soc.* **1991**, *113*, 7227−7232. [1f] D. R. Canis, M. A. Ratner, T. J. Marks, *J. Am. Chem. Soc.* **1990**, *112*, 8203−8204. [1g] D. R. Canis, M. A. Ratner, T. J. Marks, *J. Am. Chem. Soc.* **1992**, *114*, 10338−10357. [1h] D. R. Canis, M. A. Ratner, T. J. Marks, *J. Am. Chem. Soc.* **1994**, *116*, 195−242. [1i] S. Barlow, H. E. Bunting, C. Ringham, J. C. Green, G. U. Bublitz, S. G. Boxer, I. W. Perry, S. R. Marder, *J. Am. Chem. Soc.* **1999**, *121*, 3715−3723. [1j] T. J. Marks, M. A. Ratner, *Angew. Chem.* **1995**, *107*, 167; *Angew. Chem. Int. Ed. Engl.* **1995**, *34*, 155−174. [1k] N. J. Long, *Angew. Chem.* **1995**, *107*, 37−56; *Angew. Chem. Int. Ed. Engl.* **1995**, *34*, 21−38. [1l] H. S. Nalwa, *Appl. Organomet. Chem.* **1991**, *5*, 349−377. [1m] I. R. Whittall, A. M. McDonagh, M. G. Humphrey, M. Samoc, *Adv. Organomet. Chem.* **1998**, *42*, 291−362. [1n] T. Verbiest, S. Houbrechts, M. Kauranen, K. Clays, A. Persoons, *J. Mater. Chem.* **1997**, *7*, 2175−2189. [1o] B. J. Coe, S. Houbrechts, I. Asselberghs, A. Persoons, *Angew. Chem.* **1999**, *111*, 377−380; *Angew. Chem. Int. Engl. Ed.* **1999**, *38*, 366−369. [1p] T. Kondo, S. Horiuchi, I. Yagi, S. Ye, K. Uosaki, *J. Am. Chem. Soc.* **1999**, *121*, 391−398.

[2] [2a] T. Farrell, T. Meyer-Friedrichsen, J. Heck, A. R. Manning, *Organometallics* **2000**, *19*, 3410−3419. [2b] T. Farrell, A. R. Manning, T. C. Murphy, T. Meyer-Friedrichsen, J. Heck, I. Asselberghs, A. Persoons, *Eur. J. Inorg. Chem.* **2001**, 2365−2375.

[3] T. Farrell, T. Meyer-Freidrichsen, M. Malessa, C. Wittenburg, J. Heck, A. R. Manning, *J. Organomet. Chem.* **2001**, *625*, 32−39.

[4] M. B. Hall, R. F. Fenske, *Inorg. Chem.* **1972**, *11*, 768−775.

[5] C. P. Casey, M. S. Konings, S. R. Marder, Y. Takezawa, *J. Organomet. Chem.* **1988**, *358*, 347−361.

[6] S. M. LeCours, H.-W. Guan, S. G. DiMango, C. H. Wang, M. J. Therien, *J. Am. Chem. Soc.* **1986**, *118*, 1497−1503.

[7] T. Farrell, T. Meyer-Friedrichsen, M. Malessa, D. Haase, W. Saak, I. Asselberghs, K. Wostyn, K. Clays, A. Persoons, J. Heck, A. R. Manning, *J. Chem. Soc., Dalton Trans.* **2001**, 29−36.

[8] [8a] A. E. Asato, R. S. H. Liu, V. P. Rao, Y. M. Cai, *Tetrahedron Lett.* **1996**, *37*, 419−422. [8b] J. N. Woodford, C. H. Wang, A. E. Asato, R. S. H. Liu, *J. Chem. Phys.* **1999**, *111*, 4621−4628.

[9] G. Iftime, P. G. Lacroix, *Tetrahedron Lett.* **1998**, *39*, 6853−6856; P. G. Lacroix, I. Malfaut, G. Iftime, A. C. Razus, K. Nakatoni, J. A. Delaire, *Chem. Eur. J.* **2000**, *6*, 2599−2608.

[10] [10a] R. Herrmann, B. Pedersen, G. Wagner, J-H. Youn, *J. Organomet. Chem.* **1998**, *571*, 261−266. [10b] R. Herrmann, G. Wagner, C. Zollfrank, in *Electronic Conference on Trends in Chemistry* (Eds.: H. S. Rzepa, C. Leach, J. M. Goodman), CD-ROM, Royal Chem. Soc., Cambridge, **1996**, paper 49.

[11] C. P. Casey, M. S. Konings, S. R. Marder, *J. Organomet. Chem.* **1988**, *345*, 125−134.

[12] H. Wong, T. Meyer-Friedrichsen, T. Farrell, C. Mecker, J. Heck, *Eur. J. Inorg. Chem.* **2000**, 631−646.

[13] M. Nitay, W. Priester, M. Rosenblum, *J. Am. Chem. Soc.* **1978**, *100*, 3620−3622.

[14] K. Hafner, C. Bernhard, *Liebigs Ann. Chem.* **1959**, *625*, 108−123.

[15] E. C. Kirby, D. H. Reid, *J. Chem. Soc.* **1960**, 494−501.

[16] [16a] S. R. Marder, D. N. Beratan, L.-T. Cheng, *Science* **1991**, *252*, 103−106. [16b] S. R. Marder, G. B. Gorman, F. Meyers, J. W. Perry, B. Bourhill, J.-L. Brédas, B. M. Pierce, *Science* **1994**, *265*, 632−635. [16c] F. Meyers, S. R. Marder, B. M. Pierce, J.-L. Brédas, *J. Am. Chem. Soc.* **1994**, *116*, 10703−10714. [16d] S. R. Marder, B. Kippelen, A. K.-Y. Jen, N. Peyghambarian, *Nature* **1997**, *388*, 845−851. [16e] J.-L. Brédas, *Adv. Mater.* **1995**, *7*, 263−274.

[17] [17a] G. M. Dawkins, M. Green, J. C. Jeffrey, C. Sambale, F. G. A. Stone, *J. Chem. Soc., Dalton Trans.* **1983**, 499−509. [17b] M. Watanabe, I. Motoyama, T. Takayama, *J. Organomet. Chem.* **1996**, *524*, 9−18. [17c] S. Barlow, L. M. Helling, M. W. Day, S. R. Marder, *Chem. Commun.* **1999**, 1567−1568. [17d] A. I. Yanovsky, Y. T. Struchkov, A. Z. Kreindlin, M. I. Rybinskaya, *J. Organomet. Chem.* **1989**, *369*, 125−130.

[18] [18a] C. P. Casey, M. Konings, R. E. Palerm, R. E. Colborn, *J. Am. Chem. Soc.* **1985**, *107*, 5296−5297. [18b] C. P. Casey, M. S. Konings, S. R. Marder, *Polyhedron* **1988**, *7*, 881−902; M. Etienne, J. Talarmin, L. Toupet, *Organometallics* **1992**, *11*, 2058−2068.

[19] S. Barlow, S. R. Marder, *Chem. Commun.* **2000**, 1555−1562.

[20] [20a] J. L. Oudar, s. S. Chemla, *Chem. Phys.* **1977**, *66*, 2664−2668. [20b] E. Hendrickx, K. Clays, C. Dehu, J. L. Brédas, *J. Am. Chem. Soc.* **1995**, *117*, 3547−3555.

[21] K. Clays, A. Persoons, *Rev. Sci. Instrum.* **1992**, *63*, 3285−3289.

[22] J. J. Wolff, R. Wortmann, *Adv. Phys. Org. Chem.* **1999**, *32*, 121−138.

[23] S. Stadler, R. Dietrich, G. Bourhill, C. Bräuchle, A. Pawlik, W. Grahn, *Chem. Phys. Lett.* **1995**, *247*, 271−276.

[24] C. Lambert, G. Nöll, E. Schmälzlin, K. Meerholz, C. Bräuchle, *Chem. Eur. J.* **1998**, *4*, 2129−2135.

[25] K. Clays, E. Hendrickx, T. Verbiest, A. Persoons, *Adv. Mater.* **1998**, *10*, 643−655.

[26] [26a] J. J. Wolff, R. Wortmann, *J. Prakt. Chem.* **1998**, *340*, 99−111. [26b] S. Stadler, R. Dietrich, G. Bourhill, C. Bräuchle, *J. Phys. Chem.* **1996**, *100*, 6927−6934.

[27] T. Kodaira, A. Watanabe, O. Ito, M. Matsuda, K. Clays, A. Persoons, *J. Chem. Soc., Faraday Trans.* **1997**, *93*, 3039−3044.

[28] C. Lambert, W. Gaschler, E. Schmälzlin, K. Meerholz, C. Bräuchle, *J. Chem. Soc., Perkin Trans. 2* **1999**, 577−587.

[29] G. J. Kubas, *Inorg. Chem.* **1983**, *22*, 692−694.

[30] G. M. Sheldrick, *SHELXS-86 Program for crystal structure determination*, University of Göttingen, Germany, **1986**.

[31] G. M. Sheldrick, *SHELXL-93 Program for crystal structure refinement*, University of Göttingen, Germany, **1993**.

[32] G. M. Sheldrick, *SHELXL-97 Program for crystal structure refinement*, University of Göttingen, Germany, **1997**.

[33] Paralite Optical Parametrical Oscillator, LAS GmbH.

Received January 23, 2002
[I02041]

Kinetics and Mechanism of the Copper-Catalysed Oxygenation of 2-Nitropropane

Éva Balogh-Hergovich,[a] Zoltán Gréczi,[b] József Kaizer,[a] Gábor Speier,*[a] Marius Réglier,[c] Michel Giorgi,[c] and László Párkányi[d]

Keywords: 2-Nitropropane / Copper nitronates / Oxygenation / Copper / Kinetics / Dioxygenase

Primary and secondary nitro compounds react with dioxygen in the presence of copper metal and N ligands such as *N*,*N*,*N*′,*N*′-tetramethylethylenediamine (tmeda), 2,2′-bipyridine (bpy), and 1,10-phenantroline (phen) in various solvents to form aldehydes or ketones. More coordinating solvents as well as donor N ligands accelerate the reaction remarkably. The oxygenolysis of 2-nitropropane (NPH) in the presence of copper and tmeda in DMF results in acetone and acetone oxime. The amount of tmeda influences the chemoselectivity, higher tmeda concentrations preferentially lead to the formation of the oxime. The kinetics of the reaction, measured at 90 °C, resulted in a rate equation of first-order dependence on copper and dioxygen and second-order dependence on 2-nitropropane. The rate constant, activation enthalpy, and entropy at 363.16 K are as follows: k_{cat} = (5.37 ± 0.34) × 10^{-2} mol^{-3} dm^9 s^{-1}, E_a = 131 ± 4 kJ mol^{-1}, $\Delta H^{\ddagger}$ = 127 ± 4 kJ mol^{-1} and $\Delta S^{\ddagger}$ = 80 ± 13 J mol^{-1} K^{-1}. The catalytically active intermediates $Cu^{II}(NP)_2$(tmeda) and $Cu^{II}(NO_2)_2$(tmeda) in the catalytic cycle were isolated and their structures determined by X-ray crystallography. The kinetics of the stoichiometric oxygenation of $Cu^{II}(NP)_2$(tmeda) to $Cu^{II}(NO_2)_2$(tmeda) and acetone resulted in the overall second-order rate equation with a rate constant, activation enthalpy, and entropy at 313.16 K of k_s = 0.46 ± 0.02 mol^{-1} dm^3 s^{-1}, E_a = 38 ± 1 kJ mol^{-1}, $\Delta H^{\ddagger}$ = 35 ± 1 kJ mol^{-1} and $\Delta S^{\ddagger}$ = −142 ± 13 J mol^{-1} K^{-1}, respectively.
(© Wiley-VCH Verlag GmbH, 69451 Weinheim, Germany, 2002)

Introduction

The transformation of primary and secondary aliphatic nitro compounds to aldehydes or ketones is a reaction often used in organic chemistry and in biological processes as well. The Nef reaction, the classical method for this conversion, involves the hydrolysis of the conjugate bases of nitroalkanes with sulfuric acid [Equation (1)].[1]

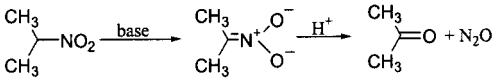

(1)

[a] Research Group for Petrochemistry, Hungarian Academy of Sciences,
8201 Veszprém, Hungary
[b] Department of Organic Chemistry, University of Veszprém,
8201 Veszprém, Hungary
Fax: (internat.) + 36-88/427-492
E-mail: speier@almos.vein.hu
[c] Université d'Aix-Marseille 1 et 3, Faculté des Sciences et Techniques de Saint-Jérome, Chimie, Biologie et Radicaux Libres, UMR CNRS, 6517,
Case 432, Avenue Escadrille Normandie-Niemen, 13397 Marseille Cedex 13, France
[d] Chemical Research Center, Hungarian Academy of Sciences,
1525 Budapest, Hungary
Supporting information for this article is available on the WWW under http://www.eurjic.com or from the author.

There are also a fair number of stoichiometric reagents for this conversion. Treatment of nitroalkanes with aqueous $TiCl_3$,[2] cetyltrimethylammonium permanganate,[3] tin complexes and $NaHSO_3$,[4] activated dry silica gel,[5] 30% H_2O_2/K_2CO_3,[6] $KMnO_4$,[7] ceric ammonium nitrate (CAN),[8] MoO_5/pyridine/HMPA,[9] ozone[10] or singlet oxygen[11] leads to oxo compounds; *t*BuOOH and a catalyst provide a catalytic process for the transformation.[12]

Biochemical degradation of aliphatic nitro compounds is also known in the literature. Glucose oxidase and D- and L-amino acid oxidase accept nitroalkane anions as substrates.[13] The flavoenzyme-catalysed oxidation of nitroalkanes and its mechanism has been established.[14,15] Electron-deficient flavins also oxidise nitroalkane anions in model reactions.[16,17]

Extracts of *Neurospora crassa* and pea seedlings oxidatively metabolise nitroethane and nitropropane,[18] and those from the hyphae of a nitrifying strain of *Aspergillus flavus* produce nitrite and nitrate from 2-nitropropane.[19] 2-Nitropropane and some other nitroalkanes are oxidatively denitrified by an intracellular enzyme of Hansenula mraki.[20] 2-Nitropropane dioxygenase has been purified and characterised as an iron-containing metalloenzyme.[21] It belongs to the peculiar class of intermolecular dioxygenases catalysing the reaction according to Equation (2).[22] That means

that the two oxygen atoms of dioxygen are incorporated into two molecules of the substrate.

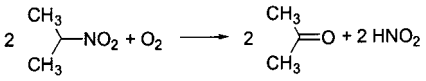

(2)

In order to gain more insight into the mechanism of these reactions we initiated studies on copper- and iron-mediated oxygenations of nitroalkanes. We could show that isopropyl nitronate, ligated to a copper ion, can be oxygenated to (nitrito)copper species and acetone,[23] and in the presence of copper metal, as a precursor, nitroalkanes are easily transformed to aldehydes or ketones by dioxygen.[24] In this paper we present kinetic and spectroscopic data on this reaction, the X-ray structures of intermediates and propose a plausible mechanism for the oxygenation as a 2-nitropropane dioxygenase mimicking reaction.

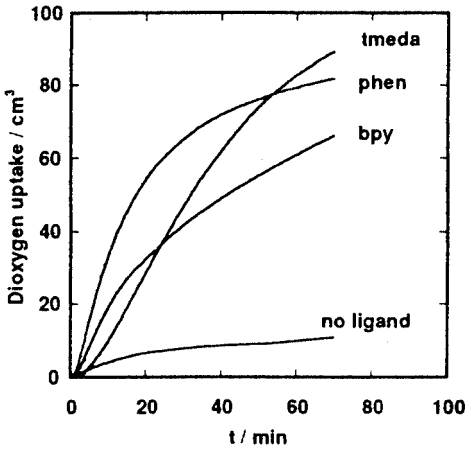

Figure 1. Time course for the stoichiometric oxygenation of 2-nitropropane in the presence of copper metal and N-containing ligands (bpy, phen, tmeda); Cu^0 = L = 1.5 mmol, NPH = 3 mmol, 90 °C, 30 mL DMF

Results and Discussion

Stoichiometric Oxygenation

To a 2-nitropropane (NPH) solution in DMF, copper metal powder was added under dioxygen. The colour of the solution slowly turned reddish and further dissolution of the solid copper resulted in a green homogeneous solution. If coordinating N ligands, such as *N*,*N*,*N*′,*N*′-tetramethylethylenediamine (tmeda), 2,2′-bipyridine (bpy), or 1,10-phenanthroline (phen) were also present, the dissolution of the copper metal proceeded even faster. According to parallel gas-volumetric (O_2), titrimetric (NO_3), spectrophotometric (NO_2) and GC (acetone) measurements (Table 1), the stoichiometry of the oxygenation reaction corresponds to Equation (3). Figure 1 shows typical dioxygen uptake vs. time curves for the oxidation process obtained by the gas-volumetric method.

$$Cu^0 + L + 2\ NPH + 2\ O_2 = Cu^{II}(L)(NO_2)(NO_3) + 2\ (CH_3)_2CO + H_2O \quad (3)$$

Table 1. Stoichiometric oxygenation of 2-nitropropane in DMF solution in the absence and presence of N ligands

Expt. no.	Ligand	Conv.[a] %	NO_3 [b] mmol	NO_2 [c] mmol	Conv.[d] %	Conv.[e] %
1	–	12	0.22	0.09	9.3	10
2	tmeda	98	0.98	1.20	73	87
3	phen	91	0.89	1.01	63	78
4	bpy	73	0.99	1.06	68	72

[a] Conversions were determined by gas volumetry. [b] Yields were determined by titrimetry. [c] Yields were determined by spectrophotometry. [d] Conversions were determined from [b] and [c]. [e] Conversions were determined by GLC.

The presence of the intermediate H_2O_2 in the reaction mixture could be demonstrated either by iodometry or oxidising triphenylphosphane to triphenylphosphane oxide. We believe that in the first step copper metal, in the presence of N ligands, reacts with the *aci* form of the secondary nitro compound to give copper nitronate complexes and H_2O_2 [Equation (4)]. Similar reactions were reported for the reaction of copper metal with acidic compounds in the presence of air.[25]

$$Cu^0 + L + 2\ NPH + O_2 = Cu^{II}(L)(NP)_2 + H_2O_2 \quad (4)$$

In the presence of molecular oxygen both copper(I) and copper(II) nitronates are probably first formed, the former is then transformed to $Cu^{II}(L)(NP)_2$, which can be oxygenated to the desired products [Equation (5)].

$$Cu^{II}(L)(NP)_2 + O_2 = Cu^{II}(L)(NO_2)_2 + 2\ (CH_3)_2CO \quad (5)$$

This is then followed by the fast consecutive formation of $Cu^{II}(L)(NO_2)(NO_3)$, which is assumed to be obtained as a product of the oxidative process between $Cu^{II}(L)(NO_2)_2$ and H_2O_2 [Equation (6)].

$$Cu^{II}(L)(NO_2)_2 + H_2O_2 = Cu^{II}(L)(NO_2)(NO_3) + H_2O \quad (6)$$

Copper-Catalysed Oxygenation of 2-Nitropropane

Previously we have reported that primary and secondary nitro compounds in the presence of copper metal and N ligands can be transformed to aldehydes or ketones and HNO_2. The reaction can also be carried out catalytically in

the presence of tmeda at high 2-nitropropane/copper ratios in a very efficient way (Figure 2).

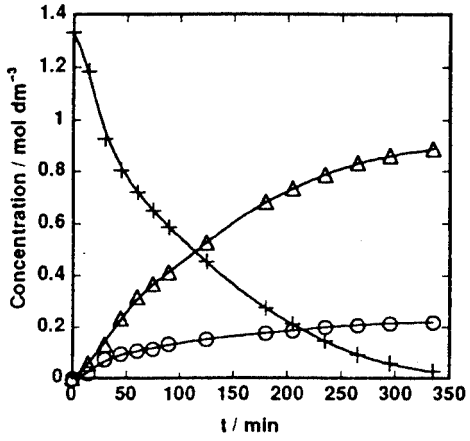

Figure 2. Time course for the copper-catalysed oxygenation of 2-nitropropane (+) [acetone (Δ); acetone oxime (o)] in DMF using tmeda as ligand (Experiment 3, Table 4)

In these experiments Cu^0, tmeda, and 2-nitropropane are first pretreated with O_2 to give a homogeneous solution in about 10−15 min and thereafter the reaction takes place in a homogeneous phase. According to simultaneous gas-volumetric and GC measurements the stoichiometry of the oxidation reaction corresponds to that shown in Equation (7).

$$2\,NPH + O_2 = 2\,HNO_2 + 2\,(CH_3)_2CO \quad (7)$$

In the reaction mixture the presence of acetone oxime is also detected (10−20%). The formation of acetone oxime is favoured at high tmeda concentrations (Figure 3). We believe that excess tmeda acts as a base and in the presence of HNO_2 the salt tmeda·HNO_2 is formed, which reacts with 2-nitropropane resulting in the oxime [Equation (8)].

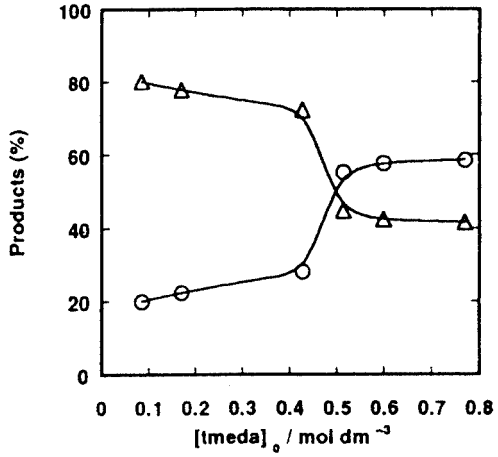

Figure 3. Plots of amounts of acetone (Δ) and acetone oxime (o) formed vs. the initial tmeda concentration at the copper-catalysed oxygenation of 2-nitropropane in DMF (Experiment 15, Table 4)

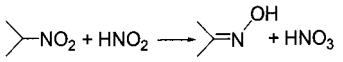

(8)

On addition of ether to the reaction mixture, a green solid precipitated from which, after recrystallisation from ethanol, green crystals of $Cu^{II}(NO_2)_2$(tmeda) were obtained. The presence of $Cu^{II}(NO_2)_2$(tmeda) in the reaction mixture clearly suggests that the first step in the catalytic oxygenation of 2-nitropropane is the formation of the fairly stable $Cu^{II}(NP)_2$(tmeda) complex from copper powder, 2-nitropropane, tmeda and dioxygen, which further rapidly reacts with dioxygen to form the more stable nitrito species $Cu^{II}(NO_2)_2$(tmeda). The complex $Cu^{II}(NP)_2$(tmeda) was prepared by the stoichiometric reaction of $Cu^{II}(OMe)_2$, 2-nitropropane and tmeda in THF under Ar.

Characterisation of $Cu^{II}(NO_2)_2$(tmeda)

$Cu^{II}(NO_2)_2$(tmeda) displays three bands at 1360, 1286 and 808 cm^{-1} in its IR spectrum assigned to the asymmetric and symmetric stretching and bending frequencies of the nitro group. There are three additional bands at 953, 845 and 593 cm^{-1} due to deformation and bending frequencies of the nitro group. Three bands at 2983, 2941 and 2899 cm^{-1} can be assigned to the ligand tmeda coordinated to the copper ion. The electronic absorption spectrum of $Cu^{II}(NO_2)_2$(tmeda) in acetonitrile showed two intense bands at 271 and 222 nm, which were assigned to LMCT bands. Further, the LMCT bands for the nitro complex at 271 nm may include contributions from the n→π* transition as well.[26] Crystallographic characterisation of Cu^{II}-(NO_2)(tmeda) shows that the molecule is monomeric. The view of the molecule depicted in Figure 4 shows that the copper(II) centre has an elongated rhombic octahedral geometry with a $CuO_2N_2O_2$ chromophore and a (4+2*)-type coordination involving two off-the-*z*-axis bonds.

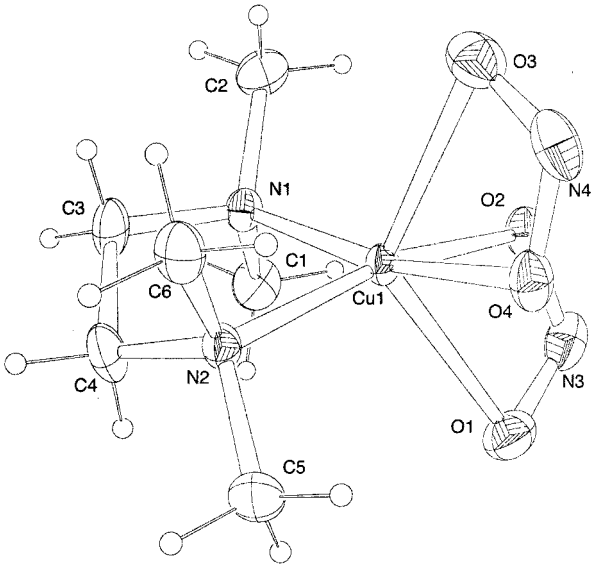

Figure 4. Molecular structure and numbering scheme of [Cu^{II}(NO_2)$_2$(tmeda)] (**1**); only one molecule is shown; hydrogen atoms are omitted for clarity, the ellipsoids represent a probability of 40%

Selected bond lengths and angles given in Table 2 show that two N atoms of the bidentate *N*,*N*,*N*′,*N*′-tetramethylethylenediamine ligand with Cu−N distances of 2.0291(4) and 2.0242(4) Å, and two O atoms of the NO_2 ligands with Cu−O distances of 2.0052(4) and 2.0087(4) Å, occupy basal positions, the other two O atoms of the NO_2 ligands with Cu−O distances of 2.3992(5) and 2.4693(5) Å being in apical positions. This is associated with the bidentate bonding mode of oxyanions to the copper(II) ion, such as the nitrite and nitrate anions, all of which form good primary ligands to the copper(II) ion as in $[Cu^{II}(pyrazine)_2(O_2NO)_2]$[27] and $[Cu^{II}(bipy)(ONO)_2]$.[28] Asymmetric bidentate copper nitrite coordination was also found in other complexes with N-donor ligands.[29,30]

Table 2. Selected bond lengths [Å] and angles [°] for $[Cu^{II}(NO_2)_2$-(tmeda)]

Cu1−O2	2.0052(4)
Cu1−O3	2.3992(5)
Cu1−O4	2.0087(4)
Cu1−N1	2.0291(4)
Cu1−N2	2.0242(4)
Cu1−O1	2.4693(5)
O1−O2	2.0898(7)
O1−N3	1.2380(7)
O2−N3	1.2700(7)
O3−O4	2.0972(6)
O3−N4	1.2279(7)
O4−N4	1.2784(7)
N1−C1	1.4805(7)
N1−C2	1.4815(8)
N1−C3	1.4851(7)
N2−C4	1.4794(7)
N2−C5	1.4830(7)
N2−C6	1.4766(7)
C3−C4	1.4838(9)
C5−C6	2.3891(10)
O2−Cu1−O3	86.99(2)
O2−Cu1−O4	89.602(15)
O2−Cu1−N1	93.13(2)
O2−Cu1−N2	166.78(2)
O3−Cu1−O4	55.98(2)
O3−Cu1−N1	111.63(2)
O3−Cu1−N2	105.41(2)
O4−Cu1−N1	167.18(2)
O4−Cu1−N2	93.57(2)
O1−Cu1−O2	54.49(2)
O1−Cu1−N1	106.08(2)
O1−Cu1−N2	112.92(2)
N1−Cu1−N2	86.61(2)
O2−O1−N3	34.06(3)
Cu1−O2−O1	74.14(2)
Cu1−O2−N3	107.18(4)
O1−O2−N3	33.09(3)
Cu1−O3−O4	52.547(15)
Cu1−O3−N4	86.48(4)
O4−O3−N4	33.96(3)
Cu1−O4−O3	71.47(2)
Cu1−O4−N4	103.89(3)
O3−O4−N4	32.45(3)
Cu1−N1−C1	111.97(3)
Cu1−N1−C2	109.26(3)
Cu1−N1−C3	106.23(3)

Characterisation of $Cu^{II}(NP)_2$(tmeda)

The green complex $Cu^{II}(NP)_2$(tmeda) was prepared in 85% yield. The IR spectrum of the complex shows intense sharp bands corresponding to the coordinated *aci*-2-nitropropanate ligands at 1612 [ν(C=N)], 1162 and 1123 [$\nu_{as}(NO_2)$], and 943 [$\nu_s(NO_2)$] cm^{-1}. The electronic spectrum of the complex shows an absorption band at 727 nm due to d-d transitions. A higher energy band at 314 nm is associated with charge transfer transition. Room-temperature magnetic measurements yielded a value of μ_{eff} = 1.92 BM for the complex consistent with a copper(II) ion. The view of the molecule in Figure 5 shows that the geometry around the copper(II) centre is similar to that of the Cu^{II}-(NO_2)(tmeda) complex with an elongated rhombic octahedral $CuO_2N_2O_2$ chromophore and a (4+2*)-type coordination, involving two off-the-*z*-axis bonds. Selected bond lengths and angles given in Table 3 show that two N atoms of the bidentate *N*,*N*,*N*′,*N*′-tetramethylethylenediamine ligand, with Cu−N distances of 2.0665(14) Å, and two O atoms of the nitronate ligands, with Cu−O distances of 1.9997(13) Å, occupy basal positions, while the other two O atoms of the nitronate ligands, with Cu−O distances of 2.3615(13) Å, are in apical positions. The carbon−nitrogen bond [1.290(2) Å] in the nitronate ligand is essentially double bond in character (C−N 1.47 Å, C=N 1.27 Å).[31] This is similar to the findings for the structures of $Cu^{I}(NP)(PPh_3)_2$ [23] and $Fe^{III}(NP)_3$.[32] The C−N distances are somewhat longer in $Cu^{II}(NP)_2$ (1.34−1.35 Å), however, its structure consists of chains of $Cu^{II}(NP)_2$ units.[33]

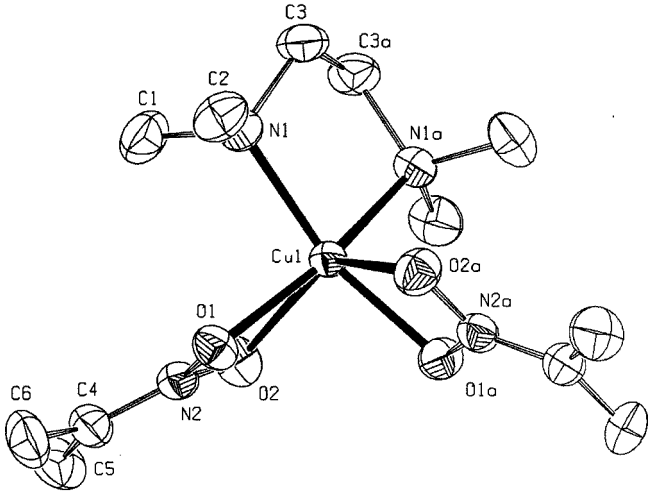

Figure 5. Molecular structure and numbering scheme of $[Cu^{II}$-$(NP)_2$(tmeda)] (**2**); only one molecule is shown; hydrogen atoms are omitted for clarity, the ellipsoids represent a probability of 40%

Kinetic Measurements

The reaction between 2-nitropropane and dioxygen in the presence of a catalytic amount of copper and tmeda were performed in DMF solution and examined in the temperature range 363.16 to 373.16 K with a ratio between initial concentrations of copper and 2-nitropropane in the range

Table 3. Selected bond lengths [Å] and angles [°] for [Cu^{II}-$(NP_2)_2$(tmeda)]

Cu1−O1	1.9997(13)
Cu1−N1	2.0665(14)
Cu1−O2	2.3615(13)
O1−N2	1.3360(18)
O2−N2	1.3205(19)
N1−C1	1.472(2)
N1−C2	1.479(2)
N1−C3	1.481(2)
N2−C4	1.290(2)
C3−C3	1.508(4)
C4−C6	1.477(3)
C4−C5	1.497(3)
O1−Cu1−O1	98.86(7)
O1−Cu1−N1	90.64(6)
O1−Cu1−N1	161.00(5)
O1−Cu1−N1	161.00(5)
O1−Cu1−N1	90.64(6)
N1−Cu1−N1	85.30(8)
O1−Cu1−O2	93.19(5)
O1−Cu1−O2	60.51(5)
N1−Cu1−O2	102.79(5)
N1−Cu1−O2	105.80(5)
O1−Cu1−O2	60.51(5)
O1−Cu1−O2	93.20(5)
N1−Cu1−O2	105.80(5)
N1−Cu1−O2	102.79(5)
O2−Cu1−O2	140.79(7)
N2−O1−Cu1	100.13(10)
N2−O2−Cu1	84.51(9)

1:6−33. Experiments were also carried out at different dioxygen concentrations. Experimental conditions are summarised in Table 4.

A simple rate law for the catalytic reaction between 2-nitropropane and dioxygen catalysed by copper in the presence of tmeda is given in Equation (9).

$$-\mathrm{d[NPH]}/\mathrm{d}t = \mathrm{d[acetone]}/\mathrm{d}t = k_{cat}[\mathrm{NPH}]^m[\mathrm{Cu}]^n[\mathrm{O_2}]^q \quad (9)$$

In order to determine the rate dependence on the various reactants, oxygenation runs were performed at different substrate concentrations (Table 4; Experiments 1−4), catalyst concentrations (Table 4; Experiments 3, 5−9), and at different dioxygen pressures (Table 4; Experiments 10−14). Assuming a constant concentration of the catalyst during each reaction, as well as a constant dioxygen pressure for the experiments, the pseudo-first-order rate law according to Equation (10) is obtained, where $k_{cat}' = k_{cat}[\mathrm{Cu}]^n[\mathrm{O_2}]^q$.

$$-\mathrm{d[NPH]}/\mathrm{d}t = k_{cat}'[\mathrm{NPH}]^m \quad (10)$$

Plots of $[\mathrm{NPH}]^{-1}$ vs. time were linear in Experiments 1−14, indicating that the reaction is second order with respect to substrate concentration. Columns k_{cat}' and R in Table 4 report slopes and the correlation coefficients obtained by the least-squares method for these linear regressions. From variations of the reaction rates, plots of $-\mathrm{d[NPH]}/\mathrm{d}t$ vs. the second exponent of the initial NPH concentration $[\mathrm{NPH}]_0^2$ (Figure S1, Supporting Information) were also linear ($R = 99.41$), reinforcing that the reaction is indeed second-order with respect to the 2-nitropropane concentration (Table 4; Experiments 1−4). This means that $m = 2$ in Equation (9).

Kinetic measurements of the reaction rate with respect to catalyst concentration (Table 4; Experiments 3, 5−9) indic-

Table 4. Kinetic data for the copper-catalysed oxygenation of 2-nitropropane in DMF solution

Expt.[a] no.	Temp. °C	$10^3[O_2]$ mol dm^{-3}	[Cu] mol dm^{-3}	[NPH] mol dm^{-3}	$10^5\ k_{cat}'$ mol^{-1} dm^3 s^{-1}	R[b] %	$10^2\ k_{cat}$ s^{-1} mol^{-3} dm^9	$10^5\ -\mathrm{d[NPH]}/\mathrm{d}t$ mol dm^{-3} s^{-1}
1	90	8.251	0.086	0.499	4.624	99.87	6.54 ± 0.19	1.469
2	90	8.251	0.086	0.853	4.579	99.58	6.47 ± 0.31	3.330
3	90	8.251	0.086	1.077	4.629	99.38	6.55 ± 0.40	4.843
4	90	8.251	0.086	1.341	2.745	99.70	3.88 ± 0.10	6.678
5	90	8.251	0.032	1.077	1.575	99.59	5.91 ± 0.22	
6	90	8.251	0.064	1.077	2.992	99.81	5.66 ± 0.18	
7	90	8.251	0.114	1.104	6.683	99.63	7.09 ± 0.30	
8	90	8.251	0.143	1.077	6.639	99.34	5.63 ± 0.29	
9	90	8.251	0.200	1.077	9.141	99.55	5.54 ± 0.21	
10	90	1.650	0.086	1.077	0.995	99.59	7.01 ± 0.31	
11	90	4.850	0.086	1.077	3.120	99.23	7.48 ± 0.37	
12	90	7.686	0.086	1.077	4.251	98.88	6.45 ± 0.38	
13	90	9.381	0.086	1.077	5.972	98.54	7.43 ± 0.63	
14	90	11.30	0.086	1.077	7.221	98.67	7.46 ± 0.58 5.37 ± 0.34[c]	
15	95	8.562	0.086	1.077	8.455	99.85	11.5 ± 0.35	
16	100	7.907	0.086	1.077	13.39	99.24	19.8 ± 0.72	
17	100	7.907	0.043	0.539	6.222	99.85	18.3 ± 0.53[d]	
18	100	7.907	0.043	0.539	7.208	99.93	21.2 ± 0.67[e]	

[a] In 30 mL of DMF, the amount of tmeda is equimolar to copper. [b] Correlation coefficients of least-squares regressions. [c] Mean value of the kinetic constant k and its standard deviation $\sigma(k)$ were calculated as $k = (\Sigma_i w_i k_i/\Sigma_i w_i)$ and $\sigma(k) = [\Sigma_i w_i(k_i - k)^2/(n-1)\Sigma_i w_i]^{1/2}$, where $w_i = 1/\sigma_i^2$. [d] $Cu^{II}(NO_2)_2$(tmeda) was used as catalyst instead of Cu^0. [e] $Cu^{II}(NP)_2$(tmeda) was used as catalyst instead of Cu^0.

ate a first-order dependence. Plots of k_{cat}' vs. [Cu] for the above experiments gave a straight line with a correlation coefficient of 99.10% (Figure S2, Supporting Information).

The experiments performed at different dioxygen concentrations (calculated from literature data assuming the validity of Dalton's law, the dissolved concentration of O_2 being 8.25×10^{-3} mol dm^{-3} at 90 °C and 760 Torr O_2 pressure) show that the reaction is first order with respect to the dioxygen concentration (Table 4; Experiments 3, 10−14). Plotting k_{cat}' against [O_2] for the above experiments resulted in a straight line with a correlation coefficient of 99.61% (Figure S3, Supporting Information). According to the kinetic data obtained the oxygenation of 2-nitropropane obeys an overall fourth-order reaction rate with $m = 2$, $n = q = 1$ in Equation (9), from which a mean value of the kinetic constant k_{cat} of $(5.37 \pm 0.34) \times 10^{-2}$ mol^{-3}·L^3 s^{-1} at 363.16 K was obtained (Table 4).

The catalytic oxygenation reactions of 2-nitropropane by $Cu^{II}(NO_2)_2$(tmeda) and $Cu^{II}(NP)_2$(tmeda) complexes as catalysts were also carried out (Table 4; Experiments 17−18). It can be seen that the mean value of the kinetic constant for $Cu^{II}(NO_2)_2$(tmeda) and $Cu^{II}(NP)_2$(tmeda) complexes are very similar to those found in the reactions, where the catalyst was prepared "in situ", suggesting that the two complexes above were involved in the catalytic process when copper metal was used as the catalyst precursor.

The activation parameters for the catalytic oxygenation reaction were determined from the temperature dependence of the kinetic constant k_{cat}. The Arrhenius plot of log k_{cat} vs. $1/T$ (Figure S4, Supporting information) using the k_{cat} values at 363.16, 368.16 and 373.16 K (Table 4; Experiments 1−14, 15−16) was linear with a correlation coefficient of 99.27%. From the slope and the ordinate intercept of this line the parameters $E_a = 131 \pm 4$ kJ mol^{-1}, $\Delta H^{\ddagger} = 127 \pm 4$ kJ mol^{-1} and $\Delta S^{\ddagger} = 80 \pm 13$ J mol^{-1} K^{-1} were calculated.

In order to shed light on the kinetic scenery of the elementary steps of these catalytic reactions we also studied the kinetics of the oxygenation of the proposed intermediate $Cu^{II}(NP)_2$(tmeda). The oxygenation of [Cu^{II}-$(NP)_2$(tmeda)] affords a stoichiometry corresponding to Equation (11) by the use of parallel gas-volumetric and GC measurements.

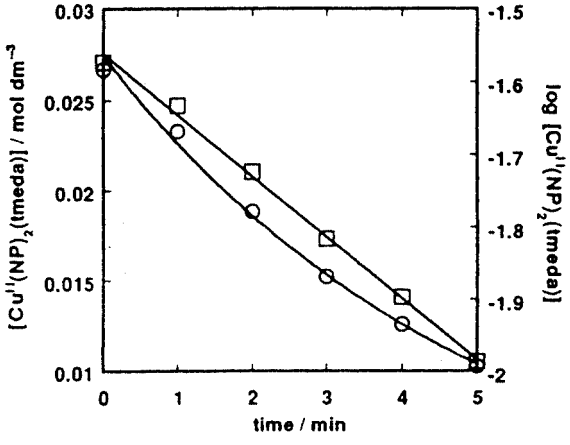

Figure 6. The time course for the oxygenation of [Cu^{II}-$(NP)_2$(tmeda)] (o) and plot of log[$Cu^{II}(NP)_2$(tmeda)] vs. time for the oxygenation of [$Cu^{II}(NP)_2$(tmeda)] (Experiment 4, Table 5)

$$Cu^{II}(NP)_2(tmeda) + O_2 = Cu^{II}(NO_2)_2(tmeda) + 2\,(CH_3)_2CO \quad (11)$$

Figure 6 shows a typical concentration vs. time curve for [$Cu^{II}(NP)_2$(tmeda)] obtained by the measured dioxygen uptake. The reaction between [$Cu^{II}(NP)_2$(tmeda)] and dioxygen was performed in DMF solution and examined in the temperature range 303.16 to 318.16 K. Experiments were also carried out at different dioxygen concentrations. The experimental conditions are summarised in Table 5.

A simple rate law for the stoichiometric reaction between [$Cu^{II}(NP)_2$(tmeda)] and dioxygen is given in Equation (12).

$$-d[Cu^{II}(NP)_2(tmeda)]/dt = k_s[Cu^{II}(NP)_2(tmeda)]^m[O_2]^n \quad (12)$$

In order to determine the rate dependence on the various reactants, oxygenation runs were performed at different [$Cu^{II}(NP)_2$(tmeda)] concentrations (Table 5; Experiments 1−4), and at different dioxygen pressures (Table 5; Experiments 4−7). Assuming a constant concentration of the dioxygen during each reaction the pseudo-first-order rate law according to Equation (13) is obtained, where $k_s' = k_s[O_2]^n$.

$$-d[Cu^{II}(NP)_2(tmeda)]/dt = k_s'[Cu^{II}(NP)_2(tmeda)]^m \quad (13)$$

Plots of log[$Cu^{II}(NP)_2$(tmeda)] vs. time were linear in Experiments 1−10, indicating that the reaction is first-order with respect to the $Cu^{II}(NP)_2$(tmeda) concentration. Columns k_s' and R in Table 5 report slopes and the correlation coefficients obtained by the least-squares method for these linear regressions. A typical first-order plot is shown in Figure 6 (Table 5; Experiment 4).

From variations of the reaction rates, plots of $-d[Cu^{II}(NP)_2(tmeda)]/dt$ (v_0) vs. [$Cu^{II}(NP)_2$(tmeda)] (Figure S5, Supporting Information) were also linear ($R = 98.46$), reinforcing that the reaction is indeed first-order with respect to the $Cu^{II}(NP)_2$(tmeda) concentration (Table 5; Experiments 1−4). This means that $m = 1$ in Equation (12).

Experiments carried out at different dioxygen concentrations (calculated from literature data assuming the validity of Dalton's law, the dissolved concentration of O_2 being 5.36×10^{-3} mol dm^{-3} at 40 °C and 760 Torr O_2 pressure) show that the reaction is first-order with respect to the dioxygen concentration (Table 5; Experiments 4−7). Plotting $-d[Cu^{II}(NP)_2(tmeda)]/dt$ (v_0) against [O_2] for the above four experiments resulted in a straight line with a correlation coefficient of 99.41% (Figure S6, Supporting Information). According to the kinetic data obtained, the oxygenation of $Cu^{II}(NP)_2$(tmeda) obeys an overall second-order rate equation with $m = n = 1$ in Equation (12), from which a mean value of the kinetic constant k_s of (0.46 ± 0.02) mol^{-1} dm^3 s^{-1}, at 313.16 K, was obtained (Table 5).

Table 5. Kinetic data for the stoichiometric oxygenation of $[Cu^{II}(NP)_2(tmeda)]$ in DMF solution

Expt.[a] no.	Temp. °C	$10^3[O_2]$ mol dm^{-3}	10^2[Cu][a] mol dm^{-3}	$10^3k_s'$ s^{-1}	R[b] %	k_s s^{-1} mol^{-1} dm^3	10^5 −d[Cu]/dt mol dm^{-3} s^{-1}
1	40	5.36	0.67	2.835 ± 0.166	99.37	0.529 ± 0.031	1.901 ± 0.11
2	40	5.36	1.33	2.604 ± 0.107	99.70	0.486 ± 0.020	3.473 ± 0.14
3	40	5.36	2.00	2.422 ± 0.123	99.45	0.452 ± 0.023	4.846 ± 0.25
4	40	5.36	2.67	2.256 ± 0.107	99.67	0.421 ± 0.020	6.015 ± 0.28
5	40	1.07	2.67	0.623 ± 0.022	99.55	0.583 ± 0.021	1.663 ± 0.06
6	40	2.68	2.67	1.283 ± 0.067	98.44	0.479 ± 0.025	3.416 ± 0.18
7	40	3.75	2.67	0.533 ± 0.041	99.85	0.409 ± 0.011 0.456 ± 0.024[c]	4.090 ± 0.11
8	30	4.84	2.67	1.050 ± 0.038	98.34	0.217 ± 0.008	2.720 ± 0.10
9	35	5.10	2.67	1.683 ± 0.076	99.60	0.330 ± 0.015	4.649 ± 0.21
10	45	5.52	2.67	2.743 ± 0.049	99.94	0.497 ± 0.009	7.314 ± 0.13

[a] In 30 mL of DMF. [b] Correlation coefficients of least-squares regressions. [c] Mean value of the kinetic constant k and its standard deviation $\sigma(k)$ were calculated as $k = (\Sigma_i w_i k_i/\Sigma_i w_i)$ and $\sigma(k) = [\Sigma_i w_i(k_i - k)^2/(n-1)\Sigma_i w_i]^{1/2}$, where $w_i = 1/\sigma_i^2$.

The activation parameters for the stoichiometric oxygenation reaction were determined from the temperature dependence of the kinetic constant k_s. The Arrhenius plot of log k_s vs. $1/T$ (Figure S7, Supporting Information) using the k_s values at 303.16, 308.16, 313.16 and 318.16 K (Table 5; Experiments 4, 8−10) was linear with a correlation coefficient of 99.48%. From the slope and the ordinate intercept of this line the parameters $E_a = 38 \pm 1$ kJ mol^{-1}, $\Delta H^{\ddagger} = 35 \pm 1$ kJ mol^{-1} and $\Delta S^{\ddagger} = -142 \pm 13$ J mol^{-1} K^{-1} were calculated. Values of the activation parameters indicate that the oxidation of $Cu^{II}(NP)_2(tmeda)$ is a bimolecular reaction involving the associative transition state of $Cu^{II}(NP)_2(tmeda)$ and molecular oxygen; k_{cat} is substantially smaller than k_s since in the former the pre-equilibrium constants K_1 and K_2 are also involved, and K_1 and K_2 are small. The equilibria according to Equations (15) and (16) are shifted to the left side. A comparison of the activation enthalpies and entropies of the catalytic and stoichiometric reactions clearly shows that the stoichiometric reaction is enthalpy-driven while in the case of the catalytic reaction the positive $\Delta S^{\ddagger}$ and the larger $\Delta H^{\ddagger}$ values show a different situation. Here the contribution of the entropy seems to be more and the enthalpy less dominant. This may be explained by the effect of the pre-equilibrium according to Equation (15), since K_1 is involved in k_{cat} thus causing this difference.

Based on the kinetic data on the copper-catalysed oxygenation of 2-nitropropane to acetone, a probable mechanism is proposed as shown in Scheme 1. According to that, the first step is the formation of the complex Cu^{II}(tmeda)$(NP)_2$ (**2**) from copper powder, 2-nitropropane, tmeda, and dioxygen [Equation (14)] or from $Cu^{II}(tmeda)(NO_2)_2$ through substitution of NO_2^- by NP^- in a pre-equilibrium in the catalytic cycle [Equation (15)]. This is then followed by an intramolecular electron transfer [Equation (16)] from the ligand 2-nitropropanate to the copper(II) ion resulting in a (2-nitropropyl radical)copper(I) complex $Cu^{I}(tmeda)(NP)(NP^{\bullet})$ (**3**). This equilibrium is largely shifted to the left (K_2 is rather small). All attempts to detect the radical by EPR spectroscopy failed. The 2-nitropropanate anion does not react with $^3O_2$.[34] The absence of the electron transfer from $Cu^{II}(tmeda)(NP)_2$ to dioxygen could also be proved by the test for free $O_2^{\bullet-}$ with nitroblue tetrazolium (NBT), where no reduction of the added dye to the blue formazan took place excluding the formation of free $O_2^{\bullet-}$.[35]

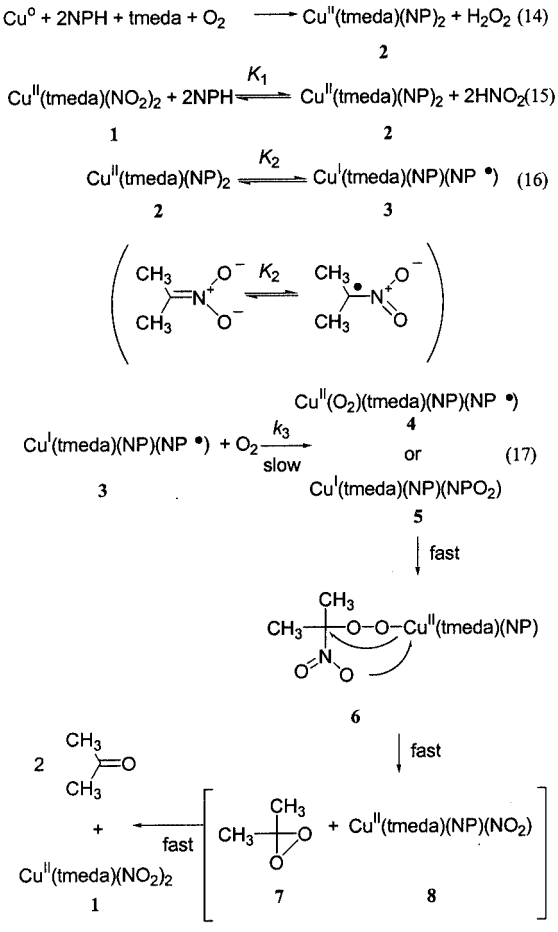

Scheme 1

In the complex Cu^{I}(tmeda)(NP)(NP$^{\cdot}$) (**3**) there are two redox-active centres, namely the nitropropanyl radical NP$^{\cdot}$ and the copper(I) ion.

The biradical dioxygen may react at both redox-active sites of the complex Cu^{I}(tmeda)(NP)(NP$^{\cdot}$), in a radical-radical reaction with the coordinated radical ligand NP$^{\cdot}$ leading to the peroxo intermediate **5**, or in an oxidative addition of O_2 to the copper(I) ion giving the (superoxo)copper(II) complex **4**, as found in the case of many other copper(I) complexes.[36] Both mechanistic assumptions satisfy the kinetic data, but we believe that the reaction of the copper(I) centre of **3** with O_2 is more probable. We have observed earlier that radical ligands bound to metal ions that cannot be oxidised (e.g. Cu^{II}, Fe^{III}, etc)[37] do not react with O_2 at all, or undergo very slow reactions only. The (superoxo)copper(II) complex **4** then undergoes an intramolecular radical-radical reaction of the coordinated ligands $O_2^{\cdot-}$ and NP$^{\cdot}$ resulting in the peroxide species **6**. This then decomposes to the mixed-ligand copper(II) complex **8** and 1,1-dimethyldioxirane (**7**). The 1,1-dimethyldioxirane (**7**) then oxygen ates the coordinated NP^{-} in **8** resulting in Cu^{II}(tmeda)-$(NO_2)_2$ and acetone. The 2-nitropropane once again replaces the nitrito ligand in **1** and so closes the catalytic cycle. Previous studies have shown, that dimethyldioxirane oxidation of nitronate anions affords the corresponding carbonyl product.[38]

As a conclusion it can be said, that the present work provides further support to the key role of redox-active ions in these oxygenation reactions, which may be regarded as functional models for 2-nitropropane dioxygenase. We believe that there is a valence tautomerism between Cu^{II}(NP) and Cu^{I}(NP$^{\cdot}$) due to intramolecular electron transfer from the ligand to the metal ion (Scheme 2a). In this sense of the activation process the ligand is transformed to a radical and copper(II) to copper(I). The latter then reacts with dioxygen to form a peroxidic species, which transforms to the (nitrito)copper(II) complex and acetone. At the intradiol cleavage of catechols either by iron-[39] or copper-containing[40] catechol 1,2-dioxygenases along with model studies[41] it has been proven that valence isomerism plays an important role (Scheme 2b). The molecular orbitals involved in this process are close to each other in energy and so the electron transfer is easily feasible. The equilibrium depends of course on auxiliary ligands as shown in the case of copper catecholate complexes, whereas soft ligands prefer the lower oxidation state of the metal ion.[42] A similar behaviour with (nitropropane)iron complexes is also to be expected as a key step in these oxygenations. Further work is in progress on the design and elucidation of iron-containing functional 2-nitropropane dioxygenase models.

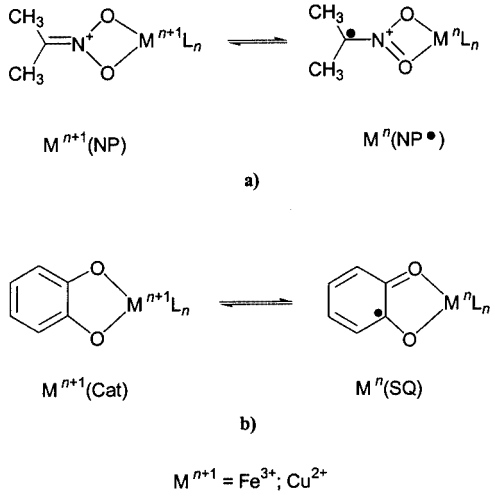

Scheme 2

Experimental Section

Materials and Methods: Analytical-grade reagents were used throughout. Copper powder (Aldrich), 2-nitropropane (Fluka), *N*,*N*,*N*′,*N*′-tetramethylethylenediamine (Aldrich), 2,2′-bipyridine (Aldrich), and 1,10-phenanthroline (Aldrich) were used as supplied. DMF (Aldrich) was purified by azeotropic distillation with benzene and water and stored under argon.[43] Gaseous dioxygen from Messer Griesheim was 99.6% and passed through P_2O_5 and Blaugel in order to remove traces of water and other impurities. IR spectra were recorded with a Specord IR-75 (Carl Zeiss) spectrometer on either Nujol or KBr pellets. Electronic spectra were measured with a Shimadzu UV-160A spectrophotometer using quartz cells. GC analyses were performed with HP 5830A and HP 5890 gas chromatographs equipped with a flame ionisation detector and CP SIL 8CB column. GC-MS measurements were recorded with an HP 5890II/5971 GC/MSD instrument at 75 eV.

Stoichiometric Oxygenation: In a typical stoichiometric reaction 2-nitropropane (0.36 mL, 3 mmol), copper metal (0.10 mg, 1.5 mmol) and tmeda (0.225 mL, 1.5 mmol) in DMF (30 mL) were stirred at 90 °C under dioxygen for 60 min. The stoichiometry of the reactions was investigated by gas volumetric (O_2), spectrophotometric (NO_2),[44] titrimetric (NO_3)[45] and GC measurements (acetone), and the presence of H_2O_2 was determined by iodometry[46] (Table 1.). Then diethyl ether was layered on the solution and left at −20 °C for 2 h to afford a green solid, which was filtered off and recrystallised from acetonitrile to give [Cu(tmeda)$(NO_3)(NO_2)$] as green crystals (0.11 g, 25%). M.p. 172 °C (dec.). $C_6H_{16}CuN_4O_5$ (287.7): calcd. C, 25.03, H 5.60, Cu 22.07, N 19.46; found C 25.4, H 5.49, Cu 22.43, N 19.31. UV/Vis (DMF): λ_{max} (log ε/mol^{-1} dm^3 cm^{-1}) = 276 (3.66), 365 (3.16), 642 nm (2.300). IR (KBr): $\tilde{\nu}_{max}$ = 2976 m, 2938 w, 2888 w, 1567 m, 1470 vs, 1387 s, 1361 vs, 1284 m, 1161 vs, 1046 s, 1020 s, 1001 m, 956 s, 846 m, 814 s, 769 cm^{-1} m. μ_{eff} = 2.07 BM. The ratio NO_3^-/NO_2^- in the complex was 1:1.2.

Preparation of [$Cu^{II}(NP)_2$(tmeda)]: [$Cu(OMe)_2$] (3.14 g, 25 mmol) was dissolved in MeOH (20 mL); tmeda (3.78 mL, 25 mmol) and 2-nitropropane (4.5 mL, 50 mmol) were added and the mixture was stirred under argon at room temperature for 20 h. The solvent was then removed in vacuo and the remaining oily residue was treated with diethyl ether, filtered off and dried to give a green powder (7.60 g, 85%). M.p. 95 °C (dec.). $C_{12}H_{28}CuN_4O_4$ (355.9): calcd. C 39.88, H 7.45, N 15.49; found C 40.50, H 7.93, N 15.74. IR (KBr): $\tilde{\nu}$ = 2925 w, 1612 vs, 1464 vs, 1393 w, 1291 w, 1162 vs, 1123 vs, 1059 m, 1033 m, 956 m, 943 s, 814 s, 782 m, 634 m, 402 cm^{-1} m. UV/Vis (DMF): λ_{max} (ε/ʟ mol^{-1} cm^{-1}) = 314 (978.5), 727 nm (76.7). μ_{eff} = 1.92 BM. On recrystallisation from THF green single

crystals of $[Cu^{II}(NP)_2(tmeda)]$ were formed suitable for X-ray diffraction.

Kinetic Experiments: Kinetic measurement were carried out at atmospheric pressure, at constant partial pressure of dioxygen with vigorous stirring in a thermostatted reaction vessel equipped with a syringe inlet for taking samples at regular time intervals. The samples taken were chilled, stored at dry-ice temperature and then submitted for GC or GC-MS analysis. Dioxygen uptakes were also measured in a constant-pressure gas-volumetric apparatus. The volume of absorbed dioxygen was read periodically using a gas burette. The amount of nitrous acid was determined spectrophotometrically[44] after diazotization of sulfanylic acid and successive coupling with 1-aminonaphthalene, and was found in each case to be nearly equal to that of acetone. The catalytic reactions were carried out by preparing the catalyst from copper metal, tmeda, and 2-nitropropane in DMF under dioxygen. After about 10−15 min, the mixture gave a green homogeneous solution by dissolving the copper metal. Thereafter, the reaction was monitored by analysing the amount of products (acetone and acetone oxime) and the starting 2-nitropropane by GLC. In a typical oxygenation of 2-nitropropane to acetone and acetone oxime, the copper metal (191 mg, 3 mmol), 2-nitropropane (3.6 mL, 40 mmol), tmeda (0.45 mL, 3 mmol) and DMF (30 mL) were stirred under dioxygen at 95 °C. After dissolution of the copper powder (10 min), samples were taken at ca. 10-min intervals, cooled to dry-ice temperature and then subjected to GLC analysis. The solubility of dioxygen in DMF at 95 °C was taken as 8.56×10^{-3} M.[47] The validity of Dalton's law was assumed for the calculation of dioxygen concentration at different partial pressures.[48] Diethyl ether was layered on the solution and left at −20 °C for 2 h to afford a green solid, which was filtered off and recrystallised from ethanol to give $[Cu^{II}(tmeda)(NO_2)_2]$ as green crystals. M.p.197 °C (dec.). $C_6H_{16}CuN_4O_4$ (271.7): calcd. C 26.51, H 5.93, N 20.62; found C 25.7, H 5.72, N 19.91. UV/Vis (DMF): λ_{max} (log ε/mol^{-1} dm^3 cm^{-1}) = 271 (3.66), 222 (3.43) and 648 nm (2.17). IR (KBr): $\tilde{\nu}_{max}$ = 2983 m, 2941 m, 2899 m, 1477 s, 1468 s, 1360 vs, 1286 m, 1249 m, 1165 vs, 1101 m, 1041 m, 1021 m, 1000 m, 953 s, 845 m, 808 s, 770 m, 593 cm^{-1} m. The stoichiometric oxygenation of $[Cu^{II}(NP)_2(tmeda)]$ was carried out in a thermostatted constant-pressure gas-volumetric apparatus. The volume of absorbed dioxygen was read periodically using a gas burette.

X-ray Crystallography: Crystallographic and experimental details of the data collection and refinement of the structures of $Cu^{II}(NO_2)_2(tmeda)$ and $Cu^{II}(NP)_2(tmeda)$ are reported in Table 6, while the molecular structures are depicted in Figures 4 and 5. The intensity data of $Cu^{II}(NO_2)_2(tmeda)$ were collected with a KappaCCD single-crystal diffractometer, using the graphite-monochromated Mo-K_α radiation and φ-scan technique. The structure was solved by direct and difmap methods (SIR92),[49] and refined on F^2 using full-matrix least-squares methods (Maxus).[50] The intensity data of $Cu^{II}(NP)_2(tmeda)$ were collected with an Enraf−Nonius CAD-4 single-crystal diffractometer, using graphite-monochromated Mo-K_α radiation and ω/2θ-scan technique. The structure was solved by direct and difmap methods (SHELXS-97),[51] and refined with full-matrix least-squares refinement on F^2 (SHELXL-97).[52] CCDC-167599 (**1**) and -167598 (**2**) contain the supplementary crystallographic data for this paper. These data can be obtained free of charge at www.ccdc.cam.ac.uk/conts/retrieving.html or from the Cambridge Crystallographic Data Centre, 12, Union Road, Cambridge CB2 1EZ, UK [Fax: (internat.) + 44-1223/336-033; E-mail: deposit@ccdc.cam.ac.uk].

Table 6. Crystal data, data collection parameters and structure refinement of compounds $Cu^{II}(NO_2)_2(tmeda)$ (**1**) and $Cu^{II}(NP)_2(tmeda)$ (**2**)

	1	**2**
Empirical formula	$C_6H_{16}CuN_4O_4$	$C_{12}H_{31}CuN_4O_6$
Crystal system	monoclinic	tetragonal
Space group	$P21/n$	$P42_1c$
Z	4	4
Temperature [K]	293(2)	293(2)
$d_{calcd.}$ [g/cm^3]	1.555	1.314
a [Å]	7.5758(2)	11.862(1)
b [Å]	12.5094(7)	11.862(1)
c [Å]	12.5291(6)	14.047(1)
α [°]	90	90
β [°]	102.091(3)	90
γ [°]	90	90
V [Å]	1161.0(1)	1976.5(3)
μ [mm^{-1}]	1.88	1.135
$F(000)$	564	832
Index ranges	$0 \le h \le 8$	$-19 \le h \le 19$
	$0 \le k \le 15$	$-19 \le k \le 19$
	$-15 \le l \le 15$	$-22 \le l \le 22$
Data collected	2263	9518
Reflections [$I > 3\sigma(I)$]	1894	2134
Parameters	136	109
$R = \Sigma\|\|F_o\| - \|F_c\|\|/\Sigma\|F_o\|$	0.032	0.0323
$wR = [w(F_o^2 - F_c^2)^2/w(F_c^2)^2]^{1/2}$	0.045	0.0682
GOF	1.537	0.814

Supporting Information: Kinetic diagrams for stoichiometric and catalytic oxygenations are available (see also footnote on the first page of this article).

Acknowledgments

Financial support of the Hungarian National Research Fund (OTKA T-30400) and Ministry of Education (FKFP-0446/1999) is gratefully acknowledged.

[1] H. W. Pinnick, *Org. React.* **1990**, *38*, 655.
[2] [2a] J. E. McMurry, J. Melton, *Canad. J. Org. Chem.* **1973**, *38*, 4367. [2b] J. E. McMurry, *Acc. Chem. Res.* **1974**, *7*, 281. [2c] R. Kirchoff, *Tetrahedron Lett.* **1976**, *17*, 2533.
[3] P. S. Vankar, R. Rathore, S. Chandrasekaran, *Synth. Commun.* **1987**, *17*, 195.
[4] F. Urpi, J. Vilarrasa, *Tetrahedron Lett.* **1990**, *31*, 7499.
[5] E. Keinan, Y. Mazur, *J. Am. Chem. Soc.* **1977**, *99*, 3861.
[6] G. A. Olah, M. Arvanahi, Y. D. Vankar, G. K. S. Prakash, *Synthesis* **1980**, 662.
[7] [7a] H. Schechter, F. T. Williams, *J. Org. Chem.* **1962**, *27*, 3699. [7b] F. Freeman, A. Yeramyan, *J. Org. Chem.* **1970**, *35*, 2061. [7c] F. Freeman, D. K. Lin, *J. Org. Chem.* **1971**, *36*, 1335. [7d] N. Kornblum, A. S. Erickson, W. J. Kelly, B. Henggeler, *J. Org. Chem.* **1982**, *47*, 4534. [7e] K. Steliou, M. A. Poupart, *J. Org. Chem.* **1985**, *50*, 4971.
[8] G. A. Olah, B. G. B. Gupta, *Synthesis* **1980**, 44.
[9] M. R. Galobardes, H. W. Pinnick, *Tetrahedron Lett.* **1981**, *22*, 5235.
[10] J. E. McMurry, J. Melton, H. Padgett, *J. Org. Chem.* **1974**, *39*, 259.
[11] J. R. Williams, L. R. Ungler, R. H. Moore, *J. Org. Chem.* **1978**, *43*, 1271.

[12] P. A. Bartlett, F. R. Green, T. R. Webb, *Tetrahedron Lett.* **1977**, *18*, 331.
[13] D. J. T. Porter, H. J. Bright, *J. Biol. Chem.* **1977**, *252*, 4361.
[14] D. J. T. Porter, J. G. Voet, H. J. Bright, *J. Biol. Chem.* **1973**, *248*, 4400.
[15] T. W. Chan, T. C. Bruice, *Biochemistry* **1978**, *17*, 4784.
[16] I. Yokoe, T. C. Bruice, *J. Am. Chem. Soc.* **1975**, *97*, 450.
[17] T. C. Bruice, *Adv. Chem. Ser.* **1980**, *191*, 89.
[18] [18a] H. N. Little, *J. Biol. Chem.* **1951**, *193*, 347. [18b] H. N. Little, *J. Biol. Chem.* **1957**, *229*, 231.
[19] J. A. E. Molina, M. Alexander, *J. Bacteriol.* **1971**, *105*, 489.
[20] T. Kido, T. Yamamoto, K. Soda, *Arch. Microbiol.* **1975**, *106*, 165.
[21] T. Kido, T. Yamamoto, K. Soda, *J. Bacteriol.* **1976**, *126*, 1261.
[22] T. Kido, K. Soda, T. Suzuki, K. Asada, *J. Biol. Chem.* **1976**, *251*, 6994.
[23] É. Balogh-Hergovich, G. Speier, G. Huttner, L. Zsolnai, *Inorg. Chem.* **1998**, *37*, 6535.
[24] É. Balogh-Hergovich, J. Kaizer, G. Speier, *Chem. Lett.* **1996**, 573.
[25] [25a] R. T. Stibrany, J. A. Potenza, H. S. Shugar, *Inorg. Chim. Acta* **1996**, *33*, 243. [25b] R. A. Leising, S. A. Kubow, L. F. Szceptura, T. J. Takeuchi, *Inorg. Chim. Acta* **1996**, *167*, 245. [25c] M. A. Andrew, T. C-T Chang, C-W. F. Cheng, L. V. Kapustay, K. P. Kelly, M. J. Zweifel, *Organometallics* **1984**, *3*, 1479. [25d] M. Green, T. A. Kuc, S. H. Taylor, *J. Chem. Soc.* **1971**, 2334. C. A. Bignozzi, C. Chiorboli, Z. Murtaza, V. E. Jones, T. J. Meyer, *Inorg. Chem.* **1993**, *32*, 1036.
[26] A. Santoro, A. D. Mighell, C. W. Reimann, *Acta Crystallogr., Sect. B* **1970**, *26*, 979.
[27] F. S. Stephens, *J. Chem. Soc. A* **1969**, 2081.
[28] M. Gargano, N. Ravasio, M. Rossi, A. Tiripicchio, C. M. Tiripicchio, *J. Chem. Soc., Dalton Trans.* **1989**, 921.
[29] S. Youngme, S. Tonpho, K. Chinnakali, S. Chantrapromma, H. Fun, *Polyhedron* **1999**, *18*, 851.
[30] A. J. Blake, S. J. Hill, P. Hubberstey, *Chem. Commun.* **1998**, 1587.
[31] L. Pauling, *The Nature of the Chemical Bond*, 3rd ed., Cornell University Press, Ithaca, New York, **1960**.
[32] T. Kovács, G. Speier, M. Réglier, M. Giorgi, A. Vértes, G. Vankó, *Chem. Commun.* **2000**, 469.
[33] O. Simonsen, *Acta Crystallogr., Sect. B* **1973**, *29*, 2600.
[34] J. R. Williams, L. R. Unger, R. H. J. Moore, *J. Org. Chem.* **1978**, *43*, 1271.
[35] B. H. J. Bielski, H. W. Richter, *J. Am. Chem. Soc.* **1977**, *99*, 3019.
[36] K. D. Karlin, S. Kaderli, A. D. Zuberbühler, *Acc. Chem. Res.* **1997**, *30*, 139.
[37] G. Speier, B. Tapodi, unpublished results.
[38] W. Adam, M. Makosza, C. R. Saha-Moller, C. G. Zhao, *Synlett* **1998**, *12*, 1335.
[39] L. Que, Jr., R. Y. N. Ho, *Chem. Rev.* **1996**, *96*, 2607.
[40] G. Speier, *New J. Chem.* **1994**, *18*, 143.
[41] G. Speier, Z. Tyeklár, L. Szabó, P. Tóth, C. G. Pierpont, D. N. Hendricson, "Evidence for Substrate Activation of Copper Catalyzed Intradiol Cleavage in Catechols", in *The Activation of Dioxygen and Homogeneous Catalytic Oxidation* (Eds.: D. H. R. Barton, A. E. Martell, D. T. Sawyer), Plenum Press, New York, **1993**, pp. 423−436.
[42] J. Rall, M. Wanner, M. Albrecht, F. M. Hornung, W. Kaim, *Chem. Eur. J.* **2000**, *5*, 2802.
[43] D. D. Perrin, W. L. Armarego, D. R. Perrin, *Purification of Laboratory Chemicals*, 2nd ed., Pergamon, New York, **1990**.
[44] E. Sawicki, *Talanta* **1963**, *10*, 641.
[45] A. Steyermark, *Quantitative Organic Microanalysis*, 2nd ed., Academic Press, New York, **1961**, p. 188.
[46] A. I. Vogel, *A Text Book of Quantitative Inorganic Analysis*, 3rd ed.,Wiley, New York, **1961**, p. 343.
[47] A. Kruis, *Landolt-Börnstein*, Springer, Berlin, **1976**, vol. 4, part 4, p. 269.
[48] G. Ram, A. R. Sharaf, *J. Ind. Chem. Soc.* **1968**, *45*, 13.
[49] S. Mackay, C. J. Gilmore, C. Edwards, N. Stewart, K. Shankland, *Maxus Computer Program for the Solution and Refinement of Crystal Structures*, Nonius (The Netherlands), MacScience (Japan), The University of Glasgow (UK), **1999**.
[50] *SIR92:* A. Altomare, G. Cascarano, C. Giacovazzo, A. Guagliardi, M. C. Burla, G. Polidori, M. Camalli, *J. Appl. Crystallogr.* **1994**, *27*, 435.
[51] G. M. Sheldrick, *SHELXS-97, Program for crystal structure refinement*, Universität Göttingen, Germany, **1997**.
[52] G. M. Sheldrick, *SHELXL-97, Program for crystal structure refinement*, Universität Göttingen, Germany, **1997**.

Received October 10, 2001
[I01401]

Synthesis and Characterization of Dihydrogen(olefin)osmium Complexes with (E)-$Ph_2P(CH_2)_2CH{=}CH(CH_2)_2PPh_2$

Sheng Hua Liu,[a] Xin Huang,[a] Zhenyang Lin,*[a] Chak Po Lau,*[b] and Guochen Jia*[a]

Keywords: Dihydrogen / Diphosphane / Hydride / Osmium

Treatment of $[OsClH_3(PPh_3)_3]$ with (*E*)-$Ph_2P(CH_2)_2CH{=}CH(CH_2)_2PPh_2$ produced $[OsClH(PPh_3)\{Ph_2P(CH_2)_2CH{=}CH(CH_2)_2PPh_2\}]$, which reacted with HOTf to give the dihydrogen(olefin) complex $[OsCl(H_2)(PPh_3)\{Ph_2P(CH_2)_2CH{=}CH(CH_2)_2PPh_2\}]OTf$. Treatment of the latter complex with H_2 did not result in hydrogenation of the olefin double bond, but gave the (hydrido)dihydrogen complex $[OsH(H_2)(PPh_3)\{Ph_2P(CH_2)_2CH{=}CH(CH_2)_2PPh_2\}]OTf$. A density functional theory study suggested that hydrogenation of the double bond in $[OsCl(H_2)(PPh_3)\{Ph_2P(CH_2)_2CH{=}CH(CH_2)_2PPh_2\}]OTf$ was thermodynamically feasible but kinetically unfavorable.
(© Wiley-VCH Verlag GmbH, 69451 Weinheim, Germany, 2002)

Introduction

Since the first report of dihydrogen complexes by Kubas and his co-workers in 1984,[1] this unique class of complexes has been intensively investigated, especially with regard to their preparation, characterization, and structural and catalytic properties.[2−4] Previous studies have established that dihydrogen complexes may have their own individual reactivity and play active roles in catalytic reactions. In catalytic hydrogenation reactions, there are several possible ways in which dihydrogen complexes may play active roles. Among them, intramolecular hydrogen transfer from a coordinated dihydrogen ligand to the α-carbon atom of a σ-bonded carbon ligand has been recognized as one of the key steps in the catalytic cycles. In particular, (alkyl)dihydrogen and (alkenyl)dihydrogen complexes have been proposed or inferred as the key intermediates in the hydrogenation of olefins and acetylenes under catalysis by group-8 metal complexes such as $[MH(H_2)(PP_3)]^+$ [M = Fe, Ru; PP_3 = $P(CH_2CH_2PPh_2)_3$],[5] $[OsClH(CO)\{P(iPr)_3\}_2]$,[6] $[RuClH(PPh_3)_3]$,[7] and $[RuH(Tp)(L)(PPh_3)]$ [Tp = hydrotris(1-pyrazolyl)borate; L = PPh_3, CH_3CN].[8] As model complexes for reactions involving intramolecular hydrogen transfer from a coordinated dihydrogen ligand to the α-carbon atom of a σ-bonded carbon ligand, several well-characterized dihydrogen complexes containing σ-bonded carbon ligands (such as alkynyl,[9] alkenyl,[10] and aryl[11]) have been synthesized in recent years.

In addition, there are reports that hydrogenation may also proceed through hydrogen transfer from a coordinated dihydrogen ligand to an olefin ligand. The complexes $[M(H_2)(\eta^4\text{-NBD})(CO)_3]$ and $[M(H_2)(\eta^2\text{-NBD})(CO)_4]$ (M = Cr, Mo, and W) have been proposed as the intermediates in the photocatalytic hydrogenation of norbornadiene with $[M(CO)_6]$.[12,13] Dihydrogen(olefin) complexes have also been proposed (but not detected) as the intermediates in catalytic hydrogenation of olefins with $[Ru(Tp)(PPh_3)_x(CH_3CN)_{3-x}]^+$ (x = 1, 2),[8] and in the protonation reaction of [Ru(Cp*)H(NBD)].[14a] However, well-characterized dihydrogen(olefin) complexes are rare.[12−14] Reported dihydrogen(olefin) complexes include $[M(H_2)(\eta^2\text{-NBD})(CO)_4]$ (M = Mo and W),[12] $[M(H_2)(\eta^4\text{-NBD})(CO)_4]$ (M = Cr, Mo, and W),[12] and $[Fe(H_2)(CO)_3(MeO_2CCH{=}CHCO_2Me)]$,[13] which have been detected by IR spectroscopy, and $[Ru(Cp^*)(H_2)(COD)]^+$, which has been detected by NMR spectroscopy.[14a] In this paper we wish to report the synthesis and characterization of new dihydrogen(olefin) complexes.

Results and Discussion

Synthesis and Characterization of $[OsClH(PPh_3)\{Ph_2P(CH_2)_2CH{=}CH(CH_2)_2PPh_2\}]$

Complexes of the type $[MCl(H_2)L_4]^+$ (M = Ru, Os; L = phosphane, CO, pyridine) are known to contain a dihydrogen ligand.[15,16] One might therefore expect that protonation of $[MClH(olefin)(PR_3)_3]$ might produce dihydrogen complexes $[MCl(H_2)(olefin)(PR_3)_3]^+$. To test this possibility, we prepared the hydrido(olefin) complex $[OsClH(PPh_3)(Ph_2P(CH_2)_2CH{=}CH(CH_2)_2PPh_2]$, hoping that subsequent protonation would produce the corres-

[a] Department of Chemistry, The Hong Kong University of Science and Technology,
Clear Water Bay, Kowloon, Hong Kong
[b] Department of Applied Biology & Chemical Technology, The Hong Kong Polytechnic University,
Hung Hom, Kowloon, Hong Kong

ponding dihydrogen(olefin) complex. Osmium metal and the bidentate phosphane ligand with an olefinic functionality in the backbone were used in the project because of the expectation that such systems may give thermally stable dihydrogen(olefin) complexes.

The ligand (*E*)-$Ph_2P(CH_2)_2CH{=}CH(CH_2)_2PPh_2$ (**2**)[17] was prepared by treatment of (*E*)-$Br(CH_2)_2CH{=}CH(CH_2)_2Br$ (**1**) with excess $KPPh_2$ in THF (Scheme 1). Ligand **2** was characterized by ^1H, $^{13}C\{^1H\}$, and $^{31}P\{^1H\}$ NMR spectroscopy and by elemental analysis. In particular, the ^1H NMR spectrum (in C_6D_6) showed the olefinic proton signal at $\delta = 5.4$ ppm, while the $^{31}P\{^1H\}$ NMR spectrum (in C_6D_6) showed a singlet at $\delta = -17.0$ ppm. The closely related ligand (*E*)-$(t\mathrm{Bu})_2P(CH_2)_2CH{=}CH(CH_2)_2P(t\mathrm{Bu})_2$ has also been reported previously.[18]

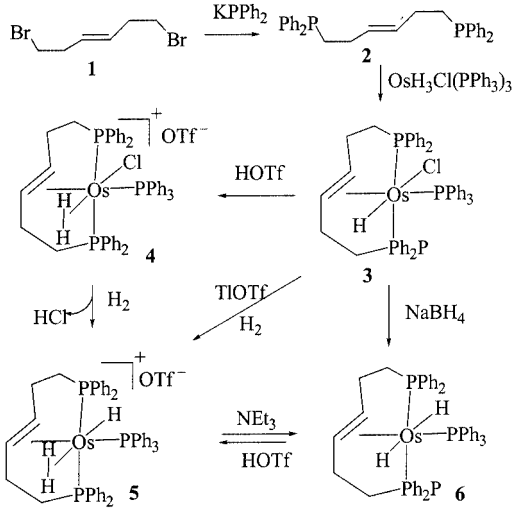

Scheme 1

Treatment of a benzene solution of $[OsClH_3(PPh_3)_3]$ with ligand **2** for 5 h produced $[OsClH(PPh_3)\{Ph_2P(CH_2)_2CH{=}CH(CH_2)_2PPh_2\}]$ (**3**), which was isolated as a gray solid in ca. 79% yield. The structure of complex **3** could readily be assigned by its ^1H, $^{13}C\{^1H\}$, $^{31}P\{^1H\}$, and ^1H-^{31}P-COSY NMR spectra and by elemental analysis. The $^{31}P\{^1H\}$ NMR spectrum (in C_6D_6) showed three doublets of doublets at $\delta = -7.7$, 7.3, and 23.8 ppm. A large $^2J_{P,P}$ coupling (290.6 Hz) for the ^{31}P signals at $\delta = 7.3$ and 23.8 ppm was observed, indicating that two of the phosphorus atoms in **3** were *trans* to each other. A ^1H-^{31}P-COSY NMR experiment suggested that the two *trans*-disposed phosphorus atoms were associated with the two PPh_2 groups of ligand **2**. In the ^1H NMR spectrum (in C_6D_6), the olefinic proton signals appeared at $\delta = 3.88$ ppm, significantly upfield from their counterparts in free ligand **2**, confirming that the olefin double bond was coordinated to the osmium center. Complex **3** exhibited a hydride signal at $\delta = -16.40$ ppm (dt, $^2J_{P,H} = 27.0$, 15.0 Hz). The magnitude of the coupling constants indicated that the hydride ligand was *cis* to the three phosphorus atoms. The chemical shift of the hydride signal was quite strongly upfield, consistently with a structure in which the hydride ligand is *trans* to a chloride ligand. During the course of this work, the closely related complex $[OsClH(PPh_3)(Ph_2P{-}C_6H_3Me{-}CH{=}CH{-}C_6H_3Me{-}PPh_2)]$ was reported.[19]

Synthesis and Characterization of $[OsCl(H_2)(PPh_3)\{Ph_2P(CH_2)_2CH{=}CH(CH_2)_2PPh_2\}]OTf$

Protonation of complex **3** with HOTf produced the dihydrogen(olefin) complex $[OsCl(H_2)(PPh_3)(Ph_2P(CH_2)_2CH{=}CH(CH_2)_2PPh_2)]OTf$ (**4**). Complex **4** was unstable and decomposed under vacuum. The compound could therefore not be isolated as a pure solid, so it was characterized in situ. The $^{31}P\{^1H\}$ NMR spectrum of complex **4** (in CD_2Cl_2) exhibited the PPh_3 signal at $\delta = -8.9$ ppm and the PPh_2 signals at $\delta = 14.2$ and 16.8 ppm. The ^{31}P signals of the PPh_2 groups at $\delta = 14.2$ and 16.8 ppm had a large $^2J_{P,P}$ coupling constant (243.6 Hz), indicating that the PPh_2 groups were *trans* to each other in **4**. The ^1H NMR spectrum (in CD_2Cl_2) exhibited a broad signal attributable to a dihydrogen ligand at $\delta = -9.57$ ppm. The broad hydride signal had a T_1 (min) of 27.0 ms (at 300 MHz) at 258 K. The short T_1 (min) value strongly suggested that complex **4** contained a dihydrogen ligand. Further support for the existence of the dihydrogen ligand in **4** was provided by the ^1H NMR spectrum of the HD isotopomer $[OsCl(HD)(PPh_3)\{Ph_2P(CH_2)_2CH{=}CH(CH_2)_2PPh_2\}]^+$, which was generated in situ by protonation of complex **3** with DOTf. The ^1H NMR spectrum of the HD isotopomer (in CD_2Cl_2) displayed the HD signal as a 1:1:1 triplet at $\delta = -9.58$ ppm, with a $^1J(HD)$ coupling constant of 14.1 Hz. A $d(HH)$ of 1.18 Å was obtained by application of the relationship $d(HH) = -0.0167J(HD) + 1.42$ and $^1J(HD) = 14.1$ Hz.[15a] On the basis of the T_1 (min) of 27 ms, the H−H bond length was calculated to be 1.13 Å for a nonspinning H_2 or 0.98 Å for a spinning dihydrogen ligand.[20]

Treatment of $[OsCl(H_2)(PPh_3)\{Ph_2P(CH_2)_2CH{=}CH(CH_2)_2PPh_2\}]OTf$ with H_2

We tried to hydrogenate the coordinated olefin double bond in **4** by storing a solution of **4** in CD_2Cl_2 under H_2. However, the expected hydrogenated product $[OsClH_x(PPh_3)\{Ph_2P(CH_2)_6PPh_2\}]^+$ was apparently not produced from the reaction, as indicated by in situ NMR studies. Instead, the fluxional (hydrido)dihydrogen complex $[OsH(H_2)(PPh_3)\{Ph_2P(CH_2)_2CH{=}CH(CH_2)_2PPh_2\}]OTf$ (**5**) was slowly produced under these reaction conditions. A molecule of HCl in **4** was thus apparently replaced by a H_2 molecule in the reaction. Mechanistically, complex **5** could be formed by initial displacement of Cl^- in **4** with an H_2 molecule to give the dicationic dihydrogen complex $[Os(H_2)_2(PPh_3)\{Ph_2P(CH_2)_2CH{=}CH(CH_2)_2PPh_2\}]^{2+}$, followed by deprotonation.

The presence of a coordinated CH=CH moiety in **5** was supported by the ^{13}C NMR spectrum (in CD_2Cl_2), which displayed the coordinated olefinic CH carbon signals at $\delta = 56.9$ and 65.7 ppm. The $^{31}P\{^1H\}$ NMR spectrum (in CD_2Cl_2) at 230 K showed the PPh_3 signal at $\delta = 4.0$ ppm

and the PPh_2 signals at δ = 29.1 and 36.5 ppm. The two PPh_2 groups in **5** had to be *trans* to each other for the large $^2J_{P,P}$ coupling constant (201.7 Hz) observed for the PPh_2 signals at δ = 29.1 and 36.5 ppm. In the room-temperature ^1H NMR spectrum (in CD_2Cl_2), a broad hydride signal was observed at δ = −5.30 ppm. When the temperature was below 275 K, the hydride signal was split into two with a relative intensity ratio of 1:2. For example, the ^1H NMR spectrum at 230 K showed a doublet of triplets at δ = −6.70 ppm ($^2J_{P,H}$ = 33.0, 19.5 Hz) and a broad singlet at δ = −4.74 ppm, corresponding to one and two hydrogen atoms, respectively. T_1 measurements showed that the broad hydride signal at δ = −4.74 ppm had a T_1 (min) of 10.1 ms (on 300 MHz) at 232 K. The short T_1 (min) value strongly suggested that complex **5** contained a dihydrogen ligand. Furthermore, a partially deuterated sample of $[OsD_{3-x}H_x(PPh_3)\{Ph_2P(CH_2)_2CH{=}CH(CH_2)_2PPh_2\}]^+$ (in CD_2Cl_2 at 235 K) showed a 1:1:1 triplet at δ = −4.69 ppm with a ^1J(HD) coupling constant of 26.7 Hz. The *d*(HH) value in **5** was estimated to be 0.97 Å by application of the relationship *d*(HH) = −0.0167 *J*(HD) + 1.42 and ^1J(HD) = 26.7 Hz.[15a] On the basis of the T_1 (min) of 10.1 ms, the H−H bond length was calculated to be 1.04 Å for a nonspinning H_2 or 0.83 Å for a spinning H_2 ligand.[20] The H−H distance in the (hydrido)dihydrogen complex **5** was shorter than that in the (chloro)dihydrogen complex **4**; a similar trend has been observed for $[MX(H_2)(dppe)_2]^+$ (M = Ru, Os; X = H, Cl).[15a]

Deprotonation of complex **5** with NEt_3 produced the neutral dihydride complex *trans*-$[OsH_2(PPh_3)\{Ph_2P(CH_2)_2CH{=}CH(CH_2)_2PPh_2\}]$ (**6**), which could also be obtained by treatment of complex **3** with $NaBH_4$. Complex **5** was regenerated when **6** was treated with HOTf. The geometry of complex **6** could readily be assigned from its NMR spectroscopic data. In particular, the ^1H NMR spectrum (in CD_2Cl_2) displayed only one hydride signal at δ = −9.13 ppm, indicating that the molecule had high symmetry. Consistently with the structure, the $^{31}P\{^1H\}$ NMR spectrum (in CD_2Cl_2) showed a doublet at δ = 41.2 ppm for the PPh_2 groups and a triplet at δ = 17.6 ppm for the PPh_3 ligand; the $^{13}C\{^1H\}$ NMR showed the coordinated olefinic CH carbon signal at δ = 37.6 ppm.

Structural Study Using Quantum Chemical Calculations

To obtain a better understanding of the interesting chemistry described above, we calculated the structures of complexes $[OsClH(PH_3)\{H_2P(CH_2)_2CH{=}CH(CH_2)_2PH_2\}]$ (**3′**), $[OsCl(H_2)(PH_3)\{H_2P(CH_2)_2CH{=}CH(CH_2)_2PH_2\}]^+$ (**4′**), and $[OsH(H_2)(PH_3)\{H_2P(CH_2)_2CH{=}CH(CH_2)_2PH_2\}]^+$ (**5′**), by the density functional theory B3LYP technique. The calculated structures of complexes **3′**, **4′**, and **5′** should provide enlightening geometric information regarding complexes **3**, **4**, and **5**. We also calculated the structure of $[OsCl(H_2)(PH_3)\{H_2P(CH_2)_6PH_2\}]^+$ (**7′**), a model complex for a hydrogenated product of complex **4**. The optimized structures are shown in Figure 1. Complex **3′** is a typical hydrido(olefin) complex with strong Os−olefin interaction. The protonated species **4′** is confirmed to be a dihydrogen complex. The H−H distance in the dihydrogen complex is calculated to be 1.011 Å, which is close to the experimentally predicted value in **4** based on the ^1J(HD) coupling constant and T_1 (min) value. In a similar manner to complex **4′**, complex **5′** is another dihydrogen(olefin) species. In **5′**, the H−H distance is significantly shorter (0.853 Å), due to the presence of the strongly *trans*-influencing hydride ligand, which gives weaker Os−H_2 interaction.

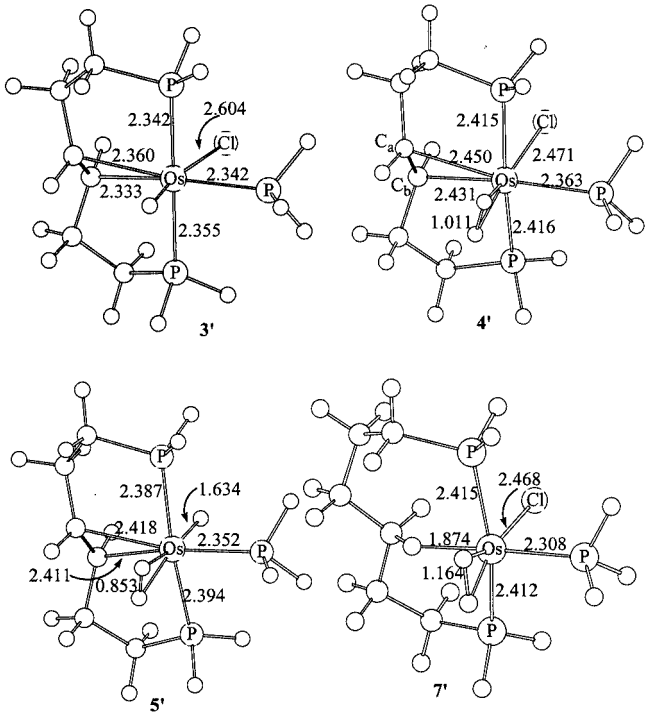

Figure 1. Optimized structures together with selected bond lengths [Å]

Experimentally, it is interesting that under H_2 the coordinated η^2-H_2 did not hydrogenate the olefin unit. The calculated free energy change (ΔG^0) for the process of **4′** + H_2 → **7′** (see Figure 1 for **7′**, the hydrogenated product featuring an agostic interaction) is ca. −1.0 kcal/mol. This result suggests that the hydrogenation is thermodynamically feasible, and we therefore feel that kinetic factors are probably responsible for the hydrogenation not occurring. Careful examination of the structure of complex **4′** (Figure 1) allows one to see that the orientation of the coordinated −HC=CH− unit is in such a manner that one olefinic carbon atom (C_a) is closer to the η^2-H_2 ligand while the other is further away. The hydrogenation of a coordinated olefin by an η^2-H_2 unit can occur through the formation of an agostic intermediate by transfer of one hydrogen atom of the H_2 ligand to one of the two olefinic carbon atoms. A reductive elimination then follows, to complete the hydrogenation process. If the transfer of one H atom from the η^2-H_2 ligand to the closer olefinic carbon atom (C_a) in **4′** is regarded as the first step, it is found that the assumed agostic species does not correspond to a stationary point in the potential energy surface. An agostic structure can be calculated (optimized) by fixing the C_a−H bond length at 1.20 Å.

However, the partially optimized structure is 20 kcal/mol higher in energy than complex **4′** and adopts a pseudopentagonal-bipyramidal (PB) structure in which the equatorial plane is formed by one hydride ligand, the chloride ion, the PH_3 molecule, the C_a-H agostic ligand, and the bonded C_b alkyl moiety. In the PB structure, the hydride ligand and the bonded C_b alkyl moiety are separated by the C_a-H agostic ligand. In such a ligand arrangement, reductive elimination starting from the high-energy partially optimized structure is difficult. Considering the PB structure, one might also take account of the possibility of pushing the C_a-H agostic ligand away and then binding an additional H_2 molecule so that reductive elimination becomes possible. Calculations showed that such a structure was again not a stationary point and had an even higher energy, due to the crowded ligand environment. When the transfer of one H atom from the η^2-H_2 ligand to the further olefinic carbon atom (C_b) was considered as the first step, we found that the activation energy (50 kcal/mol) was too high for such a transfer under the given reaction conditions. The high activation energy for such a process was not surprising, because of the geometric separation of the H and the C_b atoms. A concerted process in which both hydrogen atoms in the η^2-H_2 ligand would transfer simultaneously to the two olefinic carbon atoms seemed unlikely on the basis of our previous calculations on related systems.[21]

Conclusion

The dihydrogen(olefin) complex $[OsCl(H_2)(PPh_3)\{Ph_2P(CH_2)_2CH=CH(CH_2)_2PPh_2\}]OTf$ has been prepared and characterized by NMR spectroscopy. Treatment of $[OsCl(H_2)(PPh_3)\{Ph_2P(CH_2)_2CH=CH(CH_2)_2PPh_2\}]OTf$ with H_2 produced the (hydrido)dihydrogen complex $[OsH(H_2)\{Ph_2P(CH_2)_2CH=CH(CH_2)_2PPh_2\}]OTf$ rather than the hydrogenated products. A computational study suggested that the hydrogenation was thermodynamically feasible but kinetically unfavorable. This work provides rare examples of dihydrogen(olefin) complexes that are characterizable by NMR spectroscopy.

Experimental Section

General: All manipulations were carried out at room temperature under nitrogen by standard Schlenk techniques unless otherwise stated. Solvents were distilled under nitrogen from sodium/benzophenone (hexane, diethyl ether, THF, benzene) or calcium hydride (dichloromethane, $CHCl_3$). The starting materials $Br(CH_2)_2CH=CH(CH_2)_2Br$[22] and $[OsClH_3(PPh_3)_3]$[23] were prepared by literature methods. Microanalyses were performed by M-H-W Laboratories (Phoenix, AZ). ^1H, $^{13}C\{^1H\}$, and $^{31}P\{^1H\}$ NMR spectra were measured with a Bruker ARX 300 spectrometer (300 MHz). ^1H and ^{13}C NMR chemical shifts are relative to TMS, and ^{31}P NMR chemical shifts are relative to 85% H_3PO_4.

(*E*)-$Ph_2P(CH_2)_2CH=CH(CH_2)_2PPh_2$ (2): A THF solution of $KPPh_2$ (50 mL, 0.50 M, 25 mmol) was added slowly to a solution of (*E*)-$Br(CH_2)_2CH=CH(CH_2)_2Br$ (3.00 g, 12.4 mmol) in 30 mL of THF. The reaction mixture was stirred at room temperature for 3 h. A deep red solid was obtained after the solvent had been removed. Addition of water (10 mL) and methanol (40 mL) to the reaction mixture gave a pale yellow solid. The solid was collected on a filter frit, washed with MeOH/H_2O (4:1, 6 × 50 mL) and MeOH (4 × 40 mL), and dried under vacuum. Yield, 4.2 g, 76%. ^1H NMR (300.13 MHz, C_6D_6): δ = 2.03−2.08 (m, 4 H, $CH_2CH_2PPh_2$), 2.14−2.24 (m, 4 H, CH_2PPh_2), 5.38−5.41 (m, 2 H, *H*C=C*H*), 7.12−7.52 ppm (m, 20 H, Ph). $^{31}P\{^1H\}$ NMR (121.5 MHz, C_6D_6): δ = −17.0 ppm (s, PPh_2). $^{13}C\{^1H\}$ NMR (75.48 MHz, C_6D_6): δ = 28.0 (d, $J_{P,C}$ = 12.8 Hz, $CH_2CH_2PPh_2$), 28.9 (d, $J_{P,C}$ = 17.7 Hz, $CH_2CH_2PPh_2$), 128.1 (s, *p*-Ph), 128.2 (d, $J_{P,C}$ = 6.2 Hz, *m*-Ph), 130.2 (d, $J_{P,C}$ = 13.3 Hz, =CH), 132.6 (d, $J_{P,C}$ = 18.6 Hz, *o*-Ph), 139.2 ppm (d, $J_{P,C}$ = 14.6 Hz, *ipso*-Ph). $C_{30}H_{30}P_2$ (452.52): calcd. C 79.63, H 6.68; found C 79.72, H 6.56.

$[OsClH(PPh_3)\{Ph_2P(CH_2)_2CH=CH(CH_2)_2PPh_2\}]$ (3): A mixture of $[OsClH_3(PPh_3)_3]$ (1.37 g, 1.35 mmol) and (*E*)-$Ph_2P(CH_2)_2CH=CH(CH_2)_2PPh_2$ (0.71 g, 1.6 mmol) in benzene (110 mL) was stirred for 5 h. The volume of the reaction mixture was reduced to ca. 7 mL under vacuum. A gray solid was formed when hexane (60 mL) was added. The solid was collected by filtration, washed with hexane (3 × 15 mL), and dried under vacuum. Yield: 1.0 g, 79%. ^1H NMR (300.13 MHz, C_6D_6): δ = −16.40 (dt, $J_{P,H}$ = 27.0, 15.0 Hz 1 H, Os−*H*), 1.96−3.88 [m, 10 H, $Ph_2PCH_2)_2CH=CH(CH_2)_2PPh_2$], 6.87−8.55 ppm (m, 35 H, Ph). $^{31}P\{^1H\}$ NMR (121.50 MHz, C_6D_6): δ = −7.7 (dd, $J_{P,P}$ = 15.0, 14.2 Hz PPh_3), 7.3 (dd, $J_{P,P}$ = 290.6, 15.0 Hz, PPh_2), 23.8 ppm (dd, $J_{P,P}$ = 290.6, 14.2 Hz, PPh_2). $^{13}C\{^1H\}$ NMR (75.48 MHz, C_6D_6): δ = 28.1−33.5 (m, $CH_2CH_2PPh_2$), 56.4 (m, H*C*=), 56.7 (d, $J_{P,C}$ = 21.9 Hz, =*C*H), 126.8−143.0 ppm (m, Ph). $C_{48}H_{46}ClP_3Os$ (941.47): calcd. C 61.24, H 4.93; found C 61.06, H 5.13.

$[OsCl(H_2)(PPh_3)\{Ph_2P(CH_2)_2CH=CH(CH_2)_2PPh_2\}]OTf$ (4): Because of its low stability, the compound was not isolated but was characterized in situ. HOTf (5 μL, 0.06 mmol) was added to a CD_2Cl_2 solution (0.5 mL) containing $[OsClH(PPh_3)\{Ph_2P(CH_2)_2CH=CH(CH_2)_2PPh_2\}]$ (20 mg, 0.021 mmol) in an NMR tube. ^1H, ^{13}C, and ^{31}P NMR spectra were measured immediately. ^1H NMR (300.13 MHz, CD_2Cl_2): δ = −9.57 (br, Os−H_2), 2.15−3.10 (m, 8 H, $CH_2CH_2PPh_2$), 4.77 (br, 1 H, *H*C=), 5.58 (br, 1 H, =C*H*), 6.86−7.82 ppm (m, 35 H, Ph). $^{31}P\{^1H\}$ NMR (121.50 MHz, CD_2Cl_2): δ = −8.9 (dd, $J_{P,P}$ = 14.1, 15.5 Hz, PPh_3), 14.2 (dd, $J_{P,P}$ = 243.6, 15.5 Hz, PPh_2), 16.8 ppm (dd, $J_{P,P}$ = 243.6, 14.1 Hz, PPh_2). $^{13}C\{^1H\}$ NMR (75.48 MHz, CD_2Cl_2): δ = 28.6−37.4 (m, $CH_2CH_2PPh_2$), 89.0 (br, H*C*=), 96.0 (br, =*C*H), 118.8−137.2 ppm (m, Ph). T_1 [ms] of Os(H_2) (300 MHz, CD_2Cl_2) (temperature) = 35.2 (298 K), 31.3 (273 K), 29.1 (263 K), 27.0 (258 K), 27.5 (253 K), 29.5 (243 K), 32.5 (233 K).

$[OsCl(HD)(PPh_3)\{Ph_2P(CH_2)_2CH=CH(CH_2)_2PPh_2\}]OTf$ ($[D_1]$-4): The compound was prepared similarly, except that DOTf was used instead of HOTf. The η^2-HD signal was observed after cancellation of the η^2-H_2 peak at δ = −9.57 ppm by the inversion-recovery method. ^1H NMR (300.13 MHz, CD_2Cl_2): δ = −9.58 ppm [1:1:1 triplet, J(HD) = 14.1 Hz, Os(HD)].

Characterization of $[OsH(H_2)(PPh_3)\{Ph_2P(CH_2)_2CH=CH(CH_2)_2PPh_2\}]OTf$ (5): Because of its low stability, this compound was not isolated but was characterized in situ. **Method A:** HOTf (5 μL, 0.06 mmol) was added to a CD_2Cl_2 solution (0.5 mL) containing $[OsH_2(PPh_3)\{Ph_2P(CH_2)_2CH=CH(CH_2)_2PPh_2\}]$ (20 mg, 0.020 mmol) in an NMR tube. NMR spectra were then measured immediately. **Method B:** A CD_2Cl_2 solution (0.5 mL) containing $[OsClH(PPh_3)\{Ph_2P(CH_2)_2CH=CH(CH_2)_2PPh_2\}]$ (20 mg,

0.021 mmol) and TlOTf (20 mg, 0.057 mmol) in an NMR tube was stored under H_2 for 5 h. ^1H, ^{13}C, and ^{31}P NMR spectra were then measured. **Method C:** A CD_2Cl_2 solution of **4** was stored under H_2 for 18 h, and ^1H and $^{31}P\{^1H\}$ NMR spectra were then measured. ^1H NMR (300.13 MHz, CD_2Cl_2, 230 K): δ = −6.70 (dt, $J_{P,H}$ = 33.0, 19.5 Hz, 1 H, Os−*H*), −4.74 (br, 2 H, OsH_2), 1.60−3.80 [m, 10 H, $Ph_2P(CH_2)_2CH=CH(CH_2)_2PPh_2$], 6.86−7.70 ppm (m, 35 H, Ph). ^1H NMR (300.13 MHz, CD_2Cl_2, 298 K): δ = −5.30 (br, 3 H, Os−*H*, Os−H_2), 1.60−3.80 [m, 12 H, $Ph_2P(CH_2)_2CH=CH(CH_2)_2PPh_2$], 6.86−7.64 ppm (m, 35 H, Ph). $^{31}P\{^1H\}$ NMR (121.50 MHz, CD_2Cl_2, 230 K): δ = 4.0 (dd, $J_{P,P}$ = 11.0, 12.8 Hz, PPh_3), 29.1 (dd, $J_{P,P}$ = 201.7, 12.8 Hz, PPh_2), 36.5 ppm (dd, $J_{P,P}$ = 201.7, 11.0 Hz, PPh_2). $^{31}P\{^1H\}$ NMR (121.50 MHz, CD_2Cl_2, 298 K): δ = 4.4 (dd, $J_{P,P}$ = 12.4, 12.5 Hz, PPh_3), 29.8 (br. d $J_{P,P}$ = 181.5 Hz, PPh_2), 36.2 ppm (br. d, $J_{P,P}$ = 181.5 Hz, PPh_2). $^{13}C\{^1H\}$ NMR (75.48 MHz, CD_2Cl_2, 233 K): δ = 28.6−35.1 (m, CH_2CH_2P), 56.9 (br, H*C*=), 65.7 (br, =*C*H), 128.2−138.8 ppm (m, Ph). T_1 [ms] (300 MHz, CD_2Cl_2) (temperature): δ = −4.80: 13.8 (272 K), 12.2 (252 K), 10.1 (232 K), 14.2 (213 K); δ = −6.58: 14.9 (272 K), 65.16 (252 K), 204.9 (232 K), 301.5 (213 K).

$[OsD_{3-x}H_x(PPh_3)\{Ph_2P(CH_2)_2CH=CH(CH_2)_2PPh_2\}]BF_4$: CD_3OD (0.05 mL) was added to a solution of $[OsH(H_2)(PPh_3)\{Ph_2P(CH_2)_2CH=CH(CH_2)_2PPh_2\}]BF_4$ in CD_2Cl_2, prepared by protonation of **6** (20 mg, 0.020 mmol) with $HBF_4{\cdot}Et_2O$ (5 μL, 0.04 mmol). The mixture was stored at room temperature for 2 h, and ^1H NMR spectrum was measured at 235 K. The η^2-HD signal was observed after cancellation of the η^2-H_2 peak at δ = −4.74 ppm by the inversion-recovery method. ^1H NMR (300.13 MHz, CD_2Cl_2, 235 K): δ = −4.69 ppm [1:1:1 triplet, J(HD) = 26.7 Hz, Os(HD)].

***trans*-$[OsH_2(PPh_3)\{Ph_2P(CH_2)_2CH=CH(CH_2)_2PPh_2\}]$ (6):** A mixture of $NaBH_4$ (0.20 g, 5.3 mmol) and $[OsClH(PPh_3)\{Ph_2P(CH_2)_2CH=CH(CH_2)_2PPh_2\}]$ (0.50 g, 0.53 mmol) in 20 mL of ethanol was stirred at room temperature for 30 min. The solvent was removed under vacuum and the residue was extracted with benzene (20 mL). The volume of the extracted solution was reduced to ca 3 mL. A yellow solid was formed when hexane (40 mL) was added. The solid was collected by filtration, washed with hexane (3 × 15 mL), and dried under vacuum. Yield: 0.25 g, 52%. The complex was also produced when complex **5** was treated with NEt_3. ^1H NMR (300.13 MHz, CD_2Cl_2): δ = −9.13 (dt, $J_{P,H}$ = 29.7, 12.6 Hz, 2 H, Os−*H*), 1.80−2.74 [m, 10 H, $Ph_2P(CH_2)_2CH=CH(CH_2)_2PPh_2$], 6.74−7.80 ppm (m, 35 H, Ph). $^{31}P\{^1H\}$ NMR (121.50 MHz, CD_2Cl_2): δ = 17.6 (t, $J_{P,P}$ = 15.1 Hz, PPh_3), 41.2 ppm (d, $J_{P,P}$ = 15.0 Hz, PPh_2). ^{13}C NMR (75.48 MHz, CD_2Cl_2): δ = 30.4 (t, $J_{P,C}$ = 13.5 MHz, CH_2P), 34.2 (t, $J_{P,C}$ = 7.3 MHz, CH_2CH_2P), 37.6 (d, $J_{P,C}$ = 12.1 MHz, H*C*=), 126.8−143.1 ppm (m, Ph). $C_{48}H_{47}P_3Os{\cdot}3H_2O$ (961.06): calcd. C 59.99, H 5.56 (the water was probably from the solvents); found C 59.98, H 6.00.

Computational Details: In our calculations, the Ph group on the phosphorus ato was modeled by an H atom. Geometry optimizations and frequency calculations were carried out for all species involved in the reactions with the Gaussian 98 program[24] installed on Pentium III personal computers with Linux (Red Hat) operating systems. Molecular geometries of the model complexes were optimized at the Becke3LYP (B3LYP) level of density functional theory.[25] The LANL2DZ effective core potentials and basis sets[26] were used to describe Os, P, and Cl. Polarization functions [ξ(*d*) = 0.340][27] were added for P and [ξ(*d*) = 0.514][27] for Cl. Additionally, better to describe the electronic properties of both hydride and dihydrogen ligands, polarization functions with ξ(p) = 0.11[27] were also added to the standard basis set for H atoms of these two ligands. The standard 6−31G basis set was used for all other atoms.

Acknowledgments

The authors acknowledge financial support from the Hong Kong Research Grants Council.

[1] G. J. Kubas, R. R. Ryan, B. I. Swanson, P. J. Vergamini, H. J. Wasserman, *J. Am. Chem. Soc.* **1984**, *106*, 451−452.
[2] [2a] R. H. Crabtree, *Angew. Chem. Int. Ed. Engl.* **1993**, *32*, 789−805. [2b] D. M. Heinekey, W. J. Oldham, Jr., *Chem. Rev.* **1993**, *93*, 913−926. [2c] P. G. Jessop, R. H. Morris, *Coord. Chem. Rev.* **1992**, *121*, 155−284.
[3] M. A. Esteruelas, L. A. Oro, *Chem. Rev.* **1998**, *98*, 577−588.
[4] [4a] G. J. Kubas, *Dihydrogen and σ bond Complexes*, Kluwer Academic/Plenum Press, New York, **2001**. [4b] *Recent Advances in Hydride Chemistry* (Eds.: M. Peruzzini, R. Poli), Elsevier, Amsterdam, The Netherlands, **2001**. [4c]Y. Nishibayashi, I. Takei, M. Hidai, *Angew. Chem. Int. Ed.* **1999**, *38*, 3047−3050.
[5] [5a] C. Bianchini, A. Meli, M. Peruzzini, P. Frediani, C. Bohanna, M. A. Esteruelas, L. A. Oro, *Organometallics* **1992**, *11*, 138−145. [5b] C. Bianchini, C. Bohanna, M. A. Esteruelas, P. Frediani, A. Meli, L. A. Oro, M. Peruzzini, *Organometallics* **1992**, *11*, 3837−3844.
[6] [6a] A. Andriollo, M. A. Esteruelas, U. Meyer, L. A. Oro, R. A. Sánchez-Delgado, E. Sola, C. Valero, H. Werner, *J. Am. Chem. Soc.* **1989**, *111*, 7431−7437. [6b] M. A. Esteruelas, L. A. Oro, C. Valero, *Organometallics* **1992**, *11*, 3362−3369.
[7] R. H. Crabtree, *The Organometallic Chemistry of the Transition Metals*, 2nd ed., John Wiley & Sons, New York, **1994**, p. 221.
[8] W. C. Chan, C. P. Lau, Y. Z. Chen, Y. Q. Fang, S. M. Ng, G. Jia, *Organometallics* **1997**, *16*, 34−44.
[9] [9a] M. J. Tenorio, M. C. Puerta, P. Valerga, *J. Chem. Soc., Chem. Commun.* **1993**, 1750−1751. [9b] J. Espuelas, M. A. Esteruelas, F. J. Lahoz, L. A. Oro, C. Valero, *Organometallics.* **1993**, *12*, 663−670.
[10] S. H. Liu, S. T. Lo, T. B. Wen, Z. Y. Zhou, C. P. Lau, G. Jia, *Organometallics* **2001**, *20*, 667−672.
[11] [11a] G. Barea, M. A. Esteruelas, A. Lledós, A. M. López, E. Oñate, J. I. Tolosa, *Organometallics* **1998**, *17*, 4065−4076. [11b] R. H. Crabtree, M. Lavin, L. Bonneviot, *J. Am. Chem. Soc.* **1986**, *108*, 4032−4037. [11c] A. C. Albeniz, M. Heinekey, R. H. Crabtree, *Inorg. Chem.* **1991**, *30*, 3632−3635. [11d] A. C. Albeniz, G. Schulte, R. H. Crabtree, *Organometallics* **1992**, *11*, 242−249. [11e] D. G. Gusev, F. M. Dolgushin, M. Y. Antipin, *Organometallics* **2001**, *20*, 1001−1007. [11f] J. N. Coalter, III, J. C. Huffman, K. G. Caulton, *Organometallics* **2000**, *19*, 3569−3578.
[12] [12a] S. A. Jackson, P. M. Hodges, M. Poliakoff, J. J. Turner, F. W. Grevels, *J. Am. Chem. Soc.* **1990**, *112*, 1221−1233. [12b] A. Thomas, M. Haake, F. W. Grevels, J. Bargon, *Angew. Chem. Int. Ed. Engl.* **1994**, *33*, 755−757.
[13] G. I. Childs, A. I. Cooper, T. F. Nolan, M. J. Carrott, M. W. George, M. Poliakoff, *J. Am. Chem. Soc.* **2001**, *123*, 6857−6866.
[14] [14a] G. Jia, W. S. Ng, C. P. Lau, *Organometallics* **1998**, *17*, 4538−4540. [14b] P. H. M. Budzelaar, N. N. P. Moonen, R. de Gelder, J. M. M. Smits, A. W. Gal, *Eur. J. Inorg. Chem.* **2000**, 753−769.
[15] [15a] P. A. Maltby, M. Schlaf, M. Steinbeck, A. J. Lough, R. H. Morris, W. T. Klooster, T. F. Koetzle, R. C. Srivastava, *J. Am. Chem. Soc.* **1996**, *118*, 5396−5407. [15b] B. Chin, A. J. Lough, R. H. Morris, C. T. Schweitzer, C. D′Agostino, *Inorg. Chem.* **1994**, *33*, 6278−6288. [15c] E. Rocchini, A. Mezzetti, H. Rüegger, U. Burckhardt, V. Gramlich, A. Del Zotto, P. Martinuzzi, P. Rigo, *Inorg. Chem.* **1997**, *36*, 711−720. [15d] A. Mezzetti, A. Del Zotto, P. Rigo, E. Farnetti, *J. Chem. Soc., Dalton Trans.* **1991**, 1525−1530.

[16] G. Jia, H. M. Lee, I. D. Williams, C. P. Lau, Y. Z. Chen, *Organometallics* **1997**, *16*, 3941−3949.
[17] P. W. Clark, *J. Organomet. Chem.* **1977**, *137*, 235−256.
[18] C. Crocker, R. J. Errington, R. Markham, C. J. Moulton, K. J. Odell, B. L. Shaw, *J. Am. Chem. Soc.* **1980**, *102*, 4373−4379.
[19] W. Baratta, E. Herdtweck, P. Martinuzzi, P. Rigo, *Organometallics* **2001**, *20*, 305−308.
[20] [20a] D. G. Hamilton, R. H. Crabtree, *J. Am. Chem. Soc.* **1988**, *110*, 4126−4133. [20b] M. T. Bautista, K. A. Earl, P. A. Maltby, R. H. Morris, C. T. Schweitzer, A. Sella, *J. Am. Chem. Soc.* **1988**, *110*, 7031−7036. [20c] P. J. Desrosiers, L. Cai, Z. Lin, R. Richards, J. Halpern, *J. Am. Chem. Soc.* **1991**, *113*, 4173−4184.
[21] S. H. Liu, S. Y. Yang, S. T. Lo, Z. T. Xu, W. S. Ng, T. B. Wen, Z. Y. Zhou, Z. Lin, C. P. Lau, G. Jia, *Organometallics* **2001**, *20*, 4161−4169.
[22] P. G. Gassman, S. M. Bonser, K. Mlinaric-Majerski, *J. Am. Chem. Soc.* **1989**, *111*, 2652−2662.
[23] G. Ferrando, K. G. Caulton, *Inorg. Chem.* **1999**, *38*, 4168−4170.
[24] M. J. Frisch, G. W. Trucks, H. B. Schlegel, G. E. Scuseria, M. A. Robb, J. R. Cheeseman, V. G. Zakrzewski, J. A. Montgomery, R. E. Stratmann, J. C. Burant, S. Dapprich, J. M. Millam, A. D. Daniels, K. N. Kudin, M. C. Strain, O. Farkas, J. Tomasi, V. Barone, M. Cossi, R. Cammi, B. Mennucci, C. Pomelli, C. Adamo, S. Clifford, J. Ochterski, G. A. Petersson, P. Y. Ayala, Q. Cui, K. Morokuma, D. K. Malick, A. D. Rabuck, K. Raghavachari, J. B. Foresman, J. Cioslowski, J. V. Ortiz, B. B. Stefanov, G. Liu, A. Liashenko, P. Piskorz, I. Komaromi, R. Gomperts, R. L. Martin, D. J. Fox, T. Keith, M. A. Al-Laham, C. Y. Peng, A. Nanayakkara, C. Gonzalez, M. Challacombe, P. M. W. Gill, B. G. Johnson, W. Chen, M. W. Wong, J. L. Andres, M. Head-Gordon, E. S. Replogle, J. A. Pople, GAUSSIAN98 (Revision A.7), Gaussian, Inc., Pittsburgh, PA, **1998**.
[25] [25a] A. D. Becke, *J. Chem. Phys.* **1993**, *98*, 5648−5652. [25b] B. Miehlich, A. Savin, H. Stoll, H. Preuss, *Chem. Phys. Lett.* **1989**, *157*, 200−206. [25c] C. Lee, W. Yang, G. Parr, *Phys. Rev. B* **1988**, *37*, 785−789.
[26] P. J. Hay, W. R. Wadt, *J. Chem. Phys.* **1985**, *82*, 299−310.
[27] S. Huzinaga, *Gaussian Basis Sets for Molecular Calculations*, Elsevier Science Pub. Co., Amsterdam, **1984**.

Received November 11, 2001
[I01449]

Kinetics and Equilibria of Nickel(II)−Schiff Base Adducts Formation

Ivo Cacelli,[a] Laura Carbonaro,*[a] and Piero La Pegna[a]

Keywords: Kinetics / Nickel / Schiff base / Adducts / Substituent effects

The interactions between Ni^{II} cations and bidentate Schiff base ligands, *N*-alkyl-5-X-salicylaldimine HL (X = H; R = Et, *n*Pr, *t*Bu; X = Cl, OMe, NO_2; R = *n*Pr), and bis(*N*-*n*-alkyl-5-X-salicylaldiminato)nickel(II) complexes [NiL_2] (X = H; R = Et, *n*Pr, *n*Bu; X = Cl, OMe, Me; R = *n*Pr) were investigated by UV/Vis spectrophotometry in acetonitrile. The kinetics for the formation of Ni^{II}/HL 1:1 adducts was studied by stopped-flow techniques, which showed that the process followed a two-consecutive mechanism. Experimental evidence and theoretical calculations indicated the formation of an unidentate intermediate in the first step, according to a dissociative interchange mechanism. Ring-closure occurs in the second step and its rate is slower for electron-withdrawing-substituted Schiff bases. Nickel(II) cations interact with [NiL_2] affording $[NiL]^+$ and $[Ni_2L_3]^+$ species; the associated equilibrium constants were found to be related to the electronic effects of the 5-X ligand substituents.

(© Wiley-VCH Verlag GmbH, 69451 Weinheim, Germany, 2002)

Introduction

Metal adducts of Schiff bases are an important class of compounds. Metal complexes [ML_2] of Schiff bases derived from salicylaldehyde can form adducts with different ions,[1,2] and even with DNA.[3] Examples of $MA_n{\cdot}mHL$ adducts (A = anion) between neutral HL Schiff base ligands and metal ions have also been reported.[4] The nature and the factors influencing the observed stoichiometries of individual adducts have been investigated mainly with regard to the steric hindrance of the imine group. In spite of the interest in these compounds, not much information is available on both the stability constants and the kinetics for the formation of these compounds. This is the first investigation of the mechanism for the formation of 1:1 Ni^{II}/HL adducts in acetonitrile, and of the equilibria between Ni^{II} cations and [NiL_2] complexes (HL = 5-X-salH-R) for various 5-X aromatic ring substituents and nitrogen-bound aliphatic chains R of the Schiff base ligand, see Scheme1.

The mechanism of solvent exchange and ligand substitution involving octahedral nickel(II) ions has been shown to be dissociative in character and generally to proceed by the fast formation of an outer-sphere complex followed by the loss of a solvent molecule in the rate-determining step,[5] see Equations (1a and b). Thus, the pseudo-first-order rate constant is generally expressed by Equation (2), where K_0 is the equilibrium constant for the formation of the outer-sphere complex, k_2 can be approximated to the rate constant for solvent exchange k_{ex}, and k_{-2} is the first-order rate constant for the reverse dissociation process.

$$Z{\cdots}Y + [NiS_6]^{2+} \overset{K_0}{\rightleftharpoons} [NiS_6{\cdot}Z{\cdots}Y]^{2+} \quad (1a)$$

$$[NiS_6{\cdot}Z{\cdots}Y]^{2+} \underset{k_{-2}}{\overset{k_2}{\rightleftharpoons}} [S_5Ni{-}Z{\cdots}Y]^{2+} + S \quad (1b)$$

$$[S_5Ni{-}Z{\cdots}Y]^{2+} \underset{k_{-3}}{\overset{k_3}{\rightleftharpoons}} [S_4Ni\begin{matrix}Z\\|\\Y\end{matrix}]^{2+} + S \quad (1c) \qquad (1)$$

$$k_{obs} = k_f[Ni^{2+}] + k_d = K_0k_2[Ni^{2+}] + k_{-2} \qquad (2)$$

This mechanism can be extended to bidentate ligands by introducing an additional, usually fast, ring-closure step, see Equation (1c). It can be anticipated that bidentate 5-X-salH-R ligands give rise to ring-closure inhibition in the coordination reaction to nickel(II) cations, as they can form hydrogen bonds between their chelating sites, and may exist[6,7] in zwitterionic forms $HL^{\pm}$ in polar solvents (see Scheme 1). Differing from most of the kinetics studies reported in the literature on solvent substitution reactions by bidentate ligands, the steps according to Equations (1b and c) can be studied kinetically, and the substituent effects on the ring-closure step can be examined.

The interactions between [NiL′] tetradentate complexes (Scheme 1) and alkaline, alkaline-earth or Ni^{II} cations were previously studied by our group.[8] Adducts of stoichiometry 1:1 and/or 1:2 form in acetonitrile, see **1** and **2** of Scheme 2. Metal ions are coordinated by means of the O···O bite offered by the [NiL′] complex.

Solid-state examples of adducts formed between metal ions and bidentate [NiL_2] complexes (Scheme 1) are re-

[a] Dipartimento di Chimica e Chimica Industriale, Università di Pisa,
Via Risorgimento 35, 56126 Pisa, Italy
Fax: (internat.) + 39-050/918260
E-mail: laucb@dcci.unipi.it

Supporting information for this article is available on the WWW under http://www.eurjic.com or from the author.

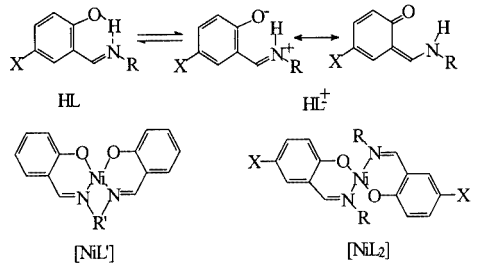

HL = 5-X-salH-R X = H; R = Et, *n*Pr; *t*Bu
X = Cl, OMe, NO_2; R = *n*Pr;
[NiL'] R' = $(CH_2)_2$, $(CH_2)_3$, 1,2-Phenyl
$[NiL_2] = [Ni(5\text{-X-sal-R})_2]$ X = H; R = Et, *n*Pr, *n*Bu
X = Cl, OMe, Me; R = *n*Pr;

Scheme 1

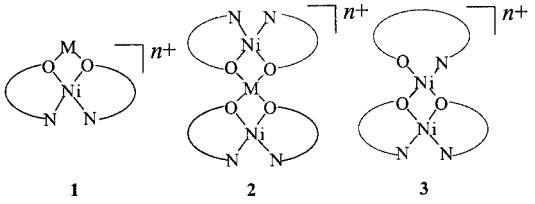

Scheme 2. Schematic representation of the interactions between tetradentate [NiL'] (N−N bridge is omitted) or bidentate $[NiL_2]$ complexes with different ions (M = alkali, alkaline earth or Ni^{II} ions; n = 1 or 2)

stricted to a few cases.[8] In solution *trans*-planar $[NiL_2]$ complexes are in equilibrium with their tetrahedral isomers when R is a bulky substituent.[9] The formation of adducts with metal ions may induce a *cis* geometry having an oxygen bite similar to that of tetradentate complexes. It has been confirmed[10,11] that 1:1 adducts are formed with Na^+ and Ba^{2+}, and 2:1 adducts with Ba^{2+} (**1** and **2** of Scheme 2) in the solid state, as well as in solution when R = H and a second pendant arm is *ortho* to the phenolato oxygen atom. From the present study it appears that $[NiL_2]$ complexes with R = alkyl group and *para* aromatic-ring substituents, may exhibit a different behaviour in the presence of Ni^{II} cations.

Results and Discussion

Reaction between HL = 5-X-salH-R and Ni^{II} Cations

The equilibrium between solvated octahedral nickel(II) and 5-X-salH-R Schiff bases for R = Et, X = H was studied in an acetonitrile solution. The spectrophotometric data were consistent with the formation of a 1:1 Ni^{II}/ligand adduct at high Ni^{II}/ligand molar ratios. A value of $\log K$ = 2.3 ± 0.01 was determined for the apparent equilibrium constant for the formation of the adduct.[12] Values of $\log K$ = 1.21 ± 0.02 and $\log K$ = 1.98 ± 0.03 were found for the formation of 1:1 adducts with Ba^{2+} and Sr^{2+}, respectively. On the basis of these findings and of the kinetic results (see below), only a 1:1 Ni^{II}/ligand product was assumed to form at the concentrations used in the kinetic measurements.

UV/Vis spectra recorded during the reaction of Ni^{II} cations with 5-X-salH-R Schiff bases (X = H, R = Et, *n*Bu; X = H, Cl, OMe, R = *n*Pr) showed different isosbestic points for the initial and final spectra, see Figure 1. At the initial reaction times a band at about 400 nm appears, while the final spectrum exhibits a maximum in the 360−370 nm range, depending on the 5-X substituent.

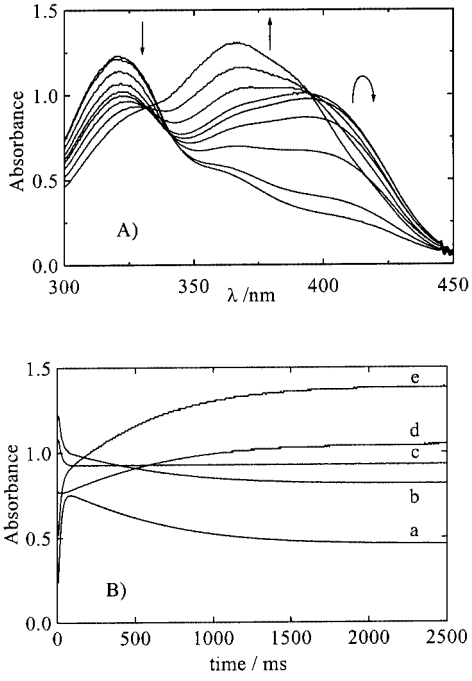

Figure 1. Spectral changes A) and kinetic traces B) at different wavelengths recorded for the reaction of 5-MeO-salH-*n*Pr (3×10^{-4} M) and nickel cations ($[Ni(CH_3CN)_6(ClO_4)_2] = 3.3 \times 10^{-2}$ M) in acetonitrile within 2500 ms at 25.0 °C (optical path = 1 cm); A) following the arrows, the spectra were recorded at 5, 10, 25, 50, 100, 250, 500, 1000, 2500 ms after mixing the reactants; B) λ = a) 416 nm, b) 332 nm, c) 322 nm, d) 394 nm, e) 366 nm

The kinetic traces could be fitted to the two-exponential Equation (10) (Exp. Sect.), which is characteristic of a two-consecutive step reaction.[13] The sum and the product of the exponential constants λ_1 and λ_2 were found to be linearly dependent on the nickel(II) concentration, Figures 2 and 3 (Figures 1*i* and 2*i*, Supporting Information). These kinetic results are in agreement with Equation (1): in the first step [Equation (1b)] the Schiff base replaces one solvent ligand leading to a mono-chelating complex; in the second step [Equation (1c)] ring closure occurs. Assuming $K_0[Ni^{2+}] << 1$, the rate constants of Equation (1) can be calculated from the slopes and the intercepts of Equations (3) and (4) (see Table 1).

$$\lambda_1 + \lambda_2 = k_f[Ni^{2+}] + (k_{-2} + k_3 + k_{-3}) \quad (3)$$

$$\lambda_1\lambda_2 = k_f(k_3 + k_{-3})[Ni^{2+}] + k_{-2}k_{-3} \quad (4)$$

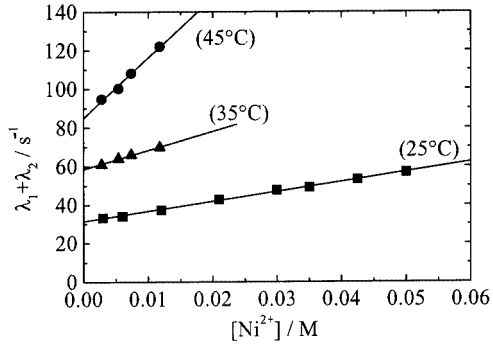

Figure 2. Plots of $\lambda_1 + \lambda_2$ [Equations (3) and (10)] against [Ni^{2+}] for the reaction between 5-H-salH-*n*Pr (ca. 10^{-4} M) and nickel(II) cations in acetonitrile at three different temperatures

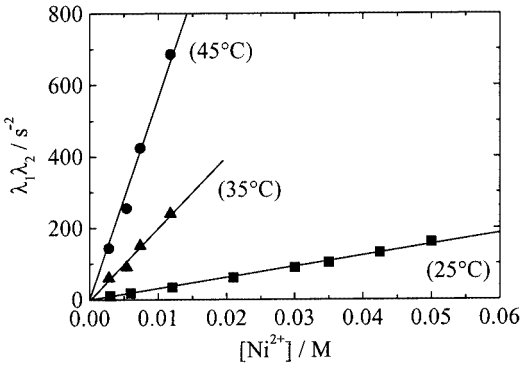

Figure 3. Plots of $\lambda_1\lambda_2$ [Equations (4) and (10)], against [Ni^{2+}] for the reaction between 5-H-salH-*n*Pr (ca. 10^{-4} M) and nickel(II) cations in acetonitrile at three different temperatures

As expected for a dissociative mechanism, the k_f rate constants were only slightly dependent on the substituent 5-X, and are close to those found for other uncharged monodentate ligands, e.g. pyridine[14] (k_f = 830 $M^{-1}s^{-1}$) and isoquinoline[15] (k_f = 709 m^{-1} s^{-1}).

The equilibrium constants K_0 for the outer-sphere complex formation were calculated from the measured k_f values as $k_f = fK_0k_{ex}$, where $k_{ex} = 3.1 \times 10^3$ s^{-1} is the rate constant of acetonitrile exchange[16] between the nickel(II) cations and the bulk solvent, and f = 3/4 is a statistical factor taking into account the number of solvent molecules in the outer-sphere complex competing with the entering ligand.[17] The theoretical K_0 values derived from the electrostatic theory, see Table 2, as well as from theoretical calculations, vide infra, were in excellent agreement.

Table 2. Calculated dipole moments of HL= 5-X-salH-R ligands, interaction energies, and theoretical and experimental equilibrium constants related to the formation of the outer-sphere complex between Ni^{II} cations and Schiff bases [Equation (1a)]

X	R	μ/Debye[a]	U[b]/kJ mol^{-1}	K_0 [c]/M^{-1}	K_0 [d]/M^{-1}
H	Et	2.44	−0.679	0.21	0.24
H	*n*Pr	2.89	−0.760	0.22	0.22
H	*t*Bu	3.63	−0.735	0.22	0.12
Cl	*n*Pr	3.31	−0.463	0.20	0.22
O_2N	*n*Pr	5.45	−0.642	0.21	0.18
MeO	*n*Pr	3.56	−0.774	0.22	0.19

[a] Dipole moment of the ligand (see text). [b] Interaction electrostatic energy between the dipole of the ligand and the charge of the nickel(II) cation. See Equation (15). [c] Theoretical K_0 values calculated by Equations (14) to (16). [d] Experimental K_0 values calculated from the ratio k_f/fk_{ex} (the values of k_f are from Table 1).

For the reaction of 5-H-salH-*n*Pr with Ni^{II} cations (Table 1), the activation parameters were $\Delta H^{\neq}$ = 34.7 ± 1.7 kJ mol^{-1} and $\Delta S^{\neq}$ = −100.4 ± 4.2 J mol^{-1} K^{-1} for k_{-2}, and $\Delta H^{\neq}$ = 71.1 ± 4.2 kJ mol^{-1}, $\Delta S^{\neq}$ = 38.5 ± 3.3 J mol^{-1} K^{-1} for k_f. The latter values compare quite satisfactorily with the activation parameters reported for solvent exchange:[17] $\Delta H^{\neq}$ = 60.8 ± 1.1 kJ mol^{-1} and $\Delta S^{\neq}$ = 25.8 J ± 2.8 J mol^{-1} K^{-1}, thus confirming a dissociative mechanism.

For X = NO_2 two well-distinct pseudo-first-order steps were confirmed. The pseudo-first-order kinetic rate constant for the first step is linearly dependent on the nickel(II) concentration, see Equation (2). For the second step, by neglecting k_{-3} and with $K_2 = k_2/k_{-2}$, Equation (5) was applied along with Equation (1). Thus the rate constants for Equation (1b) and Equation (1c) could be determined, see

Table 1. Rate constants (errors expressed as standard deviations) for the formation of 1:1 adducts between Ni^{II} cations and Schiff bases HL = 5-X-salH-R, see Equation (1)

X	R	T/°C	k_f/M^{-1} s^{-1}	k_{-2}/s^{-1}	k_3/s^{-1}	k_{-3}/s^{-1}	ΔpK_a[a]
H	Et	25.0	(5.5 ± 0.3) × 10^2 [b]	24.8 ± 0.9[b]	5.6 ± 0.4[b]	0.10 ± 0.07	
H	*n*Pr	25.0	(5.1 ± 0.1) × 10^2 [b]	25.2 ± 0.4[b]	5.6 ± 0.3[b]	0.13 ± 0.07	0.64
H	*n*Pr	35.0	(9.7 ± 0.5) × 10^2 [b]	38 ± 1[b]	20 ± 1[b]	[d]	
H	*n*Pr	45.0	(3.2 ± 0.2) × 10^3 [b]	66 ± 2[b]	18 ± 1[b]	[d]	
Cl	*n*Pr	25.0	(5.0 ± 0.2) × 10^2 [b]	40.1 ± 0.6[b]	4.4 ± 0.2[b]	[d]	0.37
O_2N	*n*Pr	25.0	(4.2 ± 0.2) × 10^2 [c]	25.2 ± 0.5[c]	0.31 ± 0.03[c]	[d]	−1.48
MeO	*n*Pr	25.0	(4.5 ± 0.1) × 10^2 [b]	33.1 ± 0.5[b]	7.5 ± 0.6[b]	0.36 ± 0.08	0.98
H	*t*Bu	25.0	(2.7 ± 0.4) × 10^2 [e]	12.5 ± 0.3[e]			
H	*t*Bu	35.0	(7.7 ± 0.6) × 10^2 [e]	19.3 ± 0.5[e]			
H	*t*Bu	45.0	(19.5 ± 0.7) × 10^2 [e]	31.8 ± 0.6[e]			

[a] $\Delta pK_a = (pK_{OH} - pK_{NH^+})$, difference between the pK_a of *p*-X-phenols[18] and *m*-X-benzylammonium[19] in water at 25 °C. [b] Calculated by Equations (10), (3) and (4). [c] Calculated according to Equations (9), (2) and (5). [d] The value of k_{-3} was neglected within the experimental error. [e] Calculated by Equations (9) and (2).

Figure 4 and Table 1, and their values confirmed the previous assumptions made on Equations (3) and (4) for the other ligands.

$$1/k_{obs(2)} = 1/(K_0K_2k_3[Ni^{2+}]) + 1/k_3 \quad (5)$$

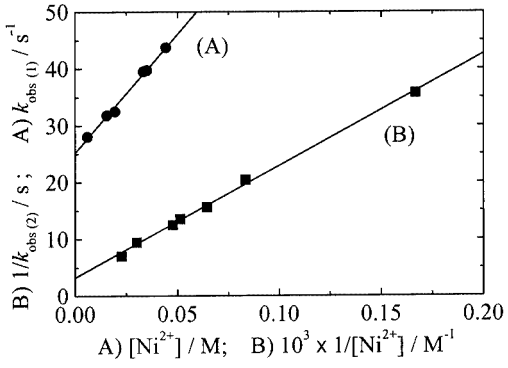

Figure 4. Plot of (A) $k_{obs(1)}$ against [Ni^{2+}] for the first reaction step [Equation (1b)] according to Equations (2) and (9), and plot of (B) $1/k_{obs(2)}$ against 1/[Ni^{2+}] for the second reaction step [Equation (1c)] according to Equations (5) and (9), for the reaction between 5-NO_2-salH-*n*Pr (ca. 10^{-4} M) and nickel(II) cations in acetonitrile at 25.0 °C

For X = H, R = *t*Bu, only one rate-determining step was seen, the final spectrum exhibits a maximum at about 390 nm. The observed pseudo-first-order rate constant depends linearly on the Ni^{II} concentration (see Figure 5) and, according to Equation (2), it could be related to the formation of the unidentate complex. The values of k_f and k_{-2} at different temperatures (Table 1) are slightly smaller than the rate constants quoted for the other ligands examined. The activation parameters, $\Delta H^{\neq}$ = 75.3 ± 1.2 kJ mol^{-1} and $\Delta S^{\neq}$ = 54.4 ± 4.2 J mol^{-1} K^{-1} for k_f and $\Delta H^{\neq}$ = 34.3 ± 2.1 kJ mol^{-1} and $\Delta S^{\neq}$ = −108.8 ± 8.4 J mol^{-1} K^{-1} for k_{-2}, are close to those found for the 5-H-salH-*n*Pr ligand. Ring closure for R = *t*Bu might be insignificant due to steric hindrance.

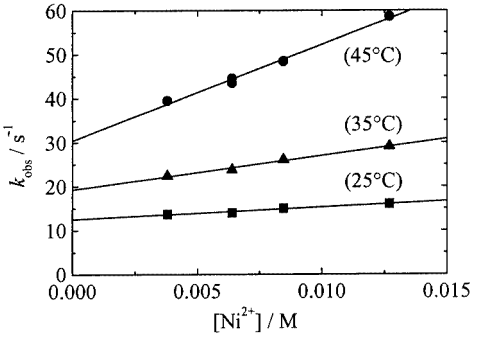

Figure 5. Plot of k_{obs} [Equations (2) and (9)] against [Ni^{2+}] for the reaction between 5-H-salH-*t*Bu (ca. 10^{-4} M) and nickel(II) cations in acetonitrile at three different temperatures

From Table 1, the rate constant k_3 for the ring-closure step depends on the substituents 5-X and increases with increasing electron-donor properties of 5-X. A linear relationship was found (slope = 0.58; correlation coefficient r = 0.999) when logk_3 is plotted vs. ΔpK_a ($\Delta pK_a = pK_{OH} - pK_{NH^+}$, where pK_{OH} [18] and pK_{NH^+} [19] are the pK_a values in water of the *p*-substituted phenols and of the *m*-substituted benzylammonium ions related to the 5-X-salH-R ligand, respectively). The positive slope suggests that migration of hydrogen from nitrogen to oxygen occurs in the ring-closure step. This agrees with a quinonic structure for the unidentate intermediate, rather than an enolic structure. The band at about 400 nm identified in the early stages of the reaction, which is characteristic[20] of the quinonic form of the ligand, confirms this proposal. Nickel(II) may be coordinated to the oxygen or the nitrogen atom of the quinonic form of the ligand, while an NH···O or N···HO intramolecular hydrogen bond is retained, respectively. Both these structures have been documented for some $MA_n \cdot mHL$ (A = anion)[4] Schiff base adducts similar to the present ones. Theoretical calculations on 5-X-salH-R ligands indicated that Ni^{II} coordination to oxygen is favoured (vide infra). A plausible mechanism for the formation of 5-X-salH-R adducts with Ni^{II} cations is depicted in Scheme 3, where solvent molecules are omitted for clarity. It is worth noting that for X = NO_2, a strong resonance stabilisation of the quinonic intermediate may account for the significantly smaller k_3 value than that observed for the other ligands.

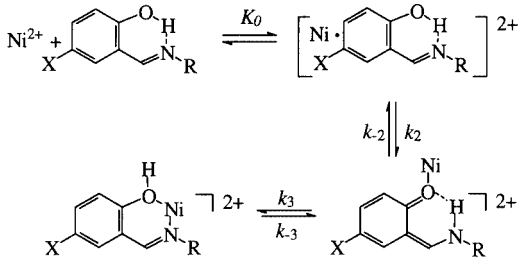

Scheme 3

Theoretical Results

The quantum-mechanical geometry optimisation shows that all the free ligands have a virtually planar geometry and that the O−H and N−H distances are 0.99 Å and 1.75−1.77 Å, respectively. These are consistent with the enolic form of HL, see Scheme 1. The computed dipole moments for the 5-X-salH-R ligands are reported in Table 2.

The most favourable arrangements for the Ni^{II}/HL outer-sphere complexes are depicted in Figure 6. In all cases the centre of the cation sphere (R = 4 Å) almost lies on the plane of the aromatic ring.

When X is an electron-donating group, the dipole moment is roughly parallel to the (HO)C−C(CH=NR) bond and the cation sphere approaches the molecule toward the oxygen atom. When X = Cl, and more so when X = NO_2, the dipole moment is rotated toward the R group and the most favourable position of the cation moves toward the aromatic ring.

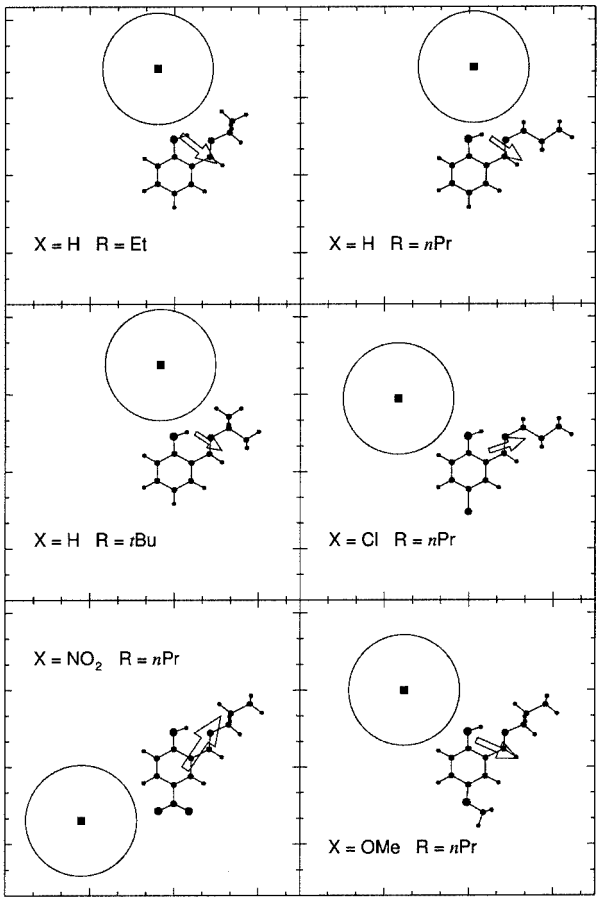

Figure 6. Schematic representation of the 5-X-salH-R/Ni^{II} outer-sphere complexes as determined by theoretical calculations; the distance between two nearest ticks of both axes is 2 Å; the molecular geometry is projected on the aromatic plane; the length of the arrow on the ligand is proportional to the dipole moment vector and indicates its position as specified in the text

When using Equations (6) and (7), a good agreement between the experimental and theoretical K_0 values (Table 2) was found. The overestimation of the theoretical K_0 value for X = H, R = *t*Bu may be of significance. The R groups are far away from the sphere of the Ni^{II} ion; nevertheless, the formation of a tighter inner-sphere complex requires the steric hindrance, that arises as a result of R, to be reduced by assuming a more favourable conformation. This cannot be achieved for R = *t*Bu.

$$K_0 = \frac{4\pi}{3000} Na^3 \times \exp(-U/k_B T) \quad (6)$$

$$U = -\frac{\mu Q \cos\alpha}{Dd^2} \quad (7)$$

In order to gain some information about the structure of the monodentate intermediate of Equation (1), we carried out a theoretical calculation on the 5-HsalH-Et ligand interaction with a cation. The effect of metal ion coordination by the ligand was studied by a simplified model system in which the NiS_5^{2+} cation was mimicked by the Na^+ cation. The cation was initially assumed to be equidistant (9 Å) from both the O and N atoms in the molecular plane of the enolic ligand. As expected, during the geometry optimisation the cation moves towards the O−H−N group, the H atom simultaneously migrates towards the N atom. The final optimised geometry (O−H = 2.09 Å, N−H = 1.03 Å) clearly shows that the presence of a cation such as Na^+ favours the quinonic form of the ligand.

Equilibria between $[NiL_2]$ = [Ni(5-X-sal-R)$_2$] Complexes and Ni^{II} Cations

The equilibria between the $[NiL_2]$ complexes and the Ni^{II} cations were studied spectrophotometrically in acetonitrile solution. On increasing the amounts of Ni^{II} cations, the characteristic MLCT and $\pi\rightarrow\pi\delta$ absorption bands[21] at ca. 400 and ca. 330 nm decrease and a new band at 370 nm appears. At high metal/ligand ratios the observed maximum shifts to longer wavelengths. (Figure 3*i*, Supporting Information). For the 5-O_2N-substituted complex, absorbance changes were too small to obtain reliable results.

Several equilibrium schemes were tested by refining the spectrophotometric data by a nonlinear least-squares program, and the formation of 1:1 or 1:2 $Ni^{II}/[NiL_2]$ adducts similar to those mentioned[2] in the introduction (see Scheme2) could be excluded. Fit residues were within the absorbance measurement error, and gave a statistical distribution at all the wavelengths examined only by applying Equation (8) (solvent molecules are omitted for clarity). In the equilibrium according to Equation (8a) the starting complex dissociates into two $[NiL]^+$ moieties. In the equilibrium according to Equation (8b) a dinuclear species $[Ni_2L_3]^+$ is formed by the interaction of $[NiL_2]$ and $[NiL]^+$.

$$[NiL_2] + Ni^{2+} \overset{K_4}{\rightleftharpoons} 2[NiL]^+ \quad (8a)$$

$$[NiL]^+ + [NiL_2] \overset{K_5}{\rightleftharpoons} [Ni_2L_3]^+ \quad (8b)$$

The related equilibrium constants, calculated as average values for at least three independent experiments, are reported in Table 3. In the present measurements, according to these values, the concentration of $[Ni_2L_3]^+$ was at most 8−10% of the total concentration of the other species.

Figure 7 shows an example of calculated spectra for the species involved in the equilibria of Equation (8) for the $Ni^{II}/[Ni(5\text{-MeO-sal-}n\text{Pr})_2]$ system; the spectrum of $[Ni_2L_3]^+$ is similar to that of $[NiL]^+$ but shows a threefold absorptivity, which is in agreement with three nearly equivalent ligands.

The ^1H NMR spectra of acetonitrile solutions of $[NiL_2]$ and Ni^{II} cations did not show detectable signals, most likely due to the presence of paramagnetic species.

A linear free energy relationship was found between the equilibrium constants $\log K_4$ of Equation (8a) and Taft's substituent constant[22] σ_p° which is related to the Schiff base oxygen atom, but not to the imine site (slope ρ° = +2.04; correlation coefficient r = 0.995) (Table 3). It is likely that an initial charge−dipole interaction between Ni^{II}

Table 3. Equilibrium constants for Equation (8) and λ_{max} [nm] of the species in solution after reaction between $[NiL_2]$ = [Ni(5-X-sal-R)$_2$] and Ni^{II} cations in acetonitrile at 25 °C

$[NiL_2]$= [Ni(5-X-sal-R)$_2$]	logK_4	logK_5	(σ°_p)[a]	$(\sigma^\circ_p - \sigma^+)$[a]	λ_{max} [b]/nm $[NiL_2]$	λ_{max} [c]/nm $[NiL^+]$	λ_{max} [c]/nm $[Ni_2L_3^+]$
[Ni(5-H-sal-Et)$_2$]	1.16 ± 0.03	3.61 ± 0.01	−	−	412	370	355
[Ni(5-H-sal-*n*Bu)$_2$]	1.03 ± 0.04	3.48 ± 0.02	−	−	413	371	360
[Ni(5-H-sal-*n*Pr)$_2$]	1.02 ± 0.03	3.50 ± 0.01	0	0	413	370	352
[Ni(5-Cl-sal-*n*Pr)$_2$]	1.64 ± 0.05	3.67 ± 0.02	0.27	0.16	420	383	355
[Ni(5-Me-sal-*n*Pr)$_2$]	0.76 ± 0.05	3.68 ± 0.02	−0.15	0.19	420	377	354
[Ni(5-MeO-sal-*n*Pr)$_2$]	0.87 ± 0.05	4.15 ± 0.01	−0.12	0.62	434	392	367

[a] Substituents constants.[22] [b] Experimental. [c] Calculated.

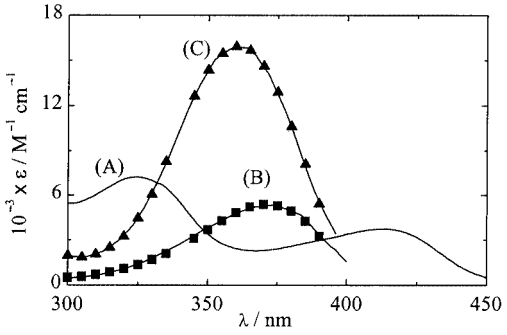

Figure 7. Experimental absorbance spectrum of $[NiL_2]$ = [Ni(5-MeO-sal-*n*Pr)$_2$] (A) and calculated absorbance spectra of $[NiL]^+$ (B), and $[Ni_2L_3]^+$ (C) in acetonitrile at 25.0 °C

cations like that in **1** in Scheme 2, yields two $[NiL]^+$ species, with electron-withdrawing substituents favouring their formation.

For logK_5, a good linear correlation was found by using the equation $\log K_5 = \rho(\sigma^\circ_p - \sigma^+)$ (slope = 0.973; r = 0.999). The interpretation of this behaviour is not straightforward since the $[Ni_2L_3]^+$ structure in solution is not known. It is likely that $[Ni_2L_3]^+$ forms by direct interaction of the starting complex $[NiL_2]$, by means of its O···O bite with the charged species $[NiL]^+$, see Scheme 2 (species **3**). This might be achieved by adopting a hindered *cis*-planar, or more likely a tetrahedral geometry. Hence, electron-withdrawing substituents on $[NiL]^+$ (which can be related to the σ^+ term) and electron-donor substituents on $[NiL_2]$ (which can be related to the σ°_p term) favour the right side of the equilibrium according to Equation (10b), accounting for the above logK_5 equation.

Experimental Section

Physical Measurements: IR and UV/Vis spectra were recorded with Perkin−Elmer 983 and Perkin−Elmer Lambda9 instruments, respectively. A Dionex Chromatograph S4000 instrument and an ICP/AES Varian Liberty 200 instrument were used for ionic chromatographic and plasma analyses, respectively. ^{1}H NMR spectra were recorded with a Varian Gemini 200 instrument.

Materials: Bis(*N*-alkyl-5-X-salicylaldiminato)nickel(II) = [Ni(5-X-sal-R)$_2$] complexes (X = H, R = Et, *n*Pr, *n*Bu; X = Cl, OMe, Me, NO_2; R = *n*Pr) were prepared and purified according to the literature.[23] *N*-Alkyl-5-X-salicylaldimine Schiff bases,[24] 5-X-salH-R (X = H; R = Et, *n*Pr, *t*Bu; X = Cl, OMe, NO_2; R = *n*Pr), were prepared by condensation of salicylaldehyde with the appropriate amine and purified by distillation under reduced pressure. Acetonitrile was purified and dried by standard methods.[25]

Caution!*: Perchlorates are potentially explosive. Only small amounts should be dried and used at once.* Alkaline earth perchlorates (Aldrich products) were dried at 100 °C under reduced pressure. Ionic HPLC and plasma analyses confirmed the purity of each salt. $[Ni(CH_3CN)_6](ClO_4)_2$ was prepared and purified according to literature methods[26] and characterised by elemental and plasma analyses.

Equilibrium and Kinetic Measurements: Spectrophotometric kinetic measurements were carried out by a stopped-flow technique previously described[27] (dead time = 6−7 ms) under dry nitrogen at different temperatures (± 0.2 °C). $[Ni(CH_3CN)_6](ClO_4)_2$ was used in a large excess (from 3×10^{-3} to 5×10^{-2} M) relative to the Schiff base ligand (ca. 10^{-4} M). The reactions were monitored by a diode-array detector (time resolution 5 ms) or a photomultiplier in the 300−500-nm UV/Vis region (time resolution 0.1 ms). Experimental kinetic traces were selected at one or more wavelengths (365, 383, 430 nm) corresponding to the largest absorbance changes. Up to six traces of absorbance (A) vs. time (t) for each kinetic run were computer-fitted to the appropriate one-exponential Equation (9), or two-exponential Equation (10). A_0 and A_∞ are the initial and final absorbances respectively, and A_1 and A_2 are pre-exponential factors. Kinetic experiments with different amounts of (nBu$_4$N)-(ClO_4) showed that the rates were not affected by ionic strength.

$$A = A_\infty + (A_0 - A_\infty) \exp(-k_{obs}t) \quad (9)$$

$$A = A_\infty + A_1 \exp(-\lambda_1 t) + A_2 \exp(-\lambda_2 t) \quad (10)$$

Equilibrium measurements were carried out as previously described.[2] 20−40 solutions of the $[NiL_2]$ complex at constant concentration (ca. 10^{-4} M) and increasing concentrations of $[Ni(CH_3CN)_6](ClO_4)_2$ were used. An inverse procedure was adopted to determine the equilibria between 5-H-salH-Et Schiff base (up to ca. 10^{-4} M) and the metal ions (ca. 10^{-3} M). The experimental absorbance $A(\lambda)$ was expressed as a function of the total concentrations C of the reactants, the absorptivities ε_λ of the species in solution and the equilibrium constants K_i according to the equilibrium scheme to be tested. Equilibrium constants and molar absorptivities at about 25 wavelengths in the range of 300 to 500 nm were simultaneously optimised using a nonlinear least-squares program.[28] Standard deviations accepted were less than 2.5×10^{-3}. Equilibria involving species at concentrations less than 2% of the total reactant were rejected.

According to Equation (8), the absorbance of an $Ni^{II}/[NiL_2]$ solution at a given wavelength λ is expressed by Equation (11), where the dependence of the ε values on the wavelength has been omitted for brevity. The mass balance equations allow to relate the concentrations of the Ni^{II} cations and $[NiL_2]$ to the total concentrations $C_{[NiL]_2}$ and $C_{[Ni^{2+}]}$.

$$A(\lambda) = \varepsilon_{Ni^{2+}}[Ni^{2+}] + \varepsilon_{NiL_2}[NiL_2] + \varepsilon_{(NiL)^+}(K_4[NiL_2][Ni^{2+}])^{1/2} + \varepsilon_{(Ni_2L_3)} + K_5[NiL_2](K_4[NiL_2][Ni^{2+}])^{1/2} \quad (11)$$

Ion pairs involving ClO_4^- anions were neglected in the acetonitrile solution.[29] In order to evaluate the activity coefficients of the charged species, the Debye−Hückel law was applied in its complete form, by taking the distance for the closest approach of the ions as $a = 5$ Å. Hence, the effect of ionic strength can be neglected for the present measurements on complexation reactions of neutral macrocyclic ligands with cations,[2] and/or for total $M(ClO_4)_2$ concentrations not exceeding 0.001 M.

Computational Details: The geometry of the 5-X-salH-R ligands was optimised by employing the Density Functional Theory based on the B3LYP functional.[30]The triple zeta with polarisation 6−311G* basis set was employed and the calculations were carried out with the Gaussian98[31] package. Other calculations concerning some species involved in the reaction of Ni^{II} cations with HL ligands were performed in the same way.

With the aim to evaluate the $[NiS_6]^{2+}$/HL (S = solvent) interaction energy of the outer-sphere complex, we resorted to the Fuoss association theory[32,33] (originally developed for ions in a solvent), represented as a polarizable continuum and adapted to the case of an ion interacting with a dipole. If the cation is considered as a point charge at the centre of a sphere of radius a, then the equilibrium constant K_0 can be approximated as in Equation (6), where a is expressed in cm, N is the Avogadro number, and U is the charge−dipole electrostatic interaction energy. By considering the solvent as a continuum of permittivity D, the energy U may be approximated to the lowest power of the charge−dipole distance d as in Equation (7), where μ is the dipole moment and α is the angle between the dipole vector and the electric field generated by the charge Q at the dipole centre. Unfortunately, this simple theoretical approach, in which the ligand dipole is placed at a fixed distance from the positive sphere and is directed towards the more favourable direction, cannot properly account for the geometrical factors of the ligands. Thus, we use a more sophisticated approach, in which each atom both of the $[NiS_6]^{2+}$ and of the ligand has been represented as a hard sphere with the appropriate van der Waals radius. The energy was calculated again using Equation (7), by placing the ligand dipole in the middle of the segment connecting the centre of the charge originated by the positively charged atoms of the ligand, to the centre of the charge arising from the negatively charged atoms [Equation (12)], where c is the centre of the dipole and k runs over the positively charged ligand atoms.

$$\vec{c} = 2\left(\sum_j^{pos} q_j\right)^{-1} \sum_k^{all} q_k \vec{R}_k \quad (12)$$

The atomic charges q were determined by the Mulliken population analysis method. The most favourable conformations were determined by starting from a large number of geometrical arrangements of the cation−ligand system and moving the molecules along the energy gradient until an energy minimum was found.

Supporting Information: See footnote on the first page of this article. Plots of $\lambda_1 + \lambda_2$ and of $\lambda_1\lambda_2$ against $[Ni^{2+}]$ for the reaction between 5-X-salH-R (ca. 10^{-4} M) and nickel(II) cations in acetonitrile at 25.0 °C; 5-X-salH-R = 5-Cl-salH-*n*Pr; 5-H-salH-Et; 5-MeO-salH-*n*Pr. UV/Vis spectra of $[Ni(5\text{-H-sal-Et})_2]$ in the presence of different amounts of $Ni(CH_3CN)_6(ClO_4)_2$ in an acetonitrile solution.

Acknowledgments

These studies were supported by the Consiglio Nazionale delle Ricerche (CNR, Roma) and by the Ministero dell'Università e della Ricerca Scientifica e Tecnologica, Ricerche di Rilevante Interesse Nazionale 2000−1. We thank Prof. F. Calderazzo for helpful discussions.

[1] A. Mederos, S. Dominguez, R. Hernandez-Molina, J. Sanchiz, F. Brito, *Coord. Chem. Rev.* **1999**, *193−195*, 857.
[2] L. Carbonaro, M. Isola, P. La Pegna, L. Senatore, *Inorg. Chem.* **1999**, *38*, 5519, and references therein.
[3] J. G. Muller, L. A. Kayser, S. J. Paikoff, V. Duarte, N. Tang, R. J. Perez, S. E. Rokita, C. J. Burrows, *Coord. Chem. Rev.* **1999**, *185−186*, 761.
[4] A. D. Garnovskii, A. L. Nivorozhkin, V. I. Minkin, *Coord. Chem. Rev.* **1993**, *126*, 1.
[5] [5a] J. Burgess in *Metal Ions in Solution*, Ellis Horwood, Chichester, **1978**, chapters 11 and 12. [5b]C. P. Kulatilleke, S. N. Goldie, M. J. Heeg, L. A. Ochrymowyez, D. B. Rorabacher, *Inorg. Chem.* **2000**, *39*, 1444, and references therein.
[6] C. M. Metzler, A. Cahill, D. Metzler, *J. Am. Chem. Soc.* **1980**, *102*, 6075.
[7] Z. Rozwadowski, E. Majewski, T. Dziembowska, P. E. Hansen, *J. Chem. Soc., Perkin Trans. 2* **1999**, 2809.
[8] [8a] R. J. Butcher, J. Jasinski, G. M. Mockler, E. Sinn, *J. Chem. Soc., Dalton Trans.* **1976**, 1099. [8b] O. F. Shall, K. Robinson, J. L. Atwood, G. W. Gokel, *J. Am. Chem. Soc.* **1991**, *113*, 7434. [8c] O. F. Shall, K. Robinson, J. L. Atwood, G. W. Gokel, *J. Am. Chem. Soc.* **1993**, *115*, 5962.
[9] R. H. Holm, M. J. O'Connor in *Progress in Inorganic Chemistry*, Wiley-Interscience, New York, **1971**, vol. 14, p. 241.
[10] J. P. Costes, F. Dahan, J. P. Laurent, *Inorg. Chem.* **1994**, *33*, 2738.
[11] J. P. Costes, J. P. Laurent, P. Chabert, G. Commenges, F. Dahan, *Inorg. Chem.* **1997**, *36*, 656, and references cited therein.
[12] The apparent equilibrium constant K is defined as $K = K_0K_2 + K_0K_2K_3$ in the case that Equation (1) applies to the reaction. For Ni^{II}/5-H-salH-Et, by introducing the kinetic rate constants k_2, k_{-2}, k_3 (see below), a calculated value of $k_{-3} = 0.73 \pm 0.63$ s^{-1} can be compared with the value of 0.10 ± 0.07 s^{-1} determined kinetically, see text.
[13] R. G. Wilkins, in *Kinetics and Mechanism of Reactions of Transition Metal Complexes*, 2nd ed., VCH, Weinheim, **1991**.
[14] P. K. Chattopadhyay, J. F. Coetzee, *Inorg. Chem.* **1973**, *12*, 113.
[15] The rate constant is reported in the molal scale as originally expressed by: K. Ishihara, S. Funahashi, M. Tanaka, *Inorg. Chem.* **1983**, *22*, 2567.
[16] Y. Yano, M. T. Fairhurst, T. W. Swaddle, *Inorg. Chem.* **1980**, *19*, 3267.
[17] J. Neely, R. Connick, *J. Am. Chem. Soc.* **1970**, *92*, 3476.
[18] A. Brändström, *J. Chem. Soc., Perkin Trans. 2* **1999**, 1847, and references therein.
[19] L. F. Blackwell, A. Fischer, I. J. Miller, R. D. Topsom, J. Vaugham, *J. Chem. Soc.* **1964**, 3588.
[20] K. K. Chatterjee, B. E. Douglas, *Spectrochim. Acta* **1964**, 1625.
[21] S. Di Bella, I. Fragalà, I. Ledoux, M. Diaz-Garcia, T. J. Marks, *J. Am. Chem. Soc.* **1997**, *119*, 9550.
[22] R. W. Taft, Jr., *J. Phys. Chem.* **1960**, *64*, 1805.
[23] [23a] L. Sacconi, M. Ciampolini, N. Nardi, *J. Am. Chem. Soc.*

1964, *86*, 819; E. Frasson, C. Panattoni, L. Sacconi, *J. Phys. Chem.* **1959**, *63*, 1908. [23b] R. H. Holm, *J. Am. Chem. Soc.* **1961**, *83*, 4683.
[24] H. Schiff, *Ann. Chem. Pharm.* **1869**, *150*, 193.
[25] J. F. Coetzee, *Progress in Physical Organic Chemistry*, Interscience, New York, **1967**, vol. 4.
[26] A. E. Wickenden, R. A. Krause, *Inorg. Chem.* **1965**, *4*, 404.
[27] L. Carbonaro, L. Guogang, M. Isola, L. Senatore, *Inorg. Chim. Acta* **2000**, *303*, 40.
[28] R. Ambrosetti, D. Ricci, R. Bianchini, *Gazz. Chim. Ital.* **1997**, *127*, 567.
[29] W. Libus, H. Strzelecki, *Electrochim. Acta* **1970**, *15*, 703.
[30] A. D. Becke, *J. Chem. Phys.* **1993**, *98*, 5648.
[31] M. J. Frisch, G. W. Trucks, H. B. Schlegel, G. E. Scuseria, M. A. Robb, J. R. Cheeseman, V. G. Zakrzewski, J. A. Montgomery, R. E. Stratmann, J. C. Burant, S. Dapprich, J. M. Millam, A. D. Daniels, K. N. Kudin, M. C. Strain, O. Farkas, J. Tomasi, V. Barone, M. Cossi, R. Cammi, B. Mennucci, C. Pomelli, C. Adamo, S. Clifford, J. Ochterski, G. A. Petersson, P. Y. Ayala, Q. Cui, K. Morokuma, D. K. Malick, A. D. Rabuck, K. Raghavachari, J. B. Foresman, J. Cioslowski, J. V. Ortiz, B. B. Stefanov, G. Liu, A. Liashenko, P. Piskorz, I. Komaromi, R. Gomperts, R. L. Martin, D. J. Fox, T. Keith, M. A. Al-Laham, C. Y. Peng, A. Nanayakkara, C. Gonzalez, M. Challacombe, P. M. W. Gill, B. G. Johnson, W. Chen, M. W. Wong, J. L. Andres, M. Head-Gordon, E. S. Replogle, J. A. Pople, *Gaussian 98* (Revision A.7), Gaussian, Inc., Pittsburgh, PA, **1998**.
[32] R. M. Fuoss, *J. Am. Chem. Soc.* **1958**, *80*, 5059.
[33] J. Williams, S. Petrucci, B. Sesta, M. Battistini, *Inorg. Chem.* **1974**, *13*, 1968.

Received November 23, 2001
[I01475]

Rate and Mechanism of the Oxidative Addition of Benzoic Anhydride to Palladium(0) Complexes in DMF

Anny Jutand,*[a] Serge Négri,[a] and Johannes G. de Vries[b]

Keywords: Palladium / Kinetics / Electrochemistry / Benzoic anhydride / Oxidative addition

The rate constant of the oxidative addition of the benzoic anhydride $(PhCO)_2O$ to $[Pd^0(PPh_3)_4]$ has been determined in DMF and compared to that of phenyl halides and phenyl triflate. The following reactivity order has been established: PhI >> $(PhCO)_2O$ > PhOTf > PhBr. The oxidative addition of $(PhCO)_2O$ proceeds by activation of one C–O bond. Two acyl-Pd^{II} complexes are formed: a neutral complex *trans*-$[(PhCO)Pd(OCOPh)(PPh_3)_2]$ and a cationic complex *trans*-$[(PhCO)PdS(PPh_3)_2]^+$ (S = DMF) showing that the decarbonylation process is highly endergonic. The exchange of PPh_3 by the bidentate ligand dppp does not favor the decarbonylation process.

Introduction

Aromatic carboxylic anhydrides $(ArCO)_2O$ were first used by Sakamoto et al. as *acylating* agents in palladium-catalyzed cross-coupling reactions [Equation (1)]:[1]

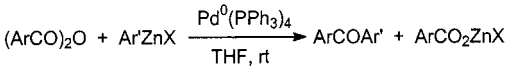

(1)

Recently, they have also been used by de Vries et al. as *arylating* agents in palladium-catalyzed Heck reactions [Equation (2)]:[2]

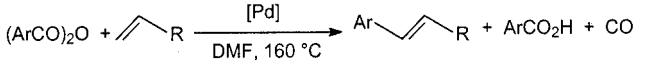

(2)

When compared to the aryl halides or triflates more commonly used as arylating agents in Heck reactions,[3–5] aromatic carboxylic anhydrides appear to be more attractive since they are a cheap aryl source and they do not lead to the formation of environmentally wasteful halide salts. Moreover, no base is required, as it usually is in Heck reactions, since benzoate anions are released in the reaction. They serve as a base by forming aromatic carboxylic acid, which can be recycled back to the aromatic carboxylic anhydride. CO is then the only by-product of the Heck reaction [Equation (2)].

[a] Ecole Normale Supérieure, Département de Chimie, UMR CNRS 8640,
24, Rue Lhomond, 75231 Paris, Cedex 5, France
Fax: (internat.) +33-1/4432-3325
E-mail: Anny.Jutand@ens.fr
[b] University of Groningen, Laboratory for Organic and Molecular Inorganic Chemistry,
Nijenborgh 4, 9747 AG Groningen, The Netherlands

By analogy to aryl halides and triflates,[3–5] the first step of the catalytic cycle of the Heck reaction must be an oxidative addition of the aromatic carboxylic anhydride to the palladium(0) catalyst, giving a palladium(II) complex. Further transformation of this complex gives an intermediate aryl-Pd^{II} complex able to react with the alkene. The oxidative addition of carboxylic anhydrides to palladium(0) complexes has been reported by Yamamoto et al.[6–8] It proceeds by cleavage of one C–O bond and *trans*-acyl(carboxylato)palladium(II) complexes have been isolated and characterized with the PMe_3 ligand [Equation (3), (R = alkyl or phenyl)].[6,7]

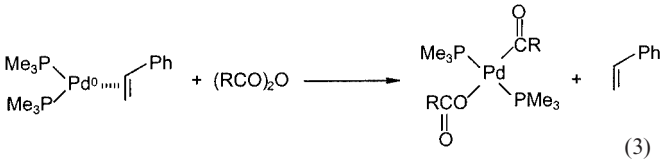

(3)

The reactivity of such complexes has been investigated by the same group. Hydrogenation gives RCHO and RCO_2H, establishing that no decarbonylation occurs in the acyl(carboxylato)palladium(II) complex formed in the oxidative addition.[6,7] Hydrogenation of $(PhCO)_2O$ to form PhCHO and $PhCO_2H$ has been successfully developed in THF with $[Pd^0(PPh_3)_4]$ as a catalyst.[6–8] Only one reaction in the aromatic series is reported (phthalic anhydride, PMe_3 as the ligand), where CO is released from the acyl(carboxylato)-palladium(II) complex, giving rise to the formation of an aryl(carboxylato)Pd^{II} complex.[7]

Grushin and Alper have characterized in solution the complex *trans*-$[(PhCO)Pd(OCOPh)(PCy_3)_2]$ formed by reacting $(PhCO)_2O$ with $[Pd^0(PCy_3)_2]$ (Cy = cyclohexyl).[9] Decarbonylation was observed in the course of the oxidative addition as a very minor process (5–10%).

We report here a mechanistic investigation of the oxidative addition of benzoic anhydride $(PhCO)_2O$ to $[Pd^0(PPh_3)_4]$ in DMF (solvent of the Heck reaction). The objective is to compare its reactivity to that of phenyl halides and phenyl triflate and to characterize the Pd^{II} complex(es) generated in the oxidative addition.

Results and Discussion

Rate of the Oxidative Addition of Benzoic Anhydride $(PhCO)_2O$ to $Pd^0(PPh_3)_4$ in DMF

The kinetics of the oxidative addition of $(PhCO)_2O$ to $[Pd^0(PPh_3)_4]$ (C_0 = 1.33 mM) in DMF (containing nBu$_4$NBF$_4$, 0.3 M) was monitored by amperometry at a rotating gold disk electrode, as reported for aryl halides[10] and triflates.[11] $[Pd^0(PPh_3)_3]$, the main complex generated in DMF from $[Pd^0(PPh_3)_4]$ [Equation (4)], exhibited an oxidation peak at +0.11 V vs. SCE. The rotating disk electrode was polarized at +0.35 V, on the plateau of the oxidation wave of $[Pd^0(PPh_3)_3]$. The kinetics of the oxidative addition of $(PhCO)_2O$ was monitored by recording the decay of the oxidation current, i, of $[Pd^0(PPh_3)_3]$ (proportional to the Pd^0 concentration) as a function of time, up to 100% conversion. The reaction was rather slow at 25 °C and the kinetic investigation was then performed at 40 °C.

$$Pd^0(PPh_3)_4 \longrightarrow Pd^0(PPh_3)_3 + PPh_3 \quad (4)$$

It is well established that when $[Pd^0(PPh_3)_4]$ is the Pd^0 precursor, any oxidative addition (e.g. of aryl halides or triflates) proceeds from the 14-electron complex $[Pd^0(PPh_3)_2]$ [Equation (5) and (6)].[10,11] The Pd^{II} complex formed in the oxidative addition is tentatively written as [(PhCO)Pd(OCOPh)$(PPh_3)_2$] after cleavage of one C−O bond, by analogy to the complex obtained when the Pd^0 is ligated by PMe_3 [6,7] or by PCy_3.[9] Its structure will be established in the second part of this work.

$$Pd^0(PPh_3)_3 \underset{}{\overset{K}{\rightleftharpoons}} Pd^0(PPh_3)_2 + PPh_3 \quad (5)$$

$$Pd^0(PPh_3)_2 + (PhCO)_2O \xrightarrow{k} (PhCO)Pd(OCOPh)(PPh_3)_2 \quad (6)$$

Overall reaction:

$$Pd^0(PPh_3)_4 + (PhCO)_2O \xrightarrow{k_{app}} (PhCO)Pd(OCOPh)(PPh_3)_2 + 2\,PPh_3 \quad (7)$$

The kinetic investigation allows the determination of the apparent rate constant k_{app} of the overall oxidative addition [Equation (7)]. Due to the continuous release of PPh_3 in the fast equilibrium (5) during the course of the oxidative addition, the kinetic law is expressed in Equation (8) {C_0: initial concentration of $[Pd^0(PPh_3)_4]$, $(PhCO)_2O$ in large excess}.[10]

$$2\ln([Pd^0]/[Pd^0]_0) + 1 - [Pd^0]/[Pd^0]_0 = -Kk[(PhCO)_2O]t/C_0 = -k_{app}[(PhCO)_2O]t = -k_{obs}t \quad (8)$$

The plot of $2\ln(i/i_0) + 1 - i/i_0 = 2\ln([Pd^0]/[Pd^0]_0) + 1 - [Pd^0]/[Pd^0]_0$ versus time is a straight line (Figure 1a) (i: oxidation current of Pd^0 at t; i_0: initial oxidation current). The value of k_{obs} was calculated from the slope of the regression line [Equation (8)]. The benzoic anhydride concentration was varied in the range 0.01−0.4 M and the plot of the corresponding k_{obs} value versus the benzoic anhydride concentration gave a straight line (Figure 1b). The reaction order in benzoic anhydride is thus +1 [Equation (8)]. This establishes that the mechanism of the oxidative addition of the benzoic anhydride to $[Pd^0(PPh_3)_4]$ [Equations (4−7)] is the same as that already established for aryl halides and triflates.[10,11] The value of $Kk = 3.6 \times 10^{-5}\ s^{-1}$ was calculated from the slope of the regression line of Figure 1b and allows the calculation of the apparent rate constant of the overall reaction [Equation (7)]: $k_{app} = Kk/C_0$ (in $M^{-1}s^{-1}$)

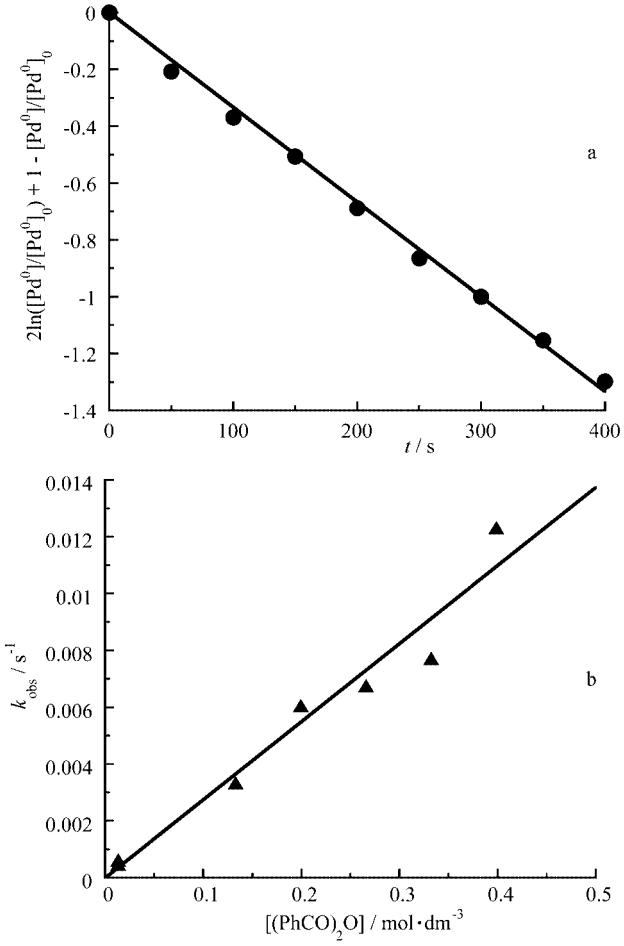

Figure 1. Oxidative addition of $(PhCO)_2O$ in DMF (containing nBu$_4$NBF$_4$ 0.3 M) to $[Pd^0(PPh_3)_4]$ (1.33 mM) at 40 °C, monitored by amperometry at a rotating gold disk electrode (diameter: 2 mm, ω = 105 rad s^{-1}) polarized at +0.35 V vs. SCE; a) $[(PhCO)_2O]$ = 0.133 M; plot of $2\ln(i/i_0) + 1 - i/i_0 = 2\ln([Pd^0]/[Pd^0]_0) + 1 - [Pd^0]/[Pd^0]_0$ *versus* time (i: oxidation current of $[Pd^0(PPh_3)_3]$ at t; i_0: initial oxidation current). k_{obs} (s^{-1}) is calculated from the slope [Equation (8)]; b) Plot of k_{obs} (s^{-1}) *versus* $(PhCO)_2O$ concentration

Table 1. Comparative reactivity of $(PhCO)_2O$, PhI, PhBr and PhOTf in their oxidative addition to $[Pd^0(PPh_3)_4]$ (2 mM) in DMF [Equation (7) for $(PhCO)_2O$]

	T (°C)	PhI	$(PhCO)_2O$	PhOTf	PhBr
k_{app} ($M^{-1}s^{-1}$)	25	25	3.1×10^{-3}	–	–
k_{app} ($M^{-1}s^{-1}$)	40	–	1.8×10^{-2}	1.2×10^{-2}	10^{-2}

[Equation (8)], for any value of C_0 (Table 1). It is worthwhile to note that, even at the lowest benzoic anhydride concentration investigated here (0.013 M), the oxidation current of Pd^0, and therefore the concentration of Pd^0, dropped to almost zero. This indicates that the oxidative addition went to completion and that the reverse reaction, the formation of $(PhCO)_2O$ and a Pd^0L_2 complex by reductive elimination from $[(PhCO)Pd(OCOPh)(PPh_3)_2]$,[9,12] was much slower than the rate of the oxidative addition and did not interfere in the kinetics investigated herein.

Since aromatic carboxylic anhydrides appear to be an alternative to the use of aryl halides and triflates in Heck reactions,[2] it was of interest to compare their reactivity in the oxidative addition, which may be rate determining in the case of poorly reactive aryl derivatives. The apparent rate constant k_{app} of the oxidative addition of PhOTf and PhBr to $[Pd^0(PPh_3)_4]$ has also been determined at 40 °C, in DMF, to allow comparison with that of $(PhCO)_2O$ (Table 1). The order of reactivity in DMF has been established to be:

$$PhI >> (PhCO)_2O > PhOTf > PhBr$$

When considering the oxidative addition, $(PhCO)_2O$ is thus slightly more reactive than PhOTf and PhBr and may therefore be a good alternative to the use of PhOTf or PhBr in any reaction where the oxidative addition is rate determining, provided the subsequent decarbonylation takes place.

Palladium(II) Complexes Generated in the Oxidative Addition of Benzoic Anhydride $(PhCO)_2O$ to $Pd^0(PPh_3)_4$ in DMF

The oxidative addition of $(PhCO)_2O$ to $[Pd^0(PPh_3)_4]$ in DMF at 40 °C was monitored by conductivity measurements, which allows the characterization of ionic complexes as well as their rate of formation.[11] Starting with a residual conductivity $\kappa_0 = 5\ \mu S{\cdot}cm^{-1}$, we observed that the conductivity of the solution increased as soon as $(PhCO)_2O$ (100 equiv.) was added to $[Pd^0(PPh_3)_4]$ (C_0 = 1.33 mM) in DMF, attesting that an ionic complex was formed in the very first stages of the oxidative addition (Figure 2). From the kinetic curve of Figure 2, we see that at least two different ionic species are formed successively, at different time scales, the first complex being formed on a shorter time scale ($t < 800$ s) than the second one. The first time scale is compatible with that of the oxidative addition when monitored independently by amperometry ($t_{1/2}$ = 250 s, see Figure 1a). This suggests that the neutral complex $[(PhCO)Pd(OCOPh)(PPh_3)_2]$, initially formed in the oxidative addition [Equation (7)], dissociates to give a cationic complex $[(PhCO)PdS(PPh_3)_2]^+$ (S = DMF) [Equation (9)] in a reaction which is faster than the oxidative addition.[13,14] A second ionic species is then generated in a subsequent reaction. This latter might be a decarbonylation as in Equation (10) or any decomposition process leading to more conductive ionic species {e.g., formation of a phosphonium salt $PhCOO\text{-}PPh_3^+$ via a reductive elimination from $[(PhCO)Pd(OCOPh)(PPh_3)_2]$,[15] reaction of dioxygen with $[(PhCO)PdS(PPh_3)_2]^+$,[16] etc.}.

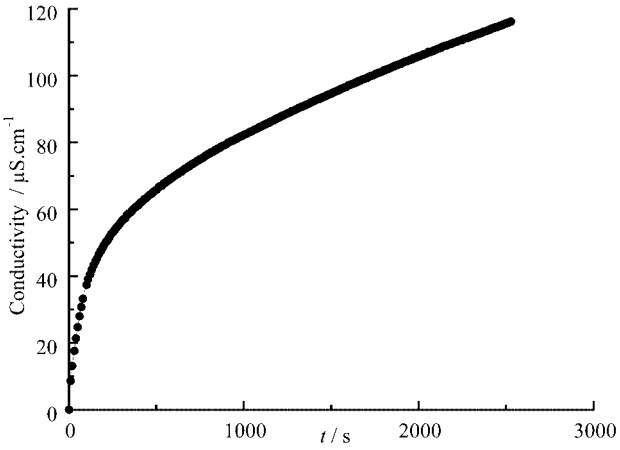

Figure 2. Oxidative addition of $(PhCO)_2O$ (0.133 M) to $[Pd^0(PPh_3)_4]$ (1.33 mM) in DMF at 40 °C, monitored by conductivity measurements; variation of the conductivity *versus* time

$$(PhCO)Pd(OCOPh)(PPh_3)_2 \rightleftharpoons (PhCO)PdS(PPh_3)_2^+ + PhCO_2^- \quad (9)$$

$$(PhCO)PdS(PPh_3)_2^+ \rightleftharpoons CO + PhPdS(PPh_3)_2^+ \quad (10)$$

To test the hypotheses formulated in Equation (9) and (10), the oxidative addition of $(PhCO)_2O$ to $[Pd^0(PPh_3)_4]$ was monitored by ^{31}P NMR spectroscopy[17] in DMF to characterize the formed Pd^{II} complexes. The ^{31}P NMR spectroscopy was first investigated after the amperometry experiment, i.e., when the oxidative addition, performed with $[Pd^0(PPh_3)_4]$ (C_0 = 1.33 mM) and $(PhCO)_2O$ (100 equiv.) in DMF at 40 °C, was over (experiment A). The ^{31}P NMR spectrum exhibited three main singlets: one singlet at $\delta = -5.4$ ppm characteristic of free PPh_3 released during the oxidative addition [Equation (7)], one singlet at $\delta = 25.6$ ppm characteristic of $(O)PPh_3$ [16] and one singlet at δ_1 = 19.9 ppm, which then characterizes the major complex formed in the oxidative addition. Two smaller singlets were also observed at δ_2 = 20.4 ppm and δ_3 = 24.1 ppm (each with a magnitude of ca. 15% of that of the singlet at δ_1). In a second experiment, the oxidative addition was monitored in an NMR tube at room temperature, starting from a more concentrated solution of $[Pd^0(PPh_3)_4]$ (C_0 = 7 mM) and $(PhCO)_2O$ (100 equiv.) in DMF (experiment B). After 30 min, the ^{31}P NMR spectrum exhibited, besides some un-

changed $[Pd^0(PPh_3)_3]$ (δ = 10.7 ppm), the two singlets δ_1 and δ_2 already observed in experiment A, although here the singlet at δ_2 was the major one (relative integration of 0.4:1). After 3 hours, the two singlets δ_1 and δ_2 had almost the same magnitude. This indicates that the signal at δ_2 = 20.4 ppm characterizes the first complex formed in the oxidative addition, which then gives a second complex at δ_1 = 19.9 ppm. Those two complexes are ligated by two PPh_3 ligands sitting in a *trans* position in the Pd^{II} complexes because only singlets were detected. The signal at δ_3 = 24.1 ppm was also detected with a magnitude of half that of δ_1, i.e., in larger amount than in experiment A.

In order to assign the signals at δ_1 and δ_2 to the complexes postulated in Equation (9) and (10), i.e., [(PhCO)-Pd(OCOPh)$(PPh_3)_2$], $[(PhCO)PdS(PPh_3)_2]^+$ or $[PhPdS(PPh_3)_2]^+$, these complexes were synthesized independently in DMF following known procedures. An oxidative addition was performed with PhOTf (100 equiv.) and $[Pd^0(PPh_3)_4]$ (C_0 = 7 mM) in DMF and monitored by ^{31}P NMR spectroscopy. Such a reaction is known to give, in DMF, the cationic complex *trans*-$[PhPdS(PPh_3)_2]^+ \cdot [OTf]^-$ [Equation (11)].[11] This complex exhibits a singlet at δ = 21.9 ppm (Table 2, entry 1) different from δ_1 and δ_2. We can already assume, therefore, that the cationic complex *trans*-$[PhPdS(PPh_3)_2]^+$, postulated in Equation (10), is not formed in the oxidative addition of $(PhCO)_2O$ under the experimental conditions used above. When CO was bubbled into the NMR tube, a new singlet appeared at higher field at δ = 20.0 ppm and was assigned to *trans*-$[(PhCO)PdS(PPh_3)_2]^+$ [Equation (12), Table 2, entry 2].[18,19] This latter signal is very similar to the signal at δ_1 observed when the oxidative addition was performed with $(PhCO)_2O$ (experiments A and B, Table 2, entry 3). When $PhCO_2^- \cdot Li^+$ was then added in large excess into the NMR tube, a singlet appeared at δ = 20.4 ppm and was assigned to *trans*-[(PhCO)Pd(OCOPh)$(PPh_3)_2$] [Equation (13)].[20] This latter signal is the same as the signal at δ_2 observed when the oxidative addition was performed with $(PhCO)_2O$ (experiment A and B, Table 2, entry 4).

$$Pd^0(PPh_3)_4 + PhOTf \longrightarrow \textit{trans}\text{-}PhPdS(PPh_3)_2^+ + TfO^- + 2PPh_3 \quad (11)$$

$$\textit{trans}\text{-}PhPdS(PPh_3)_2^+ + CO \longrightarrow \textit{trans}\text{-}(PhCO)PdS(PPh_3)_2^+ \quad (12)$$

$$\textit{trans}\text{-}(PhCO)PdS(PPh_3)_2^+ + PhCO_2^- \rightleftharpoons \textit{trans}\text{-}(PhCO)Pd(OCOPh)(PPh_3)_2 \quad (13)$$

Consequently, two complexes are formed in the oxidative addition of $(PhCO)_2O$ to $[Pd^0(PPh_3)_4]$: *trans*-[(PhCO)-Pd(OCOPh)$(PPh_3)_2$] and *trans*-$[(PhCO)PdS(PPh_3)_2]^+$ {see Equation (5) and Equation (14) and (15) for the mechanism of the oxidative addition of benzoic anhydride to $[Pd^0(PPh_3)_4]$ in DMF}.

$$Pd^0(PPh_3)_3 \overset{K}{\rightleftharpoons} Pd^0(PPh_3)_2 + PPh_3 \quad (5)$$

$$Pd^0(PPh_3)_2 + (PhCO)_2O \overset{k}{\longrightarrow} \textit{trans}\text{-}(PhCO)Pd(OCOPh)(PPh_3)_2 \quad (14)$$

$$\textit{trans}\text{-}(PhCO)Pd(OCOPh)(PPh_3)_2 \rightleftharpoons \textit{trans}\text{-}(PhCO)PdS(PPh_3)_2^+ + PhCO_2^- \quad (15)$$

The fact that *trans*-$[(PhCO)PdS(PPh_3)_2]^+$ was detected in larger amounts than *trans*-[(PhCO)Pd(OCOPh)$(PPh_3)_2$] in experiment A as opposed to experiment B (vide supra) is due to the difference of concentration. In experiment B, the concentration of $[Pd^0(PPh_3)_4]$ was higher than that in experiment A. Consequently the concentration of the released $PhCO_2^-$ was higher in experiment B and Equation (15) was shifted more towards the left hand-side, i.e., to the formation of *trans*-[(PhCO)Pd(OCOPh)$(PPh_3)_2$]. This is why *trans*-$[(PhCO)PdS(PPh_3)_2]^+$ appeared as the major complex at low $[Pd^0(PPh_3)_4]$ concentration (experiment A).

The singlet at δ = 24.3 ppm remained unassigned. Two phenyl-Pd^{II} complexes *trans*-$[PhPdS(PPh_3)_2]^+$ and *trans*-[PhPd(OCOPh)$(PPh_3)_2$] could have been formed by decarbonylation of *trans*-$[(PhCO)PdS(PPh_3)_2]^+$ and *trans*-[(PhCO)Pd(OCOPh)$(PPh_3)_2$], respectively, but the cationic complex *trans*-$[PhPdS(PPh_3)_2]^+$ was not detected in the NMR spectrum (vide supra). We have independently

Table 2. ^{31}P NMR shifts δ (101 MHz, DMF, [D_6]acetone (10%), H_3PO_4) of phenyl- and acyl-palladium(II) complexes

Entry	Complexes (S = DMF)	δ
1	*trans*-$[PhPdS(PPh_3)_2]^+$ [a]	21.9 (s)
2	*trans*-$[(PhCO)PdS(PPh_3)_2]^+$ [b]	20.0 (s)
3	*trans*-$[(PhCO)PdS(PPh_3)_2]^+$ [c]	19.9 (s)
4	*trans*-[(PhCO)Pd(OCOPh)$(PPh_3)_2$][d]	20.4 (s)
5	*trans*-[PhPd(OCOPh)$(PPh_3)_2$][e]	21.6 (s)
6	$[PhPdS(dppp)]^+$ [f]	25.2 (d, $J_{P,P}$ = 51 Hz), −2.2 (d, $J_{P,P}$ = 51 Hz)
7	$[(PhCO)PdS(dppp)]^+$ [g]	5.1 (br. d, $J_{P,P}$ = 74 Hz), −8.4 (br. d, $J_{P,P}$ = 74 Hz)
8	$[(PhCO)PdS(dppp)]^+$ [h]	5.1 (d, $J_{P,P}$ = 74 Hz), −8.8 (d $J_{P,P}$ = 74 Hz)
9	[(PhCO)Pd(OCOPh)(dppp)][i]	12.5 (d, $J_{P,P}$ = 72 Hz), −7.9 (d, $J_{P,P}$ = 72 Hz)
10	[PhPd(OCOPh)(dppp)][j]	18.9 (d, $J_{P,P}$ = 51 Hz),−6.5 (d, $J_{P,P}$ = 51 Hz)

[a] Authentic sample with OTf^- as the counter anion. [b] Formed by reaction (12) with OTf^- as the counter anion. [c] Formed in the oxidative addition of benzoic anhydride and $[Pd(PPh_3)_4]$ with $PhCO_2^-$ as the counter anion. [d] Formed in the oxidative addition of benzoic anhydride and $[Pd(PPh_3)_4]$ [Equation (7)] and by reaction (13). [e] Formed by reaction of benzoate anion with $[PhPdBr(PPh_3)_2]$. [f] Authentic sample with BF_4^- as the counter anion. [g] Formed by reaction (16) with BF_4^- as the counter anion. [h] Formed by reactions (17−19) with $PhCO_2^-$ as the counter anion. [i] Formed by ligand exchange (Scheme 1) and by reaction (18). [j] Formed by reaction (17).

checked that the complex *trans*-[PhPd(OCOPh)(PPh_3)$_2$] was not formed in the oxidative addition, by reacting *trans*-[PhPdBr(PPh_3)$_2$] (δ = 24.2 ppm) with $PhCO_2^-\cdot Li^+$ in DMF to induce the $Br^-/PhCO_2^-$ substitution.[21] Indeed, a new singlet assigned to *trans*-[PhPd(OCOPh)(PPh_3)$_2$][23] appeared at δ = 21.6 ppm (Table 2, entry 5), which was never observed in the course of the oxidative addition of the benzoic anhydride. Consequently, the decarbonylation must be a very endergonic process, since even at 100 °C for 1 h, under continuous degassing, none of the signals of either *trans*-[PhPd(OCOPh)(PPh_3)$_2$] or *trans*-[PhPd*S*(PPh_3)$_2$]$^+$ were detected. In contrast, carbonylation of [PhPd(OCOPh)(PPh_3)$_2$][20] or *trans*-[PhPd*S*(PPh_3)$_2$]$^+$ [Equation (12)] proved to be efficient.[22] Consequently, the singlet at δ = 24.3 ppm, which must be due to a decomposition product, remains unassigned.

The influence of the ligand on the decarbonylation process was tested by switching from the monodentate ligand PPh_3 investigated above to the bidentate bisphosphane ligand 1,3-bis(diphenyl)phosphanylpropane (dppp). Whereas the acyl group of acyl-Pd^{II} complexes ligated by two monophosphane ligands sits in a *cis* position relative to each monophosphane ligand, it must sit in a *trans* position relative to one P of a bidentate bisphosphane ligand. This may affect the decarbonylation process. The oxidative addition of $(PhCO)_2O$ to [Pd^0(dba)(dppp)] generated from Pd^0(dba)$_2$ + 1 equiv. dppp was very sluggish. Consequently, one equiv. dppp was added to the solution of *trans*-[PhCOPd*S*(PPh_3)$_2$]$^+$ and *trans*-[PhCOPd(OCOPh)(PPh_3)$_2$], generated from the oxidative addition of $(PhCO)_2O$ to [Pd(PPh_3)$_4$], in DMF, to test the effect of the bidentate ligand on the decarbonylation process. The two singlets δ_1 = 19.9 ppm and δ_2 = 20.4 ppm of *trans*-[PhCOPd*S*(PPh_3)$_2$]$^+$ and *trans*-[PhCOPd(OCOPh)(PPh_3)$_2$], respectively, disappeared. The signal of free PPh_3 was observed at δ = −5.4 ppm but not that of dppp (δ = −17.0 ppm), confirming the ligand exchange. As a result of this exchange, a single complex was observed, characterized by two doublets at δ_4 = 12.5 ppm (d, J_{PP} = 72 Hz) and δ_5 = 7.9 ppm (d, J_{PP} = 72 Hz) (Scheme 1).

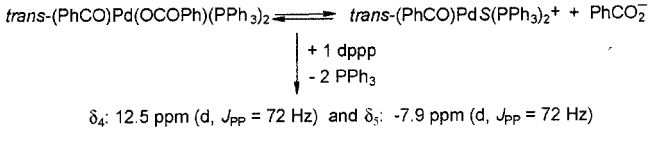

Scheme 1. Exchange of two PPh_3 ligands by one dppp in DMF

At least four complexes might be formed in DMF: [(PhCO)Pd(OCOPh)(dppp)], [(PhCO)Pd*S*(dppp)]$^+$ and the complexes formed by decarbonylation {[PhPd(OCOPh)(dppp)] and/or [PhPd*S*(dppp)]$^+$}. The ^{31}P NMR signals of an authentic sample of [PhPd*S*(dppp)]$^+$[BF_4]$^-$ in DMF (two doublets at δ = 25.2 ppm and δ = −2.2 ppm, Table 2, entry 6) showed that such a complex was not formed in the exchange reaction of Scheme 1. When CO was bubbled into an NMR tube containing the authentic sample of the cationic complex [PhPd*S*(dppp)]$^+$[BF_4]$^-$ in DMF, two new broad doublets were detected at δ = 5.1 and −8.4 ppm (Table 2, entry 7) and assigned to [(PhCO)Pd*S*(dppp)$^+$] [Equation (16)].[24] Such a complex did not appear when PPh_3 was exchanged by dppp in Scheme 1.

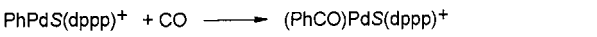

(16)

In order to discriminate between [(PhCO)Pd(OCOPh)(dppp)] and [PhPd(OCOPh)(dppp)], a series of experiments was then performed independently. To a solution of [PhPdI(PPh_3)$_2$] in DMF was first added one equiv. of dppp to generate [PhPdI(dppp)] characterized by two ^{31}P NMR doublets (δ = 12.4 ppm, $J_{P,P}$ = 53 Hz and δ = −8.6 ppm, $J_{P,P}$ = 53 Hz). Addition of 10 equiv. $PhCO_2^-\cdot Li^+$ to the NMR tube resulted in the formation of a new complex assigned to [PhPd(OCOPh)(dppp)][21] (2 doublets at δ = 18.9 ppm and δ = −6.5 ppm, Table 2, entry 10) [Equation (17)]. This complex did not appear when PPh_3 was exchanged by dppp in Scheme 1.

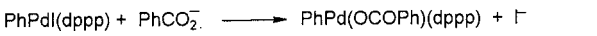

(17)

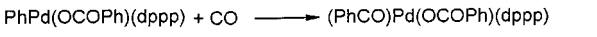

(18)

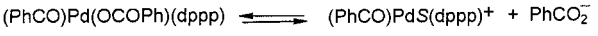

(19)

When CO was bubbled into the NMR tube, the two doublets of [PhPd(OCOPh)(dppp)] disappeared, confirming the CO insertion [Equation (18)]. Two sets of two doublets were detected (relative integration of 1:4): a first set of two major doublets at δ_4 = 12.5 ppm and δ_5 = −7.9 ppm, assigned to [(PhCO)Pd(OCOPh)(dppp)] [Equation (18)] and already observed after the ligand exchange in Scheme 1, and a second set of two minor doublets at δ = 5.1 ppm and δ = −8.8 ppm (Table 2, entry 8) similar to [(PhCO)Pd*S*(dppp)$^+$] previously characterized [vide supra, Table 2, entry 7, Equation (19)].

Consequently, the ligand exchange in Scheme 1 generated an acyl-Pd^{II} complex [(PhCO)Pd(OCOPh)(dppp)] but no phenyl-Pd^{II} complexes [PhPd(OCOPh)(dppp)] or [PhPd*S*(dppp)]$^+$ that would be formed by a decarbonylation process. The decarbonylation is definitively an endergonic process when phosphane ligands (monodentate or bidentate) are considered, which strongly stabilize neutral and cationic acyl-Pd^{II} complexes in DMF.

Conclusion

In DMF, the oxidative addition of benzoic anhydride to [Pd(PPh_3)$_4$] is slower than that of PhI but slightly faster than that of PhOTf and PhBr. This reaction gives two acyl-Pd^{II} complexes: the cationic complex *trans*-[(PhCO)Pd*S*(PPh_3)$_2$]$^+$ and the neutral complex *trans*-[(PhCO)Pd(OCOPh)(PPh_3)$_2$]. Aryl-Pd^{II} complex(es)

formed by decarbonylation of the two above acyl-Pd^{II} complexes have not been detected. Changing the monodentate PPh_3 ligand to the bidentate dppp does not favor the decarbonylation process either. This is why the Heck reaction, which requires the formation of an aryl-Pd^{II} complex, is much more efficient using catalytic Pd salts (in the absence of ligand) than catalytic phosphane-ligated Pd complexes when it is performed from benzoic anhydride.[2] The phosphane-ligated aryl-Pd^{II} complex must be present at very low concentration in an endergonic equilibrium with the major acyl-Pd^{II} complex(es) but be nevertheless more reactive with alkenes than the acyl-Pd^{II} complex(es). The decarbonylation of the acyl-Pd^{II} complex(es) ligated to the alkene, before the carbopalladation steps, appears more improbable.

Experimental Section

General Remarks: ^{31}P NMR spectra were recorded on a Bruker spectrometer (101 MHz) using H_3PO_4 as an external reference. Amperometry was performed with a generator Tacussel GSTP4. Conductivity was measured on a Radiometer Analytical CDM210 conductivity meter (cell constant: 1 cm^{-1}).

Chemicals: DMF was distilled from calcium hydride under vacuum. Commercial benzoic anhydride, phenyl triflate, PPh_3 and dppp (Acros) were used without any purification. $[Pd(PPh_3)_4]$,[25] $[PhPdBr(PPh_3)_2]$,[26] $[PhPdI(PPh_3)_2]$,[26] and $[PhPd(dppp)]^+[BF_4]^-$ [27] were prepared according to described procedures.

Electrochemical Set-Up and Procedure for Kinetic Measurements: Experiments were carried out in a thermostatted three-electrode cell connected to a Schlenk line. The counter electrode was a platinum wire of ca. 1 cm^2 apparent surface area. The reference was a saturated calomel electrode (Radiometer Analytical) separated from the solution by a bridge filled with 3 mL of DMF containing n-$Bu_4N{\cdot}BF_4$ (0.3 M). The kinetic measurements were performed at a rotating gold disk electrode (Radiometer analytical, EDI 65109, diameter: 2 mm, angular velocity: 105 $rad{\cdot}s^{-1}$) polarized at +0.35 V vs. SCE. $[Pd(PPh_3)_4]$ (23.1 mg, 0.02 mmol) was introduced into 15 mL of DMF containing n-$Bu_4N{\cdot}BF_4$ (0.3 mol dm^{-3}) followed by the appropriate amount of benzoic anhydride. The decay of the oxidation current was recorded as a function of time, up to 100% conversion.

Acknowledgments

This work has been supported by CNRS, Centre National de la Recherche Scientifique (CNRS, UMR 8640) and the Ministère de la Recherche (Ecole Normale Supérieure). Johnson Matthey PLC is gratefully thanked for a loan of Na_2PdCl_4.

[1] T. Sakamoto, Y. Kondo, N. Murata, H. Yamanaka, *Tetrahedron* **1993**, *49*, 9713−9720.
[2] M. S. Stephan, A. J. J. M. Teunissen, G. K. M. Verzijl, J. G. de Vries, *Angew. Chem. Int. Ed.* **1998**, *37*, 662−664.
[3] A. de Mejeire, F. E. Meyer, *Angew. Chem. Int. Ed. Engl.* **1994**, *106*, 2473−2506.
[4] W. Cabri, I. Candiani, *Acc. Chem. Res.* **1995**, *28*, 2−7.
[5] I. Beletskata, A. V. Cheprakov, *Chem. Rev.* **2000**, *100*, 3009−3066.
[6] K. Nagayama, F. Kawataka, M. Sakamoto, I. Shimizu, A. Yamamoto, *Chem. Lett.* **1995**, 367−368.
[7] K. Nagayama, F. Kawataka, M. Sakamoto, I. Shimizu, A. Yamamoto, *Bull. Chem. Soc. Jpn.* **1999**, *72*, 573−580.
[8] A. Yamamoto, Y. Kayaki, K. Nagayama, I. Shimizu, *Synlett* **2000**, 925−937.
[9] V. V. Grushin, H. Alper, *J. Am. Chem. Soc.* **1995**, *117*, 4305−4315.
[10] C. Amatore, A. Jutand, F. Khalil, M. A. M′Barki, L. Mottier, *Organometallics* **1993**, *12*, 3168−3178.
[11] A. Jutand, A. Mosleh, *Organometallics* **1995**, *14*, 1810−1817.
[12] Reductive elimination with formation of $(PhCO)_2O$ would occur from a *cis*-$[(PhCO)Pd(OCOPh)(PPh_3)_2]$ complex first formed in the oxidative addition before its isomerization to the *trans* complex, the final complex (see the second part of this work). Reductive elimination is usually inhibited by extra phosphanes, which favor the *cis*/*trans* isomerization. For a reductive elimination from $[(PhCO)Pd(OCOPh)(PPh_3)_2]$ synthesized in situ by reacting CO with $[PhPd(OCOPh)(PPh_3)_2]$ in the absence of extra phosphane, see ref.[9] and the comments on the deceleration of the reductive elimination due to the release of PPh_3 by decomposition of $[Pd^0(PPh_3)_2]$ also generated in the course of the reductive elimination process. In the present work, free phosphanes were generated as the oxidative addition proceeded [Equation (7)]. Moreover, it seems that the reductive elimination is favored in the presence of CO for PPh_3 or PCy_3 ligands.[9]
[13] This situation has been observed in the oxidative addition of aryl triflates to $[Pd(PPh_3)_4]$.[11]
[14] The kinetic treatment of the curve in Figure 2, featuring the kinetics of formation of the ionic species could not be done with high accuracy, since the value of the intrinsic conductivity κ_{lim} of *trans*-$[(PhCO)PdS(PPh_3)_2]^+$ could not be determined, due to the equilibrium (9) and to the "decomposition" process occurring at longer times. The first part of the curve ($t < 500$ s) featuring the kinetics of formation of the cationic complex *trans*-$[(PhCO)PdS(PPh_3)_2]^+$ was nevertheless analyzed after an estimation of $\kappa_{lim} = 110$ $\mu S{\cdot}cm^{-1}$ and by neglecting the reverse reaction of equilibrium (9) over short time periods. The plot of $\ln((\kappa_{lim} - \kappa)/\kappa_{lim})$ *versus* time was not a straight line (κ: conductivity at t). The first linear part of the curve ($t < 100$ s) gives a value of $k_{obs} = 0.0039$ s^{-1}, not far from the value of $k_{obs} = 0.0034$ s^{-1} determined for the oxidative addition by amperometry (see a in Figure 1).
[15] For reductive elimination in Pd^{II} complexes ligated by a carboxy group and PPh_3, see: C. Amatore, E. Carré, A. Jutand, A. M. M′Barki, G. Meyer, *Organometallics.* **1995**, *14*, 5605−5614.
[16] J. Vicente, J.-A. Abad, A. D. Frankland, M.-C. Ramirez de Arellano, *Chem. Commun.* **1997**, 959−960.
[17] Acyl or arylcarboxy groups ligated to Pd^{II} complexes may be characterized by ^{31}P, ^{13}C NMR and IR spectroscopy.[6,7,9] However, our purpose was to investigate the structure of the complexes formed in the oxidative addition in the conditions of a Heck reaction, i.e., in solution in DMF. ^{13}C NMR spectroscopy cannot be performed in DMF. Moreover, since the oxidative addition was slow, a large excess of benzoic anhydride was required. The presence of DMF and benzoic anhydride in large amount excludes any characterization of the complexes formed in solution by IR spectroscopy.
[18] For a reaction of CO with cationic monoorgano-Pd^{II} complexes ligated by monodentate phosphanes, see ref.[8] and references therein.
[19] Cationic MeCO-Pd^{II} complexes formed by reaction of CO with the corresponding cationic Me-Pd^{II} complexes exhibit ^{31}P NMR signals at higher field than the starting complex, see: P. Braunstein, C. Frison, X. Morise, *Angew. Chem. Int. Ed.* **2000**, *39*, 2867−2870 and references therein.
[20] Grushin and Alper have reported that the ^{31}P NMR signal of $[(PhCO)Pd(OCOPh)(PPh_3)_2]$ synthesized in situ by reacting CO with a $[D_6]$benzene solution of $[PhPd(OCOPh)(PPh_3)_2]$ was

a singlet at δ = 18.3 ppm.[9] In our case (solvent: DMF containing 10% [D_6]acetone) the singlet of [(PhCO)Pd(OCOPh)(PPh_3)$_2$] was located at δ = 20.4 ppm. This difference is due to the solvent since we observed that the singlet of *trans*-[PhPd(OCOPh)(PPh_3)$_2$] at δ = 23 ppm in [D_6]benzene reported by Grushin and Alper[9] was located at δ = 21.6 ppm in DMF containing 10% [D_6]acetone (Table 2, entry 5).

[21] For the substitution of X by carboxylate anions in *trans*-[PhPdX_2] (X = I, Br) see the reference given in ref.[15] and I. Ishiyama, M. Murata, N. Miyaura, *J. Org. Chem.* **1995**, *60*, 7508−7510.

[22] Reaction of CO with monoorgano-Pd^{II} complexes to form acyl-Pd^{II} complexes has been widely developed and is reported to be faster with cationic complexes than with neutral complexes.[8,19]

[23] Grushin and Alper have reported the synthesis of [PhPd(OCOPh)(PPh_3)$_2$] by reacting [PhPd(μ-OCOPh)(PPh_3)]$_2$ with 2 PPh_3.[9] For its ^{31}P NMR characterization see the last part of the note in ref.[20].

[24] For reaction of CO with cationic monoorgano-Pd^{II} complexes ligated by bidentate phosphanes, see ref.[8] and G. P. C. M. Dekker, C. J. Elsevier, K. Vrieze, *Organometallics.* **1992**, *11*, 1598−1603.

[25] D. T. Rosevear, F. G. H. Stone, *J. Chem. Soc. A* **1968**, 164−167.

[26] P. Fitton, E. A. Rick, *J. Organomet. Chem.* **1971**, *28*, 287−291.

[27] L. M. Ludwig, S. Strömberg, B. Swensson, B. Åkermark, *Organometallics* **1999**, *18*, 970−975.

Received November 26, 2001
[I01479]

Synthesis, Spectroscopic and Structural Characterization of Novel Diiodine Adducts with the Heterocyclic Thioamides, Thiazolidine-2-thione (tzdtH), Benzothiazole-2-thione (bztzdtH) and Benzimidazole-2-thione (bzimtH)

Vasiliki Daga,[a] Sotiris K. Hadjikakou,[a] Nick Hadjiliadis,*[a] Maciej Kubicki,[b] João H. Z. dos Santos,[c] and Ian S. Butler[d]

Keywords: Bioinorganic chemistry / Charge-transfer complexes / Iodine / S ligands / Sulfur heterocycles

Direct reaction of thiazolidine-2-thione (tzdtH), an anti-thyroidal agent with diiodine in a molar ratio of 1:2 caused the heterolytic cleavage of diiodine and formation of $[\{(tzdtH)_2I^+\}\cdot I_3^-\cdot 2I_2]$ (**1**), whereas the reaction of benzothiazole-2-thione (bztzdtH) with diiodine in a molar ratio of 1:2 and 1:1 resulted in the formation of the $[\{(bztzdtH)I_2\}\cdot I_2]$ (**2**) and $[(bztzdtH)I_2]$ (**3**) charge-transfer (c.t.) complexes. In addition, the reaction between benzimidazole-2-thione (bzimtH) with diiodine in a molar ratio 1:2 yielded the c.t. complex $[\{(bzimtH)I_2\}_2\cdot I_2\cdot 2H_2O]$ (**4**). All reactions were carried out in dichloromethane. The molecules have been characterized by m.p., elemental analyses, and FT-Raman, FT-IR, UV/Vis and ^{1}H NMR spectroscopy. Crystal structures of the named complexes have been determined by X-ray diffraction at –103 °C (**1**), 20 °C (**2** and **3**) and –168 °C (**4**). The charge-transfer nature of the bonds of the adducts (**1**–**4**) has been verified by the lengthening of the I–I bond lengths as compared to the S–I bond lengths, by the characteristic c.t. bands observed in the UV spectra and by the shifts of frequencies measured for the I–I bond vibration in the FT-Raman spectra of the complexes. Compound **1** ($C_3H_5NS_2I_4$) is monoclinic with a space group $P2_1/n$ and a = 9.145(2) Å, b = 13.259(2) Å, c = 10.615(2) Å, β = 106.30(2)°, Z = 4. The complex is ionic, containing an S–I$^+$–S linkage and an I_3^- counter anion. Compound **2** [$C_7H_5NS_2I_4$, monoclinic, space group $P2_1/n$, a = 8.357(2) Å, b = 17.829(4) Å, c = 9.603(2) Å, Z = 4, β = 94.39(3)°] consists of a benzothiazole-2-thione ligand bonded with an iodine atom through a sulfur atom. A neutral diiodine molecule is also co-crystallized. A benzothiazole-2-thione ligand is also bonded through its sulfur atom to an iodine atom in molecule **3** [$C_7H_5NS_2I_2$, orthorhombic, space group $P2_12_12_1$, a = 4.189(1) Å, b = 9.770(3) Å, c = 27.704(8) Å, Z = 4]. Extended intramolecular N–H···I contacts link the molecules forming a supramolecular assembly. The crystal structure of **4** ($C_7H_6N_2SI_3\cdot H_2O$) reveals a monoclinic space group $P2_1/c$ and a = 13.4828(14) Å, b = 4.6704(4) Å, c = 21.267(2) Å, β = 101.029(8)°, Z = 4. It consists of a benzimidazole-2-thione ligand bonded to an iodine atom through a sulfur atom. An extended intramolecular linkage via I(2)···H(4)[C(4)] leads to the formation of dimers, while an extended hydrogen-bonding network {H(12w)[O(12)w]···N(3), O(1w)···N(3)} links the alternate parallel dimers forming a supramolecular assembly. Attempts to draw conclusions on the behavior of a thione, when used as an anti-thyroidal agent, towards diiodine have been made.
(© Wiley-VCH Verlag GmbH, 69451 Weinheim, Germany, 2002)

1. Introduction

Among the most widely anti-thyroidal agents used for the treatment of hyper-thyroidism (Graves' decease) over the years are thioamides such as *N*-methylimidazoline-2-thione (methimazole), 3-methyl-2-thioxo-4-imidazoline-1-carboxylate (carbimazole) and propylthiouracil.[1] Mercaptothiazoline (thiazolidine-2-thione) has also been used[1] for this purpose. Thioamides inhibit the formation of 3,5,3′-triiodothyronine (T3) and 3,5,3′,5′-tetraiodothyronine (T4) hormones by depressing the incorporation of oxidized iodides to tyrosine, a precursor of T3 and T4 hormones.[2] In addition, a good correlation between the anti-thyroid activity in vivo and the formation constants of diiodine complexes with organic bases has been found.[2c] Therefore, there is an increasing interest in the study of the charge transfer complexes of iodine with thioamides or thiones [3–18] not

[a] Section of Inorganic and Analytical Chemistry, Department of Chemistry, University of Ioannina,
45110 Ioannina, Greece
Fax: (internat.) + 30-651/44831
E-mail: nhadjil@cc.uoi.gr
[b] Department of Chemistry, A. Mickiewicz University,
ul. Grunwaldzka 6, 60-780 Poznan, Poland
[c] Instituto de Quimica, Universidade Federal do Rio Grande do Sul,
Porto Alegre, Brazil
[d] Department of Chemistry, McGill University,
801 Sherbrooke, Montreal Quebec, Canada H2A 2K6

only for the clarification of the iodine-binding mechanism but also for the development of new anti-thyroidal agents as well. Moreover, the sulfur−iodine charge transfer complexes have been shown to possess promising electrical properties such as superconducting ability.[14,16,19]

The adduct bond formation between a donor (sulfur atom in the present case) and diiodine stabilizes the lone pair of electrons of the donor by mixing its orbital with the σ* anti-bonding orbital of I_2.[20] As a result a sulfur−iodine dative bond forms and the double bond of the thione group and also the iodine−iodine bonds[4,6] are lengthened. A direct relationship was found to exist between these three bond lengths: if *d*(S−I) is short, then *d*(C−S) and *d*(I−I) will be long and the donation is considered strong; for weak complexes, the situation is reversed.[4,6] In addition the ν(I−I) frequencies are linearly correlated with *d*(I−I) bond lengths.[12]

It is also worth noting that a partial positive charge is imparted to the rest of the molecule by the lengthening of the double bond of the thione group *d*(C−S).[4] Therefore, thioamides are particularly good donors; the positive charge is easily supported by nitrogen atoms (especially if it contains alkyl groups). Generally, the greater the stabilizing ability of the *N*-alkyl or -aryl groups, the stronger the resulting diiodine complex will be.[4] Similar behavior is expected in the case of molecules containing 1,3-dithiole sulfur atoms, such that the positive charge is delocalized over the S−C−S fragment of the ring, forming a 6π pseudo-aromatic system.[7]

In this paper, we report the structural and spectroscopic characterization of four new diiodine complexes with the heterocyclic thioamides, thiazolidine-2-thione or mercaptothiazoline (tzdtH, **I**), benzothiazole-2-thione (bztzdtH, **II**) and benzimidazole-2-thione (bzimtH, **III**) of formulae $[\{(tzdtH)_2I^+\}\cdot I_3^-\cdot 2I_2]$ (**1**), $[\{(bztzdtH)I_2\}\cdot I_2]$ (**2**), $[(bztzdtH)I_2]$ (**3**) and $[\{(bzimtH)I_2\}_2\cdot I_2\cdot 2H_2O]$ (**4**).

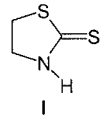
I

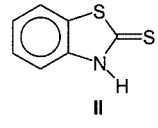
II

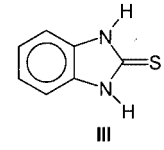
III

TzdtH (**I**) has been used in the treatment of hyper-thyroidism and our aim was to investigate its behavior in the reaction with diiodine. The ligands bztzdtH (**II**) and bzimtH (**III**), on the other hand, were also used for comparison purposes. Formation constant measurements of all these ligands with diiodine have been reported previously[8,9,21,22] in organic solvents, but always assuming the formation of 1:1 complexes in solution. No structural and/or spectroscopic studies have ever been reported previously. The structure of compound **1** shows that the ligand tzdtH, with anti-thyroidal activity, easily forms iodonium salts and is able to retain a total of four diiodine molecules per ligand molecule, thus acting as an iodine sponge. This is the first anti-thyroidal agent ever reported which contains an I_3^- counterion and interacts and retains two more diiodine molecules.

2. Results and Discussion

2.1. General Aspects

Studies on the interaction of thione donors with diiodine have established three types of adducts in the solid state, as proposed by Deplano et al.[5,10,23] These are type D···I−I (**A**) with long D···I and short I−I bond lengths,[24,25] type D−I−I (**B**) with comparable D−I and I−I distances[14,26] and type $D-I^+\cdots I^-$ (**C**) with short D−I and long I···I distances.[16] In type **A**,[5,10] the UV/Vis spectra show both the known charge-transfer band and the blue-shifted diiodine and donor bands, while the Raman ν(I−I) band appears in the range 180−140 cm^{-1}. In type **B**,[5,10] two peaks due to ν_{asym}(I−I) and ν_{sym}(I−I) are observed in the Raman spectra while in type **C** there is only one peak due to the ν(D−I) vibration.

In addition, reduction of iodine to polyiodides by electron transfer to the diiodine from the donor may also take place, together with the formation of iodonium salts with I^+ linearly bound to two donor molecules.[11,12,17] D·*n*I_2 complexes may also form where the bonded I_2 molecule interacts with the other diiodine molecules.[11,16,27,28]

In our case, thiazolidine-2-thione causes the heterolytic cleavage of the I−I bond resulting in the formation of the $S-I^+-S$ and I_3^- as a counter anion. This is a rather rare structure and the second according to the best of our knowledge of an anti-thyroidal agent, the first being the one with thiourea (tu).[29] The two other ligands, benzothiazole-2-thione and benzimidazole-2-thione form compounds of stoichiometry DI_2 and $(DI_2)I_2$ (D is the thione donor) of **B** and **C** types.

Thiazolidine-2-thione could be considered as a strong donor towards diiodine, while benzothiazole-2-thione or benzimidazole-2-thione as weaker such donors. This is expected,[8] since in the last two cases, the sulfur atom is part of an aromatic system.

The formulae of the synthesized complexes **1**, **2**, **3** and **4** were first deduced from elemental analyses and spectroscopic data. All complexes were highly soluble in organic solvents and their crystals were stable in air but were stored in darkness in a refrigerator.

2.2. Crystal and Molecular Structures

[{(tzdtH)$_2$I$^+$}·I$_3^-$·2I$_2$] (1)

An ORTEP diagram of compound **1** is shown in Figure 1 while selected bond lengths and angles are given in Table 1. There are only a few crystal structures reported in the literature containing $S-I^+-S$ dimers. These include 1,3-dimethyl-2-thiourea (dmtu), ethylenethiouria (etu) thiourea (tu) and *N*-methylbenzothiazole-2-thione (mbzttH).[4,12,16,29]

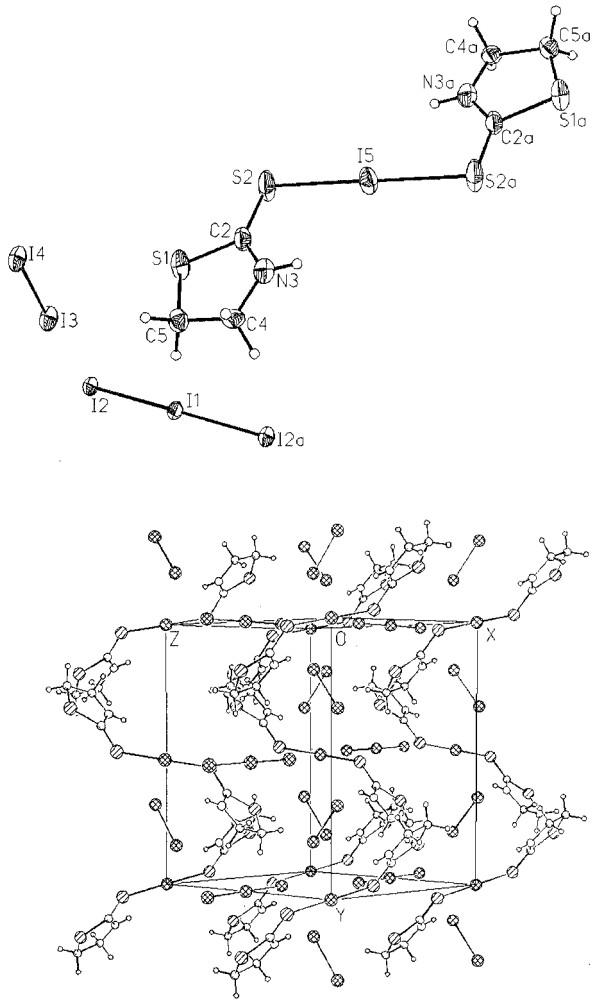

Figure 1. ORTEP diagram and unit cell of **1** together with the atomic numbering scheme

Table 1. Selected bond lengths [Å] and angles [°] for **1** with e.s.d. values in parentheses

Bond lengths:	
I(1)−I(2)	2.9195(14)
I(3)−I(4)	2.741(2)
I(5)−S(2)	2.654(6)
N(3)···I(4)[a]	3.82(2)
N(3)−H(3)	0.860(19)
H(3)[N(3)]···I(5)	2.9336(6)
N(3)···I(5)	3.495(19)
Bond angles:	
I(2)−I(1)−I(2)[b]	180.0
S(2)−I(5)−S(2)[c]	180.0
N(3)−H(3)···I(4)[a]	140

[a] $x + 1, y, z$. [b] $-x, -y, -z + 1$. [c] $-x + 1, -y + 1, -z + 1$.

The structure of compound **1** consists of three residues, one cationic $\{(tzdtH)_2I^+\}$, containing the linear S−I$^+$−S linkage, one I_3^- counter anion and two independent diiodine molecules, shown only in the packing diagram of Figure 1. More similar structures including metal complexes have also been reported.[12] Comparison of various structural parameters of known iodonium complexes are reported in Table 2.

Both S−I bond lengths are equal to 2.654(6) Å. These bond lengths compare well with the corresponding distances found in $\{[(dmtu)_2I]\}$ [2.602(4) and 2.654(4) Å],[4] in $[(tu)_2I^+]$ 2.629 Å [29] and in $[(mbzttH)_2I^+]$ [I−S = 2.600(2) and 2.634(2) Å].[12] They are, however, significantly longer than the ones in (etu)·I$^+$ of 2.487(3) Å.[16] The S(2)−C(2) bond length of the complex **1** (Figure 1) is only 1.65(3) Å which is among the shortest such distances ever reported (Table 2).

The N(3)−C(2)−S(2)−I(5) torsion angle (Figure 1) is 9(3)° indicating an almost co-planar arrangement of the iodine atom towards the plane of N−C=S bond. The corresponding torsion angle found in $\{[(tu)_2I^+]I^-\}$ is 17°, again almost co-planar, presumably due to the short intramolecular I···H or I···N distances.[29]

An intramolecular hydrogen bond between the imino NH proton and the sulfur atom coordinated to the iodine atom is formed in **1** (Figure 1) {H(3)[N(3)]···I(5) = 2.9336(6) and N(3)···I(5) = 3.495(19) Å}.[30] This hydrogen bonding favors the planar structure.[9]

The I(1)−I(2) bond length (Figure 1) of the linear I_3^- counter anion is 2.9195(14) Å, slightly longer than the corresponding bond lengths measured in $\{[(dmtu)_2I][I_3^-]\}$ [I−I = 2.8874(14) and 2.9082(14) Å[4]]. Two diiodine mole-

Table 2. Structural parameters of known iodonium complexes

Compound	Counterion	S−I [Å]	C=S [Å]	I−I−I [Å]	I−I [Å]	I_3^-···I_2 or I^-···I_2 [Å]	S−I−S [°]	X−C−S−I [°]	Ref.
$(tzdtH)_2I^+$	$I_3^-\cdot 2I_2$	2.654(6)	1.65(3)	2.9195(14)	2.741(2)	3.4220 3.4120	180.00	9(3) (X = N) 169.7(12) (X = S)	[a]
$(dmtu)_2\cdot I^+$][b]	I_3^-	2.602(4)/ 2.654(4)	1.728(13)/ 1.715(14)	2.8874(14)/ 2.9440(13)	−		177.77(4)	−	[4]
$(etu)\cdot I^+$][b]	I_3^-	2.487(3)	1.73(1)	3.004(1)/ 2.850(1)	−		−	−	[16]
$[(tu)_2I^+)_{[b]}$	I^-	2.629	1.723	−	−		180.0	17	[31]
$(mbzttH)_2I^+$ [b]	$I^-\cdot 3I_2$	2.600(2)/ 2634(2)	1.694(7)/ 1.682(7)		2.771(1)/ 2.746(1)/ 2.766(1)	3.237(1) 3.260(1) 3.242(1)	174.97(7)	−	[12]

[a] This work. [b] dmtu = 1,3-dimethyl-2-thiourea, etu = ethylenethiourea, tu = thiourea, mbzttH = *N*-methylbenzothiazole-2-thione.

cules are also co-crystallized with an I(3)−I(4) bond length of 2.741(2) Å (Figure 1). Weak intermolecular interactions ($I_3^-\cdots I_2$), shorter than the sum of iodine van der Waals radii have been measured[30] between I(3)···I(2) (3.4220 Å) and I(4)···I(2) (3.4120 Å) and are longer than the corresponding $I^-\cdots I$ interactions between I^- and I_2 species found in $\{[(mbzttH)_2I^+][I^-\cdot 3I_2]\}$ [3.237(1), 3.260(1) and 3.242(1) Å].[12]

[{(bztzdtH)I_2}·I_2] (2), [(bztzdtH)I_2] (3) and [{(bzimtH)I_2}$_2$·I_2·H_2O] (4)

ORTEP diagrams of molecules **2**, **3** and **4** are shown in Figures 2−4, respectively, while selected bond lengths and angles are given in Tables 3−5.

The crystal structures of molecules **2**, **3** and **4** consist of a thione ligand, bonded with a diiodine atom through a sulfur atom with S−I = 2.587(5) Å in **2** (Figure 2), S−I = 2.728(6) Å in **3** (Figure 3) and 2.571(6) Å in **4** (Figure 4), respectively. The corresponding I−I bonds are lengthened with values of I−I = 2.969(2) Å in **2** (Figure 2), I−I = 3.077(2) Å in **3** (Figure 3) and I−I = 2.989(2) Å in **4** (Figure 4) as compared with the I−I distances in the gas phase (2.677 Å),[14,31] or in crystalline diiodine (2.717 Å at 110 K),[14,32] as a result of the S···I interaction. Table 6 compares structural parameters of compounds **2**, **3** and **4** with other compounds of similar structures.

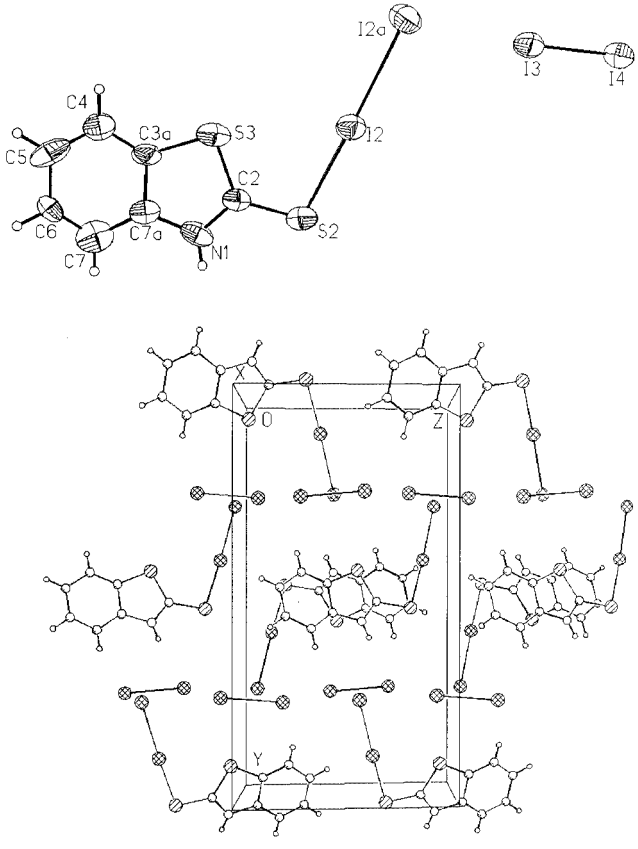

Figure 2. ORTEP diagram and unit cell of **2** together with the atomic numbering scheme

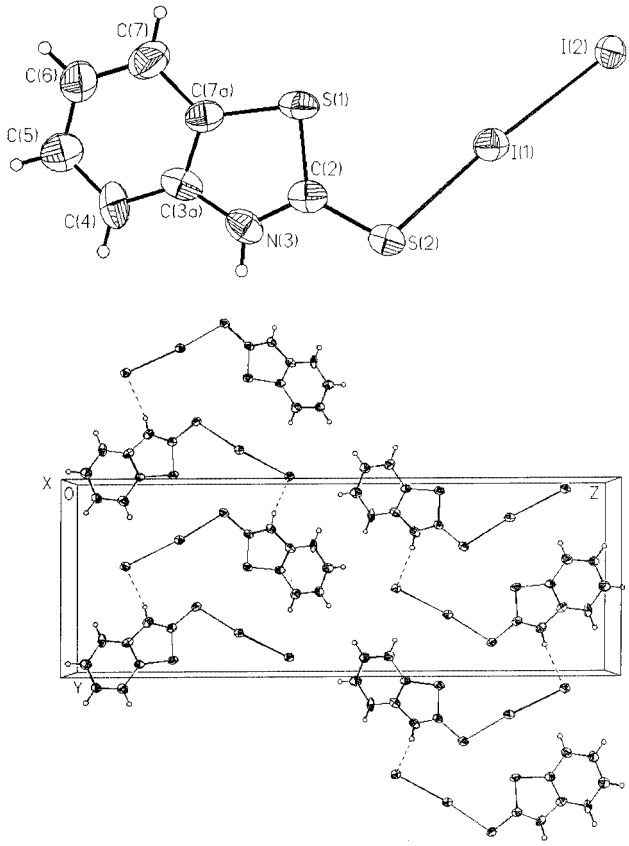

Figure 3. ORTEP diagram and unit cell of **3** together with the atomic numbering scheme

All bond lengths are within the expected ranges, however, the S−I bond length of molecule **2** is the shortest ever reported. The ligand donation leads to the formation of a neutral complex. The I−I bond lengths, all longer than the corresponding distance in free diiodine, are the longest ever measured for compounds **3** and **4**.

An extended intramolecular hydrogen bonding H(3)[N(3)]···I(2) = 2.7865(16) with N(3)···I(2) = 3.597(19) Å (Figure 3) is also formed in complex **3**. In the case of complex **4**, an intramolecular I(2)···H(4)[C(4)] = 3.2540 Å interaction[30] (Figure 4) leads to the formation of dimers, while an extended hydrogen-bonding network H(12w)[O(12)w]··· N(3) = 1.9033 Å, O(1w)··· N(3) = 2.846(19) Å[30] (Figure 4) links the alternate parallel dimers forming a supramolecular assembly.

The X−C=S···I torsion angles for the complexes were S(3)−C(2)−S(2)−I(2) = −2.3(12)° for **2** , S(1)−C(2)−S(2)−I(2) = −15.6(14)° for **3** and N(1)−C(2)−S(1)−I(3) = 3.0(19)° for **4**. Thus, all compounds, including **1** can be considered of almost coplanar arrangements of iodine atoms towards the N−C=S bond planes.

Finally, the values for the S−I−I angles (Table 6) also imply an almost linear arrangement.

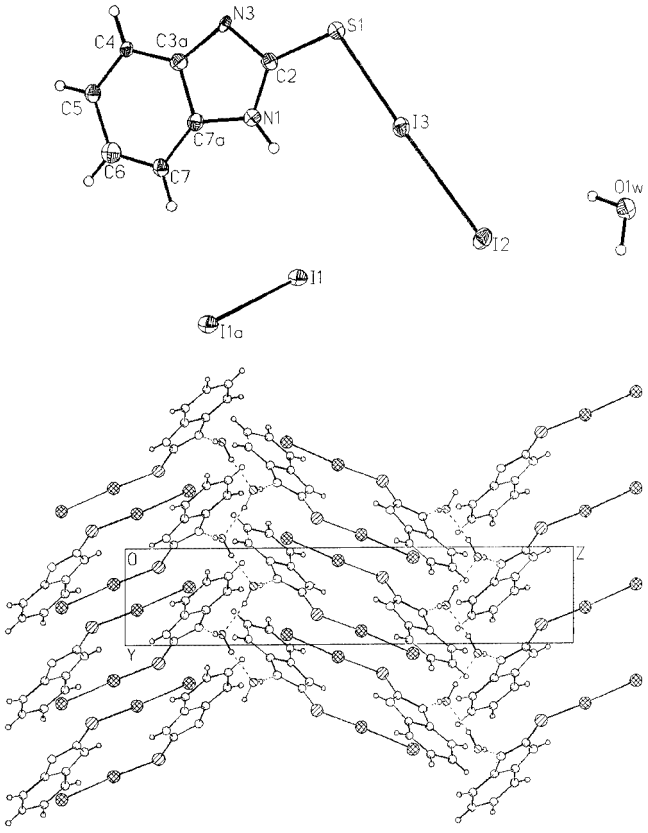

Figure 4. ORTEP diagram and unit cell of **4** together with the atomic numbering scheme

Table 3. Selected bond lengths [Å] and angles [°] for **2** with e.s.d. values in parentheses

Bond lengths:	
I(3)−I(4)	2.7504(18)
I(2)−I(2A)	2.969(2)
S(2)−I(2)	2.587(5)
N(1)···I(3)[a]	3.76(2)
Bond angles:	
C(2)−S(2)−I(2)	101.4(6)
S(2)−I(2)−I(2A)	177.78(13)
N(1)−H(1)···I(3)[a]	145

[a] $-x+1, -y, -z+1$.

Table 4. Selected bond lengths [Å] and angles [°] for **3** with e.s.d. values in parentheses

Bond lengths:	
I(1)−I(2)	3.077(2)
I(1)−S(2)	2.728(6)
N(3)···I(2)[a]	3.597(18)
Bond angles:	
S(2)−I(1)−I(2)	174.18(14)
C(2)−S(2)−I(1)	109.2(7)
N(3)−H(3)···I(2)[a]	158

[a] $-x+1, y+1/2, -z+3/2$.

2.3. Spectroscopy

UV/Vis

The visible spectra of the thione−diiodine adducts in dichloromethane or chloroform exhibit one distinct absorption band at 495−505 nm which is assigned to the "blue-shift" band of I_2,[18] which occurs at 504 nm in free I_2 in CH_2Cl_2.[14] A shoulder in the range of 310−360 nm could be assigned to a charge-transfer band from the HOMO of the donor to the diiodine LUMO (σ_π*)[5,8−10,17]. Complex **1** exhibits a c.t. band at 317 nm, while complex **4** shows a c.t. band at 356 nm. It should be noted that the c.t. bands are not recognizable for complexes **2−3**, most probably as a result of interference from the intraligand transitions occurring at almost the same wavelength. The bands, however, are enhanced in intensity, increasing their coefficients, in the complexes.

Table 5. Selected bond lengths [Å] and angles [°] for **4** with e.s.d. values in parentheses

Bond lengths:	
I(1)−I(1)[a]	2.767(3)
I(2)−I(3)	2.989(2)
I(3)−S(1)	2.571(6)
N(1)···I(3)	3.471(8)
O(1)W···O(1)W[b]	2.78(2)
O(1)W···N(3)[c]	2.77(3)
Bond angles:	
S(1)−I(3)−I(2)	176.76(14)
C(2)−S(1)−I(3)	102.3(8)
N(1)−H(1)···I(3)	119
O(1)W−H(1)W(1)···O(1)W[b]	171
O(1)W−H(1)W(2)···N(3)[c]	170

[a] $-x, -y+1, -z+1$. [b] $1-x, -1/2+y, 3/2-z$. [c] $x, 3/2-y, 1/2+z$.

According to the assumption of Laurence et al.,[9] c.t. absorption bands of I_2−thioamide complexes have been correlated with an in-plane or a perpendicular arrangement of the I_2 moiety towards the plane of N−C=S and this hypothesis is also followed by the thiocarbonyl−I_2 adduct studied by Essefar et al.[3] Thus, complexes of thiocarbonyl−I_2 or I_2−thioamide with in-plane conformation, where the X−C=S···I torsion angle was close to 0°, have shown the c.t. band at 295−305 nm while those with perpendicular arrangements with the angle near 90° have shown this band around 320−350 nm.[3,9] Generally, perpendicular complexes are expected when the substituents around the thiocarbonyl group are bulky[9] while a planar arrangement is expected when an NH group *cis* to the thiocarbonyl group exists.[3] Thus, for all our complexes coplanar arrangements are expected since they all contain the *cis*-NH group, able to form hydrogen bonds with I_2.

Since the X−C=S···I torsion angle for compound **1** is 9(3)° and for **4** is 3.0(19)°, the results of Laurence et al.[9] as well as Esseffar et al.[3] seem to be confirmed for **1** but unexpectedly not for **4**. The absorption band at 283 nm in the spectrum of complex **1**, at 329 nm in the case of complex **2**, at 329.5 nm for **3** and at 309.5 nm for **4** are attributed to intraligand (π→π*) transitions.

Vibrational Spectroscopy

Characteristic infrared bands of the complexes and the ligands are listed in Table 7. The spectra of the complexes

Table 6. Structural parameters of known iodine complexes

Compound	S−I [Å]	N−H [Å]	H(N)···I [Å]	N···I [Å]	C=S [Å]	I−I [Å] coord./ uncoord.	I···I [Å]	S−I−I [°]	X−C−S−I [°]	Ref.
[{(bztzdtH)I_2}·I_2]	2.587(5)	0.8595	−	−	1.706(18)	2.969(2)/ 2.7504(18)	3.423(2)/ 3.445(2)	177.79(13)	−2.3(12) (X = S) 174.7(13) (X = N)	[a]
[(bztzdtH)I_2]	2.728(6)	0.861(19)	2.7865(16)	3.597(19)	1.75(2)	3.077(2)	−	174.19(14)	−15.6(14) (X = S) 166.5(15) (X = N)	[a]
[{(bzimtH)I_2}$_2$· I_2·H_2O]	2.571(6)	0.8603	3.0397	3.545(8)	1.722(19)	2.989(2)/ 2.767(3)	3.4464(19)	176.84(13)	3.0(19) (X = N) −179.7(13) (X = N)	[a]
[ptc·I_2][b]	2.755(2)	−	−	−	1.690(6)	2.812(1)	−	175.42(4)	−	[5]
[ttb·I_2][b]	2.805(3)	−	−	−	1.663(8)	2.812(2)	−	175.43(6)	−	[5]
[mdtt·I_2][b]	2.716(3)	−	−	−	1.666(11)	2.8083(14)	−	177.46(7)	−1.5(9)	[7]
mbit·I_2][b]	2.683(2)	−	−	−	1.721(4)	2.897(1)	−	175.71(3)	−96.4(4)	[10]
bzoxtH·I_2][b]	2.874(2)		3.09	−	1.689(7)	2.769(1)	3.453(1)	178.44(4)	−	[11]
dmimdtH ·I_2][b]	2.748(1)	−	−	−	1.678(3)	2.817(1)	−	176.89(2)	−	[13]

[a] This work. [b] ptc = 1,3-dithiacyclohexane-2-thione, ttb = 4,5-ethylenedithio-1,3-dithiole-2-thione, mdtt = 4,5-bis(methylsulfanyl)-1,3-dithiole-2-thione, mbit = 1,1-methylenebis(3-methyl-4-imidazoline-2-thione), bzoxtH = benzoxazole-2-thione and dmimdtH = 5,5-dimethylimidazoline-2,4-dithione.

Table 7. Characteristic vibration bands [cm^{-1}] in infrared spectra of complexes or ligands

Complex	ν(N−H) solid state	ν(N−H) CH_2Cl_2 solution	Thioamide I	Thioamide II	Thioamide III	Thioamide IV	FT-Raman free I_2	Coordinated I_2	I_3^- ions	Ref.
[{$(tzdtH)_2I^+$} I_3^-·2I2] (**1**)	3296	3325	1512	1300	994	−	181.5, 178.5,		116.8	[a]
[{(bztzdtH)I_2}·I_2] (**2**)	3271	3372	1480	1329	1010	845	172.8	143.7		[a]
[(bztzdtH)I_2] (**3**)	3116	3372	1489	1327	1011	848		147		[a]
[{(bzimtH)I_2}$_2$·I_2·H_2O] (**4**)	3325	3379	1508	1212	−	747	170			[a]
ThzdtH	3131	3396, 3233	1490	1245	990	650−690				[33a]
BzthzdtH	3108	3379, 3204	1490	1320	1010	860				[33b−33c]
BzimtH	3155	3434	1513	1339	1016	743				[33d−33e]

[a] This work.

show distinct vibrational bands between 1520−1480 and 1330−1210 cm^{-1}, which can be assigned to ν(CN) vibrations (thioamide I and II bands) and 1020−990 and 850−740 cm^{-1}, which can be attributed to the ν(CS) vibrations (thioamide III and IV bands). Amide N−H bond vibrations were observed at 3434−3204 cm^{-1} in CH_2Cl_2. According to Laurence et al.,[9] the ν(NH) band of I_2−thioamide complexes in CH_2Cl_2 shifts to lower wavenumbers and it is more intense in the planar complexes than in the perpendicular ones (torsion angle X−C=S···I). This is due to the amphoteric behavior of I^+, which can simultaneously accept electrons from the sulfur atom and offer electrons to the hydrogen atom of the N−H group, thus forming an intramolecular hydrogen bond.[9]

In our case, N−H···I hydrogen bonds exist in complexes **1**, **3** and **4**. In CH_2Cl_2 solutions, the band assignable to ν(N−H) appears in the IR spectrum of complex **1** at 3325 cm^{-1}, while the ligand tzdtH shows also two bands for the same vibration at 3396, and 3233 cm^{-1} assigned to its free and associated forms.[9] The band of the free form shifts by 71 cm^{-1} to lower wavenumbers in **1**. In **4** the shift of 55 cm^{-1} is towards lower wavenumbers (3379 cm^{-1} for **4**, 3434 cm^{-1} for bzimtH), in accordance with its structure. However, the ν(N−H) band of the free form of the ligand bztzdtH at 3379 cm^{-1} ν(N−H) appears as a unique band at 3372 cm^{-1} in both **2** and **3** complexes shifted again to lower wavenumbers (7 cm^{-1}) in accordance with the literature.[9] In the solid state the situation is even more complicated, since all bands shift to higher wavenumbers on passing from the free ligands to the complexes.

New bands appearing at 155 cm^{-1} in the far-IR spectra of the compounds may be assigned to the ν(I−I) stretching vibration modes.[34] The corresponding ν(I−S) bond vibration for the dithian−I_2 complex, was observed at 212 cm^{-1}.[34] In our compounds, new bands appear around 281−280 cm^{-1} and 255−254 cm^{-1} which can be similarly assigned (Figure 5).

Characteristic Raman frequencies of the compounds are also included in Table 7. Diiodine vapor gives a strong band at 216 cm^{-1} ν(I−I) which appears at 180 cm^{-1} in the solid state.[35] This shifts to lower wavenumbers upon coordination to a donor atom, reflecting the reduction in the I−I bond order and the strengthening of the complex formed.[5,10,12]

Thus, the Raman spectrum of complex **1**, recorded in the 300−50 cm^{-1} region, shows a doublet at 181.5 and 178.0

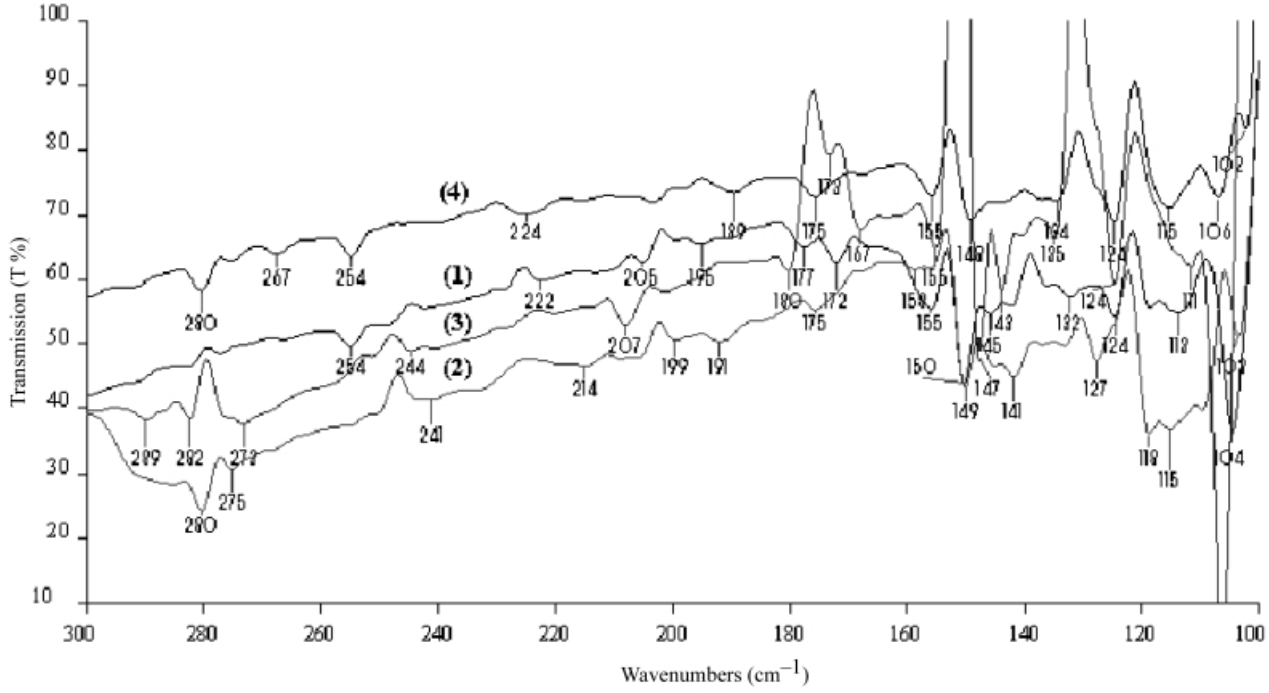

Figure 5. Far-IR spectra of the complexes

cm^{-1}, very close to that usually reported for the symmetric stretching [ν_1(I−I)] of I_2 in the solid state, which may be attributed to the uncoordinated I_2 that cocrystallizes. The I−I bond length of 2.715 Å, measured in free diiodine,[32] is slightly lengthened to 2.741 Å in **1**, justifying this shifting (Table 2). It is worth mentioning that bands around 110 cm^{-1} are normally attributed to the ν_1 symmetric stretching of I_3^-, which being a symmetrical ion normally exhibits only one Raman-active band. Antisymmetric stretching and bending is only infrared-active. When a distortion of I_3^- occurs, the antisymmetric stretching may become Raman-active and additional bands of medium intensity near 140−130 and 80−70 cm^{-1} can be observed, assigned to antisymmetric stretching (ν_3) and ν_2 deformation, respectively.[24,26] Thus, the intense band at 116.8 cm^{-1} is indicative of the presence of I_3^- ions. Similar assignments have also been reported in the literature: 172 cm^{-1} [strong, ν(I−I)], 150 (medium) and 105cm^{-1} [strong, $\nu(I_3^-)$][15,36] for interacting I_3^- and I_2 units. Furthermore the shoulder at 153.3 cm^{-1} might be attributed to the δ(C−S−I) bend, which has already been reported at 150 cm^{-1}.[37] Moreover, δ(C−S−I) bends are reported to be less intense than [ν_1(I−I)]. Therefore, it is very likely that the shoulder at 153.5 cm^{-1} might also be attributed to I, bridging both of the (tzdtH) moieties, in our case.

The Raman spectrum of complex **2** is characterized by an intense band at 172.8 cm^{-1}, attributed to ν_1(I−I) of the I_2 counterpart [I(3)−I(4), Figure 2]. The band at 143.7 cm^{-1} may also be attributed, to coordinated I_2 moieties (Figure 2). Structural assignments from Raman spectra indicate that complex **2** follows the pattern of the D−I−I (**B**-type) adducts[5] which is also in agreement with the relatively shorter S−I and longer I−I bonds measured for **2** by X-ray crystallography (see section 2.2).

The Raman spectrum of complex **3** shows a band at 147 cm^{-1} which can be attributed to ν_1(I−I) symmetric stretching. Considering the magnitude of the shift from free I_2 of 33 cm^{-1} for complex **3** and of 36.3 cm^{-1} for complex **2**, it can be said that the species generated in adduct formation are much effective.

Bands around 150 cm^{-1} were also reported in the literature for I_2 adducts: 152 cm^{-1} (5,5-dimethylimidazolidine-2,4-dithionediiodine),[24] 147 cm^{-1} {4,5,6,7-tetrathiocino[1,2-*b*:3,4-*b'*]diimidazolyl-1,3,8,10-tetraethyl-2,9-dithionebis(diiodine)},[38] 158 cm^{-1} (5,5-dimethyl-4-oxoimidazolidine-2-thionediiodine),[24] 152 and 158 cm^{-1} (5,5-dimethylimidazoline-2,4-dithione and 5,5-dimethyl-4-oxo-2-thioxoimidazolidium, respectively).[24] Finally, the presence of free I_2 is detected in the Raman spectrum of complex **4** as a shoulder at 170 cm^{-1}.

Resonance Raman (RR) uses visible laser excitation sources − which may induce fluorescence, sample pyrolysis, and photoreactions − and spurious peaks, could appear in the spectrum.[39a] Studies comparing FT-Raman and RR spectroscopy have shown remarkable advantages of the former since it eliminates or strongly reduces the pyrolysis of the samples.[39b]

The RR spectra of complex **1** were obtained, using laser sources, 488.0 and 514.5 nm. Bands at 220 cm^{-1} observed in RR have been attributed to I_2 in the gas phase arising from decomposition.[39c] The band observed in the present case (256.8 cm^{-1}) at a much higher frequency, is attributed to I_2 (vapor).

The large band centered at 100 cm^{-1} can be attributed to I_3^- species. In the case of the 514.5 nm line, the spectrum is dominated by a peak at 112.6 cm^{-1} (I_3^-). A large band centered at 167.9 cm^{-1} might be attributed to an I_2 interacting species. The high intensity observed for the 112.6 cm^{-1} band could be due to I_2 disproportionation. Nevertheless, enhancement of this band has already been reported in the literature and attributed to the resonance effect.[39c]

The RR spectra of complex **2** at 488.0 nm showed very low intensity, presenting a cut-off below 50 cm^{-1}. At 514.5 cm^{-1}, we observed an enhancement of the peak at 107 cm^{-1} ($2\nu = 212$ cm^{-1}), and a shoulder at 158.2 cm^{-1}. Once again, the detection of a band relating to I_3^- could either be considered as an RR effect or as the generation of I_3^- species by decomposition. As in the previous case, the RR spectrum using the 488.0-nm line led to a very low intensity spectrum in the case of complex **3**, presenting a cut-off below 50 cm^{-1}. In the case of 514.5-nm excitation, bands at 172 cm^{-1} and 107 cm^{-1} dominate the spectrum in the low-frequency region. It is worth noting the presence of the band at 172 cm^{-1} attributed to I_2, which was absent when an NIR source was used. For this system, the ν(C−H) region as well as the skeleton region (not shown) seemed to be unaffected. The spectra of complex **4** showed no band in the case of the 488.0-nm source. With the 514.5-nm line, an intense band was observed at 107.0 cm^{-1} ($2\nu = 214.9$ cm^{-1}; $3\nu = 328.3$ cm^{-1}), attributable to an I_3^- species which may be generated by the decomposition of complex **4**. As in the previous case, a cut-off below 50 cm^{-1} was shown in the case of 663 nm line.

2.4. Correlations

The S−I bond strength of the iodine charge transfer complexes could be classified by the graphical plots of *d*(C=S) vs. *d*(S−I) [see (a) in Figure 6] or *d*(I−I) vs. *d*(S−I) [see (b) in Figure 6].[4] Ionic complexes exhibit short S−I bond lengths, due to the strong interaction between the iodine and sulfur atoms [see (a) in Figure 6], which seems to be independent from the C=S bond length. For charge transfer complexes with an S−I−I structure, a hyperbolic correlation between *d*(S−I) vs. *d*(I−I) has been proposed[16] which is also confirmed for the complexes **2** and **4** but not for **3** [see (b) in Figure 6]. Additionally *d*(I−I) is linearly correlated to the FT-Raman ν(I−I) frequencies[24] confirmed for complexes **2** and **3** (Figure 7).

According to the value of the I−I bond order (*n*) defined by the Pauling Equation,[31] where d_o is the I−I bond length of I_2 in the gas phase, which is 2.67 Å,[40] Deplano et al.[24] and Bigoli et al.[5] classified I_2 adducts in three classes, type **A** (D···I−I), **B** (D−I−I) and **C** (D−I···I).[10,24]

$$d(\mathrm{I{-}I}) = d_o - 0.85\cdot\log(n)$$

If the value of the I−I bond order $n \geq 0.6$ [d(I−I) < 2.85 Å] the adduct could be classified as a type **A**, while if $n \leq 0.4$ [d(I−I) > 3.01 Å] as a type **C**. The I−I bond order values calculated for the complexes studied in this work are 0.445, 0.332 and 0.421 for the complexes **2**, **3**, and **4**, re-

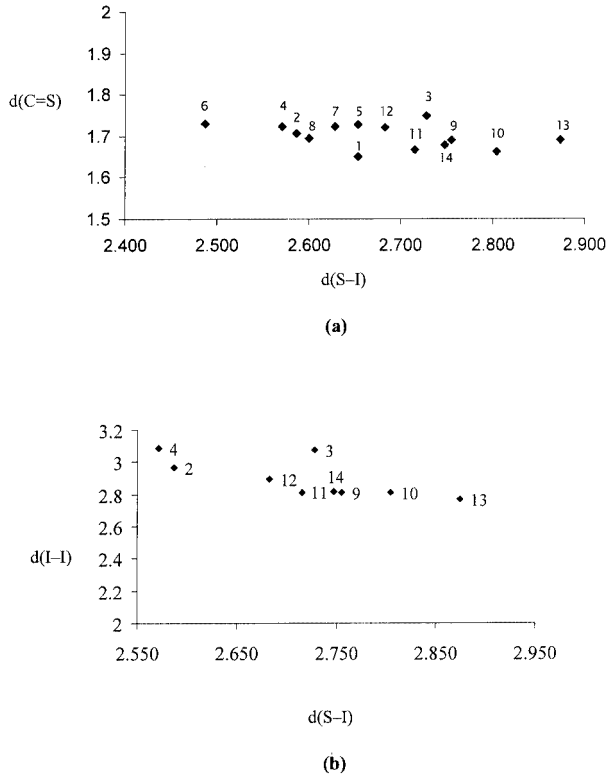

Figure 6. Plot of *d*(S−C) against *d*(S−I) (a) and *d*(I−I) against *d*(S−I) (b) for thione−iodine adducts **5** [{(dmtu)$_2$·I^+}·I_3^-][4] (dmtu = 1,3-dimethyl-2-thiourea), **6** [{(etu)·I^+}·I_3^-][16] (etu = ethylenethiouria), **7** [{(tu)$_2$$I^+$}·$I^-$][29] (tu = thiourea), **8** [(mbzttH)$_2$$I^+$·$I^-$·3$I_2$][12] (mbzttH = *N*-methylbenzothiazole-2-thione), **9** [ptc·I_2][5] (ptc = 1,3-dithiacyclohexane-2-thione), **10** [ttb·I_2],[5] (ttb = 4,5-ethylenedithio-1,3-dithiole-2-thione), **11** [mdtt·I_2][7] [mdtt = 4,5-bis(methylsulfanyl)-1,3-dithiole-2-thione], **12** [mbit·I_2][10] [mbit = 1,1-methylenebis(3-methyl-4-imidazoline-2-thione)], **13** [bzoxtH·I_2][11] (bzoxtH = benzoxazole-2-thione), **14** [dmimdtH·I_2][13] (dmimdtH = 5,5-dimethylimidazoline-2,4-dithione), including our compounds **1**−**4**

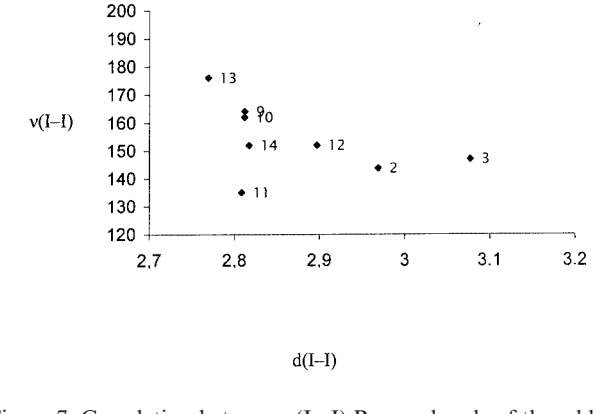

Figure 7. Correlation between ν(I−I) Raman bands of the adducts **9** [ptc·I_2][5] (ptc = 1,3-dithiacyclohexane-2-thione) [ν(I−I) = 164 cm^{-1}], **10** [ttb·I_2][5] (ttb = 4,5-ethylenedithio-1,3-dithiole-2-thione) [ν(I−I) = 162 cm^{-1}], **11** [mdtt·I_2][7] [mdtt = 4,5-bis(methylsulfanyl)-1,3-dithiole-2-thione] [ν(I−I) = 136 cm^{-1}], **12** [mbit·I_2][10] [mbit = 1,1-methylenebis(3-methyl-4-imidazoline-2-thione] [ν(I−I) = 152 cm^{-1}], **13** [bzoxtH·I_2][11] (bzoxtH = benzoxazole-2-thione) [ν(I−I) = 176 cm^{-1}], **14** [dmimdtH·I_2][13] (dmimdtH = 5,5-dimethylimidazoline-2,4-dithione) [ν(I−I) = 152 cm^{-1}], including compounds **2**−**4**

spectively. Therefore, complex **3** could be classified as a type **C** adduct, and complexes **2** and **4** as types **B**.

3. Conclusions

Using the anti-thyroidal agent thiazolidine-2-thione, together with benzothiazole-2-thione or benzimidazole-2-thione, we have tried to compare their behavior towards I_2 coordination and possibly throw some light on the anti-thyroidal activity and mechanism of reaction of these types of molecules. The structure of compound **1** is the second such example of an anti-thyroidal agent.

Laurence et al.[9] also tried to reach similar conclusions by using the anti-thyroidal drugs methimazole, carbimazole and propylthiouracil. No crystal structure of their I_2 adducts was reported, however.[9,41] These authors[9,41] concluded that the action of the anti-thyroidal drugs involved diiodine sponges trapping I_2, I^+ or HOI[42] which were produced during the oxidation of iodide ions taken up by the thyroid. Thus, the agents should be able to form stable complexes with diiodine, diverting iodides from their second oxidation step ($I_2 \rightarrow 2\ I^+ + 2\ e^-$) and in this way prevent the electrophilic substitution of I^+ on the tyrosine residue of thyroglobulin.[2c,43]

This conclusion seems to be substantiated in our work, because (i) like methimazole,[9] thiazolidine-2-thione forms the most stable complexes with I_2 in CH_2Cl_2 solution, compared with the other two ligands[8,9,22] assuming the formation of 1:1 complexes; (ii) the data shows that thiazolidine-2-thione can be classified as a strong donor ligand, in contrast to the non-anti-thyroidal activity of the two other ligands; (iii) thiazolidine-2-thione is such a strong donor that it causes heterolytic cleavage of the diiodine molecule to form $[\{D_2I^+\}I_3^-\cdot 2I_2]$ species and is able to carry two more neutral I_2 molecules in the solid state, which the two other ligands cannot.

Therefore, new anti-thyroidal agents might be found among the strong donors towards diiodine, having the ability to absorb as many molecules of diiodine as possible. Also, these agents should be able to reduce iodine to polyiodides by causing cleavage of the I−I bond.

4. Experimental Section

4.1. Materials and Instruments: All solvents used were reagent grade. Diiodine (Aldrich), thiazolidine-2-thione, benzothiazole-2-thione and benzimidazole-2-thione (Merck) were used with no further purification. Elemental analyses for C,H,N,S were carried out with a Carlo−Erba EA model 1108 elemental analyzer. Melting points were measured in open tubes with a Stuart scientific apparatus and are uncorrected. Infra-red spectra in the region of 4000−370 cm^{-1} were obtained from KBr discs while far-infrared spectra in the region of 400−50 cm^{-1} were obtained from polyethylene discs, with a Perkin−Elmer Spectrum GX FT-IR spectrophotometer. A Jasco UV/Vis/NIR V 570 series spectrophotometer was used to obtain the electronic absorption spectra. The ^1H NMR spectra were recorded with a Bruker AC250 MHFT NMR instrument in $CDCl_3$ solutions. Chemical shifts δ are given in ppm referenced to internal TMS (^1H).

4.2. Synthesis and Crystallization of the Molecules: Complexes $[\{(tzdtH)_2I^+\}\cdot I_3^-\cdot 2I_2]$ (**1**), $[\{(bztzdtH)I_2\}\cdot I_2]$ (**2**), $[(bztzdtH)I_2]$ (**3**) and $[\{(bzimtH)I_2\}_2\cdot I_2\cdot 2H_2O]$ (**4**) were prepared by mixing dichloromethane solutions of diiodine with dichloromethane solution of the appropriate thione in molar ratios of 2:1 in the case of complexes **1**, **2** and **4** or 1:1 for complex **3** in air at 0 °C under continuous stirring for 2−3 h. The solutions were then filtered and the resulting clear solutions were kept in the refrigerator for several days. Dark crystals of the complexes suitable for single-crystal analysis by X-ray crystallography were then grown and filtered off.

Complex 1: Yield 0.060 g, (20%); m.p. 50−52 °C. UV/Vis (CH_2Cl_2): λ_{max} (log ε) = 497 (3.59), 283 (4.50), 227.5 (4.39). ^1H NMR ($CDCl_3$): δ = 7.9441 [s, 1 H, HN−C(5)], 4.1884−4.1481 [t, CH_2−C(4)], 3.7081−3.6688 [t, 2 H, CH_2−C(5)]. $C_6H_{10}IN_2S_4\cdot I_3\cdot 2I_2$ (1253.60): calcd. C 5.75, H 0.80, N 2.23, S 10.23; found C 5.57, H 0.50, N 2.09; S 9.46.

Complex 2: Yield 0.105 g (30%); m.p. 112 °C. UV/Vis (CH_2Cl_2): λ_{max} (log ε) = 503 (2.82), 329 (3.90), 229 (3.92). ^1H NMR ($CDCl_3$): δ = 10.542 [s, 1 H, HN−C(2) of bztzdtH], 7.597−7.384 (m, 4 H, bz of bztzdtH). $C_7H_5I_2NS_2\cdot I_2$ (674.84): calcd. C 12.46, H 0.75, N 2.08, S 9.50; found C 12.96, H 0.47, N 1.91, S 6.28.

Complex 3: Yield 0.256 g (61%), m.p. 110 °C. UV/Vis (CH_2Cl_2): λ_{max} (log ε) = 506.5 (3.02), 329.5 (4.46), 229 (4.30). ^1H NMR ($CDCl_3$): δ = 10.6 [br, 1 H, HN−C(2) of bztzdtH], 7.935−7.379 (m, 4 H, bz of bztzdtH). $C_7H_5I_2NS_2$ (421.06): calcd. C 19.97, H 1.20, N 3.33; S 15.23; found C 19.78; H 1.12, N 3.19, S 15.68.

Complex 4: Yield 0.045 g (12%); m.p. 165 °C. UV/Vis ($CHCl_3$): λ_{max} (log ε) = 499, (3.56), 309.5, (4.91), 239 (4.60). ^1H NMR ($CDCl_3$): δ = 7.4055−7.3099 (m, 4 H, bz of bzimtH). $C_{14}H_{12}I_6N_4S_2\cdot 2H_2O$ (1097.83): calcd. C 15.32, H 1.47, N 5.10, S 5.84; found C 15.91, H 0.94, N 5.11, S 6.74.

4.3. Raman Measurements: Micro FT-Raman measurements were carried out by using near-infrared laser radiation (Nd^{3+}:YAG, 1064.1 nm). FT-Raman spectra (2.6 cm^{-1} resolution) were recorded with a Bruker IFS-88 FT-IR/FRA-105 Raman module fitted with a Ge proprietary detector and coupled via two 1.0-m photooptic cables to a Nikon Optiphot-II optical microscope equipped with a Nikon 20X, super long-range objective. Near-IR laser radiation was directed onto the sample through the objective and collected along the same optical pathway in a 180° backscattering mode. Samples were measured as solid powders dispersed on a glass slide. Resonance Raman spectra were measured by means of a Renishaw 3000 Ramanscope spectrometer. A typical acquisition time was 10 s, with a slit of 25 μ. Measurements were performed using 488.0- and 514.5-nm sources.

4.4. X-ray Structure Determination: Data were collected by the ω-scan technique in the range $3° < 2\theta < 23°$ for **1** and **4**, and $3° < 2\theta < 25°$ for **2** and **3** with a KUMA KM4CCD four-circle diffractometer[44a] with CCD detector, using graphite-monochromated Mo-K_α (λ = 0.71073Å) at −103 °C (**1**), 20 °C (**2** and **3**) and −168 °C (**4**). Cell parameters were determined by a least-squares fit[44b] of 655, 444, 807, and 3156 reflections for **1**, **2**, **3** and **4**, respectively. All data were corrected for Lorentz-polarization effects and absorption.[44b] Totals of 4672 (**1**), 5771 (**2**), 4699 (**3**) and 6939 (**4**) reflections were collected of which 1603, 2207, 1484 and 1691, respectively, were unique; of these 1175, 1159, 1311 and 1631 were observed [$I > 2\sigma(I)$]. The structures were solved with direct

Table 8. Crystal data and the structure refinement details for complexes **1**, **2**, **3** and **4**

	1	**2**	**3**	**4**
Empirical formula	$C_3H_5I_4NS_2$	$C_7H_5I_4NS_2$	$C_7H_5I_2NS_2$	$C_7H_6I_3N_2S{\cdot}H_2O$
Formula mass	626.80	674.84	421.04	548.91
Crystal size [mm]	0.3 × 0.15 × 0.1	0.4 × 0.2 × 0.1	0.2 × 0.2 × 0.1	0.3 × 0.2 × 0.05
Crystal system	monoclinic	monoclinic	orthorhombic	monoclinic
Space group	$P2_1/n$	$P2_1/n$	$P2_12_12_1$	$P2_1/c$
a [Å]	9.145(2)	8.357(2)	4.189(1)	13.4828(14)
b [Å]	13.259(2)	17.829(4)	9.770(3)	4.6704(4)
c [Å]	10.615(2)	9.603(2)	27.704(8)	21.267(2)
β [°]	106.30(2)	94.39(3)		101.029(8)
V [Å^3]	1235.4(5)	1426.6(6)	1133.8(5)	1376.3(2)
Z	4	4	4	4
$\rho_{calcd.}$ [g cm^{-3}]	3.37	3.14	2.47	2.64
μ [mm^{-1}]	10.38	9.00	5.87	6.94
R[a], $wR2$[b] [$I > 2\sigma(I)$] (%)	5.06, 13.49	6.54, 12.76	6.33, 13.05	6.53, 14.50

[a] $R = \Sigma||F_o| - |F_c||/\Sigma|F_o|$. [b] $wR2 = [\Sigma w(F_o^2 - F_c^2)^2/\Sigma w(F_o^2)^2]^{1/2}$.

methods using SHELXS97[45] and refined by full-matrix least-squares procedures on F^2. All non-hydrogen atoms were refined anisotropically, hydrogen atoms were located at calculated positions and refined as a "riding model" with isotropic thermal parameters fixed at 1.2 times the U_{eq} values of the appropriate carrier atom. Selected crystal data are listed in Table 8. Bond lengths and angles for the complexes are given in Tables 2−5, while the displacement ellipsoid representation of the complexes and their unit cell diagrams are shown in Figures 1−4. CCDC-172151 (**1**), -172154 (**2**), -172153 (**3**) and -172152 (**4**) contain the supplementary crystallographic data for this paper. These data can be obtained free of charge at www.ccdc.cam.ac.uk/conts/retrieving.html or from the Cambridge Crystallographic Data Centre, 12, Union Road, Cambridge CB2 1EZ, UK [Fax: (internat.) + 44-1223/336-033; E-mail: deposit@ccdc.cam.ac.uk].

Acknowledgments

This work was carried out in partial fulfillment of the requirements for an M.Sc. thesis of V. D. within the graduate program EPEAEK in Bioinorganic Chemistry financed by the Ministry of Education of Greece and coordinated by N. H. The NATO grant awarded to N. H. and I. S. B. is also acknowledged.

[1] [1a] Martidale, *The Extra Pharmacopoeia*, 28th ed., The Pharmaceutical Press, London, **1982**. [1b] J. Buxeraud, *Traite de Chimie Therapeutique*, Tec et Doc Lavoisier, Paris, **1995**, vol. 4, chapter 18.

[2] [2a] J. Leclerc, J. Orgiazzi, B. Rousser, J. L. Schlienger, J. L. Wemeau, *La Thyroide*, Expansion Scientifique Francaise, Paris, **1992**. [2b]C. Raby, J. Claude, C. Moesch, J. Buxeraud, C. R. Hebd, *C. R. Seances Acad. Sci., Ser. C* **1979**, *288*, 319. [2c] J. Buxeraud, A. B. Absil, J. Claude, C. Raby, G. Catazano, C. Beck, F. Claude, *Eur. J. Med Chem.-Chim. Ther.* **1985**, *20*, 43. [2d] K. C. Lob, *Postgrad. Med. J.* **2000**, *76*, 133. [2e] D. R. Doerge, C. J. Decker, R. S. Takazawa, AR. Jefferson, *Biochemistry* **1993**, *32*, 58.

[3] M. Esseffar, W. Bouab, A. Lamsabhi, J. L. M. Abboud, R. Notario, M. Yanez, *J. Am. Chem. Soc.* **2000**, *122*, 2300.

[4] P. D. Boyle, J. Christie, T. Dyer, S. M. Godfrey, I. R. Howson, C. McArthur, B. Omar, R. G. Pritchard, G. R. Williams, *J. Chem. Soc., Dalton Trans.* **2000**, 3106.

[5] F. Bigoli, P. Deplano, A. Ienco, C. Mealli, M. L. Mercuri, M. A. Pellinghelli, G. Pintus, G. Saba, E. F. Trogu, *Inorg. Chem.* **1999**, *38*, 4626.

[6] F. Demartin, F. A. Devillanova, A. Garau, F. Isaia, V. Lippolis, G. Verani, *Polyhedron* **1999**, *18*, 3107.

[7] N. Bricklebank, P. J. Skabara, D. E. Hibbs, M. B. Hursthouse, K. M. A. Malik, *J. Chem. Soc., Dalton Trans.* **1999**, 3007.

[8] M. C. Aragoni, M. Arca, F. A. Devillanova, A. Garau, F. Isaia, V. Lippolis, G. Verani, *Coord. Chem. Rev.* **1999**, *184*, 271.

[9] C. Laurence, M. J. El Ghomari, J-Y. Le Questel, M. Berthelot, R. Mokhlisse, *J. Chem. Soc., Perkin Trans. 2* **1998**, 1545.

[10] F. Bigoli, P. Deplano, M. L. Mercuri, M. A. Pellinghelli, A. Sabatini, E. F. Trogu, A. Vacca, *J. Chem. Soc., Dalton Trans.* **1996**, 3583.

[11] F. Cristiani, F. A. Devillanova, F. Isaia, V. Lippolls, G. Verani, F. Demartin, *Polyhedron* **1995**, *14*, 2937.

[12] F. Demartin, P. Deplano, F. A. Devillanova, F. Isaia, V. Lippolis, G. Verani, *Inorg. Chem.* **1993**, *32*, 3694.

[13] F. Cristiani, F. Demartin, F. A. Devillanova, F. Isaia, G. Saba, G. Verani, *J. Chem. Soc., Dalton Trans.* **1992**, 3553.

[14] F. Freeman, J. W. Ziller, H. N. Po, M. C. Keindl, *J. Am. Chem. Soc.* **1988**, *110*, 2586.

[15] D. Arzei, P. Deplano, E. F. Trogu, F. Bigou, M. A. Pellinghelli, A. Vacca, *Can. J. Chem.* **1988**, *66*, 1483.

[16] F. H. Herbstein, W. Schwotzer, *J. Am. Chem. Soc.* **1984**, *106*, 2367; F. H. Herbstein, W. Schwotzer, *Angew. Chem. Int. Ed. Engl.* **1982**, *21*, 219.

[17] D. L. Nosco, M. J. Heeg, M. D. Glick, R. C. Elder, E. Deutsch, *J. Am. Chem. Soc.* **1980**, *102*, 7784.

[18] F. A. Devillanova, G. Verani, *Tetrahedron* **1979**, *35*, 511.

[19] [19a] H. Temkin, A. Watanabe, J. Tanaka, *Bull. Chem. Soc. Jpn.* **1980**, *53*, 645. [19b] Z. Iqbal, R. H. Baughmann, J. Kleppinger, A. B. McDiarmid, *Solid State Commun.* **1978**, *25*, 409.

[20] K. F. Purcell, J. C. Kotz, *An Introduction to Inorganic Chemistry*, Saunders College, Philadelphia, USA, **1980**, pp. 140−141.

[21] F. Cristiani, F. A. Devillanova, A. Diaz, G. Verani, *J. Chem. Soc., Perkin Trans. 2* **1984**, 1383.

[22] F. A. Devillanova, G. Verani, *J. Heterocycl. Chem.* **1979**, *16*, 945; F. A. Devillanova, G. Verani, *Tetrahedron* **1981**, *37*, 1803.

[23] P. Deplano, J. R. Ferraro, M. L. Mercuri, E. F. Trogu, *Coord. Chem. Rev.* **1999**, *188*, 71.

[24] P. Deplano, F. A. Devillanova, J. R. Ferraro, F. Isaia, V. Lippolis, M. L. Mercuri, *Appl. Spectrosc.* **1992**, *46*, 1625.

[25] F. Bigoli, P. Deplano, M. L. Mercuri, A. M. Pellinghelli, A. Sabatini, E. F. Trogu, A. Vacca, *Can J. Chem.* **1995**, *73*, 380.

[26] F. Bigoli, A. M. Pellinghelli, P. Deplano, F. A. Devillanova, V. Lippolis, M. L. Mercuri, E. F. Trogu, *Gazz. Chim. Ital.* **1994**, *124*, 445.

[27] F. Cristiani, F. Demartin, F. A. Devillanova, F. Isaia, V. Lippolis, G. Verani, *Inorg. Chem.* **1994**, *33*, 6315.

[28] J. W. Bransforrd, E. A. Meyers, *Cryst. Struct. Commun.* **1978**, *7*, 697.
[29] H. Hope, H. Y. G. Lin, *J. Chem. Soc., Chem. Commun.* **1970**, 169; H. Y. G. Lin, H. Hope, *Acta Crystallogr., Sect. B*, **1972**, *28*, 643.
[30] PLATON: A. L. Spek, *Acta Crystallogr., Sect. A* **1990**, *46*, C34.
[31] L. Pauling, *The Nature of the Chemical Bond*, 3rd ed., Cornell University Press, Ithaca, New York, **1960**.
[32] F. Van Bolhuis, P. B. Koster, T. Migchelsen, *Acta Crystallogr.* **1967**, *23*, 90.
[33] [33a] C. Preti, G. Tosi, *Can. J. Chem.* **1976**, *54*, 1558. [33b] P. J. Cox, P. Aslanidis, P. Karagiannidis, S. K. Hadjikakou, *Polyhedron* **1999**, *18*, 1501. [33c] J. P. Khullar, U. Agarwala, *Can. J. Chem.* **1975**, *53*, 1165. [33d] B. Singh, M. M. Rukhaivar, R. J. Sinha, *J. Inorg. Nucl. Chem.* **1977**, *39*, 29. [33e] E. S. Raper, J. L. Brooks, *J. Inorg. Nucl. Chem.* **1977**, *39*, 2163.
[34] P. J. Hendra, N. Sadasivan, *Spectrochim. Acta* **1965**, *21*, 1127.
[35] A. Anderson, T. S. Sun, *Chem. Phys. Lett.* **1970**, *6*, 61.
[36] R. C. Teitelbaum, S. L. Ruby, T. J. Marks, *J. Am. Chem. Soc.* **1979**, *101*, 7568.
[37] R. Minkwitz, J. Nowicki, B. Jahnkow, M. Koch, *Z. Anorg. Allg. Chem.* **1991**, *596*, 77.
[38] D. Atzei, F. Bigoli, P. Deplano, M. A. Pellinghelli, A. Sabatini, E. F. Trogu, A. Vacca, *Can. J. Chem.* **1989**, *67*, 1416.
[39] [39a] S. K. Freeman, *Application of Laser Raman Spectroscopy*, Wiley, New York, **1974**, chapter 1. [39b] P. Deplano, F. A. Devillanova, J. R. Ferraro, M. L. Mercuri, V. Lippolis, E. L. Trogu, *Appl. Spectrosc.* **1994**, *48*, 1236. [39c] E. M. Nour, L. H. Chen, J. Laane, *J. Phys. Chem.* **1986**, *90*, 2841.
[40] H. B. Burgi, *Angew. Chem. Int. Ed. Engl.* **1975**, *14*, 460.
[41] C. Laurence, M. J. El Ghomari, M. Berthelot, *J. Chem. Soc., Perkin Trans.* **1998**, *2*, 1163.
[42] [42a] L. M. Abboud, R. Notario, L. Santos, C. Lopez-Mardomingo, *J. Am. Chem. Soc.* **1989**, *111*, 8960. [42b] H. L. Holland, *Organic syntheses with oxidative enzymes*, VCH Publishers, New York, **1991**. [42c] S. L. Neidelman, J. Gregert, *Biohalogenation*, Ellis Horwood, Chichester, **1986**. [42d] J. Pommier, L. Sokoloff, J. Nunez, *Eur. J. Biochem.* **1973**, *38*, 497. [42e] R. P. Magnusson, A. Taurog, *Biochem. Biophys. Res. Commun.* **1983**, *112*, 475.
[43] C. Raby, J. F. Lagorce, A. C. Jambut-Absil, J. Buxeraud, G. Catanzano, *Endocrinology* **1990**, *126*, 1683.
[44] [44a] KUMA KM-4CCD user manual, KUMA Diffraction, Wroclaw, Poland, **1999**. [44b] CrysAlis, program for reduction of the data from KUMA CCD diffractometer, KUMA Diffraction, Wroclaw, Poland, **1999**.
[45] G. M. Sheldrick, Programs for Crystal Structure Analysis (Release 97−2), Institut für Anorganische Chemie der Universität, Tammanstrasse 4, 3400 Göttingen, Germany, **1998**.

Received December 11, 2001
[I01503]

Reactions of Pentafulvene Complexes of Titanium with Carbonyl Compounds − Diastereoselective Synthesis of σ,π-Chelate Complexes with Cp~O Ligands

Jörg Stroot,[a] Rüdiger Beckhaus,*[a] Wolfgang Saak,[a] Detlev Haase,[a] and Arne Lützen[a]

Keywords: Titanium / Fulvene complexes / Reaction mechanism / Substituent effects / Stereoselectivity / O ligands / Cyclopentadienyl ligands

The compound Cp*Ti[η^6-$C_5H_4C(H)(t$Bu)]Cl (**1**) reacts with ketones, aldehydes, and esters to give σ,π-chelate complexes with Cp~O ligands through insertion of the carbonyl group into the Ti–C(H)(*t*Bu) bond. Starting from diastereomerically pure **1**, the reaction with symmetric ketones R_2CO led to the formation of two diastereomeric products. The diastereomeric ratio could be controlled by steric and electronic properties of the substituent R. Thus, this procedure provides an easy approach to complexes with Cp~O ligands where new chiral centres are formed directly in the coordination sphere of the metal atom through a side-differentiated attack of the carbonyl compound at the titanium atom. All products were thoroughly characterized. Crystal structure determinations were carried out on **2a**, **3a**, **5**, **6b**, and **9a**.
(© Wiley-VCH Verlag GmbH, 69451 Weinheim, Germany, 2002)

Introduction

Complexes with functionalized cyclopentadienyl chelate ligands have gained great importance in organo transition metal chemistry because they have been demonstrated to be useful catalysts (or precatalysts) in different kinds of reactions.[1] Generally, chelating Cp~O ligands can be classified as two principal types, ligands functionalized with a neutral O donor (mostly an ether group) (**A**) − forming a hemilabile ligand − and ligands with an anionic O donor (**B**) − leading to cyclopentadienylalkoxide σ,π-chelate complexes (Scheme 1). Diels−Alder reactions,[2] hydrogenations,[3] or the polymerization of olefins[4] and dienes,[5] as well as ring-opening metathesis polymerization reactions[6] are described for complexes of early transition metals exhibiting Cp~O ligands. However, in comparison to related *N*-functionalized cyclopentadienyl complexes, which proved to be remarkably successful in catalytic applications,[7] the use of *O*-functionalized species still seems to be underdeveloped.

Usually these complexes are available by two synthetic routes. Either a suitable transition metal ion is complexed by an already preformed *O*-functionalized cyclopentadienyl ligand,[8] or the ligand is prepared directly in the coordination sphere of the metal centre from a suitable precursor ligand. While the first route is well described,[4b,9] examples for the second one are rather rare.[10] Here we report on new titanium complexes with Cp~O ligands of the alkoxide type (**B**), which we were able to synthesize very efficiently by treating the diastereomerically pure pentafulvene complex Cp*Ti(η^6-$C_5H_4C(H)(t$Bu)]Cl (**1**) with various carbonyl compounds. This approach offers the opportunity to control the stereochemistry of the desired coordination compounds by steric and electronic effects of the carbonyl species, and that can be explained by a proposed mechanism.

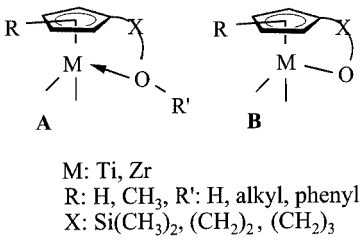

Scheme 1

Results and Discussion

The reaction of diastereomerically pure Cp*Ti[η^6-$C_5H_4C(H)(t$Bu)]Cl (**1**)[11] with benzophenone in *n*-hexane at room temperature proceeded smoothly to give complex **2** as a mixture of diastereomers (Scheme 2), which could easily be separated by a simple filtration since diastereomer **2b** precipitated as a yellow nacreous solid, whereas **2a** proved to be well soluble and remained in solution. Thus, **2b** could be obtained as a yellow powder (81%) by washing the precipitate with a small amount of *n*-hexane. Complex **2a** was isolated as yellow-orange cube-shaped crystals (18%) by

[a] Department of Chemistry, Carl von Ossietzky Universität Oldenburg
26111 Oldenburg, Germany
Fax: (internat.) + 49-(0)441/798-3581
E-mail: ruediger.beckhaus@uni-oldenburg.de
Supporting information for this article is available on the WWW under http://www.eurjic.com or from the author.

concentrating the filtrate and cooling to −20 °C. Complexes **2a** and **2b** differ in the relative arrangement of the exocyclic fulvene proton (6-H) to the titanium-bonded chlorine atom; **2a** was found to have a *trans*-arrangement and is therefore called the "*trans* diastereomer" and **2b** a *cis* arrangement and therefore named the "*cis* diastereomer".

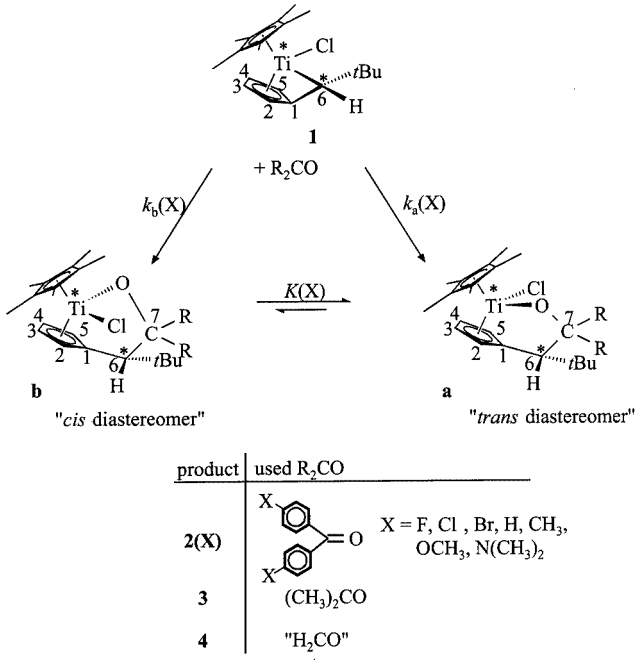

Scheme 2

The two diastereomeric products were thermally stable and could be exposed to air for several hours. However, diastereomerically pure **2a** or **2b** underwent a very slow rearrangement upon storing as a solution in [D_6]benzene for several weeks to give noticeable amounts of the other diastereomer, respectively. After about 12 months these solutions of **2a** and **2b** had equilibrated. However, this equilibrium could be reached considerably faster in the presence of Lewis acids such as $AlMe_3$ or $B(C_6F_5)_3$.

X-ray Crystal Structure Analysis of Complex 2a

Crystals of **2a** suitable for X-ray structural analysis were obtained from a concentrated solution of **2a** in *n*-hexane at 0 °C, and the results are depicted in Figure 1. Two crystallographically independent, but remarkably similar, molecules of **2a** are present within the asymmetric unit. Due to this similarity only one molecule will be discussed in the following section.

The crystal structure reveals a characteristically bent metallocene arrangement of the ligands around the titanium atom. Distances from the metal atom to the ring centroids are 2.050 Å for the functionalized cyclopentadienyl group and 2.111 Å for the Cp* ring. The angle between the geometrical centres of both rings and the titanium atom is 132.9°. These data are in good agreement with those reported for other titanium complexes.[12] The distance Ti−O1 is 1.881(2) Å, similarly as short as those reported

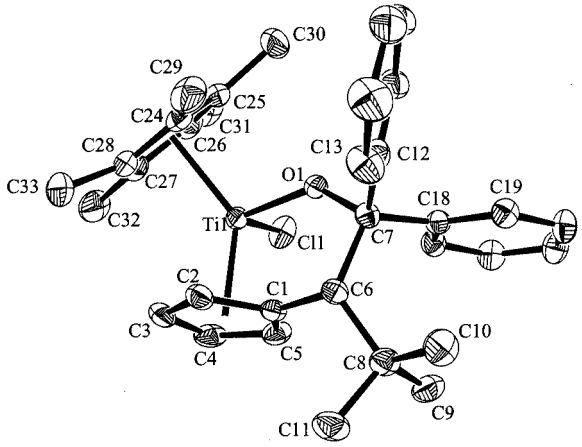

Figure 1. Molecular structure of **2a**; hydrogen atoms have been omitted for clarity; ORTEP ellipsoids represent 50% probability; selected bond lengths [Å] and angles [°]: Ti1−Cl1 2.398(1), Ti1−O1 1.881(2), O1−C7 1.439(3), C6−C7 1.601(3), C1−C6 1.515(3), Ti1−Ct1 2.050, Ti1−Ct2 2.111; Ti1−O1−C7 137.1(1), O1−C7−C6 106.8(2), C1−C6−C7 107.8(2), O1−Ti1−Cl1 100.1(1), Ct1−Ti1−Ct2 132.9; Ct1 = ring centroid of C1 to C5, Ct2 = ring centroid of C24 to C28)

for Ti−OH bonds in titanocene hydroxides,[13] and indicates metal−oxygen double-bond character caused by $O(p_\pi)\rightarrow Ti(d_\pi)$ interactions.[14] It is known from other *x*-membered metallacycles that a general correlation exists between the Ti−O bond length, the Ti−O−C angle, and the ring size. This is due to the attractive interaction between the oxygen lone pairs (located in the p_z orbital) and the lowest unoccupied molecular orbital (LUMO) of the metal atom, which increases with increasing Ti−O−C angle. In the case of the five-membered metallacycle **2a**, with its Ti−O bond length of 1.881(2) Å and its Ti−O−C angle of 137.1(1)°, there is a good agreement with these findings.[15] Furthermore, the significant elongation of the Ti−Cl distance in **2a** [2.398(1) Å] compared with the one found in **1** [2.354(1) Å][11] is noticeable, because it indicates a weakening of $Cl(d_\pi)\rightarrow Ti(d_\pi)$ interactions caused by a raised electron density at the titanium atom by $O(p_\pi)\rightarrow Ti(d_\pi)$ interactions. Whereas the O−C7 and C1−C6 distances are close to typical O−C and C−C single bonds, respectively,[16] the new C6−C7 bond shows a length [1.601(3) Å] that is significantly larger than a typical C−C single bond. This most probably indicates a higher ring strain. The hypothesis that this elongation of the C6−C7 bond is induced rather by ring strain than by steric effects of the substituents at the C6 and C7 atoms is further supported by the reaction products of **1** with several other ketones and aldehydes bearing substituents of varying steric bulkiness (Table 2). In all cases this C−C bond was significantly elongated.

Complex **2b** crystallised from all the usual solvents as fine needles, unsuitable for X-ray structure analysis. However, it could be identified unambiguously by NMR and MS data as well as elemental analysis.

Diastereoselectivity of the Insertion Reaction

In order to obtain an idea about the sense of the stereochemical induction and the underlying mechanism we

studied the reactions shown in Scheme 2 more closely by ^{1}H NMR spectroscopy. Benzophenone proved to be an especially suitable substrate for our purposes, because the proton signals of the pentamethylcyclopentadienyl ligand of **1** and the two diastereomeric products (**2a** and **2b**) were well separated from each other (Figure 2) and the reaction with **1** proceeded sufficiently slowly when we used starting concentrations of $c_{\mathbf{1}} = c_{\text{benzophenone}} = 0.071$ mol L^{-1}.[17] Thus, the concentration of all species involved in the reaction (**1**, **2a**, and **2b**) could be determined at any point during the reaction.

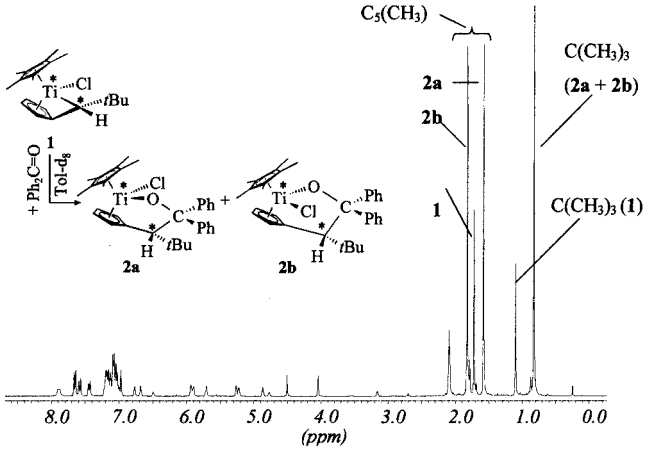

Figure 2. ^{1}H NMR spectra (300 MHz, [D$_8$]toluene) of the reaction of **1** with benzophenone after about 24 h

Furthermore, it was possible to insert activating (electron-donating) or deactivating (electron-accepting) substituents at the phenyl rings in the *para* position to the carbonyl group to study the influence of electronic effects on the reaction. As a preliminarily result,[18] the quotients of rate constants $k_b(X)/k_a(X)$ (cf. Scheme 2) for several disubstituted benzophenones [X = F, Cl, Br, (H), CH_3, OCH_3, $N(CH_3)_2$], which indicate the quantities of obtained "*cis* diastereomer" **2b(X)** and "*trans* diastereomer" **2a(X)**, are listed in Table 1.

Table 1. Ratio of single rate constants k_a and k_b at 300 K for the reactions shown in Figure 1 leading to "*trans* and *cis* diastereomers" **2a(X)** and **2b(X)**, respectively, and difference of the Gibbs energies between **2a(X)** and **2b(X)** [kJ mol^{-1}] at 298 K, showing the dependence on the benzophenone *para* substituent X

	F	Cl	Br	H	CH_3	OCH_3	$N(CH_3)_2$
$k_b(X)/k_a(X)$	3.67	1.74	–	1.39	0.95	0.69	0.23
$\Delta\Delta G_{(b-a)}$	−4.65	−4.85	−4.97	−4.90	−5.04	−5.11	−6.18

As mentioned above, **2a(X)** and **2b(X)** equilibrate after about 12 months with **2b(X)** being the thermodynamically more stable diastereomer in all cases. From equilibrium constant K ($K = c_{\mathbf{2b(X)},\infty}/c_{\mathbf{2a(X)},\infty}$) at 298 K the difference of free Gibbs energies between **2a(X)** and **2b(X)** could be calculated as given in Table 1. The *para* substituents in Table 1 are arranged in a manner that the activating effect increases to the right.

These data suggest two possible pathways for controlling the diastereomeric ratio, namely thermodynamic and kinetic control. While the thermodynamic effect is relatively small − the equilibrium between **2a(X)** and **2b(X)** shifts towards **2b(X)** with rising electron-donating effect of the *para* substituent − the kinetic effect is distinctively larger. The insertion, for example, of a benzophenone derivative with fluorine substituents, which remove electron density from the carbonyl group, led mainly to the "*cis* diastereomer" **2b(F)** ($k_{\mathbf{2b(F)}}/k_{\mathbf{2a(F)}} = 3.67$, according to Table 1), whereas the reaction with a benzophenone carrying the electron-donating Me_2N group yielded the "*trans* diastereomer" **2a(N(CH$_3$)$_2$)** as the major product ($k_{\mathbf{2b(NMe2)}}/k_{\mathbf{2a(NMe2)}} = 0.23$, according to Table 1). However, the diastereomeric ratio could be influenced, not only by electronic, but also by steric effects. In this context, reaction of **1** with small carbonyl compounds like acetone and formaldehyde led exclusively to "*trans* diastereomers" **3a** and **4a**, respectively. The "*cis* diastereomers" **3b** and **4b** could not be detected until the equilibration reaction was performed. However, the reaction with bulky *R*-(+)-camphor gave rise to the "*cis* diastereomers" **5b′** and **5d′** only (Scheme 3), and the "*trans* diastereomers" were not observed, even under the conditions mentioned above to reach equilibrium of the other insertion products.

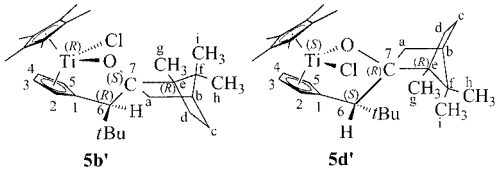

Scheme 3

Structural analyses of three of these insertion products (**3a**, **5b′**, and **5d′**) revealed the bond lengths and angles of the metallacycle to be similar to those found for **2a** (Table 2). Corresponding ORTEP plots are depicted in the Supporting Information.

According to these results, the reaction of **1** with methyl isobutyrate, which has a significantly reduced electron density at the carbonyl oxygen atom, gave exclusively the "*cis* diastereomer" **6b** after β-elimination of MeOH (Scheme 4).

However, released MeOH also reacted with **1** to form compound **11**. Furthermore, since the primary insertion step of the carbonyl group into the Ti−C6 bond is comparatively slow, while the following β-elimination is very fast, the primary product was not observed, even in a ^{1}H NMR experiment. However, both products **6b** and **11** could be isolated by fractional crystallization.

Mechanistic Reflections

In pseudo-tetrahedral bent metallocene complexes of the Cp_2MR_2 type, eight out of the nine metal valence orbitals are used for coordinating the ligands. Two opposed spatial arrangements for the remaining ninth orbital, which determines the chemical reactivity of such complexes to a considerable content, have been discussed in a number of previous

Table 2. Selected bond lengths [Å] and angles [°] in **2a**, **3a**, **5**, **6b**, and **9a**

	2a	**3a**	**5b′**	**5d′**	**6b**	**9a**
Ti−O	1.881(2)	1.854(1)	1.860(3)	1.862(3)	1.889(1)	1.870(2)
O−C7	1.439(3)	1.436(3)	1.438(5)	1.441(5)	1.371(2)	1.417(3)
C7−C6	1.601(3)	1.569(3)	1.612(6)	1.604(6)	1.534(2)	1.569(5)
C6−C1	1.515(3)	1.507(3)	1.524(6)	1.533(5)	1.515(2)	1.508(4)
Ti−Cl	2.398(1)	2.388(1)	2.407(2)	2.394(1)	2.369(1)	2.398(1)
Ti−Ct1	2.050	2.059	2.058	2.058	2.070	2.069
Ti−Ct2	2.111	2.094	2.138	2.114	2.085	2.110
Ti−O−C7	137.1(1)	132.0(1)	138.4(2)	134.4(2)	121.6(1)	134.9(2)
O−C7−C6	106.8(2)	105.1(2)	106.1(3)	106.8(3)	111.5(1)	107.5(2)
C1−C6−C7	107.8(2)	107.2(2)	107.2(3)	106.1(3)	103.4(1)	108.5(2)
Ct1−Ti−Ct2	132.9	133.2	131.9	133.4	134.4	134.2
O−Ti−Cl	100.1(1)	97.8(1)	98.1(1)	100.8(1)	95.8(1)	99.3(1)

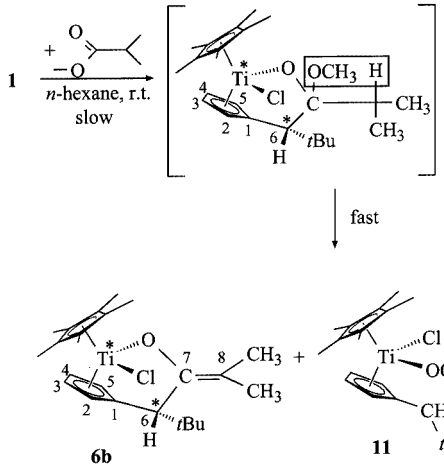

Scheme 4

publications (Scheme 5). Whereas Ballhausen and Dahl favoured a central position between the σ ligands R (**IB**),[19] Alcock et al. postulated a lateral position aligned along the *z* axis (**IA**).[20] Nowadays, recent results from several spectroscopic and theoretical studies unanimous support the lateral arrangement.[21]

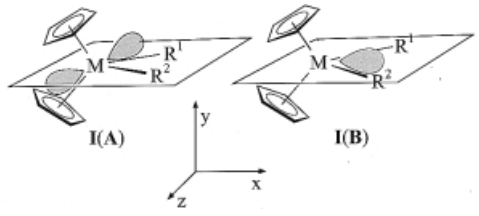

Scheme 5

In case of metallocenes of group-IV metals (16 electron species) this "ninth" orbital is unoccupied (acceptor orbital). Assuming that the spatial arrangement of the acceptor orbital of **1** (16-electron species) is also in the lateral position, the nucleophilic attack of the lone pairs of the carbonyl oxygen atom at the titanium centre and the resulting interactions with the acceptor orbital can in principle proceed from two different sites (Scheme 6). Whereas the "frontal" attack leads to the "*trans* diastereomer", the "backside" attack results the "*cis* diastereomer".

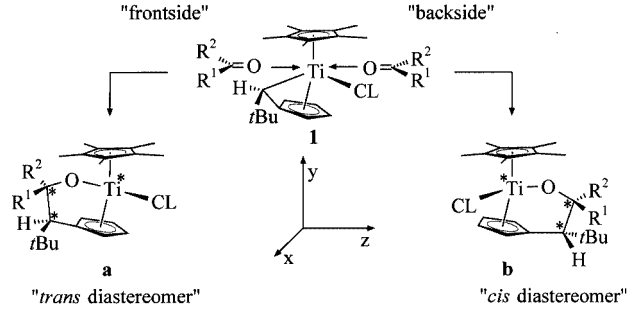

Scheme 6

Calculations of the electrostatic potential[22] of **1** indicate a high electron density at the "backside" induced by the lone pairs of the chlorine atom (Figure 3). This suggests that from the electronic point of view the nucleophilic attack of the carbonyl oxygen atom from the "backside" is strongly disfavoured compared with the "frontal" attack, because the lone pairs of the oxygen and chlorine atoms should repel each other.

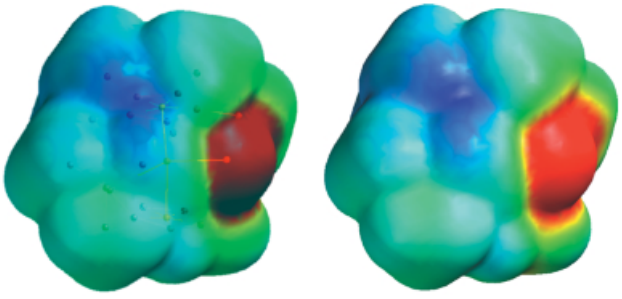

Figure 3. Electrostatic potential, molecular surface of **1** in colour-code form, red representing the negative, blue the positive maximum in charge density in relative terms (left hand semitransparent illustration)

On the other hand, the crystal structure of **1**[11] shows a slight deviation of both rings with respect to each other, and in consequence the titanium centre is sterically shielded from the "front" (Figure 4).

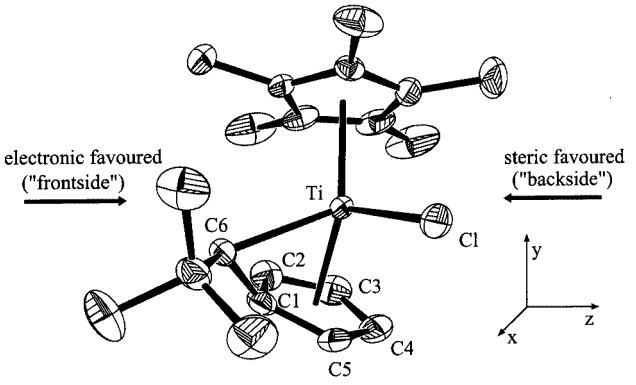

Figure 4. Molecular structure of **1**; hydrogen atoms have been omitted for clarity; ORTEP ellipsoids represent 50% probability

In solution (C_6D_6) strong NOE contacts between the pentamethylcyclopentadienyl protons and the protons at C2 and C3 atoms are observed,[11] indicating a similar deviation in solution. In consequence, an attack from the "front" should be disfavoured from a steric point of view. Thus, **1** is characterized by an electronically favoured "frontal" and a sterically favoured "backside". Therefore, benzophenone derivatives with activating (electron-donating) *para* substituents, e.g. X = NMe_2, attack mainly from the electronically favoured "front", whereas derivatives with deactivating (electron-accepting) substituents, e.g. F, attack from the sterically favoured "backside" [cf. $k_b(X)/k_a(X)$, Table 1]. Likewise, bulky carbonyl compounds like *R*-(+)-camphor approach the titanium centre from the sterically favoured, but electronically disadvantageous "backside", while small carbonyl compounds like acetone or formaldehyde from the electronic favoured "front". The "medium-sized" benzophenone attacks from both sides. According to these results, methyl isobutyrate, which has a considerably lower electron density at the carbonyl oxygen atom, reacts in terms of a "backside" attack exclusively to the "*cis* diastereomer" **6b**.

In order to further corroborate our proposed mechanism, we substituted the chlorine atom in **1** with a methyl group, which led to Cp*Ti[η^6-$C_5H_4C(H)(t\text{Bu})$]Me (**7**). If our mechanism is correct, this should eliminate the electronic disadvantages of the sterically favoured "backside", and in consequence the "*cis* diastereomer" **8b**, resulting from the "backside" attack, should be the main product of the reaction with "medium-sized" benzophenone. Indeed, only **8b** was found and **8a** could only be observed later as a consequence of the equilibration reaction. Insertion products in the Ti−Me bond of **7** were not observed.

Even the stereochemistry of the products, resulting from the reaction of **1** with asymmetric (prochiral) benzaldehyde, could be explained by our proposed mechanism if we take a pre-coordination[10b] of the carbonyl compound (Scheme 6 with R^1 = phenyl, R^2 = H) into account, which has already been suggested by Erker et al. Due to the deviation of the rings in **1**, the orientation of the benzaldehyde phenyl group out of the front of the *xz* plane is very likely, and thus leads to "*trans* and *cis* diastereomers" **9a** and **9b**, respectively.

Rearrangement of Diastereomers

As mentioned above all insertion products, except complexes **5b′** and **5d′**, slowly rearranged to give the corresponding diastereomer and finally reached an equilibrium after about 12 months. However, addition of stoichiometric as well as catalytic amounts of Lewis acids like $AlMe_3$ or $B(C_6F_5)_3$ made this equilibration reaction become considerably faster.[23] We found kinetics of pseudo-first order for the reaction **2b** → **2a** in the presence of $AlMe_3$, suggesting that the Lewis acid (LA) acts as a catalyst whose concentration does not change with time (Scheme 7). Furthermore, ^{1}H NMR spectra indicated that all involved species (**2a**, **2b**, and $AlMe_3$) existed unchanged in solution − since we did not see any permanent agglomeration products of $AlMe_3$. Also, the difference in the Gibbs free energy between the diastereomers [$\Delta\Delta G_{(b-a)}$] did not change.

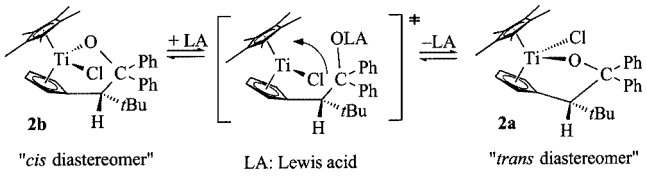

Scheme 7

In principle, one could think of two different mechanisms for this rearrangement. An intramolecular rearrangement involving only a temporary cleavage of the Ti−O bond or an intermolecular exchange of carbonyl compounds between two titanium complexes which would need the permanent cleavage of the Ti−O bond and a C−C bond. Although the latter one seemed unlikely anyway, we further proved this assumption through cross-over experiments with **2a** or **2b** and **7**, as well as with **8a** or **8b** and **1**, which clearly showed, that there was no exchange of carbonyl compounds between two titanium complexes because all complexes remained unchanged even after several months.

However, we were able to confirm the kinetic lability of the Ti−O bond in **2a** and **2b**, respectively, which is the key factor for the probability of the intramolecular rearrangement mechanism proposed in Scheme 7. This was determined by ^{1}H NMR experiments made with **11**-type complexes and free alcohols. A fast exchange of the alkoxy group (methoxy versus ethoxy group) was observed upon addition of stoichiometric amounts of ethyl alcohol to a solution of **11** in [D_6]benzene.[24] Furthermore, no chloride/alkoxy exchange was observed, neither in experiments described above nor in a mixture of Cp*Ti($C_5H_4CH_2t\text{Bu}$)Cl_2 (**15**)[25] and EtOH, hence, also supporting the proposed mechanism.

Conclusion

A simple approach to complexes with Cp~O ligands has been presented, starting from diastereomerically pure Cp*Ti[η^6-$C_5H_4C(H)(t$Bu)]Cl (**1**) and several carbonyl compounds, and it has been demonstrated how the diastereomeric ratio of the product complexes could be controlled in a rather sensitive manner by the nature, nucleophilicity, and steric properties of the utilized carbonyl compounds. In all cases, the stereochemical outcome of this insertion could be explained by a side-differentiated attack of the carbonyl compound at the titanium atom. Thus, this procedure provides a convenient access to complexes with Cp~O ligands where the new chiral centres are formed directly in the coordination sphere of the metal atom in a well-defined manner.

Experimental Section

General Remarks: All operations were performed in nitrogen with rigorous exclusion of oxygen and moisture using glove-box or Schlenk techniques. Solvents were thoroughly dried and saturated with nitrogen. ^{1}H NMR and ^{13}C NMR spectra were recorded with a Bruker AVANCE 500 spectrometer (^{1}H, 500.1 MHz; ^{13}C, 125.8 MHz) or a Bruker AVANCE 300 spectrometer (^{1}H, 300.1 MHz; ^{13}C, 75.8 MHz), chemical shifts were referenced to residual protons or carbon atoms of the solvent. The notation of the nuclei follows the numbering in Scheme 2 and 3. Electron impact (EI) mass spectra were taken with a Finnigan-MAT 95 spectrometer. IR spectra were recorded with a BIO-RAD FTS-7 Spectrometer using KBr pellets. Elemental analyses were carried out by the Analytische Laboratorien in Lindlar (Germany). The complexes Cp*Ti[η^6-$C_5H_4C(H)t$Bu]Cl (**1**)[11] and Cp*Ti[η^6-$C_5H_4C(H)t$Bu]Me (**7**)[26] were prepared according to reported procedures. All carbonyl compounds were purchased from Aldrich and used as received. Diastereomers **3b**, **4b**, and **8a** resulted from the described equilibration reaction between the corresponding diastereomers and could not be isolated, but were characterized by NMR spectroscopy of the respective diastereomeric mixtures.

Complex 2: A solution of benzophenone (0.911 g, 5.0 mmol) in *n*-hexane (10 mL) was added dropwise to a stirred solution of Cp*Ti[η^6-$C_5H_4C(H)t$Bu]Cl (**1**) (1.764 g, 5.0 mmol) in *n*-hexane (20 mL) at room temperature. A yellow nacreous solid began to precipitate after about 8 h. After stirring for additional 52 h, the suspension was filtered. Washing the residue with *n*-hexane (4 × 10 mL) and drying in vacuo led to **2b** as a yellow powder (2.167 g, 81%). Concentration of the filtrate to 10 mL and cooling to −20 °C resulted in the isolation of **2a** as yellow-orange, cube-shaped crystals (0.321 g, 18%).

2a: M.p. 104 °C. ^{1}H NMR (500 MHz, C_6D_6, 300 K): δ = 0.84 [s, 9 H, $C(CH_3)_3$], 1.57 [s, 15 H, $C_5(CH_3)_5$], 4.03 (s, 1 H, 6-H), 5.21 (m, 1 H, C_5H_4), 5.24 (m, 1 H, C_5H_4), 6.01 (m, 1 H, C_5H_4), 6.78 (m, 1 H, C_5H_4), 7.00−7.24 (m, 6 H, *m*-H_{Ph}, *p*-H_{Ph}), 7.47 (m, 2 H, *o*-H_{Ph}), 7.68 (m, 2 H, *o*-H_{Ph}). ^{13}C NMR (125 MHz, C_6D_6, 300 K): δ = 12.5 [$C_5(CH_3)_5$], 30.1 [$C(CH_3)_3$], 34.5 [$C(CH_3)_3$], 58.0 (C6), 109.3 (C_5H_4), 110.8 (C_5H_4), 112.8 (C7), 117.1 (C_5H_4), 121.2 (C_5H_4), 124.8 [$C_5(CH_3)_5$], 127.0, 127.1, 127.3, 128.3, 130.2, 131.2 (CH_{Ph}), 149.0, 149.4 (*i*-C_{Ph}), 152.2 (C1). IR (KBr): ṽ = 3047 (m), 2957 (m), 2907 (m), 2894 (m), 1729 (s), 1660 (s), 1443 (s), 1261 (vs), 1095 (vs), 1024 (s), 995 (vs), 815 (s), cm^{-1} 801 (vs). EI MS: *m*/*z* (%) = 534 (5) [M$^+$], 399 (100) [M$^+$ − Cp*], 352 (6) [M$^+$ − $(Ph)_2CO$], 316 (36) [M$^+$ − $(Ph)_2CO$ + HCl], 218 (38) [M$^+$ − ($C_{10}H_{14}$ + Ph_2CO)], 182 (22) [Ph_2CO^+], 135 (30) [Cp*$^+$]. $C_{33}H_{39}ClOTi$ (534.99): calcd. C 74.09, H 7.35; found C 72.45, H 7.42 (lower carbon value due to e.g. TiC formation).

2b: Decomposition without melting at 244 °C. ^{1}H NMR (500 MHz, C_6D_6, 300 K): δ = 0.84 [s, 9 H, $C(CH_3)_3$], 1.81 [s, 15 H, $C_5(CH_3)_5$], 4.56 (s, 1 H, 6-H), 4.87 (m, 1 H, C_5H_4), 5.71 (m, 1 H, C_5H_4), 5.86 (m, 1 H, C_5H_4), 6.89 (m, 1 H, C_5H_4), 7.04−7.31 (m, 8 H, H_{Ph}), 7.68 (m, 2 H, H_{Ph}). ^{13}C NMR (125 MHz, C_6D_6, 300 K): δ = 12.8 [$C_5(CH_3)_5$], 30.4 [$C(CH_3)_3$], 30.2 [$C(CH_3)_3$], 59.3 (C6), 102.9 (C_5H_4), 109.5 (C_5H_4), 109.8 (C7), 117.9 (C_5H_4), 124.7 [$C_5(CH_3)_5$], 135.8 (C_5H_4), 126.6, 127.0, 127.5, 128.3, 129.2, 130.2 (CH_{Ph}), 139.1 (C1), 148.8 (both *i*-C_{Ph}). IR (KBr): ṽ = 3052 (m), 2955 (m), 2905 (m), 2892 (m), 1493 (s), 1488 (s), 1445 (s), 1393 (s), 1007 (vs), 1000 (vs), 899 (s), 880 (s), 824 (vs), 799 (vs), 783 (s), 764 (vs), 716 (vs), 698 (vs), cm^{-1} 687 (vs). EI MS: *m*/*z* (%) = 534 (2) [M$^+$], 399 (100) [M$^+$ − Cp*], 352 (4) [M$^+$ − $(Ph)_2CO$], 316 (38) [M$^+$ − $(Ph)_2CO$ + HCl], 218 (90) [M$^+$ − ($C_{10}H_{14}$ + Ph_2CO)], 182 (22) [Ph_2CO^+], 135 (30) [Cp*$^+$]. $C_{33}H_{39}ClOTi$ (534.99): calcd. C 74.09, H 7.35; found C 73.94, H 7.40.

Complex 3: A mixture of acetone (0.290 g, 5.0 mmol) in *n*-hexane (10 mL) was added dropwise to a stirred solution of Cp*Ti[η^6-$C_5H_4C(H)t$Bu]Cl (**1**) (1.764 g, 5.0 mmol) in *n*-hexane (20 mL) at room temperature. After 5 min, the colour of the solution turned from dark green to orange. After stirring for an additional 2 h, the solution was concentrated to 10 mL and cooled to −20 °C, **3a** was isolated as yellow-orange, cube-shaped crystals (1.397 g, 68%). M.p. 104 °C. ^{1}H NMR (500 MHz, C_6D_6, 300 K): δ = 0.97 [s, 9 H, $C(CH_3)_3$], 1.29 (s, 3 H, CH_3), 1.53 (s, 3 H, CH_3), 1.81 [s, 15 H, $(C_5(CH_3)_5$], 2.35 (s, 1 H, 6-H), 4.97 (m, 1 H, 2-H), 5.34 (m, 1 H, 3-H), 5.54 (m, 1 H, 4-H), 6.72 (m, 1 H, 5-H). ^{13}C NMR (125 MHz, C_6D_6, 300 K): δ = 12.6 [$C_5(CH_3)_5$], 27.1 (CH_3), 30.4 [$C(CH_3)_3$], 33.1 [$C(CH_3)_3$], 37.6 (CH_3), 63.6 ($^1J_{C,H}$ = 124.5 Hz, C6), 105.4 (C7), 109.5 (C2), 111.8 (C3), 114.3 (C4), 119.0 (C5), 123.9 [$C_5(CH_3)_5$], 148.3 (C1). IR (KBr): ṽ = 3088 (m), 2969 (m), 2911 (m), 2870 (m), 1478 (s), 1452 (s), 1437 (s), 1375 (s), 1358 (s), 1146 (s), 1123 (vs), 1020 (m), 974 (s), 826 cm^{-1} (vs). EI MS: *m*/*z* (%) = 410 (10) [M$^+$], 352 (22) [M$^+$ − $(CH_3)_2CO$], 316 (22) [M$^+$ − $(CH_3)_2CO$ + HCl], 275 (100) [M$^+$ − Cp*], 218 (90) [M$^+$ −$C_{10}H_{14}$ + $(CH_3)_2CO$], 135 (16) [Cp*$^+$]. $C_{23}H_{35}ClOTi$ (410.86): calcd. C 67.24, H 8.59; found C 67.06, H 8.47.

3b: ^{1}H NMR (500 MHz, C_6D_6, 300 K): δ = 0.95 [s, 9 H, $C(CH_3)_3$], 1.25 (s, 3 H, CH_3), 1.40 (s, 3 H, CH_3), 1.81 [s, 15 H, $C_5(CH_3)_5$], 3.12 (s, 1 H, 6-H), 4.94 (m, 1 H, 4-H), 5.18 (m, 1 H, 2-H), 5.67 (m, 1 H, 3-H), 6.85 (m, 1 H, 5-H). ^{13}C NMR (125 MHz, C_6D_6, 300 K): δ = 12.6 [$C_5(CH_3)_5$], 29.6 (CH_3), 30.1 [$C(CH_3)_3$], 33.3 [$C(CH_3)_3$], 33.7 (CH_3), 62.7 (C6), 103.5 (C4), 103.7 (C7), 106.0 (C2), 116.3 (C3), 123.9 [$C_5(CH_3)_5$], 134.6 (C5), 139.6 (C1).

Complex 4: Powdered paraformaldehyde 0.300 g, 10.0 mmol) was added to a solution of Cp*Ti[η^6-$C_5H_4C(H)t$Bu]Cl (**1**) (1.764 g, 5.0 mmol) in THF (20 mL). The suspension was stirred under reflux. After 2 h, the colour of the solution turned from dark green to orange. The reaction mixture was stirred for an additional 2 h. After the THF had been removed, the residue was dissolved in 20 mL of *n*-hexane and separated from insoluble excessive paraformaldehyde by filtration. The filtrate was concentrated to 10 mL and cooled to −20 °C. Complex **4a** could be isolated as a yellow-orange, microcrystalline solid (1.340 g, 70%). **4a:** M.p. 108 °C. ^{1}H NMR (500 MHz, C_6D_6, 300 K): δ = 0.88 [s, 9 H, $C(CH_3)_3$], 1.83 [s, 15 H, $C_5(CH_3)_5$], 2.37 (dd, $^3J_{H6,H7}$ = 11.8, $^3J_{H6,H7'}$ = 6.1 Hz, 1 H, 6-H), 4.71 (dd, $^2J_{H7,H7'}$ = −9.1 Hz, 1 H, 7′-H), 5.10 (m, 1 H,

2-H), 5.34 (m, 1 H, 3-H), 5.50 (dd, 1 H, 7-H), 5.62 (m, 1 H, 4-H), 6.78 (m, 1 H, 5-H). ^{13}C NMR (125 MHz, C_6D_6, 300 K): δ = 12.5 [$C_5(CH_3)_5$], 29.0 [$C(CH_3)_3$], 32.3 [$C(CH_3)_3$], 55.7 (C6), 91.3 (C7), 109.6 (C2), 111.8 (C3), 115.8 (C4), 120.5 (C5), 124.5 [$C_5(CH_3)_5$], 148.2 (C1). IR (KBr): ṽ = 3094 (m), 2951 (m), 2889 (m), 2870 (m), 1489 (s), 1466 (s), 1447 (s), 1385 (s), 1364 (vs), 1045 (vs), 1022 (s), 1005 (s), 822 (vs), 791 cm^{-1} (s). EI MS: *m*/*z* (%) = 382 (34) [M$^+$], 352 (24) [M$^+$ − H_2CO], 316 (100) [M$^+$ − (H_2CO + HCl)], 247 (18) [M$^+$ − Cp*], 218 (72) [M$^+$ − ($C_{10}H_{14}$ + H_2CO)], 135 (66) [Cp*$^+$]. $C_{21}H_{31}ClOTi$ (382.86): calcd. C 65.89, H 8.16; found C 65.71, H 8.25.

4b: ^{1}H NMR (500 MHz, C_6D_6, 300 K): δ = 0.84 [s, 9 H, $C(CH_3)_3$], 1.81 [s, 15 H, $C_5(CH_3)_5$], 3.23 (dd, 1 H, 6-H), 4.94 (dd, 1 H, 7′-H), 5.02 (dd, 1 H, 7-H), 5.03 (m, 1 H, 4-H), 5.06 (m, 1 H, 2-H), 5.65 (m, 1 H, 3-H), 6.95 (m, 1 H, 5-H). ^{13}C NMR (125 MHz, C_6D_6, 300 K): δ = 12.3 [$C_5(CH_3)_5$], 28.4 [$C(CH_3)_3$], 31.7 [$C(CH_3)_3$], 54.2 (C6), 91.2 (C7), 105.6 (C4), 106.7 (C2), 116.2 (C3), 124.2 [$C_5(CH_3)_5$], 133.4 (C5), 148.2 (C1).

Complex 5: A solution of *R*-(+)-camphor (0.761 g, 5.0 mmol) in *n*-hexane (10 mL) was added dropwise to a stirred solution of Cp* Ti(η^6-$C_5H_4C(H)tBu$)Cl (**1**) (1.764 g, 5.0 mmol) in *n*-hexane (20 mL) at room temperature. The reaction mixture was stirred under reflux for 7 d. The colour of the solution turned from dark green to orange. The solution was concentrated to 10 mL and cooled to −20 °C. A mixture of diastereomers **5b′** and **5d′** was isolated as yellow-orange, cube-shaped crystals (1.843 g, 73%; **5b′/5d′** = 50:50). M.p. 161 °C.

5b′: ^{1}H NMR (500 MHz, C_6D_6, 300 K): δ = 0.86 (s, 3 H, $CH_{3,h}$), 1.13 (m, 1 H, H_d), 1.17 [s, 9 H, $C(CH_3)_3$], 1.27 (s, 3 H, $CH_{3,i}$), 1.31 (m, 1 H, H_d), 1.46 (s, 3 H, $CH_{3,g}$), 1.54 (m, 1 H, H_c), 1.59 (m, 1 H, H_c), 1.68 (m, 1 H, H_b), 1.83 [s, 15 H, $C_5(CH_3)_5$], 2.12 (m, 1 H, H_a), 2.23 (m, 1 H, H_a), 3.48 (s, 1 H, 6-H), 5.44 (m, 1 H, 3-H), 5.54 (m, 2 H, 2-H, 4-H), 6.49 (m, 1 H, 5-H). ^{13}C NMR (125 MHz, C_6D_6, 300 K): δ = 13.1 [$C_5(CH_3)_5$], 14.4 ($CH_{3,g}$), 22.8 ($CH_{3,h}$), 23.7 ($CH_{3,i}$), 27.6 (C_c), 31.9 [$C(CH_3)_3$], 32.6 (C_d), 34.4 [$C(CH_3)_3$], 46.4 (C_a), 46.7 (C_b), 48.1 (C_f), 55.9 (C6), 61.1 (C_e), 105.6 (C2), 113.2 (C3), 113.3 (C4), 122.0 (C5), 123.8 [$C_5(CH_3)_5$], 126.1 (C7), 152.4 (C1).

5d′: ^{1}H NMR (500 MHz, C_6D_6, 300 K): δ = 0.90 (s, 3 H, $CH_{3,h/i}$), 0.96 (s, 3 H, $CH_{3,h/i}$), 1.22 [s, 9 H, $C(CH_3)_3$], 1.41 (m, 1 H, $H_{c/d}$), 1.43 (m, 1 H, $H_{c/d}$), 1.49 (s, 3 H, $CH_{3,g}$), 1.55 (m, 1 H, H_a), 1.64 (m, 1 H, H_b), 1.84 [s, 15 H, $C_5(CH_3)_5$], 2.57 (m, 1 H, H_a), 3.48 (s, 1 H, 6-H), 5.44 (m, 3 H, 3 C_5H_4), 6.66 (m, 1 H, C_5H_4). ^{13}C NMR (125 MHz, C_6D_6, 300 K): δ = 12.7 [$C_5(CH_3)_5$], 15.5 ($CH_{3,g}$), 21.0 ($CH_{3,h/i}$), 23.7 ($CH_{3,h/i}$), 28.4 ($C_{c/d}$), 28.8 ($C_{c/d}$), 31.9 [$C(CH_3)_3$], 35.8 [$C(CH_3)_3$], 46.3 (C_b), 48.9 (C_a), 50.4 (C_f), 56.7 (C6), 61.9 (C_e), 105.4 (C_5H_4), 111.7 (C_5H_4), 113.5 (C_5H_4), 123.1 (C7), 123.6 (C_5H_4), 123.6 [$C_5(CH_3)_5$], 151.1 (C1). Diastereomeric mixture **5b′/5d′**: IR (KBr): ṽ = 3097 (w), 2946 (m), 2909 (m), 1486 (s), 1474 (s), 1444 (s), 1372 (s), 1306 (w), 1038 (vs), 1022 (s), 1007 (s), 830 cm^{-1} (vs). EI MS: *m*/*z* (%) = 504 (20) [M$^+$], 468 (42) [M$^+$ − HCl], 369 (100) [M$^+$ − Cp*], 352 (5) [M$^+$ − $C_{10}H_{16}O$], 316 (100) [M$^+$ − ($C_{10}H_{16}O$ + HCl)], 218 (36) [M$^+$ − ($C_{10}H_{14}$ + $C_{10}H_{16}O$)], 135 (8) [Cp*$^+$]. $C_{30}H_{45}ClOTi$ (505.01): calcd. C 71.35, H 8.98; found C 71.36, H 8.97.

Complex 6: A solution of methyl isobutyrate (0.106 g, 2.5 mmol) in *n*-hexane (10 mL) was added dropwise to a stirred solution of Cp* Ti[η^6-$C_5H_4C(H)tBu$]Cl (**1**) (1.764 g, 5.0 mmol) in *n*-hexane (20 mL) at room temperature. After 12 h, the colour of the solution turned from dark green to claret red. After stirring for additional 48 h, the solution was concentrated to 10 mL and cooled to 0 °C; **6b** could be isolated diastereomerically pure as ruby coloured, acicular crystals (0.655 g, 62%). M.p. 139 °C. ^{1}H NMR (500 MHz, C_6D_6, 300 K): δ = 1.02 [s, 9 H, $C(CH_3)_3$], 1.71 (s, 3 H, CH_3), 1.78 (s, 3 H, CH_3), 1.83 [s, 15 H, $C_5(CH_3)_5$], 3.86 (s, 1 H, 6-H), 5.35 (m, 1 H, 2-H), 5.37 (m, 1 H, 4-H), 5.53 (m, 1 H, 3-H), 6.46 (m, 1 H, 5-H). ^{13}C NMR (125 MHz, C_6D_6, 300 K): δ = 12.6 [$C_5(CH_3)_5$], 17.7 (CH_3), 20.7 (CH_3), 29.8 [$C(CH_3)_3$], 35.2 [$C(CH_3)_3$], 51.5 (C6), 99.0 (C8), 107.1 (C2), 112.4 (C4), 114.7 (C3), 124.9 [$C_5(CH_3)_5$], 127.1 (C5), 145.6 (C1), 169.9 (C7). IR (KBr): ṽ = 2962 (m), 2948 (m), 2903 (m), 1653 (s), 1493 (s), 1480 (s), 1464 (s), 1438 (s), 1383 (s), 1169 (s), 1138 (vs), 1099 (s), 1022 (s), 937 (s), 827 (vs), 809 cm^{-1} (vs). EI MS: *m*/*z* (%) = 422 (80) [M$^+$], 386 (22) [M$^+$ − HCl], 352 (8) [M$^+$ − C_4H_6O], 329 (100) [M$^+$ − HCl + $C(CH_3)_3$], 316 (18) [M$^+$ − (C_4H_6O + HCl)], 218 (34) [M$^+$ − ($C_{10}H_{14}$ + C_4H_6O)], 135 (16) [Cp*$^+$]. $C_{24}H_{35}ClOTi$ (422.87): calcd. C 68.17, H 8.34; found C 68.08, H 8.26.

Complex 8: A solution of benzophenone (0.456 g, 2.5 mmol) in *n*-hexane (10 mL) was added dropwise to a stirred solution of Cp* Ti[η^6-$C_5H_4C(H)tBu$]Me (**7**) (0.831 g, 2.5 mmol) in *n*-hexane (10 mL) at room temperature. After 2 h, a yellow nacreous solid began to precipitate. After stirring for an additional 58 h, the suspension was filtered. Washing of the residue with *n*-hexane (4 × 10 mL) and drying in vacuo led to **8b** as a yellow powder (0.836 g, 65%).

8a: ^{1}H NMR (500 MHz, C_6D_6, 300 K): δ = 0.66 (s, 3 H, CH_3), 0.93 [s, 9 H, $C(CH_3)_3$], 1.48 [s, 15 H, $C_5(CH_3)_5$], 4.05 (s, 1 H, 6-H), 4.64 (m, 1 H, C_5H_4), 5.36 (m, 1 H, C_5H_4), 5.58 (m, 1 H, C_5H_4), 6.54 (m, 1 H, C_5H_4), 7.01−7.24 (m, 8 H, H_{Ph}), 7.43 (m, 2 H, H_{Ph}). ^{13}C NMR (125 MHz, C_6D_6, 300 K): δ = 11.7 [$C_5(CH_3)_5$], 30.4 [$C(CH_3)_3$], 34.5 [$C(CH_3)_3$], 37.4 (CH_3), 58.6 (C6), 106.5 (C_5H_4), 113.6 (C_5H_4), 114.6 (C_5H_4), 116.2 (C_5H_4), 108.2 (C7), 119.4 [$C_5(CH_3)_5$], 125.6, 126.7, 126.9, 128.3, 128.5, 130.3 (CH_{Ph}), 136.8 (C1), 149.6, 152.6 (*i*-C_{Ph}).

8b: Decomposition without melting at 235 °C. ^{1}H NMR (500 MHz, C_6D_6, 300 K): δ = −0.05 (s, 3 H, CH_3), 0.91 [s, 9 H, $C(CH_3)_3$], 1.72 [s, 15 H, $C_5(CH_3)_5$], 4.32 (s, 1 H, 6-H), 4.53 (m, 1 H, C_5H_4), 5.39 (m, 1 H, C_5H_4), 5.86 (m, 1 H, C_5H_4), 6.41 (m, 1 H, C_5H_4), 7.04−7.24 (m, 8 H, H_{Ph}), 7.59 (m, 2 H, H_{Ph}). ^{13}C NMR (125 MHz, C_6D_6, 300 K): δ = 12.1 [$C_5(CH_3)_5$], 30.5 [$C(CH_3)_3$], 34.4 [$C(CH_3)_3$], 34.7 (CH_3), 59.4 (C6), 102.4 (C_5H_4), 106.7 (C7), 107.3 (C_5H_4), 113.6 (C_5H_4), 119.2 [$C_5(CH_3)_5$], 128.9 (C_5H_4), 126.5, 126.8, 126.9, 128.7, 128.9, 130.2 (CH_{Ph}), 136.8 (C1), 149.1, 150.5 (*i*-C_{Ph}). IR (KBr): ṽ = 3053 (m), 2943 (m), 2908 (m), 2889 (m), 1492 (s), 1477 (s), 1443 (s), 1392 (s), 1035 (s), 1013 (vs), 808 (vs), 800 (vs), 763 (vs), 713 (vs), 700 (vs), 686 cm^{-1} (vs). EI MS: *m*/*z* (%) = 514 (24) [M$^+$], 261 (100), 135 (20) [Cp*$^+$]. $C_{34}H_{42}OTi$ (514.58): calcd. C 79.36, H 8.23; found C 79.09, H 8.09.

Complex 9: A mixture of benzaldehyde (0.531 g, 5.0 mmol) in *n*-hexane (10 mL) was added dropwise to a stirred solution of Cp* Ti[η^6-$C_5H_4C(H)tBu$]Cl (**1**) (1.764 g, 5.0 mmol) in *n*-hexane (20 mL) at room temperature. After 15 min, the colour of the solution turned from dark green to orange. After stirring for an additional 4 h, the solution was concentrated to 10 mL and cooled to −20 °C. A mixture of diastereomers **9a** and **9b** was isolated as a yellow-orange, microcrystalline solid (1.308 g, 57%; **9a/9b** = 25:75).

9a: ^{1}H NMR (500 MHz, C_6D_6, 300 K): δ = 0.82 [s, 9 H, $C(CH_3)_3$], 1.76 [s, 15 H, $C_5(CH_3)_5$], 3.22 (d, $^3J_{H6,H7}$ = 8.5 Hz, 1 H, 6-H), 5.23 (m, 1 H, 2-H), 5.24 (m, 1 H, 3-H), 6.01 (m, 1 H, 4-H), 6.38 (d, 1 H, 7-H), 6.84 (m, 1 H, 5-H), 6.96−7.24, 7.89 (m, 5 H, H_{Ph}). ^{13}C NMR (125 MHz, C_6D_6, 300 K): δ = 12.4 [$C_5(CH_3)_5$], 29.3 [$C(CH_3)_3$], 33.5 [$C(CH_3)_3$], 61.0 (C6), 107.2 (C7), 109.7 (C3), 111.1

Table 3. Crystal data and structure refinement for **2a**, **3a**, **5**, **6b**, and **9a**

	2a	**3a**	**5**	**6b**	**9a**
Empirical formula	$C_{33}H_{39}ClOTi$	$C_{23}H_{35}ClOTi$	$C_{30}H_{45}ClOTi$	$C_{24}H_{35}ClOTi$	$C_{27}H_{35}ClOTi$
M_r	534.99	410.86	505.01	422.87	458.90
Cryst. size [mm]	0.55 × 0.36 × 0.31	0.50 × 0.40 × 0.20	0.47 × 0.41 × 0.36	0.65 × 0.32 × 0.25	0.69 × 0.14 × 0.04
Cryst. system	triclinic	monoclinic	triclinic	monoclinic	monoclinic
Space group	$P\bar{1}$	$P2_1/c$	P1	$P2_1/c$	$P2_1/c$
a [Å]	12.8007(9)	9.9744(4)	12.6661(14)	15.2868(7)	9.8168(5)
b [Å]	15.0494(11)	14.2277(8)	12.6773(15)	9.7894(4)	15.5485(11)
c [Å]	15.7150(13)	16.0204(6)	18.539(2)	16.0150(6)	15.2835(6)
α [°]	94.852(9)		70.535(14)		
β [°]	109.293(9)	100.635(4)	73.276(13)	113.114(5)	93.984(6)
γ [°]	99.189(9)		84.906(14)		
V [Å^3]	2789.9(4)	2234.45(18)	2687.9(5)	2204.23(16)	2327.2(2)
Z	4	4	4	4	4
$\rho_{calcd.}$ [g cm^{-3}]	1.274	1.221	1.248	1.274	1.310
μ [mm^{-1}]	0.426	0.511	0.438	0.521	0.499
F(000)	1136	880	1088	904	976
Θ_{range} [°]	2.10 to 26.17	2.08 to 26.04	2.33 to 25.86	2.50 to 25.88	2.46 to 25.92
Reflections coll.	34105	16309	32224	16754	17428
Independ. reflect.	10180 (R_{int} = 0.1012)	4076 (R_{int} = 0.0388)	19099 (R_{int} = 0.0793)	4037 (R_{int} = 0.0489)	4257 (R_{int} = 0.0959)
Observed reflect. [$I > 2\sigma(I)$]	7222	3135	14166	3274	2304
Refined parameters	601	235	1189	384	271
GOF	0.978	1.007	0.917	0.975	0.784
R_1	0.0410	0.0364	0.0474	0.0288	0.0396
wR_2	0.1064	0.0976	0.1061	0.0721	0.0788
Largest diff. peak/hole [eÅ^{-3}]	0.567/−0.359	0.760/−0.349	0.303/−0.580	0.381/−0.217	0.378/−0.277

(C2), 117.8 (C5), 120.3 (C4), 124.3 [$C_5(CH_3)_5$], 145.2 (C1), 127.7−128.3, 129.5 (CH_{Ph}), 147.7 (i-C_{Ph}).

9b: ^{1}H NMR (500 MHz, C_6D_6, 300 K): δ = 0.78 [s, 9 H, $C(CH_3)_3$], 1.78 [s, 15 H, $C_5(CH_3)_5$], 2.50 (d, $^3J_{H6,H7}$ = 10.4 Hz, 1 H, 6-H), 5.07 (m, 1 H, 5-H), 5.44 (m, 1 H, 4-H), 5.62 (m, 1 H, 3-H), 6.24 (d, 1 H, 7-H), 6.89 (m, 1 H, 2-H), 6.96−7.24 (m, 5 H, H_{Ph}). ^{13}C NMR (125 MHz, C_6D_6, 300 K): δ = 12.7 [$C_5(CH_3)_5$], 29.9 [$C(CH_3)_3$], 33.4 [$C(CH_3)_3$], 60.1 (C6), 102.0 (C7), 108.8 (C5), 112.2 (C4), 115.3 (C3), 120.3 (C2), 124.8 [$C_5(CH_3)_5$], 147.0 (C1), 127.7−128.3, 129.5 (CH_{Ph}), 146.9 (i-C_{Ph}).

Crystal Structure Determinations. Single crystals of **2a**, **3a**, **5**(**b**′+**d**′), **6b**, and **9a** were obtained from saturated *n*-hexane solutions upon cooling to 0 °C. The crystal data were collected with a STOE-IPDS diffractometer with graphite-monochromated Mo-K_α radiation (λ = 0.71073). Intensity measurements were performed at 193(2) K on crystals in sealed glass capillaries. The structures of all complexes were solved by direct phase determination (SHELXS-97) and refined on F^2 (SHELXS-97)[27] with anisotropic thermal parameters for all non-hydrogen atoms. All hydrogen atoms in **2a**, **3a**, **5**(**b**′+**d**′), and **6b** were calculated and refined as riding atoms; hydrogen atoms in **9a** refined freely. Details of data collection parameters and refinements results are listed in Table 3. CCDC-174560 (**2a**), -174562 (**3a**), -174561 (**5**), -174559 (**6b**) and -174563 (**9a**) contain the supplementary crystallographic data for this paper. These data can be obtained free of charge at www.ccdc.cam.ac.uk/conts/retrieving.html or from the Cambridge Crystallographic Data Centre, 12, Union Road, Cambridge CB2 1EZ, UK [Fax: (internat.) + 44-1223/336-033; E-mail: deposit@ccdc.cam.ac.uk].

Acknowledgments

This work was supported by the Bundesministerium für Bildung und Forschung (BMBF, 03C0276G/4), the Fonds der Chemischen Industrie and the Karl-Ziegler-Stiftung of the GDCh.

[1] Cp~O ligands reviewed in: U. Siemeling, *Chem. Rev.* **2000**, *100*, 1495−1526.
[2] A. A. H. van der Zeijden, C. Mattheis, *J. Organomet. Chem.* **1998**, *555*, 5−15.
[3] Y. Qian, K. Hong, H. Zong, J. Huang, *Polym. Adv. Technol.* **1996**, *7*, 619−624.
[4] [4a] R. Beckhaus, J. Heinrichs, S. Becke (BAYER AG Leverkusen), US 6,214,762 B1. [4b] P. Foster, M. D. Rausch, J. C. W. Chien, *J. Organomet. Chem.* **1997**, *527*, 71−74. [4c] Y. Qian, J. Huang, T. Huang, S. Chen, *Transition Met. Chem.* **1996**, *21*, 393−397. [4d] A. Rau, S. Schmitz, G. Luft, *J. Organomet. Chem.* **2000**, *608*, 71−75. [4e] E. E. C. G. Gielens, J. Y. Tiesnitsch, B. Hessen, J. H. Teuben, *Organometallics* **1998**, *17*, 1652−1654.
[5] [5a] M. Nakamura, T. Fukahori, T. Shibuya (Nippon Zeon Co., Ltd., Japan), JP2000086813. [5b] M. Nakamura, T. Fukahori, T. Shibuya (Nippon Zeon Co., Ltd., Japan), JP2000086814. [5c] M. Nakamura, T. Fukahori, T. Shibuya (Nippon Zeon Co., Ltd., Japan), JP2000086819.
[6] Y. L. Qian, D. F. Zhang, J. L. Huang, H. Y. Ma, A. S. C. Chan, *J. Mol. Catal. A: Chem.* **1998**, *133*, 135−138.
[7] [7a] J.-F. Carpentier, V. P. Maryin, J. Luci, R. F. Jordan, *J. Am. Chem. Soc.* **2001**, *123*, 898−909. [7b] K. Kunz, G. Erker, S. Döring, R. Fröhlich, G. Kehr, *J. Am. Chem. Soc.* **2001**, *123*, 6181−6182. [7c] D. van Leusen, D. J. Beetstra, B. Hessen, J. H. Teuben, *Organometallics* **2000**, *19*, 4084−4089. [7d] J. Okuda, T. Eberle, T. P. Spaniol, V. Piquet-Faure, *J. Organomet. Chem.* **1999**, *591*, 127−137. [7e] H. Hagihara, T. Shiono, R. Ikeda, *Macromol. Rapid Commun.* **1999**, *10*, 200−202. [7f] R. Gomez, P. Gomez-Sal, P. A. del Real, P. Royo, *J. Organomet. Chem.* **1999**, *588*, 22−27. [7g] T. Shiono, S. Yoshida, H. Hagihara, T. Ikeda, *Appl. Catalysis A − General* **2000**, *200*, 145−152.
[8] [8a] D. W. Macomber, W. P. Hart, M. D. Rausch, *Adv. Organomet. Chem.* **1982**, *21*, 1−55. [8b] M. I. Bruce, A. H. White, *Aust. J. Chem.* **1990**, *43*, 949.
[9] [9a] A. A. H. van der Zeijden, C. Mattheis, R. Fröhlich, *Organometallics* **1997**, *16*, 2651−2658. [9b] Q. Qian, Y. Hunag, G. Li, Y. Tang, *Transition Met. Chem.* **1990**, *15*, 483. [9c] J. Zhang, Y.

Hunag, Q. Huang, Y. Qian, *Inorg. Chem. Commun.* **1999**, *2*, 104. [9d] Y. Qian, G. Li, W. Chen, B. Li, X. Jin, *J. Organomet. Chem.* **1989**, *373*, 185.

[10] [10a] J. W. Pattiasina, C. E. Hissink, J. L. de Boer, A. Meetsma, J. H. Teuben, A. L. Spek, *J. Am. Chem. Soc.* **1985**, *107*, 7758−7759. [10b] G. Erker, U. Korek, *Z. Naturforsch., Teil B* **1989**, *44*, 1593−1598.

[11] R. Beckhaus, A. Lützen, D. Haase, W. Saak, J. Stroot, S. Becke, J. Heinrichs, *Angew. Chem.* **2001**, *113*, 2112−2115; *Angew. Chem. Int. Ed.* **2001**, *40*, 2056−2058.

[12] [12a] T. C. McKenzie, R. D. Sanner, J. E. Bercaw, *J. Organomet. Chem.* **1975**, *102*, 457−466. [12b] A. Clearfield, D. K. Warner, C. H. Saldarriaga-Molina, R. Ropal, I. Bernal, *Can. J. Chem.* **1975**, *53*, 1622−1629. [12c] R. D. Rogers, M. M. Benning, L. K. Kurihara, K. J. Moriarty, M. D. Rausch, *J. Organomet. Chem.* **1985**, *293*, 51−60.

[13] [13a] J. Stroot, D. Haase, W. Saak, R. Beckhaus, *Z. Kristallogr. NCS* **2002**, *217*, 47−48. [13b] P.-M. Pellny, V. V. Burlakov, W. Baumann, A. Spannenberg, U. Rosenthal, *Z. Anorg. Allg. Chem.* **1999**, *625*, 910−918. [13c] U. Thewalt, B. Honold, *J. Organomet. Chem.* **1988**, *348*, 291−303. [13d] M. Bochmann, A. J. Jaggar, L. M. Wilson, M. B. Hursthouse, M. Motevalli, *Polyhedron* **1989**, *8*, 1838−1843.

[14] [14a] A. Gomez-Carrera, M. Mena, P. Royo, R. Serrano, *J. Organomet. Chem.* **1986**, *315*, 329−336. [14b] R. Bortolin, V. Patel, I. Munday, N. J. Taylor, A. J. Carty, *J. Chem. Soc., Chem. Commun.* **1985**, 456−458.

[15] Ti−O distances [Å] and Ti−O−C angels [°] in *x*-membered titanacycles: *x* = 4: Ti−O−C 91.7(1), Ti−O 1.992(4),[15a] Ti−O−C 96.7(2), Ti−O 1.983(2),[15b] Ti−O−C 97.5(3), Ti−O 1.966(3);[15c] *x* = 6: Ti−O−C 146.1(1), Ti−O 1.767(1);[15d] *x* = 8: Ti−O−C 154.6(2), Ti−O 1.738(2):[15e] [15a] D. J. Schwartz, M. R. Smith, III, R. A. Andersen, *Organometallics* **1996**, *15*, 1446−1450. [15b] R. Beckhaus, I. Strauß, T. Wagner, P. Kiprof, *Angew. Chem.* **1993**, *105*, 281−283; *Angew. Chem. Int. Ed. Engl.* **1993**, *32*, 264−266. [15c] R. Beckhaus, I. Strauß, T. Wagner, *Z. Anorg. Allg. Chem.* **1997**, *623*, 654−658. [15d] R. Fandos, A. Meetsma, J. H. Teuben, *Organometallics* **1991**, *10*, 59−60. [15e] R. Fandos, J. H. Teuben, G. Helgesson, S. Jagner, *Organometallics* **1991**, *10*, 1637−1639.

[16] J. March, *Advanced Organic Chemistry*, 4th ed., John Wiley & Sons, New York, **1992**.

[17] After about 26 h, 80% of **1** and benzophenone are transformed.

[18] Unpublished results.

[19] C. J. Ballhausen, J. P. Dahl, *Acta Chem. Scand.* **1961**, *15*, 1333−1336.

[20] N. W. Alcock, *J. Chem. Soc.* **1967**, 2001−2009.

[21] [21a] J. C. Green, M. L. H. Green, C. K. Prout, *J. Chem. Soc., Chem. Commun.* **1972**, 421−422. [21b] G. Erker, *Acc. Chem. Res.* **1984**, *17*, 103−109. [21c] M. L. H. Green, *Pure Appl. Chem.* **1972**, *30*, 373−388. [21d] J. C. Green, S. E. Jackson, B. Higginson, *J. Chem. Soc., Dalton Trans.* **1975**, 403−409. [21e] J. L. Petersen, L. F. Dahl, *J. Am. Chem. Soc.* **1975**, *97*, 6416−6422. [21f] J. W. Lauher, R. Hoffmann, *J. Am. Chem. Soc.* **1976**, *98*, 1729−1742. [21g] F. De Angelis, A. Sgamellotti, N. Re, *Organometallics* **2000**, *19*, 4904−4911.

[22] M. C. W. Chan, J. M. Cole, V. C. Gibson, J. A. K. Howard, C. Lehmann, A. D. Poole, U. Siemeling, *J. Chem. Soc., Dalton Trans.* **1998**, 103−112.

[23] For $c_{AlMe3} = c_{\mathbf{2b}} = 1 \cdot 10^{-3}$ mol L^{-1} and $c_{B(C6F5)3} = c_{\mathbf{2b}} = 1 \cdot 10^{-3}$ mol L^{-1} equilibrium state is reached in 1 h and 5 min.

[24] Further details are given in the Supporting Information.

[25] J. Stroot, D. Haase, W. Saak, R. Beckhaus, *Z. Kristallogr. NCS* **2002**, *217*, 49−50.

[26] J. Stroot, M. Friedemann, A. Lützen, W. Saak, R. Beckhaus, *Z. Anorg. Allg. Chem.*, in press.

[27] G. M. Sheldrick, *SHELXL-97, A Program for Refining Crystal Structures*, University of Göttingen, Germany, **1997**.

Received December 17, 2001
[I01512]

Structural and Chiroptical Properties of Acyclic and Macrocyclic 1,5-Bis(oxazoline) Ligands and Their Copper(I) and Silver(I) Complexes

Miklos Hollosi,[a] Zsuzsa Majer,[a] Elemér Vass,[a] Zlata Raza,[b] Vladislav Tomišić,[c] Tomislav Portada,[b] Ivo Piantanida,[b] Mladen Žinić,[b] and Vitomir Šunjić*[b]

Keywords: Circular dichroism / Conformation analysis / Copper / Silver / Bis(oxazoline) ligands / Macrocyclic ligands

C_2-symmetric acyclic ligands **1a**–**1e**, macrocyclic ligands **2a**–**2d** and **3**, and their copper(I) and silver(I) complexes were studied by UV, NMR and CD spectroscopy. The stability constants of the metal–**1a** and –**1b** complexes with 1:1 and 1:2 stoichiometries in acetonitrile were determined by spectrometric titrations. Evidence of tetrahedral coordination for complex $[Ag(\mathbf{1a})_2]^+$ was obtained from the complexation induced shifts (CIS) and NOEs, and corroborated by molecular modeling. Ligands with phenyl rings on the stereogenic centers (**1a**,**c** and **2**) exhibit a strong Cotton effect (CE) in the region of the ^1B_b band, which is absent in the ligands with benzyl groups on the stereogenic center (**1b**, **3**). This effect is ascribed to the exciton coupling (EC) of two aromatic chromophores on the stereogenic center. For ligands **1a** and **2a** the EC changes the sign on complexation to Cu^+, revealing opposite helicity of the free and complexed ligand.
(© Wiley-VCH Verlag GmbH, 69451 Weinheim, Germany, 2002)

Introduction

Chiral bis(oxazoline)−metal complexes have received a great deal of attention through their use in various asymmetric catalytic processes.[1−4] Among them the complexes with 1,5-bis(oxazoline) ligands having one carbon spacer between the oxazoline rings and able to form six-membered metal chelates, are the most frequently utilized as chiral catalytic complexes in various enantioselective transformations.

The most explored catalytic complexes are those of copper(I)[5−14] (enantioselective cyclopropanation of alkenes,[5−11] aziridation of olefins[12] and imines,[13] allylic oxidation of cycloalkenes[14]), copper(II)[15−24] (Diels−Alder reaction,[15−19] Mukaiyama aldol reaction,[20] Mukaiyama−Michael addition reaction,[21,22] Friedel−Crafts reaction,[23] Canizzaro reaction[24]), palladium(II)[25−27] (allylic substitution reaction), and zinc(II)[28−30] (allylation reaction). We have recently reported on very high cumulative enantio- and diastereoselectivity in cyclopropanation of styrene catalyzed by copper(I) complexes of macrocyclic ligands **2a**−**2c** (Figure 1).[31] These results are in line with our previous observation,[32,33] that enantioselectivity enhancement can be achieved by restricting conformational mobility of the ligand by repulsive or attractive π−π interactions.[34−36]

Structural studies of the ligand−metal complexes often provide valuable information regarding transition state assembly in the catalytic transformation. Already, the solid-state structures of various bis(oxazoline)−metal complexes have been elucidated on the basis of X-ray diffraction analysis,[5,9,19,26,27,37−44] but only a few were determined in solution based on NMR[26,38,43−45] and CD[44,45] spectroscopic investigations. To the best of our knowledge, the spectroscopic study of 1,5-bis(oxazoline)−copper(I) and −silver(I) complexes in solution, aimed at elucidating their structure and stability, has not been performed to date. Herewith we report the results of the combined achiral (UV, fluorimetric, ES-MS, NMR) and chiroptical (CD) spectroscopic studies of the acyclic (**1**) and macrocyclic ligands (**2**, **3**) (Figure 1) as well as their Cu^+ and Ag^+ complexes, corroborated by molecular modeling of some selected complexes. The study was expected to give insight into the topology of the free ligands and complexes, identify the stoichiometry, stability and structure of the complexes, and consequently to shed more light on the origin of stereoselectivity exhibited by this type of bisoxazoline ligands.

After this study was completed, a paper of Walsh et al.[46] appeared reporting on the study of the conformation of flexible macrocyclic catalysts in solution. The results support that bis(sulfonamido) ligands, derived from (*R*,*R*)-1,2-

[a] Eötvös Loránd University, Department of Organic Chemistry
P. O. Box 32, 1518 Budapest, Hungary
[b] Department of Organic Chemistry and Biochemistry, "Rudjer Bošković" Institute,
P. O. Box 180, 10002 Zagreb, Croatia
Fax: (internat.) + 385-1/468-0195
E-mail: sunjic@rudjer.irb.hr
[c] Laboratory of Physical Chemistry, Faculty of Science, University of Zagreb,
P. O. Box 163, 10001 Zagreb, Croatia

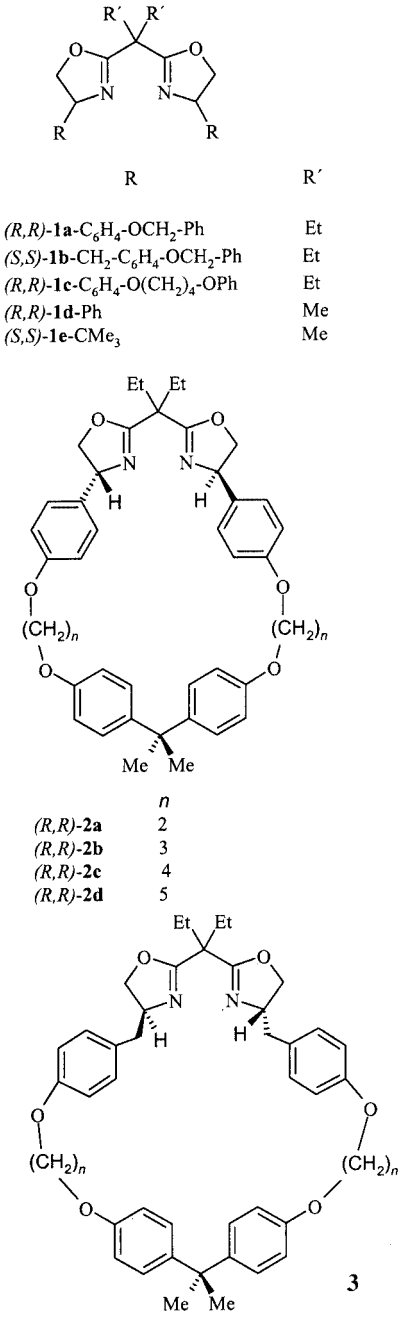

Figure 1. Formulae **1**−**3**

diaminocyclohexane, are bound to the catalytic metal ion in a C_2-symmetric conformation in the transition state of the asymmetric addition of Et_2Zn to benzaldehyde.

Results and Discussion

Spectrometric Studies of Copper(I) and Silver(I) Complexes of 1a and 1b

The copper(I) and silver(I) complexing properties of ligands **1a** and **1b** have been investigated by spectrometric (UV, NMR, and fluorimetric) titrations. The obtained spectrometric data were processed using the SPECFIT program.[47] The addition of Cu^+ into the MeCN solutions of both **1a** and **1b** caused a hyperchromic effect in the corresponding UV spectra (Figure 2). Among several chemically reasonable speciations used in the fitting of the spectrophotometric data, two (set by assuming the presence of $[CuL]^+$ and $[CuL_2]^+$ or $[CuL_2]^+$ and $[Cu_2L_2]^{2+}$; L standing for either **1a** or **1b**) gave satisfactory results. However, the electrospray mass spectrometry (ES-MS) experiments indicated formation of $[CuL]^+$ and $[CuL_2]^+$ complexes and no evidence of the presence of $[Cu_2L_2]^{2+}$ species was observed. The mass spectra of MeCN solutions of Cu^+/**1a** with various $c(Cu^+)/c(\mathbf{1a})$ ratios showed peaks at m/z = 678 $\{[Cu(\mathbf{1a})(MeCN)]_n^{n+}\}$ and 1212 $\{[Cu(\mathbf{1a})_2]^+\}$, while in the case of Cu^+/**1b** peaks were observed at 665 $\{[Cu(\mathbf{1b})]_n^{n+}\}$ and 1268 $\{[Cu(\mathbf{1b})_2]^+$, a very weak signal, presumably due to the fragmentation in the mass spectrometer$\}$. The isotopic abundances of the peaks at m/z = 678 and 665 showed peak separation of 1 Da, supporting the presence of singly charged species, i.e. $[CuL]^+$. The stability constants of the Cu^+ complexes calculated from the spectrophotometric titration data are collected in Table 1. Both, **1a** and **1b** form quite stable 1:1 ($K_{CuL} \approx 10^5$ M^{-1}) and 1:2 ($K_{CuL2} \approx 10^4$ M^{-1}) complexes with Cu^+ in MeCN.

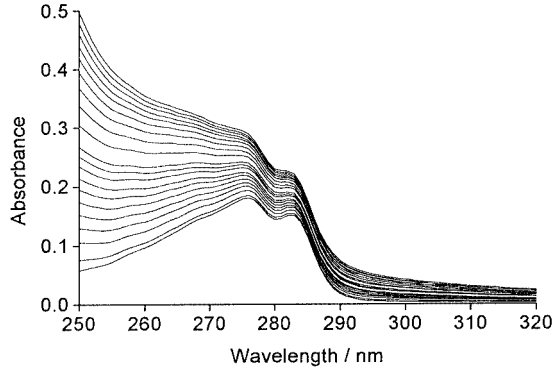

Figure 2. Spectrophotometric titration of **1a** ($c = 5\cdot10^{-5}$ mol·dm^{-3}) with $[(CH_3CN)_4Cu]PF_6$ in MeCN; l = 1 cm; φ = 25 °C; $c(Cu^+)$ = 0 (bottom curve) to $1.7\cdot10^{-4}$ mol·dm^{-3} (top curve); the spectra are corrected for dilution

Table 1. Stability constants of Cu^+ and Ag^+ complexes with **1a** and **1b** in MeCN determined by UV, ^{1}H NMR, and fluorimetric titrations; numbers in parentheses are estimated errors of the last digit

Species	log K[a] UV	^{1}H NMR	Fluorimetry
Cu(**1a**)	5.23(5)		
Cu(**1a**)$_2$	4.2(2)		
Cu(**1b**)	5.07(3)		
Cu(**1b**)$_2$	4.2(1)		
Ag(**1a**)		3.49(7)	3.45(6)
Ag(**1a**)$_2$		3.27(8)	
Ag(**1b**)		3.92(7)	3.63(4)
Ag(**1b**)$_2$		3.1(2)	

[a] $K = [ML_n]/([ML_{n-1}][L])$; M standing for Cu^+ or Ag^+ and L for **1a** or **1b**; n = 1, 2.

The UV spectral changes recorded during the titrations of **1a** and **1b** with Ag^+ in MeCN had qualitatively the same trend as in the case of Cu^+, but were insufficient to enable accurate analysis. Therefore, the formation of Ag^+ complexes was studied by means of ^1H NMR and fluorimetric titrations. The ^1H NMR spectra of **1a** and **1b** in [D$_3$]MeCN are concentration-independent in the range of $2\cdot10^{-3}$ to $2\cdot10^{-2}$ mol·dm^{-3}. The addition of $AgBF_4$ to **1a** up to the ratio $c(Ag^+)/c(\mathbf{1a}) = 0.5$ induced shielding of all protons except that of C(5)−H$_{trans}$ (Figures 3 and 4, a). Further addition [$c(Ag^+)/c(\mathbf{1a}) = 0.5-2.0$] resulted in a deshielding effect. The shielding/deshielding effect changed at the ratio $c(Ag^+)/c(\mathbf{1a}) = 0.5$ indicating the initial formation of $[Ag(\mathbf{1a})_2]^+$ species. Accordingly, the titration data were best fitted with a model including $[Ag(\mathbf{1a})]^+$ and $[Ag(\mathbf{1a})_2]^+$ complexes. The addition of Ag^+ to the solution of **1b** caused deshielding of all proton signals except for those of the methyl groups, which were shielded. However, the data were again best fitted with the model including two complex species, $[Ag(\mathbf{1b})]^+$ and $[Ag(\mathbf{1b})_2]^+$. Comparison of the determined stability constants of Ag^+ complexes with those of Cu^+ complexes (Table 1) shows that the former are more than one order of magnitude less stable for both ligands **1a** and **1b**.

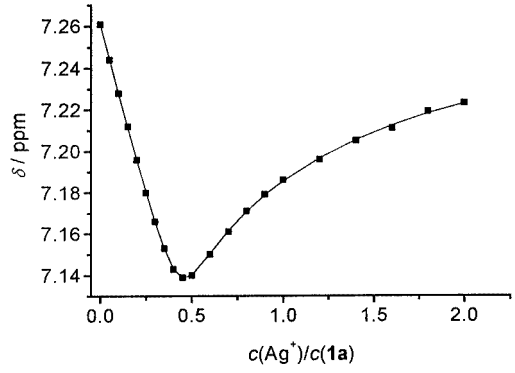

Figure 3. Experimental (dots) and calculated (line) chemical shifts of C(2′)−H of **1a** induced by addition of $AgBF_4$ (solvent: [D$_3$]MeCN)

The stabilities of the **1a**− and **1b**−Ag^+ complexes were also determined by means of fluorimetry. In MeCN ligands **1a** and **1b** exhibited a concentration-independent fluorescence up to the concentration of $2\cdot10^{-5}$ mol·dm^{-3}. The addition of Ag^+ quenched the fluorescence of **1a** and **1b** for ca. 90%. Processing of the titration data gave good fits when only the $[AgL]^+$ complex formation was taken into account for both compounds. The absence of $[AgL_2]^+$ could be explained assuming that fluorimetric properties of this species are similar to those of the free ligand causing insignificant spectral changes. On the other hand, the $[AgL]^+$ complexes exhibit a much weaker emission than free **1a** and **1b**. Consequently, titration data were collected mostly under conditions preferable for 1:1 stoichiometry and only the formation of $[Ag(\mathbf{1a})]^+$ and $[Ag(\mathbf{1b})]^+$ was observed. As can be seen in Table 1, the stability constants of these complexes determined by fluorimetric and ^1H NMR titrations are in

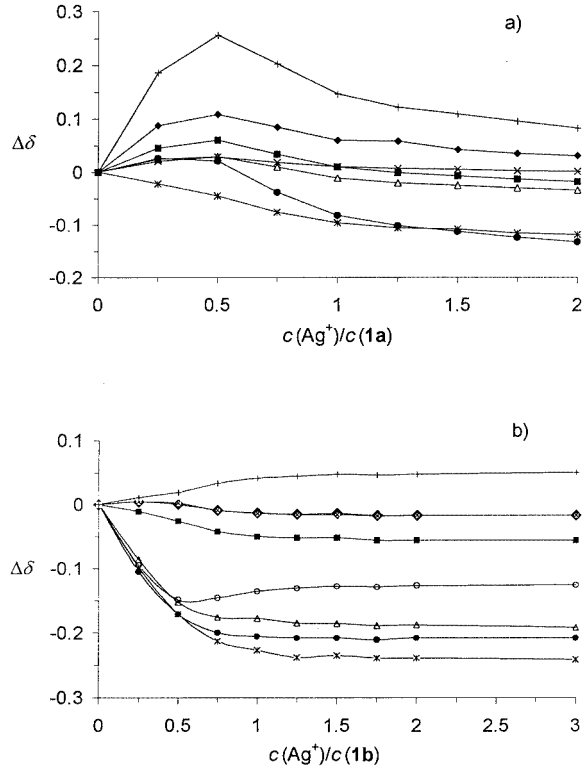

Figure 4. Complexation-induced shifts for **1a**− and **1b**−Ag^+ complexes; a): (+) CH_3; (◆) C(2′)−H; (×) C(4′)−OCH_2; (■) C(3′)−H; (Δ) C(4)−H; (*) C(5)−H$_{trans}$; (•) C(5)−H$_{cis}$; b): (O) C(4)−CH_2

rather good agreement. The stoichiometries of the Ag^+ complexes were additionally confirmed by electrospray mass spectrometry which showed peaks at m/z = 683 $\{[Ag(\mathbf{1a})]_n^{n+}\}$, 1258 $\{[Ag(\mathbf{1a})_2]^+\}$ and 711 $\{[Ag(\mathbf{1b})]_n^{n+}\}$. The exception was the absence of the signals of the $[Ag(\mathbf{1b})_2]^+$ species that could be attributed to the fragmentation in the mass spectrometer and to the equilibrium in solution (see next paragraph and Figure 6). The isotopic abundances of the peaks at m/z = 683 and 711 showed peak separation of 1 Da, corresponding to the singly charged species $[Ag(\mathbf{1a})]^+$ and $[Ag(\mathbf{1b})]^+$, respectively.

Complexation-Induced Shifts (CIS) and NOEs in the ^1H NMR Spectra of the Ag−1a,b Complexes

Structure of Complex $[Ag(1a)_2]^+$

Addition of Ag^+ to **1a** produced significant shifts of all the resonances of **1a**, without line broadening. This indicates fast equilibrium kinetics on the NMR time scale. The observed complexation induced shifts of **1a**, expressed as $\Delta\delta = \delta H i_{lig} - \delta H i_{compl}$ (ppm), were plotted against the $c(Ag^+)/c(\mathbf{1a})$ ratio (Figure 4, a). Ag^+ was added until a ratio of 0.5 was reached for the induced upfield shifts of all **1a** resonances except that of C(5)−H$_{trans}$; further additions of the cation produced downfield shifts of all resonances. A clear maximum at a $c(Ag^+)/c(\mathbf{1a})$ value of 0.5 suggests initial formation of the Ag^+−**1a** complex in a 1:2 stoichiometry which at higher ratios transforms to the 1:1 com-

plex. The methyl groups at the bis(oxazoline) bridge as well as the aromatic C(2′)−H and C(3′)−H groups experience the strongest shielding effects in the $[Ag(\mathbf{1a})_2]^+$ complex, which strongly suggests formation of the tetrahedral Ag^+ complex with the cation bound to 4 nitrogen atoms of the two orthogonally oriented bis(oxazoline) units of the **1a** molecules. The molecular models (see next paragraph and Figure 7, a) shows that in such a complex each bis(oxazoline) unit is located between two phenyl groups of the second ligand molecule. The C(4)-phenyl groups of two ligands end up close to one another, which results in the shielding of C(2′)−H and C(3′)−H. The methyl groups and the C(4)−H and C(5)−H_{cis} atoms of each bis(oxazoline) unit are also shielded by C(4)-phenyl groups of the second ligand. Additional support for the occurrence of such a 1:2 complex comes from the analysis of the NOESY spectrum at a $c(Ag^+)/c(\mathbf{1a})$ ratio of 0.5. The observed NOE interactions are shown in Figure 5. The molecular model of **1a** shows that the majority of the observed NOE crosspeaks could be explained by the favorable distances between respective hydrogen atoms in a single **1a** molecule. However, a clear crosspeak corresponding to NOE interactions between C(4′)−OCH_2 and methyl protons of the bis(oxazoline) bridge is observed. The closest possible distance between these protons in the model of **1a** is ca. 8 Å, well exceeding the limiting value of 4−5 Å, necessary for observation of NOE interactions. The additional proof for the structure of the $[Ag(\mathbf{1a})_2]^+$ complex is also provided by the observed trend of the complexation induced shifts in the $c(Ag^+)/c(\mathbf{1a})$ range of 0.5 and 2.0 (Figure 4, a), where all ligand resonances underwent downfield shifts. This trend could be explained by the disappearance of the $[Ag(\mathbf{1a})_2]^+$ complex and predominant formation of the $[Ag(\mathbf{1a})]^+$ complex. The ligand protons close to the metal center [C(4)−H, C(5)−H and C(2′)−H] of the 1:1 complex should be more deshielded by Ag^+ coordination through bond effects than those in the 1:2 complex, where these effects are distributed between two bis(oxazoline) units. Indeed, deshielding effects were observed for the C(4)−H and C(5)−H protons on going from a 1:2 to a 1:1 complex. However, the strongest deshielding experienced was of the methyl groups on the bridge, being four bonds away of the Ag^+ coordination site (Figure 4, a). Therefore, the latter effect must come from the shielding of the methyl groups in the 1:2 complex by the π-system of the C(4)-phenyl groups of the second molecule of the ligand **1a**.

In contrast to **1a**, the addition of Ag^+ to a CD_3CN solution of **1b** produced deshielding of all proton resonances but only slight shielding of the methyl protons; no clear indication of a 1:2 complex could be observed (Figure 4, b). However, processing of the NMR titration data gave the best fit for the formation of Ag^+−**1b** complexes of 1:2 and 1:1 stoichiometries (see previous paragraph). Comparison of the stability constants determined for Ag^+−**1a** and −**1b** complexes (Table 1) shows that the 1:1 complex of **1b** is around seven times more stable than the 1:2 complex, whereas the equivalent complexes of **1a** are of approximately the same stability, with the 1:1 complex being marginally more stable. This is reflected in the distribution diagrams of Ag^+−**1b** and Ag^+−**1a** systems shown in Figure 6, a, b. At a $c(Ag^+)/c(\mathbf{1b})$ ratio of 0.5 in the first system the concentration of the 1:1 complex is close to twice that of the 1:2 complex (Figure 6, a). For Ag^+−**1a** at this concentration ratio, a 1:2 complex is present in approximately four times higher concentration than the 1:1 complex (Figure 6, b). Consequently, the presence of an Ag^+−**1a** 1:2 complex can be detected through pronounced shielding effects. However, this is not the case for an Ag^+−**1b** system where the complexation induced shifts are dominated by the prevailing 1:1 complex at low and high $c(Ag^+)/c(\mathbf{1b})$ ratios. Nevertheless, the observation of shielding effects of methyl groups on the bridge in **1b** indicates similar structures of 1:2 Ag^+−**1a** and Ag^+−**1b** complexes.

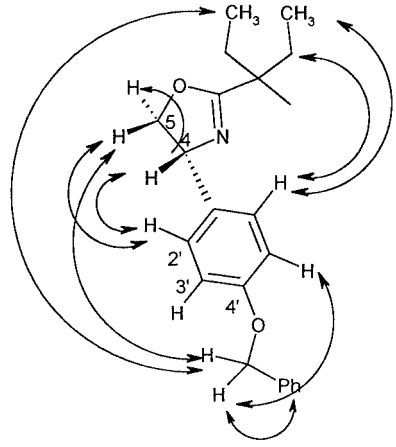

Figure 5. NOE interactions observed in the NOESY spectrum of $[Ag(\mathbf{1a})_2]^+$

Molecular Modeling

The $[Ag(\mathbf{1a})_2]^+$ complex was modeled[48] using 3−5 Å distance constrains between Me and OCH_2Ph protons in accordance with observed NOE interactions. The fully minimized final structure gives N−Ag^+ distances of 1.700, 1.704, 1.704, and 1.710 Å, Me to C(4)−Ph centroid distances of 3.12 Å and Me−OCH_2Ph C−C distances of 3.89 Å, in agreement with observed strong Me shielding and NOEs in the ^1H NMR spectra. The planes containing two bis(oxazoline) units form an angle of 71°, showing pseudotetrahedral coordination (Figure 7, a). The conformational space of the $[Ag(\mathbf{1a})]^+$ complex was then searched using the systematic search procedure at 30° increments for rotations of 8 rotatable bonds of PhO−CH_2Ph fragments. Five different low-energy conformations with energies within 5 kcal/mol were selected and each was fully minimized (Figure 7, b). The calculated structure reveals high conformational mobility of C(4′)−OCH_2Ph fragments and the absence of possible intramolecular aromatic π−π interactions between terminal phenyl groups, is in complete accordance with all experimental results.

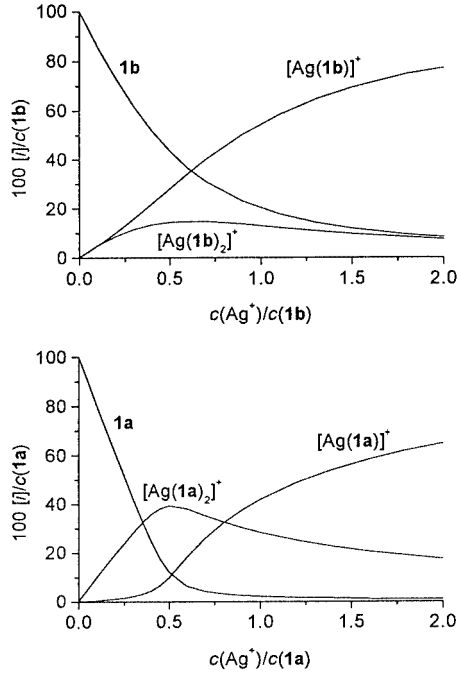

Figure 6. Distribution diagrams of the Ag^+/**1a** and Ag^+/**1b** systems in MeCN; *c* denotes total concentration, while [*i*] stands for equilibrium concentration of *i* = L (**1a** or **1b**), $[ML]^+$ and $[ML_2]^+$ species, respectively

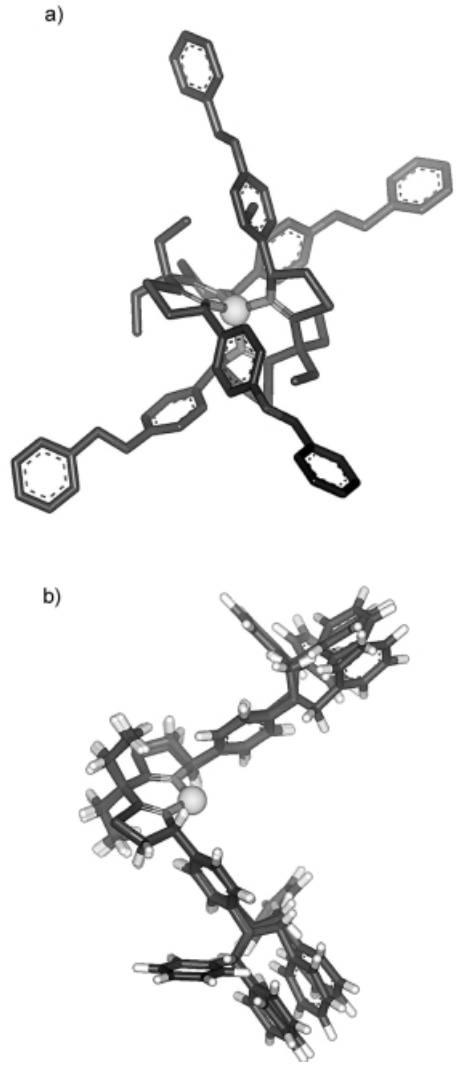

Figure 7. a) Structure of $[Ag(\mathbf{1a})_2]^+$ generated by molecular modeling; hydrogen atoms are omitted for the sake of clarity; b) five superpositioned low-energy conformations of $[Ag(\mathbf{1a})]^+$ generated by the systematic search of the conformational space

Chiroptical (CD) Study of the Acyclic and Macrocyclic Ligands and Their Copper(I) and Silver(I) Complexes

UV and CD Spectra of Acyclic Bis(oxazolines) 1

The short-wavelength band (λ_{max} = 194 nm) can be assigned to the $\pi_{C=N}-\pi^*_{C=N}$ transition in C_2-symmetric **1e**, whereas in **1d** it (λ_{max} = 190 nm) comprises superimposed ^1L_a bands of the phenyl chromophore. The weak long-wavelength band at λ_{max} = 264 nm in the UV spectrum of **1e** is assigned to the conjugated $\pi-\pi^*$ transition, based on the ab initio 6-31G* calculations and analysis of photoelectronic spectra;[49] **1a** and **1b** show similar UV spectra. However, the spectrum of **1d** is strikingly different showing much less intense bands at 264, 258, and 252 nm corresponding to phenyl substituents. The much more intense band observed at 275 nm for **1a** (ε = 4700 $M^{-1}\cdot cm^{-1}$) as compared to the band at 264 nm for **1d** (ε = 360 $M^{-1}\cdot cm^{-1}$), belongs to the phenoxy group on the stereogenic center.

Absolute configuration of acyclic bis(oxazolines) are (*R*,*R*) for **1a**,**c**,**d** and (*S*,*S*) for **1b**,**e**. In the CD spectra of **1a** and **1c** the intense positive band at 205 nm and 204 nm, respectively, is accompanied by a negative band near 192 nm as a sign of exciton interaction between the ^1B_b transitions. Ligand **1c** with an $O(CH_2)_4O$ bridge between the *para*-phenylene and phenyl rings shows some blue-shift and decreased intensity, presumably due to the increased conformational mobility of the side chains. The third ligand with a phenyl group attached to a stereogenic center (**1d**) shows a ca. 10 times decreased negative band at 190 nm ($\Delta\varepsilon < -5\ M^{-1}\cdot cm^{-1}$), and a positive band at 198 nm ($\Delta\varepsilon$ = 46.2 $M^{-1}\cdot cm^{-1}$), only ca 50% less intense then the positive 205-nm band of **1a** and **1c** (Table 2). One can argue that this shift in position and intensity is because of the absence of electron-donating *para*-alkoxy groups in **1d**. In the CD spectra of chiral bis(oxazolines) **1b** and **1e**, having no aromatic substituent at the stereogenic center the bands at 204 and 190 nm, respectively, belong to the π-π^* transition of the C=N chromophore (Table 2). The possibility of a weak exciton interaction between the ^1B_b transitions of the phenyl chromophores cannot be excluded either.

CD Spectra of Macrocyclic Bis(oxazolines) 2 and 3

As expected, in the CD spectrum of (*R*,*R*)-**2a** with oppositely configured chiral centers, as compared to **1b** and **3**, the ^1L_a band (ca. 230 nm) is positive. However, instead of one, there are two extremely strong bands of opposite sign in the ^1B_b region of the spectrum. In the UV spectrum a strong absorption was measured at 195 nm that supports the above

Table 2. CD and UV spectroscopic data for acyclic bis(oxazolines) **1a**−**1e** and their metal complexes in MeCN

Ligand (+ Metal)	Configuration	CD (1st line): λ/nm (Δε/м$^{-1}$ cm^{-1}) UV (2nd line): λ/nm (ε ×10^{-4}/м$^{-1}$ cm^{-1}) ^1B_b	^1L_a, π−π*(C=N)	^1L_b, π−π* or charge transfer
1a	(*R*,*R*)	192 (−73.6), 205 (64.22) 190 (12.1), 196 sh	229.5(41.2) 227 (2.81)	277(−0.79) 275(0.47)
1a + Ag^+, $r_{Ag,1a}$ = 1[a]		192 (−24.0), 205 (15.0)	226 (12.0), 237 (−2.0)	
1a + Cu^+, $r_{Cu,1a}$ = 1		196 (20.5), 204.5 (−13.0)	219.5(7.80), 235 (−34.0)	284.5 (0.20)
1b	(*S*,*S*)	204 (−16.8) 190.5 (12.7), 195.5 sh	≈ 229sh 225.5(2.7)	282 (0.31) 275.5 (0.51)
1b + Ag^+, $r_{Ag,1b}$ = 1[a]		196.5 (1.02)	206 (−4.05), 237 (−1.78)	
1b + Cu^+, $r_{Cu,1b}$ = 1		198 (−7.23)	207 (−4.23), 229.5 (5.83)	281 (−0.69)
1c	(*R*,*R*)	190.5 (−58.2), 204 (64.7) 195(11.7)	229 (37.6) 224.5 (2.75)	277 (−0.94)
1c + Cu^+, $r_{Cu,1c}$ = 1		196 (7.50), 202.5 (−6.98)	213sh 221(10.8) 235(−23.2)	285 (0.095)
1d	(*R*,*R*)	< 190 (< −5), 198 (46.2) < 190 (> 12)	214 (31.9) 207 (3.17)	256 (0.50) 252 (0.043), 258 (0.048), 264 (0.036)
1e	(*S*,*S*)	190 (−10.0) 194 (0.88)	229 sh (−3.13) 222 sh (0.09)	[b] 264 (very weak)

[a] Continuous spectral changes up to $r_{Ag,L} \approx 5$. [b] No band could be measured even with a 1-cm cell.

assignment. Clearly, the strong bands at 204 and 194 nm are due to the *para*-substituted phenyl chromophores attached to the stereogenic centers (Table 3). Notably, a couplet in the ^1B_b band spectral region was observed for **1a** with *para*-alkoxyphenyl substituents but not for **1b** with *para*-alkoxylbenzyl groups.

Regardless of the length of the alkyl chain (n = 2−5), the macrocyclic ligands **2a**−**d** with *para*-alkoxy-substituted phenyl groups attached to the stereogenic centers show CD spectra marked by an almost symmetric exciton couplet in the ^1B_b region. The most intense bands turn up in the spectrum of (*R*)-**2b** (n = 3) [204 nm (90.5 м$^{-1}$·cm^{-1}) and 193 nm (−73.0 м$^{-1}$·cm^{-1}), respectively]. The positive sign of the couplet is compatible with the orientation of the ^1B_b electric transition moment vectors, as discussed in the final section. On the basis of the increased intensity of the ^1L_a bands, a weaker exciton interaction between the ^1L_a transitions cannot be excluded either. However, instead of the expected negative band near 220 nm, the spectra of all macrocycles of type **2** have a positive CD (mostly two positive shoulders) between 225 and 205 nm. The lack of an exciton couplet in the ^1L_a region can be attributed to the nearly parallel orientation of the electric transition vector (Table 3). A positive band appears in the spectrum of **2b** at 220 nm. The complexity of the spectrum clearly indicates that the CD contribution of the "lower half" of the molecule cannot be completely neglected. Because of the increased flexibility, this part of the molecule likely occurs as a mixture of conformers but the dominant one(s) are expected to have the same sign of helical twist of the *para*-alkoxyphenyl rings attached to the $C(Et)_2$ bridge.

The CD spectrum of (*S*,*S*)-**3** is dominated by two negative bands at 203.5 and 228 nm which can be assigned to the ^1B_b and ^1L_a band, respectively, of the *para*-alkoxybenzyl chromophores attached to stereogenic centers. A weak positive and some weaker negative bands are seen in the ^1L_b region of the spectrum (Table 3). In the spectrum of the related acyclic analog (*S*,*S*)-**1b** (R = Bzl−O−Bzl) the cor-

Table 3. CD and UV spectroscopic data for macrocyclic bis(oxazolines) **2a**−**2d** and **3** and their metal complexes in MeCN

Ligand (+ metal)	CD (1st line): λ/nm (Δε/м$^{-1}$ cm^{-1}) UV (2nd line): λ/nm (ε ×10^{-4}/м$^{-1}$ cm^{-1}) ^1B_b	^1L_a, π−π*(C=N)	^1L_b
(*R*,*R*)-**2a**	194 (−71.0), 204 (83.9) 195 (12.6)	≈ 211 sh, ≈ 218 sh, 233 (37.0) 226 (3.18)	283 (−0.61) 276 (0.61)
(*R*,*R*)-**2b**	193 (−73.00), 204 (90.5) 195 (12.9)	220 (25.8), 232 (37.8) 226 (3.27)	284.5 (−0.62) 276 (0.73)
(*R*,*R*)-**2c**	191.5 (−65.5), 204 (75.2) 196 (13.5)	≈ 212 sh, 231 (38.2) 227 (3.40)	277 (−0.83), 290−325 (weak positive bands) 276 (0.77)
(*R*,*R*)-**2d**	191.5 (−66.6), 203.5 (81.2) 196 (13.8)	≈ 211 sh, ≈ 222 sh 232 (37.0) 227 (3.69)	276 (−1.07) 276.5 (0.83)
(*S*,*S*)-**3**	203.5 (−19.8) 194.5 (15.3)	228 (−6.40) 226 (3.66)	277 (−0.072), 282.5 (0.07), 299.5 (−0.05)
+ Ag^+, $r_{Ag,3}$ = 1[a]	203.5 (−14.9)	229 (−6.50)	273.5 sh (−0.29) weak positive bands above 300 nm
+ Cu^+, $r_{Cu,3}$ = 1	209 (−6.80)	≈ 222 sh	261 (0.68), 287 sh, 311.5 (−0.145)

[a] Continuous spectral changes up to $r_{Ag,3} \approx 4$.

responding bands turn up at 204 nm (-16.8 $M^{-1}\cdot cm^{-1}$), 229 nm (sh) and 282 nm. The lack of exciton splitting in the far-UV spectral region of **1b** and **3** is attributed to the difference in geometry and the greater conformational freedom of the *para*-alkoxybenzyl chromophores.

CD Spectra of Copper(I) and Silver(I) Complexes

In order to study their complexation by CD, acyclic ligands **1a−c** as well as the corresponding macrocyclic analogs **2a−d** and **3** were titrated with Ag^+ and Cu^+ ions.

In the spectrum of the acyclic ligand **1a** the exciton couplet of the ^1B_b transition was destroyed by Cu^+ complexing. A strong negative and a weaker positive band replaced the positive ^1L_a band at 229.5 nm (Figure 8). The spectrum showed only small changes between $r_{Cu,\mathbf{1a}} = 1$ and 2 [$r_{M,L} = c(M)/c(L)$] that suggests formation of a 1:1 complex of significant stability, in accordance with the results of the UV titration. Titration of **1a** with Ag^+ ions gave rise to a gradual decrease of the band intensities of the couplet. Significant spectral changes were observed also in the ^1L_a band region: a relatively strong negative band appeared at $r_{Ag,\mathbf{1a}} \geq 1$, while position and intensity of the band at 205 nm in the spectrum of **1a** varied gradually up to $r_{Ag,\mathbf{1a}} = 5$ (Figure 9). This spectral behavior can be explained by the formation of a 1:1 complex of lower stability compared to $[Cu(\mathbf{1a})]^+$. Ligand **1c** showed a similar spectral response to Ag^+ as **1a**. Cu^+ broke the positive couplet at $r_{Cu,\mathbf{1c}} \geq 0.75$ and the titration data indicated formation of a stable 1:1 Cu^+ complex.

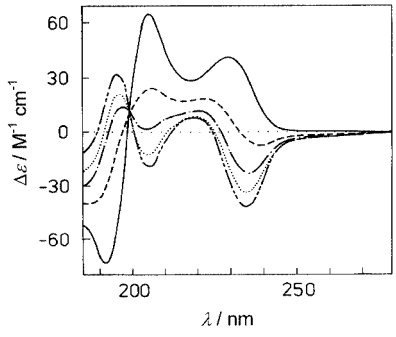

Figure 8. CD spectra of free (*R*,*R*)-**1a** (—), and on addition of Cu^+; 1:0.5 (− − −), 1:0.75 (— · —), 1:1 (·····) and 1:2 (— - - —)

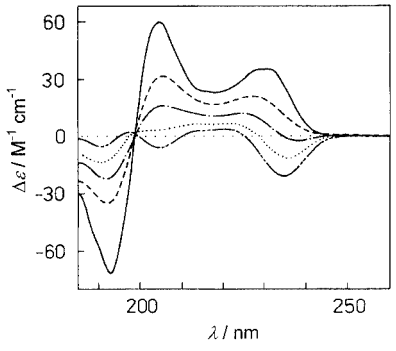

Figure 9. CD spectra of free (*R*,*R*)-**1a** (—), and on addition of Ag^+; 1:0.5 (− − −), 1:1 (— · —), 1:2 (·····), and 1:5 (— - - —)

Titration of **1b** with Ag^+ resulted in gradual spectral changes up to $r_{Ag,\mathbf{1b}} = 5$ (Figure 10). The formation of a 1:1 complex of exceeding stability could not be detected (Table 2). No definite spectral changes were seen between $r_{Ag,\mathbf{1b}} = 5$ and 10. Addition of Cu^+ caused marked spectral changes in the ^1L_a band region. Above $r_{Cu,\mathbf{1b}} = 1$ the main feature of the spectra is a positive band at ca. 230 nm. The formation of no dominant 1:1 complex could be detected (Figure 11).

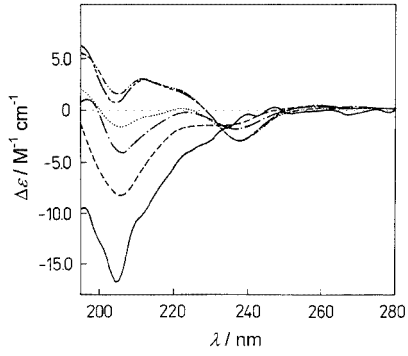

Figure 10. CD spectra of free (*S*,*S*)-**1b** (—), and on addition of Ag^+; 1:0.5 (− − −), 1:1 (— · —), 1:2 (·····), 1:5 (— - - —), and 1:10 (− · · − · ·−)

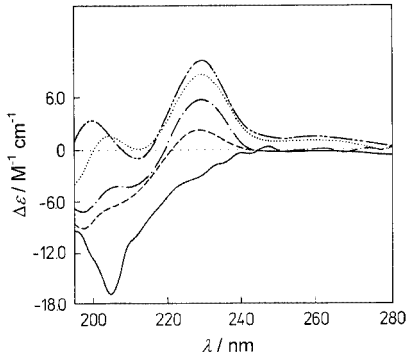

Figure 11. CD spectra of free (*S*,*S*)-**1b** (—), and on addition of Cu^+; 1:0.5 (− − −), 1:1 (— · —), 1:2 (·····), and 1:5 (— - - —)

Macrocyclic ligands **2a−d** showed a similar behavior against Ag^+. The couplet was completely destroyed at an $r_{Ag,\mathbf{2}} \geq 2$ ratio in the case of $n = 2$ and 5 (Figure 12); Cu^+ proved to be a more efficient breaker of the couplet. The spectra reflected no exciton interaction at $r_{Cu,\mathbf{2}} \geq 1$ for ligands **2**, $n = 2$ and 4. At $r_{Cu,\mathbf{2}} > 1$ the ^1L_a band appeared as a pair of negative and positive bands. The ^1B_b couplet, characteristic for the spectra of ligands **2a−d**, was replaced by a shoulder at ca. 210 nm and a pair of weaker blue-shifted oppositely signed bands (Figure 13) at $r_{Cu,\mathbf{2}} > 1$. Increasing the amount of Cu^+ gave rise to further spectral shifts, both below and above 250 nm. This spectral behavior can be interpreted as the consequence of the formation of a 1:1 complex of lower stability. However, the occurrence of complexes of other stoichiometry cannot be excluded either.

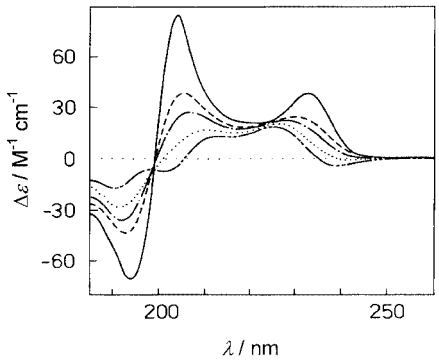

Figure 12. CD spectra of free (*R*,*R*)-**2a** (—), and on addition of Ag^+; 1:0.5 (– – –), 1:1 (— · —), 1:2 (·····), and 1:5 (— - - —)

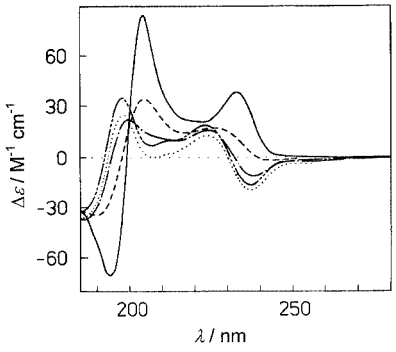

Figure 13. CD spectra of free (*R*,*R*)-**2a** (—), and on addition of Cu^+; 1:0.5 (– – –), 1:1 (— · —), 1:2 (·····), and 1:5 (— - - —)

Addition of Ag^+ to the macrocyclic ligand **3** resulted in an almost continuous spectral change (Figure 14). The position and intensity of the ^1L_a band at 228 nm were less influenced than that of the more intense ^1B_b band at 203.5 nm. Interestingly, the weak negative band at 299.5 nm of **3** with vibrational fine structure changed only to a small extent, while the weak positive band at 282.5 nm of **3** was blue-shifted, changed sign and appeared with increased intensity upon addition of Ag^+ (Table 3). Accordingly, the latter band can be assigned to the n–π* transition of the C=N groups, the nitrogen atoms of which coordinate to a central cation. Addition of Cu^+ to **3** changed the spectrum continuously up to a 2:1 metal/ligand molar ratio ($r_{Cu,3}$ = 2) (Figure 15). Complexing of Cu^+ by **3** gave rise to an increase in the intensity of both long-wavelength bands. The negative band showed a red-shift while the positive one a more definite (> 20 nm) blue-shift (Table 3). The weak negative band at ca. 310 nm of the 1:1 Cu^+ complex likely belongs to the complexed Cu^+ ion. In the far-UV region, both bands showed definite intensity and wavelength shifts up to $r_{Cu,3}$ = 2.

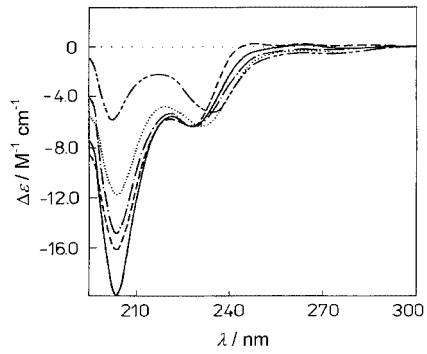

Figure 14. CD spectra of free (*S*,*S*)-**3** (—), and on addition of Ag^+; 1:0.5 (– – –), 1:1 (— · —), 1:2 (·····), and 1:7.8 (— - - —)

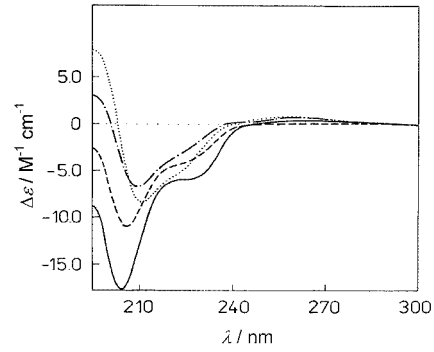

Figure 15. CD spectra of free (*S*,*S*)-**3** (—), and on addition of Cu^+; 1:0.5 (– – –), 1:1 (— · —), and 1:2 (·····)

Conformations of Free Ligand 1a and Its Copper(I) and Silver(I) Complexes in Solution

There are few reports on comparative spectroscopic study of (poly)nitrogen ligands and their metal complexes. In an early study Bosnich has observed the split of π–π* transitions and the nearly equal positive and negative CD bands (couplet) for Zn^{2+} complexes with 1,4-*N*,*N*-bidentate ligands derived from salicylaldehyde (salene), comprising strong conjugated chromophores, and the presence of exciton interaction was demonstrated;[50,51] *transoid* conformation of the free ligand was observed in solution of 6,6′-disubstituted 2,2-bipyridine,[52,53] and its rotation into a *cisoid* conformer on complexation with Co^{2+}, affording a complex of C_2 symmetry, is documented by X-ray analysis of the complex.[54] Williams et al. have recently reported on the enantiopure helicates, complexes of chiral 2,6-bis(oxazolyl)pyridines as tridentate nitrogen ligands and an Ag^+ ion.[44,45] They had observed large changes in the CD spectrum of the ligand upon complex formation. The free ligand shows a weak negative band in the UV region of the spectrum ($\Delta\varepsilon_{296} = -0.4\ M^{-1}\cdot cm^{-1}$), whereas the complex shows a strong positive band ($\Delta\varepsilon_{301} = 10.15\ M^{-1}\cdot cm^{-1}$, for one metal center), corresponding to a new shoulder in the UV/Vis spectrum ($\varepsilon = 1547\ M^{-1}\cdot cm^{-1}$). This CD activity was attributed to a fixed helical conformation of the ligand in the complex, whereas free ligands may adopt different con-

formations that cancel out each other in the CD spectrum. Similar phenomena have been observed for several ligands[55−57] and metal complexes,[44][58][59] and explained by the exciton theory.

For the free bis(oxazoline)-type ligands, the conformation in solution is not known. We have therefore performed MM calculations[48] for an analog of **1a** (for better visualization methyl substituents are attached instead of benzyl), and the most stable conformation found was the helically twisted *transoid* one. In this conformation two phenyl groups form a positive (*P*) twist, and therefore a positive CE for the ^1B_b band is expected, (Scheme 1, Figure 16). In the 1:1 complex Cu^+−**1a** two halves of bis(oxazoline) are fixed in the nearly coplanar *cis* position with two large groups on the stereogenic centers forming a "picket-fence" topology, important for high enantioselectivity in catalytic reactions.[60]

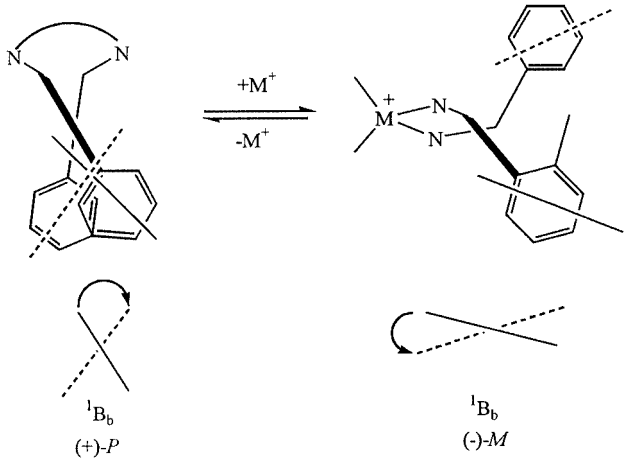

Scheme 1. Schematic presentation of interacting chromophores in **1a** and **1a**−metal complex, and position of their ^1B_b transition vectors in the free ligand and in the complex

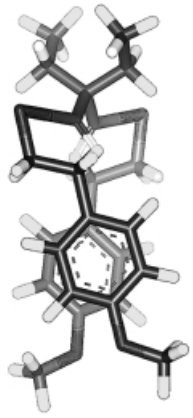

Figure 16. Ball-and-stick model of the non-hydrogen atoms of an analog of **1a** based on MM2 calculations

It is interesting that no such straight-forward change of the CD of **1a** is observed on titration with Ag^+ ions (Figure 9). The inflection point at ca. 195 nm is maintained, revealing formation of an $[Ag(\mathbf{1a})_2]^+$ complex, as confirmed by the NMR titration, but only partial inversion of the sign of the two bands of the couplet is observed. This reveals different influence of Cu^+ and Ag^+ on conformational change of **1a** upon complexation.

Generally, diminished intensity of the short-wavelength band on complexation of **1a** and **1b** is presumably raised by depleting π- and n-electron density in the C=N group on coordination to the metal ion. Since any stronger exciton coupling between two C=N chromophores, which are nonplanar in the free ligand, seems to be absent, coplanarization of the 4π system on complexation should result in an enhanced intramolecular charge transfer, and consequently could influence only the long-wavelength transition band at ca 280 nm.

Conclusion

Combined achiral and chiral spectroscopic study of 1,5-dinitrogen ligands with C_2-symmetic **1a** and **1b** and their copper(I) and silver(I) complexes has shown that they form stable 1:2 metal/ligand complexes, which transform on ulterior addition of metal ions to 1:1 complexes. Modeling experiments indicate pseudotetrahedral arrangement of coordinating N atoms around the central metal ion in the $[Ag(\mathbf{1a})_2]^+$ complex. The stability constants (Table 1) were determined for Cu^+− and Ag^+−**1a** and −**1b** complexes of 1:2 and 1:1 stoichiometries. At low cation/ligand molar ratios, 1:2 complexes are formed with Cu^+. The stabilities of 1:1 complexes exceed those of 1:2 complexes for one order of magnitude. The catalytic 1:1 Cu^+ complexs of **1a** and **1b** used in stereoselective cyclopropanations have stability constants of ca. 10^5 M^{-1} in acetonitrile. A ^1H NMR study of the **1a**−Ag^+ complexation reveals the formation of an $[Ag(\mathbf{1a})_2]^+$ complex with a stability constant of ca. 10^3 M^{-1}. The observed complexation induced shifts and NOEs together with molecular modeling suggest formation of a pseudotetrahedral complex. The comparative CD study of free acyclic (**1a−e**) and macrocyclic (**2a−d**, **3**) ligands and their Cu^+ and Ag^+ complexes provided insight into conformational changes occurring upon formation of the complexes. For free ligands **1a**, **1c** and **2a−d** strong exciton coupling in the ^1B_b region was observed and explained by a positive helicity of the alkoxyphenyl substituents on the stereogenic centers. Addition of a Cu^+ ion destroys the couplet and leads to opposite CE. The latter is the consequence of the ligand conformational change from *transoid* in the free ligand to *cisoid* in the Cu^+ complex and formation of a negative helicity between two alkoxyphenyl substituents. Such spectral properties are not observed for **1b** and **3** possessing more flexible benzyl substituents at the stereogenic centers.

Experimental Section

General: Compounds **1d** and **1e** are commercially available. Preparation of the compounds **2a−d** is reported in ref.[31] and the pre-

paration of the compounds **1a−c** and **3** will be published elsewhere. Reagents were purchased from Aldrich or Fluka and were used without further purification. All solvents were purified and dried according to standard procedures.

Spectrometric Titrations: UV titrations were performed at (25±0.1) °C by means of a Varian Cary 5 spectrophotometer equipped with a thermostating device. The spectral changes of **1a** and **1b** solutions ($c = 5{\cdot}10^{-5}$ mol·dm^{-3}) in MeCN were recorded upon stepwise addition of copper(I) ions directly into the measuring quartz cell (1 cm). Copper(I) ions were added as $[(CH_3CN)_4Cu]PF_6$ solution ($c = 2.6{\cdot}10^{-4}$ mol dm^{-3}) in MeCN. Spectra were sampled at 1-nm intervals. Fluorimetric titrations (λ_{exc} = 277 nm, λ_{em} = 285−330 nm, filter = 290 nm) were carried out using a Perkin−Elmer LS-50 spectrofluorimeter at ambient temperature. The MeCN solutions of **1a** and **1b** ($c = 1.32{\cdot}10^{-5}$ mol·dm^{-3}) were placed in the measuring quartz cell (1 cm) and titrated with an MeCN solution of $AgBF_4$ (c = 0.0116 mol·dm^{-3} and 0.116 mol·dm^{-3}). ^{1}H NMR titrations of **1a** and **1b** were performed at ambient temperature in CD_3CN (data taken as Δδ/ppm according to the signal of solvent used as internal standard) with Varian Gemini 300 MHz [c(**1a**) = 0.02 mol·dm^{-3}, V_0 = 0.5 mL, $c(AgBF_4)$ = 0.1 mol·dm^{-3}] and a Bruker 500 MHz instruments [c(**1b**) = 0.001 mol·dm^{-3}, V_0 = 0.5 mL, $c(AgBF_4)$= 0.005 mol·dm^{-3}]. Aliquots of the metal ion solution were added into the solution of the ligand in an NMR probe with Hamilton syringes. The obtained spectrometric data were processed using the SPECFIT program.[47] CD titrations: UV/Vis and CD spectra were recorded in acetonitrile with a Jobin−Yvon VI dichrograph calibrated with epiandrosterone. The ligands were titrated with $AgBF_4$ and $[(CH_3CN)_4Cu]PF_6$, respectively, in both the long-wavelength (> 240 nm) and short-wavelength UV regions. Measurements were performed at room temperature in 0.02- and 0.1-cm cells. The spectral changes of ligand solutions ($c = 4.5{-}6.0{\cdot}10^{-4}$ mol·dm^{-3}) in MeCN were recorded upon addition of silver(I) ($c = 2.0{\cdot}10^{-2}$ mol·dm^{-3}) and copper(I) ($c = 8.0{\cdot}\ 10^{-3}$ mol·dm^{-3}) solutions in MeCN, respectively.

Molecular Modeling: The metal-free bis(oxazoline) ligand was docked on the complex Ag^+/**1d** and the low-energy structure obtained modified by adding two additional N−heavy atom bonds to obtain the tetracoordinated complex. The metal−N bonds of 2.18 Å were used as distance constraints and the complex was fully minimized. In the next step, a benzyloxy group was attached in the *para* position to the stereogenic center of each phenyl ring to generate the 1:2 Ag^+/**1a** complex. The molecular modeling of the 1:2 Ag^+/**1a** complex and the search of the conformational space of the 1:1 Ag^+/**1a** complex was performed using the SYBYL molecular modeling software, version 6.3 of TRIPOS Inc. 4,4′-Diphenylbis(oxazoline) complex **1d**−Ag^+ was constructed using the Builder module. Instead of the Ag^+ ion, a heavy atom parameter available in the SYBYL package was used together with N−heavy atom distance constraints of 2.18 Å corresponding to an N−Ag^+ bond length found in the X-ray structure of some tetracoordinated Ag^+−bis(oxazoline) helicates.[44] The Gasteiger−Hückel charges were used with +1 formal charge of the heavy atom and the complex was minimized.

Acknowledgments

The financial support from the Croatian Ministry of Science and Technology (Program 009807) and the Hungarian Scientific Research Fund (OTKA Nr.T034866) is gratefully acknowledged.

[1] *Comprehensive Asymmetric Catalysis* (Eds.: E. N. Jacobsen, A. Pfaltz, H. Yamamoto), Springer, Berlin, Heidelberg, **1999**.
[2] R. Noyori, *Asymmetric Catalysis in Organic Synthesis*, J. Wiley & Sons, New York, **1993**.
[3] F. Fache, E. Schulz, M. L. Tommasino, M. Lemaire, *Chem. Rev.* **2000**, *100*, 2159−2231.
[4] A. K. Ghosh, P. Mathivanan, J. Cappiello, *Tetrahedron: Asymmetry* **1998**, *9*, 1−45.
[5] A. Pfaltz, *Acta Chem. Scand.* **1996**, *50*, 189−194.
[6] R. E. Lowenthal, A. Abiko, S. Masamune, *Tetrahedron Lett.* **1990**, *31*, 6005−6008.
[7] R. E. Lowenthal, S. Masamune, *Tetrahedron Lett.* **1991**, *32*, 7373−7376.
[8] D. A. Evans, K. A. Woerpel, M. M. Hinman, M. M. Faul, *J. Am. Chem. Soc.* **1991**, *113*, 726−728.
[9] D. A. Evans, K. A. Woerpel, M. J. Scott, *Angew. Chem. Int. Ed. Engl.* **1992**, *31*, 430−432.
[10] C. Pique, B. Fahndrich, A. Pfaltz, *Synlett* **1995**, 491−492.
[11] O. Hoarau, H. Ait-Haddou, M. Castro, G. G. A. Balavoine, *Tetrahedron: Asymmetry* **1997**, *8*, 3755−3764.
[12] D. A. Evans, M. M. Faul, M. T. Bilodeau, B. A. Anderson, D. M. Barnes, *J. Am. Chem. Soc.* **1993**, *115*, 5328−5329.
[13] K. B. Hansen, N. S. Finney, E. N. Jacobsen, *Angew. Chem. Int. Ed. Engl.* **1995**, *34*, 676−678.
[14] A. S. Gokhale, A. B. E. Minidis, A. Pfaltz, *Tetrahedron Lett.* **1995**, *36*, 1831−1834.
[15] D. A. Evans, S. J. Miller, T. Lectka, *J. Am. Chem. Soc.* **1993**, *115*, 6460−6461.
[16] D. A. Evans, D. M. Barnes, *Tetrahedron Lett.* **1997**, *38*, 57−58.
[17] D. A. Evans, E. A. Shaughnessy, D. M. Barnes, *Tetrahedron Lett.* **1997**, *38*, 3193−3196.
[18] D. A. Evans, J. S. Johnson, *J. Org. Chem.* **1997**, *62*, 786−787.
[19] D. A. Evans, J. S. Johnson, C. S. Burgey, K. R. Campos, *Tetrahedron Lett.* **1999**, *40*, 2879−2882.
[20] D. A. Evans, J. A. Murry, M. C. Kozlowski, *J. Am. Chem. Soc.* **1996**, *118*, 5814−5815.
[21] A. Bernardi, G. Colombo, C. Scolastico, *Tetrahedron Lett.* **1996**, *37*, 8921−8924.
[22] D. A. Evans, T. Rovis, M. C. Kozlowski, J. S. Tedrow, *J. Am. Chem. Soc.* **1999**, *121*, 1994−1995.
[23] N. Gathergood, W. Zhaang, K. A. Jorgensen, *J. Am. Chem. Soc.* **2000**, *122*, 12517−12522.
[24] A. E. Russell, S. P. Miller, J. P. Morken, *J. Org. Chem.* **2000**, *65*, 8381−8383.
[25] D. Mueller, G. Umbricht, B. Weber, A. Pfaltz, *Helv. Chim. Acta* **1991**, *74*, 232−240.
[26] P. von Matt, G. C. Lloyd-Jones, A. B. E. Minidis, A. Pfaltz, L. Macko, M. Neuburger, M. Zehnder, H. Ruegger, P. S. Pregosin, *Helv. Chim. Acta* **1995**, *78*, 265−284.
[27] O. Hoarau, H. Ait-Haddou, J.-C. Daran, D. Cramailere, G. G. A. Balavoine, *Organometallics* **1999**, *18*, 4718−4723.
[28] J. Wu, R. Radinov, N. A. Porter, *J. Am. Chem. Soc.* **1995**, *117*, 11029−11030.
[29] M. Nakamura, M. Arai, E. Nakamura, *J. Am. Chem. Soc.* **1995**, *117*, 1179−1180.
[30] S. Hanessian, R.-Y. Yang, *Tetrahedron Lett.* **1996**, *37*, 8997−9000.
[31] T. Portada, M. Roje, Z. Raza, V. Čaplar, M. Žinić, V. Šunjić, *Chem. Commun.* **2000**, 1993−1994.
[32] Z. Raza, S. Đaković, V. Vinković, V. Šunjić, *Croat. Chem. Acta* **1996**, *69*, 1545−1559.
[33] S. Đaković, L. Liščić-Tumir, S. I. Kirin, V. Vinković, Z. Raza, A. Šuste, V. Šunjić, *J. Mol. Catal. A* **1997**, *118*, 27−31.
[34] V. Šunjić, D. Šepac, B. Kojić-Prodić, R. Kiralj, K. Mlinarić-Majerski, V. Vinković, *Tetrahedron: Asymmetry* **1993**, *4*, 575−590.
[35] S. I. Kirin, V. Vinković, V. Šunjić, *Chirality* **1995**, *7*, 115−120.
[36] Zs. Majer, M. Hollosi, S. I. Kirin, V. Šunjić, *Chirality* **1996**, *8*, 244−248.
[37] M. Onishi, K. Isagawa, *Inorg. Chim. Acta* **1991**, *179*, 155−156.

[38] C. Bolm, K. Weickhardt, M. Zehnder, T. Rauff, *Chem. Ber.* **1991**, *124*, 1173−1180.
[39] J. Hall, J.-M. Lehn, A. DeCian, J. Fischer, *Helv. Chim. Acta* **1991**, *74*, 1−6.
[40] H. Nishiyama, K. Aoki, H. Itoh, T. Iwamura, N. Sakata, O. Kurihara, Y. Motoyama, *Chem. Lett.* **1996**, 1071−1072.
[41] S. Kanemasa, Y. Oderaotoshi, H. Yamamoto, J. Tanaka, E. Wada, D. P. Curran, *J. Org. Chem.* **1997**, *62*, 6454−6455.
[42] R. P. Singh, *Synth. React. Inorg. Met.-Org. Chem.* **1997**, *27*, 155−166.
[43] C. J. Fahrni, A. Pfaltz, M. Neuburger, M. Zehnder, *Helv. Chim. Acta* **1998**, *81*, 507−524.
[44] C. Provent, S. Hewage, G. Brand, G. Bernardinelli, L. J. Charbonniere, A. F. Williams, *Angew. Chem. Int. Ed. Engl.* **1997**, *36*, 1287−1289.
[45] C. Provent, E. Rivara-Minten, S. Hewage, G. Brunner, A. F. Williams, *Chem. Eur. J.* **1999**, *5*, 3487−3494.
[46] J. Balsells, J. M. Betancort, P. J. Walsh, *Angew. Chem. Int. Ed.* **2000**, *39*, 3428−3430.
[47] R. A. Binstead, A. D. Zuberbühler, *SPECFIT Program, Global Least-Squares Fitting by Factor Analysis and Marquart Minimization*, Spectrum Software Associates, Chapel Hill, NC, **1994**.
[48] *SYBYL, Molecular Modeling Software*, version 6.3, TRIPOS Inc.
[49] B. Kovać, L. Klasinc, Z. Raza, V. Šunjić, *J. Chem. Soc., Perkin. Trans. 2* **1999**, 2455−2459.
[50] S. F. Mason, *Quart. Rev.* **1963**, *17*, 20−66.
[51] B. Bosnich, *J. Am. Chem. Soc.* **1968**, *90*, 627−632.
[52] A. Castelano, H. Guenther, S. Ebensole, *J. Phys. Chem.* **1965**, *12*, 4166−4176.
[53] T. McL. Spotswood, C. I. Tanzer, *Aust. J. Chem.* **1967**, *20*, 1227−1242.
[54] C. Bolm, "Optically Active Bipyridines in Enantioselective Catalysis" in: *Organic Synthesis via Organometallics* (Eds.: K. H. Doetz, R. W. Hoffmann), Vieweg, Braunschweig, **1991**, pp. 223−240.
[55] N. C. Fletcher, F. R. Keene, M. Ziegler, H. Stoeckli-Evans, H. Viebrock, A. von Zelewsky, *Helv. Chim. Acta* **1996**, *79*, 1192−1202.
[56] N. Harada, K. Nakanishi, *Circular Dichroic Spectroscopy. Exciton Coupling in Organic Chemistry*, University Science Books, Mill Villay, CA, **1983**.
[57] V. Buss, S. Falzewski, K. Kolster, *J. Org. Chem.* **1999**, *64*, 1071−1073.
[58] O. Mamula, A. von Zelewsky, G. Bernardinelli, *Angew. Chem. Int. Ed.* **1998**, *37*, 290−293.
[59] O. Mamula, A. von Zelewsky, T. Bark, H. Stoeckli-Evans, A. Neels, G. Bernardinelli, *Chem. Eur. J.* **2000**, *6*, 3575−3585.
[60] M. P. Doyle, "Asymmetric Cyclopropanation", in: *Catalytic Asymmetric Synthesis* (Ed.: I. Ojima), VCH, **1993**, pp. 63−99.

Received January 8, 2002
[I02008]

Vanadium(IV/V) Complexes Containing $[VO]^{2+}$, $[VO]^{3+}$, $[VO_2]^+$ and $[VO(O_2)]^+$ Cores with Ligands Derived from 2-Acetylpyridine and *S*-Benzyl- or *S*-Methyldithiocarbazate

Mannar R. Maurya,*[a] Shilpa Khurana,[a] Wenjian Zhang,[b] and Dieter Rehder[b]

Keywords: Malonate / Oxo transfer / Sulfur ligands / Hydrazones / Vanadium

Vanadium complexes containing $[VO]^{2+}$, $[VO]^{3+}$, $[VO_2]^+$ and $[VO(O_2)]^+$ cores with ligands (LH) derived from 2-acetylpyridine and *S*-benzyldithiocarbazate (Hacpy-sbdt, **I**) or *S*-methyldithiocarbazate (Hacpy-smdt, **II**) are introduced. The dioxovanadium(V) complexes $[VO_2L]$ [HL = **I** (**2**), **II** (**5**)] were isolated from the reaction between LH and $[VO(acac)_2]$ in the presence of air and KOH in dry methanol. Treatment of **II** with aerated $[VO(acac)_2]$ in *wet* methanol yielded the malonato complex [VO(acpy-smdt)mal] (**6**), with the malonate ligand originating from acetylacetonate. Under anaerobic reaction conditions, LH replaced one of the acac(1−) ligands to yield the oxovanadium(IV) complexes [VO(acac)L] [HL = **I** (**1**), **II** (**4**)]. Treatment of these complexes with H_2O_2, catechol or benzhydroxamic acid gave rise to oxo(peroxo)vanadium complexes $[VO(O_2)L]$ [HL = **I** (**3**), **II** (**7**)], catecholato complexes [VOL(cat)] [HL = **I** (**8**), **II** (**9**)] or benzhydroxamato complexes [VOL(bha)] [HL = **I** (**10**), **II** (**11**)]. Compounds **3** and **7** were capable of transferring an oxo group to PPh_3. In the presence of L-ascorbic acid under aerobic conditions, **8** and **11** were converted into **2** and **5**, possibly through intermediate reduction. Acidification of **2** with HCl in methanol afforded a hydroxo(oxo) complex. The crystal and molecular structures of **2** and **6** were determined, confirming the *NNS* (enethiolate) binding mode of L^-, and the bidentate coordination of the malonate ligand in **6**. The geometrical arrangement of the ligand set in **2** is intermediate between a trigonal bipyramid and a tetragonal pyramid.

(© Wiley-VCH Verlag GmbH, 69451 Weinheim, Germany, 2002)

Introduction

The coordination chemistry of oxovanadium(IV), oxovanadium(V) and dioxovanadium(V) has acquired new interest as these complexes can serve as good models for vanadium-containing biomolecules.[1−3] Potential therapeutic applications,[4−6] studies on the metabolism and detoxification of vanadium compounds under physiological conditions,[7] and the stability and speciation of vanadium complexes in biofluids[8] have further influenced the study of the coordination chemistry of vanadium. In this context, vanadium complexes containing thiofunctional ligands have received less attention.[9−11] Complexes with *OS* coordination [such as bis(1-oxy-2-pyridinethiolato)oxovanadium(IV)] have been found to be orally active insulin mimetic agents in the treatment of diabetic model animals.[12] In addition, coordination of a sulfur atom to the vanadium centre has been well established in vanadium nitrogenase found in nitrogen-fixing bacteria of the genus *Azotobacter*.[13,14] Vanadium complexes that model parts of the structure of the enzyme have been designed (cf. ref.[9]). Vanadium−sulfur coordination is also of interest for the inhibition of phosphatases (interaction between the vanadium centre and the active site cysteinate)[15,16] and the enantioselective oxidation of prochiral thioethers to sulfoxide by vanadate-dependent haloperoxidases.[17,18]

Unless bulky groups are attached to the ligand to provide sufficient steric hindrance, interaction between monobasic tridentate ligands and $[VO(acac)_2]$ under aerobic conditions generally produces dimeric, pseudo-octahedral complexes with the $[VO_2]_2$ core.[19−22] In the current work, we have employed less bulky ligands (cf. Scheme 1) with an *NNS* donor set, which stabilise monomeric dioxovanadium(V) ($[VO_2]^+$) complexes with the vanadium centre in a tetragonal-pyramidal array, strongly distorted towards a trigonal bipyramid. Other complexes, with $[VO]^{2+}$, $[VO]^{3+}$ and $[VO(O_2)]^+$ cores, have also been prepared. The hitherto unknown coordination of malonate to oxovanadium(V) has been achieved by the unprecedented preparation of the complex [VO(acpy-smdt)mal] by oxidative removal of the methyl groups from one of the acetylacetonates in $[VO(acac)_2]$ in the presence of the supporting *NNS* ligand. In all cases reported here, the ligands coordinate from their thioenolate form; cf. refs.[23−31] for other examples of stable oxo- and dioxovanadium(V) complexes with this coordination mode. Apart from their interesting coordination beha-

[a] Department of Chemistry, Indian Institute of Technology, Roorkee 247 667, India
[b] Institut für Anorganische und Angewandte Chemie, Universität Hamburg
20146 Hamburg, Germany

viour, our motivation to use these particular ligands (**I** and **II**, Scheme 1) also arises from the recently assessed antiamoebic activity of their ruthenium(II) and palladium(II) complexes against *Entamoeba histolytica* (strain HK-9).[32,33]

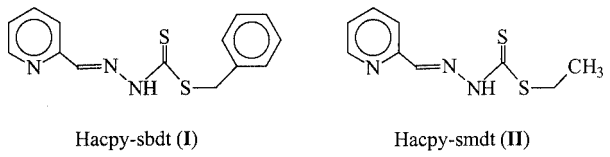

Scheme 1

Results and Discussion

Synthesis, Reactivity and Solid-State Characteristics

Direct treatment of the ligands Hacpy-sbdt (**I**) and Hacpy-smdt (**II**) (Scheme 1) with methanolic solutions of $[VO(acac)_2]$ in equimolar amounts under anaerobic conditions provided the oxovanadium(IV) complexes [VO(acac)L] [**1** and **4**, Scheme 2, Equation (1)].

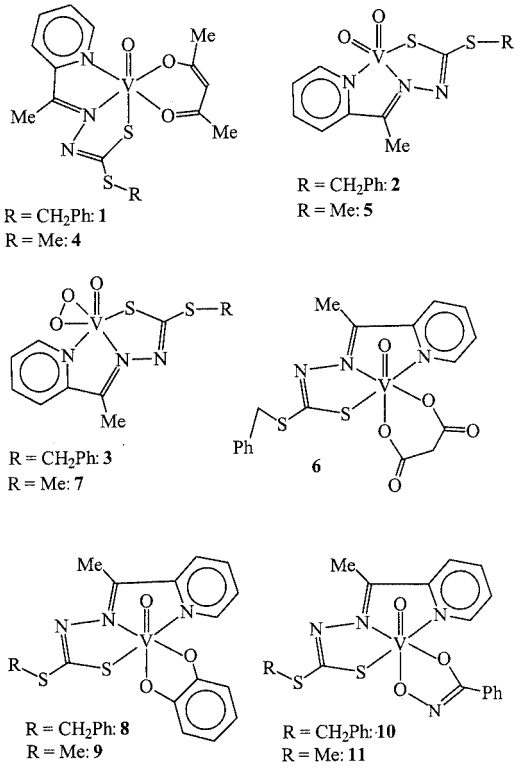

Scheme 2

Solutions of $[VO(acac)_2]$ in organic solvents undergo rather slow oxidation under aerobic conditions.[34] In methanolic KOH, however, oxidation occurred within 8−10 h, possibly to a complex of composition $K[VO_2(acac)_2]$ [Equation (2a)]. Treatment of **I** or **II** with this species, generated in situ, under aerobic conditions yielded the monomeric pentacoordinated dioxovanadium(V) complexes **2** and **5**, respectively [Scheme 2, Equation (2b)]. A pentacoordinated vanadium(V) complexes with the dioxo groupe may have either tetragonal-pyramidal or trigonal-bipyramidal coordination geometry. The former tend to dimerise through oxo bridges to produce pseudo-octahedral coordination environments.[19] With bulky substituents on the ligand, the formation of tetragonal-pyramidal species, and thus dimerisation, can be circumvented, and trigonal-bipyramidal species can be stabilised.[20−22] The procedure employed here, refraining from bulky substituents, directly provided monomeric, square-pyramidal complexes.

$$\underset{\mathbf{1,4}}{[VO(acac)_2]} + HL \rightarrow \underset{\mathbf{1,4}}{[VO(acac)L]} + Hacac \quad (1)$$

$$2[VO(acac)_2] + 2KOH + \tfrac{1}{2}O_2 \rightarrow \text{“}2K[VO_2(acac)_2]\text{”} + H_2O \quad (2a)$$

$$K[VO_2(acac)_2] + HL \rightarrow \underset{\mathbf{2,5}}{[VO_2L]} + Hacac + Kacac \quad (2b)$$

On addition of a few drops of water to solutions of $[VO(acac)_2]$ in methanol plus KOH, followed by addition of Hacpy-smdt in the presence of air, the malonato(oxo)vanadium(V) complex **6** was obtained. This unprecedented formation of malonate from acetylacetonate was apparently a consequence of oxidative removal of the methyl groups from acetylacetone, activated by coordination, and catalysed by OH^-, as depicted in Scheme 3. The malonic acid thus formed ultimately reacted with the oxidised vanadium species in the presence of Hacpy-smdt to give **6**.

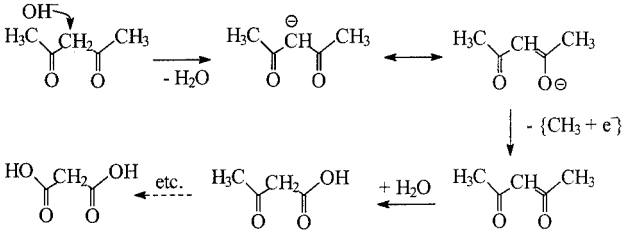

Scheme 3

Complexes **1**, **2**, **4** and **5** served as good starting materials for the preparation of other oxovanadium(V) complexes. For example, **1** and **4** were oxidised in the presence of the strong oxidant H_2O_2 to give the corresponding oxo(peroxo)vanadium(V) complexes, as shown by Equations (3) and (4).

$$\underset{\mathbf{1}}{2[VO(acac)(acpy\text{-}sbdt)]} + 3H_2O_2 \rightarrow \underset{\mathbf{3}}{2[VO(O_2)(acpy\text{-}sbdt)]} + 2Hacac + 2H_2O \quad (3)$$

$$\underset{\mathbf{4}}{2[VO(acac)(acpy\text{-}smdt)]} + 3H_2O_2 \rightarrow \underset{\mathbf{7}}{2[VO(O_2)(acpy\text{-}smdt)]} + 2Hacac + 2H_2O \quad (4)$$

These complexes could also be prepared from the corresponding dioxo species as shown for **3** by Equation (5).

$$\underset{\mathbf{2}}{[VO_2(acpy\text{-}sbdt)]} + H_2O_2 \rightarrow \underset{\mathbf{3}}{[VO(O_2)(acpy\text{-}sbdt)]} + H_2O \quad (5)$$

Treatment of catechol or benzhydroxamic acid with **1** and **4** under aerobic conditions resulted in the formation of the mixed chelate oxovanadium(V) complexes **8**, **9**, **10** and **11**, as represented by the general Equations (6) and (7). For proposed structures, cf. Scheme 2.

$$2[VO(acac)L] + 2H_2cat + \tfrac{1}{2}O_2 + 2H^+ \rightarrow 2[VO(cat)L] + 2Hacac + H_2O \quad (LH = \mathbf{I}: \mathbf{8}; LH = \mathbf{II}: \mathbf{9}) \quad (6)$$

$$2[VO(acac)L] + 2H_2bha + \tfrac{1}{2}O_2 + 2H^+ \rightarrow 2[V^{V}OL(bha)] + 2Hacac + H_2O \quad (LH = \mathbf{I}: \mathbf{10}; LH = \mathbf{II}: \mathbf{11}) \quad (7)$$

Analytical and IR spectroscopic data of the complexes are included in the Exp. Sect. All complexes were fairly soluble in CH_3CN, DMF and DMSO; peroxo complexes were sparingly soluble in CH_3CN only. Complexes **1** and **4** were paramagnetic with magnetic moments of $\mu = 2.10$ and 2.16 BM, respectively, while all other complexes were diamagnetic, as to be expected for $3d^0$ systems.

Thermogravimetric Studies

The mixed-ligand complexes **1**, **4** and **8**−**11** lost about 1−3% weight (due to residual water of crystallisation) between 80 and 135 °C. The weight loss in the temperature range 195−225 °C corresponded to the loss of acac, cat or bha, minus one oxygen atom, thus giving rise to the formation of dioxo intermediates as shown by Equation (8) for **1** and **4**.

$$[V^{IV}O(acac)L] \rightarrow [V^{V}O_2L] + \{acac - O\} \quad (8)$$

The peroxo complexes **3** and **7** lost some weight (about 3%) below 150 °C. The main decomposition process took place above 180 °C, and corresponded to the simultaneous loss of an oxygen atom plus part of the ligand, possibly forming $[VO_2L']$ and $[VOL']$ intermediates, where L′ is a fragment of L. The dioxo complexes **2** and **5** decomposed in three major steps. Between 190 and 330 °C the weight loss corresponded to $SCH_2C_6H_5$ (in **2**) or SCH_3 (in **5**), followed by a second step between 330 and 500 °C corresponding to the loss of the SCN group. On further heating, the remaining residue decomposed to yield V_2O_5 as the end product. The final residue always weighed a little more than expected, probably due to incomplete oxidation of the end-product.

Structure Descriptions

The molecular structure of $[VO_2(acpy\text{-}sbdt)]$ (**2**) together with the atom-numbering scheme is shown in Figure 1, with selected bond lengths and angles in Table 1. The geometry of this neutral, five-coordinated mononuclear complex can be described either in terms of a trigonal bipyramid, distorted towards a tetragonal pyramid, or in terms of a tetragonal pyramid, distorted towards a trigonal bipyramid. The τ value, which is 0 for ideal tetragonal and 1 for ideal trigonal arrangements, amounts to $\tau = (N1-V-S1 - O2-V-N2)/60 = 0.47$. This is significantly more than in the related thiohydrazone complex [VO(OEt)(*ONS*)], in which $\tau = 0.27$.[31] The two alternative views are depicted in Scheme 4. In both views, the distortion comes about from the steric requirements resulting from the small bite angles of the bicyclic structure constituted by the two five-membered chelate rings.

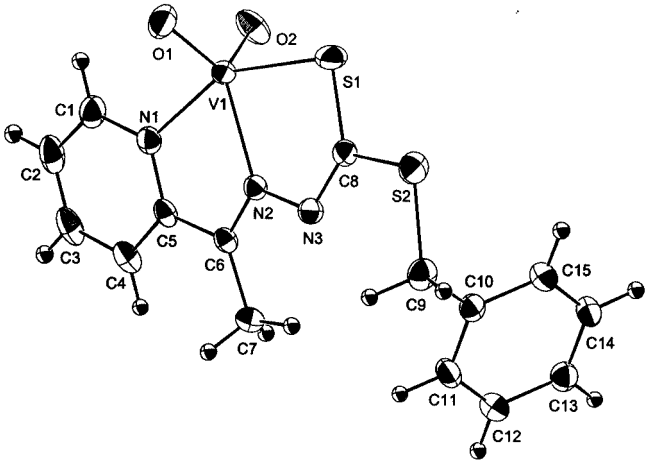

Figure 1. ORTEP plot (30% probability level) of $[VO_2(acpy\text{-}sbdt)]$ (**2**) with atom-numbering scheme

Table 1. Bond lengths [Å] and bond angles [°] for $VO_2(acpy\text{-}sbdt)$ (**2**)

Bond	Length	Bond	Angle
V(1)−O(1)	1.6148(13)	O(1)−V(1)−O(2)	109.58(8)
V(1)−O(2)	1.6152(13)	O(1)−V(1)−N(1)	97.97(6)
V(1)−N(1)	2.1038(14)	O(2)−V(1)−N(1)	95.98(6)
V(1)−N(2)	2.1454(14)	O(1)−V(1)−N(2)	127.49(6)
V(1)−S(1)	2.3852(5)	O(2)−V(1)−N(2)	122.70(7)
S(1)−C(8)	1.7273(17)	N(1)−V(1)−N(2)	73.47(5)
S(2)−C(8)	1.7406(16)	O(1)−V(1)−S(1)	100.15(5)
S(2)−C(9)	1.8113(19)	O(2)−V(1)−S(1)	99.25(5)
N(1)−C(1)	1.338(2)	N(1)−V(1)−S(1)	150.79(4)
N(1)−C(5)	1.350(2)	N(2)−V(1)−S(1)	77.32(3)
N(2)−C(6)	1.2991(19)	C(8)−S(1)−V(1)	98.61(5)
N(2)−N(3)	1.3904(17)	C(8)−S(2)−C(9)	103.22(8)
N(3)−C(8)	1.294(2)	C(1)−N(1)−C(5)	119.69(16)
		C(1)−N(1)−V(1)	122.07(13)
		C(5)−N(1)−V(1)	117.75(10)
		C(6)−N(2)−N(3)	115.40(13)
		C(6)−N(2)−V(1)	119.42(10)
		N(3)−N(2)−V(1)	125.07(10)
		N(3)−C(8)−S(1)	126.62(13)
		N(3)−C(8)−S(2)	119.95(13)
		S(1)−C(8)−S(2)	113.42(9)
		C(10)−C(9)−S(2)	115.12(12)

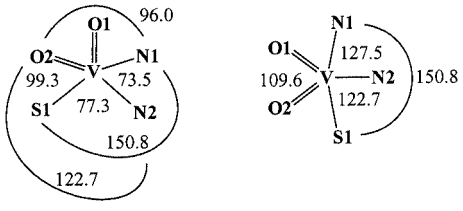

Scheme 4

The N_2SO_2 coordination in **2** is supplied by the pyridine nitrogen, the imine nitrogen and the thiolate sulfur atom of the monobasic tridentate ligand acpy-sbdt(1−), and by the two oxo groups. If viewed as a tetragonal pyramid, O1 is at the apex, while the three ligand functions and O2 form the tetragonal plane. If viewed as a trigonal bipyramid, N1 and S1 are in axial positions (N1−V−S1 = 150.8°), with the remaining ligand function (N2) plus the two doubly bonded oxygen atoms in the trigonal plane. This arrangement is similar to that reported for other $[VO_2L]$ compounds in which LH is a Schiff base derived from 2-hydroxy-1-naphthaldehyde and 8-aminoquinoline (Hsal-amq)[21] or *N*-anisoyl-*N′*(picolinylidene)hydrazine (Hpic-anh).[22] The V=O distance of 1.615(1) Å (for both oxo groups) is typical of V=O groups not involved in hydrogen bonding and other weak intermolecular contacts.[35] Furthermore, the bond lengths *d*(V1−N1) [2.1038(14) Å], *d*(V1−N2) [2.1454(14) Å] and *d*(V1−S1) [2.3852(5) Å] are in agreement with literature values for aromatic ring and imine nitrogen atoms[36] and for thioamide sulfur atoms coordinating to the vanadium centre.[29−31] The bond lengths *d*(N2−N3) [1.3904(17) Å], *d*(N3−C8) [1.294(2) Å] and *d*(S1−C8) [1.7273(17) Å] are consistent with the enethiolate mode of coordination.

For the structures of the closely related complex **5** and the peroxo complexes **3** and **7**, we assume a ligand arrangement corresponding to that in **2**; cf. Scheme 2.

The ORTEP drawing of $[VO(acpy\text{-}smdt)\{CH_2(COO)_2\}]$ (**6**) along with its atom-labelling scheme is presented in Figure 2, with selected structure parameters in Table 2. The coordination environment around vanadium is distorted octahedral, with malonate(2−) in axial/equatorial and the tridentate acpy-smdt(1−) in equatorial positions. The second axial position is occupied by the oxo group. The vanadium atom is displaced from the equatorial plane defined by N1, N2, S1 and O2 by 0.2415(9) Å towards the oxo ion O1. At 176.79(8)°, the O=V−O(malonate) axis is almost linear. Because of the strong *trans* influence of the oxo group, *d*(V−O3) [2.1387(17) Å] is significantly elongated with respect to the second, equatorial V−carboxylate bond, *d*(V−O2) = 1.9933(18) Å. Such elongation has previously been observed in other complexes with similar structures.[37−40] Bond lengths *d*(V1−N1) [2.125(2) Å] and *d*(V1−N2) [2.068(2) Å] are well within the common range.[37] The range of V−S bond length generally reported in the literature for oxovanadium(V) complexes of ligands derived from *S*-benzyldithiocarbazate is 2.343−2.365 Å.[29−31] The bond length *d*(V1−S1) = 2.4364(7) Å found here is somewhat longer. The distances *d*(N3−C8) [1.306(3) Å] and *d*(S1−C8) [1.736(3) Å] again support thioenolisation in the coordinated ligand. The bite angles in the two five-membered rings formed by the tridentate ligand are 75.77(7)° (N1−V1−N2) and 79.70(6)° (S1−V1−N2), and thus compare with the bite angles in **2**. The two "open" angles N1−V1−O2 and S1−V1−O2 amount to 95.43(8) and 106.05(6)°, respectively.

From the structural evidence provided for **6**, with the bidentate, dianionic malonato ligand occupying an axial and an equatorial position, the structures for other mixed-ligand complexes containing dianionic oxygen-functional ligands, [VO(cat)L] (**8** and **9**) and [VO(bha)L] (**10** and **11**) have been formulated accordingly in Scheme 2. For the complexes [VO(acac)L] (**1** and **4**), an axial coordination of the sulfur atom has been assumed on the basis of EPR results (see below).

IR Spectra

IR spectra of the ligands exhibited two bands at 3175 and 1064 cm^{-1} (in Hacpy-sbdt, **I**) and at 3150 and 1062 cm^{-1} (in Hacpy-smdt, **II**) due to ν(NH) and ν(C=S) stretches. The presence of both bands in the ligands was indicative of their thionic nature [−NHC(=S)− functionality] in the solid state. Absence of these bands in the spectra of the complexes indicates that the tautomeric enethiol form of the ligand [−N=C(SH)− functionality] is the preferred one on coordination to vanadium. A strong ligand band in the 1579−1600 cm^{-1} region was assigned to the ν(C=N) azomethine stretch, and this band underwent a shift to higher wave numbers by 5−42 cm^{-1} on complexation, indicating the participation of the azomethine nitrogen atom in coordination.[32,33] A sharp band appearing at ca. 1020 cm^{-1} was within the 990−1050 cm^{-1} range commonly observed for monodentate coordination of the >N−N< residue, though this band could not be located unequivocally in the ligands.[41] The band due to the coordinated pyridine nitrogen atom could not be assigned because of the strong absorption of ν(C=N) in this region. The coordination of the pyridine nitrogen atom has, however, been confirmed by single-crystal X-ray studies of, for example, $[VO_2(pic\text{-}anh)]_2$,[16] and in the complexes **2** and **6** reported here.

All of the monooxo complexes displayed one sharp band in the 945−967 cm^{-1} region, due to the ν(V=O) mode, while the dioxo compounds **2** and **5** showed two sharp bands at 930−939 and 947 cm^{-1}, corresponding to the $\nu_{sym}(O=V=O)$ and $\nu_{antisym}(O=V=O)$ modes. The existence of two sharp bands in the dioxo complexes suggested a *cis*-VO_2 arrangement, as verified by the structure results of **2**. The peroxo complexes **3** and **7** showed three IR-active vibrational modes associated with the peroxo moiety at ca. 928, 775 and 620 cm^{-1} and assigned to the O−O intrastretch (ν_1), the antisymmetric $V(O_2)$ stretch (ν_3), and the symmetric $V(O_2)$ stretch (ν_2), respectively.[42] These bands confirmed the η^2-coordination of the peroxo group.

Solution Studies

NMR and EPR Studies

The typical ^1H NMR chemical shifts of the ligands and complexes are shown in Table 3. The Schiff bases each exhibited a signal due to the NH proton at δ = 9.90−9.95, indicating their presence as their thionic tautomers. The absence of this signal in the complexes further supported the thioenolisation of the thione group and consequent replacement of H by the metal ion. A downfield shift of the signal for the methyl protons of the acetylpyridine residue from

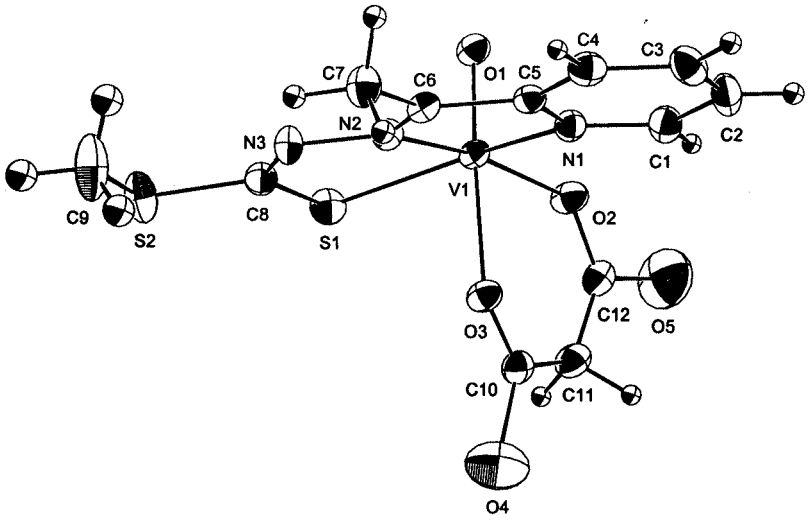

Figure 2. ORTEP plot (30% probability level) of [VO(acpy-smdt)$CH_2(COO)_2$] (**6**) with atom-numbering scheme

Table 2. Bond lengths [Å] and angles [°] for [VO(acpy-smdt)$CH_2(COO)_2$] (**6**)

Bond	Length	Bond	Angle
V(1)−O(1)	1.6132(17)	O(1)−V(1)−O(2)	93.83(8)
V(1)−O(2)	1.9933(18)	O(1)−V(1)−N(2)	99.19(8)
V(1)−N(1)	2.125(2)	O(2)−V(1)−N(2)	164.96(8)
V(1)−N(2)	2.086(2)	O(1)−V(1)−N(1)	96.25(8)
V(1)−O(3)	2.1386(17)	O(2)−V(1)−N(1)	95.43(8)
V(1)−S(1)	2.4364(7)	N(2)−V(1)−N(1)	75.77(7)
S(1)−C(8)	1.736(3)	O(1)−V(1)−O(3)	176.79(8)
S(2)−C(8)	1.743(2)	O(2)−V(1)−O(3)	83.45(7)
S(2)−C(9)	1.807(4)	N(2)−V(1)−O(3)	83.29(7)
O(3)−C(10)	1.264(3)	N(1)−V(1)−O(3)	82.35(7)
O(2)−C(12)	1.287(3)	O(1)−V(1)−S(1)	97.87(7)
O(5)−C(12)	1.513(4)	O(2)−V(1)−S(1)	106.05(6)
O(4)−C(10)	1.516(3)	N(2)−V(1)−S(1)	79.70(6)
N(1)−C(1)	1.336(3)	N(1)−V(1)−S(1)	153.32(6)
N(1)−C(5)	1.360(3)	O(3)−V(1)−S(1)	84.54(5)
N(3)−C(8)	1.306(3)	C(8)−S(1)−V(1)	94.95(8)
N(3)−N(2)	1.386(3)	C(8)−S(2)−C(9)	101.78(14)
N(2)−C(6)	1.299(3)	C(10)−O(3)−V(1)	128.08(15)
C(12)−C(11)	1.379(3)	C(12)−O(2)−V(1)	132.48(16)
C(10)−C(11)	1.406(3)	C(1)−N(1)−C(5)	119.0(2)
C(1)−C(2)	1.389(4)	C(1)−N(1)−V(1)	125.82(17)
C(2)−C(3)	1.379(4)	C(5)−N(1)−V(1)	114.96(14)
		C(6)−N(2)−V(1)	119.56(15)
		N(3)−N(2)−V(1)	124.19(15)

δ = 2.55−2.60 in the ligand to δ = 2.73−2.79 in the complex indicated coordination of the azomethine nitrogen atom. The aromatic protons of the coordinated catecholate groups (in **8** and **9**) resonated as two multiplets between δ = 6.59 and δ = 6.72, while the aromatic protons of the benzylhydroxamate groups (in **10** and **11**) appeared along with other aromatic protons (Table 3). Signals due to the methyl protons of the *S*-methyldithiocarbazate and methylene protons of the *S*-benzyldithiocarbazate residue all appeared well within the expected ranges and did not shift significantly with respect to those of the free ligands. Complexes **8**, **9**, **10** and **11** exhibited two signals both for the methyl and for the methylene protons. One set of signals corresponded to the complexes of composition [VO(cat/bha)L], while the other set belonged to the dioxo complexes $[VO_2L]$, which formed by slow decomposition in the DMSO solvent (see also below).

The ^{13}C NMR spectra of the dioxo complexes and ligands (Table 4) provided a useful diagnostic tool for the elucidation of the structures of the complexes. Assignments were based on the chemical shift and intensity patterns, and on the coordination-induced shift δΔ = δ(complex) − δ(free ligand) of the signals for the carbon atoms in the vicinity of the coordinating atoms.[43] A large coordination shift was observed for the signal of the carbon atom (C7) bearing the enethiolate sulfur atom, and for the azomethine carbon atom (C1). Even the methyl carbon signals associated with the azomethine group experienced some downfield shift.

To characterise the compounds further in solution, ^{51}V NMR spectra of **2**, **5**, **6**, **8**, **9**, **10** and **11** were also recorded; for data see Table 5. The resonances were somewhat broadened as a consequence of the nuclear quadrupole moment of the spin 7/2 nucleus ^{51}V; line widths at half height were approximately 200 Hz, which is still considered narrow in ^{51}V NMR spectroscopy.[44−46] Each dioxo complex showed one strong resonance at δ = −444.0 (**2**) or −442.5 (**5**). The ^{51}V nucleus was thus less shielded than commonly observed with dioxovanadium(V) complexes with a mixed *ON* donor set; the chemical shifts, however, were well within the range expected for coordination of a soft (thio) function in addition to *O* and *N*.[31,48−50] The catecholato complexes **8** and **9** displayed two resonances: the lowfield signals at δ = +368.4 (**9**) and +373.7 (**8**) (peak 1) were indicative of catecholate coordination and thus belonged to the mixed-ligand complexes [VO(cat)L], while the signal at δ = −434.0 (peak 2) corresponded to the decomposition product $[VO_2L]$. Similarly, the hydroxamate complexes **10** and **11** each exhibited a lowfield resonance at δ = +135.6 (**11**) or +143.0 (**10**) along with a signal in the upfield region

Table 3. ^{1}H NMR spectroscopic data of ligands and complexes

Compound[a]	NH	CH_2	CH_3	Aromatic
Hacpy-sbdt	9.95 (s, 1 H)	4.57 (s, 2 H)	2.55 (s, 3 H)	7.30 (m, 2 H), 7.44 (m, 1 H), 7.59 (d, 1 H), 7.67 (dt, 1 H), 7.90 (td, 1 H), 8.14 (d, 1 H), 8.58 (d, 1 H), 8.77 (d, 1 H)
[VO_2(acpy-sbdt)] (**2**)		4.49 (s, 2 H)	2.73 (s, 3 H)	7.36 (m, 3 H), 7.45 (d, 2 H), 7.79 (t, 1 H), 8.32 (m, 2 H), 8.74 (d, 1 H)
[$VO(O_2)$(acpy-sbdt)] (**3**)		3.38 (s, 2 H)	2.06 (s, 3 H)	7.89 (t, 3 H), 8.09 (d, 2 H), 8.38 (t, 2 H), 9.60 (d, 3 H)
[VO(acpy-sbdt)cat] (**8**)		4.46, 4.48 (s, 2 H)	2.57, 2.79 (s 3 H)	6.59 (m, 2 H), 6.71 (m, 2 H), 7.32 (m, 2 H), 7.43 (d, 2 H), 7.75 (q, 1 H), 8.09 (d, 1 H), 8.31 (bd, 1 H), 8.83 (s, 1 H)
[VO(acpy-sbdt)bha] (**10**)		4.47, 4.49 (s, 2 H)	2.73, 2.76 (s, 3 H)	7.3 (m, 4 H), 7.45 (m, 4 H), 7.77 (q, 1 H), 7.84 (d, 1 H), 8.03 (d, 1 H), 8.15 (d, 1 H), 8.35 (m, 2 H)
Hacpy-smdt	9.90 (s, 1 H)		2.25 (s, 3 H), 2.60 (s, 3 H)	6.94 (d, 1 H), 7.10 (d, 1 H), 7.32 (m, 1 H),7.5 (d,1 H)
[VO_2(acpy-smdt)] (**5**)			2.62, 2.73 (s,3 H)	7.78 (m, 1 H), 8.30 (d, 1 H), 8.37 (m, 1 H), 8.73 (m, 1 H)
[$VO(O_2)$(acpy-sbdt)] (**7**)			2.48 (s,3 H), 2.50 (s,3 H)	7.89 (t, 1 H), 8.09 (d, 1 H), 8.35 (dt, 1 H), 9.60 (d, 1 H)
[VO(acpy-smdt)cat] (**9**)			2.61, 2.63 (s, 3 H), 2.74, 2.78 (s,3 H)	6.60 (m, 2 H), 6.72 (m, 2 H), 7.77 (m, 1 H), 8.12 (d, 1 H), 8.33 (m, 1 H), 8.82 (s, 1 H)
[VO(acpy-smdt)bha] (**11**)			2.62, 2.63 (s, 3 H), 2.72, 2.74 (s, 3 H)	7.47 (m, 4 H), 7.78 (m, 1 H), 7.84 (d, 1 H), 8.05 (d, 1 H), 8.16 (d, 1 H), 8.39 (d, 1 H)

[a] Letters given in parentheses indicate the signal structure: s = singlet, d = doublet, t = triplet, td = triplet of doublets, m = multiplet, b = broad (not resolved).

Table 4. ^{13}C NMR spectroscopic data

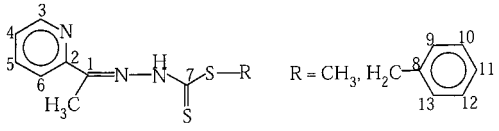

Compounds[a]	CH_3/S−CH_3	CH_2	C1	C2/C3	C6	C4/C5	C7	C8−C13
Hacpy-smdt	13.7, 17.6		144.9	142.2	129.0	127.3, 127.8	200.6	
[VO_2(acpy-smdt)] (**5**)	14.8, 18.2		166.8	153.1, 155.1	143.3	126.5, 127.7	184.7	
δΔ[b]	1.1		21.9				−15.9	
Hacpy-sbdt	13.7	38.6	154.4	149.2, 152.6	120.8	137.1, 137.2	199.2	125.1−129.6
[VO_2(acpy-sbdt)] (**2**)	15.5	38.3	167.7	154.3	143.5	137.6	189.8	127.1−129.4
δΔ[b]	2.2		18.3				−9.4	

[a] For atom labelling see scheme above. Assignments of the aromatic carbon atoms 4−6 and 8−13 are preliminary. [b] δΔ = [δ(complex) − δ(free ligand)].

at δ = −430 and −434, again due to dioxo species [VO_2L] formed by decomposition. An additional decomposition band at δ = −508 indicated either an oxo- or a dioxovanadium(V) complex with only *O*/*N* coordinating functions. The substantial downfield shift of the ^{51}V resonances (peak 1) in the catecholate and benzhydoxamate complexes has been reported previously and traced back to strong ligand-to-metal charge transfer (LMCT);[47] cf. also the UV/Vis spectra. The downfield shift of peak 2 (the resonance corresponding to the decomposition product) by ca. 10 ppm with respect to solutions containing authentic **2** or **5** is a medium effect, imparted by the presence of catechol in the solution in contact with [VO^2L].

Room-temp. EPR spectra of the two vanadium(IV) (d^1) complexes [VO(acac)L] (**1** and **4**) in DMSO provided a g_0 value of 1.965, and a comparatively large hyperfine coup-

Table 5. ^{51}V NMR chemical shifts

Complex	Chemical shifts	
	Peak 1	Peak 2[a]
$[VO_2$(acpy-sbdt)] (**2**)	−444.0	
$[VO_2$(acpy-smdt)] (**5**)	−442.5	
[VO(acpy-smdt)mal] (**6**)	−432.4	
[VO(acpy-sbdt)cat] (**8**)	373.7	−434.3
[VO(acpy-smdt)cat] (**9**)	368.4	−434.1
[VO(acpy-sbdt)bha] (**10**)	143.0	−429.5, −508.3
[VO(acpy-smdt)bha] (**11**)	135.6	−433.3, −508.4

[a] Corresponds to decomposition product(s); cf. text.

ling constant $A_0 = 93 \cdot 10^{-4}$ cm^{-1}. For the anisotropic spectrum at 97 K, the following parameters were obtained: $g_{zz} = 1.938$, $g_{xy} = 1.978$; $A_{zz} = 178.5$, $A_{xy} = 50.3 \cdot 10^{-4}$ cm^{-1}. These values were essentially in the expected range.[48] The large A_{zz} component accounts for the diminished delocalisation of electron density into the ligand system, which may be a consequence of steric strains in the bicyclic chelate structure, and of a weak bonding contribution in the axial position, provided by coordination of the thio function subjected to the *trans* influence of the oxo group.

Electronic Absorption Spectra

The UV/Vis spectroscopic data of the ligands and complexes recorded in acetonitrile are presented in Table 6. All of the complexes displayed a medium to intense electronic spectral band at $\lambda = 410.5-416$ nm, attributable to LMCT arising from the N_2S^- ligand. Coordinated benzhydroxamate and catecholate induce strong charge transfer to the metal centre in complexes with high-valent metal ions. Thus, a strong band at $\lambda = 565$ nm for **10** and **11**, and two intense bands at $\lambda \approx 500$ and 766 nm for **8** and **9** were assigned to LMCT originating from lone-pair p orbitals on the hydroxamato[49] and catecholato oxygen atoms,[50] respectively, into an empty d orbital of the vanadium ion. As vanadium(V) complexes are d^0 systems, d−d bands were not expected in these complexes. In the oxovanadium(IV) complexes **1** and **4**, however, a weak band at $\lambda \approx 590$ nm was probably due to a d−d transition, as this band slowly disappeared on oxidation of **1** and **4** to the corresponding peroxo complexes by H_2O_2 (vide infra). Other spectral features of the complexes (intraligand bands in the UV region) were nearly identical to those of the free ligands.

Stability and Reactivity Studies

The stabilities of the complexes **8**, **9**, **10** and **11** were studied in various solvents. Complexes **9**, **10** and **11** were stable in solvents such as CH_2Cl_2, MeOH and CH_3CN, while they slowly decomposed in DMF and DMSO. A rather slow loss of coordinated catechol followed by conversion into the respective dioxo species has been noticed in dry solvents, while addition of few drops of water facilitated this conversion, as observed by electronic absorption spectroscopy (Figure 3). Addition of 1 drop of water to 5 mL of a ca.10^{-4} M solution of [VO(acpy-sbdt)cat] (**8**) in DMSO caused the gradual loss of the LMCT bands belonging to coordinated catecholate, which disappeared within 8 h. Complexes **10** and **11** gave comparable results. Similar observations have also been noted for [VO(sal-amq)cat].[21] The suggested reaction is formulated in Equation (9).

$$[VOL(cat)] + H_2O \rightarrow [VO_2L] + H_2cat \quad (9)$$

Oxovanadium(V) complexes generally undergo redox reactions with reducing agents such as L-ascorbic acid, cysteine and cysteine derivatives.[51,52] A model redox reaction with L-ascorbic acid was carried out for complexes **8** and **11**. In a typical reaction, 9 mL of a 10^{-4} M solution of **8** or **11** was treated with 1 mL of a 10^{-1} M solution of L-ascorbic acid in acetonitrile, and the reaction was monitored by electron absorption spectroscopy (Figure 4). The absorption bands at $\lambda = 765.5$ and 501.5 nm for complex **8** slowly disappeared. The band at $\lambda = 410.5$ shifted to $\lambda = 415$ nm with a marginal reduction in intensity, while the band at $\lambda = 338$ nm underwent a blue shift to appear at $\lambda = 331$ nm with a marginal increase in intensity. An additional new band appeared at $\lambda = 277$ nm. For complex **11** (not shown), the bands at $\lambda = 564.5$ and 257 nm slowly disappeared. The band at $\lambda = 411.5$ nm remained unchanged, while the band at $\lambda = 338$ nm shifted to $\lambda = 331$ nm with a slight increase in intensity. As L-ascorbic acid has reducing properties, reduction of **8** and **11** might be anticipated along with the removal of coordinated catecholate/benzhydroxamate. However, the match of the spectral features with those of solutions of **2** and **5**, with only minor deviations in the UV region, indicated that the reduced species was rapidly reoxidised to the dioxo complex $[VO_2L]$, and not to the original mixed ligand compound. The slight deviations in the UV were probably due to factors arising from the presence of uncoordinated catecholate or hydroxamate. L-Ascorbic acid was thus simply involved in electron transfer, without formation of any long-lived complex with **8** or **11**.

Treatment of complexes **1** and **4** with H_2O_2 around 0 °C yielded the oxo(peroxo)vanadium(V) complexes **3** and **7** (cf. Exp. Sect.). These reactions, involving dropwise addition of 30% H_2O_2 to 10 mL of ca. 10^{-4} M solutions of **1** or **4** in acetonitrile at ca. 10 ° C, were also monitored by electron absorption spectroscopy. The spectral changes during the reaction are shown in Figure 5 for complex **4**. In each case, the band appearing at $\lambda = 410.5$ nm slowly disappeared, while a red shift to $\lambda = 350.5$ nm was observed for the band at $\lambda = 338.5$ nm of **1**, with a corresponding red shift for the band at $\lambda = 336.5$ nm to $\lambda = 345.5$ nm in the case of **4**. The features of the final spectra were similar to those of the corresponding isolated peroxo complexes **3** and **7**.

The peroxo complexes underwent oxygen transfer with PPh_3 in CH_3CN to give the corresponding dioxovanadium(V) complexes **2** and **5**. During the reaction, PPh_3 possibly inserts directly into one of the metal−peroxo bonds, followed by the transfer of an oxo group from the peroxo

Table 6. Electronic spectroscopic data of ligands and complexes

Compound	λ_{max} [nm]
Hacpy-sbdt	218(9561), 290(4154), 322(11069)
[VO(acac)(acpy-sbdt)] (**1**)	338.5(15278), 407(9320), 590(35)
[VO_2(acpy-sbdt)] (**2**)	207.5(33737), 255(15760), 295(7866), 345.5(10939), 416(7776)
[$VO(O_2)$(acpy-sbdt)] (**3**)	268.5, 336, 446
[VO(acpy-sbdt)cat] (**8**)	336(17755), 411.5(10447), 501(8407), 766(6682)
[VO(acpy-sbdt)bha] (**10**)	211(47630), 340(14529), 410.5(8962), 565(6180)
Hacpy-smdt	216(6806), 285(4167), 331(14331).
[VO(acac)(acpy-smdt)] (**4**)	248(10487), 277(7408), 336.5(9149), 411(5554), 586(48)
[VO_2(acpy-smdt)] (**5**)	208.5(52865), 252.5(31278), 299(17497), 343(23197), 416(17325)
[$VO(O_2)$(acpy-smdt)] (**7**)	270, 334, 433
[VO(acpy-smdt)cat] (**9**)	207(37628), 337(13846), 413(9126), 499.5(6278), 765.5(5017)
[VO(acpy-smdt)bha] (**11**)	208(42090), 256(23362), 337(18650), 412(12129), 565(8324)

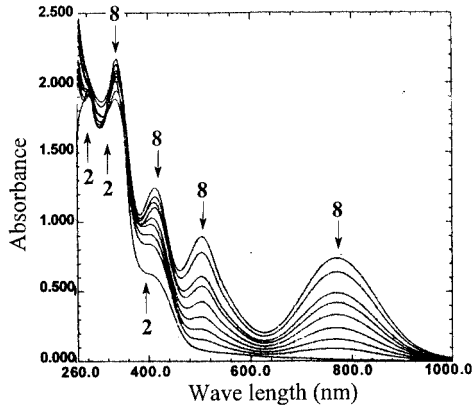

Figure 3. Decomposition of [VO(acpy-sbdt)cat] (**8**) in 5 mL of DMSO after addition of one drop of water, as a function of time

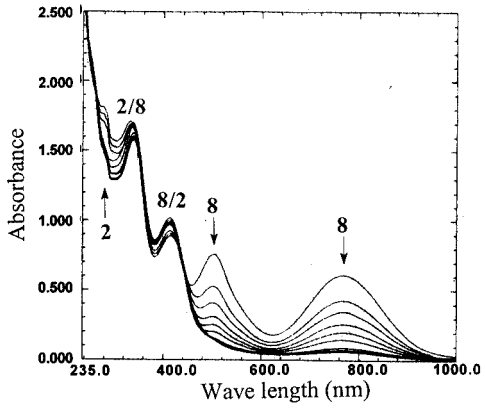

Figure 4. Absorption spectra of a ca. 10^{-4} M solution of [VO(acpy-sbdt)cat] (**8**) in CH_3CN in the presence of L-ascorbic acid (ca. 1:2 molar ratio) as a function of time, over periods of 120 min

ligand to PPh_3. The reaction mechanism in depicted in Scheme 5.

Addition of acetonitrile saturated with HCl gas to an acetonitrile solution of [VO_2(acpy-sbdt)] (**2**) resulted in a colour change from orange-red to dark red, with a reduction in intensity of the bands at λ = 416 and 251.5 nm and a shift of the band at λ = 343 nm to λ = 350.5 nm (Figure 6). An increase in the concentration of the original solution of **2** and addition of HCl/acetonitrile generated a new band at

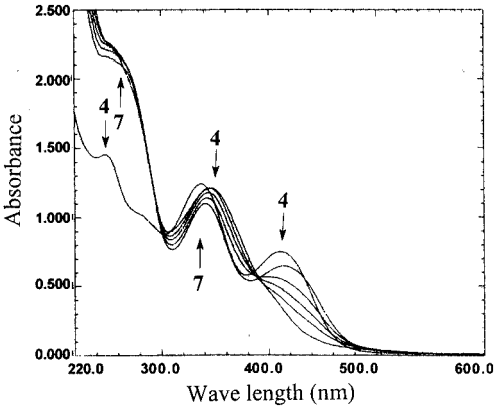

Figure 5. Titration of [VO(acac)(acpy-smdt)] (**4**) with 30% H_2O_2; spectra were recorded after successive addition of 2 drops H_2O_2 to 5 mL of ca. 10^{-4} M solution of the complex in CH_3CN

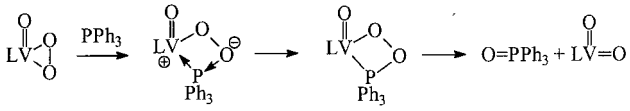

Scheme 5

λ = 585 nm. We preliminarily interpret these results in terms of the formation, on acidification, of a hydroxo complex of composition $[VO(OH)(acpy\text{-}sbdt)]^+$, similar to the hydroxo(oxo) complex $[VO(OH)(LH)]^+$, where LH_2 = *N*-[{(*o*-hydroxyphenyl)methyl}-*N*′-(2-hydroxyethyl)ethylenediamine][53] or *N*-salicylidene-*N*′-(2-hydroxyethyl)ethylenediamine,[54] generated in a similar manner from the respective dioxyvanadium(V) dimer. {See also [VO(OH)Tp(H_2O)] [Tp = tris(3,5-diisopropyl-1-pyrazolyl)borate][55] and [VO(OH)(8-oxyquinolinato)$_2$][56] for other characterised oxo-hydroxovanadium complexes.} On allowing the above solution to stand overnight, or on addition of KOH dissolved in acetonitrile, the solution reacquired its original character; the reaction was hence reversible and gave the spectrum of **2**. The reversibility of such reactions is an important observation in the context of the vanadate-dependent haloperoxidases, for which a hydroxo group in an apical position has been confirmed by X-ray diffraction analysis.[57]

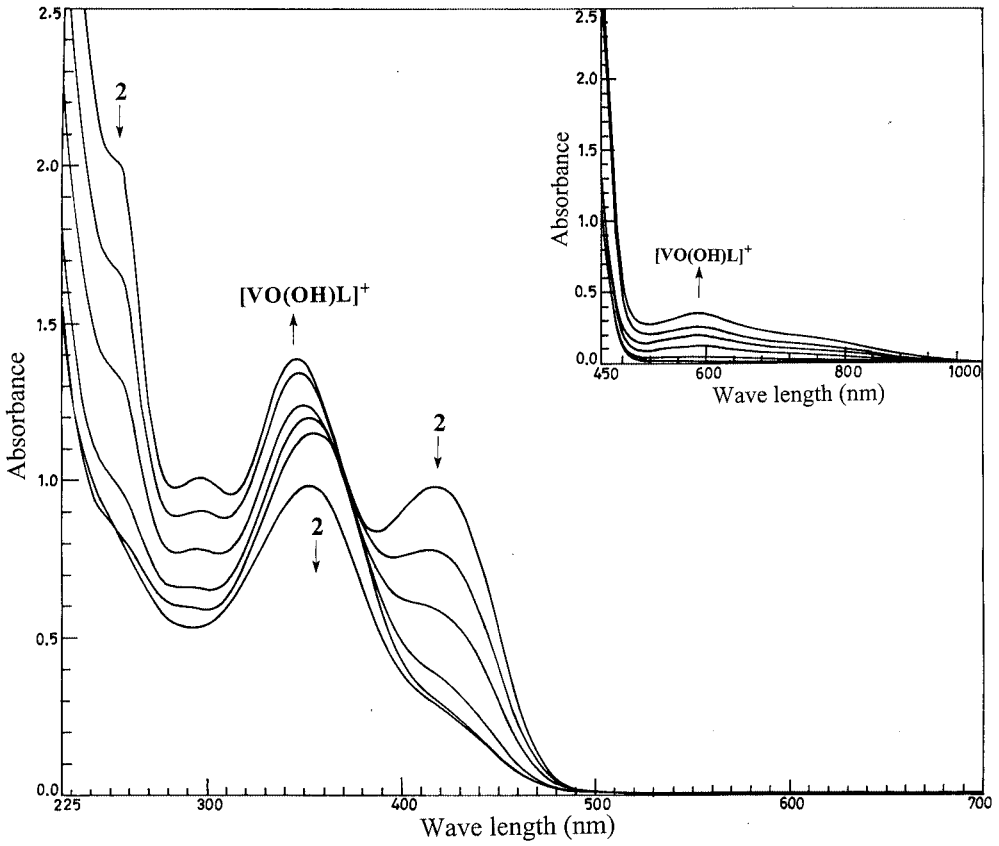

Figure 6. Titration of $[VO_2(acpy\text{-}sbdt)]$ (**2**) with a saturated solution of HCl in CH_3CN; spectra were recorded after the addition of 3 drops of CH_3CN/HCl to 10 mL of a ca. 10^{-4} M CH_3CN solution of **2**

Conclusion

The preparation and characterisation of monomeric dioxovanadium(V) complexes with a structure between a square-pyramidal and a trigonal-bipyramidal ligand arrangement is described, together with octahedral monooxovanadium complexes. A tridentate N_2S^- ligand system derived from acetylpyridine and dithiocarbazine, acpy-sbdt and acpy-smdt, was used. These complexes model part of the structure of vanadium nitrogenase and the active site of vanadate-dependent haloperoxidases. The model includes intermediate species with $[VO(OH)]^{2+}$ and $[VO(O_2)]^+$ cores, as postulated for catalytic turnover by the peroxidases, and which have been generated and characterised in this work. Additional reactions − such as the reversibility of the formation of a hydroxo(oxo) complex from a dioxo complex, the transfer of a peroxo oxygen atom from the (oxo)peroxo complex to triphenylphosphane, and the role of water or ascorbic acid in the conversion of monooxo- to dioxovanadium(V) complexes − are of interest from the perspective of vanadium speciation under physiological conditions, the mechanism by which vanadate-dependent haloperoxidases catalyse oxo transfer to halide and thioethers, and also a possible general role of vanadium in oxotransferases. The oxidative conversion of acetylacetonate in $[VO(acac)_2]$ to malonate, and concomitant oxidation of V^{IV} to V^V under mild basic conditions and in the presence of Hacpy-sbdt afforded the complex [VO(acpy-sbdt)malonate], underlining the versatile reaction patterns accompanying this interesting ligand system.

Experimental Section

Materials and Methods: V_2O_5 (Loba Chemie, India), methyl iodide (Spectrochem, India), benzhydroxamic acid (Merck, Germany), catechol (s. d. fine chemicals, India), acetylacetone and 2-acetylpyridine (Aldrich, U.S.A.) were used as obtained. Other reagents and solvents used were of AR grade. *S*-Benzyldithiocarbazate,[58] *S*-methyldithiocarbazate [59] and $[VO(acac)_2]$ [60] were prepared according to methods reported in the literature. The Schiff bases Hacpy-sbdt (**I**) and Hacpy-smdt (**II**) (cf. Scheme 1) were prepared as reported in a previous paper.[32,33] Elemental analyses were carried out by The Central Drug Research Institute, Lucknow, India. UV/Vis spectra were recorded in acetonitrile and methanol with a UV-1601 PC UV/Vis spectrophotometer. IR spectra were recorded as KBr pellets with a Perkin−Elmer model 1600 FT-IR spectrometer. EPR spectra of the paramagnetic complexes were measured with a Bruker ESP 300E spectrometer at ca. 9.6 GHz (X-band) in ca. 2 mM DMSO solution. Magnetic susceptibilities of oxovanadium(IV) complexes were measured by the Scientific Instrumentation Centre of the Indian Institute of Technology, Roorkee. ^1H NMR spectra were obtained with a Bruker 200 MHz spectrometer, ^{13}C and ^{51}V NMR spectra with a Bruker AM 360 spectrometer at 90.56 and 94.73 MHz, respectively, in $[D_6]$DMSO with the usual parameter settings. The $\delta(^{51}V)$ values have been referenced and are

quoted relative to $VOCl_3$. Thermogravimetric analyses of the complexes were carried out on a simple, manually operated thermobalance as described by us previously. Crystal Structure Determinations: Data were collected with a Siemens/Bruker SMART Apex CCD diffractometer with a graphite monochromator and Mo-K_α radiation (λ = 0.71073 Å) at 153(2) K. Hydrogen atoms were placed in calculated positions and included in the last cycles of refinement. Crystal data and details of the data collection and refinement are collected in Table 7. The programme systems SHELXS 86 and SHELXL 93 were used throughout.[61] CCDC-177111 (**2**) and -177112 (**6**) contain the supplementary crystallographic data for this paper. These data can be obtained free of charge at www.ccdc.cam.ac.uk/conts/retrieving.html or from the Cambridge Crystallographic Data Centre, 12 Union Road, Cambridge CB2 1EZ, UK [Fax: int. code + 44-1223/336-033; E-mail: deposit@ccdc.cam.ac.uk].

Preparation of Complexes

[VO(acac)(acpy-sbdt)] (1): [VO(acac)$_2$] (0.53 g, 2 mmol) was added to a stirred solution of Hacpy-sbdt (0.60 g, 2 mmol) in 20 mL of dry methanol, and the resulting mixture was refluxed for 4 h. On cooling the reaction flask to ambient temperature, a dark green solid separated and was filtered off, washed with methanol and dried in vacuo to give 0.84 g (90%) of **1**. $C_{20}H_{21}N_3O_3S_2V$ (466.47): calcd. C 51.50, H 4.51, N 9.01; found C 51.42, H 4.54, N 9.20. IR: $\tilde{\nu}$ = 1586 (C=N, C=C), 1022 (N−N), 947 (V=O), 440, 410 cm^{-1} (V−O, V−N).

[VO$_2$(acpy-sbdt)] (2): [VO(acac)$_2$] (0.53 g, 2 mmol) was dissolved in 40 mL of dry methanol, and KOH (0.11 g, 2 mmol) was added. The resulting solution was stirred for 2 h and then left for ca. 10 h in air. The solution slowly changed to red-brown. A solution of Hacpy-sbdt (0.60 g, 2 mmol) in 15 mL of methanol was added slowly, and the mixture was stirred magnetically for 4 h. A lustrous yellow solid separated; it was filtered off, washed with methanol and dried in vacuo to give **2**. Yield 0.42 g (55%). X-ray quality single crystals were grown by slow concentration of an acetonitrile solution of the complex in air. $C_{15}H_{14}N_3O_2S_2V$ (383.36): calcd. C 47.0, H 3.66, N 10.96; found C 47.0, H 3.54, N 10.83. IR: $\tilde{\nu}$ = 1600, 1580, 1557 (C=N, C=C), 1019 (N−N), 947, 939 (O=V=O sym and antisym), 461, 422 cm^{-1} (V−O, V−N).

[VO(O$_2$)(acpy-sbdt)] (3). Method A: Compound **2** (0.192 g, 0.5 mmol) was dissolved in 30 mL of acetonitrile while heating on a water bath, and filtered. The filtrate was treated with H_2O_2 (30%, 4 mL) while stirring and maintaining the reaction mixture at 10 °C. The colour changed from yellow to dark red. After 4 h, the solution was refrigerated (ca. 10 °C) overnight, whereupon orange-red crystalline **3** separated. The product was filtered off and dried in vacuo at ambient temperature. Yield: 70 mg (35%). $C_{15}H_{14}N_3O_3S_2V$ (399.36): calcd. C 45.11, H 3.51, N 10.53; found C 45.20, H 3.63, N 10.68. IR: $\tilde{\nu}$ = 1632, 1580, 1569 (C=N, C=C), 1023 (N−N), 951 (V=O), 929 (O−O), 777 (VO_2 antisym), 617 (VO_2 sym), 435, 414 cm^{-1} (V−O, V−N). **Method B:** Compound **1** (0.466 g, 1 mmol) was dissolved in 60 mL of acetonitrile, and H_2O_2 (30%, 8 mL) was added while stirring. The reaction mixture was stirred for 4 h at 10 °C and then left overnight at the same temp. The orange-red crystals that had separated were filtered and dried in vacuo. Yield: 0.16 g (40%). IR and electronic spectroscopic data matched well with **3** prepared according to method A.

[VO(acac)(acpy-smdt)] (4): Complex **4** was prepared in 85% yield by the procedure described for **1**. $C_{14}H_{17}N_3O_3S_2V$ (390.37): calcd. C 43.07, H 4.36, N 10.77; found C 43.13, H 4.47, N 10.91. IR: $\tilde{\nu}$ = 1588 (C=N, C=C), 1021 (N−N), 951 (V=O), 440, 409 cm^{-1} (V−O, V−N).

Table 7. Crystal data and structure refinement parameters for [VO$_2$(acpy-sbdt)] (**2**) and [VO(acpy-smdt)malonate] (**6**)

	2	**6**
Empirical formula	$C_{15}H_{14}N_3O_2S_2V$	$C_{12}H_{12}N_3O_5S_2V$
Formula mass	383.35	393.31
Temperature [K]	153(2)	153(2)
Wavelength [Å]	0.71073	0.71073
Crystal system, space group	monoclinic, $P2_1/c$	monoclinic, $P2_1/n$
Unit cell dimensions		
a [Å], α [°]	7.8794(2), 90	8.2949(3), 90
b [Å], β [°]	25.7527(7), 99.2860(10)	19.6498(7), 102.72(10)
c [Å], γ [°]	8.0071(2), 90	10.7717(4), 90
Cell volume [Å^3]	1603.47(7)	1727.61(11)
Z	4	4
Calculated density [g/cm^3]	1.588	1.525
Absorption coefficient [mm^{-1}]	0.890	0.848
F(000)	784	800
Crystal size [mm]	0.2 × 0.3 × 0.65	0.8 × 0.4 × 0.2
θ range for data collection [°]	2.62 to 32.57	2.20 to 32.50
Limiting indices	$-11 \le h \le 11$, $-32 \le k \le 38$, $-11 \le l \le 12$	$-12 \le h \le 12$, $-29 \le k \le 28$, $-15 \le l \le 16$
Reflections collected/unique	23468/5629	24869/5933
R_{int}	0.0346	0.0418
Max./min. transmission	1.0/0.7924	1.0/0.7935
Data/restraints/parameters	5629/0/208	5933/0/208
Goodness of fit on F^2	0.990	1.072
R indices [$I > 2\sigma(I_0)$]: R_1/wR_2	0.0417/0.1095	0.0581/0.1764
R indices (all data): R_1/wR_2	0.0554/0.1143	0.0664/0.1827
Largest diff. peak/hole(e Å^{-3})	0.732/−0.502	0.885/−1.176

$[VO_2$(acpy-smdt)] (5): An oxidized red-brown methanolic solution of $[VO(acca)_2]$ (0.53 g, 2 mmol) was produced as described for complex **2**. A solution of Hacpy-smdt (0.23 g, 2 mmol), dissolved in 15 mL of methanol, was added with stirring. Workup was carried out as described for **2**. Yield: 0.31 g (50%). $C_9H_{10}N_3O_2S_2V$ (307.26): calcd. C 35.18, H 3.26, N 13.68; found C 35.36, H 3.31, N 13.70. IR: $\tilde{\nu}$ = 1583, 1561 (C=N, C=C), 1033(N−N), 947, 930 (O=V=O sym and antisym), 461, 424 cm^{-1} (V−O, V−N).

[VO(acpy-smdt)malonate] (6): $[VO(acac)_2]$ (0.53 g, 2 mmol) was dissolved in 30 mL of methanol, and two drops of water and KOH (0.11 g, 2 mmol) were added. The resulting solution was stirred for 2 h and then left for ca. 10 h in air. The solution slowly changed to red-brown with the deposition of some white solid on the wall of the flask. A solution of Hacpy-smdt (0.23 g, 2 mmol) in 15 mL of methanol was added, and the mixture was stirred for 2 h. A light green product that gradually precipitated was redissolved by heating the reaction mixture on a water bath, and the mixture was then left in air at ambient temperature. Over ca. 5 h, a light red solid precipitated and was filtered off, washed with methanol and dried. The product was recrystallised from hot acetonitrile. Orange crystals were obtained within 2−3 d on slow evaporation of the solvent in air. Yield: 0.24 g (30%). The elemental analysis showed that the bulk product was a mixture of **6** and **4**. The S/N ratio was reproduced correctly, indicating that the ligand had remained intact.

$[VO(O_2)$(acpy-smdt)] (7): Complex **7** was prepared from **4** and from **5** with H_2O_2 as described for **3**, in ca. 50% yield. $C_9H_{10}N_3O_3S_2V$ (323.26): calcd. C 33.44, H 3.09, N 13.0; found C 33.52, H 3.24, 13.0. IR: $\tilde{\nu}$ = 1628, 1580 (C=N, C=C), 950 (V=O), 928 (O−O), 775 (VO_2 antisym), 620 (VO_2 sym), 435, 410 cm^{-1} (V−O, V−N).

[VO(acpy-sbdt)cat] (8): Compound **1** (0.47 g, 1 mmol) was dissolved in hot methanol (40 mL). After the mixture had cooled to room temp., catechol (0.11 g, 1 mmol) was added and the reaction mixture was stirred for 6 h. The volume of the solvent was reduced to ca. 10 mL and the mixture was kept in the refrigerator overnight, whereupon brown-black solid **7** separated. This was filtered off, washed with cold methanol and dried in vacuo at ambient temp. Yield: 0.19 g (40%). $C_{21}H_{18}N_3O_3S_2V$ (475.45): calcd. C 53.05, H 3.79, N 8.84; found C 53.19, H 3.83, N 8.82. IR: $\tilde{\nu}$ = 1600, 1576 (C=N, C=C), 1020 (N−N), 950 (V=O), 460, 414 cm^{-1} (V−O, V−N).

[VO(acpy-smdt)cat] (9): Complex **9** was prepared analogously to **8** in 52% yield, by replacing **1** with **4**. $C_{15}H_{14}N_3O_3S_2V$ (399.36): calcd. C 45.11, H 3.51, N 10.52; found C 45.38, H 3.56, N 10.47. IR: $\tilde{\nu}$ = 1600, 1577 (C=N, C=C), 1030 (N−N), 950 (V=O), 460, 441, 415 cm^{-1} (V−O, V−N).

[VO(acpy-sbdt)bha] (10): Compound **1** (0.47 g, 1 mmol) was dissolved in 40 mL of hot methanol, and after the reaction flask had cooled to room temp., benzohydroxamic acid (0.137 g, 1 mmol) was added. The resulting reaction mixture was stirred for 6 h. After reduction of the volume to ca. 10 mL, the solution was kept at 10 °C overnight, during which brown solid **10** separated. This was filtered off, washed with methanol, and dried in vacuo. Yield: 0.19 g (38%). $C_{22}H_{20}N_4O_3S_2V$ (503.49): calcd. C 52.48, H 3.97, N 11.13; found C 52.53, H 4.11, N 11.05. IR: $\tilde{\nu}$ = 1600, 1580 (C=N, C=C), 1031 (N−N), 967 (V=O), 473, 420 cm^{-1} (V−O, V−N).

[VO(acpy-smdt)bha] (11): Compound **11** was prepared in 42% yield analogously to **10**, by replacing **1** by **4**. $C_{16}H_{16}N_4O_3S_2V$ (427.39): calcd. C 44.96, H 3.76, N 13.11; found C 45.0, H 3.91, N 13.23. IR: $\tilde{\nu}$ = 1585, 1562 (C=N, C=C), 1025 (N−N), 963 (V=O), 463, 414 cm^{-1} (V−O, V−N).

Treatment of 3 and 7 with PPh_3: PPh_3 (0.195 g, 0.75 mmol) was added to a suspension of **3** or **7** (0.05 mmol) in 15 mL of hot CH_3CN, and the reaction mixture was refluxed on an oil bath for 4 h, during which the complex slowly dissolved. After reduction of the solvent volume to ca. 10 mL, the heating was discontinued, and the flask was kept at ca. 10 °C overnight, whereupon a crystalline solid separated out within 5−6 h. This was filtered off and dried in vacuo. Yield 45%. Analytical and spectroscopic data of the complexes thus obtained matched well with **2** and **5**, respectively

Acknowledgments

This work was supported by the Deutsche Forschungsgemeinschaft and the Fonds der Chemischen Industrie. M. R. M. and S. K. thank the Council of Scientific and Industrial Research, New Delhi, for funding. We also acknowledge C,H,N analyses carried out by RSIC, Central Drug Research Institute, Lucknow.

[1] *Vanadium in biological systems* (Ed.: N. D. Chasteen), Kluwer, Dordecht, **1990**.
[2] *Vanadium and its role in life* [*Metal ions in biological systems*, vol. 31 (Eds.: H. Sigel, A. Sigel)], Marcel Dekker, New York, **1995**.
[3] H. Sakauri, A. Tsuji, in *Vanadium in the environment*, part 2: *Health effects* (Ed.: J. O. Nriagu), Wiley, New York, **1998**.
[4] H. Sakauri, K. Fujii, S. Fujimoto, K. Fujsawa, K. Takechi, H. Yasui, *Vanadium compounds Chemistry, biochemistry and therapeutic applications* (Eds.: A. S. Tracey, D. C. Crans), ACS Symp. Ser. 711, **1998**, p. 344.
[5] D. Rehder, J. Costa Pessoa, C. F. G. C. Geraldes, M. M. C. A. Castro, T. Kabanos, T. Kiss, B. Meier, G. Micera, L. Pettersson, M. Rangel, A. Salifoglou, I. Turel, Dongren Wang, *J. Biol. Inorg. Chem.* **2002**, *7*, 384.
[6] K. H. Thompson, J. H. McNeill, C. Orvig, *Chem. Rev.* **1999**, *99*, 2561.
[7] E. J. Baran, *J. Inorg. Biochem.* **2000**, *80*, 1.
[8] T. Kiss, T. Jakusch, M. Kilyen, E. Kiss, A. Lakatos, *Polyhedron* **2000**, *19*, 2389.
[9] D. Rehder, *Coord. Chem. Rev.* **1999**, *182*, 297.
[10] D. Rehder, *Transition metals in biology and their coordination chemistry* (Ed.: A. X. Trautwein), Wiley-VCH, Weinheim, **1997**, p. 491.
[11] D. Rehder, *J. Inorg. Biochem.* **2000**, *80*, 133.
[12] H. Sakurai, H. Sano, T. Takino, H. Yasui, *J. Inorg. Biochem.* **2000**, *80*, 99.
[13] *Biology and biochemistry of nitrogen fixation* (Ed.: J. M. Dilworth, A. R. Glenn), Elsevier, Amsterdam, **1991**.
[14] R. R. Eady, G. J. Leigh, *J. Chem. Soc., Dalton Trans.* **1994**, 2739.
[15] M. Zhang, M. Zhou, R. L. van Etten, C. V. Staufacher, *Biochemistry* **1997**, *36*, 15.
[16] J. E. Banabe, L. A. Echegoyen, B. Pastrona, M. Martinez-Maldonado, *J. Biol. Chem.* **1987**, *262*, 9555.
[17] H. B. ten Brink, A. Tuynman, H. L. Dekker, W. Hemrika, Y. Izumi, T. Oshiro, H. E. Schoemaker, R. Wever, *Inorg. Chem.* **1998**, *37*, 6780.
[18] H. B. ten Brink, H. L. Holland, H. E. Schoemaker, H. van Lingen, R. Wever, *Tetrahedron: Asymmetry* **1999**, *10*, 4563.
[19] X. Li, M. S. Lah, V. L. Pecoraro, *Inorg. Chem.* **1988**, *27*, 4657.
[20] L. M. Mokry, C. J. Carrano, *Inorg. Chem.* **1993**, *32*, 6119.
[21] G. Asgedom, A. Sreedhara, J. Kivikoski, E. Kolehmainen, C. P. Rao, *J. Chem. Soc., Dalton Trans.* **1996**, 93.
[22] S. N. Pal, S. Pal, *J. Chem. Crystalogr.* **2000**, *30*, 329.
[23] D. C. Crans, C. M. Simone, *Biochemistry* **1991**, *30*, 6734.
[24] C. R. Cornman, T. C. Stauffer, P. D. Boyle, *J. Am. Chem. Soc.* **1997**, *119*, 5986.
[25] A. J. Tasiopoulos, A. T. Vlahos, A. D. Keramidas, T. A. Kabanos, Y. G. Deligiannakis, C. P. Raptopoulos, A. Terzis, *Angew. Chem. Int. Ed. Engl.* **1996**, *35*, 2531.

[26] S. C. Sendlinger, J. R. Nicholson, E. B. Lobkovsky, J. C. Huffman, D. Rehder, G. Christou, *Inorg. Chem.* **1993,** *32*, 204.
[27] K. K. Nanda, E. Sinn, A. W. Addison, *Inorg. Chem.* **1996**, *35*, 2.
[28] S. C. Davies, D. L. Hughes, Z. Janas, L. B. Jerzykiewicz, R. L. Richards, J. R. Sanders, J. E. Silverston, P. Sobota, *Inorg. Chem.* **2000**, *39*, 3485.
[29] S. K. Dutta, S. B. Kumar, S. Bhattacharya, E. R. T. Tiekink, M. Chaudhury, *Inorg. Chem.* **1997**, *36*, 4954.
[30] M. Milanesio, D. Viterbo, R. P. Hernandez, J. D. Rodriguez, J. Ramirez-Ortiz, J. Valdes-Martinez, *Inorg. Chim. Acta* **2000**, *306*, 125.
[31] D. Wang, M. Ebel, C. Schulzke, C. Grüning, S. K. S. Hazari, D. Rehder, *Eur. J. Inorg. Chem.* **2001**, 935.
[32] N. Bharati, M. R. Maurya, F. Naqvi, A. Azam, *Bioorg. Med. Chem. Lett.* **2000**, *10*, 2243.
[33] N. Bharti, M. R. Maurya, F. Naqvi, A. Bhattacharya, S. Bhattacharya, A. Azam, *Eur. J. Med. Chem.* **2000**, *35*, 481.
[34] S. S. Amin, K. Cryer, B. Zhang, S. K. Dutta, S. S. Eaton, O. P. Anderson, S. M. Miller, B. A. Reul, S. M. Brichard, D. C. Crans, *Inorg. Chem.* **2000**, *39*, 406.
[35] C. J. Carrano, C. M. Nunn, R. Quan, J. A. Bonadies, V. L. Pecoraro, *Inorg. Chem.* **1992**, *29*, 944.
[36] C. R. Cornman, G. J. Colpas, J. D. Hoeschele, J. Kampf, V. L. Pecoraro, *J. Am. Chem. Soc.* **1992**, *114*, 9925.
[37] S. Mondal, S. P. Rath, S. Dutta, A. Chakravorty, *J. Chem. Soc., Dalton Trans.* **1996**, 99.
[38] S. Mondal, S. P. Rath, K. K. Rajak, A. Chakravorty, *Inorg. Chem.* **1998**, *37*, 1713.
[39] S. P. Rath, K. K. Rajak, S. Mondal, A. Chakravorty, *J. Chem. Soc., Dalton Trans.* **1998**, 2097.
[40] S.-X. Liu, S. Gao, *Inorg. Chim. Acta* **1998**, *282*, 149.
[41] M. R. Maurya, S. Gopinathan, C. Gopinathan, R. C. Maurya, *Polyhedron* **1993**, *12*, 159.
[42] A. D. Westland, F. Haque, A-M. Bouchard, *Inorg. Chem.* **1980**, *19*, 2255.
[43] A. D. Keramidas, A. B. Papaioannou, A. Vlahas, T. A. Kabanos, G. Bonas, A. Makriyannis, C. P. Rapropoulou, A. Terzis, *Inorg. Chem.* **1996**, *35*, 357.
[44] D. Rehder, C. Weidemann, A. Duch, W. Priebsch, *Inorg. Chem.* **1988**, *27*, 584.
[45] D. Rehder, in *Transition Metal Nuclear Magnetic Resonance* (Ed.: P. S. Pregosin), Elsevier, New York, **1991**, p. 1.
[46] O. W. Howarth, *Prog. Magn. Reson. Spectrosc.* **1990**, *22*, 453.
[47] C. R. Cornman, G. J. Colpas, J. D. Hoeschele, J. Kampf, V. L. Pecoraro, *J. Am. Chem. Soc.* **1992**, *114*, 9925.
[48] A. J. Tasiopoulos, A. N. Troganis, A. Evangelou, C. P. Raptopoulou, A. Terzis, Y. Deligiannakis, T. A. Kabanos, *Chem. Eur. J.* **1999**, *5*, 910.
[49] S. Gao, Z.-Q. Wenig, S.-X Liu, *Polyhedron* **1998**, *17*, 3595.
[50] G. Asgedom, A. Shreedhara, C. P. Rao, *Polyhedron* **1996**, *15*, 3731.
[51] G. Asgedom, A. Shreedhara, C. P. Rao, *Polyhedron* **1995**, *14*, 1673.
[52] H. Degani, M. Gochin, S. J. D. Karlish, Y. Shechter, *Biochemistry* **1981**, *20*, 5795.
[53] G. J. Colpas, B. J. Hamstra, J. W. Kampf, V. L. Pacoraro, *Inorg. Chem.* **1994**, *33*, 4669.
[54] X. Li, M. S. Lah, V. L. Pecoraro, *Inorg. Chem.* **1988**, *27*, 4657.
[55] M. Kosugi, S. Hikitchi, M. Akita, Y. Moro-oka, *Inorg. Chem.* **1999**, *38*, 1173.
[56] A. Giacomelli, C. Floriani, A. O. De Souza Duarte, A. Chiesi-Villa, C. Guastino, *Inorg. Chem.* **1982**, *21*, 3310.
[57] M. Weyand, H.-J. Hecht, M. Keiß, M.-F. Liaud, H. Vilter, D. Schomburg, *J. Mol. Biol.* **1999**, *293*, 595.
[58] M. A. Ali, M. T. H. Tarafder, *J. Inorg. Nucl. Chem.* **1977**, *39*, 1785.
[59] M. Das, S. E. Livingstone, *Inorg. Chim. Acta* **1976**, *19*, 5.
[60] R. A. Row, M. M. Jones, *Inorg. Synth.* **1957**, *5*, 113.
[61] G. M. Sheldrick, *SHELXS 86*, University of Göttingen, **1986**; G. M. Sheldrick, *SHELXS 93*, University of Göttingen, **1993**.

Received January 10, 2002
[I02013]

Gold(I) Thiolates as Metalloligands for the Synthesis of the First Zirconocene−Gold Complexes

Barbara Wenzel,[a] Peter Lönnecke,[a][‡] and Evamarie Hey-Hawkins*[a]

Dedicated to Professor Dr. Peter Welzel on the occasion of his 65th birthday

Keywords: Metallocenes / Zirconium / Gold / O,S ligands / Bridging ligands

The reactions of the mercaptocarboxylic acids $HOOC(CH_2)_nSH$ (n = 1, 2) with $H[AuCl_4]$ followed by treatment with PMe_2Ph led to the (phosphane)gold thiolates $[Au\{S(CH_2)_nCOOH\}(PMe_2Ph)]$ [n = 1, (**1**) 2 (**2**)], which can act as metalloligands towards complex fragments of a second metal. Compounds **1** and **2** react with $[Cp^\circ{}_2ZrMe_2]$ (Cp° = C_5EtMe_4) to give the trinuclear Zr/Au complexes $[Cp^\circ{}_2Zr\{\kappa^1O\text{-}OOC(CH_2)_nSAu(PMe_2Ph)\}\{\kappa^2O,O'\text{-}OOC(CH_2)_n\text{-}SAu(PMe_2Ph)\}]$ [n = 1 (**3**), n = 2 (**4**)]. Complexes **1**–**4** were characterized by ^1H, ^{13}C, ^{31}P NMR and IR spectroscopy. The crystal structure of **4** shows mono- and bidentate coordination of two metalloligands to one zirconocene fragment. In solution at room temperature **3** and **4** are dynamic, and the carboxylato groups alternate between the mono- and bidentate bonding modes. Complex **4** shows catalytic activity in the oxidation of PPh_3 with O_2.
(© Wiley-VCH Verlag GmbH, 69451 Weinheim, Germany, 2002)

Introduction

Research in early/late heterobimetallics (ELHBs) has grown in the last few years and has been the subject of numerous reports.[1−4] The reasons for the interest include their relevance to bioinorganic bimetallic systems and their potential in homogeneous catalysis. The pairing of two electronically different metals in a single compound may lead to cooperative interactions between them, such as those observed in heterogeneous catalysis, and there is also the possibility for stereo- or regioselective catalysis. Heterogeneous catalysts in which late transition metals are dispersed on a Lewis acid (TiO_2 or Al_2O_3) support often show increased catalytic activity.[5−9] Such strong metal−support interactions (SMSI) are not well understood but have been attributed to the electronic communication between the metals and cooperative activation of substrates by the different metal centers.[10,11]

For the synthesis of related homogeneous systems we have used an early transition metal complex of a bifunctional ligand as a so-called metalloligand for a late transition metal. For example we reported on the synthesis of a monomeric (mercaptoacetato)zirconocene complex that acted as metalloligand to form heterobimetallic Zr/Ni and Zr/Pd complexes.[12] Furthermore, we described the synthesis of macrocyclic, dimeric zirconocene complexes as metalloligands by using thioglycolates as bridging ligands, and the formation of a tetranuclear Zr/Mo complex.[13] In the present study, we prepared Au^I-based metalloligands. Thus, we describe the synthesis of phosphanylgold thiolates from mercaptoacetic and mercaptopropionic acid and their reactions with $[Cp^\circ{}_2ZrMe_2]$ to give trinuclear Zr/Au complexes. The formation of linearly coordinated thiolato complexes is a well-known property of Au^I that is also important for our purposes, since an attempt to prepare a related bis(phosphane)nickel thiolate as a metalloligand led only to formation of the energetically stable chelate complex.[14]

Results and Discussion

Gold(I) Thiolates $[Au\{S(CH_2)_nCOOH\}]$ (n = 1, 2)

Gold(I) thiolates are well known.[15] Their preparation usually starts from gold(III), in the form of sodium tetrachloroaurate(III) or the corresponding acid, which then requires a reduction step. Bishop et al.[16] described the synthesis of $[Au(SCH_2COOH)]$ using ethyl 2-hydroxyethyl sulfide as reducing agent. We found that $HSCH_2COOH$ and $HS(CH_2)_2COOH$ also function as reductants to give nearly quantitative yields of the thiolates $[Au(SCH_2COOH)]$ and $[Au(SCH_2CH_2COOH)]$.

(Phosphane)gold(I) Thiolates $[Au\{S(CH_2)_nCOOH\}(PMe_2Ph)]$ [n = 1 (1), n = 2 (2)]

Bishop et al.[16] also reported the synthesis of $[Au(SCH_2COOH)(PPh_3)]$, which is only sparingly soluble in ethanol.

[a] Institut für Anorganische Chemie der Universität Leipzig
Johannisallee 29, 04103 Leipzig, Germany
[‡] Crystal structure determinations

To increase the solubility in common solvents, which is important for the introduction of the second metal in subsequent reactions, we used PMe_2Ph instead of PPh_3. $[Au(SCH_2COOH)(PMe_2Ph)]$ (**1**) and $[Au(SCH_2CH_2COOH)(PMe_2Ph)]$ (**2**) were obtained by treating the gold(I) thiolates $[Au(SCH_2COOH)]$ and $[Au(SCH_2CH_2COOH)]$ with 1 equiv. of PMe_2Ph in ethanol at room temperature; **1** was obtained as a pale yellow solid, but **2** was only obtained as a yellow oil. Both complexes are soluble in THF and were characterized by ^1H, ^{31}P, ^{13}C NMR and IR spectra. In the ^1H NMR spectra the protons of the carboxyl groups were observed as very broad signals in a range of δ = 10−12 ppm owing to exchange processes. The IR spectrum of **1** shows two strong bands at 1690 and 1303 cm^{-1} for the C=O and C−O stretching vibrations of the COOH group.

Trinuclear Gold(I)−Zirconocene Complexes $[Cp^\circ_2Zr\{\kappa^1O\text{-}OOC(CH_2)_nSAu(PMe_2Ph)\}\{\kappa^2O,O'\text{-}OOC(CH_2)_n\text{-}SAu(PMe_2Ph)\}]$ [n = 1 (3), n = 2 (4)]

The trinuclear Zr/Au complexes **3** and **4** were obtained by reaction of the metalloligands **1** and **2** with $[Cp^\circ_2ZrMe_2]$ in a molar ratio of 2:1 (Scheme 1). Both complexes were obtained as pale yellow solids, and X-ray quality crystals of **4** were grown from a concentrated solution in THF at room temperature.

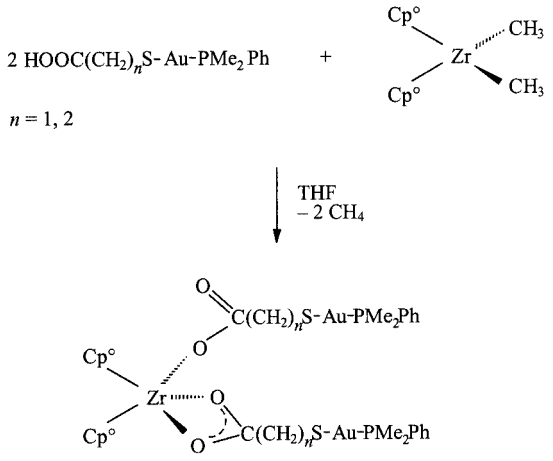

Scheme 1

Structural Studies on 4

An ORTEP plot of **4** is shown in Figure 1. The trinuclear complex crystallizes in the triclinic space group $P\bar{1}$ with two molecules of the complex and three THF molecules in the unit cell. One of the THF molecules is disordered and lies on the inversion center. The zirconium atom is coordinated by two η^5-cyclopentadienyl rings, as well as one monodentate and one bidentate carboxylato group, so that the Zr atom has 18 valence electrons. This bonding mode was also observed in related zirconocene bis(carboxylates)[17−19] and in a zirconocene mercaptoacetate[12] and the Zr−O bond lengths and O−Zr−O bond angles are similar to these complexes. Both Au atoms are almost linearly coordinated by one P and one S donor [S1−Au1−P1 174.63(6), S2−Au2−P2 176.83(6)°]. The Au−S and Au−P bond lengths are similar to those in related Au^I complexes, e.g., $[Au(SCH_2COOH)(PPh_3)]$, $[Au(SCMe_2COOH)(PPh_3)]$[16] and $[Au(SPh)(PPh_3)]$.[20] The Au1−Au2 distance of 3.2992(4) Å suggests intramolecular gold−gold interaction. Intermolecular Au−Au contacts are very common and are also found for other gold(I) complexes with sulfur-containing ligands; the distances observed range from 2.9 to 3.5 Å[21] and are attributed to relativistic effects in the valence orbitals of gold atoms,[22] e.g., $[Au(SPh)(PPh_3)]$ [Au−Au 3.1355(3) Å].[20] To facilitate this interaction the S−Au−P fragments in **4** have an almost perpendicular arrangement [torsion angles: P1−Au1−Au2−P2 116.5(3), S1−Au1−Au2−S2 118.9(3)°; see Figure 2]. This arrangement is similar to that in $[Au(SPh)(PPh_3)]$, in which torsion angles of 96.1 and 110.8° were observed.[20] Depending on the structural properties of the ligands, in other complexes the "head-to-head" or "head-to-tail" arrangements were found.

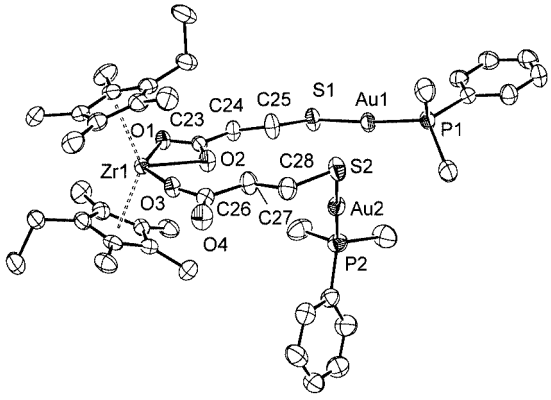

Figure 1. ORTEP plot of **4** (50% probability thermal ellipsoids are shown; hydrogen atoms are omitted for clarity); selected bond lengths [Å] and angles [°]: Zr1−O1 2.352(4), Zr1−O2 2.213(4), Zr1−O3 2.067(4), Au1−S1 2.302(2), Au1−P1 2.265(2), Au2−S2 2.306(2), Au2−P2 2.268(2), O1−C23 1.260(7), O2−C23 1.279(6), O3−C26 1.291(7), O4−C26 1.226(7); O1−Zr1−O2 56.5(1), O2−Zr1−O3 78.9(1), S1−Au1−P1 174.63(6), S2−Au2−P2 176.83(6), O1−C23−O2 117.0(5), O3−C26−O4 123.2(6)

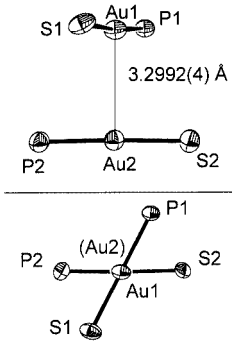

Figure 2. Front and top view of the S−Au−P fragments in **4**

Spectroscopic Studies on 3 and 4

The IR spectra of **3** and **4** exhibit two strong bands for the C=O and C−O stretching vibrations of the monodentate ligand, and two strong bands for the asymmetric and symmetric vibrations of the bidentate ligand. Compared to the free carboxyl group in **1**, the C=O and C−O vibration bands in the heterobimetallic complexes are shifted to lower wavenumbers owing to coordination to the Lewis acidic zirconium atoms.

In the NMR spectra of **3** and **4** the CH_2 groups of the two metalloligands next to the carboxylate groups were observed as one signal for both complexes. On the basis of the molecular structure of **4** in the solid state, we would expect at least two signals for these CH_2 groups owing to the different bonding mode of the ligands. Therefore the NMR spectroscopic data suggest a rapid dynamic process in which the carboxylato groups alternate between mono- and bidentate bonding. Such dynamics are well known and were observed for most zirconocene bis(carboxylates)[17−19] and in a zirconocene mercaptoacetate[12] and dimeric zirconocene thioglycolates.[13] Low-temperature NMR experiments on **3** and **4** down to −70 °C failed to freeze out this dynamic process, and we only observed slight broadening of the signals.

Preliminary catalytic investigations in oxidation reactions were performed with **4**. We used the model system O_2/PPh_3, and the ratio PPh_3/PPh_3O was determined by ^{31}P NMR spectroscopy. Complex **4** catalyzes the oxidation of PPh_3 in a molar ratio of 1:10 without apparent decomposition (only the PMe_2Ph ligands are partly oxidized) over 1.5 h at 50 °C. On the basis of earlier investigations on the catalytic properties of a similar zirconocene mercaptoacetato complex,[12] we assume that the catalytic activity of **4** is due to the Lewis acidic Zr atom, which is coordinatively unsaturated in solution. Investigations on possible interactions between the two metals in these complexes are in progress.

Experimental Section

General Details: All operations except the synthesis of the gold thiolates were carried out under dry nitrogen using standard Schlenk techniques. The reagents and solvents were purified by standard procedures. The ^1H, ^{13}C and ^{31}P NMR spectra were recorded with an AVANCE DRX 400 spectrometer. The IR spectra were recorded with an FT-IR spectrometer Perkin−Elmer System 2000 in the range 400−4000 cm^{-1}. [Cp°$_2$ZrMe$_2$][23] was prepared by a literature procedure. Mercaptoacetic and mercaptopropionic acid were purchased from Fluka. $H[AuCl_4]$ was donated by Degussa.

[Au{S(CH$_2$)$_n$COOH}] (n = 1, 2): An aqueous solution of $H[AuCl_4]$ was treated with an aqueous solution of a mercaptocarboxylic acid ($HOOCCH_2SH$, $HOOCCH_2CH_2SH$) in a molar ratio of 1:3. Both gold thiolates were obtained as pale yellow solids in nearly quantitative yields and were characterized by elemental analyses.

[Au(SCH$_2$COOH)(PMe$_2$Ph)] (1): 0.31 mL (2.2 mmol) of PMe_2Ph was added to a suspension of 0.64 g (2.2 mmol) of [Au(SCH$_2$COOH)] in 20 mL of ethanol. After about 30 min, the yellow solution became clear. Complete removal of the solvent gave a yellow oil, which was dissolved in 10 mL of THF. At −20 °C, **1** was obtained as a nearly colorless precipitate. Yield: 0.70 g (73%); m.p. 134−136 °C. ^1H NMR ($CDCl_3$, 25 °C, 400 MHz): δ = 1.81 [d, $^2J_{H,P}$ = 9.7 Hz, 6 H, P(CH_3)$_2$Ph], 3.68 (s, 2 H, SCH_2COOH), 7.49 (br. m, 3 H, $PMe_2C_6H_5$), 7.51 (m, 2 H, $PMe_2C_6H_5$) ppm, OH signal not observed. $^{13}C\{^1H\}$ NMR ($CDCl_3$, 25 °C, 100.6 MHz): δ = 16.3 [d, $^1J_{C,P}$ = 35.9 Hz, P(*C*H$_3$)$_2$Ph], 32.1 (s, S*C*H$_2$COOH), 130.0 (d, $^3J_{C,P}$ = 11.3 Hz, *m*-C of PC_6H_5), 132.3 (br. s, *p*-C of PC_6H_5), 132.5 (s, *o*-C of PC_6H_5), 132.6 (d, $^1J_{C,P}$ = 57.3 Hz, *ipso*-C of PC_6H_5), 176.5 (s, SCH$_2$*C*OOH) ppm. Signals for THF are observed in the ^1H and ^{13}C NMR spectrum. $^{31}P\{^1H\}$ NMR ($CDCl_3$, 25 °C, 162 MHz): δ = 11.2 (s, *P*Me$_2$Ph). IR (KBr pellet): $\tilde{\nu}$ = 1690 (C=O), 1303 (C−O) cm^{-1}. $C_{10}H_{14}AuO_2PS\cdot1/4THF$ (444.25): calcd. C 29.7, H 3.6, S 7.2; found C 29.1, H 4.3, S 6.9.

[Au(SCH$_2$CH$_2$COOH)(PMe$_2$Ph)] (2): 0.21 mL (1.4 mmol) of PMe_2Ph was added to a suspension of 0.44 g (1.4 mmol) of [Au(SCH$_2$CH$_2$COOH)] in 20 mL of ethanol. After about 30 min, the yellow solution became clear. Complete removal of the solvent gave a yellow oil which was dissolved in 20 mL of THF. However, in contrast to **1**, complex **2** could only be isolated as an oil. Yield: 0.45 g (85%). ^1H NMR ($CDCl_3$, 25 °C, 400 MHz): δ = 1.75 [d, $^2J_{H,P}$ = 8.8 Hz, 6 H, P(CH_3)$_2$Ph], 2.70 (t, $^3J_{H,H}$ = 7.2 Hz, 2 H, SCH_2CH$_2$COOH), 3.07 (t, $^3J_{H,H}$ = 7.2 Hz, 2 H, SCH$_2$CH_2COOH), 7.44 (br. s, 3 H, $PMe_2C_6H_5$), 7.62 (m, 2 H, $PMe_2C_6H_5$) ppm, OH signal not observed. $^{13}C\{^1H\}$ NMR ($CDCl_3$, 25 °C, 100.6 MHz): δ = 16.4 [d, $^1J_{C,P}$ = 32.8 Hz, P(*C*H$_3$)$_2$Ph], 23.4 (s, S*C*H$_2$CH$_2$COOH), 42.0 (s, SCH$_2$*C*H$_2$COOH), 129.7 (d, $^3J_{C,P}$ = 10.8 Hz, *m*-C of PC_6H_5), 131.9 (d, $^4J_{C,P}$ = 1.8 Hz, *p*-C of PC_6H_5), 132.2 (d, $^2J_{C,P}$ = 13.5 Hz, *o*-C of PC_6H_5), 133.8 (d, $^1J_{C,P}$ = 51.3 Hz, *ipso*-C of PC_6H_5), 177.2 (s, SCH$_2$*C*OOH) ppm. $^{31}P\{^1H\}$ NMR ($CDCl_3$, 25 °C, 162 MHz): δ = 7.2 (s, *P*Me$_2$Ph) ppm.

[Cp°$_2$Zr{κ^1*O*-OOCCH$_2$SAu(PMe$_2$Ph)}{κ^2*O*,*O*′-OOCCH$_2$SAu(PMe$_2$Ph)}] (3): A solution of 0.08 g (0.2 mmol) of [Cp°$_2$ZrMe$_2$] in 5 mL of THF was added to a solution of 0.17 g (0.4 mmol) of **1** in 5 mL of THF. The reaction mixture was stirred overnight at room temperature. Concentration of the solution to about half of its volume and addition of 10 mL of petroleum ether gave a pale yellow precipitate of **3** at −20 °C. Yield: 0.21 g (85%); m.p. 163−169 °C. ^1H NMR ($CDCl_3$, 25 °C, 400 MHz): δ = 0.84 (t, $^3J_{H,H}$ = 7.6 Hz, 6 H, $C_5Me_4CH_2CH_3$), 1.82 [d, $^2J_{H,P}$ = 10.0 Hz, 12 H, P(CH_3)$_2$Ph], 1.88 [s, 12 H, $C_5Et(CH_3)_4$], 1.90 [s, 12 H, $C_5Et(CH_3)_4$], 2.38 (q, $^3J_{H,H}$ = 7.6 Hz, 4 H, $C_5Me_4CH_2CH_3$), 3.74 (s, 4 H, SCH_2COO), 7.46 (br. m, 6 H, $PMe_2C_6H_5$), 7.77 (m, 4 H, $PMe_2C_6H_5$) ppm. $^{13}C\{^1H\}$ NMR ($CDCl_3$, 25 °C, 100.6 MHz): δ = 11.7, 11.9 [s, $C_5Et(CH_3)_4$], 15.0 (s, $C_5Me_4CH_2CH_3$), 16.6 [d, $^1J_{C,P}$ = 35.1 Hz, P(*C*H$_3$)$_2$Ph], 19.7 (s, $C_5Me_4CH_2CH_3$), 32.9 (s, S*C*H$_2$COO), 121.4, 122.2, 127.1 (s, C_5EtMe_4), 129.7 (d, $^3J_{C,P}$ = 11.1 Hz, *m*-C of PC_6H_5), 132.0 (s, *p*-C of PC_6H_5), 132.5 (d, $^2J_{C,P}$ = 13.1 Hz, *o*-C of PC_6H_5), 133.6 (d, $^1J_{C,P}$ = 55.3 Hz, *ipso*-C of PC_6H_5), 183.1 (s, SCH$_2$*C*OO) ppm. $^{31}P\{^1H\}$ NMR ($CDCl_3$, 25 °C, 162 MHz): δ = 10.7 (s, *P*Me$_2$Ph) ppm. IR (KBr pellet): $\tilde{\nu}$ = 1635 (C=O), 1523, 1323 (O−C−O), 1191 (C−O) cm^{-1}. $C_{42}H_{60}Au_2O_4P_2S_2Zr$ (1240.15): calcd. C 40.6, H 4.8, S 5.1; found C 38.2, H 4.9, S 4.2.

[Cp°$_2$Zr{κ^1*O*-OOC(CH$_2$)$_2$SAu(PMe$_2$Ph)}{κ^2*O*,*O*′-OOC(CH$_2$)$_2$SAu(PMe$_2$Ph)}] (4): A solution of 0.16 g (0.39 mmol) of [Cp°$_2$ZrMe$_2$] in 10 mL of THF was added to a solution of 0.35 g (0.79 mmol) of **2** in 10 mL of THF. The reaction mixture was stirred overnight at room temperature. Concentration of the solution to about half of its volume gave a pale yellow precipitate of **4** at −20 °C. Suitable crystals for a structure analysis were obtained from a saturated THF solution at room temperature. Yield: 0.38 g (77%); m.p. 95−98 °C. ^1H NMR ($CDCl_3$, 25 °C, 400 MHz): δ =

Table 1. Crystal data and data collection parameters for **4**

Empirical formula	$C_{44}H_{64}Au_2O_4P_2S_2Zr\cdot1.5THF$
Mr	1376.32
T [K]	223(2)
λ [Å]	0.71073
Crystal system	triclinic
Space group	$P\bar{1}$ (no. 2)
a [Å]	11.2310(14)
b [Å]	15.5919(19)
c [Å]	15.895(2)
α [°]	89.650(2)
β [°]	73.971(2)
γ [°]	86.307(2)
V [Å^3]	2669.5(6)
Z	2
Density (calcd.) [Mg/m^3]	1.712
Absorption coefficient [mm^{-1}]	5.855
F(000)	1360
Θ range [°]	1.31−28.71
Reflections collected	27960
Independent reflections [$R_{(int)}$ = 0.0597]	12413
Refinement method	full-matrix least squares on F^2
Data/restraints/parameters	12413/8/562
GOF on F^2	0.976
Final *R* indices [$I > 2\sigma(I)$]	R_1 = 0.0411, wR_2 = 0.1026
R indices (all data)	R_1 = 0.0636, wR_2 = 0.1213
Largest difference peak/hole [e·Å^{-3}]	1.989/−1.876

0.82 (t, $^3J_{H,H}$ = 7.6 Hz, 6 H, $C_5Me_4CH_2CH_3$), 1.82−1.79 [overlapping signals, 36 H, $P(CH_3)_2Ph$ and $C_5Et(CH_3)_4$], 2.26 (q, $^3J_{H,H}$ = 7.6 Hz, 4 H, $C_5Me_4CH_2CH_3$), 2.71 (t, $^3J_{H,H}$ = 8.8 Hz, 4 H, SCH_2CH_2COO), 3.29 (t, $^3J_{H,H}$ = 8.8 Hz, 4 H, SCH_2CH_2COO), 7.46 (m, 6 H, $PMe_2C_6H_5$), 7.75−7.69 (m, 4 H, $PMe_2C_6H_5$) ppm. $^{13}C\{^1H\}$ NMR ($CDCl_3$, 25 °C, 100.6 MHz): δ = 11.5, 11.7 (s, $C_5Et(CH_3)_4$], 14.9 (s, $C_5Me_4CH_2CH_3$), 16.4 (d, $^1J_{C,P}$ = 34.8 Hz, $P(CH_3)_2Ph$), 19.6 (s, $C_5Me_4CH_2CH_3$), 25.0 (s, SCH_2CH_2COO), 46.7 (s, SCH_2CH_2COO), 121.3, 122.0, 127.1 (s, C_5EtMe_4), 129.8 (d, $^3J_{C,P}$ = 11.0 Hz, *m*-C of PC_6H_5), 132.1 (d, $^4J_{C,P}$ = 2.3 Hz, *p*-C of PC_6H_5), 132.4 (d, $^2J_{C,P}$ = 13.2 Hz, *o*-C of PC_6H_5), 133.5 (d, $^1J_{C,P}$ = 54.4 Hz, *ipso*-C of PC_6H_5), 181.4 (s, SCH_2CH_2COO) ppm. $^{31}P\{^1H\}$ NMR ($CDCl_3$, 25 °C, 162 MHz): δ = 11.6 (s, PMe_2Ph) ppm. IR (KBr pellet): $\tilde{\nu}$ = 1644 (C=O), 1538, 1353 (O−C−O), 1186 (C−O) cm^{-1}. $C_{44}H_{64}Au_2O_4P_2S_2Zr\cdot1.5THF$ (1376.32): calcd. C 43.6, H 5.6, S 4.6; found C 44.1, H 5.1, S 4.2.

Data Collection and Structural Refinement of 4: The X-ray diffraction data[24] were measured with a Siemens diffractometer of the type SMART CCD (Mo-K_α = 0.71073 Å). All observed reflections were used for refinement (SAINT) of the unit cell parameters. Empirical absorption correction with SADABS.[24] The structures was solved by direct methods (SHELXTL PLUS).[24] Zr, Au, P, S, O, and C atoms were refined anisotropically; H atoms were refined isotropically in calculated positions. Table 1 lists crystallographic details. CCDC-177457 contains the supplementary crystallographic data for this paper. These data can be obtained free of charge at www.ccdc.cam.ac.uk/conts/retrieving.html or from the Cambridge Crystallographic Data Centre, 12, Union Road, Cambridge CB2 1EZ, UK [Fax: (internat.) + 44-1223/336-033; E-mail: deposit@ccdc.cam.ac.uk].

Acknowledgments

We gratefully acknowledge support from the Deutsche Forschungsgemeinschaft (Graduiertenkolleg 378) and we thank the Degussa AG for a generous donation of $H[AuCl_4]$.

[1] D. W. Stephan, *Coord. Chem. Rev.* **1989**, *95*, 42.
[2] T. A. Wark, D. W. Stephan, *Organometallics* **1989**, *8*, 2836.
[3] P. Kalck, C. Serra, C. Machet, R. Broussier, B. Gautheron, G. Delmas, G. Trouve, M. Kubicki, *Organometallics* **1993**, *12*, 1021.
[4] A. Schneider, L. H. Gade, M. Breuning, G. Bringmann, I. J. Scowen, M. McPartlin, *Organometallics* **1998**, *17*, 1643.
[5] S. Naito, *J. Chem. Soc., Chem. Commun.* **1985**, 1212.
[6] J. H. Sinfelt, *Sci. Am.* **1985**, *235*, 90.
[7] T. E. Whyte, R. A. Dalla Betta, *Catal. Rev.-Sci. Eng.* **1982**, *24*, 567.
[8] A. T. Bell, *Catal. Rev.-Sci. Eng.* **1981**, *23*, 203.
[9] I. E. Maxwell, *Adv. Catal.* **1981**, *30*, 1.
[10] *Metal Support Interactions in Catalysis, Sintering and Redispersion* (Eds.: S. A. Stephenson, J. A. Dumesic, R. T. K. Baker, E. Ruckenstein), Van Nostrand Reinhold Co., New York, **1987**.
[11] *Strong Metal Support Interactions* (Eds.: R. T. K. Baker, S. J. Tauster, J. A. Dumesic), American Chemical Society, Washington, DC, **1986**.
[12] B. Wenzel, P. Lönnecke, M. Stender, E. Hey-Hawkins, *J. Chem. Soc., Dalton Trans.* **2002**, 478.
[13] B. Wenzel, P. Lönnecke, E. Hey-Hawkins, *Organometallics*, in press.
[14] B. Wenzel, P. Lönnecke, M. Stender, E. Hey-Hawkins, *Z. Anorg. Allg. Chem.,* accepted.
[15] J. Vicente, M. T. Chicote, C. Rubio, *Chem. Ber.* **1996**, *129*, 327; P. J. Bonasia, D. E. Gindelberger, J. Arnold, *Inorg. Chem.* **1993**, *32*, 5126; R. M. Dávila, A. Elduque, T. Grant, R. J. Staples, J. P. Fackler, Jr., *Inorg. Chem.* **1993**, *32*, 1749; and references cited therein.
[16] P. Bishop, P. Marsh, A. K. Brisdon, B. J. Brisdon, M. F. Mahon, *J. Chem. Soc., Dalton Trans.* **1998**, 675; and references cited therein.
[17] W. A. Howard, T. M. Trnka, M. Waters, G. Parkin, *J. Organomet. Chem.* **1997**, *528*, 95.
[18] U. Thewalt, T. Güthner, *J. Organomet. Chem.* **1989**, *361*, 309.
[19] H.-M. Gau, C.-T. Chen, T.-T. Jong, M.-Y. Chien, *J. Organomet. Chem.* **1993**, *448*, 99.
[20] M. Nakamoto, W. Hiller, H. Schmidbaur, *Chem. Ber.* **1993**, *126*, 605; and references cited therein.
[21] P. G. Jones, *Gold Bull.* **1981**, *14*, 102; **1983**, *16*, 114; **1986**, *19*, 46; and references cited therein.
[22] P. Pyykkö, J. P. Desclaux, *Acc. Chem. Res.* **1979**, *12*, 276.
[23] R. S. Threlkel, J. E. Bercaw, *J. Organomet. Chem.* **1977**, *136*, 1.
[24] Absorption correction with SADABS (G. M. Sheldrick, *SADABS, Program for Scaling and Correction of Area-detector Data*). Structure solution with SHELXS-97 (G. M. Sheldrick, *SHELXS-97, Program for Crystal Structure Solution*, Universität Göttingen, **1997**) and refinement with SHELXL-97 (G. M. Sheldrick, *SHELXL-97, Program for the Refinement of Crystal Structures*, Universität Göttingen, **1997**).

Received January 16, 2002
[I02030]

Syntheses, Characterization, X-ray Crystal Structure, Redox and Photophysical Properties of Polypyridylruthenium(II) Complexes Containing Carboxylate-Substituted Pyridyltriazoles

Bedri Mehmetaj,[a][‡] Jaap G. Haasnoot,*[a] Luisa De Cola,[b] Gerard A. van Albada,[a] Ilpo Mutikainen,[c] Urho Turpeinen,[c] and Jan Reedijk[a]

Keywords: Ruthenium / N ligands / Crystal structure / Photophysical properties / Redox potentials

The syntheses and properties of two novel $[Ru(bpy)_2(L–L')]^{n+}$ complexes with **L–L′** = 3-carboxy-5-(pyrid-2′-yl)-1,2,4-triazole (**H_2cpt**) or 3-(ethoxycarbonyl)-5-(pyrid-2′-yl)-1,2,4-triazole (**Hcept**) ligands are described. Previous publications on Ru^{II} complexes containing (pyrid-2′-yl)-1,2,4-triazoles revealed that their coordination is possible via N1 and N4 of the triazole ring. ^{1}H NMR spectroscopic data and the crystal structure of $[Ru(bpy)_2(cept)]PF_6{\cdot}H_2O$ (**2**) indicate that the coordination of the **Hcpt**$^-$ and **cept**$^-$ occurs via N1 of the triazole ring. The crystals of **2** are monoclinic and belong to the space group $P2_1/n$ with a = 12.339(7), b = 16.512(7), c = 16.802(8) Å, β = 110.29(4)°, and Z = 4. A water molecule is hydrogen-bonded to the carbonyl oxygen atom of the ethoxycarbonyl group with an O···O distance of 2.891 Å. Spectroscopic measurements reveal that **H_2cpt** and **Hcept** are strong σ-donor ligands. When coordinated to a ruthenium(II) centre, both triazole ligands reported in this study lost their acidic triazole hydrogen atoms and became negatively charged, resulting in even stronger σ-donor ligands, as demonstrated by a negative shift of their redox potentials compared to the complexes containing the neutral ligand. The complexes reported in this study showed ^{3}MLCT-based luminescence emission, both at room temperature and at 77 K.
(© Wiley-VCH Verlag GmbH, 69451 Weinheim, Germany, 2002)

Introduction

A considerable number of $[Ru(bpy)_2(L\text{-}L')]^{n+}$ systems with **L−L′** = substituted (pyrid-2′-yl)-1,2,4-triazole ligands have been reported by Hage et al.[1−14] Electrochemical, absorption, and emission measurements revealed that triazoles are strong σ-donor and weak π-acceptor ligands, thus lowering the oxidation potential of the metal ion. Additionally, due to a higher π* level of the triazole compared with the π* level of the **bpy** ligand, both the first reduction and the lowest exited states of these complexes are **bpy**-based.[1] Therefore, a study towards the related ligands with a variety of substituents is relevant.

In this paper the synthesis and properties of a $Ru(bpy)_2$ moiety with 3-carboxy-5-(pyrid-2′-yl)-1,2,4-triazole (**H_2cpt**) and 3-(ethoxycarbonyl)-5-(pyrid-2′-yl)-1,2,4-triazole (**Hcept**) ligands is described. The selection of the **H_2pct** and **Hpcet** ligands was made to study the effect of electron-withdrawing groups in the photophysical and electrochemical properties of the ruthenium(II) complexes. Previous publications, mainly from our laboratory[1−14] of a number of ruthenium(II) complexes containing (pyrid-2′-yl)-1,2,4-triazoles showed that coordination is possible via N1 and via N4 of the triazole ring. A crystal structure of the $Ru(bpy)_2(cept)](PF_6){\cdot}H_2O$ (**2**) revealed that the triazole ring is coordinated to ruthenium(II) via N1. This coordination mode was also observed for the 3-methyl-5-(pyrid-2′-yl)-1,2,4-triazole (**3Meptz**),[1] and is predicted for the **H_2cpt**-based complex. The structure and properties of the complexes were investigated with the use of ^{1}H NMR spectroscopy, ESI MS, CV measurements, UV/Vis absorption, and time-resolved emission spectroscopy.

[‡] Current address: Delft University of Technology − Laboratory for Materials Science, Rotterdamseweg 137, 2628 AL Delft, The Netherlands
[a] Leiden Institute of Chemistry, Gorlaeus Laboratories, Leiden University,
P. O. Box 9502, 2300 RA Leiden, The Netherlands
Fax: (internat.) + 31-71/527-4451
E-mail: haasnoot@chem.leidenuniv.nl
[b] Institute of Molecular Chemistry, Molecular Photonics Group, University of Amsterdam,
Nieuwe Achtergracht 166, 1018 WV Amsterdam, The Netherlands
[c] Laboratory of Inorganic Chemistry, Department of Chemistry, University of Helsinki,
P. O. Box 55 (A. I. Virtasen aukio 1), 00014 Finland

Results and Discussion

Ligand Syntheses

Synthesis of the ligands (structures given in Figure 1) was straightforward by starting from pyridylamidrazone and diethyl oxalate, in a ratio 1:4 to avoid possible formation of a dimer, and heating under reflux in absolute ethanol for 1 h (modified procedure[15]). However, contrary to the results reported in the literature, two different products were obtained. The ratio was found to be close to 1:1. The first fraction appeared to be a hydrolysed ester (acid), while the second fraction was the ester itself.

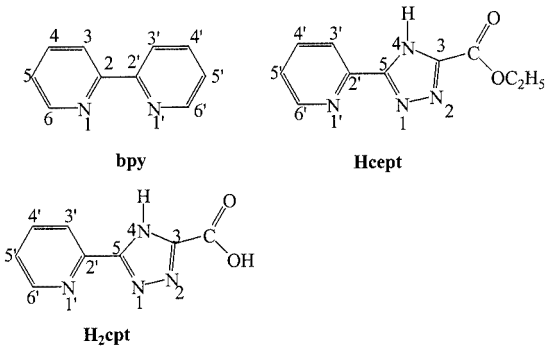

Figure 1. Structural formula of the ligands used in this study

The chemistry of amidrazones is diverse,[15−28] and offers the possibility of obtaining different products with a slight change in the experimental conditions. It is not clear how the reaction for obtaining the hydrolysed ligand may proceed. A possible reaction route is shown in Scheme 1. The triazole hydrogen atom forms a hydrogen bond to the free oxygen atom of the ethoxycarbonyl group, reducing the electron density in its carbon centre. The water molecule then attacks the partially positive carbon atom, followed by the hydrolysis of the ester. A supporting factor could be the activation of a water molecule by hydrogen-bonding to N2 of the triazole (see Scheme 1). In order to testify to these hypotheses, the same reaction was performed with an *N*-substituted triazole. The reaction was unsuccessful, and no products could be isolated. However, there are several possible routes for the hydrolysis of the ester, and more experiments would be needed to prove this mechanism.

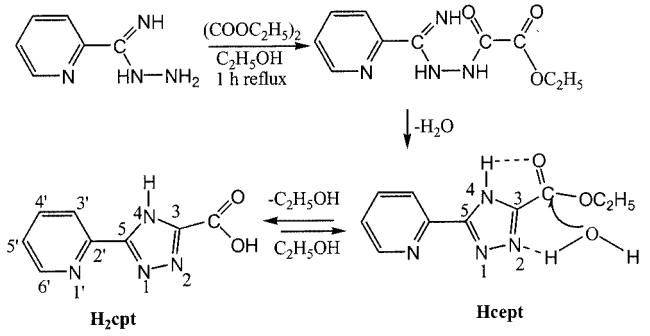

Scheme 1. Reaction route and mechanism for the **H_2cpt** and **Hcept** ligand syntheses

Syntheses and Characterization of the Complexes

The synthesis of the metal complexes was achieved by using an excess of one of the ligands and *cis*-Ru(bpy)$_2$Cl$_2$. The **Hcept** ligand lost its triazole hydron and acquired a negative charge upon coordination to the ruthenium(II) centre. This phenomenon was known from previous studies[1,10,14] and has been attributed to the increased acidity of the coordinated triazole ligands. In the **H_2cpt**-based complex, both triazole and carboxylic hydrons were found to be ionised.

The mass of the complexes was determined using mass spectrometry. Both complexes reported showed mono-positively charged complex ions [M$^+$].

Another important technique for elucidating the structure of the ruthenium(II) complexes is ^{1}H NMR spectroscopy. The chemical shifts of complex **2** are shown in Table 1. For the sake of comparison the ^{1}H NMR chemical shifts of [Ru(bpy)$_2$(3Meptz)]$^+$ are also presented. The assignment of the ^{1}H NMR spectra of the complex presented in Table 1 was made based on literature data of the related pyridyltriazole complexes,[1,14] and the difference in coupling constants (^3J) of 3-H and 6-H of the pyridine ring.

The ^{1}H NMR spectrum of [Ru(bpy)$_2$(Hcpt)]$^+$ is rather complex and the assignment is difficult. There are two sets of peaks with the same coupling constants, but different intensities (approximately 3:1 for the ones with higher chemical shifts), which suggests that the **H_2cpt** ligand is partially dehydronated (higher chemical shift). Such a claim is also supported by CV data (see next section).

Description of the X-ray Structure of [Ru(bpy)$_2$(cept)]-(PF$_6$)·H$_2$O (2)

A projection of the structure of the title compound, the atom numbering, and the position of the hydrogen bonds is presented in Figure 2. Selected bond lengths and angles, and hydrogen-bond information are presented in Table 2. The ruthenium(II) ion coordinates to two **bpy** molecules in the *cis* configuration and one **cept**$^-$ ion. The "bite angles" of the coordinated ligands are 78−79°, similar to the chelating angles observed for similar complexes.[1,10,12] The Ru−N distances, 2.04−2.06 Å, are in the normal range for this type of ruthenium(II) complexes.[1,13,29] The relatively long distance between the ruthenium(II) centre and the nitrogen atom of the pyridine ring of the **cept**$^-$ ligand might be caused by the limited π backbonding of the pyridyltriazole-containing ruthenium(II) complexes. Steric factors might also play a role in these bond lengths. Similar distances were found for the analogous mononuclear **bpt**$^-$-containing ruthenium complex.[13]

As can be seen in Figure 2, the **cept**$^-$ ligand is coordinated to ruthenium(II) via N111 and N121. This coordination mode was observed for other pyridyltriazoles containing bulky groups bound to the remaining carbon atom of the triazole ring.[1] A water molecule is relatively strongly hydrogen-bonded via H1 to O2 with an O1···O2 distance of 2.89 Å, and via H2 to F1 and F2 of a neighbouring PF$_6^-$ ion with an O1···F1 distance of 2.91 Å (see Table 2). No

Table 1. The ^{1}H NMR chemical shifts versus TMS of the **Hcept** and **3Meptz** ligands in $[Ru(bpy)_2(L-L')]^+$ complexes; values between parentheses present the difference in chemical shift of the pyridyltriazole ligands upon coordination

Compound[a]	3′-H	4′-H	5′-H	6′-H	CH_2	CH_3
$[Ru(bpy)_2(cept)]^+$	8.01 (−0.11)	7.49 (−0.07)	7.35 (−0.66)	7.79 (−0.93)	4.25 (−0.05)	1.28 (−0.05)
$[Ru(bpy)_2(3Meptr)]^+$	8.02 (+0.00)	7.99 (+0.09)	7.23 (−0.20)	7.67 (−0.96)		2.20 (−0.16)

[a] From ref.[14]

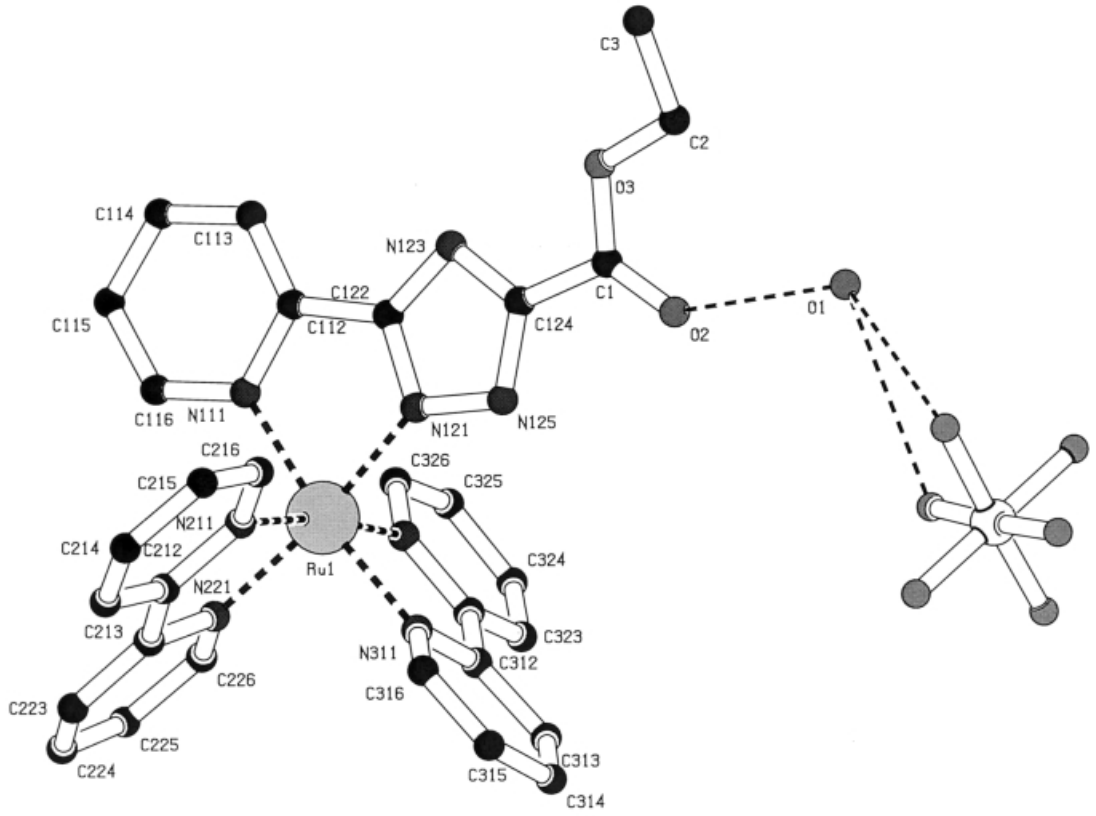

Figure 2. PLUTON drawing and numbering system of the $[Ru(bpy)_2(cept)](PF_6)\cdot H_2O$; the hydrogen atoms were omitted for reasons of clarity; hydrogen bonds from the water molecule to carboxylate and PF_6 are indicated by dashed lines

hydrogen bonds were found in which N123 and N125 of the triazolate ring were involved.

Electrochemical Properties

The highest occupied molecular orbitals (HOMOs) of most of the polypyridylruthenium(II) complexes are metal-centred, while their lowest unoccupied molecular orbitals (LUMOs) are known to be ligand-centred.[30] The oxidation of these complexes leads to the formation of the low-spin ruthenium(III) complexes $[\pi_M\ (t_{2g})^5]$, while the reduction primarily takes place in the π* orbital of the polypyridine ligands.[30]

The redox potentials of the studied complexes and of some similar complexes taken from the literature are reported in Table 3. The complexes were hydronated by addition of a drop of 1 M $HClO_4$ solution in acetonitrile. The oxidation potentials of the hydronated species occurred at higher potentials. This increase in the oxidation potential was caused by the decreased σ-donor capacity of the hydronated triazoles, which led to the stabilisation of the dπ metal orbitals.

The redox behaviour of **2** is similar to complexes of analogous pyridyltriazoles reported in the literature,[1,14] with a small shift to higher values. The reason for that is a decreased σ-donor ability of the **Hcept** ligand. This is due to the presence of an electron-withdrawing group ($COOC_2H_5$) at C-3 of the triazole ring. The cyclic voltammogram of **2** is shown in Figure 3 (**2** and **2a**). The first reduction potentials are attributed to **bpy** ligands.

The redox behaviour of **1** is rather complicated. Both, triazole ring and acid hydrons of the **H_2cpt** ligand are partially dehydronated (see **1** in Figure 3). When a drop of 1 M $HClO_4$ was added to a solution, the first oxidation peak disappeared (see **1a** in Figure 3) and the carboxy group be-

Table 2. Selected bond lengths [Å], angles [°], and hydrogen-bond information for complex $[Ru(bpy)_2cept](PF_6)\cdot H_2O$

Bond lengths [Å]					
Ru(1)−N(111)	2.104(6)	C(112)−C(113)	1.375(10)	N(123)−C(124)	1.348(9)
Ru(1)−N(121)	2.039(5)	C(112)−C(122)	1.465(10)	C(124)−N(125)	1.348(9)
Ru(1)−N(211)	2.063(5)	C(113)−C(114)	1.379(11)	C(124)−C(1)	1.473(10)
Ru(1)−N(221)	2.052(6)	C(114)−C(115)	1.392(11)	C(1)−O(2)	1.202(9)
Ru(1)−N(311)	2.061(6)	C(115)−C(116)	1.398(11)	C(1)−O(3)	1.343(9)
Ru(1)−N(321)	2.051(6)	N(121)−C(122)	1.347(8)	O(3)−C(2)	1.452(9)
N(111)−C(116)	1.338(9)	N(121)−N(125)	1.351(8)	C(2)−C(3)	1.489(13)
N(111)−C(112)	1.367(8)	C(122)−N(123)	1.324(9)		
Bond angles [°]					
N(121)−Ru(1)−N(321)	90.1(2)	N(221)−Ru(1)−N(311)	91.6(2)	N(121)−Ru(1)−N(111)	78.3(2)
N(121)−Ru(1)−N(221)	172.3(2)	N(121)−Ru(1)−N(211)	96.7(2)	N(321)−Ru(1)−N(111)	96.4(2)
N(321)−Ru(1)−N(221)	94.9(2	N(321)−Ru(1)−N(211)	171.1(2)	N(221)−Ru(1)−N(111)	95.3(2)
N(121)−Ru(1)−N(311)	95.1(2)	N(221)−Ru(1)−N(211)	78.9(2)	N(311)−Ru(1)−N(111)	172.0(2)
N(321)−Ru(1)−N(311)	78.9(2)	N(311)−Ru(1)−N(211)	94.8(2)	N(211)−Ru(1)−N(111)	90.6(2)
Hydrogen bond information D−H	*d*(D−H)	*d*(H···A)	DHA [°]	*d*(D···A)	A
O1−H1	0.840	2.105	155.59	2.891	O2
O1−H2[a]	0.840	2.134	153.01	2.908	F1[b]
		2.498	149.4	3.250	F2[b]

[a] Bifurcated H bond. [b] Symmetry operation: $3/2 - x, -1/2 + y, 1/2 - z$.

Table 3. Electrochemical properties of ruthenium(II) complexes containing **H_2cpt** and **Hcept** ligands; values in V, derived from CV measurements in CH_3CN versus Ag/AgCl reference; the scan rate was 100 mV/s

Compound	Oxidation potentials	Reduction potentials (site)	Ref.
$[Ru(bpy)_2(cpt)]$	0.90	−1.51 (bpy), −1.84 (bpy, cpt)	this work
$[Ru(bpy)_2(cept)]^+$	1.09	−1.43 (bpy), −1.69 (bpy)	this work
$[Ru(bpy)_2(Hcpt)]^+$	1.04	−1.51 (bpy), −1.84 (bpy, cpt)	this work
$[Ru(bpy)_2(Hcept)]^{2+}$	1.26	−1.43 (bpy), −1.69 (bpy)	this work
$[Ru(bpy)_2(H_2cpt)]^{2+}$	1.33	not observable	this work
$[Ru(bpy)_2(3Meptr)]^+$	0.8	−1.46 (bpy), −1.72 (bpy), −2.25 (3Meptr)	[1]
$[Ru(bpy)_2(H3Meptr)]^{2+}$	1.2	−1.53 (bpy), −1.86 (bpy),	[1]

came hydronated. Due to the presence of an electron-withdrawing group (COOH) at C-3 of the triazole ring, the remaining triazole hydrogen atom will only be partially ionized (see **1a** in Figure 3, the smaller peak at 1.33 V). The reduction parts of the voltammograms are not clear and an accurate assignment is quite difficult and was not attempted.

The fine-tuning of the electrochemical properties of **1** was possible by changing the pH of the solution. It is anticipated that in a strong acidic environment **H_2cpt** becomes a stronger π-acceptor than **bpy**, and the first reduction poten-

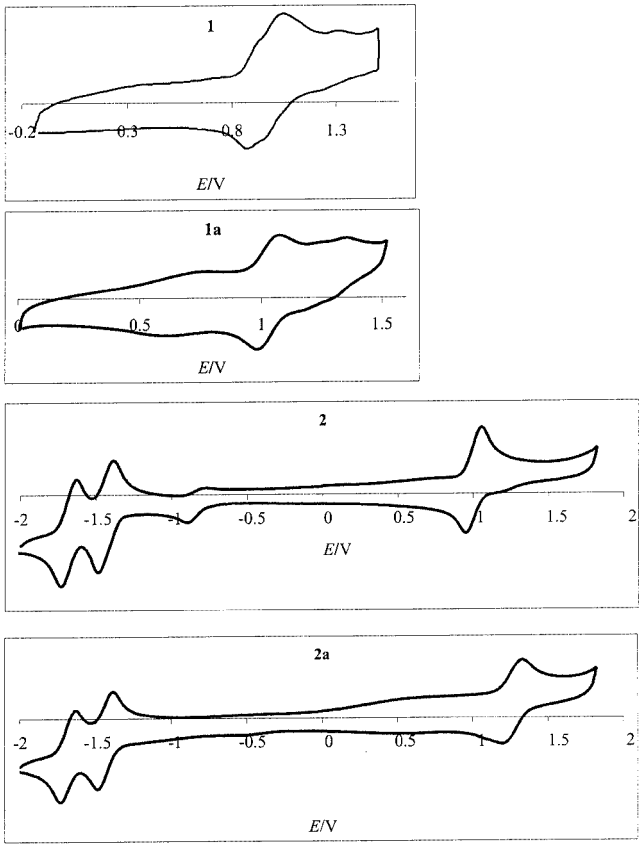

Figure 3. Cyclic voltammograms of the $[Ru(bpy)_2(cpt)]^+$ (**1**), $[Ru(bpy)_2(Hcpt)]^+$ (**1a**) $[Ru(bpy)_2(cept)]^+$ (**2**), and $[Ru(bpy)_2(Hcept)]^{2+}$ (**2a**) referenced against Ag/AgCl

tial, as well as the lowest exited state of **1** could be located at the **H_2cpt** ligand.

Absorption and Emission Spectra

The absorption and emission spectra of **1** and **2** in acetonitrile at room temperature are shown in Figure 4. The wavelengths and extinction coefficients of the lowest energy absorption maxima at 298 K, the wavelengths of the emission maxima at 77 K and 298 K, the luminescence lifetimes at 77 K and 298 K and the luminescence quantum yields at 298 K are summarized in Table 4, where the luminescence properties of the $[Ru(bpt)(bpy)_2]^+$ complex,[7] taken as model compound, are also displayed for comparison.

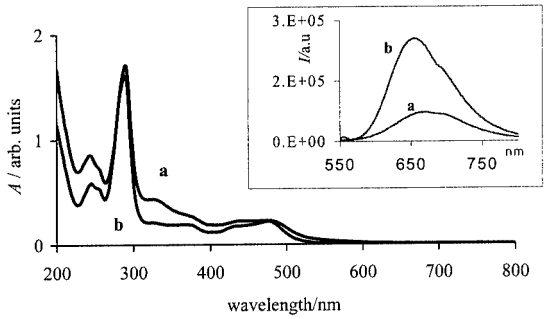

Figure 4. Absorption spectra in acetonitrile solutions at 298 K of $[Ru(bpy)_2(Hcpt)]^+$ (**a**) and $[Ru(bpy)_2(cept)]^+$ (**b**); inset: emission spectra measured at room temperature in acetonitrile approximately 2 10^{-5} M

For the complexes examined, the intense absorption bands in the UV region are due to ligand−centre transitions, and the moderately intense broad bands in the visible region (Figure 4) can be assigned to metal-to-ligand charge-transfer (^{1}MLCT) transitions. When deprotonated, both **H_2cpt** and **Hcept** are expected to be better donors and worse acceptors than **bpy**. The absorption and emission spectra of the two complexes are in agreement with this expectation. Replacement of a **bpy** ligand of $[Ru(bpy)_3]^{2+}$ by an **L−L′** ligand to give $[Ru(L-L')(bpy)_2]^+$ caused an increase in the electronic charge of the metal atom with a consequent red shift of the metal-to-ligand charge-transfer (Ru→bpy) absorption and emission band (Figure 4 and inset). A similar behaviour has been observed for complexes containing imidazole-type bridging ligands.[1,7,10,14]

The luminescence intensity was found to exhibit a mono-exponential decay in all cases. The state responsible for luminescence is likely the lowest ^{3}MLCT excited state, which corresponds to a spin-forbidden (Ru→bpy) transition. Experiments have also been performed in butyronitrile rigid matrix at 77 K and the results obtained are also summarized in Table 4.

All the photophysical properties for the reported compounds are pH-sensitive, and can be tuned by hydronation and dehydronation of the ligands.

Conclusion

In this paper ruthenium(II) mixed-ligand complexes with the newly synthesized ligands **H_2cpt** and **Hcept** are described. The crystal structure of $[Ru(bpy)_2(cept)](PF_6)\cdot H_2O$ has revealed that the **cept$^-$** ligand is coordinated to ruthenium(II) via N1 of the triazole ring. The coordination mode of the related **Hcpt$^-$** ligand is likely to take place via N1 as well. Such a coordination mode results from the presence of the bulky groups at C-3 of the triazole ring, generating steric hindrance to the N4 binding site of the triazole ring.

The CV measurements revealed that the redox potentials for the complexes discussed in this paper are altered with changing pH. The redox potentials of the complexes shift to lower values after dehydronation, which is attributed to the increased σ-donor capacity of the negatively charged ligands. Both photophysical and electrochemical data for the above-mentioned complexes suggest that **Hcpt$^-$** and **cept$^-$** are stronger σ-donor ligands than **bpy**, and that the first reduction processes involve the late ligands. **Hcpt$^-$** and **cept$^-$** play a role of spectator ligands. Both complexes show a moderate emission, which occurs from the lowest-lying triplet excited state ^{3}MLCT.

Experimental Section

Synthesis of the Ligands: A mixture of diethyl oxalate (43 g, 0.29 mol) and 2-pyridylamidrazone (10 g, 0.07 mol) in ethanol (50 mL), prepared as reported by Hage,[1] was heated under reflux for 1 h (modified procedure[15]). Two fractions were obtained in an approximate 1:1 ratio. The first fraction, 3-carboxy-5-(pyrid-2′-yl)-1,2,4-triazole (**H_2cpt**), precipitated immediately, while the second, 3-(ethoxycarbonyl)-5-(pyrid-2′-yl)-1,2,4-triazole (**Hcept**), precipitated after standing for one night at −20 °C. The second fraction was purified by recrystallisation from a acetone/methanol mixture (2:1, v/v). The yield (including both fractions) based on 2-pyridylamidrazone was 4.8 g, 30%.

Table 4. Photophysical properties of ruthenium(II) complexes containing **Hcpt$^-$**, **cept$^-$**, and **bpt$^-$** ligands compared with $[Ru(bpy)_3]^{2+}$

Compound	Absorption λ/nm (ε/10^4 M^{-1}cm^{-1})[a]	Emission (room temp.) λ/nm (τ/ns)[a]	$\varphi_{em(room\ temp.)} \times 10^3$	Emission (77 K) λ/nm (τ/μs)[b]
$[Ru(bpy)_2(Hcpt)]^+$	480 (1.3)	670 (55)	0.83	620 (2.97)
$[Ru(bpy)_2(cept)]^+$	476 (1.1)	656 (93)	2.6	610 (4.00)
$[Ru(bpy)_2(bpt)]^+$	475 (1.13)	678 (160)[c]	3[d]	628 (2.80)
$[Ru(bpy)_3]^{2+}$ [d]	452 (1.30)	620 (0.17)		582 (4.8)

[a] Measured in an aerated acetonitrile solution. [b] Measured in a butyronitrile solution. [c] Measured in a de-aerated acetonitrile solution. [d] Taken from ref.[7]

I. 3-Carboxy-5-(pyrid-2′-yl)-1,2,4-triazole (H_2cpt): M.p. 292 °C. MS: *m/z* = 191 [MH^+]. $C_8H_6N_4O_2$ (190.2): calcd. C 50.53, H 3.20, N 29.46; found C 49.57, H 3.30, N 28.52. IR: $\tilde{\nu}$ = 3271.1 (νN−H, sharp), 3128.2 (νO−H, broad), 1700.2 cm^{-1} (νC=O). ^1H NMR (300 MHz, DMSO): δ = 7.97 (d, 3′-H), 7.54 (m, 4′-H), 8.00 (t, 5′-H), 8.66 (d, 6′-H).

II. 3-(Ethoxycarbonyl)-5-(pyrid-2′-yl)-1,2,4-triazole (Hcept): M.p. 164 °C. MS: *m/z* = 219 [MH^+]. $C_{10}H_{10}N_4O_2$ (218.2): calcd. C 55.04, H 4.62, N 25.67; found C 54.93, H 4.53, N 25.63. IR: $\tilde{\nu}$ = 3161.1 (νN−H, broad), 1733.8 cm^{-1} (νC=O). ^1H NMR (300 MHz, DMSO): δ = 1.33 (t, CH_3), 4.30 (q, CH_2), 8.12 (d, 3′-H), 7.56 (t, 4′-H), 8.01 (t, 5′-H), 8.72 (d, 6′-H).

Synthesis of the Ruthenium Complexes

[Ru(bpy)$_2$(Hcpt)]PF$_6$ (1): *cis*-[Ru(bpy)$_2$Cl$_2$]·2H$_2$O (520 mg, 1 mmol), prepared as reported in the literature,[31] and **H_2cpt** (380 mg) were added to a 50 mL ethanol/water (1:1, v/v) mixture. The mixture was heated under reflux for 4 h. After cooling, the solvent was removed by rotary evaporation. The remaining solid was dissolved in 10 mL of water and added to a saturated NH_4PF_6 (4 mmol) solution. The precipitate was filtered off and dried. The solid was recrystallised from a 50 mL acetone/water (1:1, v/v) mixture. The yield based on *cis*-[Ru(bpy)$_2$Cl$_2$]·2H$_2$O was 0.5 g (65%). The complex was purified further by column chromatography using neutral alumina and acetone followed by ethanol as eluents. MS: *m/z* = 603 [M^+].

[Ru(bpy)$_2$(cept)](PF$_6$)·H$_2$O (2): This complex was prepared and purified as with **1**, except that for column chromatography acetone was used as eluent. The yield based on *cis*-[Ru(bpy)$_2$Cl$_2$]·2H$_2$O was 0.75 g (90%). Crystals of [Ru(bpy)$_2$(cept)](PF$_6$)·H$_2$O, suitable for X-ray structural determination, were obtained by slow concentration at room temperature of a diluted solution of **2** in a mixture of methanol/water (1:1, v/v). MS: *m/z* = 632 [M^+].

Physical Measurements: Infrared spectra of the compounds in the region 4000−200 cm^{-1} were measured with a Perkin−Elmer Paragon 1000 FTIR spectrophotometer using pressed KBr pellets. ^1H NMR spectra were recorded with a Bruker WM 300 MHz NMR spectrometer. The ^1H NMR spectra of the ligands were obtained in $(CD_3)_2SO$ solvent, while those of the ruthenium(II) complexes were recorded in $(CD_3)_2CO$. The peak positions are relative to TMS. Mass spectra were obtained with a Finnigan MAT TSQ-70 equipped with a custom-made electrospray interface (ESI). Spectra were collected by constant infusion of the analyte, dissolved in a methanol/water (80:20) solution with 1% acetic acid. Elemental C, H, N analyses were carried out with a Perkin−Elmer 2400 Series II analyser. Cyclic voltammograms were recorded using an Autolab PG Stat10 potentiostat controlled by a GPES4 software. A home-made three-compartment cell was used, containing an Ag/AgCl electrode as a reference electrode, a platinum wire as counter electrode, and a glassy carbon electrode as working electrode. All the CV measurements were carried out in spectroscopic grade acetonitrile, using 0.1 M tetrabutylammonium hexafluorophosphate as a supporting electrolyte. The scan rate was 100 mV/s. Prior to each run the solution was purged with argon for 30 s. Absorption and emission spectra at room temperature were performed in air-equilibrated spectroscopic grade acetonitrile solutions in 1-cm quartz cells using a Perkin−Elmer Lambda 900 spectrophotometer and Fluorolog equipment, respectively. The standard compound used for determining the emission quantum yields of the complexes was $[Ru(bpy)_3]^{2+}$ in an aerated water solution (φ_{em} = 0.028).[32] The quantum yields were calculated according to Equation (1).[33,34]

$$\phi_{em} = \phi'_{em} * \left(\frac{I}{I'}\right) * \left(\frac{A'}{A}\right) * \left(\frac{\eta}{\eta'}\right)^2 \quad (1)$$

In Equation (1), I (sample) and I' (standard) are the integrated emission intensities, A and A' the absorptions at the excitation wavelength, and η and η′ the refractive indices of the solvents. Time-resolved emission spectra were obtained using a Hamamatsu C-5680 streak camera equipped with an M 5677 sweep unit. Excitation at 337 nm was achieved by a pulsed (fwhm 600 ps) nitrogen laser (LTB, MGS 405 TD) operating at a repetition rate of 20 Hz. The time resolution of this set was ca. 200 ps, as limited by the laser pulse width. For measurements at 77 K in a rigid matrix, freshly distilled butyronitrile as a solvent was used. All the values for emission maxima are uncorrected for the phototube response. Estimated errors are as follows: band maxima, ±2 nm; relative luminescence intensity ±20%; lifetimes, ±10%.

X-ray Crystallographic Study of [Ru(bpy)$_2$(cept)](PF$_6$)·H$_2$O (2): A red needle-shaped crystal was selected and mounted on a glass fibre using the oil-drop method.[35] X-ray data were collected with a Rigaku AFC-7S diffractometer (graphite-monochromated Mo-K_α radiation, λ = 0.71073 Å, ω-2θ scans). The intensity data were corrected for Lorentz and polarisation effects, for absorption (ψ-scan absorption correction) and extinction. All non-H atoms were refined anisotropically. The water H atoms were located from a Fourier-difference map. All other H atoms were introduced in calculated positions and refined with fixed geometry with respect to their carrier atoms. The structure was solved by direct methods. The programs TEXSAN,[36] SHELXS-97,[37] and SHELXL-97[38] were used for data reduction, structure solution, and structure refinement, respectively. Refinement of F^2 was done against all reflections. The weighted R factor, wR, and goodness of fit, S, are based on F^2. Conventional R factors, R, are based on F, with F set to zero for negative F^2. Selected crystal data and numerical details of the structure determination are given in Table 5. The supple-

Table 5. Crystal data and details of the structure determination for [Ru(bpy)$_2$(cept)](PF$_6$)·H$_2$O {weighting schemes: $w = 1.0/[\sigma^2(F_o^2) + (0.0871P)^2 + 4.0317P]$}

Crystal data:	
Empirical formula	$RuC_{30}H_{27}F_6N_8O_3P$
Formula mass	793.64
Crystal system	monoclinic
Space group	$P2_1/n$
a [Å]	12.339(7)
b [Å]	16.512(7)
c [Å]	16.802(8)
β [°]	110.29(4)
V [Å^3]	3211(3)
Z	4
$D_{calcd.}$ [g cm^{-3}]	1.642
F(000)	1600
μ [cm^{-1}]	0.620
Crystal size [mm]	0.50 × 0.20 × 0.15
Data collection/refinement:	
Temperature [K]	193(2)
$\theta_{min.}$, $\theta_{max.}$ [°]	2.52, 26.49
Total data collected	5303
Observed refl. [$I > 2\sigma(I)$]	3861
Independent refl. (R_{int})	5053 (0.0539)
No.of refined params.	445
Final $R1$, $wR2$ [$I > 2\sigma(I)$]	0.0657, 0.1544
Goodness-of-fit on F^2	1.042
Min. and max. residual electron density [e·Å^{-3}]	0.878, −0.629

mentary crystallographic data for this paper is contained within publication CCDC-164043. These data can be obtained free of charge at www.ccdc.cam.ac.uk/conts/retrieving.html or from the Cambridge Crystallographic Data Centre, 12, Union Road, Cambridge CB2 1EZ, UK [Fax: (internat.) + 44-1223/336-033; E-mail: deposit@ccdc.cam.ac.uk].

Acknowledgments

B. M. wishes to acknowledge the Leiden University "Curatorenfonds" for the student Scholarship for the 1999 academic year.

[1] R. Hage, Ph. D. Thesis, Leiden University, **1991**.
[2] R. Hage, J. G. Haasnoot, J. Reedijk, J. G. Vos, *Chemtracts Inorg. Chem.* **1992**, *4,* 75.
[3] R. Hage, A. H. J. Dijkhuis, J. G. Haasnoot, R. Prins, J. Reedijk, B. E. Buchanan, J. G. Vos, *Inorg. Chem.* **1988**, *27*, 2185.
[4] R. Hage, R. Prins, J. G. Haasnoot, J. Reedijk, J. G. Vos, *J. Chem. Soc., Dalton Trans.* **1987**, 1389.
[5] R. Hage, J. G. Haasnoot, J. Reedijk, J. G. Vos, *Inorg. Chim. Acta* **1986**, *118*, 73.
[6] R. Hage, J. G. Haasnoot, D. J. Stufkens, T. L. Stoeck, J. G. Vos, J. Reedijk, *Inorg. Chem.* **1989**, *28*, 1413.
[7] V. Barigelletti, L. De Cola, V. Balzani, R. Hage, J. G. Haasnoot, J. Reedijk, J. G. Vos, *Inorg. Chem.* **1989**, *28*, 4344.
[8] R. Hage, J. G. Haasnoot, J. Reedijk, R. Wang, J. G. Vos, *Inorg. Chem.* **1991**, *30*, 3263.
[9] R. Hage, J. G. Haasnoot, H. A. Nieuwenhuis, J. Reedijk, R. Wang, J. G. Vos, *J. Chem. Soc., Dalton Trans.* **1991**, 3271.
[10] E. Buchanan, J. G. Vos, M. Kaneko, W. J. M. van der Putten, J. M. Kelly, R. Hage, R. A. G. de Graaff, R. Prins, J. G. Haasnoot, J. Reedijk, *J. Chem. Soc., Dalton Trans.* **1990**, 2425.
[11] R. Wang, J. G. Vos, R. H. Schmehl, R. Hage, *J. Am. Chem. Soc.* **1992**, *114*, 1964.
[12] R. Hage, J. G. Haasnoot, J. Reedijk, R. Wang, E. Ryan, J. G. Vos, A. L. Spek, A. J. M. Duisenberg, *Inorg. Chim. Acta* **1990**, *174*, 77.
[13] R. Hage, R. A. G. de Graaff, J. G. Haasnoot, J. P. Turkenburg, J. Reedijk, J. G. Vos, *Acta Crystallogr., Sect. C* **1989**, *45*, 381.
[14] T. E. Keyes, J. G. Vos, J. A. Kolnaar, J. G. Haasnoot, J. Reedijk, R. Hage, *Inorg. Chem. Acta* **1996**, *245*, 237.
[15] A. Spasov, G. Demirov, *Chem. Ber.* **1969**, *102*, 2530.
[16] H. Reimlinger, W. R. F. Lingier, J. J. M. Vandewalle, *Chem. Ber.* **1971**, *104*, 639.
[17] S. Kucota, M. Uda, T. Nakagawa, *J. Heterocycl. Chem.* **1975**, *12*, 855.
[18] S. S. Novikov, V. M. Brusnikina, V. A. Rudenko, *Khim. Geterotsikl. Soedin.* **1969**, *5*, 157; *Chem. Heterocycl. Compd.,* **1969**, *5*, 121.
[19] K. M. Doyle, F. Kurzer, *Tetrahedron* **1976**, *32*, 1031.
[20] K. M. Doyle, F. Kurzer, *Tetrahedron* **1976**, *32*, 2343.
[21] R. A. Bowie, M. D. Garden, D. G. Neilson, K. M. Watson, S. Mahmod, V. Ridd, *J. Chem. Soc., Perkin Trans. 1* **1973**, 1972.
[22] M. S. Neelima, A. P. Bhaduri, *Indian J. of Chem.* **1983**, *22B*, 79.
[23] P. Westermann, *Chem. Ber.* **1964**, *97*, 523.
[24] H. Paul, G. Hilgetag, G. Jänchen, *Chem. Ber.* **1968**, *101*, 2033.
[25] J. L. Marshall, K. C. Erickson, T. K. Folson, *Tetrahedron Lett.* **1970**, *46*, 4011.
[26] J. F. Geldard, F. Lions, *J. Org. Chem.* **1965**, *30*, 318.
[27] R. G. Jones, C. Ainsworth, *J. Am. Chem. Soc.* **1955**, *77*, 1538.
[28] J. de Mendoza, J. M. Ontoria, M. C. Ortega, T. Torres, *J. Synth. Org. Chem.* **1992**, 398.
[29] D. P. Rillema, T. G. Taghdiri, D. S. Jones, C. D. Keller, L. A. Worl, T. J. Meyer, H. A. Levy, *Inorg. Chem.* **1987**, *26*, 578.
[30] A. Juris, V. Balzani, F. Barigelletti, S. Campagna, P. Belser, A. von Zelewsky, *Coord. Chem. Rev.* **1988**, *84*, 85.
[31] B. P. Sullivan, D. J. Salmon, T. J. Meyer, *Inorg. Chem.* **1978**, *17*, 3334.
[32] K. Nakamura, *Bull. Chem. Soc. Jpn.* **1982**, *55*, 2697.
[33] J. N. Demas, G. A. Grosby, *J. Phys. Chem.* **1971**, *75*, 991.
[34] A. Credi, L. Prodi, *Spectrochim. Acta, Part A* **1998**, *54*, 159.
[35] T. Kottke, D. Stalke, *J. Appl. Crystallogr.* **1993**, *26*, 615.
[36] *TEXSAN, Single Crystal Structure Analysis Software*, version 1.6, Molecular Structure Corporation, The Woodlands, TX 77381, USA, **1993**.
[37] G. M. Sheldrick, *SHELXS-97, Program for crystal structure determination*, University of Göttingen, Germany, **1997**.
[38] G. M. Sheldrick, *SHELXL-97, Program for the Refinement of Crystal Structures*, University of Göttingen, Germany, **1997**.

Received August 6, 2001
[I01295]

Peralkylated Four- and Five-Membered Cyclosilanes Containing a Heteroatom: Synthesis, Structure, and Properties

Hamao Watanabe,*[a] Hideo Suzuki,[a] Syuji Takahashi,[a] Kiichiro Ohyama,[a] Yuji Sekiguchi,[a] Hideki Ohmori,[a] Michio Nishiyama,[a] Michihiro Sugo,[a] Minoru Yoshikawa,[a] Nobuo Hirai,[a] Yoichi Kanuma,[a] Takahiro Adachi,[a] Masami Makino,[a] Katsura Sakata,[b] Kentaro Kobayashi,[b] Takako Kudo,*[b] Haruo Matsuyama,[c] Nobumasa Kamigata,[c] Michio Kobayashi,[c] Masashi Kijima,*[d] Hideki Shirakawa,[d] Kazumasa Honda,[e] and Midori Goto*[e]

Keywords: HOMO−LUMO interactions / Photolysis / Small ring systems / Silicon / Strained molecules

Seventeen peralkylated four- and five-membered heteroatom-containing silacycles $[R^1R^2Si]_nX$ [R^1 = *i*Pr and/or R^2 = *t*BuCH$_2$; *n* = 3; X = CH$_2$ (**1a**, **1b**), NR^3 (R^3 = C_6H_{11}) (**3a**–**d**), O (**5a**–**c**), and *n* = 4; X = CH$_2$ (**2a**, **2b**), NR^3 (R^3 = C_6H_{11} or Pr) (**4a**–**d**), and O (**6a**, **6b**)] have been synthesized and characterized. The structural features of twelve compounds – **1b**, **3a**–**d**, and **5b** (Si_3X) and **2a**, **4a**–**c**, **6a**, and **6b** (Si_4X) – determined by X-ray analysis have been investigated and geometrical differences between the silacycles bearing neopentyl groups and those with isopropyl groups as bulky substituents on silicon atoms have been identified. The ring strain energies for the compounds $[R_2Si]_nX$ [*n* = 3, 4; R = Me, *i*Pr; X = CH$_2$, N(*i*Pr), NMe, O, SiH$_2$], estimated by theoretical calculations at the PM3 level, are discussed in relation to experimentally ascertained structural features of the silacycles $[R_2Si]_nX$ (*n* = 3, 4; R = *i*Pr; X = CH$_2$, NC_6H_{11}, O, SiR$_2$). ^{29}Si NMR spectra for **1**–**6** showed that the resonances for the α-silicon atoms attached to the heteroatoms X in the two ring-size series were shifted downfield by a deshielding effect due to an electronegative atom X; larger electronegativity (*En*) of X caused this effect at lower field. The chemical shifts of the Si^{α} atoms showed a good linear correlation with the electronegativities of the heteroatoms X in the $[R_2Si]_nX$ cycles. In the UV spectra for **1**–**6**, little difference in the longest-wavelength absorption (LWA) maxima was observed for $[(iPr)_2Si]_nX$ and $[(tBuCH_2)_2Si]_nX$ of the same ring size. The LWA bands for **1**–**6** and related compounds could be roughly classified into four groups: (a) $[R_2Si]_3X$ (X = SiR$_2$, GeR′$_2$) λ = 286–300 nm; (b) $[R_2Si]_3X$ (X = CH$_2$, NR^3, O) (**1**, **3**, **5**), λ = 230–250 nm; (c) $[R_2Si]_4X$ (X = SiR$_2$, GeR′$_2$) λ = 274–280 nm; (d) $[R_2Si]_4X$ (X = CH$_2$, NR^3, O) (**2**, **4**, **6**), λ = 250–260 nm. With the aid of the ionization potentials and the transition energies (E_T), the HOMO and LUMO levels for the series of compounds and the related ones were experimentally evaluated. The HOMO and LUMO levels thus obtained for $[R_2Si]_3X$ and $[R_2Si]_4X$ (R = *i*Pr and *t*BuCH$_2$; X = SiR$_2$, GeR′$_2$, CH$_2$, NC_6H_{11}, O) are discussed in terms of the calculated values and frontier orbitals on the basis of PM3 levels. The theoretical prediction for bond scission in the silacycles $[(iPr)_2Si]_nX$ (*n* = 3, 4; X = CH$_2$, NMe, O) in which the HOMOs and LUMOs have Si–Si bonding and antibonding character, respectively, was corroborated by the good agreement with experimental results from photolysis of the silacycles $[R_2Si]_nX$ (*n* = 3, 4; R = *i*Pr and *t*BuCH$_2$; X = CH$_2$, NC_6H_{11}, O), with bond scission occurring only at the Si–Si bonds, and not at the Si–X bonds.

(© Wiley-VCH Verlag GmbH, 69451 Weinheim, Germany, 2002)

[a] Department of Materials Science, Faculty of Engineering, Gunma University,
Kiryu, Gunma 376-8515, Japan
Fax: (internat.) + 81-277/47-5453
E-mail: hwatanab@chem.gunma-u.ac.jp
[b] Department of Fundamental Studies, Faculty of Engineering, Gunma University,
Kiryu, Gunma 376-8515, Japan
[c] Department of Chemistry, Faculty of Science, Tokyo Metropolitan University,
Hachioji, Tokyo, 192-0397, Japan
[d] Institute of Materials Science, University of Tsukuba,
Tsukuba, Ibaraki, 305-8571, Japan
[e] National Institute of Materials and Chemical Research,
Tsukuba, Ibaraki, 305-8565, Japan

Supporting information for this article is available on the WWW under http://www.eurjic.com or from the author.

Introduction

The chemistry of silacycles containing a heteroatom such as oxygen, nitrogen, etc. comprises an intriguing subject worthy of study regarding their properties. Although a large number of studies of homosilacycles Si_n[1] and of heteroatom-containing silacycles such as Si_nGe,[2] Si_nC,[3] Si_nN,[4] and Si_nO[5] have appeared, there are only limited systematic studies focusing on the series of heteroatom-containing silacycles Si_nX from the perspective of properties arising from the presence of X as a heteroatom.[6] We have previously studied some properties of various peralkylated cyclosilanes $[R^1R^2Si]_n$ ($n = 3-7$)[7] and have also reported

preliminary results for $[R_2Si]_3O$.[8] Recently, we described the synthesis, molecular structure, and photolysis of the $[R_2Si]_nGeR'_2$ series [n = 2: R = tBuCH$_2$, R′ = Me$_3$SiCH$_2$;[9] n = 3: R = iPr, tBuCH$_2$, R′ = Me$_3$SiCH$_2$ (**C**, **D**);[10] and n = 4: R = iPr, tBuCH$_2$, R′ = Me$_3$SiCH$_2$, Ph (**G**−**I**)[11]].

This paper deals with a full account of the series of heteroatom-containing four- and five-membered cyclosilanes $[R^1R^2Si]_nX$ [n = 3, 4; R^1, R^2 = iPr, tBuCH$_2$; X = CH$_2$ (**1**, **2**), NR^3 (R^3 = C$_6$H$_{11}$ or Pr) (**3**, **4**), O (**5**, **6**)], as shown in Scheme 1, including molecular structures determined by X-ray crystal analysis, some properties such as ^{29}Si NMR and UV spectra, and oxidation and ionization potentials. We have performed semiempirical PM3[12] molecular orbital calculations for a series of heterosubstituted silacycles $[R_2Si]_nX$ [n = 3, 4; R = Me, iPr; X = SiH$_2$, CH$_2$, NMe, N(iPr), O] in order to estimate the ring strain energies. The energy levels and character of their frontier orbitals are also discussed in relation to their molecular structures, oxidation and ionization potentials, and photochemical reactions of the series of heterosilacycles obtained experimentally in the current study.

Results and Discussion

Synthesis

Compounds **1** and **2** were synthesized in good yields (72−92%) by reductive coupling of the corresponding α,ω-dichlorocarbosilanes with lithium in THF at room temperature [Scheme 2, (a)]. Compounds **3** and **4** were synthesized in moderate yields (35−69%) by treatment of the corresponding α,ω-dichlorosilanes with lithium alkylamides [Scheme 2, (b) and (c)]. Compounds **5** and **6** were synthesized by hydrolytic cyclization with the corresponding α,ω-dichlorosilanes, in good yields (88−96%) except in the case of **5a** (28%) [Scheme 2, (d)]. Compound **E** was also prepared from the corresponding 1,4-dilithiotetrasilane and dichlorosilane in a reasonable yield [Scheme 2, (e)]. All the compounds **1**−**6** obtained were found to be air- and moisture-stable liquids (**1a**, **5c**) or crystals (the others) and were identified in the usual manner (NMR, IR, and MS data, as well as elemental analysis), while $[Me_2Si]_3CH_2$[3a] and $[Ph_2Si]_4X$ (X = NMe, NEt, O)[6e] have been reported to be air- and moisture-sensitive compounds.

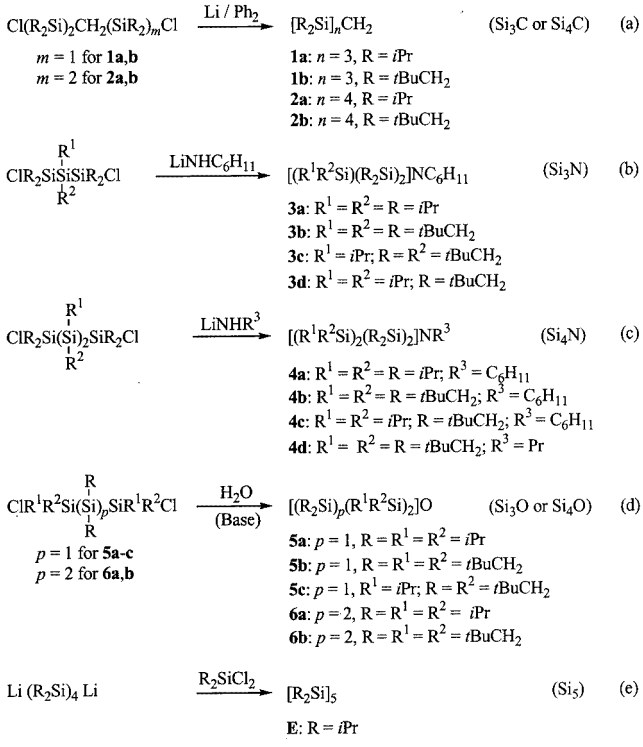

Scheme 2. (a−e) Synthetic methods for heteroatom-containing silacycles Si_nX [n = 3, 4; X = CH$_2$, NR^3 and O; n = 4, X = Si(iPr)$_2$]

Molecular Structures

Except for Si_3C[3a] and Si_4O,[5g] there are no precedents for structural studies on the ring systems Si_4C, Si_nN (n = 3, 4), and Si_nO (n = 3, 4). The molecular structures of **1b**,

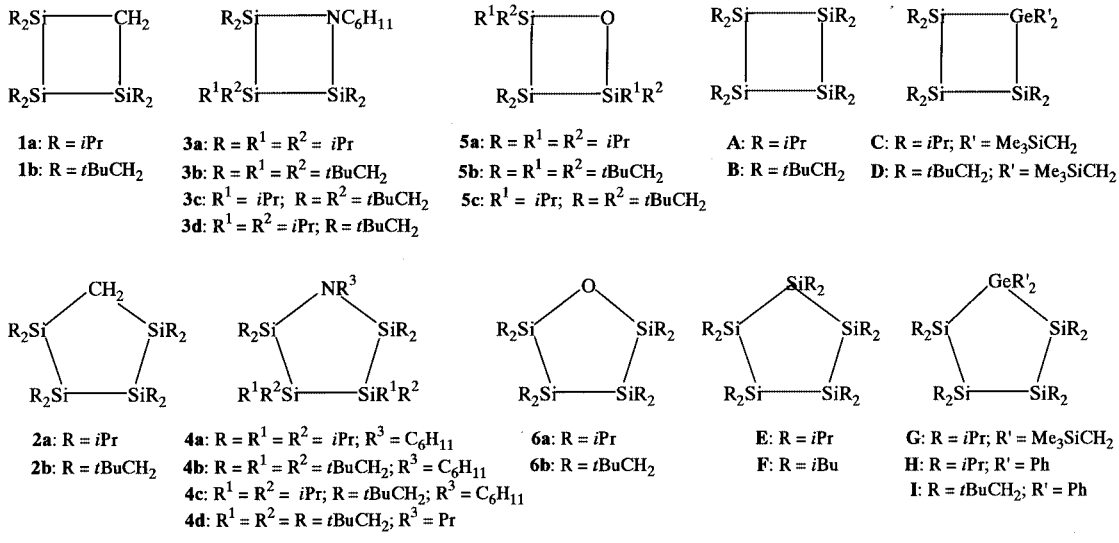

Scheme 1. Molecular formula of heteroatom-containing silacycles and related compounds

2a, **3a−d**, **4a−c**, **5b**, **6a**, and **6b** were determined by X-ray crystal analysis; structural data for **1a** and **5a** could not be obtained by X-ray analysis. Selected bond lengths and bond and torsion angles for these compounds are listed in Tables 1−12, and the pertinent geometrical data needed for structural discussion of $[R_2Si]_3X$ and $[R_2Si]_4X$ (X = C, N O) and the related compounds **A**−**E**, **H**, and **I** are summarized in Tables 13 and 14.

(1) Bond Lengths and Angles

The Si_3C ring of **1b** was found to be moderately puckered, with a dihedral angle of 25.5°, and the Si_4C ring of **2a** to be a slightly deformed envelope conformation. The structural data for four known Si_3C ring compounds[3b−3d]

Table 1. Selected bond lengths [Å], bond angles [°], and torsion angles [°] in **1b**

Bond distances					
Si(1)-Si(2)	2.400(2)	Si(2)-Si(3)	2.387(4)	Si(1)-C(1)	1.882(5)
Si(3)-C(1)	1.895(6)	Si(1)-C(2)	1.882(7)	Si(1)-C(7)	1.905(6)
Si(2)-C(12)	1.906(6)	Si(2)-C(17)	1.914(6))	Si(3)-C(22)	1.890(6)
Si(3)-C(27)	1.900(6)				
Bond angles					
Si(1)-Si(2)-Si(3)	75.9(1)	Si(2)-Si(3)-C(1)	88.0(2)		
Si(2)-Si(1)-C(1)	87.9(2)	Si(1)-C(1)-Si(3)	102.3(3)		
C(2)-Si(1)-C(7)	113.0(3)	C(12)-Si(2)-C(17)	115.4(3)		
C(22)-Si(3)-C(27)	115.8(3)				
Torsion angles					
Si(1)-Si(2)-Si(3)-C(1)	-16.2(1)	Si(2)-Si(3)-C(1)-Si(1)	20.7(2)		
Si(3)-C(1)-Si(1)-Si(2)	-20.6(2)	C(1)-Si(1)-Si(2)-Si(3)	16.3(1)		

Table 2. Selected bond lengths [Å], bond angles [°], and torsion angles [°] in **2a**

Bond distances					
Si(1)-Si(2)	2.384(2)	Si(2)-Si(3)	2.391(2)	Si(3)-Si(4)	2.403(2)
Si(1)-C(1)	1.896(4)	Si(4)-C(1)	1.877(5)	Si(1)-C(2)	1.880(6)
Si(1)-C(5)	1.906(6)	Si(2)-C(8)	1.917(5)	Si(2)-C(11)	1.910(6)
Si(3)-C(14)	1.921(5)	Si(3)-C(17)	1.906(6)	Si(4)-C(20)	1.891(5)
Si(4)-C(23)	1.940(7)				
Bond angles					
Si(1)-Si(2)-Si(3)	96.9(1)	Si(2)-Si(3)-Si(4)	98.0(1)		
Si(3)-Si(4)-C(1)	105.4(1)	Si(2)-Si(1)-C(1)	99.9(1)		
Si(1)-C(1)-Si(4)	117.7(2)	C(2)-Si(1)-C(5)	113.9(3)		
C(8)-Si(2)-C(11)	110.4(3)	C(14)-Si(3)-C(17)	109.8(3)		
C(20)-Si(4)-C(23)	114.4(3)				
Torsion angles					
Si(1)-Si(2)-Si(3)-Si(4)	-28.5(1)	Si(2)-Si(3)-Si(4)-C(1)	7.3(2)		
Si(3)-Si(4)-C(1)-Si(1)	26.4(3)	Si(4)-C(1)-Si(1)-Si(2)	-47.1(3)		
C(1)-Si(1)-Si(2)-Si(3)	43.6(2)				

Table 3. Selected bond lengths [Å], bond angles [°], and torsion angles [°] in **3a**

Bond distances					
Si(1)-Si(2)	2.362(2)	Si(1)-Si(3)	2.377(2)	Si(2)-N(1)	1.757(4)
Si(3)-N(1)	1.757(4)	Si(2)-C(21)	1.898(6)	Si(2)-C(22)	1.903(7)
Si(1)-C(11)	1.904(6)	Si(1)-C(12)	1.907(6))	Si(3)-C(31)	1.901(5)
Si(3)-C(32)	1.919(6)	N(1)-C(41)	1.485(7)		
Bond angles					
Si(2)-Si(1)-Si(3)	74.5(1)	Si(1)-Si(2)-N(1)	88.2(1)		
Si(1)-Si(3)-N(1)	87.7(1)	Si(2)-N(1)-Si(3)	109.5(2)		
C(21)-Si(2)-C(22)	108.2(3)	C(11)-Si(1)-C(12)	112.0(3)		
C(31)-Si(3)-C(32)	103.9(2)	Si(2)-N(1)-C(41)	120.3(3)		
Si(3)-N(1)-C(41)	130.1(3)				
Torsion angles					
Si(3)-Si(1)-Si(2)-N(1)	2.1(1)	Si(2)-Si(1)-Si(3)-N(1)	-2.1(1)		
Si(1)-Si(2)-N(1)-Si(3)	-2.9(2)	Si(1)-Si(3)-N(1)-Si(2)	2.9(2)		

Table 4. Selected bond lengths [Å], bond angles [°], and torsion angles [°] in **3b**

Bond distances					
Si(1)-Si(2)	2.365(2)	Si(2)-Si(3)	2.395(2)	Si(1)-N(1)	1.758(3)
Si(3)-N(1)	1.768(3)	Si(1)-C(27)	1.907(4)	Si(1)-C(32)	1.899(5)
Si(2)-C(17)	1.908(5)	Si(2)-C(22)	1.917(6)	Si(3)-C(7)	1.906(6)
Si(3)-C(12)	1.903(7)	N(1)-C(1)	1.485(4)		
Bond angles					
Si(1)-Si(2)-Si(3)	74.3(1)	Si(2)-Si(3)-N(1)	85.8(1)		
Si(2)-Si(1)-N(1)	86.9(1)	Si(1)-N(1)-Si(3)	109.3(2)		
C(27)-Si(2)-C(32)	113.0(2)	C(17)-Si(2)-C(22)	114.0(2)		
C(7)-Si(3)-C(12)	111.0(3)	Si(1)-N(1)-C(1)	121.7(2)		
Si(3)-N(1)-C(1)	129.0(3)				
Torsion angles					
Si(1)-Si(2)-Si(3)-N(1)	-12.2(1)	Si(2)-Si(3)-N(1)-Si(1)	16.9(1)		
Si(3)-N(1)-Si(1)-Si(2)	-17.1(2)	N(1)-Si(1)-Si(2)-Si(3)	12.3(1)		

Table 5. Selected bond lengths [Å], bond angles [°], and torsion angles [°] in **3c**

Bond distances					
Si(1)-Si(2)	2.373(1)	Si(2)-Si(3)	2.394(1)	Si(1)-N(1)	1.755(2)
Si(3)-N(1)	1.770(2)	Si(1)-C(1)	1.909(3)	Si(1)-C(6)	1.902(3)
Si(2)-C(11)	1.911(3)	Si(2)-C(16)	1.927(4)	Si(3)-C(19)	1.907(4)
Si(3)-C(24)	1.907(3)	N(1)-C(29)	1.484(3)		
Bond angles					
Si(1)-Si(2)-Si(3)	74.0(1)	Si(2)-Si(3)-N(1)	85.4(1)		
Si(2)-Si(1)-N(1)	86.4(1)	Si(1)-N(1)-Si(3)	108.9(1)		
C(11)-Si(2)-C(16)	109.0(1)	C(1)-Si(1)-C(16)	111.6(1)		
C(19)-Si(3)-C(24)	108.3(1)	Si(1)-N(1)-C(29)	122.0(1)		
Si(3)-N(1)-C(29)	128.9(1)				
Torsion angles					
Si(1)-Si(2)-Si(3)-N(1)	-14.6(8)	Si(2)-Si(1)-N(1)-Si(3)	-20.4(1)		
Si(1)-N(1)-Si(3)-Si(2)	20.2(1)	Si(3)-Si(2)-Si(1)-N(1)	-14.7(9)		

Table 6. Selected bond lengths [Å], bond angles [°], and torsion angles [°] in **3d**

Bond distances					
Si(1)-Si(2)	2.399(3)	Si(2)-Si(3)	2.360(3)	Si(1)-N(1)	1.778(5)
Si(3)-N(1)	1.757(5)	Si(1)-C(7)	1.912(8)	Si(1)-C(12)	1.901(9)
Si(2)-C(17)	1.900(8)	Si(2)-C(20)	1.921(8)	Si(3)-C(23)	1.902(7)
Si(3)-C(28)	1.907(7)	N(1)-C(1)	1.487(8)		
Bond angles					
Si(1)-Si(2)-Si(3)	74.3(1)	Si(2)-Si(3)-N(1)	87.3(2)		
Si(3)-N(1)-Si(1)	108.7(3)	N(1)-Si(1)-Si(2)	85.6(2)		
C(7)-Si(1)-C(12)	105.6(4)	C(17)-Si(2)-C(20)	111.6(4)		
C(23)-Si(3)-C(28)	112.3(3)	Si(1)-N(1)-C(1)	128.8(4)		
Si(3)-N(1)-C(1)	122.5(4)				
Torsion angles					
Si(1)-Si(2)-Si(3)-N(1)	13.2(2)	Si(3)-Si(2)-Si(1)-N(1)	-12.9(2)		
Si(2)-Si(1)-N(1)-Si(3)	17.8(2)	Si(1)-N(1)-Si(3)-Si(2)	-18.0(2)		

Table 7. Selected bond lengths [Å], bond angles [°], and torsion angles [°] in **4a**

Bond distances					
Si(1)-Si(2)	2.410(2)	Si(2)-Si(3)	2.402(3)	Si(3)-Si(4)	2.393(4)
Si(1)-N(1)	1.766(6)	Si(4)N(1)	1.753(6)	Si(1)-C(7)	1.939(7)
Si(1)-C(10)	1.906(7)	Si(2)-C(13)	1.930(7)	Si(2)-C(16)	1.918(8)
Si(3)-C(19)	1.929(8)	Si(3)-C(22)	1.945(8)	Si(4)-C(25)	1.937(10)
Si(4)-C(28)	1.923(9)	C(1)-N(1)	1.517(10)		
Bond angles					
Si(1)-Si(2)-Si(3)	97.0(1)	Si(2)-Si(3)-Si(4)	95.4(1)		
Si(3)-Si(4)-N(1)	106.9(2)	Si(2)-Si(1)-N(1)	105.2(2)		
Si(1)-N(1)-Si(4)	125.6(3)	C(7)-Si(1)-C(10)	104.9(3)		
C(13)-Si(2)-C(16)	109.5(3)	C(19)-Si(3)-C(22)	110.6(3)		
C(25)-Si(4)-C(28)	106.0(5)	C(1)-N(1)-Si(1)	121.9(4)		
C(1)-N(1)-Si(4)	112.5(5)				
Torsion angles					
Si(1)-Si(2)-Si(3)-Si(4)	27.3(10)	Si(2)-Si(3)-Si(4)-N(1)	-26.9(13)		
Si(3)-Si(4)-N(1)-Si(1)	13.3(20)	Si(4)-N(1)-Si(1)-Si(2)	8.3(20)		
N(1)-Si(1)-Si(2)-Si(3)	-24.7(13)				

Table 8. Selected bond lengths [Å], bond angles [°], and torsion angles [°] in **4b**

Bond distances					
Si(1)-Si(2)	2.408(3)	Si(2)-Si(3)	2.377(3)	Si(3)-Si(4)	2.405(3)
Si(1)-N(1)	1.763(7)	Si(4)-N(1)	1.787(6)	Si(1)-C(7)	1.910(12)
Si(1)-C(12)	1.912(10)	Si(2)-C(17)	1.932(13)	Si(2)-C(22)	1.908(15)
Si(3)-C(27)	1.947(11)	Si(3)-C(32)	1.925(10)	Si(4)-C(37)	1.894(14)
Si(4)-C(42)	1.891(14)	C(1)-N(1)	1.518(11)		
Bond angles					
Si(1)-Si(2)-Si(3)	94.4(1)	Si(2)-Si(3)-Si(4)	93.6(1)		
Si(3)-Si(4)-N(1)	105.8(2)	Si(2)-Si(1)-N(1)	101.6(2)		
Si(1)-N(1)-Si(4)	123.2(4)	C(7)-Si(1)-C(12)	109.8(5)		
C(17)-Si(2)-C(22)	117.3(12)	C(27)-Si(3)-C(32)	117.4(5)		
C(37)-Si(4)-C(42)	113.5(6)	C(1)-N(1)-Si(1)	126.0(5)		
C(1)-N(1)-Si(4)	110.8(5)				
Torsion angles					
Si(1)-Si(2)-Si(3)-Si(4)	37.7(1)	Si(2)-Si(3)-Si(4)-N(1)	-27.8(2)		
Si(3)-Si(4)-N(1)-Si(1)	-2.0(5)	Si(4)-N(1)-Si(1)-Si(2)	30.9(4)		
N(1)-Si(1)-Si(2)-Si(3)	-43.5(2)				

Table 9. Selected bond lengths [Å], bond angles [°], and torsion angles [°] in **4c**

Bond distances					
Si(1)-Si(2)	2.408(3)	Si(2)-Si(3)	2.372(2)	Si(3)-Si(4)	2.395(2)
Si(1)-N(1)	1.775(4)	Si(4)-N(1)	1.758(3)	Si(1)-C(7)	1.900(7)
Si(1)-C(12)	1.912(5)	Si(2)-C(17)	1.908(6)	Si(2)-C(20)	1.935(6)
Si(3)-C(23)	1.894(12)	Si(3)-C(26)	1.939(9)	Si(4)-C(29)	1.900(6)
Si(4)-C(34)	1.936(6)	C(1)-N(1)	1.522(6)		
Bond angles					
Si(1)-Si(2)-Si(3)	94.3(1)	Si(2)-Si(3)-Si(4)	94.4(1)		
Si(3)-Si(4)-N(1)	103.4(1)	Si(4)-N(1)-Si(1)	124.4(2)		
N(1)-Si(1)-Si(2)	104.7(1)	C(7)-Si(1)-C(12)	112.3(3)		
C(17)-Si(2)-C(20)	110.3(3)	C(23)-Si(3)-C(26)	113.3(4)		
C(29)-Si(4)-C(34)	111.3(3)	Si(1)-N(1)-C(1)	110.0(3)		
Si(4)-N(1)-C(1)	125.4(3)				
Torsion angles					
Si(1)-Si(2)-Si(3)-Si(4)	-36.9(1)	Si(3)-Si(2)-Si(1)-N(1)	30.8(2)		
Si(2)-Si(1)-N(1)-Si(4)	-5.8(3)	Si(2)-Si(3)-Si(4)-N(1)	38.9(1)		
Si(3)-Si(4)-N(1)-Si(1)	-22.8(3)				

Table 10. Selected bond lengths [Å], bond angles [°], and torsion angles [°] in **5b**

Bond distances					
Si(1)-Si(2)	2.445(5)	Si(2)-Si(3)	2.421(5)	Si(1)-O(1)	1.646(11)
Si(3)-O(1)	1.665(12)	Si(1)-C(1)	1.893(16)	Si(1)-C(2)	1.888(16)
Si(2)-C(3)	1.882(14)	Si(2)-C(4)	1.907(13)	Si(3)-C(5)	1.862(13)
Si(3)-C(6)	1.862(13)				
Bond angles					
Si(1)-Si(2)-Si(3)	68.2(2)	Si(2)-Si(3)-O(1)	90.5(4)		
Si(2)-Si(1)-O(1)	90.1(4)	Si(1)-O(1)-Si(3)	111.1(5)		
C(1)-Si(1)-C(2)	115.5(8)	C(3)-Si(2)-C(4)	117.3(5)		
C(5)-Si(3)-C(6)	115.0(7)				
Torsion angles					
Si(1)-Si(2)-Si(3)-O(1)	-1.7(4)	Si(1)-O(1)-Si(3)-Si(2)	2.6(6)		
Si(2)-Si(1)-O(1)-Si(3)	-2.5(6)	Si(3)-Si(2)-Si(1)-O(1)	1.7(4)		

Table 11. Selected bond lengths [Å], bond angles [°], and torsion angles [°] in **6a**

Bond distances					
Si(1)-Si(2)	2.402(2)	Si(2)-Si(3)	2.389(2)	Si(3)-Si(4)	2.386(2)
Si(1)-O(1)	1.638(3)	Si(4)-O(1)	1.654(3)	Si(1)-C(1)	1.901(6)
Si(1)-C(4)	1.887(5)	Si(2)-C(7)	1.917(5)	Si(2)-C(10)	1.901(6)
Si(3)-C(13)	1.900(5)	Si(3)-C(16)	1.892(6)	Si(4)-C(19)	1.896(6)
Si(4)-C(22)	1.880(7)				
Bond angles					
Si(1)-Si(2)-Si(3)	95.4(1)	Si(2)-Si(3)-Si(4)	95.2(1)		
Si(3)-Si(4)-O(1)	100.8(1)	Si(2)-Si(1)-O(1)	103.1(1)		
Si(1)-O(1)-Si(4)	133.6(2)	C(1)-Si(1)-C(4)	114.2(2)		
C(7)-Si(2)-C(10)	109.5(3)	C(13)-Si(3)-C(16)	109.8(3)		
C(19)-Si(4)-C(22)	115.0(3)				
Torsion angles					
Si(1)-Si(2)-Si(3)-Si(4)	-25.9(1)	Si(2)-Si(3)-Si(4)-O(1)	32.1(1)		
Si(3)-Si(4)-O(1)-Si(1)	-30.5(3)	Si(4)-O(1)-Si(1)-Si(2)	9.8(3)		
O(1)-Si(1)-Si(2)-Si(3)	16.5(1)				

Table 12. Selected bond lengths [Å], bond angles [°], and torsion angles [°] in **6b** (molecule A and molecule B)

molecule A					
Bond distances					
Si(1)-Si(2)	2.450(4)	Si(2)-Si(3)	2.413(4)	Si(3)-Si(4)	2.404(4)
Si(1)-O(1)	1.610(8)	Si(4)-O(1)	1.667(8)	Si(1)-C(1)	1.93(1)
Si(1)-C(6)	1.89(1)	Si(2)-C(11)	1.89(1)	Si(2)-C(16)	1.90(1)
Si(3)-C(21)	1.89(1)	Si(3)-C(26)	1.91(1)	Si(4)-C(31)	1.91(1)
Si(4)-C(36)	1.91(1)				
Bond angles					
Si(1)-Si(2)-Si(3)	92.0(1)	Si(2)-Si(3)-Si(4)	93.8(1)		
Si(3)-Si(4)-O(1)	102.4(3)	Si(2)-Si(1)-O(1)	103.4(3)		
Si(1)-O(1)-Si(4)	132.5(4)	C(1)-Si(1)-C(6)	111.3(5)		
C(11)-Si(2)-C(16)	112.4(5)	C(21)-Si(3)-C(26)	112.4(4)		
C(31)-Si(4)-C(36)	109.6(6)				
Torsion angles					
Si(1)-Si(2)-Si(3)-Si(4)	33.3(2)	Si(2)-Si(3)-Si(4)-O(1)	-33.1(3)		
Si(3)-Si(4)-O(1)-Si(1)	15.1(6)	Si(4)-O(1)-Si(1)-Si(2)	12.2(7)		
O(1)-Si(1)-Si(2)-Si(3)	-31.5(3)				
molecule B					
Bond distances					
Si(5)-Si(6)	2.414(4)	Si(6)-Si(7)	2.419(4)	Si(7)-Si(8)	2.383(4)
Si(5)-O(2)	1.583(10)	Si(8)-O(2)	1.664(10)	Si(5)-C(41)	1.94(1)
Si(5)-C(46)	1.91(2)	Si(6)-C(51)	1.89(1)	Si(6)-C(56)	1.91(1)
Si(7)-C(61)	1.94(1)	Si(7)-C(66)	1.94(1)	Si(8)-C(71)	1.91(1)
Si(8)-C(76)	1.90(1)				
Bond angles					
Si(5)-Si(6)-Si(7)	92.2(2)	Si(6)-Si(7)-Si(8)	93.6(1)		
Si(6)-Si(5)-O(2)	104.9(3)	Si(7)-Si(8)-O(2)	102.6(3)		
Si(5)-O(2)-Si(8)	132.0(5)	C(41)-Si(5)-C(46)	113.5(7)		
C(51)-Si(6)-C(56)	112.8(5)	C(61)-Si(7)-C(66)	115.0(5)		
C(71)-Si(8)-C(76)	113.6(5)				
Torsion angles					
Si(5)-Si(6)-Si(7)-Si(8)	-31.9(1)	Si(6)-Si(7)-Si(8)-O(2)	33.3(3)		
Si(7)-Si(8)-O(2)-Si(5)	-19.0(8)	Si(8)-O(2)-Si(5)-Si(6)	-7.6(8)		
O(2)-Si(5)-Si(6)-Si(7)	28.7(4)				

have been reported previously (dihedral angles: 0−14°, Si−Si−Si: 77.2−82.9°, Si−C−Si: 100.8−107.8°, Si−Si distances: 2.389−2.500 Å, Si−$C_{(ring)}$ distances: 1.936−1.983 Å). If the data listed in Tables 1 and 13 for **1b** are compared with those for the known compounds,[3b−3d][6a] the dihedral angle in **1b** is seen to be the largest, and both the Si−Si−Si angle and Si−$C_{(ring)}$ distance in **1b** are the smallest. The Si−Si bond length (2.394 Å) in **1b** is in the range between the known Si_3C cycles.[3b−3d] Among the four inner angles for the Si_3C ring of **1b**, Si−Si−Si (75.9°) is the smallest and Si−C−Si (102.3°) the largest. A similar trend was also observed for the five inner angles of the Si_4C ring of **2a**. The bond lengths of Si−Si (2.393 Å) and Si−$C_{(ring)}$ (1.888 Å)[13] in the Si_4C of **2a** are within the normal ranges.

The four-membered Si_3N cycles of **3a−d** are planar or puckered structures (dihedral angles 21−23°). The five-membered Si_4N cycles of **4a−c** are in distorted half-chair or envelope conformations. The Si−Si bond lengths in **3a−d** are 2.370−2.384 Å. Compound **3a** has nearly the same distance as in cyclotetrasilane **A** (2.373 Å), while those in compounds **3b−d** (average 2.381 Å) are shorter than those in cyclotetrasilane **B** (2.409) by 0.028 Å. On the other hand, the Si−Si bond lengths (2.397−2.402 Å) in the five-membered compounds **4a−c** are, except for the Si^2-Si^3 bond (2.372 Å) in **4c**, very close to each other. The three distances are longer than those in the corresponding four-membered compounds **3a−d**, but shorter than that (2.422 Å) in the related homosilacycle **E**.[14] The Si−N bond lengths in the two sets Si_3N (**3a−d**, 1.757−1.768 Å) and Si_4N (**4a−c**, 1.760−1.775 Å) are comparable with the typical value of 1.70−1.76 Å,[13] those involving neopentyl groups on the silicons being longer than those with isopro-

Table 13. Geometrical data of four-membered heteroatom-containing silacycles $[R_2Si]_3X$

			bond dist. [Å]			bond angle [deg.]			dihedral
compd	X	R	Si-Si	Si-X	Si^{α}---$Si^{\alpha'}$[a]	Si-Si-Si	Si-Si-X	Si-X-Si	angle [deg.]
1b	CH_2	$tBuCH_2$	2.394	1.889	2.95	75.9	88.0	102.3	25.5
3a	NC_6H_{11}	*i*Pr	2.370	1.757	2.90	74.5	88.0	109.5	0
3b	"	$tBuCH_2$	2.380	1.763	2.73	74.3	86.4	109.3	21
3c	"	$tBuCH_2$ *i*Pr	2.384	1.768	2.86	74.0	85.9	108.9	23
3d	"	$tBuCH_2$ *i*Pr	2.380	1.768	2.86	74.3	86.5	108.7	21
5b	O	$tBuCH_2$	2.433	1.656	2.73	68.2	90.3	111.1	3
A[b]	SiR_2	*i*Pr	2.373	2.373	3.30	87.0	87.0	87.0	37
B[c]	"	$tBuCH_2$	2.409	2.409	3.30	86.7	86.7	86.7	39
C[d]	$Ge(CH_2SiMe_3)_2$	*i*Pr	2.386	2.457	3.38	90.4	88.8	87.1	24
D	"	$tBuCH_2$	2.393	2.444	3.35	88.7	86.8	86.4	36

[a] Non-bonding distances. [b] Ref.[7f]. [c] Ref.[16]. [d] Ref.[10]

Table 14. Geometrical data of five-membered heteroatom-containing silacycles $[R_2Si]_4X$

			bond dist. [Å]		bond angle [deg.]			sum of int.	ring torsion
compd	X	R	Si-Si	Si-X	Si-Si-Si	Si-Si-X	Si-X-Si	angle [deg.]	angle [deg.]
2a	CH_2	*i*Pr	2.393	1.888	97.5	102.7	117.7	517.9	30.6 (7.3-47.1)
4a	NC_6H_{11}	*i*Pr	2.402	1.760	96.2	106.1	125.6	530.1	20.1 (8.3-27.3)
4b	"	$tBuCH_2$	2.397	1.775	94.0	103.7	123.2	518.6	28.4 (2.0-43.5)
4c	"	$tBuCH_2$	2.402[a]	1.767	94.4	104.1	124.4	521.2	27.0 (5.8-38.9)
		*i*Pr	2.372[b]						
6a	O	*i*Pr	2.392	1.646	95.3	102.0	133.6	528.1	23.0 (9.8-32.1)
6b[c]	"	$tBuCH_2$	2.414	1.631	92.9	103.3	132.3	524.7	24.6 (7.6-33.3)
E[d]	SiR_2	*i*Pr	2.422	2.422	101.9	101.9	101.9	509.5	--
H[e]	$GePh_2$	*i*Pr	2.414	2.434	106.0	102.5	110.5	527.5	22.7 (2.9-34.5)
I[e]	"	$tBuCH_2$	2.414	2.449	102.3	100.3	109.7	514.9	32.3 (14.1-51.7)

[a] Average value of the distances of Si(1)−Si(2) and Si(3)−Si(4). [b] Distance Si(2)−Si(3). [c] Average value from molecules A and B. [d] Ref.[14] [e] Ref.[11]

pyl groups in each set. Comparison of the four angles between the two ring sets identifies some interesting features. The sizes of the corresponding angles fall in the order: Si−N−Si (109.5°, **3a**; 108.7−109.3°, **3b−d**) > Si−Si−N (88.0°, **3a**; 85.9−86.5°, **3b**) > Si−Si−Si (74.5°, **3a**; 74.0−74.3°, **3b−d**). This trend is also observed in the five-membered Si_4N rings of **4a−c**. Interestingly, it could be shown that all the nitrogen atoms in **3** and **4** were of almost sp^2 geometry, from the sums (359.8−360°) of the three angles around the nitrogen atoms, as has also been shown in various silylamines[13] and a calculated cycle $[H_2Si]_3NH$.[6a]

The Si_3O cycle in **5b** and the Si_4O cycles in **6a** and **6b** are almost planar (dihedral angle 3°) and a slightly distorted envelope (dihedral angle 23°−25°), respectively, but **6b** has a distorted half-chair form. The Si−Si bond length in **5b** is 2.433 Å, which is the longest in all the Si_3X rings and considerably longer than that (2.409 Å) in the related cyclotetrasilane **B**. The long Si−Si distance in the small-membered rings is reminiscent of the fact that the presence of the bulky substituents on the highly strained planar Si_3O ring should result in remarkably stretched Si−Si distances, as has been discussed previously for cyclosilanes $[R_2Si]_n$ (n = 3, 4) bearing bulky substituents such as Me_3Si and *t*Bu groups.[7f] The Si−Si bond lengths in **6a** and **6b** are 2.392−2.414 Å, which is comparable with those (2.393−2.402 Å) in the other Si_4X rings of **2** and **4** in Table 14. It is of interest to note that the longer Si−Si bond length in **6b**, relative to those in **6a** and in the other heterosilacyles Si_3X, is similar to the situation in the five-membered rings **E**, **H**, and **I**. The Si−O bond lengths in **5b**, **6a**, and **6b** are in the 1.631−1.656 Å range, around the typical values of 1.64±0.03 Å.[13] The distance (1.656 Å) in **5b** is slightly short relative to those (1.663−1.721 Å) in the similar four-membered compounds cyclo-1,3-disiloxanes $[R_2SiO]_2$.[15] The Si−Si−Si bond angles in **5b**, **6a**, and **6b** are 68.2, 95.3, and 92.9°, respectively, and are the smallest in each set of the two types of rings (68.2−90.4°, Si_3X; 92.9−106.0°, Si_4X), as seen in Tables 13 and 14. Surprisingly, the angle (68.2°) in **5b**, with a planar structure, is unusually small and much closer to the inner angle (60°) of a three-membered ring rather than that (90°) of a planar four-membered one. This compound may thus have quite large angular and Pitzer strains, for which supporting results were obtained by theoretical calculations of the ring strain energies by the PM3 method (vide infra). The Si−O−Si bond angle in **5b** (111.1°) is comparable with those (106.3 and 112.1°) of the calculated $[H_2Si]_3O$,[6a] respectively. However, the Si−O−Si bond angles (133.6 and 132.3°) for **6a** and **6b** are significantly large compared to those (119.9−124.6°) in calculated $[R_2Si]_4O$ (R = H, Me).

Finally, the Si−Si bond lengths in **A−I** (except for **F**) and **1−6** in Tables 13 and 14 fall in the 2.370−2.433 Å range, and are considerably longer than the sums of the covalent

radii (2.34 Å), suggesting that the four- and five-membered rings are fairly strained because of steric repulsion between the bulky substituents (*i*Pr or *t*BuCH$_2$) on the silicons and the angular strains.

(2) Geometries

Firstly, the geometrical features show the following behavior with increasing bulkiness of substituent from an isopropyl to a neopentyl group in each pair of heterosilacycles [R$_2$Si]$_n$X (R = *i*Pr, *t*BuCH$_2$; X = CH$_2$, NC$_6$H$_{11}$, O, SiR$_2$, GeR′$_2$) (Tables 13 and 14):

i. The dihedral angles in the four-membered cycles increase (**3a**, **3b**; **A**, **B**; **C**, **D**).

ii. In the five-membered cycles, the ring torsion angles increase (**4a**, **4b**; **6a**, **6b**; **H**, **I**), whereas the sums of the internal angles decrease (**4a**, **4b**; **6a**, **6b**; **H**, **I**).

iii. In all cases, the Si−Si and Si−X bond lengths increase, except for Si−Ge in Si$_3$Ge, Si−Si in Si$_4$N, and Si−X in Si$_4$O cycles.

iv. The Si−Si−Si, Si−Si−X, and Si−X−Si bond angles decrease, except for Si−Si−O in the Si$_4$O cycle.

Consequently, the above results probably reflect the fact that the compounds bearing neopentyl groups release the steric repulsions between the bulky substituents through elongation of the bond lengths and expansion of the dihedral angles or torsion angles, while the compounds carrying isopropyl groups avoid steric repulsion (Pitzer strains) through expansion of the internal bond angles and distortion of the molecular shape. The bond elongation with increasing bulkiness of the substituents on the silicon atoms was also confirmed by the fact that the Si−Si bond lengths in the four- and five-membered [R$_2$Si]$_3$X and [R$_2$Si]$_4$X are longer − except in only one case (X = SiR$_2$)[14,16] − than those in the corresponding calculated cycles [R$_2$Si]$_3$X (R = H, Me, etc., X = SiH$_2$, CH$_2$, NH, O).[6a]

Secondly, the types of heteroatoms X in the four- and five-membered cycles [R$_2$Si]$_n$X also affect the geometrical parameters as follows:

i. The dihedral angles vary depending on the different combinations of heteroatom X, substituent R, and ring size; that is, Si$_n$X rings with NC$_6$H$_{11}$ or O as X prefer planar conformations (**3a**, **5b**), while the other silacyles have puckered (n = 3) or distorted conformations (n = 4).

ii. For heterosilacycles [R$_2$Si]$_n$X [n = 3, 4; R = *i*Pr, *t*BuCH$_2$; X = Ge(CH$_2$SiMe$_3$)$_2$, CH$_2$, NC$_6$H$_{11}$, O], as can be seen in Tables 13 and 14, the Si−Si−Si bond angles and Si$^{\alpha}$···Si$^{\alpha'}$ nonbonding distances in Si$_3$X decrease with decreasing atomic radii of the heteroatoms X and Si−X bond lengths, whereas the Si−X−Si bond angles increase. Alternatively, with increasing electronegativity[18] of X, decreases in the Si−Si−Si angles and the Si$^{\alpha}$···Si$^{\alpha'}$ nonbonding distances and increases in the Si−X−Si angles were observed. Interestingly, similar results from calculations for [H$_2$Si]$_3$X (X = SiH$_2$, PH, S, CH$_2$, NH, O) have previously been reported by another group of workers,[19] who explained their results in terms of a concept, the σ-bridged-π-bonding concept, by which the structural properties were correlated with the electronegativities[18] of the heteroatoms X in the rings. Thus, if this idea is applicable to the current systems for explaining the geometrical properties of such types of small rings, the results shown in Tables 13 and 14 seem virtually to substantiate this concept for the relationship between parameters such as the electronegativity of X, the Si−X bond length, and the Si−X−Si angle.

In terms of the molecular structures of heterosilacycles [R$_2$Si]$_n$X (n = 3, 4; R = *i*Pr, *t*BuCH$_2$; X = CH$_2$, NC$_6$H$_{11}$, O) (**1**−**6**), it is of considerable interest to discuss the molecular shapes on the basis of the steric repulsions arising from the bulky substituents on the ring silicon atoms and the steric requirements around the heteroatoms X, including their atomic sizes. Scheme 3 shows schematic diagrams of four-membered silacycles consisting of X = CH$_2$, NC$_6$H$_{11}$, O (see Table 13). Silacycles **3a** (X = NC$_6$H$_{11}$; R = *i*Pr) and **5b** (X = O; R = *t*BuCH$_2$) are planar rings, while **1b** (X = CH$_2$; R = *t*BuCH$_2$) and **3b**−**d** (X = NC$_6$H$_{11}$; R = *t*BuCH$_2$) are folded ones. The results show that when bulky neopentyl groups (steric substituent constant, *Es* = −1.74)[17] are attached to the two α-silicon atoms (**1b**, **3b**−**d**, **5b**), heterosilacycle **5b** containing (the smallest) oxygen (covalent atomic radius, 0.66 Å) as X (or X group), is planar, whereas the other silacycles, containing nitrogen (0.70 Å; **3b**−**d**) and carbon (0.77 Å; **1b**), are folded. However, in **3a**, which contains the medium-sized nitrogen (0.70 Å) as X and less bulky isopropyl substituents (*Es* = −0.47[17]) on the α-silicon atoms, the ring shape is also planar. In addition, the strongly electronegative X atoms, such as X = O (*En* = 3.50[18]) and N (*En* = 3.07[18]) in silacycles **3a**−**d** and **5b** strongly attract the neighboring silicon atoms (*En* = 1.74[18]) to produce an Si−X bond length shorter than that calculated on the basis of the normal covalent radii of silicon and X when there is a large electronegativity difference between them.[19] Furthermore, so-called (p−d)π bonding produced by back-donation of the lone-pair electrons from X to the d-orbitals of α-silicon atoms is also possible. From these observations, it is thus reasonable to consider that the ring shapes of the heterosilaycles may be attributable to the result of a compromise between parameters: steric repulsions due to the congestion imposed by the bulky substituents on the silicon atoms, especially α-silicon atoms, the steric requirement around the heteroatoms X (or X groups) in Si−X−Si systems, the ring strain energies, and the electronegativity differences between heteroatom X (or heteroatom group) and silicon.

For five-membered rings (R$_2$Si)$_n$X (n = 4; R = *i*Pr; *t*BuCH$_2$) (**2**, **4**, **6**), on the other hand, detailed investigation of the molecular shapes is apparently necessary to explain their structural features in Table 14 fully.

^{29}Si NMR Spectra

The ^{29}Si NMR spectroscopic data for **1**−**6** are summarized in Table 15, together with those for the related compounds **A**−**I** (except for **F**). Various features relating to variation in ring size, heteroatom X, silicon atom (Si$^{\alpha}$ or Si$^{\beta}$), and substituents on the silicon atoms [see Scheme 1, (a)−(e)] are observed, as follows:

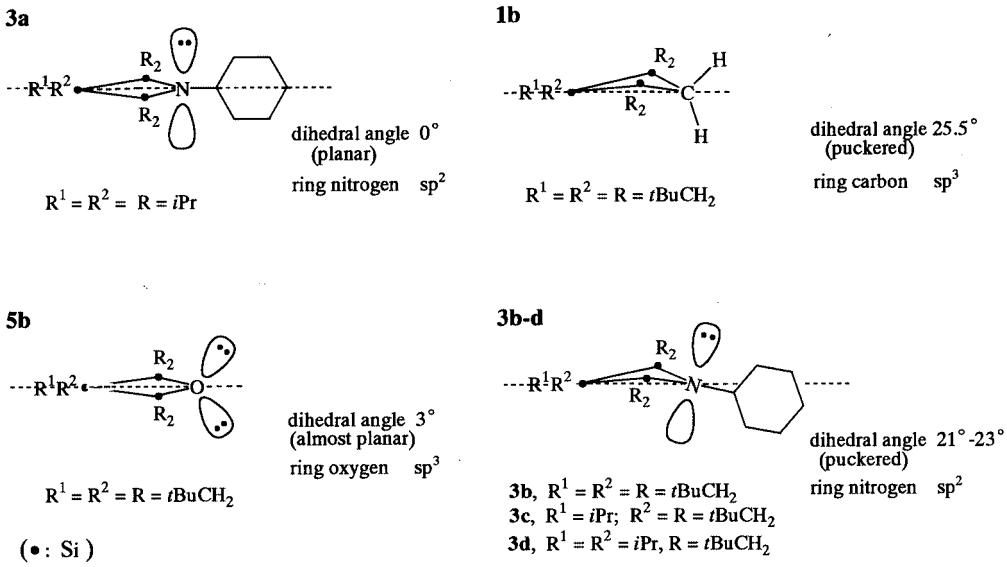

Scheme 3. Schematic diagrams of four-membered heteroatom-containing silacycles **1b**, **3a**−**d**, and **5b** (side views)

1) The resonances for the α-silicon atoms attached to the heteroatoms X are shifted downfield by a deshielding effect due to the electronegative atom X, and − as shown in Figure 1 − the larger the electronegativity (*En*)[18] of X, the lower the field of the chemical shifts.

2) The resonance for the β-silicon atoms generally occurs at higher fields than those for the α-silicon atoms, and there is no relationship between the chemical shift of the β-silicon atoms and the electronegativity[18] of X.

3) In the $[(i\mathrm{Pr})_2\mathrm{Si}]_n\mathrm{X}$ and $[(\mathrm{R^1R^2Si})_n\{(t\mathrm{BuCH_2})_2\mathrm{Si}\}_2]\mathrm{X}$ types (n = 1, 2), the resonances for the α- and β-silicon atoms appeared at higher fields with increasing ring size, due to a shielding effect with decreasing ring strain, as has previously been shown in various cyclosilanes.[20]

4) In each system of $\mathrm{Si}_n\mathrm{X}$ cycles, the resonances for both α- and β-silicon atoms of the compounds bearing neopentyl groups are shifted to higher fields than those bearing isopropyl groups, since the silicon atom at the γ-position from the terminal methyl carbon atom in an $\mathrm{SiCH_2C(CH_3)_3}$ group is subject to a high-field shielding effect due to the terminal carbon atom.[21]

Interestingly, it can be seen from Table 15 that the trend towards an increasing deshielding effect on the Si^α chemical shifts with increasing electronegativity[18] of X is substantially present, regardless of the presence or absence of a substituent on the heteroatom X. Indeed, as shown in Figure 1, the chemical shifts of the Si^α atoms in each series showed a good linear correlation with the electronegativity[18] of the heteroatom X, with good correlation coefficients (γ = 0.95−0.99). This is the first example in which a good linear correlation of $\delta\mathrm{Si}^\alpha$ with the electronegativity[18] of X in the $[\mathrm{R_2Si}]_n\mathrm{X}$ cycles has been found.

Table 15. ^{29}Si NMR spectroscopic data for $[(\mathrm{R^1R^2Si})_p(\mathrm{R_2Si})_2]\mathrm{X}$[a] and related compounds

ring size	p	$\mathrm{R^1;R^2}$	X	compd	δSi [ppm][b] Si^α	δSi [ppm][b] Si^β	ref.
4	1	$(i\mathrm{Pr})_2$	$\mathrm{SiR_2}$	**A**[c]	-5.5	-5.5	[7f]
			$\mathrm{Ge(CH_2SiMe_3)_2}$	**C**[c]	5.8	2.2	[10]
			$\mathrm{CH_2}$	**1a**	9.1	5.1	this work
			$\mathrm{NC_6H_{11}}$	**3a**	17.2	-8.6	"
			O	**5a**[c]	31.4	11.3	"
		$(t\mathrm{BuCH_2})_2$	$\mathrm{SiR_2}$	**B**[c]	-23.6	-23.6	[16]
			$\mathrm{Ge(CH_2SiMe_3)_2}$	**D**[c]	-11.8	-23.5	[10]
			$\mathrm{CH_2}$	**1b**	-4.0	-18.6	this work
			$\mathrm{NC_6H_{11}}$	**3d**	7.7	-8.6	"
			$\mathrm{NC_6H_{11}}$	**3c**	8.5	-18.0	"
			$\mathrm{NC_6H_{11}}$	**3b**	9.5	-30.9	"
			O	**5b**	29.4	-22.1	"
5	2	$(i\mathrm{Pr})_2$	$\mathrm{SiR_2}$	**E**[c]	-14.8	-14.8	[14]
			$\mathrm{GePh_2}$	**H**[c]	-12.1	-13.8	[11]
			$\mathrm{Ge(CH_2SiMe_3)_2}$	**G**[c]	-10.7	-12.5	"
			$\mathrm{CH_2}$	**2a**	1.9	-18.6	this work
			$\mathrm{NC_6H_{11}}$	**4a**[c]	1.8	-34.8	"
			O	**6a**	15.7	-20.4	"
		$(t\mathrm{BuCH_2})_2$	$\mathrm{GePh_2}$	**I**[c]	-24.0	-29.0	[11]
			$\mathrm{CH_2}$	**2b**	-8.7	-39.9	this work
			$\mathrm{NC_6H_{11}}$	**4c**	0.0	-26.0	"
			NPr	**4d**	2.3	-42.5	"
			$\mathrm{NC_6H_{11}}$	**4b**	2.7	-42.2	"
			O	**6b**	13.6	-44.3	"

[a] $\mathrm{R^2}$ = *i*Pr or $t\mathrm{BuCH_2}$. [b] In $\mathrm{CDCl_3}$. [c] In $\mathrm{C_6D_6}$.

Electronic Spectra

The UV spectra for $[\mathrm{R_2Si}]_n\mathrm{CH_2}$ (**1**, **2**), $[\mathrm{R^1R^2Si}]_n\mathrm{NR^3}$ ($\mathrm{R^3}$ = $\mathrm{C_6H_{11}}$ or Pr) (**3**, **4**), and $[\mathrm{R^1R^2Si}]_n\mathrm{O}$ (**5**, **6**) are listed in Table 16. In the UV spectra of **1a** and **1b** and of **2a** and **2b**, the longest-wavelength absorptions occur at λ = 234, 231 and 261, 254 nm, respectively, with varying extinction coefficients. The absorption maxima for the $\mathrm{Si_3C}$ cycles (**1**) consisting of peralkylated ring silicon atoms are substantially different from those (λ = 502−538 nm) for known $\mathrm{Si_3C}$ cycles with rather particular substituents,[3b][3c] such as trisilacyclobutaimines $[t\mathrm{Bu_2Si}]_3\mathrm{C{=}NAr}$. The absorption maxima of $\mathrm{Si_4C}$ (**2**) occur in almost the same region as that (λ = 258 nm) of peralkylated compound $[\mathrm{Me_2Si}]_4\mathrm{CH_2}$[3j] and are fairly different from that (λ = 443 nm) of perphenylated tetrasilacyclopentaimine $[\mathrm{Ph_2Si}]_4\mathrm{C{=}NPh}$[3f] and that (λ = 325 nm) of partially phenylated allenic tetrasilacy-

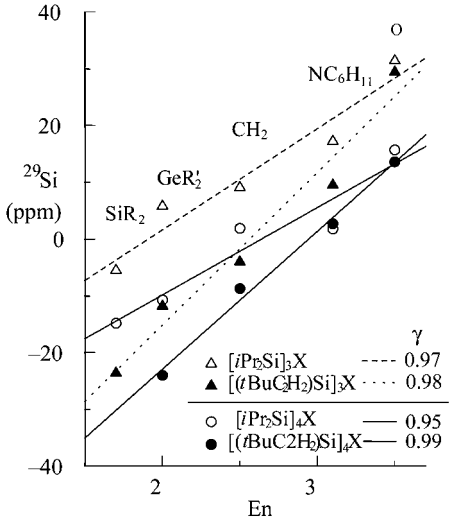

Figure 1. Correlation of $^{29}Si^{\alpha}$ chemical shifts with the electronegativities (*En*, see ref.[18]) of heteroatom X in $[R_2Si]_nX$ (n = 3, 4; R = *i*Pr, *t*BuCH$_2$)

clopentane $[Me_2Si]_4C{=}C{=}CPh_2$.[3e] It is worth noting that the UV absorption spectra of **1** are the first results for the peralkylated four-membered Si_3C cycle, since no such spectroscopic data have been described even for the only known peralkylated compound $[Me_2Si]_3CH_2$.[3a]

Table 16. UV data for $[R_2Si]_nX$ and related compounds

ring size	n	X	R	compd	λ_{max} / nm [ε / mol^{-1}dm^3 cm^{-1}][a]
4	3	CH_2	*i*Pr	**1a**	234 (8800)
			*t*BuCH$_2$	**1b**	231 (9400)
		NC_6H_{11}	*i*Pr	**3a**	233 (12000)
			*t*BuCH$_2$	**3b**	237 (10000)
			*i*Pr, *t*BuCH$_2$	**3c**	236 (8800)
			*i*Pr, *t*BuCH$_2$	**3d**	236 (10500)
		O	*i*Pr	**5a**	247 (10100), 203 (13600)
			*t*BuCH$_2$	**5b**	250 (11400), 205 (12000)
			*i*Pr, t-BuCH$_2$	**5c**	245 (11000), 213 (7400)
		SiR_2	*i*Pr	**A**	290 (200)[b]
			*t*BuCH$_2$	**B**	286 (440)[c]
		$Ge(CH_2SiMe_3)_2$	*i*Pr	**C**	300 (320)[d]
			*t*BuCH$_2$	**D**	286 (590)[d]
5	4	CH_2	*i*Pr	**2a**	261 (1100)
			*t*BuCH$_2$	**2b**	254 (1500), 233sh (6500)
		NC_6H_{11}	*i*Pr	**4a**	252sh (1600)
			*t*BuCH$_2$	**4b**	252sh (4100)
			*i*Pr, *t*BuCH$_2$	**4c**	252sh (2800)
		NPr	*t*BuCH$_2$	**4d**	252sh (3700)
		O	*i*Pr	**6a**	260sh (1800), 239 (9800) 220 (15500), 203 (18400)
			*t*BuCH$_2$	**6b**	255sh (3900), 242 (5800) 217 (16400)
		SiR_2	*i*Pr	**E**	274 (1700), 265 (1800)[e,f]
			*i*Bu	**F**	260sh (1500)[b]
		$Ge(CH_2SiMe_3)_2$	*i*Pr	**G**	280sh (1100), 262 (2000)[g]
		$GePh_2$	*i*Pr	**H**	280sh (5700), 252 (16000) 240 (18000)[g]
			*t*BuCH$_2$	**I**	280sh (7600), 245 (19000)[g]

[a] In *c*-C_6H_{12}. [b] Ref.[7d] [c] Ref.[16] [d] Ref.[10] [e] See also ref.[14] [f] Our data. [g] Ref.[7d]

The *N*-substituted four- and five-membered cycles **3** and **4** showed the longest-wavelength absorption bands at λ = 233−240 nm and 252 nm (sh), respectively. The absorption (252 nm) for **4** occurred at a longer wavelength region than that (235 nm) for $[Me_2Si]_4NMe$,[6b−6d] but shorter than that (282 nm) for $[Ph_2Si]_4NR^3$ (R^3 = Me, Et).[6e]

In the UV spectra of the *O*-substituted four- and five-membered compounds **5** and **6**, the longest-wavelength absorption bands occurred at λ = 245−250 and 255−260 nm, respectively. The absorption maxima for the Si_4O cycles (**6**) are comparable with those (λ = 253−258 nm) for $[Me_2Si]_4O$,[6d] $[Ph_2Si]_4O$,[6e] and $[Me(tBu)Si]_4O$.[5d] The UV data for the four-membered compounds **3** and **5** are the first examples for the Si_3N and Si_3O ring systems, respectively.

The UV data for **1**−**6** in Table 16, together with those for the related compounds **A**−**I**, showed various interesting features, as follows:

i. Little difference was observed in the UV data for $[iPr_2Si]_nX$ and $[(tBuCH_2)_2Si]_nX$ of the same ring size.

ii. With respect to the longest-wavelength absorption bands, compounds **1**−**6** and **A**−**I** could be roughly classified by a combination of ring size and heteroatom X into four groups: (a) $[R_2Si]_3X$ [X = SiR_2, $Ge(CH_2SiMe_3)_2$] (**A**−**D**), λ = 280−300 nm; (b) $[R_2Si]_3X$ (X = CH_2, NC_6H_{11}, O) (**1**, **3**, **5**), λ = 230−250 nm; (c) $[R_2Si]_4X$ (X = SiR_2, GeR'_2; R′ = CH_2SiMe_3, Ph) (**E**, **G**−**I**), λ = 270−300 nm; (d) $[R_2Si]_4X$ [X = CH_2, NR^3 (R^3 = C_6H_{11}, Pr), O] (**2**, **4**, **6**), λ = 250−260 nm. Compounds belonging to the same group showed absorption bands in almost the same region with nearly the same molar extinction coefficients, regardless of the nature of X and the substituents on the silicon atoms.

iii. As the ring size increased, the absorption maxima for the *Ge*-substituted compounds **C**−**D** and **G**−**I** hypsochromically shifted by 8−10 nm with increased extinction coefficients, as expected by analogy with the peralkylcyclosilanes such as $[R_2Si]_n$ (R = Me[22a,22b] and Et[22c]), while those for the *C*-, *N*-, and *O*-substituted compounds **1**−**6** bathochromically shifted by 10−20 nm with decreased extinction coefficients. This trend resembles that observed with increasing chain length for linear permethylpolysilanes $Me(Me_2Si)_nMe$,[23] rather than the cyclosilanes[22] mentioned above. Similarly, bathochromic shifts with increasing ring size have previously been observed for the *N*-substituted compounds $[Me_2Si]_nX$ (n = 4−6).[6b]

iv. The molar extinction coefficients (ε = 200−4100 $dm^3cm^{-1}mol^{-1}$) for compounds **A**−**I**, **2**, **4**, **6**, containing one germanium or four silicon atoms in the ring systems, were very small relative to those (ε = 8800−12000 $dm^3{\cdot}cm^{-1}{\cdot}mol^{-1}$) for **1**, **3**, and **5**, containing three silicon atoms. The large difference in the ε values between the two sets of ring systems may be due to differences in the forbidden σ−π* or allowed σ−σ* transitions[1a][3j] (vide infra).

Ring Strain Energies by Theoretical Calculation

The ring strain energies of homosilacycles or silicon cluster compounds are a very interesting subject, not only experimentally but also theoretically. We have previously experimentally determined the ring strain energies for a series of peralkylated homosilacycles $[R^1R^2Si]_n$ as 41, 23, 6, and 0 kcal/mol for n = 3−6, respectively.[7e] From the theoretical perspective, on the other hand, the homodesmotic ring strain energies for $(SiH_2)_4$ and $(SiH_2)_5$ at HF (Hartree−Fock) or MP2 levels with the basis sets of double

zeta plus polarization functions quality were calculated to be ca. 17.0 and 6.0 kcal/mol, respectively.[24] Similar results (18.7 and 5.7 kcal/mol) have been obtained at the higher MP4SDTQ/6-31G** level.[25] The calculated values thus seem to be slightly underestimated for the four-membered ring, although the data for the five-membered ring agree well with the above experimentally determined values.

Although some theoretical studies on the types of homosilacycles $(SiH_2)_n$[24,25] mentioned above and on $(SiH_2)_nX$ (X = PH and S)[19,26] are thus available, alkyl-substituted homosilacycles $(SiR_2)_n$ and alkyl-substituted heteroatom-containing silacycles have not so far been reported. In a preliminary study,[27] we estimated the ring strain energies for the alkylated four- and five-membered heterosilacyles $[R_2Si]_nX$ [R = Me, *i*Pr; *n* = 3, 4; X = CH_2, NMe, N(*i*Pr), O, SiH_2], on the basis of the homodesmotic reaction energies.[28] The magnitudes of the calculated strain energies for the series R = *i*Pr, listed in Table 17, were found to be in the order: *n* = 3: X = O (**5a**, 12.8 kcal/mol) > CH_2 (**1a**, 8.7) > SiH_2 (8.1) > N(*i*Pr) (6.4) > NMe (2.2); *n* = 4: X = N(*i*Pr) (11.4) > O (**6a**, 8.3) > SiH_2 (3.9) > CH_2 (**2a**, 3.1) > NMe (−2.1). In the four-membered cycle with SiH_2 as X, it was shown that the PM3 strain energy (8.1 kcal/mol) was much less than the above result (18.7 kcal/mol) obtained by the ab initio method,[25] and also the experimentally determined one (23 kcal/mol). The strain energies calculated for the four-membered rings are much larger than those for the five-membered rings for all kinds of heteroatom (or heteroatom group) X except for X = N(*i*Pr), in which the two kinds of silacycles are reversed in the magnitude of their strain energies. This may be explained in terms of the steric repulsions between the bulky groups including the Si−N(R^3)−Si system (R^3 = *i*Pr; see Table 17, footnote) in the Si_4N cycle, as such an effect is apparently more severe in the five-membered cycle than in the four-membered one, as shown and discussed previously for homosilacycles.[7f] This order of the magnitude in the two series of silacycles seems to be reasonable, although more advanced calculations are necessary.[27] In the four-membered rings, it is noteworthy that the strain energy (12.8 kcal/mol) for **5a** (X = O) is the largest and that the results agree well with prediction from the structural features of this molecule, that is, the highly strained conformation, as shown in Table 13 and discussed in the previous section. For the silacycles with X = CH_2 and SiH_2 as X, the strain energies of Si_3X (8.7, 8.1 kcal/mol) and Si_4X (3.1, 3.9) are fairly close to each other, while those for Si_3X and Si_4X cycles where X = NMe (2.2, −2.1, respectively) are the smallest. However, the considerable strain energy for Si_3X, X = N(*i*Pr) (6.4 kcal/mol) is of interest, because the conformation of the silacycle, including the steric requirements around the Si−N(R^3)−Si system, seems to be similar to that of X = NC_6H_{11} (**3a**, see also Table 17, footnote). The large strain energy calculated for Si_4X (X = O, **6a**) (8.3 k/cal) may also be in agreement with the experimental results shown in Table 2, in which the conformation, consisting of the relatively small angles Si−Si−Si (95°) and Si−Si−O (102°), the large angle Si−O−Si (134°), the short distance Si−O (1.65 Å), and the small ring-torsion angle (23°), would be a fairly strained molecule. It is worthwhile to note that a similar consideration may be applicable to the large strain energy (11.4 kcal/mol) for the heterosilacycles containing X = N(*i*Pr) if the X group can accommodate the NC_6H_{11} group of **4a** (see Table 17, footnote).

Table 17. Estimated strain energies [kcal/mol] of $[R_2Si]_nX$ at PM3 level

ring size	n	X	R: Me	R: *i*Pr
4	3	CH_2	7.9	8.7 (**1a**)
		NMe	9.0	2.2
		N(*i*Pr)[a]	...	6.4
		O	10.8	12.8 (**5a**)
		SiH_2	5.1	8.1
5	4	CH_2	0.9	3.1 (**2a**)
		NMe	-2.0	-2.1
		N(*i*Pr)[a]	...	11.4
		O	-0.9	8.3 (**6a**)
		SiH_2	0.5	3.9

[a] For convenience, the bulkiness of the two β-carbon atoms of the isopropyl group is assumed to be close to those of the cyclohexyl group; polar substituent constant σ*(*i*Pr) = −0.190, σ*(C_6H_{11}) = −0.15 (see ref.[17])

Oxidation Potentials

The oxidation potentials (E_{pa} vs. SCE) of the homo- and heterosilacycles were determined by cyclic voltammetry in MeCN or CH_2Cl_2. The results are summarized in Table 18[7h,29] and Table 19, respectively, together with those for the related compounds **A**−**I** (except for **E**). Firstly, it should be noted that this is the first report describing the oxidation potentials for silacycles containing a heteroatom in the ring system $[R_2Si]_nX$ (X = CH_2, O, NR^3, GeR'_2). The silacycles also gave irreversible voltammograms similar to those obtained for the homosilacycles, as shown in the previous work,[7h] suggesting the formation of their unstable cation-radicals produced from the starting silacycles. Interestingly, the oxidation potentials thus obtained from the four- and five-membered silacycles **1**, **3**, **5**, **A**−**D** and **2**, **4**, **6**, **F**−**I** roughly fall into nearly the same potential ranges as found for the homosilacycles Si_4 and Si_5[7h] in the two solvents. Thus, the potentials for the Si_3X rings were 0.8−1.0 V in MeCN and 0.96−1.24 V in CH_2Cl_2, while those for the Si_4X rings were 1.0−1.24 V in MeCN and 1.16−1.53 V in CH_2Cl_2. As described in the previous work,[7h] solvation of the cation radicals produced by the oxidations may account for the lower potentials in MeCN than in CH_2Cl_2 for **1**−**6**. Furthermore, it is also apparent from Table 19 that the potentials for the Si_3X system decreased relative to those for the Si_4X system in each solvent system. The results are in accord with the trend of the oxidation potentials in a series of homosilacycles $[R^1R^2Si]_n$ (*n* = 3−7).[7h,29] The silacycles of smaller ring size have larger ring strain energies and more strongly electron-donating natures than those with larger ring sizes.[7e] It was thus found that the oxidation potentials were primarily affected by the ring size, regardless of the types of heteroatom X and the substituents on the silicon

atoms, and − in addition − the presence or absence of a substituent on the heteroatom X.

Table 18. Oxidation and ionization potentials and HOMO and LUMO levels for homosilacycles $[R^1R^2Si]_m$ and related silacycles

no.	m	compd	Epa [V vs. SCE][a] CH_3CN	Epa [V vs. SCE][a] CH_2Cl_2	λ_{max}[b] [nm]	Ip, HOMO [eV] [c]	Ip, HOMO [eV] [d]	LUMO[e] [eV]	E_T[f] [eV]
1	3	$[(t\text{BuCH}_2)_2\text{Si}]_3$	0.44	0.72	310sh	-6.90[g]		-2.90	4.00
"				0.58[h]					
2		$[(t\text{BuCH}_2)_2\text{Si}]_2\text{GeR'}_2$[i]	0.37	0.57	312sh		-6.78	-2.81	3.97
3	4	$[i\text{Pr}_2\text{Si}]_4$	1.00	1.24	290sh	-7.22[h]		-2.94	4.28
4		$[s\text{Bu}_2\text{Si}]_4$	1.10	1.23	290sh		-7.44	-3.16	4.28
5		$[\text{Me}(t\text{Bu})\text{Si}]_4$	0.94	1.08	300	-7.42[j]		-3.29	4.13
"				1.21[h]					
6		$[(t\text{BuCH}_2)_2\text{Si}]_4$	1.10	1.19	298sh[l]		-7.40	-3.06	4.34
7		$[(\text{Me}_3\text{Si})_2\text{Si}]_4$		1.11[h]	286[k]	-7.10[g]		-2.94	4.26
8		$[i\text{Pr}_2\text{Si}]_3\text{GeR'}_2$[i]	0.80	0.96	300		-7.17	-3.05	4.12
9		$[(t\text{BuCH}_2)_2\text{Si}]_3\text{GeR'}_2$[i]	0.80	0.97	286		-7.18	-2.84	4.34
10	5	$[\text{Me}_2\text{Si}]_5$	1.08	1.26	275	-7.94[m]		-3.43	4.51
"				1.54[h]					
11		$[\text{Et}_2\text{Si}]_5$	1.48	1.36[h]	265sh		-7.57	-2.89	4.68
12		$[\text{Pr}_2\text{Si}]_5$	1.42	1.45	260		-7.66	-2.89	4.87
13		$[\text{Bu}_2\text{Si}]_5$	1.40	1.30	262		-7.51	-2.78	4.73
14		$[i\text{Bu}_2\text{Si}]_5$	1.36	1.38	260sh		-7.59	-2.68	4.91
15		$[i\text{Pr}_2\text{Si}]_4\text{GeR'}_2$[i]	1.04	1.23	280sh		-7.44	-3.01	4.43
16	6	$[\text{Me}_2\text{Si}]_6$	1.45	1.65	258sh	-7.79[m]		-2.98	4.81
"				1.54[h]					
17		$[\text{PrMeSi}]_6$	1.22		257sh				
18	7	$[\text{Pr}_2\text{Si}]_7$	1.40	1.40	242		-7.61	-2.49	5.12

[a] The first anodic peak potentials; scan rate, 250 mV/s; see also ref.[7h] [b] Longest-wavelength absorption band. [c] Reported values from UPS measurements. [d] Calculated values based on the regression line (Figure 2) obtained from the relationship between the ionization (UPS) and oxidation potentials (CV, E_{pa} in CH_2Cl_2) determined experimentally for runs number 1, 3, 5, 7, 10, and 16, respectively. [e] Values calculated by using the HOMO levels and the transition energies obtained from the longest-wavelength absorption bands. [f] Transition energy. [g] Ref.[31] [h] Ref.[29]; scan rate, 500 mV/s. [i] R′ = Me_3SiCH_2. [j] Ref.[32] [k] Ref.[16] [l] Ref.[34] [m] Ref.[35]

Table 19. Oxidation and ionization potentials and HOMO and LUMO levels for four- and five-membered silacycles $[R_2Si]_nX$

ring size	n	X	R	compd	Epa [V vs. SCE][a] CH_3CN	Epa [V vs. SCE][a] CH_2Cl_2	HOMO[b] [eV]	LUMO[c] [eV]	E_T[d] [eV]
4	3	CH_2	*i*Pr	**1a**	0.86	1.00	-7.21	-1.91	5.30
	"		$t\text{BuCH}_2$	**1b**	0.85	1.06	-7.27	-1.90	5.37
		NC_6H_{11}	*i*Pr	**3a**	0.94	1.19	-7.40	-2.08	5.32
	"		$t\text{BuCH}_2$	**3b**	0.89	1.04	-7.25	-2.02	5.23
	"		*i*Pr, $t\text{BuCH}_2$	**3c**	0.94	1.19	-7.40	-2.15	5.25
	"		*i*Pr, $t\text{BuCH}_2$	**3d**	0.94	1.22	-7.43	-2.17	5.26
		O	*i*Pr	**5a**	0.86	1.05	-7.26	-2.24	5.02
	"		$t\text{BuCH}_2$	**5b**	0.97	1.20	-7.41	-2.45	4.96
		SiR_2	*i*Pr	**A**	1.00	1.24	-7.22[e]	-2.94	4.28
	"		$t\text{BuCH}_2$	**B**	1.00	1.19	-7.40	-3.06	4.34
		$Ge(CH_2SiMe_3)_2$	*i*Pr	**C**	0.80	0.96	-7.17	-3.03	4.14
	"		$t\text{BuCH}_2$	**D**	0.80	0.97	-7.18	-2.84	4.34
5	4	CH_2	*i*Pr	**2a**	1.17	1.43	-7.64	-2.89	4.75
	"		$t\text{BuCH}_2$	**2b**	1.02	1.20	-7.41	-2.53	4.88
		NC_6H_{11}	*i*Pr	**4a**	1.11	1.29	-7.50	-2.58	4.92
	"		$t\text{BuCH}_2$	**4b**	1.05	1.16	-7.37	-2.45	4.92
	"		*i*Pr, $t\text{BuCH}_2$	**4c**	1.07	1.28	-7.49	-2.57	4.92
		NPr	$t\text{BuCH}_2$	**4d**	1.07	1.23	-7.43	-2.51	4.92
		O	*i*Pr	**6a**	1.22	1.34	-7.55	-2.78	4.77
	"		$t\text{BuCH}_2$	**6b**	1.08	1.23	-7.44	-2.57	4.87
		SiR_2	*i*Bu	**F**	1.36	1.38	-7.59	-2.68	4.91
		$Ge(CH_2SiMe_3)_2$	*i*Pr	**G**	1.04	1.23	-7.44	-3.01	4.43
		$GePh_2$	*i*Pr	**H**	1.27	1.53	-7.73	-3.30	4.37
	"		$t\text{BuCH}_2$	**I**	1.13	1.34	-7.55	-3.12	4.43

[a] The first anodic peak potentials; scan rate, 250 mV/s; see also ref.[7h] [b] Values calculated using the regression line (Figure 2) obtained from the experimental data of the oxidation (E_{pa}, CH_2Cl_2) and ionization potentials (Table 18). [c] Values calculated by using the HOMO levels and the transition energies obtained from the longest-wavelength absorption bands (Table 16). [d] Transition energy. [e] Ref.[31]

Molecular Frontier Orbitals

Generally, it is well known that oxidation potentials obtained by cyclic voltammetry (CV) for various compounds are linearly correlated to their ionization potentials,[30] which are useful for evaluation of HOMO levels. Accordingly, the oxidation potentials for this series of heteroatom-containing silacycles are applicable to estimation of their HOMO levels, from which their LUMO levels can also be estimated.

(1) Observed Results

Firstly, in order to determine the HOMO levels for a series of homosilacyles, we obtained a regression line for the relationship, with a good correlation coefficient (γ = 0.86 in Figure 2), between the reported ionization potentials (eV) of some homosilacycles measured by photoelectron spectroscopy (PES)[31−33,35] and their oxidation potentials (E_{pa}, in V vs. SCE in CH_2Cl_2) determined by the CV method, as listed in Table 18 (numbers 1, 3, 5, 7, 10, and 16). Interestingly, it should be pointed out that, in the current study, the E_{pa} value of $(Me_2Si)_5$ was shown to be 1.26 V (number 10), whereas the reported value is 1.54 V.[29] Although a better correlation (γ = 0.92) can be obtained if the former value is disregarded, the reason why the relatively large discrepancy occurred could not be clarified and remains to be investigated.

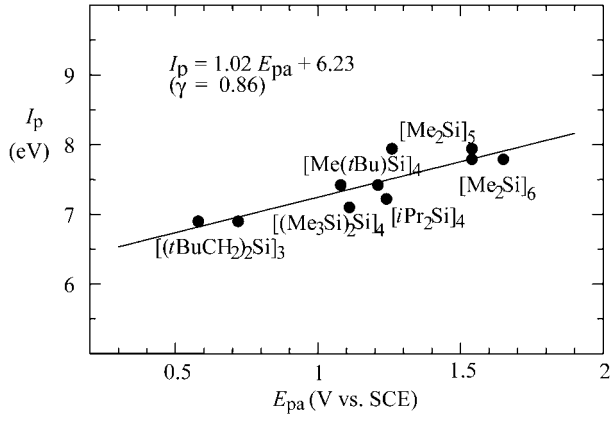

Figure 2. Correlation of the ionization potentials (PES) with the oxidation potentials (CV) of peralkylated homosilacycles $[R_2Si]_n$ (n = 3−7)

Next, with the aid of the regression line (Figure 2), the frontier HOMO levels of all the homosilacycles $(R_2Si)_m$ were estimated, from the oxidation potentials listed in Table 18, as approximately −6.8, −7.3, −7.7, −7.8, −7.6 eV for m = 3−7 (numbers 1−18), respectively. The

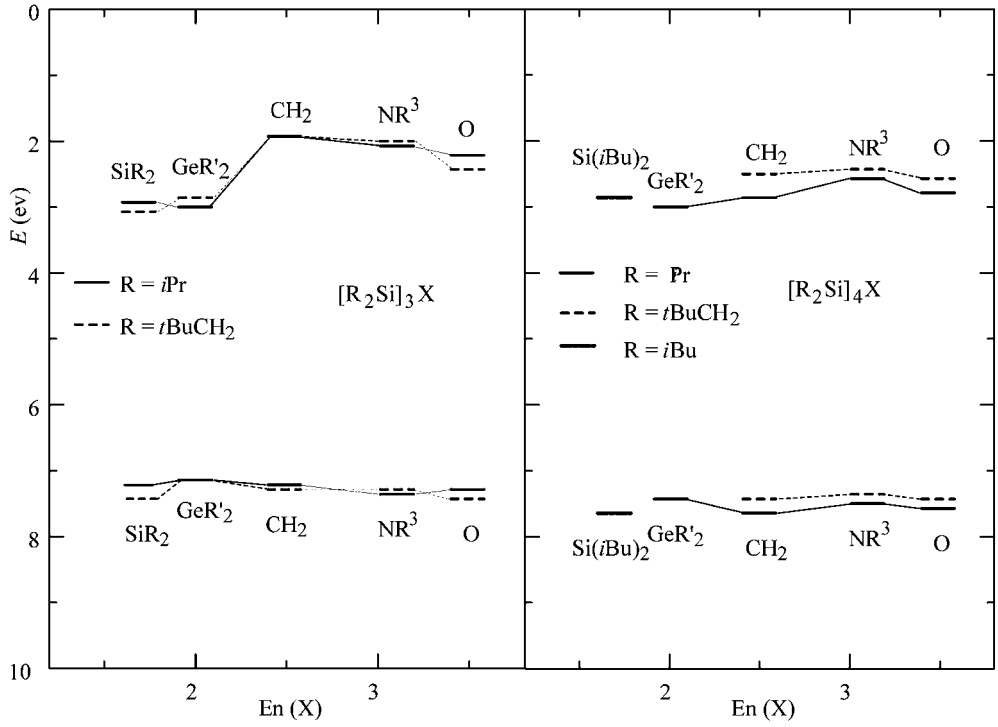

Figure 3. HOMO and LUMO levels for four- and five-membered heteroatom-containing silacycles $[R_2Si]_nX$ (n = 3, 4; R = *i*Pr, *t*BuCH$_2$)

results clearly exhibit decreasing levels with increasing ring size, except for m = 7, which is similar to that of m = 5. However, the LUMOs of m = 3−6 fall within a narrow range (numbers 1−17, −2.81 to −3.29 eV), and the level for the ring size m = 7 (number 18, −2.5 eV) appears to be slightly higher than those for m = 3−6.

In a similar manner, the two frontier levels for the series of heteroatom-containing silacycles $[R_2Si]_nX$ (R = *i*Pr, *t*BuCH$_2$; n = 3, 4; X = CH$_2$, O, NR^3, SiR$_2$, GeR′$_2$) were then estimated as listed in Table 19 and shown in Figure 3. Of interest is the fact that, in the four-membered cycles (n = 3), the HOMO levels were found to be very close to each other (ca. 7.2−7.4 eV), due to the close values of their oxidation potentials (E_{pa} = 0.96−1.24 V). The results suggest that the HOMOs of the $[R_2Si]_3X$ series lie at very close levels, probably arising from similar bonding character in the four-membered heterosilacycles at the HOMO levels. For the frontier orbitals of the five-membered cycles Si$_4$X, on the other hand, the HOMO levels are also very close to each other (Figure 3), but, as would be expected from their oxidation potentials, are at slightly lower levels than those for the Si$_3$X cycles.

With regard to the LUMO levels for the Si$_3$X cycles, the experimentally determined results can apparently be classified by the size of the energy gaps (E_T) into two groups: X = CH$_2$, NR^3, O (**1**, **3**, **5**) and X = SiR$_2$, GeR′$_2$ (**A**, **D**), as shown in Table 19 and Figure 3. Interestingly, as can be seen in Figure 4 at the LUMOs, including both the first LUMO and the second LUMO levels, which are in a very narrow range (vide infra), it is likely that the enhanced LUMO levels of the former group in comparison to those of the latter may be attributable to the contribution of the heteroatom (or heteroatom group) X to the frontier orbitals, especially the LUMOs, associated with the conformations due to the four-membered ring systems. In addition, the transition probabilities from the HOMOs to the LUMOs (ε = 8800−12000 dm^3·cm^{-1}·mol^{-1}for **1**, **3**, **5**; "allowed" transition[36]) for the former definitely appear different from those for the latter (ε = 200−590 dm^3·cm^{-1}·mol^{-1} for **A**−**D**; "forbidden" transition[36]), as shown in the longest-wavelength UV absorption bands in Table 16.

For the five-membered Si$_4$X (X = SiR$_2$, GeR′$_2$, CH$_2$, NR^3, O), on the other hand, the LUMOs are close to each other in all ring types, showing lower levels than those seen for the corresponding Si$_3$X, except for X = SiR$_2$. Thus, the contribution of the heteroatom (or heteroatom group) X to the LUMOs mentioned above cannot be observed in Figure 5 in the heterosilacycles containing X = CH$_2$, NR^3, O (**2**, **4**, **6**), which is related to their conformations. The values for the transition probabilities (ε = 1100−4100 dm^{3}cm^{-1}mol^{-1} for **2**, **4**, **6**, **E**, **F**, **G**; "partially allowed" transition[36]) in Table 16 fall in the mid-range between the two cases in the transitions, including compounds **H** and **I** (ε = 5700−7600 dm^{3}cm^{-1}mol^{-1}) which contain phenyl rings that provide resonance effects on the germanium atom in the rings.

From the above observations it should therefore be noted that the concept of a contribution through the heteroatom (or heteroatom group) X in the Si−X−Si systems to the LUMOs derived from theoretical calculations for the

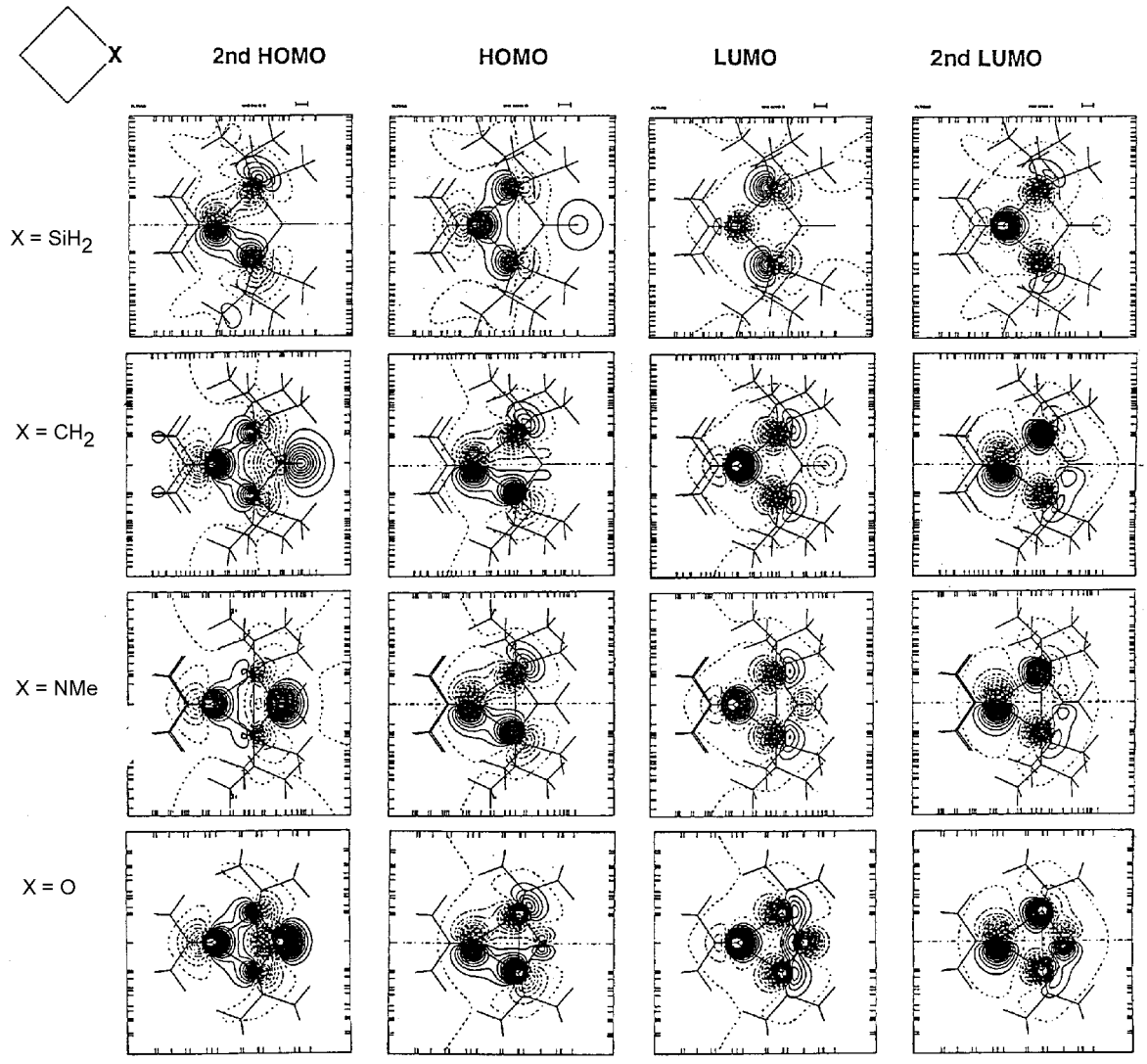

Figure 4. Orbital pictures of the frontier orbitals of $[(i\mathrm{Pr})_2\mathrm{Si}]_3\mathrm{X}$ (X = SiH_2, CH_2, NMe, and O)

HOMOs and LUMOs of the heterosilacycles Si_3X and Si_4X (X = CH_2, NR^3, O) may account for the above experimental results, although detailed studies are necessary.[27]

(2) Theoretical Calculations

The frontier orbital levels determined by PM3 are listed in Table 20. There seems to be no clear trend in the transition energies or energy gaps (E_T) of the molecules of interest. In the case of X = SiH_2, both HOMO and LUMO levels lie slightly lower in energy than in the other compounds with heteroatoms (or heteroatom groups). Both energy levels are almost the same in both sizes of rings, but the energy gaps seem to be slightly smaller in the five-membered rings than in the four-membered ones. Interestingly, the trend of the calculated E_T values in Table 20 for the series of compounds $[(i\mathrm{Pr})_2\mathrm{Si}]_n\mathrm{X}$ [n = 3, 4; X = CH_2, NMe, N(iPr), O, SiH_2] is in good agreement with those for the series of experimental results obtained from the corresponding (or similar) heterosilacycles $[R_2Si]_nX$ [n = 3, 4; X = CH_2 (**1a**; **2a**), NC_6H_{11} (**3a**; **4a**), O (**5a**; **6a**), SiR_2 (**A**; **E**)], respectively (see Table 19 and Figure 3).

The frontier orbitals for the four- and five-membered rings containing X = CH_2, NMe, SiH_2, and O are displayed in Figures 4 and 5, respectively. The orbital levels of the HOMO and the second HOMO, and the LUMO and second LUMO are very close to each other, so that the order of levels can vary depending on the kinds of heteroatom (or heteroatom group). However, the character of the orbitals is independent of the natures of X, as the HOMOs are almost localized on the ring frames. This is also true even if the kinds of substituents are changed. Interestingly enough, it was shown from Figures 4 and 5 that photochemical bond scission in the heteroatom-containing silacycles $[(i\mathrm{Pr})_2\mathrm{Si}]_n\mathrm{X}$ would occur at the Si−Si bonds and not at the Si−X bonds, as the HOMOs and LUMOs have Si−Si bonding and antibonding character, respectively.

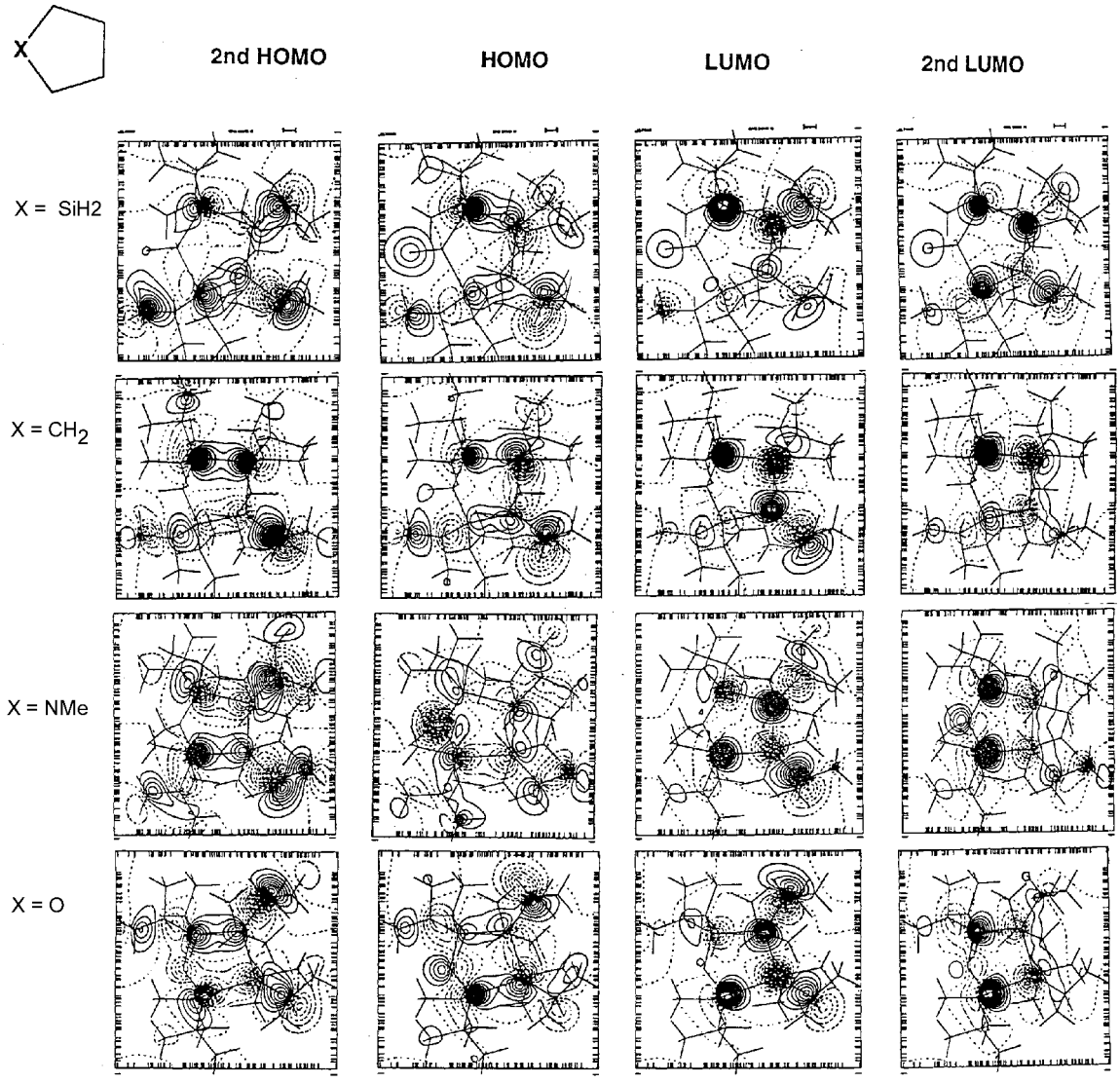

Figure 5. Orbital pictures of the frontier orbitals of $[(i\text{Pr})_2\text{Si}]_4\text{X}$ (X = SiH_2, CH_2, NMe, and O)

Table 20. Frontier orbital levels [eV] of $[(i\text{Pr})_2\text{Si}]_n\text{X}$ at PM3 level

ring size	n	X	compd	HOMO	LUMO	E_T[a]
4	3	CH_2	**1a**	-8.00	-1.29	6.71
		NMe	··	-7.97	-1.20	6.77
		N(*i*Pr)[b]	··	-7.95	-1.22	6.73
		O	**5a**	-7.84	-1.18	6.66
		SiH_2	··	-8.55	-1.58	6.97
5	4	CH_2	**2a**	-8.39	-1.19	7.20
		NMe	··	-8.01	-1.48	6.53
		N(*i*Pr)[b]	··	-7.76	-1.41	6.35
		O	**6a**	-7.79	-1.48	6.31
		SiH_2	··	-8.50	-1.69	6.81

[a] Transition energy. [b] For convenience, the bulkiness of the two β-carbon atoms of the isopropyl group is assumed to be close to that of the cyclohexyl group; polar substituent constant σ*(*i*Pr) = −0.190, σ*(C_6H_{11}) = −0.15 (see ref.[17]).

It seemed quite interesting to compare the theoretical prediction with experimental results obtained by photochemical cleavage of the heteroatom-containing silacycles Si_nX (n = 3, 4; X = CH_2, NC_6H_{11}, O).[8,37] We therefore investigated photochemical decomposition of the series of silacycles in a hydrocarbon solvent at room temperature or at 77 K under various reaction conditions in the absence or presence of reactants to trap reactive intermediates produced during the reactions.[1b] With a low-pressure mercury lamp (λ = 254 nm light)[8,37a] or a halogen lamp (λ > 390 nm light) in the presence of a photosensitizer such as 9,10-dicyanoanthracene,[37b] various photochemical decompositions were carried out to give the corresponding products, which were characterized, identified, and quantitatively analyzed (**1**, **3**, **5**, **7**, **8**, **9**, **10**, and final products). The results, summarized in Scheme 4, clearly show that the bond scissions occurred exclusively at the Si−Si bonds, and not at the Si−X bonds, which indicated good agreements with the above predictions. Finally, it should be noted that the strain energies in the series of silacycles Si_nX (n = 3, 4; X = CH_2, NR^3, O, GeR'_2) probably affect the differences between their reaction rates, as has been previously shown for thermal reactions of homosilacycles.[1b,38]

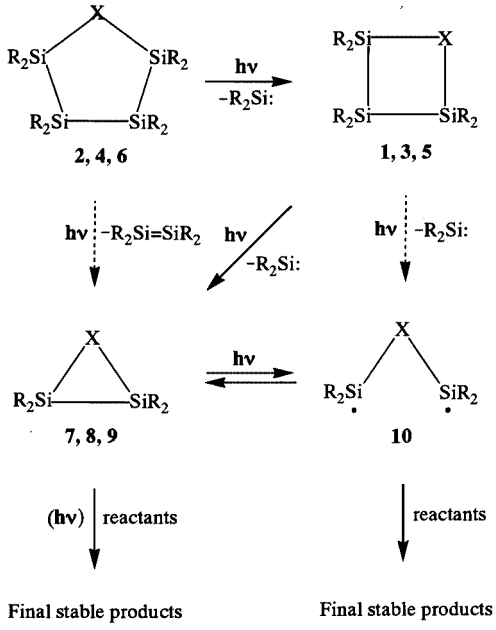

Scheme 4. Photochemical decompositions of heteroatom-containing silacycles Si_nX (n = 3, 4; X = CH_2, NR^3, and O) to give products; the paths shown with a dotted arrow do not seem to exist

Experimental Section

General Procedure: All reactions were carried out in dry flasks under an inert gas (N_2 or Ar). A commercially available 30% lithium dispersion in mineral oil was employed and was usually washed with the same solvent as used in subsequent reactions unless otherwise noted. In all preparations, the progress of the reaction in each step was monitored by GLC analysis. All melting points (uncorrected) were determined in sealed tubes, and for high melting point measurements a block heating apparatus equipped with a microscope were used. ^{1}H NMR spectra were recorded with Varian EM 360 A (60 MHz) (for **3b** and **5**), Hitachi 90H (90 MHz) and Varian Gemini 200M (200 MHz) spectrometers (for **1**, **2**, **3a**, **3c**, **3d**, **4**, and **6**) in $CDCl_3$ or C_6D_6 with Me_4Si as an internal standard. ^{13}C NMR spectra were recorded with Hitachi 90H (for **3a**, **3b**, **5**, and **6**) and Varian Gemini 200M (for **1**, **2**, **3c**, **3d**, and **4**) spectrometers in $CDCl_3$ or C_6D_6 with Me_4Si as an internal standard. For convenience, some spectroscopic data signals include the multiplicities in parentheses determined by the off-resonance technique. ^{29}Si NMR spectra were recorded in $CDCl_3$ or C_6D_6 with Hitachi 90H (for **3**−**6**) and JEOL ALPHA 500 (for **1** and **2**) spectrometers. Mass spectra were recorded with a JEOL DX 302 spectrometer (Ip = 30 or 70 eV). UV spectra were obtained with a Hitachi 200-10 spectrometer. GLC analysis was performed with an Ohkura GC-103 gas chromatograph equipped with a glass column (1 m) packed with SE-30 (10%) on Celite 545-AW (60−80 mesh). Cyclic voltammetry was performed with a Hokuto Denko Model HB-107A function generator and a Hokuto Denko Model HA-101 potentiostat. A cyclic voltammogram obtained at a scan rate of 250 mV/s was recorded with a Rikadenki X-Y recorder Model BW 133. For high-speed recording, a two-channel wave memory (NF Model MW-812A) was employed.

Materials: Tetrahydrofuran and benzene used in synthesis were dried with sodium wire and then freshly distilled out from a flask containing benzophenone/ketyl radical before use. Hexane, cyclohexane, and pentane were dried with lithium aluminum hydride and freshly distilled before use. Butyllithium solution in pentane (ca. 1.78 M) was commercially available. Spectrochemical grade cyclohexane was used for the determination of UV spectra. For cyclic voltammetry, spectrochemical grade acetonitrile and dichloromethane were dried by heating under reflux with P_2O_5 and freshly distilled under nitrogen before use. Other solvents and materials were commercially available.

Synthesis of *C*-Substituted Compounds 1 and 2: Compounds **1** and **2** were synthesized by reductive coupling of the corresponding α,ω-dichlorocarbosilanes with lithium as shown in Scheme 2, (a).

Synthesis of 2,2,3,3,4,4-Hexaisopropyl-2,3,4-trisilacyclobutane (1a): Typically, a solution of 1,4-dichloro-1,1,2,2,4,4-hexaisopropyl-1,2,4-trisilabutane $Cl(R_2Si)_2CH_2SiR_2Cl$ (R = *i*Pr) (**1a-1**, 0.161 g, 0.38 mmol) in a solvent mixture of THF (1.9 mL) and hexane (10.1 mL) was slowly added over 8 min at room temperature with stirring to a green suspension of lithium (69 mg, 2.98 mmol) and biphenyl (23 mg, 0.15 mmol) in THF (3.8 mL). After 2 h of stirring and addition of hexane, the unchanged lithium was filtered off. Purification by short column chromatography (silica gel, hexane) gave **1a** (0.134 g, 93% purity by GLC) as a colorless liquid, which was isolated by preparative GLC. ^{1}H NMR ($CDCl_3$): δ = 0.03 (s, 2 H, $C_{(ring)}H_2$), 1.09−1.12 [m, 24 H, $Si^{\alpha}CH(CH_3)_2$], 1.24 [d, 12 H, $Si^{\beta}CH(CH_3)_2$], 1.13−1.20 (m, 4 H, $Si^{\alpha}CHMe_2$), 1.41−1.50 (m, 2 H, $Si^{\beta}CHMe_2$). ^{13}C NMR ($CDCl_3$) −4.0 ($C_{(ring)}H_2$), 13.6 ($Si^{\beta}CHMe_2$), 14.9 ($Si^{\alpha}CHMe_2$), 19.7 and 20.0 [$Si^{\alpha}CH(CH_3)_2$], 22.5 [$Si^{\beta}CH(CH_3)_2$]. MS: *m*/*z* (%) = 356 (100) [M^+], 313 (60) [M − (*i*Pr)]$^+$, 271 (80) [M − (*i*Pr) − C_3H_6]$^+$. $C_{19}H_{44}Si_3$: calcd. C 63.96, H 12.43; found C 64.18, H 12.63. The above 1,4-dichlorotrisilabutane (**1a-1**) was prepared by a method similar to that used for the preparation of the methyl analogue $Br(Me_2Si)_2CH_2SiMe_2Br$,[3a] starting from R_2SiHCl (R = *i*Pr) via HR_2SiCH_2Cl (GLC yield, 36%), $HR_2SiCH_2SiR_2Ph$ (74%), $ClR_2SiCH_2SiR_2Ph$ (100%), $PhR_2SiSiR_2CH_2SiR_2Ph$ (100%), and then $ClR_2SiSiR_2CH_2SiR_2Cl$ (**1a-1**) (70%) (overall yield based on R_2SiHCl used, 19%); Colorless liquid; b.p. 103−105 °C/0.2 Torr. ^{1}H NMR ($CDCl_3$): δ = 0.28 (s, 2 H, $SiCH_2Si$), 1.11−1.50 [m, 42 H, $SiCH(CH_3)_2$]. ^{13}C NMR ($CDCl_3$): δ = 7.6 ($SiCH_2Si$), 13.5 (Si^2CHMe_2), 16.5 (Si^1CHMe_2), 17.0 (Si^4CHMe_2), 17.7 [$Si^2CH(CH_3)_2$], 18.1 and 18.6 [$Si^1CH(CH_3)_2$], 19.6 [$Si^4CH(CH_3)_2$]. MS: *m*/*z* (%) = 383 (5) [M − (*i*Pr)]$^+$, 341 (3) [M − (*i*Pr) − C_3H_6]$^+$, 274 (100) [M − (*i*Pr)$_2$SiCl]$^+$. $C_{19}H_{44}Cl_2Si_3$: calcd. C 53.35, H 10.37; found C 53.27, H 10.36.

Synthesis of 2,2,3,3,4,4-Hexaneopentyl-2,3,4-trisilacyclobutane (1b): This compound was synthesized by a method similar to that used for **1a**, by treatment of 1,4-dichloro-1,1,2,2,4,4-hexaneopentyl-1,2,4-trisilabutane $Cl(R_2Si)_2CH_2SiR_2Cl$ (**1b-1**: R = *t*$BuCH_2$; 0.599 g, 1.00 mmol, THF 5 mL/hexane 15 mL) with lithium (0.220 g, 9.5 mmol) and biphenyl (33 mg, 0.21 mmol, THF 10 mL) for 2.5 h. Compound **1b** (recrystallized from ethanol/pentane): 0.379 g, 72% yield; m.p. 138−140 °C. ^{1}H NMR ($CDCl_3$): δ = 0.44 (s, 2 H, $C_{(ring)}H_2$), 1.05 [s, 18 H, $Si^{\beta}CH_2C(CH_3)_3$], 1.06 [s, 36 H, $Si^{\alpha}CH_2C(CH_3)_3$], 1.15−1.19 [m, 12 H, $SiCH_2(t$Bu)]. ^{13}C NMR ($CDCl_3$) δ = −6.7 ($C_{(ring)}H_2$), 29.5 [$Si^{\beta}CH_2(t$Bu)], 31.4 ($Si^{\beta}CH_2CMe_3$), 32.0 ($Si^{\alpha}CH_2CMe_3$), 33.6 [$Si^{\alpha}CH_2(t$Bu)], 33.8 [$Si^{\alpha}CH_2C(CH_3)_3$], 33.9 [$Si^{\beta}CH_2C(CH_3)_3$]. MS: *m*/*z* (%) = 524 (28) [M^+], 453 (45) [M − (*t*$BuCH_2$)]$^+$, 397 (13) [M − (*t*$BuCH_2$) − C_4H_8]$^+$, 341 (10) [M − (*t*$BuCH_2$) − $(C_4H_8)_2$]$^+$. $C_{31}H_{68}Si_3$: calcd. C 70.90, H 13.10; found C 70.52, H 13.05. The above 1,4-dichlorotrisilabutane (**1b-1**) was prepared by a method similar to that used for **1a-1**, starting from $R_2SiPhCl$ (R = *t*$BuCH_2$) via PhR_2SiCH_2Cl (GLC yield, 86%), $PhR_2SiCH_2SiR_2Ph$ (61%), $ClR_2SiCH_2SiR_2Cl$ (78%), $PhR_2SiSiR_2CH_2SiR_2Cl$ (100%), and then $ClR_2SiSiR_2CH_2$-SiR_2Cl (**1b**−**1**) (84%) (overall yield based on $R_2SiPhCl$ used, 34%);

m.p. 55−57 °C. ^{1}H NMR ($CDCl_3$): δ = 0.50 (s, 2 H, $SiCH_2Si$), 1.06, 1.08 and 1.11 [54 H, $SiCH_2C(CH_3)_3$], 1.13−1.32 [m, 12 H, $SiCH_2(tBu)$]. ^{13}C NMR ($CDCl_3$): δ = 4.8 ($SiCH_2Si$), 32.0, 34.4, and 37.3 [$CH_2(tBu)$], 31.6, 31.7, and 32.0 (CH_2CMe_3), 33.2, 33.3, and 34.0 [$CH_2C(CH_3)_3$]. MS: *m*/*z* (%) = 523 (9) [M − (tBuCH$_2$)]$^+$, 389 (100) [M − (tBuCH$_2$)$_2$SiCl]$^+$, 333 (10) [M − (tBuCH$_2$)$_2$SiCl − C_4H_8]$^+$. $C_{31}H_{68}Cl_2Si_3$: calcd. C 62.47, H 11.50; found C 62.20, H 11.42.

Synthesis of 2,2,3,3,4,4,5,5-Octaisopropyl-2,3,4,5-tetrasilacyclopentane (2a): This compound was synthesized by a similar method to that used for **1a**, by treatment of 1,5-dichloro-1,1,2,2,4,4,5,5-octaisopropyl-1,2,4,5-tetrasilapentane $Cl(R_2Si)_2CH_2(SiR_2)_2Cl$ (**2a**−**1**: R = *i*Pr; 0.175 g, 0.32 mmol, THF 6 mL/hexane 5 mL) with lithium (0.127 g, 5.5 mmol) and biphenyl (42 mg, 0.28 mmol) in THF (3.5 mL) for 30 min. Compound **2a** (recrystallized from ethanol): 0.130 g, 87% yield; m.p. 249 −263 °C. ^{1}H NMR ($CDCl_3$): δ = −0.09 (s, 2 H, $C_{(ring)}H_2$), 1.14 [d, 24 H, $Si^{\alpha}CH(CH_3)_2$], 1.21−1.26 [m, 28 H, $Si^{\alpha}CHMe_2$ and $Si^{\beta}CH(CH_3)_2$], 1.41−1.56 (m, 4 H, $Si^{\beta}CHMe_2$). ^{13}C NMR ($CDCl_3$) δ = −5.9 ($C_{(ring)}H_2$), 13.6 ($Si^{\beta}CHMe_2$), 15.3 ($Si^{\alpha}CHMe_2$), 20.3 and 20.4 [$Si^{\alpha}CH(CH_3)_2$], 22.5 and 22.8 [$Si^{\beta}CH(CH_3)_2$]. MS: *m*/*z* (%) = 470 (20) [M$^+$], 427 (100) [M − (*i*Pr)]$^+$, 385 (35) [M − (*i*Pr) − C_3H_6]$^+$. $C_{25}H_{58}Si_4$: calcd. C 63.74, H 12.41; found C 63.79, H 12.25. The 1,5-dichlorotetrasilapentane (**2a-1**) mentioned above was prepared by HCl bubbling in the presence of $AlCl_3$ catalyst (2.33 mmol) in benzene (17 mL), by chlorination of $Ph(R_2Si)_2CH_2(SiR_2)Cl$ (R = *i*Pr; 2.27 mmol), which was obtained in quantitative yield by treatment of **1a-1** (2.27 mmol in 7 mL of THF) with PhR_2SiLi (R = *i*Pr; 3.76 mmol in 4 mL of THF). Compound **2a-1**: 1.27 g, purity 86%; yield 89%; Preparative GLC separation gave analytical samples; viscous liquid. ^{1}H NMR ($CDCl_3$): δ = 0.25 (s, 2 H, $SiCH_2Si$), 1.1−1.4 [m, 56 H, $SiCH(CH_3)_2$]. ^{13}C NMR ($CDCl_3$) δ = −7.9 ($SiCH_2Si$), 14.5 ($CH_2SiCHMe_2$), 17.2 ($ClSiCHMe_2$), 18.3 and 18.8 [$CH_2SiCH(CH_3)_2$], 19.8 and 20.2 [$ClSiCH(CH_3)_2$]. MS: *m*/*z* (%) = 391 (100) [M − (*i*Pr$_2$SiCl)]$^+$, 349 (40) [M − (*i*Pr$_2$SiCl)− C_3H_6]$^+$. $C_{25}H_{58}Cl_2Si_4$: calcd. C 55.40, H 10.79; found C 54.97, H 10.80.

Synthesis of 2,2,3,3,4,4,5,5-Octaneopentyl-2,3,4,5-tetrasilacyclopentane (2b): This compound was synthesized by a method similar to that used for **1a**, by treatment of 1,5-dichloro-1,1,2,2,4,4,5,5-octaneopentyl-1,2,4,5-tetrasilapentane $Cl(R_2Si)_2CH_2(SiR_2)_2Cl$ (**2b**−**1**: R = tBuCH$_2$; 0.153 g, 0.20 mmol, THF 1 mL/hexane 3 mL) with lithium (44 mg, 1.9 mmol) and biphenyl (7 mg, 0.047 mmol) in THF (2 mL) for 1.5 h. Compound **2b** (recrystallized from ethanol): 0.107 g, 77% yield; m.p. 354−364 °C. ^{1}H NMR ($CDCl_3$): δ = 0.47 (s, 2 H, $C_{(ring)}H_2$), 1.07 [s, 36 H, $Si^{\beta}CH_2C(CH_3)_3$], 1.08 [s, 36 H, $Si^{\alpha}CH_2C(CH_3)_3$], 1.14−1.36 [m, 16 H, $SiCH_2(tBu)$]. ^{13}C NMR ($CDCl_3$): δ = 1.5 ($C_{(ring)}H_2$), 30.1 [$Si^{\beta}CH_2(tBu)$], 32.3 ($Si^{\beta}CH_2CMe_3$), 32.6 ($Si^{\alpha}CH_2CMe_3$), 33.1 [$Si^{\alpha}CH_2(tBu)$], 34.1 [$Si^{\alpha}CH_2C(CH_3)_3$], 34.5 [$Si^{\beta}CH_2C(CH_3)_3$]. MS: *m*/*z* (%) = 694 (31) [M$^+$], 623 (21) [M − (tBuCH$_2$)]$^+$, 453 (13) [M − (tBuCH$_2$)$_3$Si]$^+$. $C_{41}H_{90}Si_4$: calcd. C 70.81, H 13.04; found C 70.40, H 12.94. The 1,5-dichlorotetrasilapentane (**2b-1**) mentioned above was prepared by a method similar to that used for **2a-1**, from $Ph(R_2Si)_2CH_2(SiR_2)_2Cl$ (R = tBuCH$_2$; 0.74 mmol), $AlCl_3$ catalyst (1.23 mmol in 6 mL of benzene), and HCl gas, as a crude product, 0.820 g (purity 63% by GLC; yield 91%). Recrystallization from hexane afforded analytical samples; m.p. 128−129 °C. ^{1}H NMR ($CDCl_3$): δ = 0.31 (s, 2 H, $SiCH_2Si$), 1.07 and 1.12 [72 H, $SiCH_2C(CH_3)_3$], 1.14−1.49 [m, 16 H, $SiCH_2(tBu)$]. ^{13}C NMR ($CDCl_3$): δ = 2.9 ($SiCH_2Si$), 33.0 and 34.2 [$CH_2(tBu)$], 31.7 and 32.8 (CH_2CMe_3), 33.4 and 34.1 [$CH_2C(CH_3)_3$]. MS: *m*/*z* (%) = 693 (6) [M − (tBuCH$_2$)]$^+$, 559 (100) [M − (tBuCH$_2$)$_2$SiCl]$^+$. $C_{41}H_{90}Cl_2Si_4$: calcd. C 64.25, H 11.84; found C 64.16, H 11.79.

Synthesis of *N*-Substituted Compounds 3 and 4: Compounds **3** and **4** were synthesized by treatment of the corresponding α,ω-dichlorosilanes with lithium alkylamide as shown in Scheme 2, (b) or (c).

Synthesis of 1-Cyclohexyl-2,2,3,3,4,4-hexaisopropyl-1-aza-2,3,4-trisilacyclobutane (3a) [Scheme 2, (b)]**:** Typically, a pentane solution of butyllithium (1.59 mL, 2.83 mmol) was added dropwise to a solution of cyclohexylamine (0.25 mL, 2.18 mmol) in THF (11 mL) at −75 to −60 °C. With stirring at the same temperature, the reaction progress was monitored by GLC for the peak intensity of the amine. When the intensity had decreased to a minimum, a solution of 1,3-dichloro-hexaisopropyltrisilane[5a] (0.50 g, 1.21 mmol) in THF (1 mL) was added to the reaction mixture at the same temperature. After additional stirring for 1 h at that temperature, 1 h at room temperature, and then heating under reflux for 10 h, the solvents were evaporated to give a solid, to which cyclohexane was added. After filtration, the resulting solution was concentrated, treated with water, and extracted with cyclohexane. The extracts were dried with calcium chloride, filtered, and concentrated to give a solid product, which was recrystallized from ethanol to afford colorless crystals of **3a** (0.36 g, 57% based on the dichlorotrisilane used); m.p. 208−213 °C. ^{1}H NMR ($CDCl_3$): δ = 1.08−1.15 [m, 24 H, $Si^{\alpha}CH(CH_3)_2$], 1.29−1.32 [m, 12 H, $Si^{\beta}CH(CH_3)_2$], 1.50−1.77 (m, 6 H, $SiCHMe_2$), 0.7−2.0 (m, 10 H, $C^{2-5}H_2$ in C_6H_{11}), 2.7−2.9 (m, 1 H, C^1H in C_6H_{11}). ^{13}C NMR ($CDCl_3$): δ = 14.8 (d, $Si^{\beta}CHMe_2$), 17.0 (d, $Si^{\alpha}CHMe_2$), 19.2 [q, $Si^{\alpha}CH(CH_3)_2$], 19.8 [q, $Si^{\alpha}CH(CH_3)_2$], 23.3 [q, $Si^{\beta}CH(CH_3)_2$]; 25.9 (t, C^4 in C_6H_{11}), 26.7 (t, $C^{3,5}$ in C_6H_{11}), 37.8 (t, $C^{2,6}$ in C_6H_{11}), 57.6 (d, C^1 in C_6H_{11}). MS: *m*/*z* (%) = 439 (8) [M$^+$], 396 (100) [M − (*i*Pr)]$^+$, 354 (7) [M − (*i*Pr) − C_3H_6]$^+$. $C_{24}H_{53}NSi_3$: calcd. C 65.52, H 12.14; found C 64.95, H 11.97.

Synthesis of 1-Cyclohexyl-2,2,3,3,4,4-hexaneopentyl-1-aza-2,3,4-trisilacyclobutane (3b): This compound was synthesized by a method similar to that used for **3a**, by treatment of 1,3-dichloro-1,1,2,2,3,3-hexaneopentyltrisilane $Cl(R_2Si)_3Cl$ (R = tBuCH$_2$; 2.00 g, 3.44 mmol)[10] with lithium cyclohexylamide (twice), prepared from cyclohexylamine (0.79 mL, 6.88 mmol in 20 mL of THF) and butyllithium (6.2 mL, 11.25 mmol in pentane). Compound **3b** (recrystallized from ethanol): 1.43 g, 69% yield; m.p. 228−238 °C. ^{1}H NMR ($CDCl_3$): δ = 1.08 [s, 36 H, $Si^{\alpha}CH_2C(CH_3)_3$], 1.11 [s, 18 H, $Si^{\beta}CH_2C(CH_3)_3$], 1.22 [broad s, 8 H, $Si^{\alpha}CH_2(tBu)$], 1.32 [broad s, 4 H, $Si^{\beta}CH_2(tBu)$], 1.0−1.9 (m, 10 H, $C^{2-5}H_2$ in C_6H_{11}), 2.5−2.9 (m, 1 H, C^1H in C_6H_{11}). ^{13}C NMR ($CDCl_3$): δ = 31.2 [t, $Si^{\beta}CH_2(tBu)$], 31.4 (s, $Si^{\alpha}CH_2CMe_3$), 33.4 (s, $Si^{\beta}CH_2CMe_3$), 33.9 [q, $Si^{\alpha}CH_2C(CH_3)_3$], 34.2 [q, $Si^{\beta}CH_2C(CH_3)_3$], 37.5 [t, $Si^{\alpha}CH_2(tBu)$], 26.8 (t, C^4 in C_6H_{11}), 28.7 (t, $C^{3,5}$ in C_6H_{11}), 37.8 (t, $C^{2,6}$ in C_6H_{11}), 59.2 (d, C^1 in C_6H_{11}). MS: *m*/*z* (%) = 607 (60) [M$^+$], 536 (100) [M − (tBuCH$_2$)]$^+$, 436 (45) [M − (tBuCH$_2$)$_2$SiH]$^+$, 365 (45) [M − (tBuCH$_2$)$_3$SiH]$^+$. $C_{36}H_{77}NSi_3$: calcd. C 71.09, H 12.76; found C 71.13, H 12.62.

Synthesis of 1-Cyclohexyl-3-isopropyl-2,2,3,4,4-pentaneopentyl-1-aza-2,3,4-trisilacyclobutane (3c): This compound was synthesized by a method similar to that used for **3a**, by treatment of 1,3-dichloro-2-isopropyl-1,1,2,3,3-pentaneopentyltrisilane $ClSiR_2SiRR'SiR_2Cl$ (**3c-1**: R = tBuCH$_2$, R′ = *i*Pr; 0.679 g, 1.23 mmol) with lithium cyclohexylamide (twice), prepared from cyclohexylamine (0.278 mL, 2.46 mmol in 15 mL of THF) and butyllithium (2.2 mL, 3.20 mmol in pentane). Compound **3c** (recrystallized from ethanol): 0.386 g, 54% yield; m.p. 219−225 °C. ^{1}H NMR ($CDCl_3$): δ = 1.03 [s, 2 H, $Si^{\beta}CH_2(tBu)$], 1.09 [s, 36 H, $Si^{\alpha}CH_2C(CH_3)_3$], 1.20−1.35 [m, 34 H, $CH(CH_3)_2$, $Si^{\alpha}CH_2(tBu)$, $Si^{\beta}CH_2C(CH_3)_3$, $C^{2-6}H_2$ in C_6H_{11}], 2.7−2.9 (m, 1 H, C^1H in C_6H_{11}). ^{13}C NMR ($CDCl_3$): δ = 13.6 ($SiCHMe_2$), 21.2 [$SiCH(CH_3)_2$], 28.6

[Si$^{\beta}$*C*H$_2$(*t*Bu)], 31.1 and 31.6 (Si$^{\alpha}$CH$_2$*C*Me$_3$), 31.9 (Si$^{\beta}$CH$_2$*C*Me$_3$), 33.7 [Si$^{\beta}$CH$_2$C(*C*H$_3$)$_3$], 34.2 [Si$^{\alpha}$CH$_2$C(*C*H$_3$)$_3$], 37.1 and 38.1 [Si$^{\alpha}$*C*H$_2$(*t*Bu)], 26.1 (C^4 in C$_6$H$_{11}$), 26.9 (C^{3,5} in C$_6$H$_{11}$), 39.7 (C^{2,6} in C$_6$H$_{11}$), 59.5 (C^1 in C$_6$H$_{11}$). MS: *m*/*z* (%) = 579 (5) [M$^+$], 536 (3) [M − (*i*Pr)]$^+$, 508 (100) [M − (*t*BuCH$_2$)]$^+$. $C_{34}H_{73}NSi_3$: calcd. C 70.38, H 12.68; found C 69.90, H 12.69. The 1,3-dichlorotrisilane (**3c-1**) mentioned above was prepared by chlorination of the corresponding trisilane HSiR$_2$SiRR′SiR$_2$H (**3c-2**; R = *t*BuCH$_2$, R′ = *i*Pr). Phosphorus pentachloride (0.37 g, 1.74 mmol) was added portionwise and slowly to a solution of **3c-2** (0.27 g, 0.56 mmol in 10 mL of benzene), and the mixture was stirred for ca. 18 h at room temperature. After evaporation of the solvent, hexane was added to the resulting mixture, which was then filtered. The filtrate, on evaporation of the solvents, gave **3c-1**, viscous liquid: 0.26 g, 0.83% yield. MS: *m*/*z* (%) = 552 (1) [M$^+$], 509 (1) [M − (*i*Pr)]$^+$, 481(100) [M − (*t*BuCH$_2$)]$^+$, 347 (100) [M − (*t*BuCH$_2$)$_2$SiCl]$^+$. The trisilane **3c-2** was prepared by lithium-mediated (0.46 g, 66 mmol in 50 mL of THF) cross-coupling with chlorodineopentylsilane (5.16 g, 25 mmol) and dichloro(isopropyl)(neopentyl)silane (2.37 g, 11 mmol) in THF (80 mL) (with magnetic stirring and ultrasound irradiation in a hot water bath). Compound **3c-2** (recrystallized from ethanol): 1.1 g, 20% yield; m.p. 57−58 °C. ^{1}H NMR (C$_6$D$_6$) δ = 1.13(s), 1.15(s), and 0.85−2.1(m) [62 H, SiC*H*(CH$_3$)$_2$, SiCH(C*H*$_3$)$_2$, SiCH$_2$C(C*H*$_3$)$_3$, SiC*H*$_2$(*t*Bu)], 4.38 (m, 2 H, Si*H*). ^{13}C NMR (C$_6$D$_6$) δ = 13.6 (Si*C*HMe$_2$), 21.3 [SiCH(*C*H$_3$)$_2$], 29.0 [Si^2*C*H$_2$(*t*Bu)], 30.1 (Si^{2}CH$_2$*C*Me$_3$), 30.7 [Si^{1,3}*C*H$_2$(*t*Bu)], 31.6 (Si^{1,3}CH$_2$*C*Me$_3$), 32.9 [Si^{1,3}CH$_2$C(*C*H$_3$)$_3$], 33.8 [Si^{2}CH$_2$C(*C*H$_3$)$_3$]. MS: *m*/*z* (%) = 484 (7) [M$^+$], 441 (4) [M − (*i*Pr)]$^+$, 413 (10) [M − (*t*BuCH$_2$)]$^+$, 313 (100) [M − (*t*BuCH$_2$)$_2$SiH]$^+$. $C_{28}H_{64}Si_3$: calcd. C 69.33, H 13.30; found C 69.01, H 13.32.

Synthesis of 1-Cyclohexyl-3,3-diisopropyl-2,2,4,4-tetraneopentyl-1-aza-2,3,4-trisilacyclobutane (3d): This compound was synthesized by a method similar to that used for **3a**, by treatment of 1,3-dichloro-2,2-diisopropyl-1,1,3,3-tetraneopentyltrisilane ClSiR$_2$-SiR′$_2$SiR$_2$Cl (**3d-1**: R = *t*BuCH$_2$, R′ = *i*Pr; 0.55 g, 1.0 mmol) with lithium cyclohexylamide, prepared from cyclohexylamine (1.2 mL, 10.4 mmol in 7 mL of THF) and butyllithium (8.2 mL, 13.5 mmol in pentane). Compound **3d** (recrystallized from 2-propanol): 0.23 g, 42% yield; m.p. 291−297 °C. ^{1}H NMR (CDCl$_3$): δ = 1.09 [s, 36 H, CH$_2$C(C*H*$_3$)$_3$], 0.76−1.95 [m, 32 H, C*H*(CH$_3$)$_2$, C*H*$_2$(*t*Bu), C$^{2-6}$*H*$_2$ in C$_6$H$_{11}$], 2.70−2.85 (m, 1 H, C^1*H* in C$_6$H$_{11}$). ^{13}C NMR (CDCl$_3$): δ = 12.9 (Si*C*HMe$_2$), 21.6 [SiCH(*C*H$_3$)$_2$], 31.1 (CH$_2$*C*Me$_3$), 34.0 [CH$_2$C(*C*H$_3$)$_3$], 37.6 [Si*C*H$_2$(*t*Bu)], 25.9 (C^4 in C$_6$H$_{11}$), 26.8 (C^{3,5} in C$_6$H$_{11}$), 38.2 (C^{2,6} in C$_6$H$_{11}$), 59.0 (C^1 in C$_6$H$_{11}$). MS: *m*/*z* (%) = 651 (10) [M$^+$], 508 (25) [M − (*i*Pr)]$^+$, 482 (100) [M − (*t*BuCH$_2$)]$^+$. $C_{32}H_{69}NSi_3$: calcd. C 69.61, H 12.60; found C 69.42, H 12.46. The 1,3-dichlorotrisilane (**3d-1**) mentioned above was prepared by chlorination of the corresponding trisilane HSiR$_2$SiR′$_2$SiR$_2$H (**3d-2**: R = *t*BuCH$_2$, R′ = *i*Pr; 0.52 g, 1.13 mmol) with phosphorus pentachloride (1.67 g, 7.97 mmol) in benzene (7 mL). Compound **3d-1**: viscous liquid; 0.55 g, 92% yield. MS: *m*/*z* (%) = 481 (4) [M − (*i*Pr)]$^+$, 453 (20) [M − (*t*BuCH$_2$)]$^+$, 319 (100) [M − (*t*BuCH$_2$)$_2$SiCl]$^+$. The trisilane **3d-2** was prepared by lithium-mediated (0.62 g, 89 mmol in 13 mL of THF) cross-coupling with chlorodineopentylsilane (5.71 g, 28 mmol) and dichlorodiisopropylsilane (2.38 g, 13 mmol) in THF (15 mL). Compound **3d-2** (recrystallized from ethanol): 2.37 g, 40% yield; m.p. 67−68 °C. ^{1}H NMR (CDCl$_3$): δ = 1.02 [s, 36 H, CH$_2$C(C*H*$_3$)$_3$], 0.78−1.50 [m, 22 H, C*H*(CH$_3$)$_2$, C*H*$_2$(*t*Bu)], 4.10−4.17 (m, 2 H, Si*H*). ^{13}C NMR (CDCl$_3$): δ = 14.7 (*C*HMe$_2$), 23.0 [CH(*C*H$_3$)$_2$], 31.8 [*C*H$_2$(*t*Bu)], 33.2 (CH$_2$*C*Me$_3$), 34.5 [CH$_2$C(*C*H$_3$)$_3$]. MS: *m*/*z* (%) = 456 (3) [M$^+$], 413 (6) [M − (*i*Pr)]$^+$, 385 (8) [M − (*t*BuCH$_2$)]$^+$, 285 (100) [M − (*t*BuCH$_2$)$_2$SiH]$^+$. $C_{26}H_{60}Si_3$: calcd. C 68.33, H 13.23; found C 68.39, H 13.39.

Synthesis of 1-Cyclohexyl-2,2,3,3,4,4,5,5-octaisopropyl-1-aza-2,3,4,5-tetrasilacyclopentane (4a): This compound was synthesized by a method similar to that used for **3a** [Scheme 2, (c)], by treatment of 1,4-dichloro-1,1,2,2,3,3,4,4-octaisopropylcyclotetrasilane[11] Cl(R$_2$Si)$_4$Cl (R = *i*Pr; 1.4 g, 2.6 mmol) with lithium cyclohexylamide, prepared from cyclohexylamine (0.9 mL, 7.9 mmol in 5 mL of THF) and butyllithium (6.5 mL, 10.2 mmol in hexane). Compound **4a** (recrystallized from 2-propanol): 0.51 g, 35% yield; m.p. 346−350 °C. ^{1}H NMR (δ, C$_6$D$_6$) 1.22−1.34 [m, 24 H, Si$^{\alpha}$CH(C*H*$_3$)$_2$], 1.36−1.48 [m, 24 H, Si$^{\beta}$CH(C*H*$_3$)$_2$], 1.60−1.76 (m, 8 H, SiC*H*Me$_2$), 1.2−2.0 (m, 10 H, C$^{2-6}$*H*$_2$ in C$_6$H$_{11}$), 3.0−3.2 (m, 1 H, C^1*H* in C$_6$H$_{11}$). ^{13}C NMR (C$_6$D$_6$) δ = 15.2 (Si$^{\beta}$*C*HMe$_2$), 17.8 (Si$^{\alpha}$*C*HMe$_2$), 20.4 and 20.6 [Si$^{\alpha}$CH(*C*H$_3$)$_2$], 24.1 and 24.4 [Si$^{\beta}$CH(*C*H$_3$)$_2$]; 26.3 (C^4 in C$_6$H$_{11}$), 27.9 (C^{3,5} in C$_6$H$_{11}$), 38.9 (C^{2,6} in C$_6$H$_{11}$), 59.0 (C^1 in C$_6$H$_{11}$). MS: *m*/*z* (%) = 559 (7) [M$^+$], 510 (100) [M − (*i*Pr)]$^+$, 468 (20) [M − (*i*Pr) − C$_3$H$_6$]$^+$, 446 (20) [M − (*i*Pr) − (C$_3$H$_6$)$_2$]$^+$. $C_{30}H_{67}NSi_4$: calcd. C 65.01, H 12.19; found C 64.50, H 11.98.

Synthesis of 1-Cyclohexyl-2,2,3,3,4,4,5,5-octaneopentyl-1-aza-2,3,4,5-tetrasilacyclopentane (4b): This compound was synthesized by a method similar to that used for **3a**, by treatment of 1,4-dichloro-1,1,2,2,3,3,4,4-octaneopentyltetrasilane[11] Cl(R$_2$Si)$_4$Cl (R = *t*BuCH$_2$; 0.58 g, 0.77 mmol) with lithium cyclohexylamide, prepared from cyclohexylamine (1.4 mL, 12.3 mmol in 3 mL of THF) and butyllithium (10.1 mL, 16.0 mmol in pentane). Compound **4b** (recrystallized from 2-propanol): 0.23 g, 38% yield; m.p. 379−383 °C. ^{1}H NMR (CDCl$_3$): δ = 1.12 (s), and 1.13 (s) [72 H, SiCH$_2$C(C*H*$_3$)$_3$], 0.7−1.0 (m), 1.15−1.30 (m), and 1.30−2.2 (m) [26 H, C$^{2-6}$*H*$_2$ in C$_6$H$_{11}$, SiC*H*$_2$(*t*Bu)$_3$], 3.0−3.2 (m, 1 H, C^1*H* in C$_6$H$_{11}$). ^{13}C NMR (CDCl$_3$) (tentative) δ = 30.3 [t, Si$^{\beta}$*C*H$_2$(*t*Bu)], 31.7 (s, Si$^{\beta}$CH$_2$*C*Me$_3$), 32.1 (s, Si$^{\alpha}$CH$_2$*C*Me$_3$), 34.4 [q, Si$^{\beta}$CH$_2$C(*C*H$_3$)$_3$], 34.5 [q, Si$^{\alpha}$CH$_2$C(*C*H$_3$)$_3$], 36.9 [t, Si$^{\alpha}$*C*H$_2$(*t*Bu)], 26.0 (t, C^4 in C$_6$H$_{11}$), 27.1 (t, C^{3,5} in C$_6$H$_{11}$), 37.8 (t, C^{2,6} in C$_6$H$_{11}$), 59.5 (d, C^1 in C$_6$H$_{11}$). MS: *m*/*z* (%) = 777 (3) [M$^+$], 706 (100) [M − (*t*BuCH$_2$)]$^+$, 536 (30) [M − (*t*BuCH$_2$)$_3$Si]$^+$. $C_{46}H_{99}NSi_4$: calcd. C 70.78, H 12.82; found C 70.96, H 12.82.

Synthesis of 1-Cyclohexyl-3,3,4,4-tetraisopropyl-2,2,5,5-tetraneopentyl-1-aza-2,3,4,5-tetrasilacyclopentane (4c): This compound was synthesized by a method similar to that used for **3a**, by treatment of 1,4-dichloro-2,2,3,3-tetraisopropyl-1,1,4,4-tetraneopentyltetrasilane ClSiR$_2$(SiR′$_2$)$_2$SiR$_2$Cl (**4c-1**: R = *t*BuCH$_2$, R′ = *i*Pr; 0.59 g, 0.90 mmol) with lithium cyclohexylamide, prepared from cyclohexylamine (3.46 mL, 28.7 mmol in 8 mL of THF) and butyllithium (17.1 mL, 27.9 mmol in pentane). Compound **4c** (recrystallized from 2-propanol): 0.28 g, 47% yield; m.p. 364−366 °C. ^{1}H NMR (C$_6$D$_6$) δ = 1.09 [s, 36 H, CH$_2$C(C*H*$_3$)$_3$], 0.78−2.10 [m, 51 H, C*H*(CH$_3$)$_2$, C*H*$_2$(*t*Bu), C$^{2-6}$*H*$_2$ in C$_6$H$_{11}$], 3.10−3.25 (m, 1 H, C^1*H* in C$_6$H$_{11}$). ^{13}C NMR (CDCl$_3$): δ = 14.5 (Si*C*HMe$_2$), 23.3 and 23.8 [SiCH(*C*H$_3$)$_2$], 31.7 (CH$_2$*C*Me$_3$), 34.1 [CH$_2$C(*C*H$_3$)$_3$], 36.7 [*C*H$_2$(*t*Bu)], 26.0 (C^4 in C$_6$H$_{11}$), 27.0 (C^{3,5} in C$_6$H$_{11}$), 37.6 (C^{2,6} in C$_6$H$_{11}$), 60.0 (C^1 in C$_6$H$_{11}$). MS: *m*/*z* (%) = 665 (3) [M$^+$], 622 (10) [M − (*i*Pr)]$^+$, 594 (100) [M − (*t*BuCH$_2$)]$^+$. $C_{38}H_{83}NSi_4$: calcd. C 68.49, H 12.55; found C 68.49, H 12.46. The 1,4-dichlorotrisilane (**4c-1**) mentioned above was prepared by chlorination of the corresponding tetrasilane HSiR$_2$(SiR′$_2$)$_2$SiR$_2$H (**4c-2**: R = *t*BuCH$_2$, R′ = *i*Pr; 1.00 g, 1.75 mmol) with phosphorus pentachloride (1.30, 6.19 mmol) in benzene (15 mL). Compound **4c-1** (recrystallized from hexane): 0.53 g, 47% yield; m.p. 65−66 °C. MS: *m*/*z* (%) 569 (10) [M − (*t*BuCH$_2$)]$^+$, 433 (100) [M − (*t*BuCH$_2$)$_2$SiCl]$^+$. The tetrasilane **4c-2** was prepared by lithium-mediated (1.51 g,

270 mmol in 80 mL of THF) cross-coupling with 1,2-dichlorotetraisopropyldisilane (7.36 g, 24.6 mmol) and chlorodineopentylsilane (14.24 g, 68.3 mmol) in THF (20 mL). Compound **4c-2** (recrystallized from pentane/ethanol): 10.6 g, 69% yield; m.p. 94−95 °C. ^{1}H NMR ($CDCl_3$): δ = 1.04 [s, 36 H, $CH_2C(CH_3)_3$], 0.82−1.50 [m, 36 H, $CH(CH_3)_2$, $CH_2(t$Bu)], 4.20−4.28 (m, 2 H, Si*H*). ^{13}C NMR ($CDCl_3$): δ = 13.9 (*C*HMe_2), 22.2 [$CH(CH_3)_2$], 29.8 (CH_2CMe_3), 31.5 [$CH_2(t$Bu)], 32.7 [$CH_2C(CH_3)_3$]. MS: *m*/*z* (%) = 570 (1) [M^+], 527 (10) [M − (*i*Pr)]$^+$, 499 (20) [M − (tBuCH_2)]$^+$, 399 (100) [M − (tBuCH_2)$_2$SiH]$^+$. $C_{32}H_{74}Si_4$: calcd. C 67.28, H 13.06; found C 67.06, H 13.07.

Synthesis of 1-Propyl-2,2,3,3,4,4,5,5-octaneopentyl-1-aza-2,3,4,5-tetrasilacyclopentane (4d): This compound was synthesized by a method similar to that used for **3a**, by treatment of 1,4-dichlorooctaneopentyltetrasilane[11] $Cl(R_2Si)_4Cl$ (R = tBuCH_2; 0.52 g, 0.69 mmol) with lithium propylamide, prepared from propylamine (0.44 g, 5.34 mmol in 3 mL of THF) and butyllithium (4.0 mL, 7.01 mmol in pentane). Compound **4d** (recrystallized from 2-propanol): 0.18 g, 35% yield; m.p. 396−399 °C. ^{1}H NMR ($CDCl_3$): δ = 0.83 (t, 3 H, $NCH_2CH_2CH_3$), 1.07 [s, 36 H, $Si^{\alpha}CH_2C(CH_3)_3$], 1.12 [s, 36 H, $Si^{\beta}CH_2C(CH_3)_3$], 1.17 (s), 1.24 (s), 1.31 (s), 1.38 (s), 1.43 (s), and 1.46−1.75 (m) [18 H, $NCH_2CH_2CH_3$, $Si^{\alpha}CH_2(t$Bu), $Si^{\beta}CH_2(t$Bu)], 2.90−3.10 (m, 2 H, $NCH_2CH_2CH_3$). ^{13}C NMR ($CDCl_3$): δ = 30.0 [$Si^{\beta}CH_2(t$Bu)], 31.6 ($Si^{\alpha}CH_2CMe_3$), 32.0 ($Si^{\beta}CH_2CMe_3$), 34.2 [$Si^{\beta}CH_2C(CH_3)_3$], 34.4 [$Si^{\alpha}CH_2C(CH_3)_3$], 36.5 [$Si^{\alpha}CH_2(t$Bu)], 11.7 (C^3 in C_3H_7), 27.8 (C^2 in C_3H_7), 51.6 (C^1 in C_3H_7). MS: *m*/*z* (%) = 737 (3) [M^+], 666 (100) [M − (tBuCH_2)]$^+$, 497 (15) [M − (tBuCH_2)$_4$Si$_2$]$^+$. $C_{43}H_{95}NSi_4$: calcd. C 69.93, H 12.96; found C 69.57, H 12.80.

Synthesis of *O*-Substituted Compounds 5 and 6: Compounds **5** and **6** were synthesized by treatment of the corresponding α-ω-dichlorosilanes with H_2O or NaOH as shown in Scheme 2, (d).

Synthesis of 2,2,3,3,4,4-Hexaisopropyl-1-oxa-2,3,4-trisilacyclobutane (5a): Typically, H_2O (1 mL, 56 mmol) was added at 53 °C with stirring to a solution of 1,3-dichlorohexaisopropyltrisilane[5a] (3.50 g, 8.5 mmol) in degassed triethylamine (20 mL). After the mixture had been stirred for 1 h at this temperature, degassed cyclohexane was added, and the mixture was extracted and dried with calcium chloride. After filtration, the filtrate was concentrated to give a solid product, which was recrystallized from methanol to afford colorless crystals of **5a** (see also ref.[8]) (0.85 g, 28%); m.p. 100−103 °C. ^{1}H NMR (C_6D_6) δ = 1.0−1.6 [m, 42 H, $SiCH(CH_3)_2$, $SiCH(CH_3)_2$]. ^{13}C NMR (C_6D_6) δ = 13.7 (d, $Si^{\beta}CHMe_2$), 16.6 (d, $Si^{\alpha}CHMe_2$), 17.9 [q, $Si^{\alpha}CH(CH_3)_2$], 22.7 [q, $Si^{\beta}CH(CH_3)_2$]. MS: *m*/*z* (%) = 358 (40) [M^+], 315 (100) [M − (*i*Pr)]$^+$, 273 (35) [M − (*i*Pr) − C_3H_6]$^+$. $C_{18}H_{42}OSi_3$: calcd. C 60.26, H 11.80; found C 59.58, H 11.72.

Synthesis of 2,2,3,3,4,4-Hexaneopentyl-1-oxa-2,3,4-trisilacyclobutane (5b): 1,3-Dichlorohexaneopentyltrisilane[10] $Cl(R_2Si)_3Cl$ (R = tBuCH_2; 0.59 g, 1.0 mmol in 10 mL of THF) was added to a mixture of NaOH (0.16 g, 4.0 mmol), THF (5 mL), and EtOH (5 mL). The mixture was stirred for 20 min at room temperature. After addition of hexane and filtration, the filtrate was concentrated and cyclohexane was then added. The solution was washed with dilute hydrochloric acid solution and water, dried, and then concentrated to give a crude product. Compound **5b** (recrystallized from ethanol/pentane) (see also ref.[8]): 0.41 g, 77% yield; m.p. 151−153 °C. ^{1}H NMR (C_6D_6) δ = 0.97 [s, 18 H, $Si^{\beta}CH_2C(CH_3)_3$], 1.03 [s, 36 H, $Si^{\alpha}CH_2C(CH_3)_3$], 1.22 [s, 4 H, $Si^{\beta}CH_2(t$Bu)], 1.28 [s, 8 H, $Si^{\alpha}CH_2(t$Bu)]. ^{13}C NMR ($CDCl_3$): δ = 29.0 [t, $Si^{\beta}CH_2(t$Bu)], 31.5 (s, $Si^{\alpha}CH_2CMe_3$), 31.8 (s, $Si^{\beta}CH_2CMe_3$), 33.7 [q, $Si^{\alpha}CH_2C(CH_3)_3$], 34.0 [q, $Si^{\beta}CH_2C(CH_3)_3$], 36.5 [t, $Si^{\alpha}CH_2(t$Bu)]. MS: *m*/*z* (%) = 526 (30) [M^+], 511 (25) [M − Me]$^+$, 455 (90) [M − (tBuCH_2)]$^+$, 399 (80) [M − (tBuCH_2) − C_4H_8]$^+$. $C_{30}H_{66}OSi_3$: calcd. C 68.36, H 12.62; found C 68.24, H 12.63.

Synthesis of 2,4-Diisopropyl-2,3,3,4-tetraneopentyl-1-oxa-2,3,4-trisilacyclobutane (5c): This compound was synthesized by a method similar to that used for **5a**, by hydrolysis of 1,3-dichloro-1,3-diisopropyltetraneopentyltrisilane ClSiRR′SiR_2SiRR′Cl (**5c-1**: R = tBuCH_2, R′ = *i*Pr; 0.50 g, 0.95 mmol) with H_2O (1 mL) in triethylamine (15 mL), followed by workup of the resulting mixture. Compound **5c**: 0.39 g (purity: 92%) 87% yield, liquid; analytical samples were isolated by GLC purification. ^{1}H NMR (C_6D_6) δ = 1.05−1.30 (m) (composed of four peaks at 1.16, 1.19, 1.22, 1.25) [48 H, $SiCH(CH_3)_2$, $SiCH_2C(CH_3)_3$], 1.48 (broad s, 2 H, $SiCHMe_2$), 1.60 [broad s, 8 H, $SiCH_2(t$Bu)]. $C_{26}H_{58}OSi_3$: calcd. C 66.30, H 12.41; found C 66.10, H 12.42. The 1,3-dichlorotrisilane (**5c-1**) mentioned above was prepared by chlorination of the corresponding trisilane HSiRR′SiR_2SiRR′H (**5c-2**: R = tBuCH_2, R′ = *i*Pr; 6.5 g, 14 mmol/CCl_4 30 mL) by chlorine gas bubbling. Compound **5c-1**: b.p. 185−195 °C/3 Torr; 3.8 g, 52% yield. ^{1}H NMR (C_6D_6) δ = 1.16 (s), and 1.18 (s) [48 H, $CH(CH_3)_2$, $CH_2C(CH_3)_3$], 1.35 [m, 4 H, $Si^{1,3}CH_2(t$Bu)], 1.50 [broad s, 4 H, $Si^2CH_2(t$Bu)], 1.73 (m, 2 H, $CHMe_2$). $C_{26}H_{58}Cl_2Si_3$: calcd. C 59.38, H 11.12; found C 59.41, H 11.15. The trisilane **5c-2** was prepared by lithium-mediated (fine cut, 0.4 g, 58 mmol in 40 mL of THF) cross-coupling with dichlorodineopentylsilane (2.4 g, 10.0 mmol) and chloro(isopropyl)-(neopentyl)silane (4.2 g, 23.6 mmol) in THF (15 mL). Compound **5c-2**: b.p. 124−127 °C/5 Torr; 1.8 g, 39% yield. ^{1}H NMR ($CDCl_3$):

Table 21. Crystal data, data collection, and refinement for four- and five-membered silacycles $[R_2Si]_nX$ (X = CH_2)

	Compd **1b**	Compd **2a**
	Crystal data	
formula	$C_{31}H_{68}Si_3$	$C_{25}H_{58}Si_4$
mol wt	525.135	471.075
crystal size/mm	0.3×0.1×0.1	0.3×0.2×0.2
cryst syst	Triclinic	Monoclinic
space group	$\bar{P}1$	$\bar{P}2_1/n$
a/Å	10.076(3)	20.860(3)
b/Å	11.900(4)	14.273(1)
c/Å	16.619(6)	10.487(1)
α/degree	102.04(2)	
β/degree	92.03(2)	95.36(2)
γ/degree	103.70(2)	
V/Å^3	1885(1)	3108.7(5)
Z	2	4
D_{calcd} (gcm^{-3})	0.924	1.006
	Data collection	
diffractmeter	Enraf-Nonius CAD4	Mac Science MXC18K
radiation (λ/Å)	1.5418(CuKα)	0.7107(MoKα)
temp/°C	23	23
scan mode	ω scan	ω scan
scan range (2θ)	4°∽120°	4°∽55°
no. of reflns collected	5986	7318
used ($\|Fo\| \geqq \|3\sigma\|Fo\|$)	5617	7122
μ/cm^{-1}	12.45	2.0
abs cor method	ψ scan	no
transmission factor (min/max)	0.8235/0.9988	no
	Solution and refinement	
system used	UNICS III	Crystan
method	MULTAN 78	SIR 92
refinement method	full-matrix least squares	full-matrix least squares
R (Rw)	0.083(0.086)	0.061(0.083)
wrighting scheme	[a]	[b]
goodness of fit (S)	1.19	2.59
peaks in diff Fourier map (e/Å^3)	0.45/-0.52	0.53/-0.39

[a] $w = 1/\sigma^2 |F_o|$. [b] $w = 1/\sigma^2 |F_o|$.

δ = 0.61−1.96 (m), and 1.06 (m) [58 H, C*H*(CH_3)$_2$, CH_2C(CH_3)$_3$], 3.88 (m, 2 H, Si*H*). $C_{26}H_{60}Si_3$: calcd. C 68.33, H 13.23; found C 67.80, H 13.18.

Synthesis of 2,2,3,3,4,4,5,5-Octaisopropyl-1-oxa-2,3,4,5-tetrasilacyclopentane 6a: This compound was synthesized by a method similar to that used for **5b**, by hydrolysis of 1,4-dichlorooctaisopropyltetrasilane[11] Cl(R_2Si)$_4$Cl (R = *i*Pr; 1.02 g, 1.9 mmol) with H_2O (3 mL) in THF (7 mL) at 50−60 °C for 15 h. Compound **6a** (recrystallized from methanol/ethanol): 0.88 g, 96% yield; m.p. 308−315 °C. ^{1}H NMR ($CDCl_3$): δ = 1.0−1.15 [m, 24 H, Si$^{\alpha}$CH(CH_3)$_2$], 1.20−1.35 [m, 24 H, Si$^{\beta}$CH(CH_3)$_2$], 1.35−1.56 (m, 8 H, SiC*H*Me$_2$). ^{13}C NMR ($CDCl_3$): δ = 13.4 (d, Si$^{\beta}$*C*HMe$_2$), 17.5 (d, Si$^{\alpha}$*C*HMe$_2$), 18.2 [q, Si$^{\alpha}$CH(*C*H_3)$_2$] and 18.8 [q, Si$^{\alpha}$CH(*C*H_3)$_2$], 22.6 [q, Si$^{\beta}$CH(*C*H_3)$_2$] and 22.9 [q, Si$^{\beta}$CH(*C*H_3)$_2$]. MS: *m*/*z* (%) = 472 (15) [M$^+$], 429 (100) [M − (*i*Pr)]$^+$, 387 (50) [M − (*i*Pr) − C_3H_6]$^+$, 345 (35) [M − (*i*Pr) − (C_3H_6)$_2$]$^+$. $C_{24}H_{56}OSi_4$: calcd. C 60.29, H 11.90; found C 60.94, H 11.93.

Synthesis of 2,2,3,3,4,4,5,5-Octaneopentyl-1-oxa-2,3,4,5-tetrasilacyclopentane (6b): This compound was synthesized by a method similar to that used for **5a**, by treatment of 1,4-dichlorooctaneopentyltetrasilane[11] Cl(R_2Si)$_4$Cl (R = *t*BuCH_2; 0.58 g, 0.77 mmol) with NaOH (ca. 1 mL of 1 M aq. solution) in THF (15 mL) at 50−60 °C for 20 h. Compound **6b** (recrystallized from hexane/ethanol): 0.5 g, 93% yield; m.p. 377−380 °C. ^{1}H NMR ($CDCl_3$): δ = 1.08 [s, 36 H, Si$^{\beta}$CH$_2$C(CH_3)$_3$], 1.10 [s, 36 H, Si$^{\alpha}$CH$_2$C(CH_3)$_3$], 1.16 [s, 8 H, Si$^{\beta}$CH_2(*t*Bu)], 1.29 [s, 8 H, Si$^{\alpha}$CH_2(*t*Bu)]. ^{13}C NMR ($CDCl_3$): δ = 29.6 [t, Si$^{\beta}$*C*H$_2$(*t*Bu)], 31.8 (s, Si$^{\alpha}$CH$_2$*C*Me$_3$), 32.0 (s, Si$^{\beta}$CH$_2$*C*Me$_3$), 34.0 [q, Si$^{\alpha}$CH$_2$C(*C*H_3)$_3$], 34.3 [q, Si$^{\beta}$CH$_2$C(*C*H_3)$_3$], 36.0 [t, Si$^{\alpha}$*C*H$_2$(*t*Bu)]. MS: *m*/*z* (%) = 696 (100) [M$^+$], 625 (65) [M − (*t*BuCH_2)]$^+$, 525 (50) [M − (*t*BuCH_2)$_3$Si]$^+$, 340 (70) [(*t*BuCH_2)$_4$Si$_2$]$^+$. $C_{40}H_{88}OSi_4$: calcd. C 68.88, H 12.72; found C 68.58, H 12.81.

Synthesis of Decaisopropylpentasilane E: This compound was synthesized (not optimized) by treatment of 1,4-dilithiooctaisopropyltetrasilane (in place of 1,4-dipotassiooctairopropyltetrasilane[14] with dichlorodiisopropylsilane [Scheme 2, (e)]. Freshly distilled anhydrous HMPA (1.1 mL) was added to a mixture of octaisopropylcyclotetrasilane **A** (168 mg, 0.368 mmol) and lithium (51 mg, 0.735 mmol). The mixture was stirred at room temperature for 2 h to afford a dark red-brown solution containing 1,4-dilithiooctaisopropyltetrasilane, to which benzene (5 mL) was then added. This solution, containing the 1,4-dilithiotetrasilane, was added dropwise by hypodermic syringe to a separate flask containing dichlorodiisopropylsilane (70 μL, 0.401 mmol) in benzene (2.5 mL) in an ice/water bath. After stirring at 0 °C for 30 min, the reaction mixture was mixed well with hexane (60 mL) and water (80 mL). After separation of the organic layer, it was washed well with water, dried with calcium chloride, and then filtered. The solution obtained was concentrated to give a solid product mixture, from which the reaction product, decaisopropylcyclopentasilane **E**, was isolated by repeated fractional recrystallization from a mixture of pentane/ethanol to afford 40 mg, 19% yield, m.p. 357−366 °C. It was found

Table 22. Crystal data, data collection, and refinement for four-membered silacycles [R_2Si]$_3$X (X = NR_3)

	Compd			
	3a	**3b**	**3c**	**3d**
	Crystal data			
formula	$C_{24}H_{53}NSi_3$	$C_{36}H_{77}NSi_3$	$C_{34}H_{73}NSi_3$	$C_{32}H_{69}NSi_3$
mol wt	439.946	608.268	580.214	552.160
crystal size/mm	0.4×0.4×0.2	0.5×0.3×0.2	0.65×0.6×0.1	0.06×0.06×0.7
cryst syst	Monoclinic	Monoclinic	Monoclinic	Monoclinic
space group	$P2_1/n$	$P2_1/n$	$P2_1/n$	$P2_1/n$
a/Å	8.563(2)	19.505(5)	18.108(7)	10.732(4)
b/Å	18.828(3)	11.709(1)	12.104(1)	10.947(4)
c/Å	17.978(3)	20.858(6)	19.458(6)	31.78(1)
α/degree				
β/degree	101.79(3)	117.80(1)	110.54(2)	92.29(2)
γ/degree				
V/Å^3	2837.2(2)	4212.6(2)	3994.0(2)	3729(2)
Z	2	4	4	4
D_{calcd} (gcm^{-3})	1.030	0.96	0.97	0.98
	Data collection			
diffractometer	Rigaku AFC-4	Enraf-Nonius CAD4	Enrauf-Nonius CAD4	Enrauf-Nonius CAD4
radiation (λ/Å)	0.7107(MoKα)	0.7107(MoKα)	0.7107(MoKα)	1.5418(CuKα)
temp/°C	23	23	23	23
scan mode	2θ/ω	ω scan	2θ/ω	2θ/ω
scan range (2θ)	4°∽55°	4°∽55°	4°∽55°	4°∽55°
no. of refins				
collected	6646	10588	10234	6037
used ($\|Fo\| \geqq 3\sigma\|Fo\|$)	2855	5945	6890	3782
μ/cm^{-1}	1.64	1.34	1.40	12.486
abs cor method	no	no	ψ scan	ψ scan
transmission factor (min/max)	no	no	0.9650/0.999	0.85/1.00
	Solution and refinement			
system used	MULTAN 78 UNICS III	MULTAN 78 UNICS III	UNICS III MULTAN 78	UNICS III MULTAN 78
method				
refinement method	full-matrix least squares	full-matrix least squares	full-matrix least squares	full-matrix least squares
R (Rw)	0.063(0.070)	0.079(0.082)	0.060(0.060)	0.095(0.099)
wrighting scheme	[a]	[b]	[c]	[d]
goodness of fit (S)	2.04	2.03	1.31	2.64
peaks in diff Fourier map (e/Å^3)	0.35/-0.31	0.51/-0.34	0.38/-0.31	0.64/-0.36

[a] $w = 1/[84.2\cdot(\sin\theta/\lambda)^2 - 51.4\cdot(\sin\theta/\lambda) + 8.9]$. [b] $w = 1/(0.0078\cdot|F_o|^2 - 0.432\cdot|F_o| + 7.88)$. [c] $w = 1/(0.0078\cdot|F_o|^2 - 0.06402\cdot|F_o| + 1.54216)$. [d] $w = 1/(0.00788\cdot|F_o|^2 - 0.21670\cdot|F_o| + 6.00345)$.

that crystalline materials obtained from the filtrates contained the product **E** (ca. 20 mg, calculated), the unchanged starting compound (**A**), and a small amount of unidentified material. Compound **E** (see also ref.[14]): ^{1}H NMR ($CDCl_3$): δ = 1.33 [d, 60 H, $SiCH(CH_3)_2$], 1.43−1.62 (m, 10 H, $SiCHMe_2$). ^{13}C NMR ($CDCl_3$): δ = 15.9 ($SiCHMe_2$), 23.8 [$SiCH(CH_3)_2$]. MS: *m*/*z* (%) = 570 (5) [M^+], 527 (100) [$M - i$Pr]$^+$, 485 (15) [$M - i$Pr − C_3H_6]$^+$, 413 (10) [$M - i$Pr − 2(C_3H_6)]$^+$. $C_{30}H_{70}Si_5$: calcd. C 62.25, H 12.45; found C 63.07, H 12.35.

Oxidation Potentials: Measurements of the oxidation potentials[7h,41] for **1**−**6** (10^{-3} M) by cyclic voltammetry were performed under N_2 (purified) in an anhydrous solvent (MeCN or CH_2Cl_2) containing Bu_4NClO_4 (TBAP, 0.1 M) as supporting electrolyte with a specially devised cell equipped with a working electrode (Pt inlay type, Beckmann 32273), counterelectrode (Pt wire), and saturated calomel electrode as a reference, connected to the cell through two salt bridges (saturated KCl solution), and the acetonitrile or dichloromethane solution of the sample. All runs were made at room temperature after a 15 min purge with N_2 and within 30 min of preparing the solution, experimental error ±0.02 V. All the results are summarized in Tables 18 and 19, together with those for the related compounds **A**−**D**, **F**−**I**.

Methods of Theoretical Calculations for Geometries, Frontier Molecular Orbitals, and Ring Strain Energies: Geometries of all molecules considered here were fully optimized at the PM3 level with the Gaussian 98 program.[42] They were then characterized as minima or transition states by calculation and diagonalization of the Hessian matrix of energy second derivatives at the same level of theory. The orbital pictures were drawn with the Gamess program.[43] The optimized structures for all four-membered rings are found to have C_s symmetry with a σ plane involving one silicon atom and heteroatom, except for X = N(*i*Pr) which is in a C_1 conformation. On the other hand, none of the five-membered rings have a symmetry higher than C_1. The ring strain energies for the four- and five-membered ring compounds (R = *i*Pr) were estimated on the basis of the homodesmotic reaction energies[28] [Equations (1) and (2)].

$$Si^1R_2{-}X{-}SiR_2Si^3R_2(Si^1\text{-}Si^3) + 2\,SiHR_2{-}SiHR_2 + 2\,SiHR_2{-}XH \rightarrow SiHR_2{-}X{-}SiHR_2 + SiHR_2{-}SiR_2{-}SiHR_2 + 2\,SiHR_2{-}SiR_2{-}XH \quad (1)$$

$$Si^1R_2{-}X{-}SiR_2SiR_2{-}Si^4R_2(Si^1\text{-}Si^4) + 3\,SiHR_2{-}SiHR_2 + 2\,SiHR_2{-}XH \rightarrow SiHR_2{-}X{-}SiHR_2 + 2\,SiHR_2{-}SiR_2{-}SiHR_2 + 2\,SiHR_2{-}SiR_2{-}XH \quad (2)$$

X-ray Crystal Analysis of 1−6: Crystals obtained from alcohols such as methanol, ethanol, and 2-propanol were used for X-ray analysis. Intensity data were obtained with an Enraf−Nonius CAD-4 diffractometer equipped with graphite-monochromated Cu-K_α (λ = 1.5418 Å) or Mo-K_α (λ = 0.7107 Å) radiation and by the ω-2θ scan technique. Structures of **1**−**6** were solved by direct methods with the MULTAN 78 program[39] and refined by full-matrix least squares. All the calculations were performed with the UNICS III system.[40] The molecular structures of **1b**, **2a**, **3a**−**d**,

Table 23. Crystal data, data collection, and refinement for five-membered silacycles $[R_2Si]_4X$ (X = NR^3)

	Compd 4a	4b	4c
		Crystal data	
formula	$C_{30}H_{67}NSi_4$	$C_{46}H_{99}NSi_4$	$C_{38}H_{83}NSi_4$
mol wt	554.208	778.637	666.422
crystal size/mm	0.4×0.3×0.2	0.4×0.4×0.4	0.36×0.36×0.13
cryst syst	Monoclinic	Orthorhombic	Monoclinic
space group	Pn	$P2_12_12_1$	$P2_1$
a/Å	10.550(1)	20.692(1)	11.157(1)
b/Å	10.964(1)	18.367(2)	16.375(1)
c/Å	15.551(1)	14.058(1)	13.068(2)
α/degree			
β/degree	97.70(1)		113.01(1)
γ/degree			
V/Å^3	1782.6(3)	5342.8(7)	2197.6(4)
Z	2	4	2
D_{calcd} (gcm^{-3})	1.032	0.9709	1.0072
		Data collection	
diffractmeter	Enraf-Nonius CAD4	Enraf-Nonius CAD4	Enraf-Nonius CAD4
radiation (λ/Å)	1.5418(CuKα)	1.5418(CuKα)	1.5418(CuKα)
temp/°C	23	23	23
scan mode	ω scan	ω scan	ω scan
scan range	4°⌣120°	4°⌣120°	4°⌣120°
no. of reflns			
collected	2650	4413	3487
used (|Fo| ≧ 3σ |Fo|)	2532	3561	3227
μ/cm^{-1}	16.428	11.844	13.68
abs cor method	ψ scan	ψ scan	ψ scan
transmission factor (min/max)	0.9212/0.9998	0.8577/0.9991	0.9164/0.9994
		Solution and refinement	
system used	UNICS III	SDP-package and UNICS III	UNICS III
method	MULTAN 78	MULTAN 78	MULTAN 78
refinement method	full-matrix least squares	full-matrix least squares	full-matrix least squares
R (Rw)	0.058(0.071)	0.083(0.083)	0.052(0.073)
wrighting scheme	[a]	[b]	[c]
goodness of fit (S)	1.298	0.943	1.42
peaks in diff Fourier map (e/Å^3)	0.50/-0.50	0.7/-0.2	0.4/-0.4

[a] $w = 1/(0.047\cdot|F_o|^2 - 0.0280\cdot|F_o| + 0.4783)$. [b] $w = 1/(0.00295\cdot|F_o|^2 + 0.0781\cdot|F_o| + 1.929)$. [c] $w = 1/(0.0068\cdot|F_o|^2 - 0.118\cdot|F_o| + 1.113)$.

Table 24. Crystal data, data collection, and refinement for four- and five-membered silacycles $[R_2Si]nX$ (X = O)

	Compd 5b	6a	6b
Crystal data			
formula	$C_{30}H_{66}OSi_3$	$C_{24}H_{56}OSi_4$	$C_{40}H_{88}OSi_4$
mol wt	527.107	473.048	697.477
crystal size/mm	0.2×0.2×0.2	0.4×0.3×0.2	0.3×0.2×0.1
cryst syst	Monoclinic	Monoclinic	Triclinic
space group	$P2_1$	$P2_1/n$	$\bar{P}1$
a/Å	11.250(2)	10.549(1)	20.742(2)
b/Å	16.015(1)	14.498(1)	21.454(1)
c/Å	11.715(4)	20.387(3)	11.431(1)
α/degree			97.06(1)
β/degree	119.28(2)	95.73(1)	100.96(1)
γ/degree			91.38(1)
V/Å^3	1841.3(9)	3102.1(5)	4950.2(5)
Z	2	4	4
D_{calcd} (gcm^{-3})	0.950	0.9355	0.936
Data collection			
diffractmeter	Rigaku AFC-4	Enraf-Nonius CAD4	Rigaku RAXIS
radiation (λ/Å)	0.7107(MoKα)	1.5418(CuKα)	0.7107(MoKα)
temp/°C	23	23	15
scan mode	2θ/ω	ω scan	ω scan
scan range	4°∽55°	4°∽120°	4°∽55°
no. of refins collected	4438	4978	14760
used ($\|Fo\| \geqq 3\sigma\|Fo\|$)	1568	4208	4866
μ/cm^{-1}	1.47	17.86	1.44
abs cor method	no	ψ scan	no
transmission factor (min/max)	no	0.9367/0.9977	no
Solution and refinrment			
system used	UNICS III	UNICS III	Texsan
method	MULTAN 78	MULTAN 78	SIR 92
refinement method	block diagonal least squares	full-matrix least squares	full-matrix least squares
R (Rw)	0.070(0.073)	0.074(0.083)	0.082(0.096)
wrighting scheme	[a]	[b]	[c]
goodness of fit (S)	2.33	1.959	2.38
peaks in diff Fourier map (e/Å^3)	0.42/-0.44	1.0/-0.64	0.40/-0.23

[a] $w = 1/\sigma^2 \cdot |F_o|$. [b] $w = 1/(0.00341 \cdot |F_o|^2 + 0.0961 \cdot |F_o| + 1.427)$. [c] $w = 1/\sigma^2 \cdot |F_o|$.

4a−**c**, **5b**, **6a**, and **6b** are given in the electronic supporting information. Selected bond lengths and bond and torsion angles are given in Tables 1−12, respectively. The crystallographic data for twelve four- and five-membered compounds are summarized in Tables 21−24. CCDC-169794 (**1b**), -169795 (**2a**), -169796 (**3a**), -169797 (**3b**), -169798 (**3c**), -169799 (**3d**), -169800 (**4a**), -169801 (**4b**), -169802 (**4c**), -169803 (**5b**), -169804 (**6a**), and -169805 (**6b**) contain the supplementary crystallographic data for this paper. These data can be obtained free of charge at www.ccdc.cam.ac.uk/conts/retrieving.html or from the Cambridge Crystallographic Data Centre, 12, Union Road, Cambridge CB2 1EZ, UK [Fax: (internat.) + 44-1223/336-033; E-mail: deposit@ccdc.cam.ac.uk].

Supporting Information: Supporting information for this article (Figures 6−17 with ORTEP drawings of molecular structures for **1**−**6**, and Figures 18−21 with UV spectral curves for **1**−**6**) is available (see also footnote on the first page of this article).

Acknowledgments

The authors are grateful to Toshiba Silicone Co., Ltd., and Shin-Etsu Chemical Co., Ltd., for a generous gift of chlorosilanes. The authors express their deep gratitude to the late Professor Yoichiro Nagai for helpful discussions at the early stage of this work, and also express thanks to Professors Hiroshi Hiratsuka and Shigefumi Tobita for helpful suggestions from the photochemical viewpoint. This work was partially supported (for H. W.) by Sansen Co., Ltd., Colcoat Co., Ltd., and the Gunma University Foundation for Promotion of Science and Technology.

[1] For reviews and references cited therein see: [1a] R. West, E. E. Carberry, *Science* **1975**, *189*, 179−186. [1b] H. Watanabe, Y. Nagai, in: *Organosilicon and Bioorganosilicon Chemisry* (Eds.: H. Sakurai), John Wiley & Sons, Inc., New York, **1985**, chapter 9, p. 105−114. [1c]T. Tsumuraya, A. Batcheller, S. Masamune, *Angew. Chem. Int. Ed. Engl.* **1991**, *30*, 902−930; *Angew. Chem.* **1991**, 103, 916. [1d] M. Weidenbruch, *Chem. Rev.* **1995**, *95*, 1479−1493. [1e] E. Hengge, R. Janoschek, *Chem. Rev.* **1995**, *95*, 1495−1526.

[2] [2a] A. Heine, D. Stalke, *Angew. Chem. Int. Ed. Engl.* **1994**, *33*, 113−115; *Angew. Chem.* **1994**, *106*, 121. [2b] E. Hengge, U. Brychy, *Monatsh. Chem.* **1966**, *97*, 1309−1317. [2c] E. Carberry, B. D. Dombek, *J. Organomet. Chem.* **1970**, *22*, C43−C47.

[3] [3a] G. Grunert, B. Fritz, *Z. Anorg. Allg. Chem.* **1981**, *473*, 59−79. [3b] M. Weidenbruch, J. Hamann, K. Peters, H. G. von Schnering, H. Marsmann, *J. Organomet. Chem.* **1992**, *441*, 185−195. [3c] M. Weidenbruch, J. Hamann, S. Pohl, W. Saak, *Chem. Ber.* **1992**, *125*, 1043−1046. [3d] D. Bravo-Zhivotovskii, Y. Apeloig, Y. Ovchinnikov, V. Igonin, Y. T. Struckov, *J. Organomet. Chem.* **1993**, *446*, 123−129. [3e] W. Ando, F. Hojo, S. Sekigawa, N. Nakayama, T. Shimizu, *Organometallics* **1992**, *11*, 1009−1011. [3f] M. Weidenbruch, E. Krobe, K. Peters, H. G. von Schnering, *J. Organomet. Chem.* **1993**, *461*, 35−38. [3g] S. A. Petrich, Y. Pang, G. Y. Young, Jr, T. J. Barton, *J. Am. Chem. Soc.* **1993**, *115*, 1591−1593. [3h] Y. Pang, S. A. Petrich, V. G. Young, Jr., M. S. Gordon, T. J. Barton, *J. Am. Chem. Soc.* **1993**, *115*, 2534−2536. [3i] H. Sanji, H. H. Hanao, H. Sakurai,

Chem. Lett. **1997**, 1121−1122. [3j] R. Imhof, H. Teramae, J. Michl, *Chem. Phys. Lett.* **1997**, *270*, 500−505. [3k] For Si_2C cycles, see ref.[1d]

[4] For Si_2N and Si_4N cycles, see refs.[1d,2b]

[5] [5a] H. Watanabe, T. Muraoka, M. Kageyama, Y. Nagai, *J. Organomet. Chem.* **1981**, *216*, C45−C47. [5b] S. Masamune, H. Tobita, S. Murakami, *J. Am. Chem. Soc.* **1983**, *105*, 6524−6525. [5c] M. Weidenbruch, A. Schaefer, *J. Organomet. Chem.* **1984**, *209*, 231−234. [5d] C. W. Carlson, R. West, *Organometallics.* **1983**, *2*, 1801−1807. [5e] B. J. Helmer, R. West, *Organometallics* **1982**, *1*, 1463−1466. [5f] L. Parkanyi, E. Hengge, H. Stuger, *J. Organomet. Chem.* **1983**, *251*, 167−174. [5g] S. Willms, A. Grybat, W. Saak, M. Weidenbruch, *Z. Anorg. Allg. Chem.* **2000**, *626*, 1148−1152. [5h] For Si_2O cycles, see ref.[1d] and references cited therein.

[6] [6a] Calculated geometries of $[H_2Si]_nX$ (n = 2, 3; X = SiH_2, CH_2, O, S, PH, NH): S. R. Grev, H. F. Schaefer III, *J. Am. Chem. Soc.* **1987**, *109*, 6577−6585. [6b] UV spectra of $[Me_2Si]_nX$ (n = 4−6; X = NMe, PMe): R. West, *Pure Appl. Chem.* **1982**, *54*, 1041−1050. [6c] UV spectra of $[Me_2Si]_nX$ (n = 4−6; X = NMe, PMe): T. H. Newman, R. West, R. F. Oakley, *J. Organomet. Chem.* **1980**, *197*, 159−168. [6d] UV and NMR spectra of $[Me_2Si]_nX$ (n = 4−6; X = O, S, Se, NMe, PMe): H. Stuger, M. Eibl, E. Hengge, *J. Organomet. Chem.* **1992**, *431*, 1−15. [6e] UV spectra of $[Ph_2Si]_{4-}X$ (X = $BNMe_2$, O, NMe, NEt): E. Hengge, D. Wolfer, *J. Organomet. Chem.* **1974**, *66*, 413−424.

[7] [7a] H. Watanabe, M. Kato, T. Okawa, Y. Nagai, M. Goto, *J. Organomet. Chem.* **1984**, *271*, 225−233. [7b] H. Watanabe, T. Okawa, M. Kato, Y. Nagai, *J. Chem. Soc., Chem. Commun.* **1983**, 781−782. [7c] H. Watanabe, Y. Kougo, Y. Nagai, *J. Chem. Soc., Chem. Commun.* **1984**, 66−67. [7d] H. Watanabe, T. Muraoka, M. Kageyama, M. Yoshizumi, Y. Nagai, *Organometallics* **1984**, *3*, 141−147. [7e] H. Watanabe, H. Shimoyama, T. Muraoka, T. Okawa, M. Kato, Y. Nagai, *Chem. Lett.* **1986**, 1057−1058. [7f] H. Watanabe, M. Kato, O. Okawa, Y. Kougo, Y. Nagai, M. Goto, *Appl. Organomet. Chem.* **1987**, *1*, 157−169. [7g] H. Watanabe, Y. Kougo, M. Kato, H. Kuwabara, H. Okawa, Y. Nagai, *Bull. Chem. Soc. Jpn.* **1984**, *57*, 3019−3020. [7h] H. Watanabe, K. Yoshizumi, M. Kato, T. Muraoka, Y. Nagai, T. Sato, *Chem. Lett.* **1985**, 1683−1686.

[8] H. Watanabe, E. Tabei, M. Goto, Y. Nagai, *Chem. Commun.* **1987**, 522−523.

[9] H. Suzuki, K. Okabe, S. Uchida, H. Watanabe, M. Goto, *J. Organomet. Chem.* **1996**, *509*, 177−188.

[10] H. Suzuki, K. Okabe, R. Kato, N. Sato, Y. Fukuda, H. Watanabe, M. Goto, *Organometallics* **1993**, *12*, 4833−4842.

[11] H. Suzuki, K. Tanaka, B. Yoshizoe, T. Yamamoto, N. Kenmotsu, S. Matuura, T. Akabane, H. Watanabe, M. Goto, *Organometallics* **1998**, *17*, 5091−5101.

[12] [12a] J. J. P. Stewart, *J. Comput. Chem.* **1989**, *10*, 209−220. [12b] J. J. P. Stewart, *J. Comput. Chem.* **1989**, *10*, 221−264.

[13] W. S. Sheldrick, in: *The Chemistry of Organic Silicon Compounds* (Eds.: S. Patai, Z. Rappoport), John Wiley & Sons, Inc., New York, **1989**, chapter 3, pp. 227−303 and references cited therein.

[14] R. Tanaka, M. Unno, H. Matsumoto, *Chem. Lett.* **1999**, 595−596.

[15] M. J. Michalczyk, M. J. Fink, K. J. Haller, R. West, M. Michl, *Organometallics* **1986**, *5*, 531−538.

[16] H. Matsumoto, M. Minemura, K. Takatsuna, Y. Nagai, M. Goto, *Chem. Lett.* **1985**, 1005−1006.

[17] R. W. Taft, Jr., in: *Steric Effects in Organic Chemistry* (Ed.: M. S. Newman), John Wiley & Sons, Inc., Tokyo Maruzen Co. Ltd., **1956**, chapter 13, pp. 559−675.

[18] [18a] A. T. Gordon, R. A. Ford (Eds.), *The Chemist's Companion, A Handbook of Practical Data, Techniques, and References*, John Wiley & Sons, Inc., New York, **1972**, pp. 82−87 and references cited therein; A. L. Allred, E. G. Rochow, *J. Inorg. Nucl. Chem.* **1958**, *5*, 264−268, 269−288. [18b] A. L. Allred, *J. Inorg. Nucl. Chem.* **1961**, *17*, 215−221.

[19] C. Liang, L. C. Allen, *J. Am. Chem. Soc.* **1991**, *113*, 1878−1884.

[20] E. A. Williams, in: *The Chemistry of Organic Silicon Compounds* (Eds.: S. Patai, Z. Rappoport), John Wiley & Sons, Inc., New York, **1989**, chapter 8, pp. 511−554 and references cited therein.

[21] R. K. Harris, B. J. Kimber, *Adv. Mol. Relax. Processes* **1976**, *8*, 23−35.

[22] [22a] M. Biernbaum, R. West, *J. Organomet. Chem.* **1977**, *131*, 179−188. [22b] E. Carberry, R. West, G. E. Gross, *J. Am. Chem. Soc.* **1969**, *91*, 5446−5451. [22c] C. W. Carlson, R. West, *Organometallics* **1983**, *2*, 1792−1797.

[23] H. Gilman, W. H. Atwell, G. L. Schwebke, *J. Organomet. Chem.* **1964**, *2*, 369−371.

[24] [24a] A. F. Sax, *Chem. Phys. Lett.* **1986**, *127*, 163−168. [24b] S. Nagase, M. Nakano, T. Kudo, *J. Chem. Soc., Chem. Commun.* **1987**, 60−62. [24c] R. S. Grev, H. F. Schaefer III, *J. Am. Chem. Soc.* **1987**, *109*, 6569−6585. [24d] D. B. Kitchen, J. E. Jackson, L. C. Allen, *J. Am. Chem. Soc.* **1990**, *112*, 3408−3414. [24e] M. Zhan, B. M. Gimarc, *Inorg. Chem.* **1996**, *35*, 5378−5386.

[25] M.-C. Ou, S.-Y. Chu, *J. Mol. Struct. (Theochem).* **1995**, *357*, 141−146.

[26] [26a] S. Inagaki, K. Yoshikawa, Y. Hayano, *J. Am. Chem. Soc.* **1993**, *115*, 3706−3709. [26b] S. Inagaki, Y. Ishitani, T. Kakefu, *J. Am. Chem. Soc.* **1994**, *116*, 5954−5958.

[27] Preparations for advanced calculations are currently underway.

[28] [28a] P. George, M. Trachtman, C. W. Bock, A. M. Brett, *Tetrahedron* **1976**, *32*, 317−323. [28b] P. George, M. Trachtman, C. W. Bock, A. M. Brett, *J. Chem. Soc., Perkin Trans. 2* **1976**, 1222−1227. [28c] P. George, M. Trachtman, A. M. Brett, C. W. Bock, *J. Chem. Soc., Perkin Trans. 2* **1997**, 1036−1047.

[29] F. Shafiee, R. West, *Silicon, Germanium, Tin Lead Compd.* **1986**, *9*, 1−10.

[30] For organometallic compounds: [30a] H. C. Gardner, J. K. Kochi, *J. Am. Chem. Soc.* **1975**, *97*, 1855−1865. [30b] R. J. Klingler, J. K. Kochi, *J. Am. Chem. Soc.* **1980**, *102*, 4790−4798. [30c] K. Mochida, A. Itani, M. Yokoyama, T. Tsuchiya, S. D. Worley, J. K. Kochi, *Bull. Chem. Soc. Jpn.* **1985**, *58*, 2149−2150. [30d] H. Bock, U. Lechner-Knoblauch, *J. Organomet. Chem.* **1985**, *294*, 295−304.

[31] [31a] T. Takami, S. Masuda, K. Ohno, Y. Harada, Y. Yagihashi, H. Matsumoto, Y. Nagai, *The 56th National Meeting of the Japan Chemical Society*, Tokyo, **1988**, Abstracts 1IVB27, p. 513. [31b] Y. Yagihashi, Master Thesis, The Graduate School of Engineering, Gunma University, March **1988**.

[32] T. F. Block, M. Biernbaum, R. West, *J. Organomet. Chem.* **1977**, *131*, 199−205.

[33] T. F. Block, M. Biernbaum, R. West, *J. Organomet. Chem.* **1974**, *77*, C13−C14.

[34] H. Shizuka, K. Murata, Y. Arai, K. Tonokura, H. Tanaka, H. Matsumoto, Y. Nagai, G. Gillette, R. West, *J. Chem. Soc., Faraday Trans. 1* **1989**, *85*, 2369−2377.

[35] H. Bock, W. Ensslin, *Angew. Chem.* **1971**, *83*, 435−437; *Angew. Chem. Int. Ed. Engl.* **1971**, *10*, 404−405.

[36] N. J. Turro, *Modern Molecular Photochemistry*, The Benjamain/Cummings Publishing Co., Inc., Menlo Park, California, **1978**, pp. 103−117.

[37] Unpublished work: [37a] H. Watanabe, E. Tabei, N. Hirai, M. Yoshikawa, H. Ohmori, M. Nishiyama, M. Sugo, S. Takahashi, K. Ohyama: Photochemical decompositions of $(R_2Si)_nX$ (R = *i*Pr, *t*BuCH_2; n = 3, 4; X = C, N, O; see ref.[8]). [37b] H. Watanabe, T. Adachi: Photosensitized decompositions of $(R_2Si)_nX$ (R = *i*Pr, *t*BuCH_2; n = 3, 4; X = C, N, O) by electrontransfer.

[38] H. Watanabe, H. Shimoyama, T. Muraoka, Y. Kougo, Y. Kato, Y. Nagai, *Bull. Chem. Soc. Jpn.* **1987**, *60*, 769−770.

[39] P. Main, S. E. Hull, L. Lessinger, G. Germain, J. Declercq, M. M. Woolfson, *MULTAN 78, A System of Computer Programs for the Automatic Solution of Crystal Structures for the X-ray Diffraction Data*, University of York, England, and Louvain, Belgium, **1978**.

[40] T. Sakurai, K. Kobayashi, *Rikagakukenkyujyo Houkoku* **1979**, *55*, 69−77.
[41] H. Watanabe, M. Aoki, H. Matsumoto, Y. Nagai, *Bull. Chem. Soc. Jpn.* **1977**, *50*, 1019−1020.
[42] M. J. Frish, G. W. Trucks, H. B. Schlegel, G. E. Scuseria, M. A. Robb, J. R. Cheeseman, V. G. Zakrzewski, J. A. Montogomery, R. E. Stratmann, J. C. Burant, S. Dapprich, J. M. Millam, A. D. Daniels, K. N. Kudin, M. C. Strain, O. Farkas, J. Tomasi, V. Barone, M. Cossi, R. Cammi, B. Mennuecci, C. Ponmelli, C. Adamo, S. Clifford, J. Ochterski, G. A. Petersson, P. Y. Ayala, Q. Cui, K. Morokuma, D. K. Malick, A. D. Rabuck, K. Raghavachari, J. B. Foresman, J. Cioslowski, J. V. Ortiz, B. B. Stefanov, G. Liu, A. Liashenko, P. Piskorz, I. Komaromi, D. J. Fox, R. L. Martin, R. Gomperts, T. Keith, M. A. Al-Laham, A. Nanayakkara, C. Y. Peng, A. Nanayakkara, C. Gonzalez, M. Challacombe, P. M. W. Cill, B. G.Jonson, W. Chen, M. W. Wong, J. L. Andres, M. Head-Gordon, E. S. Replogle, J. A. Pople, *GAUSSIAN98*, Gaussian, Inc., Pittsburgh, PA, **1998**.
[43] M. W. Schmidt, K. K. Baldridge, J. A. Boatz, S. T. Elbert, M. S. Gordon, J. H. Jensen, S. Koseki, N. Matsunaga, K. A. Nguyen, S. Su, T. L. Windus, M. Dupuis, J. A. Montgomery, Jr., *J. Comput. Chem.* **1993**, *14*, 1347−1363.

Received September 10, 2001
[I01354]

Phase Diagram and Impedance Spectroscopy Study of the $La_{0.5+x-y}Bi_yLi_{0.5-3x}TiO_3$ System

M.-L. Martínez-Sarrión,*[a] L. Mestres,[a] M. Herráiz,[a] O. Maqueda,[a] A. Bakkali,[a] and N. Fernández[b]

Keywords: Phase diagrams / Perovskite phases / Conducting materials / Lanthanides

The phase diagram of the system $Li_2O/La_2O_3/TiO_2/Bi_2O_3$ has been studied. Using powder X-ray diffraction, five distinct areas have been found in the triangle $Bi_{0.5}Li_{0.5}TiO_3/La_{2/3}TiO_3/La_{0.5}Li_{0.5}TiO_3$. A region of perovskite-like solid solutions was obtained when the bismuth content in the general formula $La_{0.5+x-y}Bi_yLi_{0.5-3x}TiO_3$ was less than y = 0.10. Two two-phase regions, one of them consisting of a perovskite-like phase and $La_2Ti_2O_7$, and the other a perovskite-like phase and Li_2TiO_3, were obtained. One four-phase region, consisting of a perovskite-like phase, Li_2TiO_3, $Bi_4Ti_3O_{12}$ and $La_4Ti_3O_{12}$, was also obtained. The fifth area corresponds to the melting of the initial mixtures. The microstructures of these phases were studied by SEM/EDS. The compounds of general formula $La_{0.5+x-y}Bi_yLi_{0.5-3x}TiO_3$ are ionic conductors. Their ionic conductivity increases when the amount of lithium rises up to x = 0.075, and decreases when the amount of bismuth increases.

(© Wiley-VCH Verlag GmbH, 69451 Weinheim, Germany, 2002)

Introduction

With the development of advanced materials in which the fine-tuning of composition is often required in order to optimize properties, phase diagrams take on the increasingly important role of representing phase stoichiometries. The phase diagram contains qualitative structural information as well as quantitative compositional information, and together they provide a powerful basis for understanding and optimising relationships between stoichiometry, structure and properties.

Research into solid ionic conductors and lithium cathodes is important for the development of solid-state lithium batteries. Some time ago, fast ion conductors with the general formula $RE_{0.5+x}Li_{0.5-3x}TiO_3$, where RE = La, Pr, Nd, and Sm, were reported.[1−3] The maximum bulk conductivity was found in the lanthanum system, with a value of 1.1×10^{-3} S·cm^{-1} for $x = 0.07$, although the total conductivity (bulk and grain boundary conductivity), was less than 10^{-6} S·cm^{-1}. More recently, the phase diagram, crystal chemistry and ion conductivity of the systems $RE_{0.5+x}Li_{0.5-3x}TiO_3$, (RE = La, Pr, Nd),[4−7] which show a similar total conductivity, have been reported.

In recent years, the phase diagrams, crystal chemistry and conductivity study of $Pr_{0.5+x+y}Li_{0.5-3x}Ti_{1-3y}Cr_{3y}O_3$,[8] $La_{0.5+x+y}Li_{0.5-3x}Ti_{1-3y}Mn_{3y}O_3$,[9] and $La_{0.5+x+y}Li_{0.5-3x}Ti_{1-3y}Cr_{3y}O_3$,[10] have been reported.

Systems containing Bi_2O_3 are now becoming increasingly important in the technology of new materials used by the electronics industry. Levin and Roth[11] studied 33 systems with bismuth oxide as one of the components. The content of the other components was never higher than 10−15 mol %. The binary systems Bi_2O_3/Li_2O, Bi_2O_3/TiO_2, and Bi_2O_3/La_2O_3 were described.

Bi_2O_3 has two stable crystalline forms: a low-temperature monoclinic form and a high-temperature cubic form, and the conversion of one form into the other takes place at 730 °C. Many systems typically form solid solutions based on bismuth oxide.

Doped $Bi_4V_2O_{11}$ materials are currently under intensive study in several laboratories because of their attractive electrical properties. They are, however, complex materials both structurally and compositionally as the $Bi_4V_2O_{11}$ phase has a variable Bi:V ratio.[12−14]

The aim of the present work was to investigate the synthesis and the stoichiometry range of the new compounds of general formula $La_{0.5+x-y}Bi_yLi_{0.5-3x}TiO_3$ and to establish the phase diagram at room temperature of the system $La_{2/3}TiO_3$-$Bi_{0.5}Li_{0.5}TiO_3$-$La_{0.5}Li_{0.5}O_3$. The substitution of lanthanum by bismuth in $La_{0.5+x}Li_{0.5-3x}TiO_3$ may affect the ionic conductivity of these compounds, therefore changes in the electric behaviour of the

[a] Departament de Química Inorgànica, Universitat de Barcelona
Martí i Franquès 1−11, 08028 Barcelona, Spain
Fax: (internat.) + 34-93/490-7725
E-mail: marialuisa.martinez@qi.ub.es
[b] Departamento de Química Inorgánica, Universidad de La Habana,
La Habana, Cuba

Table 1. Sample composition

Starting composition				Experimental composition				Phase
La	Bi	Li	Ti	La	Bi	Li	Ti	
0.55	0.00	0.35	1.00	0.59	0.00	0.32	1.00	Perovskite-like phase
0.57	0.00	0.30	1.00	0.60	0.00	0.27	1.00	Perovskite-like phase
0.58	0.00	0.25	1.00	0.63	0.00	0.23	1.00	Perovskite-like phase
0.60	0.00	0.20	1.00	0.64	0.00	0.18	1.00	Perovskite-like phase
0.57	0.010	0.25	1.00	0.60	0.008	0.24	1.00	Perovskite-like phase
0.59	0.010	0.33	1.00	0.55	0.009	0.32	1.00	Perovskite-like phase
0.55	0.02	0.29	1.00	0.55	0.018	0.29	1.00	Perovskite-like phase
0.57	0.040	0.17	1.00	0.59	0.038	0.15	1.00	Perovskite-like phase
0.53	0.040	0.27	1.00	0.53	0.038	0.26	1.00	Perovskite-like phase
0.52	0.040	0.32	1.00	0.55	0.037	0.30	1.00	Perovskite-like phase
0.54	0.046	0.36	1.00	0.51	0.047	0.25	1.00	Perovskite-like phase
0.50	0.055	0.35	1.00	0.46	0.056	0.33	1.00	Perovskite-like phase
0.47	0.060	0.42	1.00	0.50	0.057	0.40	1.00	Perovskite-like phase
0.50	0.10	0.20	1.00	0.47	0.098	0.17	1.00	Perovskite-like phase
0.46	0.070	0.42	1.00	0.48	0.065	0.41	1.00	Perovskite-like phase
0.51	0.075	0.25	1.00	0.52	0.072	0.22	1.00	Perovskite-like phase
0.49	0.075	0.30	1.00	0.47	0.073	0.29	1.00	Perovskite-like phase
0.46	0.075	0.40	1.00	0.48	0.072	0.37	1.00	Perovskite-like phase

$La_{0.5+x-y}Bi_yLi_{0.5-3x}TiO_3$ system are expected, even though bismuth is only a minority element.

Results and Discussion

Phase Diagram

The triangle $Bi_{0.5}Li_{0.5}TiO_3$-$La_{2/3}TiO_3$-$La_{0.5}Li_{0.5}TiO_3$ in the Li_2O-La_2O_3-TiO_2-Bi_2O_3 system was chosen for detailed study since the $La_{2/3}TiO_3$-$La_{0.5}Li_{0.5}TiO_3$ join has been reported previously.[3,15] This triangle was studied by synthesizing compounds of general formula $La_{0.5+x-y}Bi_yLi_{0.5-3x}TiO_3$ by heating, as described in the Exp. Sect. More than 50 different compositions were prepared. The results of X-ray powder diffraction and the results of ICP analysis (Table 1), were used to construct the composition diagram (Figure 1).

Five distinct areas were found on this triangle. A region, (A), resulting from the melting of the initial mixture, a region, (D), of perovskite-like solid solutions (Figure 2a), and three mixed-phase regions (B, C, E). Region C is a mixture of the perovskite-like phase and peaks belonging to $La_2Ti_2O_7$ (identified from PDF 28-517; Figure 2b). Region E is a mixture of the perovskite-like phase and peaks which belong to Li_2TiO_3 (identified from PDF 33-0831; Figure 2c). Region B is a mixture of the perovskite-like phase and peaks identified as Li_2TiO_3 (from PDF 33-0831), $Bi_4Ti_3O_{12}$ (PDF 73-2181) and $La_4Ti_3O_{12}$ (PDF 33-727; Figure 2d) (PDF compiled by JCPDS).

Table 2 shows the X-ray powder diffraction data for $La_{0.51}Bi_{0.047}Li_{0.25}TiO_3$ (region D). This compound has an orthorhombic perovskite-type structure. Table 3 shows the X-ray diffraction data for $La_{0.56}Bi_{0.047}Li_{0.08}TiO_3$ (region C), containing reflections corresponding to an orthorhombic perovskite-type structure, reflections corresponding to $La_2Ti_2O_7$ and some peaks associated with a superstructure.

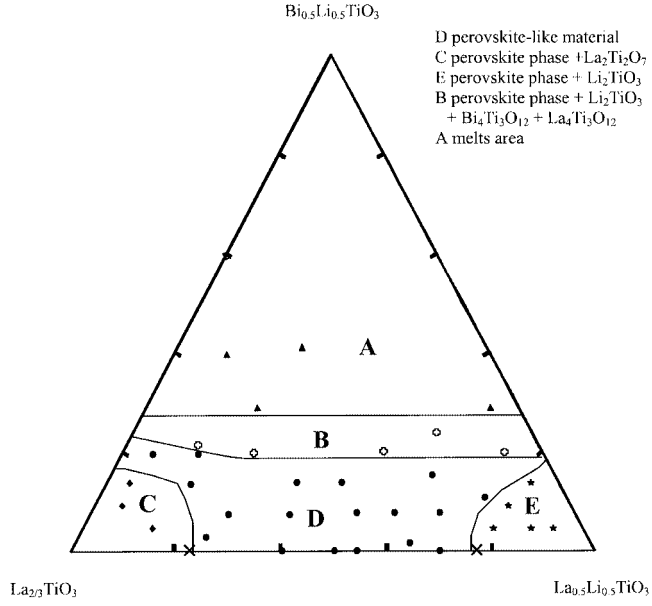

Figure 1. Composition triangle of the system $La_{0.5+x-y}Bi_yLi_{0.5-3x}TiO_3$ at 1250 °C; the samples marked with × are taken from the literature[4]

This superstructure depends on the lithium content and is related to the lanthanum and vacant A-sites that alternates along the *c*-axis. This ordering becomes progressively disordered when the lithium content increases.[16]

Table 4 shows the X-ray powder diffraction data for $La_{0.48}Bi_{0.023}Li_{0.43}TiO_3$ (region E). We observed reflections corresponding to a cubic perovskite-type structure and reflections corresponding to Li_2TiO_3. Finally, Table 5 shows X-ray powder diffraction data for $La_{0.40}Bi_{0.112}Li_{0.47}TiO_3$ (region B). In this region reflections corresponding to a cubic perovskite-type structure, Li_2TiO_3, $Bi_4Ti_3O_{12}$, and $La_4Ti_3O_{12}$ appear.

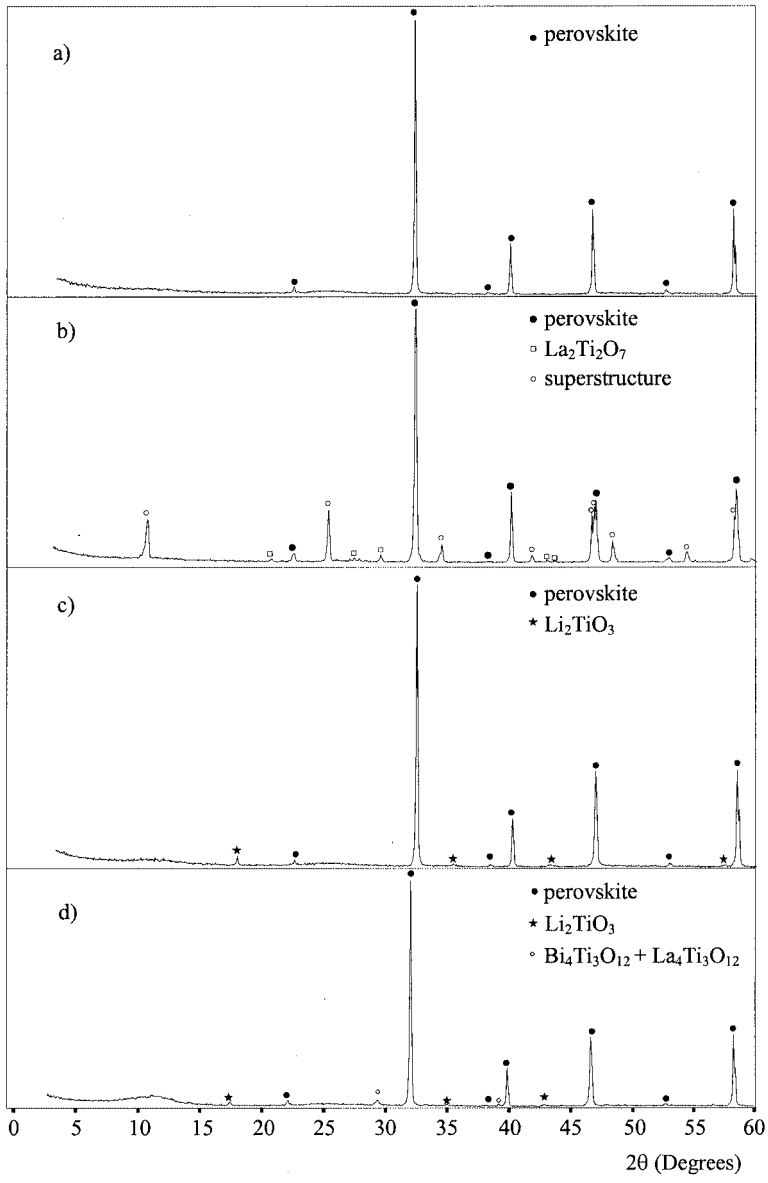

Figure 2. XRD patterns of the five regions on the composition triangle

Table 2. Indexed powder pattern of the single phase $La_{0.51}Bi_{0.047}Li_{0.25}TiO_3$; orthorhombic system: a = 5.487(2) Å, b = 5.472(1) Å, c = 7.739(2) Å, V = 232.38(5) Å^3, Z = 4

hkl	d_{obs}/Å	d_{calc}/Å	I/I_0
002	3.862	3.869	3
200	2.740	2.744	100
112	2.736	2.738	26
103	2.326	2.333	1
202	2.239	2.238	19
022	2.237	2.234	8
004	1.930	1.935	64
222	1.728	1.732	1
114	1.727	1.731	1
204	1.578	1.583	23
132	1.577	1.581	33

Some melting occurs in the compositions in area A. These compositions have a greater content of bismuth (as Bi_2O_3), and as bismuth oxide melts at about 830 °C the formation of the perovskite-like phase is prevented. Some systems containing Bi_2O_3 reported in the literature, such as Bi_2O_3-Li_2O, Bi_2O_3-TiO_2, and Bi_2O_3-La_2O_3, show the *liquidus* area at about 900 °C.[11]

Perovskite-like phases mixed with titanium compounds are obtained in the areas C and E. In the area close to the vertex $La_{2/3}TiO_3$ (area C), $La_2Ti_2O_7$ is segregated along with the perovskite-like phase. On progressing towards the join $La_{2/3}TiO_3$/$La_{0.5}Li_{0.5}TiO_3$ the lithium content increases and Li_2TiO_3 is segregated along with the perovskite-like phase near the $La_{0.5}Li_{0.5}TiO_3$ vertex (area E).

In area B, on increasing the lithium content, the number of species mixed with the perovskite-like phase increases, as

Table 3. Indexed powder pattern of $La_{0.56}Bi_{0.047}Li_{0.08}TiO_3$

d_{obs} [a]	Perovskite		$La_2Ti_2O_7$	
	d/Å	*hkl*	*d*/Å	*hkl*
7.738*		001		
4.192			4.201	−210
3.885	3.862	002		
3.447*		101		
3.208			3.217	400
2.988			2.995	−212
2.752	2.740	200		
2.743	2.736	112		
2.574*		111		
2.336	2.326	103		
2.246	2.239	202		
2.240	2.237	022		
2.148*		103		
2.094			2.101	420
2.069			2.071	−322
1.940	1.930	004		
1.933*		200		
1.878*		201		
1.738	1.728	222		
1.735	1.727	114		
1.686*		211		
1.584	1.578	204		
1.583	1.577	132		

[a] * Superstructure lines.

Table 4. Indexed powder pattern of $La_{0.48}Bi_{0.023}Li_{0.43}TiO_3$

d_{obs}	Perovskite		Li_2TiO_3	
	d/Å	*hkl*	*d*/Å	*hkl*
4.824			4.800	002
3.868	3.862	002		
2.737	2.740	200		
2.733	2.736	112		
2.521			2.502	−131
2.332	2.326	103		
2.235	2.239	202		
2.232	2.237	022		
2.089			2.075	−133
1.933	1.930	004		
1.730	1.728	222		
1.729	1.727	114		
1.579	1.578	204		
1.578	1.577	132		

do their relative amounts. For instance, the maxima of Li_2TiO_3 are not observed and the reflections of the $Bi_4Ti_3O_{12}$ and $La_4Ti_3O_{12}$ components are very weak in the sample of starting composition $La_{0.45}Bi_{0.10}Li_{0.35}TiO_3$. On increasing the lithium content, for example for starting composition $La_{0.41}Bi_{0.10}Li_{0.48}TiO_3$, the perovskite-like phase is mixed with Li_2TiO_3, $Bi_4Ti_3O_{12}$ and $La_4Ti_3O_{12}$, with an increase in the relative intensities.

The cell volume was obtained for two joins on the composition triangle. Along join 1, $La_{0.46+x}Bi_{0.04}Li_{0.5-3x}TiO_3$, the amount of bismuth remained constant, while along join 2, $La_{0.57-y}Bi_yLi_{0.29}TiO_3$, the amount of lithium was constant. The cell volume was measured against the amount of lanthanum along these two joins (Figure 3). For the same

Table 5. Indexed powder pattern of $La_{0.40}Bi_{0.112}Li_{0.47}TiO_3$

d_{obs}	Perovskite		Li_2TiO_3		$Bi_4Ti_3O_{12}$		$La_4Ti_3O_{12}$	
	d/Å	*hkl*	*d*/Å	*hkl*	*d*/Å	*hkl*	*d*/Å	*hkl*
4.811			4.800	002				
4.060			4.050	021				
3.868	3.862	002						
2.969					2.9703	117	2.960	107
2.738	2.740	200						
2.734	2.736	112						
2.640					2.6442	−119		
2.515			2.502	−131				
2.330	2.326	103						
2.270					2.2701	208		
2.235	2.239	202						
2.232	2.237	022						
2.087			2.075	−133				
2.025							2.020	119
1.934	1.930	004						
1.774					1.7714	0214		
1.732	1.728	222						
1.730	1.727	114						
1.581	1.578	204						
1.579	1.577	132						

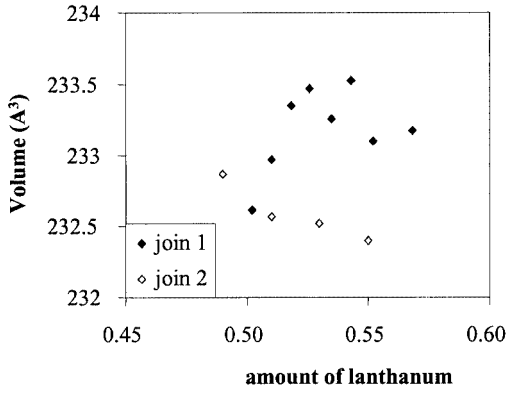

Figure 3. Cell volume vs. La content along the two joins on samples quenched from 1250 °C

amount of bismuth, the cell volume decreases as the lanthanum content decreases, due to the substitution of lanthanum by a smaller cation such as lithium in the 12-coordinate sites. Along join 2, the substitution of lanthanum by bismuth leads to a small increase in the cell volume because of the different ionic radii.

The composition with the highest conductivity in the join $La_{2/3}TiO_3$-$La_{0.5}Li_{0.5}TiO_3$ is $La_{0.57}Li_{0.29}TiO_3$.[1−3] The new conductors should occur in the join $La_{0.57}Li_{0.29}TiO_3$-$Bi_{0.5}Li_{0.5}TiO_3$. The compositions of the new phases containing bismuth should have lanthanum and lithium contents close to $La_{0.57}Li_{0.29}TiO_3$, with low bismuth contents. This is indeed the case, since the only one-phase compositions with the perovskite structure are those with bismuth contents less than 0.10 in the general formula $La_{0.5+x-y}Bi_yLi_{0.5-3x}TiO_3$.

Scanning Electron Microscopy (SEM, EDS)

A selection of ceramic samples from both within and outside the perovskite single-phase region was analysed by

SEM/EDS. Elemental analyses were carried out with a fixed beam of 10 kV and 20 nA over different points of the sample surface.

Scanning electron micrographs were obtained for samples from each of the four regions observed in the composition triangle, and in all the phases we checked the presence of the different elements by SEM and EDS.

Figure 4a shows the back-scattered electron image (BEI) of the sample $La_{0.51}Bi_{0.047}Li_{0.25}TiO_3$. In this case, homogeneous crystals were observed, which agrees with the XRD pattern shown in Figure 2a. The EDS spectrum of this zone (Figure 5a) shows the presence of lanthanum, bismuth and titanium in a perovskite-like phase for this composition obtained when different crystals of the sample are analysed. Figure 4b shows the BEI of the sample $La_{0.56}Bi_{0.047}Li_{0.08}TiO_3$. In this case we observed similar crystals to Figure 4a (area 1 in the picture) and new gray crystals (area 2 in the picture).

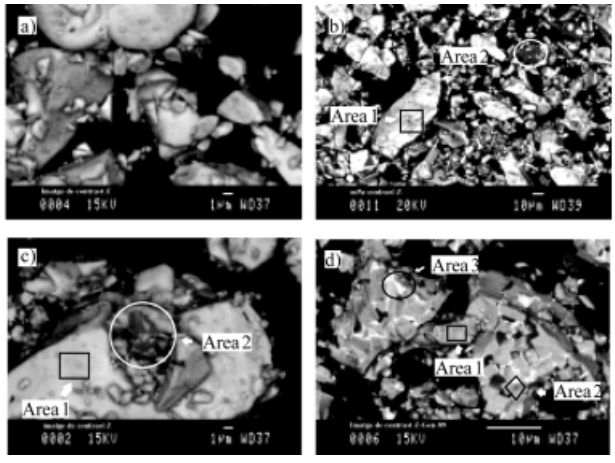

Figure 4. Scanning electron micrographs of: a) perovskite-like single-phase solid solution region; b) perovskite-like phase + $La_2Ti_2O_7$; c) perovskite-like phase + Li_2TiO_3 region; d) perovskite-like phase + Li_2TiO_3, + $Bi_4Ti_3O_{12}$ + $La_4Ti_3O_{12}$ region

The EDS spectrum of area 1 (grey line in Figure 5b) is similar to the spectrum of the previous sample. However, the EDS spectrum of area 2 does not show the peaks of bismuth (black line in Figure 5b). This confirms the results of XRD, which shows the presence of $La_2Ti_2O_7$ (Figure 2b). Figure 4c shows the BEI of the sample $La_{0.48}Bi_{0.023}Li_{0.43}TiO_3$ where two different phases co-exist. The light crystals (area 1 in the picture) correspond to the perovskite-like phase with the same distribution of the elements as in the previous cases (grey line in Figure 5c). The dark ones (area 2) belong to a titanium-rich phase, and the lines of lanthanum and bismuth do not appear in the EDS spectrum (black line in Figure 5c). This agrees with the results of XRD, which show the presence of Li_2TiO_3 (Figure 2c). Finally, Figure 4d shows the BEI of the sample $La_{0.40}Bi_{0.112}Li_{0.47}TiO_3$. We can see three zones. The greyish crystals (area 1 in the picture) belong to a perovskite-like phase with the EDS spectrum shown in Figure 5d (grey line). The dark crystals (area 2 in the picture) correspond to a titanium-rich phase with a similar EDS spectrum

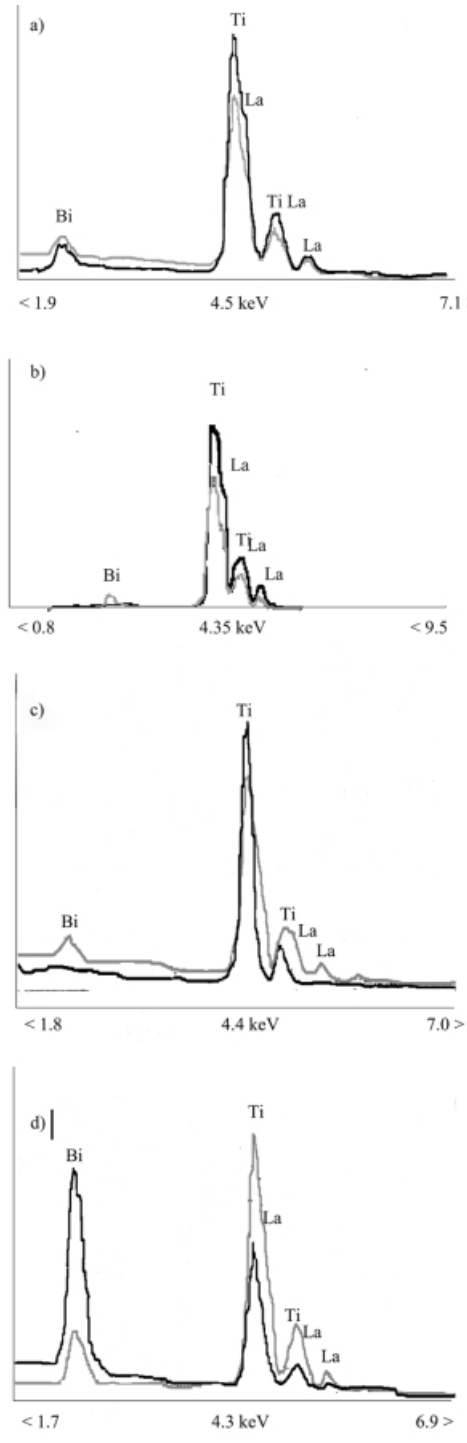

Figure 5. EDS of: a) perovskite-like single-phase solid solution region; b) perovskite-like phase + $La_2Ti_2O_7$ phase; c) perovskite-like phase + Li_2TiO_3 region; d) perovskite-like phase + Li_2TiO_3, + $Bi_4Ti_3O_{12}$ + $La_4Ti_3O_{12}$ region

(black line in Figure 5c and Li_2TiO_3 in the XRD pattern of Figure 2d). The white crystals (area 3 in the picture) are rich in bismuth and titanium but hardly contain lanthanum, as we can see from the EDS spectrum (black line in Figure 5d). This confirms the results of XRD, which showed $Bi_4Ti_3O_{12}$ (Figure 2d). The lanthanum peaks may be due to $La_4Ti_3O_{12}$, as we can see from the XRD pattern (Fig-

ure 2d), or a nearby zone corresponding to the perovskite-like phase.

ICP Analysis

ICP analyses were carried out. We assume that the oxygen content in all the samples is near to 3. For all compositions, the experimental values of Li and Bi were lower than those expected from the starting composition. The results of elemental analyses on mixed regions (Table 1) for different spots matched those for the proposed compounds in Figure 2.

Electrical Measurements (AC)

An HP 4192A Impedance Analyzer was used for AC measurements. These measurements were carried out from 25 °C to 100 °C for compounds on joins $La_{0.46+x}Bi_{0.04}Li_{0.5-3x}TiO_3$ ($0.04 < x < 0.11$) and $La_{0.57-y}Bi_yLi_{0.29}TiO_3$ ($y \leq 0.08$). Two semicircles and a spike were observed in the impedance complex plane plots in all the samples; the second semicircle becomes higher on increasing the amount of bismuth (Figure 6).

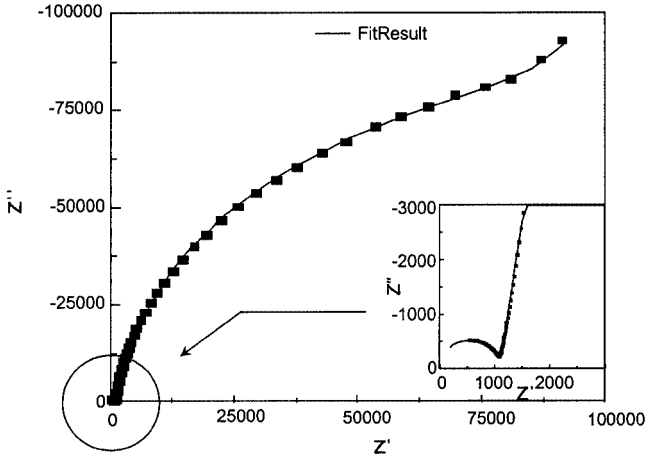

Figure 6. Impedance response at 25 °C for $La_{0.55}Bi_{0.018}Li_{0.29}TiO_3$

The centre of the semicircles was clearly depressed below the baseline, indicating a non-Debye response, which is usual in ionic conductors.[17,18] An equivalent circuit (Figure 7) with two RC and two constant phase elements (CPE)[19] has been used to fit the high frequency data; these elements are assigned to bulk and grain boundary responses with capacities around 20 $pFcm^{-1}$ and 5 $nFcm^{-1}$, respectively. An additional CPE element was used to model the low frequency spike with a capacity around 50 $nFcm^{-1}$.

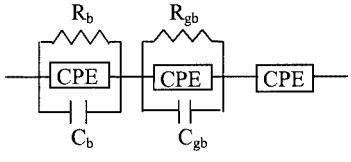

Figure 7. Equivalent circuit for fitting AC data

This value, which is too low for an electrode, has previously been reported for high Na^+ and Li^+ ion conductors,[17,5] and it is attributed to the presence of a Na^+ or Li^+ free layer on the crystal surface. All fitting used the ZView software package.[20]

Bulk conductivity data extracted from the impedance complex plane plots are shown in Arrhenius format for both joins in Figure 8 and Figure 9. Along the join $La_{0.46+x}Bi_{0.04}Li_{0.5-3x}TiO_3$, where the amount of bismuth remains constant, the conductivity is highest when $x = 0.075$, with a conductivity value at 25 °C of 7.59×10^{-4} Scm^{-1}, although the variation in conductivity with composition is quite small (Figure 10). The activation energy increased from 0.310 eV to 0.344 eV. The presence of a maximum in Figure 10 agrees with earlier results for the La system,[2] which report a conduction mechanism based on the A-site vacancies. Along the join $La_{0.57-y}Bi_yLi_{0.29}TiO_3$, where the amount of lithium remains constant, the conductivity decreases when the amount of bismuth increases (Figure 8). However, the substitution of La by Bi is not accompanied by a significant change in the cell volume of the perovskite, so this behaviour does not seem to be related to any change in the "bottleneck" size. However, it could be related to the existence of the lone-electron pair of bismuth.[21,22] Future neutron diffraction studies are underway

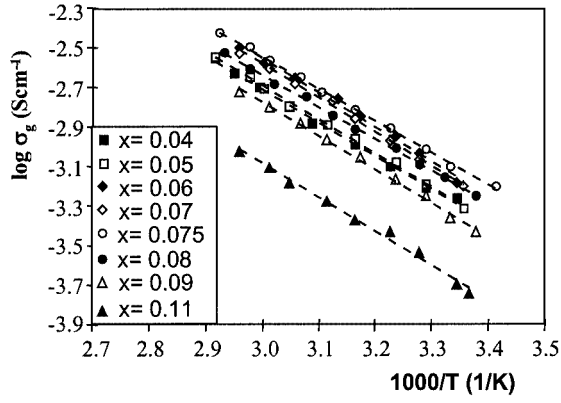

Figure 8. Arrhenius ionic conductivity plots for the join $La_{0.46+x}Bi_{0.04}Li_{0.5-3x}TiO_3$

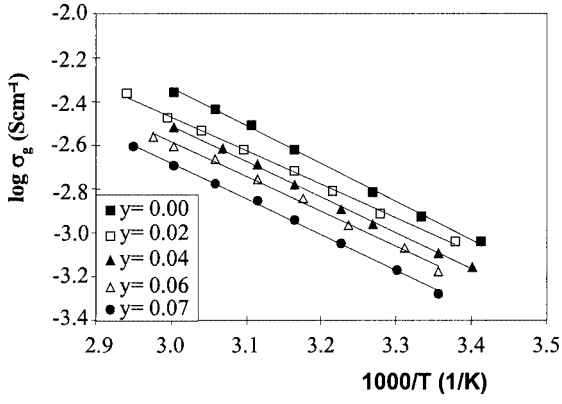

Figure 9. Arrhenius ionic conductivity plots for the join $La_{0.57-y}Bi_yLi_{0.29}TiO_3$

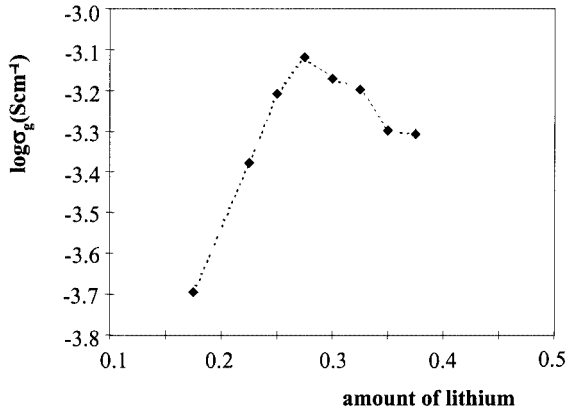

Figure 10. Plot of log σ_b vs. amount of lithium along join $La_{0.46+x}Bi_{0.04}Li_{0.5-3x}TiO_3$

which will give more information about the structure of these compounds and allow us to explain this effect better.

In spite of the good values of bulk conductivity in this system, the samples present significant boundary resistances that are three orders of magnitude higher than the resistances of the bulk, and higher activation energies, around 0.56 eV, which limit the overall conductivity.

Conclusions

Solid solutions with general formula $La_{0.5+x-y}Bi_y$-$Li_{0.5-3x}TiO_3$ have been studied and the results represented on a diagram with corners $La_{2/3}TiO_3$/$La_{0.5}Li_{0.5}TiO_3$/$Bi_{0.5}$-$Li_{0.5}TiO_3$.

Five distinct areas have been found in the diagram. Region A is a melts area, resulting from the melting of the initial mixture. Region B is a mixture of the perovskite-like compound and Li_2TiO_3, $Bi_4Ti_3O_{12}$ and $La_4Ti_3O_{12}$. Region C is a mixture of perovskite-like compounds and $La_2Ti_2O_7$. Region D is a region of perovskite-like solid solutions and region E is a mixture of perovskite-like compound and Li_2TiO_3.

The compounds of general formula $La_{0.5+x-y}Bi_y$-$Li_{0.5-3x}TiO_3$ are ionic conductors. Their ionic conductivity increases when the amount of lithium rises to $x = 0.075$, and the ionic conductivity decreases when the amount of bismuth increases.

Experimental Section

Synthesis: La_2O_3 (99.9% Fluka), TiO_2 (Aldrich 99 +%), Bi_2O_3 (99.9% Aldrich), and Li_2CO_3 (Aldrich >99%) were used as starting materials. La_2O_3 and TiO_2 were dried overnight at 900 °C prior to weighing. These chemicals were weighed, mixed in an agate mortar with acetone, dried, and heated to between 600 and 700 °C for 2 h to drive off CO_2. After grinding, the samples were pressed into pellets and covered with powder of the same composition to avoid loss of lithium and bismuth during the thermal treatment. The pellets were fired at 1100 °C for 12 h giving whitish products which were reground, re-pelleted, and fired at 1200 °C for a further 12 h. Finally, the samples were reground and re-pelleted, fired at 1250 °C for 4 h and quenched to room temperature.

X-ray Diffraction: The solid solution range, crystalline phase identification, and lattice parameters were obtained by powder X-ray diffraction on a Siemens D-500 diffractometer in reflection mode with a detector and a graphite monochromator, using Cu-K_α radiation. Lattice parameters were obtained using a silicon internal standard.

SEM and EDS: Scanning electron microscopy and EDS were obtained with an AN10000 EDS coupled to a JEOL JSM-840 microscope. Stoichiometry was obtained by ICP with a JOVIN IVON instrument.

Electrical Measurements: AC measurements were carried out using an HP 4192A Impedance Analyzer over the range 5 Hz−13 MHz, only in the single phase region. Data correction were carried out in order to avoid the stray capacitance of the jig and the stray inductance and series lead resistance associated with the leads, although data above 5×10^6 Hz were discarded.

Acknowledgments

This work was partially sponsored by financial support from 1999 SGR00044.

[1] M. Itoh, Y. Inaguma, W. Jung, L. Chen, T. Nakamura, *Solid State Ionics* **1994**, *70/71*, 203−207.
[2] H. Kawai, J. Kuwano, *J. Electrochem. Soc.* **1994**, *141*, L78−L79.
[3] Y. Inaguma, L. Chen, M. Itoh, T. Nakamura, *Solid State Ionics* **1994**, *70/71*, 196−202.
[4] A. D. Robertson, S. García Martín, A. Coats, A. R. West, *J. Mater. Chem.* **1995**, *5*, 1405−1412.
[5] M. Morales, A. R. West, *Solid State Ionics* **1996**, *91*, 33−43.
[6] J. M. S. Skakle, G. C. Mather, M. Morales, R. I: Smith, A. R. West, *J. Mater. Chem.* **1995**, *5*, 1807−1808.
[7] R. I. Smith, J. M. S. Skakle, G. C. Mather, M. Morales, A. R. West, *Mater. Sci. Forum* **1996**, *228−231*, 701−704.
[8] M. Morales, M. L. Martízez−Sarrión, *J. Mater. Chem.* **1998**, *8*, 1583−1587.
[9] I. Moreno, M. Morales, M. L. Martínez−Sarrión, *J. Solid State Chem.* **1998**, *140*, 377−386.
[10] M. L. Martínez−Sarrión, L. Mestres, M. Morales, M. Herráiz, *J. Solid State Chem.* **2000**, *154*, 280−285.
[11] E. M. Levin, R. S. Roth, *J. Res. Nat. Bur. Stand.* **1964**, *68A*, 197.
[12] F. Abraham, M. F. Debreuille−Gresse, G. Mairesse, G. Nowogrocki, *Solid State Ionics* **1988**, *28−30*, 529−532.
[13] C. K. Lee, D. C. Sinclair, A. R. West, *Solid State Ionics* **1993**, *62*, 193−198.
[14] C. K. Lee, G. S. Lim, A. R. West, *J. Mater. Chem.* **1994**, *4*, 1441−1444.
[15] Y. Inaguma, M. Itoh, *Solid State Ionics* **1996**, *86−88*, 257−260.
[16] J. L. Fourquet, H. Duroy, M. P. Crosnier-Lopez, *J. Solid State Chem.* **1996**, *127*, 283−294.
[17] A. K. Jonscher, J. M. Reau, *J. Mater. Sci.* **1978**, *13*, 563−570.
[18] P. G. Bruce, A. R. West, D. P. Almond, *Solid State Ionics* **1982**, *7*, 57−60
[19] A. K. Jonscher, in "Dielectric Relaxation in Solids", Chap. 5. Chelsea Dielectric, London (1983)
[20] ZView for windows (ver. 1.4), Scribner Assoc. Inc., Charlatesville, Virginia, USA.
[21] P. Lacorre, *Solid State Sciences* **2000**, *2*, 755−758.
[22] F. Goutenoire, O. Isnard, E. Suard, O. Bohnke, Y. Laligant, R. Retoux, P. Lacorre, *J. Mater. Chem.* **2001**, *11*, 119−124.

Received October 30, 2001
[I01428]

Synthesis and Characterization of a New Aurivillius Phase

M.-L. Martínez-Sarrión,*[a] L. Mestres,[a] M. Herraiz,[a] A M. Balagurov,[b] A. I. Beskrovniy,[b] S. G. Vasilovskij,[b,c] and L. S. Smirnov[b]

Keywords: Aurivillius phase / Neutron diffraction / Solid-state structures / Perovskite phases

Several new Aurivillius phases with the general formula $Bi_{2.5+x}Li_{0.5-3x}Nb_2O_9$ ($0.04 < x < 0.08$) were synthesized. The crystal structure of the compound with $x = 0.04$ was studied by X-ray powder diffraction at room temperature, and by neutron powder diffraction in temperature intervals from 10 to 290 K. A single-phase compound was obtained. The crystal structure can be described by a space group, $Cmc2_1$, with lattice parameters of an orthorhombic unit cell: $a = 24.840(5)$ Å, $b = 5.449(6)$ Å, $c = 5.450(9)$ Å. The atomic positions were refined by a profile method. The conductivity of $Bi_{2.53}Li_{0.29}Nb_2O_9$ ranges from 1.35×10^{-8} S/cm at 543 K to 1.46×10^{-4}S/cm at 1013 K
(© Wiley-VCH Verlag GmbH, 69451 Weinheim, Germany, 2002)

Introduction

Aurivillius phases are described by the common formula $A_2O_2(A'_{n-1}B_nO_{3n+1})$,[1] where n denotes the thickness of the perovskite layers in terms of BO_6 octahedra. Currently, compounds are known with $n = 1$, 2, 3, 4, 5 and 8. Structures of this type show a great variability in their physical properties upon substitution of different metal cations.[2] This opens up great possibilities in the synthesis of new materials.

Some Aurivillius phases exhibit pseudo-tetragonal symmetry crystallizing in orthorhombic space groups. A large number of Aurivillius phases have been structurally characterized and all of them have tetragonal or pseudo-tetragonal symmetry, with a_o ranging between 3.85 and 3.95 Å ($a_{orthorhombic} = 5.45-5.58$ Å).[3]

The Aurivillius phases Bi_2WO_6, $Bi_2SrTa_2O_9$ and $Bi_4Ti_3O_{12}$ have been known as ferroelectric materials since the work of Smolenski et al.[4] and Subbarao,[5] who extensively studied their ferroelectrical properties as a function of composition. Thin films of $Bi_2SrTa_2O_9$ have been used in the recent developments in nonvolatile computer memory applications, such as an information storage medium.

The work of Withers and co-workers[6,7] has suggested that the major cause of spontaneous polarisation in the two-layer materials is the displacement of the A site cation in the perovskite block along the *a*-direction in the polar space group $A2_1am$ and not the movement of the B site cation away from the octahedral centre. A further important question regards the possibility of anti-site defects in the cation sublattice, Bi on the A site and A on the Bi site in the system $Bi_2ATa_2O_9$ (A = Ba, Sr, Ca; B = Nb, Ta). Recent work by Ismunandar et al.[8] using powder neutron diffraction data suggests that there is no cation-site disordering in these systems, although a similar study of $Bi_2PbNb_2O_9$ by Srikanth[9] suggests that some disorder may be present.

Blake et al.[10] used simultaneous X-ray and neutron powder refinements to obtain accurate models of the structure of $Bi_2BaNb_2O_9$, which is tetragonal with space group $I4/mmm$, and the structures of $Bi_2SrNb_2O_9$ and $Bi_2CaNb_2O_9$, which are orthorhombic with space group $Cmc2_1$. All the compounds exhibit disorder between the bismuth and A sites, increasing as the A-site cation size increases. The cause of this disorder may be explained by a combination of cation size considerations and bond valence sum analysis. It is possible that the two-layer Aurivillius structure may prefer a trivalent cation on the A site.

Durán-Martín and co-workers[11] have synthesised and characterised solid solutions $Bi_{2-x}Te_xSrNb_{2-x}B_xO_9$ (B = Zr, Hf) ($0 < x < 0.5$) and $Bi_{2-y}Te_ySr_{1-y}A_yNb_2O_9$ (A = K), ($0 < y < 0.25$). These materials are stable up to 800 °C for $y = 0.25$ and 750 °C for $x = 0.5$. All compositions are ferroelectric at room temperature. The AC electric conductivity shows anomalies at temperatures close to those where the remnant polarisation disappears.

In the last few years, some Aurivillius phases have been used as cathode materials in lithium batteries.[12,13] The aim of the present work is to investigate new Aurivillius phases with the general formula $Bi_{2.5+x}Li_{0.5-3x}Nb_2O_9$. These com-

[a] Departament de Química Inorgànica, Universitat de Barcelona, Martí i Franquès, 1−11, 08028 Barcelona, Spain
Fax: (internat.) + 34-934/907-725
E-mail: marialuisa.martinez@qi.ub.es
[b] Frank Laboratory of Neutron Physics, JINR, 141980 Dubna, Russia
[c] IP SB RAS, 660049 Krasnoayrsk, Russia

pounds have vacancies in the A-sites of the perovskite blocks that could promote the lithium mobility. The stoichiometry range, crystal structure and electrical behaviour have been studied.

Results and Discussion

Four compositions with general formula $Bi_{2.5+x}Li_{0.5-3x}Nb_2O_9$ ($0.04 < x < 0.08$), corresponding to an Aurivillius phase, were prepared. The use of powder XRD at room temperature confirmed that all the samples are monophasic with orthorhombic symmetry. Table 1 shows the formula and cell parameters for the new phases.

Table 1. Sample composition and cell parameters

	a (Å)	b (Å)	c (Å)	V (Å^3)
$Bi_{2.53}Li_{0.29}Nb_2O_9$	24.82(2)	5.440(6)	5.448(9)	735.59
$Bi_{2.54}Li_{0.24}Nb_2O_9$	24.81(1)	5.442(2)	5.457(1)	736.78
$Bi_{2.56}Li_{0.22}Nb_2O_9$	24.81(1)	5.444(2)	5.460(1)	737.46
$Bi_{2.59}Li_{0.20}Nb_2O_9$	24.81(1)	5.448(4)	5.458(2)	737.73

In order to understand these compounds better, $Bi_{0.53}Li_{0.29}Nb_2O_9$ was studied by neutron diffraction at different temperatures. Figure 1 shows the X-ray and neutron powder diffraction patterns at room temperature and also shows the initial indexing of the peaks. The figure shows that only the space group $Cmc2_1$ describes all the observed peaks. The atomic positions determined for $Bi_2CaNb_2O_9$ and $Bi_2SrNb_2O_9$ [10] were used as an initial model for Rietveld refinement.

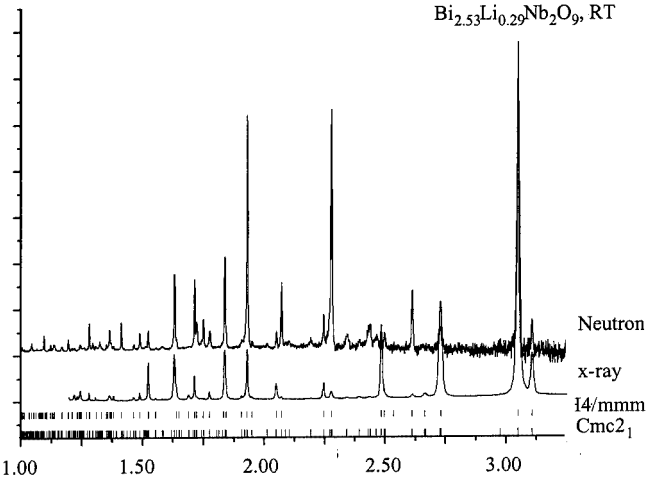

Figure 1. X-ray and neutron diffraction patterns at room temperature and initial indexing of the peaks for tetragonal *I*4/*mmm* and orthorhombic $Cmc2_1$ symmetry

Table 2 and 3 show the determined elementary cell parameters, the position of the atoms in the structure, the sites and the thermal factors in the isotropic approach, at 10 K and 290 K respectively.

Table 2. Crystallographic data for $Bi_{2.53}Li_{0.29}Nb_2O_9$ at 10K

Atom	Site	x	y	z	g	B_{iso}, Å^2
Bi(1)	4a	0.5	0.714(2)	0.274(4)	0.53	0.5
Li(1)	4a	0.5	0.546(1)	0.219(1)	0.29	0.5
Bi(2)	8b	0.2992(1)	0.7484(8)	0.258(1)	2.0	0.5
Nb	8b	0.4159(1)	0.255(1)	0.281(1)	2.0	0.2
O(1)	4a	0.5	0.208(2)	0.344(2)	1.0	0.5
O(2)	8b	0.3418(2)	0.307(1)	0.306(2)	2.0	0.5
O(3)	8b	0.7512(2)	0.506(1)	0.505(2)	2.0	0.5
O(4)	8b	0.4347(2)	0.531(1)	0.512(2)	2.0	0.5
O(5)	8b	0.4135(2)	0.053(1)	0.599(1)	2.0	0.5

R_{exp} (%) 7.7
R_p (%) 9.5
R_{wp} (%) 6.3
χ^2 3.4
Space group: $Cmc2_1$; a = 4.84373 ± 0.0019 Å, b =5.44599 ± 0.0005 Å, c =5.45467 ± 0.0005 Å

Table 3. Crystallographic data for $Bi_{2.53}Li_{0.29}Nb_2O_9$ at 290K

Atom	Site	x	y	z	g	B_{iso}, Å^2
Bi(1)	4a	0.5	0.729(2)	0.239(2)	0.53	2.65 ± 0.12
Li(1)	4a	0.5	0.694(8)	0.24(1)	0.29	1.01 ± 0.93
Bi(2)	8b	0.3000(1)	0.741	0.256(7)	2.0	2.15 ± 0.02
Nb	8b	0.4158(6)	0.2555(7)	0.2787(8)	2.0	1.76 ± 0.03
O(1)	4a	0.5	0.200(1)	0.334(1)	1.0	3.07 ± 0.09
O(2)	8b	0.3431(1)	0.3098(6)	0.312(9)	2.0	1.82 ± 0.05
O(3)	8b	0.7509(1)	0.508(6)	0.520(1)	2.0	1.61 ± 0.03
O(4)	8b	0.4325(1)	0.5326(8)	0.517(1)	2.0	3.55 ± 0.06
O(5)	8b	0.415(1)	0.0472(6)	0.5987(8)	2.0	2.52 ± 0.07

R_{exp} (%) 8.3
R_p (%) 12.5
R_{wp} (%) 7.3
χ^2 5.7
Space group:$Cmc2_1$; a = 24.849 ± 0.001 Å, b = 5.4536 ± 0.0003 Å., c = 5.4619 ± 0.0002 Å

At T = 10 K all the B_{iso} values are fixed. The results of the Rietveld refinement are shown in Figure 2. The observed neutron diffraction data are shown as a dotted line and the calculated profile as a solid line. A mark below the profile indicates the position of an allowed reflection. The lowest line near zero corresponds to the differences between observed and calculated intensities.

The possible variant of the replacement of bismuth by lithium in the bismuth oxide layer was checked during specification of the crystal structure. According to our calculations, the population of lithium in the bismuth oxide layer was nil. The bismuth oxide layer is much more inert with regard to substitution than the perovskite layer.[14,15] These data provide a basis for assuming that replacement of a bivalent ion in $Bi_2SrNb_2O_9$ or $Bi_2BaNb_2O_9$ by trivalent bismuth results in the formation of structural vacancies in the perovskite layer. The partial occupation of these vacancies

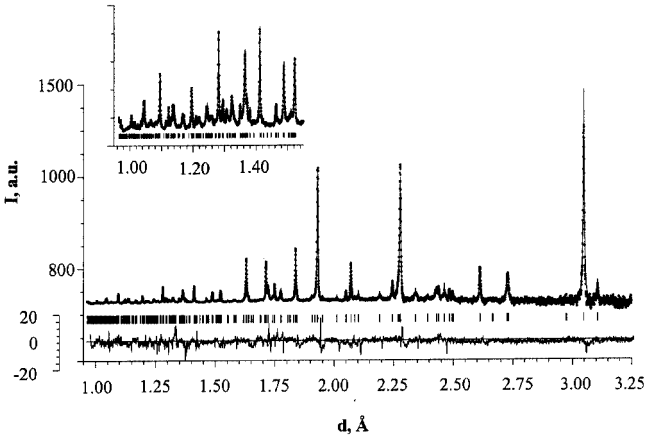

Figure 2. Observed, calculated (upper curve) and difference (lower curve) neutron profiles for $Bi_{2.53}Li_{0.29}Nb_2O_9$ obtained with an HRFD diffractometer at 290 K

by lithium ions can create favourable conditions for the development of ionic conductivity on structural vacancies.

The valences V_{ij} of the different cations were calculated from the atomic coordinates and Equation (1) (bond valence method):

$$V_{ij} = \sum_{i}^{v} s_{ij}\left(R_{ij}\right) \quad (1)$$

where v is the coordination number.

The dependence of valence strain s_{ij} on the bond length R is determined as:

$$s_{ij} = \exp\left[\left(R_{1j} - R_{ij}\right)/b\right] \quad (2)$$

where R_1 is the bond length of the individual valence, and the empirical parameter b is 0.37 Å (Table 4).

Table 4. Calculated valency for cations

Atom	Bond valence		
	T = 10 K	T = 290 K	Model
Bi	3.03	2.89	3
(Bi/Li)	1.89	1.81	1.88
Nb	4.94	5.14	5

The arrangement of octahedra in the structure is distorted. There is also a noticeable distortion of their form. Table 5 gives the bond lengths between atoms that fall into an octahedral configuration.

Table 5. Bond lengths in the NbO_6 octahedra

Bond type	L, Å	
	T = 10 K	T = 290 K
Nb−O(1)	2.131	2.136
Nb−O(2)	1.868	1.831
Nb−O(4)	1.925	1.882
	2.019	2.039
Nb−O(5)	1.957	1.992
	2.054	2.085

In order to gain a better understanding of this compound powder neutron diffraction data were collected at high temperature on a DN-2 diffractometer. On the basis of these data, the dependence of the parameters of an elementary cell on the temperature were deduced (Figure 3). From the given dependences it may be seen that orthorhombic distortion of the structure increases with temperature. This is not consistent with the data, which are given for $Bi_2(Sr, Ca)Nb_2O_9$.[10]

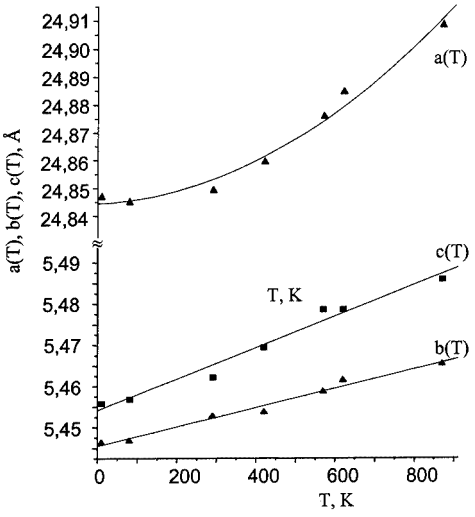

Figure 3. Dependence of the elementary cell parameters of $Bi_{2.53}Li_{0.29}Nb_2O_9$ vs. temperature

The plot of the parameters against temperature in Figure 3 shows a possible phase transition between 600 and 650 K. The small structure distortion due to the presence of lithium in the 12-coordinated positions of the perovskite part would lead to a possible phase transition at high temperature, in agreement with the small change in the slope observed in the plot.

Analysis of the results of TG and DSC analysis did not show the presence of a phase transition of these compounds in our experimental conditions, although one has to take into account that not all phase transitions carry an enthalpy variation detectable by DSC.

Figure 4 shows the structure of the new Aurivillius phase $Bi_{2.53}Li_{0.29}Nb_2O_9$, which may be described structurally as intergrowths of fluorite-like $Bi_2O_2^{2+}$ layers with perovskitic $(A'_{n-1}B_nO_{3n+1})^{2-}$ layers (n = 2). The $Bi_2O_2^{2+}$ layers are composed of a square planar net of oxygen anions with Bi^{3+} in an alternating sequence above and below, forming BiO_4-pyramids. Double perovskite layers are inserted between $Bi_2O_2^{2+}$ layers. Nb^{5+} cations are on the B-site, and Bi^{3+}, Li^+ and vacancies can be found on the A′ positions. NbO_6 octahedra in the structure are partially collapsed as a result of a cooperative tilting and rotating due to the presence of Bi^{3+}, Li^+ and vacancies placed on the larger A′ sites of the perovskite structure.

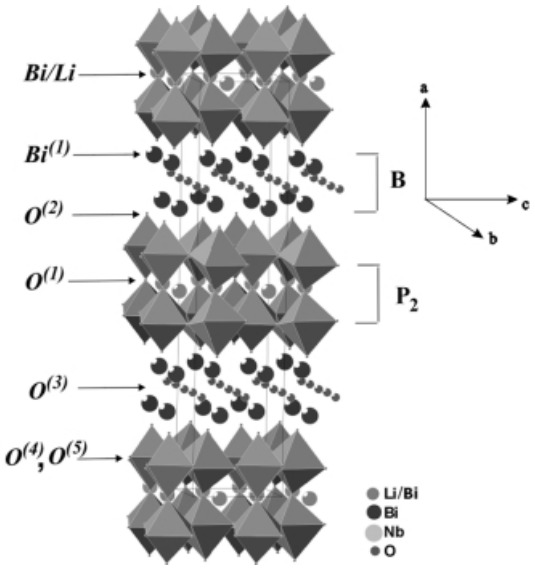

Figure 4. Crystal structure of $Bi_{2.53}Li_{0.29}Nb_2O_9$; octahedra NbO_6: large black spheres, Bi: small grey spheres O; large grey balls are Bi, Li or vacancies

AC impedance measurements were carried out on sintered pellets (diameter ≈ 6 mm and thickness ≈ 2 mm) of the sample $Bi_{2.53}Li_{0.29}Nb_2O_9$, using gold electrodes. The conductivity was measured up to 750 ΘC, the maximum temperature allowed by our sample holders. An almost perfect semicircle associated with the bulk conductivity (C ≈ 40pF) was observed (Figure 5) and the conductivity was determined from the intercepts on the real axis.

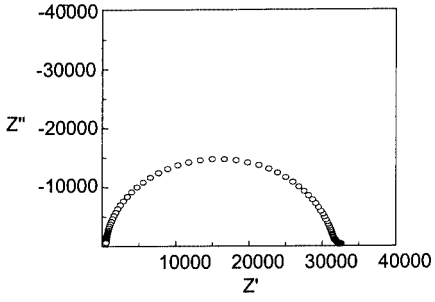

Figure 5. Impedance spectra for $Bi_{2.53}Li_{0.29}Nb_2O_9$ at 953 K

Figure 6 shows the variation of the dielectric constant (ε′) as a function of the temperature for different frequencies during the heating run. As can be seen, there are two anomalies in the behaviour of this constant; the first one at approximately 573 K and the second one at 873 K. The maximum corresponding to the first one shifts to lower temperatures with decreasing frequency. This kind of behaviour of the dielectric constant is typical of materials with a diffuse phase transition, and is also found for different ferroelectric materials.[17,18] For temperatures above 873 K a further increase of the dielectric constant was observed as the increasing electric conductivity leads to a dielectric breakdown.[19]

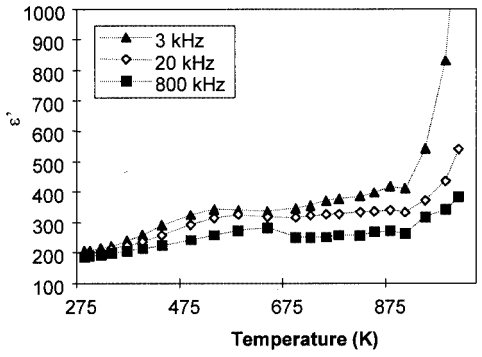

Figure 6. Dielectric constant ε′ of $Bi_{2.53}Li_{0.29}Nb_2O_9$ vs. temperature for different frequencies

Conductivity data from the impedance complex plane plots are shown in Arrhenius format in Figure 7. The plot is not linear and the slope changes around the same temperatures where the dielectric permittivity plots show anomalies that may be attributed to a phase transition. The activation energy changes from 0.57 eV to 0.93 eV, and finally 1.43 eV.

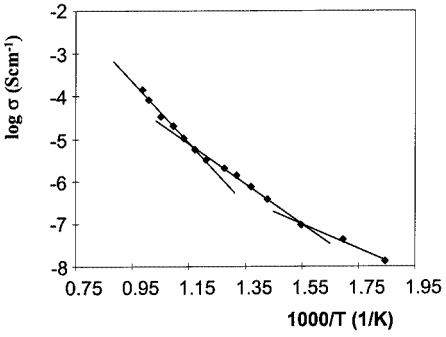

Figure 7. Arrhenius plots of conductivity for $Bi_{2.53}Li_{0.29}Nb_2O_9$

Experimental Section

Synthesis: Samples were prepared in 10 g quantities from Bi_2O_3 (Aldrich 99.9%), Li_2CO_3 (Aldrich, purity > 99.0%) and Nb_2O_5 (Aldrich 99.9%). Nb_2O_5 was dried overnight at 950 °C prior to weighing. These chemicals were weighed, mixed in an agate mortar with acetone, dried and heated to 650 °C for 3 h to drive off CO_2. After grinding, samples were pressed into pellets and covered with powder of the same composition to avoid loss of lithium during thermal treatment. The pellets were fired at 950 °C for 4 h yielding white products, which were reground, re-pelleted and fired at 1025 °C for 12 h and at 1100 °C for 6 h.

Analysis: Lithium, bismuth and niobium stoichiometries were obtained by ICP with a Jovin Ivon instrument.

X-ray Diffraction: Phase purity was checked by X-ray powder diffraction with a Siemens D-500 diffractometer in reflection mode and a secondary monochromator using Cu-K_α radiation. The program FULLPROF was used for Rietveld refinements.[20]

Neutron Diffraction: Neutron diffraction experiments were carried out in the FLNP, JINR at the IBR-2 pulse reactor using two different diffractometers. On the DN-2 diffractometer, the neutron dif-

fraction data were measured in the range from 1.5 Å to 12 Å at medium resolution. On the HRFD diffractometer, neutron diffraction data were recorded in the range from 1 Å to 3.2 Å at high resolution. The unit-cell parameters were determined using the AUTOX program for automatic indexing.[21] The atomic positions were refined by the Rietveld profile analysis using the MRIA program.[22]

Thermal Analysis: The thermal analysis for the temperature range 298−1173 K by thermogravimetry (TG), and from 123−873 K by differential scanning calorimeter (DSC) was carried out in a Mettler Toledo Star System. With TG the warming rate was 10 K/min, and the weight of the sample, was 27.4027 mg. In the DSC study the weight of the sample was 12.2430 mg from 298 K to 873 K, and 12.8800 mg, from 123 K to 298 K. The measurements were made during both heating and cooling. The reference material was alumina.

Electrical Measurements: AC measurements were carried out using a HP 4192A Impedance Analyser over the range100 Hz $< f <$ 1.3 $\times$ 10^7 Hz. Data corrections were carried out in order to avoid the stray capacitance of the jig and the stray inductance and series lead resistance associated with the leads; data above 5 $\times$ 10^6 Hz were discarded.

Acknowledgments

This work was partially sponsored by financial support from 99-SGR-00044 and INTAS-97-10177.

[1] B. Aurivillius, *Ark. Kemi* **1949**, *1*, 465−480.
[2] K. S. Aleksandrov, B. V. Beznosikov, *Crystals of Type Perovskite*, "Saince", Novosobirst, **1999**.
[3] J. F. Ackerman, *J. Solid State Chem.* **1986**, *62*, 92−104.
[4] G. A. Smolenski, V. A. Isupov, A. I. Agranovskaya, *Sov. Phys. Solid. State (Engl. Transl.)* **1959**, *3*, 651.
[5] E. C. Subbarao, *J. Phys. Chem. Solids* **1962**, *23*, 665−676.
[6] A. D. Rae, J. G. Thompson, R. L. Withers, *Acta Crystallogr., Sect. B* **1992**, *48*, 418−428.
[7] R. L. Withers, J. G. Thompson, A. D. Rae, *J. Solid State Chem.* **1991**, *94*, 404−417.
[8] Ismunandar, B. J. Kennedy, Gunawan, Marsongkohadi, *J. Solid State Chem.* **1996**, *126*, 135−141.
[9] V. Srikanth, H. Idink, W. B. White, E. C. Subbarao, H. Rajagopal, A. Sequeira, *Acta Crystallogr., Sect. B* **1996**, *52*, 432−439.
[10] S. M. Blake, M. J. Falconer, M. McCreedy, P. Lightfoot, *J. Mater. Chem.* **1997**, *7*, 1609−1613.
[11] P. Durán-Martín, B. Jiménez, P. Millán, A. Castro, *J. Phys. Chem. Solids* **2000**, *61*, 1423−1431.
[12] M. E. Arroyo y de Dompablo, F. García-Alvarado, E. Morán, *Solid State Ionics* **1996**, *91*, 273−278.
[13] J. H. Choy, J. Y. Kim, I. Chung, *J. Phys. Chem. B* **2001**, *105*, 7908−7912.
[14] A. Castro, P. Millán, M. J. Martínez-Lopez, *Solid State Ionics* **1993**, *63−65*, 897−901.
[15] P. Millán, A. Castro, J. B. Torrance, *Mater. Res. Bull.* **1993**, *28*, 117−122.
[16] V. S. Urusov, I. P. Orlov, *Crystallogr. Rep.* **1999**, *44*, 686−709.
[17] L. E. Cross, *Ferroelectric Ceramics: Tailoring Properties for Specific Applications*, Birkhäuser, Basel, **1993**.
[18] M. E. Lines and A. M. Glass, *Principles and Applications of Ferroelectrics and Related Materials* Oxford University Press, Oxford, **1977**.
[19] H. M. Rosenberg, *The Solid State* Oxford University Press, Oxford, **1988**.
[20] J. Rodríguez Carvajal, "Fullprof: A program for Rietveld refinement and pattern machine analysisi," revised version, 1994.
[21] V. B. Zlokazov, *Comput. Phys. Commun.* **1995**, *85*, 415−422.
[22] V. B. Zlokazov, V. V. Chernyshev, *J. Appl. Crystalogr.* **1992**, *25*, 447−451.

Received November 29, 2001
[I01487]

Monomeric and Dimeric Iron(III) Complexes of 5-Hydroxy-10,15,20-triphenylporphyrin: Formation of Cyano and Pyridine Complexes of (5-Oxo-10,15,20-triphenylphlorin)iron

Jacek Wojaczyński,[a] Marcin Stępień,[a] and Lechosław Latos-Grażyński*[a]

Keywords: Porphyrinoids / Oxophlorins / Iron / Electronic structure / NMR spectroscopy

The reaction of $[(TrPP)Fe^{II}(py)_2]$ (TrPP = dianion of 5,10,15-triphenylporphyrin) with hydrogen peroxide results in oxygenation of the (porphyrin)iron and the formation of (10,15,20-triphenyl-5-oxophlorin)iron $[(5\text{-}O\text{-}TrPP)Fe(py)_2]$. Coupled oxidation of $[(TrPP)Fe^{III}Cl]$ in the presence of ascorbic acid and potassium cyanide in methanol leads to oxidative hydroxylation of the porphyrin ring to form a cyclic dimer $[(5\text{-}O\text{-}TrPP)Fe^{III}]_2$. Three out of four pyrrole ^{1}H NMR resonances of the dimeric complex present the characteristic displacement with respect to the typical position for the high-spin (tetraphenylporphyrin)iron(III) complexes. The linewidths of the β-H pyrrole resonances correlate with specific locations of the respective protons within the dimeric structure. Addition of HCl to $[(5\text{-}O\text{-}TrPP)Fe^{III}]_2$ results in cleavage of the dimer producing $[(5\text{-}OH\text{-}TrPP)Fe^{III}Cl]$. $[(5\text{-}O\text{-}TrPP)Fe^{III}]_2$ is also split with acetic anhydride to give (5-acetoxy-10,15,20-triphenylporphyrin)iron(III). In the presence of $[D_5]$pyridine or a large excess of cyanide ion, $[(5\text{-}O\text{-}TrPP)Fe^{III}]_2$ undergoes cleavage to form air-sensitive $[(5\text{-}O\text{-}TrPP)Fe(py)_2]$ or $[(5\text{-}O\text{-}TrPP)Fe(CN)_2]^{2-}$. The pyrrole pattern observed for $[(5\text{-}O\text{-}TrPP)Fe(py)_2]$ is similar to that determined on the basis of an analysis carried out for four (oxophlorin)-iron regioisomers obtained from hemes. For comparison, the characteristic ^{1}H NMR features of the typical (5-substituted-10,15,20-triphenylporphyrin)iron(III) complexes have been investigated for the series of high-spin and low-spin complexes. The spin-density distribution in the (oxophlorin)iron skeleton is dominated by the radical-like electronic structure. (© Wiley-VCH Verlag GmbH, 69451 Weinheim, Germany, 2002)

Introduction

Coordinating properties of porphyrins, widely used in biomimetic chemistry and catalytic studies, can be remarkably modified by the introduction of some additional metal ion coordinating centers at the porphyrin periphery. Such substituents are suitable for coordination of the metal ion of the same or other molecular systems.[1−3] These ''hybrid'' bifunctional ligands combine properties of the porphyrin macrocycles with those of the peripheral coordinating moiety.

The hydroxy-substituted octaethylporphyrin and tetraphenylporphyrin are representative examples of polyfunctional ligands related to porphyrins. They are able to coordinate through the tetranitrogen macrocyclic center and/or through an ionized hydroxy group at the periphery. Three structurally distinct locations of the hydroxy substituents for the originally highly symmetrical model porphyrins $OEPH_2$ and $TPPH_2$ were attainable synthetically, a *meso* position for $OEPH_2$, and β-pyrrole or phenyl positions for $TPPH_2$.[4−7] Insertion of an iron ion into 5-(2-hydroxyphenyl)-10,15,20-tritolylporphyrin ($TTOPH_2$) or 5-hydroxy-octaethylporphyrin (octaethyloxophlorin, $OEPOH_2$) resulted in the formation of the high-spin doubly oxo-bridged iron(III) head-to-tail dimers $[(TTOP)Fe^{III}]_2$ and $[(OEPO)Fe^{III}]_2$, respectively.[8−10] Dimerization through phenoxide $\{[(TTOP)Fe^{III}]_2\}$ or the *meso*-oxygen atom $\{[(OEPO)Fe^{III}]_2\}$ rather than μ-oxo bridging was preferred in both cases.

The structure of $[(TTOP)Fe^{III}]_2$ was determined by X-ray crystallography and the retention of the dimeric structure in solution was demonstrated by ^{1}H NMR spectroscopy.[8,9] Goff et al. characterized the manganese(III) dimer $[(TTOP)Mn^{III}]_2$ and detected, by means of ^{1}H NMR spectroscopy, the diphenoxo-bridged heteronuclear complex $[(TTOP)Fe^{III}(TTOP)Mn^{III}]$.[9]

(Oxophlorin)iron complexes are significant in the context of their involvement as intermediates in the conversion of (porphyrin)iron to biliverdin in the oxidative heme destruction.[11,12] Masuoka and Itano characterized the (oxophlorin)iron(III) dimer $[(OEPO)Fe^{III}]_2$ by a range of spectroscopic techniques.[10] The presence of two paramagnetic centers produced marked changes of the ^{1}H NMR spectral parameters compared to monomeric analogs, including variation of the linewidths for the methylene protons.[13] The formation of $[(OEPO)Mn^{III}]_2$ has been demonstrated,[14] and the unique structure of the related indium complex determined by X-ray crystallography.[15]

[a] Department of Chemistry, University of Wrocław,
14 F. Joliot-Curie St., 50-383 Wrocław, Poland
E-mail: llg@wchuwr.chem.uni.wroc.pl

2-Hydroxy-5,10,15,20-tetraphenylporphyrin is the tetraphenylporphyrin derivative hydroxylated at a β-position. The cyclic trimers $[(2\text{-O-TPP})Fe^{III}]_3$, $[(2\text{-O-TPP})Ga^{III}]_3$, and $[(2\text{-O-TPP})Mn^{III}]_3$ were generated in a self-assembly process of monomeric (2-hydroxy-5,10,15,20-tetraphenylporphyrin)iron(III), -gallium(III), or -manganese(III).[16−18] The trivalent metal ion coordinated in the porphyrin crevice seems to be a prerequisite for the trimer formation. The paramagnetic heterometallic head-to-tail cyclic trimers of general formula $[(2\text{-O-TPP})M^{III}]_n[(2\text{-O-TPP})M_1^{III}]_{3-n}$ (M, M_1: Fe^{III}, Ga^{III}, Mn^{III}) have also been identified.[19]

In this project we introduce a new hybrid bifunctional ligand, namely 5-hydroxy-10,15,20-triphenylporphyrin (5-OH-$TrPPH_2$) which is formally derived from tetraphenylporphyrin. The molecule is "constructed" by replacement of a single *meso*-phenyl group with a hydroxy group.

5-OH-$TrPPH_2$ and the previously investigated 5-hydroxyoctaethylporphyrin contain the identical structural motif of 5-hydroxyporphyrin.[20] In analogy to 5-OH-$OEPH_2$, the coordinating properties of 5-OH-$TrPPH_2$ can be related to two tautomers, 5-hydroxyporphyrin and 5-oxophlorin, presented in Scheme 1.

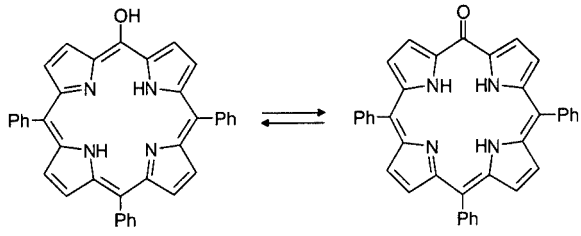

Scheme 1

In order to determine the influence of the *meso*-hydroxy group on (porphyrin)iron properties in a broader scope, a representative group of low-spin and high-spin iron(III) complexes of 5-substituted-10,15,20-triphenylporphyrin (5-X-$TrPPH_2$; X = NO_2, Br, *n*Bu, H, OMe) have been investigated in parallel. The 5-X substituents vary in their electron-donating/-withdrawing properties as measured by Hammett constants. Considering the biochemical aspects, the electronic structure and reactivity of the (5-oxo-10,15,20-triphenylphlorin)iron complex $[(5\text{-O-TrPP})FeL_2]$ (L = py, CN^-) are of particular interest.

The related (octaethyloxophlorin)Fe(pyridine)$_2$ complex {$[(OEPO)Fe(py)_2]$} has been studied extensively.[21−26] It has been found that a mechanism of coupled oxidation of $[(OEP)Fe^{II}(py)_2]$ in pyridine solution includes a *meso*-hydroxylation step producing $[(OEPO)Fe(py)_2]$.[12,27] It is widely accepted that the first step in heme degradation by heme oxygenase results in the *meso* hydroxylation of heme.[12,23,26,28,29] Direct spectroscopic evidence has been presented showing that *meso*-hydroxylated heme is formed by heme oxygenase.[30]

^{1}H NMR spectroscopy provides a uniquely useful probe for studying the structure of (porphyrin)iron complexes in solution.[31,32] The hyperfine shift patterns are particularly sensitive to the ligation, oxidation and spin state of the metal ion. For instance, the (porphyrin)iron(III) complexes bridged by ligands containing one or more oxygen atoms present ^{1}H NMR spectroscopic patterns unequivocally explainable in terms of their dimeric[8,9,13] or trimeric[16−19] structures. In this contribution our investigations have been focused on (5-hydroxy-10,15,20-triphenylporphyrin)- and (5-oxo-10,15,20-triphenylphlorin)iron(III) complexes. Four inequivalent pyrrole resonances of TrPP complexes and their *meso*-substituted derivatives provided the direct probe of the spin density around the porphyrin macrocycle, and allowed the detection of a cyclic dimeric structure.

Results and Discussion

Synthesis of [(5-X-TrPP)Fe^{III}Cl]

5,10,15-Triphenylporphyrin, $TrPPH_2$, was synthesized by the condensation of pyrrole, benzaldehyde, and paraformaldehyde. The procedure followed the methodology typically used for synthesis via a mixed aldehyde−pyrrole condensation.[33] Alternatively, $TrPPH_2$ was obtained by phenylation of 5,15-diphenylporphyrin with phenyllithium.[34]

$TrPPH_2$ was characterized by X-ray crystallography (Figure 1); the bond lengths and angles are within the range expected for a porphyrin.[35] The porphyrin macrocycle is practically flat. In the crystal, a 2_1 axis (along the *c* direction) generates a ribbon of molecules (Figure 1), which demonstrate a characteristic set of close CH−π contacts (with CH−centroid distances of 2.58 and 3.05 Å) involving Ph(5)···Ph(10)···Ph(15) *meso*-phenyl rings from adjacent triphenylporphyrins. An analogous structural motif has been observed for $TPPH_2$-based porphyrin sponges.[36,37] The periphery of $TrPPH_2$ presents a blending of structural features that are typical for $TPPH_2$ and $OEPH_2$ as the 5-*meso* position and two pyrrole rings are exposed.

5-Bromo-10,15,20-triphenylporphyrin (5-Br-$TrPPH_2$) was obtained from the reaction of $TrPPH_2$ with *N*-bromosuccinimide as described previously.[38] 5-Nitro-10,15,20-triphenylporphyrin (5-NO_2-$TrPPH_2$) was obtained by nitration of triphenylporphyrin with $AgNO_2$ in the presence of I_2 by modification of the method applied for the nitration of 5,15-diphenylporphyrin.[39]

Reaction of $[(TrPP)Zn^{II}]$ with sodium methoxide in the presence of air yielded (5-methoxy-10,15,20-triphenylporphyrin)zinc(II), which was subsequently demetallated with acid to give 5-MeO-$TrPPH_2$.

Iron insertion into 5-X-$TrPPH_2$ produced the corresponding $[(5\text{-X-TrPP})Fe^{III}Cl]$ complexes. The $[(5\text{-Br-TrPP})Fe^{III}Cl]$ complex was characterized by X-ray crystallography (Figure 2). The iron ion is five-coordinate with bonds to the four pyrrole nitrogen atoms of nearly equal lengths [2.065(4), 2.065(4), 2.071(4), and 2.076(4) Å]. The metal ion lies 0.461(2) Å out of the mean plane of the macrocycle. The Fe−N distances and the displacement from the mean plane are characteristic of five-coordinate high-spin (S = 5/2) (porphyrin)iron(III) complexes.[40−42] The Fe−Cl distance is 2.209(2) Å, which is typical for chloro(porphyrin)iron(III) complexes.[40,41]

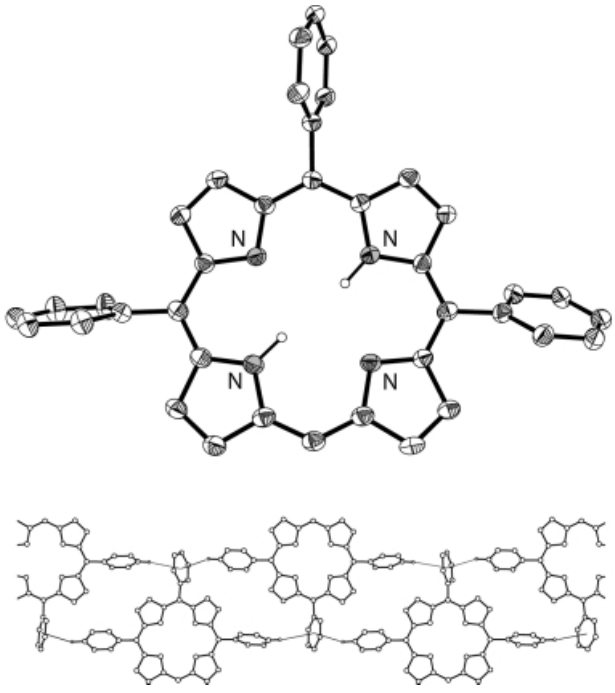

Figure 1. (top) The crystal structure of $TrPPH_2$; the vibrational ellipsoids represent 50% probability; (bottom) a view of the molecular packing demonstrating the ribbon arrangement and CH−π contacts of *meso*-phenyl rings from adjacent triphenylporphyrins

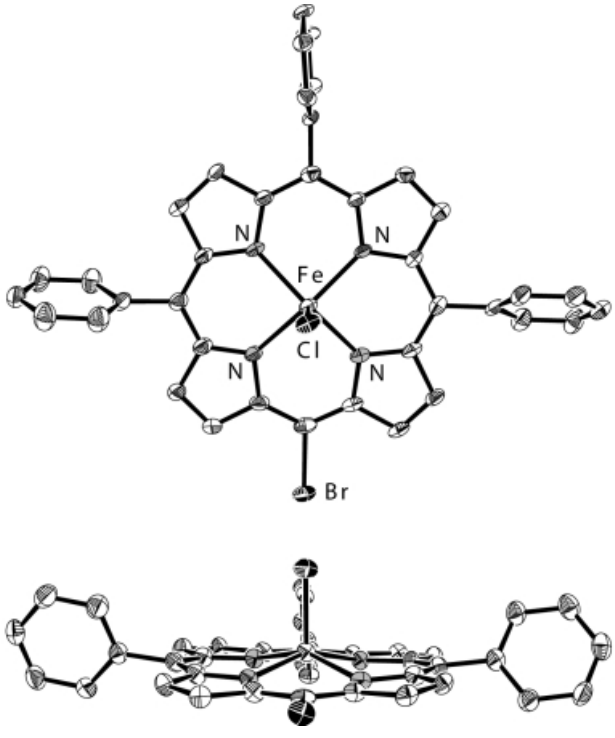

Figure 2. A perspective view of (5-Br-TrPP)$Fe^{III}Cl$ with 50% thermal contours

Reaction of Hydrogen Peroxide with [(TrPP)$Fe^{II}(py)_2$]

The standard hydroxylation procedure of $OEPH_2$ involves the reaction of [(OEP)Zn^{II}] with thallium(III) trifluoroacetate (TTFA) to produce (5-trifluoroacetoxyoctethylporphyrin)zinc(II) [(5-TFA-OEP)Zn^{II}].[4] Hydrolysis of this complex yields octaethyloxophlorin. Quite differently, the [(TrPP)Zn^{II}] complex undergoes a regiospecific C(5)−C(5′) coupling, mediated by TTFA acting solely as a two-electron oxidizing reagent to produce [5,5′-bi(10,15,20-triphenylporphyrin)]dizinc(II) [$(TrPP)_2Zn^{II}_2$].[43−45] Consequently, to obtain (5-hydroxy-10,15,20-triphenylporphyrin)iron(III), a different approach has been applied. We have taken into account that porphyrins themselves are not nearly as susceptible to initial *meso* oxygenation (hydroxylation) as are (porphyrin)iron complexes.[26,46,47] Consequently, the reaction of [(TrPP)$Fe^{II}(py)_2$] with hydrogen peroxide at −30 °C in the absence of dioxygen has been examined. Scheme 2 shows the structures and transformations involved.

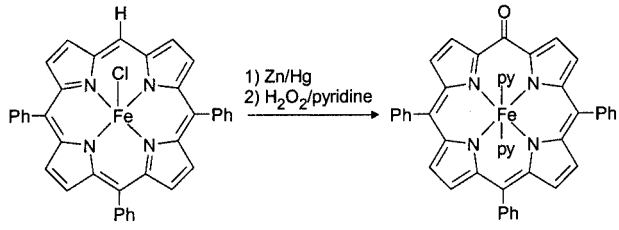

Scheme 2

A [D_5]pyridine solution of [(TrPP)$Fe^{II}(py)_2$] was prepared under dinitrogen to exclude any oxidation with dioxygen and cooled to −30 °C, at which point a dioxygen-free solution of hydrogen peroxide (30% in water)/[D_5]pyridine solution (1:60, v/v) was introduced into the sample in a stepwise manner. The red solution of [(TrPP)$Fe^{II}(py)_2$] turned brownish on addition of the hydrogen peroxide, and the ^1H NMR spectra showed the gradual growth of a new set of resonances accompanied by a lowering of the intensities of those assigned to the low-spin diamagnetic [(TrPP)Fe^{II}-$(py)_2$]. A paramagnetic product was identified as (5-oxo-10,15,20-triphenylphlorin)iron with two axially coordinated [D_5]pyridine ligands, [(5-O-TrPP)Fe$(py)_2$] (see below). Thus, the reaction had taken place exclusively at the unsubstituted *meso* position. Once formed, the solution of [(5-O-TrPP)Fe$(py)_2$] in [D_5]pyridine is stable as long as it is protected from dioxygen, the addition of which results in bleaching.

Extraction of the [D_5]pyridine solution of [(5-O-TrPP)Fe$(py)_2$] with 1 M aqueous HCl yielded high-spin [(5-OH-TrPP)Fe^{III}Cl]. Subsequently, the dichloromethane solution of [(5-OH-TrPP)Fe^{III}Cl] was subjected to chromatography on a silica column. In the course of the process the monomeric [(5-OH-TrPP)Fe^{III}Cl] complex was transformed into the cyclic dimer [(5-O-TrPP)$Fe^{III}]_2$ (Scheme 3).

Coupled Oxidation

Recently, a convenient method for the preparation of the dimeric [(OEPO)$Fe^{III}]_2$ complex has been reported in the course of coupled oxidation of [(OEP)Fe^{III}Cl] under pyridine-free conditions.[48] Herein, this procedure has been adopted with success to obtain [(5-O-TrPP)$Fe^{III}]_2$.

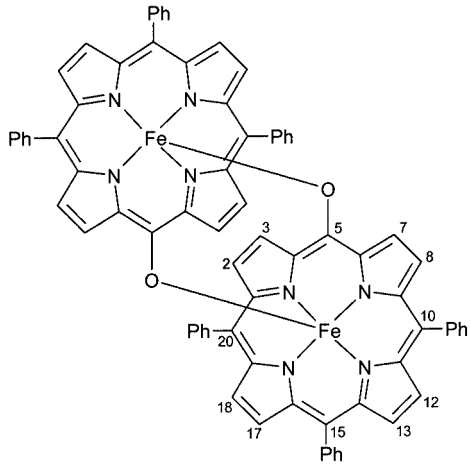

Scheme 3

Addition of [(TrPP)Fe^{III}Cl] to a methanolic solution of ascorbic acid and potassium cyanide leads to oxidative hydroxylation of the porphyrin ring to form [(5-O-TrPP)Fe^{III}]$_2$. Initially, the cyanide coordinates to [(TrPP)Fe^{III}Cl] producing [(TrPP)$Fe^{III}(CN)_2]^-$, a reaction substrate that is soluble in methanol. The reaction mixture was stirred overnight in the presence of air. In the course of the coupled oxidation we obtained [(5-O-TrPP)Fe^{III}]$_2$, which was subsequently separated using column chromatography. The yield of the process was ca. 20%. At the present stage of investigations, no effort has been made to optimize the yield and to characterize other feasible reaction products.

Characterization of [(5-O-TrPP)Fe^{III}]$_2$

The electronic spectrum of [(5-O-TrPP)Fe^{III}]$_2$ is presented in Figure 3 together with the spectrum of [(5-OAc-TrPP)Fe^{III}Cl] and [(5-O-TrPP)Fe$(CN)_2]^{2-}$ (see below). The electronic spectrum of [(5-OAc-TrPP)Fe^{III}Cl] resembles the spectra of high-spin (tetraphenylporphyrin)iron(III) complexes and other [(5-X-TrPP)Fe^{III}Cl] complexes. The electronic spectrum of [(5-O-TrPP)Fe^{III}]$_2$ is considerably different; all bands are broadened compared to [(5-OAc-TrPP)Fe^{III}Cl], and a new band is detected at 330 nm. These differences may be induced by the 5-oxygen axial ligand coordination[49] and/or from the porphyrin−porphyrin π interaction caused by the proximity of the porphyrin rings in the close-packed dimeric structure.[13,16,50−52]

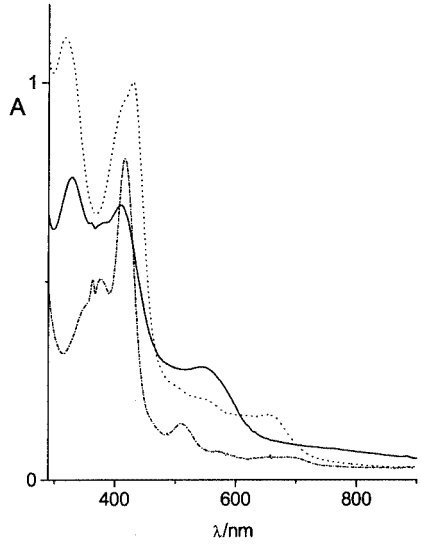

Figure 3. Electronic absorption spectra of [(5-O-TrPP)Fe^{III}]$_2$ (——), [(5-AcO-TrPP)Fe^{III}Cl] (-·-·-·) (both in CH_2Cl_2), and [(5-O-TrPP)Fe$(CN)_2]^{2-}$ (· · ·) (in methanol)

The electrospray ionization (ESI) mass spectrum of [(5-O-TrPP)Fe^{III}]$_2$ shows peaks due to the parent species [(5-O-TrPP)Fe^{III}]$_2$ at *m*/*z* (%) = 1215.4 (7) and its deoligmerization product [(5-OH-TrPP)$Fe^{III}]^+$ at *m*/*z* (%) = 608.3 (100). In our experiment the most intense peak corresponds to the monomeric unit because the technique used requires the addition of acid to the sample, which favors the formation of monomer.

^{1}H NMR Spectroscopic Studies of [(5-O-TrPP)Fe^{III}]$_2$

The downfield part of the ^{1}H NMR spectrum of [(5-O-TrPP)Fe^{III}]$_2$ is shown in Figure 4 (Trace A). The resonance assignments have been made on the basis of relative intensities and linewidth analysis. The ^{1}H NMR spectrum of [(5-O-TrPP)Fe^{III}]$_2$ shows a number of remarkable features that must arise from its unusual molecular structure. In particular, three β-pyrrolic signals are strongly displaced upfield relative to their typical position for the high-spin (tetraphenylporphyrin)iron(III) complexes at δ (linewidths in Hz) = 56.3 (400), 49.6 (650), 47.5 (2200) ppm ($CDCl_3$, 293 K). The deconvolution procedure (not shown) has been applied to this part of the spectrum in order to demonstrate that three resonances of remarkably different linewidths and identical intensities are required to reproduce the experimental spectrum. The fourth inequivalent pyrrole position produces the resonance at δ = 84.3 (linewidth 300 Hz) ppm. The phenyl resonances form a complex, unresolved pattern which is spread over the δ = 0−16 ppm range.

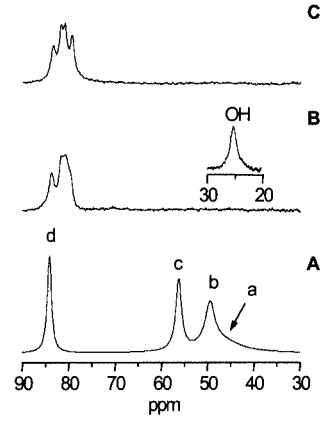

Figure 4. The downfield region of (A) 300 MHz ^{1}H NMR spectrum of [(5-O-TrPP)Fe^{III}]$_2$ at 291 K, (B) 500 MHz ^{1}H NMR spectrum of [(5-OH-TrPP)Fe^{III}Cl], (C) 500 MHz ^{1}H NMR spectrum of [(5-AcO-TrPP)Fe^{III}Cl]; resonance assignments: a: 3(7)-H; b: 2(8)-H; c: 12(18)-H; d: 13(17)-H

Molecular mechanics calculations have been used to visualize the structure of the dimer and to estimate the degree of the porphyrin distortion that is necessary to form this species. In the minimization procedure we used the standard MM+ parameterization of the HyperChem program, with the exception of the iron coordination surroundings where we imposed the constraints reflecting the high-spin state of the iron(III) ion. The characteristic features of the high-spin (tetraphenylporphyrin)iron(III) complexes and [(5-Br-TrPP)Fe^{III}Cl] included displacement of the iron ion from the plane of the four nitrogen atoms (0.45 Å), and relatively long Fe−N bonds (2.05 Å).[41−43] The spectroscopic evidence indicates that the iron(III) complex has a head-to-tail dimeric structure, with the *meso*-alkoxide groups forming the bridges from one macrocycle to the metal ion of the adjacent macrocycle. Such a dimeric structure accounts for the mass of the largest ion in the mass spectrum. The ^{1}H NMR spectrum clearly shows the equivalence of the two (porphyrin)iron(III) subunits. The upfield relocation of three β-H resonances can be explained only by the direct coordination of the O(5) atom to the external iron(III) ion, as required by the cyclic dimeric structure. Hence high-spin (5-hydroxytriphenylporphyrin)-iron(III) can be used as a building block in the dimerization.

A schematic view of the dimeric (porphyrin)iron(III) skeleton as obtained by molecular mechanics is presented in Figure 5. The closest contacts are in the range observed in the structures of other metalloporphyrins.[15,19,41]

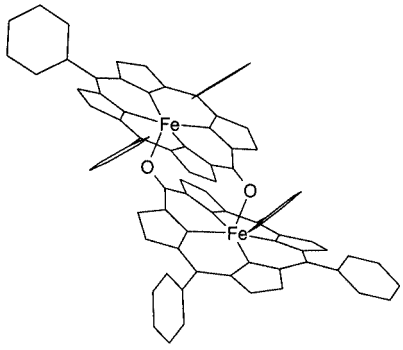

Figure 5. Drawing of the dimer [(5-O-TrPP)Fe^{III}]$_2$ obtained from the molecular mechanics calculations; hydrogen atoms have been omitted for the sake of clarity

The features of the ^{1}H NMR spectra of [(5-O-TrPP)Fe^{III}]$_2$ can be understood in the context of the presence of two high-spin iron(III) ions in the molecule. The 5-hydroxyporphyrin of each monomeric unit is coordinated simultaneously to the internal iron(III) ion through the four nitrogen atoms and to the external one by the 5-oxygen atom. The typical delocalization pathway for high-spin (tetraphenylporphyrin)iron(III) complexes shifts the pyrrole resonances downfield as a result of the dominating σ-contact contribution. Additionally, the π delocalization locates a considerable amount of the spin density at the *meso* positions,[16,31,53−55] and some at the pyrrole positions.[56] The π-spin density at the *meso*-carbon atoms produces sign alternation of the *meso*-phenyl resonances. The dipolar contribution, caused only by the ZFS effect in high-spin (porphyrin)iron complexes, is usually notably smaller than the contact contribution, and this observation has been applied in the further analysis of the hyperfine shifts.[55]

The characteristic features of the internal iron(III) ion influence are exemplified by the ^{1}H NMR spectra of [(5-X-TrPP)Fe^{III}I] (X = NO_2, Br, MeO, H; the choice of I^- as an axial ligand allowed better differentiation of the pyrrole resonances), [(5-OH-TrPP)Fe^{III}Cl], and [(5-AcO-TrPP)-Fe^{III}Cl], where the typical downfield sets of the four pyrrole resonances are found centered around δ = 80 ppm (as shown in traces B and C of Figure 4, and in Table 1). The presence of a second source of spin density in [(5-O-TrPP)Fe^{III}]$_2$, i.e., the external iron(III) ion, changes the hyperfine shifts for the β-H pyrrole protons considerably. Assuming simple additivity of contact contributions by two independent routes, we have estimated that such shifts require a downfield contribution similar to that found for [(5-OH-TrPP)Fe^{III}Cl], hence the upfield shift of ca. −30 ppm for 2(8)-H, −32 ppm for 3(7)-H, and −24 ppm for 12(18)-H. This upfield contribution to the β-H shift results mainly from the σ donation of the electron density of the 5-oxygen donor on the half-occupied d_{z^2} orbital of the iron(III) ion. The anticipated positive spin density on the σ orbital of the oxygen atom will be directly transferred into the π system of the pyrrole ring without any iron(III)−oxygen π bonding, spreading the effect up to the distant pyrrole position [12(18)-H] with respect to the coordinating oxygen atom. The σ orbital of the oxygen atom and the porphyrin π orbitals are not orthogonal, and consequently σ−π overlap permits the direct spin-density transfer.[57,58] We therefore suggest a similar delocalization mechanism to that proposed for [(2-O-TPP)Fe^{III}]$_3$, although with a different location of the external coordinating center.[16]

The linewidths of the β-H pyrrole resonances correlate with their specific locations within the dimeric structure. The dipolar contribution to linewidth broadening is presumed to be proportional to r^{-6}, where r is the distance from the paramagnetic iron(III) center to the proton in question when the ligand-centered dipolar relaxation is insignificant.[59,60] The contribution from the internal iron(III) ion by dipolar and scalar mechanisms has been approximated by the linewidths of the most downfield pyrrole resonance. The markedly larger linewidths of the β-H resonances can be split into two parts: the internal one, which is identical to the most downfield pyrrole position, and the remaining external one {100 Hz [12(18)-H], 350 Hz [2(8)-H], and 1900 Hz [3(7)-H]}. Most likely the external part derives mainly from the dominant dipolar relaxation of the neighboring external iron(III) ion. The respective $Fe_{external}$−β-H distances are estimated from the model to be: 3.5 Å (3/7-H), 5.5 Å (2/8-H), 9 Å (12/18-H), 10 Å (13/17-H). Thus, the pattern of pyrrole linewidths is qualitatively in agreement with the proposed molecular structure.

Table 1. ^{1}H NMR chemical shifts of the pyrrole resonances of *meso*-substituted high-spin (triphenylporphyrin)iron(III) complexes

Compound	δ [ppm][a]
[(5-NO_2-TrPP)Fe^{III}I]	80.0 (2 H), 80.2 (2 H), 84.5 (4 H)
[(5-Br-TrPP)Fe^{III}I]	81.1 (2 H), 82.2 (4 H), 85.3 (2 H)
[(5-MeO-TrPP)Fe^{III}I]	88.2 (2 H), 92.8 (2 H), 93.7 (2 H), 94.5 (2 H)
[(5-OH-TrPP)Fe^{III}Cl]	79.9 (2 H), 80.8 (2 H), 81.7 (2 H), 83.8 (2 H)
[(5-AcO-TrPP)Fe^{III}Cl]	79.4 (2 H), 80.9 (2 H), 81.9 (2 H), 83.5 (2 H)
[(5-O-TrPP)Fe^{III}]$_2$	47.5 (4 H), 49.6 (4 H), 56.3 (4 H), 84.3 (4 H)

[a] Conditions: T = 293 K, $CDCl_3$, 500 MHz or 300 MHz.

Cleavage of [(5-O-TrPP)Fe^{III}]$_2$

Addition of acids in excess to [(5-O-TrPP)Fe^{III}]$_2$ results in the cleavage of the dimer according to Equation (1).

$$[(5\text{-O-TrPP})Fe^{III}]_2 + 2\,HX \rightarrow 2\,[(5\text{-OH-TrPP})Fe^{III}X] \quad (X = Cl, TFA) \qquad (1)$$

Trace B of Figure 4 shows the spectrum of a [(5-O-TrPP)Fe^{III}]$_2$ sample to which gaseous HCl has been added. The spectrum is consistent with the formation of [(5-OH-TrPP)Fe^{III}Cl]. The β-H pyrrole resonances of [(5-O-TrPP)Fe^{III}]$_2$ centered at δ = 50 ppm disappeared. Four new pyrrole resonances were found (δ = 83.8, 81.7, 89.0, 79.9 ppm). They correspond to four pyrrole protons that are inequivalent because of the 5-substitution. The pyrrole resonances of [(5-OH-TrPP)Fe^{III}Cl] have similar linewidths (ca. 600 Hz). The differential broadening of the pyrrole resonances determined for the dimeric molecule is absent. A unique resonance at δ = 25.3 ppm for [(5-OH-TrPP)Fe^{III}Cl] has been assigned to the 5-hydroxy proton {the intensity of this resonance varies in the range 1−2 H depending on preparation, so the formation of [(5-H_2O-TrPP)FeCl]$^+$ remaining in the fast equilibrium with [(5-OH-TrPP)Fe^{III}Cl] seems to be of importance}. When a small amount of $CDCl_3$, saturated with deuterium oxide, was added to the solution of [(5-OH-TrPP)Fe^{III}Cl], the 5-OH resonance diminished in intensity. Addition of base to [(5-OH-TrPP)Fe^{III}Cl] caused its conversion into [(5-O-TrPP)Fe^{III}]$_2$. Actually, such a conversion was detected even when a $CDCl_3$ solution of [(5-OH-TrPP)Fe^{III}Cl] was saturated with water.

[(5-O-TrPP)Fe^{III}]$_2$ was also split with acetic anhydride into (5-acetoxy-10,15,20-triphenylporphyrin)iron(III). The relevant ^{1}H NMR spectrum of the resulting complex, [(5-AcO-TrPP)Fe^{III}Cl] is presented in trace C of Figure 4. The feasible formation of two isomeric forms, one with the carbonyl oxygen atom and the chloride ion on the same side of the porphyrin, and one with these groups on the opposite faces of the porphyrin plane cannot be excluded, although they have not been confirmed by ^{1}H NMR spectroscopy because the respective β-H resonances are not sufficiently resolved.

Cleavage of [(5-O-TrPP)Fe^{III}]$_2$ by Pyridine or Cyanide Anion

In the presence of [D_5]pyridine, [(5-O-TrPP)Fe^{III}]$_2$ undergoes a cleavage to form air-sensitive [(5-O-TrPP)Fe(py)$_2$]. Thus, treatment of a dioxygen-free chloroform solution of the dimeric complex with a 50-fold excess of [D_5]pyridine results in its immediate conversion. The overall pattern of resonances is similar to that generated in the hydroxylation of [(TrPP)Fe^{II}(py)$_2$]. The detected shift differences have been attributed to the solvent effect and/or a different concentration of the pyridine ligand remaining in equilibrium. The ^{1}H NMR spectrum of the [D_5]pyridine solution of [(5-O-TrPP)Fe(py)$_2$] is shown in Figure 6, and the chemical shifts are given in Table 2. Three of the four pyrrole resonances are found in the downfield region of the spectrum, while the other signal is located upfield. Sign alternation of isotropic shifts of *meso*-phenyl protons is also observed, with larger absolute shift values assigned to the 15-Ph position.

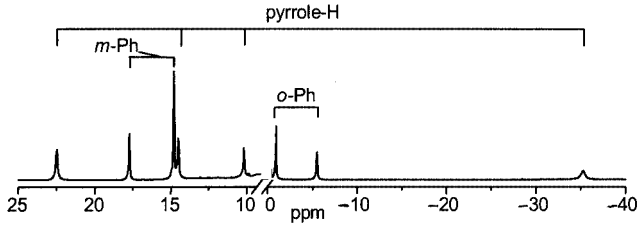

Figure 6. 500 MHz ^{1}H NMR spectrum of [(5-O-TrPP)Fe(py)$_2$] in a [D_5]pyridine solution; resonance assignment: pyrrole-H: pyrrole protons; *o*-Ph, *m*-Ph: *ortho*-, *meta*-phenyl protons

A ^{1}H NMR titration was carried out by addition of trifluoroacetic acid (solution in $CDCl_3$) to a solution of [(5-O-TrPP)Fe(py)$_2$] in [D_5]pyridine. Smooth changes of the chemical shifts in the whole titration range were observed. This fact can be attributed to a gradual protonation of the 5-oxygen atom and a fast proton exchange among two species in the system formed in the conditions of our experiment, as shown in Equation (2).

$$(5\text{-O-TrPP})Fe(py)_2 + H^+ \rightleftarrows [(5\text{-OH-TrPP})Fe^{III}(py)_2]^+ \qquad (2)$$

The direction of shift changes experienced by the pyrrole resonances indicates that protonation of the 5-O atom results in the formation of a low-spin complex [(5-OH-TrPP)Fe^{III}(py)$_2$]$^+$ with the usual $(d_{xy})^2(d_{xz},d_{yz})^3$ electronic ground state. Independently, this complex was observed in the course of [D_5]pyridine titration of [(5-OH-TrPP)Fe^{III}-(TFA)] conducted in $CDCl_3$, and is characterized by four

Table 2. ^{1}H NMR chemical shifts of bis(pyridine) and bis(cyanide) complexes[a]

Compound	δ [ppm] pyrrole-H 2(8)-H	3(7)-H	12(18)-H	13(17)-H	*ortho*-Ph 10(20)-H	15-H	*meta*-Ph 10(20)-H	15-H	*para*-Ph 10(20)-H	15-H	Solvent
[(5-O-TrPP)Fe(py)$_2$]	−35.4	22.6	10.2, 14.6[b]		−0.8	−5.5	14.9	17.8	2.2	−0.3	C_5D_5N
[(5-O-TrPP)Fe(py)$_2$]	−30.2	21.0	13.6, 14.6[b]		−0.7	−4.6	14.6	17.2	[b]	0.1	$CDCl_3$
[(5-O-TrPP)Fe(CN)$_2$]$^{2-}$	−6.0	12.9	8.1, 9.1[b]		2.2	0.2	12.9	13.7	4.1	3.0	CD_3OD
[(5-NO_2-TrPP)Fe^{III}(CN)$_2$]$^-$	−13.9	−9.6	−14.4	−15.1	6.0	4.6	7.3	6.7	6.7	6.3	CD_3OD
[(5-Br-TrPP)Fe^{III}(CN)$_2$]$^-$	−7.5	−6.9	−8.5	−7.9	5.6	5.4	8.2	8.0	6.5	6.4	CD_3OD
[(5-MeO-TrPP)Fe^{III}(CN)$_2$]$^-$ [c]	−6.6	−5.9	−7.0	−7.4	5.5	5.3	8.8	8.6	6.3	6.3	CD_3OD

[a] Conditions: T = 293 K, 500 MHz. Intensities: pyrrole resonances (2 H each); 10(20)-*ortho* and 10(20)-*meta*-Ph (4 H); 15-*ortho*, 15-*meta*, and 10-*para*-Ph (2 H); 15-*para*-Ph (1 H). [b] Not identified. [c] MeO resonance at δ = 2.9 ppm.

upfield pyrrole resonances [δ = −16.8, −19.8, −27.4, −27.8 ppm (293 K)].

In the presence of a large excess of the cyanide ion [(5-O-TrPP)Fe^{III}]$_2$, dissolved in [D_4]methanol, undergoes cleavage to form the air-sensitive [(5-O-TrPP)Fe(CN)$_2$]$^{2-}$. The ^{1}H NMR spectrum of the resulting solution is shown in Figure 7. The overall pattern of resonances with three downfield and one upfield pyrrole resonances [δ = 12.9, 9.1, 8.1, −6.0 ppm (293 K)] is similar to that of [(5-O-TrPP)Fe(py)$_2$]. The sign alternation of the isotropic shifts of the *meso*-phenyl resonances has also been detected. Since only two *ortho* resonances are observed, the axial ligation on both sides of the macrocycle is identical.

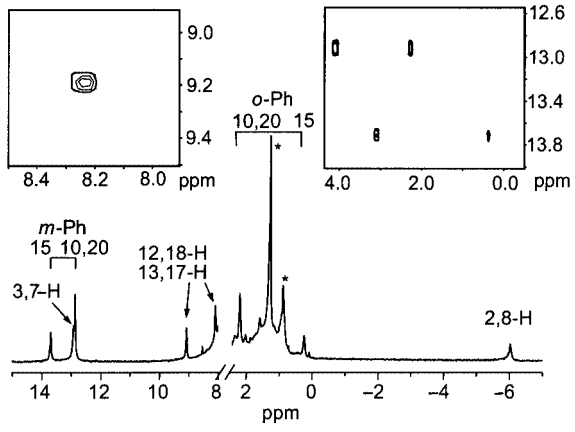

Figure 7. 500 MHz ^{1}H NMR spectrum of [(5-O-TrPP)Fe(CN)$_2$]$^{2-}$ in [D_4]methanol (293 K); the insets show the respective COSY maps; resonance assignments as in Figure 6

The insets in Figure 7 show fragments of a COSY spectrum that was obtained for [(5-O-TrPP)Fe(CN)$_2$]$^{2-}$. The individual *meso*-phenyl groups were identified by the respective cross-peaks between the *ortho*, *meta*, and *para* protons. The cross-peak detected between the pyrrole resonances at δ = 8.1 and 9.1 ppm confirms their location on the same pyrrole ring. Consequently, two other pyrrole resonances are assigned to a second scalar-coupled pair of pyrrole resonances.

The UV/Vis absorption spectrum of [(5-O-TrPP)Fe(CN)$_2$]$^{2-}$ is included in Figure 3. The spectrum displays the Soret band at 427 nm and a broad absorption at 659 nm.

Electronic Structure of [(5-O-TrPP)Fe(py)$_2$] and [(5-O-TrPP)Fe(CN)$_2$]$^{2-}$

Addition of an excess of potassium cyanide to a solution of [(5-X-TrPP)Fe^{III}Cl] in [D_4]methanol results in its conversion into the six-coordinate low-spin complex [(5-X-TPP)Fe^{III}(CN)$_2$]$^-$. The representative ^{1}H NMR spectra for [(5-X-TPP)Fe^{III}(CN)$_2$]$^-$ complexes (the pyrrole region) are shown in Figure 8, and the chemical shift values are gathered in Table 2. The characteristic sets of four upfield-shifted pyrrole resonances assigned by means of 2D NMR experiments have been observed for each compound. These resonances are accompanied by sets of upfield-shifted *ortho* and *para* proton resonances of the *meso*-phenyl groups and downfield shifted *meta* proton signals. The ^{1}H NMR spectra reflect features typical for low-spin (porphyrin)iron(III) complexes.[31,56]

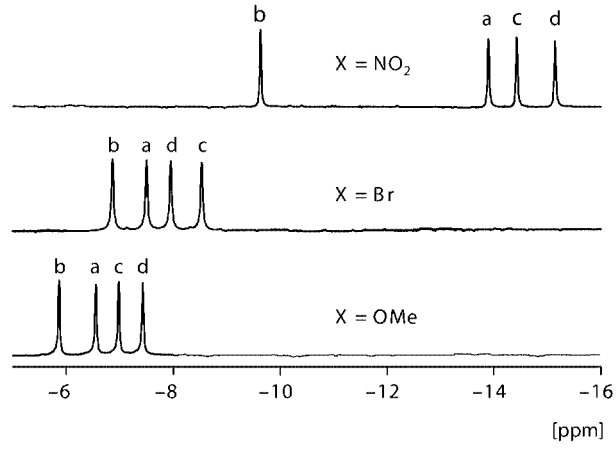

Figure 8. 500 MHz ^{1}H NMR spectra (pyrrole region) of [(5-X-TrPP)Fe^{III}(CN)$_2$]$^-$ complexes (X = NO_2, Br, MeO) in a [D_4]methanol solution at 293 K; resonance assignments follow those of Figure 4

On the contrary, the ^{1}H NMR spectrum of [(5-O-TrPP)Fe(CN)$_2$]$^{2-}$ demonstrates the remarkably different pattern revealing the sign alternation detected for the pyrrole resonances (Figure 7). The overall oxidation level of

[(5-O-TrPP)Fe(py)$_2$] or [(5-O-TrPP)Fe(CN)$_2$]$^{2-}$ is consistent with the resonance structures presented in Scheme 4.[12,21−27,48]

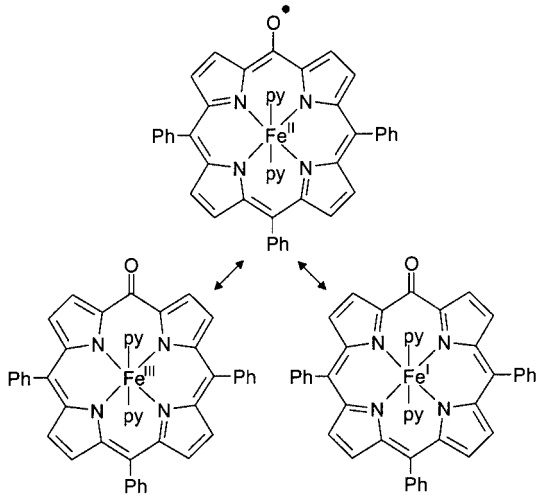

Scheme 4

The new (oxophlorin)iron complexes [(5-O-TrPP)Fe(py)$_2$] and [(5-O-TrPP)Fe(CN)$_2$]$^{2-}$ present ^{1}H NMR spectroscopic patterns that reveal a general similarity to the spectra of [(OEPO)Fe(py)$_2$], [(5-X-OEPO)Fe(py)$_2$], [(OEPO)Fe(CN)$_2$]$^{2-}$, [(Etio-I-PO)Fe(py)$_2$], [(DeuteroPO)Fe(py)$_2$], [(MesoPO)Fe(py)$_2$], and [(ProtoPO)Fe(py)$_2$] (OEPO, 5-X-OEPO, Etio-I-PO, DeuteroPO, MesoPO, and ProtoPO are trianions of oxophlorins obtained from octaethylporphyrin, 5-substituted octaethylporphyrin, etioporphyrin-I, deuteroporphyrin-IX dimethyl ester, mesoporphyrin-IX dimethyl ester, and protoporphyrin-IX dimethyl ester, respectively).[22,26,46]

Based on the chemical shifts measured for the four (deuterooxophlorin)iron isomers [(DeuteroPO)Fe(py)$_2$], the following values are anticipated for (5-oxophlorin)iron or its β-methylated derivative: pyrrole resonances: δ = −33 (2-H), 27 (3-H), 13 (12- and 13-H) ppm; methyl resonances: δ = 65 (2-CH$_3$), −14 (3-CH$_3$) ppm. Substitution of a methyl group by a proton is expected to give rise to a resonance that is subject to a hyperfine shift of opposite sign, but a magnitude similar to that of the corresponding methyl group if π-spin delocalization dominates the hyperfine shifts. Consequently, the pyrrole β-H resonances with the largest hyperfine shifts and the methyl resonances with the most upfield shift must originate from a common site (i.e., from a site with similar value and sign of the spin density) within the molecule as has been well documented for four regioisomers of [(DeuteroPO)Fe(py)$_2$].[26]

The four pyrrole protons of [(5-O-TrPP)Fe(py)$_2$] provide direct probes of the spin density around the oxophlorin macrocycle. In principle, this should allow the determination of the differences in the contact shifts for four pyrrole rings avoiding any differences due to the unsymmetrical substitution effect expected for natural porphyrins. The pyrrole pattern determined for [(5-O-TrPP)Fe(py)$_2$] was found to be very similar to that determined from the rather complex analysis carried out for four (oxophlorin)iron regioisomers obtained from hemes.[26] The relatively large paramagnetic shift of the *meso*-phenyl resonances dominated by the π-contact mechanism reflects the large spin density at the *meso* positions, as found previously for other (oxophlorin)-iron complexes. In conclusion, the spin-density distribution

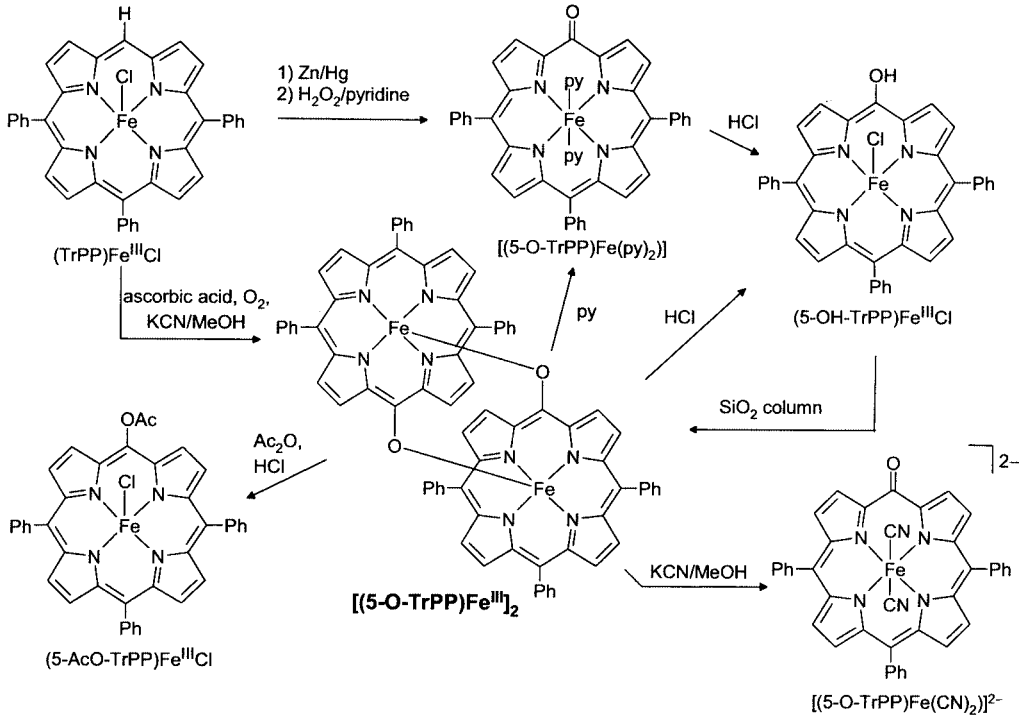

Scheme 5

in the oxophlorin skeleton is dominated by the location of the oxygenated *meso* site and that this functional group imposes a basic twofold electronic symmetry that is only moderately perturbed by the presence of other functional groups.

Conclusion

The synthetic work of this contribution is summarized in Scheme 5. In particular, this work demonstrates considerable parallels in the properties of (10,15,20-triphenyl-5-oxophlorin)iron and (oxophlorin)iron complexes completely substituted at the β-positions. Potentially, an introduction of the *meso*-phenyl groups provides a suitable means for the control and exploration of the properties of this peculiar class of (porphyrin)iron-related systems. The electronic and steric factors can be conveniently adjusted by appropriate substitution of the *meso*-phenyl rings.

Experimental Section

General: ^{1}H NMR spectra were recorded with a Bruker AMX300 and a Bruker Avance 500 spectrometer operating at 300 and 500 MHz, respectively. The residual ^{1}H resonances of the deuterated solvents were used as internal references. Absorption spectra were recorded with a diode-array Hewlett Packard 8453 spectrometer. Mass spectra were recorded with a Finnigan MAT TSQ 700 spectrometer using the ESI technique. Molecular mechanics calculations using the HyperChem software (Autodesk) were carried out and displayed with a Pentium PC. The standard MM+ force field, with the constraints set on the coordination bonds to achieve a high-spin (porphyrin)iron(III) geometry, were used as described in the text. 5,10,15-Triphenylpophyrin ($TrPPH_2$) and 5-bromo-10,15,20-triphenylporphyrin (5-Br$TrPPH_2$) were synthesized as described previously.[35,36,38,45] 5-Nitro-10,15,20-triphenylporphyrin (5-NO_2-$TrPPH_2$) was obtained by nitration of $TrPPH_2$ with $AgNO_2$ in the presence of I_2 by modification of the method applied for nitration of 5,15-diphenylporphyrin.[39]

5-Methoxy-10,15,20-triphenylporphyrin: [(TrPP)Zn^{II}] (40 mg) was dissolved in 50 mL of toluene, and sodium methoxide (1−2 g) was added along with a small amount of methanol. The mixture was refluxed in the presence of air for 6 h and then concentrated to dryness under reduced pressure. The solid residue was extracted with a small volume of CH_2Cl_2, and the dissolved crude product was column-chromatographed on basic alumina with dichloromethane. [(5-MeO-TrPP)Zn^{II}] was eluted as the second band, directly after the unchanged [(TrPP)Zn^{II}]. The zinc complex of 5-methoxy-10,15,20-triphenylporphyrin was demetallated with hydrochloric acid to yield 5-MeO-$TrPPH_2$, which was used without further purification. ^{1}H NMR ($CDCl_3$): δ = −2.70 (s, 2 H, NH), 4.95 (s, 3 H, OCH_3), 7.7 (m, 9 H, *m*,*p*-Ph), 8.2 (m, 6 H, *o*-Ph), 8.76 (d, ^3J = 4.8 Hz, 2 H, H_β), 8.81 (d, ^3J = 4.8 Hz, 2 H, H_β), 8.88 (d, ^3J = 4.8 Hz, 2 H, H_β), 9.53 (d, ^3J = 4.8 Hz, 2 H, H_β) ppm. MS (ESI): *m*/*z* (%) = 569.5 (100) [MH^+].

Iron ion insertion according to a known route yielded the corresponding [(5-X-TrPP)Fe^{III}Cl] complexes.[16,56] Usually, the dicyano-ligated complexes of the investigated (porphyrin)iron(III) complexes were prepared by dissolution of 2−3 mg of the respective high-spin complex in 0.4 mL of [D_4]methanol saturated with KCN.

[Fe^{III}(OEPO)]$_2$: Potassium cyanide (43.7 mg, 0.67 mmol) and ascorbic acid (0.53 g, 3.0 mmol) were dissolved in 50 mL of methanol. [(TrPP)Fe^{III}Cl] (41 mg, 0.065 mmol) was added to the solution, and the reaction mixture was stirred in air for 12−20 h. The resulting solution was concentrated to a volume of 5 mL, diluted with 10 mL of dichloromethane, and washed 2−3 times with water. The organic layer was dried and the solvents were evaporated to dryness. The crude sample was column-chromatographed on silica gel (0.05−0.2 mm/70−270 mesh). The dimeric complex was eluted with an ethanol/dichloromethane mixture (2:98, v/v), and recrystallized from dichloromethane/hexane. Yield: 8 mg (20%). MS (ESI): *m*/*z* (%) = 1215.4 (7) [M^+], 608.3 (100) [(5-OH-TrPP)Fe^{III}]$^+$.

X-ray Crystallographic Study: Crystals of $TrPPH_2$ were grown by slow diffusion of *n*-hexane into a dichloromethane solution of the porphyrin. Diffraction data were collected with a Kuma KM4CCD diffractometer. The data were corrected for Lorentz and polarization effects. No absorption correction was applied. The structure was solved by direct methods (SHELXS-97) and refined by full-matrix least squares (SHELXL-97). All heavy atoms were refined anisotropically and the hydrogen atoms isotropically with no constraints. Crystals of [(5-Br-TrPP)Fe^{III}Cl]·C_6H_6 were obtained by slow concentration of a CH_2Cl_2/benzene solution. The specimen chosen for analysis was twinned but the diffraction patterns of the two domains did not overlap significantly. Data collection was carried out as for $TrPPH_2$. The structure was solved using heavy-atom methods (SHELXS-97) and refined by full-matrix least squares (SHELXL-97). Heavy atoms were refined anisotropically, and the hydrogen atoms by using a riding model. Empirical absorption correction assuming an ellipsoidal crystal was applied using the routine implemented in XPREP.[61] Crystal data and details of the data collection and refinement are presented in Table 3. CCDC-173923 and -173924 contain the supplementary crystallographic data for

Table 3. Crystal data for $TrPPH_2$ and [(5-Br-TrPP)Fe^{III}Cl]·C_6H_6

	$TrPPH_2$	[(5-Br-TrPP)Fe^{III}Cl]·C_6H_6
Empirical formula	$C_{38}H_{26}N_4$	$C_{41}H_{26}N_4BrClFe$
Formula mass	538.63	745.87
a [Å]	6.5811(11)	11.341(2)
b [Å]	18.344(3)	12.994(3)
c [Å]	22.622(4)	13.626(3)
α [°]	90	107.96(3)
β [°]	90	103.66(3)
γ [°]	90	111.34(3)
V [Å^3]	2731.1(8)	1635.9(6)
Z	4	2
$D_{calcd.}$ [g·cm^{-3}]	1.310	1.514
Crystal system	orthorhombic	triclinic
Space group	$P2_12_12_1$	$P\bar{1}$
Crystal size [mm]	0.5 × 0.3 × 0.2	0.2 ×0.15 × 0.1
μ [mm^{-1}]	0.078	1.801
T_{min}, T_{max}	0.962, 0.985	0.728, 0.921
T [K]	100(2)	100(2)
θ range [°]	2.86 ≤ θ ≤ 29.07	2.66 ≤ θ ≤ 28.98
hkl range	−8 ≤ *h* ≤ 5	−11 ≤ *h* ≤ 15
	−24 ≤ *k* ≤ 24	−17 ≤ *k* ≤ 16
	−30 ≤ *l* ≤ 30	−18 ≤ *l* ≤ 18
Reflections measured	18512	12048
unique [$I \geq 2\sigma(I)$]	5117	5734
Parameters/restraints	484/1	433/0
*R*1	0.0685	0.0665
*wR*2	0.1411	0.1512
S	1.068	1.096

this paper. These data can be obtained free of charge at www.ccdc.cam.ac.uk/conts/retrieving.html or from the Cambridge Crystallographic Data Centre, 12, Union Road, Cambridge CB2 1EZ, UK [Fax: (internat.) + 44-1223/336-033; E-mail: deposit@ccdc.cam.ac.uk].

Acknowledgments

Financial support from the State Committee for Scientific Research KBN of Poland (Grant 3 T09A 155 15) and the Foundation for Polish Science is kindly acknowledged.

[1] J. Wojaczyński, L. Latos-Grażyński, *Coord. Chem. Rev.* **2000**, *204*, 113.
[2] T. Imamura, K. Fukushima, *Coord. Chem. Rev.* **2000**, *198*, 133.
[3] A. K. Burrell, D. L. Officer, P. G. Plieger, D. C. W. Reid, *Chem. Rev.* **2001**, *101*, 2751.
[4] G. H. Barnett, M. F. Hudson, S. W. McCombie, K. M. Smith, *J. Chem. Soc., Perkin Trans. 1* **1973**, 691.
[5] R. G. Little, J. A. Anton, P. A. Loach, J. A. Ibers, *J. Heterocycl. Chem.* **1975**, *12*, 343.
[6] H. Callot, *Bull. Soc. Chim. Fr.* **1974**, 1492.
[7] M. J. Crossley, L. G. King, S. M. Pyke, *Tetrahedron* **1987**, *43*, 4569.
[8] H. M. Goff, E. T. Shimomura, Y. J. Lee, W. R. Scheidt, *Inorg. Chem.* **1984**, *23*, 315.
[9] G. M. Godziela, D. Tilotta, H. M. Goff, *Inorg. Chem.* **1986**, *25*, 2142.
[10] N. Masuoka, H. A. Itano, *Biochemistry* **1987**, *26*, 3672.
[11] S. I. Beale, *Chem. Rev.* **1993**, *93*, 785.
[12] A. L. Balch, *Coord. Chem. Rev.* **2000**, *200−202*, 349.
[13] A. L. Balch, L. Latos-Grażyński, B. C. Noll, M. M. Olmstead, E. P. Zovinka, *Inorg. Chem.* **1992**, *31*, 2248.
[14] A. L. Balch, B. C. Noll, S. M. Reid, E. P. Zovinka, *Inorg. Chem.* **1993**, *32*, 2610.
[15] A. L. Balch, B. C. Noll, M. M. Olmstead, S. M. Reid, *J. Chem. Soc., Chem. Commun.* **1993**, 1088.
[16] J. Wojaczyński, L. Latos-Grażyński, *Inorg. Chem.* **1995**, *34*, 1044.
[17] J. Wojaczyński, L. Latos-Grażyński, *Inorg. Chem.* **1995**, *34*, 1054.
[18] J. Wojaczyński, L. Latos-Grażyński, *Inorg. Chem.* **1996**, *35*, 4812.
[19] J. Wojaczyński, L. Latos-Grażyński, M. M. Olmstead, A. L. Balch, *Inorg. Chem.* **1997**, *36*, 4548.
[20] P. S. Clezy, in: *The Porphyrins* (Ed.: D. Dolphin), Academic Press, New York, **1978**, vol. 2, p. 103.
[21] S. Sano, Y. Sugiura, Y. Maeda, S. Ogawa, I. Morishima, *J. Am. Chem. Soc.* **1981**, *103*, 2888.
[22] S. Sano, T. Sano, I. Morishima, Y. Shiro, Y. Maeda, *Proc. Natl. Acad. Sci. U. S. A.* **1986**, *83*, 531.
[23] I. Morishima, H. Fujii, Y. Shiro, S. Sano, *J. Am. Chem. Soc.* **1986**, *108*, 3858.
[24] I. Morishima, H. Fujii, Y. Shiro, S. Sano, *Inorg. Chem.* **1995**, *34*, 1528.
[25] A. L. Balch, R. Koerner, L. Latos-Grażyński, B. C. Noll, *J. Am. Chem. Soc.* **1996**, *118*, 2760.
[26] H. R. Kalish, L. Latos-Grażyński, A. L. Balch, *J. Am. Chem. Soc.* **2000**, *122*, 12478.
[27] T. N. St. Claire, A. L. Balch, *Inorg. Chem.* **1999**, *38*, 684.
[28] T. Yoshida, M. Noguchi, G. Kikuchi, S. Sano, *J. Biochem.* **1981**, *90*, 125.
[29] A. Wilks, P. R. Ortiz de Montellano, *J. Biol. Chem.* **1993**, *268*, 22357.
[30] Y. Liu, P. Moënne-Loccoz, T. M. Loehr, P. R. Ortiz de Montellano, *J. Biol. Chem.* **1997**, *273*, 6909.
[31] F. A. Walker, "Proton NMR and EPR Spectroscopy of Paramagnetic Metalloporphyrins", in: *The Porphyrin Handbook* (Eds.: K. M. Kadish, K. M. Smith, R. Guilard), Academic Press, New York, **2000**, vol. 5, p. 81.
[32] I. Bertini, C. Luchinat, *Coord. Chem. Rev.* **1996**, *150*, 131.
[33] J. S. Lindsey, in: *Metallopophyrins Catalyzed Oxidations* (Eds.: F. Montanari, L. Casella), Kluwer Academic Publishers, Netherlands **1994**, p. 49.
[34] M. O. Senge, X. Feng, *J. Chem. Soc., Perkin Trans. 1* **2000**, 3615.
[35] B. M. L. Chen, A. Tulinsky, *J. Am. Chem. Soc.* **1972**, *94*, 4144.
[36] M. P. Byrn, C. J. Curtis, S. I. Khan, P. A. Sawin, R. Tsurumi, C. E. Strouse, *J. Am. Chem. Soc.* **1990**, *112*, 1865.
[37] B. Sridevi, S. Jeyaprakash Narayanan, T. K. Chandrashekar, U. Englich, K. Ruhlandt-Senge, *Chem. Eur. J.* **2000**, *6*, 2554.
[38] H. J. Callot, E. Schaeffer, *J. Chem. Res. (S)* **1978**, 51; *J. Chem. Res. (M)* **1978**, 0690.
[39] D. P. Arnold, R. C. Bott, H. Eldridge, F. M. Elms, G. Smith, M. Zojaji, *Aust. J. Chem.* **1997**, *50*, 495.
[40] J. L. Hoard, G. H. Cohen, M. D. Glick, *J. Am. Chem. Soc.* **1967**, *89*, 1992.
[41] W. R. Scheidt, Y. J. Lee, *Struct. Bonding* **1987**, *64*, 1.
[42] J. Wojaczyński, L. Latos-Grażyński, T. Gowiak, *Inorg. Chem.* **1997**, *36*, 6299.
[43] K. Susumu, T. Shimidzu, K. Tanaka, H. Segawa, *Tetrahedron Lett.* **1996**, *37*, 8399.
[44] A. Osuka, H. Shmidzu, *Angew. Chem. Int. Ed. Engl.* **1997**, *36*, 135.
[45] J. Wojaczyński, L. Latos-Grażyński, P. J. Chmielewski, P. Van Calcar, A. L. Balch, *Inorg. Chem.* **1999**, *38*, 3040.
[46] H. Kalish, J. E. Camp, M. Stępień, L. Latos-Grażyński, A. L. Balch, *J. Am. Chem. Soc.* **2001**, *123*, 11719.
[47] R. Bonnett, M. J. Dimsdale, *J. Chem. Soc., Perkin Trans. 1* **1972**, 2540.
[48] A. L. Balch, R. Koerner, L. Latos-Grażyński, J. E. Lewis, T. N. St. Claire, E. P. Zovinka, *Inorg. Chem.* **1997**, *36*, 3892.
[49] S. L. Kessel, D. N. Hendrickson, *Inorg. Chem.* **1980**, *19*, 1883.
[50] A. Osuka, K. Maruyama, *J. Am. Chem. Soc.* **1988**, *110*, 4454.
[51] C. K. Chang, *Adv. Chem. Ser.* **1979**, *173*, 162.
[52] C. A. Hunter, J. K. M. Sanders, *J. Am. Chem. Soc.* **1990**, *112*, 5525.
[53] G. N. La Mar, G. R. Eaton, R. H. Holm, F. A. Walker, *J. Am. Chem. Soc.* **1973**, *95*, 63.
[54] R.-J. Cheng, L. Latos-Grażyński, A. L. Balch, *Inorg. Chem.* **1982**, *21*, 2412.
[55] D. V. Behere, R. Birdy, S. Mitra, *Inorg. Chem.* **1982**, *21*, 386.
[56] J. Wojaczyński, L. Latos-Grażyński, W. Hrycyk, E. Pacholska, K. Rachlewicz, L. Szterenberg, *Inorg. Chem.* **1996**, *35*, 6861.
[57] C. Chachaty, P. J. Rigny, *Chem. Phys.* **1982**, *79*, 203.
[58] J. Lisowski, L. Latos-Grażyński, L. Szterenberg, *Inorg. Chem.* **1992**, *31*, 1933.
[59] R. D. Arasasingham, A. L. Balch, C. R. Cornman, J. S. de Ropp, K. Eguchi, G. N. La Mar, *Inorg. Chem.* **1990**, *29*, 1847.
[60] J. Swift, in: *NMR of Paramagnetic Molecules* (Eds.: G. N. La Mar, W. D. Horrocks, Jr., R. H. Holm), Academic Press, New York **1973**, p. 53.
[61] *XPREP*, version 5.1/NT, Bruker Analytical X-ray Systems, **1997**.

Received November 14, 2001
[I01457]

Coordination Chemistry of 2,5,8-Trithia[9],(2,9)-1,10-phenanthrolinophane (L) toward Rhodium(III) at the Polarised Water/1,2-Dichloroethane Interface − A Possible New Approach to the Problem of Separating Rh^{III} from Chloride Media

Alexander J. Blake,[a] M. Helena M. Caçote,[b] Francesco A. Devillanova,[c] Alessandra Garau,[c] Francesco Isaia,[c] Vito Lippolis,*[c] Carlos M. Pereira,[b] Fernando Silva,[b] and Lorenzo Tei[c]

Keywords: Rhodium / Macrocyclic ligands / Interfaces / Cyclic voltammetry

The coordination chemistry involved in the assisted transfer of Rh^{III} by interfacial coordination with 2,5,8-trithia[9],(2,9)-1,10-phenanthrolinophane (L) has been studied at the water/1,2-dichloroethane interface by cyclic voltammetry. The dependence of the half-wave transfer potential on the ligand and metal concentrations suggests the $[Rh(L)Cl_2]^+$ formulation for the complex cation involved in the assisted transfer. In contrast, from the reaction of L in refluxing MeCN/water solution the $[Rh(L)Cl][BF_4]_2 \cdot 2MeCN$ compound has been isolated and structurally characterised. In the $[Rh(L)Cl]^{2+}$ complex cation L acts as an N_2S_3 donor encapsulating the metal centre within a cavity having a square-based pyramidal geometry. A chloride ligand completes the distorted octahedral coordination sphere around the Rh^{III} ion.
(© Wiley-VCH Verlag GmbH, 69451 Weinheim, Germany, 2002)

Introduction

The quest for new macrocyclic ligands capable of specific and effective molecular recognition of metal ions in carrier-assisted membranes or solid-state ion-selective electrodes is a topic of current interest.[1,2] Attention has mainly been focussed on the assisted transfer of group I and group II ions between two immiscible electrolyte solutions; different crown ether derivatives have been used as neutral carriers for the construction of ion-selective electrodes and for performing selective separations.[1−4] A smaller number of studies have been performed with transition and heavy metal ions, particularly precious metal ions, probably because of their greater inertness.[5,6] However, the recovery and removal of precious metals from aqueous solutions is of considerable economic and environmental concern. In particular, the separation and purification of rhodium from other platinum group metals in aqueous chloride solutions is made difficult by the complex chemistry that Rh^{III} exhibits in these media, which are largely employed because platinum group metals are usefully soluble in them. Mixed aquachloro complexes of the type $[RhCl_{6-n}(H_2O)_n]^{n-3}$ ($0 < n < 6$) are formed in different proportions depending primarily on the chloride concentration.[7] These species are highly hydrophilic and not easily isolated by direct solvent extraction. Some reagents such as $SnBr_2$, $SnCl_2$,[8,9] or SCN^- [10] can be used to enhance the extractability of the metal by forming Rh^{III} complexes with better solvent extraction properties, but once the metal is in the organic phase, the stripping process is not that easy. Despite these difficulties, the separation of Rh^{III} has been carried out by using different techniques such as solvent extraction,[11] ion exchange[9,12] and liquid membrane separation,[13−16] and particular attention is paid to research in this area is very guarded. Recently we have reported the synthesis of new mixed aza-thioether crowns containing the 1,10-phenanthroline (phen) unit as an integral part of the macrocyclic structure.[17−19] These ligands have shown a great affinity for heavier transition metal ions such as Pd^{II}, Pt^{II} and Rh^{III}, with coordination properties strictly dependent upon the conformational constraints imposed by the heteroaromatic moiety on the S-donor thioether linker of the ring. Herein we report a study by cyclic voltammetry of the assisted transfer of Rh^{III} by interfacial complexation with 2,5,8-trithia[9],(2,9)-1,10-phenanthrolinophane (L) at the polarised water/1,2-dichloroethane interface. The principal target of this work has been to study the coordination chemistry of L towards Rh^{III} at the water/1,2-dichloroethane junction; however, the results obtained could represent a useful start-

[a] School of Chemistry, The University of Nottingham, Nottingham, NG7 2RD, UK
[b] Departamento de Química, Universidade do Porto, Faculdade de Ciências do Porto, R. Campo Alegre 687, 4169−007 Porto, Portugal
[c] Dipartimento di Chimica Inorganica ed Analitica, Complesso Universitario di Monserrato, SS 554 Bivio per Sestu, 09042 Monserrato (CA), Italy

ing point for a novel way of approaching the problem of Rh^{III} separation and purification from aqueous solutions.

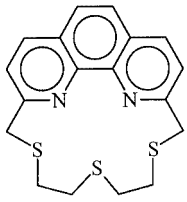

L

Results and Discussion

We reported previously[18] the reaction of L with $RhCl_3$ in refluxing MeCN/water to afford a yellow microcrystalline powder after addition of an excess of NH_4PF_6. The resulting complex was formulated as $[Rh(L)Cl][PF_6]_2 \cdot MeCN$ on the basis of elemental analysis data and IR and FAB mass spectrometry. ^{13}C NMR spectroscopic measurements in CD_3CN confirmed this formulation and indicated an octahedral stereochemistry at the Rh^{III} centre similar to that observed around Ni^{II} in $[Ni(L)Cl]^+$,[19] with all the five donor atoms of the macrocyclic ligand strongly coordinated and with a chloride completing the octahedral environment. After many attempts we have been able to grow crystals of $[Rh(L)Cl][BF_4]_2 \cdot 2MeCN$ suitable for X-ray diffraction studies by diffusion of Et_2O vapour into a MeCN solution of the complex. The structure determination confirms the rhodium(III) ion to be bound to the pentadentate macrocycle through two N-donors of the phen unit [Rh(1)−N: 2.001(3) and 1.996(3) Å] and three thioether S-donors of the thioether linker of the ligand [Rh(1)−S: 2.3361(9), 2.3219(9) (*trans* to phen) and 2.3033(9) Å (*trans* to Cl)] (Figure 1, Table 1). The octahedral coordination sphere is completed by a Cl^- ion [Rh(1)−Cl(1): 2.3456(8) Å]. The phenanthroline moiety and the two adjacent sulfur atoms S(1) and S(2) of the thioether linker lie approximately in an equatorial plane of the octahedron, with the third sulfur atom S(3) and the Cl^- ligand occupying the two apical positions [S(3)−Rh(1)−Cl(1): 178.10(3)°]. This structure demonstrates the ability of L to host the Rh^{III} ion within its ring cavity without any particular constraint of the organic framework; therefore, L is a possible candidate as a sequestering agent for the recovery of this precious metal ion from aqueous solutions.

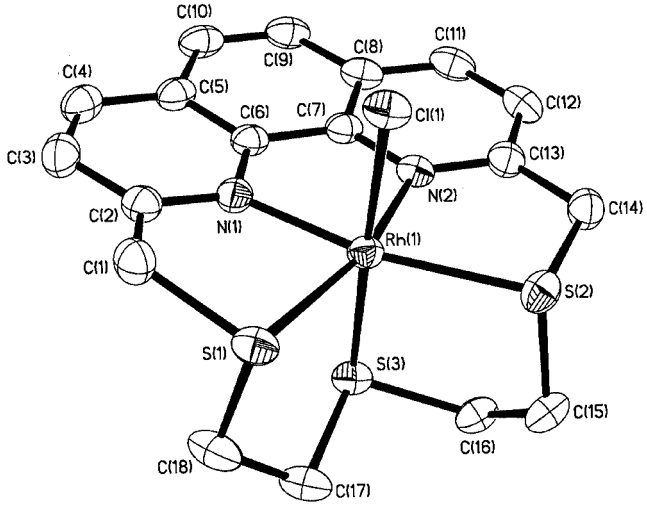

Figure 1. View of the $[Rh(L)Cl]^{2+}$ cation with the numbering scheme adopted; displacement ellipsoids are drawn at the 50% probability level and hydrogen atoms have been omitted for clarity

Table 1. Selected bond lengths (Å) and angles (°) for $[Rh(L)Cl][BF_4]_2 \cdot 2MeCN$

Rh(1)−Cl(1) 2.3456(8)	Rh(1)−S(1) 2.3361(9)
Rh(1)−S(2) 2.3219(9)	Rh(1)−S(3) 2.3033(9)
Rh(1)−N(1) 2.001(3)	Rh(1)−N(2) 1.996(3)
N(1)−Rh(1)−N(2) 82.35(11)	N(1)−Rh(1)−S(1) 82.62(8)
N(1)−Rh(1)−S(2) 166.43(8)	N(1)−Rh(1)−S(3) 92.74(8)
N(1)−Rh(1)−Cl(1) 89.16(8)	N(2)−Rh(1)−S(1) 164.88(8)
N(2)−Rh(1)−S(2) 84.36(8)	N(2)−Rh(1)−S(3) 89.80(3)
N(2)−Rh(1)−Cl(1) 90.31(8)	S(1)−Rh(1)−S(2) 110.72(3)
S(1)−Rh(1)−S(3) 89.27(3)	S(1)−Rh(1)−Cl(1) 91.12(3)
S(2)−Rh(1)−S(3) 89.94(3)	S(2)−Rh(1)−Cl(1) 88.18(3)
S(3)−Rh(1)−Cl(1) 178.10(3)	

In order to test the ability of L to assist the electrochemical extraction of Rh^{III} at the water/1,2-dichloroethane (1,2-DCE) polarised interface, we have made preliminary studies by cyclic voltammetry (CV) with an electrochemical cell as shown schematically below (Cell 1).

Cell 1

Ag	AgCl	NaCl (10 mM) NaTPB (10 mM) (H_2O)	L (0.025 mM) TOATPB (10 mM) (1,2-DCE)	$RhCl_3$ (2.8 mM) LiCl (10 mM) (H_2O)	AgCl	Ag

This type of cell has already been successfully employed to study the transfer of Cu^{II} assisted by 6,7-dimethyl-2,3-di(2-pyridyl)quinoxaline (DMDPQ),[20] and the transfer of Zn^{II}, Cd^{II} and Pb^{II} assisted by cyclic thioether ligands.[21] Previous work by Homolka,[22] Matsuda,[23] Kakiuchi and Senda,[24] and Reymond et al.[25,26] has provided a theoretical framework for the determination of parameters such as the complex stoichiometry involved in the transfer process. In the absence of L, there is no visible wave in the cyclic voltammogram within the potential window available, demonstrating the absence of any transfer process of Rh^{III} across the organic phase under these conditions (Figure 2a, dashed line). When the ligand L is present in the organic phase, the CV responses exhibit a well-defined single reversible wave (Figure 2a, full line) related to the transfer of an ionic species with $\Delta_o^w\phi_{1/2} = 30$ mV and a peak-to-peak separation of 60 mV; this is consistent with the assisted transfer of Rh^{III} by L across the water/1,2-dichloroethane interface. Measurement of the pH of the aqueous solution containing $RhCl_3$ (electrodic compartment on the right in cell 1) showed that the medium was acidic due to the hydrolysis of

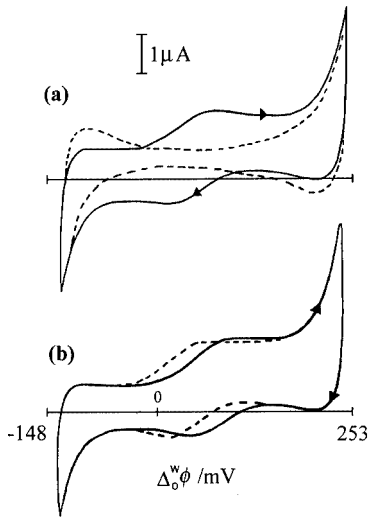

Figure 2. (a) Voltammetric responses in the absence (dashed line) and in the presence (full line) of L in the organic phase for the cell 1 system; (b) voltammetric responses for the cell 1 system in the case of acidic aqueous phase (dashed line) and neutralised aqueous phase by addition of LiOH (full line)

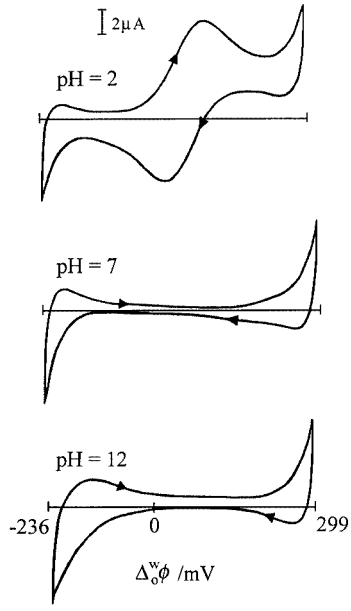

Figure 3. Voltammetric responses for the cell 2 system showing the effect of pH on the assisted transfer of H^+ by L across the water/1,2-DCE interface

Cell 2

X = HCl 10 mM (pH = 2); X = LiCl 10 mM (pH = 7); X = LiOH 10 mM + LiCl 10 mM (pH = 12)

Ag	AgCl	NaCl (10 mM) NaTPB (10 mM) (H_2O)	L (0.3 mM) TOATPB (10 mM) (1,2-DCE)		X (H_2O)	AgCl	Ag

Rh^{III} aquo/chloro complexes[7] and therefore the assisted transfer of H^+ by the ligand could also occur under these experimental conditions. The peak observed could then indicate either the facilitated transfer of the proton or the Rh^{III} ion by the ligand. In order to identify clearly the transfer of Rh^{III} assisted by L, LiOH was then added to the acidic aqueous phase containing Rh^{III} in order to neutralise it. The cyclic voltammogram recorded under neutral conditions resembles that obtained when the aqueous phase is acidic, with a single reversible wave observed at a slightly more positive $\Delta_o^w\phi_{1/2}$ (65 mV) with a peak-to-peak separation of 60 mV (Figure 2b).

We also decided to study the protonated ligand transfer across the water/1,2-DCE interface upon changing the pH of the aqueous phase. Figure 3 includes the voltammograms observed when the pH of the aqueous solution (electrodic compartment on the right in cell 2) changes from 2 to 12.

While a single well-defined peak appears in the voltammogram at pH 2, no transfer processes are observed at pH 7 and 12, indicating that the proton transfer facilitated by L across the water/1,2-DCE interface occurs only when acidic solutions are used. From the transfer potential at different pH of the aqueous phase, obtained by cyclic voltammetry using cell 2, an ionic partition diagram of the ligand was constructed as described by Reymond et al.[27] (Figure 4a). This diagram can be used to predict qualitatively the influence of the variation of the Galvani potential difference ($\Delta_o^w\phi_{1/2}$) and/or aqueous pH on the nature of the transferring species present at the water/1,2-DCE interface. Furthermore, the behaviour of the peak current on changing the pH of the aqueous phase in cell 2 (Figure 4b) allowed the assessment of the acidic constant (pK_a) in water for the ligand L, the value of which was estimated to be 4.3. This value is lower than those reported for 1,10-phenanthroline (pK_a = 4.97)[28] and 2,9-dimethyl-1,10-phenanthroline (pK_a = 5.85)[29] as determined potentiometrically in water solution. A direct pH-potentiometric determination of the pK_a of L was not possible because of the very low solubility of the ligand in water.

From these results it can be concluded that the rhodium(III)-assisted transfer by L at a polarised water/1,2-DCE interface is possible and that pH control of the aqueous phase is necessary to study the process.

The evaluation of the charge and stoichiometry of the complex involved in the transfer was carried out by studying the voltammetric behaviour of the transfer under neutral pH conditions for the aqueous phase, in the presence of excess metal with respect to the ligand in the organic phase. Cell 3 was used to carry out these studies: bis(triphenylphosphoranylidene)ammonium tetrakis(4-chlorophenyl)borate (BTPPATPBCl) was used as the organic electrolyte salt because it allows a larger potential window (and it has no effect on the voltammetric signal).

Figure 5a shows the change in mid-peak potential ($\Delta_o^w\phi_{1/2}$) when the concentration of excess metal is varied. From the slope of the line (-58 ± 6 mV) a charge of +1 for the complex is deduced.[20] The peak current (i_{pc}) is independent of the concentration of the metal. The effect on $\Delta_o^w\phi_{1/2}$ of the change of the concentration of the ligand (in the organic phase) in the presence of excess metal (in the aqueous phase) has also been monitored in order to

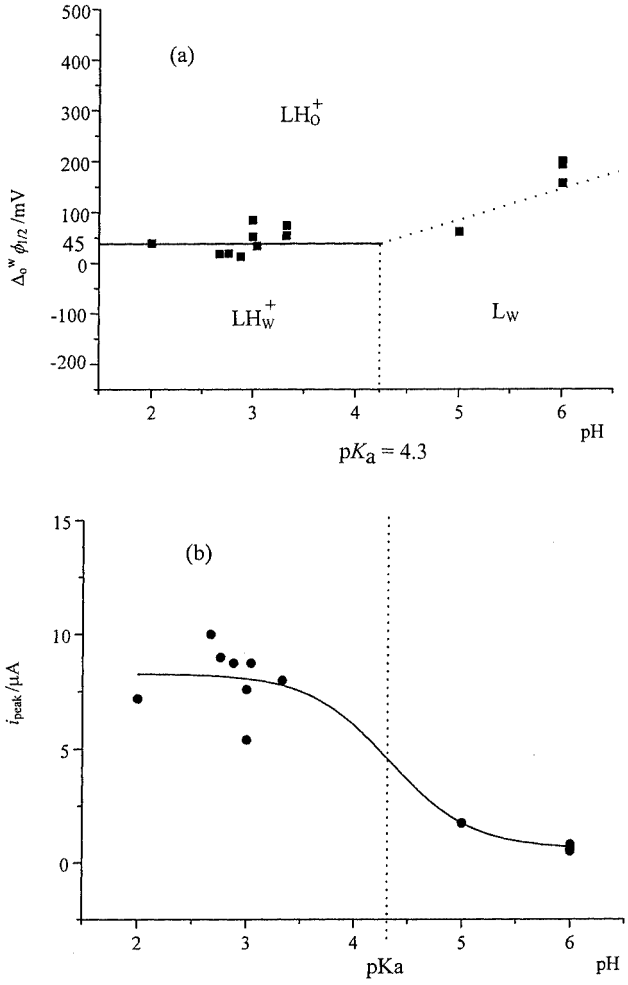

Figure 4. (a) Ionic partition diagram of L at room temperature; (b) change of the peak current upon variation of the pH of the aqueous phase in cell 2

Cell 3

Ag	AgCl	10 mM LiCl 1 mM BTPPACl (H_2O)	L 10 mM BTPPATPBCl (1,2-DCE)	$RhCl_3$ LiOH 10 mM LiCl (H_2O)	AgCl	Ag

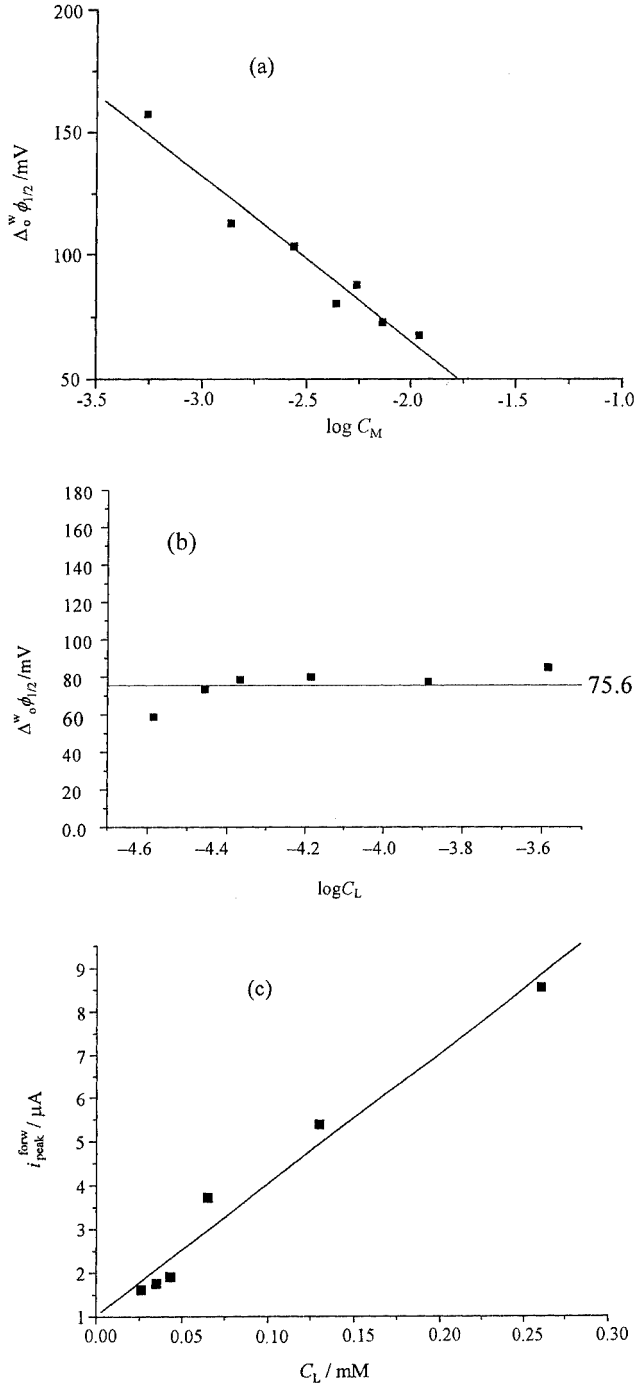

Figure 5. (a) Change in mid-peak transfer potential ($\Delta_o^w\phi_{1/2}$) when the concentration of excess metal in the aqueous phase is varied (log $C_L = -4$); (b) effect on $\Delta_o^w\phi_{1/2}$ of the change of the concentration of L in the organic phase in the presence of excess metal in the aqueous phase (log $C_M = -2.3$); (c) current forward peak intensity vs. the log of ligand concentration (C_L) (log $C_M = -2.3$, slope = 30 μA/mM); the system cell considered is cell 3

evaluate the stoichiometry of the complex.[20] Since there is no dependence of the half-wave transfer potential on log C_L (Figure 5b), according to Reymond et al.,[25,26] the stoichiometry of the complex must be 1:1. From the variation of the peak current intensity on changing the concentration of L on excess metal ion concentration (Figure 5c), and using the modified Randles−Sevcik expression,[26] it was possible to estimate the diffusion coefficient of the ligand in the organic phase (in fact, due to the metal excess, the current is limited by the diffusion of the ligand): $D_o = 5.1 \times 10^{-6}$ cm^2/s. This value is in good agreement with those reported in the literature for 1,10-phenanthroline (phen) and its bulky derivatives in 1,2-dichloroethane (D_o[phen] = 9.6×10^{-6}, D_o[4,7-diphenyl-phen] = 4.8×10^{-6} cm^2/s).[30]

As already pointed out, the studies reported so far have been conducted by cyclic voltammetry in cell 3, varying either the metal or the ligand concentration but keeping the metal-ion concentration in excess. If excess ligand is used and the metal concentration is varied, another voltammetric signal appears when $C_L > C_M$ (Figure 6), which can be assigned to the assisted transfer of a 1:2 Rh/L complex.

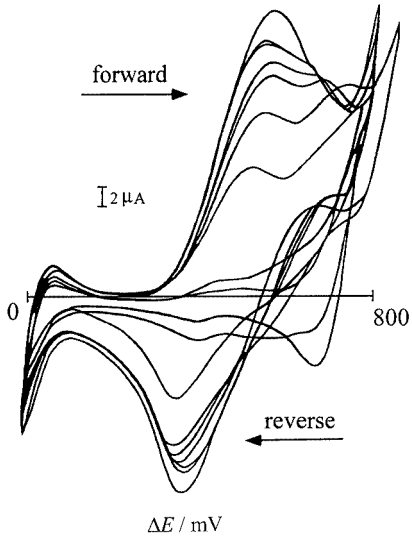

Figure 6. Cyclic voltammograms obtained for the Rh^{III} transfer assisted by L (C_L = 1.30 mM) for different metal concentrations (C_M ranging from 0.05 to 9.70 mM)

The plot of forward peak current (i_{pc}) vs. C_M for the voltammograms in Figure 6 clearly demonstrates the presence of a transition point between two limiting diffusion regimes (Figure 7). However, a study similar to that performed for the transfer of the 1:1 complex was not possible due to the poor definition of the two voltammetric signals.

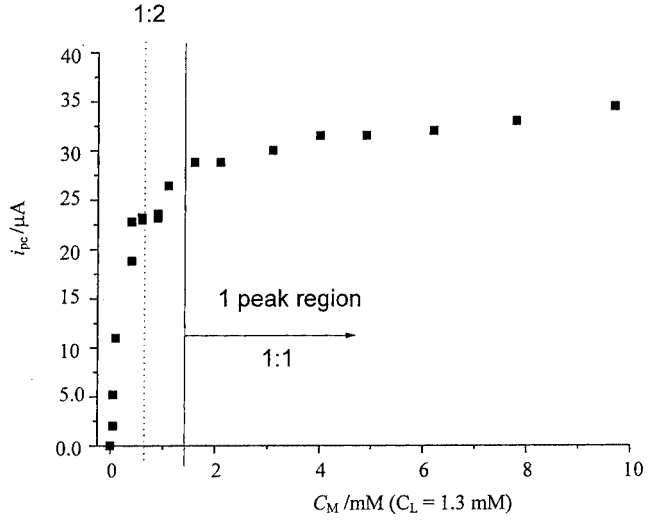

Figure 7. Plot of the forward peak current vs. C_M for the results in Figure 6

The 1:1 complex involved in the assisted transfer seems to have the formulation $[Rh(L)Cl_2]^+$. An analogous stoichiometry has been observed for the Rh^{III} complex with a structural analogue of L where S(3) (Figure 1) has been replaced by an oxygen atom. In this case, it has been shown by NMR spectroscopy that the O-donor of the ligand is not able to coordinate the octahedral metal centre and that the two chloride ligands are mutually *trans*.[31]

The unassisted transfer of Rh^{III} as $RhCl_2^+$ occurs at $\Delta_o^w\phi^{0'}$ $[RhCl_2]^+$ = 514 mV and was determined by applying the methodology proposed by Shao et al.[32] for determining the half-wave potential of the species limiting the potential window. The value of K_f^0, corresponding to the complexation of one $[RhCl_2]^+$ ion with one molecule of L, can therefore be estimated from the dependence of $\Delta_o^w\phi_{1/2}$ on the metal concentration (Figure 5a) using the methodology proposed by Reymond et al.,[26] which in the case of a metal ion excess is:

$$\Delta_o^w\phi_{1/2,ML_j^{z+}} = \Delta_o^w\phi^{0'}_{M^{z+}} - \frac{2.303RT}{zF}\log\left(\sum_{j=0}^{m} j\beta_j^0 C_{M_{init}}\left(\frac{C_{L_{init}}}{2}\right)^{j-1}\right)$$

For the case of a 1:1 complex between the $[RhCl_2]^+$ ion and L this expression can be rewritten as:

$$\Delta_o^w\phi_{1/2,ML^{z+}} = \Delta_o^w\phi^{0'}_{M^{z+}} - \frac{2.303RT}{zF}\log\left(\beta^0 C_{M_{init}}\right)$$

where j is the number of ligands in the complex, z the charge of the complex species involved in the assisted transfer, $\Delta_o^w\phi_{1/2,ML^{z+}_j}$ the half-wave Galvani potential for the transfer of the complex ML_j^{Z+}, $\Delta_o^w\phi^{0'}{}_M{}^{z+}$ the formal Galvani transfer potential for the metal ion, β_j^0 the stability constant for the complex ML_j^{z+}, and $C_{M_{init}}$, and $C_{L_{init}}$ the initial concentrations of metal ion and ligand, respectively. Taking $\Delta_o^w\phi^{0'}$ $[RhCl_2]^+$ to be 514 mV and using the intercept of Figure 5a (−69.7 mV), the value calculated for the formation constant of $[Rh(L)Cl_2]^+$ is $\log K_f^0$ = 9.7. This value, when compared with those obtained by cyclic voltammetry at the water/1,2-DCE interface for some 1:3 metal-phenanthroline complexes {$\log\beta_3^0$ $[Ca(phen)_3]^{2+}$ = 15.8, $\log\beta_3^0$ $[Sr(phen)_3]^{2+}$ =14.0},[33] clearly shows that, despite its steric hindrance, the thiacrown ring in L has an overall stabilising effect (in comparison with complexes having higher stoichiometries). This should be due to the donor properties of the S-donors in the ring.

Conclusions

The assisted transfer of Rh^{III} ion with 2,5,8-trithia[9],(2,9)-1,10-phenanthrolinophane (L) at the water/1,2-DCE interface has been demonstrated, thus pointing towards a new approach to the problem of separating Rh^{III} from chloride media. The nature of the Rh^{III} complex involved in the assisted transfer has been elucidated by cyclic voltammetry and it corresponds to the formulation $[Rh(L)Cl_2]^+$. This complex cation is different from that obtained by refluxing L with $RhCl_3$ in MeCN/water solution, which has the formulation $[Rh(L)Cl]^{2+}$, and has the same stoichiometry as the Rh^{III} complex obtained with a structural analogue of L having an O-donor instead of the S(3) atom.

Experimental Section

General Procedures and Chemicals: Cyclic voltammetry was performed using a four-electrode potentiostat (Solartron 1287) with ohmic drop compensation. The electrochemical cell was made from borosilicate glass and was of the same design as used previously;[21] with two Luggin reference probes and a geometrical area for the water/1,2-DCE interface of 0.22 cm^2. All the measurements were carried out at laboratory temperature (20 ± 3 °C), with scan rates ranging from 10 to 100 mV/s. For each experiment the addition of a fixed amount of ClO_4^- ($LiClO_4$ > 99.99% purity from Aldrich) provided a reference for all half-wave potential measurements The values measured were easily transposed to the Galvani potential scale taking into account the following relationship
$E_{1/2} - \Delta_o^w\phi^0 = E_{1/2}(ClO_4^-) - \Delta_o^w\phi^0(ClO_4^-)$
and the value of the transfer potential of perchlorate ion [$\Delta_o^w\phi^0(ClO_4^-) = -176$ mV].[34]

The organic electrolyte salts used in this study were tetraoctylammonium tetrakis(phenyl)borate (TOATPB), prepared as reported previously,[35] and bis(triphenylphosphoranylidene)ammonium tetrakis(4-chlorophenyl)borate (BTPPATPBCl), which was prepared by the metathesis of BTPPACl (Aldrich) and KTPBCl (Fluka). Rhodium(III) unassisted transfer in the absence of L was studied using 10 mM BTPPATPBCl as the supporting electrolyte in the organic phase. 2,5,8-Trithia[9],(2,9)-1,10-phenanthrolinophane (L) was synthesised according to the literature.[17] LiCl (>99% purity) and $RhCl_3 \cdot 3H_2O$ (38% Rh) were obtained from Merck. Aqueous solutions were prepared with purified water from Milli Q 185 system (Millipore). 1,2-Dichloroethane (1,2-DCE) (>99.5% purity, Merck) was used without further purification and was handled with all necessary precautions.

Crystal Structure Determination: Crystal data for $C_{22}H_{24}B_2ClF_8N_4RhS_3$, M = 752.61, orthorhombic, *Pccn*, a = 14.2317(13), b = 31.974(3), c = 12.4458(11) Å, V = 5663.4(9) $Å^3$, Mo-K_α radiation λ = 0.71073 Å, Z = 8, $D_{calcd.}$ = 1.765 g cm^{-3}, $F(000)$ = 3008. T = 150(2) K, μ(Mo-K_α) = 0.994 mm^{-1}. Yellow plate, 0.21 × 0.16 × 0.12 mm^3. Bruker SMART1000 CCD area detector diffractometer with Oxford Cryosystems open-flow cryostat,[36] ω scans, 6808 absorption-corrected reflections (SADABS,[37] T = 0.80−1.00), 5132 reflections with $I > 2\sigma(I)$. The structure was solved by direct methods using SHELXS-97[38] and full-matrix least-squares refinement on F^2 was performed using SHELXL-97.[39] All non-H atoms were refined anisotropically and H atoms were placed geometrically and thereafter allowed to ride on their parent atoms. One of the two BF_4^- anions exhibited disorder and the refinement was accomplished with restraints to the B−F distances and F−B−F angles, and to the total occupancy of the F atoms.
CCDC-175177 contains the supplementary crystallographic data for this paper. These data can be obtained free of charge at www.ccdc.cam.ac.uk/conts/retrieving.html [or from the Cambridge Crystallographic Data Centre, 12, Union Road, Cambridge CB2 1EZ, UK; Fax: (internat.) +44-1223/336-033; E-mail: deposit@ccdc.cam.ac.uk].

Acknowledgments

The authors wish to thank Dr. Pietro A. Vigato (Istituto di Chimica e Tecnologie Inorganiche e dei Materiali Avanzati, CNR, Padova, Italy) since without his contribution the realisation of this work would not have been possible. M. H. M. Caçote is grateful to Fundação para a Ciência e Tecnologia for a PRAXIS XXI Ph.D. grant. Work was carried out under INOVELREC − EU contract no. BRPR-CT95−010. L. Tei is grateful to the University of Cagliari for financial support.

[1] *Macrocyclic Compounds in Analytical Chemistry* (Ed.: Y. A. Zolotov), John Wiley & Sons, Inc.: New York, **1997**.
[2] K. Kimura, T. Shono, in *Cation Binding by Macrocycles* (Eds.: Y. Inoue, G. W. Gokel), Marcel Dekker: New York, **1990**.
[3] J. S. Bradshaw, R. M. Izatt, *Acc. Chem. Res.* **1997**, *30*, 338−345.
[4] P. Buhlmann, E. Pretsch, E. Bakker, *Chem. Rev.* **1998**, *98*, 1593−1687.
[5] A. T. Yordanov, D. M. Roundhill, *Coord. Chem. Rev.* **1998**, *170*, 93−124.
[6] G. Khayatian, M. Shamsipur, *Sep. Purif. Technol.* **1999**, *16*, 235−241.
[7] E. Benguerel, G. P. Demopoulos, G. B. Harris, *Hydrometallurgy* **1996**, *40*, 135−152.
[8] M. S. Alam, K. Inoue, *Hydrometallurgy* **1997**, *46*, 373−382.
[9] M. S. Alam, K. Inoue, K. Yoshizuka, *Hydrometallurgy* **1998**, *49*, 213−227.
[10] S. J. Al-Bazi, A. Chow, *Anal. Chem.* **1981**, *53*, 1073−1076.
[11] H. Imura, H. Takahashi, N. Suzuki, *Bull. Chem. Soc. Jpn.* **1991**, *64*, 882−887.
[12] X. Chang, X. Luo, G. Zhan, Z. Su, *Talanta* **1992**, *39*, 937−941.
[13] S. N. Ashrafizadeh, G. P. Demopoulos, *Sep. Sci. Technol.* **1996**, *31*, 895−914.
[14] S. N. Ashrafizadeh, G. P. Demopoulos, *J. Chem. Tech. Biotechnol.* **1996**, *67*, 367−375.
[15] C. Fontàs, E. Anticò, V. Salvadò, M. Valiente, M. Hildago, *Anal. Chim. Acta* **1997**, *346*, 199−206.
[16] C. Fontàs, C. Palet, V. Salvadò, M. Hildago, *J. Membrane. Sci.* **2000**, *178*, 131−139.
[17] A. J. Blake, F. Demartin, F. A. Devillanova, A. Garau, F. Isaia, V. Lippolis, M. Schröder, G. Verani, *J. Chem. Soc., Dalton Trans.* **1996**, 3705−3712.
[18] F. Contu, F. Demartin, F. A. Devillanova, A. Garau, F. Isaia, V. Lippolis, A. Salis, G. Verani, *J. Chem. Soc., Dalton Trans.* **1997**, 4401−4405.
[19] A. J. Blake, J. Casabò, F. A. Devillanova, L. Escriche, A. Garau, F. Isaia, V. Lippolis, R. Kivekas, V. Muns, M. Schröder, R. Sillampää, G. Verani, *J. Chem. Soc., Dalton Trans.* **1999**, 1085−1092.
[20] L. Tomaszewski, Z. Ding, D. J. Fermin, H. M. Caçote, C. M. Pereira, F. Silva, H. H. Girault, *J. Electroanal. Chem.* **1998**, *453*, 171−177.
[21] G. Lagger, L. Tomaszewski, M. D. Osborne, B. J. Seddon, H. H. Girault, *J. Electroanal. Chem.* **1998**, *451*, 29−37.
[22] D. Homolka, K. Holub, V. Marecek, *J. Electroanal. Chem.* **1982**, *138*, 29−36.
[23] H. Matsuda, Y. Yamada, K. Kanamori, Y. Kudo, Y. Takeda, *Bull. Chem. Soc. Jpn.* **1991**, *64*, 1497−1508.
[24] T. Kakiuchi, M. Senda, *J. Electroanal. Chem.* **1991**, *300*, 431−445.
[25] F. Reymond, P. A. Carrupt, H. H. Girault, *J. Electroanal. Chem.* **1998**, *449*, 49−65.
[26] F. Reymond, G. Lagger, P. A. Carrupt, H. H. Girault, *J. Electroanal. Chem.* **1998**, *451*, 59−76.
[27] F. Reymond, G. Steyaert, P. Carrupt, B. Testa, H. H. Girault, *J. Am. Chem. Soc.* **1996**, *118*, 11951−11957.
[28] P. Daniele, C. Rigano, *Talanta* **1985**, *32*, 78−80.
[29] H. Irving, D. Mellor, *J. Chem. Soc.* **1962**, 5222−5237.
[30] Z. Yoshida, H. Freiser, *J. Electroanal. Chem.* **1984**, *162*, 307−319.
[31] M. Arca, A. J. Blake, J. Casabo, F. Demartin, F. A. Devillanova, A. Garau, F. Isaia, V. Lippolis, R. Kivekas, V. Muns, M. Schroder, G. Verani, *J. Chem. Soc., Dalton Trans.* **2001**, 1180−1188.

[32] Y. Shao, A. A. Stewart, H. H. Girault, *J. Chem. Soc., Faraday Trans.* **1991**, *87*, 2593−2597.
[33] S. A. Dassie, L. M. Yudi, A. M. Baruzzi, *Electrochim. Acta* **1995**, *40*, 2953−2959.
[34] B. Hundhammer, T. Solomon, *J. Electroanal. Chem.* **1983**, *157*, 19−26.
[35] C. M. Pereira, W. Schmickler, F. Silva, M. Sousa, *J. Electroanal. Chem.* **1997**, *436*, 9−15.
[36] J. Cosier, A. M. Glazer, *J. Appl. Crystallogr.* **1986**, *19*, 105−107.
[37] SADABS, Bruker AXS, Madison, Wisconsin, U.S.A., **1996**.
[38] G. M. Sheldrick, *Acta Crystallogr., Sect. A* **1990**, *A46*, 467.
[39] G. M. Sheldrick, *SHELXL*-97, University of Göttingen, Germany, **1997**.

Received November 30, 2001
[I01491]

Control of Epoxidation Enantioselectivity by Axial Ligation in Manganese Chiroporphyrins with Diastereotopic Faces

Shu-Qing Liu,[a] Jacques Pécaut,[a] and Jean-Claude Marchon*[a]

Keywords: Porphyrins / Enantioselectivity / Ligand effects / Manganese

A manganese(III) chiroporphyrin with alternate pentafluorophenyl and chiral cyclopropyl meso-substituents in the αFαF conformation has been shown by X-ray crystallography to have its chloro axial ligand predominantly on the non-chiral β face. Epoxidation of 1,2-dihydronaphthalene by iodosylbenzene induced by the neat catalyst in dichloromethane solution shows a twofold increase in enantioselectivity relative to the same reaction in the presence of pyridine. These observations suggest that the location of the chloro ligand on the β face can block that face from participating in catalytic epoxidation, and direct the reaction to take place on the chiral α face.
(© Wiley-VCH Verlag GmbH, 69451 Weinheim, Germany, 2002)

Introduction

Chiroporphyrins derived from (1*R*)-*cis*-hemicaronaldehydic acid (**1**) display an αβαβ conformation of the chiral *meso*-substituents which make their two faces equivalent.[1] Their manganese(III) complexes such as chloromanganese(III) tetramethylchiroporphyrin [MnCl(TMCP)] (**2**) are mild asymmetric catalysts in olefin epoxidation by iodosylbenzene, with *ee*'s in the range 60−86% for the epoxidation of 1,2-dihydronaphthalene.[2,3] With the aim of improving the reactivity of these catalysts, we have introduced electron-withdrawing pentafluorophenyl substituents in the two opposite *meso* positions.[4] We report here that the resulting chiroporphyrin free bases have a predominant conformation (labelled αFαF) in which two opposite chiral cyclopropyl substituents are located on the same face of the macrocycle (labelled α), leaving the other face (labelled β) devoid of stereogenic groups. The enantioselectivities of 1,2-dihydronaphthalene epoxidation induced by several catalysts of this type have been measured with or without added pyridine, and the results provide new insights into the stereochemistry of the active oxidant.

Results and Discussion

Methyl and benzyl esters were obtained by deprotonation of **1** with sodium hydride followed by nucleophilic attack on methyl iodide or benzyl iodide, respectively.[5] Mixed condensation of either aldehyde ester with pentafluorobenzaldehyde and pyrrole, catalysed by trifluoroacetic acid under standard reaction conditions,[6] afforded a mixture of porphyrins (Scheme 1) from which pure products could be isolated after several consecutive separations on TLC plates. Ten types of chiroporphyrin-free bases with mixed *meso*-substitution are expected in this case, of which seven were obtained in amounts sufficient for characterization by electrospray mass spectrometry and NMR spectroscopy. The stereochemistries of the seven compounds, depicted schematically in Scheme 2, were assigned on the basis of the observed ^{1}H and ^{13}C NMR spectral multiplicities. Among the chiroporphyrins with two pentafluorophenyl groups, those with identical orientations of the chiral substituents (αFαF and ααFF) were predominant for both ester derivatives (respective yields for H_2MeCP: 4% and 4%; respective yields for H_2BzCP: 0.2% and 0.2%). Compounds of the type αβFF and βαFF were obtained in minute amounts among the benzyl ester derivatives, but they could not be separated. The αFβF stereoisomer was obtained in 0.2% yield in the H_2BzCP mixture, but it was not detected in the H_2MeCP mixture. The αβαF chiroporphyrin was obtained in 3% yield among the methyl ester derivatives, but it was not detected among the benzyl ester derivatives. The chloromanganese(III) complexes shown in Figure 1 were obtained by standard metal insertion methods, and pure samples obtained by TLC were characterized by electrospray mass spectrometry and UV/Visible spectroscopy.

The X-ray structure of the catalyst [MnCl(αFαF)MeCP] (**3**) was solved, and a stick representation is shown in Figure 2. The porphyrin macrocycle of **3** is less ruffled than that of [MnCl(TMCP)] (**2**),[2] with average out-of-plane displacements of the C_{meso} atoms with respect to the 24-atom mean-planes of 0.43(1) Å for **3** and 0.73(1) Å for **2**, consistent with the absence of steric crowding on the β face of the former. The average $Mn-N_P$ bond length is therefore

[a] Laboratoire de Chimie Inorganique et Biologique (UMR 5046 CEA-CNRS-UJF),
Département de Recherche Fondamentale sur la Matière Condensée, CEA-Grenoble, 38054 Grenoble cedex 9, France
Fax: (internat.) + 33-4/38785497
E-mail: jcmarchon@cea.fr

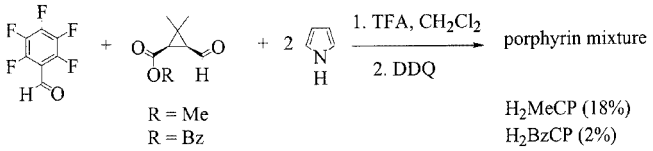

Scheme 1. Cross-condensation synthesis of the chiroporphyrin mixtures

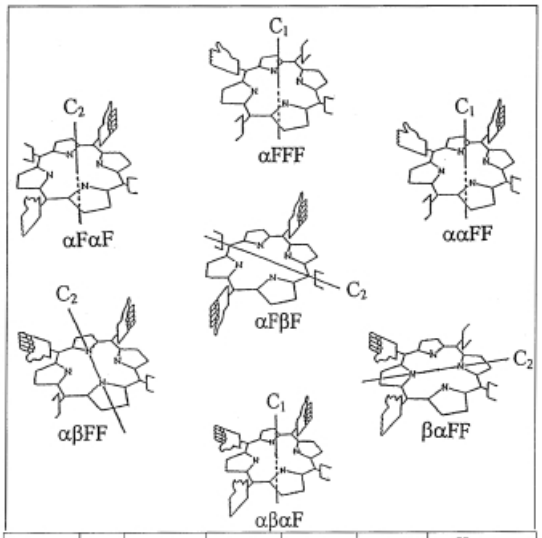

		H_β pyrr.	^{13}C pyrr.	$^{13}C_\beta$ pyrr.	$^{13}C_{meso}$	H meso substituents
αFFF	C_1	8d	8s	8s	4s	1 type
αFαF	C_2	4d	4s	4s	2s	1 type
ααFF	C_1	8d	8s	8s	4s	2 types
αFβF	C_2	4d	4s	4s	3s	1 type
αβFF	C_2	2s and 2d	4s	4s	2s	1 type
βαFF	C_2	2s and 2d	4s	4s	2s	1 type
αβαF	C_1	8d	8s	8s	4s	3 types

s = singlet; d = doublet

Scheme 2. Symmetry elements and NMR multiplicities of chiroporphyrins with mixed substitution by pentafluorophenyl and chiral cyclopropyl groups; homochiral cyclopropyl substituents are depicted as left hands

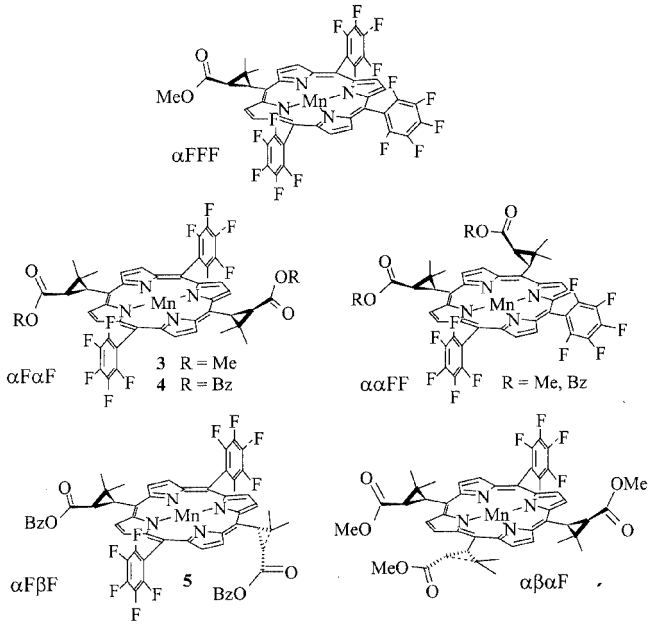

Figure 1. Stereochemistries of the five characterised types of chiroporphyrin catalysts with mixed substitution by pentafluorophenyl and chiral cyclopropyl groups

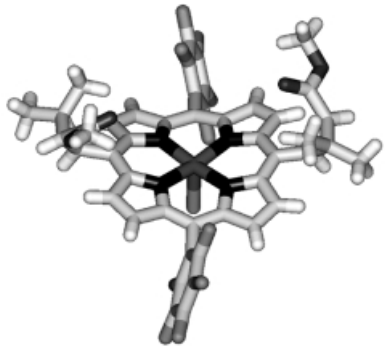

Figure 2. Stick representation of the structure of the major (90%) β-Cl conformer in the crystal lattice of [MnCl(αFαF)MeCP] (**3**), showing the moderate ruffling of the macrocycle; selected bond lengths (Å): [Mn−N_P] average 1.9972(7), Mn−Cl 2.3868(8); Mn is displaced from the porphyrin mean plane towards Cl by 0.14 Å; the C_{meso} atoms are displaced alternatively up [+0.46(1) Å] and down [−0.40(1) Å] with respect to the 24-atom mean plane

longer in **3** [1.9972(7) Å] than in **2** [1.974(2) Å], and the Mn−Cl bond length is also longer [2.3868(8) Å vs. 2.3475(9) Å]. The manganese atom of **3** is slightly displaced from the porphyrin mean plane by 0.14 Å (as compared to 0.44 Å in **2**). There is a small disorder of the chloro ligand of **3**, which is predominantly (ca. 90%) located on the open β face as shown in Figure 2 (β-Cl conformer). The presence of a small amount of α-Cl conformer in the samples of **3** (ca. 10% as indicated by the crystallographic disorder model) was confirmed by TLC on silica gel, which showed a minor, more polar spot very close to the major spot, and inseparable from it. The conformer composition of the chloromanganese(III) complex derived from the analogous benzyl ester derivative {noted [MnCl(αFαF)BzCP] (**4**)} has not been determined.

Asymmetric epoxidation of 1,2-dihydronaphthalene by iodosylbenzene with **3** as catalyst was faster than with the first-generation chiroporphyrin catalysts[3] and gave improved product yields. For example, epoxide yields obtained with **3** under our standard conditions with pyridine co-catalyst reached 96% after only 15 min, as compared to 83% after 60 min for **2** (Table 1). On the other hand, the *ee* lagged below 20% for **3**, as compared to 60% for **2**, indicating that epoxidation takes place at a significant rate on the non-chiral β face of **3**. Bulky bases such as 4-*tert*-butylpyridine, 1-(*tert*-butyldimethylsilyl)imidazole, 1,5-dicyclohexylimidazole, or diazabicyclo[2.2.2]octane had a similar effect to that of pyridine (Table 1). These observations led us to exclude the nitrogen bases and to use the neat chloromanganese(III) complexes **3** and **4** as catalysts. A remarkable improvement of the *ee* (which more than doubled from 18% to 43% for **3**, and from 17% to 35% for **4**) was obtained,

without affecting much the reaction rates and product yields, which remained satisfactory (Table 1).

Table 1. Catalytic asymmetric epoxidation of 1,2-dihydronaphthalene with manganese chiroporphyrins **3**−**5**

Axial ligand[a]	Epoxide yield (%)[b] [c]				*ee* (%, 60 min)[d]
	5 min	15 min	30 min	60 min	
	[MnCl(αFαF)MeCP] (**3**)				
py	62	96	>99	>99	18
bp	48	86	97	>99	17
bsi	80	86	92	95	2
dci	12	61	75	98	5
dabco	33	51	63	67	15
none	73	82	87	88	43
	[MnCl(αFαF)BzCP] (**4**)				
py	33	60	70	80	17
none	79	82	90	96	35
	[MnCl(αFβF)BzCP] (**5**)				
py	48	−	−		17
none	45	75	81	>99	31

[a] Axial ligands: py = pyridine; bp = 4-*tert*-butylpyridine; bsi = 1-(*tert*-butyldimethylsilyl)imidazole; dci = 1,5-dicyclohexylimidazole; dabco = 1,4-diazabicyclo[2.2.2]octane. [b] Reactions conditions: 1.0 μmol of catalyst, 100 μmol of iodosylbenzene, 250 μmol (or none) of axial ligand, and 1.00 mmol of 1,2-dihydronaphthalene in 2 mL of CH_2Cl_2, 1 h. [c] Based upon iodosylbenzene and determined by GC analysis with 20 μL of *n*-tridecane as internal standard. [d] Determined by GC (Cyclodex-B chiral capillary column). The major enantiomer had 1*S*,2*R* absolute configuration in all cases.

The detrimental effect of pyridine on enantioselectivity in this system is unexpected, since in most previous investigations the *ee* increases upon addition of a nitrogen base. A complete understanding of this effect is difficult because the nature of the active catalyst in the presence of pyridine, and that of the active oxidant, have never been established.[7,8] However, our results are consistent with a simple mechanism in which the presence of the chloro ligand on the β face favours the binding of added ligands on the vacant site of the α face. Pyridine binding on the chiral α face would, in turn, direct the formation of the active oxidant on the non-chiral β face, resulting in a poor *ee*, while iodosylbenzene binding on the α face in the absence of pyridine would generate the active oxidant on that same face and induce a good enantioselectivity. A rough calculation based on potential *ee* values of 60% for the α face (similar to that of **2**) and of 0% for the β face, and assuming equal reactivities on both faces, gives an overall *ee* value of about 50% for the mixture of conformers of **3** in a 90:10 β-Cl:α-Cl ratio. The reasonable agreement with the observed *ee* suggests that **2** and the β-Cl conformer of **3** have similar enantioselectivities.

Conclusion

In summary, although several elaborate synthetic routes to A_2B_2 porphyrins are available,[9] cross condensation is an expedient method to obtain the free-base precursors of active chiroporphyrin catalysts for a quick screening of their *ee*'s in a combinatorial sense. The two diastereotopic faces of a chiroporphyrin with mixed *meso*-substitution by pentafluorophenyl and chiral cyclopropyl groups in an αFαF conformation have widely different potential for enantiocontrol. The preference of the chloro ligand of manganese for the β face devoid of stereogenic groups in **3** directs the formation of the active oxo species on the α face and allows enantioselective olefin epoxidation. The electrophilicity of **3** allows the catalytic epoxidation to be carried out without exogenous ligand such as pyridine, which is advantageous since the latter can be a competitive substrate.[7]

Experimental Section

General Remarks: Solvents and chemicals were used without purification unless indicated. Dichloromethane was stabilized by ethanol (ACS for analysis, C_2H_5OH 0.1%). Pyrrole was purified by filtration through alumina before use. The methyl and benzyl esters of **1** (biocartol esters) were prepared according to previously published procedures.[1] Thin-layer chromatography was performed using Merck precoated silica plates 60F-254. Silica gel (230−400 mesh) and alumina (neutral, act. I) were used for column chromatography.

Spectroscopy: UV/Visible spectra were recorded on a Perkin−Elmer Lambda 9 instrument. Nuclear magnetic resonance spectra were obtained with Bruker AC 200, or Varian Avance 400 and 500 instruments. Spectra are tabulated in the following order: chemical shift (δ values), multiplicity (s = singlet, d = doublet, t = triplet, m = multiplet, br = broad singlet), number of protons, assignment [CH_{aro} (aromatic proton or carbon), $C_{aro\text{-}F}$ (pentafluorophenyl carbon), H_β (β pyrrolic protons of chiroporphyrins), C_α and C_β (α and β pyrrolic carbon of chiroporphyrins), C_{meso} (meso carbon of chiroporphyrins)]. The δ values of the C atoms connected to F atoms are not reported in the ^{13}C NMR spectra for some porphyrins because of high coupling constants.[10] Mass spectra were determined in the electrospray mode on a Finnigan MATLCQ instrument.

Typical Procedure For the Synthesis of Free Base Porphyrins: A 2.5 L commercial brown bottle filled with CH_2Cl_2 (containing 0.1% ethanol), equipped with a gas inlet, and shielded from ambient light by aluminium foil, was purged with argon for one hour. The flask was then charged with 6.4 mmol of biocartol methyl or benzyl ester, 6.4 mmol of pentafluorobenzaldehyde, and 15.4 mmol (1.2 equiv. relative to total aldehyde) of pyrrole under argon, followed 10 minutes later by the addition of 15.4 mmol (1.2 equiv.) of TFA. The resulting mixture was stirred at room temperature under gentle argon flow for 3 days. After this time, 12.8 mmol (1 equiv.) of DDQ was added to the reaction mixture which was stirred at room temperature for 4 hours. The solvents were then evaporated to dryness. The residue was chromatographed on alumina (neutral, act. I), eluting with CH_2Cl_2 containing 2% methanol under UV/Visible spectroscopic control, to afford a mixture of porphyrins. Pure compounds were obtained by preparative chromatography on successive TLC plates.

Selected Spectroscopic Data for H_2(αFαF)MeCP: ES-MS: *m*/*z* = 895.2 (calcd. 895.8 for [MH^+]). UV/Vis (CH_2Cl_2): λ_{max} = 421 nm, 519, 551, 595, 652. ^1H NMR (400 MHz, $CDCl_3$): δ = −2.26 (br, 1 H, NH), 0.99 (s, 6 H, CH_3i), 1.95 (s, 6 H, CH_3e), 2.85 [d, 2 H,

CH−C(O)], 3.13 (s, 6 H, OCH_3), 4.96 [d, 2 H, C*H*−CH−C(O)O], 8.64, 8.71, 9.31, 9.52 (4d, 8 H, H_β) ppm. ^{13}C NMR (Zn^{II} complex, 200 MHz, $CDCl_3$): δ = 18.6 (CH_3), 27.9 (C^{IV}), 29.2 (CH_3), 33.7 (CH), 38.8 (CH), 51.1 (OCH_3), 101.9, 113.7 (C_{meso}), 129.4, 129.5, 130.1, 132.0 (C_β), 133.5−144.8 (m and br, $C_{aro\text{-}F}$), 148.0, 148.1, 151.8, 152.5 (C_α), 171.2 [C(O)] ppm.

Selected Spectroscopic Data for H_2(αFβF)BzCP: ES-MS: *m*/*z* = 1047.3 (calcd. 1047.9 for [MH^+]). UV/Vis (CH_2Cl_2): λ_{max} = 422 nm, 520, 550, 594, 654. ^1H NMR (400 MHz, $CDCl_3$): δ = −2.35 (br, NH), 1.05 (s, 6 H, CH_3i), 1.96 (s, 6 H, CH_3e), 2.93 [d, 2 H, CH−C(O)], 4.38, 4.61 (2d, 4 H, OCH_2), 4.88 [d, 2 H, C*H*−CH−C(O)O], 6.65−6.85 (m, 10 H, CH_{aro}), 8.42, 8.65, 9.23, 9.42 (4d, 8 H, H_β) ppm. ^{13}C NMR (Zn^{II} complex, 400 MHz, $CDCl_3$): δ = 19.0 (CH_3), 28.3 (C^{IV}), 29.5 (CH_3), 33.9 (CH), 39.4 (CH), 66.2 (OCH_2), 101.4, 101.9, 113.5 (C_{meso}), 128.1, 128.5, 128.9 (CH_{aro}), 129.6, 130.0, 130.3, 131.9 (C_β), 136.4 (C^{IV}_{aro}), 147.8, 148.3, 152.2, 152.9 (C_α), 170.9 [C(O)] ppm.

Selected Spectroscopic Data for H_2(αβαF)MeCP: ES-MS: *m*/*z* = 855.3 (calcd. 855.9 for [MH^+]). UV/Vis (CH_2Cl_2): λ_{max} = 425 nm, 524, 563, 603, 654. ^1H NMR (400 MHz, $CDCl_3$): δ = −1.85 (br, NH), 0.90, 0.95, 1.00 (3s, 9 H, CH_3i), 1.97, 2.00, 2.01 (3s, 9 H, CH_3e), 2.86, 2.88, 2.94 [3d, 3 H, CH−C(O)], 3.15, 3.18, 3.19 (3s, 9 H, OCH_3), 4.88, 4.94, 4.96 [3d, 3 H, C*H*−CH−C(O)O], 8.57−9.42 (m, 8 H, H_β) ppm. ^{13}C NMR (400 MHz, $CDCl_3$): δ = 18.6 (CH_3), 27.8, 28.1, 28.3 (C^{IV}), 29.2 (CH_3), 33.6 (CH), 38.3, 38.4, 38.6 (CH), 51.4 (OCH_3), 99.8, 111.7, 112.1, 112.3 (C_{meso}), 127.7, 128.2, 128.6, 129.0, 129.3, 131.0, 131.4, 132.0 (C_β), 136.8 (br), 136.6 (br), 138.9 (br), 140.7 (br), 142.4 (br), 143.2 (br, $C_{aro\text{-}F}$), 147.5−150.9 (C_α), 171.0, 171.1, 171.3 [C(O)] ppm.

X-ray Crystallographic Study: Crystal data for **3**: $MnCl(C_{46}H_{30}O_4N_4F_{10})\cdot CHCl_3\cdot 0.5\,CH_2Cl_2\cdot 1.41H_2O$, M = 1170.44, monoclinic space group $P2_1$, a = 13.1971(7), b = 15.3994(8), c = 14.5274(8) Å, β = 115.8040(10)°, V = 2658.0(2) Å^3, T = 223(2) K, Z = 2, μ(Mo-K_α) = 0.583 mm^{-1}, 11678 reflections (R_{int} = 0.0202) which were used in all calculations. The final R was 0.0510, the final $wR(F^2)$ was 0.1258 [$I > 2\sigma(I)$].

CCDC-171628 contains the supplementary crystallographic data for this paper. These data can be obtained free of charge at www.ccdc.cam.ac.uk/conts/retrieving.html [or from the Cambridge Crystallographic Data Centre, 12, Union Road, Cambridge CB2 1EZ, UK; Fax: (internat.) +44-1223/336-033; E-mail: deposit@ccdc.cam.ac.uk].

Acknowledgments

This work was supported in part by a grant from the Ministère de la Recherche (postdoctoral fellowship to S.-Q. L.), for which we express our thanks.

[1] C. Pérollier, M. Mazzanti, J.-P. Simonato, F. Launay, R. Ramasseul, J.-C. Marchon, *Eur. J. Org. Chem.* **2000**, 583−589.
[2] For the X-ray structure of chloromanganese(III) tetramethylchiroporphyrin [MnCl(TMCP)] (**2**), see: J. P. Simonato, J. Pécaut, W. R. Scheidt, J. C. Marchon, *Chem. Commun.* **1999**, 989−990.
[3] M. Veyrat, O. Maury, F. Faverjon, D. E. Over, R. Ramasseul, J. C. Marchon, I. Turowska-Tyrk, W. R. Scheidt, *Angew. Chem. Int. Ed. Engl.* **1994**, *33*, 220−223; C. Pérollier, J. Pécaut, R. Ramasseul, J. C. Marchon, *Inorg. Chem.* **1999**, *38*, 3758−3759.
[4] A similar approach has been described recently: E. Rose, M. Soleilhavoup, L. Christ-Tommasino, G. Moreau, J. P. Collman, M. Quelquejeu, A. Straumanis, *J. Org. Chem.* **1998**, *63*, 2042−2044.
[5] P. E. Pfeffer, L. S. Silbert, *J. Org. Chem.* **1976**, *41*, 1373−1379.
[6] J. S. Lindsey, in *The Porphyrin Handbook* (Eds.: K. M. Kadish, K. Smith, R. Guilard), Academic Press, San Diego, CA, and Burlington, MA, **1999**, vol. 1, chapter 2.
[7] B. Meunier, *Chem. Rev.* **1992**, *92*, 1411−1456.
[8] J. P. Collman, A. S. Chien, T. A. Eberspacher, J. I. Brauman, *J. Am. Chem. Soc.* **2000**, *122*, 11098−11100.
[9] K. M. Smith, in *The Porphyrin Handbook* (Eds.: K. M. Kadish, K. Smith, R. Guilard), Academic Press, San Diego, CA, and Burlington, MA, **1999**, vol. 1, chapter 1.
[10] H. A. Wagenknecht, C. Claude, W. D. Woggon, *Helv. Chim. Acta* **1998**, *81*, 1506−1520.

Received December 21, 2001
[I01526]

Facile Oxidative Addition of C−Cl Bonds to New Neutral and Cationic Rhodium(I)-Bipyridine Complexes

Reto Dorta,[a] Linda J. W. Shimon,[b] Haim Rozenberg,[b] and David Milstein*[a]

Keywords: Rhodium / N ligands / Oxidative addition / Peroxo complexes

Neutral and cationic Rh(dmbpy) systems (dmbpy = 4,4′-dimethyl-2,2′-bipyridine) were synthesized starting from different metal precursors. [RhCl(dmbpy)(DMSO)] (**3**) was obtained either from the ethylene precursor [RhCl(dmbpy)(C_2H_4)] (**1**) or directly from [$Rh_2Cl_2(COE)_4$] (COE = cyclooctene) in DMSO. The neutral isocyanide complex [RhCl(dmbpy){CNC(CH_3)$_3$}] (**4**) was obtained by reaction of **1** with *tert*-butyl isocyanide. Reaction of dmbpy with [Rh(DMSO)$_4$]PF_6 gave the corresponding cationic complex [Rh(dmbpy)(DMSO)$_2$]PF_6 (**5**), and the cationic system [Rh(dmbpy){CNC(CH_3)$_3$}$_2$]BF_4 (**6**) was prepared starting from [Rh(dmbpy)(HD)]BF_4 (**2**) (HD = 1,5-hexadiene). All of these complexes were found to activate the C–Cl bond in benzyl chloride leading to quantitative isolation of the corresponding Rh^{III} complexes [$RhCl_2$($CH_2C_6H_5$)(dmbpy)(DMSO)] (**7**), [$RhCl_2$($CH_2C_6H_5$)(dmbpy){CNC(CH_3)$_3$}] (**9**) [RhCl(CH_2-C_6H_5)(dmbpy)(DMSO)$_2$]PF_6 (**10**) and [RhCl($CH_2C_6H_5$)-(dmbpy){CNC(CH_3)$_3$}$_2$]BF_4 (**12**). Oxidative addition of dichloromethane by complexes **3** and **5** yielded the corresponding chloromethyl complexes [$RhCl_2$(CH_2Cl)(dmbpy)(DMSO)] (**8**) and [RhCl(CH_2Cl)(dmbpy)(DMSO)$_2$]PF_6 (**11**). The reactivity of **3** towards oxygen led to the isolation of the peroxo Rh^{III} complex [RhCl(O_2)(dmbpy)(DMSO)] (**13**). Complexes **6**, **8**, **9** and **12** were characterized by X-ray crystallography.
(© Wiley-VCH Verlag GmbH, 69451 Weinheim, Germany, 2002)

Introduction

The use of transition metal catalysts that employ nitrogen-donor ligands is expanding rapidly.[1] The most widely used nitrogen ligand is the bidentate 2,2′-bipyridine unit.[2] Rh^I-bipyridine systems and closely related derivatives have been extensively investigated as catalysts in the hydrogenation and hydrogen-transfer reactions of olefins and ketones.[3] In this context, the cationic complex [Rh(bpy)(L)$_2$]X (X = PF_6^-, BF_4^-, ClO_4^-; bpy = 2,2′-bipyridine, L = acetone) is believed to be the active species in the hydrogenation of olefins.[4] Such complexes with labile additional ligands have never been isolated, the only known complexes of this type being with L = CO,[5] or with chelating ligands such as dienes[6] or bipyridine.[7] Furthermore, oxidative addition to neutral or cationic precursors of this type has never been studied in detail, the only example reported involving oxidative addition of methyl iodide to [Rh(bpy)(CO)X] (X = Cl, Br, I; bpy = 2,2′-bipyridine).[8]

The oxidative addition of carbon halides to low-valent metal complexes is involved in numerous industrially important catalytic cycles and has therefore attracted considerable academic interest. Of particular interest is the activation of the relatively inert C−Cl bond, which is more challenging than that of the C−Br and C−I bonds. Oxidative addition of C−Cl bonds, especially of dichloromethane, requires an electron-rich rhodium center. Relatively few examples of simple oxidative addition of dichloromethane to Rh^I complexes have been reported. These systems incorporate mono- or polydentate phosphorous ligands,[9−11] mono- or polydentate nitrogen ligands,[12−14] sulfur macrocycles[15] or phosphorous-nitrogen hybrid ligands,[16−18] and in several cases the starting Rh^I species were not isolated.[12,14,17,18]

Herein we report the synthesis, characterization and oxidative addition chemistry of new Rh^I complexes with the bidentate ligand 4,4′-dimethyl-2,2′-bipyridine (dmbpy).[19] The nucleophilicity of the Rh^I can be controlled by the choice of the additional ligands. We chose the loosely bound DMSO ligand and the relatively strongly bound *tert*-butyl isocyanide ligand for our study. The oxidative addition of dichloromethane at room temperature takes place in the complexes stabilized by additional DMSO ligands. Oxidative addition of the C−Cl bond of benzyl chloride is observed in all of these complexes. Reaction of the neutral Rh^I-(dmbpy)-DMSO complex with O_2 leads to the isolation of a stable peroxo-Rh^{III} compound.

Results and Discussion

Synthesis of the Rh^I-dmbpy Complexes

The new complexes **1**−**6** were prepared from different precursors. The preparation of **1** was achieved following a

[a] Department of Organic Chemistry, The Weizmann Institute of Science,
Rehovot, 76100, Israel
E-mail: david.milstein@weizmann.ac.il
[b] Department of Chemical Services, The Weizmann Institute of Science,
Rehovot, 76100, Israel

literature method published for the corresponding 2,2′-bipyridine complex.[20] Complex **1** was found to be moderately stable in a dichloromethane solution but decomposed immediately when dissolved in either acetonitrile, pyridine or methanol. Surprisingly, dissolution of **1** in DMSO resulted in quantitative formation of **3**, which was isolated by pouring the concentrated DMSO solution into a large excess of diethyl ether. Direct synthesis of **3** was achieved by treating a DMSO solution of the rhodium dimer $[Rh_2Cl_2(COE)_4]$ (COE = cyclooctene) with an equimolar amount of 4,4′-dimethyl-2,2′-bipyridine. Subsequent precipitation from diethyl ether gave **3** as a brick-red solid in high yield (Scheme 1).

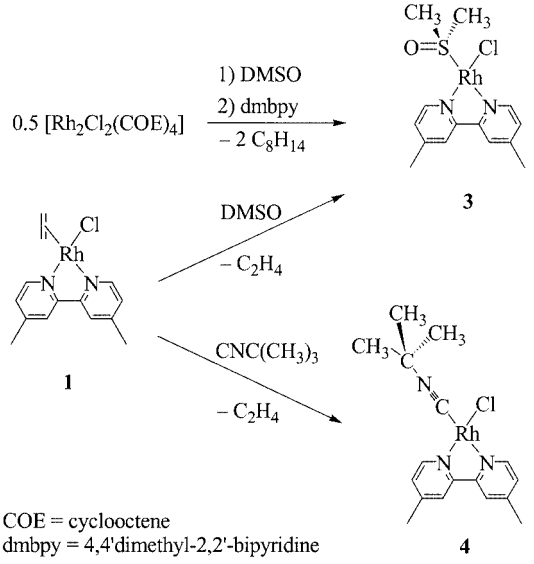

Scheme 1. Synthesis of the neutral Rh^I complexes **3** and **4**

The ^1H NMR spectrum of **3** showed six resonances in the aromatic region attributable to the nonequivalent parts of the ligand unit, one singlet at δ = 3.19 ppm for the coordinated DMSO (bound through the sulfur atom) and two singlets for the methyl groups of dmbpy at δ = 2.31 and 2.51 ppm . The corresponding neutral isocyanide complex **4** was synthesized in high yield by treating a suspension of **1** in THF with 1 equiv. of *tert*-butyl isocyanide as shown in Scheme 1. Starting with **3** and treating it with 1 equiv. of *tert*-butyl isocyanide led to a mixture of products. One of the by-products was isolated by precipitation from the solution mixture and identified by ^1H NMR spectroscopy to be the symmetrical species $[Rh(dmbpy)\{CNC(CH_3)_3\}_2]Cl$. This indicates that displacement of the DMSO molecule in **3** is much slower than that of ethylene leading to the displacement of the chloride and the formation of the more stable bis-isocyanide species. The ^1H NMR spectrum of **4** showed the expected peaks for the nonsymmetrical dmbpy ligand and a singlet at δ = 1.53 ppm for the coordinated *tert*-butyl isocyanide.

The corresponding cationic complexes, **5** and **6**, respectively, were also synthesized (Scheme 2). Compound **5** was obtained as a red solid after addition of dmbpy to a DMSO solution containing $[Rh(DMSO)_4]PF_6$.[21] As expected, the ^1H NMR spectrum in $[D_6]$DMSO showed only three peaks in the aromatic region for the ligand and one singlet for the two methyl groups of dmbpy. Complex **6** was obtained by treating a THF slurry of $[Rh(dmbpy)(HD)]BF_4$ (**2**) (HD = 1,5-hexadiene) with 2 equiv. of *tert*-butyl isocyanide. After precipitation from pentane, **6** was obtained as a deep-red solid. FT-IR spectroscopy, ^1H NMR spectroscopy and elemental analysis support its formulation, and the molecular structure of **6** was confirmed by an X-ray diffraction study of red single crystals obtained by slow evaporation of an acetone solution. An ORTEP drawing is shown in Figure 1 and the averages of selected bond lengths and angles are given in Table 1. The rhodium atom of complex **6** is located in the center of a square planar arrangement with the two

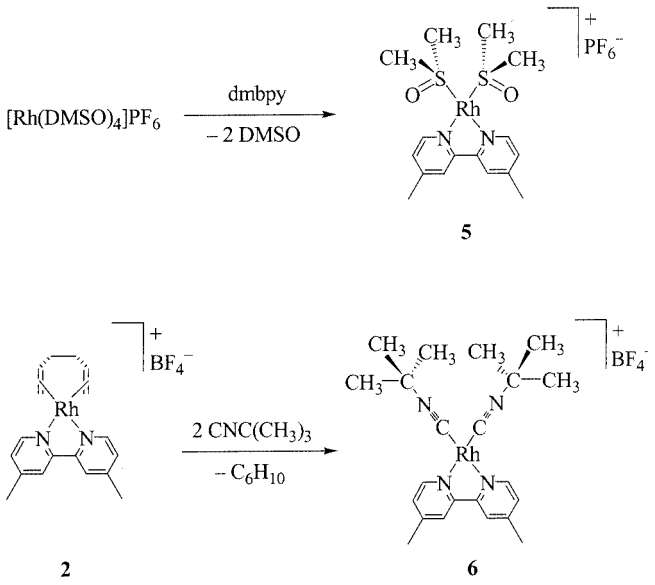

Scheme 2. Synthesis of the cationic Rh^I complexes **5** and **6**

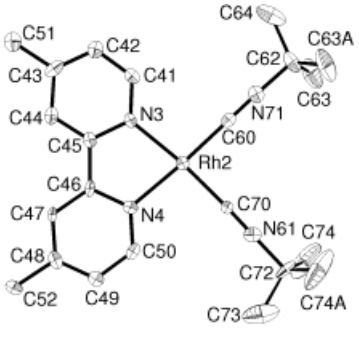

Figure 1. ORTEP drawing of a molecule of **6** (50% of probability); hydrogen atoms are omitted for clarity

Table 1. Selected bond lengths (Å) and bond angles (°) for **6**

Rh(2)−C(70)	1.909(7)	Rh(2)−N(3)	2.060(7)
Rh(2)−C(60)	1.910(8)	Rh(2)−N(4)	2.077(6)
C(70)−Rh(2)−C(60)	87.5(4)	C(70)−Rh(2)−N(4)	95.6(3)
C(70)−Rh(2)−N(3)	174.5(3)	C(60)−Rh(2)−N(4)	176.9(3)
C(60)−Rh(2)−N(3)	97.9(3)	N(3)−Rh(2)−N(4)	79.0(3)

isocyanide ligands *trans* to the corresponding pyridine moieties of dmbpy.

Oxidative Addition of C−Cl Bonds

When an acetone or DMSO solution of **3** was treated with benzyl chloride, an immediate color change from deep red to yellow took place. The ^{1}H NMR spectrum showed clean oxidative addition of the C−Cl bond, and subsequent workup of the yellow solution gave complex **7** in high yield (Scheme 3). The benzylic CH_2 group is seen as two nonequivalent proton signals showing couplings with each other (6.8 Hz) and with the rhodium metal center (3.1 Hz). In the case of dichloromethane, oxidative addition was, as expected, much slower and took 15 h for completion, giving complex **8** in quantitative yield. Following the process by ^{1}H NMR spectroscopy showed the appearance of two signals at δ = 4.31 ppm (dd, J = 5.7, 3.0 Hz) and δ = 4.75 ppm (dd, J = 5.7, 3.0 Hz) for the CH_2Cl unit (Figure 2) together with a new set of peaks for the dmbpy unit. When the reaction was performed in [D_6]DMSO, minor amounts

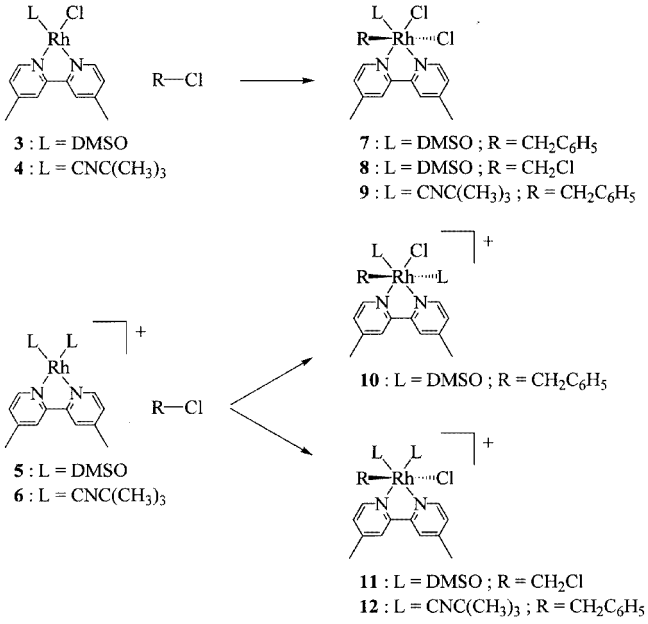

Scheme 3. Reaction of the Rh^{I} complexes **3**−**6** with R−Cl to yield the Rh^{III} complexes **7**−**12**

(<10% by integration) of an isomeric species were also present. In this case, the ligand seems to be symmetrical with three signals in the aromatic region and one singlet for the methyl group of dmbpy. The chloromethyl moiety gives rise to one doublet at δ = 5.05 ppm (d, J = 3.1 Hz). These data indicate a species with the two chloride ligands *trans* to the

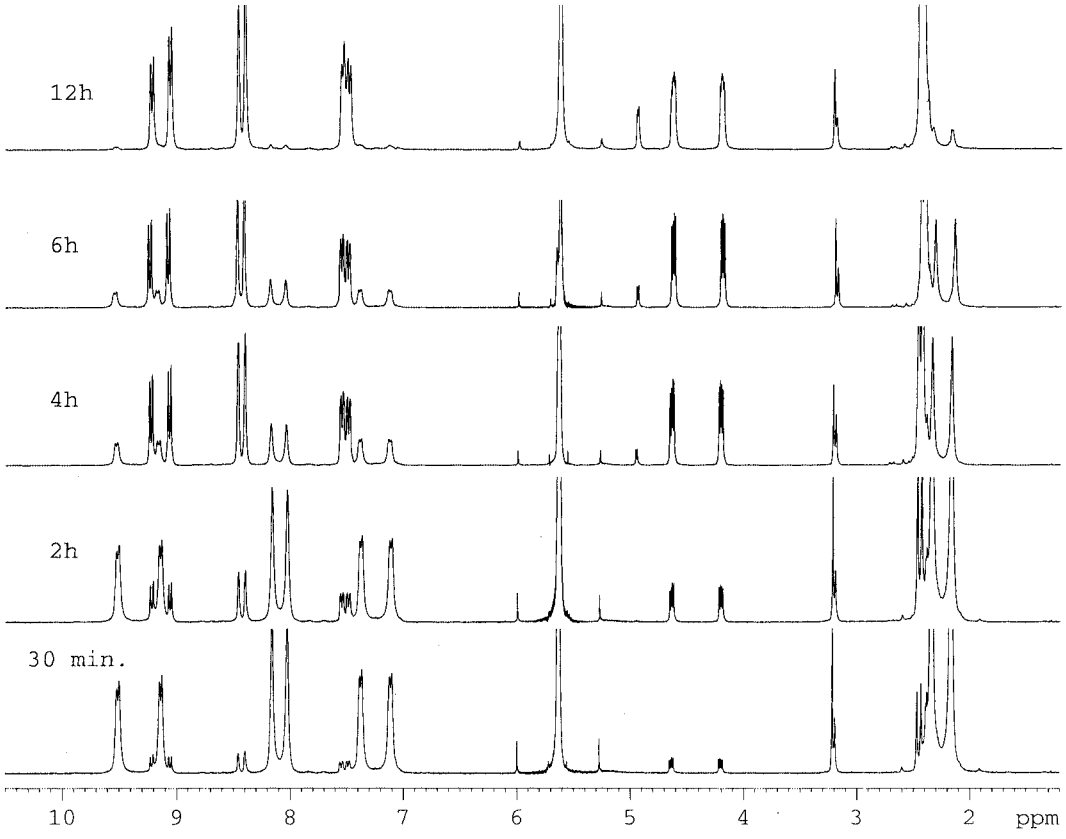

Figure 2. ^{1}H NMR follow-up experiment of the reaction between **3** and dichloromethane in [D_6]DMSO

bipyridine moiety and with the chloromethyl group and the DMSO ligand axially arranged. This compound could be removed during workup due to its higher solubility in diethyl ether. It was not observed when the reaction was performed in acetone. Trying to obtain this compound in pure form, an NMR tube sample of **8** in [D_6]DMSO was heated at 80 °C for 2 h. Indeed, the ^{1}H NMR spectrum showed 30% of this compound compared to **8** was formed.[22] Colorless single crystals of **8** suitable for X-ray diffraction were obtained by slow diffusion of diethyl ether into a concentrated DMSO solution. The geometry around the rhodium atom in this complex is distorted octahedral (Figure 3). In the equatorial plane, a chloride atom, the two N atoms of dmbpy and the S atom of DMSO are coordinated to the rhodium atom. The chloromethyl ligand and the second chloride atom occupy the axial positions. As expected, the two chloride atoms show quite different bond lengths to rhodium, the one *trans* to the N atom being significantly shorter than the chloride *trans* to the chloromethyl moiety [Rh(1)−Cl(3) = 2.3528(7) and Rh(1)−Cl(3) = 2.4891(7)] (Table 2). The Rh(1)−C(4) distance of 2.046(2) Å is very close to the value reported recently for [$RhCl_2(CH_2Cl)$\{2,6-(CH=N*i*Pr)$_2$-C_5H_3N\}].[13] The C(4)−Cl(4) bond length of 1.811(3) Å is longer than those found for other metal chloromethyl complexes, indicating a slightly higher carbene character of **8** ($Rh=CH_2^+Cl^-$).

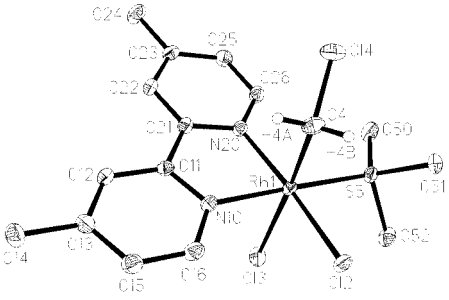

Figure 3. ORTEP drawing of a molecule of **8** (50% of probability); hydrogen atoms (except Rh−Ch_2Cl) are omitted for clarity

Table 2. Selected bond lengths (Å) and bond angles (°) for **8**

Rh(1)−C(4)	2.046(2)	Rh(1)−S(5)	2.2870(7)
Rh(1)−N(20)	2.0526(19)	Rh(1)−Cl(2)	2.3528(7)
Rh(1)−N(10)	2.0678(19)	Rh(1)−Cl(3)	2.4891(7)
C(4)−Rh(1)−N(20)	89.92(9)	N(10)−Rh(1)−Cl(2)	93.79(5)
C(4)−Rh(1)−N(10)	89.78(9)	S(5)−Rh(1)−Cl(2)	86.46(2)
N(20)−Rh(1)−N(10)	79.19(7)	C(4)−Rh(1)−Cl(3)	175.50(8)
C(4)−Rh(1)−S(5)	92.71(8)	N(20)−Rh(1)−Cl(3)	89.58(6)
N(20)−Rh(1)−S(5)	100.68(6)	N(10)−Rh(1)−Cl(3)	85.74(5)
N(10)−Rh(1)−S(5)	177.51(5)	S(5)−Rh(1)−Cl(3)	91.78(2)
C(4)−Rh(1)−Cl(2)	87.08(8)	Cl(2)−Rh(1)−Cl(3)	92.88(4)
N(20)−Rh(1)−Cl(2)	172.38(5)		

The reactivity of the corresponding *tert*-butyl isocyanide complex **4** towards C−Cl bonds was checked next. As expected, complex **4** is much less reactive due to significantly higher backbonding from the rhodium center to the *tert*-butyl isocyanide ligand and the resulting lower nucleophilicity of the metal center. Treating a deep-red acetone solution of **4** with benzyl chloride for 12 h at room temperature led to a color change to yellow. The ^{1}H NMR spectrum showed that clean oxidative addition took place also in this case, leading to quantitative isolation of complex **9**. In contrast, oxidative addition of dichloromethane to complex **4** did not occur at room temperature. Even after stirring a solution of **4** with excess CH_2Cl_2 for several days the starting complex was recovered unchanged. The crystal structure of [$RhCl_2(CH_2C_6H_5)$(dmbpy)\{$CNC(CH_3)_3$\}] (**9**) has been determined (Figure 4) and found to adopt an octahedral geometry. In the equatorial plane, the rhodium center is bound to the dmbpy, the *tert*-butyl isocyanide and to one of the chloride atoms. The benzylic moiety together with the second chloride atom adopt the apical positions. As in the case of **8**, the Rh−Cl bond length of the chloride *trans* to the pyridine of dmbpy is significantly shorter than the one *trans* to the benzyl moiety [Rh(1)−Cl(3) = 2.3573(10) and Rh(1)−Cl(2) = 2.5391(9), respectively] (Table 3).

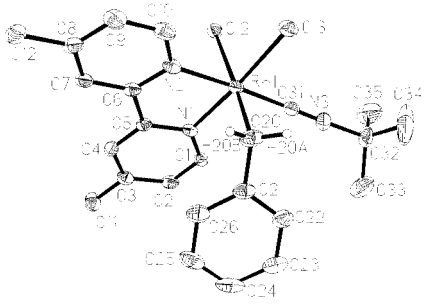

Figure 4. ORTEP drawing of a molecule of **9** (50% of probability); hydrogen atoms (except Rh−Ch_2R) are omitted for clarity

Table 3. Selected bond lengths (Å) and bond angles (°) for **9**

Rh(1)−C(31)	1.943(4)	Rh(1)−C(20)	2.100(4)
Rh(1)−N(1)	2.023(3)	Rh(1)−Cl(3)	2.3573(10)
Rh(1)−N(2)	2.070(3)	Rh(1)−Cl(2)	2.5391(9)
C(31)−Rh(1)−N(1)	98.11(13)	N(2)−Rh(1)−Cl(3)	95.57(8)
C(31)−Rh(1)−N(2)	176.73(13)	C(20)−Rh(1)−Cl(3)	86.42(11)
N(1)−Rh(1)−N(2)	79.50(11)	C(31)−Rh(1)−Cl(2)	94.09(11)
C(31)−Rh(1)−C(20)	88.59(16)	N(1)−Rh(1)−Cl(2)	84.55(8)
N(1)−Rh(1)−C(20)	94.04(13)	N(2)−Rh(1)−Cl(2)	87.93(8)
N(2)−Rh(1)−C(20)	89.35(14)	C(20)−Rh(1)−Cl(2)	177.12(12)
C(31)−Rh(1)−Cl(3)	86.84(11)	Cl(3)−Rh(1)−Cl(2)	94.76(3)
N(1)−Rh(1)−Cl(3)	175.04(8)		

The cationic complexes **5** and **6** also undergo oxidative addition of the C−Cl bond of benzyl chloride (Scheme 3). In both cases, oxidative addition occurred somewhat slower than for the corresponding neutral complexes, leading to the cationic Rh^{III} complexes **10** and **12**, respectively. Surprisingly, the benzyl methylene group in **10** shows formation of the asymmetrical species with one DMSO molecule *trans* to the benzyl methylene, giving rise to two doublets of doublets for the methylene group. Oxidative addition to complex **6** does lead to the expected symmetrical species with the methylene group appearing as one doublet at δ = 3.12 ppm, the doublet signal arising from coupling to the

rhodium center. Slow diffusion of diethyl ether into an acetone solution of **12** led to colorless crystals suitable for X-ray diffraction. As shown in Figure 5, compound **12** adopts the expected octahedral arrangement around the metal center. The bond lengths between the rhodium atom and the *tert*-butyl isocyanide and dmbpy ligands are very close to the values observed in the starting complex **6** with marginally longer Rh(1)−C(40) and Rh(1)−C(30) bond lengths (Table 4). As observed in the neutral systems, also in the cationic case the DMSO stabilized complex **5** oxidatively added dichloromethane due to its higher nucleophilicity. Reaction of **5** with excess CH_2Cl_2 resulted in a gradual color change from deep-red to yellow when left standing at room temperature for two days and gave the symmetrical complex **11** in high yield (Scheme 3).

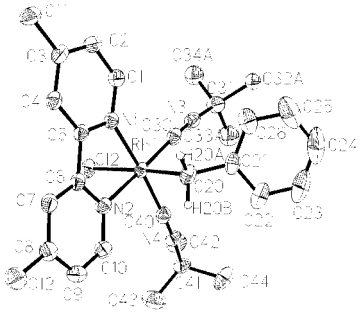

Figure 5. ORTEP drawing of a molecule of **12** (50% of probability); hydrogen atoms (except Rh−Ch_2R) are omitted for clarity

Table 4. Selected bond lengths (Å) and bond angles (°) for **12**

Rh(1)−C(40)	1.939(4)	Rh(1)−N(2)	2.066(3)
Rh(1)−C(30)	1.939(4)	Rh(1)−C(20)	2.098(3)
Rh(1)−N(1)	2.065(3)	Rh(1)−Cl(2)	2.4928(10)
C(40)−Rh(1)−C(30)	84.80(15)	N(1)−Rh(1)−C(20)	90.36(13)
C(40)−Rh(1)−N(1)	175.67(13)	N(2)−Rh(1)−C(20)	84.42(13)
C(30)−Rh(1)−N(1)	97.93(13)	C(40)−Rh(1)−Cl(2)	86.09(11)
C(40)−Rh(1)−N(2)	97.87(13)	C(30)−Rh(1)−Cl(2)	88.75(11)
C(30)−Rh(1)−N(2)	176.95(12)	N(1)−Rh(1)−Cl(2)	90.60(8)
N(1)−Rh(1)−N(2)	79.49(11)	N(2)−Rh(1)−Cl(2)	92.89(8)
C(40)−Rh(1)−C(20)	92.81(15)	C(20)−Rh(1)−Cl(2)	176.93(11)
C(30)−Rh(1)−C(20)	94.01(15)		

Oxidative Addition of Oxygen to 3

When a deep-red DMSO or acetone solution of **3** was treated with 1 equiv. or excess O_2, an immediate color change to yellow occurred. The product was identified as being the peroxo complex $[RhCl_2(O_2)(dmbpy)(DMSO)]$ (**13**) based on elemental analysis and the appearance of an IR band at $\tilde{\nu} = 870\ cm^{-1}$ for the peroxo ligand (Scheme 4). The ^1H NMR spectrum showed shifts for all the protons relative to the peaks observed for the starting complex **3**. As expected, the biggest difference is seen in one of the protons in the α-position to the nitrogen of the dmbpy ligand, the pyridine moiety being substantially more shielded by the presence of the oxygen atom *trans* to it. However, we could not determine whether the DMSO ligand or the chloride occupy the position *trans* to the second oxygen atom. With respect to the properties of **13**, we should note that O_2 is bonded strongly and did not dissociate under vacuum or by bubbling N_2 through a solution of **13**.[23] Complexes **4** and **5** also add oxygen and a detailed investigation of the reactivity of these complexes will be published in due course.

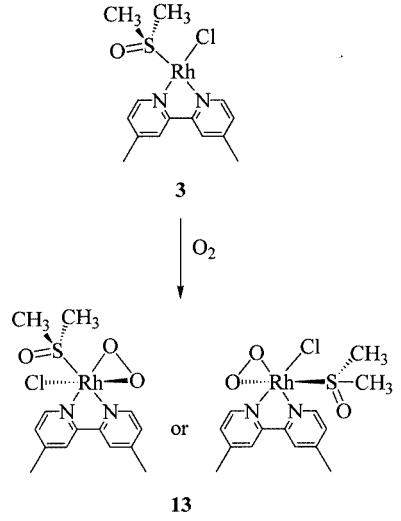

Scheme 4. Reaction of complex **3** with O_2 giving the peroxo complex **13**

Summary

New neutral and cationic rhodium complexes bearing the chelating 4,4′-dimethyl-2,2′-bipyridine (dmbpy) ligand and additional DMSO or *tert*-butyl isocyanide ligands were synthesized in high yield starting from various Rh^I precursors. These complexes underwent oxidative addition of the C−Cl bond of benzyl chloride at room temperature. The complexes bearing the additional DMSO ligands were shown to be more nucleophilic at the rhodium center and underwent C−Cl oxidative addition of dichloromethane. In addition, the oxidative addition of O_2 to one of the Rh^I complexes led to the quantitative isolation of a stable Rh^{III} peroxo species.

Experimental Section

General Procedures: All experiments were carried out under an atmosphere of purified nitrogen in a Vacuum Atmospheres glove box equipped with a MO 40-2 inert gas purifier. All solvents were reagent grade or better. All non-deuterated solvents were refluxed over sodium/benzophenone ketyl and distilled under argon atmosphere. Deuterated solvents were used as received. All the solvents were degassed with argon and kept in the glove box over molecular sieves. Commercially available reagents were used as received. The complexes $[Rh_2Cl_2(COE)_4]$,[24] $[Rh_2Cl_2(C_2H_4)_4]$,[25] and $[Rh(DMSO)_4]PF_6$ [21] were prepared according to literature procedures.

^1H NMR spectra were recorded at 250 MHz on a Bruker AMX-250 NMR spectrometer or on a Bruker AMX-400 NMR spectro-

meter. Chemical shifts are reported in ppm downfield from tetramethylsilane and are referenced to the residual hydrogen signal of the deuterated solvents (δ = 2.04 ppm, acetone; δ = 2.49 ppm, DMSO; δ = 5.32 ppm, dichloromethane). Abbreviations used in the description of NMR spectroscopic data are as follows: br., broad; s, singlet; d, doublet; t, triplet; m, multiplet. Elemental analyses were performed by H. Kolbe, Mikroanalytisches Laboratorium, 45470 Mülheim, Germany.

Synthesis of [RhCl(dmbpy)(C_2H_4)] (1): [$Rh_2Cl_2(C_2H_4)_4$] (241 mg, 0.620 mmol) was dissolved in toluene (35 mL) and filtered, affording an orange solution. 4,4′-dimethyl-2,2′-bipyridine (205 mg, 1.115 mmol) was dissolved in toluene (8 mL) and added dropwise. The color of the solution turned from orange to violet. Stirring at room temperature for 2 h resulted in the formation of a violet precipitate which was filtered off, washed with toluene and dried in vacuo. Yield: 346 mg, 89%. ^{1}H NMR (250 MHz, CD_2Cl_2, 298 K): δ = 2.27 (s, 3 H), 2.53 (s, 3 H), 3.62 (s, 4 H), 7.00 (d, *J* = 5.1 Hz, 1 H), 7.21 (d, *J* = 5.9 Hz, 1 H), 7.39 (d, *J* = 5.6 Hz, 1 H), 7.63 (s, 1 H), 7.84 (s, 1 H), 9.06 (d, *J* = 5.6 Hz, 1 H) ppm. $C_{14}H_{16}ClN_2Rh$ (350.7): C 47.95, H 4.60, N 7.99; found C 47.99, H 4.78, N 7.78.

Synthesis of [Rh(dmbpy)(HD)]BF_4 (2): A suspension of [$Rh_2Cl_2(COE)_4$] (140 mg, 0.196 mmol) in MeOH (7 mL) was treated with excess 1,5-hexadiene (1.1 mL) and the yellow suspension was stirred at room temperature for 1.5 h. Addition of a solution of 4,4′-dimethyl-2,2′-bipyridine (72 mg, 0.392 mmol) in dichloromethane (4 mL) resulted in a color change to deep red. After stirring the solution at room temperature for 1 h, a solution of $AgBF_4$ (76 mg, 0.392 mmol) in dichloromethane (4 mL) was added dropwise and the solution was stirred at room temperature for another hour. Filtration, followed by concentration of the red solution to 6 mL and addition of diethyl ether led to the precipitation of a red solid which was filtered, washed with additional diethyl ether and dried in vacuo. Yield: 173 mg, 97%. ^{1}H NMR (250 MHz, CD_2Cl_2, 298 K): δ = 1.94 (m, 2 H), 2.54 (m, 2 H), 2.61 (s, 6 H), 3.00 (d, *J* = 13.9 Hz, 2 H), 3.59 (d, *J* = 7.7 Hz, 2 H), 4.78 (m, 2 H), 7.47 (d, *J* = 5.7 Hz, 2 H), 7.66 (d, *J* = 5.8 Hz, 2 H), 8.15 (s, 2 H) ppm. $C_{18}H_{22}BF_4N_2Rh$ (456.1): C 47.40, H 4.87, N 6.14; found C 47.36, H 4.79, N 6.08.

Synthesis of [RhCl(dmbpy)(DMSO)] (3): [$Rh_2Cl_2(COE)_4$] (494 mg, 0.692 mmol, COE = cyclooctene) was dissolved in DMSO (16 mL) and the deep-orange solution was stirred at room temperature for 30 min. 4,4′-Dimethyl-2,2′-bipyridine (255 mg, 1.384 mmol) was then added as a solid in small portions resulting in a color change to deep red. The solution was stirred for 3 h at room temperature and then poured into diethyl ether (450 mL). The resulting brick-red solid was carefully decanted, washed with diethyl ether and pentane and dried in vacuo. Yield: 460 mg, 83%. ^{1}H NMR (250 MHz, [D_6]acetone, 298 K): δ = 2.31 (s, 3 H), 2.51 (s, 3 H), 3.19 (s, 6 H), 7.16 (d, *J* = 6.0 Hz, 1 H), 7.45 (d, *J* = 5.8 Hz, 1 H), 8.03 (s, 1 H), 8.18 (s, 1 H), 9.46 (d, *J* = 5.7 Hz, 1 H), 9.83 (d, *J* = 6.0 Hz, 1 H) ppm. $C_{14}H_{18}ClN_2ORhS$ (400.7): C 41.96, H 4.53, N 6.99; found C 41.78, H 4.46, N 7.06.

Synthesis of [RhCl(dmbpy){CNC(CH_3)$_3$}] (4): A solution of *tert*-butyl isocyanide (40 mg, 0.486 mmol) in THF (10 mL) was added dropwise to a violet slurry of **1** (170 mg, 0.486 mmol) in THF (14 mL). The resulting green-brown solution was stirred at room temperature for 2 h. Concentration of the THF solution to 10 mL and addition of diethyl ether (40 mL) caused the precipitation of a green-brown solid which was washed with diethyl ether and dried in vacuo. Yield: 162 mg, 83%. ^{1}H NMR (250 MHz, [D_6]acetone, 298 K): δ = 1.53 (s, 9 H), 2.23 (s, 3 H), 2.49 (s, 3 H), 7.10 (d, *J* = 5.9 Hz, 1 H), 7.46 (d, *J* = 5.7 Hz, 1 H), 7.98 (s, 1 H), 8.14 (s, 1 H), 8.85 (d, *J* = 5.6 Hz, 1 H), 9.37 (d, *J* = 5.7 Hz, 1 H) ppm. $C_{17}H_{21}ClN_3Rh$ (405.7): C 50.32, H 5.22, N 10.36; found C 50.21, H 5.29, N 10.26.

Synthesis of [Rh(dmbpy)(DMSO)$_2$]PF_6 (5): [$Rh(DMSO)_4$]PF_6 (65 mg, 0.115 mmol) and dmbpy (21 mg, 0.115 mmol) were dissolved in 4 mL DMSO and the resulting deep-red solution was stirred at room temperature for 2 h. The solution was then poured into diethyl ether (150 mL) and the brick-red precipitate was decanted, washed with additional diethyl ether and dried in vacuo. Yield: 61 mg, 90%. ^{1}H NMR (250 MHz, [D_6]DMSO, 298 K): δ = 2.52 (s, 6 H), 7.52 (d, *J* = 5.9 Hz, 2 H), 8.41 (s, 2 H), 8.70 (d, *J* = 5.8 Hz, 2 H) ppm. $C_{16}H_{24}F_6N_2O_2PRhS_2$ (588.4): C 32.66, H 4.11, N 4.76; found C 32.78, H 4.18, N 4.71.

Synthesis of [Rh(dmbpy){CNC(CH_3)$_3$}$_2$]BF_4 (6): A THF (3 mL) solution of *tert*-butyl isocyanide (33 mg, 0.401 mmol) was added dropwise to a red suspension of **2** (87 mg, 0.191 mmol) in THF (6 mL). The suspension was left stirring at room temperature for 2 h during which time the color turned deep-red with precipitation of a deep-red solid. Concentration to 3 mL, addition of pentane and subsequent washings with additional pentane afforded a deep-red solid which was dried in vacuo. Yield: 91 mg, 88%. ^{1}H NMR (250 MHz, [D_6]acetone, 298 K): δ = 1.62 (s, 18 H), 2.55 (s, 6 H), 7.56 (d, *J* = 5.6 Hz, 2 H), 8.39 (s, 2 H), 8.67 (d, *J* = 5.5 Hz, 2 H) ppm. $C_{22}H_{30}BF_4N_4Rh$ (540.2): C 48.91, H 5.60, N 10.37; found C 48.76, H 5.52, N 10.27.

Reaction of 3 with Benzyl Chloride. Formation of [$RhCl_2$-($CH_2C_6H_5$)(dmbpy)(DMSO)] (7): Complex **3** (70 mg, 0.175 mmol) was dissolved in an acetone/DMSO (3:1 mL) mixture and stirred at room temperature for 30 min giving a deep-red solution. Addition of benzyl chloride (44 mg, 0.348 mmol) led to an immediate color change to yellow. Leaving the solution at room temperature for 1 h resulted in the formation of a yellow precipitate which was carefully decanted, washed with diethyl ether and dried in vacuo. Yield: 77 mg, 84%. ^{1}H NMR (250 MHz, [D_6]DMSO, 298 K): δ = 2.39 (s, 3 H), 2.48 (s, 3 H), 3.51 (dd, *J* = 6.8 Hz and 3.0 Hz, 1 H), 4.02 (dd, *J* = 6.8 Hz and 3.1 Hz, 1 H), 6.17 (d, *J* = 6.9 Hz, 2 H), 6.50 (dd, *J* = 7.5 Hz, 2 H), 6.70 (dd, *J* = 7.3 Hz, 1 H), 7.42 (d, *J* = 5.0 Hz, 1 H), 7.52 (d, *J* = 5.0 Hz, 1 H), 8.01 (s, 1 H), 8.18 (s, 1 H), 9.12 (d, *J* = 5.9 Hz, 1 H), 9.41 (d, *J* = 5.7 Hz, 1 H) ppm. $C_{21}H_{25}Cl_2N_2ORhS$ (527.3): C 47.83, H 4.78, N 5.31; found C 47.35, H 4.76, N 5.22.

Reaction of 3 with Dichloromethane. Formation of [$RhCl_2$-(CH_2Cl)(dmbpy)(DMSO)] (8): Complex **3** (80 mg, 0.200 mmol) was dissolved in DMSO (2 mL) and five drops of CH_2Cl_2 were added. Leaving the solution at room temperature for one day led to the formation of pale yellow crystals. Addition of diethyl ether and subsequent washing with additional diethyl ether gave an off-white solid which was dried in vacuo. Yield: 82 mg, 85%. ^{1}H NMR (250 MHz, [D_6]DMSO, 298 K): δ = 2.53 (s, 3 H), 2.57 (s, 3 H), 4.31 (dd, *J* = 5.7 Hz and 3.0 Hz, 1 H), 4.75 (dd, *J* = 5.7 Hz and 3.0 Hz, 1 H), 7.60 (d, *J* = 5.0 Hz, 1 H), 7.65 (d, *J* = 5.0 Hz, 1 H), 8.51 (s, 1 H), 8.57 (s, 1 H), 9.17 (d, *J* = 5.9 Hz, 1 H), 9.33 (d, *J* = 6.0 Hz, 1 H) ppm. $C_{15}H_{20}Cl_3N_2ORhS$ (485.7): C 37.10, H 4.15, N 5.77; found C 37.27, H 4.06, N 5.71.

Reaction of 4 with Benzyl Chloride. Formation of [$RhCl_2$-($CH_2C_6H_5$)(dmbpy){CNC(CH_3)$_3$}] (9): Complex **4** (28 mg, 0.069 mmol) was dissolved in acetone (3 mL) giving a green-black solution. Addition of benzyl chloride (17 mg, 0.138 mmol) resulted in a color change to pale yellow after one day at room temperature.

Addition of diethyl ether led to the precipitation of an off-white solid which was washed with additional diethyl ether and dried in vacuo. Yield: 33 mg, 89%. ^{1}H NMR (250 MHz, [D$_6$]acetone, 298 K): δ = 1.61 (s, 9 H), 2.42 (s, 3 H), 2.48 (s, 3 H), 3.00 (dd, *J* = 7.8 Hz and 3.2 Hz, 1 H), 3.70 (dd, *J* = 7.8 Hz and 3.0 Hz, 1 H), 6.54 (m, 2 H), 6.73 (m, 3 H), 7.25 (d, *J* = 5.8 Hz, 1 H), 7.48 (d, *J* = 5.7 Hz, 1 H), 8.25 (br. s, 2 H), 8.31 (d, *J* = 5.9 Hz, 1 H), 9.35 (d, *J* = 5.7 Hz, 1 H) ppm. $C_{24}H_{28}Cl_2N_3Rh$ (532.3): C 54.15, H 5.31, N 7.89; found C 54.04, H 5.15, N 7.93.

Reaction of 5 with Benzyl Chloride. Formation of [RhCl(CH$_2$C$_6$H$_5$)(dmbpy)(DMSO)$_2$]PF$_6$ (10): Complex **5** (70 mg, 0.119 mmol) was dissolved in DMSO (2 mL) and stirred at room temperature for 30 min giving a deep-red solution. Upon addition of benzyl chloride (30 mg, 0.238 mmol) the solution turned yellow. After 12 h at room temperature, the solution was poured into diethyl ether (17 mL) and the resulting yellow precipitate was washed with additional diethyl ether and dried in vacuo. Yield: 77 mg, 91%. ^{1}H NMR (250 MHz, [D$_6$]DMSO, 298 K): δ = 2.44 (br. d, 6 H), 3.59 (dd, *J* = 6.8 Hz and 2.9 Hz, 1 H), 4.19 (dd, *J* = 6.8 Hz and 3.2 Hz, 1 H), 6.28 (d, *J* = 7.4 Hz, 2 H), 6.50 (dd, *J* = 7.5 Hz, 2 H), 6.74 (dd, *J* = 7.3 Hz, 1 H), 8.16 (s, 1 H), 8.26 (s, 1 H), 8.82 (br. s, 2 H), 9.09 (d, *J* = 5.9 Hz, 1 H), 9.30 (d, *J* = 5.9 Hz, 1 H) ppm. $C_{23}H_{31}ClF_6N_2O_2PRhS_2$ (715.0): C 38.64, H 4.37, N 3.92; found C 38.20, H 4.80, N 4.82.

Reaction of 5 with Dichloromethane. Formation of [RhCl(CH$_2$Cl)(dmbpy)(DMSO)$_2$]PF$_6$ (11): Complex **5** (80 mg, 0.136 mmol) was dissolved in DMSO (2 mL) and an excess of CH_2Cl_2 (five drops) was added. After two days at room temperature a pale yellow solution was formed. Addition of diethyl ether and subsequent washing with diethyl ether gave an off-white solid which was dried in vacuo. Yield: 71 mg, 78%. ^{1}H NMR (250 MHz, [D$_6$]DMSO, 298 K): δ = 2.59 (s, 6 H), 3.44 (br. d, 2 H), 7.66 (d, *J* = 6.0 Hz, 2 H), 7.87 (d, *J* = 6.0 Hz, 2 H), 8.89 (s, 2 H) ppm. $C_{17}H_{26}Cl_2F_6N_2O_2PRhS_2$ (673.3): C 30.33, H 3.90, N 4.16; found C 32.70, H 3.73, N 5.15.

Reaction of 6 with Benzyl Chloride. Formation of [RhCl(CH$_2$C$_6$H$_5$)(dmbpy){CNC(CH$_3$)$_3$}$_2$]BF$_4$ (12): A deep-red acetone solution (10 mL) of **6** (60 mg, 0.111 mmol) was treated with benzyl chloride (28 mg, 0.222 mmol). The color turned to orange within 1 h and leaving the solution overnight led to the precipitation of a yellow solid. Addition of diethyl ether and subsequent washing with diethyl ether gave a yellow powder which was dried in vacuo. Yield: 64 mg, 86%. ^{1}H NMR (250 MHz, [D$_6$]DMSO, 298 K): δ = 1.58 (s, 18 H), 2.57 (s, 6 H), 3.12 (d, *J* = 2.6 Hz, 2 H), 6.77 (m, 2 H), 7.00 (m, 3 H), 7.63 (d, *J* = 5.8 Hz, 2 H), 8.54 (d, *J* = 5.7 Hz, 2 H), 8.59 (s, 2 H) ppm. $C_{29}H_{37}BClF_4N_4Rh$ (666.8): C 52.24, H 5.60, N 8.40; found C 52.10, H 5.58, N 8.38.

Reaction of 3 with Oxygen. Formation of [RhCl$_2$(O$_2$)(dmbpy)(DMSO)] (13): A red DMSO solution (2 mL) of **3** (30 mg, 0.075 mmol) was treated with an equimolar amount of O_2 (1.7 mL). The solution turned yellow immediately and after 3 h at room temperature, it was poured into diethyl ether (17 mL). The pale-yellow precipitate was filtered, washed with diethyl ether and dried in vacuo. Yield: 30 mg, 93%. ^{1}H NMR (250 MHz, [D$_6$]acetone, 298 K): δ = 2.59 (s, 3 H), 2.62 (s, 3 H), 3.39 (s, 6 H), 7.53 (d, *J* = 5.9 Hz, 1 H), 7.58 (d, *J* = 5.6 Hz, 1 H), 8.38 (s, 1 H), 8.42 (s, 1 H), 8.57 (d, *J* = 5.6 Hz, 1 H), 9.56 (d, *J* = 5.5 Hz, 1 H) ppm. FT-IR (nujol): $\tilde{\nu}$ = 870 (O−O) cm^{-1}. $C_{14}H_{18}ClN_2O_3RhS$ (432.7): C 38.86, H 4.20, N 6.47; found C 38.30, H 4.26, N 6.55.

X-ray Crystal Structure Determination of 6, 8, 9 and 12: A single crystal of **6**, **8**, **9** or **12** were mounted on the nylon loop and flash frozen in a nitrogen stream at 120 K. Data were collected on a Nonius Kappa-CCD diffractometer mounted on a FR590 generator equipped with a sealed tube with Mo-K_α radiation (λ = 0.71073Å) and a graphite monochromator. The four structures were solved by direct methods with SHELXS-97 and refined by full-matrix least-squares techniques with SHELXL-97 based on F^2.[26]

Complex 6: $C_{22}H_{30}N_4Rh{\cdot}BF_4$, orange needles, 0.2 × 0.03 × 0.03 mm^3, orthorhombic, $Pmc2_1$ (No. 20), *a* = 6.861(1), *b* = 16.516(3), *c* = 21.825(4) Å, *V* = 2473.1(9) Å^3, *Z* = 4, fw = 540.22, D_c = 1.451 Mg/m^3, μ = 0.736 mm^{-1}. The final cycle of refinement based on F^2 gave an agreement factor *R* = 0.0252 for data with $I > 2\sigma(I)$ and *R* = 0.0294 for all data (2214 reflections) with a goodness-of-fit of 0.987. Idealized hydrogen atoms were placed and refined in a riding mode.

Complex 8: $C_{15}H_{20}Cl_3N_2OSRh$, yellow, thin parallelogram, 0.30 × 0.10 × 0.02 mm^3, monoclinic, $P2_1/c$ (No. 14), *a* = 7.5840(15), *b* = 10.636(2), *c* = 23.216(5) Å, β = 99.28(3)°, *V* = 1848.2(6) Å^3, *Z* = 4, fw = 485.65, D_c = 1.745 Mg/m^3, μ = 1.474 mm^{-1}. The final cycle of refinement based on F^2 gave an agreement factor *R* = 0.027 for data with $I > 2\sigma(I)$ and *R* = 0.040 for all data (4219 reflections) with a goodness-of-fit of 1.030. Idealized hydrogen atoms were placed and refined in a riding mode. Two hydrogen atoms on C4 were found and refined manually.

Complex 9: $C_{24}H_{28}N_3Cl_2Rh{\cdot}1/2(C_3H_6O){\cdot}H_2O$, yellow, bipyramidal prisms, 0.05 × 0.05 × 0.05 mm^3, tetragonal, $I4_1/a$ (No. 88), *a* = *b* = 20.722(3), *c* = 26.090(5) Å, *V* = 11203(3) Å^3, *Z* = 16, fw = 579.36, D_c = 1.374 Mg/m^3, μ = 0.824 mm^{-1}. The final cycle of refinement based on F^2 gave an agreement factor *R* = 0.0362 for data with $I > 2\sigma(I)$ and *R* = 0.0508 for all data (4291 reflections) with a goodness-of-fit of 1.054. Idealized hydrogen atoms were placed and refined in riding mode The acetone is disordered with 1/2 a molecule per asymmetric unit.

Complex 12: $C_{29}H_{37}N_4ClRh{\cdot}C_3H_6O{\cdot}BF_4$, colorless, prisms, 0.3 × 0.3 × 0.3 mm^3, monoclinic, $P2_1/n$ (No. 14), *a* = 12.623(3), *b* = 21.262(4), *c* = 14.011(3) Å, β = 105.84(3)°, *V* = 3617.7(13) Å^3, *Z* = 4, fw = 724.87, D_c = 1.331 Mg/m^3, μ = 0.596 mm^{-1}. The final cycle of refinement based on F^2 gave an agreement factor *R* = 0.0491 for data with $I > 2\sigma(I)$ and *R* = 0.0596 for all data (7146 reflections) with a goodness-of-fit of 1.035. Idealized hydrogen atoms were placed and refined in a riding mode. C32, C33 and C34 (one *tert*-butyl group) and the BF_4 are partially disordered and modeled with two alternative positions.

CCDC-176695 (**9**), -176696 (**12**), -176697 (**6**), and -176698 (**8**) contain the supplementary crystallographic data for this paper. These data can be obtained free of charge at www.ccdc.cam.ac.uk/conts/retrieving.html [or from the Cambridge Crystallographic Data Centre, 12, Union Road, Cambridge CB2 1EZ, UK; Fax: (internat.) +44-1223/336-033; E-mail: deposit@ccdc.cam.ac.uk].

Acknowledgments

This work was supported by the Israel Science Foundation, Jerusalem, Israel, and by the Tashtiyot program of the Israeli Ministry of Science. DM is the Israel Matz professor of organic chemistry.

[1] A. Togni, L. M. Venanzi, *Angew. Chem. Int. Ed. Engl.* **1994**, *33*, 497−526.
[2] C. Kaes, A. Katz, M. W. Hosseini, *Chem. Rev.* **2000**, *100*, 3553−3590.

[3] G. Zassinovich, G. Mestroni, S. Gladiali, *Chem. Rev.* **1992**, *92*, 1051−1069.
[4] G. Mestroni, R. Spogliarich, A. Camus, F. Martinelli, G. Zassinovich, *J. Organomet. Chem.* **1978**, *157*, 345−352.
[5] R. D. Gillard, K. Harrison, I. H. Mather, *J. Chem. Soc.* **1975**, 133−140, and references therein.
[6] For 1,5-cyclooctadiene, see ref.[4] and references therein; for cyclooctatetraene, see: C. Cocevar, G. Mestroni, A. Camus, *J. Organomet. Chem.* **1972**, *35*, 389−395, and references therein. For norbornadiene, see: J. J. Robertson, A. Kadziola, R. A. Krause, S. Larsen, *Inorg. Chem.* **1989**, *28*, 2097−2102, and references therein. For 1,5-hexadiene, see: G. Mestroni, G. Zassinovich, A. Camus, *J. Organomet. Chem.* **1977**, *140*, 63−72.
[7] S. Morton, J. F. Nixon, *J. Organomet. Chem.* **1985**, *282*, 123−126.
[8] G. Mestroni, A. Camus, G. Zassinovich, *J. Organomet. Chem.* **1974**, *65*, 119−129. For oxidative addition of hydrogen to $[Rh(bpy)_2]X$, see: S. G. Yan, B. S. Brunschwig, C. Creutz, E. Fujita, N. Sutin, *J. Am. Chem. Soc.* **1998**, *120*, 10553−10554.
[9] H. Werner, L. Hofmann, R. Feser, W. Paul, *J. Organomet. Chem.* **1985**, *281*, 317−347.
[10] T. B. Marder, W. C. Fultz, J. C. Calabrese, R. L. Harlow, D. Milstein, *J. Chem. Soc., Chem. Commun.* **1987**, 1543−1545.
[11] P. J. Fennis, P. H. M. Budzelaar, J. H. G. Frijns, A. G. Orpen, *J. Organomet. Chem.* **1990**, *393*, 287−298.
[12] H. Nishiyama, M. Horihata, T. Hirai, S. Wakamatsu, K. Itoh, *Organometallics* **1991**, *10*, 2706−2708.
[13] H. F. Haarman, J. M. Ernsting, M. Kranenburg, H. Kooijman, N. Veldman, A. L. Spek, P. W. N. M. van Leeuwen, K. Vrieze, *Organometallics* **1997**, *16*, 887−900.
[14] K. J. Bradd, B. T. Heaton, C. Jacob, J. T. Sampanthar, A. Steiner, *J. Chem. Soc., Dalton Trans.* **1999**, 1109−1112.
[15] T. Yoshida, T. Ueda, T. Adachi, K. Yamamoto, T. Higuchi, *J. Chem. Soc., Chem. Commun.* **1985**, 1137−1138.
[16] E. G. Burns, S. S. C. Chu, P. de Meester, M. Lattman, *Organometallics* **1986**, *5*, 2383−2384.
[17] K. Kashiwabara, A. Morikawa, T. Suzuki, K. Isobe, K. Tatsumi, *J. Chem. Soc., Dalton Trans.* **1997**, 1075−1081.
[18] R. Ziessel, L. Toupet, S. Chardon-Noblat, A. Deronzier, D. Matt, *J. Chem. Soc., Dalton Trans.* **1997**, 3777−3784.
[19] We chose this ligand over the parent 2,2′-bipyridine for reasons of solubility and easier characterization by NMR of the complexes.
[20] M. Aresta, E. Quaranta, *J. Organomet. Chem.* **1993**, *463*, 215−221.
[21] R. Dorta, H. Rozenberg, D. Milstein, *Chem. Commun.* **2002**, 710−711.
[22] Surprisingly, besides these two complexes, two new species were detected which were the only ones remaining after prolonged heating (2 weeks at 80 °C). Although these complexes were not isolated, we believe that water present in the $[D_6]$DMSO led to the formation of the trichloro compound $[RhCl_3(dmbpy)(DMSO)]$. The ^1H NMR signals of the dmbpy ligand indicate a ca. 1:1 ratio of the two possible isomers.
[23] For a similar peroxo complex, see: H. F. Haarman, F. R. Bregman, P. W. N. M. van Leeuwen, K. Vrieze, *Organometallics* **1997**, *16*, 979−985.
[24] P. Hofmann, C. Meier, U. Englert, U. Schmidt, *Chem. Ber.* **1992**, *125*, 353−365.
[25] R. Cramer, *Inorg. Chem.* **1962**, *1*, 722−723.
[26] SHELX-97, *Program for Crystal Structure Refinement*, G. M. Sheldrick, University of Goettingen, **1997**.

Received January 11, 2002
[I02016]

A Europium(II) Complex with Benzo-15-Crown-5

Przemysław Starynowicz*[a] and Krystyna Bukietyńska[a]

Dedicated to the memory of Mikołaj Starynowicz

Keywords: Europium / Crown compounds / X-ray diffraction / Luminescence / Lanthanides

The present paper reports the crystal structure and luminescent properties of bis(benzo-15-crown-5)europium(II) diperchlorate. The structure is composed of complex bis(benzo-15-crown-5)europium(II) cations and perchlorate anions. The complex cation is centrosymmetric, and the metal ion is surrounded by 10 oxygen atoms of two ligand molecules. The compound shows very bright luminescence at 23450 cm^{-1}. The emission parameters (wavelength and the average lifetime of the excited state) are compared to those previously reported for the analogous complex in methanol solutions.
(© Wiley-VCH Verlag GmbH, 69451 Weinheim, Germany, 2002)

Introduction

Complexes of divalent lanthanides (mainly Eu^{II}) with crown ethers have attracted much attention and the present state of the investigations on these complexes was excellently reviewed by Jiang et al.[1] The interest in these compounds is motivated both by the luminescent properties of the Eu^{2+} cation in the macrocyclic coordination environment and by the ligand's ability to stabilize the divalent state of the lanthanide. The luminescence quantum yield of the Eu^{II}-crown ether complexes in methanol solutions is increased relative to solutions of $EuCl_2$ and noncyclic polyethers because of encapsulation of the central ion, which in turn prevents the solvent OH groups from entering the first coordination sphere of the metal. This effect is particularly pronounced for 15-crown-5 and some of its derivatives. On the other hand the f^6d-state splittings in these systems, deduced from absorption and emission spectra, are smaller than for the $EuCl_2$-methanol system. The other interesting feature of the discussed complexes is their ability to shift the reduction potential of the Eu^{III}/Eu^{II} couple towards more positive values,[2] which may eventually lead to the application of these compounds or their derivatives as redox-sensitive shift agents in MRI tomography. It is therefore important and very interesting to gain information about the possible coordination behaviour of the macrocycles in compounds with Eu^{II} both in solution and in the solid state. Unfortunately, to the best of the authors' knowledge, there are no reports on the crystal structures of Ln^{II}-crown ether complexes, or attempts to correlate their spectroscopic properties in the solid state with their properties in solution. This work, which is an extension of our earlier work on Eu^{II} carboxylates, is intended to be such an attempt.

[a] Faculty of Chemistry, University of Wrocław,
ul. F. Joliot-Curie 14, 50-383 Wrocław, Poland
E-mail: psta@wchuwr.chem.uni.wroc.pl
[b] Faculty of Chemistry, University of Wrocław,
ul. F. Joliot-Curie 14, 50-383 Wrocław, Poland
E-mail: bk@wchuwr.chem.uni.wroc.pl

Results and Discussion

Crystal Structure

The crystals are built up from complex bis(benzo-15-crown-5)europium(II) cations and perchlorate anions, which are kept together by weak electrostatic and Van der Waals interactions. The metal ion is located at an inversion centre, between two symmetry-related ligand molecules, thus forming a sandwich-like complex cation. Such a coordination fashion for 15-crown-5-type ligands is common for K,[3] Rb,[4] Cs,[5] Sr[6] or Ba[7] (see also J. W. Steed[8] for a general review), whereas the trivalent lanthanide cations typically form 1:1 complexes.[9] The Eu^{2+} ion is accordingly surrounded by ten oxygen atoms, and the metal coordination environment may be described as a slightly distorted pentagonal antiprism with approximate point symmetry D_{5d}. The θ angles between the idealised C_5 axis and the Eu−O vectors are in the range 55.3−61.2°, with the average being 58.4°. The Eu−O distances, given in Table 1, although within the range observed in previously reported organic Eu^{II} compounds,[10] should be considered as rather long.

Table 1. The Eu−O distances (Å)

Eu−O(5)	2.662(3)
Eu−O(1)	2.688(3)
Eu−O(3)	2.694(3)
Eu−O(4)	2.718(4)
Eu−O(2)	2.728(4)

The shortest Eu−Eu distance is 9.774(2) Å. The whole macrocycle fragment is rather puckered and the aliphatic -CH_2-CH_2- chains in the macrocycle ring are disordered over two sets of positions (see the Exp. Sect.). The high values of the transversal principal components of the thermal ellipsoids may also indicate disorder within the benzo rings; however this could not be resolved during the refinement. The complex cation is drawn in Figure 1.

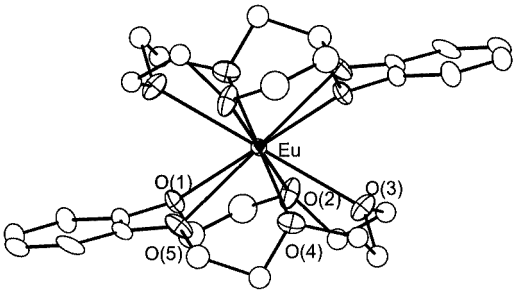

Figure 1. A DIAMOND[20] view of the complex cation; for the sake of clarity only symmetry-independent oxygen atoms have been labelled and the disordered carbon sites with the lower occupancy have been omitted

Spectroscopy

The compound shows very bright luminescence (to the point of gaining a violet hue in full daylight). The emission is observed in the form of a single peak with the maximum at 422 nm (23700 cm^{-1}) at room temperature, and at 426.5 nm (23450 cm^{-1}) at 77 K (see Figure 2). These values are slightly different from those reported for the Eu^{2+}-benzo-15-crown-5 system in methanol solution [417 nm (23980 cm^{-1})],[1,11] which may suggest a larger splitting of the excited $4f^65d^1$ state in the crystal. To identify the emitting level we decided to use the Jγ coupling method as described by Johnson and Sandoe.[12] Thus, it is commonly known that the lowest multiplet of the $4f^6$ core is ^7F, so only splitting of the 5d orbitals merits attention. To simplify our considerations we assumed that the degeneration of the 5d states is lifted by interaction with the ten oxygen atoms belonging to the first coordination sphere only, and the symmetry of the latter is D_{5d}. Following Gołębiewski,[13] the energy shift of the d orbitals in any crystal field is:

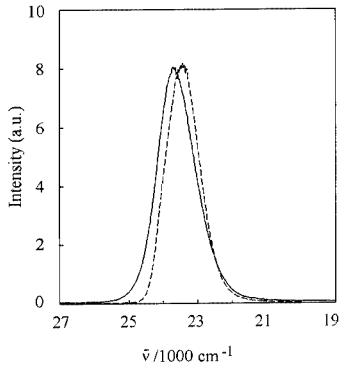

Figure 2. Emission spectrum of the complex at room temperature (solid line) and at 77 K (dashed line)

$$\Delta E(d_z2) = \frac{2}{7}L_{20}G_2+\frac{2}{7}L_{40}G_4;$$

$$\Delta E(d_{xz}) = \frac{1}{7}L_{20}G_2-\frac{4}{21}L_{40}G_4+\frac{1}{126}(9L_{22}G_2+2L_{42}G_4);$$

$$\Delta E(d_{yz}) = \frac{1}{7}L_{20}G_2-\frac{4}{21}L_{40}G_4-\frac{1}{126}(9L_{22}G_2+2L_{42}G_4); \quad (1)$$

$$\Delta E(d_x2_{-y}2) = -\frac{2}{7}L_{20}G_2+\frac{1}{21}L_{40}G_4+\frac{1}{504}L_{44}G_4;$$

$$\Delta E(d_{xy}) = -\frac{2}{7}L_{20}G_2+\frac{1}{21}L_{40}G_4-\frac{1}{504}L_{44}G_4;$$

where the L terms are angular factors in the form:

$$L_{20} = \frac{1}{2}\Sigma(3\cos^2\theta_i-1);$$

$$L_{40} = \frac{1}{8}\Sigma(35\cos^4\theta_i-30\cos^2\theta_i+3);$$

$$L_{22} = 3\Sigma\sin^2\theta_i\cos2\varphi_i; \quad (2)$$

$$L_{42} = 7\Sigma(7\cos^2\theta_i-1)\sin^2\theta_i\cos2\varphi_i;$$

$$L_{44} = 105\Sigma\sin^4\theta_i\cos4\varphi_i;$$

where θ_i and $_i$ are the angular coordinates of the i-th ligand, and the summation runs over all ligand positions. The G_2 and G_4 are (positive) radial integrals, as defined previously;[13] their detailed forms are not necessary for the reasoning below. Assuming that $\theta_i = \theta$ or $\pi-\theta$, and the φ_i angles span two regular pentagons, the last three L functions disappear. On substituting the previously obtained value of 58.4° for θ into the above equations, one gets:

$$\Delta E(d_z2) = -0.252G_2-0.928G_4 \quad (A_{1g});$$

$$\Delta E(d_{xz}) = \Delta E(d_{yz}) = -0.126G_2+0.619G_4 \quad (E_{1g}); \quad (3)$$

$$\Delta E(d_x2_{-y}2) = \Delta E(d_{xy}) = 0.252G_2-0.155G_4 \quad (E_{2g});$$

where the symbols of the relevant irreducible representations are given in parentheses.

Thus the d_{z^2} orbital will be the lowest, and the emitting states may be described as $4f^6(^7F)5d_{z^2}$. Furthermore, one may tentatively assume that the energy difference between the e_{1g} and e_{2g} orbitals will not be large because of different signs of the coefficients of G_2 and G_4; the ratio G_2/G_4 lies between 2 and 4.[13] The splitting of the $4f^6$ core must also be taken into consideration, which gives rise to a rather complicated structure of higher lying excited states that can be observed in the excitation spectra (Figure 3). The range in which the bands are observed is similar to the ranges observed in the excitation spectra of Eu^{2+} doped in $BaMg_2Si_2O_7$ [14] or MgF_2 matrices.[15] In our case the spectrum may be roughly divided into two parts: a more intense band between 270 and 400 nm (25000−37000 cm^{-1}; marked as band A in the Figure 3), and a weaker one between 220 and 270 nm (37000−45500 cm^{-1}; band B). The difference between their centres may be estimated as approximately 12000 cm^{-1}, which is similar to the energy difference between the ^7F and ^5D states in Eu^{3+} [16] or Sm^{2+}.[17] Considering this, and the earlier assumption of a small splitting of the e_{1g} and e_{2g} orbitals, one can conclude that the band B must reflect the positions of the $4f^6(^5D)5d$ states. The luminescence decay curves were monoexponen-

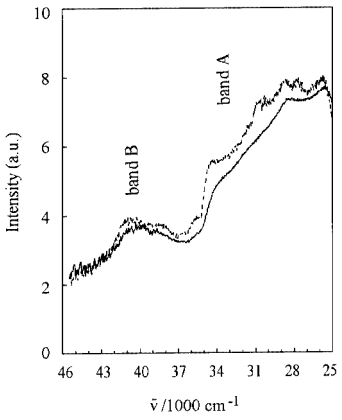

Figure 3. Excitation spectrum of the complex at room temperature (solid line) and at 77 K (dashed line)

tial, with a mean lifetime of the excited state of 0.65(2) μs at room temperature and 0.59(1) μs at 77 K. Comparison of these values with the value observed for methanol solutions (0.14 μs)[11] suggests additional relaxation processes, which could be caused by the presence of methanol OH oscillators in the first coordination sphere of the metal in solution.

Conclusion

A new complex of Eu^{II} with benzo-15-crown-5 has been obtained and characterized by X-ray diffraction and spectroscopic methods. Its properties, namely energy and the luminescence lifetime of the $4f^6 5d \rightarrow 4f^7$ transition, are different from those reported for the $EuCl_2$-benzo-15-crown-5 system in methanol solution. We can therefore conclude that the structure of the complex in the solid state is different from the labile species existing in the solution — in the latter case the solvent molecules probably enter the first coordination sphere of Eu.

Experimental Section

Preparation: Eu_2O_3 (0.663 g, 1.9 mmol) was dissolved in a small excess of 60% $HClO_4$, evaporated until white fumes appeared, cooled down and dissolved in a few millilitres of a 3:1 methanol/water mixture. To this benzo-15-crown-5 (1 g, 3.7 mmol) was added. The resulting mixture was placed in an H-shaped electrolyzer with a pool mercury cathode, platinum anode and a sintered glass diaphragm between the anode and cathode compartments. A dilute solution of $HClO_4$ in a 2:1 methanol/water mixture was the anolyte. Electrolysis was performed at a potential of −1 V with respect to the saturated calomel electrode. The first crystals appeared after half an hour. The compound is colourless, with a light violet hue in full daylight, and is rather stable in air at room temperature. $C_{28}H_{40}Cl_2EuO_{18}$: calcd. C 37.89, H 4.68, Cl 7.99, Eu 17.12; found C 37.21, H 4.54, Cl not analysed due to the explosive properties of the compound, Eu 16.30.

Spectroscopy: The luminescence and excitation spectra were measured on an SCL Aminco 500 spectrofluorimeter. The luminescence was excited with a lamp source with a wavelength of 330 nm, and the excitation spectra were recorded for the emission at 425 nm. The luminescence decay curves were detected on a device equipped with a Hamamatsu photomultiplier and Tektronix TDS-3052 digital oscilloscope. The sample was excited with the third harmonic of a neodymium laser (355 nm), and the registered output signal had a wavelength of 23460 cm^{-1}. All the measurements (luminescence, excitation and life times) were recorded at room temperature and at 77 K.

X-ray Crystallographic Study: An appropriate crystal was cut from a larger one and mounted on a Kuma KM4 diffractometer equipped with a CCD counter. The collected data were corrected for polarisation, Lorentz and absorption effects; the latter was calculated from the crystal habit captured from a photo scan. The position of Eu was found from a Patterson map, and the rest of the non-H atoms from difference Fourier maps. The positions of the hydrogen atoms were calculated geometrically. The refinement was full-matrix with all ordered atoms anisotropic. The carbon atoms belonging to the aliphatic fragment of the ligand were found to be disordered between two sets of positions [denoted with suffices A and B in the relevant atom names, with occupancies of 0.642(7) and 0.358(2), respectively], and therefore kept isotropic. The temperature factors of the H atoms were constrained to be 1.2-times the factors of the relevant C atoms.

The programs used were SHELXS-97[18] for the solution, and SHELXL-97[19] for the refinement. The data collection and refinement details are presented in Table 2.
CCDC-177469 contains the supplementary crystallographic data for this paper. These data can be obtained free of charge at www.ccdc.cam.ac.uk/conts/retrieving.html [or from the Cambridge Crystallographic Data Centre, 12, Union Road, Cambridge CB2 1EZ, UK; fax: (internat.) +44-1223/336-033; E-mail: deposit@ccdc.cam.ac.uk].

Table 2. Crystal data and structure refinement details

Empirical formula	$C_{28}H_{40}Cl_2EuO_{18}$
Molecular weight	887.46
Temperature	100(2) K
Wavelength	0.71073 Å
Crystal system, space group	monoclinic, $P2_1/n$
Unit cell dimensions	a = 9.774(2) Å
	b = 10.558(2) Å
	c = 16.989(4) Å
	β = 102.57(2)°
Volume	1711.1(6) $Å^3$
Z, Calculated density	2, 1.722 $Mg·m^{-3}$
Absorption coefficient	2.067 mm^{-1}
F(000)	898
Crystal size	0.25 × 0.2 × 0.1 mm
Theta range for data collection	3.3 to 28.5°
Index ranges	$-12 \le h \le 11$, $-13 \le k \le 13$, $-22 \le l \le 22$
Reflections collected/ unique	11102/4036 (R_{int} = 0.0378)
Completeness to 2θ = 28.5°	88.7%
Absorption correction	calculated from the crystal shape
Max. and min. transmission	0.856 and 0.609
Refinement method	full-matrix least-squares on F^2
Data/ restraints/ parameters	4036/148/216
Goodness-of-fit on F^2	1.901
Final R indices [$I > 2\sigma(I)$]	$R(F)$ = 0.0459, $R_w(F^2)$ = 0.0645
R indices (all data)	$R(F)$ = 0.0739, $R_w(F^2)$ = 0.0668
Largest diff. peak and hole	1.000 and −0.903 e·$Å^{-3}$

Acknowledgments

DSci. Z. Ciunik is thanked for his help in the diffractometric data collection, and Dr. J. Sokolnicki, Dr. S. Gołąb and Prof. W. Ryba-Romanowski are gratefully acknowledged for their help in the spectroscopic measurements

[1] J. Jiang, N. Higashiyama, K. Machida, G. Adachi, *Coord. Chem. Rev.* **1998**, *170*, 1−29.
[2] N. Higashiyama, K. Machida, G. Adachi, *Chem. Express* **1992**, *7*, 113−116.
[3] [3a] V. W. Bhagwat, H. Manohar, N. S. Poonia, *Inorg. Nuclear Chem. Lett.* **1981**, *17*, 207−2101. [3b] P. R. Mallison, M. R. Truter, *J. Chem. Soc., Perkin Trans. 2* **1972**, 1818−1823. [3c] J. Pickardt, P. Wischlinski, *Z. Anorg. Allg. Chem.* **1999**, *625*, 1527−1531. [3d] W. Xu, K. Clinger, M. L. Hackert, N. S. Poonia, *J. Inclusion Phenom. Macrocyclic Chem.* **1985**, *3*, 163−172. [3e] W. S. Sheldrick, N. S. Poonia, *J. Inclusion Phenom. Macrocyclic Chem.* **1986**, *4*, 93−98; and many others.
[4] C. Momany, K. Clinger, M. L. Hackert, N. S. Poonia, *J. Inclusion Phenom. Macrocyclic Chem.* **1986**, *4*, 61−67.
[5] [5a] A. Nurtaeva, E. M. Holt, *Acta Crystallogr., Sect. C* **1999**, *55*, 1453−1457. [5b] M. Schnock, C. Müller, P. Bottcher, *Z. Anorg. Allg. Chem.* **1996**, *622*, 655−662.
[6] V. Müller, C. Grebe, U. Müller, K. Dehnicke, *Z. Anorg. Allg. Chem.* **1993**, *619*, 416−420.
[7] [7a] L. Nuñez, R. D. Rogers, *J. Coord. Chem.* **1993**, *28*, 347−354. [7b] J. Feneau-Dupont, E. Arte, J. P. Declercq, G. Germain, M. van Meerssche, *Acta Crystallogr., Sect. B* **1979**, *35*, 1217−1220.
[8] J. W. Steed, *Coord. Chem. Rev.* **2001**, *215*, 171−221.
[9] [9a] J.-C. Bünzli, B. Klein, G. Chapuis, K. J. Schenk, *Inorg. Chem.* **1982**, *21*, 808−812. [9b] L. Yonghua, X. Yan, *Huaxue Xuebao (Acta Chim. Sinica)* **1983**, *41*, 97. [9c] L. Pinzhe, Sh. Cheng, F. Yuguo, J. Songchun, Zh. Shugong, Y. Fenglan, *Fenz. Kex. Yu Huax. Yanjiu* **1983**, *3*, 77. [9d] R. D. Rogers, L. K. Kurihara, *Inorg. Chim. Acta* **1987**, *130*, 131−137. [9e] H. Ningkai, L. Zhenxiang, Zh. Qinglian, Y. Binghu, J. Zhongsheng, N. Jaizuan, *Yingyong Huaxue (Chin. J. Appl. Chem.)* **1987**, *4*, 22. [9f] W. Rui-Yao, J. Zhong-Sheng, N. Jia-Zan, *Chinese J. Struct. Chem. (Jiegou Huaxue)* **1991**, *10*, 20.
[10] [10a] A. Lossin, G. Meyer, *Z. Anorg. Allg. Chem.* **1992**, *614*, 12−16. [10b] P. Starynowicz, *Polyhedron* **1995**, *14*, 3573−3577. [10c] P. Starynowicz, *J. Alloys Comp.* **1995**, *225*, 406−408. [10d] P. Starynowicz, *J. Alloys Comp.* **1998**, *268*, 47−49. [10e] P. Starynowicz, *J. Alloys Comp.* **1998**, *269*, 67−70. [10f] P. Starynowicz, *J. Alloys Comp.* **1998**, *275−277*, 815−817. [10g] P. Starynowicz, *J. Alloys Comp.* **2000**, *305*, 117−120. [10h] P. Starynowicz, *J. Alloys Comp.* **2001**, *323−324*, 159−163, [10i] L. Burai, E. Tóth, S. Seibig, R. Scopelliti, A. E. Merbach, *Chem. Eur. J.* **2000**, *6*, 3761−3770.
[11] G. Adachi, K. Sorita (K. Sakai), K. Kawata, K. Tomiyoko, J. Shiokawa, *J. Less-Common Met.* **1983**, *93*, 81−87.
[12] K. E. Johnson, J. N. Sandoe, *J. Chem. Soc. (A)* **1969**, 1694−1697.
[13] A. Gołębiewski, *Chemia kwantowa związków nieorganicznych*, Państwowe Wydawnictwo Naukowe, Warszawa, **1969**.
[14] G. Q. Yao, J. H. Lin, L. Zhang, G. X. Lu, M. L. Gong, M. Z. Su, *J. Mater. Chem.* **1998**, *8*, 585−588.
[15] S. Lizzo, A. H. Velders, A. Meijerink, G. J. Dirksen, G. Blasse, *J. Luminescence* **1996**, *65*, 303−311.
[16] See, for example: [16a] W. T. Carnall, P. R. Fields, K. Rajnak, *J. Chem. Phys.* **1968**, *49*, 4450−4455. [16b] W. T. Carnall, G. L. Goodman, K. Rajnak, R. S. Rama, *Report ANL-88−8*, Argonne National Laboratory, Argonne **1988**.
[17] [17a] A. Meijerink, G. J. Dirksen, *J. Luminescence* **1995**, *63*, 189−201. [17b] C. Wickleder, *J. Alloys Comp.* **2000**, *300−301*, 193−198.
[18] G. M. Sheldrick, SHELXS-97. Program for structure solution. University of Göttingen, **1997**.
[19] G. M. Sheldrick, SHELXL-97. Program for structure refinement. University of Göttingen, **1997**.
[20] DIAMOND − Visual Crystal Structure Information System, CRYSTAL IMPACT, Postfach 1251, 53002 Bonn, Germany.

Received January 14, 2002
[I02025]

Synthesis, Structures, and Redox Properties of Copper Complexes with Chiral and Achiral Amino Acid Derived Ligands

Nicole Niklas,[a] Frank Hampel,[b] Olaf Walter,[c] Günter Liehr,[a] and Ralf Alsfasser*[a]

Keywords: Amino acids / Chirality / Copper / Redox chemistry

A series of copper(II) complexes containing the amino acid derived ligands bpaAc-Gly-OEt {**1**; [bis(picolyl)amino]acylglycine ethyl ester} and bpaAc-Phe-OMe {**2**; [bis(picolyl)amino]acylphenylalanine methyl ester} were synthesized and characterized in solution and in the solid state. This was done in order to evaluate the relevance of weak aromatic interactions between a metal center and amino acid side chains in square-pyramidal or octahedral coordination environments. The results showed that the structural, spectroscopic, and electrochemical properties of the copper(II) center are not affected by the amino acid side chain structure. This is in remarkable contrast to our previous investigations on zinc(II) complexes of the same ligands, which indicate close association of the metal center and the phenyl substituent of **2** in a trigonal-bipyramidal environment.

(© Wiley-VCH Verlag GmbH, 69451 Weinheim, Germany, 2002)

Introduction

Aromatic rings are important structural and functional elements both in biological and in synthetic supramolecular architectures. They significantly contribute to the intramolecular stabilization of structures, as well as to the formation of intermolecular complexes.[1–6] This is achieved either through noncovalent ring stacking[7] or through π-cation interactions.[8,9] Furthermore, the redox-active aromatic amino acids tyrosine and tryptophan are known to participate in metalloenzyme-catalyzed substrate oxidations.[10]

The quest for synthetic metalloenzyme mimetics has stimulated much interest in the characterization of weak aromatic ring/cation interactions in small coordination complexes.[11–16] We have recently reported trigonal-bipyramidal zinc complexes of the amino acid derived ligands bpaAc-Gly-OEt (**1**) and bpaAc-Phe-OMe (**2**), shown in Scheme 1 {bpaAc = [bis(2-picolyl)amino]acyl; Gly-OEt = glycine ethyl ester; Phe-OMe = phenylalanine methyl ester}.[17] Intriguing features of the phenylalanine derivatives are: (i) the relatively short distance of 4.5 Å between the zinc ion and the center of the phenyl ring, and (ii) a rigid conformation of the benzyl side chain in solution. The latter is evidenced by analysis of the proton NMR chemical shifts and coupling constants.

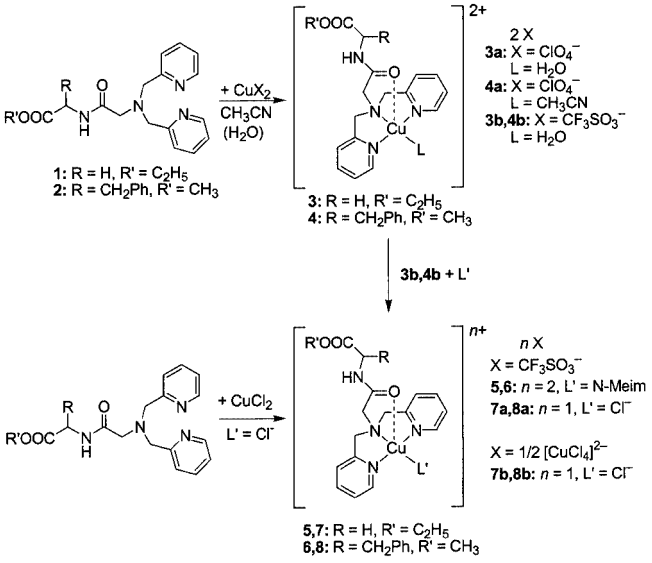

Scheme 1. Copper(II) coordination chemistry of bpaAc-Gly-OEt (**1**) and bpaAc-Phe-OMe (**2**)

Here we report the synthesis and characterization of copper(II) complexes containing **1** and **2**. This was done in order to evaluate specific geometric requirements for the occurrence of weak aromatic interactions in complexes containing our tripodal N_3O ligand framework. In contrast to our findings for trigonal-bipyramidal zinc complexes, X-ray structure analyses together with electrochemical, EPR, and

[a] Institute of Inorganic Chemistry, University of Erlangen-Nürnberg,
Egerlandstr. 1, 91058 Erlangen, Germany
Fax: (internat.) + 49-(0)9131/852-7387
E-mail: alsfasser@chemie.uni-erlangen.de
[b] Institute of Organic Chemistry, University of Erlangen-Nürnberg,
Henkestrasse 42, 91054 Erlangen, Germany
[c] ITC-CPV, Forschungszentrum Karlsruhe,
Postfach 3640, 76021 Karlsruhe

circular dichroism measurements in solution demonstrated that the phenyl ring in **2** is flexible in square-pyramidal copper(II) compounds and does not efficiently interact with the metal center.

Results

Synthesis

All reactions are summarized in Scheme 1. The complexes [(bpaAc-Gly-OEt)(H_2O)Cu](ClO_4)$_2$ (**3a**), [(bpaAc-Gly-OEt)(H_2O)Cu](OTf)$_2$ (**3b**, OTf = CF_3SO_3), [(bpaAc-Phe-OMe)(CH_3CN)Cu](ClO_4)$_2$ (**4a**), and [(bpaAc-Phe-OMe)(H_2O)Cu](OTf)$_2$ (**4b**) were readily obtained from acetonitrile solutions containing stoichiometric amounts of the respective ligand and copper(II) salt. The *N*-methylimidazole complex [(bpaAc-Gly-OEt)(*N*-Meim)Cu](OTf)$_2$ (**5**) was similarly formed in one-pot reaction mixtures containing stoichiometric amounts of the ligand **1**, *N*-Meim, and Cu(OTf)$_2$. This was not the case for the sterically more demanding ligand **2**, with only [(*N*-Meim)$_5$Cu](OTf)$_2$ and bpaAc-Phe-OMe being isolated under the same conditions. However, the complex [(bpaAc-Phe-OMe)(*N*-Meim)Cu](OTf)$_2$ (**6**) was readily obtained by substitution of the labile aquo ligand from **4b**. This method worked equally well in the synthesis of **5** from **3b**.

Ligand exchange from **3b** and **4b** was also a convenient route to generate the chloro complexes [(bpaAc-Gly-OEt)Cu(Cl)](OTf) (**7a**) and [(bpaAc-Phe-OMe)Cu(Cl)](OTf) (**8a**) in situ for spectroscopic studies in solution. As we have reported earlier for the glycine derivative **7b**,[18] the cations [LCuCl]$^+$ may also be synthesized by treatment of the respective ligand with copper(II) chloride. This method always results in the formation of chlorocuprate anions, which severely complicate spectroscopic investigations. However, the tetrachlorocuprate salt [(bpaAc-Phe-OMe)Cu(Cl)]$_2$[$CuCl_4$] (**8b**) was the only copper(II) complex of ligand **2**, other than the acetonitrile diperchlorate derivative **4a**, to yield single crystals suitable for an X-ray structure determination.

Structures

We have characterized the glycine derivatives **3a**, **3b**, and **5**, as well as the phenylalanine derivatives **4a** and **8b**, by X-ray structure analyses. ORTEP plots of the cations containing **1** are shown in Figures 1−3, and the cations containing **2** are presented in Figures 4 and 5. Crystallographic details are summarized in Table 1; the structure of **7b** has been reported elsewhere.[18] All complexes show a similar first coordination sphere with a typical Jahn−Teller-distorted octahedral geometry around the copper(II) center. The three bpa nitrogen atoms of the tripodal ligands are bound in the equatorial plane and the amide oxygen atom occupies one of the axial positions. The equatorial plane is completed by the respective monodentate coligand − water (**3a**, **3b**), CH_3CN (**4a**), *N*-Meim (**5**), or chloride (**8b**) − and a weakly coordinating anion (Cu−L > 2.5 Å) is located at the respective second axial sites in the complexes **3a**, **3b**, **4a**, and **5**. Pairs of cations are formed by **8b**, with the coordinated chloro ligand of one complex above the copper center of the other at a nonbonding distance of ca. 3.1 Å. Bond lengths and angles are compared in Table 2. The first coordination spheres within our series are very similar, and all structural parameters agree well with those of the closely related complexes described by Nishida et al.[19,20]

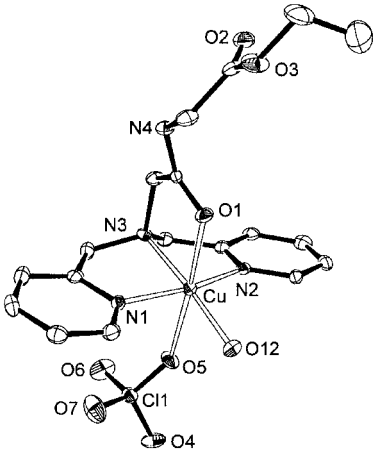

Figure 1. ORTEP plot (30% ellipsoids) of the cation [(bpaAc-Gly-OEt)(H_2O)Cu(ClO_4)]$^+$ (**3a**); hydrogen atoms are omitted for clarity

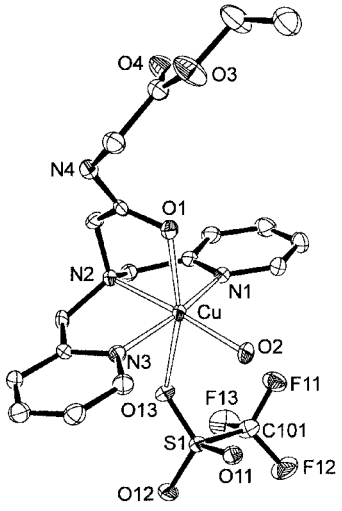

Figure 2. ORTEP plot (30% ellipsoids) of the cation [(bpaAc-Gly-OEt)(H_2O)Cu(CF_3SO_3)]$^+$ (**3b**); hydrogen atoms are omitted for clarity

Interesting are the different orientations adopted by the benzyl substituents in **4a** and **8b**. In both cases the structures are disordered. They refined best by assumption of two overlapping conformers with their phenyl rings in different orientations with respect to the equatorial plane defined by the first coordination sphere, as illustrated in Figures 4 and 5. The shortest distance between the copper(II) center and the phenyl ring center is observed in conformer B of **8b** (Figure 5; 7.24 Å). As a consequence of the disordered benzyl substituents and the disordered solvent mole-

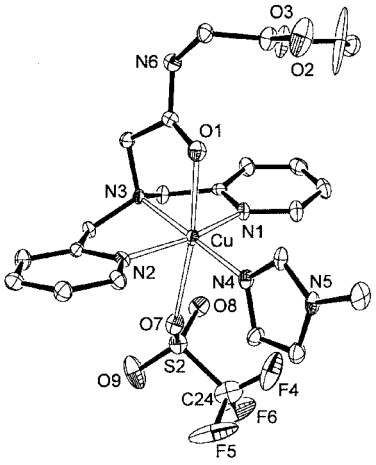

Figure 3. ORTEP plot (30% ellipsoids) of the cation [(bpaAc-Gly-OEt)(*N*-Meim)Cu(CF_3SO_3)]$^+$ (**5**); hydrogen atoms are omitted for clarity

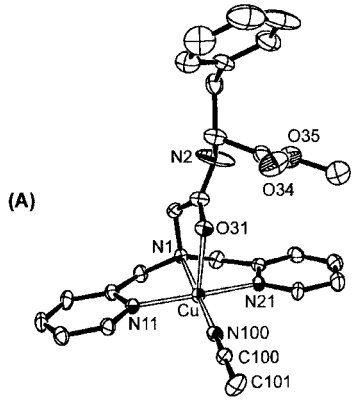

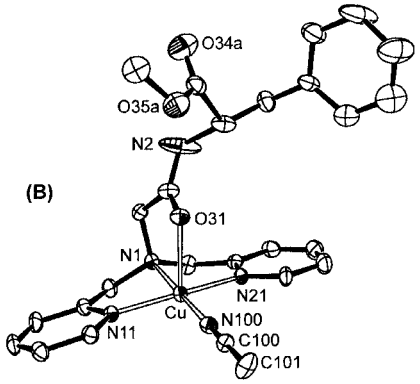

Figure 4. ORTEP plots (30% ellipsoids) of the two conformational isomers (A) and (B) of the cation [(bpaAc-Phe-OMe)(CH_3CN)Cu]$^{2+}$ (**4a**); hydrogen atoms have been omitted for clarity

cules in the asymmetric units (**4a**: CH_3CN; **8b**: 3 MeOH), both structures are of relatively poor quality. However, their similarity is striking and the data agree with the spectroscopic and electrochemical data reported below.

UV/Vis, EPR, and CD Spectroscopy

The UV/Vis spectra of our complexes in methanol were characterized by a weak metal-centered d-d band. Comparison showed that substitution of ligand **2** for ligand **1** did not significantly affect either λ_{max} or extinction coefficients. Differences were observed only between the various monodentate coligands. The spectra of the perchlorate and triflate salts **3a/3b** and **4a/4b** were very similar ($\lambda_{max} \approx 709$ nm, lg $\varepsilon \approx 1.86$), consistent with identical first coordination spheres around the copper(II) center. We therefore assume that the acetonitrile ligand in **4a** is rapidly exchanged in solution. This may also be true for the aquo ligands in **3a**, **3b**, and **4b**. With respect to the spectra of **3a**, **3b**, **4a**, and **4b**, the bands of the imidazole complexes were blue-shifted (**5**: $\lambda_{max} = 675$ nm, lg $\varepsilon = 1.93$; **6**: $\lambda_{max} = 681$ nm, lg $\varepsilon = 1.91$). The bands of the chloro complexes **7a** and **8a** appeared at longer wavelengths (**7a**: $\lambda_{max} = 725$ nm, lg $\varepsilon = 1.97$; **8a**: $\lambda_{max} = 732$ nm, lg $\varepsilon = 1.96$). Even larger red shifts and extinction coefficients were observed for the chlorocuprate salts **7b** and **8b** (**7b**: $\lambda_{max} = 757$ nm, lg $\varepsilon = 2.32$; **8b**: $\lambda_{max} = 755$, lg $\varepsilon = 2.30$). This behavior must be due to the anions, since the first coordination spheres are similar to those in **7a** and **8a**. Figure 6 illustrates the trend observed for the chloro complexes. Shown are the spectra of the aquo complexes **3b** and **4b**, their water/chloride exchange products **7a** and **8a**, and the chlorocuprate salts **7b** and **8b**.

The EPR spectra of our complexes were typical for copper(II) complexes with a $d_{x^2-y^2}$ ground state. All data obtained in frozen methanol solutions are summarized in Table 3. They confirmed that only the monodentate ligand had an effect on the *g* values and coupling constants,

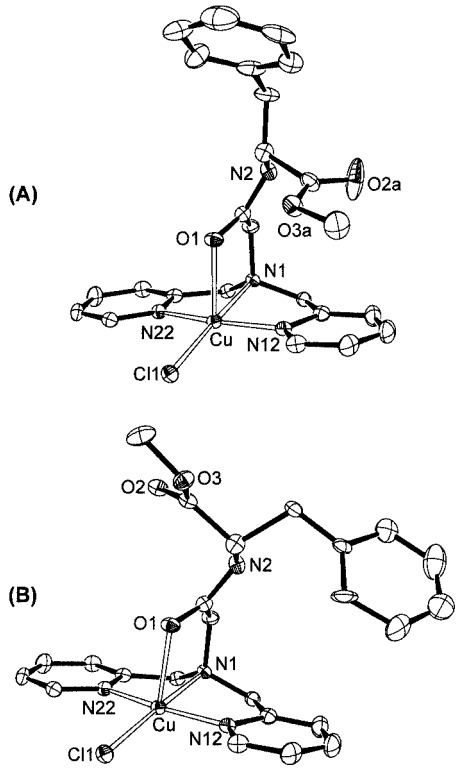

Figure 5. ORTEP plots (30% ellipsoids) of the two conformational isomers (A) and (B) of the cation [(bpaAc-Phe-OMe)Cu(Cl)]$^+$ (**8b**); hydrogen atoms have been omitted for clarity.

Table 1. Details of the X-ray structure analyses

Compound	**3a**·H_2O	**3b**·0.3CH_2Cl_2	**4a**·CH_3CN	**5**	**8b**·3CH_3OH
Empirical formula	$C_{18}H_{26}Cl_2CuN_4O_{13}$	$C_{20.3}H_{21}Cl_{0.6}CuF_6N_4O_{10}S_2$	$C_{28}H_{32}Cl_2CuN_6O_{11}$	$C_{24}H_{28}CuF_6N_6O_9S_2$	$C_{51}H_{91}Cl_6Cu_3N_8O_9$
Formula mass	640.87	743.94	763.04	786.18	1363.64
Temperature [K]	200(2)	200(2)	173(2)	200(2)	173(2)
Wavelength [Å]	0.71073	0.71073	0.71073	0.71073	0.71073
Crystal system	monoclinic	monoclinic	triclinic	monoclinic	triclinic
Space group	$P2_1/c$	$C2/c$	$P\bar{1}$	$P2_1/n$	$P\bar{1}$
a [Å]	16.82(5)	25.699(2)	7.8668(2)	8.49(5)	13.388(3)
b [Å]	9.37(5)	15.252(1)	9.2765(3)	25.95(5)	13.830(3)
c [Å]	16.23(5)	16.999(1)	24.0570(8)	14.77(5)	18.731(4)
α [°]	90	90	87.950(2)	90	89.10(3)
β [°]	95.1(2)	113.72	87.854(2)	91.3(2)	74.95(3)
γ [°]	90	90	78.381(2)	90	63.01(3)
Volume [Å^3]	2549(17)	6100.1(7)	1695.86(9)	3255(23)	2961.3(10)
Z	4	8	2	4	2
Calculated density [Mg/m^3]	1.670	1.620	1.494	1.604	1.529
Absorption coefficient [mm^{-1}]	1.139	0.998	0.867	0.892	1.398
F(000)	1316	3008	786	1604	1428
Crystal size [mm]	0.40 × 0.28 × 0.18	0.25 × 0.07 × 0.07	0.35 × 0.10 × 0.03	0.70 × 0.43 × 0.18	0.30 × 0.30 × 0.10
θ-range [°]	2.51−23.94	1.59−28.28	2.24−25.03	2.52−23.81	1.13−27.54
Index ranges	$0 \le h \le 19$	$-34 \le h \le 34$	$-9 \le h \le 9$	$0 \le h \le 9$	$-15 \le h \le 17$
	$-10 \le k = 10$	$-19 \le k \le 18$	$-11 \le k \le 11$	$-28 \le k \le 29$	$-17 \le k \le 17$
	$-18 \le l \le 18$	$-22 \le l \le 20$	$-28 \le l \le 28$	$-16 \le l \le 16$	$-24 \le l \le 24$
Reflections collected/unique	7989/4000	32657/7457	10690/5890	9832/4926	23590/13549
Refinement method	Based on F^2	Based on F^2	Based on F^2	Based on F^2	Based on F^2
Data/restraints/parameters	4000/38/343	7457/0/423	5890/34/470	4926/48/437	13549/0/893
Goodness-of-fit on F^2	1.064	1.039	1.129	1.179	1.226
Final R indices [$I > 2\sigma(I)$]	$R1 = 0.0605$	$R1 = 0.0599$	$R1 = 0.0870$	$R1 = 0.0598$	$R1 = 0.1022$
	$wR2 = 0.1509$	$wR2 = 0.1721$	$wR2 = 0.2277$	$wR2 = 0.1544$	$wR2 = 0.2583$
R indices (all data)	$R1 = 0.1146$	$R1 = 0.1281$	$R1 = 0.1128$	$R1 = 0.1096$	$R1 = 0.1253$
	$wR2 = 0.1939$	$wR2 = 0.2020$	$wR2 = 0.2402$	$wR2 = 0.1977$	$wR2 = 0.2710$
Largest diff. peak/hole [eÅ^{-3}]	1.123/−0.796	1.377/−0.796	0.828/−0.687	1.054/−0.662	1.750/−0.888

Table 2. Selected bond lengths [Å] and angles [°] with standard deviations given in parentheses

	3a	**3b**	**4a**	**5**	**8b**
$Cu-N^{am}$ [a]	2.037(11)	2.057(4)	2.048(6)	2.069(12)	2.067(6)
$Cu-N^{py}$ [b]	1.981(11)	1.981(4)	1.986(6)	2.017(12)	1.979(7)
	1.997(11)	1.992(4)	1.988(6)	2.030(12)	1.983(7)
$Cu-O^{ad}$ [c]	2.228(12)	2.278(3)	2.232(5)	2.326(14)	2.334(6)
$Cu-L^{eq}$ [d]	1.972(11)	1.985(3)	1.976(6)	1.990(12)	2.232(2)
$N^{am}-Cu-N^{py}$	83.7(2)	83.4(2)	83.2(2)	82.4(2)	83.3(3)
	82.2(2)	83.4 (2)	83.1(2)	82.4(2)	82.8(3)
$N^{am}-Cu-O^{ad}$	82.7(2)	81.9(1)	82.5(2)	81.4(2)	80.4(2)
$N^{am}-Cu-L^{eq}$	175.0(2)	176.2(2)	177.8(3)	179.4(2)	176.6(2)
$N^{py}-Cu-O^{ad}$	96.7(2)	96.0(2)	100.8(2)	90.7(2)	99.5(3)
	87.7(2)	89.6(1)	86.7(2)	91.8(2)	84.1(3)
$N^{py}-Cu-N^{py}$	164.5(2)	164.8 (2)	163.3(2)	164.0(2)	164.9(3)
$N^{py}-Cu-L^{eq}$	98.1(2)	98.7(2)	97.6(2)	98.3(2)	96.7(2)
	95.4(2)	94.1(2)	96.5(2)	97.0(2)	96.8(2)
$O^{ad}-Cu-L^{eq}$	102.2(2)	101.1 (1)	95.4(2)	98.6(2)	102.9(2)

[a] N^{am} = amine nitrogen atom of the bpa ligand fragment. [b] N^{py} = pyridine nitrogen atom of the bpa ligand fragment. [c] O^{ad} = amide oxygen atom. [d] L^{eq} = equatorial ligand atom (monodentate coligand).

whereas changes in the amino acid structures did not register. The spectra of the *N*-methylimidazole complexes **5** and **6** and the chloro complexes **7a** and **8a** were rhombic, whereas axial patterns were found for the aquo and acetonitrile species **3a**, **3b**, **4a**, and **4b**. The spectra of **7b** and **8b** appeared to be rhombic but were not well resolved, due to complications arising from the presence of different chlorocuprate anions.[18] It was therefore not possible to determine an accurate value of g_y for these complex salts.

Circular dichroism spectra were collected for the chiral L-phenylalanine derivatives **4a**, **4b**, **6**, **8a**, and **8b**. The results are shown in Figure 7. In agreement with the similarity of the structures, there was no significant observed difference between the spectra of **4a**, **4b**, and **6**. They closely resembled

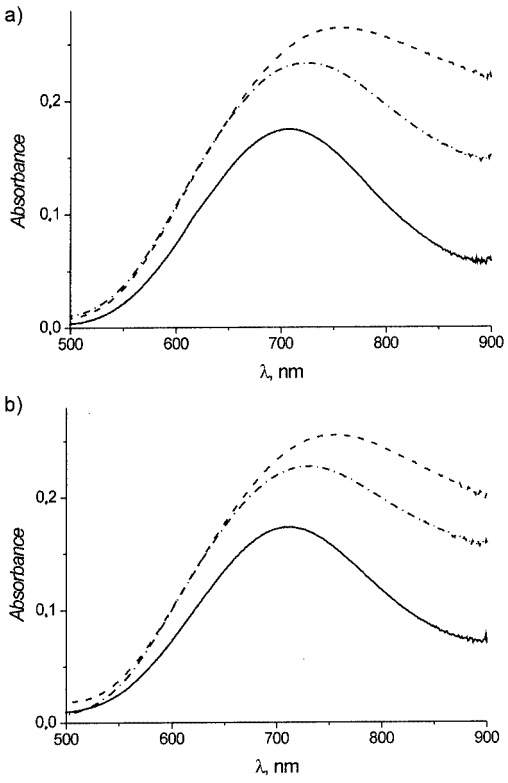

Figure 6. Vis spectra (0.002 M Cu^{2+} in methanol) of the triflate complexes **3b** (a) and **4b** (b) (——), the ligand exchange products **7a** (a) and **8a** (b) (–·–·), and the tetrachlorocuprate salts **7b** (a) and **8b** (b) (----)

Table 3. EPR spectra of the complexes in frozen methanol solutions (10^{-3} M Cu^{2+}; 120 K)

Compound	g_x	$g_\perp/g_y$	$g_\parallel/g_z$	$A_\parallel/A_z$ [10^{-4} cm^{-1}]
3a	–	2.06	2.27	170
3b	–	2.16	2.28	170
4a	–	2.05	2.26	169
4b	–	2.10	2.28	170
5	2.01	2.06	2.25	185
6	2.01	2.06	2.25	182
7a	1.94	2.03	2.23	170
7b	1.96	not resolved	2.25	175
8a	1.95	2.05	2.25	172
8b	1.96	not resolved	2.25	171

that of the free ligand **2**,[17] except for a 20 nm red shift of the pyridine ring π-π* transitions,[21] which appeared at 282 nm. In comparison, the corresponding free ligand signal is at 262 nm with a similar positive Cotton effect. Interestingly, the corresponding signal of $[(\mathbf{2})(H_2O)Zn](OTf)_2$ [17] exhibited a negative Cotton effect with a minimum at 270 nm. The chloro complexes **8a** and **8b** showed different behavior, exhibiting positive signals at ca. 289 nm significantly larger and broader than those of the other complexes studied. Though we cannot assign this band to a particular transition, it is interesting to note that the behavior is paralleled by a similar effect observed for the corresponding chlorozinc(II) complex.[22]

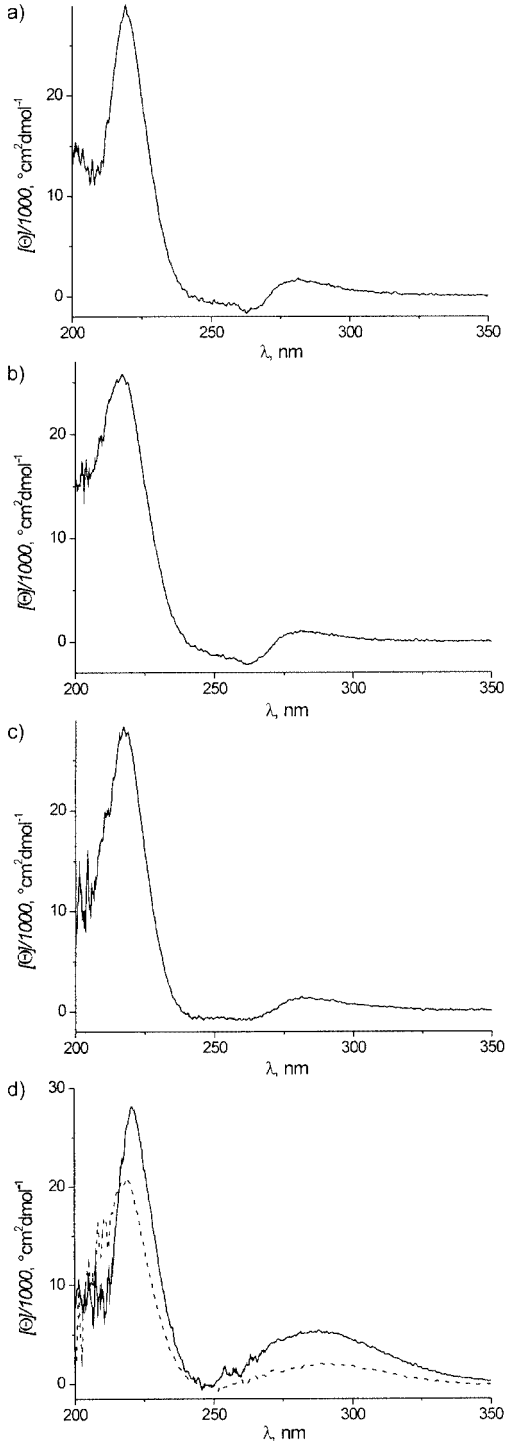

Figure 7. Circular dichroism spectra (0.001 M Cu^{2+} in methanol) of a) **4a**, b) **4b**, c) **6**, and d) **8a** (----) and **8b** (——)

Cyclic Voltammetry

The cyclic voltammograms of the complexes are shown in Figure 8 and the data are summarized in Table 4. In general, electrochemically quasireversible redox transitions were observed for all compounds. We assign these transitions to the Cu^{II}/Cu^{I} redox couple. The perchlorate and

triflate salts **3a/3b** and **4a/4b** exhibited broad shoulders at anodic potentials of ca. + 0.1 V. This feature is commonly encountered in copper(II) complexes and has been ascribed to adsorption processes at the glassy carbon working electrode.[23]

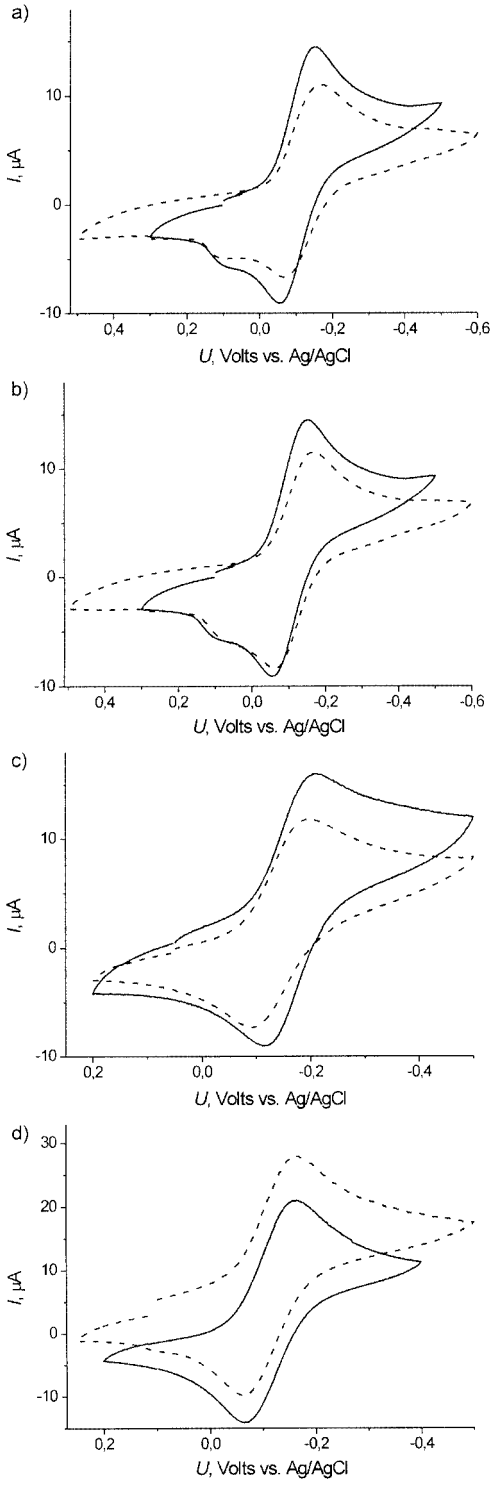

Figure 8. Cyclic voltammograms (0.1 M TBAH in methanol) of the complexes (10^{-3} M Cu^{2+}), a) **3a** and **4a**, b) **3b** and **4b**, c) **5** and **6**, d) **7b** and **8b** (——: bpaAc-Gly-OEt; ----: bpaAc-Phe-OMe)

Table 4. Electrochemical data ($E_{1/2}$ in V vs. Ag/AgCl; $\Delta E_{1/2}$ in mV) obtained for the complexes in 10^{-3} M methanol solutions at scan rates of 50 mV/s

Compd.	**3a**	**3b**	**4a**	**4b**	**5**	**6**	**7b**	**8b**
$E_{1/2}$	−0.10	−0.10	−0.10	−0.12	−0.16	−0.15	−0.11	−0.11
$\Delta E_{1/2}$	89	106	90	107	88	107	93	98

It is evident that no significant differences exist between complexes of the two ligands **1** and **2**. Considering the broad waves and the adsorption phenomena involved, the small shifts observed in $E_{1/2}$ for the triflate (**3a**, **4a**), perchlorate (**3b**, **4b**), and chloro (**7b**, **8b**) complexes are certainly well within the experimental errors. Small changes were only observed for the *N*-methylimidazole complexes **5** and **6**, which were reduced at potentials ca. −50 mV more negative than for the other compounds. In view of the accuracy of cyclic voltammetry, however, this shift may also not be significant.

Discussion

Our earlier investigations on zinc(II) complexes of ligand **2** demonstrated that a trigonal-bipyramidal coordination geometry resulted in an unusual conformational stability of the noncoordinating benzyl substituent.[17] We have now incorporated **2** in square-pyramidal copper(II) complexes. This was done in order to evaluate the effects of different geometries on the formation of noncovalent interactions between metal ions and aromatic amino acid side chains in tripodal ligand frameworks.

Both ligands **1** and **2** form copper complexes that are typical members of the tpa family [tpa: tris(picolyl)amine]. It has been generally observed that distorted square-pyramidal coordination geometries dominate when one pyridine arm of tpa is replaced by a thioether group[24] or oxygen donor ligands such as carboxylate[19] or phenolate.[25−27] In contrast, copper complexes of tris(picolyl)amine (tpa) itself are always trigonal-bipyramidal.[28−31] The amino acid side chain functionalities in **1** and **2** did not affect the structural properties of our complexes. The benzyl substituent, unlike that in the corresponding trigonal-bipyramidal zinc complexes,[17] is flexible and does not interact with the copper(II) center. This is indicated by the X-ray structure analyses of **4a** and **8b**. The distance between copper(II) and the center of the phenyl ring is always larger than 7 Å, whereas it is only 4.5 Å in $[(\mathbf{2})(H_2O)Zn]^{2+}$.

The circular dichroism spectra of **4a**, **4b**, and **6** supported these observations, no indication of a structural change affecting the chiral amino acid moiety in **2** upon copper complexation being found. This is evident on comparison with the spectra of the free ligand and its trigonal-bipyramidal zinc(II) complexes. However, there were unique features in the spectra of **8a** and **8b** that cannot yet be explained. EPR and UV/Vis spectra, as well as the cyclic voltammograms of the compounds, further confirmed that the first coor-

dination sphere was not affected by the benzyl substituent in ligand **2**. Only the monodentate coligand induced measurable changes. It is interesting to note that we did not observe an effect of the benzyl substituent on electrode processes in the electrochemical measurements. Such phenomena have been discussed with regard to a series of cobalt(III) complexes containing nitrilotriacetic acid ligands derived from different amino acids including phenylalanine.[32]

Conclusions

Our results have demonstrated that the coordination geometry of complexes with amino acid derived ligands is a crucial determinant for the occurrence of weak noncovalent interactions. The benzyl substituent in the chiral ligand **2** is closely associated with zinc(II) in trigonal-bipyramidal complexes, but does not interact at all with the copper(II) center in square-pyramidal or octahedral coordination environments. This is an important consideration for the development of synthetic chiral metal complexes intended to exhibit metalloenzyme-like properties such as the activation or recognition of substrates by interactions involving the second, noncoordinating ligand sphere.

Experimental Section

General Methods: Spectra were recorded with the following instruments: UV/Vis spectra: Varian Cary 1G spectrophotometer. Cyclic voltammetry: PAR potentiostat 263 equipped with a three-electrode cell containing a glassy carbon working electrode, an Ag/AgCl reference electrode, and a Pt counterelectrode. Methanol solutions (10^{-3} M) of the complexes containing tetrabutylammonium hexafluorophosphate (TBAH, 0.1 M) as supporting electrolyte were used. Solutions were deoxygenated by bubbling with dry nitrogen. The reported potentials have not been corrected for junction potential effects. Under the measurement conditions, the ferrocene/ferrocenium couple was observed at +0.40 V. EPR spectra: Bruker ESP 300 E spectrometer. All spectra were recorded at 120 K in frozen methanol solutions at 10^{-3} M copper concentrations. Circular dichroism: Jasco J710 Spectropolarimeter. IR: Mattson Polaris FTIR. All complexes were prepared and stored under dry nitrogen. The workup was performed under ambient laboratory conditions unless stated otherwise. Absolute solvents were purchased from Fluka and stored under nitrogen. Solvents were used without further purification. All other reagents were of commercially available reagent-grade quality. The syntheses of the ligands bpaAc-Gly-OEt (**1**) and bpaAc-Phe-OMe (**2**),[17] and of the copper complexes [(bpaAc-Gly-OEt)CuCl](OTf) (**7a**) and [(bpaAc-Gly-OEt)-$CuCl]_2[CuCl_3(MeOH)]Cl$ (**7b**)[18] are described elsewhere.

General Synthetic Procedure: The complexes **3a**, **3b**, **4a**, **4b**, and **5** were prepared by the same procedure described below. However, the subsequent workup and purification were slightly different for each compound and are therefore described separately. Solid Cu^{2+} salt was added in one portion to a stirred solution of 1 equiv. of the respective ligand in MeCN. In the case of [(bpaAc-Gly-OEt)(*N*-Meim)Cu]$(OTf)_2$ (**5**), *N*-methylimidazole was added after 15 min. Stirring was continued overnight at room temperature, followed by removal of all solvent in a vacuum.

[(bpaAc-Gly-OEt)(H_2O)Cu(ClO_4)](ClO_4)·H_2O (3a): This compound was prepared from **1** (243 mg, 0.71 mmol) and $Cu(ClO_4)_2$·$6H_2O$ (263 mg, 0.71 mmol) in MeCN (5 mL). The solid residue was suspended in a minimum of MeOH, and the resulting blue precipitate was separated from the green filtrate, dried in a vacuum, and completely dissolved in hot MeOH. The solution was left at 4 °C for several days, yielding **3a** as a blue solid that was isolated and dried in a vacuum. Single crystals suitable for an X-ray structure analysis where obtained by slow recrystallization from MeOH at 4 °C over a period of several weeks. Yield: 296 mg (0.46 mmol, 65%). $C_{18}H_{24}Cl_2CuN_4O_{12}$·$H_2O$ (640.9): calcd. C 33.74, H 4.09, N 8.74; found C 33.97, H 4.14, N 8.72. FAB-MS (nitrobenzyl alcohol): *m*/*z* = 504 [(bpaAc-Gly-OEt)Cu(ClO_4)]$^+$, 405 [(bpaAc-Gly-OEt)Cu]$^+$. IR (KBr): $\tilde{\nu}$ = 1723 cm^{-1} (COOEt), 1658 (amide I), 1105 (ClO_4). UV/Vis (MeOH): λ_{max} (lg ε) = 706 nm (1.88).

[(bpaAc-Gly-OEt)(H_2O)Cu(OTf)](OTf)·0.3CH_2Cl_2 (3b): This compound was prepared from **1** (483 mg, 1.41 mmol) and $Cu(OTf)_2$ (510 mg, 1.41 mmol) in MeCN (15 mL). The crude product was treated with CH_2Cl_2 (10 mL) and the mixture was cooled to −20 °C and filtered to remove insoluble impurities. The volume of the filtrate was reduced, and some diethyl ether was added. Storage of the solution at −20 °C and repeated addition of Et_2O afforded the product as blue needles, which were isolated by filtration and dried in a vacuum. Recrystallization from CH_2Cl_2 by slow evaporation of the solvent under dry nitrogen afforded blue crystals suitable for X-ray structure analysis. Yield: 593 mg (0.79 mmol, 56%). $C_{20}H_{24}CuF_6N_4O_{10}S_2$·0.3$CH_2Cl_2$ (747.6): calcd. C 32.62, H 3.32, N 7.49; found C 32.45, H 3.34, N 7.40. FAB-MS (nitrobenzyl alcohol): *m*/*z* = 554 [(bpaAc-Gly-OEt)Cu(OTf)]$^+$, 405 [(bpaAc-Gly-OEt)Cu]$^+$. IR (KBr): $\tilde{\nu}$ = 1749 cm^{-1} (COOEt), 1663 (amide I), 1287, 1254, 1171, 1032 (OTf). UV/Vis (MeOH): λ_{max} (lg ε) = 706 nm (1.85).

[(bpaAc-Phe-OMe)(MeCN)Cu](ClO_4)$_2$·H_2O (4a): This compound was prepared from **2** (508 mg, 1.21 mmol) and $Cu(ClO_4)_2$·$6H_2O$ (448 mg, 1.21 mmol) in MeCN (10 mL). CH_2Cl_2 (5 mL) was added to the crude product, and the resulting suspension was decanted. The residue was dried in a vacuum and dissolved in 10 mL of MeCN. Slow diffusion of Et_2O into this solution afforded the product as blue needles, which were isolated and dried in a vacuum. Some of these crystals were suitable for X-ray structure analysis. Yield: 772 mg (1.07 mmol, 88%). $C_{26}H_{31}Cl_2CuN_5O_{12}$ (740.0): calcd. C 42.20, H 4.22, N 9.46; found C 42.31, H 4.38, N 9.40. FAB-MS (nitrobenzyl alcohol): *m*/*z* = 580 [(bpaAc-Phe-OMe)Cu(ClO_4)]$^+$, 481 [(bpaAc-Phe-OMe)Cu]$^+$. IR (KBr): $\tilde{\nu}$ = 1749 cm^{-1} (COOEt), 1659 (amide I), 1103 (ClO_4). UV/Vis (MeOH): λ_{max} (lg ε) = 709 nm (1.85). CD (10^{-3} M in methanol): λ [nm] ([θ]/1000 [°cm^2dmol^{-1}]) = 219 (+28.2), 263 (−1.5), 282 (+1.6).

[(bpaAc-Phe-OMe)(H_2O)Cu](OTf)$_2$ (4b): This compound was prepared from bpaAc-Phe-OMe (713 mg, 1.70 mmol) and $Cu(OTf)_2$ (615 mg, 1.70 mmol) in MeCN (20 mL). The crude product was dissolved in 5 mL of CH_2Cl_2 and filtered. Cooling of the filtrate overnight at −20 °C yielded the complex as a blue precipitate. The suspension was decanted and the residue was dried in a vacuum. Yield: 1.133 g (1.42 mmol, 84%). $C_{26}H_{28}CuF_6N_4O_{10}S_2$ (798.2): calcd. C 39.12, H 3.54, N 7.02; found C 39.27, H 3.66, N 6.87. FAB-MS (nitrobenzyl alcohol): *m*/*z* = 630 [(bpaAc-Phe-OMe)Cu(OTf)]$^+$, 481 [(bpaAc-Phe-OMe)Cu]$^+$. IR (KBr): $\tilde{\nu}$ = 1746 (COOMe), 1657 (amide I), 1282, 1253, 1166, 1031 (OTf). UV/Vis (MeOH): λ_{max} (lg ε) = 713 nm (1.83). CD (10^{-3} M in methanol): λ [nm] ([θ]/1000 [°cm^2dmol^{-1}]) = 217 (+25.4), 262 (−2.2), 282 (+1.0).

[(bpaAc-Gly-OEt)(*N*-Meim)Cu](OTf)$_2$ (5): This compound was prepared from **1** (382 mg, 1.11 mmol), Cu(OTf)$_2$ (402 mg, 1.11 mmol), and *N*-Meim (91 mg, 1.11 mmol) in MeCN (5 mL). The residual solid was dissolved in 5 mL of CH_2Cl_2, cooled to −20 °C and filtered to yield a clear blue solution. After reduction of the filtrate, diethyl ether was added. The mixture was stored at −20 °C to precipitate the product, which was isolated by filtration and dried in a vacuum. X-ray quality crystals were grown by layering a solution of **5** in a minimum of CH_2Cl_2 with diethyl ether for several days at 4 °C. Yield: 703 mg (0.89 mmol, 80%). $C_{24}H_{28}CuF_6N_6O_9S_2$ (786.2): calcd. C 36.67, H 3.59, N 10.69; found C 36.73, H 3.78, N 10.60. FAB-MS (nitrobenzyl alcohol): *m/z* = 554 [(bpaAc-Gly-OEt)Cu(OTf)]$^+$, 405 [(bpaAc-Gly-OEt)Cu]$^+$. IR (KBr): $\tilde{\nu}$ = 1732 cm^{-1} (COOEt), 1666 (amide I), 1282, 1247, 1157, 1031 (OTf). UV/Vis (MeOH): λ_{max} (lg ε) = 675 nm (1.93).

[(bpaAc-Phe-OMe)(*N*-Meim)Cu](OTf)$_2$ (6): *N*-Methylimidazole (18 μL, 0.23 mmol) was added in one portion to a stirred solution of **4b** (187 mg, 0.23 mmol) in 10 mL of MeCN. Stirring was continued overnight at room temperature, followed by removal of all solvent in a vacuum. The resulting solid was dissolved in 5 mL of CH_2Cl_2 and stored at −20 °C overnight. After filtration, diethyl ether was added dropwise to cause a slight cloudiness. The mixture was stored again at −20 °C to afford a blue precipitate, which was isolated by decantation of the supernatant and dried in a vacuum. In order to maximize yields it was necessary to isolate the product quickly, because it redissolved at room temperature. Yield: 177 mg (0.20 mmol, 87%). $C_{30}H_{32}CuF_6N_6O_9S_2$ (862.3): calcd. C 41.79, H 3.74, N 9.75; found C 41.73, H 3.81, N 9.50. FAB-MS (nitrobenzyl alcohol): *m/z* = 630 [(bpaAc-Phe-OMe)Cu(OTf)]$^+$, 481 [(bpaAc-Phe-OMe)Cu]$^+$. IR (KBr): $\tilde{\nu}$ = 1744 (COOMe), 1661 (amide I), 1282, 1255, 1162, 1031 (OTf). UV/Vis (MeOH): λ_{max} (lg ε) = 681 nm (1.91). CD (10^{-3} M in methanol): λ [nm] ([θ]/1000 [°cm^{2}dmol^{-1}]) = 218 (+27.6), 282 (1.3).

[(bpaAc-Phe-OMe)CuCl]$_2$[CuCl$_4$]·MeOH (8b) and [(bpaAc-Phe-OMe)CuCl](OTf) (8a): Solid $CuCl_2 \cdot 2H_2O$ (189 mg, 1.11 mmol) was added in one portion to a stirred solution of **2** (309 mg, 0.74 mmol) in 20 mL of MeOH. Stirring was continued overnight at room temperature. The volume of the solution was reduced, and storage at −20 °C afforded the product as a green solid. The complex was redissolved in the minimum possible amount of MeOH and recrystallized by slow diffusion of Et_2O into the solution. Diamond-shaped, green crystals were obtained. C,H,N, elemental analysis indicated the formulation [(bpaAc-Phe-OMe)CuCl]$_2$[CuCl$_4$]·MeOH for this compound. Single crystals suitable for X-ray structure analysis were obtained by slow recrystallization from MeOH at −20 °C. It was necessary to isolate the crystals quickly, because they rapidly redissolved at room temperature. The X-ray structure analysis indicates that the single crystals contained 3 molecules of MeOH per copper complex. For spectroscopic studies, the complex salt **8a** was generated in situ by addition of aqueous NaCl (2.5 or 1 M: 10% excess; saturated solution: large excess) to a solution of **4b** in methanol. The reaction was monitored by UV/Vis, EPR, or circular dichroism spectroscopy and run to completeness. Spectroscopic data are reported for both salts **8a** and **8b**. Yield (**8b**): 405 mg (0.31 mmol, 84%). $C_{48}H_{54}Cl_6CuN_8O_7 \cdot MeOH$ (1290.4): calcd. C 45.61, H 4.53, N 8.68; found C 45.46, H 4.46, N 8.74. FAB-MS (nitrobenzyl alcohol): *m/z* = 516 [(bpaAc-Phe-OMe)CuCl]$^+$, 481 [(bpaAc-Phe-OMe)Cu]$^+$. IR (KBr): $\tilde{\nu}$ = 1743 (COOMe), 1654 (amide I). UV/Vis (MeOH): **8a:** λ_{max} (lg ε) = 732 nm (1.96); **8b:** λ_{max} (lg ε) = 755 nm (2.30). CD (10^{-3} M in methanol): **8a:** λ [nm] ([θ]/1000 [°cm^{2}dmol^{-1}]) = 216 (21.4), 289 (2.3); **8b:** λ [nm] ([θ]/1000 [°cm^{2}dmol^{-1}]) = 221 (27.6), 288 (5.3).

X-ray Data Collection and Structure Refinement Details: Crystal data and experimental conditions are listed in Table 1. The molecular structures are illustrated in Figures 1−5. Selected bond lengths and bond angles, with standard deviations in parentheses, are summarized in Table 2. Intensity data were collected with graphite-monochromated Mo-K_α radiation with a Nonius CAD MACH3 diffractometer (**3a**, **5**), with a Nonius Kappa CCD area detector (**4a**, **8b**), and with a Siemens SMART 5000 CCD-diffractometer (exposure time: 10 s/frame, Δω = 0.3°, **3b**). The collected reflections were corrected for Lorentz, polarization, and absorption effects.[33] All structures were solved by direct methods and refined by full-matrix, least-squares methods on F^2.[34−36] Non-hydrogen atoms were refined with anisotropic thermal parameters. Hydrogen atoms were calculated for idealized geometries and allowed to ride on their parent atoms with isotropic displacement parameters related to those of the adjacent atoms by a factor of 1.5. CCDC-172745 (**3a**), -173039 (**3b**), -173635 (**4a**), -172744 (**5**), and -173634 (**7b**) contain the supplementary crystallographic data for this paper. These data can be obtained free of charge at www.ccdc.cam.ac.uk/conts/retrieving.html or from the Cambridge Crystallographic Data Centre, 12, Union Road, Cambridge CB2 1EZ, UK 8Fax: (internat.) + 44-1223/336-033; E-mail: deposit@ccdc.cam.ac.uk].

Acknowledgments

The authors gratefully acknowledge financial support from the Deutsche Forschungsgemeinschaft. We also thank Professor Rudi van Eldik for his generous support.

[1] C. A. Hunter, J. K. M. Sanders, *J. Am. Chem. Soc.* **1990**, *112*, 5525−5534.
[2] C. A. Hunter, *Angew. Chem.* **1993**, *105*, 1653−1655; *Angew. Chem. Int. Ed. Engl.* **1993**, *32*, 1584−1586.
[3] K. M. Guckian, B. A. Schweitzer, R. X. F. Ren, C. J. Sheils, P. L. Paris, D. C. Tahmassebi, E. T. Kool, *J. Am. Chem. Soc.* **1996**, *118*, 8182−8183.
[4] C. Chipot, R. Jaffe, B. Maigret, D. A. Pearlman, P. A. Kollmann, *J. Am. Chem. Soc.* **1996**, *118*, 11217−11224.
[5] K. M. Guckian, B. A. Schweitzer, R. X.-F. Ren, C. J. Sheils, D. C. Tahmassebi, E. T. Kool, *J. Am. Chem. Soc.* **2000**, *122*, 2213−2222.
[6] S. D. Zaric, D. M. Popovic, E. W. Knapp, *Chem. Eur. J.* **2000**, *6*, 3935−3942.
[7] C. Janiak, *J. Chem. Soc., Dalton Trans.* **2000**, 3385−3396.
[8] S. Mecozzi, A. P. West, D. A. Dougherty, *J. Am. Chem. Soc.* **1996**, *118*, 2307−2308.
[9] J. C. Ma, D. A. Dougherty, *Chem. Rev.* **1997**, *97*, 1303−1324.
[10] J. P. Klinman, *Chem. Rev.* **1996**, *96*, 2541−2561.
[11] O. Yamauchi, *Pure Appl. Chem.* **1995**, *67*, 297−304.
[12] P. Hu, C. Sorensen, M. L. Gross, *J. Am. Soc. Mass Spectrom.* **1995**, *6*, 1079−1085.
[13] G. Maccarrone, G. Nardin, L. Randaccio, G. Tabbi, M. Rosi, A. Sgamellotti, E. Rizzarelli, E. Zangrando, *J. Chem. Soc., Dalton Trans.* **1996**, 3449−3453.
[14] L. H. Abdel-Rahman, L. Battaglia, M. R. Mahmoud, *Polyhedron* **1996**, *15*, 327−334.
[15] T. Sugimori, H. Masuda, N. Ohata, K. Koiwai, A. Odani, O. Yamauchi, *Inorg. Chem.* **1997**, *36*, 576−583.
[16] Y. Shimazaki, H. Yokoyama, O. Yamauchi, *Angew. Chem.* **1999**, *111*, 2561−2562; *Angew. Chem. Int. Ed.* **1999**, *38*, 2401−2403.
[17] N. Niklas, O. Walter, R. Alsfasser, *Eur. J. Inorg. Chem.* **2000**, 1723−1731.
[18] N. Niklas, S. Wolf, G. Liehr, C. E. Anson, A. K. Powell, R. Alsfasser, *Inorg. Chim. Acta* **2001**, *314*, 126−132.
[19] T. Okuno, S. Ohba, Y. Nishida, *Polyhedron* **1997**, *16*, 3765−3774.

[20] T. Kobayashi, T. Okuno, T. Suzuki, M. Kunita, S. Ohba, Y. Nishida, *Polyhedron* **1998**, *17*, 1553−1559.
[21] J. W. Canary, C. S. Allen, J. M. Castagnetto, Y.-H. Chiu, P. J. Toscano, Y. Wang, *Inorg. Chem.* **1998**, *37*, 6255−6262.
[22] N. Niklas, unpublished results.
[23] C. W. Lee, F. C. Anson, *Inorg. Chem.* **1984**, *23*, 837−844.
[24] Y. Nishida, K. Takahashi, *Inorg. Chem.* **1988**, *27*, 1406−1410.
[25] R. Uma, R. Viswanathan, M. Palaniandavar, M. Lakshminarayanan, *J. Chem. Soc., Dalton Trans.* **1994**, 1219−1226.
[26] H. Adams, N. A. Bailey, I. K. Campbell, D. E. Fenton, Q. Y. He, *J. Chem. Soc., Dalton Trans.* **1996**, 2233−2237.
[27] S. Ito, S. Nishino, H. Itoh, S. Ohba, Y. Nishida, *Polyhedron* **1998**, *17*, 1637−1642.
[28] K. D. Karlin, J. C. Hayes, S. Juen, J. P. Hutchinson, J. Zubieta, *Inorg. Chem.* **1982**, *21*, 4106−4108.
[29] H. Nagao, N. Komeda, M. Mukaida, M. Suzuki, K. Tanaka, *Inorg. Chem.* **1996**, *35*, 6809−6815.
[30] H. Zheng, L. Que, Jr., *Inorg. Chim. Acta* **1997**, *263*, 301−307.
[31] B. S. Lim, R. H. Holm, *Inorg. Chem.* **1998**, *37*, 4898−4908.
[32] H. Kumita, K. Jitsukawa, H. Masuda, H. Einaga, *Inorg. Chim. Acta* **1998**, *283*, 160−166.
[33] [33a] A. C. T. North, D. C. Phillips, F. S. Mathews, *Acta Crystallogr., Sect. A* **1968**, *24*, 351−359. [33b] *COLLECT*, data collection software, B. V. Nonius, **1998**. [33c] *SCALEPACK*, data processing software: Z. Otwinowski, W. Minor, *Methods Enzymol.* **1997**, *276*, 307 (Macromolecular Crystallography, Part A).
[34] A. Altomare, G. Cascarano, C. Giacovazzo, A. Guagliardi, *J. Appl. Crystallogr.* **1993**, *26*, 343−350.
[35] G. M. Sheldrick, *SHELXTL-PC*, Siemens Analytical X-ray Instruments, Inc., Madison, WI, USA, **1994**.
[36] G. M. Sheldrick, *SHELXL-97*, Universität Göttingen, **1997**.

Received November 9, 2001
[I01447]

The $[Re(CO)_6]^+$ Cation as a Ligand-Transfer Reagent with Ferrocene Derivatives

Siden Top,*[a] Stéphane Masi,[a] and Gérard Jaouen*[a]

Keywords: Carbonyl(cyclopentadienyl)rhenium / Hexacarbonylrhenium / Ferrocene / Ligand transfer

The $[Re(CO)_6]^+$ cation is a stable compound, soluble in aqueous media. We show that it can be used as a reagent in the synthesis of tricarbonyl(cyclopentadienyl)rhenium complexes. $[Re(CO)_6]^+$ reacts with ferrocene derivatives, particularly acetylferrocene, in DMSO, DMF or a water/DMSO (1:1) mixture at 160 °C to give tricarbonyl(cyclopentadienyl)rhenium derivatives with high yields.

(© Wiley-VCH Verlag GmbH, 69451 Weinheim, Germany, 2002)

Introduction

The $[Re(CO)_6]^+$ cation is a robust compound insensitive to air or moisture. It is normally prepared by one of two different standard preparation methods, either by reaction of $Re(CO)_5X$ with $AlCl_3$ under high pressure of CO gas,[1] or by treating ethyl chloroformate with $Re(CO)_5Na$ at normal atmospheric pressure, followed by addition of BF_3.[2] Unlike $Re_2(CO)_{10}$, $Re(CO)_5Br$ or $[Re(CO)_5]^-$, precursors that are often used as reagents in the synthesis of carbonyl complexes of Re, $[Re(CO)_6]^+$ is normally considered to be a relatively inert compound. To the best of our knowledge only a few rare studies have dealt with its reactivity. One example is the nucleophilic reaction with the azide ion or amines, leading to the formation of the isocyanate $Re(CO)_5(NCO)$ and of the amide $Re(CO)_5(CONRR')$, respectively.[3] The carbonyl ligands are labile in this cation, and up to three CO groups can be substituted by two-electron donor ligands, such as triphenylphosphane.[4] It is also known that $[Re(CO)_6]^+$ reacts with the metallate anions $[Fe(CO)_4]^{2-}$, $[Mn(CO)_5]^-$, $[W(CO)_5Cl]^-$ and $[W(CO)_5H]^-$ by an electron-transfer reaction to give $[Re(CO)_5]^-$, $(CO)_5MnRe(CO)_5$, $Re(CO)_5Cl$ and $HRe(CO)_5$, respectively.[5] $[Re(CO)_6]^+$ possesses several properties that are worth exploiting. Firstly, its solubility and stability allow it to be used in aqueous media. Secondly, it has been shown that hexacarbonyltungsten is accessible in its radioactive form $^{188}W(CO)_6$ and that its disintegration should lead to the formation of $[^{188}Re(CO)_6]^+$ and $[^{188}Re(CO)_5]^{\cdot}$.[6] This transformation is an important one, since ^{186}Re and ^{188}Re are now recognized as radionuclides with therapeutic applications.[7] At present, the radionuclide of rhenium is only available in the form of the perrhenate.[8] It is for this reason that rhenium-based radiopharmaceuticals have normally been prepared as chelates of the N_2S_2 or N_3S type.[9] The need for new radiopharmaceuticals with good stability has led us to consider the idea of using the tricarbonyl(cyclopentadienyl)rhenium group in place of the chelates, since it has the advantages of being lipophilic, less bulky and more robust.[10] The concept of using carbonyl organometallic compounds as radiopharmaceuticals is undergoing rapid expansion.[11] However, syntheses of cyclopentadienyl complexes of Re require multi-step reactions. The traditional methods are not available for radionuclides of rhenium. The search for an efficient preparation method has led us to propose a new synthesis for certain rhenium compounds, including $Re_2(CO)_{10}$ at normal atmospheric pressure,[12] and $(\eta^5\text{-}C_5H_4COOH)Re(CO)_3$ by a simple thermal reaction of $Re_2(CO)_{10}$.[13] Other synthetic advances have been made by Katzenellenbogen et al.[14] and by Alberto et al.[15] Recently, Alberto demonstrated the viability of preparing cyclopentadienyltechnetium complexes in aqueous media using the reagent $[Tc(CO)_3(H_2O)_3]^+$ obtained from radioactive pertechnetate.[16] However, this synthesis is limited for the moment to cyclopentadienyl compounds bearing a carbonyl substituent. There is therefore a clear need for a new source of radioactive rhenium to widen the range of organometallic radiopharmaceuticals. With this aim in mind, $[^{188}Re(CO)_6]^+$ could be generated by the decay of $^{188}W(CO)_6$, thus providing a solution to the problem and an interesting alternative to the $^{188}ReO_4^-$ generator based on $^{188}WO_3$.[8] $^{188}W(CO)_6$ decay should clearly be the most direct route to the production of the carbonyl rhenium reagent. It has already been clearly established that $[^{99m}Tc(CO)_6]^+$ can be obtained from $^{99}Mo(CO)_6$.[17] This β decay of ^{99}Mo is interesting owing to the imaging application of ^{99m}Tc as well as the recognized similarity between the chemistry of Re and Tc. We were therefore interested in examining the potential of $[Re(CO)_6]^+$ in the synthesis of

[a] Laboratoire de Chimie Organométallique, Ecole Nationale Supérieure de Chimie de Paris, UMR C.N.R.S. 7576,
11, rue Pierre et Marie Curie, 75231 Paris Cedex 05, France
Fax: (internat.) + 33-1/43260061
E-mail: Jaouen@ext.jussieu.fr

organometallic complexes. The double ligand-transfer reaction was a particular object of study with a view to preparing radiopharmaceuticals. This reaction, first reported by Wenzel,[18] has recently been enhanced by Katzenellenbogen et al.[14] We also showed that $Re_2(CO)_{10}$ can be used in ligand-transfer reactions with cyclopentadienyl complexes.[19] It may therefore be possible to use the $[Re(CO)_6]^+$ cation in this type of ligand transfer. We describe here the first results obtained with this cation.

Results and Discussion

Acetylferrocene was chosen for our first experiments with $[Re(CO)_6]^+$ since this complex has been found to give the best results in ligand-exchange reactions.[14]

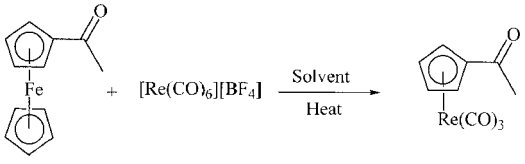

Scheme 1. Ligand-transfer reaction between acetylferrocene and hexacarbonylrhenium cation

Scheme 1 shows the synthetic route that was used. Acetylferrocene, $[Re(CO)_6][BF_4]$ and methanol were placed in a sealed tube and heated to 170 °C. After heating for 1 h and purification by chromatography, $(\eta^5\text{-}C_5H_4COMe)Re(CO)_3$ was obtained in 30% yield. We note that $CpRe(CO)_3$ is not formed under these reaction conditions. The low yield is probably due to the poor solubility of $[Re(CO)_6][BF_4]$ in methanol. Since this compound is very soluble in DMSO and DMF, the experiment was therefore repeated with DMSO in place of methanol as solvent. Owing to the high boiling point of DMSO, it was not necessary to use a sealed tube. A solution of acetylferrocene and $[Re(CO)_6][BF_4]$ in commercial DMSO was heated in an oil bath at 160 °C for 30 min. In this case, a 70% yield of $(\eta^5\text{-}C_5H_4COMe)Re(CO)_3$ was obtained. DMSO was later replaced with DMF. Under the same conditions $(\eta^5\text{-}C_5H_4COMe)Re(CO)_3$ was isolated in 64% yield. The choice of solvent has a clear influence on the outcome of the reaction. To elucidate this point, we carried out the experiments with other common solvents, such as acetonitrile, acetone, ethanol as well as water. Experimental conditions and yields obtained are summarized in Table 1.

$[Re(CO)_6][BF_4]$ is also soluble in acetonitrile. Heating a solution of the cation in acetonitrile at 95 °C for 27 h gave neither $(\eta^5\text{-}C_5H_4COMe)Re(CO)_3$ nor $CpRe(CO)_3$. The experiment was repeated using a maximum temperature of 160 °C in a sealed tube. Again, no cyclopentadienylated complex was formed, and only $[Re(CO)_3(MeCN)_3]^+$ was isolated. Heating the solution to boiling point in acetone or ethanol also failed to give $(\eta^5\text{-}C_5H_4COMe)Re(CO)_3$.

We also tried to conduct the reaction in aqueous media, because this solvent is the most commonly used for radiopharmaceutical syntheses.[16] Heating a solution of the $[Re(CO)_6]^+$ cation and acetylferrocene in water at 95 °C for 2 h gave neither $(\eta^5\text{-}C_5H_4COMe)Re(CO)_3$ nor $CpRe(CO)_3$. On the other hand, the same reaction carried out in a pressure tube gave rise to $(\eta^5\text{-}C_5H_4COMe)Re(CO)_3$ in 13% yield. The result is even more promising in a pressure tube with a water/DMSO (1:1) mixture: in this case a yield of 60% of $(\eta^5\text{-}C_5H_4COMe)Re(CO)_3$ was obtained. The use of the $[Re(CO)_6]^+$ cation in a water-based mixture of solvents could thus be envisaged. It is essential to consider this aspect when radioactive elements are handled.

The results reported below show that temperature also has a significant effect on the reaction. To study this effect, the exchange reaction was repeated using DMSO and DMF as solvents at different temperatures. The results obtained are listed in Table 2.

In DMSO, the yield of $(\eta^5\text{-}C_5H_4COMe)Re(CO)_3$ drops from 70% to 58% and then to 16% when the temperature is lowered from 160 °C to 130 °C and then 90 °C, even when the reaction is allowed to proceed for a longer time. The same pattern is observed with DMF, in which case the yield drops from 64% to 23%, and finally to 0%. This result indicates that the reaction with $[Re(CO)_6][BF_4]$ requires heating to approximately 160 °C to obtain the rhenium tricarbonyl complex in good yield.

Table 1. Reaction of acetylferrocene with $[Re(CO)_6][BF_4]$ in a variety of solvents

Entry	Solvent	Quantity of acetylferrocene	Heating time	Temperature of heating bath	Yield of $(\eta^5\text{-}C_5H_4COMe)Re(CO)_3$
1	DMSO	3.12 equiv.	30 min	160 °C	70%
2	DMF	3.12 equiv.	30 min	160 °C	64%
3	MeOH[a]	3.12 equiv.	1 h	170 °C	30%
4	MeOH	3.12 equiv.	17 h	95 °C (reflux)	0%
5	H_2O	3.12 equiv.	2 h	110 °C (reflux)	0%
6	H_2O[a]	3.12 equiv.	1 h	160 °C	13%
7	H_2O/DMSO (1:1)[a]	3.12 equiv.	1 h	160 °C	60%
6	MeCN	1.05 equiv.	27 h	95 °C (reflux)	0%
7	acetone	1.05 equiv.	17 h	75 °C (reflux)	0%
8	EtOH	3.12 equiv.	17 h	95 °C (reflux)	0%

[a] Reaction under pressure in a sealed tube.

Table 2. Reaction of acetylferrocene with $[Re(CO)_6][BF_4]$ in DMSO and DMF

Entry	Solvent	Quantity of acetylferrocene	Heating time	Temperature of heating bath	Yield of $(\eta^5\text{-}C_5H_4COMe)Re(CO)_3$
1	DMSO	3.12 equiv.	30 min	160 °C	70%
2	DMSO	3.12 equiv.	3 h	130 °C	62%
3	DMSO	1.05 equiv.	4 h 30	130 °C	58%
4	DMSO	3.12 equiv.	5 h 30	90 °C	16%
5	DMF	3.12 equiv.	30 min	160 °C	64%
6	DMF	1.05 equiv.	3 h	160 °C	71%
7	DMF	1.05 equiv.	3 h	130 °C	23%
8	DMF	1.05 equiv.	4 h 30	90 °C	0%

Table 3. Reaction of $(\eta^5\text{-}C_5H_4R)FeCp$ with $[Re(CO)_6][BF_4]$ in DMSO

Entry	R	Quantity of $(\eta^5\text{-}C_5H_4R)FeCp$	Heating time	Temperature of heating bath	Yield of $(\eta^5\text{-}C_5H_4R)Re(CO)_3$
1	COMe	1.05 equiv.	4 h 30	130 °C	58%
2	H	3.56 equiv.	5 h	180 °C	18%
3	COH	1.05 equiv.	30 min	160 °C	12%
4	COH	1.05 equiv.	3 h 20	130 °C	33%
5	COOEt	1.05 equiv.	2 h 30	160 °C	34%
6	C≡CH	1.05 equiv.	1 h 30	160 °C	0%

We also assessed how the nature of the ferrocene substituent might influence the reaction. Ferrocene, formylferrocene, ethyl ferrocenecarboxylate and ethynylferrocene were all tested in reactions in DMSO. Yields and experimental conditions are shown in Table 3.

Ferrocene gives 18% $CpRe(CO)_3$ after 5 h of heating at 180 °C. Formylferrocene and ethyl ferrocenecarboxylate give 33% and 34%, respectively of tricarbonyl(cyclopentadienyl)rhenium derivatives. Ethynylferrocene, however, gives $(\eta^5\text{-}C_5H_4COMe)Re(CO)_3$ in 48% yield instead of the expected $(\eta^5\text{-}C_5H_4C{\equiv}CH)Re(CO)_3$. This type of transformation was also observed in the reaction with the perrhenate.[14] The reaction with $[Re(CO)_6][BF_4]$ was also tested with a fairly complex molecule such as *N*-phenylferrocenecarboxamide (Scheme 2).

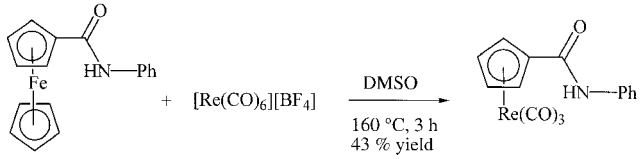

Scheme 2. Ligand-transfer reaction between *N*-phenylferrocenecarboxamide and hexacarbonylrhenium cation

Heating a solution of $[Re(CO)_6][BF_4]$ and *N*-phenylferrocenecarboxamide to 160 °C for 3 h gives tricarbonyl(*N*-phenylcyclopentadienylcarboxamide)rhenium in 43% yield.

The results obtained clearly show that $[Re(CO)_6][BF_4]$ does not react in the same way as the perrhenate.[14] The one-pot reaction between ReO_4^- and acetylferrocene in the presence of $Cr(CO)_6$ and $CrCl_2$ does not lead to the expected product in DMSO or in DMF. For this double ligand-transfer reaction, methanol was the only solvent that provided $(\eta^5\text{-}C_5H_4COMe)Re(CO)_3$ in acceptable yield (65%). This difference might be attributed to the fact that the reduction or the carbonyl transfer did not seem to proceed very well in DMSO or in DMF. By contrast, in our case, the best yields were obtained with DMSO or DMF, while methanol gave only mediocre results. It should be noted that $[Re(CO)_6][BF_4]$ is the only reagent that can react with ferrocene itself, while the perrhenate[14] and $Re_2(CO)_{10}$ [13] are inactive. To identify the real intermediate of the reaction, the $[Re(CO)_6][BF_4]$ solution in DMSO was heated to 80 °C for 3 h. The progress of the reaction was monitored using IR spectroscopy. A progressive disappearance of the peak at 2071 cm^{-1} of $[Re(CO)_6][BF_4]$ and concomitant progressive formation of two peaks at 2021 cm^{-1} and 1893 cm^{-1} were observed, characteristic of a molecule possessing C_{3v} symmetry. We postulate the formation of $[Re(CO)_3(DMSO)_3]^+$. The same transformation was also noted when $[Re(CO)_6][BF_4]$ was heated in DMF or acetonitrile under pressure. In this last case, it was possible to isolate the $[Re(CO)_3(MeCN_3)]^+$ cation which was identified by IR data.[20] Consequently, we propose that our reaction occurs in two stages (Scheme 3).

The first is the replacement of the three CO groups with solvent molecules. This exchange occurs at around 80 °C. The second step is the reaction between $[Re(CO)_3(L)_3]^+$ and the ferrocene derivative. This final reaction only begins around 130 °C and reaches full efficiency at 160 °C. Based on literature work, it has been suggested that the $\eta^5-\eta^3$ slippage of the Fe−cyclopentadienyl bond of the ferrocene

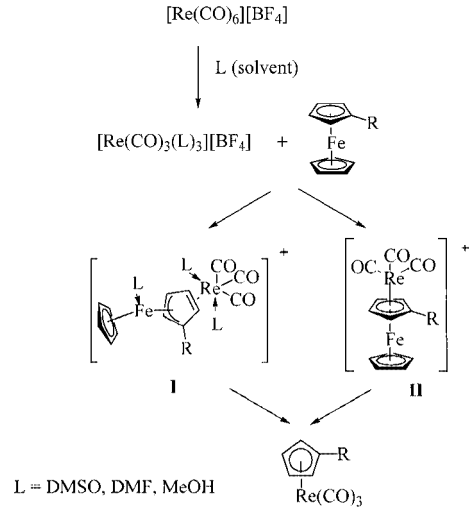

Scheme 3. Possible mechanism of cyclopentadienyl transfer reaction

derivative is responsible for its reaction with $[Re(CO)_3(MeO)(MeOH)_2]$.[14] It has also been observed that the ferrocene derivative reacts with $[(naphthalene)Mn(CO)_3]BF_4$ via the dimetallic intermediate $[Cp-Fe-Cp'-Mn(CO)_3]^+$.[21] Two mechanistic possibilities thus spring to mind for the reaction with $[Re(CO)_3(L)_3]^+$. The first is the $\eta^5-\eta^3$ slippage of the Fe−cyclopentadienyl bond, allowing the formation of the intermediate **I** which is converted into the tricarbonylrhenium compound. The second possibility is formation of the dimetallic intermediate **II**, followed by breaking of the Fe−Cp′ bond. Sweigart has shown that heating to 40 °C in dichloromethane is sufficient to cause $[(naphthalene)Mn(CO)_3]BF_4$ to react with a ferrocene derivative, leading to formation of tricarbonyl(cyclopentadienyl)manganese. Heating $[Re(CO)_3(L)_3]^+$ with the ferrocene compound to a high temperature is thus necessary to change the hapticity of the cyclopentadienyl ligand (intermediate **I**), or to drive off the three solvent molecules (intermediate **II**). Without proof of the formation of intermediates **I** and **II**, it is difficult at this stage to suggest a precise mechanism. However, the acetyl group on the cyclopentadienyl ring, acting as an electron-withdrawing group, should minimize the formation of the intermediate **II**. It is noteworthy that the reaction under pressure, using acetonitrile as the solvent, stops only at the point where $[Re(CO)_3(Me_3CN)_3]^+$ is formed indicating that this intermediate is not sufficiently reactive in the ligand-transfer reaction. To summarize, $[Re(CO)_3(Me_3CN)_3]^+$ is not an efficient intermediate, but its existence is a valuable mechanistic indicator suggesting future directions in the use of $[Re(CO)_6]^+$.

Conclusion

We have shown for the first time that the $[Re(CO)_6]^+$ cation reacts with ferrocene derivatives through a ligand-transfer reaction to give tricarbonyl(cyclopentadienyl)rhenium complexes. The reaction is rapid and in certain cases gives good yields. Due to its reactivity in water and its potential availability in a radioactive form, this reagent could be used for synthesis in water, and also in radiopharmaceutical syntheses. The reaction with $[Re(CO)_6]^+$ is both simpler and cleaner than that with the perrhenate, which requires a CO source and high pressure. We are continuing to study other types of reactions with this cation.

Experimental Section

General: The synthesis of all the compounds was performed under ambient atmospheric conditions. DMSO was used without any purification. TLC chromatography was performed on silica gel 60 GF254. Infrared spectra were obtained with an IR-FT BOMEM Michelson-100 spectrometer. ^1H and ^{13}C NMR spectra were recorded with 200 MHz and 400 MHz Bruker spectrometers. Mass spectrometry was performed with a Nermag R 10-10C spectrometer. Melting points were measured with a Kofler device. Elemental analyses were performed by the regional microanalysis department of the Université Pierre et Marie Curie.

Hexacarbonylrhenium: $[Re(CO)_6][BF_4]$ was prepared according to the procedure described in the literature.[2] IR (CH_3CN): $\tilde{\nu}$ = 2085 (ν_{CO}) cm^{-1}.

Synthesis of (Acetylcyclopentadienyl)tricarbonylrhenium in DMSO and in DMF: $[Re(CO)_6][BF_4]$ (0.073 g, 0.166 mmol) was dissolved in DMSO (1 mL) in a 5-mL round-bottom flask equipped with a magnetic stirrer bar. Acetylferrocene (0.040 g, 0.175 mmol) was added and the solution heated for 4 h 30 min at 130 °C. The mixture was allowed to warm to room temperature and then 10 mL of water was added. The product was extracted with dichloromethane (2 × 50 mL). The organic phase was washed, dried ($MgSO_4$), filtered and concentrated. The mixture was purified by chromatography on a silica gel plate (petroleum ether/ethyl acetate, 7:1) to give (acetylcyclopentadienyl)tricarbonylrhenium (0.036 g, 58%). ^1H NMR (200 MHz, $CDCl_3$): δ = 2.34 (s, 3 H, CH_3), 5.40 (t, J = 2.2 Hz, 2 H, 3,4-H of C_5H_4), 5.98 (t, J = 2.2 Hz, 2 H, 2,5-H of C_5H_4) ppm. IR (CH_2Cl_2): $\tilde{\nu}$ = 2032 s, 1939 s (ν_{CO}), 1688 w ($COCH_3$) cm^{-1}. By using DMF as solvent and by applying the same procedure (heating time: 3 h), 23% yield of (acetylcyclopentadienyl)tricarbonylrhenium was obtained.

Synthesis of (Acetylcyclopentadienyl)tricarbonylrhenium under Pressure: $[Re(CO)_6][BF_4]$ (0.073 g, 0.166 mmol) and acetylferrocene (0.118 g, 0.519 mmol) were combined in a 20-mL pressure tube containing a magnetic stirrer bar. Methanol (1 mL) was added, and the tube was sealed and heated to 170 °C. After the heating period, the tube was cooled to room temperature. The solvent was evaporated, the mixture was dissolved in a minimum volume of CH_2Cl_2 and purified by chromatography on a silica gel plate (petroleum ether/ethyl acetate, 7:1) to give (acetylcyclopentadienyl)tricarbonylrhenium (0.020 g, 30%).

Ethyl Ferrocenecarboxylate: Ferrocenecarboxylic acid (0.500 g, 2.17 mmol) was dissolved in ethanol (12 mL) in a 25-mL round-bottom flask equipped with a magnetic stirrer bar. H_2SO_4 (0.15 mL) was added, and the solution heated under reflux for 12 h. The mixture was allowed to cool to room temperature and the solvent was partially evaporated. Cold water (10 mL) was added and the product was extracted with diethyl ether (3 × 100 mL). The organic phase was washed first with saturated K_2CO_3 solution, to

eliminate the excess acid, and then with water. The organic phase was dried ($MgSO_4$), filtered and concentrated. The mixture was purified by chromatography on a silica gel plate (petroleum ether/ethyl ether, 4:1) to give ethyl ferrocenecarboxylate (0.108 g, 19%). ^1H NMR (200 MHz, $CDCl_3$): δ = 1.37 (t, J = 7.1 Hz, 3 H, CH_3), 4.21 (s, 5 H, Cp), 4.29 (q, J = 7.1 Hz, 2 H, O−CH_2−), 4.40 (t, J = 1.9 Hz, 2 H, 3,4-H of C_5H_4), 4.82 (t, J = 1.9 Hz, 2 H, 2,5-H of C_5H_4) ppm. MS (EI): m/z = 258 $[M]^+$, 230 $[M - C_2H_4]^+$, 138, 121, 56 $[Fe]^+$.

***N*-Phenylferrocenecarboxamide:** The reaction was carried out under argon in a Schlenk tube equipped with a reflux condenser. Ferrocenecarboxylic acid (0.152 g, 0.66 mmol) was placed into the Schlenk tube and cooled with an ice bath. Oxalyl chloride (3 mL, 34 mmol) was then added and the solution was kept at room temperature for 2 h. The oxalyl chloride was evaporated. The acyl chloride formed was dissolved in anhydrous THF (4 mL), and aniline (0.186 g, 2 mmol) was added dropwise. The mixture was stirred for 3 h then separated by chromatography on a silica gel plate (petroleum ether/dichloromethane, 1:1) to give *N*-phenylferrocenecarboxamide (0.114 g, 57%) m.p. 211 °C. ^1H NMR (200 MHz, $(CD_3)_2CO$): δ = 4.24 (s, 5 H, Cp), 4.42 (dd, J = 1.9 Hz, 2 H, 3,4-H of C_5H_4), 4.97 (dd, J = 1.9 Hz, 2 H, 2,5-H of C_5H_4), 7.05 (m, 1 H, Ph), 7.31 (m, 2 H, Ph), 7.76 (m, 2 H, Ph), 8.84 (s, 1 H, NH) ppm. ^{13}C NMR (50 MHz, $(CD_3)_2CO$): δ = 73.7, 74.6, 75.5, 77.8, 120.8, 123.9, 129.4, 140.5, 168.9 (CO) ppm. MS (EI): m/z = 305 $[M]^+$, 213 $[CpFeC_5H_4CO]^+$, 185 $[FeCp_2]^+$, 65 $[Cp]^+$. $C_{17}H_{15}FeNO$ (305.16): calcd. C 66.91, H 4.95, N 4.59; found. C 66.70, H 5.27, N 4.39.

Reaction in Water and in Water/DMSO: $[Re(CO)_6][BF_4]$ (0.073 g, 0.166 mmol) and acetylferrocene (0.118 g, 0.519 mmol) were combined in a 20-mL pressure tube containing a magnetic stirrer bar. Water (1 mL) was added, then the tube was sealed and heated to 160 °C. After heating for 1 h, the tube was cooled to room temperature. 10 mL of water was added. The product was extracted with dichloromethane (2 × 50 mL). The organic phase was dried ($MgSO_4$), filtered and concentrated. The mixture was purified by chromatography on a silica gel plate (petroleum ether/ethyl acetate, 7:1) to give (acetylcyclopentadienyl)tricarbonylrhenium (0.008 g, 13%). By using a water/DMSO mixture (0.5 mL/0.5 mL) as solvent and by applying the same procedure, 60% yield of (acetylcyclopentadienyl)tricarbonylrhenium was obtained.

Reaction in Acetonitrile: $[Re(CO)_6][BF_4]$ (0.073 g, 0.166 mmol) and acetylferrocene (0.040 g, 0.175 mmol) were combined in a 20-mL pressure tube containing a magnetic stirrer bar. Acetonitrile (1 mL) was added, then the tube was sealed and heated to 170 °C. After the heating period, the tube was cooled to room temperature. The solvent was evaporated, the mixture was dissolved in a minimum volume of CH_2Cl_2 and purified by chromatography on a silica gel plate (petroleum ether/ethyl acetate, 7:1) to give $[Re(CO)_3(CH_3CN)_3]^+$ (0.042 g). IR (CH_2Cl_2): $\tilde{\nu}$ = 2053 s, 1953 s (ν_{CO}) cm^{-1}.

Reaction with Ferrocene: The procedure is similar to that of the synthesis of (acetylcyclopentadienyl)tricarbonylrhenium in DMSO. Ferrocene (0.110 g, 0.591 mmol) was used in a reaction heated for 5 h at 180 °C. The compound was purified on a silica gel plate (petroleum ether/ethyl acetate, 20:1) to give tricarbonyl(cyclopentadienyl)rhenium (0.010 g, 18%). ^1H NMR (200 MHz, $CDCl_3$): δ = 5.38 (s, 5 H, Cp) ppm. IR (CH_2Cl_2): $\tilde{\nu}$ = 2024 s, 1926 vs (ν_{CO}) cm^{-1}.

Reaction with (*N*-Phenyl)ferrocenecarboxamide: The procedure is similar to that of the synthesis of (acetylcyclopentadienyl)tricarbonylrhenium in DMSO. *N*-phenylferrocenecarboxamide (0.054 g, 0.175 mmol)was used and the reaction mixture was heated for 3 h at 160 °C. The compound was purified by chromatography on a silica gel plate (ethyl acetate/petroleum ether, 2:1) to give tricarbonyl(*N*-phenylcyclopentadienylcarboxamide)rhenium (0.032 g, 43%), m.p. 179 °C. ^1H NMR (200 MHz, $(CD_3)_2CO$): δ = 5.72 (t, J = 2.3 Hz, 2 H, 3,4-H of C_5H_4), 6.41 (t, J = 2.3 Hz, 2 H, 2,5-H of C_5H_4), 7.10 (m, 1 H, Ph), 7.32 (m, 2 H, Ph), 7.67 (m, 2 H, Ph), 9.25 (s, 1 H, −NH−CO) ppm. ^{13}C NMR (100 MHz, $(CD_3)_2CO$): δ = 86.6 (C_{Cp}), 88.1 (C_{Cp}), 96.5 (C_{Cp}), 120.9 (C_{Ar}), 124.7 (C_{Ar}), 129.4 (C_{Ar}), 139.3 (C_{Ar}), 161.0 (NHC=O), 194.1 (CO) ppm. IR (CH_2Cl_2): $\tilde{\nu}$ = 2033 s, 1945 s (ν_{CO}) cm^{-1}. MS (EI): m/z = 455 $[M]^+$, 427 $[M - CO]^+$, 371 $[M - 3CO]^+$. $C_{15}H_{10}NO_4Re$ (454.45): calcd. C 39.64, H 2.22, N 3.08; found. C 40.05, H 2.00, N 3.00.

Reaction with Formylferrocene: The procedure is similar to that of the synthesis of (acetylcyclopentadienyl)tricarbonylrhenium in DMSO. Formylferrocene (0.038 g, 0.175 mmol) was used in a reaction that underwent 3 h 20 min of heating at 130 °C. The compound was purified by chromatography on a silica gel plate (petroleum ether/ethyl acetate, 5:1) to give tricarbonyl(formylcyclopentadienyl)rhenium (0.020 g, 33%). ^1H NMR (200 MHz, $CDCl_3$): δ = 5.5 (t, J = 2.4 Hz, 2 H, 3,4-H of C_5H_4), 6.0 (t, J = 2.4 Hz, 2 H, 2,5-H of C_5H_4), 9.59 (s, 1 H, −COH) ppm. IR ($CHCl_3$): $\tilde{\nu}$ = 2036 s, 1945 s (ν_{CO}), 1693 w (−CHO) cm^{-1}. IR (KBr): $\tilde{\nu}$ = 2031 s, 1920 s (ν_{CO}), 1690 w (−CHO) cm^{-1}. MS (EI): m/z = 364 $[M]^+$, 336 $[M - CO]^+$, 308 $[M - 2\ CO]^+$, 280 $[M - 3\ CO]^+$. Also isolated was $Re_2(CO)_{10}$ (0.005 g, 4%). IR ($CHCl_3$): $\tilde{\nu}$ = 2071 w, 2014 vs (ν_{CO}), 1971 w cm^{-1}.

Reaction with Ethyl Ferrocenecarboxylate: The procedure is similar to that of the synthesis of (acetylcyclopentadienyl)tricarbonylrhenium in DMSO. Ethyl ferrocenecarboxylate (0.045 g, 0.175 mmol) was used in a reaction that underwent 2 h 30 min of heating at 160 °C. The compound was purified by chromatography on a silica gel plate (petroleum ether/ethyl ether, 4:1) to give tricarbonyl(ethoxycarbonylcyclopentadienyl)rhenium (0.023 g, 34%). ^1H NMR (200 MHz, $CDCl_3$): δ = 1.32 (t, J = 7.1 Hz, 2 H, CH_3), 4.28 (q, J = 7.1 Hz, 2 H, OCH_2), 5.37 (t, J = 2.3 Hz, 2 H, 3,4-H of C_5H_4), 6.02 (t, J = 2.3 Hz, 2 H, 2,5-H of C_5H_4) ppm. IR ($CHCl_3$): $\tilde{\nu}$ = 2033 s, 1945 s (ν_{CO}), 1722 w (−CO−OEt) cm^{-1}. MS (EI): m/z = 408 $[M]^+$, 380 $[M - CO]^+$, 352 $[M - 2\ CO]^+$, 324 $[M - 3\ CO]^+$, 308, 268, 225.

Acknowledgments

Financial support from the Centre National de la Recherche Scientifique is gratefully acknowledged. We thank Barbara McGlinchey for the manuscript translation.

[1] [1a] W. Hieber, T. Kruck, *Angew. Chem.* **1961**, *73*, 580−580. [1b] W. Hieber, T. Kruck, *Z. Naturforsch., Teil B* **1961**, *16*, 709−713.
[2] D. J. Darensbourg, J. A. Froelich, *J. Am. Chem. Soc.* **1977**, *99*, 4726−4729.
[3] [3a] R. J. Angelici, G. C. Faber, *Inorg. Chem.* **1971**, *10*, 514−517. [3b] R. W. Brink, R. J. Angelici, *Inorg. Chem.* **1973**, *12*, 1062−1066.
[4] E. W. Abel, S. P. Tyfield, *Can. J. Chem.* **1969**, *47*, 4627−4633.
[5] [5a] Y. Zhen, W. G. Feighery, C-K. Lai, J. D. Atwood, *J. Am. Chem. Soc.* **1989**, *111*, 7832−7837. [5b] Y. Zhen, J. D. Atwood, *Organometallics* **1991**, *10*, 2778−2780. [5c] P. Wang, W. S. Striejewske, J. D. Atwood, *J. Coord. Chem.* **1996**, *37*, 141−149.

[6] [6a] V. D. Nefedov, M. A. Toropova, *Zhur. Neorg. Kim.* **1957**, *2*, 1667−1671. [6b] S. R. Naryan, D. R. Wiles, *Can. J. Chem.* **1969**, *47*, 1019−1024.
[7] [7a] P. Bläuenstein, *New J. Chem.* **1990**, *14*, 405−407. [7b] *Technetium and Rhenium in Chemistry and Nuclear Medicine* (Eds.: M. Nicolini, G. Bandoli, U. Mazzi), no. 3, **1990**, Cortina International, Verona, and no. 4, **1995**, SG Editoriali, Padova. [7c] R. Alberto, *Top. Curr. Chem.* **1996**, *176*, 149−187.
[8] F. F. Knapp, Jr., A. L. Beets, S. Guhlke, P. O. Zamora, H. Bender, H. Palmedo, H.-J. Biersack, *Anticancer Res.* **1997**, *17*, 1783−1796.
[9] [9a] K. E. Baidoo, S. Z. Lever, *Tetrahedron Lett.* **1990**, *31*, 5701−5704. [9b] J. P. Di Zio, C. J. Anderson, A. Davison, G. J. Ehrhardt, K. E. Carlson, M. Welch, J. A. Katzenellenbogen, *J. Nucl. Med.* **1992**, *33*, 558−569. [9c] S. K. Meegalla, K. Plössl, M-P. Kung, S. Chumpradit, D. A. Stevenson, S. A. Kushner, W. T. McElgin, P. D. Mozley, H. F. Kung, *J. Med. Chem.* **1997**, *40*, 9−17. [9d] J. L. Vanderheyden, F. M. Su, A. Fritzberg, P. Venkatesan, Patent WO 91/04057, **1991**. [9e]F. B. Van Gog, G. W. M. Visser, R. Klok, R. Van der Schors, G. B. Snow, G. A. M. S. Van Dongen, *J. Nucl. Med.* **1996**, *37*, 352−362. [9f] J. R. Dilworth, S. J. Parrott, *Chem. Soc. Rev.* **1998**, *27*, 43−55.
[10] S. Top, H. El Hafa, A. Vessieres, J. Quivy, J. Vaissermann, D. W. Hughes, M. J. McGlinchey, J-P. Mornon, E. Thoreau, G. Jaouen, *J. Am. Chem. Soc.* **1995**, *117*, 8372−8380.
[11] [11a] G. Jaouen, S. Top, A. Vessières, R. Alberto, *J. Organomet. Chem.* **2000**, *600*, 23−36. [11b] F. Le Bideau, M. Salmain, S. Top, G. Jaouen, *Chem. Eur. J.* **2001**, *7*, 2289−2294.
[12] S. Top, P. Morel, M. Pankowski, G. Jaouen, *J. Chem. Soc., Dalton Trans.* **1996**, 3611−3612.
[13] S. Top, J.-S. Lehn, P. Morel, G. Jaouen, *J. Organomet. Chem.* **1999**, *583*, 63−68.
[14] [14a] T. W. Spradau, J. A. Katzenellenbogen, *Organometallics* **1998**, *17*, 2009−2017. [14b] F. Minutolo, J. A. Katzenellenbogen, *Organometallics* **1999**, *18*, 2519−2530.
[15] [15a] R. Alberto, R. Schibli, W. A. Hermann, G. Artus, V. Abram, P. A. Schubiger, T. A. Kaden, *J. Organomet. Chem.* **1995**, *493*, 119−127. [15b] R. Alberto, R. Schibli, A. Egli, V. Abram, S. Abram, T. A. Kaden, P. A. Schubiger, *Polyhedron* **1998**, *17*, 1133−1140. [15c] R. Alberto, R. Schibli, P. A. Schubiger, V. Abram, R. Hübener, H. Berke, T. A. Kaden, *Chem. Commun.* **1996**, 1291−1292.
[16] J. Wald, R. Alberto, K. Ortner, L. Candreia, *Angew. Chem.* **2001**, *113*, 3152−3156.
[17] V. D. Nefedov, V. Mikulai, *Soviet Radiochem.* **1973**, *15*, 855−860
[18] [18a] M. Wenzel, *J. Labelled Comp. Radiopharm.* **1992**, *31*, 641−650. [18b] M. Wenzel, C. Klinge, *J. Labelled Comp. Radiopharm.* **1994**, *34*, 981−987.
[19] S. Top, C. Lescop, J.-S. Lehn, G. Jaouen, *J. Organomet. Chem.* **2000**, *593/594*, 167−174.
[20] D. R. Gard, T. L. Brown, *J. Am. Chem. Soc.* **1982**, *104*, 6340−6347.
[21] S. U. Son, K. H. Park, S. J. Lee, Y. K. Chung, D. A. Sweigart, *Chem. Commun.* **2001**, 1290−1291.

Received November 16, 2001
[I01460]

Do Divalent [{HC(CR′NR′′)$_2$}E] Compounds Contain E(I) or E(III) (E = B, Al, Ga, In)? On the Correspondence of Formal Oxidation Numbers, Lewis Structures, and Reactivity

Markus Reiher*[a] and Andreas Sundermann[b]

Dedicated to Professor Jürgen Hinze on the occasion of his 65th birthday

Keywords: Oxidation number analysis / Group-13 carbene analogs / Density functional calculations

Very recently, carbene-analogous aluminum and gallium compounds have been obtained in beautiful synthetic work giving rise to interesting theoretical questions in the framework of qualitative MO theory. We analyze the concept of oxidation numbers and the stabilities of these [{HC(CR′NR′′)$_2$}E] compounds, **1(E)**, with E being boron, aluminum, gallium, and indium. Population analyses and the electron localization function are used as analytical tools for the elucidation of the electronic density distribution. Singlet-triplet splitting energies, and model reactions probing donor and acceptor properties of the atom E, yield criteria for the reactivity of the cyclic molecules. It is demonstrated that a unique class of Lewis structures can be selected from the large number of chemically reasonable Lewis structures in order to achieve a sufficiently good mapping of the quantum chemical results on simple chemical concepts. The analysis yields that **1(E)**, where E = In, is expected to have similar properties as the experimentally known compounds **1(Al)** and **1(Ga)**, while the boron homologue is expected to be highly reactive, such that its synthesis appears to be difficult. (© Wiley-VCH Verlag GmbH, 69451 Weinheim, Germany, 2002)

1. Introduction

Recently, Cui et al.[1] synthesized a new cyclic compound **1(E)** = [{HC(CR′NR′′)$_2$}E] containing an aluminum atom bound to two neighboring nitrogen atoms. At about the same time, the corresponding gallium compound was obtained.[2] The planarity of the ring resembles a benzene-like system. This observation led both groups of authors to the conclusion that the electronic structure of the molecule may be described as a carbene analog with Al and Ga, respectively, having the formal oxidation number +I. While **1(Al)** is the first carbene-analogous aluminum compound known, a carbene-analogous gallium compound has already been characterized[3] as predicted by quantum chemical calculations.[4] A divalent boron homologue has not yet been synthesized, and the question arises whether {HC(CR′NR′′)$_2$}B might be sufficiently stable to be obtainable in bulk.

Since Cui et al. utilized quantum chemical calculations to support their conclusions,[5] the interesting problem has arisen of when and how numerical results of elaborate quantum chemical calculations can be mapped on simple qualitative chemical descriptors in order to gain transferable knowledge about the electronic structure of a new class of compounds. Is it, in particular, possible at all to determine the formal oxidation state from quantum chemical calculations? A positive answer to this question would in turn attribute substantial meaning to the concept of oxidation numbers.

Jørgensen already tried to settle this question in his book about oxidation numbers,[6] in which he introduced five different oxidation number concepts in order to account for many different chemical situations. Unfortunately, the definitions given[6] are mainly phenomenological, their number exceeds the acceptable degree, and they do not meet concepts of contemporary quantum chemical methods. For instance, Jørgensen defined a spectroscopic and a conditional oxidation state based on *atomic* orbital occupation numbers (atomic configurations). But the atomic occupation number is neither an observable property nor a decisive concept in the light of *molecular* orbitals and *configuration interaction* approaches. Atoms are no longer well-defined entities in molecules, because in all but the simplest cases molecules are treated as collections of electrons and atomic nuclei rather than as clusters of polarized atoms. Actually, this is the fundamental reason why the oxidation number concept can hardly be obtained directly as an atomic "property" in quantum chemical calculations.

[a] Theoretische Chemie, Universität Erlangen-Nürnberg, Egerlandstraße 3, 91058 Erlangen, Germany
[b] hte Aktiengesellschaft, Kurpfalzring 104, 69123 Heidelberg, Germany

Some attempts have been made to circumvent this problem and to give a definition of the oxidation number concept based on quantum chemistry. Zhan et al. founded their definition on charge transfer within molecular orbital theory.[7] However, their approach appears useless since its ingredients are not well-defined quantities (from the viewpoint of the physical foundations) such as "charge in a local region of a given atom" or "charge in the bonding region". Additionally, some electronegativity values enter their definition neglecting the importance of using clearly defined electronegativity values for an atom in a particular valence state, which gives the best resemblance to its state in the molecule, as explicated in great detail 40 years ago by Hinze and Jaffe.[8–13]

In their analysis of the oxidation state and the possible carbene-analogous character of **1(Al)**, Cui et al. followed closely an earlier work on the electronic structure of Arduengo carbene analogs of group-13 elements.[4] Here, we extend and generalize the work of Cui et al. on the aluminum compound with respect to other group-13 elements to establish a thorough oxidation number classification and stability analysis of [{HC(CR′NR″)$_2$}E], **1(E)**, with E being boron, aluminum, gallium, and indium. This permits also an assessment of the possible stability of the divalent boron compound **1(B)**.

As we demonstrate in the sequel, it is difficult to assign a most suitable Lewis structure for **1(E)** on the grounds of (chemical) common sense. We will discuss possible candidates to conclude which class of Lewis structures is the best one for the representation of the electronic structure. These reasonable Lewis structures for **1(E)** are given in the following section and extended Hückel calculations are employed for a qualitative molecular orbital discussion of the electronic situation. The structures obtained from density functional calculations are discussed thereafter and the electronic density distribution is analyzed in terms of partial charges, the electron localization function, and the Laplacian of the electron density. A discussion of reactivity on the basis of singlet-triplet splitting energies and Lewis acid-base reactions follows in Section 5. Details on the quantum chemical methods employed are given in the Appendix.

2. Qualitative Picture

Nowadays, compounds of the size of **1(E)** can be analyzed on personal computers using quantum chemical methods with sufficiently large basis sets. The aim of a theoretical study should therefore be the gain of insight rather than a reproduction of experimentally obtained quantities. Consequently, the complete knowledge about the electronic density distribution obtained from the numerical calculation should be analyzed in order to assign a characteristic set of Lewis structures. The benefit is a simplified

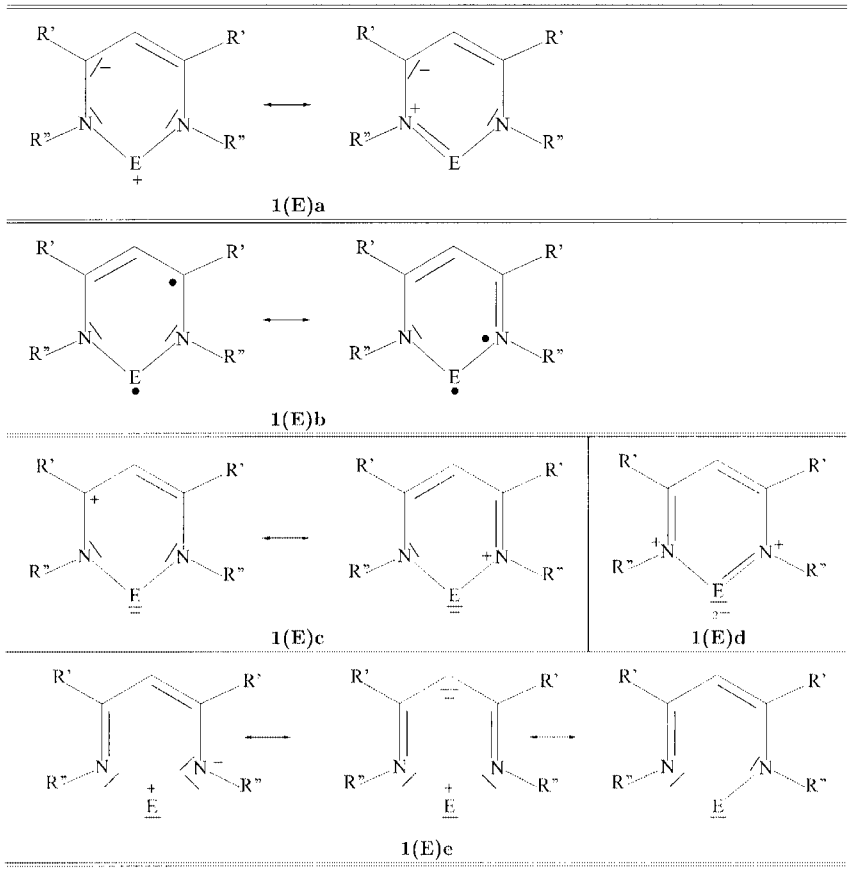

Figure 1. Three classes (the last one is subdivided into three sub-classes) of Lewis structures of [{HC(CR′NR″)$_2$E] compounds (E = B, Al, Ga, In); corresponding symmetric Lewis structures were omitted for the sake of brevity

graphical expression of the electronic structure with the most prominent features. Subsequent work should be possible on the back of an envelope rather than using large computer resources. Three different classes of Lewis structures can be constructed for **1(E)** (Figure 1).

• Class I: In **1(E)a** the element E bears a positive (formal) charge, while the corresponding negative charge is assigned to the ring carbon atoms resulting in an allyl-anion-type substructure. It is possible to delocalize the positive charge on the three-center N−E−N substructure by assuming an additional π interaction between E and the neighboring nitrogen atoms.

• Class II: The only possible electronic structure without charge separation is given by **1(E)b** yielding a diradical.

• Class III: This class is best discussed in terms of three subclasses. The structures in **1(E)c** show a similar bonding pattern like **1(E)a**, although the formal charges of the subsystems are reversed, i.e., a negatively charged atom E and an allyl cation substructure results or the positive charge is shifted towards the nitrogen atoms, respectively. Structure **1(E)d** builds up a separate subclass because a Hückel-aromatic 6π system can only be established at the cost of two negative charges localized on atom E and positive charges localized on the nitrogen atoms. Finally, the structures **1(E)e** generate the third subclass. A bidentate chelate ligand coordinates to the central atom E. Thus, **1(E)e** represents a donor-acceptor complex. This type of bonding has been extensively investigated by Schoeller and co-workers for group-13, -14, and -15 compounds with similar connectivities,[4,14−18] and others have also investigated this.[19−23]

All three classes of Lewis structures stress different qualitative aspects of the electronic structure and correspond to three different oxidation numbers. While Lewis structures and formal charges are well-defined concepts in the sense that they can be drawn without any arbitrariness, this does, in general, not hold for oxidation numbers as already discussed in the Introduction. However, in cases where electrons can be classified as "bonding" and "non-bonding" (such as in cases of lone pairs or non-bonding d electrons in transition metal complexes) the assignment of a formal oxidation number is possible. Since the Lewis structures suggest that we count 0 electron in **1(E)a**, 1 electron in **1(E)b**, and 2 electrons in **1(E)c−e** as non-bonding according to the lone-pair electrons at E [σ/π separation is possible (point group C_{2v})], we obtain the following oxidation number assignment: **1(E)c**, **1(E)d**, and **1(E)e** possess E in the formal oxidation number +I, while **1(E)b** contains E in the formal oxidation number +II and finally for **1(E)a** we have +III. This assignment is in accordance with the rules given by Pauling.[24] Pauling's rule no. 3, which states that the bonding electrons are assigned to the more electronegative atoms, leads to exactly the same oxidation number assignment. In our case, the nitrogen atoms are the more electronegative atoms when compared with E (in terms of Pauling's "averaged" electronegativity scale as well as in terms of the Mulliken−Jaffe electronegativity scale; see also ref.[8]).

The "oxidation number problem" has now been reduced to the analysis of the contribution of the Lewis structures in Figure 1 to the total electronic wavefunction. But a decision about which Lewis structure is most appropriate to describe the actual electronic structure is not straightforward. The standard textbook rules for the relative contribution of Lewis structures are difficult to apply because the stabilizing effect of several electronic and structural features (such as s−p separation in the valence shell of the isolated atom E, charge delocalization, and negative charge on electronegative atoms) is hard to estimate. Numerical results from quantum chemical calculations are needed to solve this puzzle and to achieve a better understanding and improvement of these formal concepts. It should be noted that counting the number of lone-pair electrons is complementary to counting the number of π electrons in the ring. We have 8π electrons in the case of **1(E)a** with oxidation number +III, and 6π electrons in the case of **1(E)c−d** with oxidation number +I. This gives a first hint, along the lines of Hückel's rule, which Lewis structures and thus which oxidation numbers are to be preferred.

The discussion of Lewis structures so far allows us to define descriptors for testing which of these structures are most appropriate. Firstly, we note that E^{III} always bears a positive charge while E^{II} is uncharged and E^{I} results in a more or less pronounced accumulation of negative charge on the group-13 atom. Therefore, population analyses yielding a formal separation of charges in areas of real or Hilbert space may be used to determine the partial charge on atom E.

Since a formal oxidation number of +I requires a lone-pair on atom E, approaches such as the electron localization function,[25] which are able to detect possible lone pairs, may contribute to the classification of the electronic structure in terms of the Lewis structures. Besides these methods for the direct analysis of the charge density, chemical measures for probing particular features of the electronic density distribution such as bond angles and distances, as well as reactivity-based approaches, can be considered. The latter appears to be promising because E^{I} and E^{III} compounds could be distinguished by their different affinity towards Lewis acids such as BF_3, and Lewis bases such as NH_3. Thus, the ability to form Lewis acid-base complexes could be utilized to probe for a lone-pair at the group-13 atom. Binding energies resulting from the analysis of such Lewis acid-base addition reactions are also accessible by quantum chemical calculations. A complication of this viewpoint comes from the so-called inert-pair effect: The larger the nuclear charge Z of atom E, the more important is this effect on reducing the donor property of E without changing the formal oxidation number.

To obtain a first qualitative picture of the electronic structure within molecular orbital theory, we performed Extended-Hückel Theory (EHT) calculations since they provide an *occupation number independent* view of the electronic structure. A representation of the molecular orbitals on the basis of fragment orbitals of cation E^+ and a negatively charged ligand $[HC(CR'NR'')_2]^-$ reveals some im-

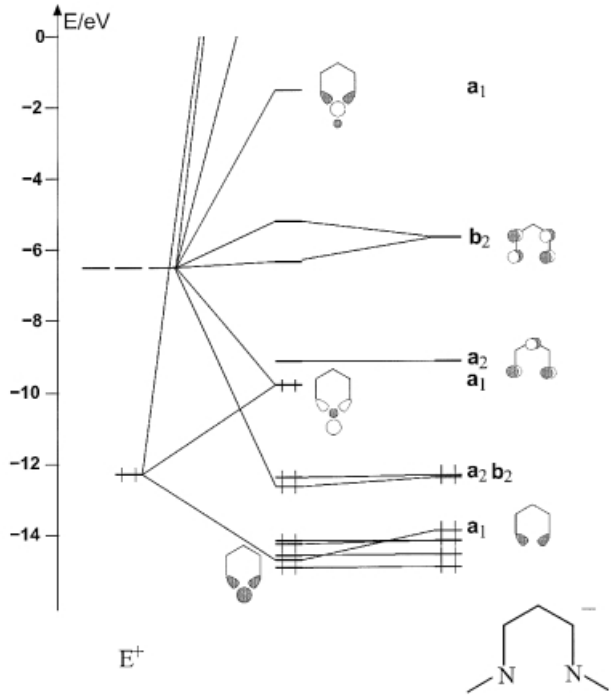

Figure 2. Simplified MO diagram from Extended-Hückel calculations; the left-hand side shows the valence atomic orbitals of the aluminum atom, whereby the highest occupied p-orbital is denoted by a small vertical line; the right-hand side gives the molecular orbitals of the remaining {HC(CR′NR′′)$_2$} chelate ligand; in the center the molecular orbitals for the total complex are depicted

portant aspects of the bonding situation (Figure 2). It should be noted that the ligand is σ- and weakly π-bonding, and element E^+ cannot back-donate.

The qualitative MO diagram from EHT calculations shows a rather small HOMO−LUMO energy splitting. The frontier orbitals can be classified as a metal−ligand nonbonding orbital of a_2 symmetry (point group C_{2v} assumed) being localized on the ligand and a weakly anti-bonding combination with nitrogen sp^2 and metal sp contributions. The latter MO has the character of a metal lone pair. Since the a_2 MO has no metal contributions for symmetry reasons, its energy is largely independent of the nature of E. The energy of the a_1 MO is expected to be the HOMO for the heavier group-13 elements, while at least for E = B a more pronounced antibonding character due to a larger π overlap may result in a_2 then becoming occupied. A decision about this ordering is beyond the scope of the qualitative EHT treatment.

3. Optimized Structures

The structures obtained with the pure density functional BP86 and the hybrid functional B3LYP are discussed in the following. For the sake of simplicity and computational efficiency and to arrive at substituent-independent conclusions we concentrate on generic models of **1(E)**. Therefore, we chose the model compound with R′ = R′′ = H. However, to test for substituent effects we also performed calculations

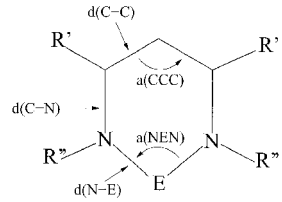

Figure 3. Definition of characteristic structural parameters

for R′′ = Me. The most important structural parameters are depicted in Figure 3 and given in Table 1. All optimized structures **1(E)** are found to be minima on the potential energy surface.

The optimized structures for the heavy elements of group-13 adopt C_{2v} symmetry in their singlet ground state, and they are thus planar. For the boron compound, a distortion to C_2 symmetry is observed, indicating a qualitatively different electronic structure of **1(B)** when compared to its higher homologues. In the triplet state, **1(Al)** and **1(B)** are planar, while the Ga and In atoms in **1(Ga)** and **1(In)**, respectively, may lie above the NCCN plane in an envelope-type structure (this depends on the density functional and on the R′′ substituent, indicating an electronic structure of the triplet state being too complicated to be accessible by density functional methods).

The C−C and N−C bond lengths deviate for Al to In slightly from the values found for the anionic $C_3H_5N_2^-$ ligand. These findings justify the fragmentation used in the qualitative EHT calculation and indicate that the Lewis structures **1(E)e** are a good representation for E = Al and an even better one for E = Ga and E = In. The heavier the group-13 element E is, the more the binding situation resembles a chelate complex.

In the case of E = B, the changes observed in the ligand are larger; the C−N bond is 5 pm longer while the C−C distance is shortened by 2.5 pm. It is interesting to note that similar values can be found for the lowest triplet states of the Al, Ga, and In complexes. This may be interpreted as an indicator for the orbital crossover discussed in the previous section.

In general, the substitution of hydrogen by a methyl group does not change the structure significantly and both compare very well with the experimental structures for E = Al and E = Ga, in which 2,6-*i*$Pr_2C_6H_3$ substituents are present, Only the N−E bond lengths deviate by 5−6 pm from the calculated distances.

4. Analysis of the Electronic Density

According to the charge separation suggested by the different Lewis structures, we calculated partial charges from two different population analyses. One was suggested by Cioslowski,[26] which is defined in real space, and the other one by Heinzmann and Ahlrichs,[27] which is defined in the Hilbert space of (modified) atomic orbitals. The two conceptually different population analyses are used since the partial charge of an atom in a molecule is not a well-defined

Table 1. Selected structural parameters of [{HC(CR′NR′′)$_2$}E] (R′ = H) for their singlet ground states (S = 0) and the lowest-lying triplet states (S = 1); the last data set contains structural parameters for the anionic ligand; distances d are given in pm and the angles a in °; the definition of parameters $a-d$ are given in Figure 3; the experimental bond lengths and angles for [{HC(CMeNAr)$_2$}E] (R′′ = Ar = 2,6-iPr$_2$C$_6$H$_3$) with E =Al, Ga are given for comparison (PG is an acronym for "point group")

E	R"	parameter	BP86/RI		B3LYP	
			S=0	S=1	S=0	S=1
B	H	d(C–C)	139.1	138.9	138.6	138.3
		d(C–N)	137.7	141.8	135.9	141.3
		d(N–E)	145.6	142.1	146.5	141.4
		a(NEN)	112.4	118.4	110.0	118.6
		a(CCC)	120.5	122.5	119.7	122.4
		PG	C_2	C_{2v}	C_2	C_{2v}
	Me	d(C–C)	139.2	138.9	138.5	138.2
		d(C–N)	137.8	141.5	136.5	141.0
		d(N–E)	144.6	142.3	144.7	141.6
		a(NEN)	115.6	120.8	114.8	121.0
		a(CCC)	120.5	122.5	120.1	122.4
		PG	C_2	C_{2v}	C_2	C_{2v}
Al	H	d(C–C)	139.8	139.4	139.2	138.8
		d(C–N)	133.3	141.3	132.4	140.9
		d(N–E)	200.6	181.9	199.6	181.0
		a(NEN)	85.8	104.5	85.9	104.5
		a(CCC)	123.0	128.1	122.7	127.9
		PG	C_{2v}	C_{2v}	C_{2v}	C_{2v}
	Me	d(C–C)	139.8	139.4	139.3	138.8
		d(C–N)	133.0	141.1	132.0	140.6
		d(N–E)	201.7	182.9	200.7	181.9
		a(NEN)	89.2	107.9	89.4	107.9
		a(CCC)	124.2	128.9	124.0	128.7
		PG	C_{2v}	C_{2v}	C_{2v}	C_{2v}
exp. [1]	Ar	d(C–C)	139.1			
		d(C–N)	134.1			
		d(N–E)	195.7			
		a(NEN)	89.9			
		a(CCC)	126.8			
Ga	H	d(C–C)	140.0	139.7	139.4	138.8
		d(C–N)	133.0	140.5	132.1	140.5
		d(N–E)	209.7	190.7	209.5	187.0
		a(NEN)	84.1	99.3	84.0	102.6
		a(CCC)	124.2	128.5	124.0	128.7
		PG	C_{2v}	C_s	C_{2v}	C_{2v}
	Me	d(C–C)	140.0	139.4	139.5	139.0
		d(C–N)	132.6	140.8	131.6	139.4
		d(N–E)	210.7	188.1	210.6	191.0
		a(NEN)	87.5	106.7	87.4	101.5
		a(CCC)	125.5	129.7	125.3	129.1
		PG	C_{2v}	C_{2v}	C_{2v}	C_s
exp. [2]	Ar	d(C–C)	140.0			
		d(C–N)	133.8			
		d(N–E)	205.5			
		a(NEN)	87.5			
		a(CCC)	127.7			
In	H	d(C–C)	140.2	141.2	139.7	140.8
		d(C–N)	132.9	138.0	132.0	136.9
		d(N–E)	229.8	222.6	229.6	226.0
		a(NEN)	79.8	84.2	79.5	82.3
		a(CCC)	126.4	130.4	126.1	130.8
		PG	C_{2v}	C_s	C_{2v}	C_s
	Me	d(C–C)	140.3	140.7	139.8	140.0
		d(C–N)	132.4	132.2	131.5	131.2
		d(N–E)	231.1	218.2	231.0	218.7
		a(NEN)	83.1	92.6	82.9	92.1
		a(CCC)	127.9	129.5	127.6	129.1
		PG	C_{2v}	C_{2v}	C_{2v}	C_{2v}
ligand	H	d(C–C)	142.1	142.5	141.5	142.5
		d(C–N)	132.0	137.6	130.8	137.6
		a(CCC)	132.1	136.5	131.6	136.5
		PG	C_{2v}	C_{2v}	C_{2v}	C_{2v}
	Me	d(C–C)	142.1	141.9	141.5	141.9
		d(C–N)	132.0	136.3	130.8	136.3
		a(CCC)	131.6	136.1	131.2	136.1
		PG	C_{2v}	C_{2v}	C_{2v}	C_{2v}

quantum mechanical quantity. Any definition of this intuitive concept is affected by a certain degree of arbitrariness. However, we aim at qualitative results and these should be reproduced by both population analyses. The results of the calculations are given in Table 2.

Table 2. Partial charges q on atom E in fractions of the elementary charge in the singlet state of **1(E)** (R′ = H) according to population analyses by Cioslowski q_C[26] and by Ahlrichs and co-workers q_A[27] (q_A includes multi-center corrections); discrepancies occur for E = In, where the general trend is not maintained; this can be traced back to the use of the ECP for In

E	R"	BP86(/RI)		B3LYP	
		q_C	q_A	q_C	q_A
B	H	−1.37	−0.34	−1.75	−0.39
	Me	−1.16	−0.35	−1.45	−0.37
Al	H	1.21	0.36	1.29	0.37
	Me	1.13	0.41	1.25	0.42
Ga	H	1.66	0.45	1.75	0.46
	Me	1.54	0.45	1.65	0.47
In	H	0.64	0.94	0.67	0.95
	Me	0.60	0.95	0.64	0.95

While Al and its higher homologues carry positive partial charges, the boron compound exhibits negative partial charges indicating that reactions of **1(B)** will be different from those of the higher homologues. The N−E bonds have substantial ionic character.

In order to visualize a potential electron-pair on element E we utilize the electron localization function (ELF).[25] The ELF is a measure for the spherically averaged Fermi-hole around a reference electron at position $\vec{r}$. As introduced by Becke and Edgecombe,[25] the function can be mapped onto an interval $0 < \mathrm{ELF} < 1$. ELF ≈ 1 indicates areas of a localized exchange potential. Such areas are occupied by electron pairs. For ELF ≈ 0 the exchange hole is strongly delocalized. The ELF reveals the presence of a lone pair at atom E for all group-13 elements (Figure 4). A polar nature of the N−E bonds is present for all heavier atoms E, i.e., E = Al, Ga, In, which is typical for donor−acceptor complexes.

In addition to ELF, we also calculated the Laplacian of the electron density in the framework of the Atoms-In-Molecules theory[28] but refrain from giving plots of the result because of the mapping which connects ELF and the Laplacian of the density.[29,30] [An advantage of ELF is that the corresponding Laplacian of the density, $\nabla^2\rho(\vec{r})$, is unbound, while ELF is not; ELF is therefore more suitable for graphical representations.] Since the Laplacian field $\nabla^2\rho(\vec{r})$ is a measure for local charge concentrations [$\nabla^2\rho(\vec{r}) < 0$] and for charge depletion [$\nabla^2\rho(\vec{r}) > 0$] in the electron distribution of a molecule, we find for the elements Al to In the N−E bonding electrons assigned to the valence shell of the nitrogen atoms as witnessed by the convex nature of the area of charge concentration/electron localization. Only for E = B is the situation less clear. Here, the bond exhibits a more covalent character.

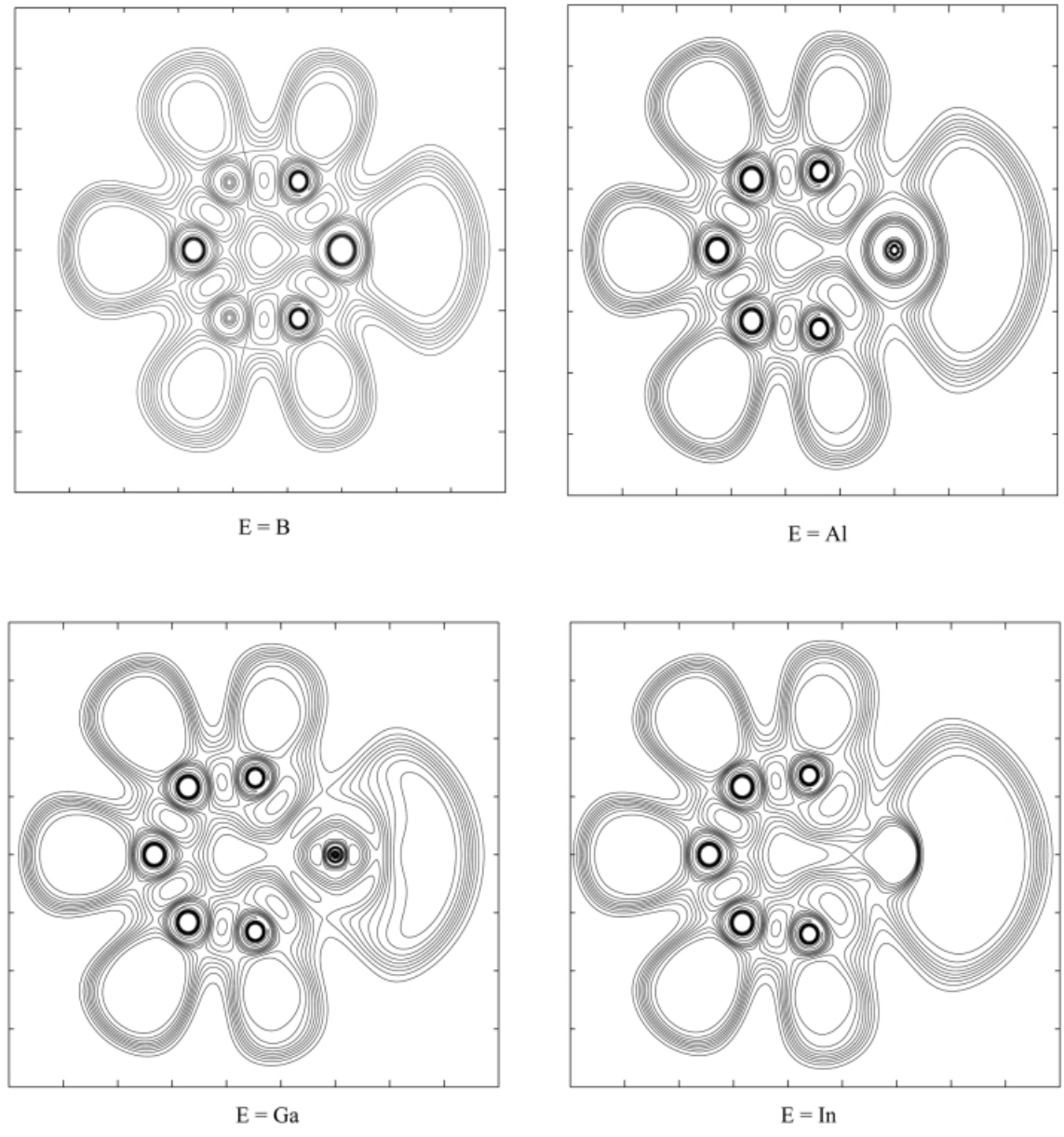

Figure 4. ELF plots for [{HC(CR′NR′′)$_2$}E], where R′ = R′′ = H; the contour lines give the increasing value for ELF in steps of 0.1 from 0.0 (no localization) outside the molecules to 1.0 (high localization) at the C−H and N−H bonds and at the lone pairs; the internal structure of the indium atom is not resolved because of the ECP

5. Reactivity − Singlet−Triplet Splittings and Addition of NH_3 and BF_3

We proceed by analyzing the singlet−triplet splitting energies given in Table 3. We find that for E = B and R′ = R′′ = H, the triplet state is almost as stable as the singlet state, indicating a high reactivity of **1(B)**. The B3LYP splitting energy favors the triplet state by about 20 kJ/mol, which is due to the fact that B3LYP always favors spin states of high multiplicities owing to the explicit consideration of Fermi correlation through exact exchange admixture.[31] If the hydrogen atoms on the ring nitrogen atoms are substituted by methyl groups, the situation becomes even less clear. DFT calculations are not sufficiently accurate to finally answer the question of the ground state multiplicity of **1(B)**. Since the knowledge of the ground state multiplicity is of minor importance to our study, we refrain from performing more elaborate calculations. The important result is that singlet and triplet states are energetically close for E = B, while this is not the case for the higher homologues, where the triplet states lie more than 150 kJ/mol above the singlet states.

This analysis of the singlet−triplet energy splittings reveals that the aluminum, gallium, and indium compounds have a similar electronic structure, while the boron compounds are different as they will exhibit a higher reactivity and are thus well represented by the Lewis structures of the biradical, **1(B)b**. This structure should also come to the fore

in a plot of the spin polarization, which is the "excess density" of the unpaired electrons. It is plotted for the triplet state of **1(B)** in Figure 5 and clearly shows a single electron at atom E and a "delocalized" electron over the four ring atoms exactly corresponding to Lewis structure **1(B)b**. It is thus most likely that the boron compound **1(E)** is not sufficiently stable to be "accessible in a flask".

Table 3. Singlet−triplet splittings $\langle E\rangle_{ST} = \langle E\rangle_{S=1} - \langle E\rangle_{S=0}$ in kJ/mol

E	R"	BP86(/RI)	B3LYP
B	H	−2	−18
	Me	12	−5
Al	H	144	148
	Me	160	164
Ga	H	217	227
	Me	233	224
In	H	245	257
	Me	271	282

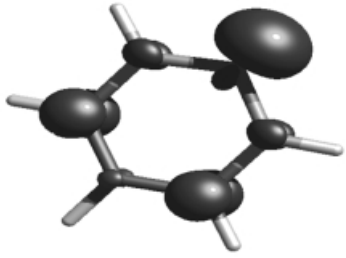

Figure 5. Spin polarization of the triplet state of **1(B)**

To analyze the electronic situation and reactivity of element E in **1(E)** further, we probe the potential lone pair or "electron-hole" on element E by addition reactions, in which an electron-pair donor such as NH_3 and an electron-pair acceptor such as BF_3 are added [Equations (1) and (2)].

Reaction (I): **1(E)** + NH_3 → **1(E)**−NH_3 (1)

Reaction (II): **1(E)** + BF_3 → **1(E)**−BF_3 (2)

Note that these addition reactions shall serve as model reactions to probe certain electronic features of **1(E)** rather than to find stable, experimentally accessible adducts. The addition of NH_3 occurs only perpendicular to the plane of the six-membered ring for E = Al, Ga, In, as one would expect for E bearing a lone-pair. An in-plane addition does not occur; the NH_3 is then rejected indicating that a lone-pair−lone-pair repulsion appears. In the case of E = B, the adduct rearranges to give a five-membered ring, where one N−H unit builds up an annulated B−C−N three-membered ring. Therefore, we restrict the discussion to the addition reactions for the higher homologues, which are all minimum structures on the potential energy surface. The general adduct structure is depicted for E = Al in Figure 6. Selected structural parameters are given in Table 4, and the reaction energetics can be found in Table 5.

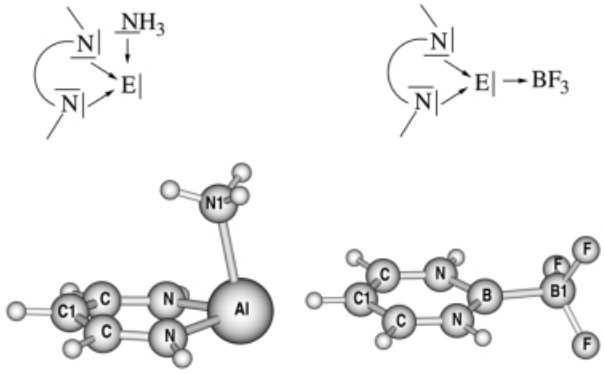

Figure 6. Structures for two possible adducts of NH_3 and BF_3 and the corresponding BP86/RI/TZVP-optimized structures for **1(Al)** + NH_3 and **1(B)** + BF_3

Table 4. Selected structural parameters of adducts $[\{HC(CR'NR'')_2\}E]NH_3$ (R′ = R″ = H) for their singlet ground state ($S = 0$): distances d are given in pm and the angles a in °; the definition of parameters $a-d$ are according to the definition for the basis systems in Figure 3; the labelling C1 and N1 is according to Figure 6; the bond lengths and angles for the boron adduct are not given since the structure rearranges drastically; all calculations have been performed with the TZVP basis set

E	parameter	BP86(/RI)	B3LYP
Al	d(C–C)	140.3	139.7
	d(C-N)	132.9	131.9
	d(N–E)	204.2	203.3
	d(E-N1)	231.1	234.1
	a(NEN)	85.6	85.7
	a(CCC)	123.2	123.0
	a(C1EN1)	79.3	79.6
Ga	d(C–C)	140.4	139.8
	d(C–N)	132.6	131.7
	d(N–E)	214.6	214.0
	d(E–N1)	252.4	260.3
	a(NEN)	83.3	83.2
	a(CCC)	124.6	124.3
	a(C1EN1)	77.6	77.5
In	d(C–C)	140.7	140.1
	d(C–N)	132.6	131.6
	d(N–E)	234.9	234.4
	d(E–N1)	266.6	271.1
	a(NEN)	79.1	78.8
	a(CCC)	126.8	126.5
	a(C1EN1)	71.4	72.1

Table 5. Energetics for the addition of NH_3 [Equation (1)]: reaction energy $\Delta\langle E\rangle$ at 0 K without zero-point vibrational energy correction (ZPVE), difference of zero point energies ΔZPVE, reaction enthalpy ΔH and free reaction enthalpy ΔG (both at 298.15 K and 1013.25 hPa) obtained for BP86/RI and B3LYP with the TZVP basis set; all energies are given in kJ/mol

	BP86(/RI)				B3LYP			
	$\Delta\langle E\rangle$	ΔZPVE	ΔH	ΔG	$\Delta\langle E\rangle$	ΔZPVE	ΔH	ΔG
Al	−20.9	5.4	−14.0	23.0	−15.1	5.3	−8.1	29.1
Ga	−13.6	4.6	−6.5	27.1	−10.2	5.3	−2.7	32.7
In	−23.5	5.5	7.9	23.4	−21.4	6.2	8.3	28.9

All three reactions are energetically very similar. They are exothermic by about 15 kJ/mol, but endergonic by about 20 kJ/mol because of the model-inherent increase of vibra-

tional entropy from the quenching of translational and rotational degrees of freedom on adduct formation. These results are almost independent of the functional used and demonstrate that **1(E)** with E = Al, Ga, In react as Lewis acids if the Lewis base approaches from above the ring plane. Upon addition, the structure of the allyl system is not changed; the C−C and C−N bond lengths as well as the C−C−C angle do not change significantly. However, the donated lone-pair of ammonia lengthens the E−N bonds in the six-membered ring by 3.6 pm for E = Al and by about 5 pm for E = Ga, In. In all adducts, the E−NH_3 distances are 30 to 40 pm longer than the in-plane E−N distances, which may be an indication for a double-bond character of the E−N bond in the ring. However, the equatorial E−N distances should be shorter because of sp^2 hybridization and for steric reasons, while the axial E−NH_3 bond should be longer because of the larger repulsion in this position.

For reaction (II) [Equation (2)], i.e., the addition of the electron acceptor BF_3, stable addition products are found for all four molecules. The general structure of the adduct is shown for E = B in Figure 6 (selected parameters see Table 6). In contrast with the NH_3 addition, the addition of BF_3 occurs in the plane of the six-membered ring as would be expected in view of the Lewis base addition of **1(E)** to BF_3.

Table 6. Selected structural parameters of adducts [{HC(CR′NR′′)$_2$}E]BF_3 (R′ = R′′ = H) for their singlet ground state (S = 0): distances d are given in pm and the angles a in °; the definition of parameters a−d are according to the definition for the basis systems in Figure 3; the labelling C1 and B1 is according to Figure 6; an asterisk, *, indicates that the BF_3 ligand tends to dissociate; all calculations have been performed with the TZVP basis set

E	parameter	BP86(/RI)	B3LYP
B	d(C–C)	139.7	138.9
	d(C–N)	133.6	132.8
	d(N–E)	147.1	146.5
	d(E–B1)	173.4	173.4
	a(NEN)	109.4	109.6
	a(CCC)	118.8	118.6
	a(C1EB1)	173.7	174.4
Al	d(C–C)	139.8	139.2
	d(C–N)	133.5	132.7
	d(N–E)	193.7	192.5
	d(E–B1)	232.6	233.9
	a(NEN)	90.6	90.8
	a(CCC)	123.5	123.2
	a(C1EB1)	177.1	179.1
Ga	d(C–C)	139.8	139.3
	d(C–N)	133.2	132.3
	d(N–E)	201.2	201.7
	d(E–B1)	237.6	250.3*
	a(NEN)	88.5	87.8
	a(CCC)	124.3	124.0
	a(C1EB1)	178.1	179.2
In	d(C–C)	140.2	139.6
	d(C–N)	132.9	132.0
	d(N–E)	226.9	227.5
	d(E–B1)	320.3*	356.4*
	a(NEN)	81.0	80.2
	a(CCC)	126.4	126.1
	a(C1EB1)	177.7	176.4

While the addition is about 140 kJ/mol exergonic for **1(B)** (Table 7) indicating that **1(B)** itself is unstable, reaction (II) is endergonic for the higher homologues, where the inert-pair effect becomes more and more important, such that the molecular orbital corresponding to the lone pair has an increased s character, which reduces the Lewis base character of the compound and reduces in turn the bond energy of the adduct. As a consequence, in the case of E = Ga and particularly for E = In, the Lewis acid BF_3 is rejected and thus does not build a donor−acceptor bond with the six-membered ring. In the case of E = B, Al, the allyl subsystem in the ring is again hardly distorted upon adduct formation, while the E−N bond lengths are shortened by about 7 pm, for aluminum it changes only little in the boron compound.

Table 7. Energetics for the addition of BF_3 [Equation (2)]: reaction energy $\Delta\langle E\rangle$ at 0 K without zero-point vibrational energy correction (ZPVE), difference of zero point energies ΔZPVE, reaction enthalpy ΔH and free reaction enthalpy ΔG (both at 298.15 K and 1013.25 hPa) obtained for BP86/RI and B3LYP with the TZVP basis set; ΔH and ΔG are not given in cases where the BF_3 tends to dissociate; all energies are given in kJ/mol

	BP86(/RI)				B3LYP			
	$\Delta\langle E\rangle$	ΔZPVE	ΔH	ΔG	$\Delta\langle E\rangle$	ΔZPVE	ΔH	ΔG
B	−196.7	8.3	−186.0	−141.5	−212.6	9.5	−201.4	−153.3
Al	−39.0	0.7	−34.3	5.03	−30.0	−0.6	−26.2	13.1
Ga	−23.7	3.4	−16.9	27.4	−13.3	1.6	—	—
In	−8.6	1.4	—	—	−8.1	2.5	—	—

6. Conclusion

To conclude, we were able to identify the formal oxidation number of atom E in **1(E)** through various descriptors and could correspond the electronic structure, stability, and reactivity with one particular class of Lewis structures for each molecule **1(E)**. This is remarkable in view of the many different classes of reasonable Lewis structures, which can be thought of for **1(E)**. All higher homologues of **1(E)** are best represented by the donor−acceptor Lewis structure **1(E)e**. For these cases we find a formal oxidation number of +I while boron is in its formal oxidation state +II in **1(B)**.

Furthermore, **1(B)** differs largely from the higher homologues: The electronic structure of **1(B)** can be characterized by the diradical Lewis structures **1(B)b**, symbolizing the low-lying triplet state, which is an indicator of high reactivity. This is supported by the finding that **1(B)** reacts with NH_3 under rearrangement, and with BF_3 to give a stable adduct with a boron−boron bond. Unfortunately, it also implies that **1(B)** with divalent boron is not a valuable synthetic target in contrast to the Arduengo-analoguous boron compound studied previously.[4]

Appendix

Quantum Chemical Methodology: For all calculations we used the density functional programs provided by the TUR-

BOMOLE 5.1 suite.[32] The Becke−Perdew functional dubbed BP86[33,34] and the hybrid functional B3LYP[35,36] were employed as implemented in TURBOMOLE. For all molecules that do not contain In, all-electron calculations have been performed. In these cases the resolution of the identity (RI) technique[37,38] was used in combination with the BP86 functional calculation. All results were obtained from fully optimized Kohn−Sham calculations using Ahlrichs' TZVP basis featuring a valence triple-zeta basis set with polarization functions on all atoms.[39] For all compounds containing indium, we tested the 46-electron effective core potential (ECP) from the Stuttgart−Bonn (SB) group,[40] which allowed us to treat only 3 electrons explicitly. It turned out that such a large-core ECP does not describe the In atom properly (i.e., the core polarization is drastically underestimated). Therefore, a 28-ECP from the SB group[41] was used, which leaves 16 electrons to be treated explicitly. The double-zeta basis set optimized for this ECP and distributed by the SB group has been employed.[42] Up to date, no optimized auxiliary basis exists for the small-core 28-ECP, therefore we did not apply the RI technique for the indium complexes. The addition reactions have not been corrected for the basis-set superposition error because it is less than 7 kJ/mol for the addition of NH_3, and less than 5 kJ/mol for the BF_3 addition, and would not change the qualitative picture. In order to analyze the electron density of the compounds, we use the population analysis by Ahlrichs and co-workers[27] as implemented in TURBOMOLE. For the vibrational analysis, the second derivatives of the total electronic energy were computed as numerical first derivatives[43,44] of analytical energy gradients (obtained from TURBOMOLE) within the harmonic approximation. The Cioslowski charges have been computed with SNF[43] as well as the thermochemical data, which were obtained in the standard way from the frequency analysis using the partition function of the harmonic oscillator in combination with the vibrational frequencies. Translational and rotational degrees of freedom were treated classically. For the EHT calculations we used YAEHMOP.[45] The ELF calculations and the analysis of the Laplacian of the electron density have been performed using the program ELF.[46] The program MOLDEN[47] has been used for the visualization of structures.

Acknowledgments

We are grateful to Prof. B. A. Hess and Prof. W. W. Schoeller for generous support and discussions. We also would like to thank Dr. E. Dobbert and Dr. G. Dembeck for drawing our attention to the Al compound. All calculations have been performed at the Chair of Theoretical Chemistry at the University of Erlangen-Nürnberg, which is gratefully acknowledged.

[1] C. Cui, H. W. Roesky, H.-G. Schmidt, M. Noltemeyer, H. Hao, F. Cimpoesu, *Angew. Chem. Int. Ed.* **2000**, *39*, 4274−4276.
[2] N. J. Hardman, B. E. Eichler, P. P. Power, *Chem. Commun.* **2000**, 1991−1992.
[3] E. S. Schmid, A. Jockisch, H. Schmidbaur, *J. Am. Chem. Soc.* **1999**, *121*, 9758−9759.
[4] A. Sundermann, M. Reiher, W. W. Schoeller, *Eur. J. Inorg. Chem.* **1998**, 305−310.
[5] M. Reiher, P. A. Netz, *Chem. Unserer Zeit* **1999**, *33*, 177−185.
[6] Chr. K. Jørgensen, *Oxidation Numbers and Oxidation States* (Molekülverbindungen und Koordinationsverbindungen in Einzeldarstellungen), Springer-Verlag, Berlin, **1969**.
[7] C.-G. Zhan, F. Zheng, G.-X. Xu, *J. Molec. Struc. (Theochem)* **1994**, *309*, 309−314.
[8] J. Hinze, H. H. Jaffé, *J. Am. Chem. Soc.* **1962**, *84*, 540−546.
[9] J. Hinze, M. A. Whitehead, H. H. Jaffé, *J. Am. Chem. Soc.* **1963**, *85*, 148−154.
[10] D. Bergmann, J. Hinze, *Struct. Bond.* **1987**, *66*, 145−190.
[11] D. Bergmann, J. Hinze, *Angew. Chem.* **1996**, *108*, 162−176.
[12] D. Bergmann, J. Hinze, *Angew. Chem. Int. Ed. Engl.* **1996**, *35*, 150.
[13] J. Hinze, "The Concept of Electronegativity of Atoms in Molecules", in: "Pauling's Legacy − Modern Modelling of the Chemical Bond", vol. 6 of: *Theoretical and Computational Chemistry*, Elsevier, Amsterdam, **1999**, p. 189.
[14] W. W. Schoeller, A. Sundermann, *Inorg. Chem.* **1998**, *37*, 3034−3039.
[15] W. W. Schoeller, A. Sundermann, M. Reiher, *Inorg. Chem.* **1999**, *38*, 29−37.
[16] W. W. Schoeller, A. Sundermann, M. Reiher, A. Rozhenko, *Eur. J. Inorg. Chem.* **1999**, 1155−1159.
[17] W. W. Schoeller, R. Schneider, U. Tubbesing, *Phosphorus, Sulfur Silicon* **1999**, *144−146*, 781−784.
[18] W. W. Schoeller, *Eur. J. Inorg. Chem.* **2000**, 369−374.
[19] W. A. Herrmann, C. Köcher, *Angew. Chem.* **1997**, *109*, 2256−2282; *Angew. Chem. Int. Ed. Engl.* **1997**, *36*, 2162−2187.
[20] N. Metzler-Nolte, *New J. Chem.* **1998**, 793−795.
[21] D. Gudat, *Eur. J. Inorg. Chem.* **1998**, 1087−1094.
[22] M. K. Denk, K. Hatano, A. J. Lough, *Eur. J. Inorg. Chem.* **1998**, 1067−1070.
[23] M. Weidenbruch, *Eur. J. Inorg. Chem.* **1999**, 373−381.
[24] L. Pauling, *General Chemistry*, Dover Publications, New York, **1988**, p. 198.
[25] A. D. Becke, K. E. Edgecombe, *J. Chem. Phys.* **1990**, *92*, 5397−5403.
[26] J. Cioslowski, *J. Am. Chem. Soc.* **1989**, *111*, 8333−8336.
[27] R. Heinzmann, R. Ahlrichs, *Theoret. Chim. Acta* **1976**, *42*, 33−45.
[28] R. F. W. Bader, "Atoms in Molecules − A Quantum Theory", vol. 22 of: *International Series of Monographs on Chemistry*, Clarendon Press, Oxford, **1990**.
[29] R. F. W. Bader, S. Johnson, T.-H. Tang, P. L. A. Popelier, *J. Phys. Chem.* **1996**, *100*, 15398−15415.
[30] R. F. W. Bader, G. L. Heard, *J. Chem. Phys.* **1999**, *111*, 8789−8798.
[31] M. Reiher, O. Salomon, B. A. Hess, *Theor. Chem. Acc.* **2001**, *107*, 48−55.
[32] R. Ahlrichs, M. Bär, M. Häser, H. Horn, C. Kölmel, *Chem. Phys. Lett.* **1989**, *162*, 165−169.
[33] A. D. Becke, *Phys. Rev. A* **1988**, *38*, 3098−3100.
[34] J. P. Perdew, *Phys. Rev. B* **1986**, *33*, 8822−8824.
[35] A. D. Becke, *J. Chem. Phys.* **1993**, *98*, 5648−5652.
[36] P. J. Stephens, F. J. Devlin, C. F. Chabalowski, M. J. Frisch, *J. Phys. Chem.* **1994**, *98*, 11623−11627.
[37] K. Eichkorn, O. Treutler, H. Öhm, M. Häser, R. Ahlrichs, *Chem. Phys. Lett.* **1995**, *240*, 283−290.
[38] K. Eichkorn, F. Weigend, O. Treutler, R. Ahlrichs, *Theor. Chem. Acc.* **1997**, *97*, 119−124.
[39] A. Schäfer, C. Huber, R. Ahlrichs, *J. Chem. Phys.* **1994**, *100*, 5829−5835.
[40] A. Bergner, M. Dolg, W. Kuechle, H. Stoll, H. Preuss, *Mol. Phys.* **1993**, *80*, 1431−1441.
[41] T. Leininger, A. Nicklass, H. Stoll, M. Dolg, P. Schwerdtfeger, *J. Chem. Phys.* **1996**, *105*, 1052−1059.

[42] B. Metz, H. Stoll, M. Dolg, *J. Chem. Phys.* **2000**, *113*, 2563−2569.
[43] C. Kind, M. Reiher, J. Neugebauer, B. A. Hess, *SNF − A program for parallelized vibrational analyses*, University of Erlangen-Nürnberg, **1999−2001**.
[44] J. Neugebauer, M. Reiher, C. Kind, B. A. Hess, *J. Comp. Chem.*, in press.
[45] G. Landrum, http://yaehmop.sourceforge.net
[46] A. Sundermann, *ELF*, University of Bielefeld, unpublished results, **1997**.
[47] G. Schaftenaar, J. H. Noordik, *J. Comput.-Aided Mol. Design* **2000**, *14*, 123−134.

Received March 7, 2001
[I01493]

Physicochemical Properties and Structural Refinement of Strontium-Lead Hydroxyapatites

Béchir Badraoui,[a] Adriana Bigi,*[b] Mongi Debbabi,[a] Massimo Gazzano,[b] Norberto Roveri,[b] and René Thouvenot[c]

Keywords: Hydroxyapatite / X-ray diffraction / IR spectroscopy / ^{31}P MAS NMR / Ionic substitution

Continuous series of solid solutions of strontium and lead apatite $Sr_{(10-x)}Pb_x(PO_4)_6(OH)_2$ ($0 \leq x \leq 10$), synthesized in aqueous media have been investigated by X-ray powder-pattern fitting, ^{31}P MAS NMR and IR spectroscopy. The lattice dimensions and the IR frequencies of the solid solutions vary linearly with the atom% of lead. The results of the Rietveld analysis indicated a clear preference of lead for the M(2) site of the apatitic structure, so that in the samples with low Pb content it is almost exclusively found in the M(2) site. ^{31}P MAS NMR spectra at 162 MHz show a unique isotropic signal at δ_{iso} between +2.9 (SrHA) and −0.7 ppm (PbHA). From the variation of δ_{iso} with the phase composition it appears that ^{31}P shielding in these mixed apatites is essentially governed by the nature of the metal in the M(1) site. The qualitative variation of the chemical shift anisotropy of the PO_4 group agrees with the deviation from ideal T_d symmetry shown by the Rietveld refinement analysis.

(© Wiley-VCH Verlag GmbH, 69451 Weinheim, Germany, 2002)

Introduction

Hydroxyapatites, $M_{10}(PO_4)_6(OH)_2$, crystallizing in the hexagonal lattice, are known for the bivalent metals M = Ca, Sr, Ba, Cd, and Pb.[1−5] Because of the high stability and flexibility of the apatitic structure, a great number of substitutions, both cationic and anionic are possible. In particular, substitution of the bivalent cations has a great influence on the structural, textural, and physical properties of these materials and justifies the increasing number of studies on this subject, which involves several research and application fields: dental and bone pathologies, bioceramics, luminescence, ionic conduction, water treatment by ionic exchange, catalysis, etc.[6−10]

A major contribution to these studies comes from the results of structural refinements of powder X-ray diffraction patterns (Rietveld methods) and of solid-state NMR spectroscopy investigations, performed at high resolution with magic-angle spinning (MAS NMR). Actually, these two methods are complementary and their combined use represents a powerful tool for investigating the localization of the substituted elements in the apatitic cell, as well as the resulting structural modifications.

The unit cell of stoichiometric crystalline apatite hosts ten cations arranged in two non-equivalent positions: four at the M(1) site aligned in the column, each surrounded by nine oxygen atoms, and six at the M(2) site arranged at the apexes of "staggered" equilateral triangles, each surrounded by seven oxygen atoms.[1,2,10]

Ca-Sr, Ca-Ba, Ca-Cd, and Ca-Pb hydroxyapatites have been widely investigated[11−15] (hereafter MHA and M′-M′′HA indicate pure or mixed-metal hydroxyapatites, respectively). The lattice parameters of these mixed apatites vary linearly with the composition, with the exception of the *c* axis of Pb-CaHA that displays a discontinuity at about 50 atom% of lead. The peculiar variation of the *c*-axis dimension has been ascribed to an inhomogeneous lead distribution in the two non-equivalent cation sites, on the basis of the results of powder pattern structure refinements of Pb-CaHA, which indicate a clear preference of lead for site M(2) of the hydroxyapatite structure.[9]

We have previously applied powder pattern fitting refinements and ^{31}P MAS NMR spectroscopy to the study of Cd-Pb and Cd-Sr systems.[16,17] CdHA and PbHA exhibit just a limited range of solubility; cadmium can replace up to 30% of the lead, whereas lead does not seem to "like" the incorporation into CdHA. The cadmium ion displays a

[a] Laboratoire de Chimie Inorganique et Industrielle, Ecole Nationale d'Ingénieurs de Monastir,
5019 Monastir, Tunisie
[b] Dipartimento di Chimica "G. Ciamician", Università degli Studi, and Istituto per la Sintesi e Fotoreattivita', CNR,
Via Selmi 2, 40126 Bologna, Italy
Fax: (internat.) + 39-051/209-9456
E-mail: bigi@ciam.unibo.it
[c] Laboratoire de Chimie Inorganique et Matériaux Moléculaires, UMR CNRS 7071, case courrier 42, Université Pierre et Marie Curie,
75252 Paris Cedex05, France
Supporting information for this article is available on the WWW under http://www.eurjic.com or from the author.

clear preference for the M(1) site of the apatite structure, in agreement with the shorter metal−metal distances in this site with respect to the M(2) site. On increasing the cadmium content, it begins to fill the M(2) site so that at the highest degree of substitution, two of the four metal ions in the M(1) site are Cd, whereas just one of the six metal ions in the equilateral triangles characteristic of site M(2) is Cd. Also $Sr_{(10-x)}Cd_xHA$ were obtained as a single phase in a limited range of composition ($x \leq 4$). In this system, in comparison with the Cd-Pb one, the relatively small Cd^{2+} ion is almost statistically distributed over both sites.

Here we report the results of a structural (Rietveld method) and spectroscopic (IR and ^{31}P MAS NMR spectroscopy) investigation carried out on strontium-lead hydroxyapatites in the whole range of lead substitution for strontium.

Results

X-ray Analysis

Preliminary structural analysis by X-ray diffraction (XRD) shows that all the samples correspond to pure apatitic phases, whatever the Sr/Pb ratio. This is confirmed by structural Rietveld refinements of six samples where the resulting formulae are: $Sr_{8.9}Pb_{1.1}HA$, $Sr_{6.9}Pb_{3.1}HA$, $Sr_{4.9}Pb_{5.1}HA$, $Sr_{4.0}Pb_{6.0}HA$, $Sr_{2.0}Pb_{8.0}HA$, and $Sr_{1.0}Pb_{9.0}HA$. From now onwards, the samples will be indicated as $Sr_{(10-x)}Pb_xHA$, where x corresponds to the stoichiometry resulting from chemical analysis.

Figure 1 displays the final plot for $Sr_{8.9}Pb_{1.1}HA$ and $Sr_{2.0}Pb_{8.0}HA$ samples, as typical comparisons between the observed and the calculated patterns. The refined structural parameters are reported in Table 1, and the data about cationic distribution are reported in Table 2.

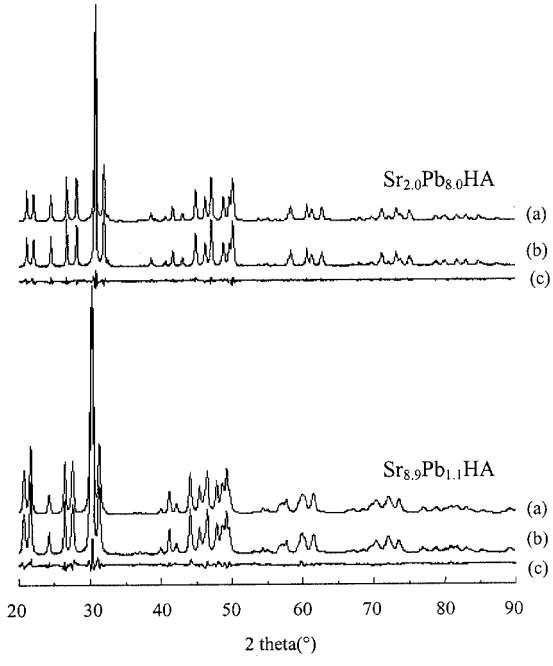

Figure 1. Comparison of the observed [curve (a)] and calculated [curve (b)] powder diffraction patterns of $Sr_{2.0}Pb_{8.0}HA$ and $Sr_{8.9}Pb1_{1.1}HA$ [curve (c)] is the difference profile

The existence of a continuous solid solution between the strontium and lead hydroxyapatite, conforms with the be-

Table 1. Fractional atomic coordinates and equivalent thermal parameters after Rietveld refinement for the mixed Sr-PbHA (e.s.d. in parentheses)

Apatite	Atom	x	y	z	B_{eq} [Å^2]
$Sr_{8.9}Pb_{1.1}$[a]	M(1)	0.3333	0.6667	0.0018(9)	0.6035
	M(2)	0.2438(3)	0.9876(3)	0.2500	0.7214
	P	0.4039(9)	0.3723(7)	0.2500	0.4225
	O(1)	0.338(2)	0.489(2)	0.2500	0.4925
	O(2)	0.583(2)	0.466(2)	0.2500	0.7246
	O(3)	0.347(1)	0.261(1)	0.073(1)	1.2854
	O(H)	0.0000	0.0000	0.325(3)	1.4251
$Sr_{6.9}Pb_{3.1}$[b]	M(1)	0.3333	0.6667	0.0040(1)	0.2351
	M(2)	0.2450(4)	0.9934(5)	0.2500	0.5958
	P	0.4039(6)	0.3726(6)	0.2500	0.9985
	O(1)	0.342(2)	0.498(3)	0.2500	0.5014
	O(2)	0.583(3)	0.470(3)	0.2500	1.009
	O(3)	0.358(2)	0.269(2)	0.073(2)	0.3987
	O(H)	0.0000	0.0000	0.413(6)	1.2514
$Sr_{4.9}Pb_{5.1}$[c]	M(1)	0.3333	0.6667	0.0102(3)	0.3385
	M(2)	0.2482(4)	0.9986(6)	0.2500	0.5924
	P	0.4097(8)	0.3781(5)	0.2500	0.9547
	O(1)	0.340(3)	0.488(3)	0.2500	0.8014
	O(2)	0.596(4)	0.467(3)	0.2500	1.3954
	O(3)	0.359(2)	0.272(2)	0.002(2)	0.5934
	O(H)	0.0000	0.0000	0.444(7)	0.3954
$Sr_{4.0}Pb_{6.0}$[d]	M(1)	0.3333	0.6667	0.0048(8)	0.8210
	M(2)	0.2505(2)	0.0026(8)	0.2500	0.8953
	P	0.4057(2)	0.3698(2)	0.2500	1.4251
	O(1)	0.363(5)	0.474(4)	0.2500	1.8004
	O(2)	0.591(5)	0.464(3)	0.2500	2.1145
	O(3)	0.359(2)	0.268(3)	0.072(2)	1.5926
	O(H)	0.0000	0.0000	0.448(5)	1.2957
$Sr_{2.0}Pb_{8.0}$[e]	M(1)	0.3333	0.6667	0.0055(5)	0.3354
	M(2)	0.2481(4)	0.9987(6)	0.2500	0.8250
	P	0.4029(2)	0.3675(1)	0.2500	0.1687
	O(1)	0.333(3)	0.506(3)	0.2500	0.5140
	O(2)	0.573(3)	0.471(3)	0.2500	0.2954
	O(3)	0.370(2)	0.280(2)	0.084(2)	0.1542
	O(H)	0.0000	0.0000	0.501(5)	0.6982
$Sr_{1.0}Pb_{9.0}$[f]	M(1)	0.3333	0.6667	0.0059(9)	0.5932
	M(2)	0.2517(3)	0.0031(5)	0.250	0.7586
	P	0.4055(2)	0.3744(4)	0.250	1.2476
	O(1)	0.336(3)	0.491(2)	0.250	1.5748
	O(2)	0.578(3)	0.475(3)	0.250	1.9507
	O(3)	0.364(2)	0.276(2)	0.079(2)	1.5842
	O(H)	0.0000	0.0000	0.394(7)	1.1957

[a] a = 9.7736(9) Å, c = 7.2958(4) Å, R_p = 7.2, R_{wp} = 9.2. [b] a = 9.8121(5) Å, c = 7.3203(6) Å, R_p = 6.4, R_{wp} = 8.4. [c] a = 9.8572(7) Å, c = 7.3352(7) Å, R_p = 7.1, R_{wp} = 9.0. [d] a = 9.8625(7) Å, c = 7.3414(8) Å, R_p = 5.6, R_{wp} = 7.8. [e] a = 9.8681(9) Å, c = 7.3616(5) Å, R_p = 7.2, R_{wp} = 9.4. [f] a = 9.8725(8) Å, c = 7.3497(5) Å, R_p = 7.2, R_{wp} = 9.4. The pattern R factor R_p is defined as $R_p = 100\{\Sigma|Y_{oi} - Y_{ci}|/\Sigma Y_{oi}\}$. The weighted pattern R factor R_{wp} is defined as $R_{wp} = 100\{\Sigma W_i(Y_{oi} - Y_{ci})^2/W_i\Sigma(Y_{oi})^2\}^{1/2}$.

Table 2. Lead substitution (atom%) in mixed Sr-PbHA (e.s.d. in parentheses)

	$Pb_1/(Pb_1 + Sr_1)$	$Pb_1/(Pb_1 + Pb_2)$	$Pb_2/(Pb_2 + Sr_2)$	Pb/(Pb + Sr)[a]	Pb/(Pb + Sr)[b]
$Sr_{8.9}Pb_{1.1}HA$	< 1	< 1	14.2(2)	8.6(5)	11.7(2)
$Sr_{6.9}Pb_{3.1}HA$	12.0(1)	15.5(3)	43.5(1)	31.0(4)	31.6(2)
$Sr_{4.9}Pb_{5.1}HA$	30.8(2)	24.0(2)	64.9(2)	51.3(2)	51(2)
$Sr_{4.0}Pb_{6.0}HA$	33.4(1)	21.9(1)	78.9(1)	60.7(1)	60.0(1)
$Sr_{2.0}Pb_{8.0}HA$	58.2(3)	29.2(1)	93.8(1)	79.5(2)	80.0(1)
$Sr_{1.0}Pb_{9.0}HA$	75.6(2)	33.9(2)	98.3(3)	89.3(1)	90.5(2)

[a] Rietveld refinement. [b] Chemical analysis.

havior of Ca-Pb and Ca-Sr apatites.[11,14] The progressive substitution of lead for strontium results in a slight increase in the lattice parameters *a* and *c*; the variation of these sizes is appreciably linear and follows the Vegard law,[18] according to the following relations:

$a = (9.7729 + 0.0122x)$ Å; $\sigma(a) = 9.3 \cdot 10^{-3}$ Å
$c = (7.2761 + 0.0011x)$ Å; $\sigma(c) = 4.7 \cdot 10^{-2}$ Å

Despite this regular variation and the similarity of the ionic radii (coord. 7: Pb^{2+} = 1.37 Å, Sr^{2+} = 1.35 Å; coord. 9: Pb^{2+} = 1.49 Å, Sr^{2+} = 1.45 Å),[19] the variation of the average values of the M(1)−O and M(2)−O distances is someway irregular. In the mixed hydroxyapatites, the phosphate group is considerably distorted by comparison with the limiting phases. A table with M−O distances and distortion indexes is reported as Supporting Information.[20]

According to the similarity of the radii of the two cations the distribution of these ions in both the M(1) and M(2) sites, should be close to a statistical occupancy. However, the refinement shows that the occupancy factor of lead in the M(2) site is always higher than that corresponding to the statistical distribution (Table 3).

Thus, small lead contents (0.86 atom per cell) go almost exclusively into the M(2) site. The difference from the statistical distribution decreases when the lead content increases. We could attribute this behavior, as well as the preferential location of lead in the M(2) site, to the relatively high electronegativity of lead, which increases the polarization of the O−H bond and strengthens the hydrogen bonds, as well as the structural stability of the apatite.[21]

Finally, we observed a good agreement between the values of the Pb/(Pb + Sr) ratios deduced from structural refinements and those obtained by chemical analyses, except for the phase $Sr_{8.9}Pb_{1.1}HA$, which exhibits an appreciably smaller lead incorporation (see Table 2).

Table 3. Statistic distribution and refinement occupancy in the metal M(1) and M(2) sites of Sr-PbHA; the occupancy parameters are normalized to one unit cell content

Pb content [atom/cell]	Refinement distribution (A)		Statistic distribution (B)		(A − B)/B	
	M(1)	M(2)	M(1)	M(2)	M(1)	M(2)
0.86	0	0.86	0.35	0.52	−1.0	+0.65
3.10	0.48	2.62	1.24	1.86	−0.61	+0.41
5.13	1.23	3.90	2.05	3.08	−0.40	+0.27
6.07	1.34	4.73	2.43	3.64	−0.44	+0.30
7.95	2.33	5.62	3.18	4.77	−0.27	+0.18
8.93	3.03	5.90	3.57	5.36	−0.15	+0.10

Infrared Absorption Spectroscopy

The infrared spectra of various mixed apatites show the characteristic absorption bands of the $(PO_4)^{3-}$ groups and OH^- ions of the apatitic structure. Weak bands characteristic of HPO_4^{2-} and CO_3^{2-} ions[22] are also present, as it which can be seen from a typical plot (Figure 2).

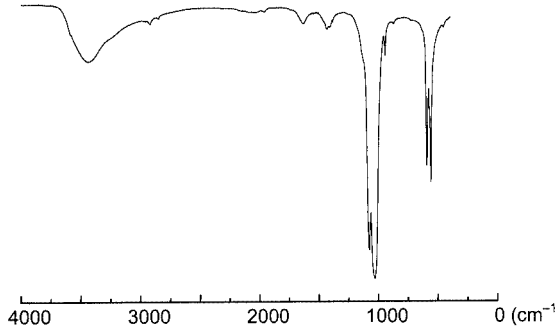

Figure 2. Infrared spectrum of $Sr_{6.9}Pb_{3.1}HA$

The progressive substitution of the lead ions for strontium induces a regular shift of the absorption bands towards smaller wavenumbers as shown in Figure 3.[20]

The shift of the absorption bands of the (PO_4) group can be attributed to the variation of the nature of the metal−oxygen interactions. The character of lead−oxygen interaction is more covalent than that of strontium−oxygen and furthermore a cation of larger mass is involved.[23] The more covalent character of the Pb−OH leads to a shift of the OH vibrational modes towards lower frequency. In particular the shift of the OH stretching mode when the Pb content increases is in agreement with the predominant role of the M−OH interaction with respect to the OH···O(PO_3) hydrogen bond.[24]

^{31}P Solid-State NMR Analysis

Table 4 shows the NMR spectroscopic data for the whole series of mixed Sr-PbHA, as well as that of the pure phases SrHA and PbHA, and Figure 4 shows parts of the 162 MHz MAS spectra obtained at relatively high spinning rates (ca. 5 kHz).

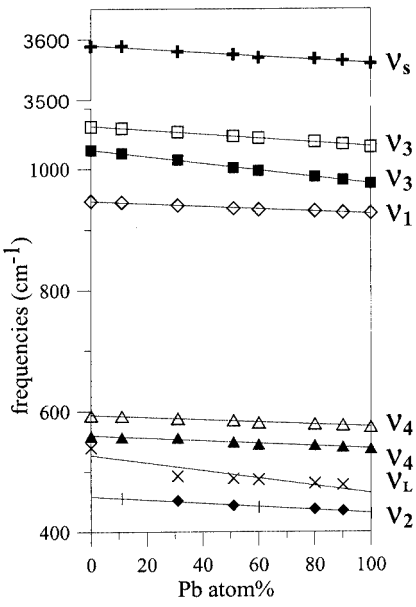

Figure 3. Infrared frequencies of the vibrational modes of strontium-lead hydroxyapatite solid solutions as a function of Pb content; ν_S, ν_L stretching and librational mode of the OH group; ν_1, ν_2, ν_3, ν_4 vibrational mode of the PO_4 group

TAble 4. ^{31}P MAS solid-state NMR spectroscopic data for strontium-lead hydroxyapatites

$Sr_{(10-x)}Pb_xHA$	δ_{iso} [a][b]	$\Delta\nu_{1/2}$ [c]	$\Delta\nu_{static}$ [d]
Sr_{10}	2.9	0.9 (150)	2.6 (16)
$Sr_{8.9}Pb_{1.1}$	3.0	1.2 (200)	2.9 (18)
$Sr_{8.0}$ $Pb_{2.0}$	3.0	1.8 (290)	3.4 (21)
$Sr_{6.9}Pb_{3.1}$	3.0	2.5 (400)	5.3 (33)
$Sr_{6.1}Pb_{3.9}$	3.0	3.0 (490)	8.6 (53)
$Sr_{4.0}Pb_{6.0}$	2.6	4.4 (710)	9.5 (59)
$Sr_{2.8}Pb_{7.2}$	1.9	5.1 (830)	12.3 (76)
$Sr_{2.0}Pb_{8.0}$	0.1	4.8 (780)	6 (37)
$Sr_{1.0}Pb_{9.0}$	−0.7	3.0 (490)	5.1 (31)
Pb_{10}	−0.7	1.2 (190)	3.1 (19)

[a] Position of the central line observed at a high spinning rate (about 5 kHz). [b] In ppm relative to 85% aqueous H_3PO_4 (±0.1 to ±0.2 ppm). [c] In ppm, with the values in Hz in parentheses. [d] Half-height bandwidth of the resonance for non-spinning sample; in kHz, with ppm values in parentheses.

The evolution of the isotropic chemical shift δ_{iso} and of the isotropic full width at half maximum (*fwhm*) as a function of the Pb content is depicted in Figures 5 and 6.

As shown in Figure 4, whatever the phase composition, only one isotropic signal is observed; however, for the samples with relatively high Pb contents, a shoulder is apparent, which cannot be resolved by resolution enhancement. This is not surprising when considering the small chemical shift difference between the limiting phases SrHA (δ_{iso} = +2.9 ppm) and PbHA (δ_{iso} = −0.7 ppm); $\Delta\delta_{iso}$ = 3.6 ppm amounts to only four times the smallest observed line width of SrHA (0.9 ppm, Table 4).

The δ_{iso} variation is far from linear; it does not vary significantly with increasing Pb content up to 60%, where it decreases abruptly, in agreement with a shielding effect of Pb^{2+} compared with Sr^{2+}. This peculiar variation has to be related to the nonstatistical distribution of Pb in both the M(1) and M(2) sites.

The isotropic signal is relatively narrow at low Pb content, it broadens significantly on increasing Pb substitution to reach a maximum value (about 5 ppm) for 70% Pb. This could also be related to the unequal site occupancy, as a

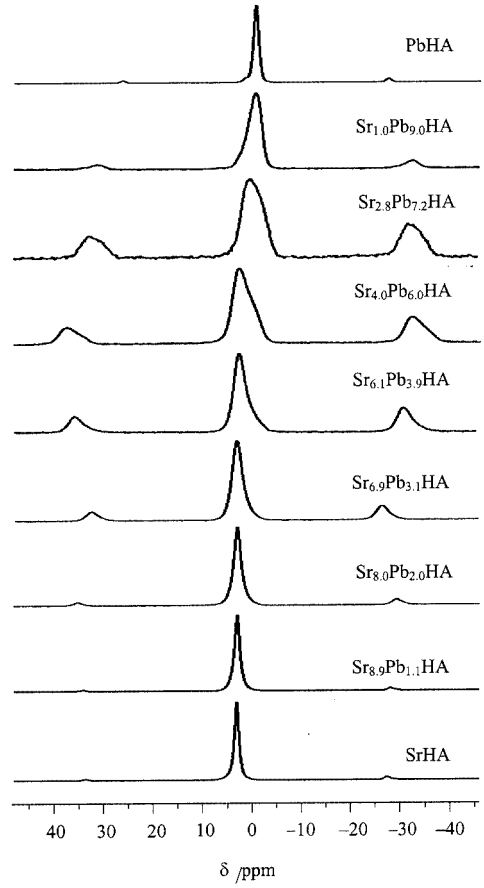

Figure 4. Part of the 162 MHz ^{31}P MAS spectra of the pure and mixed Sr-Pb hydroxyapatites, showing only the isotropic signal and the first (n = +1 and −1) spinning side bands; from bottom to top: SrHA (Ro = 5 kHz, NS = 24), $Sr_{8.9}Pb_{1.1}$ (Ro = 5.1 kHz, NS = 24), Sr_8Pb_2 (Ro = 5.2 kHz, NS = 24), $Sr_{6.9}Pb_{3.1}$ (Ro = 4.9 kHz, NS = 48), $Sr_{6.1}Pb_{3.9}$ (Ro = 5.4 kHz, NS = 48), Sr_4Pb_6 (Ro = 5.6 kHz, NS = 104), $Sr_{2.8}Pb_{7.2}$ (Ro = 5.2 kHz, NS = 72), Sr_1Pb_9 (Ro = 5.2 kHz, NS = 48), PbHA (Ro = 4.3 kHz, NS = 48)

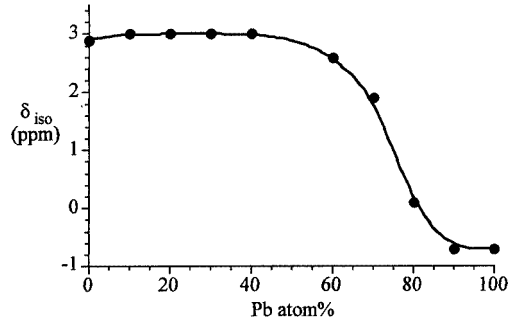

Figure 5. Variation of δ_{iso} as a function of Pb content (atom%)

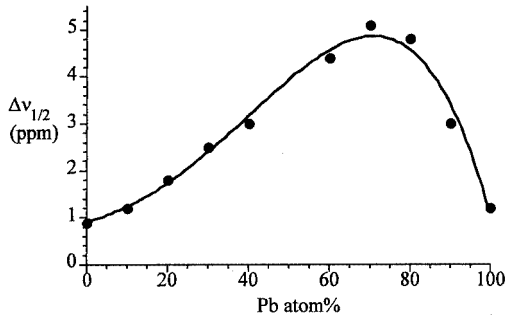

Figure 6. Variation of the full width at half maximum of the isotropic signal as a function of Pb content (atom%)

statistical distribution would have given a symmetrical shape for the $\Delta\nu_{1/2}$ variation.

The chemical shift anisotropy (CSA) of the PO_4 tetrahedron can be derived from the intensity of the spinning side bands (SSB) (see Exp. Sect.). Determination of the chemical shift tensor components and of the CSA is in principle feasible through analysis of the SSB at various spinning rates.[25] However, in the present case, this analysis is virtually impossible because of overlap of numerous unresolved resonances and because of the existence of dipolar interactions which contribute to the SSB intensity at a low spinning rate and significantly broaden the band observed in static spectra.[17] The trend in CSA variation can, however, be qualitatively appreciated from the relative intensity of the first pair of SSB depicted in Figure 4, taking into account that at any fixed spinning rate, the relative intensity of these spinning side bands increases with increasing anisotropy. It is apparent that the CSA of the PO_4 increases smoothly with increasing Pb content, reaching a maximum at around 70% Pb and decreases again with further Pb substitution. This explains the variation of the band width of the static spectra, which, in the absence of any dipolar interaction, would have allowed us a direct determination of the chemical shift anisotropy.

Discussion

The results of this study indicate that SrHA and PbHA form solid solutions over the whole range of composition. Lead substitution for strontium in the hydroxyapatite structure induces a linear expansion of the lattice constants in agreement with its slightly greater ionic radius. Furthermore, Pb is a soft acid and displays a greater tendency towards covalent interactions and directional bonding, whereas strontium can be considered a hard acid. The more covalent character of Pb−O interactions with respect to Sr−O interactions can be invoked to justify the shift of the infrared OH absorption modes towards lower frequencies when the Pb content increases.[24] The increase of lead content also induces a shift of the absorption bands, characteristic of the phosphate internal modes towards lower frequencies. This might either be due to the different ionic character of the metal or to the different anion−anion distances.[23]

The results of the powder fitting structure refinements indicate a clear preference of lead for the M(2) site of the apatitic structure, so that in the samples of low Pb content it is almost exclusively found in the M(2) site. The preference of lead for the M(2) site is in agreement with its slightly greater dimensions with respect to Sr, since in site M(2) the arrangement of the staggered equilateral triangles allows for the optimization of the packing of larger ions, in contrast to the M(1) site where the strict alignment in the columns causes a stronger repulsion. However, a contribution of the more covalent character of the M−O interaction to the cation site preference cannot be excluded, as suggested by the previous results obtained for Sr-Cd apatites[17] where cadmium displays a slight preference for the M(2) site in spite of its small dimensions which should have preferred the hexacoordination of site M(1). A clear preference of Pb for the M(2) site of the apatitic structure was previously reported on the basis of the results of the powder fitting refinements carried out on Ca-Pb apatites.[14] When substituting for calcium, lead almost exclusively fills the M(2) site, until, at Pb contents greater than 45%, it begins to fill the M(1) site, leading to a nonlinear variation of the *c* axis of the apatite structure. The ionic radii and the characters of the metal−oxygen interaction are not as different for Sr and Pb as they are for Ca and Pb. This can account for the minor modifications provoked by lead incorporation into the SrHA structure.

The preference of lead for the M(2) site becomes less evident on increasing the lead content of the solid phase. In agreement, the broadening of the NMR isotropic signal is quite small for the samples at low Pb content and increases when lead is more statistical distributed in the two cationic sites.

Numerous studies, experimental and theoretical, have shown that, among other effects, ^{31}P shielding in phosphate compounds increases − that is δ decreases − with increasing π-bond order between phosphorus and oxygen (p_π-d_π overlap) leading to shorter P−O distances.[26−31]

The shielding effect for pure PbHA (δ = −0.7 ppm) with respect to pure SrHA (δ = 2.9 ppm) can be correlated with the shortening of the mean P−O bond, which decreases from 1.54 Å in SrHA to 1.46 Å in PbHA (Table 1 in Supporting Information[20]).

For the mixed phases we have to consider the various cationic environments of the P atom, that is $PSr_{(9-y)}Pb_y$ (y = 0−9).[16,17] The isotropic resonance of each $PSr_{(9-y)}Pb_y$ environment should be observed between δ = +2.9 (PSr_9 in SrHA) and −0.7 (PPb_9 in PbHA), the shielding increasing with *y*. Accordingly, as we have already discussed for cadmium-lead hydroxyapatites,[16] the incidence in the ^{31}P MAS spectra of the progressive Pb for Sr substitution would have been in the case of a statistical distribution:

− a regular shielding of the isotropic resonance according to δ_{iso} (ppm) = [2.9·(10 − x) − 0.7·x]/10.

− a pseudo-Gaussian shape for the variation of the isotropic *fwhm*, with a maximum at $x = 5$.

On the contrary, both curves (Figures 5 and 6) present singularities for $x = 6-8$. Departure from the theoretical behavior can be accounted for by the results of the Rietveld analysis. At low Pb content, Pb is located almost exclusively in the M(2) site, this means that Sr almost exclusively occupies the M(1) site. The quasi invariance of δ_{iso} for SrPbHA up to 40% Pb could be the indication that in these series the shielding of the ^{31}P nucleus is primarily determined by the nature of the metal in M(1) and consequently influenced very little by the metal in the M(2) site. As can be seen in Table 2, more than 70% of the M(1) sites are occupied by Sr, for Pb contents of up to 60%. Therefore, the singularities observed for both δ_{iso} and $\Delta\nu_{iso}$ curves for around 60−80% Pb could easily be explained if we assume the predominant contribution of the metal in the M(1) site to the ^{31}P shielding.

Let us return to the variation of the chemical shift anisotropy, which reflects the distortion of the PO_4 tetrahedron. For the pure phases SrHA and PbHA, the geometry of the phosphate anion is quite regular and corresponds to a quasi T_d local symmetry with nearly identical P−O distances and all O−P−O angles approaching 109.47°. This explains the low intensity of the spinning side bands (Figure 4) characteristic of a small CSA. For the mixed hydroxyapatites, deviation from the T_d symmetry is evidenced by unequal bond lengths [DI(PO) > 1%] and bond angles [O−P−O between 102 and 116°, DI(O−P−O) up to 5%]. Maximal distortion occurs effectively for the mixed apatites with Pb contents around 60−80% [DI(O−P−O) ca. 0.04−0.05] which actually exhibit the largest chemical shift anisotropy (Figure 4, Table 4).

Experimental Section

Synthesis: The mixed strontium and lead hydroxyapatites with various Pb/(Pb + Sr) ratios, were obtained from a double decomposition method, in aqueous medium.[32,33] Concentrations of the solutions in lead, strontium and phosphate ions correspond to the stoichiometry of the desired apatite. 0.03 M ammonium dihydrogen phosphate [$(NH_4)H_2(PO_4)$, Merck 99%] solution (A solution) and a solution containing a mixture of lead acetate [$Pb(CH_3COO)_2{\cdot}3H_2O$, Fluka 99%] and strontium nitrate [$Sr(NO_3)_2$, Riedel−de Haën AG 98%], with a total concentration of metal cations of 0.05 M (B solution) were prepared. Solution (A) was added dropwise to solution (B), at boiling temperature under a nitrogen stream. The pH value of the slurry was maintained at approximately 12 by regular additions of small amounts of ammonia (Prolabo, $d = 0.89$; 28% aqueous solution). The resulting solid phase was kept in contact with the mother solution for 1 h, at boiling temperature. The precipitate was then filtered, washed with hot distilled water, in order to eliminate traces of ammonium, nitrate and acetate ions, dried at 100 °C for 12 h and calcined at 600 °C for 4 h to improve its crystallinity. Several B solutions, with lead cation fractions ranging from 0 to 1, were prepared and the procedure was repeated in order to obtain the mixed apatites. The compounds obtained were submitted for XRD, chemical analysis, IR spectroscopy, and ^{31}P MAS NMR spectroscopy analyses.

Characterizations: The XRD data were collected with a Philips PW1710 diffractometer, equipped with a copper anode and a graphite monochromator in the diffracted beam ($K_{\alpha 1}$ radiation, $\lambda = 1.5406$ Å). The investigated range was from 18 to 99.99° (2θ), with a step of 0.03° and a counting time of 13 s for each step. The FT-IR spectra (4000−400 cm^{-1}) were recorded with a Bio-Rad FTS 6000 spectrophotometer. 1 mg of the samples was crushed with 300 mg of KBr, and pelletized at 8 tons. The NMR experiments were performed on powdered samples at room temperature with a Bruker MSL400 spectrometer (9.4 T) operating at 162 MHz. A Doty probehead, equipped with 4-mm diameter rotors, was used for spinning rates of up to 6.5 kHz. The spinning rate was monitored by a Bruker pneumatic unit, allowing the control of bearing and drive-inlet nitrogen pressure. Because of unexpected failure of the spinning ratemeter, it was impossible to select and lock a precise spinning rate for all samples; however, bearing and drive pressures were sufficiently stable to avoid fluctuations in the spinning rate. Actually, by comparison with the isotropic signal, no significant broadening of the spinning side bands could be detected and the exact spinning rate was easily determined from the spacing of the spinning side bands. The spectra were acquired using a simple one-pulse sequence with phase cycling (CYCLOPS sequence). Pulse duration was 1 μs that corresponds to a 15° flip angle. The spectral width was 45 kHz (280 ppm). Preacquisition and interpulse delays were 22 μs and 5 s, respectively. The number of transients (NS) was chosen between 24 and about 1000, to obtain a good signal-to-noise ratio, depending on the spinning rate and of the linewidth of the signal. The 4 K free induction decay was zero-filled to the size of 8 K and Fourier-transformed after exponential multiplication of the free induction decay using a 20-Hz line-broadening factor: the final digital resolution of the real spectrum was 10 Hz (0.07 ppm). Chemical shifts are reported with respect to external 85% H_3PO_4 in the IUPAC convention, i.e. positive δ corresponds to a resonance at higher frequency (deshielding) than the reference. Chemical shift values are given with a precision ranging between ±0.1 ppm (narrow resonances) and ±0.2 ppm (broad resonances). The lead and strontium contents in the samples were determined with a Perkin−Elmer 3110 atomic absorption spectrophotometer. The phosphate ions were quantified by visible absorption spectrophotometry of the phosphovanadomolybdic complex. The measurement of the optical densities was carried out at 430 nm.[34] XRD shows that all the samples correspond to pure apatitic phases; according to the results of the chemical analyses the samples exhibit the following formulae: $Sr_{10}(PO_4)_6(OH)_2$, $Sr_{8.9}Pb_{1.1}(PO_4)_6(OH)_2$, $Sr_{8.0}Pb_{2.0}(PO_4)_6(OH)_2$, $Sr_{6.9}Pb_{3.1}(PO_4)_6(OH)_2$, $Sr_{6.1}Pb_{3.9}(PO_4)_6(OH)_2$, $Sr_{4.9}Pb_{5.1}(PO_4)_6(OH)_2$, $Sr_{4.0}Pb_{6.0}(PO_4)_6(OH)_2$, $Sr_{2.8}Pb_{7.2}(PO_4)_6(OH)_2$, $Sr_{2.0}Pb_{8.0}(PO_4)_6(OH)_2$, $Sr_{1.0}Pb_{9.0}(PO_4)_6(OH)_2$, $Pb_{10}(PO_4)_6(OH)_2$.

Structural Analysis: Rietveld full-profile refinements[35] of the mixed strontium-lead hydroxyapatites were carried out by means of the DBWS-9411 program.[36] The space group ($P6_3/m$, no. 176), the cell parameters, the atomic positions and the Debye−Waller factors of SrHA are introduced as the initial structural model for the hydroxyapatite with the lowest lead content. A five-order polynomial was used to simulate the background, while the peaks were fitted using a "pseudo-Voigt" function. Half width of the diffraction peaks as a function of 2θ was evaluated by the formulation of the Caglioti model.[37] Rietveld refinement was performed in several stages, the parameters obtained in each stage being deferred as follows. In the first cycles the scale factor and the background were refined. Refinement of the other parameters was in the following order: profile parameters, zero shift, asymmetry parameter and cell parameters. Refinement of the occupancy factors was done only

for Pb^{2+} and Sr^{2+} ions, with the assumption that these two cations were, initially, statistically located in the two cationic sites, the total contents answering to the stoichiometry obtained by chemical analysis. The apatitic structure comprises 7 independent atoms, corresponding to 21 atomic coordinates, 8 being fixed according to symmetry rules. The other 13 coordinates were refined, starting with those of the two metal sites. In the last refinement cycles, all 30 parameters were released. Then, the refined parameters were used like the initial model for apatite with the lead content immediately higher, and so on. Atomic positions, anisotropic thermal parameters, lattice parameters, reliability pattern factor R_p and weighted factor R_{wp} are gathered in Table 1. A Table in the Supporting Information[20] gives interatomic distances and distortion indices of the phosphate tetrahedron.[38] Lead ion distribution between the two metal sites and chemical analysis results are gathered in Table 3. Equivalent thermal parameters $B_{eq} = \sum_i \sum_j \beta_{ij} (\vec{a}.\vec{b})$ are calculated by the relation: $B_{eq} = 4 \cdot (a^2\beta_{11} + b^2\beta_{22} + c^2\beta_{33} + ab\beta_{12} \cdot \cos(\gamma)/3$.[4] A table with distances, angles and distortion indexes in Sr-PbHA is reported as Supporting Information.[20] Further details of the crystal-structure investigations may be obtained from the Fachinformationszentrum Karlsruhe, 76344 Eggenstein-Leopoldshafen, Germany on quoting the depository numbers CSD-412026 to -412031.

Acknowledgments

We gratefully acknowledge financial support from MURST (Italy), the University of Bologna (Funds for Selected Topics), the Direction Générale de la Recherche Scientifique et Technique (Tunisie) and the Centre National de la Recherche Scientifique (France). NMR measurements were performed at the NMR facility center (SIARE) of the Université Pierre et Marie Curie (Paris).

[1] M. I. Kay, R. A. Young, A. S. Posner, *Nature* **1964**, *204*, 1050−1052.
[2] K. Sudarsanan, R. A. Young, *Acta Crystallogr., Sect. B* **1972**, *28*, 3668−3670.
[3] O. S. Bondareva, Yu. A. Malinkovskii, *Kristallografija* **1986**, *31*, 233−236.
[4] M. Hata, K. Okada, S. Iwai, *Acta Crystallogr., Sect. B* **1978**, *34*, 3062−3064.
[5] S. Brückner, G. Lusvardi, L. Menabue, M. Saladini, *Inorg. Chim. Acta* **1995**, *236*, 209−212.
[6] P. Fourman, P. Royer, *Calcium et tissu osseux − Biologie et pathologie*, Flammarion, Paris, **1970**.
[7] T. Suzuki, Y. Hayakawa, *Proceedings of the 1st International Congress on Phosphorus Compounds*, Rabat, October 17−21, **1977**, p. 381−385.
[8] Y. Matsumura, S. Sugiyama, H. J. B. Hayashi, J. B. Moffat, *J. Solid State Chem.* **1995**, *114*, 138−145.
[9] *CRC Handbook of Bioactive Ceramics*, vol. II ("Calcium Phosphates and Hydroxyapatites Ceramics") (Eds.: T. Yamamuro, L. L. Hench, J. Wilson), CRC Press, Boca Raton, **1990**.
[10] J. C. Elliott, *Structure and Chemistry of the Apatites and Others Calcium Orthophosphates*, Elsevier Sci., The Netherlands, **1994**.
[11] I. Khattech, Degree Thesis, Univeristé de Tunis,Tunisie, **1996**.
[12] A. Bigi, E. Foresti, F. Marchetti, A. Ripamonti, N. Roveri, *J. Chem. Soc., Dalton Trans.* **1984**, 1091−1093.
[13] M. Gazzano, PhD Thesis, University of Bologna, Bologna, Italy, **1986**.
[14] A. Bigi, A. Ripamonti, S. Brückner, M. Gazzano, N. Roveri, S. A. Thomas, *Acta Crystallogr., Sect. B* **1989**, *45*, 247−251.
[15] A. Nounah, J. Szilagyi, J. L. LaCut, *Ann. Chim. Fr.* **1990**, *15*, 409−419.
[16] B. Badraoui, A. Bigi, M. Debbabi, M. Gazzano, N. Roveri, R. Thouvenot, *Eur. J. Inorg. Chem.* **2001**, *5*, 1261−1267.
[17] B. Badraoui, R. Thouvenot, M. Debbabi, *C. R. Hebd. Acad. Sc. Ser. IIC* **2000**, *3*, 107−112.
[18] L. Vegard, *Z. Physik* **1922**, *9*, 395−396.
[19] R. D. Shannon, *Acta Crystallogr., Sect. A* **1976**, *32*, 751−767.
[20] Tables given as Supporting Information (see footnote on the first page of this article).
[21] K. C. Blakeslee, A. Robert, S. R. Condrate, *J. Am. Ceram. Soc.* **1971**, *54*, 559−563.
[22] G. Engel, W. E. Klee, *J. Solid State Chem.* **1972**, *5*, 28−34.
[23] B. O. Fowler, *Inorg. Chem.* **1974**, *13*, 207−213.
[24] M. Andres-Verges, F. J. Higes-Rolando, C. Valenzuela-Calahorro, P. F. Gonzales-Diaz, *Spectrochimica Acta* **1983**, *39A*, 1077−1082.
[25] J. Herzfeld, A. E. Berger, *J. Chem. Phys.* **1980**, *73*, 6021−6030.
[26] J. H. Lechter, J. R. Van Wazer, *J. Chem. Phys.* **1965**, *44*, 815−829.
[27] A. J. R. Costello, T. Gloneck, J. R. Van Wazer, *Inorg. Chem.* **1976**, *15*, 972−974.
[28] A. R. Grimmer, *Spectrochim. Acta* **1978**, *34A*, 941.
[29] A. K. Cheetham, N. J. Clayden, C. M. Dobson, R. J. B. Jakeman, *J. Chem. Soc., Chem. Commun.* **1986**, 195−197.
[30] S. Un, M. P. Klein, *J. Am. Chem. Soc.* **1989**, *111*, 5119−5124.
[31] S. Aime, G. Digilio, R. Gobetto, A. Bigi, A. Ripamonti, N. Roveri, *Inorg. Chem.* **1996**, *35*, 149−154.
[32] A. Bigi, M. Gazzano, A. Ripamonti, E. Foresti, N. Roveri, *J. Chem. Soc., Dalton Trans.* **1986**, 241−244.
[33] A. Bigi, G. Falini, E. Foresti, M. Gazzano, A. Ripamonti, N. Roveri, *J. Inorg. Biochem.* **1993**, *49*, 69−78.
[34] K. P. Quinlan, M. A. De Sesa, *Anal. Chem.* **1955**, *27*, 1626−1629.
[35] H. M. Rietveld, *J. Appl. Crystallogr.* **1969**, *2*, 65−71.
[36] R. A. Young, *J. Appl. Crystallogr.* **1995**, *28*, 366−367.
[37] G. Caglioti, A. Paoletti, F. P. Ricci, *Nucl. Instrum.* **1958**, *3*, 223−228.
[38] W. H. Baur, *Acta Crystallogr., Sect. B* **1974**, *30*, 1195−1215.

Received September 19, 2001
[I01369]

Cooperative Effects in the Binding of Substrates to Nickel(II) and Nickel(III) Complexes with a Bis(macrocyclic) Ligand

Peter Comba,*[a] Yaroslaw D. Lampeka,*[b] Alexander Y. Nazarenko,[c] Alexander I. Prikhod'ko,[b] Hans Pritzkow,[a] and Joanna Taraszewska[d]

Keywords: Template reaction / Spin equilibrium / Recognition / Cooperative effects / Nickel / N ligands

Nickel(II) complexes of mono- and bis(macrocyclic) ligands are the products of a nickel(II)-assisted template reaction with 2,3,2-tet, melamine and formaldehyde [2,3,2-tet = bis–*N*,*N*′-(2-aminoethyl)propane-1,3-diamine; melamine = 2,4,6-triamino-1,3,5-triazine]. The structures of two four-coordinate, diamagnetic nickel(II) complexes (protonated and non-protonated form) and of a six-coordinated paramagnetic nickel(II) compound with the protonated ligand have been determined by X-ray crystallography. Electronic spectroscopy was used to analyze the equilibrium between the paramagnetic and diamagnetic forms, and the electrochemical properties have been studied extensively ($Ni^{III/II}$ and $Ni^{II/I}$ couples). The equilibrium between the paramagnetic and diamagnetic forms and the nickel(III/II) couple are strongly dependent on the electrolyte, and sulfate is found to be coordinated selectively to the apical positions of both the nickel(II) and nickel(III) centers of the dinuclear compound. The structural, thermodynamic and electrochemical studies suggest that cooperative effects, involving coordination of sulfate to one nickel center, assisted by hydrogen bonding to an axially coordinated water molecule of the other nickel center, is responsible for the recognition of this anion.
(© Wiley-VCH Verlag GmbH, 69451 Weinheim, Germany, 2002)

Introduction

Mannich-type, metal-ion-assisted condensation reactions of *cis*-disposed primary amines with formaldehyde and a nucleophile have been used extensively to prepare hexaamine cages, pendent-arm macrocyclic and open-chain ligands with N-, S-, Se- and O-donors, coordinated to copper, nickel, palladium, cobalt and a few other metal centers.[1−6] Due to the rigidity of the aromatic spacer groups and the possibility to obtain oligonuclear complexes in one-pot reactions, aromatic amines, melamine in particular (melamine = 2,4,6-triamino-1,3,5-triazine), are of interest as "capping" groups in metal-based template condensations. However, in the copper(II)-assisted condensation the poor nucleophilicity of the aniline-type amines results in low yields of the desired mono-, bis- and tris(macrocyclic) products,[7−9] and this is also the case for the nickel(II)-assisted Mannich reaction (see below). When the mono-(macrocyclic), melamine-substituted nickel(II) or copper(II) intermediates are used as capping groups in the template reactions mixed-metal oligonuclear systems may be obtained.[10]

The two factors which make the melamine-based oligomacrocyclic ligand complexes of particular interest are vacant or labile axial sites at the metal centers, with the possibility for cooperative binding and activation of substrates in the bis- and tris(macrocyclic) ligand systems, and the fact that melamine can be protonated. π-Stacking, hydrogen bonding and bonding to relatively labile axial sites of transition metal complexes have been described as important features for host-guest interactions.[11−16] Metal complex hosts which have been reported include trizinc(II) compounds and a tetrahedral tetragallium(III) complex.[17−19] A variety of possible applications, including crystal engineering, the preparation and stabilization of anionic metal complexes, as well as cooperativity and selectivity of anion binding have been described with melamine-based macrocyclic ligand complexes.[7−9,20]

Here, we present details on the syntheses and structures of nickel(II) complexes with melamine-based mono- and

[a] Universität Heidelberg, Anorganisch-Chemisches Institut, Im Neuenheimer Feld 270, 69120 Heidelberg, Germany
Fax: (internat.) + 49-(0)6221/546617
E-mail: comba@akcomba.oci.uni-heidelberg.de
[b] L. V. Pisarzhevsky Institute of Physical Chemistry, National Academy of Science of the Ukraine, Prospekt Nauki 31, 03039 Kiev 39, Ukraine
Fax: (internat.) + 38-044/2656216
E-mail: ditop@iphch.kiev.ua
[c] Department of Chemistry, State University of New York, College at Buffalo, 1300 Elmwood Ave, Buffalo, NY 14222-1095, USA
[d] Institute of Physical Chemistry, Polish Academy of Sciences, Kasprzaka 44/52, 01-224 Warsaw, Poland
Supporting information for this article is available on the WWW under http://www.eurjic.com or from the author.

bis(macrocyclic) ligands and a thorough study of the equilibria between the paramagnetic and diamagnetic forms and electrochemical reduction and oxidation processes; this leads to a detailed understanding of the importance of cooperative effects in the recognition of sulfate by the dinickel(II) and the dinickel(III) complexes.

Results and Discussion

Synthesis

The macrocyclization reaction of the open-chain copper(II) complex $[Cu(2,3,2\text{-tet})]^{2+}$ with formaldehyde and melamine yields three possible compounds of different nuclearity, $[Cu(L^1)]^{2+}$, $[Cu_2(L^2)]^{4+}$ and $[Cu_3(L^3)]^{6+}$ (Scheme 1).[7−9] Only complexes with the mono- and bis(macrocyclic) ligands, $[Ni(L^1)]^{2+}$ and $[Ni_2(L^2)]^{4+}$, can be isolated with $[Ni(2,3,2\text{-tet})]^{2+}$ as the template. These are separated by column chromatography, using 0.2 mol·L^{-1} and 0.4 mol·L^{-1} aqueous $NaClO_4$ as eluents. Melamine generally leads to lower yields of the macrocyclic ligand products than other locking groups in metal-ion-assisted Mannich condensations. The yields of the copper(II) complexes are 9%, 13% and 7% for the mono-, bis- and tris(macrocyclic) ligand complexes, respectively.[7−9] The yields of the nickel(II) compounds are even lower (see Exp. Sect.).

An aromatic nitrogen atom of melamine in $[M(L^1)]^{2+}$ and $[M_2(L^2)]^{4+}$ can be protonated (pK_{a1} = 4.2 for $[Cu(L^1)]^{2+}$ [7]). The resulting sites for hydrogen bonding are of importance for the stabilization of specific types of arrangements of the macrocyclic cations in the crystal lattices.[7−9,20]) However, since protonation does not result in significant changes of the solution spectroscopic and electrochemical properties of the nickel compounds (see below), we conclude that protonation alone does not lead to stable supramolecular assemblies in solution, similar to those observed in crystal lattices.

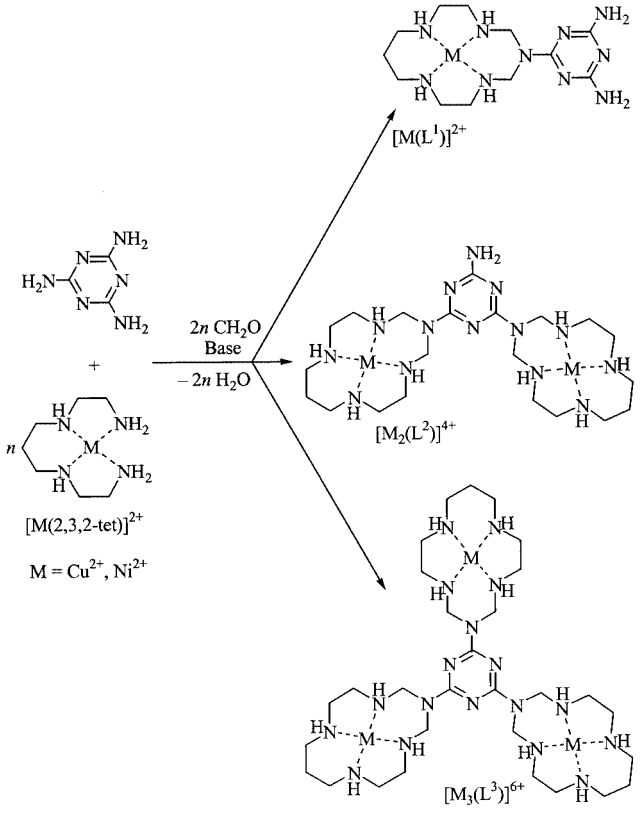

Scheme 1

Vibrational spectra of the complexes have features, which are characteristic for both the melamine fragment and the tetraazamacrocyclic ligand nickel(II) core. Similar to the copper(II) compounds,[9] the number of transitions which correspond to the out-of-plane vibrations of the aromatic amino groups [$\delta(NH_2)$, 1660 cm^{-1} in melamine] are related to the nuclearity of the complexes and, for complexes of L^1 and L^2, to the degree of protonation of the melamine fragment: three bands (1700, 1650, 1600 cm^{-1}) are observed in the nickel(II) compounds of the protonated mono(macrocyclic) ligand $(HL^1)^+$; two bands (1667 and 1600 cm^{-1}) are characteristic for complexes of the protonated bis(macrocyclic) ligand $(HL^2)^+$; one band is observed for complexes of the free bases ($[Ni(L^1)]^{2+}$, 1600 cm^{-1}; $[Ni_2(L^2)]^{4+}$, 1610 cm^{-1}).

Molecular and Crystal Structures

The structures of the mono(macrocyclic) ligand nickel(II) complexes with the non- and monoprotonated melamine fragment and diamagnetic or paramagnetic nickel(II) centers, i.e., four-coordinate nickel(II) complexes of two forms of L^1, $[Ni(L^1)](ClO_4)_2\cdot H_2O$ (**1**) and $[Ni(HL^1)](ClO_4)_2\text{-}Cl\cdot H_2O$ (**2**), and the six-coordinate complex of $(HL^1)^+$ $[Ni(HL^1)(OSO_3)(OH_2)]ClO_4\cdot 5H_2O$ (**3**) were determined by X-ray crystallography. Single crystals of the four-coordinate dinickel(II) compound $[Ni_2(L^2)](ClO_4)_4\cdot 2H_2O$ (**4**) were also obtained but were of poor quality, the preliminary data obtained were used to determine the overall conformation of the dinuclear cation. The variety of the structural data, together with the published structures of the corresponding copper(II) compounds, i.e., $[Cu(L^1)(OClO_3)_2]\cdot H_2O$ (**5**)[9] and **6**,[20] $[Cu(HL^1)(OClO_3)_2](ClO_4)\cdot H_2O$ (**7**),[9] $[Cu(HL^1)\text{-}(OClO_3)](ClO_4)_2\cdot 2H_2O$ (**8**),[7] and $\{[Cu(HL^1)(OH_2)(Cl)]\text{-}[Cu(HL^1)(OClO_3)(Cl)]\}(ClO_4)_3$ (**9**),[9] form a broad basis for a comparative analysis of the molecular and crystal structures of melamine-based macrocyclic ligand complexes [copper(II) compounds of L^2 and L^3, which have also been reported before [8,9] are not included in this analysis].

Molecular Structures

The geometries of the macrocyclic ligands L^1 and $(HL^1)^+$ in the nickel(II) complexes (Figure 1) and in the corresponding copper(II) compounds [7−9,20] are identical, i.e., *trans*-III (*RRSS*).[21] The distances and angles are typical for nickel(II) [and copper(II)] complexes of 14-membered tetraaza macrocycles.[22] The melamine rings are nearly planar (rms 0.01−0.02 Å), as observed in other 1,3,5-triazine derivatives.[23] The nickel(II) ions in **1** and **2** are coordinated in a planar chromophore to four nitrogen donors of

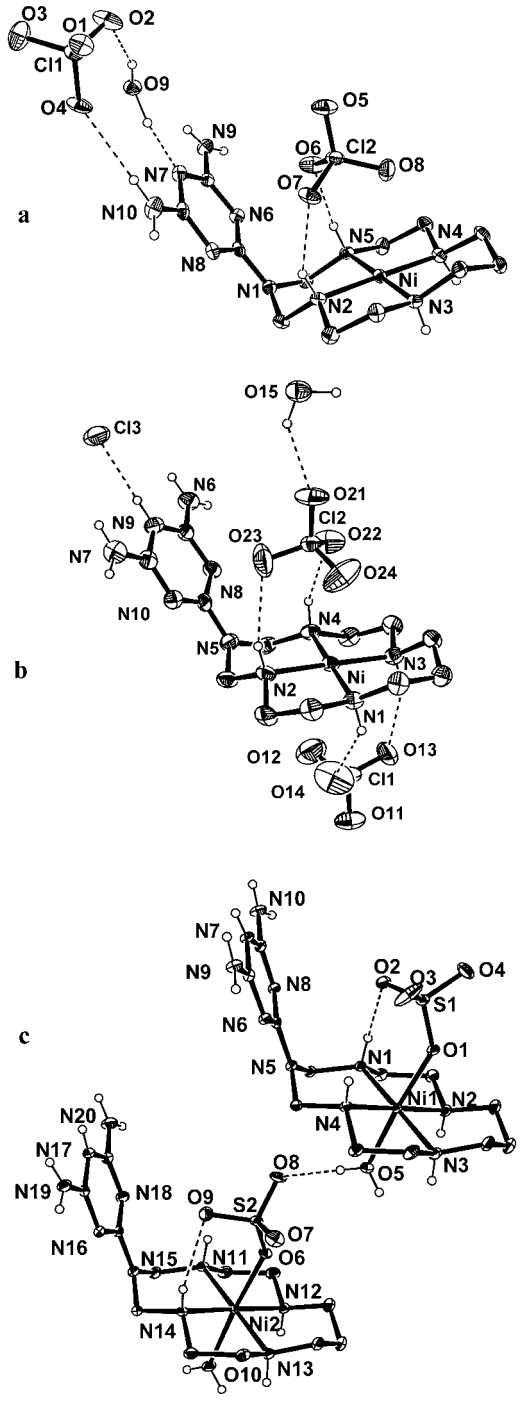

Figure 1. ORTEP[40] view (30% probability ellipsoids) of **1** (a), **2** (b) and **3** (c); C−H hydrogen atoms are omitted for clarity; selected hydrogen bond lengths are: **1**: O(4)···H−N(10) 3.278 Å, O(9)−H···O(2) 2.956 Å, O(9)−H···N(7) 2.747 Å, N(2)−H···O(7) 3.008 Å, N(5)−H···O(6) 3.047 Å; **2**: N(1)−H···O(14) 2.984 Å, N(3)−H···O(13) 3.116 Å, N(2)−H···O(23) 3.148 Å, N(4)−H···O(22) 3.071 Å, Cl(3)···H−N(9) 2.988 Å; **3**: O(5)−H···O(8) 2.680 Å, O(10)−H···O(4′) 2.630 Å O(2)···H−N(1) 2.938 Å; O(9)···H−N(14) 3.010 Å

the macrocycle with nearly identical metal−nitrogen distances, as expected for four-coordinate, diamagnetic nickel(II) compounds[22] (see Table 1). The paramagnetic nickel(II) ion in **3** is six-coordinate, with a sulfate anion and a water molecule completing the coordination sphere, in a nearly regular octahedral geometry with significantly longer metal−donor distances than observed in **1** and **2** (see Table 1).

From the structural parameters of the complexes of L^1 (see Table 1), it emerges that four-, five- or six-coordinate metal ions with a variety of metal donor distances [Ni−N < 1.95 Å in diamagnetic nickel(II); Cu−N ≈ 2.02 Å; Ni−N > 2.06 Å in paramagnetic nickel(II) complexes, 2.1 Å $<$ M−O^{ax} < 2.6 Å] are well accommodated in the macrocycle in *trans*-III configuration, with close to planar MN_4 chromophores and the expected N−M−N bite angles (ca. 95° for the six-membered and ca. 85° for the five-membered chelate rings). The flexibility in the orientation of the melamine rings with respect to the mean MN_4 planes (angles α, β, γ, see Figure 2) allows for a wide range of substrates to be stabilized (this is of specific importance for the bis- and tris(macrocyclic) compounds, see ref.[9]) and for the stabilization of specific crystal lattice patterns (see below).

In complexes with two or three macrocyclic ligands fixed on the melamine spacer group, as in L^2 and L^3, there are two possible conformations (*syn* or *anti* in L^2; *syn*,*syn* or *syn*,*anti* in L^3). Both are similar in energy[8,9] and the preference for a particular structure in a crystal lattice or in solution is a function of the substrates (or electrolytes) and the environment (lattice or solvent). Both structural types have been observed for $[Cu_3(L^3)]^{6+}$,[8,9] only the *anti* isomer was characterized structurally for the copper(II) complex with the bis(macrocyclic) ligand,[9] and the same is observed in the corresponding dinickel(II) system **4** discussed here. Also, host-guest complexation studies and preliminary computations indicate that the barrier for isomer interconversion (*syn*/*anti*) is relatively low.[9,24] The experimental structural data support this assumption (angles α, β, γ, see Table 1); there appears to be a large flexibility (shallow energy minimum) with an optimum structure of $10° < \alpha < 30°$ [planarity of the pendent amine groups of melamine would require $\alpha = 0°$, values of $\alpha > 2°$ have been observed in copper(II) complexes[9]], $70° < \beta < 90°$ and $40° < \gamma < 60°$. This flexibility is an advantage for the cooperative binding and activation of substrates at the axial sites of the metal chromophores.

Crystal Packing

Three main structural motifs have been found in crystal lattices of copper(II) complexes with the melamine-derived mono(macrocyclic) ligand,[7,9,20] i.e., infinite tapes of the molecular cations (hydrogen bonds between the free amino groups of the melamine substituents and water molecules or perchlorate anions, 5.0 Å $< d_2 <$ 5.7 Å, see Figure 3, Table 2), π-stacking interactions between the melamine rings, $d_4 \approx 3.5$ Å, $\delta \approx 0°$ (δ is the angle between the two melamine ring planes), and, for the copper(II) complexes **5** and **6** with the free-base ligand, the formation of double-stranded tapes, due to hydrogen bonding between self-complementary melamine groups (ADA, acceptor-donor-acceptor pattern). Two different types of stacked pairs are possible, depending on the orientation of the macrocyclic

Table 1. Structural parameters (distances in Å, angles in °) of metal(II) complexes with the melamine-derived macrocyclic ligand L^1

Complex	Structure of the chromophore							Conformation of the melamine macrocycle fragments[a]		
	Equatorial M−N	Axial M−O	N−M−N (av. 6-membered chelate ring)	N−M−N (av. 5-membered chelate ring)	Rms of MN_4	Deviation of M from MN_4 plane	θ[b]	α	β	γ
Non-protonated ligand L^1										
Ni (**1**)	1.936−1.943	none	94.2 ± 0.2	85.8 ± 0.2	0.01	0.01	1.1	27.2	86.2	58.6
Cu (**5**)[9]	2.015−2.025	2.458, 2.628 (ClO_4)	94.2 ± 0.4	85.7 ± 0.0	0.03	0.05	5.3	23.0	70.7	45.5
Cu (**6**)[20]	2.009−2.026	2.511, 2.617 (ClO_4)	94.3 ± 0.3	85.6 ± 0.3	0.03	0.04	4.4	12.2	80.4	36.9
Protonated ligand $(HL^1)^+$										
Ni (**2**)	1.921−1.939	none	93.3 ± 1.7	86.7 ± 0.3	0.02	0.02	2.7	11.3	86.9	48.5
Cu (**7**)[9]	2.013−2.029	2.585, 2.594 (ClO_4)	94.9 ± 2.6	85.0 ± 0.0	0.01	0.01	2.2	18.9	82.5	61.6
Cu (**8**)[7] [c]	2.008−2.019,	2.521 (H_2O)	94.8 ± 0.5,	85.1 ± 0.3,	0.01,	0.01,	1.7,	12.0,	89.1,	44.7
	2.006−2.052	none	94.7 ± 0.6	85.2 ± 0.1	0.03	0.05	5.6	12.4	86.4	46.7
Coordinated substrate, protonated ligand $(HL^1)^+$										
Ni (**3**)[c]	2.064−2.081,	2.099 (SO_4), 2.135 (H_2O)	94.6 ± 0.8,	85.4 ± 0.2,	0.01,	0.01,	1.0,	10.1,	86.7,	45.9
	2.062−2.079	2.090 (SO_4), 2.135 (H_2O)	94.6 ± 0.3	85.4 ± 0.2	0.01	0.02	1.8	12.3	86.9	46.9
Cu (**9**)[9] [c]	2.011−2.028,	2.718 (H_2O), 2.826 (Cl),	94.1 ± 3.3,	85.6 ± 0.1,	0.04,	0.04,	7.8,	9.9,	88.8,	52.3
	2.016−2.023	2.660 (Cl), 2.808 (ClO_4)	94.4 ± 2.7	85.0 ± 0.1	0.06	0.12	11.8	9.6	88.5	49.9

[a] For definition of the angles see Figure 2. [b] Average angle between two N−M−N planes (tetrahedral or pyramidal distortion of the chromophore). [c] Two independent molecules in the asymmetric unit.

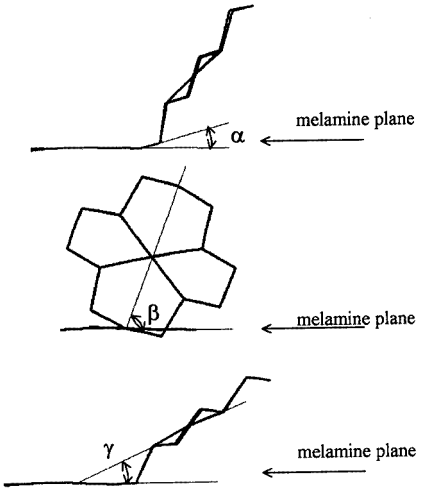

Figure 2. Definition of the structural parameters used for the analysis of the geometry of the melamine macrocycle fragments

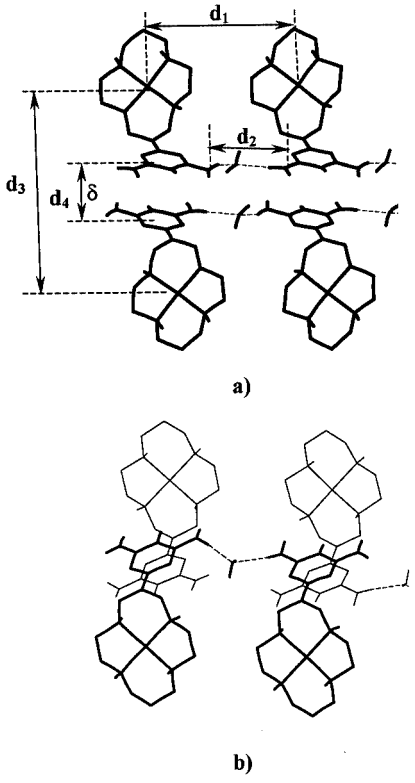

Figure 3. The two different types of stacked pairs of $[M(L^1)]^{n+}$ complexes

rings with respect to the neighboring melamine plane (see Figure 3a,b). The relevant structural parameters are given in Table 2, see Figure 3 for their definition.

Interestingly, in the crystal lattice of **1** the common features of all other structures are absent (see Figure 4a). This presumably is due to the specific location of a water molecule relative to the melamine residues; the hydrogen bonding patterns (see Figure 1a) do not allow the formation of the usual tapes and prevent a complementary hydrogen bonding interaction between pairs of melamine rings. Also, this indicates that the formation of the usually observed tapes, stabilized by hydrogen bonding and π-stacking, is, as expected, a relatively small contribution which may be overcome by other effects.

Similar to the copper(II) complexes **5**−**8**,[7,9,20] the macrocyclic cations in the crystal lattice of **2** form infinite hydrogen-bonded chains, bridged by water molecules and supported by π-interactions between the parallel and nearly coaxial melamine rings (see b in Figure 4). The metal−metal distance d_1 is slightly shorter than in the copper(II) analogues, and d_2 is intermediate between those observed in the copper(II) compounds.

Table 2. Structural parameters (distances in Å, angles in °) related to the crystal packing of complexes with the melamine-derived mono(macrocyclic) ligand

Complex	Tapes			Stacks		
	d_1	d_2	N−H···O(H_2O)	d_3	d_4	δ
Non-protonated ligand L^1						
Ni (**1**)	10.87	6.36	no H-bonds	no π-stacking		
Cu (**5**)[9]	9.54	5.11	2.86, 2.87	11.61	3.5	0
Cu (**6**)[20]	10.00	5.66	2.99, 3.05	11.64	3.5	0
Protonated ligand $(HL^1)^+$						
Ni (**2**)	9.43	4.81	2.91, 2.93	12.29	3.2	0
Cu (**7**)[9]	9.58	5.00	2.89, 2.95	13.00	av. 3.4	1.6
Cu (**8**)[7]	9.49	4.89	2.90, 3.00	12.64	3.5	0
Ni (**3**)	9.12; 9.32	4.82; 4.79	2.81, 2.96; no H-bonds	11.17;[a] 12.26;[b] 12.32[b]	av.4.2; 4.5; 4.5	4.9; 0; 0
Cu (**9**)[9]	9.67	5.10	3.01, 3.08[c]	11.28[b]	av.3.6	5.6

[a] "Open" stack (see Figure 3a). [b] "Closed" stack (see Figure 3b). [c] Bridging perchlorate anion instead of water molecule.

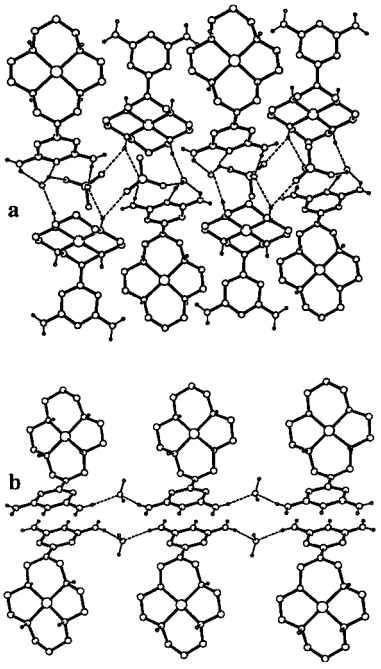

Figure 4. Crystal packing of **1** with intermolecular hydrogen bonds (a) and π-stacked cationic tapes in the crystal lattice of **2** (b)

The crystal lattice of **3** is unique, the tape structure has a "stair"-type arrangement (see a in Figure 5). This is due to the water molecule $H_2O(27)$, which not only bridges two neighboring cations in the tape but also forms a hydrogen bond to the aromatic nitrogen atom of the adjacent tape [O(27)−H···N(8), 2.988 Å]. In addition, the tape observed in **3** is not isotropic and consists of distinct hydrogen-bound dimers (d_1 = 9.32 Å, d'_1 = 9.12 Å); the distance between the melamine amino groups of the non-bonded adjacent cations is smaller than for those connected by hydrogen bonds (see Table 2). This tape interacts via π-stacking with another tape of the same structure but shifted by one macrocyclic unit, i.e., alternating hydrogen bonds hold the two tapes together (see b in Figure 5).

The melamine substituents in all examples form π-stacked pairs of cations; generally, the metal chromophores of the stacked cations are oriented at different sides of the

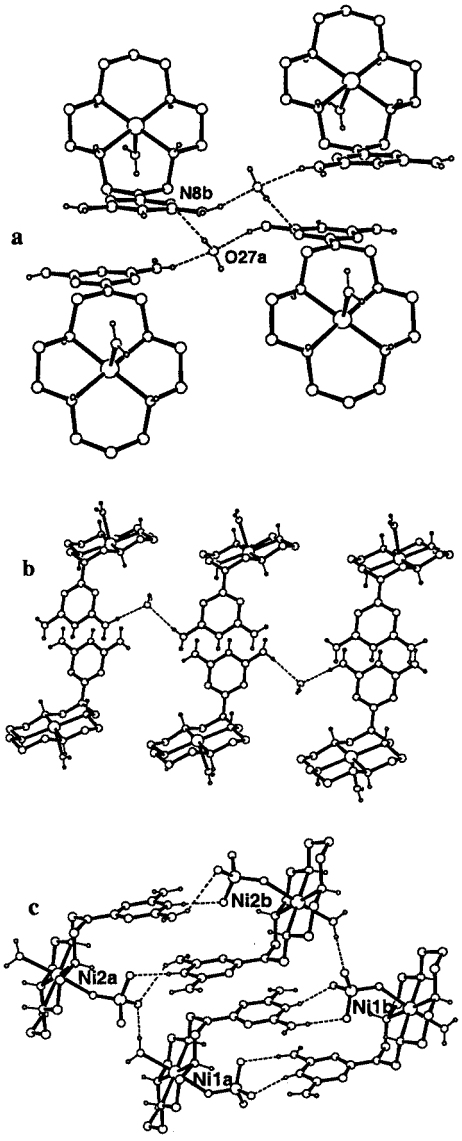

Figure 5. Pair of π-stacked cations (a), modulated tape (b) and modulated π-stacking in the crystal lattice of **3**

interaction plane (see Figure 3a, "open" stack). The only exception is the copper(II) complex **9** for which the π-π interaction plane bisects the metal chromophores (see Figure 3b, "closed" stack).[9] Both "open" [Ni(1a)−Ni(2b) pair] and "closed" stacks [Ni(na)−Ni(nb) pair] are present in the crystal lattice of **3** (Figure 5c), and the sulfate anions have the same dual function as the chloride anions in **9**, i.e., as axial donors they form strong hydrogen bonds to the acceptor centers of the protonated melamine [O(2)···H−N(9′), 2.835 Å; O(3)···H−N(7′), 2.708 Å; O(8)···H−N(19′), 3.114 Å; O(9)···H−N(17′), 2.695 Å]. Also, the stacks in **3** are not isolated and can be considered as modulated, extended chains of π-stacked molecules (see Table 2).

Solution Properties

Electronic Spectroscopy and Equilibria between Diamagnetic and Paramagnetic Compounds

Electronic spectra of the nickel(II) compounds with the mono- and bis(macrocyclic) ligands were measured in nitromethane, acetonitrile and water. The spectra in the UV region are characterized by a strong absorption centered at ca. 210 nm ($\varepsilon \approx 6\ 10^5$ L·mol^{-1}·cm^{-1}), which probably is a superposition of an MLCT band (shoulder at ca. 219 nm) and an intramolecular melamine transition (204 nm in melamine). Absorption spectra in the visible and near-infrared region consist of d-d bands at ca. 330, 455, 660 and > 910 nm, and are typical for nickel(II) complexes of tetraaza-macrocycles and for systems, where nickel(II) complexes with different electronic ground states persist simultaneously in solution [Equations (1) and (2)], i.e., a four-coordinate, planar diamagnetic form (455 nm) and a six-coordinate distorted octahedral paramagnetic form (330, 660 and > 910 nm).[25]

$$[Ni(L)]^{2+} + 2\ solv \rightleftarrows [Ni(L)(solv)_2]^{2+} \quad (1)$$

$$K_{ax} = (\varepsilon_{ls} - \varepsilon_{eff})/(\varepsilon_{eff} - \varepsilon_{hs}) \quad (2)$$

$$\varepsilon_{eff} = \{\varepsilon_{ls}[Ni(L)^{2+}] + \varepsilon_{hs}[Ni(L)(solv)^{2+}]\}/\{[Ni(L)^{2+}] + [Ni(L)(solv)^{2+}]\} \quad (3)$$

In nitromethane there is only a transition at 455 nm for $[Ni(L^1)]^{2+}$ and $[Ni_2(L^2)]^{4+}$, with a molar absorption of 64 L mol^{-1} cm^{-1} per nickel(II) center (see Table 3). Therefore, in the weakly coordinating solvent nitromethane there is no coordination of axial donors, and this allows to determine the molar absorptivity of the diamagnetic form (ε_{ls}). The apparent molar absorption coefficients [ε_{eff}, Equation (3)] of the transition at 455 nm in acetonitrile and aqueous solutions of various electrolytes are lower (see Table 3), indicating the presence of significant amounts of the six-coordinate form in equilibrium with the four-coordinate compounds.

The strength of bonding of axial donors to the nickel(II) centers (increasing K_{ax}, decreasing η) is of similar magnitude for $[Ni(L^1)]^{2+}$ and $[Ni_2(L^2)]^{4+}$ (see Table 3) and significantly higher than for $[Ni(cyclam)]^{2+}$ (cyclam = 1,4,8,11-tetraazacyclotetradecane; 0.1 mol·L^{-1} aqueous $NaClO_4$: $K_{ax} = 0.40$, η = 71%;[26] CH_3CN: η = 22% [27]). An interesting observation is that the thermodynamic parameters for the complexation to axial sites of $[Ni(Me\text{-}azacyclam)]^{2+}$ (Me-azacyclam = 3-methyl-1,3,5,8,12-pentaazacyclotetradecane) are similar to those of the cyclam complex (0.1 mol·L^{-1} aqueous $NaClO_4$: $K_{ax} < 0.5$; CH_3CN: η = 23% [28]), i.e., different to those of the structurally related azacyclam derivatives discussed here. The fact that the spectroscopic properties of all four nickel(II) complexes are similar to each other ($\lambda^{ls}_{max} \approx 455$ nm, $\lambda^{hs}_{max} \approx 330$, 670 and > 900 nm) indicates that metal-centered electronic factors are not the major reason for the drastic differences, and electronic, as well as steric factors related to the capping groups, and differences in solvation may be of importance.

A comparison of the thermodynamic parameters for the axial coordination of water (0.1 mol·L^{-1} $NaClO_4$) to $[Ni(L^1)]^{2+}$ and $[Ni_2(L^2)]^{4+}$ (see Table 3; for details see Supporting Information) with those of $[Ni(cyclam)]^{2+}$ ($\Delta H^0 = -23$ kJ mol^{-1}, $\Delta S^0 = -84$ J mol^{-1} K^{-1}) [29] indicates that the strong axial binding to nickel(II) complexes with the melamine-based ligand is primarily due to an entropy effect (less negative ΔS^0), rather than differences in bond strength (similar ΔH^0). A possible interpretation is that one of the axial water donors [H_2O(A) in Scheme 2] is, upon decomplexation to the four-coordinate form, not released to the bulk solvent, but remains in the first solvation shell. A hydrogen bond similar to that proposed in Scheme 2 was observed in the crystal lattice of **3**.

The largest fraction of the paramagnetic nickel(II) form was observed in the presence of sulfate (see Table 3). There-

Table 3. Effective molar absorptivities (ε, L mol^{-1} cm^{-1}) of the transition at 455 nm of the nickel(II) compounds and equilibria between the diamagnetic and paramagnetic forms in various solvents at 25 °C

Medium	$[Ni(L^1)]^{2+}$			$[Ni_2(L^2)]^{4+}$		
	ε_{eff}	K_{ax}	η (%)[a]	ε_{eff}	K_{ax}	η (%)[a]
CH_3NO_2	64	−	100	128	−	100
CH_3CN	10	10.80	8	21	8.92	9
H_2O; 0.1 mol·L^{-1} $NaClO_4$[b]	23	2.22[c]	28.9	48	2.05[d]	30.5
H_2O; 0.1 mol·L^{-1} $NaNO_3$ [b]	20	2.84	24.2	42	2.61	25.8
H_2O; 0.1 mol·L^{-1} NaCl[b]	19	3.10	22.7	40	2.84	24.2
H_2O; 3.33 10^{-2} mol·L^{-1} Na_2SO_4 [b]	13	6.00	13.3	22	8.15	10.1

[a] Percentage of the diamagnetic form in the equilibrium mixtures, $\eta = (\varepsilon_{eff} - \varepsilon_{hs})/\varepsilon_{ls}$. [b] pH = 7; constant ionic strength. [c] $\Delta H^0 = -23$ kJ mol^{-1}, $\Delta S^0 = -71$ J mol^{-1} K^{-1}. [d] $\Delta H^0 = -21$ kJ mol^{-1}, $\Delta S^0 = -64$ J mol^{-1} K^{-1}.

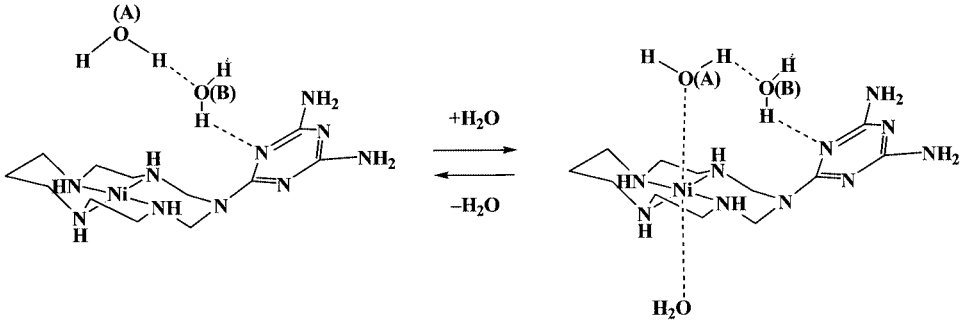

Scheme 2

fore, the stepwise complexation with sulfate was studied in aqueous solution (μ = 0.1 mol·L^{-1}; 0 mol·L^{-1} < [SO_4^{2-}] < 3.33 10^{-2} mol·L^{-1}), see Equation (4), where K_{ax}^{H2O} is the equilibrium constant in absence of sulfate [see Equation (2), 0.1 mol·L^{-1} $NaClO_4$; see Table 3) and K_{ax}^1 to K_{ax}^4 are the stepwise complexation constants with sulfate.

$$K_{ax} = K_{ax}^{H2O} + \sum_{i=1}^{4} [SO_4^{2-}]^i \prod_{j=1}^{i} K_{ax}^i \quad (4)$$

From the data analysis (see Supporting Information) it follows that K_{ax}^2 is ca. 0 for both $[Ni(L^1)]^{2+}$ and $[Ni_2(L^2)]^{4+}$, and fits with higher terms (K_{ax}^3 and K_{ax}^4 for $[Ni_2(L^2)]^{4+}$) do not lead to a significant improvement, i.e., these can be ignored. It emerges that, in sulfate-containing solutions, the mono(sulfate) adduct [per nickel(II) ion] is the primary species, and K_{ax}^1 is significantly larger for $[Ni_2(L^2)]^{4+}$ than for $[Ni(L^1)]^{2+}$ (162 ± 6 L mol^{-1} and 79 ± 10 L mol^{-1}, respectively). Part of this effect may be due to differences in ion pairing [increasing electrostatic attraction with the higher charge of the dinickel(II) complex[30]] but the increasing axial bonding may also be attributed to cooperativity, involving both nickel(II) centers and hydrogen bonding between a coordinated sulfate and an axial water molecule (see Figure 6). Qualitative models suggest that this may lead to stabilization of the sulfate/$[Ni_2(L^2)]^{4+}$ adduct in the *syn* conformation of the dinickel(II) complex.[24] A preliminary structural analysis indicates that in the crystal lattice the dinuclear complex **4** has the *anti* conformation but recent studies on the corresponding copper(II) compounds indicate that the two conformations are similar in energy and that the barrier of interconversion is low.[9,24,31]

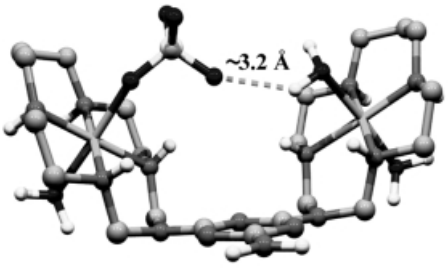

Figure 6. Model for the visualization of cooperativity in the axial bonding of sulfate

Electrochemical Properties and Recognition of Sulfate Anions

The electrochemical behavior of $[Ni(L^1)]^{2+}$ and $[Ni_2(L^2)]^{4+}$ was studied in acetonitrile and aqueous solutions of various salts. In acetonitrile (0.1 mol·L^{-1} [Bu_4N]ClO_4) a quasi-reversible redox process, assigned to the nickel(III/II) couple is observed {$[Ni(L^1)]$: E_f = 1.084 V (ΔE = 87 mV); $[Ni_2(L^2)]$: E_f = 1.027 V (ΔE = 73 mV)}. An irreversible process {E_{cat} = −1.46 V and −1.40 V for $[Ni(L^1)]^{2+}$ and $[Ni_2(L^2)]^{4+}$, respectively} is attributed to the nickel(II/I) couple; small additional peaks at ca. 0.6 V are assigned to adsorption effects and peaks at ca. 1.3 V may be assigned to ligand oxidation (see Figure 7). The data indicate that both metal centers in $[Ni_2(L^2)]^{4+}$ undergo the redox transformations independently and at the same potentials. Similar results are obtained with [Bu_4N]BF_4 as the electrolyte.

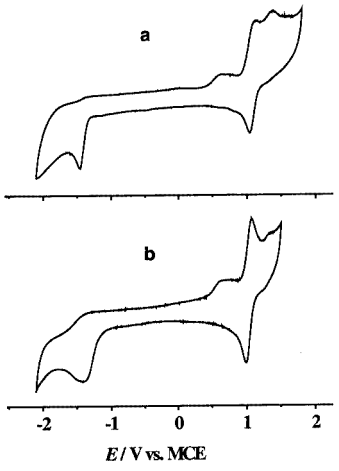

Figure 7. Cyclic voltammograms of 1 10^{-3} mol·L^{-1} solutions of $[Ni(L^1)]^{2+}$ (a) and $[Ni_2(L^2)]^{4+}$ (b) in acetonitrile (0.1 mol·L^{-1} [Bu_4N]ClO_4)

Protonation of non-coordinated nucleophiles in the ligand backbone are known to lead to a destabilization of the oxidized form of metal complexes.[32] As expected, there is approximately an inverse relationship between the destabilization of nickel(III) over nickel(II) and the distance between the nickel center and the site of protonation.[33] For [Ni(Me-azacyclam)] the change of the nickel(III/II) potential upon protonation is ca. 120 mV (0.790 V and

0.910 V in neutral solution and 9.5 mol·L^{-1} $HClO_4$, respectively).[33] The corresponding effects observed for $[Ni(L^1)]^{3+/2+}$ and $[Ni_2(L^2)]^{6+/4+}$ are much smaller (0.815 ± 0.020 V and 0.825 ± 0.010 V, respectively, 10^{-7} mol·L^{-1} < $[H^+]$ < 9.5 mol·L^{-1}). This indicates that, upon protonation of the aromatic fragment, the positive charge is delocalized over the melamine ring.

The electrochemical behavior of $[Ni(L^1)]^{2+}$ and $[Ni_2(L^2)]^{4+}$ in aqueous solution with various electrolytes was studied by cyclic voltammetry (CV) and differential pulse voltammetry (DPV). These data are listed in Table 4, relevant DPV curves of the oxidation scans are collected in Figure 8 and Figure 9. The E_f value for the single quasi-reversible redox transformation of the mono(macrocyclic) ligand complex $[Ni(L^1)]^{2+}$ is strongly anion-dependent and decreases in the order $ClO_4^- > NO_3^- > Cl^- > HSO_4^- \approx H_2PO_4^- > SO_4^{2-} > HPO_4^{2-}$. This sequence is typical for nickel(III/II) couples of azamacrocyclic ligands and reflects the increasing stabilization of nickel(III) by electrostatic effects.[34–36] The poor reversibility observed in the experiments with HPO_4^{2-} is probably related to the high pH of the solutions which leads to a destabilization of the nickel(III) complex with respect to decomposition. This is supported by significantly lower currents observed in the corresponding CV and DPV experiments.

Table 4. Redox potentials (E_f in V vs. MCE, ΔE in mV in parentheses) of the $Ni^{III/II}$ couple of melamine-derived macrocyclic ligand complexes $[Ni(L^1)]^{2+}$ and $[Ni_2(L^2)]^{4+}$ in aqueous solution, containing 0.1 mol·L^{-1} Na^+ salts (CV data, pH = 7.0, sweep rate 0.1 V s^{-1})

Anion of the electrolyte	$[Ni(L^1)]^{2+}$	$[Ni_2(L^2)]^{4+}$
ClO_4^-	0.802 (66)	0.818 (74)
NO_3^-	0.790 (76)	0.794 (78)
Cl^-	0.616 (72)	0.618 (77)
SO_4^{2-}[a]	0.545 (83)	0.488 (62), 0.609 (71)
HSO_4^-[a][b]	0.569 (68)	0.553 (60), 0.638 (60)
$H_2PO_4^-$[c]	0.553 (81)	0.534 (123)[d]
HPO_4^{2-}[e]	0.376 (120)	0.314,[f] 0.428 V[f]

[a] 3.33 10^{-2} mol L^{-1} Na_2SO_4. [b] pH = 1.0 [pK_{a1}(H_2SO_4) = 1.92]. [c] 0.1 mol L^{-1} KH_2PO_4. [d] Sweep rate 0.2 V s^{-1}. [e] pH = 8.2. [f] Anodic peaks of the irreversible oxidation process (DPV).

The behavior of the bis(macrocyclic) ligand complex $[Ni_2(L^2)]^{4+}$ in the presence of perchlorate, nitrate and chloride is similar to that of $[Ni(L^1)]^{2+}$ (see Table 4 and Figure 8). In presence of sulfate or phosphate, however, there are two separate oxidation/reduction steps for $[Ni_2(L^2)]$ (Table 4, Figure 8 and Figure 9). These are reversible in sulfate but only poorly reversible or irreversible in phosphate (similar effects were observed with the mononuclear compound, see above). The fact that the currents for the two-electron oxidation processes in $[Ni_2(L^2)]^{4+}$ in perchlorate-containing solutions are nearly equal to the sum of the two separate single-electron steps in sulfate media indicates that both single-electron oxidation steps are related to the nickel(III/II) couple. Therefore, anion coordination leads to two structurally (and electronically) different nickel centers or to strong coupling of the two metal ions. Also, the reduction potentials of the nickel(III/II) couple in the dinuclear complex are more anodic (E_{f1}) and more cathodic (E_{f2}) than that of the mononuclear compound. For a thorough analysis of the redox processes, the dependencies of the E_f values on the sulfate concentration in neutral (pH = 7.0) and acidic (pH = 1.0) aqueous solutions were studied.

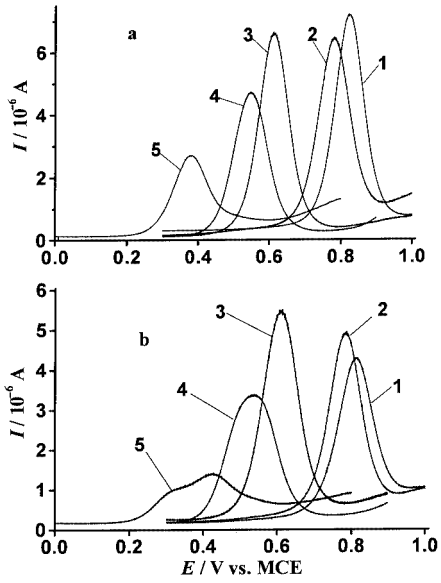

Figure 8. Differential pulse voltammograms of $1.0 \cdot 10^{-3}$ mol·L^{-1} $[Ni(L^1)]^{2+}$ (a) and $5 \cdot 10^{-4}$ mol·L^{-1} $[Ni_2(L^2)]^{4+}$ (b) in 0.1 mol·L^{-1} aqueous solutions of different electrolytes: 1: $NaClO_4$; 2: $NaNO_3$; 3: NaCl; 4: KH_2PO_4; 5: Na_2HPO_4; pulse amplitude 10 mV, potential scan rate 2 mV s^{-1}

The corresponding DPV curves are shown in Figure 9, the potentials are listed in Table 5 (CV curves are given as Supporting Information). The splitting of the redox potential depends on the concentration of the anions and, for a given concentration, it is larger for sulfate than for hydrogen sulfate. The shifts of E_{f1} and E_{f2} are also sensitive to the concentration of the anions. This indicates that sulfate forms adducts of different stability, depending on the nuclearity of the nickel(II) complex. The dependence of the reduction potential of the nickel(III/II) couple on the concentration of the anion X^{n-} is described by Equation (5), where X^{n-} is SO_4^{2-} or HSO_4^-, K_i^{II} and K_i^{III} are the stepwise stability constants of the nickel(II) and nickel(III) complexes with sulfate, and E_f^{aq} is the redox potential in absence of coordinating anions (i.e., in 0.1 mol·L^{-1} aqueous $NaClO_4$). The values of K_i^{II} are relatively small (see above); therefore Equation (5) transforms into Equation (6), where $\Delta E_f = E^X{}_f - E_f^{aq}$.[37]

$$E_f^x = E_f^{aq} - (RT/F) \ln \left(\frac{(1 + \sum_{i=1}^{4} [X^{n-}]^i \prod_{j=1}^{i} K_j^{III})}{(1 + \sum_{i=1}^{4} [X^{n-}]^i \prod_{j=1}^{i} K_j^{II})} \right) \quad (5)$$

$$\exp\{\Delta E_f(-F/RT)\} - 1 = \sum_{i=1}^{4} [X^{n-}]^i \prod_{j=1}^{i} K_j^{III} \quad (6)$$

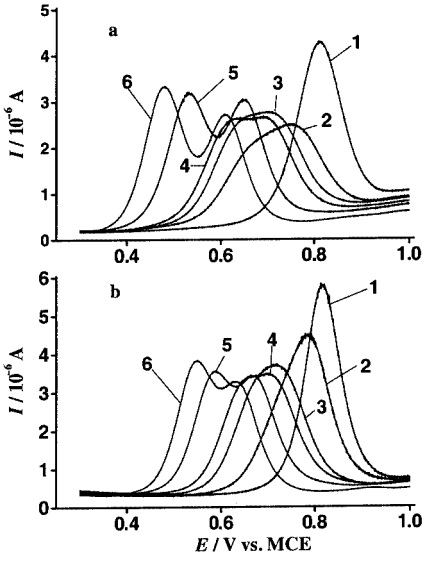

Figure 9. Differential pulse voltammograms of 5.0 10^{-4} mol·L^{-1} $[Ni_2(L^2)]^{4+}$ at various concentrations of Na_2SO_4 (a: pH = 7; 1: 0, 2: 5.0 10^{-4}, 3: 1.0 10^{-3}, 4: 1.5 10^{-3}, 5: 8.7 10^{-3}, 6: 3.3 10^{-2} mol·L^{-1}) and H_2SO_4 (b: pH = 1; 1: 0, 2: 5.0 10^{-4}, 3: 2.4 10^{-3}, 4: 4.6 10^{-3}, 5: 2.5 10^{-2}, 6: 1.0 10^{-1} mol·L^{-1}) (I = 0.1, pulse amplitude 10 mV, potential scan rate 2 mV s^{-1})

Table 5. Parameters of the oxidation of $[Ni_2(L^2)]^{4+}$ in aqueous sulfate solutions

Na_2SO_4 [mol·L^{-1}]	E_{anodic} [V]		$E_{cathodic}$ [V]		E_f [V] (ΔE [mV])	
0.0000	0.855		0.781		0.818 (74)	
0.0005	0.813		0.640		0.727 (173)	
0.0010	0.785		0.605		0.695 (180)	
0.0015	0.755		0.576		0.667 (179)	
0.0024	0.733		0.558		0.646 (175)	
0.0046	0.596	0.708	0.529	0.644	0.563 (67)	0.676 (64)
0.0087	0.573	0.687	0.505	0.619	0.539 (68)	0.653 (68)
0.0153	0.546	0.671	0.482	0.608	0.514 (64)	0.640 (63)
0.0250	0.530	0.658	0.465	0.586	0.498 (65)	0.622 (72)
0.0333	0.519	0.644	0.457	0.573	0.488 (62)	0.609 (71)
H_2SO_4 [mol·L^{-1}]						
0.0000	0.857		0.793		0.825 (64)	
0.0005	0.827		0.732		0.780 (95)	
0.0010	0.803		0.700		0.752 (103)	
0.0015	0.789		0.680		0.735 (109)	
0.0024	0.771		0.658		0.715 (113)	
0.0046	0.751		0.615		0.683 (136)	
0.0087	0.736		0.593		0.665 (143)	
0.0153	0.720		0.569		0.645 (151)	
0.0245	0.619	0.708	0.559	0.648	0.589 (60)	0.678 (60)
0.0630	0.595	0.688	0.535	0.628	0.565 (60)	0.658 (60)
0.1000	0.583	0.668	0.523	0.608	0.553 (60)	0.638 (60)

Plots of E_f^X vs. logC_X, where C_X is the total concentration of SO_4^{2-}, are linear (see Figure 10), and their slopes, divided by 0.059, give the average values of the number of anions coordinated to the metal center involved in the redox transformation (k in Table 6). Interpolation of the dependences of exp{$\Delta E_f(-F/RT)$} vs. C_X, using these values

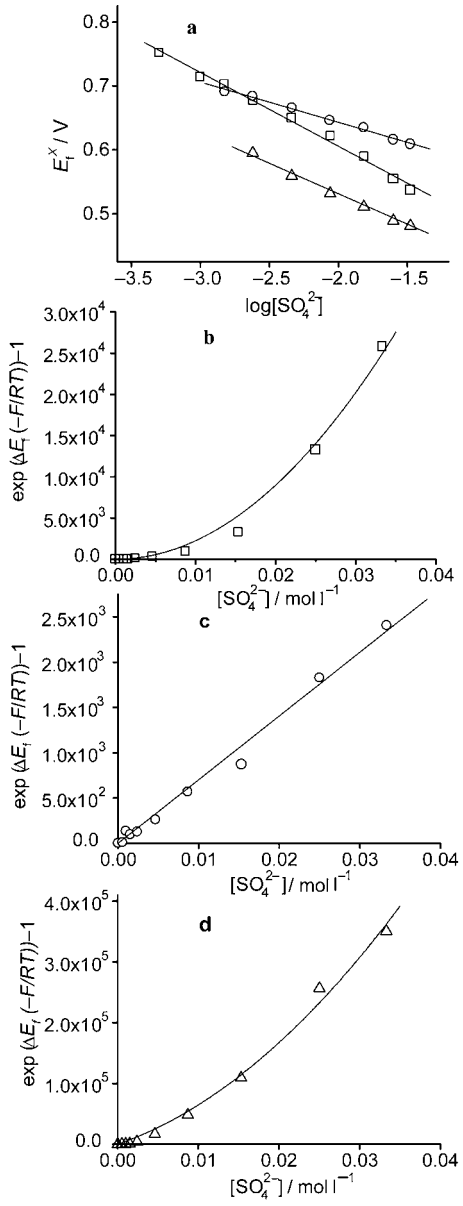

Figure 10. Plots used in the calculations of stoichiometric and thermodynamic parameters for the interaction of sulfate anion with $[Ni(L^1)]^{2+}$ (squares) and those for more anodic (E_{f1}, circles) and less anodic (E_{f2}, triangles) processes observed in $[Ni_2(L^2)]^{4+}$; the curves correspond to best fit lines based on the values presented in Table 6

of k, and assuming that $[SO_4^{2-}] = C_X$ (see Figure 10) allows to obtain values for the corresponding stability constants (see Table 6).

From Table 6 it emerges that the nickel(III) complex with the mono(macrocyclic) ligand forms a bis(sulfate) adduct, although the data analysis did not allow to separate the values of K_1^{III} and K_2^{III}. For $[Ni_2(L^2)]^{6+}$ two separate binding constants for one nickel(III) center (E_{f2}) are observed, the second nickel(III) center (E_{f1}) is coordinated to a single sulfate anion. These results agree well with the model proposed for the explanation of enhanced binding of sulfate to the nickel(II) complex with the bis(macrocyclic) ligand (see electronic spectroscopy, above, Scheme 2). Strong hydrogen

Table 6. Stoichiometric and thermodynamic parameters of the interaction of sulfate with the nickel(III) complexes with the macrocyclic ligands

Anion	$[Ni(L^1)]$	$[Ni_2(L^2)]$ E_{f2}	E_{f1}
SO_4^{2-}	$k = 1.95 \pm 0.01$ $K_1^{III} K_2^{III} = (2.25 \pm 0.02)\cdot10^7$	$k = 1.68 \pm 0.01$ $K_1^{III} = (4.59 \pm 0.02)\cdot10^6$ $K_2^{III} = 41 \pm 10$	$k = 1.06 \pm 0.01$ $K_3^{III} = (7.03 \pm 0.18)\cdot10^4$
HSO_4^-	$k = 1.82 \pm 0.01$ $K_1^{III} = (6.36 \pm 1.05)\cdot10^4$ $K_2^{III} = 28 \pm 10$	$k = 1.83 \pm 0.01$ $K_1^{III} = (2.83 \pm 0.25)\cdot10^5$ $K_2^{III} < 1$	$k = 1.02 \pm 0.01$ $K_3^{III} = (1.19 \pm 0.05)\cdot10^4$

bonding between the coordinated sulfate and an axially coordinated water molecule at the neighboring metal center leads to suppression of the substitution of the remaining water molecule by another sulfate anion. Therefore, one axial coordination site in $[Ni_2(L^2)]^{6+}$ is blocked and two independent reduction processes are observed, one with participation of the bis(sulfate) adduct (E_{f2}) and the other related to the (aqua)(sulfate) complex with the macrocyclic ligand (E_{f1}).

A similar behavior is observed for the nickel complexes in acidic media (pH = 1.0), where hydrogen sulfate is coordinated to the nickel(III) centers (see Table 6). However, the stability constants of the corresponding adducts are significantly lower. This is believed to be due to the smaller charge of the coordinating anion. All constants K_1^{III} for the complexes with the melamine-derived macrocyclic ligands are in the range expected for nickel(III) complexes with tetraaza macrocyclic ligands.[34−36]

Conclusion

The copper(II),[7−9] nickel(II) and nickel(III) complexes of the bis- and tris(macrocyclic) melamine-based ligands are versatile hosts for anionic guest molecules. This is due to the relatively labile coordination to the vacant axial sites, assisted by Jahn−Teller effects [copper(II), nickel(III)] or spin-equilibria [nickel(II)] and to some flexibility in the arrangement of the macrocyclic subunits (*syn-anti* conformations with respect to the melamine rings and relative geometry in the *syn* conformation, angles α, β, γ in Figure 2). In the case of the dinickel(II/III) complexes this leads to an enhanced stability of the coordination of sulfate to one of the axial sites, assisted by the second nickel center. With the di- and trimetal systems [nickel(II), nickel(III), copper(II) and mixed-metal] there is a variety of host systems which, in spite of or due to the limited flexibility are able to selectively bind, activate and/or stabilize anionic guest species.

Experimental Section

Syntheses: ***Caution!*** *Perchlorate salts of metal complexes with organic ligands are potentially explosive and should be handled with care.* $[Ni(2,3,2\text{-tet})](ClO_4)_2$ [2,3,2-tet = bis-*N*,*N*′-(2-aminoethyl)propane-1,3-diamine] was obtained as described,[38] all other AR grade chemicals and solvents were used as received. To a solution of $[Ni(2,3,2\text{-tet})](ClO_4)_2$ (2.0 g, 4.8 mmol) in 15 mL of water were added melamine (1.0 g, 7.9 mmol), triethylamine (5.0 mL, 35.9 mmol) and ethanol (100 mL). The resulting mixture was heated and aqueous formaldehyde (37%, 8.0 mL, 106.7 mmol) was added dropwise over a period of 1 h; refluxing of the solution was continued for an additional 24 h. The mixture was then cooled, and the dark brown precipitate that formed was removed by filtration. The resulting deep brown solution was diluted with water to 2 L and sorbed onto an SP-Sephadex C-25 cation exchange resin (Na^+ form). The column was washed with water (0.5 l) and the products were then eluted with aqueous $NaClO_4$ solutions. Two yellow bands were eluted with 0.2 mol·L^{-1} $NaClO_4$. The first contained unchanged $[Ni(2,3,2\text{-tet})](ClO_4)_2$ and was discarded. With 0.4 mol·L^{-1} $NaClO_4$ a third yellow fraction was obtained. The remaining products were eluted with NaCl or $NaNO_3$ (0.4−0.8 mol·L^{-1}) but did not contain any macrocyclic ligand products.

$[Ni(L^1)](ClO_4)_2\cdot H_2O$ (1): The second yellow band eluted with 0.2 mol·L^{-1} $NaClO_4$ was concentrated under reduced pressure to 25 mL and left cooling to room temperature. Yellow needles of the product were collected, washed with ethanol and dried under vacuum. Yield 0.38 g, 14%. $C_{12}H_{28}Cl_2N_{10}NiO_9$ (586.01): calcd. C 24.60, H 4.82, N 23.90; found C 24.51, H 4.73, N 23.94. Electronic absorption spectrum (H_2O, 0.1 mol·L^{-1} $NaClO_4$): λ_{max} (ε, L mol^{-1} cm^{-1}) = 658 (ca. 2), 455 (23), 330 sh (30), 209 nm (52000). Single crystals of **1**, suitable for X-ray analysis, were selected from the precipitate.

$[Ni(HL^1)](ClO_4)_2Cl\cdot2H_2O$: This complex was obtained with nearly quantitative yield by recrystallization of **1** from 2 mol·L^{-1} HCl. $C_{12}H_{31}Cl_3N_{10}NiO_{10}$ (640.49): calcd. C 22.50, H 4.88, N 21.87; found C 22.45, H 4.83, N 21.67. X-ray quality crystals of $[Ni(HL^1)](ClO_4)_2Cl\cdot H_2O$ (**2**) were obtained by slow concentration of an acidic aqueous solution of **1** containing NaCl.

$[Ni(HL^1)](ClO_4)SO_4\cdot3.5H_2O$: This complex was obtained in nearly quantitative yield by recrystallization of **1** from acidic 1 mol·L^{-1} Na_2SO_4. $C_{12}H_{33}ClN_{10}NiO_{11.5}S$ (627.66): calcd. C 22.96, H 5.30, N 22.32; found calcd. C 23.91, H 5.34, N 22.73. X-ray quality crystals of $[Ni(HL^1)(OSO_3)(OH_2)]_2(ClO_4)_2\cdot5H_2O$ (**3**) were obtained by slow concentration of an acidic solution of **1** containing Na_2SO_4.

$[Ni_2(HL^2)](ClO_4)_5\cdot nH_2O$: The third yellow band which contained the bis(macrocyclic) ligand complex was eluted with 0.4 mol·L^{-1} $NaClO_4$. The volume of the elute was reduced to approximately 25 mL and the hot solution was acidified to pH ≈ 1 with concentrated $HClO_4$ and then cooled. Large orange and small yellow crystals formed were collected, washed with ethanol and dried in air. Total yield: 0.08 g, 1.5%. The crystals were separated manually. Orange complex, $[Ni_2(HL^2)](ClO_4)_5\cdot6H_2O$. $C_{21}H_{59}Cl_5N_{14}Ni_2O_{26}$

Table 7. Crystallographic data for the complexes

	1	**2**	**3**
Empirical formula	$C_{12}H_{28}Cl_2N_{11}NiO_9$	$C_{12}H_{29}Cl_3N_{10}NiO_9$	$C_{12}H_{38}ClN_{10}NiO_{14}S$
Formula mass	586.05	622.51	672.74
Crystal system	monoclinic	triclinic	triclinic
Space group	$P2_1/c$	$P\bar{1}$	$P\bar{1}$
a [Å]	10.8650(14)	8.074(2)	10.9934(6)
b [Å]	8.8691(11)	8.4832(19)	13.6832(7)
c [Å]	23.8863(30)	19.055(4)	18.8799(9)
α [°]	90	93.015(18)	93.9300(10)
β [°]	92.045(3)	93.538(18)	99.8260(10)
γ [°]	90	110.598(18)	96.1030(10)
V [Å^3]	2300.3(5)	1215.5(5)	2771.6(2)
Z	4	2	4
T [K]	190(2)	293(2)	190(2)
$d_{calcd.}$ [g cm^{-3}]	1.692	1.701	1.612
Reflections: measured/unique	13669/4064	3149/2133	46023/16859
$R1$ ($I > 2\sigma$)	0.0536	0.0765	0.0401
$wR2$ (all)	0.1433	0.1843	0.1039
GOF	1.043	1.055	1.027

(1218.42): calcd. C 20.70, H 4.88, N 16.09; found C 20.71, H 4.46, N 15.94. Yellow complex, $[Ni_2(HL^2)](ClO_4)_5\cdot 2H_2O$. $C_{21}H_{51}Cl_5N_{14}Ni_2O_{22}$ (1146.36): calcd. C 22.00, H 4.48, N 17.11; found C 22.06, H 4.65, N 16.78. Recrystallization from nitromethane (diffusion of diethyl ether) of either of these complexes results in the formation of yellow crystals of the composition $[Ni_2(L^2)](ClO_4)_4\cdot 2H_2O$.

$[Ni_2(L^2)](ClO_4)_4\cdot 2H_2O$: $C_{21}H_{50}N_{14}Cl_4Ni_2O_{18}$ (1045.90): calcd. C 24.12, H 4.82, N 18.75; found C 24.05, H 4.77, N 18.63. Electronic absorption spectrum (H_2O, 0.1 mol·L^{-1} $NaClO_4$): λ_{max} (ε, L mol^{-1} cm^{-1}) = 658 (5), 455 (48), 330 (14), 214 nm (62000). Single crystals of $[Ni_2(L^2)](ClO_4)_4\cdot 2H_2O$ (**4**) were grown by vapor diffusion of diethyl ether to a nitromethane solution of $[Ni_2(HL^2)](ClO_4)_5\cdot 2H_2O$.

Crystal Structure Determinations: Reflections of representative crystals were measured with Siemens P4 (**2**) or Bruker AXS SMART 1000 (**1**, **3** and **4**) diffractometers using Mo-K_α radiation (λ = 0.71073 Å) and operating in the ω-scan mode. The structures were solved by direct methods (SHELXS-86) and refined by full-matrix least-squares methods based on F^2 (SHELXL-97),[39] using anisotropic thermal parameters for all non-hydrogen atoms. The crystallographic parameters are given in Table 7. CCDC-172715 (**1**), -172712 (**2**) and -172716 (**3**) contain the supplementary crystallographic data for this paper. These data can be obtained free of charge at www.ccdc.cam.ac.uk/conts/retrieving.html or from the Cambridge Crystallographic Data Centre, 12, Union Road, Cambridge CB2 1EZ, UK [Fax: (internat.) + 44-1223/336-033; E-mail: deposit@ccdc.cam.ac.uk].

Physical Methods: Infrared spectra (KBr pellets) were recorded with a Specord 75 IR (Carl Zeiss) spectrophotometer. Electronic absorption spectra were measured with a Cary1E (Varian) or a Specord M40 (Carl Zeiss) spectrophotometer, equipped with thermostatted cells. The electrochemical experiments (cyclic voltammetry, CV, or differential pulse voltammetry, DPV) were carried out with an Autolab (EcoChemie) system. A standard three-electrode scheme, consisting of a glassy carbon working, a calomel (1 mol·L^{-1} NaCl) reference (MCE) and a Pt plate auxiliary electrode was used. All solutions were purged with argon before measurement. The values of E_f (vs. MCE) for reversible or quasi-reversible redox transformations were calculated as the midpoints between the anodic and cathodic peaks, the distances between peaks (ΔE) were used as parameters for the characterization of the reversibility of the electrochemical transformations (ΔE = 59 mV for thermodynamically reversible process). Analytical data were obtained from the microanalytical laboratory of the chemical institutes of the University of Heidelberg.

Equilibria between Diamagnetic and Paramagnetic Forms: These were measured spectrophotometrically in a thermostatted (± 0.1°) quartz cell (only freshly prepared solutions were used). For aqueous solutions the ionic strength was kept equal at 0.1 mol·L^{-1}; when variable concentrations of sulfate were used the ionic strength was adjusted to 0.1 with $NaClO_4$ and/or $HClO_4$. ε_{ls} = 64 L mol^{-1} cm^{-1} {$[Ni(L^1)]^{2+}$} and 128 L mol^{-1} cm^{-1} {$[Ni_2(L^2)]^{4+}$} were obtained from nitromethane solutions. The ε_{ls} values were obtained from data fitting and Gaussian analyses of the experimental spectra {5 and 9 L·mol^{-1}·cm^{-1} for $[Ni(L^1)]^{2+}$ and $[Ni_2(L^2)]^{4+}$, respectively}. Stability constants for the sulfate adduct formation were calculated by iterative procedures applied to the plots of K_{ax} vs. equilibrium concentrations of sulfate. In a first step the equilibrium concentration of sulfate was assumed to be equal to its total concentration. The values of K^1_{ax} and K^2_{ax} so obtained were then used for the calculation of the equilibrium concentration of sulfate. Iterations were stopped when the difference between two consecutive equilibrium concentrations of the anion was less than $1\cdot 10^{-5}$ mol·L^{-1}.

Acknowledgments

Financial support by the German Science Foundation (DFG), the Committee for Scientific Investigation of Poland and the Foundation of Fundamental Research of the Ministry for Education and Science of the Ukraine are gratefully acknowledged.

[1] A. M. Sargeson, *Coord. Chem. Rev.* **1996**, *151*, 89.
[2] M. P. Suh, *Adv. Inorg. Chem.* **1997**, *44*, 93.
[3] P. Comba, S. M. Luther, O. Maas, H. Pritzkow, A. Vielfort, *Inorg. Chem.* **2001**, *40*, 2335.
[4] R. Bhula, A. P. Arnold, G. J. Gainsford, W. G. Jackson, *Chem. Commun.* **1996**, 143.
[5] O. Costisor, W. Linert, *Rev. Inorg. Chem.* **2000**, *20*, 63.
[6] M. Rossignoli, C. C. Allen, T. W. Hambley, G. A. Lawrance, M. Maeder, *Inorg. Chem.* **1996**, *35*, 4961.

[7] P. V. Bernhardt, E. J. Hayes, *Inorg. Chem.* **1998**, *37*, 4214.
[8] P. V. Bernhardt, E. J. Hayes, *J. Chem. Soc., Dalton Trans.* **1998**, 3539.
[9] P. Comba, Y. D. Lampeka, A. Y. Nazarenko, A. I. Prikhod'ko, H. Pritzkow, *Eur. J. Inorg. Chem.,* in press.
[10] P. Comba, Y. D. Lampeka, L. Lötzberger, A. I. Prikhod'ko, manuscript in preparation.
[11] J.-M. Lehn, *Supramolecular Chemistry: Concepts and Perspectives*, VCH, New York − Weinheim − Basel, **1995**.
[12] D. J. Cram, J. M. Cram, *Container Molecules and Their Guests*, Royal Society of Chemistry, Cambridge, **1994**.
[13] A. Müller, P. Kögerler, *Coord. Chem. Rev.* **1999**, *182*, 3.
[14] D. L. Caulder, K. N. Raymond, *Acc. Chem. Res.* **1999**, *32*, 975.
[15] L. F. Lindoy, I. M. Atkinson, *Self-Assembly in Supramolecular Systems in Monographs in Supramolecular Chemistry*, (Ed.: J. F. Stoddard), Royal Society of Chemistry, Cambridge, **2000**.
[16] E. V. Rybak-Akimova, *Rev. Inorg. Chem.* **2001**, *21*, 207.
[17] S. Aoki, M. Shiro, T. Koike, E. Kimura, *J. Am. Chem. Soc.* **2000**, *122*, 576.
[18] H.-K. Liu, W.-Y. Sun, D.-S. Ma, K.-B. Yu, W.-X. Tang, *Chem. Commun.* **2000**, 591.
[19] M. Ziegler, J. L. Brumaghim, K. N. Raymond, *Angew. Chem. Int. Ed.* **2000**, *112*, 4285.
[20] P. V. Bernhardt, *Inorg. Chem.* **1999**, *38*, 3481.
[21] B. Bosnich, C. K. Poon, M. L. Tobe, *Inorg. Chem.* **1965**, *4*, 1102.
[22] J. C. A. Boeyens, S. M. Dobson, in *Stereochemical and Stereophysical Behaviour of Macrocyclesed*, (Ed.: I. Bernal), Elsevier, Amsterdam, New York, **1987**.
[23] M. Scoponi, E. Polo, F. Pradella, V. Bertolasi, V. Carassiti, P. Goberti, *J. Chem. Soc., Perkin Trans. 2* **1992**, 1127.
[24] P. Comba, T. W. Hambley, N. Okon, G. Lauer, *MOMEC97, a molecular modeling package for inorganic compounds*, CVS Heidelberg, **1997**.
[25] A. B. P. Lever, *Inorganic Electronic Spectroscopy*, 2nd ed., Elsevier Science Publisher, Amsterdam, Oxford, New York, Tokyo, **1984**.
[26] A. Anichini, L. Fabbrizzi, P. Paoletti, R. M. Clay, *Inorg. Chim. Acta* **1977**, *24*, L21.
[27] L. Fabbrizzi, *Inorg. Chim. Acta* **1979**, *36*, L391.
[28] L. V. Tsymbal, S. V. Rosokha, Y. D. Lampeka, *J. Chem. Soc., Dalton Trans.* **1995**, 2633.
[29] L. Sabatini, L. Fabbrizzi, *Inorg. Chem.* **1979**, *18*, 438.
[30] W. G. Jackson, M. L. Hookey, M. L. Randall, P. Comba, A. M. Sargeson, *Inorg. Chem.* **1984**, *23*, 2473.
[31] P. Comba, Y. D. Lampeka, A. I. Prikhod'ko, H. Pritzkow, *Theor. Exper. Chem.* **2001**, *37*, 236
[32] P. S. Pallavicini, A. Perotti, A. Poggi, B. Seghi, L. Fabbrizzi, *J. Am. Chem. Soc.* **1987**, *109*, 5139.
[33] I. M. Maloshtan, PhD Thesis, L. V. Pisarzhevsky, Institute of Physikal Chemistry, Kiev, **1998**.
[34] E. Zeigerson, I. Bar, J. Bernstein, L. J. Kirschenbaum, D. Meyerstein, *Inorg. Chem.* **1982**, *21*, 73.
[35] J. Taraszewska, G. Roslonek, *Supramol. Chem.* **1997**, *8*, 369.
[36] I. Zilbermann, A. Meshulam, H. Cohen, D. Meyerstein, *Inorg. Chim. Acta* **1993**, *206*, 127.
[37] K. V. Gobi, T. Ohsaka, *Electrochim. Acta* **1998**, *44*, 269.
[38] I. M. Maloshtan, S. V. Rosokha, Y. D. Lampeka, *Russ. J. Inorg. Chem.* **1994**, *39*, 759.
[39] G. M. Sheldrick, *SHELXTL 5.1*, Bruker AXS, Madison, WI, **1998**.
[40] C. K. Johnson, *ORTEP, A Thermal Ellipsoid Plotting Program*, Oak National Laboratories, TN, **1965**.

Received March 5, 2002
[I02119]

Novel Ferrocene Derivatives with PH-Functionalized Phosphanylalkylcyclopentadienyl Ligands: Syntheses and Molecular Structures of *rac*-[Fe{(η^5-C_5H_4)CMe_2PHR}$_2$] (R = Ph, Mes) and *rac*-[Fe{(η^5-C_5H_4)$CMe_2PHPh(Cp^*TaCl_4)$}$_2$]

Thomas Höcher, Steffen Blaurock, and Evamarie Hey-Hawkins*

Eur. J. Inorg. Chem. **2002**, 1174−1180

In the Introduction of the article the following reference to a review was inadvertently omitted:

H. Butenschön, *Chem. Rev.* **2000**, *100*, 1537−1564.

E. Hey-Hawkins
[I01420 C]

 © WILEY-VCH Verlag GmbH, 69451 Weinheim, Germany, 2002 1434−1948/02/0707−1883 $ 17.50+.50/0

EurJIC
European Journal of Inorganic Chemistry

August 2002
Issue 8
Pages 1885–2222

COVER PICTURE

The cover picture shows the pH-dependent coordination chemistry of the potentially ambidentate ligand 2,2′-bipyridine-3,3′-diamine. A dimeric 2:2 complex is formed with copper(II) chloride in which each copper ion is bound to two pyridine nitrogen atoms and two chloride ions in a distorted square-planar arrangement, with a long axial contact from a neighbouring amino group completing a distorted square-pyramidal geometry. Under acidic conditions, both pyridine nitrogen atoms are protonated preventing coordination to the copper(II) ion and as a consequence, the two amino groups together with four chloride ions are bound to the metal ion completing an octahedral coordination sphere. Details are discussed in the article by J. D. Wallis, M. Pilkington et al. on p. 1985ff.

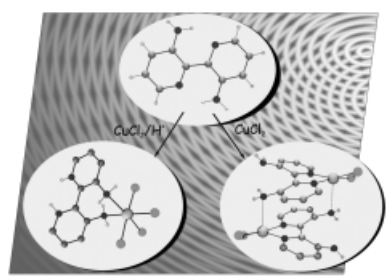

MICROREVIEW

Contents

1907 **T. J. Geldbach, P. S. Pregosin***

η^1 to η^6 Ru–Arene π Complexation: New Bonding Modes and P–C Bond Cleavage Chemistry

Keywords: P–C bond cleavage / π complexes / Unusual bonding / Stereospecific migration

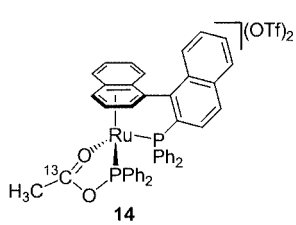

14

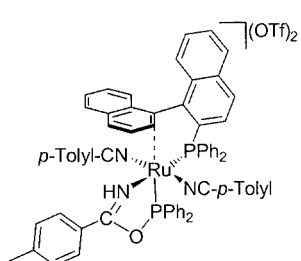

29

 © WILEY-VCH Verlag GmbH, 69451 Weinheim, Germany, 2002 1434–1948/02/0808–1889 $ 20.00+.50/0

SHORT COMMUNICATIONS

1919 **P. Klüfers,* O. Krotz, M. Oßberger**

Oxorhenium(V) Complexes of Carbohydrate Ligands

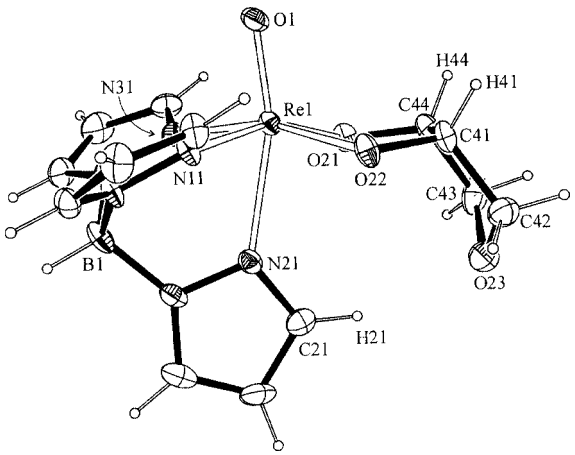

Keywords: Rhenium / Carbohydrates / Oxo ligands

1924 **E. Sondaz, J. Jaud, J.-P. Launay, J. Bonvoisin***

X-ray Structure of a Ruthenium Dinuclear Complex Incorporating 4,4′-Bis(cyanamidophenylethynyl)benzene as a Ligand, a Conjugated Bridge Two Nanometers in Length

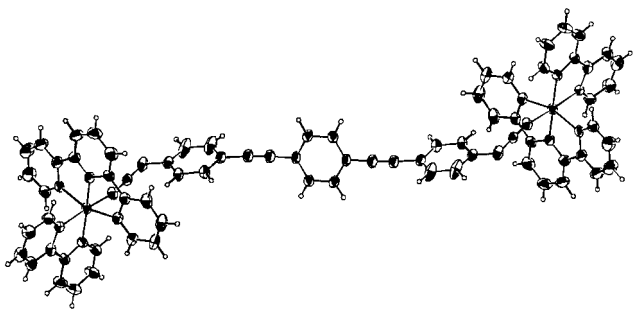

Keywords: Ruthenium / Bridging ligands / N ligands / X-ray structure

1928 **I. Turel,* M. Pečanac, A. Golobič, E. Alessio, B. Serli**

Novel Ru^{III}-DMSO Complexes of the Antiherpes Drug Acyclovir

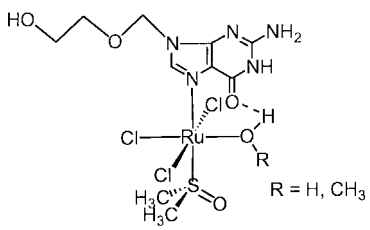

Keywords: Bioinorganic chemistry / Nucleoside analogues / Ruthenium / X-ray diffraction / Hydrogen bonds

1932 **W. Ponikwar, P. Mayer, W. Beck***

Coordinatively and Electronically Unsaturated Pentamethylcyclopentadienyliridium(III) Complexes with the Dianions of Biuret, of the Diamide of Malonic Acid and of an *N*-Acetyldipeptide Ester

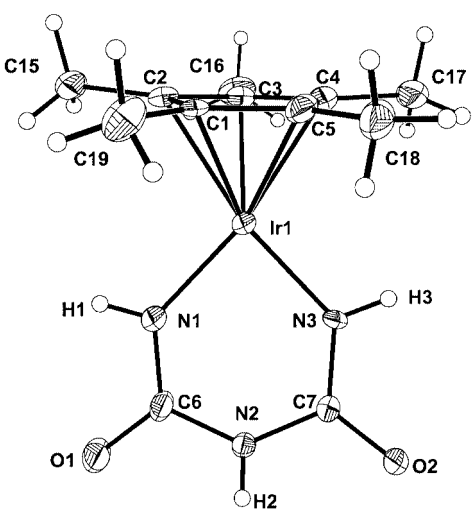

Keywords: Cyclopentadienyl ligands / Iridium / Biuret / Electron-deficient compounds

1937 **L.-H. Yin, W.-H. Gu, P. Cheng,* L. Z. Zhang, D.-Z. Liao,* J. Li, X.-L. Yang, X.-Q. Fu, S.-P. Yan, Z.-H. Jiang**

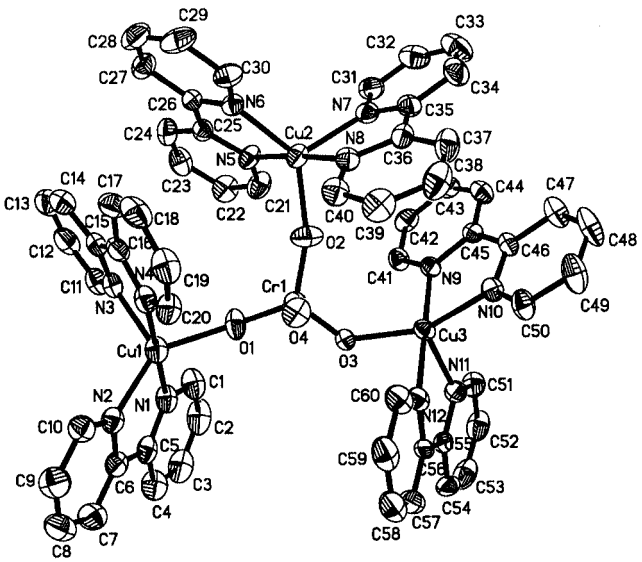

The First Tetranuclear Complex with a (μ-CrO_4-*O*,*O*′,*O*″) Bridge: Crystal Structure and Ferromagnetic Behavior of [{$Cu(bpy)_2$}$_3$(μ-CrO_4)]-(ClO_4)$_4$·H_2O

Keywords: Structure elucidation / Magnetic properties / Bridging ligands / Chromium / N,O ligands

1941 **N. Raffard-Pons Y Moll, F. Banse,* K. Miki, M. Nierlich, J.-J. Girerd***

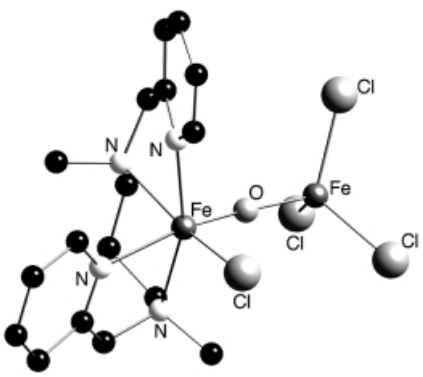

Hydroxylation of Hexane Using Dioxygen and Trimethylhydroquinone: Biomimetic Catalysis by an Unsymmetrical Diiron-μ-Oxo Complex

Keywords: Bioinorganic chemistry / Iron / Dioxygen activation / Biomimetic catalysis / N ligands

1945 **J. Y. Lu,* V. Schauss**

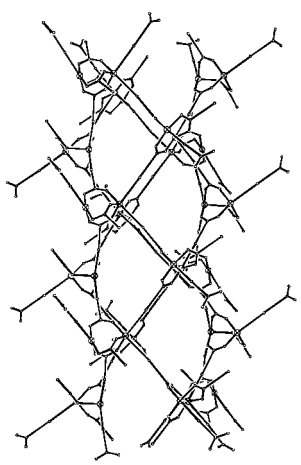

A Novel Nanostructured Open-Channel Coordination Polymer with an Included Fused-Polyiodide Ring

Keywords: Nanostructures / Hydrothermal synthesis / Copper / Iodine

1948 **A. Dumitrescu, B. Martin-Vaca, H. Gornitzka, J.-B. Cazaux, D. Bourissou,* G. Bertrand***

Zinc(II), Samarium(III) and Tin(II) Complexes Featuring a Tridentate Nitrogen Donor for the Ring-Opening Copolymerization of (D,L)-Lactide and Glycolide

Keywords: N ligands / Zinc / Samarium / Ring-opening polymerization / Copolymerization

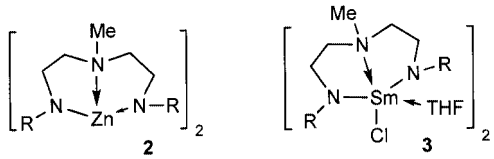

FULL PAPERS

1953 **A. Dumitrescu, H. Gornitzka, W. W. Schoeller, D. Bourissou, G. Bertrand***

A Crystalline Phosphenium Salt Featuring the Electron-Withdrawing 2,6-Bis(trifluoromethyl)-phenyl Group

Keywords: Electron-deficient compounds / Carbenoids / Phosphorus / Fluorine

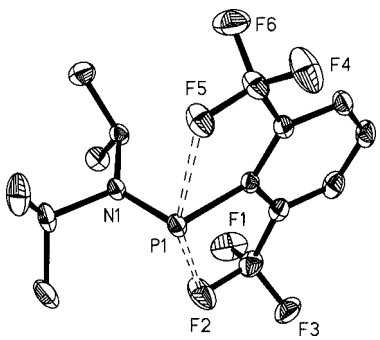

1957 **D. Herebian, P. Ghosh, H. Chun, E. Bothe, T. Weyhermüller, K. Wieghardt***

Cobalt(II)/(III) Complexes Containing *o*-Iminothiobenzosemiquinonato(1−) and *o*-Iminobenzosemiquinonato(1−) π-Radical Ligands

Keywords: Cobalt / Electrochemistry / EPR spectroscopy / N ligands / Radicals / S ligands

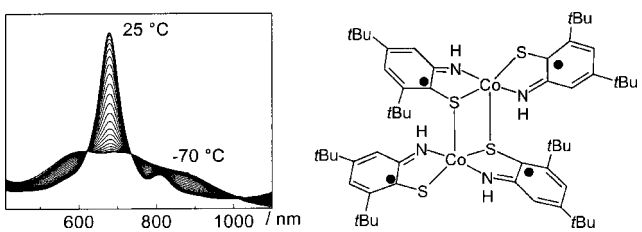

1968 **M. Lutz, C. Galka, M. Haukka, T. A. Pakkanen,* L. H. Gade***

Intramolecular Lithium Cation Solvation in the "Active Ligand Periphery" of a Tripodal Triaminostannate

Keywords: Tin / Lithium / N ligands / Metal-metal interactions / Rhodium

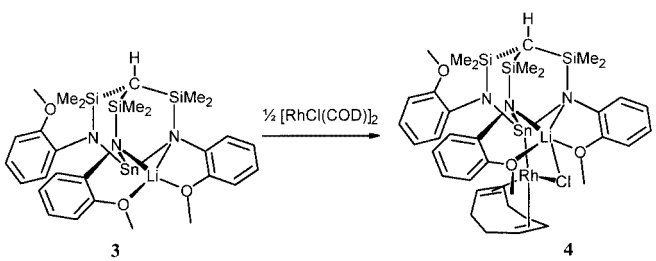

1975 **R. J. Baker, P. C. Davies, P. G. Edwards,* R. D. Farley, S. S. Liyanage, D. M. Murphy, B. Yong**

Early Transition Metal Complexes of Triphosphorus Macrocycles

Keywords: Macrocyclic ligands / P ligands / Titanium / Vanadium / Chromium

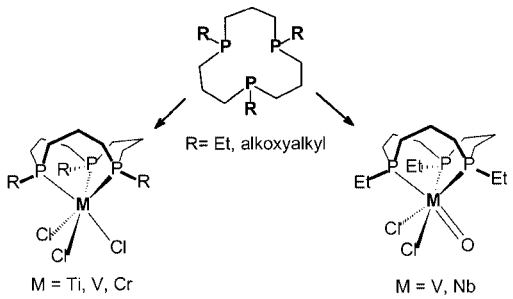

1985 **C. R. Rice, S. Onions, N. Vidal, J. D. Wallis,* M.-C. Senna, M. Pilkington,* H. Stoeckli-Evans**

The Coordination Chemistry of 3,3′-Diamino-2,2′-bipyridine and Its Dication: Exploring the Role of the Amino Groups by X-ray Crystallography

Keywords: N ligands / Hydrogen bonds / Ambidentate ligands / X-ray Crystallography / Cations

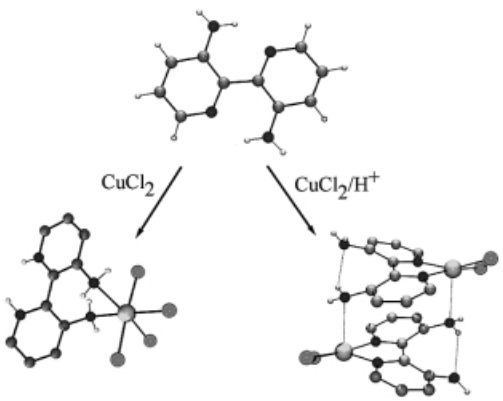

1998 **E. Lindner,* T. Salesch, S. Brugger, S. Steinbrecher, E. Plies, M. Seiler, H. Bertagnolli, H. A. Mayer**

Accessibility Studies of Sol-Gel Processed Phosphane-Substituted Iridium(I) Complexes in the Interphase

Keywords: Iridium / Immobilization / Sol-gel processes / Accessibility studies / NMR spectroscopy

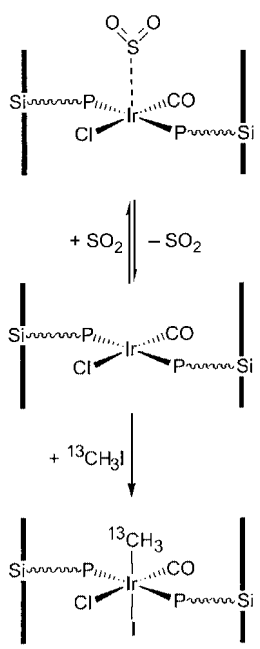

2007 **O. Sénèque, M. Campion, B. Douziech, M. Giorgi, E. Rivière, Y. Journaux, Y. Le Mest,* O. Reinaud***

Supramolecular Assembly with Calix[6]arene and Copper Ions − Formation of a Novel Tetranuclear Core Exhibiting Unusual Redox Properties and Catecholase Activity

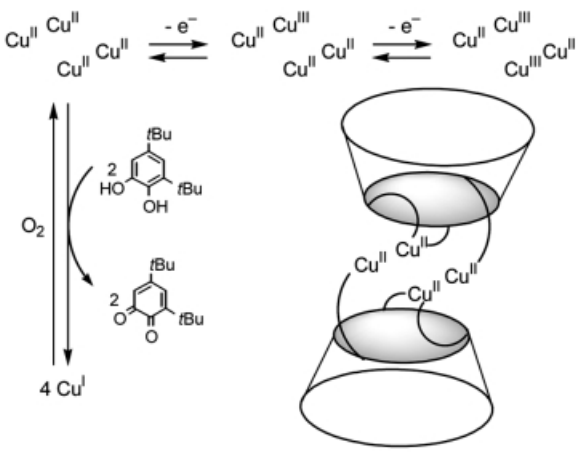

Keywords: Copper / N Ligands / Calixarenes / Bioinorganic chemistry / Electrochemistry

2015 **D. Vagedes, G. Kehr, D. König, K. Wedeking, R. Fröhlich, G. Erker,* C. Mück-Lichtenfeld, S. Grimme**

Formation of Isomeric BAr_3 Adducts of 2-Lithio-*N*-methylimidazole

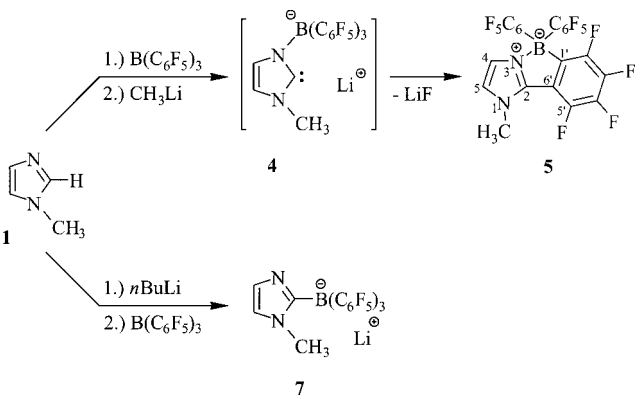

Keywords: Boranes / Carbenes / Density functional calculations / Lithium / Nucleophilic substitution

2022 **M. Rombach, H. Vahrenkamp***

Molecular Mercury Zinc Sulfides

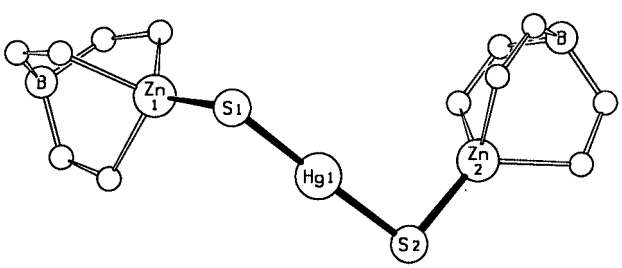

Keywords: Mercury / Zinc / S ligands / Tripod ligands

2026 **F. Guyon,* I. V. Jourdain, M. Knorr, D. Lucas, T. Monzon, Y. Mugnier, N. Avarvari, M. Fourmigué**

Synthesis of μ-$C_2S_4^{4-}$ Cobalt Complexes by Activation of the 1,3,4,6-tetrathiapentalene-2,5-dione, and Electrochemical Study of $[(Cp^*Co)_2(\mu\text{-}C_2S_4)]$

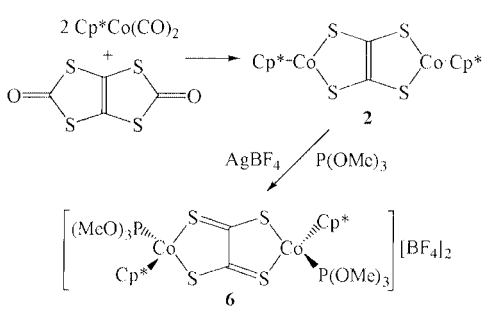

Keywords: Cobalt / S ligands / Cyclopentadienyl ligands / Electrochemistry

2034 **A. Moores, N. Mézailles, N. Maigrot, L. Ricard, F. Mathey,* P. le Floch***

Synthesis and Reactivity Towards Cationic Group 11 Metal Centers of an Extended Sila-calix-[3]-phosphinine Macrocycle

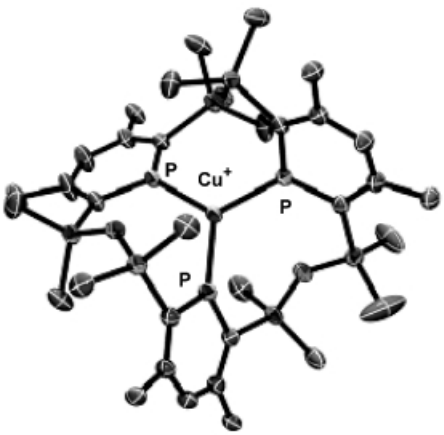

Keywords: Copper / Gold / Phosphinines / Macrocycles / Silver

2040 **J. Classen, R. Gleiter,* F. Rominger**

Oligoalkyne-Bridged (η^4-Cyclobutadiene)(η^5-cyclopentadienyl)cobalt Fragments − Syntheses and Properties

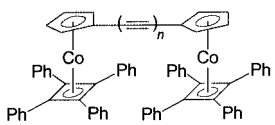

n = 2, 4, 6

Keywords: Alkynes / Conjugation / Electron transfer / Rod-like molecules / Cobalt

2047 **S. K. Mandal, G. A. N. Gowda, S. S. Krishnamurthy,* C. Zheng, S. Li, N. S. Hosmane**

Allylpalladium Complexes of Mixed-Donor Diphosphazane Ligands Bearing a Stereogenic Phosphorus Centre: Structure and Stereodynamics

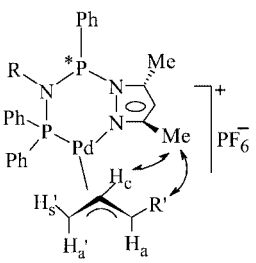

endo, syn, trans

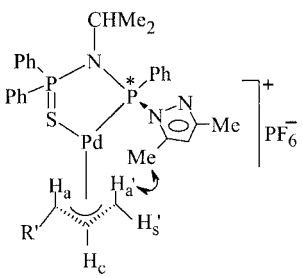

exo, syn, trans

Keywords: Allyl complexes / P ligands / Palladium / N ligands

2057 **M. González-Maupoey, G. M. Rodríguez, T. Cuenca***

μ-Imido, μ-(η^2,η^2-N,N-Hydrazido) and μ-(η^1-C:η^2-C,N-Isocyanido) Dinuclear (Fulvalene)zirconium Derivatives

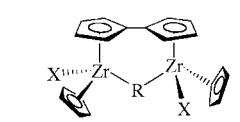

R = bis(imido), η^2,η^2-N,N-hydrazido, η^1-C:η^2-C,N-isocyanido

Keywords: Zirconium / Fulvalene ligands / Imido ligands / Hydrazido ligands / Isocyanido

2064 **A. Eckert, H. Pritzkow, W. Siebert***

Synthesis and Structure of Diboraporphyrinogenes

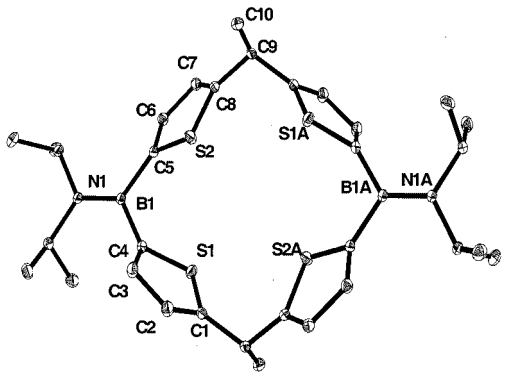

Keywords: Boranes / Boraporphyrinogenes / Porphyrins / Macrocycles

2069 **M. J. Bayer, H. Pritzkow, W. Siebert***

Synthesis, Structures, and Donor−Acceptor Adducts of Tris(3,3-dimethyl-1-butynyl)borane

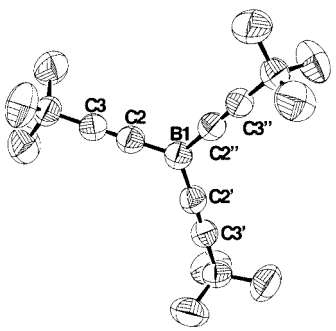

Keywords: Alkynes / Tris(alkynyl)boranes / Donors / Boron

2073 **H. Fleischer,* Y. Dienes, D. Schollmeyer**

Tellurium(IV) Tetraalkoxides and Chlorotellurium(IV) Alkoxides Derived from β-Donor Alcohols

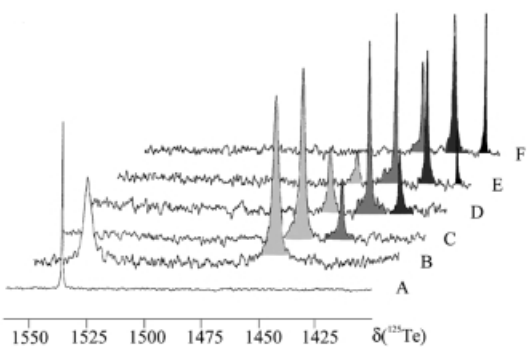

Keywords: Tellurium / Donor-acceptor systems / Ab initio calculations / X-ray diffraction / NMR spectroscopy

2082 **R.-H. Wang, M.-C. Hong,* J.-H. Luo, R. Cao,* J.-B. Weng**

Synthesis and Crystal Structures of the First Two Novel Dicarboxylate Organotin Polymers Constructed from Dimeric Tetraorganodistannoxane Units

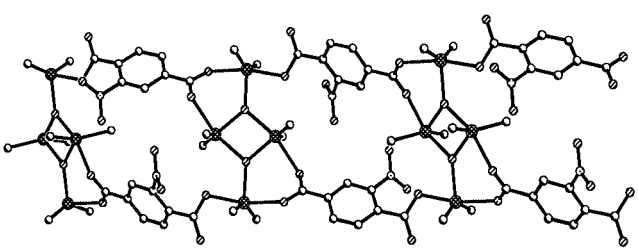

Keywords: Carboxylate ligands / Tin / X-ray diffraction / Polymers

2086 **F. Bachechi, A. Burini,* R. Galassi, B. R. Pietroni, D. Tesei**

A Single-Strand Helical Motif Induced by Self-Assembly of $[Ag(TFP)]^+$ Moieties with Nitrate Anions – ^{31}P NMR Spectroscopic and X-ray Crystal Structure Characterization of the Complexes Involved in Equilibrium Reactions of Silver Salts and TFP Ligand

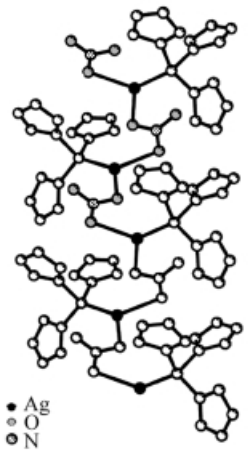

Keywords: P ligands / Silver / Helical structures / NMR spectroscopy / Equilibrium reactions

2094 **L. Gutierrez, G. Alzuet, J. A. Real, J. Cano, J. Borrás,* A. Castiñeiras**

Strong Ferromagnetic Coupling in Linear Mixed μ-Acetato, μ-Hydroxo Trinuclear Copper(II) Complexes with *N*-sulfonamide derivatives – Synthesis, Structure, EPR and Magnetic Properties

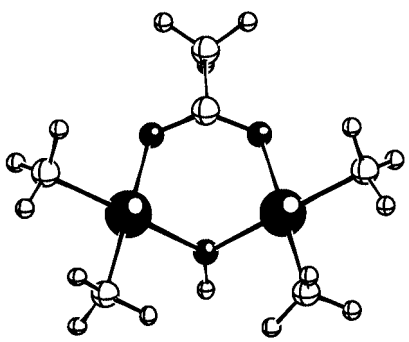

Keywords: Copper / Sulfonamide ligands / Magnetic properties / EPR spectroscopy / Density functional calculations

2103 **W.-Y. Wong,* F.-L. Ting, W.-L. Lam**

Reactivity of $[Ru_2(CO)_6(\mu\text{-}PFu_2)(\mu\text{-}\eta^1,\eta^2\text{-}Fu)]$ (Fu = 2-furyl) towards Diphosphanes – Substitution, Polymerisation, Cyclometallation and Elimination Reactions

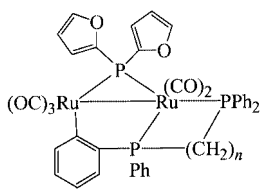

$n = 2, 3$

Keywords: Ruthenium / Phosphane ligands / Phosphido complexes

2112 **W.-Y. Wong,* K.-H. Choi, Z. Lin**

Syntheses, Structures and Photophysical Properties of Metal Carbonyl Clusters with Dansyl and Acridone Luminophores

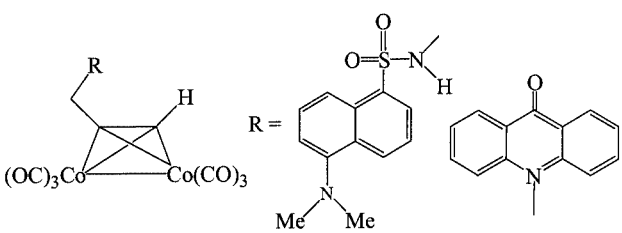

Keywords: Transition metal / Dansyl group / Acridone / Luminophores

2121

M. Allegrozzi, I. Bertini,* S.-N. Choi, Y.-M. Lee, C. Luchinat

Detecting Small Structural Changes in Metalloproteins by the Use of NMR Pseudocontact Shifts

Keywords: Metalloproteins / Pseudocontact shifts / Lanthanides / Protein structures / Temperature-dependence / Magnetic susceptibility

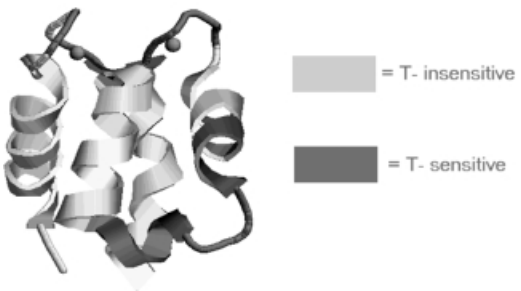

2128

M. Cindrić,* V. Vrdoljak, N. Strukan, P. Tepeš, P. Novak, A. Brbot-Šaranović, G. Giester, B. Kamenar

New Dinuclear Molybdenum(V) Complexes With β′-Hydroxy-β-enaminones Containing a 4-Hydroxy-2-pyrone Ring

Keywords: Amine ligands / Molybdenum / Nitrogen heterocycles

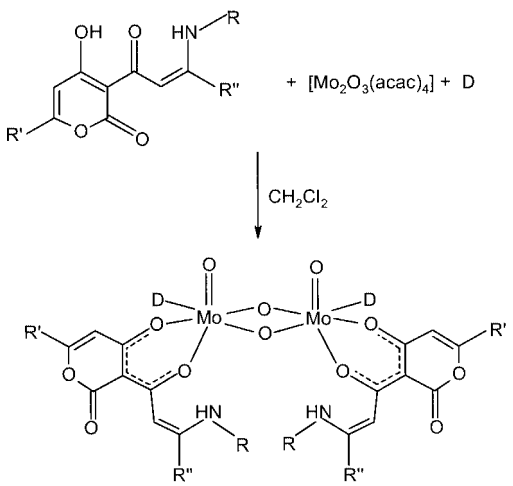

2138

D. Sellmann,* R. Prakash, F. Geipel, F. W. Heinemann

Highly Soluble Sulfur-Rich [Ni(L)($^{si}S_3$)] Complexes Containing the New Ligand Bis(2-mercapto-3-trimethylsilylphenyl) Sulfide(2−) ($^{si}S_3^{2-}$)

Keywords: Nickel / S ligands / Silicon / Hydrazine / Nicotinamide

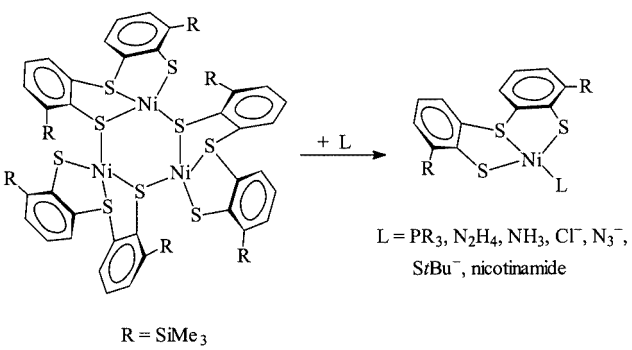

2147

R. C. van der Drift, J. W. Sprengers, E. Bouwman,* W. P. Mul, H. Kooijman, A. L. Spek, E. Drent

Ruthenium-Catalyzed Isomerization of Allylic Alcohols: Oxidation State Determines Resistance Against Diene Inhibition

Keywords: Isomerization / Allylic alcohols / Homogeneous catalysis / Ruthenium / Diene inhibition

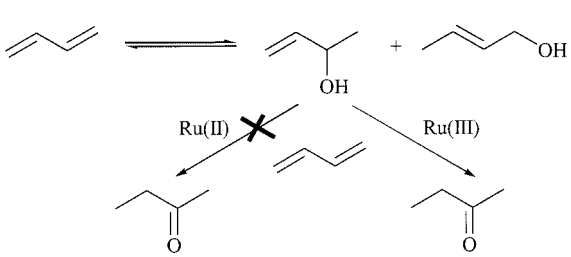

2156 **J. Prust, H. Hohmeister, A. Stasch, H. W. Roesky,* J. Magull, E. Alexopoulos, I. Usón, H.-G. Schmidt, M. Noltemeyer**

Synthesis and Structural Characterization of β-Diketoiminate Complexes Containing Three-Coordinate Zinc and Copper Atoms

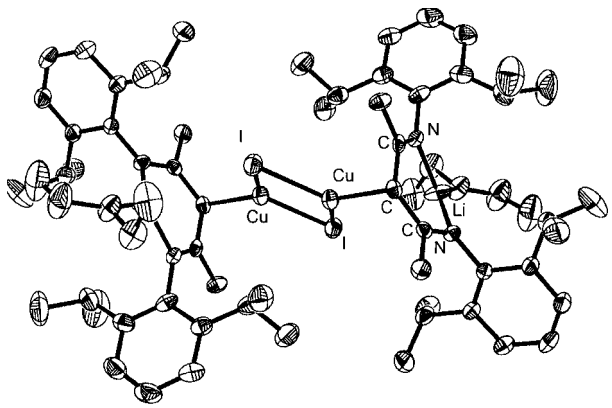

Keywords: Acetylides / Copper / N ligands / Zinc

2163 **V. G. Makhankova, O. Y. Vassilyeva,* V. N. Kokozay, J. Reedijk, G. A. van Albada, J. Jezierska, B. W. Skelton**

Formation, Structures, and Magnetic and EPR Spectroscopic Properties of Dicobalt(III)-Dicopper(II) Complexes Featuring Heterotetranuclear Cations of a Puckered Cyclic Structure with Diethanolamine and Diethanolamine(2−) as Bridging Ligands

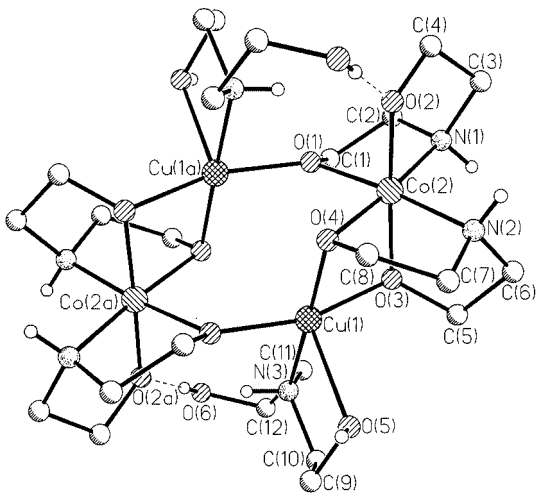

Keywords: Heterometallic complexes / Copper / Cobalt / Amino alcohols / EPR spectroscopy

2170 **Q. Liu, J. Lin, P. Jiang, J. Zhang, L. Zhu, Z. Guo***

Monitoring the Reactions of the Anticancer Drug Carboplatin with the Chemopreventive Agent Selenomethionine by Electrospray Mass Spectrometry and [^{1}H,^{15}N] HSQC NMR Spectroscopy

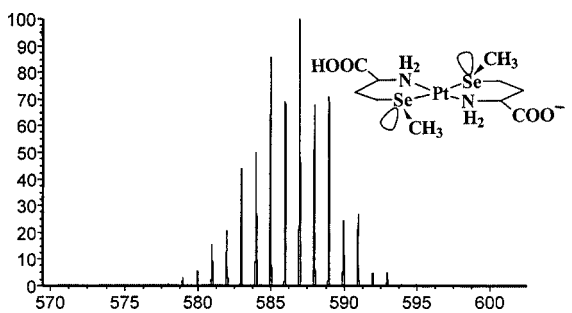

Keywords: Antitumor agents / Platinum / L-Selenomethionine / Mass spectrometry / NMR spectroscopy

2179 **A. Bacchi, M. Carcelli, C. Pelizzi, G. Pelizzi, P. Pelagatti,* S. Ugolotti**

Potentially Tridentate Ligands in the Synthesis of Methyl- and Acetylpalladium(II) Complexes

Keywords: Carbonylation / Insertion / N ligands / Palladium / Tridentate ligands

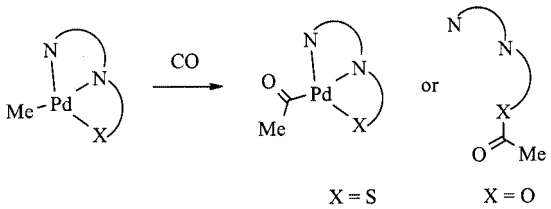

2188 **M. Aresta,* A. Dibenedetto, E. Amodio, I. Tommasi**

Oxidative Addition of Benzyliminium Tetraphenylborate to Pd(dba)(dppe): Synthesis and Catalytic Activity of [(dppe)Pd(dba){η^1(*N*)-$PhCH_2N{=}CMe_2$}]$(BPh_4)_2$

Keywords: Methyl acrylate / Dimerization / Styrene–methyl acrylate coupling / Palladium

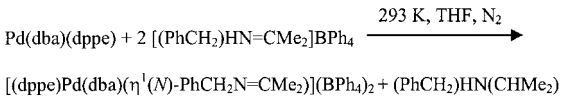

2194 **C. Comuzzi,* A. Melchior, P. Polese, R. Portanova, M. Tolazzi***

Cobalt(II) Complexes with Nitrogen Donors and Their Dioxygen Affinity in Dimethyl Sulfoxide

Keywords: Cobalt / Amine ligands / Thermodynamics / Solvent effects / Oxygen

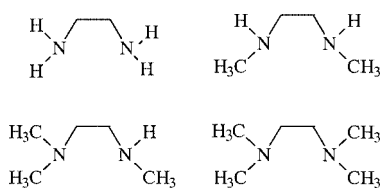

2202 **W. Schuh, H. Kopacka, K. Wurst, P. Peringer***

Homochiral Self Recognition in Gold-Phosphane-Helicates

Keywords: Self-assembly / Helical structures / Gold / X-ray diffraction / Aurophilicity

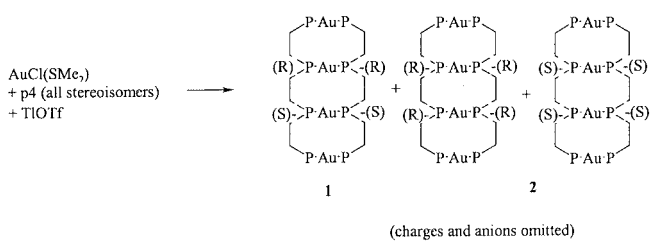

2207 **M. Dey, C. P. Rao,* P. Saarenketo, K. Rissanen, E. Kolehmainen**

Four-, Five- and Six-Coordinated Zn^{II} Complexes of OH-Containing Ligands: Syntheses, Structure and Reactivity

Keywords: N,O ligands / X-ray diffraction / Hydrogen bonds / Metalloenzymes / Zinc

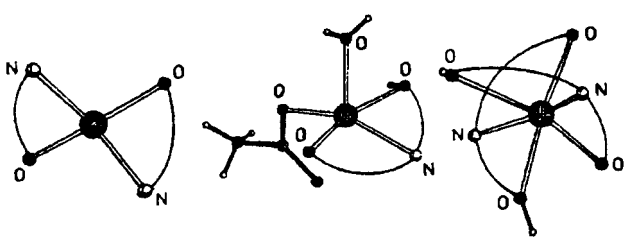

2216 **P. Aslanidis,* P. J. Cox, P. Karagiannidis, S. K. Hadjikakou, C. D. Antoniadis**

Copper(I) Halide Complexes with Triphenylphosphane and Heterocyclic Thione Ligands: The Crystal Structures of [Bis(Triphenylphosphane)(Benzimidazole-2-Thione)Copper(I) Iodide], [Bis(Triphenylphosphane)(Benzothiazole-2-Thione)Copper(I) Iodide], and Bis[μ-*S*-(Benzimidazole-2-Thione)(Triphenylphosphane)-Copper(I) Chloride]

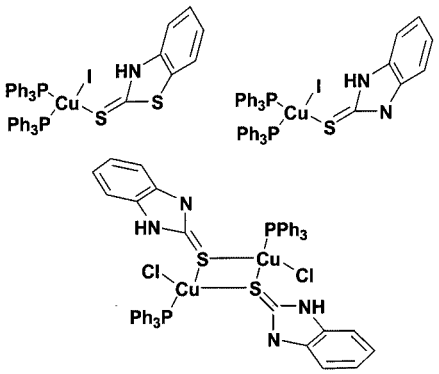

Keywords: Copper / Sulfur heterocycles / Phosphane ligands

RECRUITMENT

GROUP LEADER POSITIONS AT THE NEW INSTITUTE OF CHEMICAL RESEARCH OF CATALONIA (ICIQ)

AREAS: Homogeneous Catalysis Heterogeneous Catalysis Molecular Recognition Molecular Devices Mechanistic Organometallic Chemistry Theoretical Organometallic Chemistry

The Institute of Chemical Research of Catalonia (ICIQ), financially supported by the autonomous government of Catalonia (Generalitat de Catalunya) and sponsored by a group of chemical/petrochemical companies, has been recently created with the mission of contributting to a significant improvement of the scientific level of chemical research and of strengthening, by means of innovation and technological upgrade, competitiveness of the chemical and pharmaceutical industries in Catalonia (Spain).

Located in the town of Tarragona, 100 km south from Barcelona, nearby one of the most important chemical/petrochemical complexes in Southern Europe, the Institute will be based on a 7000 square meter building now under construction at the scientific campus of the Universitat Rovira i Virgili (URV) and will constitute, together with the Faculty of Chemistry and the School of Chemical Engineering of the URV, the nucleus of the Tarragona Research Cluster. The Institute will be equipped with highly functional laboratories and state-of-the-art scientific instruments. Research at ICIQ will be in the areas of Catalysis and Supramolecular Chemistry, with special focus on sustainable aspects of chemistry and on molecular nanotechnology. A combined theoretical/experimental approach will be followed, and dynamic collaborations for multidisciplinary approaches to relevant scientific/industrial problems will be favored.

For the start-up of research activities, planned for the 4th quarter of 2003, positions are available at ICIQ at the levels of Senior Group Leader and Junior Group Leader. The successful candidates will be responsible of leading and developing a research group of up to 16 people (Sr. group leader) or up to 8 people (Jr. group leader). Besides performing high-quality research, they should have a positive attitude towards the implication in multidisciplinary projects and in the solution of industrially relevant problems.

If you have built-up a scientific career with outstanding achievements in one of the following areas: Homogeneous Catalysis, Heterogeneous Catalysis, Molecular Recognition, Molecular Devices, Mechanistic Organometallic Chemistry, Theoretical Organometallic Chemistry

and you feel attracted by the possibility of participating in the ICIQ project from the early beginning, please submit a letter of application accompanied by a CV, a description of previous accomplishments (up to 5 pages), a brief plan of the research you would like to develop at ICIQ (up to 5 pages), and the names and contact addresses of three or more scientists willing to act as reference persons, to:

Miquel A. Pericàs, Director
Institut Català d'Investigació Química
Pg. Lluís Companys, 23
08028 Barcelona (Spain)
e-mail: mapericas@fcr.es

In addition, an electronic version of the above documents should be attached to a cover message e-mailed to: **positions@iciq.es** All the information relative to applicants will be treated confidentially. Only applications received before October 31st, 2002 will be considered, and pre-selected candidates will be notified before the end of 2002.

ICIQ
Institut Català d'Investigació Química

Young brilliant researchers now in post-doc: Tenure track positions to be announced soon.
Visit our web at: www.iciq.es

η^1 to η^6 Ru−Arene π Complexation: New Bonding Modes and P−C Bond Cleavage Chemistry

Tilmann J. Geldbach[a] and Paul S. Pregosin*[a]

Keywords: P−C bond cleavage / π complexes / Unusual bonding / Stereospecific migration

Binap and MeOBiphep biarylbis(phosphane) complexes of Ru^{II} are shown to undergo a series of stereospecific P–C bond cleavage reactions. The products are novel cationic chiral arenebis(phosphane) compounds which contain stereogenic Ru centers. Upon further solvolysis in alcohols, additional P–C cleavage reactions lead to stereogenic P atoms. Several novel olefin π-bonding modes are recognised, including one in which only a single arene carbon atom i.e. an η^1 π-bond, weakly coordinates to Ru^{II}.

(© Wiley-VCH Verlag GmbH, 69451 Weinheim, Germany, 2002)

1. Introduction

There is an increasing interest in the area of enantioselective homogeneous catalysis[1] involving relatively small quantities of chiral catalytic materials that can produce substantial amounts of an enantiopure product. Although there are numerous examples of successful chiral nitrogen chelates,[2,3] as well as mixed P,N-ligands,[4] many auxiliaries are still based on chelating tertiary phosphanes.

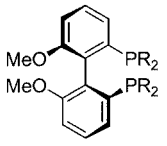

1a R = 3,5-di-*t*Bu-phenyl
1b R = Ph
1c R = *p*-tolyl
1d R = *i*Pr

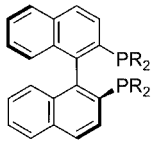

2a R = Ph
2b R = *p*-tolyl

The atropisomeric phosphanes MeO−Biphep **1**[5] and Binap **2**[6] are known to be excellent auxiliaries. These function exceptionally well in Ru-based homogeneous hydrogenation,[7,8] but can also be used in allylic alkylation,[9] and Heck reactions using palladium.[10] The syntheses of **1** and **2** are sufficiently flexible such that various R groups can be introduced and the backbone modified.[5,11] The catalyst precursor most often used in hydrogenation is the octahedral complex $Ru(OAc)_2$(**1**), $Ru(OAc)_2$(**2**), or a related trifluoroacetate complex.

Despite the widespread use of these biaryl ligands, not a great deal is known with respect to their fundamental organometallic chemistry. Several hydride compounds have been prepared,[12] e.g. $[RuH(i\text{PrOH})_2(\mathbf{1a})]BF_4$ (**3**),[13] however, olefin and alkyl compounds seem to have been neglected. Given the utility of **1** and **2**, it seems reasonable to ask how these might modify classical coordination behaviour. Moreover, if catalysts based on these ligands behave poorly or "die" in the course of the reaction, then perhaps knowledge of the possible decomposition pathways is important.

[a] Laboratorium für Anorganische Chemie, ETHZ, Hönggerberg, 8093 Zürich, Switzerland

Tilmann J. Geldbach (left) was born in Geislingen, Germany, in 1972. He began his chemistry studies in 1992 at the University of Konstanz, then spent a year at the University of Sussex at Brighton before graduating in 1998 at the Humboldt University in Berlin. He is currently preparing his PhD thesis at the ETH Zürich on the coordination chemistry of bis(phosphane)ruthenium complexes.

Professor P. S. Pregosin (right) received his PhD degree in New York City in 1970. After post-doctoral research studies at Queen Mary College, London and the University of Delaware, USA, he joined the faculty of the ETH Zürich in 1973, where he has remained. His research interests centre on NMR spectroscopy and organometallic chemistry.

MICROREVIEWS: This feature introduces the readers to the authors' research through a concise overview of the selected topic. Reference to important work from others in the field is included.

As an example, reaction of [Ru(OAc)$_2$(**1a**)] with 3 equiv. of methyllithium or trimethylsilylmethyllithium affords the dialkyl complexes [RuR$_2$(**1a**)] (**4a** or **4b**) in good yields [see Equation (1)].[14]

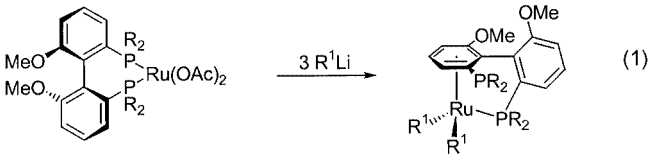

R = 3,5-di-*t*Bu-phenyl

4a R^1 = Me
4b R^1 = CH_2SiMe_3

The molecule achieves this coordinatively saturated electronic structure by dissociating one tertiary phosphane donor, thereby making room (electronically) for an η^6-arene. This reduction from a bidentate to a monodentate ligand is hardly a common occurrence; however, we believe that this propensity for the Ru atom to complex one face of the biaryl ligand is related to the observation of facile P−C bond breaking. In this Microreview, we will focus on acid- and solvent-induced P−C bond cleavage in complexes containing the bidentate phosphane ligands **1** and **2**, and the array of arene−ruthenium bonding modes that are associated with these reactions.

2. P−C Bond Cleavage

2.1 Acid-Induced Cleavage

As the starting compound in hydrogenation chemistry is often protonated to open one or more coordination positions, we begin with a discussion of the chemistry of Ru(OAc)$_2$(**1** or **2**) on addition of a strong acid. Reaction of Ru(OAc)$_2$(**1**) with 2 equiv. of HBF_4 in dichloromethane afforded product **5**, in which a P−C bond is cleaved [see Equation (2)].[15]

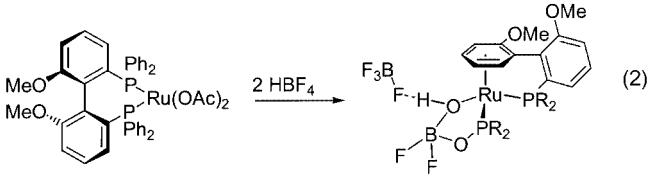

5a R = 3,5-di-*t*Bu-phenyl
5b R = Ph
5c R = *p*-tolyl

Complex **5** contains new P−O and B−O bonds, in addition to an unsymmetrical η^6 Ru−arene interaction, which arises from the complexation of the biaryl ring which loses the P-donor. The bis(phosphane) bidentate ligand has been cleaved affording two different chelating ligands.

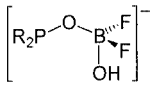

6

Formally, **5** contains the new phosphinite anion **6**, which arises by a hydrolysis reaction. The second BF_4^- ion is held close by through a hydrogen bond. The major features of the structure of **5** were determined by one- and two-dimensional multinuclear NMR spectroscopy and X-ray crystallography.[15]

A more detailed NMR spectroscopic study of this protonation was carried out for the Binap analogue **7**, and these results are summarised in Scheme 1.[16] These reactions can be shown to involve an initial 6e$^-$ donor Ru−F complex **8** (and $BF_3{\cdot}Et_2O$), followed by P−C bond splitting, yielding the monofluoro(phosphane) intermediate, whose structure is assigned as **9**. The ^{31}P and ^{19}F NMR spectra of the PR_2F ligand in **9** clearly show the expected > 900 Hz one-bond $^1J_{P,F}$ values, as well as a very high-frequency ^{31}P chemical shift due to the strongly electronegative fluorine atom. Reaction of **9** with Cl$^-$ afforded the single diastereomeric chloro complex **10**. Obviously, this reaction produces Ru complexes that are sufficiently reactive to extract a fluoride from the BF_4^- anion. Apart from their surprising structure, these compounds are noteworthy in that they demonstrate an undesirable side reaction, the potential loss of axial chirality.

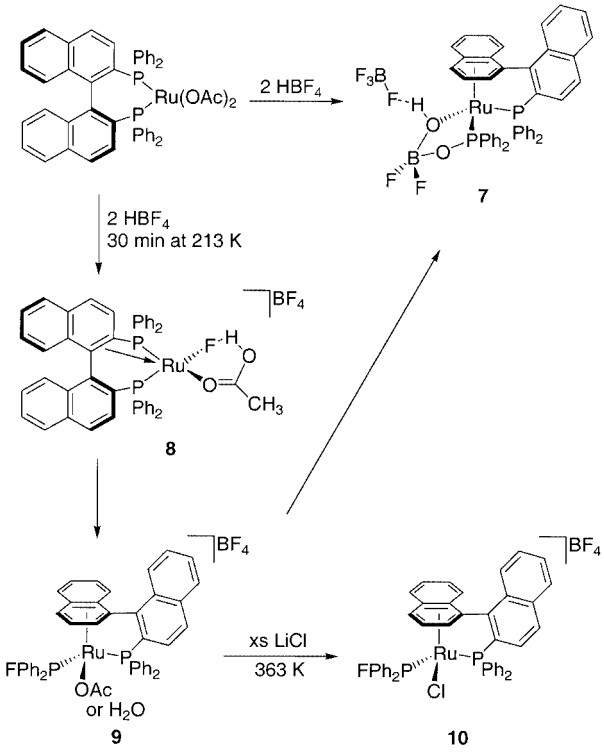

7 **8** **9** **10**

Scheme 1

The syntheses of the arene complexes **5** and **7** were complicated due to the slow, but concurrent BF_4^- anion hydrolysis. To avoid this complication, [Ru(OAc)$_2$(**1** or **2**)], was allowed to react with slightly more than 2 equiv. of wet CF_3SO_3H in 1,2-dichloroethane at 363 K [see Equations (3) and (4)].[16] These reaction conditions gave the MeO−Biphep product **11** and the Binap analogue **12** in less then 2 h and in good yields. Formally, the H$^+$ cation pro-

tonates the acetate anion and the water molecule adds across the P−C bond. Interestingly, we observed only one of the two possible diastereomers (the metal atom is a stereogenic centre), thus this reaction is stereospecific. The ligand $P(OH)Ph_2$ is not very common, but there are a number of such (and related) complexes reported in the literature.[17,18]

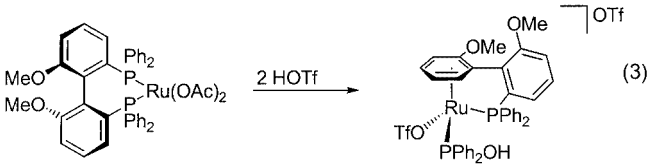

11 (3)

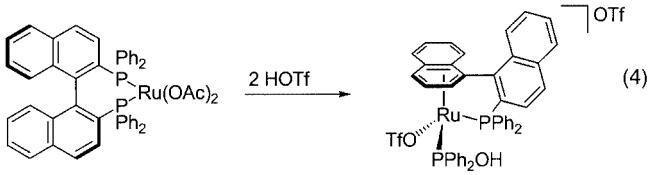

12 (4)

Apart from oxidative addition reactions,[19,20] there are not many examples of related P−C bond cleavage reactions in the literature and we show a selection of these in Scheme 2.[21−25] The first four examples involve the splitting of a P−C bond and the creation of a new P−X bond (X = electronegative group), whereas in the last reaction, a new P−C bond is formed at the expense of a P−O bond. Moreover, there are only a few examples of tethered phosphane−arene complexes,[26,27] e.g. **13** [see Equation (5)].[26a] Of course, lower valent Ru^0 clusters are also capable of cleaving P−C bonds.[28]

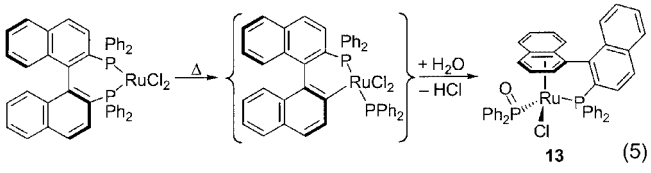

13 (5)

The structures of the new arene−phosphane compounds **11** and **12** were determined by X-ray diffraction and a view of the cation of **11** is shown in Figure 1. The six Ru−C(arene) bond lengths in both **11** and **12** are very different and seem to exist in three groups of two. Two bond lengths are relatively short [Ru−C1 and Ru−C6 (ca. 2.13−2.16 Å)] (but are fairly average),[29−33] two are slightly long [Ru−C4 and Ru−C5 (ca. 2.29−2.32 Å)], and two are quite long [Ru−C2 and Ru−C3 (ca. 2.35−2.48 Å)]. Inspection of the literature involving X-ray studies of arene complexes of Ru^{II} suggests that the usual Ru−C distances in a variety of substituted and simple Ru−arene complexes should be in the range 2.15−2.28 Å, with an average of

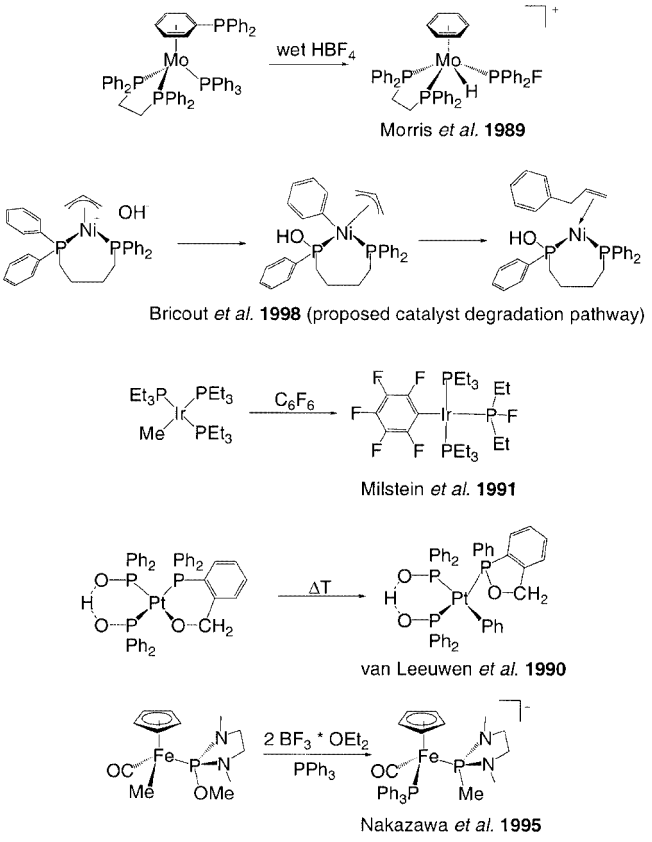

Scheme 2

ca. 2.23 Å. Specifically, the observed values of 2.480(5) and 2.477(5) Å for C2 and C3, respectively, in **11** suggest a weak interaction. The lengths of these bonds might be related to steric effects, since they involve the two sterically hindered fully substituted arene carbon atoms. We shall return to this theme in the discussion on possible flexible arene bonding in the next chapter.

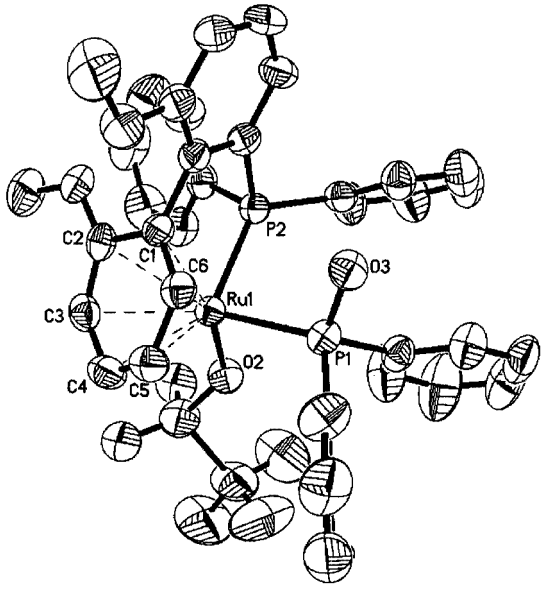

Figure 1. View of the cation of **11**

Although we reasoned that the presence of water was due to the wet triflic acid, there was another possible source. To test whether the acetate was a source of water, $Ru(OAc^*)_2(Binap)$ was synthesised containing > 98% ^{13}C-1 acetate (enriched at the carbonyl group).[34] The reaction of this complex with ca. 2.2 equiv. of high-purity (> 99%) triflic acid at 80 °C for 30 min in 1,2-dichloroethane was monitored by ^{13}C NMR spectroscopy (see Figure 2). The spectrum shows a coordinated acetate (δ ≈ 188 ppm), as well as acetic acid (δ ≈ 176 ppm) and acetic anhydride (δ ≈ 167 ppm). Clearly, the presence of acetic anhydride implies that water is produced.

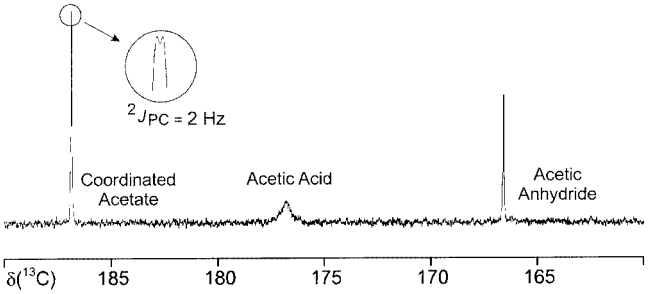

Figure 2. $^{13}C\{^1H\}$ NMR spectrum of the reaction solution after 30 min at 80 °C, with peaks for complexed acetate, acetic acid and acetic anhydride; the expanded section shows the P−C coupling, ^2J = 2.0 Hz (75 MHz, 1,2-dichloroethane with D_2O capillary as internal lock)

Warming of a fresh sample of the enriched starting material to 80 °C for 5 min afforded a small amount (< 10%) of product **12**, a parallel amount of acetic anhydride (and thus water), in addition to a large quantity of a new compound, **14** [see Equation (6)].

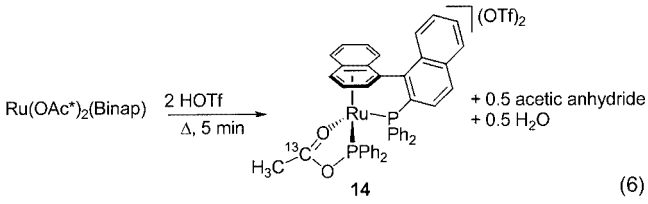

(6)

The ratio of **14** to **12** approaches unity after roughly 1 h. In the ^{31}P NMR spectrum of the new species, an AX ^{31}P spin system is seen, with one of the signals found at relatively high frequency (δ = 185.8 ppm). This new complex contains one acetate ligand as shown by ^1H and ^{13}C NMR spectroscopy. Interestingly, this intermediate species reacts quickly with water to form **12**. Indeed, workup of the NMR reaction solution, by simply pouring it into ether is sufficient to convert it immediately into **12**. The evidence for structure **14** is based on detailed NMR spectroscopic data.

2.2 Solvent-Induced Cleavage

We considered that the triflate compounds **11** and **12** might undergo solvolysis affording useful Lewis acids, so we treated these compounds with methanol. To our surprise we obtained good yields of the MeO−Biphep phenyl complex and its Binap analogue **15a**[35] [see Equation (7)].

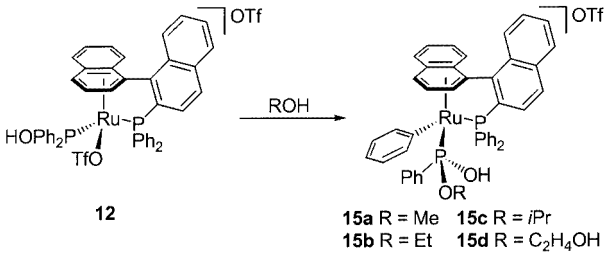

(7)

Additional compounds, **15b** and **15c**, have been prepared using EtOH and *i*PrOH, respectively. The new phenyl complexes are unique in that

a) they are produced in *only one diastereomeric form*, i.e. phenyl migration and P−O bond formation are specific,

b) they contain *three different forms of stereogenicity*: atropisomerism, from the biaryl moiety, a chiral transition metal atom and the newly formed stereogenic P atom, and

c) these are the first reported transition metal complexes of the ligands P(OH)(OR)Ph.

This kind of solvolysis and subsequent migration of a phenyl group from the phosphane group to the metal atom has been observed previously, see Equation (8).[36]

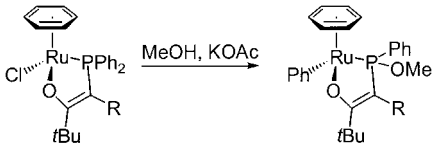

(8)

The solid-state structure of the *i*PrOH analogue **15c** was determined by X-ray diffraction methods and a view of the cation is shown in Figure 3. The immediate coordination sphere consists of the two phosphorus atoms, the π-arene and the η^1-phenyl ligand. While four of the Ru−C(arene) distances are fairly average and fall in the range

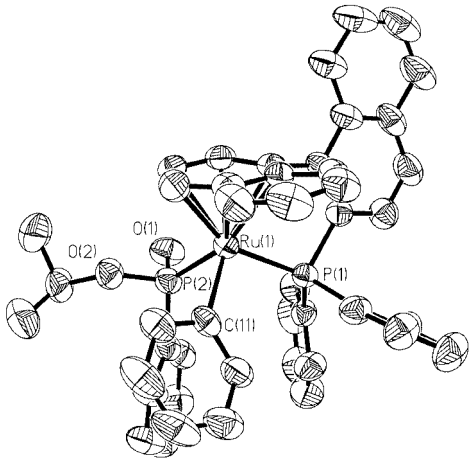

Figure 3. View of the cation of **15c**

2.217(7)−2.272(8) Å, again, the remaining two distances, involving the bridgehead carbon atoms C(2) and C(3), are quite long and suggest that little or no bonding to the metal atom occurs.

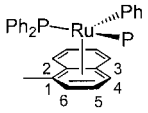

Ru–C2 = 2.433(7) Å Ru–C3 = 2.419(8) Å

The Ru{P(OH)(OR)Ph} fragment is readily deprotonated and in some cases, e.g. the ethylene glycol derivative, **16**, rather than **15d**, was isolated.

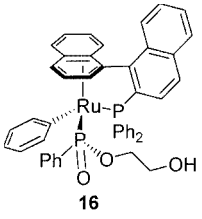

16

2.3 Stereochemistry and Protonation Studies

With a view to preparing chiral complexes with an open coordination site, two of the Ru−{P(OH)OR)Ph} compounds (**15a**: R = Me; **15c**: R = *i*Pr; both with racemic phosphane ligands), were allowed to react with excess triflic acid in dichloromethane.

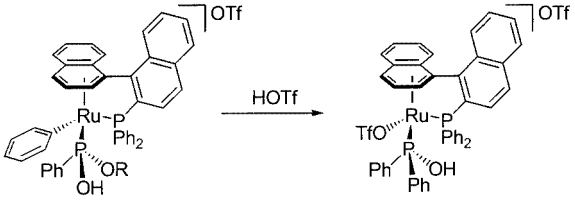

15a R = Me
15c R = *i*Pr

12

(9)

Instead of removing the Ru−phenyl ligand, the observed protonation product was either exclusively **12** (methoxy), or primarily **12** (isopropoxy).[37] For these acid reactions only a single diastereomer is observed, i.e. epimerisation at the Ru atom is not found. This type of migration reaction is known, but rare. A relevant example is shown in Equation (10).[38]

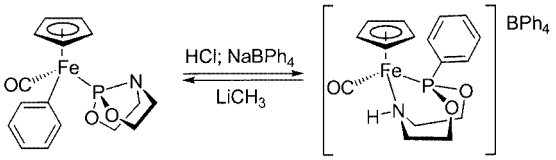

(10)

As an additional check on the stereospecificity of the transformation, we carried out several protonation reactions using the commercially available, optically pure (*S*)-(−)-*p*-tolyl−Binap **2b**. While only marginally different from **2a**, this ligand afforded yet another subset of complexes, **17**.

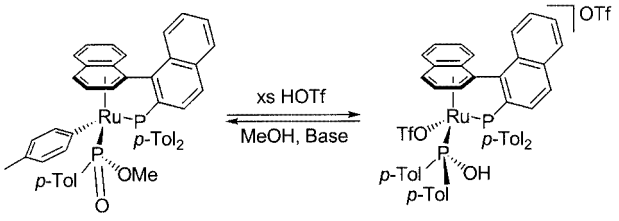

17 **18**

Addition of excess triflic acid to **17** immediately afforded only one diastereomeric form of **18**. Consequently, both the formation of the MeO analogue **15a** and the reformation of **12** proceeded stereospecifically. It was recognised that epimerisation at Ru can (but need not always) be facile.[39−41] Therefore, we repeated the protonation of **17** with excess triflic acid in dichloromethane at dry ice/acetone temperatures. After addition of HOTf to a precooled NMR probe at 220 K, we observed only a single product with a broad resonance at δ = 123.2 ppm and a sharp doublet at δ = 52.4 ppm. Slowly warming to 270 K using 10° increments, afforded a sharp peak in the ^{31}P NMR spectrum of the pure P(OH)(*p*-tolyl)$_2$ analogue of **12**. Since there is no evidence for a second diastereomer, we concluded that the reaction is very facile and, indeed, proceeds stereospecifically.

2.4 Kinetics of the Formation of 15a−c

The rates of reaction for **12** with ROH were not all identical. Consequently, these reactions were monitored by ^{31}P NMR spectroscopic methods. Reaction of **12** using either methanol or ethanol as the solvent proceeded essentially within mixing time to afford **15a** and **15b**, respectively. The difference in reaction rates as a function of the alcohol concentration becomes obvious when **12** is allowed to react using 4:1 alcohol/[D$_6$]benzene mixtures at 21 °C.

To reduce the reactivity of complex **12** with methanol and to obtain rate data at similar alcohol concentrations, 1:4 MeOH/[D$_6$]benzene mixtures were studied. The observed rate constant at 21 °C for the formation of **15a** is $k_{obs} = 6.4{\cdot}10^{-4}$ s^{-1}. For the reaction of **12** with ethanol under similar conditions, $k_{obs} = 5.6{\cdot}10^{-4}$ s^{-1}; therefore, for these somewhat more dilute alcohol solutions, the reactions with both MeOH and EtOH proceed at similar rates. In both cases, a new intermediate in the ^{31}P NMR spectrum is observed.[37] Due to its relatively slow rate, the reaction with 2-propanol was carried out at 27 °C, and not 21 °C. The major peaks observed are those of the starting material, together with a weak, unresolved resonance at δ ≈ 94 ppm. The product **15c** reacts slowly with traces of water to form a new species, which we believe to be a dinuclear complex. After 16 h, the two products are present in similar amounts. The observed reaction rate, $k_{obs} = 8.8{\cdot}10^{-5}$ s^{-1} (27 °C), was calculated using the disappearance of the substrate. Obviously, the reaction with 2-propanol can be considered to be one order of magnitude slower than with either methanol or ethanol.

We have recently managed to isolate two of the dinuclear species, **19** and **20**, and the crystallographic results for **19** are shown in Figure 4.[42]

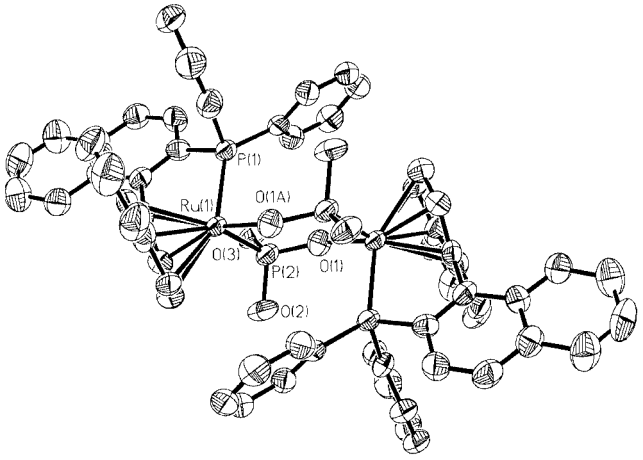

Figure 4. View of the dication of **19**

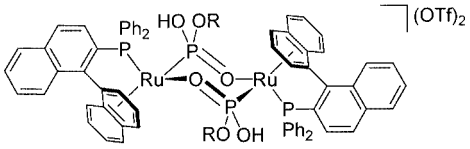

19 R = H
20 R = Me

The structures show that water from the alcohol competes favourably for the P atom, and indeed, one of these two species was prepared by a reaction involving *tert*-butyl alcohol, i.e. the *tert*-butyl alcohol reacts even more slowly than 2-propanol, relative to water.

The reaction of **12** with 2-propanol was also studied in the presence of an excess of sodium triflate. The starting material was consumed after 4 h, whereas in the same time, without added sodium triflate, ca 70% of substrate had reacted, i.e. addition of triflate increases the reaction rate. From a mechanistic point of view, if triflate dissociation was important, the rate should be slower. The kinetic data suggest that the reaction with 2-propanol, as well with methanol and ethanol, are first order with respect to complex **12**. A comparison of the values of k_{obs} obtained using different concentrations of ethanol supports a rate dependence on the concentration of the alcohol.

A possible reaction pathway, which rationalises the stereospecific transformation of complex **12** into the products is shown in Scheme 3 (only the reactive sites of these molecules are shown). Solvent substitution is followed by arene migration to afford a Ru−Ph complex. Protonation of the OR group in the Ru−Ph complex restores the $P(OH)Ph_2$ compound. Using the alcohol as the solvent favours the formation of the dicationic solvent complex (as might the presence of excess charged triflate). Presumably, these solvent complexes are the unknown compounds that appear in the ^{31}P NMR studies, when diluted with benzene. There is always solvent alcohol in close proximity, partially due to the hydrogen bonding to both the triflate anion and POH moieties (another possible source of an intermediate structure). In the transition state, the complexed solvent begins to dissociate. Simultaneously, the phenyl group bridges the Ru and P atoms and the proximate H-bonded solvent begins to form the new P−O bond through a pseudo-backside attack. Possibly, these steps occur sequentially, although the alcohol must be in the rate-determining step. This mechanism is reminiscent of the formation of a nonclassical arenium ion (a typical intermediate in 1,2 shifts of aryl rings), and would be consistent with the observed stereospecificity. Since the alcohol is involved in the transition state, it is reasonable that both its concentration and size affect the kinetics.

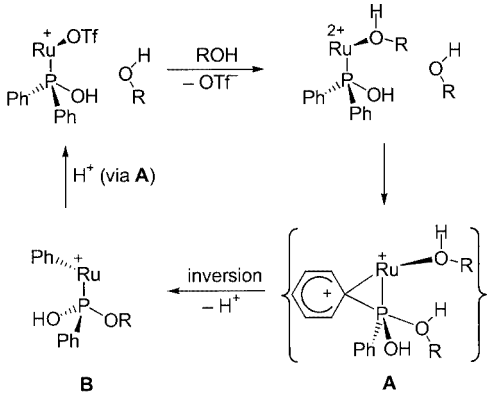

Scheme 3

To support this mechanism we have determined the 3-D solution structure of {P(=O)(OMe)(*p*-tolyl)} complex **17** in dichloromethane, using NOE methods (see Scheme 4).[37,43,44] From these and additional NOE results, it can be seen that the Ru−aryl ring is positioned in an approximately antiperiplanar position relative to the methoxy group. This structural feature allows us to rationalise both the ease and specificity of the reactions indicated in Scheme 3. The positive charge which would develop from facile protonation of the P(OR) group by the strong acid, can be stabilised by the Ru−*p*-tolyl group, again in analogy with carbon cation chemistry (see structure **A**, Scheme 3). Complete transfer of the aryl group to the P atom is then accompanied by rapid triflate capture by the ruthenium cation affording the product, e.g. **15**. Since **A** and **B** are positively charged, in dichloromethane the triflate anion will be nearby. The excess triflic acid helps to facilitate rapid capture before epimerisation.

3. Flexible Arene Bonding

3.1. Olefin-Type Coordination

We noted above, without comment, that a proximate biaryl double bond can complex the Ru^{II} atom, e.g. the middle structure in Scheme 1. We believe this type of complexation to be surprisingly common.

In dichloromethane, $Ru(OAc)_2$(**1a**) reacts with 1,5-COD and HBF_4 to afford **21** in a good yield [see Equa-

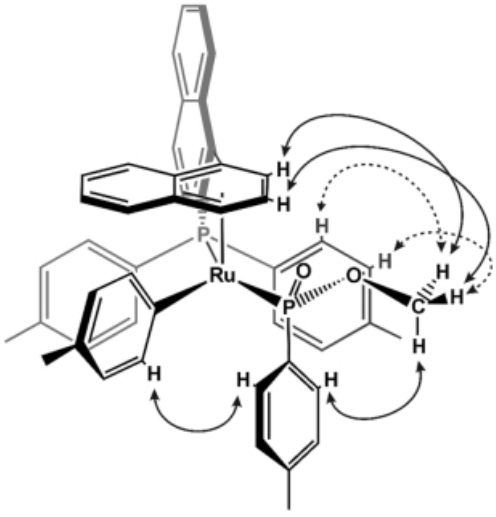

Scheme 4

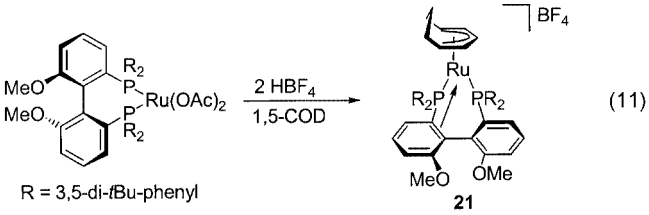

(11)

tion (11)].[45] The ^{31}P NMR spectrum shows a routine AX spin system; however, the chemical shifts at δ = 69.6 and −11.2 ppm (!) are unexpected, with the latter in a region often associated with uncoordinated phosphane. The nature of the organometallic ligand in **21** was not immediately obvious; however, a routine 2-D $^{13}C,^{1}H$-correlation showed only three aliphatic CH_2-type signals, and five CH absorptions in the region δ = 57−114 ppm. These ^{13}C chemical shift data are strongly suggestive of the cyclooctapentadienylruthenium fragment, Ru(η^6-C_8H_{11}).[46] At this point, we noted two ^{13}C resonances of *nonprotonated* carbon atoms at δ = 74.5 ppm as a strong doublet, and at δ = 95.1 ppm as a very weak triplet. A long-range $^{13}C,^{1}H$-correlation revealed connectivity between both of these nonprotonated carbon atoms and the proton *ortho* to the P atom, plus further $^{3}J(^{13}C,^{1}H)$ correlations, as indicated.

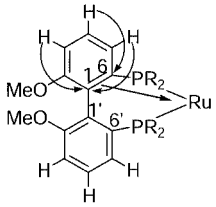

δ C(1) = 95.1 ppm δ C(6) = 74.5 ppm

The ^{13}C signals for the noncomplexed analogous carbon atoms (C1′: δ = 139.7 ppm; C6′: δ = 135.4 ppm) are at a higher frequency. Given these assignments we conclude that the C1−C6 biaryl double bond is coordinated to the metal atom, thereby affording an 18e$^-$ coordinatively saturated complex, and thus making the ligand **1a** a six-electron donor to the metal atom. The low-frequency ^{31}P signal at δ = −11.2 ppm is associated with the unexpected coordination mode.

The ^{1}H phase-sensitive NOESY spectrum[44,45] for **21** at ambient temperature reveals a slow exchange process in which the two halves of the MeO−Biphep ligand are exchanged. Since the product has exactly the same structure, one observes only one set of resonances. Presumably, the biaryl double bond dissociates, thus making room for its counterpart in the second biaryl ring [see Equation (12)].

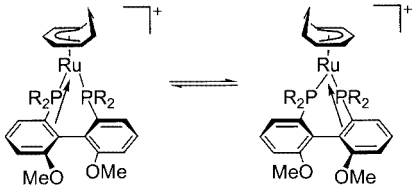

(12)

This new type of pseudo-allylic olefin bonding is unusual; however, White and co-workers reported[47] the solid-state structure for [Ru(Cp)(Binap)]CF_3SO_3, in which they found the same type of six-electron donation from the Binap ligand. They also noted widely dispersed ^{31}P chemical shifts at δ = 74.0 and 14.1 ppm. They were kind enough to provide us with samples of two Cp complexes, **22a** and **22b**, for NMR spectroscopic studies (see Scheme 5). These show both the typical ^{13}C shifts and exchange dynamics [see Equation (13)].[48]

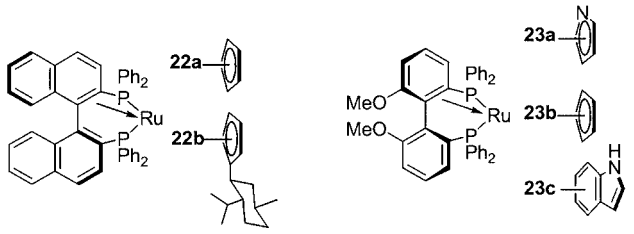

Scheme 5

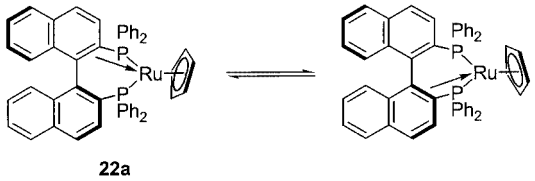

(13)

Subsequently, we prepared the complexes **23a**−**c**, and the solid-state structures of **23b** and **23c** are shown in Figure 5 and Figure 6, respectively. All of these compounds contain the complexed proximate double bond.

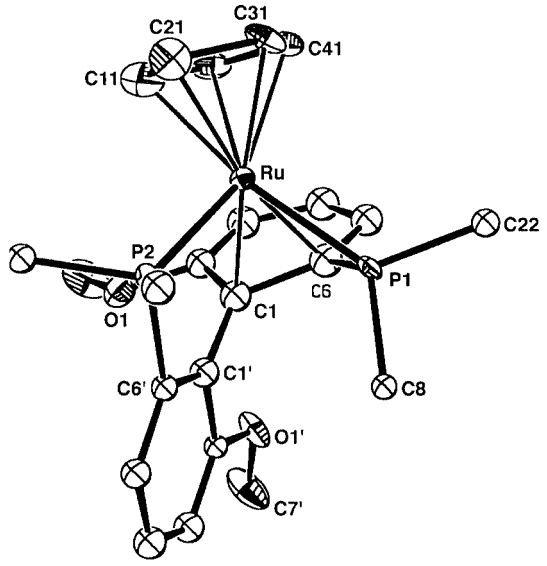

Figure 5. View of a part of the cation **23b**

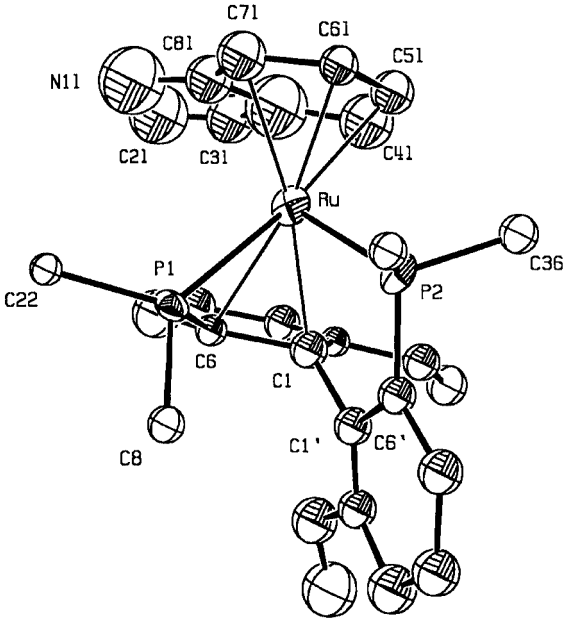

Figure 6. View of part of the cation **23c**

In recent literature reports, we found two related cases of this type of bonding: The Pt complex **24**[49] is clearly related, whereas the Mo complex **25**[50] might be of a more general nature due to the ubiquitous triphenylphosphane.

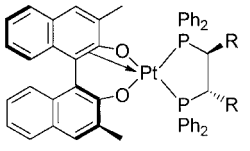

24

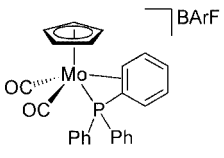

25

Once it is known that **21**−**23** are stable, then it is a relatively simple task to extend the known range of complexes showing this type of bonding by extracting chloride from [RuCl{bis(phosphane)}(arene)]Cl to afford the cymene complex **26a**.[51]

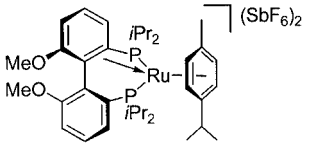

26a

Compound **26a** and related species are shown in Scheme 6, along with several other derivatives, and selected NMR spectroscopic data are given in Table 1.[51]

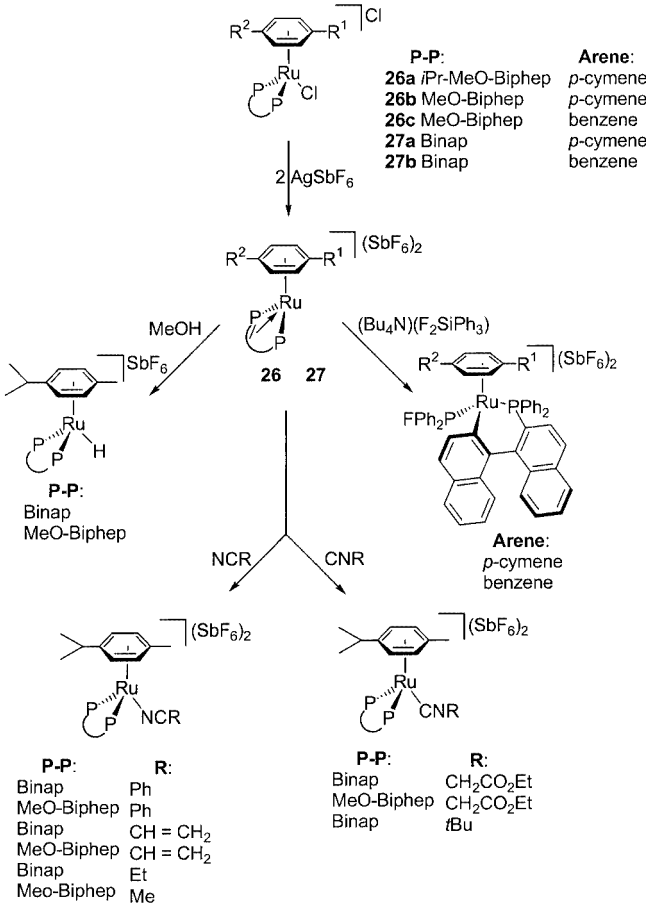

Scheme 6

Reaction of **12** with Cs_2CO_3 gave compound **28,** which also shows an η^2-olefin interaction, albeit of a different nature. Interestingly, the two carbon atoms complexed are those which can coordinate before P−C cleavage.

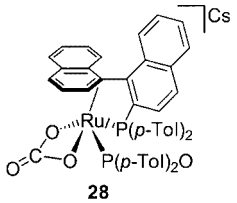

28

Table 1. Selected NMR chemical shifts for the carbon and phosphorus donors in Ru−arene complexes **26** and **27**

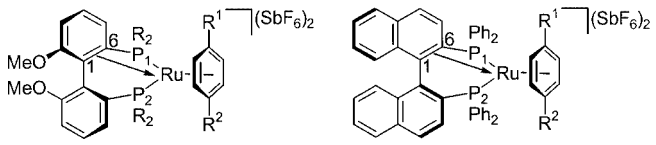

26a R = *i*Pr; *p*-cymene
26b R = Ph; *p*-cymene
26c R = Ph; benzene

27a *p*-cymene
27b benzene

	C1	C6	P1	P2
26a	102.5	79.1	27.3	82.6
26b	93.0	80.1	7.7	67.1
26c	90.9	86.0	15.4	64.7
27a	98.0	67.5	3.3	68.7
27b	101.7	73.0	19.0	64.0

A section of the ^{13}C long-range correlation for **28** is given in Figure 7 and reveals two "typical" chemical shifts for C1 and C6, the carbon atoms coordinated to the ruthenium atom. The four remaining ring carbon atoms show normal NMR characteristics.

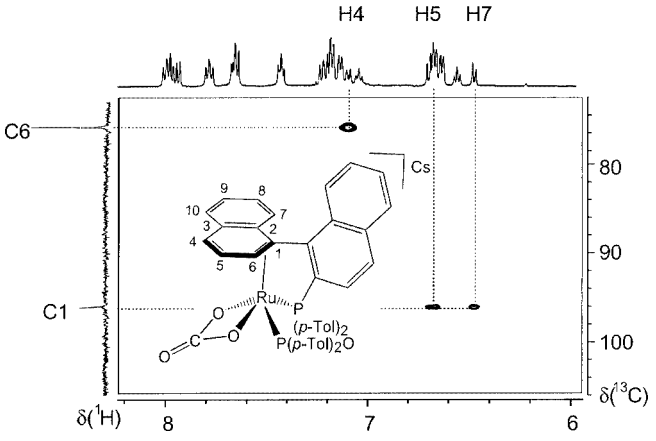

Figure 7. C,H long-range correlation for **28** showing the cross peaks for the two coordinated carbon atoms C6 and C1 stemming from the interaction of the *meta*-protons H4 and H5, and H7, respectively

3.2. Coordination from a Single Arene Carbon Atom

A number of derivatives of the [Ru−P(OH)Ph_2] complexes **11** and **12**, containing nitrile, isocyanide and phosphane donors have been prepared (see Scheme 7).[52] In these compounds the arene has either been partially or fully displaced. On the surface, all of the apparent five-coordinate nitrile complexes appear to have structures in which the η^6-arene bonding has been completely displaced. However, these nitrile complexes contain an interesting and unexpected feature as shown by their ^{13}C NMR spectroscopic data. Just *one* of the (previously η^6-arene) biaryl carbon atoms (C6) remains situated in a pseudo-sixth coordination position, and its ^{13}C resonance is shifted to δ = 105−112 ppm from that of a "normal" arene hydrocarbon, which we estimate to be at δ ≈ 127−130 ppm.[53] This difference in carbon chemical shift is much too large to arise from local anisotropic effects. The signals of the adjacent carbon atoms C1 and C5 are found at δ ≈ 130−140 ppm, i.e. in rather typical positions, so that an η^2 description is not suitable for these molecules. The protons on C6 in these nitrile compounds (δ = 7.69−8.27 ppm) are also of a routine nature.

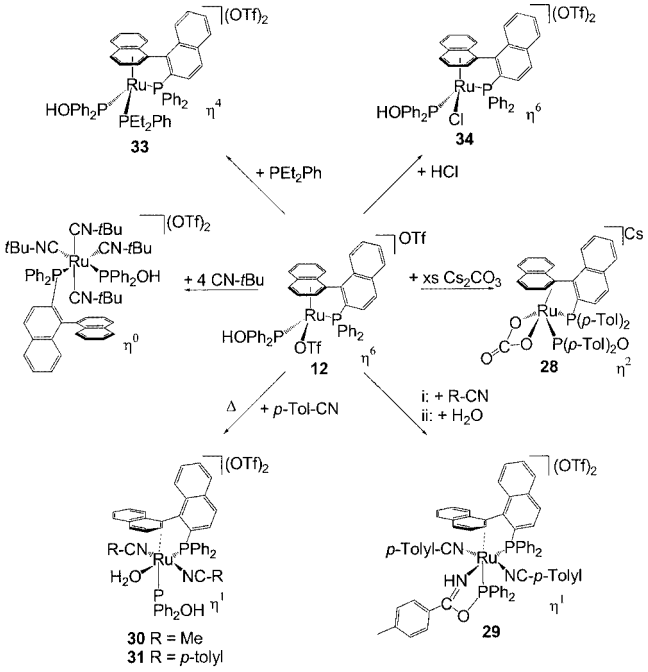

Scheme 7

Specifically, complex **29**, which arises from attack of the P−OH on a complexed nitrile ligand, shows this type of novel η^1 bonding.

One could consider the observed bonding as arising from a "remote agostic", i.e. weak, interaction of the metal atom with the biaryl C−H bond.[54,55] However, we do not believe this to be correct based on the normal observed values of $^1J_{C,H}$ (from the C,H correlations) and the H6 chemical shifts, both of which seem rather unaffected by the bonding. The most reasonable explanation involves a weak η^1-π bonding mode from a single CH biaryl arene carbon atom to the ruthenium atom. A strong interaction might induce larger coordination chemical shifts and shorter bond lengths.

Crystals of the two aquo(nitrile) complexes **30** and **31** were grown and their solid-state structures determined by X-ray diffraction. Figure 8 and Figure 9 show views of the cations and, although there is strong disorder in these crystals (the *R* values are not excellent), the coordination sphere around the ruthenium centre is clear.[52] Atom C(6) occupies the sixth position in both structures and P(2), possessing the P(OH) group, is in a pseudo-*trans* position to this arene carbon atom. The Ru−C(6) distances of 2.62 and 2.63 Å, for complexes **30** and **31**, respectively, are clearly too long for a routine σ-bond, but approach the upper end of what is known[56] for weak Ru−olefin interactions. The distances from the ruthenium atom to C(5) are both rather

long for a bonding interaction, ca 3.3 Å, which is consistent with the ^{13}C NMR results. Placing the H atom at a ca. 1 Å distance from C(6) affords Ru···H distances in the region of 2.69−2.70 Å, i.e. there is no reason to invoke a C−H agostic interaction.

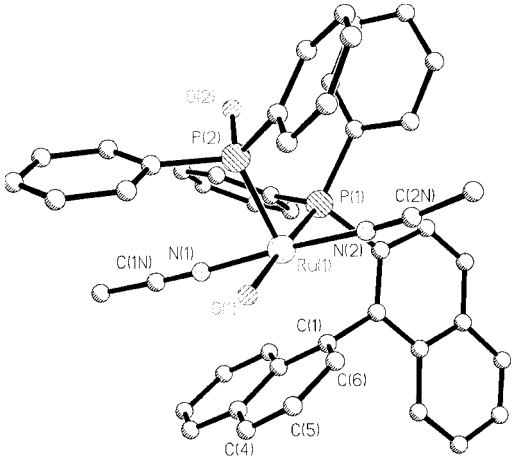

Figure 8. View of the cation **30**; note the position of C(6), occupying the 6th coordination site

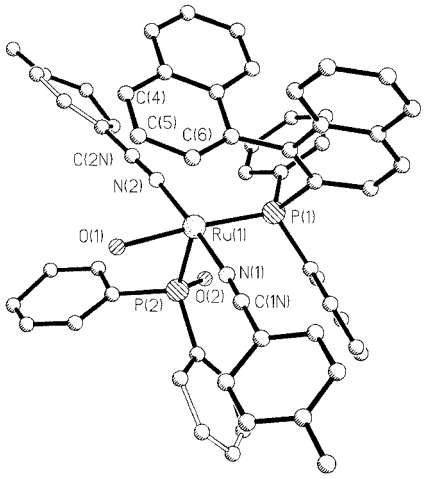

Figure 9. View of the cation **31**; note the position of C(6), occupying the 6th coordination site

We are not aware of many examples of η^1 Ru−CH bonds; however, Gusev et al.[57] have recently assigned the Ru−CH interaction in **32** as a strong agostic interaction based on the short M−C distance, ca. 2.1 Å.

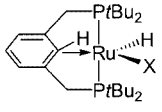

32

Indeed the reported *high frequency* carbon chemical shift of this Ru−CH carbon atom ($\delta \approx 152$ ppm) is consistent with a strong M−C σ-bond character.[58] This interaction is obviously different from those found in our Ru compounds.

3.3. η^4 or η^6 Bonding?

The PEt_2Ph complex **33** in the upper half of Scheme 7 is assigned to an η^4 diolefin structure. Although only slightly different from **12**, based on X-ray and NMR spectroscopic data, there are clearly two complexed double bonds and one remote, perhaps weak, interaction.

The question of η^6 vs. η^4 arene bonding in **12** and its derivatives is one that is discussed using ^{13}C NMR data. Despite the observed Ru−C distances (ca 2.4 Å or more), we believe that the bonding is best described as strongly asymmetric η^6. The ^{13}C chemical shifts for the two carbon atoms in question, C-2 and C-3, are shown together with three model compounds **28**, **33** and **34** (see Scheme 7).

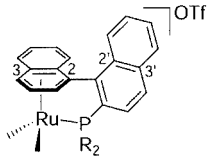

	C-2	C-3	C-2'	C-3'
28	136.6	133.7	133.8	134.8
33	116.4	116.2	131.5	134.9
34	111.6	114.0	131.8	135.1

Assuming that a "normal" ^{13}C position (pure η^4 arene bonding) would be at $\delta \approx 130$ ppm, then both C-2 and C-3 experience some effect of the proximate Ru atom. Consequently, it is somewhat superficial to draw the line between the η^6 and η^4 description; however, as expected, the presence of stronger donating groups (e.g. phosphane vs. chloride), leads to a weaker arene−Ru interaction and thus to a shift towards higher frequency for the signals of C-2 and C-3.

4. Comments

The biaryl chelating phosphanes **1** and **2** do not display "routine" coordination/organometallic chemistry. In general, for Ru complexes of **1** and **2**, the nature of the other ligands bound to the ruthenium atom determines whether these bis(phosphanes) function as $4e^-$ or $6e^-$ donors. There is a definite propensity for this metal to "reach" for the electrons of the biaryl π-system (as in **21**−**27**) as soon as the electron count for ruthenium is only $16e^-$. In order to achieve this, the biaryl is severely twisted.[43,46] Once the Ru atom has complexed the double bond next to the P atom, it is reluctant to release it, and all of the X-ray data show that the Ru−C1 and Ru−C6 distances are the shortest. When the P−C bond has been broken, and a new π-ligand formed, the nature of the different donor ligands (phosphanes, nitriles, carbonate etc.) determines whether the ring of the biaryl ligand slips from a weak six- to a normal four-, and then down to a two-atom donor. Rather than

completely forsake this nearby π-system, these complexes can adopt the novel η^1-π bonding mode, as in **29**−**31**; the weakest interaction with the π-system manageable. This interest in holding the π-cloud may well be responsible for the observed ease of P−C bond breaking in bidentate biarylphosphane compounds. In any case, the chemistry of **1** and **2** affords a variety of novel, new chiral phosphane complexes of Ru^{II} in which arene complexation plays a major role.

The undesirable second and third P−C bond breaking reactions, i.e. the formation of **19** and **20**, prohibits a controlled synthesis of $16e^-$ intermediates. Nevertheless, both **19** and **20** are unique and offer opportunities for studying interactions of these with additional harder metal centres, e.g. the preparation of phosphorus-containing chiral complexes of metals in higher oxidation states.

Acknowledgments

P. S. P. thanks the Swiss National Science Foundation, and the BBW for financial support. We also thank Johnson Matthey for a loan of precious metals and F. Hoffmann La-Roche for the gift of MeO−Biphep ligands.

[1] [1a] R. Noyori, *Asymmetric Catalysis in Organic Synthesis*, John Wiley and Sons, Inc., London, **1994**. [1b]A. Togni, L. M. Venanzi, *Angew. Chem. Int. Ed. Engl.* **1994**, *33*, 497−526. [1c] J. Tsuji, *Palladium Reagents and Catalysis*, John Wiley & Sons, Chichester, **1996**. [1d] P. S. Pregosin, M. Valentini, *Enantiomer* **1999**, *4*, 529−539.
[2] A. Pfaltz, *J. Heterocycl. Chem.* **1999**, *36*, 1437−1451.
[3] D. Tanner, *Angew. Chem. Int. Ed. Engl.* **1994**, *33*, 599−619.
[4] G. Helmchen, A. Pfaltz, *Acc. Chem. Res.* **2000**, *33*, 336−345.
[5] [5a] R. Schmid, M. Cereghetti, B. Heiser, P. Schönholzer, H. J. Hansen, *Helv. Chim. Acta* **1988**, *71*, 897−929. [5b] A. Knierzinger, P. Schönholzer, *Helv. Chim. Acta* **1992**, *75*, 1211−1220. [5c] A. Mezzetti, A. Tschumper, G. Consiglio, *J. Chem. Soc., Dalton Trans.* **1995**, 49−56. [5d] R. Schmid, E. A. Broger, M. Cereghetti, Y. Crameri, J. Foricher, M. Lalonde, R. K. Müller, M. Scalone, G. Schoettel, U. Zutter, *Pure Appl. Chem.* **1996**, *68*, 131−138. [5e] Y. Crameri, J. Foricher, U. Hengartner, C. Jenny, F. Kienzle, H. Ramuz, M. Scalone, M. Schlageter, R. Schmid, S. Wang, *Chimia* **1997**, *51*, 303−305. [5f] M. J. Fehr, G. Consiglio, M. Scalone, R. Schmid, *J. Org. Chem.* **1999**, *16*, 5768−5776.
[6] [6a] K. Mashima, K. Kusano, T. Ohta, R. Noyori, H. Takaya, *J. Chem. Soc., Chem. Commun.* **1989**, 1208−1210. [6b] H. Takaya, T. Ohta, K. Mashima, in *Homogeneous Transition Metal Catalysed Reactions*, vol. 230 (Eds.: W. R. Moser, D. W. Slocum), American Chemical Society, **1992**. [6c] T. Ohkuma, D. Ishii, H. Takeno, R. Noyori, *J. Am. Chem. Soc.* **2000**, *122*, 6510−6511. [6d] T. Ohta, H. Takaya, R. Noyori, *Inorg. Chem.* **1988**, *27*, 566−569.
[7] [7a] H. Takaya, T. Ohta, K. Mashina, R. Noyori, *Pure Appl. Chem.* **1990**, *62*, 1135−1138. [7b] J. P. Genêt, *Acros Org. Acta* **1995**, *1*, 4.
[8] [8a] J. W. Faller, J. Parr, *Organometallics* **2000**, *19*, 1829−1832. [8b] J. W. Faller, B. P. Patel, M. A. Albrizzio, M. Curtis, *Organometallics* **1999**, *18*, 3096−3104. [8c] J. W. Faller, J. Parr, *Organometallics* **2000**, *19*, 3556−3561.
[9] P. S. Pregosin, H. Rüegger, R. Salzmann, A. Albinati, F. Lianza, R. W. Kunz, *Organometallics* **1994**, *13*, 83−90.
[10] M. Tschoerner, P. S. Pregosin, A. Albinati, *Organometallics* **1999**, *18*, 670−678.
[11] D. Q. Che, N. G. Andersen, S. Y. W. Lau, M. Parvez, B. A. Keay, *Tetrahedron: Asymmetry* **2000**, 1919−1925.
[12] [12a] J. A. Wiles, C. E. Lee, R. McDonald, S. H. Bergens, *Organometallics* **1996**, *15*, 3782−3784. [12b] J. A. Wiles, S. H. Bergens, V. G. Young, *J. Am. Chem. Soc.* **1997**, *119*, 2940−2941. [12c] J. A. Wiles, S. H. Bergens, *Organometallics* **1998**, *17*, 2228−2240. [12d] J. A. Wiles, S. H. Bergens, *Organometallics* **1999**, *18*, 3709−3714.
[13] A. Currao, N. Feiken, A. Macchioni, R. Nesper, P. S. Pregosin, G. Trabesinger, *Helv. Chim. Acta* **1996**, *79*, 1587−1591.
[14] N. Feiken, P. S. Pregosin, G. Trabesinger, *Organometallics* **1997**, *16*, 3735−3736.
[15] C. J. den Reijer, H. Rüegger, P. S. Pregosin, *Organometallics* **1998**, *17*, 5213−5215.
[16] C. J. den Reijer, M. Wörle, P. S. Pregosin, *Organometallics* **2000**, *19*, 309−316.
[17] [17a] S. Neuman, D. Schomburg, R. Schmutzler, *J. Chem. Soc., Chem. Commun.* **1979**, 848. [17b] J. W. Gilje, R. Schmutzler, W. S. Sheldrick, V. Wray, *Polyhedron* **1983**, *2*, 603−606. [17c] H. J. Plinta, R. Gereke, A. Fischer, P. G. Jones, R. Schmutzler, *Z. Naturforsch., Teil B* **1993**, *48*, 737−746 and references therein.
[18] D. Hesek, G. A. Hembury, M. G. B. Drew, S. Taniguchi, Y. Inoue, *J. Am. Chem. Soc.* **2000**, *122*, 10236−10237.
[19] [19a] P. E. Garrou, *Chem. Rev.* **1985**, *85*, 171−185. [19b] P. E. Garrou, R. A. Dubois, *Organometallics* **1986**, *5*, 466−473. [19c] A. G. Abatjoglou, D. R. Bryant, *Organometallics* **1984**, *3*, 932−934. [19d] F. E. Goodson, T. I. Wallow, B. M. Novak, *J. Am. Chem. Soc.* **1997**, *119*, 12441−12453.
[20] [20a] H. Shen, S. G. Bott, M. G. Richmond, *Organometallics* **1995**, *14*, 4625. [20b] M. Sommovigo, M. Pasquali, P. Leoni, D. Braga, P. Sabatino, *Chem. Ber.* **1991**, *124*, 97−99. [20c] R. Bender, S. E. Bouaoud, P. Braunstein, Y. Dusausoy, N. Merabet, D. Rouag, *J. Chem. Soc., Dalton Trans.* **1999**, 735−741.
[21] R. H. Morris, J. F. Sawyer, C. T. Schweitzer, A. Sella, *Organometallics* **1989**, *8*, 2099−2106.
[22] H. Bricout, J-F. Carpentier, A. Montreux, *J. Mol. Catal. A* **1998**, *136*, 243−251.
[23] O. Blum, F. Frolow, D. Milstein, *J. Chem. Soc., Chem. Commun.* **1991**, 258−259.
[24] P. W. N. M. van Leeuwen, C. F. Roobeek, A. G. Orpen, *Organometallics* **1990**, *9*, 2179−2181.
[25] H. Nakazawa, Y. Yamaguchi, T. Mizuta, S. Ichimura, K. Miyoshi, *Organometallics* **1995**, *14*, 4635−4643.
[26] [26a] A. S. C. Chan, S. A. Laneman, R. E. Miller, *ACS Symp. Ser.* **1993**, *517*, 27. [26b] P. Vierling, J. G. Riess, A. Grand, *J. Am. Chem. Soc.* **1981**, *103*, 2466−2467.
[27] [27a] B. Therrien, T. R. Ward, M. Pilkington, C. Hoffmann, F. Gilardoni, J. Weber, *Organometallics* **1998**, *17*, 330−337. [27b] K. Onitsuka, Y. Ajioka, Y. Matsushima, S. Takahashi, *Organometallics* **2001**, *20*, 3274−3282.
[28] [28a] R. D. Adams, F. A. Cotton (Eds.), *Catalysis by Di- and Polynuclear Metal Cluster Complexes*, Wiley-VCH, Weinheim, **1998**. [28b]A. L. Bandini, G. Banditelli, G. Minghetti, *J. Organomet. Chem.* **2000**, *595*, 224−231.
[29] [29a] M. Bennett, A. K. Smith, *J. Chem. Soc., Dalton Trans.* **1974**, 233. [29b] M. A. Bennett, Z. Lu, X. Wang, M. Brown, D. C. R. Hockless, *J. Am. Chem. Soc.* **1998**, *120*, 10409.
[30] M. S. Röthlisberger, A. Salzer, H. B. Bürgi, A. Ludi, *Organometallics* **1986**, *5*, 298−302.
[31] A. R. Siedle, R. A. Newmark, L. H. Pignolet, D. X. Wang, T. A. Albright, *Organometallics* **1986**, *5*, 38−47.
[32] [32a] S. Bhambri, D. A. Tocher, *Polyhedron* **1996**, *15*, 2763−2770. [32b] R. F. Winter, F. M. Hornung, *Inorg. Chem.* **1997**, *36*, 6197−6204.
[33] [33a] Y. Yamamoto, R. Sato, F. Matsuo, C. Sudoh, T. Igoshi, *Inorg. Chem.* **1996**, *35*, 2329−2336. [33b] O. S. Sisodia, A. N. Sahay, D. S. Pandey, U. C. Agarwala, N. K. Jha, P. Sharma, A. Toscano, A. Cabrera, *J. Organomet. Chem.* **1998**, *560*, 35−40.
[34] T. J. Geldbach, P. S. Pregosin, *Inorg. Chim. Acta*, **2002**, *330*, 155−160.
[35] T. J. Geldbach, D. Drago, P. S. Pregosin, *Chem. Commun.* **2000**, 1629−1630.

[36] P. Crochet, B. Demerseman, C. Rocaboy, D. Schleyer, *Organometallics* **1996**, *15*, 3048−3061.
[37] T. J. Geldbach, P. S. Pregosin, M. Bassetti, *Organometallics* **2001**, *20*, 2990−2997.
[38] P. Vierling, J. G. Riess, A. Grand, *Inorg. Chem.* **1986**, *25*, 4144−4144.
[39] [39a] H. Brunner, R. Oeschey, B. Nuber, *Organometallics* **1996**, *15*, 3616−3624. [39b] H. Brunner, *Angew. Chem.* **1999**, *111*, 1248. [39c] H. Brunner, T. Zwack, *Organometallics* **2000**, *19*, 2423−2426.
[40] H. Brunner, *Eur. J. Inorg. Chem.* **2001**, 905−912.
[41] [41a] N. Gül, J. H. Nelson, *Organometallics* **1999**, *18*, 709−725. [41b] H. D. Hansen, K. Maitra, J. H. Nelson, *Inorg. Chem.* **1999**, *38*, 2150−2156. [41c] S. Attar, V. J. Catalano, J. H. Nelson, *Organometallics* **1996**, *15*, 2932−2946 and references therein.
[42] T. J. Geldbach, P. S. Pregosin, A. Albinati, F. Rominger, *Organometallics* **2001**, *20*, 1932−1938.
[43] P. S. Pregosin, R. Salzmann, *Coord. Chem. Rev.* **1996**, *155*, 35−68.
[44] [44a] P. S. Pregosin, G. Trabesinger, *J. Chem. Soc., Dalton Trans.* **1998**, 727−734. [44b] P. S. Pregosin, C. Ammann, *Pure Appl. Chem.* **1989**, *61*, 1771−1776.
[45] N. Feiken, P. S. Pregosin, G. Trabesinger, M. Scalone, *Organometallics* **1997**, *16*, 537−543.
[46] B. E. Mann, B. F. Taylor, *^{13}C NMR Spectroscopic Data for Organometallic Compounds*, Academic Press, London, **1981**.
[47] D. D. Pathak, H. Adams, N. A. Bailey, P. J. King, C. White, *J. Organomet. Chem.* **1994**, *479*, 237−245.
[48] N. Feiken, P. S. Pregosin, G. Trabesinger, A. Albinati, G. L. Evoli, *Organometallics* **1997**, *16*, 5756−5762.
[49] N. M. Brunkan, P. S. White, M. R. Gagne, *J. Am. Chem. Soc.* **1998**, *120*, 11002−11003.
[50] T. Cheng, D. J. Szalda, R. M. Bullock, *Chem. Commun.* **1999**, 1629−1930.
[51] C. J. den Reijer, P. Dotta, P. S. Pregosin, A. Albinati, *Canad. J. Chem.* **2001**, *79*, 693−704.
[52] T. J. Geldbach, D. Drago, P. S. Pregosin, *J. Organomet. Chem.* **2002**, *643−644*, 214−222.
[53] H. O. Kalinowski, S. Berger, S. Braun, *^{13}C NMR Spektroskopie*, Georg Thieme Verlag, Stuttgart, **1984**.
[54] [54a] C. G. Anklin, P. S. Pregosin, F. J. Wombacher, H. J. Rüegg, *Organometallics* **1990**, *9*, 1953−1958. [54b] A. Albinati, P. S. Pregosin, F. Wombacher, *Inorg. Chem.* **1990**, *29*, 1812−1817. [54c] A. Albinati, F. Lianza, M. Pasquali, M. Sommovigo, P. Leoni, P. S. Pregosin, H. Rüegger, *Inorg. Chem.* **1991**, *30*, 4690−4692. [54d] A. Albinati, F. Lianza, P. S. Pregosin, B. Müller, *Inorg. Chem.* **1994**, *33*, 2522−2526.
[55] T. W. Hambley, *Inorg. Chem.* **1998**, *37*, 3767−3774.
[56] A. G. Orpen, L. Brammer, F. H. Allen, O. Kennard, D. G. Watson, R. Taylor, *J. Chem. Soc., Dalton Trans.* **1989**, S1−S83.
[57] D. G. Gusev, M. Madott, F. M. Dolgushin, K. A. Lyssenko, M. Y. Antipin, *Organometallics* **2000**, *19*, 1734−1739.
[58] [58a] M. Tschoerner, R. W. Kunz, P. S. Pregosin, *Magn. Reson. Chem.* **1999**, *37*, 91−97. [58b] M. Tschoerner, P. S. Pregosin, *Inorg. Chim. Acta* **1999**, *290*, 95−99.

Received January 14, 2001
[I02018]

Oxorhenium(V) Complexes of Carbohydrate Ligands[‡]

Peter Klüfers,*[a] Oswald Krotz,[a] and Martin Oßberger[a]

Keywords: Rhenium / Carbohydrates / Oxo ligands

The reaction of anhydroerythritol (AnEryt) and methyl-β-D-galactopyranoside (Me-β-D-Gal*p*) with dichloro[hydridotris(pyrazolyl)borato]oxorhenium(V) [(tpb)ReOCl$_2$] in methanol/triethylamine results in the formation of blue crystals of the diolato complexes [(tpb)ReO(AnErytH$_{-2}$)] (**1**) and [(tpb)ReO(Me-β-D-Gal*p*3,4H$_{-2}$)] (**2**). The amounts of *anti*-**1** and *syn*-**1** isomers are investigated by means of NMR spectroscopy and depend on the solvent chosen. For **2**, the generally rigid pyranoside ligand enters the complex in a conformation that is even more heavily strained than the corresponding isopropylidene sugar in terms of torsion angles. Though *anti* and *syn* isomers are also formed in non-aqueous media initially, various synthetic procedures are given to obtain pure *syn*-**2**.

(© Wiley-VCH Verlag GmbH, 69451 Weinheim, Germany, 2002)

Introduction

Diolato complexes of the oxo-rhenium(V) moiety have attracted considerable interest in the past decade.[1−12] Most of this work has been directed towards ethylene glycol and catechol as the ligands. Unfortunately, there is no information on rhenium complexes of diol functions incorporated into a carbohydrate. A knowledge of the rules of rhenium binding to carbohydrates is of medical significance, since it would be of great advantage to couple radioactive rhenium isotopes, which are used both in tumour diagnosis and therapy, to biomolecules that specifically bind to receptor sites of a tumour. Among the biomolecules in question, glycopeptides provide carbohydrate functionalities.

In a first attempt to learn about the structural and spectroscopic properties of rhenium-carbohydrate complexes, several furanoidic and pyranoidic diols were investigated. With this work, we report on complexes of two ligands: anhydroerythritol (AnEryt), which provides the core of *cis*-configured furanosides, and methyl-β-D-galactopyranoside (Me-β-D-Gal*p*). The latter provides diol functions, which exhibit larger torsion angles as typical for pyranosides generally.

Results and Discussion

Preparation and Crystal Structures

The new compounds were prepared according to a modification of Brown and Mayer's method[7] by reaction of dichloro[hydridotris(pyrazolyl)borato]oxorhenium(V) [(tpb)ReOCl$_2$], triethylamine, and the carbohydrate in refluxing methanol (Scheme 1). To prevent formation of oligomeric rhenium complexes — obviously the main side reaction — a fourfold excess of carbohydrate over rhenium was used. Typical yields of 60% with respect to rhenium were obtained with this method. Attempts to obtain crystals were successful for both the ligands mentioned. Blue, monoclinic crystals of [(tpb)ReO(AnErytH$_{-2}$)] (**1**) are built up from equal amounts of two isomers, which differ in the orientation of the oxolanediolato ligand with respect to the (tbp)ReO fragment. Figure 1 shows the molecular structure of then *anti* isomer, highlighting an intramolecular hydrogen bond of the type C−H···O, with the ether-O atom of the ligand being the acceptor. In the *syn* isomer (Figure 2), the ligand is turned by 180° (the *syn* isomer has been defined as the one with the oxolane ring hinged towards the Re=O group). In the hydrogen-bonded *anti* form, the additional bond between the oxolanediolate and the (tpb)ReO residue results in a more perfect transfer of symmetry from the metal fragment to the ligand. Hence *anti*-**1** is close to C_s symmetry from which *syn*-**1** deviates markedly (cf. the diol torsion angles of both forms in the legends to Figure 1 and 2, the ideal angle for C_s symmetry being 0°). In the crystal structure, the ether-O atom of *syn*-**1** also acts as an acceptor in a hydrogen bond with a C−H donor; other oxygen atoms also establish weak contacts of this kind, all of which are intermolecular.

[‡] Polyol-Metal Complexes, 40. Part 39: P. Klüfers, T. Kunte, *Eur. J. Inorg. Chem.*, **2002**, 1285−1289.

[a] Department Chemie der Ludwig-Maximilians-Universität München,
Butenandtstraße 5−13, 81377 München, Germany
Fax: (internat.) + 49 (0)89/2180-7407
E-mail: kluef@cup.uni-muenchen.de

Supporting information for this article is available on the WWW under http://www.eurjic.com or from the author.

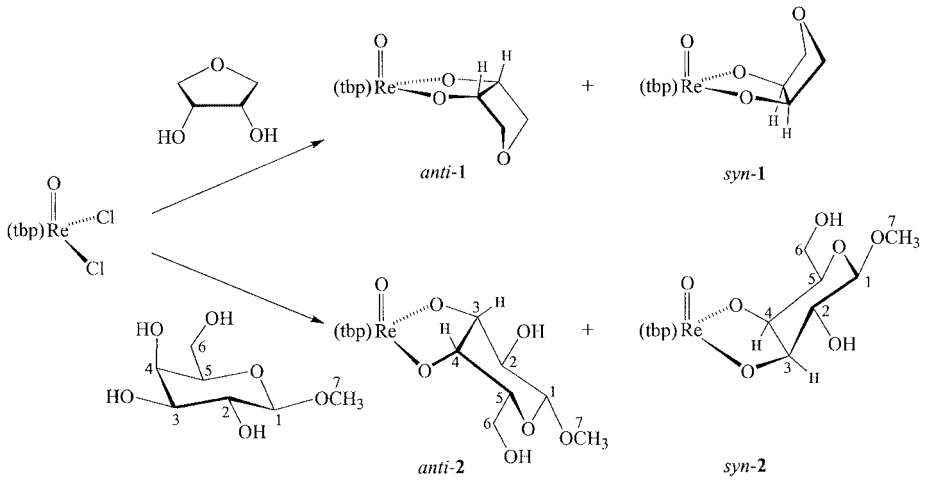

Scheme 1. Reaction scheme and numbering of carbon atoms in **2** [tpb = hydridotris(pyrazolyl)borate]

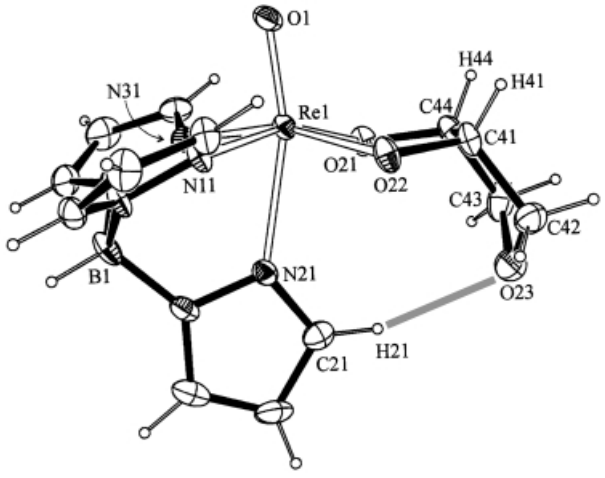

Figure 1. The structure of the H-bonded *anti* isomer of **1**; thermal ellipsoids are drawn at 40% probability; selected bond lengths (Å) and angles (°): Re1−O1 1.683(4), Re1−O21 1.929(4), Re1−O22 1.930(4), Re1−N11 2.095(4), Re1−N31 2.122(4), Re1−N21 2.291(4); O22−C41−C44−O21 −1.2(6); hydrogen bond C21−H···O23 23 3.218(7), H···O23 2.319 Å; C21−H···O23 157.8°; some of the H atoms are labelled to explain the result of an NOE experiment in the text

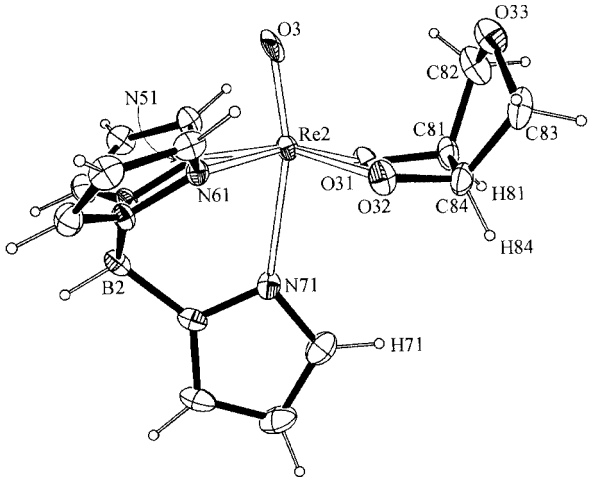

Figure 2. The structure of the *syn* isomer of **1**; thermal ellipsoids are drawn at 40% probability; selected bond lengths (Å) and angles (°): Re2−O3 1.660(4), Re2−O32 1.930(4), Re2−O31 1.932(4), Re2−N51 2.112(4), Re2−N61 2.119(4), Re2−N71 2.261(4); O31−C81−C84−O32 −19.3(6); some H atoms are labelled; in solution NMR studies, an NOE was analysed for these atoms (see text)

In a similar procedure using methyl-β-D-galactopyranoside as the polyol, blue crystals of the diolate complex [(tpb)ReO(Me-β-D-Gal*p*3,4H$_{-2}$)] (**2**) were obtained. Though the diol group with O2 and O3 is the most acidic one, a structure analysis reveals that the carbohydrate ligand binds in an O^3,O^4 bonding mode. Hence the *cis*-diol group of the pyranoside is engaged in complexation, which allows a smaller O−C−C−O torsion angle (Table 1). In **2**, the pyranose ring is found in the *syn* position (*syn* defined as in **1**). A closer inspection of the bonding parameters (Figure 3) shows the ligand to be in an unusual strained conformation. The diol torsion angles O2−C2−C3−O3 and O3−C3−C4−O4 show a 12.8° increase for the free and a 23.7° decrease for the ligating diol group with respect to the free galactoside. Hence the deviation from the unstrained conformation is much larger than would be expected from other galactopyranoside derivatives that have their O3−C3−C4−O4 fragment incorporated into a chelate ring (Table 1). For comparison, the values of the isopropylidene derivative of methyl-β-D-galactopyranoside are included in Table 1, where the differences in bond angles between metalla- (ca. 90°) and carbacycles (110−120°) are very noticeable.

The unexpectedly large distortion of the galactoside on rhenium complexation may be interpreted in terms of a mismatch between the binding sites of the metal and the diol moiety, which should result in a decreased stability of **2** with respect to **1**. In fact, **1** appears to be the product of higher stability: Batches with a 1:1 molar ratio of rhenium and galactoside hardly yielded product. On the other hand,

Table 1. Mean torsion angles τ in five-membered rings where a complex fragment L_nM (or an isopropylidene group in the last table entry) is chelated by a diolate entity derived from methyl-β-D-galactopyranoside; the torsion angles of the free galactoside are 62.9 and 56.0° for O2−C2−C3−O3 and O3−C3−C4−O4, resp.;[a] Δτ is the deviation from τ of the free galactoside; the bond length X−O (X = M or C) is given as a measure for the size of X

L_nM or Me_2C	bonding mode	X−O/Å	τ/°	Δτ/°	Ref.
(tpb)ORe^{V} (**2**)	O^3,O^4	1.944	32.3	−23.7	this work
(L-vsal)OV^{V}	O^3,O^4	2.069	44.2	−11.8	[b]
$(en)_2Co^{III}$	O^2,O^3	1.910	51.8	−11.1	[13]
isopropylidene	O^3,O^4	1.400	35.5	−20.5	[c]

[a] S. Takagi, G. A. Jeffrey, *Acta Crystallogr., Sect. B* **1978**, *34*, 2006−2010. [b] K. K. Rajak, S. P. Rath, S. Mondal, A. Chakravorty, *Inorg. Chem.* **1999**, *38*, 3283−3289; L-vsal is the salicylimide of L-valine; the galactoside ligand is the mono-anion of methyl-2,6-di-*O*-methyl-β-D-galactopyranoside, i.e. the ligand is di-*O*-methylated with respect to the other table entries. [c] P. L. Barili, G. Catelani, G. Fabrizi, D. Lamba, *Carbohydr. Res.* **1993**, *243*, 165−176.

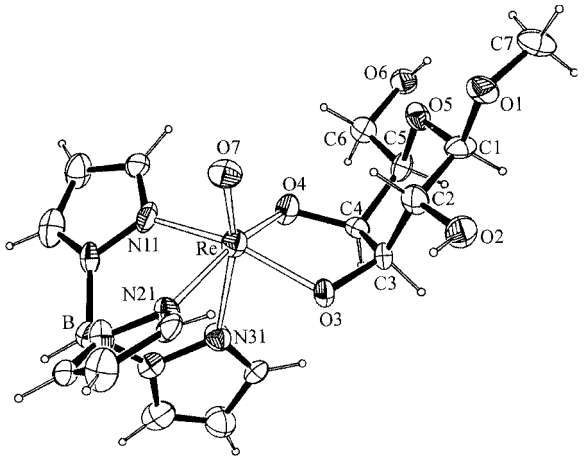

Figure 3. The molecular structure of **2**; thermal ellipsoids are drawn at 30% probability; selected bond lengths (Å) and angles (°): Re−O7 1.709(11), Re−O4 1.927(10), Re−O3 1.960(11), Re−N11 2.087(15), Re−N21 2.125(13), Re−N31 2.242(12); O3−C3−C4−O3 32.3(16), O2−C2−C3−O3 75.7(15); puckering parameters[14] of the pyranose ring: Q = 0.541(16) Å, θ = 20.3(17), φ_2 = 29(5)°

in the case of anhydroerythritol about 40% (instead of about 60% using a fourfold excess of diol) of product was obtained with the 1:1 ratio.

Solution Studies

Although *anti*-**1** and *syn*-**1** are present in equal parts in the asymmetric unit of **1**, they form in different quantities in the course of the reaction of [(tpb)$ReOCl_2$] and anhydroerythritol. After refluxing for two hours in methanol, the mixture consists of three parts of the major isomer and two parts of the minor isomer. Two sets of signals are observed in the ^1H and ^{13}C NMR spectra, and these could be assigned by means of 2D techniques as H21 and H41/H44 on one hand (Figure 1) and H71 and H81/H84 on the other (Figure 2) were well resolved. On irradiation at the frequency of the H81/H84 signal, resonance enhancement of the respective pyrazolyl-H atom (H71) was observed (the mean distance H71···H81 and H71···H84 is 3.0 Å in the crystal structure), and, likewise, irradiation at the frequency of the H71 signal resulted in resonance enhancement of the H81/H84 signal. Hence the *syn* isomer shown in Figure 2 is the minor component of the solution equilibrium. The molar ratio of the isomers depends on the solvent used. In acetonitrile, the solvent used by Brown and Mayer,[7] the *syn*/*anti* ratio increases to 4:1, whereas with water as the medium in a heterogeneous reaction, followed by dissolution of the product in dimethyl sulfoxide, a 5:1 *syn*/*anti* ratio is obtained. It should be noted, however, that due to the kinetic inertness of the complexes, these values obviously do not represent the equilibrium mixture. On prolonged heating of solutions for weeks, the isomer ratio still varies but at the same time decomposition reactions interfere with isomerization.

The ^{13}C NMR signals of both isomers were determined by a "coordination induced shift" ("CIS"), a mostly downfield shift of those carbon atoms that bear the metal-bonded oxygens. Due to the fact that rhenium(v) exhibits both a high valency and a partly filled d-shell, the CIS values are large at 28.1 ppm for *anti*-**1** and 27.1 ppm for the *syn* isomer (the methylene carbons of the oxolane ring are shifted by 3.4 and 3.0 ppm for *anti*- and *syn*-**1**, respectively).

In the case of **2**, the spectra of reaction mixtures from the methanol route consist of two signal sets, which can be assigned to *anti*-O^3,O^4- and *syn*-O^3,O^4-**2**. As with **1**, a large−although not so large−CIS is observed for C3 and C4 in the galactoside complex (Table 2). No signals have been observed that indicate O^2,O^3 isomers in solution, which are the main species in cationic complexes with the trivalent $(en)_2Co^{III}$ fragment (en = ethylenediamine).[13] An assignment of which signal set stems from the *syn* form depicted in Figure 2 was possible from NOE measurements of the same kind that have been described for **1**. These results are collected in Table 2. Despite the fact that *syn*/*anti* isomerism is also observed with **2**, all experiments support the view that no solution equilibria with significant amounts of both isomers are present for the galactoside, but instead the *syn* form is of considerably higher stability than *anti*-**2**.

Table 2. Signal positions of the methyl-β-D-galactopyranosidato(2−) ligand in ^{13}C NMR spectra of solutions of **2** in methanol; in the second and fourth numeric row Δδ, defined by $\delta_{complex} - \delta_{reference}$ is tabulated; the reference is an approximately 0.1 M solution of methyl-β-D-galactopyranoside in [D_4]methanol; Δδ values that indicate a "coordination induced shift" ("CIS") are in bold

		C1	C2	C3	C4	C5	C6	C7
syn-**2**	δ	106.0	72.4	94.8	93.0	78.0	63.7	57.5
	Δδ	−0.3	−0.4	**19.6**	**22.5**	1.1	0.9	0.0
anti-**2**	δ	105.4	71.8	94.9	91.6	78.9	62.7	57.2
	Δδ	−0.9	−1.0	**19.7**	**21.1**	2.0	−0.1	−0.3

Hence, the latter seems to be formed as an unstable intermediate only (note that *anti*-**2** is not stabilized by intramolecular hydrogen bonding). Pure *syn*-**2** is thus accessible and was obtained by several routes. Upon leaving the initial methanol solutions of both forms for about two weeks at room temperature, only *syn*-**2** is detected by NMR spectroscopy. On adding water to the reaction mixture prior to heating, only *syn*-**2** is obtained. Eventually, in a synthetic route using water as the only medium in a heterogeneous reaction, pure *syn*-**2** was also obtained. Solutions of pure *syn*-**2** in various solvents never showed formation of *anti*-**2** on heating.

Conclusion

Oxorhenium(V) complexes are kinetically inert. On reaction with a polyfunctional carbohydrate, many isomeric forms are possible in principle including isomers that are obtained by simple 180° rotation of the ligand normal to the Re=O axis (*syn*/*anti* isomers). Steric and energetic restrictions of the oxo-rhenium centre, however, reduce the number of actual species. In the case of **2**, equilibrium adjustment appears to be more rapid in aqueous media.

Experimental Section

Materials: Methyl-β-D-galactopyranoside (98%) was purchased from Fluka; anhydroerythritol was a gift from Eridania Bégin-Say; dichloro[hydridotris(pyrazolyl)borato]oxorhenium(V) was prepared according to Brown and Mayer's procedure.[7]

Spectroscopic Experiments: ^{1}H and ^{13}C NMR: Jeol EX-400. ^{1}H-^{13}C HMQC and NOE difference spectra: Jeol eclipse +500; mass spectra: Jeol JMS-700 (ionisation method: DEI$^+$). IR: Nicolet 520-FT-IR.

1: [(tpb)ReOCl$_2$] (97 mg, 0.20 mmol), anhydroerythritol (83 mg, 0.80 mmol), triethylamine (80 mg, 0.80 mmol) and 7 mL of methanol were placed in a 25 mL flask. The suspension was refluxed for 2 hours to give a dark blue solution. After cooling to room temperature, the solvent was evaporated and the residue was taken up in 3 mL of dichloromethane. The organic phase was washed

Table 3. Crystallographic data

	1	**2**
Formula	$C_{13}H_{16}BN_6O_4Re$	$C_{16}H_{22}BN_6O_7Re$
M_r/g mol^{-1}	517.322	607.400
Crystal size/mm	0.43 × 0.18 × 0.08	0.10 × 0.08 × 0.02
T/K	200(2)	200(2)
Radiation	Mo-K_α, rotating anode	Mo-K_α, rotating anode
Diffractometer	Nonius Kappa CCD	Nonius Kappa CCD
φ increment/°	1	0.3
Irradiation time/s deg^{-1}	5	80
Crystal system	monoclinic	orthorhombic
Space group	*Cc*	$P2_12_12_1$
a/Å	13.3593(2)	7.2327(8)
b/Å	8.37190(10)	14.840(2)
c/Å	29.3840(3)	19.538(3)
β/°	96.3814(5)	90
V/Å^3	3266.02(7)	2097.0(5)
Z	8	4
Calcd. density/g cm^{-3}	2.10420(5)	1.9239(5)
μ/mm^{-1}	7.474	5.846
Absorption correction	numerical (8 faces)	numerical (6 faces)
Transmission factor range	0.1651−0.5992	0.6075−0.7728
Refls. measured	13849	14707
R_{int}	0.037	0.137
Mean σ(I)/I	0.045	0.084
θ range/°	3.3−27.5	3.2−23.0
Observed refls.	6730	2290
x, y (weighting scheme)	0, 4.6734	0.0109, 22.4633
H refinement	[a]	[a]
Flack parameter	−0.017(6)	−0.02(2)
Refls. in refinement	6879	2894
Parameters	451	283
Restraints	2	0
$R(F_{obs})$	0.023	0.057
$R_w(F^2)$	0.047	0.108
S	1.045	1.115
Shift/error$_{max}$	0.001	0.001
Max. diff. density/e Å^{-3}	0.881	1.335
Min. diff. density/e Å^{-3}	−0.791	−0.747

[a] C-bonded H atoms fixed; O−H vectors were allowed to freely rotate around the C−O axis; U(H) dependent on U(pivot atom).

twice with 3 mL of water to remove triethylamine hydrochloride and unreacted anhydroerythritol, dried over magnesium sulfate and the solvents evaporated to dryness. The dark blue solid was recrystallised from toluene/*n*-pentane (ca. 1:1). Blue crystals formed within a few days at room temperature. NMR spectra of the equilibrium mixture of the two isomers of **1**: ^{1}H NMR (400 MHz, [D$_6$]DMSO, 25 °C): δ = 3.86 (m, 2 H, H82B, H83A), 4.02 (m, 2 H, H82A, H83B), 4.21 (m, 2 H, H42A, H43B), 4.51 (d, $^2J_{H,H}$ = 11 Hz, 2 H, H42B, H43A), 5.58 (m, 2 H, H41, H44), 5.67 (m, 2 H, H81, H84), 6.05 (dd, $^3J_{H,H}$ = 2 Hz, 1 H, H22), 6.06 (dd, $^3J_{H,H}$ = 2 Hz, 1 H, H72), 6.54 (m, 4 H, H12, H32, H52, H62), 7.58 (d, $^3J_{H,H}$ = 2 Hz, 1 H, H71), 7.66 (m, 2 H, H23, H73), 7.90 (m, 4 H, H11, H31, H51, H61), 8.28 (dd, $^3J_{H,H}$ = 2 Hz, 2 H, H53, H63), 8.30 (m, 3 H, H13, H21, H33) ppm. ^{13}C NMR (100.5 MHz, [D$_6$]DMSO, 25 °C): δ = 75.0 (C82, C83), 75.4 (C42, C43), 97.9 (C81, C84), 98.8 (C41, C44), 105.6 (C72), 105.7 (C22), 108.2 (C52, C62), 108.3 (C12, C32), 134.6 (C73), 134.8 (C23), 139.4 (C13, C33, C53, C63), 142.1 (C71), 142.5 (C21), 147.7 (C51, C61), 147.9 (C11, C31) ppm. MS (70 eV): *m*/*z* (%) = 518 (100) [M$^+$], 416 (27) [M$^+$ − C$_4$H$_6$O$_3$]. IR (KBr): $\tilde{\nu}$ = 967 cm^{-1} (s; Re=O). Decomposition on heating to 218−222 °C.

2: [(tpb)ReOCl$_2$] (97 mg, 0.20 mmol), methyl-β-D-galactopyranoside (155 mg, 0.80 mmol), triethylamine (80 mg, 0.80 mmol) and 7 mL of methanol were placed in a 25 mL flask. The suspension was refluxed for 2 hours to give a dark blue solution. After cooling to room temperature the solvent was evaporated and the residue was taken up in 3 mL of dichloromethane. The organic phase was washed twice with 3 mL of water to remove triethylamine hydrochloride and unreacted galactoside. Since the aqueous phase was slightly blue, it was extracted twice with 2 mL dichloromethane. The combined organic phases were dried over magnesium sulfate and the solvent was evaporated. The dark blue solid was recrystallised from chloroform/*n*-pentane (ca. 1:1). Blue crystals formed within a few days at room temperature. The crystal that was investigated by X-ray methods was obtained by this procedure.

Solutions of pure *syn*-**2** were produced by an alternative method using water as the reaction medium: [(tpb)ReOCl$_2$] (97 mg, 0.20 mmol), methyl-β-D-galactopyranoside (155 mg, 0.80 mmol), triethylamine (80 mg, 0.80 mmol) and 7 mL of deoxygenated water were placed in a 25 mL flask. The suspension was refluxed for 3 hours, its colour turning dark blue. The resulting dark blue precipitate was filtered, extracted three times with 5 mL of acetonitrile and the organic phase evaporated to dryness. NMR spectra taken from aqueous preparations: ^{1}H NMR (400 MHz, [D$_4$]MeOH, 25 °C): δ = 3.56 (dd, 2 × $^3J_{H,H}$ = 8 Hz, 1 H, H2), 3.57 (s, 3 H. C7H$_3$), 3.91 (dd, $^3J_{H,H}$ = 7, $^2J_{H,H}$ = 11 Hz, 1 H, H62), 4.01 (dd, $^3J_{H,H}$ = 5, $^2J_{H,H}$ = 11 Hz, 1 H, H61), 4.39 (d, $^3J_{H,H}$ = 8 Hz, 1 H, H1), 4.50 (ddd, $^3J_{H5,H62}$ = 7, $^3J_{H5,H61}$ = 5, $^3J_{H5,H4}$ = 2 Hz, 1 H, H5), 4.80 (dd, $^3J_{H3,H2}$ = 8, $^3J_{H3,H4}$ = 6 Hz, 1 H, H3), 5.20 (dd, $^3J_{H4,H3}$ = 6, $^3J_{H4,H5}$ = 2 Hz, 1 H, H4), 6.03 (dd, 2 × $^3J_{H,H}$ = 2 Hz, 1 H, H32), 6.45, 6.55 (dd, 2 × $^3J_{H,H}$ = 2 Hz, 2 H, H12, H22), 7.54 (d, $^3J_{H,H}$ = 2 Hz, 1 H, H33), 7.70 (d, $^3J_{H,H}$ = 2 Hz, 1 H, H31), 7.99 (d, $^3J_{H,H}$ = 2 Hz, 1 H, H21), 8.00, 8.23 (d, $^3J_{H,H}$ = 2 Hz, 2 H, H23, H13), 8.07 (d, $^3J_{H,H}$ = 2 Hz, 1 H, H11) ppm. ^{13}C NMR (100.5 MHz, [D$_4$]MeOH, 25 °C): δ = 106.7 (C32), 109.0, 109.6 (C12, C22), 136.3 (C33), 139.6, 141.0 (C13, C23), 143.0 (C31), 149.1 (C21), 149.5 (C11) ppm; the signals of the galactoside ligand are collected in Table 2. MS (70 eV): *m*/*z* (%) = 608 (97) [M$^+$], 416 (16) [M$^+$ − C$_7$H$_{12}$O$_6$]. IR (KBr): $\tilde{\nu}$ = 970 cm^{-1} (m; Re=O). Decomposition on heating to 227−235 °C. To obtain pure *syn*-**2** in a homogeneous reaction, the methanol route was slightly altered by replacing the 7 mL quantity of methanol by a mixture of 0.8 mL of water and 6.2 mL of methanol.

X-ray Structure Determinations: Details of the structure analyses are summarized in Table 3. CCDC-179747 (**1**) and CCDC-179738 (**2**) contain the supplementary crystallographic data for this paper. These data can be obtained free of charge at www.ccdc.cam.ac.uk/conts/retrieving.html [or from the Cambridge Crystallographic Data Centre, 12, Union Road, Cambridge CB2 1EZ, UK; Fax: (internat.) +44-1223/336-033; E-mail: deposit@ccdc.cam.ac.uk].

Acknowledgments

This work was supported by the Fonds der Chemischen Industrie, Frankfurt. Anhydroerythritol was gifted by Eridania Bégin-Say, Villefort, Belgium. We are indebted to Dr. P. Mayer and G. Kramer for X-ray measurements.

[1] A. Abrahams, G. Bandoli, S. Gatto, T. I. A. Gerber, J. G. H. Preez, *J. Coord. Chem.* **1998**, *43*, 297−307.
[2] D. Nunes, A. Domingos, A. Paulo, L. Patricio, I. Santos, M. F. N. N. Carvalho, A. J. L. Pombeiro, *Inorg. Chim. Acta* **1998**, *271*, 65−74.
[3] H. Sugimoto, K. Tsuge, K. Tanaka, *Chem. Lett.* **1998**, 719−720.
[4] H. Sugimoto, Y. Sasaki, *Chem. Lett.* **1997**, 541−542.
[5] P. B. Kettler, Y. D. Chang, J. Zubieta, *Inorg. Chim. Acta* **1994**, *218*, 157−165.
[6] A. Paulo, A. Domingos, A. P. Matos, I. Santos, M. F. N. N. Carvalho, A. J. L. Pombeiro, *Inorg. Chem.* **1994**, *33*, 4729−4737.
[7] S. N. Brown, J. M. Mayer, *Inorg. Chem.* **1992**, *31*, 4091−4100.
[8] J. A. Thomas, A. Davison, *Inorg. Chim. Acta* **1991**, *190*, 231−235.
[9] G. Böhm, K. Wieghardt, B. Nuber, J. Weiss, *Inorg. Chem.* **1991**, *30*, 3464−3476.
[10] J. R. Dilworth, S. K. Ibrahim, S. R. Khan, *Polyhedron* **1990**, *9*, 1323−1329.
[11] R. M. Pearlstein, A. Davison, *Polyhedron* **1988**, *7*, 1981−1989.
[12] F. Refosco, F. Tisato, U. Mazzi, *J. Chem. Soc., Dalton Trans.* **1988**, 611−615.
[13] J. Burger, P. Klüfers, *Chem. Ber.* **1995**, *128*, 75−79.
[14] D. Cremer, J. A. Pople, *J. Am. Chem. Soc.* **1975**, *97*, 1354−1358.

Received March 4, 2002
[I02107]

X-ray Structure of a Ruthenium Dinuclear Complex Incorporating 4,4′-Bis(cyanamidophenylethynyl)benzene as a Ligand, a Conjugated Bridge Two Nanometers in Length

Elodie Sondaz,[a] Joel Jaud,[a] Jean-Pierre Launay,[a] and Jacques Bonvoisin*[a]

Keywords: Ruthenium / Bridging ligands / N ligands / X-ray structure

The reaction of [Ru(bpy)(tpy)(Ipcyd)]$^+$ (bpy = 2,2′-bipyridine, tpy = 2,2′:6′,2′′-terpyridine, Ipcyd = 4-iodophenylcyanamide anion) with diethynylbenzene in a Sonogashira cross-coupling reaction gives an unprecedentedly long and conjugated dinuclear complex [{[Ru(bpy)(tpy)]$_2$(μ-dcpeb)}(BPh$_4$)$_2$]·4(PhCH$_3$) (dcpeb = dicyanamidophenylethynylbenzene dianion). The crystal structure data are as follows: crystal system monoclinic, space group $P2_1/c$, with a = 12.6960(3), b = 34.0960(10), c = 15.3540(4) Å, β = 110.7381(15)°, V = 6215.8(3) Å^3, and Z = 2. The structure was refined to a final R factor of 0.063. The metal ions are separated by a through-space distance of 24.9 Å.
(© Wiley-VCH Verlag GmbH, 69451 Weinheim, Germany, 2002)

Introduction

This work concerns the general theme of long distance electronic communication, a topic that is very important in biology[1] and also in molecular electronics.[2] One of our major preoccupations is to find a way to measure the electronic communication between redox sites through a molecular bridge (molecular wire), when the distance between these sites is long enough (>25 Å). Several methods may be followed. One such method was proposed by Crutchley, who found that NCN groups can be very efficient in ensuring a good communication between ruthenium atoms,[3] either in the mixed-valence state, by measuring the electronic coupling parameter (V_{ab}) using optical absorption techniques,[4] or in the homovalent state, by the magnetic exchange parameter (J) using magnetic susceptibility or EPR spectroscopy.[5] Following this line, we recently synthesized a mononuclear ruthenium compound which can be viewed as a starting unit.[6] In this work, we present the use of this unit to make the dinuclear ruthenium compound [{[Ru(bpy)(tpy)]$_2$(μ-dcpeb)}(BPh$_4$)$_2$]·4(PhCH$_3$) (dcpeb = dicyanamidobiphenylethynylbenzene; Scheme 1).

Very few examples of dinuclear ruthenium complexes with long conjugated bridges are known in the literature, and even rarer are those whose X-ray structures have been solved.[5,7−9] We present here the X-ray structure of the first such dinuclear ruthenium complex with a long conjugated bridge, the through-space internuclear distance reaching 24.9 Å.

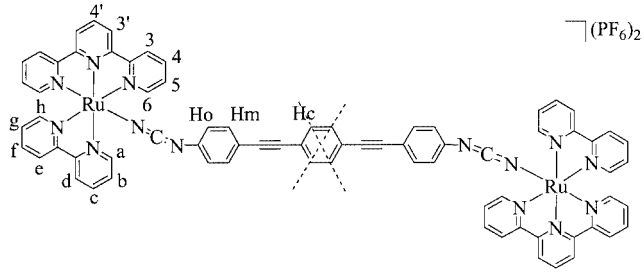

Scheme 1

Results and Discussion

The dinuclear compound was obtained by a Sonogashira cross-coupling reaction[10] adapted to the iodoruthenium complex. The use of the iodo complex was justified by its high reactivity in this kind of coupling (yield: 89%).[11]

The complex crystallises in the $P2_1/c$ space group (for crystallographic data see Table 1). The asymmetric unit consists of half a molecule of **2**, the central phenyl group lying on the inversion center. The tetraphenylborate anions are found near the angle of the bent phenylcyanamido unit, and toluene molecules fill the remaining voids of the structure.

The general shape of the molecule is a dumb-bell (see Figure 1). Interestingly, there are few reports of crystal structures containing such molecular shapes. Thus Crutchley has described the crystal structures of dinuclear complexes with dicyanamidobenzene as a bridging ligand and either [Ru(NH$_3$)$_5$]$^{3+}$,[5] *trans*-[Ru(NH$_3$)$_4$(py)]$^{3+}$ [12] or *mer*-[Ru(NH$_3$)$_3$(bpy)]$^{3+}$ [13] as terminal units (metal−metal distances 13.1, 10.9, and 13.1 Å, respectively). More recently, he has also reported the structure of [Ru(bpy)(tpy)-μ(adcp)-

[a] CEMES-CNRS, Molecular Electronics Group,
BP 4347, 29 rue Jeanne Marvig, 31055 Toulouse cedex 4, France
Fax: (internat.) + 33-5/6225-7999
E-mail: jbonvoisin@cemes.fr

Table 1. Crystal and experimental data

Formula	$C_{150}H_{122}B_2N_{14}Ru_2$
Crystal system	Monoclinic
M(g mol^{-1})	2344.38
Space group	$P2_1/c$
a, Å	12.6957(3)
b, Å	34.0958(10)
c, Å	15.3541(4)
β	110.738(2)
V, Å^3	6215.7(3)
Z	2
λ (Mo-K_α), Å	0.71074
Calculated ρ, g cm^{-3}	1.253
2θ max, °	56
No of reflections used	26985
R_{int}	0.037
No of unique reflections	9732
No of unique reflections with $I > 3\sigma(I)$	6468
Number of variables	631
Shape	Near spherical
Absorption correction	Radius 0.1
R_{int} after correction	0.035
T min/max	0.956/0.956
$R_f = \Sigma\|\|F_0\| - \|F_c\|\|/\Sigma\|F_0\|$	0.063
$R_w = [\Sigma w(\|F_0\| - \|F_c\|)^2/\Sigma\|F_0\|^2]^{1/2}$	0.068
Agreement factor	1.648

Ru(bpy)(tpy)]·$(PF_6)_2$·DMF, where adpc is the 4,4′azodi-(phenylcyanamido) dianion (metal−metal distance 19.5 Å).[9] The present molecule is longer still, with a Ru−Ru distance of 24.9 Å.

The scarcity of crystal structures with dumb-bell molecules is probably due to the fact that it is impossible to densely pack molecules made up of bulky ends connected by a thinner spacer.[14] This is why our strategy was to attempt crystallisation in the presence of a large counterion (tetraphenylborate) and also of a large solvent (toluene). Our expectation was that the large counterion and solvent molecules could fill the voids and thus stabilise the crystal structure, as already observed by Jetti et al. in the case of the dimer of 4-(triphenylmethyl)benzoic acid in the presence of either xylene or chlorobenzene.[14]

The ruthenium moiety [Ru(bpy)(tpy)(cyanamido)] is at first sight similar to the mononuclear compound described elsewhere,[6] with the NCN group in the plane of the phenylene group to which it is linked (see Figure 2). This geometry ensures a good conjugation of their π systems. The bipyridine and terpyridine planes are perpendicular, with the bipyridine plane bisecting the terpyridine. The phenylcyanamido moiety makes a dihedral angle of 79° with the bipyridine plane (see Figure 2), while this value is 28° for the mononuclear compound[6] and 58° for [Ru(bpy)(tpy)-μ(adcp)-Ru(bpy)(tpy)]$^{2+}$.[9] Since the phenylcyanamido ligand and bipyridine are not coplanar, the Ru(bpy)(tpy)-(phenylcyanamido) group is *chiral*; the two enantiomers are present in the same molecule. In solution, on the other hand, it is likely that all possible isomers are present, although because of the length of the molecule, each of the extremities of a single molecule behaves as if it were isolated with regards to the NMR spectrum.

The Ru−N(6)−C(26) moiety is slightly bent (161.5°), suggesting that the π interaction is weaker than in Ru^{III}-cyanamide complexes, for which it is almost linear.[15] The Ru−N(6) bond is shorter (2.024 Å) than in the mononuclear compound (ca. 2.08 Å), and comparable to the one observed in the complex with adpc (2.046 Å). Concerning the cyanamido group itself, one notices a short distance between the terminal nitrogen and the central carbon [N(6)−C(26) = 1.136(7) Å], showing the preponderance of the cyanamide form [$^-$N−C≡N] over the carbodiimide [-N=C=N] form.

The cyanamido groups of the $(dcpeb)^{2-}$ ligand adopt a *trans* disposition, as generally observed in dinuclear bis-cyanamido complexes,[5] and free ligands $(dicyd)(AsPh_4)_2$ [16] and $(dcpib)(AsPh_4)_2$,[17] where dcpib = 4,4′-dicyanamidobiphenyl. The only exception is $[\{Ru(NH_3)_4(py)\}_2\mu\text{-}(dicyd)]^{4+}$ where the cyanamide groups are *cis*.[12] The C(33)−C(34)

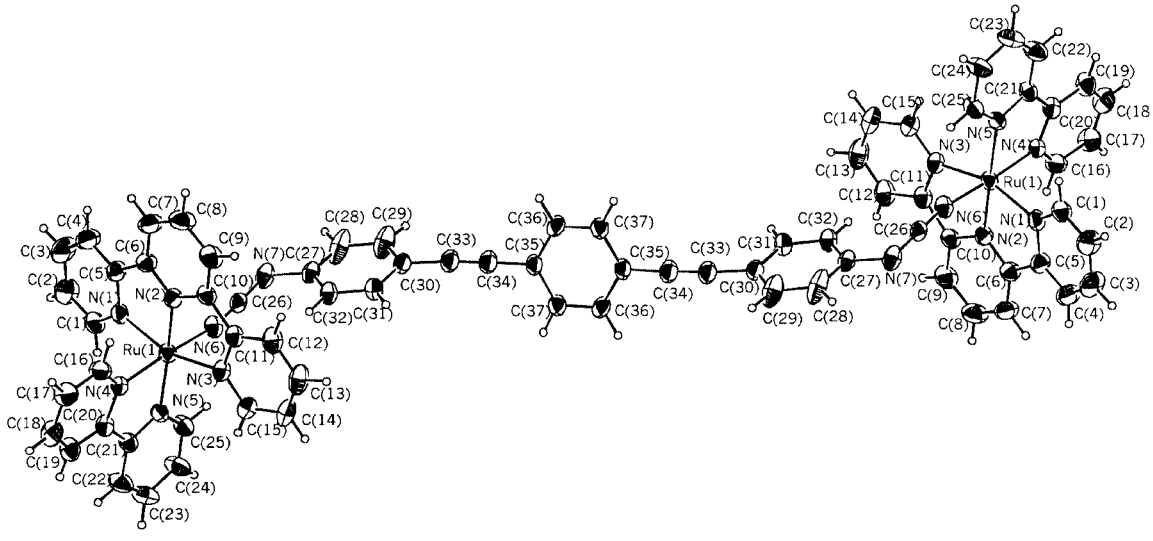

Figure 1. ORTEP drawing of the molecule of **2**

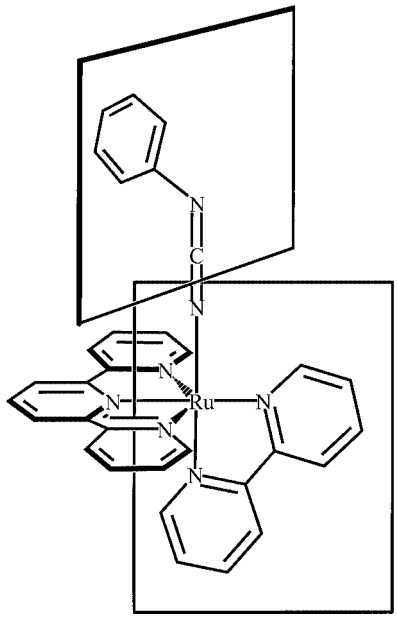

Figure 2. Coordination around ruthenium; definition of the dihedral angle between the bipyridine plane and the phenylcyanamido plane

triple bond length is 1.1863 Å, a value similar to the case of [Ru(bpy)(tpy)(pa)]$(PF_6)_2$·acetone (1.175 Å) and [Ru(bpy)(tpy)(ppa)]$(PF_6)_2$·acetone (1.187 Å) (pa = pyridylacetylene, and ppa = phenylpyridylacetylene).[18]

Of the three phenylene groups, the outer two are coplanar because of the inversion center. The dihedral angle with the central phenylene group is 65°. This value is probably not determined by intramolecular interactions, because it is known that torsion barriers around a phenylethynyl link are very small, ca. 1 kcal.[19] It is more likely determined by packing interactions. Thus, a detailed inspection of the structure shows many H···H Van der Waals contacts between the bulky Ru(bpy)(tpy) groups and tetraphenylborate and toluene molecules (H···H distances 2.60 to 2.80 Å, with an exceptionally short contact at 2.28 Å between a tpy H and a tetraphenylborate H). Consequently, the outer parts are locked in fixed positions. If free to rotate, the central phenylene group should prefer a coplanar disposition,[19] but this is prevented by a weak contact with a tetraphenylborate (H···H 2.51 Å and 2.70 Å) on one side, and with a toluene molecule on the other side.

Owing to the low torsional barrier, it is very likely that in solution there is a distribution of dihedral angles bearing on two independent torsions: between one terminal phenylene and the central one, and between the central one and the other terminal phenylene.

As far as physicochemical studies are concerned, UV/Vis spectroscopic studies of compound **1** in DMF shows two types of bands, one attributed to a $\pi\rightarrow\pi^*$ transition at 293 (94600) and 315 nm (86400 M^{-1} cm^{-1}) and the other attributed to metal-to-ligand charge-transfer bands at 397 (69800) and 493 nm (16800 M^{-1} cm^{-1}) as in similar compounds.[20,21] The cyclic voltammogram of **1** in dimethylformamide shows a quasi-reversible one-electron wave at 0.752 V vs. SCE which becomes irreversible in acetonitrile and dichloromethane. Attempts to prepare oxidized species did not lead to the appearance of any intervalence transition

Experimental Section

Physical Measurements. Electrospray (positive mode) mass spectra were obtained with a Perkin−Elmer Sciex (Nermag R10-R10) spectrometer. IR spectra were recorded as KBr pellets on a Perkin−Elmer FT-IR 1725 spectrometer. UV/Vis electronic spectra were obtained with a Shimadzu UV-3100 spectrometer. ^{1}H NMR spectra were recorded on a Bruker WF-250 spectrometer in CD_3CN solution. The solvent signal was used as internal reference at [δ_H = 1.96 ppm (CD_3CN)]. Cyclic voltammograms were obtained with an Autolab system (PGSTAT 100) (0.1 M tetrabutylammonium hexafluorophosphate, TBAH as supporting electrode) at 25 °C. A three-electrode cell was used comprising a 1 mm Pt-disk working electrode, a Pt-wire auxiliary electrode, and an aqueous saturated calomel (SCE) reference electrode.

{[Ru(bpy)(tpy)]$_2$(μ-dcpeb)}$(PF_6)_2$ (1): [Ru(bpy)(tpy)(Ipcyd)](PF_6)[6] (250 mg, 0.28 mmol) was placed in a small Schlenk tube together with [$PdCl_2(PPh_3)_2$] (4 mg, 0.007 mmol) and CuI (3 mg, 0.014 mmol). The powders were dissolved in a piperidine/DMF (1:1) mixture (3 mL) and carefully degassed under vacuum/argon several times. After stirring for 15 minutes, diethynylbenzene (18 mg, 0.14 mmol) was added to the solution. The reaction was continued all night at room temperature under argon. The solvents were then removed under vacuum and the product purified on an acidic alumina column (toluene/acetonitrile 60:40). The starting material was eliminated as a pink band, and a brown fraction of the dinuclear compound was then obtained. Recrystallisation was achieved by addition of toluene to an acetonitrile solution of **1**, which crystallised as long black needles (206 mg, 89%). IR (KBr disc): $\tilde{\nu}$ = 2160 cm^{-1} (N=C=N). ^{1}H NMR (250 MHz, CD_3CN, 20 °C, TMS): δ = 9.76 (d, *J* = 5.7 Hz, 2 H, H-a), 8.62 (d, *J* = 8.1 Hz, 2 H, H-d), 8.53 (d, *J* = 8.1 Hz, 4 H, H-3′), 8.42 (d, *J* = 8.1 Hz, 4 H, H-3), 8.32 (d, *J* = 7.9 Hz, 2 H, H-e), 8.28 (td, *J* = 8.1, 7.7 Hz, 2 H, H-c), 8.17 (t, *J* = 7.7, 8.5 Hz, 2 H, H-4′), 7.95 (t, *J* = 7.7, 8.1 Hz, 4 H, H-4), 7.95(m, 2 H, H-b), 7.73 (m, 6 H, H_{6+f}), 7.39 (s, 4 H), 7.37 (dq, *J* = 6.5 Hz, 2 H, H-h), 7.32 (dd, *J* = 5.5, 7.7 Hz, 4 H, H-5), 7.21 (d, *J* = 7.3 Hz, 2 H, H-g), 7.02 (d, *J* = 8.7 Hz, 4 H, H-m,m′), 6.07 (d, *J* = 8.7 Hz, 4 H, H-o,o′). (see Scheme 1 for atom numbering). MS (ES) for $C_{74}H_{50}F_6N_{14}PRu_2$ [M − PF_6]$^+$: *m*/*z*: calcd. 1483.2; found 1483.3; for [M − $2PF_6$]$^{2+}$/2: calcd. 669.3; found 669.1; for [M − $2PF_6$ − [Ru(bpy)(tpy)] + H^+]$^+$: calcd. 848.2; found 848.2. $C_{74}H_{50}F_{12}N_{14}P_2Ru_2(Al_2O_3)$ (1730.1): calcd. C 51.3, H 2.9, N 11.3; found C 51.4, H 2.8, N 11.0.

{[Ru(bpy)(tpy)]$_2$(μ-dcpeb)}$(BPh_4)_2$.4(Ph-CH_3) (2): Compound **1** was dissolved in acetonitrile. Subsequent addition of tetrabutylammonium bromide (in excess) precipitated the bromide salt of the complex, which was filtered and rinsed with ether. Dissolution of the bromide salt in methanol/water (1:1 mixture), followed by addition of sodium tetraphenylborate (excess) precipitated [{Ru(bpy)(tpy)]$_2$(μ-dcpeb)}]$(BPh_4)_2$. Slow diffusion of toluene into an acetonitrile solution of [{Ru(bpy)(tpy)]$_2$(μ-dcpeb)}]$(BPh_4)_2$ led to the desired complex **2**.

X-ray Crystallographic Study: Recrystallisation was performed by slow diffusion of toluene into an acetonitrile solution of the tetraphenylborate salt of the complex. Brown needles were obtained. A

single crystal was chosen to perform the X-ray diffraction measurements. Reflection data for the crystal were measured using a Nonius Kappa CCD diffractometer at room temperature, using graphite monochromated Mo-K_α radiation ($\lambda = 0.71074$ Å) at a detector distance of 4 cm and a swing angle of 20° (this type of crystal, being unfortunately very small, and showing poor quality of crystallinity, did not give observable spots at wider angles). To increase the quality of the collected data, we tried to perform measurements at low temperature, but the crystal broke due to the very poor mosaicity found at room temperature. The crystallographic cell was found by using HKL Scalepack.[22] The structure was solved using SIR92[23] and refined in the Maxus software package.[24]

The asymmetric unit contains a tetraphenylborate counteranion, and two toluene solvent molecules. The refinement was performed anisotropically for all the non-hydrogen atoms of the complex. The hydrogen atoms were localized by difference Fourier synthesis, recalculated and fixed at 0.96 Å, then their contributions were introduced in the calculations but not refined. For the toluene atoms, due to their high thermal vibration, they were refined in isotropic positions; nevertheless it was difficult to position them, so for the last refinement, they were left fixed at their last atomic positions in order not to disturb the overall geometry of the complex. 6468 reflections [$I > 3\sigma(I)$] were used for the 631 parameters and the R value dropped to 0.0634.

CCDC-179708 contains the supplementary crystallographic data for this paper. These data can be obtained free of charge at www.ccdc.cam.ac.uk/conts/retrieving.html [or from the Cambridge Crystallographic Data Centre, 12, Union Road, Cambridge CB2 1EZ, UK; Fax: (internat.) +44-1223/336-033; E-mail: deposit@ccdc.cam.ac.uk].

Acknowledgments

We thank Christine Viala for technical help, and MENRT for a thesis grant to E. S.

[1] H. B. Gray, J. R. Winkler, in *Electron Transfer in Chemistry, Vol. 3* (Ed.: V. Balzani), Wiley-VCH, Weinheim, New York, Chichester, Brisbane, Singapore, Toronto, **2001**, pp. 3−23.
[2] J.-P. Launay, *Chem. Soc. Rev.* **2001**, *30*, 386−397.
[3] R. J. Crutchley, *Adv. In Inorg. Chem.* **1994**, *41*, 273−325.
[4] A. R. Revzani, C. E. B. Evans, R. J. Crutchley, *Inorg. Chem.* **1995**, *34*, 4600−4604.
[5] M. A. S. Aquino, F. L. Lee, E. J. Gabe, C. Bensimon, J. E. Greedan, R. J. Crutchley, *J. Am. Chem. Soc.* **1992**, *114*, 5130−5140.
[6] E. Sondaz, A. Gourdon, J.-P. Launay, J. Bonvoisin, *Inorg. Chim. Acta* **2001**, *316*, 79−88.
[7] M. Beley, J.-P. Collin, R. Louis, B. Metz, J.-P. Sauvage, *J. Am. Chem. Soc.* **1991**, *113*, 8521−8522.
[8] D. J. Szalda, F. Fagalde, N. E. Katz, *Acta Crystallogr., Sect. C* **1996**, *52*, 3013−3016.
[9] P. J. Mosher, G. P. A. Yap, R. J. Crutchley, *Inorg. Chem.* **2001**, *40*, 1189−1195.
[10] K. Sonogashira, Y. Tohda, N. Hagihara, *Tetrahedron Lett.* **1975**, *50*, 4467−4470.
[11] S. Takahashi, Y. Kuroyama, N. Sonogashira, N. Hagihara, *Synthesis* **1980**, 627−630.
[12] A. R. Revzani, C. Bensimon, B. Cromp, C. Reber, J. E. Greedan, V. V. Krondatiev, R. J. Crutchley, *Inorg. Chem.* **1997**, *36*, 3322−3329.
[13] C. E. B. Evans, G. P. A. Yap, R. J. Crutchley, *Inorg. Chem.* **1998**, *37*, 6161−6167.
[14] R. K. R. Jetti, S. S. Kuduva, D. S. Reddy, F. Xue, T. C. W. Mak, A. Nangia, G. R. Desiraju, *Tetrahedron Lett.* **1998**, *39*, 913−916.
[15] R. J. Crutchley, K. McCaw, F. L. Lee, E. J. Gabe, *Inorg. Chem.* **1990**, *29*, 2576−2581.
[16] M. A. S. Aquino, R. J. Crutchley, F. L. Lee, E. J. Gabe, C. Bensimon, *Acta Crystallogr., Sect. C* **1993**, *49*, 1543−1547.
[17] M. A. S. Aquino, C. A. White, C. Bensimon, J. E. Greedan, R. J. Crutchley, *Can. J. Chem.* **1996**, *74*, 2201−2208.
[18] S. C. Rasmussen, S. E. Ronco, D. E. Mlsna, M. A. Billadeau, W. T. Pennington, J. W. Kolis, J. D. Petersen, *Inorg. Chem.* **1995**, *34*, 821−829.
[19] J. M. Seminario, A. G. Zacarias, J. M. Tour, *J. Am. Chem. Soc.* **1998**, *120*, 3970−3974.
[20] C. R. Hecker, P. E. Fanwick, D. R. McMillin, *Inorg. Chem.* **1991**, *30*, 659−666.
[21] F. R. Fletcher, F. R. Keene, *J. Chem. Soc., Dalton Trans.* **1998**, 2293−2301.
[22] Z. Otwinowski, W. Minor, in *Methods in Enzymology, Vol. 276* (Eds.: C. W. Carter, R. M. Sweet), Academic Press, New York, **1997**, pp. 307−326.
[23] A. Altomare, G. Cascarano, C. Giacovazzo, A. Guagliardi, M. C. Burla, G. Polidori, M. Camalli, *J. Appl. Cryst.* **1994**, *27*, 435−435.
[24] S. Mackay, C. J. Gilmore, C. Edwards, N. Stewart, K. Shankland, in *maXus Computer Program for the Solution and Refinement of Crystal Structures.,* Nonius, The Netherlands, MacScience, Japan & the University of Glasgow, **1999**.

Received February 18, 2002
[I02090]

Novel Ru^{III}-DMSO Complexes of the Antiherpes Drug Acyclovir

Iztok Turel,*[a] Milena Pečanac,[a] Amalija Golobič,[a] Enzo Alessio,[b] and Barbara Serli[b]

Keywords: Bioinorganic chemistry / Nucleoside analogues / Ruthenium / X-ray diffraction / Hydrogen bonds

Treatment of the anionic Ru^{III} precursor X[*trans*-$RuCl_4$(DMSO-*S*)$_2$] (X = protonated DMSO, Na^+, NH_4^+) and acyclovir (acv) in various solvents yields two new products *mer*-[$RuCl_3$(acv)(DMSO-*S*)(CH_3OH)]·0.5CH_3OH (**1**) and *mer*-[$RuCl_3$(acv)(DMSO-*S*)(H_2O)]·H_2O (**2**) in which hydrogen bonds between the acv purine oxygen and coordinated methanol or water, respectively, play an important role.

(© Wiley-VCH Verlag GmbH, 69451 Weinheim, Germany, 2002)

The antitumor properties of simple ruthenium(III) coordination compounds were discovered over 30 years ago,[1] and since then several tumor-inhibiting ruthenium complexes have been isolated and characterized,[2] with DMSO-ruthenium-N donor ligand ternary complexes being amongst the most promising. The typical example of the group, NAMI-A, [ImH] [*trans*-$RuCl_4$(DMSO-*S*)Im] (Im = imidazole), has already entered clinical phase I trials.[3] The main advantages of ruthenium-DMSO complexes are the selectivity for solid tumor metastases and the lack of significant host toxicity.

Acyclovir [9-(2-hydroxyethoxymethyl)guanine, acv] is a well-known antiviral drug used in clinical practice. The crystal structures of acv complexes with Cu,[4] Pt,[5] Ni, Co, Cd and Zn,[6] have appeared in the literature. It was found that the coordination of acv to the metal occurs in most cases through N(7) only, whereas O(6) is not directly involved in the bonding. The sole exception is [$Cu(acv)_2(H_2O)_2$](NO_3)$_2$, in which a pseudo-chelate N(7)/O(6) bonding of a purine to the metal was found.[4c]

Recently, the interactions of two Ru^{II}-DMSO precursors, *cis*- and *trans*-[$RuCl_2$(DMSO)$_4$], with acv were studied by NMR spectroscopy in aqueous solution. The authors proposed the formation of mono and bis adducts with N(7) as the preferred binding site.[7]

Our basic idea was to prepare an NAMI-A type compound of acv with the formula [*trans*-$RuCl_4$(acv)(DMSO-*S*)]$^-$. The main chemical feature of the Ru^{III} anionic precursor of NAMI-A type complexes, X[*trans*-$RuCl_4$(DMSO-*S*)$_2$] (X = protonated DMSO, Na^+, NH_4^+), is the facile dissociation of one of the two *trans* S-bonded DMSOs, attributed to the relatively large *trans* effect of this ligand.[8] The coordination position set free by DMSO is easily replaced by a nitrogen donor ligand (L) and through this synthetic procedure a wide class of derivatives with the general formula X[*trans*-$RuCl_4$(DMSO-*S*)L] (NAMI-A type complexes) have been prepared from acetone or DMSO/acetone mixtures. In these reactions it has never been observed that chloride ions were substituted; nevertheless, stepwise chloride hydrolysis occurs after dissolution of these products at physiological pH and it is thus relevant for their in vivo mechanism of action.

The generally poor solubility of acv limits the choice of solvents in which the reaction with the Ru^{III} precursor could be performed. Surprisingly, we realized that, regardless of the solvent used, coordination of acv trans to DMSO-S was always accompanied by replacement of one chloride with a molecule of a hydrogen bond donor, either H_2O (adventitious or solvent) or methanol (solvent), to give neutral species. In this paper we report the synthesis and solid-state structures of two Ru^{III}-DMSO complexes of acv:

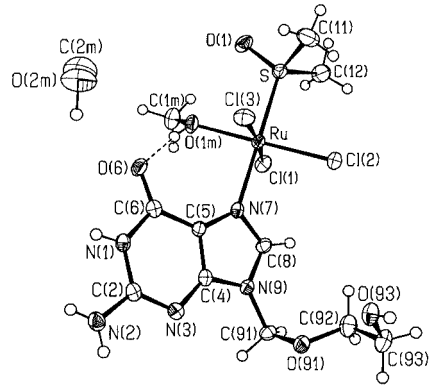

Figure 1. View of the asymmetric unit of **1**; selected bond lengths (Å): Ru−Cl(1) 2.309(2), Ru−Cl(2) 2.326(2), Ru−Cl(3) 2.362(2), Ru−S 2.270(2), Ru−O(1m) 2.072(6), Ru−N(7) 2.127(5), O(6)−C(6) 1.245(8)

[a] University of Ljubljana, Faculty of Chemistry and Chemical Technology,
Askerčeva 5, 1000 Ljubljana, Slovenia
Fax: (internat.) +386-1/241-9220
E-mail: iztok.turel@uni-lj.si
[b] University of Trieste, Department of Chemical Sciences,
Via L. Giorgieri 1, 34127 Trieste, Italy

mer-[$RuCl_3$(acv)(DMSO-*S*)(CH_3OH)]·0.5CH_3OH (**1**) and *mer*-[$RuCl_3$(acv)(DMSO-*S*)(H_2O)]·H_2O (**2**), which provide a new insight into the reactivity of the [*trans*-$RuCl_4(DMSO)_2]^-$ precursor and, in particular, show the important role of H bonds in these reactions.

Treatment of X[*trans*-$RuCl_4$(DMSO-*S*)$_2$] with acv in methanol yielded brown-red crystals of **1**; when the same reaction was performed in water or various nondried solvents (such as ethanol, propanol, acetone/DMSO mixtures, nitromethane) crystals of **2** were isolated instead. The structures of compounds **1** and **2** were determined by X-ray diffraction analysis; the asymmetric unit and selected bond lengths for each compound are reported in Figure 1 and 2, respectively, and the crystallographic data in Table 1.

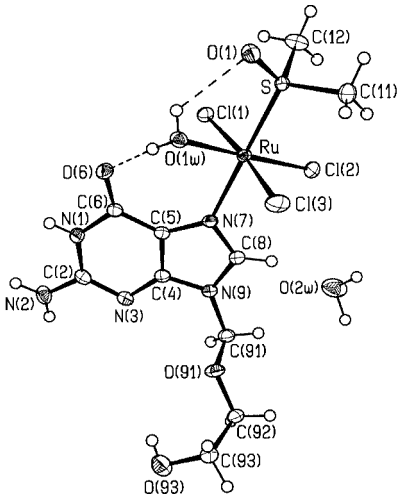

Figure 2. View of the asymmetric unit of **2**; selected bond lengths (Å): Ru−Cl(1) 2.3686(4), Ru−Cl(2) 2.3187(5), Ru−Cl(3) 2.3210(6), Ru−S 2.2677(5), Ru−O(1w) 2.077(1), Ru−N(7) 2.132(2), O(6)−C(6) 1.247(3)

In both complexes **1** and **2** the geometry about the Ru^{III} ion is distorted octahedral, as expected, with three chloride ions in a *mer*-configuration and DMSO (coordinated through S) *trans* to acv. An oxygen atom from methanol (in **1**) or water (in **2**) is additionally coordinated to ruthenium. The ruthenium-oxygen distances in both compounds are similar and are also similar to those found in the literature.[9] In both complexes one Ru−Cl bond is significantly longer than the remaining two since only that chloride ion is an acceptor of an intermolecular hydrogen bond. In **1**, Cl(3) is hydrogen bonded to an amino group of the symmetry related complex [contact distance N(2)···Cl(3) 3.298(6) Å], whereas in **2**, Cl(1) is hydrogen bonded to a noncoordinated water molecule [contact distance O(2w)···Cl(1) 3.291(2) Å] and to an amino group of the symmetry related complex [contact distance N(2)···Cl(1) 3.445(2) Å]. The shortening of the Ru−S bond in these complexes relative to the precursor (above 2.34 Å) has already been interpreted as being due to an increased π-back-bonding contribution from Ru^{III}.[8,10] All other bond lengths and angles in both compounds are also in an agreement with the corresponding data cited in the literature.[11]

Table 1. Crystallographic data for **1** and **2**

	1	**2**
Formula	$C_{11.5}H_{23}Cl_3N_5O_{5.5}RuS$	$C_{10}H_{21}Cl_3N_5O_6RuS$
Molecular weight	558.84	546.8
Crystal system	monoclinic	monoclinic
Space group	*C*2/*c*, No. 15	$P2_1/c$, No. 14
a (Å)	23.3032(4)	10.5096(1)
b (Å)	14.4930(3)	13.5455(1)
c (Å)	13.0879(3)	13.9131(1)
β (°)	110.7292(8)	104.331(1)
V (Å^3)	4134.07(15)	1919.00(3)
Z	8	4
Crystal size (mm)	0.20 × 0.10 × 0.03	0.32 × 0.30 × 0.25
Crystal description	plate	prism
Crystal colour	brown-red	brown-red
D_x (Mg m^{-3})	1.795	1.892
μ (mm^{-1})	1.283	1.381
T (K)	150(1)	150(1)
Wavelength (Å)	0.71073 (Mo-K_α)	0.71073 (Mo-K_α)
Data-collection mode	ω scans	ω scans
θ_{max} (°)	27.5	27.5
No. of integrated refl.	29217	36309
R_{int}	0.040	0.023
No. of unique refl.	4724	4393
No. of observed refl.	3948	4047
Threshold criterion	$F^2 > 2\sigma(F^2)$	$F^2 > 2\sigma(F^2)$
Final *R* and R_w	0.037, 0.034	0.026, 0.025
No. of contributing. refl.	4409	4211
No. of parameters	249	299
$(\Delta/\sigma)_{max}$	0.0005	0.004
$\Delta\rho_{max}$, $\Delta\rho_{min}$ (e Å^{-3})	0.98, −1.13	0.69, −1.20

Whereas the replacement of one DMSO-S molecule in the precursor with the N-donor ligand acv is to be expected, further replacement of one of the four chloride ions by the oxygen-bearing ligand is rare. We have tried to prevent the dissociation of the chloride ion from ruthenium by increasing the concentration of chloride in solution [by addition of $(CH_3)_4NCl$ or NaCl]. However one of the four chloride ions attached to ruthenium in the precursor was again substituted by water and the final product of this reaction was **2**. To date, syntheses performed in anhydrous solvents under inert atmosphere did not result in the isolation of the NAMI-A type acv analogue, which is another proof that such a reaction is not favourable in the case of acv.

Inspection of the crystal structures of both compounds suggests that the replacement of chloride with methanol (in **1**) or water (in **2**) is induced by the formation of intramolecular hydrogen bonds (marked with dashed lines in Figure 1 and 2). The oxygen atom O(6) from acv is hydrogen bonded to either coordinated methanol (**1**) or water (**2**). Both hydrogen bonds are strong: contact distance O(1m)···O(6) 2.517(7) Å in **1** and O(1w)···O(6) 2.573(2) Å in **2**. In **2**, the second hydrogen atom of water is additionally involved in hydrogen bonding to the oxygen atom of DMSO [contact distance O(1w)···O(1) 2.918(2) Å]. (In both structures there are additional intermolecular hydrogen bonds which are described in the CIF supplementary material deposited with the CCDC).

The neutral species **1** and **2**, which still maintain some solubility in aqueous solution, are thus good models for the first intermediate species that is expected to form upon stepwise chloride hydrolysis from NAMI-A type complexes in physiological solution. We are aware of only two examples where a similar chloride replacement was reported. The complex *mer*-[$RuCl_3(H_2O)$(DMSO-*S*)(dmtp)]·H_2O[12] was prepared by the dissolution of dmtpH[*trans*-$RuCl_4$(dmtp)(DMSO-*S*)] (dmtp = 5,7-dimethyl[1,2,4]triazolo[1,5-*a*] pyrimidine) in water, and strong hydrogen bonds between coordinated dmtp and coordinated water were also found in this case. Just recently it was reported that treatment of [$(dmso)_2H$][*trans*-$RuCl_4$(DMSO-*S*)$_2$] with 9-ethylguanine (9EtG) in methanol yielded *mer*-[$RuCl_3$(9EtG)(H_2O)(DMSO-*S*)] (**3**), in which the coordination sphere of ruthenium is very similar to that of **2**; the X-ray structure showed that the coordinated water molecule is involved in strong intramolecular hydrogen bonding with the oxygen atoms of guanine and DMSO-S.[13] The chemical difference between **3** and **2** is in the group bonded to N(9); instead of the ethyl group of **3** there is a 2-hydroxyethoxymethyl in **2** which, besides being bulkier, also acts as a donor and acceptor of intermolecular H bonds. Additionally, the crystals of **2** also contain noncoordinated water molecules and the consequence of this is that the packing of **3** and that of **2** are substantially different. In the structure of **3** there are N(1)−H···Cl(3) and N(2)−H···O(2) intermolecular H bonds, while in the structure of **2** intermolecular H bonds N(1)−H···O(1), N(2)−H···O(93), N(2)−H···Cl(1), O(93)−H···O(2w), O(2w)−H···N(3) and O(2w)−H···Cl(1) are present. Furthermore, in **3** the stacking of guanine residues was not observed. In contrast, in the structures of **1** and **2** we have observed pairs of symmetry-related acv residues for which the planes through their aromatic rings are nearly parallel. The distances between such planes are 3.25 Å in **1** and 3.50 Å in **2**, so the interactions between π electronic systems are possible.

The IR spectra of compounds **1** and **2** are very similar. In free acv the carbonyl stretching band is found at 1715 cm^{-1} whereas the bending frequency of the amino group falls at 1631 cm^{-1}.[4] Four bands are found in the spectra of both complexes in the range 1657−1630 cm^{-1}. According to the crystal structures, we assume that these absorptions can be ascribed to the stretching of the hydrogen bonded carbonyl group and to the bending of the hydrogen bonded amino group. A similar trend was previously observed in other N(7) metal-bonded complexes of acv.[4a,6]

The UV/Vis spectra of **1** and **2** were assigned according to the data of similar complexes reported in the literature.[8,12,14] The highest energy band found at 278 nm in both complexes was attributed to π-π* transitions of the ligand,[14] whereas the remaining absorptions are typical charge-transfer bands from three chlorides in a *mer*-geometry on Ru^{III}.[15]

Experiments to assess the possible cytotoxic and antiviral activity of compounds **1** and **2** are currently being planned in collaboration with other groups.

Experimental Section

***mer*-[$RuCl_3$(acv)(DMSO-*S*)(CH_3OH)]·$0.5CH_3OH$ (1):** X[*trans*-$RuCl_4$(DMSO-*S*)$_2$] (0.235 mmol) was dissolved in absolute methanol (30.0 mL) and acv (0.235 mmol) was added whilst stirring. The solution was heated at 50 °C until all acv had dissolved. The colour of the solution changed from orange to brown-yellow. Brown-red crystals appeared in the solution after one day of isothermal evaporation of the solvent in air (0.0723 g, 55.2% yield). The crystals were filtered off, washed with diethyl ether and dried in air. $C_{11.5}H_{23}Cl_3N_5O_{5.5}RuS$ (558.8): calcd. C 24.71, H 4.15, N 12.53; found C 24.61, H 4.08, N 12.59. Selected IR bands (Nujol): $\tilde{\nu}$ = 1657 cm^{-1} (s, sh), 1650 (s, sh), 1640 (vs), 1634 (vs), 1608 (s); 1082 (m, S=O for DMSO-*S*); 423 (w, Ru−*S*). UV (methanol): λ_{max} (ε) = 278 nm (6889 $dm^3 \cdot mol^{-1} \cdot cm^{-1}$), 374 (3256), 438 (1124).

***mer*-[$RuCl_3$(acv)(DMSO-*S*)(H_2O)]·H_2O (2):** This complex was prepared from several solvents following similar reaction procedures. Initially it was prepared from aqueous solution: X[*trans*-$RuCl_4$(DMSO-*S*)$_2$] (0.235 mmol) was dissolved in distilled water (30.0 mL) and acv (0.235 mmol) was added. The mixture was stirred for two hours until all the acv had dissolved. The colour of the solution changed from orange to dark green. After three days the precipitation of free acv and of a very small amount of brown-red crystals of the product occurred from the solution. These crystals were filtered off, washed with diethyl ether and dried in air. It was later found that the yield was much higher if ethanol was used as solvent (the same procedure as for compound **1**, yield 43.5%). It was also realized that this product can be isolated from many other nondried solvents such as propanol, acetone/DMSO mixtures, nitromethane. $C_{10}H_{21}Cl_3N_5O_6RuS$ (546.8): calcd. C 21.97, H 3.87, N 12.80; found C 22.27, H 3.60, N 12.63. Selected IR bands

(Nujol): $\tilde{\nu}$ = 1657 cm^{-1} (s, sh), 1650 (s, sh), 1640 (vs), 1633 (vs), 1602 (s); 1081 (m, S=O for DMSO-*S*); 426 (w, Ru−S). UV (methanol): λ_{max} (ε) = 278 nm (7182 $dm^3 \cdot mol^{-1} \cdot cm^{-1}$), 376 (3346), 438 (1138).

X-ray Crystallographic Study: X-ray diffraction data for compounds **1** and **2** were collected on a Nonius Kappa CCD diffractometer using graphite monochromated Mo-K_α radiation. Data were processed using DENZO-SMN program.[16] Both structures were solved by direct methods using SIR-97.[17] The positions of the hydrogen atoms were obtained from the difference Fourier map. Atom C(2m) from the noncoordinated methanol molecule in **1** lies on a twofold axis. The positions of three hydrogen atoms bonded to C(2m) were not determined. For both compounds we employed full-matrix least-squares refinement on *F* with anisotropic displacement factors for all non-hydrogen atoms using the Xtal3.4 program.[18] All observed and those "less than" reflections for which F_c was greater than F_0 were included in the final refinement. The hydrogen atom parameters of **1** were not refined. In the case of **2** only the coordinates of hydrogen atoms were refined while their displacement parameters were not. The resulting crystal data and details concerning data collection and refinement for both compounds are quoted in Table 1. ORTEP[19] was used for the preparation of the figures.

CCDC-178936 and CCDC-178937 contain the supplementary crystallographic data for this paper. These data can be obtained free of charge at www.ccdc.cam.ac.uk/conts/retrieving.html [or from the Cambridge Crystallographic Data Centre, 12, Union Road, Cambridge CB2 1EZ, UK; Fax: (internat.) +44-1223/336-033; E-mail: deposit@ccdc.cam.ac.uk].

Acknowledgments

This work was performed within the framework of European COST Action D20, working groups D20/0001 and D20/ 0006. We thank the International Cooperation Program between the Universities of Ljubljana and Trieste for a grant to I. T. Financial support from the Slovenian Ministry of Education, Science and Sports through grants X-2000 and PS-511-103 and from Regione Friuli-Venezia Giulia (L. R. 3/98) is gratefully acknowledged.

[1] M. J. Clarke, in *Metal Ions in Biological Systems* (Ed.: H. Sigel), Marcel Dekker, New York, **1980**; vol. 11, pp. 231−283.
[2] [2a] M. J. Clarke, in *Metal Complexes in Cancer Chemotherapy* (Ed.: B. K. Keppler), VCH, Weinheim, **1993**; pp 129−156. [2b] G. Mestroni, E. Alessio, G. Sava, S. Pacor, M. Coluccia, in *Metal Complexes in Cancer Chemotherapy* (Ed.: B. K. Keppler), VCH, Weinheim, **1993**; pp. 157−186. [2c] B. K. Keppler, K.-G. Lipponer, B. Stenzel, F. Kratz, in *Metal Complexes in Cancer Chemotherapy* (Ed.: B. K. Keppler), VCH, Weinheim, **1993**; pp. 187−220.
[3] G. Sava, E. Alessio, A. Bergamo, G. Mestroni, in *Topics in Biological Inorganic Chemistry* (Ed.: M. J. Clarke and P. J. Sadler), Springer, Berlin, **1999**; vol. 1, pp.143−170.
[4] [4a] B. Blažič, I. Turel, N. Bukovec, P. Bukovec, F. Lazarini, *J. Inorg. Biochem.* **1993**, *51*, 737−744. [4b] I. Turel, N. Bukovec, M. Goodgame, D. J. Williams, *Polyhedron* **1997**, *16*, 1701−1706. [4c] I. Turel, B. Andersen, E. Sletten, A. J. P. White, D. J. Williams, *Polyhedron* **1998**, *17*, 4195−4201.
[5] [5a] A. Sinur, S. Grabner, *Acta Crystallogr., Sect. C* **1995**, *51*, 1769−1772. [5b] S. Grabner, J. Plavec, N. Bukovec, D. Di Leo, R. Cini, G. Natile, *J. Chem. Soc., Dalton Trans.* **1998**, 1447−1451. [5c] R. Cini, S. Grabner, N. Bukovec, L. Cerasino, G. Natile, *Eur. J. Inorg. Chem.* **2000**, 1601−1607.
[6] Á. García-Raso, J. J. Fiol, F. Bádenas, R. Cons, Á. Terrón, M. Quirós, *J. Chem. Soc., Dalton Trans.* **1999**, 167−173.
[7] A. Koutsodimou, G. Natile, *Metal Based Drugs* **2000**, *7*, 325−334.
[8] E. Alessio, G. Balducci, M. Calligaris, G. Costa, W. M. Attia, G. Mestroni, *Inorg. Chem.* **1991**, *30*, 609−618.
[9] A. G. Orpen, L. Brammer, F. H. Allen, O. Kennard, D. G. Watson, R. Taylor, *J. Chem. Soc., Dalton Trans.* **1989**, S1−S83.
[10] E. Alessio, G. Balducci, A. Lutman, G. Mestroni, M. Calligaris, W. M. Attia, *Inorg. Chim. Acta* **1993**, *203*, 205−217.
[11] [11a] F. H. Allen, O. Kennard, D. G. Watson, L. Brammer, A. G. Orpen, R. Taylor, *J. Chem. Soc., Perkin Trans. 2* **1987**, S1−S19. [11b] M. Calligaris, O. Carugo, *Coord. Chem. Rev.* **1996**, *153*, 83−154. [11c] M. Calligaris, *Croat. Chem. Acta* **1999**, *72*, 147−169.
[12] A. Velders, PhD Dissertation, University of Leiden, **2000**.
[13] C. Price, M. A. Shipman, S. L. Gummerson, A. Houlton, W. Clegg, M. R. J. Elsegood, *J. Chem. Soc., Dalton Trans.* **2001**, 353−354.
[14] M. J. Clarke, H. Taube, *J. Am. Chem. Soc.* **1974**, *96*, 5413−5419.
[15] C. M. Duff, G. A. Heath, *J. Chem. Soc., Dalton Trans.* **1991**, 2401−2411.
[16] Z. Otwinowski, W. Minor, *Methods Enzymol.* **1997**, *276*, 307−326.
[17] A. Altomare, M. C. Burla, M. Camalli, G. Cascarano, C. Giacovazzo, A. Guagliardi, G. Polidori, *J. Appl. Cryst.* **1994**, *27*, 435.
[18] S. R. Hall, G. S. D. King, J. M. Stewart, *The Xtal3.4 User's Manual*, University of Western Australia: Lamb, Perth, **1995**.
[19] C. K. Johnson, ORTEPII. Report ORNL-5138. Oak Ridge National Laboratory, Tennessee, USA,**1976**.

Received February 21, 2002
[I02091]

Coordinatively and Electronically Unsaturated Pentamethylcyclopentadienyliridium(III) Complexes with the Dianions of Biuret, of the Diamide of Malonic Acid and of an *N*-Acetyldipeptide Ester[‡]

Walter Ponikwar,[a] Peter Mayer,[a] and Wolfgang Beck*[a]

Dedicated to Professor Karl Wieghardt on the occasion of his 60th birthday

Keywords: Cyclopentadienyl ligands / Iridium / Biuret / Electron-deficient compounds

The dianions of biuret, of the diamide of malonic acid and of *N*-acetyl-L-alanyl-L-alanine methyl ester give the coordinatively unsaturated 16-electron *N*,*N*′-chelate complexes [Cp*Ir[NHC(O)NHC(O)NH)] (**1**), [Cp*Ir[NHC(O)CH_2C(O)NH)] (**2**) and {Cp*Ir[N($COCH_3$)CH(CH_3)C(O)NCH(CH_3)CO_2Me]} (**3**) upon reaction with $[Cp^*IrCl_2]_2$. From $[(R_3P)PdCl_2]_2$ (R = Et, Ph) and biuret the complexes $[(Cl)(R_3P)Pd(\eta^2\text{-biureto})Pd]^-Na^+$ were obtained. The X-ray structure determinations of **1** and **3** reveal that the almost planar chelate rings lie perpendicular to the Cp* ring.
(© Wiley-VCH Verlag GmbH, 69451 Weinheim, Germany, 2002)

Introduction

The long and interesting history of biuret was reviewed by Kurzer in 1956.[2] The copper(II) complex of biuret was one of the first complexes of all,[3] and the biuret reaction, the formation of a red-violet copper compound with peptides was discovered even earlier in 1833.[4] Schiff[5] found later that the diamides of malonic acid and of oxalic acid form similar copper(II) complexes as with biuret, and the pioneers in coordination chemistry Tschugaeff[6] and Pfeiffer[7] proposed correct formulas for the biuret copper(II) chelate and analogous complexes, the structures of which were later confirmed by the X-ray diffraction studies of Freeman et al.[8]

Other chelate complexes with the dianion of biuret, including Cu^{III} and Ni^{III} complexes, have also been reported.[9] We thought it would be interesting to introduce the classical ligand biuret into organometallic chemistry. As shown below, the coordinatively unsaturated sixteen electron complexes Cp*Ir(L-L) **1**−**3** resulted from the reactions of the chloro-bridged complex $[Cp^*IrCl_2]_2$ with the dianions of biuret, its C analogue malodiamide and of an acetyldipeptide ester. Closely related to these new compounds are Grotjahn's Cp* complexes with the dianions of *N*-acyl and *N*-sulfonyl α-amino acids.[10] Other coordinatively unsaturated complexes are, for example, $[CpM(NO)R_2]$ and $[CpM(NO)L]$ (M = Mo, W),[11] $[CpMo(PR_3)_2Cl]$,[12] $[(arene)Ru(SR)_2]$,[13] [CpCo(1,2-ethylenedithiolato)],[14,15] $[Cp^*Ru(PR_3)OR]$,[16] $[Cp^*Ru(R_2NCH_2CH_2NR_2)]^+$,[17] $[M(CO)_3(O,S\text{-}C_6H_4)]^{2-}$ and $[(OC)_3MS_2C_6R_4]^{2-}$ (M = Cr, Mo, W).[18] Noyori's coordinatively unsaturated half-sandwich complex [(arene)RuNHCH(Ph)CH(Ph)-$NSO_2C_6H_4$Me] is an efficient catalyst for asymmetric hydrogen transfer to ketones.[19] The 16-electron complexes $[Cp^*M(L\text{-}L')]^+$ (M = Ru, Fe) with P,P- or P,O-donors have been studied by several groups as catalysts.[20] The geometry of coordinatively unsaturated two-legged piano-stool complexes with 16 valence electrons has been analysed theoretically.[21]

Results and Discussion

Reaction of the chloro-bridged iridium complex $[Cp^*IrCl_2]_2$ with biuret, malodiamide or *N*-acetyl-L-alanyl-L-alanine methyl ester in the presence of NaOMe gives the chelate complexes **1**−**3**.

The wine-red colour of these complexes is characteristic of 16-electron iridium complexes.[10] Addition of triphenylphosphane to **1** and **3** in methanol affords yellow solutions which show only one ^{31}P NMR signal (**1**: δ = 8.62 ppm; **3**: δ = 8.05 ppm) in the ^{31}P NMR spectra due to the corresponding 18-electron species.[10] The colour change from wine red to yellow can be explained by the π-donor function of the chelate ligands in the 16-electron complexes.[10,18]

[‡] Metal Complexes of Biologically Important Ligands, CXLV. Part CXLIV: Ref.[1]

[a] Department Chemie der Ludwig-Maximilians-Universität München,
Butenandtstr. 5−13, 81377 München, Germany
E-mail: wbe@cup.uni-muenchen.de

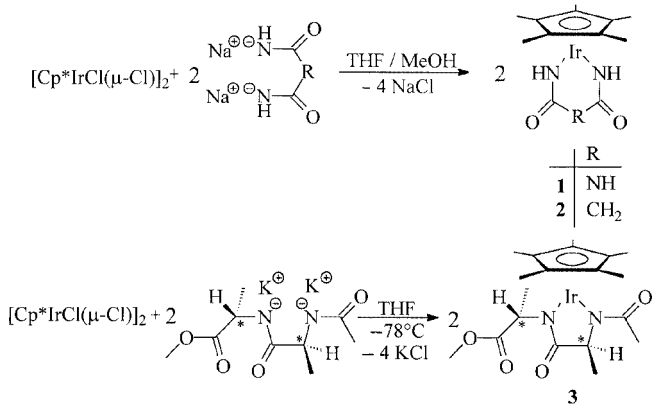

The IR, ^1H and ^{13}C NMR spectra of **1**–**3** exhibit the expected data (see Exp. Sect.). In the ^1H and ^{13}C NMR spectra of **3** only one set of signals is detected which shows that diastereoisomers of **3** were not formed. Complex **2** could not be obtained analytically pure. In the mass spectra of the product from malodiamide the ions of dimers $\{Cp_2^*\text{-}Ir_2Cl_2[NHC(O)CH_2C(O)NH)]\}^+$ (*m/z* = 826; 6%), $\{Cp_2^*\text{-}Ir_2Cl[NHC(O)CH_2C(O)NH]\}^+$ (*m/z* = 789; 4%) and $\{Cp_2^*\text{-}Ir_2[NHC(O)CH_2C(O)NH]\}^{2+}$ (*m/z* = 378; 3%) were observed.

The X-ray structure analysis of **1** (Figure 1) and **3** (Figure 2) reveals the typical geometry of a two-legged pianostool half-sandwich complex, due to the coordinatively unsaturated nature of these compounds. Although water molecules were found in the unit cells of both compounds they definitely do not coordinate because of the large distance to the iridium atoms (**1**: ≥439.8 pm, **3**: 600.7 pm). The planes formed by the Cp* ligands in **1** and **3** are almost perpendicular (**1**: 91.8°; **3**: 93.3°) to the planes formed by the two coordinating nitrogen atoms and the two carbon atoms connected to them. This has also been found in other 16-electron half sandwich complexes with chelate ligands.[10,14,19] Of great interest are the observed bond lengths for the Ir–N bonds. In compound **1** those bond lengths are 195.1(8) pm [Ir(1)–N(1)] and 197.8(6) pm [Ir(1)–N(3)]. In compound **3** these bond lengths were found to be 198.3(2) pm [Ir(1)–N(2)] and 201.3(6) pm [Ir(1)–N(1)]. A comparison with the Ir–N bond lengths (ca. 210 pm) in 18-electron complexes with monosubstituted deprotonated amide ligands,[22] for example in [Cp*(Cl)Ir(Leu-LeuOMe-H$^+$)][23] shows a significant shortening of the Ir–N bond in compounds **1** and **3**. This decrease in the Ir–N bond length is in good agreement with the decline observed by Grotjahn and Noyori in their 16-electron half-sandwich chelate complexes.[10,14] The most reasonable explanation for this bond shortening is that besides the usual σ-symmetrical interaction of a filled ligand orbital with an empty metal orbital (σ-donation), an additional π-symmetrical interaction of another filled orbital of the anionic heteroatom ligand with an empty metal orbital of suitable symmetry (π-donation) is present.[10,18] The contribution of lone-pair electrons at the anionic heteratom ligand to the π-donation explains the exceptional stability of these compounds; the dark red colour results from LMCT in those compounds. The C–N bond lengths in **1** are 2–3 pm longer than in "free" biuret.[24]

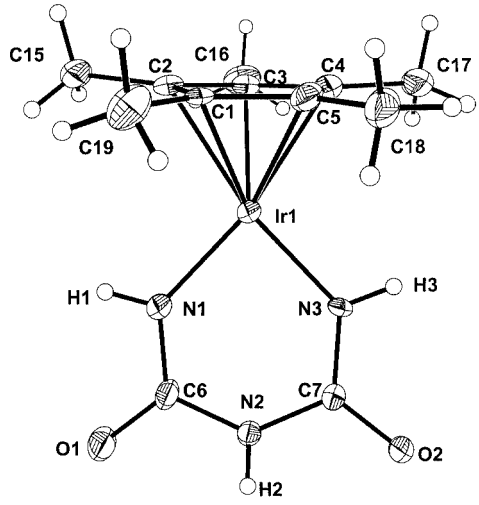

Figure 1. Molecular structure of **1** in the crystal

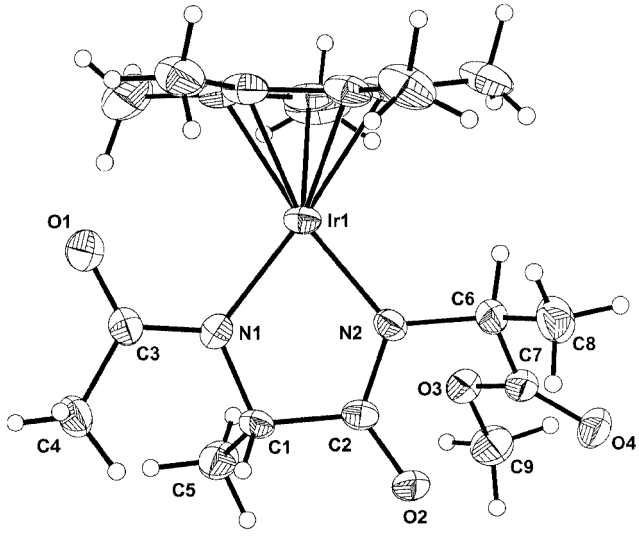

Figure 2. Molecular structure of **3** in the crystal

The chloro-bridged palladium(II) complexes $Pt_2(PR_3)_2Cl_4$ afforded the yellow anionic chelates **4** and **5** with the biuret dianion. They were characterised by their IR and NMR spectroscopic data (see Exp. Sect.). As for **1** and **2** the NH signals of CD_3OD solutions of **4** and **5** cannot be observed in the ^1H NMR spectra because of a rapid H/D exchange. The ^{31}P NMR spectra of **4** and **5** exhibit only one signal.

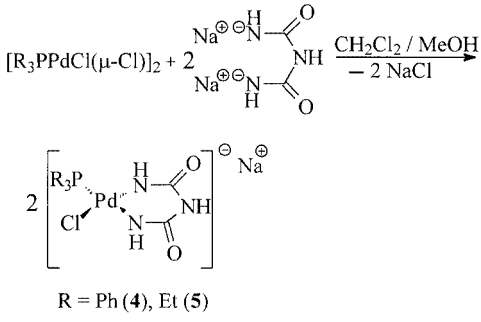

Experimental Section

The chloro-bridged complexes $[Cp^*IrCl_2]_2$ [25] and $[PdCl_2(PR_3)]_2$ [26] were obtained according to literature procedures. All reactions were carried out in Schlenk tubes under argon.

Cp*(η²-*N*,*N*-biureto)Ir^{III} (1): A solution of biuret (41.2 mg, 0.4 mmol) and 0.4 mmol of NaOMe in 10 mL of methanol was added dropwise to a suspension of $[Cp^*IrCl_2]_2$ (159.3 mg, 0.2 mmol) in 15 mL of methanol whilst stirring at room temperature. The solution turned dark red and was then stirred for 48 h. The solvent was then removed in vacuo. NaCl could not be separated from the product by chromatography. The dark red product was dried at 75 °C for 4 days. Yield 65 mg (77%). IR (KBr): $\tilde{\nu}$ = 3403 cm^{-1} s (NH sec. amide), 3294 s (NH prim. amide), 1650 vs (CO, amide I), 1635 m (NH-bending, amide II). ^{1}H NMR (270 MHz, CD_3OD): δ = 1.85 (s, 15 H, Cp*) ppm. ^{13}C NMR (67.9 MHz, CD_3OD): δ = 8.2 (s, Cp*), 88.7 (s, Cp*), 163.1 (s, CO) ppm. $C_{12}H_{18}IrN_3O_2$·2.25NaCl (559.98): calcd. C 25.74, H 3.24, N 7.50; found C 25.57, H 3.16, N 7.83.

Cp*(η²-*N*,*N*-malodiamine-2H$^+$)Ir^{III} (2): $[Cp^*IrCl_2]_2$ (159.3 mg, 0.2 mmol) in 15 mL of THF was added to a solution of malodiamide (40.8 mg, 0.4 mmol) and NaOMe (0.8 mmol) in 10 mL of methanol whilst stirring at room temperature. The solution became wine red. After stirring for 16 h at room temperature the solvent was removed in vacuo. Complex **2** was not analytically pure. Efforts to purify the compound by recrystallization from methanol led to decomposition. IR (KBr): $\tilde{\nu}$ = 3295 cm^{-1} s (NH), 2984 s (CH), 2944 s (CH), 2685 s, 2625 s, 2606 s ($HNEt_3^+$), 1676 vs (CO, amide I), 1620 m (NH-bending, amide II), 1586 w ($HNEt_3^+$), 1398 m (CH), 1384 m (CH). ^{1}H NMR (400.1 MHz, CD_3OD): δ = 1.61 (s, 15 H, Cp*), 3.35 (m, 2 H, CH_2) ppm. ^{13}C NMR (100.5 MHz, CD_3OD): δ = 5.8 (s, Cp*), 52.9 (s, CH_2), 85.2 (s, Cp*), 169.7 (s, CO, malodiamide) 178.3 (s, CO). FAB$^+$MS (*m*-NBA): *m*/*z* (%) = 429 (86) [M + H], 329 (52) [M − ligand].

Cp*(η²-*N*-acetyl-L-alanyl-L-alanine methyl ester-2H$^+$)Ir^{III} (3): [Cp*$IrCl_2]_2$ (159.3 mg, 0.2 mmol) in 15 mL of THF was stirred for 2 h at −78 °C (2-propanol/dry ice) and to this mixture was added a suspension of *N*-acetyl-L-Ala-L-Ala-OMe (86.5 mg, 0.4 mmol) and K_2CO_3 (165.8 mg, 1.2 mmol) in 15 mL of cold THF. The reaction mixture was allowed to warm to room temperature for 18 h and an almost clear wine-red suspension was formed. The solvent was then removed in vacuo and the residue treated with 15 mL of dichloromethane and stirred for 30 min. KCl and excess K_2CO_3 were centrifuged off and the solution concentrated to dryness to give a dark red microcrystalline product. Yield 88 mg (82%). IR (KBr): $\tilde{\nu}$ = 2924 cm^{-1} s (CH), 2851 s (−O-CH_3), 1738 vs (COOMe), 1630 s (CO amide I), 1375 s (−CO-CH_3). ^{1}H NMR (270 MHz, CD_2Cl_2): δ = 1.33 (d, $^3J_{H,H}$ = 10.27 Hz, 3 H, α-CH_3), 1.35 (d, $^3J_{H,H}$ = 9.99 Hz, 3 H, α-CH_3), 1.76 (s, 15 H, Cp*), 1.95 (s, 3 H, Ac-N), 3.70 (s, 3 H, Me-O), 4.50 (m, 2 H, α-H) ppm. ^{13}C NMR (67.9 MHz, CD_2Cl_2): δ = 9.9 (s, Cp*), 22.9 (s, β-C), 23.2 (s, β-C), 30.2 (s, $NCOCH_3$), 51.5 (s, $COOCH_3$), 61.4 (s, α-C), 62.6 (s, α-C), 88.9 (s, Cp*), 173.7 (s, $NCOCH_3$), 174.0 (s, $COOCH_3$), 190.5 [s, N-CO-$C(CH_3)$N] ppm. The analysed substance was recrystallised from methanol. $C_{19}H_{29}IrN_2O_4$·MeOH (573.69): calcd. C 41.87, H 5.80, N 4.88; found C 41.56, H 5.97, N 4.89.

[Cl(Ph$_3$P)(η²-biureto)Pd]$^-$Na$^+$ (4): A solution of biuret (41.2 mg, 0.4 mmol) and NaOMe (0.8 mmol) in 10 mL of methanol was added to $[(Ph_3P)PdCl_2]_2$ (176 mg, 0.2 mmol) in 10 mL of methanol whilst stirring at room temperature. After 1 h the solution turned yellow and was stirred for another 17 h at room temperature. The solvent was then removed in vacuo. The residue was treated with 15 mL of methanol, filtered over celite and the solvent was again removed in vacuo. The yellow product was washed with 10 mL of hexane , centrifuged and dried at 60 °C in vacuo for two days. IR (KBr): $\tilde{\nu}$ = 3373 cm^{-1} s (NH sec. amide), 3234 m (prim. amide), 1630 vs (CO amide I), 1601 m (NH-bending amide II). IR (PE): $\tilde{\nu}$ = 378 cm^{-1} m (Pd-Cl). ^{1}H NMR (270 MHz, CD_3OD): δ = 7.78 (m, 15 H, Ph_3P) ppm. ^{31}P NMR (109.4 MHz, CD_3OD): δ = 27.99 (s, PPh_3) ppm. $C_{20}H_{18}ClN_3NaO_2PPd$ (528.2): calcd. C 45.48, H 3.43, N 7.96; found C 45.88, H 3.66, N 8.05. FAB-MS (*m*-NBA): *m*/*z* (%) = 506 (75) [M]$^-$, 471 (24) [M − Cl], 405 (5) [M − biuret], 244 (18) [M − P(Ph)$_3$].

[(Cl)(Et$_3$P)(η²-*N*,*N*-biureto)Pd]$^-$Na$^+$ (5): A solution of biuret (20.8 mg, 0.2 mmol) and NaOMe (0.4 mmol) in 10 mL of methanol was added to a solution of $[(Et_3P)PdCl_2]_2$ (59.1 mg, 0.1 mmol) in 10 mL dichloromethane whilst stirring at room temperature. The dark red mixture turned yellow. After stirring for 30 min the solvent was removed in vacuo and the residue dissolved in 15 mL of methanol and filtered over celite. The solvent was again removed in vacuo and the residue was treated with 20 mL of *n*-pentane and stirred for 10 min. The product was then separated by centrifugation and dried in vacuo. IR (KBr): $\tilde{\nu}$ = 3429 cm^{-1} s (NH sec. amide), 3201 m (NH prim. amide), 1630 vs (CO amide I), 1597 s (NH-bending amide II). IR (PE): $\tilde{\nu}$ = 360 cm^{-1} m (Pd-Cl). ^{1}H NMR (270 MHz, CD_3OD): δ = 1.21 [m, 9 H, P(CH_2CH_3)$_3$], 1.78 [m, 6 H, P(CH_2CH_3)$_3$] ppm. ^{31}P NMR (109.4 MHz, CD_3OD): δ = 24.56 (s, Et_3P) ppm. $C_8H_{18}ClN_3NaO_2PPd$·0.75NaCl (427.90): calcd. C 21.71, H 4.10, N 9.49; found C 21.26, H 4.53, N 9.53. FAB-MS (*m*-NBA): *m*/*z* (%) = 361 (55) [M]$^-$, 325 (17) [M − Cl], 244 (16) [M − PEt_3].

Crystal Structure Determination of 1 and 3: Suitable crystals of both compounds for the X-ray structure determination were obtained by slow evaporation of a methanolic solution. The data collection for compound **1** was done on a Siemens P4 four circle X-ray diffractometer with a Single Point detector at 293 K. Compound **3** was measured on a Stoe IPDS with an Image Plate detector at 200 K. The structure solution of **1** was done with the XS program from Bruker Analytical X-ray Systems (1997 Ver. 5.10) and the structure solution of **3** with the SHELXS-97 program (Sheldrick, 1990). Structure refinement for compound **1** was done with the SHELXTL suite of programs (Bruker Analytical X-ray Systems 1997 Ver. 5.10) and for the refinement of **3** the SHELXL-97 program (G. M. Sheldrick. University of Göttingen, 97−2 version) was used. For both structure determinations graphite monochromated Mo-K_α radiation (λ = 0.71073 Å) was used. The hydrogen atoms H(1)−H(3) in compound **1** were found by difmap and refined freely. All other hydrogen atoms were inserted in idealised

Table 1. Selected experimentally observed bond lengths [pm] and angles [°] of **1**

Ir(1)−N(1)	195.1(8)	N(1)−Ir(1)−N(3)	86.5(3)
Ir(1)−N(3)	197.8(6)	C(6)−N(1)−Ir(1)	132.1(6)
N(1)−C(6)	132.9(1)	C(6)−N(2)−C(7)	130.2(7)
N(3)−C(7)	133.0(9)	N(2)−C(7)−N(3)	118.3(7)
O(1)−C(6)	124.5(1)	C(7)−N(3)−Ir(1)	132.1(5)
O(2)−C(7)	124.7(9)	O(1)−C(6)−N(1)	122.9(8)
N(2)−C(6)	136.5(1)	O(1)−C(6)−N(2)	117.0(8)
N(2)−C(7)	137.9(1)	O(2)−C(7)−N(2)	118.2(7)
		O(2)−C(7)−N(3)	123.5(7)

Table 2. Selected experimentally observed bond lengths [pm] and angles [°] of **3**

Ir(1)−N(1)	201.3(6)	N(1)−Ir(1)−N(2)	80.0(2)
Ir(1)−N(2)	198.3(2)	C(1)−N(1)−Ir(1)	115.7(4)
N(1)−C(1)	146.8(9)	N(1)−C(1)−C(2)	109.4(6)
C(1)−C(2)	149.5(1)	C(2)−N(2)−Ir(1)	118.6(5)
C(2)−N(2)	135.8(8)	Ir(1)−N(1)−C(3)	125.3(5)
O(1)−C(3)	121.3(1)	C(3)−N(1)−C(1)	119.0(6)
C(3)−N(1)	137.2(9)	Ir(1)−N(2)−C(6)	126.9(4)
N(2)−C(6)	148.5(9)	C(2)−N(2)−C(6)	114.2(6)
C(7)−O(4)	121.7(9)		
C(7)−O(3)	134.2(1)		
O(3)−C(9)	146.4(1)		

Table 3. Crystal data and structure refinements for compounds Cp*(η^2-*N*,*N*-biureto)Ir^{III} (**1**) and Cp*(η^2-*N*,*N*-[(*N*-acetyl)-L-alanyl-L-alanine-methyl ester)]Ir^{III} (**3**)

	1	**3**
Empirical formula	$C_{12}H_{18}IrN_3O_2$	$C_{19}H_{30}IrN_2O_4$
Formula weight	428.49	542.66
Temperature [K]	293(2)	200(2)
λ (Mo-K_α) [Å]	0.71073	0.7173
Crystal System	Monoclinic	Orthorhombic
Space group	$P2_1/n$	$P2_12_12_1$
a [Å]	14.147(8)	8.7398(1)
b [Å]	14.333(2)	11.2680(2)
c [Å]	15.063(2)	21.8235(4)
α [°]	90.00	90.00
β [°]	95.87(2)	90.00
γ [°]	90.00	90.00
Volume [Å^3]	3038.2(19)	2149.180(60)
Z	4	4
$\rho_{calcd.}$ [Mg/m^3]	2.048	1.70190(5)
μ [mm^{-1}]	0.809	6.239
F(000)	1792	1084
Crystal size [mm]	0.40 × 0.25 × 0.25	0.25 × 0.24 × 0.11
2θ range [°]	3.76 to 50.12	4.06 to 54.94
Index ranges	$0 \le h \le 14$	$-28 \le h \le 28$
	$-14 \le k \le 14$	$-14 \le k \le 14$
	$-14 \le l \le 14$	$-11 \le l \le 11$
Reflections collected	9631	36359
Independent reflections	4768 [R_{int} = 0.0347]	4923 [R_{int} = 0.0581]
Observed reflections	4134 [$F > 2\sigma(F)$]	4469 [$F > 2\sigma(F)$]
Max. and min. transmission	0.910 and 0.715	0.5218 and 0.2774
Refinement method	Full-matrix least-squares on F^2	Full-matrix least-squares on F^2
Data/restraints/parameters	4768/0/371	4923/0/246
Goodness-of-fit on F^2	1.067	1.168
*R*1, *wR*2 [$I > 2\sigma(I)$]	0.0338, 0.0830	0.0345, 0.0795
*R*1, *wR*2 [all data]	0.0424, 0.0879	0.0453, 0.0828
Largest diff. peak and hole [e·Å^3]	1.351 and −1.584	1.348 and −2.328

positions and were refined riding on the atoms to which they are bonded. Compound **1** crystallises in the monoclinic space group $P2_1/n$ with four molecules in the unit cell. Compound **3** crystallizes in the orthorhombic space group $P2_12_12_1$ with four molecules in the unit cell. The experimentally observed bond lengths and bond angles for **1** and **3** are compiled in Table 1 and Table 2. The crystallographic data and refinement details are summarized in Table 3. CCDC-180880 (**1**) and CCDC-181126 (**3**) contain the supplementary crystallographic data for this paper. These data can be obtained free of charge at www.ccdc.cam.ac.uk/conts/retrieving.html [or from the Cambridge Crystallographic Data Centre, 12, Union Road, Cambridge CB2 1EZ, UK; Fax: (internat.) +44-1223/336-033; E-mail: deposit@ccdc.cam.ac.uk].

Acknowledgments

Generous support by Deutsche Forschungsgemeinschaft and Fonds der Chemischen Industrie is gratefully acknowledged. We thank Degussa AG, Hanau, for chemicals.

[1] K. Haas, H. Dialer, H. Pietrowski, J. Schapp, W. Beck, *Angew. Chem.* in press.
[2] F. Kurzer, *Chem. Rev.* **1956**, *56*, 95−197.
[3] G. Wiedemann, *Ann. Chem. Pharm.* **1848**, *68*, 323−326.
[4] F. Rose, *Pogg. Ann.* **1833**, *18*, 132; P. M. H. Kroneck, V. Vortisch, P. Hemmerich, *Eur. J. Biochem.* **1980**, *109*, 603−612.
[5] H. Schiff, *Ber. Dtsch. Chem. Ges.* **1896**, *29*, 298−303; H. Schiff, *Ber. Dtsch. Chem. Ges.* **1896**, *29*, 1354−1356; H. Schiff, *Liebigs Ann. Chem.* **1897**, *299*, 236−266; H. Schiff, *Liebigs Ann. Chem.* **1901**, *319*, 300−303; H. Schiff, *Liebigs Ann. Chem.* **1906**, *352*, 73−87.
[6] L. Tschugaeff, *Ber. Dtsch. Chem. Ges.* **1907**, *40*, 1973−1980.
[7] P. Pfeiffer, S. Saure, *J. Prakt. Chem.* **1941**, *157*, 97−124.
[8] H. C. Freeman, J. E. W. Smith, J. C. Taylor, *Nature* **1959**, *184*, 707−710.
[9] See, for example: A. W. McLellan, G. A. Melson, *J. Chem. Soc. A* **1967**, 137−142; J. J. Steggerda, J. J. Bour, P. J. M. W. L. Birker, *Inorg. Chem.* **1971**, *10*, 1202−1205; P. C. Srivastava, B. K. Banerjee, *J. Ind. Chem. Soc.* **1979**, *56*, 779−781; N. Mincheva, G. Gencheva, M. Mitewa, G. Gochev, D. Mehandjiev, *Synth. React. Inorg. Met.-Org. Chem.* **1997**, *27*, 1191−1203; B. B. Kedzia, P. X. Armendarez, K. Nakamoto, *J. Inorg. Nucl. Chem.* **1968**, *30*, 849−860.
[10] D. B. Grotjahn, T. L. Groy, *J. Am. Chem. Soc.* **1994**, *116*, 6969−6970; D. B. Grotjahn, T. L. Groy, *Organometallics* **1995**, *14*, 3669−3682; D. B. Grotjahn, C. Joubran, *Tetrahedron: Asymmetry* **1995**, *6*, 745−752; D. B. Grotjahn, H. C. Lo, J. Dinoso, C. D. Atkins, C. Li, St. P. Nolan, J. L. Hubbard, *Inorg. Chem.* **2000**, *39*, 2493−2499.
[11] P. Legzdins, S. J. Rettig, L. Sanchez, *Organometallics* **1988**, *7*, 2394−2403; K. M. Smith, R. Poli, P. Legzdins, *Chem. Eur. J.* **1999**, *5*, 1598−1608.
[12] F. Abugideiri, J. C. Fettinger, D. W. Keogh, D. Webster, R. Poli, *Organometallics* **1996**, *15*, 4407−4416; D. W. Keogh, D. Webster, R. Poli, *J. Am. Chem. Soc.* **1997**, *119*, 2516−2523.
[13] K. Mashima, H. Kaneyoshi, S. Kaneko, A. Mikami, K. Tani, A. Nakamura, *Organometallics* **1997**, *16*, 1016−1025; R. I. Michelmann, G. E. Ball, R. G. Bergman, R. A. Anderson, *Organometallics* **1994**, *13*, 869−881.
[14] For an overview, see: A. Sugimori, T. Akiyama, M. Kajitani, T. Sugiyama, *Bull. Chem. Soc. Jpn.* **1999**, *72*, 879−908; M. Fourmigue, *Coord. Chem. Rev.* **1998**, *178−180*, 822−864.
[15] R. B. King, *J. Am. Chem. Soc.* **1963**, *85*, 1587−1590; S. D. Henderson, T. A. Stephenson, E. J. Wharton, *J. Organomet. Chem.* **1979**, *179*, 43−47; R. Ficker, W. Hiller, S. Drobnik, I.-P. Lorenz, *Z. Kristallogr. NCS* **1996**, *211*, 845−846; J.-H. Won, D.-H. Kim, B. Y. Kim, S.-J. Kim, C. Lee, S. Cho, J. Ko, S. O. Kang, *Organometallics* **2002**, *21*, 1443−1453.
[16] T. J. Johnson, J. C. Huffmann, K. G. Caulton, *J. Am. Chem. Soc.* **1992**, *114*, 2725−2726.
[17] C. Gemel, K. Mereiter, R. Schmidt, K. Kirchner, *Organometallics* **1997**, *16*, 5601−5603; C. Gemel, J. C. Huffmann, K. G. Caulton, K. Mauthner, K. Kirchner, *J. Organomet. Chem.* **2000**, *593−594*, 342−353.
[18] D. J. Darensbourg, J. D. Draper, B. J. Frost, J. H. Reibenspies, *Inorg. Chem.* **1999**, *38*, 4705−4714; D. Sellmann, M. Wilke, F. Knoch, *Inorg. Chem.* **1993**, *32*, 2534−2543. D. Sellmann, W. Ludwig, G. Huttner, L. Zsolnai, *J. Organomet. Chem.* **1985**, *294*, 199−207.
[19] V.-J. Haack, S. Hashiguchi, A. Fujii, T. Ikariya, R. Noyori, *Angew. Chem.* **1997**, *109*, 297−300; *Angew. Chem. Int. Ed. Engl.* **1997**, *36*, 285−288.
[20] K. Kirchner, K. Mauthner, K. Mereiter, R. Schmid, *Chem. Commun.* **1993**, 892−894; E. Lindner, M. Haustein, R. Fawzi, M. Steimann, P. Wegner, *Organometallics* **1994**, *13*, 5021−5029; E. Lindner, M. Haustein, A. Herrmann, H. Mayer, K. Gierling, R. Fawzi, M. Steimann, *Organometallics* **1995**, *14*, 2246−2252. E. Lindner, S. Pautz, M. Haustein, *Coord. Chem. Rev.* **1996**, *155*, 145−162; I. de los Rios, M. J. Tenorio, J. Padilla, M. C. Puerta, P. Valerga, *J. Chem. Soc., Dalton Trans.* **1996**, 377−381; J. W. Faller, B. P. Patel, M. A. Albrizzio, M. Curtis, *Organometallics* **1999**, *18*, 3096−3104; J. W. Faller, X. Liu, J. Parr, *Chirality* **2000**, *12*, 325−337; M. J. Tenorio, K. Mereiter, M. C. Puerta, P. Valerga, *J. Am. Chem. Soc.* **2000**, *122*, 11230−11231; G. Argouarch, P. Hamon, L. Toupet, J.-R. Hamon, C. Lapinte, *Organometallics* **2002**, *21*, 1341−1348.
[21] Th. R. Ward, O. Schafer, C. Daul, P. Hofmann, *Organometallics* **1997**, *16*, 3207−3215.
[22] R. Krämer, M. Maurus, K. Polborn, K. Sünkel, C. Robl, W. Beck, *Chem. Eur. J.* **1996**, *2*, 1518−1526.
[23] K. Polborn, W. Hoffmüller, W. Beck, *Z. Kristallogr. NCS* **2001**, *216*, 231−232.
[24] E. W. Hughes, H. L. Yakel, H. C. Freeman, *Acta Crystallogr.* **1961**, *14*, 345−352.
[25] C. White, A. Yates, P. M. Maitlis, D. M. Heinekey, *Inorg. Synth.* **1992**, *29*, 228−230.
[26] F. R. Hartley, *Organomet. Chem. Rev. Section A* **1970**, *6*, 119; W. Baratta, P. S. Pregosin, *Inorg. Chim. Acta* **1993**, *209*, 85−87.

Received March 8, 2002
[I02123]

The First Tetranuclear Complex with a (μ-CrO_4-*O*,*O*′,*O*″) Bridge: Crystal Structure and Ferromagnetic Behavior of [{$Cu(bpy)_2$}$_3$(μ-CrO_4)](ClO_4)$_4$·H_2O

Li-Hua Yin,[a] Wei-Hua Gu,[a] Peng Cheng,*[a] Lei Z. Zhang,[a] Dai-Zheng Liao,*[a] Jing Li,[a] Xiu-Lin Yang,[a] Xue-Qi Fu,[b] Shi-Ping Yan,[a] and Zong-Hui Jiang[a]

Keywords: Structure elucidation / Magnetic properties / Bridging ligands / Chromium / N,O ligands

A novel tetranuclear complex [{$Cu(bpy)_2$}$_3$(μ-CrO_4)](ClO_4)$_4$·H_2O (**1**) with a (μ-CrO_4-*O*,*O*′,*O*″) bridge has been synthesized by the reaction of K_2CrO_4 with $Cu(ClO_4)_2$·$6H_2O$ and bpy in CH_3CN/H_2O solution (bpy = 2,2′-bipyridine). A single crystal X-ray diffraction analysis showed that the chromate ion bridges three copper(II) ions showing a pesudo-C_{3v} symmetry. The coordination sphere of each copper(II) ion is best described as trigonal bipyramidal, implying that the magnetic orbital of copper(II) ion is d_{z^2}, which is also confirmed by the powder ESR spectra. Variable-temperature magnetic studies verify the validity of the chromate bridging unit to link the tricopper system with ferromagnetic coupling, with $2J = +1.8$ cm^{-1}.

(© Wiley-VCH Verlag GmbH, 69451 Weinheim, Germany, 2002)

The magnetochemistry of polynuclear metal complexes has attracted considerable interest from both physicists and chemists due to the peculiar behavior derived from the nature of these magnetic ions.[1−3] Ferromagnetic interactions can be achieved if the magnetic orbitals are orthogonal to each other.[4−6] The chromate ion has been known to act as a bridging ligand and tends to bridge metal centers to form oligo- and polymetallic systems with zero-, one-, two-dimensional structures.[7−14] Many chromate-bridged polynuclear metal complexes have been structurally and magnetically characterized. Some of them show ferromagnetic interaction due to the magnetic orbital orthogonality through the chromate bridge. For example, the one-dimensional metal(II) complexes *catena*-(μ-CrO_4-*O*,*O*′)[Ni^{II}-(cyclam)]·$2H_2O$ (cyclam = 1,4,8,11-tetraazacyclotetradecane) and *catena*-(μ-CrO_4-*O*,*O*′)[M^{II}(L)]·$5H_2O$ (M = Ni^{II}, Cu^{II}; L = 3,14-dimethyl-2,6,13,17-tetraazatricyclo[14,4,$0^{1.18}$,$0^{7.12}$]docosane) revealed an octahedral geometry about each metal(II) ion and showed weak intrachain ferromagnetic interactions [$2J = +0.6(1)$, $+1.6(1)$ and $+0.10(1)$ cm^{-1}; $H = -2J\Sigma S_i \cdot S_{i+1}$] which is explained by means of an accidental degeneracy of the σ-type frontier orbitals.[8,10] In a dinuclear copper(II) complex [{Cu^{II}(acpa)}$_2$(μ-CrO_4)] (acpa = tridentate Schiff-base ligands), the coordination geometry about the copper(II) ions is square planar, and the ferromagnetic coupling has a $2J$ value of $+14.6$ cm^{-1} ($H = -2J\Sigma S_1 \cdot S_2$).[7] Metal complexes with chromate bridge have been known to contain one, two, and three (μ-CrO_4-*O*,*O*′) ions.[7−14] However, to the best of our knowledge, no polynuclear metal complexes bridged by a chromate ion in a (μ-CrO_4-*O*,*O*′,*O*″) mode have been reported. In this paper we report the crystal structure and magnetic properties of the first tetranuclear complex [{$Cu(bpy)_2$}$_3$(μ-CrO_4)](ClO_4)$_4$·H_2O (**1**) (bpy = 2,2′-bipyridine) with a (μ-CrO_4-*O*,*O*′,*O*″) bridge.

The structure of **1** has been elucidated by X-ray crystallography. The molecular structure of **1** is presented in Figure 1. The coordination geometry about the chromium atom is a slightly distorted tetrahedron with O−Cr−O bond angles in the range 108.0(2)−111.6(2)°. The Cr−O bonds where O is also coordinated to Cu [1.648(4), 1.648(4), and 1.669(4) Å for Cu(1), Cu(2), and Cu(3), respectively] are slightly longer than the "uncoordinated" Cr−O bond [1.605(4) Å]. As can be seen from the figure, the chromate ion bridges the copper(II) ions with a pesudo-C_{3v} symmetry, with a Cu−Cr separation of 3.173−3.504 Å. The Cu−O bond lengths are 1.996(4), 1.961(4), and 1.970(3) Å, respectively. In each $Cu(bpy)_2^{2+}$ unit, the axial coordination sites of the copper(II) ion are occupied by two nitrogen atoms from bpy and the equatorial sites are occupied by two nitrogen atoms from bpy and an oxygen atom from the chromate ion. The bond angle of each axial N−Cu−N unit is almost 180° [177.5(2), 176.6(2), and 178.27(19)° for Cu(1), Cu(2), and Cu(3), respectively]. The axial Cu−N bond lengths are shorter than those of the equatorial Cu−N bonds. Thus, the coordination sphere of each copper(II) ion is best described as a trigonal bipyr-

[a] Department of Chemistry, Nankai University, Tianjin 300071, P. R. China
Fax: (internat.) +86-22/2350-2458
E-mail: pcheng@nankai.edu.cn
[b] Institute of Environmental Science and Engineering, Nankai University, Tianjin 300071, P. R. China

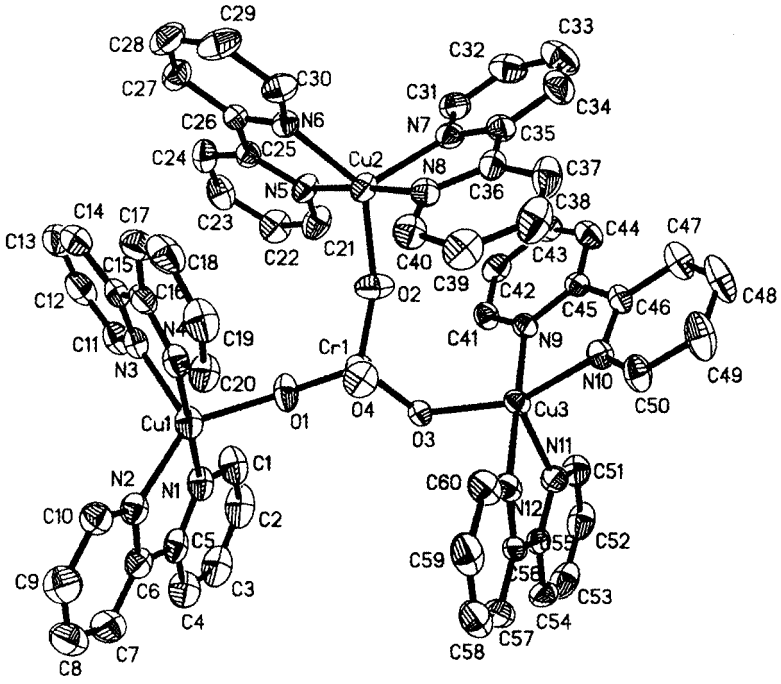

Figure 1. Molecular structure diagram of **1** (showing 30% probability ellipsoids; hydrogen atoms are omitted for clarity)

amid, which implies that the magnetic orbital of copper(II) ion is d_{z^2}.

The powder X-band ESR spectra of **1** was recorded at both room temperature and 77 K (Figure 2). The spectrum remains essentially the same down to 77 K, without any detectable alteration of the relative intensities of the peaks. The very weak ferromagnetic interaction between the copper(II) ions revealed by the magnetic measurements seems not to influence the powder ESR spectrum, where a quasi-isotropic signal centered at $g = 2.18$ is observed.

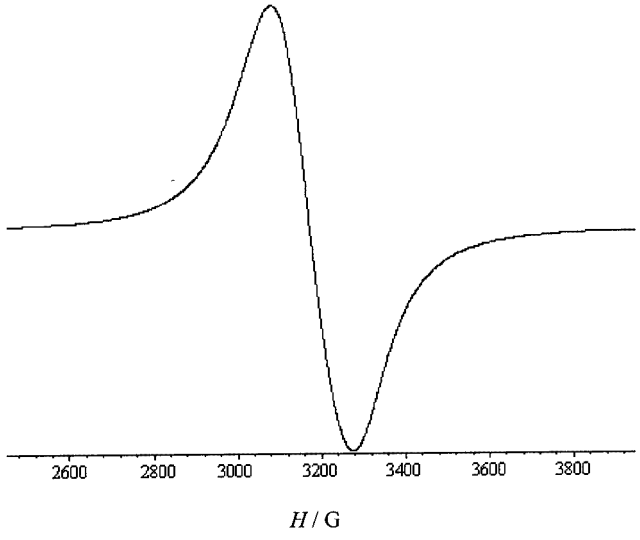

Figure 2. The powder X-band ESR spectrum of **1** at room temperature

A magnetic susceptibility measurement for **1** was carried out in the temperature range 5−300 K. The temperature dependence of the magnetic susceptibilities (χ_m) and the effective magnetic moments (μ_{eff}) versus T plot for **1** is shown in Figure 3. The tetranuclear complex has a room-temperature magnetic moment of 3.23 μ_B. The μ_{eff} value increases markedly below 20 K and reaches a maximum of 3.63 μ_B. This magnetic behavior suggests the operation of a ferromagnetic spin-exchange in the complex, which is probably due to the magnetic orbitals between copper(II) ions being orthogonal to each other through the bridging chromate ligand. The magnetic susceptibility data were fitted to the equation for a triangular unit of $S = 1/2$ spins. The parameters giving the best fit were $2J = +1.8$ cm^{-1}, $g = 2.15$, and $R = 1.4 \times 10^{-4}$ $\{R = [(\chi_m{}^{obs} - \chi_m{}^{calc})^2/(\chi_m{}^{obs})^2]\}$. These results confirmed that the spin coupling between copper(II) ions through the bridging chromate ligand is a ferromagnetic spin-exchange interaction.

Propagation of the ferromagnetic interaction in **1** can be understood from the orbital topology of the frontier orbitals (Figure 4). If we assume that the chromate ion has a tetrahedral geometry (the X-ray crystallographic analysis of **1** revealed a pesudotetrahedral symmetry), we would expect the d-orbitals of the chromium ion to be split into e- and t_2-type orbitals and the p-orbitals of the coordinated oxygen atoms to form a_1- and t_2-type orbitals.[7,8] The e pair of the d-orbitals has no matching combination of oxygen orbitals, hence these orbitals remain nonbonding. The t_2-type orbitals of the chromium ion, however, form triply degenerate bonding and antibonding orbitals with those of the oxygen p-orbitals and six electrons from the coordinated oxygen p-orbitals occupy the t_2-type bonding orbitals.

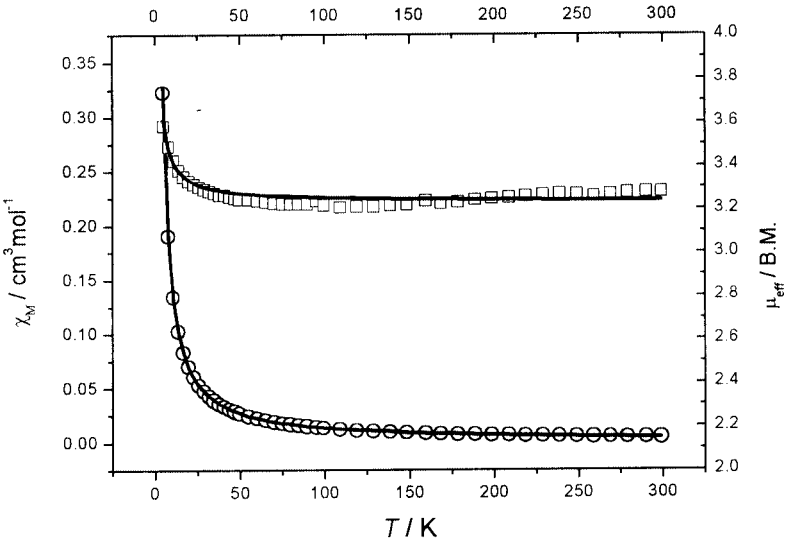

Figure 3. Plots of χ_m vs. T (O) and μ_{eff} vs. T (□) for **1**; the solid line represents the best fit of the experimental data using the parameters described in the text

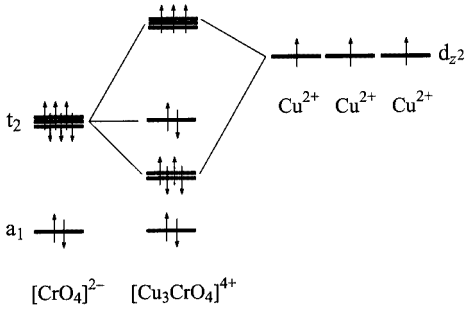

Figure 4. A proposed molecular orbital scheme for the $[Cu_3CrO_4]^{4+}$ chromophore

As revealed by previous measurements, the magnetic orbital of copper(II) ion is d_{z^2}. Thus, when the chromate anion bridges copper(II) ions, two of the t_2-type molecular orbitals of the chromate anion form two sets of σ-type bonding and antibonding orbitals with the d_{z^2} orbitals of the three copper(II) ions; the remainder of the t_2-type orbitals remains nonbonding. The d_{z^2} orbitals of the copper(II) ions and the oxygen p-orbitals interact to mix through the LMCT (O → Cu) interactions. Since the molecular geometry of the complex is pesudo-C_{3v}, orbitals do degenerate under C_{3v} symmetry. The three unpaired electrons from the d_{z^2} orbitals of copper(II) ions occupy three antibonding orbitals. The magnetic susceptibility measurement of **1** does show a ferromagnetic interaction between the copper(II) ions. Therefore, the three antibonding MOs with three spins must be energetically close enough to stabilize the high-spin state. It should be noted here that $[LFe^{III}(\mu\text{-}CrO_4)_3Fe^{III}L]$ (L = 1,4,7-trimethyl-1,4,7-triazacyclononane) shows an antiferromagnetic interaction ($2J = -15\ cm^{-1}$) between the high-spin iron(III) centers through the three chromate bridges.[12] The antiferromagnetic interaction in the iron(III) complex might be understood by an extra π-orbital overlap between $[CrO_4]^{2-}$ and Fe^{III} ions leading to the nondegenerate frontier orbitals of the $[Fe^{III}_2(\mu\text{-}CrO_4)_3]$ chromophore.

In conclusion, the first tetranuclear complex $[\{Cu(bpy)_2\}_3(\mu\text{-}CrO_4)](ClO_4)_4\cdot H_2O$ bridged by a chromate ion in a (μ-CrO_4-*O*,*O*′,*O*″) mode is reported in this paper. This complex was structurally analyzed by X-ray diffraction crystallography. Variable-temperature magnetic studies verify the validity of the chromate bridging unit linking the tricopper system with ferromagnetic interactions. These results enhance the fruitful research field of the magnetochemistry of polynuclear metal complexes.

Experimental Section

General: Infrared spectra were recorded as KBr discs on a Shimadzu IR-408 infrared spectrometer in the 4000−600 cm^{-1} region. UV/Vis absorption spectra were recorded on a Shimadzu UV-2101 spectrophotometer. The X-band ESR spectra of polycrystalline powders were collected on a Bruker ER 200 D-SRC ESR spectrometer at both room temperature and 77 K. Magnetic susceptibility data were collected in the 5−300 K range using a Quantum Design MPMS-7 SQUID magnetometer. The data were corrected for magnetization of the sample holder and for diamagnetic contributions, which were estimated from Pascal's constants.[15]

Preparation of 1: A solution of K_2CrO_4 (97 mg, 0.5 mmol) in H_2O (5 mL) was added to a solution of $Cu(ClO_4)_2\cdot 6H_2O$ (186 mg, 0.5 mmol) and bpy (78 mg, 0.5 mmol) in CH_3CN (10 mL). The reaction mixture was then stirred for 30 min. Dark green single crystals suitable for X-ray analysis were obtained by slow evaporation at room temperature over several days. Yield: 70 mg (50%). $C_{60}H_{50}Cl_4CrCu_3N_{12}O_{21}$ (1659.54): calcd. C 43.39, H 2.89, N 10.16; found C 43.15, H 2.79, N 10.07. Important IR absorptions (KBr): $\tilde{\nu}$ = 3500 (br), 1610 (s), 1090 (br), 885 (s) cm^{-1}.

X-ray Crystallographic Analysis of 1:[16] A single crystal of **1** with approximate dimensions 0.20 × 0.25 × 0.30 mm was mounted on a glass fiber. A full data collection was performed with graphite monochromatized Mo-K_α radiation (λ = 0.71073 Å) on a Bruker SMART 1000 diffractometer equipped with a CCD camera. Cell parameters were determined from a least-squares refinement. The intensities of the ±hkl reflections were measured up to θ_{max} = 25.03° using a ω-2θ scan technique. The absorption correction was performed empirically.[17] The structure was solved by direct methods using SHELXS-97,[18] and refined by full-matrix least-squares on F^2 using SHELXL-97.[19] All non-hydrogen atoms were refined anisotropically, while hydrogen atoms were set in their calculated positions and treated as riding atoms with a common fixed isotropic thermal parameter. Further data of the X-ray structure analysis are given in Table 1.

Table 1. Crystallographic data for **1**

Empirical formula	$C_{60}H_{50}Cl_4CrCu_3N_{12}O_{21}$
Molecular weight	1659.54
T [K]	298(2)
Space group	$P\bar{1}$
a [Å]	12.0788(15)
b [Å]	13.3687(18)
c [Å]	22.489(3)
α [°]	83.337(2)
β [°]	75.063(2)
γ [°]	71.994(2)
V [Å]^3	3334.3(7)
Z	2
ρ (calcd.) [g/cm^3]	1.653
F(000)	1682
μ [mm^{-1}]	1.348
θ range [°]	0.94−25.03
Index ranges	$-11 \le h \le 14$, $-15 \le k \le 14$, $-19 \le l \le 26$
Reflections collected	13897
Independent reflections	11708 (R_{int} = 0.0289)
Observed reflections [$I > 2\sigma(I)$]	6750
Data/restraints/parameters	11708/0/928
Goodness-of-fit on F^2	0.991
$R1$[a] [$I > 2\sigma(I)$]; $wR2$[b][b]	0.0572; 0.1454
Largest diff. peak/hole [e/Å^3]	0.810, −0.549

[a] $R1 = \Sigma||F_o| - |F_c||/\Sigma|F_o|$. [b] $wR2 = [\Sigma w(F_o^2 - F_c^2)^2/\Sigma(F_o^2)^2]^{1/2}$.

Acknowledgments

This work was supported by the NSFC (Nos. 90101028, 50173011, 59672015), NSF of Tianjin (013801611) and the TRAPOYT of MOE, China.

[1] *Magneto-Structural Correlations in Exchange Coupled Systems*, NATO ASI Series C140 (Eds.: R. D. Willet, D. Gatteschi, O. Kahn), D. Reidel, Dordrecht, The Netherlands, **1985**.
[2] *Magnetic Molecular Materials* (Eds.: D. Gatteschi, O. Kahn, J. S. Miller, F. Palacio), Kluwer Academic Publishers, Dordrecht, The Netherlands, **1991**.
[3] O. Kahn, *Molecular Magnetism*, VCH, New York, **1993**.
[4] C. Kollmar, O. Kahn, *Acc. Chem. Res.* **1993**, *26*, 259−265.
[5] O. Kahn, *Acc. Chem. Res.* **2000**, *33*, 647−657.
[6] J. S. Miller, A. J. Epstein, *Angew. Chem. Int. Ed. Engl.* **1994**, *33*, 385−415.
[7] H. Oshio, T. Kikuchi, T. Ito, *Inorg. Chem.* **1996**, *35*, 4938−4941.
[8] H. Oshio, H. Okamoto, T. Kikuchi, T. Ito, *Inorg. Chem.* **1997**, *36*, 3201−3203.
[9] H. Oshio, T. Kikuchi, T. Ito, *Chem. Lett.* **2000**, 1138−1139.
[10] K.-Y. Choi, I.-H. Suh, D. W. Kim, *Inorg. Chim. Acta* **1999**, *293*, 100−105.
[11] M. Harel, C. Knobler, J. D. McCullough, *Inorg. Chem.* **1969**, *8*, 11−13.
[12] P. Chaudhuri, M. Winter, K. Wieghardt, S. Gehring, W. Haase, B. Nuber, J. Weiss, *Inorg. Chem.* **1988**, *27*, 1564−1569.
[13] W. Bensch, N. Seferiadis, H. R. Oswald, *Inorg. Chim. Acta* **1987**, *126*, 113−117.
[14] Y. Hayashi, H. Mano, A. Uehara, *Chem. Lett.* **1998**, 899−890.
[15] *Theory and Application of Molecular Paramagnetism* (Eds.: E. A. Boudreaux, L. N. Mulay), Wiley and Sons, Inc., New York, **1976**.
[16] CCDC-155520 contains the supplementary crystallographic data for this paper. These data can be obtained free of charge at www.ccdc.cam.ac.uk/conts/retrieving.html [or from the Cambridge Crystallographic Data Centre, 12, Union Road, Cambridge CB2 1EZ, UK; Fax: (internat.) +44-1223/336-033; E-mail: deposit@ccdc.cam.ac.uk].
[17] G. M. Sheldrick, *SADABS*, University of Göttingen, Göttingen, Germany, **1996**.
[18] G. M. Sheldrick, *SHELXS-97*, University of Göttingen, Göttingen, Germany, **1997**.
[19] G. M. Sheldrick, *SHELXL-97*, University of Göttingen, Göttingen, Germany, **1997**.

Received December 12, 2001
[I01505]

Hydroxylation of Hexane Using Dioxygen and Trimethylhydroquinone: Biomimetic Catalysis by an Unsymmetrical Diiron-μ-Oxo Complex

Nathalie Raffard-Pons Y Moll,[a] Frédéric Banse,*[a] Keiji Miki,[b] Martine Nierlich,[c] and Jean-Jacques Girerd*[a]

Keywords: Bioinorganic chemistry / Iron / Dioxygen activation / Biomimetic catalysis / N ligands

An unusual unsymmetrical diiron(III) complex has been obtained with an amine/pyridine ligand. Its ability to catalyze the hydroxylation of *n*-hexane with O_2 and trimethylhydroquinone as reductant and proton donor, respectively, is reported in homogeneous and supported conditions. A spectroscopic study is reported to confirm the role of the reductant. A high-valent iron-oxo species is suggested.

(© Wiley-VCH Verlag GmbH, 69451 Weinheim, Germany, 2002)

Introduction

Transforming alkanes into alcohols under environmentally friendly conditions (i.e. using O_2 at room temperature) is a challenge for chemists.[1] In the area of biomimetic chemistry, complexes with porphyrins[2] or amine/pyridine ligands[3] are extensively used to model the active site of mono- or dinuclear iron-containing biological systems capable of performing the above-mentioned reaction. Among nonheme metallobiomolecules able to hydroxylate a CH bond using O_2 and electrons, one can evoke two systems: the antitumoral drug Bleomycin (BLM),[4,5] which cleaves DNA oxidatively, or the metalloenzyme methane monooxygenase (MMO),[6,7] which catalyzes the conversion of methane into methanol. In both cases, the entity responsible for the oxidation of the CH bonds has been suggested to be a high valent iron-oxo compound. In the case of MMO, the active state is an $Fe^{IV}(\mu\text{-}O)_2Fe^{IV}$ intermediate (compound Q) derived from the peroxo form $Fe^{III}(\mu\text{-}1,2\text{-peroxo})Fe^{III}$ (compound P). It has been envisioned that the so-called "activated BLM" Fe^{III}-OOH dissociates to yield $Fe^{IV}O + OH^{\cdot}$ or $Fe^{V}O + OH^{-}$.

Most of the synthetic models that mimic the oxidation reactions catalyzed by these natural systems do not react directly with O_2 plus a reductant, but with H_2O_2 instead.[3] Although some peroxo models have been obtained by reacting Fe^{II} complexes with O_2,[8,9] only a few complexes have been reported to catalyze alkane oxidation reactions with dioxygen as oxidant.[3,10] In this communication, we report a new unsymmetrical dinuclear Fe^{III} complex obtained with the ligand *N*,*N*′-dimethyl-*N*,*N*′-bis(2-pyridylmethyl)propane-1,3-diamine (L_4^3). This diiron(III) complex can be reduced to the Fe^{II} state to further react with dioxygen and converts *n*-hexane into *n*-hexanols.

Results and Discussion

The molecular structure of $[L_4^3Fe^{III}(Cl)(\mu\text{-}O)Fe^{III}Cl_3]$ (**1**) has been resolved by X-ray diffraction (cf. Figure 1).[11] The structure can be described as two different units bridged by an oxo group. The first unit is an iron center in a pseudo-octahedral environment with the L_4^3 ligand wrapping around the metal in a *cis*-β fashion; a chloro ligand and the oxo bridge complete the coordination sphere. The second unit is an Fe^{III} moiety in a tetrahedral environment with three chloro ligands and the oxo bridge. Very few examples of this type of unsymmetrical dinuclear Fe^{III} complexes have been described.[12−15] Moreover the complex described here is the first one which has been obtained with pyridine groups.

Although the possibility that the unsymmetrical diiron units can be considered as models for biological systems has been envisioned,[12−15] no reactivity studies have been carried out with these complexes. The catalytic activity of **1** towards oxidation of *n*-hexane with molecular dioxygen has been evaluated in the presence of acetic acid and trimethylhydroquinone as reductant. At the beginning of the reaction the solution is purple, although this color disappears after about 10 minutes. The results were monitored period-

[a] Laboratoire de Chimie Inorganique, UMR CNRS 8613, Université Paris-Sud, 91405 Orsay, France
[b] National Institute for Resources and Environment, 16-3 Onogawa, Tsukuba, Ibaraki, 305−8569, Japan
[c] DRECAM/SCM bat 125, CEA Saclay, 91191 Gif-sur-Yvette, France
Supporting information for this article is available on the WWW under http://www.eurjic.com or from the author.

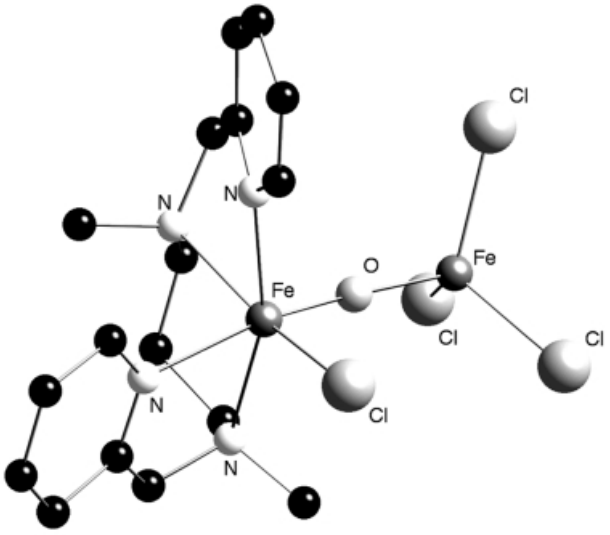

Figure 1. Molecular structure of $[L_4^3Fe^{III}(Cl)(\mu\text{-}O)Fe^{III}Cl_3]$ (**1**)

ically by GC and those recorded after 2 and 16 hours are gathered in Table 1. The total number of turnovers (ca. 10) is reached after 2 hours and further reaction time does not increase the yield nor alter the distribution of the products. Separate experiments confirmed that the presence of **1** in the reaction mixture was necessary for the oxidation of the substrate. Very interestingly, the alcohol-to-ketone ratio is much higher than 1. Such a high ratio is indicative of the absence of radical chain autoxidation, thereby suggesting the involvement of a metal-centered oxidation.[3] The evolution of this ratio from 15.5 to 50 when the reaction time increases seems artificial. Indeed, the yield of ketones decreases slightly while the yield in alcohols increases. As this phenomenon concerns a low number of turnovers, it is probably the consequence of side reactions, for example, reduction of the ketones by the excess reductant. Moreover, these side reactions take place over a period much longer than the time necessary to reach the total number of turnovers; they are therefore too slow to be responsible for the high A/K ratio observed after 2 hours.

Table 1. Oxidation of *n*-hexane by O_2 with by catalyst/trimethylhydroquinone/acetic acid[a]

System (duration)	Products (T.N.)					TTN[b]	A/K[c]
	1-ol	2-ol	3-ol	2-one	3-one		
1 in solution (2 h)	1.0	3.4	4.9	0.3	0.3	9.9	15.5
1 in solution (16 h)	1.1	3.7	5.2	0.1	0.1	10.2	50
1 on silica (2 h)	0.2	1.0	1.3	0.5	0.5	3.5	2.5
1 on silica (16 h)	5.1	17.8	22.2	1.9	2.1	49.1	11.3

[a] Yields are given as turnover numbers (T.N.) based on **1**. Reaction conditions: 1 atm. O_2 at 25 °C in 2.6 mL of dry acetonitrile; final concentration for the catalyst in the reaction mixture 0.33 mmol·L^{-1}. catalyst/*n*-hexane/trimethylhydroquinone/acetic acid 1:3000:350:250. [b] TTN stands for total number of turnovers. [c] Alcohols/ketones ratio.

Concerning the total number of turnovers and the A/K ratio, the results listed in Table 1 are of the same order as those reported for the oxidation of cyclohexane and *n*-pentane catalyzed by $[\{Fe(HBpz_3)(hfacac)\}_2O]$.[16] The same experiments were carried out without any acetic acid: the same product distribution was observed but the total yield was reduced by a factor of three. This suggests that maintaining a dimeric structure for the catalyst by means of an acetate bridge increases the lifetime of the catalyst **1**. We are currently trying to isolate the species that forms in the presence of acetate. Recently, White et al. made similar observations: they used acetate to increase the product yield and robustness of their catalyst.[17]

The same conclusion is suggested by the results obtained in heterogeneous conditions.(cf. Table 1). Upon immobilizing the L_4^3 ligand on a silica support,[18,19] the yield is increased by a factor of five after 16 hours. Contrary to the experiments in solution, these results improve drastically with time. This is not surprising if one considers that the substrate has to reach the metal center and the product has to be removed in solution before analysis. The reactivity has also been explored under slightly different conditions (results not reported in Table 1). This allows us to determine the following: i) as under homogeneous conditions, acetic acid increases the yield; ii) when the silica support was not treated with the C-18 chain (see figure in Supporting Information), the yield decreased. It appears that a hydrophobic matrix facilitates the reactivity. One can propose that, because of the long alkyl chains, the hydrophobic substrate is driven to the reactive site and the polar products are easily eliminated; iii) whatever the conditions, the heterogeneous catalyst was always more efficient than the homogeneous one for a reaction time of 16 hours.

In order to propose a mechanism for the catalytic oxidation of *n*-hexane by O_2 in the presence of trimethylhydroquinone and **1**, we have studied the reaction between **1** and the reductant in the absence of any substrate. The evolution as a function of time of a solution of equimolar amounts of **1** and trimethylhydroquinone (TMH_2Q) in acetonitrile under argon has been followed by UV/Visible spectroscopy (Figure 2). The characteristic LMCT bands of the unsymmetrical dimer **1** at 347 nm and 420 nm[20] decrease in intensity as the reaction evolves. At the same time the characteristic bands of trimethylquinone at 255 and 266 nm appear. No further change is observed after one hour. However, if dioxygen is gently bubbled through the reaction mixture for three days, the electronic spectrum reveals that the dinuclear compound **1** partly reforms (see Figure 2). With a TMH_2Q/**1** ratio of 1:1 the reoxidation by O_2 is slow. However, when using a much larger amount of reductant relative to **1**, we observed that this redox process becomes cyclic — and much faster (ca. 1 minute for each cycle) — by degassing or oxygenating the solution. It is most likely that in the presence of an excess of TMH_2Q, an Fe^{III}-TMHQ complex is formed, as indicated by the purple color (λ_{max} = 568 nm) attributed to a charge transfer between a phenolato group and Fe^{III}.[21,22] The Fe^{II}-trimethylhydroquinone complex then formed is reoxidized by O_2 much

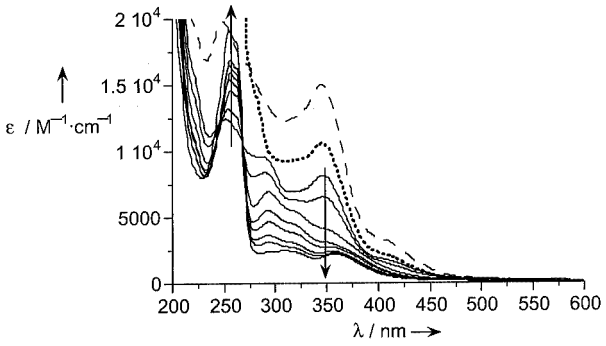

Figure 2. UV/Vis spectra of: (a) **1** + 1 equiv. of trimethylhydroquinone under argon (full line); (b) spectrum obtained after three days under O_2 at the end of evolution (a) (dotted line); spectrum of $L_4^3Fe^{III}(Cl)(\mu\text{-}O)Fe^{III}Cl_3$ **1** (dashed line)

more rapidly than the Fe^{II}-Cl complexes in the above experiment. Thus it appears that TMH_2Q plays a double role in the catalysis: reduction of Fe^{III} and displacement of the chloro ligands to give a Fe^{II}-trimethylhydroquinone complex that is more sensitive to O_2. The importance of ligation of hydroquinones to iron has already been pointed out.[23]

The observations reported above are in agreement with a mechanism implying a high-valent iron species: initial reduction of the dinuclear Fe^{III}-oxo complex **1** by trimethylhydroquinone to the Fe^{II} level allows dioxygen to interact with the metal centers to finally yield a high valent iron-oxo entity. However some questions remain to be elucidated, in particular the chemical nature (mono- or dinuclear) of the active species has to be addressed.

Conclusion

Compared to synthetic models, the pre-eminence of enzymatic systems resides in the separation of the successive steps in the catalytic cycle, whereas for model systems all the reactants are mixed together. The crucial reaction, i.e. oxidation of *n*-hexane by a putative mono- or dinuclear Fe^{IV} species, is in competition with oxidation of the excess reductant. The challenge for chemists in the coming years is therefore to devise catalytic systems in which the different steps can be timely orchestrated.

Experimental Section

The ligand L_4^3 was prepared following the method reported for the ligand bispicen[24] but using *N*,*N*′ dimethyl-1,3-propane diamine as starting material.

Synthesis of 1: A 7 mL methanolic solution of $FeCl_3{\cdot}6H_2O$ (165 mg, 0.61 mmol) was added to a solution of L_4^3 (1 equiv., 173 mg) in 10 mL of MeOH. The solution was stirred for a few minutes and a dark orange powder precipitated. The solid was filtered and washed twice with methanol (174 mg, 50%). Crystals were obtained within a few hours by diffusion of *tert*-butyl methyl ether into a solution of **1** in acetonitrile. $C_{17}H_{24}Cl_4Fe_2N_4O{\cdot}1/2CH_3OH$ (569.92 g·mol^{-1}): calcd. C 36.88, H 4.60, Cl 24.88, Fe 19.60, N 9.83; found C 36.74, H 4.50, Cl 24.77, Fe 19.34, N 9.74.

Syntheses of the grafted ligand and supported catalyst are available as Supporting information(see footnote on the first page of this article).

Acknowledgments

We thank the New Energy Development Organization and Osaka Gas Company, both in Japan, for financial support.

[1] J. M. Thomas, R. Raja, G. Sankar, R. G. Bell, *Acc. Chem. Res.* **2001**, *34*, 191.
[2] B. Meunier, A. Robert, G. Pratviel, J. Bernardou, in *The Porphyrin Handbook, Vol. 4* (Eds.: K. M. Kadish, K. Smith, E. R. Guilard), Academic Press, San Diego, **2000**, p. 119.
[3] M. Costas, K. Chen, L. Que, *Coord. Chem. Rev.* **2000**, *200−202*, 517.
[4] J. Stubbe, J. W. Kozarich, W. Wu, D. E. Vanderwall, *Acc. Chem. Res.* **1996**, *29*, 322.
[5] R. M. Burger, *Chem. Rev.* **1998**, *98*, 1153.
[6] B. J. Wallar, J. D. Lipscomb, *Chem. Rev.* **1996**, *96*, 2625.
[7] M. Merkx, D. A. Kopp, M. H. Sazinsky, J. L. Blazyk, J. Müller, S. J. Lippard, *Angew. Chem. Int. Ed.* **2001**, *40*, 2782.
[8] J. DuBois, T. J. Mizoguchi, S. J. Lippard, *Coord. Chem. Rev.* **2000**, *200−202*, 443.
[9] S. V. Kryatov, E. V. Rybak-Akimova, V. L. MacMurdo, L. Que, *Inorg. Chem.* **2001**, *40*, 2220.
[10] T. Funabiki, T. Toyoda, S. Yoshida, *Chem. Lett.* **1992**, 1279.
[11] Crystal data for **1**: $C_{17}H_{24}Cl_4Fe_2N_4O_1$, M_w = 553.90. Crystal dimensions 0.15 × 0.12 × 0.10. The data were collected at 123 K on a Nonius Kappa-CCD area detector diffractometer using graphite-monochromated Mo-K_α radiation. The structures were solved by direct methods with SHELXS-97 and refined by full-matrix least-squares on F^2 with anisotropic thermal parameters for all non-H atoms with SHELXL-97. Triclinic, space group $P\bar{1}$, a = 9.6360(19), b = 15.151(3), c = 17.665(4) Å; α = 114.77(3), β = 100.65(3), γ = 90.01(3); V = 2292.6(8) Å^3; Z = 4. 12065 measured reflections, of which 6879 were unique. CCDC-171973 contains the complete supplementary crystallographic data for this paper. These data can be obtained free of charge at www.ccdc.cam.ac.uk/conts/retrieving.html [or from the Cambridge Crystallographic Data Centre, 12, Union Road, Cambridge CB2 1EZ, UK; Fax: (internat.) +44-1223/336-033; E-mail: deposit@ccdc.cam.ac.uk].
[12] P. Gomez-Romero, G. C. DeFotis, G. B. Jameson, *J. Am. Chem. Soc.* **1986**, *108*, 851.
[13] P. Gómez-Romero, E. H. Witten, W. M. Reiff, G. Backes, J. Sanders-Loehr, G. B. Jameson, *J. Am. Chem. Soc.* **1989**, *111*, 9039.
[14] P. Gómez-Romero, E. H. Witten, W. M. Reiff, G. B. Jameson, *Inorg. Chem.* **1990**, *29*, 5211.
[15] J. Wang, M. S. Mashuta, Z. Sun, J. F. Richardson, D. N. Hendrickson, R. M. Buchanan, *Inorg. Chem.* **1996**, *35*, 6642.
[16] N. Kitajima, M. Ito, H. Fukui, Y. Moro-oka, *J. Chem. Soc., Chem. Commun.* **1991**, 102.
[17] M. C. White, A. G. Doyle, E. N. Jacobsen, *J. Am. Chem. Soc.* **2001**, *123*, 7194.
[18] K. Miki, T. Furuya, *Chem. Commun.* **1998**, 97.

[19] D. Brunel, N. Bellocq, P. Sutra, A. Cauvel, M. Laspéras, P. Moreau, F. DiRenzo, A. Galarneau, F. Fajula, *Coord. Chem. Rev.* **1998**, *178–180*, 1085.
[20] N. Raffard, F. Banse, E. Anxolabehere-Mallart, M. Nierlich, J.-J. Girerd, *Inorg. Chem.* to be submitted.
[21] P. Mialane, E. Anxolabéhère-Mallart, G. Blondin, A. Nivorojkine, J. Guilhem, L. Tchertanova, M. Césario, N. Ravi, E. Bominaar, J.-J. Girerd, E. Münck, *Inorg. Chim. Acta* **1997**, *263*, 367.
[22] B. Adam, E. Bill, E. Bothe, B. Goerdt, G. Haselhorst, P. Hildebrandt, A. Sokolowski, S. Stenken, T. Weyermüller, K. Wieghardt, *Chem. Eur. J.* **1997**, *3*, 308.
[23] T. Funabiki, T. Yokomizo, S. Suzuki, S. Yoshida, *Chem. Commun.* **1997**, 151.
[24] H. A. Goodwin, F. Lions, *J. Am. Chem. Soc.* **1960**, *82*, 5013.
Received February 19, 2002
[I02085]

A Novel Nanostructured Open-Channel Coordination Polymer with an Included Fused-Polyiodide Ring

Jack Y. Lu*[a] and Vaughn Schauss[a]

Keywords: Nanostructures / Hydrothermal synthesis / Copper / Iodine

A novel three-dimensional nanostructured open-channel metal-organic framework polymer with inclusion of a polyiodide cluster has been synthesized via an oxidation reaction mechanism under hydrothermal conditions.

(© Wiley-VCH Verlag GmbH, 69451 Weinheim, Germany, 2002)

The synthesis of new metal-organic polymers via self-assembly processes is a topical and important subject.[1] The diversities of the structures and new topologies discovered in metal-organic polymers are due to the wide variety of metal centers and organic building blocks used. Metal centers play a key role in molecular recognition processes in extended materials and biological systems.[2] We and others have recently demonstrated that copper ions and carboxylate ligands form metal-organic frameworks in which the copper(II) atoms display either a mixed octahedral/square pyramidal geometry in a triple-layer two-dimensional (2-D) open-framework,[3a] a square pyramidal coordination 2-D net in an interpenetrating 2-D/3-D structure,[3b] a square planar motif,[3c] or a trigonal bipyramidal geometry in a mixed-bonding 3-D network;[3d] the copper oxidation states are +1,[2a] +2,[4a] mixed-valence,[4b,4c] and/or with Cu−Cu bonds.[2a,4b,4c] The interest in copper arises mainly from its attractive magnetic[4b] and photoluminescence properties,[2a] novel structural features[2b,3,4a,4b] and its biological relevance in the binuclear "Cu_A" site of cytochrome oxidases and related model compounds.[4c,5] The synthetic methods used for preparing metal-organic network structures are conventional solution methodology in organic solvents or hydrothermal/solvothermal reactions under pressure. In most cases, a reduction or oxidation reaction mechanism has not been invoked during the self-assembly of metal-organic polymers. It has been found that Cu^{II} ions can be reduced to Cu^{I} by pyridine[6a] or pyridylcarboxylate[6b] under hydrothermal conditions. Often, fascinating structures and reaction chemistry can be achieved from the reduction of copper valence states.[4b,6] Hydrothermal processes are therefore considered to be necessary conditions for these reductions. It may not be surprising that the synthesis utilizing oxidation reaction route under hydrothermal conditions is hardly explored.[7] Here we report a novel open-channel framework polymer with polyiodide guests synthesized via an oxidation reaction route under hydrothermal conditions: $\{[Cu_2(IN)_3]\cdot I_5^-\cdot 2/3I_2\cdot H_2O\}_\infty$ (IN: isonicotinato) **1**.

X-ray single crystal analysis[8] revealed that compound **1** consists of a 3-D open-channel metal-organic framework with large polyiodide rings formed from fused polyiodide clusters. The metal-organic framework is comprised of two independent Cu atoms and three isonicotinato ligands. The two independent copper atoms are bridged by the oxygen atoms of three bidentate isonicotinato ligands (Figure 1). Cu(1) has a square-pyramidal geometry made up of two pyridyl groups of two IN units and three oxygen atoms from three bridging carboxylate groups of the IN units. Cu(2) has a distorted square-planar geometry consisting of one pyridyl group of an IN ligand and three oxygen atoms from three bridging carboxylate groups of IN units. This mixed square-planar/square-pyramidal binuclear unit, $[Cu_2(IN)_3]$, propagates to form an unusual nanostructured open-channel metal-organic framework polymer (Figure 2). The $[Cu_2(IN)_3]_6$ fragment displays a spiral-galaxy shape open-channel structure along the (1 1 1) direction (Figure 2). The open channel has a diameter of about 1.15 nm, similar to that of carbon nanotubes (1.2 ± 0.1 nm).[9] The association of $[Cu_2(IN)_3]_6$ fragments leads to triangular and rhombohedral units (Figure 3). These open-channel units in the structure extend in three dimensions. This complex is very different from the binuclear copper-carboxylate networks reported previously[2b,4b,10] as it can accommodate large polyiodide clusters in the open channels. The polyiodide consists of an I_5^- unit that is constructed from an I^- and two I_2 units (Figure 4). The I_2 units [I(1)−I(2), 2.774(1) Å; I(4)−I(5), 2.790(1) Å] and I^- anion have distances [I(3)−I(4), 3.115(1) Å; I(3)−I(2), 3.187(1) Å] shorter than those found in known polyiodides {I^-−I: 3.357(2) Å,[11] and 3.3 Å[12]}. It is noteworthy that every six I_5^- units are fused together around an I_2 molecule [I(6)−I(7), 2.723(7)

[a] Department of Chemistry, University of Houston-Clear Lake
Houston, TX 77058 USA
E-mail: lu@cl.uh.edu

Å] with I(5)···I(6) interactions of 3.560(10) Å (Figure 4). This distance is similar to those long range I···I interactions reported in $(Hpy)_2I_3I_7$ [3.545(13) Å].[13] The iodine molecule in the center of the fused cluster is disordered about a $\bar{3}$ site with six orientations. The fused polyiodide clusters are then linked by another I_2 molecule [I(8)−I(8), 2.759(1) Å] via long range interactions [I(3)···I(8), 3.478(1) Å]. This type of linkage results in large polyiodide rings within the open channels of the metal-organic framework (Figure 5).

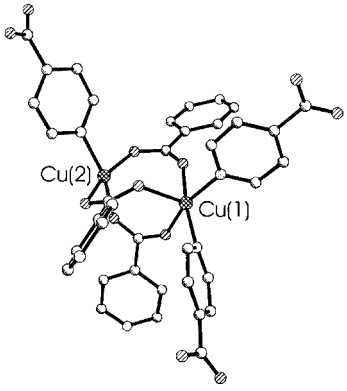

Figure 1. View of the coordination of the copper pair

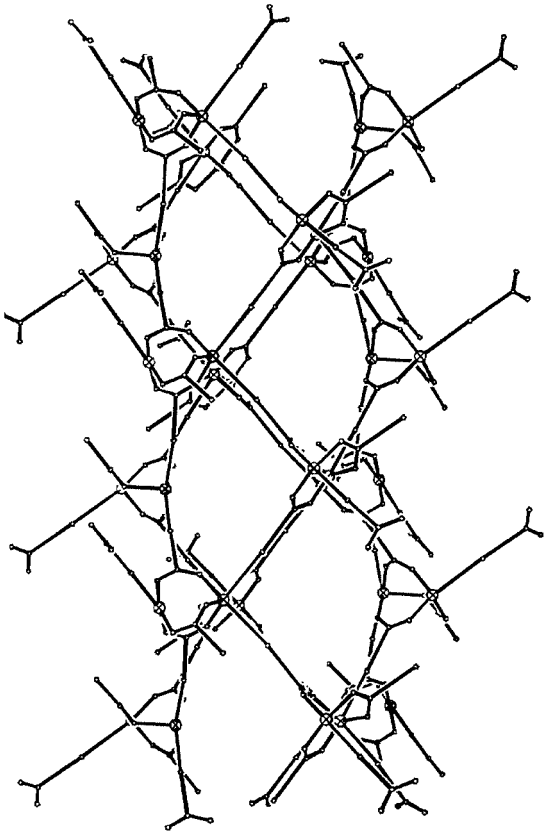

Figure 2. View of the open-channel network in **1**; isonicotinato units are represented by lines for clarity

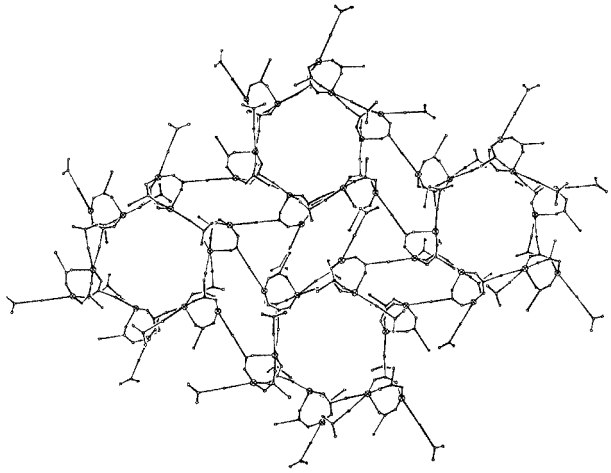

Figure 3. View of the different shape of the channels in the structure

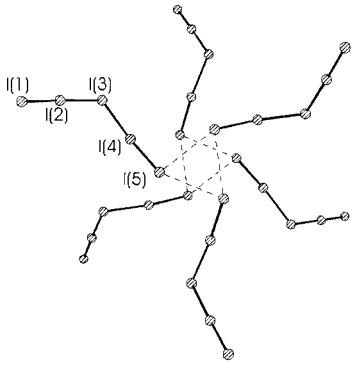

Figure 4. View of the I_5^- units in a fused polyiodide cluster; the iodine molecule with six orientations in the cluster center is not shown

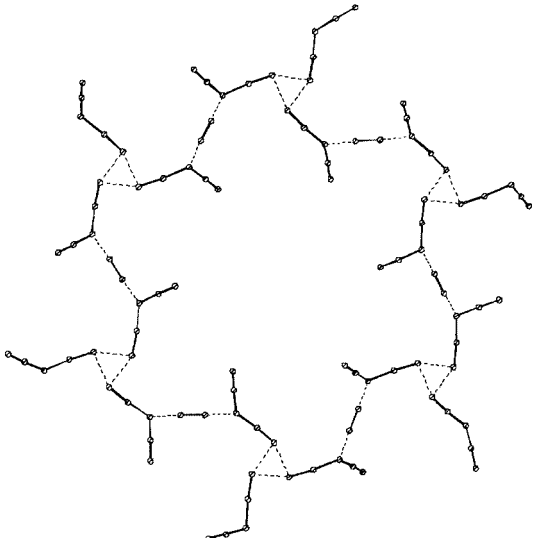

Figure 5. View of a polyiodide ring

The oxidation reaction route under hydrothermal conditions is different from that reported recently, where oxygen was used as an initiator.[7] The I_2 here acts as an oxidizer

as well as an iodine source. The half-cell potential[14] of iodine in acidic aqueous solution is +0.615 V, and that of copper is +0.153 V, based on the following half-cell reactions:

$$I_2(aq) + 2\,e \rightleftarrows 2\,I^-$$

$$Cu^{2+} + e \rightleftarrows Cu^+$$

Cu^I may also undergo disproportionation (auto-oxidation reaction) based on the following potential diagram:

$$Cu^{2+} \overset{0.153\ V}{\rightarrow} Cu^+ \overset{0.521\ V}{\rightarrow} Cu$$

Once the reaction has been initiated, the formation of the $[Cu_2(IN)_3]^+$ unit and the formation of polyiodide shifts the equilibrium of the following reaction to the right-hand side:

$$IN + CuI + I_2 \rightarrow [(Cu_2(IN)_3](I_5^-)$$

Note that the nanostructured open-channel framework in **1** is formed from the inclusion of polyiodide species. This structure is unique and unprecedented. Polyiodide species have been attracting attention recently,[11−13] and metal-organic open-framework structures templated by iodine species should be even more attractive. The synthesis of this novel polyiodide inclusion open-channel framework polymer also demonstrates that novel compounds that may not be accessible using known methods can be synthesized by an oxidation reaction route.[7] The reaction conditions are mild enough to keep the building blocks intact during the oxidation and self-assembly process.

Experimental Section

Black lustrous crystals of **1** were obtained by reacting CuI, isonicotinic acid and iodine (1:2:1) in 6 mL of water under hydrothermal conditions at 140 °C for three days. Yield: 56%.

CCDC-168434 contains the supplementary crystallographic data for this paper. These data can be obtained free of charge at www.ccdc.cam.ac.uk/conts/retrieving.html [or from the Cambridge Crystallographic Data Centre, 12, Union Road, Cambridge CB2 1EZ, UK; Fax: (internat.) +44-1223/336-033; E-mail: deposit@ccdc.cam.ac.uk].

Acknowledgments

The authors thank Dr. J. D. Korp for assistance in crystallography and financial support from the Welch Foundation and ISSO. This work made use of MRSEC/TCSUH Shared Experimental Facilities supported by the National Science Foundation under award no. DMR-9632667 and the Texas Center for Superconductivity at the University of Houston.

[1] See for example: M. J. Zaworotko, *Chem. Commun.* **2001**, 1−10; M. O'Keeffe, M. Eddaoudi, H. Li, T. Reineke, O. M. Yaghi, *J. Solid State Chem.* **2000**, *152*, 3−20; B. F. Hoskins, R. Robson, *J. Am. Chem. Soc.* **1990**, *112*, 1546−1554; L. Carlucci, G. Ciani, D. M. Proserpio, S. Rizzato, *Chem. Commun.* **2000**, 1319−1320; D.-Q. Chu, J.-Q. Xu, L.-M. Duan, T.-G. Wang, A.-Q. Tang, L. Ye, *Eur. J. Inorg. Chem.* **2001**, 1135−1137.

[2] [2a] P. C. Ford, E. Cariati, J. Bourassa, *Chem. Rev.* **1999**, *99*, 3625−3648; C.-M. Che, Z. Mao, V. M. Miskowski, M.-C. Tse, C.-K. Chan, K.-K. Cheung, D. L. Phillips, K.-H. Leung,. *Angew. Chem. Int. Ed.* **2000**, *39*, 4084−4088. [2b] B. Chen, M. Eddaoudi, T. M. Reineke, J. W. Kampf, M. O'Keeffe, O. M. Yaghi, *J. Am. Chem. Soc.* **2000**, *122*, 11559−11560. [2c] T. B. Karpishin, T. D. P. Stack, K. N. Raymond, *J. Am. Chem. Soc.* **1993**, *115*, 182−192.

[3] [3a] J. Y. Lu, A. M. Babb, *Inorg. Chem.* **2001**, *40*, 3261−3262. [3b] J. Y. Lu, A. M. Babb, *Chem. Commun.* **2001**, 821−822. [3c] J. Y. Lu, A. M. Babb, *Angew. Chem. Int. Ed.* submitted. [3d] J. Y. Lu, V. Schauss, *CrystEngComm.* **2001**, *26*, 111−113.

[4] [4a] S. S.-Y. Chui, S. M.-F. Lo, C. A. G. Orpen, I. D. Williams, *Science* **1999**, *283*, 1148−1150. [4b] S. M.-F. Lo, S. S.-Y. Chui, L.-Y. Shek, Z. Lin, X. Zhang, G. Wen, I. D. Williams, *J. Am. Chem. Soc.* **2000**, *122*, 6293−6294. [4c] S. Iwata, C. Ostermeier, B. Ludwig, H. Michel, *Nature* **1995**, *376*, 660−664. S. Ferguson-Miller, G. T. Babcock, *Chem. Rev.* **1996**, *96*, 2889−2908.

[5] K. R. Williams, D. R. Gamelin, L. B. LaCroix, R. P. Houser, W. B. Tolman, T. C. Mulder, S. de Vires, B. Hedman, K. O. Hodgson, E. I. Solomon, *J. Am. Chem. Soc.* **1997**, *119*, 613−614.

[6] [6a] O. M. Yaghi, H. Li, *J. Am. Chem. Soc.* **1995**, *117*, 10401−10402; J. Y. Lu, B. R. Cabrera, R.-J. Wang, J. Li, *Inorg. Chem.* **1998**, *37*, 4480−4481. [6b] J. Y. Lu, A. M. Babb, *Inorg. Chem.* **2002**, *41*, 1339−1341.

[7] J. Y. Lu, K. R. Runnels, *Inorg. Chem. Commun.* **2001**, *4*, 678−681.

[8] *Crystal data* for **1**: mol. wt. 1315.10; rhombohedral, space group, $R\bar{3}$; unit cell dimensions a = 20.934(1) Å, α = 115.808(1), V = 4734.3(3) Å^3, Z = 6, $D_{calcd.}$ = 2.768 gcm^{-3}, μ = 7.581 mm^{-1}, T = 223(2)K. Reflections collected: 21948; independent reflections: 4670 [R(int) = 0.0396]. Final R indices [$I > 4\sigma(I)$]: R_1 = 0.0251, wR_2 = 0.0590. The water molecule is disordered 50:50 over two different positions, and the I(6)−I(7) molecule is massively disordered about a $\bar{3}$ site.

[9] P. G. Collins, M. Ishigami, A. Zettl, *Cluster and Nanostructure Interfaces* (Ed: P. Jena et al.), Richmond, VA 25−28 October, 1999, p. 411.

[10] F. A. Cotton, E. V. Dikarev, M. A. Petrukhina, *Inorg. Chem.* **2000**, *39*, 6072−6079, and references therein.

[11] A. J. Blake, R. O. Gould, S. Parsons, C. Radek, M. Schröder, *Angew. Chem. Int. Ed. Engl.* **1995**, *34*, 2374−2376, and references therein.

[12] D. B. Morse, T. B. Rauchfuss, S. R. Wilson, *J. Am. Chem. Soc.* **1990**, *112*, 1860−1864, and references therein.

[13] T. L. Hendrixson, M. A. ter Host, R. A. Jacobson, *Acta Crystallogr., Sect. C* **1991**, *47*, 2141−2144.

[14] J. F. Rubinson, K. A. Rubinson, *Contemporary Chemical Analysis*, Prentice-Hall Inc.: New Jersey, **1998**.

Received February 25, 2002
[I02098]

Zinc(II), Samarium(III) and Tin(II) Complexes Featuring a Tridentate Nitrogen Donor for the Ring-Opening Copolymerization of (D,L)-Lactide and Glycolide

Anca Dumitrescu,[a] Blanca Martin-Vaca,[a] Heinz Gornitzka,[a] Jean-Bernard Cazaux,[a] Didier Bourissou,*[a] and Guy Bertrand*[a,b]

Keywords: N ligands / Zinc / Samarium / Ring-opening polymerization / Copolymerization

The synthesis, structure, and catalytic activity in ring-opening polymerization of zinc(II), samarium(III) and tin(II) complexes featuring a tridentate nitrogen donor are described.

(© Wiley-VCH Verlag GmbH, 69451 Weinheim, Germany, 2002)

Introduction

The design of discrete metal complexes that could be highly active and selective catalysts for the polymerization of a variety of monomer classes is of considerable current interest.[1] A significant aim is to construct less expensive catalysts while retaining the benefits of discrete metal complexes. These goals are especially important with respect to the copolymerization of lactide (L) and glycolide (G), to give poly(lactide-*co*-glycolide) (PLGA), biodegradable and biocompatible polyesters that are garnering great interest due to their biomedical, pharmaceutical, and agricultural applications.[2] To this end complexes of various metals (aluminum,[3−5] tin,[6] zinc,[7−9] iron,[10] magnesium,[7d] zirconium[11]) and lanthanides (yttrium,[12,13] lanthanum,[12,13] samarium,[13] ytterbium[13]) have been studied.

Chelating nitrogen ligands are often used for stabilizing low-valent species.[14] We have recently shown that diamidoamino ligands $[(RNCH_2CH_2)_2NR']^{2-}$, initially developed by Cloke,[15] are particularly well adapted for the stabilization of neutral as well as cationic group 13 Lewis acids.[3] Due to the formation of a rather rigid bicyclic core, these tridentate nitrogen donors enforce an approximately trigonal-monopyramidal coordination geometry around the metal, and the ensuing empty axial coordination site has been used for promoting the ring-opening polymerization of heterocycles such as propylene oxide and (D,L)-lactide.[3] We have also shown that stannylenes featuring diamidoamino ligands are monomers both in solution and in the solid state.[16] Here we report the synthesis and structural investigation of related zinc(II) and samarium(III) derivatives which adopt dimeric structures in the solid state. The catalytic activities of the zinc, samarium and previously reported tin complexes for the ring-opening copolymerization of (D,L)-lactide and glycolide are compared.

[a] Laboratoire d'Hétérochimie Fondamentale et Appliquée du CNRS (UMR 5069), Université Paul Sabatier,
118, route de Narbonne, 31062 Toulouse Cedex 04, France
Fax: (internat.) + 33-5/6155-8204
[b] UCR-CNRS Joint Research Chemistry Laboratory (UMR 2282), Department of Chemistry − University of California, Riverside, CA 92521−0403, USA
Fax: (internat.) +1-909/787-2725
E-mail: gbertran@mail.ucr.edu

Results and Discussion

Deprotonation of the triamine **1**[3] with two equivalents of *n*BuLi and treatment of the ensuing dilithium salt with anhydrous $ZnCl_2$ and $SmCl_3$ affords the neutral complexes **2** and **3** in 44 and 70% yield, respectively (Scheme 1).

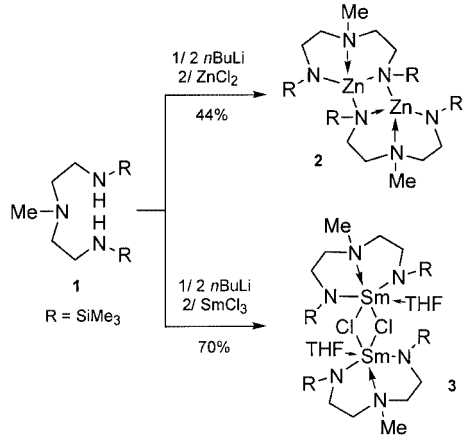

Scheme 1. Synthesis of compounds **2** and **3**

The dimeric structure of **2**, both in solution and in the solid state, was demonstrated by the presence of two sets of signals for the $SiCH_3$ groups in the ^1H and ^{13}C NMR spec-

tra and by an X-ray analysis (single crystals were obtained in pentane at −30 °C) (Figure 1). Derivative **2** contains a central rectangular $(Zn-N)_2$ four-membered ring, which is centered on the crystallographically imposed inversion center of the molecule. The Zn1−N2 [2.238(5) Å] and Zn1−N3 [1.907(0) Å] distances are in the typical range for dative (2.10−2.40 Å) and covalent (1.80−1.90 Å) Zn−N bonds,[17] respectively, while the Zn1−N1 [2.105(4) Å] and Zn1−N1a [2.025(2) Å] distances are, as expected, half-way between covalent and dative bonds. Since Zn−N and Sn−N bond lengths are very similar,[17,18] and since secondary bulky amines normally guarantee monomeric structures for both homoleptic zinc and tin amides, the dimeric structure adopted by **2** is rather surprising. It probably results from the geometry enforced by the diamidoamino ligand, which is certainly more adapted for a bent stannylene[18] than for a linear, allenic-type zinc derivative.[17]

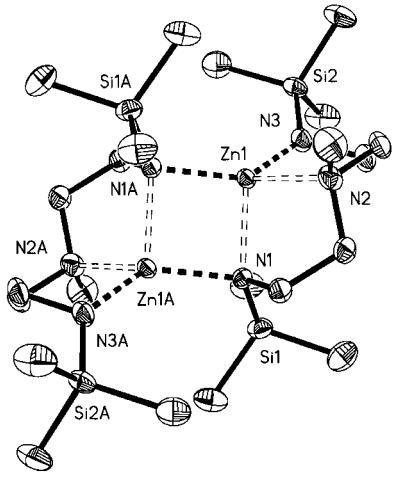

Figure 1. Molecular structure of **2** in the solid state; the hydrogen atoms are omitted for clarity; selected bond lengths (Å) and angles (°): Zn1−N1 2.105(2), Zn1−N1A 2.025(2), Zn1−N2 2.238(2), Zn1−N3 1.907(2), N1−Si1 1.736(2), N3−Si2 1.694(2); N1−Zn1−N2 85.25(6), N1−Zn1−N3 124.48(7), N1−Zn1−N1A 92.49(6), N2−Zn1−N3 86.96(7), N2−Zn1−N1A 127.35(6), N3−Zn1−N1A 133.36(6)

Complex **3** also adopts a dimeric structure but the two $[(Me_3SiNCH_2CH_2)_2NMe]Sm(THF)$ units are bridged by two chlorine atoms (Figure 2). As observed in $[(Cy_2N)_2Sm(\mu\text{-}Cl)(THF)]_2$,[19] the amido nitrogens are in a trigonal planar environment and the $(Sm-Cl)_2$ core is perfectly planar. However, each samarium atom is hexacoordinate and has a strongly distorted octahedral geometry. In other words, the coordination of the amino nitrogen to the lanthanide center does not prevent the coordination of a THF molecule: this is of particular interest for ring-opening polymerization via a coordination-insertion mechanism.[20]

The zinc, samarium and tin derivatives **2**−**4** initiate the bulk copolymerization of (D,L)-lactide and glycolide (Table 1). As estimated from ^{1}H NMR spectroscopy, complete conversion of both monomers requires about 3 h at 180 °C with the zinc complex **2**. Copolymers possessing higher molecular weight could be obtained by increasing

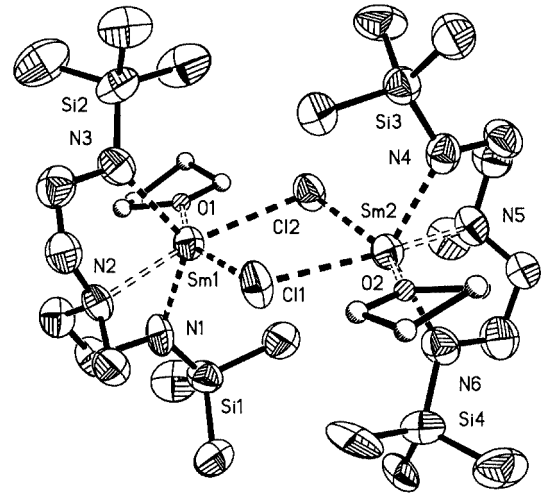

Figure 2. Molecular structure of **3** in the solid state; the hydrogen atoms are omitted for clarity; selected bond lengths (Å) and angles (°): Sm1−Cl1 2.773(3), Sm1−Cl2 2.797(3), Sm1−N1 2.290(12), Sm1−N2 2.574(9), Sm1−N3 2.299(12), Sm1−O1 2.519(8), N1−Si1 1.678(12), N3−Si2 1.695(12); N1−Sm1−N2 68.9(3), N1−Sm1−N3 124.1(4), N1−Sm1−Cl1 104.0(3), N1−Sm1−Cl2 122.1(3), N1−Sm1−O1 83.2(4), Cl1−Sm1−Cl2 75.65(9)

the reaction time but at the expense of the molecular weight distribution (from 2.3 to 3.6) (entries 1−3). However, high-molecular weight copolymers with narrow distribution and various glycolide contents could be prepared by optimizing the reaction conditions (entries 4 and 5). With the samarium derivative **3**, high conversions of both monomers are observed after only 30 minutes at 180 °C and even 160 °C (entries 6 and 7). When carrying out the copolymerization of a stoichiometric mixture of (D,L)-lactide and glycolide at 160 °C, using **3** as the initiator, a copolymer of high molecular weight and narrow molecular distribution (M_n = 26.200, M_w/M_n = 1.8) was obtained after 3.5 h (entry 9). The tin derivative $[MeN(CH_2CH_2NSiMe_3)_2]Sn$ (**4**)[16] is even more active. Conversions higher than 95% are obtained after only 30 minutes at 180 °C. Upon increasing the reaction time, the molecular weight progressively decreases, while the molecular weight distribution increases, probably due to transesterification reactions (entries 10−12).[21] At 140 °C (entries 13−15), these side reactions are significantly reduced, while the tin catalyst remains very active (conversions higher than 90% after 20 minutes); under these conditions, very high molecular weight copolymers are obtained (M_n = 85.150, M_w/M_n = 1.9) (entry 14).

Conclusion

Since the electronic and steric properties of the ligand can be tuned easily, metal complexes of type **2**−**4** are promising candidates for ring-opening polymerization of heterocycles,[22] as well as for the metal-organic vapor phase epitaxy (MOVPE)[23] and metal-organic chemical vapor deposition (MOCVD).[24]

Table 1. Bulk copolymerization of (D,L)-lactide and glycolide

Entry	Catalyst	Temp. (°C)	Time (min.)	L/cat.[a]	G/cat.[a]	Conv. L[b] (%)	Conv. G[b] (%)	G/(G+L)[b] (mol %)	M_n [c]	M_w/M_n[c]
1	**2**	180	30	800	342	31	90	55	9.200	2.3
2	**2**	180	80	800	342	76	100	48	17.200	2.7
3	**2**	180	180	800	342	98	100	38	13.000	3.6
4	**2**	180	120	580	249	87	100	34	24.900	1.9
5	**2**	180	140	702	398	79	96	49	39.400	1.7
6	**3**	180	30	130	55	86	100	33	17.800	1.7
7	**3**	160	30	130	55	71	100	39	25.650	1.6
8	**3**	160	60	150	150	44	100	58	16.600	1.7
9	**3**	160	210	150	150	96	100	51	26.200	1.8
10	**4**	180	30	800	342	95	100	30	25.800	2.8
11	**4**	180	60	800	342	96	100	30	21.100	2.9
12	**4**	180	120	800	342	99	100	27	17.700	3.0
13	**4**	140	10	800	342	85	100	32	94.450	1.8
14	**4**	140	20	800	342	93	100	31	85.150	1.9
15	**4**	140	120	800	342	97	100	30	67.100	2.2

[a] Molar ratio. [b] Obtained from ^{1}H NMR spectroscopy. [c] Obtained from GPC analysis by using polystyrene standards.

Experimental Section

General: All reactions were performed under argon atmosphere using standard Schlenk tube techniques. Solvents were dried by standard procedures and distilled prior to use. Amine **1** was prepared according to a literature procedure.[3b] ^{1}H and ^{13}C{^{1}H} NMR spectra were recorded on a Bruker AC250 spectrometer. ^{1}H and ^{13}C{^{1}H} chemical shifts are reported in ppm relative to Me_4Si as an external standard.

{[MeN(CH$_2$CH$_2$NSiMe$_3$)$_2$]Zn}$_2$ (2): An ether suspension (5 mL) of $ZnCl_2$ (0.58 g, 4.3 mmol) was added at −78 °C to an ether solution (10 mL) of the dilithium salt of *N*-methyl-*N*′,*N*′′-bis(trimethylsilyl)-diethylenetriamine (**1**) (4.3 mmol). The solution became yellow, and was allowed to warm to room temperature. After stirring overnight, removal of the solvent under vacuum and extraction with pentane (25 mL), colorless crystals of **2** were obtained at −20 °C. Yield 0.6 g (44%); m.p. 239 °C (dec.). ^{1}H NMR (250 MHz, C_6D_6): δ = 0.25 (s, 18 H, $SiCH_3$), 0.30 (s, 18 H, $SiCH_3$), 1.68−1.62 (m, 2 H, CH_2), 2.03 (m, 4 H, CH_2), 2.11 (s, 6 H, NCH_3), 2.3−2.1 (m, 2 H, CH_2), 2.98 (m, 4 H, CH_2), 3.05 (m, 4 H, CH_2) ppm. ^{13}C{^{1}H} NMR (62.9 MHz, C_6D_6): δ = 3.2 ($SiCH_3$), 3.3 ($SiCH_3$), 44.5 (NCH_3), 47.6 (CH_2), 47.7 (CH_2), 60.3 (CH_2), 65.9 (CH_2). $C_{11}H_{29}N_3Si_2Zn$ (324.9): calcd. C 40.66, H 9.00, N 12.93; found C 40.28, H 9.35, N 12.71.

{[(Me$_3$SiNCH$_2$CH$_2$)$_2$NMe]Sm(THF)Cl}$_2$ (3): A THF suspension (5 mL) of $SmCl_3$ (1.2 g, 4.7 mmol) was added at −78 °C to a tetrahydrofuran solution (10 mL) of the dilithium salt of **1** (4.7 mmol). The solution was allowed to warm to room temperature and stirred for 4 hours. After removal of the solvent under vacuum and extraction with toluene (5 mL), colorless crystals of **3** were obtained at −20 °C. Yield 1.7 g (70%); m.p. 173 °C (dec.). $C_{15}H_{37}ClN_3OSi_2Sm$ (517.5): calcd. C 34.82, H 7.21, N 8.12; found C 34.65, H 7.53, N 7.91.

X-ray Crystallography: Data for both structures were collected at low-temperatures using an oil-coated shock-cooled crystal on a Bruker-AXS CCD 1000 diffractometer with graphite-monochromated Mo-K_α (λ = 0.71073 Å) radiation. The structures were solved by direct methods using SHELXS-97[25] and refined with all data on F^2 using SHELXL-97.[26] All non-hydrogen atoms were treated anisotropically. The hydrogen atoms were geometrically idealized and refined using a riding model.

2: Monoclinic, space group $P2_1/n$; T = 173 K; a = 11.668(2), b = 11.300(2), c = 13.894(2) Å; β = 111.67(2)°; V = 1702.4(5) Å^3; Z = 4; R [$I > 2\sigma(I)$] = 0.0241, $wR2$ (all data) = 0.0646 for 2598 unique reflections, 161 parameters, GooF = 1.004.

3: Orthorhombic, space group *Pbca*; T = 173 K; a = 13.184(1), b = 18.567(2), c = 38.049(3) Å; V = 9313.9(14) Å^3; Z = 16; R [$I > 2\sigma(I)$] = 0.0543, $wR2$ (all data) = 0.1453 for 6051 unique reflections, 451 parameters, GooF = 0.820.

CCDC-183554 (**2**) and -183555 (**3**) contain the supplementary crystallographic data for this paper. These data can be obtained free of charge at www.ccdc.cam.ac.uk/conts/retrieving.html [or from the Cambridge Crystallographic Data Centre, 12, Union Road, Cambridge CB2 1EZ, UK; Fax: (internat.) +44-1223/336-033; E-mail: deposit@ccdc.cam.ac.uk].

Acknowledgments

Thanks are due to the CNRS and Beaufour-Ipsen Industrie for financial support of this work.

[1] W. Kuran, *Prog. Polym. Sci.* **1998**, *23*, 919−992.
[2] [2a] E. Chiellini, R. Solaro, *Adv. Mater.* **1996**, *8*, 305−313. [2b] M. Jacoby, *Chem. Eng. News* **2001**, *79*, 30−35.
[3] [3a] N. Emig, R. Réau, H. Krautscheid, D. Fenske, G. Bertrand, *J. Am. Chem. Soc.* **1996**, *118*, 5822−5823. [3b] N. Emig, H. Nguyen, H. Krautscheid, R. Réau, J. B. Cazaux, G. Bertrand, *Organometallics* **1998**, *17*, 3599−3608.
[4] T. Aida, S. Inoue, *Acc. Chem. Res.* **1996**, *29*, 39−48.
[5] C. P. Radano, G. L. Baker, M. R. Smith III, *J. Am. Chem. Soc.* **2000**, *122*, 1552−1553.
[6] [6a] A. P. Dove, V. C. Gibson, E. L. Marshall, A. J. P. White, D. J. Williams, *Chem. Commun.* **2001**, 283−284. [6b] K. B. Aubrecht, M. A. Hillmyer, W. B. Tolman, *Macromolecules* **2002**, *35*, 644−650.
[7] [7a] M. Cheng, E. B. Lobkovsky, G. W. Coates, *J. Am. Chem. Soc.* **1998**, *120*, 11018−11019. [7b] M. Cheng, A. B. Attygalle, E. B. Lobkovsky, G. W. Coates, *J. Am. Chem. Soc.* **1999**, *121*, 11583−11584. [7c] M. Cheng, N. A. Darling, E. B. Lobkovsky, G. W. Coates, *Chem. Commun.* **2000**, 2007−2008. [7d] B. M. Chamberlain, M. Cheng, D. R. Moore, T. M. Ovitt, E. B. Lobkovsky, G. W. Coates, *J. Am. Chem. Soc.* **2001**, *12*, 3229−3238.

[8] [8a] M. H. Chisholm, N. W. Eilerts, J. C. Huffman, S. S. Iyer, M. Pacold, K. Phomphrai, *J. Am. Chem. Soc.* **2000**, *122*, 11845−11854. [8b] M. H. Chisholm, J. C. Gallucci, H. Zhen, J. C. Huffman, *Inorg. Chem.* **2001**, *40*, 5051−5054.

[9] D. J. Darensbourg, J. R. Wildeson, J. C. Yarbrough, J. H. Reibenspies, *J. Am. Chem. Soc.* **2000**, *122*, 12487−12496.

[10] B. J. O'Keefe, S. M. Monnier, M. A. Hillmyer, W. B. Tolman, *J. Am. Chem. Soc.* **2001**, *123*, 339−340.

[11] P. Dobrzynski, J. Kasperczyk, H. Janeczek, M. Bero, *Macromolecules* **2001**, *34*, 5090−5098.

[12] [12a] W. M. Stevels, M. J. K. Ankoné, P. J. Dijkstra, J. Feijen, *Macromolecules* **1996**, *29*, 3332−3333. [12b] W. M. Stevels, M. J. K. Ankoné, P. J. Dijkstra, J. Feijen, *Macromolecules* **1996**, *29*, 6132−6138.

[13] V. Simic, N. Spassky, L. G. Hubert-Pfalzgraf, *Macromolecules* **1997**, *30*, 7338−7340.

[14] L. H. Gade, *Chem. Commun.* **2000**, 173−181.

[15] F. G. N. Cloke, P. B. Hitchcock, J. B. Love, *J. Chem. Soc., Dalton Trans.* **1995**, 25−29.

[16] J. L. Fauré, H. Gornitzka, R. Réau, D. Stalke, G. Bertrand, *Eur. J. Inorg. Chem.* **1999**, 2295−2299.

[17] [17a] A. Haaland, K. Hedberg, P. P. Power, *Inorg. Chem.* **1984**, *23*, 1972−1975. [17b] P. P. Power, K. Ruhlandt-Senge, S. C. Shoner, *Inorg. Chem.* **1991**, *30*, 5013−5015. [17c] H. Schumann, J. Gottfriedsen, F. Girgsdies, *Z. Anorg. Allg. Chem.* **1997**, *623*, 1881−1884. [17d] H. Schumann, J. Gottfriedsen, S. Dechert, F. Girgsdies, *Z. Anorg. Allg. Chem.* **2000**, *626*, 747−758.

[18] [18a] M. F. Lappert, P. P. Power, M. J. Slade, *J. Chem. Soc., Chem. Commun.* **1979**, 369−370. [18b] T. Fjeldberg, H. Hope, M. F. Lappert, P. P. Power, A. J. Thorne, *J. Chem. Soc., Chem. Commun.* **1983**, 639−340. [18c] H. Braunschweig, B. Gehrhus, P. B. Hitchcock, M. F. Lappert, *Z. Anorg. Allg. Chem.* **1995**, *621*, 1922−1928.

[19] R. K. Minhas, Y. Ma, J. I. Song, S. Gambarotta, *Inorg. Chem.* **1996**, *35*, 1866−1873.

[20] M. Ryner, K. Stridsberg, A. C. Albertsson, H. von Schenck, M. Svensson, *Macromolecules* **2001**, *34*, 3877−3881.

[21] [21a] H. R. Kricheldorf, M. Berl, N. Scharnagl, *Macromolecules* **1988**, *21*, 286−293. [21b] H. R. Kricheldorf, C. Boettcher, K. U. Tönner, *Polymer* **1992**, *33*, 2817−2824.

[22] [22a] G. Bertrand, J. B. Cazaux, J. L. Fauré, H. Nguyen, R. Réau, *Patent* WO99/02536. [22b] G. Bertrand, D. Bourissou, J. B. Cazaux, A. Dumitrescu, H. Gornitzka, B. Martin-Vaca, *Patent* WO01/00628. [22c] G. Bertrand, D. Bourissou, J. B. Cazaux, H. Nguyen, H. Gornitzka, B. Martin-Vaca, *Patent* WO01/00630.

[23] U. W. Pohl, S. Freitag, J. Gottfriedsen, W. Richter, H. Schumann, *J. Cryst. Growth* **1997**, *170*, 144−148.

[24] [24a] W. S. Rees, Jr., O. Just, H. Schumann, R. Weimann, *Angew. Chem. Int. Ed. Engl.* **1996**, *35*, 419. [24b] S. Bunge, O. Just, W. S. Rees, Jr., *Angew. Chem. Int. Ed.* **2000**, *39*, 3082−3084. [24c] H. Luten, O. Just, W. S. Rees, Jr., *Chem. Commun.* **2000**, 735−736. [24d] W. S. Rees, Jr., O. Just, S. L. Castro, J. S. Matthews, *Inorg. Chem.* **2000**, *39*, 3736−3737.

[25] G. M. Sheldrick, *Acta Crystallogr., Sect. A* **1990**, *46*, 467−473.

[26] G. M. Sheldrick, SHELXL-97; *Program for Crystal Structure Refinement*, University of Göttingen, **1997**.

Received April 10, 2002
[I02194]

A Crystalline Phosphenium Salt Featuring the Electron-Withdrawing 2,6-Bis(trifluoromethyl)phenyl Group

Anca Dumitrescu,[a] Heinz Gornitzka,[a] Wolfgang W. Schoeller,[b] Didier Bourissou,[a] and Guy Bertrand*[a,c]

Keywords: Electron-deficient compounds / Carbenoids / Phosphorus / Fluorine

The presence of a σ-withdrawing group such as the 2,6-bis-(trifluoromethyl)phenyl substituent does not prevent the isolation of a highly electrophilic phosphenium salt.

(© Wiley-VCH Verlag GmbH, 69451 Weinheim, Germany, 2002)

Introduction

Bulky hydrocarbon substituents are commonly used for the thermodynamic and kinetic stabilization of highly reactive species such as low-coordinate compounds.[1] Due to their peculiar properties,[2] related fluorinated substituents have recently attracted considerable attention, and have allowed for the isolation of several group 14 carbenoids (Figure 1). The stability of the monomeric bis(aryl)germylene,[3] -stannylene[4] and -plumbylene[5] **I**−**III** is only partly due to steric shielding,[6] the most important factor being the electron-donating ability of the fluorine lone pairs of the *o*-CF_3 groups to the electron-deficient center. Carbenes are even more reactive,[7] but using their reluctance to insert into C−F compared to C−H bonds,[8] the highly persistent triplet bis(aryl)carbene **IV**[9] and the first stable singlet (aryl)carbenes **V**[10] and **VI**[11] have been prepared. The 2,6-bis(trifluoromethyl)phenyl group Ar_F remains electronically a spectator in the (amino)(aryl)carbenes **V**,[10] while its electron-withdrawing properties are involved in the push-pull stabilization of the (aryl)(phosphanyl)carbenes **VI**.[11]

Much less is known about the group 15 carbenoids.[12] Because of their inherent electrophilicity, most of the known phosphenium salts (R_2P^+) feature two π-donor substituents such as amino groups.[13] Notable exceptions are the (amino)(mesityl)-[14] and (phosphanyl)(supermesityl)-phosphenium[15] salts, which both feature an electron-rich

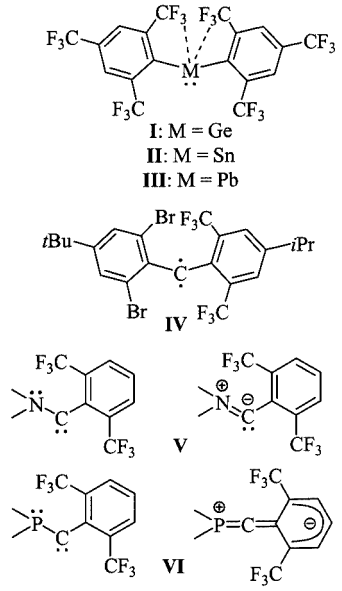

Figure 1. Structure of group 14 carbenoids **I**−**VI**

aryl substituent. Given the potential uses of phosphenium salts as strong π-acceptor ligands,[16] it was of interest to investigate the possibility of preparing a phosphenium salt featuring an electron-withdrawing group. Here we report the synthesis, structural analysis and reactivity of the [2,6-bis(trifluoromethyl)phenyl](diisopropylamino) phosphenium salt **3**.

Results and Discussion

Treatment of the chlorophosphane **1** with silver trifluoromethanesulfonate in dichloromethane, a common method for preparing phosphenium salts, led to derivative **2** (Scheme 1), which was isolated as white crystals in 70% yield. The covalent nature of **2** was suggested by the mod-

[a] Laboratoire d'Hétérochimie Fondamentale et Appliquée du CNRS (UMR 5069)
Université Paul Sabatier
118, route de Narbonne, 31062 Toulouse Cedex 04, France
Fax: (internat.) +33-5/6155-8204
[b] Fakultät für Chemie der Universität
Postfach 10 01 31, 33615 Bielefeld, Germany
Fax: (internat.) +49-(0)521/106-6467
[c] UCR-CNRS Joint Research Chemistry Laboratory (UMR 2282), Department of Chemistry − University of California, Riverside, CA 92521−0403, USA
Fax: (internat.) +1-909/787-2725
E-mail: gbertran@mail.ucr.edu

erate deshielding of the ^{31}P NMR signal (**1**: δ = 123.9 ppm; **2**: δ = 186.5 ppm), and confirmed by an X-ray analysis (Figure 2 and Table 1). Compound **2** is the first covalent (trifluoromethanesulfonate)phosphane to be structurally characterized.[17] The P(1)−N(1) bond is very short [1.626(4) Å] and the P(1)−O(1) bond is very long [1.882(2) Å], suggesting that a less coordinating anion should allow for the isolation of the highly electrophilic ionic form. Indeed, the desired phosphenium salt **3** was obtained from **1** by chloride abstraction with gallium trichloride (Scheme 1). The ionic nature of **3** in solution was unambiguously deduced from the dramatic downfield shift observed in the ^{31}P NMR spectrum (**3**: δ = 423 ppm). Single crystals of **3** suitable for an X-ray analysis were obtained from dichloromethane solution at low temperature (Figure 3 and Table 1).

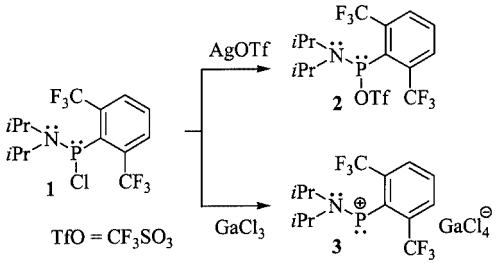

Scheme 1. Synthesis of compounds **2** and **3**

The values of the shortest P···Cl contacts [3.378(9) and 3.848(6) Å] confirm the ionic nature of **3**. The nitrogen atom is in a planar environment and the P(1)−N(1) bond is short

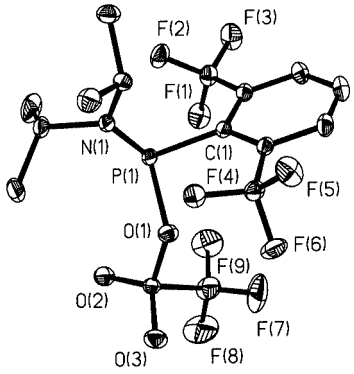

Figure 2. Thermal ellipsoid diagram (30% probability) of **2**; the hydrogen atoms have been omitted for clarity; selected bond lengths (Å) and angles (°): P(1)−N(1) 1.626(4), P(1)−C(1) 1.863(3), P(1)−O(1) 1.882(2), N(1)−P(1)−C(1) 104.15(10), N(1)−P(1)−O(1) 110.03(9), C(1)−P(1)−O(1) 91.38(12), C(9)−N(1)−C(12) 114.96(18), C(9)−N(1)−P(1) 129.06(11), C(12)−N(1)−P(1) 115.81(12)

[1.605(2) Å], as expected from the donation of the nitrogen lone pair to the vacant 3p(P) orbital. The aryl group is almost perpendicular to the plane defined by the C(9), C(12), N(1), P(1) and C(1) atoms [torsion angle N(1)−P(1)−C(1)−C(2) 94.8(2)°], which rules out any conjugation of the π system with the vacant 3p(P) orbital. Of further interest, the absence of an interaction between the phosphorus lone pair and the withdrawing aryl group is confirmed by the small C(1)−P(1)−N(1) angle [105.1(1)°] and the long P(1)−C(1) bond [1.845(2) Å]. All these data suggest that there is no π interaction between the aryl group and the phosphorus center, as observed for the (amino)(aryl)carbene

Table 1. Crystallographic data for compounds **2**, **3** and **5b**

	2	**3**	**5b**
Empirical formula	$C_{15}H_{17}F_9NO_3PS$	$C_{14}H_{17}Cl_4F_6GaNP$	$C_{33}H_{57}Cl_4F_6GaN_5P$
M_r	493.33	555.78	880.33
Crystal size [mm]	0.1 × 0.5 × 0.7	0.2 × 0.5 × 0.8	0.1 × 0.4 × 0.6
Crystal system	monoclinic	triclinic	orthorhombic
Space group	$P2_1/n$	$P\bar{1}$	$P2_12_12_1$
a [Å]	8.83(2)	9.2399(3)	13.7512(11)
b [Å]	15.74(3)	10.2700(4)	16.9623(13)
c [Å]	14.63(2)	13.7886(5)	18.4099(14)
α [°]	90	73.0520(10)	90
β [°]	92.48(9)	88.8350(10)	90
γ [°]	90	65.6620(10)	90
V [Å^3]	2032(7)	1132.89(7)	4294.1(6)
Z	4	2	4
D_x [Mg m^{-3}]	1.613	1.629	1.362
μ [mm^{-1}]	0.336	1.805	0.982
F(000)	1000	552	1832
T [K]	193(2)	193(2)	193(2)
$2\theta_{max}$ [°]	65	56	50
No. of refl. measured	24985	11644	38281
No. of refl. unique	6890	5583	7235
R_{int}	0.0526	0.0176	0.0578
Parameters	275	322	465
Restraints	0	166	0
wR_2 (all reflns.)	0.1119	0.0835	0.0871
R_1 [$I > 2\sigma I$]	0.0383	0.0316	0.0406
Max. Δρ (e·Å^{-3}]	0.414	0.459	0.430

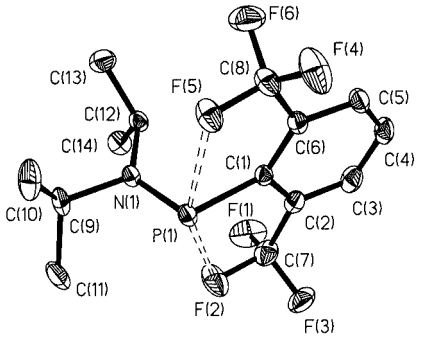

Figure 3. Thermal ellipsoid diagram (30% probability) of **3**; the hydrogen atoms and $GaCl_4^-$ counteranion have been omitted for clarity; selected bond lengths (Å) and angles (°): P(1)−N(1) 1.6050(15), P(1)−C(1) 1.8454 (18), C(1)−C(2) 1.404(3), N(1)−P(1)−C(1) 105.08(8)

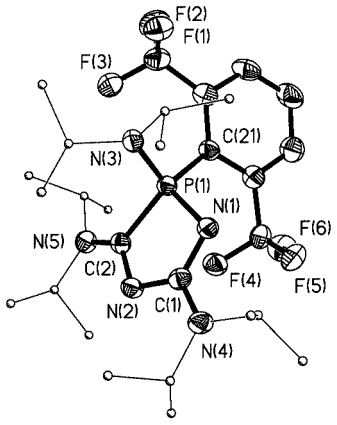

Figure 4. Thermal ellipsoid diagram (50% probability) of **5b**; for clarity the isopropyl groups have been simplified, and the hydrogen atoms and $GaCl_4^-$ counteranion omitted; selected bond lengths (Å) and angles (°): P(1)−N(3) 1.642(3), P(1)−C(21) 1.850(3), P(1)−C(2) 1.884(3), P(1)−N(1) 1.605(3), N(3)−P(1)−C(21) 112.25(15)

V. However, two close P···F contacts are present in the solid state [2.554(2) and 2.562(11) Å, sum of the van der Waals radii: 3.37 Å], as observed for the heavier group 14 carbenoids. Low-temperature experiments were prevented by the poor solubility of **3**, but the presence of a single ^{19}F NMR signal at room temperature suggests fast rotation of the *o*-CF_3 groups and thus weak P···F interactions.

The high electrophilicity of **3** is apparent from its chemical behavior. Cyanamides do not react with the bis(diisopropylamino)phosphenium salt. In marked contrast, however, dimethylcyanamide reacts smoothly with **3** (Scheme 2) The cationic five-membered heterocycle **5a** was obtained in 60% yield and characterized by multinuclear NMR spectroscopy. The formation of **5a** probably results from a [3+2] dipolar cycloaddition between the acid-base complex **4a** and a second molecule of cyanamide. This hypothesis was confirmed using diisopropylcyanamide. Steric protection allowed the characterization of the acid-base adduct **4b** when only one equivalent of cyanamide was used (Scheme 2). Addition of a second equivalent led to the cationic five-membered heterocycle **5b**, which was isolated in 65% yield as white crystals and structurally characterized (Figure 4 and Table 1).

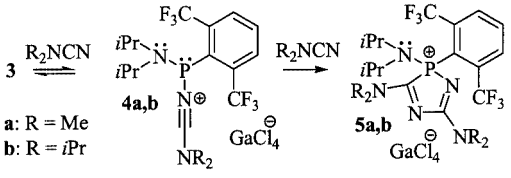

Scheme 2. Synthesis of compounds **4** and **5**

Concluding Remarks

The presence of an electron-withdrawing group such as a 2,6-bis(trifluoromethyl)-substituted aryl does not prevent the isolation of highly electrophilic phosphenium salts **3**. According to X-ray analysis, its structure is half-way between that of the related carbenes and heavier homologues. The electrophilic character of **3** is illustrated by the unusual formation of acid-base complexes **4** with cyanamides. The availability of phosphenium salts featuring a withdrawing group opens the way for new developments in the coordination chemistry of strong π-acceptor ligands.

Experimental Section

General Procedures: All reactions and manipulations were carried out under dry nitrogen in conventional glassware using standard Schlenk techniques. Solvents were dried according to standard procedures. ^1H, ^{13}C, ^{19}F and ^{31}P NMR spectra were recorded on Bruker AC200, WM250 or AMX400 spectrometers. All downfield chemical shifts are expressed with a positive sign, in ppm, relative to an external standard (Me_4Si for ^1H and ^{13}C, CF_3CO_2H for ^{19}F and 85% H_3PO_4 for ^{31}P).

Synthesis of the Chlorophosphane 1: Diisopropylamine (2 g, 19 mmol) was added to a toluene solution (15 mL) of 2,6-bis(trifluoromethyl)phenyldichlorophosphane (3 g, 9.5 mmol) and the reaction mixture was refluxed for 18 h. The solvent was then removed under vacuum and the residue extracted with pentane (30 mL). The chlorophosphane **1** was crystallized from a pentane solution at −30 °C. Yield 2.7 g (75%); m.p. 94 °C. ^1H NMR (CD_2Cl_2): δ = 1.1 (d, $^3J_{H,H}$ = 6.7 Hz, 6 H, CH_3), 1.3 (d, $^3J_{H,H}$ = 6.7 Hz, 6 H, CH_3), 3.6 (sept, $^3J_{H,H}$ = 6.7 Hz, 2 H, C*H*CH_3), 7.7 (t, $^3J_{H,H}$ = 8.2 Hz, 1 H, H_p), 8.0 (d, $^3J_{H,H}$ = 8.2 Hz, 2 H, H_m) ppm. ^{19}F NMR (CD_2Cl_2): δ = 22.4 (d, $^4J_{P,F}$ = 44 Hz) ppm. ^{31}P NMR (CD_2Cl_2): δ = 123.9 (sept, $^4J_{P,F}$ = 44 Hz) ppm. $C_{14}H_{17}ClF_9NP$ (436.7): calcd. C 38.50, H 3.92, N 3.21; found C 38.78, H 4.23, N 2.99.

Synthesis of the (Trifluoromethylsulfonyl)phosphane (2): Silver trifluoromethanesulfonate (2.1 g, 7.9 mmol) was added to a dichloromethane solution (15 mL) of the chlorophosphane **1** (3 g, 7.9 mmol) at −78 °C. After warming to room temperature and filtration, the phosphane **2** was crystallized from a dichloromethane solution at −30 °C. Yield 2.7 g (70%). ^1H NMR ($CDCl_3$): δ = 0.9 (d, $^3J_{H,H}$ = 5.4 Hz, 6 H, CH_3), 1.3 (d, $^3J_{H,H}$ = 5.4 Hz, 6 H, CH_3), 3.3 (sept, $^3J_{H,H}$ = 5.4 Hz, 1 H, C*H*CH_3), 3.4 (sept, $^3J_{H,H}$ = 5.4 Hz, 1 H, C*H*CH_3), 6.7 (t, $^3J_{H,H}$ = 6.4 Hz, 1 H, H_p), 7.4 (d, $^3J_{H,H}$ = 6.4 Hz, 2 H, H_m) ppm. ^{19}F NMR ($CDCl_3$): δ = 12.7 (s, 3 F, CF_3SO_3), 20.3 (d, $^4J_{P,F}$ = 43 Hz, 6 F, *o*-CF_3) ppm. ^{31}P NMR

($CDCl_3$): δ = 186.5 (sept, $^4J_{P,F}$ = 43 Hz) ppm. $C_{15}H_{17}F_9NO_3PS$ (493.3): calcd. C 36.52, H 3.47, N 2.84; found C 36.15, H 3.26, N 3.14.

Synthesis of the Phosphenium Salt 3: Gallium trichloride (0.46 g, 2.6 mmol) was added to a dichloromethane solution (4 mL) of the chlorophosphane **1** (1 g, 2.6 mmol) at −78 °C. After warming to room temperature, the reaction mixture was stirred for 30 minutes. The phosphenium salt **3** was crystallized from a dichloromethane solution at −30 °C. Yield 0.9 g (62%); m.p. 164 °C. ^{1}H NMR (CD_2Cl_2): δ = 1.6 (br., 12 H, CH_3), 4.4 (br., 2 H, C*H*CH_3), 8.3 (br., 3 H, H_p and H_m) ppm. ^{13}C NMR (CD_2Cl_2): δ = 25.0 (br., CH3), 62.7 (br., CHCH3), 124.3 (q, $^1J_{C,F}$ = 276 Hz, CF_3), 128.5 (d, $^1J_{C,P}$ = 78 Hz, C_{ipso}), 133.4 (s, C_m), 133.3 (q, $^2J_{C,F}$ = 32 Hz, C_o), 136.5 (s, C_p) ppm. ^{19}F NMR (CD_2Cl_2): δ = 22.4 (d, $^4J_{P,F}$ = 40 Hz) ppm. ^{31}P NMR (CD_2Cl_2): δ = 423 (br.) ppm. $C_{14}H_{17}Cl_4F_6GaNP$ (555.8): calcd. C 30.25, H 3.08, N 2.52; found C 29.87, H 2.78, N 2.35.

Synthesis of the Heterocycle 5a: Dimethylcyanamide (0.05 g, 0.68 mmol) was added at room temperature to a dichloromethane solution (4 mL) of the phosphenium salt **3** (0.2 g, 0.34 mmol). The reaction mixture was stirred for 30 minutes and the solvent was evaporated under vacuum. The heterocycle **5a** was crystallized from a 1:2 dichloromethane/diethyl ether solution at −30 °C. Yield 0.18 g (60%). ^{1}H NMR (CD_2Cl_2): δ = 1.4 (d, $^3J_{H,H}$ = 6.4 Hz, 6 H, CHC*H*$_3$), 1.5 (d, $^3J_{H,H}$ = 6.4 Hz, 6 H, CHC*H*$_3$), 3.2 (d, $J_{P,H}$ = 1.2 Hz, 3 H, NCH_3), 3.2 (s, 3 H, NCH_3), 3.3 (d, $J_{P,H}$ = 0.8 Hz, 3 H, NCH_3), 3.6 (b, 3 H, NCH_3), 3.8 (sept.d, $^3J_{H,H}$ = 6.4, $^3J_{P,H}$ = 19.2 Hz, 2 H, C*H*CH_3), 8.1 (pseudo-t, $^3J_{H,H}$ = 7.6 Hz, 1 H, H_p), 8.2 (d, $^3J_{H,H}$ = 7.6 Hz, 1 H, H_m), 8.3 (d, $^3J_{H,H}$ = 7.6 Hz, 1 H, H_m) ppm. ^{13}C NMR (CD_2Cl_2): δ = 22.0 (s, CH*C*H$_3$), 22.9 (s, CH*C*H$_3$), 37.7 (d, $J_{C,P}$ = 3.6 Hz, NCH_3), 38.2 (s, NCH_3), 43.5 (s, NCH_3), 43.6 (s, NCH_3), 52.6 (s, *C*HCH$_3$), 123.5 (q, $^1J_{C,F}$ = 275 Hz, CF_3), 126.2 (d, $^1J_{C,P}$ = 108 Hz, C_{ipso}), 133.0 (q, $^2J_{C,F}$ = 32 Hz, C_o), 133.1 (q, $^2J_{C,F}$ = 33 Hz, C_o), 133.6 (s, C_m), 133.7 (s, C_m), 135.2 (s, C_p), 166.3 (d, $J_{P,C}$ = 24 Hz, CN), 175.2 (d, $J_{P,C}$ = 37 Hz, CN) ppm. ^{31}P NMR (CD_2Cl_2): δ = 64.2 (s) ppm. $C_{26}H_{29}Cl_4F_6GaN_5P$ (768.0): calcd. C 40.66, H 3.81, N 9.12; found C 40.31, H 3.42, N 9.54.

Synthesis of the Acid-Base Adduct 4b: Diisopropylcyanamide (0.04 g, 0.34 mmol) was added at room temperature to a dichloromethane solution (4 mL) of the phosphenium salt **3** (0.2 g, 0.34 mmol). The reaction was stirred for 1 h and the solvent was evaporated under vacuum. The acid-base adduct **4b** was obtained as a colorless oil and characterized without purification. Yield 0.14 g (60%). ^{1}H NMR (CD_2Cl_2): δ = 1.1 (d, $^3J_{H,H}$ = 5.6 Hz, 6 H, CHC*H*$_3$), 1.4 (d, $^3J_{H,H}$ = 6.5 Hz, 12 H, CHC*H*$_3$), 1.5 (d, $^3J_{H,H}$ = 5.6 Hz, 6 H, CHC*H*$_3$), 3.6 (br., 1 H, C*H*CH$_3$), 3.8 (br., 2 H, C*H*CH$_3$), 3.9 (br., 1 H, C*H*CH$_3$), 8.0 (t, $^3J_{H,H}$ = 8.0 Hz, 1 H, H_p), 8.2 (d, $^3J_{H,H}$ = 8.0 Hz, 2 H, H_m) ppm. ^{13}C NMR (CD_2Cl_2): δ = 21.4 (s, CH*C*H$_3$), 22.0 (s, CH*C*H$_3$), 26.0 (d, $J_{C,P}$ = 8 Hz, CH*C*H$_3$), 49.0 (d, $J_{C,P}$ = 24 Hz, *C*HCH$_3$), 56.1 (s, *C*HCH$_3$), 56.8 (s, *C*HCH$_3$), 124.0 (q, $^1J_{C,F}$ = 276 Hz, *o*-CF_3), 129.0 (d, $^1J_{C,P}$ = 48 Hz, C_{ipso}), 132.9 (q, $^3J_{C,F}$ = 32 Hz, C_m), 134.0 (s, C_p), 134.5 (dq, $J_{C,P}$ = 17, $^2J_{C,F}$ = 30 Hz, C_o) ppm. ^{31}P NMR (CD_2Cl_2): δ = 110.9 (br.) ppm.

Synthesis of the Heterocycle 5b: Diisopropylcyanamide (0.08 g, 0.68 mmol) was added at room temperature to a dichloromethane solution (4 mL) of the phosphenium salt **3** (0.2 g, 0.34 mmol). The reaction was stirred for 2 h and the solvent was evaporated under vacuum. The heterocycle **5b** was crystallized from a 1:2 dichloromethane/diethyl ether solution at −30 °C. Yield 0.22 g (65%). ^{19}F NMR ($CDCl_3$): δ = 22.7 (s) ppm. ^{31}P NMR ($CDCl_3$): δ = 57.1 (s) ppm. $C_{28}H_{45}Cl_4F_6GaN_5P$ (808.2): calcd. C 41.61, H 5.61, N 8.67; found C 41.99, H 5.87, N 8.44.

X-ray Crystallographic Studies of Compounds 2, 3 and 5b: Crystal data for all structures are presented in Table 1. Data were collected on a Bruker-AXS CCD 1000 diffractometer with Mo-K_α radiation (λ = 0.71073 Å). The structures were solved by direct methods by means of SHELXS-97[18] and refined with all data on F^2 by means of SHELXL-97.[19] All non-hydrogen atoms were refined anisotropically. The hydrogen atoms of the molecules were geometrically idealized and refined using a riding model.
CCDC-179375 (**2**), -179376 (**3**) and -179377 (**5b**) contain the supplementary crystallographic data for this paper. These data can be obtained free of charge at www.ccdc.cam.ac.uk/conts/retrieving.html [or from the Cambridge Crystallographic Data Centre, 12, Union Road, Cambridge CB2 1EZ, UK; Fax: (internat.) +44−1223/336−033; E-mail: deposit@ccdc.cam.ac.uk].

Acknowledgments

Thanks are due to the CNRS, the DFG, the University Paul Sabatier, the University of California at Riverside and Rhodia for financial support of this work.

[1] N. Burford, J. A. C. Clyburne, M. S. W. Chan, *Inorg. Chem.* **1997**, *36*, 3204−3206.
[2] F. T. Edelmann, *Comments Inorg. Chem.* **1992**, *12*, 259−284.
[3] J. E. Bender IV, M. M. Banaszak Holl, J. W. Kampf, *Organometallics* **1997**, *16*, 2743−2745.
[4] H. Grützmacher, H. Pritzkow, F. T. Edelmann, *Organometallics* **1991**, *10*, 23−25; U. Lay, H. Pritzkow, H. Grützmacher, *J. Chem. Soc., Chem. Commun.* **1992**, 260−262.
[5] S. Brooker, J. K. Buijink, F. T. Edelmann, *Organometallics* **1991**, *10*, 25−26.
[6] A trifluoromethyl moiety almost doubles in bulk a methyl and does not fall much behind that of a *tert*-butyl group: M. Schlosser, D. Michel, *Tetrahedron* **1996**, *52*, 99−108.
[7] D. Bourissou, O. Guerret, F. P. Gabbaï, G. Bertrand, *Chem. Rev.* **2000**, *100*, 39−91.
[8] H. Tomioka, K. Taketsuji, *Chem. Commun.* **1997**, 1745−1746.
[9] K. Hirai, H. Tomioka, *J. Am. Chem. Soc.* **1999**, *121*, 10213−10214; H. L. Woodcock, D. Moran, P. v. R. Schleyer, H. F. Schaefer III, *J. Am. Chem. Soc.* **2001**, *123*, 4331−4335.
[10] S. Solé, H. Gornitzka, W. W. Schoeller, D. Bourissou, G. Bertrand, *Science* **2001**, *292*, 1901−1903.
[11] C. Buron, H. Gornitzka, V. Romanenko, G. Bertrand, *Science* **2000**, *288*, 834−836.
[12] So far, all attempts to prepare bis(aryl)carbenoids based on fluorinated aryl groups and a group 15 element have failed: N. Burford, C. L. B. MacDonald, D. J. LeBlanc, T. S. Cameron, *Organometallics* **2000**, *19*, 152−155.
[13] A. H. Cowley, R. Kemp, *Chem. Rev.* **1985**, *85*, 367−382.
[14] R. W. Reed, Z. Xie, C. A. Reed, *Organometallics* **1995**, *14*, 5002−5004.
[15] S. Loss, C. Widauer, H. Grützmacher, *Angew. Chem.* **1999**, *111*, 3546−3548; *Angew. Chem. Int. Ed.* **1999**, *38*, 3329−3331.
[16] B. Breit, *Chem. Commun.* **1996**, 2071−2072; D. Gudat, *Coord. Chem. Rev.* **1997**, *163*, 71−106.
[17] For a covalent (trifluoromethanesulfonate)iminophosphane and the corresponding iminophosphenium salt, see: E. Niecke, R. Detsch, M. Nieger, F. Reichert, W. W. Schoeller, *Bull. Soc. Chim. Fr.* **1993**, *130*, 25−31; E. Niecke, M. Nieger, F. Reichert, *Angew. Chem.* **1988**, *100*, 1781−1782; *Angew. Chem. Int. Ed. Engl.* **1988**, *27*, 1715−1716.
[18] G. M. Sheldrick, *Acta Crystallogr., Sect. A* **1990**, *46*, 467−473.
[19] SHELXL-97, *Program for Crystal Structure Refinement*, G. M. Sheldrick, University of Göttingen, **1997**.

Received April 10, 2002
[I02193]

Cobalt(II)/(III) Complexes Containing *o*-Iminothiobenzosemiquinonato(1−) and *o*-Iminobenzosemiquinonato(1−) π-Radical Ligands

Diran Herebian,[a] Prasanta Ghosh,[a] Hyungphil Chun,[a] Eberhard Bothe,[a] Thomas Weyhermüller,[a] and Karl Wieghardt*[a]

Keywords: Cobalt / Electrochemistry / EPR spectroscopy / N ligands / Radicals / S ligands

The coordination chemistry of 6-amino-2,4-di-*tert*-butylthiophenol ($H[L_S^{AP}]$) and of 2-anilino-4,6-di-*tert*-butylphenol ($H[L_O^{AP}]$) with cobalt(II) ions was investigated in the presence and absence of dioxygen. It was shown that both compounds were redox-non-innocent ligands, existing in different protonation and oxidation levels as: (i) *o*-aminophenolates(1–) $[(L_X^{AP})^{1-}]$, (ii) *o*-imidophenolates(2–) $[(L_X^{IP})^{2-}]$, and (iii) one-electron oxidized forms *o*-iminobenzosemiquinonates(1–) $[(L_X^{ISQ})^{1-}]$, which are π-radicals (X = S, O for the sulfur or oxygen derivative). The following complexes were synthesized: $[Co^{II}(L_S^{AP})_2]_2$ (**1**), $[Co^{II}(L_S^{ISQ})_2]_2$·0.5*n*-hexane (**2**·0.5*n*-hexane), $[Co^{III}I(L_S^{ISQ})_2]$ (**3**), $[Co^{III}I(L_O^{ISQ})_2]$ (**4**), and $[Co^{III}Cl(L_O^{ISQ})_2]$ (**5**). The compounds **2**·0.5*n*-hexane, **4**, and **5** were structurally characterized by X-ray crystallography. It was shown that the different protonation and oxidation levels of the ligands could readily be identified by X-ray crystallography. Complex **2** could be reversibly oxidized and reduced electrochemically, yielding a monocation and a monoanion, respectively. It was shown that these processes were metal-centered ($[Co^{III}(L_S^{ISQ})_2]^+$, $[Co^{II}(L_S^{ISQ})_2]$, and $[Co^{I}(L_S^{ISQ})_2]^-$). The electronic structures were elucidated by UV/Vis and EPR spectroscopy and magnetochemistry. Complexes **3**, **4**, and **5** were shown to be singlet diradicals.

(© Wiley-VCH Verlag GmbH, 69451 Weinheim, Germany, 2002)

1. Introduction

Despite a recent assertion to the contrary,[1] *N*,*S*-coordinated *o*-aminothiophenolate ligands are redox-non-innocent in the sense that they can exist at four distinctly different protonation and oxidation levels (Scheme 1).[2] We have recently shown that the monomeric diamagnetic, square-planar complexes $[M^{II}(L_S^{ISQ})_2]$ (M = Ni, Pd, Pt) contain two *N*,*S*-coordinated *o*-iminothiobenzosemiquinonato(1−) π-radical ligands $[(L_S^{ISQ})^{1-}]$, which are strongly antiferromagnetically coupled intramolecularly.[2] The species are thus considered to be diradicals with singlet ground states.

As shown in Scheme 2, the geometrical differences between *N*,*S*-coordinated *o*-aminothiophenolato(1−) $[(L_S^{AP})^{1-}]$, *o*-imidothiophenolato(2−) $[(L_S^{IP})^{2-}]$, and their monoanionic radical form $(L_S^{ISQ})^{1-}$ can readily be identified by X-ray crystallography. The same has been shown to hold for *O*,*N*-coordinated *o*-aminophenolates $[(L_O^{AP})^{1-}]$, *o*-imidophenolate(2−) $[(L_O^{IP})^{2-}]$, and *o*-iminobenzosemiquinonate(1−) radicals $[(L_O^{ISQ})^{1-}]$.[3−7] In these and in the current study, the ligands used were Sellmann's 6-amino-2,4-di-*tert*-butylthiophenol[8] ($H[L_S^{AP}]$) and 2-anilino-4,6-di-*tert*-butylphenol[4] ($H[L_O^{AP}]$). Here we report the coordination chemistry of cobalt(II) and -(III) with these ligands (Scheme 3).

Coordination of the unsubstituted *o*-aminothiophenol with cobalt(II) in the absence of air yielded orange-brown, paramagnetic $[Co^{II}(SC_6H_4NH_2)_2]_2$. Its dimeric nature was inferred from the temperature dependence of its magnetic moment, yielding an $S_t = 0$ ground state from two antiferromagnetically coupled high-spin Co^{II} ions ($S_{Co} = {}^3/_2$). In the presence of oxygen a deep blue material was obtained $[Co^{II}(SC_6H_4NH)_2]$, but its exact nature was not established. Finally, a diamagnetic green $[Co^{III}(SC_6H_4NH_2)_3]$ species was reported. None of these species was structurally characterized, and the problems of differing oxidation and protonation levels were not considered.[9,10] Recently, Artaud et al.[11] reported a structurally characterized dinuclear

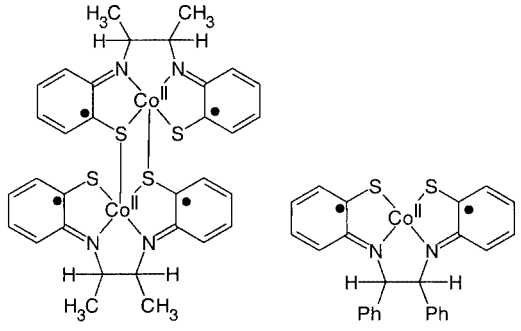

[a] Max-Planck-Institut für Strahlenchemie,
Stiftstrasse 34−36, 45470 Mülheim an der Ruhr, Germany

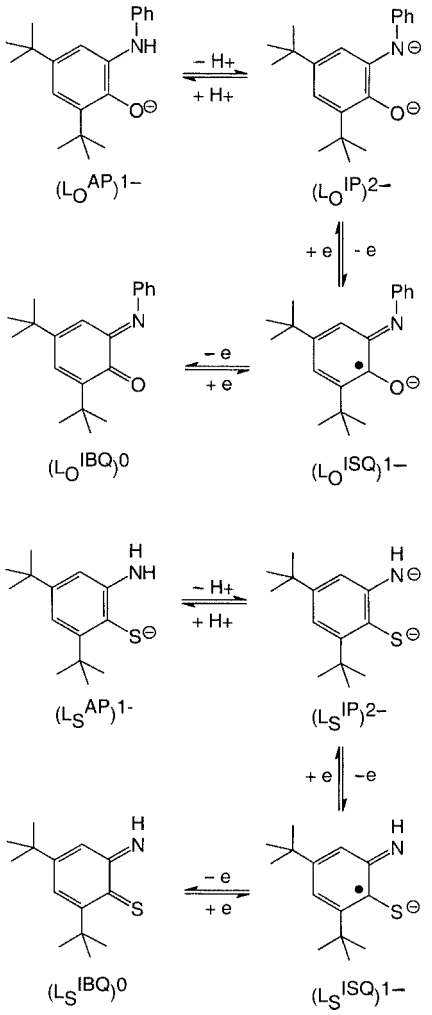

Scheme 1

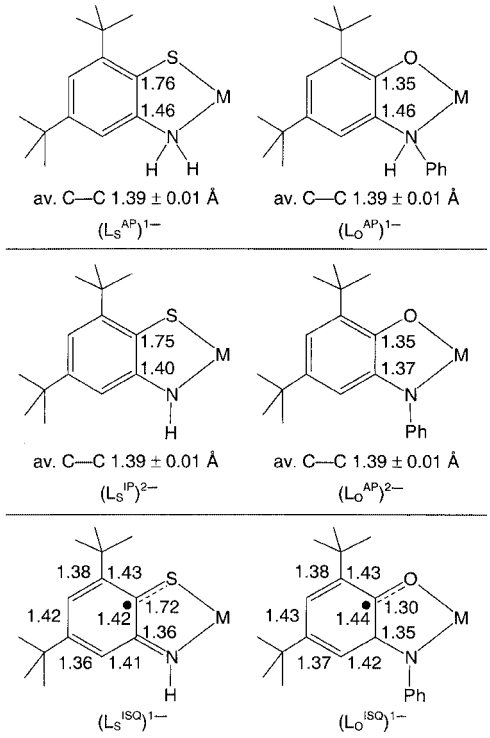

Scheme 2

Complexes:

$[Co^{II}(L_S^{AP})_2]_2$ (**1**)
$[Co^{II}(L_S^{ISQ})_2]_2$ (**2**)
$[Co^{III}I(L_S^{ISQ})_2]$ (**3**)
$[Co^{III}I(L_O^{ISQ})_2]$ (**4**)
$[Co^{III}Cl(L_O^{ISQ})_2]$ (**5**)

Scheme 3

complex of cobalt(II) with the ligand 2,3-bis(2-mercaptoanilino)butane, which is very similar to the bis(phenyl) analogue reported by Kawamoto, Kuma, and Kushi.[12] We show here for the first time that both compounds contain *N*,*S*-coordinated *o*-iminothiobenzosemiquinonate(1−) π-radicals.

2. Results and Discussion

2.1. Synthesis and Characterization of Complexes

2.1.1. Complex 1

Treatment of the ligand 6-amino-2,4-di-*tert*-butylthiophenol[8] ($H[L_S^{AP}]$) with $CoCl_2$ (2:1) in dry acetonitrile under strictly anaerobic conditions produced, upon addition of 2 equiv. of the base triethylamine, an orange precipitate of $[Co^{II}(L_S^{AP})_2]_2 \cdot 2CH_3CN$ (**1**·2CH_3CN) in good yields. This material was extremely air-sensitive even in the solid state and had to be stored under argon.

In the infrared spectrum of **1**, an antisymmetric and two symmetric ν(N−H) stretching frequencies were observed: at 3322 and at 3268 and 3246 cm^{-1}, respectively. This clearly indicated the presence of two *N*-coordinated amino groups (R−NH_2) in **1**. The electronic spectrum of **1** measured in CH_2Cl_2 solution displayed no intense absorption maxima > 450 nm (ε > 10^3 M^{-1} cm^{-1}), indicating that the ligand was aromatic and that it was *N*,*S*-coordinated as the monoanion $(L_S^{AP})^{1-}$.

Complex **1** was paramagnetic. Figure 1 displays the temperature dependence of the magnetic moment of **1**. It was possible to fit the data to a dimer model with $S_{Co} = {}^3/_2$ by use of the spin Hamiltonian $H = -2J\, S_1 \cdot S_2$ ($S_1 = S_2 = {}^3/_2$). The following parameters yielded a satisfactory fit: $g_{Co} = 2.2$, $J = -144$ cm^{-1}, $\chi_{TIP} = 0.95 \times 10^{-3}$ e.m.u., and 1% of a paramagnetic impurity ($S = {}^3/_2$). Thus, a strong intramolecular antiferromagnetic coupling between two mononuclear units $Co^{II}(L_S^{AP})_2$ prevailed, yielding an $S = 0$ ground state. In agreement with this, the X-band EPR spectrum of a toluene solution of **1** at 10 K displayed a signal ($g = 4.3$) typical for an $S = {}^3/_2$ ground state of the mononuclear unit. Thus, in solution, dimeric **1** was in equilibrium with its monomer. For the dimer in the solid state we propose one of the two following structures, depending on the

relative configuration of the two $(L_S^{AP})^{1-}$ ligands to each other in a monomer that can be *trans* or *cis*. The spectroscopic and magnetic properties of **1** were quite similar to those reported for $[Co^{II}(abt)_2]$,[9] "abt^{1-}" representing the unsubstituted *o*-aminothiophenolate(1−) anion.

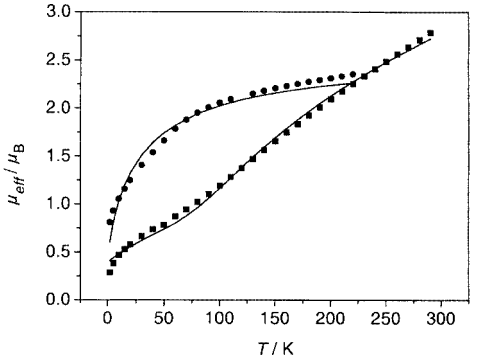

Figure 1. Temperature dependence of the magnetic moment of dinuclear **1** (■) and **2** (●); the solid lines represent best fits by use of the parameters given in the text

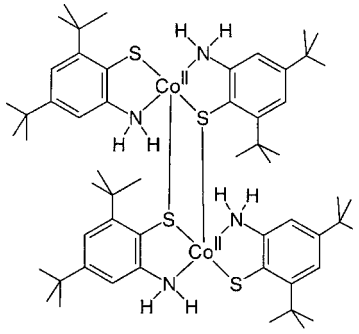

or

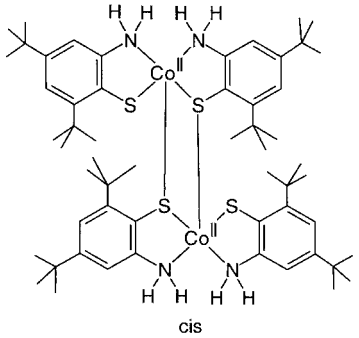

1

2.1.2. Complex 2

When orange-red crystals of **1** were exposed to air at 20 °C, a rapid color change to black was observed. Dissolution of this material in CH_2Cl_2 under argon produced a deep blue solution, from which black crystals of $[Co^{II}(L_S^{ISQ})_2]_2$·0.5*n*-hexane (**2**·0.5*n*-hexane) were obtained upon addition of *n*-hexane.

In the infrared spectrum of **2**, only a single N−H stretching frequency (at 3296 cm^{-1}) was observed, as to be expected for an imino group. The temperature dependence of the magnetic susceptibility of a solid sample of the dimeric species **2** was recorded in the range 4−240 K. The effective magnetic moment varied between 0.65 μ_B at 10 K and 1.6 μ_B at 240 K (per Co). This behavior was consistent with the presence of two Co^{II} ions with $S = {}^1/_2$, weakly antiferromagnetically coupled to yield an $S_t = 0$ ground state. From a fit of the data shown in Figure 1, $J = -7$ cm^{-1} was calculated. The X-band EPR spectrum of a frozen toluene solution of **2** at 10 K displayed an $S = {}^1/_2$ signal at $g \approx 2$, indicating that dimeric **2** existed in solution in equilibrium with its monomer. In agreement with the results of an X-ray structure determination (see below), we assigned the following structure to **2**.

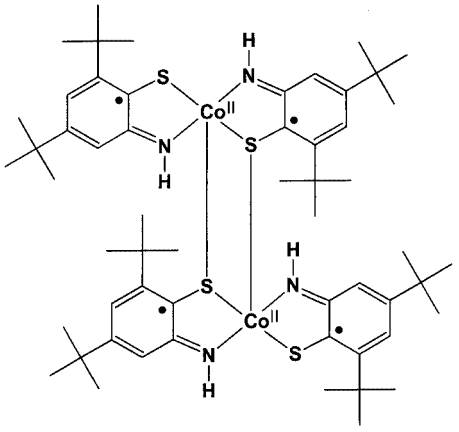

2

It thus appeared that **2** was the four-electron oxidation product of **1**, as in Equation (1).

$$[Co^{II}(L_S^{AP})_2]_2 + O_2 \rightarrow [Co^{II}(L_S^{ISQ})_2]_2 + 2\,H_2 \quad (1)$$

The electronic spectrum of **2** in CH_2Cl_2 solution at 25 °C, shown in Figure 2, displayed a very intense ($\varepsilon > 10^4$ M^{-1} cm^{-1}) absorption at 673 nm, responsible for the deep blue color of **2**, which was absent in the spectrum of **1**. This band corresponded to a spin- and dipole-allowed transition observed for all square-planar complexes containing two *cis* or *trans X*,*Y*-coordinated radicals.[2,4,13]

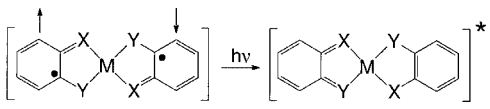

All the spectroscopic data of **2** thus pointed to the presence of two *N*,*S*-coordinated *o*-iminothiobenzosemiquinonato(1−) π-radicals in a monomeric subunit with an $S = {}^1/_2$ ground state.

Interestingly, we discovered that the electronic spectrum of **2** in CH_2Cl_2 (or in methylcyclohexane) was temperature-dependent. Upon cooling from +25 to −70 °C, the intense band at 673 nm disappeared, but was regenerated upon

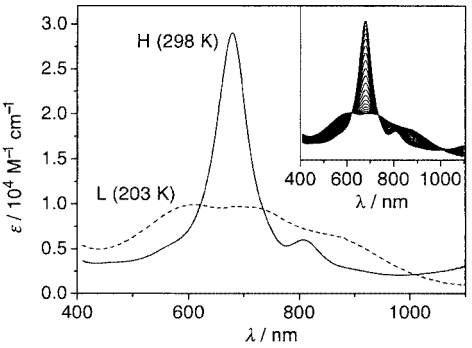

Figure 2. Electronic spectra of the high-temperature form (H) of **2** (at 25 °C) and of its low-temperature form (L) at −70 °C (absorption coefficients are calculated per cobalt ion); the inset shows the temperature dependence of the spectra between 25 and −70 °C (in 5 °C steps)

warming. Figure 2 shows the spectra of the high- and low-temperature forms. We analyzed these spectral changes on the assumption of the equilibrium shown in Equation (2) and calculated the following thermodynamic data: $\Delta G^{300} = -4.3$ kJ mol^{-1}, $\Delta H = 35 \pm 2$ kJ mol^{-1}, $\Delta S = 131 \pm 7$ J mol^{-1} K^{-1} (in methylcyclohexane) and $\Delta G^{300} = -3.6$ kJ mol^{-1}, $\Delta H = 33 \pm 2$ kJ mol^{-1}, $\Delta S = 122 \pm 9$ J mol^{-1} K^{-1} (in dichloromethane).

$$[Co^{III}(L_S{}^{IP})(L_S{}^{ISQ})]_2 \overset{K}{\rightleftharpoons} [Co^{II}(L_S{}^{ISQ})_2]_2 \quad (2)$$

Similar valence tautomeric equilibria have been reported by Pierpont et al.[14−16] for (catecholato)cobalt(III) and (semiquinonato)cobalt(II) complexes, as shown in Equation (3). For this equilibrium, $\Delta G^{300} = -3.3$ kJ mol^{-1}, $\Delta H = 33.9(1)$ kJ mol^{-1}, and $\Delta S = 124(1)$ J mol^{-1} K^{-1} were reported [bpy represents the ligand 2,2′-bipyridine, $(DBSQ)^{1-}$ is either 3,5- or 3,6-di-*tert*-butyl-1,2-benzosemiquinonate(1−), and $(DBCat)^{2-}$ is the corresponding one-electron reduced catecholate(2−)].

$$[Co^{III}(bpy)(DBSQ)(DBCat)] \rightleftarrows [Co^{II}(bpy)(DBSQ)_2] \quad (3)$$

It should be noted that the valence tautomeric equilibrium (2) was only observed in solution. In the solid state, the electronic spectrum of **2** did not change over the temperature range 10−300 K. This was also in qualitative agreement with the observations of Pierpont et al. on the $[Co^{II}(bpy)(DBSQ)_2]$ system. They reported that the transition temperature was about 50 °C higher in the solid state than in solution. They also concluded that "changes in bond energy and vibrational frequency associated with the electron transfer step are the primary contributors to the thermodynamic changes of the equilibrium". The above results for **2** represent the first example of valence tautomers of an *N*,*S*-coordinated *o*-aminothiophenolate complex.

Interestingly, Pierpont's tautomers involved octahedral cobalt(II)/(III) complexes in which the transition from a low-spin cobalt(III) (d^6, $S = 0$) to a high-spin cobalt(II) (d^7, $S = {}^3/_2$) configuration was accompanied with increasing temperature by a net change of the effective magnetic moment from 1.7 μ_B for the cobalt(III) form ($S_t = {}^1/_2$) to ca. 5.5 μ_B for the cobalt(II) form. In contrast, equilibrium (2) was not associated with a similar net change of the effective magnetic moment with increasing temperature. Both monomeric subunits $[Co^{III}(L_S{}^{IP})(L_S{}^{ISQ})]$ and $[Co^{II}(L_S{}^{ISQ})_2]$ possessed an $S = {}^1/_2$ ground state, which may antiferromagnetically couple to an overall diamagnetic ground state in the dimers.

2.1.3. Complex 3

Treatment of **2**, in CH_2Cl_2 under Ar, with I_2 (1:1) dissolved in *n*-hexane changed the blue color to dark green. From this solution a dark green microcrystalline residue of $[Co^{III}I(L_S{}^{ISQ})_2]$ (**3**) was obtained in good yields [Equation (4)].

$$[Co^{II}(L_S{}^{ISQ})_2]_2 + I_2 \rightarrow 2[Co^{III}I(L_S{}^{ISQ})_2] \quad (4)$$

Complex **3** is diamagnetic ($S = 0$), as judged from its "normal" ^{1}H NMR spectrum. In the infrared spectrum, a single N−H stretching frequency was observed at 3231 cm^{-1}, indicating the presence of two equivalent imino groups. Figure 3 shows the electronic spectrum of **3** in CH_2Cl_2 solution. The very intense absorption at 641 nm ($\varepsilon = 1.7 \times 10^4$ M^{-1} cm^{-1}) was again indicative of the presence of two $(L_S{}^{ISQ})^{1-}$ π-radical ligands. We therefore propose the following structure for **3**.

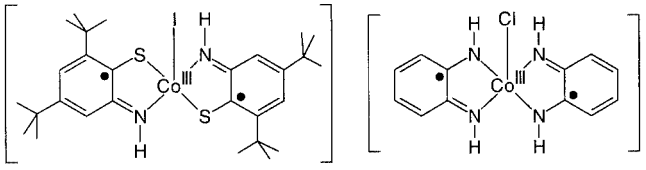

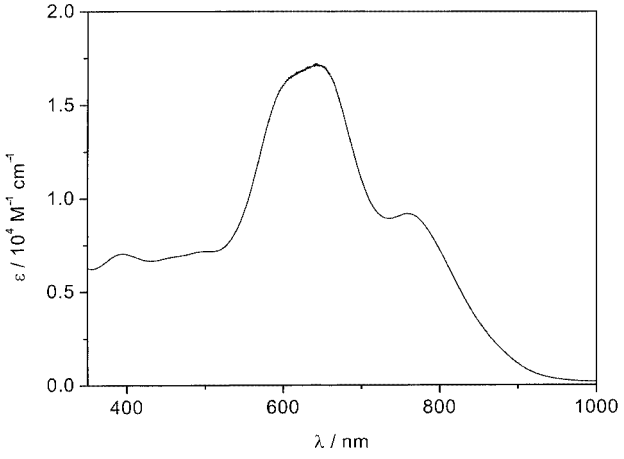

Figure 3. Electronic spectrum of **3** in CH_2Cl_2 solution at 20 °C

This complex is analogous to diamagnetic $[Co^{III}Cl(s\text{-}bqdi)_2]$, which has been structurally characterized.[17] The ligand $(s\text{-}bqdi)^{1-}$ is the *N*,*N*-coordinated *o*-diiminobenzosemiquinonate(1−) π-radical.

2.1.4. Complexes 4 and 5

Treatment of 2-anilino-4,6-di-*tert*-butylphenol ($H[L_O^{AP}]$) in acetonitrile with CoI_2 (ca. 2:1) in the presence of air and triethylamine as base resulted in the precipitation of dark microcrystalline $[Co^{III}I(L_O^{ISQ})_2]$ (**4**). This compound is the exact sulfur-free analogue of **3**. Note that, in contrast to **3**, compound **4** was formed with oxygen as the sole oxidant.

Complex **4** is also diamagnetic ($S = 0$). Figure 4 shows the electronic spectrum of **4** dissolved in CH_2Cl_2. The intense absorption maxima at 695 nm ($\varepsilon = 1.87 \times 10^4$ M^{-1} cm^{-1}) and 884 nm (1.03×10^4 M^{-1} cm^{-1}) were again indicative of the presence of two *O*,*N*-coordinated $(L_O^{ISQ})^{1-}$ π-radical ligands.

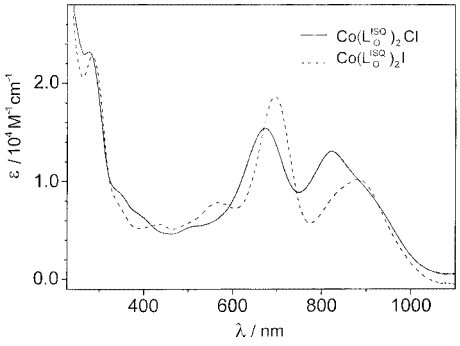

Figure 4. Electronic spectra of **4** and **5** in CH_2Cl_2 solution at 20 °C

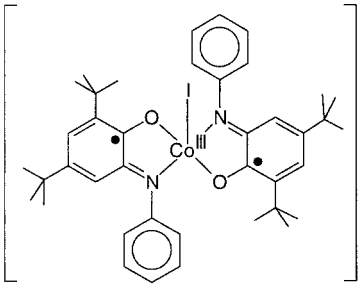

4

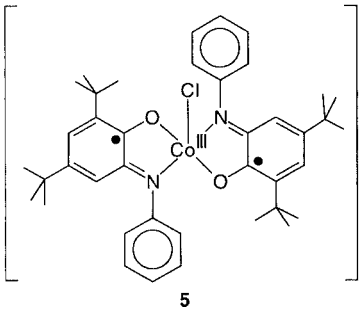

5

In an attempt to generate the exact analogue of **2**, the reaction between $[Co(H_2O)_6](BF_4)_2$ and $H[L_O^{AP}]$ (1:1) and NEt_3 in CH_3CN in the presence of air was studied. A dark solid obtained from this reaction mixture was recrystallized from a $CH_3CN/CHCl_3$ (1:1) mixture, yielding single crystals of $[Co^{III}Cl(L_O^{ISQ})_2]$ (**5**). Note that the coordinated chloride ion in **5** had to have been abstracted from chloroform. Complex **5** is also diamagnetic, and isostructural with **4**. Complex **5** could also be synthesized more straightforwardly by employment of the method used to prepare **4** by use of $CoCl_2$ as starting material. The corresponding cobalt halide for the preparation of **4** and **5** was employed only in slight excess over the amount of ligand (ca. 1:1 and not 1:2 as required stoichiometrically) in order to avoid the formation of the known octahedral complex $[Co^{III}(L_O^{ISQ})_3]$.[3]

2.2. Crystal Structures

The crystal structures of complexes **2**·0.5*n*-hexane, **4**, and **5** were determined by single-crystal X-ray crystallography at 100 K, and for **2** also at 295 K. Figure 5 shows the structure of the neutral dimer in crystals of **2**, whereas the structures of the mononuclear, neutral molecules in crystals of **4** and **5** are both displayed in Figure 6. Selected bond lengths are summarized in Table 1.

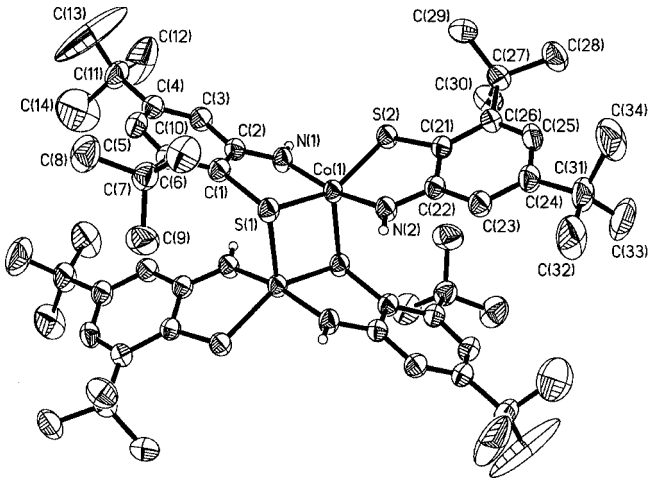

Figure 5. Structure of the neutral dimer in crystals of **2**·0.5*n*-hexane at 293 K; thermal ellipsoids are drawn at the 40% probability level; small open circles are observed hydrogen atoms of the imine groups; all other H atoms are omitted

We describe the structures of **4** and **5** first, because previous structural work on *O*,*N*-coordinated *o*-iminobenzosemiquinonato π-radical complexes such as the octahedral $[M(L_O^{ISQ})_3]$ (M = Co^{III},[3] Cr^{III},[5] Fe^{III} [5]), the square-planar $[M(L_O^{ISQ})_2]$ (M = Cu^{II}, Ni^{II}, Pd^{II}, Pt^{II}),[4] or the square-planar $[M(L_O^{ISQ})(bpy)]PF_6$ (M = Pd^{II}, Pt^{II})[7] has allowed the unequivocal structural characterization of the $(L_O^{ISQ})^{1-}$ radical anion. In all these structures the geometrical features of the ligand are identical within the small experimental error of ±0.01 Å (3σ): (i) the C−O and C−N distances are short at 1.30 Å and 1.35 Å, respectively, and (ii) the C−C distances in the six-membered ring invariably show a quinoid-type distortion, with two short C−C distances at 1.37 Å and four longer ones at ca. 1.42 Å. Furthermore, for the neutral species $[M(L_O^{IP})(bpy)]$ (M = Pd^{II},

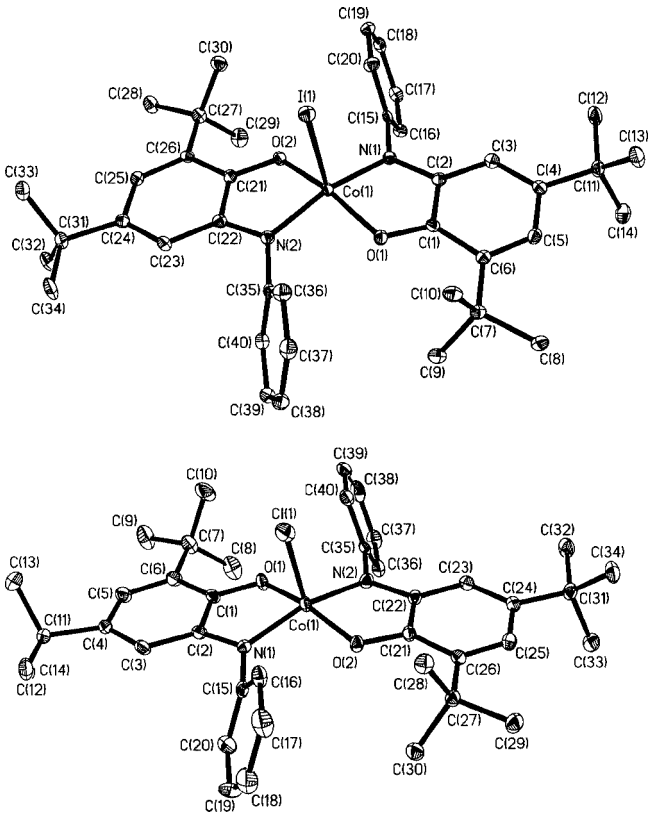

Figure 6. Structures of the neutral molecules in crystals of **4** (top) and **5** (bottom)

Table 1. Selected bond lengths [Å]

	2	**4**	**5**		
M−X	2.3506(9)	2.5784(4)	2.265(1)		
M−N1	1.866(2)	1.864(2)	1.870(3)		
M−N2	1.843(2)	1.857(2)	1.862(3)		
M−Y1	2.2015(9)	1.862(2)	1.856(2)		
M−Y2	2.1525(9)	1.873(2)	1.869(3)		
Terminal ligand(s)					
N1−C6	1.338(4)	1.355(3)	1.349(3)	1.346(5)	1.344(5)
N1−C7	−	1.433(3)	1.435(3)	1.426(5)	1.439(4)
Y1−C1	1.720(3)	1.294(3)	1.300(3)	1.301(5)	1.304(4)
C1−C6	1.419(4)	1.432(3)	1.436(3)	1.429(5)	1.429(6)
C1−C2	1.428(4)	1.444(3)	1.437(3)	1.435(5)	1.430(5)
C2−C3	1.366(4)	1.370(3)	1.372(3)	1.368(6)	1.374(6)
C3−C4	1.420(5)	1.442(3)	1.439(3)	1.422(6)	1.442(5)
C4−C5	1.363(4)	1.374(3)	1.370(3)	1.363(5)	1.366(6)
C5−C6	1.422(4)	1.418(3)	1.424(3)	1.438(5)	1.424(5)
Bridging ligand					
N1−C6	1.348(4)				
S1−C1	1.751(3)				
C1−C6	1.426(4)				
C1−C2	1.404(4)				
C2−C3	1.363(5)				
C3−C4	1.414(5)				
C4−C5	1.384(4)				
C5−C6	1.422(4)				

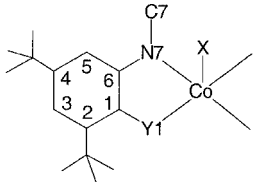

	X	Y
2	S	S
4	I	O
5	Cl	O

Pt^{II}),[7] we have clearly established by X-ray crystallography that the *O*,*N*-coordinated dianion $(L_O^{IP})^{2-}$ has distinctly different geometrical features. The C−O and C−N distances are significantly longer, at 1.35 and 1.39 Å, respectively, and the C−C distances of the now aromatic ring are equal, at 1.39 Å. These parameters are given in Scheme 2.

It is now immediately evident from the data in Table 1 and Scheme 2 that both organic ligands in **4** and **5** are *O*,*N*-coordinated, monoanionic π-radicals $(L_O^{ISQ})^{1-}$. The electronic structures of **4** and **5** may therefore correctly be described as singlet diradical, each containing a low-spin, diamagnetic, trivalent cobalt(III) ion bound to two strongly antiferromagnetically coupled π-radicals. These conclusions agree nicely with Peng's results on the *o*-diiminobenzosemiquinonate (s-bqdi) π-radical complexes $[Co^{III}(s\text{-}bqdi)_2(py)]Cl$,[18] $[Co^{III}(s\text{-}bqdi)_2(PPh_3)](ClO_4)$,[19] and $[Co^{III}Cl(s\text{-}bqdi)_2]$,[17] all of which were singlet diradicals. These authors were also able to perform the structural characterization of the mononuclear, square-planar species $[Co^{II}(s\text{-}bqdi)_2]$ ($S = {}^1/_2$),[17] which also contained two *N*,*N*-coordinated *o*-diiminobenzosemiquinonate radicals.

While the occurrence of three different oxidation levels − namely, fully aromatic, semiquinone radical, and quinone forms − has been firmly established in the literature for *o*-catecholates,[20] *o*-phenylenediamines,[21] and *o*-aminophenols,[3−7] this appears not to be the case for *o*-aminothiophenols, for which the occurrence of *o*-iminothiobenzosemiquinonate π-radicals has until very recently been questioned.[1] We have shown for a series of diamagnetic square-planar complexes $[M(L_S^{ISQ})_2]$ (M = Ni, Pd, Pt)[2] that the semiquinone oxidation level is in fact readily available for *o*-aminothiophenols and we have identified the same structural markers as described above for the *o*-aminophenol derivatives (Scheme 2). *N*,*S*-coordinated *o*-iminothiobenzosemiquinonate radicals possess short C−S bonds, at 1.72−1.74 Å, and short C−N bonds, at 1.35−1.37 Å, and two short C−C and four longer ones (semiquinone sequence). In contrast, in octahedral $[Co^{III}(en)_2(S{-}C_6H_4{-}NH_2)](ClO_4)Cl$[22] containing an *N*,*S*-coordinated *o*-aminothiophenolate(1−), the C−S distance is observed to be 1.764(4) Å and the C−N bond length 1.458(4) Å, both of which represent typical single bonds. The six C−C bonds are of equal length, at av. 1.384 Å.

The structure of **2** reveals a nearly ideal square-based pyramidal environment for both cobalt ions in the dinuclear, *S*-bridged neutral molecule (CoN_2S_3). Two *N*,*S*-coordinated, oxidized *o*-aminothiophenolato ligands are in the equatorial plane, and the two imine and the two sulfur

donors are each *trans* with respect to each other. One of the two thiolates per cobalt ion forms a bridge with an S-donor in the axial position of the other cobalt ion. The axial Co−S distance in the thiolato bridge [2.351(1) Å] is longer than the corresponding Co−S bond in the equatorial position [2.202(1) Å], and the Co−S bond in the non-bridging thiolate is the shortest at 2.152(1) Å. Thus, the dinuclear molecule in **2** possesses two terminal (nonbridging) *N*,*S*-coordinated ligands and two bridging ligands of this type. Comparison of the dimensions of the non-bridging ligand in **2** with those given in Scheme 2 for an *N*,*S*-coordinated *o*-iminothiobenzosemiquinonate radical immediately implies that this oxidation level is present: the C−S and the C−N bonds are short at 1.720(3) Å and 1.338(4) Å, respectively, and the ring clearly displays quinoid character.

For the bridging ligand, the same oxidation level appears to be appropriate, because the C−N bond is short at 1.348(4) Å and the ring exhibits quinoid character (two shorter C−C bonds and four longer ones). Only the C−S bond at 1.751(3) Å appears to be too long for an *o*-iminothionebenzosemiquinonate radical, but this sulfur atom forms the S-bridge to the second half of the molecule, which may cause the observed lengthening of the C−S bond. We therefore suggest that the molecules in **2** are correctly described as $[Co^{II}(L_S^{ISQ})_2]_2$.

Since we had discovered that **2** displayed valence tautomerism in solution, we also collected an X-ray data set of **2** at 100 K (the above results were obtained from measurements at 295 K). The two structures obtained are identical within experimental error. This is in agreement with the fact that the solid-state electronic spectrum of **2** is temperature-independent in the range 10−300 K.

It is interesting that Kawamoto[12] reported the crystal structure of the *monomer* $[Co^{II}(ddbt)]$ ($S = {}^1/_2$), where $(ddbt)^{2-}$ is the diradical-derived from 2,2′-bis(1,2-diphenylenediimine)benzenethiolate. The average C−S bond and C=N bonds here are 1.739(6) and 1.36(1) Å, respectively. The phenyl groups, in a *trans* arrangement relative to one another, effectively prevent dimer formation.

Artaud et al.[11] substituted the two bulky phenyl groups in $[Co^{II}(ddbt)]$ by methyl groups and reported the synthesis of the dinuclear cobalt complexes containing the reduced aromatic *o*-aminothiophenolate ligand (**A**) and its oxidized form (**B**). In contrast to their report, the crystal structure reported is actually that of **B**, since the average C−S and C−N bonds are short at 1.725(6) and 1.35(1) Å, respectively, both rings display quinoid character, and both nitrogen donor atoms are sp^2-hybridized and not sp^3 as required for **A**.

Ref. [11]

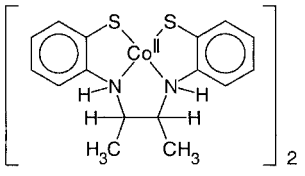

A

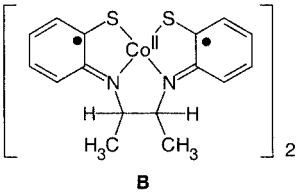

B

In our view, these authors had not prepared a pure sample of **A**. All the reported spectroscopic and magnetic properties correspond satisfactorily to those of **B** and **2**. In none of the above papers has the ligand diradical character been addressed.

As we have pointed out previously,[2] there are three interesting structures of organometallic cobalt complexes containing either an *N*,*S*-coordinated, aromatic *o*-iminothiophenolate(2−) anion or its one-electron oxidized form *o*-iminothiobenzosemiquinonate(1−). The question, then, is whether we can distinguish between the two forms **C** and **D**.

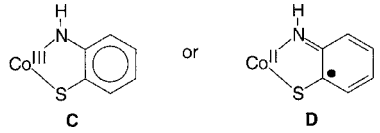

C **D**

X-ray structure determinations of $[(tripod)Co(abt)]BF_4$ [23] and $[Co\{P(OCH_3)_3\}_3(abt)]PF_6$ [24] clearly showed that the ligand abt was present as the *o*-iminothiobenzosemiquinonato π-radical, and that both compounds should therefore be viewed as singlet diradicals in which a low-spin Co^{II} ion ($S_{Co} = {}^1/_2$) is antiferromagnetically coupled to an organic π-radical, yielding the observed $S_t = 0$ ground state. The same arguments hold for the neutral complex $Co[\eta^5\text{-}C_5(CH_3)_5][(NH)SC_6H_4]$,[25] in which an *N*,*S*-coordinated *o*-iminothiobenzosemiquinonato radical (and not the reduced aromatic dianion) is also present. It should be noted that *N*,*S*-coordinated dianions $(L_S^{IP})^{2-}$ have the following geometrical features: i) the C−S bond is long at 1.755 Å, as is the C−N bond at 1.40 Å, and ii) the six C−C distances are equal at av. 1.385 Å.

2.3. Electro- and Spectroelectrochemistry

Cyclic voltammograms (CV) of complex **2** were recorded in CH_3CN solutions containing 0.10 M $[nBu_4N]PF_6$ as supporting electrolyte at a glassy carbon working electrode and

Table 2. Redox potentials in Volts of complexes in CH_2Cl_2 solutions at 20 °C

Complex[a]	$E^1_{1/2}(2-/1-)$	$E^2_{1/2}(1-/0)$	$E^3_{1/2}(0/1+)$	$E^4_{1/2}(1+/2+)$
$[Ni(L_S^{ISQ})_2]$[b]	−1.71	−0.83	0.28	0.90 (irr.)
$[Pd(L_S^{ISQ})_2]$[b]	−1.48	−0.79	0.26	0.83
$[Pt(L_S^{ISQ})_2]$[b]	−1.54	−0.70	0.51	1.20
$[Co(L_S^{ISQ})_2]_2$ [c][d]	−1.90	−0.72	−0.17	+0.4 (irr.)
$[Pd(L_O^{ISQ})_2]$[e]	−1.40	−0.99	0.08	0.47
$[Pt(L_O^{ISQ})_2]$[f]	−1.64	−1.07	0.20	0.70
$[Cu(L_O^{ISQ})_2]$[e]	−1.32	−1.02	−0.26	0.37

[a] Referenced vs. the ferrocenium/ferrocene (Fc^+/Fc) couple; [b] Ref.[2] [c] Measured in CH_3CN. [d] This work. [e] Ref.[4] [f] Ref.[7]

an $Ag/AgNO_3$ reference electrode. Ferrocene was used as an internal standard; all potentials are referenced versus the ferrocenium/ferrocene couple (Fc^+/Fc). Table 2 summarizes the results.

Since the original publications by Holm and coworkers[26−27] in the 1970s it has become well established that square-planar complexes of the type $[M(L^{ISQ})_2]$ [M = Ni, Pd, Pt; $(L^{ISQ})^{1-}$ represents *o*-iminothiobenzosemiquinonate(1−), *o*-iminobenzosemiquinonate(1−), or *o*-diiminobenzosemiquinonate(1−)] are the central members of a five-membered electron-transfer series, the component species of which (n = 2−, 1−, 0, 1+, 2+) are interrelated by reversible one-electron transfer reactions. This has also been shown to be the case for the complexes of Table 2. The reduced and oxidized forms of these neutral species have been shown to contain reduced or oxidized forms of the ligands and a divalent metal center [Equation (5)] by spectroelectrochemical methods.

$$[M^{II}(L^{IP})_2]^{2-} \underset{+e}{\overset{-e}{\rightleftharpoons}} [M^{II}(L^{ISQ})(L^{IP})]^{1-} \underset{+e}{\overset{-e}{\rightleftharpoons}} [M^{II}(L^{ISQ})_2] \underset{+e}{\overset{-e}{\rightleftharpoons}} [M^{II}(L^{IBQ})(L^{ISQ})]^{1+} \underset{+e}{\overset{-e}{\rightleftharpoons}} [M^{II}(L^{IBQ})_2]^{2+} \quad (5)$$

$E^1_{1/2}$ $E^2_{1/2}$ $E^3_{1/2}$ $E^4_{1/2}$

Figure 7 shows the CV of **2** in CH_3CN (0.10 M $[n\mathrm{Bu_4N}]PF_6$) at 20 °C over the potential range from +0.6 to −2.1 V vs. Fc^+/Fc. Three reversible electron-transfer waves were observed, at −1.90, −0.72, and −0.17 V, each wave corresponding to a one-electron transfer event per cobalt ion present, as established by coulometry. Since we have established that **2** is a dimer in the solid state, we briefly studied its solution behavior. A frozen CH_2Cl_2 solution of **2** at 10 K displayed a weak X-band EPR spectrum at $g \approx 2.0$ typical for the $S = {}^1/_2$ monomeric species $[Co^{II}(L_S^{ISQ})_2]$. Hence, the equilibrium Equation (6) exists in solution, and both the dissociation and formation rates of this equilibrium are expected to be very fast with respect to the scan rates employed in the cyclic voltammetry experiments. From the results described below we inferred that the monomers were the electroactive species.

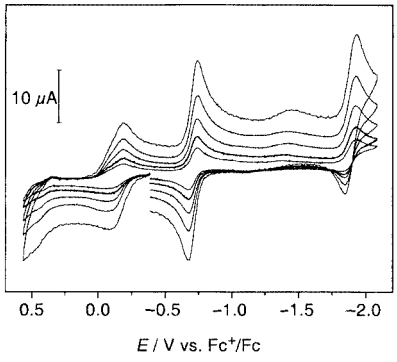

Figure 7. Cyclic voltammogram of **2** in CH_3CN solution (0.10 M $[n\mathrm{Bu_4N}]PF_6$) at 20 °C at a glassy carbon working electrode; scan rates: 50, 100, 200, 400, 500 mV s^{-1}

$$[Co^{II}(L_S^{ISQ})_2]_2 \underset{k_r}{\overset{k_f}{\rightleftharpoons}} 2\,[Co^{II}(L_S^{ISQ})_2] \quad (6)$$

Coulometric measurements established that the monomer of **2** could be reduced in a one-electron fashion at a fixed potential of −1.0 V and by another electron at −2.0 V, and oxidized by 1 e^- at 0.15 V. Thus a monocation, a monoanion, and a dianion can be reversibly generated from **2** electrochemically. The dianion proved to be too sensitive for further investigation. Figure 8 shows the electronic spectra of **2** and of its electrochemically generated monocation and monoanion in CH_3CN; Table 3 summarizes these results.

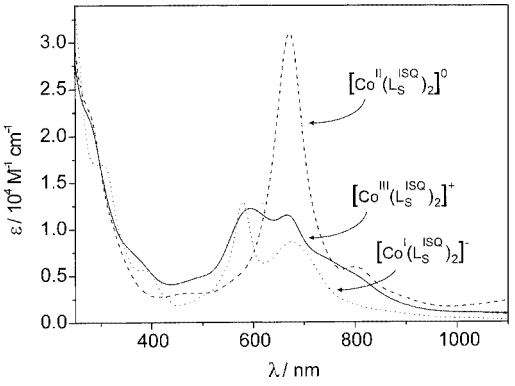

Figure 8. Electronic spectra of **2** and of its electrochemically generated monocation and monoanion in CH_3CN solution (0.10 M $[n\mathrm{Bu_4N}]PF_6$) at 20 °C

Table 3. Electronic spectra of complexes in CH_2Cl_2 solution

Complex	λ_{max} [nm] (10^4 ε [M^{-1} cm^{-1}])[a]
1	375 sh (0.4), 446 (0.42), 514 sh (0.16)
2 (H)[b]	279 sh (1.8), 458 sh (0.25), 554 sh (0.5), 678 (2.9), 806 (0.60), 901 sh (0.2), 1150 (0.6)
L[c]	611 (1.0), 712 (0.96), 885 (0.60)
$[Co^I(L_S^{ISQ})_2]^{1-}$ [d]	311 sh (1.7), 398 sh (0.52), 589 (1.3), 681 (0.80), 810 sh (0.5)
$[Co^{III}(L_S^{ISQ})_2]^{1+}$ [d]	283 sh (2.2), 380 sh (0.75), 594 (1.3), 671 (1.2), 813 sh (0.6)
3	390 (0.7), 500 sh (0.7), 600 sh (1.55), 640 (1.7), 770 (0.9)
4	283 (2.3), 434 (0.6), 566 (0.78), 695 (1.9), 884 (1.0)
5	277 (2.3), 672 (1.5), 821 (1.3)

[a] Molar absorption coefficients are given *per cobalt ion* (monomer). [b] High-temerature spectrum (20 °C). [c] Low-temperature spectrum (−70 °C). [d] Electrochemically generated in CH_3CN (0.10 M $[n\mathrm{Bu_4N}]PF_6$).

Rather surprisingly, the spectra both of the monocation and of the monoanion of **2** did not resemble those reported[2] for $[M^{II}(L_S^{IBQ})(L_S^{ISQ})]^+$ and $[M^{II}(L_S^{IP})(L_S^{ISQ})]^-$ (M = Ni, Pt), respectively. We therefore concluded that a distribution of ligand and metal oxidation levels as in these cases did not prevail for the oxidized and reduced forms of

2. In fact, it was rather remarkable that the spectra of these two species were fairly similar, both displaying two prominent absorption maxima in the visible region, at ca. 590 and 675 nm ($\varepsilon \approx 10^4$ M^{-1} cm^{-1}). Furthermore, these spectra resembled that of $[Co^{III}(L_S^{ISQ})_2I]$ (**3**), shown in Figure 3. We therefore suggest that neither the oxidation of **2** nor its reduction was ligand-centered. Instead, the spectra imply the presence of two $(L_S^{ISQ})^{1-}$ π-radical ligands and metal-centered redox activity [Equation (7)].

$$\underset{S=0}{[Co^{III}(L_S^{ISQ})_2]^+} \underset{-e}{\overset{+e}{\rightleftharpoons}} \underset{S=1/2}{[Co^{II}(L_S^{ISQ})_2]^0} \underset{-e}{\overset{+e}{\rightleftharpoons}} \underset{S=0}{[Co^{I}(L_S^{ISQ})_2]} \qquad (7)$$

$$E^3_{1/2} \qquad E^2_{1/2}$$

Note that the electronic spectrum of the valence tautomer of **2** (see above), namely $[Co^{III}(L_S^{IP})(L_S^{ISQ})]_2$, was significantly different from those reported here for the monocation and -anion, but that it did closely resemble those reported for $[Ni^{II}(L_S^{IP})(L_S^{ISQ})]^-$ and $[Pt(L_S^{IP})(L_S^{ISQ})]^-$, both of which displayed three absorption maxima, at 650, 840, 971 nm for the Ni complex and at 850, 916, 980 nm for the Pt analogue.[2] In $[Co^{III}(L_S^{IP})(L_S^{ISQ})]_2$ these bands were shifted to higher energies (611, 712, 885 nm). It is also remarkable that the electronic spectra of **4** and **5** (Figure 6) were also very similar to those of $[Co^{III}(L_S^{ISQ})_2]^+$ and $[Co^{I}(L_S^{ISQ})_2]^-$.

We would like to stress that the assignments of oxidation levels of the metal ions and the ligands for the monoanion of **2** and its monocationic form are tentative at present; they are based only on the similarity of their electronic spectra. Further investigations of these species are clearly necessary.

Experimental Section

Syntheses: The ligands 2-anilino-4,6-di-*tert*-butylphenol ($H[L_O^{AP}]$) and 6-amino-2,4-di-*tert*-butylthiophenol ($H[L_S^{AP}]$) were prepared according to published procedures.[4,8]

$[Co^{II}(L_S^{AP})_2]_2\cdot 2CH_3CN$ ($1\cdot 2CH_3CN$): A degassed solution of the ligand $H[L_S^{AP}]$ (0.50 g, 2.0 mmol) and $CoCl_2$ (0.13 g, 1.0 mmol) in dry acetonitrile (40 mL) was stirred under strictly anaerobic conditions (under Ar) for 10 min at ambient temperature. Triethylamine (0.20 g, 2.0 mmol) was added dropwise to the filtered green solution, and stirring was continued for 40 min. A microcrystalline solid precipitated from the light orange solution and was collected by filtration. The material was extremely air-sensitive and had to be stored under argon. Yield: 0.39 g (73% with respect to Co). $C_{56}H_{88}Co_2N_4S_4\cdot 2CH_3CN$ (1143.55): calcd. C 62.93, H 8.28, Co 10.31, N 7.34; found C 62.7, H 8.4, Co 10.5, N 7.2. IR (KBr disk): $\tilde{\nu}$ = 3322, 3268, 3246 [$\nu(NH_2)$] cm^{-1}.

$[Co^{II}(L_S^{ISQ})_2]_2\cdot n$-Hexane ($2\cdot n$-Hexane): When a solid sample of $1\cdot 2CH_3CN$ (0.39 g) was exposed to air, the orange microcrystals immediately turned black. Some of this black material (0.20 g) was dissolved in CH_2Cl_2 (40 mL) under argon. *n*-Hexane (20 mL) was added to the blue solution, and the solvents were allowed to evaporate slowly. Black crystals of $2\cdot n$-hexane (0.17 g, 73%) were obtained. Single crystals of this material were grown from a benzene/*n*-hexane mixture (1:1) under argon by slow evaporation. $C_{56}H_{84}Co_2N_4S_4\cdot C_6H_{14}$ (1145.61): calcd. C 65.00, H 8.62, N 4.89; found C 64.8, H 8.7, N 5.0. MS (ESI$^+$): *m*/*z* = 1059 [M$^+$]. IR (KBr disk): $\tilde{\nu}$ = 3296 [ν(N−H)] cm^{-1}.

$[Co^{III}I(L_S^{ISQ})_2]$ (3): A solution of iodine (0.05 g, 0.20 mmol) in *n*-hexane (25 mL) was added dropwise with stirring under argon to a solution of $2\cdot n$-hexane (0.225 g, 0.20 mmol) in CH_2Cl_2 (40 mL). The blue color of the solution changed to dark green. After the mixture was stirred for 15 min at 20 °C, the solvents were evaporated under reduced pressure. *n*-Hexane (20 mL) was added to the dark residue. A dark green residue was filtered off. This material was recrystallized from a mixture of CH_2Cl_2 (40 mL) and CH_3CN (25 mL) (which were allowed to slowly evaporate) in an argon stream. Yield: 0.17 g (68% based on **2**). $C_{28}H_{42}CoIN_2S_2$ (656.62): calcd. C 51.22, H 6.45, Co 8.98, I 19.33, N 4.27, S 9.77; found C 51.4, H 6.5, Co 9.2, I 18.9, N 4.2, S 10.2. MS (EI): *m*/*z* = 529 [M$^+$ − I]. ^{1}H NMR (250 MHz, $CDCl_3$, 300 K): δ = 1.73 (s, 18 H), 1.33 (s, 18 H), 7.67 (br, 2 H), 7.85 (br, 2 H), 12.85 (br, 2 H, N−H) ppm. IR (KBr disk): $\tilde{\nu}$ = 3231 [ν(N−H)] cm^{-1}.

$[Co^{III}I(L_O^{ISQ})_2]$ (4): Triethylamine (0.3 mL) was added to a solution of the ligand $H[L_O^{AP}]$ (0.30 g, 1.0 mmol) and CoI_2 (0.20 g, 0.64 mmol) in CH_3CN (25 mL). The solution was stirred in the presence of air at 20 °C for 30 min and filtered. A black precipitate formed upon standing for 12 h at ambient temperature, and was collected by filtration. Yield: 0.17 g (43% based on $H[L_O^{AP}]$). Single crystals suitable for X-ray crystallography were grown from a methanol/chloroform solution (1:2) of the above black material. $C_{40}H_{50}CoIN_2O_2$ (776.69): calcd. C 61.80, H 6.49, N 3.61; found C 62.0, H 6.5, N 3.5. MS (EI): *m*/*z* = 776 [M$^+$], 649 [M$^+$ − I]. ^{1}H NMR (400 MHz, $CDCl_3$, 300 K): δ = 8.78 (t, 2 H), 7.90 (s, 2 H), 7.57 (t, 4 H), 7.42 (s, 2 H), 7.31 (d, 4 H), 1.53 (s, 18 H), 1.10 (s, 18 H).

$[Co^{III}Cl(L_O^{ISQ})_2]$ (5): A solution of triethylamine (0.6 mL) in CH_3CN (10 mL) was added to a solution of $[Co(H_2O)_6](BF_4)_2$ (0.68 g, 2.0 mmol) and the ligand $H[L_O^{AP}]$ (0.60 g, 2.0 mmol) in CH_3CN (30 mL). The mixture was stirred in the presence of air at room temperature for 2 h and filtered. The solvent was allowed to evaporate, yielding a dark solid residue that was recrystallized from a $CH_3CN/CHCl_3$ (1:1) mixture to give a small amount (ca. 10%) of crystalline **5**. The Cl^- ligand in **5** is believed to be abstracted from the $CHCl_3$ solvent. $C_{40}H_{50}ClCoN_2O_2$ (685.24): calcd. C 70.11, H 7.35, N 4.09; found C 70.2, H 7.3, N 4.0. MS (ESI$^+$): *m*/*z* = 684 [M$^+$]; 649 [M − Cl$^+$].

X-ray Crystallographic Data Collection and Refinement of the Structures: Dark red-brown single crystals of **2**, and black crystals of **4** and **5**, were coated with perfluoropolyether. Suitable crystals were picked up with a glass fiber and were immediately mounted in the nitrogen cold stream of the diffractometers to prevent loss of solvent. Intensity data were collected at 100 K with graphite-monochromated Mo-K_α radiation (λ = 0.71073 Å); a second crystal of **2** was measured at 293(2) K. Final cell constants were obtained from a least-squares fit of a subset of several thousand strong reflections. Data collection was performed by hemisphere runs, taking frames at 0.3° (Siemens SMART) and 1.0° (Nonius Kappa-CCD) in ω. A semiempirical absorption correction was performed on the low-temperature data set of **2** by use of the program SADABS.[28] Intensity data of **2** measured at room temperature, **4**, and **5** were corrected with the Gaussian-type face-indexed absorption correction routine embedded in XPREP.[29] The ShelXTL[29] software package was used for solution, refinement, and depiction of the

Table 4. Crystallographic data for **2**·0.5hexane (293 K), **2**·hexane (100 K), **4**, and **5**

	2·0.5 hexane	**2**·hexane	**4**	**5**
Empirical formula	$C_{59}H_{91}Co_2N_4S_4$	$C_{62}H_{98}Co_2N_4S_4$	$C_{40}H_{50}CoIN_2O_2$	$C_{40}H_{50}ClCoN_2O_2$
Formula mass	1102.46	1145.54	776.65	685.20
Space group	$P\bar{1}$, no. 2	$P\bar{1}$, no. 2	$P2_1/c$, no. 14	$Pca2_1$, no. 29
a [Å]	10.5636(9)	10.496(2)	13.5489(9)	26.888(2)
b [Å]	11.4954(12)	11.145(2)	26.290(2)	12.6938(10)
c [Å]	14.5182(12)	14.513(3)	11.6662(8)	10.9282(8)
α [°]	103.73(1)	101.02(2)	90	90
β [°]	101.85(1)	103.66(2)	113.31(1)	90
γ [°]	99.13(1)	99.23(2)	90	90
V [Å]	1635.7(3)	1581.2(5)	3816.3(5)	3729.9(5)
Z	1	1	4	4
T [K]	293(2)	100(2)	100(2)	100(2)
ρ(calcd.) [g cm^{-3}]	1.119	1.203	1.352	1.220
Diffractometer used	Nonius Kappa-CCD	Siemens SMART	Siemens SMART	Siemens SMART
Refl. collected/Θ_{max}	13372/54.00	6152/46.54	33336/54.98	31976/55.00
Unique refl./$I > 2\sigma(I)$	6949/5355	4140/2730	8726/6854	6813/5395
No. of params/restraints	337/4	331/1	427/0	415/1
μ(Mo-K_α) [cm^{-1}]	6.70	6.96	12.93	5.67
$R1$[a]/goodness of fit[b]	0.0546/1.043	0.0601/0.845	0.0329/1.027	0.0548/1.026
$wR2$[c] ($I > 2\sigma(I)$]	0.1429	0.1367	0.0655	0.1268

[a] Observation criterion: $I > 2\sigma(I)$. $R1 = \Sigma||F_o| - |F_c||/\Sigma|F_o|$. [b] GooF = $\{\Sigma[w(F_o^2 - F_c^2)^2]/(n - p)\}^{1/2}$. [c] $wR2 = \{\Sigma[w(F_o^2 - F_c^2)^2]/\Sigma[w(F_o^2)^2]\}^{1/2}$ where $w = 1/\sigma^2(F_o^2) + (aP)^2 + bP$, $P = (F_o^2 + 2F_c^2)/3$.

structure. The structures were readily solved by Patterson methods and difference Fourier techniques. The hexane solvent molecule in the room-temperature structure of **2** was found to be disordered and not fully occupied. A split-atom model with restrained C−C distances and a reduced occupation factor satisfactorily described the disorder. All non-hydrogen atoms, except C atoms in disordered parts, were refined anisotropically and hydrogen atoms were placed at calculated positions and refined as riding atoms with isotropic displacement parameters. Crystallographic data of the compounds and diffractometer types used are listed in Table 4. CCDC-178090−178093 contain the supplementary crystallographic data for this paper. These data can be obtained free of charge at www.ccdc.cam.ac.uk/conts/retrieving.html or from the Cambridge Crystallographic Data Centre, 12, Union Road, Cambridge CB2 1EZ, UK [Fax: (internat.) + 44-1223/336-033; E-mail: deposit@ccdc.cam.ac.uk].

Physical Measurements: Electronic spectra of complexes and spectra of the spectroelectrochemical measurements were recorded with an HP 8452A diode array spectrophotometer (range: 190−1100 nm). Cyclic and square-wave voltammograms and coulometric experiments were performed with an EG&G potentiostat/galvanostat. Temperature-dependent (2−298 K) magnetization data were recorded with a SQUID magnetometer (MPMS Quantum design) in an external magnetic field of 1.0 T. The experimental susceptibility data were corrected for underlying diamagnetism by use of tabulated Pascal's constants. X-band EPR spectra were recorded with a Bruker ESP 300 spectrometer.

Acknowledgments

P. G. and H. C. thank the Alexander von Humboldt Foundation for fellowships. We gratefully acknowledge financial support from the Fonds der Chemischen Industrie.

[1] D. Sellmann, S. Emig, F. W. Heinemann, F. Knoch, *Angew. Chem.* **1997**, *109*, 1250; *Angew. Chem. Int. Ed. Engl.* **1997**, *36*, 1201.
[2] D. Herebian, E. Bothe, E. Bill, T. Weyhermüller, K. Wieghardt, *J. Am. Chem. Soc.* **2001**, *123*, 10013.
[3] C. N. Verani, S. Gallert, E. Bill, T. Weyhermüller, K. Wieghardt, P. Chaudhuri, *Chem. Commun.* **1999**, 1747.
[4] P. Chaudhuri, C. N. Verani, E. Bill, E. Bothe, T. Weyhermüller, K. Wieghardt, *J. Am. Chem. Soc.* **2001**, *123*, 2213.
[5] H. Chun, C. N. Verani, P. Chaudhuri, E. Bothe, E. Bill, T. Weyhermüller, K. Wieghardt, *Inorg. Chem.* **2001**, *40*, 4157.
[6] H. Chun, T. Weyhermüller, E. Bill, K. Wieghardt, *Angew. Chem.* **2001**, *113*, 2552; *Angew. Chem. Int. Ed.* **2001**, *40*, 2489.
[7] X. Sun, H. Chun, K. Hildenbrand, E. Bothe, T. Weyhermüller, K. Wieghardt, *Inorg. Chem.*, submitted.
[8] D. Sellmann, O. Kaeppler, *Z. Naturforsch., Teil B* **1987**, *42*, 1291.
[9] L. F. Larkworthy, J. M. Murphy, D. J. Phillips, *Inorg. Chem.* **1968**, *7*, 1436.
[10] S. E. Livingstone, *J. Chem. Soc.* **1956**, 1042.
[11] D. Bonnet, P. Leduc, E. Bill, G. Chottard, D. Mansuy, I. Artaud, *Eur. J. Inorg. Chem.* **2001**, 1449.
[12] T. Kawamoto, H. Kuma, Y. Kushi, *Bull. Chem. Soc. Jpn.* **1997**, *70*, 1599.
[13] A. Vogler, H. Kunkely, *Comments Inorg. Chem.* **1990**, *9*, 201.
[14] R. M. Buchanan, C. G. Pierpont, *J. Am. Chem. Soc.* **1980**, *102*, 4951.
[15] O.-S. Jung, C. G. Pierpont, *Inorg. Chem.* **1994**, *33*, 2227.
[16] C. G. Pierpont, O.-S. Jung, *Inorg. Chem.* **1995**, *34*, 4281.
[17] S.-M. Peng, C.-T. Chen, D.-S. Liaw, C. Chen, Y. Wang, *Inorg. Chim. Acta* **1985**, *101*, L31.
[18] P.-H. Cheng, H.-Y. Cheng, C.-C. Lin, S.-M. Peng, *Inorg. Chim. Acta* **1990**, *169*, 19.
[19] S. Nemeth, L. I. Simandi, G. Argay, A. Kalman, *Inorg. Chim. Acta* **1989**, *166*, 31.
[20] C. G. Pierpont, W. C. Lange, *Progr. Inorg. Chem.* **1994**, *41*, 331.
[21] A. Mederos, S. Dominguez, R. Hernandez-Molina, J. Sanchiz, F. Brito, *Coord. Chem. Rev.* **1999**, *193−195*, 913.

[22] M. H. Dickman, R. J. Doedens, E. Deutsch, *Inorg. Chem.* **1980**, *19*, 945.
[23] S. Vogel, G. Huttner, L. Zsolnai, *Z. Naturforsch., Teil B* **1993**, *48*, 641.
[24] Y.-X. Tong, B.-S. Kang, C.-Y. Su, X.-L. Yu, X.-M. Chen, *J. Chem. Crystallogr.* **1998**, *28*, 635.
[25] E. J. Miller, A. L. Rheingold, T. B. Brill, *J. Organomet. Chem.* **1985**, *282*, 399.
[26] C. E. Forbes, A. Gold, R. H. Holm, *Inorg. Chem.* **1971**, *10*, 2479.
[27] R. H. Holm, A. L. Balch, A. Davison, A. H. Maki, T. E. Berry, *J. Am. Chem. Soc.* **1967**, *89*, 2866.
[28] G. M. Sheldrick, University of Göttingen, **1994**.
[29] *ShelXTL*, V.5, Siemens Analytical X-ray Instruments, Inc., **1994**.

Received January 25, 2002
[I02043]

Intramolecular Lithium Cation Solvation in the "Active Ligand Periphery" of a Tripodal Triaminostannate

Matthias Lutz,[b] Christian Galka,[a] Matti Haukka,[b] Tapani A. Pakkanen,*[b] and Lutz H. Gade*[a]

Keywords: Tin / Lithium / N ligands / Metal-metal interactions / Rhodium

The tris(aminosilyl)methane derivative $HC\{SiMe_2NH(2\text{-}MeOC_6H_4)\}_3$ (**1**) was reacted with three molar equivalents of *n*-butyllithium in pentane to give the solvate-free trilithium triamide $HC\{SiMe_2N(Li)(2\text{-}MeOC_6H_4)\}_3$ (**2**) for which an X-ray diffraction study established the internal solvation of the lithium ions. The trilithium triamide **2** was converted to the triamidostannate $[HC\{SiMe_2N(2\text{-}MeOC_6H_4)\}_3SnLi]$ (**3**) by treatment of **2** with one molar equivalent of $SnCl_2$. Both the NMR spectroscopic data obtained in solution and an X-ray structure analysis confirmed the intramolecular coordination of the lithium cation by the peripheral *ortho*-methoxy groups. Reaction of compound **3** with 0.5 molar equivalents of the dinuclear compound $[Rh(COD)Cl]_2$ in toluene afforded the mixed heterodimetallic complex $[HC\{SiMe_2N(2\text{-}MeOC_6H_4)\}_3Sn(Li)\text{–}Rh(\eta^4\text{-}C_8H_{12})(Cl)]$ (**4**), for which a doublet resonance at high field in the ^{119}Sn NMR spectrum (δ = –196.3; $^1J_{SnRh}$ = 871.6 Hz) confirmed the formation of a Sn–Rh bond. The X-ray structure analysis revealed that the Rh centre in **4** adopts a slightly distorted, square-planar coordination mode, with a tin-rhodium bond length of 2.6048(4) Å, and that the chloro ligand is additionally bonded to the lithium cation.

(© Wiley-VCH Verlag GmbH, 69451 Weinheim, Germany, 2002)

Introduction

The structural chemistry and reactivity of neutral and anionic tin(II) compounds has attracted much attention in recent years.[1] Group 14 metal-amido and -imido derivatives, in particular, have displayed a great variety of forms of aggregation and reaction patterns.[2,3] The combination of thermodynamic stabilization of the triamidometallates by their integration into a rigid molecular cage structure along with the well-defined orientation and high variability of the peripheral N-substituents has established the tripodal triamidometallates as a versatile new class of ligands in the coordination chemistry of the transition metals.[4] The electronegative N-substituents at the divalent metal atoms render them less oxidizable than would be expected for alkyl- or aryl-substituted derivatives.

An interesting aspect of the structural chemistry of the lithium triamidometallates in solution and in the solid state is the type of interaction between the anionic cage and the countercation (in most cases solvated Li^+). Both solvent-separated salts (**I**) and contact ions have been found (Figure 1).[5] In the latter, the alkali metal ion is either bound directly to the group 14 metal (**II**), in what is thought to be primarily an ionic metal-metal bonding interaction, or attached to the amido-N atoms in a bridging coordination mode (**III**), thus breaking the overall threefold symmetry of the system.

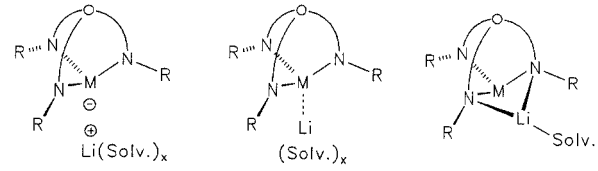

Figure 1. Different modes of cation-anion interactions in triamidostannates and their principal structural types

Which of the structural alternatives discussed above is observed in a given case has been found to be largely unpredictable. It was therefore thought that the design of an amido tripod containing a specific binding site for the metal cation in the ligand periphery would yield "ion pairs" of predefined arrangement.

In an extension of our concept of the "active ligand periphery" in polydentate amides[6,7] containing additional donor functions for cation binding, we synthesised a tripod with peripheral 2-anisyl groups. In this paper we report the

[a] Laboratoire de Chimie Organométallique et de Catalyse (CNRS UMR 7513), Institut Le Bel, Université Louis Pasteur Strasbourg,
4, rue Blaise Pascal, 67070 Strasbourg, France
Fax: (internat.) +33-390/241-531
E-mail: gade@chimie.u-strasbg.fr
[b] Department of Chemistry, University of Joensuu,
80101 Joensuu, Finland
Fax: (internat.) +358-13/251-3344
E-mail: Tapani.Pakkanen@joensuu.fi

synthesis and crystallographic characterisation of the tripodal triamine, the corresponding trilithium triamide, and its triaminostannate. The "ligand properties" of the latter are demonstrated by the characterisation of a heterobimetallic rhodium complex containing this novel type of stannate fragment.

Results and Discussion

Preparation and Crystallographic Studies of $HC\{SiMe_2NH(2\text{-}MeOC_6H_4)\}_3$ (1) and the Lithium Triamide $HC\{SiMe_2N(Li)(2\text{-}MeOC_6H_4)\}_3$ (2)

Reaction of $HC(SiMe_2Br)_3$ [8] in diethyl ether with three molar equivalents of 2-methoxyaniline in the presence of Et_3N as auxiliary base yielded the triamine $HC\{SiMe_2NH(2\text{-}MeOC_6H_4)\}_3$ (**1**) as a colourless solid (Scheme 1).

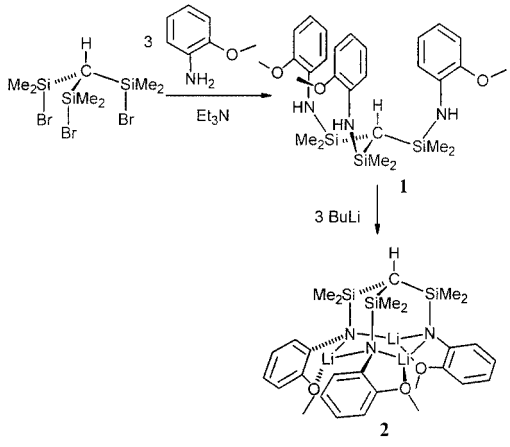

Scheme 1

The spectroscopic and analytical data are consistent with an effective threefold symmetry of **1** in solution. The low-field shift of the apical C−H proton resonance (δ = 0.93 ppm in C_6D_6) which we observed previously for aryl-substituted tris(aminosilyl)methane derivatives[9] indicated a preferred conformation of the molecule in solution that is inverted with respect to the adamantane-related arrangement found for the corresponding alkyl-substituted derivatives.[10] The peripheral groups of the ligand precursor are thus effectively turned "inside-out". This type of molecular structure is also prevalent in the solid state as was found in an X-ray diffraction study of the compound. The molecular structure of **1** is depicted in Figure 2 along with the principal bond lengths and interbond angles. The main structural features resemble those of the previously characterised triamine $HC\{SiMe_2NH(4\text{-}CH_3C_6H_4)\}_3$, the three *ortho*-anisyl groups being very regularly arranged with the aromatic rings in the same plane as the quasi-planar amine units and the methoxy groups pointing outwards.

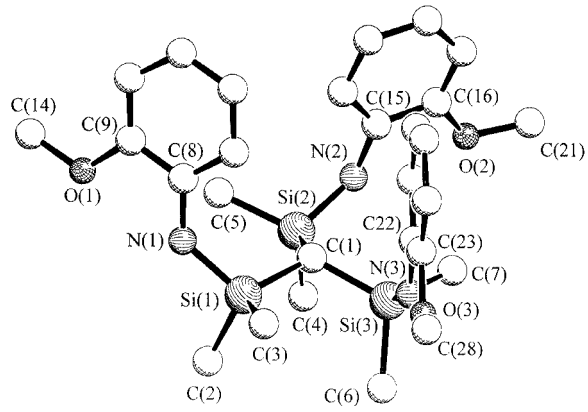

Figure 2. View of the molecular structure of **1**; principal bond lengths (Å) and angles (°): C(1)−Si(1) 1.8829(17), C(1)−Si(2) 1.8825(16), C(1)−Si(3) 1.8867(17), N(1)−Si(1) 1.7358(16), N(2)−Si(2) 1.7439(14), N(3)−Si(3) 1.7395(15), N(1)−C(8) 1.394(2), N(2)−C(15) 1.390(2), N(3)−C(22) 1.394(2); N(1)−Si(1)−C(1) 110.75(7), N(2)−Si(2)−C(1) 109.97(7), N(3)−Si(3)−C(1) 109.73(8), C(8)−N(1)−Si(1) 129.96(14), C(15)−N(2)−Si(2) 129.48(12), C(22)−N(3)−Si(3) 131.19(13)

Upon reaction of **1** with three molar equivalents of *n*-butyllithium in pentane, the solvent-free trilithium triamide $HC\{SiMe_2N(Li)(2\text{-}MeOC_6H_4)\}_3$ (**2**) was obtained as an extremely air- and moisture-sensitive compound (Scheme 1). The signal patterns in the ^1H, ^{13}C, ^{29}Si and ^7Li NMR spectra indicate a threefold symmetrical structure in solution which does not appear to undergo dynamic processes on the NMR time scale. The high molecular symmetry of the trilithium salt **2** was also found in the single crystal X-ray structure. The molecular structure is shown in Figure 3 along with the principal metric parameters.

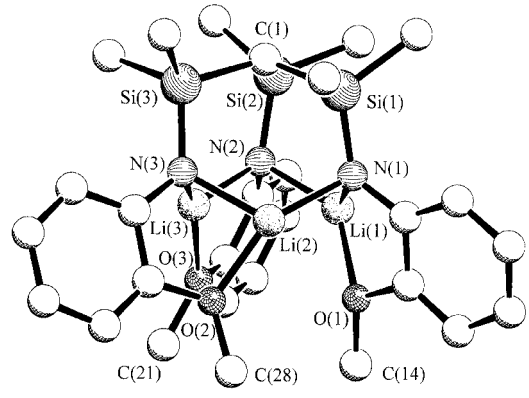

Figure 3. View of the molecular structure of **2**; principal bond lengths (Å) and angles (°): C(1)−Si(1) 1.904(2), C(1)−Si(2) 1.8902(19), C(1)−Si(3) 1.895(2), N(1)−Si(1) 1.7197(16), N(2)−Si(2) 1.7189(16), N(3)−Si(3) 1.7205(17), Li(1)−O(1) 1.963(4), Li(1)−N(1) 1.973(4), Li(1)−N(2) 1.997(4), Li(2)−O(3) 1.938(4), Li(2)−N(3) 2.000(4), Li(2)−N(1) 2.011(4), Li(3)−O(2) 1.915(4), Li(3)−N(2) 1.976(4), Li(3)−N(3) 1.992(4); N(1)−Si(1)−C(1) 107.00(8), N(2)−Si(2)−C(1) 106.40(8), N(1)−Si(1)−C(1) 106.39(8), Li(1)−N(1)−Li(2) 93.98(17), Li(3)−N(2)−Li(1) 92.76(17), Li(3)−N(3)−Li(2) 85.70(18), O(1)−Li(1)−N(1) 83.59(15), O(3)−Li(2)−N(3) 83.54(15), O(2)−Li(3)−N(2) 84.94(16)

The structural centrepiece is an adamantane-related heteroatom cage comprising three Li, N and Si atoms as well as the carbon atom C(1) at the apex of the trisilylmethane unit. This type of structural motif has been reported previously for a series of achiral[8,10] and C_3-chiral[11] tripodal lithium amides. The most remarkable feature is the internal solvation of the lithium ions which generates a rare tris-solvated lithium amide ring structure. The lithium atoms themselves attain a highly nonsymmetrical coordination geometry that is closer to a T-arrangement than to the conventional trigonal structure. In spite of this unequal distribution of the donor atoms, the lithium atoms are very symmetrically disposed vis-à-vis the negatively charged amido functions, as is evident from the approximately equal Li−N distances [overall variation: Li(1)−N(1)/N(2) 1.963(4)/1.973; Li(2)−N(1)/N(3) 2.000(4)/2.011(4); Li(3)−N(2)/N(3) 1.976(4)/1.992(4) Å]. The lithium atoms are not located within the planes defined by the two amido-N atoms they bridge and the oxygen atom of the solvating ether function but are rather displaced outside the cage structure. Due to the Li coordination, the aryl rings of the anisyl groups adopt a symmetrical propeller arrangement.

Synthesis and Structures of the Lithium Triamidostannate(II) HC{SiMe$_2$N(2-MeOC$_6$H$_4$)}$_3$SnLi (3) and the Rh−Sn Heterodimetallic Complex HC{SiMe$_2$N(2-MeOC$_6$H$_4$)}$_3$Sn(Li)−Rh(η^4-C$_8$H$_{12}$)(Cl) (4)

The trilithium triamide **2** was converted into the triamidostannate [HC{SiMe$_2$N(2-MeOC$_6$H$_4$)}$_3$SnLi] (**3**) by treatment of **2** with one molar equivalent of $SnCl_2$ in toluene at elevated temperature in an ultrasound bath. The reaction product crystallised as a colourless solid and was isolated in 63% yield (Scheme 2).

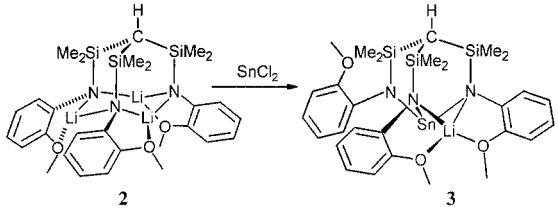

Scheme 2

The observation of three ^{1}H and ^{13}C NMR resonances for the $SiMe_2$ groups (^{1}H: δ = 0.14, 0.59, 0.62 ppm; ^{13}C: δ = 4.9, 5.6, 6.6 ppm) and two NMR resonances for the MeO groups (^{1}H: δ = 3.04, 3.34 ppm; ^{13}C: δ = 55.0, 55.6 ppm) as well as the detection of two ^{29}Si NMR signals for the $SiMe_2$ groups (δ = −1.9, −1.2 ppm) indicate a reduction of the effective symmetry in solution from C_3 to C_S. These spectral patterns are consistent with the coordination of the lithium cation to two amido N-atoms and its internal "solvation" by two of the *ortho*-anisyl groups. In order to establish the details of the molecular structure of this new type of lithium stannate(II), an X-ray diffraction study was carried out (Figure 4).

Figure 4a

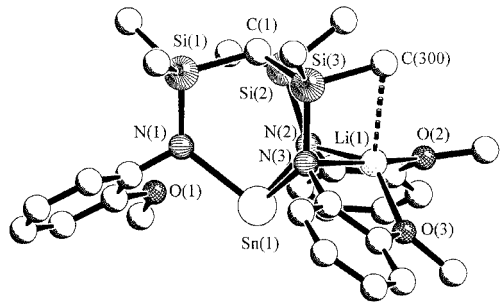

Figure 4b

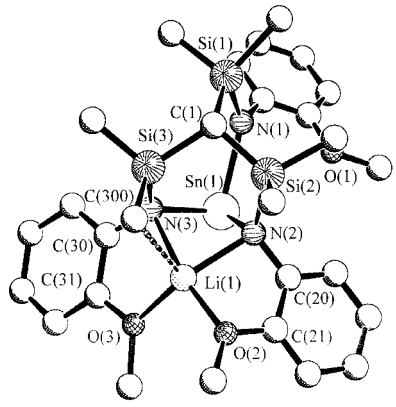

Figure 4. View of the molecular structure of **3**; principal bond lengths (Å) and angles (°): Sn(1)−N(1) 2.255(2), Sn(1)−N(2) 2.2235(19), Sn(1)−N(3) 2.096(2), Sn(1)−Li(1) 2.931(4), Li(1)−N(2) 2.039(5), Li(1)−N(3) 2.139(5), Li(1)−O(2) 1.908(5), Li(1)−O(3) 2.044(5); N(1)−Sn(1)−N(2) 94.20(7), N(1)−Sn(1)−N(3) 96.55(7), N(2)−Sn(1)−N(3) 77.84(7), N(3)−Li(1)−N(2) 81.03(17), N(2)−Li(1)−O(2) 88.2(2), N(3)−Li(1)−O(3) 85.39(18)

The lithium stannate **3** crystallises in the centrosymmetrical space group $P2_1/n$, and possesses a molecular structure in the solid which, albeit distorted, is consistent with the C_s-symmetry derived from the NMR spectroscopic data recorded in solution. The most characteristic structural feature of **3** is undoubtedly the intramolecular coordination of the lithium cation by the peripheral *ortho*-methoxy groups. The Li−O bond lengths found in **3** [1.908(5) Å and 2.044(5) Å] are similar to those found in structurally related solvated metallates, such as HC{SiMe$_2$N[(*S*)-CH(Me)Ph]}$_3$SnLi(THF) [1.95(1) Å][13b] and MeSi{SiMe$_2$N(*t*Bu)}$_3$Pb-Li(THF) [2.11(7) Å].[5b] Significantly, the lithium cation is placed above the plane, which is spanned by the atoms O2, N2, N3 and O3. This exposed position of the lithium leads to a very close contact with the adjacent methyl group C300 [*d*(Li1−C300) = 2.603(2) Å] which effectively occupies the vacant coordination site of the lithium centre. Such "agostic" interactions with hydrocarbon fragments are quite common in lithium amides provided that the coordination numbers of the lithium centres are low.[12] It is therefore surprising to observe this structural feature for four-coordinate lithium, which is probably due to the unusual coordination geometry (distorted square

planar instead of tetrahedral) imposed by the rigid caged structure of the triamidostannate(II).

It is noteworthy that compound **3** is also formed in an in situ reaction of $[HC\{SiMe_2NH(2\text{-}MeOC_6H_4)\}_3]$ (**1**) with *n*-butyllithium and $SnCl_2$ in diethyl ether, and therefore no indication for a competitive coordination of the anisyl groups vs. diethyl ether has been found. However, the formation of **3** using diethyl ether as a reaction medium is accompanied by a redox process (formation of the free ligand) and is therefore unsuitable for a high yield synthetic protocol.

Due to the efficient intramolecular cation solvation, the lithium stannate **3** can be viewed as a neutral compound. In reactions of **3** with transition metal complexes it was therefore expected to act as a neutral "ligand" and thus display a behaviour that differs from the anionic stannates we studied recently.[5,13] Reaction of compound **3** with 0.5 molar equivalents of the dinuclear compound $[Rh(COD)Cl]_2$ in toluene afforded the mixed heterodimetallic complex $[HC\{SiMe_2N(2\text{-}MeOC_6H_4)\}_3Sn(Li)-Rh(\eta^4\text{-}C_8H_{12})(Cl)]$ (**4**) in high yield (Scheme 3).

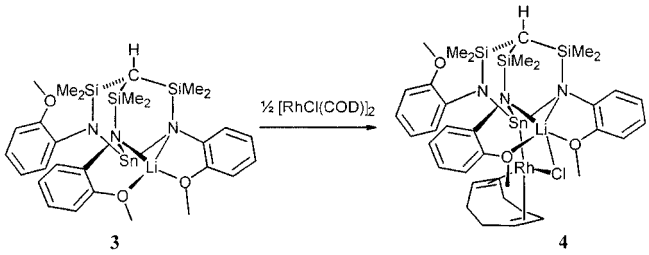

Scheme 3

The observation of a doublet resonance at high field in the ^{119}Sn NMR spectrum ($\delta = -196.3$; $^1J_{SnRh} = 871.6$ Hz) confirms the formation of a Sn−Rh bond and the elemental analysis the formulation given above. The resonance patterns attributable to the stannate fragment in the ^1H, ^{13}C, and ^{29}Si NMR spectra are very similar to those of **3** indicating the retention of the local C_S symmetry. This is consistent with the anticipated nature of the tin cage as a formally neutral ligand at the rhodium, which retains its square planar coordination geometry due to the presence of the chloro ligand and the chelating COD ligand. In order to obtain a detailed insight into the relative arrangement of the two metal complex fragments a single crystal X-ray structure analysis of complex **4** was carried out. Its molecular structure is depicted in Figure 5 along with the principal bond lengths and angles.

As can be seen in Figure 5, the overall structure of the stannate fragment in the heterodimetallic complex is the same as in the noncoordinated compound **3**. A structural effect of the transition metal coordination of the tin in **4** is the slight contraction of the Sn−N bonds relative to those in **3** [average Sn−N distance in **4** is 2.136(2) Å compared to 2.192(2) Å in **3**] which we observed in all the structurally characterised transition metal-stannate complexes. The Rh centre in **4** adopts a slightly distorted, square-planar coordination mode and the tin-rhodium bond length of

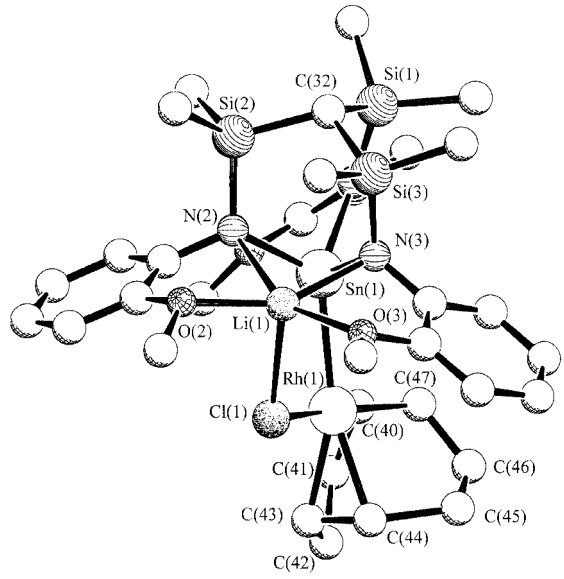

Figure 5. View of the molecular structure of **4**; principal bond lengths (Å) and angles (°): Sn(1)−N(1) 2.108(2), Sn(1)−N(2) 2.137(19), Sn(1)−N(3) 2.164(2), Sn(1)−Li(1) 2.891(5), Sn(1)−Rh(1) 2.6048(3), Rh(1)−C(43) 2.163(4), Rh(1)−C(44) 2.169(4), Rh(1)−C(40) 2.114(3), Rh(1)−C(47) 2.106(3), Li(1)−N(2) 2.371(6), Li(1)−N(3) 2.167(6), Li(1)−O(2) 1.976(5), Li(1)−O(3) 2.115(6), Li(1)−Cl(1) 2.426(5), Rh(1)−Cl(1) 2.3721(7); N(1)−Sn(1)−N(2) 99.80(9), N(1)−Sn(1)−N(3) 98.77(9), N(2)−Sn(1)−N(3) 83.35(8), N(3)−Li(1)−N(2) 77.96(18), N(2)−Li(1)−O(2) 76.76(19), N(3)−Li(1)−O(3) 77.97(19), Cl(1)−Rh(1)−Sn(1) 83.017(19), Cl(1)−Li(1)−Sn(1) 76.26(14), Rh(1)−Sn(1)−Li(1) 89.04(11), Rh(1)−Cl(1)−Li(1) 107.07(12)

2.6048(4) Å is within the range of previously characterised Rh−Sn complexes.[14] The chloro ligand is additionally bonded to the lithium cation of the stannate unit. Although the Li(1)−Cl(1) distance of 2.426(5) Å is ca. 0.2 Å greater than the Li−Cl bond length found in $[HC\{SiMe_2N(Li)[(S)\text{-}3,3\text{-dimethyl-2-butyl}]\}_3\text{-}LiCl(Et_2O)_3]$[11a] it is similar to those previously characterised in a series of Li−Cl complexes.[15]

The lithium stannate ligand has a stronger *trans* influence than the chloro ligand as is evident from the metal-carbon distances to the COD ligand [Rh(1)−C(43) 2.163(4), Rh(1)-2.169(4) Å *trans* to Sn(1) in comparison to Rh(1)−C(40) 2.114(3), Rh(1)−C(47) 2.106(3) *cis* to Sn(1)]. As a neutral ligating unit it therefore resembles the ubiquitous group 15 donor ligands.[16] The *trans* influence of the lithium stannate ligand in **4** is similar to that previously found in square-planar $[Rh(\eta^4\text{-}C_8H_{12})(\kappa^2\text{-}P,Sb\text{-}i\text{Pr}_2\text{PCH}_2\text{Sb}t\text{Bu}_2)]\text{-}PF_6$.[16a]

Conclusion

We have shown in this first study of the tin(II) chemistry of a new tripodal amido ligand containing an "active ligand periphery" that the type of lithium-stannate interaction may be controlled by secondary coordinating functions in the ligand. The stannates thus obtained can be viewed as neutral species that may serve as neutral Sn-donor "ligands" in transition metal chemistry. The scope of this ap-

proach, in particular the application of monodentate ligands with extremely large cone angles in transition metal complexes, is currently being studied in our laboratories.

Experimental Section

All manipulations were performed under nitrogen (desiccant P_4O_{10}, Granusic®, J.T. Baker) on a high vacuum line using standard Schlenk techniques, or in a glovebox. All reaction flasks were heated prior to use during three evacuation-refill cycles. Solvents and solutions were transferred by needle-septa techniques. Solvents were dried according to standard methods and saturated with nitrogen. The deuterated solvents used for the NMR spectroscopic measurements were degassed by three successive "freeze-pump-thaw" cycles and stored over 4 Å molecular sieves. Solids were separated from suspensions by filtration through dried Celite. The ^{1}H, ^{7}Li, ^{13}C, ^{19}F, ^{29}Si and ^{119}Sn NMR spectra were recorded on Bruker AC 200, Bruker Avance 250 and Bruker AMX 400 FT NMR spectrometers. ^{1}H and ^{13}C data are listed in parts per million [ppm] relative to tetramethylsilane and are referenced using the residual protonated solvent peak (^{1}H) or the carbon resonance (^{13}C). ^{7}Li data are listed in ppm relative to LiCl/D_2O (1 M, external). ^{29}Si data are listed in ppm relative to tetramethylsilane as an external standard. ^{119}Sn data are listed in ppm relative to tetramethyltin as an external standard. Infrared spectra were recorded on a Nicolet Magna IRTM 750 spectrometer. Elemental analyses were carried out with a Leco CHNS-932 microanalyzer and a CE-instruments EA 1110 CHNS-O microanalyzer, respectively. $[Rh(COD)Cl]_2$,[17] and $[HC(SiMe_2Br)_3]$[8] were prepared according to published procedures. *o*-Methoxyaniline employed in the ligand synthesis was distilled prior to use. All other chemicals used as starting materials were obtained commercially and used without further purification.

Preparation of Compounds. $[HC\{SiMe_2NH(2\text{-}MeOC_6H_4)\}_3]$ (1): At 0 °C a solution of $[HC(SiMe_2Br)_3]$ (5.22 g, 12.2 mmol) in diethyl ether (20 mL) was added dropwise to a vigorously stirred solution of 2-methoxyaniline (4.51 g, 36.7 mmol) and triethylamine (3.71 g, 36.7 mmol) in diethyl ether (50 mL). After the addition was completed the reaction mixture was stirred for another 12 h at room temperature. The solution was filtered through Celite and the residue was extracted with diethyl ether (3 × 20 mL). The solvent was removed in vacuo and the pale yellow crude product was recrystallized from diethyl ether (10 mL) at −35 °C to yield 5.61 g (83%) of a colourless powder. ^{1}H NMR (200.13 MHz, C_6D_6, 295 K): δ = 0.43 [s, 18 H, $Si(CH_3)_2$], 0.93 [s, 1 H, $HC(SiMe_2)_3$], 3.27 (s, 9 H, OCH_3), 4.60 (s, 3 H, N*H*), 6.54−6.87 (m, 12 H, aryl hydrogens) ppm. ^{13}C{^{1}H} NMR (50.32 MHz, C_6D_6, 295 K): δ = 2.9 [$Si(CH_3)_2$], 4.6 [$HC(SiMe_2)_3$], 55.1 (OCH_3), 110.6, 115.2, 117.7, 121.8, 137.4, 148.6 (aryl carbons) ppm. ^{29}Si{^{1}H} NMR (39.76 MHz, C_6D_6, 295 K): δ = 1.6 [$Si(CH_3)_2$] ppm. IR (KBr): $\tilde{\nu}$ = 3373 cm^{-1} vs, 3060 w, 2958 m, 2894 w, 2843 w, 2830 w, 1602 vs, 1519 vs, 1909 ww, 1858 ww, 1449 m, 1398 s, 1329 m, 1301 m, 1261 w, 1244 w, 1219 w, 1179 m, 1111 s, 1054 w, 1037 m, 1000 s, 900 vs, 846 vs, 767 w, 744 m, 738 m, 687 vw. $C_{28}H_{43}N_3O_3Si_3$ (553.92): calcd. C 60.71, H 7.82, N 7.59; found C 60.55, H 7.93, N 7.56.

$[HC\{SiMe_2N(Li)(2\text{-}MeOC_6H_4)\}_3]$ (2): *n*-Butyllithium (14 mL, 22.4 mmol of a 1.6 mol/L solution in hexane) was added to a slurry of $[HC\{SiMe_2NH(2\text{-}MeOC_6H_4)\}_3]$ **(1)** (4.13 g, 7.45 mmol) in pentane (50 mL) at −20 °C. The reaction mixture was slowly warmed up to ambient temperature and stirring at room temperature was continued for 2 h. The off white slurry was subsequently refluxed for 15 min and stirred for a further 12 h at room temperature. The reaction mixture was filtered through a G3 frit, washed with pentane (3 × 10 mL) and dried under vacuum to yield 4.00 g (94%) of a colourless, microcrystalline powder. ^{1}H NMR (250.13 MHz, C_6D_6, 295 K): δ = −0.59 [s, 1 H, $HC(SiMe_2)_3$], 0.61 [s, 18 H, $Si(CH_3)_2$], 3.00 (s, 9 H, OCH_3), 6.44 (dd, $^3J_{H,H}$ = 7.8, $^4J_{H,H}$ = 1.3 Hz, 3 H), 6.58 (dt, $^3J_{H,H}$ = 7.8, $^4J_{H,H}$ = 1.3 Hz, 3 H), 6.94 (dt, $^3J_{H,H}$ = 7.8, $^4J_{H,H}$ = 1.3 Hz, 3 H), 7.07 (dd, $^3J_{H,H}$ = 7.8, $^4J_{H,H}$ = 1.3 Hz, 3 H) ppm. ^{7}Li{^{1}H} NMR (97.21 MHz, C_6D_6, 295 K): δ = −0.4 ppm. ^{13}C{^{1}H} NMR (62.89 MHz, C_6D_6, 295 K): δ = 6.2 [$Si(CH_3)_2$], 12.4 [$HC(SiMe_2)_3$], 54.5 (OCH_3), 109.1, 113.7, 123.2, 123.4, 149.6, 152.8 (aryl carbons) ppm. ^{29}Si{^{1}H} NMR (49.69 MHz, C_6D_6, 295 K): δ = −1.9 [$Si(CH_3)_2$] ppm. $C_{28}H_{40}Li_3N_3O_3Si_3$ (571.72): calcd. C 58.82, H 7.05, N 7.35; found C 58.65, H 6.93, N 7.42.

$[HC\{SiMe_2N(2\text{-}MeOC_6H_4)\}_3SnLi]$ (3): Toluene (30 mL) was added to a mixture of $[HC\{SiMe_2N(2\text{-}MeOC_6H_4)\}_3Li_3]$ **(2)** (1.00 g, 1.75 mmol) and $SnCl_2$ (332 mg, 1.75 mmol) at room temperature. The resulting mixture was sonicated for 6 h at 60 °C and subsequently filtered through Celite. The residue was extracted with hot toluene (2 × 10 mL) and the solvent of the filtrate was evaporated under vacuum. The obtained off white residue was washed with diethyl ether (10 mL) and pentane (2 × 10 mL) and dried under vacuum to give 746 mg (63%) of a colourless, microcrystalline powder. ^{1}H NMR (400.13 MHz, C_6D_6, 295 K): δ = −0.49 [s, 1 H, $HC(SiMe_2)_3$], 0.14, 0.59, 0.62 [s, 18 H, $Si(CH_3)_2$], 3.04, 3.34 (s, 9 H, OCH_3), 6.52 (dd, $^3J_{H,H}$ = 7.9, $^4J_{H,H}$ = 1.2 Hz, 2 H), 6.67 (dd, $^3J_{H,H}$ = 9.7, $^4J_{H,H}$ = 1.5 Hz, 1 H), 6.82 (dt, $^3J_{H,H}$ = 7.9, $^4J_{H,H}$ = 1.8 Hz, 2 H), 6.85 (dt, $^3J_{H,H}$ = 7.9, $^4J_{H,H}$ = 1.4 Hz, 1 H), 6.93 (dt, $^3J_{H,H}$ = 7.6, $^4J_{H,H}$ = 1.5 Hz, 2 H), 7.01 (dt, $^3J_{H,H}$ = 7.3, $^4J_{H,H}$ = 1.5 Hz, 1 H), 7.34 (dd, $^3J_{H,H}$ = 7.6, $^4J_{H,H}$ = 1.8 Hz, 2 H), 7.42 (dd, $^3J_{H,H}$ = 7.6, $^4J_{H,H}$ = 1.5 Hz, 1 H) ppm. ^{7}Li{^{1}H} NMR (77.77 MHz, C_6D_6, 295 K): δ = −0.3 ppm. ^{13}C{^{1}H} NMR (100.61 MHz, C_6D_6, 295 K): δ = 4.9, 5.6, 6.6 [$Si(CH_3)_2$], 8.2 [$HC(SiMe_2)_3$], 55.0, 55.6 (OCH_3), 111.0, 111.6, 120.0, 121.2, 121.6, 123.4, 130.3, 142.5, 143.0, 154.7, 155.1 (aryl carbons) ppm. ^{29}Si{^{1}H} NMR (39.76 MHz, C_6D_6, 295 K): δ = −1.9, −1.2 [$Si(CH_3)_2$] ppm. ^{119}Sn{^{1}H} NMR (93.28 MHz, C_6D_6, 291 K): δ = −96.5 ppm. $C_{28}H_{40}LiN_3O_3Si_3Sn$ (676.53): calcd. C 49.71, H 5.96, N 6.21; found C 49.84, H 5.90, N 5.94.

$[HC\{SiMe_2N(2\text{-}MeOC_6H_4)\}_3Sn(Li)-Rh(\eta^4\text{-}C_8H_{12})(Cl)]$ (4): Toluene (10 mL) was added to a solid mixture of $[HC\{SiMe_2N(2\text{-}MeOC_6H_4)\}_3SnLi]$ **(3)** (380 mg, 0.56 mmol) and $[Rh(COD)Cl]_2$ (139 mg, 0.28 mmol) at room temperature. The orange solution was stirred for a further 12 h at room temperature and subsequently filtered through Celite. The residue was extracted with toluene (10 mL) and the filtrate was dried under vacuum. The obtained yellow residue was washed with pentane (10 mL) and diethyl ether (5 mL) and dried under vacuum to yield 410 mg (79%) of a yellow, microcrystalline powder. ^{1}H NMR (250.13 MHz, C_6D_6, 323 K): δ = −0.51 [s, 1 H, $HC(SiMe_2)_3$], 0.30, 0.40, 0.45 [s, 18 H, $Si(CH_3)_2$], 1.09−1.86 (m, 8 H, allylic hydrogens), 3.51 (s, 6 H, OCH_3), 3.78 (s, 3 H, OCH_3), 3.98 (d, $^3J_{H,H}$ = 2.8 Hz, 2 H, olefinic hydrogens), 4.33 (d, $^3J_{H,H}$ = 2.5 Hz, 2 H, olefinic hydrogens), 6.61−7.41 (m, 12 H, aryl hydrogens) ppm. ^{7}Li{^{1}H} NMR (97.21 MHz, C_6D_6, 295 K): δ = 1.5 ppm. ^{13}C{^{1}H} NMR (62.89 MHz, C_6D_6, 323 K): δ = 5.0 [$Si(CH_3)_2$], 5.6 [br, $Si(CH_3)_2$], 8.1 [$HC(SiMe_2)_3$], 28.0, 33.7 (allylic carbons), 55.0, 55.2 (OCH_3), 63.8 (d, $^1J_{RhC}$ = 13.3 Hz, olefinic carbons), 94.5 (d, $^1J_{RhC}$ = 8.3 Hz, olefinic carbons), 110.7, 110.9, 121.3, 121.8, 122.2, 122.8, 128.1, 130.9, 141.6, 141.8, 155.6, 155.9 (aryl carbons) ppm. ^{29}Si{^{1}H} NMR (49.69 MHz, C_6D_6, 295 K): δ = 1.4, 2.0 [$Si(CH_3)_2$] ppm. ^{119}Sn{^{1}H} NMR (149.19 MHz, C_6D_6, 291 K): δ = −196.3 (d, $^1J_{RhSn}$ = 871.6 Hz, N_3Sn−Rh) ppm. IR (KBr): $\tilde{\nu}$ = 3379 cm^{-1} s, 3068 vw, 2961m, 2834 vw, 2289 vw, 2019

Table 1. Crystal data and structure refinement for **1**, **2**, **3** and **4**

	1	**2**	**3**	**4**
Molecular formula	$C_{28}H_{43}N_3O_3Si_3{\cdot}C_6D_6$	$C_{28}H_{40}Li_3N_3O_3Si_3Sn{\cdot}2.5C_6D_6$	$C_{28}H_{40}LiN_3O_3Si_3Sn$	$C_{36}H_{49}ClLiN_3O_3RhSi_3Sn{\cdot}C_6D_6$
M_r	638.07	782.08	676.53	1004.19
Temperature	150(2) K	150(2) K	173(2) K	150(2) K
Wavelength	0.71073 Å	0.71073 Å	0.71073 Å	0.71073 Å
Crystal system	Monoclinic	Monoclinic	Monoclinic	Monoclinic
Space group	$P2_1/c$	$C2/c$	$P2_1/c$	$P2_1/c$
Z	4	8	4	4
Unit cell dimensions	a = 14.03350(10) Å	a = 24.5027(3) Å	a = 9.1341(18) Å	a = 12.13230(10) Å
	b = 15.1319(2) Å	b = 15.8137(3) Å	b = 14.172(3) Å	b = 19.5031(2) Å
	c = 17.0806(2) Å	c = 24.7797(4) Å	c = 24.977(5) Å	c = 18.7930(2) Å
	α = 90°	α = 90°	α = 90°	α = 90°
	β = 99.5400(6)°	β = 116.6346(6)°	β = 94.57(3)°	β = 92.2699(4)°
	γ = 90°	γ = 90°	γ = 90°	γ = 90°
Volume	3576.96(7) Å^3	8582.7(2) Å^3	3222.9(11) Å^3	4443.26(8) Å^3
$D_{calcd.}$	1.185 g cm^{-1}	1.211 g cm^{-1}	1.394 g cm^{-1}	1.501 g cm^{-1}
Absorption coefficient	0.169 mm^{-1}	0.151 mm^{-1}	0.936 mm^{-1}	1.115 mm^{-1}
F(000)	1360	3272	1392	2036
Crytal size [mm]	0.30 × 0.30 × 0.30	0.30 × 0.30 × 0.10	0.35 × 0.25 × 0.15	0.30 × 0.30 × 0.30
θ range for data collection	3.92 to 27.45°	2.58 to 27.48°	2.32 to 25.0°	3.41 to 26.37°
Limiting indices	$-18 \le h \le 18$	$-31 \le h \le 31$	$-10 \le h \le 10$	$-15 \le h \le 15$
	$-19 \le k \le 19$	$-20 \le k \le 20$	$-16 \le k \le 16$	$-24 \le k \le 24$
	$-22 \le l \le 22$	$-32 \le l \le 32$	$-29 \le l \le 29$	$-23 \le l \le 23$
Reflections collected	15821	18820	30955	53620
Independent reflections ($R_{int.}$)	8128 (0.0231)	9714 (0.0390)	5666 (0.0401)	9064 (0.0479)
Refinement method	Full-matrix least-squares on F^2	Full-matrix least-squares on F^2	Full-matrix least-squares on F^2	Full-matrix least-squares on F^2
Data/restraints/parameters	8128/0/397	9714/0/505	5666/0/361	9064/0/524
Goodness-of-fit on F^2	1.043	1.022	1.030	1.082
Final R indices	R_1 = 0.0429	R_1 = 0.0484	R_1 = 0.0268	R_1 = 0.0298
[$I > 2\sigma(I)$]	wR_2 = 0.1086	wR_2 = 0.1060	wR_2 = 0.0679	wR_2 = 0.0676
R indices (all data)	R_1 = 0.0604	R_1 = 0.0853	R_1 = 0.0335	R_1 = 0.0410
	wR_2 = 0.1212	wR_2 = 0.1209	wR_2 = 0.0698	wR_2 = 0.0725
Largest diff. peak and hole	0.298 and −0.290 e·Å^{-3}	0.249 and −0.290 e·Å^{-3}	0.659 and −0.498 e·Å^{-3}	0.676 and −0.647 e·Å^{-3}

vw, 1602 s, 1515 vs, 1444 m, 1393 m, 1332 s, 1301 s, 1240 vs, 1179 w, 1113 s, 1052 w, 1042 m, 1006 m, 904 s, 843 s, 772 w, 746 m, 690 vw. $C_{36}H_{52}ClLiN_3O_3RhSi_3Sn$ (923.07): calcd. C 46.84, H 5.68, N 4.55; found C 47.13, H 5.80, N 4.24.

X-ray Crystallographic Study of Compounds 1−4

The X-ray diffraction data were collected on a Nonius KappaCCD diffractometer (**1**, **2**, and **4**) or on an IPDS (STOE) diffractometer (**3**) using Mo-K_α radiation (λ = 0.71073 Å). The Denzo-Scalepack[18] program package or IPDS programs were used for cell refinements and data reduction. A multi-scan absorption correction, based on equivalent reflections (XPREP in SHELXTL v5.1),[19] was applied to the data of **4** (T_{max}/T_{min} 0.26648/0.21770). Structures were solved by direct methods using the SHELXS-97[20] (**1**, **3** and **4**) or SIR-97[21] (**2**) program. All structures were refined with the SHELXL-97[22] program. In **3** hydrogens were located from a difference Fourier map and refined isotropically. In **1**, **2** and **4** hydrogens were placed on an idealized position and constrained to ride on their parent atom. The crystallographic data are summarised in Table 1. The molecular structures of the complexes along with principal bond lengths and angles are presented in Figure 2−5.

CCDC-178729 (**1**), -178730 (**2**), -178731 (**3**) and -178732 (**4**) contain the supplementary crystallographic data for this paper. These data can be obtained free of charge at www.ccdc.cam.ac.uk/conts/retrieving.html [or from the Cambridge Crystallographic Data Centre, 12, Union Road, Cambridge CB2 1EZ, UK; Fax: (internat.) +44-1223/336-033; E-mail: deposit@ccdc.cam.ac.uk].

Acknowledgments

We thank the European Union (TMR program, network MECATSYN), the CNRS (France) the Deutsche Forschungsgemeinschaft (SFB 347), and the Institut Universitaire de France for financial support.

[1] Selected examples: [1a] M. Veith, R. Rösler, *Z. Naturforsch., Teil B* **1986**, *41*, 1071−1080. [1b] M. Veith, D. Käfer, V. Huch, *Angew. Chem.* **1986**, *98*, 367−368; *Angew. Chem. Int. Ed. Engl.* **1986**, *25*, 375−377. [1c] M. Veith, C. Ruloff, V. Huch, F. Töllner, *Angew. Chem.* **1988**, *100*, 1418−1419; *Angew. Chem. Int. Ed. Engl.* **1988**, *27*, 1381−1382. [1d] M. A. Beswick, M. K. Davies, P. R. Raithby, A. Steiner, D. S. Wright, *Organometallics* **1997**, *16*, 1109−1110. [1e] A. Steiner, D. Stalke, *J. Chem. Soc., Chem. Commun.* **1993**, 1702−1704. [1f] H. V. R. Dais, M. M.

Olmstead, K. Ruhlandt-Senge, P. P. Power, *J. Organomet. Chem.* **1993**, *462*, 1−6. [1g] D. Reed, D. Stalke, D. S. Wright, *Angew. Chem.* **1991**, *103*, 1539−1540; *Angew. Chem. Int. Ed. Engl.* **1991**, *30*, 1459−1460. [1h] D. R. Armstrong, M. G. Davidson, D. Moncrieff, D. Stalke, D. S. Wright, *J. Chem. Soc., Chem. Commun.* **1992**, 1413−1414. [1i] P. B. Hitchcock, M. F. Lappert, G. A. Lawless, B. Royo, *J. Chem. Soc., Chem. Commun.* **1993**, 554−555. [1j] M. A. Paver, C. A. Russel, D. S. Wright, *Angew. Chem.* **1995**, *107*, 1677−1686; *Angew. Chem. Int. Ed. Engl.* **1995**, *34*, 1545−1554.

[2] [2a] M. Veith, *Chem. Rev.* **1990**, *90*, 3−16. [2b] M. Veith, *Adv. Organomet. Chem.* **1990**, *31*, 269−300. [2c] M. Veith, *Angew. Chem. Int. Ed. Engl.* **1987**, *26*, 1−14.

[3] M. F. Lappert, P. P. Power, A. R. Sanger, R. C. Srivastava, *Metal and Metalloid Amides*; Ellis Horwood, Chichester, U. K., 1980. −

[4] Review: L. H. Gade, *Eur. J. Inorg. Chem.* **2002**, 1257−1268.

[5] [5a] K. W. Hellmann, P. Steinert, L. H. Gade, *Inorg. Chem.* **1994**, *33*, 3859−3960. [5b] K. W. Hellmann, L. H. Gade, O. Gevert, P. Steinert, J. W. Lauher, *Inorg. Chem.* **1995**, *34*, 4069−4078.

[6] H. Memmler, K. Walsh, L. H. Gade, J. W. Lauher, *Inorg. Chem.* **1995**, *34*, 4062−4068.

[7] L. H. Gade, *Chem. Commun.* **2000**, 173−182.

[8] [8a] L. H. Gade, C. Becker, J. W. Lauher, *Inorg. Chem.* **1993**, *32*, 2308−2314. [8b] C. Eaborn, P. B. Hitchcock, P. D. Lickiss, *J. Organomet. Chem.* **1983**, *252*, 281−288.

[9] H. Memmler, L. H. Gade, J. W. Lauher, *Inorg. Chem.* **1994**, *33*, 3064−3071.

[10] [10a] L. H. Gade, N. Mahr, *J. Chem. Soc., Dalton Trans.* **1993**, 489−494. [10b] M. Schubart, B. Findeis, L. H. Gade, W.-S. Li, M. McPartlin, *Chem. Ber.* **1995**, *128*, 329−334.

[11] [11a] P. Renner, C. H. Galka, L. H. Gade, S. Radojevic, M. McPartlin, *Eur. J. Inorg. Chem.* **2001**, 1425−1430. [11b] L. H. Gade, P. Renner, H. Memmler, F. Fecher, C. H. Galka, M. Laubender, S. Radojevic, M. McPartlin, J. W. Lauher, *Chem. Eur. J.* **2001**, *7*, 2563−2580.

[12] K. Gregory, P. v. R. Schleyer, R. Snaith, *Adv. Inorg. Chem.* **1991**, *37*, 47−142 and references cited therein. See also: R. E. Mulvey, *Chem. Soc. Rev.* **1999**, *27*, 339−346.

[13] [13a] K. W. Hellmann, S. Friedrich, L. H. Gade, W.-S. Li, M. McPartlin, *Chem. Ber.* **1995**, *128*, 29−34. [13b] H. Memmler, U. Kauper, L. H. Gade, D. Stalke, J. W. Lauher, *Organometallics* **1996**, *15*, 3637−3939. [13c] M. Contel, K. W. Hellmann, L. H. Gade, I. Scowen, M. McPartlin, M. Laguna, *Inorg. Chem.* **1996**, *35*, 3713−3715. [13d] B. Findeis, M. Contel, L. H. Gade, M. Laguna, M. C. Gimeno, I. J. Scowen, M. McPartlin, *Inorg. Chem.* **1997**, *36*, 2386−2390. [13e] B. Findeis, L. H. Gade, I. J. Scowen, M. McPartlin, *Inorg. Chem.* **1997**, *36*, 960−961. [13f] M. Lutz, B. Findeis, M. Haukka, T. A. Pakkanen, L. H. Gade, *Organometallics* **2001**, *20*, 2505−2509. [13g] M. Lutz, B. Findeis, M. Haukka, T. A. Pakkanen, L. H. Gade, *Eur. J. Inorg. Chem.* **2001**, 3155−3162.

[14] Examples of recently structurally characterised Rh−Sn bonds: [14a] H. Werner, O. Gevert, P. Haquette, *Organometallics* **1997**, *16*, 803−806. [14b] M. A. Garralda, E. Pinilla, M. A. Monge, *J. Organomet. Chem.* **1992**, *427*, 193−200. [14c] L. Carlton, R. Weber, D. C. Levendis, *Inorg. Chem.* **1998**, *37*, 1264−1271. [14d] D. Kruber, K. Merzweiler, C. Wagner, H. Weichmann, *J. Organomet. Chem.* **1999**, *572*, 117−123. [14e] S. Licoccia, R. Paolesse, T. Boschi, *Acta Crystallogr., Sect. C* **1995**, *51*, 833−835.

[15] [15a] W. J. Evans, J. L Shreeve, R. N. R. Broomhall-Dillard, J. W. Ziller, *J. Organomet. Chem.* **1995**, *501*, 7−11. [15b] U. Piarulli, A. J. Rogers, C. Floriani, G. Bervasio, D. Viterbo, *Inorg. Chem.* **1997**, *36*, 6127−6133. [15c] G. B. Deacon, C. M. Forsyth, P. C. Junk, B. W. Skelton, A. H. White, *J. Chem. Soc., Dalton Trans.* **1998**, 1381−1388. For recent examples of μ_3-capping halides on Li_3 faces see, for example: [15d] R. Fleischer, D. Stalke, *Coord. Chem. Rev.* **1998**, *176*, 431−450. [15e] R. Fleischer, D. Stalke, *J. Chem. Soc., Dalton Trans.* **1998**, 193−197.

[16] [16a] M. Manger, J. Wolf, M. Laubender, M. Treichert, D. Stalke, H. Werner, *Chem. Eur. J.* **1997**, *3*, 1442−1450. [16b] M. Manger, O. Gevert, H. Werner, *Chem. Ber./Recueil* **1997**, *130*, 1529−1531. [16c] H. Werner, A. Heinemann, B. Windmüller, P. Steinert, *Chem. Ber.* **1996**, *129*, 903−910. [16d] P. Schwab, N. Mahr, J. Wolf, H. Werner, *Angew. Chem. Int. Ed. Engl.* **1993**, *32*, 1480−1482.

[17] G. Giordano, R. H. Crabtree, *Inorg. Synth.* **1990**, *28*, 88−90.

[18] Z. Otwinowski, W. Minor, *Processing of X-ray Diffraction Data Collected in Oscillation Mode*, in *Methods in Enzymology, Volume 276, Macromolecular Crystallography, part A*, (Eds.: C. W. Carter, Jr. and R. M. Sweet), Academic Press, New York, **1997**, p. 307−326.

[19] G. M. Sheldrick, *SHELXTL* Version 5.1, Bruker Analytical X-ray Systems, Bruker AXS, Inc. Madison, Wisconsin, USA, **1998**.

[20] G. M. Sheldrick, *SHELS-97*, Program for Crystal Structure Determination, University of Göttingen, **1997**.

[21] A. Altomare, M. C. Burla, M. Camalli, G. L. Cascarano, C. Giacovazzo, A. Guagliardi, A. G. Moliterni, G. Polidori, R. J. Spagna, *Appl. Cryst.* **1999**, *32*, 115−119.

[22] G. M. Sheldrick, *SHELXL-97, Program for Crystal Structure Refinement*, University of Göttingen, Germany, **1997**.

Received February 6, 2002
[I02061]

Early Transition Metal Complexes of Triphosphorus Macrocycles

Robert J. Baker,[a] Philip C. Davies,[a] Peter G. Edwards,*[a] Robert D. Farley,[a] Sudantha S. Liyanage,[a] Damien M. Murphy,[a] and Ben Yong[a]

Keywords: Macrocyclic ligands / P ligands / Titanium / Vanadium / Chromium

The reactions of 1,5,9-triethyl-1,5,9-triphosphacyclododecane, [12]aneP_3Et_3, with first-row transition metal halides MCl_3 [M = Ti (**1**), V (**2**), and Cr (**3**)] or their THF adducts are reported. The oxidation of **2** gives the complex ([12]aneP_3Et_3)-$V(O)Cl_2$ (**4**). This is the first example of a phosphane ligand that is *trans* to a vanadyl moiety. Also reported are V^{III} (**5**) and Cr^{III} (**6**) complexes of the pendant ether macrocycles [12]ane$P_3(C_2H_4OEt)_3$ and 12[ane]$P_3(C_3H_6OMe)_3$ respectively. The complexes **1**–**6** have been characterised crystallographically and represent a rare class of phosphane complexes of these metals. The paramagnetic d^1 compounds are characterised by EPR and ENDOR spectroscopy, simulation of which gives valuable structural information of these species in frozen solution. With [12]aneP_3Et_3, Nb^{III} and Nb^{IV} chlorides give air-sensitive materials which could not be fully characterised although by comparison with compound **4**, EPR and ENDOR spectroscopy indicate the principal oxidation product to be ([12]aneP_3Et_3)$Nb(O)Cl_2$ (**7**).
(© Wiley-VCH Verlag GmbH, 69451 Weinheim, Germany, 2002)

Introduction

Phosphane ligands are known to readily form complexes with late transition metals. Phosphane complexes of the early transition metals, however, are still relatively uncommon and less well studied; this being predominantly due to inherent kinetic lability that limits the opportunity to obtain discrete and well-behaved complexes for further studies. The understanding of appropriate reaction conditions has led to a resurgence of interest in this field.[1] The majority of phosphane complexes of group-5 metals are stabilised by metal−metal interactions.[2] In view of the intrinsic lability of phosphane complexes of these electropositive metals, and the observation that the majority of organometallic derivatives of group-4 and -5 metals are stabilised by cyclopentadienyl and related ligands,[3] we have chosen to take advantage of the macrocyclic coordination effect and to study the coordination chemistry of 1,5,9-trialkyl-1,5,9-triphosphacyclododecane ([12]aneP_3R_3) macrocycles with early transition metals. These phosphane macrocycles[4] also bear a resemblance to the cyclopentadienyl family of ligands in that they can be considered to coordinate in a 6-electron, facial tridentate fashion. Thus the reactivity of complexes of these ligands will be of interest. In this paper we will describe the chemistry of group-4 and -5 metals with [12]aneP_3R_3 ligands and some related chemistry of chromium.

Results and Discussion

M^{III} Complexes (M = Ti, V, Cr)

Complexes of [12]aneP_3Et_3 (1,5,9-triethyl-1,5,9-triphosphacyclododecane) are readily formed by the addition of the ligand to a dichloromethane solution of MCl_3·3THF and are obtained as light blue (Ti), green (V) and blue (Cr) paramagnetic solids. The new compounds and their syntheses are outlined in Scheme 1. The chromium complex is also an intermediate in the synthesis of free [12]aneP_3Et_3 and may be formed by halogen oxidation of the $Cr(CO)_3$ adduct.[4]

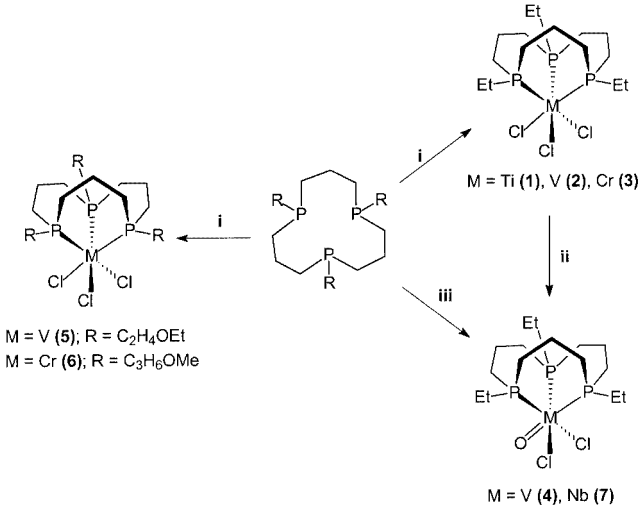

Scheme 1. i) $MCl_3(THF)_3$, CH_2Cl_2; ii) air, CH_2Cl_2; iii) $NbCl_3$(DME), air, CH_2Cl_2

[a] Department of Chemistry, Cardiff University,
P. O. Box 912, Cardiff, CF10 3TB, U.K.
E-mail: EdwardsPG@cardiff.ac.uk

The reaction of [12]aneP_3Et_3 with solutions of $TiCl_3$·3THF causes an immediate colour change to pale blue, and crystalline **1** can be isolated in good yield. Analytical and mass spectrometric data are consistent with the formula ([12]aneP_3Et_3)$TiCl_3$, and the magnetic susceptibility indicates a d^1 paramagnet. The crystal structure of **1** is shown in Figure 1 and selected bond lengths and angles are given in Table 1. The structure shows the expected octahedral geometry at the metal centre with the macrocycle capping one face. The complex shows a weak Jahn−Teller distortion, as expected for d^1 Ti^{III}. Although the quality of structural data is poor, one titanium−phosphorus bond appears marginally longer than the other two [2.623(4) Å compared to 2.608(4) Å and 2.609(4) Å] and is *trans* to the longest titanium−chlorine bond [2.371(4) Å compared to 2.331(4) Å and 2.358(3) Å]. There is no evidence of any agostic interactions in the solid-state structure or in the infrared spectrum.

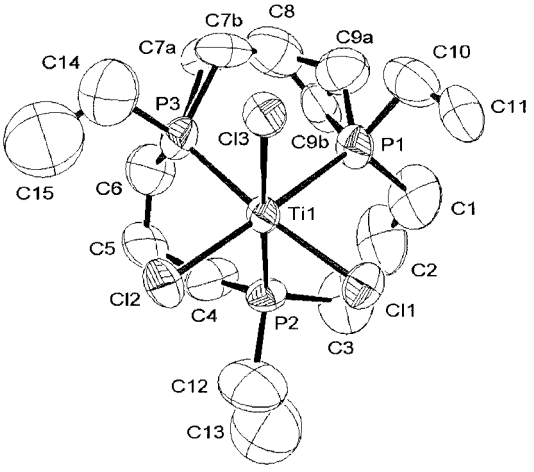

Figure 1. A view of the X-ray crystal structure and atom labelling scheme of ([12]aneP_3Et_3)$TiCl_3$ (**1**); thermal ellipsoids are set at 50% probability

There are a few examples of tris(monophosphane)titanium(III) complexes. $TiCl_3P_3$ (P = PCy_3, P*i*Pr_3, PBu_3) which have been reported to form at low temperatures, but at higher temperatures phosphane dissociation occurs and $TiCl_3P_2$ predominates.[5,6] The tridentate ligand trimpsi {trimpsi = *tert*-butyltris[(dimethylphosphanyl)methyl]silane, *t*BuSi(CH_2PMe_2)$_3$} forms a complex with $TiCl_3$ but the crystal structure has not been reported.[8] All crystallographically characterised (phosphane)Ti^{III} complexes contain cyclopentadienyl ligands except $Ti(BH_4)_3(PMe_3)_2$ which shows M−P distances of 2.571(3) and 2.539(3) Å;[9] All known titanium−phosphane distances fall within the range 2.58±0.07 Å, regardless of oxidation state or coordination number. The P−Ti−P bond angles in **1** are somewhat compressed [average 82.71(13)°] compared to those of **2** and **3** although they are similar to those reported for (trimpsi)$Ti(CO)_4$, and other chelating phosphanes more generally.[8]

The addition of [12]aneP_3Et_3 to VCl_3·3THF gives rise to ([12]aneP_3Et_3)VCl_3 (**2**) which may be isolated as a green crystalline solid in good yield. Analytical and mass spectrometric data confirm the nature of **2** and the magnetic susceptibility is consistent with d^2 V^{III}. Somewhat surprisingly, this complex is almost indefinitely stable to air as a solid, but it is moderately air-sensitive in solution. There are numerous other (phosphane)V^{III} complexes known but these contain mainly monodentate phosphanes and are stabilised by cyclopentadienyl ligands;[10] notable exceptions are [$(Me_2PCH_2CH_2)_2N$]VCl_2 (and organometallic derivatives)[11] and (trimpsi)VCl_3,[7] although neither have been structurally characterised. The crystal structure of **2** is shown in Figure 2, selected bond lengths and angles are given in Table 1. There are no related structurally characterised six-coordinate (phosphane)vanadium(III) complexes with which to make comparisons (five-coordination being more common for simple V^{III} complexes); however, the vanadium−phosphane bond lengths in **2** are similar to

Table 1. Selected bond lengths [Å] and angles [°] for compounds **1**−**6**

	1	**2**	**3**	**4**	**5**	**6**
M−P	2.608(4)	2.514(3)	2.444(2)	2.408(10)	2.465(2)	2.526(3)
	2.609(4)	2.519(3)	2.447(2)	2.451(9)	2.443(2)	2.528(3)
	2.623(4)	2.526(3)	2.450(2)	2.596(10)	2.431(2)	2.511(3)
M−Cl	2.331(4)	2.324(3)	2.328(2)	2.365(10)	2.345(2)	2.323(3)
	2.358(3)	2.325(3)	2.333(2)	2.295(10)	2.328(2)	2.324(3)
	2.371(4)	2.347(3)	2.351(2)		2.331(2)	2.302(3)
M=O	–	–	–	1.836(18)	–	–
P−M−P	81.58(12)	88.83(11)	90.72(8)	89.8(3)	89.41(8)	87.77(9)
	81.18(13)	87.22(10)	90.83(7)	81.9(3)	91.05(7)	87.46(10)
	85.38(13)	86.40(10)	91.52(8)	82.5(3)	91.02(7)	89.74(10)
Cl−M−Cl	100.77(14)	102.12(12)	98.07(8)	95.0(3)	95.84(8)	97.64(10)
	101.41(14)	95.54(12)	96.80(8)		97.47(7)	94.64(10)
	100.41(14)	100.85(11)	97.01(8)		97.51(7)	104.99(10)
P−V−O	–	–	–	92.0(6)	–	–
				91.9(6)		
				171.7(5)		
Cl−V−O	–	–	–	98.7(6)	–	–
				100.3(6)		

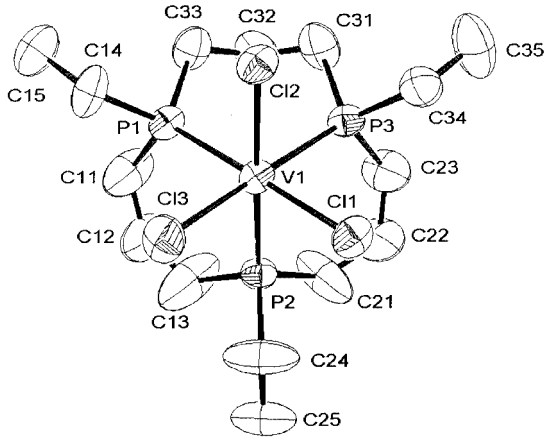

Figure 2. A view of the X-ray crystal structure and atom labelling scheme of ([12]aneP_3Et_3)VCl_3 (**2**); thermal ellipsoids are set at 50% probability

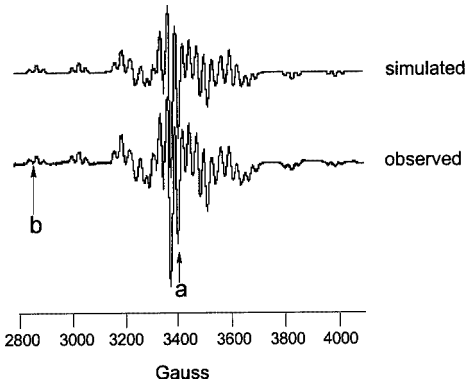

Figure 3. X-band EPR spectrum of **4** recorded in CD_2Cl_2/[D_8]toluene at 10 K

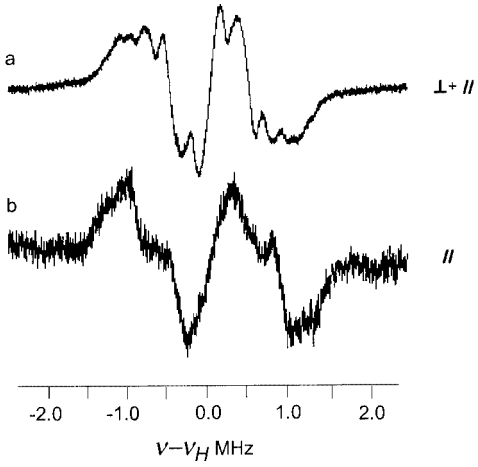

Figure 4. ^{1}H ENDOR spectrum of **4** measured at 10 K; spectrum (a) was recorded at the field position a, and spectrum (b) recorded at field position b, shown in Figure 3

those reported for $VCl_3(PMePh_2)_2$ [av. 2.527(18) Å][12] and $CpVCl_2(PMe_3)_2$ [av. 2.509(1) Å].[13] Although there is no significant difference in the V−P distances between **2** and complexes of monodentate phosphanes, the five-coordinate complexes are coordinatively unsaturated which presumably contributes to their much greater sensitivity to air and moisture. The preferential oxidation of the metal in **2** also suggests that the M−P bond is relatively inert. The majority of monodentate phosphane complexes are labile in solution (as shown by the ease in which they can be replaced with alternative σ-donor ligands), but the macrocyclic coordination effect, coupled with the coordinative saturation appears to make **2** more stable than (phosphane)vanadium complexes previously reported.

The EPR spectrum of **2** does not show a resonance due to the d^2 V^{III} centre. The absence of an observable EPR signal could also be due to relaxation effects which are not quenched even at low temperatures (10 K). Indeed, there are very few examples of EPR-active V^{III} species.[14] Exposure of solutions of **2** to air results in EPR and ENDOR spectra (Figures 3 and 4, respectively, corresponding spin Hamiltonian parameters are listed in Table 2) which can be assigned to the oxidation product of **2**, ([12]aneP_3Et_3)-$V(O)Cl_2$ (**4**). This EPR spectrum displays a characteristic superhyperfine pattern composed of a triplet of doublets, superimposed on the ^{51}V hyperfine lines (most clearly seen in the outer $m_I = \pm 7/2, \pm 5/2$ lines of the $A_{\|}$ component). As discussed in detail below, this superhyperfine pattern demonstrates the presence of two distinct phosphorus environments in **4**. Compound **4** can also be prepared and isolated in high yield by bubbling air through a dichloromethane solution of **2** containing a few drops of water. It is interesting to note that phosphane oxide is not formed by this procedure, again illustrating the relative robustness of these macrocyclic phosphane complexes. In addition to the molecular ion for **4** being observed in the mass spectrum, analytical data is consistent with the formulation and magnetic susceptibility confirms the presence of d^1 V^{IV}.

Table 2. Spin Hamiltonian parameters for **1**, **4**, and **7**

Complex	Nucleus	$g_{\|}$	$g_{\perp}$	$A_{\|}$ [G]	$A_{\perp}$ [G]
1	^{48}Ti × 1	1.9695	1.915	–	–
	^{31}P × 2	–	–	19.1	21
	^{31}P × 1	–	–	unres.	unres.
	^{35,37}Cl × 2	–	–	unres.	unres.
4	^{51}V × 1	1.978	1.984	153	50
	^{31}P × 2	–	–	24.5	27
	^{31}P × 1	–	–	6	6.1
	^{35,37}Cl × 2	–	–	0.1	3
7	^{92}Nb × 1	1.958	1.965	222	115
	^{31}P × 2	–	–	28	26

The deep blue, air-stable **4** has been structurally characterised and its crystal structure is shown in Figure 5, with selected bond lengths and angles shown in Table 1. This is the first reported complex to have an octahedral VO unit with phosphanes as ligands; the only other vanadyl species with ancillary phosphane ligands are $V(O)Cl_2(PPh_3)_2$

(which shows a trigonal-bipyramidal structure with the phosphane ligands in the axial positions[15]) and $V(O)Cl_2[P(SiMe_3)_3]_2$ [16] (which shows the same structural motif). Compound **4** can be described as a distorted octahedral complex with an unusually long V=O bond of 1.836(18) Å, and this is manifested in the infrared spectrum which shows a low-frequency V=O stretch at 936 cm^{-1}. The majority of vanadyl complexes are five-coordinate with a relatively short V=O bond (typically 1.55−1.68 Å) which is often considered to have some triple-bond character. For example $VOCl_2(NMe_3)_2$[17] has a V=O bond length of 1.590(2) Å, whilst in $V(O)Cl_2[P(SiMe_3)_3]_2$ the V=O bond length is 1.602 Å although the $V(O)Cl_2$ unit is disordered. The bond lengths in **4** show that there are two significantly different phosphorus environments (also indicated in the EPR spectrum); the V−P bond *trans* to the oxo group is longer than that to the equatorial phosphane moieties by 0.14(3) Å. Differences in V−P distances are substantially greater than those which may be attributed to Jahn−Teller distortions in **1** and **2**; this is presumably due to the high *trans* influence of the oxygen atom which commonly dictates the predominance of five-coordination in vanadyl chemistry. The relatively weak V=O bond can, in turn also be explained by a *trans* influence of the σ-donor phosphane ligand. This structure is a unique example of a V=O unit with a phosphane ligand in *trans* position and demonstrates the significance of the *trans* influence of a phosphane ligand on a bond that is commonly very strong. Recently, a structure of the first example of an imido ligand *trans* to a phosphane ligand has been reported[18] which also shows an unusually long V−P bond *trans* to the imido functionality [V−P = 2.642(2) Å]. The V−P bond length in $V(O)Cl_2(PPh_3)_2$ is 2.6217(11) Å, but this long bond length was ascribed to steric effects of the ligand. The collective shortening of the M−P bonds (in comparison to **2**) on oxidation to a more electropositive +4 state reflects the expected decrease in ionic radius upon oxidation. This feature may also indicate that the phosphane ligand is predominantly acting as a σ-donor, and back donation to the phosphane π-acceptor orbitals is of less importance.

The deep blue chromium complex ([12]aneP_3Et_3)$CrCl_3$ (**3**) is an intermediate in the liberation of free [12]aneP_3Et_3. The halogen oxidation of the tertiary phosphane macrocycle on a Cr^0 template differs to that of the molybdenum complex reported previously. Addition of chlorine to a solution of ([12]aneP_3Et_3)$Cr(CO)_3$ yields the chromium(III) complex ([12]aneP_3Et_3)$CrCl_3$, whereas under the same conditions, the molybdenum template yields seven-coordinate ([12]aneP_3Et_3)$Mo(CO)_2Cl_2$. In contrast, the secondary phosphane macrocycle complex ([12]aneP_3H_3)$Cr(CO)_3$ forms an octahedral dicarbonyl(halo)Cr^{II} halide complex.[4] Presumably the greater σ-donor ability of the tertiary phosphane macrocycle is more able to stabilise the higher oxidation state in **3**. Similar halogen oxidations of tricarbonylCr^0 complexes of linear triphosphanes have been reported to result in oxidation of the metal atom with loss of all carbonyl ligands but also with concomitant oxidation of the phosphane ligand.[18] Compound **3** can also be synthesised

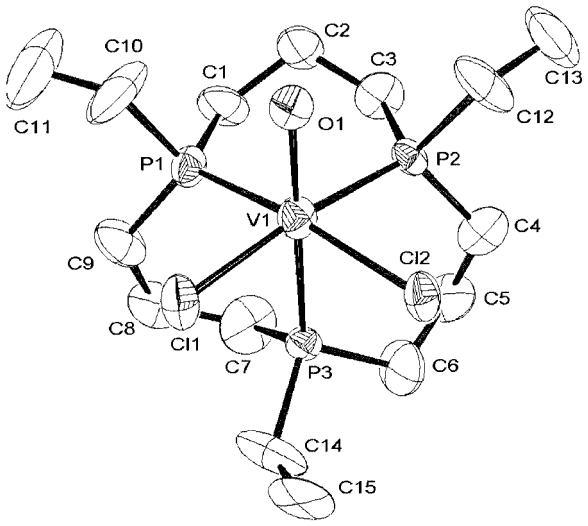

Figure 5. A view of the X-ray crystal structure and atom labelling scheme of ([12]aneP_3Et_3)$V(O)Cl_2$ (**4**); thermal ellipsoids are set at 50% probability

by the addition of [12]aneP_3Et_3 to a suspension of $CrCl_3(THF)_3$; crystals isolated by either method give rise to satisfactory analytical, mass spectrometric and magnetic susceptibility data.

The crystal structure of **3** is shown in Figure 6 and selected bond lengths and angles are shown in Table 1. The structure shows the macrocycle facially capping an octahedral metal atom, as expected. The average Cr−P bond length is 2.447(3) Å, whilst the average Cr−Cl bond length is 2.337(2) Å and variations in these distances are less than for **1** and **2** as might be expected for a d^3 metal centre. They are also similar to those reported for *fac*-[$CrCl_3$(tripod)] [Cr−P 2.456(2) Å (av.); Cr−Cl 2.306(2) Å (av.)] [tripod = $MeC(CH_2PMe_2)_3$][19] and *mer*-[$CrCl_3\{P(CH_2CH_2PPh_2)_3\}$] [av. Cr−P and Cr−Cl are 2.451(5) and 2.306(5) Å, respectively].[20] The average P−Cr−P angles in **3** [91.02(8)°] are close to the ideal values for an octahedron, unlike those in *fac*-[$CrCl_3$(tripod)] [83.47(7)°]. This difference indicates a greater flexibility in the macrocycle compared to the tripodal phosphane; restricted flexibility in tripodal ligands of this type has previously been commented on.[19]

Addition of [12]aneP_3R_3 to solutions of $TiCl_4$, $ZrCl_4$, and $HfCl_4$ resulted in coordination of the macrocycle (verified by ^{31}P NMR spectroscopy) although tractable materials could not be isolated. In the case of Zr and Hf, singlets with relatively small coordination chemical shifts were observed ($\Delta\delta$ = 15, 16 ppm, respectively) which showed only a small and linear temperature dependence and remained unchanged upon addition of excess ligand (indicating the absence of facile ligand exchange processes).

M^{III} Complexes of Pendant Ether Macrocycles

We have previously reported the synthesis of a series of ([12]aneP_3R_3)$M(CO)_3$ complexes (M = Mo, Cr; R = alkyl chain with a pendant donor function).[21] Oxidation of these chromium compounds with chlorine gives rise to ([12]aneP_3R_3)$CrCl_3$ (R = $H_3COC_3H_6$, $C_2H_5OC_2H_4$) in

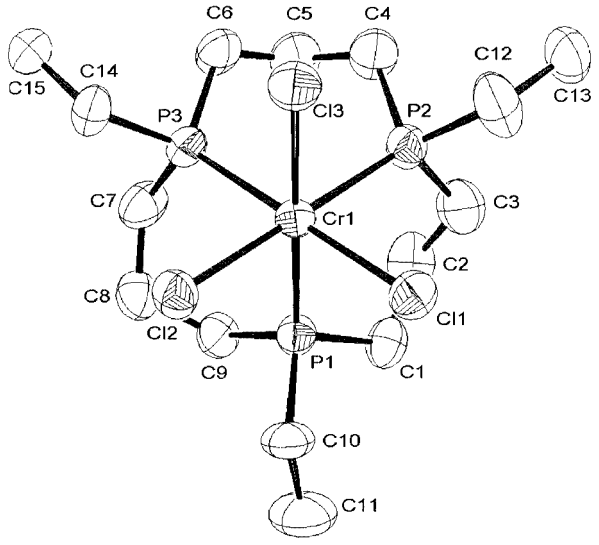

Figure 6. A view of the X-ray crystal structure and atom labelling scheme of one of the two independent molecules of ([12]aneP_3-Et_3)$CrCl_3$ (**3**); thermal ellipsoids are set at 50% probability; pyridine of crystallisation is omitted for clarity

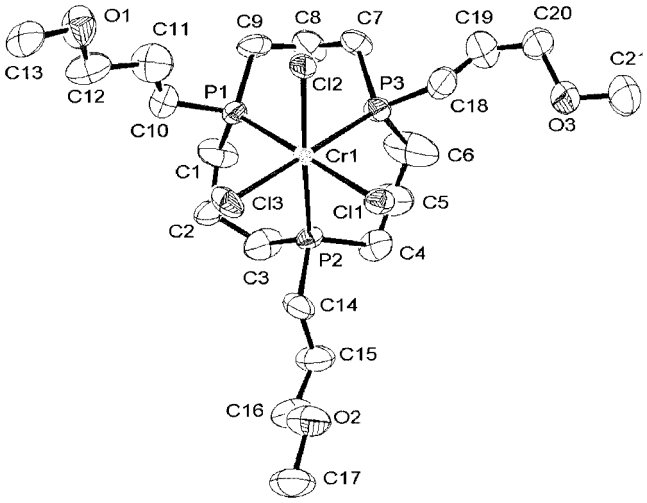

Figure 7. A view of the X-ray crystal structure and atom labelling scheme of {[12]aneP_3($C_3H_6OMe)_3$}$CrCl_3$ (**5**); thermal ellipsoids are set at 50% probability

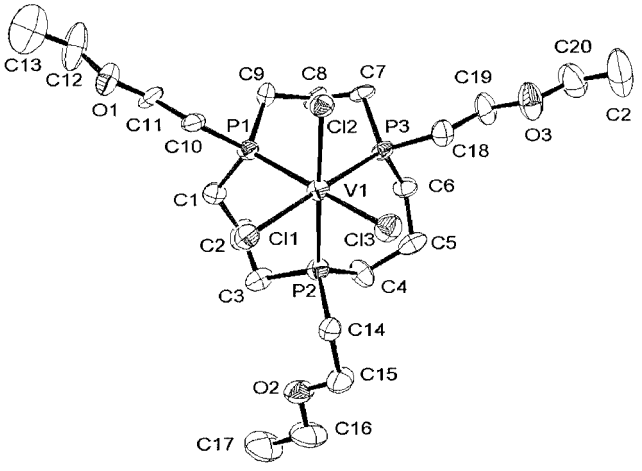

Figure 8. A view of the X-ray crystal structure and atom labelling scheme of {[12]aneP_3($C_2H_4OEt)_3$}VCl_3 (**6**); thermal ellipsoids are set at 50% probability

good yield. The crystal structure of [1,5,9-tris(3-methoxypropyl)-1,5,9-triphosphacyclododecane]chromium trichloride (**5**) is shown in Figure 7 and selected bond lengths and angles are given in Table 1. The structure (bond lengths and angles) is very similar to that of **3** which is not unexpected. Liberation of the macrocycle by digestion in strong base gives rise to the free macrocycle stereospecifically and in good yields. Reaction of the ethoxyethyl pendant donor macrocycle with $VCl_3(THF)_3$ gives rise to the green solid **6** that is similar to **2**. The crystal structure is shown in Figure 8 and selected bond lengths and angles are given in Table 1. The vanadium atom is facially capped by the macrocycle and the pendant donor atoms are well away from the metal centre, indicating that there is no bonding interaction in the solid state. The structural features are very similar to those of **2**. Attempts to force coordination of at least one pendant arm by halide abstraction have so far proved unsuccessful.

Nb^{III} and Nb^{IV} Complexes

The addition of 1 mol-equiv. of [12]aneP_3Et_3 to a frozen solution of $NbCl_3$(DME) or $NbCl_4(THF)_2$ in dichloromethane followed by warming gives rise to paramagnetic, air-sensitive solutions, manipulation of these caused decomposition (to oily materials) precluding the measurement of reliable characterisation data although EPR spectroscopy of these solutions confirmed the presence of d^2 Nb^{III} and d^1 Nb^{IV}, respectively. The Nb^{IV}-containing solution is reversibly thermochromic, being deep blue at ca. −30 °C and green at ambient temperature (20 °C). These colours are precedented for chloro(phosphane)niobium complexes and could be due to a temperature-dependent monomer/dimer equilibrium since $NbCl_4(dmpe)_2$ is blue[22] whilst $Nb_2Cl_8(PMe_3)_4$ is green.[23] The behaviour of the Nb^{III}-containing solutions is similar to those of **4** in that brief exposure to air gives rise to the loss of a resonance attributable to Nb^{III} and the appearance of a new EPR spectrum that can be attributed to the d^1 Nb^{IV} species **7** (vide infra). Attempts to grow crystals of these Nb compounds failed. Addition of [12]aneP_3Et_3 to $Nb(O)Cl_3(MeCN)_2$ gave rise to an intractable white precipitate which was not further characterised.

EPR and ENDOR Spectroscopy

The EPR spectra of **1** and **4** are shown in Figures 9 and 3, respectively. The spin Hamiltonian parameters for the Ti^{3+} and V^{4+} complexes were obtained by computer simulations (Figures 10 and 3, respectively) and the values used are presented in Table 2. Both systems are characterised by an axial g tensor of the form $g_{\|} > g_{\perp}$ which indicates that the metal ion experiences a tetragonally distorted octahedral environment. The high abundance of ^{51}V (I = 7/2) dominates the spectrum of **4**. The Ti^{3+} and V^{4+} ions have sim-

ilar d^1 electronic structures, and based on the similarities with the g values ($g_\perp = 1.915$ for Ti and 1.984 for V; $g_\parallel = 1.9695$ for Ti and 1.978 for V) both spectra are consistent with a similar crystal-field environment. Therefore, although the EPR spectra appear different, they imply very similar structures and confirm the tetragonal distortion in both **1** and **4**.

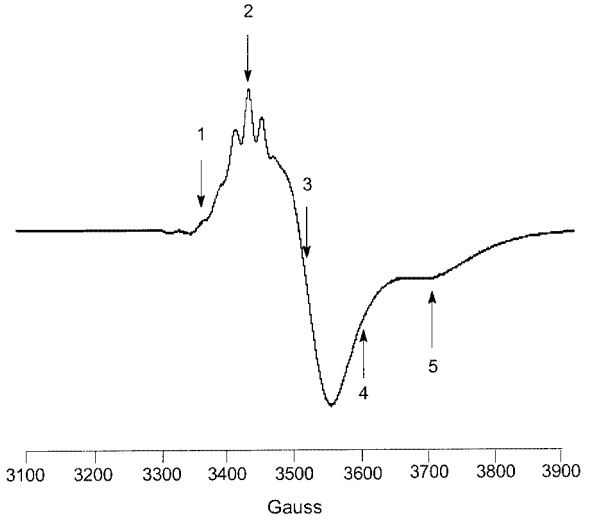

Figure 9. X-band EPR spectrum of **1** recorded in CD_2Cl_2/[D_8]toluene at 10 K

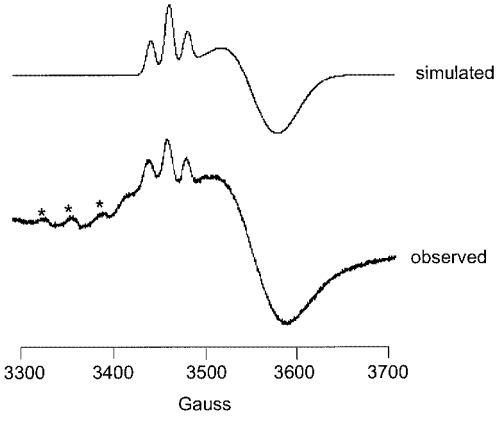

Figure 10. Computer simulation of the X-band EPR spectrum of **1**; the peaks marked * in the experimental spectrum are due to artefacts caused by the inhomogeneous nature of the sample or impurities in the complex

Due to the unpaired d^1 electron not being completely delocalised in the metal d orbitals, a weak superhyperfine interaction with the surrounding ligands can be observed; this is most clearly evident in the vanadyl spectrum (Figure 3). The outer ^{51}V hyperfine lines in Figure 3 clearly reveal a pattern composed of a triplet of doublets and this originates from the weak coupling between the d^1 electron and two equivalent phosphane moieties, and a smaller coupling to a third phosphorus nucleus. The two equivalent phosphane moities produce the triplet pattern while the third remote phosphorus nucleus creates the smaller doublet structure. Thus, the unpaired spin of the V^{4+} ion is delocalised onto the surrounding phosphorus nuclei, two of which are equivalent while the third is slightly more distant, a structural feature also observed in the crystalline state by X-ray crystallography. This EPR spectrum looks remarkably similar to that reported for $VOCl_2(PEt_3)_2$, except for the presence of the weak coupling to the third phosphorus atom, whilst the g and A values are almost identical.[13] The EPR spectrum of **4** was sufficiently resolved, that accurate values of the ^{31}P superhyperfine tensors could be obtained. The values of $^{P}A_\parallel = 24.5$ G, $^{P}A_\perp = 27$ G for the two equivalent phosphane moities and $^{P}A_\parallel = 6$ G, $^{P}A_\perp = 6.1$ G for the third inequivalent P nucleus, were tested by computer simulation (Figure 3). It was necessary to introduce a small contribution from two equivalent Cl nuclei in order to improve the quality of the fit. The satisfactory fit between the experimental and simulated spectra confirm the accuracy of the assignments (Table 2). These superhyperfine couplings were subsequently used to estimate the extent of electron delocalisation onto the P nuclei, and the results of this analysis are given in Table 3.

Based on the spin Hamiltonian parameters used in the simulations, we can suggest that the two chlorine nuclei are virtually equivalent and therefore approximately equidistant from the V centre. The s and p orbital spin density on the Cl nuclei is also found to be appreciably larger compared to the P nuclei (Table 3). This indicates, to a first approximation, that the V−Cl distances are slightly shorter compared to the V−P distances (as demonstrated from the crystal structures) and thereby produce a larger superhyperfine interaction. Although the spin densities are higher on ^{35}Cl, the A_O and B_O values for ^{31}P are larger than ^{35}Cl, so that a larger ^{31}P splitting is observed in the spectrum.

The EPR spectrum for the Ti^{3+} complex **1** was less well resolved and the lines significantly broader, so only the larger superhyperfine interaction with the phosphorus nuclei could be simulated with any degree of accuracy (seen as a triplet in the $g_\parallel$ region i.e. position 2 in Figure 9). The spin Hamiltonian parameters used in the simulations are given in Table 2. As for the vanadium case discussed above, two of the phosphane nuclei appear to be equivalent, while the third one was not resolved, presumably in part due to a relatively small superhyperfine coupling consistent with a tetragonally distorted structure. Again this feature is also confirmed by X-ray crystallography.

Electron nuclear double resonance (ENDOR) measurements were also made on **1** and **4** and the results are shown in Figures 11 and 4, respectively. Although the EPR spectrum of **4** was well resolved, it was not sufficiently intense to allow detailed ENDOR measurements to be made. The ^1H ENDOR spectra, measured at the field positions marked a and b in Figure 3, are shown in Figure 4. However, the titanium EPR spectrum (1), was sufficiently intense that a detailed magnetic angle selected ENDOR analysis could be performed as shown in Figure 11.

The ENDOR spectra of **1** and **4** (Figures 11 and 4, respectively) were recorded at positions corresponding to the z axis of the EPR framework (i.e. in **4** this is the V=O bond direction), while the perpendicular direction refers to the xy

Table 3. Calculated spin densities on surrounding nuclei for **1**, **4**, and **7**

Complex	Nucleus	A_O [G]	B_O [G]	a_{iso} [G]	B [G]	C_S^2	C_P^2	Spin density
1	$^{31}P \times 2$	3631	102	20.3	0.633	0.559%	0.62%	1.18%
4	$^{31}P \times 2$	3631	102	26.1	0.833	0.72%	0.816%	1.53%
	$^{31}P \times 1$	3631	102	6.0	0.05	0.16%	0.05%	0.21%
	$^{35,37}Cl \times 2$	1665	48.6	2.03	0.966	0.12%	1.98	2.1%
7	$^{31}P \times 2$	3631	102	26.6	1.66	0.72%	1.62%	2.024%

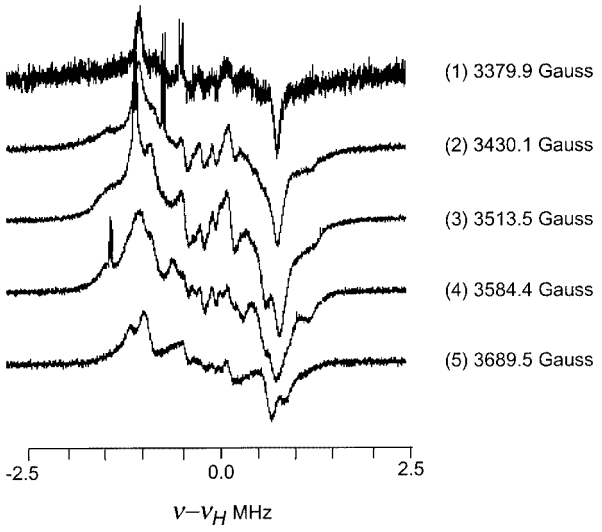

Figure 11. ^1H ENDOR spectra of **1** recorded at 10 K in CD_2Cl_2/[D_8]toluene; the spectra marked (1)−(5) were recorded using the static field positions of 3379.9 G (1), 3430.1 G (2), 3513.5 G (3), 3584.4 G (4), 3689.5 G (5), as shown in Figure 9

plane. In both ENDOR spectra, strong couplings (of approx. 1 MHz) and smaller, more poorly resolved inner couplings of less than 0.5 MHz are observed. It is interesting to note that the ENDOR spectra are slightly different for both samples. In the vanadium case a strong peak is clearly visible with a coupling of about 1 MHz but a distinctive shoulder at about 1.3 MHz, can also be seen (Figure 4, b). Based on the structures of the two complexes, two dominant groups of protons are expected, corresponding to the protons of the cyclododecane ring and those of the ethyl groups. The former set of protons are closer to the V nucleus and would therefore be expected to produce the larger ENDOR coupling compared to the more remote ethyl groups. It may therefore be suggested that the strong coupling of ca. 1 MHz corresponds to the cyclododecane protons while the inner and less well-resolved couplings of ca. 0.5 MHz are due to the ethyl groups. The differences between the titanium and vanadium ^1H ENDOR spectra are very small, however, and the implied inequivalency of the CH_2 protons cannot be confirmed by alternative spectroscopic methods (e.g. by IR spectroscopy). The ENDOR spectrum measured at position 2 in Figure 9 refers to a position in which the magnetic field is pointing "off-axis", between the z direction and the xy plane. In this case, the ENDOR spectrum becomes much more complicated as several molecular orientations are selected simultaneously, and very careful simulation is needed in order to assign each coupling to a specific CH_2 group.

The EPR spectrum of **7** (Figure 12) is strikingly similar to that of ([12]aneP_3Et_3)V(O)Cl_2 (**4**). The shape of the spectrum and the spin Hamiltonian parameters reveal that the symmetry and electronic configuration of the metal atoms must be analogous in both cases, i.e. it indicates that the overall structural features are very similar to those of ([12]aneP_3Et_3)V(O)Cl_2. The presence of two equivalent phosphane moieties is again demonstrated by the characteristic triplet pattern discussed above for **4** (Table 2), but unfortunately the slightly more distant phosphane group cannot be simulated with any degree of accuracy due to the larger EPR linewidths. The g values for the vanadyl and niobyl complexes (Table 2) are both axial in nature, and the average g values for the niobyl complex are slightly lower, which is expected considering the larger spin-orbit coupling constant for Nb compared to V. The similar shifts in g values ($\Delta g = 0.006$ for V and $\Delta g = 0.007$ for Nb), however, indicates similar symmetries for both ions. These values also suggest that the unpaired electron is either in the d_{xy} or $d_{x^2-y^2}$ orbital.

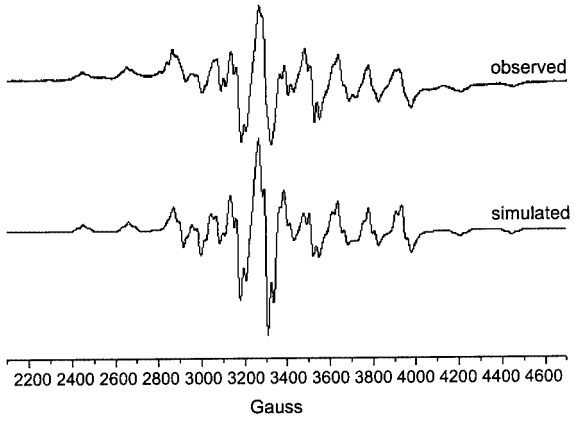

Figure 12. X-band EPR spectrum of **7** recorded in CD_2Cl_2/[D_8]toluene at 10 K

The superhyperfine interaction of the Nb nucleus with the ^{31}P nuclei can be analysed in order to extract some spatial information on the M−P (M = V, Nb) distances. This can be done by breaking the hyperfine tensor into an isotropic (a_{iso}) and anisotropic (B) component. The anisotropy is very small compared to the isotropic coupling and it can be accounted for on the basis of dipolar interactions

through space between the unpaired electron and the phosphorus nuclei. This assumption is reasonable as little backbonding is expected with the d^1 metal ions.

A simple point dipole model can be used to calculate the contribution to the anisotropic coupling from dipolar sources. With this approximation, the distance between the metal centre (V and Nb) and the interacting phosphane nucleus can be determined. Using this model and a calculated anisotropic term of 1.32 G (3.6174 MHz) and 1.66 G (4.5956 MHz) for the vanadyl and niobyl compounds, respectively, the estimated distances are calculated as V−P = 2.388 Å and Nb−P = 2.587 Å. The shortest experimentally determined V−P bond length is 2.408(10) Å (from the crystal structure of **4**), which is in good agreement with the calculated bond length based on the EPR data. The resolution of the third inequivalent P nucleus was not sufficiently good to allow an accurate estimation of the V−P bond length for this more remote phosphane group. On the basis of the EPR spectrum, its satisfactory simulation and the metrical parameters obtained, we tentatively assign the formula ([12]aneP_3Et_3)Nb(O)Cl_2 to **7**. Although incompletely characterised, **7** is only the second example of an oxo(phosphane)niobium(IV) complex, the first being Nb(O)$Cl_2(PEt_3)_2$.[24] Crystals of **7** were not obtained, and there are only three crystallographically characterised examples of phosphane complexes containing Nb=O, these being compounds of d^0 Nb^V. Nevertheless, the M−P bond length is 2.64(3) Å in Nb(O)$Cl_3(PMe_3)_3$,[25] and 2.708 Å in [Et_3PH][Nb(O)$Cl_4(PEt_3)$],[15] which compare well with the calculated bond length in **7** from the EPR data.

Conclusion

We have demonstrated that the ligand [12]aneP_3Et_3 forms relatively robust six-coordinate complexes with early transition metals. We have reported the structural characterisation of a range of complexes and shown that the EPR and ENDOR spectra of these compounds are highly informative and not only confirm the structural features determined by crystallography but also give substantial insight into the nature of paramagnetic niobium species for which other reproducible data could not be obtained. The first complex with a phosphane ligand *trans* to an oxo function in V^{IV} has been reported and the ligand effect on the V=O bond has been investigated. Preliminary results indicate that the complexes described are reactive towards alkylating agents, other metathetical reagents and are active in alkene polymerisation catalysis; details of these studies will be published in due course. The results also imply that the macrocycle coordination effect helps stabilise these phosphane complexes in relatively regular six-coordinate environments, whereas for higher coordination numbers, this effect is not as substantial as expected and tractable seven-coordinate d^0 M^{IV} complexes could not be obtained. This might result from the flexibility of the 12-membered macrocycle as well as stereochemically nonrigid (and intrinsically more reactive) seven-coordination. Consequently, smaller ring macrocycles might be expected to form more stable systems and the study of 9-,[26,27] 10-,[28] and 11-membered triphosphorus macrocycles is in progress.

Experimental Section

All reactions were carried out under nitrogen (purified by passing through a CrO column) using standard Schlenk line techniques or in a Vacuum Atmospheres drybox. Solvents were dried with standard drying agents and distilled immediately before use. Petroleum ether had a boiling range of 40−60 °C. The Zr, Hf, and Nb halides were sublimed before use. All other chemicals were dried over molecular sieves (liquids) or used as received (Aldrich). The compounds $TiCl_4(THF)_2$, $ZrCl_4(THF)_2$, $HfCl_4(THF)_2$, $TiCl_3(THF)_3$, $VCl_3(THF)_3$,[29] $NbCl_4(THF)_2$, $NbCl_3$(DME),[30] Nb(O)Cl_3(MeCN)$_2$,[26] [12]aneP_3Et_3,[4] [12]ane$P_3Et_3Cr(CO)_3$, and ([12]aneP_3R_3)$Cr(CO)_3$ (R = $CH_3OC_3H_6$. $C_2H_5OC_2H_4$)[22] were prepared by literature methods. ^1H and ^{13}C NMR spectra were recorded with a Bruker DPX400 spectrometer operating at 400.13 MHz and 100 MHz, respectively. ^{31}P NMR spectra were acquired using a JEOL FX90Q at 36.2 MHz and referenced to 85% H_3PO_4. Magnetic moments were determined by the Evans method[31] or by the Gouy method with a Johnson Matthey magnetic susceptibility balance; an experimental diamagnetic correction was measured for the free phosphane macrocycles and applied. Mass spectra (EI) were recorded with a VG Platform II Fisons mass spectrometer. Infrared spectra were recorded with a Nicolet 510 FT-IR spectrometer as a nujol mull between CsI plates. The EPR/ENDOR spectra were recorded with a CW X-band Bruker ESP 300E series spectrometer equipped with an ESP360 DICE ENDOR unit, operating at 12.5 kHz field modulation in a Bruker EN 801 cavity. All spectra (EPR and ENDOR) were recorded at 10 K using an Oxford instruments ESR 900 continuous flow He Cryostat; the ENDOR spectra were obtained at 4 mW microwave power, 8 dB RF power from a ENI A-300 RF amplifier again at 12.5 kHz modulation frequency. Computer simulations were carried out using Bruker's Simfonia program.

([12]aneP_3Et_3)$TiCl_3$ (1): To a purple solution of $TiCl_3(THF)_3$ (0.20 g, 0.51 mmol) in dichloromethane (20 mL) was added a solution of [12]aneP_3Et_3 (0.15 g, 0.51 mmol) in dichloromethane (10 mL). The solution immediately turned blue and a fine grey precipitate was observed. This was stirred for 2 h, filtered and the solvent removed in vacuo. The blue residue was washed with petroleum ether (3 × 10 mL) and recrystallised from dichloromethane/petroleum ether at −30 °C to give (0.21 g, 90%) of **1**. Crystals suitable for X-ray analysis were obtained by vapour diffusion of petroleum ether into a dichloromethane solution. $C_{15}H_{33}Cl_3P_3Ti$ (460.6): calcd. C 39.09, H 7.17; found: C 38.7, H 7.0. IR (nujol): $\tilde{\nu}_{max}$ = 1377 (sh), 1072 (br), 802 (br), 376 (br), 257 (w), 210 (w) cm^{-1}. MS: m/z = 460.57 [M^+]. μ_{eff} = 1.82 BM.

([12]aneP_3Et_3)VCl_3 (2): To a red solution of $VCl_3(THF)_3$ (0.20 g, 0.50 mmol) in dichloromethane (20 mL) was added a solution of [12]aneP_3Et_3 (0.15 g, 0.50 mmol) in dichloromethane (10 mL). The solution immediately turned green and a light green precipitate was observed. This was stirred for 2 h, filtered, and the solvent removed in vacuo. The green residue was washed with petroleum ether (3 × 10 mL) and recrystallised from dichloromethane/petroleum ether at −30 °C to give **2** (0.22 g, 94%). Crystals suitable for X-ray analysis were obtained by vapour diffusion of petroleum ether into a dichloromethane solution. $C_{15}H_{33}Cl_3P_3V$ (463.6): calcd. C 38.67, H 7.52; found: C 38.4, H 7.5. IR (nujol): $\tilde{\nu}_{max}$ = 1269 (sh), 1121

Table 4. Crystallographic data for **1**−**6**; * pent = pentane of solvation, py = pyridine of solvation

	1	**2**·1/2(pent)*	**3**·1/2(py)*	**4**	**5**	**6**
Empirical formula	$C_{15}H_{33}Cl_3P_3Ti$	$C_{17.5}H_{39}Cl_3P_3V$	$C_{17.5}H_{35.5}Cl_3CrN_{0.5}P_3$	$C_{15}H_{33}Cl_2P_3VO$	$C_{21}H_{43}Cl_3CrO_3P_3$	$C_{24}H_{52}Cl_3O_3P_3V$
Formula mass	460.57	499.69	504.22	444.16	594.81	638.86
Temp. [K]	150(2)	150(2)	293(2)	150(2)	150(2)	293(2)
Crystal system	triclinic	monoclinic	monoclinic	triclinic	monoclinic	monoclinic
Space group	$P\bar{1}$	$P2_1/n$	$P2_1/n$	$P\bar{1}$	$P2_1/a$	$P2_1/n$
a [Å]	7.774(6)	9.191(4)	14.579(3)	7.577(7)	17.743(4)	8.553(1)
b [Å]	9.381(5)	19.371(3)	12.268(3)	8.966(6)	8.5355(4)	29.386(2)
c [Å]	15.228(7)	14.048(1)	27.424(4)	15.569(15)	18.910(2)	12.683(4)
α [°]	88.320(11)	90	90	87.19(5)	90	90
β [°]	85.020(14)	102.737(5)	103.859(13)	83.70(4)	102.54(2)	92.56(1)
γ [°]	80.200(19)	90	90	80.80(6)	90	90
V [Å^3]	1090.1(11)	2439.5(11)	4762.2(16)	1037.2(15)	2795.5(6)	3184.5(11)
Z	2	4	8	2	4	4
$D_{calcd.}$ [g/cm^3]	1.403	1.361	1.407	1.422	1.413	1.332
μ	0.976	0.933	1.021	0.966	0.889	0.737
Unique reflections	2848	2186	9670	1087	4217	4564
Observed reflections [$I > 2\sigma(I)$]	1429	1449	4039	485		1181
R (obsd. data)	0.1042	0.0659	0.0694	0.1012		0.0493
R_w (wR^2) (all data)	0.2598	0.1850	0.1864	0.3061		0.1094

(sh), 1072 (sh), 798 (sh), 739 (sh), 491 (br), 385 (w), 341 (br), 278 (w), 239 (w), 217 (w) cm^{-1}. NMR (CD_2Cl_2): δ_H = 2.02 (s), −2.82 (s), −3.81 (s), −4.31 (br), −5.05 (s) ppm. MS: m/z = 463.61 [M$^+$], 444.15 [[12]ane$P_3Et_3V(O)Cl_2$]. μ_{eff} = 2.48 BM.

([12]aneP_3Et_3)$CrCl_3$·0.5py (3). Method 1: Cl_2 was bubbled through a solution of ([12]aneP_3Et_3)$Cr(CO)_3$ (2.0 g, 4.5 mmol) in dichloromethane (50 mL) for 5 min. This was stirred for 4 h and the solvent removed in vacuo to yield a violet microcrystalline solid that was recrystallised from dichloromethane to give blue **3** (1.88 g, 90%). Crystals suitable for X-ray analysis were obtained by vapour diffusion of toluene into a pyridine solution of **3**. $C_{17.5}H_{35.5}Cl_3CrN_{0.5}P_3$ (504.3): calcd. C 41.67; H,7.04; found: C 41.7, H 7.2. IR (nujol): $\tilde{\nu}_{max}$ = 310 (br), 240 (w) cm^{-1}. μ_{eff} = 3.66 BM. **Method 2:** To a purple suspension of $CrCl_3(THF)_3$ (0.10 g, 0.25 mmol) in dichloromethane (20 mL) was added a solution of [12]aneP_3Et_3 (0.08 g, 0.51 mmol) in dichloromethane (10 mL). The solution immediately turned blue. This was stirred for 4 h, filtered and the solvent removed in vacuo. The blue residue was washed with petroleum ether (3 × 10 mL) and recrystallised from dichloromethane/petroleum ether to give **3** (0.07 g, 65%).

([12]aneP_3Et_3)$V(O)Cl_2$ (4): To a dichloromethane solution of **2** (0.10 g, 0.22 mmol) was added distilled water (5 mL) and this was stirred for 2 h whilst air was slowly bubbled through the solution. The solution was dried with CaH_2, filtered, concentrated to 5 mL and cooled to −30 °C. The resulting blue crystals were isolated and dried in vacuo to yield **7** (0.08 g, 86%). Crystals suitable for X-ray analysis were obtained by slow cooling of a saturated petroleum ether solution. $C_{15}H_{33}Cl_2OP_3V$ (444.2): calcd. C 37.56, H 6.93; found: C 37.0, H 6.2. IR (nujol): $\tilde{\nu}_{max}$ = 936(V=O) cm^{-1}. MS: m/z = 444.15 [M$^+$]. μ_{eff} = 1.65 BM.

([12]aneP_3R_3)$CrCl_3$ (5): Cl_2 was bubbled through a solution of ([12]aneP_3R_3)$Cr(CO)_3$ (R = $CH_2CH_2CH_2OCH_3$) (2.0 g, 3.5 mmol) in dichloromethane (50 mL) for 5 min. This was stirred for 4 h and the solvent removed in vacuo to yield a deep blue microcrystalline solid that was recrystallised from dichloromethane/petroleum ether to give **9** (1.79 g, 86%). $C_{24}H_{52}Cl_3CrO_3P_3$ (639.9): calcd. C 42.25, H 7.28; found: C 42.7, H 7.3. IR (nujol): $\tilde{\nu}_{max}$ = 312 (br), 220 (w) cm^{-1}. μ_{eff} = 3.59 BM.

([12]aneP_3R_3)VCl_3 (6): To a red solution of $VCl_3(THF)_3$ (0.20 g, 0.50 mmol) in dichloromethane (20 mL) was added a solution of [12]aneP_3R_3 (R = $CH_2CH_2OCH_2CH_3$) (0.22 g, 0.50 mmol) in dichloromethane (10 mL). The solution immediately turned green and a light green precipitate was observed. This was stirred for 2 h, filtered and the solvent removed in vacuo. The green powder was recrystallised from dichloromethane/petroleum ether at −30 °C to give **6** (0.25 g, 84%). Crystals suitable for X-ray analysis were obtained by vapour diffusion of petroleum ether into a dichloromethane solution. $C_{24}H_{52}Cl_3O_3P_3V$ (638.9): calcd. C 45.17, H 8.20; found: C 45.0, H 8.3. IR (nujol): $\tilde{\nu}_{max}$ = 277 (w), 242 (w), 214 (w) cm^{-1}. MS: m/z = 638.86 [M$^+$]. μ_{eff} = 2.51 BM.

([12]aneP_3Et_3)$Nb(O)Cl_2$ (7): To $NbCl_3$(DME) (0.10 g, 0.34 mmol), frozen in liquid nitrogen, was added a solution of 12[ane]P_3Et_3 (0.10 g, 0.34 mmol) in dichloromethane (20 mL) and the mixture allowed to warm to room temperature with gentle agitation. The resulting dark green solution was filtered through Celite. The resulting green solution (in a Schlenk flask) was briefly exposed to air (by removing and replacing the stopper) and the inert gas was immediately reinstated. This solution was transferred to an EPR tube and the spectrum run immediately. Attempts to prepare samples of **7** by addition of water and air (as for compound **4**) resulted in complete decomposition and dissociation of the macrocyclic ligand (by NMR).

X-ray Crystallography: The crystal data for compounds **1**−**6** are given in Table 4. For compounds **1**, **2**, **4**−**6**, intensity data were collected with a FAST TV area detector diffractometer at the window of a rotating anode generator, with a molybdenum target [λ(Mo-K_α) = 0.71069 Å] and driven by MADNES[32] software (for **2** and **4**). The structures were solved by heavy atom methods (SHELXS)[33] and refined by full-matrix least squares based on F_o^2 (SHELXL 93).[34] All non-hydrogen atoms are anisotropic with H-atoms included in calculated positions (riding model) and isotropic displacement parameters which were refined. Diagrams were

drawn with SNOOPI[35] or ORTEP for Windows.[36] Sources of scattering factors are given in ref.[33] For compound **1**, the structure was finally refined to $R = 0.1042$. The quality of the crystal was very poor and it was also a very weak diffractor. One of the three $CH_2CH_2CH_2$ chains was disordered and two of its carbon atoms were refined with partial occupancies. All non-hydrogen atoms were refined anisotropically with ISOR = 0.02 restraints being applied to several carbon atoms. The C−C bond lengths were constrained at 1.52(2) Å. The H atoms of the disordered $CH_2CH_2CH_2$ chain were ignored; all others were included in calculated positions (riding model). For compound **4**, the data were collected with a small and weakly diffracting crystal and refined to a final $R = 0.1012$. The pendant ethyl carbon atoms showed high thermal motion (as is not unexpected for compounds of this nature) and correspondingly large ellipsoids although no positional disorder for these atoms could be satisfactorily modelled. Although the R factors for these two compounds are relatively high, the quality of the structures is adequate to allow comparisons of metal−ligand bond lengths and angles. Data for **3** were obtained with an Enraf−Nonius CAD4 diffractometer. The structure was solved by direct methods and refined on F^2 by full-matrix least squares (SHELX97)[37] using all unique data. Empirical absorption corrections were carried out by the DIFABS method.[38] CCDC-171468 (**1**), -143583 (**2**), -171469 (**3**), -143586 (**4**), -171471 (**5**), and -171470 (**6**) contain the supplementary crystallographic data for this paper. These data can be obtained free of charge at www.ccdc.cam.ac.uk/conts/retrieving.html or from the Cambridge Crystallographic Data Centre, 12, Union Road, Cambridge CB2 1EZ, UK [Fax: (internat.) + 44-1223/336-033; E-mail: deposit@ccdc.cam.ac.uk].

Acknowledgments

We thank Drs. D. Hibbs, S. J. Coles, K. M. A. Malik, T. Albers, and Mr. R. Haigh for assistance with the structural determinations. We also thank the EPSRC for funding (R. J. B and P. C. D), the EPSRC National ENDOR service and the Association of Commonwealth Universities and the University of Sri Jayewardenepura of Sri Lanka for a studentship (S. S. L.).

[1] M. D. Fryzuk, T. S. Haddad, D. J. Berg, *Coord. Chem. Revs.* **1990**, *99*, 137−212.
[2] L. Messerle, *Chem. Revs.* **1988**, *88*, 1229−1254.
[3] *Comprehensive Organometallic Chemistry* (Eds.: E. W. Abel, F. G. A Stone, G. Wilkinson), Pergammon Press, Oxford, UK, **1982**.
[4] P. G. Edwards, J. S. Fleming, S. S. Liyanage, *Inorg. Chem.* **1996**, *35*, 4563−4568.
[5] C. D. Schmulbach, C. H. Kolich, C. C. Hinckley, *Inorg. Chem.* **1972**, *11*, 2841−2843.
[6] N. Koide, K. Iimura, *Polym. Prepr., Am. Chem. Soc., Div. Polym. Chem.* **1979**, *20*, 558−561; *Chem. Abstr.* **1980**, *93*, 196819m.
[7] T. G. Gardner, G. S. Girolami, *Organometallics* **1987**, *6*, 2251−2256.
[8] T. G. Gardner, G. S. Girolami, *Angew. Chem. Int. Ed. Engl.* **1988**, *27*, 1693−1695.
[9] J. A. Jensen, S. R. Wilson, G. S. Girolomi, *J. Am. Chem. Soc.* **1988**, *110*, 4977−4982.
[10] P. Berno, S. Gambarotta, D. Richeson, in: *Comprehensive Organometallic Chemistry*, vol. II (Eds.: E. W. Abel, F. G. A. Stone, G. Wilkinson), Elsevier Science Ltd., Oxford, UK, **1995**.
[11] A. A. Danopoulos, P. G. Edwards, *Polyhedron* **1989**, *8*, 1339−1344.
[12] R. L. Bansemer, J. C. Huffman, K. G. Caulton, *Inorg. Chem.* **1985**, *24*, 3003−3006.
[13] J. Nieman, J. H. Teuben, J. C. Huffman, K. G. Caulton, *J. Organomet. Chem.* **1983**, *255*, 193−204.
[14] J. Lambe, C. Kikuchi, *Phys. Rev.* **1960**, *118*, 71−77.
[15] F. A. Cotton, J. Lu, *Inorg. Chem.* **1995**, *34*, 2639−2644.
[16] W. Plass, W. Schwarz, *Z. Anorg. Allg. Chem.* **1996**, *622*, 1756−1764.
[17] J. E. Drake, J. Vekris, J. S. Wood, *J. Chem. Soc. A* **1968**, 1000−1005.
[18] F. Montilla, A. Monge, E. Gutierrez-Puebla, A. Pastor, D. del Rio, N. C. Hernandez, J. F. Sanz, A. Galindo, *Inorg. Chem.* **1999**, *38*, 4462−4466.
[19] A. M. Arif, J. G. Heffner, R. A. Jones, B. R. Whittlesey, *Inorg. Chem.* **1986**, *25*, 1080−1084.
[20] L. R. Gray, A. L. Hale, W. Levason, F. P. McCullough, M. Webster, *J. Chem. Soc., Dalton Trans.* **1984**, 47−53.
[21] P. G. Edwards, J. S. Fleming, S. S. Liyanage, *J. Chem. Soc., Dalton Trans.* **1997**, 193−197.
[22] L. E. Manzer, *Inorg. Chem.* **1977**, *16*, 525−528.
[23] F. A. Cotton, M. P. Diebold, W. J. Roth, J. Wieslaw, *Polyhedron* **1985**, *4*, 1103−1108.
[24] G. Labauze, E. Samuel, J. Livage, *Inorg. Chem.* **1980**, *19*, 1384−1386.
[25] V. C. Gibson, T. P. Kee, R. M. Sorrell, M. McPartlin, *Polyhedron* **1988**, *7*, 2221−2223.
[26] P. G. Edwards, P. D. Newman, K. M. A. Malik, *Angew. Chem. Int. Ed.* **2000**, *39*, 2922−2924.
[27] P. G. Edwards, R. Haigh, M. L. Whatton, *Organometallics* **2000**, *14*, 2652−2654.
[28] P. G. Edwards, P. D. Newman, D. Hibbs, *Angew. Chem. Int. Ed.* **2000**, *39*, 2722−2724.
[29] L. E. Manzer, *Inorg. Synth.* **1982**, *21*, 135−139.
[30] S. F. Pedersen, J. B. Hartung, E. J. Roscamp, P. S. Dragovich, *Inorg. Synth.* **1992**, *29*, 119.
[31] D. F. Evans, *J. Chem. Soc.* **1959**, 2003−2005.
[32] J. W. Pflugrath, A. Messerschmidt, *MADNES*, version 11, Delft Instruments, Delft, **1989**.
[33] G. M. Sheldrick, *Acta Crystallogr., Sect. A* **1990**, *46*, 467−473.
[34] G. M. Sheldrick, University of Göttingen, **1993**.
[35] K. Davies, K. C. Prout, University of Oxford, **1993**.
[36] L. J. Farrugia, *ORTEP-3 for Windows*, University of Glasgow, **2001**.
[37] G. M. Sheldrick, *SHELX-97*, University of Göttingen, **1997**.
[38] N. P. C. Walker, D. Stuart, *Acta Crystallogr., Sect. A* **1983**, *39*, 158−166.

Received February 14, 2002
[I02077]

The Coordination Chemistry of 3,3′-Diamino-2,2′-bipyridine and Its Dication: Exploring the Role of the Amino Groups by X-ray Crystallography

Craig R. Rice,[b] Stuart Onions,[a] Natalia Vidal,[a] John D. Wallis,*[a]
Maria-Cristina Senna,[c] Melanie Pilkington,*[c] and Helen Stoeckli-Evans[d]

Keywords: N ligands / Hydrogen bonds / Ambidentate ligands / X-ray Crystallography / Cations

The synthesis and structural chemistry of a series of new divalent transition metal complexes of the bis-bidentate ligand 3,3′-diamino-2,2′-bipyridine (**L1**) and its dication $\mathbf{L1H_2}$ are described. Ligand **L1** reacts with salts of divalent transition metals to afford the (1:1) metal-ligand complexes (**2a**–**2d**) as well as the tris complexes (**3a**–**3f**). All complexes were fully characterised by spectroscopic methods and the following compounds $[Cu(\mathbf{L1})Cl_2]_2$ (**2a**), $[Cu(\mathbf{L1})(OAc)_2]$ (**2b**), $[Zn(\mathbf{L1})_3][OTf]_2$ (**3a**), and $[Zn(\mathbf{L1})_3][ZnCl_4]$ (**3e** and **3f**) were structurally characterised. Results from single crystal X-ray diffraction measurements indicate that formation of an intramolecular hydrogen bond between the two amino groups allows the ligand to coordinate divalent metal ions through their diimine binding sites. Furthermore, the structure of compound **2a** reveals that it crystallises as a dimer in which each copper ion is bound to two pyridine nitrogen atoms and two chloride ions in a distorted square planar arrangement, with a long axial contact from a neighbouring amino group completing the approximately square-pyramidal geometry at Cu^{II}. Complexation of this ligand in acidic conditions afforded the compound $[Cu(\mathbf{L1H_2})Cl_4]$ (**4**), as well as the two salts $[\mathbf{L1H_2}][CuCl_4]$ (**5a**) and $[\mathbf{L1H_2}][ZnCl_4]$ (**5b**). All three compounds have been structurally characterised and results indicate that the dication ($\mathbf{L1H_2}$) displays a different coordination preference for the chelation of metal ions. In all three cases, both of the heterocyclic N atoms of the ligand are protonated, thus preventing chelation to the metal ion, although for compound **4** crystallographic studies reveal that the two amino functionalities coordinate the copper(II) ion.

(© Wiley-VCH Verlag GmbH, 69451 Weinheim, Germany, 2002)

Introduction

The construction of multicomponent molecular systems represents an important first step in the development of novel molecular and supramolecular systems for catalysis, light-to-energy conversion, and molecule-based devices. For systems in which the components are transition metal ions, the emphasis lies in the design of the bridging ligands as well as on the choice of the metal ions. Consequently, the careful choice of bridging ligands, as suitable linkers for transition metal ions in a wide variety of oxidation states, is currently viewed as a critical element in successful design. One of the simplest but most widely used organic linkers is the bidentate ligand 2,2′-bipyridine. In recent years, this ligand has been incorporated into a huge diversity of supramolecular inorganic architectures including helices, ladders, grids and chains.[1] Furthermore, chemical modification of the 2,2′-bipyridine ligand by the introduction of additional functionality at the 4-, 5- and 6-positions is well-known, and the coordination chemistry of these compounds has been actively explored. In contrast, however, much fewer 3,3′-disubstituted bipyridines are available and the coordination chemistry of only a small number of such compounds has been studied. This is primarily due to the expectation that van der Waals repulsions between large substituents in the 3,3′-positions could prevent the pyridine rings from adopting a near *cis*-coplanar conformation, rendering them unfavourable ligands for chelation. Nevertheless, small substituents in the 3 and 3′ positions such as methyl groups,[2] carboxylic acids,[3,4] and methyl esters[5] have all been reported not to inhibit the binding of a metal ion to the diimine binding site, despite the fact that the pyridine rings in these systems are indeed displaced from co-planarity by 30−35°. Furthermore, in the early 1980's Rebek et al. were able to successfully exploit the 3,3′-substitution positions for the preparation of a novel crown ether derivative which bound transition metal ions at the diimine site, or alkali metal ions at the crown ether.[6]

Dinuclear complexes in which the metal fragments are joined by an appropriate bridging organic ligand have been of particular interest with a view to the preparation of vari-

[a] Department of Chemistry and Physics, The Nottingham Trent University,
Clifton Lane, Nottingham, NG11 8NS, England
E-mail: john.wallis@ntu.ac.uk
[b] University of Huddersfield, Department of Chemical & Biological Sciences,
Huddersfield, HD1 3DH, W. Yorkshire, England
[c] Department of Chemistry and Biochemistry, University of Berne,
Freistrasse 3, 3012, Berne, Switzerland
E-mail: melanie.pilkington@iac.unibe.ch
[d] Institute de Chemie, Université de Neuchâtel,
Avenue de Bellevaux 51, 2000, Neuchâtel, Switzerland
E-mail: helen.stoeckli-evans@ich.unine.ch

ous types of organometallic frameworks. Indeed, the dual coordinating ability of the oxalate ion (ox = $C_2O_4^{2-}$) has made it a particularly versatile bridging species for the controlled self-assembly of one-, two- and three-dimensional inorganic architectures.[7] Along these lines, with a view to prepare novel coordination polymers, we have recently turned our attention to study the coordination behaviour of the potentially ambidentate ligand 3,3′-diamino-2,2′-bipyridine (**L1**). This ligand has two possible modes for binding namely, symmetric and asymmetric (Figure 1).

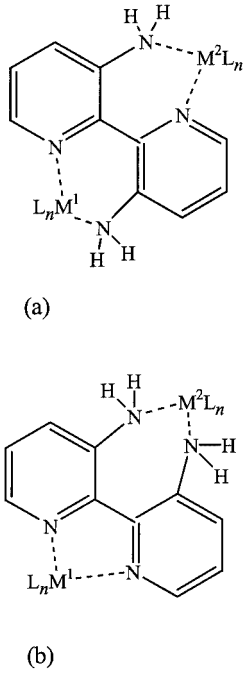

Figure 1. Potential symmetric (a) and asymmetric (b) binding modes of ligand **L1**

Since only one coordination compound incorporating ligand **L1** has been previously characterised by X-ray crystallography,[8] we have primarily set out to investigate the coordination chemistry of this compound and determine: (i) which pair of nitrogen atoms are preferred for coordination, (ii) whether the second pair of nitrogen atoms can contribute to the coordination in any way, and (iii) to what degree the substituents influence the angle between the planes of the pyridine rings.

Results and Discussion

Ligand Synthesis

The synthesis of **L1** has been achieved by two independent routes. The first method involves the preparation of 3,3′-dinitro-2,2′-bipyridine following the Ullman coupling procedure, first described by MacBride et al.[9] This was then followed by a reduction step to afford ligand **L1**. Unfortunately, the reaction conditions described by MacBride proved to be problematic, giving poor yields of a very insoluble material that was difficult to purify. After carefully monitoring the progress of the reaction, we found that it was only necessary to heat the reaction mixture for 2.5 h (cf. 15 h in the original literature).[8] The warm reaction mixture could then be poured directly into water and filtered immediately, washing with concentrated ammonia solution. This process essentially removes any insoluble impurities on the sinter, and the product which precipitates from the filtrate on cooling is easily extracted into hot dioxane, giving 3,3′-dinitro-2,2′-bipyridine in good yield. This compound is then readily reduced with Sn^{II}/HCl to afford ligand **L1**. Since the initial preparation of the dinitro precursor proved to be problematic, a second route to **L1** was also investigated. This involves the Ullman coupling of 3-acetylamino-2-chloropyridine following the route of Kaczmarek et al.,[10] followed by acidic hydrolysis to afford **L1** in substantially improved yields.

Syntheses of Metal Complexes of L1

An overview of the prepared metal complexes is provided in Scheme 1.

The complexation reactions can be divided up into three classes: (i) binding to metal salts through the diimine nitrogens, (ii) tris complexation by binding to the diimine nitrogens, and (iii) binding of the bis-protonated ligand $\mathbf{L1H_2}$ to a metal through the amino groups. The first class involves reaction of an acetonitrile solution of the ligand **L1** with one equivalent of a salt of a divalent metal, M^{II} = Cu, Mn, Zn. This afforded a range of complexes with 1:1 ligand-to-metal ratios, namely compounds **2a**−**2e**. From the microanalysis data of complex **2a**, we could deduce that ligand **L1** forms a 1:1 complex with copper(II) chloride, although the crystal structure later revealed that **2a** actually crystallises as an unusual 2:2 centrosymmetric complex of ligand **L1** and copper(II) chloride (Figure 2a).

The ligand **L1** binds copper through the diimine coordination site, and dimers are formed by a pair of bonds from neighbouring amino groups.

Copper(II) acetate forms a variety of structures with unsubstituted 2,2′-bipyridine. The formation of multinuclear systems containing two or three copper ions,[11,12,13] polymers[14] and a mononuclear cation[15] $[Cu(bipy)_2(acetate)]^+$ are facilitated by the possibility of acetate either acting as a bidentate ligand, or using one oxygen atom to bridge two metal centres. To determine in our case whether or not the amino groups of 3,3′-diamino-2,2′-bipyridine would also contribute to the coordination of the copper ion, complex **2b** was prepared and its structure determined by X-ray crystallography. The molecular structure of **2b** is shown in Figure 3.

The diimine binding site of the bipyridine together with two acetate ligands are bound to the copper ion, thus enabling us to conclude that the amino groups are not involved in coordination to the copper ion when the bidentate acetate ligands can each provide two donor atoms.

Reactions of ligand **L1** with manganese(II) chloride or manganese(II) bromide also gave compounds with 1:1 metal-to-ligand ratios, although crystals suitable for single crystal X-ray diffraction could not be grown to-date. Never-

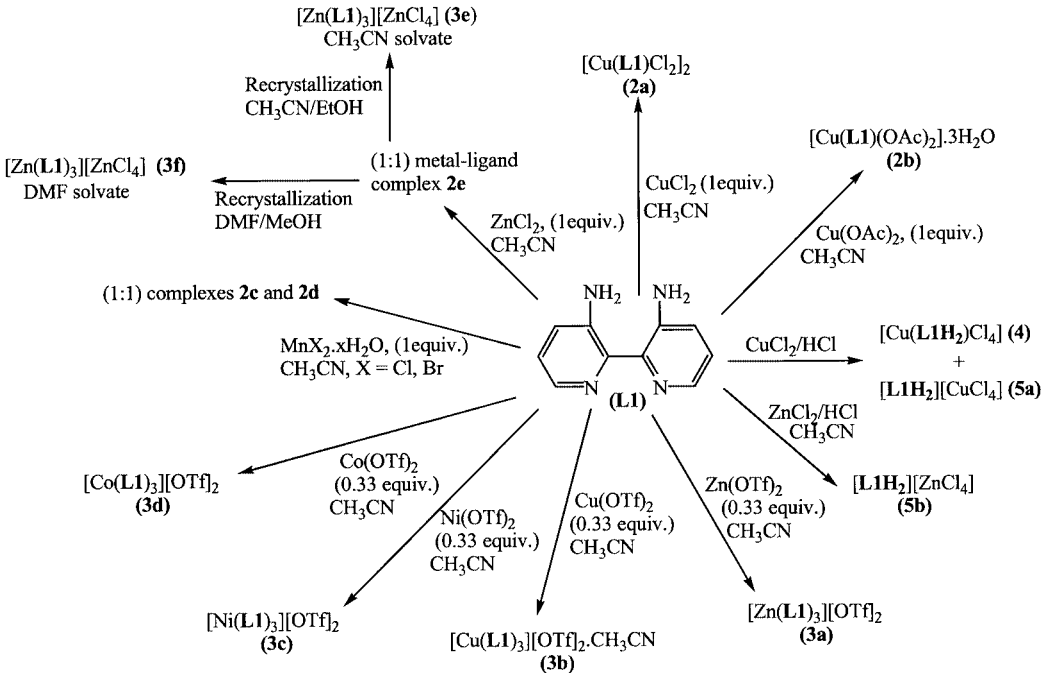

Scheme 1. An overview of the coordination chemistry of **L1**

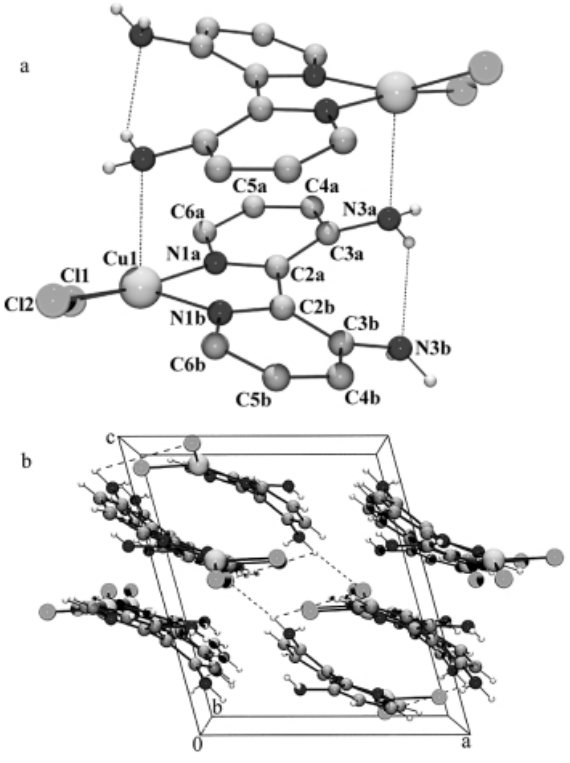

Figure 2. a) The dimeric structure of **2a**; selected distances [Å] and angles [°]: N(1A)−Cu 1.998(2), N(1B)−Cu 2.105(3), N(3A′)−Cu 2.625(3) (dotted line), Cl(1)−Cu 2.2565(10), Cl(2)−Cu 2.2880(8); N(1A)−Cu−N(1B) 80.94(10), N(1A)−Cu−Cl(1) 94.50(8), N(1A)−Cu−Cl(2) 169.32(8), N(1B)−Cu−Cl(1) 156.29(8), N(1B)−Cu−Cl(2) 94.84(7), Cl(1)−Cu−Cl(2) 93.20(3), N(1A)−Cu−N(3A′) 86.04(7), N(1B)−Cu−N(3A′) 91.62(8), Cl(1)−Cu−N(3A′) 111.36(10), Cl(2)−Cu−N(3A′) 84.27(8); b) The molecular packing arrangement for **2a**; dashed lines indicate the intermolecular hydrogen bond between H(31B) and a neighbouring chlorine atom H(31B)···Cl = 2.47 Å

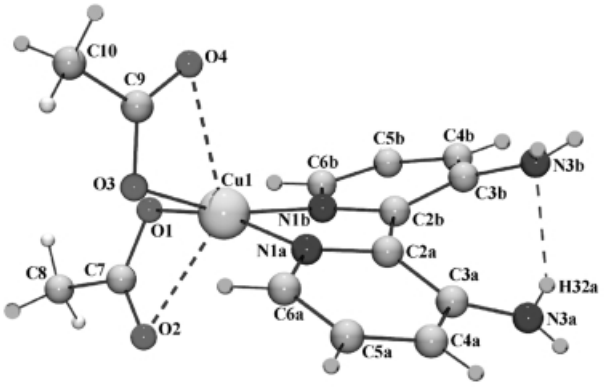

Figure 3. Molecular structure of **2b**; selected distances [Å] and angles [°]: N(1A)−Cu 1.969(5), N(1B)−Cu 1.985(5), O(1)−Cu 1.961(4), O(2)−Cu 2.616(5), O(3)−Cu 1.959(5), O(4)−Cu 2.571(6); N(1A)−Cu−N(1B) 82.05(19), N(1A)−Cu−O(1) 164.72(19), N(1A)−Cu−O(2) 110.77(17), N(1A)−Cu−O(3) 93.6(2), N(1A)−Cu−O(4) 100.45(20), N(1B)−Cu−O(1) 95.6(2), N(1B)−Cu−O(2) 104.93(18), N(1B)−Cu−O(3) 162.85(19), N(1B)−Cu−O(4) 108.32(19), O(1)−Cu−O(2) 55.10(16), O(1)−Cu−O(3) 92.9(2), O(1)−Cu−O(4) 94.64(19), O(2)−Cu−O(3) 92.14(18), O(2)−Cu−O(4) 136.85(18), O(3)−Cu−O(4) 55.99(18)

theless, we would expect the manganese(II) to favour an octahedral coordination, which could be completed by bridging halides in a similar manner to the salt formed between manganese(II) chloride and 2,2′-bipyridine, in which both chlorides bridge two neighbouring Mn^{II} ions.[16] Reactions of ligand **L1** with one equivalent of zinc(II) chloride in acetonitrile yielded complex **2e** whose chemical analysis suggested a 1:1 ratio of ligand to metal salt. These results parallel the reaction of unsubstituted 2,2′-bipyridine with zinc(II) chloride which forms a simple four-coordinate 1:1 complex.[17] In contrast, X-ray diffraction studies showed

that crystals grown from an acetonitrile/ethanol solution of the 1:1 complex **2e** belong to the second class of coordination compounds, i.e. that **3e** is the Zn^{2+} tris complex of **L1** with a tetrachlorozincate counterion. Similarly, crystals grown from **2e** in DMF/methanol were shown by X-ray crystallography to be a DMF solvate **3f** whose asymmetric unit contains three tris complexes each hydrogen bonded to one DMF solvent molecule. The closely related tris complex **3a** was prepared by reaction of zinc(II) triflate with three equivalents of **L1**. From these observations we can conclude that compound **2e** can readily rearrange in solution to afford a tris complex. Reaction of three equivalents of ligand **L1** with copper(II), nickel(II) or cobalt(II) triflates afforded the second series of 3:1 compounds, namely the tris complexes **3b**−**3d**.

Under acidic conditions it is reasonable to expect the coordination chemistry of ligand **L1** to change significantly as the more basic pair of nitrogens is protonated. Judging from the pK_b's of aniline (4.6) and pyridine (5.0) the amino nitrogen atoms would be expected to be slightly more basic; however, the crystalline salts of 3-aminopyridine are protonated on the ring nitrogen atom.[18,19] The pK_b's of the two nitrogen sites are probably quite similar. If the amino groups are protonated, metal ion binding at the diimine site may be disfavoured since there would be repulsions between the two positively charged ammonium groups in the 3- and 3′ positions. Protonation of the ring nitrogen atoms would leave open the possibility of metal ion binding to the amino groups, forming a less favourable seven-membered chelate ring.

Reaction of **L1** with copper(II) chloride in dilute hydrochloric acid yielded a third class of compound, namely complex **4**. In this case, both heterocyclic nitrogen atoms are protonated preventing coordination to the copper and, as a consequence, the two amino groups and four chloride ions are bound to the Cu^{II} completing an octahedral coordination sphere (Figure 4).

On one occasion, isomeric red crystals were also isolated from the preparation of **4**. X-ray crystallography showed that this compound was the tetrachlorocopper(II) salt of the 3,3′-diamino-2,2′-bipyridinediium dication **5a** (Figure 5). The only compound isolated from the reaction of ligand **L1** with zinc(II) chloride in a hydrochloric acid/acetonitrile mixture was shown by X-ray methods to be the corresponding tetrachlorozinc(II) salt **5b** (Figure 5).

Our findings clearly show that the pyridine rings are the favoured binding sites for coordination to divalent transition metal ions. However, by controlling the pH of the reaction mixture, it is possible to coordinate metal ions through the diamino functionality. In theory this ligand can adopt either an asymmetric or symmetric bridging mode for coordination, although the latter mode of binding has not been observed for this ligand to-date. This is in contrast to the closely related ligand 3,3′-dihydroxy-2,2′-bipyridine, which binds Ru^{II} as a mononucleating ligand through its diimine sites as well as in a symmetric "turned-around" mode presenting two N,O-donor sites to two Ru^{II} ions in an ambidentate manner.[20] For both the dihydroxy and the

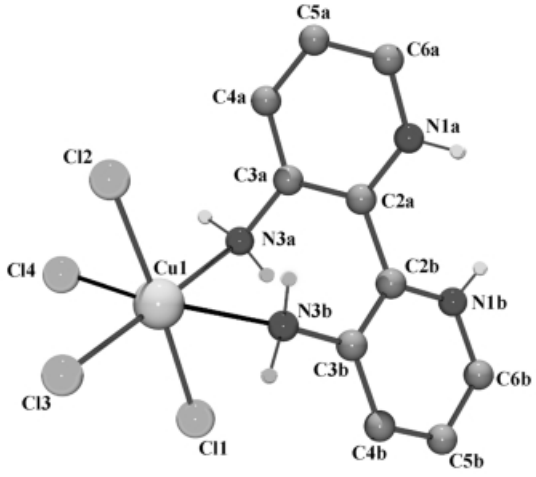

Figure 4. Molecular structure of **4**; selected distances [Å] and angles [°]: N(3A)−Cu 2.120(4), N(3B)−Cu 2.467(4), Cl(1)−Cu 2.299(2), Cl(2)−Cu 2.284(2), Cl(3)−Cu 2.3047(15), Cl(4)−Cu 3.079(2); N(3A)−Cu−N(3B) 84.3(2), N(3A)−Cu−Cl(1) 89.62(13), N(3A)−Cu−Cl(2) 88.91(13), N(3A)−Cu−Cl(3) 178.54(13), N(3A)−Cu−Cl(4) 79.03(12), N(3B)−Cu−Cl(1) 86.63(11), N(3B)−Cu−Cl(2) 100.67(11), N(3B)−Cu−Cl(3) 95.71(11), N(3B)−Cu−Cl(4) 161.43(11), Cl(1)−Cu−Cl(2) 172.37(6), Cl(1)−Cu−Cl(3) 91.84(5), Cl(1)−Cu−Cl(4) 85.23(5), Cl(2)−Cu−Cl(3) 89.67(5), Cl(2)−Cu−Cl(4) 87.14(5), Cl(3)−Cu−Cl(4) 101.21(5)

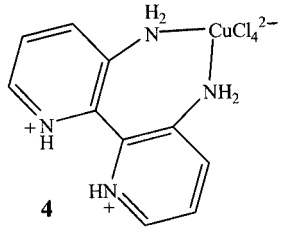

4

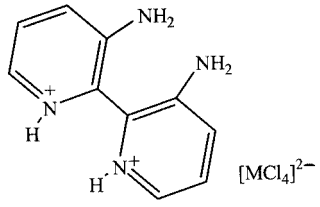

5a M = Cu
5b M = Zn

Figure 5. Compounds **4**, **5a**, and **5b**

diaminobipyridine ligands, the asymmetric mode of binding is unfavourable for dual chelation due to the fact that coordination through the diimine binding site requires an essentially planar arrangement of the two pyridine rings, whereas chelation through the diamino or dihydroxy groups requires it to be substantially twisted. As a consequence, the flexibility of the ligand is limited by the coordination requirements

of the first binding site. In this respect the bipyridine and phenanthroline families of molecules differ quite considerably. The dual chelating ability of the dipyridocatecholate (dpcat) ligand was first reported in 1975 by Balch et al.,[21] and during recent years Ward et al. have prepared dinuclear ruthenium(II) complexes of the ambidentate bridging ligand phenanthroline-5,6-diimine (pdi).[22] In this system coordination through the diamino groups of the bridging ligand is accomplished by their oxidation to the diimine state with the loss of two hydrogen atoms. Complexation by the diaminobipyridine ligand in this manner is highly unlikely since oxidation of the diamino groups would in this case occur at the expense of losing the aromaticity in both of its pyridine rings.

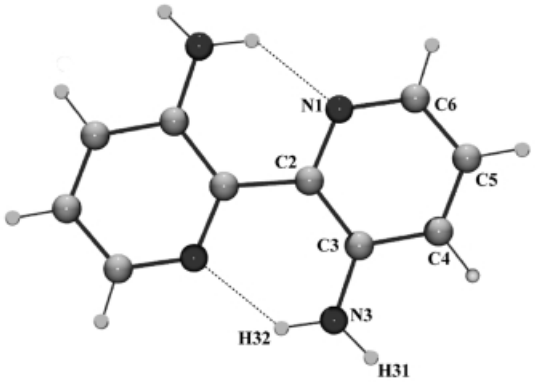

Figure 6. The molecular structure of **L1**; the dotted lines indicate the pair of intramolecular H bonds (N−H···N = 1.948 Å)

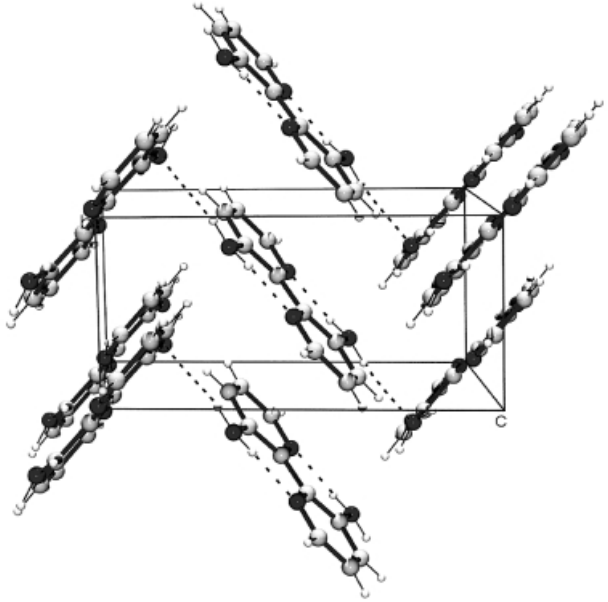

Figure 7. Molecular packing arrangement for **L1**; intra- and intermolecular H-bonding interactions are indicated by dashed lines

X-ray Structural Studies

The X-ray crystal structure of the free ligand **L1** (Figure 6) shows that the free ligand is held in a centrosymmetric *trans* conformation via a pair of intramolecular hydrogen bonds between an amino hydrogen atom and the heterocyclic nitrogen atom of the opposite ring [N−H···N = 1.948(18) Å, N−H···N = 132.7(14)°].

The molecules are packed so that the second amino hydrogen atom can participate in an intermolecular hydrogen bond to the amino N atom of another molecule, with an N···H bond length of 2.40(2) Å, and close to linear bonding at the hydrogen [N−H···N = 168.5(15)°] (Figure 7). This interaction leads to a slight pyramidalisation of the amino nitrogen atom as indicated by the sum of bond angles around nitrogen (352.5°), which enables the lone-pair electron density to participate in the intermolecular hydrogen

Table 1. Bond lengths and angles of 3,3′-diamino-2,2′-bipyridine in compounds **L1**, **2a**, **4**, **5a** and **5b**

Bond length [Å]	**L1**	**2a**[a]	**4**[a]	**5a**[a]	**5b**[a]
N(1)−C(2)	1.3502(15)	1.360(4)	1.361(6)	1.352(5)	1.374(8)
		1.374(4)	1.351(6)	1.368(5)	1.360(8)
N(1)−C(6)	1.3320(17)	1.348(4)	1.316(7)	1.324(6)	1.323(8)
		1.332(4)	1.329(7)	1.329(5)	1.330(8)
C(2)−C(3)	1.4241(18)	1.417(4)	1.388(7)	1.406(5)	1.396(8)
		1.404(4)	1.395(7)	1.402(6)	1.400(8)
N(3)−C(3)	1.3728(17)	1.387(4)	1.419(6)	1.364(4)	1.350(9)
		1.387(4)	1.384(6)	1.341(6)	1.369(8)
C(3)−C(4)	1.3984(19)	1.415(5)	1.386(7)	1.397(6)	1.392(8)
		1.403(5)	1.404(7)	1.411(6)	1.414(8)
C(4)−C(5)	1.364(2)	1.351(5)	1.383(7)	1.378(7)	1.376(9)
		1.371(5)	1.380(7)	1.373(6)	1.383(10)
C(5)−C(6)	1.375(2)	1.395(5)	1.393(8)	1.382(7)	1.376(9)
		1.388(5)	1.391(7)	1.383(7)	1.366(10)
C(2)−C(2′)	1.485(2)	1.481(4)	1.480(7)	1.465(5)	1.477(8)
Bond angle [°]					
C(2)−N(1)−C(6)	120.77(11)	121.5(3)	123.9(5)	124.6(4)	124.1(5)
		120.3(3)	123.7(5)	124.6(4)	123.6(5)
N(1)−C(2)−C(3)	119.86(11)	119.7(3)	119.5(4)	118.8(4)	118.5(5)
		119.6(3)	120.1(4)	118.7(4)	118.5(5)
N(1)−C(2)−C(2′)	116.47(13)	113.5(2)	118.9(4)	117.7(4)	116. 1(5)
		113.1(3)	118.4(4)	116.9(4)	116.8(5)
C(3)−C(2)−C(2′)	123.67(14)	126.7(3)	121.6(4)	123.5(4)	125.1(6)
		127.3(3)	121.3(4)	124.3(4)	124.7(5)
N(3)−C(3)−C(2)	123.95(12)	124.3(3)	119.9(4)	121.3(4)	122.4(6)
		123.2(3)	119.7(4)	122.7(4)	120.7(5)
N(3)−C(3)−C(4)	118.73(12)	118.5(3)	122.2(5)	121.6(4)	119.9(6)
		118.8(3)	123.4(5)	120.3(4)	121.5(6)
C(2)−C(3)−C(4)	117.29(12)	116.8(3)	117.8(5)	117.1(4)	117.7(6)
		118.0(3)	116.8(5)	117.0(4)	117.7(6)
C(3)−C(4)−C(5)	121.28(13)	121.5(3)	120.7(5)	121.0(4)	121.1(6)
		120.8(3)	121.0(5)	121.3(4)	120.2(6)
C(4)−C(5)−C(6)	118.30(13)	119.1(3)	119.6(5)	119.8(4)	120.1(6)
		118.1(3)	119.6(5)	120.1(4)	119.6(6)
N(1)−C(6)−C(5)	122.48(13)	120.6(3)	118.4(5)	118.4(4)	118.6(6)
		122.4(3)	118.6(5)	118.3(4)	119.9(6)

[a] $R1 = (F_0 - F_c)/F_0$; $wR2 = \{[w(F_0^2 - F_c^2)^2]/(F_0^2)^2]\}^{1/2}$.

Table 2. Selected molecular geometry of **L1** and its dication in complexes **2a**, **2b**, **3a**, **3e**, **4** and in salts **5a** and **5b**

Compound	**2a**	**2b**	**3a**	**3e**	**4**	**5a**	**5b**
N(3A)−H(32A) [Å]	0.78(4)	0.92(8)	0.93(6)	1.01(13)	−	−	−
H(32A)···N(3B) [Å]	2.19(4)	2.07(8)	1.97(6)	2.05(14)	−	−	−
N(3A)−H(32A)···N(3B) [°]	136(4)	135(7)	149(5)	136(11)	−	−	−
Angle between best planes of heterocyclic rings [°]	24.4(1)	28.9(2)	31.3(2) 35.3(2)	37.4(4) 37.8(4)	68.4(1)	54.5(1)	53.0(3)
Deviation of N(3A) from best plane of ring A [°]	0.374(3)	0.22(1)	0.245(4)	0.234(9)	0.072(4)	0.115(4)	0.033(7)
Deviation of N(3B) from best plane of ring B [°]	0.176(3)	0.26(1)	0.152(4)	0.133(8)	0.019(4)	0.072(5)	0.139(6)

bond. Each pyridine ring is planar, but the amino nitrogen atom is displaced to one side of this plane by 0.061(1) Å and its two hydrogen atoms are displaced by −0.12 and −0.15 Å to the other side. The molecular geometry of the pyridine rings is summarised in Table 1. In comparison with the similar *trans* conformation also adopted by 2,2′-bipyridine in the solid state,[23] differences are observed in the geometry of the pyridine rings.

For ligand **L1**, the C(2)−C(3) bond is slightly longer 1.4241(18) Å [cf. 1.394(2) for bipy] and the exocyclic C(3)−C(2)−C(2′) angle is widened from to 121.2(1)° to 123.67(14)°. This is accompanied by a consequent contraction of the endocyclic angle at C(2) by 2.7° to 119.86(11)° and an increase in the endocyclic angle at N(1) by 3.5° to 120.77(11)°. The amino group is displaced away from the opposite pyridine ring by 2.6° in the plane of the molecule. These effects enable the molecule to optimise its hydrogen bonding interactions.

The crystal structures of complexes of **L1** with copper(II) chloride (**2a**) and copper(II) acetate (**2b**), the tris complexes of **L1** with zinc(II) (**3a**, **3e** and **3f**), the complex of the dication of **L1** with copper(II) chloride (**4**) and two salts of the dication of **L1** are described. The molecular geometry of the pyridine rings for selected compounds is summarised in Table 1. Intramolecular hydrogen bonding interactions as well as the conformational geometry for ligand **L1** are listed in Table 2.

[Cu(L1)Cl$_2$]$_2$ (2a)

Remarkably, complex **2a** crystallises as a 2:2 centrosymmetric complex of ligand **L1** and copper(II) chloride (Figure 2a). The Cu^{II} metal ion adopts a near square-pyramidal geometry with two pyridine nitrogen atoms and two chloride ions bound in a distorted square-planar arrangement with angles between neighbouring atoms at copper in the range 80.9(1) to 94.8(1)°. A long axial contact from an amino nitrogen of a neighbouring bipyridine molecule to the copper metal [Cu···NH$_2$ = 2.625(3) Å] completes the five-coordinate geometry. The Cu^{II} is displaced out of the best planes of each pyridine ring by 0.482(1) and 0.468(1) Å, respectively, and the angle between the [Cl(1), Cl(2), Cu] plane and the [N(1A), N(1B), Cu] plane is 25.1(1)°. As shown in Figure 2a, these molecules are arranged in dimers as a consequence of a pair of long axial contacts between a copper ion and an amino nitrogen atom belonging to the opposite half of the dimer. A coordinating amino group approaches one face of the copper ion at angles to the other four ligating atoms in the range of 84−111°, leaving the opposite face of the copper ion exposed. The shortest contact from this face is intermolecular to a pyridine ring and is 3.785(4) and 3.626(4) Å for Cu···C(3A) of ring A and Cu···C(4A) of ring B, respectively. An intramolecular hydrogen bond [N···H = 2.19(4) Å, N···H−N = 136(3)°] leads to the best planes of the two attached pyridine rings lying at only 24.4(1)° to each other (Table 2). There is a slight folding of pyridine ring A about the C(3A)···C(6A) vector, and a slight folding of ring B about the C(2B)···C(5B) vector. This folding serves to displace the amino groups out of the best planes of their respective pyridine rings in opposite directions: N(3A) is displaced towards the copper ion to which it binds by 0.374(3) Å, while N(3B) is displaced by only 0.174(3) Å in the opposite direction. The bonding geometries at C(3A) and C(3B) remain planar. Small in-plane angular displacements of the C−N bonds at C(3A) and C(3B) in the range of 2−3° contribute to increase the distance between the amino groups, as observed in the structure of the free ligand. The molecules are packed such that there is an intermolecular hydrogen bond between H(31B) and a neighbouring chlorine atom [H(31B)···Cl = 2.47 Å] (Figure 2b). Two types of 1:1 complexes with copper(II) chloride have been reported for the unsubstituted 2,2′-bipyridine ligand.[24] The first complex is comprised of long chains in which the octahedrally bound copper(II) ions are linked by bridging chloride ions. The second complex contains a pentacoordinate Cu^{II} ion with only one bridging chloride linking adjacent metal centres. The two Cu−N bond lengths in complex **2a** [1.998(2) and 2.015(3) Å] are slightly shorter than those in the 1:1 complexes of bipyridine with copper(II) [2.026(5)−2.079(3) Å]. In contrast, the 1:1 complex of copper(II) chloride with 5,5′-diamino-2,2′-bipyridine adopts a tetracoordinate structure with even shorter Cu−N bond lengths of 1.981(1) Å.[25] Interestingly, a derivative of 3-amino-2,2′-bipyridine-6-carboxylate is reported to bind copper(II) through both a deprotonated amino group, a pyridine nitrogen and a carboxylate group.[26]

[Cu(L1)(OAc)$_2$]·3H$_2$O (2b)

To determine whether the amino groups of 3,3′-diamino-2,2′-bipyridine would still contribute to the coordination of the copper ion, the structure of the hydrated 1:1 complex **2b** with copper(II) acetate was determined by X-ray crystallography (Figure 3). The bipyridine binds to copper

through its pyridine nitrogen atoms [Cu(1)−N(3A) = 1.969(5), Cu(1)−N(3B) = 1.985(5) Å] and two acetate ligands coordinate in a bidentate manner to complete a distorted octahedral geometry. Both acetates form one short bond to copper [Cu(1)−O(1) = 1.961(4), Cu(1)−O(3) = 1.959(5) Å]. However, in contrast to **2a**, the acetate ligands make a second pair of longer contacts [Cu(1)−O(2) = 2.616(5), Cu(1)−O (4) = 2.571(6) Å] to the copper from above and below the equatorial plane. The bite angles of each acetate at the copper metal are 55.1(2) and 56.0(2)°, respectively. This mode of binding is very similar to that of the single acetate moiety in the perchlorate and tetrafluoroborate salts of the acetato-bis-bipyridinecopper(II) cation, which contain one short Cu−O bond [2.031(5) and 1.980(4) Å] and a longer Cu··O contact [2.648(5) and 2.785(5) Å].[14] The structures of the acetate ligands in **2b** are asymmetric, with longer C−O bonds [1.268(8) and 1.272(7) Å] to the oxygens which bind more tightly to the copper than for the other pair of oxygens [1.238(9) and 1.236(7) Å].

In analogy with complex **2a**, the two pyridine rings are connected by an intramolecular hydrogen bond that links the two amino groups (Table 2). The angle between the planes of the two pyridine rings is 28.9(2)° and each amino nitrogen atom is displaced by similar amounts from the plane of its attached pyridine ring, namely by 0.22(1) Å for N(3A) and 0.26(1) Å for N(3B). This serves to orient the amino groups away from each other and differs from the more asymmetric disposition of amino groups in **2a**, where one amino group coordinates the copper ion. The asymmetric unit contains two well-ordered water molecules, one of which is hydrogen bonded to an acetate oxygen O(1) and an amino hydrogen H(31B) from different molecules in the crystal structure as well as to the second water molecule.

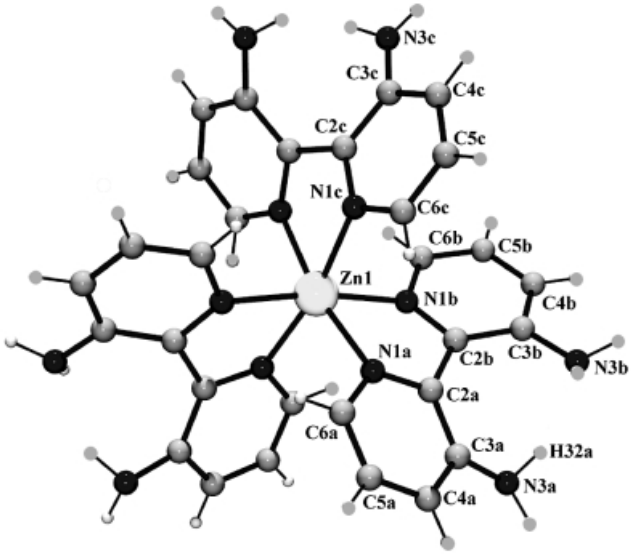

Figure 8. Molecular structure of **3a**; selected distances [Å] and angles [°]: N(1A)−Cu 2.160(3), N(1B)−Cu 2.132(3), N(1C)−Cu 2.164(3); N(1A)−Cu−N(1B) 76.1(1), N(1A)−Cu−N(1C) 169.2(1), N(1A)−Cu−N(1A′), 91.2(2), N(1A)−Cu−N(1B′) 97.9(1), N(1A)−Cu−N(1C′) 96.5(1), N(1B)−Cu−N(1C) 95.3(1), N(1B)−Cu−N(1B′) 171.5(2), N(1B)−Cu−N(1C′) 91.3, N(1C)−Cu−N(1C′) 76.9(2)

The second water molecule lies in a channel that runs through the crystal parallel to the *c* axis that contains an additional, disordered water molecule.

[Zn(L1)$_3$][CF$_3$SO$_3$]$_2$ (3a), [Zn(L1)$_3$][ZnCl$_4$]·CH$_3$CN (3e) and [Zn(L1y)$_3$][ZnCl$_4$]·DMF (3f)

The structures of the cations in all three compounds are very similar. The molecular structure of **3a** is shown in Figure 8. (NB The structures of **3a** and **3e** were solved in space groups which require the cation to lie on twofold axes, thus only one-and-a-half ligand molecules are crystallographically unique. However, the bisected ligand does not exactly conform to this twofold axis due to the asymmetry expected in the arrangement of the amino groups, where one must hydrogen bond to the other).

In all complexes three bipyridine ligands bind the zinc(II) metal through their diimine binding sites, and the cations are all octahedral with Zn−N bond lengths in the range 2.132(3)−2.164(3) Å and bond angles around the Zn^{2+} in the range 76.1(1)−97.9(1)°. The Zn−N bond lengths fall within the range typical for Zn^{2+}tris(bipyridine) complexes (2.133−2.166 Å).[27−29]

[Cu(L1H$_2$)Cl$_4$] (4)

Reaction of **L1** with copper(II) chloride in dilute hydrochloric acid yielded complex **4,** which was characterised by X-ray crystallography. The molecular structure is shown in Figure 4. Both heterocyclic nitrogen atoms are protonated and the two amino groups, which together with four additional chloride ligands complete the charge balance, are bound to the copper ion, giving an octahedral coordination sphere around the Cu^{II} ion. The endocyclic bond angles at both pyridinyl nitrogen atoms show the expected widening by 2−3° relative to the free ligand **L1** due to protonation. The Cu^{II} metal ion shows the expected Jahn−Teller distortion, namely the C−N and C−Cl bonds along one axis are longer than other similar bonds in the complex. The N(3B)−Cu bond [2.467(4) Å] is 0.35 Å longer than the N(3A)−Cu bond [2.120(4) Å], although both are shorter than the pair of bonds from amino nitrogens to coppers in the 2:2 complex **2a**. Both amino groups show a tetrahedral bonding geometry, indicative of the binding interactions between nitrogen and copper. The 1,6-bite angle of the diamino groups at the copper metal is 84.2(1)°. The molecule achieves this mode of coordination by increasing the angle between the best planes of the two pyridinium rings to 68.4(1)° from the *cis* coplanar arrangement. The amino nitrogen atoms are nearly coplanar with their pyridine rings, in contrast to the complexed neutral ligand. The two C−NH_2 bond lengths are different; this bond is longer [1.419(6) vs. 1.384(6) Å] for the amino group which binds the copper more tightly, since the nitrogen lone pair is less available for conjugation with the pyridine ring. Indeed, the shorter bond is similar in length to those in the unbound dication in **5a** and **5b**, suggesting that this amino group only binds weakly to the copper. The molecules are packed in such a way that there are intermolecular hydrogen bonds

between all six nitrogen-bonded hydrogen atoms and neighbouring chloride ions in the range of 2.24−2.67 Å.

Only a few structurally characterised examples of 2,2′-diaminobiaryl systems binding in this way have been reported in the chemical literature. 2,2′-Diaminobiphenyl and 1,2-diaminocyclohexane bind platinum(II) chloride[30] and two molecules of 2,2′-diamino-6,6′-dimethylbiphenyl bind to rhodium(III) chloride[31] with bite angles for the diamino groups at the metal atom in the 87−89° range. Several complexes of the 3-aminopyridinium cation coordinated through the amino groups to copper(II) have been reported and provide a useful comparison.[32,33] For these complexes, the Cu−N distances are in the range 2.043−2.071 Å, similar to the shorter of the Cu−N bonds in **4**, and the C−NH_2 bond lengths are in the range 1.400−1.432 Å, similar to the C(3A)−N(3A) bond length in **4**.

[L1H$_2$][CuCl$_4$] (5a) and [L1H$_2$][ZnCl$_4$] (5b)

The molecular structure of the zinc salt **5b** is presented in Figure 9. The geometry and conformation of the dication in both compounds is very similar, however the geometry of the anion in the former is intermediate between tetrahedral and square planar, whereas in the latter it is tetrahedral.

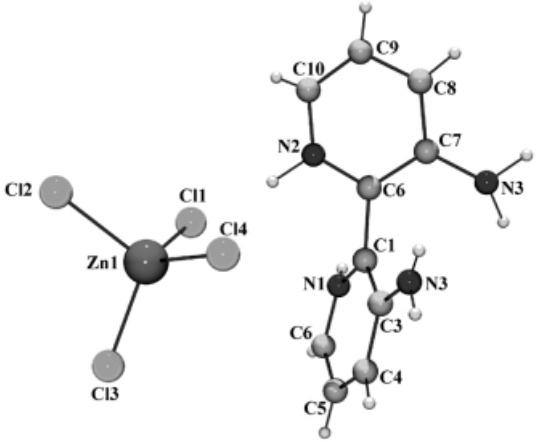

Figure 9. Molecular structure of **5b**

Protonation of the ring diimine nitrogens leads to widening of the endocyclic ring angles at these heteroatoms in the range of 123.6(5)−124.6(4)°. The best planes of the pyridinium rings lie at 54.5(1)° and 53.0(3)° from the *cis* coplanar arrangement, which serves to separate the amino nitrogen atoms at van der Waals distances of 3.063(6) Å and 3.023(9) Å. The shortest N···H separations between the two amino groups are ca. 2.7 Å, although the positions of the hydrogen atoms determined from these room temperature measurements are not very accurate. In contrast to the complexed dication in **4**, the bonding geometries at the amino nitrogen atoms are in most cases nearer to planar (the average sum of bond angles at the amino N are in the range 347−360°). The bonds between the amino nitrogen atoms and the pyridine rings are in the range 1.341(6)−1.369(8) Å (Table 1), and are shorter than in 3-aminopyridine (1.384 Å).[34] This is in accordance with the expected increase in π-overlap between each amino group's lone pair and the positively charged heterocyclic ring. The corresponding bond lengths in the complexed dication **4** are ca. 0.4 Å longer than in **5a** and **5b** since the nitrogen atoms' lone pairs are utilised in forming dative bonds.

NMR Spectroscopy

All NMR spectra were measured in [D_6]DMSO for consistency. The ^{1}H NMR chemical shifts for selected compounds are shown in Table 3.

Table 3. ^{1}H NMR spectroscopic data for selected compounds containing **L1**

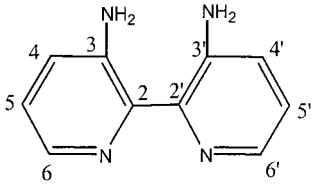

Compound	Solvent	H6, H6′	H5, H5′	H4, H4′
Free ligand (**L1**)	[D_6]DMSO	7.76	7.02	7.02
L1·2HCl	[D_6]DMSO	8.09	7.60	7.65
(**L1**H$_2$)[ZnCl$_4$] (**5b**)	[D_6]DMSO	8.07	7.55	7.55
[Dichloro(**L1**)zinc(II)] (**2e**)	[D_6]DMSO	7.80 (br)	7.04 (br)	7.14 (br)
[Zn(**L1**)$_3$][ZnCl$_4$] (**3e**)	[D_6]DMSO	7.84	7.05	7.14
[Zn(**L1**)$_3$][CF_3SO_3]$_2$ (**3a**)	[D_6]DMSO	7.62	7.16	7.40

In comparison with the free ligand **L1**, the positive charge resulting from protonation of both rings causes a downfield shift of the aromatic protons since they are now more deshielded than in **L1**. The protons in the 4- and 5-positions are shifted by approximately 0.6 ppm whereas the H-6 protons are shifted to a lesser degree by 0.3 ppm. These shifts are observed for both the HCl salt as well as compound **5b**. For the tris-zinc compound **3a**, complexation causes a small upfield shift of the protons in the 6-position, since there is a small diamagnetic interaction of the ring current with the metal ion resulting in a shielding effect of the protons α to the metal centre. The protons in the 4- and 5-positions are deshielded slightly (0.1−0.4 ppm) with respect to the free ligand **L1**. Interestingly, the ^{1}H NMR spectrum for the 1:1 complex **2e** is very broad, indicating an exchange process, and has similar chemical shifts to a solution of the tetrachlorozincate salt of the tris-zinc complex **3e**. It is notable that the ^{1}H NMR spectrum of the latter differs from that of **3a**, the triflate salt of the tris-zinc complex, which would not be expected to be involved in any exchange processes. Crystalline **3e** was initially grown from solutions of **2e**, thus it seems that the two chlorides and ligand **L1** bound to zinc in **2e** are exchanging between zinc ions.

Conclusion

Substitution at the 3,3′-positions does not prevent coordination to the pyridine rings. Compound **L1** behaves as a bidentate ligand coordinating metal ions preferentially through the nitrogen atoms of the pyridine rings. Furthermore, this ligand displays an unusual pH-dependent coordination chemistry, enabling the diamino group to participate in the coordination chemistry when both pyridine nitrogens are protonated. The second mode of binding, namely the symmetrical bridging mode, has not been observed for this ligand to-date. Attempts to prepare dinuclear complexes with ligand **L1** acting as an asymmetric bridge have so far been unsuccessful. This is most probably due to the fact that the asymmetric bridging mode is sterically difficult for divalent metal ions since chelation through the diamino functionality requires the ligand to be substantially more twisted. The above findings lead us to conclude that this ligand is not particularly well suited for linking metal ions for the assembly of coordination polymers. Tris-bipyridine complexes of selected paramagnetic ions do, however, display the phenomenon of spin-crossover. As a consequence, the preparation and magnetic studies of further derivatives of **L1** are currently in progress.[35]

Experimental Section

General: 3-Amino-2-chloropyridine, copper bronze (99%) and tin(II) chloride (98%) were purchased from Aldrich. 2-Chloro-3-nitropyridine (97%), DMF (99.8% over molecular sieves) and dioxane (99.5%) were purchased from Fluka. Solvents were dried before use. NMR spectra were measured on a JEOL GX 270 spectrometer (270 MHz for ^{1}H and 67.8 MHz for ^{13}C) using tetramethylsilane (TMS) as standard, and measured in ppm downfield from TMS, or on a Bruker AC-300 spectrometer (300 MHz for ^{1}H and 75 MHz for ^{13}C) and calibrated against the deuterated solvent. Chemical shifts δ are given in ppm and coupling constants (*J*) are given in Hz. IR spectra were recorded on an ATI Mattson Genesis Series FT-IR or a Perkin−Elmer Spectrum One FT-IR spectrophotometer as liquid films, nujol mulls or KBr pellets. Mass spectra were recorded at the EPSRC Mass Spectrometry Centre and at the University of Berne. Microanalyses were performed at the Analytical Centre, University of Kent, UK, and at the University of Fribourg, Switzerland. Flash chromatography was performed on 40−63 silica gel (Merck).

Synthesis of 3,3′-Diamino-2,2′-bipyridine (L1)

Method A: 2-Chloro-3-nitropyridine (2.00 g, 12.62 mmol) was reacted with freshly activated copper bronze (2.00 g) in dry DMF (40 mL) at 150 °C under nitrogen for 2.5 h.[8] After 2 h TLC (SiO_2, CH_2Cl_2) indicated that the starting material had been consumed. The resulting mixture was poured into water (40 mL), the solid filtered immediately and then washed with concentrated ammonia (2 × 20 mL). The remaining solid was then extracted into boiling dioxane (2 × 150 mL), stirring for about 20 min each time. After evaporating the combined extracts to dryness, the solid was recrystallised from ethanol to give 3,3′-dinitro-2,2′-bipyridine as a yellow solid (yield 1.16 g, 73%). M.p. 205−206 °C. ^{1}H NMR ($CDCl_3$): δ = 8.87 (dd, $J_{6,5}$ = 4.7 Hz, $J_{6,4}$ = 1.7 Hz, 2 H, 6-,6′-H), 8.58 (dd, $J_{4,5}$ = 8.4 Hz, $J_{4,6}$ = 1.5 Hz, 2 H, 4-,4′-H), 7.65 (m, 2 H, 5-,5′-H). ^{13}C NMR ($CDCl_3$): δ = 152.9 (6-,6′-C), 150.7 (2-,2′C), 144.0 (3-,3′-C), 133.1 (4-,4′-C), 124.6 (5-,5′-C). IR (KBr pellet): $\tilde{\nu}$ = 3084, 1590, 1561, 1534, 1440, 1417, 1366, 1048, 1038, 865, 855, 821, 790, 751, 621, 529 cm^{-1}. The dinitro product (0.8 g, 3.25 mmol) was added to a solution of tin(II) chloride dihydrate (5.6 g, 29.5 mmol) in conc. HCl (32%, 14 mL).[7] The solution was refluxed for 0.5 h, to give a yellow solution (**Important:** *do not let the solution cool, otherwise a green insoluble solid precipitates out of solution*). After adjustment of the pH to 12−13 with a solution of NaOH, the solution was extracted with chloroform, and the solvents evaporated to give **L1** as a yellow solid. (yield 0.5 g, 86%). Single crystals suitable for X-ray diffraction were grown from ethyl acetate by slow evaporation of the solvent at room temperature. M.p. 133−134 °C. ^{1}H NMR ($CDCl_3$): δ = 7.96 (dd, $J_{6,5}$ = 7.0 Hz, $J_{6,4}$ = 3.0 Hz, 2 H, 6,6′-H), 7.02 (m, 4 H, 5,5′-H and 4,4′-H), 6.27 (br. s, 4 H, 2 × NH_2). ^{13}C NMR ($CDCl_3$): δ = 143.8 (3,3′-C), 140.6 (2,2′-C), 135.7 (6,6′-C), 123.9 (4,4′-C), 122.9 (5,5′-C). IR (KBr): $\tilde{\nu}$ = 3354, 3221, 2925, 2855, 1586, 1548, 1444, 1430, 1316, 1269, 1149, 1060, 1024, 796, 729, 638 cm^{-1}.

Method B: Freshly distilled acetic anhydride (200 mL, 2.02 mol) was added to 2-chloro-3-aminopyridine (20.0 g, 0.156 mol) and the solution left to stir overnight. The excess acetic acid and acetic anhydride were both removed by distillation under reduced pressure. On cooling in ice the remaining oil produced an off-white solid which was recrystallised from toluene to give 3-acetylamino-2-chloropyridine (20.1 g, 74.0%) as white crystals, M.p. 89 °C. Activated copper bronze (18 g, 0.283 mol) was added to a solution of 3-acetylamino-2-chloropyridine (20.0 g, 0.117 mol) in dry DMF (100 mL) under nitrogen.[9] This mixture was then heated at 110 °C until TLC (SiO_2,ethyl acetate) showed the absence of starting material (3−4 h). After cooling, water (20 mL) was added and the solution filtered. The filter cake was washed with more water (20 mL), ammonium hydroxide (40 mL, 0.88 grav) and finally more water (20 mL). The cake was allowed to dry fully in a desiccator. The desired solid was then extracted with dichloromethane (5 × 200 mL) and the solvents evaporated to give crude 3,3′-diacetylamino-2,2′-bipyridine (yield 12.2 g, 76.6%). M.p. 230°C (dec.) (ref.[9] 225−226 °C), ^{1}H NMR ($CDCl_3$): δ = 9.13 (dd, $J_{4,5}$ = 8.5 Hz, $J_{4,6}$ = 1.7 Hz, 2 H, 4,4′-H), 8.35 (dd, $J_{6,5}$ = 5.9 Hz, $J_{6,4}$ = 1.5 Hz, 2 H, 6,6′-H), 7.36 (dd, $J_{5,6}$ = 13.1 Hz, $J_{5,4}$ = 4.5 Hz, 2 H, 5,5′-H), 2.20 (s, 6 H, 2 × -CH_3). ^{13}C NMR ($CDCl_3$): δ = 169.2 (C=O), 141.7 (2,2′-C), 140.3 (6,6′-C), 136.5 (4,4′-C), 129.8 (3,3′-C), 123.9 (5,5′-C), 25.4 (2 × -CH_3). IR (KBr): $\tilde{\nu}$ = 3344 (N−H str), 1691 (C=O str) cm^{-1}. This crude product (12.0 g, 44.4 mmol) was added to concentrated HCl (50 mL) and the mixture refluxed for 30 min. After cooling in ice, concentrated ammonium hydroxide was added (80 mL, 0.88 grav) to give bright yellow crystals of pure **L1** (yield 8.03 g, 95.2%).

3,3′-Diamino-2,2′-bipyridinediium Dichloride: A 2 M solution of HCl (10 mL) was added to ligand **L1** (1.0 g, 4.4 mmol) and the solution stirred for 24 h. The desired salt was precipitated from the solution by the dropwise addition of acetonitrile to give a bright yellow, amorphous solid which was washed with water and dried (yield 0.89 g, 63.9%). M.p. 181 °C (dec.), ^{1}H NMR (D_2O): δ = 8.20 (dd, $J_{6,5}$ = 5.2 Hz, $J_{6,4}$ = 1.2 Hz, 2 H, 6,6′-H), 8.01 (dd, $J_{4,5}$ = 8.9 Hz, $J_{4,6}$ = 5.4 Hz, 2 H, 4,4′-H), 7.90 (dd, $J_{5,4}$ = 8.9 Hz, $J_{5,6}$ = 5.4 Hz, 2 H, 5,5′-H). ^{13}C NMR (D_2O): δ = 146.7 (6,6′-C), 133.1 (4,4′-C), 132.9 (2,2′-C), 129.0 (5,5′-C), 122.1 (3,3′-C) IR (KBr

disc): $\tilde{\nu}$ = 3378−3207 (N−H str), 2958 (C−H, arom. str), 2631 (N^+−H str), 1546 (C=N, arom. str) cm^{-1}.

Tetrachlorobis(3,3′-diamino-2,2′-bipyridine)dicopper(II) (2a): Equimolar amounts of ligand **L1** (0.30 g) and copper(II) chloride dihydrate (0.22 g) were stirred together in acetonitrile overnight. The resulting precipitate was filtered, dried and recrystallised from water to give single crystals of **2a** as green blocks (yield 0.49 g, 97%). M.p 266−267 °C. $C_{10}H_{10}Cl_2CuN_4$ (320.7): calcd. C: 37.5, H 3.1, N 17.5; found C 37.3, H 3.1, N 17.9. IR (Nujol): $\tilde{\nu}$ = 3345, 3305, 3218, 1643, 1633, 1590, 1581, 1330, 1313, 1267, 1230, 1201, 1149, 1076, 1064, 944, 904, 823, 798,723, 713, 686 cm^{-1}.

Diacetato(3,3′-diamino-2,2′-bipyridine)copper(II)·3H_2O (2b): Following the above procedure for **2a**, reaction of ligand **L1** (0.30 g) and copper(II) acetate hydrate (0.32 g) yielded a solid which was collected, dried and recrystallised from aqueous ethanol to afford single crystals of **2b** as dark green prisms (yield 0.55 g, 93%). M.p. 212−214 °C. $C_{14}H_{16}N_4O_4Cu{\cdot}3H_2O$ (421.9): calcd. C 39.8, H 5.2, N 13.3; found C 40.0, H 4.8, N 13.5. IR (Nujol): $\tilde{\nu}$ = 3491, 3415, 3329, 3173, 1639, 1579, 1279, 1245, 1156, 1051, 1012, 922, 815, 799, 667 cm^{-1}.

Catena-dichloro(3,3′-diamino-2,2′-bipyridine)manganese(II) (2c): Reaction of **L1** (0.30 g) with manganese(II) chloride tetrahydrate (0.32 g) as for **2a** gave a dark crystalline solid tentatively assigned as **2c** (yield 0.41 g, 82%). M.p. > 330 °C. $C_{10}H_{10}Cl_2MnN_4$ (312.1): calcd. C 38.5, H 3.3, N 18.0; found C 38.3, H 3.2, N 17.7. IR (Nujol): $\tilde{\nu}$ = 3440, 3392, 3334, 3305, 3205, 1735**,** 1615, 1593, 1295, 1242, 1159, 1025, 952, 918, 817, 786, 770, 734 cm^{-1}.

Catena-dibromo(3,3′-diamino-2,2′-bipyridine)manganese(II) (2d): Reaction of **L1** (0.30 g) with manganese(II) bromide hexahydrate (0.52 g) as for **2a** gave a black solid tentatively assigned as **2d** (yield 0.47 g, 73%). M.p. dec. 280 °C. $C_{10}H_{10}Br_2MnN_4$ (401.0): calcd. C 30.0, H 2.5, N 14.0; found C 29.9, H 2.5, N 13.7. IR (Nujol): $\tilde{\nu}$ = 3330, 3301, 3203, 1712, 1627, 1589, 1314, 1263, 1207, 1156, 1012, 972, 839, 801, 737 cm^{-1}.

Tris(3,3′-diamino-2,2′-bipyridine)zinc(II) Trifluoromethanesulfonate (3a): Reaction of an acetonitrile solution of **L1** (0.56 g, 3.0 mmol) with zinc(II) trifluoromethanesulfonate tetrahydrate (0.41 g, 1.0 mmol) following the procedure as for **2a** afforded yellow single crystals of **3a** after recrystallisation from water (yield 0.84 g, 91%). M.p. 308 °C. $C_{32}H_{30}F_6N_{12}O_6S_2Zn$ (922.2): calcd. C 41.7, H 3.3, N 18.2; found C 41.3, H 3.1, N 18.5. ^{1}H NMR ([D_6]DMSO): δ = 7.84 (br. d, J = 3.4 Hz, 6 H, 3 × 6-,6′-H), 7.26 (dd, $J_{4,5}$ = 7.9 Hz, $J_{4,6}$ = 1.3 Hz, 6 H, 3 × 4-,4′-H), 7.16 (dd, $J_{4,5}$ = 8.1 Hz, $J_{5,6}$ = 4.6 Hz, 6 H, 3 × 5-,5′-H). ^{13}C NMR ([D_6]DMSO): δ = 144.1 (3,3′-C), 138.0 (2,2′-C), 135.2 (6,6′-C), 124.5 (4,4′-C), 123.2 (5,5′-C). IR (Nujol): $\tilde{\nu}$ = 3373, 3331, 3208, 1642, 1630, 1584, 1332, 1258, 1237, 1224, 1165, 1152, 1029, 804, 726, 706, 641 cm^{-1}.

Tris(3,3′-diamino-2,2′-bipyridine)copper(II) Trifluoromethanesulfonate (3b): Copper(II) trifluoromethanesulfonate (0.65 g, 1.79 mmol) was added to solution of **L1** (1.0 g, 5.38 mmol) in acetonitrile (25 mL) and stirred for 10 min. Standing overnight produced ruby red crystals of **3b** as its acetonitrile solvate (yield 0.90 g, 54%). M.p. 249 °C. $C_{32}H_{30}CuF_6N_{12}O_6S_2{\cdot}CH_3CN$ (961.7): calcd. C 42.5, H 3.5, N 18.9, Cu 6.6; found C 42.2, H 3.3, N 19.2, Cu 6.5. IR (Nujol): $\tilde{\nu}$ = 3376, 2960, 1638, 1590, 1264, 1168, 1032, 804, 724, 638 cm^{-1}.

Tris(3,3′-diamino-2,2′-bipyridine)nickel(II) Trifluoromethanesulfonate (3c): Reaction of an acetonitrile solution of **L1** (0.56 g, 3.0 mmol) with nickel(II) trifluoromethanesulfonate pentahydrate (0.41 g, 1.0 mmol) following the procedure as for **2a** gave pale-yellow single crystals of **3c** after recrystallisation from water (yield 0.89 g, 98%). M.p. 336 °C (dec.). $C_{32}H_{30}F_6N_{12}NiO_6S_2$ (915.5): calcd. C 42.0, H 3.3, N 18.4; found C 41.9, H 3.3, N 18.6. IR (Nujol): $\tilde{\nu}$ = 3369, 3331, 3209, 1643, 1632, 1590, 1257, 1234, 1165, 1028, 803, 641 cm^{-1}.

Tris(3,3′-diamino-2,2′-bipyridine)cobalt(II) Trifluoromethanesulfonate (3d): Reaction of an acetonitrile solution of **L1** (0.56 g, 3.0 mmol) with cobalt(II) trifluoromethanesulfonate tetrahydrate (0.41 g,1.0 mmol) gave dark-red single crystals of **3d** after recrystallisation from water (yield 0.82 g, 97%). M.p. 330 °C (dec. starts at 300 °C). $C_{32}H_{30}CoF_6N_{12}O_6S_2$ (915.7): calcd. C 42.0, H 3.3, N 18.4; found C 41.9, H 3.1, N 18.7. IR (Nujol): $\tilde{\nu}$ = 3372, 3330, 3209, 1642, 1602, 1590, 1258, 1235, 1224, 1165, 1029, 803, 724, 641 cm^{-1}.

Dichloro(3,3′-diamino-2,2′-bipyridine)zinc(II) (2e): Ligand **L1** (0.15 g, 0.81 mmol) was stirred with dry zinc(II) chloride (0.11 g, 0.81 mmol) in acetonitrile (10 mL) overnight. A fine, bright-yellow precipitate and was separated from the solution by centrifugation, and dried under vacuum to give **2e** (yield 0.22 g, 86%). M.p. > 310 °C. $C_{10}H_{10}Cl_2N_4Zn$ (322.5): calcd. C 37.24, H 3.13, N 17.37; found C 37.50, H 3.13, N 17.23. ^{1}H NMR ([D_6]DMSO): δ = 7.80 (br., 2 H, 6,6′-H), 7.14 (br., 2 H, 4,4′-H) 7.04 (br., 2 H, 5,5′-H), 7.00 (br., 4 H, 2 × NH_2). ^{13}C NMR ([D_6]DMSO): δ = 144.4 (3,3′-C), 139.0 (2,2′-C), 134.1 (6,6′-C), 123.1 (4,4′-C), 122.9 (5,5′-C). IR (KBr pellet): $\tilde{\nu}$ = 3409, 3327, 3234, 1638, 1626, 1593, 1583, 1467, 1440, 1344, 1331, 1271, 1248, 1203, 1157, 1102, 1075, 806, 773, 726, 710, 650, 594 cm^{-1}.

Tris(3,3′-diamino-2,2′-bipyridine)zinc(II) Tetrachlorozincate(II) (3e) and Its DMF Solvate (3f)

Slow evaporation of a 1:1 ethanol/acetonitrile mixture of the 1:1 complex **2e** yielded single crystals which were characterised by X-ray crystallography to be the tris complex **3e**. M.p > 310 °C. ^{1}H NMR ([D_6]DMSO): δ = 7.84 (dd, $J_{6,5}$ = 4.2 Hz, $J_{6,4}$ = 1.5 Hz, 6 H, 3 × 6,6′-H), 7.14 (dd, $J_{4,5}$ = 8.2 Hz, $J_{4,6}$ = 1.5 Hz, 6 H, 3 × 4,4′-H), 7.05 (dd, $J_{5,4}$ = 8.2 Hz, $J_{5,6}$ = 4.2 Hz, 6 H, 3 × 5,5′-H), 6.97 (br., 12 H, 6 × NH_2). IR (KBr pellet): $\tilde{\nu}$ = 3514, 3327, 3214, 2925, 1945, 1634, 1588, 1465, 1445, 1321, 1270, 1242, 1206, 1152, 1101, 1076, 1022, 875, 883, 806, 732, 707, 639, 589 cm^{-1}. A second set of crystals were grown by diffusion of methanol into a DMF solution of **2e**. The crystals were characterised as being compound **3f**, a DMF solvate of **3e**. M.p. 335−338 °C. ^{1}H NMR ([D_6]DMSO): δ = 7.84 (dd, $J_{6,5}$ = 4.2 Hz, $J_{6,4}$ = 1.5 Hz, 6 H 3 × 6,6′-H), 7.14 (dd, $J_{4,5}$ = 8.2 Hz, $J_{4,6}$ = 1.5 Hz, 6 H, 3 × 4,4′-H), 7.05 (dd, $J_{5,4}$ = 8.2 Hz, $J_{5,6}$ = 4.2 Hz, 6 H, 3 × 5,5′-H), 6.97 (br., 12 H, 6 × NH_2). ^{13}C NMR ([D_6]DMSO): δ = 144.39 (3,3′-C), 138.84 (2,2′-C), 134.43 (6,6′-C), 123.49 (4,4′-C), 123.04 (5,5′-C). IR (Nujol): $\tilde{\nu}$ = 3401, 3331, 3191, 1634, 1588, 1325, 1270, 1242, 1206, 1155, 1102, 1075, 806, 726, 707, 640 cm^{-1}.

3,3′-Diamino-2,2′-bipyridinium Tetrachlorocuprate(II) (4): Copper(II) chloride dihydrate (0.45 g) dissolved in 1 M HCl (5 mL) was added to a solution of **L1** (0.50 g) in acetonitrile (5 mL) and stirred for 30 min. The resulting green precipitate was collected by filtration. A second batch of green solid crystallised out of the filtrate and was collected affording compound **4** in an overall yield of 0.57 g (54%). M.p. 290−291°C. $C_{10}H_{12}Cl_4CuN_4$ (393.6): calcd. C 29.6, H 3.0, N 13.8, Cu 16.1; found C 29.7, H 3.0, N 14.2, Cu 15.7. IR (Nujol): $\tilde{\nu}$ = 3346, 3295, 3215, 1634, 1586, 1582, 1330, 1314, 1266, 1229, 1200, 1150, 904, 819, 799, 714, 684, 648 cm^{-1}.

3,3′-Diamino-2,2′-bipyridinium Tetrachlorocuprate(II) (5a): On one occasion a few red crystals were isolated on evaporation of the

above filtrate. These crystals were carefully separated from the green crystals and characterised by X-ray crystallography as being **5a**, the salt of the diprotonated ligand **L1**. M.p > 300°C. $C_{10}H_{12}Cl_4CuN_4$ (393.6): calcd. C 29.6, H 3.0, N 13.8, Cu 16.1.%; found C 29.6, H 3.0, N 14.2, Cu 15.9.

3,3′-Diamino-2,2′-bipyridinium Tetrachlorozincate(II) (5b): Aqueous HCl (10 mL, 4.77 M) was added to a solution of **L1** (150 mg) in acetonitrile (10 mL). Zinc(II) chloride (110 mg) was then added and the reaction mixture was stirred overnight. The volume of the resulting yellow solution was reduced until a solid started to precipitate. The product was then filtered, washed with ether and dried under vacuum to give **5b** (yield 0.23 g, 72%). M.p. > 310 °C. $C_{10}H_{12}Cl_4N_4Zn$ (395.4): calcd. C 30.4, H 3.1, N 14.2; found C 30.5, H 3.1, N 13.9. ^{1}H NMR ([D$_6$]DMSO): δ = 8.07 (dd, $J_{6,5}$ = 4.3 Hz, $J_{6,4}$ = 1.3 Hz, 2 H, 6,6′-H), 7.55 (m, 4 H, 4,4′-H, 5,5′-H), 3.76 (br., 6 H, 2 × NH_2, 2 × NH). ^{13}C NMR ([D$_6$]DMSO): δ = 145.4 (3,3′-C), 132.6 (6,6′-C), 128.8 (2,2′-C) 128.6 (4, 4′-C), 126.9 (5,5′-C). IR (KBr): $\tilde{\nu}$ = 3436, 3352, 3313, 3199, 3067, 2908, 1640, 1630, 1619, 1561, 1553, 1471, 1384, 1300, 1165, 1154, 945, 806, 785 cm^{-1}.

X-ray Structure Determinations: All crystal data are summarised in Table 4 and 5 unless otherwise stated. Data were collected with Mo-K_α radiation (λ = 0.71073 Å) using a graphite monochromator with the exception of compounds **L1** and **3e**, which were collected with Cu-K_α radiation (λ = 1.54178 Å). Structure solution was performed by Patterson or direct methods using SHELXS-97.[36] Refinement: Full-matrix least-squares on F^2 (SHELXL-97)[36] all non-hydrogen positions found and refined with anisotropic temperature factors. Hydrogen atoms were located from Fourier distance maps and refined isotropically. Graphics are drawn with the WINGX package for windows.[37]

CCDC-173203−173211 (**L1, 2a, 2b, 3a, 4, 5a, 5b, 3e, 3f**, respectively) contains the supplementary crystallographic data for this paper. These data can be obtained free of charge at www.ccdc.cam.ac.uk/conts/retrieving.html [or from the Cambridge Crystallographic Data Centre, 12, Union Road, Cambridge CB2 1EZ, UK; Fax: (internat.) +44-1223/336-033; E-mail: deposit@ccdc.cam.ac.uk].

Acknowledgments

This work was supported in part by the University of Nottingham Trent, University of Berne and the SNF (NRP 47, Supramolecular Functional Materials). We thank BENEFRI and EPSRC services for single crystal X-ray crystallographic measurements and the EPSRC and University of Berne mass spectrometry services for data. We thank Professor Silvio Decurtins (Ph.D Supervisor of M.-C. Senna) for his support and encouragement, and for allowing M.

Table 4. Crystal data for ligand **L1** together with complexes **2a**, **2b**, **4**, **5a**, **5b**

	L1	**2a**	**2b**	**4**	**5a**	**5b**
Empirical formula	$C_{10}H_{10}N_4$	$C_{20}H_{20}Cl_4Cu_4N_8$	$C_{14}H_{22}CuN_4O_7$	$C_{10}H_{12}Cl_4CuN_4$	$C_{10}H_{12}Cl_4CuN_4$	$C_{10}H_{12}Cl_4N_4Zn$
M (g mol^{-1})	186.2	641.4	421.9	393.6	393.6	395.4
Crystal size [mm]	0.38 × 0.30 × 0.19	0.2 × 0.10 × 0.10	0.49 × 0.42 × 0.30	0.28 × 0.20 × 0.18	0.08 × 0.25 × 0.40	0.45 × 0.25 × 0.05
Crystal description	blocks	blocks	blocks	Blocks	plates	plates
Crystal colour	yellow	green	dark blue	green	green	yellow
T [K]	293(2)	150(2)	293(2)	150(2)	293(3)	153(2)
Diffractometer	STOE AED2	Enraf Nonius Fast	STOE AED2	Enraf Nonius Fast	Enraf Nonius CAD4	STOE IPDS
2θ range [°]	13−119	4−51	4−51	5−50	4−50	5.4−52
Crystal system	monoclinic	monoclinic	monoclinic	monoclinic	orthorhombic	triclinic
Space group	$P2_1/n$	$P2_1/n$	$C2/c$	$P2_1/a$	$Pna2_1$	$P\bar{1}$
a [Å]	7.7896(7)	10.110(2)	18.819(4)	10.926(3)	17.457(9)	7.4417(11)
b [Å]	5.3100(4)	10.08122(9)	13.326(6)	8.214(1)	7.486(7)	7.6257(10)
c [Å]	11.0474(8)	11.6522(1)	15.950(3)	15.890(3)	11.213(3)	13.5058(18)
α [°]	90	90	90	90	90	85.071(16)
β [°]	100.594	105.18(2)	112.82(1)	104.37(2)	90	78.467(16)
γ [°]	90	90	90	90	90	85.088(17)
V [Å]^3	449.16(6)	1146.3(3)	3687.0(19)	1381.4(5)	1461.8(5)	746.34(18)
Z	2	2	8	4	4	2
$D_{calcd.}$ [gcm^{-3}]	1.38	1.86	1.46	1.89	1.78	1.76
μ [$^{-1}$]	7.1	23.5	12.2	23.4	22.3	23.5
Absorption correction	−	DIFABS	−	DIFABS	PSI SCANS	DIFABS
Min/max transmission	−	0.72/0.89	−	0.65/0.86	0.60/0.86	0.62/0.88
Measured reflections	2618	4854	3647	5122	1685	5313
Unique reflect. for Refinement (R_{int})	660	1766	3422	2033	1685	2702
Observed reflections [$I > 2\sigma(I)$]	633	1633	2478	1223	1462	2036
Max/minΔρ [e·Å^{-3}]	0.13/-0.10	0.55/-0.63	0.79/-0.51	0.57/-0.50	0.64/-0.38	1.09/-1.70
$R1$ [$I > 2\sigma(I)$][a]	0.035	0.038	0.069	0.034	0.026	0.073
$wR2$ (all reflections)	0.097	0.095	0.15	0.093		0.18
GOF on F^2 [b]	0.66	1.09	1.19	0.46	1.81	0.95

[a] $R1 = (F_o - F_c)/F_o$; $wR2 = \{[w(F_o^2 - F_c^2)^2]/(F_o^2)^2]\}^{1/2}$. [b] GOF = $\{[F_o^2 - F_c^2)^2]/(n - p)\}^{1/2}$; $w = 1/[\sigma 2(F_o^2) + (aP)^2 + bP$, where $P = [\max(F_o^2$ or $0 + 2F_c^2]/3$.

Table 5. Crystal data for the 3:1 Complexes **3a**, **3e, and 3f**

	3a	**3e**	**3f**
Empirical formula	$C_{32}H_{30}F_6N_{12}O_6S_2Zn$	$C_{32}H_{33}Cl_4N_{13}Zn_2$	$C_{33}H_{37}Cl_4N_{13}OZn_2$
M (g mol^{-1})	922.19	872.3	904.30
Crystal size [mm]	0.24 × 0.16 × 0.16	0.38 × 0.30 × 0.11	0.5 × 0.5 × 0.5
Crystal description	blocks	blocks	blocks
Crystal colour	yellow	yellow	yellow
T [K]	150(2)	293(3)	153(2)
Diffractometer	Enraf Nonius FAST	STOE AED2	STOE IPDS
Scan type 2θ range [°]	4-50	8-120	4-51
Crystal system	orthorhombic	orthorhombic	orthorhombic
Space group	$C222_1$	$Ama2$	$Pna2_1$
a [Å]	11.829(2)	21.721(8)	21.2015(10)
b [Å]	14.7536(7)	11.633(2)	11.7334(6)
c [Å]	21.581(5)	15.104(5)	45.956(3)
α [°]	90	90	90
β [°]	90	90	90
γ [°]	90	90	90
V [Å]^3	3766.3(2)	3816(2)	11486.2(11)
Z	4	4	12
$D_{calcd.}$ [gcm^{-3}]	1.63	1.52	1.57
μ [$^{-1}$]	8.5	44.8	15.8
Absorption correction	DIFABS	Psi scans	DIFABS
Min/max transmission	0.98/0.82	0.432/0.192	0.860/0.547
Measured reflections	6681	2974	30716
Unique reflect. for Refinement (R_{int})	2884	1505	16544
Observed reflections [$I > 2\sigma(I)$]	2632	1423	12055
Max/minΔρ [e·Å^{-3}]	0.42/−0.33	0.47/−0.31	0.535/−0.480
$R1$/$wR2$ [$I > 2\sigma(I)$][a]	0.036	0.037	0.040
$R1$/$wR2$ (all reflections)	0.085	0.096	0.102
GOF on F^2[b]	1.070	1.05	0.952

[a] $R1 = (F_o - F_c)/F_o$; $wR2 = \{[w(F_o^2 - F_c^2)^2]/(F_o^2)^2]\}^{1/2}$. [b] GOF $= \{[F_o^2 - F_c^2)^2]/(n - p)\}^{1/2}$. $w = 1/[\sigma 2(F_o^2) + (aP)^2 + bP$ where $P = [\max(F_o^2$ or $0 + 2F_c^2]/3$.

Pilkington and M.-C. Senna to participate in this collaboration. Finally, we acknowledge the ESF programme in "Molecular Magnets" for supporting a short visit for J. D. Wallis (summer 2000).

[1] J. M. Lehn, *Supramolecular Chemistry*, VCH, Weinheim, **1995**.
[2] P. N. W. Baxter, J. A. Connor, D. C. Povey, A. K. Powell, J. D. Wallis, *Polyhedron* **1992**, 1771−1777.
[3] R. Goddard, B. Hemelatha, M. V. Rajasekharan, *Acta Crystallogr., Sect. C* **1990**, *46*, 33−35; S. Menon, M. V. Rajeskharan, J. P. Tuchagues, *Inorg. Chem.* **1997**, *36*, 4341−4346; K. Ravikumar, G. Y. S. K. Swamy, N. V. Lakshmi, K. Chandramohan, *J. Chem. Cryst.* **1997**, *27*, 119−124; J. Yoo, J.-H. Kim, Y. S. Sohn, Y. Do, *Inorg. Chim. Acta* **1997**, *263*, 53−60.
[4] K. Ravikumar, G. Y. S. K. Swamy, N. V. Lakshmi, *Acta Crystallogr., Sect. C* **1995**, *51*, 608−611; G. Y. S. K. Swamy, K. Chandramohan, N. V. Lakshmi, K. Ravikumar, *Z. Kristallogr.* **1998**, *213*, 191−194; Z. J. Zhong, X-Z. You, Q.-C. Yang, *Polyhedron* **1994**, *13*, 1951−1955; Z. J. Zhong, X-Z. You, T. C. W. Mak, *Polyhedron* **1994**, *13*, 2157−2161; K. Ravikumar, G. Y. S. K. Swamy, N. V. Lakshmi, *Acta Crystallogr.* **1995**, *51*, 608−611.
[5] S. Decurtins, H. W. Schmalle, L. M. Zheng, J. Ensling, *Inorg. Chim. Acta* **1996**, *244*, 165−170; V. M. Miskowski, V. H. Houlding, C. M. Chen, Y. Wang, *Inorg. Chem.* **1993**, *32*, 2518−2524; R. V. Belzen, R. A. Klein, H. Kooijman, N. Veldman, A. L. Spek, C. J. Elsevier, *Organometallics* **1998**, *17*, 1812−1825; R. A. Klein, K. Vrieze, C. J. Elsevier, R. P. Thummel, J. Fraanje, K. Goubitz, *Coll. Czech. Chem. Commun.* **1997**, *62*, 238−256.
[6] J. Rebek Jr., J. E. Trend, R. V. Wattley, S. Chalravorti, *J. Am. Chem. Soc.* **1979**, *101*, 4333−4337; J. Rebek Jr., L. R. Marshall, *J. Am. Chem. Soc.* **1983**, *105*, 6668−6670.
[7] M. Pilkington, S. Decurtins, in *Magnetism: Molecules to Materials II* (Eds.: J. S. Miller and M. Drillon), Wiley-VCH, Weinheim, **2001**, *Chapter 10*, 339−356.
[8] S. S. Alguindigue, M. A. Kahn, M. T. Ashby, *Inorg. Chim. Acta* **2000**, *310*, 156−162.
[9] S. Kanoktanaporn, J. A. H. MacBride, *J. Chem. Soc., Perkin Trans. 1* **1978**, 1126−1131; K. Matsuda, I. Yanagisawa, Y. Isomura, *Synth. Commun.* **1997**, *27*, 2393−2402.
[10] L. Kaczmarek, P. Nantka-Namirski, *Acta Pol. Pharm.* **1979**, *36*, 629−634.
[11] G. Christou, S. P. Perlepes, E. Libby, K. Folting, J. C. Huffman, R. J. Webb, D. N. Hendrickson, *Inorg. Chem.* **1990**, *29*, 3657−3666.
[12] G. Christou, S. P. Perlepes, K. Folting, J. C. Huffman, R. J. Webb, D. N. Hendrickson, *J. Chem. Soc., Chem. Commun.* **1990**, 746−747.
[13] S. Meenakumari, S. K. Tiwary, A. R. Chakravarty, *Inorg. Chem.* **1994**, *33*, 2085−2089.

[14] S. P. Perlepes, E. Libby, W. E. Streib, K. Folting, G. Christou, *Polyhedron* **1992**, *11*, 923−936.
[15] B. J. Hathaway, N. Ray, D. Kennedy, N. O′Brien, B. Murphy, *Acta Crystallogr., Sect. B* **1980**, *36*, 1371−1377.
[16] M. Lubben, A. Meetsma, B. L. Feringa, *Inorg. Chim. Acta* **1995**, *230*, 169−172.
[17] M. A. Khan, D. G. Tuck, *Acta Crystallogr., Sect. C* **1984**, *40*, 60−62.
[18] P. Roman, A. Luque, J. I. Beitia, C. Guzman-Miralles, *Polyhedron* **1992**, *11*, 1883−1890.
[19] P. Roman, J. M. Gutierrez-Zorrilla, M. Martinez-Ripoll, S. Garcia-Blanco, *Z. Kristallogr.* **1985**, *173*, 169−178.
[20] A. M. W. Cargill Thompson, J. D. Jeffery, D. J. Liard, M. D. Ward, *J. Chem. Soc., Dalton Trans.* **1996**, 879−884.
[21] A. Y. Girgis, Y. S. Sohn, A. L. Balch, *Inorg. Chem.* **1975**, *14*, 2327−2331.
[22] N. C. Fletcher, T. C. Robinson, A. Behrendt, J. C. Jeffrey, Z. R. Reeves, M. D. Ward, *J. Chem. Soc., Dalton Trans.* **1999**, 2999−3006.
[23] H. Chisholm, J. C. Huffman, I. P. Rothwell, P. G. Bradley, N. Kress, W. H. Woodruff, *J. Am. Chem. Soc.* **1981**, *103*, 4945−4947.
[24] M. T. Garland, D. Grandjean, E. Spondine, A. M. Atria, J. Manzur, *Acta Crystallogr., Sect. C* **1988**, *44*, 1209−1212; M. Hernandez-Molina, J. Gonzalez-Platas, C. Ruiz-Perez, F. Lloret, M. Julve, *Inorg. Chim. Acta* **1999**, *284*, 258−265.
[25] C. Janiak, S. Deblon, H.-P. Wu, M. J. Kolm, P. Klufers, H. Piotrowski, P. Mayer, *Eur. J. Inorg. Chem.* **1999**, 1507−1521.
[26] G. V. Long, M. M. Harding, P. Turner, T. Hambley, *J. Chem. Soc., Dalton Trans.* **1995**, 3905−3910.
[27] R. Sieber, S. Decurtins, H. Stoeckli-Evans, C. Wilson, D. Yufit, J. A. K. Howard, S. C. Capelli, A. Hauser, *Chem. Eur. J.* **2000**, *6*, 361−368.
[28] C. C. Evans, R. Masse, J.-F. Nicoud, M. Bagieu-Beucher, *J. Mat. Chem.* **2000**, *10*, 1419−1423.
[29] E. Krausz, H. Riesen, A. D. Rae, *J. Aust. Chem.* **1995**, *48*, 929−954.
[30] C. A. Radlowski, C. F. Liu, M. J. Jun, *Inorg. Chim. Acta* **1984**, *86*, 101−106.
[31] D. Lew, I. Amer, *Tetrahedron: Asymmetry* **1993**, *4*, 2147−2148.
[32] J. T. Blanchette, R. D. Willett, *Inorg. Chem.* **1988**, *27*, 843−849.
[33] R. D. Willett, K. Halvorson, *Acta Crystallogr., Sect. C* **1988**, *44*, 2068−2071.
[34] M. Chao, E. Schempp, R. D. Rosenstein, *Acta Crystallogr., Sect. B* **1975**, *31*, 2924−2926.
[35] M-C. Senna, M. Pilkington, S. Decurtins, unpublished observations.
[36] G. M. Sheldrick, SHELXL-97, *Programme for Crystal Structure Refinement*, Göttingen 1997; SHELXS-97, *Programme for Crystal Structure Solution*, Göttingen, 1997.
[37] L. J. Farrugia, *J. Appl. Cryst.* **1999**, *32*, 837−838.

Received November 19, 2001
[I01465]

Accessibility Studies of Sol-Gel Processed Phosphane-Substituted Iridium(I) Complexes in the Interphase[‡]

Ekkehard Lindner,*[a] Thomas Salesch,[a] Stefan Brugger,[a] Stefan Steinbrecher,[b] Erich Plies,[b] Michael Seiler,[c] Helmut Bertagnolli,[c] and Hermann A. Mayer[a]

Dedicated to Professor Gottfried Huttner on the occasion of his 65th birthday

Keywords: Iridium / Immobilization / Sol-gel processes / Accessibility studies / NMR spectroscopy

The synthesis of the T-silyl functionalized, and therefore sol-gel processable, Vaska complex $[IrCl(CO)\{(C_6H_5)_2PC_6H_4(CH_2)_4Si(OMe)_3\}_2]$ **[4(T^0)]** succeeded by reaction of $[Ir(\mu\text{-}Cl)(COE)_2]_2$ (COE = cyclooctene; **1**) with the phosphane $(C_6H_5)_2PC_6H_4(CH_2)_4Si(OMe)_3$ **[3(T^0)]** in the presence of carbon monoxide. Subsequently, **4(T^0)** was co-polycondensed with five equivalents of $(MeO)_3Si(CH_2)_3C_6H_4(CH_2)_3Si(OMe)_3$ **{5[Ph(1,4-C$_3$T^0)$_2$]}** to give the polysiloxane-bound complex **X1**. For accessibility studies of the reactive centers, **X1** was reacted in the interphase systems gas/solid and liquid/solid with HCl, Cl_2, CH_3I ($^{13}CH_3I$), $Cl_2HCCHCl_2$, SO_2, O_2, and NCC≡CCN, in the course of which the xerogels **X2**–**X7** were formed. With the exception of the reversible species **X5** (SO_2) and **X6** (O_2) the reactions proceeded quantitatively. The composition of the polymers and the structures of the reactive centers were elucidated by means of multinuclear solid-state NMR (^{13}C, ^{29}Si, ^{31}P), IR, EDX, and EXAFS spectroscopy.

Introduction

In the last few years polymer-supported catalysts have evolved into an area of intensive research with the goal of combining the advantages of homogeneous and heterogeneous catalysis.[1−10] The catalysts are easily separable from the reaction products and they can be used for several runs, although frequently with some loss of activity due to metal leaching. In addition the reactive centers are very often not well defined, which also causes a decrease of the activity and selectivity. So far these drawbacks have prevented a commercial application of heterogenized catalysts. A versatile approach to reduce or even eliminate these problems is the introduction of the concept of an interphase.[11−14] Interphases are systems in which a stationary phase (comprised of a polymer, space, and reactive centers) and a mobile component (gas, liquid, or dissolved reactants) penetrate each other on a molecular scale without forming a homogeneous phase. Stationary phases are usually generated by simultaneous co-condensation of T-silyl-functionalized transition metal complexes with various bifunctionalized alkoxysilanes.[15−20] This procedure affords the possibility of modifying materials by controlling the mobility of the entire polymer, the density, and the distance of the reactive centers as well as swelling capabilities.

A major problem intrinsic to interphases is that of low diffusion, which adversely influences the activity of the catalysts as not all reactive centers are readily accessible for the substrates. Excellent model systems for accessibility studies are iridium complexes, which are much more stable than their corresponding rhodium congeners.

The objective of this work was to study the performance of organometallic model reactions in interphases. Therefore the reactive behavior of an iridium(I) complex incorporated into a stationary phase towards a series of molecules with different shapes and sizes like oxygen, sulfur dioxide, dicyanoethyne, and different halogenated substrates was examined. The resulting products were characterized by several spectroscopic methods as well as by EXAFS and EDX.

[‡] Supported Organometallic Complexes, 33. Part 32: E. Holder, D. Oelkrug, H.-J. Egelhaaf, H. A. Mayer, E. Lindner, *J. Fluorescence*, submitted for publication.

[a] Institut für Anorganische Chemie der Universität, Auf der Morgenstelle 18, 72076 Tübingen, Germany
Fax: (internat.) +49-(0)7071/295-306
E-mail: ekkehard.lindner@uni-tuebingen.de
[b] Institut für Angewandte Physik der Universität, Auf der Morgenstelle 10, 72076 Tübingen, Germany
Fax: (internat.) +49-(0)7071/295-400
E-mail: erich.plies@uni-tuebingen.de
[c] Institut für Physikalische Chemie der Universität, Pfaffenwaldring 55, 70569 Stuttgart, Germany
Fax: (internat.) +49-(0)711/685-4443
E-mail: h.bertagnolli@ipc.uni-stuttgart.de

 © WILEY-VCH Verlag GmbH, 69451 Weinheim, Germany, 2002 1434−1948/02/0808−1998 $ 20.00+.50/0 *Eur. J. Inorg. Chem.* **2002**, 1998−2006

Results and Discussion

Sol-Gel Processing of the Monomeric Iridium(I) Precursor Complex 4(T^0)

The iridium(I) complex **4(T^0)** was obtained by a modification of the synthetic pathway of Roberto et al. (Scheme 1).[21] A stoichiometric amount of the T-silyl-functionalized phosphane ligand **3(T^0)**[22] was added to an acetonitrile solution of $[Ir(\mu\text{-}Cl)(CO)_2]_2$ (**2**) to give a light brown solution of **4(T^0)** which was subjected to the sol-gel process directly. A single peak in the $^{31}P\{^1H\}$ NMR spectrum of **4(T^0)** at $\delta = 24.7$ ppm and one ν(CO) absorption in the IR spectrum at 1966 cm^{-1} indicated the completeness of the reaction.[23,24]

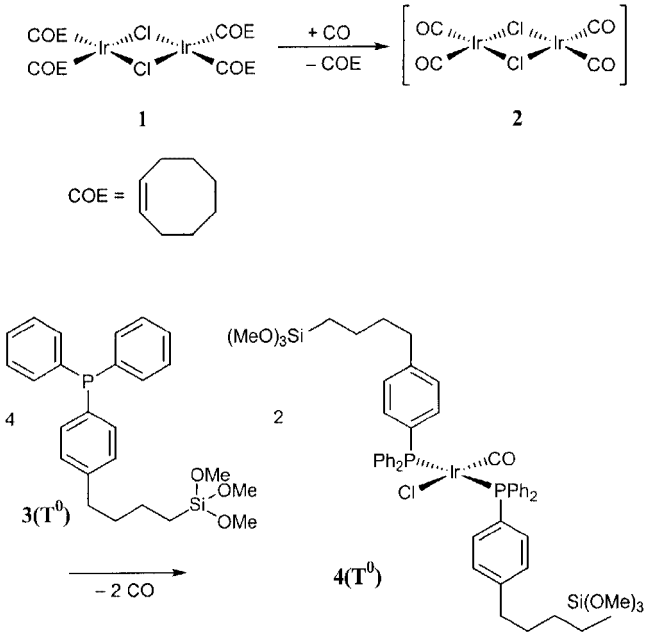

Scheme 1

A 1:5 mixture of the iridium complex **4(T^0)** and of the co-condensation agent **5[Ph(1,4-C_3T^0)$_2$]**[18] was hydrolyzed and polycondensed in water/THF in the presence of tetrabutylammonium fluoride (TBAF) as catalyst at room temperature (Scheme 2). The resulting xerogel **X1** was isolated as a pale yellow powder which is rather air stable. Only one signal, with a chemical shift of $\delta = 24.4$ ppm, is observed in the ^{31}P CP/MAS NMR spectrum of the polysiloxane-bound iridium(I) complex **X1**, in agreement with the spectrum of the monomeric complex **4(T^0)** measured in solution (Figure 1). To decide whether the phosphanes in **X1** are *cis* or *trans* oriented to each other a *J*-resolved 2D ^{31}P CP/MAS NMR spectrum according to a phase-cycled spin-echo-experiment was recorded (Figure 2).[25] The observed $^2J_{P,P}$ coupling constant of approximately 400 Hz is consistent with a *trans* configuration. In the ^{13}C CP/MAS NMR spectrum of **X1** all main signals stem from the co-condensing moiety. The missing signal for the Si–OMe function indicates a high degree of hydrolysis. All silicon atoms in the polysiloxane matrix are in the direct proximity of protons, therefore silyl species are detectable by cross polarization (CP). The signals in the ^{29}Si CP/MAS NMR spectrum of the copolymer **X1** are located in the typical range for T-silyl functions and their substructures T^2 and T^3 [$\delta = -57.3$

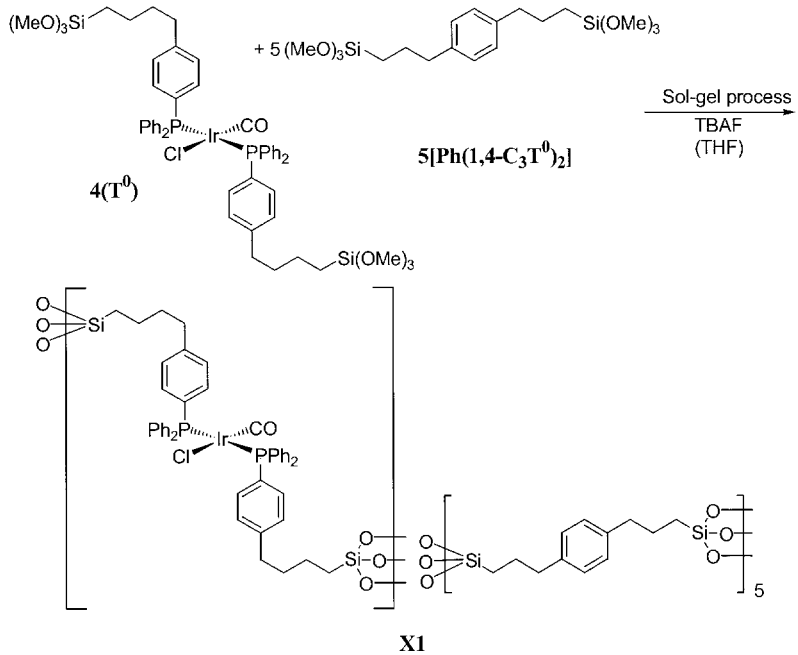

Scheme 2

(T^2), −65.7 ppm (T^3)]. The degree of condensation, which was determined by commonly used methods,[26,27] is 87%. Spin-lattice relaxation times of the protons in the rotating frame ($T_{1\rho H}$) were determined by a direct spin lock-τ-CP experiment[28] via the ^{29}Si and ^{31}P nuclei. In all cases the observed decays of the magnetization were monoexponential. Thus the relaxation mechanism is spin-diffusion controlled and the material can be considered as homogenous. The formation of domains larger than 1−2 nm in diameter is excluded.

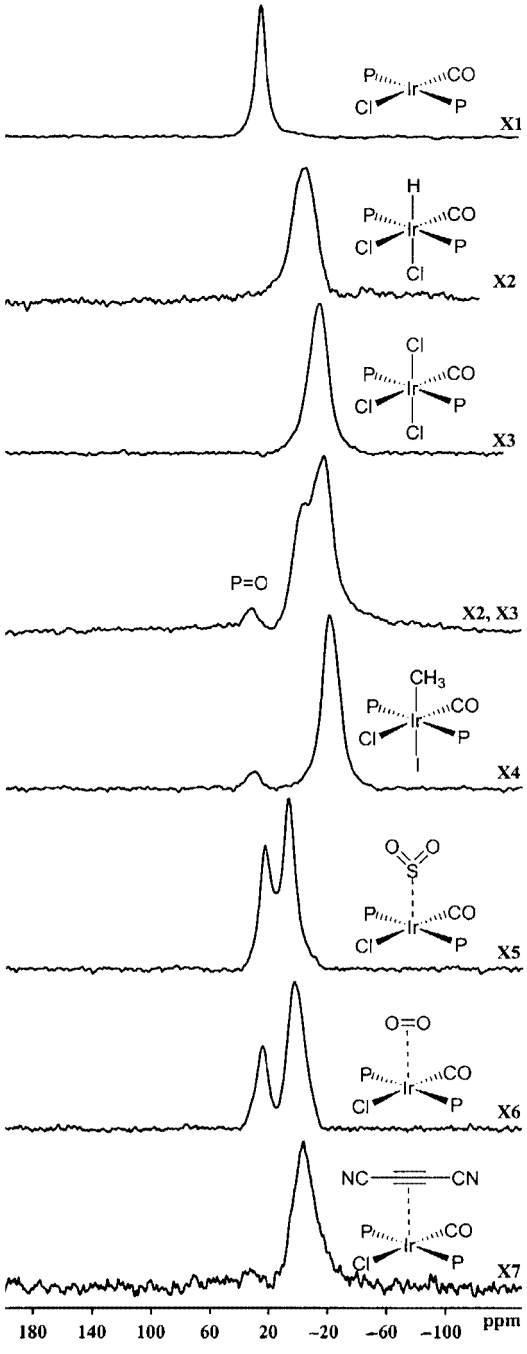

Figure 1. ^{31}P CP/MAS NMR spectra of the stationary phases **X1**−**X7**

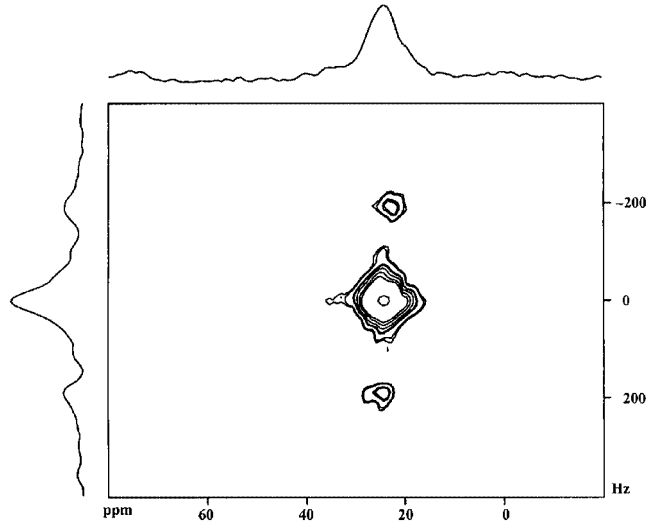

Figure 2. *J*-resolved 2D ^{31}P CP/MAS NMR spectrum of **X1**

The ν(CO) vibration (1965 cm^{-1}) in the IR spectrum of **X1** is similar to that of **4(T^0)** in solution (Figure 3). The elemental composition of the stationary phase **X1** was determined by EDX (Table 1).

Oxidative Addition Reactions on the Stationary Phase X1 with Hydrogen Chloride, Chlorine, Tetrachloroethane, and Methyl iodide (^{13}C-Methyl Iodide)

Treatment of the solid **X1** with hydrogen chloride or chlorine (interphase system: solid/gas) led to a color change from yellow to white and the polymer-anchored iridium complexes **X2** and **X3**, respectively, were formed quantitatively. The ^{31}P CP/MAS NMR and IR spectra are in full agreement with the data recorded for the corresponding monomeric complexes in solution (see Exp. Sect. and Figure 1 and 3).[29]

In the case of the reaction between **X1** and tetrachloroethane in benzene (interphase system: solid/liquid) a mixture of two different products was obtained. One component proved to be the meridional trichloroiridium(III) complex **X3**, the monomeric congener of which was described in earlier work by Al-Najjar.[30] Interestingly the second species turned out to be complex **X2**, already isolated from the reaction between hydrogen chloride and **X1**. Obviously after initial oxidative addition of the C−Cl bond both a β-C−Cl and a β-C−H elimination take place at room temperature in a competitive reaction path. The ^{31}P CP/MAS NMR spectrum reveals two resonances at δ = −3.0 (**X2**) and −18.2 ppm (**X3**) (Figure 1).[31] An unresolved broad absorption in the C≡O region between 2030 and 2080 cm^{-1} was found in the IR spectrum of this mixture (Figure 3). A direct comparison of these results with those of the known monomeric iridium(III) complexes[29] confirms the adopted structures depicted in Scheme 3.

Methyl iodide could also be oxidatively added in benzene to the iridium complex in **X1** in the interphase (solid/liquid) to give the air-stable light brown polymer **X4** (Scheme 3). The carbonyl ligand gives rise to a strong absorption band at 2042 cm^{-1}, which is in accordance with literature values

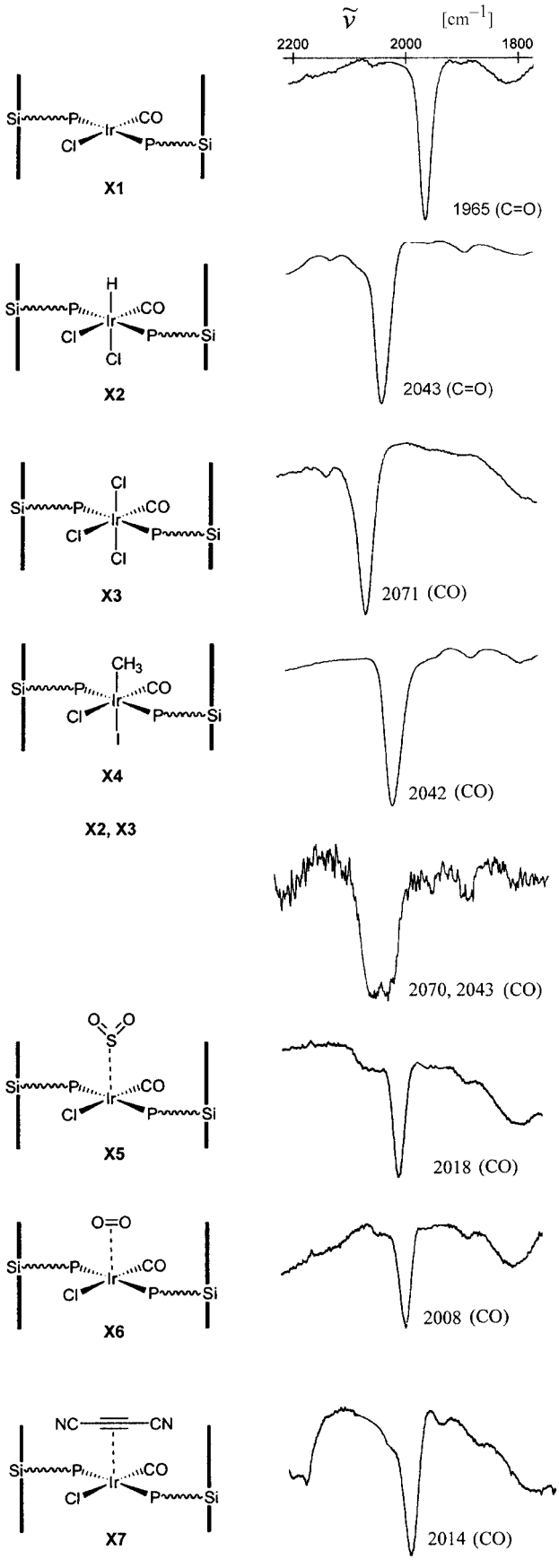

Figure 3. IR spectra of the stationary phases **X1**−**X7**

for the corresponding monomeric complex in solution.[32] Only one resonance is observed in the ^{31}P CP/MAS NMR of **X4** (Figure 1), indicating a complete conversion in the reaction. If ^{13}C-labeled methyl iodide was used an additional intense signal was observed in the ^{13}C CP/MAS NMR spectrum, which is consistent with an iridium-bound methyl group (Figure 4).

Reactions of the Stationary Phase X1 with Sulfur Dioxide, Oxygen, and Dicyanoethyne

In the solid/gas and solid/liquid interphase systems the polysiloxane-bound iridium(I) complex **X1** was reacted with sulfur dioxide, oxygen, and dicyanoethyne to give the polymeric products **X5**, **X6**, and **X7**, respectively (Scheme 3). The C≡O stretching vibration in the IR spectra of these materials confirmed a complete conversion. Absorptions at 2018, 2008, and 2014 cm^{-1} (Figure 3) were observed, which are shifted to higher wave numbers relative to **X1** (1966 cm^{-1}). These spectra were recorded under a sulfur dioxide (**X5**) or oxygen (**X6**) atmosphere. If these gases are removed, the spectrum of the starting compound **X1** appears again. However, the ^{31}P CP/MAS NMR spectra of **X5** and **X6** reveal two ^{31}P resonances (Figure 1). Since the rotors could not be packed under an oxygen or sulfur dioxide atmosphere a reversible reaction took place resulting in partial formation of the starting material **X1**. In contrast to this observation the dicyanoethyneiridium(I) complex **X7** shows only one ^{31}P signal at $\delta = -3.3$ ppm (Figure 1). These findings are in agreement with literature data[33] for the monomeric congeners in which oxygen, dicyanoethyne, and sulfur dioxide are η^2-, η^z-, and η^1-coordinated, respectively.

EXAFS and EDX Measurements of Selected Stationary Phases

One of the most powerful methods to obtain interatomic distances of amorphous materials is extended X-ray absorption fine structure spectroscopy (EXAFS). The xerogel **X4** was chosen as an example to determine the bond lengths between the metal center and the coordinating atoms of the ligand. The k^3-weighted EXAFS function (see a in Figure 5) of **X4** can be described best by six different atom shells. The first intensive peak in the corresponding Fourier transform (see b in Figure 5) is mainly due to the carbon atoms. Chlorine and phosphorus atoms were found in the case of the most intense peak, and the third intense peak belongs to the iodine and oxygen atoms. For the most intense peak of the Fourier transform (see b in Figure 5), two equivalent phosphorus atoms and one chlorine atom, with Ir−P and Ir−Cl bond lengths of 2.40 and 2.46 Å, were found. These results reveal a good agreement between the experimental and the calculated functions. A significant improvement in the fit of the first intense peak was obtained if two carbon atoms with Ir−C1 (Ir−CO bond) and Ir−C2 (Ir−CH$_3$) bond lengths of 1.86 and 2.19 Å, respectively, are considered (see b in Figure 5). Additionally, one iodine and one oxygen atom, with an Ir−I bond length of 2.63 Å and

Table 1. Elemental analysis of compounds **X1**−**X4** by EDX; hydrogen cannot be measured by X-ray emission spectroscopy therefore the reference data have been renormalized to exclude hydrogen

Xerogel	Reference data[a] Composition [%]							EDX[b] Composition [%]						
	C	O	Si	P	Cl	Ir	I	C	O	Si	P	Cl	Ir	I
X1	57.54	13.87	15.38	2.83	1.62	8.77	–	59.33	15.54	13.87	2.60	1.19	7.47	–
X2	56.62	13.65	15.13	2.78	3.18	8.63	–	56.59	11.16	17.77	3.51	2.89	8.08	–
X3	55.74	13.43	14.89	2.74	4.70	8.50	–	58.78	14.58	13.14	3.18	4.76	5.56	–
X4	54.63	13.04	14.46	2.66	1.52	8.25	5.44	54.55	13.37	14.89	2.97	1.14	8.57	4.50

[a] Calculated from theory. Complete condensation was assumed. [b] Quantified by the ZAF correction procedure.

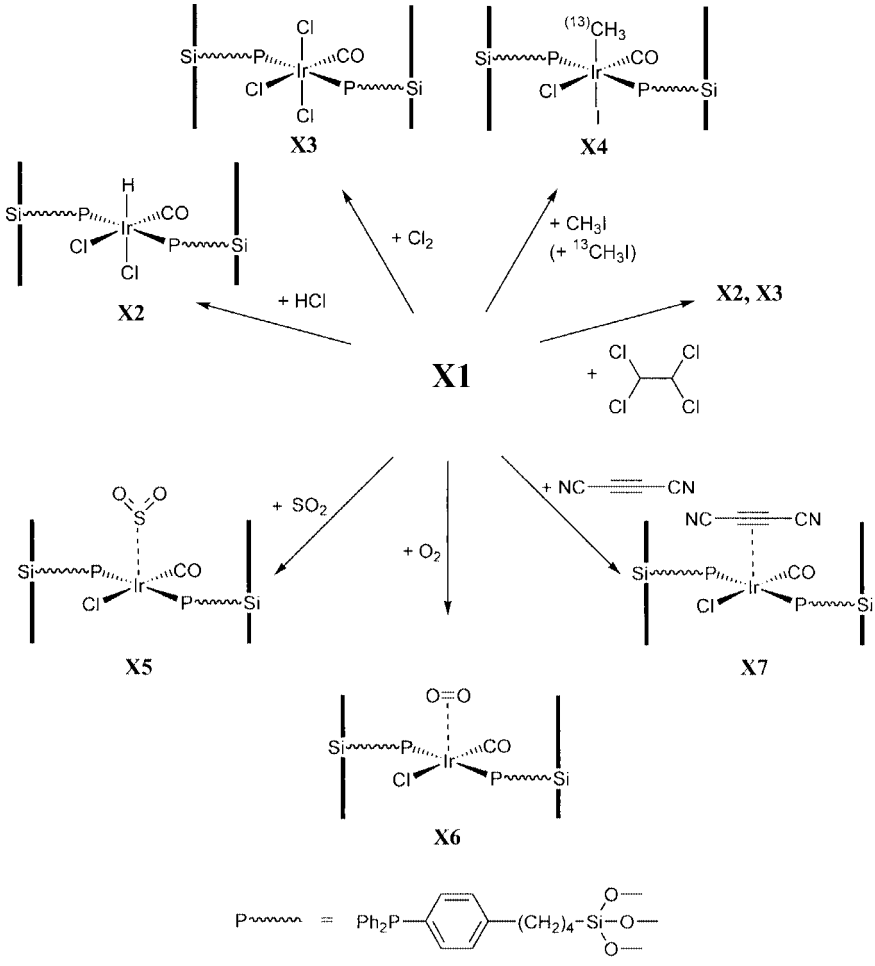

Scheme 3

an Ir−O bond length of 3.08 Å, were detected, leading to an improvement of 7.4 and 18.9% in the fit, respectively. The interatomic distances of **X4** are similar to those in similar iridium(III) complexes such as $[IrCl_3(CO)(PPh_3)_2]$,[34] $[IrCl(H)(SH)CO(PPh_3)_2]$,[35] and $[Ir(OClO_3)(CH_3)(H_2O)(CO)(PPh_3)_2]ClO_4$ [36] (Table 2).

The EDX spectra of compounds **X3** and **X4** are displayed in Figure 6. The K_α lines of carbon, oxygen, silicon, phosphorus, and chlorine and the L_α line of iridium are clearly visible. The M_α and M_β lines of iridium are overlapped by the K_α peak of phosphorus. In the case of **X4**, the L line series of iodine also appears in the spectrum. The increasing

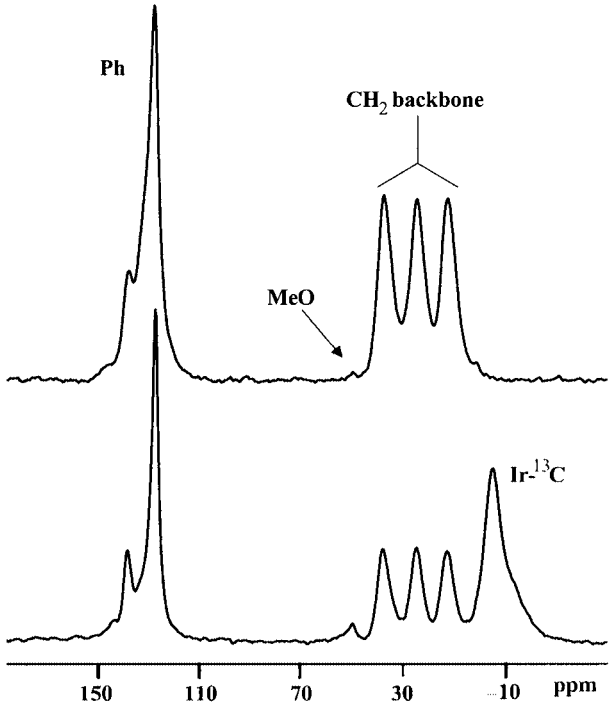

Figure 4. ^{13}C CP/MAS NMR spectra of the stationary phase **X4** (top: without ^{13}C labeling of the methyl iridium group; bottom: with ^{13}C labeling of the methyl iridium group)

content of chlorine in the xerogels **X1**−**X3** is evident as the intensity of the chlorine K line emission increases in the same direction.

Table 2. EXAFS-determined structural data of **X4**

	N[a]	r [Å][b]	σ [Å][c]
Ir−C1 (CO)[d]	1	1.86 ± 0.02	0.050 ± 0.005
Ir−C2 (CH_3)[d]	1	2.19 ± 0.02	0.095 ± 0.010
Ir−P[d]	2	2.40 ± 0.02	0.067 ± 0.010
Ir−Cl[d]	1	2.46 ± 0.03	0.097 ± 0.010
Ir−I[d]	1	2.63 ± 0.03	0.118 ± 0.012
Ir−O[d]	1	3.08 ± 0.03	0.050 ± 0.005

[a] Coordination number N. [b] Interatomic distance r. [c] Debye−Waller factor σ. [d] Absorber backscatterer.

Quantification of the EDX spectra was carried out using the ZAF correction procedure. However, as this correction procedure is valid only for flat specimens, and as the xerogels exhibit a pronounced morphology (Figure 7), special care had to be taken to find a locally flat specimen area larger than the expected electron range, which is certainly below 10 μm under the present conditions. Other sources of error, especially in light element analysis, are uncertainties in fundamental parameters and spectrometer calibration at X-ray energies below 1 keV. Spectral interference occurring between iridium and phosphorus can be corrected by peak deconvolution. Due to its high fluorescence yield, the Au-M_α line also appears under the K_β emission of phosphorus. However, the gold coating can be neglected with respect to quantification as, owing to its thickness of only 20 nm, additional absorption effects are not introduced.

Despite the numerous sources of error simultaneous quantification of all the elements present was carried out successfully. The elemental analyses by EDX are summarized in Table 1 and compared to data obtained from theory. These have been renormalized to exclude hydrogen as a

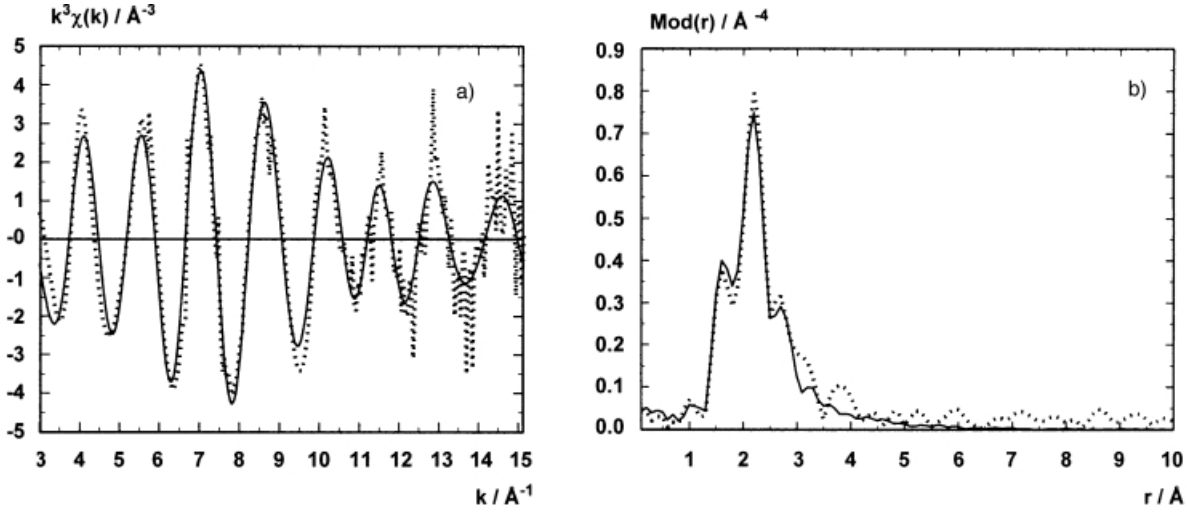

Figure 5. Experimental (dotted line) and calculated (solid line) $k^3\chi$ (k) functions (a) (k range: 2.99−15.14 $Å^{-1}$) and their Fourier transforms (b) for **X4** (Ir- L_3-edge) (see Table 2 for fit parameter)

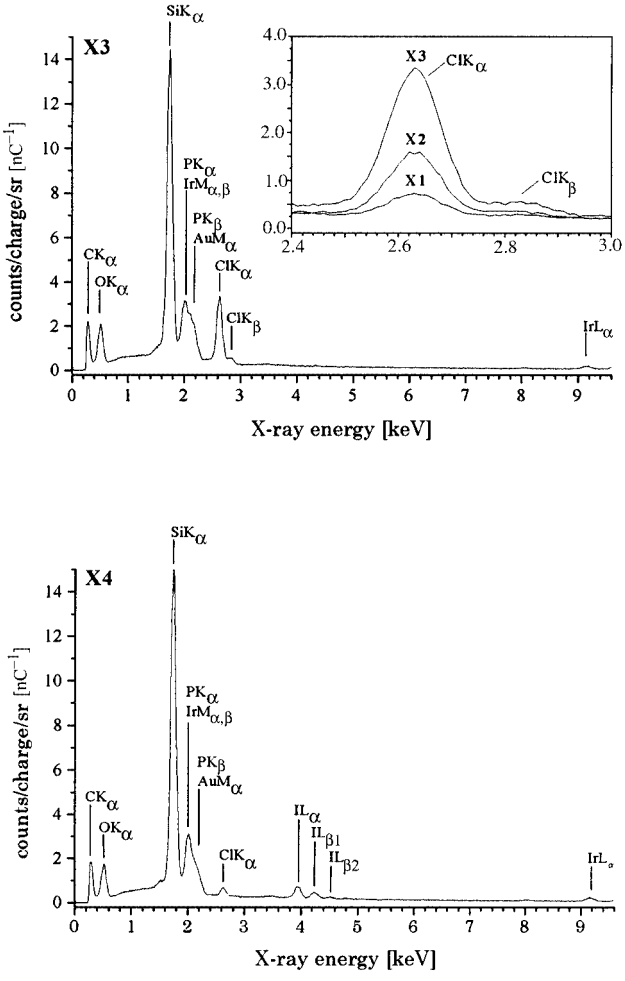

Figure 6. Energy-dispersive X-ray spectra of compounds **X3** (top) and **X4** (bottom); as shown by comparison of the Cl-K_α emission line intensities in the inlay, the chlorine content clearly increases from **X1**−**X3**; quantification results are summarized in Table 1

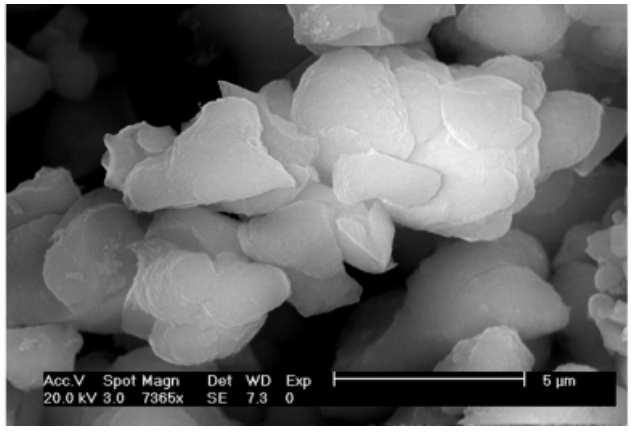

Figure 7. Scanning electron micrograph of **X1**

single-electron atom does not emit characteristic X-rays. Except for the iridium content in xerogel **X3** the elemental analyses support the reference data within the limits of error with the given samples.

Conclusion

For successful catalytic processes in interphases the polysiloxane-bound reactive centers should be completely accessible for substrate molecules. Therefore catalytic model reactions, for example the activation of small and larger molecules, are of great importance for the better understanding of catalytic reactions in interphases. To introduce reactive centers a phosphaneiridium(I) complex has been chosen because such a system is suitable for the envisaged model reactions. For the construction of a mobile stationary phase the T-silyl functionalized iridium complex **4(T^0)** was co-polycondensed with the bifunctionalized co-condensation agent $(MeO)_3Si(CH_2)_3C_6H_4(CH_2)_3Si(OMe)_3$ {**5[Ph(1,4−$C_3T^0)_2$]**} which has already been successfully employed in the rhodium-catalyzed hydroformylation of 1-hexene. The iridium-containing xerogel **X1** was then subjected to various oxidative additions and to the coordination of an alkyne. It could be unequivocally demonstrated that the iridium centers in **X1** were completely accessible for a variety of substrates with different shapes and sizes. The higher cross linkage of the T-silyl bifunctionalized co-condensation agent in the hybrid polymer matrix does not exert a disadvantageous effect on the accessibility of the metal centers. This fact presents a necessary precondition for a successful catalytic process. With the examples of the reactions with sulfur dioxide and dioxygen it could be shown that substrate molecules are also able to leave the polysiloxane matrix reversibly without any interference.

Most of these model reactions were also carried out with the corresponding rhodium(I) interphase system. However, the formed complexes proved to be unstable and partially decomposed.

Experimental Section

General: IR data were obtained on a Bruker IFS 48 FT−IR spectrometer. CP/MAS solid state NMR spectra were recorded on a Bruker DSX 200 multinuclear spectrometer equipped with a wide-bore magnet (field strength 4.7 T). Magic angle spinning was applied up to 10 kHz (4 mm ZrO_2 rotors) and 3−4 kHz (7 mm ZrO_2 rotors). Frequencies and standards: ^{31}P: 81.961 MHz (4.7 T) [85% H_3PO_4, $NH_4H_2PO_4$ (δ = 0.8 ppm) as second standard]; ^{13}C: 50.228 MHz (4.7 T), [TMS, carbonyl resonance of glycine (δ = 176.05 ppm) as second standard]; ^{29}Si: 39.73 MHz (4.7 T), (Q_8M_8 as second standard). All samples were packed with exclusion of molecular oxygen. The *J*-resolved 2D phase-cycled spin-echo-experiment was carried out according to ref.[25] [90° proton pulse length 3.8 µs, 180° proton pulse length 7.6 µs, contact time T_c 1 ms, recycle delay 1.5 s, time domain (F1) 64, time domain (F2) 2048, number of scans 512]. The cross polarization constants T_{XH} were determined by variation of the contact time T_c (14−16 experiments). The proton relaxation times in the rotating frame $T_{1\rho H}$ were measured by direct proton spin lock-τ-CP experiments[28] via ^{31}P. The relaxation parameters were obtained using Bruker software SIMFIT and WINFIT following the procedure described in ref.[15]

The EXAFS measurements were performed at the Ir−L_3-edge at 11215 eV on the beamline X1.1 at the Hamburger Synchrotron-

strahlungslabor (HASYLAB) at DESY, Hamburg at 20 °C, with a Si(111) double crystal monochromator under ambient conditions (5.46 GeV, beam current 120 mA). Data were collected in transmission mode with ion chambers. Energy calibration was monitored with 20 μm thick platinum metal foil at the L_3-edge at 11564 eV. All measurements were performed under an inert gas atmosphere. The samples were prepared from a mixture of **X4** and polyethylene. Data were analyzed with a program package specially developed for the requirements of amorphous samples.[37] The program AUTOBK of the University of Washington[38] was used for background removal, and the program EXCURV92[39] was used for the evaluation of the XAFS function. The resulting EXAFS function was weighted with k^3. Data analysis in k space was performed according to the curved-wave multiple-scattering formalism of the program EXCURV92. The mean free path of the scattered electrons was calculated from the imaginary part of the potential (VPI was set to −4.00), the amplitude reduction factor AFAC was fixed at 0.8, and an overall energy shift ΔE_0 was introduced to fit the data. In the fitting procedure the intermolecular coordination numbers were varied and the intramolecular coordination numbers were fixed according to the known values of the ligands around the iridium atom of **X4**.

Scanning electron microscopy[40] was performed on an XL 30 scanning electron microscope from Philips equipped with an DX-4 energy dispersive X-ray detection system by EDAX. This consists of a liquid-nitrogen-cooled lithium-drifted silicon detector with an active area of 10 mm^2 and the eDXi 2.11 software package. The detector resolution is 149 eV at Mn-K_α (5.984 keV) and the sample-detector distance is 50 mm in the present system. The sample powder was placed on a commercial specimen stub covered with an adhesive tab and subsequently covered with a sputtered 20 nm gold layer to ensure conductivity. The primary beam energy was 20 keV during all investigations. A probe current of 192 pA was applied for recording electron micrographs, whereas X-ray emission spectra were acquired under spot illumination applying a probe current of 569 pA for 400 live seconds (dead time approx. 33%). Measurements were repeated several times at various specimen positions to ensure reproducibility. Quantification of the X-ray spectra was carried out employing the ZAF correction procedure[41−43] after subtraction of the Bremsstrahlung background.

All reactions and manipulations were carried out under argon with usual Schlenk techniques. All solvents were distilled from sodium benzophenone or calcium hydride. H_2O was distilled under inert gas prior to use. All solvents and reagents were stored under argon. $[IrCl(COE)_2]_2$ was purchased from Aldrich, all other chemicals were bought from Fluka. The T-silyl functionalized triphenylphoshine **3(T^0)** and dicyanoethyne were prepared according to literature methods.[22,44]

Carbonylchlorobis[diphenyl{4-[4-(trimethoxysilyl)butyl]-phenyl}phosphane-κP]iridium(I) [4(T^0)]: In a three-necked flask $[IrCl(COE)_2]_2$ (350.0 mg, 0.390 mmol) was suspended in 10 mL of acetonitrile. After 10 min the argon was replaced by carbon monoxide. Undissolved $[IrCl(COE)_2]_2$ disappeared immediately, and a yellow solution was obtained, which indicated the formation of $[IrCl(CO)_2]_2$. After 10 min under an atmosphere of CO the T-silyl functionalized triphenylphosphane **3(T^0)** (684.3 mg, 156 mmol) was added. The color of the solution changed to brown yellow. According to the $^{31}P\{^1H\}$ NMR and IR spectra the reaction was finished after 20 min. The complex **4(T^0)** was sol-gel processed without further purification. $^{31}P\{^1H\}$ NMR (C_6D_6): δ = 24.7 (s) ppm. IR (KBr): $\tilde{\nu}$ = 1966 (C≡O) cm^{-1}.

Xerogel X1: In a 100 mL Schlenk-tube 5 mL of the crude solution of **4(T^0)** in acetonitrile (441.7 mg, 0.39 mmol) was added to 4 mL of THF. Subsequently, the co-condensation agent **5[Ph(1,4-C_3T^0)$_2$]** (784.9 mg, 195 mmol) was reacted with the above-mentioned mixture in the presence of 1 mL of water and 0.1 mL of a 0.1 M solution of tetrabutylammonium fluoride (TBAF) in THF as the catalyst. Stirring overnight afforded a light yellow gel. The liquid constituents were separated from the crude gel by filtration (P3) and the product was washed three times each with 10 mL of THF and 10 mL of *n*-hexane. Finally the xerogel was dried under vacuum for 4 h to give a yellow powder. Yield: 895.1 mg. ^{13}C CP/MAS NMR: δ = 139.3, 128.3 (C-phenyl, backbone and ligand), 37.9, 25.2, 12.9 (CH_2, backbone and spacer) ppm. ^{29}Si CP/MAS NMR: δ = −56.6 (T^2), −65.7 (T^3) ppm. ^{31}P CP/MAS NMR: δ = 24.4 ppm. IR (KBr): $\tilde{\nu}$ = 1965 (C≡O) cm^{-1}.

General Procedure for the Synthesis of the Xerogels X2, X3, X5, and X6 (Gas/Solid Interphases): X1 (100.0 mg) was placed in a 100 mL Schlenk tube with a magnetic stirring bar. Subsequently argon was replaced by the respective gaseous reactants at room temperature. After removal of excess reactant by argon the xerogels **X2**, **X3**, **X5**, and **X6** were obtained. In the case of the polymers **X2** and **X3** the yields were quantitative.

X2: X1 was treated with hydrogen chloride. Yield: 101.2 mg. ^{31}P CP/MAS NMR: δ = −3.2 ppm. IR (KBr): $\tilde{\nu}$ = 2043 (C≡O) cm^{-1}.

X3: X1 was treated with chlorine. Yield: 102.1 mg. ^{31}P CP/MAS NMR: δ = −20.4 ppm. IR (KBr): $\tilde{\nu}$ = 2071 (C≡O) cm^{-1}.

X5: X1 was treated with sulfur dioxide. Yield: 101.6 mg. ^{31}P CP/MAS NMR: δ = 23.9 (**X1**), 7.8 (**X5**) ppm. IR (KBr): $\tilde{\nu}$ = 2018 (C≡O) cm^{-1}.

X6: X1 was treated with oxygen. Yield: 101.6 mg. ^{31}P CP/MAS NMR: δ = 24.1 (**X1**), 3.0 (**X6**) ppm. IR (KBr): $\tilde{\nu}$ = 2008 (C≡O) cm^{-1}.

General Procedure for the Synthesis of the Xerogels X4 and X7 and Treatment of X1 with Tetrachloroethane (Liquid/Solid Interphases): A suspension of **X1** (100.0 mg) in 5 mL of benzene was treated with 0.5 mL of methyl iodide, $^{13}CH_3I$, dicyanoethyne, or tetrachloroethane, and the mixture stirred for 24 h at ambient temperature. The liquid constituents were removed by filtration (P3) and, after drying under vacuum, the respective xerogels were obtained.

X4: X1 was reacted with CH_3I or $^{13}CH_3I$. Yield: 96.4 mg (96.3 mg for $^{13}CH_3I$). ^{13}C CP/MAS NMR: δ = 139.1 (139.4*), 128.6 (128.3*) (C-phenyl, backbone and ligand), 50.1 (50.1*) (OCH_3), 37.6 (38.2*), 24.5 (24.9*), 12.5 (12.7*) (CH_2, backbone and spacer), −5.1 ($^{13}CH_3$-Ir) ppm. The asterisk indicates data for the ^{13}C labeled compound. ^{31}P CP/MAS NMR: δ = −20.2 ppm. IR (KBr): $\tilde{\nu}$ = 2042 (C≡O) cm^{-1}.

X6: X1 was reacted with dicyanoethyne. Yield: 95.8 mg. ^{31}P CP/MAS NMR: δ = −3.3 ppm. IR (KBr): $\tilde{\nu}$ = 2192 (C≡N), 2014 (C≡O) cm^{-1}.

Behavior of X1 Toward Tetrachloroethane: X1 was reacted with tetrachloroethane. Yield: 96.7. ^{31}P CP/MAS NMR: δ = −3.5 (**X2**), −18.3 (**X3**) ppm. IR (KBr): $\tilde{\nu}$ = 2070, 2043 (C≡O) cm^{-1}.

Acknowledgments

This work was supported by the Deutsche Forschungsgemeinschaft (Graduiertenkolleg "Chemie in Interphasen", Grant No. 441/2,

Bonn-Bad Godesberg, Germany) and the Fonds der Chemischen Industrie.

[1] P. Panster, S. Wieland, in *Applied Homogenous Catalysis with Organometallic Compounds* (Eds.: B. Cornils, W. A. Hermann), VCH, Weinheim, **1996**, 605.
[2] F. R. Hartley, P. N. Vezey, *Adv. Organomet. Chem.* **1977**, *15*, 189−234.
[3] P. M. Price, J. H. Clark, D. J. Macquarrie, *J. Chem. Soc., Dalton Trans.* **2000**, 101−110.
[4] S. C. Bourque, H. Alper, L. E. Manzer, P. Arya, *J. Am. Chem. Soc.* **2000**, *122*, 956−957.
[5] H. Gao, R. J. Angelici, *Organometallics* **1999**, *18*, 989−995.
[6] F. Gelman, J. Blum, D. Avnir, *J. Am. Chem. Soc.* **2000**, *122*, 11999−12000.
[7] A. J. Sandee, L. A. van der Veen, J. N. H. Reek, P. C. J. Kamer, M. Lutz, A. L. Spek, P. W. N. M. van Leeuwen, *Angew. Chem.* **1999**, *111*, 3428−3432; *Angew. Chem. Int. Ed.* **1999**, *38*, 3231−3235.
[8] A. J. Sandee, J. N. H. Reek, P. C. J. Kamer, P. W. N. M. van Leeuwen, *J. Am. Chem. Soc.* **2001**, *123*, 8468−8476.
[9] R. J. P. Corriu, C. Hoarau, A. Mehdi, C. Reye, *Chem. Commun.* **2000**, 71−72.
[10] D. W. Sindorf, G. E. Maciel, *J. Am. Chem. Soc.* **1983**, *105*, 3767−3776.
[11] E. Lindner, T. Schneller, F. Auer, H. A. Mayer, *Angew. Chem.* **1999**, *111*, 2288−2309; *Angew. Chem. Int. Ed.* **1999**, *38*, 2154−2174.
[12] E. Lindner, A. Baumann, P. Wegner, H. A. Mayer, U. Reinohl, A. Weber, T. S. Ertel, H. Bertagnolli, *J. Mater. Chem.* **2000**, *10*, 1655−1662.
[13] E. Lindner, A. Jager, F. Auer, W. Wielandt, P. Wegner, *J. Mol. Catal. A* **1998**, *129*, 91−95.
[14] E. Lindner, T. Schneller, F. Auer, P. Wegner, H. A. Mayer, *Chem. Eur. J.* **1997**, *3*, 1833−1845.
[15] E. Lindner, T. Schneller, H. A. Mayer, H. Bertagnolli, T. S. Ertel, W. Hörner, *Chem. Mater.* **1997**, *9*, 1524−1537.
[16] E. Lindner, T. Salesch, S. Brugger, F. Hoehn, P. Wegner, H. A. Mayer, *J. Organomet. Chem.* **2002**, *641*, 165−172.
[17] E. Lindner, F. Auer, A. Baumann, P. Wegner, H. A. Mayer, H. Bertagnolli, U. Reinöhl, T. S. Ertel, A. Weber, *J. Mol. Catal. A* **2000**, *157*, 97−109.
[18] E. Lindner, T. Salesch, F. Höhn, H. A. Mayer, *Z. Anorg. Allg. Chem.* **1999**, *625*, 2133−2143.
[19] E. Lindner, S. Brugger, S. Steinbrecher, E. Plies, H. A. Mayer, *Z. Anorg. Allg. Chem.* **2001**, *627*, 1731−1740.
[20] E. Lindner, S. Brugger, S. Steinbrecher, E. Plies, M. Seiler, H. Bertagnolli, P. Wegner, H. A. Mayer, *Inorg. Chim. Acta* **2002**, *327*, 54−65.
[21] D. Roberto, E. Cariati, R. Psaro, R. Ugo, *Organometallics* **1994**, *13*, 4227−4231.
[22] E. Lindner, T. Salesch, *J. Organomet. Chem.* **2001**, *628*, 151−154.
[23] K. D. Schramm, T. H. Tulip, J. A. Ibers, *Inorg. Chem.* **1980**, *19*, 3183−3185.
[24] L. Vaska, J. W. DiLuzio, *J. Am. Chem. Soc.* **1961**, *83*, 2784−2785.
[25] M. Rance, R. A. Byrd, *J. Magn. Res.* **1983**, *52*, 221−240.
[26] M. Mehring, *Principles of High Resolution NMR in Solids*, 2nd ed., Springer-Verlag, Berlin, **1983**.
[27] R. Voelkel, *Angew. Chem.* **1988**, *100*, 1525−1540; *Angew. Chem. Int. Ed. Engl.* **1988**, *27*, 1468−1483.
[28] R. S. Aujla, R. K. Harris, K. J. Packer, M. Parameswaran, B. J. Say, A. Bunn, M. E. A. Cudby, *Polym. Bull.* **1982**, *8*, 253−259.
[29] R. A. Vanderpool, H. B. Abrahamson, *Inorg. Chem.* **1985**, *24*, 2985−2989.
[30] I. M. Al-Najjar, *Inorg. Chim. Acta* **1987**, *127*, L47−L48.
[31] It is impossible to monitor the reaction in the spinner of a solid state NMR instrument at low temperature.
[32] L. Vaska, *Acc. Chem. Res.* **1968**, *1*, 335−344.
[33] G. L. McClure, W. H. Baddley, *J. Organomet. Chem.* **1971**, *27*, 155−164.
[34] F. Demartin, N. Masciocchi, *Acta Crystallogr., Sect. C* **1983**, *39*, 1225−1226.
[35] A. M. Mueting, P. Boyle, L. H. Pignolet, *Inorg. Chem.* **1984**, *23*, 44−48.
[36] C. S. Chin, M. Lee, M. Oh, G. Won, M. Kim, Y. J. Park, *Organometallics* **2000**, *19*, 1572−1577.
[37] T. S. Ertel, H. Bertagnolli, S. Hückmann, U. Kolb, D. Peter, *Appl. Spectrosc.* **1992**, *46*, 690−698.
[38] M. Newville, P. Livins, Y. Yakobi, J. J. Rehr, E. A. Stern, *Phys. Rev. B* **1993**, *47*, 14126−14131.
[39] S. J. Gurman, N. Binsted, I. Ross, *J. Phys. C* **1986**, *19*, 1845−1861.
[40] L. Reimer, *Scanning Electron Microscopy*, 2nd ed., Springer-Verlag Berlin, Heidelberg, NewYork, **1998**.
[41] V.D. Scott, G. Love, *X-ray Spectrometry* **1992**, *21*, 27−35.
[42] J. Wernisch, *X-ray Spectrometry* **1985**, *14*, 109−119.
[43] C. Poehn, J. Wernisch, W. Hanke, *X-ray Spectrometry* **1985**, *14*, 120−124.
[44] R. Faust, F. Mitzel, *J. Chem. Soc., Perkin Trans. 1* **2000**, 3746−3751.

Received December 12, 2001
[I01507]

Supramolecular Assembly with Calix[6]arene and Copper Ions − Formation of a Novel Tetranuclear Core Exhibiting Unusual Redox Properties and Catecholase Activity

Olivier Sénèque,[a] Morgan Campion,[b] Bénédicte Douziech,[b] Michel Giorgi,[c] Eric Rivière,[d] Yves Journaux,[d] Yves Le Mest,*[b] and Olivia Reinaud*[a]

Keywords: Copper / N Ligands / Calixarenes / Bioinorganic chemistry / Electrochemistry

The supramolecular biomimetic chemistry based on calix[6]arene N-ligands has been further explored. A tris(imidazole)Cu^{I} complex was treated with 1 mol-equiv. of cuprous ion under dioxygen to produce a tetranuclear cupric species. X-ray structural determination of this novel Cu_4 complex revealed that the self-inclusion of an imidazolyl coordinating arm into the hydrophobic calixarene cavity provides the base of coordination for a $\{ClImCu(OH)_2CuIm_2\}_2$ assembly. The Cu_4 core is maintained in solution and is stable even in a coordinating solvent such as acetonitrile. Magnetic susceptibility measurements evidenced a strong antiferromagnetic coupling in each $Cu(OH)_2Cu$ subunit with $J = -408\ cm^{-1}$. The complex displayed catecholase activity in the presence of 3,5-di-*tert*-butylcatechol behaving as a four-electron hole with, however, a sluggish $Cu^{I}_4 \rightarrow Cu^{II}_4$ regeneration through O_2 autooxidation. Finally, electrochemical studies revealed two oxidative reversible processes that successively gave rise to a $\{Cu^{II}Cu^{III}\}\{Cu^{II}_2\}$ and a $\{Cu^{II}Cu^{III}\}_2$ mixed-valence species that could be characterized by UV/Vis and EPR spectroscopy. The overall structure and behavior of this tetranuclear complex is reminiscent of multicopper enzymes.

(© Wiley-VCH Verlag GmbH, 69451 Weinheim, Germany, 2002)

Introduction

The synthesis of polynuclear complexes that can be studied in solution is an important topic in view of the potential role of such species in multi-metal-centered catalysis in both biological and industrial reactions. Multi-copper-containing oxygenases and oxidases have been intensively studied in recent years.[1−3] Indeed they have revealed a synergism between the copper sites on the activation of O_2. While dinuclear systems are now fairly well documented,[4] clusters of higher nuclearity appear more difficult to study. Several tetranuclear copper complexes have been described recently, displaying a wide diversity of structures of the metal cluster.[5−7] However, little information concerning their redox properties has been reported,[8] partly because of their lack of stability in solution.

In the recent past, we have been particularly interested in the synthesis, structural characterization and reactivity of copper complexes containing calix[6]arene-based N-ligands. We have shown that these supramolecular systems provide remarkable models for the type 2 active sites of copper enzymes in both Cu^{I} and Cu^{II} states.[9−11] In the process of studying the reactivity of the tris(imidazole)-based mononuclear cuprous complexes,[10] we have found that, in the presence of a second mol-equiv. of Cu^{I}, they can give rise to highly stable tetranuclear species. Here, we report the synthesis and structural characterization of a novel complex presenting a $[Cu_2(OH)_2]_2$ core with some very interesting redox properties.

[a] Laboratoire de Chimie et Biochimie Pharmacologiques et Toxicologiques, UMR CNRS 8601, Université René Descartes, 45 rue des Saints Pères, 75270 Paris cedex 06, France
Fax: (internat.) + 33-1/42862183
E-mail: reinaud@biomedicale.univ-paris5.fr
[b] Laboratoire de Chimie, Electrochimie Moléculaires et Chimie Analytique, UMR CNRS 6521, Université de Bretagne Occidentale,
BP 809, 6 Av. Victor Le Gorgeu, 29285 Brest cedex, France
Fax: (internat.) + 33-2/98017001
E-mail: yves.lemest@univ-brest.fr
[c] Laboratoire de Cristallochimie, UMR CNRS 6517, Centre Scientifique Saint-Jérôme,
Av. Escadrille Normandie-Niemen, 13397 Marseille cedex 20, France
[d] Laboratoire de Chimie Inorganique, UMR CNRS 8613, Bat 420, Université de Paris-Sud,
91405 Orsay cedex, France

Results

Synthesis and Characterization of $[Cu_4(X_6Me_3Imme_3)_2(OH)_4(Cl)_2](PF_6)_2$ (2)

Equimolar quantities of ligand $X_6Me_3Imme_3$ [12] and CuCl were first allowed to react in THF under argon to produce the cuprous complex $[Cu(X_6Me_3Imme_3)Cl]$ (**1**) that slowly precipitated out of the solution (Scheme 1). Upon

the addition of 1 mol-equiv. of $[Cu(MeCN)_4](PF_6)$ followed by dioxygen bubbling, a green solution was obtained and a blue precipitate slowly formed overnight. The isolated solid **2** was quite soluble in chlorinated solvents. Besides the absorptions characteristic of $X_6Me_3Imme_3$ and PF_6^-, the IR spectrum displayed a strong absorption at 3510 cm^{-1} that can be assigned to OH ligands. The UV/Vis spectrum in CH_2Cl_2 exhibited features at 359 and 633 nm attributed to LMCT (hydroxide or chloride to Cu^{II}) and d-d transitions, respectively. The EPR spectrum (100 K in CH_2Cl_2 or CH_2Cl_2/MeCN) showed only very weak signals at $g = 2$ and 4. The half field lines indicate the presence of exchange-coupled Cu^{II} ions,[13] whereas the signal at $g = 2$ may be attributed to traces of monomeric cupric impurities. The ^1H NMR spectrum presented both well-defined and broad peaks. However, most of the resonances were located in the diamagnetic region, suggesting an antiferromagnetic coupling between the copper ions. Elemental analysis of compound **2** was in good agreement with the formula $[Cu_4(X_6Me_3Imme_3)_2(OH)_4(Cl)_2](PF_6)_2$. Finally, the dicationic nature of complex **2** was confirmed by ES-MS analysis performed either in CH_2Cl_2 or MeCN solution. It is noteworthy that the ES-MS experiment showed that the tetranuclear entity was conserved in solution even in a dissociating and coordinating solvent such as MeCN.

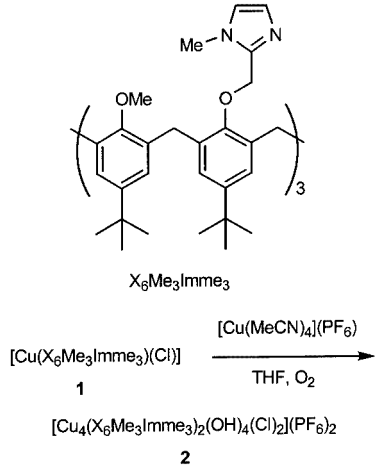

Scheme 1. Synthesis of tetranuclear complex **2**

Crystal Structure of 2

The molecular structure of this tetranuclear complex is depicted in Figure 1 and selected interatomic distances and angles are listed in Table 1. It presents an inversion center in the middle of a "stepped-cubane" Cu_4O_4 core, located between two tris(imidazolyl)calix[6]arene-based ligands that are stacked head to head. The metallic core can be viewed as two Cu_2O_2 units linked together, in which the two copper ions have a different coordination sphere.

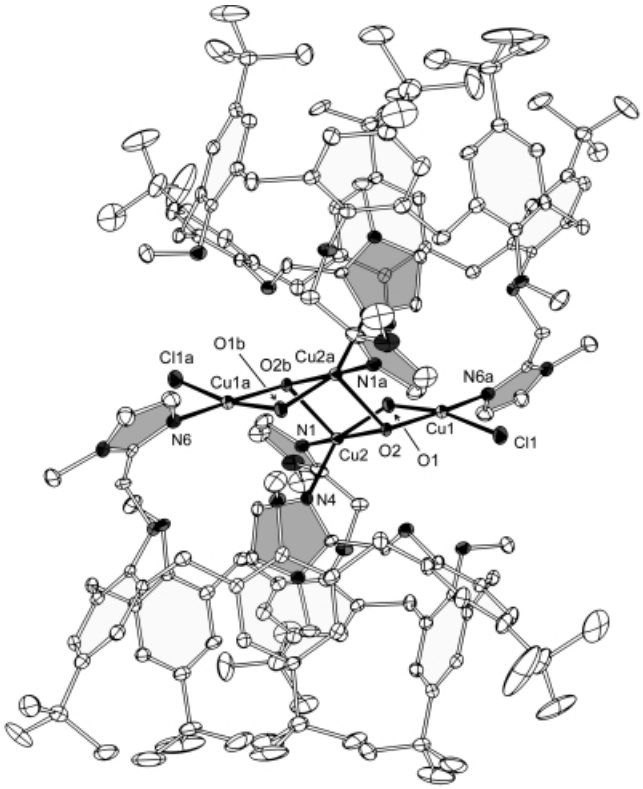

Figure 1. Crystal structure of $[Cu_4(X_6Me_3Imme_3)_2(OH)_4(Cl)_2](PF_6)_2$ (**2**) showing ellipsoids at 20% probability; hydrogen atoms, hexafluorophosphate counterions and solvent of crystallization have been omitted for clarity

Table 1. Selected interatomic distances [Å] and angles [°] for **2**

Interatomic distances[a]			
Cu1−Cl	2.230(5)	Cu2−N4	1.994(6)
Cu1−O1	1.910(6)	Cu2−O2a	2.272(7)
Cu1−O2	1.965(5)	Cu1···Cu2	2.983(1)
Cu1−N6a	1.986(7)	Cu1···Cu2a	3.770(1)
Cu2−O1	1.932(5)	Cu2···Cu2a	3.056(2)
Cu2−O2	1.988(7)	O1···O2	2.46(1)
Cu2−N1	1.97(1)	O2···O2a	2.98(2)
Angles			
Cu1−O1−Cu2	101.8(3)	Cl1−Cu1−O2	93.8(3)
Cu1−O2−Cu2	97.9(5)	N6a−Cu1−O2	170.8(3)
Cu1−O2−Cu2a	125.6(3)	N4−Cu2−O2	94.2(3)
Cu2−O2−Cu2a	91.5(3)	N4−Cu2−N1	93.5(4)
O1−Cu1−O2	78.7(3)	N1−Cu2−O2	168.1(3)
O1−Cu2−O2	77.6(3)	N1−Cu2−O1	91.4(3)
O1−Cu2−O2a	110.7(3)	N4−Cu2−O1	153.0(3)
O2−Cu2−O2a	88.5(3)	N1−Cu2−O2a	99.9(3)
Cl1−Cu1−N6a	95.1(3)	N4−Cu2−O2a	94.5(3)
Cl1−Cu1−O1	168.2(2)		

[a] Symmetry transformation for equivalent atoms: $1 - x, -y, 1 - z$.

In each discrete subunit, the Cu−O bond lengths (1.91−1.99 Å) as well as the Cu···Cu and O···O distances [d(Cu1···Cu2) = 2.98 Å; d(O1···O2) = 2.46 Å] are similar

to those reported for other bis(μ-hydroxo)dicopper(II) complexes.[14] A global charge of 2+, attested by the presence of two PF_6^- counter anions, indicates that the bridging oxygen atoms belong to hydroxo ligands (their hydrogen atoms could not be determined experimentally). The Cu_2O_2 subunit is asymmetric with bridging angles Cu1−O1−Cu2 and Cu1−O2−Cu2 angles equal to 101.8 and 97.9°, respectively. Cu1 lies in a square-planar geometry provided by one chloride ion, one calixarene-linked imidazole group and the two bridging hydroxide ions. Cu2 is coordinated in a distorted square-based pyramid ($\tau = 0.26$).[15] The base of the pyramid is constituted by the two bridging hydroxide ions and two imidazole moieties attached to the second calixarene ligand. The fifth ligand is a hydroxo group belonging to the other Cu_2O_2 core. The corresponding axial bond Cu2−O2a [2.272(7) Å] is indeed much longer than the equatorial bonds Cu2−O1 and Cu2−O2. The intersubunit distance between the two central copper ions of the tetranuclear core is only slightly longer than the Cu···Cu intrasubunit distance [*d*(Cu2···Cu2a) = 3.05 Å versus *d*(Cu1···Cu2) = 2.98 Å]. Interestingly, the calix[6]arene structures are in a cone conformation with one of the imidazole arms folded into the cavity. One C−N bond of the included imidazole ring faces an aromatic C−C bond of the host at a distance of 3.80 Å. The *N*-methyl group also stands at a relatively short distance from one of the calixarene aromatic rings (3.66 Å from the methyl group to the centroid of the aromatic ring). These observations are indicative of stabilizing π−π and CH−π host−guest interactions.[16]

Magnetism

The magnetic properties of the tetranuclear complex **2** are depicted in Figure 2. The $\chi_M T$ value at 300 K (0.66 $cm^3 \cdot K \cdot mol^{-1}$) is lower than expected for four noninteracting copper(II) ions (1.6 $cm^3 \cdot K \cdot mol^{-1}$) and decreases upon cooling. This behavior is characteristic of a strong antiferromagnetic interaction between the copper ions. The plateau of $\chi_M T$ below 70 K is due to uncoupled copper(II) impurities. As explained above, **2** can be described as two (μ-hydroxo)copper(II) binuclear subunits. As far as the magnetic properties are concerned, a weak interaction is expected between the two subunits. Let us briefly review some magneto-structural correlations concerning the bis(μ-hydroxo)-bridged copper(II) binuclear complexes. Hatfield et al. have shown that the singlet−triplet gap in such compounds varies in a regular way with the Cu−O−Cu bridging angle.[17] For bridging angles larger than 98° antiferromagnetic interactions are observed. With an average bridging angle Cu1−O−Cu2 of 99.8° in the $Cu1Cu2O_2$ subunit of **2**, a strong antiferromagnetic interaction between the copper(II) ions Cu1−Cu2 is expected. Therefore, on the first attempt, we tried to fit magnetic data using a modified Bleaney−Bowers equation taking into account the presence of two subunits. Paramagnetic impurities were accounted for by a Curie law. By least-squares fitting of the magnetic data, the following values were found: $g = 2.06$, $J = -408$ cm^{-1}, $C = 0.065$ $cm^3 \cdot K \cdot mol^{-1}$. The reliability factor $[R(\chi_M) = \Sigma(\chi_M^{obs} - \chi_M^{calc})^2/\Sigma(\chi_M^{obs})^2]$ is then $7 \cdot 10^{-5}$. On the second attempt we tried to fit the data with a tetranuclear model using complete diagonalization of the hamiltonian matrix. Interestingly, there is no improvement in the quality of the fit by using a tetranuclear model. Moreover, the *J* value for the dinuclear subunit does not change and good fits are obtained with positive and negative values for the interaction between the two central copper ions Cu2 and Cu2a. This is not unexpected; the antiferromagnetic interaction between the copper ions in the dinuclear subunits is so strong that it is not possible to measure the weakest interaction at low temperature because the dinuclear subunits are already diamagnetic at this temperature. The *J* value of -408 cm^{-1} found for the dinuclear subunit is in agreement with the theoretical calculation and the data published in the literature for an asymmetric unit.[18]

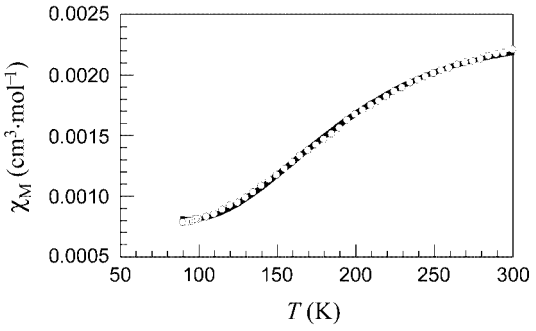

Figure 2. Plot of χ_M vs. *T* for **2**: (o) experimetal data, (−) best fit

Catecholase Activity

(μ-Hydroxo)dicopper(II) centers have been found in several active sites of enzymes.[1,2] Among the so-called type 3 copper proteins, catechol oxidase[3] catalyzes the two-electron oxidation of catechols to quinones. As complex **2** may be viewed as a dimeric form of a type 3 center, we thought of testing its activity in oxidation catalysis. Therefore, we studied the ability of compound **2** to dehydrogenate 3,5-di-*tert*-butylcatechol (dtbc) to 3,5-di-*tert*-butyl-*o*-quinone (dtbq). The reaction was conducted in a 0.088 mM dichloromethane solution of **2** with various concentrations of dtbc. Immediately after introduction of dtbc, we observed the bleaching of the initially blue solution, indicative of reduction of the four copper(II) centers to copper(I). The redox process was monitored by UV/Vis spectroscopy (see Figure 3). The absorption at 400 nm, characteristic of the *o*-quinone product ($\varepsilon = 1900$ $M^{-1} \cdot cm^{-1}$), revealed the formation of 2 equiv. of dtbq. After this first very fast process, the absorption at 400 nm only slowly increased at a rate (2.2 h^{-1}) that was independent of the dtbc concentration. This shows that the tetranuclear complex **2** is an excellent oxidant for dtbc. However, its subsequent regeneration through autooxidation of the cuprous species is slow, leading to sluggish catalytic activity.

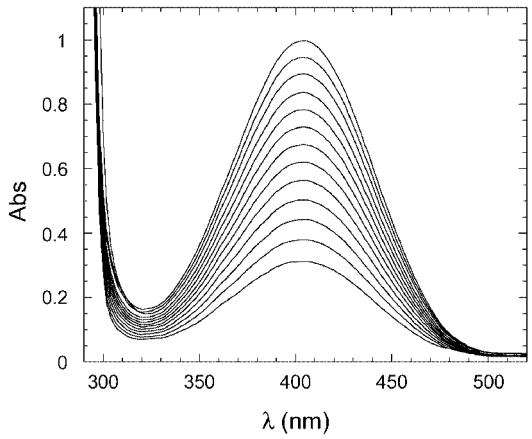

Figure 3. UV/Vis spectra of the formation of the *o*-quinone band recorded every 10 min (CH_2Cl_2 solution, [**2**] = 0.088 mM, $[dtbc]_0$ = 10.3 mM)

Electrochemistry

The electrochemical behavior of this complex has been examined in different solvents. The most interesting results were obtained in MeCN, although compound **2** is only sparingly soluble in this solvent. In pure PhCN or CH_2Cl_2 (in which **2** is highly soluble), the voltammograms displayed an elusive behavior with oxidation peaks of very low intensity. However, addition of MeCN as a co-solvent allowed the recovery of the interesting redox properties that are described as follows. On the one hand, cyclic voltammetry (CV) in the cathodic range only showed a broad peak corresponding to the reduction of some of the copper centers down to Cu^0. This is indeed indicated by the presence of an anodic redissolution peak on the reverse scan (Figure 4). In the anodic range on the other hand, two nearly reversible one-electron processes were observed at $E'°(1)$ = 0.11 V [$\Delta E_p(1)$ = 320 mV] and $E'°(2)$ = 0.66 V [$\Delta E_p(2)$ = 100 mV] with $i_{pa}/i_{pc} \approx 1$. The corresponding waves were better defined when scanning from the more anodic potential, i.e. when the totally oxidized form was generated at the surface of the electrode prior to scanning. It is noteworthy that the intensity of the peaks was much lower than those observed for the monomeric calix[6]arene-based N_3Cu family,[9,19] indicating slower diffusion processes. Rotating disk voltammetry (RDV) displayed two successive oxidation waves with a different height. The first well-defined oxidation wave was followed by a second one that was broader and 1.5 to 2 times less intense. Bulk electrolyses and coulometries gave a number of exchange electrons close to one for each oxidation step.[20] They also result in total dissolution of **2** in MeCN. After the exhaustive electrolysis of the solution (2 electrons), the RDV showed a broad composite reduction wave at a half-wave potential between the two initial oxidation waves. Evolution of the EPR spectrum was monitored after each step of the electrolysis. After a one-electron oxidation, a well-defined EPR spectrum was observed (150 K, frozen MeCN solution). The corresponding parameters ($g_\perp$ = 2.07, $g_{//}$ = 2.30, $A_{//}$ = 140 G) are typical of a magnetically isolated Cu^{II} ion sitting in a distorted square-based pyramidal environment. Interestingly, after the second one-electron exchange, an identical spectrum was recorded with double intensity, however. By UV/Vis spectrophotometry (Figure 5), the two successive oxidations resulted in the disappearance of the LMCT band and a shift of the d−d transition from 633 to 720 nm. Both oxidation steps are chemically reversible, as indicated by the restoration of the initial voltammetric and spectroscopic characteristics of the solution after counter-electrolyses.

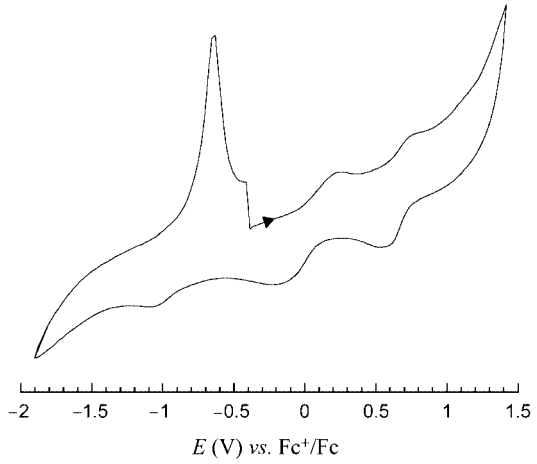

Figure 4. Cyclic voltammetry of complex **2** (1.5 mM in CH_3CN) + Bu_4NPF_6 (0.1 M) at a Pt electrode

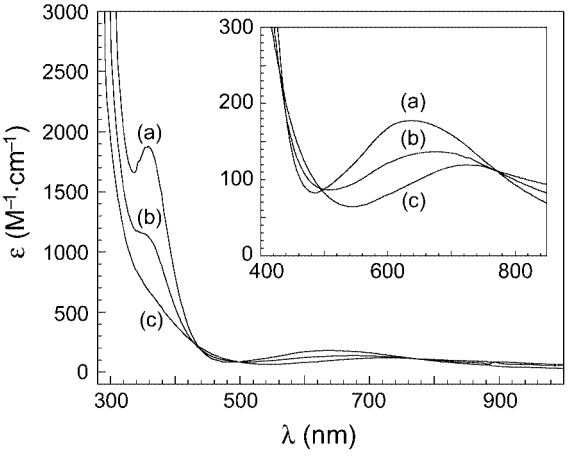

Figure 5. UV/Vis spectra of complex **2** in $MeCN/CH_2Cl_2$ (1:1) + Bu_4NPF_6 (0.1 M), before electrolysis (a), after one (b) and two (c) electron oxidation electrolysis; inset: enlarged 400−850 nm region

Discussion

The "stepped-cubane" structure of compound **2** is fairly uncommon for tetranuclear copper(II) complexes.[21] To the best of our knowledge, only one complex with similar Cu_4O_4 array has been previously reported.[22] Even more surprising is the exceptional stability of the tetranuclear

core towards coordinating solvent or redox processes. The complex results from the spontaneous assembly of two calixarene-based tridentate N-ligands, four copper atoms, one dioxygen molecule and two chloride ions. The calixarene structures seem to be frozen in a cone conformation due to the self-inclusion of one of their imidazole arms. As a result, the supramolecular assembly[23] displays interesting features: it forms a sandwich that holds and protects the Cu_4 metal core but simultaneously maintains a pathway for an external molecule to interact with it. As shown by the spontaneous dehydrogenation of 2 equiv. of dtbc into dtbq when complex **2** is introduced, the system can behave as a four-electron hole. On the other hand, the electrochemical studies showed that, in the cathodic range, complex **2** tends to decomposition after electrochemical reduction to Cu^I; this is due to the poor ability of OH^- bridges to coordinate Cu^I centers.[24] In the anodic range complex **2** can undergo two sequential one-electron oxidation processes, giving finally rise to a bis(mixed-valence) tetranuclear $[(Cu^{II}Cu^{III})]_2$ compound (**4**) (Scheme 2). Indeed, the central core of **2** is rich in anionic ligands with the two chloride and the bridging hydroxide ions. Together with the tetragonal environment of the copper ions, these features favor the stabilization of the copper(III) state. Formation of Cu^{III} derivatives, with a mixed-valence behavior, has been described in rare examples of Cu_3 and Cu_4 complexes of oxime derivatives.[25–27] The stabilization of Cu^{III} has been shown to be related to the electron-donating ability of the ligand in monomers[28] as well as in dimers.[29] In the present case, the reversibility, both electrochemical and chemical, of the redox process militates the integrity of the tetranuclearity of the system. The EPR study showed that the oxidation process gives rise to gradual apparition of magnetically isolated Cu^{II} ions. Hence, knowing that (i) the presence of MeCN is necessary for the observation of the redox systems, (ii) the spectroscopic data (NMR and UV/Vis) of **2** remained unchanged upon addition of MeCN to a CH_2Cl_2 (or $CHCl_3$) solution, and (iii) the EPR spectrum of the oxidized complex is typical of Cu^{II} sitting in a square-based pyramidal environment, we propose the sequence of reactions depicted in Scheme 2. The central copper atoms are successively oxidized to the diamagnetic Cu^{III} state leading to the formation of intermediate **3** and the final product **4**. At each step of the oxidation process, a peripheral Cu^{II} ion (Cu1) neighboring a central Cu^{III} (Cu2) becomes magnetically isolated and possibly five-coordinate due to the binding of acetonitrile in the axial position.[30] It is noteworthy that, conversely, oxidation of the peripheral Cu1 copper ions would have led to a weakly coupled dinuclear copper(II) central unit for the deoxidized species with a characteristic triplet EPR spectrum, not observed. The splitting into two one-electron redox systems, instead of a two-electron oxidation process, could result from an original cooperative/interactive phenomenon between the two dimeric units of the Cu_4 core, which should thus be considered as a pair of interacting dimers, as has been proposed in other cases.[25] This is in accordance with the dependence on the scan direction for CV and change from a two-to-one RDV wave

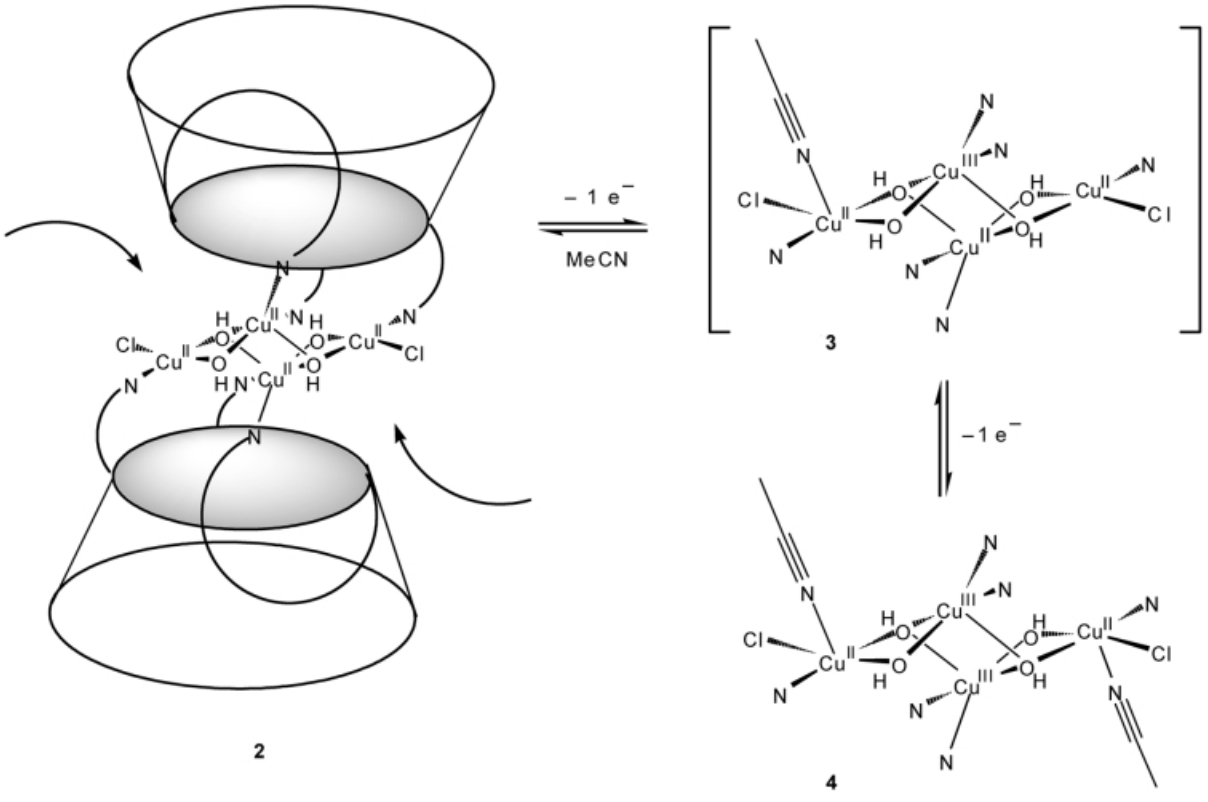

Scheme 2. Proposed electrochemical oxidation pathway for **2** in the presence of MeCN; the arrows emphasize the most accessible sites of the Cu_4O_4 core for an external molecule

after electrolysis, which is indicative of a structural rearrangement of the $[(Cu_2)_2]$ core upon oxidation.

Conclusion

Under specific conditions, reaction of the tridentate calix[6]arene-based ligand $X_6Me_3Imme_3$ with 2 mol-equiv. of copper gives rise to a tetranuclear copper(II) complex that is very stable in solution. The molecular structure of this novel compound displays a rare "stepped-cubane" Cu_4O_4 core. It also points out the self-inclusion of one imidazole arm of the calixarene ligand into its cavity. Such a self-inclusion phenomenon should be controllable by the steric hindrance of the coordinating arm. This very interesting supramolecular feature suggests that novel geometries for the coordinated metal center are actually accessible within the calix[6]arene-based tripodal systems. We are currently exploring this structural aspect. The tetranuclear complex also presents remarkable stability and redox properties that are related to its supramolecular architecture. Indeed, it can either behave as a four-electron hole, displaying catecholase activity, or itself be reversibly oxidized into mixed-valence species $Cu_3^{II}Cu^{III}$ and $Cu_2^{II}Cu_2^{III}$. In the field of biomimetic modeling, its behavior evidences an interesting similarity with multicopper enzymes in which some copper centers are specifically devoted to electron transfer and others to interaction with the substrate.[27,31] We are now actively studying the potential electrocatalytic properties of this novel Cu_4 system with promising preliminary experiments.

Experimental Section

Materials and Methods: All solvents and reagents were obtained commercially. THF was distilled from sodium/benzophenone under argon. ^{1}H NMR spectra were recorded either with a Bruker ARX 250 or a Bruker AC200 spectrometer. IR spectra were recorded with a Perkin−Elmer 783 spectrometer. Elemental analyses were performed at the Institut de Chimie des Substances Naturelles, Gif sur Yvette, France. Electrochemical experiments were carried out under dry, dioxygen-free N_2 in a dry-box manufactured by Jacomex. The electrochemical cell was specifically designed to fit the rotating disk electrode (EDI Tacussel) for a minimum volume of solution in the main compartment. The auxiliary and reference (ferrocenium/ferrocene = Fc^+/Fc) electrodes were in separate compartments connected to the main compartment through ground joints terminated by frits (Vycor tips from PAR). For voltammetric measurements, a platinum disk (diameter 2 mm) was employed, and the electrolyses were performed with the same electrode, but rotated, equipped with a disk (diameter 4 mm). A model PAR 173 potentiostat equipped with a PAR 179 digital coulometric unit, was monitored by a PAR 175 programmer. The chart recorder was a T-2Y SEFRAM ENERTEC. EPR spectra were recorded using a Bruker Elexys spectrometer (X-band). The UV/Vis spectra were recorded with a Cary 50 spectrophotometer or a Hitachi U-2010 spectrophotometer. Magnetic measurements were performed with a Quantum Design SQUID MPMS5 magnetometer. The data were collected in the range 1.8−300 K for a powdered microcrystalline sample of **2** at 0.5 T. Diamagnetic corrections were applied based on Pascal's constant.

[Cu($X_6Me_3Imme_3$)(Cl)] (1): Under argon, dry THF (2 mL) was added to a mixture of CuCl (7.0 mg, 0.067 mmol) and $X_6Me_3Imme_3$ [12] (87.0 mg, 0.067 mmol). The mixture was stirred at 40 °C for 1 h. The colorless supernatant was separated from the slightly blue precipitate by centrifugation and concentrated under vacuum. Heptane (5 mL) was added and a white precipitate formed, which was isolated by centrifugation, washed with heptane (2 mL) and dried under vacuum at 30 °C for 12 h to yield a white powder (62.8 mg, 67%). Sometimes, precipitation occurred a few minutes after addition of THF to the starting materials. In this case, the mixture was stirred at room temperature for 2 h and the precipitate was collected by centrifugation and washed with heptane. ^{1}H NMR ($CDCl_3$, 200 MHz, 25 °C): δ = 0.80 (s, 27 H, *t*Bu), 1.34 (s, 27 H, *t*Bu), 2.20 (s, 9 H, OCH_3), 3.22 (d, J = 14.2 Hz, 6 H, Ar-αCH_{eq}), 3.81 (s, 9 H, NCH_3), 4.43 (d, J = 14.7 Hz, 6 H, Ar-αCH_{ax}), 4.99 (s, 6 H, Im-αCH_2), 6.65 (s, 6 H, ArH), 6.94 (br. s, 6 H, ImH), 7.19 (s, 6 H, ArH) ppm. IR (KBr): $\tilde{\nu}$ = 1500, 1482, 1465, 1418, 1396, 1365 cm^{-1}. $C_{84}H_{108}ClCuN_6O_6$ (1396.79): calcd. C 72.23, H 7.79, N 6.02; found C 72.22, H 7.88, N 6.15.

[Cu_4($X_6Me_3Imme_3$)$_2$(OH)$_4$(Cl)$_2$](PF$_6$)$_2$ (2): Under argon, dry THF (4 mL) was added to a mixture of CuCl (12.5 mg, 0.126 mmol) and $X_6Me_3Imme_3$ (164 mg, 0.126 mmol). The mixture was stirred at room temperature for 30 min during which a white precipitate of [Cu($X_6Me_3Imme_3$)(Cl)] slowly appeared. [$Cu(CH_3CN)_4$](PF_6) (47 mg, 0.126 mmol) was added to the reaction mixture. Dry oxygen was then bubbled into the solution, which turned green. A blue precipitate slowly appeared. After 2 h, the oxygen bubbling was stopped and the mixture was stirred overnight. The green supernatant was removed and the blue precipitate was washed with THF (5 × 2 mL), dissolved in CH_2Cl_2, filtered through Celite, precipitated with pentane and dried under vacuum to yield a blue powder (131 mg, 63%). M.p. >260 °C (dec.). ^{1}H NMR ($CDCl_3$, 250 MHz, 300 K): δ = 0.5, 0.77 (s, 18 H, *t*Bu), 0.91 (s, 18 H, *t*Bu), 1.28 (s, 18 H, *t*Bu), 1.38 (s, 18 H, *t*Bu), 1.43 (s, 18 H, *t*Bu), 1.51 (s, 18 H, *t*Bu), 1.89, 2.83, 2.90, 3.75, 4.30, 4.75, 5.98, 6.12 (s, 4 H, ArH), 6.52 (s, 2 H, ArH), 6.72 (s, 2 H, ArH), 6.82 (s, 2 H, ArH), 6.85 (s, 2 H,

Table 2. Crystallographic data for **2**

Empirical formula	$C_{88}H_{120}ClCu_2F_6N_7PO_{10}$
Formula mass	1743.47
Crystal system	triclinic
Space group	$P\bar{1}$
a [Å]	15.663(1)
b [Å]	15.915(1)
c [Å]	22.803(1)
α [°]	73.72(1)
β [°]	72.36(1)
γ [°]	61.73(1)
V [Å^3]	4706.85(4)
Z	2
D_c [g cm^{-3}]	1.23
Crystal colour	blue
Crystal size [mm]	0.6 × 0.5 × 0.3
μ(Mo-K_α) [cm^{-1}]	5.65
Number of unique data	9955
Number of parameters refined	1044
Number of reflections used in refinement	9955
R [$F^2 > 4\sigma(F^2)$][34]	0.092
wR[a]	0.177
Goodness of fit	2.015
Residual Fourier [e Å^{-3}]	−0.69; 0.80

[a] $w = 1/[\sigma^2(F_o) + 0.03(F_o)^2]$.

ArH), 6.96 (s, 2 H, ArH), 7.2, 7.32 (s, 2 H, ArH), 7.70 (s, 2 H, ArH), 7.93 (s, 2 H, ArH), 8.04 (s, 2 H, ArH), 8.10 (s, 2 H, ArH), 9.85, 15.3 (br), 17, 18.1 (br), 21.9, 26.3, 30 (br), 31 (br), 32.5 (br) ppm. IR (KBr): $\tilde{\nu}$ = 3520 (OH), 1505, 1482, 1418, 1395, 1362, 1295, 1200, 842 (PF_6) cm^{-1}. UV/Vis (CH_2Cl_2, 25 °C): λ (ε) = 359 (1882), 633 (175 $M^{-1}\cdot cm^{-1}/Cu_4$) nm. ES-MS (CH_2Cl_2 or MeCN): *m/z* = 1494 [**2** − $2PF_6^-$]. $C_{168}H_{220}Cl_2Cu_4F_{12}N_{12}O_{16}P_2$ (3278.63): calcd. C 61.54, H 6.76, Cl 2.16, N 5.13; found C 61.23, H 6.61, Cl 2.56, N 4.97.

Crystal Structure Determination:[32] X-ray quality crystals of $[Cu_4(X_6Me_3Imme_3)_2(OH)_4(Cl)_2](PF_6)_2$ were obtained by slow diffusion of Et_2O into a CH_2Cl_2/MeCN or $CHCl_3$/MeCN solution of complex **2**. Data were collected at 223 K using a Nonius Kappa CCD diffractometer.[33] After a last series of Fourier analysis, two fragments remained partially resolved and were attributed to a disordered MeCN molecule and an incomplete ether solvent molecule. Crystallographic data are listed in Table 2.

Acknowledgments

The authors gratefully acknowledge financial support from the CNRS, Ministère de la Recherche (Doctoral fellowship for O. S.), and Conseil Régional de Bretagne (Doctoral fellowship for M. C.).

[1] *Multi-copper oxidases* (Ed.: A. Messerschmidt), World Scientific, Singapore, **1997**.
[2] E. I. Solomon, U. M. Sundaram, T. E. Machonkin, *Chem. Rev.* **1996**, *96*, 2563−2605.
[3] T. Klabunde, C. Eicken, J. C. Sacchettini, B. Krebs, *Nat. Struct. Biol.* **1998**, *5*, 1084−1090.
[4] [4a] K. D. Karlin, Z. Tyeklár (Eds.), *Bioinorganic Chemistry of Copper*; Champan & Hall, New York, **1993**. [4b] P. L. Holland, W. B. Tolman, *Coord. Chem. Rev.* **1999**, *190−192*, 855−869. [4c] H. C. Liang, M. Dahan, K. D. Karlin, *Curr. Opin. Chem. Biol.* **1999**, *3*, 168−175. [4d] V. Mahadevan, R. K. Gebbink, T. D. P. Stack, *Curr. Opin. Chem. Biol.* **2000**, *4*, 228−234.
[5] For some tetranuclear copper(II) complexes, see: [5a] B. J. Hathaway, in *Comprehensive Coordination Chemistry* (Eds.: G. Wilkinson, R. D. Gill, J. A. McCleverty), Pergamon Press, Oxford, U. K., **1987**, vol. 5, chapter 53. [5b] D. R. Smith, *Coord. Chem. Rev.* **1997**, *162*, 155−240. [5c] V. Tangoulis, C. P. Raptopoulou, S. Paschalidou, A. E. Tsohos, E. G. Bakalbassis, A. Terzis, S. P. Perlepes, *Inorg. Chem.* **1997**, *36*, 5270−5277. [5d] O. D. Fox, N. K. Dalley, R. G. Harrison, *Inorg. Chem.* **2000**, *39*, 620−622. [5e] Z. Xu, L. K. Thompson, C. J. Matthews, D. O. Miller, A. E. Goeta, C. Wilson, J. A. K. Howard, M. Ohba, H. Okawa, *J. Chem. Soc., Dalton Trans.* **2000**, 69−77. [5f] X. S. Tan, Y. Fujii, R. Nukada, M. Mikuriya, Y. Nakano, *J. Chem. Soc., Dalton Trans.* **1999**, 2415−2416. [5g] F. Meyer, H. Pritzkow, *Angew. Chem. Int. Ed.* **2000**, *39*, 2112−2115. [5h] E. Colacio, M. Ghazi, R. Kivekäs, J. M. Moreno, *Inorg. Chem.* **2000**, *39*, 2882−2890. [5i] B. Graham, M. T. W. Hearn, P. Junk, C. M. Kepert, F. E. Mabbs, B. Moubaraki, K. S. Murray, L. Spiccia, *Inorg. Chem.* **2001**, *40*, 1536−1543. [5j] G. Alzuet, J. A. Real, J. Borrás, R. Santiago-García, S. García-Granda, *Inorg. Chem.* **2001**, *40*, 2420−2423.
[6] For a tetranuclear copper(I) complex, see: A. F. Stange, K. W. Klinkhammer, W. Kaim, *Inorg. Chem.* **1996**, *35*, 4087−4089.
[7] For a mixed-valence tetranuclear Cu^I/Cu^{II} complex, see: P. J. van Konigsbruggen, J. G. Haasnoot, H. Kooijman, J. Reedijk, A. L. Spek, *Inorg. Chem.* **1997**, *36*, 2487−2489.
[8] For a rare example, see ref.[6]
[9] S. Blanchard, L. Le Clainche, M.-N. Rager, B. Chansou, J.-P. Tuchagues, A. F. Duprat, Y. Le Mest, O. Reinaud, *Angew. Chem. Int. Ed.* **1998**, *37*, 2732−2735.
[10] Y. Rondelez, O. Sénèque, M.-N. Rager, A. F. Duprat, O. Reinaud, *Chem. Eur. J.* **2000**, *6*, 4218−4226.
[11] L. Le Clainche, M. Giorgi, O. Reinaud, *Inorg. Chem.* **2000**, *39*, 3436−3437.
[12] O. Sénèque, M.-N. Rager, M. Giorgi, O. Reinaud, *J. Am. Chem. Soc.* **2000**, *122*, 6183−6189.
[13] R. J. M. K. Gebbink, C. F. Martens, P. J. A. Kenis, R. J. Jansen, H.-F. Nolting, V. A. Sole, M. C. Feiters, K. D. Karlin, R. J. M. Nolte, *Inorg. Chem.* **1999**, *38*, 5755−5768.
[14] [14a] N. Kitajima, T. Koda, S. Hashimoto, T. Kitagawa, Y. Moro-oka, *J. Am. Chem. Soc.* **1991**, *113*, 5664−5671. [14b] B. M. T. Lam, J. A. Halfen, V. G. Young, Jr., J. R. Hagadorn, P. L. Holland, A. Lledós, L. Cucurull-Sánchez, J. J. Novoa, S. Alvarez, W. B. Tolman, *Inorg. Chem.* **2000**, *39*, 4059−4072. [14c] S. C. Lee, R. H. Holm, *Inorg. Chem.* **1993**, *32*, 4745−4753.
[15] A. W. Addison, T. N. Rao, J. Reedijk, J. van Rijn, G. C. Verschoor, *J. Chem. Soc., Dalton Trans.* **1984**, 1349−1356.
[16] We have previously reported such CH−π interactions between the calix[6]arene moiety and a guest molecule in the case of zinc complexes: O. Sénèque, M. Giorgi, O. Reinaud, *Chem. Commun.* **2001**, 984−985.
[17] V. H. Crawford, H. W. Richardson, J. R. Wasson, D. J. Hodgson, W. E. Hatfield, *Inorg. Chem.* **1976**, *15*, 2107−2110.
[18] E. Ruiz, P. Alemany, S. Alvarez, J. Cano, *Inorg. Chem.* **1997**, *36*, 3683−3688.
[19] L. Le Clainche, Y. Rondelez, O. Sénèque, S. Blanchard, M. Campion, M. Giorgi, A. F. Duprat, Y. Le Mest, O. Reinaud, *C. R. Acad. Sci. Paris, Série IIc: Chem.* **2000**, *3*, 811−819.
[20] It is noteworthy that the number of electrons in the first step can exceed one electron up to 1.3−1.5 if the potential is maintained for a long-lasting electrolysis with a low current level (less than 10% of the initial level). This is accompanied by an increase of the first wave and a decrease of the second.
[21] Most of tetranuclear copper(II) complexes display tetrahedral or planar Cu_4 cores. See ref.[5j] and references cited therein.
[22] I. I. Matthews, H. Manohar, *J. Chem. Soc., Dalton Trans.* **1991**, 2139−2143.
[23] A *t*Bu-calix[6]arene-based tetranuclear titanium complex containing a "stepped-cubane" Ti_4O_4 core has already been described: D. D. Adreetti, G. Calestani, F. Ugozzoli, A. Arduini, E. Ghidini, A. Pochni, R. Ungaro, *J. Incl. Phenom.* **1987**, *5*, 123−126.
[24] S. Torelli, C. Belle, I. Gautier-Luneau, J. L. Pierre, E. Saint-Aman, J. M. Latour, L. Le Pape, D. Luneau, *Inorg. Chem.* **2000**, *39*, 3526−3536.
[25] E. V. Rybak-Akimova, D. H. Busch, P. K. Kahol, N. Pinto, N. Alcock, H. J. Clase, *Inorg. Chem.* **1997**, *36*, 510−520.
[26] D. Datta, A. Chakravorty, *Inorg. Chem.* **1983**, *22*, 1611−1613.
[27] A. P. Cole, D. E. Root, P. Mukherjee, E. I. Solomon, T. D. P. Stack, *Science (Washington, D. C.)* **1996**, *273*, 1848−1850.
[28] R. Ruiz, C. Surville-Barland, A. Aukauloo, E. Anxolabehere-Mallart, Y. Journaux, J. Cano, M. C. Munoz, *J. Chem. Soc., Dalton Trans.* **1997**, 745−751.
[29] For a specific case of dimeric complexes exhibiting different intensities for the two successive Cu^{II}/Cu^{III} oxidation processes, see: S. K. Mandal, L. K. Thompson, K. Nag, J. P. Charland, E. J. Gabe, *Inorg. Chem.* **1987**, *26*, 1391−1395.
[30] The possible presence of isosbestic points on the titration UV/Vis spectra (Figure 4) and the identity of the EPR data obtained after each one-electron oxidation step may be due to a relative instability of intermediate **3** compared to the fully oxidized species **4**. Indeed, it is quite possible that on the time scale of the spectroscopically coupled experiments, intermediate **3** underwent disproportionation into **2** and **4**.
[31] S. Yamanaka, H. Okawa, K.-I. Motoda, M. Yonemura, D. E. Fenton, M. Ebadi, A. B. P. Lever, *Inorg. Chem.* **1999**, *38*, 1825−1830.

[32] CCDC-176211 contains the supplementary crystallographic data for this paper. These data can be obtained free of charge at www.ccdc.cam.ac.uk/conts/retrieving. html or from the Cambridge Crystallographic Data Centre, 12, Union Road, Cambridge CB2 1EZ, UK [Fax: (internat.) + 44-1223/336-033; E-mail: deposit@ccdc.cam.ac.uk].
[33] Bruker Nonius B. V., Röntgenweg 1, 2624 BD Delft, P. O. Box 811, 2600 AV Delft, The Netherlands.
[34] S. Mackay, C. J. Gilmore, C. Edwards, M. Tremayne, N. Stewart, K. Shankland, *maXus: a computer program for the solution and refinement of crystal structures from diffraction data*, University of Glasgow, Scotland, UK, Nonius BV, Delft, The Netherlands and MacScience Co. Ltd., Yokohama, Japan, **1998**.

Received December 21, 2001
[I01527]

Formation of Isomeric BAr_3 Adducts of 2-Lithio-*N*-methylimidazole

Dominik Vagedes,[a] Gerald Kehr,[a] Dagmar König,[a] Katrin Wedeking,[a][‡] Roland Fröhlich,[a][‡] Gerhard Erker,*[a] Christian Mück-Lichtenfeld,[a][‡‡] and Stefan Grimme[a][‡‡]

Dedicated to Professor Hans J. Schäfer on the occasion of his 65th birthday

Keywords: Boranes / Carbenes / Density functional calculations / Lithium / Nucleophilic substitution

N-Methylimidazole added to the strong organometallic Lewis acid $B(C_6F_5)_3$ at the donor nitrogen atom to form the adduct **3** (characterized by X-ray diffraction). Deprotonation at the imidazole carbon atom C-2 was achieved by treatment with methyllithium to generate the reactive "Arduengo carbene anion" intermediate **4**, which underwent a rapid subsequent intramolecular nucleophilic aromatic substitution reaction at one of the adjacent C_6F_5 groups to form the tricyclic betaine-type product **5**. Rearrangement of **4** by 1,2-boron migration was not observed. The respective isomer **7** was prepared independently by deprotonation of *N*-methylimidazole, followed by C-2 addition of $B(C_6F_5)_3$. The corresponding *N*-methylimidazolide-2–$B(C_6H_5)_3$ adduct **8** was characterized by X-ray diffraction and shown to have a cyclodimeric structure made up of intermolecular bis(π-arene)(imidazole)lithium units. A DFT study revealed that the *N*-borated Arduengo carbene anions are in general very effectively kinetically protected from undergoing intramolecular rearrangement to their thermodynamically favored 2-boratoimidazole anion isomers by 1,2-BR_3 migration.
(© Wiley-VCH Verlag GmbH, 69451 Weinheim, Germany, 2002)

Introduction

The chemistry of the stable nucleophilic carbenes of the imidazol-2-ylidene type (**A**) has been developed considerably in recent years,[1−7] their use as stabilizing ligands in catalysis included.[8−11] Many other heteroatom combinations have successfully been employed for such carbene stabilization,[7d,12−14] but surprisingly little is known about the use of heteroatom-containing substituents at the nitrogen donor substituents themselves.[15−17] This would, however, be very interesting, since suitably constructed heteroatom moieties at one or both nitrogen atoms of the "Arduengo carbenes" would be expected to change the properties of such systems considerably, and would potentially open up routes to new applications of such compounds.

Siebert has recently described such a system:[17] CH deprotonation of the *N*-methylimidazole−BH_3 adduct resulted in the formation of **B** (isolated as a dimer), which may be regarded as an anionic analogue of the neutral imidazol-2-ylidine carbene species **A**. Compound **B** displayed interesting chemistry, largely determined by its nucleophilic character. Surprisingly, the analogous BEt_3 adduct **C** was reported by Siebert et al. to be unstable under the reaction conditions and to rearrange spontaneously to **D**.

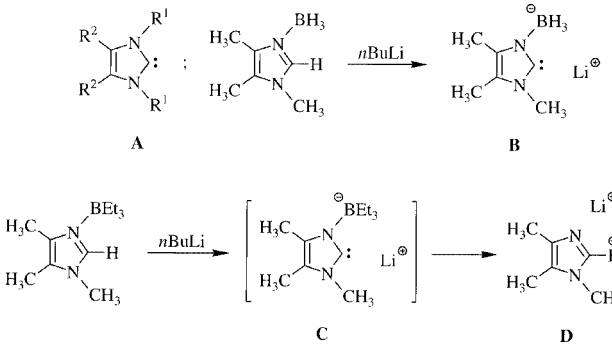

We have now developed synthetic routes to systems of types **B** and **D** by the use of triarylborane reagents and have characterized some novel chemical and structural features of such anions.

Results and Discussion

Experimental Studies

For this study, the examples of the two imidazolylborate anion types were prepared by two separate routes, since it turned out that they did not spontaneously interconvert un-

[‡] X-ray crystal structure analyses
[‡‡] Quantum chemical calculations
[a] Organisch-Chemisches Institut der Universität Münster, Corrensstraße 40, 48149 Münster, Germany

der our chosen reaction conditions. The systems described here were all derived from the parent heterocycle, the *N*-methylimidazole precursor **1**.

In the first series of experiments, the neutral starting material **1** was treated with 1 mol-equiv. of the strong organometallic Lewis acid tris(pentafluorophenyl)borane (**2a**).[18−20] The addition reaction was carried out at ambient temperature in pentane (12 h), and furnished the 1:1 addition product **3** as a white solid in > 90% yield. The ^{1}H NMR spectrum of **3** showed a singlet at δ = 7.82 ppm (1 H, 2-H), and the corresponding ^{13}C NMR C-2 resonance was observed at δ = 137.7 ppm. At ambient temperature, the "tetraarylborate" system equilibrates conformationally on the ^{19}F NMR timescale (563 MHz), and so only three ^{19}F NMR resonances were observed (at δ = −133.1, −158.6, and −164.6 ppm), in 2:1:2 ratio. The ^{11}B NMR signal at δ = −8.0 ppm indicated borate formation.

Compound **3** was characterized by X-ray diffraction. The crystal was twinned, but the structure could be solved with a sufficient accuracy. The analysis established that the bulky $B(C_6F_5)_3$ moiety was coordinated to the imidazole N1 nitrogen donor. The resulting N1−B bond length amounts to 1.605(6) Å [1.597(6) Å, the values in brackets correspond to the second independent molecule in the crystal, which is chemically equivalent]. The π-system inside the imidazole ring of the neutral adduct **3** is largely delocalized, as is evident from the respective bond lengths inside the five-membered heterocycle. The N1−C2 bond is the shortest, at 1.317(6) Å [1.303(6) Å], followed by the adjacent C2−N3 linkage at 1.336(6) Å [1.333(6) Å]. The N1−C5 [1.380(6) Å [1.389(6) Å]) and the N3−C4 bonds [1.380(6) Å [1.376(7) Å]) are almost identical in length. The C4−C5 bond is shorter [1.342(7) Å [1.350(8) Å]), whereas the exocyclic N3−C6 bond is much longer, at 1.469(6) Å [1.458(7) Å].

The conformational arrangement of **3** in the crystal is such that two of the C_6F_5 rings at the boron atom, together with the imidazole ring, form a three-bladed propeller arrangement[21] {with the dihedral angle N1−B−C11−C12 being −57.5(6)° [128.4(5)°] and N1−B−C21−C22 amounting to −65.0(5)° [106.5(5)°]}. The remaining C_6F_5 ring serves as the pivot. Its plane is rotated towards a perpendicular orientation relative to the *N*-methylimidazole ring {dihedral angles N1−B−C31−C32 179.2(4)° [+3.5(7)°], C2−N1−B−C31 −120.3(5)° [−118.3(5)°], Figure 1).

Treatment of **3** with methyllithium resulted in methane liberation, with formation of the product **5** (see Scheme 1). The ^{1}H NMR spectrum of **5** showed that the 2-H proton had been removed as expected, but the probably initially generated "anionic Arduengo carbene" product **4** proved unstable under the reaction conditions. It underwent a rapid intramolecular nucleophilic aromatic substitution with formation of a C−C bond to one of the three adjacent C_6F_5 rings at the boron atom.[22] The ^{13}C NMR resonance of the C-2 carbon atom was consequently observed at δ = 147.3 ppm (shifted ca. 50 ppm to high field from a typical value for a boron-substituted carbene **B**[23]). The remaining ^{1}H/^{13}C NMR resonances of the imidazole nucleus appeared

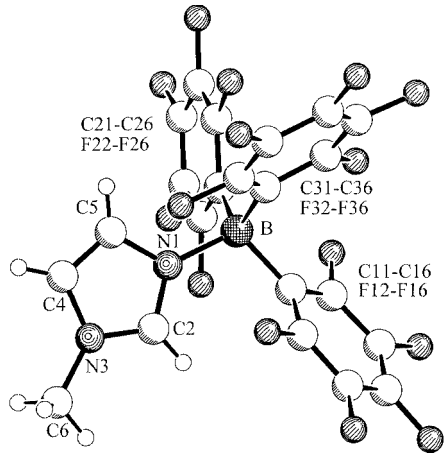

Figure 1. Projection of the molecular structure of **3**, showing the propeller-like arrangement of two C_6F_5 rings and the imidazole ring at the B−C31 pivot (only one of the two independent molecules is depicted); selected bond lengths [Å] and angles [°]: N1−C2 1.317(6)/1.303(6), N1−C5 1.380(6)/1.389(6), N1−B 1.605(6)/1.597(6), C2−N3 1.336(6)/1.333(6), N3−C4 1.380(6)/1.376(7), N3−C6 1.469(6)/1.458(7), C4−C5 1.342(7)/1.350(8), B−C11 1.640(7)/1.643(7), B−C21 1.654(7)/1.643(7), B−C31 1.632(7)/1.640(7); C2−N1−C5 106.8(4)/106.6(4), C2−N1−B 127.7(4)/129.0(4), C5−N1−B 125.5(4)/124.3(4), N1−C2−N3 110.3(4)/111.3(4), C2−N3−C4 107.7(4)/107.2(4), C2−N3−C6 125.6(4)/126.5(5), C4−N3−C6 126.7(4)/126.3(5), N3−C4−C5 106.4(4)/106.7(5), C4−C5−N1 108.8(4)/108.1(5), N1−B1−C11 108.5(4)/108.9(4), N1−B1−C21 101.8(4)/103.1(4), N1−B1−C31 112.6(4)/112.5(4), C11−B−C21 115.0(4)/116.5(4), C11−B−C31 105.2(4)/104.0(4), C21−B−C31 113.8(4)/112.0(4)

at δ = 6.99/122.2 (4-H/C-4) and δ = 6.29/126.7 (5-H/C-5). The N−CH_3 ^{1}H NMR resonance was observed as a doublet at δ = 3.08 ppm. Detailed NMR analysis, including selective ^{1}H/^{19}F decoupling, revealed that this was due to ^{1}H/^{19}F long-range coupling between the N−CH_3 protons and the 5′-F atom at the annelated C_6F_4 ring ($^6J_{H,F}$ = 4.0 Hz).[24−26] The corresponding N-CH_3/5′-F coupling was determined at $^5J_{C,F}$ = 16.7 Hz.[27−30]

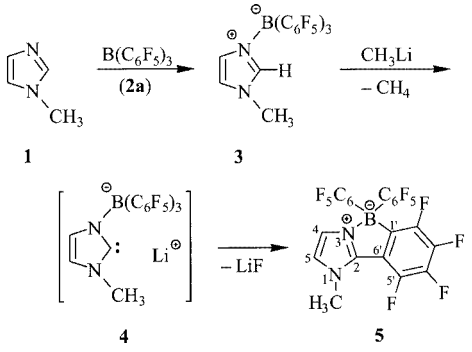

Scheme 1

The ^{11}B NMR resonance of product **5** occurred at δ = −7.6 ppm. The product exhibited the signals of a pair of symmetrically equivalent C_6F_5 substituents at the boron atom [^{19}F NMR: δ = −133.7, −157.1, −163.1 (*o*-, *p*-, *m*-F) ppm; ^{13}C NMR: δ = 148.4, 140.3, 137.6 (C-*o*, -*p*, -*m*)]

and, in addition, a typical set of four C−F signals corresponding to the annelated C_6F_4 moiety [$^{19}F/^{13}C$ NMR: δ = −131.0/148.2 (2′-F/C-2′), −151.1/140.5 (3′-F/C-3′), −156.2/142.1 (4′-F/C-4′), −135.7/141.5 (5′-F/C-5′)]. Figure 2 shows the typical appearance of the ^{19}F NMR spectrum of the product **5**.

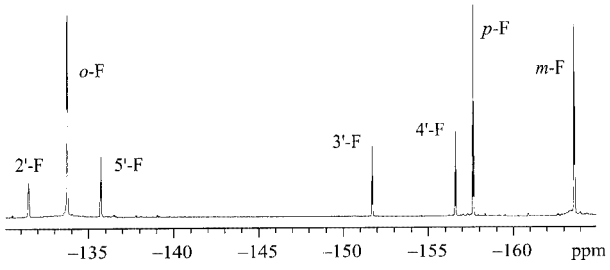

Figure 2. ^{19}F NMR spectrum of the cyclic betaine product **5** (in [D_6]benzene/[D_8]THF, 10:1, 563.6 MHz, at ambient temperature)

This experiment showed that, in this system, the *C*-borato anion **D**-type products could not be obtained by rearrangement of their Arduengo carbene anion isomers **C**. The respective system **4** was probably generated from **3** on treatment with the base methyllithium, but was shown to be unstable not with regard to rearrangement, but with regard to the much more favored intramolecular S_{NAr} reaction resulting in the observed final product **5**. In this system we therefore had to prepare the *C*-borato **D**-type isomer of the Arduengo carbene anion by a different route.

N-Methylimidazole was deprotonated at C-2 by prolonged treatment (3 d) with *n*-butyllithium at ambient temperature, as described in the literature,[31−38] to yield 2-lithio-1-methylimidazolide (**6**). This was then treated with 1 mol-equiv. of $B(C_6F_5)_3$ to yield the corresponding borate anion product **7** cleanly (see Scheme 2).

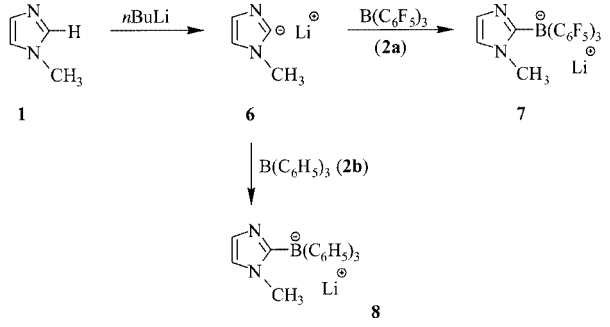

Scheme 2

Comparison of characteristic NMR spectroscopic data between compounds **6** and **7** showed that the electrophilic borane had selectively added at carbon atom C-2 of the imidazolide ring system. Most characteristically, the ^{13}C NMR resonance of the carbon atom C-2 had shifted from a very lowfield value of δ = 201.7 ppm in **6** by ca. +40 ppm to δ = 162.2 ppm in **7**. The 4-H and 5-H ^1H NMR resonances were also found at smaller values in **7** (δ = 6.61, 6.58 ppm) relative to the starting material **6** (δ = 7.23, 6.89 ppm). In addition, the ^{11}B NMR resonance of **7** was found at δ = −16.6 ppm, in the range typical for a *C*-bonded borate[39−40] [the *N*-bonded tris(pentafluorophenyl)borate systems typically show ^{11}B NMR resonances between δ = −7 and −9 ppm].

We also treated **6** with $B(C_6H_5)_3$ and obtained the salt **8** [^{13}C NMR: δ = 174.0 (C-2); ^1H NMR: δ = 6.69, 6.66 (4-H, 5-H); ^{11}B NMR: δ = −9.4]. Product **8** was characterized by X-ray crystal structure analysis. This shows the $B(C_6H_5)_3$ group attached at the imidazolide *carbon* atom C2. The C2−B bond length is found at a typical value of 1.634(2) Å. The imidazole π-system in compound **8** is delocalized, similar values as in **3** (see above) being observed: the C4−C5 bond is the shortest in the five-membered ring, at 1.334(2) Å, followed by C2−N3 [1.344(2) Å] and C2−N1 [1.367(2) Å]. The N1−C5 [1.373(2) Å] and N3−C4 bonds [1.374(2) Å] are almost equal in length. The N1−C6 linkage is much longer, at 1.453(2) Å.

The extraordinary structural feature of compound **8** is the coordinative attachment of the lithium cation to the complex anion moiety. It is bonded to N3 [Li−N3 distance: 1.922(3) Å]. One of the phenyl groups at the boron atom is rotated conformationally in such a way [θ(C2−B−C21−C22) = 86.9(2)°] that its π-face is located within bonding distance above Li. An unsymmetrical intramolecular π-arene−lithium interaction results from this orientation, with Li−C(phenyl) distances of 2.467(4) (C26), 2.641(4) (C21), 2.982(4) (C25), 3.192(4) (C22), 3.526(4) (C24), and 3.600(4) Å (C23). The coordination sphere of the lithium cation is completed by a similarly significant intermolecular π-arene−Li interaction with the C11* to C16* phenyl−B ring of an adjacent molecule of **8**. The observed *intermolecular* Li−C(phenyl)* distances are similar [2.393(4) (C15*), 2.515(4) (C16*), 2.629(4) (C14*), 2.895(4)

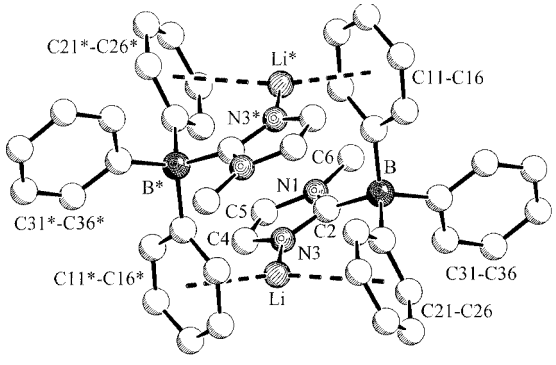

Figure 3. View of the dimeric lithiocene-type structure of **8** in the crystal; selected bond lengths [Å] and angles [°]: Li−N3 1.922(3), N1−C2 1.367(2) N1−C5 1.373(2), N1−C6 1.453(2), C2−N3 1.344(2), N3−C4 1.374(2), C4−C5 1.334(2), B−C2 1.634(2), B−C11 1.640(2), B−C21 1.650(2), B−C31 1.635(2); C2−N1−C5 108.9(1), C2−N1−C6 128.1(1), C5−N1−C6 123.0(1), N1−C2−N3 107.8(1), C2−N3−C4 107.0(1), C2−N3−Li 124.7(1), C4−N3−Li 128.3(1), N3−C4−C5 110.3(1), N1−C4−C5 106.0(1), N1−C2−B 128.1(1), N3−C2−B 124.1(1), C2−B−C11 109.3(1), C2−B−C21 106.6(1), C2−B−C31 110.8(1), C11−B−C21 111.4(1), C11−B−C31 109.9(1), C21−B−C31 108.8(1)

(C11*), 2.958(4) (C13*), and 3.066(4) Å (C12*)] to the *intramolecular* π-arene−lithium bond lengths observed in **8** (Figure 3).[41−43] The lithium−arene interaction is probably largely electrostatic in nature, as is usually observed in organolithium chemistry,[44−48] and the anionic nature of the hetaryltris(aryl)borate unit therefore facilitates the formation of this cyclodimeric structure of **8** in the solid state. Compound **8** thus represents a (dimeric) example of a distorted anionic donor ligand stabilized bis(π-arene)Li−L$^-$ lithiocene-type structure, the π-arene-derived bent lithiocene relative of the often observed Cp-derived lithiocene anions[49−51] **9**. The arene(centroid)−Li−arene(centroid) angle in **8** is 133.1°.

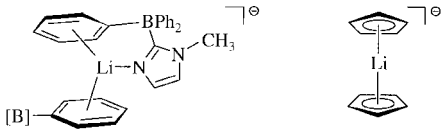

8 **9**

Theoretical Studies

Our experimental investigation had shown that the Arduengo carbene anion **4** generated in situ underwent a favored intramolecular aromatic nucleophilic substitution reaction to yield **5** rather than rearrange to the isomeric anion **7**. We were able to show by independent synthesis that **7** was stable and isolable under the applied reaction conditions. The observed resistance of **4** to rearrangement prompted us to investigate the isomerization hypersurface by theoretical methods with regard to the relative energies of the isomeric anions involved, as well as the energy profiles of their putative thermally induced interconversions with suitable model systems.

For quantum chemical investigation of the equilibrium between *N*-borane-substituted and *C*-borane-substituted imidazol-2-ylidene anions we chose the B3LYP density functional.[52−53] The structures were fully optimized without symmetry restrictions by use of the Turbomole program.[54] A triple zeta Gaussian AO basis set with additional polarization functions (TZVP)[55] was used in the optimization of the geometries and energy calculations. The calculated reaction energies for the rearrangement shown in Scheme 3 are given in Table 1.

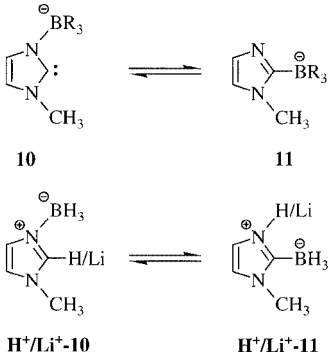

10 **11**

H$^+$/Li$^+$-10 **H$^+$/Li$^+$-11**

Scheme 3

Table 1. Reaction energies for the rearrangement of the borane (B3LYP/TZVP)

Starting compound	$\Delta_R E$ [kcal mol^{-1}]
10a (R = H)	−17.4
10b (R = CH_3)	−12.8
10c [R = (C_6H_5)]	−13.7
10d [R = (C_6F_5)]	−15.8
Li$^+$-10a	−16.9
H$^+$-10a	+5.0

Inspection of Table 1 clearly shows that the borate substituent thermodynamically prefers to be bound to C-2 of the anionic heterocyclic moiety. If the N−C fragment is regarded as an imidazolide, the Lewis acidic borane compensates the negative charge much more efficiently when bound to the carbon atom than when bound to the nitrogen atom. The different borane substituents have only a small influence on the reaction energy.

For the lithiated compound (**Li$^+$-10a**, Li at C-2), which may be viewed as a better model for the experimentally investigated situation, no significant change in the reaction energy is observed, although carbon atom C-2 is now no longer divalent. The metal atom does not change the unfavorable situation of two eclipsed vicinal sp^2 lone pairs at the carbenic center and the nitrogen atom, respectively. Only when the corresponding imidazole−borane complex (**H$^+$-10a**) is considered do we find a reversal of the equilibrium. Now the stronger boron−nitrogen interaction determines the preference for the isomer **H$^+$-10a** over the rearranged **H$^+$-11a**.

We have also localized a transition state for the intramolecular rearrangement of **10a** to **11a**.[56] The rearrangement of the borane does not proceed through the ring plane but is tilted, with a dihedral angle of 117.6° to the ring atoms (Figure 4). This is an indication of the symmetry-forbidden character of the reaction, which is also reflected in the high barrier of 40.5 kcal mol^{-1} on going from **10a** to **11a**.[57]

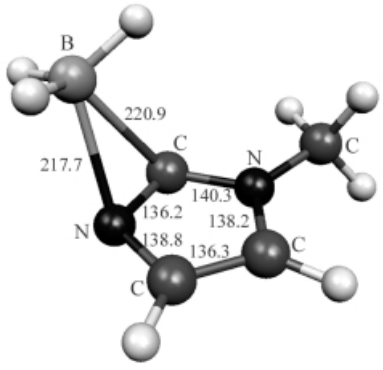

Figure 4. Transition structure of the reaction **10a** → **11a** (B3LYP/TZVP); bond lengths in pm

The nature of the transition structure was confirmed by a frequency calculation, which yielded one imaginary frequency (−119 cm^{-1}). Semiempirical (AM1) calculation of

the intrinsic reaction coordinate showed that this structure indeed linked **10a** and **11a**. By restricting the molecular symmetry to C_s, we obtained a second transition structure, with the borane in the plane, but with a much higher energy relative to **10a** (57.9 kcal mol^{-1}).

Attempts to locate a transition state for the shift of a $B(CH_3)_3$ group failed to give a similar stationary point, but ended with a loose complex of the borane with the anion (B−N 3.5 Å; B−C 3.6 Å), with a relative energy of 31.2 kcal mol^{-1} compared with **10b**. It is very likely that the $B(aryl)_3$ compounds, for which we did not try to calculate a barrier, behave in the same manner.

Our theoretical study revealed that the *C*-borated anions of type **D** (e.g. **7**) were thermodynamically favored over their "Arduengo carbene anion" isomers **B**, **C**, and, for example, **4**, but that their interconversion was practically precluded by a very high barrier of the respective 1,2-BR_3 shift. From our theoretical study it must be assumed that any such rearrangement, when experimentally observed,[17] is likely to have proceeded intermolecularly.[7d,60] Thus, we must conclude that the *N*-borato Arduengo carbene anions should exhibit their characteristic chemistry − as observed for **4** in the Experimental Study − when prepared or generated under conditions precluding *intermolecular* rearrangement pathways to their thermodynamically favored *C*-2-borated imidazole anion isomers. We expect that these findings should stimulate the use of such anionic Arduengo carbenes, especially as ligands in transition metal chemistry and catalysis, beyond the chemistry already reported for the special example of the BH_3-derived system **B**.[61]

Experimental Section

General: Reactions with organometallic compounds were carried out under argon in Schlenk-type glassware or in a glovebox. Solvents, including deuterated solvents used for NMR spectroscopy, were dried and distilled under argon prior to use. The following instruments were used for physical characterization of the compounds: Bruker AC 200 P NMR spectrometer (^{11}B: 64 MHz) at 300 K and Varian Unity plus (^{1}H: 600 MHz. ^{13}C: 150 MHz. ^{19}F: 564 MHz) NMR spectrometer at 298 K, a Nicolet 5 DXC FT-IR spectrometer, and a Micromass Quattro LC-Z mass spectrometer for HRMS determination. Elemental analyses were carried out with a Foss-Heraeus CHN-rapid elemental analyzer or a Vario El III micro elemental analyzer; melting points were determined by differential scanning calorimetry (2010 DSC, Du Pont/STA Instruments). Tris(pentafluorophenyl)borane (**2a**) was prepared according to a literature procedure.[18−20] 1-Methylimidazole (**1**) and triphenylborane (**2b**) were commercially available and were used without further purification. 1-Methylimidazole was stored over molecular sieves.

1-Methylimidazole−Tris(pentafluorophenyl)borane (3): Tris(pentafluorophenyl)borane (**2a**, 1.02 g, 2.00 mmol) was added to a suspension of 1-methylimidazole (**1**, 164 mg, 2.00 mmol) in 20 mL of pentane at 0 °C. The reaction mixture was allowed to warm to room temperature and was stirred for another 12 h. The precipitated product was collected by filtration to yield 1.08 g (91%) of **3** as a white solid, m.p. 249 °C. IR (KBr): $\tilde{\nu}$ = 3001, 1649, 1566, 1530, 1380, 1281, 1259, 1100, 991, 865, 751 cm^{-1}. ^{1}H NMR (600 MHz, [D_6]benzene): δ = 7.82 (s, 1 H, 2-H), 7.06 (s, 1 H, 4-H), 7.01 (d, $^3J_{H,H}$ = 1.2 Hz, 1 H, 5-H), 3.81 (s, 3 H, N−CH_3) ppm. ^{13}C NMR (150 MHz, [D_6]benzene): δ = 148.3 (dm, $^1J_{C,F}$ = 242 Hz, *o*-Ph), 140.2 (dm, $^1J_{C,F}$ = 247 Hz, *p*-Ph), 137.7 (CH, C-2), 137.4 (dm, $^1J_{C,F}$ = 246 Hz, *m*-Ph), 127.1 (CH, C-4), 121.9 (CH, C-5), 36.1 (CH_3, N−CH_3) ppm; *ipso*-carbon signal not detected. ^{19}F NMR (564 MHz, [D_6]benzene): δ = −133.1 (m, 6 F, *o*-Ph), −158.6 (m, 3 F, *p*-Ph), −164.6 (m, 6 F, *m*-Ph) ppm. ^{11}B NMR (64 MHz, [D_6]benzene): δ = −8.0 ($\nu_{1/2}$ = 140 Hz) ppm. $C_{22}H_6BF_{15}N_2$ (594): calcd. C 44.48, H 1.02, N 4.72; found C 43.98, H 1.08, N 5.27.

X-ray Crystal Structure Analysis of 3: Empirical formula $C_{22}H_6BF_{15}N_2$, M = 594.10, colorless crystal 0.25 × 0.20 × 0.10 mm, a = 11.222(2), b = 12.315(2), c = 16.463(3) Å, α = 88.32(1), β = 72.69(2), γ = 86.91(1)°, V = 2168.8(7) $Å^3$, $\rho_{calcd.}$ = 1.820 g cm^{-3}, μ = 18.15 cm^{-1}, empirical absorption correction from ψ scan data ($0.660 \le T \le 0.839$), Z = 4, triclinic, space group $P\bar{1}$ (no. 2), λ = 1.54178 Å, T = 223 K, ω scans, 9282 reflections collected ($-h$, $\pm k$, $\pm l$), [(sin θ)/λ] = 0.62 $Å^{-1}$, 8808 independent (R_{int} = 0.037) and 5107 observed reflections [$I \ge 2\ \sigma(I)$], 723 refined parameters, R = 0.082, wR^2 = 0.246, max. residual electron density 0.68 (−0.49) e $Å^{-3}$, crystals were always twinned (thin plates with a small tilt), by use of ω scans to collect the integrated intensities of all individuals, hydrogen atoms calculated and refined as riding atoms.

Treatment of Compound 3 with Methyllithium, Formation of the Heterocycle 5: Benzene/tetrahydrofuran (10:1, 2 mL) was added to a mixture of 1-methylimidazole−tris(pentafluorophenyl)borane (**3**, 100 mg, 168 μmol) and methyllithium (3.70 mg, 168 μmol). The resultant reaction mixture was stirred for 12 h, the solvent was removed in vacuo, and benzene was added. The LiF precipitate was removed by filtration, and evaporation of the solvent in vacuo yielded **5** as a light brown solid, yield: 83 mg (92%), m.p. 76 °C. IR (KBr): $\tilde{\nu}$ = 2966, 1647, 1616, 1519, 1486, 1467, 1382, 1287, 1266, 1098, 1058, 975, 835, 778 cm^{-1}. ^{1}H NMR (600 MHz, [D_6]benzene/[D_8]tetrahydrofuran 10:1): δ = 6.99 (d, $^3J_{H,H}$ = 1.8 Hz, 1 H, 4-H), 6.29 (d, $^3J_{H,H}$ = 1.8 Hz, 1 H, 5-H), 3.08 (d, $J_{H,F}$ = 4.0 Hz, 3 H, N−CH_3) ppm. ^{13}C NMR (150 MHz, [D_6]benzene/[D_8]tetrahydrofuran, 10:1): δ = 148.4 (dm, $^1J_{C,F}$ = 241 Hz, *o*-Ph), 148.2 (dm, $^1J_{C,F}$ = 245 Hz, C-2′), 147.3 (C, C-2), 142.1 (dm, $^1J_{C,F}$ = 257 Hz, C-4′), 141.5 (dm, $^1J_{C,F}$ = 255 Hz, C-5′), 140.5 (dm, $^1J_{C,F}$ = 251 Hz, C-3′), 140.3 (dm, $^1J_{C,F}$ = 251 Hz, *p*-Ph), 137.6 (dm, $^1J_{C,F}$ = 250 Hz, *m*-Ph), 126.7 (CH, C-5), 122.2 (CH, C-4), 116.7 (C, *ipso*-C), 35.6 (CH_3, $J_{C,F}$ = 16.7 Hz, N−CH_3) ppm; signals of C-1′ and C-6′ not detected. ^{19}F NMR (564 MHz, [D_6]benzene/[D_8]tetrahydrofuran, 10:1): δ = −131.0 (m, 1 F, 2′-F), −133.7 (m, 4 F, *o*-Ph), −135.7 (m, 1 F, 5′-F), −151.1 (m, 1 F, 3′-F), −156.2 (m, 1 F, 4′-F), −157.1 (m, 2 F, *m*-Ph), −163.2 (m, 4 F, *m*-Ph) ppm. ^{11}B NMR (64 MHz, [D_6]benzene/[D_8]tetrahydrofuran, 10:1): δ = −7.6 ($\nu_{1/2}$ = 130 Hz) ppm. $C_{22}H_5F_{14}N_{22}$ (574): calcd. C 46.03, H 0.88, N 4.88; found C 45.59, H 1.54, N 4.58.

2-Lithio-1-methylimidazole (6):[13] A solution of 1-methylimidazole (1.18 g, 14.1 mmol) in 20 mL of toluene was cooled to −78 °C and treated with an equivalent amount of *n*-butyllithium in hexane (9.00 mL, 14.4 mmol). After the mixture had stirred for 2 d at room temperature, the solvent was removed in vacuo. Pentane was added, the solid was separated by filtration, and the product was dried in vacuo to yield 1.24 g (99%) of **6**. ^{1}H NMR (600 MHz, [D_6]benzene/[D_8]tetrahydrofuran, 10:1): δ = 7.23 (s, 1 H, 4-H), 6.89 (s, 1 H, 5-H), 3.64 (CH_3, N−CH_3) ppm. ^{13}C NMR (150 MHz, [D_6]benzene/[D_8]tetrahydrofuran, 10:1): δ = 201.7 (C, C-2), 128.4 (CH, C-4), 117.8 (CH, C-5); 35.7 (CH_3, N−CH_3).

Lithium (1-Methylimidazol-2-yl)tris(pentafluorophenyl)borate (7): Tris(pentafluorophenyl)borane (**2a**, 512 mg, 1.00 mmol) was added to a suspension of 2-lithio-1-methylimidazole (**6**, 88.0 mg, 1.00 mmol) in 20 mL of pentane at room temperature. The reaction mixture was stirred for 24 h. The precipitated product was collected by filtration to yield **7** as a gray solid (380 mg, 63%), m.p. 255 °C. IR (KBr): $\tilde{\nu}$ = 1646, 1523, 1465, 1366, 1282, 1091, 981, 796, 740, 695 cm^{-1}. ^1H NMR (600 MHz, [D_6]benzene/[D_8]tetrahydrofuran, 10:1): δ = 6.61 (d, $^3J_{H,H}$ = 1.2 Hz, 1 H, 4-H), 6.58 (d, $^3J_{H,H}$ = 1.2 Hz, 1 H, 5-H), 3.17 (s, 3 H, N−CH_3) ppm. ^1H NMR (150 MHz, [D_6]benzene/[D_8]tetrahydrofuran, 10:1): δ = 162.2 (C, C-2), 148.7 (dm, $^1J_{C,F}$ = 241 Hz, *o*-Ph), 140.3 (dm, $^1J_{C,F}$ = 249 Hz, *p*-Ph), 137.3 (dm, $^1J_{C,F}$ = 250 Hz, *m*-Ph), 125.9 (CH, C-4), 121.2 (CH, C-5), 33.7 (CH_3, N−CH_3) ppm, *ipso*-carbon signal not detected. ^{19}F NMR (564 MHz, [D_6]benzene/[D_8]tetrahydrofuran, 10:1): δ = −124.6 (m, 1 F, *o*-Ph), −132.7 (m, 1 F, *o*-Ph), −133.0 (br, 3 F, *o*-Ph), −132.6 (m, 1 F, *o*-Ph), −161.6 (br, 2 F, *p*-Ph), −162.8 (m, 1 F, *p*-Ph), −165.6 (m, 1 F, *m*-Ph), −166.0 (br, 5 F, *m*-Ph) ppm. ^{11}B NMR (64 MHz, [D_6]benzene/[D_8]tetrahydrofuran, 10:1): δ = −16.6 ($\nu_{1/2}$ = 50 Hz) ppm. HRMS: calculated for $[C_{22}H_5N_2BF_{15}]^-$ 593.0310; found 593.0384.

Lithium (1-Methylimidazol-2-yl)triphenylborate (8): As described above, 2-lithio-1-methylimidazole (**6**, 264 mg, 3.00 mmol) in 20 mL of toluene was treated with triphenylborane (**2b**, 762 mg, 3.00 mmol) to yield **8** (619 mg, 62%) as a white solid, m.p. 283 °C. IR (KBr): $\tilde{\nu}$ = 3055, 1580, 1481, 1426, 1385, 1278, 1122, 1154, 1032, 943, 854, 758, 710 cm^{-1}. ^1H NMR (600 MHz, [D_6]benzene/[D_8]tetrahydrofuran, 10:1): δ = 7.55 (m, 6 H, *o*-Ph), 7.18 (m, 6 H, *m*-Ph), 7.04 (m, 3 H, *p*-Ph), 6.69 (d, $^3J_{H,H}$ = 1.2 Hz, 1 H, 5-H), 6.66 (d, $^3J_{H,H}$ = 1.2 Hz, 1 H, 4-H), 3.06 (s, 6 H, N−CH_3) ppm. ^{13}C NMR (150 MHz, [D_6]benzene/[D_8]tetrahydrofuran, 10:1): δ = 174.0 (q, $^1J_{CB}$ = 50 Hz, C-2), 160.3 (q, $^1J_{CB}$ = 57 Hz, *ipso*-C), 135.6 (CH, *o*-Ph), 127.1 (CH, *m*-Ph), 124.6 (CH, C-4), 123.5 (CH, *p*-Ph), 120.5 (CH, C-5), 35.4 (CH_3, N−CH_3) ppm. ^{11}B NMR (64 MHz, [D_6]benzene): δ = −9.4 ($\nu_{1/2}$ = 44 Hz) ppm. HRMS: calculated for $[C_{22}H_{20}N_2B]^-$ 323.1724; found 323.1781.

X-ray Crystal Structure Analysis of 8: Empirical formula $C_{22}H_{20}BLiN_2$, M = 330.15, light yellow crystal 0.45 × 0.30 × 0.30 mm, a = 10.701(1), b = 14.818(1), c = 11.104(1) Å, β = 91.65(1)°, V = 1760.0(3) $Å^3$, $\rho_{calcd.}$ = 1.246 g cm^{-3}, μ = 0.71 cm^{-1}, empirical absorption correction by SORTAV (0.969 ≤ T ≤ 0.979), Z = 4, monoclinic, space group $P2_1/n$ (no. 14), λ = 0.71073 Å, T = 198 K, ω and ψ scans, 14410 reflections collected (±h, ±k, ±l), [(sinθ)/λ] = 0.66 $Å^{-1}$, 4269 independent (R_{int} = 0.050) and 2820 observed reflections [$I \geq 2\,\sigma(I)$], 236 refined parameters, R = 0.050, wR^2 = 0.102, max. residual electron density 0.25 (−0.17) e $Å^{-3}$, hydrogen atoms calculated and refined as riding atoms.

Data sets were collected with Enraf−Nonius CAD4 and Nonius KappaCCD diffractometers, the latter equipped with a rotating anode generator (Nonius FR591). Programs used: data collection EXPRESS (Nonius B.V., 1994) and COLLECT (Nonius B.V., 1998), data reduction MolEN (K. Fair, Enraf-Nonius B.V., 1990) and Denzo-SMN (Z. Otwinowski, W. Minor, *Methods Enzymol.*, **1997**, *276*, 307−326), absorption correction for CCD data SORTAV (R. H. Blessing, *Acta Crystallogr.* **1995**, *A51*, 33−37; R. H. Blessing, *J. Appl. Crystallogr.* **1997**, *30*, 421−426), structure solution SHELXS-97 (G. M. Sheldrick, *Acta Crystallogr.* **1990**, *A46*, 467−473), structure refinement SHELXL-97 (G. M. Sheldrick, Universität Göttingen, 1997), graphics SCHAKAL (E. Keller, Universität Freiburg, 1997). CCDC-173951 (**3**) and -173952 (**8**) contain the supplementary crystallographic data for this paper. These data can be obtained free of charge at www.ccdc.cam.ac.uk/conts/retrieving.html or from the Cambridge Crystallographic Data Centre, 12, Union Road, Cambridge CB2 1EZ, UK [Fax: (internat.) + 44-1223/336-033; E-mail: deposit@ccdc.cam.ac.uk].

Acknowledgments

Financial support from the Fonds der Chemischen Industrie and the Deutsche Forschungsgemeinschaft is gratefully acknowledged.

[1] K. Öfele, *J. Organomet. Chem.* **1968**, *12*, 42.
[2] H.-W. Wanzlick, H.-J. Schönherr, *Angew. Chem.* **1968**, *80*, 154; *Angew. Chem. Int. Ed. Engl.* **1968**, *7*, 141.
[3] M. F. Lappert, *J. Organomet. Chem.* **1988**, *358*, 185.
[4] A. J. Arduengo III, R. L. Harlow, M. Kline, *J. Am. Chem. Soc.* **1991**, *113*, 361.
[5] F. E. Hahn, L. Wittenbecher, D. Le Van, R. Fröhlich, *Angew. Chem.* **2000**, *112*, 551; *Angew. Chem. Int. Ed.* **2000**, *39*, 541.
[6] Y. Liu, P. E. Lindner, D. M. Lemal, *J. Am. Chem. Soc.* **1999**, *121*, 10626.
[7] Reviews: [7a] W. A. Herrmann, C. Köcher, *Angew. Chem.* **1997**, *109*, 2256; *Angew. Chem. Int. Ed. Engl.* **1997**, *36*, 2162. [7b] A. J. Arduengo, III, *Acc. Chem. Res.* **1999**, *32*, 913. [7c] T. Weskamp, V. P. W. Böhm, W. A. Herrmann, *J. Organomet. Chem.* **2000**, *600*, 12. [7d] D. Bourisson, O. Guerret, F. Gabbäi, G. Bertrand, *Chem. Rev.* **2000**, *100*, 39.
[8] T. Weskamp, F. J. Kohl, W. Hieringer, D. Gleich, W. A. Herrmann, *Angew. Chem.* **1999**, *111*, 2573; *Angew. Chem. Int. Ed.* **1999**, *38*, 2416.
[9] J. Huang, E. D. Stevens, S. P. Nolan, J. L. Petersen, *J. Am. Chem. Soc.* **1999**, *121*, 2674.
[10] J. Jafarpour, S. P. Nolan, *Organometallics* **2000**, *19*, 2055.
[11] C. W. Bielawski, R. H. Grubbs, *Angew. Chem.* **2000**, *112*, 3025; *Angew. Chem. Int. Ed.* **2000**, *39*, 2903.
[12] A. J. Arduengo, J. R. Görlich, W. J. Marshall, *Liebigs Ann./Recueil* **1997**, 365.
[13] A. Berndt, *Angew. Chem.* **1993**, *105*, 1034; *Angew. Chem. Int. Ed. Engl.* **1993**, *32*, 985.
[14] H. Stetter, *Angew. Chem.* **1976**, *88*, 695; *Angew. Chem. Int. Ed. Engl.* **1976**, *15*, 639.
[15] I. I. Padilla-Martinez, M. de Jeses Rosalez-Hoz, R. Contreras, S. Kerschl, B. Wrackmeyer, *Chem. Ber.* **1994**, *127*, 343.
[16] K. Okuda, R. Suzuki, M. Oda, *J. Chem. Soc., Chem. Commun.* **1995**, 2069.
[17] A. Wacker, H. Pritzkow, W. Siebert, *Eur. J. Inorg. Chem.* **1998**, 843.
[18] A. G. Massey, A. J. Park, F. G. A. Stone, *Proc. Chem. Soc. London* **1963**, 212.
[19] A. G. Massey, A. J. Park, *J. Organomet. Chem.* **1964**, *2*, 245.
[20] A. G. Massey, A. J. Park, *Organometallic Syntheses* (Eds.: R. B. King, J. J. Eisch), Elsevier, New York, **1986**, vol. 3, p. 461.
[21] See for a comparison: E. L. Eliel, S. H. Wilen, *Stereochemistry of Organic Compounds*, Wiley, New York, **1994**, chapter 14-6, p. 1156−1160.
[22] For a related reaction of a $B(C_6F_5)_3$/ylide adduct see: S. Döring, G. Erker, R. Fröhlich, O. Meyer, K. Bergander, *Organometallics* **1998**, *17*, 2183.
[23] A. J. Arduengo, III, H. V. R. Dias, R. L. Harlow, M. Kline, *J. Am. Chem. Soc.* **1992**, *114*, 5530.
[24] S. Berger, S. Braun, H.-O. Kalinowski, *NMR-Spektroskopie von Nichtmetallen, ^{19}F NMR-Spektroskopie*, Thieme-Verlag, Stuttgart, New York, **1994**, p. 129.
[25] J. Hilton, L. H. Sutcliffe, *Progr. NMR Spectrosc.* **1975**, *10*, 27.
[26] F. B. Mallory, C. W. Mallory, W. M. Ricker, *J. Am. Chem. Soc.* **1975**, *97*, 4770.
[27] D. J. Sardella, E. Boger, *Magn. Reson. Chem.* **1989**, *27*, 13.
[28] L. C. Hsee, D. J. Sardella, *Magn. Reson. Chem.* **1990**, *28*, 688.

[29] I. D. Rae, A. Staffa, A. C. Diz, C. G. Giribet, M. C. Ruiz de Azua, R. H. Contreras, *Aust. J. Chem.* **1987**, *40*, 1923.
[30] H.-O. Kalinowski, S. Berger, S. Braun, *^{13}C NMR-Spektroskopie*, Stuttgart, New York, Thieme, **1984**.
[31] K. Fujita, S. Hikichi, M. Akita, M. Yoshihiko, *J. Chem. Soc., Dalton Trans.* **2000**, 117.
[32] H. G. Raubenheimer, Y. Stander, E. K. Marais, C. Thompson, G. J. Kruger, S. Cronje, M. Detlefs, *J. Organomet. Chem.* **1999**, *590*, 158.
[33] F. Chu, J. Smith, V. M. Lynch, E. V. Anslyn, *Inorg. Chem.* **1995**, *34*, 5689.
[34] H. G. Raubenheimer, S. Cronje, P. J. Olivier, *J. Chem. Soc., Dalton Trans.* **1995**, 313.
[35] D. Seyferth, L. L. Anderson, W. M. Davis, *J. Organomet. Chem.* **1993**, *459*, 271.
[36] D. P. Goldberg, S. P. Watton, A. Masshelein, L. Wimmer, S. J. Lippard, *J. Am. Chem. Soc.* **1993**, *115*, 5346.
[37] P. K. Byers, A. J. Canty, *Organometallics* **1990**, *9*, 210.
[38] A. Hassner, P. Munger, B. A. Belinka, *Tetrahedron Lett.* **1982**, *23*, 699.
[39] B. Wrackmeyer, *Annu. Rep. NMR Spectrosc.* **1988**, *20*, 61.
[40] B. Ihara, V. G. Young, Jr., R. F. Jordan, *J. Am. Chem. Soc.* **1998**, *120*, 8277.
[41] B. Schiemenz, P. P. Power, *Angew. Chem.* **1996**, *108*, 2288; *Angew. Chem. Int. Ed. Engl.* **1996**, *35*, 2150.
[42] R. J. Wehmschulte, P. P. Power, *J. Am. Chem. Soc.* **1997**, *119*, 2847.
[43] R. E. Dinnebier, U. Behrens, F. Olbrich, *J. Am. Chem. Soc.* **1998**, *120*, 1430.
[44] S. Alexandratos, A. Streitwieser, Jr., H. F. Schaefer, III, *J. Am. Chem. Soc.* **1976**, *98*, 7959.
[45] E. D. Jemmis, P. v. R. Schleyer, *J. Am. Chem. Soc.* **1982**, *104*, 4781.
[46] W. N. Setzer, P. v. R. Schleyer, *Adv. Organomet. Chem.* **1985**, *24*, 353.
[47] C. Lambert, P. v. R. Schleyer, *Angew. Chem.* **1994**, *106*, 1187; *Angew. Chem. Int. Ed. Engl.* **1994**, *33*, 1129.
[48] *Lithium Chemistry, A Theoretical and Experimental Overview* (Eds.: A. M. Sapse, P. v. R. Schleyer), Wiley, New York, **1995**, and references therein.
[49] Reviews: P. Jutzi, *J. Organomet. Chem.* **1990**, *400*, 1.
[50] D. Stalke, *Angew. Chem.* **1994**, *106*, 2256; *Angew. Chem. Int. Ed. Engl.* **1994**, *33*, 2168.
[51] P. Jutzi, N. Burford, *Chem. Rev.* **1999**, *99*, 969.
[52] A. D. Becke, *J. Chem. Phys.* **1993**, *98*, 5648.
[53] P. J. Stephens, F. J. Devlin, C. F. Chabalowski, M. J. Frisch, *J. Phys. Chem.* **1994**, *98*, 11623.
[54] Turbomole (Vers. 5.3): R. Ahlrichs, M. Bär, H.-P. Baron, R. Bauernschmitt, S. Böcker, M. Ehrig, K. Eichkorn, S. Elliott, F. Furche, F. Haase, M. Häser, H. Horn, C. Huber, U. Huniar, M. Kattannek, C. Kölmel, M. Kollwitz, K. May, C. Ochsenfeld, H. Öhm, A. Schäfer, U. Schneider, O. Treutler, M. von Arnim, F. Weigand, P. Weis, H. Weiss, Universität Karlsruhe, **2000**.
[55] A. Schäfer, C. Huber, R. Ahlrichs, *J. Chem. Phys.* **1994**, *100*, 5829.
[56] The transition structure was located with a modified version of the "TS" routine in MOPAC6, which makes use of the dscf and grad modules of the Turbomole program. The underlying procedure is based on a quasi-Newton (Eigenvector-following) algorithm: J. Baker, *J. Comp. Chem.* **1985**, *7*, 385.
[57] The reliability of the DFT results was checked by single-point ab initio calculations at the quadratic configuration interaction (QCISD) level.[58,59] These calculations yielded a barrier of 45.8 kcal mol^{-1} and a reaction energy of −15.7 kcal mol^{-1} for the process **10a** → **11a**, in good agreement with the corresponding B3LYP data.
[58] J. A. Pople, M. Head-Gordon, K. Raghavachari, *J. Chem. Phys.* **1987**, *87*, 5968.
[59] C. Hampel, K. A. Peterson, H.-J. Werner, *Chem. Phys. Lett.* **1992**, *190*, 1.
[60] For related studies see, for example: [60a] S. Solé, H. Gornitzka, O. Guerret, G. Bertrand, *J. Am. Chem. Soc.* **1998**, *120*, 9100. [60b] G. A. McGibbon, C. Heinemann, D. J. Lavorato, H. Schwartz, *Angew. Chem.* **1997**, *109*, 1572; *Angew. Chem. Int. Ed. Engl.* **1997**, *36*, 1478. [60c] G. Maier, J. Endres, H. P. Reisenauer, *Angew. Chem.* **1997**, *109*, 1788; *Angew. Chem. Int. Ed. Engl.* **1997**, *36*, 1709.
[61] A. Wacker, H. Pritzkow, W. Siebert, *Eur. J. Inorg. Chem.* **1999**, 789.

Received January 7, 2002
[I02006]

Molecular Mercury Zinc Sulfides

Michael Rombach[a] and Heinrich Vahrenkamp*[a]

Dedicated to Professor Dieter Fenske on the occasion of his 60th birthday

Keywords: Mercury / Zinc / S ligands / Tripod ligands

Reactions between $Tp^{Ph,Me}$Zn-SH and mercury bis(trimethylsilyl)amides yield the monomeric complexes $Tp^{Ph,Me}$-Zn–S–$HgCH_2Ph$ (**1**) and $Tp^{Ph,Me}$Zn–S–Hg–S–Zn$Tp^{Ph,Me}$ (**2**). The bent Zn–S–Hg and linear S–Hg–S arrays in these molecular metal sulfides were confirmed by structure determinations.
(© Wiley-VCH Verlag GmbH, 69451 Weinheim, Germany, 2002)

Introduction

The most characteristic feature of sulfur as a ligand in metal complexes is its tendency to be three- or four-coordinate by bridging several metal atoms. This has long been known for classical[1] as well as for organometallic[2] coordination chemistry. In recent years Fenske and co-workers have provided impressive examples of high-nuclearity clusters constructed by the nucleation of metal ions around sulfide ions.[3−5]

In contrast, transition metal complexes containing conventional divalent sulfur in monomeric M−S−M arrays are rare. Outside the field of plain thiometalates[6] there are only scattered examples in the literature.[7] Among the few complexes in which two metals are linked by nothing but a sulfide ligand are $[Cp(CO)_3W]_2S$,[8] $[(Ph_3P)Au]_2S$[9] and $[(triphos)Ni]_2S^{2+}$.[10] As a rule the high inertness of the L_nM units contained in these complexes has rendered their metal centers M inaccessible to aggregation triggered by loss of their ligands L.

Our present work in this field, after past experiences with polynuclear organometallic complexes,[2] results from our attempts to construct monofunctional zinc complexes for biomimetic and catalytic studies. Since sulfur ligation of zinc is a common feature of both industrially applied and biological zinc species, we have also experimented with thiolates and sulfide as ligands for zinc. Like others we experienced aggregation of the complexes[11−13] and nucleation around sulfide in the complex cores.[14,15] However, by using bulky pyrazolylborate ligands we also learnt to protect the zinc ions by encapsulation. This way zinc-hydrosulfide complexes became accessible as the very stable and versatile Tp*Zn−SH species,[16] and we could prepare $Tp^{Cum,Me}$Zn−S−Zn$Tp^{Cum,Me}$ as the first molecular zinc sulfide.[17]

After exploiting the basic chemistry of the Zn−SH function[16] we have started using the Tp*Zn−SH units as building blocks for new complexes. The present paper describes the application of $Tp^{Ph,Me}$Zn−SH for the preparation of two molecular mercury zinc sulfides.

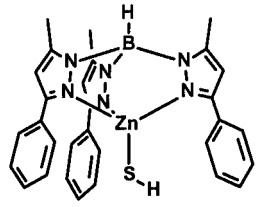

$Tp^{Ph,Me}$Zn–SH

Results and Discussion

Preparations

The most straightforward way of utilizing the Tp*Zn−S moiety for preparative purposes would be the deprotonation of Tp*Zn−SH. It turned out, however, that the "thiolates" Tp*Zn−S^- are not stable enough for this purpose.[16] Therefore we resorted to the implicit deprotonation approach, which consists in the reaction between a thiol and a metal bis(trimethylsilyl)amide. In this approach the metal-bound amide is the base for deprotonation and at the same time the ligand being substituted by the thiolate. We have used this method before for the synthesis of otherwise inaccessible zinc thiolates,[18] and we now applied it to the corresponding mercury amides.

[a] Institut für Anorganische und Analytische Chemie der Universität Freiburg
Albertstr. 21, 79104 Freiburg, Germany
Fax: (internat.) +49-761/203-6001
E-mail: vahrenka@uni-freiburg.de

The reaction between $Tp^{Ph,Me}Zn-SH$ and benzylmercury bis(trimethylsilyl)amide yielded the Zn−S−Hg complex **1**. Likewise $Tp^{Ph,Me}Zn-SH$ and mercury bis[bis(trimethylsilyl)amide] produced the Zn−S−Hg−S−Zn complex **2**. Both reactions resulted in air-stable colourless crystalline compounds in reasonable yields. While their IR data are uninformative, their ^1H NMR spectra (see Exp. Sect.) prove the presence of the Tp and Bz ligands. Compounds **1** and **2** are the first fully characterized mixed-metal sulfide complexes of the second subgroup. Mixed-metal sulfide clusters containing zinc and cadmium have been described but not isolated in a pure form.[19,20]

$Tp^{Ph,Me}Zn\text{-}S\text{-}HgCH_2Ph$
1
$Tp^{Ph,Me}Zn\text{-}S\text{-}Hg\text{-}S\text{-}ZnTp^{Ph,Me}$
2

Structures

Complex **1** (see Figure 1) contains a nearly right-angled Zn−S−Hg array. Its two constituents, the Tp*ZnS unit and the BzHgS unit, are quite normal with typical Zn−S, Hg−S and Hg−C bond lengths. Reference compounds are the Tp*Zn−SH complexes themselves[16] and the organomercury thiolates.[21] As expected for two-coordinate mercury, the S−Hg−C array is very close to being linear. The dihedral angle defined by the Zn−S and C−C bonds with respect to the Zn−S−Hg axis is 174°.

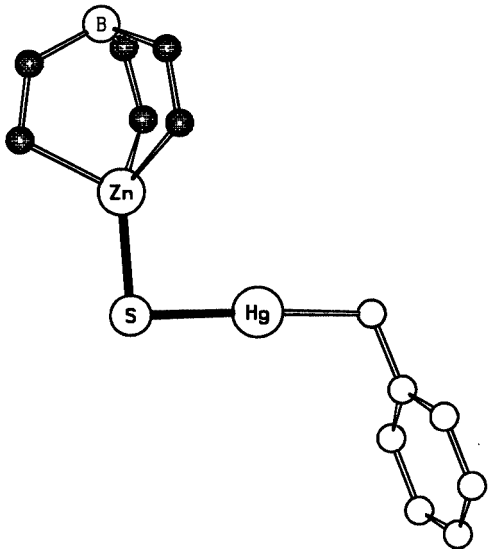

Figure 1. Molecular structure of complex **1** (for reasons of clarity the pyrazolylborate ligand is reduced to its BN_6 skeleton); important bond lengths (Å) and angles (°): Zn−N 2.065−2.092(5), Zn−S 2.221(2), Hg−S 2.316(2), Hg−C 2.115(1); Zn−S−Hg 93.41(7), S−Hg−C 176.3(5)

Complex **2** (see Figure 2) is centered around a nearly linear S−Hg−S array with Hg−S distances very similar to those in **1**. The two Hg−S−Zn angles are larger than the one in **1** and differ by 12°, probably due to steric congestion. The two Tp*Zn−S units are practically superimposable with that in **1**. While in **1** the Hg−S−Zn and Hg−C−C units define a trans array, the corresponding two Hg−S−Zn units in **2** are gauche, their dihedral angle being 95°. Complex **2** can be compared with monomeric mercury bis(thiolates), whose structures in the solid state range from linear two-coordinate to polymers with four- and five-coordinate mercury.[22] Furthermore the Zn−S−Hg−S−Zn sequence in **2** is analogous to the 1D polymeric array of mercury and sulfur in cinnabar, the thermodynamically more stable modification of HgS.[23] In cinnabar the Hg−S bond lengths are 2.37 Å and the dihedral angle is 93°.

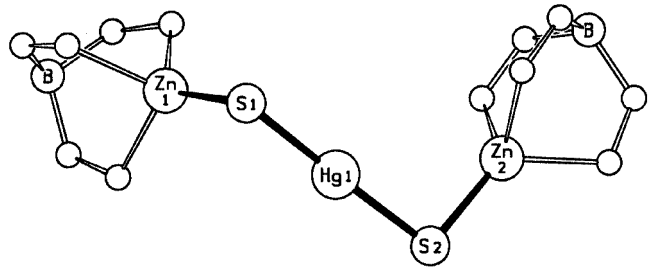

Figure 2. Molecular structure of complex **2** (for reasons of clarity the pyrazolylborate ligands are reduced to their BN_6 skeletons); important bond lengths (Å) and angles (°): Zn−N 2.070−2.086(3), Zn1−S1 2.226(1), Zn2−S2 2.219(1), Hg−S1 2.299(1), Hg−S2 2.303(1); Zn1−S1−Hg 108.70(5), Zn2−S2−Hg 96.75(5)

Conclusions

The facile preparations of **1** and **2** have proved the suitability of the Tp^*ZnS^- unit for the construction of molecular metal sulfides. Except for our Tp*Zn−S−ZnTp* [17] no such sulfides of zinc, cadmium or mercury with simple M−S−M arrays seem to have been reported, even though the standard arrangements of the types $M_3(\mu_3\text{-}S)$ and $M(\mu\text{-}S)_2M'$ are known for heterometallic mercury complexes.[24,25] Furthermore, the chain-like array of three metal and two sulfur atoms in **2** seems to be unprecedented in coordination chemistry, although the relation to cinnabar makes it understandable that it exists in complex **2**. The tendency of mercury to have a linear twofold coordination and the highly covalent nature of the mercury-ligand bonds may be important for the stabilization of these molecular metal sulfides. We believe, however, that the protection by the encapsulating Tp* ligands will stabilize similar complexes with other metals too.

Experimental Section

General: For general working and measuring procedures, see ref.[26] All reactions were performed under an inert atmosphere. $Tp^{Ph,Me}Zn-SH$[16] and the mercury silylamides[27] were prepared according to the published procedures.

Complex 1: $BzHgN(SiMe_3)_2$ (163 mg, 0.36 mmol) and $Tp^{Ph,Me}Zn-SH$ (210 mg, 0.36 mmol) in 20 mL of dichloromethane were stirred for 2 h. After removal of all volatiles in vacuo the residue was recrystallized from acetonitrile, yielding 179 mg (57%) of

Table 1. Crystallographic data

	1	**2**
Empirical formula	$C_{37}H_{35}BHgN_6SZn$ ·CH_3CN	$C_{60}H_{56}B_2HgN_{12}S_2Zn_2$ ·$2CH_3CN$
Molecular mass	872.6 + 41.0	1362.3 + 82.0
Crystal size [mm]	0.3 × 0.3 × 0.2	0.3 × 0.3 × 0.2
Space group	$P2_1/n$	$P\bar{1}$
Z	4	2
a [Å]	11.630(2)	13.501(3)
b [Å]	20.590(4)	14.077(3)
c [Å]	15.350(3)	17.529(4)
α [°]	90	101.44(3)
β[°]	96.27(3)	99.32(3)
γ [°]	90	102.91(3)
V [Å^3]	3654(1)	3108(1)
d(calc) [gcm^{-3}]	1.66	1.54
μ(Mo-K_α) [mm^{-1}]	4.95	3.35
hkl range	*h*: −14 to 9 *k*: −25 to 25 *l*: −16 to 18	*h*: −16 to 16 *k*: −16 to 16 *l*: 0 to 21
Measured reflections	14342	11318
Independent reflections	6705	11318
Observed refl. [$I > 2\sigma(I)$]	5764	10121
Parameters	451	766
Refined reflections	6705	11318
R_1 (obs.refl.)	0.073	0.041
wR_2 (all refl.)	0.209	0.101
Residual electron density [e/ Å^3]	+2.8/−4.5	+2.9/−3.0

1 as colorless crystals which turned to a powder upon drying in vacuo, M.p. 202 °C (dec.). $C_{37}H_{35}BHgN_6SZn$ (872.6): calcd. C 50.33, H 4.04, N 9.63; found C 50.73, H 4.03, N 9.61. ^{1}H NMR ($CDCl_3$): δ = 1.76 (s, 2 H, CH_2), 2.56 [s, 9 H, Me(pz)], 6.17 [s, 3 H, H(pz)], 6.69 (m, 2 H, Bz), 6.89 (m, 1 H, Bz), 7.06 (m, 2 H, Bz), 7.30 (m, 9 H, Ph), 7.61 (m, 6 H, Ph) ppm.

Complex 2: $Tp^{Ph,Me}Zn-SH$ (500 mg, 0.86 mmol) and $Hg[N(SiMe_3)_2]_2$ (224 mg, 0.43 mmol) in 30 mL of dichloromethane were stirred for 15 min, upon which the solution turned black. After removal of all volatiles in vacuo the residue was taken up in a minimum amount of hot acetonitrile, filtered hot and the filtrate kept at room temp. for one day. 210 mg (36%) of **2** were precipitated as colorless crystals, which turned to a powder upon drying in vacuo. M.p. 248 °C (dec.). $C_{60}H_{56}B_2HgN_{12}S_2Zn_2$ (1362.3): calcd. C 52.90, H 4.14, N 12.34; found C 52.72, H 4.20, N 12.42. ^{1}H NMR ($CDCl_3$): δ = 2.55 [s, 18 H, Me(pz)], 6.12 [s, 6 H, H(pz)], 7.04 (m, 18 H, Ph), 7.48 (m, 12 H, Ph).

Structure Determinations:[28] Crystals of **1** and **2** were obtained from the reaction mixtures. Diffraction data were recorded at room temp. with the ω/2θ technique on a Nonius CAD4 diffractometer fitted with a molybdenum tube (Mo-K_α, λ = 0.7107 Å) and a graphite monochromator and subjected to empirical absorption corrections. The structures were solved by direct methods and refined anisotropically with the SHELX program suite.[29] Hydrogen atoms were included with fixed distances and isotropic temperature factors 1.5-times those of their attached atoms. Parameters were refined against F^2. The R values are defined as $R_1 = \Sigma|F_o - F_c|/\Sigma F_o$ and $wR_2 = [\Sigma[w(F_0^2 - F_c^2)^2]\Sigma[w(F_0^2)^2]]^{1/2}$. Drawings were produced with SCHAKAL.[30] Table 1 lists the crystallographic data.

Acknowledgments

This work was supported by the Fonds der Chemischen Industrie.

[1] A. Müller, E. Diemann, in *Comprehensive Coordination Chemistry* (Eds.: G. Wilkinson, R. D. Gillard, J. A. McCleverty), Pergamon Press, Oxford **1987**, Vol. 2, pp 516−550.
[2] H. Vahrenkamp, *Angew. Chem.* **1975**, *87*, 363−371. *Angew. Chem. Int. Ed. Engl.* **1975**, *14*, 322−330.
[3] S. Dehnen, D. Fenske, *Chem. Eur. J.* **1996**, *2*, 1407−1416.
[4] D. Fenske, M. Bettenhausen, *Angew. Chem.* **1998**, *110*, 1288−1291; *Angew. Chem. Int. Ed.* **1998**, *37*, 1291−1294.
[5] D. Fenske, J. Ohmer, J. Hachgenei, K. Merzweiler, *Angew. Chem.* **1988**, *100*, 1300−1320: *Angew. Chem. Int. Ed. Engl.* **1988**, *27*, 1277−1296.
[6] A. Müller, H. Bögge, U. Schimanski, *Monatsh. Chem.* **1989**, *120*, 367−391, and references cited therein.
[7] S. Kuwata, M. Hidai, *Coord. Chem. Rev.* **2001**, *213*, 211−305.
[8] G. J. Kubas, H. J. Wassermann, R. R. Ryan, *Organometallics* **1985**, *4*, 419−421.
[9] C. Lensch, P. G. Jones, G. M. Sheldrick, *Z. Naturforsch., Teil B* **1982**, *37*, 944−949.
[10] C. Mealli, S. Midollini, L. Sacconi, *Inorg. Chem.* **1978**, *17*, 632−637.
[11] B. Müller, H. Vahrenkamp, *Z. Anorg. Allg. Chem.* **2001**, *627*, 1483−1486.
[12] C. Sudbrake, H. Vahrenkamp, *Eur. J. Inorg. Chem.* **2001**, 751−754.
[13] U. Brand, H. Vahrenkamp, *Z. Anorg. Allg. Chem.* **1996**, *622*, 213−218.
[14] R. Burth, M. Gelinsky, H. Vahrenkamp, *Inorg. Chem.* **1998**, *37*, 2833−2836.

[15] M. Gelinsky, H. Vahrenkamp, *Z. Anorg. Allg. Chem.* **2002**, in print.
[16] M. Rombach, H. Vahrenkamp, *Inorg. Chem.* **2001**, *40*, 6144−6150.
[17] M. Ruf, H. Vahrenkamp, *J. Chem. Soc., Dalton Trans.* **1996**, 1915−1916.
[18] U. Brand, H. Vahrenkamp, *Inorg. Chem.* **1995**, *39*, 3285−3293.
[19] I. A. Dance, *Aust. J. Chem.* **1985**, *38*, 1745−1755.
[20] T. Løver, W. Henderson, G. A. Bowmaker, J. M. Seakins, R. P. Cooney, *Inorg. Chem.* **1997**, *36*, 3711−3723.
[21] J. L. Wardell, in *Comprehensive Organometallic Chemistry* (Eds.: G. Wilkinson, F. G. A. Stone, E. W. Abel), Pergamon Press, Oxford **1982**, Vol. 2, pp 863−978.
[22] K. Brodersen, H. U. Hummel, in *Comprehensive Coordination Chemistry* (Eds.: G. Wilkinson, R. D. Gillard, J. A. McCleverty), Pergamon Press, Oxford **1987**, Vol. 5, pp 1048−1097.
[23] P. Auvray, F. Genet, *Bull. Soc. Fr. Mineral. Crystallogr.* **1973**, *96*, 218.
[24] D. Fenske, M. Bettenhausen, *Angew. Chem.* **1998**, *110*, 1288−1291; *Angew. Chem. Int. Ed.* **1998**, *37*, 1291−1294.
[25] I. Ghosh, R. Mishra, D. Poddar, A. K. Mukherjee, M. Mukherjee, R. Bhattacharyya, *Chem. Commun.* **1996**, 435−436.
[26] M. Förster, R. Burth, A. K. Powell, T. Eiche, H. Vahrenkamp, *Chem. Ber.* **1993**, *126*, 2643−2648.
[27] H. Bürger, W. Sawodny, U. Wannagat, *J. Organomet. Chem.* **1965**, *3*, 113−120.
[28] CCDC-177319 (**1**) and CCDC-177320 (**2**) contain the supplementary crystallographic data for this paper. These data can be obtained free of charge at www.ccdc.cam.ac.uk/conts/retrieving.html [or from the Cambridge Crystallographic Data Centre, 12, Union Road, Cambridge CB2 1EZ, UK; Fax: (internat.) +44-1223/336-033; E-mail: deposit@ccdc.cam.ac.uk].
[29] G. M. Sheldrick, *SHELX-86* and *SHELXL-93, Programs for Crystal Structure Determination*, Universität Göttingen, **1986** and **1993**.
[30] E. Keller, *SCHAKAL for Windows*, Universität Freiburg, **1998**.
Received January 15, 2002
[I02023]

Synthesis of μ-$C_2S_4^{4-}$ Cobalt Complexes by Activation of the 1,3,4,6-tetrathiapentalene-2,5-dione, and Electrochemical Study of [$(Cp^*Co)_2(\mu\text{-}C_2S_4)$]

Fabrice Guyon,*[a] Isabelle V. Jourdain,[a] Michael Knorr,[a] Dominique Lucas,[b] Theresa Monzon,[b] Yves Mugnier,[b] Narcis Avarvari,[c] and Marc Fourmigué[c]

Keywords: Cobalt / S ligands / Cyclopentadienyl ligands / Electrochemistry

The bimetallic complex [$Cp^{(*)}Co)_2(\mu\text{-}C_2S_4)$] in which the two metal centres are linked by an ethylenetetrathiolate $C_2S_4^{4-}$ unit, was synthesized in high yield by oxidative addition of 1,3,4,6 tetrathiapentalene-2,5-dione to [$Cp^{(*)}Co(CO)_2$]. The X-ray crystal structure of the intermediate product $Cp^*Co(dmid)$ ($dmid^{2-}$ = 4,5-disulfanyl-1,3-dithiol-2-onate) is presented. The electrochemical behaviour of the [$(Cp^*Co)_2(\mu\text{-}C_2S_4)$] complex was studied in detail in the oxidative range. This study has shown that the nature of the product obtained after oxidation depends on the presence of complexing agent in the solution. The mechanism has been elucidated in a CH_2Cl_2 solution in the presence of $P(OMe)_3$. In addition, chemical oxidation was conducted with several oxidizing agents (Br_2, $TCNQF_4$, and $AgBF_4$). The molecular structure of the tetrathiooxalate bridged complex [$(Cp^*Co\{P(OMe)_3\})_2(\mu\text{-}C_2S_4)$][$BF_4$]$_2$ was established by an X-ray diffraction study.

(© Wiley-VCH Verlag GmbH, 69451 Weinheim, Germany, 2002)

Introduction

Complexes containing the ethylenetetrathiolate $C_2S_4^{4-}$ unit as a bridging ligand between two metal centres are rather rare, despite their potential to form systems with metallic or semiconducting properties.[1] The reason for this is the lack of a general procedure to generate this sulfur-rich ligand. Most of the tetrathiolate transition metal complexes have been synthesised by metal-promoted head-to-head reductive dimerization of CS_2. Representative examples include [$(Cp_2Ti)_2(\mu\text{-}C_2S_4)$],[2] [$(Cp^*Co)_2(\mu\text{-}C_2S_4)$],[3] [$(Cp^*Ni)_2(\mu\text{-}C_2S_4)$],[4] and [{M(triphosp)}$_2(\mu\text{-}C_2S_4)$] (M = Rh or Ir).[5] However, we have found in our laboratories that the reaction of [$Cp^*Co(CO)_2$] with CS_2 leads to the formation of a mixture in which μ-dithiolene and μ-dithiocarbamate [$(Cp^*Co)_2(\mu\text{-}C_2S_4)$] isomers coexist.[6] The same result was observed in the case of the titanium complex [$(Cp_2Ti)_2(\mu\text{-}C_2S_4)$].[7] Recently, Rauchfuss et al. reported the synthesis of [$(Cp^*Rh)_2(\mu\text{-}C_2S_4)$] via an efficient reductive dechlorination of the tetrathiooxalate derivative [$(Cp^*RhCl)_2(\mu\text{-}C_2S_4)$].[8]

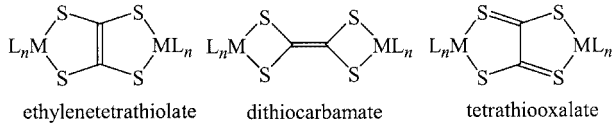

The synthesis of metal dimers containing the $C_2S_4^{4-}$ bridging ligand was also explored using the well-known reactivity of dithiocarbonate groups towards strong bases by starting from 1,3,4,6-tetrathiapentalene-2,5-dione (tpd). This method was found unsuccessful, however, or led to the desired product in low yield.[9,10] Another reactivity pattern of dithiocarbonate groups has already been employed for the synthesis of cobaltocene dithiolene complexes, used as model for the molybdenum cofactor.[11] The reaction consists of the oxidative addition of 1,3-dithiol-2-one or 1,3-dithiole-2-thione to [CpCo(cod)] (cod = cyclooctadiene).

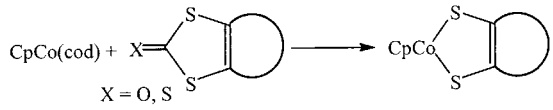

With the aim of generating dimetallic complexes, it was tempting to apply this strategy by using bis(1,3-dithiol-2-one) and bis(1,3-dithiole-2-thione) as precursors. In this paper we report on the very efficient formation of [$Cp^{(*)}Co)_2(\mu\text{-}C_2S_4)$] complexes starting from tpd. The electrochemical properties of the [$Cp^{(*)}Co)_2(\mu\text{-}C_2S_4)$] complexes have been studied in detail in CH_2Cl_2 and CH_3CN solutions. The molecular structures of the intermediate product

[a] Laboratoire de Chimie des Matériaux et des Interfaces, Université de Franche-Comté,
16 Route de Gray, 25030 Besançon, France
E-mail: fabrice.guyon@univ-fcomte.fr
[b] Laboratoire de Synthèse et d'Electrosynthèse Organométalliques, UMR 5632, Université de Bourgogne,6 Boulevard Gabriel, 21000 Dijon, France
[c] Laboratoire Chimie Inorganique, Matériaux et Interfaces, FRE 2447 CNRS Université d'Angers,
2 Boulevard Lavoisier, 49045 Angers, France

[Cp*Co(dmid)] ($dmid^{2-}$ = 4,5-disulfanyl-1,3-dithiol-2-onate) and of the oxidized species $[(Cp^*CoL)_2(\mu\text{-}C_2S_4)](BF_4)_2$ [L = $P(OMe)_3$] are also described.

Results and Discussions

Synthesis

The reaction of equimolar quantities of 1,3,4,6-tetrathiapentalene-2,5-dione (tpd) and $[Cp^*Co(CO)_2]$ in refluxing toluene afforded the intermediate complex [Cp*Co(dmid)] (**1**), which has already been isolated by the conventional metathesis of Na_2dmid and $[Cp^*Co(CO)I_2]$.[12] Recrystallization from toluene and hexane provided single crystals of **1**. The crystal structure was determined, since it has not been reported previously (see below). This intermediate **1** reacted with a second equiv. of $[Cp^*Co(CO)_2]$ under the same reaction conditions to afford the dimetallic diamagnetic complex $[(Cp^*Co)_2(\mu\text{-}C_2S_4)]$ (**2**). This compound was isolated as a green crystalline powder with a yield close to 90%, based on tpd (Scheme 1).

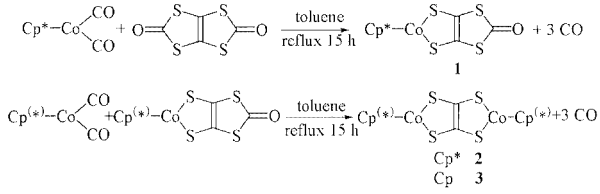

Scheme 1

Of course, this synthesis could also be achieved in one step by the reaction of 2 equiv. of $[Cp^*Co(CO)_2]$ and 1 equiv. of tpd. The isolation of **1** allowed us to deduce the dithiolene nature of the bridge instead of a dithiocarbamate core. Using an analogous procedure, we were able to synthesise the new $[(CpCo)_2(\mu\text{-}C_2S_4)]$ compound **3** in an appreciable yield (58%). In contrast to **2**, the solubility of the complex **3** was very poor in common organic solvents, which prevented any solution NMR characterization. The synthesis of **3** demonstrates the efficiency of this method, since it has not been obtained previously by the action of CS_2 on $[CpCo(CO)_2]$.[3b]

Structural Analysis of 1

The structure shown in Figure 1 is very similar to those of the structurally characterized heteroleptic cyclopentadienyl(dithiolene)cobalt complexes,[13] and particularly that of the [Cp*Co(dmit)] molecule ($dmit^{2-}$ = 4,5-disulfanyl-1,3-dithiole-2-thionate).[14] In this compound, the $Co(C_3OS_4)$ moiety is nearly planar and perpendicular to the Cp* moiety [89.3(1)°]. Selected bond lengths and angles are listed in Table 1, and have been compared with those of [Cp*Co(dmit)]. The short length of the C(1)−C(2) bond [1.337(5) Å] of the ligand is in agreement with a dithiolene structure and proves that the reaction between the tpd and the $[Cp^*Co^I(CO)_2]$ compound leads to the coordination of $dmid^{2-}$ on the Cp^*Co^{III} fragment.

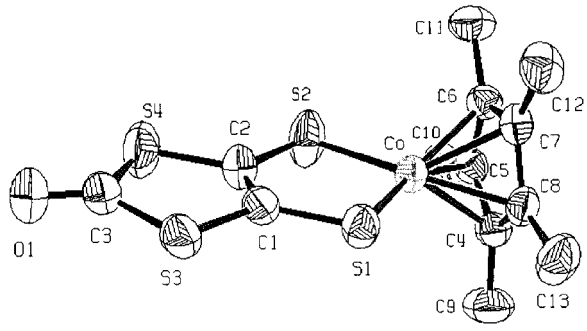

Figure 1. Molecular structure of **1**; hydrogen atoms are omitted for clarity, 50% probability ellipsoids

Table 1. Selected bonds lengths [Å] and angles [°] of **1** and [Cp*Co(dmit)] complexes

	1	[Cp*Co(dmit)][14]
Co-S1	2.1330(10)	2.138(2)
Co-S2	2.1201(10)	2.135(2)
S1−C1	1.722(3)	1.713(6)
S2−C2	1.722(3)	1.725(7)
S3−C1	1.751(3)	1.741(7)
S4−C2	1.750(3)	1.739(6)
S3−C3	1.769(4)	1.719(6)
S4−C3	1.768(4)	1.725(8)
X−C3	1.205(4) (X = O)	1.657(7) (X = S5)
C1−C2	1.337(5)	1.352(9)
Mean Co−C[a]	2.049(11)	2.050(7)
S1−Co−S2	93.16(4)	93.65(7)
C1−S1−Co1	102.54(11)	102.3(2)
C2−S2−Co1	103.08(12)	102.3(2)
S3−C3−S4	112.37(19)	113.3(4)

[a] Estimated errors on averaged Co−C distances are calculated as $\sigma = [\Sigma(d_i - d_{mean})^2/(n-1)]^{1/2}$, $n = 5$.

Electrochemical Experiments

The electrochemical behaviour of several $C_2S_4^{4-}$ bridged complexes has been studied, but the reported results point out different observations in the oxidation range. Indeed, the cyclic voltammograms of $[(Cp^*Ni)_2(\mu\text{-}C_2S_4)]$[4] and $[(Cp^*Rh)_2(\mu\text{-}C_2S_4)]$[8a] complexes in CH_2Cl_2 show a one-electron process, whereas in the case of $[\{Rh(triphosp)\}_2(\mu\text{-}C_2S_4)]$ a two electron oxidation is observed in CH_2Cl_2 or CH_3CN solutions.[5] Therefore, in order to evaluate the influence of the solvent, the redox behaviour of **2** was studied in CH_2Cl_2 and CH_3CN solutions.

The rotating-disk voltammogram in CH_2Cl_2 displays one anodic and two cathodic waves, all with nearly the same height. These were named O_1', R_1, and R_2, respectively, each associated with a one-electron transfer (Figure 2 and Table 2). In cyclic voltammetry, the first reductive step was found to be reversible, but not the second one, presumably because of the reactivity of the electrogenerated dianion $[(Cp^*Co)(\mu\text{-}C_2S_4)]^{2-}$ with the electrophilic dichloromethane (Scheme 2).[15] This is in contrast to what was observed in acetonitrile (see below). Exploring the oxidation, we ob-

served in CH_2Cl_2 solution a peak O_1' at +0.62 V versus SCE (E_p) coupled on the backward scan with a peak at +0.15 V, which is indicative of a chemical reaction following the one-electron oxidation of the neutral complex. An exhaustive controlled-potential oxidation of **2** consumed nearly 1 F/mol of the initial complex, and left the product reducible at +0.15 V; the electrolysed solution was ESR-silent, which traduces the diamagnetism of this product. We propose that the chemical reaction consists in the dimerization of the intermediate $[(Cp^*Co)_2(\mu\text{-}C_2S_4)]^+$ (Scheme 2). Indeed, this oxidation behaviour has already been observed for the analogous rhodium complex $[(Cp^*Rh)_2(\mu\text{-}C_2S_4)]$[8b] and for a dithiolene cobaltocene complex.[16] With this latter complex, it has also been shown that in the presence of a strong two-electron donor ligand the stabilization occurs via the formation of an adduct.[16] Thus, in order to explain the mechanism of the oxidation of **2** in the presence of a strong Lewis base, electrochemical experiments were conducted in CH_2Cl_2, where an excess of $P(OMe)_3$ was initially added to **2**. The resulting RDE voltammogram is depicted (see b in Figure 3). Reduction wave R_1 is still present, but with a considerably reduced height, attesting to the fact that **2** is still in solution, but in a limited amount (nearly 25% based on the relative value of $i_{d,R1}$). New oxidation waves appear at −0.62, −0.23, and +0.06 V, named $O_1{*}'$, $O_1^{\#\prime}$, and $O_2{*}'$, respectively. These can be explained by considering that **2** is able to coordinate one or two $P(OMe)_3$ moieties. As $P(OMe)_3$ is a strong σ-donor, the most negative oxidation wave, namely $O_1{*}'$, must be assigned to the two-ligand containing complex $[(Cp^*Co\{P(OMe)_3\})_2(\mu\text{-}C_2S_4)]$ (**2b**). Oxidation wave $O_1^{\#\prime}$ is attributed to the mono adduct $[(Cp^*Co)_2\{P(OMe)_3\}(\mu\text{-}C_2S_4)]$ (**2a**), which is predominant since $O_1^{\#\prime}$ is noticeably more intense than R_1 or $O_1{*}'$.

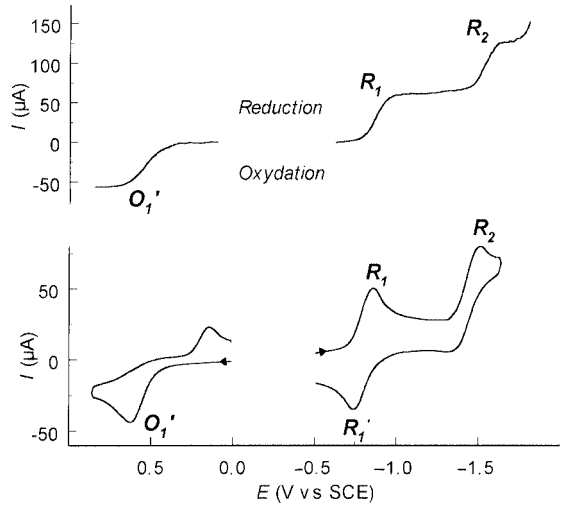

Figure 2. Rotating-disk and cyclic voltammogram of 2.7 mM of **2** in CH_2Cl_2, 0.2 M Bu_4NPF_6; CV: sweep rate = 200 $mV{\cdot}s^{-1}$, initial potential = −0.1 (anodic scan) and −0.65 V (cathodic scan); RDV: rotation speed = 15 rps

Table 2. Voltammetric data of **2** and its $P(OMe)_3$ adducts

Compound	Oxidation		Reduction	
	$E_{1/2,1}$[a][b] [V]	$E_{1/2,2}$ [V]	$E_{1/2,1}$ [V]	$E_{1/2,2}$ [V]
2 in CH_2Cl_2	+0.51		−0.9	−1.56
2 in CH_3CN	+0.25		−0.82	−1.47
2a	−0.23			
2b	−0.62	+0.06		

[a] All potentials are referred to the saturated calomel electrode. [b] Half-wave potentials are taken by RDE voltammetry.

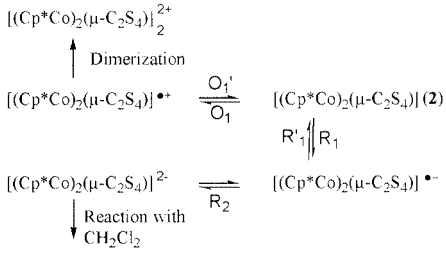

Scheme 2

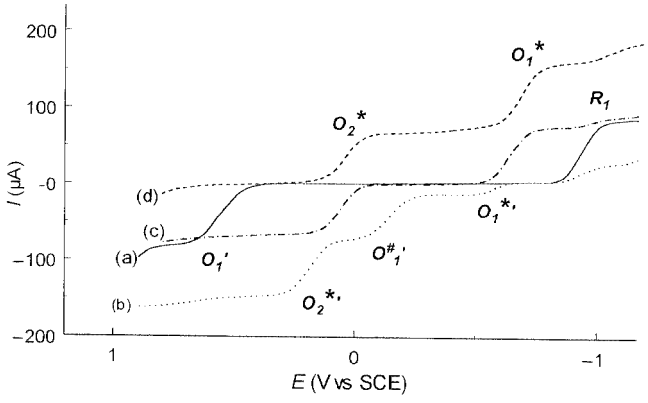

Figure 3. Rotating-disk voltammogram of 4.1 mM of **2** in CH_2Cl_2 0.2 M Bu_4NPF_6, rotation speed = 10 rps; a (——): **2** alone; b (···) after addition of 33 mol-equiv. of $P(OMe)_3$; c (·-·-) after electrolysis at −0.05 V; d (---) after electrolysis at +0.3 V

An exhaustive controlled-potential electrolysis, performed on the plateau of wave $O_1^{\#\prime}$ (E_w = −0.05 V vs. SCE), consumed nearly 1 F/mol of **2**. The resulting RDE voltammogram (see c in Figure 3) displays the anodic wave $O{*}_2'$ together with the cathodic wave $O{*}_1$, which means that at the monooxidized state, the bis(adduct) $[(Cp^*Co\{P(OMe)_3\})_2(\mu\text{-}C_2S_4)]^{+\cdot}$ (**2e**) is the only stable species. This was confirmed by ESR analysis of the electrolysed solution. The apparently complex morphology of the spectrum (Figure 4) arises from the coupling of the unpaired spin with two phosphorus and two cobalt nuclei (g_{iso} = 2.020; a_{Co} = 3.4 G; a_P = 22.6 G). Particularly, the hyperfine coupling constants are close to those found for similar complexes.[17]

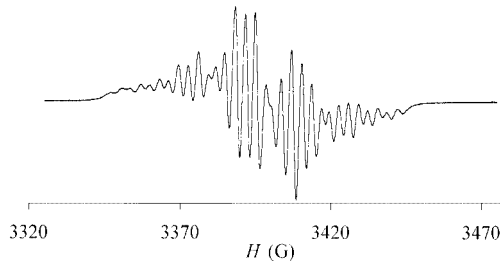

Figure 4. The ESR spectrum (X-band) of **2e**, obtained after the electrolysis (E_w = −0.05 V vs. SCE) of a CH_2Cl_2 solution of **2** in the presence of an excess of $P(OMe)_3$

The second stage of oxidation was also studied. Indeed, starting from **2e**, an electrolysis at 0.3 V (plateau of wave $O^*_2{}'$), consumed nearly 1 equiv. of electrons and quantitatively yielded $[(Cp^*Co\{P(OMe)_3\})_2(\mu\text{-}C_2S_4)]^{2+}$ (**2g**), which is evidenced in RDE voltammetry by the successive cathodic waves O^*_2 and O^*_1 (see d in Figure 3). In contrast with the first oxidation, the electron transfer is not associated herein with any chemical reaction. In summary, the detailed mechanism of the oxidation of **2** in the presence of $P(OMe)_3$ can be formalized according to Scheme 3. The overall process is governed by both electron transfer and $P(OMe)_3$ exchange reaction thermodynamics.

The electrochemical analysis of **2**, performed in acetonitrile, indicates that the dimerization does not occur, like in dichloromethane. Indeed, the rotating-disk voltammogram (Figure 5 and Table 2) exhibits a two-electron charge transfer in the oxidative range, based on the height of the oxidation wave, which is nearly twice compared to that of the reduction ones. In cyclic voltammetry, the oxidation peak O'_1, found at +0.32 V, is associated in the forward scan with a reduction peak located at +0.14V. Moreover, an exhaustive controlled-potential oxidation (E_w = +0.46 V vs. SCE) consumed 2 F/mol of initial complex, ultimately leaving the product reducible at +0.14 V. In addition, the electrolysed solution was found to be ESR-silent. We propose that the final two-electron oxidized complex incorporates two molecules of MeCN, like with $P(OMe)_3$. Within the framework of Scheme 3, the mechanism involves, after the first electron-transfer (**2** → **2c**), the addition of one molecule of solvent (**2c** → **2d**), which prevents the dimerization from occurring. At this stage, there are two possibilities, either the addition of the second molecule of solvent occurs before the second electron step (pathway **2d** → **2e** → **2g**) or after (**2d** → **2f** → **2g**). It must be outlined that this second electrochemical step occurs at the same potential as the oxidation **2** → **2c** due to the basicity of the acetonitrile, which leads to only one wave or peak in the voltammogram of **2**, with a two-electron transfer.

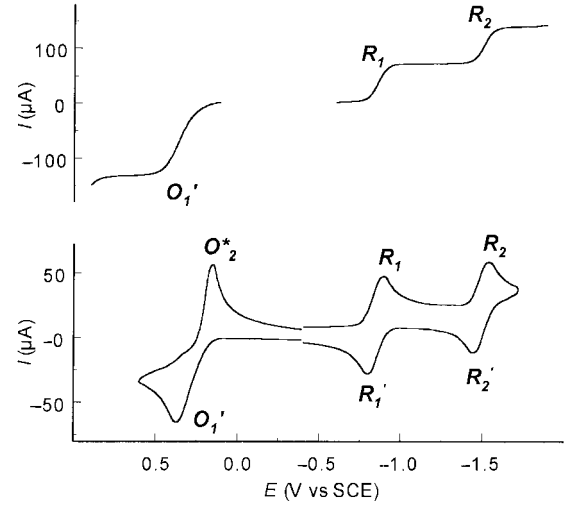

Figure 5. Rotating-disk and cyclic voltammogram of 2.8 mM of **2** in CH_3CN 0.2 M Bu_4NPF_6; CV: sweep rate = 100 $mV{\cdot}s^{-1}$, initial potential = −0.4 V (anodic and cathodic scans); RDV: rotation speed = 10 rps

It must be noted from Table 2 that going from CH_2Cl_2 to MeCN causes a strong shift in the oxidation potential (−260 mV against +80 mV in reduction), which may arise from the influence of the kinetics of the chemical reaction following the first electron transfer.[18] In any case, the potential difference between CH_2Cl_2 and MeCN cannot be explained by the complexation of MeCN in the neutral state since we have verified that there is no change at all in the UV/Vis spectra of **2** from one solvent to the other.

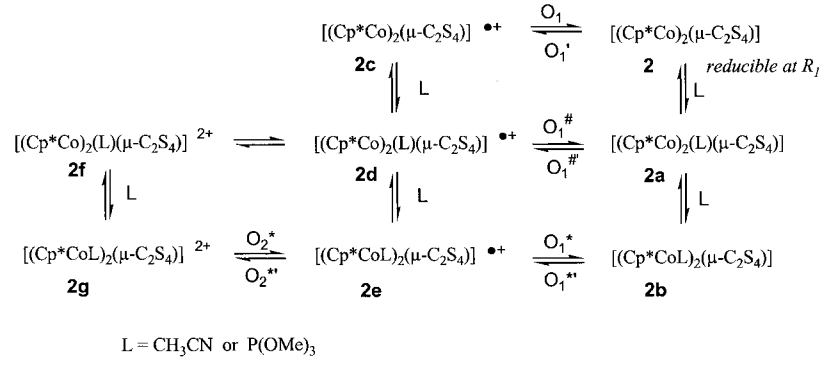

Scheme 3

Chemical Oxidation

In agreement with the results of the electrochemical studies, it can be shown that $[(Cp^*Co)_2(\mu\text{-}C_2S_4)]$ can be chemically oxidized without destroying its CoC_2S_4Co core. Oxidation of **2** by 1 equiv. of Br_2 gives the diamagnetic neutral complex $[(Cp^*CoBr)_2(\mu\text{-}C_2S_4)]$ (**4**) (Scheme 4).

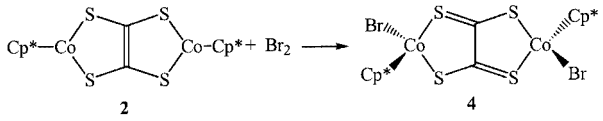

Scheme 4

The coordination of halides upon oxidation has already been observed for a (dithiolene)cobalt complex,[19] as well as for $[(Cp^*Rh)_2(\mu\text{-}C_2S_4)]$.[8a] The cyclic voltammogram of **4** (Figure 6) shows that the bromine atoms can be reductively decoordinated [Equation (1)]. Indeed, after a first reduction peak located at −0.26 V, the peak R_1 was observed at the second stage.

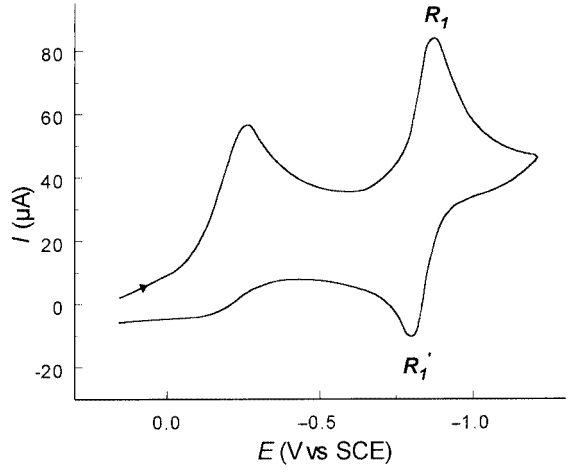

Figure 6. Cyclic voltammogram of 3.2 mM of **4** in CH_2Cl_2 of 0.2 M Bu_4NPF_6 (sweep rate = 100 $mV \cdot s^{-1}$)

$$[(Cp^*CoBr)_2(\mu\text{-}C_2S_4)] + 2\,e^- \rightarrow [(Cp^*Co)_2(\mu\text{-}C_2S_4)] + 2\,Br^- \quad (1)$$

4 **2**

Complex **2** was also oxidized by the strong oxidizer $TCNQF_4$ (perfluoro-7,7,8,8-tetracyano-*p*-quinodimethane). Indeed, treatment of an acetonitrile solution of $TCNQF_4$ with a 0.5 mol-equiv. of **2** was found to afford $[(Cp^*Co\{TCNQF_4\})_2(\mu\text{-}C_2S_4)]$ (**5**) as a blue powder (Scheme 5).

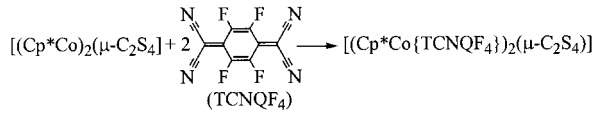

Scheme 5

The stoichiometry of **5** was ascertained from the elemental analysis. Despite the tendency of the $TCNQF_4^{-\cdot}$ to form dimeric dianionic moieties,[20] the elemental analysis suggests that the dication $[(Cp^*Co)_2(\mu\text{-}C_2S_4)]^{2+}$ is stabilized by the coordination of the anionic $TCNQF_4^{-\cdot}$ on both cobalt atoms. Unfortunately, all our attempts to grow crystals of **4** and **5** were unsuccessful.

Information about the structural changes induced by the two-electron oxidation was obtained by chemical oxidation of **2** in the presence of a Lewis base in a CH_2Cl_2 solution. Treatment with 2 equiv. of $AgBF_4$ and an excess of trimethyl phosphite induced a change of colour of the solution from green to brown. After filtration, addition of diethyl ether afforded dark brown needles of compound $[(Cp^*Co\{P(OMe)_3\})_2(\mu\text{-}C_2S_4)](BF_4)_2$ (**6**) (Scheme 6). Note that the cationic part of this salt is equivalent to compound **2g** in Scheme 3.

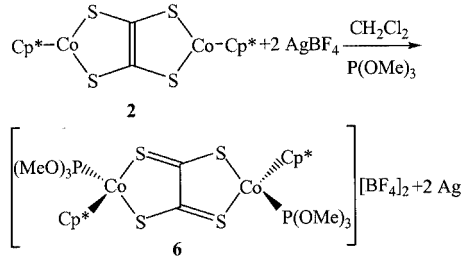

Scheme 6

The ^1H NMR spectrum of **6** consists of a single sharp signal in the C_5Me_5 region, which is consistent with a symmetric structure and a diamagnetic ground state. Integration of the C_5Me_5 fine peak vs. the $P(OMe)_3$ signal indicates that each centre is coordinated by a molecule of a trimethyl phosphite. The symmetric structure is confirmed by the $^{31}P\{^1H\}$ NMR spectrum since only one signal is observed at $\delta = 126.8$ ppm.

Electrochemical analysis of **6** provided the same RDE voltammogram as that of Figure 3d. In this there is no difference between the chemical and electrochemical approaches to the oxidation of **2**.

Structural Analysis

In addition to the NMR solution study, the solid-state structure of **6** was probed by X-ray crystallography. Crystallographic analysis established the 1:2 stoichiometry, i.e., one organometallic dication for two BF_4^- counterions. Analysis of the bond lengths shows that the C_2S_4 core is better described in **6** as tetrathiooxalate than ethylenetetrathiolate bridge. Especially since the S_2C-CS_2 distance is 0.1 Å longer in **6** than in reported complexes formulated as $C_2S_4^{4-}$ bridged complexes (Table 3). In addition, the Co–S bond is significantly lengthened in **6** in comparison to the neutral complex. Thus, the oxidation essentially affects the C_2S_4 ligand. Accordingly, with its dicationic nature, complex **6** can be described as two Co^{III} centres linked by a $C_2S_4^{2-}$ bridge. This description is similar to that of the $[(Cp^*RhCl)_2(\mu\text{-}C_2S_4)]$ compound reported by Rauchfuss et

Table 3. Selected bonds [Å] and angles [°] of μ-C_2S_4 bridged complexes

Complex	M−S	C−S	C−C	SMS	Ref.
6	2.1974(11) 2.2101(9)	1.685(4) 1.689(4)	1.460(7)	89.81(4)	this work
$[(RhCp'Cl)_2(\mu\text{-}C_2S_4)]$[a]	2.317(2) 2.334(2)	1.689(6) 1.695(7)	1.447(13)	85.08(6)	[8a]
$[(RhCp^*)_2(\mu\text{-}C_2S_4)]$	2.2432 2.2517	1.744 1.736	1.342(8)	87.33(4)	[8a]
$[(CoCp^*)_2(\mu\text{-}C_2S_4)]$	2.122(2) 2.126(2)	1.725(4) 1.725(4)	1.369(11)	91.6(1)	[3b]
$[(NiCp^*)_2(\mu\text{-}C_2S_4)]$	2.122(1)	1.718(3)	1.360(11)		[4]
$[\{Rh(triphosp)\}_2(\mu\text{-}C_2S_4)]$	2.311(6) 2.296(5)	1.76(2) 1.70(2)	1.37(3)	85.9(2)	[5]

[a] Cp′ = η^5-C_5Me_4Et.

al.[8a] The two $P(OMe)_3$ ligands are complexed in a *trans* manner giving rise to a C_{2h} structure (Figure 7). The Co−P distance [2.1693(11) Å] lies in the range of what is generally observed for this bond.[21] Due to this complexation, the C_2S_4 plane does not lie perpendicular to the Cp* plane, which is in opposition to what was observed in the case of **2**.[3b] The CoS_2 unit makes an angle of 52.1(1)° with the C_5Me_5 ring plane. The Co−C distances [2.080(4)−2.120(4) Å] are appreciably long compared with those of the neutral complex **2** [2.026(6)−2.040(6) Å].

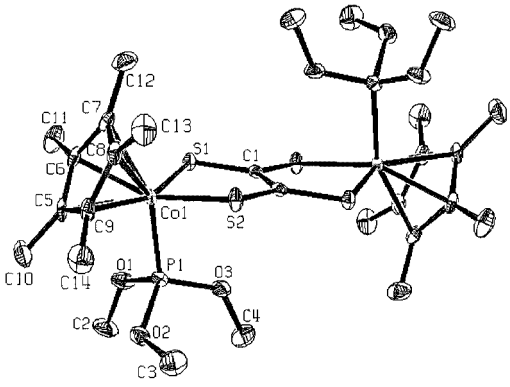

Figure 7. Molecular structure of **6**; hydrogen atoms and BF_4^- are omitted for clarity, 50% probability ellipsoids; selected bond length [Å] and angles [°]: Co(1)−P(1) 2.1693(11), P(1)−O(1) 1.575(3), P(1)−O(2) 1.587(3), P(1)−O(3) 1.575(3), Co(1)−Cp*(vertical) 1.714(2); P(1)−Co−S(2) 94.14(4), P(1)−Co−S(1) 89.04(4), C(1)−S(1)−Co(1) 104.07(12), C(1)−S(2)−Co(1) 104.63(12), O(1)−P(1)−Co(1) 109.62(11), O(2)−P(1)−Co(1) 120.10(12), O(3)−P(1)−Co(1) 110.62(11), C(1)−C(1)−S(1) 119.7(4), C(1)−C(1)−S(2) 118.9(4)

Conclusion

In summary, we have found a new efficient method for the preparation of dimetallic cobalt complexes bridged by the $C_2S_4^{4-}$ unit starting from 1,3,4,6-tetrathiapentalene-2,5-dione. Electrochemical and chemical oxidations of $[(Cp^*Co)_2(\mu\text{-}C_2S_4)]$ have shown that the loss of electrons involves mainly the bridging ligand without breaking the link between the two metal centres. The stabilization of the oxidized species results from coordination, complexation, or dimerization according to the nature of the solution in which the oxidation is conducted.

Further studies will concentrate on the formation of the first heterobimetallic complexes bridged by the $C_2S_4^{4-}$ ligand.

Experimental Section

General Comments: All reactions were carried out under dry argon using standard Schlenk techniques. Solvents were purified by standard methods and freshly distilled under nitrogen. The NMR spectra were recorded with a Bruker AC and a Bruker Avance 300 MHz spectrometer. Electron spin resonance spectra were recorded at room temperature with a Bruker ESP 300 spectrophotometer. Field calibrations were made with dpph (g = 2.0034). Elemental analyses were performed at the Université de Bourgogne with an EA 1108 Fisons instrument. The 1,3,4,6-tetrathiapentalene-2,5-dione[22] and $Cp^*Co(CO)_2$ [23] were prepared according to published literature methods and $CpCo(CO)_2$ was purchased from Aldrich. The method described by Wheland and Martin was employed for the synthesis of $TCNQF_4$.[24]

Electrochemical Experiments: Voltammetric analyses were carried out in a standard three-electrode cell with a Tacussel UAP4 unit cell. The electrolyte consisted of 0.2 M n-Bu_4NPF_6 solution in CH_2Cl_2 or in MeCN. The reference electrode was a saturated calomel electrode (SCE) separated from the analysed solution by a sintered glass disk; the auxiliary electrode was a platinum wire. For all voltammetric measurements the working electrode was a carbon disk electrode initially polished with alumina. The controlled potential electrolyses were performed with an Amel 552 potentiostat coupled to an Amel 771 integrator. A carbon gauze was used at the anode, a platinum plate as the cathode, and an SCE as the reference electrode, each electrode being separated from the others by sintered glass disks. After each measurement the reference electrode was checked against the ferrocene-ferricinium couple (+0.46 V in CH_2Cl_2 and +0.4 V in MeCN).

Synthesis of $[Cp^*Co(C_3OS_4)]$ (1): Equimolar quantities (1 mmol) of $[Cp^*Co(CO)_2]$ and 1,3,4,6-tetrathiapentalene-2,5-dione were heated under reflux in toluene (30 mL) overnight under argon. After filtration, the green solution was removed under reduced

pressure. Washing the residue by a small quantity of pentane (5 mL) afforded the complex **1** as a green powder (0.36 g, 96% yield). A single crystal of **1** was obtained by recrystallization from toluene and hexane. ^{1}H NMR (200 MHz, $CDCl_3$): δ = 1.97 (s, Me_5C_5) ppm. IR (KBr): ν̃ = 1626 and 1670 (C=O), 1340 (C=C) cm^{-1}.

Synthesis of [(Cp*Co)$_2$(μ-C$_2$S$_4$)] (2): Equimolar quantities (1 mmol) of [Cp*Co(CO)$_2$] and **1** were heated under reflux in toluene (30 mL) overnight under argon. Cooling the solution in an ice bath resulted in the precipitation of complex **2** as green needles, which were collected by filtration. Yield: 0.485 g (90%). ^{1}H NMR (200 MHz, $CDCl_3$): δ = 1.86 (s, Me_5C_5) ppm. IR (KBr): ν̃ = 1375 (C=C) cm^{-1}. UV/Vis (CH_2Cl_2): λ_{max} = 322, 809 nm. MS: *m*/*z* = 540 [M$^+$]. $C_{22}H_{30}Co_2S_4$: calcd. C 48.89, H 5.56, S 23.70; found C 48.52, H 5.65, S 23.15.

Synthesis of [(CpCo)$_2$(μ-C$_2$S$_4$)] (3): A mixture of $CpCo(CO)_2$ (0.5 mL, 3.47 mmol) and 1,3,4,6-tetrathiapentalene-2,5-dione (360 mg, 1.73 mmol) were heated under reflux in toluene overnight under argon. After cooling to room temperature, the blue reaction mixture was filtered. The collected solid afforded complex **3** as a dark blue powder. Yield: 0.400 g (58%). MS: *m*/*z* = 400 [M$^+$]. $C_{12}H_{10}Co_2S_4$: calcd. C 36.01, H 2.50, S 32.04; found C 36.25, H 2.39, S 31.67.

Synthesis of [(Cp*CoBr)$_2$(μ-C$_2$S$_4$)] (4): To a solution of MeCN (30 mL), containing 60 mg of **2** (0.111 mmol), was added 6 μL (0.117 mmol) of Br_2.The colour of the solution turned slowly from green to blue. After 12 h of stirring, the precipitate was filtered off and washed with diethyl ether to afford the complex **4** as a blue powder. Yield: 62 mg (80%). ^{1}H NMR (200 MHz, CD_2Cl_2): δ = 1.50 (s, Me_5C_5) ppm. $C_{22}H_{30}Br_2Co_2S_4$ (700): calcd. C 37.71, H 4.29, S 18.32; found C 37.42, H 4.19, S 17.66.

Synthesis of [(Cp*Co{TCNQF$_4$})$_2$(μ-C$_2$S$_4$)] (5): An MeCN solution (10 mL) of $TCNQF_4$ (60 mg, 0.214 mmol) was added to an MeCN solution (20 mL), containing 58 mg of **2** (0.107 mmol). The resulting solution was stirred overnight at ambient temperature. The complex **5** was obtained as a blue powder after filtration and washing with CH_2Cl_2. Yield: 89 mg (76%). IR (KBr): ν̃ = 2216 and 2198 (C≡N) cm^{-1}. $C_{46}H_{30}Co_2F_8S_4N_8$ (1092): calcd. C 50.55, H 2.75, N 10.26; found C 49.90, H 2.79, N 9.65.

Synthesis of [(Cp*Co{P(OMe)$_3$})$_2$(μ-C$_2$S$_4$)](BF$_4$)$_2$ (6): Complex **2** (0.070 g, 0.130 mmol) was dissolved in 20 mL of CH_2Cl_2 in the presence of $P(OMe)_3$ (0.12 mL, 1 mmol). This solution was added to a suspension of $AgBF_4$ (0.051 g, 0.260 mmol) in 5 mL of CH_2Cl_2. After 1 h of stirring, the brown solution was filtered. Addition of 10 mL of ether afforded dark brown crystalline solid of **6**, which was washed with 2 × 10 mL of ether. Yield: 0.095 g (85%). ^{1}H NMR (300 MHz, CD_2Cl_2): δ = 1.66 (s, 15 H), 3.8 (m, 9 H) ppm. ^{13}C NMR (300 MHz, CD_2Cl_2): δ = 11.8 ($C_5\mathit{Me}_5$), 58.59 [$P(OMe)_3$], 105.3 (C_5Me_5), 115 (C=C) ppm. ^{31}P{H} NMR (300 MHz, CD_2Cl_2): δ = 126.8 [$P(OMe)_3$].

Crystallographic Data Collection and Structure Determination for 1 and 6: A single crystal of each compound was mounted in a glass capillary using Araldite glue. Data were collected with a Stoe-IPDS diffractometer, with graphite-monochromated Mo-K_α radiation (λ = 0.71073 Å). Details are given in Table 4. Numerical absorption correction was applied (FACEIT, Stoe). The structure was solved by direct methods and refined by full-matrix least-squares on F^2 with anisotropic thermal parameters for all non-H atoms. H atoms were introduced at calculated positions and constrained to ride on the parent C atoms. All calculations were performed with the SHELTX package.[25] CCDC-77465 for [Cp*Co(dmid)] and -177466 for [(Cp*Co{P(OMe)$_3$})$_2$(μ-C$_2$S$_4$)](BF$_4$)$_2$ contain the supplementary crystallographic data for this paper. These data can

Table 4. Crystallographic data

Compound	**1**	**6**
Empirical formula	$C_{13}H_{15}CoOS_4$	$C_{28}H_{48}B_2Co_2F_8O_6P_2S_4$
Formula mass	374.42	962.32
Cryst size [mm]	0.2 × 0.2 × 0.15	0.16 × 0.16 × 0.08
T [K]	293(2)	293(2)
Cryst system	monoclinic	monoclinic
Space group	$P2_1/n$	$P2_1/c$
a [Å]	8.0269(16)	11.0910(11)
b [Å]	14.067(3)	14.1973(13)
c [Å]	14.386(3)	13.1834(14)
α [°]	90	90
β [°]	98.43(3)	104.303(12)
γ [°]	90	90
V [Å^3]	1606.8(6)	2011.5(3)
Z	4	2
$\rho_{calcd.}$ [g cm^{-3}]	1.548	1.589
μ [mm^{-1}]	1.576	1.187
F(000)	768	988
λ [Å]	0.71073	0.71073
θ range [°]	2.04−25.90	1.89−25.97
Index ranges	$-9 \le h \le 9$, $0 \le k \le 17$, $0 \le l \le 17$	$-13 \le h \le 13$, $0 \le k \le 17$, $0 \le l \le 16$
No. of reflections collected	3100	3872
No. of ind reflections	2243	2483
Largest diff peak and hole [e/Å^3]	−0.284/0.280	−0.409/0.517
Final *R* indices[a]	0.0349	0.0401
R indices (all data)	0.0546	0.0757
GOF on F^2	0.926	0.906

$R(F) = \Sigma||F_o| - |F_c||/\Sigma|F_o|$.

be obtained free of charge at www.ccdc.cam.ac.uk/conts/retrieving.html or from the Cambridge Crystallographic Data Centre, 12, Union Road, Cambridge CB2 1EZ, UK [Fax: (internat.) + 44-1223/336-033; E-mail: deposit@ccdc.cam.ac.uk].

Acknowledgments

We thank Dr. Hélène Cattey (LSEO, Dijon, France) and Dr. Chikako Takayama (Sophia University, Tokyo, Japan) for fruitful discussions on the EPR spectrum. Financial support from the Ministère de la Recherche et de la Technologie is gratefully acknowledged.

[1] S. Alvarez, R. Vicente, R. Hoffmann, *J. Am. Chem. Soc.* **1985**, *107*, 6253−6277.
[2] H. A. Harris, A. D. Rae, L. F. Dahl, *J. Am. Chem. Soc.* **1987**, *109*, 4739−4741.
[3] [3a] M. H. Englert, J. J. Maj, A. D. Rae, K. T. Jordan, H. A. Harris, L. F. Dahl, *Abstract of papers, 187th National Meeting of the American Chemical Society*, St. Louis, MO; American Chemical Society, Washington, DC, **1984**, INOR 280. [3b] M. H. Englert, PhD Dissertation, University of Wisconsin, Madison, **1983**.
[4] J. J. Maj, A. D. Rae, L. F. Dahl, *J. Am. Chem. Soc.* **1982**, *104*, 4278−4280.
[5] C. Bianchini, C. Mealli, A. Meli, M. Sabat, P. Zanello, *J. Am. Chem. Soc.* **1987**, *109*, 185−198.
[6] I. V. Jourdain, PhD Dissertation, Université de Franche-Comté, **1998**.
[7] See ref. [45d] cited in ref.[1]
[8] [8a] G. A. Holloway, T. B. Rauchfuss, *Inorg. Chem.* **1999**, *38*, 3018−3019. [8b] G. A. Holloway, K. K. Klausmeyer, S. R. Wilson, T. B. Rauchfuss, *Organometallics* **2000**, *19*, 5370−5375.
[9] C. E. Keefer, S. T. Purrington, R. D. Bereman, P. D. Boyle, *Inorg. Chem.* **1999**, *38*, 5437−5442.
[10] F. Guyon, C. Lenoir, M. Fourmigué, J. Larsen, J. Amaudrut, *Bull. Soc. Chim. Fr.* **1994**, *131*, 217−226.
[11] [11a] F. E. M. Amstrong, M. S. Austerberry, R. L. Beddoes, M. Helliwell, J. A. Joule, C. D. Garner, *Act. Crystallogr.* **1993**, *C49*, 1764−1766. [11b] A. Dinsmore, J. H. Birks, C. D. Garner, J. A. Joule, *J. Chem. Soc., Perkin Trans. 1* **1997**, 801.
[12] [12a] H. Ushijima, S. Sudoh, M. Kajitani, K. Shimizu, T. Akiyama, A. Sugimori, *Inorg. Chim. Acta* **1990**, *175*, 11−12. [12b] H. Ushijima, S. Sudoh, M. Kajitani, K. Shimizu, T. Akiyama, A. Sugimori, *Appl. Organomet. Chem.* **1991**, *5*, 221−228.
[13] [13a] M. R. Churchill, J. P. Fennessey, *Inorg. Chem.* **1968**, *7*, 1123−1129. [13b] H. W. Baird, B. M. White, *J. Am. Chem. Soc.* **1988**, 4744−4745. [13c] E. J. Miller, T. B. Brill, A. L. Rheingold, W. Fultz, *J. Am. Chem. Soc.* **1983**, *105*, 7580−7584.
[14] M. Fourmigué, V. Perrocheau, *Act. Crystallogr.* **1997**, *C53*, 1213−1215.
[15] A. Antinolo, M. Fajardo, A. Otero, Y. Mugnier, H. Nabaoui, H. Mourad, *J. Organomet. Chem.* **1991**, *414*, 155−164.
[16] F. Guyon, D. Lucas, I. V. Jourdain, M. Fourmigué, Y. Mugnier, H. Cattey, *Organometallics* **2001**, *20*, 2421−2424.
[17] C. Takayama, K. Takauchi, S. Ohkoshi, G. C. Janairo, T. Sugiyama, M. Kajitani, A. Sugimori, *Organometallics* **1999**, *18*, 2843−2850.
[18] M. Noel, K. I. Vasu, *Cyclic Voltammetry and the Frontiers of Electrochemistry*, Aspect Publications, Ltd., London, **1990**.
[19] H. Mori, M. Nakano, H. Tamura, G. Matsubayashi, *J. Organomet. Chem.* **1999**, *574*, 77−85.
[20] M. Fourmigué, B. Domercq, I. V. Jourdain, P. Molinié, F. Guyon, J. Amaudrut, *Chem. Eur. J.* **1998**, *4*, 1714−1723.
[21] H.-B. Bürgi, J. D. Dunitz, *Structure Correlation*, vol. 2, appendix A, VCH Weinheim, **1994**.
[22] R. R. Schumaker, V. Y. Lee, E. M. Engler, *J. Org. Chem.* **1984**, *49*, 564−566.
[23] S. A Frith, J. L. Spencer, *Inorg. Synth.* **1990**, *28*, 273−274.
[24] R. C. Wheland, E. L. Martin, *J. Org. Chem.* **1975**, *40*, 3101.
[25] G. M. Sheldrick, *Programs for the Refinement of Crystal Structures*, University of Göttingen, Germany, **1997**.

Received January 15, 2002
[I02024]

Synthesis and Reactivity Towards Cationic Group 11 Metal Centers of an Extended Silacalix-[3]-phosphinine Macrocycle

Audrey Moores,[a] Nicolas Mézailles,[a] Nicole Maigrot,[a] Louis Ricard,[a] François Mathey,*[a] and Pascal le Floch*[a]

Keywords: Copper / Gold / Phosphinines / Macrocycles / Silver

A synthetic route to a new type of phosphinine-based macrocycle has been developed. This approach involves the reaction of a phosphinine bearing two pendant $SiMe_2OSiMe_2CCR$ (R = Ph) (**5**) groups with two equivalents of a diazaphosphinine (**1**). The 2,6-bis(azaphosphininedimethylsilyl)-phosphinine (**6**) formed was then reacted under dilute conditions with a second equivalent of phosphinine **5** to produce the new macrocycle **4**. The X-ray crystal structure of **4** reveals no particular strain, and the macrocycle was fluxional in solution even at low temperature (–60 °C). Reactions of macrocycle **4** with $[Cu(MeCN)_4][BF_4]$, $[Ag][BF_4]$ and $[AuCl(SMe_2)]$ in the presence of $GaCl_3$ as chloride abstractor yielded the corresponding cationic complexes **8**, **9**, and **10**. The X-ray crystal structure of the copper complex **8** was recorded. As expected, the overall geometry around copper is trigonal planar. The macrocycle adopts a distorted arrangement to accommodate this geometry, and the phosphinines do not bind copper in a linear fashion. The examination of metric parameters suggests that the aromaticity of the rings has not been perturbed due to a weak bonding between phosphorus atoms and copper.(© Wiley-VCH Verlag GmbH, 69451 Weinheim, Germany, 2002)

Introduction

Silacalix-[*n*]-phosphinines are a new class of phosphorus macrocycles that possess unusual electronic properties relative to classical sp^3-hybridized phosphorus species.[1] Recently we showed that the combination of a rigid structure (when $n = 4$) and the presence of strong π-acceptor phosphorus atoms within these macrocycles make them suitable ligands for the stabilization of reduced transition metal centers.[2] Thus, when cationic gold(I) was encapsulated in the cavity, these macrocycles behaved as phosphorus equivalents of CO matrices and the corresponding reduced gold(0) complex proved to be particularly stable.[3]

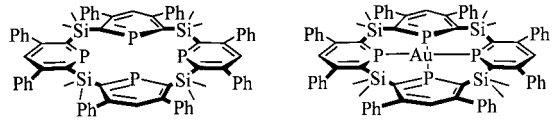

Another exciting feature of their reactivity was recently shown by studying their reduction. In the case of small macrocycles, the close vicinity of the two phosphorus atoms can be exploited to create new types of bonding. Thus, when two phosphinine units are linked by $-(Me_2Si-O-SiMe_2)-$ linkers in a cyclophane type structure, the mono-electronic reduction affords a mono-radical anion featuring a one-electron phosphorus–phosphorus single bond.[4]

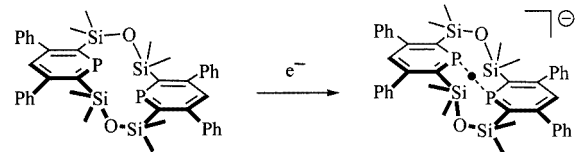

Regarding their coordinative properties, it appears that most species synthesized to date are quite rigid and allow the coordination of metal fragments that adopt a very specific geometry. Thus, silacalix-[*n*]-phosphinines incorporating $SiMe_2$ linkers are well adapted for the stabilization of metals that adopt a square planar or linear geometry ($n = 4$), or that might be coordinated through the face of an octahedron ($n = 3$).[1a] On the other hand, phosphorus analogs of cyclophane cannot incorporate metallic fragments and essentially behave as classical chelates.[5] With the aim of expanding the range of available macrocycles we recently investigated the synthesis of large and flexible species. Herein, we report on the synthesis of an extended silacalix-[3]-phosphinines and on a preliminary investigation of their coordinative properties towards cationic group 11 metals.

Results and Discussion

Among the different synthetic pathways, we deliberately chose one that relies on the reactivity of 1,3,2-diazaphosphinines towards functional alkynes. Indeed, as showed in previous studies, this method proved to be the most convenient way of assembling polyfunctional ligands and soph-

[a] Laboratoire "Hétéroéléments et Coordination" UMR CNRS 7653, Ecole Polytechnique,91128 Palaiseau Cedex, France

isticated edifices in one or two steps.[1b] In order to synthesize the extended and flexible structure **4** we focused our study on the preparation of a macrocycle incorporating $-(Me_2Si-O-SiMe_2)-$ spacer groups. Three different synthetic strategies were envisaged. The first one involved the condensation of the bidentate ligand **3** (formed from **2**), bearing two pendant $SiMe_2OSiMe_2CCPh$ groups, with one equivalent of a diazaphosphinine **1**. This approach was clearly advantageous since it could be carried out using a "one-pot sequence". The second and the third approach were different, but also utilized the same 2,6-disusbstituted phosphinine **5** as precursor. In the second approach, the macrocycle was built step by step from **5** by reacting two equivalents of **1** before closing the cavity with a third equivalent of diyne.[6] Finally, the third approach hinged on the direct condensation of **5** with the bis(monoazaphoshinine) **2**. All these pathways are summarized in the following scheme (Scheme 1).

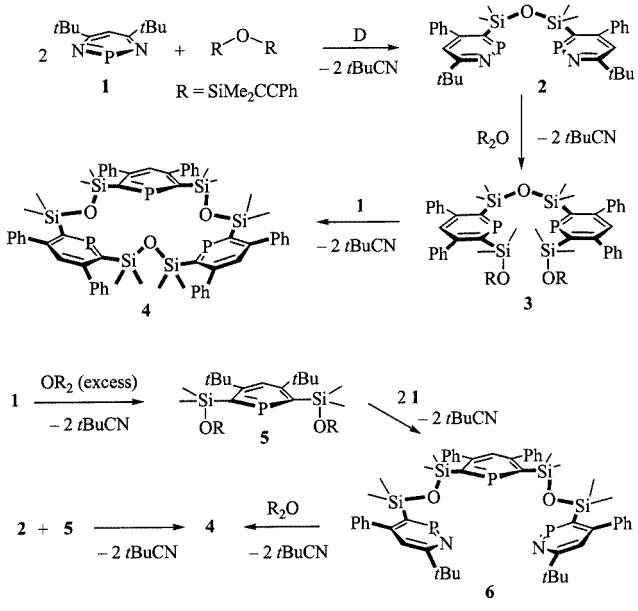

Scheme 1

In the first approach, the preparation of the intermediate **2** was easily achieved by heating the diyne with two equivalents of **1** at 80 °C for 18 hours in toluene. Bis(azaphosphinine) **2**, which is highly sensitive towards moisture, was characterized by ^{31}P NMR exclusively (δ = 305.6 ppm). Unfortunately, whatever the amount of diyne used (from 2 to 10 equiv.), the second step did not cleanly afford the expected bis(phosphinine) **3**, but mainly the diphosphacyclophane **7**[1c] and a mixture of unidentified side-compounds (Scheme 2).

As previously noted, the close vicinity of the two reacting sites clearly favors the cyclisation. The two other pathways proved to be much more adapted to the synthesis of **4**. These require as a prerequisite the synthesis of phosphinine **5**. This was readily achieved by reacting diyne in excess with one equivalent of diazaphosphinine **1** in toluene at 110 °C

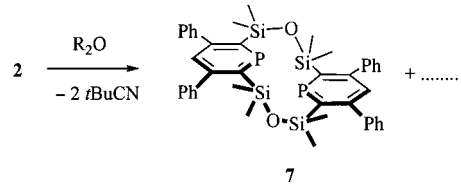

Scheme 2

for 5 hours. In the second method, reaction of **5** in toluene at 50 °C for 18 hours with two equivalents of **1** yielded compound **6** nearly quantitatively as attested by ^{31}P NMR spectroscopy (δ = 305.3 ppm). As with **2**, the high reactivity of the P=N moiety precluded the isolation and further characterization of **6**. The closing of the cavity was realized by reacting **6** with one equivalent of diyne. The use of dilute conditions turned out to be necessary to avoid the formation of linear oligomers and a series of competitive experiments showed the ideal concentration to be 5×10^{-3} mol/L. Additionally, as previously noted, we found that maintaining a steady concentration of reagents was absolutely necessary to achieve a complete conversion.[1b,1c] Unfortunately, these conditions dramatically increased the duration of experiments and the formation of **4** necessitated 2 weeks of heating. Following this experimental procedure, macrocycle **4** was isolated with an overall yield of 20% after chromatography. Finally, the third approach yielded **4** with a comparable yield. In both experiments, macrocycle **4** was easily purified by chromatography over silica gel and isolated as a very stable white powder.

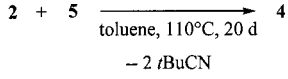

Scheme 3

As expected, ^{31}P NMR spectroscopic data suggest that the macrocycle is fluxional and its signal appeared as a singlet even at −60 °C. The formulation of **4** was also confirmed by ^{1}H and ^{13}C spectroscopy. Additional evidence was given by an X-ray crystal structure analysis. An ORTEP view of one molecule of **4** is presented in Figure 1 and the most relevant bond lengths and bond angles are listed in the corresponding legend. As can be seen, the size of the cavity is large and the distance between the two closest P atoms (P1 and P3) is 4.620 Å (P2−P3, 5.256 Å; P1−P2, 6.177 Å). No particular strain can be observed in the macrocycle and metric parameters within each ring are quite similar and roughly similar to those recorded for other silylphosphinines. Apart from these data, the structure of **4** does not deserve particular comments.

To test the coordinative ability of **4**, we logically turned our attention to cationic group 11 metal centers, which are known to accommodate a trigonal planar geometry when they are encapsulated in a suitable environment.[7] Ligand **4** was reacted with $[Cu(MeCN)_4][BF_4]$,[8] $[Ag][BF_4]$, and $[Au(Me_2S)Cl]$[9] in the presence of $GaCl_3$ as chloride ab-

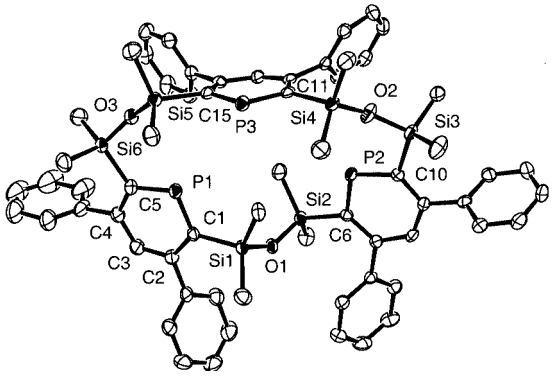

Figure 1. X-ray structure [50% TME (Thermal Motion Ellipsoids)] of one molecule of macrocycle **4**. All the hydrogen atoms and the solvents of crystallization (1 toluene, $^1/_2$ hexane and 1 H_2O) have been omitted. The numbering is arbitrary and different from that used for in the assignment of NMR spectroscopic data; selected bond lengths [Å] and angles [°]: P1−C1, 1.740(3); C1−C2, 1.411(4); C2−C3, 1.383(4); C3−C4, 1.395(4); C4−C5, 1.404(4); C5−P1, 1.742(3); C1−Si1, 1.890(3); Si1−O1, 1.638(2); O1−Si2, 1.638(2). P1−C1−C2, 121.5(2); C1−C2−C3, 122.8(3); C2−C3−C4, 126.0(3); C3−C4−C5, 123.1(3); C4−C5−P1, 121.2(2); C5−P1−C2, 105.3(1); P1−C1−Si1, 114.4(1); P1−C5−Si6, 113.9(2); C1−Si1−O1, 109.6(1); Si1−O1−Si2, 141.9(1)

stractor. All reactions cleanly proceeded at room temperature, in CH_2Cl_2 as solvent, to yield complexes **8**, **9**, and **10**, respectively, within 1 hour (Scheme 4). All three complexes were isolated as very stable powders and characterized by NMR spectroscopy and elemental analysis. The magnetic equivalency of the three phosphinine rings in each complex, which is in good agreement with a planar geometry around the metal, is evidenced by a singlet in ^{31}P NMR. Apparently, the coordination of the metal does not significantly affect the aromaticity within the phosphinine rings and, in ^{13}C NMR spectroscopic data, only minor differences can be noted between chemical shifts of the free ligand and those in complexes **8**, **9**, and **10**. A comparison between **4** and its gold derivative **10** is highly illustrative. Thus, for the carbon ring atoms, the $\Delta\delta$ ($\delta_{complex} - \delta_{ligand}$) are small: −8.74 ppm for C2, 3.3 ppm for C3 and 0.5 ppm for C4. This observation tends to show that the coordination of the macrocycle to the metal is relatively weak.

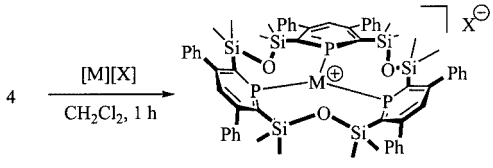

8: M = Cu, X = BF_4
9: M = Ag, X = BF_4
10: M = Au, X = $GaCl_4$

Scheme 4

In order to gain structural information, the X-ray structure of the copper complex **8** was recorded. A view of one molecule of **8** is presented in Figure 2 and the most relevant bond lengths and angles are listed in legend below. The structure consists of discrete monomeric units of the cationic copper complex and a tetrafluoroborate anion. As can be seen, the ligands adopt a highly distorted arrangement to accommodate the trigonal planar geometry around the central Cu atom. Interestingly, the copper atom is not located in the ideal axis of the phosphorus atom lone pair and in each phosphinine subunit, an important deviation is noted. Thus, the P1−Cu bond protrudes from the plane defined by the ring by 42° (34° for P2 and 22° for P3). This phenomenon is not unprecedented and reflects the important 3s character of the phosphorus atom lone pair. Similar deviations have already been observed in a helical edifice incorporating cationic biphosphinine Cu^I subunits and in chelate diphosphaferrocene based structures.[10] In P-sp^2 based ligands this geometric distortion is generally associated with a weak phosphorus−metal bonding. On the other hand, phosphorus−copper bond lengths compare with those recorded in other phosphinine[11] and tertiary phosphane Cu^I complexes.[12]

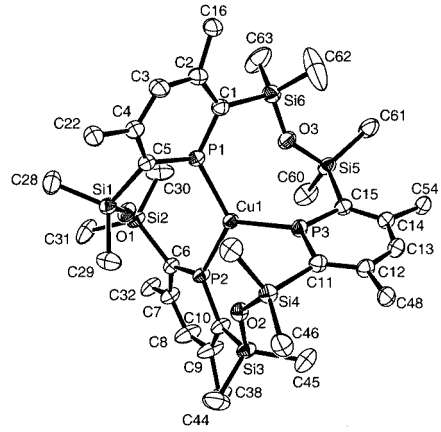

Figure 2. X-ray structure [50% TME (Thermal Motion Ellipsoids)] of one molecule of complex **8**. All the hydrogen atoms and the counter anion have been omitted for clarity. The numbering is arbitrary and different from that used in the assignment of NMR spectroscopic data.Selected bond lengths [Å] and angles [°]: P1−C1, 1.724(3); C1−C2, 1.409(4); C2−C3, 1.395(4); C3−C4, 1.399(4); C4−C5, 1.405(3); C5−P1, 1.727(3); C1−Si6, 1.890(3); Si1−O1, 1.624(2); O1−Si2, 1.628(2); C1−Si6, 1.890(3); P1−Cu1, 2.2419(7); P2−Cu1, 2.2386(7); P3−Cu1, 2.2318(7); P1−C1−C2, 118.4(2); C1−C2−C3, 123.2(2); C2−C3−C4, 126.8(2); C3−C4−C5, 121.9(3); C4−C5−P1, 119.5(2); C1−P1−C5, 108.8(1); P1−C5−Si1, 115.2(1); P1−C1−Si6, 117.1(2); C5−Si1−O1, 103.0(1); Si1−O1−Si2, 169.6(1); P1−Cu1−P2, 124.91(3); P2−Cu1−P3, 118.41(3); P3−Cu1−P1, 116.66(3)

Another interesting feature is provided by the analysis of metric parameters within the phosphinine subunits. Apart from the opening of the internal P−C−P angle, which ranges from 105.3(1) in **4** to 108.8(1) in **8** as a result of the re-hybridization at phosphorus, bond lengths and angles are not dramatically modified. In general, coordination of a phosphinine onto a metal fragment results in a lengthening of the P=C bond as a result of π-back donation in the π* LUMO, which is antibonding between P and C.[13] In **8**, P=C bond lengths compare with those of the free macrocycle **4**.

In conclusion, we have developed a straightforward route to a new type of an extended silacalix-[3]-phosphinine that

is well-tailored for the encapsulation of metal fragments adopting a trigonal planar geometry. Further studies aimed at studying the coordination of metallic centers having a catalytic activity are currently in progress in our laboratories.

Experimental Section

General: All reactions were routinely performed under an inert atmosphere of argon or nitrogen by using Schlenk and glove-box techniques with dry deoxygenated solvents. Dry THF and hexanes were obtained by distillation from Na/benzophenone and dry CH_2Cl_2 and $CDCl_3$ from P_2O_5. Dry CD_2Cl_2 was distilled and stored, like $CDCl_3$, on 4-Å Linde molecular sieves. Nuclear magnetic resonance spectra were recorded on a Bruker Avance 300 spectrometer. Solvent peaks are used as internal reference relative to Me_4Si for ^1H and ^{13}C chemical shifts (ppm). ^{31}P chemical shifts are relative to a 85% H_3PO_4 external reference. The following abbreviations are used: b; broad, singlet; d, doublet; t, triplet; m, multiplet; p, pentuplet; sext, sextuplet; sept, septuplet; v, virtual, q, quaternary. Mass spectra were obtained at 70 eV with a HP 5989B spectrometer coupled to a HP 5980 chromatograph by the direct inlet method. Elemental analyses were performed by the "Service d′analyse du CNRS", at Gif sur Yvette, France.

Synthesis of Phosphinine 5: A solution of diazaphosphinine **1** in toluene (21.7 mL, 0.0858 mmol/mL, 1.85 mmol) and 1,1,3,3-tetramethyl-1,3-bis-phenylethynyl-disiloxane (4.63 g, 13 mmol) was heated at 110 °C for 5 hours. After cooling to room temperature, celite (2 g) was added and toluene was evaporated yielding a brown powder. This solid was then added onto the top of a silica gel packed column for flash chromatography. A first fraction eluted with hexanes to yield excess diyne. A second fraction eluted with a mixture of hexane/toluene (90:10) and yielded mixed products. A third fraction gave the correct product. After evaporation of the solvents, phosphinine **5** was recovered as an orange oil. Yield: 1.13 g (85.8%). ^1H NMR (300 MHz, $CDCl_3$, 278 K): δ = 0.11 [s, 12 H, $Si(CH_3)_2OSi(CH_3)_2C{\equiv}C$], 0.24 [s, 12 H, $C{\equiv}CSi(CH_3)_2$], 7.2−7.5 (m, 21 H, phenyls and phosphinines *H*) ppm. ^{13}C NMR (75.5 MHz, $CDCl_3$, 278 K): δ = 2.8 [s, $C{\equiv}CSi(CH_3)_2$], 3.4 [d, *J* = 8.0 Hz, $Si(CH_3)_2OSi(CH_3)_2C{\equiv}C$], 94.2 (s, $C{\equiv}C{-}Si$), 104.35 (s, C_6H_5-$C{\equiv}C$), 123.3 (s, C^4 of $C{\equiv}C$-C_6H_5), 127.8 (s, C^4 of C_6H_5 on phosphinine), 128.1 (s, C^3 of C_6H_5 on phosphinine), 128.5 (s, C^3 of $C{\equiv}C$-C_6H_5), 128.9 (s, C^2 of $C{\equiv}C$-C_6H_5), 129.5 (s, C^2 of C_6H_5 on phosphinine), 132.2 (s, C^1 of $C{\equiv}C$-C_6H_5), 133.0 (d, *J* = 20.7 Hz, C^4 of phosphinine), 145.7 (d, *J* = 2.9 Hz, C^1 of C_6H_5 on phosphinine), 154.1 (d, *J* = 10.3 Hz, C^3 of phosphinine), 164.3 (d, *J* = 87.9 Hz, C^2 of phosphinine) ppm. ^{31}P NMR (121.5 MHz, $CDCl_3$, 278 K): δ = 275.6 (s) ppm. $C_{41}H_{45}O_2PSi_4$ (713.11): calcd. C 69.06, H 6.36; found C 69.36, H 6.18.

Synthesis of Macrocycle 4: Phosphinine **5** (2.07 g, 2.9 mmol) was added to a solution of diazaphosphinine **1** in toluene (79 mL, 73.5 mmol/L, 5.8 mmol) at room temperature. The volume of the solution was reduced to half and the resulting mixture was then heated at 50 °C for 18 hours. After checking the complete formation of the bis(monoazaphosphinine)phosphinine **6** by ^{31}P NMR spectroscopy, dry toluene (300 mL) was added prior to one equivalent of 1,1,3,3-tetramethyl-1,3-bis-phenylethynyl-disiloxane (0.97 g, 2.9 mmol). The resulting solution was heated at 130 °C for 20 days. After cooling to room temperature, celite (5 g) was added and the solvent was evaporated to yield a brown powder. This coated celite was the added onto the top of a silica gel packed column for flash chromatography. After eluting traces of remaining diyne with hexane, macrocycle **4** was eluted with a mixture of hexane/toluene (80:20). After evaporation of the solvents, **4** was recovered as a colorless powder. Yield: 635 mg (20%). ^1H NMR (300 MHz, $CDCl_3$, 278 K): δ = 0.00 [s, 36 H, $Si(CH_3)_3$], 7.2−7.5 (m, 33 H, C_6H_5 and H_4 of phosphinines) ppm. ^{13}C NMR (75.5 MHz, $CDCL_3$, 278 K): δ = 3.7 [s, $Si(CH_3)_3$], 127.4 (s, C_{ipso} of C_6H_5), 127.8 (s, C^3 of C_6H_5), 129.6 (s, C^2 of C_6H_5), 132.5 (d, *J* = 20.9 Hz, C^4 of phosphinines), 145.8 (s, C^1 of C_6H_5), 153.3 (d, *J* = 9.5 Hz, C^4 of phosphinines), 164.5 (d, *J* = 90.1 Hz, C^2 of phosphinines) ppm. ^{31}P NMR (121.5 MHz, $CDCl_3$, 278 K): δ = 276.9 ppm. MS (*m*/*z*, relative intensity): 1135 (M − 1, 50). $C_{63}H_{69}O_3P_3Si_6$ (1135.65): calcd. C 66.63, H 6.12; found C 66.05, H 5.94.

Synthesis of Complex 8: Macrocycle **4** (57 mg, 0.050 mmol) and $[Cu(MeCN)_4][BF_4]$ (15.8 mg, 0.050 mmol) were allowed to react in CH_2Cl_2 (3 mL) at room temperature. After one hour of stirring, the solvent was evaporated and complex **8** was washed twice with hexanes (2 × 2 mL). After filtration and drying under vacuum, **8** was recovered as a yellow powder. Yield: 62 mg (96%). ^1H NMR (300 MHz, $CDCl_3$, 278 K): δ = 0.00 [s, 36 H, $Si(CH_3)_3$], 7.2−7.5 (m, 33 H, C_6H_5 and H^4 of phosphinines) ppm. ^{13}C NMR (75.5 MHz, $CDCl_3$, 278 K): δ = 3.73 [s, $Si(CH_3)_3$], 3.79 [s, $Si(CH_3)_3$], 128.7 (s, C_{ipso} of C_6H_5), 128.8 (s, C^3 of C_6H_5), 129.1 (s, C^2 of C_6H_5), 132.9 (AXX′X′′, ΣJ = 35.6 Hz, C^4 of phosphinines), 143.5 (s, C^1 of C_6H_5), 156.4 (AXX′X′′, ΣJ = 14.9 Hz, C^3 of phosphinines), 159.2 (AXX′X′′, ΣJ = 40.2 Hz, C^2 of phosphinines) ppm. ^{31}P NMR (121.5 MHz, $CDCl_3$, 278 K): δ = 217.7 ppm. $C_{63}H_{69}BCuF_4O_3P_3Si_6$ (1286.01): calcd. C 58.84, H 5.41; found C 58.72, H 5.54.

Synthesis of Complex 9: Macrocycle 4 (50 mg, 0.044 mmol) and $AgBF_4$ (8.6 mg, 0.044 mmol) were dissolved in CH_2Cl_2 (2 mL) at room temperature. The solution was stirred for one hour. It became light brown. After evaporation of the solvent, the solid obtained was washed twice with hexanes (2 × 2 mL). Complex **9** was collected by filtration. After drying under vacuum, **9** was recovered as a beige powder. Yield: 54 mg (92%).^1H NMR (300 MHz, $CDCl_3$, 278 K): δ = 0.00 [s, 36 H, $Si(CH_3)_3$], 7.2−7.5 (m, 33 H, C_6H_5 and H^4 of phosphinines) ppm. ^{13}C NMR (75.5 MHz, $CDCl_3$, 278 K): δ = 4.11 [s, $Si(CH_3)_3$], 4.18 [s, $Si(CH_3)_3$], 128.6 (s, C_{ipso} of C_6H_5), 128.7 (s, C^3 of C_6H_5), 128.9 (s, C^2 of C_6H_5), 133.9 (AXX′X′′, ΣJ = 28.7 Hz, C^4 of phosphinines), 143.6 (s, C^1 of C_6H_5), 156.0 (AXX′X′′, ΣJ = 11.5 Hz, C^3 of phosphinines), 162.0 (AXX′X′′, ΣJ = 51.7 Hz, C^2 of phosphinines) ppm. ^{31}P NMR (121.5 MHz, $CDCl_3$, 278 K): δ = 222.3 ppm. $C_{63}H_{69}AgBF_4O_3P_3Si_6$ (1330.33): calcd. C 56.88, H 5.23; found C 57.00, H 5.42.

Synthesis of Complex 10: Macrocycle **4** (50 mg, 0.044 mmol) and [AuCl(SMe2)] (13 mg, 0.044 mmol) were dissolved in CH_2Cl_2 (2 mL) at room temperature. The resulting solution was cooled to −80 °C and a solution of $GaCl_3$ (10 mg, 0.057 mmol) in CH_2Cl_2 (prepared in the glovebox) was added into the mixture by cannula. The resulting solution was warmed to room temperature and then stirred for one hour. After evaporation of the solvent, the solid obtained was washed successively with hexanes and ether (2 × 2 mL). Complex **10** was collected by filtration. After drying under vacuum, **10** was recovered as a yellow powder. Yield: 66 mg (97%).^1H NMR (300 MHz, $CDCl_3$, 278 K): δ = 0.00 [s, 36 H, $Si(CH_3)_3$], 7.2−7.5 (m, 33 H, C_6H_5 and H^4 of phosphinines) ppm. ^{13}C NMR (75.5 MHz, $CDCl_3$, 278 K): δ = 3.90 [s, $Si(CH_3)_3$], 3.95 [s, $Si(CH_3)_3$], 128.7 (s, C_{ipso} of C_6H_5), 128.8 (s, C^3 of C_6H_5), 129.1 (s, C^2 of C_6H_5), 133.1 (AXX′X′′, ΣJ = 34.5 Hz, C^4 of phosphinines), 143.8 (s, C^1 of C_6H_5), 156.6 (AXX′X′′, ΣJ = 14.9 Hz, C^3 of phosphinines), 159.2 (AXX′X′′, ΣJ = 46.0 Hz, C^2 of phosphinines) ppm. ^{31}P NMR (121.5 MHz, CH_2Cl_2, 278 K): δ = 249.5 ppm.

Table 1. Details of X-ray structure determinations

Compound	4	8
Crystal colour	colorless	yellow
Crystal shape	plate	cube
Crystal size [mm]	0.18 × 0.18 × 0.05	0.18 × 0.18 × 0.18
Empirical formula	$C_{63}H_{69}O_3P_3Si_4.C_6H_{14}\cdot 1/2C_7H_8\cdot H_2O$	$C_{63}H_{69}BCuF_4O_3P_3Si_6\cdot 2.5CHCl_3$
Molecular mass	1285.89	1584.40
Temperature [K]	150.0(1)	150.0(1)
Radiation (graphite-monochromated)	Mo-K_α	Mo-K_α
Wavelength [Å]	0.71070	0.71069
Crystal system	Triclinic	Triclinic
Space group	$P\bar{1}$	$P\bar{1}$
a [Å]	12.1666(6)	13.775(2)
b [Å]	16.3580(6)	15.894(2)
c [Å]	18.1896(8)	18.550(3)
α [°]	104.944(2)	83.8740(10)
β [°]	98.117(2)	77.0910(10)
γ [°]	92.553(2)	77.2960(10)
V [Å]^3	3450.2(3)	3854.6(10)
Z, calcd. density [g·cm^{-3}]	2, 1.238	2, 1.365
Abs. coefficient [cm^{-1}]	0.238	0.750
$2\Theta_{max}$ [deg]	24.11	27.48
$F(000)$	1370	1630
Index ranges	$-13 \le h \le 11 - 18 \le k \le 18 - 20 \le l \le 20$	$-17 \le h \le 17 - 20 \le k \le 20 - 24 \le l \le 22$
Reflections collected/independent	17022/10952	26536/17590
Reflections used	8052	13531
R_{int}	0.0438	0.0490
Absorption correction	0.9584 min., 0.9882 max.	0.8768 min., 0.8768 max.
Parameters refined	734	794
Reflection/parameter	10	17
Final R1, $wR2$ [$I > 2\sigma(I)$]	0.0478, 0.1265	0.0534, 0.1578
Goodness-of-fit on F^2	1.020	1.103
Diff, peak and hole [e·Å^{-3}]	1.021(0.055)/−0.638(0.055)	1.524(0.076)/−1.233(0.076)

$C_{63}H_{69}AuCl_4GaO_3P_3Si_6$ (1544.15): calcd. C 49.00, H 4.50; found C 48.88, H 4.55.

X-ray Structure Determinations: Single crystals of **4** were obtained by diffusing methanol into a toluene solution of the compound. Crystals of **8** were obtained by diffusing hexane into a chloroform solution of the complex. Data were collected on a Nonius Kappa CCD diffractometer using a Mo-$K\alpha$ (λ = 0.71069 Å) X-ray source and a graphite monochromator. Experimental details are described in Table 1. The crystal structures were solved using SIR 97[14] and Shelxl-97.[15] ORTEP drawings were made using ORTEP III for Windows.[16] In the structure of **8** a 1/2 $CHCl_3$ located near a symmetry center was accounted with SQUEEZE. Analysis of the principal mean square displacements in the structure of complex **8** may indicate a slight libration or long range disorder of the BF_4 anion. CCDC-178617 (for **4**) and -178618 (for **8**) contain the supplementary crystallographic data for this paper. These data can be obtained free of charge at www.ccdc.cam.ac.uk/conts/retrieving.html [or from the Cambridge Crystallographic Data Centre, 12, Union Road, Cambridge CB2 1EZ, UK; Fax: (internat.) +44-1223/336-033; E-mail: deposit@ccdc.cam.ac.uk].

Acknowledgments

The authors thank the CNRS and the Ecole Polytechnique for financial support of this work.

[1] See for example: [1a] N. Avarvari, N. Mézailles, L. Ricard, P. Le Floch, F. Mathey, *Science* **1998**, *280*, 1587. [1b] N. Avarvari, N. Maigrot, L. Ricard, F. Mathey, P. Le Floch, *Chem. Eur. J.* **1999**, *5*, 2109. [1c] N. Mézailles, N. Maigrot, S. Hamon, L. Ricard, F. Mathey, P. Le Floch, *J. Org. Chem.* **2001**, *66*, 1054. [1d] P. Le Floch in *Phosphorus-Carbon Heterocyclic Chemistry: The Rise of a New Domain*; F. Mathey, Ed.; Pergamon: **2001**; 485.

[2] See for example: P. Rosa, N. Mézailles, L. Ricard, F. Mathey, P. Le Floch, Y. Jean, *Angew. Chem. Int. Ed.* **2001**, *40*, 1251, and references therein.

[3] N. Mézailles, N. Avarvari, N. Maigrot, L. Ricard, F. Mathey, F. Le Floch, L. Cataldo, T. Berclaz, M. Geoffroy, *Angew. Chem. Int. Ed.* **1999**, *38*, 3194.

[4] L. Cataldo, S. Choua, T. Berclaz, M. Geoffroy, N. Mézailles, L. Ricard, F. Mathey, P. Le Floch, *J. Am. Chem. Soc.* **2001**, *123*, 6654.

[5] A. Moores, N. Mézailles, L. Ricard, F. Mathey, P. Le Floch, *unpublished results.*

[6] H. Sugita, Y. Hatanaka, T. Hiyama, *Chem. Lett.* **1996**, 379.

[7] [7a] B. J. Hathaway in *Comprehensive Coordination Chemistry*; G. Wilkinson, R. D. Gillard, J. A. McClerverty, Eds.; Pergamon Press: **1987**, vol. 5, 533. [7b] R. J. Lancashire in ref.[7a], vol. 5, p. 861. [7c] R. J. Puddephatt in ref.[7a], vol. 5, p. 925. [7d] The trigonal planar geometry is relatively rare for Cu and Ag. Thus, among 9519 crystal structures reported in the Cambridge data that contain a Cu atom, only 108 (1.1%) are found in a trigonal planar geometry. In the case of Ag, 1734 structures containing an Ag atom are found, of which 33 (1.9%) feature a trigonal planar ligand field.

[8] J. G. Kubas, *Inorg. Synth.* **1990**, *25*, 68.

[9] R. Uson, A. Laguna, *Organometallic Syntheses*, (Eds.: R. B. King, J. Eisch), Elsevier Science Publishers B. V., Amsterdam, **1986**, vol. 3, 324.

[10] [10a] P. Le Floch, L. Ricard, F. Mathey, *Bull. Soc. Chim. Fr.* **1996**, *133*, 691. [10b] X. Sava, L. Ricard, F. Mathey, P. Le Floch, *Organometallics* **2000**, *19*, 4899.
[11] M. Shiotsuka, Y. Matsuda, *Chem. Lett.* **1994**, 351.
[12] See for example: M. Glöcke, K. Hübler, H.-J. Kümmerer, G. Denninger, W. Kaim, *Inorg. Chem.* **2001**, *40*, 2263.
[13] [13a] J. Waluk, H.-P. Klein, A. J. Ashe III, J. Michl, *Organometallics* **1989**, *8*, 2804. [13b] L. Nyulaszi, *Chem. Rev.* **2001**, *101*, 1229.
[14] A. Altomare, M. C. Burla, M. Camalli, G. Cascarano, C. Giacovazzo, A. Guagliardi, A. G. G. Moliterni, G. Polidori, R. Spagna, *SIR97*, an integrated package of computer programs for the solution and refinement of crystal structures using single crystal data, **1999**.
[15] G. M. Sheldrick, *SHELXL-97*; Universität Göttingen, Göttingen, Germany, **1998**.
[16] L. J. Farrugia, L. J. *ORTEP-3*, Department of Chemistry, University of Glasgow, *J. Appl. Cryst*. **1997**, *30*, 565−567.

Received February 6, 2002
[I02059]

Oligoalkyne-Bridged (η^4-Cyclobutadiene)(η^5-cyclopentadienyl)cobalt Fragments − Syntheses and Properties

Joerg Classen,[a] Rolf Gleiter,*[a] and Frank Rominger[a]

Dedicated to Professor Dwaine O. Cowan

Keywords: Alkynes / Conjugation / Electron transfer / Rod-like molecules / Cobalt

The syntheses of (η^5-cyclopentadienyl)(η^4-tetraphenylcyclobutadiene)cobalt units bridged by buta-1,3-diyne, octa-1,3,5,7-tetrayne, and dodeca-1,3,5,7,9,11-hexayne units (**15**, **18**, **21**) are reported. All three species could be obtained by Hay coupling of the corresponding mono-, di-, and triyne units **14**, **17**, and **20**. In the case of **14**–**17** and **21**, the molecular structures were confirmed on the basis of X-ray studies on single crystals. Cyclic voltammetry revealed a weak interaction between the metal centers of **15** and no interaction between the metal centers of **18** and of **21**.
(© Wiley-VCH Verlag GmbH, 69451 Weinheim, Germany, 2002)

Introduction

Transition metal complexes with two redox centers are of current interest in basic and applied research.[1] Since the first investigation of biferrocene,[1,2] biferrocenylene,[3,4] and diferrocenylacetylene[5,6] almost 30 years ago, the interest in dinuclear complexes has increased considerably.[7−20] Of current interest are species with rigid alkyne units between the metal units. The metal centers can be connected through the ligands as in **1**−**3**, or they can be connected directly to the alkyne bridges as in **4** and **5**.[13−20] In both types, voluminous termini are connected with a rigid carbon rod. The most frequent metal species to mark the end of the rod are iron- and rhenium-based fragments. In this paper we report on the synthesis, structural and spectroscopic properties of molecular wires consisting of C_4 to C_{12} chains bridging two (η^5-cyclopentadienyl)(η^4-tetraphenylcyclobutadiene)cobalt units.

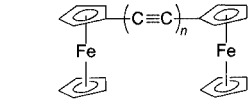

1

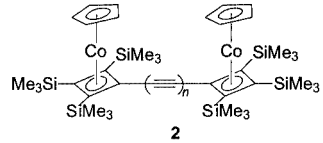

2

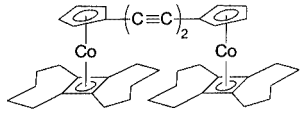

3

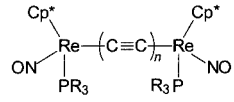

4

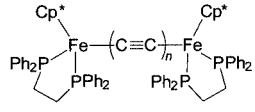

5

Syntheses of 14−20

Initiated by electrochemical studies on species with (η^4-cyclobutadiene)(η^5-cyclopentadienyl)cobalt fragments, we synthesized **3** and compared its electrochemical properties with related species. The synthesis of **3** is briefly outlined in Scheme 1 and has been described in the literature.[11] The further extension of the length of the alkyne bridges was hampered by the two low yielding steps for obtaining the starting material **8** (Scheme 1).[11] The replacement of the cyclooctadiene unit in **6** by a tricyclo[7.5.0.0^{1,7}]tetradeca-1,8-diene group could only be achieved in 22% yield.[11] Furthermore, the conversion of the acetyl group in **7**[11] to the alkyne unit according to a protocol described by Negishi, furnished **8** in only 28% yield.[11] In order to obtain higher yields of the starting material we replaced 1,8-cyclotetradecadiyne by the less expensive tolan and chose a different route to generate the alkyne unit. Our synthesis of the monoalkyne complex **14** is summarized in Scheme 2. The dicarbonyl(η^5-methoxycarbonylcyclopentadienyl)cobalt complex **9**[21] was converted into the metallocene **10**,[22,23] and subsequently reduced to the alcohol **11**[24] according to known procedures. The conversion into the aldehyde **12**[25] was accomplished with $BaMnO_4$ oxidation,[26] followed by a Wittig reaction with (chloromethyl)-triphenylphosphonium chloride, giving a 1:1 mixture of (*E*)/(*Z*)-alkenes **13**.[24] Treatment of the mixture with potassium

[a] Organisch-Chemisches Institut der Universität Heidelberg, Im Neuenheimer Feld 270, 69120 Heidelberg, Germany

tert-butoxide yielded a mixture of the (*E*) diastereomer and the alkyne **14**.[24] After separation of **14**, the (*E*) diastereomer was treated with phenyllithium at room temperature, giving **14** again. The overall yield of the five steps shown in Scheme 2 was 10%. The structure of **14** could be confirmed by a diffraction analysis on single crystals.

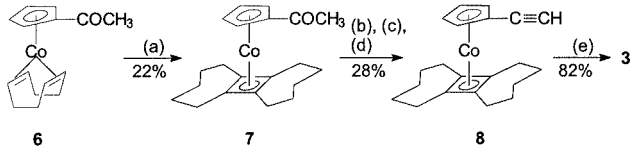

Scheme 1. Preparation of **3**: a) 1,8-cyclododecadiyne; b) LDA/THF; c) $ClPO(OEt)_2$; d) LDA, HCl; e) $Cu(OAc)_2$, pyridine

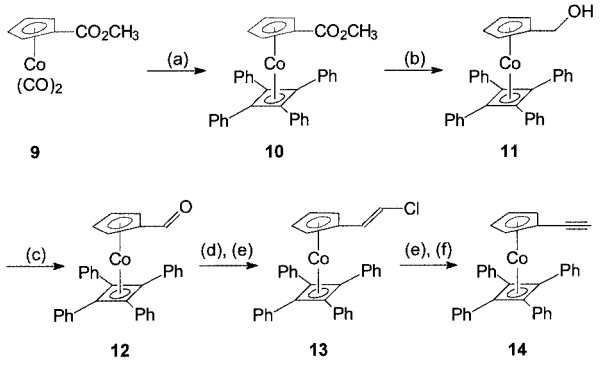

Scheme 2. Preparation of **14**: a) tolan, xylene, 120 °C; b) $LiAlH_4$/ether; c) $BaMnO_4$; d) $ClCH_2P(C_6H_5)_3{}^+Cl^-$; e) KO*t*Bu; f) C_6H_5Li

To transform **14** into its dimer **15**, we tested the protocols of Eglinton[27,28] and Hay.[29] The reaction of **14** with dry copper(II) acetate and dry pyridine at 90 °C was not successful, only decomposition of the starting material was observed. We were able to isolate 93% of the dimer **15** using the coupling reported by Hay[29] (Scheme 3). The structure of **15** could be confirmed by X-ray investigations on single crystals (see below).

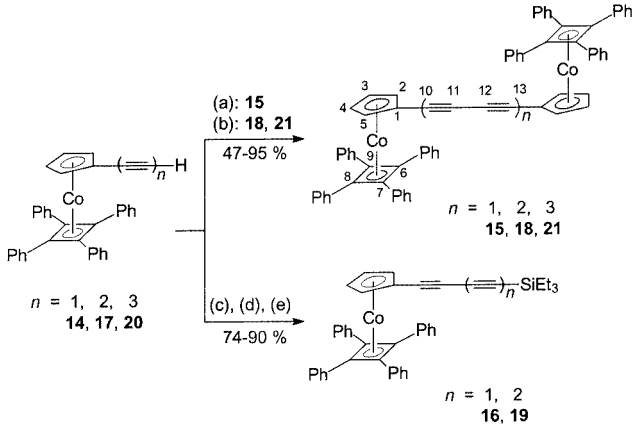

Scheme 3. Synthesis of **15**, **16**, **18**, **19**, **21**: a) CuCl/pyridine + O_2; b) CuCl/TMEDA + O_2 c) *n*BuLi; d) CuCl; e) $Br-C\equiv C-SiMe_3$, $EtNH_2$

In order to obtain longer chains we had to find a reasonable path to elongate **14** by one ethynyl unit. This could be achieved by a modified Cadiot−Chodkiewicz reaction[13,14,30−33] involving **14** and (triethylsilyl)ethynyl bromide,[32,33] as shown in Scheme 3 in 90% yield. The parent compound **17** could be obtained by solvolysis of **19** with 5 M NaOH[10,34] in DMF.

Coupling of **17** to the dimer with four alkyne units could be achieved with Cu^I in the presence of tetramethylethylenediamine (TMEDA) (Scheme 3) and oxygen. The moderate yield of this product **18** can be attributed to the instability of **17** under the coupling conditions. The yield of **18** could be increased to 95% when **17** was produced in situ and not isolated.

Compound **21** was prepared by the elongation of the alkyne chain of **17** by one unit using the homocoupling protocol as shown in Scheme 3. As a side reaction, **18** could be isolated, therefore the yield of **19** was lower (74%) relative to the coupling reaction which led to **16**. In order to obtain **21**, the triethylsilyl group of **19** was removed by NaOH in DMF in situ, followed by a Cadiot−Chodkiewicz reaction (Scheme 3). In this case the product was obtained in 47% yield. The single crystals obtained of **21** were of poor quality. Therefore, the X-ray data can only be used as proof of the constitution and conformation of the end groups.

Structural Investigations

We were able to isolate single crystals for **14**−**17** and **21**. In Figures 1 and 2 we display as examples the molecular structures of **15** and **17**. Selected bond lengths of **14**−**17** are summarized in Table 1. The asymmetric unit of **14** contains two independent molecules, one of them is disordered with respect to the position of the alkyne unit attached to the Cp ring. The alkyne unit can be located at two adjacent Cp carbon atoms with nearly the same occupancies. In the discussion only the results of the non-disordered molecule are considered.

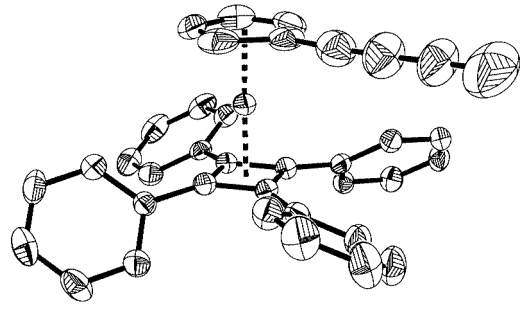

Figure 1. ORTEP plot (50% probability) of the molecular structure of **17**

The mean distances between the cobalt atom and the cyclopentadienyl (Cp) ring (1.68 Å for all structures) are slightly shorter than between the cobalt atom and the cyclobutadiene (Cb) unit (1.69 Å for all structures). These values are close to those reported for (η^4-cyclobutadiene)(η^5-

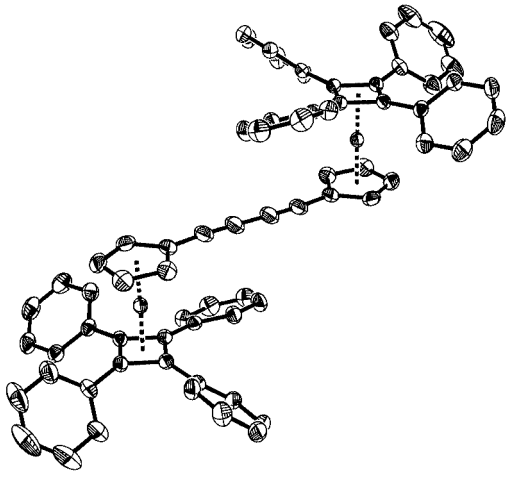

Figure 2. ORTEP plot (50% probability) of the molecular structure of **15**

Table 1. Selected bond lengths [Å] and bond angles [°] of **14**−**17**; for the numbering see Scheme 3

	14	**15**	**16**	**17**
Cp−Co (mean values)	1.675(3)	1.675(2)	1.679(2)	1.682(4)
Cb−Co (mean values)	1.691(3)	1.693(2)	1.692(2)	1.693(3)
C1−C10	1.443(6)	1.418(3)	1.422(3)	1.425(6)
C10−C11	1.143(7)	1.197(3)	1.204(3)	1.247(7)
C11−C12		1.378(4)	1.387(3)	1.319(7)
C12−C13			1.192(3)	1.275(9)
C1−C10−C11	175.6(7)	175.7(2)	178.4(2)	177.7(5)
C10−C11−C12		178.7(3)	179.4(2)	178.9(7)
C11−C12−C13			179.4(2)	176.3(8)

cyclopentadienyl)cobalt,[35] where the mean distance between the Cp ring and the cobalt atom is 1.66 Å, and the distance between the cobalt atom and the Cb ring is 1.68 Å.[34] The distances between the Cp ring and the sp carbon centers (C1−C10, Scheme 3) vary between 1.44 Å (**14**) and 1.42 Å (**15**−**17**). The bond length of the terminal triple bond in **14** [1.143(7) Å] is unrealistically short. This can be attributed to the librational shortening caused by the strong anisotropic motion of this molecular tail, which cannot be modeled correctly by an ellipsoid-shaped description. The distances found for the other triple bonds (C10−C11 and C12−C13) vary between 1.20 Å (**15**, **16**) and 1.28 Å (**17**). The angles at the triple bonds deviate slightly from 180°, as reported for other long alkyne chains.[32,33] The C−C bond lengths within the Cb and Cp rings are found to be equal. The phenyl rings are twisted out of the plane of the Cp ring in a propeller-like fashion (see Figure 2).

The molecular structure of **21** in the solid state is shown in Figure 3. In this molecule both tetraphenylcyclobutadiene units are far removed from each other, therefore they can adopt the *syn* conformation (Figure 3). The crystal data of **21** reveal *R* values that are too large to be used for a quantitative evaluation (cf. Table 2). This shortcoming is mainly due to three disordered dichloromethane molecules in the asymmetric unit. Nevertheless, **21** is the first example with a hexayne unit between two Cp ligands. It can be compared with $(CO)_2Cp^*Fe-(C\equiv C)_6-FeCp^*(CO)_2$, in which the C_{12} chain is bound directly to the metal centers.[36]

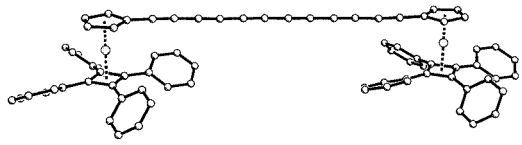

Figure 3. Molecular structure of **21** (ball-and-stick model)

Spectroscopic and Cyclovoltammetric Data

The NMR spectroscopic data of the new alkynes are listed in the Exp. Sect. The assignment of all ^{13}C signals was possible by carrying out a DEPT experiment. In Figure 4 the superimposed UV/Vis spectra of **15**, **18**, and **21** are shown. It demonstrates a shift to longer wavelengths of the absorbance bands with increasing chain length, as reported for related species.[10,13−17,36]

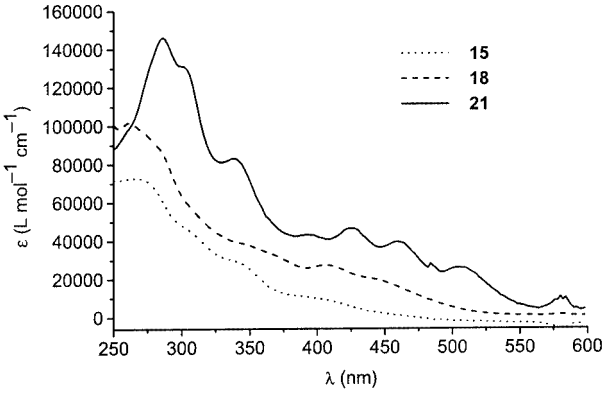

Figure 4. UV/Vis spectra of **15**, **18**, and **21**

In order to investigate the extent of metal−metal interaction in **15**, **18**, and **21**, cyclic voltammetric (CV) measurements were carried out. The uncertainty of the signals is somewhat larger (±25 mV) than usual (±15 mV), because of the low solubility of the samples in dichloromethane. As a reference, compound **14** was used, which is the simplest common building block of all three oligomers. The CV measurement of **14** shows a reversible oxidation at 540 mV (Figure 5). The CV of **15** reveals two oxidations, one at 490 mV, the second at 720 mV. The former is reversible, the latter is irreversible at different scan rates of up to 2 V/s.

The first oxidation of **15** was observed at a lower potential (by 50 mV) than that of the reference compound **14**. This result can be rationalized by assuming a lower HOMO energy due to the interaction of both metal fragments. The positive charge of the resulting radical cation is delocalized over both Co atoms through the alkyne backbone, resulting in a higher second oxidation potential. The potential separation of 230 mV suggests that the electronic interaction is relatively weak,[38] therefore, we assign **15** to class II in

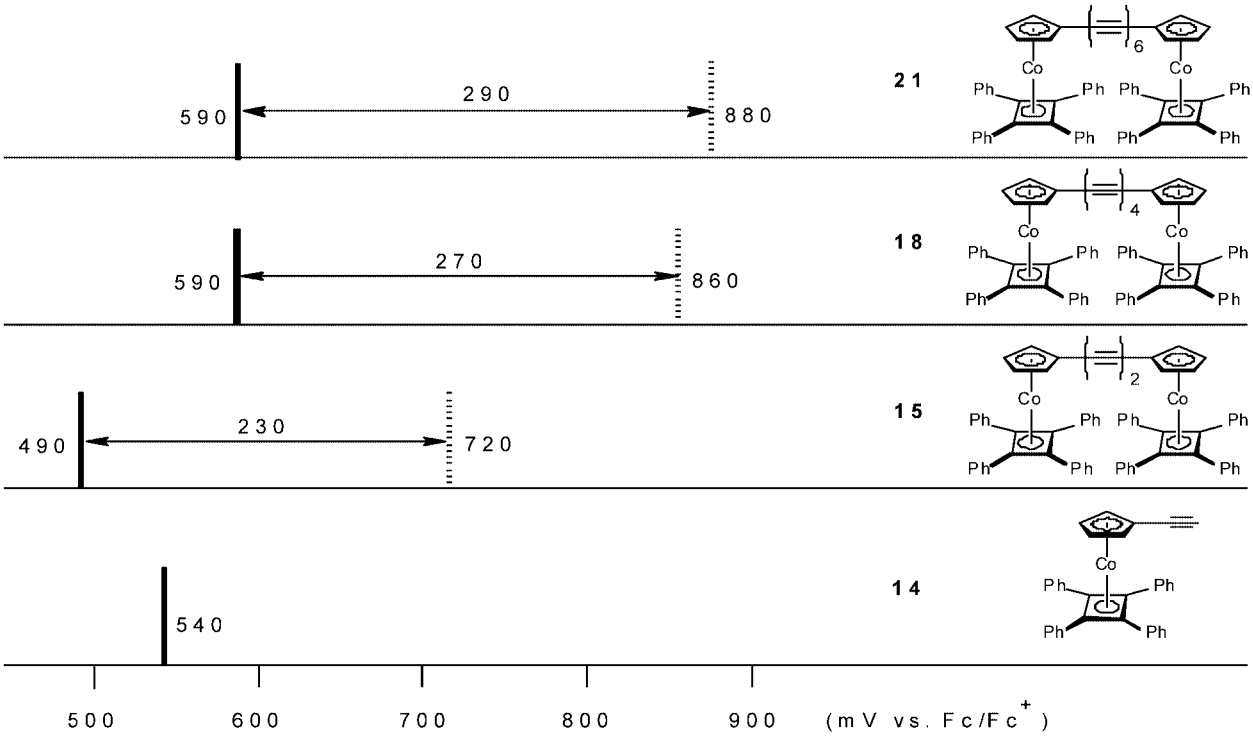

Figure 5. Comparison of the CV data of **14**, **15**, **18**, and **21**

the Robin and Day classification of mixed-valent compounds.[37]

A different situation is observed for **18** and **21**, where the first reversible oxidation potential is shifted towards a higher potential (by 50 mV) with respect to **14**. The second oxidation of **18** and **21** is irreversible at different scan rates of up to 2 V/s. The larger potential separation of 270 (**18**) and 290 mV (**21**) seems to indicate an increase in the electronic interaction with increasing alkyne chain length. However, a larger π-system is expected to result in a decrease in the HOMO energy, which in turn should cause a more facile oxidation. This contradiction can be explained by a reversible two-electron oxidation, where both Co atoms are oxidized to Co^{II} at similar potentials. At the second irreversible potential, an oxidation of one or both Co^{II} atoms to Co^{III} may occur. Another explanation is an ECE mechanism, where the first oxidation is followed by a chemical transformation, which renders the second oxidation irreversible. The latter complexes show no electronic interaction, so they can be assigned to class I in the Robin and Day classification of mixed-valent compounds.[37]

Concluding Remarks

Our goal was to find a reasonable path to prepare polyalkynes with (η^5-cyclopentadienyl)(η^4-tetraphenylcyclobutadienyl)cobalt fragments at both ends of the carbon rod. This could be achieved using **14** as a starting material. This compound was made available in five steps from **10**, with an overall yield of 10%. With **14** as the key intermediate, we were able to synthesize **15**, **18**, and **21**. The key steps were the Hay coupling reaction of the corresponding mono-, di-, and triyne units **14**, **17**, and **20**, respectively. The yields of **18** and **21** could be improved by preparing **17** and **20** in situ by deprotection of the protected diyne **16** and triyne **19**, respectively. By means of X-ray studies of the single crystals of **14**−**17** and **21** we could confirm the structure and conformation of the alkynes. For the polyyne part of all the studied samples, clear short−long C≡C−C bond alternation is observed. Our CV studies do not indicate a metal−metal interaction through the alkyne rod for **18** and **21**, whereas in **15**, where the distance between the metal centers is shorter, a slight shift with respect to **14** is observed.

Experimental Section

General Remarks: All melting points are uncorrected. The NMR spectra were measured with a Bruker Avance 500 spectrometer (^{1}H NMR at 500 MHz and ^{13}C NMR at 125.77 MHz) using the solvent as internal standard (δ). The mass spectra refer to data recorded with a JEOL JMS-700 instrument. IR spectra were recorded with a Bruker Vector 22. All reactions with CpCo(COD) were carried out in dried glassware under argon, using dried and oxygen-free solvents.

(η^5-Formylcyclopentadienyl)(η^4-tetraphenylcyclobutadienyl)cobalt(I) (12):[25] $BaMnO_4$ (2.0 g, 7.8 mmol) was added to a solution of **11** (200 mg, 0.4 mmol) in 100 mL of dichloromethane.[26] The suspen-

sion was stirred for 24 h under argon. After filtration, the solvent was removed to give 198 mg (99%) of **12** as an orange solid. ^{1}H NMR (CD_2Cl_2): δ = 4.91 (pt, 2 H, CpH), 5.23 (pt, 2 H, CpH), 7.21−7.34 (m, 12 H, *o*,*p*-ArH), 7.41−7.47 (m, 8 H, *m*-ArH), 9.31 (s, 1 H, CHO) ppm. ^{13}C NMR (CD_2Cl_2): δ = 77.5, 92.9 (s), 83.4, 88.9 (d, Cp), 127.3 (d, *p*-Ar), 128.5 (d, *o*-Ar), 129.1 (d, *m*-Ar), 135.2 (s, Ar), 190.9 (d, CHO) ppm.

[η^5-(*E*)-1-Chloroethenylcyclopentadienyl](η^4-tetraphenylcyclobutadienyl)cobalt(I) [(*E*)-13] and (η^5-Ethynylcyclopentadienyl)(η^4-tetraphenylcyclobutadienyl)cobalt(I) (14): Potassium *tert*-butoxide (106 mg, 1.0 mmol) was added to a solution of (chloromethyl)triphenylphosphonium chloride (350 mg, 1.0 mmol) in 20 mL of THF. At −70 °C, a cooled (−65 °C) solution of **12** (342 mg, 0.7 mmol) in 20 mL of THF was added to this solution. The resulting mixture was stirred for 30 min at −65 °C and then 30 min at room temperature. Subsequently, a solution of potassium *tert*-butoxide (106 mg, 1.0 mmol) in 20 mL of THF was added and the mixture refluxed for 17 h. After cooling and addition of 20 mL of distilled water, the layers were separated, and the aqueous layer was washed four times with diethyl ether. After drying ($MgSO_4$) of the combined organic layers, the solvent was removed and the crude mixture was purified by column chromatography on alumina (light petroleum ether to light petroleum ether/diethyl ether, 10:1). This procedure yielded 166 mg (46%) of (*E*)-**13** as a yellow solid. Following the isolation of (*E*)-**13**, 134 mg (39%) of the alkyne complex **14** was obtained as a yellow solid. ^{1}H NMR (CD_2Cl_2): δ = 4.63 (pt, 2 H, CpH), 4.67 (pt, 2 H, CpH), 5.84 (d, 1 H, C=CH), 5.93 (d, 1 H, C=CH), 7.19−7.30 (m, 12 H, *o*,*p*-ArH), 7.37−7.45 (m, 8 H, *m*-ArH) ppm. ^{13}C NMR (CD_2Cl_2): δ = 76.2 (s), 81.1 (d, Cp), 84.8 (d, Cp), 93.1 (s), 115.8 (d, C=C), 126.7 (d, *p*-Ar), 127.2 (d, C=C), 128.4 (d, *o*-Ar), 129.1 (d, *m*-Ar), 136.1 (s, Ar).

Transformation of (*E*)-13 to 14: Phenyllithium (0.6 mL, 1.1 mmol, 1.8 M) was added to a solution of (*E*)-**13** (500 mg, 0.9 mmol) in 20 mL of THF. After stirring for 20 h, the mixture was hydrolyzed with 25 mL of brine. The aqueous layer was extracted four times with diethyl ether, the combined organic layers were dried ($MgSO_4$) and the solvent was removed. After purification by column chromatography on alumina (neutral, grade III, light petroleum ether), 275 mg (59%) of the alkyne **14** was obtained as a yellow solid, m.p. 148 °C. ^{1}H NMR (CD_2Cl_2): δ = 2.51 (s, 1 H, CCH), 4.62 (pt, 2 H, CpH), 4.79 (pt, 2 H, CpH), 7.23−7.28 (m, 12 H, ArH), 7.45−7.49 (m, 8 H, ArH) ppm. ^{13}C NMR (CD_2Cl_2): δ = 76.4, 76.7, 78.2, 79.5 (s, cbd-C, Cp, C_{Alkyne}), 84.9 (d, Cp), 86.6 (d, Cp), 126.9 (d, *p*-Ar), 128.4 (d, *o*-Ar), 129.3 (d, *m*-Ar), 135.8 (s, Ar) ppm. IR (KBr): $\tilde{\nu}$ = 3056, 2924, 2109, 1628, 1600, 1498, 1445 cm^{-1}. HRMS (FAB): calcd. 504.1288; found 504.1273.

{μ-[Butadiynediylbis(η^5-cyclopentadienyl)]}bis(η^4-tetraphenylcyclobutadienyl)dicobalt(I) (15): A solution of CuCl (16 mg, 0.16 mmol) in 15 mL of dry pyridine, saturated with oxygen was added to a Schlenk flask. To this mixture **14** (209 mg, 0.4 mmol) was added, and oxygen was passed through the mixture for 46 h. After removal of the pyridine under vacuum, the crude product was purified by column chromatography on alumina (neutral, grade III) with light petroleum ether/diethyl ether (60:1), giving 192 mg (93%) of **15** as a yellow-orange solid, m.p. 240 °C. ^{1}H NMR (CD_2Cl_2): δ = 4.69 (pt, 4 H, CpH), 4.81 (pt, 4 H, CpH), 7.16−7.25 (m, 24 H, ArH), 7.39−7.47 (m, 16 H, ArH) ppm. ^{13}C NMR (CD_2Cl_2): δ = 74.1, 76.4, 77.1, 78.5 (s, C_{Alkyne}, cbd-C, Cp), 84.9 (d, Cp), 87.3 (d, Cp), 126.9 (d, *p*-Ar), 128.5 (d, *o*-Ar), 129.2 (d, *m*-Ar), 135.5 (s, Ar) ppm. IR (KBr): $\tilde{\nu}$ = 3056, 2924, 2148, 1604, 1497, 1446 cm^{-1}. HRMS (EI): calcd. 1006.2420; found 1006.2432.

(η^4-Tetraphenylcyclobutadienyl)[η^5-(triethylsilylbutadiynyl)cyclopentadienyl]cobalt(I) (16): *n*-Butyllithium (645 mg, 1.5 mmol, 1.6 M solution) was slowly added to a solution of **14** (695 mg, 1.4 mmol) in 100 mL of THF, at −35 °C. Subsequently, CuCl (263 mg, 1.4 mmol) was added and the mixture was stirred for 30 min at −15 °C. After stirring at room temperature for 10 min, the suspension was cooled to −25 °C and freshly distilled ethylamine (5 mL) and bromo(triethylsilyl)acetylene (330 mg, 1.5 mmol) were added. After further stirring for 18 h, the hydrolysis was carried out with 50 mL of saturated NH_4Cl solution. The workup was completed by extraction of the aqueous layer with diethyl ether and drying of the combined organic layers with $MgSO_4$. Removal of the solvent gave a crude product. Further purification by column chromatography on silica with light petroleum ether/dichloromethane (7:1) yielded 804 mg (91%) of **16** as a yellow solid, m.p. 146 °C. ^{1}H NMR (C_6D_6): δ = 0.56 (q, CH_2, 6 H), 1.01 (t, CH_3, 9 H), 4.31 (pt, CpH, 2 H), 4.61 (pt, CpH, 2 H), 7.04−7.12 (m, 12 H, ArH), 7.54−7.59 (m, 8 H, ArH) ppm. ^{13}C NMR (C_6D_6): δ = 4.7 (t, CH_2), 7.7 (q, CH_3), 73.5, 74.5, 77.0, 77.7, 86.0, 91.1 (s, Cp, C_{Alkyne}, cbd-C,), 85.1 (d, Cp), 87.4 (d, Cp), 126.9 (d, *p*-Ar), 128.4 (d, *o*-Ar), 129.2 (d, *m*-Ar), 135.6 (s, Ar) ppm. IR (KBr): $\tilde{\nu}$ = 2955, 2874, 2206, 1630, 1499, 1460 cm^{-1}. HRMS (EI): calcd. 642.2153; found 642.2159. $C_{43}H_{39}CoSi$ (642.2): calcd. C 80.35, H 6.12; found C 80.10, H 6.32.

(η^5-Butadiynylcyclopentadienyl)(η^4-tetraphenylcyclobutadienyl)cobalt(I) (17): NaOH (0.3 mL of an aqueous 5 M solution) was added to a solution of **16** (337 mg, 0.5 mmol) in 30 mL of DMF. After 5 min, 2 M HCl was added until pH < 4 (ca. 2 mL). The resulting precipitate was filtered, washed extensively with water, dissolved in diethyl ether, and dried with $MgSO_4$. Removal of the solvent yielded 264 mg (95%) of **17** as a gold-colored, oxygen-sensitive solid. ^{1}H NMR ($CDCl_3$): δ = 2.32 (s, 1 H, CCH), 4.68 (pt, 2 H, CpH), 4.82 (pt, 2 H, CpH), 7.22−7.33 (m, 12 H, ArH), 7.43−7.49 (m, 2 H, ArH) ppm. ^{13}C NMR (C_6D_6): δ = 69.3, 69.7, 72.4, 73.4, 77.1, 77.2 (s, C_{Alkyne}, cbd-C, Cp), 85.2 (d, Cp), 87.3 (d, Cp), 126.9 (d, *p*-Ar), 128.4 (d, *o*-Ar), 129.2 (d, *m*-Ar), 135.6 (s, Ar) ppm. IR (KBr): $\tilde{\nu}$ = 3060, 2209, 1609, 1499 cm^{-1}. HRMS (FAB): calcd. 528.1289; found 528.1312.

{μ-[Octatetraynediylbis(η^5-cyclopentadienyl)]}bis(η^4-tetraphenylcyclobutadienyl)dicobalt(I) (18): NaOH (0.15 mL of 1 M solution) was added to a solution of **16** (145 mg, 0.23 mmol) in 15 mL of DMF. After 5 min, HCl (1.5 mL of 2 M solution) was added. The organic layer was washed three times with water and brine. The aqueous layer was extracted twice with diethyl ether, the combined organic layers were dried with $MgSO_4$ and concentrated to 20 mL. The solution was poured into a mixture of acetone (20 mL), *N*,*N*,*N*′,*N*′-tetramethylethylenediamine (14 mg) and CuCl (12 mg). After 4 h of passing oxygen through the mixture, hydrolysis with 30 mL of saturated NH_4Cl solution was carried out. After extraction of the aqueous layer with dichloromethane, the combined layers were adsorbed on silica. The purification by column chromatography on silica with light petroleum ether/dichloromethane (4:1) yielded 113 mg (95%) of **18** as an orange-red solid, m.p. 218 °C. ^{1}H NMR ($CDCl_3$/CD_2Cl_2, 2:1): δ = 4.74 (pt, 4 H, CpH), 4.89 (pt, 4 H, CpH), 7.23−7.36 (m, 24 H, ArH), 7.42−7.49 (m, 16 H, ArH) ppm. ^{13}C NMR ($CDCl_3$/CD_2Cl_2, 2:1): δ = 63.9, 66.1, 73.6, 74.9, 75.9, 77.2 (s, C_{Alkyne}, cbd-C, Cp), 85.3 (d, Cp), 87.5 (d, Cp), 126.7 (d, *p*-Ar), 128.1 (d, *o*-Ar), 128.7 (d, *m*-Ar), 134.8 (s, Ar) ppm. IR (KBr): $\tilde{\nu}$ = 3061, 2925, 2194, 1630, 1498, 1449 cm^{-1}. HRMS (FAB): calcd. 1055.2498; found 1055.2483.

(η^4-Tetraphenylcyclobutadienyl)[η^5-(triethylsilylhexatriynyl)cyclopentadienyl]cobalt(I) (19): *n*-Butyllithium (73 mg, 0.17 mmol

of a 1.6 M solution) in *n*-hexane was slowly added to a cooled solution (−40 °C) of **17** (81 mg, 0.15 mmol) in 10 mL of THF. Subsequently, CuCl (30 mg, 0.16 mmol) was added. After stirring the mixture for a further 5 min at −30 °C, the stirring was continued at room temperature for 10 min. Subsequently, freshly distilled ethylamine (1 mL) and bromo(triethylsilyl)acetylene (70 mg, 0.25 mmol) were added at −25 °C. Stirring was continued for 50 min at that temperature and the mixture was then hydrolyzed with 15 mL of a saturated NH_4Cl solution. The extraction of the aqueous layer with diethyl ether and the removal of the solvent gave a crude product, which was further purified by column chromatography on silica with light petroleum ether/dichloromethane (5:1) gave 75 mg (74%) of **19** as a yellow-brown solid, m.p. 114 °C. ^{1}H NMR ($CDCl_3$): δ = 0.68 (q, 6 H, CH_2), 1.05 (t, 9 H, CH_3), 4.69 (pt, 2 H, CpH), 4.84 (pt, 2 H, CpH), 7.22−7.34 (m, 12 H, ArH), 7.43−7.48 (m, 8 H, ArH) ppm. ^{13}C NMR ($CDCl_3$): δ = 4.2 (CH_2), 7.4 (CH_3), 62.1, 65.3, 73.2, 74.2, 76.2, 76.9, 86.0, 89.7 (s, C_{Alkyne}, cbd-C, Cp), 85.2 (Cp), 87.3 (Cp), 126.7 (d, *p*-Ar), 128.1 (d, *o*-Ar), 128.8 (d, *m*-Ar), 134.9 (Ar) ppm. IR (KBr): $\tilde{\nu}$ = 2953, 2921, 2879, 2176, 2067, 1605, 1497, 1454 cm^{-1}. HRMS (FAB): calcd. 666.2153; found 666.2148. $C_{45}H_{39}CoSi$ (666.2): calcd. C 81.06, H 5.89; found C 81.19, H 6.15.

{μ-[Dodecahexaynediylbis(η^5-cyclopentadienyl)]}bis(η^4-tetraphenylcyclobutadienyl)dicobalt(I) (21): The removal of the protection group from **19** was achieved by adding NaOH (0.12 mL of a 5 M aqueous solution) to a solution of **19** (115 mg, 0.17 mmol) in 35 mL of DMF at room temp. After 5 min, the solution was acidified by adding HCl (35 mL of a 2 M aqueous solution). The resulting precipitate was filtered, washed extensively with water, and dissolved in diethyl ether. The aqueous layer was extracted twice with diethyl ether, the combined organic layers were dried with $MgSO_4$ and concentrated to 20 mL. The solution was poured into a solution of acetone (36 mL), *N*,*N*,*N*′,*N*′-tetramethylethylenediamine (0.053 mL) and CuCl (18 mg). After 80 min of passing oxygen through the mixture, 60 mL of diethyl ether and 50 mL of saturated NH_4Cl solution were added. The organic layer was washed twice with water. and the combined aqueous layers were washed with dichloromethane. The combined organic layers were dried with $MgSO_4$, absorbed on silica and purified by column chromatography on silica with light petroleum ether/dichloromethane (7:1), yielding 45 mg (47%) of **21** as a red solid, m.p. 210 °C. ^{1}H NMR (CD_2Cl_2: δ = 4.74 (pt, 4 H, CpH), 4.90 (pt, 4 H, CpH), 7.21−7.44 (m, 40 H, ArH) ppm. ^{13}C NMR (CD_2Cl_2): δ = 64.0, 64.2, 64.3, 65.9, 73.4, 75.3, 76.4, 77.8 (s, cbd-C, Cp, C_{Alkyne}), 86.2 (d, Cp), 88.2 (d, Cp), 127.2 (d, *p*-Ar), 128.5 (d, *o*-Ar), 129.1 (d, *m*-Ar), 135.1 (s, Ar) ppm. IR (KBr): $\tilde{\nu}$ = 2148, 2041, 1630, 1498, 1261 cm^{-1}. HRMS (FAB): calcd. 1102.2393; found 1102.2366.

Cyclovoltammetry: The electrochemical measurements were performed with an Ecochem PGStat 20. A glassy carbon disk electrode with a 3 mm diameter was used as the working electrode. The Ag/AgCl reference electrode was separated from the solution by a G4-frit and a Haber−Luggin capillary. As the electrolyte, a 0.1 M solution of nBu$_4$N$^+$PF$_6^-$ in anhydrous, degassed CH_2Cl_2 was used. All reported potentials are referred to the Fc/Fc$^+$ couple, which

Table 2. Crystal data and structure refinement for **14**−**17** and **21**

	14	**15**	**16**	**17**	**21**
Empirical formula	$C_{35}H_{25}Co$	$C_{70}H_{48}Co_2$	$C_{43}H_{39}CoSi$	$C_{37}H_{25}Co$	$C_{78}H_{48}Co_2{\cdot}3CH_2Cl_2$
Formula mass	504.48	1006.94	642.76	528.50	1357.80
Temperature [K]	200(2)	200(2)	200(2)	200(2)	150(2)
Wavelength [Å]	0.71073	0.71073	0.71073	0.71073	0.71073
Crystal system	orthorhombic	monoclinic	monoclinic	monoclinic	monoclinic
Space group	*Pna*2$_1$	*P*2$_1$/*n*	*P*2$_1$/*c*	*P*2$_1$/*c*	*P*2$_1$/*c*
Z	8	2	4	4	4
a [Å]	27.5105(2)	10.5359(3)	16.7032(2)	11.1526(2)	11.0730(1)
b [Å]	19.7683(2)	20.0926(6)	12.7019(2)	14.2496(2)	14.3480(2)
c [Å]	9.3815(1)	13.0286(4)	16.7817(1)	117.142(2)	41.4520(5)
β [°]	90	112.88(1)	106.524(1)	99.652(1)	94.286(1)
Volume [Å^3]	5102.00(8)	2540.92(13)	3413.40(7)	2685.71(7)	6567.3(1)
Density (calculated) [g/cm^3]	1.31	1.32	1.25	1.31	1.37
Absorption coefficient [mm^{-1}]	0.694	0.697	0.567	0.66	0.80
Crystal shape	polyhedron	irregular	polyhedron	lamina	lamina
Crystal size [mm]	0.38 × 0.33 × 0.11	0.4 × 0.3 × 0.2	0.42 × 0.30 × 0.30	0.46 × 0.28 × 0.03	0.38 × 0.32 × 0.10
θ range for data collection [°]	1.27 to 25.66	1.98 to 25.62	2.04 to 27.49	1.9 to 27.5	1.7 to 21.5
Index ranges	$-33 \le h \le 32$	$-12 \le h \le 12$	$-21 \le h \le 21$	$-14 \le h \le 14$	$-6 \le h \le 11$
	$-23 \le k \le 23$	$-23 \le k \le 23$	$-16 \le k \le 16$	$-8 \le k \le 8$	$-8 \le k \le 14$
	$-11 \le l \le 11$	$-15 \le l \le 15$	$-1 \le l \le 21$	$-22 \le l \le 22$	$-33 \le l \le 42$
Reflections collected	37314	18723	34497	27287	14892
Independent reflections	8350 [*R*(int) = 0.0298]	4429 [*R*(int) = 0.0274]	7828 [*R*(int) = 0.0319]	6170 [*R*(int) = 0.0594]	7505 [*R*(int) = 0.0661]
Observed reflections	7413 [$I > 2\sigma(I)$]	3813 [$I > 2\sigma(I)$]	6463 [$I > 2\sigma(I)$]	4180 [$I > 2\sigma(I)$]	6123 [$I > 2\sigma(I)$]
Absorption correction	semi-empirical from equivalents	semi-empirical from equivalents	semi-empirical from equivalents	semi-empirical from equivalents	semi-empirical from equivalents
Max. and min. transmission	0.94 and 0.83	0.89 and 0.77	0.86 and 0.74	0.98 and 0.83	0.96 and 0.65
Refinement method	Full-matrix least squares on F^2	Full-matrix least squares on F^2	Full-matrix least squares on F^2	Full-matrix least squares on F^2	Full-matrix least squares on F^2
Data/restraints/parameters	8350/221/672	4429/0/325	7828/7/424	6170/0/343	7505/73/821
Goodness-of-fit on F^2	1.03	1.09	1.02	1.03	1.26
Final *R* indices [$I > 2\sigma(I)$]	*R*1 = 0.036	*R*1 = 0.030	*R*1 = 0.037	*R*1 = 0.053	*R*1 = 0.130
	*wR*2 = 0.085	*wR*2 = 0.063	*wR*2 = 0.090	*wR*2 = 0.132	*wR*2 = 0.281
Largest diff. peak and hole [e·Å^{-3}]	0.30 and −0.38	0.23 and −0.28	0.56 and −0.39	0.94 and −0.46	1.27 and −1.48

was used as an internal calibrant. All measurements were performed at room temperature.

X-ray Crystallography and Structure Solution: The crystallographic data were recorded with a Bruker Smart CCD diffractometer at 200 K for **14**−**17** and **21**. Relevant crystal and data collection parameters are given in Table 2. The structures were solved using direct methods (**14**−**16**, **21**) or the Patterson heavy atom method (**17**), least-squares refinement, and Fourier techniques. Structure solution and refinement were performed with SHELXTL.[39] CCDC-172774 (**14**), -172775 (**15**), -172776 (**16**), -172777 (**17**), and -172778 (**21**) contain the supplementary crystallographic data for this paper. These data can be obtained free of charge at www.ccdc.cam.ac.uk/conts/retrieving.html or from the Cambridge Crystallographic Data Centre, 12, Union Road, Cambridge CB2 1EZ, UK [Fax: (internat.) + 44-1223/336-033; E-mail: deposit@ccdc.cam.ac.uk].

[1] D. Astruc, *Electron Transfer and Radical Processes in Transition Metal Chemistry*, VCH, New York, **1995**.
[2] D. B. Brown (Ed.), *Mixed Valence Compounds*, Reidel, Dordrecht, Netherlands, **1990**.
[3] D. O. Cowan, C. LeVanda, J. Park, F. Kaufman, *Acc. Chem. Res.* **1973**, *6*, 1−7.
[4] C. LeVanda, K. Bechgaard, D. O. Cowan, M. D. Rausch, *J. Am. Chem. Soc.* **1977**, *99*, 2964−2968.
[5] C. LeVanda, D. O. Cowan, C. Leitch, K. Bechgaard, *J. Am. Chem. Soc.* **1974**, *96*, 6788−6789.
[6] J. A. Kramer, D. N. Hendrickson, *Inorg. Chem.* **1980**, *19*, 3330−3337.
[7] O. Lavastre, J. Plass, P. Bachmann, S. Guesmi, C. Moinet, P. H. Dixneuf, *Organometallics* **1997**, *16*, 184−189.
[8] Z. Yuan, G. Stringer, I. R. Jobe, D. Kreller, K. Scott, L. Koch, N. J. Taylor, T. B. Marder, *J. Organomet. Chem.* **1993**, *452*, 115−120.
[9] M. Wildschek, C. Rieker, P. Jaitner, H. Schottenberger, K. E. Schwarzhans, *J. Organomet. Chem.* **1990**, *396*, 355−361.
[10] M. Altmann, V. Enkelmann, U. H. F. Bunz, *Chem. Ber.* **1996**, *129*, 269−273.
[11] H. Schimanke, R. Gleiter, *Orgonometallics* **1998**, *17*, 275−277.
[12] M. I. Bruce, B. D. Kelly, B. W. Skelton, A. H. White, *J. Organomet. Chem.* **2000**, *604*, 150−156.
[13] M. Brady, W. Weng, Y. Zhou, J. W. Seyler, A. J. Amoroso, A. M. Arif, M. Böhme, G. Frenking, J. A. Gladysz, *J. Am. Chem. Soc.* **1997**, *119*, 775−788.
[14] T. Bartik, B. Bartik, M. Brady, R. Dembinski, J. A. Gladysz, *Angew. Chem.* **1996**, *108*, 467−469; *Angew. Chem. Int. Ed. Engl.* **1996**, *35*, 414−417.
[15] F. Coat, C. Lapinte, *Organometallics* **1996**, *15*, 477−479.
[16] F. Paul, C. Lapinte, *Coord. Chem. Rev.* **1998**, *178*−*180*, 431−509.
[17] F. Paul, W. E. Meyer, L. Toupet, H. Jiao, J. A. Gladysz, C. Lapinte, *J. Am. Chem. Soc.* **2000**, *122*, 9405−9414.
[18] M. I. Bruce, *Coord. Chem. Rev.* **1997**, *166*, 91−119.
[19] M. I. Bruce, P. J. Low, K. Costuas, J.-F. Halet, S. P. Best, G. A. Heath, *J. Am. Chem. Soc.* **2000**, *122*, 1949−1962.
[20] U. H. F. Bunz, *Angew. Chem.* **1996**, *108*, 1047−1049; *Angew. Chem. Int. Ed. Engl.* **1996**, *35*, 968−971.
[21] W. P. Hart, D. Shihua, M. D. Rausch, *J. Organomet. Chem.* **1985**, *282*, 111−121.
[22] S. T. Mabrouk, M. D. Rausch, *J. Organomet. Chem.* **1996**, *523*, 111−117.
[23] A. M. Stevens, C. J. Richards, *Organometallics* **1999**, *18*, 1346−1348.
[24] A. M. Stevens, C. J. Richards, *Tetrahedron Lett.* **1997**, *38*, 7805−7808.
[25] M. D. Rausch, R. A. Genetti, *J. Org. Chem.* **1970**, *35*, 3888−3897.
[26] H. Firouzabadi, E. Ghaderi, *Tetrahedron Lett.* **1978**, *9*, 839−840.
[27] O. M. Behr, G. Eglinton, A. R. Galbraith, R. A. Raphael, *J. Chem. Soc.* **1960**, 3614−3625.
[28] G. Eglinton, W. McCrae, *Adv. Org. Chem.* **1963**, *4*, 225−328.
[29] A. S. Hay, *J. Org. Chem.* **1960**, *25*, 1275−1276; A. S. Hay, *J. Org. Chem.* **1962**, *27*, 3320−3321.
[30] P. Cadiot, W. Chodkiewicz, in: *Chemistry of Acetylenes* (Ed.: H. G. Viehe), Marcel Dekker, New York, **1969**, pp. 597−647.
[31] W. Chodkiewicz, *Ann. Chim. Paris* **1957**, *2*, 819−869.
[32] R. Dembinski, T. Lis, S. Szafert, C. L. Mayne, T. Bartik, J. A. Gladysz, *J. Organomet. Chem.* **1999**, *578*, 229−246.
[33] B. Bartik, R. Dembinski, T. Bartik, A. M. Arif, J. A. Gladysz, *New J. Chem.* **1997**, *21*, 739−750.
[34] R. Eastmond, D. R. M. Walton, *Tetrahedron* **1972**, *78*, 4591−4599.
[35] P. E. Riley, R. E. Davis, *J. Organomet. Chem.* **1976**, *113*, 157−166.
[36] A. Sakurai, M. Akita, Y. Moro-oka, *Organometallics* **1999**, *18*, 3241−3244.
[37] M. B. Robin, P. Day, *Adv. Inorg. Chem. Radiochem.* **1967**, *10*, 247−422.
[38] R. Gleiter, H. Röckel, G. Pflästerer, B. Treptow, D. Kratz, *Tetrahedron Lett.* **1993**, *34*, 8075−8078.
[39] G. M. Sheldrick, Bruker Analytical X-ray Division, Madison, WI, **1997**.

Received November 7, 2001
[I01442]

Allylpalladium Complexes of Mixed-Donor Diphosphazane Ligands Bearing a Stereogenic Phosphorus Centre: Structure and Stereodynamics

Swadhin K. Mandal,[a] G. A. Nagana Gowda,[b] Setharampattu S. Krishnamurthy,*[a] Chong Zheng,[c] Shoujian Li,[c] and Narayan S. Hosmane[c]

Keywords: Allyl complexes / P ligands / Palladium / N ligands

(η^3-Allyl)palladium complexes of general formula [Pd(η^3-R′C_3H_4){η^2-$Ph_2PN(R)PPh(N_2C_3HMe_2$-3,5)}](PF_6) (**3**–**6**) and [Pd(η^3-R′C_3H_4){η^2-$Ph_2P(S)N(CHMe_2)PPh(N_2C_3HMe_2$-3,5)}]($PF_6$) (**7**–**8**), containing pyrazolyl-substituted diphosphazane ligands bearing a stereogenic phosphorus centre, have been synthesised. NMR spectroscopic and X-ray diffraction studies showed that the diphosphazane ligand in [Pd(η^3-R′C_3H_4){η^2-$Ph_2PN(R)PPh(N_2C_3HMe_2$-3,5)}](PF_6) [R′ = Me or Ph; R = $CHMe_2$ (**3** and **5**) or (*S*)-*CHMePh (**4** and **6**)] displayed unprecedented *P,N*-coordination instead of the hitherto observed *P,P*-coordination. These complexes existed in solution as mixtures of *endo,syn,trans*, *exo,syn,trans*, and *endo,syn,cis* diastereomers. In the solid state, only the *endo,syn,trans* isomer was observed for complex **5**. Phase-sensitive 2-D NOESY and ROESY spectra showed that the complexes **3**–**5** underwent *syn,anti* isomerisation; the NMR spectroscopic data were consistent with a mechanism involving the opening of the η^3-allyl group at the *trans* position with respect to the phosphorus centre. The isomerisation thus appeared to be electronically controlled. The complexes [Pd(η^3-MeC_3H_4){η^2-$Ph_2P(S)N(CHMe_2)PPh(N_2C_3HMe_2$-3,5)}]($PF_6$) (**7**) and [Pd($\eta^3$-$PhC_3H_4$){$\eta^2$-$Ph_2P(S)N(CHMe_2)$-$PPh(N_2C_3HMe_2$-3,5)}]($PF_6$) (**8**), bearing the diphosphazane monosulfide $Ph_2P(S)N(CHMe_2)PPh(N_2C_3HMe_2$-3,5) (**1c**), displayed *P,S*-coordination and existed in solution as six and four isomers, respectively. Exchange was observed among four of the six isomers of **7** and among all the four isomers of **8** at 298 K, through the opening of the η^3-allyl moiety, which appeared to be subject to both electronic and steric control.

(© Wiley-VCH Verlag GmbH, 69451 Weinheim, Germany, 2002)

Introduction

Palladium-catalysed allylic substitution reactions have emerged as a powerful methodology in organic synthesis;[1] the use of chiral auxiliary ligands can result in the formation of optically active products. Initially, chiral diphosphane ligands were predominantly used, while in recent years, asymmetric mixed-donor ligands have proven to be advantageous. The use of P,N-,[2] P,S-,[3] and S,N-donor[4] ligands in particular has resulted in high enantiomeric excesses in allylic alkylation reactions, which is attributed to the electronic effects of two different donor centres present in these ligand systems. In contrast to most other transition metal catalysed reactions, palladium-catalysed allylic alkylations do not rely solely on a single mechanism as a source of asymmetry.[5] Differentiation of the enantiotopic faces of a π-system is one possible mechanism, but the source of the enantioselectivity is complicated by the problems associated with the regioselectivity of nucleophilic attack, possibility of various configurational isomers, and the existence of several stereodynamic processes.[6] The reaction proceeds through a (π-allyl)palladium intermediate and the configuration of the organic product strongly depends on the nature of this intermediate. There is growing interest in understanding the solution structures and the dynamic solution behaviour of the chiral (η^3-allyl)palladium intermediates, as these may be related to synthetic methods affording optically active products.[7] The situation becomes even more complicated when both the auxiliary ligands and the allyl moiety are asymmetrical; in this case, various geometrical isomers with different allyl face coordination would result, as well as allylic arrangements. As a part of our ongoing investigations into the organometallic chemistry of diphosphazane ligands,[8–9] we have recently begun a program of NMR studies of (π-allyl)palladium complexes of diphosphazane and related ligand systems based on the P−N−P motif. The diphosphazane ligands display versatile transition metal organometallic chemistry[10] and these ligand systems can be suitably modified, thus providing access to a range of mixed-donor ligands. Despite extensive studies of the reactions of diphosphazane ligands with sev-

[a] Department of Inorganic and Physical Chemistry, Indian Institute of Science,
Bangalore 560012, India
Fax: (internat.) + 91-80/360-0683 or -1552
E-mail: sskrish@ipc.iisc.ernet.in
[b] Sophisticated Instruments Facility, Indian Institute of Science, Bangalore 560012, India
[c] Department of Chemistry and Biochemistry, Northern Illinois University,
DeKalb, IL 60115, USA

eral transition metal precursors, the allylpalladium chemistry of unsymmetrical diphosphazane ligands has not been explored except for a brief report on allylpalladium complexes of $Ph_2PN(H)P(O)Ph_2$.[10d] Here we report the synthesis, solution characterisation and dynamic behaviour of (η^3-allyl)palladium complexes bearing phosphorus-stereogenic diphosphazane ligands − $Ph_2PN(R)PPh(N_2C_3HMe_2$-3,5) [R = $CHMe_2$ (**1a**) or (*S*)-*CHMePh (**1b**)] − and the diphosphazane monosulfide ligand $Ph_2P(S)N(CHMe_2)PPh(N_2C_3HMe_2$-3,5) (**1c**). In the case of **1b**, the (S_CR_P) diastereomer, the absolute configuration of which has been determined by X-ray crystallography,[8d] was used for the preparation of allylpalladium complexes.

Results and Discussion

Synthesis

The cationic allyl complexes **3**−**8** were prepared by treatment of the chloro-bridged allylpalladium dimer **2** with the appropriate ligands in the presence of NH_4PF_6 in acetone (Scheme 1). These complexes have been characterised by elemental analyses and NMR spectroscopic data (see Exp. Sect.). Several isomers are possible for complexes that contain an unsymmetrically substituted allyl group. In the first place, isomers can arise because of different modes of coordination of the ligands (e.g., *P*,*P* or *P*,*N* for **1a** or **1b**, *P*,*S* or *P*,*N* or *N*,*S* for **1c**). Secondly, geometrical isomers can be formed because the substituent on the allyl moiety can be oriented in a *cis* or *trans* position with respect to one of the phosphorus atoms. Thirdly, several allylic arrangements are also possible since the substituent on the allyl moiety can be positioned *syn* or *anti* with respect to the central allyl proton. Additionally, for each of these isomers, diastereomers can arise owing to the different face coordination (*exo* or *endo*) of the allyl group. The isomeric composition in each case was determined by NMR spectroscopy. The salient features of the spectroscopic data and dynamic behaviour are discussed below.

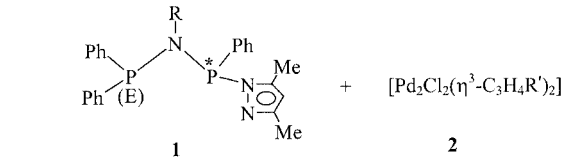

1a, R = $CHMe_2$, E = lone pair (l.p);
1b, R = (*S*)-*CHMePh, E = l.p; (S_CR_P- diastereomer)
1c, R = $CHMe_2$, E = S

NH_4PF_6

$[Pd(\eta^3\text{-}C_3H_4R')(\mathbf{1})](PF_6)$

3-8

3, R' = Me, R = $CHMe_2$, E = l.p;
4, R' = Me, R = (*S*)-*CHMePh, E = l.p;
5, R' = Ph, R = $CHMe_2$, E = l.p;
6, R' = Ph, R = (*S*)-*CHMePh, E = l.p;
7, R' = Me, R = $CHMe_2$, E = S;
8. R' = Ph, R = $CHMe_2$, E = S

Scheme 1

NMR Studies on $[Pd(\eta^3\text{-}R'C_3H_4)\{\eta^2\text{-}Ph_2PN(R)PPh(N_2C_3HMe_2$-3,5)$\}](PF_6)$ (3−6)

The $^{31}P\{^1H\}$ NMR spectra of complexes **3**−**6** in $CDCl_3$ in each case displayed six doublets (see Table 1) in different isomeric ratios, revealing the presence of three isomers. The structures proposed for these isomers are shown in Figure 1. Analysis of the ^{13}C NMR spectra of the allyl carbon nuclei pointed to *P*,*N*-coordination through the nitrogen atom at the 2-position of the pyrazole ring (see Table 2). The resonances of the central allyl carbon atoms of all the isomers appeared as doublets. For *P*,*P*-coordination, one should observe a doublet of doublets pattern in the ^{13}C NMR spectra for each of the palladium-bound allyl carbon nuclei. The signals for terminal allyl carbon nuclei appeared as two doublets and were assigned on the basis of the two-bond phosphorus-carbon coupling and a 2-D ^{13}C-^1H HSQC experiment. The doublets in the ^{13}C NMR spectra in the δ = 94−105 and 78−80 ppm ranges, with $^2J_{P,C}$ values of 28−31 Hz, were assigned to the substituted terminal allyl and unsubstituted terminal allyl carbon atom, respectively, *trans* to the coordinated phosphorus centre. On the other hand, the resonances for the substituted and unsubstituted terminal allyl carbon nuclei *trans* to the nitrogen atom appeared in more shielded regions (δ = 64−77 and

Table 1. The $^{31}P\{^1H\}$ NMR spectroscopic data for the complexes **3**−**8**

Complex[a]	−PPh($N_2C_3HMe_2$-3,5) (δ_A)	$\Delta\delta_A$	−P(E)Ph_2 (δ_X)	$\Delta\delta_X$
3a	72.7 d (31.1)	0.8	75.0 d	31.1
3b	72.4 d (28.4)	0.5	77.2 d	33.3
3c	71.1 d (29.5)	−0.8	78.9 d	35.0
4a	72.7 d (28.3)	3.9	79.3 d	32.1
4b	73.0 d (28.6)	4.2	78.1 d	30.9
4c	71.1 d (28.7)	2.3	80.0 d	32.8
5a	71.9 d (29.8)	0.0	76.9 d	33.0
5b	71.3 d (28.4)	−0.6	75.2 d	31.3
5c	71.1 d (30.8)	−0.8	78.7 d	34.8
6a	71.9 d (28.3)	3.1	79.1 d	31.9
6b	71.4 d (28.3)	2.6	79.9 d	32.7
6c	72.1 d (29.9)	3.3	77.9 d	30.7
7a	92.4 d (91.8)	21.9	76.0 d	10.7
7b	92.2 d (87.9)	21.7	75.0 d	9.7
7c	94.2 d (100.4)	23.7	79.5 d	14.2
7d	94.7 d (100.5)	24.2	78.7 d	13.4
7e	94.7[b]	24.2	78.4 d	13.1
7f	(−)[c]	(−)	78.3 d	13.0
8a	92.1 d (88.2)	21.6	74.4 d	9.1
8b	91.7 d (83.7)	21.2	73.6 d	8.3
8c	95.7 d (99.2)	25.2	78.8 d	13.5
8d	93.7 d (101.2)	23.2	79.3 d	14.0

[a] The $^{31}P\{^1H\}$ NMR spectra were recorded in $CDCl_3$ at 298 K except for **3** and **8**, in which cases a 1:1 mixture of $CDCl_3$ and CH_2Cl_2 was used. The ^{31}P-^{31}P coupling constants are given in parentheses [$\Delta\delta$ = δ(complex) − δ(free ligand)]. [b] Overlapped by signals arising from the −PPh($N_2C_3HMe_2$-3,5) phosphorus atom of isomer **7d**. [c] The signal could not be assigned unequivocally.

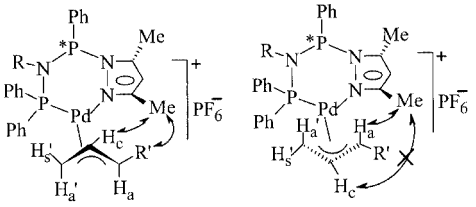

endo, syn, trans
(**3a**, **4a**, **5a** or **6a**)

exo, syn, trans
(**3b**, **4b**, **5b** or **6b**)

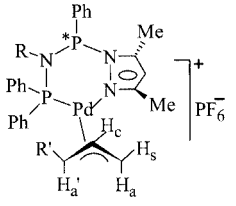

endo, syn, cis
(**3c**, **4c**, **5c** or **6c**)

Figure 1. The three isomers of (allyl)(diphosphazane)Pd^{II} complexes $[Pd(\eta^3\text{-}R'C_3H_4)\{\eta^2\text{-}Ph_2PN(R)PPh(N_2C_3HMe_2\text{-}3,5)\}](PF_6)$ [R′ = Me or Ph, R = $CHMe_2$ or (*S*)-*CHMePh] observed in solution; selective NOE contacts (shown by the arrows) revealed that, in the *endo*,*syn*,*trans* isomer, the central allyl proton and pyrazole-3-Me protons were close to each other, whereas in the *exo*,*syn*,*trans* isomer, such an NOE contact with the central allyl proton was absent

Table 2. The ^{13}C NMR spectroscopic data for the allyl carbon nuclei of complexes **3**−**8**

Complex[a]	C_t	C_t'	C_c
3a	105.0 d (29.8)[b]	51.6 d (5.4)[c]	117.2 d (6.2)
3b	94.8 d (28.9)[b]	55.4 br.	120.9 d (5.9)
4a	104.6 d (29.5)[b]	52.1 br.	117.4 d (5.5)
4b	94.6 d (28.6)[b]	55.5 br.	120.7 d (5.3)
4c	78.6 d (28.6)[b]	72.5 br.	117.4[d]
5a	103.7 d (28.5)[b]	54.8 d (3.8)[c]	112.1 d (6.8)
5b	102.5 d (27.8)[b]	54.7 d (3.9)[c]	114.6 d (6.9)
5c	79.2 d (28.1)[b]	76.8 d (4.2)[c]	117.4 d (5.9)
6a	103.0 d (29.2)[b]	53.9 (3.9)[c]	111.4 d (8.2)
6b	104.5 d (27.1)[b]	55.5 d (4.6)[c]	112.5 d (6.1)
6c	78.1 d (27.7)[b]	64.3 d (5.4)[c]	116.6 d (6.6)
7a	96.0 d (30.7)[b]	65.3 s	119.4 br. s
7b	96.9 d (34.8)[b]	65.3[e]	120.2 br. s,
7c	68.6 d (34.9)[b]	91.8 br. s	119.8 br. s
7d	70.5 d (33.3)[b]	89.4 br. s	119.8[f]
8a	96.6 d (32.2)[b]	66.5 br. s	113.7 br. s
8b	97.9 d (30.7)[b]	66.3 br. s	114.2 br. s
8c	68.5 d (33.3)[b]	94.0 br. s	113.2 br. s
8d	70.6 br. d (24.1)[b]	91.4 br. s	113.9 br. s

[a] The ^{13}C NMR spectra were recorded in $CDCl_3$ at 298 K except for **3** and **8**, in which cases a 1:1 mixture of $CDCl_3$ and CH_2Cl_2 was used. The ^{13}C-^{31}P coupling constants are given in parentheses. C_t is the terminal allyl carbon atom *trans* to the coordinated phosphorus centre. C_t' is the terminal allyl carbon atom *cis* to the coordinated phosphorus centre. C_c is the central allyl carbon atom. [b] $^2J_{P,C\ trans}$. [c] $^2J_{P,C\ cis}$. [d] Overlapped with central allyl carbon resonance of **4a**. [e] Overlapped with C_t' resonance of **7a**. [f] Overlapped with central allyl carbon resonance of **7c**.

51−56 ppm, respectively) with $^2J_{P,C}$ coupling constants in the 3−6 Hz range, typical for two-bond coupling of phosphorus and carbon nuclei in a *cis* orientation. It is well documented that in cationic allyl complexes with phosphorus ligands the ^{31}P nucleus shows a larger coupling constant with the terminal allyl carbon atom in the *trans* position than with that in the *cis* position.[11] In all the major isomers (**3a**, **4a**, **5a**, and **6a**) and in the second most abundant isomers (**3b**, **4b**, **5b**, and **6b**), the coordinated phosphorus atom and the substituent on the allyl moiety had a *trans* disposition. The remaining isomers (**3c**, **4c**, **5c**, and **6c**) were assigned structures in which the coordinated phosphorus atom and the substituent on the allyl moiety had a *cis* disposition. The *P*,*N*-coordination was also supported by the ^{31}P chemical shifts (see Table 1).

Transition metal complexes of the ligands **1a** and **1b** usually feature *P*,*P*-coordination.[9] The driving force for *P*,*N*-coordination in the (η^3-allyl)palladium complexes **3**−**6** might be the formation of a stable six-membered chelate ring around the palladium centre rather than the four-membered ring that would result from *P*,*P*-coordination. Moreover, coordination of a stronger σ-donor nitrogen atom would electronically stabilise the allyl−palladium bonding much more than coordination with a stronger π-acceptor phosphorus centre, by enhancing the metal-to-allyl back-bonding.[12] Such a pronounced electronic effect is well known[13] and is reflected in the ^{13}C NMR parameters (see Table 2).

The ^1H NMR spectra of the complexes **3**−**6** showed three sets of four nonequivalent resonances for the allylic protons at 298 K. The magnetic nonequivalence of the allylic protons arises because of the asymmetry in the ligands **1a** and **1b**. The presence of two *anti*-allyl protons in each set of signals indicated a *syn* arrangement of the allyl substituent with respect to the central allyl proton in each isomer. The major isomers of these complexes showed NOE contacts between the 3-Me protons of the pyrazole ring and the central allyl proton H_c. This result indicated that the central allyl hydrogen atom H_c pointed towards the 3-Me group of the pyrazole. Hence, the major isomers (**3a**−**6a**) have the *endo*,*syn*,*trans* arrangement.[7b,14] For the second set of isomers (**3b**−**6b**), the pyrazole 3-Me protons did not show NOE contacts to the central allyl proton H_c but there was an NOE contact to the *anti*-allyl proton H_a. The central allyl proton H_c thus pointed away from the 3-Me group of the pyrazole, and so these isomers (**3b**−**6b**) could be assigned the *exo*,*syn*,*trans* configuration. The central allyl proton resonances for the *endo* isomers **3a**−**6a** appeared at a more deshielded region (δ ≈ 5.7 ppm) than those (δ ≈ 4.5 ppm) for the *exo* isomers **3b**−**6b**. This trend has also been observed for other allylpalladium complexes $[Pd(\eta^3\text{-}1,3\text{-}R'_2C_3H_3)\{\eta^2\text{-}Ph_2PN(R)PPh(N_2C_3HMe_2\text{-}3,5)\}](PF_6)$ [R′ = H, Me or Ph; R = $CHMe_2$ or (*S*)-*CHMePh] bearing **1a** and **1b** ligands.[15] On this basis, we assigned the *endo*,*syn*,*cis* configuration (see Figure 1) to the third set of minor isomers (**4c**−**6c**) as the chemical shifts of the H_c protons in each of these isomers were close to those observed for **4a**−**6a**. The *cis* geometries and the *syn*-allylic arrangements for the minor isomers were confirmed by ^{13}C NMR (see Table 2) and 2-D NMR spectroscopy, respectively. The ^{13}C and ^1H NMR signals for isomer **3c** could not be ob-

served because of its low abundance and poor solubility in $CDCl_3$. However, the ^{31}P chemical shift and P-P coupling constant values for **3c** were similar to those of **4c**, and so an *endo*,*syn*,*cis* configuration may tentatively be assigned to **3c**. An important difference was observed between the relative abundances of the isomers of 1-methylallyl and 1-phenylallyl derivatives. For the 1-methylallyl derivatives (**3** and **4**), the *exo*,*syn*,*trans* isomers were present to an extent of 40%, whereas for the 1-phenylallyl derivatives (**5** and **6**), the *exo*,*syn*,*trans* isomers were present to an extent of less than 10%. The low relative abundances of the *exo*,*syn*,*trans* isomers in the case of 1-phenylallyl derivatives is probably related to the steric demand of the larger phenyl group on the allyl moiety.

Dynamic Behaviour of the Complexes 3−6

The dynamic behaviour of the complexes **3**−**6** was examined by ^1H-^1H NOESY and ROESY spectra. No exchange among the isomers of complexes **4**−**6** was observed in $CDCl_3$ at 298 K. For complex **3**, on the other hand, exchange between the isomers **3a** and **3b** was observed at 298 K in [D_6]acetone. The high-temperature (323 K) ^1H-^1H NOESY and ROESY spectra for the complexes **4** and **5** revealed that the major isomers **4a** and **5a** exchanged with the minor isomers **4b** and **5b**, respectively, in a way similar to that observed for the isomers **3a** and **3b** at 298 K. The phase-sensitive ^1H-^1H NOESY spectrum of complex **4** recorded at 323 K is shown in Figure 2 and the exchange results are summarised in Scheme 2. Pregosin and coworkers[16] have shown that this type of exchange can be explained in terms of a selective opening of the η^3-allyl moiety at the *trans* position with respect to the phosphorus centre to generate an η^1-bonded intermediate, followed by a rotation around the sp^3-sp^2 C−C bond and reversion to the η^3-mode of coordination by the other face of the allyl group. This type of electronic control over the interconversion process is especially well known in cases of mixed-donor P,N-, P,S-, and P,O- bidentate ligand systems.[17−19] The minor isomers (**4c** and **5c**) did not show any observable exchange even at 323 K, but their formation can be interpreted, starting from isomers **4b** and **5b**, respectively, in terms of *cis*,*trans* isomerisation by rotation around the Pd−C bond in the corresponding η^1-bonded intermediate.

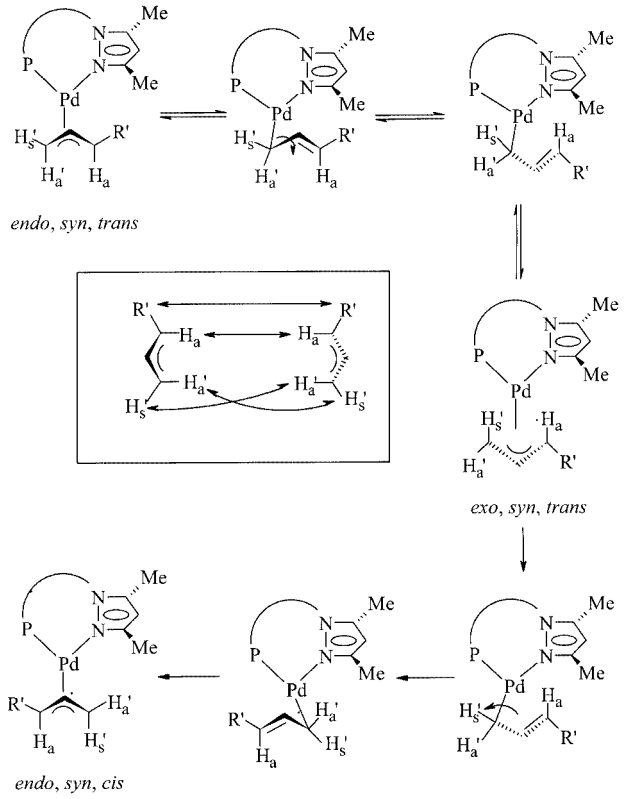

Scheme 2

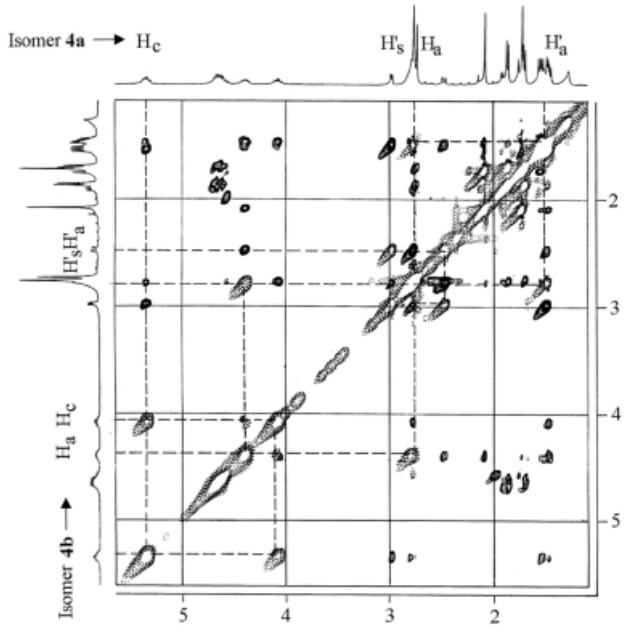

Figure 2. The ^1H-^1H phase-sensitive NOESY spectrum ($CDCl_3$, 400 MHz) of complex **4** at 323 K, showing the exchange cross-peaks in the isomers **4a** and **4b**

Solid-State Structure of Complex 5a

The details of the crystal data are presented in Table 3. The molecular structure is shown in Figure 3. The solid-state structure reveals the presence of only one isomer with *P*,*N*-coordination and a *trans* disposition of the *syn*-allylphenyl group with respect to the coordinated phosphorus centre. The central allyl carbon atom C(2) and the 3-methyl carbon atom C(10) of the pyrazole ring in **5a** lie on the same side of the coordination plane defined by P(2)−Pd(1)−N(3), thus revealing an *endo* arrangement in the solid state (*endo* refers to the relative orientation of the central C−H vector pointing towards the 3-methyl group on the pyrazole ring[7b,14]). The bonding parameters fall in the expected ranges observed for cationic allylpalladium

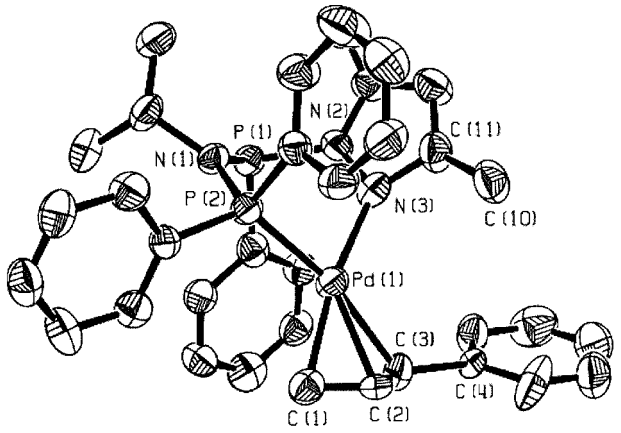

Figure 3. Molecular structure of **5a** in the solid state (the hydrogen atoms and the hexafluorophosphate anion are not shown); selected bond lengths [Å] and angles [°]: Pd(1)−C(1) = 2.075(2), Pd(1)−C(2) = 2.137(2), Pd(1)−C(3) = 2.263(2), Pd(1)−P(2) = 2.293(3), Pd(1)−N(3) = 2.075(1); N(3)−Pd(1)−P(2) = 85.4(3), C(1)−Pd(1)−C(3) = 64.0(8), N(3)−Pd(1)−C(1) = 169.8(5), C(3)−Pd(1)−P(2) = 167.8(6), P(2)−N(1)−P(1) = 122.5(6)

complexes bearing P,N-ligands.[17b,20] The coordination geometry around the metal centre is distorted square-planar, with the N(3)−Pd(1)−P(2) and C(1)−Pd(1)−C(3) bond angles 85.4(3)° and 64.0(8)°, respectively. The two terminal allyl carbon atoms are not exactly coplanar with the coordination plane formed by P(2)−Pd(1)−N(3). The distances of the terminal allyl carbon atoms C(1) and C(3) are 0.120 Å and 0.089 Å, respectively, whereas the central allyl carbon atom C(2) lies at a distance of 0.703 Å from the plane. The terminal Pd−C(allyl) bond lengths are significantly different from one another. The carbon atom *trans* to the phosphorus atom displays the expected longer bond length [Pd(1)−C(3) = 2.263(2) Å], as compared to its partner *trans* to the nitrogen atom [Pd(1)−C(1) = 2.075(2) Å]. This is consonant with the larger *trans* influence of the phosphorus donor.[13] This elongation of the Pd−C(terminal allyl) bond length *trans* to the phosphorus atom relative to that *trans* to the nitrogen atom is consistent with the proposed mechanism (Scheme 2) involving selective opening of one of the allyl termini. The six-membered chelate ring adopts a distorted boat conformation; P(2) is almost coplanar (deviation 0.168 Å) with the plane formed by N(1)−N(2)−N(3), while Pd(1) and P(1) lie on the same side of this plane at 1.063 and 0.778 Å, respectively. The P(1)−N(1)−P(2) bond angle is increased to 122.5(6)°, compared to a value of ca. 100° observed for *P,P*-coordinated complexes.[9]

NMR Studies on Complexes 7 and 8

The $^{31}P\{^{1}H\}$ NMR spectrum of an analytically pure sample of [Pd(η³-1-MeC_3H_4){η²-$Ph_2P(S)N(CHMe_2)PPh$-($N_2C_3HMe_2$-3,5)}](PF_6) (**7**) in $CDCl_3$ showed ten doublets arising from six AX spin systems. The two missing doublets (from the fifth and sixth isomers) overlapped with those arising from the major isomers, as revealed by a ^{31}P-^{31}P COSY spectrum. A 24-line spectrum was consistent with the formation of six isomers. The relative integrated intensities of the doublets indicated that the six isomers were present in the ratio 21:10:9:6:2:1. The allyl ^{13}C resonances for these isomers were assigned by recourse to a ^{13}C-^{1}H HSQC experiment. Analysis of the ^{13}C NMR spectrum showed a doublet pattern with a $^{2}J_{P,C}$ value of ca. 30 Hz for one of the two terminal allyl carbon resonances in the cases of isomers **7a**−**7d**, indicating bonding of one phosphorus atom with the palladium centre. From the ^{31}P chemical shifts (Table 1 and see also below), we were able to conclude that the pyrazolyl-bearing phosphorus atom and the sulfur atom were coordinated to the palladium centre. This conclusion was supported by the ^{13}C chemical shifts of the allyl carbon nuclei, when compared with the chemical shifts of allyl carbon nuclei of *P,N*-coordinated complexes **3**−**6** (see Table 2). It may be noted that the chemical shifts of allyl carbon nuclei *trans* to the nitrogen atom indicated that they were more shielded (by about 10−20 ppm) than the allyl carbon nuclei *trans* to the sulfur atom, if we consider the similar allyl isomers in both cases. Ligand **1c**, in contrast to **1a** and **1b**, thus did not coordinate through the nitrogen atom of the pyrazole ring, *P,S*-coordination presumably being favoured because of the formation of a stable five-membered ring around the palladium centre. The competitive *N,S*-coordination would give rise to the formation of a seven-membered chelate ring around the palladium atom. The fifth and sixth isomers (**7e** and **7f**) could not be detected by ^{13}C NMR, owing to their low relative concentrations (present at less than 5%). However, the similarity of their ^{31}P chemical shifts with those of other isomers (**7a**−**7d**) and the multiplicities of the allyl resonances in the ^{1}H NMR spectrum suggested that these isomers must be structurally closely related to **7a**−**7d**.

The ^{1}H NMR spectrum of complex **7** showed several broad signals; in addition, the chemical shifts of several allylic proton resonances were very close. However, a careful analysis of various 2-D NMR spectra (^{1}H-^{1}H DQF COSY, NOESY, and ROESY) resulted in a correct assignment of the allyl protons. The intra-allyl NOESY spectrum revealed that in the four isomers **7a**−**7d** there was a *syn* arrangement of the allylmethyl group with respect to the central allyl proton (H_c), while in the isomers **7e** and **7f** there was an *anti* arrangement of the allylmethyl group and the central allyl proton. The interligand NOE cross-peaks confirmed the configurations of these isomers. One of the methyl groups of the pyrazole ring came close to the central allyl proton H_c and to the *syn*-proton H_s' in the *endo* isomer, whereas for the *exo* isomer the *anti*-allyl proton H_a' showed NOE contact with this methyl group. The structures assigned to the six isomers on the basis of NMR measurements are shown in Figure 4. The structural assignments for **7a** and **7b** are unequivocal, while there is some uncertainty with regard to the structural assignments for the other isomers (**7c**−**7f**) because of the overlap of the pyrazole methyl proton signals arising from these minor isomers. However, studies on the exchange behaviour of the isomers (see below) lent support to the assignments.

The ^{1}H-^{1}H phase-sensitive NOESY and ROESY spectra at 298 K in $CDCl_3$ showed that isomers **7a**−**7d** were in

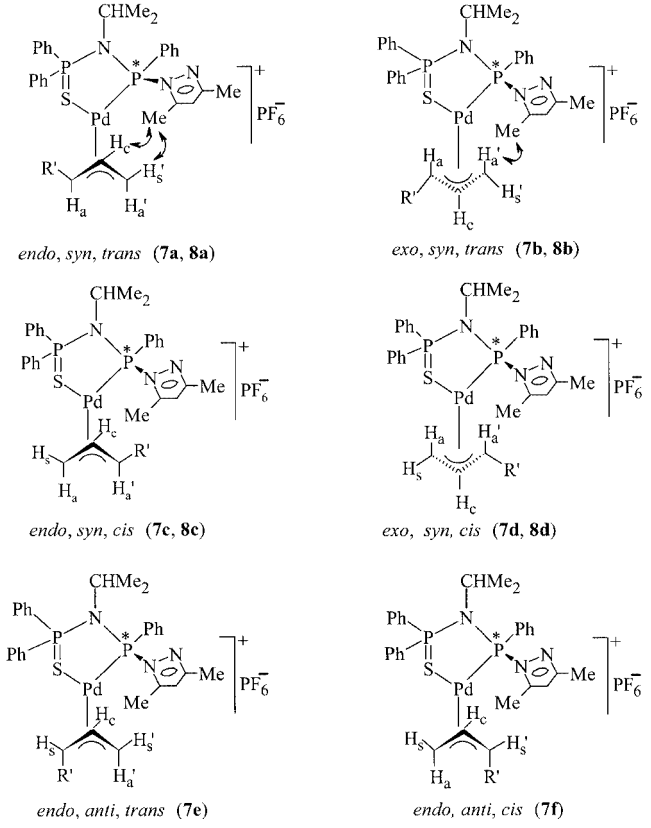

Figure 4. The six isomers for the (methylallyl)palladium complex $[Pd(\eta^3\text{-}MeC_3H_4)\{\eta^2\text{-}Ph_2P(S)N(CHMe_2)PPh(N_2C_3HMe_2\text{-}3,5)\}](PF_6)$ (**7**) and the four isomers observed in solution for the (phenylallyl)palladium complex $[Pd(\eta^3\text{-}PhC_3H_4)\{\eta^2\text{-}Ph_2P(S)N(CHMe_2)PPh(N_2C_3HMe_2\text{-}3,5)\}](PF_6)$ (**8**)

equilibrium with one another. The exchange followed an η^3-η^1-η^3 pathway, with the opening of the allyl terminus at the position *trans* with respect to the phosphorus centre. The isomer **7a** showed dynamic behaviour with isomer **7b** through a s*yn*,*anti* isomerisation process. Hence, **7b** could be assigned the *exo*,*syn*,*trans* structure, as the starting isomer **7a** had the *endo*,*syn*,*trans* structure. On the other hand, the isomer **7a** transformed into **7d** by a *cis*,*trans* isomerisation process, indicating that **7d** should be the *exo*,*syn*,*cis* isomer. The isomer **7b** showed *cis*,*trans* exchange with the isomer **7c**, and so the isomer **7c** should be *endo*,*syn*,*cis*. Exchange cross-peaks were also observed between isomers **7a** and **7c**, as well as between isomers **7b** and **7d**. The exchange equilibria may be represented schematically as in Scheme 3.

The $^{31}P\{^1H\}$ NMR spectrum of complex **8** (see Figure 5) revealed eight doublets arising from four isomers. A detailed NMR investigation (^1H NMR, ^{13}C NMR, ^1H-^1H DQF COSY, NOESY, and ROESY) indicated that all four isomers involved *P*,*S*-coordination with *syn*-allylphenyl arrangement, and that the major isomer had the *endo*,*syn*,-*trans* configuration (**8a**) as shown in Figure 4. In contrast to complex **7**, no *anti* isomer was formed in this case, owing to the presence of a relatively more bulky phenyl group on the allyl moiety. The exchange behaviour for **8a**−**8d** was similar to that observed for **7a**−**7d**; the exchanges are depicted in Scheme 4. The results can be explained in terms of the pathways shown in Scheme 5, the isomers **8a** and **8d** being related by *cis*,*trans* isomerisation and **8a** and **8b** by *syn*,*anti* isomerisation, with both processes occurring by means of a selective opening of the terminal allyl Pd−C bond located *trans* to the better π-acceptor phosphorus centre. Hence, the conversion of **8a** into **8b** or **8d** was electronically controlled.

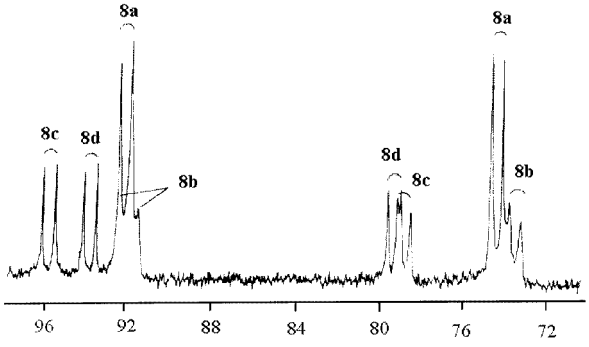

Figure 5. The $^{31}P\{^1H\}$ NMR spectrum ($CDCl_3$, 161.9 MHz) of complex **8** at 298 K, showing the presence of four isomers

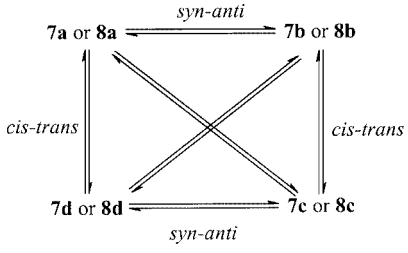

Scheme 3

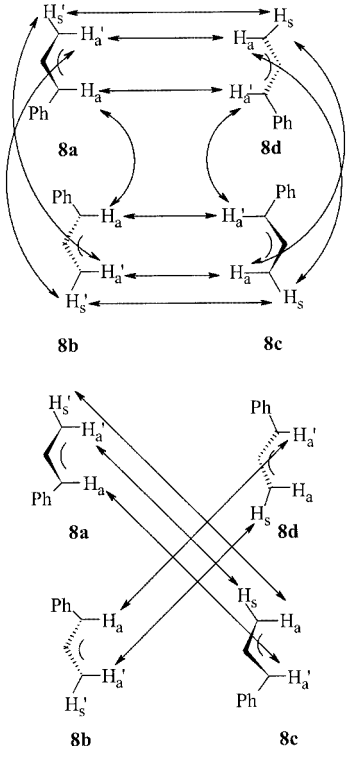

Scheme 4

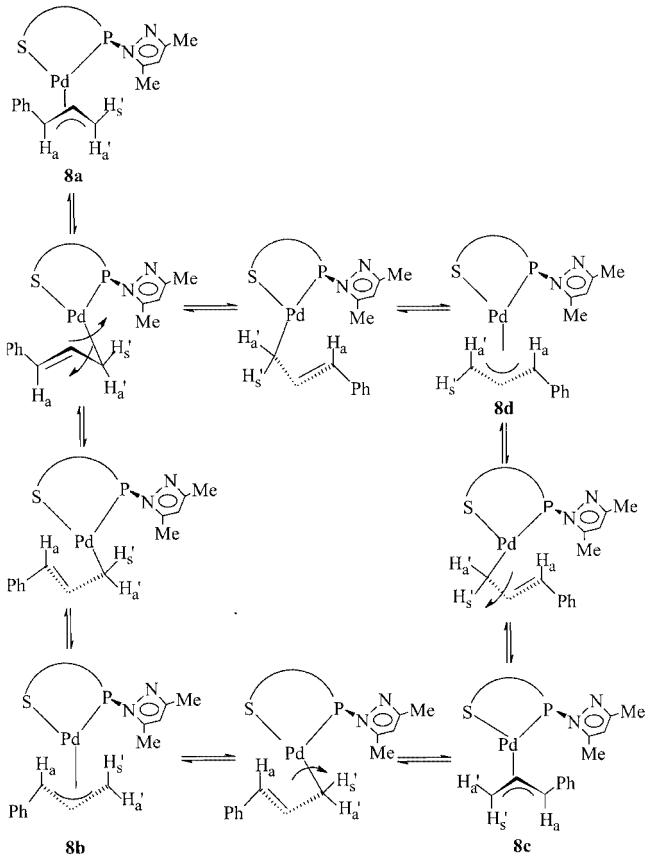

Scheme 5

In contrast, the isomerisation between **8d** and **8c** took place by a selective opening of the η^3-allyl group at the *cis* position with respect to the phosphorus centre, and hence was subject to steric control over the opening of the η^3-allyl moiety. The presence of a bulky allylphenyl group at the position *cis* to the $-PPh(N_2C_3HMe_2$-3,5) group in isomer **8d** exerted a more pronounced steric repulsion than in isomer **8a**, in which the allylphenyl group resided at the position *cis* to the sterically less demanding $-P(S)Ph_2$ group. Hence, the opening of the η^3-allyl moiety to a three-coordinated η^1-bonded intermediate in isomer **8d** relieved the steric strain. This type of steric control over *syn*,*anti* isomerisation has been observed in the case of a cationic allylpalladium complex bearing a P,S-ligand with a bulky allyl moiety.[18] Moreover, the isomer **8a** exchanged with **8c**, and **8b** exchanged with **8d**. Direct exchange between isomers **8a** and **8c** or between **8b** and **8d** should not be permitted, in view of their structural differences. However, NMR measurements clearly indicated exchange between **8a** and **8c** as well as **8b** and **8d**. The exchange information was transmitted via the intermediates **8b** or **8d**, resulting in an equilibrium among all four isomers **8a**−**8d**. The rapid dynamic processes for **7** and **8** were most probably related to the fact that the free nitrogen atom on the pyrazole ring can coordinatively interact with the palladium centre in the η^1-bonded intermediate. Such an interaction would stabilize the η^1-bonded intermediate and could accelerate the dynamic process. It is well known that catalytic amounts of anions such as chloride or fluoride or polar solvents such as DMSO and acetonitrile, which can coordinate to the palladium centre, accelerate the dynamic processes in allylpalladium complexes.[21]

Trends in ^{31}P Chemical Shifts

The ^{31}P resonances were assigned on the basis of the $\Delta\delta$ [$\Delta\delta = \delta$(complex) − δ(free ligand)] and sensitivity of the chemical shifts upon variation of the allyl moiety (see Table 1). The chemical shifts of one of the phosphorus nuclei in each of complexes **3**−**6** lay in the $\delta = 71-73$ ppm range, with $\Delta\delta$ being only 4.2−0.5 ppm. The constancy in the magnitude of chemical shifts on changing the allyl component and the low $\Delta\delta$ value suggested that this chemical shift could be assigned to the noncoordinated phosphorus atom bearing the pyrazole moiety. On the other hand, the chemical shifts of the other phosphorus nuclei showed a greater range of variation ($\delta = 75-80$ ppm). These phosphorus chemical shifts lay very much further downfield from that of the free ligand, and the magnitude of $\Delta\delta$ was in the 30.7−35.0 ppm range. Hence, this chemical shift was assigned to the coordinated $-PPh_2$ phosphorus atom. For the *P*,*S*-coordinated complexes **7** and **8**, the $-P(S)Ph_2$ and the −PPh(pyrazole) chemical shifts were assigned the values $\delta = 73.6-79.5$ and 91.7−95.7 ppm, respectively, based on the magnitude of $\Delta\delta$ and chemical shifts observed for allylpalladium complexes of the ligands $Ph_2P(S)N(CHMe_2)PPh_2$ and $Ph_2P(S)N(CHMe_2)P(S)Ph_2$, and also the chemical shifts of *P*,*P*-coordinated complexes of **1a**.[15]

With regard to P−P couplings, two observations were worthy of note:

(1) The $^2J_{P,P}$ values for *P*,*N*-coordinated complexes of **1a** and **1b** lay in the 29−31 Hz range, whereas $^2J_{P,P}$ values for *P*,*P*-coordinated allyl complexes are observed in the range of ca. 100 Hz.[15]

(2) The $^2J_{P,P}$ values for the *P*,*S*-coordinated complexes of **1c** were in the 80−100 Hz range.

Conclusions

Diphosphazane ligands of the type $Ph_2P(E)N(R)PPh(N_2C_3HMe_2$-3,5) (**1**), bearing a stereogenic phosphorus centre, exhibited diverse allylpalladium chemistry including various fluxional processes in solution. The preferred mode of coordination with the ligands $Ph_2PN(R)PPh(N_2C_3HMe_2$-3,5) [R = $CHMe_2$ (**1a**) or (*S*)-*CHMePh (**1b**)] was through the phosphorus and nitrogen atoms rather than the usually observed *P*,*P*-coordination. The former mode of coordination should electronically stabilise the allyl−palladium bonding, besides giving rise to the formation of a six-membered chelate ring. On the other hand, the monosulfide ligand $Ph_2P(S)N(R)PPh(N_2C_3HMe_2$-3,5) (**1c**) displayed *P*,*S*-coordination and also gave rise to a larger number of diastereomers with different allylic arrangements than observed in the *P*,*N*-coordinated ligands (**1a** and **1b**), which were more selective towards stabilisation of particu-

lar allyl diastereomers. In addition, in the case of *P,N*-coordinated complexes, there was a drastic decrease in the relative abundances of the *exo*,*syn*,*trans* isomers of 1-phenylallyl derivatives (below 10%) compared to those (40%) of the *exo*,*syn*,*trans* isomers of 1-methylallyl derivatives. Such a trend was not observed for the *P,S*-coordinated complexes. As far as the dynamic behaviour is concerned, the activation barriers for exchange processes among various allyl isomers bearing the P,S-ligand were less than those observed for the allyl isomers formed by P,N-ligands. The exchange pathway involved an η^1-allyl species generated by the opening of the η^3-allyl moiety at the position *trans* with respect to phosphorus atom in the case of *P,N*-coordinated complexes, and so was subject to electronic control. In the case of *P,S*-coordinated complexes, on the other hand, exchange among the allyl diastereomers occurred through the opening of the η^3-allyl moiety at either end (both *trans* with respect to the phosphorus atom as well as the sulfur atom). One possible reason for this difference is that the *trans* influences exerted by the two donor atoms − namely, phosphorus and sulfur − of the P,S-ligand (**1c**) would be reasonably similar to each other, whereas the *trans* influence of the phosphorus atom of the P,N-ligand (**1a** or **1b**) would be much larger than that of the nitrogen atom, as evident from the ^{13}C chemical shift values of the allyl termini.

Experimental Section

General Remarks: Reactions and manipulations were carried out under purified nitrogen by standard Schlenk and vacuum-line techniques. The solvents were purified by standard procedures[22] and distilled under nitrogen. The chloro-bridged allyl dimers $[Pd(\eta^3\text{-}1\text{-}MeC_3H_4)(\mu\text{-}Cl)]_2$ and $[Pd(\eta^3\text{-}1\text{-}PhC_3H_4)(\mu\text{-}Cl)]_2$ were prepared as previously described.[23] Diphosphazane ligands **1a**, the (S_CR_P) diastereomer of **1b** and diphosphazane monosulfide **1c** were prepared according to literature procedures.[8d,9c] The NMR spectra were recorded with Bruker DRX 500 MHz and Bruker AMX 400 MHz spectrometers. Chemical shifts downfield from the reference standard were assigned positive values. Elemental analyses were carried out with a Perkin−Elmer 2400 CHN analyser. The $^{31}P\{^1H\}$ and ^{13}C NMR spectroscopic data are given in Tables 1 and 2, respectively. The remaining NMR spectroscopic data are given below.

Synthesis of Palladium Complexes

$[Pd(\eta^3\text{-}1\text{-}MeC_3H_4)\{\eta^2\text{-}Ph_2PN(CHMe_2)PPh(N_2C_3HMe_2\text{-}3,5)\}](PF_6)$ (3): A mixture of $[Pd(\eta^3\text{-}1\text{-}MeC_3H_4)(\mu\text{-}Cl)]_2$ (0.039 g, $0.99\cdot10^{-4}$ mol), NH_4PF_6 (0.033 g, $2.02\cdot10^{-4}$ mol), and **1a** (0.095 g, $2.13\cdot10^{-4}$ mol) was dissolved in 20 mL of acetone. The solution was stirred for 2 h at 298 K and the white precipitate formed during the reaction was filtered off. The resulting colourless filtrate was concentrated to 10 mL under reduced pressure, and the solution was layered by addition of 5 mL of hexane (b.p. 40−60 °C) to yield colourless microcrystals. Yield: 0.140 g (93%). $C_{30}H_{36}F_6N_3P_3Pd$ (751.9): calcd. C 47.93, H 4.79, N 5.59; found C 47.56, H 4.88, N 5.53. m.p.191−194 °C (dec.). Major *endo*,*syn*,*trans* isomer (**3a**): ^1H NMR (400 MHz, CD_3COCD_3): δ = 1.41 (d, $^3J_{H,H}$ = 6.5 Hz, CH_3 $CHMe_2$), 1.66 (d, $^3J_{H,H}$ = 6.6 Hz, CH_3 $CHMe_2$), 1.74 (merged with allyl-CH_3 signal of isomer **3b**, H_a'), 1.79 (dd, $^4J_{H,P}$ = 11.6, $^3J_{H,H}$ = 6.4 Hz, allyl-CH_3), 2.20 (merged with solvent signal, 3-CH_3 $N_2C_3HMe_2$-3,5), 2.86 (s, 5-CH_3 $N_2C_3HMe_2$-3,5), 3.11 (m, H_a), 3.30 (d, $^3J_{H,H}$ = 6.6 Hz, H_s'), 4.12 (m, CH $CHMe_2$), 5.76 (m, H_c), 6.61 (br. s, CH $N_2C_3HMe_2$-3,5), 7.16−8.48 (m, aryl protons) ppm. ^{13}C NMR [100.6 MHz, $CDCl_3$ and CH_2Cl_2 (1:1)]: δ = 13.1 (d, $^3J_{C,P}$ = 5.6 Hz, CH_3 $N_2C_3HMe_2$-3,5), 14.8 (s, CH_3 $N_2C_3HMe_2$-3,5), 18.7 (br. s, allyl-CH_3), 25.3 (s, CH_3 $CHMe_2$), 25.5 (d, $^3J_{C,P}$ = 9.0 Hz, CH_3 $CHMe_2$), 52.8 (dd, $^2J_{C,P}$ = 28.05 and 6.5 Hz, CH $CHMe_2$), 110.1 (s, CH $N_2C_3HMe_2$-3,5), 129.5−157.2 (aryl carbon atoms) ppm. *exo*,*syn*,*trans* isomer (**3b**): ^1H NMR (400 MHz, CD_3COCD_3): δ = 1.12 (d, $^3J_{H,H}$ = 6.4 Hz, CH_3 $CHMe_2$), 1.39 (d, $^3J_{H,H}$ = 6.6 Hz, CH_3 $CHMe_2$), 1.69 (dd, $^4J_{H,P}$ = 11.7, $^3J_{H,H}$ = 6.8 Hz, allyl-CH_3), 2.69 (s, 3-CH_3 $N_2C_3HMe_2$-3,5), 2.73 (d, $^3J_{H,H}$ = 6.7 Hz, H_s'), 2.88 (s, 5-CH_3 $N_2C_3HMe_2$-3,5), 2.92 (d, $^3J_{H,H}$ = 12.1 Hz, H_a'), 4.25 (m, H_c), 4.91 (m, H_a), 6.81 (br. s, CH $N_2C_3HMe_2$-3,5) ppm. ^{13}C NMR [100.6 MHz, $CDCl_3$ and CH_2Cl_2 (1:1)]: δ = 13.3 (d, $^3J_{C,P}$ = 6.5, CH_3 $N_2C_3HMe_2$-3,5), 14.6 (s, CH_3 $N_2C_3HMe_2$-3,5), 17.7 (br. s, allyl-CH_3), 24.6 (d, $^2J_{C,P}$ = 16.6 Hz, CH_3 $CHMe_2$), 24.3 (d, $^2J_{C,P}$ = 19.4 Hz, Me $CHMe_2$), 110.0 (s, CH $N_2C_3HMe_2$-3,5) ppm.

The following complexes were synthesised in a way similar to that used for the preparation of complex **3**.

$[Pd(\eta^3\text{-}1\text{-}MeC_3H_4)\{\eta^2\text{-}(SR)\text{-}Ph_2PN[(S)\text{-}*CHMePh]PPh(N_2C_3HMe_2\text{-}3,5)\}](PF_6)$ (4): Starting materials: $[Pd(\eta^3\text{-}1\text{-}MeC_3H_4)(\mu\text{-}Cl)]_2$ (0.039 g, $0.99\cdot10^{-4}$ mol), NH_4PF_6 (0.033 g, $2.02\cdot10^{-4}$ mol), and **1b** (0.105 g, $2.07\cdot10^{-4}$ mol). Colourless crystals of **4** were grown from acetone solution by layering with hexane (b.p. 40−60 °C). Yield: 0.130 g (80%); m.p. 140−142 °C dec. $C_{35}H_{38}F_6N_3P_3Pd$ (814.0): calcd. C 51.66, H 4.67, N 5.16; found C 51.37, H 4.59, N 5.11. Major, *endo*,*syn*,*trans* isomer (**4a**): ^1H NMR (500 MHz, $CDCl_3$): δ = 1.46 (merged with allyl-CH_3 signal of isomer **4b**, H_a'), 1.54 (dd, $^4J_{H,P}$ = 11.2, $^3J_{H,H}$ = 6.4 Hz, allyl-CH_3), 1.72 (s, 3-CH_3 $N_2C_3HMe_2$-3,5), 1.87 [d, $^3J_{H,H}$ = 6.9 Hz, CH_3 (*S*)-*CHMePh], 2.76 (merged with 5-CH_3 $N_2C_3HMe_2$-3,5 signal, H_a), 2.77 (s, 5-CH_3 $N_2C_3HMe_2$-3,5), 3.01 (d, $^3J_{H,H}$ = 6.5 Hz, H_s'), 4.65 [m, CH (*S*)-*CHMePh], 5.35 (m, H_c), 6.22 (d, $^4J_{H,P}$ = 1.7 Hz, CH $N_2C_3HMe_2$-3,5), 6.52−7.81 (m, aryl protons) ppm. ^{13}C NMR (125.7 MHz, $CDCl_3$): δ = 13.7 (s, CH_3 $N_2C_3HMe_2$-3,5), 14.6 (s, CH_3 $N_2C_3HMe_2$-3,5), 18.9 (br. s, allyl-CH_3), 25.1 [d, $^3J_{C,P}$ = 22.2 Hz, CH_3 (*S*)-*CHMePh], 60.3 [m, CH (*S*)-*CHMePh], 110.5 (s, CH $N_2C_3HMe_2$-3,5), 126.3−157.2 (aryl carbon atoms). *exo*,*syn*,-*trans* isomer (**4b**): ^1H NMR (500 MHz, $CDCl_3$): δ = 1.45 (merged with H_a' of isomer **4a**, allyl-CH_3), 1.45 (dd, $^4J_{H,P}$ = 10.7, $^3J_{H,H}$ = 6.0 Hz, allyl-CH_3), 1.70 [d, $^3J_{H,H}$ = 7.3 Hz, CH_3 (*S*)-*CHMePh], 2.08 (s, 3-CH_3 $N_2C_3HMe_2$-3,5), 2.46 (d, $^3J_{H,H}$ = 11.9 Hz, H_a'), 2.75 (s, 5-CH_3 $N_2C_3HMe_2$-3,5), 2.77 (merged with 5-CH_3 $N_2C_3HMe_2$-3,5 signal, H_s'), 4.05 (m, H_c), 4.40 (m, H_a), 6.34 (d, $^4J_{H,P}$ = 2.3 Hz, CH $N_2C_3HMe_2$-3,5) ppm. ^{13}C NMR (125.7 MHz, $CDCl_3$): δ = 13.8 (s, CH_3 $N_2C_3HMe_2$-3,5), 14.9 (s, CH_3 $N_2C_3HMe_2$-3,5), 17.9 (br. s, allyl-CH_3), 24.8 [d, $^3J_{C,P}$ = 21.1 Hz, CH_3 (*S*)-*CHMePh], 110.6 (s, CH $N_2C_3HMe_2$-3,5) ppm. *endo*,*syn*,*cis* isomer (**4c**): ^1H NMR (500 MHz, $CDCl_3$): δ = 0.97 (t, $^3J_{H,H}$ = $^4J_{H,P}$ = 6.5 Hz, allyl-CH_3), 1.75 (s, 3-CH_3 $N_2C_3HMe_2$-3,5), 1.92 [d, $^3J_{H,H}$ = 7.1 Hz, CH_3 (*S*)-*CHMePh], 2.06 (merged with 3-CH_3 $N_2C_3HMe_2$-3,5 signal of isomer **4b**, H_a), 2.59 (m, H_a'), 2.74 (merged with 5-CH_3 $N_2C_3HMe_2$-3,5 signal of isomer **4a**, 5-CH_3 $N_2C_3HMe_2$-3,5), 4.65 [merged with CH (*S*)-*CHMePh signal, H_s], 5.35 (merged with H_c signal of isomer **4a**, H_c) ppm. ^{13}C NMR (125.7 MHz, $CDCl_3$): δ = 17.4 (s, allyl-CH_3) ppm.

$[Pd(\eta^3\text{-}1\text{-}PhC_3H_4)\{\eta^2\text{-}Ph_2PN(CHMe_2)PPh(N_2C_3HMe_2\text{-}3,5)\}](PF_6)$ (5): Starting materials: $[Pd(\eta^3\text{-}1\text{-}PhC_3H_4)(\mu\text{-}Cl)]_2$ (0.052 g, $1.00\cdot10^{-4}$ mol), NH_4PF_6 (0.033 g, $2.02\cdot10^{-4}$ mol), and **1a** (0.095 g, $2.13\cdot10^{-4}$ mol). Yellow crystals of **5** were obtained by layering with hexane (b.p. 40−60 °C). Yield: 0.135 g (83%); m.p. 193−196 °C (dec.). $C_{35}H_{38}F_6N_3P_3Pd$ (814.0): calcd. C 51.66, H 4.67, N 5.16;

found C 51.48, H 4.88, N 5.17. *endo*,*syn*,*trans* isomer (**5a**): ^{1}H NMR (400 MHz, $CDCl_3$): δ = 0.96 (s, 3-CH_3 $N_2C_3HMe_2$-3,5), 1.13 (d, $^3J_{H,H}$ = 6.5 Hz, CH_3 $CHMe_2$); 1.20 (d, $^3J_{H,H}$ = 6.4 Hz, CH_3 $CHMe_2$), 1.74 (d, $^3J_{H,H}$ = 11.6 Hz, H_a'), 2.60 (s, 5-CH_3 $N_2C_3HMe_2$-3,5), 3.17 (dd, $^3J_{H,H}$ = 6.8, $^3J_{H,P}$ = 1.7 Hz, H_s'), 3.73 (m, CH $CHMe_2$), 3.97 (dd, $^3J_{H,H}$ = 13.5, $^3J_{H,P}$ = 11.3 Hz, H_a), 6.01 (d, $^4J_{H,P}$ = 2.1 Hz, CH $N_2C_3HMe_2$-3,5), 6.12 (m, H_c), 6.85−7.71 (m, aryl protons) ppm. ^{13}C NMR (100.6 MHz, $CDCl_3$): δ = 13.3 (s, CH_3 $N_2C_3HMe_2$-3,5), 13.8 (d, $^3J_{C,P}$ = 17.8 Hz, CH_3 $N_2C_3HMe_2$-3,5), 24.9 (d, $^3J_{C,P}$ = 17.8 Hz, CH_3 $CHMe_2$), 26.1 (d, $^3J_{C,P}$ = 9.1 Hz, CH_3 $CHMe_2$), 53.4 (dd, $^2J_{C,P}$ = 27.9 and 6.1 Hz, CH $CHMe_2$), 110.1 (s, CH $N_2C_3HMe_2$-3,5), 127.7−158.7 (aryl carbon atoms). *exo*,*syn*,*trans* isomer (**5b**): ^{1}H NMR (400 MHz, $CDCl_3$): δ = 2.11 (s, 3-Me $N_2C_3HMe_2$-3,5), 2.52 (s, 5-CH_3 $N_2C_3HMe_2$-3,5), 2.59 (merged with 5-CH_3 $N_2C_3HMe_2$-3,5 signal of isomer **5a**, H_s'), 2.61 (merged with 5-CH_3 $N_2C_3HMe_2$-3,5 signal of isomer **5a**, H_a'), 4.88 (m, H_c), 5.50 (t, $^3J_{H,H}$ = $^3J_{H,P}$ = 12.5 Hz, H_a), 6.17 (merged with H_c signal of isomer **5a**, CH $N_2C_3HMe_2$-3,5). *endo*,*syn*,*cis* isomer (**5c**) ^{1}H NMR (400 MHz, $CDCl_3$): δ = 2.05 (s, 3-CH_3 $N_2C_3HMe_2$-3,5), 2.37 (dd, $^3J_{H,H}$ = 12.5, $^3J_{H,P}$ = 10.0 Hz, H_a), 2.62 (s, 5-CH_3 $N_2C_3HMe_2$-3,5), 3.29 (d, $^3J_{H,H}$ = 12.0 Hz, H_a'), 4.80 (t, $^3J_{H,H}$ = $^3J_{H,P}$ = 7.5 Hz, H_s), 5.91 (m, H_c), 6.29 (br., CH $N_2C_3HMe_2$-3,5) ppm.

[Pd(η^3-1-PhC_3H_4){η^2-(*SR*)-Ph_2PN[(*S*)-*CHMePh]PPh-($N_2C_3HMe_2$-3,5)}](PF_6) (6): Starting materials: [Pd(η^3-1-PhC_3H_4)(μ-Cl)]$_2$ (0.052 g, 1.00·10^{-4} mol), NH_4PF_6 (0.033 g, 2.02·10^{-4} mol), and **1b** (0.105 g, 2.07·10^{-4} mol). Isolation of the title compound in a pure form was unsuccessful. *endo*,*syn*,*trans* isomer (**6a**): ^{1}H NMR (400 MHz, $CDCl_3$): δ = 0.73 (s, 3-CH_3 $N_2C_3HMe_2$-3,5), 1.74 (d, $^3J_{H,H}$ = 12.9 Hz, H_a'), 1.84 [d, $^3J_{H,H}$ = 6.9 Hz, CH_3 (*S*)-*CHMePh], 2.73 (s, 5-CH_3 $N_2C_3HMe_2$-3,5), 3.22 (d, $^3J_{H,H}$ = 6.9 Hz, H_s'), 3.92 (t, $^3J_{H,H}$ = $^3J_{H,P}$ = 12.3 Hz, H_a), 4.63 [m, CH (*S*)-*CHMePh], 5.96 (d, $^4J_{H,P}$ = 2.1 Hz, CH $N_2C_3HMe_2$-3,5), 6.08 (m, H_c), 6.65−7.68 (m, aryl protons) ppm. ^{13}C NMR (100.6 MHz, $CDCl_3$): δ = 12.5 (s, CH_3 $N_2C_3HMe_2$-3,5), 13.5 (d, $^3J_{C,P}$ = 18.2 Hz, CH_3 $N_2C_3HMe_2$-3,5), 24.8 [d, $^3J_{C,P}$ = 22.9 Hz, CH_3 (*S*)-*CHMePh], 60.2 [dd, $^2J_{C,P}$ = 24.1 and 6.3 Hz, CH (*S*)-*CHMePh], 110.2 (s, CH $N_2C_3HMe_2$-3,5), 126.6−158.3 (aryl carbon atoms). *exo*,*syn*,*trans* isomer (**6b**): ^{1}H NMR (400 MHz, $CDCl_3$): δ = 2.11 (s, 3-CH_3 $N_2C_3HMe_2$-3,5), 2.52 (s, 5-CH_3 $N_2C_3HMe_2$-3,5), 2.71 (merged with 5-CH_3 $N_2C_3HMe_2$-3,5 of isomer **6a**, H_a'), 2.82 (br., H_s'), 4.81 (m, H_c), 5.41 (dd, $^3J_{H,H}$ = 13.6, $^3J_{H,P}$ = 11.2 Hz, H_a), 5.99 (br. s, CH $N_2C_3HMe_2$-3,5). *endo*,*syn*,*cis* isomer (**6c**): ^{1}H NMR (400 MHz, $CDCl_3$): δ = 2.21 (br. t, H_a), 3.20 (merged with H_s' of isomer **6a**, H_a'), 4.75 (t, $^3J_{H,H}$ = $^3J_{H,P}$ = 7.2 Hz, H_s), 5.83 (m, H_c) ppm.

[Pd(η^3-1-MeC_3H_4){η^2-Ph_2P(S)N($CHMe_2$)PPh($N_2C_3HMe_2$-3,5)}]PF_6 (7): Starting materials: [Pd(η^3-1-MeC_3H_4)(μ-Cl)]$_2$ (0.039 g, 0.99·10^{-4} mol), NH_4PF_6 (0.033 g, 2.02·10^{-4} mol), and **1c** (0.100 g, 2.09·10^{-4} mol). Colourless crystals of **7** were obtained by layering with hexane (b.p. 40−60 °C). Yield: 0.133 g (85%); m.p. 178−180 °C (dec.). $C_{30}H_{36}F_6N_3P_3PdS$ (784.0): calcd. C 45.97, H 4.59, N 5.36; found C 45.95, H 4.41, N 5.24. *endo*,*syn*,*trans* isomer (**7a**): ^{1}H NMR (500 MHz, $CDCl_3$): δ = 0.41 (d, $^3J_{H,H}$ = 6.9 Hz, CH_3 $CHMe_2$), 1.10 (d, $^3J_{H,H}$ = 6.1 Hz, CH_3 $CHMe_2$), 1.95 (merged with 5-CH_3 $N_2C_3HMe_2$-3,5 signal, allyl-CH_3), 2.40 (merged with 3-CH_3 $N_2C_3HMe_2$-3,5 signal, H_a'), 3.97 (d, $^3J_{H,H}$ = 6.1 Hz, H_s'), 4.60 (merged with CH $CHMe_2$ signal, H_a), 5.40 (m, H_c), 6.16 (br. s, CH $N_2C_3HMe_2$-3,5), 7.19−7.96 (m, aryl protons) ppm. ^{13}C NMR (100.6 MHz, $CDCl_3$): δ = 12.2 (s, CH_3 $N_2C_3HMe_2$-3,5), 13.6 (s, CH_3 $N_2C_3HMe_2$-3,5), 18.3 (br. s, allyl-CH_3), 22.9 (d, $^3J_{C,P}$ = 20.4 Hz, CH_3 $CHMe_2$), 23.1 (d, $^3J_{C,P}$ = 15.2 Hz, CH_3 $CHMe_2$), 57.8 (br. s, CH $CHMe_2$), 110.7 (s, CH $N_2C_3HMe_2$-3,5), 128.2−155.6 (aryl carbon atoms). *exo*,*syn*,*trans* isomer (**7b**): ^{1}H NMR (500 MHz, $CDCl_3$): δ = 2.15 (s, 5-CH_3 $N_2C_3HMe_2$-3,5), 1.96 (merged with allyl-CH_3 signal of isomer **7a**, allyl-CH_3), 2.91 (d, $^3J_{H,H}$ = 12.0 Hz, H_a'), 3.52 (d, $^3J_{H,H}$ = 6.4 Hz, H_s'), 4.46 (br. t, $^3J_{H,H}$ = 7.6 Hz, H_a), 5.49 (m, H_c) ppm. ^{13}C NMR (100.6 MHz, $CDCl_3$): δ = 18.3 (merged with allyl-CH_3 signal of isomer **7a**, allyl-CH_3). *endo*,*syn*,*cis* isomer (**7c**): ^{1}H NMR (500 MHz, $CDCl_3$): δ = 1.32 (dd, $^4J_{H,P}$ = 9.5, $^3J_{H,H}$ = 6.5 Hz, allyl-CH_3), 2.02 (s, 5-CH_3 $N_2C_3HMe_2$-3,5), 3.37 (m, H_a), 3.65 (m, H_a'), 4.46 (merged with H_a signal of isomer **7b**, H_s), 5.42 (merged with H_c signal of isomer **7a**, H_c) ppm. ^{13}C NMR (100.6 MHz, $CDCl_3$): δ = 17.2 (br. s, allyl-CH_3). *exo*,*syn*,*cis* isomer (**7d**): ^{1}H NMR (500 MHz, $CDCl_3$): δ = 0.98 (br. t, $^3J_{H,H}$ = $^4J_{H,P}$ = 6.6 Hz, allyl-CH_3), 2.10 (s, CH_3 $N_2C_3HMe_2$-3,5), 3.37 (merged with H_a signal of isomer **7c**, H_a), 4.02 (br. s, H_a'), 4.63 (merged with CH $CHMe_2$ signal, H_s), 5.38 (merged with H_c signal of isomer **7a**, H_c) ppm. ^{13}C NMR (100.6 MHz, $CDCl_3$): δ = 17.5 (br. s, allyl-CH_3). *endo*,*anti*,*trans* isomer (**7e**): ^{1}H NMR (500 MHz, $CDCl_3$): δ = 0.76 (br. d, allyl-CH_3), 2.80 (d, H_a'), 3.73 (br. s, H_s), 4.15 (br. d, H_s'), 5.30 (m, H_c). *endo*,*anti*,*cis* isomer (**7f**): ^{1}H NMR (500 MHz, $CDCl_3$): δ = 0.27 (t, allyl-CH_3), 3.72 (merged with H_s signal of isomer **7e**, H_a), 4.66 (merged with CH $CHMe_2$ signal, H_s), 5.05 (m, H_s'), 5.29 (merged with H_c signal of isomer **7e**, H_c).

[Pd(η^3-1-PhC_3H_4){η^2-Ph_2P(S)N($CHMe_2$)PPh($N_2C_3HMe_2$-3,5)}]-(PF_6) (8): Starting materials: [Pd(η^3-1-PhC_3H_4)(μ-Cl)]$_2$ (0.052 g, 1.00·10^{-4} mol), NH_4PF_6 (0.033 g, 2.02·10^{-4} mol), and **1c** (0.100 g, 2.09·10^{-4} mol). Yellow crystals were obtained by layering with hexane (b.p. 40−60 °C). Yield: 0.142 g (84%); m.p. 171−174 °C (dec.). $C_{35}H_{38}F_6N_3P_3PdS$ (846.1): calcd. C 49.70, H 4.49, N 4.97; found C 49.62, H 4.55, N 4.65. *endo*,*syn*,*trans* isomer (**8a**): ^{1}H NMR (400 MHz, $CDCl_3$): δ = 0.39 (br. s, CH_3 $CHMe_2$), 1.19 (br. s, CH_3 $CHMe_2$), 2.05 (s, 5-CH_3 $N_2C_3HMe_2$-3,5), 2.37 (s, 3-CH_3 $N_2C_3HMe_2$-3,5), 2.79 (br. s, H_a'), 4.23 (br. s, H_s'), 4.61 (br., CH $CHMe_2$), 5.63 (br., H_a), 6.04 (br., H_c), 6.28 (br. s, CH $N_2C_3HMe_2$-3,5), 6.52−7.98 (m, aryl protons) ppm. ^{13}C NMR [100.6 MHz, $CDCl_3$ and CH_2Cl_2 (1:1)]: δ = 13.5 (s, CH_3 $N_2C_3HMe_2$-3,5), 13.9 (br., CH_3 $N_2C_3HMe_2$-3,5), 23.0 (s, CH_3 $CHMe_2$), 58.0 (br., CH $CHMe_2$), 110.8 (s, CH $N_2C_3HMe_2$-3,5), 126.0−155.7 (aryl carbon atoms). *exo*,*syn*,*trans* isomer (**8b**): ^{1}H NMR (400 MHz, $CDCl_3$): δ = 3.23 (br. s, H_a'), 3.77 (br., H_s'), 5.49 (br. H_a), 6.11 (br., H_c). *endo*,*syn*,*cis* isomer (**8c**): ^{1}H NMR (400 MHz, $CDCl_3$): δ = 3.70 (br., H_a), 4.68 (br. t, H_s), 4.73 (br. d, H_a'), 6.18 (br., H_c). *exo*,*syn*,*cis* isomer (**8d**): ^{1}H NMR (400 MHz, $CDCl_3$): δ = 3.69 (br., H_a), 4.79 (br., H_s), 5.00 (br. d, H_a'), 6.00 (m, H_c) ppm.

X-ray Crystallography: Crystal data for complex **5a** were collected by using a Siemens SMART CCD diffractometer. The crystallographic data and details on data collection are summarised in Table 3. The structure was solved by direct methods, using the program SIR-97[24] and refined on F^2 values for all unique data by full-matrix, least squares by using SHELXTL.[25] The non-hydrogen atoms were refined anisotropically. The hydrogen atoms were fixed at their calculated geometrical positions and refined isotropically. CCDC-172846 contains the supplementary crystallographic data for this paper. These data can be obtained free of charge at www.ccdc.cam.ac.uk/conts/retrieving.html or from the Cambridge Crystallographic Data Centre, 12, Union Road, Cambridge CB2 1EZ, UK [Fax: (internat.) + 44-1223/336-033; E-mail: deposit@ccdc.cam.ac.uk].

Acknowledgments

We thank the Department of Science and Technology (DST), New Delhi for financial support.

Table 3. Crystal data and structure refinement for complex **5a**

Empirical formula	$C_{35}H_{38}F_6P_3N_3Pd$
Formula mass	813.99
Temperature	293(2) K
Wavelength	0.71073 Å
Crystal system	monoclinic
Space group	$P2_1$
Unit cell dimensions	a = 9.8783(8) Å b = 18.1125(14) Å; c = 10.2360(8) Å β = 97.223(2)°
Volume	1816.9(2) Å^3
Z	2
Density (calculated)	1.488 Mg/m^3
Absorption coefficient	0.703 mm^{-1}
F(000)	828
Crystal size	0.12 × 0.06 × 0.06 mm
θ range for data collection	2.01−23.28°.
Index ranges	$-10 \le h \le 10$, $-20 \le k \le 20$, $-11 \le l \le 9$
Reflections collected	8238
Independent reflections	4817 [R(int) = 0.0275]
Completeness to θ = 23.28°	99.7%
Refinement method	full-matrix, least squares on F^2
Data/restraints/parameters	4817/1/435
Goodness-of-fit on F^2	1.140
Final R indices [$I > 2\sigma(I)$]	$R1$ = 0.0740, $wR2$ = 0.1785
R indices (all data)	$R1$ = 0.1058, $wR2$ = 0.2102
Absolute structure parameter	0.00(7)
Extinction coefficient	0.0055(13)
Largest diff. peak and hole	2.298 and −0.676 e·Å^{-3}

[1] [1a] B. M. Trost, T. R. Verhoeven, in: *Comprehensive Organometallic Chemistry* (Eds.: G. Wilkinson, F. G. A. Stone, E. W. Abel), Pergamon Press, Oxford, **1982**, vol. 8, p. 799. [1b] P. Von Matt, A. Pfaltz, *Angew. Chem. Int. Ed. Engl.* **1993**, *32*, 566. [1c] T. Hayashi, in: *Catalytic Asymmetric Synthesis* (Ed.: I. Ojima), VCH, New York, **1993**, p. 325 and references cited therein. [1d] R. Noyori, *Asymmetric Catalysis in Organic Synthesis*, Wiley, New York, **1994**, p. 82. [1e] B. M. Trost, D. L. van Vranken, *Chem. Rev.* **1996**, *96*, 395. [1f] G. Consiglio, R. M. Waymouth, *Chem. Rev.* **1989**, *89*, 257. [1g] C. G. Frost, J. Howarth, J. M. J. Williams, *Tetrahedron: Asymmetry* **1992**, *3*, 1089. [1h] G. Helmchen, *J. Organomet. Chem.* **1999**, *576*, 203.

[2] [2a] A. Pfaltz, *Acta Chim. Scand. B* **1996**, *50*, 189 and references there in. [2b] S. Kudis, G. Helmchen, *Angew. Chem. Int. Ed.* **1998**, *37*, 3047. [2c] G. J. Dawson, G. Frost, J. M. J. Williams, *Tetrahedron Lett.* **1993**, *34*, 3149. [2d] G. Helmchen, S. Kudis, P. Sennhenn, H. Steinhagen, *Pure Appl. Chem.* **1997**, *69*, 513 and references therein.

[3] [3a] D. A. Evans, K. R. Campos, J. S. Tedrow, F. E. Michael, M. R. Gagné, *J. Org. Chem.* **1999**, *64*, 2994. [3b] D. A. Evans, K. R. Campos, J. S. Tedrow, F. E. Michael, M. R. Gagné, *J. Am. Chem. Soc.* **2000**, *122*, 7905. [3c] K. Selvakumar, M. Valentini, P. S. Pregosin, A. Albinati, *Organometallics* **1999**, *18*, 4591. [3d] A. Albinati, P. S. Pregosin, K. Wick, *Organometallics* **1996**, *15*, 2419. [3e] A. Albinati, J. Eckert, P. S. Pregosin, H. Rüegger, R. Salzmann, C. Stössel, *Organometallics* **1997**, *16*, 579.

[4] [4a] T. Morimoto, K. Tachibana, K. Achiwa, *Synlett* **1997**, 783. [4b] J. C. Anderson, D. S. James, J. P. Mathias, *Tetrahedron: Asymmetry* **1998**, *9*, 753. [4c] J. Allen, J. Bower, J. Williams, *Tetrahedron: Asymmetry* **1994**, *5*, 1895. [4d] K. Boog-Wick, P. S. Pregosin, G. Trabesinger, *Organometallics* **1998**, *17*, 3254.

[5] B. M. Trost, F. D. Toste, *J. Am. Chem. Soc.* **1999**, *121*, 4545.

[6] G. Helmchen, A. Pfaltz, *Acc. Chem. Res.* **2000**, *33*, 336.

[7] [7a] P. S. Pregosin, R. Salzmann, *Coord. Chem. Rev.* **1996**, *155*, 35. [7b] P.S. Pregosin, G. Trabesinger, *J. Chem. Soc., Dalton Trans.* **1998**, 727. [7c] J. M. Canal, M. Gómez, F. Jiménez, M. Rocamora, G. Muller, E. Duñach, D. Franco, A. Jiménez, F. H. Cano, *Organometallics* **2000**, *19*, 966. [7d] A. Gogoll, C. Johansson, A. Axén, H. Grennberg, *Chem. Eur. J.* **2001**, *7*, 396.

[8] [8a] M. Ganesan, S. S. Krishnamurthy, M. Nethaji, *J. Organomet. Chem.* **1998**, *570*, 247. [8b] R. P. K. Babu, K. Aparna, S. S. Krishnamurthy, M. Nethaji, *Phosphorus, Sulfur Silicon* **1995**, *103*, 39. [8c] M. Ganesan, S. S. Krishnamurthy, M. Nethaji, K. Raghuraman, *Phosphorus, Sulfur Silicon* **1999**, *147*, 355. [8d] R. P. K. Babu, S. S. Krishnamurthy, M. Nethaji, *Tetrahedron: Asymmetry* **1995**, *6*, 427.

[9] [9a] R. P. K. Babu, S. S. Krishnamurthy, M. Nethaji, *Organometallics* **1995**, *14*, 2047. [9b] R. P. K. Babu, S. S. Krishnamurthy, M. Nethaji, *Polyhedron* **1996**, *15*, 2689. [9c] R. P. K. Babu, S. S. Krishnamurthy, M. Nethaji, *J. Organomet. Chem.* **1993**, *454*, 157.

[10] [10a] M. S. Balakrishna, V. S. Reddy, S. S. Krishnamurthy, J. F. Nixon, J. C. T. R. Burckett St Laurent, *Coord. Chem. Rev.* **1994**, *129*, 1. [10b] M. Witt, H. W. Roesky, *Chem. Rev.* **1994**, *94*, 1163. [10c] P. Bhattacharyya, J. D. Woollins, *Polyhedron* **1995**, *14*, 3367. [10d] A. M. Z. Slawin, M. B. Smith, J. D. Woollins, *J. Chem. Soc., Dalton Trans.* **1996**, 1283.

[11] [11a] N. Baltzer, L. Macko, S. Schaffner, M. Zehnder, *Helv. Chim. Acta* **1996**, *79*, 803. [11b] J. Powell, B. L. Shaw, *J. Chem. Soc. A* **1967**, 1839. [11c] B. Åkermark, B. Krakenberger, S. Hansson, A. Vitagliano, *Organometallics* **1987**, *6*, 620.

[12] [12a] M. L. H. Green, P. L. I. Hagy, *Adv. Organomet. Chem.* **1964**, *2*, 325. [12b] R. Rossch, R. Hoffman, *Inorg. Chem.* **1974**, *13*, 2656.

[13] [13a] A. Togni, U. Burckhardt, V. Gramlich, P. S. Pregosin, R. Salzmann, *J. Am. Chem. Soc.* **1996**, *118*, 1031. [13b] U. Burckhardt, V. Gramlich, P. Hofmann, R. Nesper, P. S. Pregosin, R. Salzmann, A. Togni, *Organometallics* **1996**, *15*, 3496. [13c] T. G. Appleton, H. C. Clark, L. Manzer, *Coord. Chem. Rev.* **1973**, *10*, 335.

[14] J. W. Faller, M. E. Thomson, M. Mattina, *J. Am. Chem. Soc.* **1971**, *93*, 2642.

[15] S. K. Mandal, S. S. Krishnamurthy, unpublished results.

[16] C. Breutel, P. S. Pregosin, R. Salzmann, A. Togni, *J. Am. Chem. Soc.* **1994**, *116*, 4067.

[17] [17a] J. Sprinz, M. Kiefer, G. Helmchen, M. Reggelin, G. Huttner, O. Walter, L. Zsolnai, *Tetrahedron Lett.* **1994**, *35*, 1523. [17b] R. Fernández-Galán, F. A. Jalón, B. R. Manzano, J. R. Fuente, M. Vrahami, B. Jedlicka, W. Weissensteiner, G. Jogl, *Organometallics* **1997**, *16*, 3758.

[18] J. Hermann, P. S. Pregosin, R. Salzmann, A. Albinati, *Organometallics* **1995**, *14*, 3311.

[19] T. Hosokawa, Y. Wakabayashi, K. Hosokawa, T. Tsuji, S.-I. Murahashi, *Chem. Commun.* **1996**, 859.

[20] B. Crociani, S. Antonaroli, G. Bandoli, L. Canovese, F. Visentin, P. Uguagliati, *Organometallics* **1999**, *18*, 1137.

[21] [21a] J. M. Brown, D. I. Hulmes, P. J. Guiry, *Tetrahedron* **1994**, *50*, 4493. [21b] S. Hansson, P.-O. Norrby, M. P. T. Sjögren, B. Åkermark, M. E. Cucciolito, F. Giordano, A. Vittagliano, *Organometallics* **1993**, *12*, 4940. [21c] U. Burckhardt, M. Baumann, G. Trabesinger, V. Gramlich, A. Togni, *Organometallics* **1997**, *16*, 5252.

[22] D. D. Perrin, W. L. F. Armarego, D. R. Perrin, *Purification of Laboratory Chemicals*, 3rd ed., Pergamon Press, Oxford, U. K., **1988**.

[23] P. R. Auburn, P. B. McKenzie, B. Bosnich, *J. Am. Chem. Soc.* **1985**, *107*, 2033.

[24] A. Altomare, M.C. Burla, M. Camalli, G. L. Cascarano, C. Giacovazzo, A. Guagliardi, A. G. G. Moliterni, G. Polidori, R. Spagna, *J. Appl. Cryst.* **1999**, *32*, 115.

[25] G. M. Sheldrick, *SHELXTL*, Version 5; Bruker AXS Inc.: Madison, Wisconsin, **1997**.

Received November 19, 2001
[I01463]

μ-Imido, μ-(η²,η²-N,N-Hydrazido) and μ-(η¹-C:η²-C,N-Isocyanido) Dinuclear (Fulvalene)zirconium Derivatives

Marta González-Maupoey,[a] Gema M. Rodríguez,[a] and Tomás Cuenca*[a]

Keywords: Zirconium / Fulvalene ligands / Imido ligands / Hydrazido ligands / Isocyanido ligands

Treatment of the chloro(fulvalene)zirconium(III) compound $[Zr(\eta^5\text{-}C_5H_5)(\mu\text{-}Cl)]_2[\mu\text{-}(\eta^5,\eta^5\text{-}C_{10}H_8)]$ with an equimolar amount of azobenzene in toluene, under extremely anhydrous conditions, gives the μ-[bis(imido)] derivative $[Zr(\eta^5\text{-}C_5H_5)(\mu\text{-}NPh)]_2[\mu\text{-}(\eta^5,\eta^5\text{-}C_{10}H_8)]$ (**1**). However, when this reaction is carried out under insufficiently dry conditions a mixture of the previously reported μ-oxo complex $[Zr(\eta^5\text{-}C_5H_5)Cl]_2(\mu\text{-}O)[\mu\text{-}(\eta^5,\eta^5\text{-}C_{10}H_8)]$ and 1,2-diphenylhydrazine is obtained. When the chloro(fulvalene)zirconium(III) compound reacts with benzo[*c*]cinnoline the μ-(η²,η²-N,N-hydrazido) complex $[Zr(\eta^5\text{-}C_5H_5)Cl]_2[\mu\text{-}(NC_6H_4C_6H_4N)][\mu\text{-}(\eta^5,\eta^5\text{-}C_{10}H_8)]$ (**2a**) is obtained, which rearranges to the thermodynamically more stable **2b**. Addition of an equimolar amount of RNC (R = *n*Bu, C_6H_{11}) to a toluene solution of $[Zr(\eta^5\text{-}C_5H_5)(\mu\text{-}Cl)]_2[\mu\text{-}(\eta^5,\eta^5\text{-}C_{10}H_8)]$ gives $[Zr(\eta^5\text{-}C_5H_5)Cl]_2(\mu\text{-}CNR)[\mu\text{-}(\eta^5,\eta^5\text{-}C_{10}H_8)]$ [R = *n*Bu (**3**), C_6H_{11} (**4**)]. Reaction of $[Zr(\eta^5\text{-}C_5H_5)Cl]_2(\mu\text{-}CN\textit{t}Bu)[\mu\text{-}(\eta^5,\eta^5\text{-}C_{10}H_8)]$ with 1 equiv. of $PhCH_2MgCl$ or $(PhCH_2)_2Mg(THF)_2$ afforded the monobenzyl derivatives $[Zr(\eta^5\text{-}C_5H_5)]_2(CH_2Ph)(Cl)(\mu\text{-}CN\textit{t}Bu)[\mu\text{-}(\eta^5,\eta^5\text{-}C_{10}H_8)]$ (**5** and **6**). When this reaction was carried out with 2 equiv. or an excess of $PhCH_2MgCl$, a mixture of the monobenzyl and dibenzyl compounds $[Zr(\eta^5\text{-}C_5H_5)]_2(CH_2Ph)(Cl)(\mu\text{-}CN\textit{t}Bu)[\mu\text{-}(\eta^5,\eta^5\text{-}C_{10}H_8)]$ (**5**) and $[Zr(\eta^5\text{-}C_5H_5)(CH_2Ph)]_2(\mu\text{-}CN\textit{t}Bu)[\mu\text{-}(\eta^5,\eta^5\text{-}C_{10}H_8)]$ (**7**) is obtained. Similar reactions with 1 or 2 equiv. of $(CH_3)_3SiCH_2Li$ afford a mixture of the monoalkyl and dialkyl compounds $[Zr(\eta^5\text{-}C_5H_5)]_2[CH_2Si(CH_3)_3](Cl)(\mu\text{-}CN\textit{t}Bu)[\mu\text{-}(\eta^5,\eta^5\text{-}C_{10}H_8)]$ (**8**) and $\{Zr(\eta^5\text{-}C_5H_5)[CH_2Si(CH_3)_3]\}_2(\mu\text{-}CN\textit{t}Bu)[\mu\text{-}(\eta^5,\eta^5\text{-}C_{10}H_8)]$ (**9**) compounds. Moreover, methylation of $[Zr(\eta^5\text{-}C_5H_5)Cl]_2(\mu\text{-}CN\textit{n}Bu)[\mu\text{-}(\eta^5,\eta^5\text{-}C_{10}H_8)]$ gives the analytically pure tetramethyl derivative $[Zr(\eta^5\text{-}C_5H_5)(CH_3)]_2(\mu\text{-}CN\textit{n}Bu)[\mu\text{-}(\eta^5,\eta^5\text{-}C_{10}H_8)]$ (**10**), whereas $[Zr(\eta^5\text{-}C_5H_5)Cl]_2(\mu\text{-}CNC_6H_{11})[\mu\text{-}(\eta^5,\eta^5\text{-}C_{10}H_8)]$ reacts with MeLi to give a mixture of the monomethyl derivatives $[Zr(\eta^5\text{-}C_5H_5)]_2(CH_3)(Cl)(\mu\text{-}CNC_6H_{11})[\mu\text{-}(\eta^5,\eta^5\text{-}C_{10}H_8)]$ (**11** and **12**), as well as the dimethyl compound $[Zr(\eta^5\text{-}C_5H_5)(CH_3)]_2(\mu\text{-}CNC_6H_{11})[\mu\text{-}(\eta^5,\eta^5\text{-}C_{10}H_8)]$ (**13**).

(© Wiley-VCH Verlag GmbH, 69451 Weinheim, Germany, 2002)

Introduction

Complexes with cyclopentadienyl ancillary ligands have dominated the study of early transition metal chemistry. Mono- and dicyclopentadienyltitanium, -zirconium and -hafnium derivatives are considered the most widely studied organometallic transition compounds. The stability, solubility and reactivity of these complexes are dramatically influenced by modifying their cyclopentadienyl ligands.[1]

The presence of two metal centres in homo- and heterodimetallic complexes has generated considerable effort in recent years, with a myriad of studies on their properties as well as cooperative investigations into their reactivity, which were then compared with analogous mononuclear cyclopentadienyl compounds.[2] For such organometallic complexes, particular attention has been devoted to compounds in which two metal centres are coordinated by a fulvalene bridging ligand.[3] The fulvalene group is especially interesting as it tends to form dinuclear complexes with short distances between the two metal centres, which may even have slight metal−metal interactions, as in compound **I**. With this disposition the metal centres are in close proximity, making the possible cooperative effects capable of enhancing or modifying the chemical reactivity. Free rotation of the rings around the C−C bond in the fulvalene plane makes two *cis*,*trans* conformations (**I**, **II**) of the metal fragments possible. The preferred conformation depends mainly on electronic and steric factors. In this type of ligand each cyclopentadienyl group is substituted through one bond to a second identical group. It makes the metal centre more electron-deficient, reducing secondary reactions such as ring C−H bond activation because of the rigid system that generates the fulvalene.

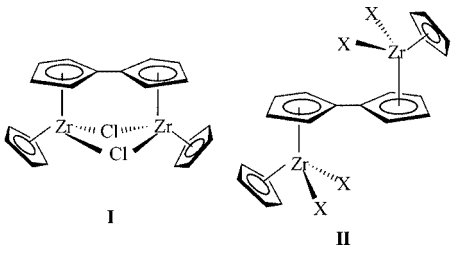

I **II**

[a] Departamento de Química Inorgánica, Universidad de Alcalá,
Campus Universitario,
28871 Alcalá de Henares, Spain
Fax: (internat.) + 34-91/885-4683
E-mail: tomas.cuenca@uah.es

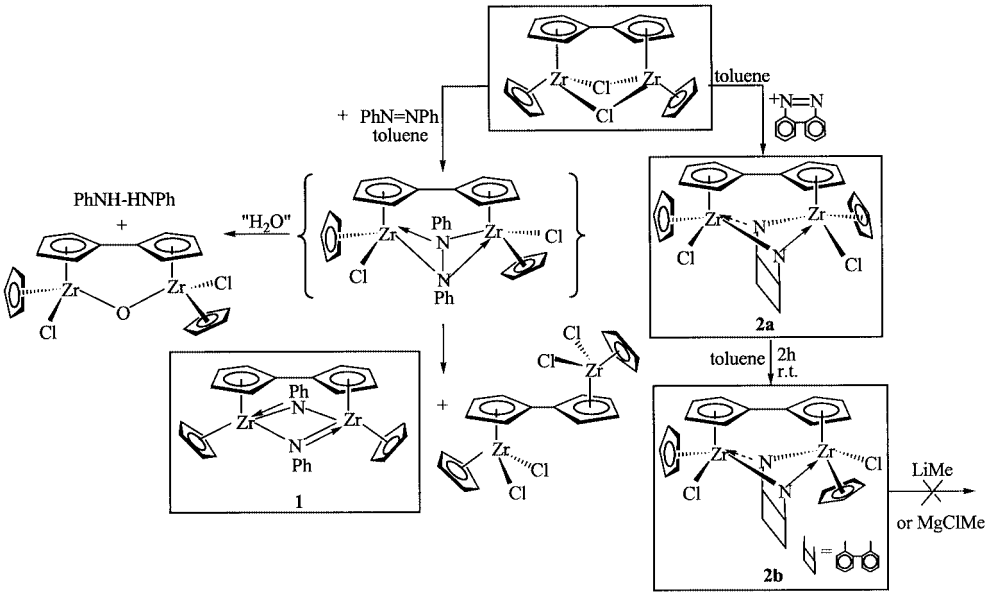

Scheme 1

To enable systematic studies of such compounds we have developed a high-yield route to titanium and zirconium compounds.[4] In recent years, the synthesis and reactivity of dinuclear organotitanium and -zirconium compounds containing the fulvalene ligand have been the focus of our research[5,6] and the study of fundamental chemical reactions with a variety of new fulvalene derivatives has been published.[7] In this paper we report the formation of dinuclear (fulvalene)zirconium complexes where both metal atoms are bridged by an additional μ-imido, μ-(η^2,η^2-N,N-hydrazido) or μ-(η^1-C:η^2-C,N-isocyanido) ligand.

Results and Discussion

μ-Imido, μ-(η^2,η^2-N,N-Hydrazido) Derivatives

Imido complexes of group-4 elements have been synthesized by different routes.[8] According to the described method using the N=N bond cleavage of an azobenzene,[9] the known chloro(fulvalene)zirconium(III) compound [Zr(η^5-C_5H_5)(μ-Cl)]$_2$[μ-(η^5,η^5-$C_{10}H_8$)][4a] reacts with an equimolar amount of PhN=NPh in toluene, under extremely anhydrous conditions, as shown in Scheme 1. The initially deep violet solution first turns dark yellow and then orange with gradual precipitation of a yellow solid. The solid was identified by elemental analysis and IR spectroscopy as the known chloro(fulvalene)zirconium(IV) complex [Zr(η^5-C_5H_5)Cl$_2$]$_2$[μ-(η^5,η^5-$C_{10}H_8$)].[5c] This compound is rather insoluble in the usual organic solvents and can be separated by simple filtration. By removing the solvent in vacuo from the resulting solution, an orange product was obtained in 46% yield, characterized as the μ-[bis(phenylimido)] derivative [Zr(η^5-C_5H_5)(μ-NPh)]$_2$[μ-(η^5,η^5-$C_{10}H_8$)] (**1**).

Complex **1** can be considered as arising from an initial interaction of the zirconium(III) compound with the organic reagent to give a hydrazido intermediate species, which evolves through N−N bond breaking and a subsequent intermolecular ligand exchange to yield the final mixture containing **1** and the chloro(fulvalene)zirconium(IV) complex. This latter step may be favoured by the low solubility of [Zr(η^5-C_5H_5)Cl$_2$]$_2$[μ-(η^5,η^5-$C_{10}H_8$)]. Attempts to isolate and characterise the hydrazido intermediate species by carrying out the reaction under milder conditions have not been successful. When this reaction is carried out under insufficiently dry conditions, the final product always contained a mixture of the previously reported μ-oxo complex [Zr(η^5-C_5H_5)Cl]$_2$(μ-O)[μ-(η^5,η^5-$C_{10}H_8$)][4a] and 1,2-diphenylhydrazine, identified by analytical and NMR spectroscopic characterisation. This is consistent with the reaction pathway shown in Scheme 1, indicating that the proposed hydrazido intermediate species reacts with water, resulting in the immediate hydrolysis of the Zr−N bonds to give a mixture of the oxo zirconium compound and hydrazine. Several studies reveal that III is an unstable oxidation state for zirconium. It rapidly reacts with oxygen through a peroxo intermediate species, which immediately transforms into the final products, probably containing oxozirconium(IV) species.[1,10] Peroxo and hydrazido are isoelectronic and their zirconium-type derivatives are rare. In order to determine whether a stable hydrazido complex could be isolated, we treated the starting chlorozirconium(III) compound with benzo[*c*]cinnoline, an organic molecule similar to azobenzene in which the biphenyl system connecting the nitrogen atoms prevents the N−N bond from breaking due to the additional C−C bond. Equimolar amounts of the two compounds reacted overnight in toluene solution to give the complex [Zr(η^5-C_5H_5)Cl]$_2$[μ-(η^2,η^2NC$_6$H$_4$C$_6$H$_4$N)][μ-(η^5,η^5-$C_{10}H_8$)] (**2a**), which converted in toluene solution into **2b** within 2 h (see Scheme 1). Compound **2b** remains unaltered under reflux in toluene

solution after 5 h. The N−N bond cleavage and intermolecular ligand exchange processes were not observed and the compound was isolated as a yellow microcrystalline solid in 60% yield.

Both compounds are air- and moisture-sensitive and must be manipulated under dry conditions. They are soluble in aromatic and chlorinated solvents and insoluble in alkanes. Formulation of **1** as an imido-bridged dinuclear compound is based on analytical and spectroscopic data and comparisons with similar structurally characterized titanium and zirconium species.[11] We propose that compound **2** is an unusual μ-(η^2,η^2-hydrazido) bridge derivative. Mass spectra confirm the dinuclear nature of these compounds. The presence of the fulvalene ligand must contribute to the formation and stabilization of the μ-(phenylimido) and μ-(η^2,η^2-hydrazido) disposition.

A medium-intensity absorption at 568 cm^{-1} in the IR spectrum of **2** can be assigned to the ν(N−N) stretching mode and implies that on coordination an important reduction in the N−N multiple-bond character has taken place which supports the bonding description given in Scheme 1. The ^1H NMR spectrum for complex **1** (C_6D_6 or $CDCl_3$, room temperature) shows one singlet and three resonances assigned to the cyclopentadienyl and the phenyl group protons, respectively. The fulvalene ligand gives two pseudotriplets corresponding to an AA′BB′ spin system. These spectroscopic features agree with the C_{2v} symmetrical arrangement depicted in Scheme 1 for a dimetallic species with the zirconium centres linked by a fulvalene ligand and two bridging phenylimido groups giving a central Ti_2N_2 heterocyclic ring. The ^1H NMR spectrum of **2a** (C_6D_6 or $CDCl_3$, room temperature) shows one singlet and four multiplets corresponding to an ABCD spin system assigned to the cyclopentadienyl and fulvalene groups, respectively. The phenyl protons appear as eight signals and are readily assignable (see Exp. Sect.). These spectroscopic data indicate the formation of a dinuclear zirconium species with a chiral ligand arrangement around each equivalent zirconium centre, with the bridging hydrazido ligand centrally disposed and located perpendicular to the C_{ipso}−C_{ipso} bond of the fulvalene unit and the cyclopentadienyl and chloro ligands in a *cis* disposition. This arrangement makes the two phenylhydrazido rings nonequivalent, generating eight resonances for the corresponding protons. When **2a** is maintained in toluene solution at room temperature, a new compound **2b** is formed within 2 h (Scheme 1). Its ^1H NMR spectrum shows the same set of resonances for the cyclopentadienyl and the fulvalene protons observed for **2a**, but they are slightly shifted (see Exp. Sect.). However, the phenyl protons appear as four signals (two doublets of doublets and two doublets of triplets with coupling constant values of $^3J_{H\text{-}H}$ = 8 Hz and $^4J_{H\text{-}H}$ = 0.97 Hz). Compounds **2a** and **2b** offer identical elemental analyses, IR and mass spectroscopic data. These observations may be explained by an enantiomeric isomerization process, if the ligands bonded to one of the zirconium centres re-coordinate in **2a** to give the thermodynamically more stable **2b**, in which the cyclopentadienyl and chloro ligands adopt a *trans* disposition. While the nature of the structure of **1** and **2** is of interest, all attempts to obtain crystals of crystallographic quality were unsuccessful.

Terminal η^1-hydrazido(2−) coordination M=N−NR_2 has been well established for transition metal complexes.[12] There has been some concern about the nature of these species and it has been noted that these compounds appear closer to isodiazene (M−N=NR_2) than hydrazido(2−) derivatives.[13] Hydrazido as a bridging dianion ligand is much less common and has been observed in a few transition metal derivatives such as the dinuclear compounds $[W(NPh)Me_3]_2[\mu\text{-}(\eta^1,\eta^1\text{-}NH_2NH_2)][\mu\text{-}(\eta^2,\eta^2\text{-}NHNH)]$[14] and $[Sm(C_5Me_5)]_2[\mu\text{-}(\eta^2,\eta^2\text{-}NRNR)]$ (R = Ph, H).[15]

No reaction was observed when **2b** was treated with MeLi or MeMgCl in THF or toluene under varying conditions; the starting substances were always recovered. The lack of reactivity reflects the stability of this type of compound, with its coordinatively saturated metal centres decreasing its electrophilicity. Compound **1** must be consistent with a formal 18 valence electron species with 4 electrons donated from each μ-imido ligand to the "Zr_2" unit. The hydrazido group in **2** is considered as a 6-electron ligand, thereby also making this compound formally an 18 valence electron species.

μ-(η^1-C:η^2-C,N-Isocyanido) Derivatives

The (fulvalene)bis[chloro(cyclopentadienyl)zirconium] fragment "$(ZrCpCl)_2(C_{10}H_8)$" can provide an excellent support to promote uncommon ligand dispositions. Particularly interesting is the μ-isocyanido bonding mode found in the compounds $[Zr(\eta^5\text{-}C_5H_5)Cl]_2(\mu\text{-}CNR)[\mu\text{-}(\eta^5,\eta^5\text{-}C_{10}H_8)]$ (R = *t*Bu;[5c,5i] 2,6-$Me_2C_6H_3$ [6a]), which have an unsymmetrical bridging ligand, a μ-(η^1-C:η^2-C,N) 4-electron ligand (σ,π), between their zirconium atoms. We have reported the synthesis of complexes of this type by RNC addition to the dinuclear zirconium(III) derivative $[Zr(\eta^5\text{-}C_5H_5)(\mu\text{-}Cl)]_2[\mu\text{-}(\eta^5,\eta^5\text{-}C_{10}H_8)]$. Analogous dicyclopentadienyl compounds have also been described.[16]

Addition of RNC (R = *n*Bu, C_6H_{11}) to a toluene solution of $[Zr(\eta^5\text{-}C_5H_5)(\mu\text{-}Cl)]_2[\mu\text{-}(\eta^5,\eta^5\text{-}C_{10}H_8)]$ (molar ratio 1:1) results in an immediate colour change from violet to bright red. After work up, compounds $[Zr(\eta^5\text{-}C_5H_5)Cl]_2(\mu\text{-}CNR)[\mu\text{-}(\eta^5,\eta^5\text{-}C_{10}H_8)]$ [R = *n*Bu (**3**), C_6H_{11} (**4**)] were isolated in high yield (ca. 80%) (Scheme 2) as red solids, characterized by analytical and spectroscopic methods. Compound **4** was obtained as a partial toluene solvate, indicated by elemental analysis and ^1H NMR spectroscopy. These compounds are air- and moisture-sensitive and must be manipulated under dry conditions. They are soluble in benzene, toluene and chloroform but insoluble in alkanes. Characteristic absorptions at $\tilde{\nu}$ = 1656 [1650(sh)] and 1637 cm^{-1} due to ν(C=N) vibrations are observed in the IR spectra of **3** and **4**, similar to those found for other compounds of this type.[5i,6a,7c] The ^1H NMR spectra in $CDCl_3$ at room temperature show the expected two ABCD spin systems for the fulvalene protons and two signals for the cyclopentadienyl rings, consistent with a dinuclear species

with two zirconium atoms each in a different coordination environment. Characteristic resonances for the cyclohexyl and *n*-butyl groups are also observed. The spectrum of **3** also shows an AB spin system for the diastereotopic "N−CH_2" protons. Similar spectroscopic features were observed in the ^{13}C NMR spectra. The resonance for the isocyanide carbon atom (CN−) is observed at δ = 295.0 ppm in compound **3** but not observed for **4**.

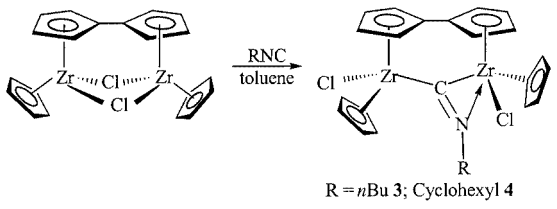

Scheme 2

Alkylation of $[Zr(\eta^5\text{-}C_5H_5)Cl]_2(\mu\text{-}CNR)[\mu\text{-}(\eta^5,\eta^5\text{-}C_{10}H_8)]$ (R = *t*Bu,[5i] *n*Bu, C_6H_{11}) with R′M [R′ = Me, $CH_2Si(CH_3)_3$, M = Li; R′ = $(PhCH_2)_2$, $(PhCH_2)Cl$, M = Mg] was also studied (Scheme 3). $[Zr(\eta^5\text{-}C_5H_5)Cl]_2(\mu\text{-}CNtBu)[\mu\text{-}(\eta^5,\eta^5\text{-}C_{10}H_8)]$ reacts with 1 equiv. of $PhCH_2MgCl$ or $(PhCH_2)_2Mg(THF)_2$ to afford an orange yellow oil. Its ^1H NMR spectrum in C_6D_6 indicated a mixture containing the two isomers of the monobenzyl derivatives $[Zr(\eta^5\text{-}C_5H_5)]_2(CH_2Ph)(Cl)(\mu\text{-}CNtBu)[\mu\text{-}(\eta^5,\eta^5\text{-}C_{10}H_8)]$ (**5** and **6**) in a 1:3 molar ratio. When the reaction was carried out with 2 equiv. or an excess of $PhCH_2MgCl$, a mixture of the monobenzyl compound **5** and the dibenzyl complex $[Zr(\eta^5\text{-}C_5H_5)(CH_2Ph)]_2(\mu\text{-}CNtBu)[\mu\text{-}(\eta^5,\eta^5\text{-}C_{10}H_8)]$ (**7**) (30%:70%) was obtained. In an attempt to isolate a pure monoalkyl complex, the bulkier $(CH_3)_3SiCH_2Li$ was used as an alkylating reagent, but the final results were similar to those found with the benzyl and the previously reported methyl reagents.[7c] The starting dichloro compound reacted with 1 or 2 equiv. of $(CH_3)_3SiCH_2Li$ in toluene at room temperature for 16 h to give a mixture of the monoalkyl complex $[Zr(\eta^5\text{-}C_5H_5)]_2[CH_2Si(CH_3)_3](Cl)(\mu\text{-}CNtBu)[\mu\text{-}(\eta^5,\eta^5\text{-}C_{10}H_8)]$ (**8**) and the dialkyl compound $[Zr(\eta^5\text{-}C_5H_5)]_2[CH_2Si(CH_3)_3]_2(\mu\text{-}CNtBu)[\mu\text{-}(\eta^5,\eta^5\text{-}C_{10}H_8)]$ (**9**). Moreover, when $[Zr(\eta^5\text{-}C_5H_5)Cl]_2(\mu\text{-}CNnBu)[\mu\text{-}(\eta^5,\eta^5\text{-}C_{10}H_8)]$ was treated in toluene with 2 equiv. of MeLi, the dimethyl complex $[Zr(\eta^5\text{-}C_5H_5)(CH_3)]_2(\mu\text{-}CNnBu)[\mu\text{-}(\eta^5,\eta^5\text{-}C_{10}H_8)]$ (**10**) was isolated as an analytically pure substance, unlike the mixture of the monomethyl and dimethyl compounds obtained in the methylation of $[Zr(\eta^5\text{-}C_5H_5)Cl]_2(\mu\text{-}CNtBu)[\mu\text{-}(\eta^5,\eta^5\text{-}C_{10}H_8)]$.[7c] Reaction of $[Zr(\eta^5\text{-}C_5H_5)Cl]_2(\mu\text{-}CNC_6H_{11})[\mu\text{-}(\eta^5,\eta^5\text{-}C_{10}H_8)]$ with MeLi in a molar ratio of 1:2 gave the dimethyl compound $[Zr(\eta^5\text{-}C_5H_5)(CH_3)]_2(\mu\text{-}CNC_6H_{11})[\mu\text{-}(\eta^5,\eta^5\text{-}C_{10}H_8)]$ (**13**), which was always obtained with small amounts of the monomethyl derivatives $[Zr(\eta^5\text{-}C_5H_5)]_2(CH_3)(Cl)(\mu\text{-}CNC_6H_{11})[\mu\text{-}(\eta^5,\eta^5\text{-}C_{10}H_8)]$ (**11** and **12**). Attempts to separate this mixture by repeated recrystallization were unsuccessful.

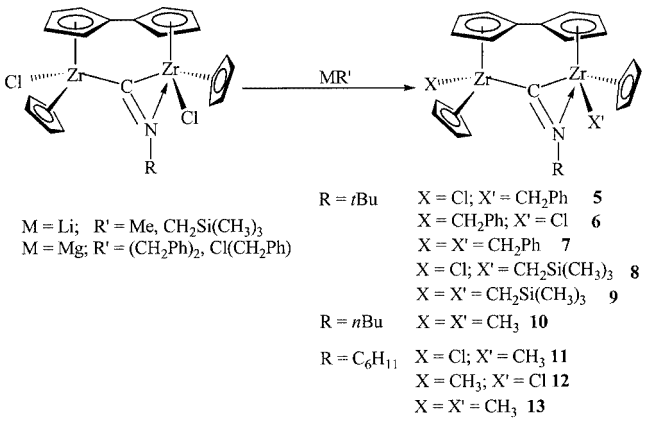

Scheme 3

Compounds **5**−**13** are moisture-sensitive but thermally stable in the solid state, allowing them to be stored under inert conditions for weeks. They are soluble in aromatic hydrocarbons, THF, dichloromethane and chloroform, but insoluble in diethyl ether and alkanes. The pairs of compounds obtained, **5/6**, **5/7** and **8/9**, and the compounds **11**−**13**, show the same solubility in all common solvents and therefore could not be separated. Consequently, they have been characterized by NMR spectroscopy but satisfactory elemental analyses were not obtained; **10** can be obtained as a pure compound and has been analytically and spectroscopically identified.

The ^1H NMR spectra of complexes **5**−**13** in C_6D_6 at room temperature show two ABCD spin systems (eight signals) for the fulvalene ligand and two signals for the cyclopentadienyl ring protons. The expected resonances for the protons of the isocyanide alkyl substituents are observed. The spectra of **5**−**9** show one singlet for the *tert*-butyl protons. Four signals are assigned to the *n*-butyl protons in **10** with the "NCH_2−" methylene groups as diastereotopic protons and four signals are assigned to the cyclohexyl protons in **13**. These spectroscopic data indicate the formation of dinuclear zirconium compounds with the metal atoms in nonequivalent coordination environments.

The "CH_2Ph" methylene group protons appear as AB spin systems with two doublets for **5** and **6** (δ = 2.05, 1.17 ppm and δ = 2.82, 2.50 ppm, respectively) and four doublets for **7** (δ = 2.82, 2.58, 2.15, 1.37 ppm) suggesting the presence of CH_2 diastereotopic groups. Two of the chemical shifts of the methylene groups in **7** (δ = 2.15 and 1.37 ppm) compare well with the signals for the same protons in **5** (δ = 2.05 and 1.17 ppm), while the other two methylene groups in **7** (δ = 2.82 and 2.58 ppm) compare with the corresponding signals in **6** (δ = 2.82 and 2.50 ppm). These spectroscopic features suggest that the CH_2 groups in each pair of compounds occupy very similar chemical environments and must be bonded to the same type of zirconium atom. The presence of the bridging isocyanido group can exert an important influence in the reactivity of these fulvalene derivatives. The η^2-side-on coordination of the isocyanido bridge[5i] to one of the zirconium atoms involves donation of the nitrogen atom's free electron pair to the metal centre to give an 18-electron valence shell. The increase of

the electronic density at this zirconium centre must cause shielding of the NMR signals for all of the directly bonded ligands.[7c] These observations allow the structures of **5** and **6** to be distinguished (Scheme 4).

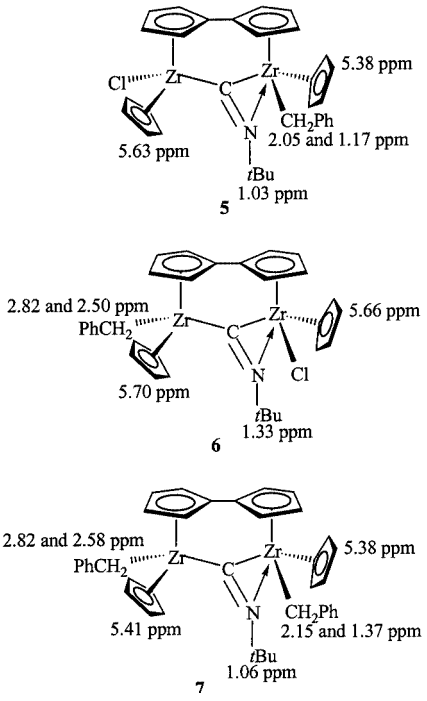

Scheme 4

Similar spectroscopic behaviour has been observed in the ^{1}H NMR spectrum (C_6D_6, room temperature) for the diastereotopic "CH_2SiMe_3" methylene group protons for compounds **8** and **9** (one and two AB spin systems respectively; see Exp. Sect.). Two markedly different chemical shifts are found for the methyl protons in the dimethyl derivatives **10** (δ = 0.29 and −0.37 ppm) and **13** (δ = 0.29 and −0.32 ppm).

These experimental results highlighted differences in the reactivity of the two Zr−Cl bonds present in the starting $[Zr(\eta^5\text{-}C_5H_5)Cl]_2(\mu\text{-}CNR)[\mu\text{-}(\eta^5,\eta^5\text{-}C_{10}H_8)]$ compounds and allow us to conclude that the ease of alkylation of the chloride ion bonded to the tetracoordinated zirconium atom is greater than the alkylation of the chloride ion bonded to the pentacoordinated zirconium atom. This proposal is consistent with the results obtained in the methylation reactions of the dichloro compound $[Zr(\eta^5\text{-}C_5H_5)Cl]_2(\mu\text{-}CN\textit{t}Bu)[\mu\text{-}(\eta^5,\eta^5\text{-}C_{10}H_8)]$.[7c]

Conclusion

This report shows that dinuclear zirconium(IV) complexes, containing one fulvalene and one additional group (imido, η^2,η^2-N,N-hydrazido or η^1-C:η^2-C,N-isocyanido) as bridging ligands, can be synthesized by adding neutral organic reagents (azobenzene, benzo[*c*]cinnoline, isocyanide) to the easily accessible zirconium(III) derivative $[Zr(\eta^5\text{-}C_5H_5)(\mu\text{-}Cl)]_2[\mu\text{-}(\eta^5,\eta^5\text{-}C_{10}H_8)]$. Alkylation reactions of the chloro(fulvalene)isocyanido complexes show important differences in the reactivity of both chloride ions present in the $[Zr(\eta^5\text{-}C_5H_5)Cl]_2(\mu\text{-}CNR)[\mu\text{-}(\eta^5,\eta^5\text{-}C_{10}H_8)]$ compounds.

Experimental Section

General Remarks: All manipulations were performed under argon using Schlenk and high-vacuum line techniques or a glovebox model HE-63. The solvents were purified by distillation under argon before use, by employing the appropriate drying/deoxygenating agent. Deuterated solvents were stored over activated 4 Å molecular sieves and degassed by several freeze-thaw cycles. Azobenzene, benzo[*c*]cinnoline, *n*-butyl isocyanide, cyclohexyl isocyanide, BzMgCl and MeLi (Aldrich) were purchased from commercial sources and used without further purification. $[Zr(\eta^5\text{-}C_5H_5)(\mu\text{-}Cl)]_2[\mu\text{-}(\eta^5,\eta^5\text{-}C_{10}H_8)]$,[4a] $[Zr(\eta^5\text{-}C_5H_5)Cl]_2(\mu\text{-}CN\textit{t}Bu)[\mu\text{-}(\eta^5,\eta^5\text{-}C_{10}H_8)]$,[5i] $(CH_3)_3SiCH_2Li$[17] and $Bz_2Mg(THF)_2$ [18] were prepared by known procedures. C,H, N microanalyses were performed with a Perkin−Elmer 240B and/or a Heraeus CHN-O-Rapid microanalyzer. IR spectra were recorded with a Perkin−Elmer Spectrum 2000 spectrophotometer by using KBr pellets; only selected IR data are reported. NMR spectra, measured at 25 °C, were recorded with a Varian Unity 300 (^{1}H at 300 MHz and ^{13}C at 75 MHz) and a 500 Plus (^{1}H at 300 MHz and ^{13}C at 125 MHz) spectrometer and chemical shifts are referenced to residual proton and carbon signals of the solvent.

$[Zr(\eta^5\text{-}C_5H_5)(\mu\text{-}NPh)]_2[\mu\text{-}(\eta^5,\eta^5\text{-}C_{10}H_8)]$ (1): 1.7 g (9.7 mmol) of PhN=NPh was added at room temperature to a solution of 5 g (9.7 mmol) of $[Zr(\eta^5\text{-}C_5H_5)(\mu\text{-}Cl)]_2[\mu\text{-}(\eta^5,\eta^5\text{-}C_{10}H_8)]$ in toluene (100 mL). The reaction mixture was heated under reflux (80 °C) and stirred for 12 h. The deep violet solution first turned dark yellow and then changed into a suspension of a yellow solid in an orange solution. After cooling, the yellow solid was separated by filtration and identified as $[Zr(\eta^5\text{-}C_5H_5)Cl_2]_2[\mu\text{-}(\eta^5,\eta^5\text{-}C_{10}H_8)]$ by IR spectroscopy and elemental analysis (1.8 g, 63% yield). The resulting solution was concentrated to 10 mL and cooled to −30 °C overnight to give compound **1** as a yellow-orange microcrystalline solid. The compound was recrystallised from toluene/hexane (1.4 g, 46% yield). ^{1}H NMR (500 MHz, C_6D_6, 25 °C): δ = 6.04, 5.65 (AA′BB′ spin system, 4 + 4 H, J = 2.7 Hz, $C_{10}H_8$), 5.97 (s, 10 H, C_5H_5), 7.18 (t, 4 H, Ph), 6.77 (t, 2 H, Ph), 6.04 (d, 4 H, Ph) ppm. ^{1}H NMR (500 MHz, $CDCl_3$, 25 °C): δ = 6.21 (s, 10 H, C_5H_5), 6.19, 6.05 (AA′BB′ spin system, 4 + 4 H, J = 2.7 Hz, $C_{10}H_8$), 7.07 (t, 4 H, Ph), 6.59 (t, 2 H, Ph), 5.95 (d, 4 H, Ph) ppm. $C_{32}H_{28}N_2Zr_2$ (623.06): calcd. C 61.69, H 4.50, N 4.50; found C 61.34, H 4.55, N 3.75.

$[Zr(\eta^5\text{-}C_5H_5)Cl]_2[\mu\text{-}(\eta^2,\eta^2\text{-}NC_6H_4C_6H_4N)][\mu\text{-}(\eta^5,\eta^5\text{-}C_{10}H_8)]$ (2): 1.2 g (6.8 mmol) of benzo[*c*]cinnoline was added at room temperature to a solution of 3.5 g (6.8 mmol) of $[Zr(\eta^5\text{-}C_5H_5)(\mu\text{-}Cl)]_2[\mu\text{-}(\eta^5,\eta^5\text{-}C_{10}H_8)]$ in toluene (100 mL). The reaction mixture was heated under reflux and stirred for 12 h. The deep violet solution slowly turned orange-yellow. After cooling and filtration, the resulting solution was concentrated to 10 mL and cooled to −30 °C overnight to give compound **2** as a yellow microcrystalline solid. The compound was recrystallised from toluene/hexane (2.8 g, 60% yield). **2a:** IR (KBr): $\tilde{\nu}$ = 568 cm^{-1} [ν(N−N)]. ^{1}H NMR (500 MHz, C_6D_6, 25 °C): δ = 6.93, 5.92, 5.82, 5.54 (ABCD spin system, 4 × 2 H, $C_{10}H_8$), 5.58 (s, 10 H, C_5H_5), 8.18 (dd, 1 H, Ph), 7.25 (dd, 1 H, Ph), 7.17 (dd, 1 H, Ph), 7.13 (t, 1 H, Ph), 7.04 (t, 1 H, Ph), 6.70

(dd, 1 H, Ph), 6.69 (t, 1 H, Ph), 6.67 (t, 1 H, Ph) ppm. ^{1}H NMR (500 MHz, $CDCl_3$, 25 °C): δ = 6.83, 6.65, 6.33, 5.83 (ABCD spin system, 4 × 2 H, $C_{10}H_8$), 5.71 (s, 10 H, C_5H_5), 7.68 (dd, 1 H, Ph), 7.59 (dd, 1 H, Ph), 7.46 (dd, 1 H, Ph), 7.27 (t, 1 H, Ph), 7.17 (t, 1 H, Ph), 7.08 (dd, 1 H, Ph), 6.91 (t, 1 H, Ph), 6.82 (t, 1 H, Ph) ppm. **2b:** IR (KBr): $\tilde{\nu}$ = 568 cm^{-1} [ν(N−N)]. ^{1}H NMR (500 MHz, C_6D_6, 25 °C): δ = 7.43, 6.97, 5.54, 5.17 (ABCD spin system, 4 × 2 H, $C_{10}H_8$), 5.51 (s, 10 H, C_5H_5), 7.61 [dd, $^3J_{H\text{-}H}$ = 8, $^4J_{H\text{-}H}$ = 0.97 Hz, 2 H, Ph(A)], 7.19 [dd, $^3J_{H\text{-}H}$ = 8, $^4J_{H\text{-}H}$ = 0.97 Hz, 2 H, Ph(D)], 7.11 [dt, $^3J_{H\text{-}H}$ = 8, $^4J_{H\text{-}H}$ = 0.97 Hz, 2 H, Ph(B)], 6.68 (dt, $^3J_{H\text{-}H}$ = 8, $^4J_{H\text{-}H}$ = 0.97 Hz, 2 H, Ph(C) ppm; the numbering assignment is shown in Scheme 5. ^{13}C NMR (125 MHz, C_6D_6, 25 °C). δ = 122.9, 121.0, 113.3, 110.4 ($C_{10}H_8$), 115.3 (C_5H_5), 101.2 (C_{ipso}, $C_{10}H_8$), 135.7, 131.6, 129.1 ppm, and signals collapsed by the C_6D_6 resonances. $C_{32}H_{26}Cl_2N_2Zr_2$ (691.95): calcd. C 55.54, H 3.79, N 4.05; found C 56.06, H 3.96, N 3.63.

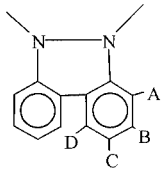

Scheme 5

[Zr(η^5-C_5H_5)Cl]$_2$(μ-CN*n*Bu)[μ-(η^5,η^5-$C_{10}H_8$)] (3): A solution of [Zr(η^5-C_5H_5)(μ-Cl)]$_2$[μ-(η^5,η^5-$C_{10}H_8$)] (1.00 g, 1.94 mmol) in 75 mL of toluene was treated at room temperature with *n*-butyl isocyanide (0.20 mL, 2.00 mmol). The violet solution turned red within an hour. After filtration, the solvent was completely removed in vacuo and the resulting red solid washed with *n*-hexane. After recrystallization from toluene/hexane, a sample of **3** suitable for analysis was obtained (1.04 g, 90%). IR (KBr): $\tilde{\nu}$ = 1656 [1650 (sh)] cm^{-1} [ν(C=N)]. ^{1}H NMR (300 MHz, $CDCl_3$, 25 °C): δ = 6.18, 5.82 (s, 2 × 5 H, C_5H_5), 6.41, 6.40, 6.28, 6.00, 5.63, 5.40, 4.83, 4.78 (two ABCD spin systems, 8 × 1 H, $C_{10}H_8$), 3.88, 3.35 (AB spin system, 2 × 1 H, N−CH_2−[CH$_2$]$_2$−CH$_3$), 1.85 (m, 2 H, N−CH$_2$−CH_2−CH$_2$−CH$_3$), 1.46 (m, 2 H, N−CH$_2$−CH$_2$−CH_2−CH$_3$), 1.03 (t, 3 H, N−CH$_2$−CH$_2$−CH$_2$−CH_3) ppm. ^{13}C NMR (75 MHz, $CDCl_3$, 25 °C): δ = 295.0 (*C*N*n*Bu), 133.2, 120.4 [C_{ipso}, $C_{10}H_8$], 122.3, 117.1, 105.4, 102.7, 101.8, 101.4, 100.1, 95.6 ($C_{10}H_8$), 109.76, 108.62 (C_5H_5), 57.7, 31.7, 20.8, 14.0 (CN*nBu*) ppm. $C_{25}H_{27}Cl_2NZr_2$ (594.87): calcd. C 50.48, H 4.57, N 2.35; found C 50.01, H 4.67, N 2.15.

[Zr(η^5-C_5H_5)Cl]$_2$(μ-CNC_6H_{11})[μ-(η^5,η^5-$C_{10}H_8$)] (4): According to the procedure described for **3**, 1.93 g (3.75 mmol) of [Zr(η^5-C_5H_5)(μ-Cl)]$_2$[μ-(η^5,η^5-$C_{10}H_8$)] and 0.48 mL (3.77 mmol) of cyclohexyl isocyanide were allowed to react in 150 mL of toluene to give **4** (2.25 g, 97%) as a partial toluene solvate, indicated by elemental analysis and ^{1}H NMR spectroscopy. IR (KBr): $\tilde{\nu}$ = 1637 cm^{-1} [ν(C=N)]. ^{1}H NMR (300 MHz, $CDCl_3$, 25 °C): δ = 6.18, 5.81 (s, 2 × 5 H, C_5H_5), 6.41, 6.37, 6.28, 5.98, 5.64, 5.42, 4.96, 4.82 (two ABCD spin systems, 8 × 1 H, $C_{10}H_8$), 3.85, 1.86, 1.29 (C_6H_{11}) ppm. ^{13}C NMR (75 MHz, $CDCl_3$, 25 °C): δ = 119.9, 113.5 (C_{ipso}, $C_{10}H_8$), 123.4, 117.5, 104.8, 102.5, 101.8, 101.1, 100.8, 95.7 ($C_{10}H_8$), 109.8, 109.0 (C_5H_5), 67.5, 32.8, 32.3, 25.2 [CN(C_6H_{11})] ppm. $C_{27}H_{29}Cl_2NZr_2$·1/2toluene (666.98): calcd. C 54.88, H 4.95, N 2.10; found C 54.74, H 5.01, N 2.06.

[Zr(η^5-C_5H_5)]$_2$(CH_2Ph)(Cl)(μ-CN*t*Bu)[μ-(η^5,η^5-$C_{10}H_8$)] (5 and 6): 1.23 mL of a 2 M solution of BzMgCl in THF (2.45 mmol) was added to a solution of [Zr(η^5-C_5H_5)Cl]$_2$(μ-CN*t*Bu)[μ-(η^5,η^5-$C_{10}H_8$)] (1.46 g, 2.45 mmol) in toluene (50 mL) at −78 °C. The reaction mixture was warmed to room temperature and stirred for 18 h with formation of an $MgCl_2$ precipitate. After filtration, the solvent was removed and an orange yellow solid was obtained which was washed with diethyl ether and hexane. Recrystallization from toluene/hexane gave an orange yellow microcrystalline solid. **5** and **6** have the same composition and therefore they must have an identical elemental analysis. However, the isolated final solid consisted mainly of **5** and **6**, but it contained a small amount of unidentified impurities that could not be removed, and satisfactory elemental analysis was not obtained. Spectroscopic data showed the presence of **5** (25%) and **6** (75%). **6:** ^{1}H NMR (500 MHz, C_6D_6, 25 °C): δ = 7.40−6.98 (m, 5 H, CH_2*Ph*), 5.70, 5.66 (s, 2 × 5 H, C_5H_5), 6.50, 6.36, 5.76, 5.65, 5.05, 4.46, 4.41, 4.40 (two ABCD spin systems, 8 × 1 H, $C_{10}H_8$), 2.82, 2.50 (AB spin system, 2 × 1 H, CH_2Ph), 1.03 (s, 9 H, *t*BuNC) ppm. **5:** ^{1}H NMR (500 MHz, C_6D_6, 25 °C): δ = 7.40−6.98 (m, 5 H, CH_2*Ph*), 5.63, 5.38 (s, 2 × 5 H, C_5H_5), 5.57, 5.55, 5.45, 5.27, 5.06, 4.86, 4.60, 4.48 (two ABCD spin systems, 8 × 1 H, $C_{10}H_8$), 2.05, 1.17 (AB spin system, 2 × 1 H, CH_2Ph), 1.33 (s, 9 H, *t*BuNC) ppm.

[Zr(η^5-C_5H_5)]$_2$(CH_2Ph)(Cl)(μ-CN*t*Bu)[μ-(η^5,η^5-$C_{10}H_8$)] (5) and [Zr(η^5-C_5H_5)(CH_2Ph)]$_2$(μ-CN*t*Bu)[μ-(η^5,η^5-$C_{10}H_8$)] (7): According to the same procedure described for the preparation of **5** + **6**, using 2.46 mL of a 2 M solution of BzMgCl in THF (4.90 mmol) and 1.46 g (2.45 mmol) of [Zr(η^5-C_5H_5)Cl]$_2$(μ-CN*t*Bu)[μ-(η^5,η^5-$C_{10}H_8$)] a mixture of **5** (30%) + **7** (70%) was obtained and spectroscopically characterized. **5** and **7** have the same solubility in all common solvents. They could not be separated and satisfactory elemental analyses were not obtained. **7:** ^{1}H NMR (500 MHz, C_6D_6, 25 °C): δ = 7.40−6.98 (m, 5 H, CH_2*Ph*), 5.41, 5.38 (s, 2 × 5 H, C_5H_5), 6.60, 6.50, 5.29, 5.14, 4.99, 4.48, 4.46, 4.40 (two ABCD spin systems, 8 × 1 H, $C_{10}H_8$), 2.82, 2.58, 2.15, 1.37 (two AB spin systems, 4 × 1 H, CH_2Ph), 1.06 (s, 9 H, *t*BuNC) ppm.

[Zr(η^5-C_5H_5)]$_2$[CH_2Si(CH_3)$_3$](Cl)(μ-CN*t*Bu)[μ-(η^5,η^5-$C_{10}H_8$)] (8) and [Zr(η^5-C_5H_5)]$_2$[CH_2Si(CH_3)$_3$]$_2$(μ-CN*t*Bu)[μ-(η^5,η^5-$C_{10}H_8$)] (9): 0.09 g (1.0 mmol) of (CH_3)$_3$SiCH_2Li was added to a solution of [Zr(η^5-C_5H_5)Cl]$_2$(μ-CN*t*Bu)[μ-(η^5,η^5-$C_{10}H_8$)] (0.6 g, 1.0 mmol) in toluene (50 mL) at −78 °C. The reaction mixture was warmed to room temperature and stirred for 16 h with the formation of an LiCl precipitate. After filtration, the solvent was removed and a red solid was obtained which was washed with diethyl ether and hexane. Recrystallization from toluene/hexane gave an orange microcrystalline solid identified as a mixture of **8** + **9** (molar ratio 2:1) with the presence of a small amount of the starting zirconium compound. When 0.19 g (2.0 mmol) of (CH_3)$_3$SiCH_2Li was used to react with 0.6 g (1.0 mmol) of [Zr(η^5-C_5H_5)Cl]$_2$(μ-CN*t*Bu)[μ-(η^5,η^5-$C_{10}H_8$)] a mixture of **8** + **9** (molar ratio 1:3) with no traces of the starting zirconium compound was obtained. **8** and **9** have the same solubility in all common solvents. They could not be separated and satisfactory elemental analyses were not obtained. Spectroscopic data showed the presence of **8** (25%) + **9** (75%). **8:** ^{1}H NMR (500 MHz, C_6D_6, 25 °C): δ = 5.64, 5.62 (s, 2 × 5 H, C_5H_5), 6.58, 6.26, 5.72, 5.50, 5.40, 5.39, 4.86, 4.70 (two ABCD spin systems, 8 × 1 H, $C_{10}H_8$), 1.37 (s, 9 H, CN*t*Bu), 0.20 (s, 9 H, SiMe_3), −0.19, −0.40 (AB spin system, CH_2SiMe$_3$) ppm. **9:** ^{1}H NMR (500 MHz, C_6D_6, 25 °C): δ = 5.65, 5.47 (s, 2 × 5 H, C_5H_5), 6.38, 6.32, 5.60, 5.44, 5.20, 4.58, 4.55, 4.40 (two ABCD spin systems, 8 × 1 H, $C_{10}H_8$), 1.08 (s, 9 H, CN*t*Bu), 0.42, 0.29 (s, 9 × 2 H, SiMe_3), 0.33, 0.11, −0.05, −0.37 (two AB spin systems, CH_2SiMe$_3$) ppm.

[Zr(η^5-C_5H_5)(CH_3)]$_2$(μ-CN*n*Bu)[μ-(η^5,η^5-$C_{10}H_8$)] (10): 1.12 mL of a 1.50 M solution of LiMe in diethyl ether (1.70 mmol) was added at −78 °C to a solution of [Zr(η^5-C_5H_5)Cl]$_2$(μ-CN*n*Bu)[μ-(η^5,η^5-

$C_{10}H_8$)] (0.50 g, 0.84 mmol) in toluene (50 mL). The reaction mixture was stirred for 30 min and warmed to room temperature. After filtration, the solvent was removed and an orange-yellow solid was obtained. Recrystallization from toluene/hexane gave **10** as a microcrystalline solid (0.21 g, 46%). IR (KBr): $\tilde{\nu}$ = 1660 [1620 (sh)] cm^{-1} [ν(C=N)]. ^1H NMR (500 MHz, C_6D_6, 25 °C): δ = 5.58, 5.44 (s, 2 × 5 H, C_5H_5), 5.97, 5.94, 5.36, 5.33, 5.13, 4.57, 4.42, 4.12 (two ABCD spin systems, 8 × 1 H, $C_{10}H_8$), 3.41, 2.89 (AB spin system, $N-CH_2-[CH_2]_2-CH_3$), 1.57 (m, $N-CH_2-CH_2-CH_2-CH_3$), 1.23 (m, $N-CH_2-CH_2-CH_2-CH_3$), 0.89 (t, $N-CH_2-CH_2-CH_2-CH_3$), 0.29, −0.37 (s, $Zr-CH_3$) ppm. ^{13}C NMR (125 MHz, C_6D_6, 25 °C): δ = 116.2, 111.9 (C_{ipso}, $C_{10}H_8$), 116.6, 110.0, 101.8, 101.0, 99.9, 97.6, 96.7, 92.8 ($C_{10}H_8$), 105.7, 105.6 (C_5H_5), 57.9, 32.3, 21.0, 14.2 (CN*nBu*), 13.4, 9.5 ($Zr-CH_3$) ppm. $C_{27}H_{33}NZr_2$ (554.04): calcd. C 58.54, H 5.96, N 2.53; found C 58.11, H 6.12, N 2.29.

$[Zr(\eta^5\text{-}C_5H_5)]_2(CH_3)(Cl)(\mu\text{-}CNC_6H_{11})[\mu\text{-}(\eta^5,\eta^5\text{-}C_{10}H_8)]$ (11 + 12) and $[Zr(\eta^5\text{-}C_5H_5)(CH_3)]_2(\mu\text{-}CNC_6H_{11})[\mu\text{-}(\eta^5,\eta^5\text{-}C_{10}H_8)]$ (13): 1.0 mL of a 1.50 M solution of MeLi in diethyl ether (1.5 mmol) was added to a solution of $[Zr(\eta^5\text{-}C_5H_5)Cl]_2(\mu\text{-}CNC_6H_{10})[\mu\text{-}(\eta^5,\eta^5\text{-}C_{10}H_8)]$ (0.5 g, 0.75 mmol) in toluene (50 mL) at −78 °C. The reaction mixture was warmed to room temperature and stirred for 16 h with formation of an LiCl precipitate. After filtration, the solvent was removed and a red solid was obtained which was washed with hexane. Recrystallization from toluene/hexane gave a red solid identified by NMR spectroscopy as a mixture of **11** + **12** + **13** (molar ratio 1:1:4). They could not be separated and satisfactory elemental analyses were not obtained. **13:** ^1H NMR (500 MHz, C_6D_6, 25 °C): δ = 5.60, 5.43 (s, 2 × 5 H, C_5H_5), 5.96, 5.94, 5.36, 5.32, 5.15, 4.60, 4.58, 4.19 (two ABCD spin systems, 8 × 1 H, $C_{10}H_8$), 3.60 (m, 1 H, *ipso*-C_6H_{11}), 2.00−1.00 (C_6H_{11}), 0.29, −0.32 (s, $Zr-CH_3$) ppm.^{13}C NMR (125 MHz, C_6D_6, 25 °C): δ = 115.9, 111.7 (C_{ipso}, $C_{10}H_8$), 117.4, 110.4, 101.7, 100.8, 99.2, 98.0, 97.7, 92.9 ($C_{10}H_8$), 106.0, 105.6 (C_5H_5), 65.8, 33.8, 33.1, 25.8 (C_6H_{11}), 14.4, 9.8 ($Zr-CH_3$) ppm.

Acknowledgments

Financial support by DGICYT (Project PB97-0776) is gratefully acknowledged. M. G. M. acknowledges Comunidad de Madrid (CAM) for the award of a Fellowship.

[1] [1a] P. C. Wailes, R. S. P. Coates, H. Weigold, *Organometallic Chemistry of Titanium, Zirconium and Hafnium*, Academic Press, New York, **1974**. [1b] D. J. Cardin, M. F. Lappert, C. L. Raston, P. I. Riley, in *Comprehensive Organometallic Chemistry* (Eds.: G. Wilkinson, F. G. A. Stone, E. W. Abel), Pergamon, Oxford, **1982**, vol. 3. [1c] D. J. Cardin, M. F. Lappert, C. L. Raston, *Chemistry of Organo-Zirconium and -Hafnium Compounds*, John Wiley & Sons, New York, **1986**.[1d] *Comprehensive Organometallic Chemistry II. A Review of the Literature* (Eds.: E. W. Abel, F. G. A. Stone, G. Wilkinson), Pergamon, Oxford, **1994**, vol. 4.

[2] [2a] S. Barlow, D. O'Hare, *Chem. Rev.* **1997**, *97*, 637−669. [2b] D. Astruc, *Acc. Chem. Res.* **1997**, *30*, 383−391.

[3] [3a] W.-q. Weng, A. M. Arif, R. D. Ernst, *Organometallics* **1998**, *17*, 4240−4248. [3b] Y. K. Kang, K. S. Shin, S.-G. Lee, I. S. Lee, Y. K. Chung, *Organometallics* **1999**, *18*, 180−186 and references cited therein. [3c] C. Elschenbroich, O. Schiemann, O. Burghaus, K. Harms, J. Pebler, *Organometallics* **1999**, *18*, 3273−3277.

[4] [4a] T. V. Ashworth, T. Cuenca, E. Herdtweck, W. A. Herrmann, *Angew. Chem. Int. Ed. Engl.* **1986**, *25*, 289−290. [4b] S. Gambarotta, M. Y. Chiang, *Organometallics* **1987**, *6*, 897−899.

[5] [5a] T. Cuenca, W. A. Herrmann, T. V. Ashworth, *Organometallics* **1986**, *5*, 2514−2516. [5b] W. A. Herrmann, T. Cuenca, U. Küsthardt, *J. Organomet. Chem.* **1986**, *309*, C15−C17. [5c] W. A. Herrmann, T. Cuenca, B. Menjón, E. Herdtweck, *Angew. Chem. Int. Ed. Engl.* **1987**, *26*, 697−699. [5d] M. M. Rohmer, M. Benard, *Organometallics* **1991**, *10*, 157−163. [5e] Y. Wielstra, S. Gambarotta, A. Meetsma, J. L. de Boer, *Organometallics* **1989**, *8*, 250−251. [5f] Y. Wielstra, S. Gambarotta, A. Meetsma, A. L. Spek, *Organometallics* **1989**, *8*, 2948−2952. [5g] Y. Wielstra, A. Meetsma, S. Gambarotta, S. Khan, *Organometallics* **1990**, *9*, 876−879. [5h] Y. Wielstra, S. Gambarotta, A. L. Spek, W. J. J. Smeets, *Organometalics* **1990**, *9*, 2142−2148. [5i] W. A. Herrmann, B. Menjón, E. Herdtweck, *Organometallics* **1991**, *10*, 2134−2142.

[6] [6a] T. Cuenca, R. Gómez, P. Gómez-Sal, G. M. Rodríguez, P. Royo, *Organometallics* **1992**, *11*, 1229−1234. [6b] L. M. Alvaro, J. C. Flores, T. Cuenca, P. Royo, M. A. Pellinghelli, A. Tiripicchio, *Organometallics* **1992**, *11*, 3301−3306. [6c] A. Cano, T. Cuenca, G. Rodríguez, P. Royo, C. Cardin, D. J. Wilcok, *J. Organomet. Chem.* **1993**, *447*, 51−57. [6d] A. Cano, T. Cuenca, M. Galakhov, G. M. Rodríguez, P. Royo, C. Cardin, M. A. Convery, *J. Organomet. Chem.* **1995**, *493*, 17−25. [6e] M. González-Maupoey, G. M. Rodríguez, T. Cuenca, *J. Organomet. Chem.* **2001**, *645*, 112−117.

[7] [7a] M. Bochmann, T. Cuenca, D. T. Hardy, *J. Organomet. Chem.* **1994**, *484*, C10−C12. [7b] T. Cuenca, M. Galakhov, G. Jiménez, E. Royo, P. Royo, *J. Organomet. Chem.* **1997**, *543*, 209−215. [7c] E. Royo, M. Galakhov, P. Royo, T. Cuenca, *Organometallics* **2000**, *19*, 3347−3353. [7d] E. Royo, M. Galakhov, P. Royo, T. Cuenca, *Organometallics* **2000**, *19*, 5559−5567. [7e] E. Royo, P. Royo, T. Cuenca, M. Galakhov, *J. Organomet. Chem.* **2001**, *634*, 177−184.

[8] D. J. Arney, M. A. Bruck, S. R. Huber, D. E. Wigley, *Inorg. Chem.* **1992**, *31*, 3749−3755 and references cited there in.

[9] [9a] J. E. Hill, R. D. Profilet, P. E. Fanwick, I. P. Rothwell, *Angew. Chem. Int. Ed. Eng.* **1990**, *29*, 664−665. [9b] J. E. Hill, P. E. Fanwick, I. P. Rothwell, *Inorg. Chem.* **1991**, *30*, 1143−1144. [9c] R. Duchateau, A. J. Willians, S. Gambarotta, M. Y. Chiang, *Inorg. Chem.* **1991**, *30*, 4863−4866.

[10] R. Gómez, T. Cuenca, P. Royo, M. A. Pellinghelli, A. Tiripichio, *Organometallics* **1991**, *10*, 1505−1510.

[11] [11a] S. Jambarotta, C. Floriani, A. Chiesi-Villa, C. Guastini, *J. Am. Chem. Soc.* **1983**, *105*, 7295−7301. [11b] P. J. Walsh, F. J. Hollander, R. G. Bergman, *J. Am. Chem. Soc.* **1988**, *110*, 8729−8731. [11c] P. J. Walsh, F. J. Hollander, R. G. Bergman, *Organometallics* **1993**, *12*, 3705−3723. [11d] W. J. Grigsby, M. M. Olmstead, P. P. Power, *J. Organomet. Chem.* **1996**, *513*, 173−180.

[12] [12a] F. A. Cotton, G. Wilkinson, C. A. Murillo, *Advanced Inorganic Chemistry*, 6th ed., John Wiley and Sons, New York, **1999**. [12b] N. N. Greenwood, A. Earnshaw, *Chemistry of the Elements*, 2nd ed., Butterworth-Heinemann, Oxford, **1998**. [12c] A. J. Blake, J. M. McInnes, P. Mountford, G. I. Nikonov, D. Swallow, D. J. Watkin, *J. Chem. Soc., Dalton Trans.* **1999**, 379−391. [12d] J. L. Thorman, L. K. Woo, *Inorg. Chem.* **2000**, *39*, 1301−1304.

[13] J. R. Dilworth, J. Zubieta, J. R. Hyde, *J. Am. Chem. Soc.* **1982**, *104*, 365−367.

[14] L. Blum, I. D. Willians, R. R. Schrock, *J. Am. Chem. Soc.* **1984**, *106*, 8316−8317.

[15] [15a] W. J. Ewans, D. K. Drummond, L. R. Chamberlain, R. J. Doedens, S. G. Bott, H. Zhang, J. L. Atwood, *J. Am. Chem. Soc.* **1988**, *110*, 4983−4994. [15b] W. J. Evans, G. Kociok-Köhn, V. S. Leong, J. W. Ziller, *Inorg. Chem.* **1992**, *31*, 3592−3600.

[16] D. Röttger, J. Pflug, G. Erker, S. Kotila, R. Fröhlich, *Organometallics* **1996**, *15*, 1265−1267.

[17] C. Tessiers-Yoyng, O. T. Beachley, Jr, *Inorg. Synth.* **1986**, *24*, 95−97.

[18] R. R. Schrock, *J. Organomet. Chem.* **1972**, *122*, 209.

Received December 5, 2001
[I01500]

Synthesis and Structure of Diboraporphyrinogenes

Anke Eckert,[a] Hans Pritzkow,[a] and Walter Siebert*[a]

Dedicated to Prof. Dr. Robert Corriu

Keywords: Boranes / Boraporphyrinogens / Porphyrins / Macrocycles

Reactions of 5,5′-dilithiated 1,1-bis(2-thienyl)ethane (**3**) with different substituted dichloroboranes led to the novel 5,15-diboraporphyrinogenes **5**–**8**, in good yields. Amino groups at the boron atoms stabilize the macrocycles **5**–**7**, whereas the first organyl-stabilized diboraporphyrinogene **8** contains the 2,3,5,6-tetramethylphenyl substituent at the boron atoms. A [3+1] approach yields the 5,10-diboraporphyrinogene **13** by treating 2,5-bis[1-(5-lithio-2-thienyl)ethyl]thiophene (**4**) with the 2,5-diborylthiophene derivative **9**. Analogously, the mixed 5,10-diboraporphyrinogenes **15** and **16** are formed from **4** and 2,5-diborylfuran **11** and 2,5-diboryl-*N*-methylpyrrole **12**, respectively. The constituents of the new compounds follow from spectroscopic and structural data.

(© Wiley-VCH Verlag GmbH, 69451 Weinheim, Germany, 2002)

Introduction

Different syntheses for porphyrins are known: 5,10,15,20-Tetraphenylporphyrin is formed in a one-pot reaction of pyrrole with benzaldehyde in the presence of a catalyst.[1] The [2+2] approach uses dipyrromethanes[2] or dipyrromethenes.[3] In a [3+1] formation of porphyrin a 2,5-difunctionalized pyrrole reacts with a tripyrrolic species to produce the macrocycle.[4] The latter two types of porphyrin formation are used for the synthesis of diboraporphyrinogenes.

The chemistry of porphyrinogenes containing thiophene, furan and *N*-protected pyrrole instead of pyrrole has been studied intensely since the isolation of the first chalcogen porphyrinogene by Johnson et al. in 1971.[5] The heteroatom analogs **A** of the porphyrin may be regarded as bridged [20]annulenes having a paratropic ring current.[6] They are oxidized to yield dicationic aromatic compounds having diatropic ring currents.[7]

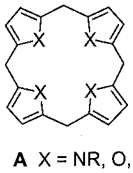

A X = NR, O, S

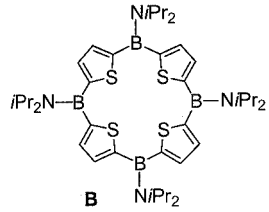

B

Different boron-containing porphyrins and porphyrinogenes have been synthesized. Recently, Corriu, Douglas, Siebert et al.[8] reported the first tetraboratetrathiaporphyrinogene **B**, and porphyrins with boron atoms in side chains have been used for BNCT (boron neutron capture therapy) studies.[9] Boryl and diborane(4)-diyl groups bridging the nitrogen atoms[10] have been incorporated into porphyrins.

The tetraboratetrathiaporphyrinogene **B** is nonplanar in the solid and has no delocalized electrons in the macrocycle. In solution a magnetic ring current or an electronic interaction of the thiophene units through the boron atoms can be ruled out. Compound **B** exhibits an ^{11}B NMR signal at δ = 40 ppm, which is expected for diaryl(dialkylamino)boranes. Attempts to reduce **B** to the dianion $\mathbf{B}^{2-}$ and to form metal complexes of the macrocycle have not been successful.

We are interested in the synthesis and characterization of diboraporphyrins, in their electronic structures and in the ligand properties of the diboraporphyrinogenes **C** and **D**, which formally derive from **A** by exchange of two *meso*-carbon atoms for two boron atoms. The empty p_z orbitals of the boron atoms may allow macrocyclic conjugation when **C** and **D** are deprotonated to give dianions. The formation of silyl- and stannyl-bridged macrocycles has been reported.[11]

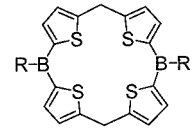

C

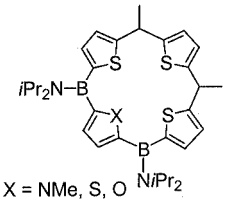

D X = NMe, S, O

[a] Anorganisch-Chemisches Institut der Universität Heidelberg, Im Neuenheimer Feld 276, 69120 Heidelberg, Germany
Fax: (internat.) + 49-(0)6221/545-609
E-mail: ci5@ix.urz.uni-heidelberg.de

Results and Discussion

Synthesis of Diboraporphyrinogenes

Liquid 1,1-bis(2-thienyl)ethane (**1**) is formed[12] in 39% yield by treating thiophene and paraldehyde with a solution of 40% HF. After distillation of **1**, a dark residue is obtained, probably a mixture of thiophene and the aldehyde condensation products (Scheme 1). Under the same conditions we obtained a mixture of **1** and **2** in a ratio of 5:7; 28.3% of thiophene reacted to give **1** and **2** in 42 and 58% yield, respectively. Deprotonation of **1** with butyllithium in diethyl ether at room temperature leads to 1,1-bis(5-lithio-2-thienyl)ethane (**3**). Under these conditions it is not necessary to use a solvent mixture of hexane and *N*,*N*,*N*′,*N*′-tetramethylethylenediamine (tmeda) as proposed.[8,13] Due to its high reactivity **3** is prepared in situ for the synthesis of the macrocycles **5**−**8**.

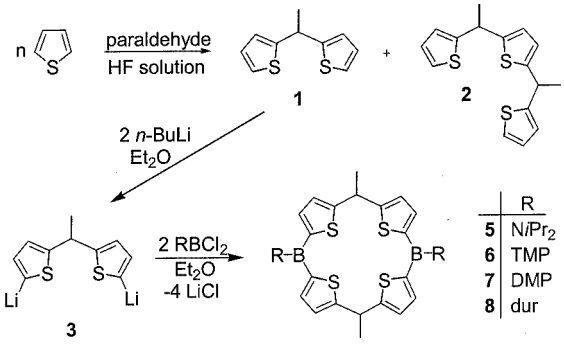

Scheme 1

Reaction of **3** with iPr_2N-BCl_2 leads to the yellow, air- and moisture-sensitive tetrathiadiboraporphyrinogene **5** in 95% yield. Its composition follows from spectroscopic data and its structure is confirmed by an X-ray diffraction analysis. In the solid **5** has a center of inversion and is nonplanar, which may prevent possible electron delocalization. The observed B−C distances of 1.58(2) Å are in the range expected for B−C single bonds (1.56−1.60 Å). The short B−N distance of 1.40(1) Å results from the donor effect of the nitrogen atom. In the thienyl ring the bond lengths C1−C2, C3−C4, C5−C6 and C7−C8 are smaller than C2−C3 and C6−C7, which may indicate a localized π system[14] and no electronic interaction between the thiophene units across the boron atoms (Figure 1).

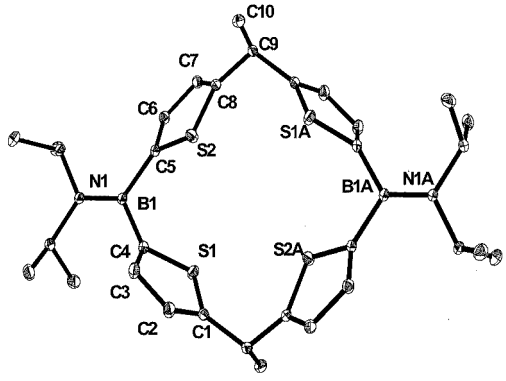

Figure 1. Molecular structure of **5** in the crystal, selected bond lengths [Å] and angles [°]: C1−C2 1.358(2), C2−C3 1.426(2), C4−B1 1.584(2), B1−N1 1.401(1), B1−C5 1.575(2); C4−B1−N1 124.56(10), C5−B1−N1 122.23(10), C5−B1−C4 113.20(9)

The ^1H NMR spectrum of **5** exhibits the expected doublet and septuplet of the isopropyl substituent, the doublet and quadruplet of the bridging $HCCH_3$ group and the two doublets of the thiophene protons at δ = 6.78 and 6.84 ppm, shifted high-field by 0.4 ppm relative to those of **1**. Similar shifts have been explained by a π interaction of the heterocycle with the boryl substituent.[15] In the ^{11}B NMR spectrum a broad signal appears at δ = 35 ppm, indicating a B−N π interaction. The ^{13}C NMR spectrum shows signals for the $HCCH_3$ groups at δ = 14.5 and 50.3 ppm, the signals of the isopropylamino substituents appear at δ = 25.3 and 37.1 ppm. For the thienyl rings three sharp and one broad signal for the *ipso*-carbon atoms are observed.

Attempts to replace the diisopropylamino substituents in **5** with $AlMe_3$ and MeOH were not successful; instead cleavage of the macrocycle occurred. We could not obtain any metal complexes of **5** with rhodium, ruthenium and silver reagents.

Treatment of **3** with dichloro(2,2′,6,6′-tetramethylpiperidyl)borane and dichloro(2,6-dimethylpiperidyl)borane yielded the yellow 5,15-diboraporphyrinogenes **6** and **7** in 51 and 60% yield, respectively. As for **5** and **8** (see below), the macrocycles **6** and **7** are air- and moisture-sensitive. Their ^{11}B NMR spectra exhibit broad signals at δ = 43 ppm (**6**) and δ = 42 ppm (**7**), which appear in the same region as that of the tetrathiatetraboraporphyrinogene **B**.[8] Because of the amino substituents at the boron atoms, the tetrathia-5,15-diboraporphyrinogenes **5**−**7** are electronically saturated due to the π interactions with the nitrogen atoms.

In order to obtain a sterically rather than an electronically stabilized macrocycle we prepared the first aryl-stabilized tetrathia-5,15-diboraporphyrinogene **8**, in 45% yield by treating **3** with dichloro(2,3,5,6-tetramethylphenyl)borane. In yellow **8** the boron atoms are sterically protected by the duryl substituents (dur), because the ring planes are perpendicular to the plane of the trigonal-planar arranged boryl groups [^{11}B NMR: δ = 70 (br)]. Compound **8** is an interesting molecule for deprotonation of the 10,20-positions. If we could deprotonate **8** to obtain the dianion $[\mathbf{8} - 2\ H^+]^{2-}$, we may create a conjugated π system in the macrocycle.

Deprotonation of **2**, analogously to **1**, forms the dilithio compound **4** as a red solution which reacts with the 2,5-bis(boryl)thiophenes **9**[16] and **10** at low temperature to give the tetrathia-5,10-diboraporphyrinogenes **13** and **14** as yellow solids in 61 and 62% yield, respectively (Scheme 2). Applying the [3+1] method for the synthesis of porphyrins it is possible to prepare mixed porphyrinogenes. The reaction of **4** with the 2,5-bis(boryl)furan **11** and 2,5-bis(boryl)-*N*-methylpyrrole **12** in diethyl ether leads to the formation of **15** and **16** in 40 and 47% yield, respectively. Their ^{11}B NMR

signals appear in the expected region (δ = 39, 43 ppm) as (amino)dithienylboranes (δ = 38 ppm).[17]

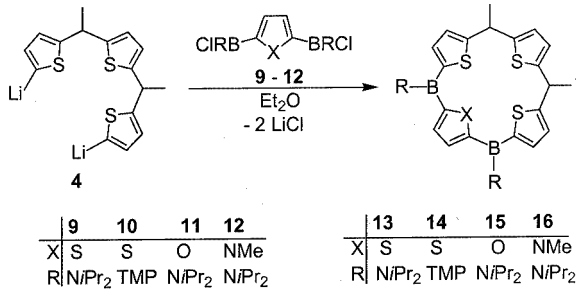

Scheme 2

The 5,10-diboraporphyrinogenes **13**−**16** are yellow solids, sensitive to air and moisture. They show similar properties to those of the 5,15-diboraporphyrinogenes **5**−**8**. It was not possible to replace the boron substituent with $AlMe_3$ or MeOH without destruction of the macrocycles. Furthermore, attempts to obtain metal complexes with ruthenium, rhodium or silver reagents were unsuccessful. Treatment of **13**−**16** with tricarbonyltris(acetonitrile)-chromium did not lead to a macrocyclic tricarbonyl(thiophene)chromium complex.

Conclusion

The synthesis of 5,15- (**5**−**7**) and 5,10-diboraporphyrinogenes **13**−**16** is possible when electron-donating amino substituents like diisopropylamino, dimethylpiperidyl and tetramethylpiperidyl reduce the Lewis acidity of the boron atoms. Despite this electronic stabilization, the yellow macrocycles are sensitive to moisture and air. The sterically active 2,3,5,6-tetramethylphenyl substituents protect the boron atoms in yellow **8**, which after deprotonation to the dianion may have better ligand properties towards transition metals than that of **5**.

Experimental Section

General: Reactions were carried out under dry nitrogen using standard Schlenk techniques. Solvents and chemicals were dried, distilled, and saturated with nitrogen. Glassware was dried with a heat-gun under high vacuum. ^1H, ^{11}B, ^{13}C NMR: Bruker DRX 200 spectrometer, NMR references are $(CH_3)_4Si$ and $BF_3{\cdot}Et_2O$. Mass spectra were obtained with a Joel JMS-700 spectrometer, using EI, CI and FAB techniques. Melting points (uncorrected) were measured with a Büchi apparatus, using a capillary, which was filled under nitrogen and sealed. Cl_2BNiPr_2,[14] Cl_2BTMP,[18] Cl_2BDMP,[19] Cl_2Bdur,[20] 2,5-bis[chlorobis(diisopropylamino)boryl]thiophene,[16] 1,1-bis(2-thienyl)ethane[12] were prepared according to literature procedures.

1 and 2: A solution of paraldehyde (52.8 g, 0.4 mol) in thiophene (101 g, 1.2 mol) was placed in a 1-L plastic flask. The flask was immersed in an ice-bath and 50 g of 40% hydrofluoric acid was added with stirring as follows: 5 g at the beginning, 10 g after 1.5 h and the rest after 3 h. Stirring was continued for 4 h at 0 °C and 3 d at room temperature. Distilled water (300 mL) and diethyl ether (200 mL) were added to the reaction mixture. After separating the organic layer, it was washed twice with a solution of NaOH (0.1 N) and dried with Na_2SO_4. Distillation gave **1** (10.3 g, 0.055 mol, 42%), b.p. 90 °C/1.0 mbar and **2** (23.5 g, 0.077 mol, 58%) as a brown, oily residue. **1:** ^1H NMR (CD_2Cl_2, 200.1 MHz): δ = 1.87 (d, $^3J_{H,H}$ = 7 Hz, 1 H, $CHCH_3$), 4.74 (q, $^3J_{H,H}$ = 7 Hz, 3 H, $CHCH_3$), 7.03 (m, 4 H, CH), 7.24 (d, 2 H, CH) ppm. ^{13}C NMR (CD_2Cl_2, 50.3 MHz): δ = 24.9 ($CHCH_3$), 36.6 ($CHCH_3$), 124.1, 127.0, 150.6 (CH) ppm. EI-MS: *m*/*z* (%) = 194 (75) $[M]^+$, 179 (100) $[M - CH_3]^+$. **2:** ^1H NMR (CD_2Cl_2, 200.1 MHz): δ = 1.75 (d, $^3J_{H,H}$ = 7 Hz, 6 H, $CHCH_3$), 4.60 (q, $^3J_{H,H}$ = 7 Hz, 2 H, $CHCH_3$), 6.80 (m, 3 H, CH), 6.90 (m, 3 H, CH), 7.15 (d, 2 H, CH) ppm. ^{13}C NMR (CD_2Cl_2, 50.3 MHz): δ = 24.4 ($CHCH_3$), 36.7 ($CHCH_3$), 124.2, 125.4, 127.3, 148.5, 150.5 (CH) ppm. EI-MS: *m*/*z* (%) = 304 (70) $[M]^+$; 289 (100) $[M - CH_3]^+$.

5: To a stirred solution of 1,1-bis(2-thienyl)ethane (**1**) (1.0 g, 5.2 mmol) in diethyl ether (20 mL), a 2.5 M solution of butyllithium in hexane (4.2 mL) was added dropwise at room temp. The colorless solution turned red within 30 min. After cooling to −30 °C, Cl_2BNiPr_2 (1.0 g, 5.5 mmol) was added dropwise and stirred for 14 h at 20 °C. The solid was then filtered and washed with diethyl ether and the solvent was removed under vacuum to give a yellow solid which was washed twice with pentane. Yield: 1.50 g (2.5 mmol, 95%) of yellow **5**, m.p. 175 °C (decomp.). ^1H NMR ($CDCl_3$, 200.1 MHz): δ = 1.20 [d, $^3J_{H,H}$ = 7 Hz, 24 H, $CH(CH_3)_2$], 1.71 (d, $^3J_{H,H}$ = 7 Hz, 3 H, $CHCH_3$), 4.03 [s, $^3J_{H,H}$ = 7 Hz, 4 H, $CH(CH_3)_2$], 4.57 (q, $^3J_{H,H}$ = 7 Hz, 2 H, $CHCH_3$), 6.76 (d, $^3J_{H,H}$ = 4.0 Hz, 4 H, H_{ar}), 6.84 (d, $^3J_{H,H}$ = 4.0 Hz, 4 H, H_{ar}) ppm. ^{11}B NMR ($CDCl_3$, 64.1 MHz): δ = 35.0 ppm. ^{13}C NMR ($CDCl_3$, 50.3 MHz): δ = 14.5 ($CHCH_3$), 25.3 [$CH(CH_3)_2$], 37.1 [$CH(CH_3)_2$], 50.3 ($CHCH_3$), 125.0, 134.0, 154.8 (C_{ar}), 143 (br, CB) ppm. FAB-MS: *m*/*z* (%) = 606 (90) $[M]^+$, 591 (43) $[M - CH_3]^+$, 507 (49) $[M - NiPr_2]^+$. HR-FAB-MS: *m*/*z* (%) = $C_{32}H_{44}N_2S_4{}^{11}B_2$ $[M]^+$ calcd. 606.2575; found 606.2615; Δ*m* = 4.0 mmu.

6: The compound was prepared, analogously to **5**, from **1** (0.95 g, 4.9 mmol), *n*-butyllithium (4.2 mL) and dichloro(2,2′,6,6′-tetramethylpiperidyl)borane (1.1 g, 4.98 mmol). Yield: 0.86 g (1.3 mmol, 51%) of yellow **6**, m.p. 185 °C (decomp.). ^1H NMR (200 MHz, $CDCl_3$): δ = 1.43 [s, 24 H, $C(CH_3)_2$], 1.68 (m, 12 H, CH_2), 1.77 (d, $^3J_{H,H}$ = 7 Hz, 6 H, $CHCH_3$), 4.63 (q, $^3J_{H,H}$ = 7 Hz, 2 H, $CHCH_3$), 6.87 (m, 8 H, H_{ar}) ppm. ^{11}B NMR (64.2 MHz, $CDCl_3$): δ = 43.3 ppm. ^{13}C NMR (50.3 MHz, $CDCl_3$): δ = 14.0 ($CHCH_3$), 24.5 [$C(CH_3)_2$], 32.1 (CH_2), 36.1 (CH_2), 55.4 [$CH(CH_3)$], 123.6; 126.5; 150.0 (C_{ar}) ppm, CB signal not detected. CI-MS: *m*/*z* (%) = 743 (10) [M + C_4H_8 gas], 687 (15) $[M]^+$, 672 (13) $[M - CH_3]^+$. HR-FAB-MS: $C_{38}H_{52}N_2S_4{}^{11}B_2$ $[M]^+$ calcd. 686.3200; found 686.3220; Δ*m* = 2.0 mmu.

7: The compound was prepared analogously to **5**, from 1,1-bis(2-thienyl)ethane (1.82 g, 9.4 mmol), *n*-butyllithium (8.3 mL) and dichloro(2,6-dimethylpiperidyl)borane (1.83 g, 9.6 mmol). Yield: 1.78 g (2.8 mmol, 60%) of yellow **7**, m.p. 185 °C (decomp.). ^1H NMR (200 MHz, $CDCl_3$): δ = 1.36−1.87 (m, 28 H, H_{dmp} and $CHCH_3$), 4.35 (q, $^3J_{H,H}$ = 7 Hz, 2 H, CH_3HC_{dmp}), 4.47 (q, $^3J_{H,H}$ = 7 Hz, 2 H, CH_3HC_{dmp}), 4.67 (q, $^3J_{H,H}$ = 7 Hz, 2 H, $CHCH_3$), 6.93−7.06 (m, H_{ar}) ppm. ^{11}B NMR (64.2 MHz, $CDCl_3$): δ = 42.3 ppm. ^{13}C NMR (50.3 MHz, $CDCl_3$): δ = 14.1 (H_3CHC_{dmp}

and $CHCH_3$), 23.1, 24.3, 26.2, 28.5, 31.6, 34.1 (CH_2), 36.2 ($CHCH_3$), 48.0, 49.1, 49.9, 52.5 (CH_3HC_{dmp}), 124.4, 134.5, 152.6 (C_{ar}), 142 (br, C−B) ppm. EI-MS: *m*/*z* (%) = 630 (15) $[M]^+$, 615 (7) $[M - CH_3]^+$. HR-EI-MS: $C_{40}H_{44}N_2S_4{}^{11}B_2$ $[M]^+$ calcd. 630.2574; found 630.2609; Δm = 3.5 mmu.

8: The compound was prepared analogously to **5**, from **1** (1.2 g, 6.2 mmol), *n*-butyllithium (5.4 mL) and dichloro(2,3,5,6-tetramethylphenyl)borane (1.3 g, 6.2 mmol). Yield: 0.92 g (1.4 mmol, 45%) of yellow **8**, m.p. 180 °C (decomp.). ^{1}H NMR (200 MHz, $CDCl_3$): δ = 1.79 (d, $^3J_{H,H}$ = 7 Hz, 6 H, $CHCH_3$), 1.95 (s, 9 H, CH_{3dur}), 2.19 (s, 15 H, H_3C_{dur}), 4.68 (q, $^3J_{H,H}$ = 7 Hz, 2 H, $CHCH_3$), 6.95 (m, 8 H, H_{ar}), 7.57 (s, 2 H, HC_{dur}) ppm. ^{11}B NMR ($CDCl_3$, 64.2 MHz): δ = 70 (br) (special parameters have been used: *SW* = 1000 ppm, *TD* = 8 k, *NS* = 1 k) ppm. ^{13}C NMR ($CDCl_3$, 50.3 MHz): δ = 19.8, 20.1 (H_3C_{dur}), 24.3 ($CHCH_3$), 37.2 ($CHCH_3$), 124.2, 127.0 (C_{ar}), 131.2, 133.0, 134.0, 134.5 (C_{dur}), 142.6 (C_{dur}), 163 (br, B−C_{ar}) ppm. FAB-MS: *m*/*z* (%) = 673 (5) $[M + H]^+$; 540 (6) $[M - dur]^+$. HR-FAB-MS: $C_{40}H_{42}B_2S_4$ $[M]^+$ calcd. 672.2355; found 672.2377; Δm = 2.2 mmu.

13: To a solution of 2,5-bis[1(2-thienyl)ethyl]thiophene (**2**) (1.0 g, 3.3 mmol) in diethyl ether (20 mL), a 2.5 M solution of butyllithium (3 mL) was added slowly. After stirring for 30 min at room temp., the red solution was cooled to −30 °C and 2,5-bis[chlorobis(diisopropylamino)boryl]thiophene (**9**) (1.23 g, 3.3 mmol) was added slowly. The solution was warmed to 20 °C over 14 h, LiCl was filtered off, and the solvent was evaporated under vacuum to give a residue, which was extracted with pentane. Evaporation of the solvent gave yellow **13**, m.p. 178 °C (decomp.), yield: 1.22 g (2.0 mmol, 61%). ^{1}H NMR ($CDCl_3$, 200.1 MHz): δ = 1.26 [d, $^3J_{H,H}$ = 7 Hz, 24 H, $CH(CH_3)_2$], 1.70 (d, $^3J_{H,H}$ = 7 Hz, 6 H, $CHCH_3$), 4.09 [sept, $^3J_{H,H}$ = 7 Hz, 4 H, $CH(CH_3)_2$], 4.53 (q, $^3J_{H,H}$ = 7 Hz, 2 H, $CHCH_3$), 6.64−6.90 (m, 6 H, H_{ar}), 7.08 (m, 2 H, H_{ar}) ppm. ^{11}B NMR ($CDCl_3$, 64.2 MHz): δ = 36.5 ppm. ^{13}C NMR ($CDCl_3$, 50.3 MHz): δ = 14.3 ($CHCH_3$), 23.3, 23.7 [$CH(CH_3)_2$], 36.6 [$CH(CH_3)_2$], 47.2 ($CHCH_3$), 123.2, 124.0, 124.3, 124.5, 129.1, 131.2 (C_{ar}), 149 (br, CB) ppm. EI-MS: *m*/*z* (%) = 606 (15) $[M]^+$, 591 (10) $[M - CH_3]^+$, 507 (20) $[M - NiPr_2]^+$.

14: The compound was prepared analogously to **13**, from **2** (0.17 g, 0.4 mmol), *n*-butyllithium (0.4 mL) and 2,5-bis[chloro(2,2′,6,6′-tetramethylpiperidyl)boryl]thiophene (**10**) (0.19 g, 0.42 mmol). Yield: 0.19 g (0.3 mmol, 62%) yellow **14**, m.p. 185 °C (decomp.). ^{1}H NMR ($CDCl_3$, 200.1 MHz): δ = 1.29 [s, 24 H, $C(CH_3)_2$], 1.62 (d, 6 H, $CHCH_3$), 1.72−1.91 (m, 12 H, CH_2), 4.54 (q, 2 H, $CHCH_3$), 6.67 (s, 2 H, CH_{thio}), 6.89−7.01 (m, 4 H, CH_{thio}), 7.16−7.27 (m, 2 H, CH_{thio}) ppm. ^{11}B NMR ($CDCl_3$, 64.2 MHz): δ = 40 (br) ppm. ^{13}C NMR ($CDCl_3$, 50.3 MHz): δ = 14.4 [$CH(CH_3)$], 30.0 [$C(CH_3)_2$], 32.2 (CH_2), 36.6 (CH_2), 46.6 [$CH(CH_3)$], 122.9; 123.8; 126.7 (C_{ar}), 148.4 (br, CB) ppm. EI-MS: *m*/*z* (%) = 684 (20) $[M - H_2]^+$, 604 (10) $[M -$ thiophene$]^+$.

15: The compound was prepared analogously to **13**, from **2** (0.30 g, 0.1 mmol), *n*-butyllithium (0.9 mL) and 2,5-bis[chlorobis(diisopropylamino)boryl]furan (**11**) (0.33 g, 1.0 mmol). Yield: 0.24 g (0.4 mmol, 40%) of yellow **15**, m.p. 187 °C (decomp.). ^{1}H NMR ($CDCl_3$, 200.1 MHz): δ = 1.27 [d, 24 H, $^3J_{H,H}$ = 5.0 Hz, $CH(CH_3)_2$], 1.49 [d, 6 H, $^3J_{H,H}$ = 4.8 Hz, $CH(CH_3)_2$], 4.01 [sept, 4 H, $^3J_{H,H}$ = 5.0 Hz, $CH(CH_3)_2$], 4.56 [q, 2 H, $^3J_{H,H}$ = 4.8 Hz, $CH(CH_3)_2$], 6.68(m, 2 H, H_{ar}), 6.87−6.93 (m, 3 H, H_{ar}), 7.14−7.23 (m, 3 H, H_{ar}) ppm. ^{11}B NMR ($CDCl_3$, 64.2 MHz): δ = 39.0 ppm. ^{13}C NMR ($CDCl_3$, 50.3 MHz): δ = 14.4 ($CHCH_3$), 23.6, 24.2 [$CH(CH_3)_2$], 36.5 [$CH(CH_3)_2$], 47.0 ($CHCH_3$), 123.3; 123.8; 123.9; 124.3; 125.4(C_{ar}), 150 (br, CB) ppm. EI-MS: *m*/*z* (%) = 590 (5) $[M]^+$, 490 (12) $[M - NiPr_2]^+$.

16: The compound was prepared analogously to **13**, from **2** (0.55 g, 1.8 mmol), *n*-butyllithium (1.6 mL) and 2,5-bis[chlorobis(diisopropylamino)boryl]-*N*-methylpyrrole (**12**) (0.67 g, 1.8 mmol). Yield: 0.51 g (0.85 mmol, 47%) of yellow **16**, m.p. 190 °C (decomp.). ^{1}H NMR ($CDCl_3$, 200.1 MHz): δ = 1.35 [d, 24 H, $^3J_{H,H}$ = 5.0 Hz, $CH(CH_3)_2$], 1.73 [d, 6 H, $^3J_{H,H}$ = 4.8 Hz, $CH(CH_3)_2$], 3.27 (s, 3 H, NCH_3), 3.75 [sept, 4 H, $^3J_{H,H}$ = 5.0 Hz, $CH(CH_3)_2$], 4.54 [q, 2 H, $^3J_{H,H}$ = 4.8 Hz, $CH(CH_3)_2$], 6.21 (m, 2 H, H_{py}), 6.63−6.68 (m, 3 H, H_{thio}), 6.83−7.11 (m, 3 H, H_{thio}) ppm. ^{11}B NMR ($CDCl_3$, 64.2 MHz): δ = 43.9 ppm. ^{13}C NMR ($CDCl_3$, 50.3 MHz): δ = 14.1 ($CHCH_3$), 23.0; 25.3 [$CH(CH_3)_2$], 36.2 [$CH(CH_3)_2$], 47.2 ($CHCH_3$), 50.7 (NCH_3), 107.1; 114.1 ($C_{ar,py}$), 122.9; 124.1; 124.8 ($C_{ar,thio}$), 148 (br, CB) ppm. CI-MS: *m*/*z* (%) = 661 (20) $[M + H + C_4H_8]^+$, 604 (45) $[M + H]^+$, 581 (8) $[M + H - Me]^+$, 524 (15) [M + H − *N*-methylpyrrole].

Crystal Structure Determination of 5: Intensity data were collected with a Bruker AXS SMART 1000 area detector (Mo-K_α radiation, λ = 0.71073, ω-scans, *T* = −83 °C). All calculations were performed using SHELXLT 5.1.[21] Non-hydrogen atoms were refined with anisotropic displacement factors. Hydrogen atoms were located in a difference Fourier synthesis and refined with isotropic displacement factors. Crystal data and details of the structure determination are given in Table 1. CCDC-175313 contains the supplementary crystallographic data for this paper. These data can be obtained free of charge at www.ccdc.cam.ac.uk/conts/retrieving.html or from the Cambridge Crystallographic Data Centre, 12, Union Road, Cambridge CB2 1EZ, UK [Fax: (internat.) + 44-1223/336-033; E-mail: deposit@ccdc.cam.ac.uk].

Table 1. Crystal data and structure refinement for **5**

Empirical formula	$C_{34}H_{48}B_2Cl_4N_2S_4$
Formula mass	776.40
Crystal system	triclinic
Space group	$P\bar{1}$
Unit cell	
a [Å]	10.438(2)
b [Å]	10.865(2)
c [Å]	10.999(2)
α [°]	72.911(3)
β [°]	65.324(2)
γ [°]	64.731(3)
V [Å^3]	1014.8(2)
Z	1
Calcd. density [g/cm^3]	1.27
Adsorption coeff. [mm^{-1}]	0.524
F(000)	408
Crystal size [mm]	0.54 × 0.28 × 0.17
Θ_{max} [°]	30
Index ranges	−13/+15, −15/+15, 0/+16
Number of reflections unique	6767
Observed [$I > 2\sigma(I)$]	5628
Parameters	313
Final *R* indices	
R1 [$I > 2\sigma(I)$]	0.0361
*wR*2	0.1025
Max. diff. peak/hole [e/Å^3]	+0.755/−0.573

Acknowledgments

This work was supported by the Deutsche Forschungsgemeinschaft and the Fonds der Chemischen Industrie.

[1] P. Rothemund, *Am. Chem. Soc.* **1935**, *57*, 2179−2180.
[2] C. H. Lee, J. S. Lindsey, *Tetrahedron* **1994**, *50*, 11427−11428.
[3] C. Brückner, V. Karunarante, S. J. Rettig, D. Dolphin, *Can. J. Chem.* **1996**, *74*, 2182−2193.
[4] K. M. Smith, G. W. Craig, *J. Org. Chem.* **1983**, *48*, 4302−4306.
[5] A. W. Johnson, *Pure Appl. Chem.* **1971**, *28*, 195−217.
[6] [6a] M. Pohl, H. Schmickler, J. Lex, E. Vogel, *Angew. Chem.* **1991**, *103*, 1737−1741, *Angew. Chem. Int. Ed. Engl.* **1991**, *30*, 1693−1697. [6b] E. Vogel, *Pure Appl. Chem.* **1990**, *62*, 557−564.
[7] E. Vogel, W. Haas, B. Knipp, J. Lex, H. Schmickler, *Angew. Chem.* **1988**, *100*, 445−448; *Angew. Chem. Int. Ed. Engl.* **1988**, *27*, 406−409.
[8] F. H. Carré, R. Corriu, T. Deforth, W. E. Douglas, W. Siebert, W. Weinmann, *Angew. Chem.* **1998**, *110*, 654−656; *Angew. Chem. Int. Ed.* **1998**, *37*, 652−654.
[9] [9a] S. B. Kahl, M. S. Koo, *J. Chem. Soc., Chem. Commun.* **1990**, 1769−1771. [9b] A. S. Phadke, A. R. Morgan, *J. Chem. Soc., Chem. Commun.* **1993**, 1725−1728. [9c] A. H. Soloway, W. Tjarks, B. A. Barnum, F.-G. Rong, R. F. Barth, I. M. Codogni, J. G. Wilson, *Chem. Rev.* **1998**, *98*, 115−1562.
[10] [10a] W. J. Belcher, M. Breede, P. J. Brothers, C. E. F. Rickard, *Angew. Chem.* **1998**, *110*, 1133−1135; *Angew. Chem. Int. Ed.* **1998**, *37*, 1112−1114. [10b] A. Weiss, H. Pritzkow, W. Siebert, P. J. Brothers, *Angew. Chem.* **2001**, *113*, 4311−4313; *Angew. Chem. Int. Ed.* **2001**, *40*, 4182−4184.
[11] [11a] B. König, M. Rödel, P. Bubenitschek, P. G. Jones, *Angew. Chem.* **1995**, *107*, 752−754; *Angew. Chem. Int. Ed. Engl.* **1995**, *34*, 661−663. [11b] B. König, M. Rödel, P. Bubenitschek, P. G. Jones, I. Thondorf, *J. Org. Chem.* **1995**, *60*, 7406−7410.
[12] T. L. Cairns, B. C. McKusick, V. Weinmayr, *J. Am. Chem. Soc.* **1951**, *73*, 1270−1273.
[13] J. Faderl, B. Deobald, R. Guilard, H. Pritzkow, W. Siebert, *Eur. J. Inorg. Chem.* **1999**, 399−404.
[14] E. Vogel, M. Röhrig, M. Sicken, B. Knipp, A. Herrmann, M. Pohl, H. Schmickler, J. Lex, *Angew. Chem.* **1989**, *101*, 1683−1687; *Angew. Chem. Int. Ed. Engl.* **1989**, *28*, 1651−1655.
[15] B. Wrackmeyer, H. Nöth, *Chem. Ber.* **1976**, *109*, 1075−1088.
[16] T. Köhler, University of Heidelberg, unpublished results, **2001**.
[17] H. Nöth, B. Wrackmeyer, *NMR-Spectroscopy of Boron Compounds*, Springer Verlag, Berlin, Heidelberg, New York, **1978**, p. 165.
[18] T. Weinschenck, Zulassungsarbeit, Universität Heidelberg, **1999**.
[19] W. Maringgele, M. Noltemeyer, H. Schmidt, A. Meller, *Main Group Metal Chem.* **1999**, *22*, 715−732.
[20] C. Präsang, personal communication, University of Marburg, **2000**.
[21] G. M. Sheldrick, *SHELXTL 5.1*, Bruker AXS, Madison, WI, **1998**.

Received December 20, 2001
[I01518]

Synthesis, Structures, and Donor−Acceptor Adducts of Tris(3,3-dimethyl-1-butynyl)borane

Michael J. Bayer,[a] Hans Pritzkow,[a] and Walter Siebert*[a]

Dedicated to Prof. Günter Schmid on the occasion of his 65th birthday

Keywords: Alkynes / Tris(alkynyl)boranes / Donors / Boron

The synthesis and properties of tris(3,3-dimethyl-1-butynyl)-borane (**1**), the first donor-free tris(alkynyl)borane, and of its adducts **2** [donor = pyridine (**2a**), triphenylphosphane (**2b**), tetrahydrofuran (**2c**)] are reported. X-ray structure analyses reveal that the B–C bond lengths in **1** are shorter than in **2**; however, the C≡C triple bond lengths are similar to those of the donor-stabilized compounds **2a**, **2b**, and **2c**.

(© Wiley-VCH Verlag GmbH, 69451 Weinheim, Germany, 2002)

Introduction

Tris(alkynyl)boranes were first obtained by Krüerke[1] as donor-stabilized compounds by the reaction of tetraphenylalkynylborates with HCl in the presence of tetrahydrofuran and trialkylamines, respectively. Another approach was described by Ashby et al.[2] who treated sodium acetylide or sodium organylacetylides with boron trifluoride−amine to yield the corresponding amine−B-$(C{\equiv}CH_3)_3$ adducts [amine = C_5H_5N, $(CH_3)_3N$, $(CH_3)_2NH$], and $H_5C_5N{-}B(C{\equiv}CC_6H_5)_3$. Köster et al.[3] prepared tris(alkynyl)borane−trimethylamine adducts by oxidizing alkynylborane adducts of trimethylamine with trimethylamine oxide, the resulting alkynylbis(alkoxy)boranes rearrange to form tris(alkynyl)borane−trimethylamine and tris(alkoxy)borane. Wheatley et al.[4] treated phenylacetylene with *n*-butyllithium and boron trifluoride−diethyl ether in tetrahydrofuran/toluene and obtained the tris-(phenylethynyl)borane−tetrahydrofuran adduct as a hydrogen-bonded dimer. Siebert, Cederbaum et al.[5] published the X-ray structure analysis of the adduct $H_5C_5N{-}B(C{\equiv}CH)_3$ and ab initio calculations on the electronic structure of the donor-free tris(ethynyl)borane. Attempts to synthesize donor-free tris(alkynyl)boranes led to polymeric products.[2]

We report here on the synthesis of tris(3,3-dimethyl-1-butynyl)borane (**1**), the first donor-free tris(alkynyl)borane. Furthermore, the NMR spectroscopic and structural data of **1** and of its pyridine, triphenylphosphane, and tetrahydrofuran adducts **2a**−**c** are described.

Results and Discussion

Synthesis

Tris(3,3-dimethyl-1-butynyl)borane (**1**) is obtained quantitatively by the reaction of deprotonated 3,3-dimethyl-1-butyne with boron trichloride at −78 °C in pentane. Treatment of **1** with pyridine, triphenylphosphane, and tetrahydrofuran leads to the donor-stabilized tris(alkynyl)boranes **2a**−**c** (Scheme 1).

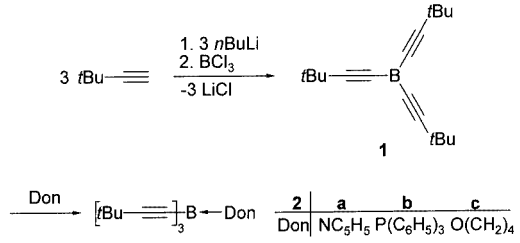

Scheme 1

The composition of the new compounds is derived from NMR and mass spectra and confirmed by X-ray structure analyses. The ^{11}B NMR signal of **1** shows a remarkable shift at δ = 38 ppm upfield from shifts for alkyl- and alkenylboranes.[6] The ^1H NMR spectrum of **1** exhibits a resonance at δ = 1.26 ppm for the methyl protons and in the ^{13}C NMR spectrum the broadened signal for the boron-bound α-carbon atoms is detected at δ = 91 ppm. In comparison

[a] Anorganisch-Chemisches Institut der Universität Heidelberg, Im Neuenheimer Feld 270, 69120 Heidelberg, Germany
Fax: (internat.) + 49-(0)6221/545609
E-mail: ci5@ix.urz.uni-heidelberg.de

to 3,3-dimethyl-1-butyne[7] [$\delta(^{13}C) = 67.3$] the signal for the α-carbon atom of **1** is shifted by 24 ppm to lower field, while the resonance of the β-carbon atoms ($\delta = 126.3$ ppm) is shifted by 32 ppm to higher field. The signals for the *tert*-butyl substituent are observed at $\delta = 30.5$ ppm for methyl groups and $\delta = 28.7$ ppm for the quaternary carbon atom. An EI mass spectrum of **1** shows the molecular ion peak [M^+] at $m/z = 254$ with an intensity of 72%, and the IR spectrum features for the C≡C triple bond a strong stretching vibration at $\tilde{\nu} = 2171.5\ cm^{-1}$ indicating that this bond is not elongated (confirmed by X-ray structure data, see below).

The ^{11}B NMR shift of **2a** at $\delta = -15$ ppm indicates a fourfold coordination of the boron atom. In the ^1H NMR spectrum the signal for *tert*-butyl group is observed at $\delta = 1.22$ ppm, and the ^{13}C NMR spectrum exhibits the resonances of the *tert*-butyl substituent at $\delta = 31.4$ ppm for the methyl groups and at $\delta = 29.7$ ppm for the quaternary carbon atom. The boron-bound α-carbon signals appear at $\delta = 106$ ppm, which is shifted to lower field than that of **1**. At $\delta = 128.2$ ppm the resonance for the β-carbon atoms is found.

The ^{11}B NMR signal of **2b** at $\delta = -26$ ppm is upfield relative to that of **2a**. In the ^1H NMR spectrum a singlet is observed for the *tert*-butyl groups at $\delta = 0.88$ ppm. The ^{13}C NMR spectrum exhibits four resonances at $\delta = 29.7$ (CMe_3), 30.9 (CH_3), 107 (broad, CB) and 125.2 ppm (β-carbon atoms). Four signals in the aromatic region are assigned to the triphenylphosphane donor. The ^{31}P NMR signal of **2b** is found at $\delta = 4.0$ ppm. The ^{11}B NMR shift of **2c** at $\delta = -9$ ppm is downfield compared with the values of **2a** and **2b**. The ^1H and ^{13}C NMR signals of complexed **1** in **2c** do not deviate significantly from the data of **2a** and **2b**. In the EI mass spectrum no peak for the molecular ion [M^+] of **2a**–**c** but that of **1** and peaks for pyridine, triphenylphosphane, and tetrahydrofuran, respectively, are detected.

Attempts to synthesize tris(alkynyl)boranes with a number of terminal alkynes (propyne, 1-butyne, trimethylsilylacetylene, phenylacetylene, mesitylacetylene) were not successful. Instead mixtures of polymeric products of unknown compositions were formed.

Crystal Structures

The molecular structure of **1** was obtained by performing a single-crystal X-ray diffraction analysis. Colorless crystals of **1** were grown from pentane at 4 °C, its molecular structure is shown in Figure 1. In **1** the C≡C triple bond lengths [1.203(2) Å] are similar, but the B–C distances [1.519(2) Å] are shorter than those of the adducts $H_8C_4O{-}B(C{\equiv}C{-}C_6H_5)_3$ [1.209(3), 1.580(4) Å][4] and $H_5C_5N{-}B(C{\equiv}CH)_3$ [1.188(2), 1.586(2) Å].[5] The catecholborylacetylene $H_4C_6O_2B{-}C{\equiv}CH$ [1.195(3), 1.520(4) Å][8] has C≡C and B–C bond lengths similar to those of **1**.

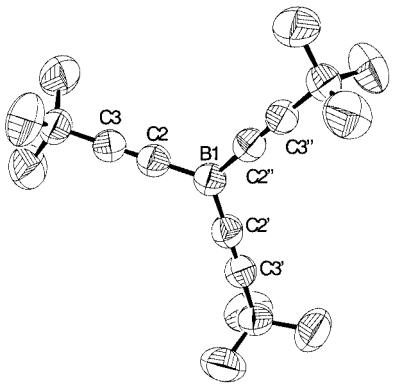

Figure 1. Molecular structure of **1** in the crystal; selected bond lengths [Å] and angles [°]: B1–C2 1.519(2), C2–C3 1.203(2), C3–C4 1.467(2), C2–B1–C2′ 120.00(1), C2–B1–C2′′ 120.00(1), C2′–B1–C2′′ 120.00(1)

Single crystals of **2a** and **2b** were grown from a solution of toluene at −30 °C, while **2c** crystallizes in tetrahydrofuran at −30 °C. Their molecular structures with distorted tetrahedral coordination at the boron atoms are shown in Figures 2–4. The lengths of the C≡C triple bonds [1.196(6)–1.212(1) Å] lie in the range of the donor-free tris(alkynyl)borane **1** [1.203(2) Å], while the B–C bond lengths [1.575(6)–1.593(2) Å] are similar to those in similar adducts of tris(alkynyl)boranes.[4,5] The B–C bonds are elongated compared with those of **1**.

Because the C≡C triple bonds in **1** are not elongated and the B–C distances are shorter in comparison to those of the donor-stabilized compounds **2a**–**c** it may be concluded that a small pπ–pπ interaction between the sp-hybridized carbon atoms and the sp^2-boron atom is present. This is supported by ab initio calculations on the unknown tris(ethynyl)borane,[5] which indicate weak π interactions between the boron atom and the C≡C triple bond. Furthermore, ab initio calculations on the model compound ethynylborane ($H_2B{-}C{\equiv}CH$) showed that a (polar) heteroallene structure with a B=C double bond is only of minor import-

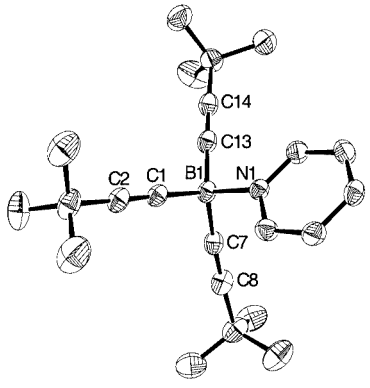

Figure 2. Molecular structure of **2a** in the crystal; selected bond lengths [Å] and angles [°]: B1–C1 1.593(2), B1–C7 1.582(2), B1–C13 1.583(2), C1–C2 1.202(2), C7–C8 1.201(2), C13–C14 1.207(2), B1–N1 1.646(2), C1–B1–N1 106.1(1), C7–B1–N1 103.6(1), C13–B1–N1 107.4(1), C1–B1–C7 111.0(1), C1–B1–C13 113.0(1), C7–B1–C13 114.9(1)

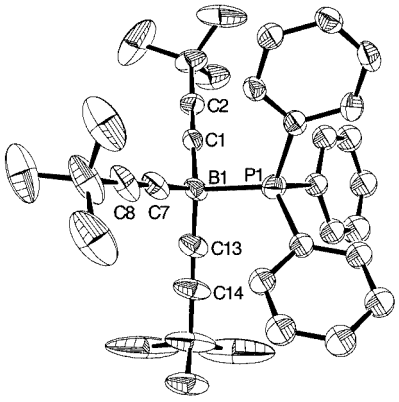

Figure 3. Molecular structure of **2b** in the crystal; selected bond lengths [Å] and angles [°]: B1−C1 1.580(5), B1−C7 1.575(7), B1−C13 1.586(6), C1−C2 1.204(5), C7−C8 1.196(6), C13−C14 1.203(6), B1−P1 2.029(4), C1−B1−P1 103.0(2), C7−B1−P1 108.7(3), C13−B1−P1 102.0(3), C1−B1−C7 114.6(4), C1−B1−C13 114.5(3), C7−B1−C13 112.6(3)

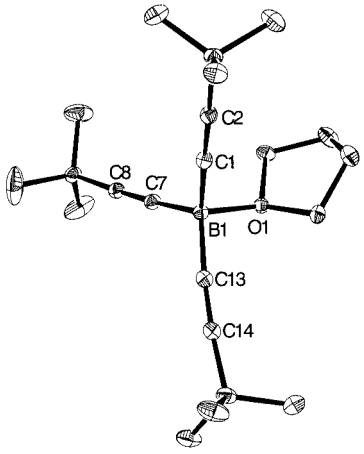

Figure 4. Molecular structure of **2c** in the crystal; selected bond lengths [Å] and angles [°]: B1−C1 1.580(1), B1−C7 1.578(1), B1−C13 1.575(1), C1−C2 1.210(1), C7−C8 1.212(1), C13−C14 1.209(1), B1−O1 1.605(1), C1−B1−O1 104.5(1), C7−B1−O1 104.2(1), C13−B1−O1 103.0(1), C1−B1−C7 112.6(1), C1−B1−C13 115.6(1), C7−B1−C13 115.2(1)

ance.[9] The observed shortening of the B−C bond length may be explained by the different boron hybridizations present in **1** (sp^2) and in the adducts **2** (sp^3).

Conclusion

In this paper we report on the synthesis of the first donor-free tris(alkynyl)borane. By treating of 3,3-dimethyl-1-butynyllithium with boron trichloride in a ratio of 3:1 tris(3,3-dimethyl-1-butynyl)borane (**1**) is formed. Reactions with several other terminal alkynes did not yield the corresponding tris(alkynyl)boranes, but mixtures of polymeric products with unknown compositions were obtained. Addition of pyridine, triphenylphosphane or tetrahydrofuran to **1** yields the donor-stabilized derivatives **2a**, **2b**, and **2c**, respectively. X-ray structure analyses of **1**, **2a**, **2b**, and **2c** show that the lengths of the C≡C triple bonds of **1** are similar to the C≡C triple bonds of **2a**−**c**, while the B−C bonds in **1** are shorter compared with the B−C bonds in **2a**−**c**. This result seems to be in agreement with the presence of a (C−B)π interaction as indicated by ab initio calculations on the nonexistent tris(ethynyl)borane[5] and by NMR studies of several alkenyl- and alkynylboranes.[6] However, the elongation of the B−C bonds more likely is a consequence of the decrease of the 2s character in the boron−carbon bonds of **2a**−**c**, rather than a (C−B)π bond in **1**.

Experimental Section

General: Reactions were carried out under dry argon or nitrogen, using standard Schlenk techniques. Solvents were dried, distilled, and saturated with nitrogen. Glassware was dried with a heat-gun under high vacuum. ^1H, ^{13}C, ^{31}P and ^{11}B NMR: Bruker DRX 200 spectrometer, $Et_2O{\cdot}BF_3$ was used as external standard for ^{11}B NMR, 30% H_3PO_4 for ^{31}P NMR. As internal references for ^1H and ^{13}C NMR spectra the signals of the deuterated solvents were used and calculated for TMS. The mass spectra were measured with a ZAB-2F VH Micromass CTD spectrometer and with a Jeol MS station JMS 700 using EI and HR-EI techniques. IR spectra were recorded with a Perkin−Elmer 983G spectrometer. Melting points (uncorrected) were measured with a Büchi apparatus using capillaries, which were filled under argon or nitrogen, and sealed.

Tris(3,3-dimethyl-1-butynyl)borane (1): To a solution of 5 g (61 mmol) of 3,3-dimethyl-1-butyne in 140 mL of pentane 61 mmol of *n*BuLi was added at −20 °C. The mixture was allowed to warm to room temp. and stirred for 1 h. Then the suspension was cooled to −78 °C and transferred to a solution of 3.3 g (28 mmol) of BCl_3 in 40 mL of pentane at −78 °C. The reaction mixture was allowed to warm slowly to room temp. and was stirred for 12 h. After filtration, the solvent was evaporated to give **1** as colorless solid (5.04 g, 97.5%, m.p. 48 °C). ^1H NMR (200 MHz, $CDCl_3$): δ = 1.26 [s, 27 H, $C(CH_3)_3$] ppm. ^{11}B NMR (64 MHz, $CDCl_3$): δ = 38 ppm ($\Delta_{1/2}$ = 580 Hz). $^{13}C\{^1H\}$ NMR (50 MHz, $CDCl_3$): δ = 28.7 [$C(CH_3)_3$], 30.5 [$C(CH_3)_3$], 91 (br., B*C*≡C), 126.3 ppm (BC≡*C*). EI-MS: *m/z* (%) = 254 (72) [M^+], 239 (38) [$M^+ - CH_3$], 197 (78) [$M^+ - C_4H_9$], 173 (20) [$M^+ - C_6H_9$], 67 (100) [$C_5H_7^+$], 57 (43) [$C_4H_9^+$], 41 (74) [$C_3H_5^+$]. HR-MS (EI): *m/z* = 254.2208 [M^+]; calcd. for $^{12}C_{18}{}^1H_{27}{}^{11}B_1$: 254.2206 (Δ = 0.2 mmu). IR: $\tilde{\nu}$ = 2171.5 cm^{-1} (C≡C).

Tris(3,3-dimethyl-1-butynyl)borane−Pyridine Adduct (2a): 133 mg (0.52 mmol) of **1** was dissolved in 15 mL of pentane and treated with 45 mg (0.57 mmol) of pyridine at −10 °C. The mixture was allowed to warm to room temp. and was stirred for 4 h. Then the solvent was removed under vacuum to yield **2a** as colorless solid (168 mg, 96.3%, m.p. 74 °C). ^1H NMR (200 MHz, $CDCl_3$): δ = 1.22 [s, 27 H, $C(CH_3)_3$], 7.62 (m, 2 H, H_{py}), 8.03 (m, 1 H, H_{py}), 9.28 ppm (m, 2 H, H_{py}). ^{11}B NMR (64 MHz, $CDCl_3$): δ = −15 ppm ($\Delta_{1/2}$ = 139 Hz). $^{13}C\{^1H\}$ NMR (50 MHz, $CDCl_3$): δ = 29.7 [$C(CH_3)_3$], 31.4 [$C(CH_3)_3$], 106 (br., B*C*≡C), 128.2 (BC≡*C*), 125.1, 140.6, 146.1 ppm (C_{py}). EI-MS: *m/z* (%) = 254 (81) [M^+ −py], 239 (49) [$M^+ - py - CH_3$], 197 (100) [$M^+ - py - C_4H_9$], 173 (22) [$M^+ - py - C_6H_9$], 79 (96) [py^+], 67 (60) [$C_5H_7^+$], 57 (36) [$C_4H_9^+$], 52 (87) [$C_4H_4^+$], 41 (86) [$C_3H_5^+$].

Tris(3,3-dimethyl-1-butynyl)borane−Triphenylphosphane Adduct (2b): 90 mg (0.35 mmol) of **1** was dissolved in 20 mL of toluene, and a solution of 93 mg (0.35 mmol) of PPh_3 in 10 mL of toluene was added at room temp. After 4 h of stirring, the solvent was

Table 1. Crystal data and details of the structure determinations

	1	2a	2b	2c
Empirical formula	$C_{18}H_{27}B$	$C_{23}H_{32}BN{\cdot}0.5\ C_7H_8$	$C_{36}H_{42}BP$	$C_{22}H_{35}BO$
Formula mass	254.22	379.37	516.51	326.31
Temperature [K]	293(2)	173(2)	173(2)	100(2)
Crystal system	hexagonal	trigonal	monoclinic	triclinic
Space group	$P6_3/m$	$P3_121$	$P2_1/n$	$P\bar{1}$
Unit cell dimensions				
a [Å]	11.530(2)	14.2708(1)	14.188(2)	10.5829(5)
b [Å]	11.530(2)	14.2708(1)	16.857(2)	10.9449(5)
c [Å]	8.552(2)	21.7049(3)	15.003(2)	11.5218(5)
α [°]	90	90	90	96.675(1)
β [°]	90	90	114.358(3)	107.182(1)
γ [°]	120	120	90	117.710(1)
Volume [Å^3]	984.6(3)	3828.11(7)	3268.9(8)	1076.84(8)
Z	2	6	4	2
Calcd. density [g/cm^3]	0.857	0.987	1.049	1.006
Absorp. coeff. [mm^{-1}]	0.047	0.055	0.105	0.058
F(000)	280	1242	1112	360
Crystal size [mm]	0.72 × 0.46 × 0.44	0.42 × 0.33 × 0.28	0.75 × 0.33 × 0.26	0.42 × 0.25 × 0.22
Θ_{max} [°]	26.33	26.37	24.41	32.00
Index ranges	−11/7, 0/14, −10/10	−17/8, 0/17, −0/27	−16/15, 0/19, 0/17	−15/14, −16/16, 0/17
No. of reflections				
Unique	717	5232	5393	7287
Observed [$I > 2\sigma(I)$]	561	4326	3810	5906
Parameters	49	399	331	357
Final R indices				
$R1$ [$I > 2\sigma(I)$]	0.0535	0.0401	0.0927	0.0472
$wR2$	0.1583	0.1101	0.2360	0.1230
Largest diff. peak/hole [e/Å^3]	+0.104/−0.127	+0.171/−0.124	+0.509/−0.475	+0.477/−0.276

removed under vacuum to give **2b** as colorless solid (143 mg, 78.3%, m.p. 96 °C). ^{1}H NMR (200 MHz, $CDCl_3$): δ = 0.88 [s, 27 H, $C(CH_3)_3$], 7.10−7.20 ppm (m, 15 H, Ar-H). ^{11}B NMR (64 MHz, $CDCl_3$): δ = −26 ppm (Δ1/2 = 174 Hz). $^{13}C\{^1H\}$ NMR (50 MHz, $CDCl_3$): δ = 29.7 [$C(CH_3)_3$], 30.9 [$C(CH_3)_3$], 107 (br., B*C*≡C), 125.3 (BC≡*C*), 128.2, 129.0, 134.0, 137.8 ppm (Ar-C). ^{31}P NMR (81 MHz, $CDCl_3$): δ = 4.0 ppm. EI-MS: *m*/*z* (%) = 262 100) [PPh_3^+], 254 (14) [$M^+ - PPh_3$], 239 (12) [$M^+ - PPh_3 - CH_3$], 197 (36) [$M^+ - PPh_3 - C_4H_9$], 108 (33) [PPh^+].

Tris(3,3-dimethyl-1-butynyl)borane−Tetrahydrofuran Adduct (2c): 169 mg (0.67 mmol) of **1** was dissolved in 15 mL of pentane and treated with 5 mL of tetrahydrofuran at −10 °C. The mixture was allowed to warm up to room temp. and was stirred for 4 h. Then the solvents were removed under vacuum to yield **2c** as colorless solid (202 mg, 92.4%, m.p. 63 °C). ^{1}H NMR (200 MHz, [D_8]THF): δ = 1.15 [s, 27 H, $C(CH_3)_3$], 1.78 (m, 4 H, β-H_{thf}), 3.63 ppm (m, 4 H, α-H_{thf}). ^{11}B NMR (64 MHz, [D_8]THF): δ = −8 ppm ($\Delta_{1/2}$ = 412 Hz). $^{13}C\{^1H\}$ NMR (50 MHz, [D_8]THF): δ = 26.5 (β-C_{thf}), 31.5 [$C(CH_3)_3$], 32.0 [$C(CH_3)_3$], 68.5 (α-C_{thf}), 89 (br., B*C*≡C), 104.6 ppm (BC≡*C*). EI-MS: *m*/*z* (%) = 254 (64) [M^+ − THF], 239 (43) [M^+ − THF − CH_3], 197 (100) [M^+ − THF − C_4H_9], 72 (84) [THF^+], 57 (14) [$C_4H_9^+$].

X-ray Crystal Structure Analyses of 1, 2a, 2b, and 2c: Crystal data and details of the structure determinations are compiled in Table 1. Intensity data were collected with a Bruker AXS Smart 1000 CCD area detector (Mo-K_α radiation, λ = 0.71073 Å, ω-scan). An empirical absorption correction was applied (SADABS). The structures were solved by direct methods and refined by full-matrix least squares based on F^2 with all measured reflections.[10] Non-hydrogen atoms were refined anisotropically. Hydrogen atoms for **2a** were located in a difference Fourier map and refined isotropically, for **1** and **2b** they were inserted in calculated positions. CCDC-179205−179209 contain the supplementary crystallographic data for this paper. These data can be obtained free of charge at www.ccdc.cam.ac.uk/conts/retrieving.html or from the Cambridge Crystallographic Data Centre, 12, Union Road, Cambridge CB2 1EZ, UK [Fax: (internat.) + 44-1223/336-033; E-mail: deposit@ccdc.cam.ac.uk].

Acknowledgments

This work was supported by the Deutsche Forschungsgemeinschaft, the Fonds der Chemischen Industrie, and the BASF AG.

[1] U. Krüerke, *Z. Naturforsch., Teil B* **1956**, *11*, 676−677.
[2] E. C. Ashby, W. E. Foster, *J. Org. Chem.* **1964**, *29*, 3225−3229.
[3] R. Köster, H.-J. Horstschäfer, P. Binger, *Justus Liebigs Ann. Chem.* **1968**, *717*, 1−20.
[4] J. E. Davies, P. R. Raithby, R. Snaith, A. E. H. Wheatley, *Chem. Commun.* **1997**, 1797−1798.
[5] A. Maderna, H. Pritzkow, W. Siebert, T. Sommerfeld, L. S. Cederbaum, *Z. Naturforsch., Teil B* **1997**, *52*, 1315−1320.
[6] B. Wrackmeyer, H. Nöth, *Chem. Ber.* **1977**, *110*, 1086−1094.
[7] G. Fraenkel, P. Pramanik, *J. Chem. Soc., Chem. Commun.* **1983**, 1527−1528.
[8] Y. Gu, H. Pritzkow, W. Siebert, *Eur. J. Inorg. Chem.* **2001**, 373−379.
[9] V. Bachler, N. Metzler-Nolte, *Eur. J. Inorg. Chem.* **1998**, 733−744.
[10] G. M. Sheldrick, SHELXTL V5.1, Bruker AXS, Madison, Wisconsin, **1998**.

Received February 14, 2002
[I02078]

Tellurium(IV) Tetraalkoxides and Chlorotellurium(IV) Alkoxides Derived from β-Donor Alcohols

Holger Fleischer,*[a] Yvonne Dienes,[a] and Dieter Schollmeyer[b]

Keywords: Tellurium / Donor-acceptor systems / Ab initio calculations / X-ray diffraction / NMR spectroscopy

$Te(OiPr)_3OCH_2CH_2XMe_n$ (**1a**–**1c**) and $Te(OCH_2CH_2NMe_2)_4$ (**2**) were synthesised by the reaction of $Te(OiPr)_4$ with $HOCH_2CH_2XMe_n$, while $TeCl_2(OCH_2CH_2OMe)_2$ (**3**) and $TeCl_3OCH_2CH_2XMe_n$ (**4a**–**4c**) resulted from the reaction of $TeCl_4$ with the corresponding silylated alcohols $Me_3SiOCH_2CH_2XMe_n$ (X = N, n = 2; X = O or S, n = 1). These compounds are the first known representatives of the hitherto unknown classes of tellurium(IV) tetraalkoxides and chlorotellurium(IV) alkoxides derived from β-donor-substituted alcohols. The donor atom X in the alkoxy ligand enables an intramolecular donor-acceptor Te···X interaction, which stabilises the di- and trichlorotellurium alkoxides, but reduces the reactivity of the tellurium atom towards nucleophiles, a result from which an associative-dissociative mechanism was inferred for the nucleophilic substitution in $TeCl_4$. In contrast to this, all O*i*Pr ligands of $Te(OiPr)_4$ can be exchanged by reaction with $HOCH_2CH_2XMe_n$. As was shown by multinuclear NMR studies, the kinetics and equilibrium of the reaction of $Te(OiPr)_4$ with $HOCH_2CH_2XMe_n$ depend substantially on X and thus demonstrate the presence of Te···X interactions in solution. The molecular and crystal structure of **3** was investigated by single-crystal X-ray diffraction. In the solid state of **3**, two kinds of molecules are present, differing in the coordination modes of the Te atoms. In each molecule, two intramolecular dative Te···O bonds [264.3(2)–267.7(2) pm] exist, approximately *trans* to the covalent Te–O bonds. Two C_1-symmetric molecules are linked by intermolecular Te···Cl contacts to a third, namely the C_2-symmetric molecule, giving coordination numbers of six and seven for the Te atoms of the C_2- and C_1-symmetric moieties, respectively. Ab initio (MP2/LANL2DZP) geometry optimizations and thermochemical calculations of the model compounds $TeCl_3OCH_2CH_2XH_n$ (**4α**–**4γ**) and $Te(OH)_3OCH_2CH_2XH_n$ (**1α**–**1γ**) as well as an analysis of the bonds in terms of natural bond orbitals were performed in order to study the nature of the Te···X bond and its dependence on conformational restraints. The donor power of the N atom was found to be greater than those of the O and S atoms and the Te···X interactions are stronger for $TeCl_3OCH_2CH_2XH_2$ than for $Te(OH)_3OCH_2CH_2XH_2$; σ-type n(X)–σ*(Te–E) interactions are important for the Te···X bond and compete with π-type n(O)–σ*(Te–E) interactions, which in turn are of importance for the E–Te–O–C conformation (E = O, Cl).

(© Wiley-VCH Verlag GmbH, 69451 Weinheim, Germany, 2002)

Introduction

In contrast to $SiCl_4$, $GeCl_4$ or $SnCl_4$, $TeCl_4$ does not react with alcohols themselves by means of partial or full exchange of the chloride ligands by alkoxy groups, but dissolves in many alcohols without decomposition.[1] In order to obtain tellurium(IV) tetraalkoxides, $Te(OR)_4$, from $TeCl_4$ and the appropriate alcohol, HOR, the latter has to be activated. This activation can either be achieved by *O*-silylation or *O*-metallation of the alcohol prior to the synthesis or by addition of tertiary amines which drive the reaction by formation of the corresponding ammonium chloride.[2−4] Alternatively, $Te(OR)_4$ can be derived from $Te(OR')_4$ and HOR by ligand exchange according to Equation (1).

$$Te(OR')_4 + 4\ HOR \rightleftarrows Te(OR)_4 + 4\ HOR' \quad (1)$$

Gottlieb and co-workers showed that the equilibrium in Equation (1) is quickly reached for R, R′ = Me, Et in chloroform or benzene as solvents. They also found out that Equation (1) showed a statistical product distribution characteristic of thermally neutral reactions.[5] The equilibrium according to Equation (1) can be shifted towards the right if HOR′ can be removed by distillation or $Te(OR)_4$ is precipitated from the reaction mixture.[6,7]

Reaction of $TeCl_4$ with silylated alcohols according to Equation (2) represents a good approach to the synthesis of chlorotellurium(IV) alkoxides, $TeCl_{4-n}(OR)_n$.[3]

$$TeCl_4 + n\ Me_3SiOR \rightarrow TeCl_{4-n}(OR)_n + n\ Me_3SiCl \quad (2)$$

The chlorotrimethylsilane which is formed as a by-product, can easily be distilled off together with the solvent. Trichlorotellurium(IV) alkoxides like trichlorotellurium(IV)

[a] Institut für Anorganische Chemie und Analytische Chemie, Johannes Gutenberg Universität Mainz, Duesbergweg 10−14, 55099 Mainz, Germany
[b] Institut für Organische Chemie, Johannes Gutenberg Universität Mainz, Duesbergweg 10−14, 55099 Mainz, Germany

2-propoxide or ethoxide, which are reported to be unstable, could be stabilised as 1:1 adducts with THF or ethyl acetate.[7]

A number of tellurium compounds exhibit intramolecular donor-acceptor interactions, i.e. a Lewis acidic Te centre.[8,9] Concerning organotellurenyl halides, for example, these interactions enable the isolation of these otherwise unstable compounds. We were thus interested to see whether tellurium(IV) alkoxides and especially chlorotellurium(IV) alkoxides could be stabilised by such intramolecular donor-acceptor interactions and how these interactions would influence structure and reactivity.

Results and Discussion

Synthesis and ^{125}Te NMR Spectra

$Te(OiPr)_3OCH_2CH_2NMe_2$ (**1a**), $Te(OiPr)_3OCH_2CH_2OMe$ (**1b**) and $Te(OiPr)_3OCH_2CH_2SMe$ (**1c**) (Scheme 1) were prepared from equimolar amounts of $Te(OiPr)_4$ and the β-donor alcohols $HOCH_2CH_2NMe_2$, $HOCH_2CH_2OMe$ and $HOCH_2CH_2SMe$, respectively, by means of stirring the reactants in benzene and distilling off all volatile products under reduced pressure. $Te(OCH_2CH_2NMe_2)_4$ (**2**) could be prepared in this way as well by treating $Te(OiPr)_4$ with 4 equiv. of $HOCH_2CH_2NMe_2$. Reactions of equimolar amounts of $TeCl_4$ and the silylated β-donor alcohols $Me_3SiOCH_2CH_2XMe_n$ (X = N, n = 2; X = O or S, n = 1) resulted in good yields of the trichlorotellurium(IV) alkoxides $TeCl_3OCH_2CH_2NMe_2$ (**4a**), $TeCl_3OCH_2CH_2OMe$ (**4b**) and $TeCl_3OCH_2CH_2SMe$ (**4c**) (Scheme 1).

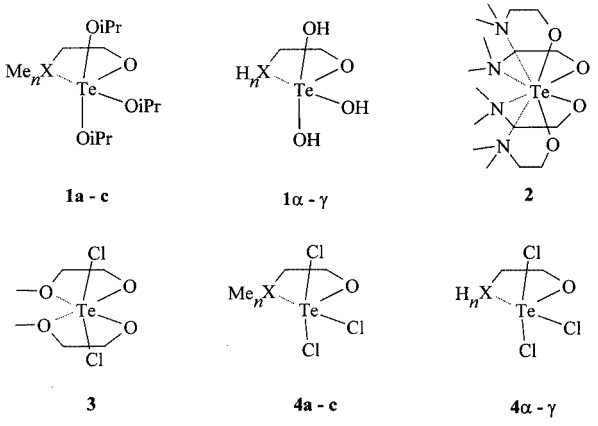

Scheme 1. Structural formulae of compounds and model compounds presented in this paper

Reaction of $TeCl_4$ with 2 or more equiv. of $Me_3SiOCH_2CH_2OMe$ resulted in the formation of $TeCl_2(OCH_2CH_2OMe)_2$ (**3**), whose crystal structure was solved and refined (see below).

At room temperature, **1a**−**c** and **2** are viscous colourless liquids that are quickly hydrolysed when exposed to air, whereas **3** and **4a**−**c** are colourless or slightly grey solids which are less sensitive to air, but decompose on melting. The positions of the ν(Te−Cl) bands in the Raman spectrum of **4a** indicate an aggregation in the solid state via Te−Cl···Te bridges. Whereas **4b** easily dissolves in chloroform, **4c** is soluble only in more polar solvents like THF. Compound **4a** is not soluble without decomposition, hence no high-resolution NMR spectra could be obtained for it.

When treating $TeCl_4$ with $Me_3SiOCH_2CH_2NMe_2$ and $Me_3SiOCH_2CH_2SMe$, no more than one Cl atom could be exchanged for an $OCH_2CH_2XMe_n$ group, even if an excess of the silylated alcohol was used and longer reaction times were applied. This is in contrast to the reaction of $Te(OiPr)_4$ with $HOCH_2CH_2NMe_2$, where all O*i*Pr groups could be substituted by $OCH_2CH_2NMe_2$ groups, leading to compound **2**. Thus, the conclusion could be drawn that the nucleophilic substitution reactions with the Te atoms in $TeCl_4$ and $Te(OiPr)_4$ proceed with different mechanisms and that the intramolecular Te···N interactions in **1a** and **4a** exhibit different strengths (see also the ab initio studies below). For $TeCl_4$, an associative-dissociative mechanism (Scheme 2) is assumed, whereas for $Te(OiPr)_4$ a dissociative-associative mechanism (Scheme 3) is more likely.

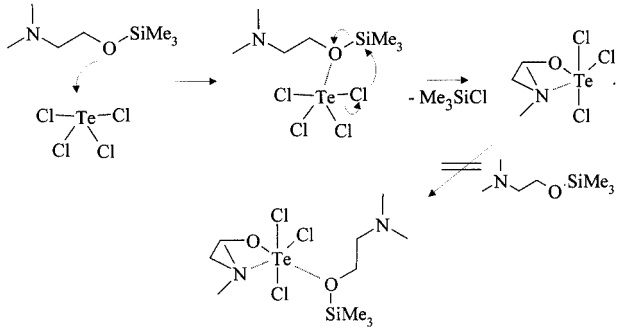

Scheme 2. Proposed associative-dissociative mechanism for the nucleophilic substitution at $TeCl_4$

In the associative-dissociative mechanism, the intramolecular Te···N bond shields the Te atom and reduces its Lewis acidity, so that interaction with the O atom of the silyl ether is not strong enough to cleave the O−Si bond.

For $Te(OiPr)_4$, a hydrogen bond assisted cleavage of a Te−O bond is supposed to precede the transfer of a proton from HOR^1 to OR^- and the addition of the thus formed OR^{1-} to $[Te(OR)_3]^+$. The different mechanisms of the nucleophilic substitution for $TeCl_4$ and $Te(OiPr)_4$ are due to a smaller Lewis acidity of $Te(OiPr)_4$ than $TeCl_4$ and a greater basicity of OR than the Cl ligand.

Whereas the ^{125}Te NMR shift of **1b** (δ = 1540 ppm) is very similar to that of $Te(OiPr)_4$ (δ = 1538 ppm), signals of **1c** (δ = 1519 ppm), **1a** (δ = 1454 ppm) and **2** (δ = 1410 ppm) exhibit a significant high-field shift. This effect is attributed to an increased coordination number of the tellurium atom due to intramolecular Te···X interactions. This interpretation is supported by the observation that on addition of an equimolar amount of H_2SO_4 to a solution of **1a** in $CDCl_3$, the ^{125}Te NMR signal undergoes a low-field shift to δ = 1558 ppm, an effect which is attributed to protonation of the nitrogen atom with subsequent cleavage of the Te···N bond, according to Equation (3).

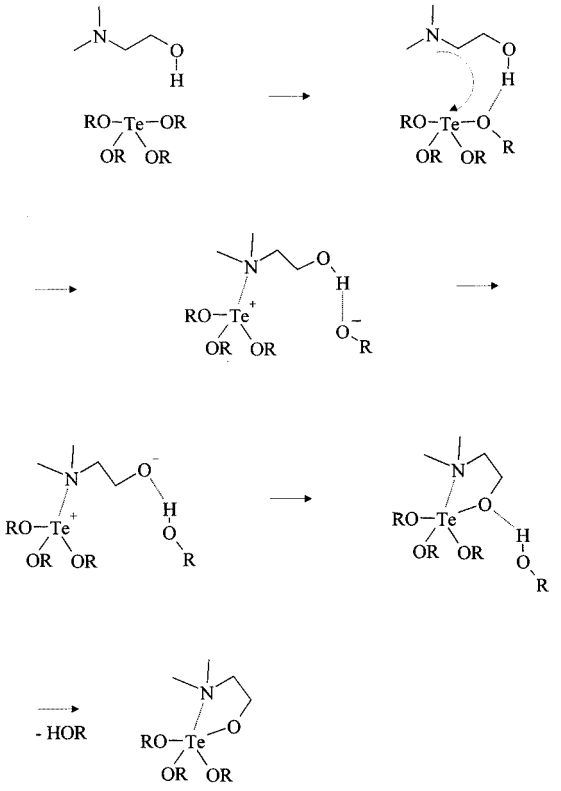

Scheme 3. Proposed dissociative-associative mechanism for the nucleophilic substitution with $Te(OiPr)_4$ (R = O*i*Pr)

$$\mathbf{1a} + H_2SO_4 \rightarrow [Te(OiPr)_3OCH_2CH_2NHMe_2][HSO_4] \quad (3)$$

The chemical shifts of **1a**, **1b** and **1c**, and their comparison with that of $Te(OiPr)_4$ indicate an increase in Te···X bond strength in the order X = N > S > O. The difference between the ^{125}Te NMR shifts of **1a** and **2** is attributed to a further increase in the coordination number of the Te atom and to the different inductive effects of the O*i*Pr and the $OCH_2CH_2NMe_2$ groups. Each of the intramolecular Te···N interactions in **2** must be weaker than the one in **1a**, since the difference in the ^{125}Te NMR shifts of **1a** and **2** is only half as much as that between **1a** and $Te(OiPr)_4$.

In order to investigate the molecular dynamics of the Te···X interactions, ^{125}Te NMR spectra of **1a**, **1b** and **1c** were recorded at different temperatures (Table 1). The data shows δ(^{125}Te) of **1a** to have a large, δ(^{125}Te) of **1c** a small, and δ(^{125}Te) of **1b** to have hardly any positive temperature gradient. As the temperature increases, the differences in δ(^{125}Te) of **1a**, **1b** and **1c** decrease, a fact attributed to a substantial weakening of the Te···X interactions at higher temperatures.

Table 1. ^{125}Te NMR shifts of **1a**−**c** at different temperatures

T/°C	**1a**	**1b**	**1c**
−30	1426	1538	1511
−10	1434	1538	1511
10	1445	1539	1516
25	1453	1540	1519
35	1458		

Ligand Exchange of $Te(OiPr)_4$ with $HOCH_2CH_2XMe_n$

The equilibria and kinetics of the ligand-exchange reactions according to Equations (4a)−(4d) were investigated by means of NMR titration of solutions of $Te(OiPr)_4$ in $CDCl_3$ with $HOCH_2CH_2XMe_n$ [X = N, *n* = 2; X = O or S, *n* = 1; in Equations (4a)−(4d), R′ = $CH_2CH_2XMe_n$].

$$Te(OiPr)_4 + HOR' \rightleftarrows Te(OiPr)_3OR' + HOiPr \quad (4a)$$

$$Te(OiPr)_3OR' + HOR' \rightleftarrows Te(OiPr)_2(OR')_2 + HOiPr \quad (4b)$$

$$Te(OiPr)_2(OR')_2 + HOR' \rightleftarrows Te(OiPr)(OR')_3 + HOiPr \quad (4c)$$

$$Te(OiPr)(OR')_3 + HOR' \rightleftarrows Te(OR')_4 + HOiPr \quad (4d)$$

With X = N, six solutions were investigated, containing a given amount of $Te(OiPr)_4$ in $CDCl_3$ but different amounts of $HOCH_2CH_2NMe_2$. Figure 1 shows the ^{125}Te NMR spectra of these solutions, marked A−F. Five different signals can be observed, attributed to the five species of $Te(OiPr)_{4-n}(OCH_2CH_2NMe_2)_n$ (*n* = 0−4), with the signals of $Te(OiPr)_4$ (*n* = 0), **1a** (*n* = 1) and **2** (*n* = 4) known from the spectra of the pure compounds. The single species of $Te(OiPr)_{4-n}(OCH_2CH_2NMe_2)_n$ are sufficiently stable on the NMR time scale towards ligand exchange among each other or with free alcohol, so that no coalescence of their ^{125}Te NMR signals occurs. Unlike these results, the ligand exchange between $Te(OiPr)_4$ and HOMe, HOEt or HO*i*Pr, respectively,[5] and that between $Te(OiPr)_4$ and $Te(OMe)_4$,[10] proceed at such a rate at room temperature that only averaged ^{125}Te NMR signals could be observed.

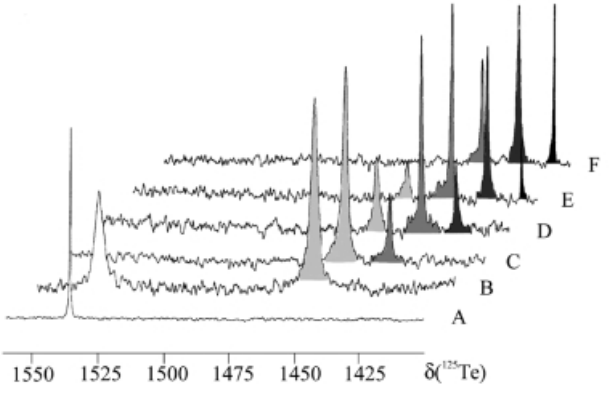

Figure 1. ^{125}Te NMR spectra of a solution of $Te(OiPr)_4$ in $CDCl_3$ with 0.00 (A), 0.65 (B), 1.26 (C), 1.97 (D), 2.77 (E) and 3.89 (F) equiv. of $HOCH_2CH_2NMe_2$; the different signals correspond to the entire species of $Te(OiPr)_{4-n}(OCH_2CH_2NMe_2)_n$ (*n* = 0−4); the darkening of the peaks' grey shadings corresponds to an increase in *n*

The ^{1}H NMR spectrum of solution B lacks any signal attributable to $HOCH_2CH_2NMe_2$, showing that the equilib-

rium according to Equation (4a) with X = N is shifted far towards the right side. Thus, formation of **1a** from Te(O-*i*Pr)$_4$ and $HOCH_2CH_2NMe_2$ is favoured thermodynamically. Since the signal of $HOCH_2CH_2NMe_2$ is missing, no equilibrium constant could be obtained from the spectral intensities.

The equilibrium constants for Equations (4b)−(4d) were estimated considering the relative abundance of Te(*i*PrO)$_{4-n}$(OCH$_2$CH$_2$NMe$_2$)$_n$, HO*i*Pr and $HOCH_2CH_2NMe_2$ in solutions C−F, derived from the intensities of their signals. Due to experimental errors, the values obtained for K_{4b}, K_{4c} and K_{4d} vary between the different solutions as described in the following: $35 < K_{4b} < 44$, $5.4 < K_{4c} < 8.1$, and $1.1 < K_{4d} < 1.4$. Hence, substitution of O*i*Pr for $OCH_2CH_2NMe_2$ is favoured for all compounds Te(O*i*Pr)$_{4-n}$(OCH$_2$CH$_2$NMe$_2$)$_n$ (n = 0−3). The more $OCH_2CH_2NMe_2$ groups, however, are bound to the Te atom, the less favourably substitution takes place.

Information about the kinetics of reactions according to Equations (4a) and (4b) was obtained from ^{1}H NMR spectra. Sample B contains the following three moieties with isopropoxy groups: Te(O*i*Pr)$_4$, **1a** and HO*i*Pr. Nevertheless, only a single set of isopropoxy signals was observed, leading to the assumption of a rapid exchange of O*i*Pr groups between the different species. As the concentration of $HOCH_2CH_2NMe_2$ increases, two sets of signals were observed for each of the O*i*Pr and the $OCH_2CH_2NMe_2$ groups. One set of each could be attributed to the free alcohols, HO*i*Pr and $HOCH_2CH_2NMe_2$, the other one was due to an O*i*Pr and $OCH_2CH_2NMe_2$ group, respectively, both being bound to the Te atom.

Hence it follows that the exchange rate of O*i*Pr between HO*i*Pr and Te(O*i*Pr)$_{4-n}$(OCH$_2$CH$_2$NMe$_2$)$_n$ decreases with increasing n, a fact attributed to the shielding of the tellurium atom by the $OCH_2CH_2NMe_2$ ligands. This is also reflected in the widths of the ^{125}Te signals, which become sharper with increasing n. It is noteworthy that each of the NMe_2, NCH_2 and OCH_2 groups of **2** gives rise to more than a single signal in the ^{1}H NMR spectrum, with the NMe_2 and OCH_2 groups also giving two signals each in the ^{13}C NMR spectrum. This is seen to be due to differences between equatorial and apical ligands and due to differences between coordinating and noncoordinating $OCH_2CH_2NMe_2$ groups.

In contrast to the NMR titration of Te(O*i*Pr)$_4$ with $HOCH_2CH_2NMe_2$, neither titration of Te(O*i*Pr)$_4$ with $HOCH_2CH_2OMe$ nor with $HOCH_2CH_2SMe$ leads to separated signals for Te(O*i*Pr)$_{4-n}$(OCH$_2$CH$_2$XMe)$_n$ (X = O or S, n = 0−4) in the ^{125}Te NMR spectra of the respective solutions (not depicted). The addition of $HOCH_2CH_2OMe$ to a solution of Te(O*i*Pr)$_4$ in $CDCl_3$ led to an enormous line broadening with hardly any change of the chemical shift. This result is presumably due to a fast exchange between the O*i*Pr and the OCH_2CH_2OMe ligands, assuming that all species Te(O*i*Pr)$_{4-n}$(OCH$_2$CH$_2$OMe)$_n$ (n = 0−4) have a similar chemical shift, which could at least be shown for n = 0 [Te(O*i*Pr)$_4$, δ = 1538 ppm] and n = 1 (**1b**, δ = 1540 ppm). Titration of a solution of Te(O*i*Pr)$_4$ in $CDCl_3$ with $HOCH_2CH_2SMe$ led to a significant broadening and a high-field shift of the ^{125}Te NMR signal. At room temperature, no signal could be observed with 5.5 equiv. of the alcohol added, while at −20 °C a single broad signal appeared at δ = 1480 ppm. These results are explained as well through a rapid exchange between the O*i*Pr and the OCH_2CH_2SMe ligands, the high-field shift being due to the different chemical shifts of Te(O*i*Pr)$_4$ and **1c** (δ = 1519 ppm). Similar to the ^{125}Te NMR spectra, the ^{1}H NMR spectra of the solutions of Te(O*i*Pr)$_4$ with either $HOCH_2CH_2OMe$ or $HOCH_2CH_2SMe$ give only averaged signals for chemically different O*i*Pr or OCH_2CH_2XMe groups.

Crystal and Molecular Structures of 3

In Figure 2, a section of the crystal structure of **3** is shown, illustrating the coordination of the Te atoms and the intermolecular association of the molecules. In the solid state, there are two nonequivalent molecules of **3**, differing in the coordination modes of the Te atoms as well as in their conformations.

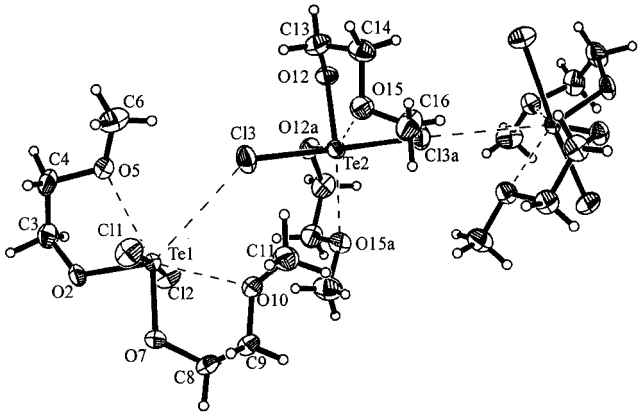

Figure 2. Molecular structure of **3** in the solid state; displacement ellipsoids are at the 50% probability level

Te1 exhibits heptacoordination with a distorted pentagonal-bipyramidal configuration (see bond angles in Table 2); Te1, O2, O5, O7 and O10 are nearly in a plane. Due to the effect of the lone pair of Te1, Cl3 lies slightly outside the plane. The two methyl groups bound to O5 and O10, respectively, are *cis* with respect to the O5−Te1−O10 plane. In contrast to Te1, Te2 is hexacoordinate with a stereochemically active lone pair, leading to a distorted pseudo-pentagonal-bipyramidal configuration; Te2 lies on a twofold axis and the entire molecule exhibits C_2 symmetry. Hence, the methyl groups bound to O15 and O15a, respectively, are *trans* with respect to the O15−Te2−O15a plane. Considering the covalent bonds of the Te atoms only, Te1 and Te2 exhibit pseudo-trigonal-bipyramidal configurations, in accordance with the VSEPR rules; the Cl atoms are in the apical positions, the O atoms and the lone pair are situated in the equatorial positions.

Table 2. Selected XRD and ab initio (MP2/LANL2DZP) atomic distances (in pm) and bonding angles (in °) of **3**

	XRD		XRD	Ab initio
Te1−O2	191.2(2)	Te2−O12	191.5(2)	193.4
Te1−O7	192.4(2)	Te2−Cl3	248.5(1)	249.0
Te1−Cl1	247.5(1)	Te2···O15	266.6(2)	268.0
Te1−Cl2	253.2(1)	O12−Te2−O12a	84.4(1)	84.2
Te1···O5	264.3(2)	Cl3−Te2−Cl3a	178.3(1)	178.2
Te1···O10	267.4(2)	O15···Te2−O12a	155.9(1)	154.7
Te1···Cl3	357.7(1)	O15···Te2···O15a	131.9(1)	133.4
O2−Te1−O7	84.4(1)	Cl3−Te2−O12	88.8(1)	89.8
Cl1−Te1−Cl2	175.1(1)			
O2−Te1···O5	71.7(1)			
O7−Te1···O10	71.8(1)			
O5···Te1···O10	130.5(1)			
Cl1−Te1−O2	88.2(1)			
Cl2−Te1−O7	89.0(1)			
Cl1−Te1···Cl3	104.1(1)			
Cl2−Te1···Cl3	80.7(1)			
O5−Te1···Cl3	69.5(1)			
O10−Te1···Cl3	67.4(1)			

The molecular structure of **3**, restrained to C_2 symmetry, was optimised by ab initio methods (MP2/LANL2DZP). The optimised molecular structure agrees quite well with that of the C_2-symmetric unit in the solid state, despite the different phases (isolated vs. solid state) and the different structural types (r_e vs. r_α). An analysis of the Te···O bonds in terms of natural bond orbital interactions shows that these bonds are mainly due to n(O)−σ*(Te−O) interactions between one nonbonding orbital of the donor O atom and the antibonding orbital of the Te−O bond in *trans* position to it. The energy for both of these interactions was estimated to be 72 kJ·mol^{-1}.

Ab initio Studies

With the model compounds $Te(OH)_3OCH_2CH_2NH_2$ (**1α**), $Te(OH)_3OCH_2CH_2OH$ (**1β**), $Te(OH)_3OCH_2CH_2SH$ (**1γ**), $TeCl_3OCH_2CH_2NH_2$ (**4α**), $TeCl_3OCH_2CH_2OH$ (**4β**), and $TeCl_3OCH_2CH_2SH$ (**4γ**), the intramolecular Te···X (X = N, O, S) interactions were investigated in detail. The following two conformations were taken into consideration for each of the model compounds: one exhibiting a Te···X bond, and the second without such an interaction. The optimised molecular structures are depicted in Figures 3 and 4, and structural and energy data are given in Tables 3 and 4.

If only the covalently bound ligands are considered, the Te atoms exhibit pseudo-trigonal-bipyramidal configurations, in accordance with the VSEPR rules. The lone pair of the Te atom occupies an equatorial position, and for **4α**, **4β** and **4γ**, the apical positions are occupied by two Cl atoms which exhibit a greater distance to the Te atom than the equatorial Cl atom. An exothermal process for all model compounds is the conversion of the conformation without the Te···X bond into the conformation with the Te···X bond. From the ΔH^{298} values given in Tables 3 and 4 it follows that Te···X bonds are stronger for the trichlorotellurium(IV) alkoxides **4α**−**4γ** than for the tellurium(IV) tetraalkoxides **1α**−**1γ**, i.e. the Te atom is a better electron-pair acceptor in the former than in the latter. Furthermore, the N atom is a much better donor than the O or the S atom.

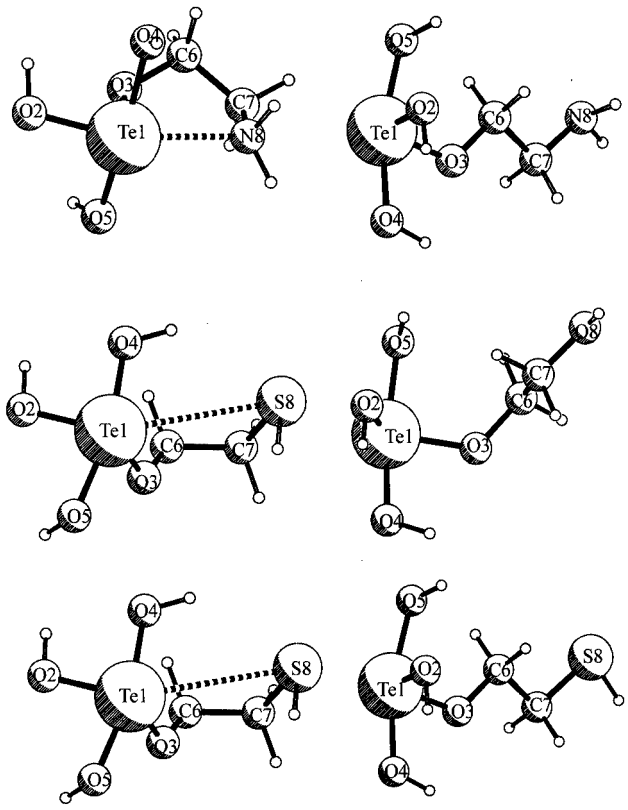

Figure 3. Ab initio molecular structures of model compounds $Te(OH)_3OCH_2CH_2NH_2$ (**1α**), $Te(OH)_3OCH_2CH_2OH$ (**1β**) and $Te(OH)_3OCH_2CH_2SH$ (**1γ**) with Te···X bond (on the left) and without Te···X bond (on the right; X = N8, O8, S8)

The results derived from thermochemical data are confirmed by an NBO analysis of the Te···X bond and by the structural parameters. The interaction of an occupied, nonbonding orbital of the donor atom, n(X), with the unoccupied, anti-bonding orbital of the Te−O or Te−Cl bond in the *trans* position, σ*(Te−O_{trans}) or σ*(Te−Cl_{trans}), is important for the Te···X bonds in $Te(OH)_3OCH_2CH_2XH_n$ and $TeCl_3OCH_2CH_2XH_n$, respectively. The energies of the n(X)−σ*(Te−Cl_{trans}) interactions in **4α**−**γ** are higher than those of the n(X)−σ*(Te−O_{trans}) interactions in **1α**−**γ**, and also higher when X is N than when X is O or S. According to second-order perturbation theory, the smaller the energy difference and the greater the overlap integral between two orbitals, the greater is the energy of their interaction. Both factors favour the interaction of n(N) compared to n(O) or n(S) with σ*(Te−Cl_{trans}) or σ*(Te−O_{trans}).

The structural parameters and their differences between the two conformations of the same model compound also serve as a measure of the strength of the Te···X bond. In the conformations of **1α**, **1β** and **4α**−**γ** with a Te···X

Table 3. Selected ab initio structural parameters (distances in pm, angles in °), $n_p(O)-\sigma^*(Te-O)$ and $n(X)-\sigma^*(Te-O)$ energies of interaction and thermochemical data (in kJ·mol^{-1}) of the model compounds **1α**, **1β** and **1γ**, with (a) and without (b) Te···X bond (X = N, O, S, see Figure 3)

(a)[a]	**1α** with Te···N bond	**1β** with Te···O bond	**1γ** with Te···S bond
Te1−O2/Te1−O3	194.2/196.6	192.8/195.8	192.6/195.5
Te1−O4/Te1−O5	205.7/198.7	202.9/196.4	203.1/195.9
Te1···X	261.4	312.3	385.6
l[b]	1.26	1.54	1.60
O2−Te1−O3	87.8	101.5	102.4
O2−Te1···X	159.6	137.9	135.1
O3−C6−C7−X	−56.0	−64.2	−63.4
C6−O3−Te1−O2	147.1	100.5	79.4
$n_p(O3)-\sigma^*(Te1-O2)$	13	29	31
$n(X)-\sigma^*(Te1-O2)$	68	[c]	[c]
ΔH^{298}[d]	−18	−15	−6

(b)	**1α** without Te···N bond	**1β** without Te···O bond	**1γ** without Te···S bond
Te1−O2/Te1−O3	194.1/194.9	194.2/195.1	193.9/195.5
Te1−O4/Te1−O5	200.3/198.0	200.2/198.2	200.0/198.1
O2−Te1−O3	103.8	104.6	104.3
O4−Te1−O5	163.5	162.8	162.9
O3−C6−C7−X	−178.2	177.2	−179.4
C6−O3−Te1−O2	−80.5	−79.1	−80.3
$n_p(O3)-\sigma^*(Te1-O2)$	32	32	31

[a] X = N8, O8 and S8 for **1α**, **1β** and **1γ**, respectively. [b] $l = (Te\cdots X)/[r_{cov}(Te) + r_{cov}(X)]$. Covalent radii, r_{kov}, according to Sutton (70, 66, 104 and 137 pm for N, O, S and Te, respectively).[11] [c] Less than 5 kJ·mol^{-1}. [d] $\Delta H^{298} = H^{298}$(with Te···X-bond) − H^{298}(without Te···X-bond).

Table 4. Selected ab initio structural parameters (distances in pm, angles in °), $n_p(O)-\sigma^*(Te-Cl)$ and $n(X)-\sigma^*(Te-Cl)$ energies of interaction and thermochemical data (in kJ·mol^{-1}) of the model compounds **4α**, **4β** and **4γ**, with (a) and without (b) Te···X bond (X = N, O, S, see Figure 4)

(a)[a]	**4α** with Te···N bond	**4β** with Te···O bond	**4γ** with Te···S bond
Te1−Cl2	236.5	232.8	233.5
Te1−Cl3/Te1−Cl4	246.7/249.3	247.8/245.0	245.7/245.8
Te1−O5	194.6	193.7	194.1
Te1···X	240.2	251.5	302.2
l[b]	1.16	1.24	1.25
Cl2−Te1−O5	85.2	88.8	89.8
Cl2−Te1···X	162.3	161.8	164.9
O3−C6−C7−X	−53.4	−57.9	−63.6
Cl2−Te1−O5−C6	161.5	161.2	149.1
$n_p(O3)-\sigma^*(Te1-Cl2)$	4	6	16
$n(X)-\sigma^*(Te1-Cl2)$	184	89	111
ΔH^{298} [c]	−84	−42	−19

(b)	**4α** without Te···N bond	**4β** without Te···O bond	**4γ** without Te···S bond
Te1−Cl2	233.1	232.9	232.9
Te1−Cl3/Te1−Cl4	245.1/241.1	244.3/241.5	241.2/244.8
Te1−O5	191.2	191.1	191.4
Cl2−Te1−O5	99.7	99.8	100.0
O3−C6−C7−X	178.9	177.8	179.1
Cl2−Te1−O5−C6	−62.5	−63.0	61.9
$n_p(O3)-\sigma^*(Te1-Cl2)$	45	45	44

[a] X = N8, O8 and S8 for **4α**, **4β** and **4γ**, respectively. [b] $l = (Te\cdots X)/[r_{cov}(Te) + r_{cov}(X)]$. Covalent radii, r_{kov}, according to Sutton (70, 66, 104 and 137 pm for N, O, S and Te, respectively).[11] [c] $\Delta H^{298} = H^{298}$(with Te···X-bond) − H^{298}(without Te···X-bond).

Table 5. Crystal data, data collection and correction, structure solution and refinement for **3**

Empirical formula	$C_6H_{14}O_4Cl_2Te$
M/g·mol^{-1}	348.67
Cryst. size/mm	0.06 × 0.19 × 0.35
Cryst. system	monoclinic
Space group	*C*2/*c*
Z	12
θ range and limiting indices	4° ≤ 2θ ≤ 54° −37 ≤ *h* ≤ 37 −9 ≤ *k* ≤ 9 −29 ≤ *l* ≤ 29
T/K	185
$\rho_{calcd.}$/g·cm^{-3}	1.958
a/nm	2.82632(4)
b/nm	0.72874(3)
c/nm	2.22623(11)
β/°	129.285(1)
V/nm^3	3.54903(11)
Reflections meas.[a]	45588
Unique reflections	4407
μ/mm^{-1}	2.95
Reflections observed	3709
Refined parameters	186
R [$\|F\| > 4\sigma(F)$][b]	0.0275
$wR2$[c]	0.0642
Goodness-of-fit on F^2	1.136
Max./min. peak in diff. Fourier synthesis/10^{-3} e·nm^{-3}	−1.55/0.78

[a] Lorentz and polarisation corrections were performed on the data. Absorption correction was performed with the MULABS program.[17] Hydrogen atoms were localised and isotropically refined by using a riding model. All non-hydrogen atoms were refined anisotropically. [b] $R = \Sigma||F_o| - |F_c||/\Sigma|F_o|$. [c] $wR2 = \{\Sigma[w(F_o^2 - F_c^2)^2]/\Sigma[w(F_o)^2]^2\}^{1/2}$.

"bond", all Te···X distances are smaller than the sum of the van der Waals radii (155, 152, 180 and 206 pm for N, O, S and Te, respectively[12]). The Te···N distance in **4α** corresponds quite well to that in *o*-$TeCl_3[C_6H_4CH(Me)NMe_2]$ [241.1(7) pm].[13] The Te···S bond in **1γ** nearly equals the sum of the van der Waals radii and the term "bond" has to be dealt with carefully. To compare the Te···X distance for different donor atoms with different covalent radii, the relative length, *l*, is used (for definition see Tables 3 and 4).[14] Since the bond with the smaller *l* is the stronger one, the Te···X bonds are again found to be stronger with X = N than with X = O or S and stronger in **4α**−**γ** than in **1α**−**γ**. Accordingly, the Te1−Cl2 bond in the *trans* position to the Te1···X8 bond is significantly longer in **4α** than in **4β** or **4γ**, demonstrating the stronger *trans* effect of the N atom compared to the O or S atom.

Optimal π-type n_p(O3)−σ*(Te1−E2) (**1α**−**γ**: E = O; **4α**−**γ**: E = Cl) interactions are not compatible with optimal σ-type n(X8)−σ*(Te1−E2) interactions (see Figure 5). In the conformation without a Te···X "bond", the absolute values of the C6−O3−Te1−E2 torsion angles are between 60 and 80° and permit a good overlap between n_p(O3) and σ*(Te1−E2). In the conformations with a Te···X "bond" the five-membered ring formed requires enlarged C6−O3−Te1−E2 torsion angles in order to obtain X in *trans* position to the Te1−E2 bond for a good σ-type n(X8)−σ*(Te1−E2) interaction. The π-type n_p(O3)−σ*(Te1−E2) interaction is significantly reduced in such a conformation (see Tables 3 and 4, b), but at least for **1α** and **4α**−**γ** it is more than compensated by the n(X8)−σ*(Te1−E2) interaction.

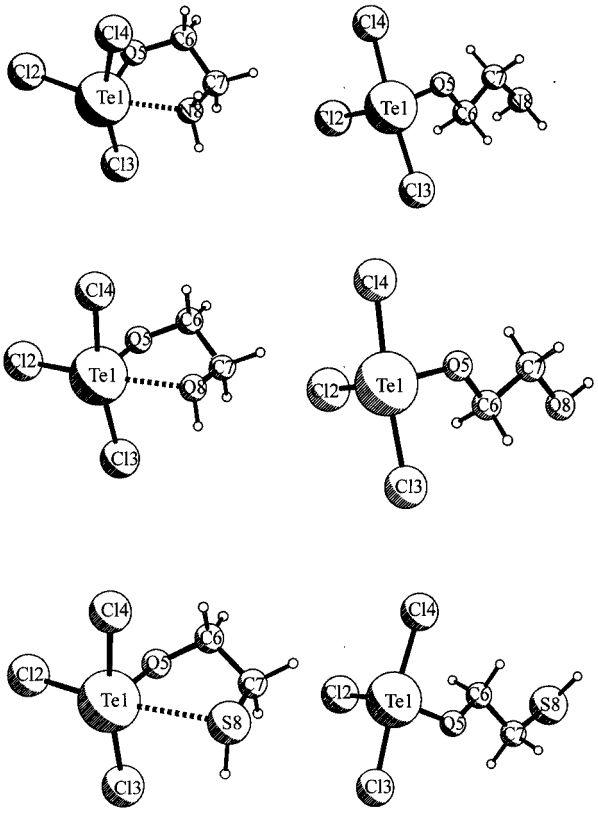

Figure 4. Ab initio molecular structures of model compounds $TeCl_3OCH_2CH_2NH_2$ (**4α**) $TeCl_3OCH_2CH_2OH$ (**4β**) and $TeCl_3OCH_2CH_2SH$ (**4γ**) with Te···X bond (on the left) and without Te···X bond (on the right; X = N8, O8, S8)

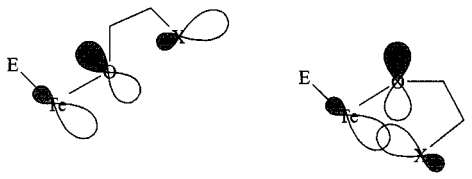

Figure 5. Conformations of the $ETeOCH_2CH_2X$ fragment for optimum π-type n_p(O)−σ*(Te−E) (on the left) and σ-type n(X)−σ*(Te−E) interactions (on the right), respectively

Conclusion

Tellurium(IV) tetraalkoxides, dichlorotellurium(IV) dialkoxides and trichlorotellurium(IV) alkoxides derived from β-donor-substituted alcohols are stabilised kinetically and thermodynamically by intramolecular Te···X interactions. In the trichlorotellurium(IV) alkoxides, this interaction re-

duces the reactivity of the Te atom towards nucleophiles and only with X = O substitution of a second Cl atom was feasible, leading to $TeCl_2(OCH_2CH_2OMe)_2$. Of all donor atoms investigated, nitrogen forms the strongest Te···X interaction. Substitution of Cl for alkoxide ligands substantially reduces the acceptor power of the Te atom; π-type $n_p(O)-\sigma^*(Te-E)$ interactions and σ-type $n(X)-\sigma^*(Te-E)$ interactions compete with each other in $TeCl_3(OCH_2CH_2XH_n)$ (E = Cl) and $Te(OH)_3(OCH_2CH_2XH_n)$ (E = O), and the stronger one determines the conformation.

Experimental Section

General Procedures: All procedures were carried out under an inert gas or under vacuum, using carefully dried glassware and solvents purified according to standard methods. $Te(OiPr)_4$ was prepared according to Mehrotra et al.[6] NMR: Bruker DRX 400, $B_1(^1H)$ = 400.000, $B_1(^{13}C)$ = 100.577, $B_1(^{125}Te)$ = 126.387 MHz; standards: TMS (^1H, ^{13}C) and $Te(CH_3)_2$ (^{125}Te). Raman: SPEX 1402, excitation with a Kr Laser (647 nm). CHNS analyses were performed with an Elemental Vario EL2.

Syntheses

Tellurium 2-(Dimethylamino)ethoxide Tris(2-propoxide), $Te(OiPr)_3OCH_2CH_2NMe_2$ (1a): A solution of 2-(dimethylamino)ethanol, $HOCH_2CH_2NMe_2$ (0.48 g, 5.3 mmol), in 30 mL of benzene was slowly added to a stirred solution of $Te(OiPr)_4$ (1.94 g, 5.3 mmol) in 50 mL of benzene. Subsequently, the benzene and 2-propanol formed during the reaction were distilled off in a slight vacuum; **1a** was isolated from the crude product by a fractionated distillation under high vacuum (113 °C/1.5 10^{-2} mbar, partial decomp.). Yield: 1.54 g (73.9%). ^1H NMR ($CDCl_3$): δ = 1.16 [d, $^3J_{H,H}$ = 6.12 Hz, 18 H, $OCH(CH_3)_2$], 2.41 [s, 6 H, $N(CH_3)_2$], 2.66 (t, $^3J_{H,H}$ = 5.2 Hz, 2 H, NCH_2), 4.17 (t, $^3J_{H,H}$ = 5.2 Hz, 2 H, OCH_2), 4.40 [m, 3 H, $OCH(CH_3)_2$] ppm. $^{13}C\{^1H\}$ NMR ($CDCl_3$): δ = 26.2 [$OCH(CH_3)_2$], 44.0 [$N(CH_3)_2$], 59.2 (NCH_2), 61.5 (OCH_2), 64.9 [$OCH(CH_3)_2$] ppm. $^{125}Te\{^1H\}$ NMR ($CDCl_3$): δ = 1454 ppm. $C_{13}H_{31}NO_4Te$ (393.00): calcd. C 39.73, H 7.95, N 3.56 ; found C 40.47, H 7.74 N 3.24.

Tellurium 2-(Methoxy)ethoxide Tris(2-propoxide), $Te(OiPr)_3OCH_2CH_2OMe$ (1b): The preparation was carried out by analogy to that of **1a**, using 2-(methoxy)ethanol, $HOCH_2CH_2OMe$ (0.28 g, 3.7 mmol), and $Te(OiPr)_4$ (1.35 g, 3.7 mmol). The colourless and viscous crude product was washed with a small amount of dietyl ether and dried in vacuo. Yield: 1.25 g (88.9%). ^1H NMR (C_6D_6): δ = 1.33 [d, $^3J_{H,H}$ = 6.1 Hz, 18 H, $OCH(CH_3)_2$], 3.13 (s, 3 H, OCH_3), 3.30 (t, $^3J_{H,H}$ = 4.7 Hz, 2 H, H_3COCH_2), 4.21 (t, $^3J_{H,H}$ = 4.7 Hz, 2 H, $TeOCH_2$), 4.76 [sept, $^3J_{H,H}$ = 6.1 Hz, 3 H, $OCH(CH_3)_2$] ppm. $^{13}C\{^1H\}$ NMR (C_6D_6): δ = 26.1 [$OCH(CH_3)_2$], 57.9 (H_3CO), 62.6 ($TeOCH_2$), 65.4 [$OCH(CH_3)_2$], 74.2 (H_3COCH_2) ppm. $^{125}Te\{^1H\}$ NMR (C_6D_6): δ = 1540 ppm. $C_{12}H_{28}O_5Te$ (379.94): C 37.94, H 7.43; found C 33.68, H 6.34%. The deviation between calculated and found data for the C,H analysis of compound **1b** is due to the thermal instability of the compound and its sensitivity to air.

Tellurium 2-(Methylsulfenyl)ethoxide Tris(2-propoxide), $Te(OiPr)_3OCH_2CH_2SMe$ (1c): The preparation was carried out by analogy to that of **1a**, using (2-methylsulfenyl)ethanol, $HOCH_2CH_2SMe$ (0.37 g, 4.0 mmol), and $Te(OiPr)_4$ (1.48 g, 4.1 mmol). The colourless and viscous crude product was washed with a small amount of diethyl ether and dried in vacuo. Yield: 1.62 g (98.2%). ^1H NMR (C_6D_6): δ = 1.30 [d, $^3J_{H,H}$ = 6.1 Hz, 18 H, $OCH(CH_3)_2$], 1.85 (s, 3 H, SCH_3), 2.54 (t, $^3J_{H,H}$ = 6.2 Hz, 2 H, SCH_2), 4.17 (t, $^3J_{H,H}$ = 6.2 Hz, 2 H, OCH_2), 4.71 [sept, $^3J_{H,H}$ = 6.1 Hz, 3 H, $OCH(CH_3)_2$] ppm. $^{13}C\{^1H\}$ NMR (C_6D_6): δ = 26.1 [$OCH(CH_3)_2$], 37.9 (SCH_2), 61.4 (OCH_2), 65.7 [$OCH(CH_3)_2$] ppm; the signal of (H_3CS) was not observed. $^{125}Te\{^1H\}$ NMR (C_6D_6): δ = 1519 ppm. $C_{12}H_{28}O_4STe$ (396.02): C 36.40, H 7.13, S 8.10; found C 35.36, H 6.70, S 8.32.

Tellurium Tetrakis[2-(dimethylamino)ethoxide], $Te(OCH_2CH_2NMe_2)_4$ (2): The preparation was carried out by analogy to that of **1a**, using $Te(OiPr)_4$ (1.15 g, 3.2 mmol), 2-(dimetylamino)ethanol, $HOCH_2CH_2NMe_2$ (1.16 g, 13.0 mmol), and 50 mL of benzene. The colourless and viscous crude product was washed with a small amount of diethyl ether and dried in vacuo. Yield: 1.21 g (80.0%). ^1H NMR ($CDCl_3$): δ = 2.36 + 2.25 + 2.21 [3 s, 24 H, $N(CH_3)_2$], 2.83 + 2.68 + 2.45 + 2.41 (4 m, 8 H, NCH_2), 4.36 + 4.09 + 4.01 + 3.54 (4 m, 8 H, OCH_2) ppm. $^{13}C\{^1H\}$ NMR ($CDCl_3$): δ = 43.5 + 44.9 [$N(CH_3)_2$], 58.4 (NCH_2), 60.3 + 62.4 (OCH_2) ppm. $^{125}Te\{^1H\}$ NMR ($CDCl_3$): δ = 1410 ppm. Raman: $\tilde{\nu}$ = 2941 [vs, ν(C−H)], 2863 [s, ν(C−H)], 2827 [s, ν(C−H)], 2784 [s, ν(C−H)], 2766 [s, ν(C−H)], 781 [m, ν(Te−O)], 711 [w, ν(Te−O)], 571 [m, ν(Te−O)], 533 [vs, ν(Te−O)] cm^{-1}. $C_{16}H_{40}N_4O_4Te$ (480.10): C 40.02, H 8.40, N 11.67; found C 41.02, H 8.48, N 11.79.

Tellurium Dichloride Bis[2-(methoxy)ethoxide], $TeCl_2(OCH_2CH_2OMe)_2$ (3): $TeCl_4$ (1.05 g, 3.9 mmol) and $Me_3SiOCH_2CH_2OMe$ (2.35 g, 15.9 mmol) were dissolved in 20 mL of benzene. The major part of the solvent together with the chlorotrimethylsilane formed during the reaction was then distilled off under normal pressure. The brown viscous residue was dissolved in 10 mL of toluene. From this solution **3** precipitated at −45 °C as colourless crystals. Yield: 1.27 g (93.3%). M.p. 102 °C. ^1H NMR ([D$_8$]THF): δ = 3.50 (s, 3 H, H_3CO), 3.65 (t, $^3J_{H,H}$ = 4.4 Hz, 2 H, H_3COCH_2), 4.58 (t, $^3J_{H,H}$ = 4.5 Hz, 2 H, $TeOCH_2$) ppm. $^{13}C\{^1H\}$ NMR ([D$_8$]THF): δ = 55.8 (OCH_3), 70.2 ($MeOCH_2$), 72.5 ($TeOCH_2$) ppm. $^{125}Te\{^1H\}$ NMR ([D$_8$]THF): δ = 1759 ppm. $C_6H_{14}Cl_2O_4Te$ (348.68): C 20.67, H 4.05; found C 18.93, H 3.72.

Tellurium Trichloride 2-(Dimethylamino)ethoxide, $TeCl_3OCH_2CH_2NMe_2$ (4a): $Me_3SiOCH_2CH_2NMe_2$ (3.20 g, 19.8 mmol) and $TeCl_4$ (5.32 g, 19.7 mmol) were dissolved in 80 mL of THF. The major part of the solvent together with the chlorotrimethylsilane formed during the reaction was then distilled off under normal pressure. A brownish solid precipitated which was isolated, washed several times with petroleum ether and dried in vacuo. Yield: 5.56 g (87.6%). M.p. 130 °C (decomp.). Raman: $\tilde{\nu}$ = 2975 [m, ν(C−H)], 2935 [w, ν(C−H)], 2919 [w, ν(C−H)], 1259 [w, δ(CH_2)], 1172 [w, δ(CH_3)], 764 [w, ρ(CH_2)], 590 (w), 560 [s, ν(Te−O)], 473 (m), 399 (m), 289 [s, ν(Te−Cl)], 270 [s, ν(Te−Cl)], 232 [m, ν(Te−Cl)] cm^{-1}. $C_4H_{10}Cl_3NOTe$ (322.08): C 14.92, H 3.13, N 4.35; found C 14.87, H 3.12, N 4.37.

Tellurium Trichloride 2-(Methoxy)ethoxide, $TeCl_3OCH_2CH_2OMe$ (4b): The preparation was carried out by analogy to that of **4a**, using $TeCl_4$ (2.51 g, 9.3 mmol), $Me_3SiOCH_2CH_2OMe$ (1.38 g, 9.3 mmol) and 30 mL of THF. The brown viscous residue was dissolved in 10 mL of toluene. From this solution **4b** precipitated at −45 °C as a colourless solid. Yield: 2.31 g (80.4%). M.p. 148−150 °C (decomp.). MS (field ionisation): *m*/*z* (%) = 309.8 (12) [M^+], 274.9 (100) [M − Cl]$^+$. ^1H NMR ($CDCl_3$): δ = 3.76 (s, 3 H, OCH_3), 4.03 (m, 2 H, $MeOCH_2$), 4.82 (m, 2 H, $TeOCH_2$) ppm. $^{13}C\{^1H\}$ NMR ($CDCl_3$): δ = 46.2 (OCH_3), 65.4 ($MeOCH_2$), 72.7

($TeOCH_2$) ppm. $^{125}Te\{^1H\}$ NMR ($CDCl_3$): δ = 1747 ppm. $C_3H_7Cl_3O_2Te$ (309.04): C 11.66, H 2.28; found C 11.98, H 2.05.

Tellurium Trichloride 2-(Methylsulfenyl)ethoxide, $TeCl_3OCH_2CH_2SMe$ (4c): The preparation was carried out by analogy to that of **4a**, using $TeCl_4$ (2.30 g, 8.5 mmol), $Me_3SiOCH_2CH_2SMe$ (1.42 g, 8.6 mmol) and 30 mL of THF. From the yellow solution, which remained after distillation of the main part of the solvent and the chlorotrimethylsilane, a colourless solid precipitated which was washed with petroleum ether and dried in vacuo. Yield: 1.71 g (61.6%). M.p. 170−173 °C (decomp.). MS (field ionisation): *m*/*z* (%) = 325.8 (100) [M^+], 288.8 (22) [M − Cl]$^+$. ^1H NMR ([D$_8$]THF): δ = 2.52 (s, 3 H, SCH_3), 3.18 (t, $^3J_{H,H}$ = 5.2 Hz, 2 H, SCH_2), 5.04 (t, $^3J_{H,H}$ = 5.2 Hz, 2 H, OCH_2) ppm. $^{13}C\{^1H\}$ NMR ([D$_8$]THF): δ = 16.4 (SCH_3), 39.2 (SCH_2), 64.7 (OCH_2) ppm. $^{125}Te\{^1H\}$ NMR ([D$_8$]THF): δ = 1693 ppm. $C_3H_7Cl_3OSTe$ (325.10): C 11.08, H 2.17, S 9.86; found C 11.36, H 2.36, S 10.04.

Single-Crystal X-ray Diffraction: The single-crystal X-ray diffraction experiment was performed with a SMART CCD (Bruker AXS) diffractometer with low-temperature unit, employing Mo-K_α radiation (λ = 71.073 pm). The crystal structure was solved with direct methods and difference Fourier analysis (SIR-92)[15] and refined against F^2 (SHELXL-97).[16] For further details, see Table 5. CCDC-173865 contains the supplementary crystallographic data for this paper. These data can be obtained free of charge at www.ccdc.cam.ac.uk/conts/retrieving.html or from the Cambridge Crystallographic Data Centre, 12, Union Road, Cambridge CB2 1EZ, UK [Fax: (internat.) + 44-1223/336-033; E-mail: deposit@ccdc.cam.ac.uk].

Theoretical Methods: The ab initio calculations were performed by using the GAUSSIAN-94 and GAUSSIAN-98 software packages.[18,19] For these the following procedure was applied: Starting from a molecular structure with reasonable atomic distances, bond and torsion angles, the energy was calculated at the Hartree Fock level, using an effective core double-zeta pseudopotential basis set,[20,21] augmented by d-type polarisation functions for all non-hydrogen atoms, with exponents for Te, S and Cl according to Höllwarth et al,[22] and 0.75, 0.80 and 0.85 for C, N and O, respectively (HF/LANL2DZP). The geometry was optimised by using energy gradients obtained according to the algorithm of Schlegel,[23] and the HF/LANL2DZP energy of the stationary point reached at the end of the optimisation was calculated. The HF/LANL2DZP-optimised geometry was re-optimised by using energy gradients from second-order perturbation calculation according to Møller and Plesset using the above-mentioned basis set (MP2/LANL2DZP). Again, the energy of the stationary point at the end of the optimisation was calculated. The chemical bonds of the optimised molecule were analysed in terms of natural bond orbitals (NBO).[24,25] The normal modes of vibration were then calculated from numerical (GAUSSIAN94) or analytical (GAUSSIAN98) force constants. By means of statistical thermodynamics, the enthalpy at 298 K, H^{298}, was calculated. Only MP2/LANL2DZP molecular structures, energies, and enthalpies are given in this paper.

Acknowledgments

H. F. would like to thank the Fonds der Chemischen Industrie and the Johannes-Gutenberg-Universität Mainz for financial support.

[1] N. N. Greenwood, B. P. Straughan, A. E. Wilson, *J. Chem. Soc. A* **1968**, 2209−2212.
[2] D. B. Denney, D. Z. Denney, P. J. Hammond, Y. F. Hsu, *J. Am. Chem. Soc.* **1981**, *103*, 2340−2347.
[3] K. C. Malhotra, N. Sharma, R. Sharma, S. C. Chaudhry, *J. Indian Chem. Soc.* **1990**, *67*, 793−795.
[4] H. Meerwein, T. Bersin, *Justus Liebigs Ann. Chem.* **1929**, *476*, 139.
[5] H. E. Gottlieb, S. Hoz, I. Elyashiv, M. Albeck, *Inorg. Chem.* **1994**, *33*, 808−811.
[6] R. C. Mehrotra, S. N. Mathur, *J. Indian Chem. Soc.* **1965**, *42*, 1−4.
[7] R. C. Mehrotra, S. N. Mathur, *J. Indian Chem. Soc.* **1967**, *44*, 216−218.
[8] N. Sudha, H. B. Singh, *Coordination Chemistry Reviews* **1994**, *135/136*, 469−515 and references cited therein.
[9] A. Panda, G. Mugesh, H. B. Singh, R. J. Butcher, *Organometallics* **1999**, *18*, 1986−1993.
[10] H. Fleischer, D. Schollmeyer, *Inorg. Chem.* **2001**, *40*, 324−328.
[11] *Tables of Interatomic Distances and Configurations in Molecules and Ions* (Ed.: L. Sutton), Spec. Publ. no. 11 and 18, The Chemical Society, London, **1958** and **1965**.
[12] A. Bondi, *J. Phys. Chem.* **1964**, *68*, 441−451.
[13] H. B. Singh, N. Sudha, R. J. Butcher, *Inorg. Chem.* **1992**, *31*, 1431−1435.
[14] H. Fleischer, *Eur. J. Inorg. Chem.* **2001**, 393−404.
[15] *SIR − A Program for the Automatic Solution fo Crystal Structures by Direct Methods:* A. Altomare, G. Cascarano, C. Giacovazzo, A. Guagliardi, M. C. Burla, G. Polidori, M. Camalli, *J. Appl. Crystallogr.* **1994**, *27*, 435−436.
[16] G. M. Sheldrick, SHELXL-97 *Program for crystal structure refinement*, University of Göttingen, Germany, **1997**.
[17] R. Blessing, *Acta Crystallogr., Sect. A* **1995**, *51*, 33−38.
[18] M. J. Frisch, G. W. Trucks, H. B. Schlegel, P. M. W. Gill, B. G. Johnson, M. A. Robb, J. R. Cheeseman, T. Keith, G. A. Petersson, J. A. Montgomery, K. Raghavachari, M. A. Al-Laham, V. G. Zakrzewski, J. V. Ortiz, J. B. Foresman, J. Cioslowski, B. B. Stefanov, A. Nanayakkara, M. Challacombe, C. Y. Peng, P. Y. Ayala, W. Chen, M. W. Wong, J. L. Andres, E. S. Replogle, R. Gomperts, R. L. Martin, D. J. Fox, J. S. Binkley, D. J. Defrees, J. Baker, J. P. Stewart, M. Head-Gordon, C. Gonzalez, J. A. Pople, *GAUSSIAN 94*, Revision E.2, Gaussian, Inc., Pittsburgh PA, **1995**.
[19] M. J. Frisch, G. W. Trucks, H. B. Schlegel, G. E. Scuseria, M. A. Robb, J. R. Cheeseman, V. G. Zakrzewski, J. A. Montgomery, Jr., R. E. Stratmann, J. C. Burant, S. Dapprich, J. M. Millam, A. D. Daniels, K. N. Kudin, M. C. Strain, O. Farkas, J. Tomasi, V. Barone, M. Cossi, R. Cammi, B. Mennucci, C. Pomelli, C. Adamo, S. Clifford, J. Ochterski, G. A. Petersson, P. Y. Ayala, Q. Cui, K. Morokuma, D. K. Malick, A. D. Rabuck, K. Raghavachari, J. B. Foresman, J. Cioslowski, J. V. Ortiz, B. B. Stefanov, G. Liu, A. Liashenko, P. Piskorz, I. Komaromi, R. Gomperts, R. L. Martin, D. J. Fox, T. Keith, M. A. Al-Laham, C. Y. Peng, A. Nanayakkara, C. Gonzalez, M. Challacombe, P. M. W. Gill, B. Johnson, W. Chen, M. W. Wong, J. L. Andres, C. Gonzalez, M. Head-Gordon, E. S. Replogle, J. A. Pople, *GAUSSIAN 98*, Revision A.6, Gaussian, Inc., Pittsburgh PA, **1998**.
[20] L. Szasz, *Pseudopotential Theory of Atoms and Molecules*, Wiley, New York, Chichester, Brisbane, Toronto, Singapore, **1985**.
[21] W. R. Wadt, P. J. Hay, *J. Chem. Phys.* **1985**, *82*, 284−298.
[22] A. Höllwarth, M. Böhme, S. Dapprich, A. W. Ehlers, A. Gobbi, V. Jonas, K. F. Köhler, R. Stegmann, A. Veldkamp, G. Frenking, *Chem. Phys. Lett.* **1993**, *208*, 237−240.
[23] H. B. Schlegel, *J. Comp. Chem.* **1982**, *3*, 214−218.
[24] A. E. Reed, R. B. Weinstock, F. Weinhold, *J. Chem. Phys.* **1985**, *83*, 735−746.
[25] A. E. Reed, L A. Curtiss, F. Weinhold, *Chem. Rev.* **1988**, *88*, 899−926.

Received January 16, 2002
[I02027]

Synthesis and Crystal Structures of the First Two Novel Dicarboxylate Organotin Polymers Constructed from Dimeric Tetraorganodistannoxane Units

Rui-Hu Wang,[a] Mao-Chun Hong,*[a] Jun-Hua Luo,[a] Rong Cao,*[a] and Jia-Bao Weng[a]

Keywords: Carboxylate ligands / Tin / X-ray diffraction / Polymers

Assembly of nitroterephthalic acid (H_2NTPA) or diphenic acid (H_2DPA) with trimethyltin chloride under hydrothermal conditions produces a one-dimensional chain polymer $[(Me_2Sn)_2(\mu_3\text{-NTPA})(\mu_3\text{-O})]_n$ (**1**) or a two-dimensional corrugated sheet polymer $[(Me_2Sn)_4(\mu_3\text{-DPA})(\mu_4\text{-DPA})(\mu_3\text{-O})_2]_n$ (**2**), respectively. Both consist of different types of dimeric dicarboxylatotetraorganodistannoxane secondary building units.

(© Wiley-VCH Verlag GmbH, 69451 Weinheim, Germany, 2002)

The design and synthesis of novel coordination polymers with unusual and tailorable structures are fundamental steps to discover and fabricate various technologically useful materials.[1−4] The majority of such species have been constructed from organic ligands and metal ions by spontaneous self-assembly. Recently, much effort has been devoted to the design and construction of new supramolecular frameworks by using metal clusters[5,6] or metal-organic secondary building units (SBUs)[7−13] as building blocks, and multifunctional organic ligands as linkers. Such assembly has resulted in a host of intriguing structural topologies and an extensive application in material science. For instance, the use of carboxylate-bridged zinc clusters as metal-organic SBUs and 1,4-benzenedicarboxylate or 1,3,5-benzenetricarboxylate as linkers by Yaghi et al. has provided several novel porous metal-organic frameworks which can absorb and desorb small gas molecules.[9−13]

It is well-known that the discrete dimeric dicarboxylatotetraorganodistannoxane complexes $\{[R_2Sn(O_2CR')_2O]_2\}$ have been extensively studied due to their wide application in biology and catalysis; most of them were obtained by the assembly of monofunctional carboxylate ligands and organotin reagents.[14−20] To the best of our knowledge, the crystal structures of only two organotin polymers containing dimeric tetraorganodistannoxane units have been reported.[21,22] It is predictable that extended structures may be obtained by using bifunctional dicarboxylate ligands instead of monofunctional carboxylate ligands as linkers and the dimeric tetraorganodistannoxane as nodes. However, the reported dicarboxylate organotin complexes exist as dinuclear[23−25] and one-dimensional zigzag chain structures.[26−29] With the aim of extending the chemistry of dimeric dicarboxylatotetraorganodistannoxane, we have recently begun to study the reactions of organotin and di- or polycarboxylic acid ligands under hydrothermal conditions. Here we report the syntheses and crystal structures of two novel organotin complexes consisting of dimeric dicarboxylatotetraorganodistannoxane SBUs, $[(Me_2Sn)_2(\mu_3\text{-NTPA})(\mu_3\text{-O})]_n$ (**1**) and $\{(Me_2Sn)_4(\mu_3\text{-DPA})(\mu_4\text{-DPA})(\mu_3\text{-O})_2\}_n$ (**2**), assembled from nitroterephthalic acid (H_2NTPA) or diphenic acid (H_2DPA) with trimethyltin chloride under hydrothermal conditions.

The hydrothermal reaction of H_2NTPA or H_2DPA, 4,4′-bipyridne and trimethyltin chloride in a molar ratio 1:1:2 at 140 °C for three days produced colorless crystals of **1** or **2**, respectively (Scheme 1). These compounds are insoluble in common solvents, such as water, methanol, acetone, acetonitrile, dichloromethane, tetrahydrofuran, *N*,*N*′-dimethylformamide and dimethyl sulfoxide. The presence of the carboxylate group was confirmed by very strong IR absorption peaks in the solid-state spectrum at 1647 and 1365 cm^{-1} for **1** and 1699 and 1680 cm^{-1} for **2**. Signals for the nitro group in **1** were identified at 1549, 1531 and 1340 cm^{-1}; these values are unchanged with respect to those of the starting acid.

A single crystal X-ray diffraction analysis reveals that complex **1** has a one-dimensional chain motif constructed from novel approximately rectangular rings. As shown in Figure 1, each ring is composed of two NTPAs and two dimeric tetraorganodistannoxane units. The dihedral angle of the two phenyl rings in the ring is 91.9° i.e. they are almost perpendicular. NTPA in a μ_3-bridging mode links two dimeric tetraorganodistannoxane units and the dimeric tetraorganodistannoxane units are shared by the approximate rectangular rings to form a one-dimensional chain coordination polymer. This structural feature of **1** is quite different from that of $\{([Me_2Sn(OAc)]_2O)_2\}_n$, the only known one-dimensional organotin polymer, in which the acetate

[a] Key Laboratory of Structural Chemistry, Fujian Institute of the Research on the Structure of Matter, Chinese Academy of Sciences,
Fuzhou, Fujian, 350002, China

Supporting information for this article is available on the WWW under http://www.eurjic.org or from the author.

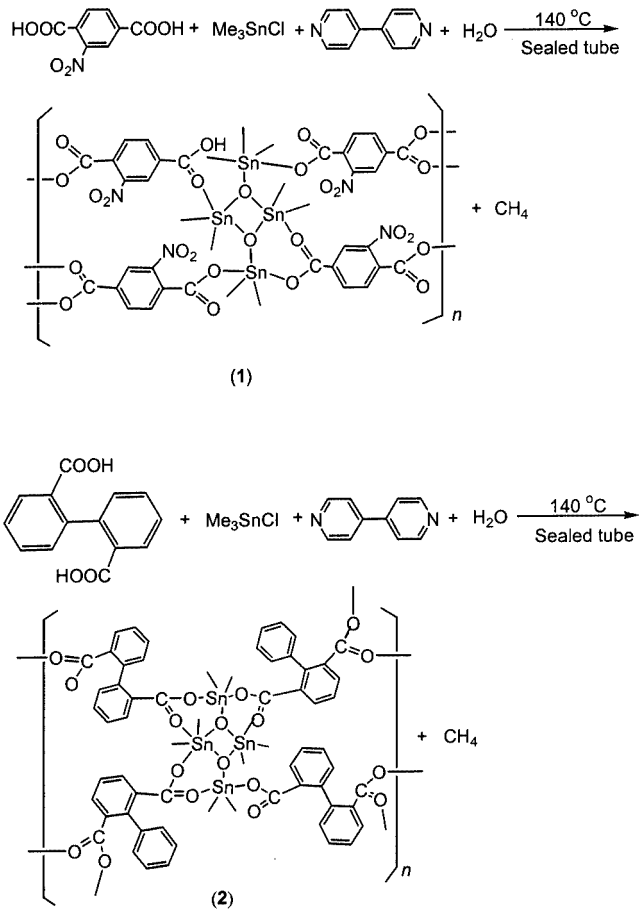

Scheme 1. Synthesis of complexes **1** and **2**

links the dimeric tetraorganodistannoxane units in a tetradentate mode.[21]

The SBU in **1** is the predominant structural form in five types of dimeric dicarboxylatotetraorganodistannoxane in which each Sn atom is in a five-coordinate geometry.[14] It consists of a central planar $(Me_2Sn)_2O_2$ four-membered ring and two peripheral Me_2Sn units attached to two μ_3-oxygen atoms. NTPA acts as a tridentate ligand which coordinates to an outer Sn atom through an oxygen atom of the carboxylate adjacent to NO_2 and chelates between exocyclic and endocyclic Sn atoms forming a stable six-membered ring through the other carboxylate oxygen atoms. The NO_2 in NTPA is not involved in coordination to Sn atoms. Thus, the Sn atoms in the SBU adopt a distorted trigonal bipyramidal geometry. The exocyclic and endocyclic Sn atoms lie 0.1442 and 0.1492 Å out of the plane defined by the three coordinated oxygen atoms, respectively.

Complex **2** is a two-dimensional corrugated sheet polymer made up of the dimeric tetraorganodistannoxane units and bridging DPA ligands. As shown in Figure 2, the SBU in **2** is different from that in complex **1**. The central four-membered ring $(Me_2Sn)_2O_2$ is connected to two independently exocyclic Sn atoms through μ_3-oxygen atoms. The distance between the two Sn atoms in the four-membered ring is 3.325 Å, which is longer than 3.264 Å in complex **1**, but smaller than the sum of the van der Waals radii of Sn^{II} (3.40 Å), suggesting the possible presence of a weak metal-metal interaction. There are two types of DPA ligands which are distinguished by their bridging fashions. One acts as a tetradentate ligand and bridges a pair of exocyclic and endocyclic Sn atoms to form two stable six-membered rings; the other adopts a μ_3-bridging mode through bonding to an exocyclic Sn atom and chelating between exocyclic and endocyclic Sn atoms. Thus, an endocyclic Sn(1) atom adopts a six-coordinate geometry with a deviation of 0.0088 Å from the plane defined by the four coordinated oxygen atoms [O(1) O(2) O(11) and O(41)], two methyl groups occupy the apical positions, with a Me−Sn(1)−Me bond angle of 157.4°, and the other endocyclic Sn(3) atom and two exocyclic Sn atoms (Sn2 and Sn4) are a five-coordinate with deviations of 0.0191, 0.1161 and 0.0110 Å from the plane defined by the coordinated oxygen atoms, respectively.

In complex **2**, DPA is a chiral ligand and the dihedral angles of two phenyl rings are 99.4° for the tridentate mode and 87.1° for the tetradentate mode. It is noteworthy that a μ_4-bridging DPA moiety links the dimeric tetraorganodist-

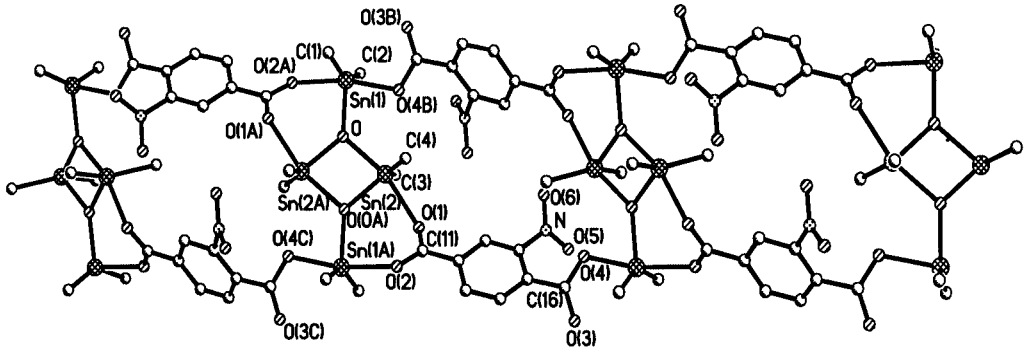

Figure 1. View of the one-dimensional chain in **1** with atomic numbering; selected bond lengths (Å): Sn(1)−C(1) 2.092(7) Sn(1)−C(2) 2.098(7), Sn(1)−O2.045(5), Sn(1)−O(2A) 2.290(5), Sn(1)−O(4B) 2.191(5), Sn(2)−C(3) 2.106(8), Sn(2)−C(4) 2.094(8), Sn(2)−O 2.137(4), Sn(2)−O(1) 2.267(5), Sn(2)−O(0A) 2.042(5), Sn(2)−Sn(2A) 3.2644(9); symmetry code: (A) $-x + 1/2, -y + 3/2, -z$; (B) $-x + 1, y, -z + 1/2$.

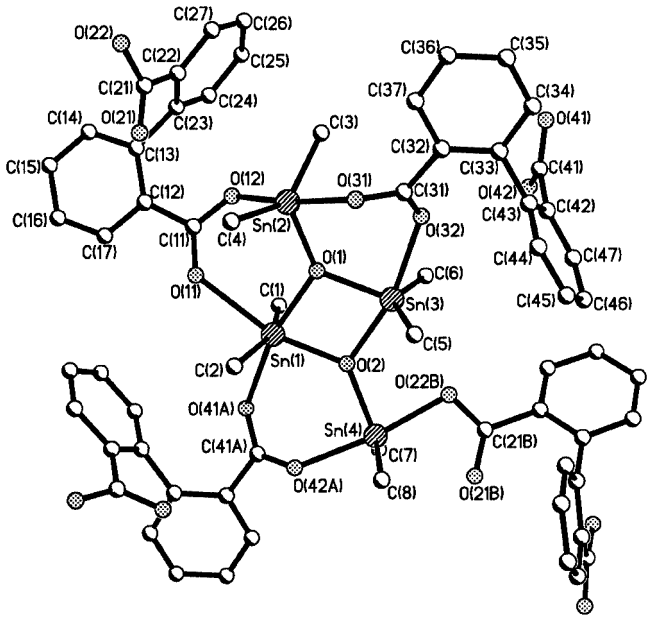

Figure 2. View of the SBU in **2** with atomic numbering; selected bond lengths (Å): Sn(1)−C(1) 2.084(9), Sn(1)−C(2) 2.106(8), Sn(1)−O(1) 2.183(5), Sn(1)−O(2) 2.078(5), Sn(1)−O(11) 2.514(7), Sn(1)−O(41A) 2.326(5), Sn(2)−C(3) 2.083(9), Sn(2)−C(4) 2.104(8), Sn(2)−O(1) 1.997(5), Sn(2)−O(12) 2.139(5), Sn(2)−O(31) 2.270(5), Sn(3)−C(5) 2.107(8), Sn(3)−C(6) 2.096(8), Sn(3)−O(1) 2.047(5), Sn(3)−O(2) 2.129(5), Sn(3)−O(32) 2.318(5), Sn(4)−C(7) 2.093(8), Sn(4)−C(8) 2.086(8), Sn(4)−O(2) 2.012(5), Sn(4)−O(22C) 2.171(5), Sn(4)−O(42A) 2.250(5); symmetry code: (A) $x + 1/2, -y + 1/2, z + 1/2$, (C) $x - 1/2, -y + 1/2, z + 1/2$.

annoxane units, forming a helical chain, and a μ_3-bridging DPA moiety links the helical chains by ligating the remaining coordination sites of the dimeric tetraorganodistannoxane units, forming a curved two-dimensional sheet structure (Figure 3). The main structural feature of **2** is quite different from that of a two-dimensional rhombohedral grid polymer composed of ladder-type dimeric tetraorganodistannoxane units and 4-hydroxyl-3-methoxybenzoic acid dianion.[22] As shown in Figure 4, the two-dimensional sheet is folded in a highly corrugated way with DPA as the turning points when viewed along *c* axis. The distance between adjacent sheets is 9.54 Å.

In summary, this work demonstrates that the assembly of dicarboxylate ligands — such as nitroterephthalic acid and diphenic acid — and trimethyltin chloride allows for the formation of organotin polymers consisting of dimeric dicarboxylatotetraorganodistannoxane units, which act as metal-organic SBUs in the extended structures. To the best of our knowledge, they are the first dicarboxylate polymers consisting of dimeric dicarboxylatotetraorganodistannoxane SBUs of which the crystal structures have been determined. Thus, our report may open a new approach for the assembly of different types of discrete dimeric dicarboxylatotetraorganodistannoxane complexes into extended polymers through using di- or polycarboxylates as linker ligands instead of monofunctional carboxylates. Extension of this work, including more di- or polycarboxylate ligands and other organotin compounds, is in progress.

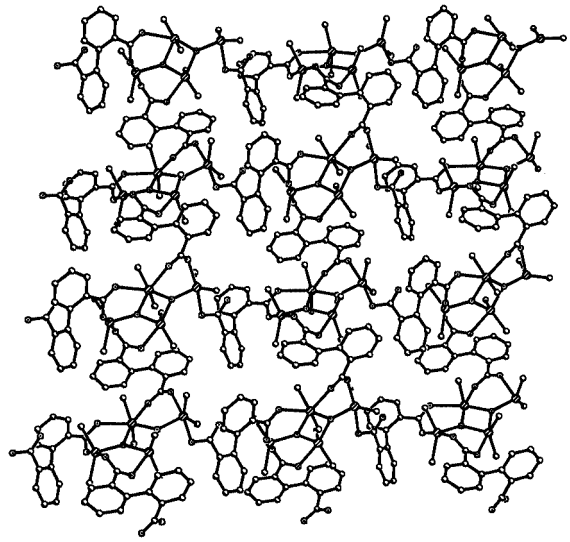

Figure 3. View of the two-dimensional sheet along the *b* axis in **2**

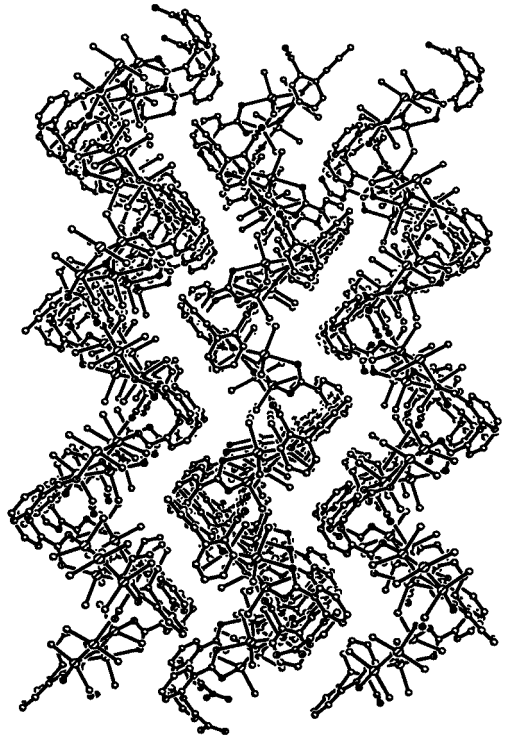

Figure 4. View of the corrugated sheet along the *c* axis in **2**

Experimental Section

Synthesis of $[(Me_2Sn)_4(\mu_3\text{-}O)_2(\mu_3\text{-}NTPA)_2]_n$ (1): A mixture of H_2NTPA (0.11 g, 0.5 mmol), 4,4′-bipyridne (0.08 g, 0.5 mmol) and

trimethyltin chloride (0.20 g, 1 mmol) in 16 mL of H_2O was placed in a Parr Teflon-lined stainless steel vessel and heated to 140 °C for 72 h, then cooled to room temperature during 5 hours. Colorless crystals were obtained and collected by filtration and washed with water. Yield: 56%. $C_{12}H_{15}NO_7Sn_2$ (522.6): calcd. C 27.58, H 2.87, N 2.68; found C 27.23, H 2.67, N 2.54. IR (KBr pellet): $\tilde{\nu}$ = 3456 (w), 3084 (vw), 2918 (vw), 1647 (s), 1591 (s), 1549 (m), 1531 (s), 1491 (m), 1412 (s), 1365 (s), 1340 (s), 1304 (m), 1254 (w), 1147 (vw), 1066 (vw), 928 (vw), 825 (w), 796 (m), 783 (m), 633 (m), 577 (m), 499 (m) cm^{-1}.

Synthesis of $\{(Me_2Sn)_4(\mu_3\text{-}O)_2(\mu_3\text{-}DPA)(\mu_4\text{-}DPA)\}_n$ (2): The procedure is similar to the synthesis of complex **1** except that H_2DPA (0.12 g, 0.5 mmol) was used instead of H_2NTPA. Yield: 70%. $C_{36}H_{40}O_{10}Sn_4$ (1107.5): calcd. C 39.04, H 3.61; found C 39.32, H 3.43%. IR (KBr pellet): $\tilde{\nu}$ = 3061 (w), 2864 (m), 2825 (m), 1699 (s), 1680 (s), 1599 (s), 1572 (m), 1539 (w), 1475 (w), 1452 (w), 1412 (w), 1360 (s), 1250 (s), 1213 (s), 1140 (m), 1099 (w), 1063 (m), 1003 (m), 939 (w), 822 (vw), 808 (m), 796 (m), 758 (m), 708 (w), 625 (m), 584 (vw) cm^{-1}.

X-ray crystallography: The crystal data and structure determination summary for **1** and **2** are listed in the Table 1. Intensity data for **1** and **2** were measured on a Siemens Smart CCD diffractometer with graphite-monochromated Mo-K_α radiation (λ = 0.71073 Å) at 298 K. Empirical absorption corrections were applied with the SADABS program. The structures were solved by direct methods and all calculations were performed using the SHELXL PC program. The positions of the H-atoms were generated geometrically (C−H bond fixed at 0.96 Å), assigned isotropic thermal parameters, and allowed to ride on their parent carbon atoms before the final cycle of refinement. The structures were refined by full-matrix least-squares minimization of $\Sigma(F_o - F_c)^2$ with anisotropic thermal parameters for all atoms except the H-atoms.
CCDC-181351 (**1**) and -181352 (**2**) contain the supplementary crystallographic data for this paper. These data can be obtained free of charge at www.ccdc.cam.ac.uk/conts/retrieving.html [or from the Cambridge Crystallographic Data Centre, 12, Union Road, Cambridge CB2 1EZ, UK; Fax: (internat.) +44-1223/336-033; E-mail: deposit@ccdc.cam.ac.uk].

Table 1. Crystallographic data for complexes **1** and **2**

	1	**2**
Empirical formula	$C_{12}H_{15}NO_7Sn_2$	$C_{36}H_{40}O_{10}Sn_4$
Mol. wt.	522.63	1107.44
Crystal system	monoclinic	monoclinic
Space group	*C*2/*c*	$P2_1/n$
a, Å	15.1164(4)	13.9872(3)
b, Å	12.6447(1)	19.0810(4)
c, Å	17.4594(5)	16.0374(4)
β, deg	90.549(2)	107.295(1)
V, Å^3	3337.08(13)	4086.69(16)
Z	8	4
D_c, g cm^{-3}	2.080	1.800
μ, cm^{-1}	30.24	24.67
*R*1 [$I > 2\sigma(I)$][a]	0.0419	0.0471
*wR*2 (all data)[b]	0.1150	0.1099

[a] $R = \|\|F_o| - |F_c\|\|/|F_o|$. [b] $wR = [w(F_o^2 - F_c^2)^2/w(F_o^2)^2]^{1/2}$.

Acknowledgments

This work was supported by the National Nature Science Foundation of China, the Nature Science Foundation of Fujian Province and the Key Project of Chinese Academy of Science.

[1] J. Makarević, M. Jokić, B. Perić, V. Tomisić, B. Kojić-Prodić, M. Zinić, *Chem. Eur. J.* **2001**, *7*, 3328−3341.
[2] H. Zhang, X. Wang, H. Zhu, W. Xiao, K. Zhang, B. K. Teo, *Inorg. Chem.* **1999**, *38*, 886−892.
[3] J. Hagrman, D. Hagrman, J. Zubieta, *Angew. Chem. Int. Ed.* **1999**, *38*, 2638−2684.
[4] L. R. MacGillivray, J. L. Reid, J. A. Ripmeester, *Chem. Commun.* **2001**, 1034−1035.
[5] F. A. Cotton, C. Lin, C. A. Murillo, *Acc. Chem. Res.* **2001**, *34*, 759−771 and references therein.
[6] D. L. Caulder, K. N. Raymond, *J. Chem. Soc., Dalton Trans.* **1999**, 1185−1200.
[7] S. A. Bourne, J. Lu, A. Mondal, B. Moulton, M. J. Zaworotko, *Angew. Chem. Int. Ed.* **2001**, *40*, 2111−2113.
[8] S. O. H. Gutschke, D. J. Price, A. K. Powell, P. T. Wood, *Eur. J. Inorg. Chem.* **2001**, 2739−2741.
[9] M. Eddaoudi, D. B. Moler, H. Li, B. Chen, T. M. Reineke, M. O'Keeffe, O. M. Yaghi, *Acc. Chem. Res.* **2001**, *34*, 319−330.
[10] M. Eddaoudi, H. Li, O. M. Yaghi, *J. Am. Chem. Soc.* **2000**, *122*, 1391−1397.
[11] H. Li, M. Eddaoudi, M. O'keeffe, O. M. Yaghi, *Nature* **1999**, *402*, 276−279.
[12] H. Li, M. Eddaoudi, T. L. Groy, O. M. Yaghi, *J. Am. Chem. Soc.* **1998**, *120*, 8571−8572.
[13] H. Li, C. E. Davis, T. L. Groy, D. G. Kelly, O. M. Yaghi, *J. Am. Chem. Soc.* **1998**, *120*, 2186−2187.
[14] E. R. T. Tiekink, M. Gielen, A. Bouhdid, M. Biesemans, R. Willem, *J. Organomet. Chem.* **1995**, *494*, 247−253.
[15] F. Ribot, C. Sanchez, A. Meddour, M. Gielen, E. R. T. Tiekink, M. Biesemans, R. Willem, *J. Organomet. Chem.* **1998**, *552*, 177−186.
[16] S. P. Narula, S. Kaur, S. K. Bharadwaj, R. K. Chadha, *J. Organomet. Chem.* **1996**, *506*, 181−190.
[17] V. S. Petrosyan, N. S. Yashina, T. V. Drovetskaia, A. V. Yatsenko, L. A. Aslanov, L. Pellerito, *Appl. Organometallic Chem.* **1996**, *10*, 523−530.
[18] C. Vatsa, V. K. Jain, T. K. Das, E. R. T. Tiekink, *J. Organomet. Chem.* **1991**, *421*, 21−28.
[19] M. Danish, S. Ali, M. Mazhar, A. Badshah, *Main Group Metal Chem.* **1996**, *19*, 121−131.
[20] J. A. Blie, R. A. Howie, J. L. Wardell, P. J. Cox, *Polyhedron* **1997**, *16*, 881−888.
[21] T. P. Lockhart, W. F. Manders, E. M. Holt, *J. Am. Chem. Soc.* **1986**, *108*, 6611−6616.
[22] R.-G. Xiong, J.-L. Zuo, X.-Z. You, H.-K. Fun, S. S. Raj, *Organometallics* **2000**, *19*, 4183−4186.
[23] B. D. James, L. M. Kivlighon, B. W. Skelton, A. H. White, *Appl. Organometallic Chem.* **1998**, *12*, 13−23.
[24] S.-I. Aizawa, T. Natsume, K. Hatano, S. Funahashi, *Inorg. Chim. Acta* **1996**, *248*, 215−224.
[25] S. W. Ng, S. S. S. Raj, I. A. Razak, H.-K. Fun, *Main Group Metal Chem.* **2000**, *23*, 193−201.
[26] S. W. Ng, V. G. K. Das, E. R. T. Tiekink, *J. Organomet. Chem.* **1991**, *403*, 111−117.
[27] J. H. Wengrovius, M. F. Garbauskas, *Organometallics* **1992**, *11*, 1334−1342.
[28] G. Stocco, G. Guli, M. A. Girasolo, G. Bruno, F. Nicolo, R. Scopelliti, *Acta Crystallogr., Sect. C* **1996**, *52*, 829−832.
[29] Z. Arifin, E. J. Filmore, J. D. Donaldson, S. M. Grimes, *J. Chem. Soc., Dalton Trans.* **1984**, 1965−1968.

Received March 11, 2002
[I02126]

A Single-Strand Helical Motif Induced by Self-Assembly of $[Ag(TFP)]^+$ Moieties with Nitrate Anions − ^{31}P NMR Spectroscopic and X-ray Crystal Structure Characterization of the Complexes Involved in Equilibrium Reactions of Silver Salts and TFP Ligand

Fiorella Bachechi,[a] Alfredo Burini,*[b] Rossana Galassi,[b] Bianca Rosa Pietroni,[b] and Dania Tesei[b]

Keywords: P ligands / Silver / Helical structures / NMR spectroscopy / Equilibrium reactions

The ability of the ligand tris(2-furyl)phosphane (TFP) to coordinate Ag^I ions has been investigated. The molar ratio and the nature of the counterions used (NO_3^-; BF_4^-) affected the reaction. Moreover, equilibrium reactions were observed and the $[Ag(TFP)_n]^+$ (n = 1–4) species involved were identified by variable-temperature ^{31}P NMR spectroscopy. The $[Ag(TFP)_3]BF_4$ complex turned out to be the more labile species in solution and it disproportionates by means of an S_N2 mechanism to yield the complexes $[Ag(TFP)_2(H_2O)]BF_4$ (**3**) and $[Ag(TFP)_4]BF_4$ (**4**). Most of the compounds detected in solution were isolated and characterized in the solid state. The molecular structures of the complexes $[Ag(TFP)NO_3]$ (**1**), $[Ag(TFP)_3NO_3]$ (**2**), and $[Ag(TFP)_2(H_2O)]BF_4$ (**3**) were determined by X-ray crystal structure diffraction confirming the solution characterization data. In these structures the TFP ligand was always only bonded to the metal centre by the phosphorous atom. It is noteworthy to underline that the molecular structure of complex **1** consists of an infinite single-strand helix arising from the ability of the bridging nitrate anions to connect the $[Ag(TFP)]^+$ units. In the structure the nitrate anions are coordinated to the metal centres in unusual modes acting simultaneously as chelating and bridging ligands.

(© Wiley-VCH Verlag GmbH, 69451 Weinheim, Germany, 2002)

Introduction

There is a growing interest in investigating the role of tris(2-furyl)phosphane (TFP) in catalytic systems[1] and a comparative study between the function of Ph_3P or TFP in palladium(0)-catalysed reactions has been reported.[2] The coordinative ability of TFP with transition metal ions is not well known and few examples of TFP complexes have been structurally characterized, i.e. $[Fe_2(CO)_5(TFP)\mu\text{-}P(2\text{-furyl})_2]$[3] and $[Rh(CO)Cl_2(TFP)_2HgCl]$.[4]

As a part of an investigation on the chemistry of late transition metal ions coordinated to tertiary phosphane ligands containing heterocycles[5,6] we have studied the ability of TFP to coordinate Ag^I.

Silver(I) is one of the metal ions involved in the formation of helical compounds obtained by the self-assembly of silver salts and appropriate ligands.[7,8] Helical motifs are of great current interest in supramolecular chemistry,[9] organic synthesis,[10] material science[11] and metal complex drugs.[12] In general, the organization in helical structures derives from coded self-assembly of metal ions and simple ligands. Here we report the formation of a single-strand helical polymer governed by the nitrate counterion instead of the ancillary ligand coordinated to the metal centre. It is well known that even weakly coordinating anions have an effect on the coordination number and on the molecular structure of the transition metal complexes.[13] Thus, as far as silver(I) derivatives are concerned, different arrangements occur depending on the anion used. Tetranuclear cubane-like compounds $[AgPR_3X]_4$ (R = Et or Ph) were isolated when strongly coordinating anions (X^-) such as Cl^- or Br^- were used,[14,15] while mononuclear derivatives (i.e. $[Ag(PCy_3)_2NO_3]$, $[Ag(PCy_3)_2ClO_4]$) have been obtained by using weakly coordinating anions. In these last examples the silver ions are tetracoordinated and tricoordinated, respectively.[16] However, bicoordinated $[Ag(PR_3)_2]X$ compounds have also been structurally characterized {e.g.$[Ag\{P(CH_2CH_2CN)_3\}_2]NO_3$,[17] $[Ag\{P(mes)_3\}_2]PF_6$ (mes = $C_6H_2Me_3$-2,4,6)}.[18] Moreover, the NO_3^- counterion influences the ring conformations and the nuclearity of cyclic silver derivatives.[5,19]

[a] Istituto di Strutturistica Chimica "G. Giacomello" CNR, Roma, Italy
[b] Dipartimento di Scienze Chimiche Università di Camerino, Via S. Agostino 1, 62032 Camerino, Italy
Fax: (internat.) + 39-0737/637345
E-mail: alfredo.burini@unicam.it

Results and Discussion

The reactions of TFP phosphane ligand with silver(I) ions were affected by the molar ratio and by the nature of

the counterion used and equilibrium reactions were observed. With $AgNO_3$ as the silver salt and a 1:1 or 1:3 Ag/TFP molar ratio, the complexes $[Ag(TFP)NO_3]$ (**1**) and $[Ag(TFP)_3NO_3]$ (**2**) were isolated. Two other species: $[Ag(TFP)_2(H_2O)]BF_4$ (**3**) and $[Ag(TFP)_4]BF_4$ (**4**) were obtained treating TFP with $AgBF_4$ in THF solution and with either a 1:1 or 1:2 Ag/TFP molar ratio. Compound **4** is insoluble in THF and for this reason it was easily separated from the reaction mixture containing the more soluble compound **3**. However, compound **4** can be obtained in good yields when the right stoichiometry is used. The silver complexes synthesized and studied are represented in Scheme 1.

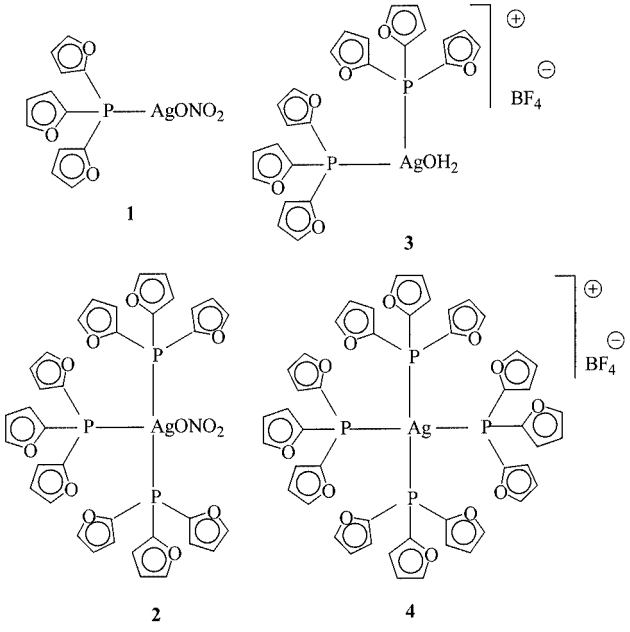

Scheme 1

The molecular structures of compounds **1**−**3** were obtained by X-ray crystal structure determinations while the species present in solution were identified by variable-temperature ^{31}P NMR investigations.

Molecular and Crystal Structure of $[Ag(TFP)NO_3]$ (1)

The molecular structure of complex **1** with the atom numbering scheme is shown in Figure 1 and selected bond lengths and angles are listed in Table 1. In the solid-state structure of **1**, the silver ion is tetracoordinated. It is only linked to the potentially bidentate TFP ligand by the phosphorus atom; with a P(1)−Ag(1) distance of 2.366(3) Å. This length is short but still in the range of the P−Ag bond lengths (2.50−2.37 Å) found in other tertiary (phosphane)-silver derivatives.[16,17,20,21] The coordination sphere around the silver ion is completed by three oxygen atoms of the nitrate anion which is coordinated to the metal centre in quite a complex and unusual mode. In fact the nitrate group is bonded to the silver ion by O(4) [Ag(1)−O(4) = 2.38(1) Å] and O(6) [Ag(1)−O(6) = 2.63(1) Å] as an asymmetric

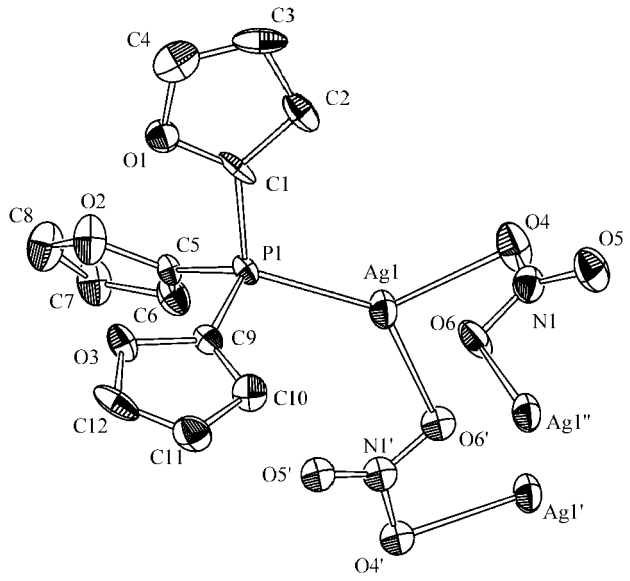

Figure 1. ORTEP plot of complex **1**, with the numbering schemes of the atoms; primed atoms are related by $P2_1$ symmetry with operators $-x$, $1/2 + y$, $1/2 - z$ for Ag(1) and $-x$, $-1/2 + y$, $1/2 - z$ for Ag(1′); thermal ellipsoids are shown at 40% probability levels

chelating ligand. In addition, O(6′) [symmetry-related by a 2_1 screw axis to O(6)] is coordinated to the same silver ion Ag(1) [Ag(1)−O(6′) = 2.35(1) Å] and O(6) is coordinated to a silver ion Ag(1′′) {symmetry-related by a 2_1 screw axis to Ag(1)} [Ag(1′′)−O(6) = 2.35(1) Å]. In this way the nitrate anion acts as both a chelating and a bridging ligand. On the whole the Ag−O distances observed in compound **1** are similar to those found in $[Ag(PPh_3)NO_3]$ showing a zigzag chain of $AgNO_3$,[20] but they are shorter than those found in the related polymeric helical complex $[Ag(pydz)NO_3]$ (pydz = pyridazine).[7] However, the most relevant feature of the structure arises from the ability of the bridging nitrate anions to connect each $[Ag(TFP)]^+$ unit, forming an infinite single-strand helix, Figure 2. The silver ion also weakly interacts with O(5) of the 2_1-symmetry-related nitrate anion through the long 2.95(1) Å distance. Neglecting this last interaction, the coordination geometry around the metal centre can be described as a distorted tetrahedron with coordination angles P(1)−Ag(1)−O(4) = 128.1(3)°, P(1)−Ag(1)−O(6′) = 132.0(2)°, O(4)−Ag(1)−O(6′) = 99.9(3)°, and a bite angle of the nitrate group O(4)−Ag(1)−O(6) = 45.9(2)°. The crystal structure consists of the packing of single helices of both chiralities, coupled by centres of symmetry running along the *b* axis, Figure 3. The period of the helix is 7.37(1) Å and along the helix the Ag atoms lie at distances of 4.890(1) Å. The distance between Ag atoms, which belong to close centrosymmetric helices, is 5.642(2) Å. It is interesting to note that, from the particular arrangement of the helices, channels are formed in the centrosymmetric unit cell where small molecules could be trapped even though this has not yet been attempted.

Table 1. Selected bond lengths [Å] and angles [°] with e.s.d. values in parentheses

Complex **1**				Complex **2**			
Ag(1)−P(1)	2.366(3)	P(1)−Ag(1)−O(4)	128.1(3)	Ag(1)−P(1)	2.508(7)	P(1)−Ag(1)−P(2)	110.2(3)
Ag(1)−O(4)	2.38(1)	P(1)−Ag(1)−O(6′)	132.0(2)	Ag(1)−P(2)	2.512(7)	P(1)−Ag(1)−P(3)	113.9(2)
Ag(1)−O(6)	2.63(1)	O(4)−Ag(1)−O(6′)	99.9(3)	Ag(1)−P(3)	2.493(7)	P(1)−Ag(1)−O(11)	92(1)
Ag(1)−O(6′)	2.35(1)	Ag(1)−P(1)−C(1)	114.2(4)	Ag(1)−O(11)	2.71(3)	P(1)−Ag(1)−O(12)	130(1)
P(1)−C(1)	1.78(1)	Ag(1)−P(1)−C(5)	114.7(4)	Ag(1)−O(12)	2.72(4)	P(2)−Ag(1)−P(3)	115.8(3)
P(1)−C(5)	1.80(1)	Ag(1)−P(1)−C(9)	110.4(4)	P(1)−C(1)	1.74(2)	P(2)−Ag(1)−O(11)	99(1)
P(1)−C(9)	1.79(1)	Ag(1)−O(4)−N(1)	101.1(7)	P(1)−C(5)	1.76(3)	P(2)−Ag(1)−O(12)	98(1)
N(1)−O(4)	1.25(1)	Ag(1)−O(6)−N(1)	111.8(7)	P(1)−C(9)	1.82(2)	P(3)−Ag(1)−O(11)	122(1)
N(1)−O(5)	1.24(1)	C(1)−P(1)−C(5)	105.2(5)	P(2)−C(13)	1.82(3)	P(3)−Ag(1)−O(12)	87(1)
N(1)−O(6)	1.27(1)	C(1)−P(1)−C(9)	104.8(5)	P(2)−C(17)	1.78(3)	O(11)−Ag(1)−O(12)	42(1)
		C(5)−P(1)−C(9)	106.8(5)	P(2)−C(21)	1.81(3)	Ag(1)−P(1)−C(1)	115(1)
		O(4)−N(1)−O(5)	123(1)	P(3)−C(25)	1.80(3)	Ag(1)−P(1)−C(5)	119(1)
		O(4)−N(1)−O(6)	119(1)	P(3)−C(29)	1.74(3)	Ag(1)−P(1)−C(9)	110(1)
		O(5)−N(1)−O(6)	118(1)	P(3)−C(33)	1.80(3)	Ag(1)−P(2)−C(13)	110(1)
Complex **3**				O(10)−N(1)	1.26(3)	Ag(1)−P(2)−C(17)	121(1)
Ag(1)−P(1)	2.425(3)	P(1)−Ag(1)−P(2)	131.2(1)	O(11)−N(1)	1.09(3)	Ag(1)−P(2)−C(21)	116(1)
Ag(1)−P(2)	2.426(2)	P(1)−Ag(1)−O(7)	117.2(2)	O(12)−N(1)	1.11(4)	Ag(1)−P(3)−C(25)	117(1)
Ag(1)−O(7)	2.36(1)	P(2)−Ag(1)−O(7)	111.0(2)			Ag(1)−P(3)−C(29)	111(1)
P(1)−C(1)	1.78(1)	Ag(1)−P(1)−C(1)	115.5(4)			Ag(1)−P(3)−C(33)	116(1)
P(1)−C(5)	1.79(1)	Ag(1)−P(1)−C(5)	111.4(4)			C(1)−P(1)−C(5)	102(1)
P(1)−C(9)	1.80(1)	Ag(1)−P(1)−C(9)	114.3(4)			C(1)−P(1)−C(9)	105(1)
P(2)−C(13)	1.79(1)	Ag(1)−P(2)−C(13)	115.7(3)			C(5)−P(1)−C(9)	103(1)
P(2)−C(17)	1.77(1)	Ag(1)−P(2)−C(17)	115.9(3)			C(13)−P(2)−C(17)	104(1)
P(2)−C(21)	1.80(1)	Ag(1)−P(2)−C(21)	110.0(4)			C(13)−P(2)−C(21)	103(1)
F(1)−B(1)	1.28(3)	C(1)−P(1)−C(5)	107.3(5)			C(17)−P(2)−C(21)	101(1)
F(2)−B(1)	1.33(2)	C(1)−P(1)−C(9)	104.6(5)			C(25)−P(3)−C(29)	104(1)
F(3)−B(1)	1.47(2)	C(5)−P(1)−C(9)	102.7(6)			C(25)−P(3)−C(33)	102(1)
F(4)−B(1)	1.33(3)	C(13)−P(2)−C(17)	102.7(5)			C(29)−P(3)−C(33)	105(1)
		C(13)−P(2)−C(21)	106.8(6)			P(1)−C(1)−O(1)	124(2)
		C(17)−P(2)−C(21)	104.7(5)			O(10)−N(1)−O(11)	122(4)
		F(2)−B(1)−F(1)	114(1)			O(10)−N(1)−O(12)	114(4)
		F(3)−B(1)−F(1)	105(1)			O(11)−N(1)−O(12)	124(4)
		F(3)−B(1)−F(2)	108(1)				
		F(4)−B(1)−F(1)	110(1)				
		F(4)−B(1)−F(2)	114(1)				
		F(4)−B(1)−F(3)	102(1)				

Molecular Structure of $[Ag(TFP)_3NO_3]$ (2)

The molecular structure of complex **2**, with the atom numbering scheme, is shown in Figure 4 and selected bond lengths and angles are listed in Table 1. As far as we know, only one other example of $[Ag(PR_3)_3X]$ complexes has been reported in the literature, namely $[Ag(PPh_3)_3Cl]$,[22] showing a distorted tetrahedral geometry. Complex **2** contains mononuclear units in which the silver ion is five-coordinated by three phosphorus atoms of three TFP ligands and by two oxygen atoms belonging to the chelate nitrate ion. The geometry around the metal centre is a distorted square-base pyramid, where the silver ion lies 0.8098 Å out of the base formed by P(1), P(3), and two O atoms. The Ag−P bond lengths are longer [2.508(7), 2.512(7), 2.493(7) Å] than those found in complex **1** but slightly shorter than the Ag−P bond lengths found in $[Ag(PPh_3)_3Cl]$ (2.52−2.56 Å). The nitrate ion is symmetrically bonded to the silver ion with a bite angle of 42(1)° and the Ag(1)−O(11) and Ag(1)−O(12) bond lengths are 2.71(3) Å and 2.72(4) Å, respectively.

Molecular Structure of $[Ag(TFP)_2(OH_2)]BF_4$ (3)

The molecular structure of complex **3**, with the atom numbering scheme, is shown in Figure 5 and selected bond lengths and angles are listed in Table 1.

The silver atom of the sixteen-electron complex **3** is tricoordinated with a distorted trigonal geometry. The metal ion is bonded to two TFP ligands by the P atoms and to one oxygen atom of a water molecule. The two Ag−P bond lengths are equivalent [2.425(3) Å and 2.426(2) Å]. They are very close to those found in $[Ag\{P(C_6H_4Me\text{-}m)_3\}_2NO_3]$[17] (2.4128 Å), shorter than those found in $[Ag(PPh_3)_2NO_3]$[23] and $[Ag(PCy_3)_2NO_3]$ (ca. 2.44 Å),[16] but longer than those found in $[Ag(PCy_3)_2ClO_4]$[16] [2.394(2), 2.393(3) Å] and in $[Ag\{P(CH_2CH_2CN)_3\}_2]NO_3$ [2.3832(9) Å].[17] The P(1)−Ag(1)−P(2) angle is 131.2(1)°. In the molecular structure of complex **3** an oxygen atom of a water molecule is coordinated to the metal ion [Ag(1)−O(7) 2.36(1) Å], revealing the poor coordinative ability of the oxygen atoms present in the furyl rings of the TFP ligand. Only one structure was recently reported,[4]

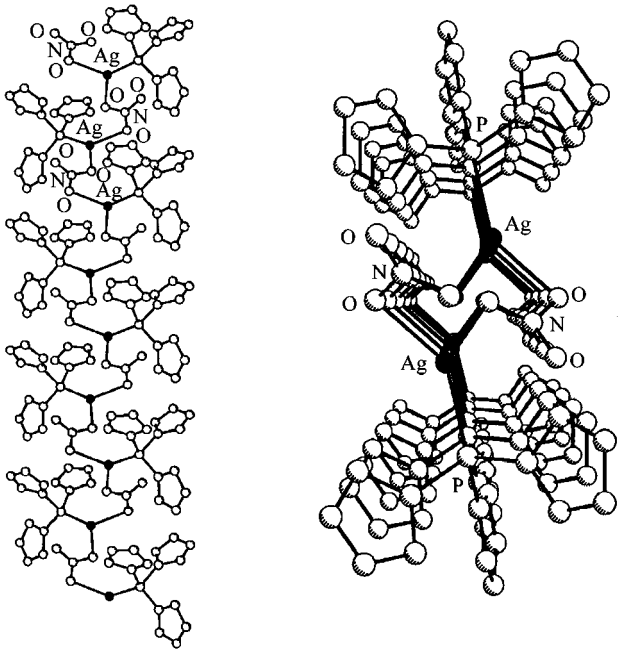

Figure 2. Complex **1**: (left) side view of the helical polymer chain extended along the crystallographic *b* axis with a helical period of 7.370(1) Å; the distance between Ag atoms is 4.891(1) Å; (right) top view along the axis of the polymer chain showing the twofold helical symmetry of the structure

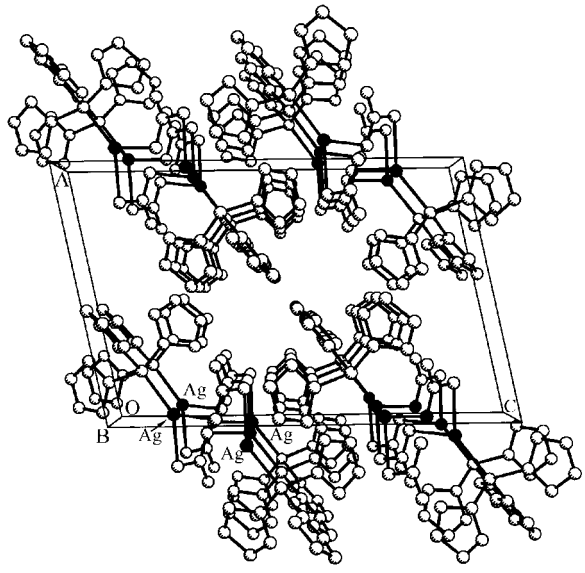

Figure 3. Unit cell content of complex **1** viewed down the *b* axis; adjacent chains are related by centres of symmetry

where the furyl rings interact through the oxygen atoms to the metal centre {i.e. $[Rh(CO)Cl_2(TFP)_2HgCl]$; Hg−O distances 2.855(3) and 3.025(3) Å}. The BF_4^- anion is present in the structure of **3** as a counterion and weakly interacts with the water molecule [O(7)···F(1) 3.09 Å and O(7)···F(2) 2.93 Å].

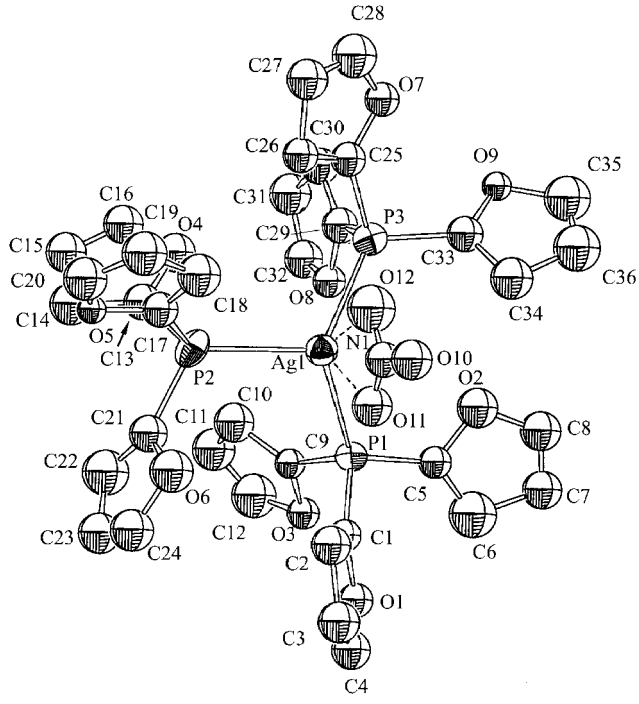

Figure 4. ORTEP plot of complex **2**, with the numbering schemes of the atoms; thermal ellipsoids are shown at 40% probability levels

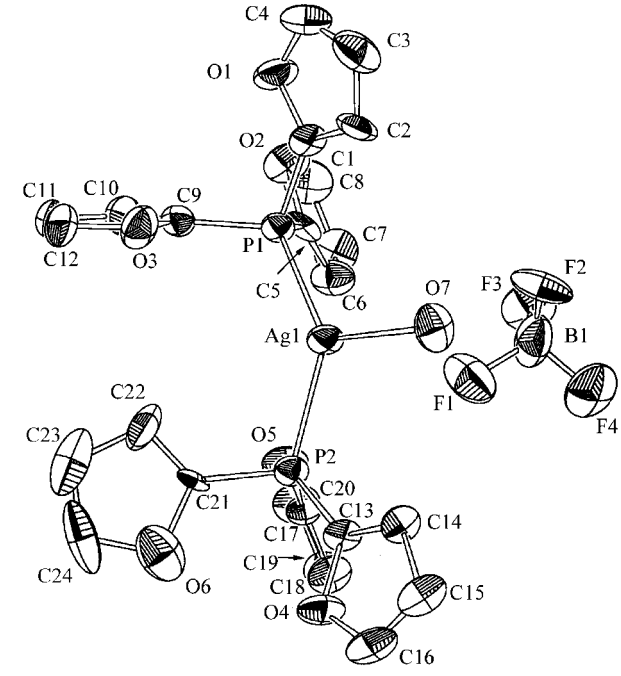

Figure 5. ORTEP plot of complex **3**, with the numbering schemes of the atoms; thermal ellipsoids are shown at 40% probability levels

^{31}P NMR Spectroscopic Investigation

The isolation in the solid state of several $[Ag(TFP)_nX]$ (n = 1−4; X = NO_3; BF_4) species highlights that equilibrium reactions could occur in solution. On the other hand silver(I) complexes are known to behave in this way when coordinated to labile monodentate ligands.[24,25] Thus to in-

Table 2. $^{31}P\{^{1}H\}$ NMR spectroscopic data of the Ag(TFP) species detected in $CDCl_3$ solution

Compound	δ (296 K)	δ (218 K)	$^{1}J(^{31}P,^{107}Ag)$ [Hz] (218 K)	$^{1}J(^{31}P,^{109}Ag)$ [Hz] (218 K)
TFP	−77.37 (s)			
TFP=O	−11.14 (s)	−10.00 (s)		
$[Ag(TFP)NO_3]$ (**1**)	−56.30 (m, br.)	−63.30 (dd)	699	803
$[Ag(TFP)_2NO_3]$		−62.40 (dd)	467	537
$[Ag(TFP)_2(OH_2)]BF_4$ (**3**)	−55.77 (s, br.)	−60.08 (dd)[a]	519[a]	573[a]
$[Ag(TFP)_3]BF_4$		−58.42 (d, br.)[a]		
$[Ag(TFP)_4]BF_4$ (**4**)	−57.48 (s, br.)	−56.74 (dd)	246	285

[a] The spectrum was recorded at 193 K in $CDCl_3$ + CF_2Br_2 solution.

vestigate this aspect, variable-temperature ^{31}P NMR spectra were recorded on compounds **1**−**4**, Table 2.

Compound **1**, that has a polymeric nature in the solid state, probably exists as a monomeric unit in solution. This hypothesis is reasonable because the silver ions forming the helical structure are held together only by bridging nitrate groups that, in solution, can easily break the bridging bonds. On the other hand the loss of the polymeric nature of compound **1** is underlined by the presence of the equilibrium reaction to be discussed.

Owing to rapid intermolecular ligand exchange in $CDCl_3$ solution, the ^{31}P NMR spectrum of compound **1**, recorded at 296 K, shows a broad signal at δ = −56.30 that is shifted to lower fields with respect to the free TFP ligand (δ = −77.37). By cooling the solution at 218 K the signal sharpened into two doublets of doublets, Figure 6. Each doublet of doublets is due to the spin-spin coupling of the phosphorus atom of the ligand with the two magnetically active isotopes of the silver ion (^{107}Ag spin 1/2, natural abundance 51.82%; ^{109}Ag spin 1/2, natural abundance 48.18%). Taking into consideration that the coupling constants decrease when the number of the phosphane ligands coordinated to the silver ion increase, the two AB systems of the ^{31}P NMR spectrum were assigned to $[Ag(TFP)NO_3]$ (**1**) and $[Ag(TFP)_2NO_3]$ complexes. Thus the signal centred at δ = −63.30, $^{1}J(^{31}P,^{107}Ag)$ = 699 Hz and $^{1}J(^{31}P,^{109}Ag)$ = 803 Hz was assigned to compound **1**; while the doublet of doublets centred at δ = −62.40, $^{1}J(^{31}P,^{107}Ag)$ = 467 Hz and $^{1}J(^{31}P,^{109}Ag)$ = 537 Hz was attributed to the compound $[Ag(TFP)_2NO_3]$. The values of the coupling constants observed for both complexes are in perfect agreement with the expected magnetogyric ratios. This interpretation of the spectrum was confirmed by the isolation in the solid state of complex $[Ag(TFP)_2(OH_2)]BF_4$ (**3**) showing the chemical shift of the ^{31}P nucleus and the Ag,P coupling constants similar to that observed for the species $[Ag(TFP)_2NO_3]$ identified only in solution (see discussion reported below). From the data the following equilibrium reaction seems to occur in solution:

$2\ [Ag(TFP)NO_3] \rightleftarrows [Ag(TFP)_2NO_3] + AgNO_3$.

The ^{31}P NMR spectrum of the analytically pure sample of $[Ag(TFP)_3NO_3]$ (**2**) recorded in $CDCl_3$ solution at 296 K shows two signals, a sharp one at δ = −11.14 and a broad one at δ = −57.00. By cooling the solution to 218 K the phosphorus, silver spin-spin coupling is solved, Figure 7. The spectrum shows a singlet at δ = −10.00 assigned to tris(2-furyl)phosphane oxide and a doublet of doublets at δ = −62.40 [$^{1}J(^{31}P,^{107}Ag)$ = 467 Hz and $^{1}J(^{31}P,^{109}Ag)$ = 537 Hz] that, as reported above, belongs to the $[Ag(TFP)_2NO_3]$ complex. Thus, we can conclude that when the complex $[Ag(TFP)_3NO_3]$ is dissolved in the presence of atmospheric oxygen, it gives rise to a dissociative process, and a fast oxidation of the free TFP ligand occurs. The lability of complex **2** in solution results in low yields of this compound.

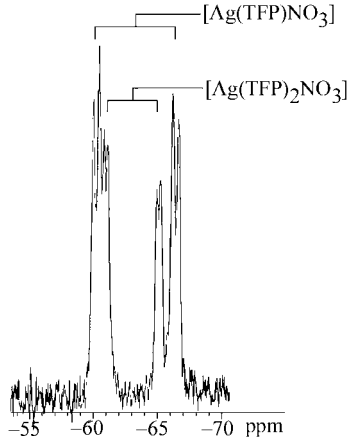

Figure 6. ^{31}P NMR spectrum recorded at 218 K; the signal centred at δ = −63.30 belongs to the complex $[Ag(TFP)NO_3]$ (**1**) while the doublet of doublets centred at δ = −62.40, was attributed to the compound $[Ag(TFP)_2NO_3]$

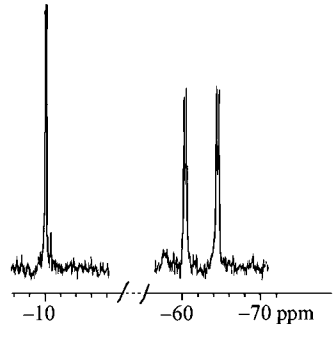

Figure 7. ^{31}P NMR spectrum recorded at 218 K; the species $[Ag(TFP)_3NO_3]$ decomposed in $CDCl_3$ solution to give tris-(2-furyl)phosphane oxide and $[Ag(TFP)_2NO_3]$ signals at δ = −10.00 and −62.40, respectively

Differing from the compounds discussed above, complexes **3** and **4** were simultaneously obtained by the same reaction mixture (see Exp. Sect.). This could be explained taking into consideration, the hypothesis, that in the first step the labile complex $[Ag(TFP)_3]BF_4$ is formed, which disproportionates to give the bis and tetrakis complexes **3** and **4**, respectively. The plausible S_N2 mechanism is reported in Scheme 2. The presence of water molecules in the reaction mixture could be due to the highly hygroscopic $AgBF_4$ salt used in the reaction.

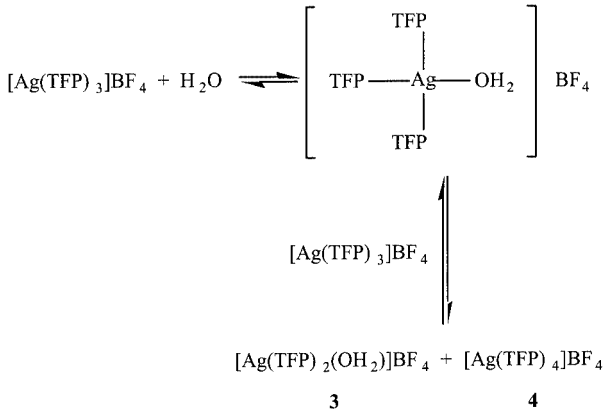

Scheme 2

The proposed mechanism and the equilibrium reactions involved were confirmed by the ^{31}P NMR spectrum obtained after dissolving an analytical sample of **3** in $CDCl_3$. The spectrum recorded at 193 K is shown in Figure 8. It consists of three systems centred at $\delta = -60.08$, -58.42, and -56.74. On the basis of the coupling constants the doublet of doublets at $\delta = -60.08$ [$^1J(^{31}P,^{107}Ag) = 519$ Hz and $^1J(^{31}P,^{109}Ag) = 573$ Hz] was assigned to complex **3**, while the doublet of doublets at $\delta = -56.74$ [$^1J(^{31}P,^{107}Ag) = 246$ Hz and $^1J(^{31}P,^{109}Ag) = 285$ Hz] was attributed to the tetrakis complex **4**. The different chemical shift (ca. 2 ppm) of **3** compared to that observed in the analogous $[Ag(TFP)_2NO_3]$ complex, could be due to the influence of the different anions of these two complexes or to the water molecule presents in the coordination sphere of **3**. The last signal of the spectrum centred at $\delta = -58.42$ consists of an unresolved doublet of doublets belonging to the species $[Ag(TFP)_3]BF_4$, that being labile, gives quite a broad signal at low temperatures. The complex was not isolated in the solid state; thus, it seems to be only a transient species in solution.

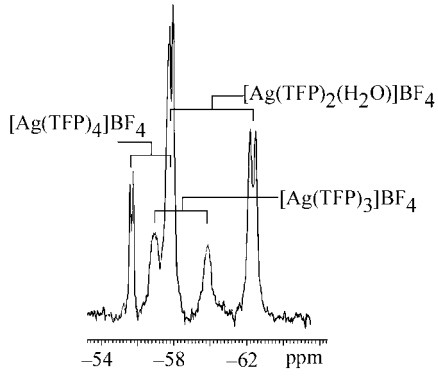

Figure 8. ^{31}P NMR spectrum recorded at 193 K; the three systems centred at $\delta = -60.08$, -58.42, and -56.74 were assigned to the complexes $[Ag(TFP)_2(H_2O)]BF_4$ (**3**) $[Ag(TFP)_3]BF_4$ and $[Ag(TFP)_4]BF_4$ (**4**), respectively

A successful attempt to obtain complex **4** in good yield was done treating the TFP ligand and $AgBF_4$ in a 4:1 molar ratio; from this reaction mixture only a small amount of complex **3** was obtained. The ^{31}P NMR spectrum of an analytical sample of **4** recorded at 296 K shows a sharpened signal at $\delta = -57.48$ that is solved in a doublet of doublets at 218 K, the chemical shifts and the coupling constants observed were the same as those reported above. The ligand lability of complex **4** is confirmed by the loss of the Ag,P coupling at temperatures above ca. 218 K.

Experimental Section

General: Elemental analyses were carried out with a Carlo Erba 1106 elemental microanalyser. ^1H and ^{31}P NMR spectra were performed in $CDCl_3$ solution with Varian VXR-300 spectrometers. Referencing is relative to TMS (^1H) and 85% H_3PO_4 (^{31}P). Variable-temperature ^{31}P NMR spectroscopic experiments were recorded over the temperature range 193−296 K. The reactions were carried out in the darkness at room temperature under nitrogen and with purified solvents.

Reaction of TFP with $AgNO_3$ (1:1 Molar Ratio); Compound 1: To a solution of TFP (0.10 g; 0.43 mmol) in THF (6 mL), crystalline $AgNO_3$ (0.074 g; 0.43 mmol) was added. Methanol (4 mL) was added to the reaction mixture to solubilize the silver salt. After 2 h, the solution was concentrated to dryness. The crude product was crystallized by slow diffusion of hexane into a dichloromethane solution. Colourless needles of **1** suitable for an X-ray crystal structure determination were formed after a few days (yield 0.104 g, 60%). $C_{12}H_9AgNO_6P$ (**1**) (402.0): calcd. C 35.85, H 2.26, N 3.48; found C 36.25, H 2.35, N 3.26. ^1H NMR ($CDCl_3$; 296 K): $\delta = 6.51$ (m, 3 H), 7.11 (m, 3 H), 7.74 (m, 3 H). $^{31}P\{^1H\}$ NMR ($CDCl_3$; 296 K): $\delta = -56.30$ (m, br.)

Reaction of TFP with $AgNO_3$ (3:1 Molar Ratio); Compound 2: To a solution of TFP (0.10 g; 0.43 mmol) in THF (6 mL), crystalline $AgNO_3$ (0.024 g; 0.14 mmol) and methanol (4 mL) were added. After 2 h, the solution was concentrated to dryness. The solid obtained was dissolved in the minimum amount of dichloromethane and, after filtration, the solution was cooled to 4 °C. Colourless crystals of **2** suitable for an X-ray crystal structure determination grew overnight (yield 0.030 g; 30%). $C_{36}H_{27}AgNO_{12}P_3$ (**2**) (866.4): calcd. C 49.91, H 3.14, N 1.62; found C 49.74, H 3.24, N 1.65. ^1H NMR ($CDCl_3$; 296 K): $\delta = 6.47$ (m, 9 H), 7.13 (m, 9 H), 7.70 (s, 9 H). $^{31}P\{^1H\}$ NMR ($CDCl_3$; 296 K): $\delta = -11.14$ (s), -57.00 (m, br.)

Reaction of TFP with $AgBF_4$ (2:1 Molar Ratio); Compounds 3 and 4: To a solution of TFP (0.15 g; 0.65 mmol) in THF (6 mL), $AgBF_4$ (0.068 g; 0.32 mmol) was added. A cloudy solution was immediately obtained. After 1 h, the white precipitate was separated from the supernatant by centrifugation, to give the analytical sample of **4** (yield 0.085 g; 47%, calculated respect to the amount of the TFP ligand used). The solution was concentrated to dryness and the crude product obtained was dissolved in hot chloroform. Crystals

of **3** suitable for an X-ray crystal structure determination (yield 0.089 g; 40%, calculated with respect to the amount of the TFP ligand used) were obtained by cooling the chloroform solution to 4 °C. With TFP and $AgBF_4$ in a 1:1 molar ratio, compounds **3** and **4** were both obtained. $C_{24}H_{20}AgBF_4O_7P_2$ (**3**) (677.0): calcd. C 42.58, H 2.98; found C 42.89, H 2.75. ^1H NMR ($CDCl_3$; 296 K): δ = 1.85 (s, 2 H), 6.48 (m, 6 H), 7.19 (m, 6 H), 7.68 (s, 6 H). $^{31}P\{^1H\}$ NMR ($CDCl_3$; 296 K): δ = −55.77 (s, br.). $C_{48}H_{36}AgBF_4O_{12}P_4$ (**4**) (1123.4): calcd. C 51.32, H 3.23; found C 51.40, H 3.11. ^1H NMR ($CDCl_3$; 296 K): δ = 6.36 (m, 12 H), 6.74 (m, 12 H), 7.38 (s, br 12 H). $^{31}P\{^1H\}$ NMR ($CDCl_3$; 296 K): δ = −57.48 (s, br.)

Reaction of TFP with $AgBF_4$ (4:1 Molar Ratio); Compound 4: To a solution of TFP (0.15 g; 0.65 mmol) in THF (6 mL), $AgBF_4$ (0.031 g; 0.16 mmol) was added. The cloudy solution was stirred for 0.5 h and a white precipitated of **4** formed (0.15 g; yield 84%). The supernatant, separated by centrifugation from the precipitate, was concentrated to dryness. The oily crude product was washed with hexane and then crystallized from $CHCl_3$; a small amount of **3** was recovered. $C_{48}H_{36}AgBF_4O_{12}P_4$ (**4**) (1123.4): calcd. C 51.32, H 3.23; found C 51.18, H 3.07. ^1H NMR ($CDCl_3$; 296 K): δ = 6.36 (m, 12 H), 6.74 (m, 12 H), 7.38 (s, br., 12 H). $^{31}P\{^1H\}$ NMR ($CDCl_3$; 296 K): δ = −57.48 (s, br.)

X-ray Crystal Structure Analyses of 1, 2, and 3: X-ray diffraction data of single crystals of the three complexes were collected with a Rigaku AFC5R diffractometer with graphite-monochromated Cu-K_α radiation and a 12-kV rotating anode generator. Intensity data were collected by the ω-2θ technique to a maximum 2θ value of about 124°. Corrections for Lorentz polarisation and absorption were applied to the data of the three compounds. A linear correction factor was applied to the data of **2** to account for the intensity decay of −61% detected in the intensities of the standard reflections. The structures were solved by Patterson methods and subsequent Fourier analyses and refined by the full-matrix least-squares method with anisotropic thermal parameters for all non-hydrogen atoms of **1** and **3** and for the heavier atoms of **2**, while the carbon and oxygen atoms of the furyl groups were refined isotropically. The hydrogen atoms were included at calculated positions and not refined for the three compounds. Crystal parameters and structure determination data are given in Table 3. Atomic scattering factors and anomalous dispersion terms were taken from the International Tables.[26] All calculations were performed by using the TEXAN crystallographic software package.[27] CCDC-164610 (**1**), -164611 (**2**) and -164612 (**3**) contain the supplementary crystallographic data for this paper. These data can be obtained free of charge at www.ccdc.cam.ac.uk/conts/retrieving.html or from the

Table 3. Crystal data

Compound	**1**	**2**	**3**
Empirical formula	$C_{12}H_9AgNO_6P$	$C_{36}H_{27}AgNO_{12}P_3$	$C_{24}H_{18}AgBF_4O_6P_2$
Molecular mass	402.05	866.40	675.02
Crystal size [mm]	0.20 × 0.30 × 0.60	0.25 × 0.50 × 0.70	0.10 × 0.20 × 0.30
Crystal system	monoclinic	orthorhombic	triclinic
a [Å]	11.274(1)	18.291(4)	13.009(5)
b [Å]	7.370(1)	24.052(5)	10.789(3)
c [Å]	17.106(2)	17.027(6)	10.839(4)
α [°]	90	90	68.50(3)
β [°]	101.58(1)	90	80.22(3)
γ [°]	90	90	75.00(4)
V [Å^3]	1392.3(4)	7491(3)	1362(1)
Space group	$P2_1/c$ (#14)	*Pbca* (#61)	$P\bar{1}$ (#2)
Z	4	8	2
$D_{calcd.}$ [g·cm^{-3}]	1.918	1.537	1.646
F(000)	792	3504	672
μ(Cu-K_α) [cm^{-1}]	132.08	61.59	7.80
Scan type	ω-2θ	ω-2θ	ω-2θ
Scan rate [°·min^{-1}]	16.00 (3 rescans)	16.00 (3 rescans)	16.00 (3 rescans)
Scan width [°]	0.94 + 0.30 tanθ	1.10 + 0.30 tanθ	1.37 + 0.30 tanθ
$2\theta_{max.}$ [°]	124.20	124.10	124.2
No. measured reflections			
total	4931	6518	4516
unique	4692	6202	4297
corrections	Lorentz polarisation	Lorentz polarisation	Lorentz polarisation
Abs. trans. factors	0.73−1.00	0.53−1.00	0.30−1.00
Decay	−61%		
Refinement	full matrix	full matrix	full matrix
Function minimised	$w(\|F_o\| - \|F_c\|)^2$	$w(\|F_o\| - \|F_c\|)^2$	$w(\|F_o\| - \|F_c\|)^2$
Least-squares weights	$4F_o^2/\sigma^2(F_o^2)$	$4F_o^2/\sigma^2(F_o^2)$	$4F_o^2/\sigma^2(F_o^2)$
p factor	0.03	0.03	0.03
No. observations [$I > 3\sigma(I)$]	1453	1538	2569
No. variables	190	233	353
Reflection/parameter ratio	7.7	6.60	7.3
Residuals: *R*; *Rw*	0.062; 0.077	0.077; 0.087	0.071; 0.085
Goodness of fit indicator	0.10	0.55	0.75
Max shift/error	0.59	0.11	0.80
Max peak diff. map [e·Å^{-3}]	0.61	0.37	0.70
Min peak diff. map [e·Å^{-3}]	−1.32	−0.26	−1.21

Cambridge Crystallographic Data Centre, 12, Union Road, Cambridge CB2 1EZ, UK [Fax: (internat.) + 44-1223/336-033; E-mail: deposit@ccdc.cam.ac.uk].

Acknowledgments

This work was supported by grants from University of Camerino and CNR (Roma).

[1] V. Farina, S. R. Baker, D. A. Benigni, S. I. Hauck, C. Sapino, Jr., *J. Org. Chem.* **1990**, *55*, 5833.
[2] C. Amatore, A. Jutand, G. Meyer, H. Atmani, F. Khalil, F. O. Chahdi, *Organometallics* **1998**, *17*, 2958 −and references therein).
[3] C. Santelli-Rouvier, C. Coin, L. Toupet, M. Santelli, *J. Organomet. Chem.* **1995**, *495*, 91.
[4] S.-M. Kuang, F. Xue, T. C. W. Mak, Z.-Z. Zhang, *Inorg. Chim. Acta* **1999**, *284*, 119.
[5] [5a] F. Bachechi, A. Burini, R. Galassi, A. Macchioni, B. R. Pietroni, F. Ziarelli, C. Zuccaccia, *J. Organomet. Chem.* **2000**, *593−594*, 392. [5b] T. S. A. Hor, S. P. Neo, C. S. Tan, T. C. W. Mak, K. W. P. Leung, R-J. Wang, *Inorg. Chem.* **1992**, *31*, 4510.
[6] C. Tejel, R. Bravi, M. A. Ciriano, L. A. Oro, M. Bordonaba, C. Graiff, A. Tiripicchio, A. Burini, *Organometallics* **2000**, *19*, 3115.
[7] [7a] L. Carlucci, G. Ciani, D. W. v. Gudenberg, D. M. Proserpio, *Inorg. Chem.* **1997**, *36*, 3812. [7b] L. Carlucci, G. Ciani, D. M. Proserpio, A. Sironi, *Inorg. Chem.* **1998**, *37*, 5941. [7c] Y. Fu, J. Sum, Q. Li, Y. Chen, W. Dai, D. Wang, T. C. W. Mak, W. Tang, H. Hu, *J. Chem. Soc., Dalton Trans.* **1996**, 2309.
[8] C. A. Hester, R. G. Baughman, H. L. Collier, *Polyhedron* **1997**, *16*, 2893.
[9] [9a] K. D. Karlin (Ed.), *Progress in Inorganic Chemistry*, John Wiley & Sons, Inc., New York, **1994**, vol. 42. [9b] J. M. Lehn, *Angew. Chem. Int. Ed. Engl.* **1990**, *29*, 1304. [9c] W. Zarges, J. Hall, J. M. Lehn, C. Bolm, *Helv. Chim. Acta* **1991**, *74*, 1843.
[10] [10a] E. J. Corey, C. L. Cymin, M. C. Noe, *Tetrahedron Lett.* **1994**, *35*, 69. [10b] K. Maruoka, N. Murase, H. Yamamoto, *J. Org. Chem.* **1993**, *58*, 2938.
[11] C. Chen, K. S. Suslick, *Coord. Chem. Rev.* **1993**, *128*, 293 and references therein.
[12] K. Nomiya, S. Takahashi, R. Noguchi, S. Nemoto, T. Takayama, M. Oda, *Inorg. Chem.* **2000**, *39*, 3301.
[13] M. Dartiguenave, Y. Dartiguenave, A. Mari, A. Guitard, M. J. Olivier, A. L. Beauchamp, *Can. J. Chem.* **1988**, *66*, 2386.
[14] B.-K. Teo, J. C. Calabrese, *Inorg. Chem.* **1976**, *15*, 2467.
[15] M. R. Churchill, J. Donahue, F. J. Rotella, *Inorg. Chem.* **1976**, *15*, 2752.
[16] M. Camalli, F. Caruso, *Inorg. Chim. Acta* **1988**, *144*, 205.
[17] C. W. Liu, H. Pan, J. P. Fackler, Jr., G. Wu, E. Wasylishen, M. Shang, *J. Chem. Soc., Dalton Trans.* **1995**, 3691.
[18] E. C. Alyea, G. Ferguson, A. Smogyvari, *Inorg. Chem.* **1982**, *21*, 1369.
[19] D. M. Ho, R. Bau, *Inorg. Chem.* **1983**, *22*, 4073.
[20] R. A. Stein, C. Knobler, *Inorg. Chem.* **1977**, *16*, 242 and references therein.
[21] G. A. Ardizzoia, G. La Monica, A. Maspero, M. Moret, N. Masciocchi, *Inorg. Chem.* **1997**, *36*, 2321.
[22] A. Cassel, *Acta Crystallogr., Sect. B* **1981**, *37*, 229.
[23] P. F. Barron, J. C. Dyason, P. C. Healy, L. M. Engelhardt, W. Skelton, B. A. H. White, *J. Chem. Soc., Dalton Trans.* **1986**, 1965.
[24] A. Del Zotto, P. Di Bernardo, M. Tolazzi, G. Tomat, P. Zanonato, *Chem. Soc., Dalton Trans.* **1993**, 3009.
[25] E. L. Muetterties, C. W. Alegranti, *J. Am. Chem. Soc.* **1972**, *94*, 6386 [exhaustive article regarding ^{31}P NMR investigation of silver(I)-phosphane and -phosphite complexes].
[26] *International Tables for X-ray Crystallography*, vol. IV, Kynoch Press, Birmingham, UK, **1974**.
[27] *TEXSAN-TEXRAY*, Structure Analysis Package, Molecular Structure Corporation, **1985**.

Received August 1, 2001
[I01284]

Strong Ferromagnetic Coupling in Linear Mixed μ-Acetato, μ-Hydroxo Trinuclear Copper(II) Complexes with *N*-sulfonamide derivatives − Synthesis, Structure, EPR and Magnetic Properties

Laura Gutierrez,[a] Gloria Alzuet,[a] Jose A. Real,[a] Joan Cano,[b] Joaquin Borrás,*[a] and Alfonso Castiñeiras[c]

Keywords: Copper / Sulfonamide ligands / Magnetic properties / EPR spectroscopy / Density functional calculations

Two new trinuclear copper(II) complexes have been synthesised and structurally characterised: $[Cu_3(L1)_2(CH_3COO)_2(OH)_2(DMF)_2]$ (**1**) [HL1 = *N*-(pyrid-2-ylmethyl)benzenesulfonylamide] and $[Cu_3(L2)_2(CH_3COO)_2(OH)_2]_\infty$ (**2**) [HL2 = *N*-(pyrid-2-ylmethyl)naphthalenesulfonylamide]. In both complexes the central copper ion has a regular square planar geometry. The coordination spheres of the terminal copper atoms are square pyramidal, the apical positions being occupied by a DMF oxygen atom in **1** and by a sulfonamido oxygen of the contiguous trimer in **2**, as a consequence the latter can be considered a chain of trinuclear species. For the two compounds the three copper atoms are in a strict linear arrangement and adjacent coppers are connected by a hydroxo bridge and a bidentate *syn-syn* carboxylato group. The mixed bridging by a hydroxide oxygen atom and a bidentate carboxylato group leads to a noncoplanarity of the adjacent basal coordination planes with a dihedral angle of 54.4(1)° for compound **1** and 58.34(3)° for compound **2**. Susceptibility measurements (2–300 K) reveal a strong ferromagnetic coupling, J = 94.0 and 59.1 cm^{-1}, respectively, in the mixed-bridged moiety leading to a quadruplet ground state that is confirmed by the EPR spectra. The ferromagnetic coupling arising from the countercomplementarity of the hydroxo and acetato bridges has been discussed on the basis of DFT calculations on model compounds.

(© Wiley-VCH Verlag GmbH, 69451 Weinheim, Germany, 2002)

Introduction

There is a great deal of interest in multimetallic complexes due to the special chemical and physical properties resulting from the mutual interaction of two or more metal centres.[1] Investigations of trinuclear transition metal complexes have been of increasing interest in recent years. One reason for this was the lack of metallobiomolecules for which the trinuclear core can act as a synthetic analogue. The MCD spectroscopic proof of a trinuclear active site in laccase,[2] the recent discovery of a ferromagnetically coupled Cu^{II} triad in a subunit of methane mono-oxygenase[3] and an X-ray structure analysis of ascorbate oxidase from zucchini,[4] which revealed an angled trimeric Cu^{II} unit as well as a mononuclear type 1 copper(II) centre, have all stimulated an increasing interest in the study of trinuclear copper systems.

Very recently we have reported a ferromagnetically coupled copper(II) triad that has been synthesised and structurally as well as magnetically characterised.[5] This compound presents a linear arrangement of the three copper(II) atoms linked by μ-hydroxo and μ-carboxylato bridges. Until now this complex and that previously reported by Haase et al.[6] are the only ferromagnetic linear trinuclear copper(II) complexes fully characterised.

The importance of these systems does not arise only from the occurrence of this bridging unit in several metalloproteins.[7] These studies are also related to the properties of quadruplet ground states, to magnetostructural correlations in mixed bridged systems, to ferromagnetic exchange coupling, and to long-range coupling effects between terminal copper centres.

Within this framework and following our current study on multiatom-bridged exchange-coupled systems we report here the synthesis, X-ray structure and magnetic properties of two trinuclear copper(II) complexes, $[Cu_3(L1)_2(CH_3COO)_2(OH)_2(DMF)_2]$ (**1**) and $[Cu_3(L2)_2(CH_3COO)_2$-

[a] Departamento de Química Inorgánica/Instituto de Ciencia Molecular. Universidad de Valencia
Avda. Vicent Estellés s/n. 46100, Burjassot, Spain
Fax: (internat.) + 34-(0)96/386-4960
E-mail: Joaquin.Borrás@uv.es
[b] Laboratoire de Chimie Inorganique, ICMO, Bât. 420. Université Paris-Sud,
91405 Orsay, France
Fax: (internat.) + 33-(0)1/6915-4754
E-mail: jocano@icmo.u-psud.fr
[c] Departamento de Química Inorgánica. Facultad de Farmacia. Universidad de Santiago
15703 Santiago de Compostela, Spain
Fax: (internat.) + 34-981/547-163
E-mail: qiac01@usc.es

$(OH)_2]_\infty$ (**2**) {HL1 = [*N*-(pyrid-2-ylmethyl)benzenesulfonylamide)] and HL2 = [*N*-pyrid-2-ylmethylnaphthalenesulfonylamide]}. In both compounds the copper atoms are bridged by hydroxo and acetate groups. In compound **2** the trinuclear units are linked by a sulfonamide oxygen atom from the HL2 ligand leading to a three dimensional network. The complexes display a linear arrangement of the copper centres and a strong ferromagnetically coupled pair of copper atoms.

Results and Discussion

Crystal Structure of $[Cu_3(L1)_2(CH_3COO)_2(OH)_2(DMF)_2]$ (1)

The trinuclear entity of compound **1** with the atomic labelling scheme used is shown in Figure 1. Selected bond lengths and angles are collected in Table 1. The complex molecule consists of a neutral symmetrical trinuclear unit and two disordered dimethylformamide molecules along with the Cu(2) at the symmetry centre. The terminal copper atoms Cu(1) and Cu(1a) have a distorted square pyramidal geometry (τ parameter 0.30) coordinated by two nitrogen atoms N(1) and N(2) of the pyridyl ring and of the sulfonamidato group of the deprotonated ligand ($L1^-$), the O(1) of the hydroxo bridge, the O(21) of the acetate bridge and the O(30) from a dimethylformamide solvent. The central Cu(2) presents a regular square plane geometry formed from the O(1), O(1a), O(22) and O(22a) atoms of the hydroxo and acetate bridging groups, respectively [deviation of the O(1), O(22), O(1a), O(22a), and Cu(2) atoms from the plane, 0.000].

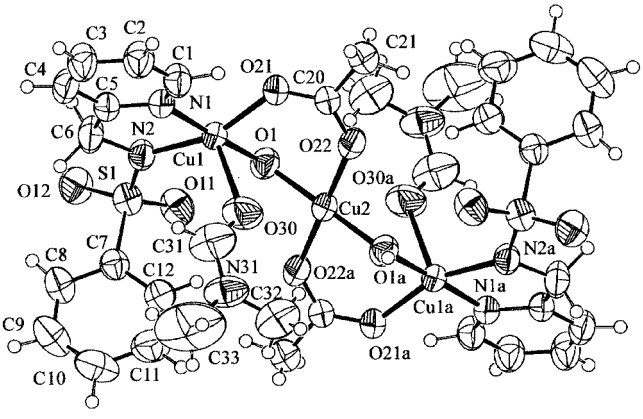

Figure 1. Molecular structure of $[Cu_3(L1)_2(CH_3COO)_2(OH)_2(DMF)_2]$ (**1**)

Adjacent copper centres are bridged by the oxygen atom of the hydroxo ligand [Cu(1)−O(1)−Cu(2) = 113.33(15)°] and two oxygen atoms of a bidentate *syn-syn* carboxylato group leading to a mixed-bridged coplanar coordination geometry with Cu(1)···Cu(2) = 3.1656(6) Å. The Cu(2)−O(1) and Cu(2)−O(22) bond lengths are 1.899(3) Å and 1.959(3) Å, respectively. The Cu(1)−N(1) and Cu(1)−N(2) lengths are 2.004(3) Å and 2005(3) Å, respectively, and the Cu(1)−O(1) and Cu(1)−O(21) bond lengths are 1.890(3) Å and 1.981(3) Å. The apical bond length Cu(1)−O(30) is 2.398(4) Å. The two O(30) and O(30a) atoms from the DMF molecules linked to the Cu(1) and Cu(1a) centres are at 2.776(5) Å from the Cu(2). The Cu(1)−O(11) and Cu(1)−O(12) distances are 3.420(2) and 4.422(3) Å indicating that the Cu^{II} ions do not interact with the oxygen atoms of the sulfonamido group. Bond lengths are similar to those of the previously reported $[Cu_3(L)_2(CH_3COO)_2(OH)_2(DMF)_2]$ [HL = *N*-(pyrid-2-ylmethyl)toluensulfonylamide] compound[5] except for the Cu−O(30) bond length, which is significantly shorter (ca. 0.12 Å) in the present compound.

The Cu(1) atom is 0.1706 Å from the square plane formed by the N(1), N(2), O(1) and O(21) atoms. The skeleton Cu(1a)−O(1)−Cu(2)−O(1a)−Cu(1) is in a zigzag with the three copper ions forming a straight line with an angle of 180°. The mixed bridging leads to a noncoplanarity of the basal N(1)N(2)O(1)O(2) and O(1)O(22)O(22A)O(21A) planes characterised by a folding angle of 54.4(1)°.

Crystal Structure of $[Cu_3(L2)_2(CH_3COO)_2(OH)_2]_\infty$ (2)

The trinuclear entity with the atomic labelling scheme used is shown in Figure 2. Selected bond lengths and angles are listed in Table 1. The polymer compound consists of trinuclear copper fragments $[Cu_3(L2)_2(CH_3COO)_2(OH)_2]$. The sites of the central and terminal copper ions are nonequivalent. The geometry around the terminal copper atoms Cu(1) and Cu(1A) is distorted square pyramidal (τ parameter 0.22) with a $CuN_2O_2\cdots O$ chromophore. The basal plane is described by the two nitrogen atoms N(1) and N(2) of the pyridyl ring and of the sulfonamidato group of the deprotonated ligand ($L2^-$), the O(1) of the hydroxo bridge and O(21) of the acetate bridge. The apical position is occupied by a sulfonamide O atom [O(11B)] of another $L2^-$ ligand pertaining to a contiguous asymmetric unit. For the central Cu(2) a regular square plane geometry is realised with the O(1), O(1A), O(22) and O(22A) atoms from the hydroxo and acetate bridging groups, respectively.

The Cu−O and Cu−N distances are similar to those found in complex **1**. The Cu(2)−O(1) and Cu(2)−O(22) bond lengths are 1.883(8) Å and 2.005(7) respectively. The Cu(1)−N(1) and Cu(1)−N(2) lengths are 2.022(10) Å and 1.991(9) Å, respectively, and the Cu(1)−O(1) and Cu(1)−O(21) bond lengths are 1.914(7) Å and 1.981(8) Å. The apical bond length Cu(1)−O(11A) is 2.460(8) Å. The Cu(1) atom lies 0.0985 Å above the square plane formed by the N(1), N(2), O(1) and O(21) atoms.

In the same way as in complex **1**, adjacent copper centres are bridged by the oxygen atom O(1) of the hydroxo ligand [Cu(1)−O(1)−Cu(2) = 112.6(4)°] and two oxygen atoms O(21) and O(22) of a bidentate *syn-syn* carboxylato group leading to a mixed-bridged non coplanar coordination geometry [dihedral angle between the mean equatorial planes N(1)N(2)O(1)O(2) and O(1)O(22)O(22A)O(21A), 58.3(3)°]. In the trinuclear entity, the three copper ions are arranged in a strict linear fashion [Cu(1)−Cu(2)−Cu(1A) = 180°]

Table 1. Selected bond lengths [Å] and angles [°] for $[Cu_3(L1)_2(CH_3COO)_2(OH)_2(DMF)_2]$ (**1**) and $[Cu_3(L2)_2(CH_3COO)_2(OH)_2]_\infty$ (**2**); symmetry transformations used to generate equivalent atoms: #1 $-x, -y + 1, -z + 1$ (compound **1**); #1 $x, -y + 1, z - 1/2$ #2 $-x + 1/2, -y + 3/2, -z$ (compound **2**)

1		**2**	
Cu(1)−O(1)	1.890(3)	Cu(1)−O(1)	1.914(7)
Cu(1)−O(21)	1.981(3)	Cu(1)−O(21)	1.981(8)
Cu(1)−N(1)	2.004(3)	Cu(1)−N(2)	1.991(9)
Cu(1)−N(2)	2.005(3)	Cu(1)−N(1)	2.022(10)
Cu(1)−O(30)	2.398(4)	Cu(1)−O(11)#1	2.460(8)
Cu(1)−Cu(2)	3.1656(6)	Cu(1)−Cu(2)	3.1589(15)
Cu(2)−O(1)#1	1.899(3)	Cu(2)−O(1)#2	1.883(8)
Cu(2)−O(1)	1.899(3)	Cu(2)−O(1)	1.883(8)
Cu(2)−O(22)#1	1.959(3)	Cu(2)−O(22)#2	2.005(7)
Cu(2)−O(22)	1.959(3)	Cu(2)−O(22)	2.005(7)
Cu(2)−O(30)#1	2.776(5)		
Cu(2)−O(30)	2.776(5)		
O(1)−Cu(1)−O(21)	90.59(13)	O(1)−Cu(1)−O(21)	89.4(3)
O(1)−Cu(1)−N(1)	177.85(13)	O(1)−Cu(1)−N(2)	102.3(4)
O(21)−Cu(1)−N(1)	88.46(12)	O(21)−Cu(1)−N(2)	162.9(4)
O(1)−Cu(1)−N(2)	98.61(13)	O(1)−Cu(1)−N(1)	176.6(4)
O(21)−Cu(1)−N(2)	159.83(13)	O(21)−Cu(1)−N(1)	87.5(4)
N(1)−Cu(1)−N(2)	81.71(13)	N(2)−Cu(1)−N(1)	81.1(4)
O(1)−Cu(1)−O(30)	87.82(15)	O(1)−Cu(1)−O(11)#1	87.8(3)
O(21)−Cu(1)−O(30)	88.58(14)	O(21)−Cu(1)−O(11)#1	94.6(4)
N(1)−Cu(1)−O(30)	94.07(15)	N(2)−Cu(1)−O(11)#	98.3(3)
N(2)−Cu(1)−O(30)	109.57(14)	N(1)−Cu(1)−O(11)#1	90.9(4)
O(1)#1−Cu(2)−O(1)	180.00(17)	O(1)#2−Cu(2)−O(1)	180.0(4)
O(1)#1−Cu(2)−O(22)#1	91.96(13)	O(1)#2−Cu(2)−O(22)#2	91.8(3)
O(1)−Cu(2)−O(22)#1	88.04(13)	O(1)−Cu(2)−O(22)#2	88.2(3)
O(1)#1−Cu(2)−O(22)	88.04(13)	O(1)#2−Cu(2)−O(22)	88.2(3)
O(1)−Cu(2)−O(22)	91.96(13)	O(1)−Cu(2)−O(22)	91.8(3)
O(22)#1−Cu(2)−O(22)	180.00(7)	O(22)#2−Cu(2)−O(22)	180.00(7)
O(1)#1−Cu(2)−O(30)#1	77.21(12)	Cu(1)#2−Cu(2)−Cu(1)	180.0
O(1)−Cu(2)−O(30)#1	102.79(12)		
O(22)#1−Cu(2)−O(30)#1	83.17(14)		
O(22)−Cu(2)−O(30)#1	96.83(14)		
O(1)#1− Cu(2)−O(30)	102.79(12)		
O(1)−Cu(2)−O(30)	77.21(12)		
O(22)#1−Cu(2)−O(30)	96.83(14)		
O(22)−Cu(2)−O(30)	83.17(14)		
O(30)#1−Cu(2)−O(30)	180.0		

with Cu(2) on the inversion centre and a Cu(1)···Cu(2) distance of 3.1589(15).

As for the coordination mode of the ligand, it is noteworthy that HL2 coordinates to one copper ion in a bidentate fashion through the pyridyl and sulfonamidato N atoms and to another copper(II) of another asymmetric unit through the sulfonamide O atom giving an infinite tridimensional network of trinuclear units. As a consequence of the coordination of the $O_{sulfonamidate}$ atom to the copper ion, there is a small difference between the S−O bond lengths [S−O(11): 1.452 Å, S−O(12): 1.434 Å] the former being larger due to the O(11) that is linked to the copper ion. However, the S−O bond lengths in compound **1** and in the compound previously reported[5] are the same, 1.443 Å, because in these complexes there is no interaction between the copper ion and the $O_{sulfanomidate}$ atom of the SO_2 group.

IR and Electronic Spectra

The IR spectra of both complexes present a similar pattern to that of the previously reported trinuclear compounds with the related *N*-(pyrid-2-ylmethyl)toluensulfonylamide ligand.[5] The IR spectrum of complex **2** shows a band at 3530 cm^{-1} characteristic of the O−H bridging group.[7] The characteristic vibrations of the acetato group in the spectra of both complexes confirm that it acts as a bridging bidentate ligand [$\Delta\nu = \nu_{asymm.}(COO) - \nu_{symm.}(COO) = 144$ and 142 cm^{-1} for compounds **1** and **2**, respectively].[8] The spectrum of complex **1** exhibits a new band at 1653 cm^{-1}, which is assigned to the ν(C=O) vibration of the dimethylformamide. As a consequence of the deprotonation and coordination of the sulfonamido N atom the characteristic bands of the SO_2 group are shifted to lower frequencies. The $\nu(SO_2)_{asymm.}$ vibrations present the

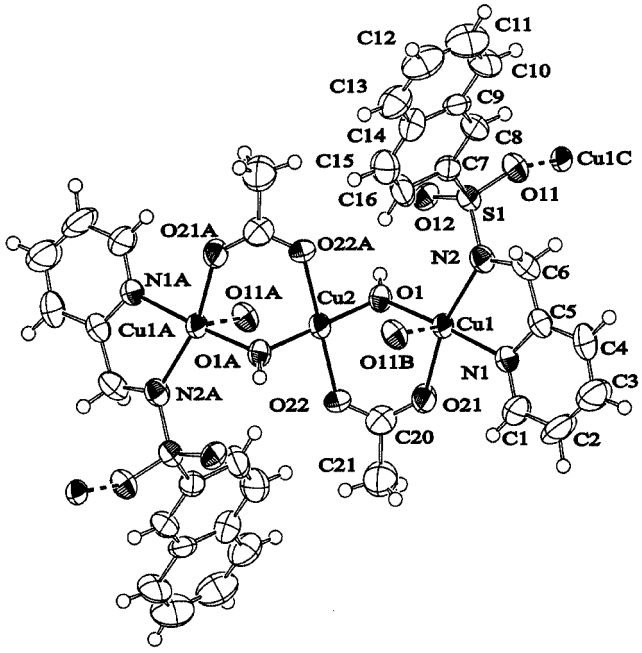

Figure 2. Molecular structure of $[Cu_3(L2)_2(CH_3COO)_2(OH)_2]_\infty$ (**2**)

same band at 1256 cm^{-1} for both complexes, however the $\nu(SO_2)_{symm.}$ vibrations are different, 1130 cm^{-1} in compound **1** and 1120 cm^{-1} in compound **2**, probably due to the interaction of one of the oxygen atoms of the sulfonamido group with the metal ion in complex **2**.

The solid-state spectra of both trinuclear complexes exhibit a broad band at about 15314 cm^{-1} (**1**) and 15873 cm^{-1} (**2**) that corresponds to the two chromophores, CuN_2O_2 and CuO_4, present in the compounds.[9] In dichloromethane solution, the d-d band of the complexes is slightly shifted. The small shift of ca. 500 cm^{-1} to lower frequencies in complex **1** and ca. 700 cm^{-1} to higher frequencies in complex **2** can be attributed to solvent effects.

Magnetic Properties

The temperature dependence of the $\chi_M T$ product for $[Cu_3(L1)_2(CH_3COO)_2(OH)_2(DMF)_2]$ (**1**) and $[Cu_3(L2)_2(CH_3COO)_2(OH)_2]_\infty$ (**2**) (χ_M being the magnetic susceptibility per trimer unit and T the absolute temperature) in the temperature range 2−300 K is shown in Figure 3. As expected, the magnetic behaviour of both complexes is similar and resembles that of the related trinuclear compound $[Cu_3(L)_2(CH_3COO)_2(OH)_2(DMF)_2]$ [HL = *N*-(pyrid-2-ylmethyl)toluensulfonylamide].[5] At room temperature $\chi_M \cdot T$ is 1.51 and 1.32 $cm^3 \cdot mol^{-1} \cdot K$, respectively, a value which is somewhat larger than that expected for a magnetically uncoupled trinuclear Cu^{II} compound (1.23 $cm^3 \cdot mol^{-1} \cdot K$, $g = 2.1$). Upon cooling of the sample, $\chi_M \cdot T$ increases and reaches a value of 2.18 $cm^3 \cdot mol^{-1} \cdot K$ (compound **1**) and of 2.00 $cm^3 \cdot mol^{-1} \cdot K$ (compound **2**) in the 6−15 K temperature range. This behaviour is indicative of strong ferromagnetic coupling between the adjacent Cu^{II} atoms in the trinuclear species. Below 5 K, $\chi_M T$ decreases rapidly down to 1.9 $cm^3 \cdot mol^{-1} \cdot K$ (compound **1**) and to 1.8 $cm^3 \cdot mol^{-1} \cdot K$ (compound **2**), which is most likely due to zero-field splitting (ZFS) within the quadruplet ground state. The occurrence of intermolecular antiferromagnetic interactions may also be operative at very low temperatures.

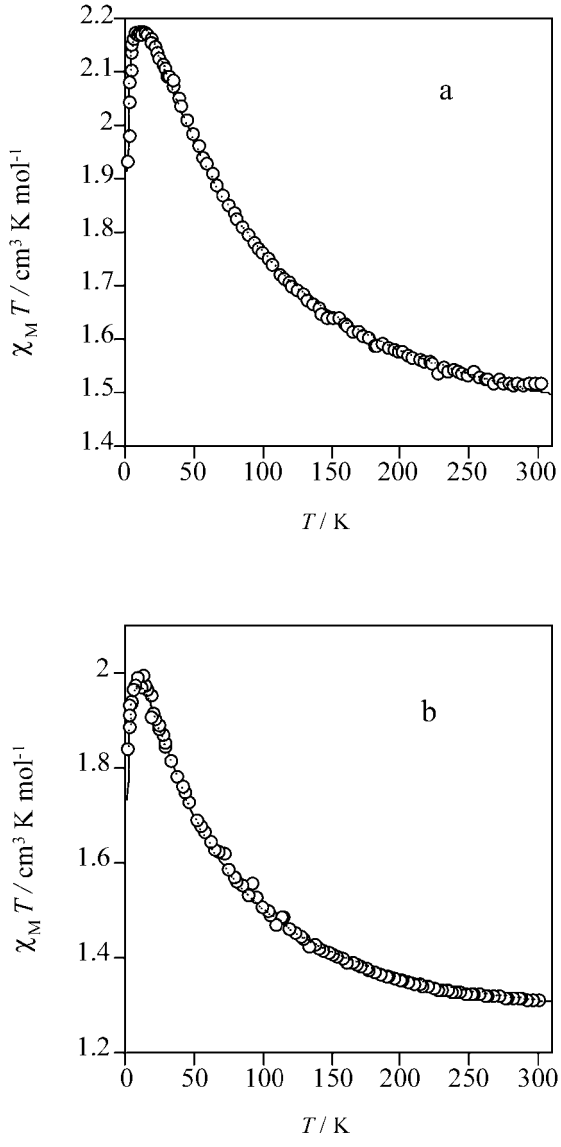

Figure 3. a) Temperature dependence of $\chi_M T$ for $[Cu_3(L1)_2(CH_3COO)_2(OH)_2(DMF)_2]$ (**1**); b) temperature dependence of $\chi_M T$ for $[Cu_3(L2)_2(CH_3COO)_2(OH)_2]_\infty$ (**2**)

The spin Hamiltonian that is appropriate for describing the exchange interaction in a linear symmetric trimer has the form:

$$H = -J(S_1S_2 + S_2S_3) - J' S_1S_3 + D[S_z^2 - S(S+1)/3] + g\beta HS \quad (1)$$

where the occurrence of axial ZFS between the ±3/2 and ±1/2 Kramer's doublets arising from the $S = 3/2$ ground state have been included. The exchange parameters J and

J' refer to the interaction between two adjacent centres and the interaction between the terminal centres, respectively. The resulting spin multiplets are two doublets ($S = 1/2$) and one quadruplet ($S = 3/2$).[10] D denotes the half energy gap between the above mentioned Kramer's doublets.

In a first step we have set $D = 0$ in expression (1). In this case, the fitting of the experimental data for $T > 10$ K to this Hamiltonian confirms that the values of J and J' are strongly correlated in determining the temperature dependence of the magnetic susceptibility, as has already been observed for other similar systems.[5,11] The fitting to the experimental data, including the low temperature region where D is operative, shows a similar correlation between J and J'. The solid and broken lines in Figure 3 represent typical fits with $J = 94$ cm^{-1}, $J' = -3.6$ cm^{-1}, $|D| = 1.76$ cm^{-1}, $g = 2.17$ and $R = 3.10-5$ (Figure 3a) and $J = 59.1$ cm^{-1}, $J' = -4.6$ cm^{-1}, $|D| = 1.76$ cm^{-1}, $g = 2.06$ and $R = 3.10-4$ (Figure 3b), respectively [R values obtained from the expression $R = \{\Sigma_i[(\chi_M T)_{obs,i} - (\chi_M T)_{calcd,i}]^2/\Sigma_i[(\chi_M T)_{obs,i}]^2\}$. These J and J' values are indicative of a strong ferromagnetic and a weak antiferromagnetic coupling, respectively.

It is well-known that in dinuclear copper(II) complexes with *syn-syn* carboxylato bridges and hydroxo bridges, with an angle at the hydroxo bridge larger than 97.5°, antiferromagnetic coupling occurs;[12] the magnetic coupling in **1** and **2** should therefore be antiferromagnetic. However, when the bridging ligands are different, the two bridges may either increase or cancel out these effects. This phenomenon is known as orbital complementarity and countercomplementarity,[13–20] respectively, and was observed by us for the previously reported $[Cu_3(L)_2(CH_3COO)_2(OH)_2(DMF)_2]$[5] [HL = *N*-(pyrid-2-ylmethyl)toluensulfonylamide]. In this case, the antiferromagnetic contributions of each bridge almost cancelled each other out (these bridges show an orbital countercomplementarity) and the ferromagnetic term dominates ($J_T = J_{AF} + J_F$ with $|J_{AF}|$ being smaller than $|J_F|$). Here, both complexes **1** and **2** are good examples of the countercomplementarity effect imposed by the carboxylato bridge, which attenuates the effect of the antiferromagnetic hydroxo bridge to the point where strong ferromagnetic behaviour is observed.

EPR Spectra

The X-band EPR spectra of complexes **1** and **2** at room temperature are dominated by a transition at 2000 and 2100 G, respectively, which identifies an $S = 3/2$ ground state. The Q-band EPR spectrum at room temperature of compound **1** is shown in Figure 4, where the strong transition at 8000 G confirms the ferromagnetic behaviour of the compound.

For the complex $[Cu_3(L)_2(CH_3COO)_2(OH)_2(DMF)_2]$[5] [HL = *N*-(pyrid-2-ylmethyl)toluensulfonylamide] we have reported variable temperature studies in detail that revealed a strong shift of this resonance towards higher fields upon raising the temperature. This effect was explained from the

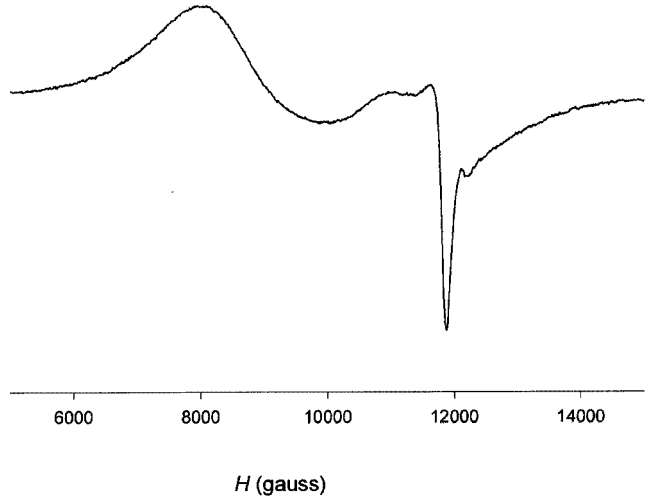

Figure 4. Q-band EPR spectrum at room temperature for $[Cu_3(L1)_2(CH_3COO)_2(OH)_2(DMF)_2]$ (**1**)

temperature-dependent contribution of the resonance fields of the three spin states to a composite EPR signal. In the present work, due to the similarity between the structures, magnetic properties and EPR spectra of the compounds $[Cu_3(L1)_2(CH_3COO)_2(OH)_2(DMF)_2]$ (**1**) and $[Cu_3(L2)_2(CH_3COO)_2(OH)_2]_\infty$ (**2**) and the complex $[Cu_3(L)_2(CH_3COO)_2(OH)_2(DMF)_2]$, we assumed a similar g-temperature dependence for **1** and **2**.

DFT Calculations

In previous work[5] we stated that the nature of the magnetic interaction in this kind of compound is governed by orbital countercomplementarity phenomena, in particular the SOMOs (Singly Occupied Molecular Orbital). In other words, two different bridging ligands can interact with the magnetic orbitals in the metal ions in a different way, destabilising the in-phase combination in one case (Φ_{AS}), and the out-of-phase (Φ_S) in the other. So, in the systems with two bridging ligands, there is a counterbalance and a compensation of their effects in the formation of the SOMOs. This leads to an increase in the energy gap, $\Delta = E_{AS} - E_S$, between the SOMOs, and therefore a reduction in the antiferromagnetic contribution to the magnetic coupling.[5] The antiferromagnetic contributions of each bridge almost cancel each other out and the ferromagnetic term dominates.

When we compare the J values of compounds **1** (94 cm^{-1}), **2** (59.1 cm^{-1}) and that of the related trinuclear complex of ref.[5] (96 cm^{-1}) and try to correlate them with the CuOCu angle φ (113.3°, 112.6° and 114.9° respectively) (Figure 5), we find that the J value of **2** is significantly smaller than the values of the other two compounds, when into account the φ angle is taken.

Several structural parameters can modify the exchange coupling constant value, J, in the family of the compounds studied. The CuOCu angle, φ, can have a dominant influence. As is well-known, there is a strong dependence be-

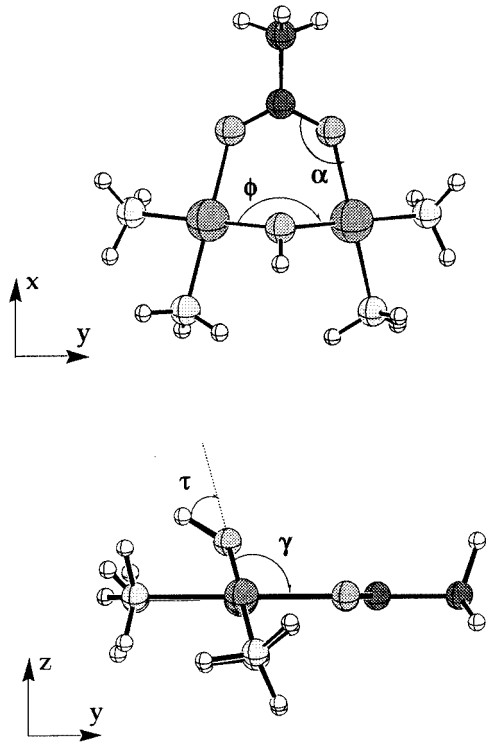

Figure 5. The structural parameters studied in the model **III**

tween the *J* constant and the φ angle in the binuclear bis(μ-hydroxo)Cu^{II} complexes[12,21] $[Cu_2(\mu\text{-}OH)_2]^{2+}$. So, in the last complexes small changes in the φ values produce important variations in the magnitude and the nature of the magnetic interaction. Wieghardt and co-workers[18] have proposed a magneto-structural correlation between the coupling constant *J* and the CuOCu angle φ for μ-hydroxo-μ-carboxylatodicopper(II) complexes. Using this correlation the values of *J* obtained for the trinuclear complexes **1** and **2** are approximately -20 cm^{-1}, which are not in agreement with the experimental results. Later, Chakravarty et al.[22] proposed a linear magneto-structural correlation [$-2J = 11.48\varphi(\text{deg}) - 1373$] for μ-alkoxo/hydroxo-μ-carboxylato dicopper(II) systems. Using this empirical relationship the value of *J* for the three compounds (**1**, **2** and that of ref.[5]) are 36.1, 40.1 and 26.9 cm^{-1}, respectively, which, as in the previous correlation, are not in agreement with the experimental measurements.

In order to understand the different *J* values found in these trinuclear compounds we have performed DFT calculations on three model compounds derived from the structure of the complexes: model **I** [two copper(II) atoms bridged by an acetato group], model **II** [two copper(II) atoms bridged by a hydroxo group] and model **III** [two copper(II) atoms bridged by an acetato and a hydroxo group]. To avoid the extra influences in the *J* constant, we have frozen most of the structural parameters in the variation of φ. Only the α angle (see Figure 5) has been varied in the φ change process. This angle (α), which governs the carboxylate-copper ion conformation (*syn-syn* or *anti-anti*), varies between 123.8 (φ = 90°) and 135.0° (φ = 130°) in the calculated models. The calculations with model **I** have shown that this small change in α causes a slight shift to weaker magnetic interactions for the smaller α values (-12.3 to -50.7 cm^{-1}) because of a loss of overlap between the magnetic orbitals in the metal ions and the HOMO's of the carboxylate ligand.

For a certain value of φ, a zero value for Δ is expected for model **II**, as in the $[Cu_2(\mu\text{-}OH)_2]^{2+}$ complexes. When this angle increases, a splitting of the SOMOs is observed. This energy gap has the opposite sign to the one found for model **I** (see Figure 6). This phenomenon is more pronounced as the φ value increases, and a stronger ferromagnetic character is expected for the magnetic interaction. So, a total counterbalance is found and a maximum ferromagnetic interaction must be observed. From here, the energy gap in the SOMOs of the hydroxo ligand will be bigger than that caused by the carboxylate ligand, and, consequently, a decrease in the ferromagnetic interaction is expected. Similar results have been found for the calculation on model **III**. All these comments are summarised in Figure 6. For model **III** a maximum of *J* is obtained for a φ value of 102.8° (see Figure 7). The more stable structure appears for a φ value of 118.7°, which is slightly bigger than that in the $[Cu_2(\mu\text{-carboxylate})(\mu\text{-}OH)]^{2+}$ complexes.

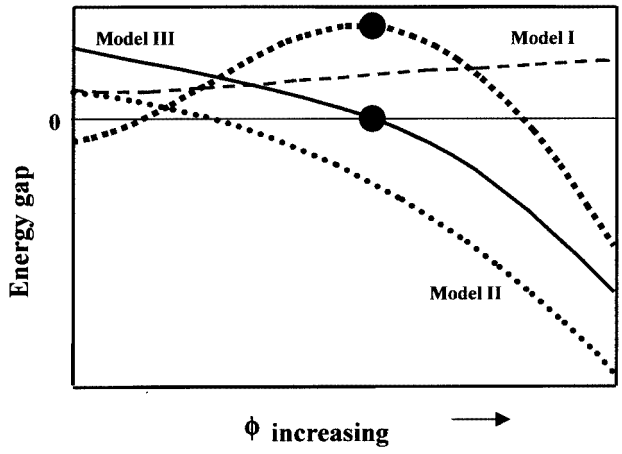

Figure 6. Theoretical dependence of Δ (energy gap) with the φ angle for the models **I** (- - -), **II** (···) and **III** (——); the variation of *J* as a function of φ is shown as a (···) line; the maximum *J* value for the model **III** coincides with the zero value in the energy gap (Δ) (black circles)

Figure 7 shows the theoretical *J* values for model **III**, the experimental ones of dinuclear copper(II) complexes reported in the literature (shown as circles), those found for the trinuclear compounds described here and that described in ref.[5] (shown as crosses). In the range from 103 to 135° the magnetic coupling becomes more antiferromagnetic when φ increases. It should be emphasised that the compounds with an aliphatic peripheral ligand [18–19,23] show φ angles bigger than those with an aromatic peripheral one.[7,24–25] However, our compounds show an intermediate φ value. This is probably due to the trinuclear topology adopted in our series of compounds. We have therefore found

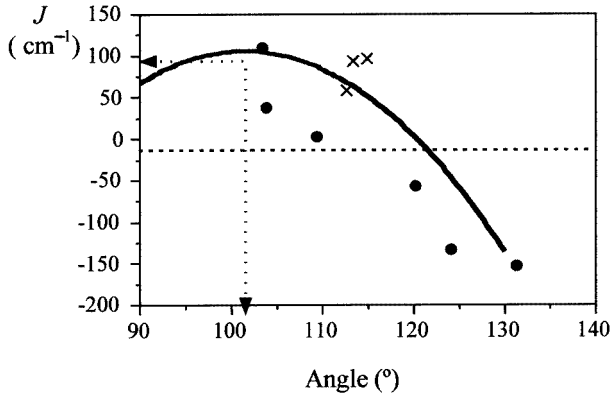

Figure 7. Calculated dependence of J with the φ angle for the model **III**; the arrows point to the maximum J value; experimental J values of dinuclear copper(II) complexes reported in the literature (·) and those of compounds **1**, **2** and that described in ref.[5] (x)

a way to tune the magnitude and the nature of the magnetic interaction through the peripheral ligand and the molecular nuclearity. On the other hand, Figure 7 shows that the experimental J values of trinuclear compounds (**1**, **2** and the compound from ref.[5]) are higher than that found experimentally in dinuclear complexes for similar φ angles. The formation of trinuclear entities implies a change in the coordination sphere. Thus, the compounds in the literature (dinuclear complexes) present a N_2O_2 environment, while the trinuclear complexes show both N_2O_2 and O_4 ones. The higher J value shown by the title compounds could be explained by taking into account the effect of the nature of the donor atoms of the peripheral ligands on the magnetic interaction magnitude.[26] Nevertheless, it is not uncommon that a relatively large range of values for the J constant is observed for a family of complexes with similar φ angles.

To explain this phenomenon, we have studied several structural distortions found in the real systems: changes in the $Cu-N_{peripheral\ ligand}$, $Cu-O_{bridging\ ligands}$ distances, the dihedral angle γ (Figure 5) between the $CuO_{hydroxo}Cu$ and $CuOO_{carboxylate}Cu$ planes, distortions in the carboxylate group, etc. No important effects on the J constant values have been found. Only the relative position of the hydrogen atom in the hydroxo group, defined by the τ angle (see Figure 5), as in the $[Cu_2(\mu\text{-}OH)_2]^{2+}$ complexes, is able to cause meaningful changes in the J constant. Although, as in the $[Cu_2(\mu\text{-}OH)_2]^{2+}$ complexes, a structural correlation can exist between the φ and τ angles[12,21] (the same electronic reasons), there are other factors, such as hydrogen bonds, that can govern the hydrogen-atom position or the τ value. Unfortunately, in many cases, the exact positions of these hydrogen atoms have not been determined by X-ray diffraction; however, it is possible to estimate this position when a solvent molecule or anion forms a hydrogen bond with the hydroxo groups. The hydrogen atom can then be placed in the direction of this bond. In this way the τ angle for these compounds lies between 0 and 51°, with a maximum value for the compound with the anomalous stronger ferromagnetic interaction. In any case, for model **III**, based on compound **2** (τ = 58.5°) and **1** (τ = 0°) we have found J values (36.4 and 85.4 cm^{-1}, respectively) that are in good agreement with the tendency found experimentally.

Although two parameters mostly govern the nature and magnitude of the magnetic interaction in this family of compounds, a lot of other structural parameters exist that have negligible influences.

Experimental Section

General Remarks: The infrared spectra ($\tilde{\nu}$ = 400−4000 cm^{-1}) were obtained on a Mattson Satellite FTIR spectrophotometer. Elemental Analyses were performed on a Carlo Erba AAS instrument. The variable temperature magnetic susceptibility measurements were carried out on a microcrystalline sample using a Quantum Design MPMS2 SQUID susceptometer equipped with a 55 kG magnet and operating at 10 kG in the range of 1.8−400 K. The susceptometer was calibrated with $(NH_4)_2Mn(SO_4)_2{\cdot}12H_2O$. The corrections for the diamagnetism were estimated from Pascal's constants. Diffuse Reflectance and UV/Vis spectra were recorded on a Shimadzu 2101 PC spectrophotometer. The EPR spectra of ground crystals were carried out at the X-band with a Bruker ELEXSYS and at the Q-band frequencies with a Bruker ESP300 spectrometer.

***N*-(pyrid-2-ylmethyl)benzenesulfonylamide (HL1) and *N*-(pyrid-2-ylmethyl)naphthalenesulfonylamide (HL2):** The ligands were obtained by condensation of 2-picolylamine and the corresponding sulfonyl chloride (benzenesulfonyl chloride or 2-naphthalenesulfonyl chloride) following the synthesis procedure previously described.[5] **HL1** (yield 1.38 g, 56%). $C_{12}H_{12}N_2O_2S$ (248): calcd. C 58.1, H 4.8, N 11.3, S 12.9; found C 57.3, H 4.7, N 11.1, S 12.7. IR (KBr): $\tilde{\nu}$ = 1330, 1160 $\nu(SO_2)$, 850 cm^{-1} ν(S−N). **HL2** (yield 2.11 g, 71%). $C_{16}H_{14}N_2O_2S$ (298): calcd. C 64.4, H 4.7, N 9.4, S 10.7; found C 61.5, H 4.8, N 8.9, S 10.4. IR (KBr): $\tilde{\nu}$ = 1329, 1162 $\nu(SO_2)$, 954 cm^{-1} ν(S−N).

Bis(μ-acetato)-bis(μ-hydroxo)-bis[*N*-(pyrid-2-ylmethyl)benzenesulfonylamidate(DMF)$_2$]tricopper(II) (1) and Bis(μ-acetato)-bis(μ-hydroxo)-bis[*N*-(pyrid-2-ylmethyl)naphthalenesulfonylamidate]-tricopper(II) (2): Both copper complexes were prepared by the reaction of the metal acetate (1 mmol in 25 mL DMF) with the ligand (1 mmol in 25 mL DMF). Slow evaporation of the resulting solution at room temperature provided well-developed blue crystals of both compounds suitable for X-ray diffraction. Microanalysis of the dried crystals was satisfactory. **1** (yield 354 mg, 24%). $C_{17}H_{22}Cu_{1.5}N_3O_6S$ (**1**) (491.75): calcd. C 41.48, H 4.47, N 8.54, S 6.50; found C 40.94, H 4.40, N 8.30, S 6.53. IR (KBr): $\tilde{\nu}$ = 3530 ν(O−H), 1567 ν_{as}(COO), 1423 ν_s(COO), 1256, 1130 $\nu(SO_2)$, 970 cm^{-1} ν(S−N). Diffuse Reflectance: (λ_{max}) = 15314 cm^{-1} (653 nm). UV/Vis (dichloromethane/THF/acetic acid): λ_{max} = 14837 cm^{-1} (674 nm), 26882 cm^{-1} (sh) (372 nm). **2** (yield 281 mg, 20%). $C_{36}H_{34}Cu_3N_4O_{10}S_2$ (**2**) (937): C 46.10, H 3.62, N 5.97, S 6.63; found C 45.91, H 3.69, N 6.02, S 6.47. IR (KBr): $\tilde{\nu}$ = 3530 ν(O−H), 1569 ν_{as}(COO), 1427 ν_s(COO), 1256, 1120 $\nu(SO_2)$, 975 cm^{-1} ν(S−N). Diffuse Reflectance: λ_{max} = 15150 cm^{-1} (660 nm). UV/Vis (dichloromethane): λ_{max} = 15873 cm^{-1} (630 nm), 27030 cm^{-1} (sh) (370 nm).

X-ray Crystallographic Study: A blue prismatic crystal of $[Cu_3(L1)_2(CH_3COO)_2(OH)_2(DMF)_2]$ (**1**) and a blue plate crystal of $[Cu_3(L2)_2(CH_3COO)_2(OH)_2]_\infty$ (**2**) were mounted on a glass fibre. Cell constants and an orientation matrix for data collection were obtained by least-squares refinement of the diffraction data from 25 reflections in the range of 15.884 < θ < 45.488° (compound **1**)

Table 2. Crystal data and structure refinement for $[Cu_3(L1)_2(CH_3COO)_2(OH)_2(DMF)_2]$ (**1**) and $[Cu_3(L2)_2(CH_3COO)_2(OH)_2]_\infty$ (**2**)

	1	**2**
Empirical formula	$C_{17}H_{22}Cu_{1.50}N_3O_6S$	$C_{36}H_{34}Cu_3N_4O_{10}S_2$
Formula weight	491.75	937.41
Temperature	293(2) K	293(2) K
Wavelength	1.54184 Å	1.54184 Å
Crystal system	Monoclinic	Monoclinic
space group	$P2_1/n$ (No. 14)	$C2/c$ (No. 15)
Unit cell dimensions	a = 11.390(2) Å	a = 29.3948(11) Å
	b = 13.6125(14) Å	b = 14.4396(7) Å
	c = 13.2216(13) Å	c = 10.7455(6) Å
	β = 93.271(7)°	β = 108.826(4)°
Volume	2046.7(5) Å^3	4316.9(4) Å^3
Z, Calculated density	2, 1.596 Mg/m^3	4, 1.442 Mg/m^3
Absorption coefficient	3.334 mm^{-1}	3.089 mm^{-1}
F(000)	1010	1908
Crystal size	0.35 × 0.25 × 0.25 mm	0.25 × 0.15 × 0.10 mm
θ range	4.67 to 75.89°	3.18 to 77.78°
Limiting indices	$-14 \le h \le 14$, $-17 \le k \le 0$, $-16 \le l \le 0$	$-33 \le h \le 37$, $-17 \le k \le 0$, $-13 \le l \le 9$
Reflections collected/unique	4454/4269 [R(int) = 0.0271]	5099/4056 [R(int) = 0.1316]
Completeness to θ	75.90, 100.0%	77.78, 87.9%
Absorption correction	ψ-scan	ψ-scan
Max. and min. transmission	0.979 and 0.922	0.979 and 0.802
Refinement method	Full-matrix least-squares on F^2	Full-matrix least-squares on F^2
Data/restraints/parameters	4269/0/310	4056/0/251
Goodness-of-fit on F^2	1.065	0.970
Final R[a] indices [$I > 2\sigma(I)$]	$R1$ = 0.0583, $wR2$ = 0.1610	$R1$ = 0.0515, $wR2$ = 0.1715
R indices (all data)	$R1$ = 0.0680, $wR2$ = 0.1698	$R1$ = 0.1242, $wR2$ = 0.2162
Largest diff. Peak and hole	0.917 and −0.525 e·A^{-3}	1.143 and −1.036 e·A^{-3}

[a] $R = ||F_o| - |F_c|| / |F_o|$; $R_w = \{[w(F_o^2 - F_c^2)^2] / [w(F_o^2)^2]\}^{1/2}$

and 16.039° < θ < 45.208° (compound **2**) on an Enraf Nonius CAD4 automatic diffractometer.[27] Data were collected at 293 K using Cu-K_α radiation (λ = 1.54184 Å) and the ω-scan technique, and corrected for Lorentz and polarisation effects.[28] A semi-empirical absorption correction (Ψ-scans) (DIFABS) was made.[29] The structure was solved by direct methods[30] and subsequent difference Fourier maps, and refined on F^2 by a full-matrix least-squares procedure using anisotropic displacement parameters.[31] For compound **1** all hydrogen atoms were located from difference Fourier maps except those of two of the phenyl group and of DMF which were located in their calculated positions (C−H 0.93−0.97 Å). The located H atoms were refined isotropically, whereas the calculated H atoms were refined using a riding model. For compound **2** all hydrogen atoms were located in their calculated positions (C−H: 0.93−0.97 Å) and were refined using a riding model. Atomic scattering factors were obtained from the International Tables for X-ray Crystallography.[32] Molecular graphics were obtained from PLATON-98[33] (compound **2**) and from PLATON-99[34] (compound **1**). A summary of the crystal data, experimental details and refinement results are listed in Table 2.

CCDC-168013 (**1**) and -168014 (**2**) contain the supplementary crystallographic data for this paper. These data can be obtained free of charge at www.ccdc.cam.ac.uk/conts/retrieving.html [or from the Cambridge Crystallographic Data Centre, 12, Union Road, Cambridge CB2 1EZ, UK; Fax: (internat.) +44-1223/336-033; E-mail: deposit@ccdc.cam.ac.uk].

Computational Details: A detailed description of the computational strategy adopted in this work has been described elsewhere[12] and is only briefly reviewed here. For the evaluation of the coupling constants of dinuclear models, two separate calculations were carried out by means of density functional theory,[35] one for the triplet state and another for the singlet state. The hybrid B3LYP method,[36] as implemented in Gaussian98,[37] was used in all calculations, mixing the exact Hartree−Fock exchange[38] with Becke's expression for the exchange and with the Lee−Yang−Parr correlation functional.[39] Double-ζ quality and triple-ζ quality basis sets proposed by Ahlrichs[40] were employed for nonmetallic and metallic atoms, respectively. Also, for the metallic atoms, we added two extra polarisation p functions. The presence of a low-energy singlet made it difficult to evaluate, accurately, the energy of the lowest singlet by a single-determinant method. To solve this problem, broken-symmetry wave functions, as proposed by Noodleman et al., were used.[41−44] Previously, it has been found among the most common functionals, that the B3LYP method combined with the broken-symmetry treatment is the strategy that provides the best results for calculating coupling constants.[5,12,45−49] It is clear that for broken-symmetry, Hartree−Fock calculations are necessary to make a correction due to the multideterminant character of the wave function of the low-multiplicity state.[48] On the other hand, for DFT calculations we adopted single-determinant wave functions for which DFT is well defined.[50−52] Then, we used the broken-symmetry energy calculated by DFT methods as the real energy of the state.

Acknowledgments

G. A. and J. B. thank CYCIT (project PM97−0105-C02−01) and A. C. thanks the Xunta de Galicia (Project XUGA20309B97) for financial support. J. A. Real thanks CYCIT (Project PB97−1397) and the TMR European Community (Contract ERBFMRXCT-

980181) for financial support. We thank Dr. L. Lezama (University of Pais Vasco) for the EPR band Q measurements.

[1] O. Kahn, *Comments Inorg. Chem.* **1984**, *3*, 105−131.
[2] D. J. Spira-Solomon, M. Allendorf, E. I. Solomon, *J. Am. Chem. Soc.* **1986**, *108*, 5316−5318.
[3] [3a] S. I. Chan, H.-H. T. Nguyen, A. K. Shiemke, M. E. Lindstrom, in *Bioinorganic Chemistry of Copper* (Eds.: K. D. Karlin, Z. Tyeklar), Chapman & Hall, New York, **1993**, p. 184. [3b]H.-H. T. Nguyen, A. K. Shiemke, S. J. Jacobs, B. J. Hales, M. E. Linstrom, S. I. Chan, *J. Biol. Chem.* **1994**, *269*, 14995−15005.
[4] [4a] A. Messerschmidt, A. Rossi, R. Ladensteins, R. Huber, M. Bolognsei, G. Gatti, A. Marchesini, R. Petruzzelli, A. Finazzi-Agró, *J. Mol. Biol.* **1989**, *206*, 513−529. [4b] A. Messerschmidt, R. Huber, *Eur. J. Biochem.* **1990**, *187*, 341−352. [4c] A. Messerschmidt, in *Bioinorganic Chemistry of Copper* (Eds.: K. D. Karlin, Z. Tyeklar), Chapman & Hall, New York, **1993**, p. 471.
[5] L. Gutierrez, G. Alzuet, J. A. Real, J. Cano, J. Borrás, A. Castiñeiras, *Inorg. Chem.* **2000**, *39*, 3608−3614.
[6] [6a] W. Haase, S. Gehring, *J. Chem. Soc., Dalton Trans.* **1985**, 2609−2613. [6b] S. Ghering, W. Haase, H. Paulus, *Acta Crystallogr., Sect. C* **1991**, *47*, 1814−1816. [6c] P. Fleischhauer, S. Gehring, W. Haase, *Ver. Bunsenges. Phys. Chem.* **1992**, *96*, 1701−1704. [6d] S. Gehring, P. Fleischhauer, H. Paulus, W. Haase, *Inorg. Chem.* **1993**, *32*, 54−60. [6e] P. Fleischhauer, S. Gehring, C. Saal, W. Haase, Z. Tomkowicz, C. Zanchini, D. Gatteschi, D. Davidof, A. L. Barra, *J. Magn. And Magn. Materials* **1996**, *159*, 166−174.
[7] G. Christou, S. P. Perlepes, E. Libby, K. Foltong, J. C. Huffman, R. J. Webb, D. N. Hendrickson, *Inorg. Chem.* **1990**, *29*, 3657−3666.
[8] G. G. B. Deacon, R. J. Phillips, *Coord. Chem. Rev.* **1980**, *33*, 227−250.
[9] B. J. Hathaway, in *Comprehensive Coordination Chemistry* (Ed.: G. Wilkinson, R. D. Gill, J. A. McCleverty), Pergamon Press, Oxford, **1987**, Vol. 5.
[10] E. A. Boudroux, L. N. Mulay, in *Theory and Applications of Molecular Paramagnetism*, John Wiley, New York, **1976**.
[11] D. B. Brown, J. R. Wasson, J. W. Hall, W. E. Hatfield, *Inorg. Chem.* **1977**, *16*, 2526−2529.
[12] E. Ruiz, P. Alemany, S. Alvarez, J. Cano, *J. Am. Chem. Soc.* **1997**, *119*, 1297−1303·
[13] Y. Nishida, M. Takeuchi, K. Takahashi, S. Kida, *Chem. Lett.* **1985**, 631−634.
[14] Y. Nishida, M. Takeuchi, K. Takahashi, S. Kida, *Chem. Lett.* **1983**, 1815−1818.
[15] V. McKee, M. Zvagulis, C. A. Reed, *Inorg. Chem.* **1985**, *24*, 2914−2919.
[16] V. McKee, M. Zvagulis, J. V. Dagdian, M. G. Patch, C. A. Reed, *J. Am. Chem. Soc.* **1984**, *106*, 4765−4772.
[17] L. K. Thompson, S. S. Tandon, F. Lloret, J. Cano, M. Julve, *Inorg. Chem.* **1997**, *36*, 3301−3606.
[18] K.-S. Burger, P. Chaudhuri, K. Wieghardt, *J. Chem. Soc., Dalton Trans.* **1996**, 247−248.
[19] C. J. Boxwell, R. Bhalla, L. Cronin, S. S. Turner, P. H. Walton, *J. Chem. Soc., Dalton Trans.* **1998**, 2449−2550.
[20] E. Kavlakoglu, A. Elmali, Y. Eleman, H. Fuess, *Z. Naturforschung, Teil B* **2000**, *55*, 561−566.
[21] E. Ruiz, P. Alemany, S. Alvarez, J. Cano, *Inorg. Chem.* **1997**, *36*, 3683−3688, and their references.
[22] K. Geetha, M. Nethaji, N. Y. Vasanthacharya, A. R. Chaktavarty, *J. Coord. Chem.* **1999**, *47*, 77−89.
[23] S. Meenakumari, S. K. Tiwari, A. R. Chakravarty, *J. Chem. Soc., Dalton Trans.* **1993**, 2175−2181.
[24] T. Tokii, N. Hamanura, N. Nakashima, Y. Muto, *Bull. Chem. Soc. Jpn.* **1992**, *65*, 1214−1219.
[25] W. B. Tolman, R. L. Rardin, S. J. Lippard, *J. Am. Chem. Soc.* **1989**, *111*, 4532−33.
[26] P. Roman, C. Guzman-Miralles, A. Luque, J. I. Beitia, J. Cano, F. Lloret, M. Julve, S. Alvarez, *Inorg. Chem.* **1996**, *35*, 3741−3751.
[27] B. V. Nonius, CAD4-Express Software, Ver. 5.1/1.2. Enraf Nonius, Delft, The Netherlands, **1994**.
[28] M. Kretschmar, GENHKL Program for the reduction of CAD4 Diffractometer data, University of Tuebingen, Germany, **1997**.
[29] A. C. T. North, D. C. Phillips, F. S. Mathews, *Acta Crystallogr., Sect. A* **1968**, *24*, 351−359.
[30] G. M. Sheldrick, *Acta Crystallogr., Sect. A* **1990**, *46*, 467−473.
[31] G. M. Sheldrick, *SHELXL-97. Program for the Refinement of Crystal Structures*, University of Goettingen, Germany, **1997**.
[32] *International Tables for X-ray Crystallography*, Kluwer Academic Publishers, Dordrecht, The Netherlands, **1995**; Vol. C.
[33] A. L. Spek, PLATON. *A Multipurpose Crystallographic Tool*, Utrecht University, Utrecht, The Netherlands, **1998**.
[34] A. L Spek, PLATON. *A Multipurpose Crystallographic Tool*, Utrecht University, Utrecht, The Netherlands, **1999**.
[35] R. G. Parr, W. Yang, *Density-Functional Theory of Atoms and Molecules*, Oxford University Press, New York, **1989**.
[36] A. D. J. Becke, *J. Chem. Phys.* **1993**, *98*, 5648−5652.
[37] Gaussian 98 (Revision A.7), M. J. Frisch, G. W. Trucks, H. B. Schlegel, G. E. Scuseria, M. A. Robb, J. R. Cheeseman, V. G. Zakrzewski, J. A. Montgomery, R. E. Stratmann, J. C. Burant, S. Dapprich, J. M. Millam, A. D. Daniels, K. N. Kudin, M. C. Strain, O. Farkas, J. Tomasi, V. Barone, M. Cossi, R. Cammi, B. Mennucci, C. Pomelli, C. Adamo, S. Clifford, J. Ochterski, G. A. Petersson, P. Y. Ayala, Q. Cui, K. Morokuma, D. K. Malick, A. D. Rabuck, K. Raghavachari, J. B. Foresman, J. Cioslowski, J. V. Ortiz, B. B. Stefanov, G. Liu, A. Liashenko, P. Piskorz, I. Komaromi, R. Gomperts, R. L. Martin, D. J. Fox, T. Keith, M. A. Al-Laham, C. Y. Peng, A. Nanayakkara, C. Gonzalez, M. Challacombe, P. M. W. Gill, B. G. Johnson, W. Chen, M. W. Wong, J. L. Andres, M. Head-Gordon, E. S. Replogle, J. A. Pople, Gaussian, Inc., Pittsburgh, PA, **1998**.
[38] A. D. J. Becke, *Phys. Rev.* **1988**, *A38*, 3098−3100.
[39] C. Lee, W. Yang, R. G. Parr, *Phys. Rev.* **1988**, *B37*, 785−789.
[40] A. Schaefer, H. Horn, R. Ahlrichs, *J. Chem. Phys.* **1992**, *97*, 2571−2574.
[41] L. Noodlemann, C. Y. Peng, D. A. Case, J. M. Mouesca, *Coord. Chem. Rev.* **1995**, *144*, 199−244.
[42] L. Noodlemann, D. A. Case, *Adv. Inorg. Chem.* **1992**, *38*, 423−470.
[43] L. Noodlemann, E. R. Davidson, *Chem. Phys.* **1986**, *109*, 131−133.
[44] L. Noodlemann, *J. Chem. Phys.* **1981**, *74*, 5737−5743.
[45] J. Cano, P. Alemany, S. Alvarez, M. Verdaguer, E. Ruiz, *Chem. Eur. J.* **1998**, *4*, 476−484.
[46] E. Ruiz, J. Cano, S. Alvarez, P. Alemany, *J. Am. Chem. Soc.* **1998**, *120*, 11122−11129.
[47] J. Cano, E. Ruiz, P. Alemany, F. Lloret, S. Alvarez, *J. Chem. Soc., Dalton Trans.* **1999**, 1669−1676.
[48] E. Ruiz, J. Cano, S. Alvarez, P. Alemany, *J. Comput. Chem.* **1999**, *20*, 1391−1400.
[49] I. Castro, M. L. Calatayud, J. Sletten, F. Lloret, J. Cano, M. Julve, G. Seitz, K. Mann, *Inorg. Chem.* **1999**, *38*, 4680−4687.
[50] J. P. Perdew, A. Savin, K. Burke, *Phys. Rev. A* **1995**, *51*, 4531−4541.
[51] B. Miehlich, H. Stoll, A. Savin, *Mol. Phys.* **1997**, *91*, 527−536.
[52] A. Goursot, J. P. Malrieu, D. R. Salahub, *Theor. Chim. Acta* **1995**, *91*, 225−236.

Received September 24, 2001
[I01376]

Reactivity of $[Ru_2(CO)_6(\mu\text{-}PFu_2)(\mu\text{-}\eta^1,\eta^2\text{-}Fu)]$ (Fu = 2-furyl) towards Diphosphanes − Substitution, Polymerisation, Cyclometallation and Elimination Reactions

Wai-Yeung Wong,*[a] Fai-Lung Ting,[a] and Wai-Lim Lam[a]

Keywords: Ruthenium / Phosphane ligands / Phosphido complexes

Thermal reaction of $[Ru_2(CO)_6(\mu\text{-}PFu_2)(\mu\text{-}\eta^1,\eta^2\text{-}Fu)]$ (Fu = 2-furyl) (**1**) with bis(diphenylphosphanyl)methane (dppm), bis(diphenylphosphanyl)amine (dppam), or bis(diphenylphosphanyl)methylamine (dppma), produces the substitution products $[Ru_2(CO)_4(\mu\text{-}PFu_2)(\mu\text{-}\eta^1,\eta^2\text{-}Fu)(\mu\text{-}L)]$ [**2** (L = dppm), **3** (L = dppam), **4** (L = dppma)] in good yields. The Ru–Ru edge is bridged by the diphosphane in each case, while the $\mu\text{-}\eta^1,\eta^2$-bound furyl fragment remains intact. When the reactions were carried out using bis(diphenylphosphanyl)ethane (dppe) or bis(diphenylphosphanyl)propane (dppp), the compounds $[Ru_2(CO)_5(\mu\text{-}PFu_2)(\mu\text{-}\eta^1\text{-}C_6H_4PPh(CH_2)_nPPh_2)]$ [**5** (n = 2), **6** (n = 3)] were isolated as the thermodynamic products in which both P atoms chelate to one Ru centre to afford five- (for **5**) and six-membered (for **6**) ruthenacycles, accompanied by orthometallation of one of the phenyl rings of the phosphane ligand. Interestingly, elimination of the coordinated furyl moiety occurs during the formation of **5** and **6**. Upon reaction with bis(diphenylphosphanyl)butane (dppb), bis(diphenylphosphanyl)pentane (dpppe), or bis(diphenylphosphanyl)ferrocene (dppf), cyclometallation is not favoured in each case. Instead, $[\{Ru_2(CO)_5(\mu\text{-}PFu_2)(\mu\text{-}\eta^1,\eta^2\text{-}Fu)\}_2(L)]$ [**7a** (L = dppb), **8a** (L = dpppe), **9a** (L = dppf)] and polymeric $[Ru_2(CO)_4(\mu\text{-}PFu_2)(\mu\text{-}\eta^1,\eta^2\text{-}Fu)(L)]_n$ [**7b** (L = dppb), **8b** (L = dpppe), **9b** (L = dppf)] were obtained with the product yield depending on the stoichiometry of the reactants. All these new diruthenium complexes are electron-precise with 34 cluster valence electrons.

(© Wiley-VCH Verlag GmbH, 69451 Weinheim, Germany, 2002)

Introduction

There is a continuing interest in the synthesis and chemistry of phosphido-bridged di- and polynuclear complexes.[1−7] Several recent developments provide a wealth of unexpected and intriguing reactivity of some dinuclear allenyl complexes of the type $[M_2(CO)_6(\mu\text{-}PPh_2)(\mu\text{-}\eta^1,\eta^1_{\alpha,\beta}\text{-}C_\alpha(R)=C_\beta=CR_2)]$ (M = Fe, Ru; R = H, Ph) towards mono- and bidentate phosphanes.[8−12] In these studies, the nature of the phosphane plays a significant role in governing the reaction pathways involved and the final products isolated.[8−12]

We are interested in the use of tris(2-furyl)phosphane (PFu_3) as a ligand in organometallic syntheses.[13,14] The recent preparation of $[Ru_2(CO)_6(\mu\text{-}PFu_2)(\mu\text{-}\eta^1,\eta^2\text{-}Fu)]$ (**1**) and its reactivity with 1-alkynes sparked our interest in the synthesis of a new class of complexes with different ligand environments.[13] In order to explore the synthetic potential of this system, we have now initiated a comprehensive study of the reactions of **1** with some diphosphane ligands. Herein, we describe results on reactions of **1** with various diphosphanes PPh_2EPPh_2 [E = $(CH_2)_n$, n = 1−5; N(H); N(Me); or $Fe(\eta^5\text{-}C_5H_4)_2$], which lead to the formation and characterisation of a range of novel carbonyl(μ-phosphido)-diruthenium complexes. These products are formed by different reaction pathways embracing (i) simple phosphane substitution with displacement of carbonyl ligands, (ii) polymerization, and (iii) phosphane coordination accompanied by cyclometallation. Another noteworthy feature of these phosphane-containing compounds is the various modes of coordination towards metal atoms which the ligands exhibit[15−18]. Three binding modes have been observed for the diphosphanes used in our studies, namely chelating, intrabridging, and interbridging (Scheme 1).

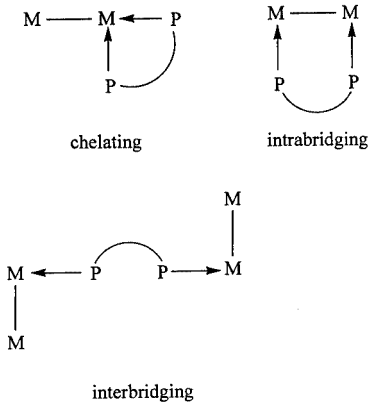

Scheme 1

[a] Department of Chemistry, Hong Kong Baptist University, Waterloo Road, Kowloon Tong, Hong Kong, P. R. China
E-mail: rwywong@hkbu.edu.hk

Results and Discussion

Synthesis and Spectroscopic Characterisation

Complex **1** reacts with an equimolar amount of the bidentate phosphane, namely bis(diphenylphosphanyl)methane (dppm), bis(diphenylphosphanyl)amine (dppam), or bis(diphenylphosphanyl)methylamine (dppma), in refluxing toluene to afford three new diruthenium compounds $[Ru_2(CO)_4(\mu\text{-}PFu_2)(\mu\text{-}\eta^1,\eta^2\text{-}Fu)(\mu\text{-dppm})]$ (**2**), $[Ru_2(CO)_4(\mu\text{-}PFu_2)(\mu\text{-}\eta^1,\eta^2\text{-}Fu)(\mu\text{-dppam})]$ (**3**), and $[Ru_2(CO)_4(\mu\text{-}PFu_2)(\mu\text{-}\eta^1,\eta^2\text{-}Fu)(\mu\text{-dppma})]$ (**4**) as the sole products after TLC purification on silica, all in reasonable yield (Scheme 2). They were isolated as bright yellow crystalline solids and are soluble in common organic solvents. These compounds display almost identical IR ν(CO) absorption patterns, suggesting a great resemblance of their structures. Each of the $^{31}P\{^1H\}$ NMR spectra of **2** and **4** consists of two separated sets of resonance signals. The resonance due to the phosphido-P atom shows equal coupling to the two coincidentally equivalent P atoms of the chelating diphosphanes, thus appearing as a pseudo-triplet ($^2J_{P-P}$ = 172 for **2** and 169 Hz for **4**). For **3**, a doublet of doublets appears around δ = 94.0 ppm, attributable to the $\mu\text{-}PFu_2$ entity and two interpenetrating sets of doublets in close proximity centred at δ = 87.16 and 87.18 ppm were also observed for the coordinated dppam ligand.

In order to further investigate, how the separation between the P donor atoms in $PPh_2(CH_2)_nPPh_2$ (i.e. the value of *n*) might affect the chemistry of such classes of complexes, we have examined the reactions that take place with the related bidentate phosphanes containing more methylene groups, namely bis(diphenylphosphanyl)ethane (dppe), bis(diphenylphosphanyl)propane (dppp), bis(diphenylphosphanyl)butane (dppb), or bis(diphenylphosphanyl)pentane (dpppe). To our surprise, two novel 34-electron phosphido-stabilised diruthenium complexes $[Ru_2(CO)_5(\mu\text{-}PFu_2)(\mu\text{-}\eta^1\text{-}C_6H_4PPhCH_2CH_2PPh_2)]$ (**5**) and $[Ru_2(CO)_5(\mu\text{-}PFu_2)(\mu\text{-}\eta^1\text{-}C_6H_4PPhCH_2CH_2CH_2PPh_2)]$ (**6**) were obtained as the thermodynamically stable products, upon reaction of **1** with dppe or dppp at elevated temperatures. In both structures, the two P atoms chelate to one Ru atom to result in five- (for **5**) and six-membered (for **6**) ruthenacycles, followed by orthometallation of one of the phenyl rings of $PPh_2(CH_2)_nPPh_2$ (*n* = 2, 3).[18] No sign of the formation of polymeric species in these reactions was observed under our experimental conditions. The transformation of these two products is illustrated in Scheme 2. Most interestingly, in marked contrast with **2**−**4**, the $\mu\text{-}\eta^1,\eta^2$-bonded furyl group was found to be detached during the formation of **5** and **6** so as to stabilize the products to retain 34 cluster valence electrons (CVE). However, the mechanism for this reaction is not yet ascertained. The IR spectral features of **5** and **6**

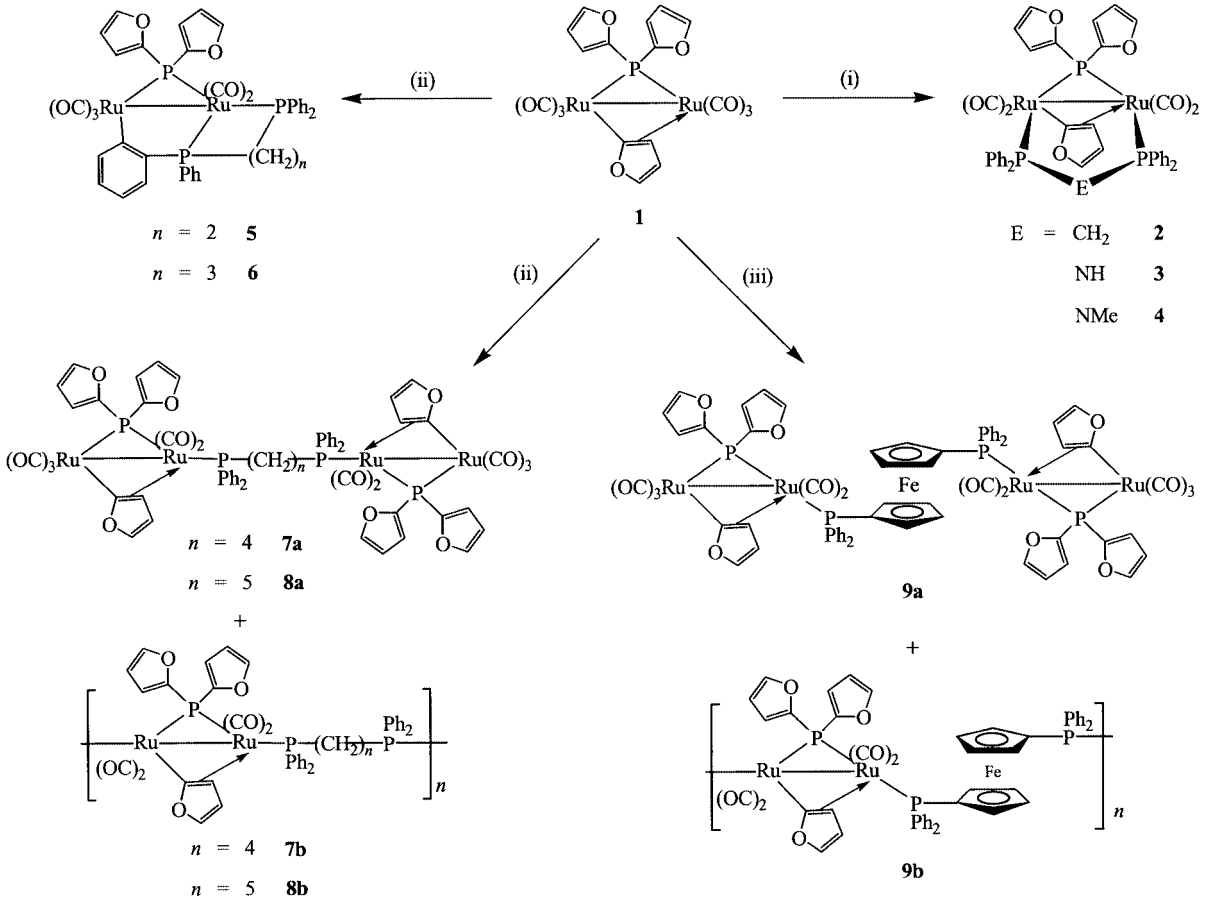

Scheme 2. (i) PPh_2EPPh_2; (ii) $PPh_2(CH_2)_nPPh_2$; (iii) dppf

are almost identical, indicative that they have similar structures. They exhibit different patterns from the dppm analogue. Their ν(CO) bands absorb at lower energies than those of **1**, in agreement with chelation of the strongly electron-donating phosphane ligands. They display three distinct sets of resonances in the $^{31}P\{^1H\}$ NMR spectra and afford a typical AMX spectrum in each case. Compound **5** gives a characteristic doublet of doublets at δ = 99.08 ppm ($^2J_{P-P}$ = 25 and 146 Hz) due to the μ-PFu_2 group and another doublet of doublets at δ = 68.36 ppm ($^2J_{P-P}$ = 25 and 146 Hz) for the orthometallated PPh moiety. We note that the resonance peak at δ = 65.67 ppm due to the PPh_2 group shows equal coupling to the other two *cis*-phosphorus atoms ($^2J_{P-P}$ = 25 Hz), thereby appearing as a virtual triplet. A similar coupling phenomenon has been observed in $[CpW_2(CO)_5(\mu\text{-}PPh_2)(\eta^2\text{-}dppe)]$.[19] The $^{31}P\{^1H\}$ NMR spectrum of **6** reveals three sets of doublets of doublets at δ = 84.27, 21.82, and 20.60 ppm with the most downfield signal corresponding to the phosphido group.

As a continuation of our effort in the study of the effect of the methylene chain length on the identity of products formed, similar reactions with dppb or dpppe were also carried out and in none of the cases was the product analogous to other $PPh_2(CH)_nPPh_2$-bridged species (n = 1−3) obtained. Complex **1** undergoes a rapid ligand substitution reaction with a 0.5 equiv. of dppb or dpppe in refluxing toluene for 1 h to give $[\{Ru_2(CO)_5(\mu\text{-}PFu_2)(\mu\text{-}\eta^1,\eta^2\text{-}Fu)\}_2(dppb)]$ (**7a**) (70%) and $[\{Ru_2(CO)_5(\mu\text{-}PFu_2)(\mu\text{-}\eta^1,\eta^2\text{-}Fu)\}_2(dpppe)]$ (**8a**) (65%) as yellow solids (Scheme 2). Their structures were firmly supported by spectroscopic data. There is also no indication of the formation of dppb- or dpppe-bridged analogues of **2**−**4**. Apparently, the long methylene bridge separating two bulky PPh_2 groups would favour the isolation of **7a** and **8a**. Although it is commonly found that the dppe and dppp can form stable five- and six-membered chelating rings with the metal centre without imposing strong steric interactions between the two PPh_2 groups,[12,19−22] chelation at the Ru atom by the dppb or dpppe is inhibited since the formation of 7- or 8-membered rings is generally not feasible. Moreover, the formation of a sterically unfavourable four-membered metallacycle for dppm would disfavour coordination via a chelating mode.

When the experiment was conducted with an equimolar amount of **1** and dppb or dpppe for 1 h, polymerisation occurred producing yellow polymers $[Ru_2(CO)_4(\mu\text{-}PFu_2)(\mu\text{-}\eta^1,\eta^2\text{-}Fu)(L)]_n$ [**7b** (L = dppb) or **8b** (L = dpppe)] in high yields and purity, which could not be isolated by TLC or column chromatography. Purification of the polymers was accomplished by extraction of the yellow residues with several portions of hot hexane, followed by repeated precipitation from their toluene solutions with methanol. Both polymers were characterized by Gel Permeation Chromatography (GPC) as low-molecular-weight substances. A prolonged heating of the reaction mixture was found to increase the extent of polymerisation, and we observed that polymer **7b** shows 23 repeating units (M_w = 24500, M_n = 22700) in the main chain when the reaction is carried out for 10 h. They are both air-stable and soluble in common organic solvents. By virtue of symmetry, they both present almost equivalent $^{31}P\{^1H\}$ NMR spectra and each shows two ^{31}P resonances at δ ≈ 34.0 and 39.0 ppm. However, no attempts have been made to fully assign these signals. The rather upfield resonances observed for the μ-phosphido atom in **7** and **8** were found to be in line with that for the disubstituted product $[Ru_2(CO)_4(PFu_3)_2(\mu\text{-}PFu_2)(\mu\text{-}\eta^1,\eta^2\text{-}Fu)]$ which gave a pseudo AX_2 $^{31}P\{^1H\}$ spectrum with a triplet at δ = 48.00 ppm and a doublet at δ = −12.28 ppm ($^2J_{P-P}$ = 23 Hz) for the μ-PFu_2 and PFu_3 groups, respectively, in an intensity ratio of 1:2.[23]

Attempts have also been made to study the interaction between **1** and the organometallic diphosphane ligand $[Fe(\eta^5\text{-}C_5H_4PPh_2)_2]$ (dppf) in view of the considerable research attention on the use of the latter in the syntheses of di- or polymetallic complexes.[24] Instead of producing a chelating complex as in **2**−**4**, thermal reaction of **1** with dppf in a 2:1 molar ratio for a short period of time (ca. 1 h) afforded the complex $[\{Ru_2(CO)_5(\mu\text{-}PFu_2)(\mu\text{-}\eta^1,\eta^2\text{-}Fu)\}_2(dppf)]$ (**9a**) in fairly good yield in which two phosphido-bridged diruthenium fragments are linked by a bridging bis(diphenylphosphanyl)ferrocene moiety (Scheme 2). The two PPh_2 groups in dppf are separated by a large ferrocenyl moiety and are free to form bidentate complex **9a**. On the contrary, the relatively short bridging length between both PPh_2 groups in PPh_2EPPh_2 [E = CH_2, N(H), N(Me)] appears to hinder the adoption of such an interbridging mode. Spectroscopic and MS data of **9a** are consistent with the formula of the product having a 2:1 stoichiometry (Ru_2/dppf) with the loss of two CO ligands. The IR spectrum of **9a** shows a rather different ν(CO) pattern from those of **2**−**4**, indicating that an intrabridging interaction probably did not happen in this case. Like the spectrum of $[\{CpW_2(CO)_6(\mu\text{-}PPh_2)\}_2(dppf)]$,[19] two phosphorus doublets were clearly shown in its $^{31}P\{^1H\}$ NMR spectrum, in agreement with the structure shown. An attempt to generate a polymeric complex was also carried out via the reaction of **1** with dppf in a 1:1 stoichiometric ratio. Only a

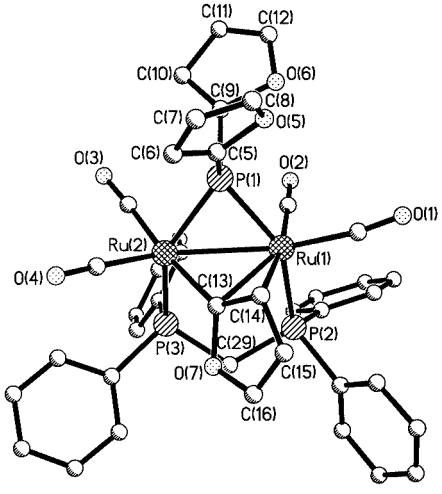

Figure 1. A perspective drawing of compound **2**; for clarity, all H atoms and the labels on the phenyl rings are omitted; the labels on the carbonyl C atoms have the same labels as the O atoms

trace quantity of **9a** was detected in this reaction and its yield was reduced as the time of reflux was increased. An air-stable polymeric substance $[Ru_2(CO)_4(\mu\text{-}PFu_2)(\mu\text{-}\eta^1,\eta^2\text{-}Fu)(dppf)]_n$ (**9b**) was obtained as the major product following similar purification procedures as for **7b** and **8b**. An analytically pure sample of **9b** was collected as an orange solid in 64% yield which is soluble in chlorinated solvents such as CH_2Cl_2 and $CHCl_3$. Analysis of **9b** by GPC revealed a low-molecular-weight polymer (M_w = 11400, M_n = 8550, average degree of polymerization = 8). Compound **9b** displays NMR spectroscopic data that is very similar to that of the model complex **9a,** except that its resonance peaks are rather broad in appearance.

Crystal Structure Analyses

Perspective drawings of the structures of **2** (Figure 1, Table 1), **3** (Figure 2, Table 1), **4** (Figure 3, Table 1), **5** (Figure 4, Table 2), **6** (Figure 5, Table 3), **8a** (Figure 6, Table 4), and **9a** (Figure 7, Table 5) are shown together with the atomic numbering schemes used and selected bond lengths and angles are given. The general structural features of **2**−**4** are very similar. Each of them possesses a difurylphosphido-bridged diruthenium skeleton and the Ru−Ru edge is spanned by a bridging PPh_2EPPh_2 {**2** (E = CH_2), **3** [E = N(H)], **4** [E = N(Me)]} ligand. In each case, the C- or N(R)-bridged (R = H, Me) diphosphane forms a nonplanar, five-membered metallacyclic ring. While the Ru−Ru distances in **2**−**4** are relatively insensitive to the nature of the bridging unit between both of the PPh_2 end groups, they are shorter than those in **1** and other related dialkyne-bridged Ru_2 complexes reported recently [ca. 2.7735(3)−2.8006(6) Å].[13] For **2**−**4**, the P(1) atom is asymmetrically bonded to Ru(1) and Ru(2). The furyl unit is σ-bonded to Ru(2) and π-bonded to Ru(1). These compounds display only slight chelate ring twisting about the Ru−Ru axis for the diphosphane ligands and the torsion angles defined by P(2)−Ru(1)−Ru(2)−P(3) are 7.3, 8.9, and 4.5° for **2**−**4**, respectively. Within the five-membered ruthenacycle in **2**, the structural parameters of the coordinated dppm are very similar to those found in other Ru_2 complexes bridged by dppm, such as in $[Ru_2(CO)_4(\mu\text{-}PPh_2)\{\mu\text{-}\eta^1,\eta^2_{\alpha,\beta}\text{-}C(Ph)=C=CPPh_2\}(\mu\text{-dppm})]$ [2.367(1) Å and 113.6(2)°],[12] $[Ru_2(CO)_3(MeCN)(\mu\text{-}O_2CMe)(\mu\text{-dppm})_2]^+$ [2.37(1) Å and 113(2)°],[25] and $[Ru_2(CO)_2(PPh_3)(\mu\text{-}PPh_2)(\mu_1\text{-}\eta^2\text{-}CH_2PPh_2)(\mu\text{-dppm})]^+$ [2.405(3) Å and 110.0(4)°].[25] The P−N−P angle for **3** is 126.0(4)°, in common with other dinuclear compounds with bridging dppam in the literature.[26–31] The corresponding angle is 121.59(15)° for **4**. These angles are slightly larger than 118.9(2) and 114.6(1)° in free dppam and dppma,[32] respectively. To date, relatively few structural data are available for metal complexes containing dppma as a bridging ligand.[32,33]

The structural characterisations of **5** and **6** provide unequivocal proof of the identity of both molecules in the solid state. Basically, both structures contain a difurylphosphido-substituted diruthenium framework with the $(CH_2)_n$-bridged diphosphane ligands (n = 2, 3) interacting with both metal atoms in an η^1-bonding mode. The furyl moiety that is originally present in **1** has been eliminated. The two P atoms chelate to Ru(1) to afford a sterically favourable five- and six-membered ruthenacycle for **5** and **6**, respectively, accompanied by orthometallation of one of the phenyl rings on the P(3) atom. The coordination around the Ru(1) and Ru(2) atoms is completed by two and three

Table 1. Selected bond lengths [Å] and angles [°] for complexes **2**, **3**·0.5MeOH, and **4**·2CH_2Cl_2

	2	**3**·0·5MeOH	**4**·2CH_2Cl_2
Ru(1)−Ru(2)	2.7443(6)	2.7292(11)	2.7339(4)
Ru(1)−P(1)	2.325(2)	2.356(3)	2.3370(9)
Ru(1)−P(2)	2.376(2)	2.348(2)	2.3728(9)
Ru(2)−P(1)	2.299(2)	2.318(3)	2.2951(9)
Ru(2)−P(3)	2.357(2)	2.327(3)	2.3416(9)
Ru(1)−C(13)	2.363(6)	2.365(9)	2.358(3)
Ru(1)−C(14)	2.504(5)	2.501(9)	2.558(3)
Ru(2)−C(13)	2.093(6)	2.090(9)	2.120(3)
C(13)−C(14)	1.390(10)	1.388(12)	1.390(5)
P(2)−X	1.843(6) [X = C(29)]	1.682(7) [X = N(1)]	1.717(3) [X = N(1)]
P(3)−X	1.869(6) [X = C(29)]	1.704(7) [X = N(1)]	1.717(3) [X = N(1)]
Ru(1)−P(1)−Ru(2)	72.80(6)	71.46(7)	72.34(3)
Ru(2)−Ru(1)−P(1)	53.16(5)	53.62(7)	53.12(2)
P(2)−Ru(1)−Ru(2)	97.17(5)	94.55(7)	92.47(2)
P(3)−Ru(2)−Ru(1)	91.45(4)	91.96(7)	93.79(2)
Ru(1)−C(14)−C(13)	67.9(3)	68.1(5)	65.81(18)
Ru(1)−C(13)−Ru(2)	75.76(19)	75.3(3)	75.05(10)
Ru(2)−Ru(1)−C(13)	47.65(15)	47.8(2)	48.51(8)
Ru(2)−Ru(1)−C(14)	75.61(13)	75.9(2)	75.31(8)
Ru(1)−C(13)−C(14)	79.1(3)	78.9(6)	81.7(2)
C(13)−Ru(1)−C(14)	33.0(2)	33.0(3)	32.54(11)
Ru(2)−C(13)−C(14)	134.5(6)	134.6(7)	133.3(2)
P(2)−X−P(3)	114.3(4) [X = C(29)]	126.0(4) [X = N(1)]	121.59(15) [X = N(1)]

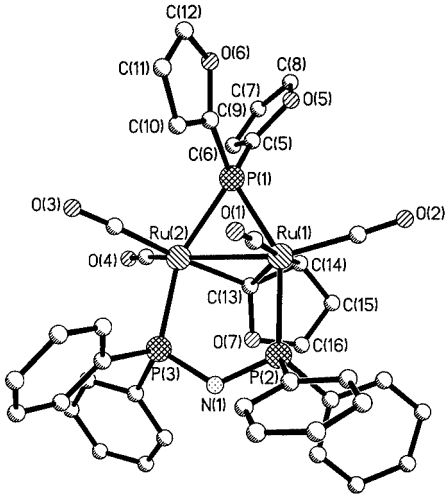

Figure 2. A perspective drawing of compound **3**; for clarity, all H atoms and the labels on the phenyl rings are omitted; the labels on the carbonyl C atoms have the same labels as the O atoms

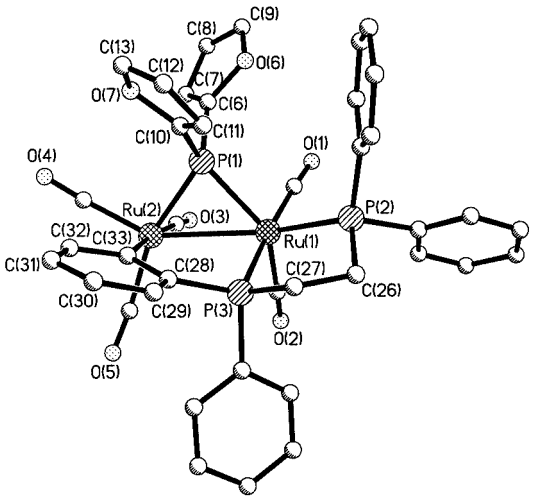

Figure 4. A perspective drawing of compound **5**; for clarity, all H atoms and the labels on the phenyl rings are omitted; the labels on the carbonyl C atoms have the same labels as the O atoms

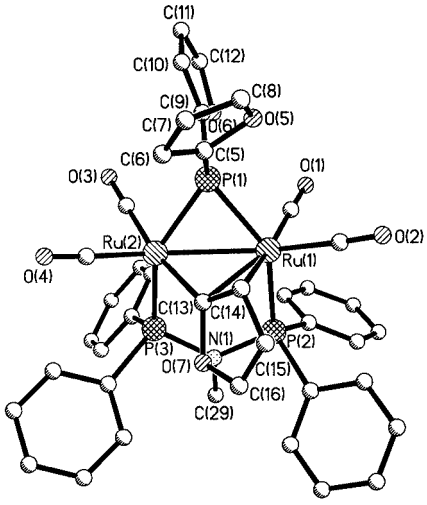

Figure 3. A perspective drawing of compound **4**; for clarity, all H atoms and the labels on the phenyl rings are omitted; the labels on the carbonyl C atoms have the same labels as the O atoms

Table 2. Selected bond lengths [Å] and angles [°] for complex **5**

Ru(1)−Ru(2)	2.8786(3)	Ru(1)−P(1)	2.3410(7)
Ru(1)−P(2)	2.3302(7)	Ru(1)−P(3)	2.3488(7)
Ru(2)−P(1)	2.3189(8)	Ru(2)−C(33)	2.156(3)
C(28)−C(33)	1.409(5)		
Ru(1)−P(1)−Ru(2)	76.30(2)	Ru(2)−Ru(1)−P(1)	51.50(2)
Ru(2)−Ru(1)−P(2)	154.39(2)	Ru(2)−Ru(1)−P(3)	79.90(2)
Ru(1)−Ru(2)−C(33)	92.74(8)	Ru(1)−P(3)−C(28)	116.20(11)
Ru(2)−C(33)−C(28)	122.4(2)	P(3)−C(28)−C(33)	116.7(2)

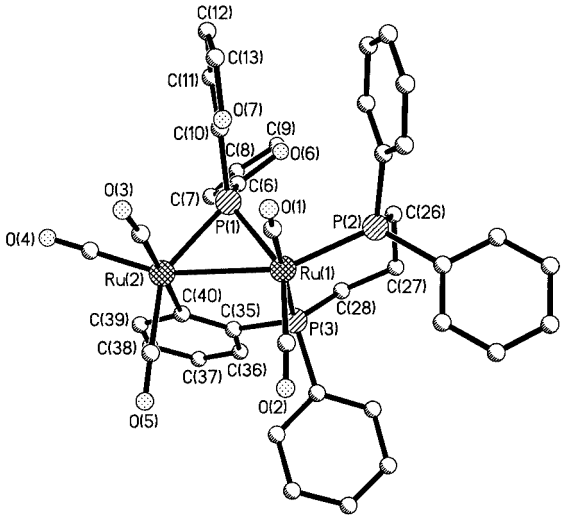

Figure 5. A perspective drawing of compound **6**; for clarity, all H atoms and the labels on the phenyl rings are omitted; the labels on the carbonyl C atoms have the same labels as the O atoms

terminal carbonyl ligands, respectively. For **5**, the dppe ligand was shown to coordinate to the Ru centres, being bonded to Ru(1) through both P(2) and P(3) atoms, and to Ru(2) through the C(33) atom of the orthometallated ring. The torsion angle defined by P(2)−C(26)−C(27)−P(3) is 45.5°. A salient structural feature observed in the structure of **6** is the formation of a six-membered ring, which adopts a stable chair conformation. The P(2) and P(3) atoms are bonded to Ru(1) within the metallacycle. The Ru(2)−C(40) distance [2.174(2) Å] is typical of a Ru−C bond.[12,13,34−36] Both compounds have 34 CVE and the EAN rule supports the metal−metal bond formation based on the three- and five-electron contribution from the phosphido and $C_6H_4PPh(CH_2)_nPPh_2$ (n = 2, 3) units, respectively.

For **8a**, the dpppe ligand links two identical $[Ru_2(CO)_5(\mu\text{-}PFu_2)(\mu\text{-}\eta^1,\eta^2\text{-}Fu)]$ units such that the two halves of the molecule are symmetrically related by an inversion centre at C(32). The C−C bonds in the aliphatic pentamethylene chain of the molecule are staggered with C−C bond lengths between 1.509(6) and 1.511(6) Å and C−C−C angles between 111.4(5) and 115.4(6)°. Complex **9a** reveals a symmetrical dppf-bridged structure in which a dppf unit is

Table 3. Selected bond lengths [Å] and angles [°] for complex **6**·0.5MeOH

Ru(1)−Ru(2)	2.8597(3)	Ru(1)−P(1)	2.3442(6)
Ru(1)−P(2)	2.3339(7)	Ru(1)−P(3)	2.3650(6)
Ru(2)−P(1)	2.3263(7)	Ru(2)−C(40)	2.174(2)
C(35)−C(40)	1.402(3)		
Ru(1)−P(1)−Ru(2)	75.51(2)	Ru(2)−Ru(1)−P(1)	51.961(17)
Ru(2)−Ru(1)−P(2)	152.630(17)	Ru(2)−Ru(1)−P(3)	86.338(16)
Ru(1)−Ru(2)−C(40)	92.06(6)	Ru(1)−P(3)−C(35)	115.16(7)
Ru(2)−C(40)−C(35)	125.70(17)	P(3)−C(35)−C(40)	120.31(17)

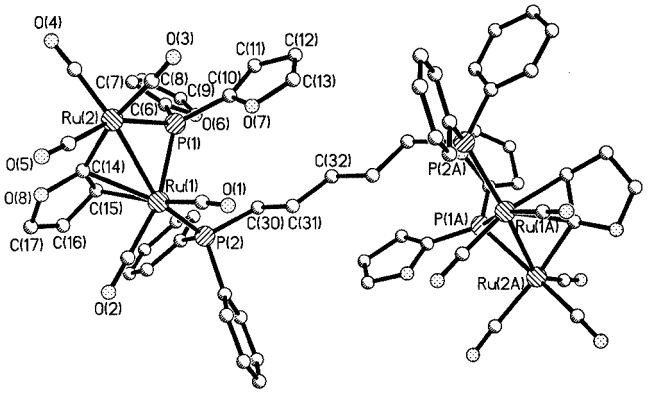

Figure 6. A perspective drawing of compound **8a**; for clarity, all H atoms and the labels on the phenyl rings are omitted; the labels on the carbonyl C atoms have the same labels as the O atoms

Table 4. Selected bond lengths [Å] and angles [°] for complex **8a**·CH_2Cl_2

Ru(1)−Ru(2)	2.7934(5)	Ru(1)−P(1)	2.3592(12)
Ru(2)−P(1)	2.3243(13)	Ru(1)−P(2)	2.3511(11)
Ru(1)−C(14)	2.347(4)	Ru(1)−C(15)	2.398(4)
Ru(2)−C(14)	2.073(4)	C(14)−C(15)	1.401(6)
Ru(1)−P(1)−Ru(2)	73.23(4)	Ru(2)−Ru(1)−P(1)	52.81(3)
Ru(2)−Ru(1)−P(2)	150.19(3)	Ru(1)−C(15)−C(14)	70.8(3)
Ru(1)−C(14)−Ru(2)	78.12(15)	Ru(2)−C(14)−C(15)	135.1(3)
Ru(2)−Ru(1)−C(14)	46.56(11)	Ru(2)−Ru(1)−C(15)	76.28(10)
C(14)−Ru(1)−C(15)	34.33(15)		

sandwiched by two μ-phosphido Ru_2 moieties to afford a heterometallic complex aggregate. The average Ru−Ru bond length is 2.7982(6) Å. The retention of the dissociated furyl fragment in the structure is highlighted by the formation of a σ and a π bonds between the furyl fragment and the Ru_2 core at both ends, similar to those mentioned before in **2**−**4**. The two PPh_2 groups are oriented in an *anti* configuration and the two P atoms are displaced from each cyclopentadienyl ring (away from the Fe atom) by 0.2461 Å for P(2) and −0.2649 Å for P(3). The two phosphanylcyclopentadienyl rings are nearly parallel (dihedral angles 4.4°), planar and deviate by 8.1° from the idealised eclipsed conformation.

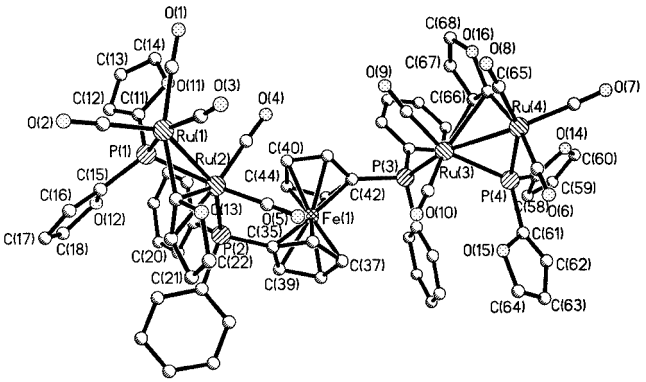

Figure 7. A perspective drawing of compound **9a**; for clarity, all H atoms and the labels on the phenyl rings are omitted; the labels on the carbonyl C atoms have the same labels as the O atoms

Table 5. Selected bond lengths [Å] and angles [°] for complex **9a**·CH_2Cl_2

Ru(1)−Ru(2)	2.8200(6)	Ru(3)−Ru(4)	2.7763(6)
Ru(1)−P(1)	2.3264(17)	Ru(2)−P(1)	2.3545(14)
Ru(2)−P(2)	2.3651(13)	Ru(3)−P(3)	2.3617(13)
Ru(3)−P(4)	2.3671(14)	Ru(4)−P(4)	2.3252(14)
Ru(1)−C(19)	2.063(6)	Ru(2)−C(19)	2.378(5)
Ru(2)−C(20)	2.419(5)	C(19)−C(20)	1.389(8)
Ru(3)−C(65)	2.362(5)	Ru(3)−C(66)	2.419(5)
Ru(4)−C(65)	2.068(6)	C(65)−C(66)	1.395(7)
Ru(1)−P(1)−Ru(2)	74.09(5)	Ru(2)−Ru(1)−P(1)	53.41(4)
Ru(1)−Ru(2)−P(2)	151.81(4)	Ru(1)−C(19)−C(20)	135.7(4)
Ru(2)−C(20)−C(19)	71.6(3)	Ru(1)−C(19)−Ru(2)	78.49(18)
Ru(1)−Ru(2)−C(19)	45.78(13)	Ru(1)−Ru(2)−C(20)	75.05(13)
Ru(2)−C(19)−C(20)	74.8(3)	C(19)−Ru(2)−C(20)	33.65(18)
Ru(3)−P(4)−Ru(4)	72.55(4)	Ru(4)−Ru(3)−P(4)	53.03(4)
Ru(4)−Ru(3)−P(3)	156.10(4)	Ru(3)−C(66)−C(65)	70.8(3)
Ru(3)−C(65)−Ru(4)	77.29(17)	Ru(4)−Ru(3)−C(65)	46.61(14)
Ru(4)−Ru(3)−C(66)	75.91(13)	Ru(3)−C(65)−C(66)	75.3(3)
C(65)−Ru(3)−C(66)	33.91(18)	Ru(4)−C(65)−C(66)	134.8(4)

Concluding Remarks

The work presented here concerns the reaction chemistry of $[Ru_2(CO)_6(\mu\text{-}PFu_2)(\mu\text{-}\eta^1,\eta^2\text{-}Fu)]$ (Fu = 2-furyl) (**1**) with various bidentate phosphane ligands. The general reactivity patterns comprise chemical transformations involving (i) substitution of CO ligands by phosphanes via intrabridging or interbridging coordination modes to afford discrete or polymeric molecules, or (ii) cyclometallation reactions accompanied by reductive elimination of the dissociated furyl moiety. In our studies, three bonding types have been encountered for the diphosphanes used: chelating, intrabridging, and interbridging. We have also investigated in detail the factors dictating the preference for a particular coordination geometry and we observe that the mode of coordination is dependent on the nature and the length of the linking chains between the terminal PPh_2 groups. Although the dominant reaction pathway involves replacement of CO li-

gands by phosphido groups to give substitution products in the majority of cases, thermolysis of **1** with dppe or dppp results in orthometallation of the phenyl ring to yield thermodynamically stable 34-electron complexes containing a $\mu\text{-}\eta^1\text{-}C_6H_4PPh(CH_2)_nPPh_2$ (n = 2, 3) moiety along with the unprecedented detachment of the original furyl fragment from precursor **1**. Work is in progress to study the reactivity of **1** with other organic and organometallic nucleophilic reagents.

Experimental Section

General Procedures: All reactions were conducted under dry nitrogen with the use of standard Schlenk techniques. Solvents for preparative work were dried and distilled before use. Unless otherwise stated all reagents were obtained from commercial suppliers and used without further purification. The syntheses of complex **1**[13] and the ligands dppam[28,29] and dppma[32] were carried out as reported previously. IR spectra were recorded as CH_2Cl_2 solutions with a Perkin−Elmer Paragon 1000 PC or Nicolet Magna 550 Series II FTIR spectrometer. NMR spectra were measured in $CDCl_3$ with a JEOL EX270 or a Varian Inova 400 MHz FT NMR spectrometer, with ^1H NMR chemical shifts quoted relative to $SiMe_4$ and ^{31}P chemical shifts relative to an 85% H_3PO_4 external standard. Fast atom bombardment (FAB) mass spectra were recorded in *m*-nitrobenzyl alcohol matrices with a Finnigan-SSQ 710 spectrometer. Separation of products was accomplished by preparative TLC plates coated with silica (Merck, Kieselgel 60). The molecular weight of each polymer sample was estimated by GPC (HP 1050 series HPLC with visible wavelength and fluorescent detectors) against polystyrene standards.

$[Ru_2(CO)_4(\mu\text{-}PFu_2)(\mu\text{-}\eta^1,\eta^2\text{-}Fu)(\mu\text{-}dppm)]$ (2): A solution of complex **1** (50 mg, 0.083 mmol) in toluene (20 mL) was refluxed with dppm (32 mg, 0.083 mmol) for 4 h. The solution gradually changed from pale yellow to dark orange-yellow. The solvent was then removed in vacuo and the residue taken up in CH_2Cl_2 for TLC separation eluting with hexane/CH_2Cl_2 (2:1, v/v). The bright yellow band (R_f = 0.34) consisting of **2** was obtained and the product was isolated in 84% yield (65 mg). Recrystallisation of the product was achieved by concentration of a hexane/CH_2Cl_2 solution at room temperature, affording bright yellow block crystals. IR (CH_2Cl_2): $\tilde{\nu}$ = 2007 s, 1985 vs, 1942 vs [ν(CO)] cm^{-1}. ^1H NMR ($CDCl_3$): δ = 3.74 (t, $^2J_{H-P}$ = 10.8 Hz, 2 H, CH_2), 4.87 (m, 1 H, Fu), 5.63 (m, 1 H, Fu), 6.33−6.46 (m, 4 H, Fu), 6.75 (s, 1 H, Fu), 7.27 (m, 16 H, Ph), 7.54 (s, 1 H, Fu), 7.67 (m, 4 H, Ph), 7.74 (s, 1 H, Fu) ppm. $^{31}P\{^1H\}$ NMR ($CDCl_3$): δ = 41.61 (d, $^2J_{P-P}$ = 172 Hz, PPh_2), 100.46 (t, $^2J_{P-P}$ = 172 Hz, PFu_2) ppm. FAB MS: m/z = 931 [M^+]. $C_{41}H_{31}O_7P_3Ru_2$ (930.75): calcd. C 52.91, H 3.36; found C 53.14, H 3.30.

$[Ru_2(CO)_4(\mu\text{-}PFu_2)(\mu\text{-}\eta^1,\eta^2\text{-}Fu)(\mu\text{-}dppam)]$ (3): White powdered dppam (32 mg, 0.083 mmol) was added to a toluene solution of **1** (50 mg, 0.083 mmol) and the mixture was stirred under reflux for 3 h to afford a bright yellow solution. The volatile materials were removed in vacuo and subsequent workup by TLC purification with hexane/CH_2Cl_2 (1:1, v/v) as eluent gave a yellow band (R_f = 0.60) which furnished compound **3** as a yellow crystalline solid in 44% (34 mg). IR (CH_2Cl_2): $\tilde{\nu}$ = 2011 s, 1989 vs, 1946 vs [ν(CO)] cm^{-1}. ^1H NMR ($CDCl_3$): δ = 4.42 (m, 1 H, NH), 4.75 (m, 1 H, Fu), 5.92 (m, 1 H, Fu), 6.31−6.40 (m, 3 H, Fu), 6.73 (s, 1 H, Fu), 7.17 (m, 1 H, Fu), 7.34 (m, 12 H, Ph), 7.48 (m, 5 H, Fu + Ph), 7.62 (m, 4 H, Ph), 7.71 (s, 1 H, Fu) ppm. $^{31}P\{^1H\}$ NMR ($CDCl_3$): δ = 87.16 (d, $^2J_{P-P}$ = 191 Hz, PPh_2), 87.18 (d, $^2J_{P-P}$ = 162 Hz, PPh_2), 93.97 (dd, $^2J_{P-P}$ = 162, 191 Hz, PFu_2) ppm. FAB MS: m/z = 876 [(M − 2 CO)$^+$]. $C_{40}H_{30}NO_7P_3Ru_2$ (931.74): calcd. C 51.56, H 3.25, N 1.50; found C 51.30, H 3.16, N 1.32.

$[Ru_2(CO)_4(\mu\text{-}PFu_2)(\mu\text{-}\eta^1,\eta^2\text{-}Fu)(\mu\text{-}dppma)]$ (4): This compound was prepared similarly as described above for **2** and **3** from **1** (50 mg, 0.083 mmol) and dppma (33 mg, 0.083 mmol). The resulting reddish-orange mixture was subjected to preparative TLC eluting with hexane/CH_2Cl_2 (3:1, v/v). From the bright yellow band (R_f = 0.21), the title compound was obtained in 42% yield (33 mg) as bright yellow block-shaped crystals upon recrystallisation from hexane/CH_2Cl_2 under ambient conditions. IR (CH_2Cl_2): $\tilde{\nu}$ = 2007 s, 1988 vs, 1944 vs [ν(CO)] cm^{-1}. ^1H NMR ($CDCl_3$): δ = 2.47 (t, $^3J_{H-P}$ = 6.4 Hz, 3 H, NMe), 5.02 (m, 1 H, Fu), 5.28 (m, 1 H, Fu), 6.34−6.38 (m, 3 H, Fu), 6.49 (m, 1 H, Fu), 6.68 (m, 1 H, Fu), 7.44 (m, 16 H, Ph), 7.66 (s, 1 H, Fu), 7.72 (m, 4 H, Ph), 7.75 (s, 1 H, Fu) ppm. $^{31}P\{^1H\}$ NMR ($CDCl_3$): δ = 91.80 (t, $^2J_{P-P}$ = 169 Hz, PFu_2), 106.92 (d, $^2J_{P-P}$ = 169 Hz, PPh_2) ppm. FAB MS: m/z = 946 [M^+]. $C_{41}H_{32}NO_7P_3Ru_2$ (945.77): calcd. C 52.07, H 3.41, N 1.48; found C 51.73, H 3.25, N 1.70.

$[Ru_2(CO)_5(\mu\text{-}PFu_2)(\mu\text{-}\eta^1\text{-}C_6H_4PPh(CH_2)_2PPh_2)]$ (5): A mixture of compound **1** (50 mg, 0.083 mmol) and dppe (33 mg, 0.083 mmol) in toluene was stirred under reflux for 5 h resulting in a reddish-brown mixture. Removal of the solvent followed by TLC separation on silica eluting with hexane/CH_2Cl_2 (2:1, v/v) gave a yellow solid of complex **5** (35 mg, 46%) after recrystallisation from a hexane/$CHCl_3$ mixture at room temperature. IR (CH_2Cl_2): $\tilde{\nu}$ = 2046 vs, 2002 vs, 1980 m, 1961 s [ν(CO)] cm^{-1}. ^1H NMR ($CDCl_3$): δ = 1.98−2.06 (m, 2 H, CH_2), 2.81−2.91 (m, 2 H, CH_2), 5.45 (m, 1 H, Fu), 5.91 (m, 1 H, Fu), 6.01 (m, 1 H, Fu), 6.19 (m, 1 H, Fu), 6.42 (t, $^3J_{H-H}$ = 7.6 Hz, 1 H, Fu), 6.70−7.63 (m, 19 H, aromatic), 8.06 (d, $^3J_{H-H}$ = 7.6 Hz, 1 H, Fu) ppm. $^{31}P\{^1H\}$ NMR ($CDCl_3$): δ = 65.67 (t, $^2J_{P-P}$ = 25 Hz, PPh), 68.36 (dd, $^2J_{P-P}$ = 25 and 146 Hz, PPh), 99.08 (dd, $^2J_{P-P}$ = 25 and 146 Hz, PFu_2) ppm. FAB MS: m/z = 850 [(M − 2 CO)$^+$]. $C_{39}H_{29}O_7P_3Ru_2$ (904.72): calcd. C 51.78, H 3.23; found C 51.42, H 3.16.

$[Ru_2(CO)_5(\mu\text{-}PFu_2)(\mu\text{-}\eta^1\text{-}C_6H_4PPh(CH_2)_3PPh_2)]$ (6): In a manner similar to compound **5**, refluxing a toluene solution (20 mL) of **1** (50 mg, 0.083 mmol) and dppp (34 mg, 0.083 mmol) in a 1:1 molar ratio for 5 h produced a dark yellowish-brown solution. The usual workup procedures afforded a colourless TLC band (hexane/CH_2Cl_2, 4:1, v/v; R_f = 0.31), which became apparent under UV light. The title complex was subsequently isolated as a pale yellow solid in 40% yield (31 mg). IR (CH_2Cl_2): $\tilde{\nu}$ = 2049 vs, 2004 s, 1985 s, 1959 s [ν(CO)] cm^{-1}. ^1H NMR ($CDCl_3$): δ = 2.03−2.42 (m, 4 H, CH_2), 2.85−3.06 (m, 2 H, CH_2), 5.57 (m, 1 H, Fu), 5.96 (m, 1 H, Fu), 6.10 (m, 1 H, Fu), 6.22 (m, 1 H, Fu), 6.56 (t, $^3J_{H-H}$ = 7.6 Hz, 1 H, Fu), 6.74−7.91 (m, 19 H, aromatic), 8.22 (d, $^3J_{H-H}$ = 7.6 Hz, 1 H, Fu) ppm. $^{31}P\{^1H\}$ NMR ($CDCl_3$): δ = 20.60 (dd, $^2J_{P-P}$ = 31 and 38 Hz, PPh), 21.82 (dd, $^2J_{P-P}$ = 4 and 38 Hz, PPh), 84.27 (dd, $^2J_{P-P}$ = 4 and 31 Hz, PFu_2) ppm. FAB MS: m/z = 919 [M^+]. $C_{40}H_{31}O_7P_3Ru_2$ (918.74): calcd. C 52.29, H 3.40; found C 52.01, H 3.19.

$[\{Ru_2(CO)_5(\mu\text{-}PFu_2)(\mu\text{-}\eta^1,\eta^2\text{-}Fu)\}_2(dppb)]$ (7a) and $[Ru_2(CO)_4(\mu\text{-}PFu_2)(\mu\text{-}\eta^1,\eta^2\text{-}Fu)(dppb)]_n$ (7b): A toluene solution (20 mL) of **1** (50 mg, 0.083 mmol) was heated at reflux in the presence of a 0.5 equiv. of dppb (18 mg, 0.042 mmol). After 1 h, the solvent was removed and the residue chromatographed. A yellow band, eluted with hexane/CH_2Cl_2 (1:1, v/v), yielded the linking cluster **7a** (46 mg, 70%) after recrystallisation from the same solvent mixture.

Mixing compound **1** with 1 mol-equiv. of dppb (0.083 mmol) in toluene (20 mL), followed by heating to reflux for 1 h, generated a deep yellow solution. TLC screening essentially revealed the absence of **7a**. The solvent was removed and the crude solid obtained after washing with hot hexane was redissolved in the minimum volume of toluene. Analytically pure sample of **7b** was isolated as a yellow solid (56 mg, 69%) by repeated precipitation from methanol, washing with hexane and drying in vacuo. **7a**: IR (CH_2Cl_2): $\tilde{\nu}$ = 2060 vs, 2006 vs, 1974 m, 1958 sh [ν(CO)] cm^{-1}. ^1H NMR ($CDCl_3$): δ = 2.09−2.57 (m, 6 H, CH_2), 3.50 (m, 2 H, CH_2), 4.83 (m, 2 H, Fu), 6.04−6.44 (m, 10 H, Fu), 7.08−7.57 (m, 26 H, Fu + Ph) ppm. $^{31}P\{^1H\}$ NMR ($CDCl_3$): δ = 34.58 (m, PFu_2 or PPh_2), 48.80 (m, PFu_2 or PPh_2) ppm. FAB MS: *m*/*z* = 1491 [(M − 3 CO)$^+$]. $C_{62}H_{46}O_{16}P_4Ru_4$ (1575.21): calcd. C 47.28, H 2.94; found C 46.95, H 2.80. **7b**: IR (CH_2Cl_2): $\tilde{\nu}$ = 2014 vs, 1982 m, 1951 s [ν(CO)] cm^{-1}. ^1H NMR ($CDCl_3$): δ = 2.00−2.50 (m, 6 H, CH_2), 3.49 (m, 2 H, CH_2), 4.52 (m, 1 H, Fu), 5.36 (m, 1 H, Fu), 5.85−6.32 (m, 4 H, Fu), 7.05−7.56 (m, 23 H, Fu + Ph) ppm. $^{31}P\{^1H\}$ NMR ($CDCl_3$): δ = 34.33 (m, PFu_2 or PPh_2), 38.60 (m, PFu_2 or PPh_2) ppm. GPC (THF as eluent): M_w = 5030, M_n = 4810 (*n* = 1.05). When the polymerization was performed for 10 h, M_w = 24500, M_n = 22700 (*n* = 1.08). $C_{44}H_{37}O_7P_3Ru_2{\cdot}0.5C_6H_{14}$ (1015.92): calcd. C 55.57, H 4.37; found C 55.79, H 4.34.

[{$Ru_2(CO)_5$(μ-PFu_2)(μ-η^1,η^2-Fu)}$_2$(dpppe)] (8a) and [$Ru_2(CO)_4$(μ-PFu_2)(μ-η^1,η^2-Fu)(dpppe)]$_n$ (8b): A mixture of **1** (50 mg, 0.083 mmol) and dpppe (19 mg, 0.042 mmol) in toluene (20 mL) was heated to reflux for 1 h. Concentration of the resulting yellow solution followed by TLC separation gave a bright yellow band (R_f = 0.55) from which compound **8a** was isolated in 65% yield (43 mg). When a similar reaction was performed using a 1:1 molar ratio of **1** and dpppe (0.083 mmol), the desired polymer **8b** formed after 1 h of reflux, which was worked up in a fashion identical to that for **7b**, to afford a yellow-orange solid (60 mg, 73%). **8a**: IR (CH_2Cl_2): $\tilde{\nu}$ = 2060 vs, 2006 vs, 1973 m, 1957 sh [ν(CO)] cm^{-1}. ^1H NMR ($CDCl_3$): δ = 2.25−2.62 (m, 8 H, CH_2), 3.48 (m, 2 H, CH_2), 4.83 (s, 1 H, Fu), 4.90 (s, 1 H, Fu), 6.21−6.33 (m, 10 H, Fu), 7.20−7.46 (m, 26 H, Fu + Ph), 7.54 (s, 2 H, Fu) ppm. $^{31}P\{^1H\}$ NMR ($CDCl_3$): δ = 34.75 (m, PFu_2 or PPh_2), 49.15 (m, PFu_2 or PPh_2) ppm. FAB MS: *m*/*z* = 1561 [(M − CO)$^+$]. $C_{63}H_{48}O_{16}P_4Ru_4$ (1589.24): calcd. C 47.61, H 3.04; found C 47.32, H 2.85. **8b**: IR (CH_2Cl_2): $\tilde{\nu}$ = 2014 vs, 1981 m, 1951 s [ν(CO)] cm^{-1}. ^1H NMR ($CDCl_3$): δ = 2.08−2.67 (m, 8 H, CH_2), 3.49 (m, 2 H, CH_2), 4.88 (m, 1 H, Fu), 5.39 (m, 1 H, Fu), 6.12−6.34 (m, 4 H, Fu), 7.10−7.89 (m, 23 H, Fu + Ph) ppm. $^{31}P\{^1H\}$ NMR ($CDCl_3$): δ = 34.22 (m, PFu_2 or PPh_2), 38.99 (m, PFu_2 or PPh_2) ppm. GPC (THF as eluent): M_w = 8550, M_n = 7270 (*n* = 1.18). $C_{45}H_{39}O_7P_3Ru_2{\cdot}0.5C_6H_{14}$ (1029.95): calcd. C 55.98, H 4.50; found C 55.97, H 4.27.

[{$Ru_2(CO)_5$(μ-PFu_2)(μ-η^1,η^2-Fu)}$_2$(dppf)] (9a) and [$Ru_2(CO)_4$(μ-PFu_2)(μ-η^1,η^2-Fu)(dppf)]$_n$ (9b): Compound **1** (50 mg, 0.083 mmol) and dppf (23 mg, 0.042 mmol) in a 2:1 molar ratio were dissolved and mixed in toluene (20 mL). After heating to reflux and stirring for about 1 h, the resulting mixture was purified by chromatography on silica plates using hexane/CH_2Cl_2 (3:1, v/v) as eluent, leading to the isolation of an orange product **9a** (R_f = 0.38, 38 mg, 53%). When an equimolar amount of **1** and dppf (0.083 mmol) was employed in the reaction whilst stirring for 1 h, an orange solution resulted and the solvent was evaporated. The crude product was then washed with several portions of hot hexane (3 × 10 mL) and the resulting solid was reprecipitated thrice from toluene/methanol to produce an orange powder of **9b** in 64% yield (59 mg) after drying in vacuo. **9a**: IR (CH_2Cl_2): $\tilde{\nu}$ = 2061 vs, 2005 vs, 1978 s, 1957 sh [ν(CO)] cm^{-1}. ^1H NMR ($CDCl_3$): δ = 3.78 (m, 4 H, C_5H_4), 4.05 (m, 2 H, C_5H_4), 4.32 (m, 2 H, C_5H_4), 4.52 (s, 2 H, Fu), 5.16 (s, 2 H, Fu), 5.96 (s, 2 H, Fu), 6.18 (m, 4 H, Fu), 6.39 (m, 2 H, Fu), 6.97−7.51 (m, 24 H, Fu + Ph), 7.66 (s, 2 H, Fu) ppm. $^{31}P\{^1H\}$ NMR ($CDCl_3$): δ = 36.13 (d, $^2J_{P-P}$ = 20 Hz, PFu_2 or PPh_2), 47.86 (d, $^2J_{P-P}$ = 20 Hz, PFu_2 or PPh_2) ppm. FAB MS: *m*/*z* = 1703 [M$^+$]. $C_{68}H_{46}FeO_{16}P_4Ru_4$ (1703.13): calcd. C 47.96, H 2.72; found C 47.52, H 2.40. **9b**: IR (CH_2Cl_2): $\tilde{\nu}$ = 2014 vs, 1981 m, 1953 s [ν(CO)] cm^{-1}. ^1H NMR ($CDCl_3$): δ = 3.48−4.56 (m, br, 9 H, Fu + C_5H_4), 5.20 (m, 1 H, Fu), 5.81−6.02 (m, 3 H, Fu), 6.30 (m, 1 H, Fu), 6.72−7.65 (m, 23 H, Fu + Ph) ppm. $^{31}P\{^1H\}$ NMR

Table 6. Summary of crystal data

	2	**3**·0.5H_2O	**4**·2CH_2Cl_2	**5**	**6**·0.5MeOH	**8a**·CH_2Cl_2	**9a**·CH_2Cl_2
Empirical formula	$C_{41}H_{31}O_7P_3Ru_2$	$C_{40}H_{30}NO_7P_3Ru_2{\cdot}0.5H_2O$	$C_{41}H_{32}NO_7P_3Ru_2{\cdot}2CH_2Cl_2$	$C_{39}H_{29}O_7P_3Ru_2$	$C_{40}H_{31}O_7P_3Ru_2{\cdot}0.5MeOH$	$C_{63}H_{48}O_{16}P_4Ru_4{\cdot}CH_2Cl_2$	$C_{68}H_{46}FeO_{16}P_4Ru_2{\cdot}CH_2Cl_2$
Formula mass	930.71	940.71	1115.58	904.67	934.72	1674.17	1787.98
Crystal system	orthorhombic	monoclinic	triclinic	triclinic	triclinic	monoclinic	triclinic
Space group	*Pna*2$_1$	*P*2$_1$/*c*	*P*$\bar{1}$	*P*$\bar{1}$	*P*$\bar{1}$	*I*2/*a*	*P*$\bar{1}$
a [Å]	21.3556(15)	18.9075(14)	12.2529(13)	9.6249(6)	10.1612(6)	22.0907(14)	11.5260(6)
b [Å]	17.0951(12)	27.521(2)	13.0394(14)	11.2508(7)	11.5813(7)	10.4004(7)	16.4507(9)
c [Å]	10.9896(8)	15.1706(11)	15.4098(16)	18.0515(11)	18.8017(11)	31.980(2)	19.0961(11)
α [°]	90	90	79.028(2)	105.9470(10)	78.5950(10)	90	81.0200(10)
β [°]	90	90.1050(10)	71.699(2)	91.0220(10)	80.1120(10)	98.4900(10)	75.8440(10)
γ [°]	90	90	87.659(2)	95.0250(10)	67.5230(10)	90	85.0760(10)
V [Å^3]	4012.0(5)	7894.1(10)	2294.3(4)	1870.5(2)	1992.8(2)	7266.9(8)	3463.5(3)
Z	4	8	2	2	2	4	2
T [K]	293	293	293	293	293	293	293
F(000)	1864	3768	1116	904	938	3328	1772
μ(Mo-$K_α$) [mm^{-1}]	0.920	0.938	1.045	0.984	0.927	1.037	1.293
Reflections collected	19431	38989	13482	11086	9946	17500	20763
Unique reflections	6147	13841	9807	8062	6870	6364	15005
R_{int}	0.0389	0.0851	0.0179	0.0154	0.0174	0.0332	0.0274
Observed reflections	6147	13841	9807	8062	6870	6364	15005
GOF on F^2	0.998	0.908	0.841	0.779	0.986	1.031	0.876
*R*1, *wR*2 [$I > 2.0σ(I)$][a]	0.0395, 0.1035	0.0582, 0.1317	0.0364, 0.0993	0.0307, 0.0851	0.0355, 0.1095	0.0433, 0.1183	0.0476, 0.1017

[a] $R1 = \Sigma||F_o| - |F_c||/\Sigma|F_o|$; $wR2 = [\Sigma w(|F_o^2| - |F_c^2|)^2/\Sigma w|F_o^2|^2]^{1/2}$.

($CDCl_3$): δ = 34.05 (m, PFu_2 or PPh_2), 41.35 (m, PFu_2 or PPh_2) ppm. GPC (THF as eluent): M_w = 11400, M_n = 8550 (n = 1.33). $C_{50}H_{37}FeO_7P_3Ru_2$ (1100.75): calcd. C 54.56, H 3.39; found C 54.10, H 3.08.

X-ray Crystallography: Except for compounds **6** and **8a**, good-quality crystals of our compounds suitable for X-ray diffraction studies were grown by slow concentration of their respective solutions in hexane/CH_2Cl_2 at room temperature. Crystals of **6**·MeOH and **8a**·CH_2Cl_2 were obtained from an MeOH/$CHCl_3$ and C_6H_{12}/CH_2Cl_2 mixture, respectively. Geometric and intensity data were collected using graphite-monochromated Mo-K_α radiation (λ = 0.71073 Å) with a Bruker AXS SMART 1000 CCD area-detector diffractometer. The collected frames were processed with proprietary software SAINT[37] and an absorption correction was applied (SADABS[38]) to the collected reflections. The space group of each crystal was determined from the systematic absences and confirmed by successful refinement of the structure. The possible alternative *Pbca* for compound **3** was tried but did not give any reasonable solution. The structures of these molecules were solved by direct methods and expanded by standard difference Fourier syntheses using the software SHELXTL.[39] Structure refinements were made on F^2 by the full-matrix least-squares technique. All non-hydrogen atoms were refined with anisotropic displacement parameters. For **2** and **3**, one of the furyl rings was refined isotropically with constrained geometry and the resulting model yielded reasonable bond lengths and angles. Hydrogen atoms were either generated from Fourier maps or placed in their idealised positions and allowed to ride on the respective carbon atoms. Pertinent crystallographic information is provided in Table 6. CCDC-168743 to -168749 contain the supplementary crystallographic data for this paper. These data can be obtained free of charge at www.ccdc.cam.ac.uk/conts/retrieving.html or from the Cambridge Crystallographic Data Centre, 12, Union Road, Cambridge CB2 1EZ, UK [Fax: (internat.) + 44-1223/336-033; E-mail: deposit@ccdc.cam.ac.uk].

Acknowledgments

W.-Y. W. thanks the Hong Kong Baptist University (FRG/01-02/I-31) for financial support and F.-L. T. acknowledges the receipt of a studentship administered by the Hong Kong Baptist University.

[1] P. Blenkiron, G. D. Enright, N. J. Taylor, A. J. Carty, *Organometallics* **1996**, *15*, 2855−2857.
[2] V. D. Patel, N. J. Taylor, A. J. Carty, *J. Chem. Soc., Chem. Commun.* **1984**, 99−100.
[3] A. J. Carty, G. Hogarth, G. D. Enright, J. W. Steed, D. Georganopoulou, *Chem. Commun.* **1999**, 1499−1500.
[4] A. J. Deeming, S. N. Jayasuriya, A. J. Arce, Y. De Sanctis, *Organometallics* **1996**, *15*, 786−793.
[5] G. García, M. E. García, S. Melón, V. Riera, M. A. Ruiz, *Organometallics* **1997**, *16*, 624−631.
[6] Y. Chi, A. J. Carty, P. Blenkiron, E. Delgado, G. D. Enright, W. Wang, S.-M. Peng, G. Lee, *Organometallics* **1996**, *15*, 5269−5271.
[7] P. Blenkiron, D. Pilette, J. F. Corrigan, N. J. Taylor, A. J. Carty, *J. Chem. Soc., Chem. Commun.* **1995**, 2165−2166.
[8] S. Doherty, M. R. J. Elsegood, W. Clegg, D. Mampe, N. H. Rees, *Organometallics* **1996**, *15*, 5302−5308.
[9] S. Doherty, G. Hogarth, M. Waugh, W. Clegg, M. R. J. Elsegood, *Organometallics* **2000**, *19*, 5696−5708.
[10] S.-M. Hsiao, S.-G. Shyu, *Organometallics* **1998**, *17*, 1151−1154.
[11] S. Doherty, M. R. J. Elsegood, W. Clegg, T. Scanlan, N. H. Rees, *Chem. Commun.* **1996**, 1545−1546.
[12] P. Blenkiron, J. F. Corrigan, N. J. Taylor, A. J. Carty, S. Doherty, M. R. J. Elsegood, W. Clegg, *Organometallics* **1997**, *16*, 297−300.
[13] W.-Y. Wong, F.-L. Ting, W.-L. Lam, *J. Chem. Soc., Dalton Trans.* **2001**, 2981−2988.
[14] N. G. Andersen, B. A. Keay, *Chem. Rev.* **2001**, *101*, 997−1030.
[15] J. A. Cabeza, J. M. Fernández-Colinas, *Coord. Chem. Rev.* **1993**, *126*, 319−336.
[16] J. A. Cabeza, J. M. Fernández-Colinas, V. Riera, M. A. Pellinghelli, A. Tiripicchio, *J. Chem. Soc., Dalton Trans.* **1991**, 371−377.
[17] J. A. Cabeza, M. A. Martínez-García, V. Riera, D. Ardura, S. García-Granda, J. F. Van der Maelen, *Eur. J. Inorg. Chem.* **1999**, 1133−1139.
[18] F. Neumann, H. Stoeckli-Evans, G. Süss-Fink, *J. Organomet. Chem.* **1989**, *379*, 151−163.
[19] W.-Y. Yeh, Y.-J. Cheng, M. Y. Chiang, *Organometallics* **1997**, *16*, 918−925.
[20] W.-Y. Wong, W.-T. Wong, *J. Chem. Soc., Dalton Trans.* **1995**, 2831−2836.
[21] Y.-Y. Choi, W.-Y. Wong, W.-T. Wong, *J. Organomet. Chem.* **1996**, *518*, 227−233.
[22] F. A. Cotton, E. V. Dikarev, W.-Y. Wong, *Polyhedron* **1997**, *16*, 3893−3898.
[23] W.-Y. Wong, F.-L. Ting, unpublished work.
[24] A. J. Deeming, *Adv. Organomet. Chem.* **1986**, *26*, 1−96.
[25] K.-B. Shiu, S.-W. Jean, H.-J. Wang, S.-L. Wang, F.-L. Liao, J.-C. Wang, L.-S. Liou, *Organometallics* **1997**, *16*, 114−119.
[26] G. Sánchez-Cabrera, E. V. García-Báez, M. J. Rosales-Hoz, *J. Organomet. Chem.* **2000**, *599*, 313−316.
[27] F. A. Cotton, F. E. Kühn, *J. Am. Chem. Soc.* **1996**, *118*, 5826−5827.
[28] D. I. Arnold, F. A. Cotton, F. E. Kühn, *Inorg. Chem.* **1996**, *35*, 4733−4737.
[29] D. I. Arnold, F. A. Cotton, F. E. Kühn, *Inorg. Chem.* **1996**, *35*, 5764−5769.
[30] F. A. Cotton, F. E. Kühn, *Inorg. Chim. Acta* **1996**, *252*, 257−264.
[31] F. A. Cotton, E. V. Dikarev, N. Nawar, W.-Y. Wong, *Inorg. Chim. Acta* **1997**, *262*, 21−32.
[32] F. A. Cotton, F. E. Kühn, A. Yokochi, *Inorg. Chim. Acta* **1996**, *252*, 251−256.
[33] C. S. Browning, D. H. Farrar, *J. Chem. Soc., Dalton Trans.* **1995**, 521−530.
[34] P. Blenkiron, D. Pilette, J. F. Corrigan, N. J. Taylor, A. J. Carty, *J. Chem. Soc., Chem. Commun.* **1995**, 2165−2166.
[35] M. I. Bruce, P. A. Humphrey, B. W. Skelton, A. H. White, *J. Chem. Soc., Dalton Trans.* **1997**, 1485−1487.
[36] E. Delgado, Y. Chi, W. Wang, G. Hogarth, P. J. Low, G. D. Enright, S.-M. Peng, G.-H. Lee, A. J. Carty, *Organometallics* **1998**, *17*, 2936−2938.
[37] *SAINT, Reference manual*, Siemens Energy and Automation, Madison, WI, **1994−1996**.
[38] G. M. Sheldrick, *SADABS, Empirical Absorption Correction Program*, University of Göttingen, Germany, **1997**.
[39] G. M. Sheldrick, *SHELXTL™, Reference manual*, version 5.1, Siemens, Madison, WI, **1997**.

Received November 19, 2001
[I010466]

Syntheses, Structures and Photophysical Properties of Metal Carbonyl Clusters with Dansyl and Acridone Luminophores

Wai-Yeung Wong,*[a] Ka-Ho Choi,[a] and Zhenyang Lin[b]

Keywords: Transition metal / Dansyl group / Acridone / Luminophores

A series of fluorescent transition metal complexes bearing the 5-(dimethylamino)naphthalene-1-sulfonyl (R^1) and acridone (R^2) frameworks have been prepared. Reactions of the fluorescent-labeled alkyne ligands $R^1CH_2C{\equiv}CH$ and $R^2CH_2C{\equiv}CH$ with various metal carbonyl compounds $[Co_2(CO)_8]$, $[Et_3NH][Fe_2(CO)_6(\mu\text{-}CO)(\mu\text{-}S\textit{t}Bu)]$ and $[M_3(CO)_{10}(NCMe)_2]$ (M = Ru, Os) readily afforded new cluster complexes of the stoichiometry $[Co_2(CO)_6(\mu\text{-}\eta^2\text{-}RCH_2CCH)]$ (**1**: R = R^1, **2**: R^2), $[Fe_2(CO)_6(\mu\text{-}S\textit{t}Bu)(\mu\text{-}\eta^2\text{-}RCH_2C{=}CH_2)]$ (**3**: R = R^1, **4**: R^2), $[Ru_3(CO)_9(\mu\text{-}CO)(\mu_3\text{-}\eta^2\text{-}RCH_2CCH)]$ (**5**: R = R^1, **6**: R^2) and $[Os_3(CO)_9(\mu\text{-}CO)(\mu_3\text{-}\eta^2\text{-}RCH_2CCH)]$ (**7**: R = R^1, **8**: R^2) in moderate to good yields. All of these new complexes have been fully characterized by FTIR, ^1H NMR spectroscopy, UV/Vis spectroscopy and fast atom bombardment mass spectrometry (FABMS). The single-crystal X-ray structural analyses and molecular orbital calculations on **1**, **2**, **4** and **8** have been performed. It was found that all of these compounds are fluorescent in solutions at room temperature and a luminescence band characteristic of the inherent fluorophore is observed in these metal structures. However, a strong quenching of the fluorescence intensity of the chromophoric groups was observed upon coordination of metal cluster moieties.

(© Wiley-VCH Verlag GmbH, 69451 Weinheim, Germany, 2002)

Introduction

Photoluminescence spectroscopy has continued to attract increasing current attention in the scientific community due to its wide applications in environmental and biological sciences and molecular electronics.[1−6] The preparation and photophysical properties of several fluorescent methylmercury acetylides carrying the anthracene, 5-(dimethylamino)naphthalene-1-sulfonyl (dansyl) and 9-acridone frameworks have recently been reported and these compounds could be exploited in the development of new analytical methods for methylmercury in environmental and biological samples.[7] Prodi and co-workers also described the use of a tripodal ligand containing the dansyl chromophore as a luminescent chemosensor for metal ions.[8]

We have a long-term interest in the design and synthesis of luminescent transition metal-containing materials[9,10] and major efforts have been devoted to the studies of organometallic acetylide complexes and polymers incorporating a vast range of aromatic and heteroaromatic spacers.[11−16] In view of the high luminescence quantum yields of the auxiliary dansyl and acridone units,[17] we expect that a properly derivatized molecule such as 5-(dimethylamino)-*N*-(2-propynyl)-1-naphthalenesulfonamide (**I**) and 10-(2-propynyl)-9-acridone (**II**) (Scheme 1) could be employed to attach a fluorescent label to the metal center through an acetylide linkage,[7,10] which is likely to exhibit rich optical and photo-electronic properties. Indeed, two novel blue luminescent platinum(II) acetylide compounds bearing these functionalities have been reported recently by us in preliminary form.[10] We therefore sought to design new molecular systems featuring these luminophores. In this context, we aim at preparing some fluorescent-labeled metal carbonyl complexes of Groups 8 and 9 transition metal elements by using properly tailored acetylenes since the interactions between alkynes and binary low-nuclearity carbonyl complexes of iron, ruthenium, osmium and cobalt have been well documented.[18−28] To the best of our knowledge, studies of luminescent transition metal carbonyl clusters bearing fluorescent labels are scarce. In this article, we describe the synthesis, as well as the spectroscopic, structural and photophysical properties of a new series of fluorescent dinuclear and trinuclear metal complexes incorporating the dansyl and acridone entities.

Results and Discussion

Synthesis

An adaptation of the literature methods was employed to obtain the fluorescent-labeled ligands **I** and **II**.[7,10] The synthetic routes to all the new compounds are shown in Scheme 2. The dinuclear cobalt carbonyl complexes **1** and

[a] Department of Chemistry, Hong Kong Baptist University, Waterloo Road, Kowloon Tong, Hong Kong, P. R. China
E-mail: rwywong@hkbu.edu.hk
[b] Department of Chemistry, The Hong Kong University of Science and Technology, Clearwater Bay, Hong Kong, P. R. China

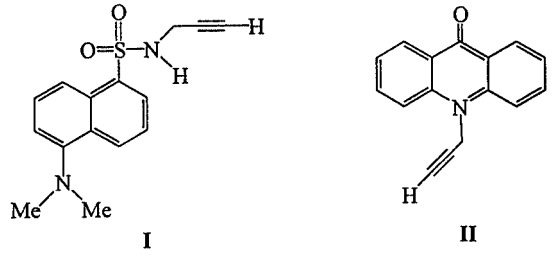

Scheme 1. Structures of **I** and **II**

2 were prepared in moderate yields by reacting $[Co_2(CO)_8]$ with one equivalent of **I** and **II**, respectively, at 0 °C.[25−28] Thermal treatment of **I** and **II** with the iron carbonyl salt $[Et_3NH][Fe_2(CO)_6(\mu\text{-}CO)(\mu\text{-}S\textit{t}Bu)]$ prepared in situ from a $[Fe_3(CO)_{12}]/NEt_3/\textit{t}BuSH$ mixture[18] in a 1:1 molar ratio in refluxing THF afforded the σ,π-vinyl complexes **3** and **4** in yields of 31 and 35%, respectively. This reaction sequence was accompanied by the formation of $[Fe_2(CO)_6(\mu\text{-}S\textit{t}Bu)_2]$ as a by-product.[18] The reactions of the freshly prepared $[Ru_3(CO)_{10}(NCMe)_2]$ with the appropriate alkynes **I** and **II** are straightforward at room temperature with the loss of MeCN to give complexes **5** and **6** as the final products. The facile displacement of two MeCN groups of $[Os_3(CO)_{10}(NCMe)_2]$ by the terminal acetylenes to afford $[Os_3(CO)_9(\mu\text{-}CO)(\mu_3\text{-}\eta^2\text{-}RCCH)]$ was successfully applied to the preparation of alkyne-substituted complexes **7** and **8** as major products.[21−23] All of these compounds were purified by preparative TLC on silica and compounds **1**−**4** were isolated as orange to red solids and products **5**−**8** as yellow solids. Complexes **1**−**8** are highly soluble in common organic solvents such as CH_2Cl_2 and $CHCl_3$ and their solutions slowly decompose when exposed to air. As solid materials they are stable at room temperature for prolonged periods even when precautions to exclude air or moisture are not taken.

Spectroscopic Properties

Collated spectroscopic data (IR, ^1H NMR and FABMS) of these new fluorophore-anchored metal complexes are in agreement with their formulation and full details are given in the Exp. Sect. The disappearance of the IR ν(C≡C) and ν(≡C−H) bands in **1**−**8** indicates that metal carbonyl fragments are coordinated to the acetylenic unit. A broad peak at 1880 cm^{-1} for the Ru complexes **5** and **6**, and 1848 cm^{-1} for the osmium derivatives **7** and **8**, was consistent with the presence of a bridging carbonyl group in each case. In the IR spectra, the band patterns between the uncomplexed and complexed chromophores are similar. Coordination of the alkyne moiety to the metal core was confirmed by the close resemblance of the IR spectral pattern in the ν(CO) region of our complexes with those observed for the reported cobalt−alkyne complexes,[25−28] $[Fe_2(CO)_6(\mu\text{-}SR)(\mu\text{-}\eta^2\text{-}R'C{=}CH_2)]$[18,29] and $'M_3(CO)_{10}'$ cores (M = Ru, Os) which coordinate an alkyne in a $\mu_3\text{-}(\eta^2\text{-}\|)$ fashion.[21−24] The ^1H NMR spectra of the new complexes display resonances stemming from the coordinated dansyl or acridone group but the signals due to −C≡CH for **I** (ca. 1.92 ppm) and **II** (ca. 2.43 ppm) were absent.[7] Except for **3** and **4**, the presence of a singlet peak in the range of δ = 5.74−9.10 is clearly resolved for the −CCH protons in these compounds. Assignments for the signals arising from the protons attached to C_β in the vinyl-bridged diiron compounds **3** and **4** could be made in their corresponding ^1H NMR spectra

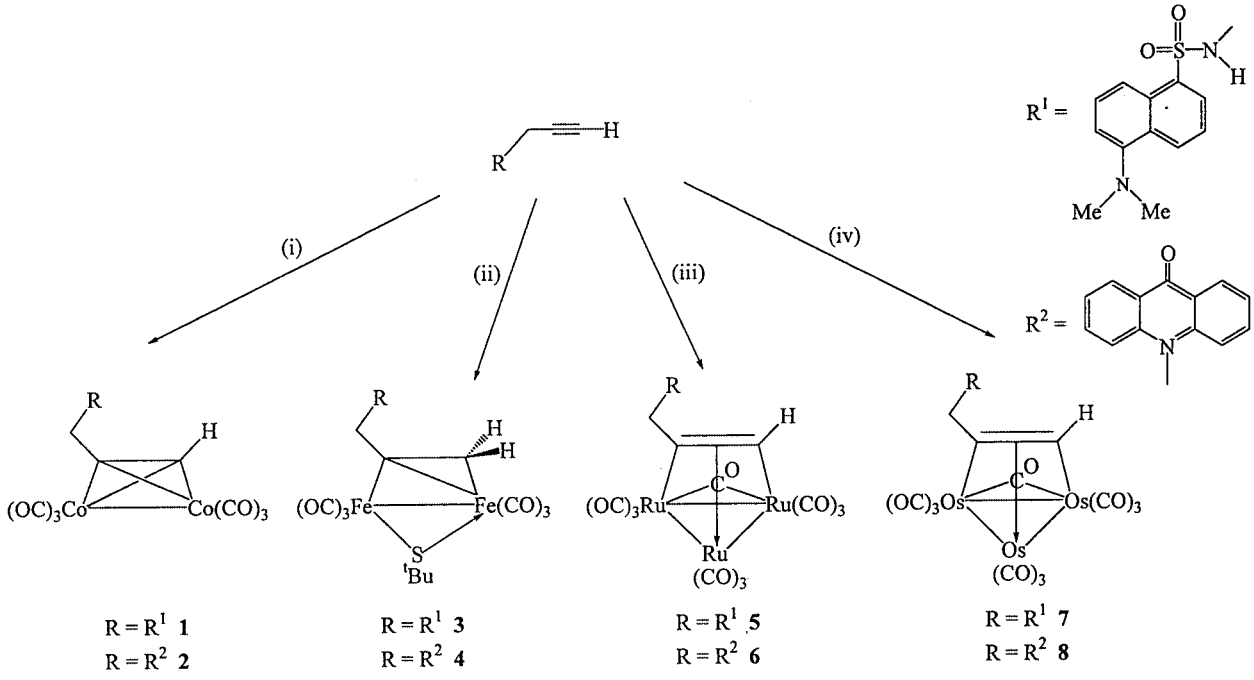

Scheme 2. (i) $[Co_2(CO)_8]$, hexane, 1 h, 0 °C; (ii) $[Et_3NH][Fe_2(CO)_6(\mu\text{-}CO)(\mu\text{-}S\textit{t}Bu)]$, THF, reflux, 5 h; (iii) $[Ru_3(CO)_{10}(NCMe)_2]$, CH_2Cl_2/MeCN, room temp., 2 h; (iv) $[Os_3(CO)_{10}(NCMe)_2]$, CH_2Cl_2, room temp., 2 h.

consistent for both structures. For **3**, the two vinyl proton resonances appear as two doublets at δ = 2.63 and 3.48 ppm with a geminal coupling constant of 2.6 Hz, whereas two doublets are apparent at δ = 2.77 and 3.13 ppm (J_{H-H} = 4.6 Hz) for **4**. These data agree with those reported for other [$Fe_2(CO)_6$(μ-SR)(μ-R′$C_α$=$C_βH_2$)] complexes and they are consistent with NMR spectroscopic data for other μ-vinyl systems as well.[18,29] The thiolate moieties in **3** and **4** display the expected singlet peak due to the *tert*-butyl group. These new compounds also gave satisfactory mass spectroscopic data and, in most cases, they showed the molecular ion peaks followed by the consecutive loss of carbonyl fragments. The parent ion peaks indicate a 1:1 (metal/ligand) stoichiometry for the complexes.

Electronic Absorption and Luminescence Spectra

The photophysical properties of complexes **1**−**8** have been studied in CH_2Cl_2 at room temperature and the results are summarized in Table 1. Both of the free alkynes **I** and **II** typically exhibit three intense absorption peaks in the near-UV region that can be ascribed to π−π* transitions within the ligand framework.[10] For the metal cluster complexes, they all show similar structured low-energy bands in the near-UV and the visible regions due to the metal-perturbed intraligand π−π* transitions of the organic units. At the lowest energy regime, absorptions probably arise from the ligand-to-cluster core charge transfer transitions for each appropriate metal cluster fragment (vide infra). Excitation of **1**−**8** in CH_2Cl_2 solutions results in a blue to greenish-blue luminescence band peaking in the range of 506−509 nm for the dansyl derivatives and of 425−431 nm for the acridone counterparts (Figure 1 and Figure 2). The emission wavelengths of the dansyl complexes remain relatively unshifted with respect to that of **I** but we observe a slight bathochromic shift in the peak maxima for the acridone congeners as compared to that of **II**. These featureless luminescence spectra are independent of the excitation wavelength used. Due to their similar structured peak pattern, we consider that the emission features between the uncomplexed and complexed fluorophores should have the same origin for each case and are most likely caused by the metal-perturbed dansyl or acridone emission. Of particular relevance here is the observation of a strong quenching of the fluorescence intensity of the luminophores upon metal coordination in all the cases studied. The fluorescence quantum yields of the metal complexes are less than those of **I** and **II** by one to two orders of magnitude. With reference to previous work on other organometallic systems, we can attribute the quenching in the luminescence intensity to the so-called heavy-atom effect, an energy-transfer or an electron-transfer mechanism.[7,8]

Crystal Structure Analyses

The single-crystal X-ray structures of **1**, **2**, **4** and **8** were established unambiguously and the perspective views are depicted in Figures 3−6, respectively. Pertinent bond

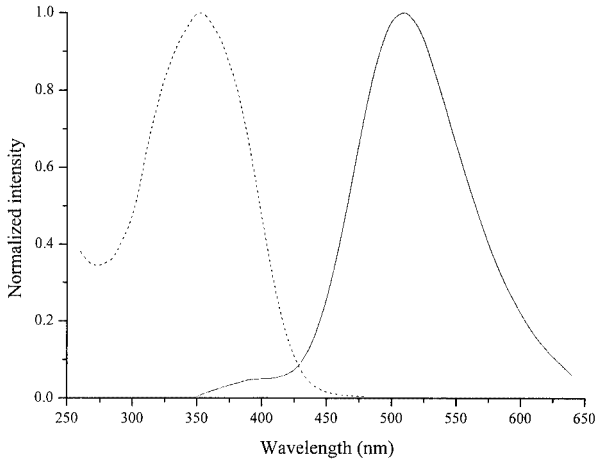

Figure 1. Excitation (---) and photoluminescence (—) spectra of **1** in CH_2Cl_2 at room temperature

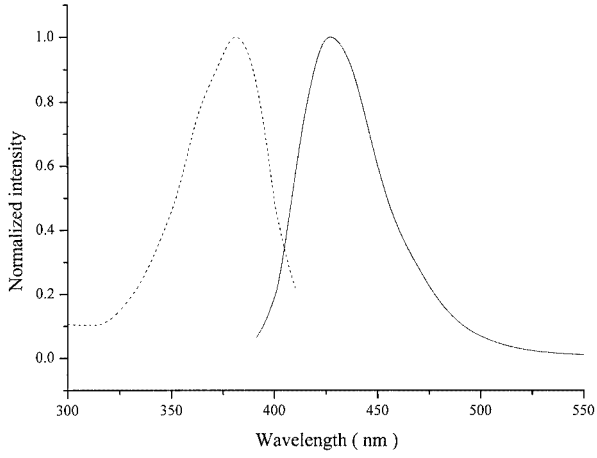

Figure 2. Excitation (---) and photoluminescence (—) spectra of **2** in CH_2Cl_2 at room temperature

lengths and angles are collected in Tables 2−5. Structurally, the essential features of both **1** and **2** are very similar in which the Co(1)−Co(2) axis forms a pseudo-tetrahedron with the C≡C bond of the alkynyl ligands **I** and **II** with the C≡C vector lying perpendicular to the Co−Co vector. In each case, the Co−Co separation [2.492(1) **1**, 2.4791(4) Å **2**] is in the region expected for other Co_2-alkyne systems.[25−28] The C(7)−C(8) bond lengths for **1** and **2** are 1.341(7) and 1.333(3) Å, respectively, suggestive of the loss of the triple bond character of the alkyne ligands upon complexation. There are no unusual structural parameters in the chromophoric groups of both molecules.

The basic structure of **4** consists of a diiron hexacarbonyl core in which the Fe−Fe edge [2.534(2) Å] is bridged by the thiolate and μ-σ-vinyl groups. The thiolate bridge itself spans the Fe−Fe bond asymmetrically with the Fe(1)−S(1) and Fe(2)−S(1) distances being 2.239(2) and 2.279(3) Å, respectively. While the iron−sulfur distances are typical of thiolate-bridged diiron compounds,[29−31] the C(7)−S(1) bond of 1.848(9) Å is slightly longer than the normal carbon−sulfur single bonds of 1.815(1) Å,[32] and this indic-

Table 1. Electronic absorption and emission data for complexes **1**−**8**

Compound	λ_{max}/nm ($\varepsilon \times 10^{-4}$/M^{-1} cm^{-1})[a]	λ_{em}/nm ($10^3 \times \Phi$)[a]
I[7]	230 (1.4), 253 (1.6), 345 (0.5)	508 (450)
II[7]	250 (3.6), 373 (1.9), 390 (2.4)	417 (8.0)
1	253 (2.9), 312 (0.8), 348 (0.9)	509 (5.0)
2	248 (3.7), 304 (0.7), 358 (0.8), 378 (1.0), 396 (1.3)	427 (0.1)
3	232 (1.8), 252 (1.8), 336 (0.6), 469 (0.1)	506 (7.5)
4	250 (2.3), 375 (1.1), 395 (1.4), 460 (0.2)	404, 425 (3.2)
5	230 (2.3), 250 (2.1), 340 sh (0.6), 477 sh (0.1)	506 (1.4)
6	230 sh (2.8), 254 (3.8), 381 (0.8), 397 (1.0), 468 sh (0.1)	429 (0.6)
7	248 (0.3), 342 sh (0.1), 440 sh (0.02)	506 (4.3)
8	232 sh (1.5), 254 (2.3), 380 (1.1), 398 (1.6), 442 sh (0.2)	431 (0.4)

[a] In CH_2Cl_2. sh = shoulder

ates some delocalization of electron density from the thiolate bridge into the metal core. The C(11)−C(12) bond is bound to Fe(2) via a π-interaction [Fe(2)−C(11) 2.131(7), Fe(2)−C(12) 2.14(1) Å] and to Fe(1) via a σ bond [Fe(1)−C(11) 1.983(8) Å]. The C(11)−C(12) bond length of 1.37(1) Å is characteristic of this type of vinylic coordination. The six carbonyl ligands are all terminally bound and essentially linear. By regarding both the vinyl and μ-SR groups as three-electron donors, complex **4** has 34 cluster valence electrons and is electron precise.

For **8**, the triosmium unit is coordinated to an alkyne moiety in a classical μ_3-(η^2-||) manner via two σ bonds through Os(1) and Os(3) and a typical π bond to Os(2). This creates the nido-octahedral M_3C_2 core geometry expected for this type of coordination. The alkyne-metal σ bonds are 2.135(7) and 2.085(6) Å long, while the relevant π-interactions are characteristically longer at 2.181(6) and 2.315(6) Å. The C(11)−C(12) edge bridges the Os(1)−Os(3) bond to afford a four-membered metallacyclic ring, which makes a dihedral angle of 58.1° with the Os_3 triangle. The observation that the C(3)−Os(1)−Os(3) and Os(1)−C(3)−O(3) bond angles of 64.7(2) and 163.3(7)°, respectively, suggests that this carbonyl ligand is tending towards a semi-bridging interaction. In **2**, **4** and **8**, the acridone ring is almost planar (mean deviation is ca. 0.016−0.047 Å) and no evidence of intermolecular stacking interaction between individual acridone units in the crystal lattice was observed in each case.

Molecular Orbital Calculations

In order to study the electronic structures for the new clusters, we have performed molecular orbital calculations on **1**, **2**, **4** and **8** at the B3LYP level of density functional theory (DFT) based on their experimental geometries from X-ray data (see Computational Details section). The characteristics of the molecular orbitals in the frontier region are comparable for these four complexes. The contour plots[33] of the highest occupied (HOMO) and lowest unoccupied (LUMO) molecular orbitals for **1** and **2** are shown in Figure 7. The DFT calculations show that the HOMO−LUMO gaps for the four clusters are close to each other (ca. 23,356 **1**, 23,354 **2**, 25,119 **4** and 23,920 cm^{-1} **8**).

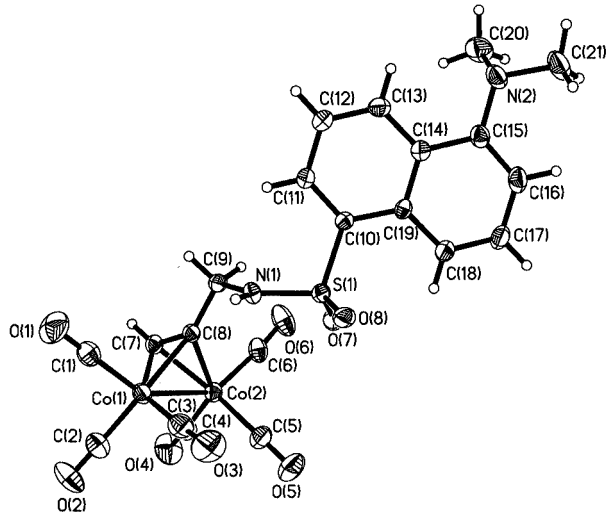

Figure 3. A perspective drawing of compound **1** with the atoms shown at the 25% probability level

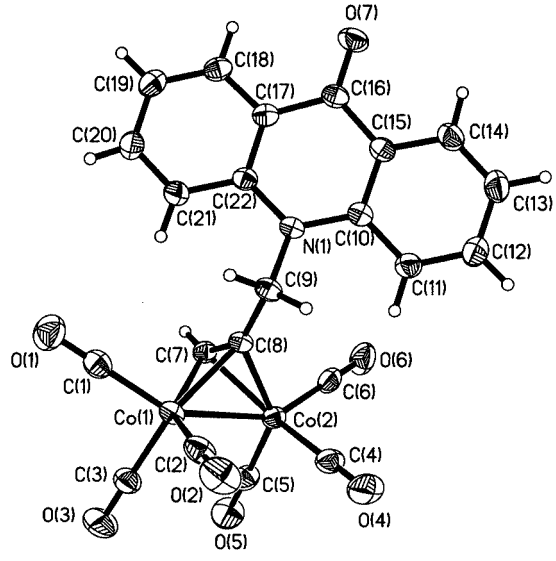

Figure 4. A perspective drawing of compound **2** with the atoms shown at the 25% probability level

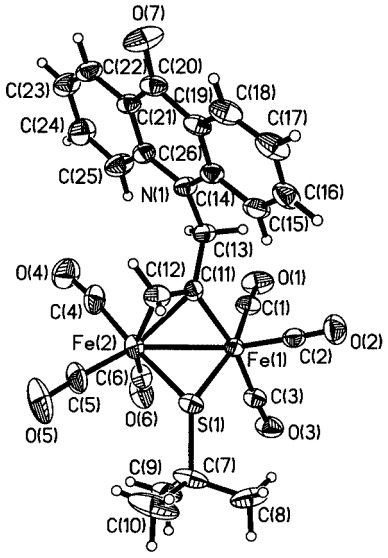

Figure 5. A perspective drawing of compound **4** with the atoms shown at the 25% probability level

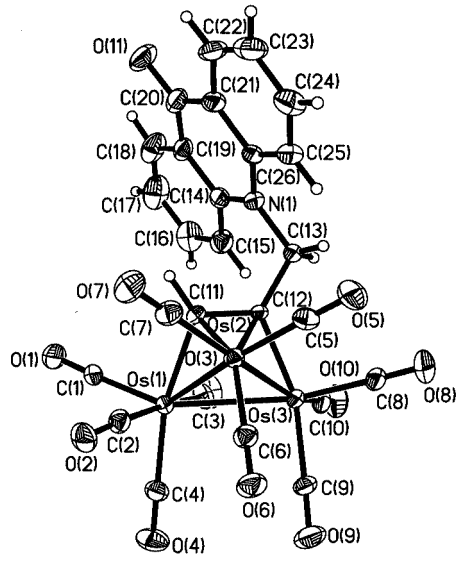

Figure 6. A perspective drawing of compound **8** with the atoms shown at the 25% probability level

Table 2. Selected bond lengths (Å) and angles (°) for complex **1**

Co(1)−Co(2)	2.492(1)	Co(1)−C(7)	1.969(6)
Co(1)−C(8)	1.953(5)	Co(2)−C(7)	1.934(6)
Co(2)−C(8)	1.962(6)	C(7)−C(8)	1.341(7)
N(1)−S(1)	1.614(5)	S(1)−O(7)	1.431(4)
S(1)−O(8)	1.444(4)		
Co(2)−Co(1)−C(7)	49.7(2)	Co(2)−Co(1)−C(8)	50.6(2)
Co(1)−Co(2)−C(7)	50.9(2)	Co(1)−Co(2)−C(8)	50.3(2)
C(7)−C(8)−C(9)	138.2(5)		

The common feature of the HOMOs and LUMOs of these metal clusters is that the HOMO corresponds to the π bonding in the aromatic unit of the bridging acetylene ligand and the LUMO involves metal−metal antibonding,

Table 3. Selected bond lengths (Å) and angles (°) for complex **2**

Co(1)−Co(2)	2.4791(4)	Co(1)−C(7)	1.974(2)
Co(1)−C(8)	1.970(2)	Co(2)−C(7)	1.972(2)
Co(2)−C(8)	1.972(2)	C(7)−C(8)	1.333(3)
Co(2)−Co(1)−C(7)	51.03(5)	Co(2)−Co(1)−C(8)	51.06(5)
Co(1)−Co(2)−C(7)	51.11(5)	Co(1)−Co(2)−C(8)	51.00(5)
C(7)−C(8)−C(9)	144.8(2)		

Table 4. Selected bond lengths (Å) and angles (°) for complex **4**

Fe(1)−Fe(2)	2.534(2)	Fe(1)−C(11)	1.983(8)
Fe(1)−S(1)	2.239(2)	Fe(2)−C(11)	2.131(7)
Fe(2)−C(12)	2.14(1)	Fe(2)−S(1)	2.279(3)
C(11)−C(12)	1.37(1)	S(1)−C(7)	1.848(9)
Fe(1)−Fe(2)−C(11)	49.4(2)	Fe(1)−Fe(2)−C(12)	79.5(3)
Fe(1)−C(11)−Fe(2)	75.9(3)	Fe(1)−S(1)−Fe(2)	68.23(8)
Fe(2)−Fe(1)−C(11)	54.7(2)	Fe(2)−C(11)−C(12)	71.8(6)
C(11)−Fe(2)−C(12)	37.3(4)	C(12)−C(11)−C(13)	116.5(8)
Fe(1)−Fe(2)−S(1)	55.14(7)	Fe(2)−Fe(1)−S(1)	56.63(7)

Table 5. Selected bond lengths (Å) and angles (°) for complex **8**

Os(1)−Os(2)	2.8276(4)	Os(1)−Os(3)	2.8983(4)
Os(2)−Os(3)	2.7194(4)	Os(1)−C(11)	2.135(7)
Os(2)−C(11)	2.181(6)	Os(2)−C(12)	2.315(6)
Os(3)−C(12)	2.085(6)	C(11)−C(12)	1.418(8)
Os(1)−Os(2)−Os(3)	62.966(9)	Os(1)−Os(3)−Os(2)	60.342(9)
Os(1)−C(11)−C(12)	108.8(4)	Os(2)−C(11)−C(12)	76.8(4)
Os(3)−C(12)−C(11)	111.3(4)	C(11)−Os(2)−C(12)	36.6(2)
C(11)−C(12)−C(13)	122.4(5)		

suggesting a dominant ligand-to-metal charge transfer character of their lowest HOMO−LUMO electronic transition. In the related work, the HOMO for **I** was found to possess a significant contribution from the pπ orbital of the NMe_2 group in addition to the π bonding feature within the aromatic unit, whereas the LUMO corresponds to the π* orbital of the aromatic moiety. The energy gap was calculated to be 33,792 cm^{-1}, which is much greater than that of **1**. Contrary to what we have observed here, previous calculations on other $[Os_3(CO)_{10}(\alpha\text{-diimine})]$ clusters[34,35] showed that the HOMOs are mainly metal orbital-based (Os−Os bonding) while the LUMOs are more localized on the α-diimine ligand. Clearly, the bridging acetylene ligands in the currently studied clusters, significantly affect the orbital structures in the HOMO−LUMO region. Examining the orbital energies in the HOMO−LUMO region for our compounds, we found that the molecular orbitals derived from metal d-orbitals (both bonding and antibonding) are shifted down to a lower energy region and the π and π* orbitals of the aromatic units in the ligands go up in energy in comparison to the corresponding MOs calculated for the $[Os_3(CO)_{10}(diimine)]$-type clusters mentioned above. It is because of these changes in the orbital energies that we observe the totally different patterns between the alkyne- and

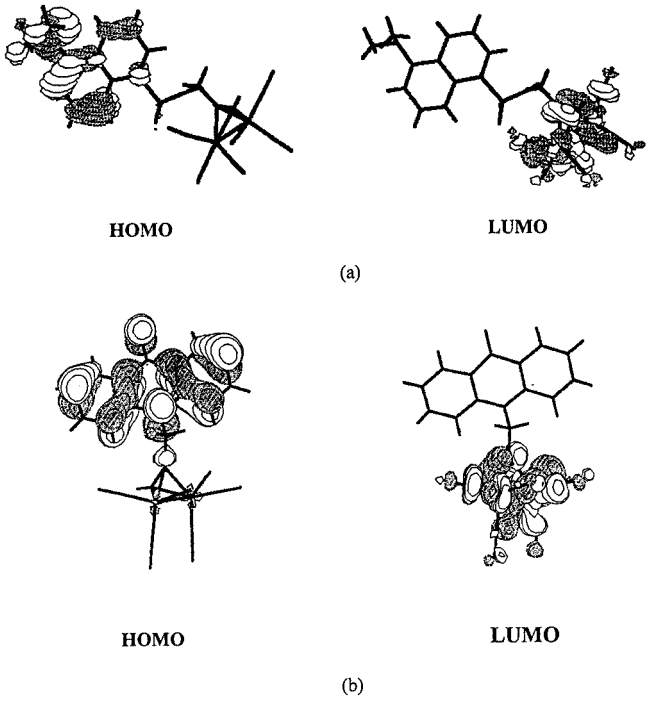

Figure 7. Spatial plots of the highest occupied (HOMO) and the lowest unoccupied molecular orbitals (LUMO) for complexes (a) **1** and (b) **2**

diimine-bridged compounds. The stabilization of the metal d-orbital-based MOs can be related to the π*-accepting properties and strong binding abilities of the bridging acetylene ligands. Since the LUMOs for these clusters involve metal−metal antibonding, and by considering the possible fragmentation, we expect that the life-time of an excited state of such clusters is much shorter when compared to other types of clusters in which there is a significant contribution of the ligands to the LUMOs. This probably results in a poor fluorescence quantum efficiency of the clusters in the present study.

Concluding Remarks

Our present work provides a simple access to a new family of alkyne-derived fluorescent-labeled metal clusters. A series of metal complexes of Groups 8 and 9 elements containing dansyl and acridone chromophores have been synthesized in moderate yields and spectroscopically and photophysically characterized. These new compounds are shown to be emissive in the blue to green-blue region in solutions at room temperature and quenched luminescence bands typical of the fluorophores are observed. In this work, we have also demonstrated how one can modulate the luminescence properties of the fluorophore in the presence of a variety of metal cluster cores and such a quenching process is particularly crucial to our understanding in the development of new molecular luminescent sensing systems. The effect of other transition metals on the luminescent behavior and a more in-depth investigation on analytical applications of these systems will be the subject of a future study.

Experimental Section

General Procedures: All reactions were conducted under an atmosphere of dry nitrogen with the use of standard Schlenk techniques. Solvents for preparative work were dried and distilled before use. Unless otherwise stated all reagents were obtained from commercial suppliers and used without further purification. The syntheses of ligand precursors **I** and **II**[7] and the complexes $[Et_3NH][Fe_2(CO)_6(\mu\text{-}CO)(\mu\text{-}S\textit{t}Bu)]$[18] and $[M_3(CO)_{10}(NCMe)_2]$ (M = Ru, Os)[36,37] were carried out as reported previously. IR spectra were recorded as CH_2Cl_2 solutions on a Perkin−Elmer Paragon 1000 PC or Nicolet Magna 550 Series II FTIR spectrometer. Proton NMR spectra were measured in $CDCl_3$ on a JEOL EX270 or a Varian Inova 400 MHz FT NMR spectrometer, with chemical shifts quoted relative to $SiMe_4$. Fast atom bombardment (FAB) mass spectra were recorded in *m*-nitrobenzyl alcohol matrices on a Finnigan-SSQ 710 spectrometer. Electronic absorption spectra were obtained with an HP 8453 or Cary 100 UV/Vis spectrometer. Corrected emission and excitation spectra were obtained in CH_2Cl_2 with a Perkin−Elmer LS50B or PTI QM1 spectrofluorimeter. The fluorescence quantum yields were determined in CH_2Cl_2 solutions at 290 K against the anthracene standard in the same solvent (Φ = 0.27).[38] Separation of products was accomplished by preparative TLC plates coated with silica (Merck, Kieselgel 60).

Computational Details: Density functional theory calculations at the B3LYP level[39−41] were performed on **1**, **2**, **4** and **8** based on their experimental geometries from X-ray crystallographic data. The basis set used for C, H N and O atoms was 6−31G[42] while effective core potentials with a LanL2DZ basis set[43] were employed for Co, Fe and Os atoms. All calculations were performed with the use of Gaussian 98.[44] In view of the large systems studied here and computing resources available to us, we did not use basis sets with higher quality. Addition of polarization functions to C, N and O would increase the number of basis functions by more than a hundred. Previous molecular orbital calculations on other related systems[45,46] showed that the medium-size basis set provides reasonable results. In addition, we are interested in obtaining the qualitative picture of orbital patterns for the clusters and in comparing the relative HOMO−LUMO gaps. We believe that the addition of polarization functions in our calculations will not alter the conclusions we have made.

$[Co_2(CO)_6(\mu\text{-}\eta^2\text{-}R^1CH_2CCH)]$ (1): $[Co_2(CO)_8]$ (32.1 mg, 0.09 mmol) was dissolved in degassed hexane (10 mL) and the solution was stirred at 0 °C under N_2. The alkyne ligand **I** (22.9 mg, 0.10 mmol) in CH_2Cl_2 (3 mL) was subsequently added. After the mixture was stirred for 1 h, the solvent was removed under reduced pressure. The residue was purified by preparative TLC on silica using hexane/CH_2Cl_2 (1:1, v/v) as eluent to furnish a major brown-red band. The title product was recrystallized from hexane−CH_2Cl_2 to give deep red crystals of **1** in 32% yield (17.3 mg). IR (CH_2Cl_2): ν(N−H) = 3384 w, ν(CO) = 2097s, 2058 vs and 2031 vs cm^{-1}. ^1H NMR ($CDCl_3$): δ = 2.88 (s, 6 H, NMe_2), 4.20 (s, 2 H, NCH_2), 4.91 (s, 1 H, NH), 5.74 (s, 1 H, CCH), 7.21 (m, 1 H, aromatic), 7.55 (t, J_{H-H} = 7.6 Hz, 2 H, aromatic), 8.30 (m, 2 H, aromatic) and 8.55 (d, J_{H-H} = 8.6 Hz, 1 H, aromatic). FAB MS: *m*/*z* = 490 [(M − 3CO)$^+$]. $C_{21}H_{16}N_2Co_2O_8S$ (574.29): calcd. C 43.92, H 2.81, N 4.88; found C 43.69, H 2.60, N 4.50.

[$Co_2(CO)_6$(μ-η²-R^2CH_2CCH)] (2): Compound **2** was prepared using the same conditions described above for **1**, but ligand **II** was used instead to produce a deep red solid of **2** (35%) after TLC separation eluting with hexane/CH_2Cl_2 (1:4, v/v). IR (CH_2Cl_2): ν(CO) = 2098s, 2059 vs and 2033 vs cm^{-1}. ^1H NMR ($CDCl_3$): δ = 5.28 (s, 2 H, NCH_2), 5.75 (s, 1 H, CCH), 7.34 (t, J_{H-H} = 7.3 Hz, 2 H, aromatic), 7.62 (d, J_{H-H} = 7.3 Hz, 2 H, aromatic), 7.76 (t, J_{H-H} = 7.3 Hz, 2 H, aromatic) and 8.59 (d, J_{H-H} = 7.3 Hz, 2 H, aromatic). FAB MS: *m*/*z* = 520 [M^+]. $C_{22}H_{11}NCo_2O_7$ (519.20): calcd. C 50.89, H 2.14, N 2.70; found C 50.75, H 2.02, N 2.32.

[$Fe_2(CO)_6$(μ-S*t*Bu)(μ-η²-$R^1CH_2C{=}CH_2$)] (3): The complex [Et_3NH][$Fe_2(CO)_6$(μ-CO)(μ-S*t*Bu)] was freshly prepared by reacting [$Fe_3(CO)_{12}$] (101 mg, 0.20 mmol), *t*BuSH (22.5 μL, 0.20 mmol) and NEt_3 (27.9 μL, 0.20 mmol) in THF (15 mL) at 25−30 °C under N_2. This reaction mixture was then treated with **I** (57.7 mg, 0.20 mmol) and the red solution was heated to reflux for 5 h. The volatile components were removed and the residue was subjected to TLC on silica using hexane/CH_2Cl_2 (2:1, v/v) as eluent to afford a major deep orange product **3** in 31% yield (40.8 mg). IR (CH_2Cl_2): ν(N−H) = 3379 w, ν(CO) = 2070 m, 2038 vs and 1996 vs cm^{-1}. ^1H NMR ($CDCl_3$): δ = 1.35 (s, 9 H, *t*Bu), 2.63 (d, J_{H-H} = 2.6 Hz, 1 H, CCH_2), 2.90 (s, 6 H, NMe_2), 3.48 (d, J_{H-H} = 2.6 Hz, 1 H, CCH_2), 4.07 (m, 2 H, NCH_2), 4.83 (t, J_{H-H} = 6.2 Hz, 1 H, NH), 7.21 (d, J_{H-H} = 7.6 Hz, 1 H, aromatic), 7.49−7.61 (m, 2 H, aromatic), 8.25−8.33 (m, 2 H, aromatic) and 8.55 (d, J_{H-H} = 8.4 Hz, 1 H, aromatic). FAB MS: *m*/*z* = 658 [M^+]. $C_{25}H_{26}N_2Fe_2O_8S_2$ (658.30): calcd. C 45.61, H 3.98, N 4.26; found C 45.29, H 3.67, N 4.01.

[$Fe_2(CO)_6$(μ-S*t*Bu)(μ-η²-$R^2CH_2C{=}CH_2$)] (4): A procedure similar to that for **3** was employed using **II** (46.7 mg, 0.20 mmol) to produce orange **4** in 35% yield (42.2 mg) following TLC purification on silica with hexane/CH_2Cl_2 (1:1, v/v) as eluent. IR (CH_2Cl_2): ν(CO) = 2068 m, 2037 vs and 1995 vs cm^{-1}. ^1H NMR ($CDCl_3$): δ = 1.41 (s, 9 H, *t*Bu), 2.77 (d, J_{H-H} = 4.6 Hz, 1 H, CCH_2), 3.13 (d, J_{H-H} = 4.6 Hz, 1 H, CCH_2), 5.01 (s, 2 H, NCH_2), 7.31 (t, J_{H-H} = 7.6 Hz, 2 H, aromatic), 7.58 (d, J_{H-H} = 7.6 Hz, 2 H, aromatic), 7.76 (t, J_{H-H} = 7.6 Hz, 2 H, aromatic) and 8.55 (d, J_{H-H} = 7.6 Hz, 2 H, aromatic). FAB MS: *m*/*z* = 603 [M^+]. $C_{26}H_{21}NFe_2O_7S$ (603.21): calcd. C 51.77, H 3.51, N 2.32; found C 51.49, H 3.36, N 2.18.

[$Ru_3(CO)_9$(μ-CO)(μ₃-η²-R^1CH_2CCH)] (5): To an orange solution of [$Ru_3(CO)_{10}(NCMe)_2$] prepared in situ from a mixture of [$Ru_3(CO)_{12}$] (51.1 mg, 0.08 mmol) and NMe_3O (12.0 mg, 0.16 mmol) in CH_2Cl_2/MeCN, **I** (23.1 mg, 0.08 mmol) was added. The resulting mixture was allowed to stir at room temperature for 2 h, after which the solution was concentrated and subjected to TLC separation with pure CH_2Cl_2 as eluent. The title complex was isolated as a deep yellow product in 23% yield (16.0 mg). IR (CH_2Cl_2): ν(N−H) = 3379 w, ν(CO) = 2100 w, 2063 sh, 2055 vs, 2031s, 2012 sh and 1880 w cm^{-1}. ^1H NMR ($CDCl_3$): δ = 2.89 (s, 6 H, NMe_2), 3.71 (d, J_{H-H} = 6.4 Hz, 2 H, NCH_2), 4.74 (t, J_{H-H} = 6.4 Hz, 1 H, NH), 7.20 (d, J_{H-H} = 7.2 Hz, 1 H, aromatic), 7.51−7.59 (m, 2 H, aromatic), 8.02 (s, 1 H, CCH), 8.20−8.23 (m, 2 H, aromatic) and 8.56 (d, J_{H-H} = 8.8 Hz, 1 H, aromatic). FAB MS: *m*/*z* = 871 [M^+]. $C_{25}H_{16}N_2O_{12}Ru_3S$ (871.68): calcd. C 34.45, H 1.85, N 3.21; found C 34.59, H 1.90, N 3.20.

[$Ru_3(CO)_9$(μ-CO)(μ₃-η²-R^2CH_2CCH)] (6): Similar to **5**, complex **6** was synthesized from **II** (18.7 mg, 0.08 mmol) and isolated as a deep yellow solid in 27% yield (17.6 mg). IR (CH_2Cl_2): ν(CO) = 2101 w, 2066 vs, 2055 vs, 2034s, 2012 sh and 1881 w cm^{-1}. ^1H NMR ($CDCl_3$): δ = 5.32 (s, 2 H, NCH_2), 7.29−7.39 (m, 4 H, aromatic), 7.67 (s, 1 H, CCH), 7.74 (t, J_{H-H} = 7.4 Hz, 2 H, aromatic) and 8.60 (dd, J_{H-H} = 7.4, 1.2 Hz, 2 H, aromatic). FAB MS: *m*/*z* = 816 [M^+]. $C_{26}H_{11}NO_{11}Ru_3$ (816.58): calcd. C 38.24, H 1.36, N 1.72; found C 38.05, H 1.13, N 1.50.

[$Os_3(CO)_9$(μ-CO)(μ₃-η²-R^1CH_2CCH)] (7): Ligand **I** (11.5 mg, 0.04 mmol) was added to a yellow solution of [$Os_3(CO)_{10}(NCMe)_2$] (37.3 mg, 0.04 mmol) in CH_2Cl_2 (15 mL). The reaction mixture turned orange and stirring was continued at room temperature for 2 h. Upon removal of solvent, the residue was purified by TLC on silica using pure CH_2Cl_2 as eluent to give a yellow-orange product

Table 6. Summary of crystallographic data ($R1 = \Sigma||F_o| - |F_c||/\Sigma|F_o|$, $wR2 = [\Sigma w(|F_o^2| - |F_c^2|)^2/\Sigma w|F_o^2|^2]^{1/2}$)

	1	2	4	8
Empirical formula	$C_{21}H_{16}N_2Co_2O_8S$	$C_{22}H_{11}NCo_2O_7$	$C_{26}H_{21}NFe_2O_7S$	$C_{26}H_{11}NO_{11}Os_3$
Formula mass	574.28	519.18	603.20	1083.96
Crystal system	Monoclinic	Triclinic	Triclinic	Monoclinic
Space group	$P2_1/n$	$P\bar{1}$	$P\bar{1}$	$P2_1/n$
a [Å]	13.741(2)	8.0188(8)	8.778(3)	9.4492(6)
b [Å]	7.158(1)	10.677(1)	9.369(4)	29.994(2)
c [Å]	26.660(4)	12.621(1)	16.362(6)	9.4818(6)
α [°]		88.141(2)	100.363(6)	
β [°]	90.563(3)	83.551(2)	96.295(7)	92.771(1)
γ [°]		76.218(2)	98.823(7)	
V [Å³]	2622.1(8)	1042.8(2)	1294.8(9)	2684.2(3)
Z	4	2	2	4
T [K]	293	293	293	293
F(000)	1160	520	616	1960
μ(Mo-K_α) [mm^{-1}]	1.389	1.635	1.247	14.229
Reflections collected	14783	6037	6499	15570
Unique reflections	5902	4403	4487	6021
R_{int}	0.0618	0.0109	0.0518	0.0477
Observed reflections	5902	4403	4487	6021
GOF on F^2	1.036	1.031	0.805	0.986
*R*1, *wR*2 [$I > 2.0\sigma(I)$]	0.0572, 0.1770	0.0299, 0.0837	0.0698, 0.1556	0.0328, 0.0865

in a moderate yield (13.7 mg, 30%). IR (CH_2Cl_2): ν(N−H) = 3383 w, ν(CO) = 2103 w, 2065 vs, 2054 sh, 2025s, 2006 sh and 1848 w cm^{-1}. ^1H NMR ($CDCl_3$): δ = 2.89 (s, 6 H, NMe_2), 3.55 (m, 1 H, NCH_2), 3.69 (m, 1 H, NCH_2), 4.64 (t, J_{H-H} = 6.8 Hz, 1 H, NH), 7.19 (d, J_{H-H} = 7.0 Hz, 1 H, aromatic), 7.49−7.60 (m, 2 H, aromatic), 8.16−8.21 (m, 2 H, aromatic), 8.55 (d, J_{H-H} = 8.6 Hz, 1 H, aromatic) and 9.10 (s, 1 H, CCH). FAB MS: *m/z* = 1139 [M^+]. $C_{25}H_{16}N_2O_{12}Os_3S$ (1139.07): calcd. C 26.36, H 1.42, N 2.46; found C 26.10, H 1.20, N 2.18.

[$Os_3(CO)_9(\mu$-CO)(μ_3-η^2-R^2CH_2CCH)] (8): Instead of using **I**, the reaction between [$Os_3(CO)_{10}(NCMe)_2$] (37.3 mg, 0.04 mmol) and **II** (9.30 mg, 0.04 mmol) in CH_2Cl_2 resulted in the formation of the desired compound as a yellow solid. Purification was accomplished by TLC on silica using hexane/CH_2Cl_2 (1:1, v/v) as eluent to afford an analytically pure sample of **8** in 39% yield (16.9 mg). IR (CH_2Cl_2): ν(CO) = 2104 w, 2067 vs, 2054 vs, 2029 s, 2005 s and 1848 w cm^{-1}. ^1H NMR ($CDCl_3$): δ = 5.00 (m, 1 H, NCH_2), 5.19 (m, 1 H, NCH_2), 7.26−7.36 (m, 4 H, aromatic), 7.74 (t, J_{H-H} = 7.8 Hz, 2 H, aromatic), 8.59 (dd, J_{H-H} = 7.8, 1.7 Hz, 2 H, aromatic) and 8.99 (s, 1 H, CCH). FAB MS: *m/z* = 1084 [M^+]. $C_{26}H_{11}NO_{11}Os_3$ (1083.97): calcd. C 28.81, H 1.02, N 1.29; found C 28.90, H 1.15, N 1.43.

X-ray Crystallography: Good-quality crystals of our compounds suitable for X-ray diffraction studies were grown by slow evaporation of their respective solutions in hexane−CH_2Cl_2 at room temperature. Geometric and intensity data were collected using graphite-monochromated Mo-K_α radiation (λ = 0.71073 Å) on a Bruker AXS SMART 1000 CCD area-detector diffractometer. The collected frames were processed with proprietary software SAINT[47] and an absorption correction was applied (SADABS[48]) to the collected reflections. The structures of these molecules were solved by direct methods and expanded by standard difference Fourier syntheses using the software SHELXTL.[49] Structure refinements were made on F^2 by the full-matrix least-squares technique. All other non-hydrogen atoms were refined with anisotropic displacement parameters. Hydrogen atoms were either generated from Fourier maps or placed in their idealized positions and allowed to ride on the respective carbon atoms. Pertinent crystallographic information is provided in Table 6.

CCDC-174709 to -174712 contain the supplementary crystallographic data for this paper. These data can be obtained free of charge at www.ccdc.cam.ac.uk/conts/retrieving.html [or from the Cambridge Crystallographic Data Centre, 12, Union Road, Cambridge CB2 1EZ, UK; Fax: (internat.) +44−1223/336−033; E-mail: deposit@ccdc.cam.ac.uk].

Acknowledgments

W.-Y.W. thanks the Hong Kong Research Grants Council (HKBU 2022/99P) and the Hong Kong Baptist University for financial support.

[1] A. Mayer, S. Neuenhofer, *Angew. Chem. Int. Ed. Engl.* **1994**, *33*, 1044−1072.
[2] A. P. de Silva, H. Q. N. Gunaratne, T. Gunnlaugsson, A. J. M. Huxley, C. P. McCoy, J. T. Rademacher, T. E. Rice, *Chem. Rev.* **1997**, *97*, 1515−1566, and references therein.
[3] L. Fabbrizzi, A. Poggi, *Chem. Soc. Rev.* **1995**, 197−202, and references therein.
[4] A. P. de Silva, H. Q. N. Gunarantne, T. Gunnlaugsson, A. J. M. Huxley, C. P. McCoy, J. T. Rademacher, T. E. Rice, *Advances in Supramolecular Chemistry,* vol. 4, Jai Press Inc., **1997**, p. 1−53.
[5] *Fluorescent Chemosensors for Ion and Molecular Recognition* (Ed.: A. W. Czarnik), American Chemical Society, Washington, DC, **1992**.
[6] L. Fabbrizzi, M. Licchelli, P. Pallavicini, L. Parodi, A. Taglietti, *Transition Metals in Supramolecular Chemistry* (Ed.: J. P. Sauvage), Wiley, **1999**, p. 93−135.
[7] F. Bolletta, D. Fabbri, M. Lombardo, L. Prodi, C. Trombini, N. Zaccheroni, *Organometallics* **1996**, *15*, 2415−2417.
[8] L. Prodi, F. Bolletta, M. Montalti, N. Zaccheroni, *Eur. J. Inorg. Chem.* **1999**, 455−460.
[9] W.-Y. Wong, K.-Y. Tsang, K.-H. Tam, G.-L. Lu, C. Sun, *J. Organomet. Chem.* **2000**, *601*, 237−245.
[10] W.-Y. Wong, K.-H. Choi, K.-W. Cheah, *J. Chem. Soc., Dalton Trans.* **2000**, 113−115.
[11] J. Lewis, N. J. Long, P. R. Raithby, G. P. Shields, W.-Y. Wong, M. Younus, *J. Chem. Soc., Dalton Trans.* **1997**, 4283−4288.
[12] J. Lewis, P. R. Raithby, W.-Y. Wong, *J. Organomet. Chem.* **1998**, *556*, 219−228.
[13] N. Chawdhury, A. Köhler, R. H. Friend, W.-Y. Wong, J. Lewis, M. Younus, P. R. Raithby, T. C. Corcoran, M. R. A. Al-Mandhary, M. S. Khan, *J. Chem. Phys.* **1999**, *110*, 4963−4970.
[14] W.-Y. Wong, W.-K. Wong, P. R. Raithby, *J. Chem. Soc., Dalton Trans.* **1998**, 2761−2766.
[15] W.-Y. Wong, S.-M. Chan, K.-H. Choi, K.-W. Cheah, W.-K. Chan, *Macromol. Rapid Commun.* **2000**, *21*, 453−457.
[16] W.-Y. Wong, K.-H. Choi, G.-L. Lu, J.-X. Shi, *Macromol. Rapid Commun.* **2001**, *22*, 461−465.
[17] S. L. Murov, I. Carmichael, G. L. Hug, *Handbook of Photochemistry* Dekker, New York, **1993**.
[18] D. Seyferth, J. B. Hoke, G. B. Womack, *Organometallics* **1990**, *9*, 2662−2672.
[19] J. Suades, R. Mathieu, *J. Organomet. Chem.* **1986**, *312*, 335−341.
[20] P. R. Raithby, M. J. Rosales, *Adv. Inorg. Chem. Radiochem.* **1985**, *29*, 169−247.
[21] L. P. Clarke, J. E. Davies, P. R. Raithby, G. P. Shields, *J. Chem. Soc., Dalton Trans.* **1996**, 4147−4148.
[22] L. P. Clarke, *Ph.D. Thesis,* University of Cambridge, **1997**.
[23] C. J. Adams, L. P. Clarke, A. M. Martin-Castro, P. R. Raithby, G. P. Shields, *J. Chem. Soc., Dalton Trans.* **2000**, 4015−4017.
[24] A. J. Deeming, A. M. Senior, *J. Organomet. Chem.* **1992**, *439*, 177−188.
[25] C. E. Housecroft, B. F. G. Johnson, M. S. Khan, J. Lewis, P. R. Raithby, M. E. Robson, D. A. Wilkinson, *J. Chem. Soc., Dalton Trans.* **1992**, 3171−3178.
[26] S. M. Draper, M. Delamesiere, E. Champeil, B. Twamley, J. J. Byrne, C. Long, *J. Organomet. Chem.* **1999**, *589*, 157−167.
[27] X. Verdaguer, A. Moyano, M. A. Pericàs, A. Riera, A. Alvarez-Larena, J.-F. Piniella, *Organometallics* **1999**, *18*, 4275−4285.
[28] W.-Y. Wong, H.-Y. Lam, S.-M. Lee, *J. Organomet. Chem.* **2000**, *595*, 70−80.
[29] D. Seyferth, J. B. Hoke, J. C. Dewan, *Organometallics* **1994**, *13*, 3452−3464.
[30] L. F. Dahl, C.-H. Wei, *Inorg. Chem.* **1963**, *2*, 328−333.
[31] D. Seyferth, G. B. Womack, J. C. Dewan, *Organometallics* **1985**, *4*, 398−400.
[32] *International Tables for X-ray Crystallography*, (Eds.: C. M. MacGillavry, G. D. Rieck), Kynoch Press, Birmingham, England, **1974**, vol. 3, p. 276.
[33] G. Schaftenaar, Molden, version 3.5, CAOS/CAMM Center Nijmegen, Toernooiveld, Nijmegen, The Netherlands, **1999**.
[34] M. J. Calhorda, E. Hunstock, L. F. Veiros, F. Hartl, *Eur. J. Inorg. Chem.* **2001**, 223−231.
[35] J. Nijhoff, F. Hartl, J. W. M. van Outersterp, D. J. Stufkens, M. J. Calhorda, L. F. Veiros, *J. Organomet. Chem.* **1999**, *573*, 121−133.
[36] J. N. Nicholls, M. D. Vargas, *Inorg. Synth.* **1990**, *28*, 292−293.
[37] A. J. Blake, P. J. Dyson, B. F. G. Johnson, C. M. Martin, J. G.

M. Nairn, E. Parisini, J. Lewis, *J. Chem. Soc., Dalton Trans.* **1993**, 981−984.
[38] W. R. Dawson, M. W. Windsor, *J. Phys. Chem.* **1968**, *72*, 3251−3260.
[39] A. D. Decke, *J. Chem. Phys.* **1993**, *98*, 5648−5652.
[40] B. Miehlich, A. Savin, H. Stoll, H. Preuss, *Chem. Phys. Lett.* **1989**, *157*, 200−206.
[41] C. Lee, W. Yang, G. Parr, *Phys. Rev. B* **1988**, *37*, 785−789.
[42] P. C. Hariharan, J. A. Pople, *Theor. Chim. Acta* **1973**, *28*, 213−222.
[43] P. J. Hay, W. R. Wadt, *J. Chem. Phys.* **1985**, *82*, 299−310.
[44] M. J. Frisch, G. W. Trucks, H. B. Schlegel, G. E. Scuseria, M. A. Robb, J. R. Cheeseman, V. G. Zakrzewski, J. A. Montgomery Jr., R. E. Stratmann, J. C. Burant, S. Dapprich, J. M. Millam, A. D. Daniels, K. N. Kudin, M. C. Strain, O. Farkas, J. Tomasi, V. Barone, M. Cossi, R. Cammi, B. Mennucci, C. Pomelli, C. Adamo, S. Clifford, J. Ochterski, G. A. Petersson, P. Y. Ayala, Q. Cui, K. Morokuma, D. K. Malick, A. D. Rabuck, K. Raghavachari, J. B. Foresman, J. Cioslowski, J. V. Ortiz, B. B. Stefanov, G. Liu, A. Liashenko, P. Piskorz, I. Komaromi, R. Gomperts, R. L. Martin, D. J. Fox, T. Keith, M. A. Al-Laham, C. Y. Peng, A. Nanayakkara, C. Gonzalez, M. Challacombe, P. M. W. Gill, B. Johnson, W. Chen, M. W. Wong, J. L. Andres, C. Gonzalez, M. Head-Gordon, E. S. Replogle, J. A. Pople, *Gaussian 98* (Revision A.5); Gaussian, Inc.: Pittsburgh (PA), **1998**.
[45] W.-Y. Wong, G.-L. Lu, K.-F. Ng, K.-H. Choi, Z. Lin, *J. Chem. Soc., Dalton Trans.* **2001**, 3250−3260.
[46] W.-Y. Wong, K.-H. Choi, G.-L. Lu, J.-X. Shi, P.-Y. Lai, S.-M. Chan, Z. Lin, *Organometallics* **2001**, *20*, 5446−5454.
[47] *SAINT, Reference manual*, Siemens Energy and Automation, Madison, WI, **1994**−**1996**.
[48] G. M. Sheldrick, SADABS, Empirical Absorption Correction Program, University of Göttingen, Germany, **1997**.
[49] G. M. Sheldrick, *SHELXTL*™, *Reference manual*, version 5.1, Siemens, Madison, WI, **1997**.

Received December 5, 2001
[I01499]

Detecting Small Structural Changes in Metalloproteins by the Use of NMR Pseudocontact Shifts

Marco Allegrozzi,[a] Ivano Bertini,*[a,b] Sung-Nak Choi,[c] Yong-Min Lee,[a] and Claudio Luchinat[a,d]

Keywords: Metalloproteins / Pseudocontact shifts / Lanthanides / Protein structures / Temperature-dependence / Magnetic susceptibility

The potential use of pseudocontact shifts (PCS) for detecting small structural changes that may occur in a protein in aqueous solution as a function of temperature is demonstrated on lanthanide-substituted calbindin D_{9k}. The protein is a dicalcium protein in which one of the calcium ions can be selectively substituted by lanthanides. The solution structure of the protein had been previously solved at 300 K. New sets of PCS that could readily be obtained at 280 and 310 K from ^{1}H-^{15}N HSQC experiments, together with the other constraints used for the 300 K structure, were used to recalculate the solution structure at the new temperatures, since the new solution structures are consistent with different sets of PCS constraints *and* a single NOE/dihedral angle set of constraints. Temperature-dependent PCS data were collected and analyzed for as many as eleven different paramagnetic lanthanides, but the relevant structural information could already be obtained by using data from only one [erbium(III)] derivative. It is found that small structural changes occur preferentially in nonhelical regions of the protein, i.e. the N- and C-terminal ends, in the linker region between the two helix-loop-helix motifs, as well as at the metal binding loops. This research shows that PCS are most sensitive to small structural rearrangements that may be within the tolerance of the NOE constraints, and can be safely used to monitor changes that would not be detectable by NOE and dihedral angle measurements. From the newly obtained structures, the parameters describing the metal magnetic susceptibility tensors at the different temperatures can be obtained, which represent a further source of information.

(© Wiley-VCH Verlag GmbH, 69451 Weinheim, Germany, 2002)

Introduction

Solution structures of proteins by NMR spectroscopy are often more cumbersome to obtain than solid state X-ray structures, and are often less resolved. However, the availability of structural information in solution is precious because the protein is closer to its native state and because dynamic information can be extracted from NMR spectroscopic parameters. Another advantage of NMR spectroscopy as a structural tool that is not often appreciated is that small structural changes, for instance those induced by denaturants at sub-denaturing conditions, by interactions with small chemical compounds or with other biomolecules, by pH changes or temperature changes, may be observed in favorable cases, while these changes may not be accessible under the conditions of crystallization. However, the most important class of NMR structural constraints, i.e. NOEs, can be safely used in a semi-quantitative way only, and small structural changes may escape detection. Paramagnetism-based constraints, such as the pseudocontact shifts (PCS)[1−3] that originate from the presence of a paramagnetic metal ion possessing magnetic susceptibility anisotropy, are more promising in this respect. This is due to the favorable functional form of the constraint, which involves both the metal-nucleus distance and the angular coordinates of the nucleus with respect to the principal axes of the magnetic susceptibility tensor, χ [Equation (1)][1,2,4]

$$\delta_i^{pc} = \frac{1}{12\pi r_i^3}\left[\Delta\chi_{ax}\left(3\cos^2\theta - 1\right) + \frac{3}{2}\Delta\chi_{rh}\left(\sin^2\theta\cos 2\Omega\right)\right] \quad (1)$$

[a] Magnetic Resonance Center (CERM), University of Florence
Via L. Sacconi, 6, 50019 Sesto Fiorentino, Italy
Fax: (internat.) +39-055/457-4271
E-mail: bertini@cerm.unifi.it
lee@cerm.unifi.it
allegrozzi@cerm.unifi.it
[b] Department of Chemistry, University of Florence
Via della Lastruccia, 5, 50019 Sesto Fiorentino, Italy
[c] Department of Chemistry, Pusan National University
Kumjeong-Ku, Pusan 609−735, Korea
E-mail: sunachoi@pusan.ac.kr
[d] Department of Agricultural Biotechnology, University of Florence
P. le delle Cascine, 24, 50144 Sesto Fiorentino, Italy
E-mail: luchinat@cerm.unifi.it
Supporting information for this article is available on the WWW under http://www.eurjic.com or from the author.

where $\Delta\chi_{ax}$ and $\Delta\chi_{rh}$ are the axial and the rhombic anisotropies of the magnetic susceptibility tensor, and r_i, θ and Ω are the polar coordinates of the nucleus *i*. Metalloproteins are ideal systems to measure PCS on nuclei around the metal ion (by taking care to avoid nuclei with contact shifts).

In this work we investigate the possibility of detecting small structural changes that may occur as a function of temperature in a suitable metalloprotein, for example the calcium-binding protein calbindin D_{9k}. The protein has two helix-loop-helix motifs, called EF-hands, joined by a linker region made more flexible by a Pro-Met (P43M) mutation. Each of the two loops hosts a calcium ion. The first EF-hand, the so called ''pseudo EF-hand'', consists of 14 residues and binds calcium by using four backbone carbonyl oxygen atoms and one side-chain carboxylic group, whereas the second EF-hand, the common EF-hand, consists of 12 residues and binds calcium by using one backbone carbonyl oxygen and four side-chain carboxylic groups. Both solution[5−7] and X-ray[8] structures of the protein are available, as well as mobility studies in solution.[9] We exploit the fact that lanthanide ions can be selectively substituted for calcium in the second calcium binding site, and in so doing generate pseudocontact shifts.[7,10,11] Indeed, the solution structure has been solved using the PCS constraints of the peptide NH nuclei, induced by as many as 11 different lanthanides.[7] Therefore, this seemed to us an ideal system to test the sensitivity of PCS towards minor temperature-dependent structural changes. Of course it is assumed (and verified a posteriori) that the structure of all of the lanthanide derivatives is the same.

In this approach two distinct types of phenomena are to be looked for: i) structural changes, occurring anywhere in the protein, causing a change in the polar coordinates of some nuclei with respect to the metal-centered tensor frame, and consequently changing their PCS values; ii) intrinsic (structure-independent) temperature-dependence of the magnetic susceptibility tensor parameters which alter the PCS values of all protein atoms.

Results and Discussion

Structure Calculations at the Three Temperatures

Thirteen sets of ^{15}N-^{1}H HSQC shifts at 280 and 310 K for the peptide ^{15}N-^{1}H nuclei of lanthanide-substituted calbindin D_{9k} have been collected, and added to the existing 300 K data.[7] The two sets of data for the diamagnetic derivatives CaLaCb and CaLuCb were used as a blank for the other 11 paramagnetic sets of data as previously reported.[7] The resulting PCS values are 966 PCS at 280 K and 1028 PCS at 310 K. These data, together with the previously determined 1097 PCS at 300 K,[7] are reported as supplementary material (Table S1). The number of observed ^{1}H-^{15}N HSQC cross-peaks at 310 K are almost the same as those at 300 K, however, there are fewer ^{1}H-^{15}N HSQC cross-peaks at 280 K than at 300 or 310 K, probably due to the increased paramagnetism at lower temperatures.

From the 11 sets of data at each temperature and from the existing solution structure at 300 K,[7] initial estimates of the magnetic susceptibility tensor anisotropies and orientations were obtained using the program FANTASIA.[12] Separate structure calculations were then performed using the program PSEUDYANA,[13] the PCS constraints at either 280 or 310 K, and all the NOEs and other diamagnetic constraints previously collected at 300 K.[14] The rationale behind this procedure is that as long as structure alterations with respect to the 300 K structure are modest, the expected violations of the NOE constraints are within the tolerance level, and this can be verified a posteriori.

After an initial family of structures was obtained at each temperature, the values of the tensors were recalculated using FANTASIA,[12] and PSEUDYANA[13] runs were repeated until convergence was obtained. Calculations were also repeated for the 300 K data, which obviously gave the same family and the same tensors as obtained previously, within the uncertainty margin. The structures at 280 and 310 K showed modest differences (which were outside the uncertainty margin) from the one at 300 K, as well as from one another. A quality factor[7,15] was determined which showed that the agreement between calculated and experimental PCS is good at all three temperatures. The global RMSD values are reported in Table 1, together with the quality factors and target functions at the three temperatures. The latter were somewhat higher than those of the structure at 300 K. This finding is important because it provides an a posteriori validation of the use of NOE constraints at one temperature as structural constraints for a different temperature. This was not completely unexpected, however, as NOE constraints are applied in the form of upper distance limits, and the structural variations are probably within their tolerance level. The final values of the five parameters for the 11 paramagnetic derivatives, together with their errors evaluated through a Monte Carlo analysis,[7] at the three temperatures are presented in Table 2. They will be discussed further, in the context of the analysis of possible structural alterations at the binding site.

Analysis of the Structural Differences

As suggested by the RMSD values in Table 1, structural differences outside the uncertainty seem to arise from changes in temperature for calbindin D_{9k}. A more detailed analysis of the nature and significance of these differences can be attempted by examining the RMSD per residue between the structures at the three temperatures. Figure 1 illustrates the pairwise RMSD per residue between each pair of structures, both referred to the backbone and to all the heavy atoms. It is clear that in several places of the sequence the agreement is significantly poorer than that within each family. This is particularly apparent in the N- and C- terminal parts, in the metal binding loops, as well as in the region of the linker between the two helix-loop-helix motifs, i.e. in all nonhelical parts of the structure. Although the nonhelical regions are those with intrinsically larger RMSD within each family, the RMSD between the families are well above the sum of the RMSD within each family in these

Table 1. Global RMSD, together with the target functions and quality factors for the families of structures at the three temperatures, and RMSD between mean structures at the two temperatures

	RMSD (bb) (2−74)		RMSD (heavy) (2−74)		Tf	Q^{pc}
	from the average	pairwise	from the average	pairwise		
280 K (30 structures)	0.32 ±0.07	0.44 ±0.10	0.79 ±0.08	1.10 ±0.11	4.2	0.14
300 K (30 structures)	0.31 ±0.07	0.43 ±0.10	0.80 ±0.07	1.11 ±0.10	1.9	0.16
310 K (30 structures)	0.34 ±0.08	0.47 ±0.11	0.81 ±0.07	1.14 ±0.10	2.6	0.16
Between 280 K and 300 K	0.80 ± 0.10		1.20 ± 0.15		–	–
Between 280 K and 310 K	0.90 ± 0.10		1.18 ± 0.11		–	–
Between 300 K and 310 K	0.88 ± 0.10		1.19 ± 0.15		–	–

Table 2. Magnetic susceptibility tensor anisotropies, $\Delta\chi_{ax}$ and $\Delta\chi_{rh}$, calculated from the solution structure at each temperature

Metal	$\Delta\chi_{ax}$ (10^{-32} m^3)[a]			$\Delta\chi_{rh}$ (10^{-32} m^3)[a]		
	310 K	300 K	280 K	310 K	300 K	280 K
Ce	1.81 ± 0.10	1.91 ± 0.13	2.34 ± 0.11	0.87 ± 0.11	0.76 ± 0.13	0.89 ± 0.14
Pr	2.69 ± 0.07	3.37 ± 0.29	3.94 ± 0.22	2.16 ± 0.07	2.31 ± 0.14	2.56 ± 0.17
Nd	1.38 ± 0.12	1.53 ± 0.14	2.22 ± 0.12	0.54 ± 0.16	0.38 ± 0.13	0.39 ± 0.22
Sm	0.19 ± 0.12	0.36 ± 0.11	0.19 ± 0.07	0.16 ± 0.06	0.12 ± 0.05	0.07 ± 0.05
Eu	1.84 ± 0.15	2.44 ± 0.17	1.78 ± 0.27	0.71 ± 0.27	1.50 ± 0.29	0.86 ± 0.43
Tb	38.2 ± 3.6	42.3 ± 3.3	52.7 ± 2.6	12.8 ± 2.1	10.0 ± 2.1	11.8 ± 1.5
Dy	34.8 ± 0.7	35.7 ± 2.1	36.5 ± 2.7	20.7 ± 0.5	21.2 ± 2.0	25.3 ± 2.1
Ho	17.1 ± 0.7	20.0 ± 0.8	20.9 ± 1.0	6.85 ± 0.95	4.68 ± 0.65	6.27 ± 0.89
Er	11.4 ± 0.2	11.6 ± 0.2	14.2 ± 0.3	5.38 ± 0.68	7.32 ± 0.40	10.2 ± 0.7
Tm	26.5 ± 0.9	27.4 ± 0.9	30.4 ± 0.6	11.3 ± 1.2	12.2 ± 0.9	14.2 ± 1.6
Yb	7.14 ± 0.51	8.03 ± 0.37	9.66 ± 0.31	3.63 ± 0.45	4.44 ± 0.50	5.05 ± 0.73

[a] The uncertainties reported correspond to the sum of the standard deviation of the tensor parameters resulting from either the fit of the individual conformers of the family, or fitting partial data sets in which 30% of the input data were randomly deleted according to a MonteCarlo analysis.

regions (Figure 1). In particular, noticeable temperature changes are shown by the φ and ψ angles of the residues in the first loop (residues 17, 18, 21, 22 and 23), in the linker and beginning of the third helix (residues 36−48) and in the second loop (residues 56−62). Furthermore, the orientations of the side-chain of residues Glu 17, Gln 22, Lys 41 and Asn 56 are somewhat different. However, the overall quality of the three structures based on Ramachandran plots[16] is very similar (about 89% of residues in most favored regions and 11% in additionally allowed regions at all temperatures). Interestingly, residues 17, 41 and 56 all precede a glycine in the sequence. The lower conformational barrier of glycine could be responsible for the temperature sensitivity of the preceding residues. The fact that significant differences among the three families are observed, despite the use of a single set of NOEs, suggests that the actual differences may be even larger. Figure 2 summarizes the regions of the protein where temperature-dependent structural changes are observed.

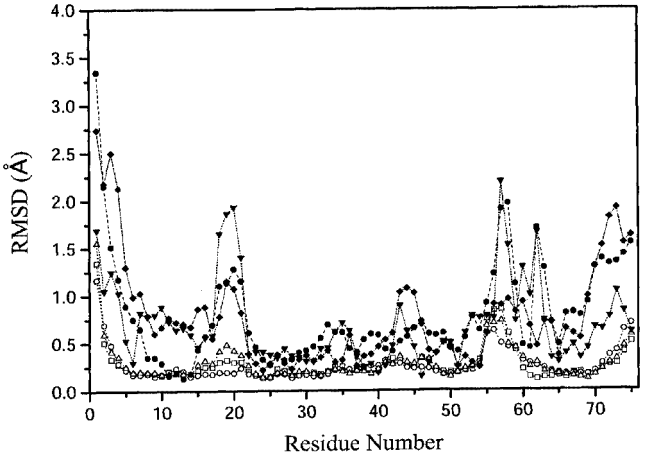

Figure 1. RMSD per residue within each family of structures at 280 K (□), 300 K (○) and 310 K (△), and between mean structures at the two temperatures, 280 K-300 K (▼), 280 K−310 K (◆) and 300 K−310 K (●)

In order to test whether the present results could still be obtained in systems where only one paramagnetic derivative is available, the solution structures at three temperatures were also calculated using the PCS of only the Er^{3+} derivative (chosen among the eleven lanthanides because it provides a sufficiently high number of ^{15}N-^{1}H HSQC cross-peaks with nonnegligible PCS values). The pairwise RMSD values of each family at each of the three temperatures for the backbone are in the range 0.71−0.77 Å, while the RMSD between the different families of structures at the three temperatures are in the range 0.80−1.07 Å. Based on Ramachandran plots,[16] the overall quality of the structures from the Er^{3+} derivative is the same as that from 11 lanthanide derivatives. In all nonhelical parts of the three

Figure 2. Schematic representation of the solution structure of calbindin D_{9k}, highlighting the residues that undergo slight temperature-dependent structural changes (shaded in dark gray)

structures of the Er^{3+} derivative at different temperatures, the agreement is sizably poorer than that within each family. In particular, the φ and ψ angles of the residues in the first loop (residues 19−22), linker (residues 41−44) and second loop (residues 54−62) were affected by variations in temperature. These results are very similar to those obtained by making use of the PCS data for all eleven lanthanide derivatives, and therefore show: i) that the assumption that the structure is lanthanide-independent is verified, and ii) that the present approach may be of general applicability for any paramagnetic metalloprotein.

The significance of the observed temperature-related changes, at least in regions far from the paramagnetic center, should be further checked by going back to the original PCS data. This practice is common in the analysis of differences between solution structures, and originates from the fact that, due to the global nature of the simulated annealing procedure and the local nature of the structural changes, the best check to ascertain the significance of the latter is to relate them to local variations of the constraints. In the present case, the simple comparison of the PCS data at different temperatures for a particular residue or group of residues is not feasible, as: i) a temperature-dependent variation of the magnitude of the tensor parameters (and therefore of the PCS values) is theoretically expected, independent of structural variations, and ii) structural changes at the metal ion site would also alter the tensors, and therefore all the PCS, simultaneously. Therefore, a way of comparing the PCS values should be found that is independent of the tensor variations. A possibility is that of examining the *ratios* between the ^{15}N and ^{1}H PCS for a given NH group for each lanthanide. This ratio should be much less sensitive to tensor variations than to changes in orientation of the N−H vector with respect to either the M−N or M−H vectors.

Therefore, again assuming the same behavior for all lanthanides, a plot of ^{15}N chemical shifts versus ^{1}H chemical shifts of a given NH group for all lanthanides at the same temperature should be a straight line. The slope, which depends on the third power of the ratio between the M−N and M−H distances, is expected not to exceed the range 0.77−1.3 for all NH groups that are farther than 12 Å from the metal.

In the absence of temperature-dependent structural variations, such straight lines for each temperature should be identical, whereas variations in the slopes should indicate a structural change. Examples of such plots are reported in Figure 3. The slopes for Ser 2, Phe 36 and Gly 42 indicate some temperature-dependent changes, whereas Leu 32 and Leu 69 are examples that exhibit structural invariance. From this qualitative analysis evidence is provided for temperature-dependent structural changes for residues Ser 2, Gly 18, Phe 36, Gly 42, Leu 46, Asp 47, Glu 48 and Gly 57, all in nonhelical regions. Despite the fact that the number of residues does not fully correspond to those which show variations in the structure, they still support the hypothesis that indeed the loops and linker undergo temperature-dependent changes. In any case, the structures at the three temperatures reliably show differences in about 25 residues, seven of which are confirmed spectroscopically.

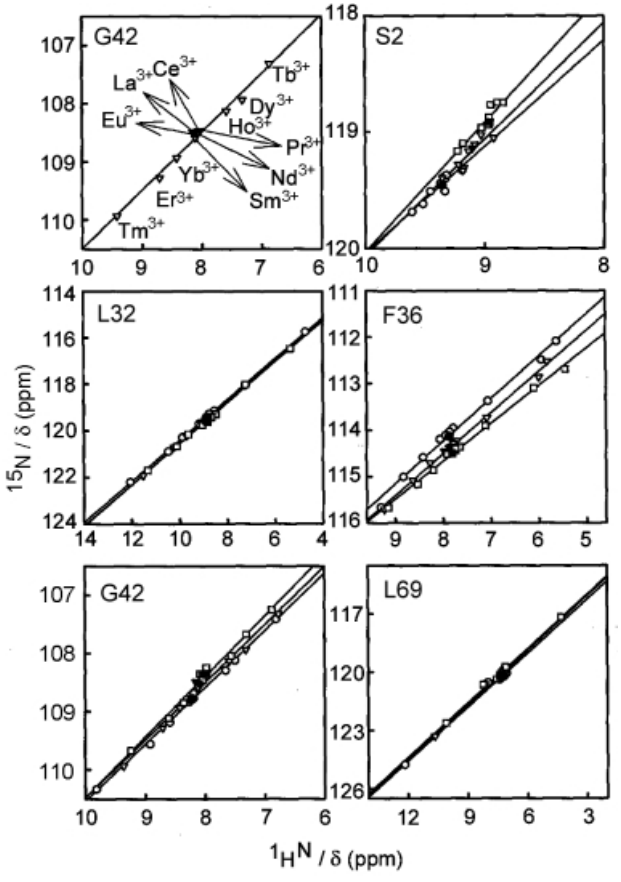

Figure 3. Observed ^{15}N versus ^{1}H chemical shifts of the G42 NH moiety (upper left) with all lanthanide ions at 300 K (▽) (diamagnetic CaLaCb values as filled symbols); analogous plots for selected residues at 280 K (○), 300 K (▽), and 310 K (□) are also shown

Temperature-Dependence of the Tensor Parameters

It is worth examining the temperature-dependence of the $\Delta\chi_{ax}$ and $\Delta\chi_{rh}$ parameters. Theory predicts that these parameters should experience a temperature dependence that is proportional to the temperature dependence of the overall magnetic susceptibility. The latter is expected to have a T^{-2} dependence, with modest positive or negative corrections from a T^{-3} term arising from the thermal population of the excited electronic states.[17–19] The $\Delta\chi_{ax}$ values for the 11 lanthanides as a function of T^{-2} are reported in Figure 4. Most lanthanides show a monotonous change with temperature, with the exception of samarium(III) and europium(III). The behavior of the latter two ions is unexpected. However, the collection of a number of experimental data at different temperatures to address this point is beyond the scope of this paper. Although a quantitative assessment of the slopes is difficult to make, some lanthanides clearly show a more marked temperature dependence [e.g. terbium(III)] and some a less marked one [e.g. dysprosium(III)]. Inspection of Table 2 reveals that some modest, but consistent, changes in the angular parameters are also observed for all lanthanides. Figure 5 illustrates such changes in the form of plots of θ vs. φ, where θ and φ are the angles defining the orientation of the principal axes of the χ tensor with respect to a fixed reference frame. The changes are on average between 5 and 10 degrees, with the largest (almost 20 degrees) being observed for the holmium(III) derivative. These changes are of the same order as the uncertainties; however they are in all cases monotonous with temperature i.e. they have a systematic character that cannot be explained by random errors. In summary, changes both in the magnitude of the susceptibility anisotropy parameters and in the principal axes orientations are detected over the temperature range investigated. The changes in axes orientation, in particular, suggest that population of excited states involving different *f*-orbitals may occur. Overall, the present analysis shows that possible structural or electronic changes at the metal site can be recognized as such and do not prevent detection of small temperature-dependent structural changes in the protein part of paramagnetic metalloproteins when using PCS.

The possibility that the present analysis may be hampered by some kind of circular argument could be considered. However, it is easy to show that the ratios of the PCS values for the ^{15}N and ^{1}H nuclei of a peptide NH moiety are much less sensitive to the orientation of the tensor axes than they are to changes in the orientations of the NH vectors. Furthermore, the tensor parameters are barely sensitive to structural variations that occur far from the metal center and that essentially compensate each other. Sample calculations show that random variations (up to ±40°) of ten different NH vector orientations (i.e. larger structural changes than those observed here) change the magnetic anisotropy parameters of the various lanthanide ions by much less (typically less than 1%) than the changes due to temperature. In another set of sample calculations, variations of ±5° in the tensor orientation for the lanthanide ions with the largest magnetic susceptibility anisotropy change the δ_N/δ_H ratios of the NH groups with the largest pseudocontact shift by less than 4%, i.e., much less than the observed changes in the slopes that have been considered meaningful indications of true structural changes.

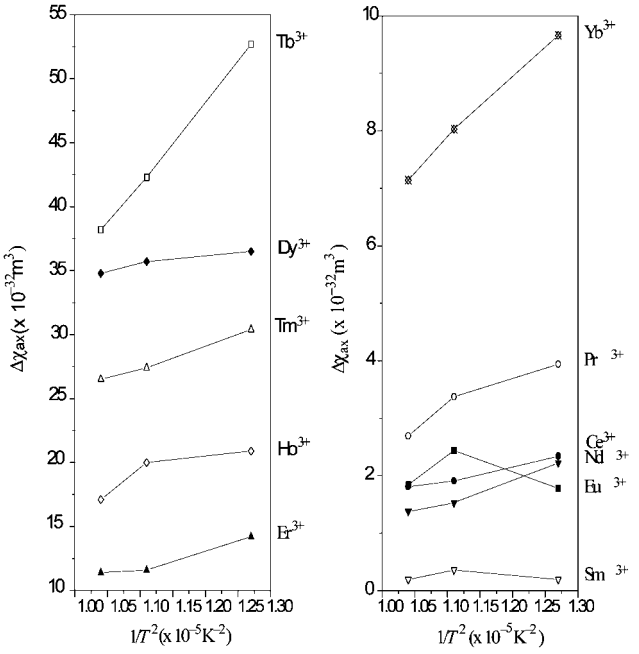

Figure 4. Plot of experimental $\Delta\chi_{ax}$ values vs. $1/T^2$ for all lanthanide ions

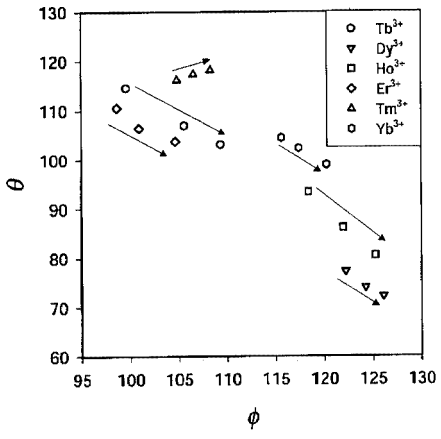

Figure 5. Temperature dependence of the θ and φ values of the principal axis of the χ tensor for the second half of the lanthanide series; the reference system is arbitrary and fixed to the molecular frame; the arrows indicate increasing temperature

Concluding Remarks

The power of PCS in determining the solution structure is proved by the finding that minor changes of PCS, for example with temperature, can be used to relate them to small structural changes, by solving the solution structure with a common set of NOEs and appropriate PCS. This is

shown through lanthanide substitution of a calcium binding protein, calbindin D_{9k}. This finding is qualitative, but is definitively confirmed by the analysis of the $^{15}N/^{1}H$ PCS ratios for NH moieties. If no temperature-dependent change occurs in the NH orientation, the above ratio is constant, even if modest temperature-dependent changes in the metal magnetic susceptibility occur. From the different solution structures, the magnetic susceptibility anisotropies at different temperatures are obtained which are additional and precious pieces of information that may be further analyzed.

Experimental Section

Materials and Methods

Sample Preparation: Protein expression and purification of the ^{15}N-enriched dicalcium form of bovine calbindin D_{9k} (P43M mutant) was performed as reported previously.[20−23] NMR samples were prepared by dissolving the lyophilized protein in 500 μL of 90% H_2O/10% D_2O to give final 2.0 mM protein solutions. The pH was adjusted to 6.0 by means of 0.1 M NaOH or 0.1 M HCl. Lanthanide-containing calbindin D_{9k} (hereafter CaLnCb) samples were obtained by titrating the dicalcium form with 0.02 M solutions of analytical grade $LnCl_3$ (Sigma, Aldrich), up to one equivalent.[7,24] Titrations were followed by 2D ^{1}H-^{15}N HSQC spectroscopy. The samples were kept at 4 °C between measurements.

NMR Spectroscopy: NMR spectra were acquired on Bruker AVANCE 800 and 400 spectrometers operating at 800.13 and 400.13 MHz, respectively. The residual water signal was suppressed by either presaturation during both the relaxation delay and mixing time, or by gradient-tailored excitation (WATERGATE).[25] The spectra were calibrated in the proton dimension at different temperatures according to the empirical relationship[26] $\delta_{HOD} = (-0.012 \times T + 5.11)$ ppm, where T is the temperature in °C. ^{1}H-^{15}N HSQC[27] spectra were recorded for all lanthanide derivatives at 280, 300 and 310 K using a spectral width of 16 ppm and 36 ppm in the ^{1}H and ^{15}N dimension, respectively. 512 increments, each with 1024 complex data points and 32 transients, were collected. The recycle delays were in the range between 0.5 s (CaTbCb) and 1.0 s (CaLaCb). All NMR spectroscopic data were processed with the Bruker XWINNMR software packages. The program XEASY was used for analysis of the 2D spectra.[28]

Computer Programs: The programs FANTASIA, PSEUDYANA are available at http://www.postgenomicNMR.net

Determination of PCS and Simultaneous Refinement of Magnetic Tensor Anisotropies and Solution Structure: Pseudocontact shifts for each paramagnetic lanthanide derivative at 280, 300 and 310 K were calculated by subtracting the shifts of either the CaLaCb or the CaLuCb diamagnetic protein. The pseudocontact shifts at 300 K have been taken from previous work without modification.[7] The variations in pseudocontact shifts for each lanthanide derivative at 280 and 310 K were directly calculated as the differences from the chemical shifts of each lanthanide derivative at 300 K.
The magnetic susceptibility tensor anisotropies for each lanthanide, $\Delta\chi_{ax}$ and $\Delta\chi_{rh}$, were obtained by simultaneously fitting all the PCS values to a family of 30 conformers obtained from solution structure calculations through Equation (1), and the error estimated through a MonteCarlo analysis.[7] These calculations were accomplished with the program FANTASIA.[12] Solution structure calculations at each temperature were performed using all diamagnetic constraints (NOEs, van der Waals) at 300 K and PCS constraints at each temperature. These diamagnetic constraints have been taken from previous work.[14] These amounted to 1793 meaningful NOEs, 191 dihedral angles, 15 hydrogen bonds and 26 T_1.
The quality factor for PCS was defined as:[7,15]

$$Q^{ax} = \frac{\sqrt{\sum_i \left(\delta_i^{obs} - \delta_i^{calc}\right)^2}}{\sqrt{\sum_i \left(\delta_i^{obs}\right)^2}} \qquad (2)$$

where δ_i^{obs} is the i-th experimental PCS value measured, δ_i^{calcd} is the corresponding calculated PCS value, and the summations span all experimental PCS.

Supporting Information Available: A table reporting the PCS values used in the solution structure calculations at three temperatures for all lanthanide derivatives (PDF); see also footnote on the first page of this article.

Acknowledgments

This research has been financially supported under the RTD project (Contracts QLG2-CT-1999−01003 for FIND structure and HPR1-1999-CT-50006 for Transient NMR). This work also has been supported partly by MIUR, ex 40%, and CNR (Contracts 97.01133.49, 98.01789.CT03, and 99.00393.49). Financial support of the EU through Contract No.: QLG2-CT-1999-01003 to Y.-M.L. is gratefully acknowledged.

[1] H. M. Mc Connell, R. E. Robertson, *J. Chem. Phys.* **1958**, *29*, 1361−1365.
[2] R. J. Kurland, B. R. McGarvey, *J. Magn. Reson.* **1970**, *2*, 286−301.
[3] I. Bertini, C. Luchinat, G. Parigi, *Solution NMR of Paramagnetic Molecules*, Amsterdam, Elsevier, **2001**.
[4] L. Banci, I. Bertini, K. L. Bren, M. A. Cremonini, H. B. Gray, C. Luchinat, P. Turano, *J. Biol. Inorg. Chem.* **1996**, *1*, 117−126.
[5] J. Kordel, N. J. Skelton, W. J. Chazin, *J. Mol. Biol.* **1993**, *231*, 711−734.
[6] D. M. E. Szebenyi, K. J. Moffat, *J. Biol. Chem.* **1986**, *261*, 8761−8777.
[7] I. Bertini, M. B. L. Janik, Y.-M. Lee, C. Luchinat, A. Rosato, *J. Am. Chem. Soc.* **2001**, *123*, 4181−4188.
[8] L. A. Svensson, E. Thulin, S. Forsén, *J. Mol. Biol.* **1992**, *223*, 601−606.
[9] I. Bertini, C. J. Carrano, C. Luchinat, M. Piccioli, L. Poggi, *Biochemistry* **2002**, *41*, 5104−5111.
[10] H. J. Vogel, T. Drakenberg, S. Forsén, J. D. O′Neil, T. Hofmann, *Biochemistry* **1985**, *24*, 3870−3876.
[11] M. Akke, S. Forsén, W. J. Chazin, *J. Mol. Biol.* **1991**, *220*, 173−189.
[12] L. Banci, I. Bertini, G. Gori Savellini, A. Romagnoli, P. Turano, M. A. Cremonini, C. Luchinat, H. B. Gray, *Proteins Struct. Funct. Genet.* **1997**, *29*, 68−76.
[13] L. Banci, I. Bertini, M. A. Cremonini, G. Gori Savellini, C. Luchinat, K. Wüthrich, P. Güntert, *J. Biomol. NMR* **1998**, *12*, 553−557.
[14] I. Bertini, A. Donaire, B. Jimenez, C. Luchinat, G. Parigi, M. Piccioli, L. Poggi, *J. Biomol. NMR* **2001**, *21*, 85−98.
[15] G. Cornilescu, J. Marquardt, M. Ottiger, A. Bax, *J. Am. Chem. Soc.* **1998**, *120*, 6836−6837.
[16] R. A. Laskowski, M. W. MacArthur, D. S. Moss, J. M. Thornton, *J. Appl. Crystallogr.* **1993**, *26*, 283−297.

[17] B. Bleaney, *J. Magn. Reson.* **1972**, *8*, 91−100.
[18] W. D. Horrocks, Jr., *J. Magn. Reson.* **1977**, *26*, 333−339.
[19] B. R. McGarvey, *J. Magn. Reson.* **1979**, *33*, 445−455.
[20] P. Brodin, T. Grundstrom, T. Hofmann, T. Drakenberg, E. Thulin, S. Forsén, *Biochemistry* **1986**, *25*, 5371−5377.
[21] C. Johansson, P. Brodin, T. Grundstrom, E. Thulin, S. Forsén, T. Drakenberg, *Eur. J. Biochem.* **1990**, *187*, 455−460.
[22] A. Malmendal, G. Carlström, C. Hambraeus, T. Drakenberg, S. Forsén, M. Akke, *Biochemistry* **1998**, *37*, 2586−2595.
[23] W. J. Chazin, J. Kördel, T. Drakenberg, E. Thulin, P. Brodin, T. Grundstrom, S. Forsén, *Proc. Natl. Acad. Sci. U. S. A.* **1989**, *86*, 2195−2198.
[24] M. Allegrozzi, I. Bertini, M. B. L. Janik, Y.-M. Lee, G. Liu, C. Luchinat, *J. Am. Chem. Soc.* **2000**, *122*, 4154−4161.
[25] M. Piotto, V. Saudek, V. Sklenar, *J. Biomol. NMR* **1992**, *2*, 661−666.
[26] I. Bertini, S. Ciurli, A. Dikiy, C. Luchinat, *J. Am. Chem. Soc.* **1993**, *115*, 12020−12028.
[27] G. Bodenhausen, D. J. Ruben, *Chem. Phys. Lett.* **1980**, *69*, 185−188.
[28] C. Eccles, P. Güntert, M. Billeter, K. Wüthrich, *J. Biomol. NMR* **1991**, *1*, 111−130.

Received November 28, 2001
[I01483]

New Dinuclear Molybdenum(V) Complexes With β′-Hydroxy-β-enaminones Containing a 4-Hydroxy-2-pyrone Ring[‡]

Marina Cindrić,*[a] Višnja Vrdoljak,[a] Neven Strukan,[a] Predrag Tepeš,[b] Predrag Novak,[b] Ana Brbot-Šaranović,[c] Gerald Giester,[d] and Boris Kamenar[a]

Keywords: Amine ligands / Molybdenum / Nitrogen heterocycles

New dinuclear molybdenum(V) complexes of the general formula $[Mo_2O_4L_2D_2]$, were prepared by the reaction of $[Mo_2O_3(acac)_4]$ (acac = acetylacetonate ion) with β′-hydroxy-β-enaminones (L). All prepared complexes consist of $Mo_2O_4^{2+}$ cores coordinated by two ligands L via two donor oxygen atoms as in the analogous β-diketonates. The usual octahedral coordination around the molybdenum atoms is completed by the monodentate solvent molecules D (methanol, ethanol, or 2-propanol). All compounds were characterized by elemental analyses, IR, one- and two-dimensional NMR spectra, and thermal analysis, and some of them by X-ray crystallography (**1a**, **4a**, **8b**, and **9a**).
(© Wiley-VCH Verlag GmbH, 69451 Weinheim, Germany, 2002)

Introduction

Metal complexes with 2-pyrone derivatives are of interest in coordination and bioinorganic chemistry because of their application in immunoassay procedures and in cytological investigations, as well as for their use as potential HIV protease inhibitors.[1−6] Dehydroacetic acid (dha = 3-acetyl-4-hydroxy-6-methyl-2-pyrone) containing a 4-hydroxy-2-pyrone ring is a frequently investigated compound due to its good complexing properties. However, only two crystal structures of complexes $[Re(dha)Cl_2(OPPh_3)(PPh_3)]\cdot EtOH$[7] and $[Co(dha)_2(dmf)_2]$[8] have been known so far. Furthermore, little is known about complexes with dehydroacetic derivatives such as the β′-hydroxy-β-enaminone, and to the best of our knowledge only the copper(II) complex $[Cu(acrp)_2(py)]\cdot H_2O$ [Hacrp = 4-hydroxy-6-methyl-3-(3-dimethylaminoacryloyl)-2*H*-pyran-2-one] has been structurally characterized.[9] Such complexes have been studied not only as models for the elucidation of interactions between flavonoides and metal ions, but they are also of interest when studying the correlation between their steric, electronic, and hydrogen bonding effects, as well as for their possible relevance to biological processes.[10,11] In addition, the enaminone derivatives are good analytical reagents for spectrofluorometric determination of beryllium.[12]

We have recently published syntheses and structures of several isomeric enaminones obtained by the reaction of ethyl 2-hydroxy-4-(4-hydroxy-6-methyl-2*H*-pyran-2-on-3-yl)-4-oxo-2-butenoate and corresponding amines (*n*-butylamine, aniline, *p*-anisidine, and α-naphthylamine).[13−16] Continuing this research, we describe here nine new dinuclear molybdenum(V) complexes obtained by the reaction of isomeric β′-hydroxy-β-enaminones and $[Mo_2O_3(acac)_4]$ (Scheme 1). All complexes have the general formula $[Mo_2O_4L_2D_2]$, where ligand L is coordinated to molybdenum in a bidentate manner through the deprotonated hydroxyl groups and ketone moieties. The typical octahedral coordination around the Mo atom is completed by the monodentate solvent molecules D.

All compounds were characterized by means of chemical analysis, high-resolution NMR and IR spectroscopy, and thermogravimetric analysis. Four of them were also characterized by X-ray crystallography (**1a**, **4a**, **8b**, and **9a**).

Results and Discussion

Synthesis and Characterization of Complexes

The reaction of ethyl 2-hydroxy-4-(4-hydroxy-6-methyl-2*H*-pyran-2-on-3-yl)-4-oxo-2-butenoate (**ehmpb**) with a suitable amine (*n*-butylamine, aniline, or α-naphthylamine)

[‡] This paper is part of our studies on molybdenum complexes with enaminones.[16]

[a] Laboratory of General and Inorganic Chemistry, Chemistry Department, Faculty of Science, University of Zagreb,
Ul. kralja Zvonimira 8, 10000 Zagreb, Croatia
Fax:(internat.) + 385-1-46 11 191
E-mail: marina@chem.pmf.hr
[b] Chemistry Department, Faculty of Science, University of Zagreb,
Strossmayerov trg 14, 10000 Zagreb, Croatia
[c] Chemistry Department, Veterinary Faculty, University of Zagreb,
Heinzelova 55, 10000 Zagreb, Croatia
[d] Institut für Mineralogie und Kristallographie, Geozentrum, Universität Wien,
Althanstraße 14, 1090 Wien, Austria

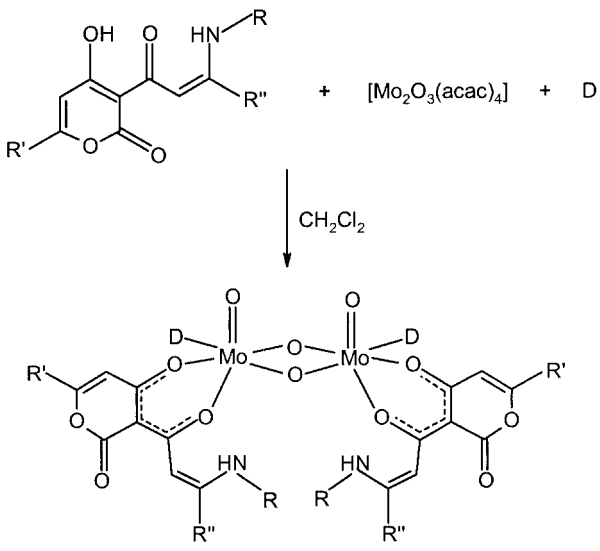

	R	R'	R''	D
1a		$CO_2C_2H_5$	CH_3	CH_3OH
2a	*n*-C_4H_9	$CO_2C_2H_5$	CH_3	CH_3CH_2OH
3a		$CO_2C_2H_5$	CH_3	$(CH_3)_2CHOH$
4a		$CO_2C_2H_5$	CH_3	CH_3OH
4b		CH_3	$CO_2C_2H_5$	CH_3OH
5a	C_6H_5	$CO_2C_2H_5$	CH_3	CH_3CH_2OH
5b		CH_3	$CO_2C_2H_5$	CH_3CH_2OH
6a		$CO_2C_2H_5$	CH_3	$(CH_3)_2CHOH$
6b		CH_3	$CO_2C_2H_5$	$(CH_3)_2CHOH$
7a		$CO_2C_2H_5$	CH_3	CH_3OH
7b		CH_3	$CO_2C_2H_5$	CH_3OH
8a	α-$C_{10}H_7$	$CO_2C_2H_5$	CH_3	CH_3CH_2OH
8b		CH_3	$CO_2C_2H_5$	CH_3CH_2OH
9a		$CO_2C_2H_5$	CH_3	$(CH_3)_2CHOH$
9b		CH_3	$CO_2C_2H_5$	$(CH_3)_2CHOH$

Scheme 1

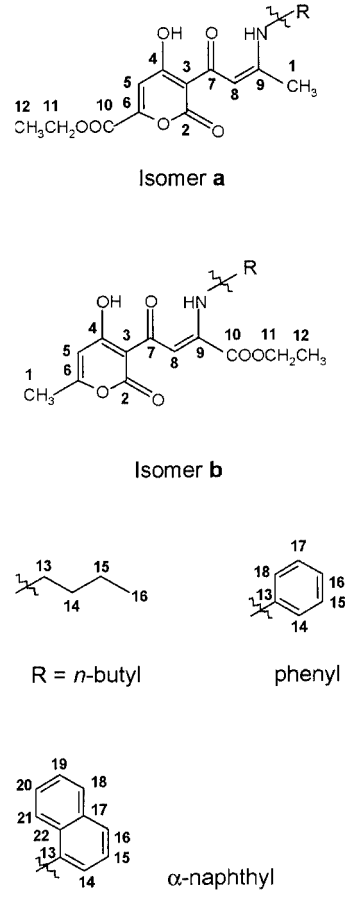

Scheme 2

resulted in the formation of two isomeric enaminones (Scheme 2), one with the 2-pyrone ring substituted at position 6 by ethoxycarbonyl group (isomer **a**) and the other one substituted by a methyl group (isomer **b**).[14,15] The reaction of **ehmpb** with *n*-butylamine gave both isomers **a** and **b**, but the obtained amount of isomer **b** was insufficient for further synthesis of molybdenum complexes.

New molybdenum(V) complexes of general formula $[Mo_2O_4L_2D_2]$ were prepared by reaction of $[Mo_2O_3(acac)_4]$ with enaminones (Scheme 1) variously substituted at the nitrogen atom (R = *n*-butyl, phenyl, or α-naphthyl). Both isomers **a** and **b** of the phenyl and α-naphthyl derivatives were used as starting reagents for the preparation of the corresponding molybdenum(V) complexes, whereas in the case of the *n*-butyl derivative only isomer **a** was used. Dichloromethane was chosen as the most suitable solvent for all preparations, followed by the addition of the corresponding alcohol D (methanol for the preparation of complexes **1**, **4**, and **7**, ethanol for **2**, **5**, and **8**, and 2-propanol for **3**, **6**, and **9**).

In all complexes, ligand L was coordinated in a bidentate fashion to molybdenum through two oxygen atoms (as in the case of β-diketonates) and not through the nitrogen atom. One neutral solvent molecule D, acting as a monodentate ligand, completed the octahedral coordination of each Mo atom. Such behaviour was expected from the previous studies of molybdenum complexes with analogous ligands.[14,17,18]

Infrared Spectra and Thermal Analyses

All complexes were characterized by IR spectroscopy (selected spectroscopic data are given in Table 1). Two bands at 1735−1720 cm^{-1} and 1650−1700 cm^{-1} can be attributed to the stretching vibrations of the carbonyl group belonging to the ester $COOC_2H_5$ and 2-pyrone, respectively. The stretching frequencies at about 1570 and 1520 cm^{-1} attributed to the coordinated C···O groups and to C···C were observed at lower values compared to those found in the free ligands.[14,15] The single strong absorption maximum at about 950 cm^{-1} belongs to Mo−O (terminal), while the band at 730 cm^{-1} to the Mo−O (bridging) stretching frequencies. The remaining frequencies in the IR spectra are due to the vibrations within the ligands.

Thermal analyses of all prepared specimens revealed two main processes: (1) loss of solvent molecules, and (2) complex decomposition (Table 2). When heated, a weight loss

Table 1. Analytical and IR data for $[Mo_2O_4L_2D_2]$ complexes.

Formula *M*r	Complex	Analysis found (calcd.)				Yield (%)	Selected IR data (cm^{-1})
		%C	%H	%N	%Mo		
$C_{34}H_{48}Mo_2N_2O_{18}$ 964.63	**1a**	42.13 (42.33)	4.92 (5.01)	3.39 (2.90)	19.64 (19.89)	46	1724, 1651, 1594, 1522, 952, 738
$C_{36}H_{52}Mo_2N_2O_{18}$ 992.68	**2a**	43.13 (43.56)	5.29 (5.28)	2.77 (2.82)	18.72 (19.32)	40	1720, 1654, 1597, 1525, 957, 738
$C_{38}H_{56}Mo_2N_2O_{18}$ 1020.73	**3a**	44.25 (44.71)	5.17 (5.53)	2.32 (2.74)	18.28 (18.80)	35	1729, 1647, 1591, 1520, 952, 738
$C_{38}H_{40}Mo_2N_2O_{18}$ 1004.61	**4a**[a]	45.30 (45.43)	3.94 (4.01)	3.00 (2.79)	18.89 (19.10)	30	1733, 1686, 1573, 1504, 952, 735
	4b	45.36 (45.43)	3.88 (4.01)	3.07 (2.79)	19.30 (19.10)	33	1732, 1684, 1577, 1518, 958, 736
$C_{40}H_{44}Mo_2N_2O_{18}$ 1032.66	**5a**	46.75 (46.52)	3.88 (4.29)	2.64 (2.71)	18.27 (18.52)	35	1727, 1670, 1572, 1523, 961, 719
	5b	46.31(46.52)	4.37 (4.29)	2.63 (2.71)	18.21 (18.52)	34	1728, 1682, 1577, 1519, 959, 734
$C_{42}H_{48}Mo_2N_2O_{18}$ 1060.71	**6a**	46.88 (47.56)	3.86 (4.56)	2.29 (2.64)	17.84 (18.09)	40	1726, 1671, 1572, 1522, 962, 720
	6b	47.68 (47.56)	4.12 (4.56)	2.69 (2.64)	17.75 (18.09)	36	1731, 1681, 1574, 1519, 946, 728
$C_{46}H_{44}Mo_2N_2O_{18}$ 1104.72	**7a**	49.27 (50.01)	3.94 (4.01)	2.43 (2.54)	17.17 (17.37)	55	1720, 1696, 1568, 1499, 956, 712
	7b	49.30 (50.01)	3.96 (4.01)	2.38 (2.54)	17.28 (17.37)	57	1735, 1681, 1573, 1519, 961, 736
$C_{48}H_{48}Mo_2N_2O_{18}$ 1132.78	**8a**	50.47 (50.89)	3.95 (4.27)	2.50 (2.47)	17.16 (16.94)	59	1720, 1675, 1566, 1498, 951, 734
	8b*	50.23 (50.89)	4.12 (4.27)	2.54 (2.47)	16.71 (16.94)	58	1736, 1681, 1574, 1520, 960, 747
$C_{56}H_{68}Mo_2N_2O_{20}$ 1220.93	**9a**	51.78 (52.50)	5.28 (5.35)	2.05 (2.18)	15.36 (14.98)	61	1732, 1654, 1570, 1505, 946, 728
$C_{50}H_{52}Mo_2N_2O_{18}$ 1160.83	**9b**	51.55 (51.73)	4.31 (4.52)	2.15 (2.41)	16.21 (16.53)	60	1742, 1681, 1573, 1514, 957, 738

[a] According to the X-ray structure analysis, complex (**4a**) is solvated with two methanol molecules, while (**8b**) is solvated with two dichloromethane molecules. The crystals were readily loosing solvent at room temperature, so that they were left in a desiccator until constant weight, and analyzed as unsolvated species.

corresponding to the loss of solvated alcohol molecules was only observed in the case of **9a**, while all other complexes were loosing solvated molecules already at room temperature. The presence of solvated molecules in $[Mo_2O_4(C_{18}H_{16}O_6N)_2(CH_3OH)_2]\cdot 2CH_3OH$ (**4a**) and dichloromethane molecules in $[Mo_2O_4(C_{22}H_{18}O_6N)_2(CH_3CH_2OH)_2]\cdot 2CH_2Cl_2$ (**8b**) is established by the crystal structure determination. In general, the first weight loss could be attributed to the loss of coordinated alcohol and the complex conversion into a stable species of the formula $[Mo_2O_4L_2]$. On further heating, significant weight losses are indicative of complex decomposition resulting in the solid residues identified as MoO_3.

NMR Spectroscopy

^1H and ^{13}C resonances were assigned by using one-dimensional proton and carbon experiments as well as two-dimensional COSY sequence combined with $^1H-^{13}C$ correlation techniques through one bond- (HSQC) and multiple bond- (HMBC) procedures. Chemical shifts of the complexes are given in Table 3. A complete and unambiguous atom assignment for complex **4b** was not possible in

Table 2. Thermoanalytical data for $[Mo_2O_4L_2D_2]$ complexes

Formula	Complex	Loss of solvent			Decomposition		
		Temperature range (°C)	Δm (%) found	(calcd.)	Temperature range (°C)	Δm (%) found	(calcd.)
$[Mo_2O_4(C_{16}H_{20}NO_6)_2(CH_3OH)_2]$	**1a**	65−126	6.32	(6.64)	169−536	62.98	(63.52)
$[Mo_2O_4(C_{16}H_{20}NO_6)_2(CH_3CH_2OH)_2]$	**2a**	55−115	8.81	(9.28)	170−535	62.68	(61.72)
$[Mo_2O_4(C_{16}H_{20}NO_6)_2\{(CH_3)_2CHOH\}_2]$	**3a**	54−114	11.09	(11.77)	169−537	60.22	(60.03)
$[Mo_2O_4(C_{18}H_{16}NO_6)_2(CH_3OH)_2]$	**4a**[a]	85−161	5.75	(6.37)	187−514	65.19	(64.97)
	4b	40−138	5.84	189−533	65.35		
$[Mo_2O_4(C_{18}H_{16}NO_6)_2(CH_3CH_2OH)_2]$	**5a**	70−150	8.62	(8.92)	187−515	63.68	(63.20)
	5b	45−145	8.52	190−531	63.69		
$[Mo_2O_4(C_{18}H_{16}NO_6)_2\{(CH_3)_2CHOH\}_2]$	**6a**	50−137	10.89	(11.33)	186−515	60.94	(61.53)
	6b	48−138	10.79	188−532	61.82		
$[Mo_2O_4(C_{22}H_{18}NO_6)_2(CH_3OH)_2]$	**7a**	60−151	5.23	(5.80)	169−510	67.74	(68.15)
	7b	83−149	5.39	193−529	68.60		
$[Mo_2O_4(C_{22}H_{18}NO_6)_2(CH_3CH_2OH)_2]$	**8a**	50−142	7.58	(8.13)	167−508	66.89	(66.46)
	8b*	95-158	7.28	189−528	67.23		
$[Mo_2O_4(C_{22}H_{18}NO_6)_2\{(CH_3)_2CHOH)\}_2]\cdot 2(CH_3)_2CHOH$	**9a**	50−153	18.31	(14.77)	170−506	58.94	(58.77)
$[Mo_2O_4(C_{22}H_{18}NO_6)_2\{(CH_3)_2CHOH)\}_2]$	**9b**	114−174	9.63	(10.35)	190−528	63.06	(62.52)

[a] According to the X-ray structure analysis, complex (**4a**) is solvated with two methanol molecules, while (**8b**) is solvated with two dichloromethane molecules. The crystals were readily loosing solvent at room temperature, so that they were left in a desiccator until constant weight, and analyzed as unsolvated species.

Table 3. ^1H and ^{13}C NMR chemical shifts (ppm) of the compounds $[Mo_2O_4(C_{16}H_{20}NO_6)_2(CH_3OH)_2]$ (**1a**), $[Mo_2O_4(C_{18}H_{16}NO_6)_2(CH_3OH)_2]$ (**4a**), $[Mo_2O_4(C_{22}H_{18}NO_6)_2(CH_3OH)_2]$ (**7a**), and $[Mo_2O_4(C_{22}H_{18}NO_6)_2(CH_3OH)_2]$ (**7b**).

Compound	**1a**		**4a**		**7a**		**7b**	
atom	^1H	^{13}C	^1H	^{13}C	^1H	^{13}C	^1H	^{13}C
1	1.97	20.49	2.28	21.30	1.86	21.71	2.11	19.61
2		161.81		160.36				162.06
3		102.10		106.47		102.11		99.53
4		179.41		176.02		179.86		181.93
5	6.94	114.07	6.37	111.10	6.27	113.91	5.38	107.25
6		148.38		150.12		148.16		163.25
7		180.22		179.52		183.49		187.23
8	6.45	96.11	6.89	99.10	6.46	98.33	6.70	99.53
9		168.69		171.12		167.38		153.07
10		160.37		159.26		160.89		165.28
11	4.39	62.70	4.39	63.12	4.47	62.68	3.96	62.04
12	1.38	14.27	1.39	14.30	1.48	14.51	0.78	13.65
13	3.16, 2.81	44.96		137.26		134.83		136.61
14	1.53, 1.43	31.76	7.21	125.60	7.33	125.70	7.05	122.15
15	1.14, 1.04	20.64	7.39	130.56	7.63		7.28	125.76
16	0.81	13.96	7.31	128.61	7.33	125.95	7.66	126.80
17			7.39	130.56		134.38		134.29
18			7.21	125.60	7.73	128.41	7.83	127.75
19					7.51	127.10	7.53	126.94
20					7.60	128.51	7.61	127.00
21					8.19	125.27	8.42	124.91
22						130.04		128.46
NH	9.98		12.21		11.58		10.48	

$[D_6]$acetone owing to its very low solubility in this solvent. In order to increase the solubility we added small amounts of DMSO, but the complex underwent rapid decomposition.

The chemical shift values listed in Table 3 are similar to those reported recently for related systems including molybdenum complexes.[13−16] Both proton and carbon chemical shifts are in the range expected for molybdenum complexes with ligands **a** and **b** [14,15] (Scheme 2). In that respect, the coordination-induced chemical shifts are the most pronounced for C-7 (up to 6 ppm), i.e. for one interacting site rather than for the other one, C-4.[14,15] The effects at C-7 atom are all upfield, as previously reported for related complexes.[16] The changes in chemical shifts for other car-

bon atoms are smaller and exhibit sign alternation as a consequence of the electron redistribution upon complexation with molybdenum.

All NMR spectroscopic data indicate that the ligand is in its enaminonic rather than iminoenolic form, which is in perfect agreement with the crystal structure determinations. The absence of hydroxyl proton resonances in the ^1H spectra confirms the complex formation. The marked downfield shifts of the NH protons ranging from 9.98 ppm up to 12.21 ppm (Table 3) are characteristic of strong hydrogen bonding in solution, as was found in the solid state.[11] The largest shift was observed for **4a**, indicating the strongest N−H···O bond in solution.

X-ray Analysis

Crystal structure determination was carried out for the nonsolvated compound $[Mo_2O_4(C_{16}H_{20}O_6N)_2(CH_3OH)_2]$, (**1a**), and for three solvated complexes $[Mo_2O_4(C_{18}H_{16}O_6N)_2(CH_3OH)_2]\cdot 2CH_3OH$ (**4a**), $[Mo_2O_4(C_{22}H_{18}O_6N)_2(CH_3CH_2OH)_2]\cdot 2CH_2Cl_2$ (**8b**), and $[Mo_2O_4(C_{22}H_{18}NO_6)_2\{(CH_3)_2CHOH)\}_2]\cdot 2(CH_3)_2CHOH$ (**9a**).

Selected interatomic distances and angles for complexes **1a**, **4a**, **8b**, and **9a** are given in Table 4−7, respectively. All four complex molecules contain the $[Mo_2O_4]^{2+}$ core, which displays a crystallographic twofold symmetry in **1a** and **9a** (Figure 1 and 4) but not in **4a** and **8b** (Figure 2 and 3). The Mo−Mo distances, ranging from 2.5319(6) Å in **9a** to 2.5561(5) Å in **4a**, correspond to a single bond between two molybdenum atoms, a result in agreement with the NMR spectroscopic data.[19,20] The molybdenum−to−molybdenum bonds established by structure analyses were confirmed by magnetic measurements.

Table 4. Selected interatomic distances (Å) and angles (°) for **1a**. Symmetry transformations used to generate equivalent atoms: *i* = $-x + 1, y, -z + 3/2$; *ii* = $-x + 1, -y, -z + 1$.

Mo1−Mo1^{i}	2.5341(6)			
Mo1−O7	1.688(1)	N1−C9	1.317(2)	
Mo1−O8	1.921(1)	N1−C13	1.463(2)	
Mo1−O8^{i}	1.934(1)			
Mo1−O3	2.086(1)	C1−C9	1.501(2)	
Mo1−O4	2.138(1)	C2−C3	1.451(2)	
Mo1−O9	2.212(1)	C3−C4	1.411(2)	
		C3−C7	1.471(2)	
O1−C6	1.349(2)	C4−C5	1.446(2)	
O1−C2	1.409(2)	C5−C6	1.332(2)	
O2−C2	1.207(2)	C6−C10	1.493(2)	
O3−C4	1.280(1)	C7−C8	1.400(2)	
O4−C7	1.293(1)	C8−C9	1.413(2)	
O5−C10	1.321(2)			
O5−C11	1.466(2)			
O6−C10	1.210(2)			
O9−C17	1.376(2)			
Hydrogen bonding				
D−H···A	*d*(D−H)	*d*(H···A)	*d*(D···A)	<(DHA)
O9−H1···O6^{ii}	0.90	1.91	2.784(2)	160
N1−H2···O4	0.86	1.95	2.611(1)	133

Table 5. Selected interatomic distances (Å) and angles (°) for **4a**. Symmetry transformations used to generate equivalent atoms: *i* = $x + 1/2, -y + 3/2, z$; *ii* = $x - 1/2, -y + 1/2, z$; *iii* = $x, y - 1, z$; *iv* = $-x, -y + 1, z + 1/2$.

Mo1−Mo2	2.5561(5)			
Mo1−O17	1.679(2)	Mo2−O27	1.685(2)	
Mo1−O18	1.929(2)	Mo2−O18	1.934(2)	
Mo1−O28	1.946(2)	Mo2−O28	1.926(2)	
Mo1−O13	2.096(2)	Mo2−O23	2.105(2)	
Mo1−O14	2.145(2)	Mo2−O24	2.155(2)	
Mo1−O19	2.191(2)	Mo2−O29	2.174(2)	
O11−C106	1.350(4)	O21−C206	1.340(4)	
O11−C102	1.398(3)	O21−C202	1.381(3)	
O12−C102	1.217(3)	O22−C202	1.229(3)	
O13−C104	1.292(3)	O23−C204	1.272(3)	
O14−C107	1.297(2)	O24−C207	1.292(2)	
O15−C110	1.329(4)	O25−C210	1.319(4)	
O15−C111	1.469(4)	O25−C211	1.460(4)	
O16−C110	1.198(4)	O26−C210	1.217(4)	
O19−C119	1.404(4)	O29−C219	1.411(5)	
N1−C109	1.338(3)	N2−C209	1.332(3)	
N1−C113	1.421(3)	N2−C213	1.421(3)	
C101−C109	1.492(4)	C201−C209	1.499(4)	
C102−C103	1.436(3)	C202−C203	1.437(3)	
C103−C104	1.403(3)	C203−C204	1.414(3)	
C103−C107	1.473(3)	C203−C207	1.466(3)	
C104−C105	1.445(3)	C204−C205	1.443(4)	
C105−C106	1.334(4)	C205−C206	1.327(4)	
C106−C110	1.499(4)	C206−C210	1.501(4)	
C107−C108	1.398(3)	C207−C208	1.398(3)	
C108−C109	1.402(3)	C208−C209	1.405(3)	
Hydrogen bonding				
D−H···A	*d*(D−H)	*d*(H···A)	*d*(D···A)	<(DHA)
O19−H11···O22^{i}	0.93	1.76	2.673(3)	168
N1−H12···O14	0.86	1.94	2.618(3)	134
O29−H21···O1^{ii}	0.92	1.84	2.537(3)	130
N2−H22···O24	0.86	1.95	2.629(3)	135
O1−H4···O12^{iii}	0.82	1.86	2.675(3)	170
O2−H8···O18^{iv}	0.82	1.89	2.696(6)	168

Each molybdenum atom is in a distorted octahedral coordination, being bonded to one terminal and two bridging oxygen atoms, two oxygens from the bidentate ligand and one from the coordinated alcohol molecule. The shortest bond lengths with the terminal oxo−O, ranging from 1.679(2) Å in **4a** to 1.688(1) Å in **1a**, agree well with the value considered as Mo=O_t double bond.[21] Mo−O_b distances range from 1.914(2) Å in **8b** to 1.946(2) Å in **4a**. Two oxygen atoms from the bidentate ligand molecules are bonded at distances ranging from 2.073(3) to 2.105(2) Å (Mo−O3), and at 2.1380(10) to 2.1893(12) Å (Mo−O4). The Mo−$O_{alcohol}$ bond lengths range from 2.182(3) to 2.242(3) Å (both values observed in **8b**). In all four complexes, the characteristic bond lengths C8=C9, ranging from 1.365(5) to 1.413(2) Å, and C9−N1, from 1.317(2) to 1.344(5) Å, are indicative of the enamine C=C−N−H form of the ligand.

According to the values of the C−N−C13−C14 torsion angle: −165.3(1)° (**1a**), 50.1(4) and 55.0(4)° (**4a**), 41.8(5) and 45.7(6)° (**8b**), and 47.8(3)° (**9a**), the N-substituents have significant flexibility around the single N−C bonds. More-

over, in **4a** the ethyl groups adopt different conformations, with the torsion angles C110−O15−C111−C112 of −82.3(4)° and C210−O25−C211−C212 of 156.3(4)°.

Table 6. Selected interatomic distances (Å) and angles (°) for **8b**. Symmetry transformations used to generate equivalent atoms: *i* = −*x* + 2,−*y* + 1,−*z*; *ii* = −*x* + 2,−*y* + 1,−*z* + 1.

Mo1−Mo2	2.5438(7)		
Mo1−O17	1.684(3)	Mo2−O27	1.682(2)
Mo1−O18	1.914(2)	Mo2−O18	1.934(3)
Mo1−O28	1.934(2)	Mo2−O28	1.920(2)
Mo1−O13	2.086(3)	Mo2−O23	2.073(3)
Mo1−O19	2.182(3)	Mo2−O24	2.147(2)
Mo1−O14	2.185(2)	Mo2−O29	2.242(3)
O11−C106	1.361(5)	O21−C206	1.367(4)
O11−C102	1.379(4)	O21−C202	1.380(4)
O12−C102	1.220(4)	O22−C202	1.229(4)
O13−C104	1.283(4)	O23−C204	1.283(4)
O14−C107	1.283(4)	O24−C207	1.297(4)
O15−C110	1.325(5)	O25−C210	1.336(5)
O15−C111	1.474(5)	O25−C211	1.468(5)
O16−C110	1.201(5)	O26−C210	1.193(4)
O19−C123	1.447(5)	O29−C223	1.509(6)
N1−C109	1.342(4)	N2−C209	1.344(5)
N1−C113	1.419(4)	N2−C213	1.418(5)
C101−C106	1.492(5)	C201−C206	1.479(5)
C102−C103	1.442(5)	C202−C203	1.431(5)
C103−C104	1.418(5)	C203−C204	1.428(5)
C103−C107	1.456(5)	C203−C207	1.437(5)
C104−C105	1.435(5)	C204−C205	1.435(5)
C105−C106	1.324(6)	C205−C206	1.332(5)
C107−C108	1.418(5)	C207−C208	1.419(5)
C108−C109	1.373(5)	C208−C209	1.365(5)
C109−C110	1.521(5)	C209−C210	1.508(5)

Hydrogen bonding				
D−H···A	d(D−H)	d(H···A)	d(D···A)	<(DHA)
O19−H11···O12^{i}	0.91	1.69	2.596(3)	177
N1−H12···O14	0.86	2.05	2.663(4)	128
O29−H21···O22^{ii}	0.94	1.76	2.673(4)	165
N2−H22···O24	0.86	2.02	2.633(4)	127

Table 7. Selected interatomic distances (Å) and angles (°) for **9a**. Symmetry transformations used to generate equivalent atoms: *i* = −*x*,*y*,−*z* + 1/2; *ii* = −*x*,−*y* + 2,−*z*.

Mo1−Mo1^{i}	2.5319(6)		
Mo1−O7	1.681(1)	N1−C9	1.337(2)
Mo1−O8	1.922(1)	N1−C13	1.427(2)
Mo1−O8^{i}	1.931(1)		
Mo1−O3	2.086(1)	C1−C9	1.507(2)
Mo1−O9	2.184(1)	C2−C3	1.451(2)
Mo1−O4	2.189(1)	C3−C4	1.413(2)
		C3−C7	1.466(2)
O1−C6	1.353(2)	C4−C5	1.448(2)
O1−C2	1.408(2)	C5−C6	1.326(2)
O2−C2	1.206(2)	C6−C10	1.488(2)
O3−C4	1.278(2)	C7−C8	1.411(2)
O4−C7	1.294(2)	C8−C9	1.386(2)
O5−C10	1.327(2)		
O5−C11	1.458(2)		
O6−C10	1.203(2)		
O9−C23	1.447(2)		

Hydrogen bonding				
D−H···A	*d*(D−H)	*d*(H···A)	*d*(D···A)	<(DHA)
O9−H1···O10	0.87	1.78	2.640(2)	172
N1−H2···O4	0.86	2.03	2.680(2)	131
O10−H27···O6^{ii}	0.82	2.00	2.765(2)	155

Owing to the strong N−H···O intramolecular hydrogen bonds, reinforced with π-delocalization along the heterodienic O=C−C=C−NH moiety [*d*(N···O) from 2.611(1) to 2.680(2) Å, *d*(H···O) from 1.95 to 2.05 Å], in all four structures, the enaminonic fragments adopt the form of a six-membered ring.[10,11] As seen from Table 4−7, all complex molecules in the crystal structures are interconnected as chains (along the *c*-axis in **1a**, **8b**, and **9a**, and along the *a*-axis in **4a**) realized through hydrogen bonds. These hydrogen bonds are formed between the coordinated methanol molecule and the carboxylato-oxygen [O9−H1···O6^{ii} of 2.784(2) Å] in **1a**, between ethanol and the keto-oxygens of 2-pyrone [O19−H11···O12^{i} of 2.596(3)

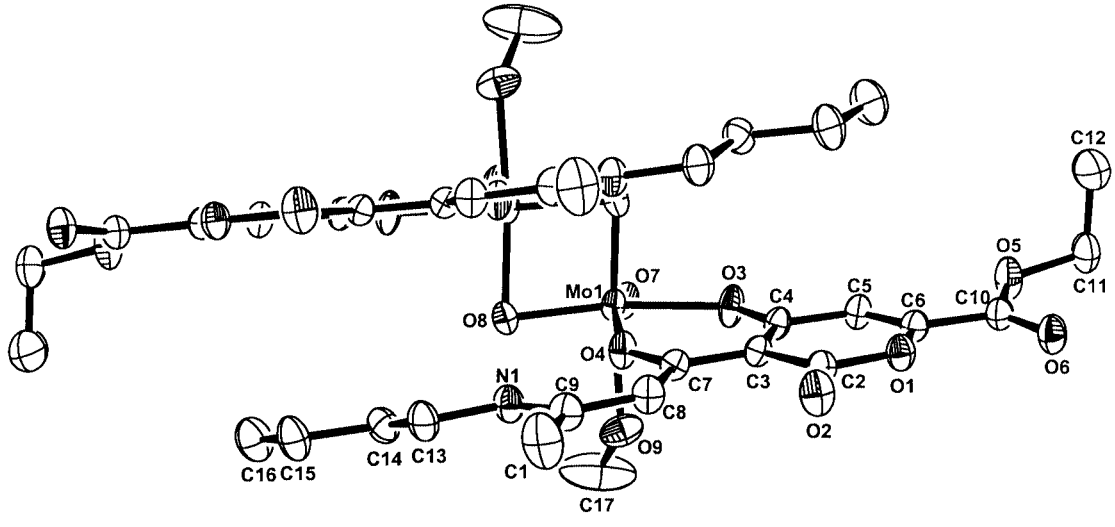

Figure 1. An ORTEP view of the dinuclear complex $[Mo_2O_4(C_{16}H_{20}NO_6)_2(CH_3OH)_2]$ in **1a** (hydrogen atoms are omitted for clarity). Ellipsoids are shown at the 50% probability level.

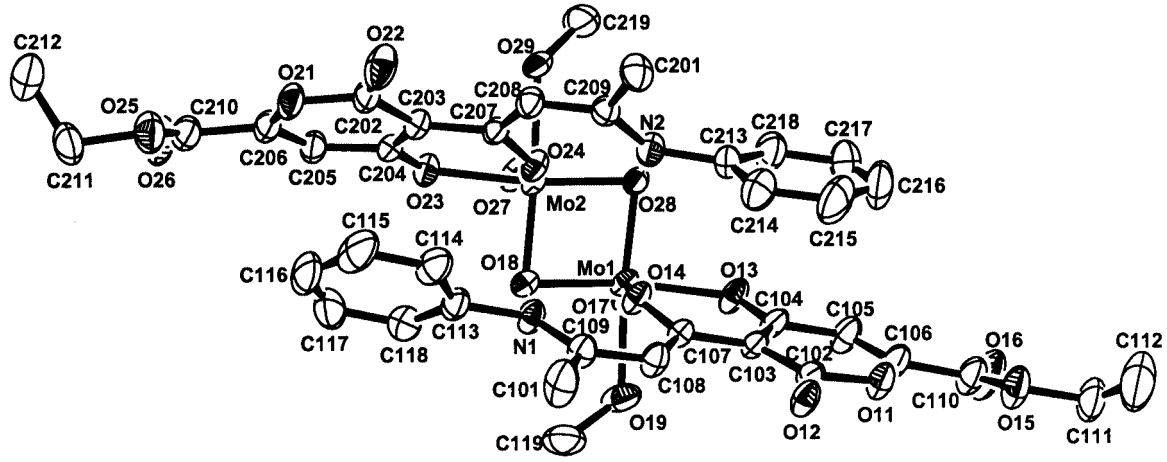

Figure 2. An ORTEP view of the dinuclear complex $[Mo_2O_4(C_{18}H_{16}NO_6)_2(CH_3OH)_2]$ in **4a** (hydrogen atoms are omitted for clarity). Ellipsoids are shown at the 50% probability level.

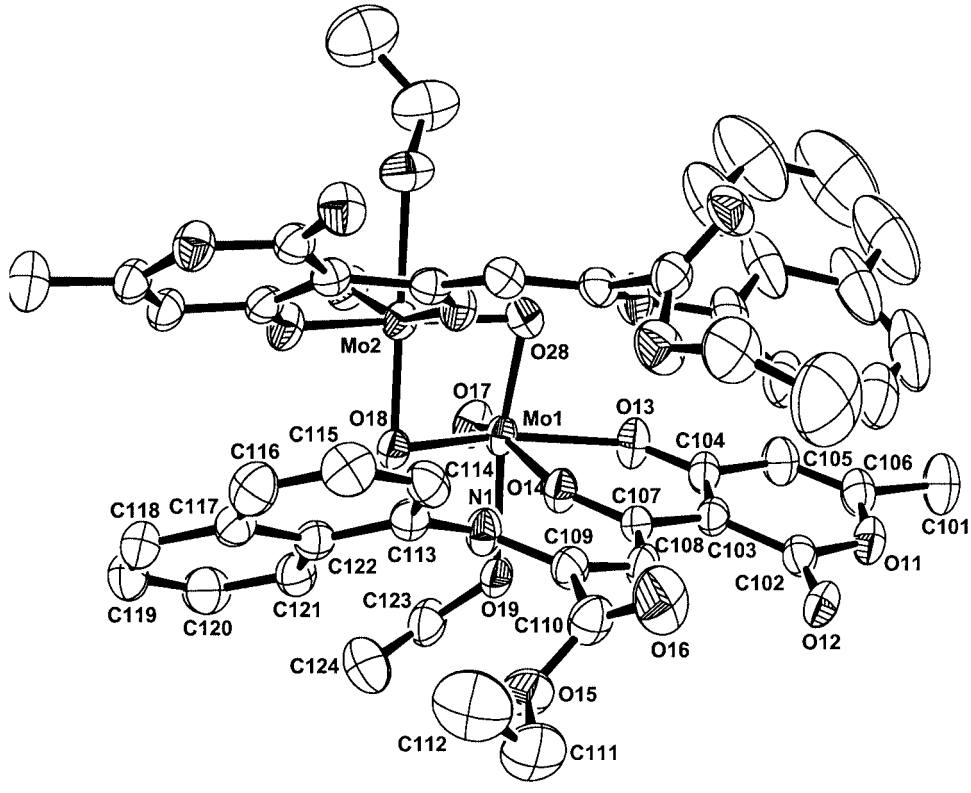

Figure 3. An ORTEP view of the dinuclear complex $[Mo_2O_4(C_{22}H_{18}NO_6)_2(CH_3CH_2OH)_2]$ in **8b**. Hydrogen atoms as well as the analogous labelling of upper part of the molecule are omitted for clarity. Ellipsoids are shown at the 50% probability level.

and O29−H21···O22^{ii} of 2.673(4) Å] in **8b**, and between methanol and the keto-oxygens [O19−H11···O22^{i} of 2.673(3) Å] in **4a**. The molecules in **4a** are further connected through solvent methanol molecule, acting as a proton donor when bonded to the keto group of the pyrone ring [O1−H4···O12^{iii} of 2.675(3) Å], and as a proton acceptor in a bond with coordinated methanol molecule [O29−H21···O1^{ii} of 2.537(3) Å]. In **9a** the complex molecules are interconnected through solvated 2-propanol molecules. Hydrogen bridges are formed between coordinated and solvated 2-propanol molecules [O9−H1···O10 of 2.640(2) Å], and between solvated 2-propanol molecule and ligand carboxylato-oxygen [O10−H27···O6^{ii} of 2.765(2) Å]. Observed values of O−H···O angles and H···O distances, ranging from 1.69 to 2.00 Å, are in the accordance with a proposed hydrogen bonding scheme. The crystal structures

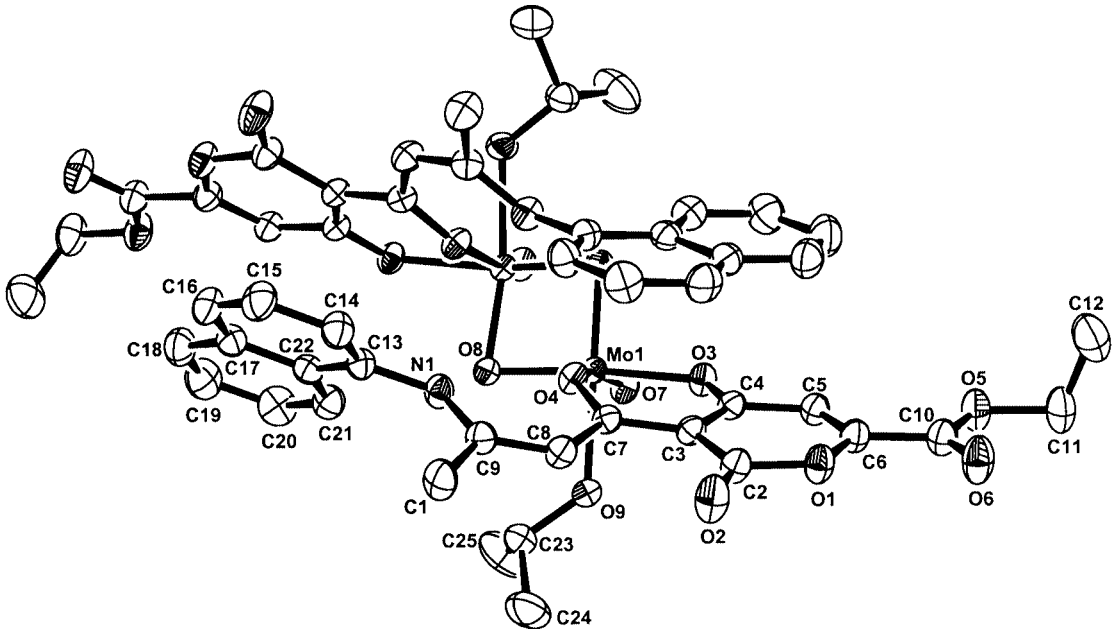

Figure 4. An ORTEP view of the $[Mo_2O_4(C_{22}H_{18}NO_6)_2\{(CH_3)_2CHOH)\}_2]$ dinuclear complex in **9a** (hydrogen atoms are omitted for clarity). Ellipsoids are shown at the 50% probability level.

of all compounds are additionally stabilized by C−H···O weak hydrogen bonds in the range from 2.745(2) to 3.358(5) Å.

Experimental Section

General: All chemicals and solvents were of reagent grade and used as purchased. The starting acetylacetonato complex $[Mo_2O_3(acac)_4]$ was prepared as described in the literature.[22,23] Ethyl 2-hydroxy-4-(4-hydroxy-6-methyl-2*H*-pyran-2-on-3-yl)-4-oxo-2-butenoate and isomeric enaminones (Scheme 2) were prepared according to previously described procedures.[13−16] Elemental analyses for C, H and N were provided by the Analytical Services Laboratory of Rudjer Bošković Institute, Zagreb. Molybdenum was determined using the usual procedure.[24] Infrared spectra were recorded in KBr with an FTIR 1600 Fourier transform spectrophotometer in the 4500−450 cm^{-1} region. Thermogravimetric (TG) analyses were measured on a Mettler TG 50 thermobalance using aluminum crucibles under oxygen atmosphere with a heating rate of 5 °C min^{-1}. For all experiments the temperature ranged from 30 to 600 °C. The results were developed by applying the GrafVare 2.1. program.

General Procedures for the Synthesis of Complexes

$[Mo_2O_3(acac)_4]$ (0.25 g, 0.4 mmol) was suspended in dry dichloromethane (25 mL) and appropriate ligand (0.4 mmol) was added. The mixture was gently warmed up for 0.5 h, the solution was filtered off, and corresponding alcohol (30 mL) added to the filtrate. Upon standing at room temperature for 5−10 days the obtained crystalline product was filtered off, washed with cold alcohol and dried. All complexes were orange-red crystalline solids very soluble in coordinating solvents such as DMF, DMSO, picoline, and pyridine, slightly soluble in dichloromethane, acetone, methanol, and ethanol. Elemental analyses, yields (based on $[Mo_2O_3(acac)_4]$) and selected IR data are given in Table 1. Thermal analysis data are given in Table 2. Since the crystals were easily loosing alcohol solvent, all analyses (elemental analyses, thermal analyses, IR, and NMR spectroscopy) were carried out with the samples left in a desiccator until constant weight.

NMR Spectra

NMR experiments were carried out on a Bruker Avance DRX500 spectrometer operating at 500.13 MHz for ^1H, with a 5 mm diameter inverse detection probe and a z-axis gradient coil. The solvent was $[D_6]$acetone and all experiments were performed at ambient temperature. TMS was used as the internal standard.

^1H NMR experiments were executed with a spectral width of 12500 Hz, 65 K data points and 8−32 scans. The sample concentration was 10−15 $mg.ml^{-1}$. The digital resolution was 0.2 Hz per point. In ^{13}C NMR spectra the spectral width was 31400 Hz, the number of data points 65 K, and the number of scans 2500−3000 per spectrum. The digital resolution was 0.5 Hz per point.

Two-dimensional absolute-value COSY spectra were recorded under the following conditions. Spectral width was 6600 Hz in both domains, 2 K data points were applied in time domain and 512 increments were collected for each data set with linear prediction and zero filling to 2 K. The relaxation delay was 1.5 s. Spectra were rocessed with sine or sine squared window functions. The digital resolution was 3.3 Hz per point in both f1 and f2 domains. The number of scans was 8.

Phase sensitive HSQC and absolute value HMBC spectra were recorded with a relaxation delay of 1.5 s and 32 scans per increment. The spectral width was 6600 Hz in acquisition domain f2 and 31000 Hz in time domain f1. Data were collected into 2048 × 256 acquisition matrix and processed by using a 2 K × 1 K transformed matrix with zero filling in f1 domain. Sine multiplication was performed prior to Fourier transformations. In HMBC spectra the delay for long range couplings was set to 60 ms.

Table 8. General and crystal data and summary of intensity data collection and structure refinement.

Compound	**1a**	**4a**	**8b**	**9a**
Formula	$C_{34}H_{48}Mo_2N_2O_{18}$	$C_{40}H_{48}Mo_2N_2O_{20}$	$C_{50}H_{52}Cl_4Mo_2N_2O_{18}$	$C_{56}H_{68}Mo_2N_2O_{20}$
M_r	964.62	1068.68	1302.62	1281.00
Crystal system and habit	Monoclinic, prism	Orthorhombic, prism	Triclinic, prism	Monoclinic, prism
Space group	$C2/c$	$Pna2_1$	$P\bar{1}$	$C2/c$
a [Å]	11.943(2)	21.252(4)	12.364(2)	20.352(4)
b [Å]	15.650(3)	9.623(2)	12.510(3)	10.184(2)
c [Å]	21.552(4)	21.524(4)	18.635(4)	28.548(6)
α [°]	90	90	89.60(3)	90
β [°]	99.26(3)	90	72.99(3)	98.20(3)
γ [°]	90	90	88.91(3)	90
Volume [Å^3]	3975.7(13)	4401.8(15)	2755.8(10)	5857(2)
Z	4	4	2	4
Density (calcd.) [gcm^{-3}]	1.612	1.613	1.570	1.453
μ (Mo-K_α) [mm^{-1}]	0.709	0.652	0.722	0.504
F(000)	1976	2184	1324	2648
2θ range for data collection [°]	5.4−66.3	4.2−66.2	4.6−52.6	4.6−66.2
h,k,l range	−18/18, −24/+23, −32/+33	−32/32, −14/14, −33/+33	−15/15, −15/15, −23/23	−31/30, −15/+12, −37/+40
Scan type	2° and ω scans	2° and ω scans	2° and ω scans	2° and ω scans
No. measured reflections	14098	16777	20231	15962
No. independent reflections	7490	16126	11114	10127
No. refined parameters	258	583	685	369
No. observed reflections, [$I \geq 2\sigma(I)$]]	6575	13397	9003	8047
g_1, g_2 in w[a]	0.0288, 3.20	0.0427, 1.68	0.0615, 4.27	0.0296, 7.01
R[b], wR[c] [$I \geq 2\sigma(I)$]	0.0247, 0.0623	0.0359, 0.0812	0.0459, 0.1166	0.0348, 0.0769
R, wR [all data]	0.0305, 0.0660	0.0502, 0.0877	0.0602, 0.1257	0.0508, 0.0838
Goodness-of-fit on F^2, S[d]	1.030	1.025	1.011	1.012
Max., min. electron density [e Å^{-3}][e]	0.889, − 0.518	0.658, − 0.499	1.297, − 1.083	0.818, −0.744
Extinction coefficients	0.0014(2)	0.0005(1)		0.00025(8)
Maximum Δ/σ	0.006	0.006	0.001	0.001

[a] According to the X-ray structure analysis, complex **4a** is solvated with two methanol molecules, while **8b** is solvated with two dichloromethane molecules. The crystals were readily loosing solvent at room temperature, so that they were left in a desiccator until constant weight, and analyzed as unsolvated species. [b] $w = 1/[\sigma^2(F_o^2) + (g_1P)^2 + g_2P]$ where $P = (F_o^2 + 2F_c^2)/3$. [c] $R = \Sigma||F_o| - |F_c||/\Sigma|F_o|$. [d] $wR = [\Sigma[w(F_o^2 - F_c^2)^2]/\Sigma[w(F_o^2)^2]]^{1/2}$. [e] $S = [\Sigma[w(F_o^2 - F_c^2)^2]/(N_{obs} - N_{param})]^{1/2}$.

X-ray Crystallography

Single crystals of the complexes **1a**, **4a**, **8b**, and **9a** were grown by slow evaporation of solutions obtained from the above described preparations. The crystals so obtained were, however, unstable as they rapidly lost solvent and decomposed. Intensity data for all four structures were collected at 200 K on a Nonius−Kappa CCD diffractometer with graphite-monochromated Mo-K_α radiation (λ = 0.7107 Å), at crystal to detector distance of 28 mm and 50 s exposure time per frame. Data were reduced using DENZO program.[25]

Crystal data, experimental conditions, details of structure determination and final refinement parameters are summarized in Table 8.

Molybdenum atoms in all structures were located by the Patterson method. The remaining non-hydrogen atoms were found in subsequent difference Fourier maps. Refinements in which all non-hydrogen atoms were treated anisotropically were performed by the full-matrix least-squares method based on the F^2 values against all reflections. The last Fourier maps revealed positions of all H atoms but some with poor geometry. Therefore all hydrogen atoms attached to carbon and nitrogen atoms were generated on geometrical grounds. The hydrogen atoms bound to the oxygen atoms of coordinated alcohol molecules were kept fixed during the refinement.

Structure **4a** was refined in noncentrosymmetric space group $Pna2_1$. However, the value of the refined Flack parameter of 0.50(2) is indicative of a racemic twinning.

All calculations were performed on an IBM THINKPAD microcomputer (Pentium II processor, 300 MHz) using SHELXS-97[26] and SHELXL-97[27] programs, and ORTEP[28] to draw the structural diagrams.

CCDC-174217 (**1a**), -174218 (**4a**), -174219 (**8b**) and -174220 (**9a**) contain the supplementary crystallographic data for this paper. These data can be obtained free of charge at www.ccdc.cam.ac.uk/conts/retrieving.html [or from the Cambridge Crystallographic Data Centre, 12, Union Road, Cambridge CB2 1EZ, UK; Fax: (internat.) +44-1223/336-033; E-mail: deposit@ccdc.cam.ac.uk].

Acknowledgments

This research was supported by the Ministry of Science and Technology of the Republic of Croatia (Grant No. 119407).

[1] J.-C. G. Bünzli, *Inorg. Chim. Acta* **1987**, *139*, 219−222.
[2] S. J. Lord, N. A. Epstein, R. L. Paddock, C. M. Vogels, T. L. Hennigar, M. J. Zaworotko, N. J. Taylor, W. R. Driedzic, T. L. Broderick, S. A. Westcott, *Can. J. Chem.* **1999**, *77*, 1249−1261.

[3] C. Bisi Castellani, O. Carugo, *Inorg. Chim. Acta* **1989**, *159*, 157−161.
[4] C. Bisi Castellani, O. Carugo, C. Tomba, A. Invernizzi Gamba, *Inorg. Chem.* **1988**, *27*, 3965−3969.
[5] A. Wlodawer, J. W. Erickson, *Annu. Rev. Biochem.* **1993**, *62*, 543−585.
[6] S. Thaisrivongs, D. L. Romero, R. A. Tommasi, M. N. Janakiraman, J. W. Strohbach, S. R. Turner, C. Biles, R. R. Morge, P. D. Johnson, P. A. Aristoff, P. K. Tomich, J. C. Lynn, M. M. Horng, K. T. Chong, R. R. Hinshaw, W. J. Howe, B. C. Finzel, K. D. Watenpaugh, *J. Med. Chem.* **1996**, *39*, 4630−4642.
[7] H. Luo, S. Liu, S. J. Rettig, C. Orvig, *Can. J. Chem.* **1995**, *73*, 2272−2281.
[8] J. Casabó, J. Marquet, M. Moreno-Mañas, M. Prior, F. Teixidor, F. Florencio, S. Martínez-Carrera, S. García-Blanco, *Polyhedron* **1987**, *6*, 1235−1238.
[9] O. Carugo, C. Bisi Castellani, M. Rizzi, *Polyhedron* **1990**, *9*, 2061−2069.
[10] G. Gilli, V. Bertolasi, V. Ferretti, P. Gilli, *Acta Crystallogr., Sect. B* **1993**, *49*, 564−576.
[11] P. Gilli, V. Bertolasi, V. Ferretti, G. Gilli, *J. Am. Chem. Soc.* **2000**, *122*, 10405−10417.
[12] V. Drevenkar, Z. Stefanac, A. Brbot, *Microchem. J.* **1976**, *21*, 402−410.
[13] A. Brbot-Šaranović, B. Katušin-Ra|158em, I. Sušnik, *Heterocycles* **1989**, *29*, 1559−1571.
[14] A. Brbot-Šaranović, G. Pavlović, M. Cindrić, *Struct. Chem.* **2000**, *11*, 65−76.
[15] A. Brbot-Šaranović, G. Pavlović, V. Vrdoljak, M. Cindrić, *Croat. Chem. Acta* **2001**, *74*, 441−454.
[16] M. Cindrić, V. Vrdoljak, T. Kajfež, P. Novak, A. Brbot-Šaranović, N. Strukan, B. Kamenar, *Inorg. Chim. Acta*, **2002**, *328*, 23−32.
[17] B. Kamenar, B. Korpar Čolig, M. Penavić, M. Cindrić, *J. Chem. Soc., Dalton Trans.* **1990**, 1125−1130.
[18] E. McCarron III, J. F. Whitney, D. B. Chase, *Inorg. Chem.* **1984**, *23*, 3275−3280.
[19] F. A. Cotton, *Inorg. Chem.* **1965**, *4*, 334−336.
[20] F. A. Cotton, *J. Less-Common Met.* **1977**, *54*, 3−12.
[21] F. A. Schröeder, *Acta Crystallogr., Sect. B* **1975**, *31*, 2294−2309.
[22] B. Kamenar, B. Korpar-Čolig, M. Cindrić, D. Matković-Čalogović, M. Penavić, *Bull. Chem. Technol. Macedonia* **1997**, *16*, 33−37.
[23] F. W. Moore, R. E. Rice, *Inorg. Chem.* **1968**, *7*, 2510−2514.
[24] G. A. Parker, Analytical Chemistry of Molybdenum, Springer-Verlag, New-York, **1983**.
[25] Z. Otwinowski, Proceedings of the CCP4 Study Weekend: Data Collection, Warington: Daresbury Laboratory, UK, **1993**.
[26] G. M. Sheldrick, *SHELXS-97, Program for the Solution of Crystal Structures*, University of Göttingen, Germany, **1997**.
[27] G. M. Sheldrick, *SHELXL-97, Program for the Refinement of Crystal Structures*, University of Göttingen, Germany, **1997**.
[28] C. K. Johnson, ORTEP-II, Rep. *ORNL-5138*, Oak Ridge National Laboratory, Oak Ridge, TN, **1976**.

Received November 29, 2001
[I01488]

Highly Soluble Sulfur-Rich [Ni(L)($^{si}S_3$)] Complexes Containing the New Ligand Bis(2-mercapto-3-trimethylsilylphenyl) Sulfide(2−) ($^{si}S_3{}^{2-}$)[‡]

Dieter Sellmann*,*[a] Raju Prakash,[a] Franz Geipel,[a] and Frank W. Heinemann[a]

Dedicated to Professor Joachim Strähle on the occasion of his 65th birthday

Keywords: Nickel / S ligands / Silicon / Hydrazine / Nicotinamide

The new organosulfur ligands $^{si}S_3$-H_2 [$^{si}S_3{}^{2-}$ = bis(2-mercapto-3-trimethylsilylphenyl) sulfide(2–)] and $^{ca}S_3$-H_2 [$^{ca}S_3{}^{2-}$ = bis(2-mercapto-3-carboxyphenyl) sulfide(2–)] were synthesized from $^{H}S_3$-H_2 [$^{H}S_3{}^{2-}$ = bis(2-mercaptophenyl) sulfide(2–)], *n*-butyllithium, and Me_3SiCl or CO_2/H^+. Reaction of $^{si}S_3$-H_2 with $Ni(ac)_2{\cdot}4H_2O$ gave the air-stable and well-soluble trinuclear complex [Ni($^{si}S_3$)]$_3$ (**1**) whose structure was determined by X-ray crystallography. Reactions of complex **1** with nucleophiles L [L = PR_3 (R = *n*Pr, Ph, Cy), N_2H_4, S*t*Bu$^-$, and Cl$^-$] yielded the corresponding neutral or anionic complexes, which were isolated as [Ni(PR_3)($^{si}S_3$)] [R = *n*Pr (**2**), Ph (**3**), Cy (**4**)], Bu_4N[Ni(Cl)($^{si}S_3$)] (**5**), Bu_4N-[Ni(S*t*Bu)($^{si}S_3$)] (**6**), and [Ni(N_2H_4)($^{si}S_3$)] (**8**). The azido complex Et_4N[Ni(N_3)($^{si}S_3$)] (**7**) was prepared from Me_3SiN_3 and the precursor chloro complex Et_4N[Ni(Cl)($^{si}S_3$)]. Reaction of **1** with NH_3 yielded labile [Ni(NH_3)($^{si}S_3$)] (**9**), which was characterized in solution by ^1H and ^{13}C NMR spectroscopy. Analogously, **1** reacts with nicotinamide (NA) or diethylnicotinamide ($NAEt_2$) to give, from equilibrium reactions, the corresponding mononuclear [Ni(L)($^{si}S_3$)] complexes with L = NA, $NAEt_2$. X-ray structure determinations showed that **1**, **3**, **4**, **5**, and **7** all exhibit tetrahedrally distorted planar [Ni(L)($^{si}S_3$)] fragments. Complex **7** is the first structurally characterized azidonickel complex with a coligand having exclusively sulfur donors.

(© Wiley-VCH Verlag GmbH, 69451 Weinheim, Germany, 2002)

Introduction

The discovery of nickel cysteinate units in the active centers of [NiFe] hydrogenases[1−3] and CO dehydrogenases[4] accounts for much of the current interest in nickel thiolate complexes. Numerous efforts have been made in order to find low molecular weight complexes that model the nickel cysteinate site and the reactivity of these enzymes.[5−10] In this context, we have recently found that [Ni(L)($^{H}S_3$)] complexes containing the [Ni($^{H}S_3$)] complex fragment[11−13] $^{H}S_3{}^{2-}$ = bis(2-mercaptophenyl) sulfide(2−) and L = $NHPnPr_3$ or $N(SiMe_3)_2{}^-$ as coligands exhibit reactions relevant to [NiFe] hydrogenases and CO dehydrogenases, e.g., catalysis of H_2/D_2O exchange[14] and deoxygenation of CO, CO_2, and SO_2.[15]

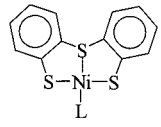

[Ni(L)($^{H}S_3$)]

The unique reactivity of these complexes could be traced back to the formation of [Ni(L′)(L)($^{H}S_3$)] intermediates (L′ = H_2, CO, CO_2, SO_2) exhibiting five-coordinate nickel centers. The heterolysis of H_2 catalyzed by [Ni($NHPnPr_3$)($^{H}S_3$)][14] prompted us to investigate the activation of H_2 by other [Ni(L)($^{H}S_3$)] complexes, and a particularly intriguing goal was to use H_2 for intramolecularly hydrogenating ligands which can exist in the hydro and dehydro form such as the nicotinamide/dihydronicotinamide couple (NA/NAH_2) [Equation (1)].

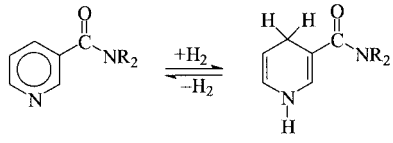

(1)

The prerequisite for corresponding experiments were [Ni(NA)($^{H}S_3$)] complexes. Although NA complexes are known

[‡] Transition Metal Complexes with Sulfur Ligands, 154. Part 153: D. Sellmann, F. Geipel, F. Lauderbach, F. W. Heinemann, *Angew. Chem.* **2002**, *114*, 654−656; Angew. Chem. Int. Ed. 2002, 41, 632−634.

[a] Institut für Anorganische Chemie der Universität Erlangen-Nürnberg,
Egerlandstrasse 1, 91058 Erlangen, Germany
Fax: (internat.) + 49-(0)9131/852-7367
E-mail: sellmann@anorganik.chemie.uni-erlangen.de

to exist,[16] they could not be obtained with [Ni($^{H}S_3$)] fragments. A major obstacle was the fact that [Ni(L)($^{H}S_3$)] complexes frequently are only very sparingly soluble in common organic solvents. A prime example is the trinuclear parent complex [Ni($^{H}S_3$)]$_3$ which is practically insoluble in all solvents. Due to this we have now tried to obtain better soluble derivatives by introducing $SiMe_3$ or CO_2H substituents into the $^{H}S_3$-H_2 ligand. This paper reports on the synthesis of two new ligands, and a series of nickel complexes with the $SiMe_3$ derivative $^{si}S_3^{2-}$ = bis(2-mercapto-3-trimethylsilylphenyl) sulfide(2−).

Results and Discussion

Synthesis of $SiMe_3$ and CO_2H Derivatives of $^{H}S_3$-H_2

The new ligands $^{si}S_3$-H_2 and $^{ca}S_3$-H_2, where "si" and "ca" denote $SiMe_3$ and CO_2H substituents in the *ortho* position to the SH functions, were obtained in one-pot reactions according to Scheme 1.

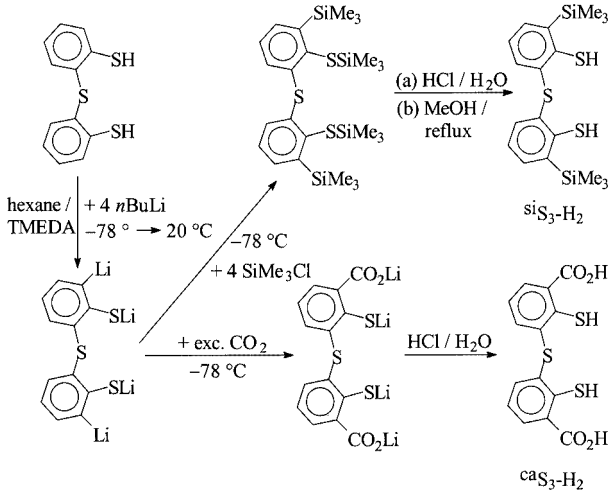

Scheme 1. Synthesis of $^{si}S_3$-H_2 and $^{ca}S_3$-H_2

The synthesis route made use of previous results obtained by other authors and us showing that aromatic sulfur compounds such as S(C_6H_5) can be lithiated with excess butyllithium.[17,11]

Treatment of $^{H}S_3$-H_2 with 4 equiv. of *n*BuLi in a hexane/TMEDA mixture (TMEDA = *N*,*N*′-tetramethylethylenediamine) yielded a white to yellow precipitate. This precipitate was not characterized in detail, and its structure, indicated in Scheme 1, was concluded only from subsequent reactions. Treatment of the heterogeneous mixture with 4 equiv. of $SiMe_3Cl$, acidification with hydrochloric acid, and extraction with Et_2O yielded a product in which the thiol functions of $^{si}S_3$-H_2 were still partially silylated by the $SiMe_3$ groups. These $SiMe_3$ groups were removed in boiling MeOH (yielding Me_3SiOMe_3) and the resultant $^{si}S_3$-H_2 was obtained as a brown viscous oil. It was identified by elemental analysis and spectroscopic methods, and could be used for synthesis of complexes without further purification.

In an analogous reaction, treatment of the heterogeneous mixture obtained from $^{H}S_3$-H_2 and butyllithium with gaseous CO_2 and subsequent acidification yielded $^{ca}S_3$-H_2. Upon recrystallization from acetone, it was obtained in green-yellow needles.

The ^{1}H NMR spectrum of $^{si}S_3$-H_2 exhibits three multiplets for the six aromatic protons, a broad singlet for the two thiols and a sharp singlet for the $SiMe_3$ protons. The ^{1}H NMR spectrum of $^{ca}S_3$-H_2 shows a similar pattern for the aromatic protons and broad peaks at δ = 7.28 and 11.85 ppm for the SH and CO_2H protons. It is worth noting that the SH proton shift is influenced by the benzene ring substituents and appears δ ≈ 4.5 ppm at lower field in $^{ca}S_3$-H_2 than in $^{si}S_3$-H_2. The number and shift of the ^{13}C resonances in the $^{13}C\{^1H\}$ NMR spectra of $^{si}S_3$-H_2 and $^{ca}S_3$-H_2 established that both of the ligands possess C_2 symmetry in solution.

Synthesis, Reaction, and Characterization of Complexes with [Ni($^{si}S_3$)] Fragments

The starting complex [Ni($^{si}S_3$)]$_3$ (**1**) was formed in a straightforward reaction from Ni(ac)$_2$·4H_2O and $^{si}S_3$-H_2 in THF/MeOH mixtures. A dark brown solution resulted from which **1** was obtained analytically pure and in high yield (87%). Complex **1** is stable towards air and moisture for extended periods of time and soluble in many common organic solvents, e.g., THF, CH_2Cl_2, acetone, Et_2O, toluene, hexane, MeCN, DMF, DMSO. In MeOH or pentane, **1** is sparingly soluble. Complex **1** fulfilled one of the expectations connected with the synthesis of $^{si}S_3$-H_2, showing good solubility in organic solvents in which the parent complex [Ni($^{H}S_3$)]$_3$ proved insoluble. The ^{1}H and $^{13}C\{^1H\}$ NMR spectra of **1** were compatible with the trinuclear structure indicated in Scheme 2. This structure was confirmed by a single-crystal X-ray structure determination.

Subsequent experiments were aimed at cleaving trinuclear [Ni($^{si}S_3$)]$_3$ and probing the coordination of σ and σ-π ligands to the [Ni($^{si}S_3$)] fragment. Scheme 2 summarizes the reactions of **1** yielding mononuclear [Ni(L)($^{si}S_3$)] complexes. Treatment of **1** with phosphanes gave [Ni(PR_3)($^{si}S_3$)] with R = *n*-Pr (**2**), Ph (**3**), and Cy (**4**). The reactions could be monitored by the practically instantaneous color change of the THF solution from red-brown to yellow-red or orange, and they took place much faster than the analogous reactions of the parent [Ni($^{H}S_3$)]$_3$ complex with the phosphanes. The phosphane derivatives **2**, **3**, and **4** proved inert with regard to substitution of the phosphane ligands.

Substitution-labile [Ni(L)($^{si}S_3$)] complexes were obtained with L = Cl^- and S*t*Bu$^-$. Treatment of **1** with an equimolar amount of Bu_4NCl yielded dark purple needles of Bu_4N[Ni(Cl)($^{si}S_3$)] (**5**). With Bu_4NS*t*Bu, brown microcrystals of Bu_4N[Ni(S*t*Bu)($^{si}S_3$)] (**6**) were obtained. The chloro derivative [Ni(Cl)($^{si}S_3$)]$^-$ enabled the synthesis of the azido complex, which was not accessible directly from **1**. For this purpose **1** was first treated with Et_4NCl to give Et_4N[Ni(Cl)($^{si}S_3$)] in situ. Subsequent addition of Me_3SiN_3 yielded Et_4N[Ni(N_3)($^{si}S_3$)] (**7**) which was isolated as violet needles. Complexes **5** and **7** demonstrated that typical σ-

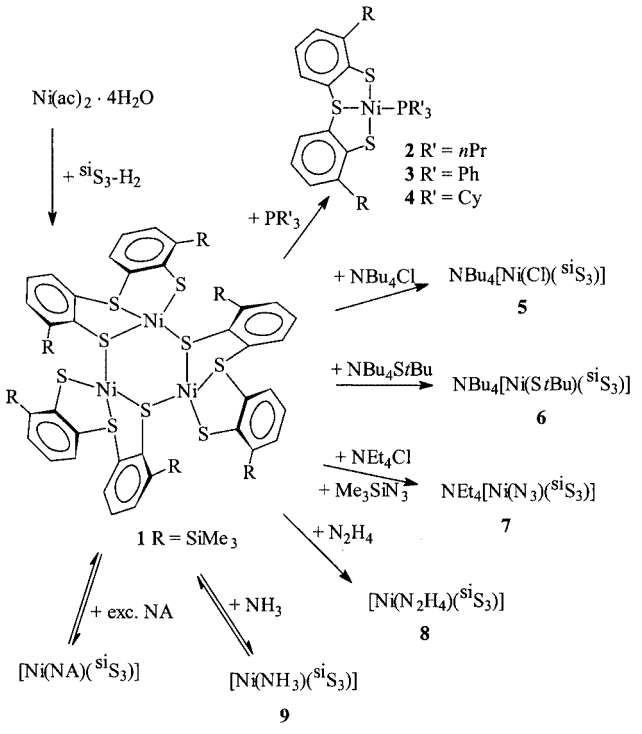

Scheme 2. Synthesis and reactions of $[Ni(^{si}S_3)]_3$ complexes

donor ligands can form stable adducts with $[Ni(^{si}S_3)]$ fragments. With hydrazine, **1** could directly be cleaved to give dark-red $[Ni(N_2H_4)(^{si}S_3)]$ (**8**). The analogous reaction with NH_3 yielded a very labile species that could be generated and characterized only in situ in an NMR tube. All attempts to isolate $[Ni(NH_3)(^{si}S_3)]$ in the solid state remained unsuccessful.

Hydride or CO derivatives of $[Ni(^{si}S_3)]$ could not be obtained. At high pressures of CO (100 bar), minor amounts of **1** were converted into $Ni(CO)_4$ in the course of 10 d. The resulting $Ni(CO)_4$ could be isolated by fractional condensation and was identified by its ν(CO) IR band at 2040 cm^{-1}.[10e]

All of the complexes **1**−**9** proved to be very soluble in THF, CH_2Cl_2, acetone, toluene, MeCN, DMF, and DMSO. As judged by their NMR spectra, they are diamagnetic. The ^1H NMR spectra of all mononuclear complexes **2**−**9** show a typical splitting pattern for the aromatic protons, consisting of three multiplets, and an $SiMe_3$ singlet. The intense $SiMe_3$ singlet is also well suited for probing the purity of the complexes. In addition, the $SiMe_3$ singlet in the ^1H NMR spectrum indicates C_s symmetry of the $[Ni(^{si}S_3)]$ fragments in **2**−**9**. This is corroborated by ^{13}C and ^{31}P NMR spectra as well as by the X-ray structure determination of **3**, **4**, **5**, and **7**. The azido complex **7** shows a characteristic $\nu(N_3)$ band at 2037 cm^{-1}in the IR spectrum, in the solid state as well as in CH_2Cl_2 solution. It is noted that **7** is the first structurally characterized azidonickel complex with a coligand exclusively having sulfur donors.

The formation and characterization of the complexes **7**, **8**, and also **9** proved the capability of the $[Ni(^{si}S_3)]$ fragment to bind σ-donor amine ligands, though the ammonia derivative **9** showed that the resulting mononuclear complexes may be labile. Nevertheless, much effort was spent on the synthesis of $[Ni(^{si}S_3)]$ complexes with nicotinamide (NA) or nicotinamide derivatives (NAR_2) as coligands. The aim of these efforts was to form species that could be hydrogenated by molecular hydrogen according to Equation (2).

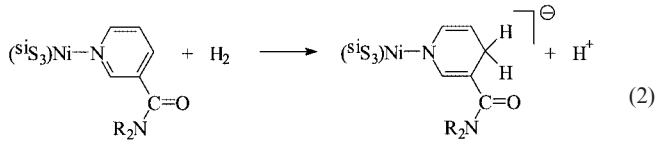

(2)

In this reaction we wanted to make use of the heterolytic cleavage of H_2 observed to be catalyzed by $[Ni(NHPnPr_3)(^{H}S_3)]$ in order to achieve the chemical "storage" of H_2 characteristic for the NAD/NADH couple. Taking the pK_a values of different nicotinamide derivatives into account,[18] we have focused on the coordination of either NA or diethylnicotinamide ($NAEt_2$), and treated **1** or the substitution-labile complexes **5** and **6** with varying amounts of NA or $NAEt_2$, ranging from 1:1 ratios to a large excess of NA or $NAEt_2$. In these experiments, mixtures of **1**, the nicotinamide $[Ni(L)(^{si}S_3)]$ complexes and uncoordinated nicotinamide derivatives were obtained that could not be separated. The color change of the THF reaction solutions from dark-brown to red indicated that a reaction took place. Using the $SiMe_3$ signals as a spectroscopic probe enabled us to monitor the reaction course by ^1H NMR spectroscopy. Figure 1 illustrates the reaction between **1** and NA. Figure 1 (a) shows the two $SiMe_3$ singlets of the starting complex **1** at δ = 0.57 and 0.09 ppm. Addition of 1 equiv. of NA gives rise to a new $SiMe_3$ singlet at δ = 0.33 ppm indicating the formation of $[Ni(NA)(^{si}S_3)]$, while the intensity of the two signals of **1** decreases. The intensity of the signal at δ = 0.33 ppm increases when more NA is added. Figure 1 (c) demonstrates that at a 1:10 ratio of **1**/NA, which equals an approximately threefold excess of NA, complex **1** has been converted almost entirely into the derivative $[Ni(NA)(^{si}S_3)]$. Analogous spectra were observed for the reaction between **1** and $NAEt_2$. However, attempts to

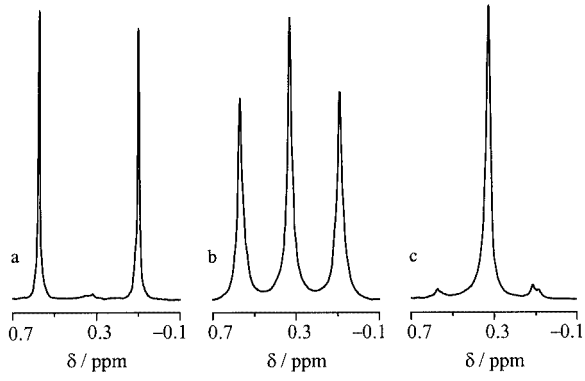

Figure 1. $SiMe_3$ region of ^1H NMR spectra of $[Ni(^{si}S_3)]_3$ in $[D_8]$THF (a) before and (b) after addition of 1 equiv. and (c) after addition of 10 equiv. of nicotinamide

crystallize the [Ni(NA)($^{si}S_3$)] or [Ni(NAEt$_2$)($^{si}S_3$)] complexes from such solutions or to remove the excess of NA or NAEt$_2$ by extraction were unsuccessful. In the latter case, the starting complex **1** was regenerated. This clearly demonstrates that the reaction between **1** and NA or NAEt$_2$ is an equilibrium reaction [Equation (3)].

$$[Ni(^{si}S_3)]_3 + 3\,NA \rightleftharpoons 3\,[Ni(NA)(^{si}S_3)] \quad (3)$$

In this regard, the reactions between **1** and NA or NAEt$_2$ compare with the reversible formation of [Ni(NH$_3$)($^{si}S_3$)] from **1** and NH$_3$. Because it proved impossible to isolate [Ni(NA)($^{si}S_3$)] or [Ni(NAEt$_2$)($^{si}S_3$)] in a pure state, mixtures of the complexes and the respective free NA or NAEt$_2$ were treated with molecular hydrogen in an autoclave at pressures ranging from 10 to 100 bar. However, in no case could the formation of dihydronicotinamide derivatives be observed. The most plausible explanation is that [Ni(NA)($^{si}S_3$)] and [Ni(NAEt$_2$)($^{si}S_3$)] complexes, unlike the phosphorane imine complex [Ni(NHP*n*Pr$_3$)($^{H}S_3$)], do not catalytically heterolyze H_2 or if they do, do not enable the necessary subsequent hydride transfer from the nickel atom to the NA ligand.

X-ray Structure Determinations

Crystal structures of [Ni($^{si}S_3$)]$_3$·0.5CD$_2$Cl$_2$ (**1**·0.5CD$_2$Cl$_2$), [Ni($^{si}S_3$)]$_3$·2THF·3MeOH (**1**·2THF·3MeOH), [Ni(PPh$_3$)($^{si}S_3$)] (**3**), [Ni(PCy$_3$)($^{si}S_3$)]·2CDCl$_3$ (**4**·2CDCl$_3$), Bu$_4$N[Ni(Cl)($^{si}S_3$)]·0.625THF·0.375Et$_2$O (**5**·0.625THF·0.375Et$_2$O), Et$_4$N[Ni(N$_3$)($^{si}S_3$)]·THF (**7**·THF) were determined by X-ray structure analysis. Figures 2 and 3 depict ORTEP diagrams of the structures, Tables 1 and 2 list selected distances and angles.

The unit cells of all compounds contain discrete molecules or ions. The unit cells of **3** and **5** each contain two

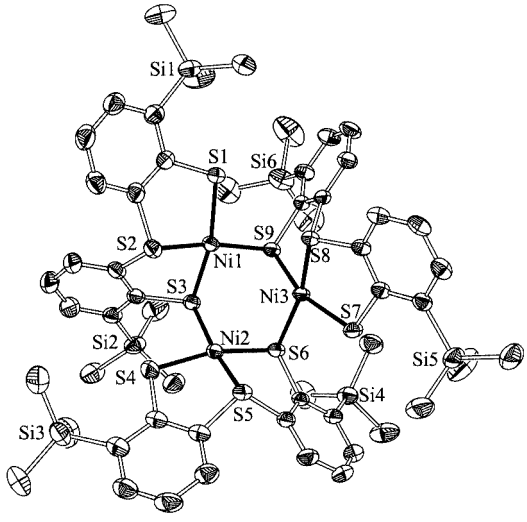

Figure 2. ORTEP diagram of [Ni($^{si}S_3$)]$_3$·0.5CD$_2$Cl$_2$ (**1**·0.5CD$_2$Cl$_2$) (50% probability ellipsoids; hydrogen atoms and solvent molecule omitted)

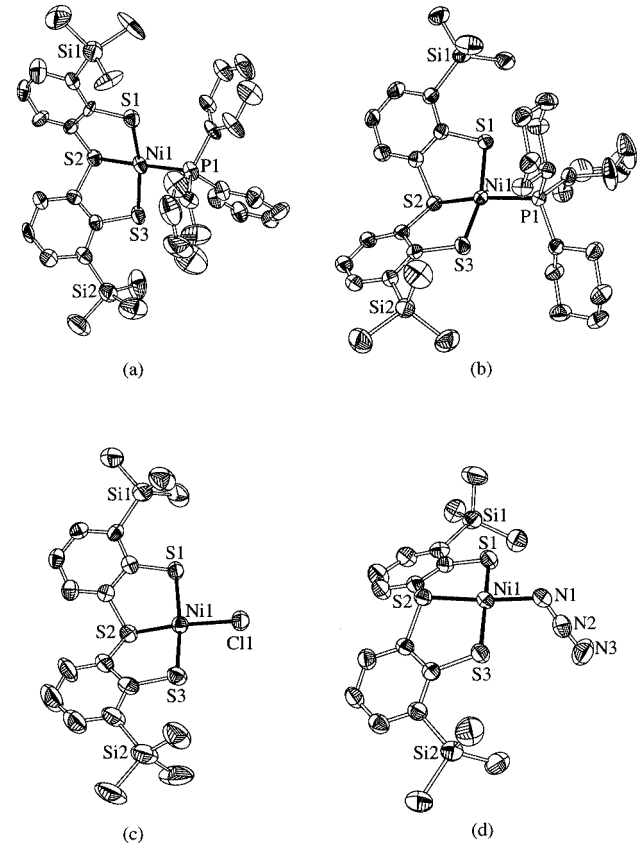

Figure 3. ORTEP diagrams of (a) [Ni(PPh$_3$)($^{si}S_3$)] (**3**), (b) [Ni(PCy$_3$)($^{si}S_3$)]·2CDCl$_3$ (**4**·2CDCl$_3$), (c) Bu$_4$N[Ni(Cl)($^{si}S_3$)]·0.625THF·0.375Et$_2$O (**5**·0.625THF·0.375Et$_2$O), and (d) Et$_4$N[Ni(N$_3$)($^{si}S_3$)]·THF (**7**·THF) (50% probability ellipsoids; hydrogen atoms, solvent molecules, and cations omitted)

Table 1. Selected distances [pm] and angles [°] for [Ni($^{si}S_3$)]$_3$·0.5CD$_2$Cl$_2$ (**1**·0.5CD$_2$Cl$_2$) (three independent [Ni($^{si}S_3$)] units; the columns refer to: a: Ni1, S1, S2, S3; b: Ni2, S4, S5, S6; c: Ni3, S7, S8, S9)

Compound	[Ni($^{si}S_3$)]$_3$ (**1**)		
	a	b	c
Ni1−S1	215.6(1)	214.9(1)	214.8(1)
Ni1−S2	214.4(1)	214.4(1)	214.3(1)
Ni1−S3	219.4(1)	220.2(1)	222.2(1)
Ni1−S9	219.8(1)	220.6(1)	221.7(1)
Ni1···Ni2	334.6(2)	321.3(6)	327.5(6)
S3···S9	305.8(1)	312.1(4)	318.7(3)
S1−Ni1−S2	91.12(4)	89.74(4)	90.89(3)
S1−Ni1−S3	159.82(4)	162.99(4)	158.06(4)
S1−Ni1−S9	95.84(3)	93.42(4)	95.25(3)
S2−Ni1−S3	88.77(3)	89.61(3)	87.46(3)
S2−Ni1−S9	167.50(4)	169.90(4)	165.23(4)
S3−Ni1−S9	88.25(3)	90.15(3)	91.75(3)
Ni1−S3−Ni2	99.00(4)	93.29(3)	95.61(3)

crystallographically independent molecules, exhibiting essentially identical bond lengths and angles, of which only one molecule is shown in Figure 2. All compounds exhibit four-coordinate nickel centers in a strongly tetrahedrally distorted planar coordination. The tetrahedral distortion

Table 2. Selected distances [pm] and angles [°] for [Ni(PPh_3)($^{si}S_3$)] (**3**), [Ni(PCy_3)($^{si}S_3$)]·2$CDCl_3$ (**4**·2$CDCl_3$), Bu_4N[Ni(Cl)($^{si}S_3$)]·0.625THF·0.375Et_2O (**5**·0.625THF·0.375Et_2O), and Et_4N[Ni(N_3)($^{si}S_3$)]·THF (**7**·THF)

Compound	**3** (Ni−PPh_3)	**4** (Ni−PCy_3)	**5** (Ni−Cl)	**7** (Ni−N_3)
Ni1−S1	216.5(3)	217.3(1)	218.3(3)	216.9(2)
Ni1−S2	213.0(4)	213.5(1)	208.7(2)	211.1(2)
Ni1−S3	219.7(4)	215.3(2)	217.3(3)	218.2(2)
Ni1−L	221.3(4)	221.7(2)	220.3(2)	191.3(4)
N1−N2				118.5(6)
N2−N3				115.8(6)
S1−Ni1−S2	90.1(2)	88.14(4)	88.1(1)	89.78(5)
S1−Ni1−S3	164.2(2)	160.00(6)	162.3(1)	167.31(6)
S1−Ni1−L	90.3(2)	93.35(4)	93.0(1)	91.4(2)
S2−Ni1−S3	86.0(2)	90.00(5)	90.3(1)	89.15(5)
S2−Ni1−L	176.9(2)	165.05(5)	165.3(1)	173.4(2)
S3−Ni1−L	94.5(2)	93.54(4)	93.1(1)	91.1(2)
Ni1−N1−N2				121.2(3)
N1−N2−N3				175.6(6)

can be traced back to the sp^3-hybridized thioether S donors of the $^{si}S_3$ ligand, leading to a butterfly-like shape of the resulting [Ni($^{si}S_3$)] fragments. The characteristic topology of the $^{si}S_3$ ligand also causes the Ni−S(thioether) distances to always be shorter than the Ni−S(thiolate) distances. In this respect, [Ni($^{si}S_3$)] complexes are analogous to [Ni($^{H}S_3$)] complexes that contain the $^{H}S_3$ parent ligand and have been described previously.[11−13]

Trimerization of [Ni($^{si}S_3$)] fragments by thiolate bridges leads to **1**. Complex **1** contains a cyclohexane-like six-membered $[NiS]_3$ ring with a chair conformation, and the structure of **1** parallels that of the parent complex $[Ni(^{H}S_3)]_3$.[12] All bridging Ni−S(thiolate) distances in the six-membered $[NiS]_3$ ring, ranging from 219.4(1) to 222.2(1) pm, are distinctly longer than the terminal Ni−S(thiolate) distances [214.3(1) to 215.6(1) pm]. This elongation of bridging Ni−S distances rationalizes the ready dissociation of **1** in solution when treated with suitable monodentate ligands.

In the complexes **3**, **4**, **5**, and **7**, the fourth coordination site of the [Ni($^{si}S_3$)] fragments is occupied by PPh_3, PCy_3, Cl^-, or N_3^-. The distances and angles in **3**, **4**, **5**, and **7** lie in the range observed for analogous [Ni(L)($^{H}S_3$)] complexes, and thus far, show no anomalies.[10−15] For example, the Ni−S(thioether) distance is always shorter than the Ni−S(thiolate) distances and the [Ni($^{si}S_3$)] fragments exhibit their typical butterfly shape. The N−N distances [118.5(6) and 115.8(6) pm] and Ni−N1−N2 angle [121.2(3)°] in **7** are characteristic for azide complexes in which the azide ligand binds end-on as a σ-donor to the metal atom.[19,20]

Conclusion

This work describes the synthesis of the new ligands $^{si}S_3$-H_2 and $^{ca}S_3$-H_2 and a series of [Ni(L)($^{si}S_3$)] complexes. The major aim of the investigations was to find complexes with [Ni($^{si}S_3$)] fragments that are well soluble in common solvents and more reactive than the [Ni($^{H}S_3$)] parent complexes. These objectives have been reached and, unlike the [Ni($^{H}S_3$)] parent fragment, the [Ni($^{si}S_3$)] complex fragment has been proved to bind even nicotinamide or diethylnicotinamide, though only in equilibrium reactions. Attempts to hydrogenate the nicotinamide complexes in solution to give dihydronicotinamide derivatives, however, remains unsuccessful.

Experimental Section

General Methods: Unless stated otherwise, all reactions and manipulations were carried out under nitrogen at room temperature using standard Schlenk techniques. All solvents were dried and distilled before use. As far as possible, reactions were monitored by IR or NMR spectroscopy. Physical measurements were carried out with the following instruments: IR (KBr discs or CaF_2 cuvettes, solvent bands were compensated), Perkin−Elmer 983, 1620 FT-IR and 16PC FT-IR; NMR: Jeol JMM-GX 270, Jeol JMM-EX 270, and Lambda LA 400 with the residual protio-solvent signal used as an internal reference. Chemical shifts are quoted in the δ scale (down field shifts are positive) relative to tetramethylsilane (^1H, $^{13}C\{^1H\}$ NMR) or 85% H_3PO_4 ($^{31}P\{^1H\}$ NMR). Mass spectra: Jeol MSTATION 700 spectrometer. Elemental analyses: Carlo Erba EA 1106 or 1108 analyzer. Me_3SiCl, Me_3SiN_3, HS*t*Bu, Bu_4NCl, Et_4NCl, N_2H_4 (1 M solution in THF), nicotinamide, *N*,*N*-diethylnicotinamide were purchased from either Aldrich or Fluka. $^{H}S_3$-H_2 was prepared as described in the literature.[11]

$^{si}S_3$-H_2: With continuous vigorous stirring under argon, *n*BuLi in hexane (2.5 M, 45 mL, 112.51 mmol) was slowly added to a suspension of $^{H}S_3$-H_2 (6.49 g, 25.92 mmol) in hexane (200 mL) at −78 °C. After addition of TMEDA (31 mL, 206.01 mmol), the temperature was raised gradually to 25 °C. Stirring was continued for another 72 h, in the course of which the color of the suspension turned from white to yellow. This suspension was cooled to −78 °C, SiMe_3Cl (15 mL, 118.03 mmol) was added slowly, and stirring was continued for 1 h at −78 °C and 24 h at 25 °C, in the course of which the color of the suspension changed back to white. H_2O (50 mL) was added, and all volatile components were removed in vacuo. A red-brown highly viscous residue remained which was dissolved in Et_2O (500 mL). The resulting Et_2O solution was washed by extraction with hydrochloric acid (5%, 3 × 200 mL) and a saturated NaCl/H_2O solution (2 × 100 mL), and dried with solid Na_2SO_4. Removal of all volatile components in vacuo yielded a yellow-red viscous residue, which was dissolved in MeOH (150 mL) and heated to reflux for 12 h. Removal of volatile components in vacuo gave a red-brown viscous oil of $^{si}S_3$-H_2, which could be used for the synthesis of complexes without further purification. Yield: 9.55 g (93%). $C_{18}H_{26}S_3Si_2$ (394.78): calcd. C 54.76, H 6.65, S 24.39; found C 55.01, H 6.58, S 24.28. MS (FD, THF): *m*/*z* = 394 [M^+]. ^1H NMR (269.7 MHz, C_6D_6): δ = 7.23 (d, 2 H, C_6H_3), 7.10 (d, 2 H, C_6H_3), 6.78 (t, 2 H, C_6H_3), 4.61 (br, 2 H, SH), 0.35 (s, 18 H, $SiMe_3$) ppm. $^{13}C\{^1H\}$ NMR (67.8 MHz, C_6D_6): δ = 141.3, 140.9, 134.6, 134.4, 133.0, 126.3 (C_6H_3), −0.2 ($SiMe_3$) ppm.

$^{ca}S_3$-H_2: To a suspension of $^{H}S_3$-H_2 (7.05 g, 28.17 mmol) in hexane (150 mL), *n*BuLi in hexanes (2.5 M, 45 mL, 112.51 mmol) was added slowly at −78 °C. Under vigorous stirring, TMEDA (31 mL, 206.01 mmol) was added and the temperature gradually raised to 25 °C. The mixture was stirred for another 72 h, in the course of

which the color of the suspension turned from white to yellow. This suspension was cooled down again to −78 °C, CO_2 was bubbled through for 30 min under vigorous stirring and the mixture was gradually warmed to 0 °C in the course of 1 h. All volatile components were removed in vacuo. The resulting mixture was treated with cold water (50 mL) and concentrated hydrochloric acid (70 mL). The resulting mixture was extracted with a mixture of Et_2O (100 mL) and THF (30 mL). The extract was dried with Na_2SO_4 and the solvents were evaporated to give a dry pale yellow residue. This was recrystallized from acetone (60 mL) at −20 °C. Green yellow needles precipitated, which were separated after 2 d, washed with cold acetone (10 mL, 0 °C) and dried in vacuo. Yield: 4.83 g (51%). $C_{14}H_{10}O_4S_3$ (338.43): calcd. C 49.69, H 2.98, S 28.42; found C 49.99, H 3.36, S 27.78. MS (FD, THF): *m*/*z* = 338 [M^+]. IR (KBr): $\tilde{\nu}$ = 2980 [ν(OH)], 2484 [ν(SH)], 1652 [ν(COOH)] cm^{-1}. ^1H NMR (399.7 MHz, [D_8]THF): δ = 11.85 (br, 2 H, COOH), 8.06 (d, 2 H, C_6H_3), 7.30 (d, 2 H, C_6H_3), 7.28 (s, 2 H, SH), 7.08 (t, 2 H, C_6H_3) ppm. $^{13}C\{^1H\}$ NMR (100.4 MHz, [D_8]THF): δ = 167.7 (COOH), 141.5, 135.3, 133.2, 131.2, 126.6, 123.6 (C_6H_3) ppm.

[Ni($^{si}S_3$)]$_3$ (1): $^{si}S_3$-H_2 (3.00 g, 7.60 mmol) in THF (40 mL) was added dropwise to a solution of $Ni(ac)_2{\cdot}4H_2O$ (1.90 g, 7.65 mmol) in MeOH (25 mL). A dark brown solution formed which was stirred for 24 h and then concentrated to dryness. The resulting dark brown residue was redissolved in hexane (20 mL), traces of insoluble particles were removed by filtration after 30 min, and the filtrate was layered with MeOH (50 mL). A dark brown powder precipitated, which was separated, washed with MeOH (30 mL) and pentane (25 mL), and dried in vacuo. Yield: 3.02 g (87%). $C_{54}H_{72}Ni_3S_9Si_6$ (1354.36): calcd. C 47.89, H 5.36, S 21.31; found C 47.58, H 5.53, S 20.98. MS (FD, THF): *m*/*z* = 1354 [M^+], 902 [Ni($^{si}S_3$)]$_2^+$. ^1H NMR (399.7 MHz, [D_8]THF): δ = 7.82 (d, 1 H, C_6H_3), 7.68 (d, 1 H, C_6H_3), 7.40 (d, 1 H, C_6H_3), 7.28 (t, 1 H, C_6H_3), 7.24 (d, 1 H, C_6H_3), 6.96 (t, 1 H, C_6H_3), 0.55 (s, 9 H, $SiMe_3$), 0.08 (s, 9 H, $SiMe_3$) ppm. $^{13}C\{^1H\}$ NMR (100.4 MHz, [D_8]THF): δ = 158.8, 146.7, 145.1, 139.3, 138.5, 135.4, 134.8, 132.2, 130.9, 127.8, 127.6, 122.1 (C_6H_3), 0.6, −0.6 ($SiMe_3$) ppm.

[Ni(P*n*Pr$_3$)($^{si}S_3$)] (2): P*n*Pr_3 (0.16 mL, 0.99 mmol) was added to a solution of **1** (400 mg, 0.30 mmol) in THF (15 mL). The solution instantaneously changed its color from dark brown to dark yellow, was filtered after 1 h, reduced in volume to 2 mL, and layered with pentane (20 mL). Orange microcrystals precipitated which were separated after 5 d, washed with pentane (10 mL), and dried in vacuo. Yield: 435 mg (80%). $C_{27}H_{45}NiPS_3Si_2$ (611.694): calcd. C 53.02, H 7.42, S 15.73; found C 53.28, H 7.24, S 15.47. MS (FD, THF): *m*/*z* = 611 [M^+]. ^1H NMR (269.7 MHz, $CDCl_3$): δ = 7.64 (d, 2 H, C_6H_3), 7.24 (d, 2 H, C_6H_3), 6.94 (t, 2 H, C_6H_3), 1.74 (m, 6 H, PCH_2), 1.06 (m, 6 H, PCH_2CH_2), 0.37 (s, 18 H, $SiMe_3$), 0.05 (t, 9 H, $PCH_2CH_2CH_3$) ppm. $^{13}C\{^1H\}$ NMR (100.4 MHz, $CDCl_3$): δ = 159.0 (d, $^3J_{P,C}$ = 13.2 Hz), 141.1, 135.1, 133.6, 129.1, 122.3 (C_6H_3), 26.7 (d, $^1J_{P,C}$ = 26.40 Hz), 18.7, 16.7 (d, $^3J_{P,C}$ = 14.1 Hz) ($PCH_2CH_2CH_3$), 0.0 ($SiMe_3$) ppm. $^{31}P\{^1H\}$ NMR (161.8 MHz, $CDCl_3$): δ = 14.6 [P*n*(C_3H_7)$_3$] ppm.

[Ni(PPh$_3$)($^{si}S_3$)] (3): Whilst stirring, a solution of PPh_3 (200 mg, 0.76 mmol) and **1** (280 mg, 0.21 mmol) in THF (10 mL) was heated to reflux for 5 min, in the course of which the color changed from dark brown to red. The red solution was stirred for another 30 min at room temperature, then combined with MeOH (30 mL), filtered, and reduced in volume to ca. 5 mL. Red microcrystals precipitated which were separated after 3 d, washed with MeOH (10 mL), and dried in vacuo. Yield: 268 mg (76%). $C_{36}H_{39}NiPS_3Si_2$ (713.72): calcd. C 60.58, H 5.51, S 13.48; found C 60.48, H 5.80, S 13.51. MS (FD, THF): *m*/*z* = 712 [M^+]. ^1H NMR (269.7 MHz, [D_6]acetone): δ = 7.94 (d, 2 H, C_6H_3), 7.83−7.52 (m, 15 H, C_6H_5), 7.28 (d, 2 H, C_6H_3), 7.04 (t, 2 H, C_6H_3), 0.12 (s, 18 H, $SiMe_3$) ppm. $^{13}C\{^1H\}$ NMR (67.8 MHz, [D_6]acetone): δ = 159.5 (d, $^3J_{PC}$ = 14 Hz), 143.0, 135.4, 135.3 (d, J_{PC} = 10.8 Hz), 133.3, 131.7, 130.4 (d, $^1J_{PC}$ = 47.4 Hz) 129.6, 129.1 (d, J_{PC} = 10.2 Hz), 122.7 [C_6H_3, $P(C_6H_5)_3$], −0.8 ($SiMe_3$) ppm. $^{31}P\{^1H\}$ NMR (161.8 MHz, [D_6]acetone): δ = 29.4 [$P(C_6H_5)_3$] ppm.

[Ni(PCy$_3$)($^{si}S_3$)] (4): A solution of PCy_3 (200 mg, 0.71 mmol) in THF (2 mL) was added dropwise to a solution of **1** (300 mg, 0.22 mmol) in THF (10 mL). Over the course of ca. 5 min, the color of the solution changed from dark brown to dark yellow. The solution was stirred for 3 h, filtered, reduced in volume to ca. 2 mL, and layered with MeOH (20 mL). Yellow-red microcrystals precipitated, which were separated after 3 d, washed with MeOH (10 mL), and dried in vacuo. Yield: 452 mg (93%). $C_{36}H_{57}NiPS_3Si_2$ (731.889): calcd. C 59.08, H 7.85, S 13.14; found C 59.32, H 7.96, S 12.69. MS (FD, THF): *m*/*z* = 731 [M^+]. ^1H NMR (399.7 MHz, $CDCl_3$): δ = 7.74 (d, 2 H, C_6H_3), 7.28 (d, 2 H, C_6H_3), 6.98 (t, 2 H, C_6H_3), 2.10−1.28 (m, 33 H, PCy_3), 0.37 (s, 18 H, $SiMe_3$) ppm. $^{13}C\{^1H\}$ NMR (100.4 MHz, $CDCl_3$): δ = 159.0 (d, $^3J_{PC}$ = 10 Hz), 141.2, 135.0, 133.1 (d, $^4J_{PC}$ = 1.6 Hz), 128.7, 122.0 (C_6H_3), 34.5 (d, $^1J_{PC}$ = 20.1 Hz), 30.7, 28.5 (d, $^3J_{PC}$ = 11 Hz), 27.1 [$P(C_6H_{11})_3$], 0.0 ($SiMe_3$) ppm. $^{31}P\{^1H\}$ NMR (161.8 MHz, $CDCl_3$): δ = 31.9 [$P(C_6H_{11})_3$] ppm.

Bu$_4$N[Ni(Cl)($^{si}S_3$)] (5): Bu_4NCl (210 mg, 0.76 mmol) was added to a dark brown solution of **1** (312 mg, 0.23 mmol) in THF (10 mL). The solution was stirred for 12 h, over the course of which its color changed to violet. The solution was filtered, reduced in volume to 2 mL, and layered with Et_2O (20 mL). Pink crystals precipitated which were separated after 7 d, washed with Et_2O (15 mL), and dried in vacuo. Yield: 410 mg (81%). $C_{34}H_{60}ClNNiS_3Si_2$ (729.377): calcd. C 55.99, H 8.29, N 1.92, S 13.19; found C 56.01, H 8.32, N 2.07, S 12.72. ^1H NMR (269.7 MHz, [D_8]THF): δ = 7.60 (d, 2 H, C_6H_3), 7.18 (d, 2 H, C_6H_3), 6.79 (t, 2 H, C_6H_3), 3.57 (m, 8 H, NCH_2), 1.76 (m, 8 H, NCH_2CH_2), 1.39 [m, 8 H, $N(CH_2)_2CH_2$], 0.87 [m, 12 H, $N(CH_2)_3CH_3$], 0.36 (s, 18 H, $SiMe_3$) ppm. $^{13}C\{^1H\}$ NMR (67.8 MHz, [D_8]THF): δ = 161.6, 139.6, 134.7, 134.6, 128.9, 120.7 (C_6H_3), 59.7, 35.1, 20.7, 14.2 [$N(CH_2)_3CH_3$], −0.2 ($SiMe_3$) ppm.

Bu$_4$N[Ni(S*t*Bu)($^{si}S_3$)] (6): Whilst stirring, NaS*t*Bu (1 mL of 1 M MeOH solution, 1.00 mmol) was added to a solution of **1** (300 mg, 0.22 mmol) in THF (10 mL). After 1 h, Bu_4NOH (0.68 mL, 1 M MeOH solution, 0.68 mmol) was added and the stirring continued for another 2 h. A dark brown solution resulted, which was filtered, concentrated in volume to 2 mL, and layered with pentane (15 mL). Dark brown microcrystals precipitated which were separated after 5 d, washed with pentane (5 mL) and dried in vacuo. Yield: 340 mg (65%). $C_{38}H_{69}NNiS_4Si_2$ (783.106): calcd. C 58.28, H 8.88, N 1.79, S 16.37; found C 58.43, H 8.97, N 1.91, S 15.89. ^1H NMR (269.7 MHz, $CDCl_3$): δ = 7.52 (d, 2 H, C_6H_3), 7.14 (d, 2 H, C_6H_3), 6.78 (t, 2 H, C_6H_3), 3.32 (m, 8 H, NCH_2), 1.59 (m, 8 H, NCH_2CH_2), 1.53 (s, 9 H, S*t*Bu), 1.31 [m, 8 H, $N(CH_2)_2CH_2$], 0.88 [m, 12 H, $N(CH_2)_3CH_3$], 0.34 (s, 18 H, $SiMe_3$) ppm. $^{13}C\{^1H\}$ NMR (67.8 MHz, $CDCl_3$): δ = 161.6, 139.5, 133.7, 133.0, 127.9, 119.7 (C_6H_3), 58.9 (NCH_2), 40.4, 36.8 (S*t*Bu), 24.2, 19.7 13.9 [$N(CH_2)_3CH_3$], −0.5 ($SiMe_3$) ppm.

Et$_4$N[Ni(N$_3$)($^{si}S_3$)] (7): A solution of Et_4NCl (95 mg, 0.57 mmol) and **1** (250 mg, 0.19 mmol) in THF (10 mL) was stirred for 3 h, over the course of which the color changed from dark brown to purple. Me_3SiN_3 (0.1 mL, 0.76 mmol) was added, whereupon the color became slightly lighter. After 1 h, all volatile materials were

removed in vacuo, the residue was redissolved in THF (10 mL). The THF solution was filtered, reduced in volume to 2 mL and layered with pentane (15 mL). Violet needles precipitated, which were separated after 4 d, washed with pentane (10 mL), and dried in vacuo. Yield: 285 mg (82%). $C_{26}H_{44}N_4NiS_3Si_2$ (623.729): calcd. C 50.07, H 7.11, N 8.98, S 15.42; found C 50.61, H 7.40, N 8.70, S 15.19 − IR (KBr): $\tilde{\nu}$ = 2037 [$\nu(N_3)$] cm^{-1}. ^1H NMR (269.7 MHz, $CDCl_3$): δ = 7.48 (d, 2 H, C_6H_3), 7.26 (d, 2 H, C_6H_3), 6.90 (t, 2 H, C_6H_3), 3.40 (m, 8 H, NCH_2), 1.20 (t, 12 H, NCH_2CH_3), 0.37 (s, 18 H, $SiMe_3$) ppm. $^{13}C\{^1H\}$ NMR (67.8 MHz, $CDCl_3$): δ = 157.9, 140.0, 134.5, 132.9, 127.8, 120.9 (C_6H_3), 52.6, 7.8 [$N(CH_2CH_3)_4$], −0.9 ($SiMe_3$) ppm.

[Ni(N_2H_4)($^{si}S_3$)] (8): Addition of N_2H_4 (2 mL of 1 M THF solution, 2.00 mmol) to a solution of **1** (250 mg, 0.19 mmol) in THF (10 mL) led to a rapid color change from dark brown to orange. The solution was stirred for 2 h and stored at −30 °C for 12 h. At this temperature, the excess free hydrazine that crystallized from the solution could be removed by filtration at −30 °C. The filtrate was reduced in volume to 2 mL and layered with pentane (20 mL). Dark red crystals precipitated which were separated, washed with pentane (10 mL) and dried in vacuo. Yield: 242 mg (90%). $C_{18}H_{28}N_2NiS_3Si_2$ (489.499): calcd. C 44.71, H 5.84, N 5.79, S 19.90; found C 45.01, H 5.88, N 5.51, S 19.43. IR (KBr): $\tilde{\nu}$ = 3350 [ν(NH)] cm^{-1}. ^1H NMR (269.7 MHz, [D_8]THF): δ = 7.62 (d, 2 H, C_6H_3), 7.25 (d, 2 H, C_6H_3), 6.90 (t, 2 H, C_6H_3), 4.83 (b, 2 H, NH_2NH_2), 3.32 (b, 2 H, NH_2), 0.39 (s, 18 H, $SiMe_3$) ppm. $^{13}C\{^1H\}$ NMR (67.8 MHz, [D_8]THF): δ = 157.6, 140.9, 135.5, 134.5, 129.9, 122.4 (C_6H_3), −0.4 ($SiMe_3$) ppm.

[Ni(NH_3)($^{si}S_3$)] (9): This compound was synthesized in an NMR tube and characterized only by ^1H and ^{13}C NMR spectra: NH_3 gas (2.5 mL, 0.15 mmol) was injected into the dark brown solution of **1** (25 mg, 0.02 mmol) in [D_8]THF contained in an NMR tube. The color of the solution immediately changed to red. The ^1H and ^{13}C NMR spectra of the solutions indicated the complete conversion of **1** into **9**. ^1H NMR (269.7 MHz, [D_8]THF): δ = 7.63 (d, 2 H, C_6H_3), 7.23 (d, 2 H, C_6H_3), 6.89 (t, 2 H, C_6H_3), 2.27 (b, 3 H, NH_3), 0.37 (s, 18 H, $SiMe_3$) ppm. $^{13}C\{^1H\}$ NMR (67.8 MHz, [D_8]THF): δ = 158.4, 140.6, 135.3, 134.5, 129.6, 122.0 (C_6H_3), −0.5 ($SiMe_3$) ppm.

[Ni(L)($^{si}S_3$)] Complexes (L = NA or $NAEt_2$): In a typical experiment, NA (0.5 g, 4.09 mmol) or $NAEt_2$ (1.0 mL, 5.95 mmol) was added to a dark brown solution of **1** (500 mg, 0.37 mmol) in THF (10 mL). The solution was stirred for 48 h, over the course of which its color changed to yellow red. The solution was filtered, reduced in volume to 2 mL, and layered with Et_2O (20 mL). Yellow red powders precipitated which were separated after 5 d, washed with Et_2O (15 mL), and dried in vacuo. Elemental analyses and IR and NMR spectra indicated that these powders were mixtures of [Ni(L)($^{si}S_3$)] and **1,** which could not be separated.

^1H NMR Spectroscopic Monitoring of the Reactions between 1 and NA or $NAEt_2$: To a dark brown solution of **1** (25 mg, 0.02 mmol) in [D_8]THF, NA, or $NAEt_2$ (1−10 equiv.) was added stepwise, and the ^1H NMR spectra were recorded after every addition. The $SiMe_3$ signals were used as a spectroscopic probe to monitor the formation of the corresponding [Ni(L)($^{si}S_3$)] complex.

X-ray Structure Determination of [Ni($^{si}S_3$)]$_3$·0.5CD_2Cl_2 (1·0.5CD_2Cl_2), [Ni($^{si}S_3$)]$_3$·2THF·3MeOH (1·2THF·3MeOH), [Ni(PPh_3)($^{si}S_3$)] (3), [Ni(PCy_3)($^{si}S_3$)]·2$CDCl_3$ (4·2$CDCl_3$), Bu_4N[Ni(Cl)($^{si}S_3$)]·0.625THF·0.375Et_2O (5·0.625THF·0.375Et_2O), Et_4N[Ni(N_3)($^{si}S_3$)]·THF (7·THF): In an NMR tube at −30 °C, black blocks of [Ni($^{si}S_3$)]$_3$·0.5CD_2Cl_2 (**1**·0.5CD_2Cl_2) crystallized in the course of 10 d from a CD_2Cl_2 solution of **1** which had been layered with MeOH. From THF/MeOH mixtures, **1** crystallized as **1**·2THF·3MeOH. The crystallographic data of this solvate have been deposited. Red cubes of **3** and orange-prisms of **4**·2$CDCl_3$

Table 3. Selected crystallographic data for [Ni($^{si}S_3$)]$_3$·0.5CD_2Cl_2 (**1**·0.5CD_2Cl_2), [Ni(PPh_3)($^{si}S_3$)] (**3**), [Ni(PCy_3)($^{si}S_3$)]·2$CDCl_3$ (**4**·2$CDCl_3$), Bu_4N[Ni(Cl)($^{si}S_3$)]·0.625THF·0.375Et_2O (**5**·0.625THF·0.375Et_2O), and Et_4N[Ni(N_3)($^{si}S_3$)]·THF (**7**·THF)

	1·0.5CD_2Cl_2	**3**	**4**·2$CDCl_3$	**5**·0.625THF·0.375Et_2O	**7**·THF
Empirical formula	$C_{54.50}H_{72}ClDNi_3S_9Si_6$	$C_{36}H_{39}NiPS_3Si_2$	$C_{38}H_{57}Cl_6D_2NiPS_3Si_2$	$C_{38}H_{68.75}ClNNiOS_3Si_2$	$C_{30}H_{52}N_4NiOS_3Si_2$
Formula mass [g/mol]	1397.79	713.71	972.61	802.21	695.83
Crystal system	monoclinic	monoclinic	orthorhombic	monoclinic	orthorhombic
Space group	*C*2/*c*	*Cc*	$P2_12_12_1$	$P2_1/c$	*Pbca*
a [pm]	3232.3(3)	2664.0(8)	1236.2(1)	1343.8(2)	1951.2(2)
b [pm]	2452.3(3)	1883.1(6)	1720.6(2)	3057.9(4)	1572.2(2)
c [pm]	1996.6(2)	1518.2(5)	2266.2(2)	2237.9(3)	2404.8(4)
α [°]	90	90	90	90	90
β [°]	118.88(1)	105.10(3)	90	95.16(1)	90
γ [°]	90	90	90	90	90
V [nm^3]	13.858(3)	7.353(4)	4.8202(8)	9.159(2)	7.377(2)
Z	8	8	4	8	8
$d_{calcd.}$[g/cm^3]	1.340	1.289	1.337	1.164	1.253
μ [mm^{-1}]	1.253	0.831	0.974	0.698	0.789
Crystal size [mm]	0.80×0.70×0.35	0.55×0.30×0.10	0.64×0.60×0.42	0.90×0.80×0.20	0.96×0.48×0.36
2θ range[°]	3.6−54.0	3.5−54.0	3.6−56.0	3.6−50.0	3.7−54.0
T_{min}/T_{max}	0.358/0.419	0.984/1.000	0.224/0.269	0.278/0.341	0.261/0.340
Measd. refl.	16730	16914	12783	19091	9574
Indep. refl.	15146	8679	11611	16114	8046
Obsd. refl.	10965	2691	8889	6482	4403
Ref. parameters	882	787	467	881	380
*R*1[a] ; *wR*2[%]	4.39; 10.57	5.09; 8.63	5.52; 13.88	8.64; 21.32	6.60; 16.67
Abs. struct. parameters		0.01(2)	0.00(2)		

[a] [$I > 2\sigma(I)$].

were grown at −20 °C over the course of 3−5 d from a concentrated THF solution which was layered with MeOH. Red-violet plates of **5**·0.625THF·0.375Et_2O formed over the course of 7 d when a saturated THF solution of **5** was layered with Et_2O at −30 °C. Red-black crystals of **7**·THF were obtained from a dilute THF/acetone mixture of **7** which was layered with pentane and stored for 8 d at −30 °C. Suitable single crystals were embedded in protective perfluoro polyether or were sealed in glass capillaries under N_2. Data were collected at 200 K (**1**·0.5CD_2Cl_2, **5**·0.625THF·0.375Et_2O, **7**·THF), 220 K (**4**·2$CDCl_3$) or 293 K (**3**) with a Siemens P4 diffractometer or a Nicolet R 3m/V diffractometer (**3**) using Mo-K_α radiation (λ = 71.073 pm), a graphite monochromator, and the ω-scan technique. For all compounds a semi-empirical absorption correction using ψ-scans has been performed. The structures were solved by direct methods, full-matrix least-squares refinement was carried out on F^2 (SHELXTL NT 5.1).[21] All non-hydrogen atoms were refined anisotropically. The hydrogen atoms of **1**·0.5CD_2Cl_2 were located from a difference Fourier map, while in all other compounds the H atoms were geometrically positioned with isotropic displacement parameters being 1.5 times U(eq) of the preceding carbon atom. One *n*-butyl group in the cation of **5**·0.625THF·0.375Et_2O was found to be disordered. Two alternative sites could be refined with occupancy factors of 57(2) and 43(2)%, respectively. One THF and one Et_2O molecule of the included solvent share a single site. These disordered molecules have been refined using several restraints. Selected crystallographic data are summarized in Table 3.[22]

Acknowledgments

Financial support of these investigations by the Deutsche Forschungsgemeinschaft and the Fonds der Chemischen Industrie is gratefully acknowledged.

[1] [1a] J. R. Lancaster, *FEBS Lett.* **1980**, *115*, 285−288. [1b] E. G. Graf, R. K. Thauer, *FEBS Lett.* **1981**, *136*, 165−169. [1c] R. Cammack, V. M. Fernandez, K. Schneider, in: *Bioinorganic Chemistry of Nickel* (Ed.: J. R. Lancaster, Jr.), VCH, Weinheim, **1988**, p. 167−190. [1d] M. W. W. Adams, *Biochem. Biophys. Acta* **1990**, *1020*, 115−145. [1e] A. F. Kolodziej, *Progr. Inorg. Chem.* **1994**, *41*, 493−598. [1f] S. P. Albracht, *Biochem. Biophys. Acta* **1994**, *1188*, 167−204. [1g] M. Y. Darensbourg, E. J. Lyon, J. J. Smee, *Coord. Chem. Rev.* **2000**, *206−207*, 553−561.

[2] [2a] A. Volbeda, M. H. Charon, C. Piras, E. C. Hatchikian, M. Frey, J. C. Fontecilla-Camps, *Nature (London)* **1995**, *373*, 580−587. [2b] R. Cammack, *Nature (London)* **1995**, *373*, 556−557. [2c] A. Volbeda, E. Garcin, C. Piras, A. L. de Lacey, V. M. Fernandes, E. C. Hatchikian, *J. Am. Chem. Soc.* **1996**, *118*, 12989−12996. [2d] Y. Higuchi, N. Yasuoka, *Structure (London)* **1997**, *5*, 1671−1680.

[3] [3a] E. Garcin, X. Vernede, E. C. Hatchikian, A. Volbeda, M. Frey, J. C. Fontecilla-Camps, *Structure (London)* **1999**, *7*, 557−566. [3b] Y. Higuchi, H. Ogata, K. Miki, N. Yasuoka, T. Yagi, *Structure (London)* **1999**, *7*, 549−556.

[4] [4a] A. S. W. Ragsdale, J. E. Clark, G. Ljungdahl, L. L. Lundie, H. L. Drake, *J. Biol. Chem.* **1983**, *258*, 2364−2369. [4b] R. B. Diekert, M. Ritter, *FEBS Lett.* **1983**, *151*, 41−44. [4c] C. Y. Ralston, H. Wang, S. W. Ragsdale, M. Kumar, N. J. Spangler, P. W. Ludden, W. Gu, R. M. Jones, D. S. Patil, S. P. Cramer, *J. Am. Chem. Soc.* **2000**, *122*, 10553−10560. [4d] A. L. De Lacey, C. Stadler, C. Cavazza, E. C. Hatchikian, V. M. Fernandez, *J. Am. Chem. Soc.* **2000**, *122*, 11232−11233. [4e] H. Dobbek, V. Svetlitchnyi, L. Gremer, R. Huber, O. Meyer, *Science* **2001**, *293*, 1281−1285.

[5] [5a] H. J. Krüger, R. H. Holm, *Inorg. Chem.* **1989**, *28*, 1148−1155. [5b] M. Kumar, G. J. Colpas, R. O. Day, M. J. Maroney, *J. Am. Chem. Soc.* **1989**, *111*, 8323−8325. [5c] M. Frey, *Struct. Bond* **1998**, 97−126. [5d] H. Wang, C. Y. Raltson, D. S. Patil, R. M. Jones, W. M. Verhagen, M. Adams, P. C. Riordan, C. A. Marganian, P. Mascharak, J. Kovacs, C. C. Miller, T. J. Collins, S. Brooker, P. D. Croucher, K. Wang, E. I. Steifel, S. P. Cramer, *J. Am. Chem. Soc.* **2000**, *122*, 10544−10552.

[6] [6a] S. Fox, Y. Wang, A. Silver, M. Millar, *J. Am. Chem. Soc.* **1990**, *112*, 3218−3220. [6b] H. J. Krüger, G. Peng, R. H. Holm, *Inorg. Chem.* **1991**, *30*, 734−742. [6c] P. Stavropoulos, M. C. Muetterties, M. Carrièe, R. H. Holm, *J. Am. Chem. Soc.* **1991**, *113*, 8485−8492. [6d] N. Baidya, M. Olmstead, P. K. Mascharak, *Inorg. Chem.* **1991**, *30*, 929−937. [6e] E. J. Lyon, I. P. Georgakaki, J. H. Reibenspies, M. Y. Darensbourg, *J. Am. Chem. Soc.* **2001**, *123*, 3268−3278.

[7] [7a] J. D. Franolic, W. Y. Wang, M. Millar, *J. Am. Chem. Soc.* **1992**, *114*, 6587−6588. [7b] G. J. Colpas, R. O. Day, M. J. Maroney, *Inorg. Chem.* **1992**, *31*, 5053−5055. [7c] M. A. Halcrow, G. Christou, *Chem. Rev.* **1994**, *94*, 2421−2481. [7d] M. T. B. Rauchfuss, S. M. Contakes, S. C. N. Hsu, M. A. Reynolds, S. R. Wikson, *J. Am. Chem. Soc.* **2001**, *123*, 6933−6934.

[8] [8a] S. A. Mirza, R. O. Day, M. J. Maroney, *Inorg. Chem.* **1996**, *35*, 1992−1995. [8b] G. Musie, P. J. Farmer, T. Tuntulani, J. H. Reibenspies, M. Y. Darensbourg, *Inorg. Chem.* **1996**, *35*, 2176−2183. [8c] F. Osterloh, W. Saak, D. Haase, S. Pohl, *Chem. Commun.* **1996**, 777−778. [8d] C-H. Lai, J. H. Reibenspies, M. Y. Darensbourg, *Angew. Chem. Int. Ed. Engl.* **1996**, *35*, 2390−2392. [8e] Th. L. James, L. Cai, M. C. Muetterties, R. H. Holm, *Inorg. Chem.* **1996**, *35*, 4148−4161.

[9] [9a] F. Osterloh, W. Saak, D. Haase, S. Pohl, *Chem. Commun.* **1997**, 979−980. [9b] G. Henkel, M. Kockerling, A. Müller, *Bioinorg. Chem.* **1997**, 456−467. [9c] J. C. A. Grapperhaus, M. Y. Darensbourg, *Acc. Chem. Res.* **1998**, *31*, 451−459. [9d] E. Bouwman, R. K. Henderson, A. L. Spek, J. Reedijk, *Eur. J. Inorg. Chem.* **1999**, *4*, 217−219.

[10] [10a] D. Sellmann, S. Fünfgelder, G. Pöhlmann, F. Knoch, M. Moll, *Inorg. Chem.* **1990**, *29*, 4772−4778. [10b] D. Sellmann, S. Fünfgelder, F. Knoch, M. Moll, *Z. Naturforsch., Teil B* **1991**, *46*, 1601−1608. [10c] D. Sellmann, H. Schillinger, F. Knoch, M. Moll, *Z. Naturforsch., Teil B* **1992**, *47*, 748−753. [10d] D. Sellmann, W. Prechtel, F. Knoch, M. Moll, *Inorg. Chem.* **1993**, *32*, 538−546. [10e] D. Sellmann, D. Häußinger, F. Knoch, M. Moll, *J. Am. Chem. Soc.* **1996**, *118*, 5368−5374. [10f] D. Sellmann, C. Allmann, F. W. Heinemann, F. Knoch, J. Sutter, *J. Organomet. Chem.* **1997**, *541*, 291−305.

[11] D. Sellmann, D. Häußinger, F. W. Heinemann, *Eur. J. Inorg. Chem.* **1999**, 1715−1725.

[12] D. Sellmann, F. Geipel, F. W. Heinemann, *Eur. J. Inorg. Chem.* **2000**, 271−279.

[13] D. Sellmann, F. Geipel, F. W. Heinemann, *Eur. J. Inorg. Chem.* **2000**, 59−63.

[14] D. Sellmann, F. Geipel, M. Moll, *Angew. Chem. Int. Ed.* **2000**, *39*, 561−563.

[15] D. Sellmann, F. Geipel, F. W. Heinemann, *Chem. Eur. J.* **2000**, *6*, 4279−658.

[16] [16a] A. Kobayashi, R. Takatori, I. Kikuchi, H. Konno, K. Sakamoto, O. Ishitani, *Organimetallics* **2001**, 3361−3363. [16b] S. Fukuzumi, K. Ohkubo, M. Fujitsuka, O. Ito, M. C. Teichmann, E. Maisonhaute, C. Amatore, *Inorg. Chem.* **2001**, *40*, 1213−1219. [16c] C. Kim, I. Novozhilova, M. Scott, G. Kimberly, A. Bagley, P. Coppens, *Inorg. Chem.* **2000**, *39*, 5791−5795. [16d] S. V. Zelenak, *Main Group Met. Chem.* **1999**, *22*, 179−184. [16e] M. Rivas, *New. J. Chem.* **1998**, *22*, 1315−1318. [16f] J. R. Burke, P. A. Fery, *J. Org. Chem.* **1996**, *61*, 530−533. [16g] B. Schiott, Ya-Jun Zheng, T. C. Bruice, *J. Am. Chem. Soc.* **1998**, *120*, 7192−7200. [16h] R. N. Mukerjee, M. S. Venkateshan, *J. Inorg. Nucl. Chem.* **1976**, *38*, 917−919.

[17] [17a] G. D. Figuly, C. K. Loop, J. C. Martin, *J. Am. Chem. Soc.* **1989**, *111*, 654−658. [17b] E. Block, V. Eswarakrishnan, M.

Gernon, G. Ofori-Okai, C. Saha, K. Tang, J. Zubieta, *J. Am. Chem. Soc.* **1989**, *111*, 658−665. [17c] K. Smith, C. M. Lindsay, G. J. Pritchard, *J. Am. Chem. Soc.* **1989**, *111*, 665−669.
[18] [18a] C. D. Johnson, I. Roberts, P. G. Taylor, *J. Chem. Soc., Perkin Trans. 2* **1981**, 409−413. [18b] *Handbook of Chemistry and Physics* (Ed.: R. C. Weast), 68th ed., CRC, Florida, **1988**, pp. D159−D163.
[19] [19a] J-P. Costes, F. Dahan, J. M. Dominguez-Vera, J-P. Laurent, J. Ruiz, J. Sotiropoulos, *Inorg. Chem.* **1994**, *33*, 3809−3813. [19b] A. Becalska, R. J. Batchelor, F. W. B. Einstein, R. H. Hill, B. J. Palmer, *Inorg. Chem.* **1992**, *31*, 3118−3123.
[20] Z. Dori, R. F. Zialo, *Chem. Rev.* **1973**, *73*, 247−254.
[21] *SHELXTL NT 5.1*, Bruker Axs, Inc., Madison, WI, U.S.A. **1998**.
[22] CCDC-170684 (**1**·0.5CD_2Cl_2), -170685 (**1**·2THF·3MeOH), -170686 (**3**), -170687 (**4**·2$CDCl_3$), -170688 (**5**·0.625THF·0.375Et_2O), and -170689 (**7**·THF) contain the supplementary crystallographic data for this paper. These data can be obtained free of charge at www.ccdc.cam.ac.uk/conts/retrieving.html or from the Cambridge Crystallographic Data Centre, 12 Union Road, Cambridge CB2 1EZ, UK [Fax: (internat.) + 44-1223/336-033; E-mail: deposit@ccdc.cam.ac.uk].

Received December 12, 2001
[I01506]

Ruthenium-Catalyzed Isomerization of Allylic Alcohols: Oxidation State Determines Resistance Against Diene Inhibition

Robert C. van der Drift,[a] Jeroen W. Sprengers,[a] Elisabeth Bouwman,*[a] Wilhelmus P. Mul,[b] Huub Kooijman,[c] Anthony L. Spek,[c] and Eite Drent[a]

Keywords: Isomerization / Allylic alcohols / Homogeneous catalysis / Ruthenium / Diene inhibition

The novel complex *mer*-[$RuCl_3$(dmso)(phen)] (**1**) has been prepared and characterized by X-ray diffraction. The ruthenium center is in a distorted octahedral environment with the three chloride ions coordinated in a *mer*-fashion and an *S*-bonded dmso ligand *trans* to one of the phen nitrogen atoms. Electrochemical experiments show two reversible waves in acetonitrile solution, corresponding to the couples $Ru^{III/II}$ (0.11 V) and $Ru^{IV/III}$ (1.73 V). The analogous Ru^{II} complex *cis*,*cis*-[$RuCl_2$(dmso)$_2$(phen)] (**2**) shows one reversible wave at 1.08 V, corresponding to the $Ru^{III/II}$ couple. Both complexes exhibit high catalytic activity in the isomerization of 3-buten-2-ol to butanone. The initial turnover frequency (TOF) for **1** in diglyme/water at 130 °C is 295 h^{-1} with a first-order k_{ini} of 0.6 h^{-1}, while **2** reaches an initial TOF of 260 h^{-1} and a k_{ini} of 0.5 h^{-1}. A cumulative turnover number (TON) of 1025 has been obtained with **1** as a catalyst precursor. The activity of **1** and **2** has been compared to that of in situ mixtures with both Ru^{III} and Ru^{II} precursors. All Ru^{II} complexes are deactivated before 100% conversion has been attained. $RuCl_3$ is a good catalyst precursor with an initial TOF of 500 h^{-1}. If $RuCl_3$ is mixed in situ with one equivalent of phen, an induction period of 40 min results and the activity thereafter is much lower than without the addition of phen. With 2 equiv. of phen, no reaction is observed in the first 6 h and only a very low activity is obtained after that. An important difference between **1** and **2** becomes apparent when a conjugated diene is added to the reaction mixture; only **1** remains active. The results demonstrate that only Ru^{III} complexes with one phen ligand are active catalyst precursors for the isomerization of allylic alcohols in the presence of conjugated dienes. The consequence of this observation is further demonstrated by applying both catalyst precursors in the direct one-pot conversion of 1,3-butadiene to butanone. In this reaction, complex **1** (TON = 2050, t = 6 h) forms a much more active precursor than complex **2** (TON = 1300, t = 7 h).

(© Wiley-VCH Verlag GmbH, 69451 Weinheim, Germany, 2002)

Introduction

Homogeneous catalysis opens new pathways to environmentally benign industrial processes. Many processes in use today produce stoichiometric amounts of inorganic salts. Transition metal catalyzed reactions on the other hand, may offer complete atom-economical routes to important industrial products. For example, butanone (methyl ethyl ketone, MEK) is a megaton-per-year scale solvent traditionally produced from butenes.[1] This process requires the use of stoichiometric amounts of concentrated sulfuric acid as shown in Scheme 1.

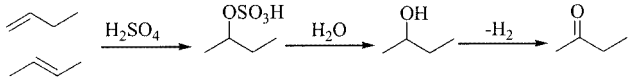

Scheme 1. Present-day synthesis of MEK from a mixture of butenes

1,3-Butadiene is an attractive alternative starting material for the preparation of MEK. A viable route would require water as the only other stoichiometric reagent. After acid-catalyzed hydration of butadiene [see (a) in Scheme 2], the 1,2-addition product 3-buten-2-ol can be isomerized to MEK [see (b) in Scheme 2].[2] The equilibrium of Scheme 2 (a) is 97% on the left-hand side, making a one-pot synthesis preferable in order to circumvent an extensive butadiene recycle. For the selective formation of MEK, this calls for catalysts that catalyze the isomerization of the secondary allylic alcohol 3-buten-2-ol but not the primary allylic alcohol 2-buten-1-ol, in the presence of dienes. Despite consid-

[a] Gorlaeus Laboratories, Leiden Institute of Chemistry, Leiden University,
P. O. Box 9502, 2300 RA Leiden, The Netherlands
Fax: (internat.) + 31-71/527-4451
E-mail: bouwman@chem.leidenuniv.nl
[b] Shell International Chemicals BV, Shell Research and Technology Center Amsterdam,
Badhuisweg 3, 1031 CM Amsterdam, The Netherlands
[c] Bijvoet Center for Biomolecular Research, Crystal and Structural Chemistry, Utrecht University,
Padualaan 8, 3584 CH Utrecht, The Netherlands
Supporting information for this article is available on the WWW under http://www.eurjic.com or from the author.

erable efforts this type of catalysts remain scarce.[3] Alternatively, other reagents such as alcohols and amines could be used instead of water to obtain higher conversions, and after isomerization and hydrolysis of the vinyl ether or enamine the carbonyl compound can be obtained.[4,5] In this case an extra, costly purification step will be required to separate MEK from butanal (or to separate the intermediates).

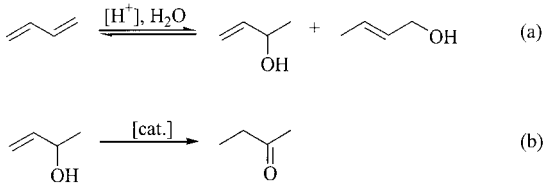

Scheme 2. (a) Acid-catalyzed hydration of 1,3-butadiene (b) followed by isomerization yields MEK in a complete atom-economical process

The feasibility of the one-pot synthesis of MEK from 1,3-butadiene was shown by Drent and co-workers.[6,7] A catalytically active species obtained by in situ mixing of [Ru(acac)$_3$] (Hacac = 2,4-pentanedione) and between 1 and 2 equiv. of 2,2′-bipyridine (bpy) or 1,10-phenanthroline (phen) catalyzes the direct conversion of 1,3-butadiene to MEK (in over 95% selectivity) with a maximum of 1200 turnovers in 32 h. Yet, this turnover number (TON) is not sufficiently high to make this route economically successful. An important catalyst deactivation route proved to be ligand redistribution that results in inactive ruthenium complexes with two and three didentate nitrogen-donor ligands (Scheme 3).[7] Indeed, it has been demonstrated recently that reducing the extent of ligand redistribution may increase the initial activity by a factor of almost ten.[8]

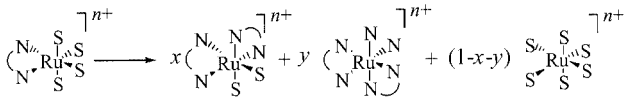

Scheme 3. Ligand redistribution of mono(phen)Ru complexes; S = vacant site or labile ligand; N$_\cup$N = phen; $2x + 3y = 1$, $n = 2, 3$

Although the catalyst precursor consists of an Ru^{III} complex, both Ru^{III} and Ru^{II} complexes can be identified with mass spectrometry (MS) in a used catalyst. This observation raises the question as to what the oxidation state of the ruthenium atom in the catalytically active species is. In this paper the synthesis and characterization of the Ru^{III} compound *mer*-[RuCl$_3$(dmso)(phen)] (**1**) and the analogous Ru^{II} complex *cis,cis*-[RuCl$_2$(dmso)$_2$(phen)] (**2**) are described. The activities of both complexes in the key step of the catalytic process, the isomerization of 3-buten-2-ol to MEK, are compared in the absence and the presence of isoprene (2-methyl-1,3-butadiene) to reveal the role of the ruthenium oxidation state in the isomerization of allylic alcohols.

Results and Discussion

Synthesis and Structure of *mer*-[RuCl$_3$(dmso)(phen)] (1) and *cis,cis*-[RuCl$_2$(dmso)$_2$(phen)] (2)

Synthesis of 1 and 2

To obtain a clear view of the influence of the ruthenium oxidation state in the catalytic process, two complexes are required with ligand environments as identical as possible. It was deduced from earlier studies[7,8] that the catalytically active species should contain only one phen ligand. Furthermore, the complexes should contain innocent ligands that are easily replaced during the catalytic cycle. Numerous ruthenium complexes with two or three phen ligands are known,[9,10] but examples of mono(phen) complexes remain scarce.[9–13] It is especially difficult to prevent ligand redistribution during synthesis.[12] The synthesis of mono(phen) complexes was attempted in our laboratory starting from [Ru(H$_2$O)$_6$](OTs)$_2$, [Ru(MeCN)$_6$](OTf)$_2$ [14] and RuCl$_3$. In all cases, it proved impractical to obtain the ruthenium atom in both the 2+ and 3+ oxidation states. The syntheses of [Ru(acac)$_2$(phen)] and [Ru(acac)$_2$(phen)]PF$_6$ were successful,[15] but the acac ligand could not be replaced under the reaction conditions.

A literature method to prepare the Ru^{II} complex **2**[12] from *cis*-[RuCl$_2$(dmso)$_4$] and phen in CHCl$_3$ gave only low yields in our hands, but changing the solvent to toluene[16] resulted in direct precipitation of the pure product from the reaction mixture [see (c) in Scheme 4]. An additional and vital advantage of this method is the complete absence of bis- and tris(phen)ruthenium complexes. Upon slow concentration of a CHCl$_3$/toluene solution of **2**, red crystals of **1** were obtained; a lead to the synthesis of the analogous Ru^{III} complex **1** was found. CHCl$_3$ is known to contain traces of HCl and recently the syntheses of several complexes with the general formula [RuCl$_3$(dmso)L], where L is triazole, thiadiazole or diamine, by oxidation with HCl were reported.[17,18] Indeed, it proved feasible to prepare **1** by oxidation of *cis*-[RuCl$_2$(dmso)$_4$] with HCl in the presence of phen [see (a) and (b) in Scheme 4]. The formation of an Ru^{III} species from an Ru^{II} precursor can be envisioned to involve simultaneous reduction of the dmso ligand to dimethyl sulfide as proposed by Cingi et al. [see Equation (1)].[17] A general path to the Ru^{II} species that does not invoke ligand participation is discussed below. The room-temperature route [see (a) in Scheme 4] results directly in analytically pure **1**, but the overall yield with the high-temperature route [see (b) in Scheme 4] is higher. It should be noted, however, that at higher reaction temperatures with longer reaction times and using concentrated HCl, other products may precipitate, which are probably oligomeric analogs of **1**.

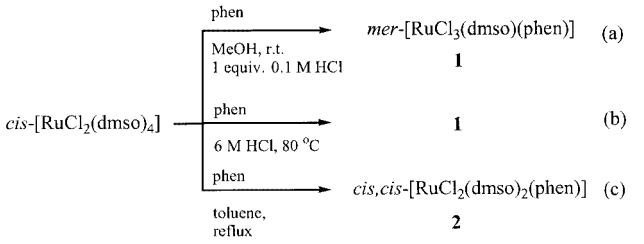

Scheme 4. Synthesis of **1** (a) (b) and **2** (c) from *cis*-$[RuCl_2(dmso)_4]$

$$2\ cis,cis\text{-}[RuCl_2(dmso)_2(phen)] + 2\ HCl \longrightarrow 2\ mer\text{-}[RuCl_3(dmso)(phen)] + Me_2S + dmso + H_2O \quad (1)$$

Crystal Structure Determination of 1

An ORTEP drawing of **1** is shown in Figure 1. Some selected bond lengths and angles are given in Table 1. The ruthenium center is in a distorted octahedral environment with coordination of one didentate phen ligand, three chloride ions and one *S*-bonded dmso ligand *trans* to one of the phen nitrogen atoms. The S−O bond is in the same plane as the phen ligand. Both ruthenium−nitrogen distances are in the range found for other ruthenium complexes with aromatic nitrogen donor ligands.[13,17] The Ru(1)−S(21) bond is longer than in analogous Ru^{II} complexes,[17] which reflects the smaller degree of π-back donation in this Ru^{III} complex. The S(21)−O(22) bond [1.478(2) Å] is slightly shorter than in free dmso [1.492(1) Å][19] indicating greater S−O double-bond character in the *S*-bonded dmso. The bonds within the phen ligand are similar to those in other (phen)ruthenium complexes.[13]

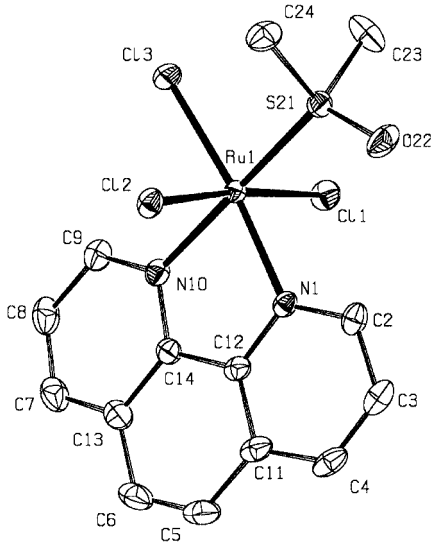

Figure 1. ORTEP plot and numbering scheme of the major component of complex **1**; hydrogen atoms and toluene solvent molecules are omitted for clarity; thermal ellipsoids are drawn at the 50% probability level

Table 1. Selected bond lengths and angles for **1**·toluene

Bond lengths [Å]			
Ru(1)−N(1)	2.099(2)	Ru(1)−Cl(3)	2.3477(8)
Ru(1)−N(10)	2.087(2)	Ru(1)−S(21)	2.2971(8)
Ru(1)−Cl(1)	2.3267(8)	S(21)−O(22)	1.478(2)
Ru(1)−Cl(2)	2.3444(8)		
Angles [°]			
N(1)−Ru(1)−N(10)	78.99(8)	N(10)−Ru(1)−S(21)	178.75(7)
N(1)−Ru(1)−Cl(1)	86.27(6)	S(21)−Ru(1)−Cl(1)	90.73(2)
N(1)−Ru(1)−Cl(2)	87.08(6)	S(21)−Ru(1)−Cl(2)	90.87(2)
N(1)−Ru(1)−Cl(3)	172.34(6)	S(21)−Ru(1)−Cl(3)	87.06(2)
N(1)−Ru(1)−S(21)	100.60(6)	Cl(1)−Ru(1)−Cl(2)	173.34(3)
N(10)−Ru(1)−Cl(1)	90.42(6)	Cl(1)−Ru(1)−Cl(3)	93.49(2)
N(10)−Ru(1)−Cl(2)	87.93(7)	Cl(2)−Ru(1)−Cl(3)	93.05(2)
N(10)−Ru(1)−Cl(3)	93.35(6)		

The Cl(1)−Ru(1)−Cl(2) angle is significantly smaller than 180° due to steric repulsion of the dmso methyl groups; the N(1)−Ru1−N(10) bond angle of 78.99(8)° is contracted compared to the ideal octahedral value by the small phen bite angle, which is somewhat smaller than in the complex where dmso is replaced by CO.[13] In this complex the phen ligand itself is boat-shaped to some extent, with angles between pairs of least-squares planes (through each of the three rings) ranging from 4.97(13) to 10.30(12)°. In the crystal packing a high degree of stacking is observed. Only two rings of each phen ligand are stacked with two rings of a phen ligand on an adjacent complex molecule (generated by symmetry operation $1 - x, -y, 1 - z$), avoiding steric repulsion between neighboring dmso groups. Approximately perpendicular to this, the cocrystallized toluene molecules form dimers, totally enclosed by molecules **1**, through stacking interactions.

Cyclic Voltammetry Studies on 1 and 2

The redox properties of both complexes have been investigated with cyclic voltammetry. In an acetonitrile solution, **1** exhibits two reversible one-electron waves (Figure 2). The first peak ($E_{1/2}$ = 0.11 V, ΔE_p = 60 mV) corresponds to the $Ru^{III/II}$ couple, whereas the second peak ($E_{1/2}$ = 1.73 V, ΔE_p = 54 mV) corresponds to the $Ru^{IV/III}$ couple. The nature of both couples has been corroborated by linear sweep voltammetry that shows the expected signs of the currents. The current for both peaks is linearly dependent on $v^{1/2}$ for the scan rates studied (0.05−1 V s^{-1}) indicating reversible diffusion-controlled processes.[20] The potential of the first wave is evidence for the ease of reduction of **1,** which plays an important role in isomerization catalysis (vide infra).

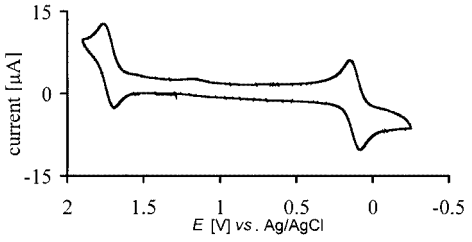

Figure 2. Cyclic voltammogram of **1** in acetonitrile at room temperature; scan rate: 0.1 V s^{-1}

The reversibility of the second peak is remarkable, demonstrating a robust Ru^{IV} complex, this was also observed in the analogous compound *mer*-[$RuCl_3$(dmso)(tmen)] (tmen = *N*,*N*,*N*′,*N*′-tetramethylethylenediamine).[18] From this peak it can be concluded that dmso in **1** is primarily a σ-donor and remains *S*-bonded even with the ruthenium atom in the 4+ oxidation state.

Complex **2** shows one reversible one-electron wave ($E_{1/2}$ = 1.08 V, ΔE_p = 56 mV), corresponding to the $Ru^{III/II}$ couple (Figure 3). In this case, the current for this peak is also linearly dependent on $v^{1/2}$ for the scan rates studied (0.05−1 V s^{-1}) and the oxidation state of **2** has been proven with linear sweep voltammetry. In the reductive part of the voltammogram (at potentials < −1.0 V) an irreversible wave is observed that can be attributed to a ligand-based reduction or reduction of the ruthenium center to Ru^0.

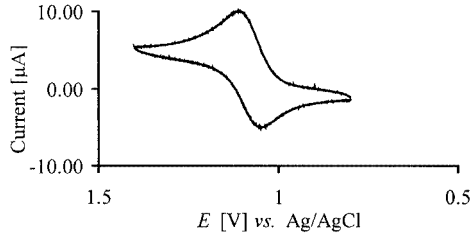

Figure 3. Part of the cyclic voltammogram of **2** in acetonitrile at room temperature showing the $Ru^{III/II}$ wave; scan rate: 0.1 V s^{-1}

Isomerization of 3-Buten-2-ol to MEK

The Influence of a Conjugated Diene

The key step in the direct conversion of 1,3-butadiene to MEK has been identified as the isomerization of 3-buten-2-ol to MEK in the presence of 1,3-butadiene.[3,7] Since 1,3-butadiene is a suspected carcinogenic and due to its high volatility (b.p. −4 °C) it is difficult to handle in standard glassware, so it was decided instead to use isoprene in this study. Isoprene is converted analogously to MIPK [methyl isopropyl ketone, Equation (2)] and can thus function as a reasonable substitute for 1,3-butadiene.[7] The results of isomerization of 3-buten-2-ol to MEK catalyzed by several Ru^{III} (Entries 1−5) and Ru^{II} catalyst precursors (Entries 6−10) both in the absence and presence of isoprene are collected in Table 2.

Table 2. Isomerization of 3-buten-2-ol to MEK catalyzed by Ru^{III} and Ru^{II} complexes

Entry[a]	Catalyst precursor	TON	TON with isoprene[b]
1	[$RuCl_3 \cdot xH_2O$]	285	95
2	[$RuCl_3 \cdot xH_2O$] + 1 equiv. phen	390	300
3	**1**	465	440
4	**1**[c]	n.d.	475
5	**1** + 3 equiv. AgOTs	410	n.d.
6	*cis*-[$RuCl_2(dmso)_4$]	325	110
7	*cis*-[$RuCl_2(dmso)_4$] + 1 equiv. phen	275	75
8	**2**	290	150
9	**2** + 2 equiv. AgOTs	295	n.d.
10	**2**[d]	270	n.d.

[a] Reactions were performed in a 25-mL sealed glass vessel at 130°C; substrate: 3-buten-2-ol (5.8 mmol); catalyst: ruthenium complex (0.011 mmol) plus ligand as appropriate; substrate/catalyst: 530; solvent: water/diglyme (1:3 mL); reaction time: 6 h; n.d. = not determined. [b] 10 mmol of isoprene was added prior to addition of the substrate. [c] 15 mmol of isoprene. [d] In Ar with standard Schlenk techniques.

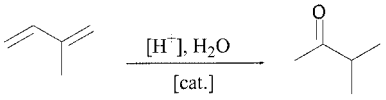

(2)

It is clear that both Ru^{III} and Ru^{II} complexes are capable of catalyzing the isomerization of 3-buten-2-ol to MEK, but Ru^{III} precursors consistently show higher conversion. The result of Entry 10 demonstrates that exclusion of air is not essential to obtaining good activity. Comparison of Entries 1 and 6 with 2 and 7, respectively, shows that the phen ligand as such is not a necessary requirement for activity. Both in situ mixing of the components and the use of preformed catalyst precursors gave comparable results. If a higher substrate/**1** ratio is applied, a TON of 1025 in 12 h can be obtained with an average TOF of 85 h^{-1}. The negative influence of an increased ligand-redistribution rate is demonstrated by successive removal of chloride ions by Ag^I salts from either **1** or **2**, which results in the same or only slightly lower catalytic activity (Entries 5 and 9). Presumably, the anticipated higher activity, as a consequence of more vacant coordination sites, is counterbalanced by an increased rate of ligand redistribution. Addition of a fourfold excess of Ag^I gives a color change of the reaction mixture to dark blue and almost complete loss of activity.

While a large number of catalysts are able to catalyze the isomerization of allylic alcohols to carbonyl compounds,[2] almost all of these fail to do so in the presence of dienes. The crucial next step therefore is to compare the catalytic systems *in the presence* of isoprene. From Table 2, it becomes apparent that isoprene indeed has a dramatic effect on the catalysis. Two factors are proven to play a role in resistance against isoprene inhibition. First, although phen is not required for activity in the absence of isoprene, the significant difference in activity of the catalyst precursors in Entries 1 and 2 shows that phen is an essential component for catalytic activity in the presence of isoprene. Second, all Ru^{II} catalyst precursors (Entries 6−9) loose 50% or more of their activity with isoprene in the reaction mixture. The presence of phen here (Entry 7) does not lead to resistance against diene inhibition. Thus, both of the requirements, a 3+ oxidation state and one phen ligand, have to be met. Complex **1** remains active, even if more isoprene is added (Entry 4, > 1300 mol-equiv. to ruthenium). These results unambiguously show, for the first time, the crucial influence of the oxidation state of the ruthenium center in allylic alcohol isomerization in the presence of a diene. Comparison of several catalytic precursors lacking or con-

taining various amounts of dmso ligands (cf. Table 2, Entries 2 and 3, 7 and 8), especially in the presence of isoprene, shows that the influence of the ligands on the difference in activity is marginal.

Isomerization Profile in Time

The difference in isomerization activity of Ru^{III} complex **1** and Ru^{II} complex **2** in the absence of isoprene is smaller than suggested by the overall results given in Table 2. The results plotted in Figure 4 clearly indicate that the reaction does not obey clean first-order kinetics. Therefore, *initial* TOFs and *initial* first-order rate constants (k_{ini}) have been calculated for both complexes.[21] The values obtained for **1** (TOF = 295 h^{-1}; k_{ini} = 0.6 h^{-1}) are similar to those found for **2** (TOF = 260 h^{-1}; k_{ini} = 0.5 h^{-1}). Although initial activity is comparable, **2** is deactivated much faster under the reaction conditions. The influence of isoprene is nicely illustrated (Figure 4). In the initial stages of the reaction, complex **2** still catalyzes the formation of MEK, but both initial TOF (75 h^{-1}) and k_{ini} (0.1 h^{-1}) are significantly lower than they are in the absence of isoprene. This remarkable finding may also explain the relatively low conversion reached by Ru^{II} complexes in the absence of isoprene: under the reaction conditions, some reversion (dehydration) occurs [see (a) in Scheme 2] that yields 1,3-butadiene as evidenced by GLC analysis of the gas cap. The increasing concentration of 1,3-butadiene in time causes a decrease of the number of active catalyst centers until finally catalysis is stopped completely.

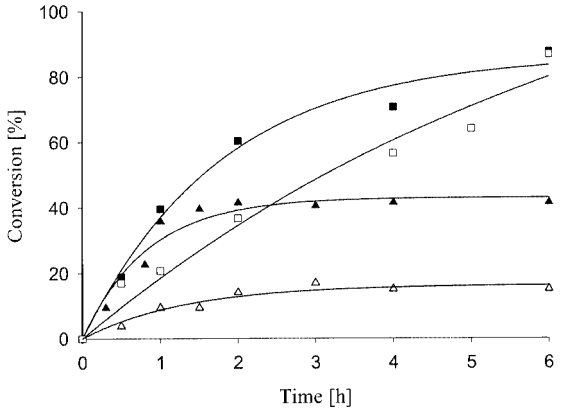

Figure 4. Isomerization of 3-buten-2-ol to MEK catalyzed by complexes **1** (squares) and **2** (triangles) at 130 °C in water/diglyme (1:3 mL) in the absence (filled symbols) and presence (open symbols) of 10 mmol of isoprene; substrate/catalyst precursor = 530

The initial rate of isomerization in the presence of isoprene is also lower with **1** as the catalyst precursor (TOF = 140 h^{-1}, k_{ini} = 0.3 h^{-1}), but deactivation in time does not occur and a high conversion can be attained in 6 h. Previous studies with $Ru(acac)_3$ and phen or bpy likewise showed a decrease in the reaction rate in the presence of 1,3-butadiene, but this system also remained active.[7]

The results of a time-dependent investigation using catalysts formed from [$RuCl_3 \cdot xH_2O$] and varying amounts of phen at 100 °C are shown in Figure 5. In the absence of phen, the isomerization is first order in 3-buten-2-ol with an initial TOF of 500 h^{-1} after a negligible induction period. When 1 equiv. of phen is added, the induction time increases to 40 min. Moreover, the initial TOF drops to 105 h^{-1}. In the original catalytic system with $Ru(acac)_3$, addition of either 1 or 2 equiv. of phen resulted in equal reactivity.[7] In sharp contrast to this, the activity of $RuCl_3$ with 2 equiv. of phen is virtually zero. After more than 16 h of reaction time, a small amount of MEK (60 turnovers) is obtained, but this must have been formed after an induction period of at least 5 h (Figure 5). The variation in lengths of the induction periods most likely originates from a kinetic difference in displacement of the various ligands involved. If isomerization is to occur with [$RuCl_3 \cdot xH_2O$] as the catalyst precursor, water has to be replaced by the substrate, which appears to be reasonably fast. Upon addition of 1 equiv. of phen, [$RuCl_3(H_2O)$(phen)] is formed. In this case, dissociation of one or more chloride ions has to take place prior to catalysis, which is considerably slower.[22] An induction period is not often observed in transition metal catalyzed isomerization of allylic alcohols and it seems to point at a cooperative effect; dissociation of the second and subsequent chloride ions is faster after dissociation of the first chloride ion. A similar effect has also been observed in isomerization of 3-buten-2-ol to MEK catalyzed by [$Ru(MeCN)_6$].[14] Increasing the polarity of the reaction mixture, by doubling the water content, should facilitate dissociation. Indeed, the induction period is reduced to 20 min, while the initial TOF is raised to 215 h^{-1}. At the higher reaction temperatures used with complexes **1** and **2** (Figure 4), chloride dissociation is much faster and only a small induction period is observed. If 2 equiv. of phen are added to $RuCl_3$, [$Ru(phen)_2Cl_2$]Cl is formed. In an analogous isomerization reaction catalyzed by $RuCl_3$ with 2 equiv. of 2,2′-bipyridine, only [$RuCl_2(bpy)_2$]Cl and related dinuclear species are observed with electrospray MS,[15] while complexes with only one bpy ligand are not found under these

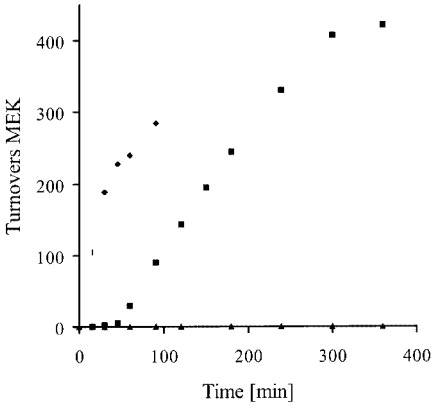

Figure 5. Isomerization of 3-buten-2-ol to MEK with $RuCl_3$ (◆) and $RuCl_3$ plus 1 (■) and 2 (▲) equiv. of phen at 100 °C in water/diglyme (1:3)

conditions. Given the slow dissociation of chloride ions from Ru^{III},[22] catalytic activity is now difficult to achieve.

Direct Conversion of 1,3-Butadiene to MEK

In the presence of *p*-toluenesulfonic acid, the preformed complex **1** is active in the direct conversion of 1,3-butadiene to MEK (Scheme 2). A TON of 2050 is reached in 6 h with a selectivity for MEK of over 95% in water/diglyme at 145 °C. Remarkably, in view of the isomerization results above, **2** also catalyzes the formation of MEK from 1,3-butadiene. The TON of 1300 in 7 h, however, is considerably lower than the TON reached with **1** as the catalyst precursor. The activity of **2** may be ascribed to the in situ oxidation of Ru^{II} to Ru^{III} by the acid present in the reaction mixture for the hydration of 1,3-butadiene. As schematically shown in Equation (3), oxidative addition of a proton initially leads to an Ru^{IV} hydride species. After protonation of the hydride yielding dihydrogen, the resulting Ru^{IV} species may comproportionate with a second Ru^{II} complex to give two Ru^{III} complexes. On the other hand, complex **1** can be reduced, under these reaction conditions, to the inactive Ru^{II} species according to Equation (4). Coordination of a substrate alkoxide followed by β-hydrogen elimination gives an Ru^{III} hydride and an aldehyde. After reductive elimination of 1 equiv. of HCl, the resulting Ru^{I} species may comproportionate with a starting Ru^{III} complex to give two Ru^{II} species.

$$\mathrm{Ru(II) + HCl \longrightarrow HRu(IV)Cl \xrightarrow[-H_2]{HCl} Ru(IV)Cl_2 \xrightarrow{Ru(II)} 2\,Ru(III)Cl} \quad (3)$$

$$\mathrm{Cl_3Ru(III) + {}^{-}OCH_2R \xrightarrow[-Cl^-]{} Cl_2Ru(III)OCH_2R \xrightarrow[-O{=}CHR]{}}$$

$$\mathrm{HCl_2Ru(III) \xrightarrow[-HCl]{} ClRu(I) \xrightarrow{Cl_3Ru(III)} 2\,Cl_2Ru(II)} \quad (4)$$

Analysis of reaction mixtures containing either catalyst precursors **1** or **2** with electrospray MS clearly shows the presence of Ru^{II} and Ru^{III} species in both cases. Since both catalyst precursors exhibit a significantly different activity, apparently an equilibrium has not been reached during the early stages of the reaction. The formation of Ru^{II} complexes, even to a significant extent in the presence of (oxidizing) acid, is unfortunate and should receive further attention in attempts to maximize catalytic activity. However, simply increasing the acid concentration to keep the ruthenium centers in the 3+ oxidation state results in an increased amount of side reactions such as 1,3-butadiene polymerization.

The direct conversion of 1,3-butadiene was previously shown to also be catalyzed by an in situ mixture of $RuCl_3$ and one phen ligand.[8] In fact, the performance of this system with an initial TOF of 960 h^{-1} and a cumulative TON of 2700 in 5 h is significantly better than the $Ru(acac)_3$/phen system.[7] In connection with the present study it is interesting to recall that electrospray MS spectra showed the presence of species with ruthenium in the oxidation state 3+ or 2+.[8] It can now be concluded that the latter species are inactive under the actual 1,3-butadiene hydration/isomerization reaction conditions used.

Mechanistic Rationale of Diene Inhibition

Two general mechanisms have been proposed for isomerization of allylic alcohols: the intramolecular π-allylmetal hydride mechanism and the intermolecular metal hydride addition/elimination mechanism.[2] Neither mechanism assigns a specific role to the oxygen moiety during the catalytic cycle. However, complexes **1** and **2** are inactive in the isomerization of unsubstituted alkenes such as 1-octene. So, a third, fundamentally different mechanism that invokes coordination of the oxygen moiety was proposed that is shown in Scheme 5.[3,23]

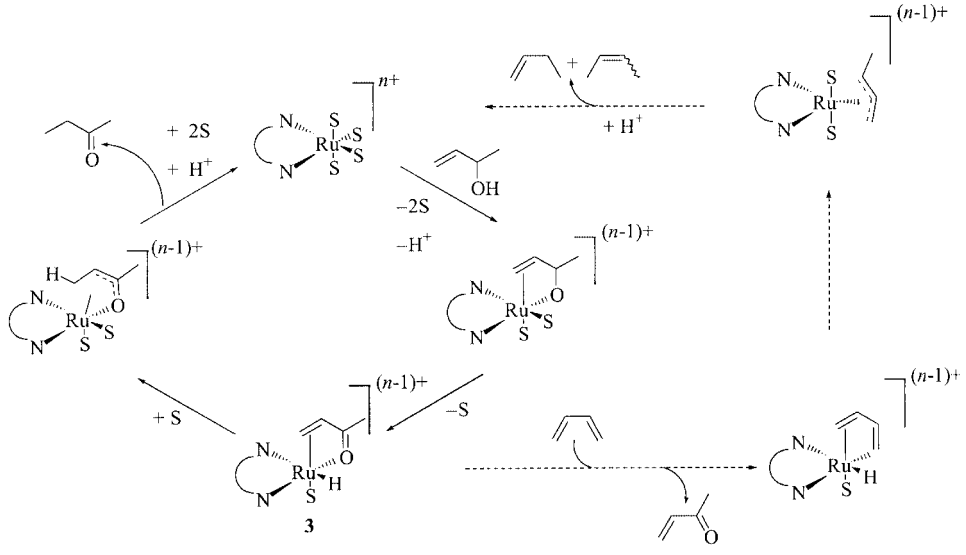

Scheme 5. Mechanism of isomerization of 3-buten-2-ol invoking oxygen coordination; indicated with dotted arrows is a possible deactivation/regeneration route involving a π-allyl species; S = labile ligand or $2e^-$ vacant site; $N_{\cup}N$ = phen, n = 2, 3

The first step is the coordination of 3-buten-2-olate to the ruthenium center after deprotonation of the substrate. This coordination can either be directly didentate as shown in Scheme 5, or occur in two consecutive steps with initial coordination of the double bond.[3] β-Hydrogen abstraction yields the (enone)ruthenium hydride species **3**. After readdition of the hydride ion to give an (oxaallyl)ruthenium complex, protonation affords MEK and regenerates the starting complex.

Two possibilities of catalyst deactivation by conjugated dienes can be envisioned. The simplest mode of action is preferential coordination; if isoprene coordinates much stronger to the ruthenium center than 3-buten-2-ol, no isomerization can take place. Although at this point we cannot completely exclude formation of a stable (isoprene)ruthenium complex with either **1** or **2**, NMR studies with ruthenium(II) complexes in our laboratory indicated a stronger initial coordination of 3-buten-2-ol.[15]

Intermediate **3** forms a second possible handle for diene inhibition as dienes are known to form stable π-allyl complexes after reaction with ruthenium hydrides.[24] Throughout a normal catalytic cycle with extremely fast intramolecular hydrogen transfer no long-lived (“free”) hydride is present. However, if methyl vinyl ketone (MVK) dissociates from **3**, the resulting ruthenium hydride may react with isoprene to form a (presumably inactive) (methylallyl)ruthenium complex. Whereas pure 1-octene is not isomerized in the presence of **1** or **2**, *trans*-2-octene (ca. 10 turnovers with either **1** or **2** as catalyst precursor) can be detected by GLC during the isomerization of 3-buten-2-ol in the presence of 1-octene, a strong support for the presence of free hydrides. Hydrides resulting from direct oxidative addition of acids to the ruthenium atom in **1** or **2** (vide supra) appear to be short-lived as 1-octene isomerization is not observed upon addition of HOTs in the absence of allylic alcohols.

The behavior of both catalyst precursors **1** and **2** is similar with the GLC detection of approximately 30 turnovers of MVK with respect to ruthenium. It should be noted that in both cases a mixture of Ru^{III} and Ru^{II} species is produced and it cannot be determined which of the two is responsible for MVK formation. The higher selectivity to MEK with catalyst precursor **1** suggests a lower rate of MVK dissociation in this case. The amount of MVK formed is more than stoichiometric and there must therefore be a way to regenerate the original catalytically active species from a ruthenium hydride or a (π-allyl)ruthenium species. A tentative route for a ruthenium hydride involves reaction of the hydride with the protic allylic alcohol to generate dihydrogen gas. Alternatively, protonation of an allylruthenium species will yield alkenes. A GLC gas-cap analysis of $RuCl_3$/phen-catalyzed isomerization of 3-buten-2-ol in the presence of isoprene demonstrates the presence of a mixture of C_5 alkenes, which is nicely explained by the protonation of π-allyl species.

Thus, the reaction of a diene with a free ruthenium hydride may explain the deactivation of the catalyst, but at this point no conclusion can be drawn as to why Ru^{III} complexes are much more resistant to this deactivation route and various explanations may be offered. Perhaps ruthenium(III) hydrides are less easily formed, as dissociation of MVK, coordinated through both the oxygen moiety and the double bond, from the higher charged Ru^{III} center may be relatively slower than from Ru^{II}. Alternatively, the removal of a π-allyl species by protonation might be faster with (allyl)Ru^{III} species. We currently favor the former explanation as more plausible, but molecular modeling aided by well-designed experiments should further clarify the peculiar difference in reactivity between Ru^{III} and Ru^{II} complexes.

Conclusion

In conclusion, the novel ruthenium(III) complex **1** has been synthesized and characterized by X-ray diffraction. The comparison with its Ru^{II} analog **2** revealed an important difference in catalytic activity in isomerization of allylic alcohols. Whereas both complexes show high activity in the isomerization of 3-buten-2-ol to MEK, only **1** remains active in the presence of the conjugated diene isoprene. Comparison with other catalyst precursors demonstrated that not only an Ru^{III} oxidation state is required for activity in the presence of isoprene, but also that one phen ligand has to be present in the complex. This is the first time that the role of the oxidation state has been pinpointed, implying that a second major deactivation route is discovered in the ruthenium-catalyzed direct conversion of 1,3-butadiene to MEK, next to ligand redistribution. In fact, while **1** gives high turnovers of MEK (up to 2050), **2** is less active (TON = 1300). The activity of **2** is most likely caused by in situ oxidation to **1** by the acid present in the reaction mixture. The reduction potential of **1** (0.11 V, $Ru^{III/II}$) and the oxidation potential of **2** (1.08 V, $Ru^{III/II}$) indicate that under the applied reaction conditions a delicate balance between both Ru^{III} and Ru^{II} complexes will be present in solution, which is confirmed by MS. Further studies are aimed at complexes with higher redox potentials with ligands that may provide stabilization of Ru^{III}.

Experimental Section

General Remarks: *cis*-$[RuCl_2(dmso)_4]$[12] was prepared according to a literature procedure. $[RuCl_3{\cdot}xH_2O]$ (Aldrich), 3-buten-2-ol (Aldrich), isoprene (Acros) and other reagents and solvents were commercially available and used as received, except 1-octene, from which peroxides were removed by flash chromatography on alumina immediately prior to use. Quantitative gas liquid chromatography (GLC) analyses were carried out with a Chrompack apparatus equipped with a CP wax 58 (FFAP) CB column (25 m × 1.2 μm) with toluene as internal standard. Melting points were measured with a Büchi apparatus and are uncorrected. Matrix Assisted Laser Desorption Ionization (MALDI) Time of Flight (TOF) mass spectra were recorded with a Finnigan MAT Vision 2000 spectrometer. The analytes were mixed with a 2,5-dihydroxybenzoic acid (DHB) or a α-cyano-4-hydroxycinnamic acid (α-CHCA) matrix. Elemental analyses were performed with a Perkin−Elmer series II 2400 CHNS/O analyzer. IR spectra were

obtained with a Perkin−Elmer Paragon 1000 FT-IR spectrophotometer equipped with a golden gate ATR device, using the reflectance technique (4000−300 cm^{-1}). ^1H NMR spectra (300.1 MHz) were measured with a Bruker 300 DPX. Chemical shifts (δ) are reported in ppm. Proton chemical shifts are relative to TMS.

***mer*-[$RuCl_3$(dmso)(phen)] (1):** A bright yellow solution of [$RuCl_2(dmso)_4$] (1.0 g, 2.1 mmol) and phen (0.39 g, 2.2 mmol) in 6 M HCl was heated at 80 °C for 2.5 h, after which time the resulting orange-red mixture was filtered. The filtrate was concentrated in a rotary evaporator. Flash chromatography of the red-brown solid on Al_2O_3 with CH_2Cl_2/MeOH (10:1) as eluent gave **1** as a dark red solid. Yield: 0.71 g, 74%. Alternatively, **1** can be prepared in situ from *cis*-[$RuCl_2(dmso)_4$] and phen at room temperature in MeOH with 1 equiv. of 0.1 M HCl (yield: 30%). Crystals suitable for X-ray analysis can be obtained from slow concentration of an MeOH solution at room temperature. M.p. 182 °C (decomp.). Paramagnetic ^1H NMR ($CDCl_3$): δ = −17.3 (br. s, 6 H, dmso), −8.9 (br. s, 1 H, phen), 2.2 (br. s, 1 H, phen), 8.2 (br. s, 1 H, phen), 8.5 (br. s, 1 H, phen), 11.5 (br. s, 1 H, phen) ppm. Other phen peaks were too broad to be observed. MALDI-TOF MS: *m*/*z* = 497 [M − 2 Cl − dmso + (α-CHCA−H)]$^+$. IR: $\tilde{\nu}$ = 3055 (νC−H), 2923 (νC−H), 1429−1411 (δC−H), 1342−1309 (δC−H), 1106 (νS−O), 1094 (νS−O), 328 (νRu−Cl). $C_{14}H_{14}Cl_3N_2ORuS$ (465.5): calcd. C 36.1, H 3.0, N 6.0, S 6.9; found C 36.9, H 2.9, N 6.0, S 7.0.

***cis*,*cis*-[$RuCl_2(dmso)_2$(phen)] (2):** This complex was prepared analogous to the method described in ref.[16] from *cis*-[$RuCl_2(dmso)_4$] (0.20 g, 0.41 mmol) and phen (0.07 g, 0.4 mmol). Yield: 0.18 g, 86%; m.p. > 300 °C (decomp.). ^1H NMR ($CDCl_3$): δ = 2.44 (s, dmso), 3.12 (s, dmso), 3.59 (s, dmso), 3.62 (s, dmso), 7.76 (dd, 1 H, ArH^3 or ArH^8, ^3J = 5.1, ^3J = 8.1 Hz), 7.87 (dd, 1 H, ArH^3 or ArH^8, ^3J = 5.1, ^3J = 8.1 Hz), 7.92 (d, 1 H, ArH^5 or ArH^6, ^3J = 9.0 Hz), 7.98 (d, 1 H, ArH^5 or ArH^6, ^3J = 9.0 Hz), 8.37 (d, 1 H, ArH^4 or ArH^7, ^3J = 8.1 Hz), 8.47 (d, 1 H, ArH^4 or ArH^7, ^3J = 8.1 Hz), 9.98 (d, 1 H, ArH^2 or ArH^9, ^3J = 5.1 Hz), 10.07 (d, 1 H, ArH^2 or ArH^9, ^3J = 5.1 Hz) ppm. MALDI-TOF MS: *m*/*z* = 435 [M − 2Cl + (DHB−H)]$^+$. IR (cm^{-1}): $\tilde{\nu}$ = 3049 (νC−H), 2924 (νC−H), 1418 (δC−H), 1302 (δC−H), 1082 (νS−O), 930 (νS−O), 328 (νRu−Cl). $C_{16}H_{20}Cl_2N_2O_2RuS_2$·0.1toluene (517.3): calcd. C 38.7, H 4.0, N 5.4, S 12.4; found C 38.4, H 3.9, N 5.7, S 11.5.

Cyclic Voltammetry Experiments: The electrochemistry measurements were performed with an Autolab PGstat 10 potentiostat controlled by GPES4 software. A three-electrode system was used, consisting of a platinum (Pt) working electrode, a platinum (Pt) auxiliary electrode and an Ag/AgCl reference electrode. The experiments were carried out in acetonitrile at room temperature under argon with tetrabutylammonium hexafluorophosphate as electrolyte (0.1 M). Under these conditions the ferrocenium/ferrocene couple was located at +0.436 V with a peak separation of 0.099 V. All potentials are reported relative to Ag/AgCl. Linear voltammograms were obtained with a rotating (500 rpm) platinum disc as working electrode at a scan rate of 0.005 V s^{-1}.

Isomerization Experiments: Catalytic reactions were performed in a closed glass vessel under air. The reaction vessel was charged with ruthenium precursor (0.011 mmol), ligand as appropriate (0.011 mmol, see text) and substrate (5.8 mmol). In some experiments an Ag^I salt (silver tosylate and silver triflate gave identical results) was added in the required stoichiometric amount. After addition of the solvent mixture water/diglyme (1:3 mL) and internal standard (toluene, 0.3 mL), the vessel was closed and the mixture was stirred in a pre-heated oil bath at 130 °C for 6 h. After cooling to room temperature, the mixture was analyzed by GLC. Several time-dependent measurements were performed at 100 °C under argon by using standard Schlenk techniques (see Figure captions). In isoprene inhibition experiments the amount of isoprene [typically 1.0 mL (10 mmol)] was added prior to the addition of the substrate. All reported values for TONs and TOFs are the arithmetic means of two or more reproducible experiments. Experiments are considered reproducible when the deviation of the obtained results are less than 15% of the arithmetic mean.

Direct Conversion of 1,3-Butadiene to MEK: In a typical experiment, a high-pressure autoclave was filled with 0.09 mmol of **1** or **2** and 3.5 mmol of *p*-toluenesulfonic acid (for the acid-catalyzed hydration of 1,3-butadiene). After addition of 100 mL of diglyme/water (70/30) solvent mixture, the autoclave was closed and purged three times with dinitrogen. Next, 1,3-butadiene (10 mL) was added as a liquid using an ISCO high-pressure pump and the autoclave was heated to 145 °C. After 10 h, the autoclave was cooled to room temperature and the contents were analyzed with GLC.

X-ray Crystallographic Study of 1: Crystals of **1** suitable for X-ray analysis were obtained by slow concentration of a $CHCl_3$/toluene solution of **2** at room temperature. Pertinent data for **1**: $C_{14}H_{14}Cl_3N_2ORuS$·C_7H_8, M_r = 557.90, red, block-shaped crystal (0.2 × 0.3 × 0.3 mm), triclinic, space group $P\bar{1}$ with *a* = 7.7503(10), *b* = 12.046(2), *c* = 12.872(3) Å, α = 73.972(10), β = 80.949(10), γ = 79.691(10)°, *V* = 1128.9(4) $Å^3$, *Z* = 2, D_c = 1.641 g cm^{-3}, μ(Mo-K_α) = 1.157 mm^{-1}. 20526 Reflections were measured (5133 independent, R_{int} = 0.0442, 1.6° < θ < 27.48°, *T* = 150 K, Mo-K_α radiation, graphite monochromator, λ = 0.71073 Å) with a Nonius Kappa CCD diffractometer with a rotating anode; no absorption correction was applied. The structure was solved by automated direct methods.[25] The structure displays relatively high residual density peaks in the area around Ru (peak height up to 2.7 e $Å^{-3}$ at 0.78 Å from Ru). The peaks appear to be related to the heavy atoms positions (Ru, Cl and S) by a noncrystallographic twofold rotation, approximately parallel to the local twofold rotation axis of the phenanthroline ligand. The rotation images of some heavy atoms coincide with existing atom sites. Similar peaks were observed in data sets collected on two other crystals. There are no signs of twinning. Rough models, describing these peaks as the result of orientational disorder of the Ru complex, indicated a disorder fraction of approximately 3%. In view of the low occupation factor of the minor component, the disorder model was abandoned. Hydrogen atoms were introduced on calculated positions and included riding on their carrier atoms. Non-hydrogen atoms were described with anisotropic displacement parameters. The isotropic displacement parameters of the hydrogen atoms were coupled to the equivalent isotropic displacement parameters of their carrier atoms. Full-matrix least-squares refinement[26] of 265 parameters on F^2 resulted in a final *R*1 value of 0.0306 [for 4914 reflections with $I > \sigma(I)$], *wR*2 = 0.0729, GoF = 1.044. The final residual density was in the range of −1.09 to 2.66 e $Å^{-3}$. Geometric calculations and molecular graphics were performed with the PLATON package.[27] CCDC-176535 contains the supplementary crystallographic data for this paper. These data can be obtained free of charge at www.ccdc.cam.ac.uk/conts/retrieving.html or from the Cambridge Crystallographic Data Centre, 12, Union Road, Cambridge CB2 1EZ, UK [Fax: (internat.) +44-1223/336-033; E-mail: deposit@ccdc.cam.ac.uk].

Acknowledgments

This research was supported by the Technology Foundation STW, applied science division of NWO and the technology program of

the Ministry of Economic Affairs. This work was supported in part (A. L. S.) by the Council for Chemical Sciences of the Netherlands Organization for Scientific Research (CW-NWO). The authors are indebted to Mr. W. W. Jager (SRTCA, The Netherlands) for his skilful technical assistance and to Dr. W. J. L. Genuit (SRTCA, The Netherlands) for recording the mass spectra. Dr. J. G. de Vries (DSM, The Netherlands) and Mr. W. G. Reman (SRTCA, The Netherlands) are thanked for stimulating discussions.

[1] *Ullmann's Encyclopedia of Industrial Chemistry*, 6th electronic release ed., Wiley-VCH, Weinheim, **2000**.
[2] R. C. Van der Drift, E. Bouwman, E. Drent, *J. Organomet. Chem.* **2002**, *650*, 1−24.
[3] R. C. Van der Drift, M. Vailati, E. Bouwman, E. Drent, *J. Mol. Catal. A: Chem.* **2000**, *159*, 163−177.
[4] J. Kanand, R. Paciello, M. Roper, U.S. Pat. No. 6166265, **2000**.
[5] J. Kanand, M. Roper, R. Paciello, A. Thome, U.S. Pat. No. 5892125, **1999**.
[6] E. Drent, Eur. Pat. No. 457387, **1991**.
[7] F. Stunnenberg, F. G. M. Niele, E. Drent, *Inorg. Chim. Acta* **1994**, *222*, 225−233.
[8] R. C. Van der Drift, W. P. Mul, E. Bouwman, E. Drent, *Chem. Commun.* **2001**, 2746−2747.
[9] E. A. Seddon, K. R. Seddon, *The Chemistry of Ruthenium*, Elsevier, Amsterdam, **1984**.
[10] X. Meddin in *Comprehensive Coordination Chemistry* (Ed.: G. Wilkinson), Pergamon Press, Oxford, **1987**, vol. 4, p. 277.
[11] F. P. Dwyer, H. A. Goodwin, E. C. Gyarfas, *Aust. J. Chem.* **1963**, *16*, 42−50.
[12] I. P. Evans, A. Spencer, G. Wilkinson, *J. Chem. Soc., Dalton Trans.* **1973**, 204−209.
[13] F. P. Pruchnik, E. Galdecka, Z. Galdecki, A. Kowalski, *Polyhedron* **1999**, *18*, 2091−2097.
[14] R. C. Van der Drift, M. Van Meurs, W. P. Mul, E. Bouwman, E. Drent, manuscript in preparation.
[15] R. C. Van der Drift, E. Bouwman, E. Drent, unpublished results.
[16] H. A. Hudali, J. V. Kingston, H. A. Tayim, *Inorg. Chem.* **1979**, *18*, 1391−1394.
[17] M. B. Cingi, M. Lanfranchi, M. A. Pellinghelli, M. Tegoni, *Eur. J. Inorg. Chem.* **2000**, 703−711.
[18] J. J. Rack, H. B. Gray, *Inorg. Chem.* **1999**, *38*, 2−3.
[19] M. Calligaris, O. Carugo, *Coord. Chem. Rev.* **1996**, *153*, 83−154.
[20] D. H. Evans, K. M. O′Connell, R. A. Petersen, M. J. Kelly, *J. Chem. Educ.* **1983**, *60*, 290−293.
[21] It is assumed that all reactions are first order in 3-buten-2-ol. In view of any deactivation, initial k values have been determined by fitting straight lines through ln(1 − TON) vs. time curves over the first 20 min of the reactions rather than fitting power curves through the complete turnover vs. time plots. Initial TOF values have been determined by using k_{ini} and the final TON after 6 h.
[22] R. G. Wilkins in *Kinetics and Mechanism of Reactions of Transition Metal Complexes*, 2nd ed., VCH, Weinheim, **1991**, p. 400.
[23] B. M. Trost, R. J. Kulawiec, *J. Am. Chem. Soc.* **1993**, *115*, 2027−2036.
[24] M. A. Bennett, M. I. Bruce, T. W. Matheson in *Comprehensive Organometallic Chemistry*, 1st ed. (Ed.: G. Wilkinson), Pergamon Press, Oxford, **1982**, vol. 4, p. 691.
[25] G. M. Sheldrick, *SHELXS-86 Program for crystal structure determination*, University of Göttingen, Germany, **1986**.
[26] G. M. Sheldrick *SHELXL-97 Program for crystal structure refinement*, University of Göttingen, Germany, **1997**.
[27] A. L. Spek, *PLATON A multi-purpose crystallographic tool*, Utrecht University, The Netherlands, **2000**; internet: http//www.cryst.chem.uu.nl/platon

Received January 7, 2002
[I02004]

Synthesis and Structural Characterization of β-Diketoiminate Complexes Containing Three-Coordinate Zinc and Copper Atoms

Jörg Prust,[a] Holger Hohmeister,[a] Andreas Stasch,[a] Herbert W. Roesky,*[a] Jörg Magull,[a] Eftichia Alexopoulos,[a] Isabel Usón,[a] Hans-G. Schmidt,[a] and Mathias Noltemeyer[a]

Dedicated to Professor Dieter Naumann on the occasion of his 60th birthday

Keywords: Acetylides / Copper / N ligands / Zinc

The reaction of the lithium β-diketoiminate complex (dipp)NacNacLi·OEt_2 {(dipp)NacNac = 2-[(2,6-diisopropylphenyl)amino]-4-[(2,6-diisopropylphenyl)imino]pent-2-enyl} with $ZnCl_2$ yielded the corresponding (dipp)NacNacZnCl (**1**) and (dipp)NacNacZn(μ-Cl)$_2$Li$(OEt_2)_2$ (**1a**). Treatment of **1** with LiC≡CPh and $NaBH_4$ in diethyl ether gave (dipp)NacNacZnC≡CPh (**2**) and (dipp)NacNacZn(μ-H)$_2BH_2$ (**3**). The core element of compounds **1a**–**3** is a six-membered ZnN_2C_3 ring. The structure of **1a** shows the β-diketoiminate backbone in a boat conformation with the tetrahedrally coordinated metal centre in **1a** at the prow and the opposing carbon atom at the stern. The zinc atoms in **2** and **3** show a planar arrangement to the β-diketoiminate plane. The zinc atom in **2** is three-coordinated and that in **3** four-coordinated. Treatment of (dipp)NacNacLi·OEt_2 with CuI in diethyl ether yielded {[Li(OEt_2)][(dipp)NacNacCuI]}$_2$ (**4**). In contrast to **1a**–**3**, compound **4** contains a dimetallic system. The core of compound **4** consists of two six-membered LiN_2C_3 rings and one four-membered Cu_2I_2 ring. In addition to bonds to the two iodine atoms, the three-coordinated copper atom has a further bond to the γ-carbon atom of the six-membered LiN_2C_3 ring.
(© Wiley-VCH Verlag GmbH, 69451 Weinheim, Germany, 2002)

Introduction

Recent reports have indicated increasing interest in the β-diketoiminate ligand, due to its sterically demanding and chelating properties.[1,2] Vinamidines are useful for the stabilization of low oxidation states of group-13 elements. Recently, we reported the preparation of (dipp)NacNacAl^{I}, the first example of a monomeric Al^{I} compound[3] stable at room temperature. Power et al. described the synthesis of the first compound containing a Ga−N double bond, by using a β-diketoiminate ligand.[4] We have also reported on the synthesis of a β-diketoiminate boranate complex of magnesium, in which the magnesium centre is six-coordinated and octahedral.[5]

While the first metals to have a prominent role in organic synthesis were magnesium and lithium, several of the transition metals have also become very important.[6] Organozinc[7] and organocopper[8] complexes are extensively used in both organic and organometallic synthesis. In particular, these complexes offer valuable alternatives to the corresponding magnesium and lithium reagents. Dialkylzinc complexes exist as monomeric molecules with two-coordinate zinc atoms.[9] However, the corresponding dialkylcopper complexes, such as $[LiCuMe_2]_2$, exist as dimers.[10,11] Only discrete R_2Cu^- anions have been observed in crystals in which the lithium cation is complexed by crown ethers.[12] Recent reports have indicated increasing interest in zinc hydrides as reducing agents.[13−15] We have reported the synthesis of $[(dipp)NacNacZnH]_2$ by means of the reaction between $[(dipp)NacNacZnF]_2$ and Et_3SiH.[16]

Although the chemistry of organozinc complexes with four-coordinate zinc atoms has been developed, the synthesis of the corresponding acetylides is not well known. Wright et al. synthesized the first zinc acetylide derivatives in 1996,[17] and Dehnicke et al. have prepared a number of zinc acetylide derivatives.[18,19] Monomeric compounds with three-coordinate zinc are still quite rare; only a few examples have been reported in the literature.[20−27]

Here we report on the formation of a monomeric zinc acetylide complex with a three-coordinate zinc atom. We used the bulky β-diketoiminate 2-[(2,6-diisopropylphenyl)amino]-4-[(2,6-diisopropylphenyl)imino]pent-2-enyl ligand [(dipp)NacNac]. In summary, we prepared four new β-diketoiminate zinc derivatives − (dipp)NacNacZnCl (**1**), (dipp)NacNacZn(μ-Cl)$_2$Li$(OEt_2)_2$ (**1a**), (dipp)NacNacZnC≡CPh (**2**), and (dipp)NacNacZn(μ-H)$_2BH_2$ (**3**) − and also one β-diketoiminate copper derivative, {[Li(OEt_2)][(dipp)NacNacCuI]}$_2$ (**4**).

[a] Institut für Anorganische Chemie der Georg-August-Universität, Göttingen
Tammannstrasse 4, 37077 Göttingen, Germany
Fax: (internat.) + 49-(0)551/39-3373
E-mail: hroesky@gwdg.de

Results and Discussion

Compounds **1** and **1a** were prepared in high yield (92%) by the addition of (dipp)NacNacLi·OEt_2 to a $ZnCl_2$ suspension in diethyl ether (Scheme 1). Compounds **2** and **3** were obtained by addition of LiC≡CPh and $NaBH_4$, respectively, to a solution of **1**. LiCl and NaCl, respectively, were eliminated, and the monomeric zinc complexes **2** and **3** were isolated in high yields (83% **2**, 79% **3**) (Scheme 2).

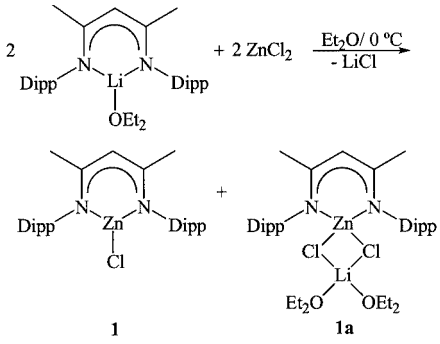

Scheme 1

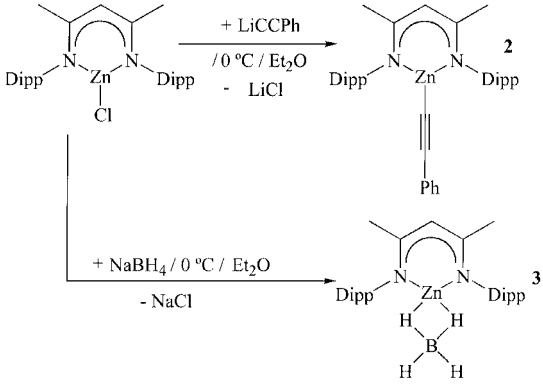

Scheme 2

Compounds **1**, **2**, and **3** were characterized by EI-MS spectrometry, ^1H and ^{13}C NMR and elemental analysis. All compounds are moisture- and air-sensitive. The ^1H NMR spectra of **1**, **2**, and **3** showed the typical resonances of the β-diketoiminate unit, with two non-equivalent resonances for the methyl groups of the isopropyl substituents due to the hindered rotation about the Ar−N bonds, as observed for related metal systems.[1−3,28] The ^1H NMR spectroscopic data were consistent with the solid-state structures of **2** and **3**. Single crystals suitable for X-ray structural analysis were only obtained for **1a**, but the ^1H NMR spectrum was not consistent with the solid-state structure, with no resonances assignable to protons of the diethyl ether molecules being observed. From the predominance of **1** in the NMR and EI-MS spectra (m/z = 516 [M^+]) **1a** is obviously a by-product that crystallises more rapidly than the main product. The EI-MS spectra of **2** and **3**, however, showed the molecular fragments for **2** (m/z = 582 [M^+]) and for **3** (m/z = 482 [$M - BH_3]^+$), respectively.

Reactions with transition metal compounds are widely used in organic chemistry, organocopper compounds being important starting materials for new reactions in synthetic chemistry.[5] Compound **4** was therefore prepared in high yields (76%) by the addition of (dipp)NacNacLi·OEt_2 to a suspension of CuI in diethyl ether at −78 °C (Scheme 3).

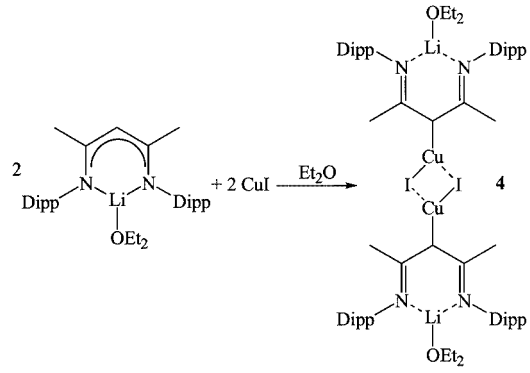

Scheme 3

Compound **4** was characterized by EI-MS spectrometry, ^1H, ^{13}C, and ^7Li NMR and elemental analysis. Like compounds **1**−**3**, compound **4** is air- and moisture-sensitive. The ^1H NMR spectrum of **4** showed the typical resonances of the β-diketoiminate unit, the resonances at δ = 0.75 and 2.98 ppm corresponding with the protons of the coordinated ether molecules. The ^{13}C and ^7Li NMR spectroscopic data were consistent with the solid-state structure of **4**. The EI-MS showed a fragment of **4** minus one iodine atom (m/z = 1251 [$M - I]^+$).

Because of the similarity of compounds **1**−**7** to β-acetylacetonate complexes, a few examples and their physical properties are listed in Table 1 for comparison.

Table 1. Physical data of compounds **1**−**9**; acac = acetylacetonate, tmtch = 3,3,6,6-tetramethyl-1-thia-4-cycloheptyne, Tp* = hydrotris(3-cumyl-5-methylpyrazolyl)borate

	M.p. [°C]	^1H NMR of γ-C*H* (δ [ppm])
(dipp)NacNacZnCl (**1**)	205	4.88
(dipp)NacNacZnC≡CPh (**2**)	154	5.00
(dipp)NacNacZn(μ-H)$_2$BH_2 (**3**)	182−186	4.71
[{Et_2O)Li}{(dipp)NacNacCuI}]$_2$ (**4**)	165	4.24
(dipp)NacNacZnPh (**5**)[2]	155	5.04
(dipp)NacNacMg*i*Pr·Et_2O (**6**)[5]	165	4.85
(dipp)NacNacAl (**7**)[3]	> 150 (dec.)	5.18
(Tp*)Zn(cumoylacetonate) (**8**)[29]	183	5.43
(acac)Cu(tmtch) (**9**)[30]	116	5.37

The compounds **8** and **9** used for the comparison have coordination numbers at their metal centres of three for **8** and of five for **9**. It can be seen that the melting points of the β-acetylacetonate complexes (**8**, **9**) range from 116 to 183 °C, while those of compounds **1**−**4** ranged from 154 to 205 °C. The resonances for γ-CH in **8** and **9** were shifted

downfield [δ = 5.43 (**8**), 5.37 (**9**) ppm] relative to the β-diketoiminate compounds **1**−**7**.

Molecular Structures

The central core of compounds **1a**−**3** is a (dipp)NacNacZn unit. The β-diketoiminate ligand acts as a chelating ligand through its two nitrogen atoms, forming a six-membered ring with the zinc atom. The six-membered ZnN_2C_3 ring in **1a** is not planar, but displays a boat conformation with the metal atom at the prow and the opposite carbon atom at the stern, whereas the ZnN_2C_3 rings in **2** and **3** are planar. This deviation from planarity is imposed by the metal centre, as the planar arrangement implies more distortion of its coordination sphere. Nevertheless, the π-electrons of the β-diketoiminate ligand are delocalised, since the C(1)−C(2), C(2)−C(3), C(1)−N(1), and C(3)−N(2) bond lengths in each compound are equal within experimental errors and correspond to those in conjugated systems.[26] Moreover, the two N−Zn bond lengths are equal as well. The Zn−N distances {**1a**: 1.979(2) and 1.982(2) Å; **2** [$(C_7H_8)_{0.5}$]: 1.941(2) and 1.929(2) Å; **3**: 1.917(6) and 1.911(6) Å} are shorter than those in comparable Zn−N derivatives.[28,32−34] The N−Zn−N angles are 97.8° in compound **1a**, 98.8° in **2** and 101.9° in **3**.

The tetrahedral coordination sphere of the zinc atom is completed in compound **1a** by two chlorine atoms and in compound **3** by two hydrogen atoms, whereas the zinc atom in compound **2** adopts a trigonal-planar environment through an additional bond to one C≡CPh moiety.

The central core of **4** is made up of two (dipp)NacNacLi units. As in **1a**−**3**, the β-diketoiminate ligand acts as a chelating ligand through its two nitrogen atoms, forming a six-membered ring with the lithium atom. The LiN_2C_3 rings in **4** are not planar, but display boat conformations with the metal atom at the prow and the opposite γ-carbon atom at the stern. Surprisingly, the copper atom forms a bond to the γ-carbon atom of the β-diketoiminate ligand. In contrast, Tolman et al. recently reported the preparation of a copper(I) compound with the β-diketoiminate ligand in which the copper formed a six-membered CuN_2C_3 ring.[35] A possible explanation for this different behaviour might be that the soft Cu^{I} prefers coordination with the soft carbon atom while the harder Cu^{II} prefers coordination with the harder nitrogen atoms. The Cu−C bond length of 2.089(6) Å is similar to those found in the literature.[36,37] The trigonal environment of the copper atom is completed by two iodine atoms. The copper atoms form a four-membered Cu_2I_2 ring with the two iodine atoms. The C(1)−C(2) and C(2)−C(3) bond lengths [1.443(8) and 1.455(8) Å] correspond to C−C single bonds, whereas the C−N bond lengths [1.295(8) and 1.299(8) Å] are in the range of C−N double bonds.

The crystallographic data for **1a**, **2**, **3**, and **4** are summarized in Table 6.

Molecular Structure of 1a

Compound **1a** crystallises in the monoclinic space group $P2_1/n$ with one molecule in the asymmetric unit (Figure 1). Selected bond lengths and angles for **1** are given in Table 2.

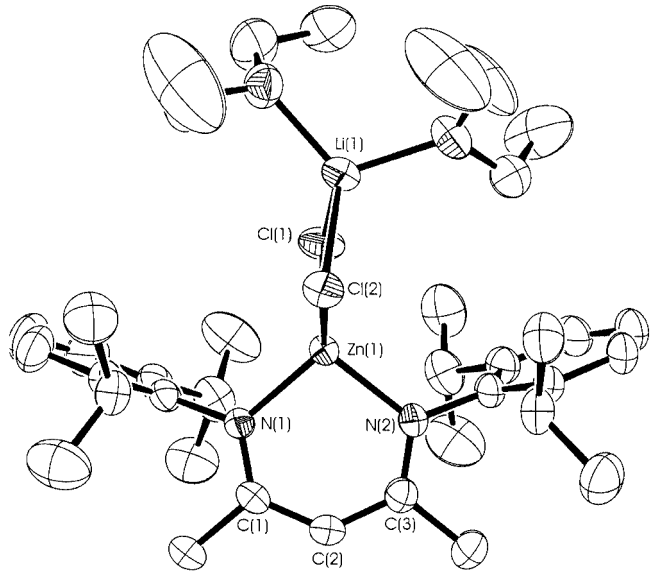

Figure 1. Crystal structure of **1a** (hydrogen atoms are omitted for clarity)

Table 2. Selected bond lengths [Å] and angles [°] of **1a**

Zn(1)−Cl(1)	2.2858(8)	N(1)−Zn(1)−N(2)	97.88(8)
Zn(1)−Cl(2)	2.3144(8)	C(1)−N(1)−Zn(1)	120.42(16)
Zn(1)−N(1)	1.979(2)	C(3)−N(2)−Zn(1)	19.75(17)
Zn(1)−N(2)	1.982(2)	N(1)−C(1)−C(2)	124.0(2)
N(1)−C(1)	1.324(3)	C(3)−C(2)−C(1)	130.1(2)
N(2)−C(3)	1.326(3)	N(2)−C(3)−C(2)	124.3(2)
C(1)−C(2)	1.398(4)	N(1)−Zn(1)−Cl(1)	115.20(6)
C(2)−C(3)	1.409(4)	N(2)−Zn(1)−Cl(1)	117.82(6)
Cl(1)−Li(1)	2.371(5)	N(1)−Zn(1)−Cl(2)	116.71(6)
Cl(2)−Li(1)	2.384(5)	N(2)−Zn(1)−Cl(2)	113.02(6)
		Zn(1)−Cl(1)−Li(1)	84.52(11)
		Zn(1)−Cl(2)−Li(1)	83.63(12)

Molecular Structure of 2

Compound **2** crystallises in the monoclinic space group $P2_1/n$ with one molecule in the asymmetric unit. Besides the two nitrogen atoms of the (dipp)NacNac ligand, the zinc atom coordinates to one phenylacetylide group, a trigonal coordination sphere of the zinc atom thus being formed (Figure 2). Furthermore, the Zn−C≡C backbone deviates from linearity [Zn−C(30)−C(31): 168.18(19)°]. This deviation from linearity has been reported for corresponding transition metal complexes[32−34] and also found in aluminium compounds.[38] Selected bond lengths and angles for **2** are given in Table 3.

Molecular Structure of 3

Compound **3** crystallises in the monoclinic space group $P2_1/n$ (Figure 3). The B−H(b1 and b2) bond lengths are nearly equal [1.211(8) and 1.214(8) Å]. Compound **3** is thus

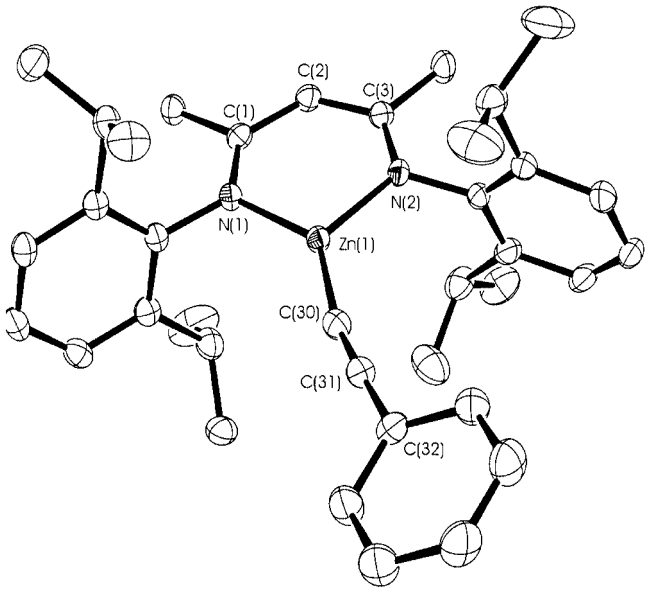

Figure 2. Crystal structure of **2** (hydrogen atoms are omitted for clarity)

Table 3. Selected bond lengths [Å] and angles [°] of **2**

Zn(1)−C(30)	1.906(2)	Zn(1)−C(30)−C(31)	168.18(19)
Zn(1)−N(1)	1.941(2)	C(30)−C(31)−C(32)	177.1(2)
Zn(1)−N(2)	1.929(2)	N(1)−Zn(1)−N(2)	98.85(7)
N(1)−C(1)	1.333(3)	N(1)−Zn(1)−C(30)	124.14(8)
N(2)−C(3)	1.335(3)	N(2)−Zn(1)−C(30)	137.01(8)
C(1)−C(2)	1.403(3)	N(1)−C(1)−C(2)	123.55(18)
C(2)−C(3)	1.406(3)	N(2)−C(3)−C(2)	123.87(19)
C(30)−C(31)	1.207(3)	C(3)−C(2)−C(1)	129.56(19)
C(31)−C(32)	1.439(3)		

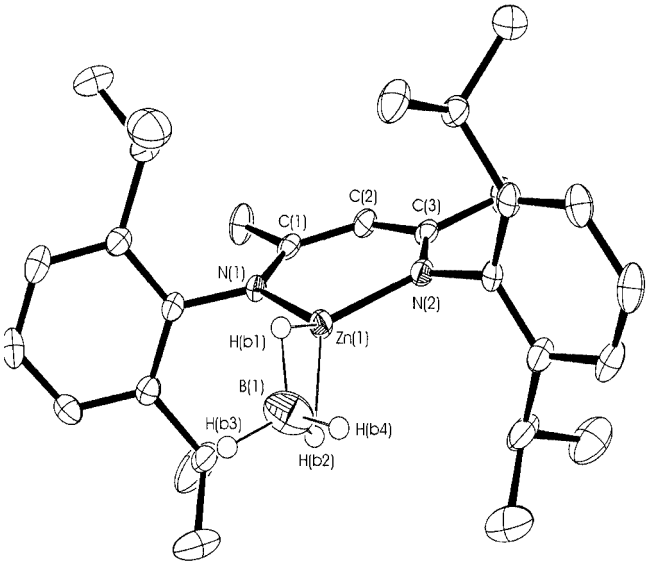

Figure 3. Crystal structure of **3** (hydrogen atoms are omitted for clarity)

a boranate complex but not an adduct of BH_3. The terminal B−H bond lengths correspond to those found in the literature.[13−15] Selected bond lengths and angles for **3** are given in Table 4.

Molecular Structure of 4

Compound **4** crystallises in the monoclinic space group $P2_1/n$ with half a molecule in the unit cell (Figure 4). Selected bond lengths and angles for **4** are given in Table 5.

Table 4. Selected bond lengths [Å] and angles[°] of **3**

Zn(1)−N(1)	1.917(6)	N(1)−Zn(1)−N(2)	101.96(3)
Zn(1)−N(2)	1.911(6)	B(1)−H(b1)−Zn(1)	91.08(7)
Zn(1)−H(b1)	1.754(9)	B(1)−H(b2)−Zn(1)	91.47(7)
Zn(1)−H(b2)	1.744(9)	H(b1)−Zn(1)−N(1)	120.91(12)
B(1)−H(b1)	1.211(8)	H(b1)−Zn(1)−N(2)	123.50(12)
B(1)−H(b2)	1.214(8)	H(b2)−Zn(1)−N(1)	119.80(12)
B(1)−H(b3)	1.059(8)	H(b2)−Zn(1)−N(2)	121.03(12)
B(1)−H(b4)	1.052(8)	Zn(1)−N(1)−C(1)	119.48(6)
N(1)−C(1)	1.333(4)	Zn(1)−N(1)−C(3)	119.78(6)
N(2)−C(3)	1.334(4)	N(1)−C(1)−C(2)	124.21(4)
C(1)−C(2)	1.394(3)	C(1)−C(2)−C(3)	130.66(4)
C(2)−C(3)	1.404(3)		

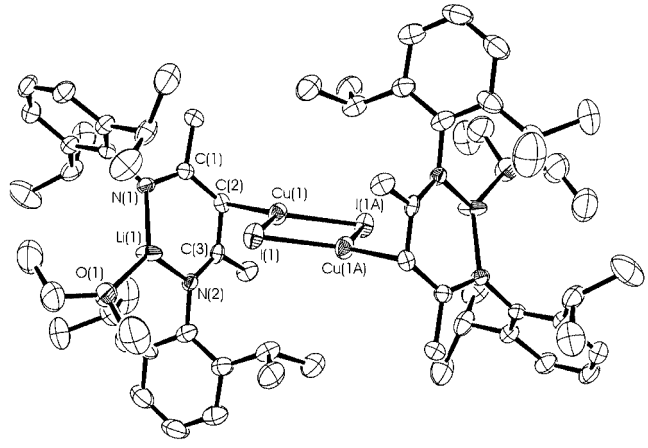

Figure 4. Crystal structure of **4** (hydrogen atoms are omitted for clarity)

Table 5. Selected bond lengths [Å] and angles [°] of **4**

Cu(1)−C(2)	2.089(6)	C(2)−Cu(1)−I(1)	117.4(2)
Cu(1)−I(1)	2.5711(2)	C(1)−C(2)−Cu(1)	91.8(3)
N(1)−Li(1)	1.969(10)	C(3)−C(2)−Cu(1)	110.8(4)
N(2)−Li[(1)	1.973(11)	C(1)−N(1)−Li(1)	117.5(5)
N(1)−C(1)	1.295(8)	C(3)−N(2)−Li(1)	117.5(5)
N(2)−C(3)	1.299(8)	C(3)−N(2)−Li(1)	114.9(5)
C(1)−C(2)	1.443(8)	N(1)−C(3)−C(2)	123.3(5)
C(2)−C(3)	1.455(8)	N(2)−C(3)−C(2)	124.4(5)

Conclusions

The sterically demanding β-diketoiminate ligand (dipp)NacNac facilitates the stabilization of compounds with low-coordination sites at the metal centre. We have synthesized three zinc β-diketoiminate complexes and one copper β-diketoiminate complex with novel structural motifs generated through substitution of the chlorine and iodine atom, respectively. We are at present investigating these compounds as alternatives for Grignard reagents in organic syntheses.

Experimental Section

General: All reactions were performed by standard Schlenk and dry-box techniques. Solvents were appropriately dried and distilled under dinitrogen prior to use. All NMR spectra were recorded in 5-mm tubes with dry degassed [D_6]benzene as a solvent, referenced externally to $SiMe_4$. Elemental analyses were performed by the Analytisches Chemisches Laboratorium des Instituts für Anorganische Chemie, Göttingen, and (dipp)NacNacH and (dipp)NacNacLi·OEt_2 were prepared by literature procedures.[3]

(dipp)NacNacZnCl (1): A solution of (dipp)NacNacLi·OEt_2 (3.11 g, 1.55 mmol) in Et_2O (20 mL) was slowly added at −78 °C to a suspension of $ZnCl_2$ (420 mg, 1.55 mmol) in Et_2O (20 mL). The mixture was allowed to warm to room temperature and then stirred for an additional 3 h and filtered. The solution was reduced in vacuo to 10 mL and stored at −24 °C to yield **1** and **1a** [(dipp)NacNacZn(μ-Cl)$_2$LiOEt$_2$)$_2$]$_2$ as colourless crystalline solids after 2 d. Data for **1**: Yield 1.48 g, 92%. M.p. 205 °C. ^{1}H NMR (500 MHz, C_6D_6): δ = 1.15 [d, J = 6.8 Hz, 12 H, CH(CH_3)$_2$], 1.16 [d, J = 6.8 Hz, 12 H, CH(CH_3)$_2$], 1.18 [d, J = 6.8 Hz, 12 H, CH(CH_3)$_2$], 1.20 [d, J = 6.8 Hz, 12 H, CH(CH_3)$_2$], 1.70 (s, 6 H, CH_3), 1.75 (s, 6 H, CH_3), 3.02 (sept, J = 6.8 Hz, 3.07 [sept, J = 6.8 Hz, 4 H, CH(CH$_3$)$_2$], 4.87 (s, 1 H, CH), 4.89 (s, 1 H, CH), 7.12 (m, 6 H, ArH) ppm. ^{13}C NMR (125 MHz, C_6D_6): δ = 23.3 [NC(CH$_3$)], 25.4 [CH(CH$_3$)$_2$], 28.8 [CH(CH$_3$)$_2$], 94.2 (γ-C), 123.8 (ArC), 125.2 (ArC), 141.2 (ArC), 142.3 (ArC), 165.4 (NC) ppm. MS (EI): m/z (%) = 481 (21) [M − Cl]$^+$, 516 (100) [M$^+$]. $C_{29}H_{41}ClN_2Zn$ (518.49): calcd. C 67.18, H 7.97, N 5.40; found C 67.0, H 7.6, N 5.3. Molecular mass (cryoscopic in THF in g/mol): calcd. 518.49; found 505. Only single crystals of **1a** were suitable for X-ray structural analysis.

(dipp)NacNacZnC≡CPh (2): A solution of LiC≡CPh (2.34 mL of a 1.0 M solution in THF, 2.34 mmol) was slowly added at −78 °C to a stirred solution of (dipp)NacNacZnCl (1.21 g, 2.34 mmol) in Et_2O (20 mL). The reaction mixture was stirred for an additional 3 h and allowed to warm to room temperature. The residue was filtered and the solution was concentrated to 10 mL under reduced pressure. Storage at −24 °C afforded colourless crystals of **2**: Yield 1.13 g (1.94 mmol), 83%. M.p. 154 °C. ^{1}H NMR (500 MHz, C_6D_6): δ = 1.17 [d, J = 6.8 Hz, 12 H, CH(CH_3)$_2$], 1.40 [d, J = 6.8 Hz,12 H, CH(CH_3)$_2$], 1.67 (s, 6 H, CH_3), 3.19 [sept, J = 6.8 Hz, 4 H, CH(CH$_3$)$_2$], 5.00 (s, 1 H, CH), 6.72−7.28 (m, 11 H, ArH) ppm. ^{13}C NMR (125 MHz, C_6D_6): δ = 20.5 [NC(CH$_3$)], 23.7 [CH(CH$_3$)$_2$], 24.5 CH(CH$_3$)$_2$, 28.3 [CH(CH$_3$)$_2$], 77.7 (C≡C), 83.8 (C≡C), 94.3 (γ-C), 123.3 (ArC), 123.5 (ArC), 124.5 (ArC), 125.1 (ArC), 128.2 (ArC), 139.2 (ArC), 142.6 (ArC), 161.9 (NC) ppm. MS (EI): m/z (%) = 202 (100) [DippNCCH$_3$], 481 (29) [M − C≡CPh]$^+$, 582 (59) [M$^+$]. $C_{37}H_{46}N_2Zn$ (584.16): calcd. C 76.08, H 7.94, N 4.80; found C 75.5, H 7.94, N 4.6.

(dipp)NacNacZn(μ-H)$_2$BH$_2$ (3): A solution of (dipp)NacNacZnCl (1.59 g, 3.10 mmol) in Et_2O (20 mL) was slowly added at −78 °C to a suspension of $NaBH_4$ (0.117 g, 3.10 mmol) in Et_2O (10 mL).

Table 6. Crystallographic data of **1a**, **2**, **3**, and **4**

	1a	**2**·(C_7H_8)$_{0.5}$	**3**	**4**
Empirical formula	$C_{37}H_{61}Cl_2LiN_2O_2Zn$	$C_{40.5}H_{54}N_2Zn$	$C_{29}H_{45}BN_2Zn$	$C_{66}H_{102}Cu_2I_2Li_2N_4O_2$
Formula mass	709.09	634.23	497.85	1378.28
Temperature [K]	203	133(2)	133(2)	203(2)
Wavelength [Å]	0.71073	0.71073	0.71073	0.71073
Crystal system	monoclinic	monoclinic	monoclinic	monoclinic
Space group	$P2_1/n$	$C2/c$	$P2_1/n$	$P2_1/n$
Unit cell dimensions	a = 12.0841(17) Å	a = 18.0736(6) Å	a = 12.344(3) Å	a = 10.622(3) Å
	b = 21.2125(5) Å	b = 19.2773(9) Å	b = 17.605(4) Å	b = 26.509(16) Å
	c = 15.896(3) Å	c = 21.1298(8) Å	c = 13.884(3) Å	c = 12.542(3) Å
	β = 99.961(16)°	β = 104.969°	β = 104.93(3)	β = 107.77(2)°
Volume [Å^3]	6031(13)	7112.0(5)	2914.4(10)	3363.0(23)
Z	4	8	4	2
Density (calculated) [Mg/m^3]	1.168	1.185	1.135	1.361
Absorption coefficient [mm^{-1}]	0.772	0.720	0.860	1.593
F(000)	1520	2728	1072	1424
Crystal size [mm]	0.8 × 0.6 × 0.3	0.4 × 0.3 × 0.4	0.2 × 0.2 × 0.1	0.8 × 0.6 × 0.3
θ range for data collection	3.55 to 25.00°	1.57 to 24.79°	2.06 to 24.44°	3.52 to 24.99°
Reflections collected	9210	53140	35772	5885
Independent reflections	7073 [R_{int} = 0.0547]	6097 [R_{int} = 0.0489]	4800 [R_{int} = 0.1107]	5874 [R_{int} = 0.0474]
Data/restraints/parameters	7073/0/420	6097/0/417	4800/3/324	5868/0/364
Goodness-of-fit on F^2	1.039	1.077	1.027	1.166
Final R indices [$I > 2\sigma(I)$]	$R1$ = 0.0488	$R1$ =0.0344	$R1$ = 0.0446	$R1$ = 0.0594
	$wR2$ = 0.1380	$wR2$ = 0.1091	$wR2$ = 0.1097	$WR2$ = 0.1682
R indices (all data)	$R1$ = 0.0551	$R1$ = 0.0380	$R1$ = 0.0578	$R1$ = 0.0652
	$wR2$ = 0.1380	$wR2$ = 0.1108	$wR2$ = 0.1189	$WR2$ = 0.1762
Largest diff. peak and hole [e·Å^{-3}]	0.979 and −1.066	1.127 and −0.346	0.288 and −0.448	0.954 to −1.089

The mixture was allowed to warm to room temperature and then stirred for an additional 12 h and filtered. The solution was reduced to 5 mL in vacuo and stored at −24 °C to yield colourless crystals of **3**: Yield 1.21 g, 79%. M.p. 182−186 °C. ^{1}H NMR (500 MHz, C_6D_6): δ = 1.15 [d, *J* = 6.8 Hz, 12 H, CH(CH_3)$_2$], 1.19 [d, *J* = 6.8 Hz, 12 H, CH(CH_3)$_2$], 1.59 (s, 6 H CH_3), 3.48 [sept, *J* = 6.8 Hz, 4 H, C*H*(CH$_3$)$_2$], 4.71 (s, 1 H, C*H*), 7.12−7.19 (m, 6 H, Ar*H*) ppm. ^{13}C NMR (125 MHz, C_6D_6): δ = 23.1 [NC(*C*H$_3$)], 24.7 [CH(*C*H$_3$)$_2$], 25.2 [CH(*C*H$_3$)$_2$], 28.6 [*C*H(CH$_3$)$_2$], 97.9 (γ-*C*), 124.8 (Ar*C*), 125.1 (Ar*C*), 142.1 (Ar*C*), 168.1 (N*C*) ppm. MS (EI): *m*/*z* (%) = 417 (100) [M − ZnBH$_4$]$^+$, 482 (43) [M − BH$_3$]$^+$. $C_{29}H_{45}BN_2Zn$ (497.85): calcd. C 69.96, H 9.12, N 5.63; found C 68.2, H 7.9, N 4.8.

[{Et$_2$O)Li}{(dipp)NacNacCuI}]$_2$ (4): A solution of (dipp)NacNacLi·OEt$_2$ (1.18 g, 2.28 mmol) in Et$_2$O (20 mL) was slowly added at −78 °C to a suspension of CuI (434 mg, 2.28 mmol) in Et$_2$O (20 mL). The mixture was allowed to warm to room temperature and then stirred for an additional 24 h and filtered. The solution was concentrated to 5 mL under reduced pressure. Storage at −24 °C afforded colourless crystals of **4**. Yield 1.19 g, 76%. M.p. 165 °C (decomp.). ^{1}H NMR (500 MHz, C_6D_6): δ = 0.75 (t, *J* = 6.8 Hz, 12 H, OCH$_2$CH_3), 1.12 [d, *J* = 6.8 Hz, 24 H, CH(CH_3)$_2$], 1.21 [d, *J* = 6.8 Hz, 24 H, CH(CH_3)$_2$], 1.78 (s, 12 H, CH_3), 2.98 (q, *J* = 6.8 Hz, 8 H, OCH_2CH$_3$), 3.13 [sept, *J* = 6.8 Hz, 4 H, C*H*(CH$_3$)$_2$], 4.24 (s, 2 H, C*H*), 7.08−7.14(m, 12 H, Ar*H*) ppm. ^{7}Li NMR (97 MHz, C_6D_6): δ = 0.64 ppm. ^{13}C NMR (C_6D_6): δ = 14.6 (*C*H$_3$CH$_2$O), 23.3 [NC(*C*H)$_3$], 24.0 [CH(*C*H$_3$)$_2$], 24.4 [CH(*C*H$_3$)$_2$], 28.1 [*C*H(CH$_3$)$_2$], 64.3 (γ-*C*), 124.1 (Ar*C*), 125.3 (Ar*C*), 141.9 (Ar*C*), 144.8 (Ar*C*), 163.5 (N*C*) ppm. MS (EI): *m*/*z* (%) = 202 (100) [DippNCCH$_3$], 417 (30) [(dipp)$_2$NacNac], 1251 (40) [M − I]$^+$. $C_{66}H_{102}Cu_2I_2Li_2N_4O_2$ (1378.28): calcd. C 57.51, H 7.46, N 4.06; found C 58.7, H 8.5, N 5.2.

Crystal Structure Determination: All crystals were mounted on glass fibres in a rapidly cooled perfluoropolyether.[39] Diffraction data for **1a** and **4** were collected with a Stoe-Siemens-Huber four-circle diffractometer at 203(2) K, with graphite-monochromated Mo-K_α radiation (λ = 0.71073 Å), while diffraction data for **2** and **3** were collected with a Stoe IPDS-II at 133(2) K, again with graphite-monochromated Mo-K_α radiation (λ = 0.71073 Å). The structures were solved by direct methods with SHELXS-97 and refined against F^2 on all data by full-matrix, least squares with SHELXS-97.[40,41] All non-hydrogen atoms were refined anisotropically. The hydrogen atoms were included in the model at geometrically calculated positions and refined with a riding model if not otherwise stated (Table 6). Atomic coordinates, thermal parameters, bond lengths and angles: CCDC-175030 (**1a**), -175031 (**2**), 175033-(**3**), and -175032 (**4**) contain the supplementary crystallographic data for this paper. These data can be obtained free of charge at www.ccdc.cam.ac.uk/conts/retrieving.html or from the Cambridge Crystallographic Data Centre, 12, Union Road, Cambridge CB2 1EZ, UK [Fax: (internat.) + 44-1223/336-033; E-mail: deposit@ccdc.cam.ac.uk].

Acknowledgments

The financial support of the Deutsche Forschungsgemeinschaft and the Göttinger Akademie der Wissenschaften is very gratefully acknowledged.

[1] Y. Q. Ding, H. W. Roesky, M. Noltemeyer, H.-G. Schmidt, P. P. Power, *Organometallics* **2001**, *20*, 1190−1194.
[2] J. Prust, A. Stasch, W. Zheng, H. W. Roesky, E. Alexopoulos, I. Usón, D. Böhler, T. Schuchardt, *Organometallics* **2001**, *20*, 3825−3828.
[3] C. Cui, H. W. Roesky, H.-G. Schmidt, M. Noltemeyer, H. Hao, F. Cimpoesu, *Angew. Chem.* **2000**, *112*, 4444−4446; *Angew. Chem. Int. Ed.* **2000**, *39*, 4274−4276.
[4] N. J. Hardman, C. Cui, H. W. Roesky, W. H. Fink, P. P. Power, *Angew. Chem.* **2001**, *113*, 2230−2232; *Angew. Chem. Int. Ed.* **2001**, *40*, 2172−2174.
[5] J. Prust, K. Most, I. Müller, E. Alexopoulos, A. Stasch, I. Usón, H. W. Roesky, *Z. Anorg. Allg. Chem.* **2001**, *627*, 2032−2037.
[6] F. A. Carey, R. J. Sundberg, *Organische Chemie*, VCH Verlagsgesellschaft, Weinheim, **1995**.
[7] C. Elschenbroich, A. Salzer, *Organometallics: A Concise Introduction*, 2nd ed., VCH Publisher, New York, **1992**.
[8] B. H. Lipshutz, *Organometallics in Synthesis*, Wiley, Chichester, **1994**.
[9] F. J. Bickelhaupt, *J. Organomet. Chem.* **1994**, *475*, 1−14.
[10] R. G. Pearson, C. D. Gregory, *J. Am. Chem. Soc.* **1976**, *98*, 4098−4104.
[11] B. H. Lipshutz, J. A. Kozlowski, C. M. Breneman, *J. Am. Chem. Soc.* **1985**, *107*, 3197−3204.
[12] H. Hope, M. M. Olmstead, P. P. Power, J. Sandell, X. Xu, *J. Am. Chem. Soc.* **1985**, *107*, 4337−4338.
[13] N. A. Bell, A. L. Kassyk, *J. Organomet. Chem.* **1988**, *345*, 245−251.
[14] Y. Gao, K. Harada, T. Hata, H. Urabe, F. Sato, *J. Org. Chem.* **1995**, *60*, 290−291.
[15] N. A. Bell, A. L. Kassyk, *Inorg. Chim. Acta* **1996**, *250*, 345−349.
[16] H. Hao, C. Cui, H. W. Roesky, G. Bai, H.-G. Schmidt, M. Noltemeyer, *Chem. Commun.* **2001**, 1118−1119.
[17] A. J. Edwards, A. Fallaize, P. R. Raithby, M.-A. Rennie, A. Steiner, K. L. Verhorevoort, D. S. Wright, *J. Chem. Soc., Dalton Trans.* **1996**, 133−137.
[18] M. Krieger, R. O. Gould, B. Neumüller, K. Harms, K. Dehnicke, *Z. Anorg. Allg. Chem.* **1998**, *624*, 1434−1442.
[19] M. A. Putzer, B. Neumüller, K. Dehnicke, *Z. Anorg. Allg. Chem.* **1997**, *623*, 539−544.
[20] A. N. Chernega, M. Y. Antipin, M. Y. Struchkov, V. D. Romanenko, *Koord. Chim.* **1989**, *15*, 894−901.
[21] A. J. Arduengo III, H. V. R. Dias, F. Davidson, R. L. Harlow, *J. Organomet. Chem.* **1993**, *462*, 13−18.
[22] M. Steiner, H. Grützmacher, H. Pritzkow, L. Zsolnai, *Chem. Commun.* **1998**, 285−286.
[23] A. Looney, R. Han, I. B. Gorrell, M. Cornebise, K. Yoon, G. Parkin, A. L. Rheingold, *Organometallics* **1995**, *14*, 274−288.
[24] I. B. Gorrell, A. Looney, G. Parkin, A. L. Rheingold, *J. Am. Chem. Soc.* **1990**, *112*, 4068−4069.
[25] M. M. Olmstead, W. J. Grigsby, D. R. Chacon, T. Hascall, P. P. Power, *Inorg. Chim. Acta* **1996**, *251*, 273−284.
[26] M. Westerhausen, B. Rademacher, W. Schwarz, *Z. Anorg. Allg. Chem.* **1993**, *619*, 675−689.
[27] G. C. Forbes, A. R. Kennedy, R. E. Mulvey, R. B. Rowlings, W. Clegg, S. T. Liddle, C. C. Wilson, *Chem. Commun.* **2000**, 1759−1760.
[28] M. Westerhausen, T. Bollwein, N. Makropoulos, T. M. Rotter, T. Habereder, M. Suter, H. Nöth, *Eur. J. Inorg. Chem.* **2001**, 851−857.
[29] M. Ruf, K. Weis, I. Brasack, H. Vahrenkamp, *Inorg. Chim. Acta* **1996**, *250*, 271−281.
[30] G. Schmidt, U. Behrens, *J. Organomet. Chem.* **1996**, *509*, 49−55.
[31] "3D Search and Research Using the Cambridge Structural Database": F. H. Allen, O. Kennard, *Chemical Design Automation News* **1993**, *8*, 1 and 31.
[32] N. L. Narvor, L. Toupet, C. Lapinte, *J. Am. Chem. Soc.* **1995**, *117*, 7129−7138.
[33] T. Yamagata, H. Imoto, T. Saito, *Acta Crystallogr., Sect. C* **1997**, *53*, 859−862.

[34] R. Beckhaus, M. Wagner, V. V. Burlakov, W. Baumann, N. Peulecke, A. Spannenberg, R. Kempe, U. Rosenthal, *Z. Anorg. Allg. Chem.* **1998**, *624*, 129−134.
[35] B. A. Jazdzewski, P. L. Holland, M. Pink, V. G. Young, Jr., D. J. E. Spencer, W. B. Tolman, *Inorg. Chem.* **2001**, *40*, 6097−6107.
[36] P. Schulte, G. Gröger, U. Behrens, *J. Organomet. Chem.* **1999**, *584*, 1−10.
[37] D. Fortin, M. Drouin, M. Turcotte, P. D. Harvey, *J. Am. Chem. Soc.* **1997**, *119*, 531−541.
[38] W. Zheng, N. Mösch-Zanetti, H. W. Roesky, M. Hewitt, F. Cimpoesu, T. R. Schneider, A. Stasch, J. Prust, *Angew. Chem.* **2000**, *112*, 3229−3231; *Angew. Chem. Int. Ed.* **2000**, *39*, 3099−3101.
[39] T. Kottke, D. Stalke, *J. Appl. Crystallogr.* **1993**, *26*, 615−619.
[40] G. M. Sheldrick, *Acta Crystallogr., Sect. A* **1990**, *46*, 467−473.
[41] G. M. Sheldrick, *SHELX 97*, Universität Göttingen, **1997**.

Received January 10, 2002
[I02012]

Formation, Structures, and Magnetic and EPR Spectroscopic Properties of Dicobalt(III)-Dicopper(II) Complexes Featuring Heterotetranuclear Cations of a Puckered Cyclic Structure with Diethanolamine and Diethanolamine(2−) as Bridging Ligands

Valeriya G. Makhankova,[a] Olga Yu. Vassilyeva,*[a] Volodymyr N. Kokozay,[a] Jan Reedijk,[b] Gerard A. van Albada,[b] Julia Jezierska,[c] and Brian W. Skelton[d]

Keywords: Heterometallic complexes / Copper / Cobalt / Amino alcohols / EPR spectroscopy

The compounds $[Cu^{II}_2Co^{III}_2(H_2dea)_2(dea)_4]X_2(Solv)_n$ [X = Cl (**1**), Br (**2**), SCN (**3**), O_2CMe (**4**), I (**5**); Solv = H_2O or/and CH_3OH, DMF, n = 1–4] were synthesised by the reaction of zero-valent copper with cobalt(II) salts in non-aqueous (CH_3OH, DMF, DMSO) solutions of diethanolamine (H_2dea) in air. Crystallographic investigations of **1**–**4** reveal that the complexes contain the centrosymmetric cation $[Cu_2Co_2(H_2dea)_2(dea)_4]^{2+}$ in which the four metal atoms are linked together by bridging oxygen atoms of the six ligand groups to form a parallelogram with the length of the short edge (Cu···Co) being ca. 2.83 Å and a short diagonal distance (Cu···Cu) at approximately 3.23–3.29 Å. The copper atom is five-coordinate with a square-pyramidal geometry; the geometry at the trivalent cobalt ion is almost octahedral. The tetranuclear units are further stabilized by intramolecular O–H···O and N–H···O hydrogen bonds. The hydrogen-bonded network that involves the OH and NH groups of the ligands, uncoordinated anions, and solvent molecules links the tetranuclear units together and results in the formation of extended two- and three-dimensional networks. Variable-temperature magnetic susceptibility measurements of **1**–**3** and **5** show no significant exchange coupling between the copper centres. The frozen-solution and solid-state EPR spectra at 77 K are characteristic of a triplet state with the hyperfine structure distinctly resolved in solution. On the assumption of noncoaxiality of the g and D tensors the spectra were interpreted with the zero-field-splitting parameters D = 0.0560(1) (**2**–**5**) and D = 0.0712(1), E= 0.0028(2) cm^{-1} (**1**). Dominant contributions to the observed EPR zero-field splitting are presumed to be dipole-dipole in origin.
(© Wiley-VCH Verlag GmbH, 69451 Weinheim, Germany, 2002)

Introduction

The development of new approaches to the preparation of mixed-metal complexes plays an important role in synthetic coordination chemistry. Our current research in this field has been focused on the synthesis of Cu/M (M = Co,[1] Zn,[2] Ni) compounds. Investigation of their physico-chemical and catalytic properties may elucidate features found in polynuclear biologically active molecules, in which copper ions play an essential role in processes such as electron transfer, oxidation and dioxygen transport.[3]

A convenient synthetic pathway to such complexes has proven to be the use of zero-valent copper, a metal salt, and an amino alcohol as starting materials in solution in air. As we showed earlier, metal powders (Cu^0, Ni^0, Zn^0) dissolved to form metal complexes in the presence of an ammonium salt (a proton donating agent) and dioxygen from the air via Equation (1)

$$M^0 + 2\,NH_4^+ + 1/2\,O_2 \rightarrow M^{2+} + H_2O + NH_3 \quad (1)$$

in which copper oxidation occurs in the two-step process $Cu \rightarrow Cu^+ \rightarrow Cu^{2+}$.[4] The concept of the need for a proton-donating agent in syntheses of coordination compounds from elemental metals in air was further developed into a methodology for the preparation of mixed-metal complexes.[5] We believed that coordinatively unsaturated copper aminoalkoxides generated in situ could easily interact with other metal ions present in solution to afford the formation of a mixed-metal compound, due to the estab-

[a] Department of Inorganic Chemistry, National Taras Shevchenko University,
Volodimirska str. 64, Kyiv 01033, Ukraine
Fax: (internat.) +380-44/296-2467
E-mail: vassilyeva@chem.univ.kiev.ua
[b] Leiden Institute of Chemistry, Gorlaeus Laboratories, Leiden University,
P. O. Box 9502, 2300 RA Leiden, The Netherlands
[c] Faculty of Chemistry, University of Wroclaw,
14 Joliot-Curie Str., 50-383 Wroclaw, Poland
[d] Department of Chemistry, University of Western Australia,
Crawley, Western Australia 6009, Australia

lished ability of amino alcohols to form polynuclear metal complexes.[6]

A unique pentanuclear mixed-valence complex[1a] $[Cu^{II}_2Co^{II}Co^{III}_2(O_2CMe)_4(H_2tea)_2(tea)_2]\cdot 2(HO_2CMe)$ was obtained by the reaction of copper powder with cobalt(II) acetate and triethanolamine (H_3tea) in DMF solution in air. A marked decrease of the χT value below 40 K for this compound was attributed to antiferromagnetic exchange coupling between the Cu^{II} and Co^{II} magnetic centres interacting through the diamagnetic Co^{III} ions. We therefore started systematic investigations into the reactions of zerovalent copper and a cobalt(II) salt in the presence of another amino alcohol, diethanolamine [H_2dea, $NH(C_2H_4OH)_2$], and wish to report here the synthesis, crystal structures, spectroscopic investigations and magnetochemistry of the compounds $[Cu^{II}_2Co^{III}_2(H_2dea)_2(dea)_4]X_2(Solv)_n$ [X = Cl (**1**), Br (**2**), SCN (**3**), O_2CMe (**4**), I (**5**); Solv = H_2O or/and CH_3OH, DMF, n = 1−4].

Results and Discussion

Synthesis

When copper powder and cobalt(II) salts (chloride, bromide, iodide, thiocyanate, or acetate) were treated with nonaqueous (CH_3OH, DMF, DMSO) solutions of diethanolamine in air, dissolution of copper occurred within several hours whilst stirring at 50−60 °C, resulting in the formation of dark green solutions. These solutions slowly precipitated green crystalline products that were isolated as the corresponding solvates or hydrates in high yields. Crystals of an iodide complex formed in methanol appeared to lose solvent and crystallinity within minutes if left to stand exposed to a solvent-free atmosphere. The compounds showed analytical data accounting for the presence of Cu^{II} and Co^{III} in a 1:1 stoichiometry. Their formation can be understood if one considers the reaction scheme in Equation (2).

$$2\,Cu^0 + 2\,CoX_2 + 8\,H_2dea + 1.5\,O_2 + n\,Solv \rightarrow [Cu^{II}_2Co^{III}_2(H_2dea)_2(dea)_4]X_2\cdot n\,Solv + 2\,H_2dea\cdot HX + 3\,H_2O \quad (2)$$

The assumption of neutral and doubly deprotonated amino alcohols that follows from counting the electrostatic charges was verified structurally. A similar tetranuclear cation was found for the mixed-valence dark green cobalt complex $[Co^{II}_2Co^{III}_2(H_2dea)_2(dea)_4](ClO_4)_2$ (**6**),[7] prepared from a Co^{II} salt in air. This observation suggests that the structure and nuclearity of these complexes are governed by the ligand nature of diethanolamine in its interaction with Co^{II} ions in solution. The presence of the amino alcohol facilitates partial air oxidation of the initial Co^{II} to Co^{III} in the case of **6**. When metallic copper is involved the formation of a mixed-metal complex becomes more favourable and all the initial Co^{II} ions oxidise to Co^{III}.

Spectroscopic Characterization

The IR spectra of complexes **1**−**5** in the range 4000−400 cm^{-1} are quite similar, and show all the characteristic ligand peaks. The spectra indicate the presence of hydrogen-bonded (3300−3400 cm^{-1}) OH groups only; free (≈ 3600 cm^{-1}) OH groups are not observed.[8] Compound **3** shows the sharp, intense ν(CN) absorption at 2090 cm^{-1} and a weak band for ν(CS) of a thiocyanate group at 745 cm^{-1}. The δ(NCS) mode is obscured by other vibrations. The frequencies of the observed bands suggest a terminal N-bonded thiocyanate,[9] although this is not supported by the X-ray structural study (vide infra). Participation of the uncoordinated NCS^- group in the intermolecular hydrogen bonding may account for this observation (the $N_{NCS}\cdots O_{solvent}$ contacts of about 2.8 Å support such hydrogen bonding).

The IR spectrum of **4** displays two bands at 1600 and 1380 cm^{-1} of higher and lower intensity (Δ = 220 cm^{-1}), respectively, not observed in the spectra of **1**−**3** and **5** and therefore assigned to ν(CO_2) vibrations. The Δ values above 200 cm^{-1} for the acetato complexes appear generally to be associated with unidentate coordination.[8,10] This criterion is not applicable to **4**, as the results of the X-ray structural study show that the acetate oxygen atoms are not coordinated to metals. However, those oxygens are strongly hydrogen bonded to methanol and the NH groups of the amino alcohol, giving what may be regarded as a "pseudo-bridging" arrangement responsible for the observed spectral pattern. Also, the possibility of anion exchange in a KBr disc and pressure-induced changes cannot be ruled out in the case of **3** and **4**.

The absorption spectra of **1**−**5** in DMF are dominated by the low-energy broad absorption at approximately 600 nm, attributable to a superposition of transitions in the visible region of a low-spin cobalt(III) ion in an octahedral geometry and a five-coordinate copper(II) centre, as revealed in the crystal structure.[11] The high energy, very intense band lower than 330 nm is associated with a charge-transfer transition.

Molecular and Crystal Structures of 1−4

All four complexes consist of the tetranuclear cation $[Cu_2Co_2(H_2dea)_2(dea)_4]^{2+}$, which has a puckered cyclic structure, two anions, and several solvent molecules in the crystal lattice. The overall structural configurations of the cation for **1**−**4** are similar. The important differences show up as relatively small changes in bond lengths and angles (Table 1) as well as in the hydrogen bonding. The molecular diagram and numbering scheme of **1** is shown in Figure 1, which illustrates the general geometry of the compounds.

The existence of an inversion centre induces all metal centres to lie in the same plane. The four metal atoms are linked together by the bridging oxygen atoms of the six diethanolamine groups to form a parallelogram with the length of the short edge [Cu(1)−Co(2)] being ca. 2.83 Å and a short diagonal distance [Cu(1)−Cu(1′)] at approximately 3.23−3.29 Å (Table 1). Our assignments of the positions of the metal ions are based on the relative metal−N(O) bond lengths and the geometric features of the two chromophores. The atom Cu(1) is five-coordinate with a square-pyramidal geometry. The four copper-ligand

Table 1. Selected bond lengths (Å) and angles (°) for **1**−**4**[a]

	1	**2**	**3**	**4**
Cu(1)−O(1′)	1.945(1)	1.941(6)	1.94(2)	1.9453(7)
Cu(1)−O(3)	1.981(1)	1.978(6)	1.96(2)	1.9547(7)
Cu(1)−O(5)	2.356(2)	2.352(11)	2.37(2)	2.408(1)
Cu(1)−O(4)	1.974(1)	1.966(7)	1.93(2)	1.9843(6)
Cu(1)−N(3)	2.029(1)	2.017(9)	2.00(2)	2.0151(7)
Co(2)−O(2)	1.893(1)	1.885(8)	1.92(1)	1.9061(7)
Co(2)−O(4)	1.904(1)	1.901(7)	1.91(2)	1.9116(8)
Co(2)−N(2)	1.939(2)	1.924(11)	1.91(3)	1.952(1)
Co(2)−O(1)	1.904(1)	1.895(9)	1.89(2)	1.9074(8)
Co(2)−O(3)	1.926(1)	1.915(8)	1.91(2)	1.9116(7)
Co(2)−N(1)	1.955(2)	1.950(9)	1.96(3)	1.949(1)
Cu(1)···Co(2)	2.8445(3)	2.818(2)	2.820(6)	2.8294(2)
Cu(1)···Cu(1′)	3.2955(4)	3.261(3)	3.237(6)	3.2308(2)
O(1′)−Cu(1)−O(4)	92.99(5)	93.3(3)	94.7(7)	94.86(3)
O(4)−Cu(1)−O(3)	82.12(5)	82.2(3)	82.7(7)	81.98(3)
O(4)−Cu(1)−N(3)	177.90(7)	177.8(4)	177.4(9)	176.78(5)
O(1′)−Cu(1)−O(5)	92.42(5)	93.4(3)	91.3(8)	90.69(3)
O(3)−Cu(1)−O(5)	105.06(5)	104.7(3)	106.1(8)	106.83(3)
O(1′)−Cu(1)−O(3)	162.48(6)	161.9(4)	162.6(8)	162.47(4)
O(1′)−Cu(1)−N(3)	86.53(5)	87.3(3)	85.4(8)	86.58(3)
O(3)−Cu(1)−N(3)	97.73(5)	96.6(3)	96.5(8)	95.78(3)
O(4)−Cu(1)−O(5)	102.67(5)	101.9(3)	103.8(8)	101.56(3)
N(3)−Cu(1)−O(5)	79.40(6)	80.2(4)	78.7(8)	81.27(4)
O(2)−Co(2)−O(1)	92.11(5)	92.7(4)	91.9(7)	91.83(3)
O(1)−Co(2)−O(4)	89.29(6)	89.0(3)	90.1(8)	90.27(3)
O(1)−Co(2)−O(3)	91.86(5)	90.5(4)	91.0(8)	89.66(3)
O(2)−Co(2)−N(2)	91.67(6)	93.0(4)	90.0(9)	91.84(4)
O(4)−Co(2)−N(2)	87.43(6)	87.1(4)	87.0(1)	84.83(4)
O(2)−Co(2)−N(1)	86.74(5)	87.0(4)	87.9(8)	86.85(3)
O(4)−Co(2)−N(1)	174.36(7)	174.8(4)	176(1)	175.56(4)
N(2)−Co(2)−N(1)	98.21(7)	98.1(4)	97.0(1)	99.60(4)
O(2)−Co(2)−O(4)	93.03(5)	92.0(3)	93.3(7)	93.21(3)
O(2)−Co(2)−O(3)	175.72(6)	176.0(4)	176.4(9)	177.71(5)
O(4)−Co(2)−O(3)	85.44(5)	85.6(3)	84.6(7)	85.04(3)
O(1)−Co(2)−N(2)	175.12(5)	173.2(4)	176(1)	174.04(4)
O(3)−Co(2)−N(2)	84.28(6)	83.7(4)	87.0(9)	86.54(3)
O(1)−Co(2)−N(1)	85.09(6)	85.9(4)	86.0(1)	85.29(4)
O(3)−Co(2)−N(1)	95.18(5)	95.7(4)	94.5(8)	95.01(4)

[a] Symmetry transformations used to generate equivalent atoms (indicated by ′): $1 - x$, $1 - y$, $1 - z$.

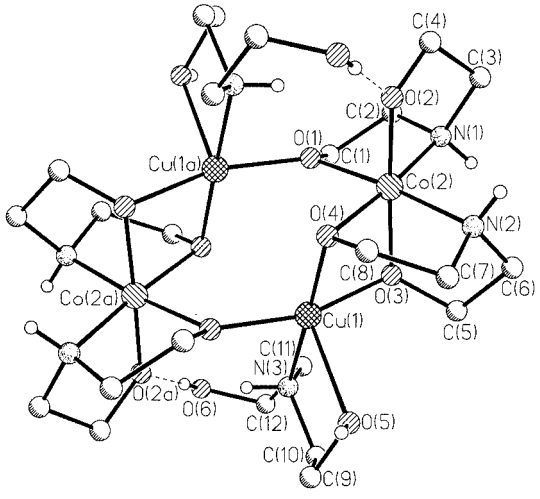

Figure 1. Molecular structure of the tetranuclear cation of **1**

bonds in the plane have normal bond lengths (average Cu−O and Cu−N distances of 1.96 and 2.02 Å, respectively), while the axial Cu−O(5) bond is elongated [2.352(11)−2.408(1) Å] due to the Jahn−Teller effect in the d^9 electronic configuration (Table 1). This long distance also allows one to infer the existence of the hydroxo donor function of the O(5) oxygen atom. The geometry at the trivalent cobalt ion, Co(2), is almost octahedral with Co(2)−O(N) distances in the range 1.885(8)−1.955(2) Å (Table 1), similar to those of low-spin cobalt(III) in an octahedral environment.[12] The structure of the tetranuclear cation is similar to that found for the mixed-valence cobalt complex **6**[7] in which the positions of the Co^{II} ions correspond to those of Cu^{II} in **1**−**4**.

The uncoordinated ethanol group of the neutral diethanolamine ligand forms an intramolecular hydrogen bond with the ethanolato group of the dea^{2-} ligand, as evidenced by the O(6)···O(2′) distances and O−H···O angles (Table 2, Figure 1). There is also a weaker intramolecular H bond between N(3) and O(2′) atoms (Table 2).

Table 2. Parameters of the intramolecular H-bonding for **1**−**4**, bond lengths (Å) and angles (°)[a]

	1	**2**	**3**	**4**
H(6O)−O(2′)	1.87(3)	1.35		1.97(2)
O(6)···O(2′)	2.592(2)	2.60(1)	2.62	2.731(1)
O(6)−H(6O)−O(2′)	178(4)	168		172(3)
H(3N)···O(2′)	2.12(2)	1.93	2.00	2.06(2)
N(3)···O(2′)	2.931(2)	2.90(1)	2.88(3)	2.911(1)
N(3)−H(3N)−O(2′)	163(3)	164	158	170(2)

[a] Symmetry transformations used to generate equivalent atoms (indicated by ′): $-x + 1$, $-y + 1$, $-z + 1$.

Intermolecular hydrogen bonding involving the OH and NH groups of the ligands, the uncoordinated anions, and solvent molecules, links the tetranuclear units together and results in the formation of extended two- and three-dimensional networks. A fragment of the solid-state structure of **4** is given in Figure 2 as a representative example. We believe that the participation of solvent molecules in the hydrogen-bonded network is essential for the complex integrity in the solid state.

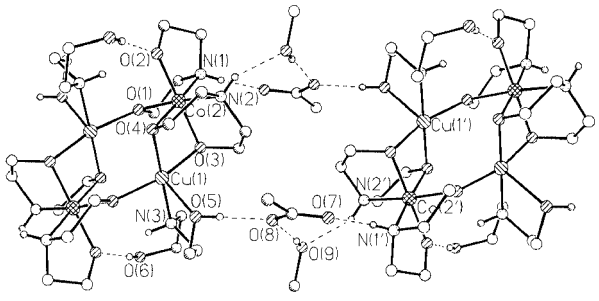

Figure 2. View of **4** showing the hydrogen-bonded network involving the noncoordinating acetate groups and methanol molecules

All bond lengths and angles within neutral and deprotonated diethanolamine are normal, and these data are given as supplementary material. Thiocyanate [d(N−C) 1.14(6), d(S−C) 1.59(4) Å, ∠N−C−S 170(4)°] and acetate groups [d(O−C) ca. 1.256(2), d(C−C) 1.519(2) Å, ∠O−C−O 124.9(1), ∠C−C−O 117.5(1)°] are structurally normal.[12]

Magnetic Properties

Experimental magnetic data for **1**−**3** and **5** are displayed in Figure 3 as μ_{eff} vs. T plots. The experimental data are presented as solid lines to distinguish between different plots. These show that in all cases the magnetic behaviour is paramagnetic. On the assumption that the Co^{III} ions are diamagnetic, the room temperature magnetic moment for each copper atom, ca. 1.8−1.9 B.M., is in the normal range for isolated $S = 1/2$ ions. The drop in the effective magnetic moment below 6 K indicates the onset of a weak antiferromagnetic coupling; this is not unexpected for systems in which H-bond contacts are important. It can be concluded that -O−Co−O- bridges effectively prevent any exchange interactions between copper centres.

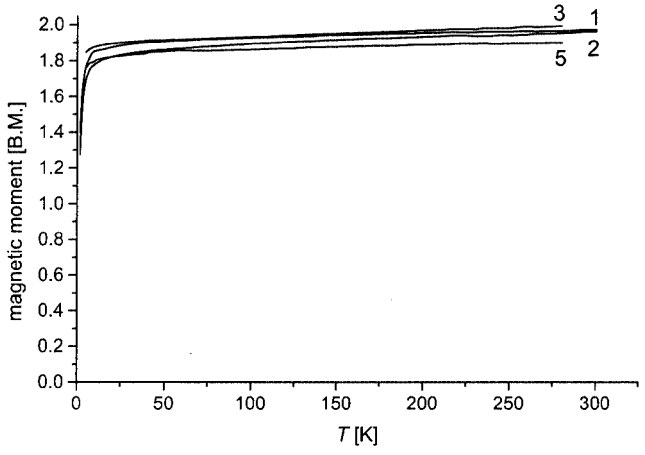

Figure 3. Plots of the effective magnetic moment per copper atom vs. T for **1**−**3** and **5**

The polycrystalline powder EPR spectra of **1**−**5** (Figure 4), which are essentially similar, show characteristic features of the spin-triplet state with the half-field signal observed (ca. 160 mT).[13] Fine structure components due to $\Delta M_S = 1$ transitions are distinctly visible for compounds **2** and **5**, and partly for **3** and **4**. In the case of compound **1** the $\Delta M_S = 1$ triplet-state components are not resolved. The spectra contain an isotropic signal in the $g \approx 2$ region, indicating crystal defects or monomeric impurities of different contribution. No sharpening of the lines or hyperfine splitting was observed upon cooling from room temperature to 77 K.

Nicely resolved spectra of the complexes showing almost identical triplet-state patterns were obtained from fresh solutions in DMF and methanol (77 K) (see Figure 5 for a representative example). The hyperfine structure from the two coupled Cu^{II} centres is clearly observed for the $\Delta M_S = 1$ and $\Delta M_S = 2$ signals and also partly resolved on the line present in frozen solution spectra only at ca. 375 mT, which is attributed to a high-field "parallel" line (Figure 5). Careful examination of the $\Delta M_S = 2$ signals (using the accumulation procedure) reveals two sets of "parallel" orientation lines for compounds **3** and **5** in DMF (Figure 5). One of them corresponds to that observed for all other compounds; the second is most likely associated with the additional spin-triplet line seen at 397 mT for **3** and **5** in DMF, suggesting a very small contribution of other triplet-state species.

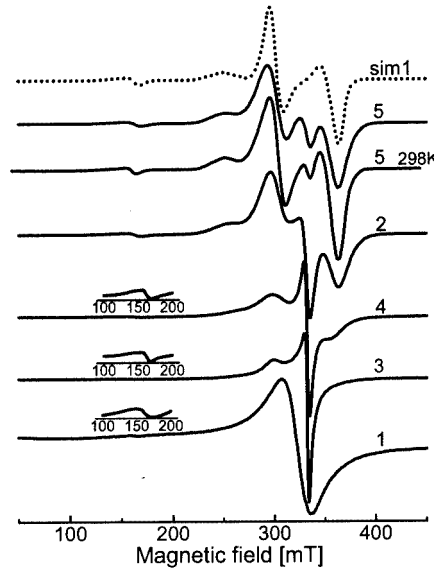

Figure 4. EPR spectra of polycrystalline complexes **1**−**5** measured at 77 K (solid lines), the dotted line being the simulated (sim1) spectrum obtained with parameters reported in the text

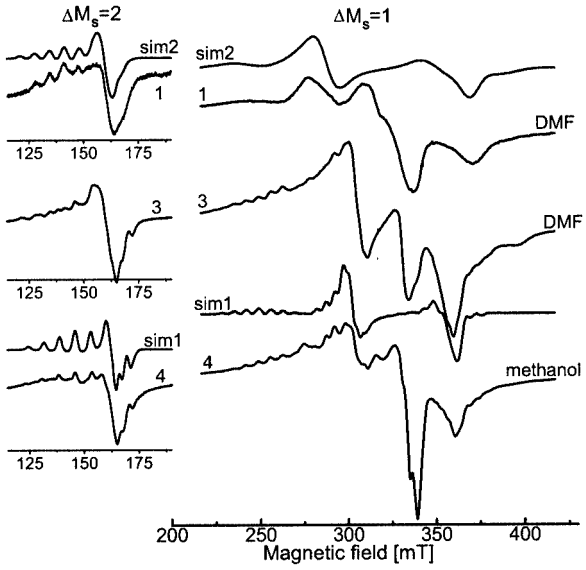

Figure 5. EPR spectra of frozen solutions of **1** and **3** in DMF and **4** in methanol (77 K); sim1 and sim2 are the fits obtained for the frozen solution spectra for **2**−**5** in DMF and methanol and for **1** in DMF, respectively, using parameters reported in the text

No substantial variation of the zero-field splitting for the different complexes was observed in both DMF and methanol frozen solutions, except compound **1**. However, the relative intensities of the fine-structure signals and signals due to paramagnetic species vary for the two solvents. The former signals are much more intense in DMF, indicating that tetranuclear $[Cu_2Co_2(H_2dea)_2(dea)_4]^{2+}$ cations are destroyed by the alcohol to a greater extent. The triplet-state spectra became weaker with time and the paramagnetic species contribution substantially increased.

The triplet EPR spectra are described by the spin Hamiltonian shown in Equation (3):[14]

$$H = \mu_B B\{g\}\, S + I\{A\}S + D[S_z^2 - 1/3\, S(S+1)] + E(S_x^2 - S^2{}_y) \qquad (3)$$

The experimental spectra have been fitted with nonparallel g and D tensors through a computer simulation procedure as described in refs.[15−17] The main features of the solid-state and frozen solution (methanol, DMF) spectra of compounds **2**−**5** were well simulated with the same set of spin-Hamiltonian parameters ("sim1" in Figure 4 and 5), $g_z = 2.305(5)$, $g_x = 2.063(2)$, $g_y = 2.063(2)$, $A_z = 0.0070(2)$, $A_x = 0.0014(4)$, $A_y = 0.0010(4)$ cm^{-1}, $D = 0.0560(1)$ cm^{-1} and an angle (α) between g_{zz} and D_{zz} directions of 25(1)°. In the polycrystalline powder spectrum of **1** the high intensity of the isotropic signal and the low resolution of the triplet signals make a determination of the g and D values impossible. Dissolution of the compound in DMF afforded the triplet-state spectrum (77 K) with the following spin-Hamiltonian parameters ("sim2" in Figure 5): $g_z = 2.350(5)$, $g_x = 2.068(2)$, $g_y = 2.068(2)$, $A_z = 0.0070(2)$, $A_x = 0.0012(4)$, $A_y = 0.0012(4)$ cm^{-1}, $D = 0.0712(1)$ cm^{-1}, $E = 0.0028(2)$ cm^{-1}, $\alpha = 30(1)°$.

These results clearly indicate that the configuration of the tetranuclear cations is retained in solution. Since no significant exchange coupling between copper centres is involved, according to the solid-state magnetic susceptibility studies for the reported compounds, the dominant interaction that brings about the characteristic shape of the EPR spectra is presumed to be dipole-dipole in origin.[13] Assuming only dipolar contributions to the observed EPR zero-field splitting, the empirical formula[18] would yield a separation of 3.4 (**2**−**5**) and 3.2 Å (**1**) for the Cu−Cu distance, which are in nice — although not very accurate — agreement with the solid-state distances (Table 1). The following observation also provides support for such a conclusion. In the case of dominant dipolar effects, the largest component of the zero-field-splitting tensor, D_{zz}, is parallel to the Cu−Cu direction; the largest g value for a square pyramidal copper(II) is expected to be orthogonal to the plane of equatorial ligands.[19] According to the crystallographic studies of compounds **1**−**4** the normal to the least-squares plane provided by N(3), O(3), O(4), and O(1′) makes an angle of ca. 30° with the axis joining the two copper centres. The value obtained is in good agreement with the values of α derived from the assumption of the noncoaxiality of the g and D tensors.

Concluding Remarks

Once again, employing zero-valent metals as a source of one of the metals in the synthesis of mixed-metal compounds allowed the generation of remarkable crystal structures, such as the heterotetranuclear dicobalt(III)dicopper(II) complexes containing diethanolamine.

Magnetic susceptibility measurements and EPR triplet spectra of the complexes showed evidence that the zero-field splitting parameter D originates from dipole-dipole interactions. The structure of the tetranuclear cations is fully preserved in solution and magnetic dipole-dipole coupling between the copper(II) ions is maintained.

Experimental Section

General: All chemicals were of reagent grade, and were used as received. All experiments were carried out in air. Elemental analyses for metals were performed by atomic absorption spectroscopy, and potentiometric titration with a solution of $K_3[Fe(CN)_6]$ for Co^{II},[20] using standard titrimetric methods for anions and a Carlo Erba Strumentazion Analyzer (for C, H and N). Infrared spectra were recorded as KBr discs or as Nujol mulls on a UR-10 spectrophotometer in the 4000−400 cm^{-1} region using conventional techniques. UV/Vis DMF solution spectra were recorded on a Perkin−Elmer Lambda 12 spectrometer. The EPR spectra were recorded on a Bruker ESP 300E (Bruker, Germany) spectrometer operating at X-band and equipped with a Bruker NMR gaussmeter ER 035M and a Hewlett−Packard microwave frequency counter HP 5350B. Variable-temperature magnetic measurements on complexes **1** and **2** in the region 1.8−300 K were made using a SQUID magnetometer (Quantum Design) with samples sealed in capsules. Magnetic susceptibility measurements for compounds **3** and **5** were recorded in the temperature range 4−300 K with a fully automated Manics DSM-8 susceptometer equipped with a TBT continuous-flow cryostat and a Drusch EAF 16 NC electromagnet, operating at ca. 1.4 T. In all cases, diamagnetic corrections for the sample holders were applied to the data. Diamagnetic corrections for the samples were determined from Pascal's constants.[21]

General Procedure for the Synthesis of 1−5: Copper powder (0.32 g, 5 mmol), $Co(X)_2{\cdot}nH_2O$ (5 mmol) (X = Cl, Br, I, NCS, O_2CMe; n = 1−6), CH_3OH (10 cm^3, DMF in the case of **5**) and H_2dea (4 cm^3) were heated to 50−60 °C and stirred magnetically until total dissolution of Cu was observed (several hours). The resulting solutions were allowed to stand at room temperature for one week during which time dark-green crystalline products of **1**−**5** precipitated. They were filtered off, washed with dry 2-propanol and finally dried in vacuo at room temperature.

$[Cu_2Co_2(H_2dea)_2(dea)_4]Cl_2{\cdot}2H_2O$ (1): Mass collected: 1.36 g, yield 56%. IR (KBr): $\tilde{\nu}$ = 3370 br, 3145 s, 3105 s, 2970 sh, 2940 m, 2900 m, 2885 m, 2860 m, 1660 br, 1450 m, 1375 w, 1350 sh, 1340 w, 1270 w, 1250 w, 1235w, 1220 w, 1185 w, 1165 w, 1115 sh, 1105 s, 1080 m, 1060 vs, 1040 sh, 1020 sh, 925 w, 915 w, 900 w, 880 w, 865 w, 830 w, 680 w, 645 m, 600 w, 570 sh, 560 m, 535 m, 500 w, 480 w, 445 w. $C_{24}H_{62}Cl_2Co_2Cu_2N_6O_{14}$ (974.65): calcd. Cu 13.04, Co 12.09, Cl 7.27, C 29.58, H 6.41, N 8.62; found Cu 13.4, Co 12.0, Cl 7.6, C 28.8, H 6.6, N 8.1.

$[Cu_2Co_2(H_2dea)_2(dea)_4]Br_2{\cdot}2H_2O{\cdot}2CH_3OH$ (2): Mass collected: 1.20 g, yield 43%. IR (KBr): $\tilde{\nu}$ = 3400 br, 3160 s, 3115 s, 2940 m,

2890 w, 2880 m, 2850 m, 1650 br, 1450 m, 1375 w, 1350 sh, 1340 w, 1270 w, 1250 w, 1235 w, 1215 w, 1180 w, 1150 w, 1110 sh, 1100 s, 1080 m, 1055 vs, 1040 sh, 1020 sh, 925 w, 915 w, 900 w, 880 w, 865 w, 825 w, 720 w, 680 w, 645 m, 595 w, 570 sh, 560 m, 535 m, 495 w, 480 w, 445 w cm^{-1}. $C_{26}H_{70}Br_2Co_2Cu_2N_6O_{16}$, (1127.64): calcd. Cu 11.27, Co 10.45, Br 14.17, C 27.69, H 6.26, N 7.45; found Cu 11.8, Co 10.9, Br 14.6, C 27.8, H 6.3, N 7.8.

$[Cu_2Co_2(H_2dea)_2(dea)_4](NCS)_2\cdot 2CH_3OH$ (3): Mass collected: 0.73 g, yield 28%. IR (KBr): $\tilde{\nu}$ = 3400 br, 3300−3100 br, 2935 m, 2870 m, 2830 sh, 2090 s, 1630 br, 1450 m, 1425 m, 1380 w, 1365 w, 1270 w, 1250 w, 1215 w, 1155 w, 1120 sh, 1095 m, 1060 vs, 1045 vs, 1015 sh, 920 w, 915 w, 885 w, 860 w, 830 w, 745 w, 665 w, 645 m, 595 w, 570 w, 555 m, 520 m, 500 w, 480 w, 465 w cm^{-1}. $C_{28}H_{66}Co_2Cu_2N_8O_{14}S_2$ (1047.95): calcd. Cu 12.13, Co 11.25, NCS 11.08, C 32.09, H 6.35, N 11.36; found Cu 12.7, Co 11.6, NCS 11.0, C 31.2, H 6.1, N 10.7.

$[Cu_2Co_2(H_2dea)_2(dea)_4](O_2CMe)_2\cdot 2CH_3OH$ (4): Mass collected: 1.25 g, yield 48%. IR (KBr): $\tilde{\nu}$ = 3430 br, 3220−3100 br, 2935 m, 2870 m, 2830 m, 1600 s, 1435 m, 1390 sh, 1380 m, 1330 m, 1275 w, 1250 w, 1220 w, 1180 w, 1120 w, 1100 m, 1055 vs, 1035 sh, 1020 sh, 920 w, 915 sh, 890 w, 880 w, 860 w, 820 w, 675 w, 645 m, 615 w, 600 w, 590 w, 570 m, 555 m, 520 m, 500 w, 480 w, 465 w cm^{-1}. $C_{30}H_{72}Co_2Cu_2N_6O_{18}$ (1049.89): calcd. Cu 12.11, Co 11.23, C 34.32, H 6.91, N 8.00; found Cu 12.3, Co 11.4, C 33.5, H 7.0, N 7.9.

$[Cu_2Co_2(H_2dea)_2(dea)_4]I_2\cdot 2DMF$ (5): Mass collected: 1.53 g, yield 48%. IR (KBr): $\tilde{\nu}$ = 3450 br, 3300−3050 br, 2935 m, 2875 m, 2835 sh, 1660 s, 1440 m, 1400 m, 1370 w, 1350 w, 1250 w, 1185 w, 1160 w, 1110 sh, 1100 m, 1060 vs, 1030 sh, 1020 sh, 920 w, 900 w, 880 w, 855 sh, 830 w, 675 w, 645 m, 600 w, 570 m, 555 m, 525 m, 500 m, 480 w, 450 w cm^{-1}. $C_{30}H_{72}Co_2Cu_2I_2N_8O_{14}$ (1267.73): calcd. Cu 10.03, Co 9.30, I 20.02, C 28.42, H 5.72, N 8.84; found Cu 9.9, Co 9.0, I 20.3, C 29.2, H 5.9, N 8.8.

X-ray Crystallographic Investigations: Diffraction experiments were performed on a Bruker SMART CCD diffractometer (ω rotation scans with narrow frames) (**1**, **4**) and an Enraf−Nonius CAD-4 diffractometer operating in the ω/2θ scan mode (**2**, **3**) equipped with graphite-monochromated Mo-K_α radiation (λ = 0.71073 Å) (**1**, **2**, **4**) and Cu-K_α radiation (λ = 1.54178 Å) (**3**). The data were corrected for Lorentz polarisation effects and for the effects of absorption [multi-scan (**1**, **4**), Gaussian (**2**, **3**)]. The structures were solved by direct methods using the XTAL3.5[22] (**1**, **4**) and SHELXS-86[23] (**2**, **3**) programs, and refined by full-matrix least-squares methods on *F* using SHELXL-93[24] and XTAL3.5.[22] Details of the structural investigations and crystallographic data are summarized in Table 3.

In most cases (**1**, **2**, **4**), the non-hydrogen atoms were refined anisotropically (full-matrix least-squares). For both **1** and **4** all hydrogen atoms were located in a difference Fourier synthesis and refined isotropically. For **2** hydrogen atoms were included in their calculated positions, except hydroxyl hydrogen atoms, which were located but not refined. The ethanol solvent OH hydrogen atom was not located. For **3**, carbon atoms were refined with isotropic displacement parameters. The solvent methanol was refined with two disordered components with site occupancy factors set at 0.75 and 0.25 after initial trial refinement. Hydrogen atoms were included in

Table 3. Crystallographic data and relevant data referring to the structure solution and refinement

Compound	**1**	**2**	**3**	**4**
Empirical Formula	$C_{24}H_{62}Cl_2Co_2Cu_2N_6O_{14}$	$C_{26}H_{70}Br_2Co_2Cu_2N_6O_{16}$	$C_{28}H_{66}Co_2Cu_2N_8O_{14}S_2$	$C_{30}H_{72}Co_2Cu_2N_6O_{18}$
Molecular mass	974.65	1127.64	1047.97	1049.89
Cryst. size [mm]	0.5 × 0.28 × 0.24	0.25 × 0.45 × 0.45	0.40 × 0.29 × 0.27	0.4 × 0.4 × 0.15
Space group	$P2_1/c$	$P\bar{1}$	$P2_1/n$	$P\bar{1}$
CCDC deposit no.	164276	164275	164274	164273
a [Å]	11.338(1)	10.092(2)	11.048(2)	8.4439(5)
b [Å]	17.831(2)	10.749(2)	15.913(3)	11.4758(7)
c [Å]	10.229(1)	11.477(2)	13.023(3)	11.9843(7)
α [°]	90	67.89(3)	90	76.183(1)
β [°]	112.644(2)	67.80(3)	109.45(3)	89.700(1)
γ [°]	90	88.63(3)	90	69.540(1)
V [$Å^3$]	1908.6(3)	1057.7(5)	2158.9(8)	1052.6(1)
Z	2	1	2	1
$\rho_{calcd.}$ [g/cm^3]	1.696	1.77	1.612	1.656
μ [mm^{-1}]	2.161	3.721	8.512	1.85
F(000)	1012	578	1092	550
Index range	$-15 \le h \le 13$	$0 \le h \le 10$	$0 \le h \le 11$	$-14 \le h \le 14$
	$0 \le k \le 24$	$-12 \le l \le 12$	$0 \le k \le 16$	$-19 \le k \le 19$
	$0 \le l \le 13$	$-12 \le l \le 12$	$-13 \le l \le 13$	$0 \le l \le 20$
θ_{min}, θ_{max} [°]	1.95, 29.03	2.06, 23.92	4.55, 55.94	2.6, 38.54
T [K]	150	293	293	150
Refl. collected	18379	2860	2133	22000
Refl. unique	4738	2643	2022	11175
R_{int}	0.021	0.04	0.078	0.024
Refl. observed	4304	2122	1048	9343
	[$F > 4.00\sigma(F)$]	[$I > 2\sigma(I)$]	[$I > 2\sigma(I)$]	[$F > 4.00\sigma(F)$]
R	0.025	0.066	0.102	0.026
wR	0.033	0.077	0.136	0.032
No. of variable	351	244	191	406
GoF	1.168	1.165	1.205	0.998
Larg. res. Peak [$e/Å^3$]	0.579; −0.510	1.192; −1.396	1.031; −0.917	0.977; −0.798

their calculated positions where possible. OH hydrogen atoms were not located.

CCDC-164273 (**4**), -164274 (**3**), -164275 (**2**), and -164276 (**1**) contain the supplementary crystallographic data for this paper. These data can be obtained free of charge at www.ccdc.cam.ac.uk/conts/retrieving.html [or from the Cambridge Crystallographic Data Centre, 12, Union Road, Cambridge CB2 1EZ, UK; Fax: (internat.) +44-1223/336-033; E-mail: deposit@ccdc.cam.ac.uk].

Acknowledgments

The work was in part supported by the Science and Technology Center in Ukraine (Project Gr-32j). A Royal Society Ex-Agreement Visit − FSU grant (O.Yu.V.) is gratefully acknowledged.

[1] [1a] V. G. Makhankova, O. Yu. Vassilyeva, V. N. Kokozay, B. W. Skelton, J. Reedijk, G. A. van Albada, L. Sorace, D. Gatteschi, *New J. Chem.* **2001**, *25*, 685. [1b] V. G. Makhankova, O. Yu. Vassilyeva, V. N. Kokozay, B. W. Skelton, G. A. van Albada, J. Reedijk, *Z. Naturforsch., Teil B* **2001**, *56*, 931.

[2] [2a] E. A. Vinogradova, O. Yu. Vassilyeva, V. N. Kokozay, P. J. Squattrito, J. Reedijk, G. A. van Albada, W. Linert, S. K. Tiwary, P. R. Raithby, *New J. Chem.* **2001**, *25*, 949. [2b] E. A. Vinogradova, O. Yu. Vassilyeva, V. N. Kokozay, *Inorg. Chem. Commun.* **2002**, *5/1*, 19.

[3] E. Fenton, H. Okawa, *Chem. Ber. Recueil* **1997**, *130*, 433.

[4] [4a] V. A. Pavlenko, V. V. Skopenko, V. N. Kokozay, *Dopov. Akad. Nauk Ukr. RSR, Ser. B.* **1983**, 47. [4b] V. A. Pavlenko, V. N. Kokozay, V. V. Skopenko, *Dopov. Akad. Nauk Ukr. RSR, Ser. B* **1985**, 42. [4c] O. Yu. Vassilyeva, N. D. Nevesenko, V. V. Skopenko, Yu. S. Gerasimenko, V. N. Kokozay, *Dopov. Akad. Nauk Ukr. RSR, Ser. B* **1988**, 36. [4d] O. Yu. Vassilyeva, V. N. Kokozay, *Ukr. Khim. Zh. (Russ. Ed.)* **1993**, *59*, 176.

[5] [5a] L. A. Kovbasyuk, O. Yu. Vassilyeva, V. N. Kokozay, W. Linert, J. Reedijk, B. W. Skelton, A. G. Oliver, *J. Chem. Soc., Dalton Trans.* **1998**, 2735. [5b] L. A. Kovbasyuk, O. Yu. Vassilyeva, V. N. Kokozay, W. Linert, B. W. Skelton, A. G. Oliver, *New J. Chem.* **1998**, 931, and refs. therein.

[6] [6a] K. Smolander, *Annales Academiae Scientirum Finnicae*, Series A **1983**, *2*, 1. [6b] J. A. Bertrand, P. G. Eller, *Progr. Inorg. Chem.* **1976**, *21*, 29. S. Wang, Z. Pang, K. D. L. Smith, M. J. Wagner, *J. Chem. Soc., Dalton Trans.* **1994**, 955. [6c] A. Lehtonen, R. Sillanpaa, *J. Chem. Soc., Dalton Trans.* **1995**, 2701.

[7] J. A. Bertrand, E. Fujita, D. G. VanDerveer, *Inorg. Chem.* **1979**, *18*, 230.

[8] K. Nakamoto, *Infrared and Raman Spectra of Inorganic and Coordination Compounds*, 4th ed.; John Wiley & Sons: New York, **1986**.

[9] [9a] G. A. van Albada, R. A. G. de Graaff, J. G. Haasnoot, J. Reedijk, *Inorg. Chem.* **1984**, *23*, 1404. [9b] J. G. Haasnoot, W. L. Driessen, J. Reedijk, *Inorg. Chem.* **1984**, *23*, 2803. [9c] E. Bouwman, P. Evans, R. A. G. de Graaff, H. Kooijman, R. Poinsot, P. Rabu, J. Reedijk, A. L. Spek, *Inorg. Chem.* **1995**, *34*, 6302. [9d] *Chemistry of Pseudohalides* (Eds.: A. Golub, H. Kohler, V. Skopenko), Elsevier, Amsterdam, **1986**.

[10] G. B. Deacon, R. J. Phillips, *Coord. Chem. Rev.* **1980**, *33*, 227.

[11] B. J. Hathaway, D. E. Billing, *Coord. Chem. Rev.* **1970**, *5*, 143.

[12] A. F. Wells, *Structural Inorganic Chemistry*, 5th edn., Clarendon Press, Oxford, **1986**.

[13] [13a] T. D. Smith, J. R. Pilbrow, *Coord. Chem. Rev.* **1974**, *13*, 173. [13b] W. M. E. Koomen-van Oudenniel, R. A. G. de Graaff, J. G. Haasnoot, R. Prins, J. Reedijk, *Inorg. Chem.* **1989**, *28*, 1128. [13c] G. J. A. A. Koolhaas, W. L. Driessen, J. Reedijk, J. L. van der Plas, R. A. G de Graaff, D. Gatteschi, H. Kooijman, A. L. Spek, *Inorg. Chem.* **1996**, *35*, 1509. [13d] J. Jezierska, A. Ożarowski, G. Vučković, *Nukleonika* **1997**, *42*, 475. [13e] V. K. Voronkova, G. Vučković, J. Jezierska, J. Mroziński, Yu. V. Yablokov, *Inorg. Chim. Acta* **1997**, *262*, 147. [13f] J. Jezierska, T. Głowiak, A. Ożarowski, Yu. V. Yablokov, S. Rzaczyńska, *Inorg. Chim. Acta* **1998**, *275*, 28.

[14] A. Abragam, B. Bleaney, *Electron Paramagnetic Resonance of Transition Ions*, Clarendon Press, Oxford, **1970**.

[15] A. Ożarowski, unpublished program.

[16] J. Baranowski, T. Cukierda, B. Jeżowska-Trzebiatowska, H. Kozłowski, *Chem. Phys. Lett.* **1976**, *39*, 606.

[17] A. Ożarowski, D. Reinen, *Inorg. Chem.* **1986**, *25*, 1704.

[18] N. Sreehari, P. T. Manoharan, *Mol. Phys.* **1988**, *63*, 1077.

[19] F. E. Mabbs, D. Collison, *Electron Paramagnetic Resonance of d Transition Metal Compounds*, Elsevier, Amsterdam, **1992**.

[20] V. V. Udovenko, V. N. Evreev, *Izv. Vyssh. Uchebn. Zaved., Khim. Khim. Tekhnol.* **1963**, *6*, 8.

[21] C. J. O'Connor, *Prog. Inorg. Chem.* **1982**, 29.

[22] S. R. Hall, G. S. D. King, J. M. Stewart, XTAL3.5. User's Manual, University of Western Australia: Lamb, Perth, **1995**.

[23] G. M. Sheldrick, SHELXS-86, *Acta Crystallogr., Sect. A* **1990**, *46*, 467.

[24] G. M. Sheldrick, *SHELXL-93, Program for the Crystal Structure Refinement*, University of Göttingen, **1993**.

Received January 11, 2002
[I02017]

Monitoring the Reactions of the Anticancer Drug Carboplatin with the Chemopreventive Agent Selenomethionine by Electrospray Mass Spectrometry and [^{1}H,^{15}N] HSQC NMR Spectroscopy

Qin Liu,[a,b] Jun Lin,[a] Pengju Jiang,[a] Junyong Zhang,[a] Longgen Zhu,[a] and Zijian Guo*[a]

Keywords: Antitumor agents / Platinum / L-Selenomethionine / Mass spectrometry / NMR spectroscopy

The reactions of the second-generation platinum anticancer drug carboplatin with L-selenomethionine (L-Se-MetH) and L-methionine (L-MetH) (abbreviations used: L-Se-MetH: L-selenomethionine; L-Se-Met: deprotonated L-selenomethionine; L-MetH: L-methionine; L-Met: deprotonated L-methionine) were studied by ESMS and 2D [^{1}H,^{15}N] HSQC NMR spectroscopy. The combination of the two techniques provided the unambiguous assignment of [Pt(NH_3)$_2$(CBDCA-*O*)(L-Se-MetH-*Se*)] (**1**), the long-lived ring-opened adduct, [Pt(NH_3)(CBDCA-*O*)(L-Se-Met-*Se*,*N*)] (**2**), [Pt(CBDCA-*O*,*O*)(L-Se-MetH-*Se*,*N*)] (**3**) and [Pt(L-Se-Met-*Se*,*N*)$_2$] (**4**). The reaction of carboplatin with L-MetH is very similar to that with L-Se-MetH, except for a slower reaction rate. Interestingly, we observed the dimer and polymer forms of carboplatin in solution by electrospray mass spectrometry. This work demonstrates that carboplatin differs from cisplatin in that both reactions with L-Se-MetH and L-MetH form [Pt(L-Se-Met-*Se*,*N*)$_2$] or [Pt(L-Met-*S*,*N*)$_2$] as the dominant adducts.
(© Wiley-VCH Verlag GmbH, 69451 Weinheim, Germany, 2002)

Introduction

Carboplatin, [Pt(NH_3)$_2$(CBDCA)] (CBDCA: cyclobutane-1,1-dicarboxylate, Scheme 1), is now a widely used second-generation platinum anticancer drug. The major advantage of carboplatin compared with cisplatin ([$PtCl_2(NH_3)_2$]) [1] is its much lower toxicity, which may be attributed to its low reactivity caused by the presence of the chelating CBDCA ligand. [2]

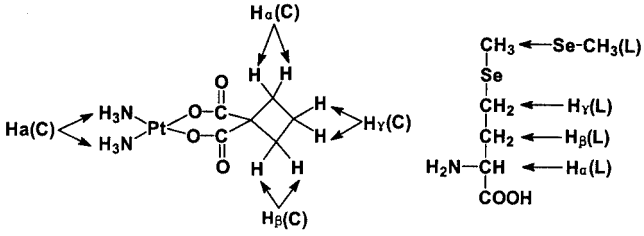

Carboplatin **L-Se-MetH**

Scheme 1. Schematic drawing of carboplatin and L-Se-MetH and the labeling scheme used in the ^{1}H NMR spectra

The in vivo activation of carboplatin has been a subject of much interest. [3,4] Although early studies suggested that carboplatin is merely a prodrug of cisplatin, [5] the aquation rate is too slow to account for its in vivo activity. [6] The amino acid L-methionine (L-MetH) has been shown to react rapidly with carboplatin to form long-lived ring-opened complexes. [7] It has been therefore postulated that L-methionine may play a role in the mechanism of the reaction of the platinum drug. [8] More interestingly, a similar ring-opened complex has been detected in the urine of animals treated with carboplatin. [9] Since the complex [Pt(Met-*S*,*N*)$_2$] was identified as the in vivo metabolite of cisplatin, many studies on the interactions of platinum drugs with methionine and its derivatives have been carried out. [10–14]

L-Selenomethionine (L-Se-MetH, Scheme 1), the selenium analogue of L-methionine, is currently on clinical trials as a potential cancer chemopreventive agent in reducing both environmentally and genetically determined cancer. [15,16] It was also recently reported that L-Se-MetH is able to protect against cisplatin-induced renal and other toxicities in mice and rats. [17] We have recently investigated the reactions between cisplatin and L-selenomethionine, and demonstrated that the combination of ESMS and NMR spectroscopy could provide valuable information on the mechanism of the reactions. [18] Here, we extend our study to the interactions of L-selenomethionine and the second-generation anticancer drug carboplatin. The reaction be-

[a] State Key Laboratory of Coordination Chemistry, Coordination Chemistry Institute,
Nanjing University, 210093 Nanjing, P. R.China
Fax: (internat.) + 86-25/331-4502
E-mail: zguo@netra.nju.edu.cn
[b] Department of Food Sciences and Engineering, Nanjing College of Economics,
210003 Nanjing, P. R. China
Supporting information for this article is available on the WWW under http://www.eurjic.com or from the author.

tween carboplatin and L-methionine is also carried out in order to compare the results with those studied by NMR spectroscopy.[7]

Results and Discussion

Results

(1) ESMS Investigation of Carboplatin in Solution: Detection of Dimer and Polymer Forms

A solution of carboplatin (2.68 mmol/mL) was studied at pH = 5.00 (no buffer solution was used) by ESMS. As shown in Figure 1, apart from the positive ion of protonated carboplatin (m/z = 372.1) and {[Pt(NH_3)$_2$(CBDCA)] + Na^+} (m/z = 394.1), three pairs of peaks at m/z = 743.1, 765.1; 1114.1, 1136.1; and 1486.0, 1508.0 were observed. These ions correspond to the formation of the dimer, trimer, and tetramer forms of carboplatin, respectively, and their corresponding sodium adducts (Table 1). These forms of carboplatin have never been detected previously in solution by other methods, although they may be formed only during the ionization process (vide infra). As can be seen from Figure 1, the intensity of the peaks decrease with the increase in the molecular size.

(2) The Time-Dependent Reaction of Carboplatin with L-Se-MetH in a 1:1 Molar Ratio

The reaction between carboplatin and L-Se-MetH was monitored for 22 h. The first ESMS spectrum was measured 2 min after mixing of the solutions of carboplatin and L-Se-MetH. Figure 2 shows the representative spectra of the reaction recorded after 25 min, 3 h and 22 h. As noted, all the isotopic peaks were separated by 1 unit and can be assigned to complexes with one positive charge. After 2 min, two new peaks (peak 1 and 12) appeared in the spectrum. Peak 1 at m/z = 567.9 can be assigned to

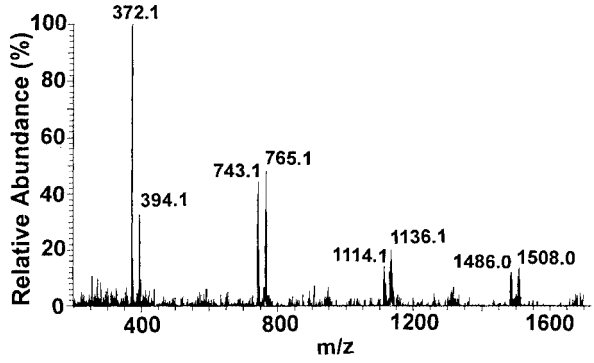

Figure 1. ESMS spectrum of a carboplatin solution (2.68 mmol/mL) at pH = 5.00

[Pt(NH_3)$_2$(CBDCA)(L-Se-MetH)]$^+$ (**1**), in which L-Se-MetH is likely to be coordinated to Pt via the selenium atom and the CBDCA chelate ring is opened. This is confirmed by 2D [^{1}H,^{15}N] HSQC NMR spectroscopy (vide infra). Peak 12 (m/z = 939.9) can be assigned to {[Pt(NH_3)$_2$(CBDCA)]$_2$ (m/z = 742.5) + L-Se-MetH + H^+}. The calculated molecular mass (Table 2) and isotopic distribution match perfectly with the formulae (Figure 1 of Supporting Information). It is worth noting that the intensity of the peak assigned to the carboplatin dimer (m/z = 743.1, 765.1) decreased with time. However, it could still be seen at the end of the reaction (Figure 2c). The intensity of peak 1 increased with time for the first 3 h, then decreased after 4 h, and finally disappeared after 22 h.

Peak 2 (m/z = 553.0), which is assigned to [Pt(NH_3)(CBDCA)(L-Se-MetH)]$^+$ (**2**), appeared 15 min after the reaction began. The intensity of this peak increased gradually, but decreased after 9 h of the reaction. Peak 3 (m/z = 532.3) appeared after 50 min with a low intensity, and is assigned to [Pt(CBDCA)(L-Se-MetH)]$^+$ (**3**). It finally disappeared completely after 12 h of the reaction. Peak 4 (m/z = 587.0), assigned to [Pt(L-Se-MetH)(L-Se-

Table 1. Observed and calculated molecular masses of the complexes for the reaction of carboplatin with L-Se-MetH

Peak	Compound	Observed mass[a]	Calculated mass
1	[Pt(NH_3)$_2$(CBDCA)(L-Se-MetH)] + H^+	564.0−569.9	568.4
2	[Pt(NH_3)(CBDCA)(L-Se-MetH)] + H^+	548.1−556.1	551.3
3	[Pt(CBDCA)(L-Se-MetH)] + H^+	531.1−538.2	533.3
4	[Pt(L-Se-MetH)(L-Se-Met)]$^+$	582.9−590.9	587.0
5	[Pt(NH_3)(L-Se-MetH)(L-Se-Met)]$^+$	−	603.3
6	[Pt(L-Se-Met)$_2$] + Na^+	604.9−612.9	609.0
7	[Pt(NH_3)$_2$(L-Se-Met)]$^+$	421.9−427.9	424.2
8	[Pt(NH_3)$_2$(CBDCA)] + H^+	371.1−375.2	372.3
9	[Pt(NH_3)$_2$(CBDCA)] + Na^+	392.1−397.1	394.3
10	[Pt(NH_3)$_2$(CBDCA)]$_2$ + H^+	741.1−747.1	743.5
11	[Pt(NH_3)$_2$(CBDCA)]$_2$ + Na^+	763.1−769.1	765.5
12	[Pt(NH_3)$_2$(CBDCA)]$_2$ + L-Se-MetH + H^+	933.9−943.9	939.6
13	[Pt(L-Se-MetH)(L-Se-Met)]$^+$ + carboplatin	952.9−964.9	958.3
14	[Pt(NH_3)$_2$(CBDCA)]$_3$ + H^+	1112.0−1118.2	1114.2
15	[Pt(NH_3)$_2$(CBDCA)]$_3$ + Na^+	1132.1−1140.1	1136.2
16	[Pt(NH_3)$_2$(CBDCA)]$_4$ + H^+	1482.9−1491.9	1489.9
17	[Pt(NH_3)$_2$(CBDCA)]$_4$ + Na^+	1502.7−1512.7	1511.9

[a] The Peaks are separated by m/z = 1 in the mass region indicated.

Met)]$^+$ (**4**), began to appear after 1 h 40 min. It had the highest relative intensity after 3 h 10 min (Figure 2b) and became the dominant complex in the final stage of the reaction (Figure 2c). Peaks 6 (m/z = 608.8) and 7 (m/z = 423.1), assigned to the adduct of complex **4** + Na^+ (Figure 2 of the Supporting Information) and complex [$Pt(NH_3)_2$(L-Se-MetH)]$^+$ (**7**), respectively, began to appear after 3 h and could be observed until the end of the reaction (Figures 2b and c). Peak 13 at m/z = 956.9 in the final stage of the reaction (see Figure 2c) can be assigned to {[$Pt(NH_3)_2$(CBDCA)] + [Pt(L-Se-Met)$_2$] + H^+} (Table 1). As shown in Figure 2c, after 22 h of the reaction less products were observed for this reaction than for the reaction of cisplatin with L-Se-MetH,[18] and the major species is peak 4 which corresponds to [Pt(L-Se-MetH)(L-Se-Met)]$^+$ (**4**). This result is rather similar to the reaction of cisplatin with L-Se-MetH in a 1:2 molar ratio, in which the bis(chelated) adduct was the dominant product. No further changes were observed in the ESMS spectra after 22 h. In contrast to the reaction of cisplatin, no dinuclear adducts were observed during the course of the reaction.

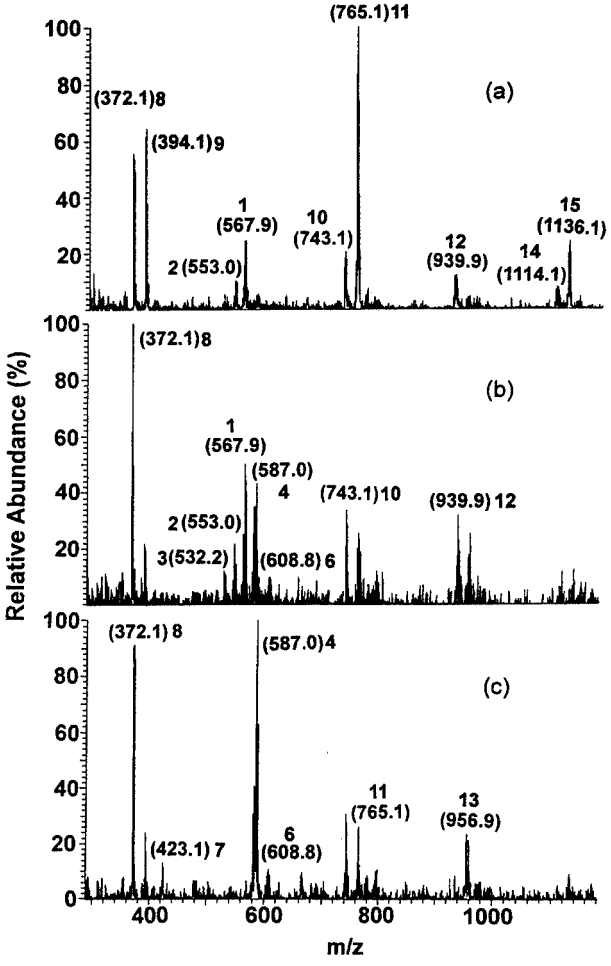

Figure 2. ESMS spectra of the reaction of L-Se-MetH with carboplatin (1:1, 310 K), recorded at different reaction times: (a) 25 min, (b) 3 h, (c) 22 h

(3) ESMS Study of the Time-Dependent Reaction of Carboplatin with L-MetH in a 1:1 Molar Ratio

The above reaction was conducted in order to compare the results with those previously reported.[7] Three typical ESMS spectra recorded after 40 min, 12 h and 38 h of the reaction are shown in Figure 3. Three new peaks (1′, 8′ and 9′) appeared in the spectra immediately after mixing the two reactants. Peak 1′ (m/z = 520.9) corresponds to the ring-opened complex [$Pt(NH_3)_2$(CBDCA)(L-MetH)]$^+$ (**1′**), peak 8′ (m/z = 669.9) is assigned to {[$Pt(NH_3)_2$(CBDCA)(L-MetH)] + L-MetH}$^+$ (Figure 3 of the Supporting Information) and peak 9′ (m/z = 892.0) to {[$Pt(NH_3)_2$(CBDCA)]$_2$ + L-MetH}$^+$ (Figure 4 of the Supporting Information). In these two latter complexes, the existing status of L-MetH is not clear. The hydrogen bonding between the carboxylate and amino groups may play a role in the formation of the two adducts. Peak 1′ remained to be the dominant species for ca. 15 h and then began to decrease in intensity after 18 h, and finally disappeared after 38 h. Peak 2′ (m/z = 504.1), which is assigned to the complex [$Pt(NH_3)$(CBDCA)(L-MetH)]$^+$ (**2′**), appeared after 40 min of the reaction (Figure 3a), and its intensity increased in the following 8 h, then decreased after 10 h. Peak 3′ (m/z = 486.1) is assigned to [Pt(CBDCA)(L-MetH)]$^+$ (**3′**) and appeared after 50 min but remained with a low intensity until it disappeared after 24 h. Peak 7′ (m/z = 377.1), which is assigned to [$Pt(NH_3)_2$(L-Met)]$^+$ (**7′**), appeared after 2 h, reached its maximum intensity after 10 h and then

Table 2. Observed and calculated molecular masses of the complexes for the reaction of carboplatin with L-MetH

Peak	Compound	Observed mass[a]	Calculated mass
1′	[$Pt(NH_3)_2$(CBDCA)(L-MetH)] + H^+	520.0−524.0	521.5
2′	[$Pt(NH_3)$(CBDCA)(L-MetH)] + H^+	503.1−507.1	503.4
3′	[Pt(CBDCA)(L-MetH)] + H^+	486.2−490.1	486.4
4′	[Pt(L-MetH)(L-Met)]$^+$	491.1−495.1	492.5
5′	[$Pt(NH_3)$(L-Met)(L-MetH)]$^+$	−	509.5
6′	[Pt (L-Met)$_2$] + Na^+	513.1−517.1	514.5
7′	[$Pt(NH_3)_2$(L-Met)]]$^+$	376.1−379.1	377.4
8′	[$Pt(NH_3)_2$(CBDCA)(L-MetH)] + H^+ + MetH	668.9−672.9	670.7
9′	[$Pt(NH_3)_2$(CBDCA)]$_2$ + L-MetH + H^+	890.1−898.1	892.7
10′	[Pt(L-MetH)(L-Met)]$^+$ + carboplatin	861.9−867.9	863.8

[a] The Peaks are separated by m/z = 1 in the mass region indicated.

remained constant for 38 h. Peak 4′ (m/z = 491.2), which appeared after 3 h and is assigned to $[Pt(L\text{-MetH})(L\text{-Met})]^+$ (**4′**), increased in intensity with time and became the major species in the final stage. It should be noted that complex $[Pt(NH_3)(L\text{-MetH})(L\text{-Met})]^+$ (**5′**) which is similar to complex **5** and should have an m/z value of 509.5 was not observed in this reaction. Similar to peak 6, peak 6′ at m/z = 514.1 can be assigned to complex **4′** + Na^+. Peak 10′ at m/z = 863.2 (see Figure 3c) can be assigned to $\{[Pt(NH_3)_2(CBDCA)] + [Pt(L\text{-Met})_2] + H^+\}$ (Table 2). Similar to the reaction with L-Se-MetH, the species observed after 38 h were the unchanged carboplatin and the adducts corresponding to peaks 4′ and 7′. From the ESMS results, it can be seen that the final intensity of the peak assigned to carboplatin is much weaker than that of peak 8 in the reaction with L-Se-MetH.

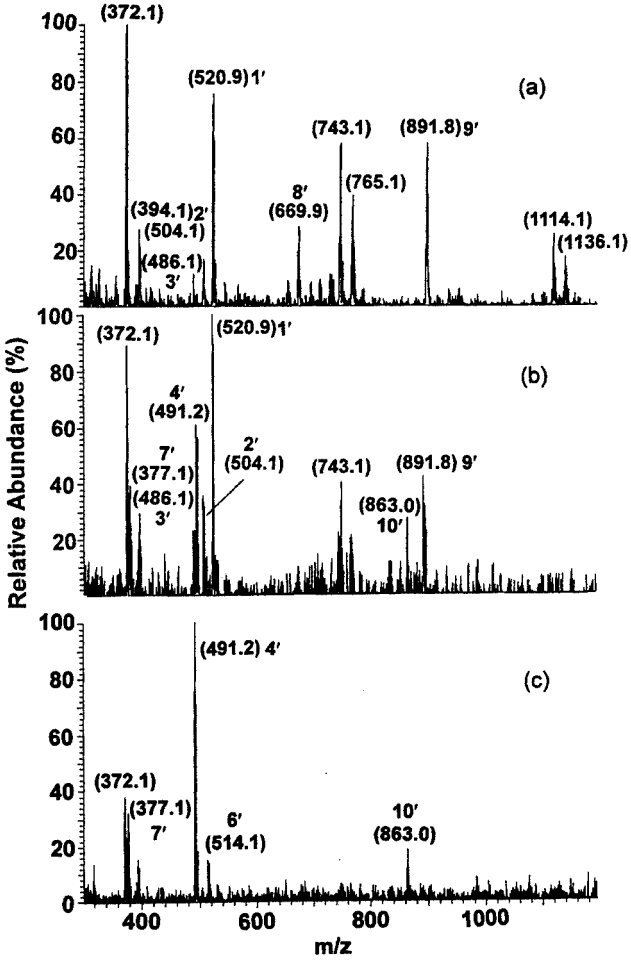

Figure 3. ESMS spectra of the reaction of L-MetH with carboplatin (1:1, 310 K), recorded at different reaction times: (a) 40 min, (b) 12 h, (c) 38 h

We also performed the reactions of carboplatin with L-Se-MetH or L-MetH at 290 K; the spectra recorded after 7 d are shown in Figure 4. As can be seen, complex **7** and **7′** were more abundant than in the reactions at 310 K, suggesting their lower stability at higher temperatures.

(4) NMR Spectroscopic Study of the Reaction of Carboplatin with L-Se-MetH in a 1:1 Molar Ratio

The reaction was initially monitored by ^1H NMR spectroscopy. The spectra recorded at 40 min, 5 h and 10 h are

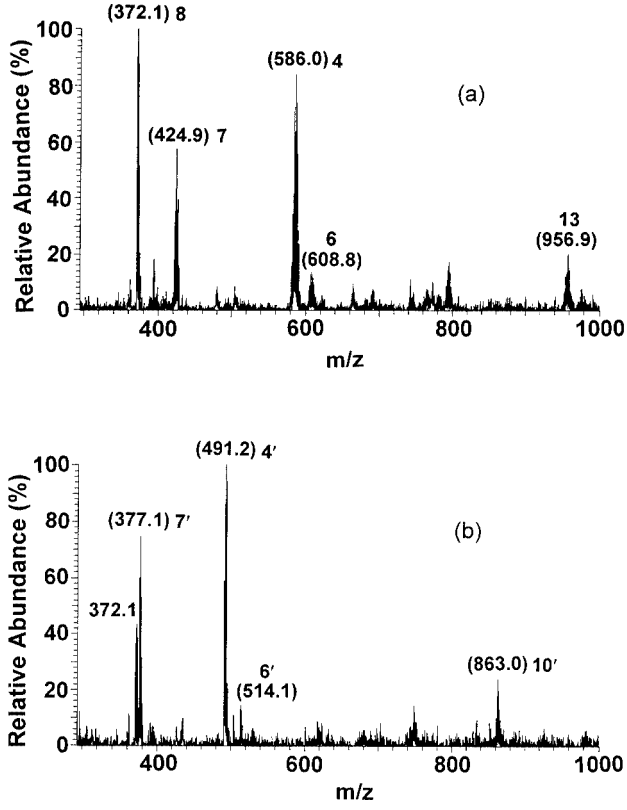

Figure 4. (a) Final ESMS spectra of the reaction of carboplatin with L-Se-MetH (1:1, 290 K); (b) final ESMS spectra of the reaction of carboplatin with L-MetH (1:1, 290 K)

shown in Figure 5. Initially, apart from the signals of free L-Se-MetH and carboplatin, four new singlets appeared between δ = 2.55 and 2.65 ppm. These signals can be assigned to the CH_3 group of the *Se*-bound L-Se-MetH. During the course of the reaction, the signals assigned to free carboplatin and L-Se-MetH decreased in intensity, whilst the signals assigned to free CBDCA increased (Figures 4b, c). After 22 h of the reaction, the signal of the CH_3 group of free L-Se-MetH disappeared completely, while the signals for carboplatin could still be observed (Figure 5 of the Supporting Information). These data are consistent with those observed by ESMS.

The same reaction was then monitored by 2 D [^1H,^{15}N] HSQC NMR spectroscopy. Figure 6 shows the spectra of the reaction recorded after 2 h, 10 h and 22 h. After 1 h, apart from the cross-peak of carboplatin at δ = 4.19/−82.0 ppm (Table 3), four new cross-peaks at δ = 4.33/−84.0 ppm (1a), δ = 4.30/−84.0 ppm (1a′), δ = 4.28/−45.5 ppm (1b), and δ = 4.28/−45.3 ppm (1b′) appeared. The ^{15}N chemical shifts of 1a, 1a′ are consistent with species that have an

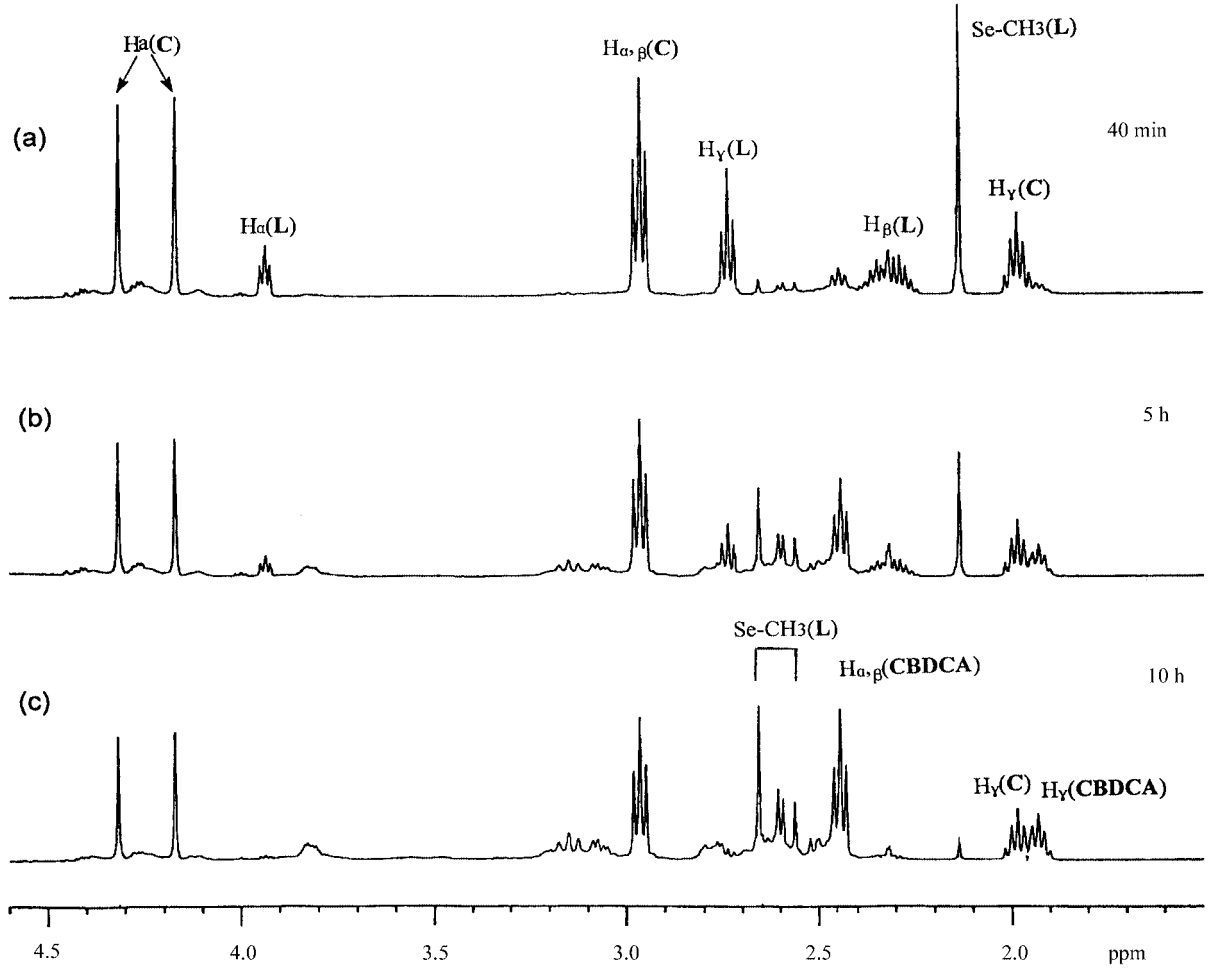

Figure 5. ^{1}H NMR spectra of the reaction of ^{15}N-carboplatin with L-Se-MetH in a 1:1 molar ratio and at 310 K, recorded at different reaction times: (a) 40 min, (b) 5 h, (c) 10 h

amine group *trans* to the oxygen atom, and the ^{15}N chemical shifts of 1b, 1b′ are consistent with species that have an amine group *trans* to the selenium atom. It is likely that these cross-peaks correspond to the formation of $[Pt(NH_3)_2(CBDCA)(L\text{-Se-MetH})]$, which contains a monodentate CBDCA and L-Se-MetH. This agrees well with the ESMS results. The splitting of the cross-peaks (1a and 1a′; 1b and 1b′) in the ^{1}H dimension is similar to that observed in the reaction of carboplatin and L-MetH,[7,19] which can be explained by the slow inversion of the methyl group at the coordinated chiral selenium atom of L-Se-MetH. In the following 3 h, these two cross-peaks increased in intensity, and then disappeared after 14 h. After 1.5 h of the reaction, a new cross-peak at $\delta = 4.16/-67.0$ ppm (2a) appeared, which has a ^{15}N chemical shift in the region of the NH_3 group *trans* to N. After ca 2.5 h, the cross-peaks at $\delta = 4.44/-42.1$ (2b) and $\delta = 4.41/-42.4$ (2b′), which have the NH_3 group *trans* to the selenium atom, began to appear. These cross-peaks were observed even after 22 h. Comparing these with the result of the mass spectrum, cross-peaks 2a and 2b, 2b′ can be assigned to complex $[Pt(NH_3)_2(L\text{-Se-Met})]$ (**7**). However, from the structure of complex **7**, the cross-peak 2a should be split into a doublet in the ^{1}H dimension, similar to the cross-peaks 2b, 2b′, due to the slow inversion of the methyl group at the chiral selenium atom. Therefore, we performed the NMR experiment at 283 K (Figure 5 of the Supporting Information). In the spectrum, cross-peak 2a became two cross-peaks with different chemical shifts in the ^{1}H dimension. The intensity of cross-peaks 2a and 2a′ was equal to that of 2b and 2b′. This showed that the two pairs of cross-peaks are related to the same species. The earlier appearance of cross-peak 2a than cross-peaks 2b, 2b′ may be due to the splitting of cross-peaks 2b, 2b′.

(5) NMR Spectroscopic Study of the Reaction between L-MetH and Carboplatin

An NMR investigation of the reaction between L-MetH and carboplatin was carried out, monitored by 2 D [^{1}H,^{15}N] HSQC NMR spectroscopy. The results obtained could then be compared with the ESMS results and those of a previous NMR study at a different pH. Figure 7 shows the spectra recorded after 2 h, 12 h and 38 h. After 1 h of the reaction,

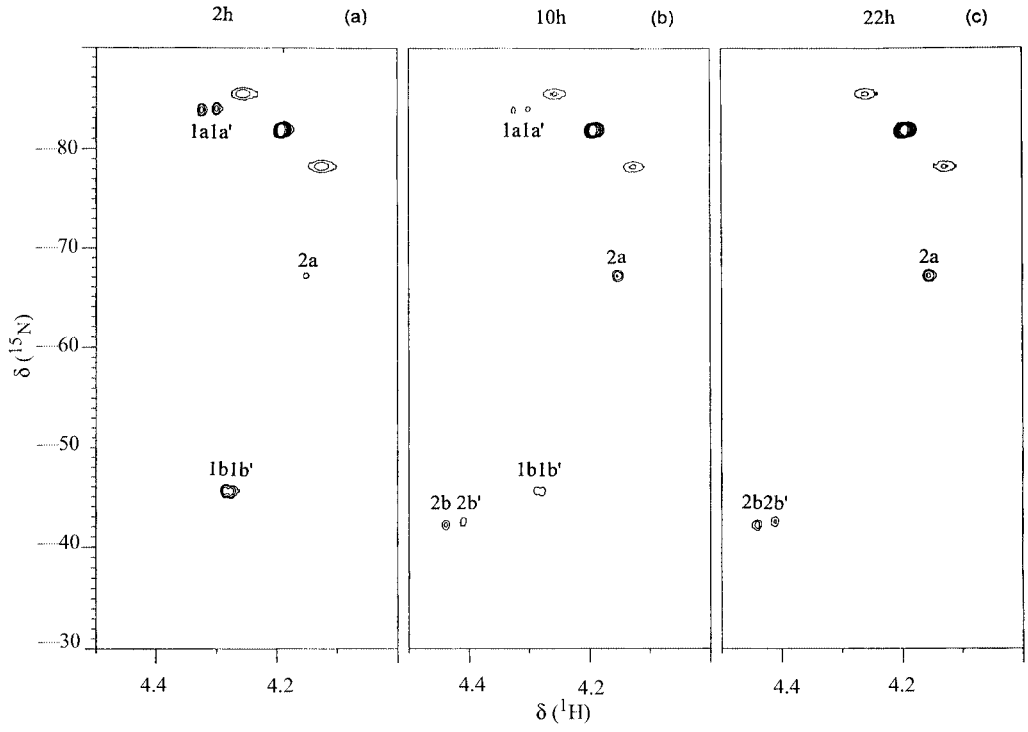

Figure 6. 2D [^{1}H,^{15}N] HSQC NMR spectrum of the reaction of ^{15}N-carboplatin with L-Se-MetH in a 1:1 molar ratio at 310 K, recorded after (a) 2 h, (b) 10 h, (c) 22 h

Table 3. ^{1}H and ^{15}N NMR chemical shifts of carboplatin and its adducts with L-Se-MetH and L-MetH

Complexes	δ(^{1}H)/δ(^{15}N) for Pt−NH_3	Pt−NH_3 *trans* to
[Pt(NH_3)$_2$(CBDCA)]	4.19/−82.0	O
[Pt(NH_3)$_2$(CBDCA)(L-Se-Met)]$^+$	4.33/−84.0; 4.30/−84.0	O
	4.28/−45.5; 4.28/−45.3	Se
[Pt(NH_3)(L-Se-Met)(L-Se-MetH)]$^+$	4.16/−67.0	N
	4.44/−42.1; 4.41/−42.2	Se
[Pt(NH_3)$_2$(CBDCA)(L-Met)]$^+$	4.36/−79.5; 4.34/−79.5	O
	4.29/−46.0	S
[Pt(NH_3)$_2$(L-Met)]$^+$	4.21/62.6; 4.18/−62.5	N
	4.44/−43.0; 4.39/−42.5	S

apart from the cross-peak of carboplatin, two sets of new cross-peaks (1a, 1a′, 1b) with similar intensities appeared at δ = 4.36/−79.5 ppm (1a), δ = 4.34/−79.5 ppm (1a′), and δ = 4.29/−46.09 ppm (1b). These three cross-peaks (1a, 1a′, 1b) can be assigned to [Pt(NH_3)$_2$(CBDCA)(L-MetH)] (**1′**), based on their known shifts.[20] The split of cross-peaks 1a and 1a′ can be attributed to the slow inversion of the coordinated chiral sulfur atom. The intensity of these peaks increased in the following 7 h and decreased after 8 h of the reaction. After 30 h, the peaks disappeared completely, which is consistent with the result by mass spectrometry. After ca. 7 h, two new cross-peaks at δ = 4.21/−62.6 ppm (2a) and δ = 4.44/−43.0 ppm (2b) appeared, and 2 h later another pair of cross-peaks could be seen at δ = 4.18/−62.5 ppm (2a′) and δ = 4.39/−42.5 ppm (2b′). From their ^{15}N chemical shifts these cross-peaks (2a, 2a′ and 2b, 2b′) can be assigned to the NH_3 group *trans* to N and S, respectively. These two pairs of cross-peaks correspond to complex [Pt(NH_3)$_2$(L-Met)] (**7′**), and the splitting of the cross-peaks in the ^{1}H dimension can be attributed to the slow inversion of the methyl group at the coordinated chiral sulfur atom.[7] These adducts could be observed even after 38 h. The final product [Pt(L-Met)(L-MetH)]$^+$ (**4′**) which was observed in the ESMS study could not be observed in the 2 D [^{1}H,^{15}N] HSQC NMR study due to the elimination of ammonia. This result is different from those reported previously[7] in which, apart from the complex **7′**, complexes **1′** and **5′** were also observed even after 3 d at 293 K and at pH = 7.

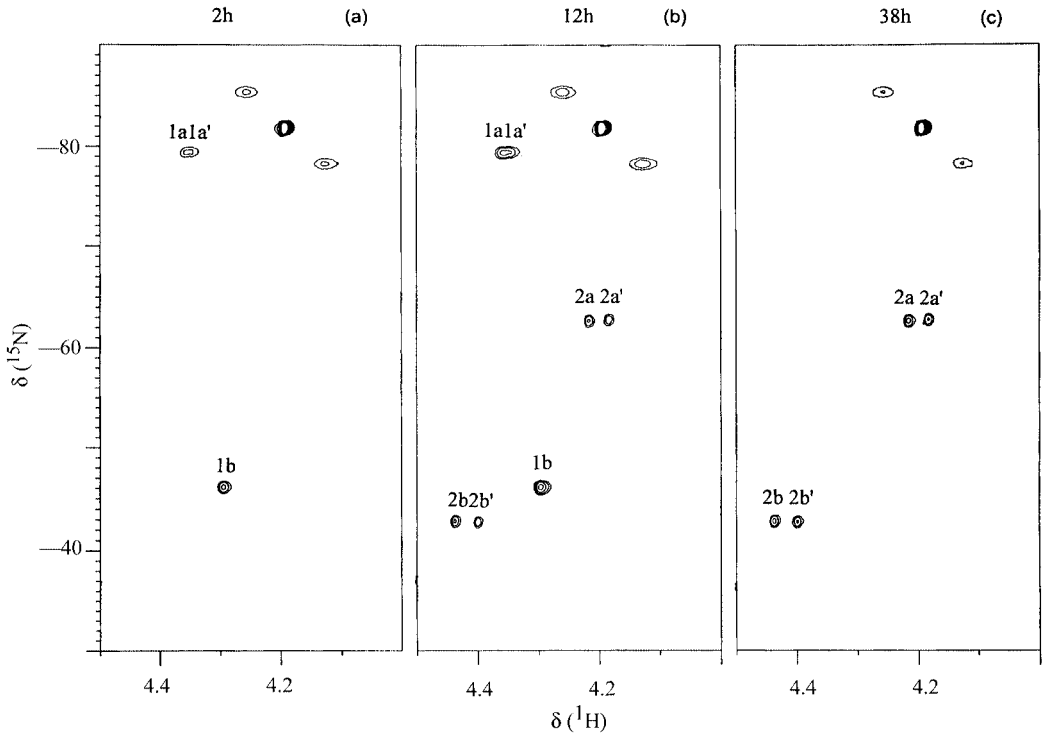

Figure 7. 2D [^{1}H,^{15}N] HSQC NMR spectrum of the reaction of ^{15}N-carboplatin with L-MetH in a 1:1 molar ratio at 310 K, recorded after (a) 2 h, (b) 12 h, (c) 38 h

Discussion

Our recent work on the investigation of the reaction of cisplatin with L-Se-MetH and L-MetH using the combined techniques of ESMS and 2D [^{1}H,^{15}N] NMR has further clarified the reaction pathways.[18] Here we extend our study to the reaction of the second-generation anticancer drug carboplatin with L-Se-MetH and L-MetH, and compared the different reactivities of the two drugs towards the two ligands.

We have detected the dimer, trimer and tetramer forms of carboplatin by ESMS. Although they are not stable in the presence of L-Se-MetH, the dimer form of carboplatin (either as the H^+ or Na^+ form) can be observed for quite a long period of time. Recently, it has been reported that polynuclear Pt complexes can be formed in aqueous solution.[21,22] However, it is possible that these complexes may be formed only in the capillary device of the mass spectrometer due to the high temperature.[23]

Based on the ESMS and 2D [^{1}H,^{15}N] NMR results, the reaction pathway between carboplatin and L-Se-MetH is summarized in Scheme 2.

As can be seen from the ESMS results, the reaction between L-Se-MetH and carboplatin initially gave rise to a ring-opened species [Pt(NH_3)$_2$(CBDCA)(L-Se-MetH)] (**1**) which is very stable and can be observed for ca 18 h in the ESMS experiment (peak 1) and for ca 13 h in the 2D [^{1}H,^{15}N] HSQC NMR experiment (1a, 1a′; 1b, 1b′). The appearance of two pairs of cross-peaks 1a, 1a′, 1b, 1b′ may be due to the hydrogen bonding between the NH_3 group and the oxygen atom of CBDCA similar to that reported in *cis*-[Pt(CBDCA)(NH_3)$_2$(L-Met-*S*)][7] and [Pt(en)(Me-Mal-O)(Ac-Met-*S*)].[24] The high *trans* effect of selenium labilizes the NH_3 group, and L-Se-MetH undergoes ring-closure to form [Pt(CBDCA)(NH_3)(L-Se-Met-*N*,*Se*)] (**2**). The complex [Pt(NH_3)$_2$(L-Se-Met-*Se*,*N*)] (**7**) is also formed. This species corresponds to the cross-peaks 2a and 2b, 2b′ in the 2D NMR spectrum. Most of complex **2** was converted into complex **5**, [Pt(NH_3)(L-Se-MetH-*Se*)(L-Se-MetH-*Se*,*N*)], the rest was converted into complex **3**, [Pt(CBDCA)(L-Se-MetH-*Se*,*N*)] (peak 3 in the ESMS spectrum). Complex **3** could only be observed in the ESMS spectrum with a low intensity for ca. 9 h. However, complex **5** could be observed neither in the ESMS nor in the NMR spectrum, which may be due to its fast conversion into the final product, complex **4**. As can be seen from the ESMS data, the dominant adduct at the end of the reaction is [Pt(L-Se-Met-*Se*,*N*)$_2$] (complex **4**, peak 4 in the ESMS spectrum). There should be two geometrical isomers (*cis* and *trans*) of complex **4**. Previous studies on [Pt(L-Met-*S*,*N*)$_2$] showed that both isomers were present in solution, and that the dominant one was the *cis* isomer. A similar situation may occur in the current work. This result is different from that between cisplatin and L-Se-MetH. In the latter case the final product has one L-Se-MetH coordinated group, i.e. the final product is the complex [Pt(NH_3)Cl(L-Se-MetH)], and there is a low abundance of complex **4**.[18]

Similarly, the reaction of carboplatin with L-MetH gives rise to [Pt(L-Met-*N*,*S*)$_2$] as the final adduct, which is differ-

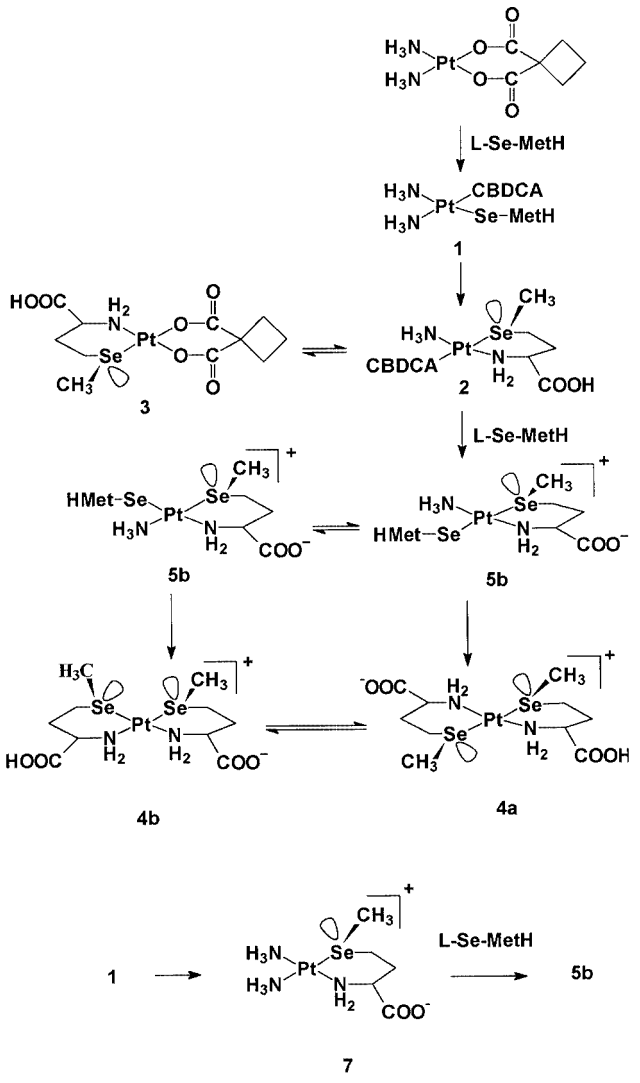

Scheme 2. Reaction pathway of carboplatin with L-Se-MetH in a 1:1 molar ratio at pH = 5.40

ent from the previous 2D [^{1}H,^{15}N] NMR study.[7] However, it should be noted that the temperature and pH of the two studies are different. The lower temperature and high pH may facilitate the stabilization of the ring-opened adduct and slow down the rate of elimination of the ammonia ligand. It can be concluded from the comparison between the reactions of cisplatin and carboplatin with L-Se-MetH and L-MetH that under the same conditions the bis(chelated) adducts [Pt(L-Se-Met)$_2$] or [Pt(L-Met)$_2$] can be formed more easily in the reaction with carboplatin than in that the reaction with cisplatin.

It is interesting to note that under the same experimental conditions the inversion rate of Se−CH$_3$ in complex **7** is faster than that of S−CH$_3$ in complex **7′**. This is rather intriguing because a reversal of the inversion rate would be expected.

Conclusion

The self-association of carboplatin in aqueous solution was detected by ESMS for the first time. From the ESMS and 2D [^{1}H,^{15}N] HSQC NMR results of this work, the major species [Pt(NH$_3$)$_2$(CBDCA)(L-SeMetH)] (**1**), [Pt(NH$_3$)$_2$(CBDCA)(L-MetH)] (**1′**); [Pt(NH$_3$)(CBDCA)-(L-SeMetH)] (**2**), [Pt(NH$_3$)(CBDCA)(L-MetH)] (**2′**); [Pt(CBDCA)(L-MetH)](**3**), [Pt(CBDCA)(L-MetH)] (**3′**); [Pt(NH$_3$)$_2$(L-SeMet)]$^+$ (**7**), [Pt(NH$_3$)$_2$(L-Met)]$^+$ (**7′**); [Pt (L-Se-Met)$_2$] (**4**) and [Pt(L-Met)$_2$] (**4′**) were found. Due to the elimination of the ammonia group and the abundance of the species, only complex **1**, **1′** and complex **7**, **7′** can be observed by 2D [^{1}H,^{15}N] HSQC NMR spectroscopy. A detailed pathway of the reaction was provided and compared with that of cisplatin. The bis(chelated) adducts [Pt(L-Se-Met)$_2$] or [Pt(L-Met)$_2$] can be formed more easily in the reaction with carboplatin than in the reaction with cisplatin under the same reaction conditions. It remains to be seen whether this observation can be related to in vivo activity and metabolism of the drug.

Experimental Section

General: Carboplatin and [^{15}N]carboplatin were prepared and recrystallized according to a published procedure,[25] L-selenomethionine (L-Se-MetH) and L-methionine (L-MetH) were purchased from Sigma.

Spectroscopy

ESMS: Electrospray mass spectra were recorded using an electron mass spectrometer (ESMS, Finnigan) by loading 1.0 μL of solution into the injection valve of the LCQ unit, and then injecting into the mobile phase solution (50% of aqueous methanol) which was carried through the electrospray interface into the mass analyzer at a rate of 200μL min^{-1}. The voltage employed at the electrospray needles was 5 kV, and the capillary was heated to 200 °C. A maximum injection time of 200 ms, along with 10 scans was set. Positive ion mass spectra were obtained. The predicted isotope distribution patterns for each of the complexes were calculated using the Isopro 3.0 program.[26]

NMR: NMR spectroscopic data were acquired with 500-MHz Bruker DMX and DRX spectrometers. One-dimensional spectra were typically acquired with 128 transients and 32 K data points over a spectral width of 10 kHz by using standard pulse sequences. Two-dimensional [^{1}H,^{15}N] HSQC NMR (Heteronuclear Single Quantum Coherence) data were acquired and processed according to previously reported methods.[27] The ^{15}N chemical shifts are externally referenced to 1.5 M NH_4Cl in 1 M HCl. The indirect referencing method resulted in slightly different ^{15}N chemical shifts to those in previous reports for similar species, and no corrections have been made.

pH Measurements: The pH measurements were carried out using a pHS-3C pH meter equipped with a Phoenix Ag/AgCl reference electrode, calibrated with phosphate buffer solutions at pH = 4.00 and 10.00. The values reported are those measured after the reactions were finished.

Sample Preparations: Samples for the ESMS studies were prepared using double-distilled water. Due to the limitation of the ESMS, no phosphate buffer solution was employed in these studies so as to avoid the potential blockage of the capillary of the instrument. (1) [Pt(NH$_3$)$_2$(CBDCA)] (1.00 mg) was dissolved in 1 mL of water. The pH of the solution was 5.00. The ESMS spectra were recorded

at this pH value. (2) $[Pt(NH_3)_2(CBDCA)]$ (1.00 mg) and L-Se-MetH (0.53 mg) were dissolved in 1 mL of water. The solution was monitored by ESMS for a period of 22 h at 310 K. The pH value after 22 h was 5.40. (3) $[Pt(NH_3)_2(CBDCA)]$ (1.00 mg) was mixed with L-MetH in a 1:1 molar ratio. The reaction was monitored by ESMS for 38 h at 310 K. The pH of the solution after 38 h was 5.41. All the reactions were carried out at 310 K unless otherwise stated. Samples for the NMR study were prepared as follows. $[Pt(NH_3)_2(CBDCA)]$ (2.68 mmol) and L-Se-MetH (2.68 mmol) or L-MetH (2.68 mmol) were dissolved in a 500-μL solution of 90% H_2O and 10% D_2O. The final concentration of carboplatin and L-Se-MetH or L-MetH was 2.68 mmol/mL. To be consistent with the conditions used in the ESMS study, no buffer solution was employed in the NMR study. The reaction was also conducted at 310 K.

Acknowledgments

We thank the National Natural Science Foundation of China for the Distinguished Young Scientists Fund (Grant No. 29925102) and the Major State Basic Research Development Program (Grant No. G200007750). We thank Prof. P. J. Sadler (Edinburgh) for access to his NMR spectrometer with which a part of the experiments were carried out.

[1] [1a] *Cisplatin: Chemstry and Biochemistry of a Leading Anticancer Drug* (Ed.: B. Lippert), Wiley-VCH, Weinheim. [1b] *Platinum and Other Metal Complexes in Cancer Chemotherapy* (Ed.: S. B. Howell), Plenum Press, New York, **1991**.
[2] S. Neidle, I. M. Ismail, P. J. Sadler, *J. Inorg. Biochem.* **1980**, *13*, 205−212.
[3] J. D. Ranford, P. J. Sadler, K. Balmanno, D. R. Newell, *Magn. Reson. Chem.* **1991**, *29*, S125−S129.
[4] R. J. Knox, F. Friendlos, D. A. Lydall, J. J. Roberts, *Cancer Res.* **1986**, *46*, 1972−1979.
[5] N. D. Tinker, H. L. Sharma, C. A. McAuliffe, in *Platinum and other Metal Coordination Compounds in Cancer Chemotherapy* (Ed.: M. Nicolini), Martinus Nijhoff, Boston, MA, **1988**, pp. 144−159.
[6] L. Canovese, L. G. Cattalini, M. L. Chessa Tobe, *J. Chem. Soc., Dalton Trans.* **1988**, 2135−2140.
[7] K. J. Barnham, M. I. Djuran, P. del Socorro Murdoch, J. D. Ranford, P. J. Sadler, *Inorg. Chem.* **1996**, *35*, 1065−1072.
[8] S. S. G. E. van Boom, J. Reedijk, *J. Chem. Soc., Chem. Commun.* **1993**, 1397−1398.
[9] K. J. Barham, V. Frey, P. del Socorro Murdoch, J. D. Ranford, P. J. Sadler, D. R. Newell, *J. Am. Chem. Soc.* **1994**, *116*, 11175−11176.
[10] J. Reedijk, *Inorg. Chim. Acta* **1992**, *198−200*, 873−881.
[11] R. E. Norman, J. D. Ranford, P. J. Sadler, *Inorg. Chem.* **1992**, *31*, 877−888.
[12] A. F. M. Siebert, W. S. Sheldrick, *J. Chem. Soc., Dalton Trans.* **1997**, 4411−4420.
[13] J. M. Teuben, J. Reedjik, *J. Biol. Inorg. Chem.* **2000**, *5*, 463−468.
[14] M. Hahn, M. Kleine, W. S. Sheldrick, *J. Biol. Inorg. Chem.* **2001**, *6*, 556−566
[15] H. E. Ganther, J. R. Lawrence, *Tetrahedron* **1997**, *53*, 12299−12310.
[16] I. P. Clement, *J. Nutr.* **1998**, *128*, 1845−1854.
[17] M. Rao, M. A. Rao, *J. Pharm. Pharmacol.* **1998**, *50*, 687−691.
[18] Q. Liu, J. Y. Zhang, X. K. Ke, Y. H. Meu, L. G. Zhu, Z. J. Guo, *J. Chem. Soc., Dalton Trans.* **2001**, 911−916.
[19] P. del Socorro Murdoch, J. D. Ranford, P. J. Sadler, S. J. Berners-Price, *Inorg. Chem.* **1993**, *32*, 2249−2255.
[20] K. J. Barnham, M. I. Djuran, P. del Socorro Murdoch, J. D. Ranford, P. J. Sadler, *J. Chem. Soc., Dalton Trans.* **1995**, 3721−3726.
[21] K. J. Fisher, I. G. Dance, G. D. Willett, R. Zhang, E. C. Alyea, *Eur. J. Mass Spectrom.* **2000**, *6*, 23−30.
[22] P. Zollner, A. Zenker, M. Galanski, B. K. Keppler, W. Lindner, *J. Mass Spectrom.* **2001**, *36*, 742−753.
[23] M. T. Caudle, R. D. Stevens, A. L. Crumbliss, *Inorg. Chem.* **1994**, *33*, 6111−6115.
[24] Z. J. Guo, T. W. Hambley, P. del Socorro Murdoch, P. J. Sadler, U. Frey, *J. Chem. Soc., Dalton Trans.* **1997**, 469−478.
[25] C. J. Boreham, J. A. Broomhead, D. P. Fairlie, *Aust. J. Chem.* **1981**, *34*, 659−664.
[26] J. A. Yergey, *Int. J. Mass Spectrom. Ion Phys.* **1983**, *52*, 337−349.
[27] K. J. Barnham, S. J. Berners-Price, T. A. Frenkiel, F. U. Frey, P. J. Sadler, *Angew. Chem. Int. Ed. Engl.* **1995**, *34*, 1874−1877.

Received January 9, 2002
[I02019]

Potentially Tridentate Ligands in the Synthesis of Methyl- and Acetylpalladium(II) Complexes

Alessia Bacchi,[a] Mauro Carcelli,[a] Corrado Pelizzi,[a] Giancarlo Pelizzi,[a] Paolo Pelagatti,*[a] and Silvia Ugolotti[a]

Keywords: Carbonylation / Insertion / N ligands / Palladium / Tridentate ligands

The two protic tridentate ligands HNN′O (**1**) and HNN′S (**2**) were treated with [(COD)Pd(Me)Cl], and the corresponding methylpalladium(II) complexes [Pd(η^2-HNN′)(Me)Cl] (**1a** and **2a**) were isolated. The neutral ligands in these complexes coordinated the metal in an NN′ bidentate mode, through the pyridine and imine nitrogens, excluding the O or S atom from the coordination. This behavior was confirmed by X-ray diffraction analysis of the dichloro complex of **1**, [Pd(η^2-HNN′)Cl_2] (**1c**). Complexes **1a** and **2a** easily transformed quantitatively into the corresponding three-coordinate complexes [Pd(η^3-NN′X)(Me)] (**1b**: X = O, **2b**: X = S) in basic medium, with elimination of HCl. The complexes **1a** and **1b** were treated with PPh_3 and $P(CD_3)_3$, respectively, resulting in **1e** and **1h**; **1a** reacted further with a double quantity of PPh_3 to give rise to the diphosphane complex [*trans*-$(PPh_3)_2$Pd(Me)Cl] (**1g**) and free **1**. The three-coordinate complexes **1b** and **2b** were subjected to CO bubbling at room temperature. In the case of **1b**, acylation of the ligand on the phenolic oxygen was observed, with the formation of an organic acetate and release of palladium black. In the case of **2b**, besides the acylated ligand on the thiolic sulfur, the acetylpalladium(II) complex [Pd(η^3-NN′S)(MeCO)] (**2c**) was isolated. The X-ray structures of **1c**·THF, **1b**·1/2$C_6H_6O_2$, **2b**, **2c**·1/2CH_2Cl_2, and **1g** have been solved.
(© Wiley-VCH Verlag GmbH, 69451 Weinheim, Germany, 2002)

Introduction

There is ongoing interest in the study of CO insertion into Pd−C bonds, because of its importance as a key step in many metal-catalyzed reactions.[1] Much work has been done with both non-hybrid[2] and hybrid[3] bidentate ligands. In contrast, little has been done with tridentate ligands,[4] and there is a lack of data concerning the use of protic tridentate ligands.[5] We have recently shown that the use of protic tridentate HNN′O acylhydrazonic ligands (Scheme 1) resulted in the isolation of two different types of methylpalladium(II) complexes: [Pd(η^2-HNN′)(Me)Cl] and [Pd(η^3-NN′O)(Me)].[6] These complexes showed different reactivities towards CO: the first, in fact, gave rise to the isolation of the corresponding acetyl complexes [Pd(η^2-HNN′)(MeCO)Cl] in excellent yields, whereas the second resulted in the acetylation of the ligands on the hydrazonic nitrogen, with concomitant formation of palladium black; conversion was also quantitative in this case. The presence of the basic hydrazone nitrogen was considered to be responsible for the instability of the complexes under CO atmosphere. With the aim of verifying this hypothesis, we prepared the methylpalladium(II) complexes of the Schiff base ligands 2-[(pyridin-2-ylmethylene)amino]phenol (**1**, HNN′O) and 2-(1-pyridin-2-yl-ethylideneamino)benzenethiol (**2**, HNN′S) (see b in Scheme 1). These chelating agents are potentially tridentate and do not contain a hydrazone nitrogen. Compounds **1** and **2** were treated with [(COD)Pd(Me)Cl], resulting in the isolation, under appropriate conditions, of two different kinds of methylpalladium(II) complexes: [Pd(η^2-HNN′)(Me)Cl] (**1a** and **2a**) and [Pd(η^3-NN′X)(Me)] (**1b**: X = O, **2b**: X = S), which were fully characterized. The reactivity of **1a**−**b** towards phosphanes and, in particular, the reactivity of the three-coordinate complexes **1b** and **2b** towards CO was investigated.

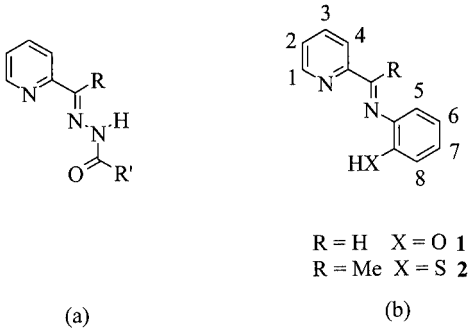

Scheme 1

[a] Dipartimento di Chimica Generale ed Inorganica, Chimica Analitica, Chimica Fisica, Università degli Studi di Parma
Parco Area delle Scienze 17/A, 43100 Parma, Italy
Fax: (internat.) +39-0521/905-557
E-mail: paolo.pelagatti@unipr.it

Results and Discussion

Synthesis of the Methyl Complexes 1a and 2a

The ligands HNN′O (**1**) and HNN′S (**2**) reacted with [(COD)Pd(Me)Cl] in diethyl ether at room temperature to afford the complexes [Pd(η^2-HNN′)(Me)Cl] (**1a** and **2a** in Scheme 2). The reactions proceed with rapid displacement of the labile diolefin COD by the incoming chelating pyridylimine ligands. These ligands coordinate to the metal in a bidentate mode through the pyridine and imine nitrogen atoms. The bidentate behavior of the ligand was confirmed by the X-ray structure of the dichloro complex [Pd(η^2-HNN′)Cl_2] (**1c**) (see crystallographic discussion). As previously reported for other methylpalladium(II) complexes containing protic ligands,[6] diethyl ether is the solvent of choice as the fast precipitation of **1a** and **2a** prevents methane elimination caused by ligand deprotonation, a process that takes place easily in solution (vide infra). Complex **1a** is a yellow powder, while complex **2a** is a gray powder. The neutral character of the ligand was indicated by the IR stretching bands of the OH and SH bonds, centered at 3377 cm^{-1} and 3229 cm^{-1}, respectively. The structure of **1a** proposed in Scheme 2 agrees with the ^{1}H NMR spectrum: the sequence of the pyridine protons is normal for pyridylimine ligands in which both nitrogens are involved in coordination.[2b,6] A single isomer was detected, probably that with the methyl ligand *cis* to the imino function. This is in fact the preferred configuration for this type of complex.[2] Moreover, the chemical shift of the methyl group is unusually low (δ = 0.41 ppm in $CDCl_3$ and δ = 0.54 ppm in MeOD, as compared to δ = 0.8−1.1 ppm normally), probably because of the shielding effect of the neighboring aromatic ring.[7] The ^{1}H NMR spectrum of complex **2a** recorded in [D_6]Me_2SO shows a complicated pattern, which prevents unambiguous assignment of the aromatic signals. In the aliphatic region, however, three different species can be distinguished: the expected complex **2a** [singlets at δ = 2.50 and 0.81 ppm, belonging to the C(Me)=N and Pd−Me groups, respectively], and the products of solvent-assisted ligand deprotonation [Pd(η^3-NN′O)(Me)] (**2b**, singlets at δ = 2.70 and 0.20 ppm) and [Pd(η^3-NN′O)Cl] (**2d**, singlet at δ = 2.84 ppm). As far as complex **2a** is concerned, it was not possible to establish the disposition of the methyl and chloride ligands around the metal unequivocally, but we assume that **1a** and **2a** have the same stereochemistry. As a matter of fact, complex **1a** is also not completely stable in solution: in deuterated methanol or dimethyl sulfoxide it slowly converts into the chloride complex [Pd(η^3-NN′O)Cl] (**1d**) with elimination of methane (Scheme 2). This elimination is faster for **2a** than for **1a**, because **2** is more acidic than **1**. Interestingly, methane elimination also takes place in the solid state, as confirmed by TGA analyses (**1a**: 158.3−198.1 °C, weight loss 6%; **2a**, 103.3−149.0 °C, weight loss 5%).

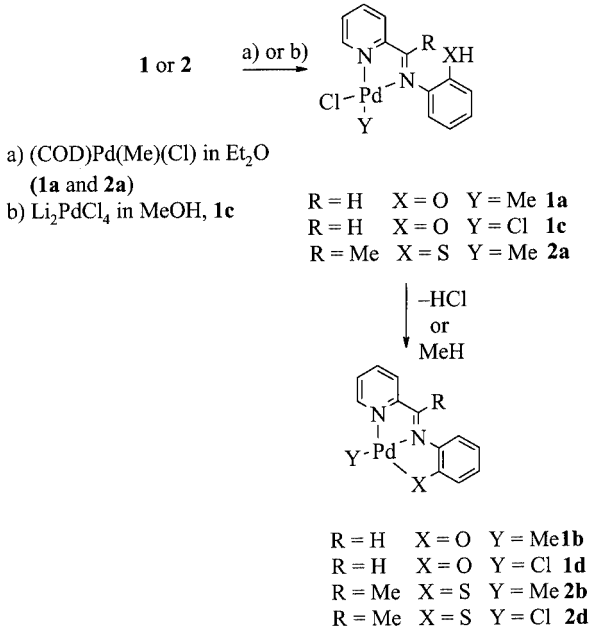

Scheme 2

Synthesis of the Methyl Complexes 1b and 2b

When the reaction between **2** and (COD)Pd(Me)Cl was carried out in THF in the presence of a slight excess of a base, such as NaOMe or Et_3N, elimination of HCl took place and the reaction proceeded with a drastic color change, from yellow to green. During the stirring the solution released the three-coordinate methyl complex [Pd(η^3-NN′S)(Me)] (**2b**) as a green powder (Scheme 2). The anionic character of the ligand was attested to by the disappearance of the IR and ^{1}H NMR signals of the SH group. The methyl ligand resonates at δ = 0.15 ppm, a value similar to those found for other methylpalladium(II) complexes in which the metal is bound to an anionic tridentate ligand.[6]

With **1**, the corresponding process had to be carried out in the presence of *n*BuLi instead of NaOMe or Et_3N. In this way, the deprotonation of the ligand was complete and the reaction was able to proceed smoothly, with a drastic color change from yellow to purple. The three-coordinate methyl complex [Pd(η^3-NN′O)(Me)] (**1b**) precipitated from the solution as a purple solid (Scheme 2). The same product could be obtained by deprotonation of **1a** by *n*BuLi or NaOMe in THF. The tridentate character of the ligand was corroborated by the disappearance of the spectroscopic OH signals; the methyl ligand is found at δ = 0.60 ppm, a higher value than found for **2a**, but still shielded with regard to the value usually found for methylpalladium(II) complexes with bidentate nitrogen ligands.[2b,3,8] The *trans* influence of the methyl attached to palladium is well attested to by the shielding undergone by the imine proton relative to the free ligand: δ = 7.88 ppm for **1b** and δ = 8.71 ppm for **1**.

Single-crystal diffraction analysis of **1b**·1/2$C_6H_6O_2$ and **2b** confirmed the proposed structures (see crystallographic discussion).

Reactions of 1a and 1b with Phosphanes

In order to investigate the complexation strength of the ligand **1**, and before dealing with the carbonylation reactions, the complexes **1a** and **1b** were treated with PPh_3 and $P(CD_3)_3$. When complex **1a** was treated with a stoichiometric amount of PPh_3 in [D_6]DMSO, an immediate color change took place. The ^{31}P NMR spectrum of the reactant mixture showed a strong signal at $\delta = 40.5$ ppm, a value characteristic for a phosphane coordinated to palladium, and a second, much less intense, singlet at $\delta = 32.5$ ppm. No signals belonging to free PPh_3 were visible. The first resonance was attributable to a species in which the ligand was monodentate through a nitrogen atom and the square-planar coordination was completed by the methyl ligand, the chlorine atom, and PPh_3 (**1e** in Scheme 3). The second signal was tentatively attributed to the chloro(phosphane)-palladium complex **1f** (Scheme 3) , with the deprotonated ligand coordinating palladium through the imine nitrogen and the oxygen, and the square-planar coordination being completed by a PPh_3 molecule and a chlorine atom. Complex **1f** is formed by the reaction between PPh_3 and **1d**, the formation of which has previously been described in Me_2SO solution. The addition of double quantities of PPh_3 resulted in the immediate precipitation of *trans*-[$(PPh_3)_2$Pd(Me)Cl] and the consequent displacement of **1** (Scheme 3). The diphosphane complex is completely soluble in chlorinated solvents, the ^1H NMR spectrum recorded in $CDCl_3$ showing a triplet for the methyl ligand at $\delta = -0.03$ ppm with a $J_{P,H}$ of 5.9 Hz, while in the ^{31}P NMR spectrum the phosphanes generate a singlet centered at $\delta = 27.7$ ppm. The structure of this complex was definitely established by X-ray analysis. Crystals of *trans*-[$(PPh_3)_2$Pd(Me)Cl] were obtained by slow diffusion of *n*-hexane into a refrigerated dichloromethane solution. The methyl is *trans* to the chloride; coordination is planar within 0.08 Å. Relevant coordination features are: Pd−P1 = 2.3272(5), Pd−P2 = 2.3225(6), Pd−Cl = 2.4248(5), Pd−C = 2.0574(4)Å; P1−Pd−P2 = 177.49(2), P1−Pd−Cl = 88.85(1), P1−Pd−C = 91.69(1), P2−Pd−Cl = 89.17(1), P2−Pd−C = 90.43(1), Cl−Pd−C = 174.86(1)°.

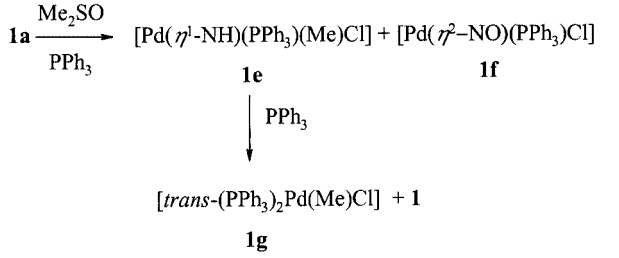

Scheme 3

The three-coordinate methyl complex **1b** was treated with a slight excess of $P(CD_3)_3$ in [D_6]DMSO, and the reaction was monitored by ^1H and ^{31}P NMR spectroscopy. After the addition of the phosphane, the signals of an uncoordinated pyridine ring appeared: in fact, the sequence of the hydrogen resonances, from low to high field, was 1-H, 4-H, 3-H, 2-H [Scheme 1(b)].[2b,6] The methyl ligand now resonates at $\delta = 0.25$ ppm ($\delta = 0.60$ ppm in **1b**) as a singlet, while the singlet of a coordinated phosphorus is now present in the ^{31}P NMR spectrum at $\delta = 41.3$ ppm. In conclusion, the phosphane replaces the pyridine ring in the coordination sphere, giving rise to the complex [Pd(η^2-NO){$P(CD_3)_3$}(Me)] (**1h**, Scheme 4). On the basis of literature spectroscopic data,[9] we assume that the methyl is *trans* to the oxygen and the phosphane *trans* to the imine nitrogen (Scheme 4).

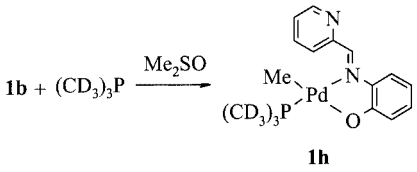

Scheme 4

Carbonylation Reactions

Dichloromethane solutions of **1b** and **2b** were subjected to CO bubbling at room temperature. In both cases the formation of palladium black was observed. As in the case of the methyl complexes of NN′O acylhydrazone ligands studied previously,[6] the decomposition of **1b** was very fast, and after 5 min the solution was completely bleached. A different behavior was observed in the case of **2b**: after 3.5 h of exposure to CO the solution was still light purple. After removal of palladium, the resulting solutions were analyzed by mass spectrometry: peaks relating to the acylated ligands [$m/z = 240$ (**3**) and 270 (**4**), respectively] were present in both cases (Scheme 5). In the mass spectrum of the carbonylated solution of **1b**, no signals belonging to the starting complex or to an acetylpalladium complex were observed, whereas the peak of the acetylpalladium complex [Pd(η^3-NN′S)(MeCO)] (**2c** in Scheme 4, $m/z = 378$) was present in the corresponding mass spectrum of **2b**. Such a complex was isolated in a crystalline form by slow diffusion of *n*-hexane into the refrigerated mother liquor; X-ray analysis confirmed the proposed structure (see crystallographic discussion). Unfortunately, the few collected crystals did not allow the spectroscopic characterization of the complex.

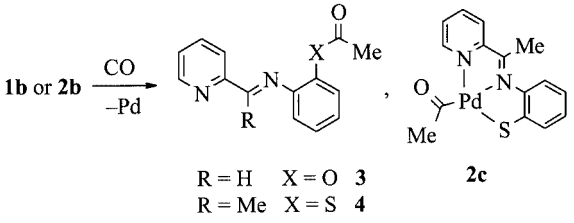

Scheme 5

The different reactivities shown by the two three-coordinate methyl complexes are due in the case of **2b** to the presence of a *soft* donor (the S atom), making the isolation of

the acetyl complex **2c** possible. This can definitely be viewed as an intermediate in the acetylation of the ligand, as already proposed by other groups for methyl(alkoxo) and methyl(thiolato)palladium(II) and nickel(II) complexes[10] and by us for hydrazonic palladium(II) complexes.[6] On the basis of the reactivity shown by **1b** toward $P(CD_3)_3$ (see complex **1h**), it is plausible to suppose that the CO coordination occurs with concomitant pyridine displacement. The subsequent step could be the migration of the methyl onto the coordinated CO molecule, followed by coupling between the ligand and the acetyl group.

Structures of Complexes 1c·THF, 1b·1/2$C_6H_6O_2$, 2b, and 2c·1/2CH_2Cl_2

Complex **1c** (Figure 1) crystallizes as a 1:1 THF solvate. The ligand is NN′-bidentate [bite angle N1−Pd−N2: 80.1(2)°], the metal square-planar coordination being completed by two chloride ligands. The OH group is not involved in the coordination. The terminal phenyl ring is nearly perpendicular to the chelation plane [Pd−N−C−C(OH): 72.2(8)°], due to the hindrance of the chloride ligand in the coordination plane [Cl2···O1 3.446(5) Å]. The coordination geometry can be summarized as follows: Pd−N2: 2.018(6) Pd−N1: 2.034(6), Pd−Cl1: 2.290(2), Pd−Cl2: 2.300(2) Å; N2−Pd−N1: 80.1(2), N2−Pd−Cl1: 174.0(2), N1−Pd−Cl1: 94.2(2), N2−Pd−Cl2: 94.8(2), N1−Pd−Cl2: 173.4(2), Cl1−Pd−Cl2: 90.93(8)°.

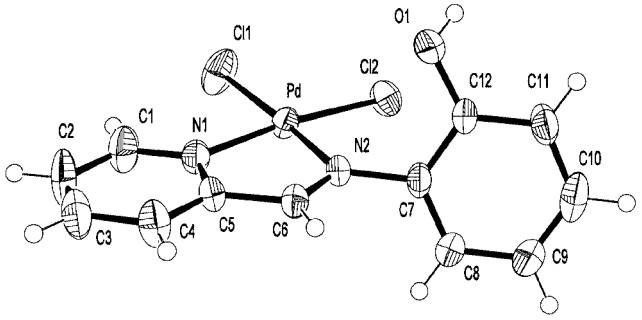

Figure 1. Perspective view of molecule **1c**·THF; thermal ellipsoids are drawn at the 50% probability level; the solvent has been omitted

The molecular structure of **1b**, shown in Figure 2, features NN′O-tridentate coordination for the ligand, with the methyl group *trans* to the iminic nitrogen. The whole complex molecule is perfectly planar (maximum displacement less than 0.08 Å), and two pentaatomic chelation rings are formed upon coordination. Table 1 lists the main bonding features for **1b**. The bite angles involved in the chelation are typical for tridentate chelation in these systems. A survey of the crystal structures of molecules containing a pyridineiminic pentaatomic N(py)−C(py)−C(iminic)−N(iminic)−Pd chelation ring was performed on the Cambridge Crystallographic Database (release of October 2001). The N1−Pd−N2 and Pd−N2−C6 angles appear in the ranges 77.2−82.3° and 108.6−119.2°, respectively, and, as a general trend, they tend to be wider (>80° and >117° respectively) for tridentate NN′X (X = O, S) systems containing two five-membered chelated rings, as in the case of these complexes, than for NN-bidentate systems containing only the Pd−N1−C5−C6−N2 chelation ring (<80° and <116°, respectively). The enlargement of the endocyclic angles upon tridentate coordination correlates well with a shortening of the Pd−N2 bond, ranging between 1.92 and 1.98 Å for tridentate complexes and 1.98 and 2.28 Å for bidentate complexes (with the exception of two NNN-tridentate compounds in which the third donor atom belongs to a flexible six-membered chelation ring). The elongation of the Pd−N2 distance in **1b** [2.009(3) Å] compared to those (1.917−1.944 Å) observed in similar NNO Pd^{II} halogen complexes of phenyl 2-pyridyl ketone benzoylhydrazone[11] is consistent with the *trans* influence of the methyl group, as also attested to by the NMR spectroscopic data. The Pd−O1 distance [2.037(2) Å] is in agreement with those found for the above hydrazone complexes (Pd−O: 2.017−2.033 Å). The growth of good quality crystals of **1b** was favored by co-crystallization with hydroxyquinone, present in traces in the THF used for recrystallization. In the crystal structure, the hydroxyquinone is positioned on a crystallographic center of inversion and bridges two symmetry-related complex molecules through strong O2−H···O1 hydrogen bonds [O2···O1: 2.697(4) Å, O−H···O: 176(3)°], as shown in Figure 3.

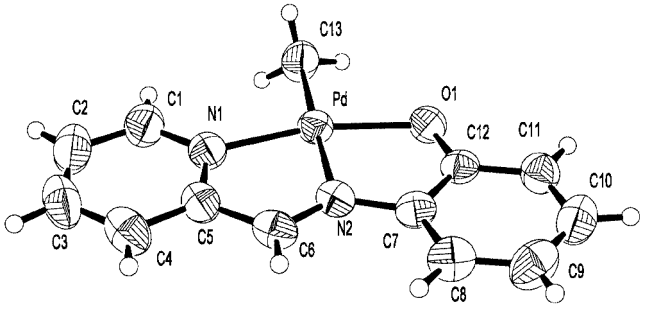

Figure 2. Perspective view of molecule **1b**·1/2$C_6H_6O_2$; thermal ellipsoids are drawn at the 50% probability level

The molecular structure of **2b** is shown in Figure 4, while the most relevant geometric features are listed in Table 1. The coordination is square-planar, with the ligand behaving as NN′S-tridentate, and the methyl *trans* to the iminic N2. The hindrance of the methyl substituent at C6 produces a minor deviation from planarity involving a slight rotation of the benzenethiol group around the C8−N2 bond [C6−N2−C8−C9: −8.0(5)°]. The overall planarity is conserved (maximum deviation 0.16 Å). The presence of the soft and bulkier S donor in the ligand has the effect of opening the S−Pd−N2 angle relative to the analogous O−Pd−N2 angle in **1b** [88.21(6) and 82.7(1)° for **2b** and **1b**, respectively], with a consequent slight weakening of the Pd−N2 bond [2.069(2) for **2b** and 2.009(3) Å for **1b**]. The *trans* effect of the S atom also results in a lengthening of the Pd−N1 bond [2.060(2) in **2b** and 2.033(3) Å for **1b**]. The dimensions of the S atom also seem to induce a compression of the Pd−N2−C6 angle [115.2(2)°] from the usual

Table 1. Selected bond lengths (Å) and angles (°) for compounds **1b**·1/2$C_6H_6O_2$, **2b**, and **2c**·1/2CH_2Cl_2

	1b·1/2$C_6H_6O_2$		**2b**	**2c**·1/2CH_2Cl_2 (two molecules)	
Pd−N1	2.033(3)	Pd−N1	2.060(2)	2.070(7)	2.062(8)
Pd−N2	2.009(3)	Pd−N2	2.069(2)	2.088(7)	2.062(8)
Pd−O1	2.037(2)	Pd−S	2.2382(9)	2.251(3)	2.241(3)
Pd−C13	2.061(4)	Pd−C14	2.045(3)	1.91(1)	1.936(9)
O1−C12	1.327(4)	S−C13	1.762(3)	1.750(9)	1.761(8)
N1−C5	1.350(5)	N1−C5	1.365(3)	1.37(1)	1.36(1)
N2−C6	1.278(4)	N2−C6	1.290(3)	1.27(1)	1.28(1)
N2−C7	1.410(4)	N2−C8	1.436(3)	1.41(1)	1.41(1)
C5−C6	1.474(5)	C5−C6	1.498(4)	1.46(1)	1.47(1)
C7−C12	1.418(5)	C8−C13	1.402(4)	1.36(1)	1.40(1)
N2−Pd−N1	80.9(1)	N2−Pd−N1	80.22(8)	78.7(3)	79.1(3)
N2−Pd−O1	82.7(1)	N2−Pd−S	88.21(6)	86.7(2)	86.8(2)
N1−Pd−O1	163.6(1)	N1−Pd−S	168.43(6)	163.7(3)	165.5(2)
N2−Pd−C13	177.3(1)	N2−Pd−C14	178.3(1)	177.6(4)	173.3(4)
N1−Pd−C13	101.1(1)	N1−Pd−C14	98.3(1)	100.2(4)	100.5(4)
O1−Pd−C13	95.3(1)	S−Pd−C14	93.2(1)	94.0(3)	93.1(3)
C12−O1−Pd	110.1(2)	C13−S−Pd	96.69(9)	96.4(3)	97.9(4)
C5−N1−Pd	111.8(2)	C5−N1−Pd	112.6(2)	110.8(6)	111.0(6)
C6−N2−Pd	115.6(3)	C6−N2−Pd	115.2(2)	114.4(6)	114.0(6)
C7−N2−Pd	112.4(2)	C8−N2−Pd	116.0(2)	114.8(6)	116.1(6)
N1−C5−C6	116.0(3)	N1−C5−C6	115.9(2)	117.5(9)	118.0(9)
N2−C6−C5	115.7(3)	N2−C6−C5	115.9(2)	115.1(9)	114.5(9)
N2−C7−C12	113.0(3)	N2−C8−C13	115.5(2)	117.5(9)	116.7(8)
O1−C12−C7	121.7(3)	S−C13−C8	123.6(2)	123.6(8)	122.3(8)

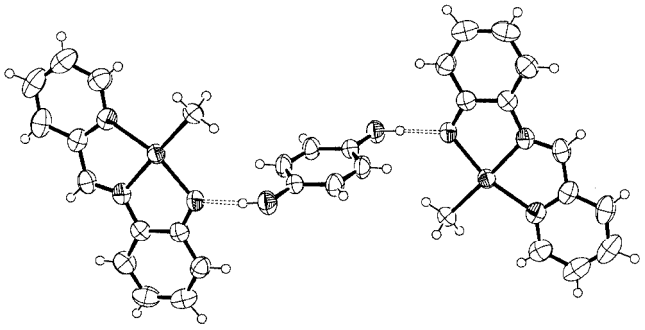

Figure 3. Molecular assembly through hydrogen bonds in the cocrystallization of **1b** with hydroxyquinone

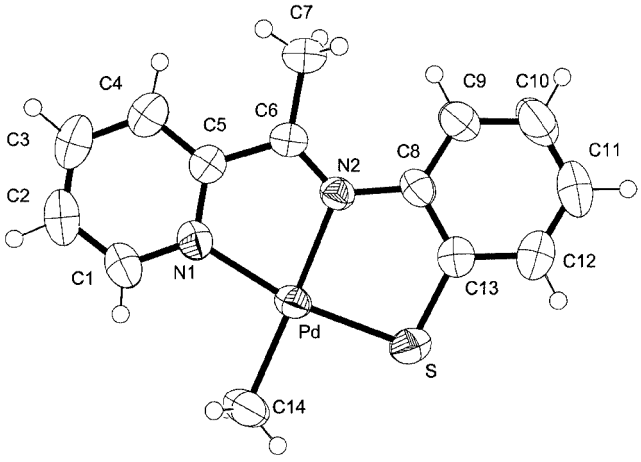

Figure 4. Perspective view of molecule **2b**; thermal ellipsoids are drawn at the 50% probability level

value for tridentate complexes; this has also been observed in some other cases of similar complexes [115.8° in chloro(-pyridine-2-carbaldehyde thiosemicarbazone-*N*,*N*′,*S*)palladium(II),[12] and chloro(2-formylpyridine 3-hexamethylene iminyl thiosemicarbazone-*N*,*N*′,*S*)palladium(II)[13]].

Compound **2c** crystallizes with two independent molecules in the asymmetric unit, one of which is shown in Figure 5. A dichloromethane molecule is also present in the asymmetric unit. The two complex molecules have similar geometries, and their relevant bonding features are listed in Table 1. The insertion of the CO into the Pd−CH_3 bond of **2b** produces a remarkable modification in the geometry of the resulting acylated complex **2c**, the resulting ligand structure being significantly distorted, with deviations from planarity as large as 0.75 Å, due to a rotation of the terminal benzenethiol group around the C−N bond [C6−N2−C8−C9: 33(1) and C21−N4−C23−C24: −30(1)°]. The metal coordination planes (N, N S, C, Pd) are also affected, with maximum deviations from planarity of 0.22 and 0.14 Å, respectively, for the two molecules. The bite geometry of the Pd−N−C−C−S chelation ring is not influenced by this conformational modification, as can be seen by comparison of the corresponding bond angles of **2b** and **2c** (Table 1), whereas angular strains are induced in the Pd−N−C−C−N chelation ring, which in **2c** are generally narrower than in **2b**. In particular, the N−Pd−N bite angle is reduced to values typical for bidentate systems [78.7(3) and 79.1(3)° for the two molecules of **2c**]. The modification

of the coordination geometry upon introduction of the acetyl ligand may be due to a larger *trans* effect determining the elongation of the Pd−N2 bond than in the methyl complex [Pd−C: 2.090(7) and 2.097(7) Å in **2c** and 2.069(2) Å in **2b**], and also to steric reasons involving the orientation of the acetyl group around the Pd−C bond. It has been shown that acetyl groups coordinated to square-planar Pd or Pt atoms tend to orient themselves perpendicularly to the coordination plane, with dihedral angles between the acetyl and the coordination planes varying in the 68−90° range, and Pd−C bonds falling between 1.947 and 2.001 Å.[6] In **2c**, the Pd−C bonds [1.91(1) and 1.936(9) Å] are significantly shorter than average, and the acetyl groups are closer to the coordination planes [dihedral angles of 51.4(4) and 31.7(7)°], thus increasing the steric crowding in the average molecular plane. In both molecules the acetyl optimizes electrostatic interactions with **2** through an orientation of the methyl towards the ligand sulfur atom and the oxygen towards the pyridine C1−H [CH_3(acyl)···S: 3.35(1) and 3.15(1) Å; O(acyl) ···C(py) =3.19(1) and 3.11(1) Å].

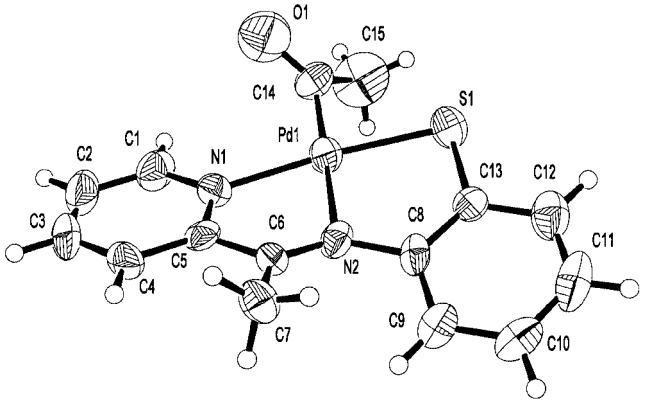

Figure 5. Perspective view of one of the two independent molecules in the crystal structure of **2c**·1/2CH_2Cl_2; thermal ellipsoids are drawn at the 50% probability level; the solvent has been omitted

Conclusions

We have reported the preparation of methylpalladium(II) complexes containing protic tridentate ligands of the HNN′O and HNN′S types. These ligands can adopt two different coordination modes around palladium: η^2-HNN′ when neutral, η^3-NN′X (X = O or S) when deprotonated. The reactivity of the three-coordinate complexes towards phosphanes and CO has been investigated. As far as carbonylation was concerned, in the absence of *soft* donors (**1b**) it was not possible to isolate the corresponding acetyl complex, and the reaction product was an organic molecule derived from the acetylation of the ligand (**3**). In the presence of a *soft* donor (the sulfur atom in **2b**), however, isolation of the carbonylated complex was successful, although the major product of the reaction was the thioacetate **4**, derived from acetylation of the ligand. The formation of the organic derivatives was accompanied by the release of palladium black. According to the results of a study on the reactivity of **1b** toward trimethylphosphane, it seems likely that the CO coordination proceeds by the breaking of the Pd-py bond. The possibility of making such a reaction catalytic is under investigation in our laboratories.

Experimental Section

General: All reactions were performed under an atmosphere of nitrogen by standard Schlenk techniques. Solvents were dried prior to use and stored under nitrogen. Elemental analyses (C, H, N, and S) were performed with a Carlo Erba Mod. EA 1108 apparatus. Infrared spectra were recorded with a Nicolet 5PCFT-IR spectrophotometer in the 4000−400 cm^{-1} range, as KBr disks. ^{1}H NMR spectra were obtained on a Bruker 300 FT spectrometer with $SiMe_4$ as internal standard at 25 °C, while $^{31}P\{^1H\}$ NMR spectra were recorded on a Bruker CPX 200 FT with H_3PO_4 (85%) as external standard at 25 °C. MS-CI spectra (methane) were recorded on a Finnigan SSQ 710 spectrometer, collecting negative ions; the relative intensities are reported in brackets. The thermogravimetric analyses were carried out under nitrogen atmosphere on a Perkin−Elmer Delta Series TGA7 apparatus, with a programmed temperature increment of 5 °C/min. The ligands HNN′O (**1**)[14] and HNN′S (**2**)[15] were synthesized by slightly modified literature procedures. The reagents used in the syntheses of the ligands — PPh_3, $P(CD_3)_3$ and *n*BuLi (1.6 M solution in *n*-hexane) — were commercial grade and were used without further purification. [(COD)Pd(Me)Cl] was synthesized as reported in the literature.[4b]

[Pd(η^2-HNN′)(Me)Cl] (1a): Compound **1** (0.050 g, 0.252 mmol) was dissolved in 30 mL of diethyl ether and [(COD)Pd(Me)Cl] (0.066 g, 0.250 mmol) was added. The immediate precipitation of a yellow powder was observed. The mixture was stirred at room temperature for 1 h and then filtered, and the solid was washed repeatedly with diethyl ether and dried under vacuum. Yield: 0.083 g (94%). ^{1}H NMR ([D_6]Me_2SO): δ = 0.41 (s, 3 H, Pd-Me), 6.89 (t, 1 H, 7-H), 6.98 (d, 1 H, 8-H), 7.08 (d, 1 H, 5-H), 7.16 (t, 1 H, 6-H), 7.91 (t, 1 H, 2-H), 8.14 (d, 1 H, 4-H), 8.27 (t, 1 H, 3-H), 8.82 (d, 1 H, 1-H), 8.88 [s, 1 H, C(H)=N], 9.84 (s, 1 H, O−H) ppm. IR: ṽ = 3377 m (OH), 1597 m−1589 m (C=N) cm^{-1}. $C_{13}H_{13}ClN_2OPd$ (355.1): calcd. C 43.97, H 3.69, N 7.89; found C 44.00, H 3.71, N 7.85.

[Pd(η^2-HNN′)(Me)Cl] (2a): Complex **2** (0.050 g, 0.219 mmol) was dissolved in 20 mL of diethyl ether and [(COD)Pd(Me)Cl] (0.058 g, 0.219 mmol) was added. The rapid formation of a gray powder was observed, and this was filtered off after two hours of stirring at room temperature. The filtered solid was washed repeatedly with diethyl ether and then dried under vacuum. Yield: 0.060 g 71%. ^{1}H NMR ([D_6]Me_2SO): δ = 0.81 (s, Pd-Me), 2.50 [s, C(Me)=N] ppm. The other signals overlapped with the signals of **2b** and **2d**. IR: ṽ = 3229 m (SH), 1587 m (C=N) cm^{-1}. $C_{14}H_{15}ClN_2PdS$ (385.2): calcd. C 43.65, H 3.92, N 7.27, S 8.32; found C 43.63, H 3.85, N 7.19, S 8.17.

[Pd(η^3-NN′O)(Me)] (1b). Method a: Complex **1** (0.050 g, 0.252 mmol) was dissolved in 10 mL of THF and [(COD)Pd(Me)Cl] (0.067 g, 0.252 mmol) was added, resulting in a yellow solution that was stirred at room temperature for 5 min. *n*BuLi (0.016 g, 0.252 mmol, 158 μL) was then added, to produce a purple solution that was stirred for 3 h, filtered, concentrated, and then treated with an excess of *n*-hexane. A purple solid was filtered off, washed with *n*-hexane, and then dried under vacuum. Yield: 0.072 g (90%). On slow evaporation of a THF solution of **1b**,

crystals of **1b**·1/2$C_6H_6O_2$ suitable for X-ray analysis were collected.

Method b: Complex **1a** (0.050 g, 0.141 mmol) was dissolved in 10 mL of THF, and NaOMe (0.011 g, 0.211 mmol) or *n*BuLi (0.008 g, 0.141 mmol, 88 μL) was added; the purple solution was stirred at room temperature for 2 h, then filtered and concentrated, and the product was precipitated with *n*-hexane and worked up as described above. Yield: 0.039 g (85%). ^{1}H NMR ([D$_6$]DMSO): δ = 0.60 (s, 3 H, Pd-Me), 6.37 (t, 1 H, 6-H), 6.72 (d, 1 H, 8-H), 7.00 (m, 2 H, 5-H−7-H), 7.21 (t, 1 H, 2-H), 7.38 (d, 1 H, 4-H), 7.76 (t, 1 H, 3-H), 7.88 [s, 1 H, C(H)=N], 8.15 (d, 1 H, 1-H) ppm. IR: $\tilde{\nu}$ = 1600 s (C=N) cm^{-1}. MS: *m*/*z* (%) = 317 (43) [**1b**]$^-$, 301 (19) [**1b** − Me]$^-$, 198 (100) [**1**]$^-$. $C_{13}H_{12}N_2OPd$ (318.7): calcd. C 49.00, H 3.79, N 8.79; found C 49.09, H 3.85, N 8.75.

[Pd(η^3-NN′S)(Me)] (2b): Complex **2** (0.100 g, 0.438 mmol) was dissolved in 30 mL of THF. [(COD)Pd(Me)Cl] (0.116 g, 0.438 mmol) was then added, and the resulting yellow solution was stirred at room temperature for 5 min. NaOMe (0.035 g, 0.656 mmol) or Et_3N (0.066 g, 0.656 mmol, 91 μL) was added, producing a deep green solution that was stirred for 1.5 h and from which a green solid was released. The solid was filtered off, washed with cold methanol and diethyl ether, and then dried under vacuum. Yield: 0.115 g (75%). On slow evaporation of a THF solution of **2b**, crystals suitable for X-ray analysis were collected. ^{1}H NMR ([D$_6$]DMSO): δ = 0.15 (s, 3 H, Pd-Me), 2.70 [s, 3 H, C(Me)=N], 6.78 (t, 1 H, 7-H), 6.91 (t, 1 H, 6-H), 7.15 (d, 1 H, 5-H), 7.23 (d, 1 H, 8-H), 7.66 (t, 1 H, 2-H), 8.01 (d, 1 H, 4-H), 8.13 (t, 1 H, 3-H), 8.35 (d, 1 H, 1-H) ppm. IR: $\tilde{\nu}$ = 1595 m (C=N) cm^{-1}. MS: *m*/*z* (%) = 349 (100) [**2b**]$^-$. $C_{14}H_{14}N_2PdS$ (348.7): calcd. C 48.21, H 4.05, N 8.03, S 9.19; found C 48.25, H 4.10, N 8.05, S 9.14.

[Pd(η^2-HNN′)Cl$_2$] (1c): 1 (0.076 g, 0.383 mmol) was dissolved in 30 mL of methanol, and a methanol solution (30 mL) of Li_2PdCl_4 (0.100 g, 0.383 mmol) was added. The mixture was stirred at room temperature for 2 h, producing a brown solid, which was filtered off, washed with methanol, and dried under vacuum. Yield: 0.111 g (77%). On slow evaporation of a THF solution of **1c**, crystals of **1c**·THF suitable for X-ray analysis were collected. ^{1}H NMR ([D$_6$]DMSO): δ = 6.83 (t, 1 H, 7-H), 6.92 (d, 1 H, 8-H), 7.19 (m, 2 H, 5-H−6-H), 7.95 (t, 1 H, 2-H), 8.20 (d, 1 H, 4-H), 8.39 (t, 1 H, 3-H), 8.72 [s, 1 H, C(H)=N], 9.06 (d, 1 H, 1-H), 10.01 (s, 1 H, O−H) ppm. IR: $\tilde{\nu}$ = 3423 s (O−H), w (C=N) 1615 cm^{-1}. $C_{12}H_{10}Cl_2N_2OPd$·THF (447.62): calcd. C 42.93, H 4.05, N 6.26; found C 42.95, H 4.10, N 6.24.

[Pd(η^3-NN′O)Cl] (1d): Characterization was performed only in solution. ^{1}H NMR ([D$_6$]DMSO): δ = 6.48 (m, 2 H, 7-H−8-H), 7.05 (t, 1 H, 6-H), 7.39 (d, 1 H, 5-H), 7.61 (t, 1 H, 2-H), 7.77 (d, 1 H, 4-H), 8.16 (t, 1 H, 3-H), 8.43 (d, 1 H, 1-H) ppm; the C(H)=N signal was obscured.

Reactions of 1a and 1b with Phosphanes: The complex (0.020 g, 0.056 mmol for **1a** and 0.063 mmol for **1b**, respectively) was dissolved in 0.75 mL of [D$_6$]DMSO in a 5-mm NMR tube. The desired amount of phosphane was added quickly, with the progress of the reaction being monitored by ^{1}H or ^{31}P NMR spectroscopy at 25 °C.

Treatment of 1a with PPh_3: PPh_3 (stoichiometric, 0.015 g, 0.056 mmol) was added; the solution instantaneously turned from yellow to green. **1e:** ^{31}P NMR: δ = 40.5 (s) ppm. **1f:** ^{31}P NMR: δ = 32.5 (s) ppm; (excess of PPh_3): Additional PPh_3 (0.015 g) was added, resulting in the immediate precipitation of a white solid (*trans*-[$(PPh_3)_2$Pd(Me)Cl]), which was filtered off, washed with Me_2SO and diethyl ether, and then dried under vacuum. Yield: 0.035 g (92%). ^{1}H NMR ($CDCl_3$): δ = −0.03 (t, $J_{P\text{-}H}$ = 5.9 Hz, 3 H, Pd−Me), 7.71−7.38 (m, 30 H, Ph) ppm. ^{31}P NMR ($CDCl_3$): δ = 27.7 (s) ppm. Crystals suitable for X-ray analysis were collected from a refrigerated THF/*n*-hexane mixture of *trans*-[$(PPh_3)_2$Pd(Me)Cl]. $C_{37}H_{33}ClP_2Pd$ (681.5): calcd. C 65.21, H 4.88, N 4.11; found C 65.20, H 4.85, N 4.10.

Treatment of 1b with $P(CD_3)_3$: $P(CD_3)_3$ (0.007 g, 0.112 mmol, 8.7 μL) was added to the complex solution by micropipette, without observation either of color changes or of solid formation. **1h:** ^{31}P NMR: δ = 43.1 (s) ppm. ^{1}H NMR: δ = 0.25 (s, 3 H, Pd-Me), 6.13 (t, 1 H, 6-H), 6.46 (d, 1 H, 8-H), 6.75 (t, 1 H, 7-H), 7.08 (d, 1 H, 5-H), 7.31 (t, 1 H, 2-H), 7.81 (t, 1 H, 3-H), 8.02 (d, 1 H, 4-H), 8.57 (d, 1 H, 1-H), 9.70 [s, 1 H, C(H)=N] ppm.

Carbonylations of 1b and 2b: The complex (0.050 g, 0.157 mmol for **1b** and 0.144 mmol for **2b**) was placed in a Schlenk tube and dissolved under nitrogen in 15 mL of dichloromethane. CO was bubbled through a glass capillary until complete saturation of the solution (at least 5 min), the vessel was closed, and the CO atmosphere was maintained for the required time. The solution was filtered through Celite in order to remove palladium black, and analyzed by mass spectrometry.

Carbonylation of 1b (3): The formation of palladium black was practically instantaneous, as was the bleaching of the solution. The CO was released after 10 min. MS: *m*/*z* (%) = 241 (48) [**3**]$^-$, 199 (32) [**1**]$^-$.

Carbonylation of 2b (2c and 4): The formation of palladium black was much slower then in the case of **1b**. The CO was released after 2 h. MS: *m*/*z* (%) = 378 (2) [**2c**]$^-$, 270 (100) [**4**]$^-$, 228 (37) [**2**]$^-$. A portion of the solution was dried and redissolved in the minimum amount of dichloromethane, and *n*-hexane was slowly diffused into it at −18 °C; crystals of **2c**·1/2CH_2Cl_2 suitable for X-ray analysis were collected.

Crystal Structure Determinations of 1b·1/2$C_6H_6O_2$, 1c·THF, 2b, 2c·1/2CH_2Cl_2, and *trans*-[$(PPh_3)_2$Pd(Me)Cl]: Single crystals were mounted on glass fibers, and X-ray diffraction data were collected at room temperature on a Bruker−Siemens SMART AXS 1000 equipped with a CCD detector for compounds **1b**·1/2$C_6H_6O_2$, **2b**, and **2c**·1/2CH_2Cl_2, and a Philips PW1100 diffractometer equipped with a scintillation counter for compounds *trans*-[$(PPh_3)_2$Pd(Me)Cl] and **1c**·THF. Graphite-monochromated Mo-K_α radiation (λ = 0.71069 Å) was used in all cases. Data collection details for **1b**, **2b**, and **2c** are: crystal to detector distance: 5.0 cm, hemisphere mode, time per frame: 30 s, oscillation Δω = 0.300°. Data reduction was performed by use of the SAINT package[16] and data were corrected for absorption effects by the SADABS[17] procedure. For *trans*-[$(PPh_3)_2$Pd(Me)Cl] and **1c**·THF, data were processed with a peak-profile procedure and corrected for Lorentz, polarization, and absorption effects (Ψ-scan method). Crystal decay was negligible in all cases. The phase problem was solved by direct methods[18] and the structures were refined by full-matrix, least-squares on all F^2,[19] by use of the WinGX package.[20] Anisotropic displacement parameters were refined for all non-hydrogen atoms, while hydrogen atoms were partly located from Fourier maps and refined isotropically, and partly introduced at calculated positions. Use was made of the Cambridge Crystallographic Database[21] facilities for structure discussion. Final maps were featureless. Data collection and refinement results are summarized in Table 2.

CCDC-178202 (**1b**·1/2$C_6H_6O_2$), -178203 (**2b**), -178204 (**2c**·1/2CH_2Cl_2), -178205 (**1g**), and -178206 (**1c**·THF) contain the

Table 2. Crystal data and structure refinement for **1b**·1/2$C_6H_6O_2$, **2b**, **2c**·1/2CH_2Cl_2, **1g** and **1c**·THF

	1b·1/2$C_6H_6O_2$	**2b**	**2c**·1/2CH_2Cl_2	**1g**	**1c**·THF
Empirical formula	$C_{16}H_{15}N_2O_2Pd$	$C_{14}H_{14}N_2PdS$	$C_{15.5}H_{15}N_2ClOPdS$	$C_{37}H_{33}ClP_2Pd$	$C_{16}H_{18}Cl_2N_2O_2Pd$
Molecular mass	373.70	348.73	419.21	681.47	447.62
Crystal system	Triclinic	Monoclinic	Monoclinic	Monoclinic	Monoclinic
Space group	$P\bar{1}$	$P2_1/c$	$P2_1/a$	$P2_1/n$	$P2_1/n$
Unit cell dimensions (Å, °)	a = 7.124(2) α = 95.40(1) b = 9.301(2) β = 95.43(1) c = 11.408(3) γ = 104.26(1)	a = 7.353(3) b = 18.063(5) β = 107.45(1) c = 10.417(3)	a = 20.188(5) b = 7.665(3) β = 98.66(2) c = 20.209(5)	a = 12.367(3) b = 23.433(5) β = 111.93(2) c = 11.891(3)	a = 10.576(4) b = 15.753(6) β= 103.49(2) c = 10.938(4)
Volume (Å^3)	723.9(3)	1319.9(8)	3091(2)	3197(1)	1772(1)
Z	2	4	8	4	4
$D_{calcd.}$ (Mg/m^3)	1.714	1.755	1.801	1.416	1.678
Absorption coefficient (mm^{-1})	1.287	1.546	1.508	0.789	1.358
F(000)	374	696	1672	1392	896
θ range (°)	1.81−28.22	2.25−28.08	2.04−21.96	3.13−26.10	3−30
Reflections collected	4404	7770	11579	6620	5376
Independent reflections	3068 [R(int) = 0.0161]	2915 [0.0231]	3769 [0.0763]	6320 [0.0572]	5145 [0.3492]
Observed reflections	2579	2378	1959	1434	2644
Data/restraints/ parameters	3068/2/239	2915/0/219	3769/0/392	6320/0/371	5145/0/209
Goodness-of-fit	0.964	0.945	0.810	0.621	0.888
Final R indices [$I > 2\sigma(I)$]	$R1$ = 0.0316, $wR2$ = 0.0751	0.0258, 0.0582	0.0402, 0.0732	0.0536, 0.1283	0.0735, 0.1770
R indices (all data)	$R1$ = 0.0408, $wR2$ = 0.0790	0.0361, 0.0625	0.1038, 0.0882	0.2031, 0.1565	0.1380, 0.2037
ΔF maximum/ minimum (e/Å^3)	0.482/-0.440	0.528/-0.653	0.537/−0.604	1.164/-0.576	2.440/-4.537

supplementary crystallographic data for this paper. These data can be obtained free of charge at www.ccdc.cam.ac.uk/conts/retrieving.html [or from the Cambridge Crystallographic Data Centre, 12, Union Road, Cambridge CB2 1EZ, UK; Fax: (internat.) +44−1223/336−033; E-mail: deposit@ccdc.cam.ac.uk].

Acknowledgments

The C.I.M. (Centro Interfacoltà di Misure "Giuseppe Casnati") is thanked for technical assistance.

[1] J. P. Collman, L. S. Hegedus, J. R. Norton, R. G. Finke, *Principles and Applications of Organotransition Metal Chemistry*; University Science Books, Mill Valley, California (US), **1987**.

[2] [2a] G. P. C. M. Dekker, C. J. Elsevier, K. Vrieze, P. W. N. M. van Leeuwen, C. F. Roobeek, *J. Organomet. Chem.* **1992**, *430*, 357−372. [2b] R. E. Rülke, J. P. G. Delis, A. M. Groot, C. J. Elsevier, P. W. N. M. van Leeuwen, K. Vrieze, K. Goubitz, H. Schenk, *J. Organomet. Chem.* **1996**, *508*, 109−120. [2c] J. H. Groen, M. J. M. Vlaar, P. W. N. M. van Leeuwen, K. Vrieze, H. Kooijman, A. L. Spek, *J. Organomet. Chem.* **1998**, *551*, 67−79. [2d] J. H. Groen, B. J. de Jong, J.-M. Ernsting, P. W. N. M. van Leeuwen, K. Vrieze, W. J. J. Smeets, A. L. Spek, *J. Organomet. Chem.* **1999**, *573*, 3−13.

[3] [3a] G. P. C. M. Dekker, A. Bujis, C. J. Elsevier, K. Vrieze, P. W. N. M. van Leeuwen, W. J. J. Smeets, A. L. Spek, Y. F. Wang, C. H. Stam, *Organometallics* **1992**, *11*, 1937−1948. [3b] P. W. N. M. van Leeuwen, C. F. Roobeek, H. van der Heijden, *J. Am. Chem. Soc.* **1994**, *116*, 12117−12118. [3c] H. A. Ankersmit, B. H. Løken, H. Kooijman, A. L. Spek, K. Vrieze, G. van Koten, *Inorg. Chim. Acta* **1996**, *252*, 141−155. [3d] L. Crociani, G. Bandoli, A. Dolmella, M. Basato, B. Corain, *Eur. J. Inorg. Chem.* **1998**, 1811−1820. [3e] M. J. Green, G. J. P. Britovsek, K. J. Cavell, F. Gerhards, B. F. Yates, K. Frankcombe, B. W. Skelton, A. H. White, *J. Chem. Soc., Dalton Trans.* **1998**, 1137−1144.

[4] [4a] R. E. Rülke, I. M. Han, C. J. Elsevier, K. Vrieze, P. W. N. M. van Leeuwen, C. F. Roobeek, M. C. Zoutberg, Y. F. Wang, C. H. Stam, *Inorg. Chim. Acta* **1990**, *169*, 5−8. [4b] R. E. Rülke, J. M. Ernsting, A. L. Spek, C. J. Elsevier, P. W. N. M. van Leeuwen, K. Vrieze, *Inorg. Chem.* **1993**, *32*, 5769−5778. [4c] R. E. Rülke, V. E. Kaasjager, D. Kliphuis, C. J. Elsevier, P. W. N. M. van Leeuwen, K. Vrieze, K. Goubitz, *Organometallics* **1996**, *15*, 668−677. [4d] H. A. Ankersmit, N. Veldman, A. L. Spek, K. Vrieze, G. van Koten, *Inorg. Chim. Acta* **1996**, *252*, 339−354. [4e] R. E. Rülke, V. E. Kaasjager, P. Wehman, C. J. Elsevier, P. W. N. M. van Leeuwen, K. Vrieze, J. Fraanje, K. Goubitz, A. L. Spek, *Organometallics* **1996**, *15*, 3022−3031. [4f] G. J. P. Britovsek, K. J. Cavell, M. J. Green, F. Gerhards, B. W. Skelton, A. H. White, *J. Organomet. Chem.* **1997**, *533*, 201−212.

[5] J. Andrieu, B. R. Steele, C. G. Screttas, C. J. Cardin, J. Fornies, *Organometallics* **1998**, *17*, 839−845.

[6] P. Pelagatti, M. Carcelli, F. Franchi, C. Pelizzi, A. Bacchi, A. Fochi, H.-W. Frühauf, K. Goubitz, K. Vrieze, *Eur. J. Inorg. Chem.* **2000**, 463−475.

[7] S. P. Meneghetti, P. J. Lutz, J. Kress, *Organometallics* **1999**, *18*, 2734−2737.

[8] [8a] J. G. P. Delis, J. H. Groen, K. Vrieze, P. W. N. M. van Leeuwen, N. Veldman, L. Spek, *Organometallics* **1997**, *16*, 551−562. [8b] A. Satake, H. Koshino, T. Nakata, *J. Organomet. Chem.* **2000**, *595*, 208−214.

[9] J. L. Hoare, K. J. Cavell, R. Hecker, B. W. Skelton, A. White, *J. Chem. Soc., Dalton Trans.* **1996**, 2197−2206.

[10] [10a] S. Komiya, Y. Akai, K. Tanaka, T. Yamamoto, A. Yamamoto, *Organometallics* **1985**, *4*, 1130−1136. [10b] Y.-J. Kim, H. Osakada, K. Sugita, T. Yamamoto, A. Yamamoto, *Organometallics* **1988**, *7*, 2182−2188.
[11] A. Bacchi, M. Carcelli, M. Costa, P. Pelagatti, C. Pelizzi, G. Pelizzi, *J. Chem. Soc., Dalton Trans.* **1996**, 4239−4244.
[12] D. Kovala-Demertzi, J. R. Miller, N. Kourkoumelis, S. K. Hadjikakou, M. A. Demertzis, *Polyhedron* **1999**, *18*, 1005−1013.
[13] D. Kovala-Demertzi, M. A. Demertzis, A. Castineiras, D. X. West, *Polyhedron* **1998**, *17*, 3739−3745.
[14] C. G. Pitt, Y. Bao, J. Thompson, M. C. Wani, H. Rosenkrantz, J. Metterville, *J. Med. Chem.* **1986**, *29*, 1231−1237.
[15] J. R. Dilworth, S. D. Howe, A. J. Huston, J. R. Miller, J. Silver, R. M. Thompson, M. Harman, M. B. Hursthouse, *J. Chem. Soc., Dalton Trans.* **1994**, 3553−3562.
[16] SAINT: SAX, *Area Detector Integration*, Siemens Analytical instruments Inc., Madison, Wisconsin, USA.
[17] SADABS: *Siemens Area Detector Absorption Correction Software*, G. Sheldrick, University of Göttingen, Germany, **1996**.
[18] Sir97: *A new Program For Solving And Refining Crystal Structures* − A. Altomare, M. C. Burla, M. Camalli, G. Cascarano, C. Giacovazzo, A. Guagliardi, A. G. Moliterni, G. Polidori, R. Spagna, Istituto di Ricerca per lo Sviluppo di Metodologie Cristallografiche C. N. R., Bari, **1997**.
[19] Shelxl97. *Program for structure refinement.* G. Sheldrick, University of Göttingen, Germany, 1997.
[20] L. J. Farrugia, *J. Appl. Crystallogr.* **1999**, *32*, 837−838.
[21] F. H. Allen, O. Kennard, R. Taylor, *Acc. Chem. Res.* **1983**, *16*, 146−153.

Received January 29, 2002
[I02048]

Oxidative Addition of Benzyliminium Tetraphenylborate to Pd(dba)(dppe): Synthesis and Catalytic Activity of [(dppe)Pd(dba)-{η^1(*N*)-$PhCH_2N{=}CMe_2$}]$(BPh_4)_2$

Michele Aresta,*[a] Angela Dibenedetto,[a] Eliana Amodio,[a] and Immacolata Tommasi[a]

Keywords: Methyl acrylate / Dimerization / Styrene−methyl acrylate coupling / Palladium

The synthesis and catalytic activity of the new dicationic Pd^{II} complex [(dppe)Pd(dba){η^1(*N*)-$PhCH_2N{=}CMe_2$}]$(BPh_4)_2$ from the Pd^0 complex Pd(dba)(dppe) and $[(PhCH_2)HN{=}CMe_2]BPh_4$ are described. $[(PhCH_2)HN{=}CMe_2]BPh_4$ adds to Pd(dba)(dppe) under mild conditions through a selective N–H activation. The resulting species further reacts with $[(PhCH_2)HN{=}CMe_2]BPh_4$ and generates *N*-benzyl-*N*-isopropylamine and [(dppe)Pd(dba){η^1(*N*)-$PhCH_2N{=}CMe_2$}]$(BPh_4)_2$. The latter catalyzes the dimerization of methyl acrylate (MA) and the co-oligomerization of MA with styrene. Significant changes of the selectivity in the dimerization of MA have been found, e.g. changing the solvent from methyl acrylate (mostly tail-to-tail, T-T, coupling) to the ionic liquid $[bmim]BF_4$ (T-T and head-to-tail, H-T, coupling).
(© Wiley-VCH Verlag GmbH, 69451 Weinheim, Germany, 2002)

Introduction

We have recently reported that $[(PhCH_2)HN{=}CMe_2]BPh_4$ (**1**)[1] oxidatively adds to $(PCy_3)_2N{-}N{\equiv}NNi(PCy_3)_2$ (**2**)[2] through a selective N−H activation,[3] affording [*trans*-$(H)Ni(PCy_3)_2${η^1(*N*)-$PhCH_2N{=}CMe_2$}]BPh_4 (**3**) [Equation (1)].

$$2\,[(PhCH_2)HN{=}CMe_2]BPh_4\ (\mathbf{1}) + (PCy_3)_2NiN{\equiv}NNi(PCy_3)_2\ (\mathbf{2}) \xrightarrow{293\ K,\ THF,\ N_2} 2\,[(H)Ni(PCy_3)_2(\eta^1(N)\text{-}PhCH_2N{=}CMe_2)]BPh_4\ (\mathbf{3}) + N_2 \quad (1)$$

Compound **3** promotes the head-to-tail (H-T) oligomerization of methyl acrylate (**4**), with 100% selectivity, to give dimethyl 2-methyleneglutarate (**5**), accompanied by traces of the trimer 2,4,6-tris(methoxycarbonyl)-1-hexene (**6**), which is still an H-T coupling product.[4] Conversely, $(CH_2{=}CHCH_2NH_3)BPh_4$ (**7**)[1] adds to Ni^0 complexes, such as **2**[3] or $(PCy_3)_2Ni(\eta^2\text{-}CO_2)$ (**8**),[5] through the selective activation of the C−N allyl bond, affording $[(\eta^3\text{-}C_3H_5)Ni(PCy_3)(NH_3)]BPh_4$ (**9**).[4] Compound **9**, in the presence of dihydrogen (0.1 MPa) as a cocatalyst, shows the same 100% selectivity towards the H-T oligomerization of **4**, affording **5**.[4] As we have demonstrated, in both cases the formation of (hydrido)Ni species is the key factor for catalysis to occur. In order to ascertain if such a reaction also occurs with other metal systems, we have investigated the reaction of **1** with [1,2-bis(diphenylphosphanyl)ethane][(*E*,*E*)-dibenzylideneacetone]palladium (**10**) and found a completely different behavior with respect to Ni^0. Compound **1** reacts with **10** in a multistep reaction, giving the dicationic Pd^{II} complex [(dppe)Pd(dba){η^1(*N*)-$PhCH_2N{=}CMe_2$}]$(BPh_4)_2$ (**11**), that has been proved to catalyze the dimerization of **4** and the co-oligomerization of **4** with styrene (**12**). The reaction takes place in either the neat monomer(s), or in the ionic liquid 1-butyl-3-methylimidazolium tetrafluoroborate ($[bmim]BF_4$) (**13**),[6,7] but with different yields and selectivities (Figure 1).

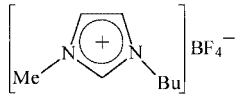

13

Figure 1. 1-Butyl-3-methylimidazolium tetrafluoroborate, $[bmim]BF_4$ (**13**)

The interest in ionic liquids, such as $[bmim]BF_4$, as solvents in biphasic processes such as Pd-catalyzed oligomerization, hydroformylation and hydrogenation of olefins is growing.[8,9] Most Pd complexes are perfectly stable and soluble in these solvents. Moreover, biphasic systems allow for easier product isolation and catalyst recycling.

Results and Discussion

Reaction of Pd(dba)(dppe) (10) with $[(PhCH_2)HN{=}CMe_2]BPh_4$ (1)

The iminium salt **1** reacts with the palladium(0) species Pd(dba)(dppe) (**10**), in THF at 293 K, to give the dicationic

[a] Dipartimento di Chimica, Campus Universitario, Università di Bari, and Centro METEA,
Via Celso Ulpiani 27, 70126 Bari, Italy
Fax: (internat.) + 39-080/544-2429
E-mail: aresta@metea.uniba.it

Pd^{II} complex **11** [Equation (2)] as ultimate product. This implies a different reaction pathway to that of the addition of **1** to Ni^0 [Equation (1)].

$$\underset{\mathbf{1}}{2\,[(PhCH_2)HN{=}CMe_2]BPh_4} + \underset{\mathbf{10}}{Pd(dba)(dppe)} \xrightarrow{293\ K,\ THF,\ N_2} \underset{\mathbf{11}}{[(dppe)Pd(dba)(\eta^1(N)\text{-}PhCH_2N{=}CMe_2)](BPh_4)_2} + \underset{\mathbf{20}}{(PhCH_2)HN(CHMe_2)} \quad (2)$$

It is known that **10** exists in solution in equilibrium with a small amount of (S)Pd(dppe) (**10′**) (S = solvent) and dba. Compound **10′** undergoes the oxidative addition of reagents such as chloroform (**14**)[10] and phenyl iodide (**15**).[11] Pd(dba)(dppe) also reacts; however, the reaction is slower than that of (S)Pd(dppe). The result is the formation of a Pd^{II} species, with the release of dba [Equations (3) and (4)].

$$Pd(dba)(dppe) + CHCl_3 \rightarrow Pd(dppe)(Cl)(CHCl_2) + dba \quad (3)$$

$$Pd(dba)(dppe) + PhI \rightarrow PhPdI(dppe) + dba \quad (4)$$

In order to ascertain if **11** is formed by an initial addition of **1** to Pd^0 with the formation of a hydride species, we have continuously monitored the reaction depicted in Equation (2) by ^1H NMR spectroscopy at 293 K, over a period of 1 h (Scheme 1).

The iminium tetraphenylborate salt (**1**) does not add to the metal center, as observed with the Ni^0 complexes.[3] As a matter of fact, neither hydrides nor free dba have been detected during the reaction. This excludes the complication added by the presence of **10′** in the addition process. It seems that both the presence of dba as a potential proton acceptor and the lower stability of the palladium hydride species with respect to Ni[3,12b] and Pt,[12] may favor a different reaction path for Pd. Rarely have Pd−H species been isolated,[13] and often the formation of cationic (hydrido)Pd compounds have been inferred on the basis of the products that can originate by H-transfer.[14,15] Recently, we have reported that **1** reacts with $Pd(dppe)_2$ (**21**) to afford the unstable hydride $[HPd(dppe)_2]BPh_4$ (**22**), which has been detected in solution and characterized by ^1H (quint at δ = −7.37 ppm) and ^{31}P NMR spectroscopy (d at δ = 32.98 ppm).[15] The reaction of **1** with Pd(dba)(dppe) (**10**) was monitored by ^1H NMR spectroscopy. Soon after the addition of **1** to Pd(dba)(dppe) (**10**), a new resonance signal appears at δ = 4.75 ppm, which is assigned to an N−H moiety (**16** or **17**), as demonstrated by D_2O exchange. In principle, either the protonation of dba may occur to give **18** or the organometallic species **17** (possibly in equilibrium with the amido complex **17′**), derived from the coordination of the iminium cation to the palladium atom. The appearance of a new signal at δ = 2.65 ppm seems to support the

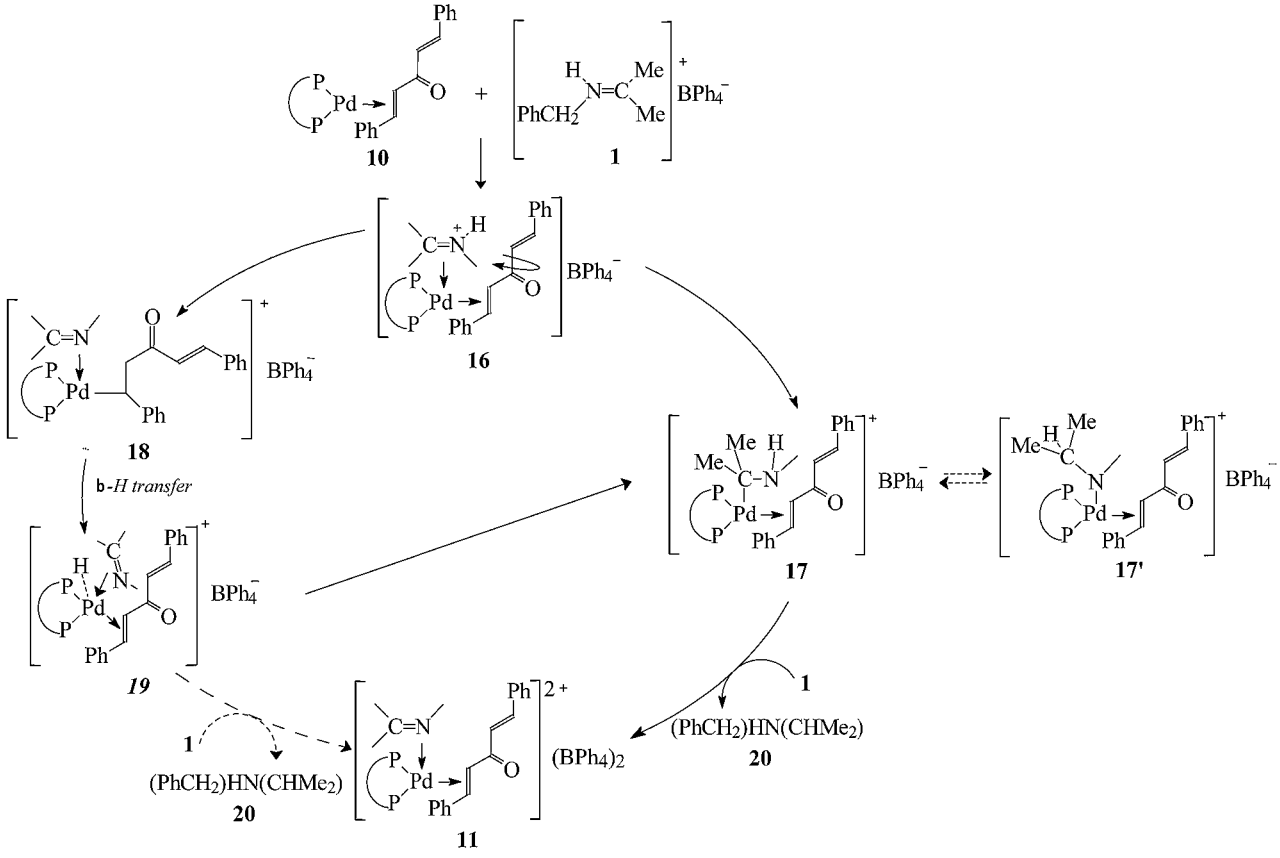

Scheme 1. The lifetime of **19** is not long enough to record the ^1H NMR spectrum

formation of **18**. This assignment agrees well with the ^1H resonance of alkyl moieties bonded to Pd {such as those in cationic complexes of the type $[(N-N)Pd(CH_3)(acetonitrile)]BF_4$} that commonly fall in the δ = 2.32−2.71 ppm range (CD_3CN, 293 K).[16] Compound **18** can be converted into **17** (or **17′**), probably through the formation of the unstable palladium hydride species (**19**), not observed by ^1H NMR spectroscopy. Compound **17** (or **17′**) can easily be protonated by the benzyliminium salt **1** affording the saturated amine *N*-benzyl-*N*-isopropylamine (**20**), which is found free in solution as revealed by GC-MS analysis, and the final complex **11**, in which dba is π-coordinated to the palladium atom, as suggested by two broad resonances at δ = 4.77 and 5.98 ppm, assigned to the nonequivalent protons of the C=C double bond.[10] Therefore, both Pd(dba)(dppe) and $Pd(dppe)_2$ react with the iminium salt **1**, affording the saturated amine **20** and a dicationic Pd^{II} complex, but by a different reaction path.[15] The ^{31}P NMR spectrum of the isolated complex **11** at 293 K shows that the two original resonances at δ = 34.79 and 37.07 ppm, characteristic of the asymmetric complex Pd(dba)(dppe), shift downfield and are found at δ = 35.31 and 38.00 ppm, respectively. The observed shift agrees with the greater electrophilicity of the metallic center that is oxidized to Pd^{II} after the reaction occurs. During the reaction such signals appear as broad resonances as a result of the dynamic behavior of the system Pd(dba)(dppe)/$[(PhCH_2)HN{=}CMe_2]BPh_4$ in solution. Unfortunately, solubility properties do not allow a low-temperature investigation. Complex **11** is stable in solution at 293 K, while above 353 K it decomposes to give benzene (**23**), generated from the BPh_4^- moiety, as already observed with rhodium[17a] and nickel[4] complexes. The cleavage of the B−C bond may be promoted by the preliminary coordination of the tetraphenylborate unit to the metal atom through one of its phenyl rings. However, **23** can also be formed by the direct protolysis of one of the B−C bonds of BPh_4^- by the iminium cation [Equation (5)]. The latter reaction has been proved to occur when the benzyliminium tetraphenylborate is heated in a solvent in the absence of any metal system.[17b]

$$H^+ + BPh_4^- \rightarrow BPh_3 + PhH \quad (5)$$

We have used **11** as a catalyst in the oligomerization of methyl acrylate (**4**) and discovered that the different properties and reactivity of the system Pd(dba)(dppe)/$[(PhCH_2)HN{=}CMe_2]BPh_4$, relative to the nickel complexes, greatly modifies the catalytic activity towards **4**.

Catalytic Activity of 11 in the Dimerization of Methyl Acrylate (4)

Interest in the dimerization of methyl acrylate (**4**) arises from the utility, at an industrial level, of the products that can be formed by C_3-C_3 or C_3-C_2 coupling (Figure 2).

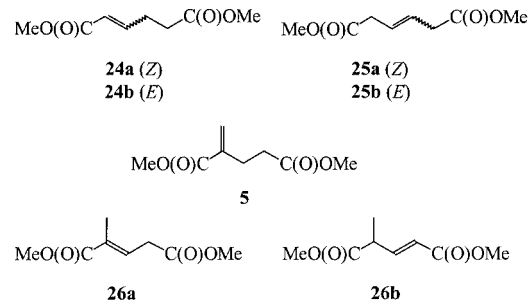

Figure 2. Tail-to-tail (**24a**−**b**, **25a**−**b**) and head-to-tail (**5**, **26a**−**b**) dimers of methyl acrylate

The dimethyl (*Z*)- and (*E*)-hex-2-enedioates (**24a**, **24b**), and dimethyl (*Z*)- and (*E*)-hex-3-enedioates (**25a**, **25b**), obtained by C_3-C_3 coupling of two methyl acrylate units,[18] are used principally as precursors for the synthesis of adipic acid, which is used in the Nylon-6,6 production. Conversely, head-to-tail dimers dimethyl 2-methyleneglutarate (**5**) and dimethyl methylpentenedioates (**26a**, **26b**), obtained by C_3-C_2 coupling of two methyl acrylate units, find their application essentially as monomers in co-polymerization reactions.[19] As mentioned above, in a recent study[4] we have shown that **3**[1] and **9**,[4] in the presence of H_2 as a cocatalyst, catalyze the selective (100%) H-T oligomerization of **4** giving dimer **5** and traces of trimer **6**. We have now studied the catalytic activity of complex **11**; typically, a **4**/**11** ratio of 1000:1 was used either in methyl acrylate as the solvent or in the ionic liquid $[bmim]BF_4$. We have found that the solvent drives both the rate of conversion and the selectivity of the process towards the T-T dimer dimethyl (*E*)-hex-2-enedioate (**24b**). The conversion yield of methyl acrylate in $[bmim]BF_4$ is four times higher than in methyl acrylate as the solvent. In $[bmim]BF_4$, **11** catalyzes the formation of the T-T product dimethyl (*E*)-hex-2-enedioate (**24b**) (41%), followed by the H-T product dimethyl 4-methylpent-2-enedioate (**26b**) (36%). Minor amounts of T-T dimers dimethyl (*Z*)-hex-2-enedioate (**24a**) (4%) and dimethyl (*E*)-hex-3-enedioate (**25b**) (5%), and the H-T dimers dimethyl 2-methyleneglutarate (**5**) (4%) and dimethyl 2-methylpent-2-enedioate (**26a**) (10%) were also obtained. In methyl acrylate, **11** catalyzes the dimerization of **4** affording the T-T dimer dimethyl (*E*)-hex-2-enedioate (**24b**) with a selectivity of 82%. Smaller amounts of the T-T dimer dimethyl (*E*)-hex-3-enedioate (**25b**) (2%) and the H-T dimers dimethyl 2-methyleneglutarate (**5**) (5%), dimethyl 2-methylpent-2-enedioate (**26a**) (9%) and dimethyl 4-methylpent-2-enedioate (**26b**) (2%) were also obtained. In both cases, traces of methyl 3-phenyl-2-propenoate (**27**) are also formed that are produced by the reaction of the phenyl moiety, formed by thermal degradation of complex **11**, with **4**. The trend shown by Pd catalysts is quite different from that characteristic of analogous Ni complexes. It has been proved[4] that the H-T coupling of **4** requires a hydride catalyst[4,20] or monodentate phosphorus ligands.[21] In the present case, the instability of Pd−H represses H-T coupling

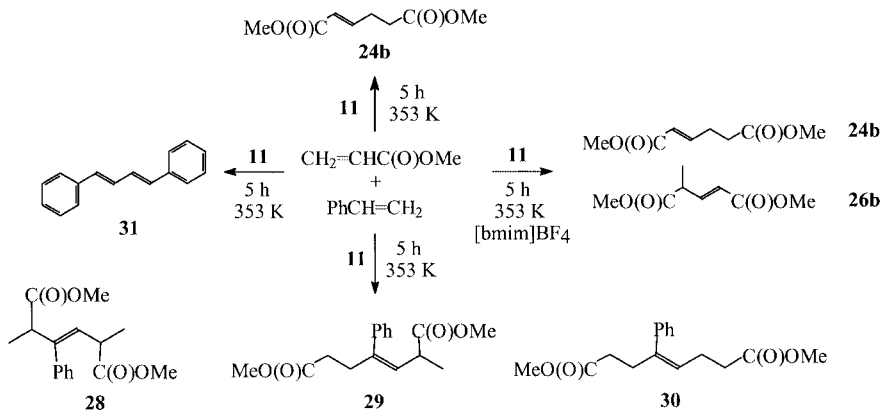

Scheme 2

and favors the formation of T-T dimers of **4** that do not require M−H species.[18k] Also the nature of the solvent can favor or disfavor the formation of Pd−H systems and, thus, promote or prevent H-T coupling.

Catalytic Activity of 11 in the Co-Oligomerization of Methyl Acrylate (4) with Styrene (12)

Complex **11** has also been found to be active in the co-oligomerization of **4** with **12** (**11**/**4**/**12** = 1:1000:1000), when both the monomers are used as the solvent, or in [bmim]BF_4. The reaction affords the co-trimers dimethyl 2,5-dimethyl-3-phenylhex-3-enedioate (**28**), dimethyl 2-methyl-4-phenylhept-3-enedioate (**29**) and dimethyl 4-phenyloct-4-enedioate (**30**) (Scheme 2).

These co-oligomerization products are accompanied by the dimers of **4**, dimethyl (*E*)-hex-2-enedioate (**24b**) and dimethyl 4-methylpent-2-enedioate (**26b**) in the presence of [bmim]BF_4, or dimethyl (*E*)-hex-2-enedioate (**24b**) in methyl acrylate and styrene as the solvents. In each case, the dimer of styrene 1,4-diphenyl-1,3-butadiene (**31**) is also formed in traces. In [bmim]BF_4, the conversion of methyl acrylate is higher than in the neat reagents as the solvent, but the **4**/**12** co-trimers are present in minor amounts and the dimers of **4** are the major products. However, when the reagents methyl acrylate and styrene are used as the solvent, **4**/**12** co-trimers are predominantly formed. These results agree with those reported in the literature[22] that showed that the co-dimerization of **12** with **4**, catalyzed by [Pd(C_6H_5CH=CH_2)Cl_2]$_2$, gives the co-dimers of **12** and **4**, and the dimers of **4** or **12**. Ethylbenzene (**32**) is also formed in traces, which is produced by H-transfer to **12**, as a result of the reductive coupling of two units of **12** which gives 1,4-diphenyl-1,3-butadiene (**31**) that is found in the reaction medium. Small amounts of methyl 3-phenyl-2-propenoate (**27**) and stilbene (**33**) are also generated, most likely by the reaction of the phenyl moiety, a thermal degradation product of **11**, with **4** or **12**.[17]

Conclusions

[($PhCH_2$)HN=CMe_2]BPh_4 (**1**) reacts with palladium(0) complex Pd(dba)(dppe) (**10**) to afford the dicationic Pd^{II} complex [(dppe)Pd(dba){η^1(*N*)-$PhCH_2N$=CMe_2}](BPh_4)$_2$ (**11**), through a complex path that starts with the protonation of the coordinated dba. Complex **11** has been proved to be catalytically active in the dimerization of methyl acrylate (**4**) and in the co-oligomerizations of **4** with styrene (**12**). No polymerization products have been observed. In neat methyl acrylate, the selective (84%) T-T coupling of **4** affording dimethyl (*E*)-hex-2-enedioate (**24b**) with a regioselectivity of 82% has been observed. In the ionic liquid [bmim]BF_4, a selectivity of 50% was found towards the T-T coupling of **4**, affording dimethyl (*E*)-hex-2-enedioate (**24b**). The H-T dimethyl 4-methylpent-2-enedioate (**26b**) is formed with a regioselectivity of ca. 40%. In neat methyl acrylate/styrene, co-trimers are formed in higher yields than in [bmim]BF_4, which favors the homocoupling of **4**.

Experimental Section

General Comments: Unless otherwise stated, all reactions and manipulations were conducted under dinitrogen by using vacuum-line techniques. All solvents were dried as described in the literature[23] and stored under N_2. MA was purchased from Fluka and stored under N_2. [($PhCH_2$)HN=CMe_2]BPh_4,[1] Pd(dba)(dppe)[10a,24] and [bmim]BF_4 [6,25] have been prepared as previously reported. Elemental C,H,N microanalyses were performed with an Euro EA 3000 analyser, P analyses were performed using a UV Shimadzu 1601 (λ = 460 nm), Pd was dosed using a Perkin−Elmer Atomic Absorption Spectrometer 3110. NMR spectra were run with a Varian XL-200 instrument. ^{1}H NMR chemical shifts are in ppm vs. TMS and referenced to the solvent peak. ^{31}P NMR chemical shifts are in ppm vs. 85% H_3PO_4. GC-MS analyses were carried out with a Shimadzu GC-17A linked to a Shimadzu GCMS-QP5050 selective mass detector (capillary column: 60 m × 0.25 mm Supelco MDN-5S, 0.25 μm film thickness). Temperature program: 343 K (3 min) → 21 min → 553 K (30 min). GC analyses were performed by using an HP 5890 Series II GC (capillary column: 30 m × 0.25 mm Altech AT-5, 0.25 μm film thickness). Temperature program: 318 K (5 min) → 7.5 min → 393 K (1 min) → 9.5 min → 583 K (30 min).

Synthesis of [(dppe)Pd(dba){η^1(*N*)-$PhCH_2N$=CMe_2}](BPh_4)$_2$ (11): [($PhCH_2$)HN=CMe_2]BPh_4 (0.140 g, 0.30 mmol), dissolved in THF (10 mL), was added to a solution of Pd(dba)(dppe) (0.183 g,

0.25 mmol) in THF (10 mL), prepared under dinitrogen at 293 K. The resulting mixture was stirred at room temperature (293 K) for 5 h, until its color turned to yellowish orange. The reaction mixture was filtered, concentrated in vacuo, and, after addition of diethyl ether (20 mL), cooled to 253 K. The red oil obtained was isolated, washed with diethyl ether (2 × 3 mL), dried in vacuo, and characterized as [(dppe)Pd(dba){η^1(*N*)-$PhCH_2N{=}CMe_2$}]$(BPh_4)_2$ (**11**) (0.219 g, 58%). ^{1}H NMR ([D$_8$]THF, 293 K): δ = 2.02 (s, 3 H, $-CH_3$), 2.07 (s, 3 H, $-CH_3$), 2.50 (br. s, 4 H, $-CH_2CH_2-$), 4.42 (s, 2 H, $-CH_2Ph$), 4.77 (br. s, 1 H, $-HC{=}CH-$), 5.98 (br. s, 1 H, $-HC{=}CH-$), 6.70 (t, J_{ortho} = 7.10 Hz, 2 × 4 H, H_{para} BPh_4^-,), 6.80 (t, J_{ortho} = 7.44 Hz, 2 × 8 H, H_{meta} BPh_4^-), 6.93−7.82 (m, 53 H, 2 × 8 H, H_{ortho} BPh_4^-, $H_{ortho,meta,para}$ $PhCH_2-$, dppe, $H_{aromatic,olefinic}$ dba) ppm. ^{31}P NMR ([D$_8$]THF, 293 K): δ = 35.31 (m), 38.00 (m) ppm. $C_{101}H_{91}B_2NOP_2Pd$ (1524.80): calcd. C 79.56, H 6.02, N 0.92, Pd 6.98, P 4.06; found C 79.77, H 6.05, N 1.08, Pd 6.85, P 4.07. Water must be avoided in order to prevent the hydrolysis of benzyliminium tetraphenylborate to afford acetone and benzylammonium tetraphenylborate.

Reaction of Pd(dba)(dppe) (10) with [(PhCH$_2$)HN=CMe$_2$]BPh$_4$ (1) Monitored by ^{1}H NMR Spectroscopy: A water-free [D$_8$]THF solution (0.75 mL) of Pd(dba)(dppe) (13.20 mg, 0.018 mmol), prepared under N_2, was introduced into an NMR tube, avoiding contact with air. The iminium tetraphenylborate was added (8.20 mg, 0.018 mmol), the tube sealed and the solution continuously monitored by ^{1}H NMR spectroscopy at 293 K (Scheme 1). **18:** ^{1}H NMR ([D$_8$]THF, 293 K): δ = 1.95 (s, 3 H, $-CH_3$), 2.05 (s, 3 H, $-CH_3$), 2.20 (br. s, 4 H, $-CH_2CH_2-$), 2.65 (br. s, Pd−alkyl), 4.43 (s, 2 H, $-CH_2Ph$), 4.75 (br. s, 1 H, N−*H*), 6.70 (t, J_{ortho} = 7.10 Hz, 2 × 4 H, H_{para} BPh_4^-), 6.80 (t, J_{ortho} = 7.44 Hz, 2 × 8 H, H_{meta} BPh_4^-), 6.93−7.82 (m, 53 H, 2 × 8 H, H_{ortho} BPh_4^-, $H_{ortho,meta,para}$ $PhCH_2-$, dppe, $H_{aromatic,olefinic}$ dba) ppm. The formation of *N*-benzyl-*N*-isopropylamine (**20**) was confirmed by analyzing the reaction mixture by GC-MS: $C_{10}H_{15}N$: *m*/*z* = $[M]^+$ (not observed), 134, 106, 91, 77, 65, 41, 39.

Dimerization of Methyl Acrylate (4) Promoted by 11 in Methyl Acrylate: Methyl acrylate (1 mL, 11.10 mmol) was added to [(dppe)Pd(dba){η^1(*N*)-$PhCH_2N{=}CMe_2$}]$(BPh_4)_2$ (13.75 mg, 0.009 mmol) under N_2. The reaction mixture was then stirred at 353 K for 5 h and, after cooling to 293 K, the products were diluted in toluene. They were analyzed by GC and GC-MS, that showed that dimethyl (*E*)-hex-2-enedioate (**24b**) was the main product (82%) and **26a** (9%), **5** (5%), **25 b** (2%) and **26b** (2%) were the minor products. **24b:** GC-MS: $C_8H_{12}O_4$: *m*/*z* = $[M]^+$ (not observed), 157 [$M^+ - CH_3$], 140 [$CH_3O(O)C-CH{=}CH-CH-CH_2-CO$], 108 [$OC-CH{=}CH-CH{=}CH-CO$], 97 [$H_2C{=}CH-CH{=}CH-C(O)O$], 81 [$H_2C{=}CH-CH{=}CH-CO$], 71 [$H_2C{=}CH-C(O)O$], 59 [$C(O)OCH_3$], 53 [$H_2C{=}CH-CH{=}CH$], 41 [$H_2C{=}CH-CH_2$], 39 [$HC-CH{=}CH$], 31 [$OCH_3$].

Dimerization of Methyl Acrylate (4) Promoted by 11 in [bmim]BF$_4$: Methyl acrylate (0.47 mL, 5.22 mmol) and the ionic liquid [bmim]BF_4 (0.25 mL) were added to [(dppe)Pd(dba){η^1(*N*)-$PhCH_2N{=}CMe_2$}]$(BPh_4)_2$ (6.40 mg, 0.004 mmol) under N_2. The reaction mixture was then stirred at 353 K for 5 h and, after cooling to 293 K, the products were isolated by extraction in toluene. They were analyzed by GC and GC-MS, that showed that dimethyl (*E*)-hex-2-enedioate (**24b**) (41%) and dimethyl 4-methylpent-2-enedioate (**26b**) (36%) were the main products and **24a** (4%), **25b** (5%), **5** (4%) and **26a** (10%) were the minor products. **26b:** GC-MS: $C_8H_{12}O_4$: *m*/*z* = $[M]^+$ (not observed), 140 [$M^+ - CH_3OH$], 112 [$H_2C{=}CH-CH{=}CH-C(O)OCH_3$], 97 [$H_2C{=}CH-CH{=}CH-C(O)O$], 85 [$CH{=}CH-C(O)OCH_3$], 81 [$H_2C{=}CH-CH{=}CH-CO$], 71 [$H_2C{=}CH-C(O)O$], 59 [$C(O)OCH_3$], 53 [$H_2C{=}CH-CH{=}CH$], 41 [$H_2C{=}CH-CH_2$], 39 [$HC-CH{=}CH$].

Co-Oligomerization of Methyl Acrylate (4) and Styrene (12) Promoted by 11 in Methyl Acrylate and Styrene: Methyl acrylate (0.46 mL, 5.11 mmol) and styrene (0.59 mL, 5.13 mmol) were added to [(dppe)Pd(dba){η^1(*N*)-$PhCH_2N{=}CMe_2$}]$(BPh_4)_2$ (6.20 mg, 0.004 mmol) under N_2. The reaction mixture was then stirred at 353 K for 5 h and, after cooling to 293 K, the products were diluted in toluene and analyzed by GC and GC-MS. Three different isomers of methyl acrylate/styrene trimers were isolated, dimethyl 2,5-dimethyl-3-phenylhex-3-enedioate (16%) (**28**), dimethyl 2-methyl-4-phenylhept-3-enedioate (14%) (**29**) and dimethyl 4-phenyloct-4-enedioate (35%) (**30**), and the dimer of methyl acrylate dimethyl (*E*)-hex-2-enedioate (32%) (**24b**). **28:** GC-MS: $C_{16}H_{20}O_4$: *m*/*z* = $[M]^+$ (not observed), 244 [$M^+ - CH_3OH$], 216 [$H_2C{=}CH-C(Ph){=}CH-CH(CH_3)C(O)OCH_3$ or $H_2C{=}CH-CH{=}C(Ph)-CH(CH_3)C(O)OCH_3$], 207, 185 [$H_2C{=}CH-C(Ph){=}CH-CH(CH_3)CO$ or $H_2C{=}CH-CH{=}C(Ph)-CH(CH_3)CO$], 143 [$HC-C(Ph){=}CH-CH-CH_3$ or $CH-CH{=}C(Ph)-CH(CH_3)$], 129 ($Ph-C{=}CH-CH{=}CH_2$), 115 ($Ph-C{=}CH-CH$), 96, 77 (C_6H_5), 59 [$C(O)OCH_3$), 51 (C_4H_3). **29:** GC-MS: $C_{16}H_{20}O_4$: *m*/*z* = $[M]^+$ (not observed), 244 [$M^+ - CH_3OH$], 216 [$H_2C{=}CH-CH{=}C(Ph)-CH_2-CH_2C(O)OCH_3$ or $H_2C{=}CH-C(Ph){=}CH-CH(CH_3)C(O)OCH_3$], 207, 185 [$H_2C{=}CH-CH{=}C(Ph)-CH_2-CH_2CO$ or $H_2C{=}CH-C(Ph){=}CH-CH(CH_3)CO$], 143 [$HC-CH{=}C(Ph)-CH_2-CH_2$ or $CH-C(Ph){=}CH-CH-CH_3$], 129 [$HC-CH{=}C(Ph)-CH_2$], 115 [$HC-CH{=}C-Ph$], 96, 77 [C_6H_5], 59 [$C(O)OCH_3$], 51 [C_4H_3]. **30:** GC-MS: $C_{16}H_{20}O_4$: *m*/*z* = $[M]^+$ (not observed), 244 [$M^+ - CH_3OH$], 216 [$H_2C{=}CH-CH{=}C(Ph)-CH_2CH_2C(O)OCH_3$ or $H_2C{=}CH-C(Ph){=}CH-CH_2CH_2C(O)OCH_3$], 207, 157 [$Ph-C{=}CH-CH-CH_2CO$], 141, 129 [$Ph-C{=}CH-CH{=}CH_2$], 115 [$Ph-C{=}CH-CH$], 88, 77 [$C_6H_5$], 59 [$C(O)OCH_3$], 51 [$C_4H_3$].

Co-Oligomerization of Methyl Acrylate (4) and Styrene (12) Promoted by 11 in [bmim]BF$_4$: Methyl acrylate (0.911 g, 10.58 mmol), styrene (1.028 g, 9.87 mmol) and the ionic liquid [bmim]BF_4 (1 mL) were added to [(dppe)Pd(dba){η^1(*N*)-$PhCH_2N{=}CMe_2$}]$(BPh_4)_2$ (12.30 mg, 0.008 mmol) under N_2. The reaction mixture was then stirred at 353 K for 5 h and, after cooling to 293 K, the products were isolated by extraction in toluene and analyzed by GC and GC-MS. Three different isomers of methyl acrylate/styrene trimers were isolated, dimethyl 2,5-dimethyl-3-phenylhex-3-enedioate (4%) (**28**), dimethyl 2-methyl-4-phenylhept-3-enedioate (3%) (**29**) and dimethyl 4-phenyloct-4-enedioate (16%) (**30**), and the dimers of methyl acrylate dimethyl (*E*)-hex-2-enedioate (36%) (**24b**) and dimethyl 4-methylpent-2-enedioate (25%) (**26b**).

Acknowledgments

We gratefully acknowledge financial support from MURST (Project no. MM03027791) and Università di Bari.

[1] M. Aresta, E. Quaranta, *J. Organomet. Chem.* **1995**, *488*, 211−222.
[2] M. Aresta, C. F. Nobile, A. Sacco, *Inorg. Chim. Acta* **1975**, *12*, 167−178.
[3] M. Aresta, E. Quaranta, A. Dibenedetto, P. Giannoccaro, I. Tommasi, M. Lanfanchi, A. Tiripicchio, *Organometallics* **1997**, *16*, 834−841.
[4] M. Aresta, A. Dibenedetto, E. Quaranta, M. Lanfranchi, A. Tiripicchio, *Organometallics* **2000**, *19*, 4199−4207.

[5] M. Aresta, C. F. Nobile, V. G. Albano, E. Forni, M. Manassero, *J. Chem. Soc., Chem. Commun.* **1975**, 636−637.
[6] [6a] J. D. Holbrey, K. R. Seddon, *J. Chem. Soc., Dalton Trans.* **1999**, 2133−2139. [6b] P. A. Z. Suarez, J. E. L. Dullius, S. Einloft, R. De Souza, J. Dupont, *Polyhedron* **1996**, *15*, 1217−1219.
[7] J. E. L. Dullius, P. A. Z. Suarez, S. Einloft, R. F. De Souza, J. Dupont, *Organometallics* **1998**, *17*, 815−819.
[8] T. Welton, *Chem. Rev.* **1999**, *99*, 2071−2083.
[9] P. Wasserscheid, W. Keim, *Angew. Chem. Int. Ed.* **2000**, *39*, 3772−3789.
[10] [10a] W. A. Herrmann, W. R. Thiel, C. Broßmer, K. Öfele, T. Priermeier, W. Scherer, *J. Organomet. Chem.* **1993**, *461*, 51−60. [10b] S. M. Reid, J. T. Mague, M. J. Fink, *J. Organomet. Chem.* **2000**, *616*, 10−18.
[11] [11a] C. Amatore, A. Jutand, *Coord. Chem. Rev.* **1998**, *178−180*, 511−528. [11b] C. Amatore, A. Jutand, *J. Organomet. Chem.* **1999**, *576*, 254−278.
[12] [12a] W. W. Ellis, C. J. Curtis, D. E. Berning, D. H. Gibson, D. L. DuBois, *ICCDU VI*, September 9−14, **2001**, Breckenridge, Colorado, USA, Book of Abstracts, O-28. [12b]D. E. Berning, B. C. Noll, D. L. DuBois, *J. Am. Chem. Soc.* **1999**, *121*, 11432−11447.
[13] [13a] E. H. Brooks, F. Glockling, *J. Chem. Soc. A* **1967**, 1030−1034. [13b] R. H. Cragg, J. P. N. Husband, A. F. Weston, *J. Chem. Soc., Chem. Commun.* **1970**, 1701−1702. [13c] T. Yoshida, S. Otsuka, *J. Am. Chem. Soc.* **1977**, *99*, 2134−2140. [13d] H. Werner, W. Bertleff, *Chem. Ber.* **1983**, *116*, 823−826.
[14] [14a] T. Hosokawa, P. M. Maitlis, *J. Am. Chem. Soc.* **1973**, *95*, 4924−4931. [14b] D. J. Mabbott, P. M. Maitlis, *J. Organomet. Chem.* **1975**, *102*, C34−C36. [14c] D. J. Mabbott, P. M. Maitlis, *J. Chem. Soc. D* **1976**, 2156−2160. [14d] V. N. Zudin, V. D. Chinakov, V. M. Nekipelov, V. A. Likholobov, Yu. I. Yermakov, *J. Organomet. Chem.* **1985**, *289*, 425−430.
[15] [15a] M. Aresta, E. Quaranta, G. D'Andola, *Euro-Hydrides 2000*, September 6−9, **2000**, Université de Bourgogne, Dijon, France, Book of Abstracts, OC7. [15b] E. Quaranta, manuscript in preparation.
[16] R. E. Rülke, J. G. P. Delis, A. M. Groot, C. J. Elsevier, P. W. N. M. van Leeuwen, K. Vrieze, K. Goubitz, H. Schenk, *J. Organomet. Chem.* **1996**, *508*, 109−120.
[17] [17a] M. Aresta, E. Quaranta, I. Tommasi, *New J. Chem.* **1997**, *21*, 595−613. [17b] M. Aresta, E. Quaranta, I. Tommasi, *Gazz. Chim. Ital.* **1993**, *123*, 271−278.
[18] [18a] M. G. Barlow, M. J. Bryant, R. N. Haszeldine, A. G. Mackie, *J. Organomet. Chem.* **1970**, *21*, 215−226. [18b] G. Z. Oehme, H. Pracejus, *Tetrahedron Lett.* **1979**, 343−344. [18c] G. Z. Oehme, H. Pracejus, *J. Prakt. Chem.* **1980**, *322*, 798−808. [18d] G. Z. Oehme, H. Pracejus, *J. Organomet. Chem.* **1987**, *320*, C56−C58. [18e] W. A. Nugent, F. W. Hobbs, *J. Org. Chem.* **1983**, *48*, 5364−5366. [18f] W. A. Nugent, U. S. Patent 4,451,665, **1984**. [18g]W. A. Nugent, R. J. McKinney, *J. Mol. Catal.* **1985**, *29*, 65−76. [18h] W. A. Nugent, F. W. Hobbs, *Org. Synth.* **1987**, *66*, 52−59. [18i] P. Grenouillet, D. Neibecker, I. Tkatchenko, *Organometallics* **1984**, *3*, 1130−1132. [18j] P. Grenouillet, D. Neibecker, I. Tkatchenko, Fr. Patent Appl. 86.04644 (Rhône Poulenc, 26.03.**1986**). [18k] I. Guibert, D. Neibecker, I. Tkatchenko, *J. Chem. Soc., Chem. Commun.* **1989**, 1850−1852.
[19] D. C. Trumbo, R. A. Zander, *J. Polym. Sci. Polym. Chem.* **1991**, *29*, 1053−1059.
[20] [20a] G. Wilke, K. Sperling, L. Stehling, U. S. Patent 4 594 447, **1986**. [20b] G. Wilke, *Angew. Chem. Int. Ed. Engl.* **1988**, *27*, 185−206.
[21] [21a] J. D. McClure, *J. Org. Chem.* **1970**, *35*, 3045−3048. [21b] M. M. Baizer, J. D. Anderson, *J. Org. Chem.* **1965**, *30*, 1357−1360. [21c] G. L. Tembe, A. R. Bandyopadhyay, P. A. Ganeshpure, S. Satish, *Catal. Rev.-Sci. Eng.* **1996**, *38*, 299−327.
[22] K. Kawamoto, A. Tatani, T. Imanaka, S. Teranishi, *Bull. Chem. Soc. Jpn.* **1971**, *44*, 1239−1243.
[23] D. D. Perrin, W. L. F. Armarego, D. R. Perrin, Purification of Laboratory Chemicals, 3rd ed., Pergamon, Oxford, **1988**.
[24] [24a] Y. Takahashi, Ts. Ito, S. Sakai, Y. Ishii, *J. Chem. Soc., Chem. Commun.* **1970**, 1065−1066. [24b] M. F. Rettig, P. M. Maitlis, *Inorg. Synth.* **1977**, *17*, 134−137.
[25] [25a] J. G. Huddleston, H. D. Willauer, R. P. Swatloski, A. E. Visser, R. D. Rogers, *Chem. Commun.* **1998**, 1765−1766. [25b] P. J. Dyson, M. C. Grossel, N. Srinivasan, T. Vine, T. Welton, D. J. Williams, A. J. P. White, T. Zigras, *J. Chem. Soc., Dalton Trans.* **1997**, 3465−3469. [25c] J. S. Wilkes, J. A. Levisky, R. A. Wilson, C. L. Hussey, *Inorg. Chem.* **1982**, *21*, 1263−1264.

Received January 30, 2002
[I02054]

Cobalt(II) Complexes with Nitrogen Donors and Their Dioxygen Affinity in Dimethyl Sulfoxide

Clara Comuzzi,*[a] Andrea Melchior,[a] Pierluigi Polese,[a] Roberto Portanova,[a] and Marilena Tolazzi*[a]

Keywords: Cobalt / Amine ligands / Thermodynamics / Solvent effects / Oxygen

The formation of Co^{II} complexes with differently methylated N-donor ligands ethylenediamine (en), *N*,*N*′-dimethylethylenediamine (dmen), *N*,*N*,*N*′-trimethylethylenediamine (trmen), and *N*,*N*,*N*′,*N*′-tetramethylethylenediamine (tmen), has been studied at 298 K in both the aprotic solvent dimethyl sulfoxide (dmso) and in an ionic medium set to 0.1 mol dm^{-3} with Et_4NClO_4 under anaerobic conditions. UV/Vis spectrophotometric and calorimetric measurements were carried out to obtain the thermodynamic parameters for the systems investigated. Only mononuclear CoL_j^{2+} complexes were formed (j = 1–3 for en, j = 1, 2 for dmen; and j = 1 for trmen and tmen) where the diamines act as bidentate agents. All the complexes are enthalpy-stabilized whereas the entropy changes counteract the complex formation. The results are discussed in terms of different basicities and steric requirements both of the ligands and the complexes formed. Voltammetric measurements were carried out to correlate the electrochemical properties of the anaerobic complexes with their different dioxygen affinities. The X-ray structure of the starting adduct $[Co(dmso)_6][ClO_4]_2$, determined on a monocrystal, is also reported.

(© Wiley-VCH Verlag GmbH, 69451 Weinheim, Germany, 2002)

Introduction

A wide variety of cobalt(II) complexes are known to bind dioxygen more or less reversibly and are therefore frequently studied as model compounds for natural oxygen carriers and for their use in O_2 storage, as well as in organic syntheses due to their catalytic properties under mild conditions.[1−7] In this respect, Co^{II} complexes with N-donor ligands containing binding units suitable either for the coordination of a single metal ion or for assembling dimetallic centres have proven to be particularly useful, and have been extensively investigated especially in aqueous solutions.[8−14]

Minor attention has been devoted to the behaviour of such complexes in aprotic solvents[15−21] where their activity as oxidation catalysts can be of great interest. In a previous paper,[21] as result of an initial study focused on thermodynamics of complex formation of Co^{II} with linear, cyclic polyaza or mixed N−O ligands in aprotic solvents, the interactions of Co^{II} with the monoamine *n*-butylamine (n-but) and the triamines diethylenetriamine (dien), *N*,*N*′′-dimethyldiethylenetriamine (dmdien), and *N*,*N*,*N*′,*N*′′,*N*′′-pentamethyldiethylenetriamine (pmdien) were presented in dimethyl sulfoxide (dmso). In this work it was shown that the Co^{II} complex stabilities were greatly dependent on the degree of *N*-alkylation of the triamines, and that their dioxygen affinity varied concomitantly; thus, the tertiary pmdien was not able to take up O_2 whilst dmdien and dien were.

Strong σ-donor ligands are known to increase the dioxygen affinity.[6] In fact, in the oxygenation reaction, the dioxygen donates an electron into the appropriate Co d orbital while the metal centre is thought to donate an electron from the d_{z^2} orbital into the π* orbital of the electrophilic molecular dioxygen, thus forming a complex. This electron transfer should depend on the available electron density at the central metal atom. This density, however, is greatly affected by the electron donor properties of the ligands in the coordination sphere; as the ligand basicity increases, its electron donating ability also increases facilitating such a transfer.[1]

As an extension of the previous work and with the aim of systematically tuning the influence of the introduction of methyl groups on amino groups we have investigated the Co^{II} complex formation in dimethyl sulfoxide (dmso) with the following diamines: ethylenediamine (en), *N*,*N*′-dimethylethylenediamine (dmen), *N*,*N*,*N*′-trimethylethylenediamine (trmen), and *N*,*N*,*N*′,*N*′-tetramethylethylenediamine (tmen), which are gradually increasingly methylated, so varying the basicity of the amino group in the order $-NH_2 > -NHR > -NR_2$.[22] The study presented in this paper refers in detail to the determination of the thermodynamic parameter of Co^{II} complex formation under anaerobic con-

[a] Dipartimento di Scienze e Tecnologie Chimiche, Università di Udine,
Via Cotonificio 108, 33100 Udine, Italy
Fax: (internat.) + 39-0432/558803
E-mail: comuzzi1@dstc.uniud.it
tolazzi@dstc.uniud.it

ditions, as the knowledge of the properties of the starting complexes are fundamental to extending this investigation to aerobic conditions.

The values of the stability constants of the various systems investigated were determined by UV/Vis spectroscopic measurements using Cd^{II} as auxiliary metal ion,[23] for the reasons discussed in a previous paper.[21] The stability constants of this latter ion with the same ligands were previously determined by potentiometric measurements using the ion-selective cadmium electrode.[24] The enthalpy values were obtained by direct calorimetric titrations.

Also, preliminary remarks concerning dioxygen uptake are reported; in particular voltammetric measurements were carried out in order to obtain a correlation between the electrochemical properties of the anaerobic complexes with the diamines and the triamines previously investigated[21] and their dioxygen affinity in dmso.

All the spectrophotometric, calorimetric, and voltammetric measurements were performed at 298 K and in an ionic medium adjusted to 0.1 mol dm^{-3} with Et_4NClO_4 as the neutral salt, taking extreme care to obtain and maintain the lowest possible water and oxygen contents in the systems.

The X-ray structure of $[Co(dmso)_6][ClO_4]_2$, determined on a monocrystal, is also reported. This structural study is interesting in itself, taking into account the considerable interest of transition metal complexes with dmso for their role as possible intermediates in homogeneous catalysis, as antitumoural agents, or radiosensitizers in medicinal chemistry.[25] Finally, it is important because few X-ray structural evidences are to date available for cobalt−dmso complexes.[26−29]

Results and Discussion

The best fit of the spectrophotometric data was obtained when the species reported in Table 1 were taken into ac-

Table 1. Overall stability constants and thermodynamic functions for the reaction $Co^{2+} + j\ L \rightleftarrows CoL_j^{2+}$ in dmso at 298 K and $I = 0.1$ mol dm^{-3} and in water; the errors quoted correspond to three standard deviations.

	Complex	$\log\beta_j$	$-\Delta G°_{\beta j}$/kJmol^{-1}	$-\Delta H°_{\beta j}$/kJmol^{-1}	$-T\Delta S°_{\beta j}$/kJmol^{-1}
n-but[a]	CoL	1.91	10.8	23	12.2
	CoL_2	3.2	18.3	62	43.7
	CoL_3	4.1	23	88	65
en	CoL	6.41(0.09)	36.5(0.5)	53.5(1.2)	17
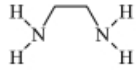	CoL_2	12.2(0.2)	70.1(0.6)	106.2(1.6)	36.1
	CoL_3	15.8(0.3)	90(1)	172.0(2.2)	82
dmen	CoL	5.70(0.05)	32.5(0.3)	48.3(1.1)	15.8
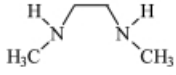	CoL_2	9.90(0.12)	56.5(0.9)	99.0(0.9)	42.5
trmen	CoL	4.28(0.22)	4.4(0.5)	45.7(0.5)	21.3
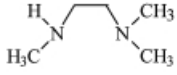					
tmen	CoL	3.07(0.04)	17.5(2)	36(1)	18.5
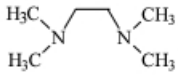					
en $_{water}$[b]	CoL	5.94	33.86	28.87	–4.99
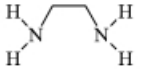	CoL_2	11.66	60.86	58.37	–2.49
	CoL_3	14.68	78.06	92.68	14.62

[a] Ref.[21] [b] Ref.[32]

count. In Table 1, the overall stability constants and the free energies of formation, with the limits of error indicated, are listed for the reactions $Co^{2+} + j\ L \rightleftarrows CoL_j^{2+}$ (where L is the amine concerned and $j = 1-3$). No polynuclear or mixed Co−L−Cd complexes were observed within the concentration range investigated.

As an example, in Figure 1(a) typical UV/Vis spectral changes observed during the reaction of Co^{2+} with dmen are reported in terms of absorbances vs. wavelengths. In Figure 1(b) the spectral modification due to dioxygen uptake is also inserted for the $[Co(dmen)_2]^{2+}$ system.

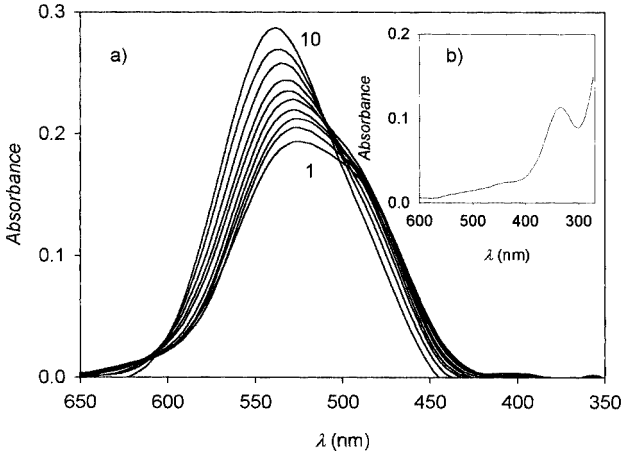

Figure 1. (a) Spectral changes observed during the reaction of Co^{2+} with dmen in dmso: $C^0_{Co} = 25.3$; $C^0_{Cd} = 27.7$ mmol dm^{-3} (spectrum 1); C^0_{dmen} varied from 0 (spectrum 1) to 65.6 (spectrum 10) mmol dm^{-3}; (b) UV/Vis spectrum of a solution of $[Co(dmen)_2]^{2+} = 0.4$ mmol dm^{-3} in air after 5 min

The experimental data obtained from the calorimetric measurements for all the systems investigated are reported in Figure 2 as Δh_t, the total heats of reaction per mol of metal ion, as a function of $R_C = C_L/C_M$, the ratio between the amount (mol) of ligand and the amount (mol) of cobalt(II) in the calorimetric vessel. The enthalpy curves are fully consistent with the information obtained from the analysis of spectrophotometric data. In fact, the curves representing the complexation of Co^{II}−trmen and −tmen indicate formation of complex(es) of relatively low stability(-ies), whereas the Co^{II}−en and −dmen data are consistent with the formation of 3 and 2 complexes, respectively, of relatively high stability.

The lack of evolved heat for $R_C > 2$ for the Co^{II}−dmen system clearly indicates that no more complexes are formed beyond the second one. The fit between experimental and calculated (full lines in Figure 2) curves is quite good.

In Figure 3 the FT-IR spectra of a series of solutions containing the same concentration (about 50 mmol dm^{-3}) of Co^{2+} and different ligand-to-metal ratios R_C, are reported for the Co^{II}−dmen system, chosen as significant example.

In Table 2, the data obtained from electrochemical measurements are summarized in terms of E_{pc}, the cathodic potential at maximum diffusion current, for the Co^{II}/Co^0 redox couple, and in terms of $E_{1/2}$ [$E_{1/2} = (E_{pc} + E_{pa})/2$] for

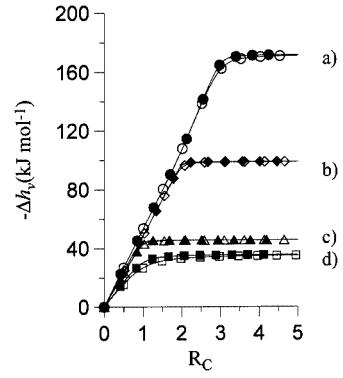

Figure 2. The total molar enthalpy changes, Δh_t, as a function of $R_C = C_L/C_M$ for Co^{II}−diamine systems in dmso: (a) en: (○) 5.05, (●) 19.91 mmol dm^{-3} in Co^{2+}; (b) dmen: (◇) 5.12, (◆) 19.96 mmol dm^{-3} in Co^{2+}; (c) trmen: (△) 5.09, (▲) 19.97 mmol dm^{-3} in Co^{2+}; (d) tmen: (□) 5.04, (■) 20.01 mmol dm^{-3} in Co^{2+}; only some of the experimental points, chosen at random, have been plotted; the solid lines were calculated from the values of β_j and $\Delta H°_{\beta j}$ in Table 1

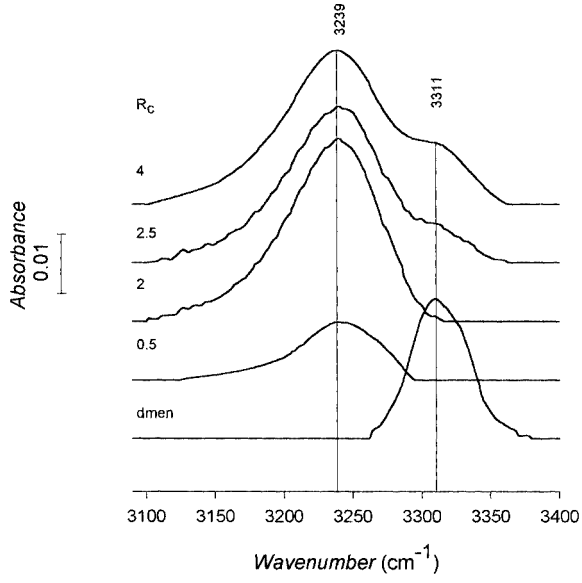

Figure 3. FT-IR spectra of solutions containing 50 mmol dm^{-3} of cobalt(II) and different dmen/metal ratios, R_C

the $Co^{II}L_j/Co^{III}L_j$ couple. The relative reactions [Equations (1) and (2)] are written in the direction in which the experiments were carried out.

$$Co^{II}L_j + 2e \rightarrow Co^0 + jL \quad (1)$$

$$Co^{II}L_j \rightarrow Co^{III}L_j + e \quad (2)$$

For comparison, the measurements have been extended to the triamines dien, dmdien, and pmdien, and the data obtained are also inserted in Table 2. The signals relative to Equation (2) consisted of a pair of irreversible oxidation/reduction waves, but were only detected for some of the systems investigated; no better results could be obtained by

Table 2. Redox potentials [V] of the cobalt(II) complexes vs. sat. Ag/AgCl electrode

	E_{pc} Reaction 1	$E_{1/2}$ Reaction 2
$Co(en)^{2+}$	−1.50	
$Co(en)_2^{2+}$	−1.56	
$Co(en)_3^{2+}$	−1.62	−0.44
$Co(dmen)^{2+}$	−1.46	
$Co(dmen)_2^{2+}$	−1.58	
$Co(trmen)^{2+}$	−1.42	
$Co(tmen)^{2+}$	−1.38	
$Co(dien)^{2+}$	−1.54	
$Co(dien)_2^{2+}$	−1.70	−0.34
$Co(dmdien)^{2+}$	−1.53	
$Co(dmdien)_2^{2+}$	−1.63	0.25
$Co(pmdien)^{2+}$	−1.44	

working with different electrodes, Au or glassy carbon. The cyclic voltammograms related to the Co^{II}/Co^0 couple show only the reduction peak corresponding to reaction (1).

Figure 4 shows an arbitrary view of the crystal unit of the cationic $[Co(dmso)_6]^{2+}$ unit along with the labelling scheme. Selected interatomic distances and angles are listed in Table 3. Crystal data and data collection summary are reported in Table 4.

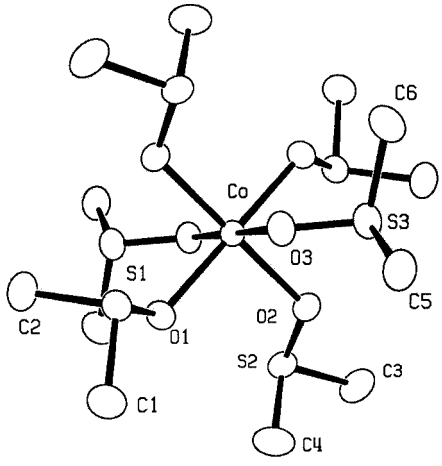

Figure 4. ORTEP view of the asymmetric unit of the $[Co(dmso)_6]^{2+}$; perchlorate anions and hydrogen atoms are omitted

Equilibrium Studies under Anaerobic Conditions

The complexes listed in Table 1 are all characterized by negative enthalpy and entropy values, which is typical of reactions involving complexation of metal ions by neutral ligands in aprotic solvents.[30,31] The desolvation of the species is here rather small and, given the relatively weak ligand−solvent interactions, the enthalpy change associated with the complex formation is therefore essentially a measure of the difference in bond energy toward the metal ion between the ligand and the coordinated molecules of the solvent. Thus, the enthalpy stabilization found here emphasizes the importance of the Co^{II}−nitrogen interaction in the aprotic solvent dmso.

The data for the analogous complexes formed by the Co^{II}−en system in aqueous solution have also been inserted in Table 1;[32] no data in water are available in the literature for the other diamine systems.[33] Lower stabilities are observed in water than in dmso; in a previous work,[21] as no information concerning the heat of transfer of Co^{2+} from water to any other solvent were available,[34] we reasonably supposed that this ion would be more strongly solvated by dmso than by water on the basis of some comparisons between Zn^{2+} and Co^{2+}, characterized by similar charge density.[35] The X-ray structural data reported here for the $[Co(dmso)_6]^{2+}$ species show that, in the solid state, interactions more akin to Co−dmso than to Zn−dmso are at play;

Table 3. Selected bond lengths [Å] and angles [°] for $[Co(dmso)_6][ClO_4]_2$

Bonds	[Å]	Angles	[°]
Co−O(1)	2.0934(15)	O(1)−Co−O(2)	92.31(6)
Co−O(2)	2.0887(15)	O(2)−Co−O(3)	90.11(6)
Co−O(3)	2.0833(17)	O(1)−Co−O(3)	90.72(6)
S(1)−O(1)	1.5203(16)	S(1)−O(1)−Co	117.26(8)
S(2)−O(2)	1.5352(17)	S(2)−O(2)−Co	118.95(9)
S(3)−O(3)	1.5304(16)	S(3)−O(3)−Co	117.42(9)
S(1)−C(1)	1.787(2)	O(1)−S(1)−C(1)]	104.15(11)
S(1)−C(2)	1.785(3)	O(1)−S(1)−C(2)	105.27(12)
S(2)−C(3)	1.780(3)	O(2)−S(2)−C(3)	102.83(12)
S(2)−C(4)	1.786(3)	O(2)−S(2)−C(4)	104.36(14)
S(3)−C(5)	1.784(2)	O(3)−S(3)−C(5)	104.01(10)
S(3)−C(6)	1.780(3)	O(3)−S(3)−C(6)	105.19(12)
		C(1)−S(1)−C(2)	99.03(14)
		C(3)−S(2)−C(4)	99.36(15)
		C(5)−S(3)−C(6)	98.89(14)

Table 4. Crystal data and data collection summary

Empirical formula	$C_{17.32}H_{48}Cl_2CoO_{16}S_{6.68}$
Formula mass [g mol^{-1}]	856.39
Crystal dimensions [mm]	0.45 × 0.3 × 0.3
T [K]	120.0
Crystal system	monoclinic
Space group	$P21/c$
a [Å]	8.606(4)
b [Å]	15.147(4)
c [Å]	15.230(3)
β [°]	76.05(2)
V [Å^3]	1985.3(12)
Z	2
$D_{calcd.}$ [g cm^{-3}]	1.433
μ [mm^{-1}]	0.974
Limiting indices	$h = -12/12$, $k = -21/21$, $l = -21/21$.
R_{int}	0.0366
R	0.0496
$wR2$	0.1363
GOF	1.032
Parameters	232
Reflections/unique reflections/$I > 2\sigma(I)$	10771/5933/5160
ρ_{max}, ρ_{min}	0.848, −0.848

this seems to confirm our previous hypothesis. Therefore, the trend in the complexes stabilities in water and dmso, at variance with what might be expected on the basis of Co^{II} solvation in the two solvents, is to be attributed to a greater solvation of amines in water than in dmso[30] through hydrogen bonding.

The electronic spectra of CoL_j complexes are similar to those observed for the octahedral $[Co(H_2O)_6]^{2+}$ complex[35] and to those previously reported for octahedral $[Co(dmso)_6]^{2+}$ and Co^{II}−triamine systems[21] in dmso [see (a) in Figure 1] and clearly indicate that also for Co^{II}−diamine systems the octahedral structure is retained after the coordination of the ligands. Thermodynamic data confirm that no change of coordination occurs at any step of complexation. If the change occurred, in fact, abnormally less unfavourable entropy and less favourable enthalpy values would be expected.[30]

A comparison between the stability constant associated with the first complexation step for the Co^{II}−en and −n-but systems (Table 1) shows that it is much higher for the former ligand, indicating that the en ligand behaves as bidentate; the very exothermic value of the $\Delta H^\circ_{\beta 1}$ and the unfavourable entropy terms are in line with this hypothesis, which is further confirmed by FT-IR spectra run on solutions containing Co^{II}−en in a molar ratio 1:0.5 where no bands typical of free $-NH_2$ groups[36,37] were detected.

Similar considerations can be applied for the successive complexation steps; coming to the conclusion that hexacoordination is saturated by nitrogen groups when the $[Co(en)_3]^{2+}$ species is formed. It is interesting to note that the third stepwise complexation step is slightly more exothermic than the preceding ones and that the stepwise entropy term is more unfavourable: the coordination of the third en ligand evidently has no great effects on the desolvation of the central metal ion. The data for the other diamines investigated also indicate that bidentation is achieved for all the systems investigated.

The log β_1 values decrease smoothly for Co^{II}−dmen system with respect to the primary en, whereas this decrease is much more evident when one (trmen) or two (tmen) tertiary groups are present. The trend in thermodynamic stabilities primarily reflects the different basicities of the N atoms, which decrease in the order $-NH_2 > -NHR > -NR_2$,[22] whereas, when tertiary amino groups are involved, the greater steric crowding also contributes to a marked elongation of the M−N bonds.[38] In addition, *N*-methylation inhibits the formation of hydrogen bonds of the type M−N−H−O, decreasing the outer-sphere solvation energy of the complexes.[38] It is to note that *N*-alkylation strongly influences not only the stabilities but also the stoichiometry of the species formed; in fact, despite the borderline acid character, cobalt(II) is expected to become harder in dmso,[30] enhancing its affinity for the hard N atom, no more complexes beyond ML_2 or even ML could be detected when dmen or trmen and tmen, respectively, were concerned. In addition to the steric requirements of the more bulky ligands, certainly a role is also played by the small ionic radius of Co^{II} [35] as for example dmen and trmen ligands were found to be able to form three and two complexes, respectively, when octahedral Cd^{II} complexes were considered in dmso. Likely, large metal ions such as Cd^{II} can better minimize steric hindrances and repulsions when more than two bulky $-N(CH_3)_2$ moieties are involved in the complex formation. This is confirmed by the observation that the drop in complex stability by methylation is indeed more evident for Co^{II}− than for Cd^{II}−diamino complexes[24] ($\Delta\log K_{1[Co\text{-}(en)]\rightarrow[Co(trmen)]} = 2.13$; $\Delta\log K_{1[Co(en)]\rightarrow[Co(tmen)]} = 3.34$; $\Delta\log K_{1[Cd(en)]\rightarrow[Cd(trmen)]} = 1.76$; $\Delta\log K_{1[Cd(en)]\rightarrow[Cd(tmen)]} = 2.78$). Also, the increasing soft nature of the nitrogen donors should be responsible of this behaviour in this latter case.[38] The same trend was found for Co^{II} and Cd^{II} complexes with 1,4,8,11-tetraazacyclotetradecane (cyclam) and tetramethylcyclam.[39]

Independent FT-IR measurements were carried out in order to ascertain both the maximum stoichiometry and the coordination mode of the dmen ligand. Figure 3 shows the spectra of a series of solutions containing Co^{II} and different dmen-to-metal ratios, R_C It can be observed that up to $R_C = 2$, only the band due to the bonded secondary amine (at 3239 cm^{-1}) is present, whereas the band due to the free amino groups (at 3311 cm^{-1}) is also present when $R_C > 2$. This confirms both the bidentation in the ML_2 complex and the absence of higher species beyond the ML_2 one, as evidenced also by calorimetry studies.

As mentioned in the introduction, particular interest was devoted to the tuning of the behaviour of different methylated diamines in Co^{II} complexation under anaerobic conditions, in order to clarify their successive role in the affinities for molecular dioxygen. As a matter of fact, it was found[21] that in the case of the Co^{II} complexes with the triamines dien, dmdien, and pmdien, the affinity for dioxygen varied with the number of methyl groups present in the ligands; pmdien was in fact not able to promote dioxygen binding, dmdien promoted a certain amount of binding and release, and dien caused an irreversible dioxygen uptake.[21,40]

A similar behaviour is shown by en, dmen, and tmen; CoL_j complexes with en and dmen ($j \geq 2$) were able to take up dioxygen (see also Electrochemical and UV/Vis Data), with a certain degree of reversibility ascertained for the secondary dmen system, whereas $[Co(tmen)]^{2+}$ was not able to do the same. Unfortunately, the trmen ligand, chosen for its σ-donor properties (intermediate between that of dmen and tmen), was unexpectedly unable to form higher complexes beyond the first one, thus not reaching a minimum of three nitrogen donors per cobalt ion which appears to be necessary to form an oxygenated species as supposed in a previous work[41] and suggested by a comprehensive view of the results reported here and previously.[21] Therefore, we systematically searched for a correlation between the electron density of the metal ion in the complexes and the dioxygen uptake, by means of cyclic voltammetry.

Electrochemical and UV/Vis Data

The signals relative to the $Co^{II}L_j/Co^{III}L_j$ couples were visible only for the $[Co(en)_3]^{2+}/[Co(en)_3]^{3+}$ and $[Co(L)_2]^{2+}/[Co(L)_2]^{3+}$ (L = dien or dmdien) systems (Table 2). Con-

sidering the basicity order of the amino groups,[22] one should expect that the electron density on the cobalt ion decreases in the order $Co(en)_3 > Co(dien)_2 > Co(dmdien)_2$, which is reflected (see Table 2) in the concomitant increase in the $E_{1/2}$ values of the corresponding CoL_j^{2+}/CoL_j^{3+} couples.[38,42,43] This finding agrees with previous reports that *N*-alkylation of amine ligands shifts the redox potentials of the couples $M^{n+1/n}L_m$ anodically relative to those of the corresponding non-alkylated systems.[38] The voltammograms for the other di- and triamine systems should be, according to this trend in electron density, shifted anodically,[38] likely in the potential range where the solvent signals overcome those of the investigated couples.

The values of E_{pc} for reaction (2) are, on the other hand, easily evaluated for all the systems investigated; taking into account that the reaction for the uptake of dioxygen by a given Co^{II} complex is a charge-transfer process, a correlation between E_{pc} values for reaction (1) and Co^{II} charge density, and therefore the $Co^{II}L_j$ dioxygen affinity, should be observed. The higher the charge density is, the more difficult the reduction process to Co^0 should be and the more negative the expected E_{pc} values should be. The E_{pc} values for reaction (1) are in fact shifted anodically as secondary or, even more, tertiary diamines and triamines are considered.

These data are combined with UV/Vis results, obtained both for the Co^{II}−diamine systems studied in this paper and for previously investigated Co^{II}−triamine systems, dien, dmdien, and pmdien,[21] which show that: (i) no changes are observed in the spectra of deaerated and aerated solutions of all the 1:1 Co^{II}−diamine and Co^{II}−triamine (exept dien) species in the range 650−300 nm; (ii) all the aerated spectra of the other complexes show the origin of a charge-transfer band in the range 380−300 nm as shown in Figure 1(b) for the $[Co(dmen)_2]^{2+}$ system. The species mentioned in (i) are clearly not able to bind dioxygen whereas the others are. Therefore, the data reported in Table 2 for reaction (1) suggest an interesting correlation between the E_{pc} values of the Co^{II} complexes related to Equation (1) and their dioxygen affinity; one can in fact foresee that when $E_{pc} \geq -1.54$ V for the $Co^{II}L_j/Co^0$ couple the uptake of dioxygen is not possible in dmso.

Structural Data

Few crystal structures of cobalt(II)−dmso solvates are available in the literature,[26−29] due to the difficulty of obtaining single crystals suitable for X-ray investigation. Despite numerous attempts to improve their quality, also the crystals here investigated show a relative degree of disorder that does not in any case invalidate the overall features of the structure.

Co^{II} is a hard acceptor in dmso preferring hard donor atoms like oxygen, the bonds being mainly of electrostatic character.[30] In the solid-state structure reported in Figure 4, six solvent molecules are coordinated to the metal centre through the oxygen atom in a distorted octahedral geometry. The mean Co−O distance of 2.088(5) Å (Table 3) is consistent with the value found for an octahedral Co^{II}−oxygen coordination[25] and a little shorter than the analogous distance found for the Zn^{II} ion (Zn−O 2.11 Å) in $[Zn(dmso)_6][ClO_4]_2$,[44] shown for comparison for the similar charge density values of these ions. This datum indicates that slightly stronger interactions exist in the solid state between Co and dmso than between Zn and dmso.

Sulfur−oxygen average bond lengths [1.5286(16) Å], are in agreement with those present in the literature[25] for metal−sulfoxide complexes and greater than the S−O bond length in free dmso [1.495(4) Å]. The O−S−C angles [104.08(20)°] are also average for corresponding angles found in the literature for 400 related metal−sulfoxide complexes and less than that in free dmso [105.7(2) °], whereas the C−S−C bond angles (Table 3) are almost similar to the corresponding values in free dmso (98.6°).[25] The perchlorate anions are not coordinated to the central Co^{II} ion and therefore they are not reported in Figure 4. This feature is also maintained in dmso solution as $Co(ClO_4)_2$ has been found to be completely dissociated in dmso.[21]

Concluding Remarks

Important information have been obtained on how different donor properties of the ligands influence the stability and stoichiometry of the Co^{II} complexes; in fact the addition of only one $-CH_3$ group to dmen is shown to cause a drastic change in the number of complexes formed and strongly influence their dioxygen affinity. This result should be taken into account to suitably modify N-donors in order to obtain Co^{II} complexes able to promote a more or less reversible dioxygen binding.

The electrochemical properties, correlated with the number of methyl substituents, point to an interesting result, i.e. that an E_{pc} value of −1.54 V, related to reaction (1), should be at least overcome by the Co^{II}−amino complexes to be able to bind dioxygen. Finally, the structural data of the $[Co(dmso)_6][ClO_4]_2$ adduct are fully consistent with a distorted octahedral geometry of the hexasolvate and provide additional data on cobalt(II)−dmso complexes.

Experimental Section

Warning: Although metal perchlorates solvated by dmso are generally explosive under certain conditions,[45] no problems were encountered when handling $M(ClO_4)_2 \cdot 6dmso$ (M = Co or Cd). Anyway, as a precaution, only small quantities of the salts should be prepared each time. Great caution was exercised when handling dmso solutions of poisonous cadmium salts, since they are easily carried through the skin by dmso, which penetrates lipid tissues at an astonishing rate.

Chemicals: $Co(ClO_4)_2 \cdot 6dmso$ and $Cd(ClO_4)_2 \cdot 6dmso$ were prepared and standardised as before.[21,24] Dimethyl sulfoxide (Fluka; > 99%) was purified by distillation according to the described procedures,[46] degassed by a pumping-freezing procedure and stored over 4-Å molecular sieves. The ligands en, dmen, trmen, and tmen (Aldrich; > 97%) were purified by fractional distillation.[47] Perchlorate

stock solutions of Cd^{II} and Co^{II} ions were prepared by dissolving weighed amounts of the adducts in anhydrous degassed dmso, and their concentrations were checked by titration with EDTA.[48]

The background salt Et_4NClO_4 was recrystallised twice from methanol and dried at 110 °C. Solutions of the ligands were prepared as described.[24] All standard solutions were prepared and stored in an MB Braun 150 glove box under a controlled atmosphere containing less than 1 ppm of water and less than 1 ppm of oxygen. The water content in the solutions, typically 10−20 ppm, was determined by a Metrohm 684 KF Coulometer.

Spectrophotometric Measurements: UV/Vis spectra were recorded with a Varian Cary 50 Spectrophotometer directly inside the glove box using optic fibre probes and a quartz cuvette with a pathlength of 1 cm (117.100 Bracco cell). The data were recorded over the wavelength range 300−650 nm. Different types of titrations were carried out in order to obtain the best competition between Cd^{II} and Co^{II} for the same ligand and/or to evidence possible formation of mixed or polynuclear species. The absorption maximum for $Co(ClO_4)_2$ in dmso occurs at 535 nm with an extinction molar coefficients $\varepsilon = 11.9$ mol^{-1} dm^3 cm^{-1}. The absorption maximum of CoL_j complexes are shifted to lower wavelengths, in line with an increase in the ligand field strength, with the maximum ε values being of the same order of magnitude as that of the starting salt; therefore the dmso solutions always contained at least 20.00 mmol dm^{-3} of the $Co(ClO_4)_2$ starting salt in order to obtain reliable values for absorbance data.[23] The fact that equilibrium was attained was supported by the observation that addition of a titrant solution produced an immediate spectral change with no further change noted after several hours. The absorbance data at about 20 different wavelengths in the range 450−550 nm were analysed and the formation constants of the CoL_j complexes ($j = 1-3$) were determined, together with the molar extinction coefficients of the complexes at each relevant wavelength, using the Hyperquad program.[49]

Calorimetric Measurements: A Tronac model 87-558 precision calorimeter was employed to measure the heats of reaction. The cover of the titration vessel and its connection to the calorimeter were modified in order to make a gas-proof closure. To be sure of operating in absence of O_2, both the vessel and the burette were filled inside the glove box, joined together, taken out of the glove box and connected to the calorimeter for the measurements. The calorimeter was checked by titration of tris(hydroxymethyl)aminomethane (tham) with a standard solution of HCl in water. The experimental value of the heat of neutralization of tham was found to be $\Delta H° = -47.48$ kJ mol^{-1}, in good agreement with the accepted value of -47.53 ± 0.13 kJ mol^{-1}.[33] The procedure for the calorimetric titration was described before.[46] The heats of dilution of the reactants, determined in separate runs, were found to be negligible. The least-squares computer program Letagrop Kalle[50] was used for the calculation of the enthalpy changes.

FT-IR Spectroscopy: The FT-IR spectra were obtained using a Bio-Rad FTS 40 spectrometer (maximum resolution 4 cm^{-1}; 16 scans). A cell with barium fluoride windows (thickness of 25μm) was used. The cells were filled and closed in a glove box and quickly transferred to the spectrometer. The C^0_{Co} in the dmso solutions was about 50 mmol dm^{-3}.

Cyclic Voltammetry: The cyclic voltammograms of CoL_j complexes were carried out using an EG&G Princeton Applied Research Model 263A potentiostat controlled by a Win/PC based program. A saturated Ag/AgCl electrode was employed as reference and a Pt electrode was used as working electrode, being a Pt wire present as auxiliary electrode. The measurements were carried out with a scan rate of 100 mV/s.

X-ray Crystallography: Small violet crystals of the $[Co(dmso)_6][ClO_4]_2$ adduct were obtained from an anhydrous dmso solution of $Co(ClO_4)_2$ by the solvent-diffusion method with acetone. Data collection was carried out on a crystal of dimensions 0.45 × 0.30 × 0.30 mm by using a Nonius DIP-1030H system with Mo-K_α radiation, at 120 K by a nitrogen stream cryo-cooler. A total of 30 frames were collected, each with an exposure time of 10 min, over half of the reciprocal space with a rotation of 6° about , the detector being at a distance of 80 mm from the crystal. Data reduction and cell refinement was carried out by using the program Mosflm.[51] The structure was solved by Patterson and Fourier analyses[52] and refined by the full-matrix least-squares method based on F^2 with all observed reflections.[53] Of three crystallographic independent dmso ligands, two were found to be disordered, and the S−C moiety refined over two positions (occupancies of 88 and 12%, respectively, with hydrogen atoms omitted for the methyl group at lower occupancy). A solvent molecule of dmso and of acetone, sharing the methyl groups and the oxygen atom, were disordered on the same site. Occupancy factor of the S atom (dmso) and of the central C atom (acetone) refined to 0.68 and 0.32, respectively. All the calculations were performed using the WinGX System, Ver 1.64.[54] Additional material is available from the Cambridge Crystallographic Data Center as supplementary material comprising H-atom coordinates, thermal parameters, and remaining bond lengths and angles. CCDC-178439 contains the supplementary crystallographic data for this paper. These data can be obtained free of charge at www.ccdc.cam.ac.uk/conts/retrieving.html or from the Cambridge Crystallographic Data Centre, 12, Union Road, Cambridge CB2 1EZ, UK [Fax: (internat.) + 44-1223/336-033; E-mail: deposit@ccdc.cam.ac.uk].

Acknowledgments

This work has been supported by the Ministero dell'Università e della Ricerca Scientifica e Tecnologica (MURST, Rome) within the program COFIN 2000. We thank Prof. Ennio Zangrando for fruitful discussion on the X-ray structure.

[1] A. F. Martell, D. T. Sawyer, *Oxygen Complexes and Oxygen Activation by Transition Metals*, Plenum, New York, **1988**; G. McLendon, A. E. Martell, *J. Chem. Soc., Chem. Commun.* **1975**, 223−225.
[2] H. Sugimoto, T. Nagayama, S. Maruyama, S. Fujinami, Y. Yasuda, M. Suzuki, A. Uehara, *Bull. Chem. Soc. Jpn.* **1998**, *71*, 2267−2279.
[3] G. McLendon, A. E. Martell, *Coord. Chem. Rev.* **1976**, *19*, 1−39.
[4] R. D. Jones, D. A. Summerville, F. Basolo, *Chem. Rev.* **1979**, *79*, 139−179.
[5] T. D. Smith, J. T. Pilbrow, *Coord. Chem. Rev.* **1981**, *39*, 295−383.
[6] E. C. Niederhoffer, J. H. Timmons, A. Martell, *Chem. Rev.* **1984**, *84*, 137−203.
[7] L. I. Simandi, in *Dioxygen Activation and Homogeneous Catalytic Oxidation*, Elsevier, Amsterdam, **1991**.
[8] S. Cabani, N. Ceccanti, M. R. Tinè, *Pure Appl. Chem.* **1991**, *63*, 1455−1464.
[9] A. Bencini, A. Bianchi, C. Giorgi, P. Paoletti, B. Voltancoli, N. Ceccanti, R. Pardini, *Polyhedron* **2000**, *19*, 2441−2445.
[10] N. Ceccanti, R. Pardini, F. Secco, M. R. Tinè, M. Venturini, A. Bianchi, P. Paoletti, *Polyhedron* **2000**, *19*, 2447−2455.
[11] Z.-L. Lu, M. S. A. Hamza, R. van Eldik, *Eur. J. Inorg. Chem.* **2001**, 503−510.

[12] N. Ceccanti, M. Formica, V. Fusi, L. Giorgi, M. Micheloni, R. Pardini, R. Pondetteri, M. R. Tinè, *Inorg. Chim. Acta* **2001**, *321*, 153−161.
[13] D. H. Busch, N. W. Alcock, *Chem. Rev.* **1994**, *94*, 585−623.
[14] S. Cabani, *React. Funct. Polym.* **1996**, *28*, 167−182.
[15] D. P. Rillema, C. M. Wicker, R. D. Morgan, *J. Phys. Chem.* **1983**, *87*, 5151−5158.
[16] G. Costa, C. Tavagnacco, *Gazz. Chim. Ital.* **1995**, *125*, 243−261.
[17] D. K. Chand, P. K. Bharadway, *Inorg. Chem.* **1997**, *36*, 5658−5660.
[18] W. B. Tolman, *Acc. Chem. Res.* **1997**, *30*, 227−237.
[19] S. Schindler, C. D. Hubbard, R. van Eldik, *Chem. Soc. Rev.* **1998**, *27*, 387−393 and refs. therein.
[20] K. J. Franz, S. J. Lippard, *J. Am. Chem. Soc.* **1999**, *121*, 10504−10512.
[21] C. Comuzzi, M. Grespan, P. Polese, R. Portanova, M. Tolazzi, *Inorg. Chim. Acta* **2001**, *321*, 49−55.
[22] [22a] A. Mucci, R. Domain, R. L. Benoit, *Can. J. Chem.* **1980**, *58*, 953−958. [22b] R. L. Benoit, M. J. Mackinnon, L. Bergeron, *Can. J. Chem.* **1981**, *59*, 1501−1504.
[23] F. J. C. Rossotti, H. Rossotti, in *The determination of Stability Constants*, McGraw-Hill, New York, **1961**.
[24] C. Comuzzi, M. Grespan, A. Melchior, R. Portanova, M. Tolazzi, *Eur. J. Inorg. Chem.* **2001**, *12*, 3087−3094.
[25] M. Calligaris, O. Arugo, *Coord. Chem. Rev.* **1996**, *153*, 83−154.
[26] A. Ciccarese, D. A. Clemente, A. Marzotto, G. Valle, *J. Cryst. Spectrosc. Res.* **1993**, *23*, 223−228.
[27] V. Vtkachev, E. A. Lavrent'eva, O. S. Rosschupkina, I. P. Lavrent'ev, L. O. Atovmyan, *Koord. Khim.* **1994**, *20*, 636−638.
[28] D. A. House, P. J. Steel, *Inorg. Chim. Acta* **1998**, *269*, 229−234.
[29] L. Öhrström, G. Svensson, *Inorg. Chim. Acta* **2000**, *305*, 157−162.
[30] S. Ahrland, in *The Chemistry of Non-aqueous Solvents* (Ed.: J. J. Lagowsky), Academic Press, New York, **1978**, vol. 5a.
[31] A. Cassol, P. Di Bernardo, R. Portanova, M. Tolazzi, P. L. Zanonato, *Inorg. Chim. Acta* **1997**, 1−8 and refs. therein
[32] S. Cabani, N. Ceccanti, G. Conti, *J. Chem. Soc., Dalton Trans.* **1983**, 1247−1251.
[33] [33a] A. E. Martell, R. M. Smith, R. J. Motekaitis, *Critically Selected Stability Constants of Metal Complexes Database*, **1998**, version 5.0. [33b] L. D. Pettit, H. K. Powell, *IUPAC Stability Constants Database*, Academic Software, U. K., **2000**, vers. 5.10.
[34] C. Halidas, G. Heffer, Y. Marcus, *Chem. Rev.* **2000**, *100*, 819−852.
[35] F. A. Cotton, G. Wilkinson, *Advanced Inorganic Chemistry*, 4th ed., Wiley, New York, **1980**.
[36] R. M. Silverstein, G. C. Bassler, T. C. Morrill, in *Spectrometric Identification of Organic Compounds*, 3rd ed., Wiley, New York, **1974**.
[37] A. Cassol, P. Di Bernardo, R. Portanova, M. Tolazzi, G. Tomat, P. L. Zanonato, *J. Chem. Soc., Dalton Trans.* **1992**, 469−474.
[38] D. Meyerstein, *Coord. Chem. Rev.* **1999**, *185−186*, 141−147.
[39] A. E. Martell, R. D. Hancock, R. J. Motekaitis, *Coord. Chem. Rev.* **1994**, *133*, 39−65.
[40] Our group; work in progress.
[41] M. S. Michailidis, R. B. Martine, *J. Am. Chem. Soc.* **1969**, *91*, 4683−4689.
[42] M. J. Carter, D. P. Rillema, F. Basolo, *J. Am. Chem. Soc.* **1974**, *23*, 392−400.
[43] K. Araki, T. Kuboki, M. Otohata, N. Kishimoto, M. Yamada, S. Shiraishi, *J. Chem. Soc., Dalton Trans.* **1993**, 3647−3651.
[44] I. Persson, *Acta Chem. Scand., Ser. A* **1982**, *36*, 7−13.
[45] D. Martin, H. G. Hauthal, *Dimethyl Sulfoxide*, van Nostrand Reinhold, Wokingham, Berkshire, **1975**, pp.448−449.
[46] A. Cassol, P. Di Bernardo, P. L. Zanonato, R. Portanova, M. Tolazzi, *J. Chem. Soc., Dalton Trans.* **1987**, 657− 659.
[47] D. D. Perrin, W. L. F. Armarego, D. R. Perrin, in *Purification of Laboratory Chemicals*, 2nd ed., Pergamon, Oxford, **1980**.
[48] A. I. Vogel, in *Textbook of Quantitative Chemical Analysis*, 5th ed., Longman Group UK, **1989**.
[49] P. Gans, A. Sabatini, A. Vacca, *Talanta* **1996**, *43*, 1739−1753.
[50] R. Arnek, *Ark. Kemi* **1970**, *32*, 81−88.
[51] A. G. W. Leslie, *Joint CCP4 + ESF EACMB Newsletter on Protein Crystallography* **1992**, p. 26.
[52] *SHELXS-86, Program for structure solution:* G. M. Sheldrick, *Acta Crystallogr., Sect. A* **1990**, *46*, 467−473.
[53] G. M. Sheldrick, SHELXL-97, *Program for crystal structure refinement*, University of Göttingen, Germany, **1997**.
[54] L. J. Farrugia, *WinGX − A Windows Program for Crystal Structure Analysis*, University of Glasgow, Glasgow, **1998**.

Received February 1, 2002
[I02055]

Homochiral Self Recognition in Gold-Phosphane-Helicates

Walter Schuh,[a] Holger Kopacka,[a] Klaus Wurst,[a] and Paul Peringer*[a]

Keywords: Self-assembly / Helical structures / Gold / X-ray diffraction / Aurophilicity

Treatment of $Au(SMe_2)Cl$ with a mixture of (R^*,S*)- and (R^*,R*)-(±)-p4 (p4 = 1,1,4,7,10,10-hexaphenyl-1,4,7,10-tetraphosphadecane) and TlOTf produces $[Au_4(R,S\text{-p4})_2](OTf)_4$ (**1**) and a racemic compound of $[Au_4(R,R\text{-p4})_2](OTf)_4$ and $[Au_4(S,S\text{-p4})_2](OTf)_4$ (**2**). Compounds **1** and **2** were isolated as colorless crystals and characterized by single crystal X-ray diffraction. In both **1** and **2**, four gold atoms are bridged by two p4 ligands. The structure of **1** is a *meso*-helicate composed of a P, an M and a central achiral domain. The ligands exhibit a head-to-head arrangement. The structures of **2** consist of a non-palindromic double helix. In both **1** and **2** the *R* centers induce a left-handed (M) and the *S* centers a right-handed (P) helicity. The helical elements of both **1** and **2** are unsaturated and show Au···Au interactions.
(© Wiley-VCH Verlag GmbH, 69451 Weinheim, Germany, 2002)

Introduction

Most of the activity in the area of helical complexes has been concentrated on achiral ligands.[1,2] More recently, however, chiral ligands have been used and interest has become focused towards stereoselective helical induction by enantiopure ligands.[3] One report deals with the stereospecific assembly of a racemic compound of homochiral dinuclear helicates from a racemic tetradentate nitrogen donor ligand.[4]

The object of this paper is the investigation of chiral self-recognition during the assembly of double stranded helicates in the presence of all stereoisomers of a ligand containing two chiral centers. The linear tetraphosphane ligand p4 (1,1,4,7,10,10-hexaphenyl-1,4,7,10-tetraphosphadecane, $Ph_2P-CH_2-CH_2-PPh-CH_2-CH_2-PPh-CH_2-CH_2-PPh_2$) exists as ($R$*,S*) and ($R$*,R*)-(±) stereoisomers. In this ligand, the chiral phosphorus centers act as donor atoms, whilst most other chiral ligands used in helicate architecture contain achiral donor atoms and some non-coordinating chiral centers attached to the ligand. We report here on the reaction of $Au(SMe_2)Cl$ with p4 in a stoichiometry that provides two phosphorus donor atoms per gold center. A complex with the ratio Au:P = 2:8, $[Au_2\{(R,R)\text{-p4}\}_2](PF_6)_2$ has been synthesized previously using enantiopure p4.[5] The structure consists of a *parallel helix*,[6] in which the two ligands form two helices whose helical axes are not defined by the metal ions but run parallel to the Au−Au vector. The Au centers are coordinated by four phosphorus atoms. As far as we know this, and the related silver complex,[5] are the sole published complexes containing more than one p4 ligand. A complex of the composition [$(AuCl)_4$(p4)], whose stereochemistry was not specified, has been patented as an antitumor agent.[7]

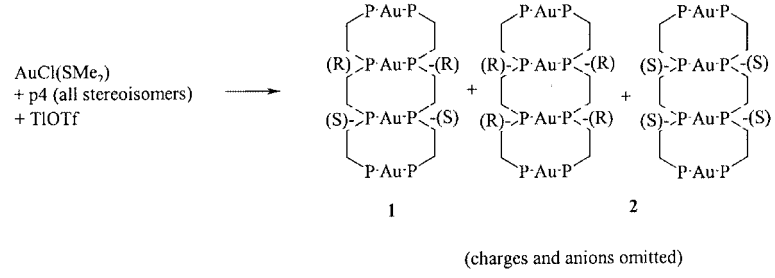

Scheme 1

Results and Discussion

The reaction of $Au(SMe_2)Cl$ with a mixture of all stereoisomers of p4 and TlOTf in the molar ratio of 4:2:4 in MeOH produces two compounds of the composition [Au_4-

[a] Institut für Allgemeine, Anorganische und Theoretische Chemie, Universität Innsbruck,
Innrain 52a, 6020 Innsbruck, Austria

$(p4)_2](OTf)_4$ which were separated by fractional crystallization from MeOH and isolated as colorless crystals. The less soluble isomer contains exclusively (*R*,*S*)-p4 ligands (**1**) and the other contains p4 with the configurations (*R*,*R*)- or (*S*,*S*)-(**2**) (Scheme 1).

Crystals of **1**·2MeOH or **1**·2EtOH were grown by slow evaporation of solutions of **1** in MeOH or EtOH. The EtOH solvate shows a more compact packing, whilst the structures of the cations are almost identical for both solvates. The cation of **1**·2EtOH (shown in Figure 1, selected distances and angles are presented in Table 1 and the data for **1**·2MeOH are provided as supporting information) contains four gold atoms bridged by two p4 ligands. The assembly is stereoselective in view of the coordination of two (*R*,*S*)-p4 ligands and the head-to-head arrangement of the ligands, i.e. one gold center is coordinated by two *R* phosphorus atoms and another by two *S* phosphorus atoms. The stereoselective coordination of four gold atoms is reflected by a center of symmetry in the cation $[Au_4(\mu^4\text{-}R,S\text{-p4})_2]^{4+}$ in the crystal lattice.

The structure of the cation of **1**·2EtOH shown in Figure 1 is a *meso*-helicate: The two terminal $(Au-P-CC-P)_2$ rings form double helices whose axes pass through the gold atoms. In keeping with the center of symmetry, these domains exhibit opposite helicities: The *R* centers induce an M handedness and the S centers a P sense. The central $(Au-P-CC-P)_2$ element is achiral and adopts a centrosymmetric chair-like geometry. The Au−Au distance of the helical domains [2.9802(4) Å] indicates a 1,6-transannular Au−Au d^{10}-d^{10} interaction in the 10-membered $(Au-P-CC-P)_2$ rings while there is no contact between the inner gold atoms 2 and 2A [4.1062(5) Å]. The axes of the two helical domains are not co-linear.

Crystals of **2**·2MeOH were grown by slow evaporation of a solution of **2** in MeOH. There are two crystallographically

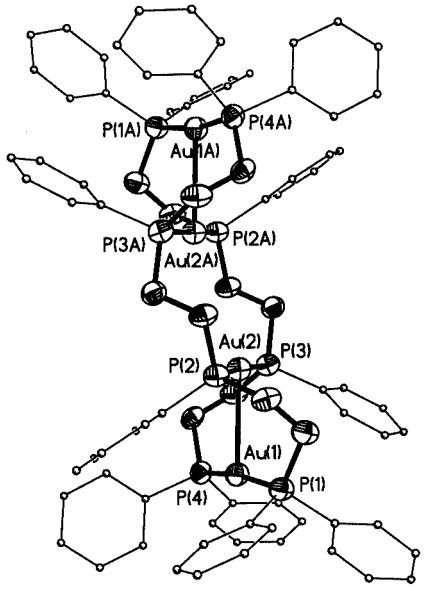

Figure 1. Structure of the cation of **1**

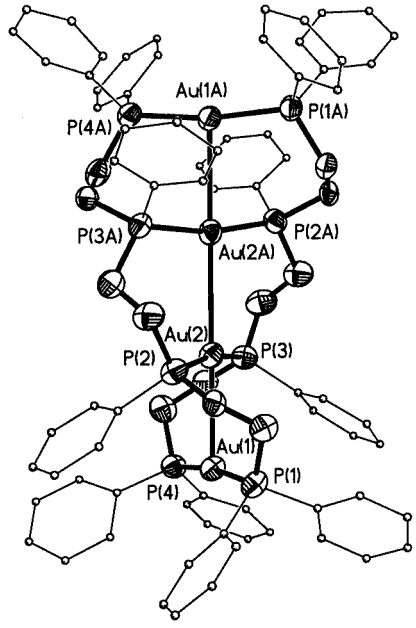

Figure 2. Structure of the M-$[Au_4(\mu\text{-}(R,R)\text{-p4})_2](OTf)_4$ isomer of the first of two crystallographically independent helicates of **2**

Table 1. Selected distances (Å) and angles (°) of **1** and the two crystallographically independent complexes of **2**

1		**2**		**2**	
Au1−Au2	2.9802(4)	Au1−Au2	3.0898(9)	Au11−Au22	3.0955(14)
Au2−Au2A	4.1062(5)	Au2−Au2A	3.3292(13)	Au22−Au33	3.3404(14)
Au1−P1	2.324(2)	Au1−P1	2.317(5)	Au33−Au44	3.071(2)
Au1−P4	2.319(2)	Au1−P4	2.317(5)	Au11−P11	2.313(4)
Au2−P2	2.310(2)	Au2−P2	2.313(4)	Au22−P22	2.322(4)
Au2−P3	2.309(2)	Au2−P3	2.323(5)	Au33−P33	2.321(5)
P1−Au1−P4	170.14(6)	P1−Au1−P4	171.0(2)	Au44−P44	2.323(5)
P2−Au2−P3	173.76(6)	P2−Au2−P3	168.0(2)	P11−Au11−P11A	170.9(2)
Au1−Au2−Au2A	160.676(13)	Au1−Au2−Au2A	179.62(3)	P22−Au22−P22A	168.4(2)
P1−Au1−Au2−P2	47.64(7)	P1−Au1−Au2−P2	53.71(17)	P33−Au33−P33A	168.0(2)
P4−Au1−Au2−P3	49.28(6)	P4−Au1−Au2−P3	53.08(17)	P44−Au44−P44A	170.0(3)
		P2−Au2−Au2A−P3A	28.66(17)	P11−Au11−Au22−P22	52.52(17)
				P22−Au22−Au33−P33	28.61(17)
				P33−Au33−Au44−P44	53.43(17)

independent complexes with very similar structures which are shown in different perspectives in Figure 2 and 3. The structures consist of two ligand strands wrapped as a double helix around a linear Au_4 rod. The helices stereoselectively contain either two *R*,*R*- or two *S*,*S*-p4 ligands.

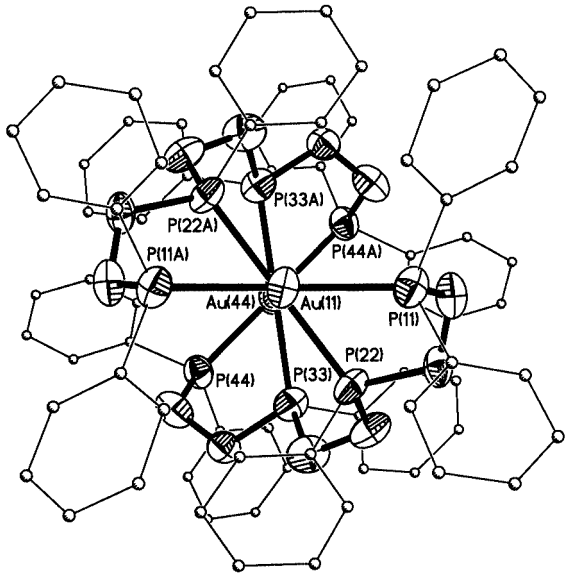

Figure 3. View of the P-$[Au_4(\mu\text{-}(S,S)\text{-p4})_2](OTf)_4$ isomer of the second of two crystallographically independent helicates of **2** along the Au_4 chain

The configuration of the helices is dictated by that of the ligands analogously to **1**: the *R* centers are related to an M helix and the S centers to P. In keeping with the centrosymmetric space group, crystals of **2** are a racemic compound of equal amounts of P and M helices. The helices are nonpalindromic (see Figure 3): the pitch angle of the outer $(Au-P-CC-P)_2$ segments of **2** amounts to 53.2° (mean value), and the inner $(Au-P-CC-P)_2$ segments display a significantly smaller helical twist of 28.6° (mean value). The helical twist in the trinuclear helicate $[Au_3(\mu^3\text{-pp2})_2](OTf)_3$ (pp2 = $PhP(CH_2CH_2PPh_2)_2$] is between 50.66(7)° and 54.57(6)°.[8]

The helicates are unsaturated in view of the gold-gold distances, which all are within the range of Au−Au d^{10}-d^{10} interactions.[9] The separation of the inner Au centers (3.33 Å, mean value) is significantly larger than the contact between inner and outer gold atoms (3.09 Å, mean value).

The stereoselective coordination of the four gold atoms by two ligand strands in **2** is reflected in the symmetry of the complexes in the crystal lattice: The different $[Au_4(\mu^4\text{-}R^*,R^*\text{-p4})_2]^{4+}$ cations in **2** both show internal C_2 symmetry: The twofold axis in one complex is essentially perpendicular to the helical axis bisecting it between the two inner gold atoms; in the other complex it coincides with the Au_4 chain forming the helical axis. Both crystallographically independent cations display idealized D_2 point symmetry. The symmetry of $[Au_4(\mu^4\text{-}R^*,R^*\text{-p4})_2]^{4+}$ in the solid state is remarkable because the existence of different crystallographic symmetry elements in the same helicate seems to be uncommon and because there are no precedents for a twofold symmetry parallel to the helical axis in the space group *C*2/*c*, which is the most frequently occurring space group for helicates.[2]

The crystal packing of **2** is unusual. Because of their cylindrical shape, helicates tend to align themselves along to the helical axis.[2] In contrast, the crystal packing of **2** (Figure 4) produces a sheet of alternatingly parallel and perpendicular helices. Two of the four OTf anions of **2** are located between the terminal gold atoms of one helicate and the two central Au atoms of the neighboring helicates within this sheet; the nearest Au···O and Au···F distances are 3.1 and 3.3 Å, respectively. The sequence of the sheets along *c* is an AB arrangement: In one sheet (A) all helices parallel to the twofold crystallographic axis are built from ligands with an *R*,*R* configuration and the helices perpendicular to the twofold crystallographic axis contain *S*,*S* ligands; the reverse is true for the next sheet (B). The remaining two OTf anions are between the sheets without any contacts to gold atoms.

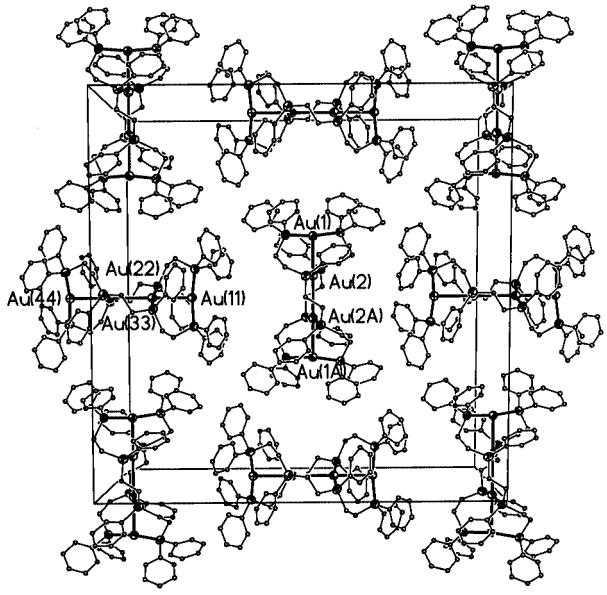

Figure 4. Structure **2** packed along *c*; the anions and solvate molecules have been omitted for clarity

Although the structures of **1** and **2** are essentially different, they display some similarities. The conformation of the substituents of the diagonal phosphorus donor atoms at each gold atom is eclipsed in the view along the P−Au−P axis, the outer phosphorus atoms display a torsion angle C(phenyl)−P−Au−P−C(phenyl) of ca. 0° whereas the inner phosphorus atoms show corresponding angles of approximately 120°. The mean dihedral P−C−C−P angles of the ligand backbone in the different $(Au-P-CC-P)_2$ segments increase in the order 67.9° (**1**, outer segment) < 69.5° (**2**, outer segment) < 104.6° (**2**, inner segment) < 127.14° (**1**, inner segment) and roughly correlate with the Au−Au distances.

Steric reasons may control the formation of helicates or *meso*-helicates: A geometrical extrapolation of $[Au_3(\mu^3\text{-pp2})_2](OTf)_3$ [8] does not exclude the formation of a helical structure from (*R*,*S*)-p4 ligands. In fact, a *meso*-helicate is observed for **1**. Possible factors of strain are different steric requirements concerning the coordination geometry of gold and the conformation of the p4 ligands. A possible indicator of such a strain is that all Au atoms are shifted slightly towards the center of the complex cations (P−Au−P = 173.76−168.0°). This shift is particularly pronounced for the inner gold atoms in compound **2**. Related effects are present in $[Au_3(\mu^3\text{-pp2})_2](OTf)_3$.[8] More data is available on the control of the formation of triple-stranded helicates or *meso*-helicates from achiral ligands. This is related to the rigidity and the form (S or C type) of the ligands, the nature of the spacer (even or odd number of alkylene chains and the chirality of the spacers) and the presence of suitable templates.[10]

Chiral self-recognition has been attributed firstly to the conformational rigidity of the ligand and secondly to the tendency of a more compact structure resulting in maximal intramolecular van der Waals interactions.[4] The first aspect does not apply to the present system in view of the flexibility of the p4 ligand used, whereas the second is thought to control the chiral self-recognition described in this paper.

Experimental Section

The ligand p4 was obtained commercially [(*R**,S*)/(*R**,R*)-(±) ratio ca. 5:1]. Chemical analyses were performed by the Institut für physikalische Chemie, Universität Wien.

Synthesis of 1·2EtOH and 2·2MeOH: A mixture of $Au(SMe_2)Cl$ (58.9 mg, 0.200 mmol), p4 (67.1 mg, 0.100 mmol) and TlOTf (70.7 mg, 0.200 mmol) in MeOH (1 mL) was stirred for 2 h. The TlCl precipitate was removed and the solvent evaporated to a volume of ca. 0.2 mL resulting in a colorless precipitate, which was collected, dried and dissolved in EtOH. Crystals of X-ray quality of **1**·2EtOH were obtained from the first fraction by slow evaporation of this solution. Yield 30 mg (21%, not optimized). $C_{88}H_{84}Au_4F_{12}O_{12}P_8S_4$·2EtOH: calcd. C 39.22, H 3.43; found C 39.1, H 3.3.

The mother liquor mentioned above (MeOH solution) was reduced to a volume of ca. 0.1 mL. Further evaporation of the mother liquor gave X-ray quality crystals of **2**·2MeOH. Yield 6 mg, (4%, not optimized). $C_{88}H_{84}Au_4F_{12}O_{12}P_8S_4$·2MeOH: calcd. C 38.75, H 3.32; found C 38.8, H 3.2.

X-ray Crystallography: The data collection was performed on a Nonius Kappa CCD equipped with graphite-monochromatized Mo-K_α radiation (λ = 0.71073 Å) and a nominal crystal-to-area-detector distance of 36 mm. Intensities were integrated using DENZO and scaled with SCALEPACK.[11] Several scans in the φ and ω direction were made to increase the number of redundant reflections, which were averaged over the refinement cycles. This procedure replaces an empirical absorption correction. The structures were solved with direct methods and refined against F^2 using the SHELX program suite.[12,13] Hydrogen atoms were added geometrically and refined using a riding model. All non-hydrogen atoms of compound **1** were refined with anisotropic displacement parameters. In compound **2** nearly all OTf anions and the solvent molecules MeOH are highly disordered and were refined isotropically. Five OTf anions are found in the asymmetric unit, three in a general position and two with occupancy of 0.5 near a crystallographic twofold rotation axis, which passes in a sloping manner through the C−S axis of the OTf anions. Only one OTf anion in a general position is well ordered and could be refined anisotropically. The two others, which are placed between the layers, are 1:1 disordered by a small movement of the complete anion with two common oxygen atoms for both positions. The disorder of these anions leads partly to overlying positions and bond restraints must be used to minimize correlation effects.

CCDC-179094 (**1**·EtOH), -179095 (**1**·2MeOH) and -179096 (**2**·2MeOH) contain the supplementary crystallographic data for this paper. These data can be obtained free of charge at www.ccdc.cam.ac.uk/conts/retrieving.html [or from the Cambridge Crystallographic Data Centre, 12, Union Road, Cambridge CB2 1EZ, UK; Fax: (internat.) +44-1223/336-033; E-mail: deposit@ccdc.cam.ac.uk].

Table 2. Crystallographic data for new complexes

	1·2EtOH	**2**·2MeOH
Empirical formula	$C_{92}H_{96}Au_4F_{12}O_{14}P_8S_4$	$C_{90}H_{92}Au_4F_{12}O_{14}P_8S_4$
Formula mass (g mol^{-1})	2817.55	2789.50
Temperature (K)	223(2)	223(2)
Wavelength (Å)	0.71073	0.71073
Space group	$P2_1/c$ (No. 14)	$C2/c$ (No. 15)
a (Å)	11.1975(2)	28.4795(7)
b (Å)	26.9696(7)	28.5089(7)
c (Å)	17.1861(5)	25.0645(6)
β (deg)	100.900(2)	97.390(1)
V (Å^3)	5096.4(2)	20181.3(9)
Z	2	8
D (g cm^{-3})	1.836	1.836
μ (mm^{-1})	6.028	6.088
Final *R*1[a] $[I > 2\sigma(I)]$	0.0330	0.0545
*wR*2[a] (all data)	0.0781	0.1288

[a] $R1 = \Sigma||F_0| - |F_c||/\Sigma|F_0|$, $wR2 = \{\Sigma[w(F_0^2 - F_c^2)^2]/\Sigma[w(F_0^2)^2]\}^{1/2}$.

[1] J. M. Lehn, *Supramolecular Chemistry*, VCH Verlagsgesellschaft, Weinheim, **1995**.

[2] C. Piguet, G. Bernardinelli, G. Hopfgartner, *Chem. Rev.* **1997**, *97*, 2005−2062.

[3] For example and references cited in: [3a] G. Baum, E. C. Constable, D. Fenske, C. E. Housecroft, T. Kulke, M. Neuburger, M. Zehnder, *J. Chem. Soc., Dalton Trans.* **2000**, 945−959. − [3b] R. Annunziata, M. Benaglia, M. Cinquini, F. Cozzi, C. R. Woods, J. S. Siegel, *Eur. J. Org. Chem.* **2001**, *1*, 173−180. − [3c] O. Mamula, F. J. Monlien, A. Porquet, G. Hopfgartner, A. E. Merbach, A. von Zelewsky, *Chem. Eur. J.* **2001**, *7*, 533−539. − [3d] M. Albrecht, K. Witt, H. Röttele, R. Fröhlich, *Chem. Commun.* **2001**, 1330−1331.

[4] M. A. Masood, E. J. Enemark, T. D. P. Stack, *Angew. Chem.* **1998**, *110*, 973−977; *Angew. Chem. Int. Ed.* **1998**, *37*, 928−932.

[5] A. L. Airey, G. F. Swiegers, A. C. Willis, S. B. Wild, *Inorg. Chem.* **1997**, *36*, 1588−1597.
[6] V. C. Cook, A. C. Willis, J. Zank, S. B. Wild, *Inorg. Chem.* **2002**, *41*, 1897−1906.
[7] D. T. Hill, R. K. Johnson, USP-A 4698422, **1986**.
[8] W. Schuh, H. Kopacka, K. Wurst, P. Peringer, *Chem. Commun.* **2001**, 2186−2187.
[9] P. Pyykkö, *Chem. Rev.* **1997**, *97*, 597−636.
[10] M. Albrecht, *Chem. Eur. J.* **2000**, *6*, 3485−3489.
[11] Z. Otwinowski, W. Minor, *Methods Enzymol.* **1997**, *276*, 307−317.
[12] G. M. Sheldrick, *SHELXS-86* Universität Göttingen, **1986**.
[13] G. M. Sheldrick, *SHELXL-93* Universität Göttingen, **1993**.

Received February 8, 2002
[I02068]

Four-, Five- and Six-Coordinated Zn^{II} Complexes of OH-Containing Ligands: Syntheses, Structure and Reactivity

Mishtu Dey,[a] Chebrolu Pulla Rao,*[a] Pauli Saarenketo,[b] Kari Rissanen,[b] and Erkki Kolehmainen[b]

Keywords: N,O ligands / X-ray diffraction / Hydrogen bonds / Metalloenzymes / Zinc

Four-, five- and six-coordinated complexes of Zn^{II} with OH-rich molecules possessing an ONO binding core were synthesized, characterized and their structures were established by single-crystal X-ray diffraction. The corresponding metal ion geometries were found to be distorted tetrahedral, square pyramidal and octahedral, respectively. The complexes exhibit interesting lattice structures such as layered and corrugated sheets owing to the presence of a number of weak intermolecular interactions. The five-coordinated, water-bound Zn^{II} complex was studied because of its putative hydrolysis property towards *p*-nitrophenyl acetate.

(© Wiley-VCH Verlag GmbH, 69451 Weinheim, Germany, 2002)

Introduction

Zinc is an essential element for all forms of life and is present at the active site of various enzymes.[1] Zn^{II} is known to exhibit both catalytic and structural roles in its proteins and enzymes.[2−4] The diversity in the functions of Zn^{II} is attributed to its versatile coordination chemistry. Hence, coordination compounds of Zn^{II} are used as biomimetic models.[5−8] It is therefore important to understand how the Zn^{II} center controls the function of metalloenzymes.[9] It may be noted that generally the geometry around the catalytic zinc is distorted and the coordination number varies between four, five and at times even six, along with the presence of labile ligands including a water molecule.[2] While the biological functions of zinc in metalloproteins vary considerably, the active sites exhibit some common structural features.[1] In several zinc enzymes, the metal center is coordinated through the N of histidine and O of aspartic or glutamic acid.[10−12] The role of Zn^{II} in the active centers of hydrolytic metalloenzymes, such as carbonic anhydrase, carboxypeptidase and phosphatase, has constantly been a subject of interest in bioinorganic chemistry.[13−15] Therefore we have chosen a series of hydroxy-rich molecules possessing tridentate ONO donor sites to study their coordination chemistry with Zn^{II}. The coordination behavior of OH-rich molecules has been demonstrated by us in the case of *cis*-VO_2^+, *cis*-MoO_2^{2+} and *trans*-UO_2^{2+} and Ti^{IV}, and by others in the case of iron and manganese, as reported recently in the literature.[16−20] The present paper deals with the results of syntheses, characterization and crystal structure determinations of four-, five-, and six-coordinated Zn^{II} complexes of molecules possessing an ONO core. The ligands used in the study are shown in Scheme 1. A five-coordinated $Zn^{II}-OH_2$ complex was studied for its hydrolytic activity towards *p*-nitrophenyl acetate.

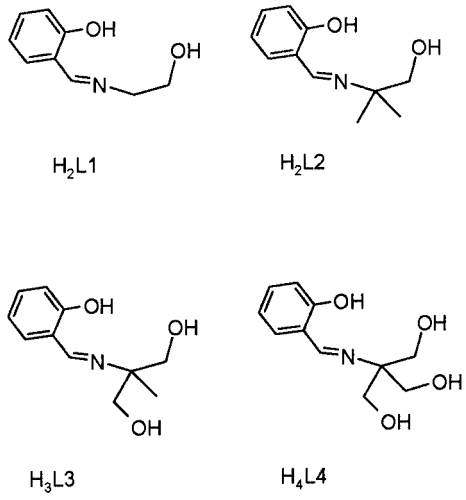

Scheme 1. Schematic representation of the ligands used

Results and Discussions

The reactions of Zn^{II} yielded complexes possessing one or two ligand moieties in its coordination sphere depending

[a] Bioinorganic Laboratory, Department of Chemistry, Indian Institute of Technology Bombay,
Mumbai 400 076, India
Fax: (internat.) +91-22/572-3480
E-mail: cprao@chem.iitb.ac.in
[b] Department of Chemistry, University of Jyväskylä,
Jyvaskyla, 40351, Finland

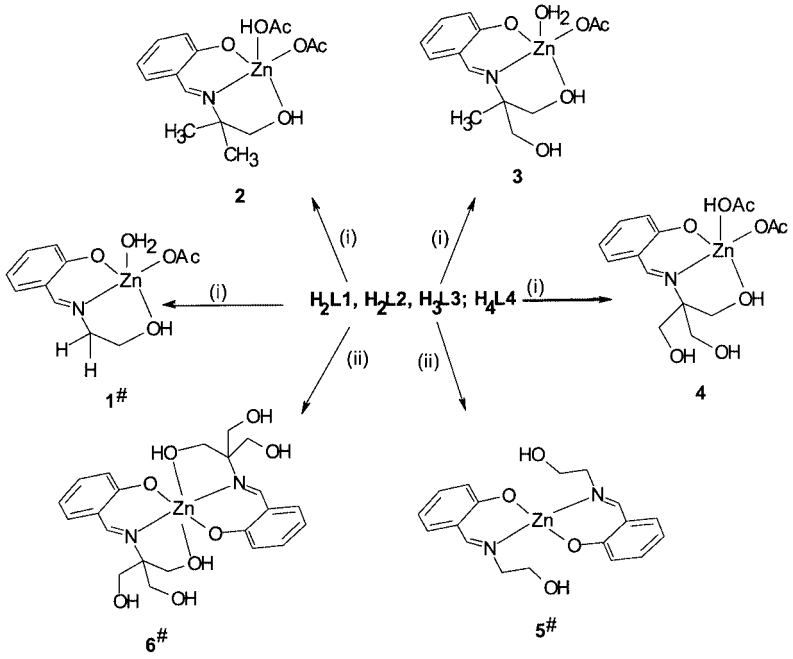

Scheme 2. Zn^{II} complexes of OH-rich molecules; # structure was established by a single crystal XRD study; reaction conditions: (i) $Zn(OAc)_2{\cdot}2H_2O$; Zn/L (1:1), CH_3OH; (ii) $Zn(OAc)_2{\cdot}2H_2O$; Zn/L (1:2), CH_3OH

upon the ratio of metal to ligand (H_2L1 – H_4L4) used (1:1 or 1:2) as shown in Scheme 2. However, H_2L2 and H_3L3 resulted in the formation of the same type of complex, possessing only one ligand per metal ion whether the reaction was carried out in a 1:1 or 1:2 ratio. All the products exhibited similar types of coordination features among the 1:1 reactions no matter how many -OH groups were present in the ligands, H_2L1 (one), H_2L2 (one), H_3L3 (two) and H_4L4 (three). The complexes were all characterized by FTIR, UV/Vis, ^1H and ^{13}C NMR spectroscopy, FAB mass spectrometry, and the structures of **1**, **5** and **6** were also established by single crystal XRD. The crystallographic data is given in Table 1. Further studies were performed on **1** to determine its effect on the hydrolysis of *p*NPA.

IR and UV/Vis Spectra

The IR spectra of the compounds **1**–**6** show ν_{OH} and $\nu_{C=N}$ vibrations at 3321–3390 and 1624–1638 cm^{-1}, respectively and the binding of the imine nitrogen was revealed by the lowering of the frequency (13–15 cm^{-1}). The ν_{asym} and ν_{sym} vibrations of the acetate group were observed in the regions, 1550–1570 and 1407–1445 cm^{-1}, respectively, with $\Delta\nu$ being 105–120 cm^{-1}, suggesting a monodentate binding of the acetate group.[21] These were further confirmed from the single crystal XRD structure of **1**. An intense absorption band around 360 nm, due to the phenolate π-π* transition, was observed in all cases. The π-π* transition associated with the azomethine moiety showed a 10 nm blue shift in the complexes.

^1H NMR Spectroscopic Studies

The phenolic-OH proton signal disappeared from the spectra of all the complexes **1**–**6** due to the binding of this moiety as Ph-O^- to Zn^{II}. The spectra also indicated a downfield shift in the azomethine (–CH=N) proton signal by about 0.2–0.3 ppm, suggesting the binding of this nitrogen to Zn^{II}. Complexes **1**–**4** and **6** exhibited one bound -CH_2OH (δ = 5.2–6.0 ppm, $\Delta\delta$ = 0.5 to 1.3 ppm), **2**, **4** and **6** exhibited one bound -CH_2OH and one or two free -CH_2OH groups (δ = 4.7–5.1 ppm, $\Delta\delta$ = 0.02 to 0.3 ppm), and **5** exhibited one free -CH_2OH (δ = 5.1 ppm). The signal at δ = 1.82 ppm indicates the presence of an acetate moiety in **1**–**4**. Thus, based on ^1H NMR spectra, it was possible to derive the primary coordination about Zn^{II}.

^{13}C NMR Spectroscopic Studies

In **1**–**6** the azomethine (H*C*=N) carbon shifts downfield ($\Delta\delta$ = 6–14 ppm) relative to the corresponding ligand. Downfield shifts were also observed with the tertiary carbon ($\Delta\delta$ = 3–7 ppm) and with the bound -*C*H_2OH signals ($\Delta\delta$ = 0.7–4.2 ppm). In **1**–**4**, the presence of an acetate moiety was identified.

Mass Spectral Studies

The FAB mass spectra of all the complexes showed molecular ion peaks corresponding to their molecular weights as mentioned in the Exp. Sect.. The peak pattern and the intensity ratio confirms the isotopic ratio of M/M + 2/M + 4 peaks as 2.6:1.5:1.

Molecular and Crystal Lattice Structure of 1

Complex **1** is neutral, five-coordinate and has the molecular formula [Zn(HL1)(OAc)(H_2O)], where HL1 acts as a tridentate ligand bound through O_{phen}, O_{alk} and N_{imi} groups. The fourth and fifth coordination sites are occupied

Table 1. Summary of crystallographic data for the complexes **1**, **5** and **6**

	1	**5**	**6**
Empirical formula	$C_{11}H_{15}NO_5Zn$	$C_{18}H_{20}N_2O_4Zn$	$C_{23}H_{32}N_2O_9Zn$
Molecular mass	306.61	393.73	545.88
T/K	173(2)	173(2)	123(2)
Crystal system	Orthorhombic	Monoclinic	Orthorhombic
Space group	*Pbca* (No. 61)	*Cc* (No. 9)	*Pbca*
a (Å)	10.797(1)	9.777(2)	11.166(10)
b (Å)	12.484(1)	10.522(2)	18.735(2)
c (Å)	17.997(1)	16.454(3)	22.496(2)
β (°)		90.66(2)	
V (Å^3)	2425.8(3)	1692.6(6)	4705.8(8)
Z	8	4	8
Absorption coefficient (m)/mm^{-1}	2.037	2.241	1.101
$D_{calcd.}$ (gcm^{-3})	1.679	1.545	1.541
Total reflections	8785	1826	49183
Unique reflections	2762	1826	4142
Parameters	223	306	337
Final *R* [$I > 2\sigma(I)$]	0.0339	0.0270	0.0281
R_w [a]	0.0732	0.0692	0.0673

[a] Weighting scheme is as follows: **1:** calcd. $w = 1/[s^2(F_o^2) + (0.0172P)^2 + 1.4009P]$, where $P = (F_o^2 + 2F_c^2)/3$. **5**: calcd. $w = 1/[s^2(F_o^2) + (0.0583P)^2 + 0.8186P]$, where $P = (F_o^2 + 2F_c^2)/3$. **6**: calcd. $w = 1/[s^2(F_o^2) + (0.0275P)^2 + 5.0231P]$, where $P = (F_o^2 + 2F_o^2)/3$.

by an acetate group and a water molecule (Figure 1). The $Zn-O_{phe}$, $Zn-O_{water}$, $Zn-N_{imi}$, $Zn-O_{acetate}$ and $C-O_{acetate}$ distances were found to be consistent with those reported in the literature.[21–24] In **1**, the trans angle [167.5(1)°], the angles in the basal plane [98.0(1) – 143.7(1)°] and the apical to basal angles [76.3(1) – 100.9(1)°], all indicate a distorted square-pyramidal geometry around the Zn^{II} center (Table 2). A $Zn-O_{alk}$ distance of 2.419 Å observed for $Zn-OHCH_2$- binding in **1** is rather long when compared to that generally found in the literature for similar coordination. It is attributable to a weak binding as well as an increase in the coordination number from four to five. It has been noticed from O,N-bound Zn^{II} complexes in the literature that the common coordination number is four and when this number increases the additional coordinations are found to be generally weak with $Zn^{II}\cdots O$ distances ranging from 2.34 to 2.91 Å; the corresponding geometries are highly distorted.[25–29] Such observations include a $Zn^{II}\cdots O_{phosphato}$ distance of 2.71 Å observed in the case of the Zn^{II}-ATP complex[25] (distorted octahedral), $Zn^{II}\cdots O_{carboxylato}$ distances of 2.91 Å and 2.79 Å observed in the case of two Zn^{II}-histidino complexes,[26,27] (distorted octahedral), $Zn^{II}\cdots O_{perchlorato}$ distances of 2.528 and 2.818 Å observed with the two crystallographically independent molecules present in the lattice of a Zn^{II}-triazacyclododecane complex[28] (distorted trigonal bipyramidal), $Zn^{II}\cdots O_{crownether}$ distances of 2.34, 2.56 and 2.60 Å observed in the case of the Zn-crown ether complex[29] (highly distorted trigonal bipyramidal).

Each molecule in the lattice of **1** interacts with three other neighbor molecules via two hydrogen bonds, resulting in a total of six hydrogen bonds. The phenoxy oxygen accepts a hydrogen bond from the $-CH_2OH$ of a neighboring molecule. The Zn^{II}-bound water molecule exhibits two H-bond interactions as donors towards two different neighboring molecules. These H-bonds are accepted by the unbound oxygen of the acetate in the one case and the $-CH_2OH$ group in the other case. Thus, both H_2O and $-CH_2OH$ groups are involved in two H-bonds each (Figure 2). The packing of the molecules in the lattice is reminiscent of a layer type structure where the molecules are arranged to result in columns.

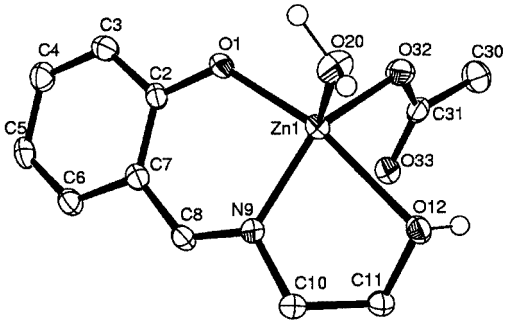

Figure 1. Molecular structure of **1** showing 50% probability thermal ellipsoids (ORTEP)

Molecular and Crystal Lattice Structure of 5

Molecule **5** is neutral, having a molecular formula $[Zn(HL1)_2]$ where each ligand is bidentately bound through O_{phen} and N_{imi} groups, thereby resulting in a distorted tetrahedral geometry around Zn^{II} (Table 2, Figure 3). In this structure, the $-CH_2OH$ groups are not bound to the Zn^{II} center, with $Zn\cdots OH-CH_2$ distances being 3.735 and 4.084 Å. In the crystal lattice of **5**, each Zn^{II} complex is involved in four intermolecular hydrogen bonds with four different

Table 2. Selected bond lengths (Å) and bond angles (deg)

1	5	6
Zn(1)−O(32) 1.960(2)	Zn(1)−O(1A) 1.923(2)	Zn(1)−O(1′) 2.011(1)
Zn(1)−O(20) 2.006(2)	Zn(1)−O(1B) 1.929(2)	Zn(1)−O(1) 2.014(1)
Zn(1)−O(1) 2.025(2)	Zn(1)−N(9B) 2.001(2)	Zn(1)−N(7) 2.056(2)
Zn(1)−O(12) 2.419(2)	Zn(1)−N(9A) 1.984(2)	Zn(1)−N(7′) 2.068(2)
Zn(1)−N(9) 2.017(2)		Zn(1)−O(11) 2.259(1)
		Zn(1)−O(11′) 2.315(1)
O32−Zn1−O20 98.0(1)	O1A−Zn1−O1B 112.7(1)	O(1′)−Zn(1)−O(1)···92.7(1)
O32−Zn1−N9 143.7(1)	O1A−Zn1−N9B 117.6(1)	O(1′)−Zn(1)−N(7) 103.6(1)
O20−Zn1−N9 114.0(2)	O1B−Zn1−N9B 96.5(1)	O(1)−Zn(1)−N(7) 90.8(1)
O32−Zn1−O1 100.9(1)	O1A−Zn1−N9A 97.3(1)	O(1′)−Zn(1)−N(7′) 91.5(1
O20−Zn1−O1 98.3(1)	O1B−Zn1−N9A 114.3(1)	O(1)−Zn(1)−N(7′) 99.7(1)
N9−Zn1−O1 91.4(1)	N9B−Zn1−N9A 119.5(1)	N(7)−Zn(1)−N(7′) 161.2(1)
O32−Zn1−O12 88.4(1)		O(1′)−Zn(1)−O(11) 86.5(1)
O20−Zn1−O12 88.6(1)		O(1)−Zn(1)−O(11) 168.2(1)
N9−Zn1−O12 76.3(1)		N(7)−Zn(1)−O(11) 78.0(1)
O1−Zn1−O12 167.5(1)		N(7′)−Zn(1)−O(11) 92.1(1)
		O(1′)−Zn(1)−O(11′) 164.8(1)
		O(1)−Zn(1)−O(11′) 97.2(1)
		N(7)−Zn(1)−O(11′) 87.9(1)
		N(7′)−Zn(1)−O(11′) 75.5(1)
		O(11)−Zn(1)−O(11′) 86.2(1)

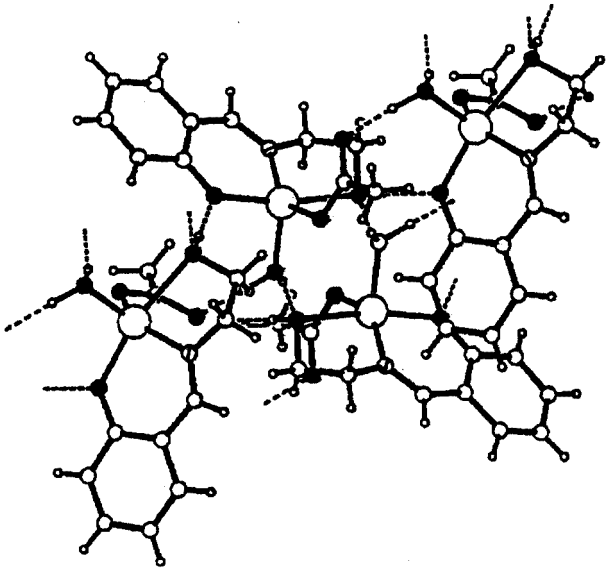

Figure 2. Lattice structure of **1** showing intermolecular hydrogen bond interaction (----); filled circles refer to oxygen,; circles with a line refer to nitrogen and large circles refer to Zn^{II}

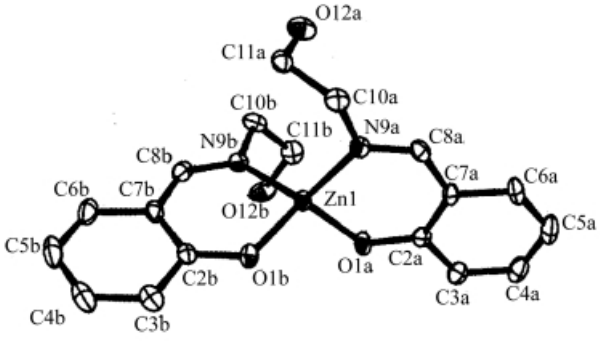

Figure 3. Molecular structure of **5** showing 50% probability thermal ellipsoids using ORTEP

neighbors, of which two are of a donor type and the other two are of an acceptor type. While the O_{phe} acts as an acceptor, the -CH_2OH group acts as a donor in these intermolecular interactions (Figure 4). The lattice structure of **5** shows a corrugated sheet pattern with the presence of channels as shown in Figure 5.

Molecular and Crystal Lattice Structure of 6

Both the H_4L4 ligands act as monoanionic and tridentate binding through the O_{phen}, O_{alk} and N_{imi} groups to result in a distorted octahedral Zn^{II} complex, **6**, with the formula $[Zn(H_3L4)_2]$ (Figure 6). Selected bond lengths and bond angles are shown in Table 2. Of the three -CH_2OH groups, only one is bound to the zinc center (Zn−O distances being 2.259 and 2.315 Å), whereas the other two remain free (Zn−O distances being 4.25 to 5.41 Å); all these -OH groups are involved in hydrogen-bonding interactions in the lattice. In the crystal lattice of **6**, all four of the oxygen atoms of each ligand are involved in hydrogen bond interactions. Compound **6** participates in intermolecular hydrogen bonds of the O−H···O type with five different neighbors in the lattice (Figure 7). While the O_{phe} acts as an acceptor, the -CH_2OH groups act both as a donor and an acceptor. Both of the free CH_2OH groups exhibit two hydrogen bonds each whereas the bound CH_2OH group and O_{phe} exhibit only one hydrogen bond interaction. The lattice MeOH is involved in two H-bond interactions connecting two neighboring zinc complex units. Weak interactions present in all of these complexes exhibited a linear correlation between *d*(D···A) vs. *d*(H···A) as shown in Figure 8.

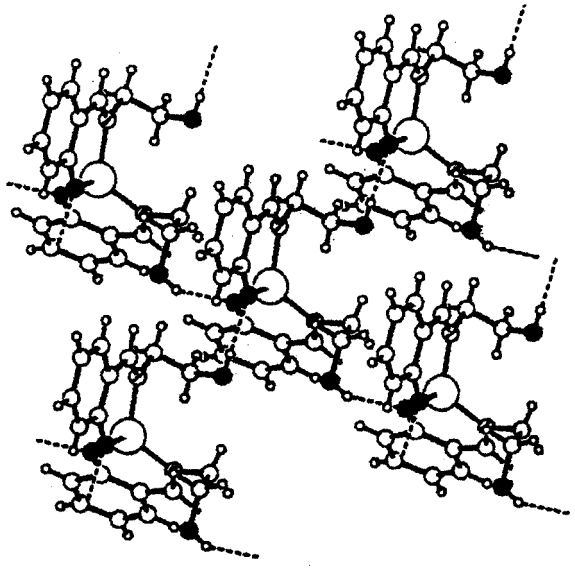

Figure 4. Lattice structure of **5** showing intermolecular hydrogen bond interactions (----); filled circles refer to oxygen, circles with a line refer to nitrogen and the large circles to the Zn^{II}

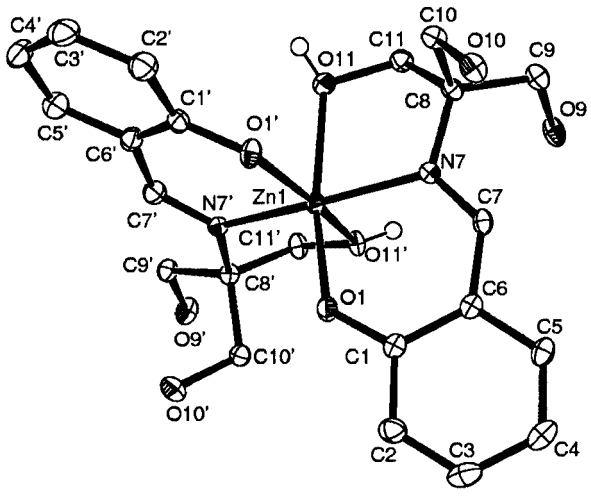

Figure 6. Molecular structure of **6** showing 50% probability of thermal ellipsoids using ORTEP

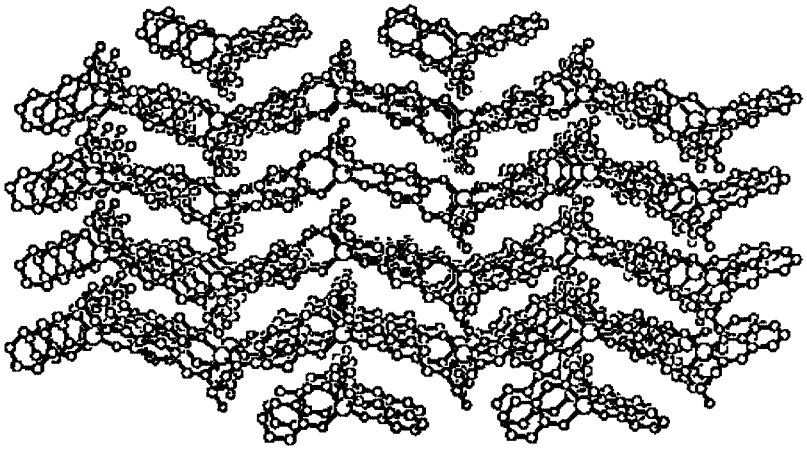

Figure 5. Lattice structure of **5** exhibiting corrugated sheet pattern

pH Titration

The potentiometric pH titration curves of H_2L1 in MeOH/water solution in the absence and in the presence of one equivalent of $Zn(OAc)_2$ are shown in Figure 9. A 0.1 M NaOH solution was used to titrate the Zn^{II}-coordinated water. The precursor ligand H_2L1 exhibited one sharp inflection with a pK_a of 9.14 corresponding to the phenolic moiety. On the other hand, the titration of $H_2L1+Zn(OAc)_2$ exhibited two inflection points. The first inflection observed at a pK_a of 6.93 corresponds to the deprotonation of the phenolic-OH followed by formation of a stable complex at pH $>$ 6. This pK_a value for phenolate agrees well with that reported in the literature wherein deprotonation of the phenol was promoted by Zn^{II} coordination, with the pK_a shifting from 9.2 (without zinc) to 6.8 (with zinc).[13] The second inflection point observed at pK_a 8.61 corresponds to the deprotonation of Zn^{II}-bound water in the complex. This value was similar to the pK_a of 8.7 reported for bound H_2O in the case of a macrocyclic tetraamine Zn^{II} complex,[30] a model for carbonic anhydrase. A potentiometric pH titration experiment carried out under similar conditions with the isolated complex **1** also indicated an inflection point at a pK_a of 9.07, corresponding to the deprotonation of the Zn^{II}-bound aquo species.

Kinetics of the Hydrolysis of p-Nitrophenyl Acetate

The kinetics of *p*NPA hydrolysis in the presence and in the absence of zinc complex **1** was studied. The initial rate of the reaction was determined from the slope of a straight line obtained from the plot of the absorbance of *p*-nitrophenolate vs. time. The slope was calculated for the first 10% of the conversion from which the initial rate (v) of the

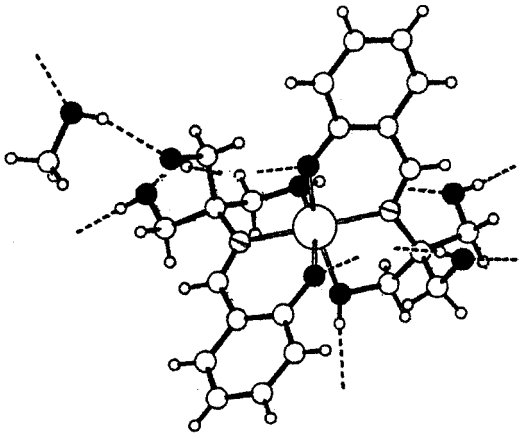

Figure 7. Structure of **6** showing intermolecular hydrogen bond interactions (---); filled circles refer to oxygen, circles with a line refer to nitrogen and the large circles to Zn^{II}

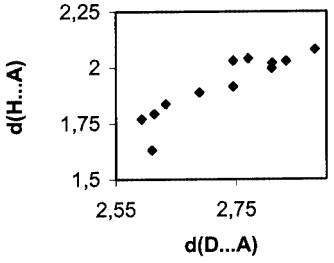

Figure 8. Plot of d(D···A) vs. d(H···A) using the hydrogen bond interaction data obtained in the lattices of **1**, **5** and **6**; d(D···A) and d(H···A) are in Å.

reaction was determined. Thus, these reactions yielded initial rates of 0.183×10^{-4}, 0.80×10^{-4} and 2.28×10^{-4} Ms^{-1} at pH values of 7.2, 8.0 and 9.0, respectively, at 25 °C. The initial rate of hydrolysis increased when the pH of the reaction solution increased, owing to an increase in the concentration of the $Zn-OH^-$ species. The rate of hydrolysis was found to increase to 2.35×10^{-4} Ms^{-1} at 35 °C and pH 8.0 as expected. The experimental results obtained at each stage were compared with the results of the corresponding control experiments.

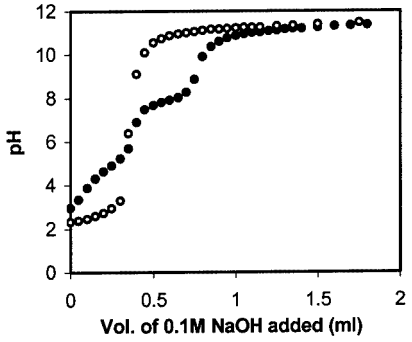

Figure 9. Experimental titration curves of 1.0×10^{-3} M H_2L1 in the presence of 4.0×10^{-3} M HCl in aqueous methanol (33%, v/v) at 25 °C and $I = 0.1$ M ($NaNO_3$); (o) in the absence of Zn^{2+} and (•) in the presence of an equimolar amount of Zn^{2+}

Experiments were also carried out at a fixed concentration of **1** and variable concentrations of *p*NPA (C) and vice versa. The plot of ln v vs. ln C showed that the hydrolysis kinetics is first order with respect to the substrate as well as the zinc complex **1**, and second order overall. The second order rate constants (k_{obs}) were found to be 0.967×10^{-3} and 6.88×10^{-3} $M^{-1}s^{-1}$ at pH 8.0 and 9.0, respectively. Based on the present studies it has been proposed that the water coordinated to the Zn^{II} center plays an important role in the hydrolysis process as indicated in Scheme 3. Four- or five-coordinated mononuclear Zn^{II} complexes of the type $L-Zn-OH_2$ have been used in the literature as model molecules for hydrolytic enzymes.[31,32]

Conclusions

Complexes synthesized from the reaction of Zn^{II} with −OH rich molecules exhibited varied structures and geometry. All these ligands are monoanionic and are bound to the zinc center, either in a bi- or tridentate fashion. This resulted in the formation of distorted geometries of tetrahedral (**5**), square pyramidal (**1**) and octahedral complexes (**6**). Thus, as we go from four- to five- to six-coordinated species, the coordination environment changes from N_2O_2

Table 3. Hydrogen bond interaction data for **1, 5** and **6**

D−H···A	d(H···A)	d(D···A)	<DHA	Symmetry
1				
O12−H12A···O1	1.837	2.633	176.9	$[x - 1/2, -y + 1/2, -z]$
O20−H20A···O33	1.631	2.610	169.0	$[x + 1/2, -y + 1/2, -z]$
O20−H20B···O12	2.030	2.745	168.7	$[-x, -y, -z]$
5				
O(12A)−H(12A)···O(1A)#1	2.02(6)	2.801(3)	164(5)	$[x + 1/2, y - 1/2, z]$
O(12B)−H(12B)···O(1B)#2	2.04(7)	2.770(3)	151(6)	$[x - 1/2, y - 1/2, z]$
6				
O(9)−H(9)···O(1′)#1	1.770(17)	2.593(2)	170(3)	$x - 1/2, -y + 3/2, -z + 1$
O(10)−H(10)···O(9)#2	1.889(17)	2.689(2)	170(2)	$x + 1/2, -y + 3/2, -z + 1$
O(11)−H(11)···O(1M)	1.997(17)	2.809(2)	173(2)	
O(9′)−H(9′)···O(1)#3	1.793(17)	2.614(2)	171(2)	$x - 1/2, y, -z + 3/2$
O(10′)−H(10′)···O(9′)#4	1.915(17)	2.745(2)	173(2)	$x + 1/2, y, -z + 3/2$
O(11′)−H(11′)···O(10)#1	2.028(17)	2.833(2)	172(2)	$x - 1/2, -y + 3/2, -z + 1$
O(1M)−H(1M)···O(10′)#5	2.08(2)	2.881(2)	169(3)	$-x + 1, y + 1/2, -z + 3/2$

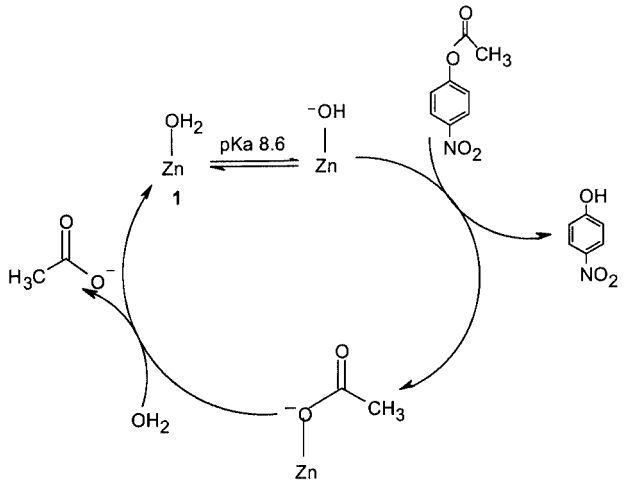

Scheme 3. Possible mechanism for *p*-nitrophenyl acetate hydrolysis by **1**

to NO_4 to N_2O_4 as derived from the crystal structures of **1**, **5** and **6,** respectively. The primary coordination spheres of these complexes are shown in Figure 10 for comparison. The number of chelate rings formed in these complexes increases from two (**5**) to three (**1**) to four (**6**) in the respective complexes. Interestingly, the five-coordinated zinc complex (HL1−Zn−OH_2) (**1**) exhibited an increased rate of hydrolysis of *p*NPA and hence is expected to possess a relationship with the Zn^{II} center, of relevance in zinc hydrolytic enzymes.

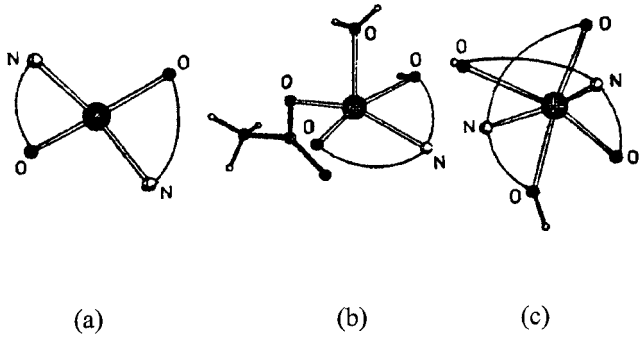

Figure 10. Structures representing primary coordination spheres of **1**, **5** and **6**; (a), (b) and (c) stand for **5**, **1** and **6,** respectively; big circles represent Zn

Experimental Section

General: Elemental analysis was carried out on a Carlo−Erba elemental analyzer. FTIR spectra were recorded on a Nicolet Impact 400 machine in a KBr matrix. UV/Vis spectrophotometric experiments were performed on a Shimadzu UV2101PC instrument equipped with a temperature controlled cell holder (TCC-260). ^1H and ^{13}C NMR spectra were recorded on JEOL JNM GSX-270 FT or Varian XL-300 spectrometer in $(CD_3)_2SO$. The FAB mass spectra were recorded on a JEOL SX 102/DA-6000 Mass Spectrometer/Data System using Argon/Xenon (6 kV, 10 mA) as the carrier gas. The accelerating voltage was 10 kV and the spectra were recorded at room temperature. *m*-Nitrobenzyl alcohol (NBA) was used as the matrix. All the chemicals used were procured from local sources and purified before use. All the solvents were purified and dried immediately before use. All complexes were isolated and purified by recrystallization before performing further studies.

Syntheses

H_2L1: 2-Amino-1-ethanol (1.05 g, 10 mmol) dissolved in MeOH (15 mL) was added to salicylaldehyde (1.0 mL, 10 mmol) in MeOH (15 mL). The reaction mixture was heated to 40 °C for 1 h and then cooled to room temperature followed by concentrating the resulting mixture to a liquid product. FTIR (KBr): $\tilde{\nu}$ = 3411 (ν_{OH}), 1639 ($\nu_{C=N}$) cm^{-1}. ^1H NMR ([D_6]DMSO): δ = 8.50 (s, 1 H, *H*C=N), 7.43 (d, 1 H, Ar *H*), 7.31 (t, 1 H, Ar *H*), 6.87 (m, 2 H, Ar *H*), 4.79 (s, 1 H, CH_2OH), 3.64 (s, 4 H, CH_2OH). The ligands **H_2L2**, **H_3L3** and **H_4L4** were synthesized adopting a similar procedure. The products were obtained as yellow solids by trituration with hexane and were further recrystallized from MeOH and then characterized.[20]

[Zn(HL1)(CH_3COO)(H_2O)] (1): The reaction was carried out using a 1:1 mol ratio of the zinc acetate to the ligand. Zn(acetate)$_2$·$2H_2O$ (0.2195 g, 1.0 mmol) in MeOH (10 mL) was added dropwise to H_2L1 (0.140 mL, 1 mmol) in MeOH (10 mL), and the resultant pale yellow reaction mixture was stirred at room temperature for an hour and then refluxed for 4 h. The reaction mixture was then cooled to room temperature and was concentrated to give a yellow mass, which was triturated with hexane resulting in an off-white product. The crude product was recrystallized from a methanol/hexane mixture (1:2 v/v) resulting in the formation of single crystals of **1** suitable for X-ray diffraction (XRD) studies. Yield: 0.269 g (88%); m.p. 128−132 °C. FTIR (KBr): $\tilde{\nu}$ = 3301 (ν_{OH}), 1638 ($\nu_{C=N}$) cm^{-1}. ^1H NMR ([D_6]DMSO): δ = 8.30 (s, 1 H, *H*C=N), 7.19 (d, 2 H, Ar *H*), 6.60 (d, 1 H, Ar *H*), 6.49 (t, 1 H, Ar *H*), 5.25 (br, 1 H, CH_2OH), 3.54 (m, 4 H, CH_2OH), 1.81 (s, 3 H, CH_3COO) ppm. ^{13}C NMR: δ = 171.5 (H*C*=N), 176.8 (CH_3COO), 170.1, 135.8, 133.9, 122.2, 118.3, 113.1 (six Ar ***C***), 61.4 (CH_2), 60.0 (CH_2OH), 22.6 (CH_3COO). $C_{11}H_{15}NO_5Zn$ (306.6): calcd. C 43.09, H 4.93, N 4.57; found C 42.20, H 4.98, N 4.54%.

[Zn(H_3L4)(CH_3COO)(CH_3COOH)] (2): This compound was synthesized by adopting the procedure given for **1**, except that the ligand used was H_4L4. Yield: 0.445 g (77%); m.p. >200 °C. FTIR (KBr): $\tilde{\nu}$ = 3390 (ν_{OH}), 1638 cm^{-1} ($\nu_{C=N}$). ^1H NMR ([D_6]DMSO): δ = 8.28 (s, 1 H, *H*C=N), 7.14 (m, 2 H, Ar *H*), 6.52 (d, 1 H, Ar *H*), 6.40 (t, 1 H, Ar *H*), 5.99 (br, 1 H, CH_2OH), 5.13 (br, 1 H, CH_2OH), 4.73 (br, 1 H, CH_2OH), 3.47 (s, 6 H, CH_2), 1.82 (s, 3 H, CH_3COO) ppm. ^{13}C NMR: δ = 176.9 (H*C*=N), 170.3 (CH_3COO), 168.3, 136.3, 133.4, 122.3, 118.9, 112.3 (six Ar *C*), 65.4, (*tert C*), 64.6, (CH_2OH), 63.3, (CH_2OH), 23.1, (CH_2OH), 18.4, (CH_3COO). $C_{15}H_{21}NO_8Zn$ (408.7): calcd. C 44.11, H 5.15, N 3.43; found C 44.40, H 4.90, N 3.50. FAB MS: *m*/*z* = 409 (10) [M^+].

[Zn(HL2)(CH_3COO)(H_2O)] (3): Compound **3** was synthesized by adopting the procedure given for **1** but using H_2L2. Yield: 0.240 g (72%); m.p. >200 °C. FTIR (KBr): $\tilde{\nu}$ = 3231, (ν_{OH}), 1634 cm^{-1} ($\nu_{C=N}$). ^1H NMR ([D_6]DMSO): δ = 8.38 (s, 1 H, *H*C=N), 7.21 (d, 1 H, Ar *H*), 7.12 (t, 1 H, Ar *H*), 6.56 (d, 1 H, Ar *H*), 6.42 (t, 1 H, Ar *H*), 5.76 (s, 2 H, CH_2OH, CH_3OH), 3.42 (s, 2 H, CH_2OH), 1.82 (s, 3 H, CH_3COO), 1.20 (s, 6 H, CH_3), 1.09 (s, 3 H, CH_3) ppm. ^{13}C NMR: δ = 170.2 (H*C*=N), 177.9 (CH_3COO), 167.0, 136.3, 133.9, 122.5, 119.3, 113.4 (six Ar C), 68.1 (*tert C*), 60.8 (CH_2OH), 53.4 (CH_3OH), 24.9 (CH_3COO), 24.0, 23.6 (CH_3) ppm. $C_{13}H_{19}NO_5Zn$ (334.7): calcd. C 46.66, H 5.72, N 4.19; found C 46.41, H 5.86, N 4.17. FAB MS: *m*/*z* = 334 (50) [M^+].

[Zn(H$_2$L3)(CH$_3$COO)(CH$_3$COOH)] (4): Compound **4** was synthesized by adopting the procedure given for **1** with the use of H$_3$L3. Yield: 0.354 g (65%); m.p. >200 °C. FTIR (KBr): $\tilde{\nu}$ = 3388 (ν_{OH}), 1637 cm^{-1} ($\nu_{C=N}$). ^{1}H NMR ([D$_6$]DMSO): δ = 8.29 (s, 1 H, *H*C=N), 7.16 (m, 2 H, Ar *H*), 6.57 (d, 1 H, Ar *H*), 6.46 (t, 1 H, Ar *H*), 5.40 (br, 1 H, CH$_2$O*H*), 4.82 (br, 1 H, CH$_2$O*H*), 3.43 (d, 4 H, C*H*$_2$OH), 1.82 (s, 3 H, C*H*$_3$COO), 1.16 (s, 3 H, C*H*$_3$) ppm. ^{13}C NMR: δ = 177.0 (H*C*=N), 170.3, (CH$_3$*C*OO), 167.9, 136.2, 132.7, 122.3, 118.8, 112.5 (six Ar *C*), 65.4, (*tert C*), 64.6, (*C*H$_2$OH), 63.4 (*C*H$_2$OH), 23.2 (CH$_3$COO), 17.9 (CH$_3$). C$_{15}$H$_{21}$NO$_7$Zn (392.6): calcd. C 45.89, H 5.39, N 3.57; found C 46.29, H 5.42, N 4.00. FAB MS: *m*/*z* = 392 (20) [M$^+$].

[Zn(HL1)$_2$] (5): This reaction was carried out using a 1:2 mol ratio of zinc acetate to ligand. Zn(acetate)$_2$·2H$_2$O (0.5 mmol, 0.110 g) in MeOH (25 mL) was added to H$_2$L1 (1 mmol, 0.140 mL) in MeOH (10 mL), and the resultant golden-yellow solution was refluxed for 4 h and then cooled to room temperature. The solvent was removed under vacuum and the resultant yellow residue was redissolved in MeOH (3 mL) and kept at room temperature, whereupon **5** separated out. Single crystals of **5** suitable for X-ray diffraction studies were grown from the methanolic solution of the product. Yield: 0.357 g (91%); m.p. 210−212 °C. FTIR (KBr): $\tilde{\nu}$ = 3328 (ν_{OH}), 1624 cm^{-1} ($\nu_{C=N}$). ^{1}H NMR ([D$_6$]DMSO): δ = 8.38 (s, 1 H, *H*C=N), 7.23 (m, 2 H, Ar *H*), 6.62 (m, 1 H, Ar *H*), 6.53 (m, 1 H, Ar *H*), 5.05 (s, 1 H, CH$_2$O*H*), 3.59 (m, 4 H, C*H*$_2$OH) ppm. ^{13}C NMR: δ = 172.0 (H*C*=N), 170.1, 135.9, 134.1, 122.2, 118.3, 113.4 (Ar *C*), 61.9 (*C*H$_2$OH), 59.9 (*C*H$_2$) ppm. C$_{18}$H$_{20}$N$_2$O$_4$Zn (393.7): calcd. C 54.91, H 5.12, N 7.12; found C 55.40, H 5.21, N 6.74. FAB MS: *m*/*z* = 393 (70) [M$^+$].

[Zn(H$_3$L4)$_2$] (6): A similar procedure was adopted for synthesizing compound **6** using the ligand H$_4$L4. Crystallization of the crude product from methanol resulted in single crystals of **6** suitable for XRD studies. Yield: 0.333 g (65%); m.p. >200 °C. FTIR (KBr): $\tilde{\nu}$ = 3333 (ν_{OH}), 1625 cm^{-1} ($\nu_{C=N}$). ^{1}H NMR ([D$_6$]DMSO): δ = 8.35 (s, 1 H, *H*C=N), 7.10 (m, 1 H, Ar *H*), 6.77 (d, 1 H, Ar *H*), 6.41 (d, 2 H, Ar *H*), 5.16 (br, 1 H, CH$_2$O*H*), 4.74 (br, 1 H, CH$_2$O*H*), 4.11 (br, 1 H, CH$_2$O*H*), 3.62 (s, 6 H, C*H*$_2$) ppm. ^{13}C NMR: δ = 170.1 (H*C*=N), 168.9, 136.2, 132.1, 122.3, 118.5, 112.0 (Ar *C*), 67.1 (*C*H$_2$OH), 61.5 (*C*H$_2$OH), 61.4 (*C*H$_2$OH), 48.6 (*tert-C*) ppm. C$_{22}$H$_{28}$N$_2$O$_8$Zn (513.9): calcd. C 51.43, H 5.49, N 5.45; found C 51.16, H 6.07, N 4.73. FAB MS: *m*/*z* = 513 (95) [M$^+$].

However, when 1:2 reactions were carried out using ligands H$_2$L2 and H$_3$L3 the products obtained were similar to the products of the 1:1 reaction (**3** and **4**).

Potentiometric pH Titration

Titrations were carried out at 25 ± 0.2 °C by means of a Control Dynamics pH meter with a combined glass electrode. The electrode was calibrated using standard aqueous buffers immediately before use. Solutions were made of aqueous methanol (33%, v/v) and the ionic strength was adjusted to 0.1 M using NaNO$_3$. A solution of H$_2$L1 (1.00 mM) with four equivalents of HCl (4.00 mM) in the absence and in the presence of one equivalent of zinc(II) ion was titrated with 0.1 M NaOH aqueous solution. For the titration, every increment of NaOH (50 μL) was added with an equilibration time of 60 s after each addition.

Hydrolysis of *p*-Nitrophenyl Acetate (*p*NPA): The hydrolysis rate of *p*NPA in the presence of [Zn(HL1)(acetate)(H$_2$O)] (**1**) was measured by an initial-slope method following the absorbance increase in the 400 nm band of the released *p*-nitrophenolate species at 25 °C. Such experiments were carried out at a solution pH of 7.2, 8.0 and 9.0 and these were maintained using tris(hydroxymethyl)-aminomethane (20 mM) with an ionic strength of 0.1 mM KNO$_3$. To increase the solubility of *p*NPA, 10% CH$_3$CN/H$_2$O solution was used. In a typical experiment, *p*NPA (c = 0.02−0.5 mM) and the complex, [Zn(HL^1)(acetate)(H$_2$O)] (c = 0.01−0.1 mM) in 10% CH$_3$CN/H$_2$O solution, were mixed at the appropriate pH (the control experiment does not contain the Zn^{II} complex) and the UV/Vis absorption spectra were measured as a function of time until no substantial increase was observed in the absorbance of the 400 nm band. Hydrolysis of *p*NPA was also studied at 35 °C at pH 8.00. Initial slopes were determined from the plots of the measured absorbance at 400 nm versus time.

X-ray Crystallography: Diffraction data were collected for **1** and **6** on a Nonius Kappa CCD machine in the φ scan + ω scan mode (Mo-K_α) and data for **5** were collected on a MACH3 detector in the psi scan mode (Cu-K_α). The structures were routinely solved using SHELXS 97/SIR92 and refined using the SHELXL 97 program packages.[33,34] The diagrams were generated using the ORTEP 3 and PLUTON 98 programs.[35] The data were corrected for empirical absorption. Full-matrix least-squares refinement with anisotropic thermal parameters for all non-hydrogen atoms was used. The hydrogen atoms were treated as riding atoms with fixed thermal parameters. Other details of data collection and structure refinement are provided in Table 1.

CCDC-183936 (**1**), -183937 (**5**) and -183938 (**6**) contain the supplementary crystallographic data for this paper. These data can be obtained free of charge at www.ccdc.cam.ac.uk/conts/retrieving.html [or from the Cambridge Crystallographic Data Centre, 12, Union Road, Cambridge CB2 1EZ, UK; Fax: (internat.) +44-1223/336-033; E-mail: deposit@ccdc.cam.ac.uk].

Acknowledgments

CPR acknowledges the financial support from the Department of Science and Technology, New Delhi and the Council of Scientific and Industrial Research (CSIR), New Delhi. MD acknowledges the SRF fellowship from CSIR. We thank RSIC, CDRI Lucknow for Mass Spectral measurements and Mr. Kuppinen for some experimental help. We thank all three of the referees for their constructive suggestions.

[1] W. N. Lipscomb, N. Straeter, *Chem. Rev.* **1996**, *96*, 2375.
[2] B. L. Vallee, D. S. Auld, *Biochemistry* **1990**, *29*, 5647; B. L. Vallee, D. S. Auld, *Biochemistry* **1993**, *32*, 6493.
[3] *Hydrolytic Enzymes* (Eds.: A. Neuberger, K. Brocklehurst), Elsevier Science: Amsterdam, **1987**.
[4] *Zinc Enzymes* (Eds.: I. Bertini, C. Luchinat, W. Maret, M. Zeppezauer), Birkhäuser: Boston, **1986**.
[5] R. H. Prince, in *Comprehensive Coordination Chemistry* (Eds.: G. Wilkinson, R. D. Gillard, J. A. McCleverty), Pergamon Press: Oxford, U. K., **1987**, *5*, 925.
[6] E. Kimura, T. Koike, *Chem. Commun.* **1998**, 1495, and references therein.
[7] M. Ruf, K. Weis, H. Vahrenkamp, *J. Am. Chem. Soc.* **1996**, *118*, 9288.
[8] A. Looney, G. Parkin, R. Alsfasser, R. Ruff, H. Vahrenkamp, *Angew. Chem. Int. Ed. Engl.* **1992**, *31*, 92.
[9] J. E. Coleman, *Zinc Enzymes*, Birkhauser, Boston, **1986**, 49.
[10] D. C. Rees, M. Lewis, W. N. Lipscomb, *J. Mol Biol.* **1983**, *168*, 367.
[11] E. E. Kim, H. W. Wyckoff, *J. Mol Biol.* **1991**, *218*, 449.
[12] P. A. Frey, S. A. Whitt, J. B. Tobin, *Science* **1994**, *264*, 1927.
[13] E. Kimura, *Acc. Chem. Res.* **2001**, *34*, 171.
[14] H. Sigel, R. B. Martin, *Chem. Soc. Rev.* **1994**, *94*, 83.

[15] J. P. Glusker, *Adv. Protein Chem.* **1991**, *42*, 1.
[16] [16a] C. R. Cornman, G. J. Colpas, J. D. Hoeschele, J. Kampf, V. L. Pecoraro, *J. Am. Chem. Soc.* **1992**, *114*, 9925. [16b] C. J. Carrano, C. M. Nunn, R. Quan, J. A. Bonadies, V. L. Pecoraro, *Inorg. Chem.* **1990**, *29*, 944. [16c] X. Li, M. S. Lah, V. L. Pecoraro, *Inorg. Chem.* **1998**, *27*, 4567.
[17] J. A. Bonadies, C. J. Carrano, *J. Am. Chem. Soc.* **1986**, *108*, 4088.
[18] [18a] D. Rehder, C. Weidemann, A. Duch, W. Priebsch, *Inorg. Chem.* **1988**, *27*, 584. [18b] V. Vergopolous, W. Priebsch, M. Fritzsch, D. Rehder, *Inorg. Chem.* **1993**, *32*, 1844.
[19] [19a] D. C. Crans, R. A. Felty, O. P. Anderson, M. M. Miller, *Inorg. Chem.* **1993**, *32*, 247. [19b] D. C. Crans, R. W. Marshman, M. S. Gottlieb, O. P. Anderson, M. M. Miller, *Inorg. Chem.* **1992**, *31*, 4939. [19c] D. C. Crans, H. Chen, O. P. Anderson, M. M. Miller, *J. Am. Chem. Soc.* **1993**, *115*, 6769. [19d] D. C. Crans, P. M. Ehde, P. K. Shin, L. Pettersson, *J. Am. Chem. Soc.* **1991**, *113*, 3728. [19e] D. C. Crans, P. K. Shin, *J. Am. Chem. Soc.* **1994**, *116*, 1305. [19f] D. C. Crans, H. Chen, R. A. Felty, *J. Am. Chem. Soc.* **1992**, *114*, 4543.
[20] [20a] G. Asgedom, A. Sreedhara, J. Kivikoski, J. Volkonen, E. Kolehmainen, C. P. Rao, *Inorg. Chem.* **1996**, *35*, 5674. [20b] G. Asgedom, A. Sreedhara, J. Kivikoski, J. Volkonen, C. P. Rao, *J. Chem. Soc., Dalton Trans.* **1995**, 2459. [20c] C. P. Rao, A. Sreedhara, P. V. Rao, B. M. Verghese, K. Rissanen, E. Kolehmainen, N. K. Lokanath, M. A. Sridhar, J. S. Prasad, *J. Chem. Soc., Dalton Trans.* **1998**, 2383 and refs. therein. [20d] P. V. Rao, C. P. Rao, E. K. Wegelius, K. Rissanen, E. Kolehmainen, *J. Chem. Soc., Dalton Trans.* **1999**, 4469. [20e] P. V. Rao, C. P. Rao, A. Sreedhara, E. K. Wegelius, K. Rissanen, E. Kolehmainen, *J. Chem. Soc., Dalton Trans.* **2000**, 1213.
[21] G. B. Deacon, R. J. Phillips, *Coordn. Chem. Rev.* **1980**, *33*, 227.
[22] C. O. Rodriguez, C. O. R. de Barbarin, N. A. Bailey, D. E. Fenton, Q.-Y. He, *J. Chem. Soc., Dalton Trans.* **1997**, 161.
[23] A. Erxleben, J. Hermann, *J. Chem. Soc., Dalton Trans.* **2000**, 569.
[24] A. Abufarag, H. Vahrenkamp, *Inorg. Chem.* **1995**, *34*, 2207.
[25] P. Orioli, R. Cini, D. Donati, S. Mangani, *J. Am. Chem. Soc.* **1981**, *103*, 4446.
[26] M. M. Harding, S. J. Cole, *Acta Crystallogr.* **1963**, *16*, 643.
[27] R. H. Kretsinger, F. A. Cotton, R. F. Bryan, *Acta Crystallogr.* **1963**, *16*, 651.
[28] S. C. Rawle, A. J. Clarke, P. Moore, N. W. Alcock, *J. Chem. Soc., Dalton Trans.* **1992**, 2755.
[29] A. B. Charette, J.-F. Marcoux, F. Bélanger-Gariépy, *J. Am. Chem. Soc.* **1996**, *118*, 6792.
[30] P. Woolley, *Nature* (London) **1975**, *258*, 677.
[31] T. Koike, E. Kimura, *J. Am. Chem. Soc.* **1991**, *113*, 8935.
[32] E. Kimura, I. Nakamura, T. Koike, M. Shionoya, Y. Kodama, T. Ikeda, M. Shiro, *J. Am. Chem. Soc.* **1994**, *116*, 4764.
[33] *SHELX97 Programs for Crystal Structure Analysis (Release 97−2)*, G. M. Sheldrick, Institut für Anorganische Chemie der Universität, Tammanstrasse 4, 3400 Göttingen, Germany, **1998**.
[34] SIR92 − A *program for crystal structure solution:* A. Altomare, G. Cascarano, C. Giacovazzo, A. Guagliardi, *J. Appl. Crystallogr.* **1993**, *26*, 343.
[35] [35a] M. N. Burnett, C. K. Johnson, ORTEP III, Report ORNL-6895, Oak Ridge National Laboratory, Oak Ridge, TN, **1996**. [35b] A. L. Spek, *Acta Crystallogr., Sect. A* **1990**, *46*, C34.

Received December 19, 2001
[I01514]

Copper(I) Halide Complexes with Triphenylphosphane and Heterocyclic Thione Ligands: The Crystal Structures of [Bis(Triphenylphosphane)(Benzimidazole-2-Thione)Copper(I) Iodide], [Bis(Triphenylphosphane)(Benzothiazole-2-Thione)Copper(I) Iodide], and Bis[μ-*S*-(Benzimidazole-2-Thione)(Triphenylphosphane)Copper(I) Chloride]

Paraskevas Aslanidis,*[a] Phil J. Cox,[b] Petros Karagiannidis,[a] Sotiris K. Hadjikakou,[c] and Constantinos D. Antoniadis[c]

Dedicated to Prof. Joseph Grobe on the occasion of his 70th birthday

Keywords: Copper / Sulfur heterocycles / Phosphane ligands

While the reaction of benz-1,3-imidazole-2-thione ($bzimtH_2$) or benz-1,3-thiazole-2-thione (bztztH) with copper(I) iodide in the presence of two equivalents of triphenylphosphane led to mononuclear complexes of the type $[CuI(PPh_3)_2(L)]$, the reaction of benz-1,3-imidazole-2-thione with copper(I) chloride gave a dimeric complex $[CuCl(PPh_3)(bzimtH_2)]_2$. These three compounds were characterized by IR, UV/Vis, and ^1H NMR spectroscopy, and the crystal structures determined by single-crystal X-ray diffraction methods. Vibrational, electronic, and ^1H NMR spectroscopic data of the complexes are discussed in relation to the structures.

(© Wiley-VCH Verlag GmbH, 69451 Weinheim, Germany, 2002)

Introduction

The great interest, currently in copper(I) coordination chemistry is due to the participation of this cation in certain biochemical redox reactions,[1] and also because of its ability to adopt various coordination modes.[2] With tertiary phosphanes as ligands, copper(I) halides produce complexes with ligand to copper halide ratios 2:1, 2:2, 3:1, 3:2, 4:2, and 4:4, with the geometry normally being determined by steric rather than by electronic properties of the phosphane ligands.[3]

During our previous work on the interaction of univalent group IB metal cations with biologically interesting molecules, a number of mixed-ligand coordination compounds of copper(I) halides with heterocyclic thiones and triarylphosphanes were prepared and structurally characterized.[4,5] In these complexes, the neutral thione molecules with both nitrogen and sulfur as donating atoms always adopted the monodentate coordination mode, binding the metal centres exclusively through the exocyclic sulfur atom in a terminal or bridging mode. Nonetheless, a remarkable variety of structures ranging from mononuclear three or four-coordinate species with trigonal planar and tetrahedral Cu(I), respectively, to dimers with pseudo-tetrahedral geometry formed by bridging halogen or thione ligands was obtained, even within a closely related series of thione ligands.[6]

As for the factors governing the stoichiometric and structural preferences of these complexes, the bulk of the ligands seemed to be the main factor that determined the coordination number of the metal atom, since the steric demands of the *ortho*-methyl groups clearly lead to three-coordination in the copper(I) halide complexes of tri-*o*-tolylphosphane.[6] On the other hand, the interplay of several other parameters like the geometrical flexibility of the coinage metals, electronic properties on the part of the ligands, as well as the preparation conditions might also be expected to be of major importance, causing significant changes to the coordination geometry of the metal atom. Thus, for example, the cause of dimerization as well as the reasons for the formation of two different types of binuclear copper(I) halide complexes of general formula $[CuX(PR_3)thione]_2$, in which the two copper centers are linked either by a double halide or by a double thione-sulfur bridge, are still not fully understood. On the basis of our earlier observations on dimeric species of the above-mentioned type, the coordination

[a] Aristotle University of Thessaloniki, Faculty of Chemistry, Inorganic Chemistry Laboratory
P. O. Box 135, 541 24, Thessaloniki, Greece
E-mail: aslanidi@chem.auth.gr
[b] School of Pharmacy, The Robert Gordon University
Schoolhill, Aberdeen AB10 1FR, Scotland
E-mail: p.j.cox@rgu.ac.uk
[c] Section of Inorganic and Analytical Chemistry, Department of Chemistry, University of Ioannina
45110 Ioannina, Greece
E-mail: shadjika@cc.uoi.gr

behavior (terminal or bridging mode) of each ligand seems to depend on the nature of the halogen present. In particular, formation of halogen-bridges has been found to be preferred for the "soft" iodine but not for the "harder" chlorine base,[7,8,9] whereas both bridging and terminal bonding modes were observed for bromo ligands[10,11] since bromide lies on the borderline between soft and hard. However, the information obtained so far is insufficient to establish the above supposition, so we now report on the synthesis and X-ray crystal structure of three novel copper(I) halide complexes in an attempt to obtain further insight into this problem.

Results and Discussion

General Considerations

The complexes were prepared by reacting equimolar quantities of copper(I) halide and triphenylphosphane (PPh_3) followed by the addition of one equivalent of the appropriate thione (L) in dry acetonitrile solution. This procedure, frequently used for the preparation of copper(I) halide complexes containing both heterocyclic thiones and triphenyl- or tritolylphosphane ligands, gave, in the case of copper(I) iodide, the monomeric complexes $[CuI(PPh_3)_2(bzimtH_2)]$ (**1**) and $[CuI(PPh_3)_2(bztztH)]$ (**2**). In contrast, copper(I) chloride, used exactly in the same manner, gave the dimer $[CuCl(PPh_3)(bzimtH_2)]_2$ (**3**) with the two copper centres being double bridged by the thione-S atom.

Crystals of the complexes, prepared by slow evaporation of the solution remaining after filtration of the initial product deposited from the reactions, were coloured solids, soluble in chloroform, methanol, ethanol, acetone, and acetonitrile. They were stable to air and moisture, and could be manipulated in air after their isolation without appreciable decomposition. Their solutions were non-conducting in acetone and chloroform. Room temperature magnetic measurements confirmed the diamagnetic nature of the compounds.

The electronic absorption spectra of the three complexes in chloroform, which are very similar, are dominated by two broad bands with maxima at 240 nm and in the 310−340 nm region. The first one can be attributed to intraligand transitions of the phosphane ligand, since the uncoordinated triphenylphosphane reveals a strong absorption at 245 nm, which usually remains non-shifted upon coordination to Cu^I.[12,13] The lower energy band lies in the region where the free thiones absorb, expressing a small red shift as a consequence of the coordination to Cu^I and should therefore be considered as a thione-originating intraligand transition with some MLCT character.[12,13]

The infrared spectra of the compounds, recorded in the range 4000−250 cm^{-1} show, apart from the existence of strong phosphane bands, the usual four "thioamide bands" required by the presence of the heterocyclic thione ligands, as well as the characteristic NH stretching vibrations observed in the 3050−3160 cm^{-1} region. The shifts observed for these bands due to coordination (upward shifts of 15−35 cm^{-1} for thioamide I, downward shifts of 10−30 cm^{-1} for thioamide II and III) in combination with the lack of ν(SH) bands at ca. 2500−2600 cm^{-1}, signify the exclusive S-coordination mode of the thione ligands.

The prevalence of the thione tautomer in the complexes is further confirmed by the ^1H NMR spectra of the compounds, which display, apart from the signals expected for the phosphane and thione ligands, a single resonance at $\delta \approx 12-14$, attributed to the NH proton.

Description of the Structures

$[CuI(PPh_3)_2(bzimtH_2)]$ (1) and $[CuI(PPh_3)_2(bztztH)]$ (2)

The main bond lengths and angles for compounds **1** and **2** are given in Tables 1 and 2. Molecular plots showing the atom numbering schemes are shown in Figures 1 and 2, re-

Table 1. Selected bond lengths [Å] and angles [°] for **1**

Cu(1)−P(1)	2.2839 (10)	P(1)−C(14)	1.831 (3)
Cu(1)−P(2)	2.2796 (9)	P(1)−C(20)	1.818 (3)
Cu(1)−S(1)	2.3692 (9)	P(2)−C(26)	1.827 (3)
Cu(1)−I(1)	2.6901 (6)	P(2)−C(32)	1.826 (3)
S(1)−C(1)	1.691 (3)	P(2)−C(38)	1.828 (3)
P(1)−C(8)	1.834 (3)		

P(2)−Cu(1)−P(1)	122.45(4)	C(14)−P(1)−Cu(1)	114.16(10)
P(2)−Cu(1)−S(1)	104.55(3)	C(8)−P(1)−Cu(1)	113.46(11)
P(1)−Cu(1)−S(1)	105.97(3)	C(32)−P(2)−C(26)	101.23(13)
P(2)−Cu(1)−I(1)	105.70(3)	C(32)−P(2)−C(38)	103.76(13)
P(1)−Cu(1)−I(1)	106.14(3)	C(26)−P(2)−C(38)	103.76(13)
S(1)−Cu(1)−I(1)	112.10(3)	C(32)−P(2)−Cu (1)	114.83(10)
C(20)−P(1)−C(14)	104.63(14)	C(26)−P(2)−Cu(1)	117.99(9)
C(20)−P(1)−C(8)	104.03(14)	C(38)−P(2)−Cu(1)	113.88(10)
C(14)−P(1)−C(8)	103.42(14)	C(1)−S(1)−Cu(1)	111.34(10)
C(20)−P(1)−Cu(1)	115.80(10)		

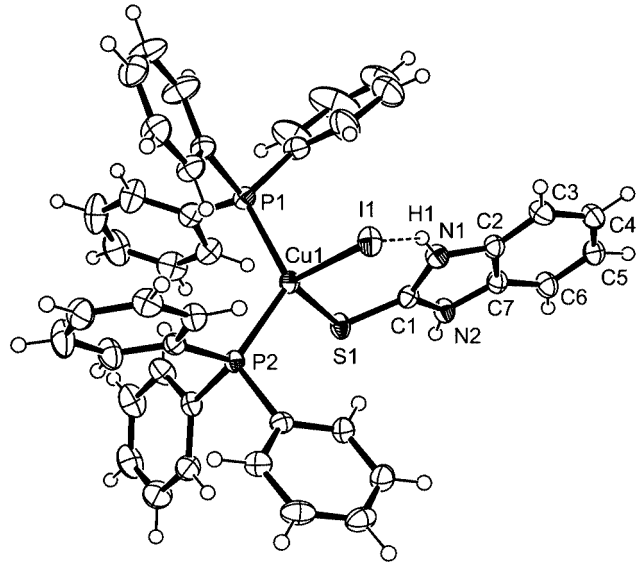

Figure 1. A view of compound **1** with atom labels. Displacement ellipsoids are shown at the 50% probability level

spectively, and details of the hydrogen bonding are shown in Table 3. Both complexes are mononuclear with the copper atom being surrounded by two P, one S, and one I atom in a distorted tetrahedral coordination. It should be noted that copper(I) iodide usually tends to form dimeric complexes with two iodine atoms serving as bridges between the two copper atoms, while only one single representative of mononuclear species with a $CuIP_2S$ core exists among the structures characterized by us so far.[5] The largest deviation from the ideal geometry is reflected by the P−Cu−P angles with values of 122.45(4)° (**1**) and 125.33(2)° (**2**). These higher angles are counterbalanced by the bond angles I−Cu−P(1), I−Cu−P(2), S−Cu−P(1), and S−Cu−P(2), whose values are all lower than the tetrahedral value of 109.4°. This tetrahedral distortion may be attributed to steric interactions between the bulky phosphane ligands, which is common among a large series of monomeric copper(I) halide complexes containing one heterocyclic thione

Table 2. Selected bond lengths [Å] and angles [°] for **2**

Cu(1)−P(1)	2.2822 (6)	P(1)−C(14)	1.818 (2)
Cu(1)−P(2)	2.2796 (6)	P(1)−C(20)	1.827 (2)
Cu(1)−S(1)	2.3660 (6)	P(2)−C(26)	1.822 (2)
Cu(1)−I(1)	2.6807 (3)	P(2)−C(32)	1.832 (2)
S(1)−C(1)	1.668 (2)	P(2)−C(38)	1.830 (2)
P(1)−C(8)	1.824 (2)		
P(2)−Cu(1)−P(1)	125.33(2)	C(8)−P(1)−C(20)	101.74(10)
P(2)−Cu(1)−S(1)	104.44(2)	C(14)−P(1)−Cu(1)	115.99(7)
P(1)−Cu(1)−S(1)	98.82(2)	C(8)−P(1)−Cu(1)	113.97(7)
P(2)−Cu(1)−I(1)	107.053(17)	C(20)−P(1)−Cu(1)	112.95(7)
P(1)−Cu(1)−I(1)	108.907(18)	C(26)−P(2)−C(38)	103.53(10)
S(1)−Cu(1)−I(1)	111.740(18)	C(26)−P(2)−C(32)	102.60(9)
C(1)−S(1)−Cu(1)	115.65(8)	C(38)−P(2)−C(32)	102.86(10)
C(2)−S(2)−C(1)	91.69(11)	C(26)−P(2)−Cu(1)	111.53(7)
C(14)−P(1)−C(8)	104.79(10)	C(38)−P(2)−Cu(1)	116.77(7)
C(14)−P(1)−C(20)	106.03(10)	C(32)−P(2)−Cu(1)	117.68(7)

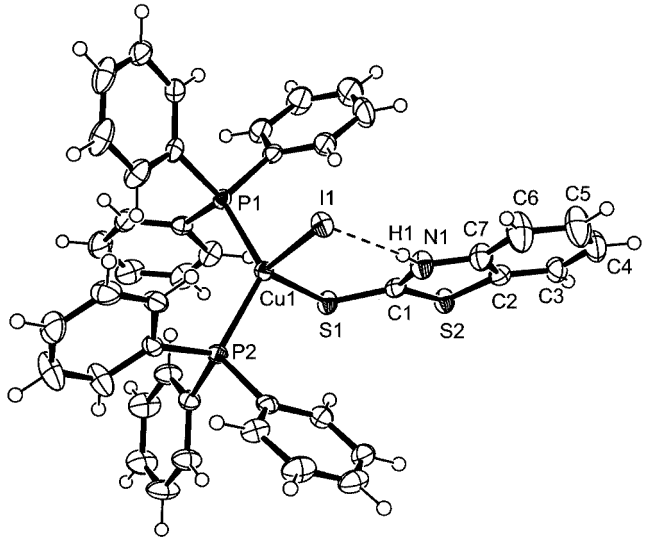

Figure 2. A view of compound **2** with atom labels. Displacement ellipsoids are shown at the 50% probability level

Table 3. Selected bond lengths [Å] and angles [°] for **3**

Cu(1)−P(1)	2.236(3)	P(1)−C(8)	1.813(9)
Cu(1)−S(1)^{1} [a]	2.332(2)	P(1)−C(20)	1.819(8)
Cu(1)−C1(1)	2.347(2)	P(1)−C(14)	1.855(8)
Cu(1)−S(1)	2.555(3)	P(2)−C(33)	1.828(9)
Cu(1)−Cu(1)^{1}	2.919(2)	P(2)−C(45)	1.840(8)
Cu(2)−P(2)	2.234(3)	P(2)−C(39)	1.844(9)
Cu(2)−S(2)^{2}	2.352(3)	N(1)−C(1)	1.366(10)
Cu(2)−Cl(2)	2.357(2)	N(1)−C(2)	1.378(10)
Cu(2)−S(2)	2.448(3)	N(2)−C(1)	1.342(10)
Cu(2)−Cu(2)^{2}	2.943(2)	N(2)−C(7)	1.381(10)
S(1)−C(1)	1.708(8)	N(3)−C(26)	1.326(12)
S(1)−Cu(1)^{1}	2.332(2)	N(3)−C(27)	1.391(11)
S(2)−C(26)	1.745(10)	N(4)−C(26)	1.363(12)
S(2)−Cu(2)^{2}	2.352(3)	N(4)−C(32)	1.409(12)
P(1)−Cu(1)−S(1)^{1}	116.05(10)	P(2)−Cu(2)−Cu(2)^{1}	134.28(8)
P(1)−Cu(1)−Cl(1)	114.53(9)	S(2)^{1}−Cu(2)−Cu(2)^{2}	53.67(7)
S(1)^{1}−Cu(1)−Cl(1)	112.81(9)	Cl(2)−Cu(2)−Cu(2)^{2}	119.05(10)
P(1)−Cu(1)−S(1)	110.90(9)	S(2)−Cu(2)−Cu(2)^{2}	50.71(7)
S(1)^{1}−Cu(1)−S(1)	106.79(7)	C(1)−S(1)−Cu(1)^{1}	107.7(3)
Cl(1)−Cu(1)−S(1)	93.06(8)	C(1)−S(1)−Cu(1)	110.4(3)
P(1)−Cu(1)−Cu(1)^{1}	131.53(8)	Cu(1)^{1}−S(1)−Cu(1)	73.21(7)
S(1)^{1}−Cu(1)−Cu(1)^{1}	56.92(7)	C(26)−S(2)−Cu(2)^{2}	105.7(3)
Cl(1)−Cu(1)−Cu(1)^{1}	110.88(9)	C(26)−S(2)−Cu(2)	105.2(4)
S(1)−Cu(1)−Cu(1)^{1}	49.87(6)	Cu(2)^{2}−S(2)−Cu(2)	75.62(8)
P(2)−Cu(2)−S(2)^{2}	116.23(9)	C(8)−P(1)−Cu(1)	117.7(3)
P(2)−Cu(2)−Cl(2)	105.96(10)	C(20)−P(1)−Cu(1)	111.5(3)
S(2)^{2}−Cu(2)−Cl(2)	112.93(10)	C(14)−P(1)−Cu(1)	117.6(3)
P(2)−Cu(2)−S(2)	114.52(9)	C(33)−P(2)−Cu(2)	114.7(3)
S(2)^{2}−Cu(2)−S(2)	104.38(8)	C(45)−P(2)−Cu(2)	112.5(3)

[a] Symmetry transformations used to generate equivalent atoms: #^{1}: $-x+1, -y+1, -z+1$; #^{2}: $-x, -y, -z$.

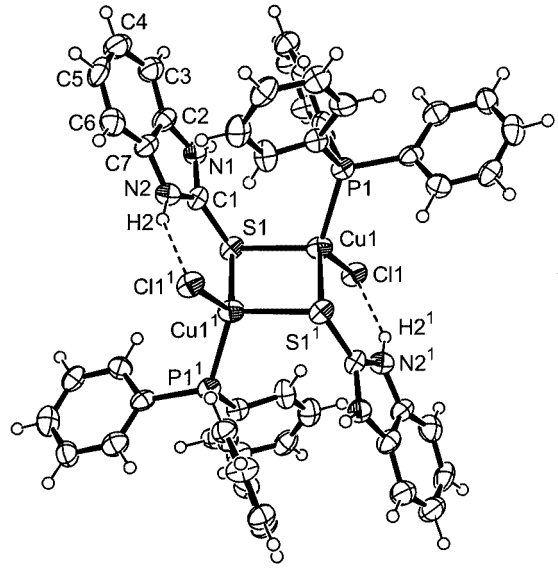

Figure 3. A view of compound **3** with atom labels. Displacement ellipsoids are shown at the 50% probability level

and two monodentate triphenylphosphane ligands, and exhibiting the same $CuSP_2X$ core.[11,14,15]

The Cu−I and Cu−S bonds in **1** and **2** are both somewhat longer, while the two individual Cu−P distances are

Table 4. Hydrogen bonding in the three complexes

Compd.	Donor (D)	H	Acceptor (A)	DH [Å]	HA [Å]	DA [Å]	DHA [°]
1	N1	H1	I1	0.88	2.73	3.526(2)	151
1	N2	H2	O1^{i} [a]	0.88	2.06	2.860(3)	150
2	N1	H1	I1	0.88	2.63	3.493(2)	167
2	C31	H31	S1	0.95	2.87	3.719(2)	149
2	C40	H40	S1^{ii}	0.95	2.83	3.648(2)	146
3	N1	H1	Cl2^{iii}	0.88	2.56	3.227(7)	133
3	N2	H2	Cl1^{iv}	0.88	2.30	3.105(7)	153
3	N3	H3	Cl2^{v}	0.88	2.18	3.036(8)	165
3	N4	H4	Cl1	0.88	2.36	3.198(9)	159
3	C15	H15	N2	0.95	2.48	3.25(1)	137
3	C49	H49	Cl1	0.95	2.80	3.53(1)	134

[a] Atom coordinates transposed by: **i**: x, 0.5 − y, 0.5 + z; **ii**: −1 + x, y, z; **iii**: 1 − x, 1 − y, 1 − z; **iv**: −x, 1 − y, −z; **v**: 1 + x, y, z.

slightly shorter than those found in [CuI(PPh_3)$_2$(pymtH)]. This represents, according to the Cambridge Structural Database, a unique known structure of a monomeric, tetrahedrally coordinated copper(I) iodide complex with terminal iodine and thione-sulfur donors.[5] These bond lengths all lie within the range of the corresponding values previously reported for a number of related tetracoordinated copper(I) complexes.

[CuCl(PPh_3)(bzimtH$_2$)]$_2$ (3)

The asymmetric unit of the crystal cell contains two half-molecules. The atoms in molecule **3a** are Cu1, S1, Cl1, C1−C25, H1, H2, H3A, H4A, H5−H24, and their equivalent primed atoms. The atoms in molecule **3b** are Cu2, S2 Cl2, N3, N4, C26−C50, H3, H4, H26−H50, and their equivalent primed atoms. The main bond lengths and angles for both molecules are given in Table 4, and an ORTEP view of molecule **3a** showing the atom numbering is given in Figure 3. There are some significant differences in bond lengths and angles between the two molecules which will be mentioned in the subsequent discussion. The basic structural unit of [CuCl(PPh_3)(bzimtH$_2$)]$_2$ is a dimer in which the two copper atoms are doubly bridged by two S atoms of the thione ligands to form a strictly planar four-membered Cu_2S_2 core. The slightly distorted tetrahedral coordination around copper is completed by one P atom from the phosphane ligand and one chlorine atom.

Three structurally determined analogues, [CuCl(tmtp)(bzimtH$_2$)]$_2$ (tmtp = tri-*m*-tolylphosphane), [CuCl(tptp)(tzdtH)]$_2$ (tptp = tri-*p*-tolylphosphane, tzdtH = 1,3-thiazolidine-2-thione), and [CuCl(tptp)(pmtH)]$_2$ (pmtH = pyrimidine-2-thione) will be used for the subsequent comparative discussion (hereafter referred to as complexes **A**, **B**, and **C**, respectively).

Each of the two non-equivalent Cu−S bonds of 2.332(2) and 2.555(3) Å in **3a** and 2.322(3) and 2.448(3) Å in **3b**, respectively, are within the range expected for binuclear Cu^{I} complexes with double bridging sulfur atoms. The asymmetry in the two bridging distances in molecule **3a**, however, is remarkably larger than in the three already known analogues. As in the other dimers, the two bulky phosphane ligands are *trans* disposed with a Cu−P bond length of 2.236(3) Å, somewhat longer than the values observed in **B** and **C**, but clearly shorter than the "long" one [2.251(1) Å] in **A**. Likewise, the Cu−Cl bond length of 2.347(2) Å in **3a** and 2.357(2) Å in **3b**, lies well above the corresponding values 2.283(1) and 2.300(1) Å found in **C** and **B**, but is significantly shorter than that in **A** [2.391(2) Å]. As previously demonstrated, this Cu−Cl bond appears to be associated with the S−Cu−S angle, namely an opening up of the S−Cu−S angle from 92.48(2)° in **B** to 93.24(2)° in **C** and 110.2(1)° in **A** results in an elongation of the Cu−Cl bond.[16] As for the complex under consideration, it fits well into the above mentioned series, even when the mean values for the Cu−Cl bond length and the S−Cu−S angle for **3a** and **3b** are taken into consideration.

The S−Cu−S and Cu−S−Cu angles [106.79(7) and 73.21(7)° for **3a** and 104.38(8) and 75.62(8)° for **3b**], which are close to the ideal values (109.5 and 70.5°) for symmetric dimers, deviate significantly from those found in **B** and **C**, but are not far from those observed in **A**. The value of the Cl−Cu−S angle of 102.10(10)° in **3b** is similar to the corresponding values observed in the previous complexes **B** and **C**, whereas the same angle in **3a** [93.06(8)°] is strongly distorted and very close to that observed in complex **A**. Finally, the value of the P−Cu−Cl angle of 114.53(9)° in **3a** is similar to the corresponding values observed in the previous complexes **A**, **B**, and **C**, but the same angle in **3b** is surprisingly much smaller [105.96(10)°].

Computational Study

It is generally accepted that the local metal environment in monovalent copper coordination compounds is mainly determined by steric effects as well as by the Lewis basicity of the ligands, but additional considerations may be useful in explaining the situation in some specific cases. The dimerization often realized in copper(I) halide complexes containing heterocyclic thione and triarylphosphane ligands as well as the bridging or terminal bonding mode of each ligand in such dimers, for instance, are of unknown origin. The contribution of electronic factors, however, is suspected to be important. The computations performed in the present paper are an attempt to unravel any such electronic factor.

The lowest unoccupied molecular orbitals (LUMO) for **3A** and **3B** are 3.346 eV and 3.349 eV higher, respectively, than their highest occupied molecular orbitals (HOMO), while the LUMO energies in complexes **2** and **1** are higher than their HOMO energies by 3.518 and 3.432 eV, respect5-ively. This indicates that the monomers are more stable than the dimers. An overlap population of 0.005 e in **3A** and 0.001 e in **3B** between the two metal centres, which are separated by 2.919(2) Å and 2.943(2) Å, respectively, has been calculated for the dimeric structures, whereby the corresponding value for $CuI(pytH)(tmtp)]_2$,[9] with a Cu···Cu distance of 3.119(1) Å, was found to be 0.006 e. The bonding nature of these metal−metal interactions is, of course, too small to be considered as the crucial factor for the domination of the dimeric structures. The stabilizing effect of a metal−metal interaction could be important only for Cu···Cu separations below the value of 2.80 Å proposed to be the sum of two copper covalent van der Waals radii. In the case of $[CuCl(bztzdtH)(tmtp)]_2$ or $[CuBr(pytH)(tmtp)]_2$,[16] where the Cu···Cu distances are 2.764 and 2.691 Å (both shorter than the sum of the copper−copper van der Waals radius by 0.046 and 0.109 Å, respectively), the corresponding overlap populations are 0.019 e and 0.026 e.

The calculated overlap populations for the Cu(1)−S(1) and Cu(1)−S(1)[1] bonds in **3** are 0.384 e and 0.178 e, respectively. The calculated overlap populations for the Cu(1)−P(1) and Cu(1)−Cl(1) bonds are 0.607 and 0.330 e, respectively. The calculated overlap populations, for the Cu(1)−I(1) and Cu(1)−S(1) bonds are 0.244 and 0.348 e, respectively, in complex **2** and 0.255 and 0.344 e in complex **1**, while the values for the overlap population calculated for the two Cu(1)−P(1) and Cu(1)−P(2) bonds are 0.566 and 0.565 e in complex **2** and 0.561 and 0.571 e, respectively, in complex **1**.

Conclusion

The coordination chemistry of copper(I) with heterocyclic thiones and tertiary phosphanes as ligands offers opportunities for the detailed examination of the factors governing the stereochemical preferences of copper(I) compounds. According to our previous investigations, the stoichiometry may be one of these factors, especially in association with the solvent used for the preparation. The three new copper(I) complexes investigated in this work were prepared in an acetonitrile/methanol mixture, whereby two different types of structures were formed, tetrahedral monomeric and pseudo-tetrahedral dimeric with the halogen acting as bridging ligand. However,

Table 5. Crystal data and structure refinement

	1	**2**	**3**
Chemical formula	$C_{43}H_{36}CuIN_2P_2S{\cdot}CH_3OH{\cdot}0.85CH_3CN{\cdot}0.27H_2O$	$C_{43}H_{35}CuINP_2S_2$	$C_{50}H_{42}Cl_2Cu_2N_4P_2S_2$
Molecular weight	934.4	882.22	1022.92
Temperature	150(2) K	150(2) K	150(2) K
Wavelength	0.71073 Å	0.71073 Å	0.71073 Å
Crystal system	Monoclinic	Monoclinic	Triclinic
Space group	$P2_1/c$	$P2_1/n$	$P\bar{1}$
a	12.528(3) Å	9.6250(10) Å	12.4251(8) Å
b	18.573 (4) Å	22.9400 (10) Å	13.6559 (10) Å
c	18.639 (4) Å	17.9130 (10) Å	13.9637 (13) Å
α	90°	90°	95.533 (3)°
β	91.49 (3)°	95.025 (5)°	91.756 (3)°
γ	90°	90°	104.047 (7)°
Volume	4335.7 (15) Å^3	3939.9 (5) Å^3	2284.2 (3) Å^3
Z	4	4	2
Density (calculated)	1.424 Mg/m^{3}Å	1.487 Mg/m^{3}Å	1.487 Mg/m^{3}Å
Absorption coefficient	1.375 mm^{-1}	1.556 mm^{-1}	1.250 mm^{-1}
F(000)	1873	1776	1048
Crystal size	0.24 × 0.22 × 0.06 mm	0.34 × 0.22 × 0.18 mm	0.07 × 0.05 × 0.01 mm
Theta range for data collection	2.27 to 27.48°	2.28 to 27.48°	2.43 to 25.06°
Index ranges	$-16 \le h \le 15$ $-21 \le k \le 24$ $-24 \le l \le 24$	$-12 \le h \le 12$ $-26 \le k \le 29$ $-22 \le l \le 23$	$-14 \le h \le 14$ $-16 \le k \le 16$ $-16 \le l \le 16$
Reflections collected	37460	34765	25382
Independent reflections	9838 [R(int) = 0.0525]	8940 [R(int) = 0.0484]	7977 [R(int) = 0.1828]
Completeness to theta = 27.48°	99.0%	98.8%	98.5%
Data [$I > 2\sigma(I)$] / restrains / parameters	7872 / 6 / 481	7266 / 0 / 452	3776 / 0 / 559
Max. and min. transmission	0.9220 and 0.7337	0.7670 and 0.6197	0.9876 and 0.9176
Refinement method	Full-matrix l.s. on F^2	Full-matrix l.s. on F^2	Full-matrix l.s. on F^2
Goodness-of-fit on F^2	1.024	1.039	0.945
Final R indices [$I > 2\sigma(I)$]	$R1$=0.0390, $wR2$=0.0999	$R1$=0.0315, $wR2$=0.0727	$R1$=0.0784, $wR2$=0.1710
R indices (all data)	$R1$=0.0547, $wR2$=0.1091	$R1$=0.0452, $wR2$=0.0775	$R1$=0.1873, $wR2$=0.2203
Final weighting scheme	Calc $w = 1/[\sigma^2(F_0^2) + (0.0582P)^2 + 4.5196P)$, where $P = (F_0^2 + 2F_c^2)/3$	Calc $w=1/[\sigma^2(F_0^2) + (0.0420P)^2 + 0.0789P)$, where $P = (F_0^2 + 2F_c^2)/3$	Calc $w = 1/[\sigma^2(F_0^2) + (0.0989P)^2 + 0.0000P)$, where $P = (F_0^2 + 2F_c^2)/3$
Largest diff peak and hole	1.103 and −1.496 e/Å^3	0.488 and −1.240 e/Å^3	0.823 and −0.597 e/Å^3

since the softness of the halogen decisively affects its donor properties, reaction stoichiometry and solution media cannot be considered as the only reason for the structural preferences of copper(I), at least in the case of complexes investigated in this work. Consequently, this phenomenon needs more extensive studies in consideration of further structures of this series. Finally, extended Hückel calculations could not provide any evidence for significant interaction between the two copper(I) centres, despite the short Cu−Cu distance, in the case of the dimeric complex $[CuCl(PPh_3)(bzimtH_2)]_2$ (**3**).

Experimental Section

Materials and Instruments: Copper(I) chloride, copper(I) iodide, and all solvents are commercially available and were used as obtained, while the thiones (Merck or Aldrich) were recrystallized from hot ethanol prior to their use. Elemental analyses for C, H, N, and S were carried out with a Carlo erba EA MODEL 1108. Melting points were measured in open tubes with a STUART scientific instrument and are uncorrected. Infra-red spectra in the region of 4000−370 cm^{-1} were obtained in KBr discs while far-infrared spectra in the region of 400−50 cm^{-1} were obtained in polyethylene discs, with a Perkin−Elmer Spectrum GX FT-IR spectrometer. A Jasco UV/Vis/NIR V 570 series spectrophotometer was used to obtain the electronic absorption spectra.

Computational: Extended Hückel calculations were performed using the CACAO program.[17] The calculations were carried out using crystallographic data from the studied molecules. The EHT parameters for Cu were those established in the literature.

Synthesis of the Complexes: The complexes were prepared according to the following general procedure. A suspension of copper(I) halide (0.5 mmol) and triphenylphosphane (132 mg, 0.5 mmol) in 10 cm^3 of acetonitrile was stirred until a white precipitation of the intermediate $[Cu_nX_n(PPh_3)_m]$ (X = Cl or I) complex was formed. A solution of the appropriate thione (0.5 mmol beznimidazoline-2-thione (bzimtH) or benzthiazoline-2-thione (bztzdtH) in methanol was then added and the new suspension was stirred until clear (15 min). The resulting solution was filtered off and the clear solution was kept in darkness at room temperature. After 24 hours, crystals of the complexes suitable for single crystal analysis by X-ray crystallography were obtained by filtration.

$[CuI(PPh_3)_2(bzimtH)]$ (1): Pale yellow crystals. Yield 340 mg (72%), m.p. 221−222 °C; $C_{43}H_{36}CuIN_2P_2S{\cdot}CH_3OH{\cdot}0.85CH_3CN{\cdot}0.27H_2O$: C 59.36, H 4.77, N 4.42; found C 59.55, H 4.63, N 4.30%. IR $\tilde{\nu}$ (cm^{-1}): 3050 w, 1619 m, 1493 s, 1434 vs, 1161 s, 1093 s, 742 vs, 694 vs, 603 s, 517 vs, 490 vs; far-IR $\tilde{\nu}$ (cm^{-1}): 218 m, 200 m, 174 s, 162 s, 151vs, 146 m, 121 s. UV-Vis, λ_{max} (logε), $CHCl_3$: 241 (4.373), 310 (4.412).

$[CuI(PPh_3)_2(bztzdtH)]$ (2): Orange crystals. Yield 335 mg (76%), m.p. 218−219 °C; $C_{43}H_{35}CuINP_2S_2$: C 58.54, H 3.99, N 1.59; found C 58.84, H 3.88, N 1.70%. IR $\tilde{\nu}$ (cm^{-1}): 3052 w, 1488 s, 1424 vs, 1322 s, 1094 s, 1029 s, 743 vs, 695 vs, 515 vs, 503 vs; far-IR $\tilde{\nu}$ (cm^{-1}): 219 m, 205 m, 200 m, 174 s, 164 s, 151 vs, 146 m, 121 s. UV-Vis, λ_{max} (logε), $CHCl_3$: 243 (4.471), 329.5 (4.304).

$[CuCl(PPh_3)(bzimtH)]_2$ (3): Pale yellow crystals. Yield 395 mg (77%), m.p. 249−250 °C; $C_{50}H_{42}Cl_2CuN_2P_2S_2$: C 58.71, H 4.13, N 5.48; found C 58.79, H 4.01, N 5.52%. IR $\tilde{\nu}$ (cm^{-1}): 3193 m, 3053 s, 1502 vs, 1459 vs, 1446 s, 1179 vs, 1095 s, 743 vs, 694 vs, 598 s, 520 vs, 501 vs; far-IR $\tilde{\nu}$ (cm^{-1}): 217 w, 200 w, 174 s, 163 s, 151 vs, 146 m, 121 s. UV-Vis, λ_{max} (logε), $CHCl_3$: 240.5 (4.358), 310.5 (4.530).

X-ray Crystallographic Study: The unit cell and intensity data were collected on a Delft Instruments FAST diffractometer using the routines ENDEX, REFINE, and MADONL in the MADNES software suite[18] and processed using ABSMAD;[19] detailed procedures are described by Darr, Drake, Hursthouse, and Malik.[20] Absence of crystal decay in the X-ray beam was confirmed by checking equivalent reflections at the beginning and end of data collection, which lasted about 8 hours. The structures were solved with SIR92[21] and refined with SHELX93.[22] Details are given in Table 5. The copper, bromine, chlorine, iodine, sulfur, phosphorus, nitrogen, and carbon atoms were refined with anisotropic temperature factors. The hydrogen atoms were allowed to ride on their attached atoms with common isotropic temperature factors for methyl and non-methyl hydrogens. An absorption correction was made with DIFABS.[23]

CCDC-174528 (**1**), -174529 (**2**), and -174526 (**3**) contain the supplementary crystallographic data for this paper. These data can be obtained free of charge at www.ccdc.cam.ac.uk/conts/retrieving.html [or from the Cambridge Crystallographic Data Centre, 12, Union Road, Cambridge CB2 1EZ, UK; Fax: (internat.) +44−1223/336-033; E-mail: deposit@ccdc.cam.ac.uk].

Acknowledgments

We thank the EPSRC X-ray crystallographic service at the University of Wales, Cardiff, (now based in Southampton) for data collection.

[1] K. B. Karlin, J. Zubieta (Eds.), *Copper Coordination Chemistry. Biochemical and Inorganic Perspectives*, Adenine, New York, **1983**.
[2] E. S. Raper, *Coord. Chem. Rev.* **1994**, *129*, 91−156.
[3] A. Baiada, F. H. Jardine, D. Willett, *Inorg. Chem.* **1990**, *29*, 3042−3046.
[4] P. Aslanidis, S. K. Hadjikakou, P. Karagiannidis, B. Kojic-Prodic, M. Luic, *Polyhedron* **1994**, *13*, 3119−3125.
[5] P. Aslanidis, S. K. Hadjikakou, P. Karagiannidis, M. Gdaniec, Z. Kosturkiewicz, *Polyhedron* **1993**, *12*, 2221−2226 and references therin.
[6] S. K. Hadjikakou, P. Aslanidis, P. Karagiannidis, A. Aubry, S. Skoulika, *Inorg. Chim. Acta* **1992**, *193*, 129−135.
[7] P. Karagiannidis, S. K. Hadjikakou, P. Aslanidis, A. Hountas, *Inorg. Chim. Acta* **1990**, *178*, 27−34.
[8] S. K. Hadjikakou, P. Aslanidis, P. Karagiannidis, D. Mentzafos, A. Terzis, *Polyhedron* **1991**, *10*, 935−840.
[9] S. K. Hadjikakou, P. Aslanidis, P. Karagiannidis, A. Hountas, A. Terzis, *Inorg. Chim. Acta* **1991**, *184*, 161−166.
[10] P. Karagiannidis, P. Aslanidis, D. P. Kessissoglou, B. Krebs, M. Dartmann, *Inorg. Chim. Acta* **1989**, *156*, 47−56.
[11] C. Lecomte, S. Skoulika, P. Aslanidis, P. Karagiannidis, S. Papastefanou, *Polyhedron* **1989**, *8*, 1103−1109.
[12] A. A. Del Paggio, D. R. McMillin, *Inorg. Chem.* **1983**, *22*, 691−692.
[13] C. Kutal, *Coord. Chem. Rev.* **1990**, *99*, 213−252.
[14] P. Karagiannidis, P. Aslanidis, S. Papastefanou, D. Mentzafos, A. Hountas, A. Terzis, *Polyhedron* **1990**, *9*, 981−986.
[15] P. Aslanidis, S. K. Hadjikakou, P. Karagiannidis, P. J. Cox, *Inorg. Chim. Acta* **1998**, *271*, 243−247.
[16] S. K. Hadjikakou, P. Aslanidis, P. D. Akrivos, P. Karagiannidis, B. Kojic-Prodic, M. Luic, *Inorg. Chim. Acta* **1992**, *197*, 31−38.
[17] C. Mealli, D. Proserpio, C. A. C. A. O. (Computer Aided Com-

position of Atomic Orbitals) PC Ver. 4.0, *J. Chem. Education* **1990**, *67*, 399−402.
[18] J. W. Pflurgrath, A. Messerschmidt, *MADNES*, Version 11, September **1989**. Distributed by Delft Instruments, Delft, The Netherlands.
[19] A. I. Karaulov, *ABSMAD*, Program for FAST data Processing, University of Wales, Cardiff, **1992**.
[20] J. A. Darr, S. R. Drake, M. B. Hursthouse, K. M. A. Malik, *Inorg. Chem.* **1993**, *32*, 5704−5708.
[21] A. Altomare, M. C. Burla, M. C. Camalli, G. Cascarano, C. Giacovazzo, A. Guagliardi, G. Polidori, *J. Appl. Cryst.* **1994**, *27*, 435−436.
[22] G. M. Sheldrick, *SHELXL-93*, Program for the Refinement of Crystal Structures, University of Goettingen, Germany, **1994**.
[23] N. Walker, D. Stuart, *Acta Crystallogr., Sect. A* **1983**, *39*, 158−166.

Received January 25, 2002
[I02044]

EurJIC
European Journal of Inorganic Chemistry

September 2002
Issue 9
Pages 2223–2518

COVER PICTURE

The cover picture shows the structures of several vanadium(III) complexes that contain η^2-pyrazolato ligands, along with orbital interactions that stabilize the η^2-pyrazolato ligand bonding mode. Details are discussed in the article by C. H. Winter et al. on p. 2327 ff.

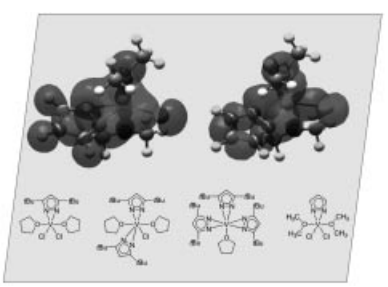

MICROREVIEW

Contents

2239 **D. Carmona,* M. P. Lamata, L. A. Oro**

Half-Sandwich Complexes with Aminocarboxylate Ligands and Their Use as Enantioselective Hydrogen Transfer Catalysts

Keywords: Chiral-at-metal complexes / Asymmetric hydrogen transfer catalysis / Rhodium / Ruthenium / Iridium / Osmium / Aminocarboxylate ligands

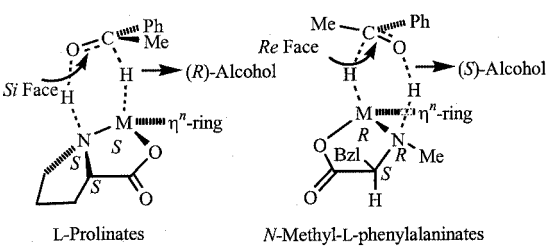

 © WILEY-VCH Verlag GmbH, 69451 Weinheim, Germany, 2002 1434–1948/02/0909–2227 $ 20.00+.50/0

SHORT COMMUNICATIONS

2253 A. Eichhöfer,* E. Tröster

Synthesis and Structure of the new cluster $[Hg_{10}Se_4(SePh)_{12}(PPh_2nPr)_4]$ and its Conversion into $[Hg_{32}Se_{14}(SePh)_{36}]$

Keywords: Cluster compounds / Mercury / Selenium / UV/Vis spectroscopy

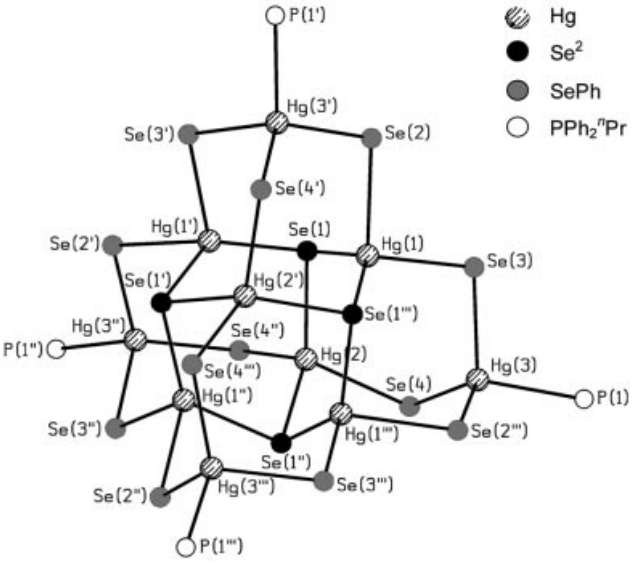

2257 P. J. Steel,* N. C. Webb

Diels–Alder Synthesis of Rigid 60° Angular Bridging Ligands and X-ray Crystal Structures of their Silver Nitrate Complexes

Keywords: Silver / Coordination polymers / Bridging ligands / Self-assembly / N ligands

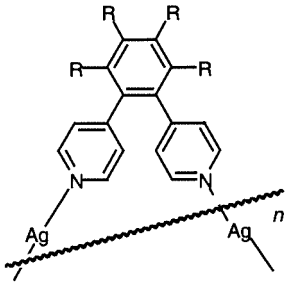

2261 L. Wesemann,* S. Hagen, T. Marx, I. Pantenburg, M. Nobis, B. Drießen-Hölscher*

Reactivity of Platinum Stanna-*closo*-dodecaborate Complexes: First Hydroformylation Studies

Keywords: Boranes / Cluster compounds / Homogeneous catalysis / Platinum / Tin

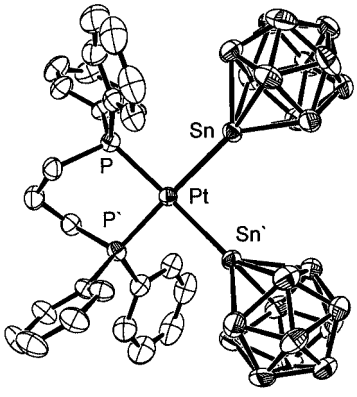

$[(dppp)Pt(SnB_{11}H_{11})_2]^{2-}$

2266 T. Chivers,* G. Schatte

A New Coordination Mode for the Tripodal $[Te(NtBu)_3]^{2-}$ Dianion: Preparation and Structures of $\{ClIn[Te(NtBu)_3]\}_2$ and $\{LiIn[Te(NtBu)_3]_2\}\cdot LiCl$

Keywords: Indium / Tellurium / Imido compound / Tridentate ligand

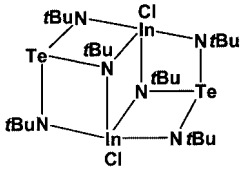

FULL PAPERS

2271 **J. Beck,* A. Hormel, M. Koch**

1,2-Dichalcogenolylium Ions $(C_3Cl_3E_3)^+$ from Equilibria Involving Dichalcogen Dichlorides E_2Cl_2 (E = S, Se, Te) − Syntheses and Crystal Structures of $(C_3Cl_3S_2)Cl$, $(C_3Cl_3Se_2)Cl$, and $(C_3Cl_3Te_2)_2[Te_2Cl_{10}]$

Keywords: Chalcogens / Heterocycles / Cations / Solvothermal synthesis

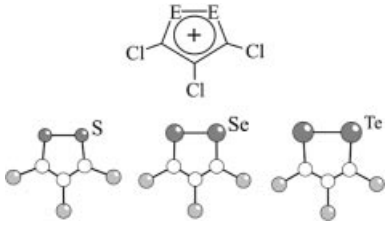

2276 **J. Hermann, D. Schumacher, A. Erxleben***

Anion-Dependent Substitution of Zinc by Magnesium in Mononuclear Schiff Base Complexes

Keywords: Schiff bases / Zinc / Magnesium / Crystal structures

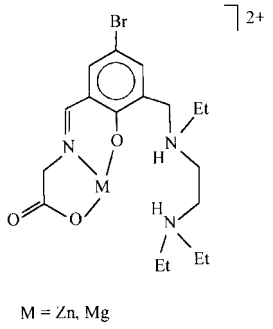

M = Zn, Mg

2281 **R. Andrés,* E. de Jesús,* F. J. de la Mata, J. C. Flores, R. Gómez**

Titanocene and Zirconocene Complexes containing Dendrimer-Substituted Cyclopentadienyl Ligands − Synthesis and Ethylene Polymerization

Keywords: Metallocenes / Dendrimers / Titanium / Zirconium / Substituent effects

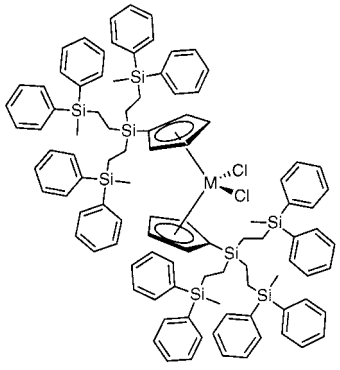

2287 **E. Balogh-Hergovich, J. Kaizer, J. Pap, G. Speier,* G. Huttner, L. Zsolnai**

Copper-Mediated Oxygenolysis of Flavonols via Endoperoxide and Dioxetan Intermediates; Synthesis and Oxygenation of $[Cu^{II}(Phen)_2(Fla)]ClO_4$ and $[Cu^{II}(L)(Fla)_2]$ [FlaH = Flavonol; L = 1,10-Phenanthroline (Phen), 2,2′-Bipyridine (Bpy), *N*,*N*,*N*′,*N*′-Tetramethylethylenediamine (TMEDA)] Complexes

Keywords: Enzyme models / Copper / Peroxides / Kinetics

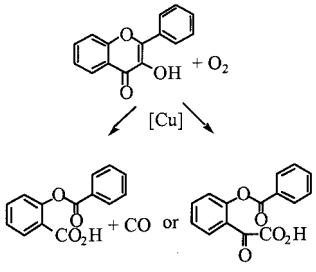

2296 **R. J. Schaller, G. Haberhauer, R. Gleiter,* F. Rominger**

Synthesis and Properties of Donor/Acceptor-Substituted Metal-Capped Twofold-Sila-Bridged Cyclobutadieno Superphanes

Keywords: Donor-acceptor systems / Phanes / Cyclic voltammetry / Electron transfer / Cobalt

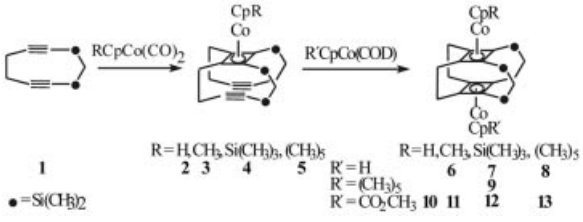

2305 **F. Stöhr, D. Sturmayr, G. Kickelbick, U. Schubert***

C−Cl and Si−Cl Activation by *P,N*-Chelated Pt^{II} Complexes

Keywords: Platinum / Silicon / Hemilabile ligands / Oxidative addition / Halogen compounds

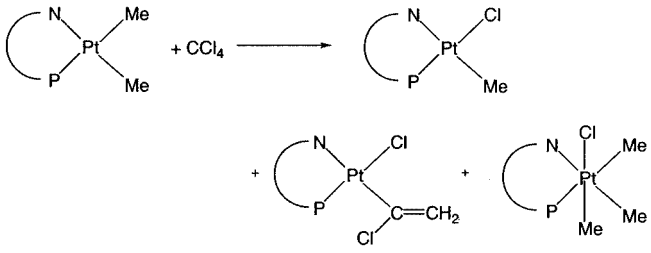

2312 **M. Robitzer, C. Sirlin,* N. Kyritsakas, M. Pfeffer***

Molecular Recognition of Anions by a Novel Organocobalt Receptor: Oxyanion versus Halide Selectivity in Water

Keywords: Host-Guest Systems / Cobalt / N,C ligand / Anions / Allosterism

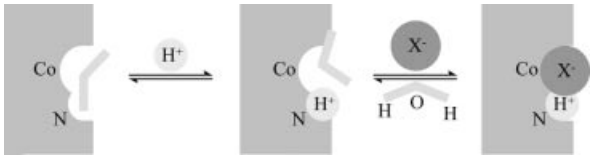

2320 **B. Štíbr,* J. Holub, M. Bakardjiev, D. Hnyk, O. L. Tok, W. Milius, B. Wrackmeyer**

Phosphacarborane Chemistry: The Synthesis of the Parent Phosphadicarbaboranes *nido*-7,8,9-$PC_2B_8H_{11}$ and [*nido*-7,8,9-$PC_2B_8H_{10}$]$^-$, and Their 10-Cl Derivatives − Analogs of the Cyclopentadienide Anion

Keywords: Ab initio calculations / Boranes / Clusters / Phosphorus

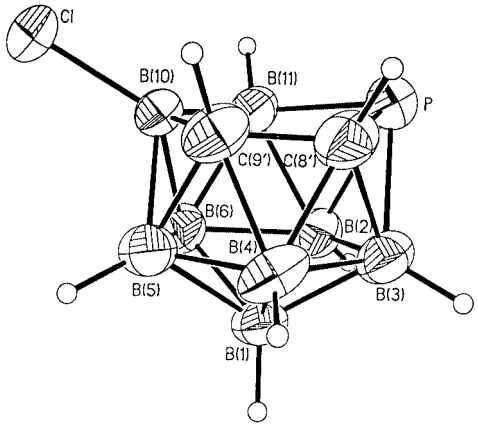

2327 **K. R. Gust, J. E. Knox, M. J. Heeg, H. B. Schlegel, C. H. Winter***

Synthesis, Structure, and Molecular Orbital Calculations of (Pyrazolato)vanadium(III) Complexes − Understanding η^2-Pyrazolato Ligand Coordination on d^2 Metal Centers

Keywords: Vanadium / Pyrazolato ligands / Ab initio calculations / N ligands / Coordination modes

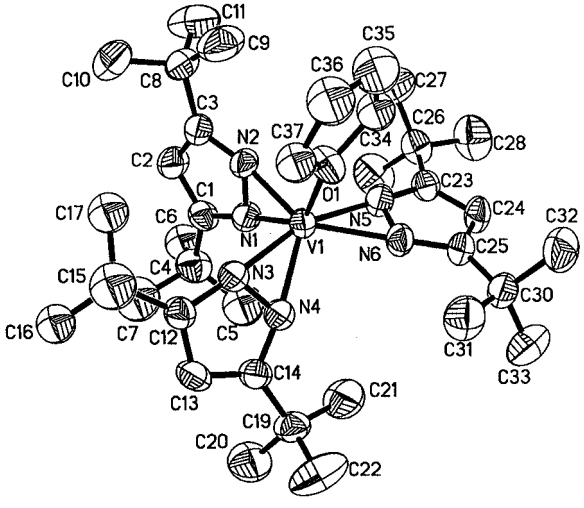

2335 **A. L. Rheingold, G. P. A. Yap, L. N. Zakharov, S. Trofimenko***

Homoscorpionate Ligands Based on 3-(Cyclobutyl)pyrazole and 3-(Cyclopentyl)pyrazole

Keywords: Scorpionates / Cobalt / Borates / N ligands

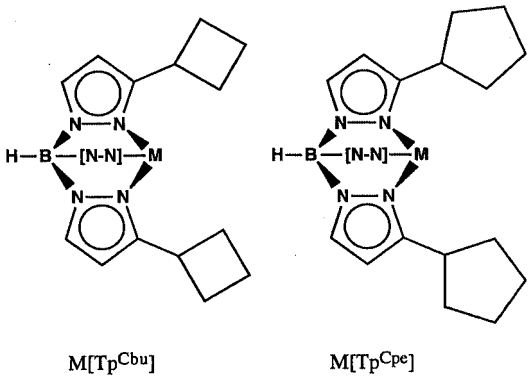

2344 **P. Starynowicz,* K. Bukietyńska, S. Gołąb, W. Ryba-Romanowski, J. Sokolnicki**

Europium(II) Complexes With Benzo-18-Crown-6

Keywords: Europium / Lanthanides / Crown compounds / X-ray diffraction / Luminescence

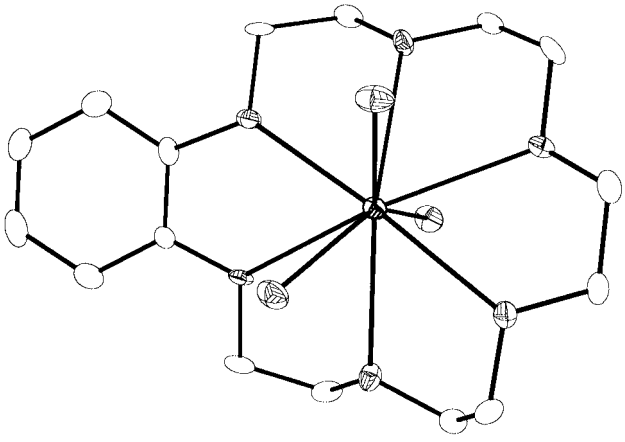

2348 **M. L. Durán, J. A. García-Vázquez,* C. Gómez, A. Sousa-Pedrares, J. Romero, A. Sousa***

Electrochemical Synthesis of Cobalt Complexes with 4-Methyl-*N*-(2-pyridylmethyl)benzenesulfonamide (HL) − Crystal Structures of HL, $[Co^{II}L_2]$ and $[Co^{III}L_2L^o]$ [L^o = {HNC-$(CH_3)\}_2C(CN)$

Keywords: Cobalt / Electrochemistry / N ligands / X-ray crystal structures

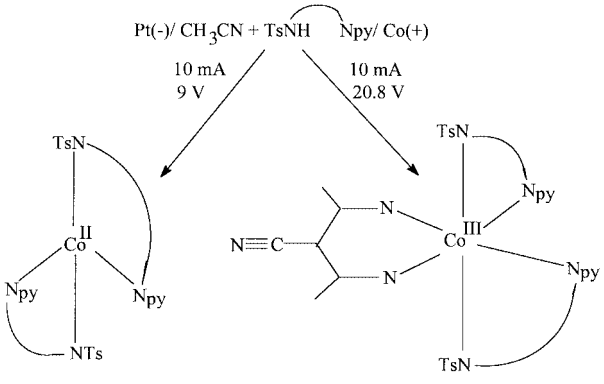

2355 **O. Kristiansson**

Structures of Complexes of Thallium(I) and Functionalized Benzoate Ligands with Pronounced Stereoactivity of the Lone Pair of Electrons and Metal−Phenyl π-Bonding

Keywords: Thallium(I) / Stereoactive inert pair / Thallophilic interaction / Coordination polymer / Metal−phenyl π-bonding

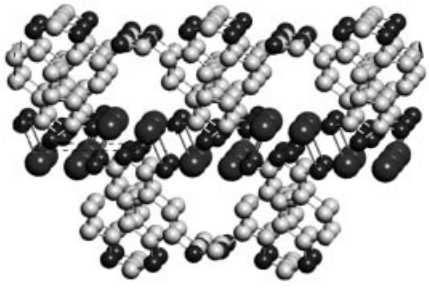

2362 M. M. Corradi, M. A. D. McGowan, P. C. McGowan,* M. Thornton-Pett

The Synthesis and Structure of Bis- and Tris(amino)-Functionalised Cyclopentadienylyttrium DerivativesBis- and Tris(amino)-Functionalised Cyclopentadienylyttrium Derivatives

Keywords: N ligands / Cyclopentadienyl ligands / Yttrium

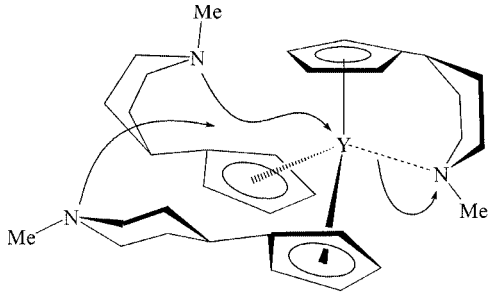

2367 S. Youngme, G. A. van Albada, H. Kooijman, O. Roubeau, W. Somjitsripunya, A. L. Spek, C. Pakawatchai, J. Reedijk*

A Unique Dinuclear Cu^{II} Compound with Two Phase Transitions Clearly Visible from Thermal and Magnetic Behaviour; Synthesis, Magnetism and X-ray Structures at Three Temperatures of Bis(di-2-pyridylamine)bis(μ-hydroxo)bis(μ-perchlorato-*O*,*O*)dicopper(II)

Keywords: Copper / Bridging ligands / Magnetic properties / Phase transitions / X-ray structure

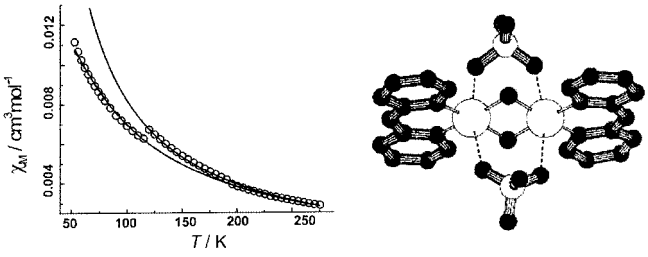

2375 B. A. J. Jansen, P. Wielaard, H. den Dulk, J. Brouwer, J. Reedijk*

Oxa-aza Crown Ethers as Ligands for Mixed-Ligand Cisplatin Derivatives and Dinuclear Platinum Anticancer Drugs

Keywords: Anticancer drugs / Platinum / DNA binding / Crown ethers / A2780 human ovarian cancer

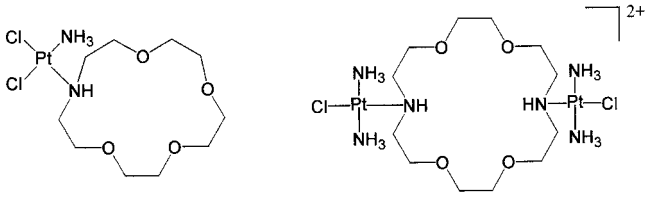

2380 D. G. Samsonenko, J. Lipkowski, O. A. Gerasko, A. V. Virovets, M. N. Sokolov, V. P. Fedin,* J. G. Platas, R. Hernandez-Molina, A. Mederos

Cucurbituril as a New Macrocyclic Ligand for Complexation of Lanthanide Cations in Aqueous Solutions

Keywords: Lanthanides / Solid-state structures / Supramolecular chemistry / Aqua complexes / Cucurbituril

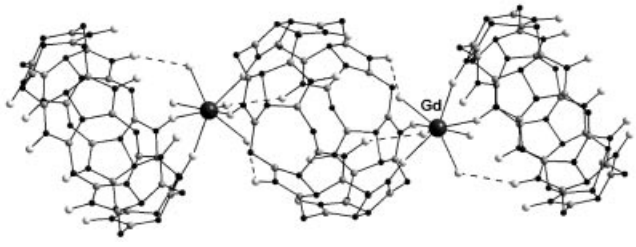

2389 **A. Fernández,* D. Vázquez-García, J. J. Fernández, M. López-Torres, A. Suárez, S. Castro-Juiz, J. M. Vila***

The First Crystal and Molecular Structure of a *syn*-Acetato-Bridged Dinuclear Cyclometallated Complex $[Pd\{2,3,4\text{-}(MeO)_3C_6HC(H)=NCH_2\text{-}CH_2OH\}(\mu\text{-}OAc)]_2$

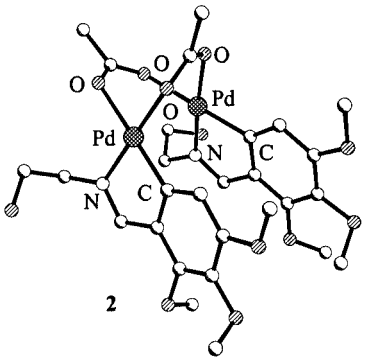

2

Keywords: C-H activation / Cyclometallation / P ligands / Schiff bases / Palladium

2402 **E. Palma, J. D. G. Correia, Â. Domingos, I. Santos***

New Mixed-Ligand Re^V Complexes with Bis-(2-mercaptoethyl) Sulfide and Functionalized Thioimidazolyl Ligands

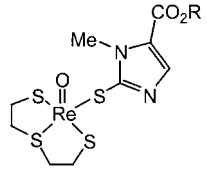

1 (R = Me), **3** (R = GlyGly)

Keywords: S ligands / Rhenium / Peptides / N ligands

2408 **S. M. Aucott, A. M. Z. Slawin, J. D. Woollins***

Synthesis and Late Transition Metal Complexes of the Heterofunctional Phosphane *o*-$Ph_2PNHC_6H_4P(S)Ph_2$

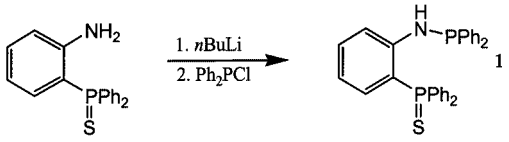

Keywords: Phosphorus−sulfur ligands / Monodentate complexes / Chelate complexes

2419 **M. Knorr,* I. Jourdain, G. Crini, K. Frank, H. Sachdev, C. Strohmann**

Synthesis, Reactivity and Molecular Structures of Bis(diphenylphosphanyl)methane-Bridged Heterobimetallic Iron−Platinum Isocyanide Complexes: Breaking and Formation of Metal−Metal Bonds

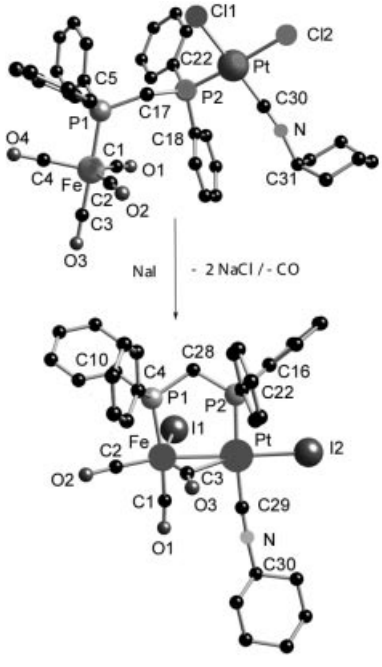

Keywords: Heterobimetallics / Isocyanide ligands / Metal−metal interactions / Iron / Platinum

2427 E. Solomon-Rapaport, A. Masarwa,* H. Cohen, J. S. Valentine, D. Meyerstein

The Case of (2,3,9,10-Tetramethyl-1,4,8,11-tetraazacyclotetradeca-1,3,8,10-tetraene)(H_2O)-$Co^{III}-OOR^{2+}$ (R = CH_2OH, CH_2CN, CCl_3) and Reactions with the Methylperoxyl Radical

Keywords: Cobalt / Peroxides / Radicals / Radiation chemistry

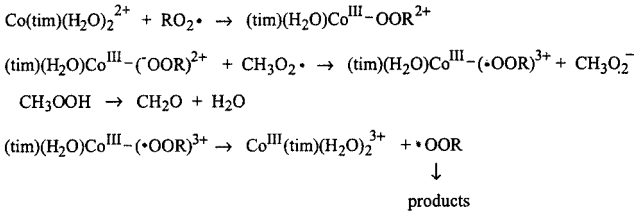

2433 J. Mathieu, A. Marsura,* N. Bouhmaida, N. Ghermani

Selective Self-Assembly of a Sequential Bipyridine−Bipyrazine Ligand Strand into a Double-Stranded Cu^I Helicate

Keywords: Helicates / Self-assembly / Copper / NMR spectroscopy / N ligands

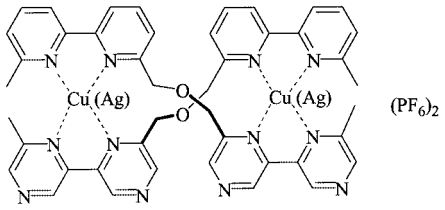

5 (6)

2438 L. Weber,* A. Rausch, H. B. Wartig, H.-G. Stammler, B. Neumann

Chiral 2,3-Dihydro-1*H*-1,3,2-diazaboroles

Keywords: Boron / Chirality / Diazaboroles / Heterocycles / Crystal structure

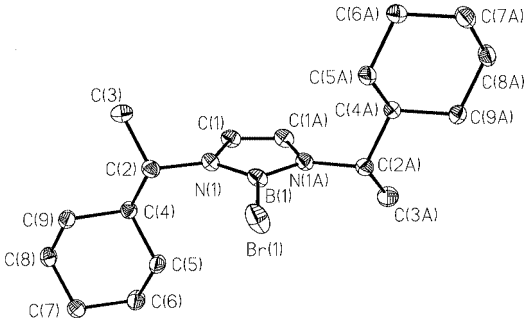

2447 Y. Yamamoto,* H. Settu, K. Nishiyama, K. Kuge, K. Tatsumi

Unprecedented Formation of Dinuclear Macrocyclic Complexes by Insertion of 2,3,5,6-Tetrafluoro-7,7,8,8-tetracyanoquinodimethane (F4-Tcnq) into a C−H Bond and Subsequent Coordination to Metal Atoms

Keywords: Cyclopentadienyl ligands / Rhodium / Iridium / Lithium / Macrocyclic ligands

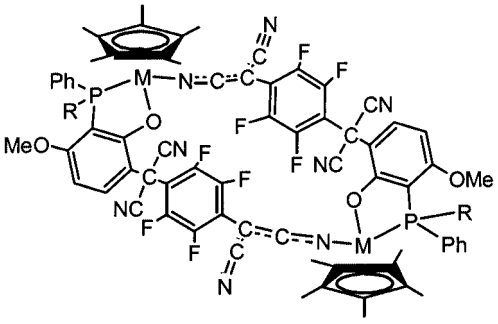

2453 L. Mimassi, C. Guyard-Duhayon, L. Raehm, H. Amouri*

Serendipity and Rational Design of One-Dimensional Doubly Stranded Chains with Nanometric Cavities Based on Ag^I Coordination Chemistry

Keywords: Coordination chemistry / Polymers / Silver / Self-assembly / Supramolecular chemistry

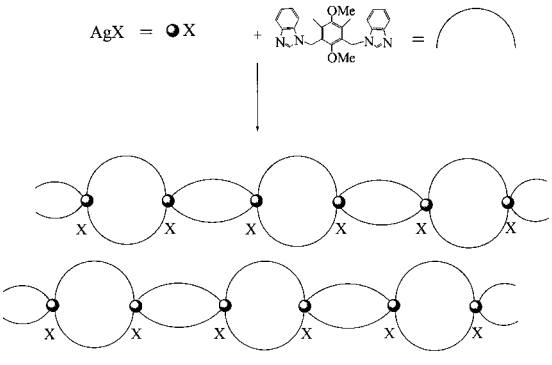

X = $CF_3SO_3^-$ (**3a**); BF_4^- (**3b**)

2458 **M. Gelinsky, H. Vahrenkamp***

Zinc Complexes of a Helical 22-mer Peptide with Two Histidine Donors

Keywords: Zinc / Peptides / Bioinorganic chemistry / Enzyme mimics

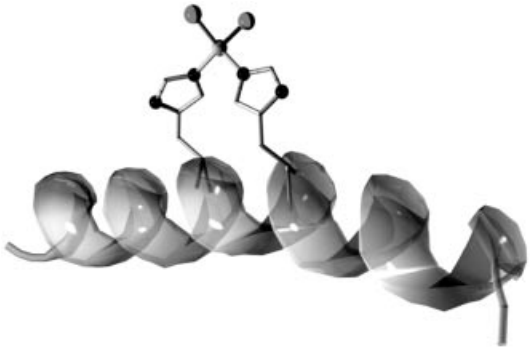

2463 **M. J. Martínez-Lope, J. A. Alonso,* M. T. Casais, M. T. Fernández-Díaz**

Preparation, Crystal and Magnetic Structure of the Double Perovskites Ba_2CoBO_6 (B = Mo, W)

Keywords: Perovskite structure / Neutron diffraction / Magnetic properties / Antiferromagnetic ordering / Cobalt

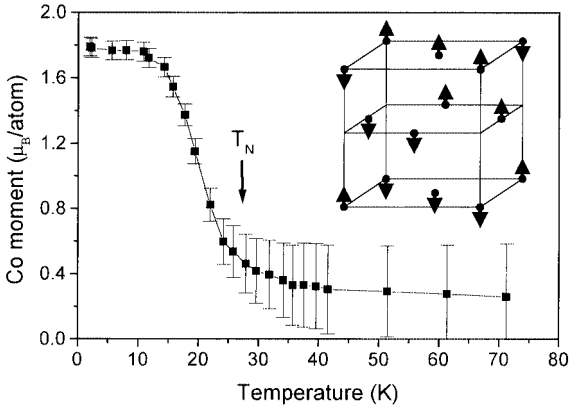

2470 **A. Antiñolo, R. Fernández-Galán, I. Orive, A. Otero,* S. Prashar**

New Group 4 Metallocene and Niobocene Complexes Containing Phosphane-Functionalized *ansa*-Ligands

Keywords: Metallocenes / Niobium / Phosphane ligands / Homogeneous catalysis / Insertion

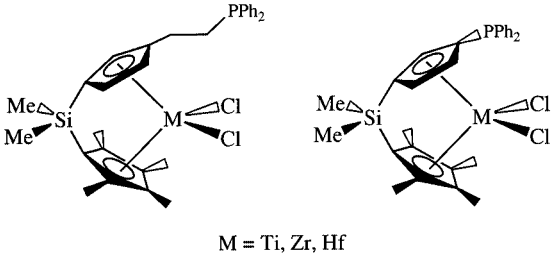

2477 **M. Benito, O. Rossell,* M. Seco, G. Muller, J. I. Ordinas, M. Font-Bardia, X. Solans**

Palladium and Platinum Units Grafted on the Periphery of Carbosilane Dendrimers

Keywords: Dendrimers / Alkynes / Homogeneous catalysis / Palladium / Platinum

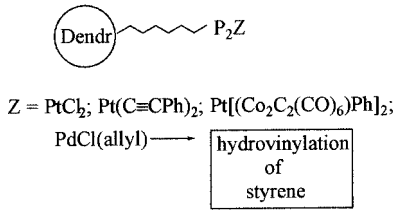

2488 **G. S. Papaefstathiou, R. Vicente, C. P. Raptopoulou, A. Terzis, A. Escuer, S. P. Perlepes***

A One-Dimensional Manganese(II) Coordination Polymer Derived from Zerovalent Manganese and 1-Hydroxybenzotriazole − Synthesis, Characterization, Crystal Structure and Magnetic Properties

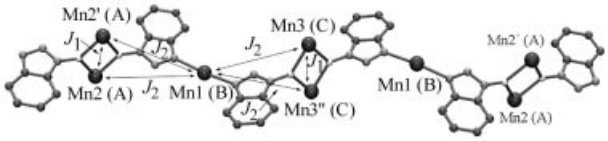

Keywords: Coordination polymers / Nitrogen heterocycles / Magnetic properties / Manganese / X-ray crystal structure

2494 **H. Brunner,* J. Klankermayer, M. Zabel**

Synthesis, Stereochemistry and Molecular Structures of Chiral-at-Metal (Cycloheptatrienyl)-molybdenum Complexes Containing the Diphosphane Prophos

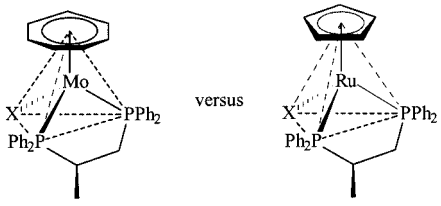

Keywords: Chirality / Molybdenum / Half-sandwich complexes / Configuration determination

2502 **G. Fernández, M. Corbella,* J. Mahía, M. A. Maestro**

Polynuclear Mn^{II} Complexes with Chloroacetate Bridge − Syntheses, Structure, and Magnetic Properties

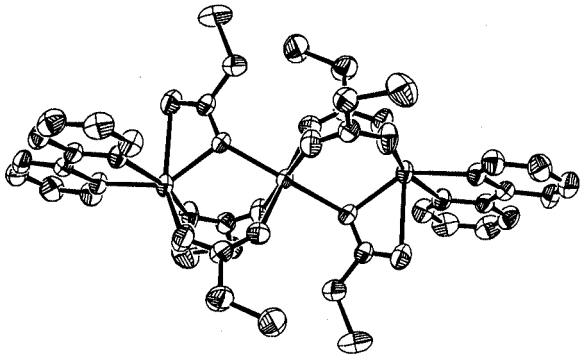

Keywords: Manganese / Crystal structures / Magnetic properties / EPR spectroscopy / Bridging ligands

2511 **T. M. Klapötke,* H. Nöth, T. Schütt, M. Suter**

Mixed Chloride/Azide Complexes of Arsenic and Antimony

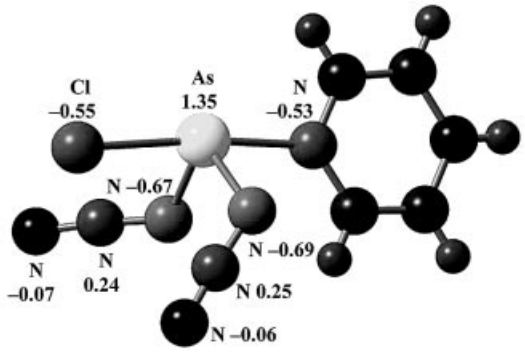

Keywords: Azides / Antimony / Arsenic / Lewis acids / Lewis bases / Density functional calculations

Half-Sandwich Complexes with Aminocarboxylate Ligands and Their Use as Enantioselective Hydrogen Transfer Catalysts

Daniel Carmona,*[a] María Pilar Lamata,[b] and Luis A. Oro[a]

Keywords: Chiral-at-metal complexes / Asymmetric hydrogen transfer catalysis / Rhodium / Ruthenium / Iridium / Osmium / Aminocarboxylate ligands

Chiral-at-metal half-sandwich complexes of rhodium, iridium, ruthenium, or osmium of the general formula [(η^n-ring)M(Aa)Cl] [(η^n-ring)M = (η^5-C_5Me_5)Rh, (η^5-C_5Me_5)Ir, (η^6-*p*-MeC_6H_4*i*Pr)Ru, (η^6-*p*-MeC_6H_4*i*Pr)Os; Aa = L-α-aminocarboxylate] can readily be prepared from the corresponding dimers [{(η^n-ring)MCl}$_2$(μ-Cl)$_2$]. The compounds have been prepared as diastereomeric mixtures of the two epimers at the metal center. In general, alkynyl aminocarboxylate derivatives [(η^n-ring)M(Aa)(C≡CR)] are obtained by treating the aforementioned chlorides with the corresponding alkynes in basic media. However, the reaction of the (alaninato)rhodium chloride [(η^5-C_5Me_5)Rh(Ala)Cl] with the alkynes HC≡CR (R = Ph, *p*-tolyl) produced the alkynylcyclobutadiene complexes [(η^5-C_5Me_5)Rh(η^4-C_4HR_2C≡CR)] (R = Ph, *p*-tolyl). Treatment of the chlorides [(η^n-ring)M(Aa)Cl] with $AgBF_4$ afforded the cationic trimers [{(η^n-ring)M(Aa)}$_3$](BF_4)$_3$. Trimerization occurs with chiral self-recognition: only the (*R*,*R*,*R*) or (*S*,*S*,*S*) configuration at the metal trimers can be detected. The trimers [{(η^n-ring)M(Aa)}$_3$](BF_4)$_3$ reacted with tertiary phosphanes, leading to the cationic mononuclear complexes [(η^n-ring)M(Aa)(PR_3)](BF_4). The assignment of the configuration at the metal center was accomplished by X-ray diffraction, circular dichroism and NMR spectroscopy. Most of the aminocarboxylate derivatives epimerized at the metal center. On the basis of kinetic and spectroscopic data, a general mechanism is proposed for the epimerization process. Neutral [(η^n-ring)M(Aa)Cl] and cationic [{(η^n-ring)M(Aa)}$_3$](BF_4)$_3$ complexes are active catalysts for the hydrogen transfer reaction from 2-propanol to acetophenone. Conversions of up to 97% and enantioselectivities up to 75% were achieved. A proposal about the origins of the enantioselectivity is given.
(© Wiley-VCH Verlag GmbH, 69451 Weinheim, Germany, 2002)

1. Introduction

Organometallic complexes containing stereogenic metal centers are ideally suited to obtain mechanistic information about the stereochemical course of reactions.[1−5] Most of these complexes posses half-sandwich geometries and contain chiral chelating ligands of C_1 symmetry.[6] Among

[a] Facultad de Ciencias, Instituto de Ciencia de Materiales de Aragón (Universidad de Zaragoza − CSIC)
50009 Zaragoza, Spain
Fax: (internat.) + 34-976/761187
E-mail: dcarmona@posta.unizar.es
[b] Escuela Universitaria de Ingeniería Técnica Industrial, Instituto de Ciencia de Materiales de Aragón (Universidad de Zaragoza − CSIC), 50009 Zaragoza, Spain

Daniel Carmona (top, left) obtained his PhD degree in chemistry in 1980 at the University of Zaragoza under the supervision of Prof. Usón. After a postdoctoral stay at the E.T.H. of Zürich with Prof. Venanzi he returned to the University of Zaragoza joining Prof. Oro's group. Since 1988 he is a Research Scientist (Spanish Council for Scientific Research) at the Instituto de Ciencia de Materiales de Aragón. His current research interest is focused on the development of chiral transition metal catalysts, as well as in their application to asymmetric catalysis.

María Pilar Lamata (top, right) obtained her PhD degree in chemistry in 1983 at the University of Zaragoza under the supervision of Drs. Carmona and Oro. In 1986, she was appointed Associate Professor of Inorganic Chemistry at the University of Zaragoza. Her current research interests concern the study of chiral transition metal complexes and their use as enantioselective catalysts.

Luis A. Oro (bottom, left) received his PhD in 1970. After postdoctoral studies at Cambridge University he has served on the faculties of the University of Zaragoza, Madrid Complutense, and Santander. He was appointed to the Chair of Inorganic Chemistry in Zaragoza in 1982. His main research interests are in the field of organometallic and coordination chemistry and homogeneous catalysis, with particular focus on late transition metals. He has been co-author of a book on Homogeneous Hydrogenation, and more recently co-editor of a book on Metal Clusters in Chemistry. He is President of the Spanish Royal Society of Chemistry and member of the editorial board of several scientific journals, including the European Journal of Inorganic Chemistry.

MICROREVIEWS: This feature introduces the readers to the authors' research through a concise overview of the selected topic. Reference to important work from others in the field is included.

them, transition-metal complexes with α-aminocarboxylates as ligands constitute an important class of compounds as they are closely related to both biochemistry and organometallic chemistry.[7]

In this context, Dersnah and Baird reported[8] in 1977 that the dimer $[\{(\eta^6\text{-}C_6H_6)RuCl\}_2(\mu\text{-}Cl)_2]$ reacted with glycinate or alaninate anions to form the pseudotetrahedral complexes $[(\eta^6\text{-}C_6H_6)Ru(Aa)Cl]$ (Aa = glycinate, L,D-alaninate), in which the ruthenium ion is chiral. After a strikingly dormant period, over the last decade several (η^6-arene)ruthenium[9–11] or -osmium[12] compounds, as well as (η^5-pentamethylcyclopentadienyl)rhodium,[9,13,14] -iridium[9,13–18] or -ruthenium[19,20] complexes with a variety of α-aminocarboxylate ligands have been reported.

On the other hand, half-sandwich compounds with chiral chelate ligands have been successfully employed as enantioselective catalysts. In particular, chiral (arene)ruthenium(II) complexes with α-aminocarboxylates,[21] L-prolinamide derivatives,[22] or *N*-(*p*-toluenesulfonyl)-1,2-diphenylethylenediamine[23] as chiral ligands have achieved high levels of enantioselectivity in asymmetric transfer hydrogenations with 2-propanol as the hydrogen donor. The prolinamide complexes are also active catalysts for the asymmetric hydrogen transfer reduction of aromatic ketones in aqueous media.[24,25]

Our contribution to this field started with the publication in 1990 of a series of optically active pseudotetrahedral rhodium(III), iridium(III), and ruthenium(II) complexes with L-alaninato and L-prolinato ligands.[26] Since then, we have continued with the study of this type of compounds, including their application in enantioselective hydrogen transfer reactions. This Microreview presents our results in this area.

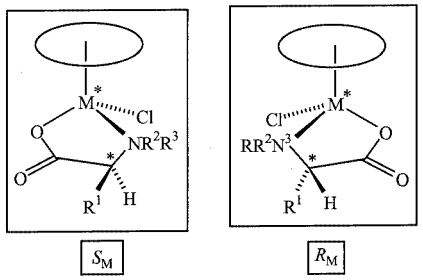

M = η^5-(C_5Me_5)M, (M = Rh, Ir); η^6-(*p*-MeC_6H_4iPr)M, (M = Ru, Os)

R^1	R^2	R^3	Abbrv.
Me	H	H	Ala
Et	H	H	Abu
*n*Pr	H	H	Ape
*i*Pr	H	H	Val
*n*Bu	H	H	Ahx
*s*Bu	H	H	Ile
*i*Bu	H	H	Leu
*t*Bu	H	H	Tle
Ph	H	H	Pgl
Bzl	H	H	Phe
Bzl	H	Me	MePhe
$(CH_2)_2$	H		Aze
$(CH_2)_3$	H		Pro
$(CH_2)_4$	H		Pip
$(CH_2)_3$	Me		MePro
$CH_2CHOHCH_2$	H		Hyp

Ala = Alaninate; Abu = 2-Aminobutyrate; Ape = 2-Aminopentanoate (norvalinate); Val = Valinate; Ahx = 2-Aminohexanoate (norleucinate); Ile = Isoleucinate; Leu = Leucinate; Tle = *tert*-leucinate; Pgl = Phenylglycinate; Phe = Phenylalaninate; MePhe = *N*-Methylphenylalaninate; Aze = 2-Azetidinecarboxylate; Pro = Prolinate; Pip = 2-Piperidinecarboxylate; MePro = *N*-Methylprolinate; Hyp = 4-Hydroxyprolinate

Scheme 1. L-α-Aminocarboxylato complexes

2. Chloro Complexes

The acetylacetonato complexes $[(\eta^n\text{-ring})M(acac)Cl]$ [$(\eta^n$-ring)M = (η^5-C_5Me_5)Rh, (η^5-C_5Me_5)Ir, (η^6-*p*-MeC_6H_4-*i*Pr)Ru; Hacac = acetylacetone], easily prepared from the corresponding dimer $[(\eta^n\text{-ring})MCl\}_2(\mu\text{-}Cl)_2]$ and Hacac,[27,28] reacted with stoichiometric amounts of free L-α-amino acids to give the neutral complexes $[(\eta^n\text{-ring})M(Aa)Cl]$ as a mixture of epimers at the metal center in an almost quantitative yield [Equation (1), Scheme 1].[29] The osmium analogues $[(\eta^6\text{-}p\text{-}MeC_6H_4iPr)Os(Aa)Cl]$ were prepared starting from $[\{(\eta^6\text{-}p\text{-}MeC_6H_4iPr)OsCl\}_2(\mu\text{-}Cl)_2]$, the amino acid and KOH [Equation (2)].[9,26,30–33]

$$[(\eta^n\text{-ring})M(acac)Cl] + HAa \rightarrow [(\eta^n\text{-ring})M(Aa)Cl] + Hacac \quad (1)$$

$$1/2\,[\{(\eta^6\text{-}p\text{-}MeC_6H_4iPr)OsCl\}_2(\mu\text{-}Cl)_2] + HAa + KOH \rightarrow [(\eta^6\text{-}p\text{-}MeC_6H_4iPr)Os(Aa)Cl] + KCl + H_2O \quad (2)$$

In solution, the diastereomeric composition of these compounds ranges from 0 to 100% *de*. In general, the lowest values correspond to aminocarboxylates such as Ala [*de* = 0 (Rh, Ir), 36% (Ru), 20% (Os)], Abu [*de* = 0 (Rh, Ir)], Val [*de* = 0 (Rh, Ir), 20% (Ru)] or Leu [*de* = 20% (Rh, Ir), 12% (Ru)], and the greatest to the conformationally more rigid cyclic amino acids [Pro = 90% (Rh, Ir), 80% (Ru), 86% (Os); MePro = 100% (Rh, Ir, Ru), 80% (Os)]. However, the complexes are configurationally labile at the metal center.[34] In this regard, the case of iridium prolinate [(η^5-C_5Me_5)Ir(Pro)Cl] is typical. A single crystal of the complex shows the presence of both epimers at the metal center in the unit cell in a 1:1 ratio (Figure 1). Nevertheless, for the same sample, a diastereomeric excess of 90% was measured by ^{1}H NMR spectroscopy in solution at room temperature, as stated above. The composition of the solid is maintained if the crystals are dissolved at −90 °C, but diastereomeric excesses of 30 and 90% were measured immediately after heating the sample to −35 °C and room temperature, respectively. The rhodium analogue [(η^5-C_5Me_5)Rh(Pro)Cl] behaves similarly. These facts indicate that (i) the epimerization process requires a low activation energy and proceeds at a high rate even at low temperatures and (ii) at room temperature, the measurements reflect thermodynamic compositions. A careful analysis of the crystal structures reveals that there is an intermolecular hydrogen-bond network. Thus, for example, in the iridium complex

(Figure 2), this network involves the NH group of the (R_{Ir}) isomer with the oxygen atoms of the carboxylate group of the (S_{Ir}) epimer [N(1b)···O(1a) = 3.196(11) Å, N(1b)H(1b)O(1a) = 140.9(9)°; N(1b)···O(2a) = 3.069(12) Å, N(1b)H(1b)O(2a) = 146.1(8)°], and the chloride ion of the (R_{Ir}) isomer with the NH group of the (S_{Ir}) epimer of the next unit cell [Cl(1b)···N(1a) = 2.510(8) Å, Cl(1b)H(1a)N(1a) = 145.2(7)°]. Most probably, the energy released from the formation of this network is the driving force for the observed epimerization on going from solution to the solid and, therefore, it would be precluded in *N*-substituted prolinates. In fact, we have only detected one diastereomer for the *N*-methylprolinates in both solid state and solution, and determined, from NOE measurements in solution and/or from X-ray diffraction analyses in the crystal, that it has an (*S*) configuration at the metal center for the four metals (Figure 3). On comparison of the circular dichroism (CD) spectrum of the *N*-methylprolinates with those of enriched mixtures of the remaining aminocarboxylates, we propose that the (*S*) configuration at the metal center is adopted for the major component of the mixtures, in all cases.

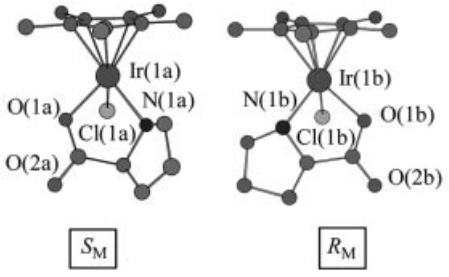

Figure 1. Molecular structure of [(η^5-C_5Me_5)Ir(Pro)Cl]

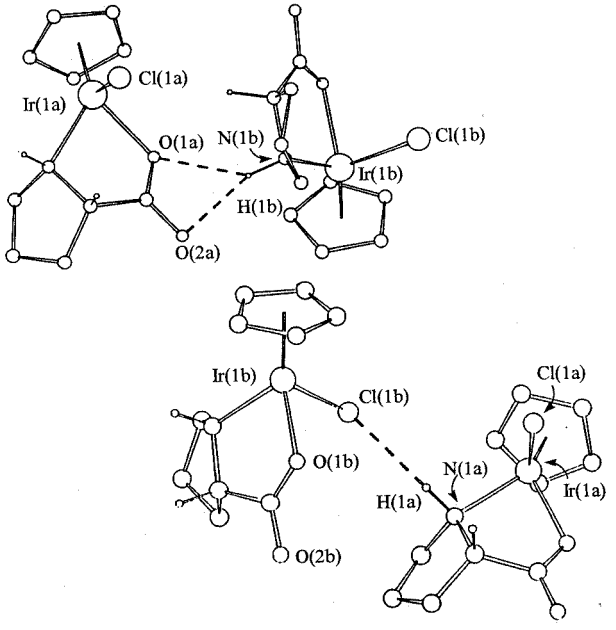

Figure 2. Hydrogen-bond network present in the iridium prolinate [η^5-C_5Me_5)Ir(Pro)Cl]

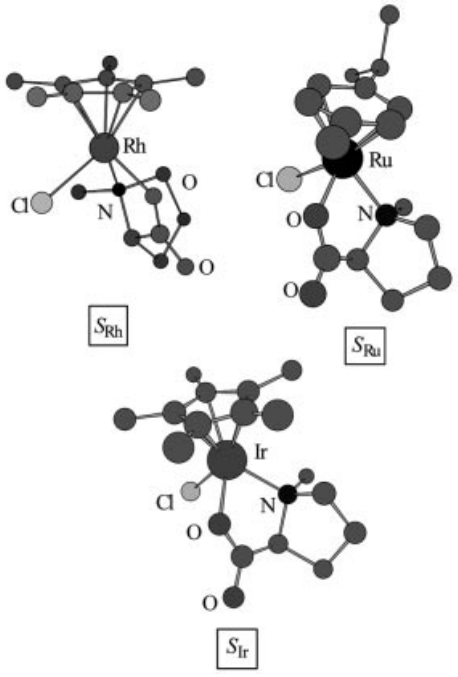

Figure 3. Molecular structures of *N*-methylprolinates

3. Alkynyl Compounds

The aforementioned aminocarboxylate compounds [(η^n-ring)M(Aa)Cl] reacted with terminal alkynes HC≡CR (R = CMe_3, $SiMe_3$, Ph, CO_2Me) in basic media (KOH or NEt_3), affording the corresponding alkynyl compounds [(η^n-ring)M(Aa)(C≡CR)] (Scheme 2).[35,36] In the preparation of the rhodium derivatives, it is necessary that KOH be used as the base. For the rhodium and iridium prolinate complexes, as well as for the ruthenium alaninate [{(η^6-*p*-MeC_6H_4*i*Pr)Ru(Ala)(C≡CPh)] two epimers at the metal center were detected. These complexes slowly epimerize in chloroform, acetone or methanol, the equilibrium composition is dependent on the metal, aminocarboxylate and alkynyl ligand. In particular, the equilibrium constant for the process (R_{Ir},S_C,S_N)-[(η^5-C_5Me_5)Ir(Pro)(C≡$CCMe_3$)] ⇆ (S_{Ir},S_C,S_N)-[(η^5-C_5Me_5)Ir(Pro)(C≡$CCMe_3$)] is 2.70 ± 0.41, in methanol at 20 °C. However, for the other alkynyl complexes only one epimer at the metal center was detected, their CD and NMR spectra remained essentially unchanged over several days.

Although the reaction between aminocarboxylate compounds [(η^n-ring)M(Aa)Cl] and terminal alkynes in basic media usually affords alkynyl compounds of the formula [(η^n-ring)M(Aa)(C≡CR)], the reaction of the (alaninato)-rhodium chloride [(η^5-C_5Me_5)Rh(Ala)Cl] with the monosubstituted alkynes HC≡CR (R = Ph, *p*-tolyl) takes a completely different route. From the reaction medium the alkynylcyclobutadiene complexes [(η^5-C_5Me_5)Rh(η^4-C_4HR_2C≡CR)] (R = Ph, *p*-tolyl) can be isolated (Scheme 3).[37] Their formation implies a novel type of rhodium-mediated trimerization reaction. The most common trimerization process that alkynes undergo is cycloaddition,

$$[(\eta^n\text{-ring})M(Aa)Cl] + HC{\equiv}CR + Base \rightarrow [(\eta^n\text{-ring})M(Aa)(C{\equiv}CR)] \quad (3)$$

$(\eta^n$-ring)M	aa	R
$(\eta^5$-$C_5Me_5)Rh$	Pro	CMe_3
$(\eta^5$-$C_5Me_5)Rh$	Pro	$SiMe_3$
$(\eta^5$-$C_5Me_5)Ir$	Pro	CMe_3
$(\eta^5$-$C_5Me_5)Ir$	Pro	$SiMe_3$
$(\eta^5$-$C_5Me_5)Ir$	MePro	CMe_3
$(\eta^5$-$C_5Me_5)Ir$	MePro	$SiMe_3$
$(\eta^6$-*p*-MeC_6H_4iPr)Ru	Ala	Ph
$(\eta^6$-*p*-MeC_6H_4iPr)Ru	Ala	CO_2Me
$(\eta^6$-*p*-MeC_6H_4iPr)Ru	Pro	Ph
$(\eta^6$-*p*-MeC_6H_4iPr)Ru	Pro	CO_2Me

Scheme 2. Alkynyl aminocarboxylate complexes of Rh, Ir, and Ru

rendering arenes; however, as far as we know, cyclobutadiene-containing transition metal complexes have never been the result of an alkyne trimerization process.[38,39] Figure 4 displays the molecular structure of the phenyl complex. The structure of the cyclobutadiene ligand indicates that both oligomerization and cyclization steps have to be involved in its formation. In agreement with previously reported alkyne oligomerization processes, the pathway shown in Scheme 4 is suggested. The reaction could start with the protonation of the α-alaninato ligand by one alkyne molecule. Subsequently, a second alkyne molecule could substitute the chloride anion. At this point, the reductive tail-to-tail coupling of the two alkynyl ligands at the rhodium center could take place, rendering intermediate **B**. This reductive coupling is a key step since it has been proposed that in the absence of the amino acid ligand, $[(\eta^5\text{-}C_5Me_5)Rh(C_2Ph)_2(NCMe)]$ inserts acetylenes into the rhodium−acetylide bond in a series of stepwise *cis* insertions, which ultimately yields the rhodium complexes depicted in Scheme 5.[40] The substitution of the alanine by an alkyne molecule in **B**, followed by the oxidative coupling of the two alkyne ligands in **C**, may occur to give the unsaturated metallacyclopentadiene **D**. Finally, compound **D** could, through a reductive elimination, give the cyclobutadiene product.

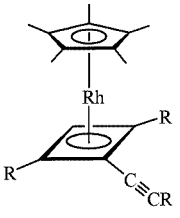

R = Ph, *p*-Tolyl

Scheme 3. Alkynylcyclobutadiene complexes

4. Cationic Trimers

The α-aminocarboxylate chloride complexes $[(\eta^n\text{-ring})M(Aa)Cl]$ (M= Ir, Rh, Ru, Os) were found to behave as ionic conductors in polar solvents such as methanol or

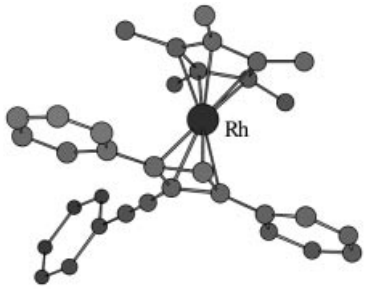

Figure 4. X-ray molecular structure of $[(\eta^5\text{-}C_5Me_5)Rh(\eta^4\text{-}C_4HPh_2C{\equiv}CPh)]$

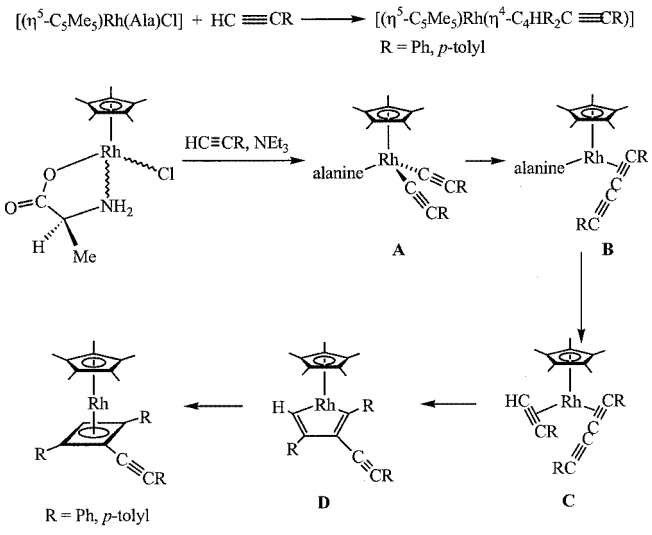

Scheme 4. Suggested pathway for the formation of the (cyclobutadiene)rhodium complexes

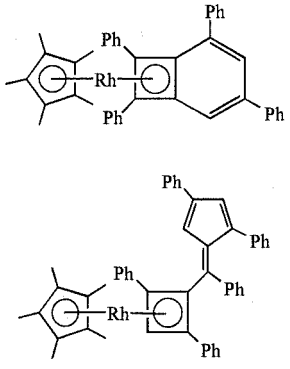

Scheme 5. Related (cyclobutadiene)rhodium complexes

water. Molar conductances greater than 60 $\Omega^{-1}cm^2mol^{-1}$ were achieved in the latter solvent. This behavior was explained by assuming a reversible ionization of the chloride ligand.[26,41] However, conductance measurements in water gave values for the slope of the Onsager equation that clearly pointed to a molecular complexity greater than that of univalent electrolytes.[41] To obtain further insights into the actual nature of this ionic species, the reactions of a variety of the aforementioned chloro complexes with $AgBF_4$ were carried out. The reactions resulted in the preparation of a family of chiral-at-metal trimers of the general formula

$[\{(\eta^n\text{-ring})M(Aa)\}_3](BF_4)_3$ (Scheme 6). Two members of this family, namely $[\{(\eta^5\text{-}C_5Me_5)Rh(Phe)\}_3](BF_4)_3$ and $[\{(\eta^5\text{-}C_5Me_5)Ir(Pro)\}_3](CF_3SO_3)_3$, have been previously reported by Beck et al.[42−45] Figure 5 shows the X-ray molecular structures of four members of this series. The aminocarboxylate ligand acts as a tridentate bridging group. The nitrogen atom and one of the carboxylic oxygen atoms of each amino acid are bonded to a metal center in a chelated fashion forming a five-membered metallacycle; the remaining oxygen atom coordinates to a second, different metal center and confers an additional intermetallic bridging nature to the amino acid anion ligand. The coordination environment confers a chiral nature to each metal center and, interestingly, only the two diastereomers with the same absolute configuration for the three metal centers, i.e. the ($R_MR_MR_M$) or the ($S_MS_MS_M$) isomers, were detected. Thus, the cyclization process occurs *with chiral self-recognition* among the mononuclear fragments. Solution studies revealed that in highly polar solvents isomerization of the trimers readily takes place. The rates of diastereomerization are strongly metal-dependent, increasing in the sequence Ru ≈ Os << Ir < Rh. Furthermore, while in solvents of low polarity, such as dichloromethane or acetone, the ($R_MR_MR_M$) isomer is thermodynamically preferred, in water the ($S_MS_MS_M$) isomer is thermodynamically favored. A theoretical analysis carried out at a supramolecular level for the trimer $[\{(\eta^5\text{-}C_5Me_5)Ir(Ala)\}_3](BF_4)_3$ led us to suggest a plausible explanation for the different stabilities encountered: the low number and the relatively restrained localization of the polar groups (amino hydrogen atoms) on the molecular surface of the ($R_{Ir}R_{Ir}R_{Ir}$) diastereomer (Figure 6) could sterically constrain the accessibility of solvent molecules to this area, thus reducing the number of polar trimer−solvent intermolecular interactions formed.[41] On the other hand, for the ($S_{Ir}S_{Ir}S_{Ir}$) diastereomer, the change in the metal configuration is associated to a change in the

$$[(\eta^n\text{-ring})M(Aa)Cl] + AgBF_4 \rightarrow$$
$$1/3\ [\{(\eta^n\text{-ring})M(Aa)\}_3](BF_4)_3 + AgCl \qquad (4)$$

Aa =	(η^n-ring)M =
Ala	[Rh], [Ir], [Ru], [Os]
Abu	[Rh]
Val	[Rh], [Ir], [Ru]
Tle	[Rh], [Ir], [Ru]
Phe	[Rh], [Ir], [Ru], [Os]
MePhe	[Ru], [Os]
L-Pro	[Rh], [Ir], [Ru], [Os]
D-Pro	[Rh], [Ir], [Ru]
Aze	[Ru], [Os]
Pip	[Ru], [Os]
MePro	[Rh], [Ir]
Hyp	[Rh], [Ir], [Ru]

Scheme 6. Cationic aminocarboxylate trimers

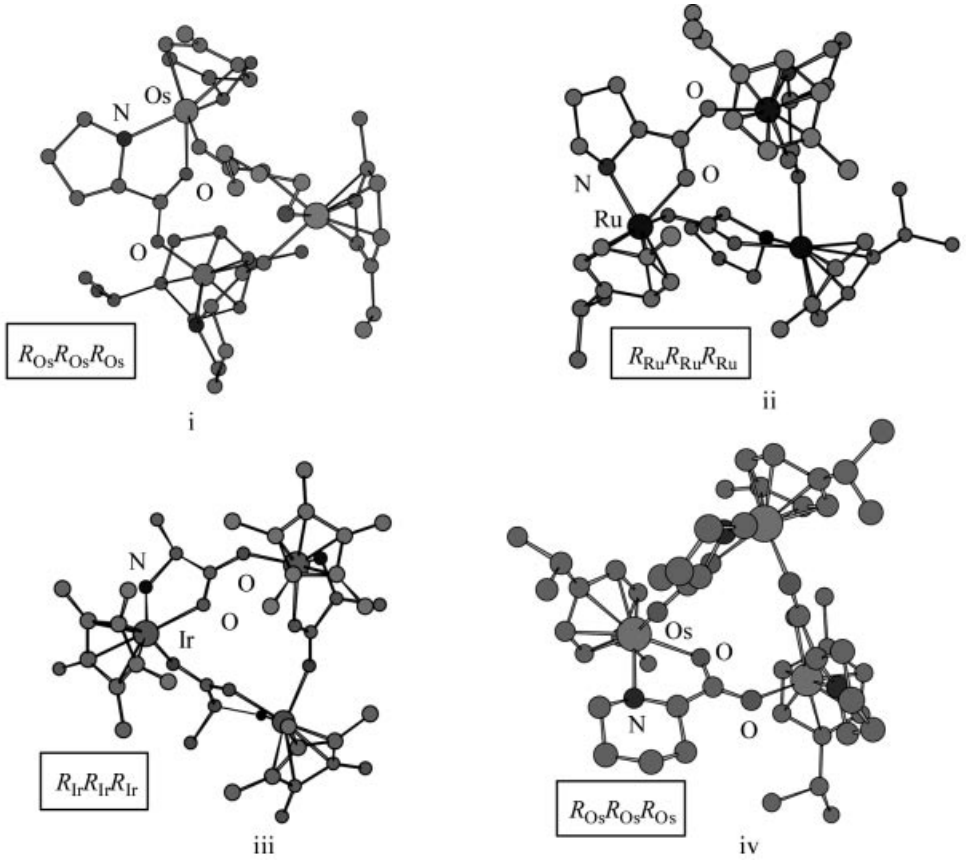

Figure 5. Molecular representations of the trinuclear cations of i) $[\{(\eta^6\text{-}p\text{-}MeC_6H_4iPr)Os(Pro)\}_3]^{3+}$, ii) $[\{(\eta^6\text{-}p\text{-}MeC_6H_4iPr)Ru(Pro)\}_3]^{3+}$, iii) $[\{(\eta^5\text{-}C_5Me_5)Ir(Ala)\}_3]^{3+}$, and iv) $[\{(\eta^6\text{-}p\text{-}MeC_6H_4iPr)Os(Pip)\}_3]^{3+}$

localization of amino hydrogen atoms on the surface of the molecule. They are dispersed on the molecular surface allowing interaction with solvent molecules when dissolved, with no apparent steric constrain. This major accessibility of the polar groups in the ($S_MS_MS_M$) diastereomers compared with that of the ($R_MR_MR_M$) isomers seems to be responsible for the greater stability of the ($S_MS_MS_M$) diastereomers in solution as the polarity of the solvent molecules is increased.

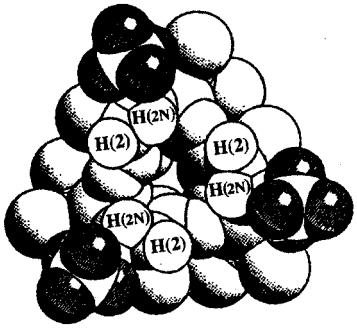

Figure 6. Space-filling model of the ($R_{Ir}R_{Ir}R_{Ir}$)-[{(η^5-C_5Me_5)Ir(Ala)}$_3$](BF_4)$_3$ compound showing the location of one of the amino hydrogen atoms [H(2N)] which is hydrogen-bonded to the BF_4 groups (shaded spheres: carbon atoms; open spheres: hydrogen atoms; black spheres: fluorine atoms of the BF_4 anions)

The equilibrium constant for Equation (5) was determined in methanol, for the range 270−318 K, by integration of corresponding ^{1}H NMR signals of the equilibrated solutions. The equilibrium obeys a simple van't Hoff dependence on the temperature, with $\Delta H^\circ = 23.4 \pm 0.5$ kJ mol^{-1} and $\Delta S^\circ = 80.6 \pm 1.7$ JK^{-1} mol^{-1}.

$$(R_{Rh}R_{Rh}R_{Rh})\text{-}[\{(\eta^5\text{-}C_5Me_5)Rh(Tle)\}_3](BF_4)_3 \leftrightarrows (S_{Rh}S_{Rh}S_{Rh})\text{-}[\{(\eta^5\text{-}C_5Me_5)Rh(Tle)\}_3](BF_4)_3 \quad (5)$$

5. Cationic Phosphane Complexes

Attempts to prepare [(η^n-ring)M(Aa)L]$^+$ compounds by treating [{(η^n-ring)M(Aa)}$_3$]$^{3+}$ trimers with ligands L, such as carbon monoxide, olefins or alkynes, proved to be unsuccessful. However, reaction with tertiary phosphanes readily produces the corresponding cationic monometallic compounds [(η^n-ring)M(Aa)(PR_3)]$^+$ [Equation (6), Scheme 7].[9,26,30,31]

$$1/3\,[\{(\eta^n\text{-ring})M(Aa)\}_3](BF_4)_3 + PR_3 \rightarrow [(\eta^n\text{-ring})M(Aa)(PR_3)]BF_4 \quad (6)$$

The phosphane complexes have been prepared as mixtures of (S_M) and (R_M) epimers. The assignment of the absolute configuration of the metal center was accomplished by a combination of X-ray diffraction (Figure 7), CD and

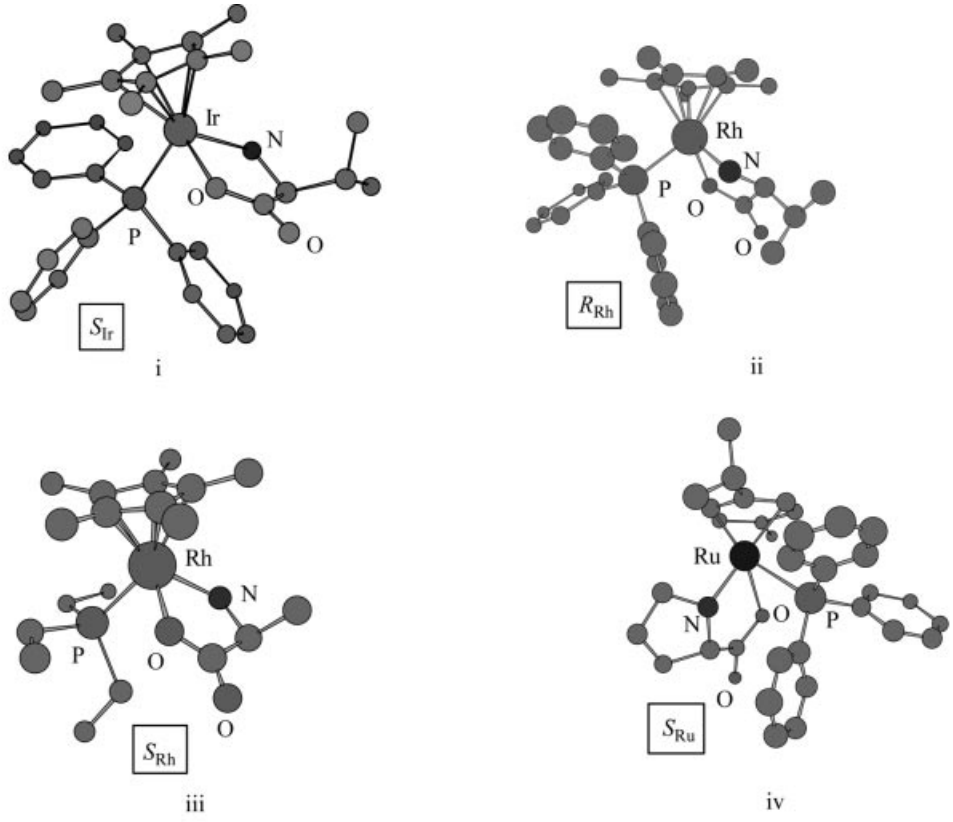

Figure 7. Molecular structures of the cationic phosphane complexes i) [(η^5-C_5Me_5)Ir(Val)(PPh_3)]$^+$, ii) [(η^5-C_5Me_5)Rh(Val)(PPh_3)]$^+$, iii) [(η^5-C_5Me_5)Rh(Ala)(PEt_3)]$^+$, and iv) [(η^6-*p*-MeC_6H_4*i*Pr)Ru(Pro)(PPh_3)]$^+$

NMR spectroscopic measurements. The isolated compounds were always enriched in the (S_M) isomer, which is the kinetically preferred epimer. In alcoholic solutions the (S_M) isomers epimerize at the metal center, the (R_M) isomers are thermodynamically preferred. The kinetic formation of the (S_M) isomers can be accounted for by assuming the preferential attack of the PR_3 ligand through the *Re*-face (hydrogen-shielded), rather than the *Si*-face (R^1- and R^2-shielded),[46] of a planar intermediate derived from the cleavage of the metal−oxygen bridging bonds of the trimers (Scheme 8). Support for this proposal stems from the measured diasteroselectivities. Thus, the kinetic diastereoselectivity in the (triphenylphosphane)rhodium series [(η^5-C_5Me_5)Rh(Aa)(PPh_3)](BF_4), Aa = Ala (R^1, Me), Abu (R^1, Et), Val (R^1, *i*Pr), and Tle (R^1, *t*Bu)] is 46, 50, 70, and 78% *de*, respectively, reflecting the increase in the size of the R^1 group.

The epimerization rate strongly depends on the metal and on the phosphane. Again, it increases in the sequence Ru < Ir < Rh. Table 1 presents the values of the rate constant for a series of (*tert*-leucinato)rhodium complexes with different tertiary phosphanes. The epimerization rate increases as the phosphane basicity decreases. Thus, arylphosphanes with electron-withdrawing substituents have the largest rate constants.

6. Epimerization Processes

As stated above, most of the aminocarboxylate derivatives epimerized at the metal center. To gain a better insight into the epimerization mechanism some kinetic and scrambling experiments have been performed. Thus, for example: (i) Kinetic measurements for the epimerization of (R_{Ir},S_C,S_N)-[(η^5-C_5Me_5)Ir(Pro)(C≡CCMe$_3$)] in chloroform for the temperature range 293−318 K revealed that the epimerization obeys a first-order rate law, with derived rate constants ranging from (2.74 ± 0.02) × 10^{-5} s^{-1} ($t_{1/2}$ = 6 h, 293 K) to (61.7 ± 5.3) × 10^{-5} s^{-1} ($t_{1/2}$ = 0.25 h, 318 K); the activation parameters are $\Delta H^{\neq}$ = 91.4 ± 3.4 kJmol^{-1} and $\Delta S^{\neq}$ = −20.8 ± 10.8 JK^{-1}mol^{-1}. (ii) The rate of isomerization of the iridium compound [{(η^5-C_5Me_5)Ir(MePro)}$_3$](BF_4)$_3$ at 51°C in methanol, was adequate to be monitored by ^{1}H NMR spectroscopy; a first-order rate law was obtained with a rate constant *k* of 2.45 ± 0.01 × $10^{-5}$$s^{-1}$. (iii) Epimerization of the triphenylphosphane complex [(η^5-C_5Me_5)Rh(Tle)(PPh_3)]BF_4 in methanol also follows a first-order rate law, and from the dependence of its rate constant on the temperature in the 296−307 K interval, activation parameters of $\Delta H^{\neq}$= 88.7 ± 0.6 kJmol^{-1} and $\Delta S^{\neq}$ = −24.9 ± 1.7 JK^{-1}mol^{-1} have been obtained.[31]

On the other hand, an equimolar mixture of (R_{Ir},S_C,S_N)-[(η^5-C_5Me_5)Ir(Pro)(C≡CCMe$_3$)] and (S_{Ru},S_C)/(R_{Ru},S_C)-[(η^6-*p*-MeC_6H_4*i*Pr)Ru(Ala)(C≡CPh)] [(S_{Ru},S_C)/(R_{Ru},S_C) = 70:30 molar ratio] was allowed to epimerize in methanol at 22 °C (Scheme 9). The processes were monitored by ^{1}H NMR spectroscopy and this technique clearly showed that both compounds epimerize independently to the corresponding (S_{Ir},S_C,S_N) and (R_{Ru},S_C) derivatives. Thus, no intermolecular processes rendering compounds containing Ru(Pro), Ru(C≡CCMe$_3$), Ir(Ala) or Ir(C≡CPh) moieties have been observed.

However, when equimolar amounts of the cationic complexes with an (*S*) configuration at the ruthenium center, [(η^6-*p*-MeC_6H_4*i*Pr)Ru(Val)(PPh_3)]BF_4 and [(η^6-*p*-MeC_6H_4-

α-Amino-carboxylate	Phosphane	(η″-ring)M
Ala	P(4-$MeOC_6H_4$)$_3$	[Rh], [Ir], [Ru]
	P(4-MeC_6H_4)$_3$	[Rh], [Ir], [Ru]
	PPh_3	[Rh], [Ir], [Ru]
	P(4-FC_6H_4)$_3$	[Rh], [Ir], [Ru]
	P(4-ClC_6H_4)$_3$	[Rh], [Ir], [Ru]
	P(3-MeC_6H_4)$_3$	[Rh], [Ir], [Ru]
	P(3-ClC_6H_4)$_3$	[Rh], [Ir]
	P(2-MeC_6H_4)$_3$	[Ir]
	PEt_3	[Rh], [Ir]
Abu	PPh_3	[Rh]
Val	P(4-$MeOC_6H_4$)$_3$	[Ru]
	P(4-MeC_6H_4)$_3$	[Ru]
	PPh_3	[Rh], [Ir], [Ru]
	P(4-FC_6H_4)$_3$	[Ru]
	P(4-ClC_6H_4)$_3$	[Ru]
	P(3-MeC_6H_4)$_3$	[Ru]
	P(3-ClC_6H_4)$_3$	[Ru]
Leu	P(4-$MeOC_6H_4$)$_3$	[Ru]
	P(4-MeC_6H_4)$_3$	[Ru]
	PPh_3	[Ru]
	P(4-FC_6H_4)$_3$	[Ru]
	P(4-ClC_6H_4)$_3$	[Ru]
Ile	PPh_3	[Ru]
Tle	P(4-$MeOC_6H_4$)$_3$	[Rh]
	P(4-MeC_6H_4)$_3$	[Rh]
	PPh_3	[Rh], [Ir]
	P(4-FC_6H_4)$_3$	[Rh]
	P(4-ClC_6H_4)$_3$	[Rh]
	P(3-MeC_6H_4)$_3$	[Rh]
	P(3-ClC_6H_4)$_3$	[Rh]
	$PMePh_2$	[Rh]
Phe	PPh_3	[Rh], [Ir], [Ru]
Pro	P(4-$MeOC_6H_4$)$_3$	[Rh], [Ir], [Ru]
	P(4-MeC_6H_4)$_3$	[Rh], [Ir], [Ru]
	PPh_3	[Rh], [Ir], [Ru]
	P(4-FC_6H_4)$_3$	[Rh], [Ir], [Ru]
	P(4-ClC_6H_4)$_3$	[Rh], [Ir], [Ru]
	P(3-MeC_6H_4)$_3$	[Rh], [Ir], [Ru]
	P(3-ClC_6H_4)$_3$	[Ir], [Ru]
	PEt_3	[Rh], [Ir]
Hyp	PPh_3	[Ru]

Scheme 7. Cationic (aminocarboxylato)(phosphane) complexes

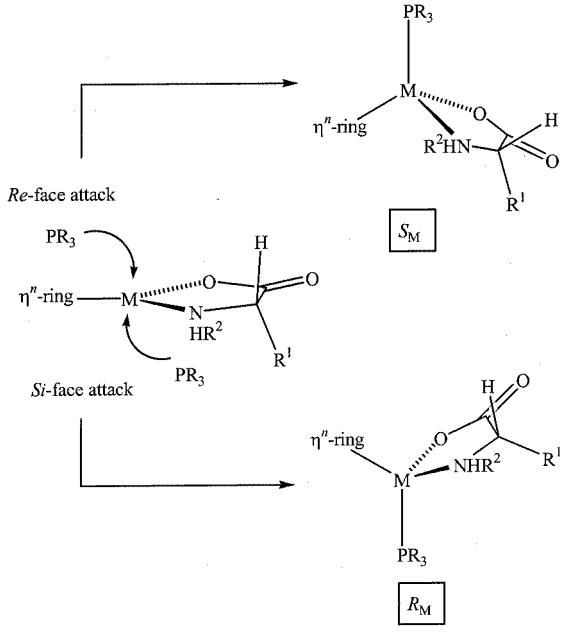

Scheme 8. Proposed formation of the two epimers for the cationic phosphane complexes

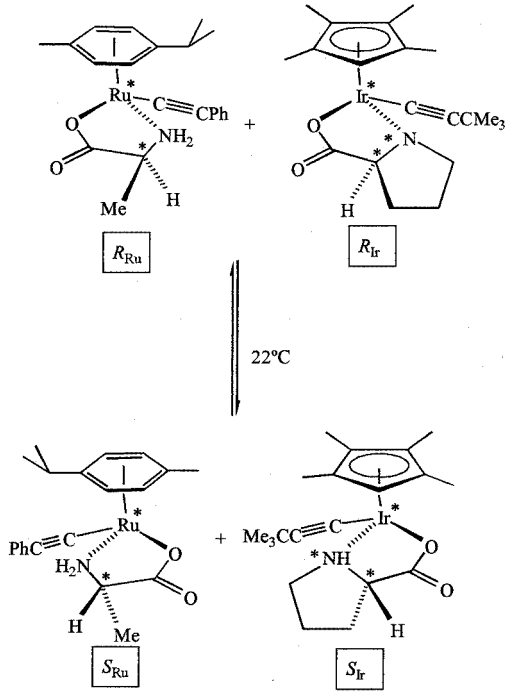

Scheme 9. Epimerization of an equimolar mixture of (R_{Ir},S_C,S_N)-[(η^5-C_5Me_5)Ir(Pro)(C≡CCMe$_3$)] and (S_{Ru},S_C)/(R_{Ru},S_C)-[(η^6-*p*-Me-C_6H_4*i*Pr)Ru(Ala)(C≡CPh)] [(S_{Ru},S_C)/(R_{Ru},S_C) = 70:30 molar ratio]

Table 1. Rate constant k at 296 K in methanol for the (S_{Rh}) → (R_{Rh}) epimerization process

Compound	$k \times 10^5$ [s^{-1}]
[(η^5-C_5Me_5)Rh(Tle){P(4-MeOC$_6$H$_4$)$_3$}]BF_4	4.22 ± 0.09
[(η^5-C_5Me_5)Rh(Tle)(PMePh$_2$)]BF_4	5.63 ± 0.09
[(η^5-C_5Me_5)Rh(Tle){P(4-MeC$_6$H$_4$)$_3$}]BF_4	5.06 ± 0.06
[(η^5-C_5Me_5)Rh(Tle){P(3-MeC$_6$H$_4$)$_3$}]BF_4	6.00± 0.07
[(η^5-C_5Me_5)Rh(Tle)(PPh$_3$)]BF_4	13.6 ± 0.4
[(η^5-C_5Me_5)Rh(Tle){P(4-FC$_6$H$_4$)$_3$}]BF_4	66.1 ± 0.6
[(η^5-C_5Me_5)Rh(Tle){P(4-ClC$_6$H$_4$)$_3$}]BF_4	209.8 ± 6.6
[(η^5-C_5Me_5)Rh(Tle){P(3-ClC$_6$H$_4$)$_3$}]BF_4	262.8 ± 6.0

*i*Pr)Ru(Pro){P(4-MeOC$_6$H$_4$)$_3$}]BF_4, were allowed to epimerize, the formation of the (phosphane)metal scrambling products [(η^6-*p*-MeC$_6$H$_4$*i*Pr)Ru(Val){P(4-MeOC$_6$H$_4$)$_3$}]BF_4 and [(η^6-*p*-MeC$_6$H$_4$*i*Pr)Ru(Pro)(PPh$_3$)]BF_4 [(*R*)- and (*S*)-metal epimers] was also observed (Scheme 10). Therefore, epimerization occurs with the dissociation of the phosphane ligand.

In a related experiment, an equimolar mixture of the (*tert*-leucinato)rhodium and -iridium complexes [{(η^5-C_5Me_5)M(Tle)}$_3$]$(BF_4)_3$ was dissolved in CD_3OD at −77 °C and the reaction monitored by ^{1}H NMR spectroscopy. An initial ^{1}H NMR spectrum was immediately recorded at −84 °C and it revealed that only the two starting compounds were present in solution, but after 5 min at the same temperature, new signals emerged in the C_5Me_5 region. At room temperature the spectrum showed nine new resonances in this region (most probably due to a mixture of diastereomers of heterometallic trimers), and an FAB$^+$ mass spectrum of the solution revealed peaks at *m*/*z* values of 828, 1196, and 1285, which are assigned to [(η^5-C_5Me_5)$_2$RhIr(Tle)$_2$]$^+$, [(η^5-C_5Me_5)$_3$Rh$_2$Ir(Tle)$_3$]$^+$, and [(η^5-C_5Me_5)$_3$RhIr$_2$(Tle)$_3$]$^+$ fragments, respectively (Scheme 11). Thus, most likely diastereomerization implies the dissociation of the trimers into monomers.

The data collected from all these experiments are compatible with a common epimerization pathway that is outlined in Scheme 12. Dissociation of the chloride ion in the aminocarboxylates [(η^n-ring)M(Aa)Cl], or of the phosphane ligand in the cationic complexes [(η^n-ring)M(Aa)(PR$_3$)]BF_4, and cleavage of the M−O or M−N bonds in the alkynyl compounds [(η^n-ring)M(Aa)(C≡CR)], or of the M−O(bridging) bond in the trimers [{(η^n-ring)M(Aa)}$_3$]$(BF_4)_3$ produce an unsaturated pyramidal species **A** which is in equilibrium with its metal center epimer **C** through a planar achiral intermediate **B**. Subsequent re-coordination of the separated moiety from the other side of the intermediate completes the process. This path accounts for all the experimental observations.

7. Asymmetric Hydrogen Transfer Reactions

Enantioselective transfer hydrogenation of prochiral ketones is a major catalytic procedure for the synthesis of chiral nonracemic secondary alcohols. The results obtained in this field have been reviewed[47] and considerable efforts have recently been paid to elucidate the operating mechanism(s).[48−57]

We have found that both the neutral (aminocarboxylato)(chloro) compounds [(η^n-ring)M(Aa)Cl] and the cationic

trimers $[\{(\eta^n\text{-ring})M(Aa)\}_3](BF_4)_3$ are active catalysts for the hydrogen transfer reaction from 2-propanol to acetophenone (Scheme 13).[41,58] 2-Propanol was used as a hydrogen donor and the solvent; reactions were carried out at refluxing temperature and sodium formate was used as the base. Both conversion and enantioselectivity were measured by gas chromatography. Table 2 presents the results achieved after treating acetophenone under the aforementioned conditions with some selected catalysts.

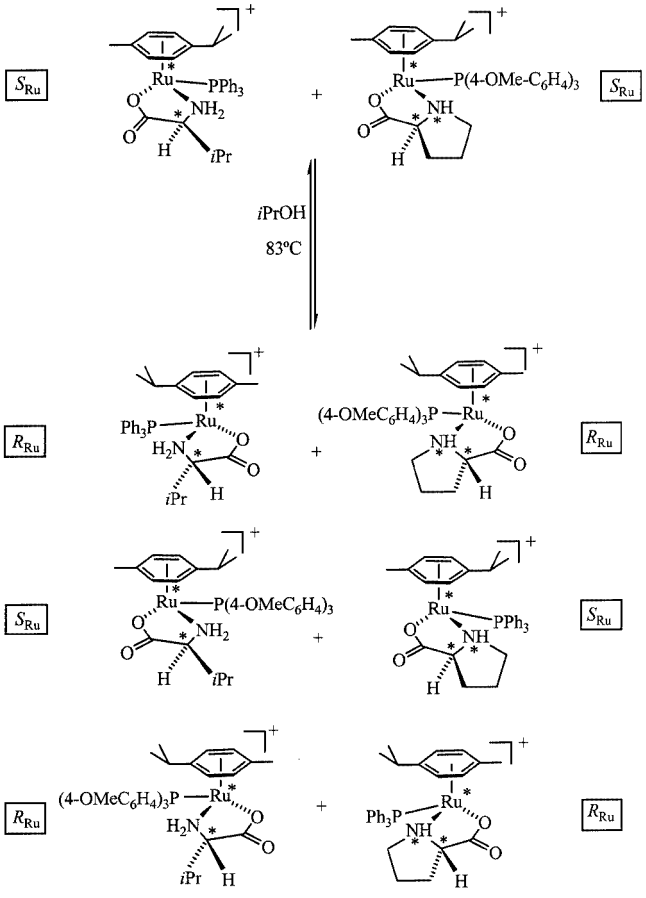

Scheme 10. Epimerization of an equimolar mixture of (S_{Ru},S_C)-$[(\eta^6\text{-}p\text{-}MeC_6H_4iPr)Ru(Val)(PPh_3)](BF_4)$ and (S_{Ru},S_C,S_N)-$[(\eta^6\text{-}p\text{-}MeC_6H_4iPr)Ru(Pro)\{P(4\text{-}MeOC_6H_4)_3\}](BF_4)$

The results deserve some comments:

(i) The best conversions, as well as enantioselectivities were obtained with ruthenium or osmium catalysts. Compare, for example, Entries 1 and 2 (rhodium and iridium prolinate trimers as catalysts) with Entries 3 and 4 (ruthenium and osmium analogues as catalysts).

(ii) Catalysts based on cyclic aminocarboxylates produced the best enantioselectivities. Entries 1−4 correspond to cyclic aminocarboxylates, while entries 5−8 correspond to linear aminocarboxylates. Probably, the greater conformational rigidity of the cyclic aminocarboxylates with respect to the linear ones, accounts for the apparent changes in *ee*.

(iii) For a fixed metal and aminocarboxylate, mononuclear chloro complexes and cationic trimers afforded very similar conversions and enantioselectivities. Compare Entries 5 and 7 or Entries 2 and 10. Most probably both species catalyze through a common solvate intermediate $[(\eta^n\text{-ring})M(Aa)S]$, formed by cleavage of the M−O(bridging) bonds in the trimers and halogen abstraction in the chloride ions.

(iv) Catalysts without the NH functionality were almost inactive. Very poor conversions and enantioselectivities have been achieved with *N*,*N*-dimethylphenylalaninate (Entry 15) or *N*-methyl-substituted prolinate (Entries 16 and 17) catalysts. Very recently, Noyori and co-workers have proposed a new metal−ligand bifunctional mechanism that operates for ruthenium-based catalysts containing primary or secondary amines (Scheme 14). The catalyst **A** incorporates hydrogen from the hydrogen donor molecule to form an NH-containing hydride **B** which, in turn, simultaneously transfers the NH proton and RuH hydride to the unsatur-

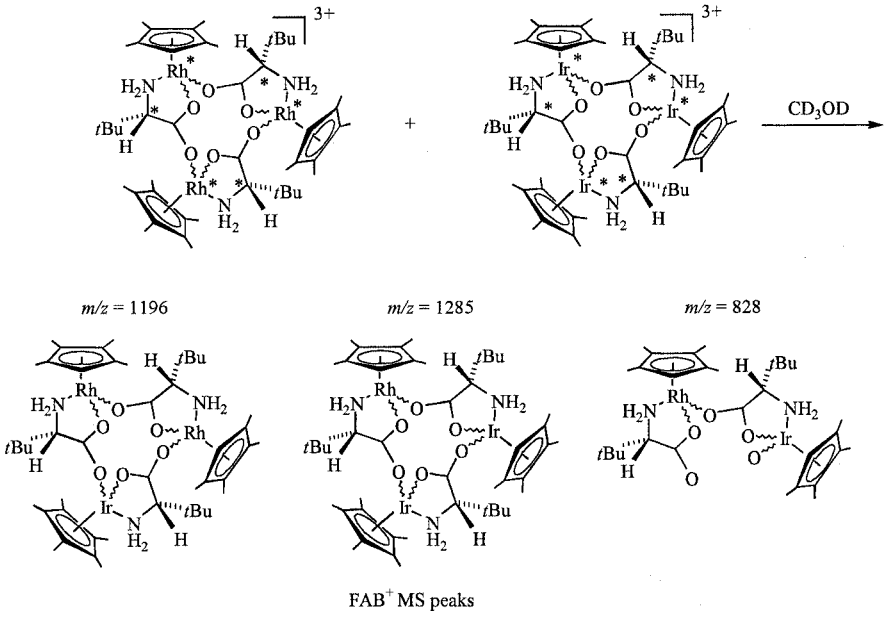

Scheme 11. Epimerization of a mixture of the complexes $[\{(\eta^5\text{-}C_5Me_5)M(Tle)\}_3](BF_4)_3$ (M = Rh, Ir) in CD_3OD

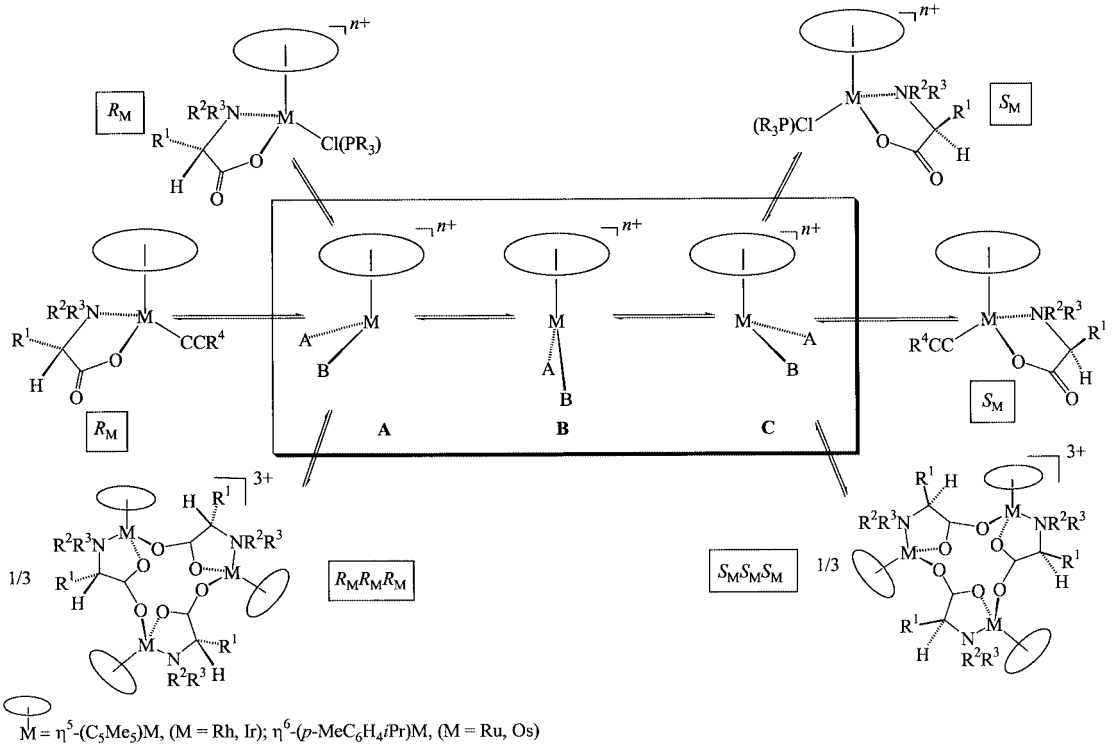

Scheme 12. Proposed pathway for the epimerization processes

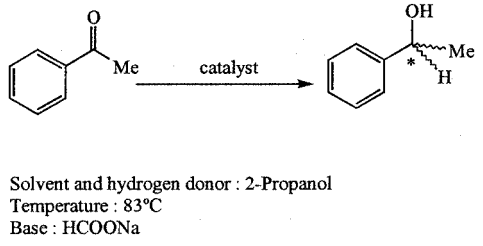

Scheme 13. Standard conditions for the hydrogen transfer reactions

ated substrate through a six-membered cyclic intermediate **C**.[23,59] Probably, this mechanism is operating in the aminocarboxylate catalysts and, therefore, aminocarboxylates, not containing NH groups, are almost inactive.

(v) The (*R*)-alcohols were selectively obtained, except for the piperidine-2-carboxylates (Entries 12 and 14) and *N*-methylphenylalaninate derivatives (Entry 18) which preferentially rendered (*S*)-configured alcohols. When *N*-substituted α-aminocarboxylates coordinate to a metal center through the nitrogen atom, this atom becomes a chiral

Table 2. Reduction of acetophenone by hydrogen transfer from 2-propanol

Entry	Catalyst	M/Base/Subst.	*t* [h]	Conv. (%)	TOF	*ee* (%)
1	$[\{(\eta^5\text{-}C_5Me_5)Rh(Pro)\}_3][BF_4]_3$	1:2:214	1	8.7	19	60
2	$[\{(\eta^5\text{-}C_5Me_5)Ir(Pro)\}_3][BF_4]_3$	1:2:214	1	15.6	33	64
3	$[\{(\eta^6\text{-}p\text{-}MeC_6H_4iPr)Ru(Pro)\}_3][BF_4]_3$	1:1:100	1	97	97	75
4	$[\{(\eta^6\text{-}p\text{-}MeC_6H_4iPr)Os(Pro)\}_3][BF_4]_3$	3:4:200	1.25	70	37	72
5	$[\{(\eta^6\text{-}p\text{-}MeC_6H_4iPr)Ru(Phe)\}_3][BF_4]_3$	1:2:214	1	86	184	22
6	$[\{(\eta^6\text{-}p\text{-}MeC_6H_4iPr)Os(Ala)\}_3][BF_4]_3$	3:4:200	1.5	74	33	14
7	$[(\eta^6\text{-}p\text{-}MeC_6H_4iPr)Ru(Phe)Cl]$	1:2:214	1	87.5	187	23
8	$[(\eta^6\text{-}p\text{-}MeC_6H_4iPr)Os(Ala)Cl]$	3:6:200	1	87	58	8
9	$[(\eta^6\text{-}p\text{-}MeC_6H_4iPr)Os(Pro)Cl]$	3:6:200	1	86	57	66
10	$[(\eta^5\text{-}C_5Me_5)Ir(Pro)Cl]$	1:2:214	1	17	36	58
11	$[\{(\eta^6\text{-}p\text{-}MeC_6H_4iPr)Ru(Aze)\}_3][BF_4]_3$	1:1:100	1	70	70	55
12	$[\{(\eta^6\text{-}p\text{-}MeC_6H_4iPr)Ru(Pip)\}_3][BF_4]_3$	1:1:100	0.5	48	97	60 (*S*)
13	$[\{(\eta^6\text{-}p\text{-}MeC_6H_4iPr)Os(Aze)\}_3][BF_4]_3$	3:4:200	1.25	35	19	50
14	$[\{(\eta^6\text{-}p\text{-}MeC_6H_4iPr)Os(Pip)\}_3][BF_4]_3$	3:4:200	1.75	70	27	52 (*S*)
15	$[(\eta^6\text{-}p\text{-}MeC_6H_4iPr)Os(Me_2Phe)Cl]$	3:6:200	2	16	5	–
16	$[(\eta^5\text{-}C_5Me_5)Ir(MePro)Cl]$	1:2:214	1	1.8	4	–
17	$[(\eta^6\text{-}p\text{-}MeC_6H_4iPr)Os(MePro)Cl]$	3:6:200	1.5	3	1	–
18	$[(\eta^6\text{-}p\text{-}MeC_6H_4iPr)Ru(MePhe)Cl]$	3:6:200	1	90	30	37 (*S*)

center. This is the case for the metal piperidine-2-carboxylates, prolinates or azetidine-2-carboxylates (Scheme 15A, n = 2, 1, or 0, respectively) or for the *N*-methylphenylalaninates (Scheme 15B).

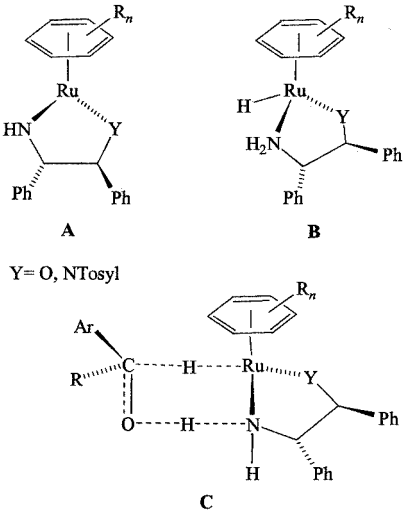

Scheme 14. Metal−ligand bifunctional mechanism

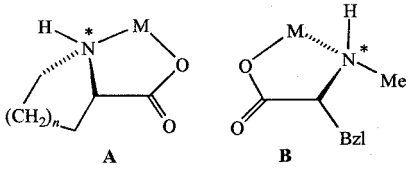

Scheme 15. Chiral nitrogen centers generated by coordination of *N*-substituted aminocarboxylates

Several molecular structures of prolinato complexes determined by X-ray diffraction have been reported and, interestingly, the nitrogen atom always adopts the same configuration as the asymmetric aminocarboxylate carbon atom.[46] Similarly, only diastereomers with the same configuration at both carbon and nitrogen atoms have been detected in the crystal structures for azetidine-2-carboxylate complexes.[9,60]

In sharp contrast, the molecular structures of the L-piperidine-2-carboxylato-containing osmium compounds, [(η^6-*p*-MeC_6H_4*i*Pr)Os(Pip)Cl] and [(η^6-*p*-MeC_6H_4*i*Pr)Os(Pip)]$_3$[BF_4]$_3$, as well as those of the *N*-methyl-L-phenylalaninates, [(η^6-*p*-MeC_6H_4*i*Pr)M(MePhe)Cl] (M = Ru, Os), show that the nitrogen and the asymmetric carbon atoms of the aminocarboxylate adopt opposite configurations, (S_C,R_N) (Figure 8).[61,62]

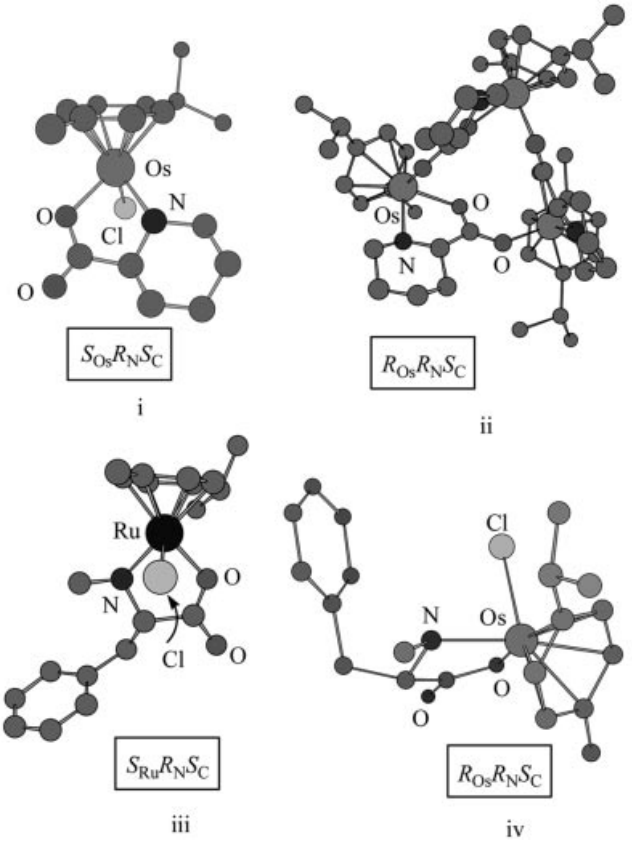

Figure 8. Molecular structures of the (L-piperidine-2-carboxylato)osmium compounds i) [(η^6-*p*-MeC_6H_4*i*Pr)Os(Pip)Cl] and ii) [(η^6-*p*-MeC_6H_4*i*Pr)Os(Pip)]$_3$[BF_4]$_3$, and those of the *N*-methyl-L-phenylalaninates [(η^6-*p*-MeC_6H_4*i*Pr)M(MePhe)]Cl with iii) M = Ru, iv) M = Os

At this point, we suspect that the enantioselection would be related to the different configuration adopted by the nitrogen atom when it coordinates. In fact, we can explain the observed *ee* assuming that the concerted mechanism proposed by Noyori and co-workers is being used.[23,59] Scheme 16 shows the proposed six-membered cyclic intermediate. L-Prolinates (type **A**) and *N*-methyl-L-phenylalaninates (type **B**) have been selected as representative examples of the two types of enantioselection. The cyclic intermediate can only be formed when the metal center and the nitrogen atom adopt the same configuration, i.e. for (S_M) epimers of the **A**-type (S_C,S_N), or for (R_M) epimers of the **B**-type (S_C,R_N). To account for the obtained results [(*R*)-alcohol for the former and (*S*)-alcohol for the latter] the acetophenone phenyl group has to eclipse the *p*-MeC_6H_4*i*Pr ring. In this disposition the carbonyl group interacts with catalysts of type **A** through its *Si* face, but via its *Re* face with those of type **B**, which is in good agreement with the stereochemical outcome. Most probably, recognition of carbonyl enantiofaces is possible through attractive CH−π interactions between the arene ligand and the aromatic acetophenone group, as Noyori et al. have recently proposed, based on theoretical calculations for related (arene)ruthenium systems.[56,57]

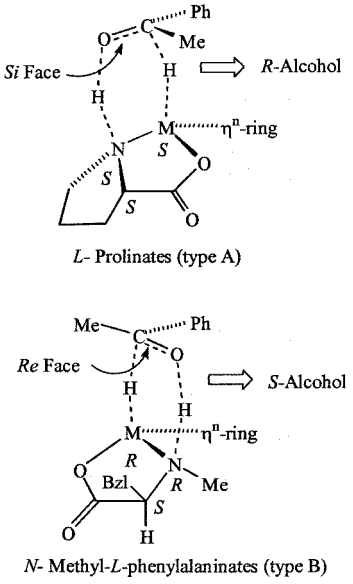

Scheme 16. The two possible types of six-membered cyclic intermediates

To obtain further evidence for this proposal we have attempted the reduction of the dialkyl ketone 4-phenyl-2-butanone. Using this substrate, we tried to disrupt the CH−π interactions and then, on the basis of steric grounds, to reverse the enantioselection for both types of catalysts. The results presented in Table 3 strongly support this hypothesis. The L-prolinates [(η^6-*p*-MeC_6H_4*i*Pr)M(Pro)Cl] (M = Ru, Os) afforded (*S*)-4-phenyl-2-butanol, whereas *N*-methyl-L-phenylalaninates produced (*R*)-4-phenyl-2-butanol, preferentially. Thus, the assumption of Noyori's mechanism for the hydrogen transfer reaction from 2-propanol to acetophenone or 4-phenyl-2-butanone, catalyzed by α-aminocarboxylate complexes, explains the *ee* obtained.

Table 3. Reduction of 4-phenyl-2-butanone by hydrogen transfer from 2-propanol

Entry	Catalyst	*t* [h]	TOF	*ee* (%)
1	[(η^6-*p*-MeC_6H_4*i*Pr)Ru(Pro)Cl]	1.5	42	32 (*S*)
2	[(η^6-*p*-MeC_6H_4*i*Pr)Ru(MePhe)Cl]	1	56	14 (*R*)
3	[(η^6-*p*-MeC_6H_4*i*Pr)Os(Pro)Cl]	3	45	30 (*S*)
4	[(η^6-*p*-MeC_6H_4*i*Pr)Os(MePhe)Cl]	6	36	5 (*R*)

8. Conclusions

In this Microreview, we have described half-sandwich aminocarboxylato compounds of rhodium, iridium, ruthenium or osmium with a chlorine atom, alkynyl groups or tertiary phosphanes as ancillary ligands. The neutral chloro compounds [(η^n-ring)M(Aa)Cl] reacted with $AgBF_4$, most probably yielding the corresponding mononuclear solvates [(η^n-ring)M(Aa)S]$^+$. Whichever metal was used and whatever the aminocarboxylate was, the solvates rearranged to trinuclear compounds through the coordination of the free oxygen atom of the carboxylate group. This trimerization takes place with chiral self-recognition; from the four possible diastereomers only the formation of trimers with equally configured metal centers, that is (*R*,*R*,*R*) or (*S*,*S*,*S*)trimers, was observed. Most of the new aminocarboxylate derivatives epimerized at the metal center following the epimerization pathway outlined in Scheme 12. Chloro compounds [(η^n-ring)M(Aa)Cl] and cationic trimers [{(η^n-ring)M(Aa)}$_3$]$(BF_4)_3$ are active catalysts for the hydrogen transfer reaction from 2-propanol to acetophenone. Finally, it is possible to rationalize that the recognition of the carbonyl enantiofaces of the ketone for the ruthenium catalysts occurs as a result of attractive CH−π interactions between the arene ligand and the aromatic acetophenone group, a mechanistic proposal recently suggested by Noyori et al.

[1] H. Brunner, *Adv. Organomet. Chem.* **1980**, *18*, 151−206.
[2] G. Consiglio, F. Morandini, *Chem. Rev.* **1987**, *87*, 761−778.
[3] S. G. Davies, *Pure Appl. Chem.* **1988**, *60*, 13−20.
[4] V. I. Sokolov, *Chirality and Optical Activity in Organometallic Compounds*, Gordon and Breach Science Publishers, New York, **1990**.
[5] J. A. Gladysz, B. J. Boone, *Angew. Chem.* **1997**, *109*, 566−602; *Angew. Chem. Int. Ed. Engl.* **1997**, *36*, 550−583.
[6] D. Carmona, C. Vega, F. J. Lahoz, S. Elipe, M. P. Lamata, F. Viguri, R. García-Correas, C. Cativiela, M. P. López-Ram de Víu, *Organometallics* **1999**, *18*, 3364−3371, and references therein.
[7] K. Severin, R. Bergs, W. Beck, *Angew. Chem. Int. Ed.* **1998**, *37*, 1634−1654.
[8] D. F. Dersnah, M. C. Baird, *J. Organomet. Chem.* **1977**, *127*, C55−C57.
[9] R. Krämer, K. Polborn, H. Wanjek, I. Zahn, W. Beck, *Chem. Ber.* **1990**, *123*, 767−778.
[10] W. S. Sheldrick, S. Heeb, *Inorg. Chim. Acta* **1990**, *168*, 93−100.
[11] L. C. Carter, D. L. Davies, K. T. Duffy, J. Fawcett, D. R. Russell, *Acta Crystallogr., Sect. C* **1994**, *50*, 1559−1561.
[12] H. Werner, T. Daniel, O. Nürnberg, W. Knaup, U. Meyer, *J. Organomet. Chem.* **1993**, *445*, 229−235.
[13] I. Zahn, B. Wagner, K. Polborn, W. Beck, *J. Organomet. Chem.* **1990**, *394*, 601−614.
[14] I. Zahn, K. Polborn, B. Wagner, W. Beck, *Chem. Ber.* **1991**, *124*, 1065−1073.
[15] D. B. Grotjahn, T. L. Groy, *J. Am. Chem. Soc.* **1994**, *116*, 6969−6970.
[16] T. Hauck, K. Sünkel, W. Beck, *Inorg. Chim. Acta* **1995**, *235*, 391−396.
[17] D. B. Grotjahn, T. L. Groy, *Organometallics* **1995**, *14*, 3669−3682.
[18] D. B. Grotjahn, C. Joubran, J. L. Hubbard, *Organometallics* **1996**, *15*, 1230−1235.
[19] W. S. Sheldrick, A. Gleichmann, *J. Organomet. Chem.* **1994**, *470*, 183−187.
[20] U. Koelle, K. Bücken, U. Englert, *Organometallics* **1996**, *15*, 1376−1383.
[21] T. Ohta, S.-i. Nakahara, Y. Shigemura, K. Hattori, I. Furukawa, *Chem. Lett.* **1998**, 491−492.
[22] J. W. Faller, A. R. Lavoie, *Organometallics* **2001**, *20*, 5245−5247.
[23] K.-J. Haack, S. Hashiguchi, A. Fujii, T. Ikayira, R. Noyori, *Angew. Chem.* **1997**, *109*, 297−300; *Angew. Chem. Int. Ed. Engl.* **1997**, *36*, 285−288.

[24] H. Y. Rhyoo, H.-J. Park, Y. K. Chung, *Chem. Commun.* **2001**, 2064−2065.
[25] H. Y. Rhyoo, H.-J. Park, W. H. Suh, Y. K. Chung, *Tetrahedron Lett.* **2002**, *43*, 269−272.
[26] D. Carmona, A. Mendoza, F. J. Lahoz, L. A. Oro, M. P. Lamata, E. San José, *J. Organomet. Chem.* **1990**, *396*, C17−C21.
[27] W. Rigby, H.-B. Lee, P. M. Bailey, J. A. McCleverty, P. M. Maitlis, *J. Chem. Soc., Dalton Trans.* **1979**, 387−394.
[28] D. Carmona, J. Ferrer, L. A. Oro, M. C. Apreda, C. Foces-Foces, F. H. Cano, J. Elguero, M. L. Jimeno, *J. Chem. Soc., Dalton Trans.* **1990**, 1463−1476.
[29] Isoleucinate (Ile) stands for the (2*S*,3*S*) isomer and the configuration at the HC(OH) carbon atom of the 4-hydroxyprolinate (Hyp) is (*R*).
[30] A. Mendoza, PhD Dissertation, Univ. of Zaragoza, **1993**.
[31] E. San José, PhD Dissertation, Univ. of Zaragoza, **1994**.
[32] C. Vega, PhD Dissertation, Univ. of Zaragoza, **2001**.
[33] P. Lombarte, Proyecto Fin de Carrera, Escuela Universitaria de Ingeniería Técnica Industrial, Univ. de Zaragoza, **2000**.
[34] H. Brunner, *Eur. J. Inorg. Chem.* **2001**, 905−912.
[35] D. Carmona, F. J. Lahoz, R. Atencio, L. A. Oro, M. P. Lamata, E. San José, *Tetrahedron: Asymmetry* **1993**, *4*, 1425−1428.
[36] D. Carmona, C. Vega, F. J. Lahoz, R. Atencio, L. A. Oro, M. P. Lamata, F. Viguri, E. San José, *Organometallics* **2000**, *19*, 2273−2280.
[37] M. P. Lamata, E. San José, D. Carmona, F. J. Lahoz, R. Atencio, L. A. Oro, *Organometallics* **1996**, *15*, 4852−4856.
[38] M. J. Winter, in *The Chemistry of the Metal-Carbon Bond* (Eds.: F. R. Hartley, S. Patai), Wiley, Chichester, England, **1985**, vol. 3, p. 259.
[39] N. E. Schore, *Chem. Rev.* **1988**, *88*, 1081−1119.
[40] J. Moretó, K.-I. Maruya, P. M. Bailey, P. M. Maitlis, *J. Chem. Soc., Dalton Trans.* **1982**, 1341−1347.
[41] D. Carmona, F. J. Lahoz, R. Atencio, L. A. Oro, M. P. Lamata, F. Viguri, E. San José, C. Vega, J. Reyes, F. Joó, Á. Kathó, *Chem. Eur. J.* **1999**, *5*, 1544−1564.
[42] R. Krämer, K. Polborn, C. Robl, W. Beck, *Inorg. Chim. Acta* **1992**, *198−200*, 415−420.
[43] K. Sünkel, W. Hoffmüller, W. Beck, *Z. Naturforsch., Teil B* **1998**, *53*, 1365−1368. See also ref. 44 and 45.
[44] S. Ogo, H. Chen, M. M. Olmstead, R. H. Fish, *Organometallics* **1996**, *15*, 2009−2013.
[45] T. Poth, H. Paulus, H. Elias, C. Dücker-Benfer, R. van Eldik, *Eur. J. Inorg. Chem.* **2001**, 1361−1369.
[46] In the prolinate derivatives the nitrogen atom always adopts the same configuration as the asymmetric aminocarboxylate carbon atom: H. Kolowski, L. D. Pettit, in *Chemistry of the Platinum Metals* (Ed.: F. R. Hartley), Elsevier, New York, **1991**, chapter 15, p. 530.
[47] M. J. Palmer, M. Wills, *Tetrahedron: Asymmetry* **1999**, *10*, 2045−2061.
[48] M. Bernard, V. Guiral, F. Delbecq, F. Fache, P. Sautet, M. Lemaire, *J. Am. Chem. Soc.* **1998**, *120*, 1441−1446.
[49] M. Yamakawa, H. Ito, R. Noyori, *J. Am. Chem. Soc.* **2000**, *122*, 1466−1478.
[50] V. Guiral, F. Delbecq, P. Sautet, *Organometallics* **2000**, *19*, 1589−1598.
[51] M. Bernard, F. Delbecq, P. Sautet, F. Fache, M. Lemaire, *Organometallics* **2000**, *19*, 5715−5722.
[52] Y. R. S. Laxmi, J.-E. Bäckvall, *Chem. Commun.* **2000**, 611−612.
[53] C. P. Casey, S. W. Singer, D. R. Powell, R. K. Hayashi, M. Kavana, *J. Am. Chem. Soc.* **2001**, *123*, 1090−1100.
[54] V. Guiral, F. Delbecq, P. Sautet, *Organometallics* **2001**, *20*, 2207−2214.
[55] O. Pàmies, J.-E. Bäckvall, *Chem. Eur. J.* **2001**, *7*, 5052−5058.
[56] M. Yamakawa, I. Yamada, R. Noyori, *Angew. Chem.* **2001**, *113*, 2900−2903; *Angew. Chem. Int. Ed.* **2001**, *40*, 2818−2821.
[57] R. Noyori, M. Yamakawa, S. Hashiguchi, *J. Org. Chem.* **2001**, *66*, 7931−7944.
[58] Á. Kathó, D. Carmona, F. Viguri, C. D. Remacha, J. Kovács, F. Joó, L. A. Oro, *J. Organomet. Chem.* **2000**, *593−594*, 299−306.
[59] R. Noyori, S. Hashiguchi, *Acc. Chem. Res.* **1997**, *30*, 97−102.
[60] E. Voureka, J. M. Tsangaris, A. Terzis, C. P. Raptopoulou, *Transition Met. Chem.* **1996**, *21*, 244−249.
[61] D. Carmona, M. P. Lamata, F. Viguri, I. Dobrinovich, F. J. Lahoz, L. A. Oro, *Adv. Synth. Catal.*, in press.
[62] As far as we know, there is no previously reported any crystal structure for (*N*-methyl-L-phenylalaninato)metal complexes. In the three crystal structures reported for (L-piperidine-2-carboxylato)Co^{III} compounds the nitrogen atom adopts the (*R*) configuration.[63−65]
[63] J. N. Brown, R. J. Majeste, L. D. Chung, L. M. Trefonas, *Cryst. Struct. Comm.* **1977**, *6*, 65−68.
[64] K.-I. Okamoto, M. Okabayashi, M. Ohmasa, H. Einaga, J. Hidaka, *Chem. Lett.* **1981**, 725−726.
[65] W. S. Sheldrick, E. Hanck, S. Korn, *J. Organomet. Chem.* **1994**, *467*, 283−292.

Received January 10, 2002
[I02014]

Synthesis and Structure of the new cluster $[Hg_{10}Se_4(SePh)_{12}(PPh_2nPr)_4]$ and its Conversion into $[Hg_{32}Se_{14}(SePh)_{36}]$

Andreas Eichhöfer*[a] and Emma Tröster[a]

Keywords: Cluster compounds / Mercury / Selenium / UV/Vis spectroscopy

The reaction of $HgCl_2$ and PPh_2nPr with $PhSeSiMe_3$ and $Se(SiMe_3)_2$ in THF at –30 °C results in the formation of yellow octahedral crystals of $[Hg_{10}Se_4(SePh)_{12}(PPh_2nPr)_4]$. The molecular structure of the cluster is similar to structures of other $[M_{10}Se_4(SePh)_{12}(PR_3)_4]$ (M = Cd, Zn; R = organic group) cluster compounds although it is the first of its type with mercury as the group 12 metal atom. Dissolving $[Hg_{10}Se_4(SePh)_{12}(PPh_2nPr)_4]$ in benzene at 10 °C leads to the rapid formation of a dark red solution from which red crystals of the larger cluster $[Hg_{32}Se_{14}(SePh)_{36}]$ could be crystallized in 50% yield upon layering with pentane.

(© Wiley-VCH Verlag GmbH, 69451 Weinheim, Germany, 2002)

Introduction

Systematic studies of the size-dependent optical and electronic properties of CdSe cluster molecules such as $[NPr_4]^+_2[Cd_4(SePh)_6Cl_4]^{2-}$, $[Cd_{10}Se_4(SePh)_{12}(PPr_3)_4]$, $[Cd_{17}Se_4(SePh)_{24}(PPh_2Pr)_4]^{2+}[Cd_8Se(SePh)_{12}Cl_4]^{2-}$ and $[Cd_{32}Se_{14}(SePh)_{36}(PPh_3)_4]$ (Ph = phenyl, Pr = *n*-propyl) show that the absorption and low temperature photoluminescence excitation onset of the clusters shifts systematically to the blue in smaller clusters,[1] thus confirming that the quantum confinement effect that is well-known for larger CdSe nanocrystals is also valid in these small molecular systems. The synthesis and structural characterization of group 12/16 cluster molecules has mostly been focused on ZnS,[2] ZnSe,[3] ZnTe,[4] CdS,[5,6] and CdSe[7] compounds. In contrast, chalcogenide cluster compounds with mercury are rare and $[Hg_{32}Se_{14}(SePh)_{36}]$ (**2**) is, to the best of our knowledge, the only example of such a compound containing selenido ligands as well as selenolato ones.[8] Nonetheless, these materials possess interesting properties as bulk or nano-materials. The alloy $Cd_{1-x}Hg_xTe$ is a well-known material for long-wavelength IR detector technologies, and HgTe nanoparticles have been proposed to act as potential amplifiers operating at wavelengths of 1.3 μm and 1.55 μm for telecommunication device.[9,10] Furthermore, optical investigations on small cluster molecules of bulk materials with smaller band gaps have advantages over those which possess larger ones due to the fact that for smaller clusters the mixing of ligand transitions with those of the cluster core are more pronounced in materials with a large band gap. Therefore in order to extend optical investigations on group 12/16 cluster molecules we began to investigate the synthesis and crystallisation of further mercury selenide cluster molecules.

[a] Institut für Nanotechnologie, Forschungszentrum Karlsruhe, Postfach 3640, 76021 Karlsruhe, Germany
Fax: (internat.) +49-(0)7247/82-6368
E-mail: eichhoefer@int.fzk.de

Results and Discussion

The reaction of $HgCl_2$ and PPh_2nPr with $PhSeSiMe_3$ and $Se(SiMe_3)_2$ in THF at −30 °C results in the formation of yellow octahedral crystals of $[Hg_{10}Se_4(SePh)_{12}(PPh_2nPr)_4]$ (**1**; Scheme 1).

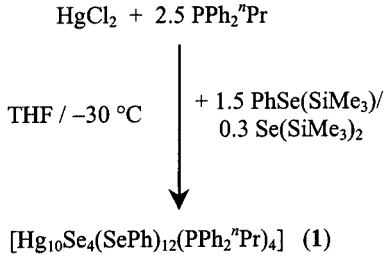

Scheme 1

Figure 1 shows the X-ray crystal structure of the $[Hg_{10}Se_{16}P_4]$ cluster core. The compound crystallizes in the tetragonal space group $I4_1/a$. The core of the cluster, which comprises four HgSe adamantane cages, is a macrotetrahedral fragment of the sphalerite structure, which is also found in HgSe.[11] The tetrahedron with the four phosphane atoms at the apex positions displays edge lengths of 1221.4−1293.4 pm. The Hg atoms Hg1−Hg3 have distorted tetrahedral environments, coordinated by the Se atoms of the μ_2-$SePh^-$ (Se2, Se3, Se4) and the μ_3-Se^{2-} (Se1) atoms as well as the P atoms of the PPh_2nPr (P1) ligands [Se−Hg−Se: 92.17−130.73(5); P−Hg−Se: 103.31−112.98(7)°]. The Hg−SePh bond lengths range

from 262.09 to 277.69(12) pm and the Hg−Se bond lengths from 256.03 to 262.81(10) pm; these distances are similar to those in HgSe (262 pm).[11] The value for the Hg−P1 bond length of the four outer Hg1 atoms coordinated by the PPh_2nPr ligands is 257.5(3) pm. The structure is therefore similar to structures of other $[M_{10}Se_4(SePh)_{12}(PR_3)_4]$ (M = Cd, Zn; R = organic group)[3,7] cluster compounds although it is the first of this type with mercury as the group 12 metal atom.

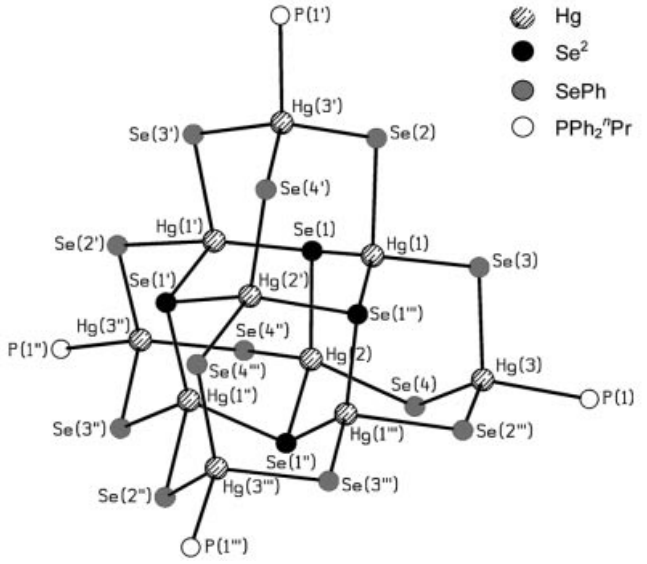

Figure 1. The $Hg_{10}Se_{16}P_4$ cluster core as a section of the molecular structure of **1**; Hg atoms (hatched circles), Se^{2-} atoms (black), $SePh^-$ (grey), P atoms (open circles); C and H atoms are omitted for clarity

Filtration of **1** at −30 °C and subsequent drying under vacuum results in a yellow powder which is stable under nitrogen at room temperature. A reflectance spectrum of microcrystalline **1** between two quartz plates (Figure 2, straight line) displays an absorption onset at 475 nm and two shoulders at approximately 410 nm and 382 nm. If **1** is dissolved in benzene at 10 °C one observes the rapid formation of a deep red solution and a small amount of black precipitate. The UV/Vis absorption spectrum of the supernatant solution (Figure 2, dashed line) displays the bands characteristic of the larger cluster $[Hg_{32}Se_{14}(SePh)_{36}]$ (**2**).[8] Upon concentration at room temperature yellow crystals of $Hg(SePh)_2$ are formed in the red solution. Layering of the filtered solution with pentane yields red crystals of **2**, sometimes accompanied by a small amount of $[Hg(SePh)_2]$. Both compounds were characterized by the determination of the lattice parameters and comparison to literature data {$[Hg(SePh)_2]$,[12] **2**: hexagonal, $a = b = 22.863$, $c = 53.390$ Å, $V = 24256$ Å^3 [8]} and **2** also by elemental analysis. Additionally the UV/Vis absorption spectrum of the red crystalline powder is in perfect agreement with the published one of **2**.[8] The black precipitate displays the three main reflections $2\theta_{111} = 25.4°$, $2\theta_{220} = 42.1°$ and $2\theta_{311} = 49.8°$ of cubic HgSe in its powder diffraction pattern.[13] Following these observations the schematic reaction equation in Scheme 2 can be established.

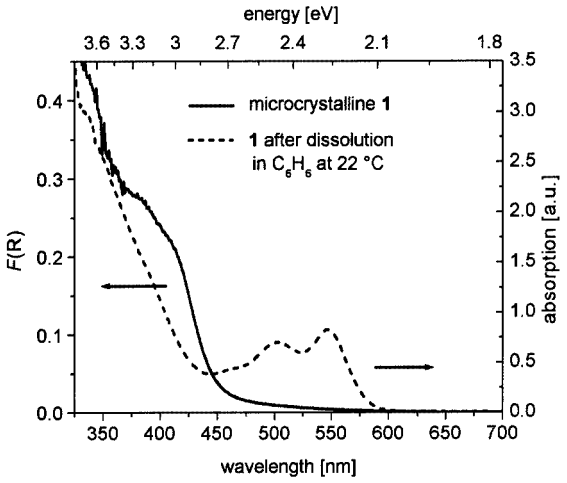

Figure 2. Reflectance spectra of **1** as a microcrystalline powder between two quartz plates (straight line) and UV/Vis absorption spectra of **1** after dissolution in C_6H_6 at 22 °C (dashed line)

$$[Hg_{10}Se_4(SePh)_{12}(PPh_2{}^nPr)_4] \quad \mathbf{(1)}$$

$$\downarrow \; C_6H_6 \,/\, 22\ °C$$

$$[Hg_{32}Se_{14}(SePh)_{36}] \quad \mathbf{(2)}$$

$$+$$

$$Hg(SePh)_2 + HgSe$$

Scheme 2

The conversion of the smaller cluster to the larger one is not induced by light as confirmed by experiments in benzene in the dark. This is in contrast to the experiment of Corrigan et al. who observed the formation of $[Cu_{50}(TePh)_{20}Te_{17}(PEtPh_2)_8][PEtPh_3]$ from $[Cu_6(TePh)_6(PEtPh_2)_5]$ by a light-induced conversion of tellurolate to telluride.[14] Furthermore we could not find any proof for the formation of $SePh_2$ in the reaction solutions similar to the formation of $TePh_2$ in Corrigan's experiment. In the present case temperature seems to play an important role for the induction of the conversion. Because of the high melting point of benzene (5 °C) the progress of the reaction could only be followed in other solvents. Compound **1** is not soluble in toluene at −60 °C. Upon warming, the solution gradually becomes coloured; it is pale yellow at −45 °C, yellow-orange at −15 °C and then becomes turbid at 0 °C with the formation of a black precipitate. The UV/Vis absorption spectrum of the supernatant pale red solution displays the bands typical for **2**. Upon layering with pentane only a few tiny crystals of **2** could be grown. In THF **1** is hardly soluble at −60 °C leading to a pale yellow solution. Upon warming, this solution also gradually turns dark remaining yellow up to −30 °C changing to brown at −10 °C and finally becoming black and turbid at room temperature. This solution shows a strong band at 256 nm prob-

ably originating from transitions related to the phenyl ligands, followed by a continuous decay to 800 nm with no indication of the formation of **2**. These results indicate that the solvent used has also an important influence on the formation of **2**.

Although **2** consists of a core built up from Hg−Se adamantane cages its formation cannot be explained in terms of a direct condensation reaction of the [$Hg_{10}Se_4(SePh)_{12}$] cluster cores of **1**. Because the outer Se−Ph ligands cannot act as bridging ligands inside the cluster cage of **2** larger rearrangements of the cluster core in **1** must take place which could also include the temporary formation of other cluster compounds. These larger rearrangements are also suggested by the formation of $Hg(SePh)_2$ and HgSe, which indicate partial decomposition of **1** during the reorganisation to **2**. The driving force of the conversion reaction could therefore be the complete formation of bulk HgSe and $Hg(SePh)_2$. Accordingly, heating a benzene solution for several hours results in a pale yellow solution with a black precipitate. However the additional formation of elemental mercury and the proof of the formation of $SePPh_2nPr$ by GC-MS and ^{31}P NMR spectroscopy suggests that the decomposition process is a more complex one as is also suggested by the yield of approximately 50% for **2** with respect to the theoretical yield based on the reaction in Scheme 2.

In summary we have shown that the new cluster [$Hg_{10}Se_4(SePh)_{12}(PPh_2nPr)_4$] (**1**) is a metastable compound that converts to $Hg(SePh)_2$, HgSe and the larger cluster [$Hg_{32}Se_{14}(SePh)_{36}$] (**2**) in benzene at room temperature. This is therefore an interesting example of controlled cluster growth in solution induced by thermal energy and suggests also the possible use of these clusters as precursor compounds in the synthesis of nanoparticles. Whether the treatment of **2** with other solvents such as THF and toluene leads to the formation of different cluster compounds and whether this conversion reaction is also valid for cluster compounds with composition [$M_{10}E_4(EPh)_{12}(PR_3)_4$] (M = Zn, Cd; E = Se, Te; R = organic group) is the focus of current investigations.

Experimental Section

General: Standard Schlenk techniques were employed throughout the syntheses using a double-manifold vacuum line with high purity dry nitrogen. Tetrahydrofuran and benzene were dried over sodium/benzophenone, pentane with $LiAlH_4$ and distilled under nitrogen. Anhydrous $HgCl_2$ was purchased from Aldrich. $PhSeSiMe_3$ [15] and $Se(SiMe_3)_2$ [16] were prepared according to standard literature procedures.

X-ray powder diffraction patterns (XRD) were measured on a STOE STADI P diffractometer (Cu-K_α radiation, Ge monochromator, Debye−Scherrer geometry) in sealed glass capillaries.

Absorption spectra of cluster molecules in solution were measured on a Varian Cary 500 spectrophotometer in quartz cuvettes. Solid-state reflectance spectra were measured on micron-sized crystalline powders between quartz plates with a Labsphere integrating sphere.

Synthesis of 1: $HgCl_2$ (0.18 g, 0.66 mmol) was dissolved in 30 mL of THF and PPh_2nPr (0.30 mL, 1.33 mmol) was added. Then $PhSeSiMe_3$ (0.19 mL, 0.99 mmol) was added at 0 °C and the resulting clear yellow solution stirred overnight at room temperature. Addition of $Se(SiMe_3)_2$ (0.045 mL, 0.2 mmol) at −60 °C led to the formation of a pale yellow solution from which [$Hg_{10}Se_4(SePh)_{12}(PPh_2nPr)_4$] (**1**) could be crystallized at −30 °C (60% yield). $C_{132}H_{128}Hg_{10}P_4Se_{16}$ (5107.6): calcd. C 31.04, H 2.53; $C_{132}H_{128}Hg_{10}P_4Se_{16}{\cdot}6C_4H_8O$: calcd. C 33.8, H 3.02; found C 31.60, H 2.44%. Most of the solvent molecules in the crystal therefore evaporate upon drying under vacuum (10^{-3} mbar). Suitable crystals for X-ray diffraction were obtained by warming the reaction solution to 0 °C and recooling to −35 °C.

Synthesis of 2: Compound **1** (0.18 g, 0.035 mmol) was dissolved in 20 mL of benzene at 10 °C to give a dark red solution with a small amount of black precipitate of HgSe. After two days at room temperature the solution was concentrated to 10 mL. Yellow platelet-like crystals of $Hg(SePh)_2$ grow together with a small amount of red crystals of **2**. These were filtered after two days and subsequent layering of the clear red solution with benzene/pentane led to the formation of red crystals of **2** (yield 49% calculated for Scheme 2). $C_{216}H_{180}Hg_{32}Se_{40}$ (12353.1): calcd. C 19.74, H 1.38; found C 21.87, H 1.58. The deviations in the C H analysis probably indicate the presence of $Hg(SePh)_2$ in the red crystalline powder.

Crystallographic Data for $1{\cdot}6C_4H_8O$: M_r = 5514.91, tetragonal, space group $I4_1/a$ (No. 88), $a = b$ = 23.059(3), c = 37.757(8) Å, V = 20077 Å^3, Z = 4, D_c = 1.825 g·cm^{-3}, μ(Mo-K_α) = 10.59 mm^{-1}. The data collection was carried out on a STOE IPDS II diffractometer using graphite-monochromated Mo-K_α (l = 0.71073 Å) radiation at 170 K. The structure solution and full-matrix least square refinement based on F^2 were performed with the SHELX-97 program package,[17] giving a final $R1$ value of 0.0466 for 406 parameters and 7061 unique reflections with $I \geq 2\sigma(I)$ and a $wR2$ value of 0.1588 for all 37265 reflections.

CCDC-178317 contains the supplementary crystallographic data for this paper. These data can be obtained free of charge at www.ccdc.cam.ac.uk/conts/retrieving.html [or from the Cambridge Crystallographic Data Centre, 12 Union Road, Cambridge CB2 1EZ, UK; fax: (internat.) +44-1223/336-033; E-mail: deposit@ccdc.cam.ac.uk].

[1] V. Soloviev, A. Eichhöfer, D. Fenske, U. Banin, *J. Am. Chem. Soc.* **2001**, *123*, 2354−2364.
[2] B. Ali, I. G. Dance, D. C. Craig, M. L. Scudder, *J. Chem. Soc., Dalton Trans.* **1998**, 1661−1667; M. D. Nyman, M. J. Hampden-Smith, E. N. Duesler, *Inorg. Chem.* **1996**, *35*, 802−803.
[3] A. Eichhöfer, D. Fenske, H. Pfistner, M. Wunder, *Z. Anorg. Allg. Chem.* **1998**, *624*, 1909−1914.
[4] H. Pfistner, D. Fenske, *Z. Anorg. Allg. Chem.* **2001**, *627*, 575−582.
[5] G. S. H. Lee, K. J. Fisher, D. C. Craig, M. L. Scudder, I. G. Dance, *J. Am. Chem. Soc.* **1990**, *112*, 6435−6437; G. S. H. Lee, D. C. Craig, I. Ma, M. L. Scudder, T. D. Bailey, I. G. Dance, *J. Am. Chem. Soc.* **1988**, *110*, 4863−4864; I. G. Dance, A. Choy, M. L. Scudder, *J. Am. Chem. Soc.* **1984**, *106*, 6285−6295.
[6] T. Vossmeyer, G. Reck, L. Katsikas, E. T. K. Haupt, B. Schulz, H. Weller, *Science* **1995**, *267*, 1476−1479; T. Vossmeyer, G. Reck, B. Schulz, L. Katsikas, H. Weller, *J. Am. Chem. Soc.* **1995**, *117*, 12881−12882.

[7] S. Behrens, M. Bettenhausen, A. Eichhöfer, D. Fenske, *Angew. Chem.* **1997**, *109*, 2874−2876; *Angew. Chem. Int. Ed. Engl.* **1997**, *24*, 2797; S. Behrens, D. Fenske, *Ber. Bunsenges. Phys. Chem.* **1997**, *101*, 1588−1592.
[8] S. Behrens, M. Bettenhausen, A. C. Deveson, A. Eichhöfer, D. Fenske, A. Lohde, U. Woggon, *Angew. Chem.* **1996**, *108*, 2360−2363; *Angew. Chem. Int. Ed. Engl.* **1996**, *35*, 2215−2218.
[9] A. Rogach, S. Kershaw, M. Burt, M. Harrison, A. Kornowski, A. Eychmüller, H. Weller, *Adv. Mater.* **1999**, *11*, 552−555.
[10] M. Harrison, S. Kershaw, A. Rogach, A. Kornowski, A. Eychmüller, H. Weller, *Adv. Mater.* **2000**, *12*, 123−125.
[11] Landolt-Börnstein, Gruppe III: Kristall und Festkörperphysik, Band 17: Halbleiter (Gesamtherausgabe: O. Madelung), Springer, Berlin, **1982**, p. 236.
[12] E. Schulz Lang, M. Müller Dias, U. Abram, E. M. Vázquez-López, *Z. Anorg. Allg. Chem.* **2000**, *626*, 784−788.
[13] J. W. Early, *Am. Mineral.* **1950**, *35*, 337−364.
[14] J. F. Corrigan, D. Fenske, *Angew. Chem.* **1997**, *109*, 2070−2072; *Angew. Chem. Int. Ed. Engl.* **1997**, *36*, 1981−1983.
[15] N. Miyoshi, H. Ishii, K. Kondo, S. Mui, N. Sonoda, *Synthesis* **1979**, 301−304.
[16] H. Schmidt, H. Ruf, *Z. Anorg. Allg. Chem.* **1963**, *321*, 270−273.
[17] G. M. Sheldrick SHELX-97, Program for X-ray crystal structure determination and refinement, Göttingen University, Germany, **1997**.

Received March 22, 2002
[I02153]

Diels–Alder Synthesis of Rigid 60° Angular Bridging Ligands and X-ray Crystal Structures of their Silver Nitrate Complexes

Peter J. Steel*[a] and Nicholas C. Webb[a]

Keywords: Silver / Coordination polymers / Bridging ligands / Self-assembly / N ligands

Using Diels–Alder chemistry, three bridging ligands (**2**–**4**) have been synthesised, each of which contains two pyridine nitrogen donors disposed at a 60° angle. X-ray crystal structures are reported for ligand **4** and two coordination polymers formed by the reaction of **2** and **3** with silver nitrate.

(© Wiley-VCH Verlag GmbH, 69451 Weinheim, Germany, 2002)

Introduction

The controlled self-assembly of two- and three-dimensional metallosupramolecular species has been the subject of enormous study in recent years.[1] The most common synthetic approach to such compounds has been to employ logical combinations of rigid linear and angular components in order to construct rationally designed architectures.[1] Within this context, molecular squares have proved to be particularly popular synthetic targets as they are readily assembled from combinations of linear, bridging ligands (such as pyrazine or 4,4′-bipyridine) and right-angular (90°) metal linkages (such as is provided by *cis*-coordination in a square-planar metal centre).[2] Similarly, molecular pentagons and hexagons are available using tetrahedral and trigonal linking components.[1] This concept has been extended into the third dimension with reports of molecular cubes,[3] dodecahedra,[4] and other polyhedra.[1]

Of the two-dimensional molecular polygons, triangles pose a particular problem.[1] Metal centres are not suitable for use as the angular components, since the requisite 60° angle is not readily provided by the subset of angular geometries offered by ligand coordination to transition metals. Consequently, the construction of metallosupramolecular triangles necessitates an inversion of approach, such that the metal provides the linear bridge (e.g. *trans* coordination to a square-planar metal centre) and the organic ligand provides the angular component (Figure 1a). A limited number of such species have been reported, the most common of which have employed pyrazolates as angular bridges linking linear metal centres, such as silver or gold (Figure 1b).[5] Intrinsically, the use of pyrazolates as the angular components allows no control over the dimension of the triangles assembled. Loeb and co-workers[6] have used 4,7-naphthyridine to construct larger molecular triangles in which the organic ligand provides the necessary 60° angular bridge linking doubly cyclometallated palladium-based linear bridges. However, such ligands are not amenable to control of the distance between the donor centres, and hence the size of the triangle produced. More recently, a number of isolated examples of metastable distorted triangles have been reported that used pyrazine[7] or larger, more flexible bridging ligands.[8]

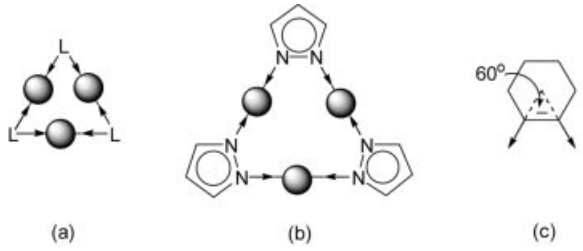

Figure 1. Molecular triangle components

Since the internal angle subtended by adjacent corners of a hexagon is 60°, we reasoned that a diverse range of triangular building blocks would be provided by organic ligands that incorporate donor groups with adjacent substitution in a cyclohexene or benzene ring (Figure 1c). We now report the synthesis of three such ligands that contain two 4-pyridyl substituents, each of which provides two nitrogen donors disposed at a 60° angle. Using a similar conceptual approach, Espinet and co-workers[9] recently reported the synthesis of an organometallic triangle derived from 1,2-phenylene diisocyanide, despite the fact that the corresponding diacetylide had led to an organometallic molecular square.[10] As we,[11] and others,[12] have found, reactions of bridging ligands with silver(I) species have led to a rich array of metallosupramolecular architectures. Thus, we have initially explored the coordination chemistry of these new

[a] Department of Chemistry, University of Canterbury, Christchurch, New Zealand
Fax: (internat.) +64-3/364-2110
E-mail: p.steel@chem.canterbury.ac.nz

ligands by examining their reactions with silver nitrate. Accordingly, we also report the synthesis and X-ray crystal structures of complexes formed from these ligands by reactions with silver nitrate.

Results and Discussion

The three ligands **2**−**4** were prepared by procedures based on the Diels−Alder reaction, as shown in Scheme 1. Di(4-pyridyl)acetylene (**1**) was prepared in 55% overall yield from commercially available 1,2-di(4-pyridyl)ethylene by bromination and dehydrobromination, according to a literature procedure.[13] In order to improve the dienophilicity of this compound, the pyridyl substituents were made more electron-withdrawing by conversion into the pyridinium species, through reaction with tetrafluoroboric acid. This methodology has previously been employed for the Diels−Alder reaction of **1** with cyclopentadiene.[14] Reaction of **1** with cyclohexa-1,3-diene gave the bicyclooctadiene **2**, albeit in a disappointing 12% yield.[15] Since mass spectrometry showed that this compound readily undergoes a retro-Diels−Alder reaction, with expulsion of ethylene, this strategy was used to prepare the disubstituted ligand **3**. Thus, heating **2** to 280 °C resulted in its smooth conversion into ligand **3**, which was isolated in 49% yield. This compound has previously been prepared by a Stille coupling procedure in the course of the synthesis of a large series of poly(4-pyridyl)-substituted aromatics.[16] The tetraphenyl derivative **4** was prepared by reaction of **1** with tetracyclone. In this case the free base was used, as Diels−Alder reactions of tetracyclone are well-known to proceed with inverse electron demand.[17] The intermediate adduct **5** underwent spontaneous expulsion of carbon monoxide to give the new ligand **4**.[18]

In order to confirm the structure of **4**, and to examine the relative orientations of the aryl rings, a single crystal X-ray crystal structure determination was carried out.[19] Figure 2 shows a perspective view of this new ligand, along with selected bond lengths and angles. Whereas the six peripheral aryl rings are all planar (to within 0.007 Å), the central ring displays an interesting distortion into a boat conformation, with C(3) and C(6) each displaced ca. 0.04 Å above the plane of the other four atoms of the ring. This in turn points the two attached phenyl rings above the plane of the central ring. As is the case in the crystal structure of hexaphenylbenzene,[20] the planes of the six external rings display a cooperatively correlated inclination with respect to the central benzene ring. The two pyridine rings are inclined at angles of 63.2 and 68.8° to the central ring, whereas the four phenyl rings are twisted by angles ranging from 65.9 to 76.1°. With respect to the centre of the central ring the two pyridine nitrogen donors subtend an angle of 62.6°.

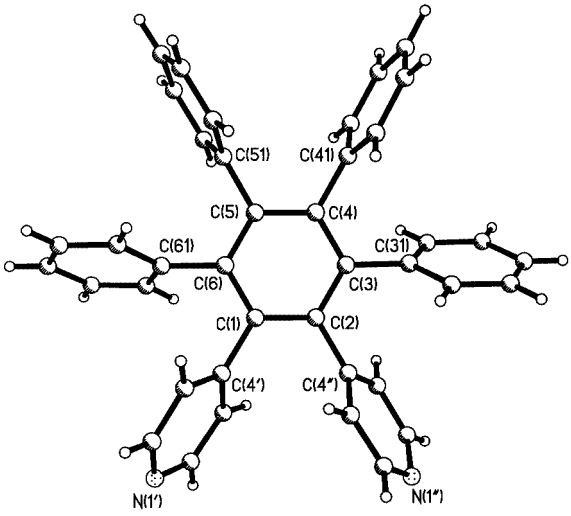

Figure 2. Perspective view of the X-ray crystal structure of ligand **4**; selected bond lengths (Å) and angles (°): C1−C2 1.411(3); C1−C6 1.409(3), C1−C4′ 1.501(3), C2−C3 1.408(3); C2−C4′′ 1.496(3), C3−C4 1.406(3), C3−C31 1.495(3), C4−C5 1.413(3), C4−C41 1.502(3); C5−C6 1.400(3), C6−C61 1.515(3); C2−C1−C6 119.9(2), C1−C2−C3 120.2(2), C2−C3−C4 119.4(2), C3−C4−C5 120.2(2), C4−C5−C6 120.1(2), C1−C6−C5 119.8(2)

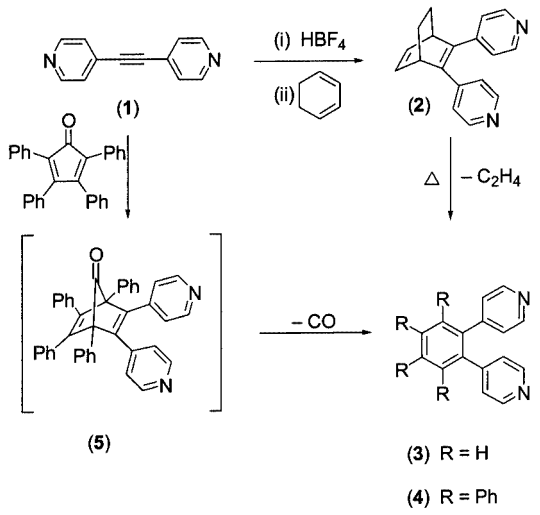

Scheme 1

Ligands **2** and **3** were reacted with silver(I) nitrate in acetonitrile to give quantitative formation of complexes **6** and **7**, respectively, which on slow evaporation of the solutions furnished crystals suitable for an X-ray structure determination. In the case of the hexasubstituted ligand **4**, the low solubility of the ligand in acetonitrile required that the reaction be performed in methanol solution, which did not lead to X-ray quality crystals.

The structure[19] of the complex (**6**) formed from the bicyclo[2.2.2]octa-2,5-diene ligand **2** is surprisingly intricate. Figure 3 shows a perspective view of the contents of the asymmetric unit, which contains two silver atoms, two molecules of **2**, two nitrate anions and an acetonitrile solvate molecule. Each of the two independent ligands is bonded to three silver atoms through its two nitrogen donors and to the endo face of the more exposed double bond of the bicyclo[2.2.2]octa-2,5-diene moiety. Similarly, each silver atom is coordinated to three different ligands and also in-

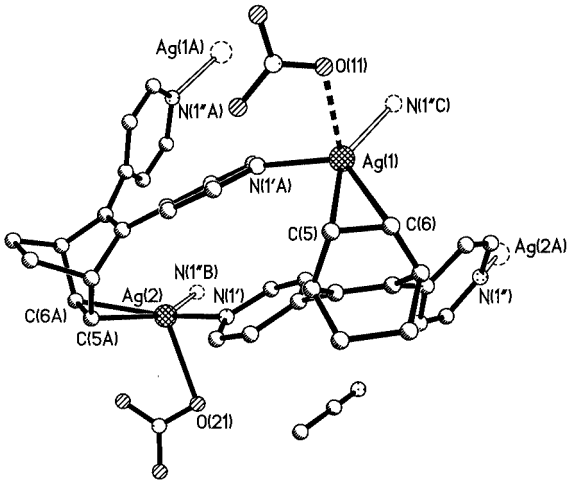

Figure 3. Perspective view of the contents of the asymmetric unit of the crystal structure of **6**; hydrogen atoms have been omitted for clarity; selected bond lengths (Å): Ag1–N1′A 2.328(5), Ag1–N1′′C 2.260(5), Ag1–C5 2.342(7), Ag1–C6 2.468(8), Ag1–O11 2.653(5), C5–C6 1.371(10), Ag2–N1′ 2.328(5), Ag2–N1′′B 2.292(5), Ag2–C6A 2.443(6), Ag2–C5A 2.457(7), Ag2–O21 2.565(5), C5A–C6A 1.403(8)

teracts weakly with one of the oxygen atoms of a nitrate counterion. The bridging nature of both the ligand and the metal results in an extension into a complex coordination polymer that propagates along the *a* axis.

Thus ligand **2** bridges three silver atoms with coordination to both the pyridine donors as well as a double bond of the bicyclooctadiene unit. To the best of our knowledge the only previously reported X-ray crystal structure which incorporates both of these features, is that of an ethylene adduct of a silver complex of a tris-pyrazolylborate.[21] As expected the nitrogen donors subtend angles [66.7(5) and 69.1(5)°] at the centroids of their attached bicyclooctane units which would be compatible with the formation of molecular triangles in the absence of these additional interactions.

The complex (**7**) formed from 1,2-di(2-pyridyl)benzene (**3**) is a zigzag coordination polymer. Figure 4 shows a perspective view of a section of this polymer, with selected atom labelling. In the crystal structure,[19] ligand **2** bridges two silver atoms, with an angle subtended at the centre of the benzene ring of 67.8°. The plane of the benzene ring is inclined to the planes of the attached pyridine rings at angles of 54.1 and 46.9°. By virtue of the coordination to the nitrate anion the silver atom deviates significantly from linear geometry.

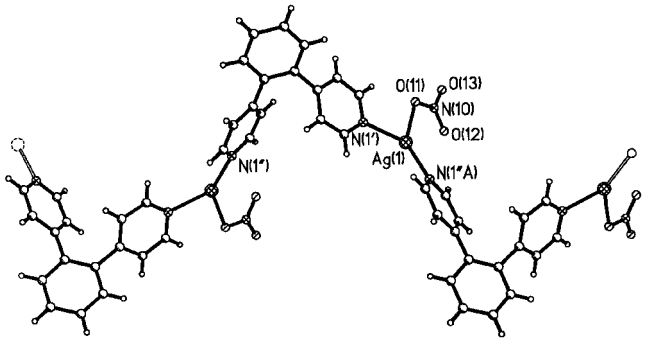

Figure 4. Crystal structure of a segment of the coordination polymer **7**; selected bond lengths (Å) and angles (°): Ag1–N1′ 2.279(2), Ag1–N1′′A 2.210(2), Ag1–O11 2.408(2); N1′–Ag1–N1′′A 132.13(6), N1′–Ag1–O11 87.90(5), N1′′A–Ag1–O11 138.23(5)

Table 1. X-ray crystal data and details of data collections and structure refinements

Compound	**4**	**6**	**7**
Formula	$C_{40}H_{28}N_2$	$C_{38}H_{35}Ag_2N_7O_6$	$C_{16}H_{12}AgN_3O_3$
Molecular weight	536.64	901.47	402.16
Crystal system	monoclinic	triclinic	monoclinic
Space group	*Cc*	$P\bar{1}$	$P2_1/n$
a (Å)	12.261(6)	10.738(7)	9.514(2)
b (Å)	21.343(11)	13.050(9)	10.940(3)
c (Å)	11.239(6)	13.825(10)	14.296(4)
α (°)	90	89.693(9)	90
β (°)	98.432(7)	67.692(9)	100.332(3)
γ (°)	90	87.084(10)	90
V (Å^3)	2909(3)	1790(2)	1463.8(6)
Z	4	2	4
D_c (Mg m^{-3})	1.225	1.673	1.825
F(000)	1128	908	800
Temperature (K)	168(2)	168(2)	168(2)
Crystal form	colourless prism	colourless needle	colourless block
Crystal size (mm)	0.36 × 0.16 × 0.12	0.64 × 0.03 × 0.02	0.86 × 0.21 × 0.17
μ (mm^{-1})	0.071	1.673	1.396
$2\theta_{max}$ (°)	50	50	53
Unique reflections	5111	6264	2989
Parameters	380	491	208
R[a] [$I > 2\sigma(I)$][a]	0.0386	0.0431	0.0201
wR[b] (all data)	0.0809	0.0814	0.0534

[a] $R = \Sigma(|F_0| - |F_c|)/\Sigma|F_0|$. [b] $wR = (\Sigma[w(F_0^2 - F_c^2)^2]/\Sigma[w(F_0^2)^2])^{1/2}$.

In conclusion, we have prepared three bridging ligands, each of which possesses two pyridine nitrogen donors disposed at a 60° angle, suitable for the self-assembly of molecular triangles. In their reactions with silver nitrate coordination polymers are formed as a result of the fact that the silver atoms do not behave as linear bridges due to additional interactions with the nitrate anions.

Acknowledgments

We thank the Royal Society of New Zealand Marsden Fund and the University of Canterbury Summer Scholarship Scheme for financial support.

[1] For recent reviews, see: S. Leininger, B. Olenyuk, P. J. Stang, *Chem. Rev.* **2000**, *100*, 853−908; G. F. Swiegers, T. J. Malefetse, *Chem. Rev.* **2000**, *100*, 3483−3538; B. Moulton, M. J. Zaworotko, *Chem. Rev.* **2001**, *101*, 1629−1658; M. Fujita, K. Umemoto, M. Yoshizawa, N. Fujita, T. Kusukawa, K. Biradha, *Chem. Commun.* **2001**, 509−518; D. W. Johnson, K. N. Raymond, *Supramol. Chem.* **2001**, *13*, 639−659; B. J. Holliday, C. A. Mirkin, *Angew. Chem. Int. Ed.* **2001**, *40*, 2022−2043; G. F. Swiegers, T. J. Malefetse, *Coord. Chem. Rev.* **2002**, *225*, 91−121.

[2] G. F. Swiegers, T. J. Malefetse, *Chem. Eur. J.* **2001**, *7*, 3637−3643.

[3] S. Roche, C. Haslam, H. Adams, S. L. Heath, J. A. Thomas, *Chem. Commun.* **1998**, 1681−1682; K. K. Klaumeyer, T. B. Rauchfuss, S. R. Wilson, *Angew. Chem. Int. Ed.* **1998**, *37*, 1694−1696.

[4] B. Olenyuk, M. D. Levin, J. A. Whiteford, J. E. Shield, P. J. Stang, *J. Am. Chem. Soc.* **1999**, *121*, 10434−10435.

[5] H. H. Murray, R. G. Raptis, J. P. Fackler, *Inorg. Chem.* **1988**, *27*, 26−33; R. G. Raptis, J. P. Fackler, *Inorg. Chem.* **1990**, *29*, 5003−5006.

[6] J. R. Hall, S. J. Loeb, G. K. H. Shimizu, G. P. A. Yap, *Angew. Chem. Int. Ed.* **1998**, *37*, 121−123.

[7] X.-Y. Yu, M. Maekawa, M. Kondo, S. Kitagawa, G.-X. Jin, *Chem. Lett.* **2001**, 168−169; M. Schweiger, S. R. Seidel, A. M. Arif, P. J. Stang, *Angew. Chem. Int. Ed.* **2001**, *40*, 3467−3469.

[8] R.-D. Schnebeck, E. Freisinger, F. Glabe, B. Lippert, *J. Am. Chem. Soc.* **2000**, *122*, 1381−1390; S.-S. Sun, A. J. Lees, *J. Am. Chem. Soc.* **2000**, *122*, 8956−9867; A. Sautter, D. G. Schmid, G. Jung, F. Wurthner, *J. Am. Chem. Soc.* **2001**, *123*, 5424−5430; Z. Qin, M. C. Jennings, R. J. Puddephatt, *Chem. Commun.* **2001**, 2676−2677; M. Schweiger, S. R. Seidel, A. M. Arif, P. J. Stang, *Inorg. Chem.* **2002**, *41*, 2556−2559.

[9] P. Espinet, K. Soulantica, J. P. H. Charmant, A. G. Orpen, *Chem. Commun.* **2000**, 915−916.

[10] K. Onitsuka, S. Yamamoto, S. Takahashi, *Angew. Chem. Int. Ed.* **1999**, *38*, 174−176.

[11] C. M. Hartshorn, P. J. Steel, *Inorg. Chem.* **1996**, *35*, 6902−6903; C. M. Hartshorn, P. J. Steel, *J. Chem. Soc., Dalton Trans.* **1998**, 3927−3934; C. M. Hartshorn, P. J. Steel, *J. Chem. Soc., Dalton Trans.* **1998**, 3935−3940; R. J. Anderson, P. J. Steel, *Acta Crystallogr., Sect. C* **1998**, *54*, 223−225; B. J. O'Keefe, P. J. Steel, *Inorg. Chem. Commun.* **1998**, *1*, 147−149; C. Richardson, P. J. Steel, *Inorg. Chem. Commun.* **1998**, *1*, 260−262;; D. A. McMorran, P. J. Steel, *Inorg. Chem. Commun.* **1999**, *2*, 368−370; B. J. O'Keefe, P. J. Steel, *Inorg. Chem. Commun.* **2000**, *3*, 473−475; C. M. Hartshorn, P. J. Steel, *Inorg. Chem. Commun.* **2000**, *3*, 476−481; C. M. Fitchett, P. Steel, *New J. Chem.* **2000**, *24*, 945−947; C. M. Fitchett, P. J. Steel, *Inorg. Chim. Acta* **2000**, *310*, 127−132; P. J. Steel, C. J. Sumby, *Chem. Commun.* **2002**, 322−323; P. J. Steel, C. J. Sumby, *Inorg. Chem. Commun.* **2002**, *5*, 323−327.

[12] M. Munakata, L. P. Wu, T. Kuroda-Sowa, *Adv. Inorg. Chem.* **1999**, *46*, 173−303.

[13] M. Tanner, A. Ludi, *Chimia* **1980**, *34*, 23−24.

[14] Y. Yamashita, T. Hanaoka, Y. Takeda, T. Mukai, T. Miyashi, *Bull. Chem. Soc. Jpn.* **1988**, *61*, 2451−2458.

[15] Preparation of **2**: Di(4-pyridyl)acetylene (500 mg) was converted into its di-HBF_4 salt by addition of 1 mL of 50% HBF_4 solution to a stirred solution of the acetylene in 350 mL diethyl ether. The white precipitate was filtered off, and dried under vacuum. This was added to 3.5 mL of cyclohexa-1,3-diene in 60 mL of dry acetonitrile and the mixture refluxed for 18 h. The solvent was removed in vacuo, leaving a brown/black residue, which was dissolved in 100 mL water, containing a small amount of HBF_4. This was washed with 4 × 45 mL dichloromethane, neutralised with $NaHCO_3$, then extracted with 4 × 60 mL dichloromethane. The dichloromethane solution was dried over $MgSO_4$ and the solvent removed in vacuo. After chromatography on alumina (10% methanol in ethyl acetate) the isolated product was recrystallised from petroleum ether/ethyl acetate to give 86.6 mg of a yellow solid. M.p. 124−126 °C. ^{1}H NMR ($CDCl_3$): δ = 8.44 (d, 4 H), 6.95 (d, 4 H), 6.53 (dd, 2 H), 3.97 (br. s, 2 H), 1.62 (dd, 2 H), 1.53 (dd, 2 H) ppm. ^{13}C NMR ($CDCl_3$): δ = 149.8, 146.7, 141.9, 134.4, 122.8, 43.7, 25.0. $C_{18}H_{16}N_2$ (260.3): calcd. C 83.04, H 6.20, N 10.76; found C 82.97, H 6.18, N 10.92.

[16] M. Fujita, H. Oka, K. Ogura, *Tetrahedron Lett.* **1995**, *36*, 5247−5250.

[17] M. A. Ogliaruso, M. G. Romanelli, E. I. Becker, *Chem. Rev.* **1965**, *65*, 261−367.

[18] Selected data for **4**: M.p. > 340 °C. ^{1}H NMR ($CDCl_3$): δ = 8.13 (d, 4 H), 6.88 (m, 12 H), 6.81 (m, 8 H), 6.78 (d, 4 H).

[19] The crystal data, data collection and refinement parameters for the X-ray structures are listed in Table 1. Data were collected with a Siemens SMART CCD area detector, using graphite monochromatized Mo-K_α radiation (λ = 0.71073 Å). The structures were solved by direct methods, and refined on F^2 using all data by full-matrix least-squares procedures.
CCDC-182307 to CCDC-182309 contain the supplementary crystallographic data for this paper. These data can be obtained free of charge at www.ccdc.cam.ac.uk/conts/retrieving.html [or from the Cambridge Crystallographic Data Centre, 12, Union Road, Cambridge CB2 1EZ, UK; Fax: (internat.) +44-1223/336-033; E-mail: deposit@ccdc.cam.ac.uk].

[20] J. C. J. Bart, *Acta Crystallogr., Sect. B* **1968**, *24*, 1277−1287.

[21] H. V. R. Dias, Z. Wang, W. Jin, *Inorg. Chem.* **1997**, *36*, 6205−6215.

Received April 2, 2002
[I02170]

Reactivity of Platinum Stanna-*closo*-dodecaborate Complexes: First Hydroformylation Studies

Lars Wesemann,*[a] Siegbert Hagen,[a] Thiemo Marx,[a] Ingo Pantenburg,[a] Markus Nobis,[b] and Birgit Drießen-Hölscher*[b]

Dedicated to Professor Dieter Naumann on the occasion of his 60th birthday

Keywords: Boranes / Cluster compounds / Homogeneous catalysis / Platinum / Tin

The synthesis and characterization of two (dppp)Pt complexes with the stannaborate ligand $SnB_{11}H_{11}$ is described. In the case of the salt $[Bu_3MeN]_2[(dppp)Pt(SnB_{11}H_{11})_2]$ the structure in the solid state was determined by X-ray crystal structure analysis. As a result of comparative catalysis studies between $SnCl_3$ and $[SnB_{11}H_{11}]^-$-substituted platinum complexes we found selective hydroformylation of 1-octene catalysed by the $[(dppp)PtPh(SnB_{11}H_{11})]^-$ and $[(dppp)Pt(SnB_{11}H_{11})_2]^{2-}$ complexes.

(© Wiley-VCH Verlag GmbH, 69451 Weinheim, Germany, 2002)

Introduction

We are interested in the coordination abilities of the hetero-*closo*-dodecaborate clusters $[EB_{11}H_{11}]^{2-}$ of the group 14 elements.[1,2] The first example of the complexation of these *closo*-borates at a transition metal centre was the copper compound $\{[Bu_4N]_2[ClCu(CB_{11}F_{11})]\}$ reported by Strauss et al.[3] For E = Sn we have synthesised coordination compounds of the type $L_nM\text{-}(SnB_{11}H_{11})$ for a wide variety of transition metals (Fe, Mo, Rh, Ir, Ni, Pd, Pt).[4−7] Characterization of the hydride complex $[Bu_3MeN][trans\text{-}(Et_3P)_2PtH(SnB_{11}H_{11})]$ led us to the conclusion that the stannaborate ligand has a higher *trans* influence than the trichlorostannyl ligand ($SnCl_3$).[7] Furthermore, we found that the tin ligand $[SnB_{11}H_{11}]^-$ activates Pt−C bonds towards isocyanide insertion.[8] In the field of carbonylation hydroformylation is one of the most important reactions catalysed homogeneously by transition metal complexes, with cobalt and rhodium complexes being amongst the most important.[9] The mechanistic aspects of platinum-catalysed hydroformylation have been studied extensively.[10] In particular, the insertion of the carbon monoxide molecule and the effect of the bite angle of the chelating phosphane have been investigated.

Asymmetric hydroformylation using chiral phosphanes has been carried out successfully with platinum complexes.[11] Most of the platinum complexes studied so far in hydroformylation experiments are of the type L_2PtCl_2 and have to be reacted with $SnCl_2$ to provide hydroformylation activity;[12,13] tin(II) chloride inserts into the Pt−Cl bond and forms the trichlorostannyl ligand.[14] The role of this ligand is the subject of many studies and it appears that the lability of the $SnCl_3$ group is one reason for the activation of platinum complexes.[15] Besides these trichlorostannyl complexes several very interesting alternative platinum catalysts have been developed ($[Pt(C_2H_4)$(chelating phosphane)$]/CH_3SO_3H$;[16] platinum-diphenylphosphinous acid complex catalyst).[17] The easily accessible stanna-*closo*-dodecaborate cluster is resistant towards moisture and air and reacts with most of the transition metal electrophiles studied so far by complexation and formation of a metal-tin bond. Since (phosphane)Pt-$(R)SnCl_3$ complexes are well known for their catalytic activity in hydroformylation reactions we started a comparative study on the hydroformylation activity of $SnCl_3$ and $SnB_{11}H_{11}$ complexes of platinum.

Results and Discussion

At the beginning of our stannaborate complex synthesis we decided to use the 1,3-bis(diphenylphosphanyl)propane (dppp) as the chelating ligand. Following our standard procedure two stannaborate complexes were synthesised in high yield by nucleophilic substitution of the chloride anion with the stannaborate dianion (Scheme 1 and 2).

[a] Institut für Anorganische Chemie, Universität zu Köln
Greinstr. 6, 50939 Köln, Germany
Fax: (internat.) + 49-(0)221/470-4899
E-mail: lars.wesemann@uni-koeln.de
[b] Institut für Makromolekulare und Technische Chemie der Technischen Hochschule Aachen,
Worringerweg 1, 52074 Aachen, Germany

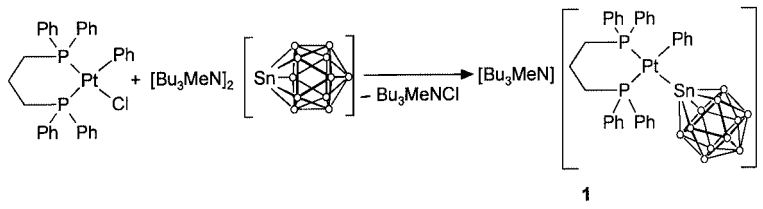

Scheme 1

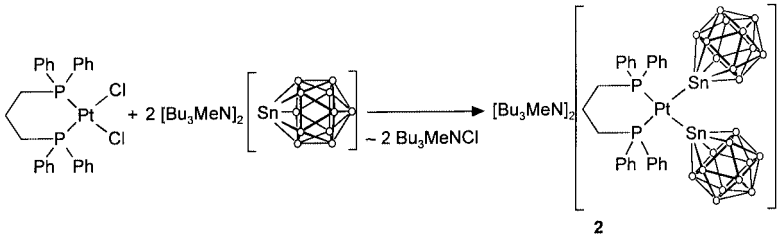

Scheme 2

The salts **1** and **2** were characterised by elemental analysis, NMR spectroscopy and in the case of **2** by a single-crystal structure analysis. It is well established that the $^2J_{SnP}$ coupling constant permits unambiguous assignment of the stereochemistry in Pt^{II} complexes. Indirect coupling between ligand atoms is known to be much larger for *trans* than for *cis* related ligands.[18] Here the $^2J_{SnP}$ of the signal at $\delta = 2.40$ ppm (*trans* to Sn) is around 10 times larger than the respective coupling of the signal at $\delta = -5.40$ ppm (*cis* to Sn).

Single crystals of complex **2** were obtained at room temperature from acetone and methanol solution. The salt crystallises as yellow-green octahedra in the orthorhombic space group *Pbcn* with the dianion $[(dppp)Pt(SnB_{11}H_{11})]^{2-}$ lying on a twofold rotation axis.[19] Figure 1 shows the molecular structure of the dianion of **2**.

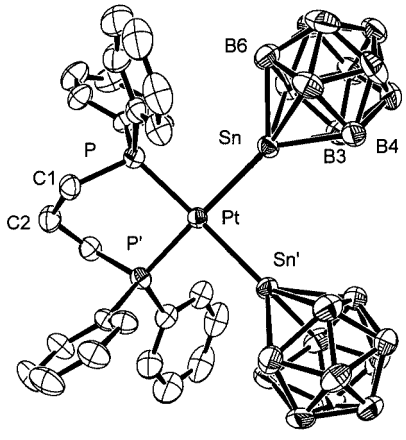

Figure 1. Molecular structure of the $[(dppp)Pt(SnB_{11}H_{11})_2]^{2-}$ dianion in the crystal structure of **2**; bond lengths [Å] and angles [°] (with estimated standard deviations in parentheses): Pt−Sn 2.596(1), Pt−P 2.279(2), Sn−B2 2.288(8), Sn−B3 2.322(8), Sn−B4 2.285(8), Sn−B5 2.308(9), Sn−B6 2.299(9), P−C1 1.821(7), P−Pt−P′ 91.07(8), Sn−Pt−Sn′ 88.87(2), P−Pt−Sn 91.32(4)

Due to steric crowding around the platinum centre the square-planar coordination is slightly distorted towards a tetrahedral arrangement with a torsion angle (P−P′−Sn−Sn′) of 17°. The interatomic distances are similar to those in other stannaborate complexes.

Hydroformylation experiments were carried out with 1-octene in CH_2Cl_2 with four different (dppp)Pt complexes: **1**, **2**, [(dppp)Pt(Ph)$SnCl_3$] (**3**) and [(dppp)Pt($SnCl_3$)$_2$] (**4**). Due to isomerization of 1-octene during the catalysis four different aldehydes are the expected products of this conversion (Scheme 3).

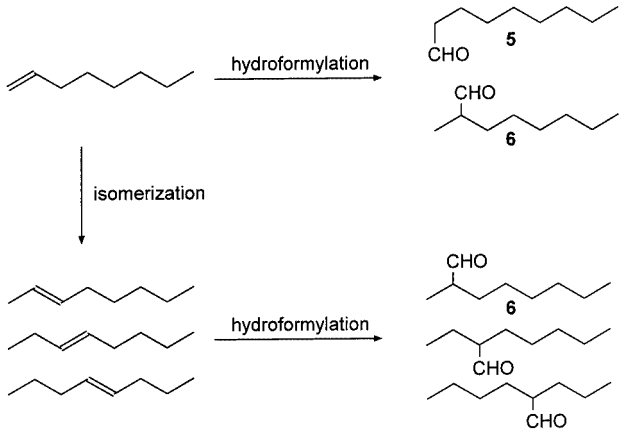

Scheme 3. Products of the hydroformylation of 1-octene and the olefins 2-, 3- and 4-octene, which result from preceding isomerization (isomerized olefins were drawn without considering the stereochemistry).

Besides other criteria the importance of olefin hydroformylation arises, of course, from the selectivity of the aldehyde formation. The *n*/*iso* ratio, which is always an important parameter in hydroformylation catalysis, refers to the amount of *n*-nonanal (**5**) and *iso*-nonanal (**6**), which is usually determined by gas chromatography. Table 1−4 show the results of the catalysis experiments with complexes

1−**4**. From comparative catalysis studies between $SnCl_3$- and $[SnB_{11}H_{11}]^-$-substituted platinum complexes we found the highest activity at 100 °C for the $SnCl_3$-substituted derivative. However, at 120 °C the activity of the stannaborate complex **1** is the highest and rises upon increasing the temperature. Thus, complexes **1** and **2** are thermally stable at 140 °C whereas their $SnCl_3$ counterparts decompose at this temperatures. In the range of temperature studied the *n*/*iso* selectivity is much higher with the borate complex, although upon increasing the temperature the amount of isomerized olefins also increases. Only a slight pressure dependence of the *n*/*iso* ratio in the case of the reactions with complex **2** was observed (Table 4). In our opinion it is very interesting that the isomerized olefins (Table 3) which were formed during catalysis were not hydroformylated by the stannaborate complexes. Instead 1-octene is selectively transformed into the aldehydes **5** and **6**. The olefin selectivity observed is presumably due to the higher steric crowding in the cluster compounds **1** and **2**. Furthermore, no reaction products from aldol condensation of the produced aldehydes were detected in the experiments with **1** and **2**.

Table 1. Initial TOF[a] [h^{-1}] for the hydroformylation of 1-octene with (dppp)Pt complexes **1**−**4** at different temperatures[b]

Pt compound	100 °C	120 °C	140 °C	160 °C
1	11.0	62.1	72.8	23.6[c]
2	19.3	34.1	73.9	52.7
3	50.5	46.6[c]	[c]	[c]
4	31.6	10.2	[c]	[c]

[a] Turnover frequencies were calculated as mol of aldehyde per mol of Pt per hour. [b] Reactions were carried out in 10 mL of CH_2Cl_2 under 50 bar of CO/H_2 with an octene/Pt catalyst ratio of 250 (0.02 mmol cat.) and reaction times of 2 h. [c] Decomposition of the catalyst.

Table 2. Influence of the temperature of the hydroformylation experiments on the *n*/*iso* ratio of nonanal[a]

Pt compound	100 °C	120 °C	140 °C	160 °C
1	7.8	8.4	8.2	6.0[b]
2	8.8	9.1	9.2	7.8
3	1.7	1.6[b]	[b]	[b]
4	1.4	1.6	[b]	[b]

[a] Reactions were carried out in 10 mL of CH_2Cl_2 under 50 bar of CO/H_2 with an octene/Pt catalyst ratio of 250 (0.02 mmol cat.) and reaction times of 2 h. [b] Decomposition of the catalyst.

Table 3. Degree of isomerization of 1-octene in hydroformylation reaction with complex **1** and **2**[a][b]

Pt compound	100 °C	120 °C	140 °C	160 °C
1	2.5%	13.7%	27.5%	55.3%
2	3.9%	8.5%	26.7%	46.1%

[a] Reactions were carried out in 10 mL of CH_2Cl_2 under 50 bar of CO/H_2 with an octene/Pt catalyst ratio of 250 (0.02 mmol cat.) and reaction times of 2 h. [b] In the case of complexes **3** and **4** the isomerized olefins were partially hydroformylated.

Table 4. Hydroformylation results of 1-octene with complex **2**[a] and their dependence on the CO/H_2 pressure at 140 °C

Pressure [bar]	*n*/*iso*	TOF [h^{-1}]	iso. Olefins[b]
20	8.9	25.4	43.0%
30	10.1	41.4	24.8%
40	9.7	63.7	27.6%
50	9.2	73.9	26.7%

[a] Reactions were carried out in 10 mL of CH_2Cl_2 under 50 bar of CO/H_2 with an octene/Pt catalyst ratio of 250 (0.02 mmol cat.) and reaction times of 2 h. [b] The isomerized olefins were detected by GC analysis.

In order to study the olefin selectivity, in a separate experiment the hydroformylation of *trans*-4-octene at 140 and 160 °C was investigated with complex **2**. Here the formation of 3-propyl-1-hexanal was not detected; olefin isomerization took place. The internal olefins thus formed did not undergo hydroformylation, and the only aldehydes obtained were *n*-nonanal (1-nonanal, **5**) and *iso*-nonanal (2-methyl-1-octanal, **6**).

Conclusion

To conclude, with the stanna-*closo*-dodecaborate dianion we have found a new ligand for the activation of platinum complexes for hydroformylation. The $Pt(SnB_{11}H_{11})$ derivatives studied here have a higher thermal stability and are more selective in hydroformylation experiments than their $SnCl_3$ analogues. *n*- and *iso*-nonanal (**5**, **6**) are the only aldehydes formed during the catalysis.

Experimental Section

General: All manipulations were carried out under dry N_2 in Schlenk glassware; solvents were dried and purified by standard methods and were stored under N_2; NMR Bruker AC 200 (^1H: 200 MHz, int. TMS. $^{31}P\{^1H\}$: 81 MHz, ext. H_3PO_4. $^{11}B\{^1H\}$: 64 MHz, ext. $BF_3{\cdot}Et_2O$); Elemental analysis: Institut für Anorganische Chemie der Universität zu Köln, Heraeus C,H,N,O-Rapid elemental analyser.

$[Bu_3MeN][(dppp)PtPh(SnB_{11}H_{11})]$ (1): At room temperature (dppp)Pt(Ph)Cl (360 mg, 0.50 mmol) was dissolved in 10 mL of CH_2Cl_2 and reacted with a CH_2Cl_2 solution of $[Bu_3MeN]_2[SnB_{11}H_{11}]$ (341 mg, 0.53 mmol). The solution turned yellow immediately and was stirred for 24 h. The solvent was then evaporated and the remaining solid was washed with water to give **1** (493 mg, 87%). Since we were not able to recrystallise this salt, an elemental analysis of the crude product was carried out. ^1H NMR (CD_2Cl_2, 200 MHz, TMS, without the signals for $[Bu_3MeN]^+$): δ = 2.00 (m, 2 H, dppp), 2.50 (m, 4 H, dppp), 6.40 (m, 1 H, Pt-Ph), 6.53 (m, 2 H, Pt-Ph), 6.92 (m, 2 H, Pt-Ph), 7.2−7.4 (m, 12 H, P-Ph), 7.8−7.9 (m, 8 H, P-Ph) ppm. $^{11}B\{^1H\}$ NMR (CD_2Cl_2, 64 MHz, ext. BF_3Et_2O): δ = −16.1 (s, B2−B11), −10.9 (s, B12) ppm. $^{31}P\{^1H\}$ NMR (CD_2Cl_2, 81 MHz, ext. H_3PO_4): δ = −5.4 (d, $^2J_{P\text{-}P}$ = 26.2, $^1J_{P\text{-}Pt}$ = 1733.0, $^2J_{P\text{-}Sn}$ = 204.9 Hz), 2.4 (d, $^2J_{P\text{-}P}$ = 26.2, $^1J_{P\text{-}Pt}$ = 3167.3, $^2J_{P\text{-}Sn}$ = 2419.5 Hz) ppm. $C_{46}H_{72}B_{11}NP_2PtSn$

(1133.7): calcd. C 48.73, H 6.40, N 1.24; found C 49.51, H 6.01, N 1.59.

$[Bu_3MeN]_2[(dppp)Pt(SnB_{11}H_{11})_2]$ (2): At room temperature a solution of $[(dppp)PtCl_2]$ (250 mg, 0.37 mmol) in 20 mL of CH_2Cl_2 was added to a solution of $[Bu_3MeN]_2[SnB_{11}H_{11}]$ (479 mg, 0.74 mmol) also in 20 mL of CH_2Cl_2. The colour of the reaction mixture turned orange immediately and after 14 h stirring the solvent was evaporated. The resulting solid was washed with water (two times with 30 mL). Crystallization from acetone/methanol at room temperature yielded yellow-green crystals of **2** (498 mg, 90%). ^1H NMR (CD_2Cl_2, 200 MHz, TMS, without the signals for $[Bu_3MeN]^+$): δ = 2.08 (m, 2 H, dppp), 2.42 (m, 4 H, dppp), 7.48 (m, 12 H, Ph), 7.85 (m, 8 H, Ph) ppm. $^{11}B\{^1H\}$ NMR (CD_2Cl_2, 64 MHz, ext. BF_3Et_2O): δ = −15.8 (s, B2−B11), −9.5 (s, B12) ppm. $^{31}P\{^1H\}$ NMR (CD_2Cl_2, 81 MHz, ext. H_3PO_4): δ = −1.1 (s, $^1J_{Pt\text{-}P}$ = 2820.7, $^2J_{P\text{-}Sn}$ = 2127.5 Hz)] ppm. $C_{53}H_{108}B_{22}N_2P_2PtSn$ (1387.0): calcd. C 42.28, H 7.23, N 1.86; found C 42.11, H 7.32, N 2.12.

Experimental Setup: All hydroformylations were carried out in a 75 mL steel autoclave which was built in the workshop of the Institut für Makromolekulare und Technische Chemie der Technischen Hochschule Aachen. The autoclave possesses a 25 mL dropping funnel equipped with a pressure release, a valve connected to a steel capillary with a diameter of 1 mm to take samples, a manometer and two other valves. The reaction mixture was stirred by a cross magnetic stirrer.

Experimental Procedure for Hydroformylations: The reactor was evacuated and filled with argon three times. The catalyst solution, prepared previously in a Schlenk vessel, was then introduced (the exact amount was determined by a syringe). The exact amounts of 1-octene and of GC standard (di-*n*-butyl ether) were transferred to the dropping funnel. The autoclave was pressurized with synthesis gas (CO/H_2) and was heated to reaction temperature by placing it in an oil bath. The reaction mixture was stirred at 750 rpm and kept for 30 minutes at the reaction temperature in order to ensure the preformation of the active catalyst species before the mixture of 1-octene and GC standard was added. Finally the autoclave was cooled in an ice bath, slowly vented and the mixture was analysed by GC.

Analytical Methods for Hydroformylations: The GC chromatograms were recorded on a Sichromat 2 apparatus (Siemens) equipped with a FID detector and an HP-LAS 3359 integrator. Column: 50m Pona-HP-FS; temperature program: 5 min isotherm at 80 °C; 8 °C per minute to 25 °C; temperature of the evaporator: 250 °C; He, 1.5bar; volume of the sample: 0.2 to 1.0 μL.

[1] R. W. Chapman, J. G. Kester, K. Folting, W. E. Streib, L. J. Todd, *Inorg. Chem.* **1992**, *31*, 979−983.

[2] W. H. Knoth, *J. Am. Chem. Soc.* **1967**, *89*, 1274−1275.

[3] S. V. Ivanov, J. J. Rockwell, O. G. Polyakov, C. M. Gaudinski, O. P. Anderson, K. A. Solntsev, S. H. Strauss, *J. Am. Chem. Soc.* **1998**, *120*, 4224−4225.

[4] L. Wesemann, T. Marx, U. Englert, M. Ruck, *Eur. J. Inorg. Chem.* **1999**, *9*, 1563−1566.

[5] T. Marx, L. Wesemann, *J. Organomet. Chem.* **2000**, *614−615*, 137−143.

[6] T. Marx, L. Wesemann, S. Dehnen, *Z. Anorg. Allg. Chem.* **2001**, *627*, 1146−1150.

[7] T. Marx, L. Wesemann, S. Dehnen, I. Pantenburg, *Chem. Eur. J.* **2001**, *7*, 3025−3032.

[8] T. Marx, L. Wesemann, I. Pantenburg, *Organometallics* **2001**, *20*, 5241−5244.

[9] [9a] *Applied Homogeneous Catalysis with Organometallic Compounds* (Ed.: B. Cornils, W. A. Herrmann), Wiley-VCH, Weinheim, **2000**. [9b] P. W. N. M. van Leeuwen, P. C. J. Kamer, J. N. H. Reek, P. Dierkes, *Chem. Rev.* **2000**, *100*, 2741−2769.

[10] [10a] L. A. van der Veen, P. K. Keeven, P. C. J. Kamer, P. W. N. M. van Leeuwen, *J. Chem. Soc., Dalton Trans.* **2000**, *13*, 2105−2112. [10b] J.-T. Chen, Y.-S. Yeh, C.-S. Yang, F.-Y. Tsai, G.-L. Huang, B.-C. Shu, T.-M. Huang, Y.-S. Chen, G.-H. Lee, M.-C. Cheng, C.-C. Wang, Y. Wang, *Organometallics* **1994**, *13*, 4804−4824. [10c] I. Tóth, T. Kégl, C. J. Elsevier, L. Kollár, *Inorg. Chem.* **1994**, *33*, 5708−5712.

[11] [11a] P. Haelg, G. Consiglio, P. Pino, *Helv. Chim. Acta* **1981**, *64*, 1865−1869. [11b] J. K. Stille, H. Su, P. Brechot, G. Parrinello, L. S. Hegedus, *Organometallics* **1991**, *10*, 1183−1189. [11c] I. Tóth, I. Guo, B. E. Hanson, *Organometallics* **1993**, *12*, 848−852. [11d] A. Scrivanti, V. Beghetto, A. Bastianini, U. Matteoli, G. Menchi, *Organometallics* **1996**, *15*, 4687−4694. [11e] J. Bakos, S. Cserepi-Szucs, A. Gomory, C. Hegedus, L. Marko, A. Szollosy, *Can. J. Chem.* **2001**, *79*, 725−730.

[12] C. Y. Hsu, M. Orchin, *J. Am. Chem. Soc.* **1975**, *97*, 3553−3554.

[13] I. Schwager, J. F. Knifton, *J. Catal.* **1976**, *45*, 256−263.

[14] [14a] M. S. Holt, W. L. Wilson, J. H. Nelson, *Chem. Rev.* **1989**, *89*, 11−49. [14b] J. D. Donaldson, *Prog. Inorg. Chem.* **1968**, *8*, 287−356. [14c] F. Glocking, in *Chemistry of Tin* (Ed.: P. G. Harrison), Chapman and Hall, New York, **1989**, pp. 245−293.

[15] [15a] G. K. Anderson, H. C. C. Clark, J. A. Davies, *Organometallics* **1982**, *1*, 64−70. [15b] G. K. Anderson, H. C. Clark, J. A. Davies, *Inorg. Chem.* **1983**, *22*, 427−433. [15c] G. K. Anderson, H. C. Clark, J. A. Davies, *Inorg. Chem.* **1983**, *22*, 434−438. [15d] G. K. Anderson, C. Billard, H. C. Clark, J. A. Davies, C. S. Wong, *Inorg. Chem.* **1983**, *22*, 439−443.

[16] [16a] C. Botteghi, S. Paganelli, U. Matteoli, A. Scrivanti, R. Ciorciaro, L. M. Venanzi, *Helv. Chim. Acta* **1990**, *73*, 284−287. [16b] C. Botteghi, S. Paganelli, *J. Organomet. Chem.* **1991**, *417*, C41−C45. [16c] C. Botteghi, S. Paganelli, A. Perosa, R. Lazzaaroni, G. Uccello-Barretta, *J. Organomet. Chem.* **1993**, *447*, 153−157.

[17] [17a] P. W. N. M. van Leeuwen, C. F. Roobeek, R. L. Wife, J. H. G. Frijns, *J. Chem. Soc., Chem. Commun.* **1986**, 31−33. [17b] P. W. N. M. van Leeuwen, C. F. Roobeek, R. L. Wife, J. H. G. Frijns, A. G. Orpen, *Organometallics* **1990**, *9*, 1211−1222.

[18] G. Butler, C. Eaborn, A. Pidcock, *J. Organomet. Chem.* **1979**, *181*, 47−53.

[19] X-ray crystal structure analysis of **2**: $C_{53}H_{108}B_{22}N_2P_2PtSn_2$; M_r = 1505.64; orthorhombic space group *Pbcn* (no. 60); *a* = 20.2352(6), *b* = 19.5630(7), *c* = 17.9094(7) Å, *V* = 7089.6(4) Å^3, *Z* = 4, $\rho_{calcd.}$ = 1.411 g cm^{-3}; $\mu_{lin.}$ = 2.748 mm^{-1}; Stoe IPDS II diffractometer; Mo-K_α (λ = 0.71073 Å); graphite monochromator, data collection at 170 K in 323 frames with ω-scans (0 ≤ ω ≤ 180°, φ = 0°; 0 ≤ ω ≤ 180°, φ = 60°; 0 ≤ ω ≤ 180°, φ = 90°; 0 ≤ ω ≤ 106°, φ = 180°; Δω = 2°, exposition time of 1 min) in the 2θ range of 2.3 to 59.5° on a single crystal 0.7 × 0.4 × 0.5 mm; 233603 reflections measured, 9587 independent, 7492 observed with $I > 2\sigma(I)$; corrections for Lorentz and polarisation factors; numerical absorption correction, max./min. transmission 0.3371/0.1674; structure solution with direct methods[20] and difference Fourier synthesis, F^2 refinement;[21−23] anisotropic parameters for non-hydrogen atoms, and hydrogen atoms placed in calculated positions (C−H = 0.98 Å, B−H = 1.1 Å). Due to partial disorder the Bu_3MeN cations were refined using an isotropic structure model without hydrogen positions. Convergence obtained for 374 variables with *R*1(all) = 0.076 *wR*2(all) = 0.169, GooF = 1.176; max./min. residual electron density +2.31/−1.78 e Å^{-3}. CCDC-177990 contains the supplementary crystallographic data for this paper. These data can be obtained free of charge at www.ccdc.cam.ac.uk/conts/retrieving.html [or from the Cambridge Crystallographic Data Centre, 12, Union Road,

Cambridge CB2 1EZ, UK; Fax: (internat.) +44-1223/336-033; E-mail: deposit@ccdc.cam.ac.uk].
[20] [20a] Fa. Stoe & Cie, X-RED 1.22, Data Reduction for STAD4 and IPDS, Darmstadt **2001**. [20b] Fa. Stoe, & Cie, X-Shape 1.06, *Crystal Optimization for Numerical Absorption Correction*, Darmstadt **1999**.
[21] WINGX 1.63: L. J. Farrugia, *J. Appl. Crystallogr.* **1999**, *32*, 837−838.
[22] SIR 92 − A program for crystal structure solution, A. Altomare, G. Cascarano, C. Giacovazzo, A. Guagliardi, *J. Appl. Crystallogr.* **1993**, *26*, 343−350.
[23] G. M. Sheldrick, *SHELXL 93, Program for the Refinement of Crystal Structures*, Göttingen **1993**.

Received March 19, 2002
[I02142]

A New Coordination Mode for the Tripodal $[Te(NtBu)_3]^{2-}$ Dianion: Preparation and Structures of $\{ClIn[Te(NtBu)_3]\}_2$ and $\{LiIn[Te(NtBu)_3]_2\}\cdot LiCl$

Tristram Chivers*[a] and Gabriele Schatte[a]

Keywords: Indium / Tellurium / Imido compound / Tridentate ligand

The complexes $\{ClIn[Te(NtBu)_3]\}_2$ (**1**) and $\{LiIn[Te(NtBu)_3]_2\}\cdot LiCl$ (**2**) are formed from the reaction of $InCl_3$ (or InCl) with $\{Li_2[Te(NtBu)_3]\}_2$ in toluene. The $[Te(NtBu)_3]^{2-}$ dianions in the centrosymmetric dimer **1** act as tridentate [bis(*N*,*N*′-monodentate), μ_2-*N*′′] ligands bridging two indium atoms. Complex **2** involves a spirocyclic indium centre bis(*N*,*N*′-chelated) by two $[Te(NtBu)_3]^{2-}$ ions.

(© Wiley-VCH Verlag GmbH, 69451 Weinheim, Germany, 2002)

Introduction

The pyramidal tris(imido) chalcogenite anions $[E(NtBu)_3]^{2-}$ (E = S, Se, Te),[1−3] isoelectronic with EO_3^{2-}, are potentially interesting tridentate ligands.[4] The tellurium congener $[Te(NtBu)_3]^{2-}$ acts as an *N*,*N*′-bidentate ligand in $PhB(\mu\text{-}NtBu)_2TeNtBu$[1] and in the anions $[M(\mu\text{-}NtBu)_2TeNtBu]^-$ (M = Sb, Bi).[5] The formation of coordination complexes is often accompanied by redox processes.[1,6,7] For example, the reaction of $[Te(NtBu)_3]^{2-}$ with $PhPCl_2$ produces the spirocycle $Te[(\mu\text{-}NtBu)_2P(Ph)NtBu]_2$, formally a tellurium(IV) complex of the $[PhP(NtBu)_3]^{2-}$ dianion, and elemental tellurium.[1] More dramatically, the stannatellurone $[tBuNSn(\mu\text{-}NtBu)_2TeNtBu](\mu_3\text{-}SnTe)$ is produced from $[Te(NtBu)_3]^{2-}$ and $SnCl_2$.[8] We report here the synthesis and structures of the neutral, dimeric complex $\{ClIn[Te(NtBu)_3]\}_2$ (**1**), in which the $[Te(NtBu)_3]^{2-}$ dianion adopts a novel, tridentate bonding mode, and the lithium chloride adduct $\{LiIn[Te(NtBu)_3]_2\}\cdot LiCl$ (**2**) with a spirocyclic indium centre.

Results and Discussion

Synthesis

The reaction of $\{Li_2[Te(NtBu)_3]\}_2$ with indium trichloride produces two complexes $\{Cl[InTe(NtBu)_3]\}_2$ (**1**) and $\{LiIn[Te(NtBu)_3]_2\}\cdot LiCl$ (**2**) as extremely moisture-sensitive, yellow solids. The relative amounts of **1** and **2** are determined by the stoichiometry. Thus, **1** is obtained in ca. 60% yield from the 1:2 reaction [Equation (1)] while **2** is best prepared by using a 2:3 stoichiometry. The separation of **1** and **2** is difficult because of their similar solubilities, but **2** may be isolated in modest yields by fractional crystallization from benzene.

$$\{Li_2[Te(NtBu)_3]\}_2 + 2\,InCl_3 \rightarrow \{Cl[InTe(NtBu)_3]\}_2 + 4\,LiCl \quad (1)$$

Complex **1** may also be obtained (ca. 65% yield with respect to Te) from the reaction of $\{Li_2Te(NtBu)_3\}_2$ with indium monochloride. However, this process is inefficient with respect to the use of indium, $^2/_3$ of which is reduced to In metal [Equation (2)].

$$\{Li_2[Te(NtBu)_3]\}_2 + 6\,InCl \rightarrow \{Cl[InTe(NtBu)_3]\}_2 + 4\,In + 4\,LiCl \quad (2)$$

Complexes **1** and **2** were characterised by multinuclear (^1H, ^{13}C, ^{125}Te, ^7Li) NMR spectra. However, the ^1H NMR spectra were structurally uninformative. Thus, both **1** and **2** exhibit singlets at δ = 1.558 and 1.407 ppm, respectively, in $[D_8]THF$ at 23 °C indicative of fluxional processes. These resonances broaden upon lowering the temperature, but resolution of these signals was precluded by the low solubility of **1** and **2** at low temperature.

X-ray Crystal Structures of 1 and 2

An X-ray crystallographic study revealed that **1** is a centrosymmetric dimer with a "deck-chair" structure (Figure 1).[9] As illustrated in Scheme 1, the dimer **1** may be viewed to form by association of the putative monomer $ClIn(\mu\text{-}NtBu)_2TeNtBu$, cf. $PhB(\mu\text{-}NtBu)_2TeNtBu$.[1] The $[Te(NtBu)_3]^{2-}$ dianion in **1** behaves as a tridentate ligand. Two of the nitrogen atoms, N(2) and N(3), are coordinated in a monodentate fashion to different indium atoms, while the third [N(3)] bridges those two indium atoms. Selected bond lengths and angles are given in the Figure caption. The mean Te−N bond length of 198.2 pm may be compared with the values of 208.1 and 187.8 pm for the bridging and terminal Te−N bonds, respectively, in $PhB(\mu\text{-}NtBu)_2TeNtBu$.[1] The Te−N bond length involving the

[a] Department of Chemistry, University of Calgary, Calgary, Alberta T2N 1N4, Canada
E-mail: chivers@ucalgary.ca

bridging (four-coordinate) nitrogen atom is slightly longer (by ca. 4 pm) than those involving three-coordinate nitrogen atoms. The geometry about the indium atom is a highly distorted trigonal bipyramid. The mean axial In−N bond length of 215.4(3) pm is significantly shorter than the mean value of 223.7 pm observed for the related five-coordinate monomeric complex $[CyNC(tBu)NCy]_2InCl$.[10] There is a large disparity in the bridging In−N bond lengths of the four-membered In_2N_2 ring. The In−N(1) distance of 220.5(3) pm is in the range reported for five-coordinate indium,[10,11] whereas the In−N(1)* separation of 250.9(3) pm is typical of a long-range intramolecular interaction.[12] This disparity leads to a substantial difference in the geometries of the two InN_2Te rings. The distortion of the tbp geometry is reflected in the bond angles at the indium centre. The axial bond angle N−In−N of 157.14(13)° deviates substantially from linearity. The sum of the bond angles in the equatorial plane is ca. 359°, but there is a notable difference between the values of Cl−In−N(1) and Cl−In−N(1)*, 164.89(8) and 110.19(9)°. The In−Cl distance of 2.4464(13) Å is slightly longer than the values of 2.383(9) and 2.405(1) Å found for related five-coordinate complexes,[10,11] probably as a result of weak Te···Cl interactions [374.67(13) pm, cf. sum of the van der Waals radii is 381[13a] or 400 pm],[13b] which give rise to a tetrameric array of dimeric molecules in the unit cell.

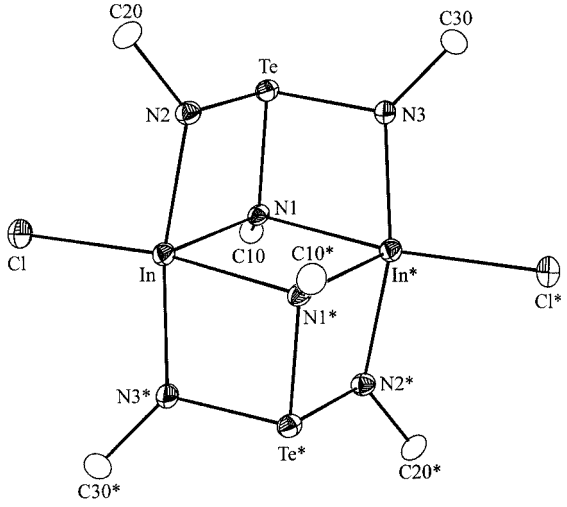

Figure 1. ORTEP diagram (30% probability ellipsoids) for **1**; only the α-carbon atoms of *t*Bu groups are shown; selected bond lengths [pm] and bond angles [°]: Te−N(1) 201.0(3), Te−N(2) 197.3(3), Te−N(3) 196.3(4), In−N(1) 220.5(3), In−N(1)* 250.9(3), In−N(2) 217.3(3), In−N(3)* 213.5(3), In−Cl 244.64(13); N(2)−In−N(3)* 157.14(3), N(1)−In−Cl 110.19(9), N(1)−In−N(1)* 84.90(12), Cl−In−N(1)* 164.89(8); symmetry transformations used to generate equivalent atoms: *: $-x + 1, -y, -z$

An X-ray analysis revealed that $\{Li\{In[Te(NtBu)_3]_2\}\}\cdot LiCl$ (**2**) is a centrosymmetric dimer (Figure 2). Important structural parameters are given in the Figure caption. Each monomeric unit consists of an indium centre bis(*N*,*N*′-chelated) by two $[Te(NtBu)_3]^{2-}$ dianions in a distorted tetrahedral arrangement. Charge balance is provided

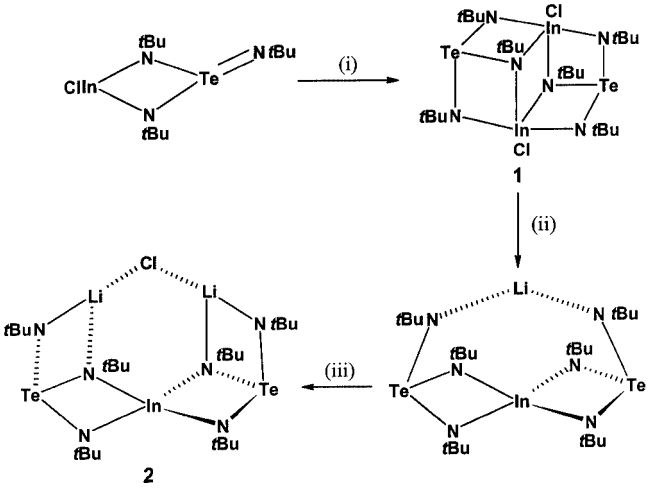

Scheme 1. (i) Dimerization, (ii) $\{Li_2[Te(NtBu)_3]\}_2$, (iii) incorporation of LiCl

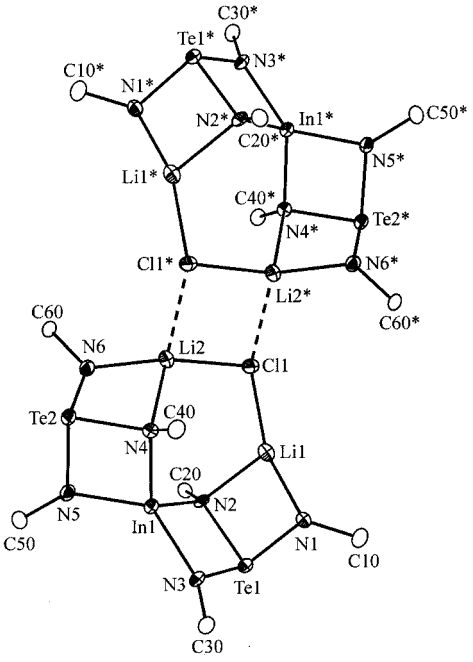

Figure 2. ORTEP diagram (30% probability ellipsoids) for **2** showing the intermolecular Li···Cl interactions; only the α-carbon atoms of *t*Bu groups are shown; symmetry transformations used to generate equivalent atoms: *: $-x + 2, -y + 1, -z + 1$; selected bond lengths [pm] and bond angles [°]: $|Te-N_{endo}|$ 199.2(3), $|Te-N_{exo}|$ 191.8(1), $|In-N_{axial}|$ 216(1), $|In-N_{eq}|$ 208(1), Li−N 195.0(16)−218.4(16), Li(1)−Cl(1) 220.3(15), Li(2)−Cl(1) 238.1(13); N(2)−In(1)−N(3) 77.3(2), N(2)−In(1)−N(5) 130.9(3), N(3)−In(1)−N(5) 131.4(3), N(5)−In(1)−N(4) 78.2(2), N(3)−In(1)−N(4) 131.2(2), N(2)−In(1)−N(4) 114.4(2)

by an Li^+ counterion. In addition, one molecule of LiCl is incorporated into the structure so that an $[Li-Cl-Li]^+$ unit bridges the spirocyclic $\{In[Te(NtBu)_3]_2\}^-$ anion, which is *N*,*N*′-chelated to both lithium centres.[14] The asymmetry in this bridge is the result of dimer formation through a weak Li···Cl interaction [Li(2)···Cl(1) = 247.9(3) pm]. A similar dimeric structural arrangement has been reported recently for $[(THF)_2Li_3Cl\{(NtBu)_3\}S]_2$.[15] The spirocyclic structure of **2**, prior to entrapment of LiCl (Scheme 1), is reminiscent

of the structures of the group-15 derivatives $Li\{M[Te(NtBu)_3]_2\}$ (M = Sb, Bi).[5] However, the bond angles of 84.6(2) and 83.5(3)° subtended at the indium atom are significantly larger than the corresponding bond angles in $Li\{M[Te(NtBu)_3]_2\}$ [72.7(3)° (M = Bi) and 75.4(5)° (M = Sb)].[5] The smaller angles presumably reflect the influence of the lone-electron pair located on the group-15 metal atoms. The geometry at the Te atoms is distorted trigonal-pyramidal with a mean Te−N bond length of 196.7(7) pm, cf. $|d(Te-N)|$ = 197.6(2) pm in $\{Li_2[Te(NtBu)_3]\}_2$.[1] As expected, the Li−N and In−N bond lengths involving the four-coordinate nitrogen atoms, N(2) and N(4), are significantly longer than the corresponding bond lengths involving the three-coordinate nitrogen atoms, N(1)/N(6) and N(3)/N(5), respectively. Curiously, however, this disparity is not observed for the Te−N bonds within the TeN_2In rings, which are equal within the experimental error.

In summary, complex **1** represents the first example of the bridging tridentate bonding mode [bis(*N*,*N*′-monodentate), μ$_2$-*N*′′] for the $[Te(NtBu)_3]^{2-}$ dianion. It is also the first complex of the tris(imidotellurite) dianion that contains an element−halogen bond, which may be utilized for further metathetical reactions.

Experimental Section

General Procedures: Indium(III) chloride and indium(I) chloride (Aldrich, 99.999%) were used as received. $\{Li_2[Te(NtBu)_3]\}_2$ was prepared by a literature procedure.[1,14b] Solvents were dried with the appropriate drying agents and distilled onto molecular sieves before use. All reactions and the manipulation of moisture-sensitive products were carried out under argon or under vacuum. ^{1}H NMR spectra were recorded with Bruker ACE 200 and AM 400 spectrometers, and chemical shifts are reported relative to Me_4Si in $CDCl_3$. ^{13}C and ^{125}Te NMR spectra were measured with a Bruker AM 400 spectrometer using a 5-mm broadband probe operating at 100.594 and 126.393 MHz, respectively. The samples were externally referenced to K_2TeO_3 in D_2O referred to Me_2Te and Me_4Si in $CDCl_3$, respectively. Relaxation delays of 3 and 1.5 s were applied for the measurement of the ^{13}C and ^{125}Te NMR spectra, respectively.

Synthesis of $\{ClIn[Te(NtBu)_3]\}_2$ (1): (a) A suspension of $InCl_3$ (0.250 g, 1.128 mmol) in toluene (20 mL) was added to a pale yellow solution of $\{Li_2[Te(NtBu)_3]\}_2$ (0.400 g, 0.564 mmol) in toluene (10 mL) at −78 °C. THF (10 mL) was added and the yellow slurry was stirred for 10 min at −78 °C and then allowed to reach 23 °C. After 24 h, the intense yellow solution was filtered and the volatile material was removed from the filtrate under vacuum. The solid residue was extracted with *n*-hexane (10 mL) to give **1** as a pale yellow solid (0.339 g, 0.345 mmol, 61%). ^{1}H NMR ([D$_8$]THF): δ = 1.56 [C(C*H*$_3$)$_3$] ppm. ^{13}C NMR ([D$_8$]THF): δ = 37.4 [C(*C*H$_3$)$_3$], 59.9 [*C*(CH$_3$)$_3$] ppm. ^{125}Te NMR ([D$_8$]THF): δ = 1570.6 ppm. $C_{24}H_{54}Cl_2In_2N_6Te_2$ (982.47): calcd. C 29.34, H 5.54, N 8.55; found C 28.64, H 5.98, N 8.09; the product was recrystallised from THF to give **1**·(THF)$_{0.5}$: calcd. C 30.66, H 5.74, N 8.25; found C 30.18, H 6.42, N 8.61. **(b)** A solution of $\{Li_2[Te(NtBu)_3]\}_2$ (0.110 g, 0.155 mmol) in toluene (10 mL) was added to a suspension of InCl (0.093 g, 0.620 mmol) in THF (10 mL) at 23 °C. The formation of indium metal was observed. After 1.5 h, the volume of the solution was reduced to 4 mL and X-ray quality, yellow crystals of **1** (0.098 g, 0.099 mmol, 64% based on Te) were obtained after 1 d at −20 °C.

Synthesis of $\{LiIn[Te(NtBu)_3]_2\}\cdot LiCl$ (2): A suspension of $InCl_3$ (0.169 g, 0.764 mmol) in toluene (10 mL) was added to a pale yellow solution of $\{Li_2[Te(NtBu)_3]\}_2$ (0.400 g, 0.563 mmol) in toluene (10 mL) at −78 °C. The suspension was stirred for 15 min at −78 °C and then allowed to reach 23 °C. After 3 h, the yellow solution was filtered and the solvent was removed from the filtrate under vacuum. The solid residue was extracted with *n*-hexane (5 mL) to give **2** as a yellow solid (0.238 g, 0.109 mmol, 19%). ^{1}H NMR (C_6D_6): δ = 1.29 [C(C*H*$_3$)$_3$, 9 H], 1.38 [C(C*H*$_3$)$_3$, 9 H] ppm. ^{1}H NMR ([D$_8$]THF): δ = 1.41 ppm. ^{13}C NMR ([D$_8$]THF): δ = 38.1 [C(*C*H$_3$)$_3$], 53.7 [*C*(CH$_3$)$_3$] ppm. ^{7}Li NMR ([D$_8$]THF): δ = 2.06 ppm. ^{125}Te NMR ([D$_8$]THF): δ = 1589 ppm. The presence of hexane and small amounts of **1** was evident from the NMR spectra. **2**·(C$_7$H$_{14}$)$_{0.5}$: calcd. C 36.46, H 6.91, N 9.45; found C 35.73, H 7.68, N 9.30.

X-ray Analyses: All measurements were made with a Bruker AXS SMART 1000 CCD. A yellow prismatic crystal of **1** (0.21 × 0.20 × 0.15 mm) was coated with Paratone oil and mounted on a glass fibre. $C_{24}H_{54}Cl_2In_2N_6Te_2$, *M* = 982.47, monoclinic, space group $P2_1/n$, *a* = 10.1689(18), *b* = 15.684(3), *c* = 11.874(2) Å, β = 110.650(2)°, *V* = 1768.0(5) Å, D_c = 1.845 Mg m^{-3}, *Z* = 2, μ(Mo-K_α) = 3.095 mm^{-1}, *T* = 193(2) K. Of a total of 5507 collected reflections 3301 were unique and 2771 had $I > 2\sigma(I)$. The data were corrected for absorption by semi-empirical methods. The structure was solved by direct methods[16] and refined by full-matrix least-squares methods on F^2.[17] A yellow plate-like crystal of **2** (0.21 × 0.16 × 0.10 mm), obtained by fractional crystallization from C_6D_6, was coated with Paratone oil and mounted on a glass fibre. $C_{24}H_{54}ClInLi_2N_6Te_2$, *M* = 846.08, triclinic, space group $P\bar{1}$, *a* = 10.6736(15), *b* = 13.483(2), *c* = 14.357(2) Å, α = 98.885(3), β = 113.036(2), γ = 106.574(2)°, *V* = 1737.5(4) Å^3, D_c = 1.617 Mg m^{-3}, *Z* = 2, μ(Mo-K_α) = 2.424 mm^{-1}, *T* = 193(2) K. Of a total of 14227 collected reflections 6963 were unique and 4782 had $I \geq 2\sigma(I)$. A faced-indexed absorption correction was applied. The structure was solved by the heavy-atom method[18] and refined by full-matrix least-squares methods on F^2.[17] CCDC-183320 (**1**) and -183321 (**2**) contain the supplementary crystallographic data for this paper. These data can be obtained free of charge at www.ccdc.cam.ac.uk/conts/retrieving.html or from the Cambridge Crystallographic Data Centre, 12, Union Road, Cambridge CB2 1EZ, UK [Fax: (internat.) + 44-1223/336-033; E-mail: deposit@ccdc.cam.ac.uk].

Acknowledgments

This work received financial support from the NSERC (Canada). We thank Dr. R. MacDonald (University of Alberta) for the X-ray data collections of **1** and **2**.

[1] T. Chivers, X. Gao, M. Parvez, *Angew. Chem.* **1995**, *107*, 2756−2758; *Angew. Chem. Int. Ed. Engl.* **1995**, *34*, 2549−2551.
[2] R. Fleischer, S. Freitag, F. Pauer, D. Stalke, *Angew. Chem.* **1996**, *108*, 208−211; *Angew. Chem. Int. Ed. Engl.* **1996**, *35*, 204−207.
[3] T. Chivers, M. Parvez, G. Schatte, *Inorg. Chem.* **1996**, *35*, 4094−4095.
[4] For complexes of the related pyramidal anion $TeSe_3^{2-}$ see: [4a] D-Y. Chung, S-P. Huang, K-W. Kim, M. G. Kanatzidis, *Inorg. Chem.* **1995**, *34*, 4292−4293. [4b] X. Zhang, M. G. Kanatzidis, *J. Am. Chem. Soc.* **1994**, *116*, 1890−1898. [4c] X. Zhang, M. G.

Kanatzidis, *Inorg. Chem.* **1994**, *33*, 1238−1240. [4d] T. J. McCarthy, X. Zhang, M. G. Kanatzidis, *Inorg. Chem.* **1993**, *32*, 2944−2948.
[5] T. Chivers, M. Parvez, G. Schatte, G. P. A. Yap, *Inorg. Chem.* **1999**, *38*, 1380−1381.
[6] R. Fleischer, D. Stalke, *Organometallics* **1998**, *17*, 832−838.
[7] R. Fleischer, D. Stalke, *Coord. Chem. Rev.* **1998**, *176*, 431−450.
[8] T. Chivers, G. Schatte, *Chem. Commun.* **2001**, 2264−2264.
[9] For use of the term "deck-chair" see: A. J. Edwards, M. A. Paver, P. R. Raithby, M.-A. Rennie, C. A. Russell, D. C. Wright, *Angew. Chem.* **1994**, *106*, 1334−1336; *Angew. Chem. Int. Ed. Engl.* **1994**, *33*, 1277−1279.
[10] Y. Zhou, D. S. Richeson, *Inorg. Chem.* **1996**, *35*, 2448−2451.
[11] Y. Zhou, D. S. Richeson, *Inorg. Chem.* **1996**, *35*, 1423−1424.
[12] [12a] H. Schumann, T. D. Seuss, O. Just, R. Weiman, H. Hemling, F. H. Görlitz, *J. Organomet. Chem.* **1994**, *479*, 171. [12b] H. Schumann, F. H. Görlitz, T. D. Seuss, W. Wassermann, *Chem. Ber.* **1992**, *125*, 3. [12c] H. Schumann, W. Wassermann, A. Dietrich, *J. Organomet. Chem.* **1989**, *365*, 11.
[13] [13a] N. W. Alcock, *Adv. Inorg. Chem. Radiochem.* **1972**, *15*, 1. [13b] L. Pauling, *The Nature of the Chemical Bond*, 3rd ed., Cornell University Press, Ithaca, NY, **1960**, chapter 7, p. 260.
[14] For some recent examples of the entrapment of lithium halides by lithiated complexes see: [14a] T. Chivers, A. Downard, M. Parvez, *Inorg. Chem.* **1999**, *38*, 4347−4353. [14b] T. Chivers, X. Gao, M. Parvez, *Inorg. Chem.* **1996**, *35*, 4336−4341.
[15] B. Walfort, T. Auth, B. Degel, H. Helten, D. Stalke, *Organometallics* **2002**, *21*, 2208−2214.
[16] G. M. Sheldrick, *SHELXS-97, Program for the Solution of Crystal Structures*, Universität of Göttingen, Göttingen, Germany, **1997**.
[17] G. M. Sheldrick, *SHELXL-97-2, Program for the Refinement of Crystal Structures*, Universität of Göttingen, Göttingen, Germany, **1997**.
[18] P. T. Beurskens, G. Beurskens, W. P. Bosman, R. de Gelder, S. Garcia-Granda, R. O. Gould, R. Israel, J. M. M. Smits, *DIRDIF96 Program System*, Crystallography Laboratory, University of Nijmegen, The Netherlands, **1996**.

Received April 22, 2002
[I02207]

1,2-Dichalcogenolylium Ions $(C_3Cl_3E_3)^+$ from Equilibria Involving Dichalcogen Dichlorides E_2Cl_2 (E = S, Se, Te) − Syntheses and Crystal Structures of $(C_3Cl_3S_2)Cl$, $(C_3Cl_3Se_2)Cl$, and $(C_3Cl_3Te_2)_2[Te_2Cl_{10}]$

Johannes Beck,*[a] Andreas Hormel,[a] and Michael Koch[a]

Keywords: Chalcogens / Heterocycles / Cations / Solvothermal synthesis

The reaction of tetrachlorocyclopropene with $SeCl_4$ or $TeCl_4$ in CH_2Cl_2 under solvothermal conditions at 120 °C and 90 °C, respectively, is a suitable route to 1,2-dichalcogenolylium ions. Yellow crystals of $(C_3Cl_3Se_2)^+Cl^-$ or red crystals of $\{(C_3Cl_3Te_2)^+\}_2[Te_2Cl_{10}]^{2-}$ are formed in such reactions. The reaction of hexachloropropene with elemental sulfur — the well-known route to 3,4,5-trichloro-1,2-dithiolylium chloride $(C_3Cl_3S_2)Cl$ — turned out not to be transferable to selenium and tellurium chemistry. NMR investigations of the reaction solutions allowed to set up reaction equilibria also involving hexachloropropene and dichalcogen dichlorides E_2Cl_2. The crystal structures of all three compounds were determined by X-ray diffraction. All contain planar, five-membered ring shaped cations $(C_3Cl_3E_2)^+$ (E = S, Se, Te). Short E–E bonds (S–S 201, Se–Se 231, Te–Te 266 pm) indicate substantial π-bonding and charge delocalisation. The anion in $(C_3Cl_3Te_2)_2[Te_2Cl_{10}]$ consists of two tetragonal pyramidal $[TeCl_5]^-$ units linked by long Te–Cl bridges to centrosymmetric dimers in the form of edge-sharing double octahedra.

(© Wiley-VCH Verlag GmbH, 69451 Weinheim, Germany, 2002)

Introduction

The 1,2-dithiolylium ion is a well-known aromatic planar five-membered ring system. Molecular orbital calculations were carried out on the unsubstituted 1,2-dithiolylium ion by Bergson,[1] and these showed that one 3p electron pair of each sulfur atom is involved in a 6π-electron aromatic system.

Syntheses leading to a variety of differently substituted 1,2-dithiolylium ions have been developed. The reaction of hexachloropropene with sulfur at 160 °C was described by Boberg[2] to yield 3,4,5-trichloro-1,2-dithiolylium chloride (Scheme 1), a stable yellow solid with a decomposition temperature of 235 °C but unknown crystal structure.

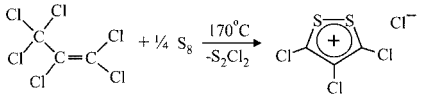

Scheme 1. Synthesis of 1,2-dithiolium chloride from hexachloropropene and sulfur

Although a lot of stable 1,2-dithiolylium salts are known much less work has been done on the respective 1,2-ditellurolylium ions. Bender et al. obtained the unsubstituted 1,3-ditellurolylium ion $(C_3H_3Te_2)^+$ by oxidation of 1,3-ditellurol at low temperatures.[3] NMR studies at ambient temperature indicated a rapid rearrangement to the 1,2-ditellurolylium ion (Scheme 2). Alkyl or aryl substituents caused an acceleration of the rearrangement from 1,3- to 1,2-ditelluroles with the consequence that the intermediate 1,3-ditellurolylium ions could not be detected on the NMR time scale. The 1,2-ditellurolylium ion was supposed to be planar with a delocalized positive charge. Above room temperature rapid decomposition with precipitation of tellurium occurs for solutions containing alkyl- or aryl-substituted $(C_3R_3Te_2)^+$ ions. No reports on 1,2-diselenolylium ions have been published.

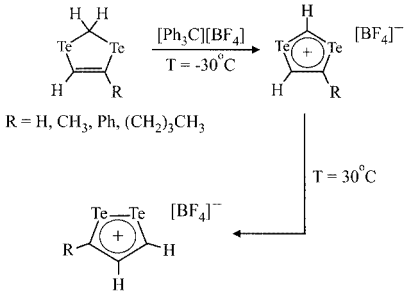

Scheme 2. Synthesis of 1,3-ditellurolylium salts by oxidation of 1,3-ditelluroles, and their rearrangement to 1,2-ditellurolylium salts

In our studies on the reactivity of tetrachlorocyclopropene toward Lewis acidic metal halides we discovered a straightforward method for the synthesis of 1,2-dichalcogenolylium ions, including the previously unknown diseleno derivative.

[a] Institut für Anorganische Chemie der Rheinischen Friedrich-Wilhelms-Universität,
Gerhard-Domagk-Str. 1, 53121 Bonn, Germany
E-mail: j.beck@uni-bonn.de

Results and Discussion

Synthesis of $(C_3Cl_3E_2)^+$ Ions (E = Se, Te) from Tetrachlorocyclopropene and ECl_4

Heating $SeCl_4$ and tetrachlorocyclopropene in CH_2Cl_2 under solvothermal conditions in a molar ratio of 1:2 yields yellow crystals of 3,4,5-trichloro-1,2-diselenolylium chloride, $(C_3Cl_3Se_2)Cl$, as well as a black precipitate of elemental selenium. The composition of the crystals was checked by energy dispersive X-ray fluorescence. ^{77}Se NMR spectroscopy of the filtered red reaction solution showed one signal with a chemical shift of $\delta = 1257$ ppm, which is ascribed to Se_2Cl_2.[4] The ^{13}C NMR spectrum showed the signals of hexachloropropene ($\delta = 92.7$, 127.4, and 131.8 ppm[5]), and tetrachlorocyclopropene ($\delta = 62.4$ and 122.6 ppm[5]). Due to the very low solubility, signals attributable to the Se atoms of the 1,2-diselenolylium cation could not be detected. A two-step reaction mechanism is supposed: the first step is a redox equilibrium between tetrachlorocyclopropene/$SeCl_4$ and hexachloropropene/selenium (Scheme 3), and the second step yields $(C_3Cl_3Se_2)Cl$ and Se_2Cl_2 analogous to the reaction of hexachloropropene and sulfur described by Boberg.[3]

$$2\,C_3Cl_4 + ECl_4 \rightleftharpoons 2\,C_3Cl_6 + E$$

$$C_3Cl_6 + 4\,E \rightleftharpoons (C_3Cl_3E_2)Cl + E_2Cl_2$$

$$C_3Cl_4 + E_2Cl_2 \rightleftharpoons C_3Cl_6 + 2\,E$$

Scheme 3. Equilibria in the reactions between chalcogen tetrachlorides and tetrachlorocyclopropene (E = Se, Te)

Heating equimolar amounts of $TeCl_4$ and tetrachlorocyclopropene in CH_2Cl_2 yields deep-red 3,4,5-trichloro-1,2-ditellurolylium pentachlorotellurate(IV) $(C_3Cl_3Te_2)_2[Te_2Cl_{10}]$. Energy dispersive X-ray fluorescence confirmed the composition. The ^{125}Te NMR spectrum of the deep-red solution shows one signal at $\delta = 1830$ ppm and a second very weak signal at $\delta = 1000$ ppm. It was verified by comparative measurements that the signal occurring at $\delta = 1830$ ppm was not from $TeCl_4$. This signal can therefore be assigned to tellurium in $(C_3Cl_3Te_2)^+$. Only one signal for both tellurium atoms is expected for chemically equivalent nuclei, consistent with the mirror symmetry of the cation. The second signal might be due to Te_2Cl_2 as an intermediate in the reaction equilibrium. Te_2Cl_2 has recently been prepared from Te, $LiBHEt_3$ and $TeCl_4$,[6] and a ^{125}Te NMR resonance at $\delta = 1336$ pm in CS_2 and $\delta = 1287$ ppm in toluene has been reported. Since it is known that ^{125}Te NMR signals are very dependent on the solvent, we can tentatively propose that the reaction of $TeCl_4$ and C_3Cl_4 incorporates the same equilibria as for the reaction of $SeCl_4$ (Scheme 3). In the ^{13}C NMR spectrum four resonances between $\delta = 172.4$ and 160.3 ppm were present, indicating equilibria between cationic species. The unsubstituted dithiolylium cation $(C_3H_3S_2)^+$ shows two signals at $\delta = 142.6$ and 176.7 ppm in this region, corresponding to the central and the terminal carbon atoms of the allylic group.[7]

While $(C_3Cl_3S_2)Cl$ can readily be obtained from hexachloropropene and sulfur, neither $(C_3Cl_3Se_2)Cl$ nor $(C_3Cl_3Te_2)Cl$ could be synthesized in this way with the respective elemental chalcogen; only the reaction of tetrachlorocyclopropene and the respective chalcogen tetrahalide yields the cyclic cations incorporating Se and Te. This is probably caused by the insolubility of selenium and tellurium in organic solvents. The stability of the chalcogen tetrachlorides ECl_4 (E = S, Se, Te) increases from S to Te, while the stability of the dichalcogen dichlorides E_2Cl_2 decreases. The equilibria set up according to Scheme 3 are thus strongly dependent on the kind of chalcogen used. S_2Cl_2 is a favored product in the reaction of C_3Cl_6 with sulfur and it is not reduced to the element by tetrachlorocyclopropene. In the case of selenium this reduction occurs, since a precipitate of finely dispersed elemental selenium is observed. More complex equilibria are present in the case of tellurium. $(C_3Cl_3Te_2)Cl$ could not be isolated, only the less soluble $(C_3Cl_3Te_2)_2[Te_2Cl_{10}]$, formed from $(C_3Cl_3Te_2)Cl$ and $TeCl_4$; no precipitation of elemental tellurium was observed at temperatures below 100 °C. Temperatures higher than 110 °C generated a mixture of products which could not be separated or individually characterized.

Crystal Structures

The crystal structures of $(C_3Cl_3S_2)Cl$, $(C_3Cl_3Se_2)Cl$ and $(C_3Cl_3Te_2)_2[Te_2Cl_{10}]$ all contain nearly planar, five-membered ring shaped cations $(C_3Cl_3E_2)^+$ (E = S, Se, Te; Figure 1). Only $(C_3Cl_3Se_2)^+$ has a crystallographic mirror plane bisecting the ion. $(C_3Cl_3S_2)^+$ and $(C_3Cl_3Te_2)^+$, however, do not deviate substantially from C_s symmetry despite not possessing crystallographic symmetry. In all three ions the C−C and C−Cl bond lengths are almost identical, except for the central C2−Cl2 bond, which increases slightly from S to Te (Table 1). As expected, the chalcogen-C and chalcogen-chalcogen bonds increase in the same direction; they are all shorter than expected for single bonds. In the dithiolylium ion the S−S bond is 200.93(7) pm long, shorter than the expected bond length for a *cis*-planar S−S single bond (210 pm),[8] although it is similar to the bond lengths found in square-planar S_4^{2+} polycations ($S_4[Sb_9F_{39}]$ 197.5−199.5 pm,[9] $S_4[AsF_6]\cdot SO_2$ 201.4 pm[10]) and even shorter than in differently substituted 1,2-dithiolylium ions (3,5-diamino-1,2-dithiolylium iodide 208 pm,[11] 3,5-dimethyl-1,2-dithiolylium tetrachlorocobaltate 202 pm,[12] phenyl-1,2-dithiolylium chloride 202 pm [13]). In the homologous 1,2-diselenolylium ion the Se−Se bond length measures 231.1(2) pm. This is shorter than a normal Se−Se single bond (e.g. 233 pm in Se_8 [14]) and in the typical region for Se_4^{2+} cluster ions ($Se_4[Sb_9F_{39}]$ 224.7−227.6 pm;[15] $Se_4[MoOCl_4]_2$ 226−230 pm[16]). In the 1,2-tellurolylium ion the Te−Te bond is 265.6(2) pm long, which is shorter than in Te_4^{2+} polycations (266−270 pm[17]). The remarkably short chalcogen-chalcogen bonds in this series of trichlorodichalcogenolylium ions indicate bond orders higher than one. The presence of electron-withdrawing substituents strengthens the partial double bond character: on going from E = S to Te in the series $(C_3Cl_3E_2)^+$ the bonding

character changes from an almost equally delocalized system to a separation of a partially localized E−E double bond and the formation of an allylic system [RC=C(R)−CR]$^+$.

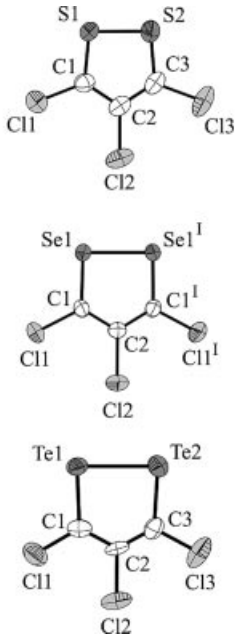

Figure 1. The cations in the structure of $(C_3Cl_3S_2)Cl$ (top), $(C_3Cl_3Se_2)Cl$ (middle), and $(C_3Cl_3Te_2)_2$ $[Te_2Cl_{10}]$ (bottom).; the molecules are drawn to the same scale; the displacement ellipsoids represent a probability density of 50%; the $(C_3Cl_3Se_2)^+$ ion is located with its atoms C2 and Cl2 in a mirror plane, the exponent I refers to the symmetry operation x, $0.5 - y$, z.

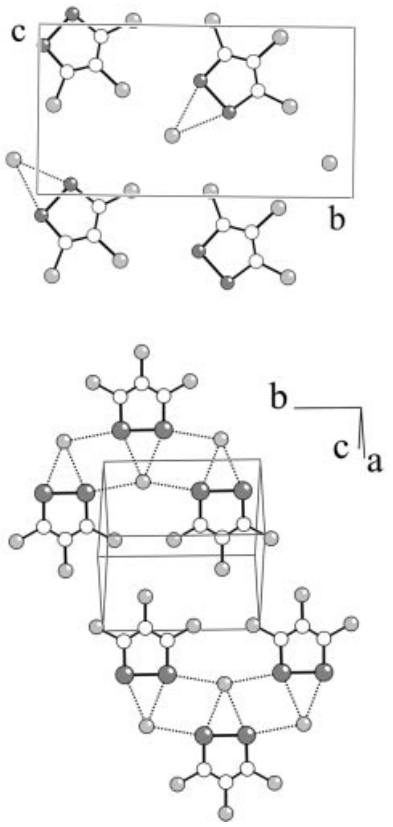

Figure 2. The crystal structures of $(C_3Cl_3S_2)Cl$ (top) and $(C_3Cl_3Se_2)Cl$ (bottom); for both structures only one layer of cations and chloride ions is shown

Table 1. Selected distances (pm) and angles (°) in the $(C_3Cl_3E_2)^+$ (E = S, Se, Te) cations

	$(C_3Cl_3S_2)^+$	$(C_3Cl_3Se_2)^+$	$(C_3Cl_3Te_2)^+$
E−E	200.93(7)	231.1(2)	265.6(2)
E−C	169.1(2); 169.9(2)	184.1(3)	205(2); 206(2)
C−C	138.9(3); 137.9(3)	138.3(3)	137(2); 141(2)
C−Cl(terminal)	168.6(2); 169.1(2)	169.2(3)	169(2); 168(2)
C−Cl(central)	170.8(2)	171.5(4)	174(2)
E−E−C	95.31(7); 95.05(8)	90.93(8)	87.5(4); 86.2(4)
C−C−C	113.6(2)	118.0(3)	123(2)
E−C−C	118.0(2); 118.11(2)	120.0(2)	122.4(9); 121(1)

In the structure of $(C_3Cl_3S_2)Cl$ the cations are arranged in layers. The chloride ions are located in the layers which are stacked with an interlayer distance of 341 pm along the crystallographic *a*-axis in an ABAB.... sequence (Figure 2). The chloride ion interacts with the cation via short, nearly symmetrical contacts to the sulfur atoms of the disulfide group, with S−Cl distances of 292.5 and 293.3 pm. Additionally, the chloride ion is η^5-coordinated by two cations belonging to adjacent planes with distances of 341 pm to the centres of the rings.

The structure of $(C_3Cl_3Se_2)Cl$ is substantially different from the structure of its sulfur-containing congener. Again, the cations and the chloride anions are located in planes. These planes are stacked along the [101] direction in an ABCABC... sequence with an interlayer distance of 342 pm (Figure 2). Three chloride ions approach the diselenide group of each cation giving rise to triangular Se_2Cl groups with Se−Cl contacts of 305.3 pm lengths and to almost linear $ClSe_2Cl$ groups with Se−Cl distances of 320.7 pm. These interactions link the cations to bands running along the crystallographic *b*-axis. An equivalent arrangement was found in the structure of 4-phenyl-1,2-dithiolylium chloride.[18]

The structure of $(C_3Cl_3Te_2)_2[Te_2Cl_{10}]$ contains binuclear $[Te_2Cl_{10}]^{2-}$ ions (Figure 3). Two tetragonal pyramidal $[TeCl_5]^-$ units are linked via long Te−Cl bridges (Te3−Cl4 290.0 pm) to centrosymmetric dimers. The Cl−Te3−Cl angles deviate by a maximum of 6° from rectangularity. The Te−Cl bonds, however, show marked differences. There is always a short Te−Cl bond (Te3−Cl6, Te3−Cl7, Te3−Cl8 234.1−244.3 pm) in the *trans* position to a long bond (Te3−Cl4, Te3−Cl4^I, Te3−Cl5 261.6−290.0 pm). The structure of the $[Te_2Cl_{10}]^{2-}$ ion in $(C_3Cl_3Te_2)_2$ $[Te_2Cl_{10}]$ is almost identical to the respective ion in $[Ph_4As]_2$ $[Te_2Cl_{10}]$.[19]

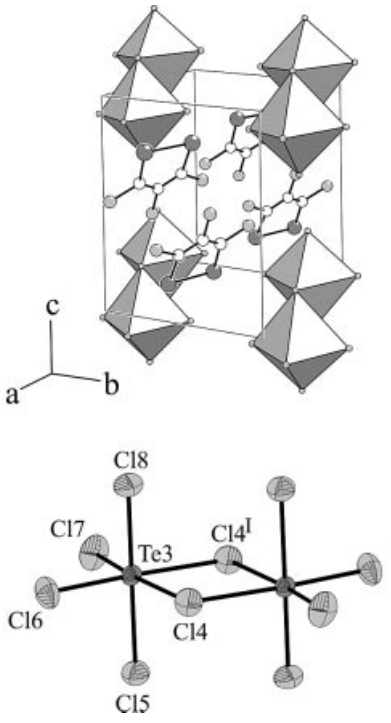

Figure 3. The unit cell of $(C_3Cl_3Te_2)_2[Te_2Cl_{10}]$ and a detailed view of the dinuclear $[Te_2Cl_{10}]^{2-}$ anion.; the displacement ellipsoids represent a probability density of 50%; the exponent I refers to the symmetry operation $-x + 1, -y, -z$; selected bond lengths [pm] and angles [°]: Te3−Cl4^{I} 290.0(3); Te3−Cl4 274.5(4); Te3−Cl5 261.6(3); Te3−Cl6 238.5(3); Te3−Cl7 234.1(3); Te3−Cl8 244.3(4); Te3−Cl4−Te3^{I} 94.8(1)

Experimental Section

General Techniques: All reactions were carried out in thick-walled glass ampoules of 10 cm length and 10 mm diameter. The ampoules were heated under vacuum to remove traces of water and filled with the starting materials under argon, the solvent was added with a syringe. The contents were frozen with liquid nitrogen, the ampoules were flame-sealed under vacuum and placed in horizontally aligned tube furnaces. Since the products are sensitive towards moisture and oxygen they were opened after the reaction under an argon atmosphere. Liquids were removed with a syringe. Single crystals were prepared under paraffin and mounted in glass capillaries under an argon atmosphere. Tetrachlorocyclopropene (>98%, Fluka) and $SeCl_4$ (Aldrich) were used as purchased. $TeCl_4$ was obtained by chlorinating tellurium powder according to literature procedures.[20] CH_2Cl_2 was dried with P_4O_{10} and freshly distilled before use.

$(C_3Cl_3S_2)Cl$: Heating hexachloropropene (0.1 mL, 7.1 mmol) and sulfur (105 mg, 3.3 mmol) to 170 °C for one day produced yellow needles of $(C_3Cl_3S_2)Cl$. Although the stoichiometry of the reaction (Scheme 1) affords one equivalent of C_3Cl_6 for two equivalents of sulfur, a crystalline product could not be obtained unless a twofold excess of hexachloropropene was used. The yield approached about 70% based on the amount of sulfur used.

$(C_3Cl_3Se_2)Cl$: $SeCl_4$ (270 mg, 1.2 mmol), tetrachlorocyclopropene (0.3 mL, 2.6 mmol), and 1 mL of CH_2Cl_2 were heated slowly at a rate of 10 °C/h to 120 °C. At about 70 °C the $SeCl_4$ dissolved completely with formation of an orange solution. Keeping the temperature at 120 °C for 24 hours and cooling at 10 °C/h to ambient temperature yielded a greyish-black precipitate of elemental selenium and yellow crystals of $(C_3Cl_3Se_2)Cl$. On the basis of $SeCl_4$ the yield reached about 50%.

$(C_3Cl_3Te_2)_2[Te_2Cl_{10}]$: $TeCl_4$ (150 mg, 0.56 mmol), tetrachlorocyclopropene (0.75 mL, 0.65 mmol), and 1.5 mL of CH_2Cl_2 were heated slowly at a gradient of 10 °C/h to 90 °C. After 45 hours the reaction ampoule was cooled to room temperature with a gradient of 5 °C/day. $(C_3Cl_3Te_2)_2[Te_2Cl_{10}]$ was obtained as dark-red, needle-shaped crystals in low yield (not exceeding 10%). Pure samples could only be obtained by mechanical separation from unchanged starting materials and by-products. UV/Vis (saturated filtered reaction solu-

Table 2. Crystal data and details of data collection for $(C_3Cl_3S_2)Cl$, $(C_3Cl_3Se_2)Cl$, and $(C_3Cl_3Te_2)_2[Te_2Cl_{10}]$

	$(C_3Cl_3S_2)Cl$	$(C_3Cl_3Se_2)$	$(C_3Cl_3Te_2)_2[Te_2Cl_{10}]$
Empirical formula	$C_3Cl_4S_2$	$C_3Cl_4Se_2$	$C_6Cl_{16}Te_6$
Molecular mass/gmol^{-1}	241.97	335.77	1404.91
Space group	$P2_1/n$	$P2_1/m$	$P\bar{1}$
Crystal system	monoclinic	monoclinic	triclinic
a/pm	682.0(1)	542.1(3)	839.77(6)
b/pm	1487.7(1)	861.8(4)	857.9(1)
c/pm	804.5(1)	846.2(5)	1092.12(7)
α/°	90	90	96.940(7)
β/°	96.79(1)	92.77(6)	102.295(7)
γ/°	90	90	99.65(1)
V/10^{6}pm^3	810.6(2)	394.9(4)	748.8(2)
Z	4	2	1
$D_{calcd.}$/gcm^{-3}	1.983	2.824	3.119
μ/cm^{-1}	18.8	106.2	72.0
$2\theta_{max}$	55.7	70.1	50.0
Data(total)	7206	6963	6719
Data(independent)	1830	1845	2625
Refined parameters	82	47	128
Final electron density/e10^{-6}pm^{-3}	+0.37/−0.24	+0.58/−0.48	+2.01/−2.52
$R(\|F\|)$	0.036	0.060	0.077
$wR(F^2)$	0.071	0.071	0.149

tion): λ_{max} = 260 nm, 238, 214. MS (EI): *m/z* (%) = 358 (7) $[C_2Cl_2Te_2]^+$, 200 (65) $[TeCl_2]^+$, 165 (65) $[TeCl]^+$, 130 (100) $[Te]^+$, 117 (40) $[CCl_3]^+$, 94 (40) $[C_2Cl_2]^+$.

Energy Dispersive X-ray fluorescence: The composition of all three compounds, $(C_3Cl_3S_2)Cl$, $(C_3Cl_3Se_2)Cl$, and $(C_3Cl_3Te_2)_2[Te_2Cl_{10}]$ was checked by electron beam X-ray fluorescence spectra. Crystals were selected in an argon-filled glove box, mechanically broken, placed on a conductive carbon-plated sample holder and transferred into the vacuum chamber of the spectrometer (Zeiss DSM 940, EDAX PV 9800) via an argon-filled gate. Spectra were recorded with a 15 kV acceleration voltage targeting the freshly broken faces of several crystals. Standard deviations are given in brackets and were estimated by the mean error of 10 independent measurements.

$(C_3Cl_3S_2)Cl$, calcd. C 33.3, S 22.2, Cl 44.4; found C 32(2), S 23.8(7), Cl 44(1)

$(C_3Cl_3Se_2)Cl$, calcd. C 33.3,Se 22.2, Cl 44.4; found C 33(2), Se 23(1), Cl 45(2)

$(C_3Cl_3Te_2)_2[Te_2Cl_{10}]$, calcd. C 21.4, Cl 57.1, Te 21.4; found C 20(2), Cl 58(1), Te 22.2(8)

Crystal Structure Analyses: Crystals of all three compounds were tested for diffraction quality by precession photographs. Data were collected at ambient temperature with a STOE Image Plate diffractometer for $(C_3Cl_3S_2)Cl$ and with a STOE AED 2 four circle diffractometer for $(C_3Cl_3Se_2)Cl$ and $(C_3Cl_3Te_2)_2[Te_2Cl_{10}]$ using graphite monochromated Mo-K_α radiation (λ = 71.073 pm). An empirical absorption correction was applied to the data set of $(C_3Cl_3Se_2)Cl$. Structure models were obtained by direct methods using SHELXS-86[21] and were refined based on F^2 by least-squares full-matrix refinements with anisotropic displacement parameters for all atoms using SHELXL-93.[22] Table 2 contains the crystallographic data and further details of data collection and refinement. CCDC-170239 [$(C_3Cl_3S_2)Cl$], CCDC-170240 [$(C_3Cl_3Se_2)Cl$) and CCDC-170241 [$(C_3Cl_3Te_2)_2[Te_2Cl_{10}]$) contain the supplementary crystallographic data for this paper. These data can be obtained free of charge at www.ccdc.cam.ac.uk/conts/retrieving.html [or from the Cambridge Crystallographic Data Centre, 12, Union Road, Cambridge CB2 1EZ, UK; Fax: (internat.) +44-1223/336-033; E-mail: deposit@ccdc.cam.ac.uk].

Acknowledgments

The support of our work by the Deutsche Forschungsgemeinschaft and the Fonds der Chemischen Industrie is gratefully acknowledged. We thank Dr. A. Fischer, Stockholm University, Sweden, for ^{125}Te NMR measurements.

[1] G. Bergson, *Arkiv Kemi* **1962**, *19*, 181−194.
[2] F. Boberg, *Justus Liebigs Ann. Chem.* **1964**, *679*, 109−118.
[3] S. L. Bender, M. R. Detty, N. P. Haley, *Tetrahedron Lett.* **1982**, *23*, 1531−1534.
[4] J. B. Milne, *Can. J. Chem.* **1992**, *70*, 693−699.
[5] G. E. Hawkes, R. A. Smith, J. D. Roberts, *J. Org. Chem.* **1974**, *39*, 1276−1290.
[6] J. Pietikäinen, R. S. Laitiuen, *Chem. Commun.* **1998**, 2381−2382.
[7] C. Th. Pedersen, *Sulfur Rep.* **1980**, *1*, 1−96.
[8] A. Hordvik, *Acta Chem. Scand.* **1966**, *20*, 1885−1891.
[9] R. Faggiani, R. J. Gillespie, J. F. Sawyer, J. E. Vekris, *Acta Crystallogr., Sect. C* **1989**, *45*, 1847−1853.
[10] J. Passmore, G. Sutherland, P. S. White, *J. Chem. Soc., Chem. Commun.* **1980**, 330−331.
[11] A. Hordvik, *Acta Chem. Scand.* **1965**, *19*, 1039−1044.
[12] G. Heath, P. Murray-Rust, J. Murray-Rust, *Acta Crystallogr., Sect. B* **1977**, *33*, 1209−1301.
[13] F. Grundvik, A. Hordvik, *Acta Chem. Scand.* **1971**, *25*, 1567−1575.
[14] P. Cherin, P. Unger, *Acta Crystallogr., Sect. B* **1972**, *28*, 313−317.
[15] G. Cardinal, R. J. Gillespie, J. F. Sawyer, J. E. Vekris, *J. Chem. Soc., Dalton Trans.* **1982**, 765−779.
[16] J. Beck, *Z. Anorg. Allg. Chem.* **1995**, *621*, 131−136.
[17] J. Beck, G. Bock, *Z. Naturforsch., Teil B* **1996**, *51*, 119−126.
[18] F. Grundtvik, A. Hordvik, *Acta Chem. Scand.* **1971**, *25*, 1567−1575.
[19] B. Krebs, F. P. Ahlers, *Adv. Inorg. Chem. Radiochem.* **1990**, *35*, 235−317.
[20] B. Krebs, B. Buss, W. Berger, *Z. Anorg. Allg. Chem.* **1973**, *397*, 1−15.
[21] G. M. Sheldrick, SHELXS-86, *A program for solving crystal structures*, University of Göttingen, **1986**.
[22] G. M. Sheldrick, SHELXS-93, *A program for solving crystal structures*, University of Göttingen, **1990**.

Received September 10, 2001
[I01353]

Anion-Dependent Substitution of Zinc by Magnesium in Mononuclear Schiff Base Complexes

Jolante Hermann,[a] Dinah Schumacher,[a] and Andrea Erxleben*[a]

Keywords: Schiff bases / Zinc / Magnesium / Crystal structures

The zinc and magnesium Schiff-base complexes $[ZnL(H_2O)(NO_3)]NO_3$ (**1**) and $[MgL(H_2O)_3](NO_3)_2{\cdot}H_2O$ (**2**) (L = Schiff base derived from 4-bromo-2-[(2-diethylaminoethyl)ethylaminomethyl]-6-formylphenol and glycine) have been prepared and structurally characterized. The reaction of **1** with Mg^{2+} has been studied in water, methanol and DMSO. Substitution of Zn by Mg^{2+} was observed in DMSO and methanol and the amount of Mg complex formed was found to be strongly dependent on the nature and concentration of the anions in solution: Cl^- and $CH_3CO_2^-$ mediate conversion of **1** into **2**, while ClO_4^-, NO_3^-, F^-, Br^-, I^- and SO_4^{2-} are ineffective.
(© Wiley-VCH Verlag GmbH, 69451 Weinheim, Germany, 2002)

Introduction

In previous papers we outlined our interest in Mg coordination chemistry.[1,2] Mg is an essential cofactor in biology, yet, compared with other biologically relevant metal ions, its coordination chemistry has received little attention.[3−10] Recently, we have studied the reaction of mononuclear Zn complexes derived from binucleating Schiff-base ligands like L′ with $MgCl_2$ and observed substitution of Zn by Mg in DMSO, which appeared to contradict the order of stability predicted by the Irving−Williams series.[11] However, the low solubility of the compounds prevented more detailed studies, for example, the use of different solvents. Furthermore, only $MgCl_2$ was used as the Mg salt, and salts with other anions were not considered. We have now studied the Schiff-base ligand derived from 4-bromo-2-[(2-diethylaminoethyl)ethylaminomethyl]-6-formylphenol and glycine (L) that forms the mononuclear Zn complex $[ZnL(H_2O)(NO_3)]NO_3$ (**1**) with Zn binding to the glycine side arm, while the protonated ammonium nitrogens render the complex soluble. Besides the effect of the solvent we have also investigated the reaction of **1** with different Mg salts and found that the metal ion exchange is strongly dependent on the anions present in solution.

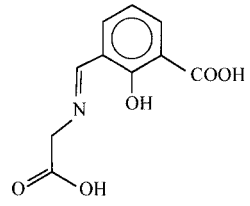

L'

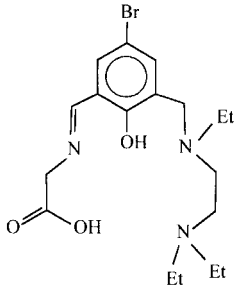

L

Results and Discussion

Synthesis and Characterisation of $[ZnL(H_2O)(NO_3)]NO_3$ (1) and $[MgL(H_2O)_3](NO_3)_2{\cdot}H_2O$ (2)

The zinc complex $[ZnL(H_2O)(NO_3)]NO_3$ (**1**) was prepared in situ by Schiff base condensation of 4-bromo-2-[(2-diethylaminoethyl)ethylaminomethyl]-6-formylphenol with glycine in the presence of $Zn(NO_3)_2{\cdot}6H_2O$. X-ray suitable crystals were obtained from methanol/water at pH 5.4. As shown in Figure 1, the ligand coordinates to zinc in a tridentate manner through the deprotonated phenolic oxygen,

[a] Fachbereich Chemie der Universität Dortmund,
Otto-Hahn-Str. 6, 44227 Dortmund, Germany
Fax: (internat.) + 49-(0)231/755-3797
E-mail: aerx@platon.chemie.uni-dortmund.de

the carboxylate group and the imine nitrogen. The amine nitrogens are both protonated and remain uncoordinated. The coordination sphere of Zn is completed by a water molecule and a nitrate ion that binds in an asymmetric chelating mode [Zn(1)−O(4) 2.470(9) Å, Zn(1)−O(5) 2.076(6) Å]. In the crystal packing hydrogen bonding interactions occur that involve the aqua ligand, the carboxylate and nitrate oxygens as well as the ammonium nitrogens (Table 1).

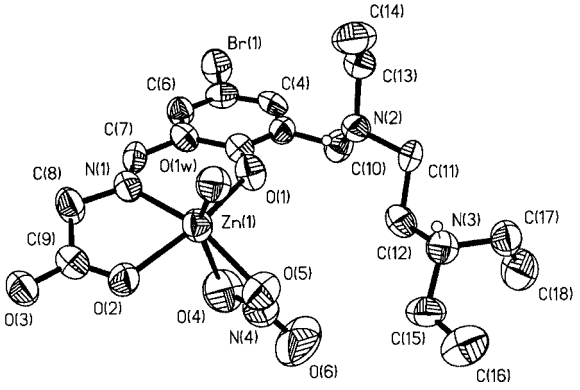

Figure 1. View of the cation of $[ZnL(H_2O)(NO_3)]NO_3$ (**1**) with atom numbering scheme; except for the ammonium protons, hydrogen atoms are omitted for clarity

Table 1. Selected bond lengths (Å), angles (°) and hydrogen bonding interactions (Å) for **1**

Zn(1)−N(1)	2.091(7)	Zn(1)−O(1)	2.017(6)
Zn(1)−O(2)	2.108(6)	Zn(1)−O(4)	2.470(9)
Zn(1)−O(5)	2.076(6)	Zn(1)−O(1w)	2.035(6)
N(1)−Zn(1)−O(1)	89.2(3)	N(1)−Zn(1)−O(2)	77.5(3)
N(1)−Zn(1)−O(1w)	110.3(3)	N(1)−Zn(1)−O(5)	152.7(3)
O(1)−Zn(1)−O(2)	165.5(2)	O(1)−Zn(1)−O(1w)	94.0(2)
O(1w)−Zn(1)−O(4)	151.5(3)	O(5)−Zn(1)−O(4)	55.4(3)
O(1w)···O(3)[a]	2.675(8)	O(1w)···O(7)[a]	2.71(1)
N(2)···O(3)[b]	3.17(1)	N(3)···O(2)[b]	2.779(9)

[a] $1/2 + x, -1/2 - y, 1/2 + z$. [b] $-1/2 + x, -1/2 - y, -1/2 + z$.

As described below the reaction of **1** with Mg^{2+} leading to the conversion of the Zn complex into the Mg complex of L was studied in solution by NMR spectroscopy; for an unambiguous assignment of the NMR resonances the Mg complex was prepared on a preparative scale. Reaction of 4-bromo-2-[(2-diethylaminoethyl)ethylaminomethyl]-6-formylphenol with sodium glycinate in the presence of $Mg(NO_3)_2{\cdot}6H_2O$ and NaOH yielded the Schiff-base complex of composition $[MgL(H_2O)_3](NO_3)_2{\cdot}H_2O$ (**2**), the X-ray structure of which is depicted in Figure 2. Mg binds to the phenolate oxygen, one carboxylate oxygen and the imine nitrogen and to three water ligands. Again, both amine nitrogens are protonated and noncoordinating. Due to the narrow bite angle of the chelating ligand, Mg adopts a distorted octahedral coordination geometry with the angles around Mg ranging from 76.7 to 100.0° (Table 2).

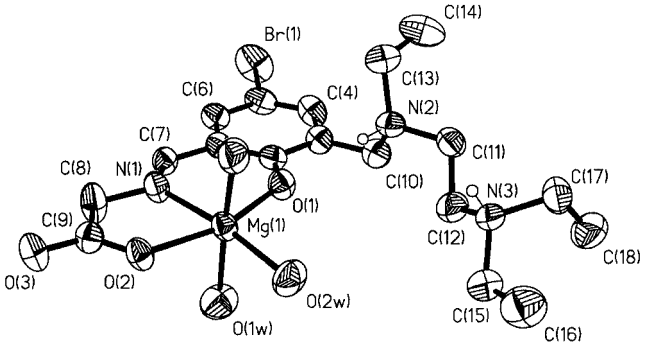

Figure 2. View of the cation of $[MgL(H_2O)_3](NO_3)_2{\cdot}H_2O$ (**2**) with atom numbering scheme; except for the ammonium protons, hydrogen atoms are omitted for clarity

Table 2. Selected bond lengths (Å) and angles (°) for **2**

Mg(1)−N(1)	2.144(5)	Mg(1)−O(1)	2.007(5)
Mg(1)−O(2)	2.120(4)	Mg(1)−O(1w)	2.119(5)
Mg(1)−O(2w)	2.068(4)	Mg(1)−O(3w)	2.046(5)
N(1)−Mg(1)−O(1)	86.3(2)	N(1)−Mg(1)−O(2)	76.7(2)
N(1)−Mg(1)−O(1w)	87.8(2)	N(1)−Mg(1)−O(2w)	172.4(2)
N(1)−Mg(1)−O(3w)	98.9(2)	O(1)−Mg(1)−O(2)	162.3(2)
O(1)−Mg(1)−O(1w)	93.6(2)	O(2)−Mg(1)−O(3w)	87.2(2)
O(1w)−Mg(1)−O(3w)	172.2(2)		

Solution Studies

Mg^{2+} shows a strong tendency to bind six water molecules in its inner coordination sphere so that in aqueous solution no reaction of **1** with Mg salts was observed. Consequently it was not unexpected that addition of one equivalent of $Zn(NO_3)_2$ to a solution of **2** in D_2O (pD 9.7) resulted in complete conversion into **1**. Even in the presence of 10 equivalents of $MgCl_2$ (for the choice of Cl^- ions see below) the percentage of **2** is less than 5%. We note that there is no indication for metal binding to the second coordination site of the ligand even under basic conditions.

By contrast, Zn is replaced by Mg when **1** is treated with $MgCl_2$ in DMSO, as observed before for related Schiff-base ligands.[1,2] Addition of three equivalents of $MgCl_2$ leads to approximately 44% conversion of **1** into **2**. The NMR spectra of the reaction solution reveal no change with time. In MeOD 11 equivalents of $MgCl_2$ are required to give an approximately 1:1 mixture of **1** and **2**. Consequently, the concentration of the Mg complex in DMSO is significantly reduced upon addition of MeOD, as shown in Figure 3. In the presence of 10 and 20% MeOD the percentage of **2** decreases to 33 and 22%, respectively. The effect of D_2O is even more pronounced: Upon addition of 20% D_2O the equilibrium is completely shifted towards the Zn complex. Exchange of Zn with Mg in DMSO can be attributed to the low dielectric constant of DMSO that stabilizes Mg binding to the N,O-ligand.

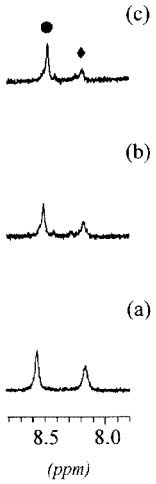

Figure 3. Reaction of **1** with 3 equiv. $MgCl_2$ in [D_6]DMSO solutions containing increasing amounts of MeOD; ^1H NMR spectra (δ = 7.8−8.8 ppm, resonance of the azomethine proton) for (a) 0, (b) 10 and (c) 20% MeOD; (•) $[ZnL]^{2+}$ (◆) $[MgL]^{2+}$

Apart from the effect of the solvent the equilibrium between the Zn and Mg complex is dependent on the anions present in solution. When **1** is treated with $Mg(NO_3)_2$, $Mg(ClO_4)_2$ or $MgSO_4$ instead of $MgCl_2$, no metal-ion substitution is observed in DMSO, while two equivalents of $Mg(CH_3CO_2)_2$ yield 38% of **2**. Addition of NaCl to a 1:1 mixture of **1** and $Mg(ClO_4)_2$ mediates formation of **2**. As shown in Figure 4 the concentration of **2** increases with increasing concentrations of NaCl until ca. 40% of the Mg complex is formed in the presence of 20 equivalents of NaCl.

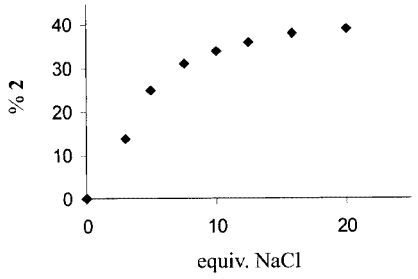

Figure 4. Percentage of **2** upon addition of increasing amounts of NaCl to a 1:1 mixture of **1** and $Mg(ClO_4)_2$ in DMSO

Analogously, addition of $NaCH_3CO_2$ triggers the substitution of Zn by Mg in a 1:1 mixture of $Mg(ClO_4)_2$ and **1**. Acetate is even more effective than Cl^- in promoting replacement of Zn by Mg: Addition of 7.5 equivalents to an equimolar solution of **1** and $Mg(ClO_4)_2$ gives 43% conversion of **1** into **2** in comparison with 31% in the case of Cl^-. Unfortunately, the limited solubility of sodium acetate in DMSO prevents a further increase of the amount of Mg complex formed. No Zn/Mg exchange is observed in the presence of F^-, Br^- and I^- ions. In line with the effect of the anions described so far, Mg is completely substituted by Zn when **2** is treated with one equivalent of $Zn(NO_3)_2$ in the absence of Cl^- or $CH_3CO_2^-$, while treatment of **2** with one equivalent of $Zn(CH_3CO_2)_2$ gives a mixture of 68% **1** and 32% **2**. Elias et al. have studied the replacement of Cu by Ni in [Cu(amben)] [H_2amben = *N,N′*-ethylenebis(2-aminobenzaldimine)].[12] They found a catalytic effect of the anion with the rate of the substitution reaction increasing as follows: $ClO_4^- < Br^- < SCN^- << Cl^-$. In our case, the reaction of **1** with $MgCl_2$ and $Mg(CH_3CO_2)_2$ is fast, the NMR spectra of the reaction mixtures (including those with counterions where no exchange is observed) do not change with time. In other words, the equilibrium is reached immediately and the lack of observation of a reaction in the absence of Cl^- and acetate is clearly not the result of a much slower reaction rate.

The reaction of [$Zn(L'^{2-})(H_2O)_2$] (**3**) with $MgCl_2$ has been described recently by us,[2] and in continuation of this work we have now investigated the anion dependence of the reaction for comparison with the system **1**/Mg^{2+}. Similarly to the reaction behavior of **1**/Mg^{2+}, $MgCl_2$ substitutes Zn in **3**, while $Mg(NO_3)_2$, $Mg(ClO_4)_2$ and $MgSO_4$ are ineffective. Furthermore, no substitution takes place in the presence of iodide, bromide or fluoride ions. Again, the effect of chloride ions can be confirmed by treating mixtures of **3** and $Mg(ClO_4)_2$ with NaCl. Addition of four equivalents of NaCl to a 1:2 mixture of **3** and $Mg(ClO_4)_2$ induces formation of the Mg complex of L′ (**4**) in 67% yield. Complete conversion is achieved with four equivalents of $Mg(ClO_4)_2$ and eight equivalents of NaCl. Thus, as observed for the direct reaction with $MgCl_2$, exchange of Zn with Mg occurs more easily in **3** than in **1**, where the substitution reaction does not go to completion. Investigation of the reaction of **3** with $Mg(CH_3CO_2)_2$ was hampered by the deprotonation of the aromatic carboxylate group by acetate.[13] An NMR spectrum displaying several imine signals indicates the formation of dinuclear complexes that will be isolated and characterized in future work.

Replacement of Zn by Mg in the coordination sphere of the Schiff-base ligand apparently contradicts the order of stability predicted by the Irving−Williams series and, interestingly, the substitution strongly depends on the nature of the anions present in solution. One plausible explanation for the effect of the anions is their interaction with Zn^{2+} in solution. Non- or weakly coordinating ions like ClO_4^-, NO_3^- and SO_4^{2-} do not interact with metal ions in solution — coordination of NO_3^- to Zn in the X-ray structure of **1** is a feature of the solid-state structure and is unlikely to be maintained in solution.[14] By contrast, Cl^- and $CH_3CO_2^-$ do interact with Zn^{2+} in DMSO, and Zn^{2+} is released when a solution of **3** is treated with NaCl as evident from the appearance of a signal set for the free ligand as well as that of **3** in the NMR spectrum. After addition of 2.3 equivalents of NaCl, the intensities of the resonances of **3** and L correspond to a 4:3 ratio of Zn complex and free ligand. The existence of distinct sets of resonances for the free ligand and for the Zn complex shows that the Zn complex is nonlabile on the NMR time-scale in DMSO. This behavior is in contrast to the kinetic properties of the majority of Zn complexes, although it has been observed previously for related Zn Schiff base complexes.[1,15] Coor-

dination of acetate to Zn^{2+} and Mg^{2+} in DMSO solutions can easily be followed by the change in the chemical shift of the acetate resonance in the NMR spectra of solutions of $NaCH_3CO_2$ containing increasing amounts of Mg^{2+} or Zn^{2+} ions. Addition of $Mg(ClO_4)_2$ or $Zn(NO_3)_2$ shifts the methyl signal of the acetate ion to lower fields ($\Delta\delta$ = 0.20 ppm with 1 equiv. Mg^{2+} and 0.24 ppm with 1 equiv. Zn^{2+}). Addition of NaCl to mixtures of $NaCH_3CO_2$ and $Mg(ClO_4)_2$ or $Zn(NO_3)_2$ gives slight upfield shifts of the acetate resonance indicating that Cl^- competes weakly with acetate for metal-ion coordination in DMSO.

In conclusion, in the case of ClO_4^-, NO_3^- and SO_4^{2-} the equilibrium in DMSO

$$[ZnL(DMSO)_x]^{2+} + [Mg(DMSO)_6]^{2+} + nY^- \leftrightarrows [MgL(DMSO)_3]^{2+} + [Zn(DMSO)_m]^{2+} + nY^-$$

lies to the left-hand side due to the coordination properties of Zn and Mg. When coordinating anions are present, the equilibrium

$$[ZnL(DMSO)_x]^{2+} + [Mg(DMSO)_{6-n}X_n]^{(2-n)+} \leftrightarrows [MgL(DMSO)_3]^{2+} + [Zn(DMSO)_mX_y]^{(2-y)+}$$

is to be considered and the position of the equilibrium is determined by the affinities of the metal ions for the Schiff-base ligand *and* for the counterions (solvent effects are also present, see above). For both Zn complexes **1** and **3**, the equilibrium lies further to the right-hand side in the presence of acetate than in the presence of Cl^-. For reaction mixtures containing two equivalents of the respective counterion equilibrium constants of $K = 0.01 \pm 0.03$ (Cl^-) and $K = 0.07 \pm 0.04$ (acetate) can be estimated from the relative intensities of the NMR resonances. In the case of F^-, Br^- and I^-, coordination of Zn to the Schiff-base ligands is favored (100% **1** and **3**).

Although the primary coordination sphere of the metal ion is identical for L and L′ (O_2N), Zn is considerably more susceptible to exchange by Mg in **3** than in **1** as evident from an equilibrium constant of $K \approx 0.18 \pm 0.06$ for the reaction of **3** with Mg^{2+} in the presence of two equivalents of Cl^-. This can be attributed to the presence of the ammonium groups in **1**. Compared with aqueous solutions, the acidity of the ammonium groups is increased in organic solvents, while the acidity of phenols and carboxylic acids decreases significantly.[16] Thus, the metal ions have to compete with the protons of the two tertiary ammonium nitrogens for the binding sites of the ligand. Due to the coordination properties of Zn and Mg, the Mg complex is probably destabilized, while Zn competes efficiently with the protons. This interpretation is in accordance with the observation that upon treating 1:1 mixtures of **1** and **2** with NH_4NO_3 the equilibrium is shifted further towards the Zn complex. On addition of six equivalents of NH_4NO_3 the percentage of **2** is decreased by 25%. Since acetate acts as a relatively strong base in DMSO,[16] deprotonation of the ammonium groups may contribute to the effect of acetate in favoring the formation of the Mg complex.

Conclusions

In conclusion we have isolated and structurally characterized a Zn and Mg complex with the Schiff-base ligand derived from 4-bromo-2-[(2-diethylaminoethyl)ethylaminomethyl]-6-formylphenol and glycine. These can be interconverted and the position of the equilibrium is determined by the solvent and the nature of the anions added to the reaction mixture.

Experimental Section

Materials and Methods: 4-Bromo-2-[(2-diethylaminoethyl)ethylaminomethyl]-6-formylphenol was prepared according to the literature procedure.[17] The Zn complex of L′ (**3**) was synthesized as previously described.[1] All chemicals and solvents were reagent grade and used without further purification. ^1H NMR spectra (200.13 MHz) were recorded on a Varian Mercury spectrometer. Spectra were run in [D_6]DMSO, MeOD or D_2O solutions using sodium 3-(trimethylsilyl)propanesulfonate as internal reference. The pD values of D_2O solutions were obtained by use of a glass electrode and addition of 0.4 to the pH meter reading. The CHN analyses were carried out on an Element Analyzer CHNS 932 (LECO). Infrared spectra of KBr pellets were taken on a Bruker IFS 28 FT-spectrometer.

CAUTION: *Perchlorate salts are potentially explosive and should be handled carefully in small quantities only.*

Complex 1: Glycine (141 mg, 1.89 mmol) was dissolved in water (20 mL) and added to a solution of 4-bromo-2-[(2-diethylaminoethyl)ethylaminomethyl]-6-formylphenol (675 mg, 1.89 mmol) and $Zn(NO_3)_2{\cdot}6H_2O$ (1178 mg, 3.96 mmol) in MeOH (9 mL). The solution was stirred at room temperature for 24 h. Slow evaporation of the solution yielded yellow needles of $[ZnL(H_2O)(NO_3)]NO_3{\cdot}nH_2O$ (elemental analysis $n = 1$, X-ray analysis $n = 0$) in 81% yield. Selected IR data (KBr): $\tilde{\nu}$ = 3002, 1640 (C=N), 1604, 1551, 1452, 1384 (NO_3^-), 1309, 1288, 1201, 1074, 1020, 879, 824 (NO_3^-), 769 cm^{-1}. ^1H NMR [D_2O, pD = 6.8]: δ = 1.14 (t, ^3J = 7.58 Hz, 6 H, CH_3), 1.27 (t, ^3J = 7.58 Hz, 3 H, CH_3), 2.96−3.26 (m, 10 H, CH_2-N), 3.96 (br. s, 2 H, CH_2-COO), 4.21 (s, 2 H Ar-CH_2), 7.49 (s, 1 H, H_{ar}), 7.55 (s, 1 H, H_{ar}), 8.35 (s, 1 H, HC=N). $C_{18}H_{32}BrN_5O_{11}Zn$ (639.78): calcd. C 33.8, H 5.0, N 11.0; found C 33.7, H 4.8, N 11.3.

Complex 2: 4-Bromo-2-[(2-diethylaminoethyl)ethylaminomethyl]-6-formylphenol (258 mg, 0.72 mmol), $Mg(NO_3)_2{\cdot}6H_2O$, (923 mg, 3.60 mmol), sodium glycinate hydrate (105 mg, 0.913 mmol) and NaOH (85 mg, 2.13 mmol) were reacted in methanol/water (5:1, 12 mL) at room temperature. After stirring overnight some insoluble precipitate was filtered off. From the filtrate small needles of composition $[MgL(H_2O)_3](NO_3)_2{\cdot}H_2O{\cdot}CH_3OH$ (**2·CH$_3$OH**) were obtained. Yield: 27%. Selected IR data (KBr): $\tilde{\nu}$ = 3391, 1655 (C=N), 1604, 1545, 1384 (NO_3), 1237, 1199, 1147, 1094, 1037, 829 (NO_3^-), 771 cm^{-1}. ^1H NMR [$(CD_3)_2SO$]: δ = 1.03 (br. s, 6 H, CH_3), 1.22 (br. s, 3 H, CH_3), 2.6−3.1 (br. m, 10 H, CH_2-N), 3.92 (br. s, 2 H, CH_2-COO), 4.04 (br. s, 2 H, Ar-CH_2), 7.38 (s, 2 H, H_{ar}), 8.16 (br. s, 1 H, HC=N). $C_{19}H_{40}BrMgN_5O_{14}$ (666.78): calcd. C 34.2, H 6.1, N 10.5; found C 33.9, H 5.7, N 10.1. Recrystallization yielded X-ray suitable crystals of $[MgL(H_2O)_3](NO_3)_2{\cdot}H_2O$ (**2**).

Table 3. Crystallographic data and experimental details of the X-ray studies of **1** and **2**

	1	**2**
Empirical formula	$C_{18}H_{30}BrN_5O_{10}Zn$	$C_{18}H_{36}BrMgN_5O_{13}$
Molecular mass	621.75	634.74
Crystal system	monoclinic	monoclinic
Space group	*Cc*	*Cc*
a [Å]	9.814(1)	9.915(1)
b [Å]	20.444(1)	23.395(1)
c [Å]	12.811(1)	12.411(1)
β [°]	100.49(1)	102.85
V [Å^3]	2527.4(3)	2806.8(4)
Z	4	4
$\rho_{calcd.}$ [g cm^{-3}]	1.634	1.502
No. measured reflections	2240	2666
No. observed reflections [$I > 2\sigma(I)$]	1266	1782
R_1 [$I > 2\sigma(I)$][a]	0.048	0.050
wR_2 [$I > 2\sigma(I)$][b]	0.078	0.117

[a] $R_1 = \Sigma \, ||F_o| - |F_c|| / \Sigma \, |F_o|$. [b] $wR_2 = [\Sigma(F_o^2 - F_c^2)^2 / \Sigma w(F_o^2)^2]^{0.5}$; $w^{-1} = \sigma^2(F_o^2) + (aP)^2$; $P = (F_o^2 + 2F_c^2)/3$ with $a = 0.0473$ for **1** and 0.0843 for **2**.

X-ray Crystallography: Crystal data for compounds **1** and **2** (Table 3) were recorded at room temperature on an Enraf−Nonius-KappaCCD diffractometer[18] using graphite-monochromated Mo-K_α radiation ($\lambda = 0.71069$ Å). For data reduction and cell refinement the programs DENZO and SCALEPACK were applied.[19] The structures were solved by conventional Patterson (**1**) and direct methods (**2**) and subsequent Fourier syntheses and refined by full-matrix least-squares on F^2 using the SHELXTL PLUS and SHELXL-93 programs.[20] The scattering factors were those given in the SHELXL programs. Transmission factors were calculated with SHELXL-97.[20] All non-hydrogen atoms except for the oxygen of water of crystallization in **2** were refined anisotropically. Hydrogen atoms were generated geometrically and given fixed isotropic U values.

CCDC-177901 (**1**) and -177902 (**2**) contain the supplementary crystallographic data for this paper. These data can be obtained free of charge at www.ccdc.cam.ac.uk/conts/retrieving. html [or from the Cambridge Crystallographic Data Centre, 12, Union Road, Cambridge CB2 1EZ, UK; Fax: (internat.) +44-1223/336-033; E-mail: deposit@ccdc.cam.ac.uk].

Acknowledgments

We thank Prof. Bernhard Lippert for the continuous support of our work. Financial support by the Ministerium für Schule, Wissenschaft und Forschung, NRW (Lise-Meitner-Habilitationsstipendium to A. E.) and the Deutsche Forschungsgemeinschaft is gratefully acknowledged.

[1] A. Erxleben, D. Schumacher, *Eur. J. Inorg. Chem.* **2001**, *12*, 3039−3046.
[2] J. Hermann, A. Erxleben, *Inorg. Chim. Acta* **2000**, *304*, 125−129.
[3] D. E. Fenton, in *Comprehensive Coordination Chemistry* (Ed.: G. Wilkinson), Pergamon Press: Oxford, 1987; Vol. 3, pp 1−80 and references therein.
[4] J. W. Yun, T. Tomoaki, L. E. Pence, S. J. Lippard, *J. Am. Chem. Soc.* **1995**, *117*, 4407−4408.
[5] H. Schmidbaur, I. Bach, D. L. Wilkinson, G. Müller, *Chem. Ber.* **1989**, *122*, 1433−1438.
[6] P. Ghosh, G. Parkin, *Inorg. Chem.* **1996**, *35*, 1429−1430.
[7] B.-H. Ye, T. Mak, I. D. Williams, X.-Y. Li, *J. Chem. Soc., Dalton Trans.* **1998**, 1935−1936.
[8] J. Huskens, A. D. Sherry, *Inorg. Chem.* **1996**, *35*, 5137−5143.
[9] L. B. Cole, E. M. Holt, *Inorg. Chim. Acta* **1989**, *160*, 195−203.
[10] S. R. Drake, K. D. Sanderson, M. B. Hursthouse, K. M. A. Malik, *Inorg. Chem.* **1993**, *32*, 1041−1044.
[11] H. Irving, R. J. P. Williams, *J. Chem. Soc.* **1953**, 3192−3200.
[12] S. Busse, H. Elias, J. Fischer, M. Poggemann, K. J. Wannowius, R. Boca, *Inorg. Chem.* **1998**, *37*, 3999−4005.
[13] Deprotonation of the second binding site of the ligand by acetate in aprotic, non-aqueous solution should also take place in the case of ligand L. However, there is no evidence for the formation of homo- or heterodinuclear complexes of L under the reaction conditions used. For acid-base properties in aprotic organic solvents see ref.[16]
[14] Interaction of NO_3^- with Zn^{2+} ions in solution is ruled out, since no dissociation of the complex is observed. As discussed below, interaction with coordinating anions result in the release of Zn^{2+} ions.
[15] A. Erxleben, J. Hermann, *J. Chem. Soc., Dalton Trans.* **2000**, 569−575.
[16] K. Izutsu, *IUPAC Chemical Data Series No. 35, Acid−Base Dissociation Constants in Dipolar Aprotic Solvents*, Blackwell Scientific Publications, Oxford, 1990.
[17] J. D. Crane, D. E. Fenton, J. M. Latour, A. J. Smith, *J. Chem. Soc., Dalton Trans.* **1991**, 2979−2987.
[18] KappaCCD package, Nonius, Delft, The Netherlands, 1997.
[19] Z. Otwinowsky, W. Minor, DENZO and SCALEPACK, *Methods Enzymol.* **1996**, *276*, 307−326.
[20] G. M. Sheldrick, SHELXTL-PLUS (VMS), Siemens Analytical X-ray Instruments, Inc., Madison, WI, 1990; SHELXL-93, *Program for crystal structure refinement*, University of Göttingen, Germany, 1993; SHELXL-97, Program for the Refinement of Crystal Structures, University of Göttingen, 1997.

Received January 23, 2002
[I02039]

Titanocene and Zirconocene Complexes containing Dendrimer-Substituted Cyclopentadienyl Ligands − Synthesis and Ethylene Polymerization

Román Andrés,*[a] Ernesto de Jesús,*[a] F. Javier de la Mata,[a] Juan C. Flores,[a] and Rafael Gómez[a]

Keywords: Metallocenes / Dendrimers / Titanium / Zirconium / Substituent effects

This paper describes the synthesis of a series of titanium and zirconium metallocenes bearing one or two first-generation silane dendritic wedges as bulky substituents at their cyclopentadienyl rings. Wedges $(R_2R'SiCH_2CH_2)_3SiCl$ [R = R′ = Et (**1**); R = Ph, R′ = Me (**2**)] were prepared by hydrosilylation of chlorotrivinylsilane with $R_2R'SiH$. They were reacted with $K(C_5H_5)$ and, subsequently, with KH to give $K[(R_2R'SiCH_2CH_2)_3Si(C_5H_4)]$ [R = R′ = Et (**3**); R = Ph, R′ = Me (**4**)]. The dendronized cyclopentadienides **3** and **4** were the starting materials for preparation of the mixed-ring titanocenes $[\{(R_2R'SiCH_2CH_2)_3SiC_5H_4\}(C_5R''_5)TiCl_2]$ [R = R′ = Et, R′′ = H (**5**), R′′ = Me (**6**); R = Ph, R′ = Me, R′′ = H (**7**), R′′ = Me (**8**)] or the symmetrically substituted metallocenes $[\{(Ph_2MeSiCH_2CH_2)_3SiC_5H_4\}_2MCl_2]$ [M = Ti (**9**), Zr (**10**)]. Cyclic voltammograms and catalytic behavior of all the new metallocenes in ethylene polymerization, using MAO as a cocatalyst, have been studied and compared to that of related non-dendritic complexes. Polyethylene polydispersities increase with the number of dendritic wedges in the catalyst, while activities decrease. Bimodal molecular weight distributions were clearly observed for the bis-dendritic titanocene **9**.

(© Wiley-VCH Verlag GmbH, 69451 Weinheim, Germany, 2002)

Introduction

The modification of cyclopentadienyl (Cp) ligands has played a crucial role in improving the usefulness of group 4 metallocenes as catalysts in olefin polymerization. It has proved to be especially relevant to the microstructure of polymers obtained from α-olefins.[1] Control of the stereochemistry requires some conformational constraint because it arises mainly from steric interactions between the incoming olefin monomer and the Cp ligand; bridged cyclopentadienyl ligands (*ansa*-metallocenes) have often been used for this purpose.[2] However, some degree of stereocontrol is in principle possible without a rigid ligand framework if rotation of the Cp ligands is hindered,[3] for example by means of sterically demanding substituents.[4]

We are currently studying the chemistry of titanium and zirconium metallocenes located at the focal point of one or two dendritic wedges. Our interest is focused on their use as precursors for olefin polymerization. In these complexes, the dendrimers[5] act as ligand modifiers that introduce steric hindrance around the cyclopentadienyl rings, and their behavior can be compared to that of other sterically encumbered metallocenes.

Cyclopentadienyl complexes have been employed for the peripheral functionalization of dendrimers and, in particular, group 4 derivatives have been already synthesized[6,7] and tested in olefin polymerization.[6a,7c] We have observed[7c] that, in such cases, dendrimers are more than mere supports of active sites and may significantly modify activities and molecular weights. Less attention has been paid to dendrimers, such as those reported here, that are metallated at their core or focal-point with cyclopentadienyl complexes.[8] However, the ability of dendritic shells to encapsulate functional core moieties and to create specific site-isolated nanoenvironments,[9] a concept taken from biological systems, has already been exploited in catalysis using a variety of metal complexes.[9,10]

In the present report, we describe the syntheses of titanium and zirconium metallocenes bearing one or two first generation carbosilane dendritic wedges, together with their behavior in ethylene polymerization using MAO as a cocatalyst.

Results and Discussion

The new dendritic titano- and zirconocenes were synthesized following the pathway depicted in Scheme 1. The reactions described below fulfil two conditions in order to warrant pure final products: high yields in every step and at least one step involving enough differences in solubility between the target compound and by-products. These conditions are required since the separation of by-products accumulated in these multistep preparations is complicated by

[a] Departamento de Química Inorgánica, Universidad de Alcalá, Campus Universitario,
28871 Alcalá de Henares (Madrid), Spain
Fax: (internat.) +34-91/885-4683
E-mail: ernesto.dejesus@uah.es

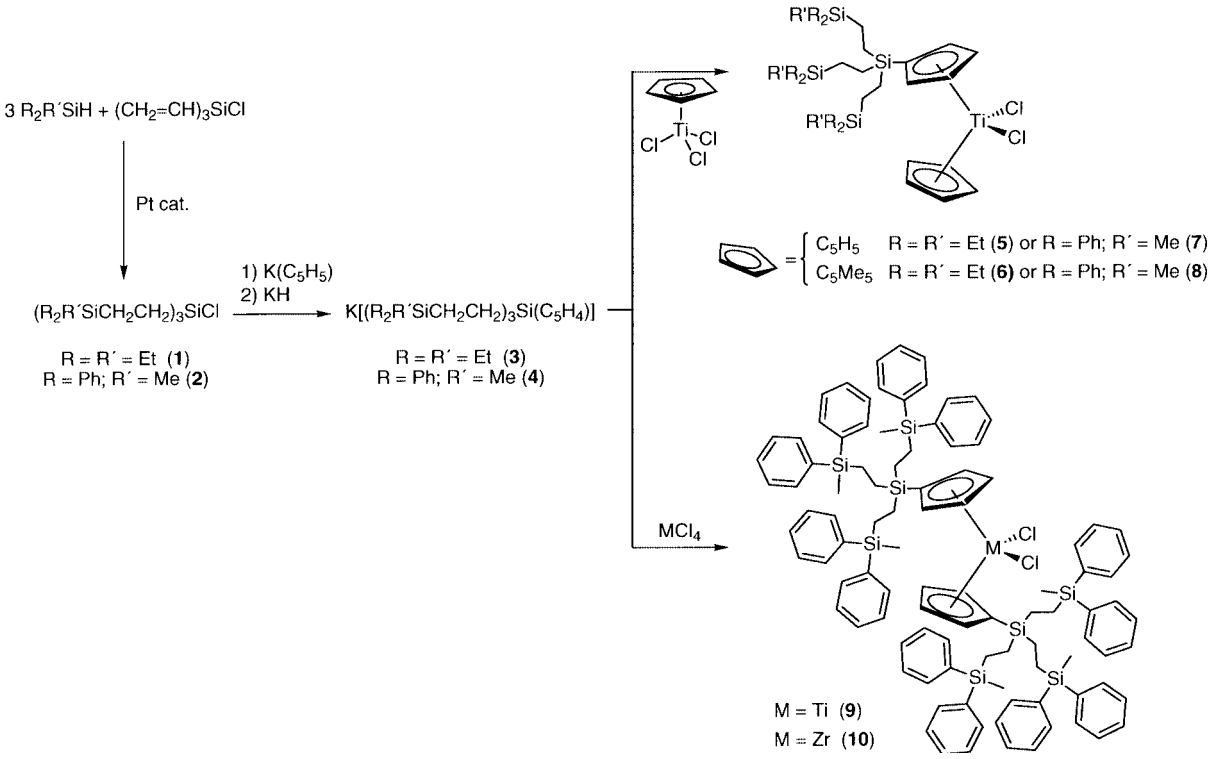

Scheme 1

the high solubility and oily nature of these dendritic compounds.

The chlorosilanes $(R_2R'SiCH_2CH_2)_3SiCl$ [R = R′ = Et (**1**); R = Ph, R′ = Me (**2**)] were obtained from a solvent-free reaction in which chlorotrivinylsilane was hydrosilylated with an excess of the corresponding silane $R_2R'SiH$, using hydrogen hexachloroplatinate(IV) as a catalyst (Scheme 1). Only the formation of β-silylated compounds was observed. Silane **1** was obtained as a colorless oil after removal of volatiles in vacuo, whereas compound **2** was recrystallized from pentane at −30 °C as an off-white solid. The dendronized cyclopentadienides **3** and **4** were synthesized as their potassium salts by reaction of **1** or **2** with $K(C_5H_5)$ in THF and subsequent treatment of the cyclopentadienes with KH. Compound **3** separated from pentane at −30 °C as an oily pale yellow product whereas **4** was precipitated from hexane at room temperature as a white solid.

The mixed-ring titanocenes **5**−**8** were prepared by reaction of **3** or **4** and one equiv. of $[(C_5H_5)TiCl_3]$ or $[(C_5Me_5)TiCl_3]$. The symmetrically substituted metallocenes **9** (Ti) and **10** (Zr) were obtained from the reaction of **4** and $TiCl_4$ or $[ZrCl_4]\cdot 2THF$ in a 2:1 ratio. The reactions were carried out in THF and products were initially isolated as oils. Complexes **5**−**8** crystallized after workup whereas all attempts to crystallize **9** and **10** failed. Compounds **5**−**10** are rather stable to air and the analytical and spectroscopic data are in agreement with their proposed structure (see Exp. Sect.).

Among electrochemical methods, cyclic voltammetry has been widely used to study the influence of substituents on the electronic density at the metal center of complexes.[11,12] Cyclic voltammograms of metallocene derivatives **5**−**10** were recorded in THF solution. Each complex shows a quasi-reversible electrode process due to a one-electron reduction of the titano- and zirconocene derivatives at the potentials summarized in Table 1 vs. the ferricinium/ferrocene couple. The potential of the reference complex $[(C_5H_5)_2TiCl_2]$ is within the narrow range in which potentials of C_5H_5 complexes **5**, **7**, and **9** are observed (1.34−1.40 V). The same is true for $[(C_5H_5)(C_5Me_5)TiCl_2]$ and the range of C_5Me_5 compounds **6** and **8** (1.64−1.66 V), and for $[(C_5H_5)_2ZrCl_2]$ and **10**. These data can be interpreted in the sense that dendritic silane substituents have a minor influence on the electron-donating properties of the cyclopentadienyl ring and therefore on the electronic density of the metal center. Similar results have been obtained for the $SiMe_3$-substituted complexes $[(C_5H_4SiMe_3)_2TiCl_2]$ and $[(C_5H_3(SiMe_3)_2]_2TiCl_2]$, whose potentials are not shifted from those observed for $[(C_5H_5)_2TiCl_2]$.[13] It has been pointed out that steric hindrance between cyclopentadienyl substituents, when they are placed at the hinge positions of titanocene dichlorides, decreases the dihedral angle (φ) formed by the ring planes. This change results in LUMO orbitals of lower energy, and therefore in the observation of a decreased absolute value of the reduction potential.[12] The absence of a significant shift in the potential values of the dendritic titanocenes **5**−**9** (and for **10**) compared to their non-dendritic counterparts {$[(C_5H_5)_2MCl_2]$ or $[(C_5H_5)(C_5Me_5)TiCl_2]$} is compatible with a dynamic model in which the rotating Cp ligands are preferentially accommodated in conformations in which the intramolecular

steric strain is relieved; obviously these conformations are those with the dendritic wedges occupying the lateral positions of the molecule. However, the rotation of the Cp rings is far from being fully stopped in solution, as demonstrated by the fact that only two types of cyclopentadienyl protons are observed in the ^{1}H NMR spectrum of **9** even at −90 °C.

Upon activation with an excess of methylaluminoxane (MAO), complexes **5**−**10** catalyze the polymerization of ethylene. These results are summarized in Table 2 and details of the polymerization procedure are given in the Exp. Sect. As a reference, polymerization with $[(C_5H_5)_2MCl_2]$ (M = Ti, Zr) and $[(C_5H_5)(C_5Me_5)TiCl_2]$ was also carried out under the same conditions. Every dendritic catalyst displayed a lower activity than its reference complex.

For the titanium series, we can establish the following order of activity according to the type of cyclopentadienyl ligands: $(C_5H_5)_2$ > $(C_5H_4R)(C_5H_5)$ >> $(C_5H_4R)_2$ ≈ $(C_5H_5)(C_5Me_5)$ >> $(C_5H_4R)(C_5Me_5)$, where each >> corresponds to an activity reduction of one order of magnitude. What it is remarkable in these data is that replacement of a $C_5H_5^-$ ligand by a dendritic cyclopentadienide in **5** and **7** only causes a moderate decrease in activity (from 4320 in $[(C_5H_5)_2TiCl_2]$ to 2064 and 1728 kg/mol·h, respectively). Steric hindrance might cause the later decrease and an argument for this hypothesis is based on the CV results (see above) that show slight electronic density differences between their metal centers. The lower activity of bis-dendritic Cp system **9** might be interpretable in steric terms assuming that interaction between both dendritic wedges restricts the conformations in which they are kept far away from the metal center. In the case of zirconium, much less appreciable effects might be expected because of the bigger size of the metal center. In fact, the activity of the bis-dendritic Zr complex **10** is similar to that of $[(C_5H_5)_2ZrCl_2]$ with a decrease (from 8016 to 5472 kg/mol·h) far away from the one order of magnitude decrease observed for the analogous pair of titanium complexes. This result seems to contradict the data reported by Alt and Köppl in a recent review on the polymerization activity of ethylene with metallocenes. For complex $[(C_5H_4SiMe_2Ph)_2ZrCl_2]$ the activity found was less than 10% that of $[(C_5H_5)_2ZrCl_2]$.[1f] However, in this case an interaction of the aromatic end group of the substituent with the Lewis-acid center of the catalyst could be responsible for such an effect because of the additional stabilization of the active site. In the above discussion, it has been assumed that the concentration of active centers is the same for all the compared catalysts (and ideally equal to the precursor concentration). This is a general obstacle in the discussion of results in polymerization with metallocene/MAO catalysts.[14,15] In any case, the practical question is that dendritic wedges can be used as cyclopentadienyl substituents without hindering the closest metal environment to such an extent that the polymerization process is prevented.

Table 1. Cyclic voltammetric data for metallocene derivatives **5**−**10** in THF/Bu_4NPF_6[a]

Complex	Half-wave potentials[b]
$[(C_5H_5)_2TiCl_2]$	−1.39
$[\{(Et_3SiCH_2CH_2)_3SiC_5H_4\}(C_5H_5)TiCl_2]$ (**5**)	−1.34
$[\{(Ph_2MeSiCH_2CH_2)_3SiC_5H_4\}(C_5H_5)TiCl_2]$ (**7**)	−1.39
$[\{(Ph_2MeSiCH_2CH_2)_3SiC_5H_4\}_2TiCl_2]$ (**9**)	−1.40
$[(C_5H_5)(C_5Me_5)TiCl_2]$	−1.65
$[\{(Et_3SiCH_2CH_2)_3SiC_5H_4\}(C_5Me_5)TiCl_2]$ (**6**)	−1.66
$[\{(Ph_2MeSiCH_2CH_2)_3SiC_5H_4\}(C_5Me_5)TiCl_2]$ (**8**)	−1.64
$[(C_5H_5)_2ZrCl_2]$	−2.26
$[\{(Ph_2MeSiCH_2CH_2)_3SiC_5H_4\}_2ZrCl_2]$ (**10**)	−2.20

[a] Concentration 2×10^{-4} M; scan rate 0.1 V s^{-1}. [b] $(E_p^{red} + E_p^{ox})/2$ in volts vs. $(C_5H_5)_2Fe^+/(C_5H_5)_2Fe$.

The polyethylene samples generated with complexes **5**, **7**, **9**, and **10** were analyzed by gel-permeation chromatography (GPC). The molecular weights of the polymers obtained with dendritic systems are near to 400×10^3, a normal region for metallocenes, although the titanium dendrimers **5**−**9** gave polymers somewhat larger than those produced with $[(C_5H_5)_2TiCl_2]$/MAO. More remarkable are the molecular weight distributions of the samples obtained from the titanium complexes: the polydispersity values increase with the number of dendritic substituents on the catalyst precursor (from 1.86 for non-dendritic to 5.81 for bis-dend-

Table 2. Ethylene Polymerization results with complexes **5**−**10**[a]

Precatalyst	Yield (mg)	Activity (kg_{PE}/mol_M h)	M_w ($\times 10^{-3}$)	M_w/M_n
$[(C_5H_5)_2ZrCl_2]$	1670	8016	380	2.18
$[\{(Ph_2MeSiCH_2CH_2)_3SiC_5H_4\}_2ZrCl_2]$ (**10**)	1140	5472	410	2.80
$[(C_5H_5)_2TiCl_2]$	900	4320	244	1.86
$[\{(Et_3SiCH_2CH_2)_3SiC_5H_4\}(C_5H_5)TiCl_2]$ (**5**)	430	2064	434	2.51
$[\{(Ph_2MeSiCH_2CH_2)_3SiC_5H_4\}(C_5H_5)TiCl_2]$ (**7**)	360	1728	398	3.33
$[\{(Ph_2MeSiCH_2CH_2)_3SiC_5H_4\}_2TiCl_2]$ (**9**)	120	576	376	5.81
$[(C_5H_5)(C_5Me_5)TiCl_2]$	118	566	–	–
$[\{(Et_3SiCH_2CH_2)_3SiC_5H_4\}(C_5Me_5)TiCl_2]$ (**6**)	11	53	–	–
$[\{(Ph_2MeSiCH_2CH_2)_3SiC_5H_4\}(C_5Me_5)TiCl_2]$ (**8**)	10	48	–	–

[a] Conditions: MAO cocatalyst, Al/M = 1000, 1.25 μmol of catalyst dissolved in 50 mL of toluene, 10 minutes, 293 K, 1 bar of constant monomer pressure.

ritic). As shown in Figure 1, these values reflect the appearance of bimodal molecular weight distributions, especially for polymer yielded by the bis-dendritic system **9**. In contrast, the zirconium complex **10** produces polyethylene of low polydispersity. Bimodal distributions may result for several reasons, such as a multistate catalyst with slow interconversion of states,[16] or the presence of traces of impurities (for example, unsubstituted metal complexes).

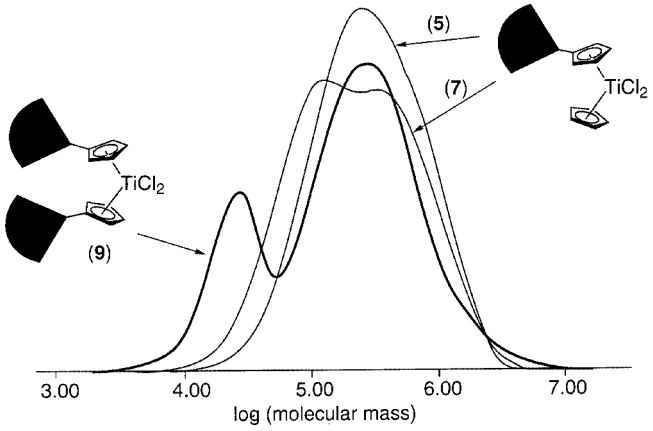

Figure 1. Molecular weight distributions for polyethylene samples obtained from **5**, **7**, and **9**/MAO catalytic systems

Conclusion

In this paper, we have modified the metal environment in titanium and zirconium metallocenes by the incorporation of first-generation carbosilane dendritic wedges into Cp ligands. An effect of such a modification in ethylene polymerization is the observed correlation between polyethylene polydispersities and the number of dendritic wedges in the titanium catalysts. Bimodal molecular weight distributions have been observed for several of the reported complexes, especially for the bis-dendritic titanocene **9**. On the other hand, the activity decreases caused by the bulky substituents are moderate, especially for zirconium complex **10**, suggesting that the metal centers remain quite accessible. In contrast to other bulky substituents, the long range of their space-filling properties is a distinctive feature of dendritic wedges (Figure 2) that may be truly useful for polymer stereocontrol. Work on the effects of growing dendritic generations on the polymerization of α-olefins is under way in our laboratory.

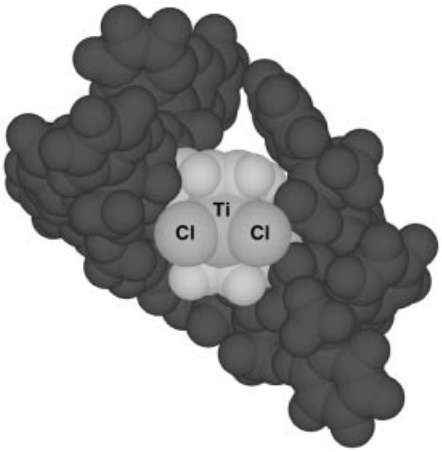

Figure 2. Space-filling model for complex [{($Ph_2MeSiCH_2CH_2)_3SiC_5H_4$}$_2$$TiCl_2$] (**9**) in a bis-lateral arrangement; the wedges are shown in dark colors

Experimental Section

Reagents and General Techniques: All operations were performed under an argon atmosphere using Schlenk or dry box techniques. Solvents were dried and distilled under argon as described elsewhere.[17] Unless otherwise stated, reagents were obtained from commercial sources and used as received. MAO was obtained in toluene solution 1.5 M from Witco. $K(C_5H_5)$ was prepared from freshly distilled cyclopentadiene and KH in THF. [$M(C_5H_5)_2Cl_2$] (M = Ti, Zr),[18] [$Ti(C_5H_5)(C_5Me_5)Cl_2$],[19] [$Ti(C_5H_5)Cl_3$],[20] and [$Ti(C_5Me_5)Cl_3$][21] were prepared according to reported procedures. ^1H, ^{13}C, and ^{29}Si NMR spectra were recorded on Varian Unity 300 or 500 Plus spectrometers. Chemical shifts (δ, ppm) are relative to $SiMe_4$ and were measured by internal referencing to the deuterated solvent (^{13}C and residual ^1H resonances), or by the substitution method from the ^{29}Si resonance of $SiMe_4$. C, H and N analyses were performed in a Heraeus CHN-O-Rapid microanalyzer by the Microanalytical Services of the Universidad de Alcalá. Cyclic voltammograms were obtained with an AMEL 553 Potentiostat, an AMEL 567 Wave Generator, and a three-platinum-electrode cell. [Bu_4N][PF_6] (0.2 M in THF) was used as supporting electrolyte and potentials were zeroed to the ferricinium/ferrocene couple used as internal reference.

Synthesis of ($Et_3SiCH_2CH_2)_3SiCl$ (1): A mixture of trivinylchlorosilane (2.0 mL, 13 mmol), an excess of Et_3SiH (8.2 mL, 52 mmol), and a hydrosilylation Pt catalyst (4 drops of a 2×10^{-3} M solution of H_2PtCl_6 in 2-propanol) was stirred for 24 h at 70 °C. After completion of the reaction (^1H NMR monitoring) the volatiles were removed under vacuum to give **1** (5.7 g, 89%) as a colorless oil. The sample was not analytically pure but was suitable for further preparations. ^1H NMR (300 MHz, $CDCl_3$, 25 °C): δ = 0.91 (t, 27 H, CH_3CH_2), 0.70 and 0.46 [A and B parts of an A_2B_2 spin system, 12 H, $Si(CH_2)_2Si$], 0.50 (quart, 18 H, CH_3CH_2) ppm. $^{13}C\{^1H\}$ NMR (300 MHz, $CDCl_3$, 25 °C): δ = 7.4 (CH_3CH_2), 7.0 [$Si(CH_2)_2Si$], 2.8 (CH_3CH_2), 2.5 [$Si(CH_2)_2Si$] ppm. $^{29}Si\{^1H\}$ NMR (500 MHz, $CDCl_3$, 25 °C): δ = 35.2 (*Si*Cl), 8.5 (Et_3Si) ppm.

Synthesis of ($Ph_2MeSiCH_2CH_2)_3SiCl$ (2): This compound was prepared by the procedure described above for **1** from trivinylchlorosilane (1.9 mL, 12.5 mmol) and Ph_2MeSiH (10 mL, 50 mmol). After completion of the reaction, pentane (50 mL) was added to the solution and then cooled at −30 °C overnight. Sometimes an oil, instead of a solid, separated from the solution. In that case, the mixture was shaken vigorously, cooled again to −30 °C for several hours, and the process repeated until precipitation of a white solid. The mixture was filtered and the solid dried in vacuo and characterized as **2**. Further crops of **2** were collected from the pentane solution by repeated (2−3 times) concentration and crystallization, giving an overall yield of 7.0 g (76%). $C_{45}H_{51}ClSi_4$ (739.7): calcd. C 73.07, H 6.95; found C 72.68, H 7.17. ^1H NMR (300 MHz, $CDCl_3$, 25 °C): δ = 7.45 (m, 12 H, C_6H_5), 7.31 (m, 18 H, C_6H_5), 0.91 and 0.73 [A and B parts of an A_2B_2 spin system, 12 H, $Si(CH_2)_2Si$], 0.51 (s, 9 H, CH_3) ppm. $^{13}C\{^1H\}$ NMR (300 MHz, $CDCl_3$, 25 °C): δ = 136.5 (C_{ipso}, C_6H_5), 134.4 (C_{meta}, C_6H_5), 129.2 (C_{para}, C_6H_5), 127.8 (C_{ortho}, C_6H_5), 7.2 and 5.7 [$Si(CH_2)_2Si$], −5.0

(CH_3) ppm. $^{29}Si\{^1H\}$ NMR (500 MHz, $CDCl_3$, 25 °C): δ = 35.8 (*Si*Cl), −5.5 (Ph_2MeSi) ppm.

Synthesis of K[(Et$_3$SiCH$_2$CH$_2$)$_3$Si(C$_5$H$_4$)] (3): This compound was prepared by the same procedure described below for **4** from potassium cyclopentadienide (0.58 g, 6.0 mmol), **1** (3.0 g, 6.0 mmol) and KH (0.24 g, 6.0 mmol). However, its high solubility in hexane prevented its crystallization. Compound **3** was obtained as a pale yellow oil by evaporation of the final solution in vacuo to dryness (2.8 g, 85% yield). ^1H NMR (300 MHz, C_6D_6, 25 °C): δ = 6.07 and 6.04 (AA′ and BB′ parts of an AA′BB′ spin system, 4 H, C_5H_4), 1.20 (t, 27 H, CH_3CH_2), 1.06 and 0.68 [A and B parts of an A_2B_2 spin system, 12 H, $Si(CH_2)_2Si$], 0.79 (quart, 18 H, CH_3CH_2) ppm. $^{13}C\{^1H\}$ NMR (300 MHz, C_6D_6, 25 °C): δ = 114.2 and 109.3 (C_5H_4), 8.2 (CH_3CH_2), 7.8 and 5.9 [$Si(CH_2)_2Si$], 3.5 (CH_3CH_2) ppm; C_{ipso} of C_5H_4 not found.

Synthesis of K[(Ph$_2$MeSiCH$_2$CH$_2$)$_3$Si(C$_5$H$_4$)] (4): Potassium cyclopentadienide (0.42 g, 4.0 mmol) was added to a solution of **2** (3.0 g, 4.0 mmol) in THF (50 mL). The mixture was stirred for 24 h at room temperature. Then the mixture was treated with solid KH (0.16 g, 4.0 mmol) and stirred until evolution of H_2 ceased. After addition of hexane (10 mL), the mixture was filtered off and the solution was concentrated (up to ca. 5 mL). Hexane (100 mL) was added again to the metastable solution, and the stirring continued until precipitation of **4** as a white solid. The precipitate was filtered, washed with hexane and dried in vacuo (2.3 g, 72%). ^1H NMR (300 MHz, C_6D_6, 25 °C): δ = 7.67 (m, 12 H, C_6H_5), 7.22 (m, 18 H, C_6H_5), 5.85 and 5.71 (AA′ and BB′ parts of an AA′BB′ spin system, 4 H, C_5H_4), 1.15 and 0.85 [A and B parts of an A_2B_2 spin system, 12 H, $Si(CH_2)_2Si$], 0.71 (s, 9 H, CH_3) ppm. $^{13}C\{^1H\}$ NMR (300 MHz, C_6D_6, 25 °C): δ = 137.8 (C_{ipso}, C_6H_5), 135.1 (C_{meta}, C_6H_5), 129.5 (C_{para}, C_6H_5), 128.3 (C_{ortho}, C_6H_5), 114.2 (C_5H_4), 109.1 (C_5H_4), 7.7 and 5.9 [$Si(CH_2)_2Si$], −4.51 (CH_3) ppm; C_{ipso} of C_5H_4 not found.

Synthesis of [{(Et$_3$SiCH$_2$CH$_2$)$_3$SiC$_5$H$_4$}(C$_5$H$_5$)TiCl$_2$] (5): [$(C_5H_5)TiCl_3$] (0.50 g, 2.3 mmol) was added to a solution of the substituted potassium cyclopentadienide **3** (1.30 g, 2.3 mmol) in THF (20 mL). The mixture was stirred at room temperature for 4 h. After filtration, the THF solution was evaporated in vacuo to dryness. The crude red oil was dissolved in the minimum amount of pentane and **5** was crystallized as a red solid (0.97 g, 61%) at −30 °C. $C_{34}H_{66}Cl_2Si_4Ti$ (706.0): calcd. C 57.84, H 9.42; found C 57.54, H 9.48. ^1H NMR (300 MHz, $CDCl_3$, 25 °C): δ = 6.83 and 6.60 (AA′ and BB′ parts of an AA′BB′ spin system, 4 H, C_5H_4), 6.51 (s, 5 H, C_5H_5), 0.90 (t, 27 H, CH_3CH_2), 0.70 and 0.42 [A and B parts of an A_2B_2 spin system, 12 H, $Si(CH_2)_2Si$], 0.50 (quart, 18 H, CH_3CH_2) ppm. $^{13}C\{^1H\}$ NMR (300 MHz, $CDCl_3$, 25 °C): δ = 132.3 (C_{ipso}, C_5H_4), 128.6 (C_5H_4), 121.6 (C_5H_4), 120.0 (C_5H_5), 7.5 (CH_3CH_2), 4.6 and 3.6 [$Si(CH_2)_2Si$], 2.8 (CH_3CH_2) ppm. $^{29}Si\{^1H\}$ NMR (500 MHz, $CDCl_3$, 25 °C): δ = 8.3 (Et_3Si), 0.0 (*Si*C_5H_4) ppm.

Synthesis of [{(Et$_3$SiCH$_2$CH$_2$)$_3$SiC$_5$H$_4$}(C$_5$Me$_5$)TiCl$_2$] (6): This complex was prepared by the same procedure described for **5**, starting from [$(C_5Me_5)TiCl_3$] (0.49 g, 1.7 mmol) and **3** (0.95 g, 1.7 mmol) in THF (20 mL). Due to its high solubility in pentane, compound **6** was obtained as a dark red oil (1.0 g, 78%) by removal of the solvent in vacuo. Crystals grew inside the oily samples when stored at room temperature for several days. Unfortunately, they were not suitable for X-ray diffraction studies. $C_{39}H_{76}Cl_2Si_4Ti$ (776.2): calcd. C 60.35, H 9.87; found C 60.60, H 10.09. ^1H NMR (300 MHz, $CDCl_3$, 25 °C): δ = 6.40 and 6.07 (AA′ and BB′ parts of an AA′BB′ spin system, 4 H, C_5H_4), 2.02 (s, 15 H, C_5Me_5), 0.88 (t, 27 H, CH_3CH_2), 0.76 and 0.43 (A and B parts of an A_2B_2 spin system, 12 H, $Si(CH_2)_2Si$), 0.47 (quart, 18 H, CH_3CH_2) ppm. $^{13}C\{^1H\}$ NMR (300 MHz, $CDCl_3$, 25 °C): δ = 136.0 (C_{ipso}, C_5H_4), 129.4 (C_5Me_5), 128.7 and 117.3 (C_5H_4), 13.5 (C_5Me_5), 7.5 (CH_3CH_2), 4.3 and 3.5 [$Si(CH_2)_2Si$], 2.8 (CH_3CH_2) ppm. $^{29}Si\{^1H\}$ NMR (500 MHz, $CDCl_3$, 25 °C): δ = 8.3 (Et_3Si), −0.6 (*Si*C_5H_4) ppm.

Synthesis of [{(Ph$_2$MeSiCH$_2$CH$_2$)$_3$SiC$_5$H$_4$}(C$_5$H$_5$)TiCl$_2$] (7): This complex was prepared by the same procedure described for **5**, from [$(C_5H_5)TiCl_3$] (0.13 g, 0.62 mmol) and **4** (0.50 g, 0.62 mmol) in THF (20 mL). Due to its high solubility in pentane, compound **7** was obtained by removal of the solvent in vacuo as a dark red oil, which solidified after several weeks at room temperature (0.48 g, 81%). $C_{55}H_{60}Cl_2Si_4Ti$ (952.2): calcd. C 69.38, H 6.35; found C 69.22, H 6.63. ^1H NMR (300 MHz, $CDCl_3$, 25 °C): δ = 7.53 (m, 12 H, C_6H_5), 7.40 (m, 18 H, C_6H_5), 6.63 and 6.51 (AA′ and BB′ parts of an AA′BB′ spin system, 4 H, C_5H_4), 6.29 (s, 5 H, C_5H_5), 0.91 and 0.81 [A and B parts of an A_2B_2 spin system, 12 H, $Si(CH_2)_2Si$], 0.53 (s, 9 H, CH_3) ppm. $^{13}C\{^1H\}$ NMR (300 MHz, $CDCl_3$, 25 °C): δ = 136.8 (C_{ipso}, C_6H_5), 134.5 (C_{meta}, C_6H_5), 130.5 (C_{ipso}, C_5H_4), 129.1 (C_{para}, C_6H_5), 128.5 (C_5H_4), 127.8 (C_{ortho}, C_6H_5), 121.7 (C_5H_4), 119.9 (C_5H_5), 6.5 and 4.5 [$Si(CH_2)_2Si$], −5.1 (CH_3) ppm. $^{29}Si\{^1H\}$ NMR (500 MHz, $CDCl_3$, 25 °C): δ = 0.7 (*Si*C_5H_4), −5.7 (Ph_2MeSi) ppm.

Synthesis of [{(Ph$_2$MeSiCH$_2$CH$_2$)$_3$SiC$_5$H$_4$}(C$_5$Me$_5$)TiCl$_2$] (8): This complex was prepared by the same procedure described for **5**, from [$(C_5Me_5)TiCl_3$] (0.18 g, 0.62 mmol) and **4** (0.50 g, 0.62 mmol) in THF (20 mL). Due to its high solubility in pentane, compound **8** was obtained, after removal of the solvent in vacuo, as a dark red oil, which solidified after several weeks at room temperature (0.54 g, 86%). $C_{60}H_{70}Cl_2Si_4Ti$ (1022.4): calcd. C 70.49, H 6.90; found C 70.31, H 6.99. ^1H NMR (300 MHz, $CDCl_3$, 25 °C): δ = 7.40 (m, 12 H, C_6H_5), 7.25 (m, 18 H, C_6H_5), 6.26 and 6.00 (AA′ and BB′ parts of an AA′BB′ spin system, 4 H, C_5H_4), 1.95 (s, 15 H, C_5Me_5), 0.88 and 0.81 [A and B parts of an A_2B_2 spin system, 12 H, $Si(CH_2)_2Si$], 0.48 (s, 9 H, CH_3) ppm. $^{13}C\{^1H\}$ NMR (300 MHz, $CDCl_3$, 25 °C): δ = 137.4 (C_{ipso}, C_6H_5), 134.6 (C_{meta}, C_6H_5), 129.54 (C_5Me_5), 129.48 (C_{ipso}, C_5H_4), 129.0 (C_{para}, C_6H_5), 128.8 (C_5H_4), 127.7 (C_{ortho}, C_6H_5), 117.2 (C_5H_4), 13.5 (C_5Me_5), 6.4 and 4.5 [$Si(CH_2)_2Si$], −5.01 (CH_3) ppm. $^{29}Si\{^1H\}$ NMR (500 MHz, $CDCl_3$, 25 °C): δ = 0.2 (*Si*C_5H_4), −5.8 (Ph_2MeSi) ppm.

Synthesis of [{(Ph$_2$MeSiCH$_2$CH$_2$)$_3$SiC$_5$H$_4$}$_2$TiCl$_2$] (9): [$TiCl_4$] (68 mL, 0.62 mmol) was added via syringe to a solution of **4** (1.00 g, 1.24 mmol) in toluene (25 mL). The solution was stirred overnight at room temperature. After filtration of the KCl precipitate, the solution was evaporated in vacuo to dryness yielding **9** (0.94 g, 92%) as a dark red oil. $C_{100}H_{110}Cl_2Si_8Ti$ (1655.5): calcd. C 72.55, H 6.70; found C 72.61, H 6.79. ^1H NMR (300 MHz, $CDCl_3$, 25 °C): δ = 7.40 (m, 12 H, C_6H_5), 7.25 (m, 18 H, C_6H_5), 6.39 and 6.17 (AA′ and BB′ parts of an AA′BB′ spin system, 4 H, C_5H_4), 0.85 and 0.75 [A and B parts of an A_2B_2 spin system, 12 H, $Si(CH_2)_2Si$], 0.49 (s, 9 H, CH_3) ppm. $^{13}C\{^1H\}$ NMR (300 MHz, $CDCl_3$, 25 °C): δ = 136.9 (C_{ipso}, C_6H_5), 134.4 (C_{meta}, C_6H_5), 129.1 (C_{para}, C_6H_5), 131.5 (C_{ipso}, C_5H_4), 128.5 (C_5H_4), 127.8 (C_{ortho}, C_6H_5), 120.2 (C_5H_4), 6.6 and 4.7 [$Si(CH_2)_2Si$], −5.0 (CH_3) ppm. $^{29}Si\{^1H\}$ NMR (500 MHz, $CDCl_3$, 25 °C): δ = 0.6 (*Si*C_5H_4), −5.7 (Ph_2MeSi) ppm.

Synthesis of [{(Ph$_2$MeSiCH$_2$CH$_2$)$_3$SiC$_5$H$_4$}$_2$ZrCl$_2$] (10): This complex was obtained as a colorless oil (0.49 g, 94%) by the same procedure described for **9** from $ZrCl_4$·2THF (0.12 g, 0.31 mmol) and **4** (0.50 g, 0.62 mmol) in toluene (25 mL). $C_{100}H_{110}Cl_2Si_8Zr$ (1698.8):

calcd. C 70.70, H 6.53; found C 70.53, H 6.62. ^{1}H NMR (300 MHz, $CDCl_3$, 25 °C): δ = 7.42 (m, 12 H, C_6H_5), 7.26 (m, 18 H, C_6H_5), 6.28 and 6.14 (AA′ and BB′ parts of an AA′BB′ spin system, 4 H, C_5H_4), 0.85 and 0.74 [A and B parts of an A_2B_2 spin system, 12 H, $Si(CH_2)_2Si$], 0.49 (s, 9 H, CH_3) ppm. $^{13}C\{^1H\}$ NMR (300 MHz, $CDCl_3$, 25 °C): δ = 136.9 (C_{ipso}, C_6H_5), 134.4 (C_{meta}, C_6H_5), 129.1 (C_{para}, C_6H_5), 127.7 (C_{ortho}, C_6H_5), 125.3 (C_5H_4), 124.3 (C_{ipso}, C_5H_4), 116.3 (C_5H_4), 6.5 and 4.6 [$Si(CH_2)_2Si$], −5.0 (CH_3) ppm. $^{29}Si\{^1H\}$ NMR (500 MHz, $CDCl_3$, 25 °C): δ = 0.0 (SiC_5H_4), −5.7 (Ph_2MeSi) ppm.

Ethylene Polymerization: A 250 mL flask charged with toluene (50 mL) and equipped with a magnetic stirrer was evacuated four times and refilled with pre-dried ethylene gas. Keeping the flask pressurized with ethylene (1 bar) and stirred at room temperature, a toluene solution of methylaluminoxane (MAO, 0.83 mL, 1.5 M) was syringed through a septum. After 5 min, a toluene solution of the catalyst (0.50 mL, 2.5 mM) was injected into the flask with simultaneous starting of a stopwatch. The polymerization was quenched 10 min later by closing the ethylene feed, release of the overpressure and addition of acidified methanol (4% v/v HCl). The mixture was stirred for 6 h and the polymer was filtered, washed with copious amounts of methanol, and dried in an oven to constant weight. Molecular weights were determined by gel-permeation chromatography (GPC).

Acknowledgments

We acknowledge the DGESIC-Ministerio de Educación y Cultura (Project PB97-0765) and the University of Alcalá (project E043/2001) for financial support.

[1] Some recent reviews: [1a] H. H. Brintzinger, D. Fischer, R. Mülhaupt, B. Rieger, R. M. Waymouth, *Angew. Chem.* **1995**, *107*, 1255−1283; *Angew. Chem. Int. Ed. Engl.* **1995**, *34*, 1143−1170. [1b] M. Bochmann, *J. Chem. Soc., Dalton Trans.* **1996**, 255−270. [1c] A. L. McKnight, R. M. Waymouth, *Chem. Rev.* **1998**, *98*, 2587−2598. [1d] H. G. Alt, E. Samuel, *Chem. Soc. Rev.* **1998**, *27*, 323−329. [1e] W. Kaminsky, *J. Chem. Soc., Dalton Trans.* **1998**, 1413−1418. [1f] H. G. Alt, A. Köppl, *Chem. Rev.* **2000**, *100*, 1205−1222. [1g] G. W. Coates, *Chem. Rev.* **2000**, *100*, 1223−1252. [1h] L. Resconi, L. Cavallo, A. Fait, F. Piemontesi, *Chem. Rev.* **2000**, *100*, 1253−1345.

[2] [2a] W. Kaminsky, K. Külper, H. H. Brintzinger, F. R. W. P. Wild, *Angew. Chem.* **1985**, *97*, 507−508; *Angew. Chem. Int. Ed. Engl.* **1985**, *24*, 507−508. [2b] J. A. Ewen, *J. Am. Chem. Soc.* **1984**, *106*, 6355−6364.

[3] Selected references: [3a] G. Erker, R. Nolte, R. Aul, S. Wilker, C. Krüger, R. Noe, *J. Am. Chem. Soc.* **1991**, *113*, 7594−7602. [3b] G. Erker, M. Aulbach, M. Knickmeier, D. Wingbermühle, C. Krüger, M. Nolte, S. Werner, *J. Am. Chem. Soc.* **1993**, *115*, 4590−4601. [3c] G. Erker, B. Temme, *J. Am. Chem. Soc.* **1992**, *114*, 4004−4006. [3d] G. Erker, C. Mollenkopf, *J. Organomet. Chem.* **1994**, *483*, 173−181. [3e] O. Gobley, P. Meunier, B. Gautheron, J. C. Gallucci, G. Erker, M. Dahlmann, J. D. Schloss, L. A. Paquette, *Organometallics* **1998**, *17*, 4897−4903. [3f] S. Knüppel, J. L. Fauré, G. Erker, G. Kehr, M. Nissinen, R. Fröhlich, *Organometallics* **2000**, *19*, 1262−1268. [3g] G. W. Coates, R. M. Waymouth, *Science* **1995**, *267*, 217−219. [3h] M. D. Bruce, G. W. Coates, E. Hauptman, R. M. Waymouth, J. W. Ziller, *J. Am. Chem. Soc.* **1997**, *119*, 11174−11182. [3i] K. Kimura, K. Takaishi, T. Matsukawa, T. Yoshimura, H. Yamazaki, *Chem. Lett.* **1998**, 571−572.

[4] J. Okuda, *Top. Curr. Chem.* **1992**, *160*, 97−145 (review of complexes with sterically demanding cyclopentadienyl ligands).

[5] Some recent general reviews about metallodendrimers: [5a] C. Gorman, *Adv. Mater.* **1998**, *10*, 295−308. [5b] G. R. Newkome, E. He, C. N. Moorefield, *Chem. Rev.* **1999**, *99*, 1689−1746. [5c] I. Cuadrado, M. Morán, C. M. Casado, B. Alonso, J. Losada, *Coord. Chem. Rev.* **1999**, *193−195*, 395−445. [5d] F. J. Stoddart, T. Welton, *Polyhedron* **1999**, *18*, 3575−3591.

[6] [6a] D. Seyferth, R. Wryrwa, U. W. Franz, S. Becke, *PCT Int. Appl.* WO 97/32908, 1997; *Chem. Abstr.* **1997**, *127*, 263179p. [6b] K. Brüning, H. Lang, *J. Organomet. Chem.* **1999**, *575*, 153−157. [6c] V. Cadierno, A. Igau, B. Donnadieu, A. M. Caminade, J. P. Majoral, *Organometallics* **1999**, *18*, 1580−1582. [6d] V. Cadierno, M. Zablocka, B. Donnadieu, A. Igau, J. P. Majoral, A. Skowronska, *Chem. Eur. J.* **2001**, *7*, 221−229.

[7] [7a] S. Arevalo, J. M. Benito, E. de Jesús, F. J. de la Mata, J. C. Flores, R. Gómez, *J. Organomet. Chem.* **2000**, *602*, 208−210. [7b] S. Arevalo, E. de Jesús, F. J. de la Mata, J. C. Flores, R. Gómez, *Organometallics* **2001**, *20*, 2583−2592. [7c] S. Arevalo, E. de Jesús, F. J. de la Mata, J. C. Flores, R. Gómez, unpublished results.

[8] Fe, Co, and Ni complexes containing dendritic cyclopentadienyl ligands have been reported. See [8a] G. E. Oosterom, R. J. van Hareen, J. N. H. Reek, P. C. J. Kamer, P. W. N. M. van Leeuwen, *Chem. Commun.* **1999**, 1119−1120. [8b] C. M. Cardona, A. E. Kaifer, *J. Am. Chem. Soc.* **1998**, *120*, 4023−4024. [8c] C. M. Cardona, T. D. McCarley, A. E. Kaifer, *J. Org. Chem.* **2000**, *65*, 1857−1864. [8d] D. Vos, A. Salmon, H. G. Stammler, B. Neumann, P. Jutzi, *Organometallics* **2000**, *19*, 3874−3878. [8e] B. García, C. M. Casado, I. Cuadrado, B. Alonso, M. Morán, J. Losada, *Organometallics* **1999**, *18*, 2349−2356.

[9] [9a] S. Hecht, J. M. J. Fréchet, *Angew. Chem.* **2001**, *113*, 76−94; *Angew. Chem. Int. Ed.* **2001**, *40*, 74−91. [9b] D. K. Smith, F. Diederich, *Chem. Eur. J.* **1998**, *4*, 1353−1361. [9c] H. Brunner, *J. Organomet. Chem.* **1995**, *500*, 39−46.

[10] Recent reviews about dendrimers in catalysis: [10a] G. E. Oosterom, J. N. H. Reek, P. C. J. Kamer, P. W. N. M. van Leeuwen, *Angew. Chem.* **2001**, *113*, 1878−1901; *Angew. Chem. Int. Ed.* **2001**, *40*, 1828−1849. [10b] D. Astruc, F. Chardac, *Chem. Rev.* **2001**, *101*, 2991−3023.

[11] [11a] Y. Mugnier, A. Fakhr, M. Fauconet, C. Moise, E. Laviron, *Acta Chem. Scand., Ser. B* **1983**, *37*, 423−427. [11b] Y. Mugnier, C. Moïse, E. Laviron, *Nouv. J. Chim.* **1982**, *6*, 197−200.

[12] J. Langmaier, Z. Samec, V. Varga, M. Horácek, K. Mach, *J. Organomet. Chem.* **1999**, *579*, 348−355.

[13] G. L. Soloveichik, A. B. Gavrilov, V. V. Strelets, *Metalloorg. Khimia* **1989**, *2*, 431.

[14] W. Spaleck, F. Küber, A. Winter, J. Rohrmann, B. Bachmann, M. Antberg, V. Dolle, E. F. Paulus, *Organometallics* **1994**, *13*, 954−963.

[15] It has been estimated that only a maximum of ca. 10% of the titanium centers are active in C_5Me_5 complexes **6** and **8**. Poor yields prevented analysis of their polyethylene samples and we have assumed similar parameters to those of the polyethylene samples obtained from **5**, **7**, or **9** for this calculation.

[16] M. Nele, S. Collins, M. L. Dias, J. C. Pinto, S. Lin, R. M. Waymouth, *Macromolecules* **2000**, *33*, 7249−7260.

[17] D. D. Perrin, W. L. F. Armarego, *Purification of Laboratory Chemicals*, 3rd ed., Butterworth-Heinemann Ltd, Oxford, **1988**.

[18] R. B. King, in *Organometallic Syntheses*, Vol. 1 (Eds.: J. J. Eisch, R. B. King), Academic Press, New York, **1965**, p 75.

[19] R. D. Rogers, M. M. Benning, L. K. Kurihara, K. J. Moriarty, M. D. Rausch, *J. Organomet. Chem.* **1985**, *293*, 51−60.

[20] A. M. Cardoso, R. J. H. Clark, S. Moorhouse, *J. Chem. Soc., Dalton Trans.* **1980**, 1156−1160.

[21] G. Hidalgo, M. Mena, F. Palacios, P. Royo, R. Serrano, in *Synthetic Methods of Organometallic and Inorganic Chemistry*, Vol. 1, (Eds.: W. A. Herrmann, A. Salzer), Thieme-Verlag, Stuttgart, **1996**, pp 95−97.

Received February 15, 2002
[I02080]

Copper-Mediated Oxygenolysis of Flavonols via Endoperoxide and Dioxetan Intermediates; Synthesis and Oxygenation of $[Cu^{II}(Phen)_2(Fla)]ClO_4$ and $[Cu^{II}(L)(Fla)_2]$ [FlaH = Flavonol; L = 1,10-Phenanthroline (Phen), 2,2′-Bipyridine (Bpy), *N*,*N*,*N*′,*N*′-Tetramethylethylenediamine (TMEDA)] Complexes

Éva Balogh-Hergovich,[a] József Kaizer,[a] József Pap,[b] Gábor Speier,*[b] Gottfried Huttner,[c] and László Zsolnai[c]

Keywords: Enzyme models / Copper / Peroxides / Kinetics

$[Cu(phen)_2(fla)]ClO_4$ was prepared by treating $[Cu(CH_3CN)_4]$-ClO_4 with flavonol (flaH) in the presence of 1,10-phenanthroline (phen) as a co-ligand. Its oxygenation in DMF (or CH_3CN) solution at elevated temperature gave the (*O*-benzoylsalicylato)copper(II) complex $[Cu(phen)_2(O\text{-bs})]ClO_4$ (bs = benzoylsalicylato) and carbon monoxide via an endoperoxide intermediate. Crystallographic characterisation of $[Cu(phen)_2(O\text{-bs})]ClO_4$ as the CH_2Cl_2 solvate [triclinic, space group $P\bar{1}$, a = 10.499(3) Å, b = 12.556(4) Å, c = 17.094(5) Å, α = 72.69(2), β = 89.35(2), γ = 69.19(2)°, V = 1999.7(10) Å^3, Z = 2, $R1$ = 0.0962] shows that the molecule has a distorted trigonal-bipyramidal structure (τ = 0.96). The oxygenolysis was monitored by spectrophotometry, and the pseudo-first-order rate constant k'_{phen} was found to be $(2.47 \pm 0.11) \times 10^{-4}$ s^{-1} at 120 °C. Complexes of $[Cu(L)(4'R\text{-fla})_2]$ (L = phen, bpy, TMEDA; R = H, OCH_3, CH_3, Cl) were also prepared by treating the complexes $Cu(4'R\text{-fla})_2$ with nitrogen-containing co-ligands. Their oxygenation resulted in the corresponding complexes $Cu(L)(2HOpg)_2$ (2HOpg =2-hydroxyphenylglyoxylate) derived by spontaneous hydrolysis of $Cu(L)(bpg)_2$ (bpg = 2-benzoatophenylglyoxylate). The (phenylglyoxylato)-copper complexes were probably formed via 1,2-dioxetan intermediates, since the oxygenation of $Cu(phen)(fla)_2$ showed chemiluminescence with bands at 506, 546, and 578 nm in the emission spectrum due to the decomposition of a 1,2-dioxetan species. Labelling experiments with an $^{18}O_2/^{16}O_2$ mixture (1:3) showed the incorporation of both ^{18}O atoms of $^{18}O_2$ into the flavonolate ligand. The kinetics of the oxygenolysis of $Cu(L)(fla)_2$ gave rate constants according to the rate law $-d[Cu(L)(4'R\text{-fla})_2]/dt = k[Cu(L)(4'R\text{-fla})_2][O_2]$: k/m^{-1} s^{-1} = $(9.50 \pm 0.60) \times 10^{-2}$ (L = phen), $(2.40 \pm 0.10) \times 10^{-2}$ (L = bpy), $(2.00 \pm 0.10) \times 10^{-2}$ (L = TMEDA) m^{-1} s^{-1} at 353.16 K. The oxygenolysis of the complexes $Cu(phen)(4'R\text{-fla})_2$ fits a Hammett linear free energy relationship and an increase of the electron density on the copper ion makes the oxygenation reaction faster.

(© Wiley-VCH Verlag GmbH, 69451 Weinheim, Germany, 2002)

Introduction

Flavonols are widely distributed in vascular plants,[1,2] and flavonoids form active constituents of a number of herbal and traditional medicines.[3] Flavonols are readily degraded by microorganisms, especially by fungi such as *Aspergillus* or *Pullularia* species.[4] Flavonol 2,4-dioxygenase (quercetinase), which catalyses the oxidative degradation of flavonols (**1**) to a depside (phenolic carboxylic acid esters, **2**) with concomitant evolution of carbon monoxide [Equation (1)], was purified from culture filtrate of *Aspergillus niger*.[4b]

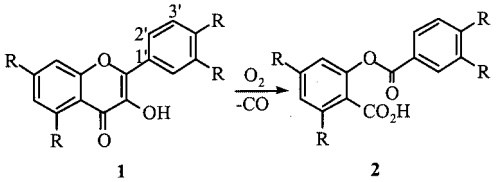

1 **2** (1)

This reaction is rather exceptional as it involves the oxygenolytic cleavage of two carbon−carbon bonds. Carbon monoxide forming enzymes are rare. To date, three prokaryotic dioxygenases are known that catalyse a dioxygenolytic release of CO in a manner analogous to that of fungal quer-

[a] Research Group for Petrochemistry, Hungarian Academy of Sciences,
8201 Veszprém, Hungary,
[b] Department of Organic Chemistry, University of Veszprém,
8201 Veszprém, Hungary,
Fax: (internat.) + 36-88/427-492
E-mail: speier@almos.vein.hu
[c] Anorganisch Chemisches Institut, Universität Heidelberg,
69120 Heidelberg, Germany

Supporting information for this article is available on the WWW under http://www.eurjic.org or from the author.

cetinase, these being 3-hydroxyquinaldin-4(1*H*)-one 2,4-dioxygenase, 3-hydroxyquinolin-4(1*H*)-one 2,4-dioxygenase,[5] and 1,2-dihydroxy-5-(methylthio)pent-1-en-3-one anion 1,3-dioxygenase.[6] These prokaryotic enzymes were claimed not to contain any metal ion or organic cofactor[5b] and thus differ fundamentally from the copper-containing flavonol 2,4-dioxygenase. However, it was reported recently, that the 1,2-dihydroxy-5-(methylthio)pent-1-en-3-one anion 1,3-dioxygenase is a Ni-containing enzyme.[6c]

For the oxidative cleavage reaction of the heterocycle in flavonols, two pathways have been proposed (Scheme 1),[7] the first via an endoperoxide **3** (route a) and the other via a 1,2-dioxetan **4** (route b).

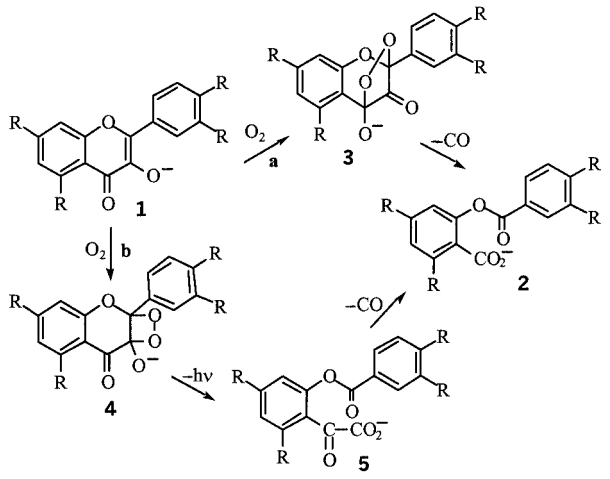

Scheme 1

Since flavonol 2,4-dioxygenase is a copper-containing metalloenzyme, metal complexes of copper[8,9] and cobalt[10] have been used in model reactions. Autoxidation reactions of potassium[11] and zinc flavonolates[12] have also resulted in enzyme-like products, and some efforts have been made to elucidate the mechanism of the reaction. From our earlier results obtained both with redox and non-redox metal-containing systems, the conclusion could be drawn that the oxygenolysis of the flavonolate ion in aprotic solvents takes place via an endoperoxide intermediate.[9e−9h,11,12]

Flavonol 2,4-dioxygenase has been claimed to contain nonblue type 2 Cu^{II} ions at its active site.[4b] Recent crystal structure determination of quercetin 2,3-dioxygenase from *Aspergillus japonicus* reveal that it forms homodimers. The mononuclear type 2 copper centre displays two distinct geometries: a distorted tetrahedral coordination, formed by three histidine residues and one water molecule, and a distorted trigonal-bipyramidal environment, which additionally comprises a glutamate.[4i] In this paper we report details for the synthesis and characterisation of $[Cu(phen)_2(fla)]ClO_4$ (**6**) and $[Cu(L)(4'R\text{-}fla)_2]$ [L = phen (**7**), bpy (**8**), TMEDA (**9**); R = H (a), OCH_3 (**7b**), CH_3 (**7c**), Cl (**7d**)] complexes, which are models for the enzyme−substrate (ES) complex. Spectrophotometric and kinetic studies aimed at elucidating the mechanism of the stoichiometric oxygenation of the two systems are also reported on.

Results and Discussion

Synthesis and Characterisation of the Complex $[Cu(phen)_2(fla)]ClO_4$

Complex $[Cu(phen)_2(fla)]ClO_4$ was isolated as a green solid by the reaction of $[Cu(CH_3CN)_4]ClO_4$, flavonol (**1**) and 1,10-phenanthroline monohydrate at room temperature in acetonitrile under dioxygen. Its IR spectrum shows the principal band corresponding to the coordinated flavonolate at 1581 cm^{-1}. The decrease of approximately 20 cm^{-1} of the ν(CO) band compared to that of free flavonol [ν(CO): 1602 cm^{-1}] is due to chelation and formation of a stable five-membered ring.[13] The absorption bands at 1082 and 626 cm^{-1} can be assigned to the perchlorate anion. A very strong band at 1608 cm^{-1} [ν(C=N)] is due to the coordinated 1,10-phenanthroline. The electronic spectrum of the complex in the charge transfer region exhibits a band of the coordinated flavonolate ligand at 419 nm. The band at 702 nm is associated with the d−d transition of Cu^{II}. Room-temperature magnetic measurements yielded a value of μ_B = 1.92, consistent with a copper(II) ion.

Synthesis and Characterisation of $Cu(L)(4'R\text{-}fla)_2$

$Cu(4'R\text{-}fla)_2$ (R = H, CH_3, OCH_3, Cl) complexes reacted with 1,10-phenanthroline at room temperature in acetonitrile under argon to give the corresponding complexes $Cu(phen)(4'R\text{-}fla)_2$ in fairly good yields. Similarly, in the presence of TMEDA or bpy co-ligands $Cu(TMEDA)(fla)_2$ or $Cu(bpy)(fla)_2$ was obtained. Satisfactory elemental analyses were obtained for all of the new complexes. Compounds $Cu(L)(fla)_2$ have very similar IR and electronic spectra. The IR spectrum shows the principal bands corresponding to the coordinated flavonolate in the 1560−1580 cm^{-1} region. Decreases of approximately 40 cm^{-1} of the ν(CO) bands compared to that of the 4′-substituted flavonols [ν(CO): ca. 1605 cm^{-1}] are due to chelation and formation of a stable five-membered ring.[13] In the case of complexes with 2,2′-bipyridine and 1,10-phenanthroline, a strong band in the 1590−1600 cm^{-1} region is seen due to the coordinated nitrogen donor ligands ν(C=N). The π−π* transitions in the 420−435 nm region arise from the coordinated flavonolate ligands.

Oxygenation of $[Cu(phen)_2(fla)]ClO_4$

Treatment of $[Cu(phen)_2(fla)]ClO_4$ with dioxygen in DMF or CH_3CN solution at elevated temperature led to the corresponding (*O*-benzoylsalicylato)copper complex $[Cu(phen)_2(O\text{-}bs)]ClO_4$ (**10**) and carbon monoxide contaminated with a small amount of CO_2 [Equation (2)]. The formation of **10** from **6** required dioxygen, which was measured by volumetry (no apparent dioxygen uptake was observed, because the absorption of dioxygen and the liberation of CO compensate each other).

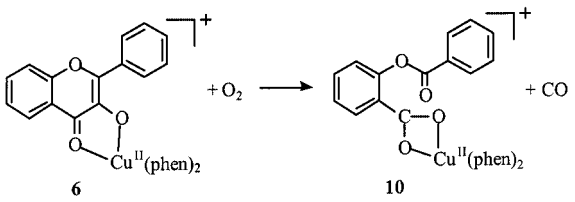

6 10 (2)

The oxygenation of **6** was monitored by UV/Vis spectroscopy. The time course of the variation of $[Cu(phen)_2(fla)]ClO_4$ (**6**) in DMF solution at 120 °C is shown in Figure 1. Plots of $\log[Cu(phen)_2(fla)]ClO_4$ vs. time show a linear dependence under pseudo-first-order conditions[14] (constant dioxygen pressure), in agreement with a rate equation of first-order dependence with respect to the complex **6**. The pseudo-first-order rate constant k' was found to be $(2.47 \pm 0.11) \times 10^{-4}$ s^{-1} at 120 °C. This value is very close to that found for the oxygenation of $[Cu(idpaH)(fla)]ClO_4$ [idpaH = 3,3′-iminobis(*N*,*N*-dimethylpropylamine)] in DMF [$k'_{120\ °C} = (1.45 \pm 0.06) \times 10^{-4}$ s^{-1})].[9g]

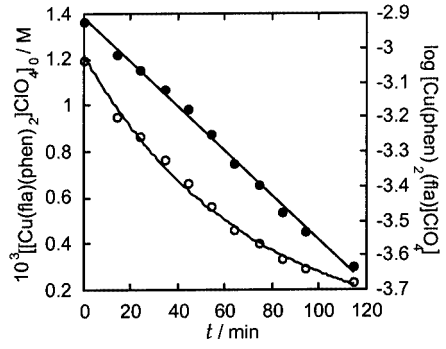

Figure 1. Time course for the oxygenation of $[Cu(phen)_2(fla)]ClO_4$ in DMF (o) and plot of $\log[\{Cu(phen)_2(fla)]ClO_4\}]$ (•) vs. reaction time for the oxygenation of $[Cu(phen)_2(fla)]ClO_4$ ($[\{Cu(phen)_2(fla)]ClO_4\}]_0 = 1.35 \times 10^{-3}$ M, $[O_2] = 6.1 \times 10^{-3}$ M, 120 °C)

Characterisation of $[Cu(phen)_2(O\text{-bs})]ClO_4$

The complex $[Cu(phen)_2(O\text{-bs})]ClO_4$ can also be prepared by the reaction of $[Cu(CH_3CN)_4]ClO_4$, *O*-benzoylsalicylic acid and 1,10-phenanthroline monohydrate at room temperature in acetonitrile under dioxygen. Its IR spectrum shows bands corresponding to the coordinated *O*-benzoylsalicylate at 1741 [ν(CO), indicating that the carbonyl group of the benzoyl group is not coordinated], 1572 and 1388 [$\nu(CO_2)$] cm^{-1}. The difference between the asymmetric and symmetric stretching frequencies of the carboxylato group [$\Delta\tilde{\nu} = \nu_{as}(CO_2) - \nu_s(CO_2)$] is 184 cm^{-1}, rendering these to a monodentate carboxylate bonding mode. Absorption bands at 1068 and 635 cm^{-1} are associated with the perchlorate anion. In the UV/Vis spectrum the d−d transition may be assigned to the 694 nm absorption and the ligand-to-metal charge transfer at 271 and 294 nm. The magnetic moment of $\mu_B = 2.06$ is in agreement with a d^9 Cu^{II} ion without magnetic interactions.

X-ray Crystal Structure of $[Cu(phen)_2(O\text{-bs})]ClO_4$

The molecular structure and atom numbering scheme for $[Cu(phen)_2(O\text{-bs})]ClO_4$ is shown in Figure 2, and selected bond lengths and angles are listed in Table 1. The copper ion has a slightly distorted trigonal-bipyramidal geometry with $\tau = 0.96$.[9g] Two nitrogen atoms of the 1,10-phenanthroline ligands [Cu(1)−N(1) 2.176(5), Cu(1)−N(3) 2.074(5) Å] and one oxygen atom of the *O*-benzoylsalicylate ligand [Cu(1)−O(1) 1.993 Å] occupy basal positions. The two other nitrogen atoms of the phenanthroline ligands [Cu(1)−N(2) 1.992(5) and Cu(1)−N(4) 1.987(5)] are in apical positions. The Cu−N distances in the basal plane are longer than those in apical positions.

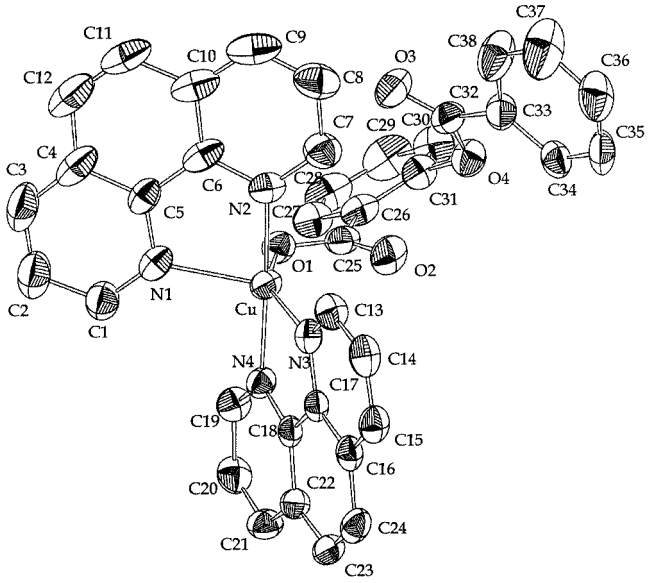

Figure 2. Molecular structure of $[Cu(phen)_2(O\text{-bs})]ClO_4\ 1.5CH_2Cl_2$

Table 1. Selected bond lengths [Å] and angles [°] for $[Cu(phen)_2(O\text{-bs})]ClO_4 \cdot 1.5CH_2Cl_2$

Cu(1)−N(4)	1.987(5)	Cu(1)−N(3)	2.074(5)
Cu(1)−N(2)	1.992(5	Cu(1)−N(1)	2.176(5)
Cu(1)−O(1)	1.993(4)		
N(4)−Cu(1)−N(2)	176.4(2)	N(4)−Cu(1)−O(1)	90.7(2)
N(2)−Cu(1)−O(1)	92.5(2)	N(4)−Cu(1)−N(3)	81.4(2)
N(2)−Cu(1)−N(3)	96.8(2)	O(1)−Cu(1)−N(3)	148.0(2)
N(4)−Cu(1)−N(1)	97.5(2)	N(2)−Cu(1)−N(1)	80.6(2)
O(1)−Cu(1)−N(1)	92.9(2)	N(3)−Cu(1)−N(1)	118.8(2)

Oxygenation of the Complexes $Cu(L)(4'R\text{-fla})_2$

Treatment of the complexes $Cu(L)(4'R\text{-fla})_2$ (L = bpy, phen, TMEDA; R = H, CH_3, OCH_3, Cl) with dioxygen in DMF or CH_3CN solution at elevated temperature led to the corresponding (2-hydroxyphenylglyoxylato)copper complexes $Cu(L)(2HOpg)_2$ and 4-substituted benzoic acids [Equation (3)]. According to gas-volumetric and GC measurements, the stoichiometry of the oxygenation reactions

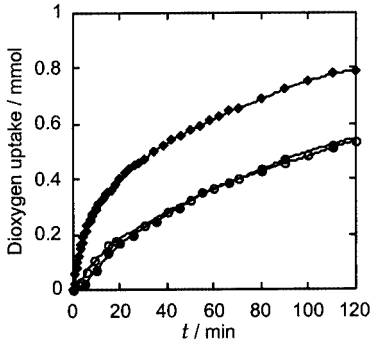

Figure 3. Time course for the oxygenation of the complexes Cu(L)-(fla)$_2$ (**7**−**9**) (L = phen (◆), bpy (●), TMEDA (○); [Cu(L)(fla)$_2$]$_0$ = 0.4 mmol in 50 mL of DMF, [O_2] = 6.91 × 10^{-3} M, 80 °C)

corresponds to Equation (3). Figure 3 shows typical dioxygen uptakes vs. time curves for the complexes [Cu(L)(fla)$_2$] (L = bpy, phen, TMEDA). No other oxidation products could be detected.

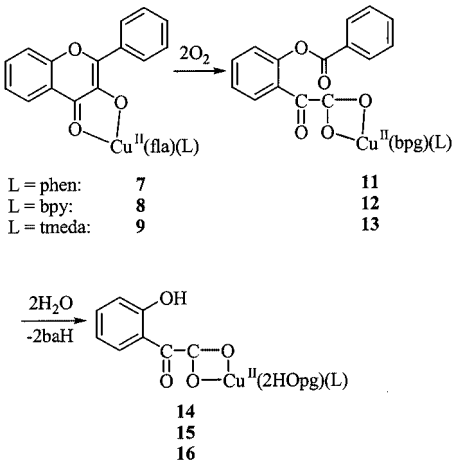

(3)

The GC and GC-MS analyses of the reaction mixture obtained by the oxygenation of Cu(phen)(fla)$_2$, after treatment with dilute HCl solution (10%) and ethereal diazomethane, show the presence of methyl benzoate {136 (23) [M^+], 105 (100), 77 (87)}, coumaronedione {148 (3) [M^+], 120 (100), 92 (59), 64 (22), 63 (14)}, and methyl 2-hydroxyphenylglyoxylate {180 (7) [M^+], 121 (100), 93 (11), 65 (11)}. In the case of complex Cu(phen)(fla)$_2$, during the oxygenation reaction chemiluminescence was observed, which is crucial evidence for the decomposition of a 1,2-dioxetan[15] intermediate to carbonyl compounds. Figure 4 shows the electron spectrum of the emitted light (λ = 506, 546, 578 nm). Compound Cu(phen)(2HOpg)$_2$ does not seem to be involved in the chemiluminescence process since its fluorescence spectrum in DMF excited by 430 nm shows bands at 480 and 535 nm with a shoulder at 557 nm (Figure 5), which does not match the spectrum of the emitted light of the chemiluminescence process. It seems likely that the real emitter is Cu(phen)(bpg)$_2$ (**11**), which could not be isolated due to its extreme sensitivity toward hydrolysis.

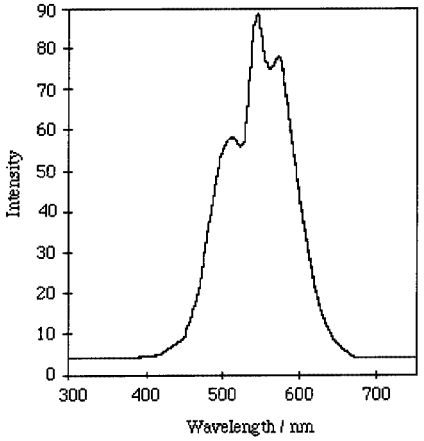

Figure 4. Electron spectrum of the emitted light during the oxygenation of Cu(phen)(fla)$_2$ in DMF

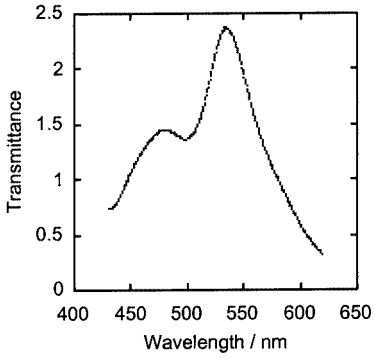

Figure 5. Fluorescence spectrum of Cu(phen)(2HOpg)$_2$ in DMF

Characterisation of the Complexes Cu(L)(2HOpg)$_2$ (L = phen, bpy, TMEDA)

Satisfactory elemental analyses were obtained for the three new (2-hydroxyphenylglyoxylato)copper complexes, namely Cu(phen)(2HOpg)$_2$ (**14**), Cu(bpy)(2HOpg)$_2$ (**15**), and Cu(TMEDA)(2HOpg)$_2$ (**16**). The IR spectrum shows the presence of the coordinated α-oxocarboxylato ligand {ca. 1616 [ν(CO)], ca. 1575, ca. 1375 [ν(CO_2)] cm^{-1}, respectively}.

Kinetic Measurements

The kinetics of the oxygenation of Cu(phen)(fla)$_2$ were monitored by electron spectroscopy at 432 nm. Experimental conditions are summarised in Table S1 (Supporting Information). To determine the rate dependence on the two reactants, oxygenation runs were performed at various initial Cu(phen)(fla)$_2$ concentrations and different dioxygen pressures. A simple rate law for the reaction between Cu-(phen)(fla)$_2$ and O_2 is as shown in Equation (4).

$$-d[Cu(phen)(fla)_2]/dt = d[Cu(phen)(2HOpg)_2]/dt = k_{phen}[Cu(phen)(fla)_2]^m[O_2]^n \quad (4)$$

Under pseudo-first-order conditions (constant dioxygen concentration) for the oxygenation of **7** a typical time course and first-order plot are shown in Figure 6; the reaction remained first-order in **7** during the whole time in which the experiment was monitored (81% conversion, 0.6 h). The first-order dependence on the reaction rate on **7** could also be confirmed by plotting the initial reaction rate $-d[Cu(phen)(fla)_2]/dt$ vs. initial substrate concentration. The straight line obtained [as shown in Figure S1 (Supporting Information)] validates the first-order dependence in $Cu(phen)(fla)_2$ with the pseudo-first-order rate constant $k'_{phen} = 6.86 \times 10^{-4}\ s^{-1}$ and a correlation coefficient of 99.5%.

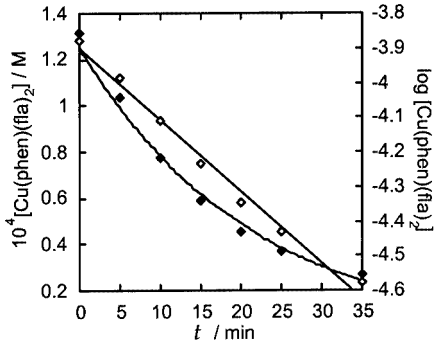

Figure 6. Time course for the oxygenation of $Cu(phen)(fla)_2$ in DMF (◆) and plot of $\log[Cu(phen)(fla)_2]$ (□) vs. reaction time for the oxygenation of $Cu(phen)(fla)_2$

Experiments made at different dioxygen pressures show that p_{O2} appreciably influences the rate of the reaction. Kinetic measurements of the reaction rate indicate a first-order dependence with respect to the dioxygen concentration. Plots of k'_{phen} vs. $[O_2]$ for the above experiments give a straight line with $k_{phen} = 0.10\ M^{-1}\ s^{-1}$ and a correlation coefficient of 99.1% (Figure 7). On the basis of the results above, it can be concluded that the reaction follows the rate law of Equation (4) with $m = n = 1$, from which a mean value of the kinetic constant k_{phen} of $(9.50 \pm 0.60) \times 10^{-2}\ M^{-1}\ s^{-1}$ at 353.16 K can be obtained. In the case of the oxygenation of $Cu(bpy)(fla)_2$ and $Cu(TMEDA)(fla)_2$ the mean values of the kinetic constants at 353.16 K were found to be $k_{bpy} = (2.40 \pm 0.10) \times 10^{-2}\ M^{-1}\ s^{-1}$ and $k_{TMEDA} = (2.00 \pm 0.10) \times 10^{-2}\ M^{-1}\ s^{-1}$.

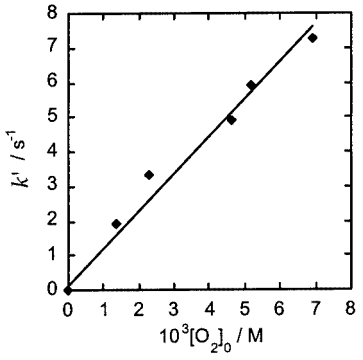

Figure 7. Plot of pseudo-first-order rate constant k' vs. O_2 pressure

The activation parameters for the oxygenation reactions were determined from the temperature dependence of the kinetic constant k_{phen} in the temperature range of 348.16−363.16 K. From the straight line in the Eyring plot [Figure S2 (Supporting Information)], with a correlation coefficient of 99.7% the activation parameters $\Delta H^{\ddagger} = 79 \pm 16\ kJ\ mol^{-1}$ and $\Delta S^{\ddagger} = -40 \pm 44\ J\ mol^{-1}\ K^{-1}$ were calculated at 353.16 K.

Reaction rates on the oxygenation of the 4′-substituted complexes $Cu(phen)(4'R\text{-}fla)_2$ under identical conditions were also determined (with various electron-withdrawing or releasing substituents R) in order to find out electronic effects on the reaction rate. The Hammett plot obtained is shown in Figure 8. Electron-releasing substituents enhanced the reaction rate, and the reaction constant ρ_{phen} was found to be −1.03 (R = 98.3%).

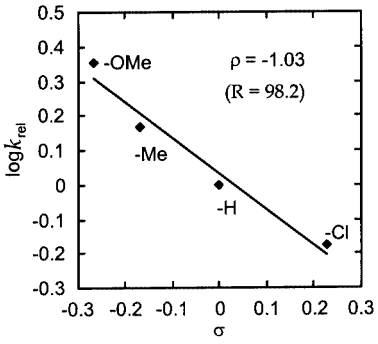

Figure 8. Hammett plot for the oxygenation of $Cu(phen)(4'R\text{-}fla)_2$ complexes

$^{18}O_2$ Labelling Experiments

Oxygenation of $Cu(phen)_2(fla)$ was also carried out with a mixture of $^{16}O_2$ and $^{18}O_2$ (3:1) in acetonitrile. After stirring the reactants at 25 °C for 48 h, the unchanged starting material was filtered off (ca. 50%), and the green solution was concentrated to dryness, giving a mixture of $Cu(phen)(^{16}O\text{-}bpg)_2$ and $Cu(phen)(^{18}O\text{-}bpg)_2$ {IR (Nujol): 1685 [$\nu(C^{18}O)$], 1716 [$\nu(C^{16}O)$] cm^{-1}}, $Cu(phen)(^{18}O\text{-}2HOpg)_2$ and $Cu(phen)(^{16}O\text{-}2HOpg)_2$, respectively. The GLC-MS analysis of the residue, after treatment with ethereal diazomethane, showed the presence of ^{16}O- and ^{18}O-containing methyl benzoate: *m/z* (%) = 136 (23) [M^+], 105 (100), 77 (87); 138 (8) [$M^+ + 2$], 181 (9), 107 (26), 105 (100), 77 (87); methyl 2-methoxyphenylglyoxylate: *m/z* (%) = 194 (32) [M^+], 179 (22), 135 (100), 120 (29), 105 (15), 92 (15); 196 (12) [$M^+ + 2$], 181 (9), 135 (100), 120 (29), 105 (15), 92 (28); methyl 2-hydroxyphenylglyoxylate: *m/z* (%) = 180 (7) [M^+], 121 (100), 93 (17), 65 (23); 182 (2.2) [$M^+ + 2$], 121 (100), 93 (17), 65 (23); and coumaronedione: *m/z* (%) = 148 (4.3) [M^+], 120 (100), 92 (69), 64 (27), 63 (30); 138 (8) [$M^+ + 2$], 107 (26), 105 (100), 77 (87); in the appropriate ratio. On the bases of the above results it can be said that both ^{18}O atoms of $^{18}O_2$ are incorporated into the primary oxygenated product 2-benzoatophenylglyoxylic acid from molecular oxygen (Scheme 2).

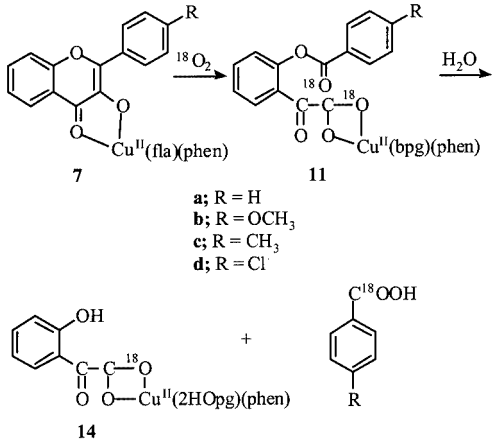

Scheme 2

All experimental data reported in the previous sections can be used for the interpretation of the mechanism of copper-assisted oxygenolysis of coordinated flavonolate to *O*-benzoylsalicylate or 2-benzoatophenylglyoxylate. Flavonolate as a chelating ligand forms stable complexes with copper ions. In most cases they are stable toward dioxygen in the solid form or even in solution at ambient conditions. At elevated temperatures the oxygenolysis proceeds reasonably rapidly. Recently, we have found that copper(II) flavonolate complexes with simple N-containing tridentate ligands reacted with dioxygen to the corresponding enzyme-like (*O*-benzoylsalicylato)copper complexes and CO. On the basis of kinetic measurements of the reaction of the complexes above with dioxygen, a mechanism was proposed to proceed via an endoperoxide intermediate according to route a in Scheme 1.[9g,9h] Treatment of the (flavonolato)copper complex $[Cu(phen)_2(fla)]ClO_4$ with dioxygen in DMF or CH_3CN solution at elevated temperature leads also to an (*O*-benzoylsalicylato)copper complex $[Cu(phen)_2(O\text{-}bs)]ClO_4$ and carbon monoxide, indicating that the mechanism of this reaction is the same as that proposed for copper-containing model systems investigated earlier by us.

Recently, we have published that the oxygenolysis of $Cu(fla)_2$ in DMF resulted in the $Cu(O\text{-}bs)_2$ complex and CO.[9e] We found that this reaction proceeded in a bimolecular step via an endoperoxide intermediate (Scheme 1, route a), and the kinetic constant k_{obs} was found to be $9.90 \pm 0.80 \times 10^{-3}$ mol^{-1} dm^3 s^{-1} at 90 °C.[9e] This value is much smaller than that obtained for the oxygenolysis for $Cu(phen)(fla)_2$ ($21.3 \pm 1.8 \times 10^{-2}$ mol^{-1} dm^3 s^{-1} at 90 °C). This difference in the reaction rates indicates that there are two different pathways for the above reactions. The formation of (oxocarboxylato)copper(II) complexes **14**−**16** in the oxygenation of the complexes $Cu(L)(fla)_2$ (L = phen, bpy, TMEDA) also suggest that the oxidative cleavage reaction of the coordinated flavonolate ligand can only proceed via a 1,2-dioxetan intermediate, which, upon the usual decomposition and hydrolysis of the ester linkage, leads to the corresponding (oxocarboxylato)copper complexes **14**−**16**. The $^{18}O_2$ labelling experiments on the oxygenation of $Cu(phen)(fla)_2$ revealed that both ^{18}O atoms of the $^{18}O_2$ molecule are incorporated into the substrate. A reaction mechanism that nicely fits the chemical, photochemical, spectroscopic, labelling, kinetic, and thermodynamic data is shown in Scheme 3.

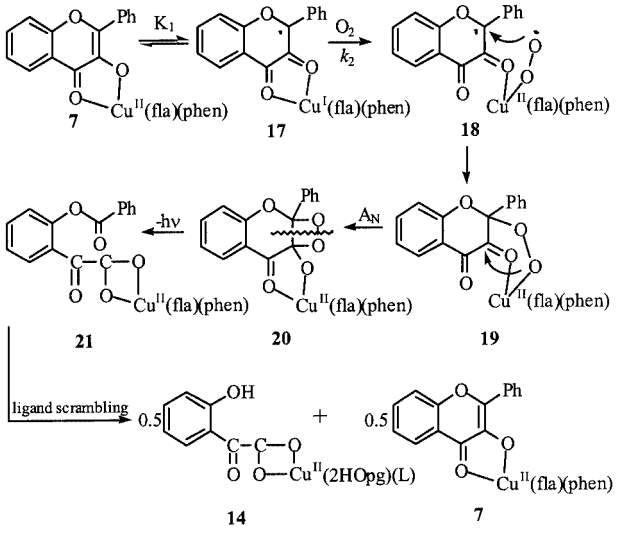

Scheme 3

The second-order overall rate expression for the oxygenation of the flavonolato complexes **7** supports the proposal that in a fast pre-equilibrium the copper(II) flavonolate complex **7** undergoes intramolecular electron transfer from the ligand fla^- to Cu^{II}, resulting in the copper(I) flavonoxy radical complex **17**. The equilibrium is largely shifted to the left (K_1 is rather small). In **17** there are two redox-active centres, the radical ligand and the copper(I) ion. The biradical dioxygen may react at both sites; in an oxidative addition to the copper ion [leading to a (superoxo)copper(II) complex **18**], or in a radical-radical reaction with the flavonoxy ligand. We believe that the former is the rate-determining step. The Hammett relationship shows that higher electron density at the copper ion enhances the rate of the reaction. This is consistent with an electrophilic attack of dioxygen at the copper(I) centre.

The reaction constant of the oxygenation reaction is almost the same ($\rho_{phen} = -1.03$, $R = 98.2\%$) as that found for the oxygenation of copper(I) chloride in pyridine ($\rho = -1.24$).[16] The crucial evidence for a bimolecular reaction step is the negative $\Delta S^{\ddagger}$ value (−40.3 J mol^{-1} K^{-1}). The (superoxo)copper(II) complex **18** is possibly then transformed in a fast consecutive coupling reaction to **19**, which reacts by an intramolecular nucleophilic addition on C3 to give the 1,2-dioxetan **20**. The main difference between the two types of mechanistic routes can be explained by this step. The nucleophilic attack of the bound peroxide could also take place on the 4-C=O group as well giving rise to an endoperoxide intermediate, but in that case the higher electron density on the 4-C=O carbon atom compared to that on the 3-C=O carbon atom renders this pathway unlikely. The 1,2-dioxetan **20** is then believed to decompose in a fast step to the (oxocarboxylato)copper complex **21**. Ow-

ing to a ligand scrambling reaction, the starting copper flavonolate complex **7** and the product (2-hydroxyphenylglyoxylato)copper complex **14** are formed by hydrolysis of the ester linkage in complex **11**. In order to prove the formation of 1,2-dioxetan during the oxygenolysis the chemiluminescence of the reaction was tested. In the emission spectrum bands at 506, 546, and 578 nm were found, which were assigned to the decomposition of the 1,2-dioxetan species.[15] Light emission is a result of the transition of the exited complex **21** to its ground state. Assuming steady-state conditions for species **17** the rate according to Equation (5) can be deduced, which after some simplification ($k_2[O_2] << k_1 + k_{-1}$ and [Cu] means the total copper concentration) is in good agreement with an overall second-order dependence according the experimental data obtained in the kinetic measurements.

$$-\frac{d[Cu]}{dt} = \frac{k_1 k_2 [Cu][O_2]}{k_1 + k_{-1} + k_2[O_2]} = \frac{k_1 k_2 [Cu][O_2]}{k_1 + k_{-1}} = k_{obs}[Cu][O_2] \quad (5)$$

Conclusion

From the results obtained the conclusion may be drawn that the oxidative ring-cleavage reaction of the flavonolate ligand coordinated to the copper ion may take place by two different reaction routes, namely through an endoperoxide or a 1,2-dioxetan intermediate. We believe that the coordination mode and the ligand environment around the metal centre, and the Lewis acidity of the copper ion influence the mechanism of this unusual reaction. Both complexes $Cu(phen)(fla)_2$ and $[Cu(phen)_2(fla)]ClO_4$ are sterically very crowded so that the discrimination of the intramolecular nucleophilic peroxide group between the 4-C=O and 3-C=O carbon atoms seems to be governed by the different electron densities on the carbon atoms, which is influenced by changing the ligand environment. Further work is in progress to better understand the reasons and factors affecting the selectivity between this two types of C−C cleavage reactions.

Experimental Section

General Remarks: Solvents used for the reactions were purified using literature methods[17] and stored under argon. Flavonol,[18] 4′-methoxyflavonol,[18] 4′-methylflavonol,[19] 4′-chloroflavonol,[19] O-benzoylsalicylic acid,[20] $Cu(OCH_3)_2$,[21] $[Cu(CH_3CN)_4]ClO_4$,[22] and $Cu(fla)_2$ [9b] were prepared using literature methods. The ligands 1,10-phenanthroline, 2,2′-bipyridine, and *N*,*N*,*N*′,*N*′-tetramethylethylenediamine (Aldrich) were used as provided.

CAUTION: Perchlorate salts of metal complexes with organic ligands are potentially explosive. Only small amounts of material should be prepared, and these should be handled with great care.

Preparation of $[Cu(phen)_2(fla)]ClO_4$ (6): $[Cu(CH_3CN)_4]ClO_4$ (0.328 g, 1 mmol) was dissolved in acetonitrile (60 mL), and flavonol (0.238 g, 1 mmol) and 1,10-phen·H_2O (0.396 g, 2 mmol) were added and stirred under argon for 1 h, and then under dioxygen (0.1 MPa) for 2 h. A green solid formed, which was filtered, washed with acetonitrile, and dried under vacuum (0.66 g, 87%). The product was recrystallised from acetonitrile. M.p. 195 °C. IR (KBr): $\tilde{\nu}$ = 1608 (vs, C−N), 1581 (vs, C−O), 1511, 1493, 1416, 1207, 1141, 1082 (vs, ClO_4), 845, 756, 719, 626 cm^{-1} (vs, ClO_4). UV/Vis (DMF): λ_{max} (ε/L mol^{-1} cm^{-1}) = 229 (67608), 269 (69183), 419 (8318), 702 nm (51). μ_B = 1.92. $C_{39}H_{25}ClCuN_4O_7$ (760.7): calcd. C 61.58, H 3.31, N 7.36; found C 61.04, H 3.16, N 7.18.

Preparation of $Cu(phen)(fla)_2$ (7a): To a solution of $Cu(fla)_2$ (0.538 g, 1 mmol) in acetonitrile (35 mL) was added 1,10-phen·H_2O (0.198 g, 1 mmol) and the reaction mixture stirred under argon for 4 h. A green precipitate formed, which was filtered off, washed with ether, and dried under vacuum (0.65 g, 90%). M.p. 236 °C. IR (KBr): $\tilde{\nu}$ = 3059 vw, 3044 vw, 1595 vs, 1564 vs, 1508 s, 1485 m, 1465 m, 1408 vs, 1350 m, 1310 s, 1221 vs, 1187 m, 1144 m, 1109 m, 1077 m, 1033 m, 995 w, 913 m, 859 s, 774 s, 747 s, 735 m, 721 w, 698 s, 571 m, 533 m, 499 m cm^{-1}. UV/Vis (DMF): λ_{max} (ε/L mol^{-1} cm^{-1}) = 265 (64125), 432 nm (63658). μ_B = 1.98. $C_{42}H_{26}CuN_2O_6$ (718.2): calcd. C 70.24, H 3.64, N 3.90; found C 69.88, H 3.48, N 3.98.

$Cu(phen)(4'OCH_3\text{-}fla)_2$ (7b): Yield 0.66 g (85%). M.p. 200 °C. IR (KBr): $\tilde{\nu}$ = 3052 vw, 2924 vw, 2823 w, 1591 vs, 1568 vs, 1542 s, 1491 s, 1416 vs, 1355 m, 1305 s, 1249 vs, 1216 vs, 1181 s, 1116 s, 1046 s, 1003 m, 923 m, 852 s, 761 s, 742 s, 691 m, 642 m, 578 m, 529 m cm^{-1}. UV/Vis (DMF): λ_{max} (ε/L mol^{-1} cm^{-1}) = 271 (70018), 434 (67844) nm. μ_B = 2.01. $C_{44}H_{30}CuN_2O_8$ (778.3): calcd. C 67.90, H 3.38, N 3.82; found C 67.29, H 3.48, N 3.98.

$Cu(phen)(4'CH_3\text{-}fla)_2$ (7c): Yield 0.62 g (83%). M.p. 197 °C. IR (KBr): $\tilde{\nu}$ = 3030 vw, 2895 vw, 2841 wv, 1590 vs, 1576 vs, 1495 vs, 1476 s, 1412 vs, 1353 m, 1312 s, 1217 vs, 1189 s, 1147 m, 1112 s, 1050 w, 1029 w, 1001 m, 916 s, 861 s, 834 s, 766 s, 738 s, 689 m, 663 w, 638 m, 514 s cm^{-1}. UV/Vis (DMF): λ_{max} (ε/L mol^{-1} cm^{-1}) = 271 (80041), 429 (63062) nm. μ_B = 1.86. $C_{44}H_{30}CuN_2O_6$ (746.3): calcd. C 70.81, H 4.05, N 3.75; found C 69.84, H 3.89, N 3.88.

$Cu(phen)(4'Cl\text{-}fla)_2$ (7d): Yield 0.59 g (75%). M.p. 238 °C. IR (KBr): $\tilde{\nu}$ = 3048 vw, 1595 vs, 1568 vs, 1510 m, 1483 vs, 1410 vs, 1355 m, 1316 s, 1219 vs, 1149 m, 1109 s, 1093 m, 1022 m, 1003 m, 916 s, 849 s, 758 s, 736 s, 691 w, 661 w, 616 m, 551 w, 505 m. UV/Vis (DMF): λ_{max} (ε/L mol^{-1} cm^{-1}) = 271 (73578), 424 (60173) nm. μ_B = 1.81. $C_{42}H_{28}Cl_2CuN_2O_6$ (788.1): calcd. C 64.01, H 3.67, N 3.56; found C 63.68, H 3.89, N 3.66.

$Cu(bpy)(fla)_2$ (8): Yield 0.22 g (40%). M.p 280 °C. IR (KBr): $\tilde{\nu}$ = 3023 vw, 1588 vs, 1578 vs, 1513 m, 1484 m, 1465 s, 1438 m, 1405 vs, 1348 m, 1305 vs, 1239 vs, 1142 w, 1117 w, 1078 m, 1057 vw, 1032 m, 997 w, 913 m, 857 vw, 765 vs, 742 w, 719 w, 703 s, 671 m, 591 vw, 532 m, 507 s cm^{-1}. UV/Vis (DMF): λ_{max} (ε/L mol^{-1} cm^{-1}) = 273 (67640), 431 (58829) nm. μ_B = 1.89. $C_{40}H_{26}CuN_2O_6$ (694.2): calcd. C 69.21, H 3.77, N 4.04; found C 68.79, H 3.92, N 4.11.

$Cu(TMEDA)(fla)_2$ (9): Yield 0.43 g (65%). M.p. 160 °C (dec.). IR (KBr): $\tilde{\nu}$ = 3055 vw, 2999 vw, 2873 vw, 2827 vw, 1573 vs, 1524 m, 1473 s, 1440 m, 1427 vs, 1352 m, 1318 vs, 1298 w, 1256 w, 1226 vs, 1188 w, 1150 w, 1124 w, 1086 m, 1061 vw, 1037 w, 973 w, 937 vw, 918 m, 863 vw, 822 m, 783 s, 751 vs, 749 vw, 724 w, 705 s, 692 vw, 674 m, 612 vw, 537 m, 501 s cm^{-1}. UV/Vis (DMF): λ_{max}(ε/L mol^{-1} cm^{-1}) = 272 (51368), 430 (59979), 674 (380) nm. μ_B = 1.91. $C_{36}H_{34}CuN_2O_6$ (654.2): calcd. C 66.09, H 5.24, N 4.28; found C 65.79, H 4.95, N 4.21.

Preparation of [Cu(phen)$_2$(*O*-bs)]ClO$_4$ (10): [Cu(CH$_3$CN)$_4$]ClO$_4$ (0.328 g, 1 mmol) was dissolved in acetonitrile (30 mL), then *O*-benzoylsalicylic acid (0.242 g, 1 mmol) and 1,10-phen·H$_2$O (0.360 g, 2 mmol) were added and the reaction mixture was stirred under argon for 1 h and then under dioxygen (0.1 MPa) for 4 h. A blue crystalline solid formed, which was filtered, washed with acetonitrile, and dried under vacuum (0.69 g, 90%). Recrystallisation of the product from dichloromethane gave blue crystals. The dichloromethane solution produced crystals suitable for X-ray analysis upon standing at room temperature for a few days. M.p. 262 °C. IR (KBr): $\tilde{\nu}$ = 741 (vs, C−O), 1600 (vs, C−N), 1572 (vs, CO$_2$), 1420, 1388 (vs, CO$_2$), 1253, 1200, 1143, 1094, 1068 (vs, ClO$_4$), 841, 800, 731, 719, 635 (vs, ClO$_4$) cm^{-1}. UV/Vis (DMF): λ_{max} (ε/L mol^{-1} cm^{-1}) = 271 (52481), 294 (17783), 331 (2042), 694 (115) nm. μ_B = 2.06. $C_{38}H_{25}ClCuN_4O_8$ (764.6): calcd. C 59.70, H 3.29, N 7.33; found C 58.62, H 2.98, N 7.21. The complex was also prepared by stirring (0.76 g, 1 mmol) Cu(fla)(phen)$_2$]ClO$_4$ in acetonitrile (30 mL) at room temperature under dioxygen (0.1 MPa) for 25 h (0.61 g, 80%).

Oxygenation of Cu(L)(fla)$_2$ (7a−d, 8−9): In a typical experiment, [Cu(phen)(fla)$_2$] (**7a**) (0.57 g, 0.8 mmol) in DMF (50 cm^3) was treated with dioxygen (0.1 MPa) until dioxygen uptake ceased at 80 °C. The dioxygen uptake was measured by a gas-volumetric method. The GC-MS analyses of the reaction mixture, after treatment with dilute HCl solution (10%) and ethereal diazomethane showed the presence of methyl benzoate: *m*/*z* (%) = 136 (23) [M$^+$], 105 (100), 77 (87); coumaronedione: *m*/*z* (%) = 148 (3) [M$^+$], 120 (100), 92 (59), 64 (22), 63 (14); and methyl 2-hydroxyphenylglyoxylate: *m*/*z* (%) = 180 (7) [M$^+$], 121 (100), 93 (11), 65 (11). Addition of excess Et$_2$O resulted in the deposition of [Cu(phen)(2HOpg)$_2$] (**14**) as a green microcrystalline solid: Yield 0.20 g (43%). M.p. 204 °C (dec.). IR (KBr): $\tilde{\nu}$ = 3037 w, 1616 vs, 1575 vs, 1516 s, 1462 m, 1423 s, 1375 m, 1346 m, 1326 m, 1265 w, 1213 vs, 1158 s, 1110 m, 1039 vw, 908 w, 858 vs, 785 s, 752 m, 733 s, 688 m, 629 w, 575 m. UV/Vis (DMF): λ_{max} (ε/L mol^{-1} cm^{-1}) = 273 (42213), 398 (5262) nm. μ_B = 1.91. $C_{28}H_{18}CuN_2O_8$ (574.0): calcd. C 58.59, H 3.16, N 4.88; found C 57.89, H 3.33, N 5.12.

Cu(bpy)(2HOpg)$_2$ (15): Yield 0.18 g (41%). M.p. 176 °C. IR (KBr): $\tilde{\nu}$ = 3057 w, 1618 vs, 1577 vs, 1550 s, 1516 s, 1496 s, 1448 m, 1428 s, 1387 m, 1352 w, 1326 m, 1258 w, 1217 vs, 1156 s, 1041 w, 770 vs, 668 m, 629 w, 573 m. UV/Vis (DMF): λ_{max} (ε/L mol^{-1} cm^{-1}) = 268 (29960), 305 (46121) nm. μ_B = 1.94. $C_{26}H_{18}CuN_2O_8$ (550.0): calcd. C 56.78, H 3.30, N 5.09, found C 56.49, H 3.16, N 5.12.

Cu(TMEDA)(2HOpg)$_2$ (16): Yield 0.12 g (30%). M.p 195 °C (dec.). IR (KBr): $\tilde{\nu}$ = 3126 vw, 3084 vw, 3068 vw, 3045 vw, 2871 vw, 2827 vw, 1616 vs, 1571 vs, 1519 s, 1478 w, 1465 w, 1445 s, 1421 s, 1407 m, 1362 m, 1320 m, 1258 m, 1207 s, 1147 s, 1084 vw, 1062 w, 1035 m, 990 w, 913 w, 861 m, 845 w, 769 s, 758 s, 745 s, 735 m, 720 m, 671 m, 558 m. UV/Vis (DMF): λ_{max} (ε/L mol^{-1} cm^{-1}) = 266 (14207), 302 (19828), 349 (7650) nm. μ_B = 1.91. $C_{22}H_{26}CuN_2O_8$ (510.0): calcd. C 51.81, H 5.14, N 5.49; found C 52.23, H 4.95, N 5.57.

X-ray Data Collection: Crystal data for [Cu(*O*-bs)(phen)$_2$]ClO$_4$·1.5 CH$_2$Cl$_2$: crystal dimensions 0.20 × 0.25 × 0.30 mm, triclinic, space group $P\bar{1}$, a = 10.499(3) Å, b = 12.556(4) Å, c = 17.094(5) Å, α = 72.69(2), β = 89.35(2), γ = 69.19(2)°, V = 1999.7(10) Å^3, Z = 2, $\rho_{calcd.}$ = 1.481 g·cm^{-3}, 2 Θ_{max} = 48.0°, radiation Mo-K_α (λ = 0.71073 Å), ω-scan, T = 200 K. Of the 6861 measured reflections, 6160 were independent, and 4838 observed for $I > 2\sigma(I)$. Lorentz and polarisation factors and experimental absorption correction (ψ scan, μ = 0.870 mm^{-1}). Data were collected with a Siemens (Nicolet Syntex) R3m/V diffractometer and the structure was solved by direct methods and refined by full-matrix least-squares techniques against F^2 (SHELXL-93,[23] SHELXS-86[24]), hydrogen atoms located geometrically, R_1 = 0.0962, ωR_2 = 0.2614 (all data) for 540 parameters, min/max residual electron density = −0.642/1.448 e Å^{-3}. CCDC-179746 contains the supplementary crystallographic data for this paper. These data can be obtained free of charge at www.ccdc.cam.ac.uk/conts/retrieving.html or from the Cambridge Crystallographic Data Centre, 12, Union Road, Cambridge CB2 1EZ, UK [Fax: (internat.) + 44-1223/336-033; E-mail: deposit@ccdc.cam.ac.uk].

Physical Measurements: Electronic spectra were recorded with a Shimadzu UV-160 (Carl Zeiss) spectrometer, infrared spectra with a Specord IR-75 (Carl Zeiss) spectrometer. Magnetic susceptibilities were determined at room temperature with a Bruker B-E 10B8 magnetic balance. GC analyses were performed with an HP 5830A gas chromatograph equipped with a flame ionization detector and a CP SIL8CB column. GC-MS measurements were recorded with an HP 5890 II, 5971 GC/MSD at 75 eV.

Kinetic Measurements: Reactions of copper flavonolate complexes with O$_2$ were performed in DMF solutions. In a typical experiment Cu^{II}(phen)(fla)$_2$ was dissolved under argon in a thermostatically controlled reaction vessel with an inlet for taking samples with a syringe, and connected to a mercury manometer to maintain a constant pressure. The solution was then heated to the appropriate temperature, a sample was taken by syringe, and the initial concentration of Cu^{II}(phen)(fla)$_2$ was determined by UV/Vis spectroscopy measuring the absorbance of the reaction mixture at 432 nm (63 658) {λ_{max} of a typical band of Cu^{II}(phen)(fla)$_2$}. The argon was then replaced by dioxygen, and the consumption of Cu^{II}(phen)(fla)$_2$ was analysed periodically (ca. every 10 min). Experimental conditions are summarised in Table 1. The temperature was determined with an accuracy of ±0.5 °C and the pressure of dioxygen with an accuracy of ±0.5%. The O$_2$ concentration was calculated from literature data,[25] taking into account the partial pressure of DMF[26] and assuming the validity of Dalton's law.

Supporting Information: Kinetic data and diagrams for the oxygenations are available (see also footnote on the first page of this article).

Acknowledgments

Financial support of the Hungarian National Research Fund (OTKA T-30400) and Ministry of Education (FKFP-0446/1999) is gratefully acknowledged.

[1] E. Wollenweber, in *Flavonoids: Advances in Research* (Eds.: J. B. Harborne, T. J. Mabry), Chapman & Hall, London, New York, **1982**, pp. 189−259.
[2] J. B. Harborne, C. A. Williams, in *Flavonoids: Advances in Research* (Eds.: J. B. Harborne, T. J. Mabry), Chapman & Hall, London, New York, **1982**, pp. 261−311.
[3] E. Wollenweber, *Prog. Clin. Biol. Res.* **1988**, *2850*, 45−55.
[4] [4a] S. Hattori, I. Noguchi, *Nature* **1959**, *184*, 1145−1146. [4b] H. K. Hund, J. Breuer, F. Lingens, J. Hüttermann, R. Kappl, S. Fetzner, *Eur. J. Biochem.* **1999**, *263*, 871−878. [4c] W. Barz, *Arch. Mikrobiol.* **1971**, *78*, 341−352. [4d] D. W. S. Westlake, G. Talbot, E. R. Blakley, F. J. Simpson, *Can. J. Microbiol.* **1959**, *5*, 621−629. [4e] D. W. S. Westlake, J. M. Roxburgh, G. Talbot, *Nature* **1961**, *189*, 510−511. [4f] T. Oka, F. J. Simpson, *Biochem. Biophys. Res. Commun.* **1971**, *43*, 1−5. [4g] H. G. Krishnamurty, F. J. Simpson, *J. Biol. Chem.* **1970**, *245*, 1467−1471. [4h] T. Oka, F. J. Simpson, H. G. Krishnamurty, *Can. J. Microbiol.* **1972**, *18*, 493−508. [4i] F. Fusetti, K. H. Schröter, R. A. Steiner, P. I.

van Noort, T. Pijning, H. J. Rozeboom, K. H. Kalk, M.R. Egmond, B. W. Dijkstra, *Structure* **2002**, *10*, 259−268.
[5] [5a] I. Bauer, A. de Beyer, B. Tshisuaka, S. Fetzner, F. Lingens, *FEMS Microbiol. Lett.* **1994**, *117*, 299−304. [5b] I. Bauer, N. Max, S. Fetzner, F. Lingens, *Eur. J. Biochem.* **1996**, *240*, 576−583.
[6] [6a] J. W. Wray, R. H. Abeles, *J. Biol. Chem.* **1993**, *268*, 21 466−469. [6b] J. W. Wray, R. H. Abeles, *J. Biol. Chem.* **1995**, *270*, 3147−3153. [6c] Y. Dai, T. C. Pochapsky, R. H. Abeles, *Biochemistry* **2001**, *40*, 6379−6387.
[7] T. Matsuura, *Tetrahedron* **1977**, *33*, 2869−2905.
[8] [8a] M. Utaka, M. Hojo, Y. Fujii, A. Takeda, *Chem. Lett.* **1984**, 635−636. [8b] M. Utaka, A. Takeda, *J. Chem. Soc., Chem. Commun.* **1985**, 1824−1825.
[9] [9a] G. Speier, V. Fülöp, L. Párkányi, *J. Chem. Soc., Chem. Commun.* **1990**, 512−513. [9b] É. Balogh-Hergovich, G. Speier, G. Argay, *J. Chem. Soc., Chem. Commun.* **1991**, 551−552. [9c] É. Balogh-Hergovich, J. Kaizer, G. Speier, *Inorg. Chim. Acta* **1997**, *256*, 9−14. [9d] I. Lippai, G. Speier, G. Huttner, L. Zsolnai, *Chem. Commun.* **1997**, 741−742. [9e] É. Balogh-Hergovich, J. Kaizer, G. Speier, G. Argay, L. Párkányi, *J. Chem. Soc., Dalton Trans.* **1999**, 3847−3854. [9f] É. Balogh-Hergovich, J. Kaizer, G. Speier, V. Fülöp, L. Párkányi, *Inorg. Chem.* **1999**, *38*, 3787−3795. [9g] É. Balogh-Hergovich, J. Kaizer, G. Speier, G. Huttner, L. Zsolnai, *Inorg. Chim. Acta* **2000**, *304*, 72−77. [9h] É. Balogh-Hergovich, J. Kaizer, G. Speier, G. Huttner, A. Jacobi, *Inorg. Chem.* **2000**, *39*, 4224−4229. [9i] É. Balogh-Hergovich, J. Kaizer, G. Speier, *J. Mol. Catal. A: Chem.* **2000**, *159*, 215−224.
[10] [10a] A. Nishinaga, T. Tojo, T. Matsuura, *J. Chem. Soc., Chem. Commun.* **1974**, 896−897. [10b] A. Nishinaga, T. Kuwashiga, T. Tsutsui, T. Mashino, K. Maruyama, *J. Chem. Soc., Dalton Trans.* **1994**, 805−810.
[11] L. Barhács, J. Kaizer, G. Speier, *J. Org. Chem.* **2000**, *65*, 3449−3452.
[12] L. Barhács, J. Kaizer, G. Speier, *J. Mol. Catal. A: Chem.* **2001**, *172*, 117−125.
[13] L. M. Bellamy, *Ultrarot-Spektrum und chemische Konstitution*, Dr. Dietrich Steinkopff Verlag, Darmstadt, **1966**, p. 12.
[14] J. H. Espenson, *Chemical Kinetics and Reaction Mechanism*, 2nd ed., McGraw-Hill, New York, **1995**.
[15] R. Hiatt, *Organic Peroxides* (Ed.: D. Swern), Wiley Interscience, New York, **1971**, vol. III, p. 70.
[16] É. Balogh-Hergovich, G. Speier, *Trans. Met. Chem.* **1982**, *7*, 177−180.
[17] D. D. Perrin, W. L. Armarego, D. R. Perrin, *Purification of Laboratory Chemicals*, 2nd ed., Pergamon, New York, **1990**.
[18] A. Nishinaga, T. Tojo, T. Matsuura, *J. Chem. Soc., Perkin. Trans. I* **1979**, 2511− 2516.
[19] M. A. Smith, R. M. Newman, R. A. Webb, *J. Heterocycl. Chem.* **1966**, *5*, 425.
[20] A. Einhorn, L. Rothlauf, R. Seuffert, *Ber. Dtsch. Chem. Ges.* **1911**, *44*, 3309.
[21] R. W. Adams, E. Bishop, R. L. Martin, G. Winter, *Aust. J. Chem.* **1966**, *19*, 207.
[22] B. J. Hathaway, D. G. Holah, J. D. Postlethwaite, *J. Chem. Soc.* **1961**, 3215−3216.
[23] G. M. Sheldrick, *SHELXL-93: Program for Crystal Structure Refinement*, University of Göttingen, **1993**.
[24] G. M. Sheldrick, *SHELXS-86: Program for Crystal Structure Solution*, University of Göttingen, **1990**.
[25] A. Kruis, in *Landolt-Börnstein*, Springler-Verlag, Berlin, **1976**, vol. 4, part 4, p. 269.
[26] G. Ram, A. R. Sharaf, *J. Indian Chem. Soc.* **1968**, *45*, 13.

Received February 20, 2002
[I02087]

Synthesis and Properties of Donor/Acceptor-Substituted Metal-Capped Twofold-Sila-Bridged Cyclobutadieno Superphanes

Rolf Jens Schaller,[a] Gebhard Haberhauer,[a] Rolf Gleiter,*[a] and Frank Rominger[a]

Dedicated to Professor Gottfried Huttner on the occasion of his 65th birthday

Keywords: Donor-acceptor systems / Phanes / Cyclic voltammetry / Electron transfer / Cobalt

The synthesis of the tetrasilasuperphanes **10**–**18** can be achieved from 1,1,3,3-tetramethyl-1,3-disilacyclonona-4,8-diyne (**7**), 1,1,2,2-tetramethyl-1,2-disilacyclonona-3,8-diyne (**8**) or 1,1,4,4-tetramethyl-1,4-disilacyclodeca-5,9-diyne (**9**) by heating with [RCpCoL$_2$] [R = H, Si(CH$_3$)$_3$, (CH$_3$)$_5$, CO$_2$CH$_3$; L$_2$ = COD, (CO)$_2$, (C$_2$H$_4$)$_2$]. The reaction of **7** with [RCpCo(CO)$_2$] [R = H, CH$_3$, Si(CH$_3$)$_3$, (CH$_3$)$_5$] produces the tricyclic cobalt-stabilized cyclobutadienediynes **20**–**23**, whereas reaction with [R′CpCo(L$_2$)] [R′ = H, (CH$_3$)$_5$, CO$_2$CH$_3$; L$_2$ = COD, (CO)$_2$] leads to the donor/acceptor superphanes **24**–**31**. X-ray investigations on the superphanes **10**, **13**–**15** and **18** reveal distances between the two cyclobutadiene units in the range of 2.65 Å and 3.79 Å. Investigations by means of cyclic voltammetry of the superphanes **10**–**18** show a dependence of the oxidation potentials on the nature of the bridges. A comparison between the first oxidation potentials of **10/28**, **24/29**, and **26/31** gives evidence for a partial charge delocalization over both CpCoCbd fragments of the superphanes.

(© Wiley-VCH Verlag GmbH, 69451 Weinheim, Germany, 2002)

Introduction

Rigid metallorganic species with two or more metal centers are often used as model systems for generating intervalence compounds. Attractive examples are biferrocene[1–3] and related species as well as metal-capped cyclophanes with benzene[4] or cyclobutadiene rings[5] as π-systems. For such intervalence compounds Robin and Day suggested a classification scheme 35 years ago[6] which is based on the extent of electron transfer between the metal fragments. According to this classification the charge can either be localized (class I), fully delocalized (class III) or partly delocalized (class II). The latter two classes deserve special interest because the delocalization promises new properties of the radical cations as compared to the localized species. Those systems on the interface of class II and class III with a relatively low barrier to intramolecular electron transfer have been called "almost delocalized" and are currently of considerable interest.[7]

Our recent studies of a series of superphanes with two[5] or four[8] cobalt centers revealed that for larger bridges between the metal fragments (**2**, **3**) the mixed valent monocations are valence trapped with very weak interactions between the metal centers.

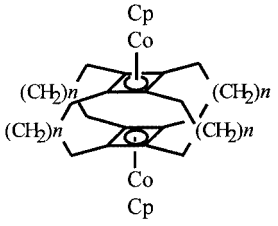

n = 1, 2, 3
1 2 3

For **1** we found strong interactions between the molecular halves which suggested classifying this system as an "almost delocalized" intervalence compound.[9] This finding encouraged us to synthesize related superphanes with smaller bridges between the metal fragments. In this paper we report on the synthesis, structural and electrochemical properties of CpCo-capped cyclobutadieno superphanes derived from **A**, **B** or **C**.

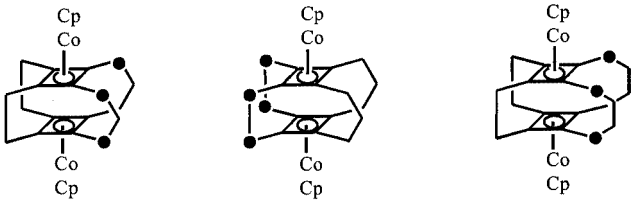

[a] Organisch-Chemisches Institut der Universität Heidelberg, Im Neuenheimer Feld 270, 69120 Heidelberg, Germany
Fax: (internat.) +49-(0)6221-544205
E-mail: rolf.gleiter@urz.uni-heidelberg.de

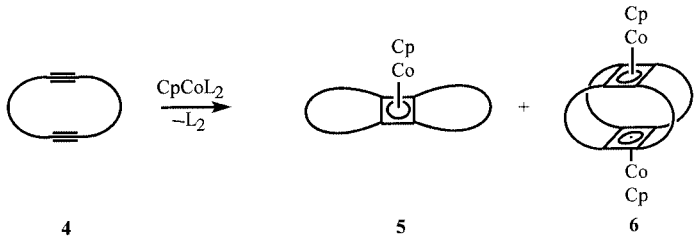

Scheme 1

Results and Discussion

Synthesis

Our studies on the reactivity of cyclic diynes with (η^5-cyclopentadienyl)cobalt complexes at 150 °C revealed two major products:[5] the intramolecular tricyclic system **5** and the intermolecular product **6** (Scheme 1).

If one side of the two alkyne units in **4** is tethered by an ethano or tetramethyldisilano bridge only superphanes **6** are obtained.[10] To prepare the target systems **A**−**C** we used 1,1,3,3-tetramethyl-1,3-disilacyclonona-4,8-diyne (**7**),[11] 1,1,2,2-tetramethyl-1,2-disilacyclonona-3,8-diyne (**8**)[11] and 1,1,4,4-tetramethyl-1,4-disilacyclodeca-5,9-diyne (**9**)[11] as starting materials (Scheme 2).

Heating these alkynes with [RCpCo(COD)] [R = H, $Si(CH_3)_3$, $(CH_3)_5$, CO_2CH_3] at 150 °C in cyclooctane afforded the superphanes **10**−**18** in yields between 10% and 68%. Especially noteworthy are the high yields (>60%) of **10**, **12**, **13** and **18**.

Donor/Acceptor Superphanes

In view of the mechanism of the formation of the superphanes[5] shown in Scheme 2 it was of interest to try and isolate some reaction intermediates. When we heated the diyne **7** with various substituted (η^5-cyclopentadienyl)(dicarbonyl)cobalt complexes (Scheme 3) at 100 °C[10] instead of 150 °C we were able to isolate the intermediates **20**−**23**. In all cases the bulky silyl groups are found adjacent to each other.[5,12] We ascribe this observation to the intermediate metallacycle[13] **19** in which the bulky groups are pointing away from each other. The yields of **20**−**23** vary between 20% and 30%.

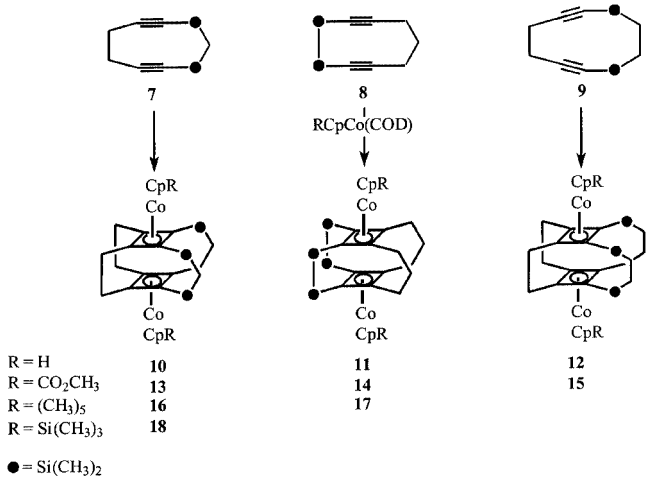

Scheme 2

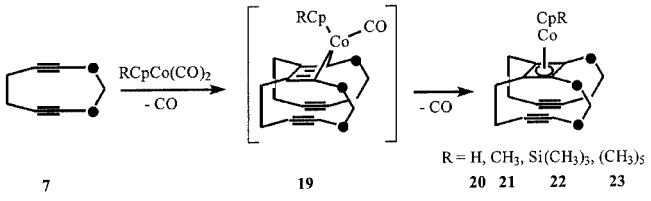

Scheme 3

In the case of **23** we were able to isolate single crystals which confirm the assigned stereochemistry (Figure 1). The two triple bonds are nearly parallel to each other with an intermolecular distance of 4.7 Å on the ethano-tethered side and 5.3 Å on the other side.

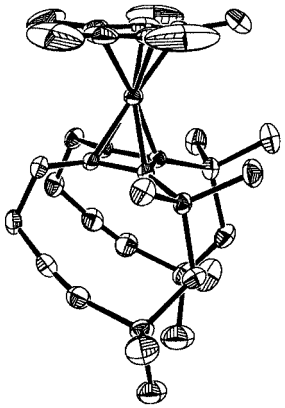

Figure 1. Molecular structure of **23** (ORTEP drawing, 50% probability ellipsoids); the hydrogen atoms have been omitted for clarity

Having in our hands the intermediates **20**−**23** prompted us to synthesize the donor- and acceptor-substituted superphanes **24**−**31** (Scheme 4) in order to compare their electronic properties with those of **10**−**18**.

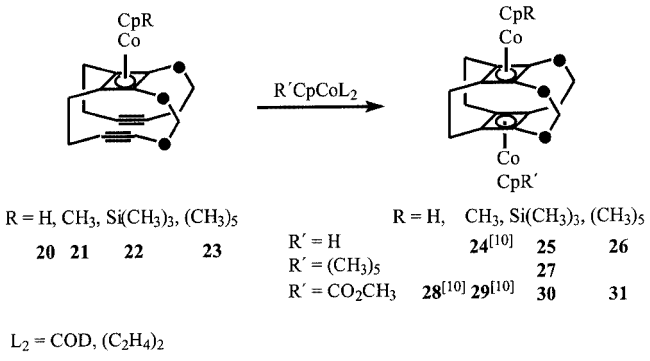

Scheme 4

The species **24**−**31** were obtained in a straightforward way by heating **20**−**23** with [R′CpCoL$_2$] [L$_2$ = COD, (C$_2$H$_4$)$_2$] [R′ = H, (CH$_3$)$_5$, CO$_2$CH$_3$] in cyclooctane. The yields of **24**−**31** vary from 24% up to 97%.

Structural Studies on the Superphanes

We were able to grow single crystals of **10**, **13**−**15** and **18** which allowed us to study the molecular structures of these species in the solid state. In Figure 2 we compare the molecular structures of **13**−**15** as examples.

In this series the tilting of the planes of the cyclobutadiene rings varies considerably. To demonstrate this we have listed the intramolecular distance at the short-bridged (*c*) and the long-bridged side (*d*) of the two cyclobutadiene units as well as the interplanar angle γ in Table 1. The disilano and propano bridges in **14** provide approximately the same intramolecular distance giving rise to a small value for γ (6.2°) and almost equal lengths for *c* and *d* (Table 1). For **10**, **13** and **18** the differences between *c* and *d* amount to ca. 0.7 Å and the interplanar angle γ varies between 24° and 25°. The deviation is largest for **15** with about 1.1 Å difference between *c* and *d* and a γ value of 41°.

The average distances between the ligands and the cobalt atom (*a*, *b*) are close to those found for other (η^5-cyclopentadienyl)(cyclobutadiene)cobalt complexes.[14−19]

Cyclovoltammetric Investigations

To probe the interactions between the [RCpCoCbd] units in **10**−**18** we carried out cyclic voltammetry studies (CV).[20] As reference we used the oxidation potentials of **1** and **32**.[21] The latter species serves as a model for systems

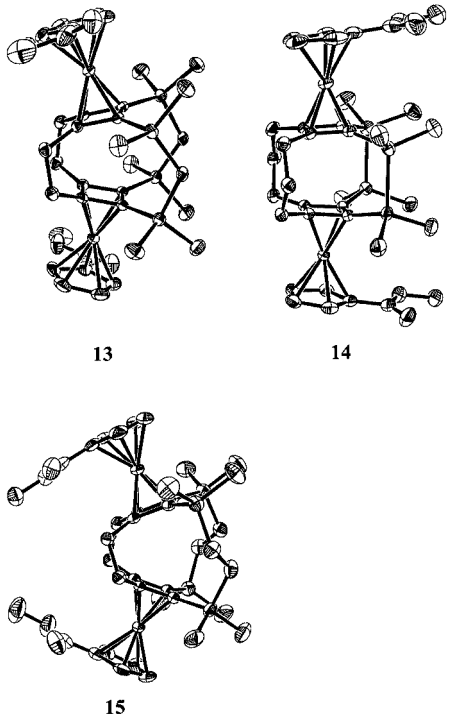

Figure 2. Molecular structures of **13**−**15** (ORTEP drawing 50% probability ellipsoids); the hydrogen atoms have been omitted for clarity

that are not influenced by the interaction of a second CpCo(Cbd) unit.

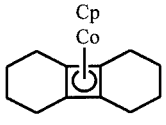

32

Compound **32** shows only one oxidation potential (Table 2) whereas for **1** two oxidation steps are observed. The one at $E^1_{1/2}$ = 656 mV was found to be reversible, whereas the second one at E^{ox}_{2p} = 1101 mV is irreversible.[9,21] The observed half-wave potentials for the reversible redox steps ($E^1_{1/2}$ and $E^2_{1/2}$) and the oxidation peak potentials for the irreversible steps (E^{ox}_{1p} and E^{ox}_{2p}) of **10**−**18** are compiled in Table 2.

We found that the differences $\Delta E = E^2_{1/2} - E^1_{1/2}$ are, with the exception of **12** and **16**, close to that found for **1**. As anticipated the oxidation potentials are highest for **13**−**15**

Table 1. Average distances [Å] between the metal and the C(Cp) atoms (*a*) and the C(Cbd) atoms (*b*), respectively, the distances between the cyclobutadiene rings on the short-bridged side (*c*) and opposite (*d*) as well as the average angle (γ) [°] between the planes of both cyclobutadiene units of **10**, **13**−**15** and **18**

Compound	a	b	c	d	γ
10	2.06 ± 0.01	1.98 ± 0.01	2.64 ± 0.02	3.29 ± 0.02	25.3 ± 0.5
13	2.07 ± 0.01	2.00 ± 0.01	2.65 ± 0.02	3.27 ± 0.02	24.5 ± 0.5
14	2.06 ± 0.01	1.99 ± 0.01	3.00 ± 0.02	3.16 ± 0.02	6.2 ± 0.5
15	2.06 ± 0.01	1.99 ± 0.01	2.72 ± 0.02	3.79 ± 0.02	41.4 ± 0.5
18	2.06 ± 0.01	1.99 ± 0.01	2.65 ± 0.02	3.27 ± 0.02	24.0 ± 0.5

Table 2. Half wave potentials ($E^1_{1/2}$ and $E^2_{1/2}$) or oxidation peak potentials (E^{ox}_{1p} and E^{ox}_{2p}) of **1**, **10**−**18** and **32**; the values are given in mV vs. Ag/AgCl[a]

Compound	$E^1_{1/2}$	E^{ox}_{1p}	$E^2_{1/2}$	E^{ox}_{2p}
32	801			
1	656			1101[b]
10	857		1260	
11	742		1278	
12	889		1218	
13	1119			1520[b]
14		1196[b]		1596[b]
15	1176			1567[b]
16		682[b]		1032[b]
17	835		1233	
18	856		1279	

[a] Solvent: CH_2Cl_2, 0.1 M of NBu_4PF_6. [b] Irreversible oxidation.

due to the electron-withdrawing effect of the methoxycarbonyl group. The difference between ΔE correlates approximately with the average distance [$(c + d)/2$] of the cyclobutadiene moieties: it is largest for **11** and smallest for **15**. To probe any transannular interactions between the molecular halves we carried out further cyclovoltammetric studies on the donor/acceptor superphanes **24** and **26**−**31**. The measured half wave potentials ($E^1_{1/2}$ and $E^2_{1/2}$) or the oxidation peak potentials (E^{ox}_{1p} and E^{ox}_{2p}) are compared in Table 3.

Table 3. Half wave potentials ($E^1_{1/2}$ and $E^2_{1/2}$) or oxidation peak potentials (E^{ox}_{1p} and E^{ox}_{2p}) of **24** and **26**−**31**; the values are given in mV vs. Ag/AgCl[a]

Compound	$E^1_{1/2}$	E^{ox}_{1p}	$E^2_{1/2}$	E^{ox}_{2p}
24	851		1270	
26		737[b]		1260[b]
27		733[b]		1316[b]
28	941			1505[b]
29	899			1382[b]
30	916		1430	
31		803[b]		1485[b]

[a] Solvent: CH_2Cl_2, 0.1 M of NBu_4PF_6. [b] Irreversible oxidation.

We noticed that the first oxidation step is reversible with the exception of the superphanes containing the $(CH_3)_5Cp$ ligand (**26**, **27** and **31**). The second oxidation step was found to be irreversible in most cases, possibly indicating an electrochemical-chemical-electrochemical (ECE) mechanism.

A comparison between the first oxidation potentials of **10** (857 mV), **24** (851 mV) and **26** (737 mV) as well as **28** (941 mV), **30** (916 mV), **29** (899 mV) and **31** (803 mV) shows a decrease of the first oxidation step in both series. This was anticipated since the donor character of one Cp ring increases in both series.[22] This finding suggests that the first electron is removed from the RCpCo fragment where R is either CH_3, $Si(CH_3)_3$ or $(CH_3)_5$. The assumption that the electrochemical oxidation removes the first electron from the donor-substituted unit allows us to probe the intramolecular interaction in the radical cation. A comparison of the first oxidation potentials of the pairs **10/28**, **24/29** and **26/31** shows in all three cases that the methoxycarbonyl substituent causes a shift of the first oxidation potential to higher values: $E^1_{1/2}$(**10**) − $E^1_{1/2}$(**28**) = −84 mV, $E^1_{1/2}$(**24**) − $E^1_{1/2}$(**29**) = −48 mV and E^{ox}_{1p}(**26**) − E^{ox}_{1p}(**31**) = −66 mV. Due to the irreversibility the values obtained for **26** and **31**, their differences have to be taken with a grain of salt. This increase of the oxidation potential is indicative of the delocalization of the positive charge between the two π-fragments of the cyclophanes. These results demonstrate the same tendency as for the carbocyclic systems.

Conclusion

The use of cyclic diynes with a short bridge on one side enabled us to synthesize and characterize the superphanes **10**−**18** and **24**−**31**. Structural investigations reveal that the two planes of the cyclobutadiene rings deviate from being parallel due to the different lengths of the bridges. The CV data indicate that the intramolecular distance of the cyclobutadiene rings affects the potential difference between the first two oxidation potentials. The comparison between the pairs of donor/acceptor superphanes **10/28**, **24/29** and **26/31** shows a clear substituent effect of the distant ester group on the electron-rich part of the molecule. This result corroborates the model of charge delocalization for the superphanes investigated.

Experimental Section

General: All melting points are uncorrected. The NMR spectra were measured with a Bruker WH 300 or Avance 500 spectrometer (^{1}H NMR at 200, 300 or 500 MHz and ^{13}C NMR at 50, 75 or 125 MHz) using the solvent as internal standard (δ). The mass spectra refer to data from a JEOL JMS-700 instrument. IR spectra were recorded with a Bruker Vector 22 FT-IR-spectrometer. UV/Vis absorption data were recorded using a Hewlett Packard HP 8452A Diode Array-spectrometer. Elemental analysis: Microanalytical laboratory of the University of Heidelberg. All reactions were carried out under an argon atmosphere using dried and oxygen-free solvents.

X-ray Crystallography and Structure Solution: Data were collected on a Siemens CCD-diffractometer at 200 K. Relevant crystal and data collection parameters are given in Table 4. The structures were solved by direct methods and refined against F^2 with a full-matrix least-square algorithm by using SHELXTL-97[23] software. An empirical absorption correction was applied by using SADABS,[24] based on the Laue symmetry of the reciprocal space.
CCDC-179719 (**10**), CCDC-179720 (**13**), CCDC-179721 (**14**), CCDC-179722 (**15**), CCDC-179723 (**18**) and CCDC-179724 (**23**) contain the supplementary crystallographic data for this paper. These data can be obtained free of charge at www.ccdc.cam.ac.uk/conts/retrieving.html [or from the Cambridge Crystallographic Data Centre, 12, Union Road, Cambridge CB2 1EZ, UK; Fax: (internat.) +44−1223/336−033; E-mail: deposit@ccdc.cam.ac.uk].

Electrochemistry: A traditional three-electrode, three-compartment cell was employed for cyclic voltammetry experiments with a Ag/AgCl reference electrode in CH_2Cl_2 separated from the test solution by a Haber−Luggin capillary. The $E^1_{1/2}$ and $E^2_{1/2}$ values reported for

Table 4. Crystal data and structural refinement for **10**, **13**, **14**, **15**, **18** and **23**

	10	**13**	**14**	**18**	**15**	**23**
Empirical formula	$C_{32}H_{46}Co_2Si_4$	$C_{36}H_{50}Co_2O_4Si_4$	$C_{36}H_{50}Co_2O_4Si_4$	$C_{38}H_{62}Co_2Si_6$	$C_{38.50}H_{54}Cl_{1.50}Co_2O_4Si_4$	$C_{32}H_{51}CoSi_4$
Mol. wt.	660.91	776.98	776.98	805.28	864.21	607.02
Wavelength [Å]	0.71073	0.71073	0.71073	0.71073	0.71073	0.71073
Crystal system	monoclinic	monoclinic	monoclinic	triclinic	triclinic	triclinic
Space group	*C*2/*c*	*P*2/*n*	$P2_1/n$	$P\bar{1}$	$P\bar{1}$	$P\bar{1}$
Temp [K]	200(2)	200(2)	200(2)	200(2)	200(2)	200(2)
Z	4	4	4	2	8	2
a [Å]	23.6960(4)	20.7948(4)	9.3517(1)	9.3254(1)	18.8837(2)	9.1911(2)
b [Å]	8.5413(1)	8.4898(1)	21.6918(2)	14.7928(1)	22.5698(2)	13.3105(3)
c [Å]	18.1854(3)	20.8561(4)	18.4924(2)	17.1732(2)	22.6874(1)	13.9913(3)
α [deg]	90	90	90	67.525(1)	66.6690(10)	97.282(1)
β [deg]	113.010(1)	93.4340(10)	94.3120(10)	78.383(1)	73.0420(10)	90.167(1)
γ [deg]	90	90	90	74.740(1)	89.7280(10)	92.351(1)
V [Å^3]	3387.78(9)	3675.40(11)	3740.66(7)	2098.37(4)	8424.89(12)	1696.38(6)
$D_{calcd.}$ [g/m^3]	1.30	1.40	1.38	1.27	1.36	1.19
Abs coeff μ [mm^{-1}]	1.14	1.07	1.05	0.99	1.03	0.67
Crystal shape	polyhedron	polyhedron	block	polyhedron	polyhedron	polyhedron
Crystal size [mm^3]	0.38 × 0.19 × 0.10	0.50 × 0.10 × 0.06	0.48 × 0.18 × 0.16	0.40 × 0.30 × 0.20	0.48 × 0.30 × 0.16	0.55 × 0.20 × 0.04
θ range for data coll [deg]	1.9 to 25.6	2.0 to 27.5	1.9 to 27.4	1.3 to 27.5	1.9 to 27.5	1.5 to 26.4
Index ranges	$-27 \le h \le 28$ $-10 \le k \le 10$ $-21 \le l \le 20$	$-26 \le h \le 26$ $-10 \le k \le 11$ $-27 \le l \le 26$	$-12 \le h \le 12$ $-28 \le k \le 28$ $-23 \le l \le 23$	$-12 \le h \le 12$ $-19 \le k \le 19$ $-22 \le l \le 22$	$-24 \le h \le 24$ $-29 \le k \le 29$ $-29 \le l \le 29$	$-11 \le h \le 11$ $-16 \le k \le 16$ $-17 \le l \le 17$
Reflns collected	12193	36700	38155	21918	87422	16324
Indep reflns [*R*(int)]	2943 (0.023)	8382 (0.0859)	8527 (0.0402)	9545 (0.0282)	38545 (0.0522)	6912 (0.0361)
Observed reflns	2545 [$I > 2\sigma(I)$]	5546 [$I > 2\sigma(I)$]	6819 [$I > 2\sigma(I)$]	7936 ($I > 2\sigma(I)$]	22537 ($I > 2\sigma(I)$]	4984 ($I > 2\sigma(I)$]
Max. and min. transm.	0.92 and 0.79	0.95 and 0.77	0.86 and 0.64	0.86 and 0.75	0.87 and 0.76	0.97 and 0.81
Data/restraints/params.	2942/110/222	8382/15/454	8527/0/425	9545/0/42	38545/154/1911	6912/0/347
Goodness-of-fit on F^2	1.08	1.00	1.02	1.04	1.00	1.02
R(*F*)	0.026	0.042	0.034	0.030	0.053	0.040
$R_W(F^2)$	0.067	0.079	0.080	0.076	0.117	0.094
(Δp)max, (Δp)min [e Å^{-3}]	0.39 and −0.21	0.45 and −0.50	0.92 and −0.42	0.60 and −0.36	0.94 and −0.95	0.42 and −0.37

chemically reversible systems are an average of the observed anodic and cathodic peak potentials, whereas the E_{1p}^{ox} and E_{2p}^{ox} values for chemically irreversible systems are the absolute values of the anodic peak potential. A supporting electrolyte concentration of 0.1 M of NBu_4PF_6 was employed unless otherwise noted. The working electrode for cyclic voltammetry was a glassy carbon disk GC disk of 3 mm diameter. The potential of the ferrocene/ferrocenyl system was set with an error of 5 mV at 721 mV vs. SCE at a scan rate of 100 mVs^{-1} and of 200 mVs^{-1}.

1,1,2,2-Tetramethyl-1,2-disilacyclonona-3,8-diyne (8): 1,6-Heptadiyne (0.46 g, 5.0 mmol) was dissolved in 50 mL of THF. At −20 °C a butyllithium solution (1.6 M in hexane; 7.5 mL, 12.0 mmol) was added and the mixture was stirred for 30 minutes at this temperature. After warming the mixture to room temperature it was cooled again (−20 °C) and 1,2-dichloro-1,1,2,2-tetramethyldisilane (0.94 g, 5.0 mmol) dissolved in 25 mL of THF was added over two hours. While stirring for a further hour the reaction mixture reached room temperature. After removal of the solvent the crude product was purified by column chromatography (silica gel/CCl_4) to give 0.10 g (10.0%) of colorless crystals; m.p. 49 °C. ^{1}H NMR (300 MHz, $CDCl_3$): δ = 2.40 (m, 4 H, CH_2), 1.85 (m, 2 H, CH_2), 0.21 [s, 12 H, $Si(CH_3)_2$] ppm. ^{13}C NMR (75 MHz, $CDCl_3$): δ = 114.8 [$Si(CH_3)_2$], 88.1 ($C_{\equiv}$), 28.4 (CH_2), 21.2 (CH_2), −2.4 (CH_2) ppm. HRMS (positive EI) calcd. for $C_{11}H_{18}Si_2$ ([M]$^+$): 206.0947; found 206.0959 (+1.2 mmu). IR (KBr): $\tilde{\nu}$ = 2955 cm^{-1}, 2896, 2157, 1428, 1320, 1244. UV/Vis (CH_2Cl_2) (log ε): λ_{max} = 226 nm (3.88). $C_{11}H_{18}Si_2$ (206.4): calcd. C 64.00, H 8.79; found C 63.89, H 8.81.

Superphane 10: A solution of 1,1,3,3-tetramethyl-1,3-disilacyclonona-4,8-diyne (**7**) (93 mg, 0.45 mmol) and [CpCo(COD)] (130 mg, 0.55 mmol) in 8 mL of cyclooctane was heated to 150 °C. The reaction progress was checked by TLC and after 8 hours the reaction mixture was allowed to cool to room temperature. After removal of the solvent the crude product was purified by column chromatography (silica gel/CCl_4) to give 104 mg (70.0%) of yellow crystals; m.p. > 250 °C. ^{1}H NMR (300 MHz, $CDCl_3$): δ = 4.70 (s, 10 H, CpH), 2.25−2.00 (m, 8 H, CH_2), 0.09 [s, 24 H, $Si(CH_3)_2$], −0.19 (m, 4 H, $SiCH_2$) ppm. ^{13}C NMR (75 MHz, $CDCl_3$): δ = 90.1 (C_{Cbd}), 77.9 (CH), 64.4 (C_{Cbd}), 24.5 (CH_2), 7.0 ($SiCH_2$), 3.0 [$Si(CH_3)_2$], 0.0 [$Si(CH_3)_2$] ppm. HRMS (positive EI) calcd. for $C_{32}H_{46}Co_2Si_4$ ([M]$^+$): 660.1340; found 660.1340 (±0.0 mmu). IR (KBr): $\tilde{\nu}$ = 2949 cm^{-1}, 2848, 1624, 1478, 1407, 1248. UV/Vis (CH_2Cl_2) (log ε): λ_{max} = 224 nm (4.62), 294 (4.64), 336 (3.59), 392 (3.08). $C_{32}H_{46}Co_2Si_4$ (660.9): calcd. C 58.15, H 7.02; found C 58.29, H 7.15.

Superphane 11: A solution of 1,1,2,2-tetramethyl-1,2-disilacyclonona-3,8-diyne (**8**) (93 mg, 0.45 mmol) and [CpCo(COD)] (130 mg, 0.55 mmol) in 8 mL of cyclooctane was heated to 150 °C. The reaction progress was checked by TLC and after 8 hours the reaction mixture was allowed to cool to room temperature. After removal of the solvent the crude product was purified by column

chromatography (alumina III/petroleum ether) to give 16 mg (11.0%) of yellow crystals; m.p. > 250 °C. ^{1}H NMR (200 MHz, $CDCl_3$): δ = 4.68 (s, 10 H, CpH), 2.13−1.26 (m, 12 H, CH_2), 0.21 (s, 12 H, $SiCH_3$), 0.12 (s, 12 H, $SiCH_3$) ppm. ^{13}C NMR (75 MHz, $CDCl_3$): δ = 93.0 (C_{Cbd}), 78.2 (CH), 65.3 (C_{Cbd}), 28.4 (CH_2), 26.9 (CH_2), −1.5 [$Si(CH_3)_2$], −1.7 [$Si(CH_3)_2$] ppm. HRMS (FAB+) calcd. for $C_{32}H_{46}Co_2Si_4$ ([M]$^+$): 660.1340; found 660.1306 (−3.6 mmu). IR (KBr): $\tilde{\nu}$ = 3095 cm^{-1}, 2941, 2900, 1631, 1245. UV/Vis (CH_2Cl_2) (log ε): λ_{max} = 234 nm (4.53), 300 (4.49), 404 (3.04). $C_{32}H_{46}Co_2Si_4$ (660.9): calcd. C 58.15, H 7.02; found C 58.54, H 7.33.

Superphane 12: A solution of 1,1,4,4-tetramethyl-1,4-disilacyclodeca-5,9-diyne (**9**) (100 mg, 0.45 mmol) and [CpCo(COD)] (130 mg, 0.55 mmol) in 8 mL of cyclooctane was heated to 150 °C. The reaction progress was checked by TLC and after 8 hours the reaction mixture was allowed to cool to room temperature. After removal of the solvent the crude product was purified by column chromatography (silica gel/CCl_4) to give 94 mg (61.0%) of yellow crystals; m.p. > 250 °C. ^{1}H NMR (200 MHz, $CDCl_3$): δ = 4.60 (s, 10 H, CpH), 2.36−1.94 (m, 8 H, CH_2), 0.45 (s, 8 H, $SiCH_2$), 0.00 [s, 12 H, $Si(CH_3)_2$], −0.08 [s, 12 H, $Si(CH_3)_2$] ppm. ^{13}C NMR (50 MHz, $CDCl_3$): δ = 90.5 (C_{Cbd}), 79.0 (CH), 64.3 (C_{Cbd}), 26.7 (CH_2), 8.6 ($SiCH_2$), 0.1 [$Si(CH_3)_2$], −0.4 [$Si(CH_3)_2$] ppm. HRMS (positive EI) calcd. for $C_{34}H_{50}Co_2Si_4$ ([M]$^+$): 688.1654; found 688.1659 (+0.5 mmu). IR (KBr): $\tilde{\nu}$ = 2943 cm^{-1}, 2898, 1624, 1473, 1408, 1246. UV/Vis (CH_2Cl_2) (log ε): λ_{max} = 224 nm (4.62), 284 (4.66), 322 (3.70), 394 (3.23). $C_{34}H_{50}Co_2Si_4$ (689.0): calcd. C 59.27, H 7.31; found C 59.41, H 7.42.

Superphane 13: A solution of 1,1,3,3-tetramethyl-1,3-disilacyclonona-4,8-diyne (**7**) (93 mg, 0.45 mmol) and [H_3CO_2CCpCo(COD)] (160 mg, 0.55 mmol) in 8 mL of cyclooctane was heated to 150 °C. The reaction progress was checked by TLC and after 12 hours the reaction mixture was allowed to cool to room temperature. After removal of the solvent the crude product was purified by column chromatography (silica gel/CH_2Cl_2, petroleum ether/diethyl ether 5:1) to give 116 mg (66.0%) of yellow crystals; m.p. > 250 °C. ^{1}H NMR (300 MHz, $CDCl_3$): δ = 5.26 (pseudo t., 4 H, CpH), 4.90 (pseudo t., 4 H, CpH), 3.72 (s, 6 H, OCH_3), 2.10−1.93 (m, 8 H, CH_2), 0.08 [s, 24 H, $Si(CH_3)_2$], −0.20 (m, 4 H, $SiCH_2$) ppm. ^{13}C NMR (75 MHz, $CDCl_3$): δ = 168.0 (CO), 92.0 (C_{Cp}), 83.5 (C_{Cbd}), 81.3 (CH), 80.2 (CH), 67.3 (C_{Cbd}), 50.9 (OCH_3), 23.4 (CH_2), 6.8 ($SiCH_2$), 2.8 [$Si(CH_3)_2$], −0.3 [$Si(CH_3)_2$] ppm. HRMS (FAB+) calcd. for $C_{36}H_{50}Co_2O_4Si_4$ ([M]$^+$): 776.1450; found 776.1411 (−3.9 mmu). IR (KBr): $\tilde{\nu}$ = 2951 cm^{-1}, 1710, 1464, 1281, 1247. UV/Vis (CH_2Cl_2) (log ε): λ_{max} = 222 (4.66), 282 (4.45), 298 (4.62), 344 (3.67), 414 (2.32). $C_{36}H_{50}Co_2O_4Si_4$ (777.0): calcd. C 55.65, H 6.49; found C 55.76, H 6.65.

Superphane 14: A solution of 1,1,2,2-tetramethyl-1,2-disilacyclonona-3,8-diyne (**8**) (54 mg, 0.26 mmol) and [H_3CO_2CCpCo(COD)] (88 mg, 0.30 mmol) in 6 mL of cyclooctane was heated to 130 °C. The reaction progress was checked by TLC and after 5 hours the reaction mixture was allowed to cool to room temperature. After removal of the solvent the crude product was purified by column chromatography (silica gel/petroleum ether/diethyl ether 10:1) to give 15 mg (14.7%) of orange crystals; m.p. 242 °C. ^{1}H NMR (300 MHz, $CDCl_3$): δ = 5.23 (pseudo t., 4 H, CpH), 4.89 (pseudo t., 4 H, CpH), 3.73 (s, 6 H, OCH_3), 2.00−1.97 (m, 8 H, CH_2), 1.71−1.65 (m, 4 H, CH_2), 0.20 [s, 12 H, $Si(CH_3)_2$], 0.11 [s, 12 H, $Si(CH_3)_2$] ppm. ^{13}C NMR (75 MHz, $CDCl_3$): δ = 168.5 (CO), 94.8 (C_{Cp}), 83.5 (C_{Cbd}), 81.5 (CH), 80.4 (CH), 68.3 (C_{Cbd}), 51.2 (OCH_3), 27.9 (CH_2), 26.0 (CH_2), −1.9 [$Si(CH_3)_2$] ppm. HRMS (FAB+) calcd. for $C_{36}H_{51}Co_2O_4Si_4$ ([M + H]$^+$): 777.1528; found 777.1481 (−4.7 mmu). IR (KBr): $\tilde{\nu}$ = 2955 cm^{-1}, 1710, 1630, 1466, 1361, 1256. UV/Vis (CH_2Cl_2) (log ε): λ_{max} = 282 nm (4.35), 300 (4.46).

Superphane 15: A solution of 1,1,4,4-tetramethyl-1,4-disilacyclodeca-5,9-diyne (**9**) (230 mg, 1.04 mmol) and [(H_3CO_2CCp)Co(COD)] (350 mg, 1.20 mmol) in 25 mL of cyclooctane was heated to 130 °C. The reaction progress was checked by TLC and after 7 days the reaction mixture was allowed to cool to room temperature. After removal of the solvent the crude product was purified by column chromatography (silica gel/CH_2Cl_2, CH_2Cl_2/EtOAc 20:1) to give 38 mg (9.0%) of orange crystals; m.p. 176 °C. ^{1}H NMR (500 MHz, $CDCl_3$): δ = 5.23 (pseudo t., 4 H, CpH), 4.90 (pseudo t., 4 H, CpH), 3.74 (s, 6 H, OCH_3), 2.25−2.23 (m, 4 H, CH_2), 2.01−1.99 (m, 4 H, CH_2), 0.54 (s, 8 H, $SiCH_2$), 0.10 [s, 12 H, $Si(CH_3)_2$], 0.00 [s, 12 H, $Si(CH_3)_2$] ppm. ^{13}C NMR (125 MHz, $CDCl_3$): δ = 168.7 (CO), 93.0 (C_{Cp}), 85.0 (C_{Cbd}), 82.8 (CH), 81.9 (CH), 68.0 (C_{Cbd}), 51.9 (OCH_3), 26.0 (CH_2), 9.2 ($SiCH_2$), 0.4 [$Si(CH_3)_2$], 0.0 [$Si(CH_3)_2$] ppm. HRMS (FAB+) calcd. for $C_{38}H_{54}Co_2O_4Si_4$ ([M]$^+$): 804.1763; found 804.1793 (+3.0 mmu). IR (KBr): $\tilde{\nu}$ = 2949 cm^{-1}, 2896, 1712, 1633, 1465, 1325, 1282. UV/Vis (CH_2Cl_2) (log ε): λ_{max} = 288 nm (4.39), 318 (3.56), 400 (2.91). $C_{38}H_{54}Co_2O_4Si_4$ (805.1): calcd. C 56.69, H 6.76; found C 56.10, H 7.04.

Superphane 16: A solution of 1,1,3,3-tetramethyl-1,3-disilacyclonona-4,8-diyne (**7**) (81 mg, 0.39 mmol) and [$(CH_3)_5CpCo(C_2H_4)_2$] (113 mg, 0.45 mmol) in 10 mL of cyclooctane was heated to 50 °C. The reaction progress was checked by TLC and after 4 hours the reaction mixture was allowed to cool to room temperature. After removal of the solvent the crude product was purified by column chromatography (silica gel/petroleum ether/diethyl ether 10:1) to give 17 mg (10.8%) of orange crystals; m.p. 226 °C. ^{1}H NMR (500 MHz, C_6D_6): δ = 1.89 (s, 30 H, $CpCH_3$), 1.85 (m, 8 H, CH_2), 0.26 [s, 12 H, $Si(CH_3)_2$], 0.17 [s, 12 H, $Si(CH_3)_2$], −0.02 (d, 2 H, $SiCH_2$), −0.31 (d, 2 H, $SiCH_2$) ppm. ^{13}C NMR (125 MHz, C_6D_6): δ = 88.3 (C_{Cbd}), 88.3 (C_{Cp}), 86.2 (C_{Cbd}), 23.9 (CH_2), 11.4 [$(CH_3)_5$], 11.0 ($SiCH_2$), 3.1 [$Si(CH_3)_2$], 0.7 [$Si(CH_3)_2$] ppm. HRMS (FAB+) calcd. for $C_{42}H_{66}Co_2Si_4$ ([M]$^+$): 800.2899; found 800.2902 (+0.3 mmu). IR (KBr): $\tilde{\nu}$ = 2951 cm^{-1}, 2903, 1633, 1245. UV/Vis (CH_2Cl_2) (log ε): λ_{max} = 242 nm (4.75), 252 (4.77), 308 (4.85). $C_{42}H_{66}Co_2Si_4$ (801.2): calcd. C 62.96, H 8.31; found C 62.96, H 8.21.

Superphane 17: A solution of 1,1,2,2-tetramethyl-1,2-disilacyclonona-3,8-diyne (**8**) (54 mg, 0.26 mmol) and [$(CH_3)_5CpCo(C_2H_4)_2$] (75 mg, 0.30 mmol) in 6 mL of cyclooctane was heated to 55 °C. The reaction progress was checked by TLC and after 4 hours the reaction mixture was allowed to cool to room temperature. After removal of the solvent the crude product was purified by column chromatography (alumina III/petroleum ether) to give 41 mg (39.1%) of orange crystals; m.p. > 250 °C. ^{1}H NMR (300 MHz, C_6D_6): δ = 1.92 [s, 30 H, $Cp(CH_3)_5$], 1.94−1.67 (m, 12 H, CH_2), 0.35 [s, 12 H, $Si(CH_3)_2$], 0.28 (s, 12 H, $Si(CH_3)_2$ ppm. ^{13}C NMR (75 MHz, C_6D_6): δ = 88.1 (C_{Cbd}), 88.0 (C_{Cp}), 64.0 (C_{Cbd}), 28.9 (CH_2), 25.3 (CH_2), 11.2 [$(CH_3)_5$], −1.5 [$Si(CH_3)_2$], −2.0 [$Si(CH_3)_2$] ppm. HRMS (FAB+) calcd. for $C_{42}H_{66}Co_2Si_4$ ([M]$^+$): 800.2938; found 800.2922 (−1.6 mmu). IR (KBr): $\tilde{\nu}$ = 2902 cm^{-1}, 1629, 1244. UV/Vis (CH_2Cl_2) (log ε): λ_{max} = 318 nm (4.96), 364 (3.79), 408 (3.13). $C_{42}H_{66}Co_2Si_4$ (801.2): calcd. C 62.97, H 8.30; found C 62.46, H 8.53.

Superphane 18: A solution of 1,1,3,3-tetramethyl-1,3-disilacyclonona-4,8-diyne (**7**) (93 mg, 0.45 mmol) and [$(CH_3)_3Si$ $CpCo(CO)_2$] (107 mg, 0.55 mmol) in 8 mL of cyclooctane was heated to 150 °C. The reaction progress was checked by TLC and

after 6 hours the reaction mixture was allowed to cool to room temperature. After removal of the solvent the crude product was purified by column chromatography (silica gel/petroleum ether) to give 105 mg (68.0%) of yellow crystals; m.p. > 250 °C. ^{1}H NMR (300 MHz, $CDCl_3$): δ = 4.63 (m, 4 H, CpH), 4.56 (m, 4 H, CpH), 2.2−2.0 (m, 8 H, CH_2), 1.9 (s, 6 H, CH_3), 0.1 [s, 24 H, $Si(CH_3)_2$], −0.2 (m, 4 H, $SiCH_2$) ppm. ^{13}C NMR (75 MHz, $CDCl_3$): δ = 92.7 (C_{Cp}), 89.2 (C_{Cbd}), 79.0 (CH), 76.8 (CH), 64.0 (C_{Cbd}), 24.5 (CH_2), 13.5 (CH_3), 7.3 ($SiCH_2$), 3.1 [$Si(CH_3)_2$], 0.0 [$Si(CH_3)_2$] ppm. HRMS (FAB+) calcd. for $C_{34}H_{50}Co_2Si_4$ ([M]$^+$): 688.1654; found 688.1664 (+1.0 mmu). IR (KBr): $\tilde{\nu}$ = 2947 cm^{-1}, 2923, 2850, 1632, 1473, 1246. UV/Vis (CH_2Cl_2) (log ε): λ_{max} = 224 nm (4.68), 296 (4.69), 376 (3.22). $C_{34}H_{50}Co_2Si_4$ (689.0): calcd. C 59.27, H 7.31; found C 59.33, H 7.45.

{(1,2,10,11-η)-3,3,5,5,16,16,18,18-Octamethyl-3,5,16,18-tetrasilatricyclo[9.7.0.0^{2,10}]octadeca-1,10-diene-6,14-diyne}(η^5-cyclopentadienyl)cobalt (20): A solution of 1,1,3,3-tetramethyl-1,3-disilacyclonona-4,8-diyne (**7**) (290 mg, 1.40 mmol) and [$CpCo(CO)_2$] (126 mg, 0.70 mmol) in 20 mL of cyclooctane was heated to 100 °C. The reaction progress was checked by TLC and after 7 days the reaction mixture was allowed to cool to room temperature. After removal of the solvent the crude product was purified by column chromatography (silica gel/CCl_4, CCl_4/CH_2Cl_2 10:1) to give 140 mg (37.0%) of orange crystals; m.p. 152 °C. ^{1}H NMR (300 MHz, $CDCl_3$): δ = 4.71 (s, 5 H, CpH), 2.34−2.11 (m, 8 H, CH_2), 0.34 [s, 6 H, $Si(CH_3)_2$], 0.22 [s, 6 H, $Si(CH_3)_2$], 0.10 [s, 12 H, $Si(CH_3)_2$], 0.05 (d, 2 H, $SiCH_2$), −0.16 (d, 2 H, $SiCH_2$) ppm. ^{13}C NMR (75 MHz, $CDCl_3$): δ = 109.6 ($C_{\equiv}$), 89.7 ($C_{\equiv}$), 88.7 (C_{Cbd}), 79.5 (C_{Cp}), 68.7 (C_{Cbd}), 27.5 (CH_2), 20.9 (CH_2), 5.7 ($SiCH_2$), 5.1 [$Si(CH_3)_2$], 1.2 [$Si(CH_3)_2$], 0.6 [$Si(CH_3)_2$], 0.5 [$Si(CH_3)_2$] ppm. HRMS (FAB+) calcd. for $C_{27}H_{41}CoSi_4$ ([M]$^+$): 536.1617; found 536.1603 (−1.4 mmu). IR (KBr): $\tilde{\nu}$ = 2950 cm^{-1}, 2904, 2176, 1624, 1474, 1432, 1250. UV/Vis (CH_2Cl_2) (log ε): λ_{max} = 222 nm (4.32), 276 (4.43), 306 (3.33), 398 (3.16). $C_{27}H_{41}CoSi_4$ (536.9): calcd. C 60.40, H 7.70; found C 60.58, H 7.98.

{(1,2,10,11-η)-3,3,5,5,16,16,18,18-Octamethyl-3,5,16,18-tetrasilatricyclo[9.7.0.0^{2,10}]octadeca-1,10-diene-6,14-diyne}(η^5-methylcyclopentadienyl)cobalt (21): A solution of 1,1,3,3-tetramethyl-1,3-disilacyclonona-4,8-diyne (**7**) (206 mg, 1.00 mmol) and [$(CH_3)CpCo(CO)_2$] (97 mg, 0.50 mmol) in 15 mL of cyclooctane was heated to 100 °C. The reaction progress was checked by TLC and after 7 days the reaction mixture was allowed to cool to room temperature. After removal of the solvent the crude product was purified by column chromatography (silica gel/CCl_4, CCl_4/CH_2Cl_2 10:1) to give 82 mg (30.0%) of orange crystals; m.p. 113 °C. ^{1}H NMR (200 MHz, $CDCl_3$): δ = 4.58 (m, 2 H, CpH), 4.37 (m, 2 H, CpH), 2.34−2.05 (m, 8 H, CH_2), 1.82 (s, 3 H, CH_3), 0.22−0.00 [m, 26 H, $Si(CH_3)_2$, $SiCH_2$], −0.26 (d, 2 H, $SiCH_2$) ppm. ^{13}C NMR (50 MHz, $CDCl_3$): δ = 109.8 ($C_{\equiv}$), 93.4 ($C_{\equiv}$), 88.9 (C_{Cbd}) 88.6 (C_{Cbd}), 80.6 (CH), 78.5 (CH), 68.2 (C_{Cp}), 27.1 (CH_2), 21.0 (CH_2), 13.3 (CH_3), 6.1 ($SiCH_2$), 5.3 [$Si(CH_3)_2$], 1.4 [$Si(CH_3)_2$], 0.80 [$Si(CH_3)_2$], 0.76 [$Si(CH_3)_2$] ppm. HRMS (FAB+) calcd. for $C_{28}H_{43}CoSi_4$ ([M]$^+$): 550.1774; found 550.1804 (+3.0 mmu). IR (KBr): $\tilde{\nu}$ = 2957 cm^{-1}, 2905, 2173, 1631, 1472, 1431, 1251. UV/Vis (CH_2Cl_2) (log ε): λ_{max} = 232 (4.23), 278 (4.42), 308 (3.31), 390 (2.87). $C_{28}H_{43}CoSi_4$ (550.9): calcd. C 61.04, H 7.87; found C 60.78, H 7.93.

{(1,2,10,11-η)-3,3,5,5,16,16,18,18-Octamethyl-3,5,16,18-tetrasilatricyclo[9.7.0.0^{2,10}]octadeca-1,10-diene-6,14-diyne}(η^5-trimethylsilylcyclopentadienyl)cobalt (22): A solution of 1,1,3,3-tetramethyl-1,3-disilacyclonona-4,8-diyne (**7**) (206 mg, 1.00 mmol) and [$(CH_3)_3SiCpCo(CO)_2$] (126 mg, 0.50 mmol) in 11 mL of cyclooctane was heated to 100 °C. The reaction progress was checked by TLC and after 7 days the reaction mixture was allowed to cool to room temperature. After removal of the solvent the crude product was purified by column chromatography (silica gel/petroleum ether/diethyl ether 10:1) to give 78 mg (23.7%) of an orange solid; m.p. 135 °C. ^{1}H NMR (500 MHz, C_6D_6): δ = 5.07 (pseudo t., 2 H, CpH), 4.55 (pseudo t., 2 H, CpH), 2.15−1.81 (m, 8 H, CH_2), 0.52 [s, 6 H, $Si(CH_3)_2$], 0.39 [s, 6 H, $Si(CH_3)_2$], 0.29 [s, 6 H, $Si(CH_3)_2$], 0.24 [s, 6 H, $Si(CH_3)_2$], 0.20 [s, 9 H, $Si(CH_3)_3$], 0.20 (d, 2 H, $SiCH_2$), −0.17 (d, 2 H, $SiCH_2$) ppm. ^{13}C NMR (125 MHz, C_6D_6): δ = 110.1 ($C_{\equiv}$), 90.2 (C_{Cbd}), 89.2 (C_{Cbd}), 87.1 (C_{Cp}), 84.7 (CH), 82.7 (CH), 70.3 ($C_{\equiv}$), 28.6 (CH_2), 21.3 (CH_2), 8.7 ($SiCH_2$), 5.7 [$Si(CH_3)_2$], 1.8 [$Si(CH_3)_2$], 1.1 [$Si(CH_3)_2$], 0.2 [$Si(CH_3)_3$] ppm. HRMS (FAB+) calcd. for $C_{30}H_{49}CoSi_5$ ([M]$^+$): 608.2012; found 608.1996 (−1.6 mmu). IR (KBr): $\tilde{\nu}$ = 2957 cm^{-1}, 2904, 2177, 1477, 1429, 1406, 1247. UV/Vis (CH_2Cl_2) (log ε): λ_{max} = 280 nm (4.38), 312 (3.36), 398 (3.12).

{(1,2,10,11-η)-3,3,5,5,16,16,18,18-Octamethyl-3,5,16,18-tetrasilatricyclo[9.7.0.0^{2,10}]octadeca-1,10-dien-6,14-diyne}(η^5-pentamethylcyclopentadienyl)cobalt (23): A solution of 1,1,3,3-tetramethyl-1,3-disilacyclonona-4,8-diyne (**7**) (206 mg, 1.00 mmol) and [$(CH_3)_5CpCo(CO)_2$] (125 mg, 0.50 mmol) in 11 mL of cyclooctane was heated to 100 °C. The reaction progress was checked by TLC and after 7 days the reaction mixture was allowed to cool to room temperature. After removal of the solvent the crude product was purified by column chromatography (silica gel/petroleum ether/diethyl ether 10:1) to give 82 mg (27.1%) of yellow crystals; m.p. 231 °C. ^{1}H NMR (500 MHz, C_6D_6): δ = 2.07−1.61 (m, 8 H, CH_2), 1.76 (s, 15 H, $CpCH_3$), 0.49 [s, 6 H, $Si(CH_3)_2$], 0.40 [s, 6 H, $Si(CH_3)_2$], 0.32 [s, 6 H, $Si(CH_3)_2$], 0.26 [s, 6 H, $Si(CH_3)_2$], 0.20 (d, 2 H, $SiCH_2$), −0.16 (d, 2 H, $SiCH_2$) ppm. ^{13}C NMR (125 MHz, C_6D_6): δ = 110.6 ($C_{\equiv}$), 89.2 (C_{Cbd}), 88.6 (C_{Cp}), 84.5 (C_{Cbd}), 67.1 ($C_{\equiv}$), 26.9 (CH_2), 21.1 (CH_2), 11.1 [$(CH_3)_5$], 8.2 ($SiCH_2$), 4.8 [$Si(CH_3)_2$], 1.9 [$Si(CH_3)_2$], 1.2 [$Si(CH_3)_2$], 1.0 [$Si(CH_3)_2$] ppm. HRMS (FAB+) calcd. for $C_{32}H_{51}CoSi_4$ ([M]$^+$): 606.2400; found 606.2384 (−1.6 mmu). IR (KBr): $\tilde{\nu}$ = 2952 cm^{-1}, 2904, 2862, 2176, 1248. UV/Vis (CH_2Cl_2) (log ε): λ_{max} = 296 nm (4.54), 330 (3.44), 400 (2.92).

Superphane 24: A solution of **20** (30 mg, 0.056 mmol) and [$(CH_3)CpCo(CO)_2$] (28 mg, 0.14 mmol) in 3 mL of cyclooctane was heated to 150 °C. The reaction progress was checked by TLC and after 4 hours the reaction mixture was allowed to cool to room temperature. After removal of the solvent the crude product was purified by column chromatography (silica gel/CH_2Cl_2, petroleum ether) to give 22 mg (58.0%) of yellow crystals; m.p. > 250 °C. ^{1}H NMR (300 MHz, $CDCl_3$): δ = 4.71 (s, 5 H, CpH), 4.62 (m, 2 H, CpH), 4.56 (m, 2 H, CpH), 2.27−2.01 (m, 8 H, CH_2), 1.93 (s, 3 H, CH_3), 0.10 [s, 12 H, $Si(CH_3)_2$], 0.09 [s, 12 H, $Si(CH_3)_2$], −0.21 (m, 4 H, $SiCH_2$) ppm. ^{13}C NMR (75 MHz, $CDCl_3$): δ = 92.7 (C_{Cbd}), 90.1 (C_{Cbd}), 89.2 (C_{Cbd}), 79.0 (CH), 77.1 (CH), 76.8 (CH), 64.4 (C_{Cp}), 64.0 (C_{Cbd}), 24.5 (CH_2), 24.0 (CH_2), 13.5 (CH_3), 7.2 ($SiCH_2$), 3.0 [$Si(CH_3)_2$], 0.0 [$Si(CH_3)_2$] ppm. HRMS (FAB+) calcd. for $C_{33}H_{48}Co_2Si_4$ ([M]$^+$): 674.1497; found 674.1490 (−0.7 mmu). IR (KBr): $\tilde{\nu}$ = 2949 cm^{-1}, 2848, 2362, 1632, 1479, 1247. UV/Vis (CH_2Cl_2) (log ε): λ_{max} = 222 nm (4.60), 278 (4.38), 296 (4.63), 334 (3.82). $C_{33}H_{48}Co_2Si_4$ (675.0): calcd. C 58.72, H 7.17; found C 58.81, H 7.45.

Superphane 25: A solution of **22** (50 mg, 0.08 mmol) and [CpCo(COD)] (48 mg, 0.21 mmol) in 5 mL of cyclooctane was heated to 150 °C. The reaction progress was checked by TLC and after 6 hours the reaction mixture was allowed to cool to room temperature. After removal of the solvent the crude product was purified

by column chromatography (silica gel/CH_2Cl_2/petroleum ether 1:2) to give 27 mg (44.9%) of an orange solid; m.p. 172 °C. ^{1}H NMR (500 MHz, $CDCl_3$): δ = 4.93 (pseudo t., 2 H, CpH), 4.72 (s, 7 H, CpH), 2.24 (s, 4 H, CH_2), 2.04 (s, 4 H, CH_2), 0.12 [(br, 33 H, $Si(CH_3)_3/Si(CH_3)_2$], 0.18 (s, 4 H, $SiCH_2$) ppm. ^{13}C NMR (125 MHz, $CDCl_3$): δ = 90.6 (C_{Cbd}), 90.5 (C_{Cbd}), 86.0 (C_{Cbd}), 83.1 (CH), 81.1 (CH), 78.4 (CH), 64.6 (C_{Cp}), 64.0 (C_{Cbd}), 25.6 (CH_2), 25.1 (CH_2), 7.7 ($SiCH_2$), 3.5 [$Si(CH_3)_2$], 3.4 [$Si(CH_3)_2$], 0.5 [$Si(CH_3)_2$], 0.4 [$Si(CH_3)_2$], 0.0 [$Si(CH_3)_3$] ppm. HRMS (FAB+) calcd. for $C_{35}H_{54}Co_2Si_5$ ([M]$^+$): 732.1736; found 732.1740 (+0.4 mmu). IR (micro pellet): 2951 cm^{-1}, 2851, 1631, 1248. UV/Vis (CH_2Cl_2) (log ε): λ_{max} = 280 nm (4.04), 314 (3.89), 460 (3.02). $C_{35}H_{54}Co_2Si_5$ (733.1): calcd. C 57.34, H 7.42; found C 57.61, H 7.67.

Superphane 26: A solution of **23** (16 mg, 0.03 mmol) and [CpCo(COD)] (14 mg, 0.06 mmol) in 2 mL of cyclooctane was heated to 150 °C. The reaction progress was checked by TLC and after 7 hours the reaction mixture was allowed to cool to room temperature. After removal of the solvent the crude product was purified by column chromatography (silica gel/CH_2Cl_2, petroleum ether) to give 11 mg (57.6%) of a yellow solid. ^{1}H NMR (500 MHz, $CDCl_3$): δ = 4.71 (s, 5 H, CpH), 2.19 (m, 8 H, CH_2), 1.79 (s, 15 H, $CpCH_3$), 1.54 (cyclooctane), 0.39 (s, 4 H, $SiCH_2$), −0.01 [s, 24 H, $Si(CH_3)_2$] ppm. ^{13}C NMR (125 MHz, $CDCl_3$): δ = 96.0 (C_{Cbd}), 88.3 (C_{Cbd}), 86.0 (C_{Cbd}), 78.2 (CH), 63.7 (C_{Cp}), 26.7 (cyclooctane), 24.7 (CH_2), 23.7 (CH_2), 11.1 [$(CH_3)_5$], 9.1 ($SiCH_2$), 1.1 [$Si(CH_3)_2$] ppm. HRMS (FAB+) calcd. for $C_{37}H_{56}Co_2Si_4$ ([M]$^+$): 730.2123; found 730.2142 (+1.9 mmu). IR (KBr): $\tilde{\nu}$ = 2922 cm^{-1}, 2852, 1632, 1445, 1378, 1247. UV/Vis (CH_2Cl_2) (log ε): λ_{max} = 282 nm (4.01), 306 (4.22), 352 (3.34), 382 (3.04).

Superphane 27: A solution of **22** (41 mg, 0.07 mmol) and [$(CH_3)_5$CpCo(COD)] (49 mg, 0.17 mmol) in 4 mL of cyclooctane was heated to 150 °C. The reaction progress was checked by TLC and after 7 hours the reaction mixture was allowed to cool to room temperature. After removal of the solvent the crude product was purified by column chromatography (silica gel/CH_2Cl_2/petroleum ether 1:2) to give 13 mg (24.1%) of an orange solid. ^{1}H NMR (500 MHz, $CDCl_3$): δ = 4.96 (pseudo t., 2 H, CpH), 4.71 (s, 2 H, CpH), 2.23 (s, 4 H, CH_2), 1.90 (s, 4 H, CH_2), 1.56 (s, 15 H, $CpCH_3$), 0.11 [br, 33 H, $Si(CH_3)_3/Si(CH_3)_2$], −0.20 (d, 4 H, $SiCH_2$) ppm. ^{13}C NMR (125 MHz, $CDCl_3$): δ = 90.9 (C_{Cbd}), 88.6 (C_{Cbd}), 86.3 (C_{Cbd}), 83.1 (CH), 81.3 (CH), 63.8 (C_{Cp}), 27.1 (CH_2), 25.7 (CH_2), 11.4 [$(CH_3)_5$], 9.6 ($SiCH_2$), 3.8 [$Si(CH_3)_2$], 2.9 [$Si(CH_3)_2$], 1.4 [$Si(CH_3)_3$], 0.6 [$Si(CH_3)_2$], 0.3 [$Si(CH_3)_2$] ppm. HRMS (FAB+) calcd. for $C_{40}H_{64}Co_2Si_5$ ([M]$^+$): 802.2519; found 802.2507 (−1.2 mmu). IR (KBr): $\tilde{\nu}$ = 2962 cm^{-1}, 2853, 1638, 1261, 1244. UV/Vis (CH_2Cl_2) (log ε): λ_{max} = nm 284 (4.21), 306 (4.41), 348 (3.57), 398 (2.12).

Superphane 28: A solution of **20** (30 mg, 0.056 mmol) and of [H_3CO_2CCpCo(COD)] (41 mg, 0.14 mmol) in 3 mL of cyclooctane was heated to 150 °C. The reaction progress was checked by TLC and after 4 hours the reaction mixture was allowed to cool to room temperature. After removal of the solvent the crude product was purified by column chromatography (silica gel/CH_2Cl_2) to give 32 mg (79.0%) of orange crystals; m.p. 225 °C. ^{1}H NMR (300 MHz, $CDCl_3$): δ = 5.28 (pseudo t., 2 H, CpH), 4.90 (pseudo t., 2 H, CpH), 4.71 (s, 5 H, CpH), 3.72 (s, 3 H, OCH_3), 2.27−1.88 (m, 8 H, CH_2), 0.09 [s, 12 H, $Si(CH_3)_2$], 0.08 [s, 12 H, $Si(CH_3)_2$], −0.19 (m, 4 H, $SiCH_2$) ppm. ^{13}C NMR (75 MHz, $CDCl_3$): δ = 168.4 (CO), 92.6 (C_{Cp}), 90.2 (C_{Cbd}), 83.7 (C_{Cbd}), 81.5 (CH), 80.4 (CH), 78.4 (CH), 67.7 (C_{Cbd}), 64.6 (C_{Cbd}), 51.1 (OCH_3), 24.6 (CH_2), 24.0 (CH_2), 7.2 ($SiCH_2$), 3.4 [$Si(CH_3)_2$], 3.0 [$Si(CH_3)_2$], 0.3 [$Si(CH_3)_2$], 0.0 [$Si(CH_3)_2$] ppm. HRMS (FAB+) calcd. for $C_{34}H_{48}Co_2O_2Si_4$ ([M]$^+$): 718.1395; found 718.1371 (−2.4 mmu). IR (KBr): $\tilde{\nu}$ = 2950 cm^{-1}, 2850, 2362, 1715, 1632, 1465, 1281, 1249. UV/Vis (CH_2Cl_2) (log ε): λ_{max} = 224 nm (4.67), 282 (4.51), 296 (4.61). $C_{34}H_{48}Co_2O_2Si_4$ (719.0): calcd. C 56.80, H 6.73; found C 56.96, H 7.01.

Superphane 29: A solution of **21** (25 mg, 0.045 mmol) and [(H_3CO_2CCp)Co(COD)] (33 mg, 0.11 mmol) in 3 mL of cyclooctane was heated to 150 °C. The reaction progress was checked by TLC and after 4 hours the reaction mixture was allowed to cool to room temperature. After removal of the solvent the crude product was purified by column chromatography (silica gel/CH_2Cl_2) to give 32 mg (97.0%) of yellow crystals; m.p. 198 °C. ^{1}H NMR (300 MHz, $CDCl_3$): δ = 5.28 (m, 2 H, CpH), 4.90 (m, 2 H, CpH), 4.62 (m, 2 H, CpH), 4.55 (m, 2 H, CpH), 3.72 (s, 3 H, OCH_3), 2.18−2.02 (m, 8 H, CH_2), 1.92 (s, 3 H, CH_3), 0.09 [s, 12 H, $Si(CH_3)_2$], 0.08 [s, 12 H, $Si(CH_3)_2$], −0.19 (m, 4 H, $SiCH_2$) ppm. ^{13}C NMR (75 MHz, $CDCl_3$): δ = 168.1 (CO), 92.9 (C_{Cp}), 92.3 (C_{Cbd}), 89.1 (C_{Cbd}), 83.4 (C_{Cbd}), 81.2 (CH), 80.1 (CH), 79.1 (CH), 77.0 (CH), 67.4 (C_{Cbd}), 63.9 (C_{Cp}), 50.8 (OCH_3), 23.7 (CH_2), 23.6 (CH_2), 13.5 (CH_3), 7.1 ($SiCH_2$), 3.1 [$Si(CH_3)_2$], 2.7 [$Si(CH_3)_2$], 0.0 [$Si(CH_3)_2$], −0.3 [$Si(CH_3)_2$] ppm. HRMS (FAB+) calcd. for $C_{35}H_{50}Co_2O_2Si_4$ ([M]$^+$): 732.1552; found 732.1550 (−0.2 mmu). IR (KBr): $\tilde{\nu}$ = 2950 cm^{-1}, 2850, 2362, 1714, 1632, 1466, 1281, 1247. UV/Vis (CH_2Cl_2) (log ε): λ_{max} = 222 nm (4.74), 280 (4.55), 296 (4.69). $C_{35}H_{50}Co_2O_2Si_4$ (733.0): calcd. C 57.35, H 6.88; found C 57.42, H 6.92.

Superphane 30: A solution of **22** (33 mg, 0.05 mmol) and [H_3CO_2CCpCo(COD)] (40 mg, 0.14 mmol) in 3 mL of cyclooctane was heated to 150 °C. The reaction progress was checked by TLC and after 4 hours the reaction mixture was allowed to cool to room temperature. After removal of the solvent the crude product was purified by column chromatography (silica gel/CH_2Cl_2/petroleum ether 1:2) to give 34 mg (79.1%) of a yellow solid; m.p. 146 °C. ^{1}H NMR (500 MHz, $CDCl_3$): δ = 5.28 (pseudo t., 2 H, CpH), 4.92 (m, 4 H, CpH), 4.68 (pseudo t., 2 H, CpH), 3.74 (s, 3 H, OCH_3), 2.14−1.95 (m, 8 H, CH_2), 0.13 [br, 33 H, $Si(CH_3)_3/Si(CH_3)_2$], −0.18 (s, 4 H, $SiCH_2$) ppm. ^{13}C NMR (125 MHz, $CDCl_3$): δ = 168.5 (CO), 92.7 (C_{Cp}), 90.4 (C_{Cbd}), 86.2 (C_{Cbd}), 83.2 (CH), 81.7 (CH), 81.2 (CH), 80.0 (CH), 67.6 (C_{Cbd}), 63.9 (C_{Cp}), 51.3 (OCH_3), 25.4 (CH_2), 24.1 (CH_2), 7.6 ($SiCH_2$), 3.6 [$Si(CH_3)_2$], 3.1 [$Si(CH_3)_2$], 0.5 [$Si(CH_3)_2$], 0.1 [$Si(CH_3)_2$], 0.0 [$Si(CH_3)_3$] ppm. HRMS (FAB+) calcd. for $C_{37}H_{56}Co_2O_2Si_5$ ([M]$^+$): 790.1791; found 790.1788 (−0.3 mmu). IR (micro pellet): 2952 cm^{-1}, 2850, 1712, 1637, 1462, 1248. UV/Vis (CH_2Cl_2) (log ε): λ_{max} = 252 nm (4.08). $C_{37}H_{56}Co_2O_2Si_5$ (791.1): calcd. C 56.17, H 7.13; found C 56.62, H 7.39.

Superphane 31: A solution of **23** (100 mg, 0.40 mmol) and [H_3CO_2CCpCo(COD)] (130 mg, 0.45 mmol) in 3 mL of cyclooctane was heated to 150 °C. The reaction progress was checked by TLC and after 4 hours the reaction mixture was allowed to cool to room temperature. After removal of the solvent the crude product was purified by column chromatography (silica gel/CH_2Cl_2/petroleum ether 1:2) to give 22 mg (55.0%) of an orange solid; m.p. 212 °C. ^{1}H NMR (500 MHz, $CDCl_3$): δ = 5.28 (pseudo t., 2 H, CpH), 4.91 (pseudo t., 2 H, CpH), 3.74 (s, 3 H, OCH_3), 2.11 (s, 4 H, CH_2), 2.00 (s, 4 H, CH_2), 1.86 (s, 15 H, $CpCH_3$), 0.09 [s, 24 H, $Si(CH_3)_2$], −0.22 (s, 4 H, $SiCH_2$) ppm. ^{13}C NMR (125 MHz, $CDCl_3$): δ = 168.6 (CO), 92.6 (C_{Cp}), 88.4 (C_{Cbd}), 85.8 (C_{Cbd}), 83.6 (C_{Cbd}), 81.5 (CH), 80.4 (CH), 67.3 (C_{Cbd}), 63.6 (C_{Cp}), 51.2 (OCH_3), 23.7 (CH_2), 23.4 (CH_2), 11.1 [$(CH_3)_5$], 8.8 ($SiCH_2$), 2.6 [$Si(CH_3)_2$], 2.3 [$Si(CH_3)_2$], 0.3 [$Si(CH_3)_2$], −0.1 [$Si(CH_3)_2$] ppm. HRMS

(FAB+) calcd. for $C_{39}H_{58}Co_2O_2Si_4$ ([M]$^+$): 788.2178; found 788.2135 (−4.3 mmu). IR (KBr): $\tilde{\nu}$ = 2948 cm^{-1}, 2902, 2849, 1714, 1628, 1465, 1279, 1248. UV/Vis (CH_2Cl_2) (log ε): λ_{max} = 286 nm (4.50), 306 (4.58), 396 (3.26).

Acknowledgments

We are grateful to the Deutsche Forschungsgemeinschaft, the Fonds der Chemischen Industrie and the BASF Aktiengesellschaft, Ludwigshafen, for their continuing support of our studies. The authors are grateful to Dr. J. Classen and A. Flatow for recording the cyclovoltammetric data.

[1] D. O. Cowan, F. Kaufman, *J. Am. Chem. Soc.* **1970**, *92*, 219−220.
[2] D. O. Cowan, D. Le Vanda, J. Park, F. Kaufman, *Acc. Chem. Res.* **1973**, *6*, 1−7.
[3] U. T. Mueller-Westerhoff, *Angew. Chem.* **1986**, *98*, 700−716; *Angew. Chem. Int. Ed. Engl.* **1986**, *25*, 702−718.
[4] R. H. Voegeli, H. C. Kang, R. G. Finke, V. Boekelheide, *J. Am. Chem. Soc.* **1986**, *108*, 7010−7016.
[5] R. Gleiter, M. Merger, *Angew. Chem.* **1997**, *109*, 2532−2546; *Angew. Chem. Int. Ed. Engl.* **1997**, *36*, 2426−2439.
[6] M. Robin, P. Day, *Adv. Inorg. Radiochem.* **1967**, *10*, 247−422.
[7] S. F. Nelson, *Chem. Eur. J.* **2000**, *6*, 581−588 and references therein.
[8] R. Roers, J. Hofmann, J. Classen, R. Gleiter, *Tetrahedron Lett.* **2001**, *42*, 5871−5873.
[9] M. E. Stoll, S. R. Lovelace, W. E. Geiger, H. Schimanke, I. Hyla-Kryspin, R. Gleiter, *J. Am. Chem. Soc.* **1999**, *121*, 9343−9351.
[10] G. Haberhauer, R. Gleiter, *Tetrahedron Lett.* **1998**, *39*, 6695−6698.
[11] G. Haberhauer, R. Roers, R. Gleiter, *Tetrahedron Lett.* **1997**, *38*, 8679−8682.
[12] R. Gleiter, H. Stahr, B. Nuber, *Tetrahedron Lett.* **1995**, *36*, 4607−4610.
[13] Y. Wakatsuki, O. Nomura, K. Kitaura, K. Morokuma, H. Yamazaki, *J. Am. Chem. Soc.* **1983**, *105*, 1907−1912 and references therein.
[14] R. Gleiter, M. Karcher, M. L. Ziegler, B. Nuber, *Tetrahedron Lett.* **1987**, *28*, 195−198.
[15] P. E. Riley, R. E. Davis, *J. Organomet. Chem.* **1976**, *113*, 157−166.
[16] A. Efraty, *Chem. Rev.* **1977**, *77*, 691−744.
[17] A. C. Villa, L. Coghi, A. G. Manfredotti, C. Guastini, *Acta Crystallogr., Sect. B* **1974**, *30*, 2101−2112.
[18] A. Clearfield, R. Gopal, M. D. Rausch, E. F. Tokas, F. A. Higbie, I. Bernal, *J. Organomet. Chem.* **1977**, *135*, 229−248.
[19] M. D. Rausch, G. F. Westhofer, E. Mintz, G. M. Reisner, I. Bernal, A. Clearfield, J. M. Troup, *Inorg. Chem.* **1979**, *18*, 2605−2615.
[20] J. Heinze, *Angew. Chem.* **1984**, *96*, 823−840; *Angew. Chem. Int. Ed. Engl.* **1984**, *23*, 831−848.
[21] R. Gleiter, H. Röckel, G. Pflästerer, B. Treptow, D. Kratz, *Tetrahedron Lett.* **1993**, *34*, 8075−8078.
[22] R. Gleiter, R. Roers, J. Classen, A. Jacobi, G. Huttner, T. Oeser, *Organometallics* **2000**, *19*, 147−151.
[23] SHELXTL V5.10 G, M. Sheldrick, Bruker Analytical X-ray-Division, Madison, Wisconsin **1997**.
[24] G. Sheldrick, **1996**, unpublished work based on the method described in: R. H. Blessing, *Acta Crystallogr., Sect. A* **1995**, S1−S33.

Received February 22, 2002
[I02092]

C−Cl and Si−Cl Activation by *P,N*-Chelated Pt^{II} Complexes

Frank Stöhr,[a] Dietmar Sturmayr,[a] Guido Kickelbick,[a] and Ulrich Schubert*[a]

Keywords: Platinum / Silicon / Hemilabile ligands / Oxidative addition / Halogen compounds

The complex [(κ²-*P,N*)-$Ph_2PCH_2CH_2NMe_2$]$PtMe_2$ reacts with chlorinated hydrocarbons such as CCl_4, $CHCl_3$, CH_2Cl_2, and CH_3Cl by oxidative addition of the C–Cl bond. In the reaction with CCl_4, the complexes [(κ²-*P,N*)-$Ph_2PCH_2CH_2NMe_2$]-Pt(Me)Cl, [(κ²-*P,N*)-$Ph_2PCH_2CH_2NMe_2$]$Pt(Me)_3Cl$, and [(κ²-*P,N*)-$Ph_2PCH_2CH_2NMe_2$]$Pt(CCl{=}CH_2)Cl$ are obtained. The analogous *P,P*-chelated complex [(κ²-*P,P*)-$Ph_2CH_2CH_2PPh_2$]-$PtMe_2$ does not react under the same conditions. Reaction of [(κ²-*P,N*)-$Ph_2PCH_2CH_2NMe_2$]$PtMe_2$ with $ClSiMe_2Ph$ results in the formation of $Ph_2Me_4Si_2$ along with [(κ²-*P,N*)-$Ph_2PCH_2CH_2NMe_2$]Pt(Me)Cl and [(κ²-*P,N*)-$Ph_2PCH_2CH_2NMe_2$]$Pt(Me)_3Cl$.
(© Wiley-VCH Verlag GmbH, 69451 Weinheim, Germany, 2002)

Introduction

The oxidative addition of organic halides to several complexes of the type (*N,N*-chelate)$PtMe_2$ to form Pt^{IV} derivatives has been described. While bromides and iodides react readily, simple alkyl chlorides were not employed since they react poorly.[1] The reason is probably the carbon−halogen bond strength, which increases in the sequence C−I (56 kcal·mol^{-1} for CH_3I), C−Br (70 kcal·mol^{-1}), C−Cl (84 kcal·mol^{-1}), and C−F (109 kcal·mol^{-1}). While the *thermal* reaction of chlorocarbons is not straightforward, Zelewsky et al. reported *photochemical* oxidative additions of chlorinated hydrocarbons to Pt^{II} complexes with hemilabile C,N ligands.[2]

In previous studies on the oxidative addition of organosilanes to Pt^{II} complexes, we found that the reactivity the complexes is strongly enhanced by hemilabile *P,N*-chelating ligands.[3,4] In this paper, we report that this is also true for reactions with chlorocarbons. The presence of the hemilabile ligands allows the *thermal* reactions of chloromethane derivatives with Pt^{II} complexes.

Results and Discussion

Reaction of (P∩N)$PtMe_2$ with CCl_4

When CCl_4 was added to a solution of [(κ²-*P,N*)-$Ph_2PCH_2CH_2NMe_2$]$PtMe_2$ (**1**) (the chelating ligand $Ph_2PCH_2CH_2NMe_2$ is abbreviated as P∩N) in C_6D_6 at room temperature, a colorless precipitate was immediately formed. The reaction was complete within 2 min. In contrast, no reaction occurred with the bis(phosphane) complexes [(κ²-*P,P*)-$Ph_2PCH_2CH_2PPh_2$]$PtMe_2$ or $(PhMe_2P)_2$-$PtMe_2$.

The course of the reaction was monitored by ^{31}P, ^{1}H, and ^{195}Pt NMR spectroscopy. Three new sets of signals are observed in the ^{31}P and ^{195}Pt NMR spectra, with characteristic coupling constants (Table 1).

Table 1. ^{31}P and ^{195}Pt NMR spectra of complexes **2**−**4** (in [D_6]acetone; δ in ppm, *J* in Hz)

Complex	δ(^{195}Pt)	$^{1}J_{PtP}$	δ(^{31}P)
2	−4243	4678	27.29
3	−3905	4363	25.5
4	−2976	1213	9.33

The precipitate was spectroscopically characterized as (P∩N)Pt(Me)Cl (**2**) and independently synthesized by reaction of (P∩N)$PtMe_2$ with HCl or from (norbornadiene)Pt(Me)Cl and $Ph_2PCH_2CH_2NMe_2$, as described for [(κ²-*P,P*)-$Ph_2PCH_2CH_2CH_2PPh_2$]Pt(Me)Cl.[5] Complex **2** was only sparingly soluble in benzene, and therefore part of the formed **2** precipitated from the reaction solution.

After separation of **2** and addition of petroleum ether to the clear solution, the additional complex **3** crystallized. Compound **3** was identified by an X-ray crystal structure analysis as (P∩N)Pt($CCl{=}CH_2$)Cl (Figure 1 and Table 2). The vinylic protons in the ^{1}H NMR spectrum of isolated **3** have chemical shifts and $^{3}J_{PtH}$ coupling constants similar to those reported in the literature.[6,7] $^{4}J_{PH}$ and geminal $^{2}J_{H,H}$ were not observed.

In **3**, Pt^{II} has the typical square-planar coordination. The Pt−P(1) distance of 220.19(8) pm and the Pt−N(16) distance of 218.1(2) pm are in the same range as observed for (silyl)Pt^{II} complexes with such ligands.[4] The chloro ligand is located *trans* to the phosphorus atom; the Pt−Cl(1) distance of 236.64(8) pm is typical for this arrangement.[8] The only other related structure is a methyl-substituted complex (PTFA)$Pt(CH_3)Cl$ [PTFA: (η⁵-cyclopentadienyl)(η⁵-4-*endo*-

[a] Institut für Materialchemie, Technische Universität Wien, Getreidemarkt 9, 1060 Wien, Austria

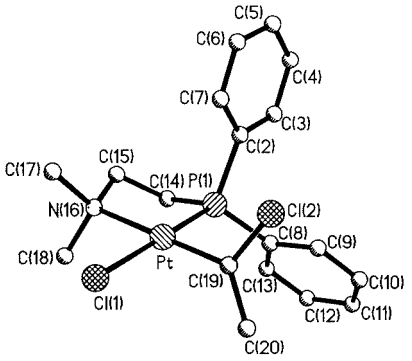

Figure 1. Molecular structure of $[(\kappa^2\text{-}P,N)\text{-}Ph_2PCH_2CH_2NMe_2]Pt(CCl{=}CH_2)Cl$ (**3**); the asymmetric unit also contains three benzene molecules that are not shown in this figure

Table 2. Selected bond lengths [pm] and angles [°] for **3**

Pt−Cl(1)	236.64(8)	C(19)−Pt−Cl(1)	89.61(8)
Pt−P(1)	220.19(8)	Cl(1)−Pt−P(1)	175.28(2)
Pt−N(16)	218.1(2)	C(2)−P(1)−C(8)	105.66(13)
Pt−C(19)	200.2(3)	C(2)−P(1)−C(14)	104.03(13)
P(1)−C(2)	181.6(3)	C(8)−P(1)−C(14)	107.84(13)
P(1)−C(8)	181.1(3)	C(15)−N(16)−C(17)	107.9(2)
P(1)−C(14)	182.8(3)	C(17)−N(16)−C(18)	108.7(2)
Cl(2)−C(19)	168.9(4)	C(15)−N(16)−C(17)	108.9(2)
N(16)−Pt−P(1)	85.32(7)	C(20)−C(19)−Pt	124.7(2)
C(19)−Pt−P(1)	94.03(8)	C(20)−C(19)−Cl(2)	117.7(2)
C(19)−Pt−N(16)	179.34(9)	Cl(2)−C(19)−Pt	117.61(18)
N(16)−Pt−Cl(1)	91.04(7)		

dimethylamino-3-diphenylphosphanyl-4,5,6,7-tetrahydro-1*H*-indenyl)iron].[9] A chlorovinyl-substituted bis(phosphane)Pt^{II} complex $(Me_2PhP)_2Pt(CCl{=}CH_2)_2$ was reported in the literature with a Pt−C bond length of 205.3(5) pm.[10] In comparison, the Pt−C bond length in **3** is rather short [Pt−C(19), 200.2(3) pm]. However, the accuracy of the bond lengths in the chlorovinyl ligand of **3** is rather low because the Cl and C positions are disordered. The position Cl(2) (Figure 1) has an occupation of 70% Cl and 30% C, and that of C(20) vice versa.

The ^{1}H NMR spectrum of the original reaction solution shows four Pt−CH_3 signals with characteristic $^2J_{PtH}$ and $^3J_{PH}$ coupling constants. One of them is assigned to the PtMe group of complex **2**. Since **3** contains no methyl ligands, the remaining three signals with equal intensity must belong to a single complex. This complex is spectroscopically identified as (P∩N)$Pt(Me)_3Cl$ (**4**) by comparison with an authentic sample of **4** obtained by another route (see below). An X-ray structure analysis of **4** was performed.

The postulated sequence of reactions starting with **1** and CCl_4 is shown in Scheme 1.

CCl_4 probably attacks (P∩N)$PtMe_2$ (**1**) by oxidative addition of one C−Cl bond in the first step of the reaction. Kuyper reported the oxidative addition of CCl_4 to (bpy)$PtMe_2$ yielding the stable product (bpy)$Pt(Me)_2Cl(CCl_3)$.[11] In contrast, we did not observe the corresponding Pt^{IV} complex **5**. It can therefore be assumed that subsequent reductive elimination to Pt^{II} complexes is fast. It appears that the hemilabile (P∩N)-chelate ligand facilitates both the oxidative addition and the reductive elimination from the Pt complex. There are three possibilities of reductive elimination from complex **5**: (i) Elimination of Me−CCl_3 to give complex **2**. This possibility can be excluded because there is no NMR spectroscopic evidence for $MeCCl_3$. (ii) Elimination of MeCl to give complex **6**. (iii) Elimination of ethane. There is no experimental evidence for the formation of ethane.

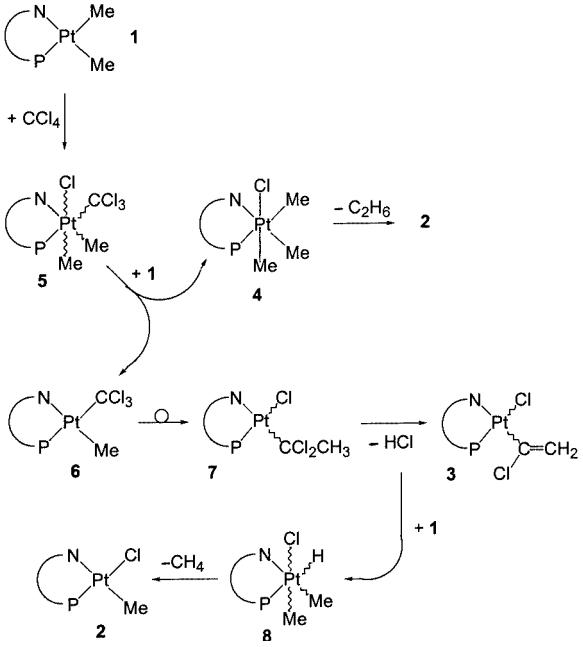

Scheme 1

A bis(phosphane) complex analogous to **6**, $[(\kappa^2\text{-}P,P')\text{-}Ph_2PCH_2CH_2PPh_2]Pt(CCl_3)Me$, was reported to rearrange by a CCl_2 shift, followed by the elimination of HCl.[12] The same mechanism leads to the formation of **7** and the isolated vinylidene complex **3**. The eliminated HCl can react with the starting complex **1** to give complex **8**, followed by the elimination of methane to give complex **2**. The latter reaction sequence was confirmed by the reaction of (P∩N)$PtMe_2$ (**1**) with a solution of HCl in diethyl ether, which resulted in the formation of **2**.

Complex **1** does not react with the methyl chloride eliminated in the second step under the conditions at which the reaction with CCl_4 was performed (room temperature) to form the observed product **4** (**4** is only formed at elevated temperatures, see below). We therefore propose a methyl transfer reaction between complexes **1** and **5** to give **4** and **6**. The elimination of ethane from **4** can be assumed as another source of complex **2** in the reaction scheme above. This was proven by another experiment described below.

Due to the different donor/acceptor properties of the two Lewis basic centers of the (P∩N) ligand, the reactions described above are highly selective, and no isomers of the complexes **2**−**4** were observed.

When the deuterated complex (P∩N)$Pt(CD_3)_2$ is used for the reaction with CCl_4, the ^{31}P NMR spectrum is unchanged. The Pt−CH_3 signals of complexes **2** and **4** and the $=CH_2$ signals of complex **3** are not detected in the ^{1}H

NMR spectrum. The ^2H NMR spectrum shows three $Pt-CD_3$ signals of equal intensity for the deuterated complex **4**, and one $Pt-CD_3$ signal for deuterated **2**. There is one additional peak at $\delta = 0.11$ ppm in the ^1H NMR spectrum. This may belong to deuterated ethane, proving the formation of **2** from **4** by reductive elimination. Only one $=CD_2$ signal of the deuterated form of **3** is detected. The experiment was repeated in C_6H_6 since the second peak may be hidden by the broad signal of the solvent C_6D_6. However, no further peak is detected. The lack of the second $=CD_2$ signal may be due to exchange effects.[13]

Reaction of $(P^{\frown}N)PtMe_2$ with $CHCl_3$

$(P^{\frown}N)PtMe_2$ was much more reactive towards CCl_4 than towards $CHCl_3$. While the reaction with CCl_4 was complete within 2 min at room temperature, no reaction was observed with $CHCl_3$ after 1 d under the same conditions. However, $(P^{\frown}N)Pt(Me)Cl$ (**2**) crystallized from a $CHCl_3$/petroleum ether solution of $(P^{\frown}N)PtMe_2$ after several weeks. For a reasonable reaction rate, it was necessary to heat the mixture to 60 °C. At this temperature, the reaction was complete in about 10 h.

Three new signals are observed in the ^{31}P NMR spectrum when a mixture of $(P^{\frown}N)PtMe_2$ and $CHCl_3$ in a 1:2 ratio was heated in C_6D_6. Comparison of the spectra with those of the products obtained in the reaction of $(P^{\frown}N)PtMe_2$ with CCl_4 shows that complexes **2** and **4** are also formed in the reaction with $CHCl_3$. The concentrations of **2** and **4** increase simultaneously, while the concentration of **1** decreases. The new complex **9** with a large $^1J_{PtP}$ coupling constant, indicating a chlorine atom *trans* to the phosphorus atom, is detected in small quantities only after a reaction time of about 6 h. No Pt−Me resonances are observed in the ^1H NMR spectrum, other than those of complexes **4** and **2**. According to the reaction mechanism shown in Scheme 1, complex **9** could be $(P^{\frown}N)Pt(Cl)(CH=CH_2)$. There are signals between $\delta = 5$ and 6 ppm in the ^1H NMR spectrum, which may arise from the vinyl group of **9**. The signals are very weak probably due to the H−H, H−P, and H−Pt coupling, and unequivocal identification is therefore not possible. We were not able to separate **9** from the reaction mixture.

When $(P^{\frown}N)Pt(CD_3)_2$ is treated with $CHCl_3$, no $Pt-CH_3$ signals are observed in the ^1H NMR spectrum, and the ^2H NMR spectrum shows a signal for deuterated **2** and three signals of equal intensity for deuterated **4**.

Reaction of $(P^{\frown}N)PtMe_2$ with CH_2Cl_2

The reactivity of CH_2Cl_2 was lower than that of $CHCl_3$. At 60 °C in C_6D_6, **2** and **4** were formed after a few days, along with decomposition products, which were not identified, and a black precipitate. In contrast to the reaction with CCl_4 and $CHCl_3$, no other P-containing platinum complex is observed by ^{31}P NMR spectroscopy.

The sequence of reactivity of the halogenated hydrocarbons, i.e. $CCl_4 > CHCl_3 > CH_2Cl_2$, is related to the C−Cl bond strength in these compounds (CCl_4 −248 kJ·mol^{-1}, $CHCl_3$ −280 kJ·mol^{-1}, CH_2Cl_2 −304 kJ·mol^{-1}, CH_3Cl −328 kJ·mol^{-1}).

Reaction of $(P^{\frown}N)PtMe_2$ with CH_3Cl

CH_3Cl does not fit into the sequence as it reacted with $(P^{\frown}N)PtMe_2$ in a hot C_6D_6 solution to form complex **4** and traces of **2**. The reaction was complete within 12 h. The amount of **2** increased on further heating, indicating reductive elimination of ethane from **4**. At room temperature no reaction occurred after 1 h (see above). Again, the analogous *P,P*-chelated complex $(dppe)PtMe_2$ did not react with CH_3Cl at 60 °C in C_6D_6 after 24 h.

Complex **4** was structurally characterized and has a distorted octahedral geometry (Figure 2 and Table 3). The asymmetric unit contains only half of the molecule with Pt, C(20), C(21), C(8) N(10), and P(1) in a crystallographic mirror plane. Therefore, the positions of Cl and C(22A) are disordered and hence have a mixed occupancy. The C(9) atom of the ethylene bridge is also disordered. The Pt−C distances of the equatorial methyl substituents [Pt−C(20):

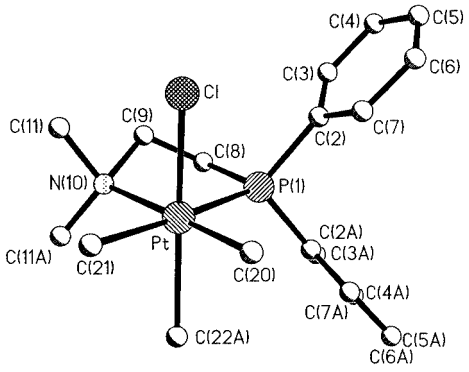

Figure 2. Molecular structure of $[(\kappa^2\text{-}P,N)\text{-}Ph_2PCH_2CH_2NMe_2]\text{-}Pt(Me)_3Cl$ (**4**)

Table 3. Selected bond lengths [pm] and angles [°] measured for **4** and calculated for **4b**. The asterisks refer to symmetry-equivalent atoms

	4	**4b**
Pt−C(20)	206.3(10)	207.2
Pt−C(21)	208.2(9)	208.6
Pt−N(10)	230.4(8)	230.8
Pt−P(1)	236.9(2)	244.7
Pt−Cl	240.9(3)	252.8
Pt−C(22)*	240.9(3)	208.3
C(20)−Pt−C(21)	85.4(5)	87.9
N(10)−Pt−C(20)	178.1(4)	177.6
N(10)−Pt−C(21)	92.7(4)	91.7
P(1)−Pt−C(20)	99.5(3)	100.0
P(1)−Pt−C(21)	175.1(4)	171.5
P(1)−Pt−N(10)	82.4(2)	80.2
Cl−Pt−C(20)	87.55(8)	94.7
Cl−Pt−C(21)	88.36(7)	90.1
Cl−Pt−N(10)	92.40(8)	82.9
Cl−Pt−P(1)	91.84(7)	86.1
C(2)−P(1)−C(8)	105.9(3)	
C(11)−N(10)−C(11)*	105.4(10)	
C(9)−N(10)−C(11)	87.3(9)	

206.3(10) pm; Pt−C(21): 208.2(9) pm] are in the same range as for corresponding Pt^{II} complexes with a P−N-chelating ligand.[14] Due to the disorder of the axial positions, an average distance of only 240.9(3) pm was found.

In order to estimate the Pt−Cl and Pt−C distances, in spite of the disorder of the axial ligands, an ab initio calculation was performed. The phenyl and methyl groups of the chelate ligand were substituted by hydrogen to reduce calculation time. The geometry optimization of this simplified molecule **4b** resulted a Pt−C(22) distance of 208.3 pm and a Pt−Cl distance of 252.8 pm. Additional bond lengths and angles are given in Table 2. Most bond lengths and angles are in good agreement with the measured values of complex **4**. The calculated bond lengths are typical for hexacoordinated Pt compounds and are in agreement with those found in an iodotrimethylplatinum(IV) complex.[15]

Elimination of Ethane from (P⌒N)Pt(Me)$_3$Cl (4) on Heating

A sample of the isolated complex **4** was dissolved in [D_8]toluene and heated in an NMR tube. At 60 °C, formation of **2** was detected in the ^{1}H and ^{31}P NMR spectra, but the reaction rate was quite low. Therefore, the temperature was increased to 90 °C, at which temperature the reaction was complete in about 12 h. At this temperature the two Pt−CH_3 signals of **4** at δ = 0.59 and 1.92 ppm are extremely broad, while the third Pt−CH_3 signal of **4** at δ = 1.49 ppm remains unchanged. Comparison of the Pt−CH_3 resonances of **4** with that of complexes **1**, **2**, and a $(PhMe_2P)_2PtMe_3Cl$ isomer[16] analogous to **4**, allows for the assignment of the Pt−Me signal at δ = 0.59 ppm to the methyl group *trans* to Cl, the signal at δ = 1.92 ppm to the methyl group *trans* to the nitrogen atom, and the signal at δ = 1.49 ppm to the methyl group *trans* to the phosphorus atom. The broadening of the two methyl resonances appears to be related to the start of the reductive elimination of ethane, i.e. ethane is probably formed from the methyl groups *trans* to the nitrogen atom and *trans* to the chlorine atom. The formation of ethane was proven by mass spectrometry.

(P⌒N)Pt(CD_3)$_2$ was analogously treated to check whether the addition of CH_3Cl is stereospecific. However, no difference is seen in the ^{31}P NMR spectra compared with those of the experiments with (P⌒N)PtMe_2. The ^{1}H NMR spectrum shows three Pt−CH_3 signals of **4** with equal intensities. Instead of three singlets with satellites, there are three doublets of doublets with satellites. The additional line splitting may be due to an H−D coupling, or due to the different chemical shifts of the structural isomers. Corresponding signals, also with equal intensity, are seen in the ^{2}H NMR spectrum, indicating a statistical distribution of the added CH_3 group to the three possible positions of complex **4**. An intermolecular exchange reaction, or rearrangement via a five-coordinate complex with an intermediate and the reversible opening of the (P⌒N)-chelate ligand may be responsible for the scrambling reaction. Thermolysis of (P⌒N)Pt(CD_3)$_2$(Me)Cl results in the formation of both C_2H_6 and $C_2H_3D_3$, as found by mass spectrometry.

Reaction of (P⌒N)PtMe$_2$ with ClSiMe$_2$Ph

(P⌒N)PtMe_2 not only exhibited a strongly increased reactivity towards C−Cl bonds in comparison with related (P⌒P)PtMe_2 complexes, but was also able to activate the stronger Si−Cl bond of $ClSiMe_2Ph$. When a solution of (P⌒N)PtMe_2 was heated in C_6D_6 with a stoichiometric amount of $ClSiMe_2Ph$, the disilane $Ph_2Me_4Si_2$ was the only silicon-containing product. Complexes **4** and **2** were formed in this reaction in a ratio of about 1:4. The amount of **2** increased after complete conversion of the chlorosilane, indicating a reductive elimination of ethane from **4**, forming **2**. The products were identified by spectroscopic comparison with independently prepared samples. A possible reaction mechanism is shown in Scheme 2. Although the intermediate complex **10** was not observed, this mechanism appears plausible because the formation of both **4** and **10** would correspond to the formation of complexes **4**−**5** in the reaction of **1** with CCl_4 (Scheme 1). A rearrangement similar to **6** → **7** is obviously less favored than the substitution of the second methyl ligand.

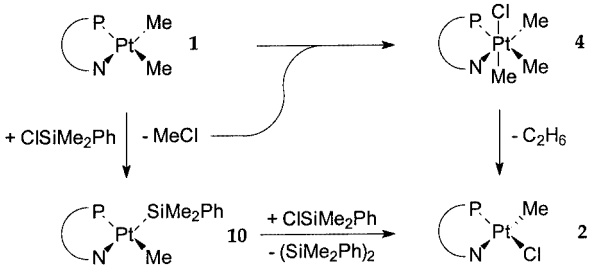

Scheme 2

Conclusions

The reactivity of Pt^{II} complexes with the chelating P⌒N ligands towards chlorinated hydrocarbons and chlorinated silanes is greatly enhanced relative to the corresponding chelating bis(phosphane) complexes. This reactivity enhancement may have two reasons: (i) The nitrogen donor group of the P⌒N ligands can be reversibly de-coordinated, i.e. the ligand is hemilabile. In comparison, the de-coordination of a phosphorus donor center chelating bis(phosphane) complexes is much more difficult. Hemilabile ligands are known to promote both oxidative addition and reductive elimination reactions. (ii) Due to the different donor/acceptor properties of the two Lewis basic centers in the P⌒N ligands, the electronic difference *trans* to the nitrogen atom is different to that *trans* to the phosphorus atom, i.e. the bond strengths of the *trans* ligands are greatly influenced.

Experimental Section

General: All reactions were performed under dried argon. All reagents were of best commercial grade. The complexes (P⌒N)PtMe_2,

$(P^{\frown}P)PtMe_2$, and $(PhMe_2P)_2PtMe_2$ were prepared as previously described.[4] Solids were used without further purification, liquids were dried with molecular sieves (4 Å) for 24 h and argon-saturated by freeze-pump-thaw. NMR spectra were recorded with a Bruker DPX 300 Avance spectrometer (^1H and ^{29}Si NMR spectroscopy, TMS as an external standard. ^{31}P NMR spectroscopy, 85% H_3PO_4 as an external standard; ^{195}Pt NMR spectroscopy, Na_2PtCl_6 in D_2O as an external standard). ^{29}Si NMR spectra were recorded with an INEPT pulse sequence.

Computational Details: The geometry optimization of the equilibrium geometry of **4b** was carried out using the B3LYP version of DFT, which is comprised of Becke's hybrid three-parameter exchange functional,[17] and the correlation functional of Lee, Yang, and Parr.[18] The structure was characterized as minima by computing the Hessian matrices. The ab initio calculation was performed with the Gaussian98 program package.[19] From the available ECP basis sets in Gaussian98, the SDD basis set was used for platinum and the 6-311++G(d) basis set for all the other atoms.

General Procedure for the Reaction of Pt Complexes with Halogenated Compounds: All reactions were performed under argon in NMR or Schlenk tubes. The reaction vessels were flame-dried and argon-saturated before addition of the Pt complex. After addition of the solvent and the liquid halogenated compound, the vessel was closed and put into a thermostatically controlled oil bath or into the thermostatically controlled NMR spectrometer immediately. Experiments with silanes were performed in an NMR Teflon liner.

Reaction of $(P^{\frown}N)PtMe_2$ with CCl_4 in C_6D_6: CCl_4 (11.4 μL, 0.12 mmol) was added to a solution of **1** (28.7 mg, 0.06 mmol) in 0.7 mL of C_6D_6. A colorless solid precipitated immediately. It was separated by decanting the liquid phase and washed twice with cold benzene. The NMR spectra were identical with that of an independently prepared sample of **2** (see below). The supernatant solution was decanted and analyzed by NMR spectroscopy. ^1H NMR (C_6D_6, 27 °C): δ = 0.61 (d, $^3J_{PH}$ = 7.7, $^2J_{PtH}$ = 71 Hz, Pt−CH_3, **4**), 1.39 (d, $^3J_{PH}$ = 3.0, $^2J_{PtH}$ = 75 Hz, Pt−CH_3, **2**), 1.61 (d, $^3J_{PH}$ = 8.1, $^2J_{PtH}$ = 57 Hz, Pt−CH_3, **4**), 1.89 (s, $^3J_{PtH}$ = 13.8 Hz, NMe_2, **4**), 2.03 (d, $^3J_{PH}$ = 7.0, $^2J_{PtH}$ = 73 Hz, Pt−CH_3, **4**), 2.56 (s, $^3J_{PtH}$ = 13 Hz, NMe_2, **3**), 2.64 (s, $^3J_{PtH}$ = 11 Hz, NMe_2, **2**), 2.69 (s, $^3J_{PtH}$ = 10 Hz, NMe_2, **4**), 5.04 (s, $^3J_{PtH}$ = 34 Hz, *cis* =CH, **3**), 6.18 (s, $^3J_{PtH}$ = 89 Hz, *trans* =CH, **3**) ppm. $^{31}P\{^1H\}$ NMR (C_6D_6, 27 °C): δ = 8.11 (s, $^1J_{PtP}$ = 1185 Hz, **4**), 24.43 (s, $^1J_{PtP}$ = 4375 Hz, **3**), 26.45 (s, $^1J_{PtP}$ = 4677 Hz, **2**) ppm. $^{195}Pt\{^1H\}$ NMR (C_6D_6, 27°C): δ = −4243 (d, $^1J_{PtP}$ = 4678 Hz, **2**), −3905 (d, $^1J_{PtP}$ = 4363 Hz, **3**), −2976 (d, $^1J_{PtP}$ = 1213 Hz, **4**) ppm. After the addition of some petroleum ether (boiling range 30−50°C)) to the decanted reaction solution, crystals of **3** suitable for a crystal structure analysis were formed within a few days. **3**: ^1H NMR ([D_6]acetone, 27 °C): δ = 2.65−2.85 (m, 4 H, CH_2), 2.87 (s, $^3J_{PtH}$ = 14 Hz, 6 H, NCH_3), 4.39 (s, $^3J_{PtH}$ = 36 Hz, 1 H, *cis* =CH), 5.43 (s, $^3J_{PtH}$ = 90 Hz, 1 H, *trans* =CH), 7.50−7.95 (m, 10 H, C_{arom}) ppm. $^{31}P\{^1H\}$ NMR (C_6D_6, 27 °C): δ = 24.33 (s, 4376 Hz) ppm. $^{31}P\{^1H\}$ NMR ([D_6]-acetone, 27°C): δ = 25.5 (s, $^1J_{PtP}$ = 4369 Hz) ppm.

Synthesis of $(P^{\frown}N)Pt(Cl)Me$ (2) by Reaction of $(P^{\frown}N)PtMe_2$ with HCl: A solution of HCl (0.1 mL, 0.10 mmol) in diethyl ether was added to a solution of $(P^{\frown}N)PtMe_2$ (23.9 mg, 0.05 mmol) in 0.7 mL of C_6D_6. The volatile compounds were then removed from the solution, and $(P^{\frown}N)Pt(Me)Cl$ (**2**) remained as a colorless powder in a quantitative yield. ^1H NMR ($CDCl_3$, 27 °C): δ = 0.63 (d, $^3J_{PH}$ = 2.8, $^2J_{PtH}$ = 73 Hz, Pt−CH_3, **2**), 2.3−2.7 (m, CH_2CH_2), 2.87 (s, $^3J_{PtH}$ = 11 Hz, NMe_2), 7.4−7.8 (m, PPh_2) ppm. $^{31}P\{^1H\}$ NMR ($CDCl_3$, 27 °C): δ = 27.28 (s, $^1J_{PtP}$ = 4700 Hz) ppm. $C_{17}H_{23}ClNPPt$ (475.4): calcd. C 40.61, H 4.70, N 2.56; found C 41.39, H 4.70, N 2.56.

Synthesis of $(P^{\frown}N)Pt(Cl)Me$ (2) by Reaction of (nbd)PtMeCl[5] with $P^{\frown}N$: A solution of [2-(diphenylphosphanyl)ethyl]dimethylamine ($P^{\frown}N$)[20] (282 mg, 1.09 mmol) in 10 mL of CH_2Cl_2 was added slowly to a solution of (nbd)Pt(Me)Cl (365 mg, 1.08 mmol) in 40 mL of CH_2Cl_2. After the mixture was stirred for 1 h, the colorless product was filtered and washed with benzene (3 × 5 mL) and pentane (3 × 5 mL). Yield 543 mg (85%).

Reaction of $(P^{\frown}N)Pt(CD_3)_2$ with CCl_4 in C_6D_6: CCl_4 (8.7 μL, 0.09 mmol) was added to a solution of $(P^{\frown}N)Pt(CD_3)_2$ (22 mg, 0.045 mmol) in 0.7 mL of C_6D_6. ^1H NMR (C_6D_6, 27 °C): δ = 1.83 (s, $^3J_{PtH}$ = 14.3 Hz, NMe_2, **4**), 2.59 (s, $^3J_{PtH}$ = 13 Hz, NMe_2, **3**), 2.64 (s, $^3J_{PtH}$ = 10.7 Hz, NMe_2, **2**), 2.69 (s, $^3J_{PtH}$ = 9.6 Hz, NMe_2, **4**) ppm. $^2H\{^1H\}$ NMR (C_6D_6, 27 °C): δ = 0.43 (s, $^2J_{PtD}$ = 10.1 Hz, Pt−CD_3, **4**), 1.18 (s, $^2J_{PtD}$ = 10.0 Hz, Pt−CD_3, **2**), 1.40 (s, $^2J_{PtD}$ = 7.5 Hz, Pt−CD_3, **4**), 1.83 (s, $^2J_{PtD}$ = 10.9 Hz, Pt−CD_3, **4**), 4.89 (s, =CD_2, **3**) ppm. $^{31}P\{^1H\}$ NMR (C_6D_6, 27 °C): δ = 8.67 (s, $^1J_{PtP}$ = 1180 Hz, **4**), 24.72 (s, $^1J_{PtP}$ = 4381 Hz, **3**), 26.89 (s, $^1J_{PtP}$ = 4679 Hz, **2**) ppm.

Reaction of $(P^{\frown}N)PtMe_2$ with $CHCl_3$ in C_6D_6: $CHCl_3$ (7.8 μL, 0.095 mmol) was added to a solution of **1** (23 mg, 0.05 mmol) in 0.7 mL of C_6D_6. After addition, the sample was heated to 60 °C. ^1H NMR (C_6D_6, 60 °C): δ = 0.59 (d, $^3J_{PH}$ = 7.7, $^2J_{PtH}$ = 71.0 Hz, Pt−CH_3, **4**), 1.34 (d, $^3J_{PH}$ = 3.5, $^2J_{PtH}$ = 75.1 Hz, Pt−CH_3, **2**), 1.53 (d, $^3J_{PH}$ = 8.3, $^2J_{PtH}$ = 58.0 Hz, Pt−CH_3, **4**), 1.91 (s, $^3J_{PtH}$ = 14.1 Hz, NCH_3, **4**), 1.94 (d, $^3J_{PH}$ = 6.9, $^2J_{PtH}$ = 73.1 Hz, Pt−CH_3, **4**), 2.60 (s, $^3J_{PtH}$ = 12.6 Hz, NCH_3, **9**), 2.64 (s, $^3J_{PtH}$ = 11.5 Hz, NMe_2, **2**), 2.70 (s, $^3J_{PtH}$ = 9.3 Hz, NMe_2, **4**) ppm. $^{31}P\{^1H\}$ NMR (C_6D_6, 60 °C): δ = 7.57 (s, $^1J_{PtP}$ = 1175 Hz, **4**), 26.15 (s, $^1J_{PtP}$ = 4657 Hz, **2**), 27.95 (s, $^1J_{PtP}$ = 4559 Hz, **9**) ppm.

Reaction of $(P^{\frown}N)Pt(CD_3)_2$ with $CHCl_3$ in C_6D_6: $CHCl_3$ (19.5 μL, 0.24 mmol) was added to a solution of **1** (58.6 mg, 0.12 mmol) in 0.7 mL of C_6D_6. The sample was then heated to 60 °C. ^1H NMR (C_6D_6, 60 °C): δ = 1.93 (s, $^3J_{PtH}$ = 13.9 Hz, NCH_3, **4**), 2.59 (s, $^3J_{PtH}$ = 12.4 Hz, NCH_3, **9**), 2.64 (s, $^3J_{PtH}$ = 11.8 Hz, NMe_2, **2**), 2.72 (s, $^3J_{PtH}$ = 9.2 Hz, NMe_2, **4**). $^2H\{^1H\}$ NMR (C_6D_6, 60 °C): 0.45 (s, $^2J_{PtD}$ = 10.4 Hz, Pt−CD_3, **4**), 1.26 (s, $^2J_{PtD}$ = 10.0 Hz, Pt−CD_3, **2**), 1.48 (s, $^2J_{PtD}$ = 7.5 Hz, Pt−CD_3, **4**), 1.86 (s, $^2J_{PtD}$ = 11.0 Hz, Pt−CD_3, **4**) ppm. $^{31}P\{^1H\}$ NMR (C_6D_6, 60 °C): δ = 7.93 (s, $^1J_{PtP}$ = 1180 Hz, **4**), 26.63 (s, $^1J_{PtP}$ = 4679 Hz, **2**), 28.41 (s, $^1J_{PtP}$ = 4562 Hz, **9**) ppm.

Reaction of $(P^{\frown}N)PtMe_2$ with CH_2Cl_2 in C_6D_6: CH_2Cl_2 (29.4 μL, 0.445 mmol) was added to a solution of **1** (21.5 mg, 0.045 mmol) in 0.7 mL of C_6D_6. After addition, the sample was heated to 60 °C. $^{31}P\{^1H\}$ NMR (C_6D_6, 60 °C): δ = 7.33 (s, $^1J_{PtP}$ = 1167 Hz, **4**), 26.60 (s, $^1J_{PtP}$ = 4681 Hz, **2**) ppm.

Formation of $(P^{\frown}N)Pt(Me)_3Cl$ (4) by Reaction of $(P^{\frown}N)PtMe_2$ with CH_3Cl in C_6D_6: A gentle stream of methyl chloride was bubbled through a solution of **1** (108 mg, 0.22 mmol) in 2 mL of C_6D_6. After 1 h, the ^1H NMR spectrum showed an intensive CH_3Cl signal at δ = 2.48 ppm, but no formation of new complexes. The CH_3Cl saturated solution was then heated to 60 °C and a finely divided colorless solid precipitated. After 12 h, the conversion into **4** was approximately 95%. After 24 h, conversion was complete and only traces of **1** were observed. Crystallization from a saturated benzene solution yielded pure **4** as colorless crystals, some of them suitable for a X-ray structure analysis. ^1H NMR (C_6D_6, 60 °C): δ = 0.59 (d, $^3J_{PH}$ = 7.7, $^2J_{PtH}$ = 70.8 Hz, Pt−CH_3), 1.51 (d, $^3J_{PH}$ = 8.2, $^2J_{PtH}$ = 57.6 Hz, Pt−CH_3), 1.89 (s, $^3J_{PtH}$ = 14.1 Hz, NCH_3), 1.93

Table 4. Crystallographic data for **3** and **4**

Compound	**3**	**4**
Empirical formula	$C_{30}H_{26}Cl_2NPPt$	$C_{19}H_{22}ClNPPt$
Formula mass	697.48	525.89
Crystal system	triclinic	orthorhombic
Space group	$P\bar{1}$	*Pnma*
Unit cell dimensions		
a [pm]	832.3(3)	900.36(4)
b [pm]	1300.8(4)	1359.59(6)
c [pm]	1492.4(5)	1655.71(7)
α [°]	68.069(5)°	90
β [°]	81.566(6)°	90
γ [°]	81.455(6)°	90
Volume [pm^3]	1474.8(8)×10^6	2026.79(15)×10^6
Z	2	4
Calculated density [g cm^{-3}]	1.571	1.723
Absorption coefficient [mm^{-1}]	5.011	7.132
F(000)	680	1012
Crystal size [mm]	0.60 × 0.16 × 0.16	0.32 × 0.28 × 0.08
θ range [°]	1.81−28.35	1.94−26.37
Reflections collected/unique	10116/7137 [*R*(int) = 0.0183]	11350/2143 [*R*(int) = 0.0373]
Completeness to θ [%]	97.0	99.0
Max. and min. transmission	0.5011, 0.1530	0.5992, 0.2087
Data/restraints/parameters	7137/0/317	2143/0/119
Goodness-of-fit on F^2	1.033	1.213
Final *R* indices [$I > 2\sigma(I)$]	R_1 = 0.0208, wR_2 = 0.0534	R_1 = 0.0312, wR_2 = 0.0792
R indices (all data)	R_1 = 0.0229, wR_2 = 0.0543	R_1 = 0.0335, wR_2 = 0.0803
Weighting scheme $P = (F_o^2 + 2F_c^2)/3$	$w = 1/[\sigma^2(F_o^2) + (0.0299P)^2 + 0.16P]$	$w = 1/[\sigma^2(F_o^2) + 9.69\ P]$
Extinction coefficient	0.0014(2)	0.00040(15)
Largest diff. peak/hole [e·A^{-3}]	1.147/−1.131	0.888/−1.130

(d, $^2J_{PtH}$ = 7.2, $^3J_{PH}$ = 73.1 Hz, Pt−CH_3), 2.70 (s, $^3J_{PtH}$ = 9.4 Hz, NCH_3) ppm. $^{31}P\{^1H\}$ NMR (C_6D_6, 60 °C): δ = 8.01 (s, $^1J_{PtP}$ = 1166 Hz) ppm. $C_{19}H_{29}ClNPPt$ (525.9): found C 42.82, H 5.48, N 2.63; found C 42.81, H 5.37, N 2.65.

Reaction of (P⌒N)Pt(CD$_3$)$_2$ with CH$_3$Cl in C$_6$D$_6$: A gentle stream of methyl chloride was bubbled through a solution of (P⌒N)Pt$(CD_3)_2$ (27.5 mg, 0.056 mmol) in 0.6 mL of C_6D_6. The CH_3Cl-saturated solution was heated to 60 °C for 24 h. The conversion was complete yielding (P⌒N)Pt$[(CH_3)/(CD_3)]_3Cl$, with a statistical distribution of the added CH_3 group. (P⌒N)Pt$(CH_3)(CD_3)_2Cl$: ^1H NMR (C_6D_6, 60 °C): δ = 0.59 (dd, *J* = 1.0, $^3J_{PH}$ = 7.7, $^2J_{PtH}$ = 71.0 Hz, Pt−CH_3), 1.49 (dd, *J* = 1.1, $^3J_{PH}$ = 8.1, $^2J_{PtH}$ = 57.0 Hz, Pt−CH_3), 1.92 (dd, *J* = 1.0, $^3J_{PH}$ = 7.0, $^2J_{PtH}$ = 72.6 Hz, Pt−CH_3) ppm. ^2H NMR (C_6D_6, 27 °C): δ = 0.45 ($^3J_{PD}$ = 1.1, $^2J_{PtD}$ = 10.7 Hz, Pt−CD_3), 1.36 ($^3J_{PD}$ = 1.7, $^2J_{PtD}$ = 6.9 Hz, Pt−CD_3), 1.84 ($^3J_{PD}$ = 1., $^2J_{PtD}$ = 10.8 Hz, Pt−CD_3) ppm. $^{31}P\{^1H\}$ NMR (C_6D_6 60 °C): δ = 8.01 (s, $^1J_{PtP}$ = 1161 Hz) ppm.

Reaction of (P⌒N)PtMe$_2$ with ClSiMe$_2$Ph in C$_6$D$_6$: $ClSiMe_2Ph$ (26 μL, 0.156 mmol) was added to a solution of (P⌒N)$PtMe_2$ (37.5 mg, 0.078 mmol) in 0.5 mL of C_6D_6 in a Teflon liner. The sample was then heated to 60 °C. Because of the Teflon liner, the resolution of the ^1H NMR spectrum was very low, and resolution of the Pt complexes was not possible. ^1H NMR (C_6D_6, 60 °C): δ = 0.39 [s, $(SiMe_2Ph)_2$] ppm. $^{29}Si\{^1H\}$ NMR (C_6D_6, 60 °C): δ = −21.45 ppm. $^{31}P\{^1H\}$ NMR (C_6D_6, 60 °C): δ = 7.87 (s, $^1J_{PtP}$ = 1168 Hz, **4**), 26.24 (s, $^1J_{PtP}$ = 4665 Hz, **2**) ppm.

X-ray Structure Analyses: Crystal data and experimental details are given in Table 4. The X-ray data were collected at 294 K with a Siemens SMART CCD area detector diffractometer using graphite-monochromated Mo-K_α radiation (λ = 0.71073 Å), a nominal crystal-to-detector distance of 4.40 cm and 0.3° ω-scans frames. Corrections for Lorentz polarization, and an empirical absorption correction with the program SADABS were applied. The structures were solved by direct methods (SHELXS-86) and refined by the full-matrix least-squares method based on F^2 (SHELXL-93). All non-hydrogen atoms were refined anisotropically, and the hydrogen atoms were included in idealized positions. CCDC-174589 (**3**) and -174590 (**4**) contain the supplementary crystallographic data for this paper. These data can be obtained free of charge at www.ccdc.cam.ac.uk/conts/retrieving.html or from the Cambridge Crystallographic Data Centre, 12, Union Road, Cambridge CB2 1EZ, UK [Fax: (internat.) + 44-1223/336-033; E-mail: deposit@ccdc.cam.ac.uk].

Acknowledgments

We thank the Fonds zur Förderung wissenschaftlicher Forschung (FWF) for the support of this work.

[1] V. de Felice, B. Giovannitti, A. de Renzi, D. Tesauro, P. Panunzi, *J. Organomet. Chem.* **2000**, *593/594*, 445.
[2] L. Chassot, A. v. Zelewsky, *Helv. Chim. Acta* **1986**, *69*, 1855. L. Chassot, A. v. Zelewsky, D. Sandrini, M. Maestri, V. Balzani, *J. Am. Chem. Soc.* **1986**, *108*, 6084. C. Deuschel-Corioley, R. Lüönd, A. v. Zelewsky, *Helv. Chim. Acta* **1989**, *72*, 377. A. v. Zelewsky, A. P. Suckling, H. Stoeckli-Evans, *Inorg. Chem.* **1993**, *32*, 4585.
[3] J. Pfeiffer, U. Schubert, *Organometallics* **1999**, *18*, 3245.
[4] J. Pfeiffer, U. Schubert, *Organometallics* **2000**, *19*, 62.
[5] G. P. C. M. Dekker, A. Buijs, C. J. Elsevier, K. Vrieze, *Organometallics* **1992**, *11*, 1937.
[6] R. A. Bell, M. H. Chisholm, *J. Chem. Soc., Chem. Commun.* **1976**, 200.
[7] R. A. Bell, M. H. Chisholm, *Inorg. Chem.* **1977**, *16*, 687.
[8] R. Argazzi, P. Bergamini, E. Costa, V. Gee, J. K. Hogg, A. Martin, A. G. Orpen, P. G. Pringle, *Organometallics* **1996**, *15*, 5591.
[9] B. Jedlicka, R. E. Rulke, W. Weissensteiner, R. Fernandez-Galan, F. A. Jalon, B. R. Manzano, J. R. de la Fuente, N. Veldman, H. Kooijman, A. L. Spek, *J. Organomet. Chem.* **1996**, *516*, 97.
[10] D. A. Piering, J. M. Malin, *J. Am. Chem. Soc.* **1976**, *98*, 19. D. A. Piering, J. M. Malin, *J. Am. Chem. Soc.* **1976**, *98*, 6046.
[11] J. Kuyper, *Inorg. Chem.* **1977**, *17*, 77.
[12] P. W. N. M. van Leeuwen, C. F. Roobeck, R. Huis, *J. Organomet. Chem.* **1977**, *142*, 243.
[13] R. A. Bell, M. H. Chrisholm, *Inorg. Chem.* **1977**, *16*, 698.
[14] U. Schubert, J. Pfeiffer, F. Stöhr, D. Sturmayr, S. Thompson, *J. Organomet. Chem.*, **2002**, *646*, 53.
[15] F. S. M. Hassan, S. J. Higgins, G. B. Jacobsen, B. L. Shaw, M. Thornton-Pett, *J. Chem. Soc., Dalton Trans.* **1988**, 3011.
[16] J. D. Ruddick, B. L. Shaw, *Inorg. Phys. Theor.* **1969**, 2801.
[17] A. D. Becke, *J. Chem. Phys.* **1993**, *98*, 5648.
[18] C. Lee, W. Yang, R. G. Parr, *Phys. Rev. B* **1988**, *37*, 785. B. Miehlich, A. Savin, H. Stoll, H. Preuss, *Chem. Phys. Lett.* **1989**, *157*, 200.
[19] M. J. Frisch, G. W. Trucks, H. B. Schlegel, G. E. Scuseria, M. A. Robb, J. R. Cheeseman, V. G. Zakrzewski, J. A. Montgomery, Jr., R. E. Stratmann, J. C. Burant, S. Dapprich, J. M. Millam, A. D. Daniels, K. N. Kudin, M. C. Strain, O. Farkas, J. Tomasi, V. Barone, M. Cossi, R. Cammi, B. Mennucci, C. Pomelli, C. Adamo, S. Clifford, J. Ochterski, G. A. Petersson, P. Y. Ayala, Q. Cui, K. Morokuma, D. K. Malick, A. D. Rabuck, K. Raghavachari, J. B. Foresman, J. Cioslowski, J. V. Ortiz, A. G. Baboul, B. B. Stefanov, G. Liu, A. Liashenko, P. Piskorz, I. Komaromi, R. Gomperts, R. L. Martin, D. J. Fox, T. Keith, M. A. Al-Laham, C. Y. Peng, A. Nanayakkara, C. Gonzalez, M. Challacombe, P. M. W. Gill, B. G. Johnson, W. Chen, M. W. Wong, J. L. Andres, M. Head-Gordon, E. S. Replogle, J. A. Pople, *Gaussian 98*, Revision A.3, Gaussain, Inc., Pittsburgh, PA, **1998**.
[20] R. Malet, M. Morena-Manas, T. Parella, R. Pleixats, *J. Org. Chem.* **1996**, *61*, 758.

Received March 7, 2002
[I02122]

Molecular Recognition of Anions by a Novel Organocobalt Receptor: Oxyanion versus Halide Selectivity in Water

Mike Robitzer,[a] Claude Sirlin,*[a] Nathalie Kyritsakas,[b] and Michel Pfeffer*[a]

Keywords: Host-Guest Systems / Cobalt / N,C ligand / Anions / Allosterism

The dissolution of $[Co\{2,6\text{-}(Me_2NCH_2)_2C_6H_3\}(\eta^5\text{-}C_5H_5)(H_2O)]PF_6$ (**1a**) in dry methanol or dry acetonitrile affords compounds **1b** and **1c**, respectively, in which the water ligand of **1a** has been substituted by MeOH or by CH_3CN. The crystal structure analysis of **1b** established that a strong intramolecular interaction exists between the methanolic proton and the NMe_2 group that was interacting with H_2O in **1a**. For **1c** no interaction could be found between the Co-bound acetonitrile ligand and this NMe_2 as it has changed its position in order to be as far away from the cobalt atom as possible. Whereas no reaction takes place between **1a** and an excess of sodium iodide in water or in methanol, in acetone I^- easily substitutes the water ligand of **1a** to afford high yields of the neutral compound **3**. Here also ^1H NMR spectroscopic data are in favour of a structure with no interaction between the NMe_2 and the iodide ligand as in **1c**. Protonation of the free NMe_2 unit of **1a** by adding increasing amounts of HPF_6 in water leads to the synthesis of **4a**. The p*K*a of **1a** in D_2O was found to be 6.1. Treating **1a** with acidic buffered water solutions (pH = 5.5) leads to the in situ formation of **4a**. From these solutions, association constants were determined for Cl^-, Br^-, I^-, AcO^-, $H_2PO_4^-$ and NO_3^-. Significant selectivity in water for AcO^- and $H_2PO_4^-$ vs. halide anions has been established.
(© Wiley-VCH Verlag GmbH, 69451 Weinheim, Germany, 2002)

Introduction

The molecular recognition of anions[1−3] emerged with the discovery of a multiprotonated hollow, called katapinate,[4] which was the first host for a chloride ion. Crystal structure determinations established that the anion is indeed encapsulated within the macrobicyclic cavity of the host molecule.[5] Important results were reported when chloride and azide were selectively complexed in water by tetraprotonated macrotricyclic[6,7] and hexaprotonated macrobicyclic[8] molecules, respectively. In all these examples the anions were found to have formed hydrogen-bonding interactions with the protonated ammonium derivatives. It was therefore thought that complexation of anions should also be feasible with metallic cations located in related cavities.[9,10] A macrobicyclic biscopper cryptate complex was thus synthesised which was shown by potentiometric studies to display the expected interactions between the bis-metallic centres and a chloride anion. Another related compound containing one copper atom only displayed a chloride anion interacting with the Cu centre and the ammonium moieties of the ligand.[11] Until then only very rare examples derived from organometallic compounds had been reported to exhibit a related behaviour.[12−14]

We have recently described the synthesis and the preliminary behaviour of a simple organocobalt compound[15] which was built with the well-known mono-anionic pincer ligand extensively studied by van Koten et al.[16,17] In our compound, however, the N,C,N ligand is only coordinated to the cobalt centre in a bidentate fashion as one N atom does not interact directly with the metal. In fact we found that these organometallic species are interesting Brønsted acid receptors as a series of such acids were indeed coordinated to the (N,C,N)metal moiety without any hydrolysis of the Co−C bond being observed. It thus appeared that in these species the anions associated with the acids were interacting both with a metal cation *and* an ammonium unit as in the anion hosts mentioned above. We thus embarked on a project aimed at defining both the mechanism of the acid complexation by our cobalt complex and the thermodynamic data associated with the protonation of the amine unit that is not directly bound to Co in **1a**. This study allowed us to determine the association constants between the organocobalt host and various anions and to compare their selectivity with related known systems.

Results and Discussion

The key compound of this study is the aquo derivative **1a** in which an intramolecular hydrogen bond between one

[a] Laboratoire de Synthèses Métallo-Induites, UMR 7513 du CNRS, Université Louis Pasteur,
4, rue Blaise Pascal, 67070 Strasbourg, France
Fax: (internat.) + 33-390/241-526
E-mail: pfeffer@chimie.u-strasbg.fr
sirlin@chimie.u-strasbg.fr
[b] Service Commun de Rayon-X, FR 2351 du CNRS, Université Louis Pasteur,
4, rue Blaise Pascal, 67070 Strasbourg, France

of the aquo protons and the noncoordinated nitrogen atom of the pincer ligand was established. The reaction of **1a** with acids affords the complexes **2a**−**e**, which display a related intramolecular H-bond between the dimethylammonium unit and the X atoms (see Scheme 1). These intramolecular H-bonds in both **1a** and **2a**−**e** contribute to the stability of the complexes by forming pseudo seven-membered organometallic rings.

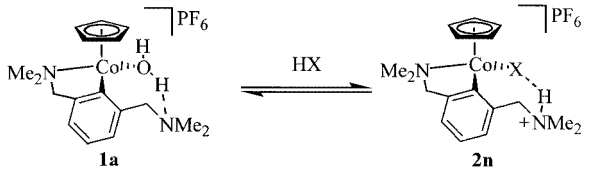

1a **2n**

Scheme 1. Complexation of HX by **1a** affords **2a**−**e** [**a** (X = F), **b** (X = Cl), **c** (X = Br), **d** (X = I), **e** (X = OAc)]

This stabilisation seems to play a key role for the coordination of the anion to the cobalt centre as, when treating **1a** *in water* with excess (up to 10^3 equivalents) of NaI, for instance, no complexation of the iodide was observed. Changing water for methanol in order to increase the solubility of **1a**, with the same excess of sodium iodide, did not lead to the coordination of I^- to cobalt. However, following this reaction by UV/Vis spectroscopy, we noticed the presence of new absorption bands at λ = 459, 560 and 675 nm vs. one band only for **1a** in water at λ_{max} = 465 nm. The ^{1}H NMR spectrum of **1a** in CD_3OD displays only slight modifications of the chemical shifts of the various signals of **1a** as compared to the same spectrum in [D_6]acetone. Single crystals of **1b** were obtained from a methanol/hexane solution of **1a**. The molecular structure of **1b** was determined by means of an X-ray diffraction study on one of these crystals (Figure 1 and Table 1). It was at once apparent that, in **1b**, a molecule of methanol has substituted the water molecule in **1a**. Importantly, a strong intramolecular OH···N bond is also found between the coordinated methanol and the free NMe_2 unit. The ^{1}H NMR spectrum of **1b** in [D_6]acetone containing traces of water showed the spectrum of **1a**, confirming that the coordination of methanol is easily reversed even by small amounts of water.

In dry CD_3CN, **1a** displays a ^{1}H NMR spectrum which allows the identification of both unmodified **1a** and a new species **1c** in ratios depending on the concentration of **1a**. The ^{1}H NMR spectrum of **1c** shows the presence of one singlet for the NMe_2 group not interacting with the cobalt centre at δ = 2.30 ppm, together with the expected two singlets for the diastereotopic Co-bound NMe_2 unit. These features suggest that **1c** is a derivative of **1a** in which the water molecule has been substituted by a MeCN ligand. The X-ray diffraction study of a single crystal of **1c** (Figure 1 and Table 1) confirmed that **1c** is a MeCN adduct of **1a**. The conformation of the five-membered cyclometallated ring of the pincer ligand is very similar to that found for this ligand in **1a**. The only difference between **1a** and **1c** is a different orientation of the second NMe_2 group with respect to Co: it is now as far away from the acetonitrile ligand as possible, this being achieved by a rotation of ca. 90° around the C_{13}−C_{15} vector.

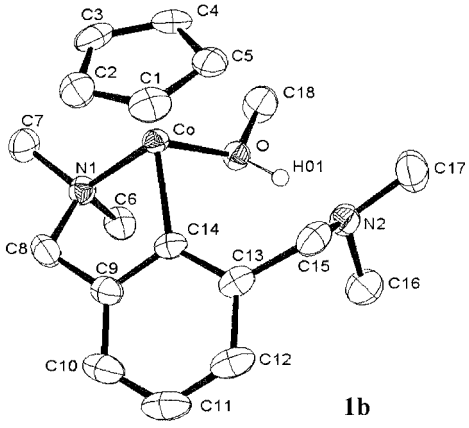

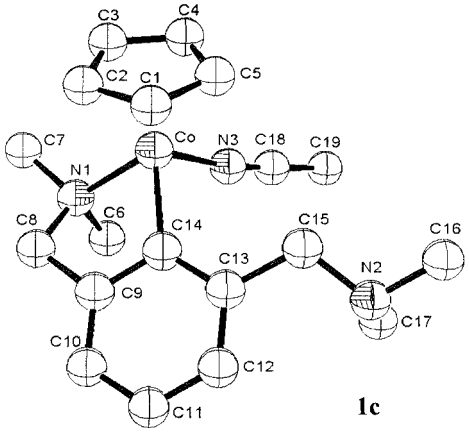

Figure 1. ORTEP representation of the cationic parts of **1b** and **1c**

As NaI is not soluble in CD_3CN we added one equivalent of NBu_4I to a solution of **1a** in order to check whether I^- can substitute the MeCN ligand in **1c**. We noticed no such complexation unless we increased the concentration of I^-: when adding more than 10 equivalents of NBu_4I a new species **3** was observed together with **1a** and **1c** (**3**:**1a**:**1c** = 0.07:0.16:0.77 with 12 equiv. of NBu_4I). The ^{1}H NMR spectroscopic data of **3** show significant high-field shifts for all the protons of the pincer ligand. Moreover the $\Delta\delta$ of the NMe_2 group bound to Co drops to 0.5 ppm as compared to its value in **1a**, **1b**, and **1c** (2.15, 2.11 and 1.47 ppm respectively). In the latter three compounds displaying these rather important $\Delta\delta$ values, the molecular structure shows a similar ring puckering of the five-membered cobaltacyclic ring, whereby one of the N−Me bonds eclipses either the Co−O or the Co···NCMe bond. The $\Delta\delta$ value found for **3** militates in favour of a staggered conformation in which the NMe_2 has now rotated around the C_8−N_1 vector by ca. 60° as shown in Figure 2. This latter feature is probably due to steric interactions between the bulky I^- ligand and the N−Me bond.

Table 1. Selected bond lengths and angles in complexes **1b** and **1c**

Bond lengths [Å]		Compound **1b**	Angles [°]	
Co−Cp# [a]	1.713(2)		N_1−Co−C_{14}	82.7(9)
Co−C(Cp)$_{av}$	2.091(2)		N_1−Co−O	93.5(7)
Co−O	1.950(2)		O−Co−C_{14}	88.9(8)
Co−N_1	2.050(2)		Cp#−Co−N_1	128.0(4)
Co−C_{14}	1.952(2)		Cp#−Co−C_{14}	124.0(1)
N_1−C_8	1.489(3)		Cp#−Co−O	126.6(3)
C_8−C_9	1.497(4)		Co−N_1−C_8	103.8(1)
C_9−C_{14}	1.402(3)		N_1−C_8−C_9	107.9(2)
N_2−H_{01}	1.600(2)		C_8−C_9−C_{14}	115.4(2)
N_2−O	2.582(2)		C_9−C_{14}−Co	111.8(2)
			N_2−H_{01}−O	170.2(2)
			C_6−N_1−Co−O	−8.9(2)
			C_{14}−C_{13}−C_{15}−N_2	67.2(2)
		1c		
Co−Cp#[a]	1.712(2)		N_1−Co−C_{14}	82.4(8)
Co−C(Cp)$_{av}$	2.089(2)		N_1−Co−N_3	95.3(8)
Co−N_1	2.051(2)		N_3−Co−C_{14}	93.9(9)
Co−N_3	1.902(2)		Cp#−Co−N_1	128.4(3)
Co−C_{14}	1.960(2)		Cp#−Co−C_{14}	123.9(3)
N_1−C_8	1.493(3)		Cp#−Co−N_3	122.1(3)
C_8−C_9	1.502(4)		Co−N_1−C_8	103.1(1)
C_9−C_{14}	1.409(3)		N_1−C_8−C_9	107.3(2)
N_2−N_3	4.403(3)		C_8−C_9−C_{14}	114.7(2)
			C_9−C_{14}−Co	111.6(2)
			C_6−N_1−Co−N_3	−15.1(2)
			C_{14}−C_{13}−C_{15}−N_2	153.5(2)

[a] Cp#: centroid of the cyclopentadienyl ring.

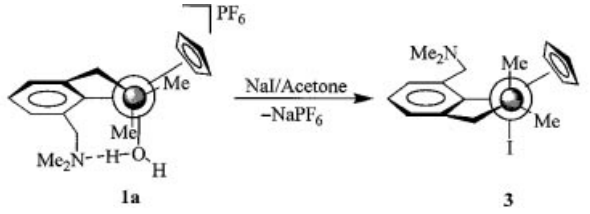

Figure 2. Newman representation of **3** around the Co−N_1 bond

This latter experiment showed unambiguously that iodide can indeed be coordinated to cobalt by displacement of the water *provided that the reaction is run in a non-protic solvent*. Indeed, the synthesis of **3** can be better achieved in acetone as, in this poorly coordinating solvent, **3** is obtained in almost quantitative yields. It is most likely that coordination of I^- takes place from an acetone solvate derivative **1d** akin to **1c** in which MeCN is substituted by acetone, knowing that cobalt has a much higher affinity for I^- than for acetone. We assume that in this solvent, **1a** might well be in equilibrium with the hypothetical acetone adduct **1d**, although the concentration of this latter species is far too low to be detected by ^{1}H NMR spectroscopy.

We have seen that the "CpCo(pincer)" moiety could be a host for HX, as HF, HCl, HBr, HI or HOAc could substitute the water ligand when an excess of one of these Brønsted acids is added to solutions of **1a** in methanol.[15] From the results discussed above, it appears that the coordination of the X^- anions to Co is probably only possible once the NMe_2 unit of the pincer ligand not coordinated to cobalt in **1a** has been protonated by HX. We have indeed checked that a solution of **1a** and 10^3 equiv. of NaCl in water leads to the formation of **2b** only when decreasing the pH of the solution by addition of HPF_6.

We have also studied the protonation of **1a** in D_2O as a function of [H^+]. In this respect we have run the ^{1}H NMR spectra of several solutions of **1a** in D_2O to which various amounts of HPF_6 had been added. The correlation between the chemical shifts of certain protons of **1a** and the pH of the solutions allowed the determination of the pK_a of the species **4a**. The equilibrium between **1a** and **4a** (Scheme 2) must be fast on the ^{1}H NMR time scale, as only one signal is observed for the two species. Most of the signals of **1a** experience a decrease of chemical shifts upon lowering the pH of the D_2O solutions. However, the signal of one proton of a CH_2 group (at δ = 3.89 ppm) displays a behaviour that is worthy of further discussion. At pH 8.0 the intensity of this doublet starts to decrease, it then gradually becomes broader as the pH drops and finally disappears when the pH is in the range 6.5 to 7.0. Surprisingly, at pH 4.05 it reappears as a doublet but at a very different chemical shift (δ = 5.02 ppm). During this process the chemical shift of the second CH associated to the previous one does not change (δ = 4.59 vs. 4.57 ppm). One explanation for this dynamic behaviour could be that the reversible protonation of the NMe_2 unit induces the cleavage of the OH···NMe_2 bond in **1a** and rotation around the C_{13}−C_{15} vector as in **1c**. Since the chemical shifts of the two protons of the CH_2 group resonate at very different chemical shifts in the two exchanging position it is reasonable to observe a broadening of the high-field shifted proton as it is known that the broadness of any given signal that is exchanging with another one is proportional to the square of the difference of the chemical shifts of both signals.[18] At pH < 4.5 the protonation of the NMe_2 close to this CH_2 is complete and thus exchange of the CH_2 group is no longer possible.

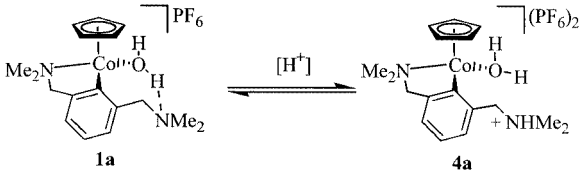

Scheme 2. Equilibrium between **1a** and **4a**

At pH ≥ 8.5 the NMe_2 interacting with H_2O is a broad singlet because this species is rapidly exchanging the two diastereotopic methyl groups by a fast coordination-decoordination of the N atom to the O−H group. We found good evidence for this while studying the behaviour of **1a** in [D_6]acetone. At room temperature the signal of the "free" NMe_2 group is a broad singlet at δ = 2.20 ppm, but when the temperature is lowered (< −20 °C) the diastereotopic nature of this NMe_2 group is recovered, the difference

in chemical shift between the two methyls being more than 0.6 ppm. At lower pH (4.05) the NMe_2, which until then is a broad singlet, appears as two broad signals, showing that the NMe_2 group is indeed completely protonated: the N atom can no longer invert its configuration and hence the exchange process is not detectable anymore. The pK_a value of **4a** in D_2O follows from the results reported in Figure 3, leading to a value of 6.1 ± 0.1.

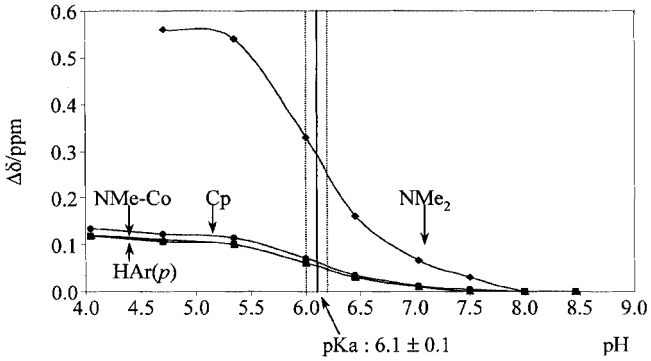

Figure 3. Variation of Δδ for significant signals as a function of pH

Association Constant Determinations

As we have seen that **1a** becomes a good host for anions at slightly acidic pH, we looked for the best buffer solutions to determine the thermodynamic data for the various complexations of anions by our system. We have thus chosen MES (2-[*N*-morpholino]ethanesulfonic acid) which leads to a pH of 5.5 in water. The K_{ass} values were obtained by following the addition of various amounts of anions (as their NH_4^+ or NEt_3H^+ derivatives)[19] to a buffered solution of **1a** by standard UV/Vis spectroscopy; the spectra of **4a** and **2b**−**d** are shown in Figure 4.

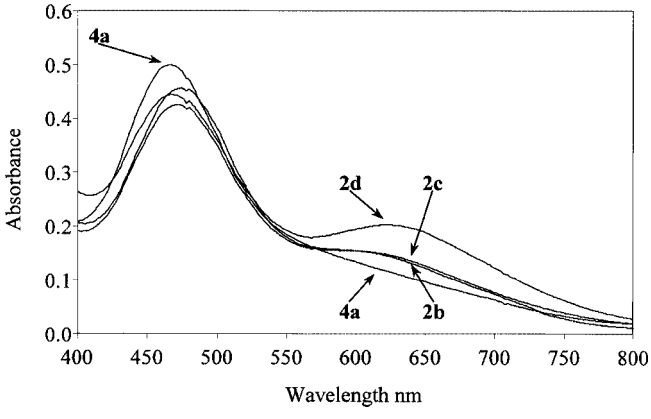

Figure 4. Superposition of UV/Vis of **4a** and **2b**−**d**

As the concentrations of the species **2b**−**d** are proportional to the absorption around 620−650 nm we used this modification to determine the association constants according to Equation (1). These constants are given in Table 2.

The constant for the fluoride anion could not be measured by any of these techniques because this anion reacts with the buffer leading to the formation of an uncharacterised insoluble material.

Table 2. log K_{ass} for compounds **2b**−**g** in various solvents

Entry	Anion	Complexes	log K_{ass} in water pH = 5.5[b]	log K_{ass} in M/W[a] pH = 5.4[b]	log K_{ass} in methanol pH = 6.4[c]
1	Cl^-	**2b**	1.8[d] [e]	3.9[e]	3.4[e]
2	Br^-	**2c**	1.5[d,e]	3.1[e]	2.7[e]
3	I^-	**2d**	1.7[d,e]	3.2[e]	2.9[e]
4	CH_3COO^-	**2e**	3.0[e]	1.7[e]	1.9[e]
5	$H_2PO_4^-$	**2f**	3.1[e]	ns[f]	ns[f]
6	NO_3^-	**2g**	1.0[e]	1.4[e]	1.5[e]

[a] M/W = methanol/water (95:5). [b] MES. [c] MOPS. [d] UV/Vis. [e] ^{1}H NMR spectroscopy. [f] Not soluble.

$$\mathbf{4a} + NR_3HX \underset{MES,\ D_2O}{\overset{K_{ass}}{\rightleftharpoons}} \mathbf{2b\text{-}g} + D_2O + NR_3 \qquad (1)$$

$$K_{ass} = \frac{[\mathbf{2b\text{-}g}]}{[\mathbf{4a}][X^-]}$$

R = Et X = Cl, Br
R = H X = I, OAc, H_2PO_4, NO_3

This technique could not be applied to oxygen-containing anions such as acetate, nitrate or dihydrogenophosphate because the UV/Vis spectra of the complexes obtained by trapping of these latter ions do not display significant differences with the aquo derivative **4a**.

We checked that the K_{ass} obtained by analysis of the ^{1}H NMR spectra for the halide anions afforded results in line with those obtained by the UV/Vis technique. An example of the spectra obtained for different concentrations of iodide is shown in Figure 5 and 6, in which the chemical shift of the Cp ring in both **4a** and **2d** is represented. A related study was then performed for the $CH_3CO_2^-$, NO_3^- and $H_2PO_4^-$ anions, which led to the results reported in Table 2.

In order to be able to compare these data with related values for different anion hosts reported in the literature, we also determined these K_{ass} values in pure CD_3OD and

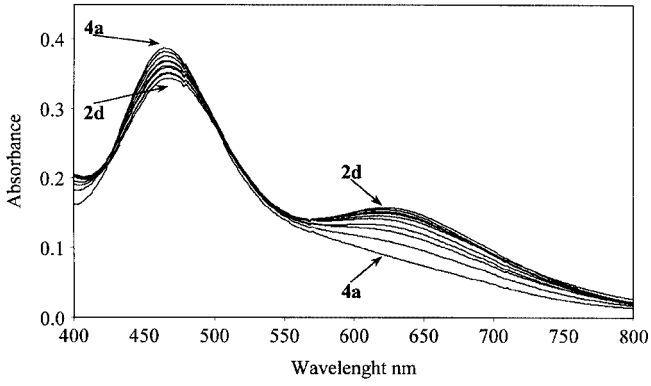

Figure 5. Evolution of the UV/Vis spectra of **4a** with increasing amounts of NH_4I (10, 20, 30, 40, 50, 60, 80 and 100 equiv.)

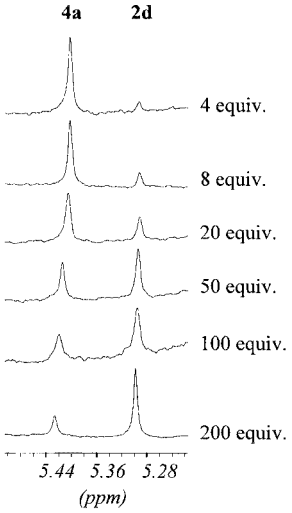

Figure 6. Evolution of the ^{1}H NMR spectra of **4a** with increasing amounts of NH_4I

in a 95:5 mixture of CD_3OD and D_2O. The relative concentration of **1a** and **1b**, as anticipated, is dependent on the amount of water present. In dry CD_3OD ($HDO/D_2O <$ 0.03%) the ratio of **1a** to **1b** is 5:95, whereas in CD_3OD/D_2O (95:5) this ratio is 40:60. These data are another illustration of a much stronger complexation of water to cobalt as opposed to methanol. In order to determine the pK_a of **1b** in pure CD_3OD and in CD_3OD/D_2O (95:5), we used the same procedure as described above for **1a** in D_2O. Addition of DPF_6 in CD_3OD resulted in a duplication of most of the signals of **1a** and **1b** in the ^{1}H NMR spectrum. We believe that the explanation for this phenomenon is due to the occurrence of four species, namely **1a**, **1b**, **4a** and **4b** (**4b** is the N-protonated derivative of **1b**). Particularly diagnostic of the existence of **4a** and **4b** are the presence of two pairs of CH_2 signals at chemical shifts analogous to those observed for **4a** in D_2O (see above).

As MES is poorly soluble in pure methanol, we decided to use MOPS (3-[*N*-morpholino]propanesulfonic acid) whose pH is slightly higher than that of MES (6.4 vs. 5.5). Solutions of **1a** in both solvents display the same ^{1}H NMR spectra, i.e. the Cp ring appears as three resonances. We believe that three different species should exist in these solutions, i.e. **1a**, **1b** and a compound in which the sulfonic group of the buffers has been trapped by the cobalt receptor. This compound is found in very low yield (< 5%) and it is always present in methanol solution whatever the concentration of the anions. A likely explanation for the occurrence of this species in methanol is based upon a different solvation of the sulfonic group, which is more solvated in water than in methanol. The occurrence of **1a** and **1b** in these solutions must be due to a very small degree of protonation of the nitrogen atom of either **1a** or **1b** by the buffer protons. However, despite the fact that it is not visible in the ^{1}H NMR spectrum, a small amount of the protonated form must exist to enable the trapping of the anions to take place. The presence of large quantities of buffer must be therefore be a strong enough driving force for the anion complexation to occur. The K_{ass} in this case was determined using a slightly different equation [Equation (2)] than above:

$$\mathbf{1a} + \mathbf{1b} + NR_3HX \underset{\text{i or ii}}{\overset{K_{ass}}{\rightleftharpoons}} \mathbf{2b\text{-}g} + D_2O + CD_3OD + NR_3$$

$$K_{ass} = \frac{[\mathbf{2b\text{-}g}]}{([\mathbf{1a}]+[\mathbf{1b}])[X^-]}$$

R = Et X = Cl, Br
R = H X = I, OAc, H_2PO_4, NO_3
i : MES, MeOD:D_2O (95:5)
ii : MOPS, MeOD

(2)

Several interesting comments can be made with respect to the K_{ass} values obtained in water or in methanol. There is an obvious important difference between the K_{ass} values measured for the halides and those obtained for the oxyanions. Whereas these values are much higher on going from water to methanol for the halides, the opposite is found for the oxyanions (see below). Schmidtchen has found a similar trend for the halide series when changing water for methanol.[20] However, in marked contrast to our results the complexation of the halide was somehow parallel to their sizes, iodide being by far the best complexed species. In our case K_{ass} for chloride is ca. five times higher than that for iodide. Our receptor is a competitive Cl^- host in methanol as compared to those reported elsewhere.[6,20] It is, however, important to note that the previously reported receptors were usually built from several ammonium units, whereas in our case this result was obtained by interaction of the Cl^- with Co^+ and one NH^+ moiety only. Our organocobalt receptor displays an interesting behaviour with respect to the oxyanions such as acetate and dihydrogenophosphate, since the stability of **2e**−**f** is higher than that of **2b**−**d** by at least one order of magnitude. The only previous data in water concerning these two anions are those of Schmidtchen who reported values of 1.86 and 2.1, respectively.[20] Upon comparing the selectivity of our receptor for oxyanions vs. chloride with that of other hosts (cf. Table 3) it appeared that the organocobalt complex is 10 times more selective than the better such hosts in water.

Table 3. Selectivity of hosts for oxyanions vs chloride

Entry	NO_3^-	CH_3COO^-	$H_2PO_4^-$	Receptors
1	0.2	15	20	**4a**
2	0.6	0.2[a]	−	Bis-Tren[8]
3	−	1.5	2.5	Macrotricyclic quaternary ammonium salt[20]

[a] $HCOO^-$ value.

Our result is without precedent in the literature. The only known examples of a better complexation of the oxyanions have been found for non-protic solvents such as CH_3CN, DMSO and $CHCl_3$.[21−24]

As the respective hydration free energies of the chloride and the acetate anions are similar [$\Delta G_H(Cl^-) = -365$ kJ·mol^{-1}, $\Delta G_H(AcO^-) = -340$ kJ·mol^{-1}][3] the better acetate vs. chloride complexation can be rationalized

by means of both a stronger coordination of an oxygen-containing anion to a cobalt(III) center and a stronger hydrogen bond between an NH^+ and an oxygen atom. In the case of the dihydrogenophosphate, a rather strong hydration energy has been reported [$\Delta G_H(H_2PO_4^-) = -465$ kJ·mol^{-1}].[3] Thus the arguments given above cannot be sufficient to explain the stronger complexation of this anion vs. halides. We suggest that in this case the H_2PO_4 anion coordinated to the outer surface of the organocobalt receptor is partially solvated by several water molecules, thus contributing to the somehow surprising selectivity disclosed for this substrate.

Conclusion

Our organocobalt compound can be a genuine host for anion in water or in methanol provided that a source of protons is present in the solution. We have observed that a too-acidic medium can cause decomposition of the complex. This anion host is therefore most efficient in solutions whose pH is slightly acidic through the presence of a buffer. When no source of protons is present the aquo ligand cannot be displaced by any anions. This behaviour is reminiscent of an allosteric behaviour[25−27] of our molecule, as the bonding of the anion to the cobalt receptor is somehow modulated by prior protonation at another part of the molecule. This behaviour is represented schematically in Scheme 3.

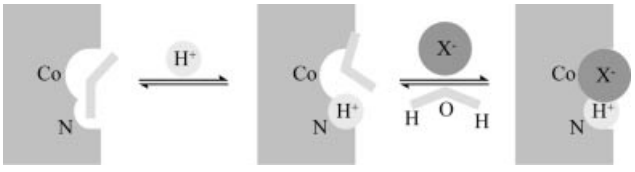

Scheme 3. Representation of the allosteric phenomenon

Further work in line with this property, as well as modification of the cobalt complexes, is being actively pursued.

Experimental Section

General Remarks: All chemicals used [NEt_3·$(HF)_3$, NEt_3·HCl, NEt_3·HBr, NH_4I, NH_4OAc, NH_4NO_3 and $NH_4H_2PO_4$] were of analytical grade and dried under vacuum before use. Buffer solutions were prepared from 3-[*N*-morpholino]propanesulfonic acid (MOPS, hemisodium salt) or 2-[*N*-morpholino]ethanesulfonic acid (MES, 2 equivalents of hemisodium salt and 3 equivalents of acid). In water the pH of the thus obtained solutions is 7.1 and 5.5, respectively, whereas in methanol the pH is 6.4 and 5.4, respectively.

UV/Vis experiments were carried out in distilled water or in spectrophotometer UV-fluo methyl alcohol quality (Carlo Erba). Absorption spectra were recorded on a Uvikon XL spectrometer. pH was determined using a PHN78 (Tacussel electronique) with an ECS electrode.^{1}H NMR spectra were recorded at 300.13 MHz and $^{13}C\{^1H\}$ NMR spectra at 75.47 MHz on a Bruker FT instrument (AV-300). Chemical shifts (δ) and coupling constants (*J*) are expressed in ppm and Hz, respectively, and referenced to external TMS. The starting materiel $[CpCo(NCN)H_2O]^+$·PF_6^- (**1a**) was prepared according to a published method.[15] Elemental analyses were performed by the Service Central d′Analyse de l′Institut de Chimie (Strasbourg). Association constants were determined from a Scatchard plot [2n/X = f(2n)]. The respective concentrations of **4a** and **2n** in water or **1a**, **1b** and **2n** in methanol or methanol/water were determined by ^{1}H NMR integrations or UV/Vis Δabs variations. Reproducibility of multiple experiments afforded in general the same values for a determined anion within a 10% variation. All the selected values have an R^2 value greater than 0.90 and errors were estimated to be between 5 and 10%.

[Co{2,6-(Me_2NCH_2)$_2$$C_6H_3$}(η^5-$C_5H_5$)($H_2O$)]$PF_6$ (1a): ^{1}H NMR spectra of **1a** (5×10^{-4} M) in D_2O at pH 8.5: δ = 7.30 (d, $^3J_{H\text{-}H}$ = 7.1, 1 H, Ar), 7.21 (t, $^3J_{H\text{-}H}$ = 7.1, 1 H, Ar), 7.14 (d, $^3J_{H\text{-}H}$ = 7.1, 1 H, Ar), 5.26 (s, 5 H, C_5H_5), 4.59 and 3.87 (AB spin system, $^2J_{H\text{-}H}$ = 12.4, 2 H, CH_2N), 4.23 and 3.63 (AB spin system, $^2J_{H\text{-}H}$ = 14.0, 2 H, CH_2N-Co), 3.33 and 1.26 (2s, 6 H, Co-NMe_2), 2.31 (br. s, 6 H, NMe_2).

[Co{2,6-(Me_2NCH_2)$_2$$C_6H_3$}(η^5-$C_5H_5$)(MeOH)]$PF_6$ (1b): *n*-Hexane (80 mL) was slowly added to a solution of **1a** (0.240 g, 0.5 mmol) in CH_3OH (20 mL) and the solution was cooled to 0 °C for two days. This afforded **1b** as brown crystals, which were collected by filtration, washed with hexane and dried in vacuo (quantitative yield). ^{1}H NMR (CD_3OD): δ = 7.24 (d, $^3J_{H\text{-}H}$ = 7.2, 1 H, Ar), 7.16 (t, $^3J_{H\text{-}H}$ = 7.2, 1 H, Ar), 7.07 (d, $^3J_{H\text{-}H}$ = 7.2, 1 H, Ar), 5.37 (s, 5 H, C_5H_5), 4.50 and 3.63 (AB spin system, $^2J_{H\text{-}H}$ = 12.4, 2 H, CH_2N), 4.29 and 3.57 (AB spin system, $^2J_{H\text{-}H}$ = 14.0, 2 H, H_2N-Co), 3.40 and 1.29 (2s, 6 H, Co-NMe_2), 2.26 (br. s, 6 H, NMe_2) ppm. $^{13}C\{^1H\}$ NMR (CD_3OD): δ = 152.8, 148.0, 131.2, 126.2 and 12.7 (C_6H_3), 85.9 (C_5H_5), 77.7 (CH_2N-Co), 68.2 (CH_2N), 59.1 and 49.2 (Co-NMe_2), 30.7 (NMe_2). $C_{18}H_{28}CoF_6N_2OP$ (492.33): calcd. C 43.91, H 5.73, N 5.69; found C 44.03, H 5.73, N 5.62.

[Co{2,6-(Me_2NCH_2)$_2$$C_6H_3$}(η^5-$C_5H_5$)($NCCH_3$)]$PF_6$ (1c): Et_2O (80 mL) was slowly added to a solution of **1a** (0.240 g, 0.5 mmol) in CH_3CN (20 mL) and this solution was cooled to 0 °C for two days. This afforded **1c** as red crystals, which were washed with hexane and dried in vacuo (quantitative yield). ^{1}H NMR (CD_3CN): δ = 7.33 (m, 1 H, Ar), 7.09 (t, $^3J_{H\text{-}H}$ = 7.3, 1 H, Ar), 6.96 (m, 1 H, Ar), 5.38 (s, 5 H, C_5H_5), 4.12 and 3.47 (AB spin system, $^2J_{H\text{-}H}$ = 14.0, 2 H, CH_2N), 3.81 and 3.33 (AB spin system, $^2J_{H\text{-}H}$ = 13.0, 2 H, CH_2N-Co), 3.14 and 1.67 (2s, 6 H, Co-NMe_2), 2.30 (br. s, 6 H, NMe_2) ppm. $^{13}C\{^1H\}$ NMR (CD_3CN): δ = 153.2, 150.5, 150.2, 129.5, 125.7, 122.7 (C_6H_3), 135.4 (N*C*CH$_3$), 88.3 (C_5H_5), 76.7 (CH_2N-Co), 65.9 (CH_2N), 59.0 and 52.7 (Co-NMe_2), 45.7 (NMe_2), 1.1 (NC*C*H3) ppm. $C_{19}H_{27}CoF_6N_3P$ (501.34): calcd. C 45.52, H 5.43, N 8.38; found C 45.54, H 5.41, N 8.30.

[CoI{2,6-(Me_2NCH_2)$_2$$C_6H_3$}(η^5-$C_5H_5$)] (3): NaI (0.750 g, 5.0 mmol) was added to a solution of **1a** (0.240 g, 0.5 mmol) in acetone (10 mL). The colour of the solution turned from purple to green in 5 minutes. After removal of insoluble material by filtration, the product was precipitated by addition of *n*-hexane. Yield: 2.21 g (75%). ^{1}H NMR ([D$_6$]acetone): δ = 7.13 (d, $^3J_{H\text{-}H}$ = 7.1, 1 H, Ar), 6.71 (t, $^3J_{H\text{-}H}$ = 7.1, 1 H, Ar), 6.66 (d, $^3J_{H\text{-}H}$ = 7.1, 1 H, Ar), 5.22 (s, 5 H, C_5H_5), 4.18 and 3.42 (AB spin system, $^2J_{H\text{-}H}$ = 12.2, 2 H, CH_2N), 3.74 and 3.18 (AB spin system, $^2J_{H\text{-}H}$ = 13.0, 2 H, H_2N-Co), 3.00 and 2.53 (2s, 6 H, Co-NMe_2), 2.22 (s, 6 H, NMe_2).

[Co{2-(Me_2NCH_2)-6-($Me_2ND^+CH_2$)C_6H_3}(η^5-C_5H_5)(D_2O)]$(PF_6)_2$ (4a): HPF_6 (pH 2.2 in D_2O) was added to a solution of **1a** (5×10^{-4} M) in D_2O, leading to a pH of ca. 4.0. ^{1}H NMR (D_2O): δ = 7.39 (d, $^3J_{H\text{-}H}$ = 7.2, 1 H, Ar), 7.32 (t, $^3J_{H\text{-}H}$ = 7.2, 1 H, Ar), 7.18

Table 4. X-ray diffraction data

	1b	**1c**
Formula	$C_{18}H_{28}CoN_2O.PF_6$	$C_{19}H_{27}CoN_3.PF_6$
Molecular weight	492.33	501.34
Crystal system	monoclinic	triclinic
Space group	$P2_{1/c1}$	$P\bar{1}$
a [Å]	14.229(1)	7.942(1)
b [Å]	10.291(1)	9.728(1)
c [Å]	15.290(1)	14.770(1)
α [°]		95.02(1)
β [°]	105.92(1)	102.46(1)
γ [°]		94.03(1)
V [Å^3]	2153.2(2)	1105.3(1)
Z	4	2
Color	brown	red
Crystal dim [mm]	0.20 × 0.20 × 0.05	0.12 × 0.10 × 0.08
$\rho_{calcd.}$ [g cm^{-3}]	1.52	1.51
F_{000}	1016	516
μ [mm^{-1}]	0.934	0.909
T [K]	173	173
λ [Å]	0.71073	0.71073
Radiation	Mo-K_α	Mo-K_α
Diffractometer	KappaCCD	KappaCCD
Scan mode	φ scans	φ scans
hkl limits	−19/20, −13/14, −21/21	−10/10, −11/12, −18/19
θ limits [°]	2.5/30.04	2.5/27.47
Data measured	10827	7449
Data with $I > 3\sigma(I)$	3956	3556
Number of variables	298	271
R	0.038	0.035
R_w	0.060	0.050
GOF	1.052	1.016
Largest peak in final difference [e Å^{-3}]	0.612	0.357

(d, $^3J_{H\text{-}H}$ = 7.2, 1 H, Ar), 5.40 (s, 5 H, C_5H_5), 5.01 and 4.57 (AB spin system, $^2J_{H\text{-}H}$ = 13.6, 2 H, CH_2ND$^+$), 4.24 and 3.70 (AB spin system, $^2J_{H\text{-}H}$ = 14.5, 2 H, CH_2N-Co), 3.45 and 1.47 (2s, 6 H, Co-NMe$_2$), 3.09 and 2.81 (2 br. s, 6 H, $^+$NDMe_2).

[Co{2-(Me_2NCH_2)-6-($Me_2ND^+CH_2$)C_6H_3}(η^5-C_5H_5)(CD_3OD)]-(PF_6)$_2$ (4b): HPF_6 (pH 0.7 in CD_3OD/D_2O 95:5) was added to a solution of **1a** (1×10^{-2} M) in CD_3OD/D_2O, leading to a pH of ca. 3.9. ^{1}H NMR (CD_3OD/D_2O 95:5): δ = 7.35−7.05 (m, 3 H, Ar), 5.36 (s, 5 H, C_5H_5), 5.10 and 4.50 (AB spin system, $^2J_{H\text{-}H}$ = 12.8, 2 H, CH_2ND$^+$), 4.34 and 3.72 (AB spin system, $^2J_{H\text{-}H}$ = 14.0, 2 H, CH_2N-Co), 3.58 and 1.21 (2s, 6 H, Co-NMe$_2$), 2.98 and 2.23 (2 s, 6 H, $^+$NDMe_2).

X-ray Crystallographic Study: Single crystals suitable for X-ray diffraction analysis were obtained as described above. Data were collected on a Nonius KappaCCD diffractometer, using Mo-K_α graphite-monochromated radiation (λ = 0.7107 Å), and ω scans. Absorption corrections were partially included in the data reduction procedure. The structures were solved by direct methods and refined against |F|. Hydrogen atoms were introduced in structure factor calculations as fixed contributors by their computed coordinates [d(C-H) = 0.95 Å, B(H) = 1.3*Beqv Å^2 of the attached carbon atom] except for the OH protons of **1a**, which were located in difference Fourier maps. The absolute structures were determined by refinement of Flack's x parameter. For all computations, the Nonius OpenMoLeN package[28] was used. Further experimental details are given in Table 4.

CCDC-181527 (**1b**) and -181526 (**1c**) contain the supplementary crystallographic data for this paper. These data can be obtained free of charge at www.ccdc.cam.ac.uk/conts/retrieving.html [or from the Cambridge Crystallographic Data Centre, 12, Union Road, Cambridge CB2 1EZ, UK; Fax: (internat.) +44-1223/336-033; E-mail: deposit@ccdc.cam.ac.uk].

Acknowledgments

M.R. thanks the Ministère de l'Education Nationale for a PhD fellowship.

[1] F. P. Schmidtchen, M. Berger, *Chem. Rev.* **1997**, *97*, 1609−1646.
[2] P. D. Beer, P. A. Gale, *Angew. Chem. Int. Ed.* **2001**, *40*, 486−516.
[3] *Supramolecular Chemistry of Anions* (Eds: A. Bianchi, K. Bowman-James, E. Garcia-Espana), Wiley-VCH, New York, **1997**.
[4] C. H. Park, H. E. Simmons, *J. Am. Chem. Soc.* **1968**, *90*, 2431−2432.
[5] R. A. Bell, G. G. Christoph, F. R. Fonczek, R. E. Marsh, *Science* **1975**, 151−152.
[6] E. Graf, J.-M. Lehn, *J. Am. Chem. Soc.* **1976**, *98*, 6403−6405.
[7] B. Metz, J. M. Rosalky, R. Weiss, *J. Chem. Soc., Chem. Commun.* **1976**, 533−534.
[8] B. Dietrich, J. Guilhem, J.-M. Lehn, C. Pascard, E. Sonveaux, *Helv. Chim. Acta* **1984**, *67*, 91−104.
[9] J.-M. Lehn, J. Simon, *Helv. Chim. Acta* **1977**, *60*, 141−151.

[10] J.-M. Lehn, *Pure Appl. Chem.* **1980**, *52*, 2441−2459.
[11] R. J. Motekaitis, A. E. Martell, B. Dietrich, J.-M. Lehn, *Inorg. Chem.* **1984**, *23*, 1588−1591.
[12] P. B. Beer In *Transition Metals in Supramolecular Chemistry*, (Eds: L. Fabbrizzi, A. Poggi), Kluwer Academic Publishers, Dordrecht, Boston, London, **1994**, pp 33−54.
[13] P. D. Beer, M. G. B. Drew, D. K. Smith, *J. Organomet. Chem.* **1997**, *543*, 259−262.
[14] D. M. Rudkevich, W. Verboom, D. N. Reinhoudt, *Journal of Organic Chemistry* **1994**, *59*, 3683−3686.
[15] M. R. Meneghetti, M. Grellier, M. Pfeffer, A. De Cian, J. Fischer, *Eur. J. Inorg. Chem.* **2000**, 1539−1547.
[16] G. Van Koten, *Pure Appl. Chem.* **1989**, *61*, 1681−1694.
[17] M. Albrecht, G. Van Koten, *Angew. Chem.* **2001**, *113*, 3866−3898; *Angew. Chem. Int. Ed.* **2001**, *40*, 3750−3781.
[18] J. Sandström, *Dynamic NMR Spectroscopy*, Academic Press Inc, New York, **1982**.
[19] We have first checked that in this buffered solution Cl^- was indeed trapped while adding NaCl in the reaction medium.
[20] F. P. Schmidtchen, *Chem. Ber.* **1981**, *114*, 597−607.
[21] D. M. Rudkevich, W. Verboom, Z. Brzozka, M. J. Palys, S. P. R. V. Stauthamer, G. J. Van Hummel, S. M. Franken, S. Harkema, J. F. J. Engbersen, D. N. Reinhoudt, *J. Am. Chem. Soc.* **1994**, *116*, 4341−4351.
[22] E. Fan, S. A. Van Arman, S. Kincaid, A. D. Hamilton, *J. Am. Chem. Soc.* **1993**, *115*, 369−370.
[23] P. Azenbacher, Jr., K. Jursíková, J. L. Sessler, *J. Am. Chem. Soc.* **2000**, *122*, 9350−9351.
[24] P. D. Beer, S. W. Dent, *Chem. Commun.* **1998**, 825−826.
[25] D. E. Koshland, Jr., G. Némethy, D. Filmer, *Biochemistry* **1966**, *5*, 365−385.
[26] E. Brunet, O. Juanes, M. J. De La Mata, J. C. Rodríguez-Ubis, *Eur. J. Org. Chem.* **2000**, 1913−1922.
[27] E. Graf, M. W. Hosseini, *Coord. Chem. Rev.* **1998**, 1193−1209.
[28] B. V. Nonius In *OpenMoleN*, Interactive Structure Solution, Delft, The Netherlands, **1997**.

Received March 8, 2002
[I02124]

Phosphacarborane Chemistry: The Synthesis of the Parent Phosphadicarbaboranes *nido*-7,8,9-$PC_2B_8H_{11}$ and [*nido*-7,8,9-$PC_2B_8H_{10}$]$^-$, and Their 10-Cl Derivatives − Analogs of the Cyclopentadienide Anion

Bohumil Štíbr,*[a,b] Josef Holub,[a] Mario Bakardjiev,[a] Drahomír Hnyk,[a] Oleg L. Tok,[b] Wolfgang Milius,[b] and Bernd Wrackmeyer[b]

Keywords: Ab initio calculations / Boranes / Clusters / Phosphorus

The reaction of the carborane *nido*-5,6-$C_2B_8H_{12}$ (**1**) with PCl_3 in dichloromethane in the presence of a "proton sponge" [PS = 1,8-bis(dimethylamino)naphthalene], followed by hydrolysis of the reaction mixture, resulted in the isolation of the eleven-vertex *nido*-phosphadicarbaboranes 7,8,9-$PC_2B_8H_{11}$ (**2**) and 10-Cl-7,8,9-$PC_2B_8H_{10}$ (**10-Cl-2**), depending on the ratio of the reactants. Both of these compounds can be deprotonated by PS to give the *nido* anions [7,8,9-$PC_2B_8H_{10}$]$^-$ (**2**$^-$) and [10-Cl-7,8,9-$PC_2B_8H_9$]$^-$ (**10-Cl-2**$^-$). The molecular geometries of all compounds were optimized by ab initio methods at a correlated level of theory [RMP2(fc)] using the 6-31G* basis set and their correctness was assessed by a comparison of the experimental ^{11}B NMR chemical shifts with those calculated by the GIAO-SCF/II//RMP2(fc)/6-31G* method. Moreover, the structure of **10-Cl-2**$^-$ was determined by an X-ray diffraction analysis. The anionic compounds **2**$^-$ and **10-Cl-2**$^-$ are analogs of the Cp (Cp = η^5-$C_5H_5^-$) anion.
(© Wiley-VCH Verlag GmbH, 69451 Weinheim, Germany, 2002)

Introduction

There is current interest in the synthesis and chemistry of phosphacarboranes since the presence of P as a B-cluster constituent gives borane clusters carborane character. The cluster P atom in these species contributes three electrons and three orbitals into the cluster bonding, as does a carborane CH group, while the remaining two electrons reside in the exopolyhedral P sp^3 orbital.[1] Recent efforts are dominated by successful attempts at the isolation of phosphacarborane analogues of tricarbollides (11-vertex *nido*-tricarbaboranes).[2] In this field of chemistry, one of our groups has recently reported preliminary results on the synthesis of the *nido*-phosphadicarbaboranes 7,8,11-$PC_2B_8H_{11}$ and [7,8,11-$PC_2B_8H_{10}$]$^-$ based on the reaction between [6,9-$C_2B_8H_{10}$]$^{2-}$ and PCl_3.[3] The first species is an analog of the neutral tricarbollide 7,8,9-$C_3B_8H_{12}$ and the second anion is analogous to [7,8,9-$C_3B_8H_{11}$]$^-$.[4] Both anions, [7,8,11-$PC_2B_8H_{10}$]$^-$ and [7,8,9-$C_3B_8H_{11}$]$^-$ are also regarded[2] as perfect Cp analogs as they are monoanionic and contain an open pentagonal face which can donate five electrons for the η^5-type coordination to metal ions. As shown in structures **I** and **II**, the presence of the P vertex in the open pentagonal face of an eleven-vertex phosphadicarbaborane anion with the general formula [$PC_2B_8H_{10}$]$^-$ allows for two possible configurations of open-face heteroatoms in adjacent positions. While Cp analogs of configuration **I** are known,[3] those of structure **II** have not yet been reported. Although Sneddon et al. have prepared neutral compounds 7-R-7,8,9-$PC_2B_8H_{10}$ (R = Me and Ph)[5] adopting configuration **II**, these cannot be regarded as Cp analogs as they are not monoanionic. We report here a simple and efficient method for the synthesis of the missing Cp analogs of structure **II**, specifically the preparation of the neutral compound 7,8,9-$PC_2B_8H_{11}$ and the anionic [7,8,9-$PC_2B_8H_{10}$]$^-$, and their 10-Cl derivatives.

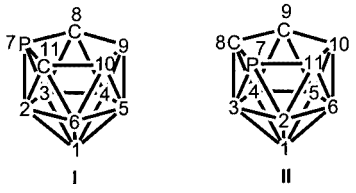

Results and Discussion

Syntheses

As shown in Scheme 1 [path *i)*] (C = CH, vertices of individual polyhedra denote BH groups), treatment of *nido*-

[a] Institute of Inorganic Chemistry, Academy of Sciences of the Czech Republic, Research Centre for New Inorganic Compounds and Advanced Materials, University of Pardubice
25068 Rez, Czech Republic
Fax: (internat.) + 420-2/20941502
E-mail: stibr@iic.cas.cz
[b] Laboratorium für Anorganische Chemie der Universität Bayreuth,
Postfach 101251, Bayreuth, 95440, Germany
Fax: (internat.) + 49-(0)921/552157
E-mail: B.Wrack@uni-bayreuth.de

5,6-$C_2B_8H_{12}$ (**1**)[6] with excess PCl_3 in the presence of a proton sponge [PS = 1,8-bis(dimethylamino)naphthalene] (molar ratio **1**/PS = 1:1.5) in CH_2Cl_2, at room temperature for 48 h, followed by hydrolysis and chromatographic purification of the products, resulted in the isolation of the 11-vertex phosphadicarbaborane *nido*-7,8,9-$PC_2B_8H_{11}$ (**2**) in a yield of 38% (based on **1**). One of the chromatographic fractions contained the dicarbaborane *closo*-1,2-$C_2B_8H_{10}$, which justifies the overall stoichiometry as in Equation (1); otherwise the formation of **2** could not be explained [Equation (1)].

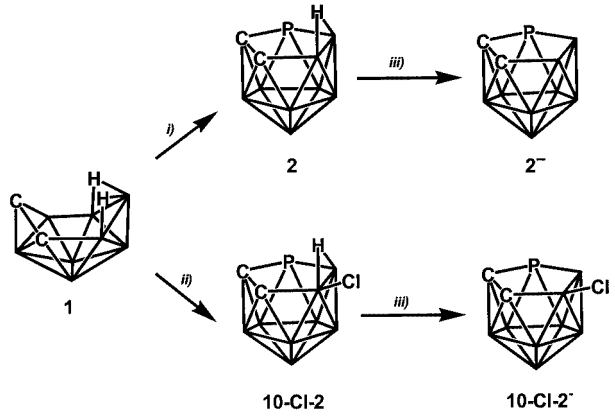

Scheme 1

$$2\,C_2B_8H_{12}\,(\mathbf{1}) + PCl_3 + 3\,PS \rightarrow PC_2B_8H_{11}\,(\mathbf{2}) + C_2B_8H_{10} + 3\,PSH^+Cl^- \quad (1)$$

We assume that 1 equiv. of **1** is oxidized to give *closo*-1,2-$C_2B_8H_{10}$ under the formation of transient $[PHCl_2]$ [Equation (2)] which then reacts with **1** according to Equation (3) to produce the phoshacarborane **2**.

$$C_2B_8H_{12} + PCl_3 + PS \rightarrow C_2B_8H_{10} + [PHCl_2] + PSH^+Cl \quad (2)$$

$$C_2B_8H_{12} + [PHCl_2] + 2\,PS \rightarrow PC_2B_8H_{11} + 2\,PSH^+Cl^- \quad (3)$$

In contrast to the reaction according to Equation (1), the same reaction of **1** with an excess of PCl_3, but using a different **1**/PS ratio (1:2) [Scheme 1, path *ii)*], leads to the formation of the 10-Cl-substituted derivative 10-Cl-*nido*-7,8,9-$PC_2B_8H_{10}$ (**10-Cl-2**) as a predominant product (yield 30%).

$$C_2B_8H_{12}\,(\mathbf{1}) + PCl_3 + 2\,PS \rightarrow PC_2B_8H_{10}Cl\,(\mathbf{10\text{-}Cl\text{-}2}) + 2\,PSH^+Cl^- \quad (4)$$

From the mechanistic viewpoint, reactions according to Equations (1) and (4) are consistent with the insertion of the P vertex into the area identified by the C(6), B(7), B(8), and B(9) vertices in structure **1** (see Scheme 1). Interestingly, in the reaction corresponding to Equation (4), the Cl substituent enters a position not adjacent to the P vertex, as observed earlier in the case of the $P_2C_2B_7H_8Cl$ derivatives.[7] Both **2** and **10-Cl-2** can easily be deprotonated by reactions with stoichiometric amounts of PS in CH_2Cl_2 to give the crystalline salts PSH^+ [*nido*-7,8,9-$PC_2B_8H_{10}$]$^-$ (compound $PSH^+\mathbf{2}^-$) and PSH^+ [10-Cl-*nido*-7,8,9-$PC_2B_8H_9$]$^-$ (compound $PSH^+\mathbf{10\text{-}Cl\text{-}2}^-$) upon careful addition of pentane onto the surface of the solution. The deprotonation reaction thus generates a bare pentagonal face, a favorable feature for employing these anions as Cp analogs for metal complexation.

NMR Spectroscopic Studies

The asymmetrical structure with a contiguous P−C−C string in the open face of an 11-vertex framework (see Scheme 1) is in agreement with the NMR-spectroscopic data of all the compounds described above. The ^{11}B NMR spectra of all the isolated compounds consist of eight different resonances with some incidental overlaps. All of them are doublets, except that the spectra of the substituted compounds **10-Cl-2** and **10-Cl-2**$^-$ contain one B(10) singlet, the resonances being shifted downfield ($\Delta\delta$ = 11.4 and 11.8 ppm, respectively) in comparison to the unsubstituted counterparts. It is also obvious that the ^{11}B NMR signals of the anionic compounds **2**$^-$ and **10-Cl-2**$^-$ are all shifted upfield ($\Delta\delta$ = 11.2 and 11.0 ppm, respectively) in comparison to those of the neutral compounds **2** and **10-Cl-2**. Graphical comparisons of the ^{11}B NMR shifts of **2**, **10-Cl-2**, and the isostructural tricarbaboranes *nido*-7,8,9-$C_3B_8H_{12}$ (compound **3**)[4] are given in Figure 1 (bottom part) together with similar comparisons for the corresponding anionic species **2**$^-$, **10-Cl-2**$^-$, and [*nido*-7,8,9-$C_3B_8H_{11}$]$^-$ (**3**$^-$)[4] (top diagrams).

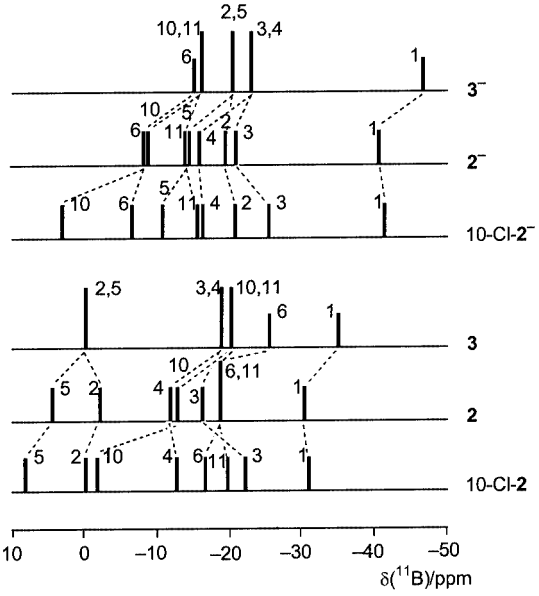

Figure 1. Stick representation and intercomparison of the $\delta(^{11}B)$ chemical shifts for neutral *nido* compounds 7,8,9-$PC_2B_8H_{11}$ (**2**), 10-Cl-7,8,9-$PC_2B_8H_{10}$ (**10-Cl-2**), and 7,8,9-$C_3B_8H_{12}$ (**3**) (bottom diagrams) and their anionic counterparts [7,8,9-$PC_2B_8H_{10}$]$^-$ (**2**$^-$), [10-Cl-7,8,9-$PC_2B_8H_9$]$^-$ (**10-Cl-2**$^-$), and [7,8,9-$C_3B_8H_{11}$]$^-$ (**3**$^-$) (top diagrams)

Figure 1 clearly shows that the δ(^{11}B) data of individual isostructural couples **2/3** and **2**$^-$**/3**$^-$ are very similar (spectrum span δ = 36.4/35.5 and 35.2/31.9 ppm, respectively), but all signals of the P compounds are shifted downfield by an increment of Δδ ≈ 5 ppm. Similar deshielding effects are also observed in the corresponding ^{1}H NMR spectra. These straightforward NMR similarities between tricarbaboranes and the corresponding phosphadicarbaborane counterparts reflect the isolobal relationship between CH and bare P vertices, which is that each contribute three electrons to the cluster bonding scheme. The characteristic feature of the ^{1}H NMR spectra of all compounds isolated is the presence of one CH(9) singlet and one CH(8) doublet ($^2J_{PH}$ coupling). The spectra of the neutral compounds **2** and **10-Cl-2** contain a typical broad, high-field μH(10,11) resonance at δ = −2.48 and −1.12 ppm, respectively. The ^{31}P NMR spectra of all compounds show one singlet and the ^{13}C NMR spectra display one doublet ($^1J_{P-C}$ splitting) and one broader singlet (with fine multiplet $^1J_{CB}$ splitting) due to C(8) and C(9) resonances, respectively. As in the ^{11}B NMR spectra, there are similar upfield shifts of both CH(9) (Δδ = 1.58 [9.3] and 1.79 [9.8] ppm) and CH(8) (Δδ = 1.75 [27.7] and 1.82 [28.9] ppm) resonances, in the corresponding ^{1}H and ^{13}C (data in square brackets) NMR spectra of anions **2**$^-$ and **10-Cl-2**$^-$, with respect to those of the neutral **2** and **10-Cl-2**. This effect is copied in the ^{31}P NMR spectra in which the singlet resonances of the anionic species **2**$^-$ and **10-Cl-2**$^-$ again exhibit shielding (Δδ = 33.1 and 27.7 ppm) with respect to those of the neutral compounds **2** and **10-Cl-2**. As shown in Figure 2, there is a linear correlation between δ(^{13}C) and δ(^{1}H) shifts for CH(8) (line A) and CH(9) (line B) cluster units which can be useful for further NMR-spectroscopic considerations in the fields of carborane and heterocarborane chemistry.

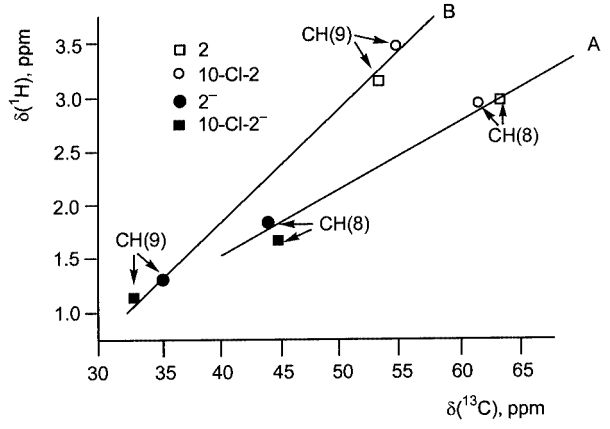

Figure 2. Plot of δ(^{1}H) versus δ(^{13}C) chemical shifts for CH(8) (line A) and CH(9) (line B) cluster units for the *nido*-phosphadicarbaboranes 7,8,9-$PC_2B_8H_{11}$ (**2**), 10-Cl-7,8,9-$PC_2B_8H_{10}$ (**10-Cl-2**), [7,8,9-$PC_2B_8H_{10}$]$^-$ (**2**$^-$), and [10-Cl-7,8,9-$PC_2B_8H_9$]$^-$ (**10-Cl-2**$^-$)

Geometry Optimization

Gimarc's topological stabilization rule[8] suggests that elements with higher electronegativity than boron, such as e.g. C and P, occupy cluster sites of the highest electronegativity of a parent boron hydride from which a corresponding isostructural heteroborane is formally derived. Indeed, the contiguous P−C−C string substitutes the analogous B−B−B string of the hypothetical [*nido*-$B_{11}H_{11}$]$^{4-}$ in its open pentagonal belt [RMP2(fc)/6-31G* natural population analysis (NPA) charge is −0.334, in contrast to −0.170 attributed to the B_5 girdle capped by B(1)].[7] The experimental NMR spectra indicate a total lack of symmetry in all compounds and, consequently, their geometries were fully optimized (see Figure 3) without any symmetry constraints beginning at the SCF level with 3-21G and 6-31G* basis sets. Frequency calculations confirmed the structures to be minima on the corresponding 6-31G* potential energy hypersurfaces. The final level of optimization was second-order Møller−Plesset perturbation theory in frozen core approximation (fc). These geometries were used for GIAO-SCF/II//RMP2(fc)/6-31G* (level of NMR theory// geometry) calculations of the ^{11}B and ^{13}C NMR shifts. Comparisons of these shifts with experimental values are in satisfactory agreement [see Exp. Sect., maximum differences for δ(^{11}B) fall within the range of 5 ppm with the exception of B(4) in **2** (δ = 7 ppm), δ(^{13}C) calculations performed slightly worse but these usually show strong dependence on the theory and basis set used[9]] and thus provide evidence for believing that the RMP2(fc)/6-31G* internal coordinates can be deemed as good representations of the molecular geometries of **2** and **10-Cl-2** and of the anionic species **2**$^-$ and **10-Cl-2**$^-$ in their solutions. The calculated geometries are depicted in Figure 3 and Table 1 offers salient computed geometrical parameters. Apparently, the presence of the P vertex is a principal source of the distortion from a regular "icosahedral-like" shape. The carbon atoms contribute to such a deformation to a lesser extent.

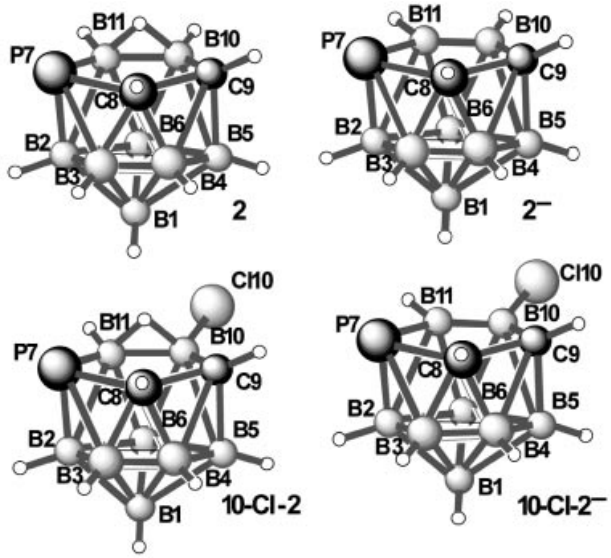

Figure 3. RMP2(fc)/6-31G*-optimized structures of the phosphadicarbaboranes 7,8,9-$PC_2B_8H_{11}$ (**2**), 10-Cl-7,8,9-$PC_2B_8H_{10}$ (**10-Cl-2**), [7,8,9-$PC_2B_8H_{10}$]$^-$ (**2**$^-$), and [10-Cl-7,8,9-$PC_2B_8H_9$]$^-$ (**10-Cl-2**$^-$)

Table 1. Salient internal coordinates at the RMP2(fc)/6-31G* level

	2	**10-Cl-2**	**2$^-$**	**10-Cl-2$^-$**
Bond lengths [Å]				
$[B(1)-B]_{mean}$ [a]	1.772	1.774	1.774	1.774
$(B-B)_{mean}$ [b]	1.777	1.776	1.777	1.776
2−7	2.028	2.026	2.051	2.051
3−7	2.025	2.023	2.060	2.057
3−8	1.748	1.747	1.748	1.743
4−8	1.712	1.713	1.710	1.711
4−9	1.700	1.701	1.726	1.726
5−9	1.693	1.698	1.719	1.724
5−10	1.795	1.799	1.787	1.790
6−10	1.797	1.796	1.788	1.783
2−11	1.826	1.823	1.821	1.816
6−11	1.778	1.784	1.768	1.776
7−8	1.888	1.890	1.871	1.871
8−9	1.528	1.529	1.528	1.527
9−10	1.658	1.647	1.620	1.612
10−11	1.834	1.837	1.741	1.727
7−11	2.027	2.035	1.949	1.950
$(B-H)_{mean}$	1.189	1.188	1.198	1.195
$(C-H)_{mean}$	1.088	1.189	1.090	1.089
10-Cl		1.790		1.834
10-H_b	1.329	1.347		
11-H_b	1.305	1.290		
Bond angles [°]				
7-8-9	120.0	120.1	113.4	113.6
8-9-10	112.8	112.7	114.7	113.8
8-7-11	91.5	91.4	94.8	94.8
Dihedral angles [°]				
7−8−9−10	−3.2	−3.4	−7.8	−7.9
9−8−7−11	8.7	8.6	13.1	13.0
8−9−10−11	−5.0	−4.8	−2.8	−2.6

[a] For atomic numbering, see Figure 3. [b] Lower pentagon.

The most remarkable features of the computed molecular structures of these systems are the considerable deformations of the open pentagonal belts. For instance, the C(8)−P(7)−B(11) angles for **2** and **10-Cl-2** are 91.5 and 91.4°, respectively. Such deviations from a regular pentagonal angle of 108° are by far the largest noticed so far in the family of heteroboranes that contain a third-row element.[7,10] In the case of the corresponding anions, **2$^-$** and **10-Cl-2$^-$**, these angles are opened by ca. 3.5° with respect to **2** and **10-Cl-2**, but still deviate substantially from 108°. On the other hand, such a pronounced narrowing in **2** and **10-Cl-2** is likely to be compensated by opening of the P(7)−C(8)−C(9) angles when compared with their smaller values for both anions. Moreover, these pentagons are not planar, as exemplified by some dihedral angles in Table 1, although such a nonplanarity is less marked in the neutral species. As found in other phosphaboranes,[7,11] the Cl-substitution brings about only marginal effects in the molecular cage geometry relative to an unsubstituted compound (see Table 1). The P−C, P−B, C−C, and B−B nearest-neighbor separations in the open pentagonal belts resemble those determined for the four $P_2C_2B_7H_9$ isomers and their Cl derivatives[7], at the same level of theory [e.g. *r*(C−C), retain their aliphatic single-bond character, which is also revealed by their Wiberg bond indices (WBI, natural atomic bond orders) calculated for **2** and **2$^-$**: 0.962 (0.833) and 0.946 (0.817), respectively]. Whereas the WBI for the remaining four linkages of the open pentagonal face of **2$^-$** span a narrow interval of <0.773, 0.866> (<0.688, 0.823>), the presence of the hydrogen bond in **2** considerably decreases electron delocalization in the open pentagonal face {WBI for *r*[B(10)−B(11)] = 0.457 (0.619)}.

X-ray Diffraction Studies

The structure of PSH^+**10-Cl-2$^-$** was determined unambiguously by an X-ray diffraction analysis (for selected crystallographic parameters see Tables 2 and 3). As seen from Figure 4, the structure of the anionic part **10-Cl-2$^-$** is consistent with all NMR-spectroscopic data and compares well with the calculated RMP2(fc)/6-31G* geometrical parameters. The computed and experimental structural parameters in Tables 1 and 2, respectively, are generally in good agreement. The cage P−C, P−B, C−C and C−B, B−B distances in the open pentagonal face are 1.866(4), 1.939(4), 1.517(4) and 1.596(5), 1.723(4) Å, respectively, similar to those found crystallographically for the diphosphadicarbaboranes $P_2C_2B_7H_9$, the other cluster C−B and P−B, B−B, and B−Cl separations fall within usual limits.[7] The structure determination also confirms the asymmetrical arrangement of the C and P heteroatoms within a distorted open pentagonal face. As also exhibited in the calculated structure, the distortion is due to relatively long P−B and P−C separations as demonstrated, e.g., by the torsion angle B(11)−P−C(8′)−C(9′) −13.3(2)°. Also the C(8′)−P−B(11) angle shows at 94.92(14)°, a remarkable deviation from the ideal 108° in a regular pentagon. We were even able to localize the bridging N−H−N hydrogen in the cationic (PSH^+) part of the molecule, which is closer to one of the nitrogen atoms by 0.7454(3) Å than to the other.

Conclusions

The neutral compound 7,8,9-$PC_2B_8H_{11}$ (**2**) and its chlorinated derivative **10-Cl-2** can now easily be prepared by phosphorus insertion from the readily available 5,6-$C_2B_8H_{12}$ (**1**) dicarbaborane.[6] We have demonstrated that the constitution of **2** is analogous to that of the neutral tricarbollide 7,8,9-$C_2B_8H_{12}$ (**3**) as the bare P vertex is isolobal with the cage CH group. The bridging hydrogen atom in **2** can be removed by deprotonation to generate anion **2$^-$**. This anion is analogous to the Cp anion as it is monoanionic, contains a bare pentagonal face and would then be capable of donating five electrons for η^5-type complexation of suitable metal centers. This is also justified by similar electron densities in the linkages forming the PCCBB pentagon in terms of the Wiberg and natural bond orders. Indeed, recent experiments in our laboratories[12] point to facile formation of the isomeric (cyclopentadienyl)-ferraphosphadicarbaboranes of general formula $CpFePC_2B_8H_{10}$, analogues of ferrocene and the earlier reported[2] ferratricarbollides. Apart from extending metal complexation reactions of **2$^-$**, we are also exploring various

Table 2. Selected intracluster bond lengths [Å] and angles [°] for $PSH^+[10\text{-Cl-}nido\text{-}7,8,9\text{-}PC_2B_8H_9]^-$ (PSH^+**10-Cl-2**$^-$)

Cl−B(10)	1.844(3)	P−C(8′)	1.866(4)
P−B(2)	2.041(3)	P−B(3)	2.038(4)
P−B(11)	1.939(4)	B(1)−B(2)	1.767(5)
B(1)−B(3)	1.761(5)	B(1)−B(4)	1.791(5)
B(1)−B(5)	1.787(4)	B(1)−B(6)	1.800(5)
B(2)−B(3)	1.812(5)	B(2)−B(6)	1.776(4)
B(2)−B(11)	1.805(4)	B(3)−B(4)	1.830(5)
B(3)−C(8′)	1.740(4)	B(4)−B(5)	1.766(5)
B(4)−C(8′)	1.749(5)	B(4)−C(9′)	1.743(4)
B(5)−B(6)	1.748(5)	B(5)−C(9′)	1.729(5)
B(5)−B(10)	1.783(5)	B(6)−B(10)	1.787(4)
B(6)−B(11)	1.770(5)	C(8′)−C(9′)	1.517(4)
C(9′)−B(10)	1.596(5)	B(10)−B(11)	1.723(4)
C(8′)−P−B(11)	92.92(14)	C(8′)−P−B(3)	52.70(13)
B(11)−P−B(3)	95.44(14)	C(8′)−P−B(2)	90.93(14)
B(11)−P−B(2)	53.84(13)	B(3)−P−B(2)	52.74(14)
C(9′)−C(8′)−B(3)	112.6(2)	C(9′)−C(8′)−B(4)	64.1(2)
B(3)−C(8′)−B(4)	63.26(19)	C(9′)−C(8′)−P	113.4(2)
B(3)−C(8′)−P	68.72(17)	B(4)−C(8′)−P	123.7(2)
C(8′)−C(9′)−B(10)	113.9(3)	C(8′)−C(9′)−B(5)	113.1(2)
B(10)−C(9′)−B(5)	64.7(2)	C(8′)−C(9′)−B(4)	64.4(2)
B(10)−C(9′)−B(4)	116.8(2)	B(5)−C(9′)−B(4)	61.1(2)
C(9′)−B(10)−B(11)	109.8(2)	C(9′)−B(10)−B(5)	61.2(2)
B(11)−B(10)−B(5)	110.1(2)	C(9′)−B(10)−B(6)	106.4(2)
B(11)−B(10)−B(6)	60.55(18)	B(5)−B(10)−B(6)	58.61(18)
B(10)−B(11)−B(6)	61.51(18)	B(10)−B(11)−B(2)	106.3(2)
B(6)−B(11)−B(2)	59.56(18)	B(10)−B(11)−P	105.8(2)
B(6)−B(11)−P	114.4(2)	B(2)−B(11)−P	65.97(15)

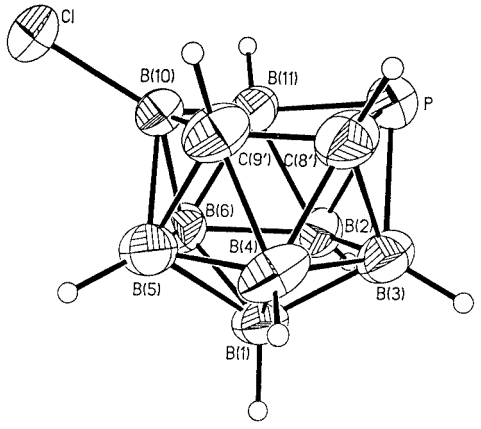

Figure 4. ORTEP representation of the crystallographically determined molecular structure of the $[10\text{-Cl-}nido\text{-}7,8,9\text{-}PC_2B_8H_9]^-$ (**10-Cl-2**$^-$) anion

isomerization and substitution reactions of the phosphadicarbaborane species outlined in this paper. Moreover, phosphorus insertion reactions with other borane and carborane compounds are also being studied with the aim of generating new types of chemically versatile heteroborane cages.

Experimental Section

General Procedures: All reactions were carried out with the use of standard vacuum or inert-gas techniques as described by Shriver,[13] although some operations, such as column LC, were carried out in air. The starting carborane **1** was prepared according to the literature.[6] Dichloromethane and hexane (both from Fluka) were dried with CaH_2 and freshly distilled before use. Other chemicals were reagent- or analytical grade and were used as purchased. Column chromatography was carried out using silica gel (Aldrich, 130−270 mesh) as the stationary phase. The purity of individual chromatographic fractions was checked by analytical TLC on Silufol (silica gel on aluminum foil; detection by diiodine vapor, followed by 2% aqueous $AgNO_3$ spray). Melting points were measured in sealed capillaries under argon and are uncorrected. Low-resolution mass spectra were obtained using a Finnigan MAT MAGNUM ion trap quadrupole mass spectrometer equipped with a heated inlet option, as developed by Spectronex AG, Basel, Switzerland (70 eV, EI ionisation). Proton (^1H) and boron (^{11}B), and phosphorus (^{31}P) NMR spectroscopy was performed at 11.75 and 5.88 Tesla with Varian XL-500, and ARX 250 instruments and the ^{13}C NMR spectra were measured with a Bruker DRX 500 spectrometer, equipped for heteronuclear $^{13}C\{^1H,^{11}B\}$ triple-resonance experiments. The [^{11}B-^{11}B]-COSY[14] and ^1H-{^{11}B(selective)}[15] NMR experiments were essentially as described in other related papers from our laboratories.[16] Chemical shifts are given in ppm to high frequency (low field) of Ξ = 32.083971 MHz (nominally $F_3B{\cdot}OEt_2$ in $CDCl_3$) for ^{11}B (quoted ±0.5 ppm), Ξ = 25.144 MHz ($SiMe_4$) for ^{13}C (quoted ±0.5 ppm), Ξ = 40.4805 MHz (H_3PO_3) for ^{31}P (quoted ±0.5 ppm), and Ξ = 100 MHz ($SiMe_4$) for ^1H (quoted ±0.05 ppm), Ξ being defined as in ref.[17] Solvent resonances were used as internal secondary standards. Coupling constants $^1J(^{11}B$-$^1H)$ are taken from resolution-enhanced ^{11}B spectra with digital resolution ±8 Hz and are given in Hz. The ^{11}B and ^1H NMR spectra of all phosphacarborane compounds discussed in this work can easily be assigned using two-dimensional [^{11}B-^{11}B]-COSY spectroscopy[14] combined with $^1H\{^{11}B$(selective)$\}$[15] measurements. Moreover, all $^1H\{^{11}B\}$ resonances of individual BH and CH vertices adjacent to the cluster P vertex are spit into doublets due to $^2J_{PH}$ coupling, which helps all cluster resonances to be assigned. IR spectra were obtained with an EU 9512 Pye−Unicam Fourier transform spectrometer.

***nido*-7,8,9-$PC_2B_8H_{11}$ (2):** A solution of compound **1** (5.0 g, 40.2 mmol) in CH_2Cl_2 (50 mL) was cooled to 0 °C and treated with PS (10.0 g, 46.7 mmol) whilst stirring for 15 min. To this solution, PCl_3 (3.5 mL, 40.4 mmol) was added dropwise over a period of 15 min and the mixture was then stirred for 24 h at ambient temperature. The mixture was then cooled again to 0 °C and decomposed carefully with water (50 mL) whilst stirring. The CH_2Cl_2 layer was separated, the solvent evaporated and the residual materials were separated by chromatography on a silica gel column (30 × 2.5 cm) to collect a pure fraction of R_f = 0.22 which was identified by NMR spectroscopy as **2** (2.42 g, 39%). Crystallization of an analytical sample of **2** by slow concentration of a pentane solution. R_f (hexane) = 0.22; m.p. 260 °C. ^{11}B NMR ($CDCl_3$, ppm): δ = 5.7 (d, $^1J_{B-H}$ = 162 Hz, 1 B, B^5), 2.2 (d, $^1J_{B-H}$ = 158 Hz, 1 B, B^2), −12.8 (d, 1 B, B^4), −13.6 (d, $^1J_{B-\mu H}$ = 42 Hz, 1 B, B^{10}), −17.2 (d, 1 B, B^3), ca. −18.0 (d, 1 B, B^6), −18.3 (d, 1 B, B^{11}), −30.9 (d, $^1J_{B-H}$ = 158 Hz, 1 B, B^1), all theoretical [^{11}B-^{11}B]-COSY cross-peaks observed. ^{11}B NMR [calcd., GIAO-SCF/II/RMP2(fc)/6-31G*, ppm]: δ = 9.5 (B^5), 7.0 (B^2), −11.1 (B^4), −13.9 (B^{10}), −14.2 (B^3), −17.0 (B^6), −17.5 (B^{11}), −30.2 (B^1). $^1H\{^{11}B\}$ NMR ($CDCl_3$, ppm): δ = 3.22 (s, 1 H, H^9), 3.02 (d, $^2J_{P-H}$ = 17 Hz, 1 H, H^8),. 2.96 (s, 1 H, H^5), 2.68 (d, $^2J_{P-H}$ = 23 Hz, 1 H, H^2), 2.35 (d, $^2J_{P-H}$ = 23 Hz, 1 H, H^3), 2.34 (s, 1 H, H^4),. 2.29 (s, 1 H, H^{10}), 1.88 (s, 1 H, H^1), 1.73 (s, 1 H, H^{11}), 1.72 (s, 1 H, H^6), −2.73 (q, $^2J_{H-H}$ = 12 Hz, 1 H, $\mu H^{10,11}$). $^{13}C\{^1H\}$ NMR ($CDCl_3$, ppm): δ =

63.3 (d, $^1J_{P-C}$ = 72 Hz, 1 C, C^8), 53.4 (s, 1 C, C^9). ^{13}C NMR [calcd., GIAO-SCF/II/RMP2(fc)/6-31G*, ppm]: δ = 58.3 (C^8), 44.8 (C^9). $^{31}P\{^1H\}$ NMR ($CDCl_3$, ppm): δ = −60.1 (s, 1 P, P^7). IR (KBr, cm^{-1}): $\tilde{\nu}$ = 2926 (C−H), 2576 (B−H). MS (70 eV, EI): *m*/*z* (%) = 154 (9) $[M]^+$, 150 (100) $[M - 4\ H]^+$; elemental analysis: calcd. (%) for $C_2H_{11}B_8P$ (152.64): B 56.71, found B 55.11.

10-Cl-*nido*-7,8,9-$PC_2B_8H_{10}$ (10-Cl-2): To a solution of **1** (2.00 g, 16.1 mmol) in CH_2Cl_2 (40 mL) was added PS (7.00 g, 32.7 mmol), followed by dropwise addition of PCl_3 (5 mL, 57.7 mmol) whilst stirring and cooling to 0 °C. The mixture was then stirred at ambient temperature for 24 h and carefully treated with water (50 mL) at 0 °C and the CH_2Cl_2 layer was concentrated to dryness. The residual solid was then separated by LC on a silica gel column (2.5 × 35 cm) using hexane as a mobile phase to collect three pure fractions of R_f (hexane) = 0.22, 0.13, and 0.07 which were concentrated to dryness and identified by ^{11}B NMR spectroscopy as **2** (130 mg, 5%), 1,2-$C_2B_8H_{10}$ (125 mg, 6%), and **10-Cl-2** (910 mg, 30%), respectively. Crystallization of **10-Cl-2** by slow concentration of a pentane solution gave an analytically pure sample. R_f (hexane) = 0.07; m.p. 150 °C. ^{11}B NMR ($CDCl_3$, ppm): δ = 7.8 (d, $^1J_{B-H}$ = 165 Hz, 1 B, B^5), −0.4 (d, $^1J_{B-H}$ = 154 Hz, 1 B, B^2), −2.2 (s, 1B, B^{10}), −13.1 (d, $^1J_{B-\mu H}$ = 177 Hz, 1 B, B^4), −16.9 (d, $^1J_{B-H}$ = 154 Hz, 1 B, B^6), ca. −19.9 (d, $^1J_{B-H}$ = 158 Hz, 1 B, B^{11}), −22.8 (d, $^1J_{B-H}$ = 173 Hz, 1 B, B^3), −31.2 (d, $^1J_{B-H}$ = 154 Hz, 1 B, B^1), all theoretical [^{11}B-^{11}B]-COSY cross-peaks observed. ^{11}B NMR [calcd., GIAO-SCF/II/RMP2(fc)/6-31G*, ppm]: δ = 11.4 (B^5), 4.9 (B^2), −2.0 (B^{10}), −11.7 (B^4), −15.5 (B^6), −18.5 (B^3), −18.8 (B^{11}), −30.7 (B^1). $^1H\{^{11}B\}$ NMR ($CDCl_3$, ppm): δ = 3.48 (s, 1 H, H^9), 3.35 (s, 1 H, H^5), 2.96 (d, $^2J_{P-H}$ = 28 Hz, 1 H, H^8), 2.61 (d, $^2J_{P-H}$ = 21 Hz, 1 H, H^2), 2.39 (s, 1 H, H^4), 2.20 (d, $^2J_{P-H}$ = 14 Hz, 1 H, H^3), 1.98 (s, 1 H, H^6), 1.85 (d, $^2J_{P-H}$ = 55 Hz, 1 H, H^{11}), 1.80 (s, 1 H, H^1), −1.12 (q, $^2J_{H-H}$ = 9 Hz, 1 H, $\mu H^{10,11}$). $^{13}C\{^1H\}$ NMR ($CDCl_3$, ppm): δ = 61.5 (d, $^1J_{P-C}$ = 72 Hz, 1 C, C^8), 54.6 (q, $^1J_{C-B} \approx$ 33 Hz, 1 C, C^9). ^{13}C NMR [calcd., GIAO-SCF/II/RMP2(fc)/6-31G*, ppm]: δ = 56.1 (C^8), 47.6 (C^9). $^{31}P\{^1H\}$ NMR ($CDCl_3$, ppm): δ = −67.7 (s, 1 P, P^7). IR (KBr, cm^{-1}): $\tilde{\nu}$ = 2932 (C−H), 2581 (B−H). MS (70 eV, EI), *m*/*z* (%) = 189 (5) $[M]^+$, 185 (100) $[M - 4\ H]^+$. $C_2H_{10}B_8ClP$ (187.13): calcd. B 46.26; found B 45.12.

PSH$^+$[*nido*-7,8,9-$PC_2B_8H_{10}$]$^-$ (PSH$^+$2$^-$): To a solution of **2** (129 mg, 0.85 mmol) in CH_2Cl_2 (10 mL) was added PS (193 mg, 0.9 mmol) whilst stirring and cooling to 0 °C. Onto the surface of the solution, a layer of hexane (20 mL) was carefully added and the mixture was left to crystallize for 48 h. The colorless crystals were then isolated by filtration, washed with hexane, and vacuum-dried at room temperature to give PSH$^+$**2**$^-$ (290 mg, 93%). Crystallization of an analytical sample was achieved by diffusion of pentane vapors into a CH_2Cl_2 solution. R_f (CH_2Cl_2) = 0.1; m.p. 230 °C. ^{11}B NMR ($CDCl_3$, ppm): δ = −8.0 (d, 1 B, B^6), −8.3 (d, 1 B, B^{10}), −13.6 (d, 1 B, B^{11}), −14.4 (d, $^1J_{B-H} \approx$ 150 Hz, 1 B, B^{10}), −15.5 (d, $^1J_{B-H} \approx$ 165 Hz, 1 B, B^4), −19.0 (d, $^1J_{B-H}$ = 143 Hz, 1 B, B^2), −20.9 (d, $^1J_{B-H}$ = 158 Hz, 1 B, B^3), −41.1 (d, $^1J_{B-H}$ = 142 Hz, 1 B, B^1), all theoretical [^{11}B-^{11}B]-COSY cross-peaks observed. ^{11}B NMR [calcd., GIAO-SCF/II/RMP2(fc)/6-31G*, ppm]: δ = −3.7 (B^6), −10.4 (B^{10}), −13.8 (B^5), −14.4 (B^{11}), −14.7 (B^4), −17.5 (B^2), −19.6 (B^3), −42.7 (B^1). $^1H\{^{11}B\}$ NMR ($CDCl_3$, ppm): δ = 2.16 (d, $^2J_{P-H}$ = 10 Hz, 1 H, H^3), 2.15 (s, 1 H, H^6), 2.13 (s, 1 H, H^4), 2.03 (s, 1 H, H^9), 1.81 (s, 1 H, H^5), 1.80 (s, 1 H, H^{10}), 1.46 (d, $^2J_{P-H}$ = 30 Hz, 1 H, H^8), 1.18 (d, $^2J_{P-H}$ = 40 Hz, 1 H, H^{11}), 1.18 (d, $^2J_{P-H}$ = 20 Hz, 1 H, H^2), 1.02 (s, 1 H, H^1). $^{13}C\{^{11}B,^1H\}$ NMR (CD_3CN, ppm): δ = 44.1 (s, 1 C, C^9), 35.4 (d, $^1J_{C-P}$ = 55 Hz, 1 C, C^8). $^{13}C\{^{11}B\}$ NMR (CD_3CN, ppm): δ = 44.1 (d, $^1J_{C-H}$ = 162 Hz, 1 C, C^9), 35.4 (dd, $^1J_{C-H}$ = 169, $^1J_{C-P} \approx$ 60 Hz, 1 C, C^8). ^{13}C NMR [calcd., GIAO-SCF/II/RMP2(fc)/6-31G*, ppm]: δ = 38.2 (C^9), 28.6 (C^8). $^{31}P\{^1H\}$ NMR (CD_3CN, ppm): δ = −91.0 (s, 1 P, P^7). IR (KBr, cm^{-1}): $\tilde{\nu}$ = 2574 (B−H). $C_{16}H_{29}B_8N_2P$ (366.95): calcd. B 23.59; found B 22.70.

PSH$^+$[10-Cl-*nido*-7,8,9-$PC_2B_8H_9$]$^-$ (PSH$^+$10-Cl-2$^-$): To a solution of **10-Cl-2** (200 mg, 1.1 mmol) in hexane (20 mL), a solution of PS (300 mg, 1.4 mmol) in hexane was added whilst stirring and cooling to 0 °C. The colorless crystals that deposited were filtered, washed with hexane, and vacuum dried at room temperature to give PSH$^+$**10-Cl-2**$^-$ (390 mg, 91%). Crystallization of an analytical sample by diffusion of pentane vapors into a CH_2Cl_2 solution. R_f (CH_2Cl_2) = 0.04; m.p. 155 °C. ^{11}B NMR (CD_3CN, ppm): δ = 3.0 (s, 1 B, B^{10}), −7.3 (d, $^1J_{B-H}$ = 138 Hz, 1B, B^6), −11.8 (d, $^1J_{B-H}$ = 147 Hz, 1B, B^5), −16.4 (d, 1B, B^{11}),−17.2 (d, $^1J_{B-H} \approx$ 165 Hz, 1 B, B^4), −20.8 (d, $^1J_{B-H}$ = 142 Hz, 1 B, B^2), −25.6 (d, $^1J_{B-H}$ = 154 Hz, 1 B, B^3), −42.2 (d, $^1J_{B-H}$ = 139 Hz, 1 B, B^1), all theoretical [^{11}B-^{11}B]-COSY cross-peaks observed. ^{11}B NMR [calcd., GIAO-SCF/II/RMP2(fc)/6-31G*, ppm]: δ = 3.0 (B^{10}), −2.3 (B^6), −10.3 (B^5), −15.8 (B^{11}), −16.1 (B^4), −18.8 (B^2), −22.8 (B^3), −43.2 (B^1). $^1H\{^{11}B\}$ NMR (CD_3CN, ppm): δ = 1.91 (s, 1 H, H^6), 1.84 (s, 1 H, H^4), 1.69 (s, 1 H, H^9), 1.64 (s, 1 H, H^5), 1.54 (d, $^2J_{P-H}$ = 32 Hz, 1 H, H^{11}), 1.80 (s, 1 H, H^{10}), 1.14 (d, $^2J_{P-H}$ = 32 Hz, 1 H, H^8), 0.78 (d, $^2J_{P-H}$ = 40 Hz, 1 H, H^2), 0.60 (d, $^2J_{P-H}$ = 20 Hz, 1 H, H^3), 0.44 (s, 1 H, H^1). $^{13}C\{^{11}B,^1H\}$ NMR (CD_3CN, ppm): δ = 44.8 (s, 1 C, C^9), 33.0 (d, $^1J_{C-P}$ = 56 Hz, 1 C, C^8). $^{13}C\{^{11}B\}$ NMR (CD_3CN, ppm): δ = 44.8 (d, $^1J_{C-H}$ = 163 Hz, 1 C, C^9), 33.0 (dd, $^1J_{C-H}$ = 170, $^1J_{C-P}$ = 56 Hz, 1 C, C^8). ^{13}C NMR [calcd., GIAO-SCF/II/RMP2(fc)/6-31G*, ppm]: δ = 40.0 (C^9), 26.0 (C^8). $^{31}P\{^1H\}$ NMR (CD_3CN, ppm): δ = −91.0 (s, 1 P, P^7). IR (KBr, cm^{-1}): $\tilde{\nu}$ = 2579 (B−H). $C_{16}H_{28}B_8ClN_2P$ (401.44): calcd. B 21.56; found B 19.90.

X-ray Crystallography: A colorless crystal of PSH$^+$**10-Cl-2**$^-$ of dimensions 0.30 × 0.21 × 0.18 mm was sealed into a glass capillary under argon and measured with a Siemens P4 four-circle diffractometer at 293(2) K with Mo-K_α radiation (graphite monochromator). The crystallographic details are summarized in Table 3 and selected interatomic distances are listed in Table 2. The structure was solved by the direct methods and refined by a full-matrix least-squares procedure based on F^2 (SHELXLTL V.5.1: G. M. Sheldrick, program package SHELXTL, Göttingen). The absorption was neglected. Hydrogen atoms were localized on a difference Fourier map and refined isotropically. The final difference map had no peaks of chemical significance. Scattering factors were those implemented in the SHELXLTL V.5.1 programs. CCDC-175954 contains the supplementary crystallographic data for this paper. These data can be obtained free of charge at www.ccdc.cam.ac.uk/conts/retrieving.html or from the Cambridge Crystallographic Data Centre, 12, Union Road, Cambridge CB2 1EZ, UK [Fax: (internat.) + 44-1223/336-033; E-mail: deposit@ccdc.cam.ac.uk].

Computational Details: Geometry optimizations and frequency calculations employed standard ab initio methods incorporated[18] in the Gaussian94 suite of programs[19] and were performed with the Power Challenge XL computer of the Supercomputing Center of the Charles University in Prague. This program package also enabled us to compute both the Wiberg bond indices (WBI),[20] overlap-weighted natural atomic orbital (NAO) bond orders[21] and the chemical shifts, the latter being calculated at an SCF level using the GIAO (gauge-invariant atomic orbital) method and employing a II Huzinaga basis set[22] well-proven for the calculations of shielding tensors.[23]

Table 3. Crystal data and structure refinement for PSH^+ [10-Cl-*nido*-7,8,9-$PC_2B_8H_9$]$^-$ (PSH^+**10-Cl-2**$^-$)

Empirical formula	$C_{16}H_{28}B_8ClN_2P$
M_r	401.30
λ [Å]	0.71073
Crystal system	monoclinic
Space group	$P2_1/c$
a [Å]	6.4573(4)
b [Å]	24.5282(17)
c [Å]	13.8020(9)
β [°]	94.626
V [Å^3]	2178.9(2)
Z	4
$\rho_{calcd.}$ [Mg/m^3]	1.223
μ [mm^{-1}]	0.254
F(000)	840
θ range [°]	2.22−24.99
h,*k*,*l* collected	$-1 \le h \le 7$, $-1 \le k \le 29$, $-16 \le l \le 16$
No. of reflections collected	5131
No. of independent reflections	3806 [*R*(int) = 0.0336]
Completeness to θ = 24.99° [%]	99.0
Data/restraints/parameters	3806/0/246
GoF on F^2	1.020
Final *R* indices [$I > 2\sigma(I)$]	*R*1 = 0.0502, *wR*2 = 0.1391
R indices (all data)	*R*1 = 0.0701, *wR*2 = 0.1531
Extinction coefficient	0.0046(14)
max/min Δρ [e·Å^{-3}]	0.358/−0.345

Acknowledgments

This work was supported by the Alexander von Humboldt Stiftung (FRG) (B. S.), the Deutsche Forschungsgemeinschaft (B. W., O. L. T.), the Fonds der Chemischen Industrie (B. W.), the Ministry of Education of Czech Republic (project no. LN00A028). We also thank the Grant Agency of the Charles University (grant no. 203/00/B-CH/PrF) and the Supercomputing Center of the Charles University in Prague for granting computer time, and Drs. J. Fusek, Z. Plzák, and E. Vecerníková for partial NMR-spectroscopic measurements, mass and IR spectra.

[1] [1a] L. J. Todd, in: *Comprehensive Organometallic Chemistry* (Eds.: G. Wilkinson, F. G. A. Stone, E. Abel), Pergamon, **1982**, part I, chapter 5.6, pp. 543−553. [1b] L. J. Todd, in: *Metal Interactions with Boron Clusters* (Ed.: R. N. Grimes), Plenum, New York, **1982**, pp. 145−171.

[2] [2a] B. Štíbr, *Chem. Rev.* **1992**, *92*, 225−250, and references therein. [2b] B. Stíbr, J. Holub, F. Teixidor, in: *Advances in Boron Chemistry* (Ed.: W. Siebert), Royal Society of Chemistry, Cambridge, **1997**, pp. 333−340.

[3] J. Holub, D. L. Ormsby, J. D. Kennedy, R. Greatrex, B. Štíbr, *Inorg. Chem. Commun.* **2000**, *3*, 178−181.

[4] [4a] B. Štíbr, J. Holub, F. Teixidor, C. Vinňas, *J. Chem. Soc., Chem. Commun.* **1995**, 795−796. [4b] J. Holub, B. Štíbr, D. Hnyk, J. Fusek, I. Císařová, F. Teixidor, C. Viňas, Z. Plzák, P. v. R. Schleyer, *J. Am. Chem. Soc.* **1997**, *119*, 7750−7759.

[5] M. Shedlow, L. G. Sneddon, *Inorg. Chem.* **1998**, *37*, 5269−5277.

[6] B. Štíbr, J. Holub, T. Jelínek, B. Grüner, J. Fusek, Z. Plzák, F. Teixidor, C. Viňas, J. D. Kennedy, *Collect. Czech. Chem. Commun.* **1997**, *62*, 1229−1238.

[7] J. Holub, T. Jelínek, D. Hnyk, Z. Plzák, I. Císařová, M. Bakardjiev, B. Štíbr, *Chem. Eur. J.* **2001**, *7*, 1546−1554.

[8] J. J. Ott, B. M. Gimarc, *J. Am. Chem. Soc.* **1986**, *108*, 4303−4308.

[9] M. Bühl, P. v. R. Schleyer, *J. Am. Chem. Soc.* **1992**, *114*, 477−491.

[10] D. Hnyk, M. Hofmann, P. v. R. Schleyer, M. Bühl, D. W. H. Rankin, *J. Phys. Chem.* **1996**, *100*, 3435−3440.

[11] B. Grüner, D. Hnyk, I. Císarová, Z. Plzák, B. Stíbr, *J. Chem. Soc., Dalton Trans.*, submitted for publication.

[12] J. Holub, B. Stíbr, M. Bakardjiev, I. Císarová, O. L. Tok, B. Wrackmeyer, *Abstracts of the 2nd European Symposium on Boron Chemistry (EUROBORON 2)*, Dinard (France), 2.−6.9.**2001**, O18.

[13] D. F. Shriver, M. A. Drezdon, *Manipulation of Air Sensitive compounds*, 2nd ed., Wiley, New York, **1986**.

[14] [14a] J. D. Kennedy, in: *Multinuclear N. M. R.* (Ed.: J. Mason), Plenum Press, New York, **1987**, p. 221. [14b] W. C. Hutton, T. L. Venable, R. N. Grimes, *J. Am. Chem. Soc.* **1984**, *106*, 29−37. [14c] Schraml, J. M. Bellama, *Two-Dimensional NMR Spectroscopy*, Wiley, New York, **1982**.

[15] X. L. R. Fontaine, J. D. Kennedy, *J. Chem. Soc., Dalton Trans.* **1987**, 1573.

[16] J. Plešek, B. Štíbr, X. L. R. Fontaine, J. D. Kennedy, S. Heřmánek, T. Jelínek, *Collect. Czech. Chem. Commun.* **1991**, *56*, 1618−1635.

[17] W. McFarlane, *Proc. R. Soc. London, Ser. A* **1968**, *306*, 185.

[18] W. Hehre, L. Radom, P. v. R. Schleyer, J. A. Pople, *Ab initio Molecular Orbital Theory*, Wiley, New York, **1986**.

[19] M. J. Frisch, G. W. Trucks, H. B. Schlegel, P. M. W. Gill, B. G. Johnson, M. A. Robb, J. R. Cheeseman, T. Keith, G. A. Petterson, J. A. Montgomery, K. Raghavachari, M. A. Al-Laham, V. G. Zahrzewski, J. V. Ortiz, J. B. Foresman, J. Cioslowski, B. B. Stefanov, A. Nanayakkra, M. Challacombe, C. Y. Peng, P. Y. Ayala, Y. Chen, M. W. Wong, J. L. Andres, E. S. Replogle, R. Gomprets, R. L. Martin, D. J. Fox, J. S. Binkley, D. J. Defrees, L. Baker, J. P. Stewart, M. Head-Gordon, C. Gonzales, J. A. Pople, *Gaussian94*, Revision B.2. Gaussian Inc., Pittsburg, PA, **1995**.

[20] K. Wiberg, *Tetrahedron* **1968**, *24*, 325.

[21] [21a] A. E. Reed, R. B. Weinstock, F. Weinhold, *J. Phys. Chem.* **1985**, *83*, 735. [21b] A. E. Reed, F. Weinhold, *Chem. Rev.* **1988**, *88*, 899. [21c] A. E. Reed, P. v. R. Schleyer, *J. Am. Chem. Soc.* **1990**, *112*, 1434.

[22] S. Huzinaga, *Approximate Atomic Wave Functions*, University of Alberta, Edmonton, Canada, **1971**.

[23] W. Kutzelnigg, M. Schindler, U. Fleischer, *NMR, Basic Principles and Progress*, Springer-Verlag, Berlin, New York, **1990**; vol. 23.

Received March 14, 2002
[I02133]

Synthesis, Structure, and Molecular Orbital Calculations of (Pyrazolato)vanadium(III) Complexes − Understanding η^2-Pyrazolato Ligand Coordination on d^2 Metal Centers

Karl R. Gust,[a] John E. Knox,[a] Mary Jane Heeg,[a] H. Bernhard Schlegel,[a] and Charles H. Winter*[a]

Keywords: Vanadium / Pyrazolato ligands / Ab initio calculations / N ligands / Coordination modes

Treatment of trichlorotris(tetrahydrofuran)vanadium(III) with (3,5-di-*tert*-butylpyrazolato)potassium (1, 2, or 3 equiv.) in tetrahydrofuran afforded V(*t*Bu$_2$Pz)Cl$_2$(THF)$_2$ (48%), V(*t*Bu$_2$Pz)$_2$Cl(THF)$_2$ (67%), and V(*t*Bu$_2$Pz)$_3$(THF) (77%), respectively, as purple crystalline solids. The X-ray crystal structures of V(*t*Bu$_2$Pz)Cl$_2$(THF)$_2$, V(*t*Bu$_2$Pz)$_2$Cl(THF)$_2$, and V(*t*Bu$_2$Pz)$_3$(THF) reveal six- and seven-coordinate vanadium centers with η^2-pyrazolato ligands. Molecular orbital calculations were carried out to understand the electronic nature of pyrazolato coordination to transition metal centers containing d electrons. It is demonstrated that η^2-pyrazolato ligand coordination occurs through interaction of filled symmetric and antisymmetric combinations of the nitrogen lone pairs with empty d_z^2 and d_{yz} orbitals. The complexes described herein are the first examples of η^2-pyrazolato ligand coordination to a d^2 metal center.
(© Wiley-VCH Verlag GmbH, 69451 Weinheim, Germany, 2002)

Introduction

Pyrazolato ligand coordination has been extensively investigated among complexes of the main-group, d-block, and lanthanide metals.[1−6] Structurally documented coordination modes in mid to late d-block metals have been restricted to η^1-bonding to a single metal ion,[1] μ-η^1:η^1-bonding between two metal centers,[1] and our recent report of η^5-bonding in a ruthenium complex.[7] Prior to 1997, only one example of η^2-pyrazolato coordination to a d-block metal had been reported.[3] Since 1997, we have reported many examples of η^2-pyrazolato ligand coordination among d^0 group-4 and -5 complexes.[4,5]

Until recently, η^2-pyrazolato ligand coordination in d-block metals was limited to systems with empty d shells.[1,3−5] In our original report of titanium complexes containing η^2-pyrazolato ligands,[4] molecular orbital calculations demonstrated that the η^2-coordination occurs through interaction of symmetric and antisymmetric combinations of the nitrogen lone pairs with empty d orbitals on titanium. A significant open question relates to the occurrence of η^2-pyrazolato ligands among d-block metal complexes with partially filled d shells, where repulsions between the filled d orbitals and pyrazolato nitrogen atoms might destabilize η^2-pyrazolato coordination in favor of other coordination modes. In this vein, Mösch-Zanetti has reported the synthesis and structure of tris(3,5-di-*tert*-butylpyrazolato)titanium(III) and several other (pyrazolato)titanium(III) complexes, and found η^2-coordination of the pyrazolato ligands in these d^1 systems.[8] In addition, we have recently described the synthesis, structure, and bonding of tris(3,5-di-*tert*-butylpyrazolato)chromium(III) and -iron(III).[9] These d^3 and d^5 complexes contain η^2-pyrazolato ligands, and suggest that many transition metal complexes with partially filled d shells may be able to support η^2-pyrazolato ligands. As part of our general studies, we sought to explore pyrazolato ligand coordination to d^2 metal centers.

Herein, we report the synthesis, structure, and characterization of a series of vanadium(III) complexes that exhibit η^2-pyrazolato ligand coordination. Molecular orbital calculations performed on a model vanadium(III) complex demonstrate that η^2-pyrazolato ligand coordination is preferred over η^1-coordination by 4.1 kcal/mol. The η^2-coordination occurs through overlap of symmetric and antisymmetric combinations of the nitrogen lone pairs with empty d orbitals on the vanadium(III) centers. These complexes are the first examples of η^2-pyrazolato ligand coordination to a d^2 metal center.

Results and Discussion

Synthesis of New Complexes

Treatment of trichlorotris(tetrahydrofuran)vanadium(III) with 1, 2, or 3 equiv. of (3,5-di-*tert*-butylpyrazolato)potas-

[a] Department of Chemistry, Wayne State University, 5101 Cass Avenue, Detroit, Michigan 48202, USA
Fax: (internat.) + 1-313/577-1377
E-mail: chw@chem.wayne.edu
Supporting information for this article is available on the WWW under http://www.eurjic.com or from the author.

sium afforded dichloro(3,5-di-*tert*-butylpyrazolato)bis-(tetrahydrofuran)vanadium(III) (**1**), chlorobis(3,5-di-*tert*-butylpyrazolato)bis(tetrahydrofuran)vanadium(III) (**2**), and tris(3,5-di-*tert*-butylpyrazolato)tetrahydrofuranvanadium(III) (**3**), respectively, as purple crystalline solids (Scheme 1). Compounds **1**−**3** are air-sensitive in solution and in the solid state, but are thermally stable indefinitely at ambient temperature under argon. The structures of **1**−**3** were assigned by ^{1}H NMR spectroscopy, IR spectroscopy, microanalysis, and by X-ray structure determinations (vide infra). Complexes **1**−**3** are paramagnetic, and exhibited broad resonances in the ^{1}H NMR spectra. Magnetic moments (μ_{eff}) of **1**−**3** were also determined and ranged between 2.60 and 2.82 BM. These values are close to the spin-only magnetic moment expected for the two unpaired electrons of a vanadium(III) center (μ_s = 2.83 BM).[10] EPR spectra were not recorded, since even-electron systems generally do not give useful spectra.[11]

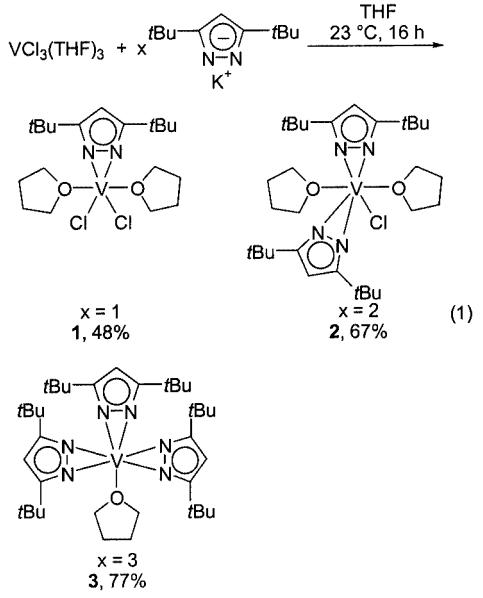

Scheme 1

X-ray Crystal Structures of 1−3

The X-ray crystal structures of **1**−**3** were determined to establish the geometry about the metal center and the bonding modes of the pyrazolato ligands. Experimental crystallographic data are summarized in Table 4, selected bond lengths and angles are given and perspective views are presented for **1** (Figure 1, Table 1), **2** (Figure 2, Table 2), and **3** (Figure 3, Table 3).

Complex **1** contains one η^2-pyrazolato, two chloride, and two tetrahydrofuran ligands. The coordination sphere about the vanadium atom possesses approximate trigonal-bipyramidal geometry, if the center of the nitrogen−nitrogen bond in the 3,5-di-*tert*-butylpyrazolato ligand is considered as a monodentate donor. The tetrahydrofuran ligands comprise the axial substituents, with an oxygen−vanadium−oxygen angle of 177.88(13)°. The

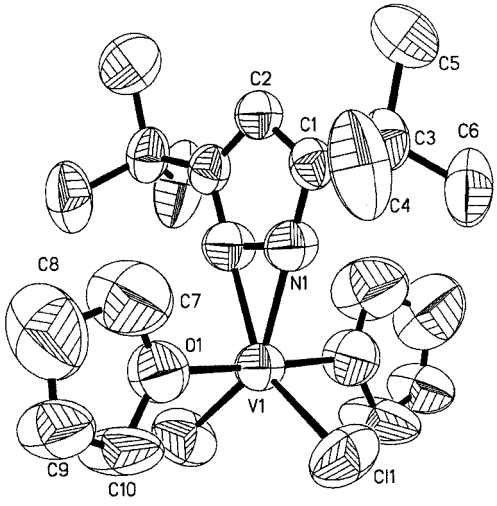

Figure 1. Perspective view of V(tBu$_2$Pz)Cl$_2$(THF)$_2$ (**1**) with thermal ellipsoids at the 50% probability level

Table 1. Selected bond lengths [Å] and angles [°] for **1**

V−N(1)	2.021(3)	V−Cl(1)	2.2655(9)
V−O(1)	2.097(2)	N(1)−N	1.356(5)
V−centroid[N(1),N(1′)]	1.904(3)		
N(1)−V−N	39.19(12)	N(1)−V−O(1)	90.27(11)
N−V−O(1)	87.73(10)	N−V−O	90.27(11)
N(1)−V−O	87.73(10)	O(1)−V−O	177.88(13)
N−V−Cl(1)	142.84(7)	N(1)−V−Cl(1)	103.78(7)
N(1)−V−Cl	142.84(7)	N−V−Cl	103.78(7)
O(1)−V−Cl(1)	90.03(8)	O−V−Cl(1)	91.14(8)
O−V−Cl	90.03(8)	O(1)−V−Cl	91.14(8)
Cl(1)−V−Cl	113.36(6)	N−N(1)−V	70.41(7)
Cl(1)−V−centroid[N(1),N(1)′]	123.3(1)		
Cl(1)−V−centroid[N(1),N(1)′]	88.9(1)		

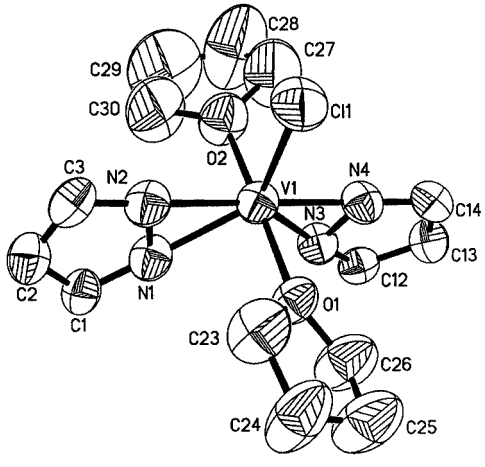

Figure 2. Perspective view of V(tBu$_2$Pz)$_2$Cl(THF)$_2$ (**2**) with *tert*-butyl groups removed for clarity; thermal ellipsoids are at the 50% probability level

vanadium−oxygen bond length is 2.097(2) Å. The pyrazolato ligand lies in the equatorial plane, with nitrogen−vanadium−oxygen angles ranging from 87.73(10) to 90.27(11)°. The two chlorine atoms also lie in the equatorial plane, with oxygen−vanadium−chlorine angles ran-

Table 2. Selected bond lengths [Å] and angles [°] for **2**

V−N(1)	2.094(4)	V−N(2)	2.040(4)
V−N(3)	2.106(4)	V−N(4)	2.014(4)
V−O(1)	2.112(3)	V−O(2)	2.118(3)
V−Cl	2.3338(14)	N(1)−N(2)	1.354(4)
N(3)−N(4)	1.367(4)		
V−centroid[N(1),N(2)]	1.953(4)		
V−centroid[N(3),N(4)]	1.944(4)		
N(1)−V−N(2)	38.20(12)	N(3)−V−N(4)	38.68(12)
O(1)−V−O(2)	174.49(13)		
N(1)−V−O(1)	86.70(13)	N(1)−V−O(2)	91.17(15)
N(2)−V−O(1)	91.29(13)	N(2)−V−O(2)	90.18(14)
N(3)−V−O(1)	90.35(13)	N(3)−V−O(2)	85.28(13)
N(4)−V−O(1)	86.62(13)	N(4)−V−O(2)	92.03(14)
N(1)−V−Cl	127.33(11)	N(2)−V−Cl	89.22(11)
N(3)−V−Cl	127.77(11)	N(4)−V−Cl	89.56(11)
O(1)−V−Cl	93.40(9)	O(2)−V−Cl	91.94(11)
N(1)−N(2)−V	73.1(3)	N(2)−N(1)−V	68.7(2)
N(3)−N(4)−V	74.3(2)	N(4)−N(3)−V	67.0(2)
Cl(1)−V−centroid[N(1),N(2)]	108.5(1)		
Cl(1)−V−centroid[N(3),N(4)]	109.1(1)		
O(1)−V−centroid[N(1),N(2)]	88.9(1)		
O(1)−V−centroid[N(3),N(4)]	88.4(1)		
O(2)−V−centroid[N(1),N(2)]	90.7(1)		
O(2)−V−centroid[N(3),N(4)]	88.5(1)		
centroid[N(1),N(2)]−V−centroid[N(3),N(4)]	142.3(1)		

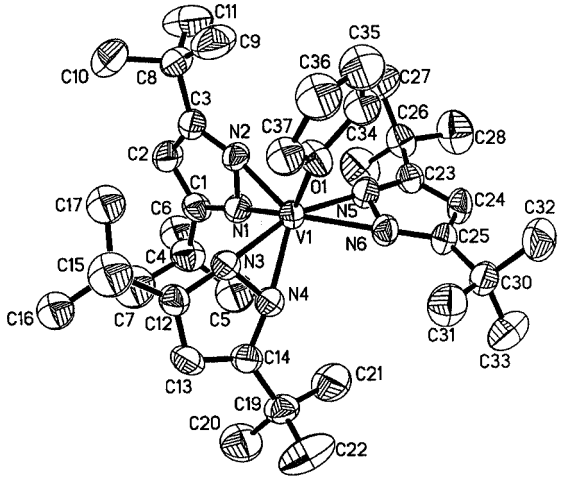

Figure 3. Perspective view of V(tBu$_2$Pz)$_3$(THF) (**3**) with thermal ellipsoids at the 50% probability level

ging from 90.03(8) to 91.14(8)°. The vanadium−chlorine bond length is 2.2655(9) Å. The pyrazolato ligand displays symmetric η^2-coordination with a vanadium−nitrogen bond length of 2.021(3) Å. The nitrogen−nitrogen distance [1.356(5) Å] and the bite angle [39.19(13)°] of the pyrazolato ligand in **1** are similar to the corresponding values found in η^2-pyrazolato complexes of the early transition metals.[5]

Complex **2** contains two η^2-pyrazolato, one chloride, and two tetrahydrofuran ligands. The coordination sphere about the vanadium atom possesses approximate trigonal bipyramidal geometry, if the centers of the nitrogen−nitrogen bonds in both 3,5-di-*tert*-butylpyrazolato ligands are considered to be monodentate donors. The tetrahydrofuran ligands comprise the axial ligands, with an oxygen−vanadium−oxygen angle of 174.49(13)°. The vanadium−oxygen distances are 2.112(3) and 2.118(3) Å. The chlorine atom lies in the equatorial plane, with chlorine−vanadium−oxygen angles of 93.40(9) and 91.94(11)°. The vanadium−chlorine bond length of 2.3338(14) Å is longer than the vanadium−chlorine bond length in **1**, due to the coordination number of seven in **2** compared to six in **1**. The two pyrazolato ligands are approximately coplanar and lie in the equatorial plane. The nitrogen−vanadium−oxygen angles range from 85.28(13) to 92.03(14)°. The pyrazolato ligands exhibit η^2-coordination to the vanadium atom, with vanadium−nitrogen bond lengths ranging from 2.014(4) to 2.106(4) Å. The longer vanadium−nitrogen bond lengths [to N(1) and N(3)] are farthest from the chlorine atom, and are the result of steric crowding between the *tert*-butyl groups containing C(4) and C(15). The nitrogen−nitrogen bond lengths [1.354(4) and 1.367(4) Å] and bite angles [38.20(12) and 38.68(12)°] of the pyrazolato ligands in **2** are similar to the corresponding values found in η^2-pyrazolato complexes of the early transition metals.[5]

Complex **3** contains three η^2-pyrazolato and one tetrahydrofuran ligands. The coordination sphere about the vanadium atom possesses a pseudo-tetrahedral geometry, if the centers of the nitrogen−nitrogen bonds in the 3,5-di-*tert*-butylpyrazolato ligands are considered as monodentate donors. The vanadium−nitrogen bond lengths range from 2.035(2) to 2.102(2) Å. The pyrazolato ligand containing N(1) and N(2) exhibits symmetric η^2-bonding to the vanadium atom within 5σ. However, the pyrazolato ligands containing N(3)−N(6) show a slight (0.062−0.066 Å) asymmetry in the vanadium−nitrogen bond lengths. In the pyra-

Table 3. Selected bond lengths [Å] and angles [°] for **3**

V−N(1)	2.053(2)	V−N(2)	2.043(2)
V−N(3)	2.097(2)	V−N(4)	2.035(2)
V−N(5)	2.036(2)	V−N(6)	2.102(2)
V−O	2.1289(17)	N(1)−N(2)	1.382(2)
N(3)−N(4)	1.374(3)	N(5)−N(6)	1.368(3)
V−centroid[N(1),N(2)]	1.928(2)		
V−centroid[N(3),N(4)]	1.948(2)		
V−centroid[N(5),N(6)]	1.953(2)		
N(1)−V−N(2)	39.44(7)	N(3)−V−N(4)	38.82(7)
N(5)−V−N(6)	38.56(8)		
N(1)−V−N(3)	91.71(9)	N(1)−V−N(4)	96.91(9)
N(1)−V−N(5)	94.96(9)	N(1)−V−N(6)	126.81(9)
N(2)−V−N(3)	97.56(9)	N(2)−V−N(4)	124.39(9)
N(2)−V−N(5)	97.95(9)	N(2)−V−N(6)	135.96(9)
N(3)−V−N(5)	162.37(9)	N(3)−V−N(6)	126.48(9)
N(1)−V−O	136.86(8)	N(2)−V−O	97.51(8)
N(3)−V−O	92.11(8)	N(4)−V−O	112.31(8)
N(5)−V−O	94.12(8)	N(6)−V−O	82.99(7)
N(1)−N(2)−V	70.68(13)	N(2)−N(1)−V	69.89(13)
N(3)−N(4)−V	73.02(13)	N(4)−N(3)−V	68.16(13)
N(5)−N(6)−V	68.12(13)	N(6)−N(5)−V	73.32(13)
O(1)−V−centroid[N(1),N(2)]	117.2(1)		
O(1)−V−centroid[N(3),N(4)]	102.6(1)		
O(1)−V−centroid[N(5),N(6)]	88.4(1)		
centroid[N(1),N(2)]−V−centroid[N(3),N(4)]	103.6(1)		
centroid[N(1),N(2)]−V−centroid[N(5),N(6)]	116.0(1)		
centroid[N(3),N(4)]−V−centroid[N(5),N(6)]	127.9(1)		

zolato ligand containing N(3) and N(4), the slightly longer bond to N(3) can be rationalized as arising through steric repulsion between the *tert*-butyl group containing C(15) and the tetrahydrofuran ligand. Similarly, the pyrazolato ligand containing N(5) and N(6) shows a slightly longer bond from the vanadium atom to N(6) due to steric crowding between the *tert*-butyl groups containing C(19) and C(30). This steric crowding causes these two pyrazolato ligands to be canted with respect to each other, as opposed to the coplanar pyrazolato ligands observed in **2**. The vanadium−oxygen bond length is 2.1289(17) Å. This value is similar to the related bond lengths in seven-coordinate **2**. The nitrogen−nitrogen bond lengths range from 1.368(3) to 1.382(2) Å. The pyrazolato bite angles range from 38.56(8) to 39.44(7)°. These values are similar to those found in **1**, **2**, and other complexes containing η^2-pyrazolato ligands.[5]

Molecular Orbital Calculations

To understand the nature of the pyrazolato ligand bonding to vanadium(III), ab initio calculations were performed using the Gaussian suite of programs.[12] The simplified models used in this study are the η^1- and η^2-pyrazolato complexes **4** and **5**. A previous study of ours has shown that a simplified model (pyrazolato)titanium(IV) complex does not significantly change the electronic distribution relative to homoleptic pyrazolato complexes.[4] Model complexes **4** and **5** optimized using the B3LYP/6−311G* level of theory.[13] The bond lengths and angles associated with the pyrazolato ligand in the optimized structure of **5** are in good agreement with the X-ray crystal structures of **1**−**3** [V−N(calcd) = 2.040, 2.042 Å versus V−N (X-ray) = 2.014−2.106 Å; N−N(calcd) = 1.350 Å versus N−N(X-ray) = 1.354−1.382 Å; N−N−V(calcd) = 70.86° versus N−N−V(X-ray) 67.0−74.3°]. Complex **5** is calculated to be 4.09 kcal/mol more stable than the η^1 complex **4**.

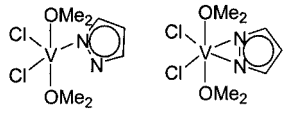

4 **5**

Natural population analysis[14] shows that the charges on the pyrazolato ligands are −0.556 in **4** and −0.561 in **5**. These values can be compared to charges of −0.32 for (η^2-Me_2pz)$TiCl_3$[4] and −0.75 in (η^2-pz)$YCl_2(NH_3)_2$[15a] that have been previously reported by our group. Natural bond order analysis[14] indicates that there is very little interaction between the occupied vanadium d orbitals and the unoccupied pyrazolato ligand orbitals. A more significant stabilization occurred by the symmetric and antisymmetric occupied nitrogen lone pair orbitals interacting with empty vanadium d orbitals. The fragment orbitals involved are shown in Figure 4. The symmetric combination of the nitrogen lone pair combines with the empty d_z^2 vanadium orbital and appropriate in-plane orbitals based on the carbon and chlorine atoms. The antisymmetric combination of the nitrogen lone pairs interacts with an antisymmetric combination of vanadium−chlorine σ* orbitals. These vanadium−chlorine orbitals consist primarily of the metal d_{yz} orbital and a smaller, antibonding contribution from a chlorine p orbital.

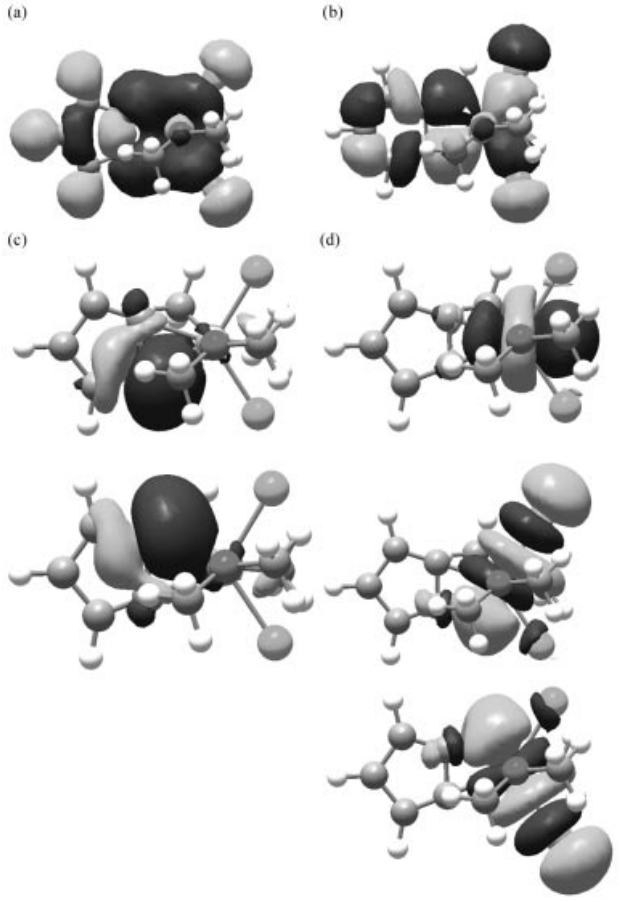

Figure 4. Calculated molecular orbitals of **5**: (a) symmetric combination of the nitrogen lone pairs that interact with the empty d_{z^2} fragment; (b) antisymmetric combination of the nitrogen lone pairs that interact with the empty d_{yz} fragment; (c) pyrazolato nitrogen atom lone pair fragments that add together to form symmetric and antisymmetric combinations; (d) empty d_{z^2} and d_{yz} fragments that interact with the symmetric and antisymmetric combinations of the pyrazolato nitrogen atom lone pair fragments

Additionally, there is some mixing between the HOMO π orbital on the pyrazolato fragment and an occupied d_{xz} orbital, but the NBO analysis indicates that this does not stabilize the complex significantly. Thus, the most important orbital contributions to the bonding between the pyrazolato ligand and the vanadium center are the symmetric and antisymmetric combinations of the nitrogen lone pairs interacting with the unoccupied vanadium d_{z^2} and d_{yz} orbitals.

Discussion

The central discovery highlighted herein is the η^2-pyrazolato ligands bonded to the d^2 vanadium(III) centers in **1**−**3**. These are the first examples of η^2-pyrazolato ligand coordination to a metal center with a d^2 electronic configuration. In addition, **1**−**3** constitute rare examples of η^2-pyrazolato ligand coordination to d-block metal centers with partially filled d shells.[8,9] There has been one previous report of a (pyrazolato)vanadium complex, [(Tp*i*Pr^{2}V(O)(μ-OH)(μ-Pz*i*Pr^2)V(O)(μ-OH)(μ-Pz*i*Pr^2)V(O)Tp*i*Pr^2)], which was obtained by partial hydrolysis of a vanadium(IV) hydrotris(3,5-diisopropyl-1-pyrazolyl)borate complex.[16] The 3,5-diisopropylpyrazolato ligands in this complex bridge between two vanadium(IV) ions with the well-documented μ-η^1:η^1-coordination mode. There have been 70 tris(pyrazolyl)borate complexes of vanadium whose structures are listed in the Cambridge Crystallographic Database (version 5.22; October 2001).[17] These complexes contain μ-η^1:η^1-pyrazolato ligands bridged between boron(III) and vanadium ions in various oxidation states. Traditional wisdom[1] holds that the lone pairs of electrons on each nitrogen atom within a pyrazolato ligand are pointed in geometrically inappropriate directions to allow η^2-coordination to a small metal ion such as vanadium(III), and the μ-η^1:η^1 coordination mode is therefore favored. Instead, our theoretical studies[4,14] demonstrate that η^2-pyrazolato ligand coordination occurs through overlap of symmetric and antisymmetric combinations of the nitrogen-based lone pairs with empty d orbitals on the metal center. Recent reports of η^2-pyrazolato ligands among main-group metal and d^0, d^1, d^3, and d^5 transition metal complexes,[2−5,8,9] together with the present work, suggest that this previously rare coordination mode may be generally accessible among the transition metals. In particular, most of the known η^2-pyrazolato complexes contain the bulky 3,5-di-*tert*-butylpyrazolato ligand. Molecular orbital calculations described above demonstrate that η^2-pyrazolato ligand coordination is thermodynamically preferred over η^1 coordination, even in the absence of steric effects. However, very bulky pyrazolato ligands or extremely bulky ancillary ligands may be required to destabilize the μ-η^1:η^1 coordination mode and make η^2-pyrazolato ligands feasible.

There is an analogy between **1**−**3** and related vanadium(III) complexes containing other bidentate, monoanionic donor ligands.[18−21] In particular, vanadium(III) complexes containing amidinate or formamidinate ligands are highly relevant, since these ligands are bidentate nitrogen donors that are similar to η^2-pyrazolato ligands. The complexes V(RNCR′NR)$_3$ (R = *p*-tol, R′ = H;[18] R = C_6H_{11}, R′ = CH_3[19]) contain six-coordinate metal centers with distorted D_3 geometries. Unlike seven-coordinate **3**, which contains a coordinated tetrahydrofuran molecule in addition to the η^2-pyrazolato ligands, V(RNCR′NR)$_3$ did not crystallize with coordinated tetrahydrofuran. The smaller bite angle of the η^2-pyrazolato ligands (38−40°), compared to the related values for V(RNCR′NR)$_3$ (63−64°), make the vanadium(III) center in **3** more accessible sterically and allows tetrahydrofuran coordination. The benzamidinate complex VCl[N(SiMe$_3$)CPhN(SiMe$_3$)]$_2$ is related structurally to **2**.[20] However, **2** contains two tetrahydrofuran ligands, while VCl[N(SiMe$_3$)CPhN(SiMe$_3$)]$_2$ does not contain any neutral donor ligands. Again, tetrahydrofuran coordination in **2** occurs due to the more open coordination sphere, compared to VCl[N(SiMe$_3$)CPhN(SiMe$_3$)]$_2$.

Experimental Section

General Considerations: All reactions were performed under argon using either glovebox or Schlenk line techniques. Toluene was distilled from sodium, tetrahydrofuran was distilled from sodium benzophenone ketyl, and hexane was distilled from P_2O_5. Trichlorotris(tetrahydrofuran)vanadium(III) was purchased from Aldrich Chemicals, Inc. (3,5-Di-*tert*-butylpyrazolato)potassium was prepared by a literature procedure.[22] ^1H and $^{13}C\{^1H\}$ NMR were obtained at 300 or 75 MHz in [D_6]benzene. IR spectra were obtained using Nujol as the medium. Elemental analyses were performed by Midwest Microlab, Indianapolis, IN. Melting points were obtained with a Haake−Buchler HBI digital melting point apparatus and are uncorrected. Magnetic susceptibility measurements were determined using a Johnson−Matthey magnetic susceptibility balance.

Preparation of Dichloro(3,5-di-*tert*-butylpyrazolato)bis(tetrahydrofuran)vanadium(III) (1): A 100-mL Schlenk flask was charged with trichlorotris(tetrahydrofuran)vanadium(III) (0.856 g, 2.29 mmol), (3,5-di-*tert*-butylpyrazolato)potassium (0.502 g, 2.29 mmol), and tetrahydrofuran (50 mL). The resultant purple solution was stirred for 16 h. The solvent was then removed under reduced pressure to yield a purple solid. This solid was extracted with hexane (50 mL), and the resultant solution was filtered through a 2-cm pad of Celite on a coarse glass frit. The filtrate was concentrated to a volume of about 20 mL, and was then placed in a −20 °C freezer for 36 h. Decanting of the solvent, followed by vacuum drying for 1 h, afforded **1** as purple crystals (0.49 g, 48%), m.p. 115 °C (dec). IR (Nujol, cm^{-1}): $\tilde{\nu}$ = 1589 (w), 1563 (w), 1250 (s), 1030 (s), 862 (w), 795 (m). ^1H NMR (C_6D_6, 22 °C, ppm): δ = 2.86 (broad, C_4H_8O), 1.49 [broad, $C(CH_3)_3$]. μ_{eff} = 2.82 BM. $C_{19}H_{35}Cl_2N_2O_2V$ (445.3): calcd. C 51.24, H 7.92, N 6.29; found C 51.27, H 8.12, N 6.26.

Preparation of Chlorobis(3,5-di-*tert*-butylpyrazolato)bis(tetrahydrofuran)vanadium(III) (2): In a fashion similar to the preparation of **1**, trichlorotris(tetrahydrofuran)vanadium(III) (1.189 g, 3.18 mmol) was treated with (3,5-di-*tert*-butylpyrazolato)potassium (1.388 g, 6.36 mmol) to afford **2** as purple crystals (1.26 g, 67%), m.p. 117 °C. IR (Nujol, cm^{-1}): $\tilde{\nu}$ = 1515 (m), 1498 (m), 1415 (m), 1361 (s), 1312 (w), 1251 (s), 1234 (s), 1208 (w), 1171 (w), 1030 (s), 919 (w), 874 (s), 792 (s), 725 (m), 712 (m). ^1H NMR (C_6D_6, 22 °C, ppm): δ = 1.63 [broad, C_4H_8O and $C(CH_3)_3$]. μ_{eff} = 2.60 BM. $C_{30}H_{65}N_6OV$ (1589.2): calcd. C 61.16, H 9.24, N 9.51; found C 61.42, H 9.27, N 9.36.

Preparation of Tris(3,5-di-*tert*-butylpyrazolato)tetrahydrofuranvanadium(III) (3): In a fashion similar to the preparation of **1**, trichlorotris(tetrahydrofuran)vanadium(III) (0.804 g, 2.15 mmol) was treated with (3,5-di-*tert*-butylpyrazolato)potassium (1.500 g, 6.87 mmol) to afford **3** as purple crystals (1.11 g, 77%), m.p. 149 °C dec. IR (Nujol, cm^{-1}): $\tilde{\nu}$ = 1567 (w), 1515 (m), 1310 (w), 1251 (s), 1278 (m), 1202 (w), 1017 (m), 874 (w), 783 (m), 715 (m). ^1H NMR (C_6D_6, 22 °C, ppm): δ = 4.80 (broad, C_4H_8O), 2.26 [broad, $C(CH_3)_3$]. μ_{eff} = 2.71 BM. $C_{37}H_{65}N_6OV$ (660.9): calcd. C 67.24, H 9.91, N 12.72; found C 67.36, H 10.01, N 12.73.

X-ray Crystallography for 1−3: The crystalline samples were mounted in thin-walled glass capillaries under nitrogen. All crystallographic data were collected at room temperature with a Siemens/Bruker automated P4/CCD diffractometer with monochromated Mo radiation. 1650 frames were collected at 10 s/frame and integrated with the manufacturer's SMART and SAINT software. Absorption corrections were applied with Sheldrick's SADABS program and the structure was solved and refined using the programs of SHELX-97. The molecules crystallize as neutral complexes. Hydrogen atoms were calculated and assigned to ride on the carbon atoms to which they are bound. CCDC-178824 (**1**), -178825 (**2**), and -178826 (**3**) contain the supplementary crystallographic data for this paper. These data can be obtained free of charge at www.ccdc.cam.ac.uk/conts/retrieving.html or from the Cambridge Crystallographic Data Center, 12, Union Road, Cambridge CB2 1EZ, UK [Fax: (internat.) + 44-1223/336-033; E-mail: deposit@ccdc.cam.ac.uk]. Complex **1** crystallized as purple rods in *C*2/*c* with *Z* = 4. The vanadium atoms occupy a crystallographic twofold axis. Atoms C9 and C10 in the coordinated THF were assigned alternate partial positions to model the disorder. Complex **2** crystallized as purple rods in *P*4(2)/*n* with *Z* = 8. All atoms in the vanadium complex occupied general positions, but there is an indeterminate solvent region near the twofold axis. Any placement and refinement of atoms in this solvent region becomes unreasonable. There was no evidence for any solvate inclusion in the C,H,N microanalysis. The coordinated THF exhibits typically large thermal parameters. Complex **3** crystallized as purple rectangles in $P2_1/c$ with *Z* = 4. All atoms occupy general positions. Partially occu-

Table 4. Experimental crystallographic data for **1−3**

	1	**2**	**3**
Empirical formula	$C_{19}H_{35}Cl_2N_2O_2V$	$C_{30}H_{54}ClN_4O_2V$	$C_{37}H_{65}N_6OV$
Formula mass	445.33	589.16	660.89
Space group	*C*2/*c*	*P*4(2)/*n*	$P2_1/c$
a [Å]	16.2481(17)	25.754(3)	9.8014(11)
b [Å]	15.1194(16)	25.754(3)	22.247(3)
c [Å]	9.9232(9)	10.8091(15)	18.857(2)
β [°]	96.968(2)	90	101.448(2)
V [Å^3]	2419.7(4)	7169.4(15)	4030.0(8)
Z	4	8	4
T [K]	295(2)	295(2)	295(2)
λ [Å]	0.71073	0.71073	0.71073
ρ(calcd.) [g·cm^3]	1.222	1.092	1.089
μ [mm^{-1}]	0.645	0.379	0.280
$R(F) = \Sigma\|\|F_o\| - \|F_c\|\|/\Sigma\|F_o\|$ (%)	5.69	5.74	4.80
$Rw(F^2) = [\Sigma w(F_o^2 - F_c^2)^2/\Sigma w(F_o^2)^2]^{1/2}$ (%)	17.43	16.60	10.87

pied positions (60:40) and isotropic parameters were assigned to C5−7, C16−18, and C34−37 to describe their positional disorder; all other non-hydrogen atoms were defined anisotropically.

Acknowledgments

We are grateful to the National Science Foundation (grant no. CHE-9807269) for support of this research.

[1] For reviews, see: [1a] A. P. Sadimenko, *Adv. Heterocycl. Chem.* **2001**, *80*, 157−240. [1b] J. E. Cosgriff, G. B. Deacon, *Angew. Chem. Int. Ed.* **1998**, *37*, 286−287; *Angew. Chem.* **1998**, *110*, 298−299. [1c] G. La Monica, G. A. Ardizzoia, *Progr. Inorg. Chem.* **1997**, *46*, 151−238. [1d] A. P. Sadimenko, S. S. Basson, *Coord. Chem. Rev.* **1996**, *147*, 247−297. [1e] S. Trofimenko, *Progr. Inorg. Chem.* **1986**, *34*, 115−210. [1f] S. Trofimenko, *Chem. Rev.* **1972**, *72*, 497−508.

[2] [2a] G. B. Deacon, A. Gitlits, P. W. Roesky, M. R. Burgstein, K. C. Lim, B. W. Skelton, A. H. White, *Chem. Eur. J.* **2001**, *7*, 127−138. [2b] A. Steiner, G. T. Lawson, B. Walfort, D. Leussser, D. Stalke, *J. Chem. Soc., Dalton Trans.* **2001**, 219−221. [2c] W. J. Zheng, H. W. Roesky, M. Noltemeyer, *Organometallics* **2001**, *20*, 1033−1035. [2d] W. J. Zheng, N. C. Mösch-Zanetti, T. Blunck, H. W. Roesky, M. Noltemeyer, H. G. Schmidt, *Organometallics* **2001**, *20*, 3299−3303. [2e] W. Zheng, H. Hohmeister, N. C. Mösch-Zanetti, T. Blunck, H. W. Roesky, M. Noltemeyer, H-G. Schmidt, *Inorg. Chem.* **2001**, *40*, 2363−2367. [2f] G. B. Deacon, E. E. Dellbridge, C. M. Forsyth, B. W. Skelton, A. H. White, *J. Chem. Soc., Dalton Trans.* **2000**, 745−751. [2g] D. Pfeiffer, M. J. Heeg, C. H. Winter, *Inorg. Chem.* **2000**, *39*, 2377−2384. [2h] G. B. Deacon, E. E. Delbridge, C. M. Forsyth, B. W Skelton, A. H. White, *J. Chem. Soc., Dalton Trans.* **2000**, 745−751. [2i] W. Zheng, N. C. Mösch-Zanetti, H. W. Roesky, M. Hewitt, F. Cimpoesu, T. R. Schneider, A. Stasch, J. Prust, *Angew. Chem. Int. Ed.* **2000**, *39*, 3099−3101; *Angew. Chem.* **2000**, *112*, 3229−3231. [2j] E. E. Pullen, D. Rabinovich, C. D. Incarvito, T. E. Concolino, A. L. Rheingold, *Inorg. Chem.* **2000**, *39*, 1561−1567. [2k] G. B. Deacon, E. E. Delbridge, C. M. Forsyth, P. C. Junk, B. W. Skelton, A. H. White, *Aust. J. Chem.* **1999**, *52*, 733−739. [2l] E. E. Pullen, A. L. Rheingold, D. Rabinovich, *Inorg. Chem. Commun.* **1999**, *2*, 194−196. [2m] H. Witte-Abel, C. Drost, U. Klingebiel, M. Noltemeyer, *J. Organomet. Chem.* **1999**, *585*, 341−347. [2n] J. Lewinksi, J. Zachara, T. Kopec, I. Madura, I. Prowotorow, *Inorg. Chem. Commun.* **1999**, *2*, 131−134. [2o] D. Pfeiffer, M. J. Heeg, C. H. Winter, *Angew. Chem. Int. Ed.* **1998**, *37*, 2517−2519; *Angew. Chem.* **1998**, *110*, 2674−2676. [2p] M. V. Capparelli, P. Hodge, B. Piggot, *Chem. Commun.* **1997**, 937−938.

[3] D. Röttger, G. Erker, M. Grehl, R. Frölich, *Organometallics* **1994**, *13*, 3897−3902.

[4] I. A. Guzei, A. G. Baboul, G. P. A. Yap, A. L. Rheingold, H. B. Schlegel, C. H. Winter, *J. Am. Chem. Soc.* **1997**, *119*, 3387−3388.

[5] [5a] C. Yélamos, K. R. Gust, A. G. Baboul, M. J. Heeg, H. B. Schlegel, C. H. Winter, *Inorg. Chem.* **2001**, *40*, 6451−6462. [5b] K. R. Gust, M. J. Heeg, C. H. Winter, *Polyhedron* **2001**, *20*, 805−813. [5c] C. Yélamos, M. J. Heeg, C. H. Winter, *Inorg. Chem.* **1999**, *38*, 1871−1878. [5d] C. Yélamos, M. J. Heeg, C. H. Winter, *Organometallics* **1999**, *18*, 1168−1176. [5e] I. A. Guzei, G. P. A Yap, C. H. Winter, *Inorg. Chem.* **1997**, *36*, 1738−1739.

[6] [6a] G. B. Deacon, A. Gitlits, P. W. Roesky, M. R. Burgstein, K. C. Lim, B. W. Skelton, A. H. White, *Chem. Eur. J.* **2001**, *7*, 127−138. [6b] G. B. Deacon, A. Gitlits, B. W. Skelton, A. H. White, *Chem. Commun.* **1999**, 1213−1214. [6c] G. B. Deacon, E. E. Delbridge, B. W. Skelton, A. H. White, *Eur. J. Inorg. Chem.* **1999**, 751−761. [6d] J. G. Cederberg, T. D. Culp, B. Bieg, D. Pfeiffer, C. H. Winter, K. L. Bray, T. F. Kuech, *J. Appl. Phy.* **1999**, *85*, 1825−1831. [6e] J. G. Cederberg, T. D. Culp, B. Bieg, D. Pfeiffer, C. H. Winter, K. L. Bray, T. F. Kuech, *J. Cryst. Growth* **1998**, *195*, 105−111. [6f] T. D. Culp, J. G. Cederberg, B. Bieg, T. F. Kuech, K. L. Bray, D. Pfeiffer, C. H. Winter, *J. Appl. Phys.* **1998**, *83*, 4918−4927. [6g] G. B. Deacon, E. E. Delbridge, B. W. Skelton, A. H. White, *Angew. Chem. Int. Ed.* **1998**, *37*, 2251−2252; *Angew. Chem.* **1998**, *110*, 2372−2373. [6h] J. E. Cosgriff, G. B. Deacon, B. M. Gatehouse, *Aust. J. Chem.* **1993**, *46*, 1881−1896. [6i] D. S. Black, G. B. Deacon, G. L. Edwards, B. M. Gatehouse, *Aust. J. Chem.* **1993**, *43*, 1323−1336. [6j] J. E. Cosgriff, G. B. Deacon, B. M. Gatehouse, H. Hemling, H. Schumann, *Angew. Chem. Int. Ed. Engl.* **1993**, *32*, 874−875; *Angew. Chem.* **1993**, *105*, 906−907.

[7] J. R. Perera, M. J. Heeg, H. B. Schlegel, C. H. Winter, *J. Am. Chem. Soc.* **1999**, *121*, 4536−4537.

[8] N. C. Mösch-Zanetti, R. Kratzner, C. Lehmann, T. R. Schneider, I. Uson, *Eur. J. Inorg. Chem.* **2000**, 13−16.

[9] K. R. Gust, J. E. Knox, M. J. Heeg, H. B. Schlegel, C. H. Winter, *Angew. Chem. Int. Ed.*, **2002**, *41*, 1591−1594. *Angew. Chem.*, **2002**, *114*, 1661−1664.

[10] R. H. Crabtree, *The Organometallic Chemistry of the Transition Metals*, 3rd ed., Wiley, New York, **2001**, pp. 454−461.

[11] For leading references, see: [11a] P. L. W. Tregenna-Piggott, H. Weihe, J. Bendix, A.-L. Barra, H.-U. Güdel, *Inorg. Chem.* **1999**, *38*, 5928−5929. [11b] T. Weyermuller, K. Weighardt, P. Chaudhari, *J. Chem. Soc., Dalton Trans.* **1998**, 3805−3813. [11c] R. S. Drago, *Physical Methods for Chemists*, 2nd ed., Surfside Scientific Publishers, Gainesville, Florida, **1992**, pp. 559−603.

[12] M. J Frisch, G. W. Trucks, H. B. Schlegel, G. E. Scuseria, M. A. Robb, J. R. Cheeseman, V. G. Zakrewski, J. A. Montgomery, Jr., R. E. Stratmann, J. C. Burant, S. Dapprich, J. M. Millam, A. D. Daniels, K. N. Kudin, M. C. Strain, O. Farkas, J. Tomasi, V. Barone, B. Mennuci, M. Cossi, C. Adamo, J. Jaramillo, R. Cammi, C. Pomelli, J. Ochterski, G. A. Peterson. P. Y. Ayala, K. Morokuma, D. K. Malick, A. D. Rabuck, K. Raghavachari, J. B. Foresman, J. V. Ortiz, Q. Cui, A. G. Baboul, S. Clifford, J. Cioslowski, B. B. Stefanov, G. Liu, A. Liashenko, P. Piskorz, I. Komaromi, R. Gomperts, R. L. Martin, D. J. Fox, T. Keith, M. A. Al-Laham, C. Y. Peng, A. Nanayakkara, M. Challacombe, P. M. W. Gill, B. Johnson, W. Chen, M. W. Wong, J. L. Andres, C. Gonzalez, M. Head-Gordon, E. S. Replogle, J. A. Pople, *Gaussian 99, Development Version (Revision B.08+)*, Gaussian, Inc., Pittsburgh, PA, **2000**.

[13] [13a] D. A. Becke, *Phys. Rev. A* **1988**, *38*, 3098−3100. [13b] C. Lee, R. D. Parr, *Phys. Rev. B* **1988**, *37*, 785−789. [13c] D. A. Becke, *J. Chem. Phys.* **1993**, *98*, 5648−5652. [13d] A. J. H. Wachters, *J. Chem. Phys.* **1970**, *52*, 1033−1036. [13e] P. J. Hay, *J. Chem. Phys.* **1977**, *66*, 4377−4384.

[14] [14a] J. E. Carpenter, F. Weinhold, *J. Mol. Struct. (Theochem)* **1988**, *46*, 41−62. [14b] J. E. Carpenter, Ph. D. Thesis, University of Wisconsin, **1987**. [14c] J. P. Foster, F. Weinhold, *J. Am. Chem. Soc.* **1980**, *102*, 7211−7218. [14d] A. E. Reed, F. Weinhold, *J. Chem. Phys.* **1983**, *78*, 4066−4073. [14e] A. E. Reed, F. Weinhold, *J. Chem. Phys.* **1985**, *83*, 1736−1740. [14f] A. E. Reed, R. B. Weinstock, F. Weinhold, *J. Chem. Phys.* **1985**, *83*, 735−746. [14g] A. E. Reed, L. A. Curtiss, F. Weinhold, *Chem. Rev.* **1988**, *88*, 899−926. [14h] F. Weinhold, J. E. Carpenter, *The Structure of Small Molecules and Ions*, Plenum, Amsterdam, **1988**, p. 227.

[15] [15a] D. Pfeiffer, B. J. Ximba, L. M. Liable-Sands, A. L. Rheingold, M. J. Heeg, D. M. Coleman, H. B. Schlegel, T. F Kuech, C. H. Winter, *Inorg. Chem.* **1999**, *38*, 4539−4548. [15b] C. Yélamos, K. R. Gust, A. G. Baboul, M. J. Heeg, H. B. Schlegel, C. H. Winter, *Inorg. Chem.* **2001**, *40*, 6451−6462.

[16] M. Kosugi, S. Hikichi, M. Akita, Y. Moro-oka, *Inorg. Chem.* **1999**, *38*, 2567−2578.

[17] For leading recent references, see: [17a] M. Kosugi, S. Hikichi, M. Akita, Y. Moro-Oka, *J. Chem. Soc., Dalton Trans.* **1999**, 1369−1371. [17b] P. J. Bonitatebus Jr., W. H. Armstrong, *Chem. Commun.* **1999**, 55−56. [17c] T. Oshiki, K. Mashima, S. Kawa-

mura, K. Tani, K. Kitaura, *Bull. Chem. Soc. Jpn.* **2000**, *73*, 1735−1748.
[18] F. A. Cotton, L. M. Daniels, C. A. Murillo, *Inorg. Chem.* **1993**, *32*, 2881−2885.
[19] S. Hao, P. Berno, R. K. Minhas, S. Gambarotta, *Inorg. Chim. Acta* **1996**, *244*, 37−49.
[20] E. A. C. Brussee, A. Meetsma, B. Hessen, J. H. Teuben, *Organometallics* **1998**, *17*, 4090−4095.
[21] See also: [21a] A. Spannenberg, A. Tillack, P. Arndt, R. Kirmse, R. Kempe, *Polyhedron* **1998**, *17*, 845−850. [21b] B. Morosin, H. Montgomery, *Acta Crystallogr., Sect. B* **1969**, *25*, 1354−1359.
[22] C. Yélamos, M. J. Heeg, C. H. Winter, *Inorg. Chem.* **1998**, *37*, 3892−3894.

Received February 7, 2002
[I02064]

Homoscorpionate Ligands Based on 3-(Cyclobutyl)pyrazole and 3-(Cyclopentyl)pyrazole

Arnold L. Rheingold,[a] Glen P. A. Yap,[b] Lev N. Zakharov,[a] and Swiatoslaw Trofimenko*[a]

Keywords: Scorpionates / Cobalt / Borates / N ligands

The novel scorpionate ligands hydrotris[3-(cyclobutyl)pyrazol-1-yl]borate (Tp^{Cbu}), hydrotris[3-(cyclopentyl)pyrazol-1-yl]borate (Tp^{Cpe}), tetrakis[3-(cyclobutyl)pyrazol-1-yl]borate (pz^oTp^{Cbu}), tetrakis[3-(cyclopentyl)pyrazol-1-yl]borate (pz^oTp^{Cpe}), have been synthesized, converted into a variety of homo- and heteroleptic complexes, and studied by NMR spectroscopy. The complexes $Tl[Tp^{Cbu}]$ (**1**), $Tl[Tp^{Cpe}]$ (**2**), $Co[Tp^{Cbu}]_2$ (**3**), $Co[Tp^{Cpe*}]_2$ (**4**), $Co[Tp^{Cpe}][Tp]$ (**5**), $Co[pz^oTp^{Cbu}]_2$ (**6**), and $Co[pz^oTp^{Cpe}]_2$ (**7**) have been structurally characterized by X-ray crystallography. The coordination behavior of Tp^{Cpe} is similar to that of Tp^{Cy} or Tp^{iPr} in producing stable tetrahedral $Tp^{Cpe}MX$ complexes, but octahedral homoleptic complexes only with ligand rearrangement, yielding $M[Tp^{Cpe*}]_2$. By contrast, Tp^{Cbu} is unusual in forming both tetrahedral $Tp^{Cbu}MX$, and homoleptic $M[Tp^{Cbu}]_2$ complexes, without rearrangement. The complex **6** is tetrahedral in solution but octahedral in the crystal, while complex **7** is tetrahedral in solution and in the crystal.
(© Wiley-VCH Verlag GmbH, 69451 Weinheim, Germany, 2002)

Introduction

Among the many known homoscorpionate [tris(pyrazolyl)borate] ligands of the type Tp^R,[1] where the R substituent is in the 3-position, there are only two in which R is a cycloalkyl group. One is Tp^{Cpr},[2,3] where R is cyclopropyl, and the other Tp^{Cy},[4–7] where R is cyclohexyl. Their coordinative behavior is strikingly different. Tp^{Cpr} coordinates very much like the parent Tp ligand, forming octahedral $M[Tp^{Cpr}]_2$ complexes with great ease, as does its tetrakis analog, pz^oTp^{Cpr} {= $[B(pz^{Cpr})_4]^-$} and, conversely, it is very reluctant to form stable tetrahedral species $M[Tp^{Cpr}]X$. By contrast, Tp^{Cy} readily forms stable tetrahedral complexes $M[Tp^{Cy}]X$, and its $M[Tp^{Cy}]_2$ complexes are not octahedral but tetrahedral, containing κ^2-Tp^{Cy} ligands. It is only through thermally induced rearrangement, which converts one 3-(cyclohexyl)pyrazolyl arm to 5-(cyclohexyl)pyrazolyl, that octahedral complexes are obtained.[7] We decided to study the coordination chemistry of scorpionates with 3-R = cycloalkyl substituents intermediate in size between cyclopropyl and cyclohexyl, in order to determine where the transition from one type of behavior to the other occurs.

That the variations in the size and geometry of 3-R substituents have a pronounced effect on the coordination chemistry, and on the catalytic effectiveness of specific Tp^R metal complexes, has been conclusively demonstrated in the studies, where a series of Tp^R copper(I) complexes was used in achieving carbene transfer, and C-bond activation. Thus, in the cyclopropanation reaction by way of carbene transfer from ethyl diazoacetate to styrene and to other olefins, the by far most active ligand was Tp^{Ms} (Ms = mesityl).[8] On the other hand, in the rather similar cyclopropenation of acetylenes, catalysts derived from Tp^{Ms} gave only mediocre results, but catalysts based on Tp^{Cy} were stellar performers.[9]

We have, therefore, synthesized Tp^R ligands where R was 3-cyclobutyl (= Tp^{Cbu}) or 3-cyclopentyl (= Tp^{Cpe}), as well as their tetrakis analogs pz^oTp^{Cbu} and pz^oTp^{Cpe}, and have examined their coordination chemistry in high-spot fashion.

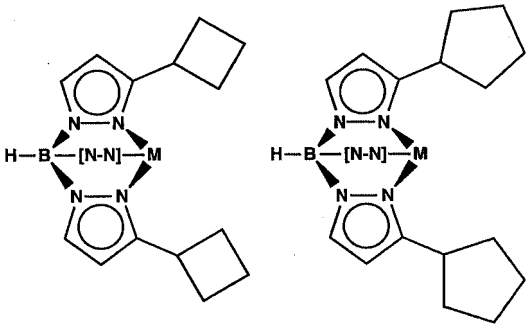

$M[Tp^{Cbu}]$ $M[Tp^{Cpe}]$

-(N-N)- is the third, hidden, 3-cycloalkylpyrazolyl ring

[a] Department of Chemistry and Biochemistry, University of Delaware,
Newark, DE 19716, USA
E-mail: trofimen@udel.edu
[b] Department of Chemistry, University of Ottawa
10 Marie Curie Street, Ottawa K1N 6N5, Canada

Results and Discussion

The two new pyrazoles, 3-(cyclobutyl)pyrazole and 3-(cyclopentyl)pyrazole, were synthesized by way of formylating cyclobutyl methyl ketone, and cyclopentyl methyl ketone, respectively, and treatment of the resulting dicarbonyl intermediates with hydrazine. Reaction of these pyrazoles with KBH_4 produced the respective ligands, characterized as their Tl derivatives, Tl[Tp^{Cbu}] (**1**) and Tl[Tp^{Cpe}] (**2**). Comparing the cone and wedge angles of the structurally

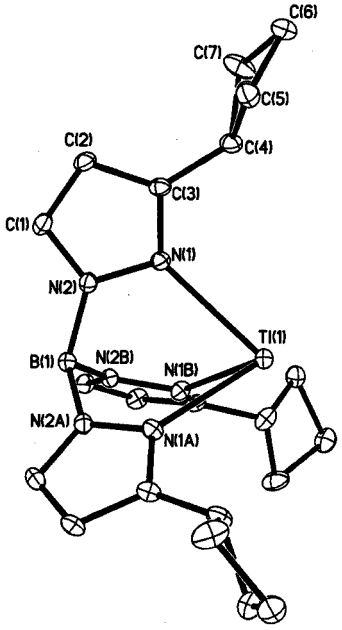

Figure 1. ORTEP plot of the structure of Tl[Tp^{Cbu}] (**1**); selected bond length [Å] and angle [°]: Tl−N(1) 2.562(2); N(1)−Tl−N(1A) 75.20(7)

characterized compounds **1** and **2** (Figure 1 and 2), which were 234 and 253°, respectively,[11] with those of Tl[Tp^{Cpr}] (223°) and Tl[Tp^{Cy}] (281°), one can see that the cone angle of **1** is still relatively close to Tl[Tp^{Cpr}], in differing by only 11°, but the cone angle of **2** is roughly midway between those of Tl[Tp^{Cpr}] and Tl[Tp^{Cy}]. One could expect, therefore, at first approximation, the ligand [Tp^{Cbu}] to be somewhat similar in terms of its coordination behavior to [Tp^{Cpr}], while [Tp^{Cpe}] might resemble [Tp^{Cy}]. The average Tl−N bond lengths of **1** and **2** were both 2.562 Å, although in the case of **1** all lengths were exactly equal, while in **2** they ranged from 2.530 to 2.607 Å. The respective N−Tl−N angles averaged 75.2 and 75.5°, again being all identical in the case of **1**, but ranging from 72.3 to 77.3° in the case of **2**. Both, the Tl−N bond lengths and N−Tl−N bond angles fall right into the middle range of known Tl[Tp^R] complexes.[12]

The cyclopropyl group in Tp^{Cpr} compounds has the angle between its 2- and 3-C atoms very close to the theoretical 60°.[2,3] The cyclopropyl ring is thus very constrained, as compared to an isopropyl (or cyclohexyl) group, the two methylene groups being pinned back and offering little in terms of steric hindrance. Hence, the coordination behavior

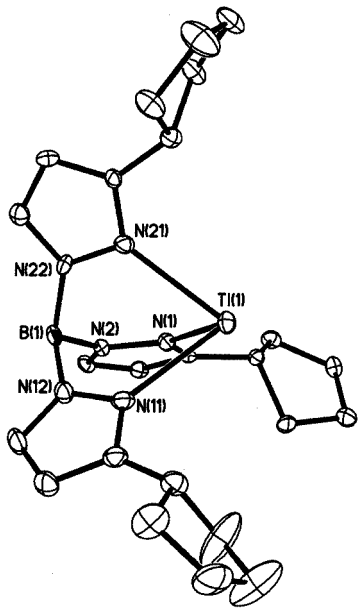

Figure 2. ORTEP plot of the structure of Tl[Tp^{Cpe}] (**2**); selected bond lengths [Å] and angles [°]: Tl−N(1) 2.530(10), Tl−N(11) 2.607(10), Tl−N(21) 2.59(9); N(1)−Tl−N(11) 77.3(3), N(1)−Tl−N(21) 76.7(3), N(1)−Tl−N(11) 72.6(3)

of Tp^{Cpr} resembles that of the parent Tp or of Tp^{Me}. Going to the less tight angle between the 2- and 4-C atoms in the cyclobutyl group, which was 86.4° in Co[Tp^{Cbu}]$_2$ (**3**) and 86.7° in Co[pz^oTp^{Cbu}]$_2$ (**6**) for the cyclobutyl groups in the equatorial belt, such small contraction of the angle is perhaps necessary in order to accommodate there the six cyclobutyl groups. The angle was 96° for the cyclobutyl groups in **6** on the uncoordinated pyrazolyl ring. Clearly, one would expect an increase in steric hindrance in Tp^{Cbu}, as compared to Tp^{Cpr}. A further increase in steric hindrance is anticipated in the case of Tp^{Cpe}, where the angle between the 2- and 5-C atoms of a planar cyclopentyl group would be 108°, and thus almost equal to the tetrahedral angle of 109° present in isopropyl or cyclohexyl groups. In the Co[Tp^{Cpe*}]$_2$ complex **4** the angle in the inner cyclopentyl groups was 101°, while it was 103° in the cyclopentyl group on the rearranged pz^{Cpe} arm. This increased loosening of the 2- and 5-methylene groups would make the cyclopentyl substituent even closer, in terms of steric effects, to a cyclohexyl or isopropyl group.

The Tp^{Cbu} ligand was found to form isolable tetrahedral M[Tp^{Cbu}]X complexes, differing in this respect from Tp^{Cpr}, where such complexes with transition metals were spontaneously converted into octahedral homoleptic species, M[Tp^{Cpr}]$_2$.[3] At the same time homoleptic complexes M[Tp^{Cbu}]$_2$ could also be prepared. In the case of the paramagnetic Co[Tp^{Cbu}]$_2$ (**3**) its NMR spectrum was extremely sharp and indicated all pz^{Cbu} arms to be identical, which meant that no rearrangement of the ligands to Tp^{Cbu*} had taken place. The structure of **3** was determined by X-ray crystallography, and showed the molecule to be of D_{3d} symmetry (Figure 3). There appeared to be no problem of accommodating the six cyclobutyl groups in the equatorial

belt of the molecule. The N−Co distances averaged 2.142 Å, and this is very close to the values found in $Co[Tp]_2$ (2.129 Å),[13] $Co[Tp^*]_2$ (2.143 Å),[14] and to the N−Co distances of the Tp^{Cpr} component in $Co[Tp^{Cpr}][Tp^{Ph}]$, where the N−Co distances average 2.121 Å for Tp^{Cpr}, and 2.223 Å for Tp^{Ph}.[3]

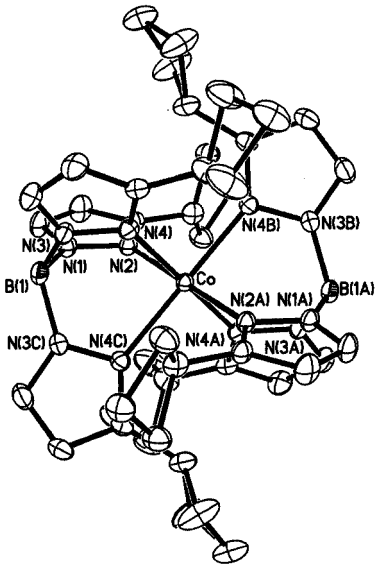

Figure 3. ORTEP plot of the structure of $Co[Tp^{Cbu}]_2$ (**3**); selected bond lengths [Å] and angle [°]: Co−N(2) 2.139(5), Co−N(4) 2.143(4); N(2)−Co−N(4) 88.7(1)

As an example of heteroleptic complexes, $Co[Tp^{Cbu}][Tp]$ was synthesized by the reaction of $Co[Tp^{Cbu}]Cl$ with Tl[Tp]. The NMR of this complex was very sharp and indicative of C_{3v} symmetry for the molecule, with each proton readily identifiable, even to the point of separating the *cis*- and *trans*-protons of the cyclobutyl ring. We assumed that the protons nearer to the metal center would exhibit the larger chemical shift.[15]

The ligand $[Tp^{Cpe}]^-$ readily formed tetrahedral $Co[Tp^{Cpe}]X$ complexes, which were stable, yet reactive enough to serve as precursors to a variety of heteroleptic compounds of the type $Co[Tp^{Cpe}][Tp^R]$, as discussed further on.

The homoleptic complex $Co[Tp^{Cpe}]_2$ was prepared readily from $Tl[Tp^{Cpe}]$ and $Co(ClO_4)_2$. It was purple in solution, but wine-red in the solid state. Heating in hydrocarbon solvents, such as toluene or xylene produced a purple solution, suggestive of tetrahedral coordination, and on concentration the wine-red solid was recovered unchanged. However, when $Co[Tp^{Cpe}]_2$ was refluxed briefly in benzonitrile, the purple color changed to amber, and layering of the solution with heptane resulted in the formation of bright yellow crystals, m.p. 286−288 °C. This color is typical of octahedral cobalt homoscorpionates, and so the crystals were assumed to be $Co[Tp^{Cpe*}]_2$ (**4**). Heating of $Co[Tp^{Cpe}]_2$ in a melting point tube, resulted in a purple melt at 142−144 °C, resolidification with a color change to amber at around 166−168 °C, and melting of that solid at around 280 °C. That this, indeed, involved rearrangement of $Co[Tp^{Cpe}]_2$ to **4**, containing one 5-(cyclopentyl)pyrazolyl group per ligand, was suggested by the proton NMR spectrum. It was rather complicated, as each proton of the two 3-(cyclopentyl) rings was unique [*cis* and *trans*, inner and outer protons with respect to the C_2 axis, plus the tertiary one for a total of nine peaks for the two 3-(cyclopentyl) rings], the 5-(cyclopentyl) ring had four pairs of 2,5- and 3,4-protons, plus the tertiary one for a total of five peaks. In addition, there were the pyrazolyl protons (three 4-H, two 5-H, and one 3-H), for a total of 19 peaks. Nevertheless, they all could be assigned, on the basis of the protons closer to the cobalt center exhibiting the greater shifts.[15] The four 2,5-protons of the 3-(cyclopentyl) rings were well separated in the $\delta = -32$ to -49 ppm range, while those of the 3,4-protons were closely bunched together in the $\delta = -14$ to -15 ppm area. Such thermal rearrangements [Equation (1)] have been observed before as, for instance, in converting $Co[Tp^{Np}]_2$ to $Co[Tp^{Np*}]_2$,[16] or $Co[Tp^{Cy}]_2$ to $Co[Tp^{Cy*}]_2$.[7]

$$M[HB(3\text{-}Rpz)_3]_2 \rightarrow M[HB(3\text{-}Rpz)_2(5\text{-}Rpz)]_2 \quad (1)$$

The rearranged structure of **4** was confirmed by X-ray crystallography. In this structure (Figure 4) the two pyrazolyl arms with the 5-(cyclopentyl) group are *trans* to each other, and their Co−N bond lengths are 2.11 Å, while those with the 3-(cyclopentyl) group have Co−N bond lengths of 2.16 Å, thus being significantly longer (see Table 1).

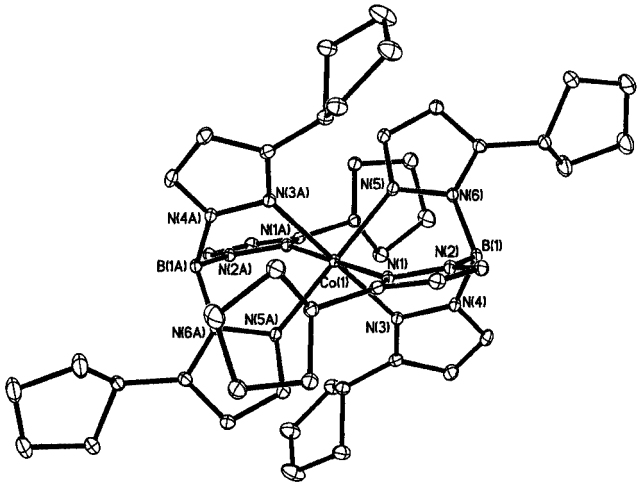

Figure 4. ORTEP plot of the structure of $Co[Tp^{Cpe*}]_2$ (**4**); selected bond lengths [Å] and angles [°]: Co−N(5) 2.1154(14), Co−N(3) 2.1576(13), Co−N(1) 2.11619(13); N(5)−Co−N(3) 88.18(5), N(5)−Co−N(1) 87.21(5), N(1)−Co−N(3) 84.44(5)

A series of heteroleptic complexes $Co[Tp^{Cpe}][Tp^R]$ was also prepared, to check how large an R group in 3-position of the Tp^R ligand can still be accommodated in such complexes without causing rearrangement of $[Tp^{Cpe}]$ to $[Tp^{Cpe*}]$, or altering the octahedral structure. Three such compounds were prepared: $Co[Tp^{Cpe}][Tp]$ (**5**), $Co[Tp^{Cpe}][Tp^*]$ and $Co[Tp^{Cpe}][Tp^{Cpr}]$. In each of them, the octahedral structure was maintained without rearrangement of the Tp^{Cpe} ligand, as was clearly indicated by the NMR spectra of these paramagnetic complexes. All the

Table 1. Average Co−N bond lengths in octahedral homoleptic $Co[Tp^x]_2$ and heteroleptic $Co[Tp^x][Tp^y]$ complexes

Tp^R ligand	Co−N [Å]	Found in complex	Ref.
Tp	2.129(7)	$Co[Tp]_2$	[13]
Tp	2.129(4)	$Co[Tp^{Cpe}][Tp]$	this work
Tp	2.131(5)	$Co[Tp^{\alpha Nt}][Tp]$	[19]
Tp	2.143(2)	$Co[Tp^{\beta Nt}][Tp]$	[19]
Tp	2.142(3)	$Co[Tp^{CHPh2}][Tp]$	[21]
Tp	2.124(3)	$Co[Tp^{Ph,4Me}][Tp]$	[21]
Tp	2.122(2)	$Co[Tp^{Ph,4Et}][Tp]$	[21]
Tp	2.124(2)	$Co[Tp^{Tol}][Tp]$	[21]
Tp^4tBu	2.165(6)	$Co[Tp^{CHPh2}][Tp^{4tBu}]$	[21]
Tp^4tBu	2.129(2)	$Co[Tp^{Np}][Tp^{4tBu}]$	[21]
Tp*	2.144(2)	$Co[Tp^*]_2$	[14]
Tp*	2.141(5)	$Co[Tp^{\alpha Nt}][Tp^*]$	[19]
Tp^{Cpr}	2.121(6)	$Co[Tp^{Cpr}][Tp^{Ph}]$	[3]
Tp^{Cbu}	2.142(2)	$Co[Tp^{Cbu}]_2$	this work
Tp^{Cbu}	2.124(3)	$Co[pz^oTp^{Cbu}]_2$	this work
Tp^{Cpe}	2.160(2)[a]	$Co[Tp^{Cpe*}]_2$	this work
Tp^{Cpe}	2.168(3)	$Co[Tp^{Cpe}][Tp]$	this work
Tp^{iPr}	2.167(2)[b]	$Co[Tp^{iPr*}]$	[10]
$Tp^{iPr,4Br}$	2.179(3)[c]	$Co[Tp^{(iPr,4Br)*}]$	[10]
Tp^{Np}	2.167(6)	$Co[Tp^{Np}][Tp^{4tBu}]$	[21]
Tp^{Np}	2.175(4)	$Co[Tp^{Np}][Tp^{Br3}]$	[22]
Tp^{Np}	2.137(7)	$Co[Tp^{Np}][Tp^{3Bo,7Me}]$	[20]
Tp^{Np}	2.172(3)	$Co[Tp^{Np}][Tp^{Me,mt3}]$	[23]
Tp^{Np}	2.153(15)	$Co[Tp^{Np}][Tp^{a*,3Me}]$	[20]
$Tp^{Me,mt3}$	2.149(3)[d]	$Co[Tp^{Np}][Tp^{Me,mt3}]$	[23]
$Tp^{a*,3Me}$	2.207(2)	$Co[Tp^{Np}][Tp^{a*,3Me}]$	[20]
$Tp^{3Bo,7Me}$	2.236(7)[e]	$Co[Tp^{Np}][Tp^{3Bo,7Me}]$	[20]
Tp^{Br3}	2.139(2)	$Co[Tp^{Br3}]_2$	[21]
Tp^{Br3}	2.128(3)	$Co[Tp^{Br3}][Tp^{Np}]$	[21]
Tp^{Tn}	2.155(3)	$Co[Tp^{Tn}]_2(CHCl_3)$	[18]
Tp^{Tn}	2.170(2)	$Co[Tp^{Tn}]_2(C_6H_6)$	[18]
Tp^{Ph}	2.223(6)	$Co[Tp^{Cpr}][Tp^{Ph}]$	[3]
$Tp^{Ph,4Me}$	2.223(3)	$Co[Tp^{Ph,4Me}][Tp]$	[21]
$Tp^{Ph,4Et}$	2.222(2)	$Co[Tp^{Ph,4Et}][Tp]$	[21]
Tp^{Tol}	2.226(2)	$Co[Tp^{Tol}][Tp]$	[21]
$Tp^{a*,3Me}$	2.207(15)[f]	$Co[Tp^{Np}][Tp^{a*,3Me}]$	[20]
$Tp^{\alpha Nt}$	2.238(5)	$Co[Tp^{\alpha Nt}][Tp]$	[19]
$Tp^{\alpha Nt}$	2.233(4)	$Co[Tp^{\alpha Nt}][Tp^*]$	[19]
$Tp^{\beta Nt}$	2.228(2)	$Co[Tp^{\beta Nt}][Tp]$	[19]
Tp^{CHPh2}	2.214(4)	$Co[Tp^{CHPh2}][Tp]$	[21]
Tp^{CHPh2}	2.206(1)	$Co[Tp^{CHPh2}][Tp^{4tBu}]$	[21]

[a] Values taken from the two 3-cyclopentylpyrazolyl arms per ligand. [b] Values taken from the two 3-isopropylpyrazolyl arms per ligand. [c] Values taken from the two 4-bromo-3-isopropylpylpyrazolyl arms per ligand. [d] $Tp^{Me,mt3}$ = hydrotris(3-methyl-4,5-propylenepyrazol-1-yl)borate. [e] $Tp^{3Bo,7Me}$ = hydrotris(7-methylindazol-1-yl)borate. [f] $Tp^{a*,3Me}$ = hydrotris(3-methyl-2*H*-benz[*g*]indazol-2-yl)borate.

spectra were extremely sharp, as is the case with octahedral cobalt(II) bis(homoscorpionates), and showed each proton to be in a specific environment, with assignments based on the previously established ranges for the chemical shifts of the pyrazolyl ring protons, and protons of pyrazolyl substituents in the various positions. The structure of **5** was determined by X-ray crystallography (Figure 5). It was of C_{3v} symmetry, and contained slightly longer Co−N bonds for the Tp^{Cpe} ligand than for Tp (2.168 versus 2.129 Å).

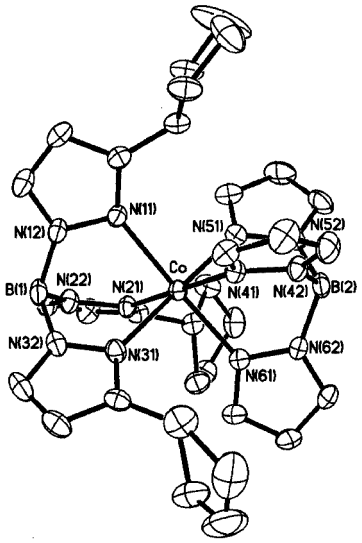

Figure 5. ORTEP plot of the structure of $Co[Tp^{Cpe}][Tp]$ (**5**); selected bond lengths [Å] and angles [°]: Co−N(11) 2.173(3), Co−N(21) 2.167(3), Co−N(31) 2.165(4), Co−N(41) 2.132(3), Co−N(51) 2.130(4), Co−N(61) 2.126(4); N(11)−Co−N(21) 87.4(1), N(11)−Co−N(31) 87.5(1), N(31)−Co−N(21) 87.3(1), N(41)−Co−N(51) 85.7(1), N(41)−Co−N(61) 84.7(1), N(51)−Co−N(61) 85.2(1)

When the reaction of KBH_4 with 3-(cyclobutyl)pyrazole or 3-(cyclopentyl)pyrazole was carried out without solvent, and long reaction times were employed, the tetrakis ligands $[B(pz^{Cbu})_4]^-$ (= pz^oTp^{Cbu}) and $[B(pz^{Cpe})_4]^-$ (= pz^oTp^{Cpe}) were obtained and were converted into their thallium derivatives, $Tl[pz^oTp^{Cbu}]$ and $Tl[pz^oTp^{Cpe}]$. While $Tl[pz^oTp^{Cbu}]$ could be isolated in crystalline form and characterized, $Tl[pz^oTp^{Cpe}]$ was very difficult to crystallize and, for this reason, the crude K salt was used to prepare $[pz^oTp^{Cpe}]$ complexes. The coordination chemistry of the two new ligands fitted neatly between that of pz^oTp^{Cpr} and pz^oTp^{Cy}. Whereas pz^oTp^{Cpr}, just like the parent pzTp,[17] coordinated only in a κ^3-fashion, forming with first-row transition metals octahedral complexes $M[Tp^{Cpr}]_2$, in which the three-coordinated and one uncoordinated pz^{Cpr} arms did not exchange, giving rise to NMR signals for each pyrazolyl arm in 3:1 ratio, the ligand pz^oTp^{Cy} coordinated only in a κ^2-fashion, yielding tetrahedral complexes, as was also the case with the ligand pz^oTp^{iPr}.[10] This distinction between octahedral and tetrahedral complexes is most apparent in the $Co[pz^oTp^R]_2$ species, where the octahedral complexes are yellow, while the tetrahedral ones are deep purple.

The solid complex $Co[pz^oTp^{Cbu}]_2$ (**6**) was yellow, but when in solution, be it in chloroform at room temperature or in boiling toluene, the color changed to deep purple, indicating dissociation of one of the pz^{Cbu} arms per ligand, and formation of a dynamic tetrahedral structure. Upon crystallization of the complex from the purple solution, the resulting crystals were again bright yellow, indicative of octahedral coordination. The NMR of this compound was quite different from that of $Co[pz^oTp^{Cpr}]_2$ in which the signals corresponding to the three-coordinated and one uncoordinated pyrazolyl arms per ligand were sharp and well separated, consistent with a lack of exchange between the coordinated and uncoordinated pyrazolyl arms. The NMR spectrum of **6**, by contrast, contained broad peaks at positions averaging the peaks of the two-coordinated and two uncoordinated pyrazolyl arms per ligand. Nevertheless, the structure determination of **6** (Figure 6) confirmed the octahedral nature of the complex in the crystal, with each ligand being κ^3-coordinated, and the fourth pz^{Cbu} arm remaining free.

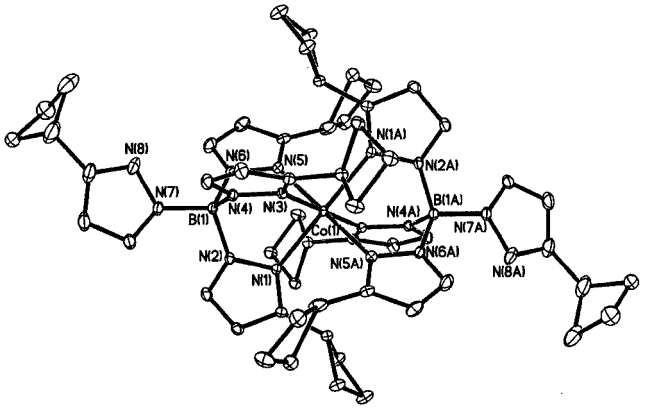

Figure 6. ORTEP plot of the structure of $Co[pz^oTp^{Cbu}]_2$ (**6**); selected bond lengths [Å] and angles [°]: Co−N(1) 2.1317(18), Co−N(3) 2.0923(18), Co−N(5) 2.1469(18), N(1)−Co−N(3) 88.33(7), N(1)−Co−N(5) 88.14(7), N(5)−Co−N(3) 88.41(7)

The $[pz^oTp^{Cpe}]$ ligand also formed a 2:1 cobalt complex, $Co[pz^oTp^{Cpe}]_2$ (**7**), which was purple in solution, and remained purple on concentration suggestive of a tetrahedral structure throughout, with κ^2-coordination of each ligand. It is similar, in this regard, to the ligands $[pz^oTp^{iPr}]$ and $[pz^oTp^{Cy}]$. The NMR spectrum of **7** showed broad peaks, indicative of exchange of all four pyrazolyl arms at room temperature. In the crystal (Figure 7) the complex also exhibited a tetrahedral structure, similar to that found in the case of $Co[pz^oTp^{Cy}]_2$ and $Co[pz^oTp^{iPr}]_2$. The Co−N distances for the coordinated pz^{Cpe} arms averaged 1.997 Å, and were thus considerably shorter than the values of 2.158 Å found in **4** or 2.168 Å encountered in **5**, implying a lesser degree of congestion in the tetrahedral structure.

The steric hindrance imposed on Tp^R ligands by the R substituents in 3-position manifests itself in the slight, but persistent, M−N bond lengthening in their octahedral homo- and heteroleptic complexes. In Table 1 we have collected Co−N bond length data from structurally determined $Co[Tp^R]_2$ and $Co[Tp^R][Tp^{R'}]$ complexes. As can be seen there, the parent Tp ligand is indeed, and expectedly, the least hindered, while the ligand Tp^{Cbu} resembles Tp*, in terms of steric hindrance, as expressed in terms of Co−N bond lengths. The Tp^{Cpe} ligand appears closest in its Co−N bond length values to Tp^{iPr}, which is also in consonance with its observed coordination chemistry.

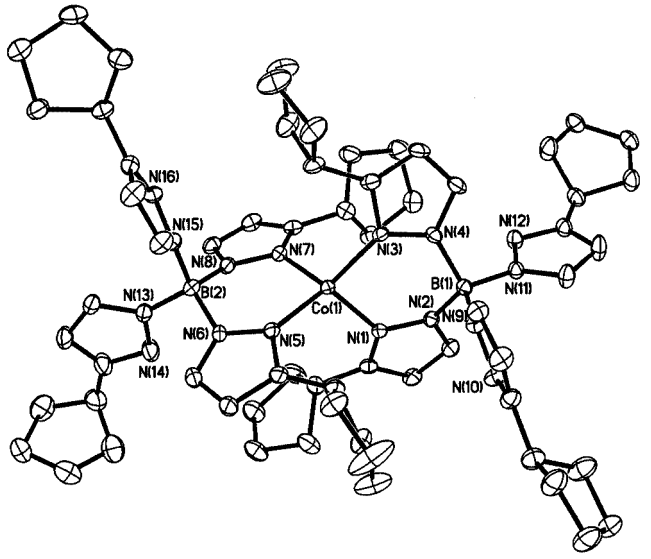

Figure 7. ORTEP plot of the structure of $Co[pz^oTp^{Cpe}]_2$ (**7**); selected bond lengths [Å] and angles [°]: Co−N(1) 1.991(3), Co−N(3) 1.986(3), Co−N(5) 1.985(3), Co−N(7) 1.984(3); N(1)−Co−N(3) 96.79(13), N(1)−Co−N(5) 115.56(13), N(5)−Co−N(3) 125.76(15), N(1)−Co−N(7) 109.01(14), N(3)−Co−N(7) 112.82(13)

We also compared the propensity for dynamic exchange of the coordinated and uncoordinated pyrazolyl arms in a series of $[pz^oTp^R]$ ligands by examining the NMR spectra for the 4- and 5-protons in a series of diamagnetic zinc complexes $Zn[pz^oTp^R]_2$, where R was methyl, cyclopropyl, cyclobutyl, cyclopentyl and cyclohexyl. For the complexes where R was methyl or cyclopropyl, there were only two very sharp peaks for the 4- and 5-protons, implying very rapid exchange of all the pyrazolyl arms. When R was cyclobutyl, there were still only two peaks present, but they ceased to be sharp, with one of them being more of a hump than a peak and the other significantly broadened. The broadest peak was the one for 5-H, as was the C-5 peak in the ^{13}C NMR spectrum of this compound. When R was cyclopentyl, there were already four peaks for the 4- and 5-protons, although they could not be discerned as doublets, implying still a small degree of exchange. In the case where R was cyclohexyl, the four peaks were narrow and sharp with their doublets clearly resolved. These comparisons indicate that the ligand $[pz^oTp^{Cbu}]$ exhibits a hybrid type of behavior which, in turn, implies that the energy difference in solution between the tetrahedral and octahedral forms is quite small.

Conclusion

In summary, we have prepared and characterized new Tp^{Cbu} and Tp^{Cpe} ligands and their tetrakis analogs, [pz^oTp^{Cbu}] and [pz^oTp^{Cpe}], establishing the main features of their coordination chemistry. The ligands Tp^{Cpe} and [pz^oTp^{Cpe}] act very much like the more hindered analogs Tp^{Cy} and [pz^oTp^{Cy}]. However, the Tp^{Cbu} and [pz^oTp^{Cbu}] ligands are, in some ways, special. Tp^{Cbu} is a Tp^R ligand with the largest cycloalkyl group which still permits the formation of homoleptic $Co[Tp^R]_2$ complexes without rearrangement of the ligand to Tp^R*, while [pz^oTp^{Cbu}] exhibits a very facile conversion from octahedral to tetrahedral when going into solution. Being relatively unhindered, this tetrahedral form of [pz^oTp^{Cbu}] might interact/coordinate with some small molecules and, perhaps, exhibit interesting catalytic properties. We are planning to investigate these aspects in the future.

Experimental Section

General: All chemicals were of the highest commercial reagent grade and were used as received. Cyclobutyl methyl ketone and cyclopentylmagnesium chloride were purchased from Aldrich. Elemental analyses were done by Microanalysis, Inc., Wilmington, DE. Infrared spectra were obtained as Nujol mulls of KBr pellets with a Perkin−Elmer 1625 FTIR infrared spectrophotometer, using 16 scans. Proton NMR spectra were obtained with a Nicolet NT360WB spectrometer. The compounds were studied with typical conditions of 16 K data points, a sweep width of 3000−4000 Hz, 90° pulse angles, and a recycle time of 4−5 s.

3-(Cyclobutyl)pyrazole: This compound was prepared by formylation of cyclobutyl methyl ketone (125 g 1.27 mol) with methyl formate, and anhydrous sodium methoxide, followed by the reaction with hydrazine, as has been done in the synthesis of 3-isopropylpyrazole.[10] The product, b.p. 123 °C/1.7 Torr, was obtained in 98 g (63%) yield. ^{1}NMR: δ = 7.49 (d, J = 2.0 Hz, 1 H, 5-H), 6.12 (d, J = 2.0 Hz, 1 H, 4-H), 3.59 (quint, 1 H, tertiary H), 2.14 (m, 2 H, cyclobutyl), 2.20 (quint of d, 2 H, cyclobutyl), 2.1−1.8 (m, 4 H, cyclobutyl) ppm. ^{13}C NMR: δ = 18.8 (unique methylene), 29.6 (2 methylenes), 32.5 (tertiary C), 102.0 (C-4), 135 (C-5), 151.6 (C-3) ppm. $C_7H_{10}N_2$ (122.09): calcd. C 68.9, H 8.20, N 23.0; found C 68.8, H 8.29, N 22.8.

3-(Cyclopentyl)pyrazole: Cyclopentyl methyl ketone was prepared by adding 1.20 mol of cyclopentylmagnesium chloride to a solution of 1.35 mol of acetic anhydride in 1 L of THF. After completion of the addition and another hour of stirring, saturated aqueous ammonium chloride was added, and the two layers were separated. The upper layer was passed through alumina, and the filtrate was stripped and distilled in vacuo, saving the cut with b.p. 163−165 °C. The yield was 56 g (41%). 3-(Cyclopentyl)pyrazole was prepared from the above cyclopentyl methyl ketone, methyl formate, and anhydrous sodium methoxide, followed by the reaction with hydrazine as has been done in the case of 3-isopropylpyrazole.[10] The redistilled pyrazole, b.p. 145−150 °C/5.8 Torr, was obtained in 26 g (42%) yield. ^{1}H NMR: δ = 12.4 (br., 1 H, NH), 7.47 (d, J = 2.0, 1 H, 5-H), 6.06 (d, J = 2.0, 1 H, 4-H), 3.14 (quint, 1 H, tertiary H), 2.07 (m, 2 H, cyclopentyl), 1.5−1.9 (m, 6 H, cyclopentyl) ppm. ^{13}C NMR: δ = 15.1, 33.2, 37.5 (tertiary C), 101.6 (C-4), 135.0 (C-5), 151.4 (C-3) ppm. $C_8H_{12}N_2$ (136.10): calcd. C 70.6, H 8.82, N 20.6; found C 70.6, H 8.94, N 20.6%.

Thallium Hydrotris[3-(cyclobutyl)pyrazol-1-yl]borate, Tl[Tp^{Cbu}] (1): A mixture of 96 g (0.79 mol) of 3-(cyclobutyl)pyrazole and 11.6 g (0.215 mol) of KBH_4 was stirred and refluxed in 200 mL of 4-methylanisole. Hydrogen evolution was steady, and the theoretical amount was evolved within 4 h. The solvent was distilled off under vacuum, and the residue was boiled with 300 mL of heptane, and the solution was filtered hot. The crude K[Tp^{Cbu}] had a B−H band at $\tilde{\nu}$ = 2383 cm^{-1}. The compound was converted into Tl[Tp^{Cbu}] in standard fashion, and this product was obtained in 58 g (48%) overall yield. M.p. 132−134 °C. IR: $\tilde{\nu}$ = 2428 (B−H) cm^{-1}. ^{1}H NMR: δ = 7.54 (d, J = 2.0, 3 H, 5-H), 6.05 (d, J = 2.0, 3 H, 4-H), 3.65 (quint, 3 H, tertiary H), 2.33 (m, 6 H, cyclobutyl), 2.16 (m, 6 H, cyclobutyl), 1.99 (m, 3 H, cyclobutyl), 1.86 (m, 3 H, cyclobutyl) ppm; the BH signal of intensity 1 is visible by integration in the δ = 3.6−5.2 ppm region. ^{13}C NMR: δ = 18.9 (Cbu C-3), 30.0 (Cbu C-2,4), 33.9 (Cbu C-1), 101.6 (C-4), 135.9 (C-5), 157.8 (C-3) ppm. $C_{21}H_{28}BN_6Tl$ (579.67): calcd. C 43.5, H 4.84, N 14.5; found C 43.6, H 4.98, N 14.3.

Thallium Hydrotris[3-(cyclopentyl)pyrazol-1-yl]borate, Tl[Tp^{Cpe}] (2): This compound was prepared as above from 50 g (0.37 mol) of 3-(cyclopentyl)pyrazole and 5.6 g (0.10 mol) of KBH_4 in 75 mL of 4-methylanisole. The residue, after removal of the solvent in vacuo, was converted into Tl[Tp^{Cpe}], which was obtained in 30 g (47%) overall yield. IR: $\tilde{\nu}$ = 2438 (B−H) cm^{-1}. ^{1}H NMR: δ = 7.51 (3 H, 5-H), 5.98 (3 H, 4-H), 3.21 (3 H, quint, Cpe 1-H), 2.07 (6 H, Cpe), 1.75 (m, 6 H, Cpe), 1.64 (m, 12 H, Cpe) ppm; the BH (1 H) signal is visible by integration in the δ = 3.6−5.2 ppm region. ^{13}C NMR: δ = 25.4, 34.1, 38.9 (Cpe, C-1), 101.1 (C-4), 135.8 (C-5), 157.9 (C-3) ppm. $C_{24}H_{34}BN_6Tl$ (621.75): calcd. C 46.4, H 5.48, N 13.5; found C 46.3, H 5.56, N 13.4.

Co[Tp^{Cbu}]Cl: A solution of Tl[Tp^{Cbu}] (1.2 g, 2.0 mmol) in 50 mL of dichloromethane was stirred vigorously with a large excess of anhydrous $CoCl_2$. After 2 h, the blue slurry was filtered through a pad of Celite, and the filtrate was concentrated, yielding a blue solid in 0.64 g (68%) yield. It was obtained after recrystallization from a toluene/heptane mixture as dark blue crystals, m.p. 148−150 °C. IR: $\tilde{\nu}$ = 2504 (B−H) cm^{-1}. $C_{21}H_{28}BClCoN_6$ (469.46): calcd. C 53.6, H 5.96, N 17.9; found C 54.0; H 6.14, N 17.7.

Co[Tp^{Cpe}]Cl: This compound was synthesized in the same way as Co[Tp^{Cbu}]Cl, and was obtained in 63% yield as dark blue crystals, m.p. 161−163 °C. IR: $\tilde{\nu}$ = 2478 (B−H) cm^{-1}. $C_{24}H_{34}BClCoN_6$ (505.49): calcd. C 56.3, H 6.64, N 16.4; found C 56.4, H 6.83, N 16.3.

Zn[Tp^{Cpe}]NCS: The compound was prepared by stirring vigorously in dichloromethane Tl[Tp^{Cpe}] with a large excess of zinc perchlorate and potassium thiocyanate (1:4 mol ratio) in a minimum amount of water. After 2 h, the organic layer was separated, passed through alumina, and the solvents were evaporated, yielding the product in 64% yield. M.p. 160−162 °C. IR: $\tilde{\nu}$ = 2496 (B−H), 2063 (NCS) cm^{-1}. ^{1}H NMR: δ = 7.54 (3 H, 5-H), 6.03 (d, 3 H, 4-H), 3.24 (3 H, quint, Cp 1-H), 2.13 (m, 6 H, Cpe), 1.77 (m, 12 H, Cpe), 1.58 (m, 6 H, Cpe) ppm. $C_{35}H_{34}BN_7SZn$ (660.63): calcd. C 55.6, H 6.30, N 18.2; found C 55.7, H 6.41, N 18.0.

Co[Tp^{Cbu}]$_2$ (3): To a stirred solution of Tl[Tp^{Cbu}] (1.2 g, 2.0 mmol) in 50 mL of THF was added dropwise a concentrated aqueous solution of 0.26 g (1 mmol) of $Co(ClO_4)_2 \cdot (H_2O)_6$ followed, after 1 h, by 200 mL of water and 100 mL of chloroform. The layers were separated, and the chloroform layer was passed through a shallow

bed of alumina, and the solvents were evaporated, yielding 0.67 g (83%) of yellow Co[Tp^{Cbu}]$_2$, which was purified by recrystallization from xylene. M.p. 254−256 °C. IR: $\tilde{\nu}$ = 2439, 2467 cm^{-1}. ^{1}H NMR: δ = 97 (1 H, BH), 74.0 (3 H, 5-H), 48.9 (3 H, 4-H), −12.0 (6 H, 3′-H), −26.1 and 26.7 (6 H each, *cis* and *trans* 2′-H), −92.5 (3 H, 1′-H) ppm. $C_{42}H_{56}B_2CoN_{12}$ (809.50): calcd. C 62.3, H 6.92, N 20.8; found C 62.5, H 7.14, N 20.6.

Co[Tp^{Cpe*}]$_2$ (4): The complex Co[Tp^{Cpe}]$_2$ was prepared as above, but using Tl[Tp^{Cpe}] instead of Tl[Tp^{Cbu}], and it was obtained in 76% yield, as a pale purplish-red solid. It melted to a purple melt at 142−144 °C, then the melt resolidified with a color change to amber at around 166−168 °C, melting again at around 280 °C. Boiling of a sample of the product in benzonitrile resulted in an amber solution, after passing through a deep purple stage. Overlayering this solution with heptane resulted, on standing, in the formation of bright yellow needles, m.p. 286−288 °C. NMR: δ = 84.9 (2 H, 5-H of 3-Cpe), 59.2 (1 H, 4-H of 5-Cpe), 49.5 (2 H, 4-H of 3-Cpe), 38.6 (1 H, tertiary H of 5-Cpe), 24.8 (2 H, *trans*-2,4-H of 5-Cpe), 16.9 (2 H, *cis*-2,4-H of 5-Cpe), 13.5 (2 H, *trans*-3,4-H of 5-Cpe), 9.12 (2 H, *cis*-3,4-H of 5-Cpe), −14.104 (2 H, 3,4-H of 3-Cpe), −14.7 (2 H, 3,4-H of 3-Cpe), −14.7 (2 H, 3,4-H of 3-Cpe) −15.0 (2 H, 3,4-H of 3-Cpe), −31.9 (2 H, *trans*-2,5-H of 3-Cpe), −36.3 (2 H, *trans*-2,5-H of 3-Cpe), −40.9 (2 H, *cis*-2,5-H of 3-Cpe, −46.8 (2 H, *cis*-2,5-H of 3-Cpe), −94 (1 H, 3-H), −108 (2 H, tertiary H of 3-Cpe) ppm. $C_{48}H_{68}B_2CoN_{12}$ (893.69): calcd. C 64.5, H 7.61, N 18.8; found C 65.1, H 7.80, N 19.0.

Zn[Tp^{Cbu}]$_2$: M.p. 186−188 °C. IR: $\tilde{\nu}$ = 2466, 2438 (B−H) cm^{-1}. ^{1}H NMR: δ = 7.57 (d, *J* = 2.0, 3 H, 5-H), 6.16 (d, *J* = 2.0, 3 H, 4-H), 2.73 (quint, 3 H, tertiary H), 1.81 (m, 6 H, cyclobutyl), 1.62 (m, 6 H, cyclobutyl), 1.57 (m, 6 H, cyclobutyl) ppm; the BH (1 H) signal can be discerned by integration in the δ = 3.5−5.0 ppm range. ^{13}C NMR: δ = 18.1 (C-3′), 30.1 (C-2′), 32.9 (C-1′), 102.1 (C-4), 135.9 (C-5), 159.3 (C-3) ppm. $C_{42}H_{56}B_2N_{12}Zn$ (815.55): calcd. C 61.8, H 6.87, N 20.6; found C 62.0, H 7.01, N 20.5.

Zn[Tp^{Cpe}]$_2$: M.p. 182−184 °C. ^{1}H NMR: δ = 7.31 (d, 3 H, 5-H), 6.06 (d, 3 H, 4-H), 2.60 (3 H, quint, Cpe 1-H), 1.63 (m, 12 H, Cpe), 1.47 (m, 12 H, Cpe) ppm. ^{13}C NMR: δ = 25.3, 33.8, 38.9, 102.0, 137.5, 161.0 ppm. $C_{48}H_{68}B_2N_{12}Zn$ (899.61): calcd. C 64.1, H 7.56, N 18.7; found C 64.2, H 7.69, N 18.5.

Preparation of Heteroleptic Co[Tp^R][$Tp^{R'}$] Complexes. A: One method to synthesize octahedral cobalt complexes containing two different Tp^R ligands was to stir equimolar amounts of Co[Tp^R]Cl (R = Cbu, Cpe) and Tl[$Tp^{R'}$] (R′ = H, Me, cyclopropyl) in dichloromethane until the disappearance of the characteristic blue color of Co[Tp^R]Cl. This took from a few minutes to several hours, depending on the steric hindrance of $Tp^{R'}$. The slurry was then filtered through a bed of Celite to remove TlCl, and the filtrate was chromatographed on alumina, collecting the yellow band. Concentration of the eluate yielded the crude product, which was recrystallized from toluene or xylene. **B:** An alternative way was to stir Tl[Tp^R] in dichloromethane with a large excess of anhydrous $CoCl_2$, to filter the blue slurry after 4 h, and without isolation of Co[Tp^R]Cl, adding an equimolar amount of the appropriate Tl[$Tp^{R'}$] salt. When the color of the slurry changed from blue to yellowish, the slurry was filtered to remove TlCl, the filtrate was chromatographed on alumina, and concentration of the eluate yielded the crude Co[Tp^R][$Tp^{R'}$] complex, which was purified by recrystallization. The unoptimized yields in these reactions ranged from 55 to 82%.

Co[Tp^{Cbu}][Tp]: This complex was prepared by method A, was obtained in 82% yield, and recrystallized from toluene. M.p. 267−268 °C. IR: $\tilde{\nu}$ = 2469, 2445 (B−H) cm^{-1}. ^{1}H NMR: δ = 114.2 and 111.8 (1 H each, BH), 90.4 and 82.5 (3 H each, 5-H), 44.8 and 41.5 (3 H each, 4-H), −14.5 and − 15.0 (3 H each, *cis*- and *trans*-3′-H), −31.5 and −35.4 (6 H each, *cis*- and *trans*-2′-H), −102.1 (3 H, 1′-H), −124.3 (3 H, 3-H) ppm. $C_{30}H_{38}B_2CoN_{12}$ (646.97): calcd. C 55.6, H 5.87, N 26.0; found C 55.5, H 6.01, N 25.7.

Co[Tp^{Cpe}][Tp] (5): This complex was prepared by method A and was obtained in 77% yield. M.p. 278−280 °C. IR: $\tilde{\nu}$ = 2473, 2440 (B−H) cm^{-1}. ^{1}H NMR: δ = 118.5 and 115.7 (1 H each, BH and BH′), 92.9 and 93.4 (3 H each, 5-H and 5′-H), 45.3 and 42.0 (3 H each, 4-H and 4′-H), −13.6 and − 14.5 (6 H each, Cp 3-H, *cis* and *trans*), −35.5 (6 H, Cp 2-H, *trans*) −45.6 (6 H, Cp 2-H, *cis*), −106.3 (3 H, Cp 1-H), −131.7 (3 H, 3-H) ppm. $C_{33}H_{44}B_2N_{12}$ (689.40): calcd. C 57.5, H 6.39, N 24.4; found 57.8, H 6.48, N 24.1.

Co[Tp^{Cpe}][Tp*]: This complex was prepared by method B and was obtained in 69% yield. M.p. 282−284 °C. IR: $\tilde{\nu}$ = 2515, 1475, 2443 (B−H) cm^{-1}. ^{1}H NMR: δ = 105.5 (2 H, BH and BH′), 77.6 (3 H, 5-H), 48.1 and 44.8 (3 H each, 4-H and 4′-H), 42.9 (9 H, 5-Me), −12.3 and −12.9 (6 H each, Cp 3-H, *cis* and *trans*), −31.5 (6 H, Cp 2-H, *trans*), −38.4 (6 H, Cp 2-H, *cis*), −75.7 (9 H, 3-Me), −113.6 (3 H, Cp 1-H) ppm. $C_{39}H_{56}B_2CoN_{12}$ (773.06): calcd. C 60.5, H 7.24, N 21.7; found C 60.4, H 7.31, N 21.6.

Co[Tp^{Cpe}][Tp^{Cpr}]: This complex was prepared by method B and was obtained in 55% yield. M.p. 247−248 °C. IR: $\tilde{\nu}$ = 2438, 2473 (B−H) cm^{-1}. ^{1}H NMR: δ = 99.6 and 97.2 (1 H each, BH and BH′), 76.0 and 69.4 (3 H each, 5-H and 5′-H), 47.6 and 45.4 (3 H each, 4-H and 4′-H), −11.2 (12 H, Cpr 3-H), −23.8 (3 H, Cpr 2-H, *trans*), −25.6 (6 H, Cpr 2-H, *cis*), −28.9 (6 H, Cpr 2-H, *trans*) −32.4 (6 H Cpe 2-H, *cis*), −97.3 and −100.0 (3 H each, Cpr and Cpe 1-H) ppm. $C_{42}H_{56}B_2CoN_{12}$ (809.09): calcd. C 56.6, H 6.92, N 20.8; found C 56.5, H 7.04, N 20.7.

Preparation of the [pz^oTp^{Cbu}] and [pz^oTp^{Cpe}] Ligands: These ligands were prepared by heating with stirring the appropriate pyrazole and KBH_4 in a 5:1 mol ratio, bringing the oil-bath temperature slowly up to 250−270 °C, and maintaining this temperature under a gentle nitrogen stream for 24 h. After some cooling, the excess pyrazoles were distilled off in vacuo, and the residues were refluxed for 1 h in heptane, cooled and filtered, yielding the crude K salts K[pz^oTp^{Cbu}] and K[pz^oTp^{Cpe}], respectively. Samples of each were converted into the Tl salts, Tl[pz^oTp^{Cbu}] and Tl[pz^oTp^{Cpe}]. However, only Tl[pz^oTp^{Cbu}] could be recrystallized, as the resinous Tl[pz^oTp^{Cpe}] resisted all attempts at crystallization. For this reason, the crude K[pz^oTp^{Cpe}] salt was employed for preparing M[pz^oTp^{Cpe}] complexes.

Tl[pz^oTp^{Cbu}]: It was recrystallized from octane. M.p. 129−132 °C. ^{1}H NMR: δ = 7.41 (d, *J* = 2 Hz, 1 H, 5-H), 6.15 (d, *J* = 2 Hz, 1 H, 4-H), 3.65 (quint, 1 H, tertiary H), 2.34 (m, 2 H, Cbu), 2.18 (m, 2 H, Cbu), 1.8−2.1 (m, 2 H, Cbu) ppm. ^{13}C NMR: δ = 18.8 (Cbu C-3), 29.7 (Cbu C-2), 33.9 (Cbu C-1), 102.7 (C-4), 136.0 (C-5), 158.9 (C-3) ppm. $C_{28}H_{36}BN_8Tl$ (699.55): calcd. C 48.1, H 5.15, N 16.0; found C 48.2, H 5.23, N 15.8.

Co[pz^oTp^{Cbu}]$_2$ (6): This complex was prepared from Tl[pz^oTp^{Cbu}] and $Co[ClO_4]_2{\cdot}(H_2O)_6$. It turns gradually deep purple above 150 °C, and melts at around 250 °C. ^{1}H NMR: δ = 63.9 (1 H), 34.8 (1 H), −5.0 (1 H), − 5.6 (1 H), −14.8 (16 H), −57 (1 H) ppm. $C_{56}H_{72}B_2CoN_{16}$ (1049.85): calcd. C 64.1, H 6.86, N 21.4; found C 63.9, H 6.92, N 21.2.

Co[pz^oTp^{Cpe}]$_2$ (7): This complex was prepared from Tl[pz^oTp^{Cpe}] and $Co[ClO_4]_2{\cdot}(H_2O)_6$. M.p. 251−253 °C. ^{1}H NMR: very broad

Table 2. Crystallographic data of compounds **1**−**7**

	1	**2**	**3**	**4**	**5**	**6**	**7**
Empirical formula	$C_{21}H_{28}BN_6Tl$	$C_{24}H_{34}BN_6Tl$	$C_{42}H_{56}B_2CoN_{12}$	$C_{48}H_{68}B_2CoN_{12}$	$C_{33}H_{44}B_2CoN_{12}$	$C_{56}H_{72}B_2CoN_{16}$	$C_{64}H_{88}B_2CoN_{16}$
Formula mass	579.67	621.75	809.5	893.69	689.4	1049.85	1162.05
Space group	$Pa\bar{3}$	$P2_1/c$	$Pnnm$	$P\bar{1}$	$P2_1/n$	$P2_1/c$	$P2_1/n$
a [Å]	16.5976(1)	26.5969(2)	11.932(5)	9.1733(5)	13.741(4)	10.9923(4)	10.4526(5)
b [Å]	???	16.3566(1)	12.580(6)	11.3770(6)	15.592(3)	19.0910(7)	41.7982(19)
c [Å]	???	18.3532(2)	13.669(8)	11.7241(6)	17.279(4)	12.9080(5)	14.9597(7)
α [°]	???	???	???	76.188(1)	???	???	???
β [°]	???	105.793(1)	???	78.193(1)	104.93(2)	98.674(1)	109.851(1)
γ [°]	???	???	???	87.916(1)	???	???	???
V [Å^3]	4572.31(5)	7682.88(11)	2052(2)	1163.0(1)	3577(2)	2677.8(2)	6147.3(5)
Z/Z'	24/8	4/12	8/2	2/1	4/4	4/2	4/4
Crystal color, habit	colorless, block	colorless, block	yellow, block	yellow, block	yellow, cube	yellow, block	purple, plate
D(calcd.) [g cm^{-3}]	1.684	1.613	1.310	1.276	1.280	1.302	1.256
μ(Mo-K_α) [cm^{-1}]	7.083	6.329	4.66	4.17	5.22	3.75	3.34
T [K]	173(2)	203(2)	298	120.0(0.1)	298	120.0(0.1)	173.0(0.1)
Diffractometer	Siemens P4	Siemens P4	Siemens P4	Bruker Smart Apex CCD	Siemens P4	Bruker Smart Apex CCD	Bruker Smart Apex CCD
Radiation	Mo-K_α (λ = 0.71073 Å)	Mo-K_α (λ = 0.71073 Å)	Mo-K_α (λ = 0.71073 Å)	Mo-K_α (λ = 0.71073 Å)	Mo-K_α (λ = 0.71073 Å)	Mo-K_α (λ = 0.71073 Å)	Mo-K_α (λ = 0.71073 Å)
$R(F)$ (%)[a]	2.32	6.82	5.80	4.08	3.81	5.94	9.37
$R(wF^2)$ (%)[b]	4.85[c]	16.06	9.09[c]	10.65	4.00[c]	15.98	21.92

[a] $R=\|\|F_o\| - |F_c\|\|/|F_o|$. [b] $R(wF^2)=\{[w(F_o^2 - F_c^2)^2]/[w(F_o^2)^2]\}^{1/2}$; $w=1/[\sigma^2(F_o^2) + (aP)^2 + bP]$, $P = [2F_c^2 + \max(F_o,0)]/3$. [c] $R(wF)=\{[w(|F_o| - |F_c|)^2]/[wF_o^2]\}^{1/2}$; $w=1/\sigma^2(F_o)$.

peaks at δ = 70, 36, 30, 16, −10, −26 ppm, with a very large indistinct hump centered at δ = 5 ppm. $C_{64}H_{88}B_2CoN_{16}$ (1162.05): calcd. C 66.1, H 7.58, N 19.3; found C 65.9, H 7.70, N 19.0.

Zn[pz^{o}Tp^{Cbu}]$_2$: This complex was prepared from Tl[pz^{o}Tp^{Cbu}] and $Zn[ClO_4]_2{\cdot}(H_2O)_6$. M.p. 266−268 °C. ^{1}H NMR: δ = 6.86 (br. hump, 1 H, 5-H), 6.20 (d, 1 H, 4-H), 2.97 (very br. hump, 1 H, tertiary H), 1.66−2.10 (m, 6 H, cyclobutyl) ppm. ^{13}C NMR: δ = 18.5 (Cbu C-4), 29.7 (Cbu C-2,3), 33.7 (Cbu C-1), 102.9 (C-4), 138 (C-5), 161.1 (C-4) ppm. $C_{56}H_{72}B_2N_{16}Zn$ (1055.73): calcd. C 63.7, H 6.82, N 21.2; found C 64.0, H 6.98, N 21.0.

Zn[pz^{o}Tp^{Cpe}]$_2$: This complex was prepared from Tl[pz^{o}Tp^{Cpe}] and $Zn[ClO_4]_2{\cdot}(H_2O)_6$. M.p. 221−223 °C. ^{1}H NMR: δ = 7.15 (d, 2 H, 5-H), 6.33 (d, 2 H, 5-H), 6.07 (d, 2 H, 4-H), 5.94 (d, 2 H, 4-H), 3.08 (2 H, quint, Cpe 1-H), 2.17 (2 H, quint, Cpe 1-H), 1.95 (m, 4 H, Cpe), 1.4−1.8 (m, 20 H, Cpe), 1.27 (m, 8 H, Cpe) ppm. ^{13}C NMR: δ = 25.4, 33.6, 34.2, 37.7, 39.4, 102.1, 102.3, 133.4, 140.4, 159.5, 163.6 ppm. $C_{64}H_{88}B_2N_{16}Zn$ (1.167.81): calcd. C 65.8, H 7.54, N 19.2; found C 66.0, H 7.71, N 19.1.

X-ray Crystal Structure Determinations: Diffraction intensity data were collected with Siemens P4 (**1**−**3**, **5**) and Bruker Smart Apex CCD (**4**, **6**, **7**) diffractometers. Crystal, data collection, and refinement parameters are given in Table 2. The systematic absences in the diffraction data of **1**−**3**, **5**−**7** structures are uniquely consistent with the reported space groups. The space group for **4** has been chosen by intensity statistics. The structures were solved by direct methods (**1**−**6**) and the Patterson function (**7**), completed by subsequent Fourier syntheses and refined by full-matrix, least-squares procedures on reflection intensities (F^2). SADABS absorption corrections were applied to the data of **1**, **3**−**6** and DIFABS[22] corrections to the data of **2** (T_{min} = 0.48, T_{max} = 1.00) and **7** (T_{min} = 0.28, T_{max} = 1.00).[23] All non-hydrogen atoms were refined with anisotropic displacement coefficients, and hydrogen atoms were treated as idealized contributions. In the structure of **6**, two C_4 rings are disordered in two positions with occupation multiplicity μ = 0.60, 0.40 and 0.59, 0.41, respectively. All software and sources scattering factors are contained in the SHELXTL (5.10) program package (G. Sheldrick, Bruker XRD, Madison, WI). CCDC-178940 (**1**), -178941 (**2**), -178942 (**3**), -178943 (**4**), -178944 (**5**), -178945 (**6**) and -178946. (**7**) contain the supplementary crystallographic data for this paper. These data can be obtained free of charge at www.ccdc.cam.ac.uk/conts/retrieving.html or from the Cambridge Crystallographic Data Centre, 12, Union Road, Cambridge CB2 1EZ, UK [Fax: (internat.) + 44-1223/336-033; E-mail: deposit@ccdc.cam.ac.uk].

[1] S. Trofimenko, *Scorpionates: The Coordination Chemistry of Polypyrazolylborate Ligands*, Imperial College Press, London, **1999**.
[2] A. L. Rheingold, L. M. Liable-Sands, S. Trofimenko, *Chem. Commun.* **1997**, 1691−1962.
[3] A. L. Rheingold, G. P. A. Yap, L. M. Liable-Sands, I. A. Guzei, S. Trofimenko, *Inorg. Chem.* **1997**, *36*, 6261−6265.
[4] A. L. Rheingold, B. S. Haggerty, S. Trofimenko, *Angew. Chem. Int. Ed. Engl.* **1994**, *33*, 1983−1985.
[5] X. Liu, L. M. L. Chia, C. A. Kilner, L. J. Yellowlees, M. Thornton-Pitt, S. Trofimenko, M. A. Halcrow, *Chem. Commun.* **2000**, 1947−1948.
[6] M. A. Halcrow, C. A. Kilner, M. Thornton-Pett, *Acta Crystallogr., Sect. C* **2001**, *57*, 711−713.
[7] S. Trofimenko, A. L. Rheingold, L. M. Liable-Sands, *Inorg. Chem.* **2002**, *41*, 1889−1896.
[8] M. M. Díaz-Requejo, T. R. Belderraín, S. Trofimenko, P. Pérez, *J. Am. Chem. Soc.* **2001**, *123*, 3167−3168.
[9] M. M. Díaz-Requejo, M. A. Mairena, T. R. Belderraín, N. C. Nicasio, S. Trofimenko, P. Pérez, *Chem. Commun.* **2001**, 1804−1805.
[10] S. Trofimenko, J. C. Calabrese, P. J. Domaille, J. S. Thompson, *Inorg. Chem.* **1989**, *28*, 1091−1101.
[11] L. M. Liable-Sands, PhD Dissertation, University of Delaware, **2000**.

[12] C. Janiak, *Coord. Chem. Rev.* **1997**, *163*, 107−216.
[13] M. R. Churchill, K. Gold, C. E. Maw, Jr., *Inorg. Chem.* **1970**, *9*, 1597−1604.
[14] A. L. Rheingold, L. M. Liable-Sands, C. L. Incarvito, S. Trofimenko, *J. Chem. Soc., Dalton Trans.,* in press.
[15] The sensitivity of the chemical shifts of protons in octahedral Tp-derived Co^{II} complexes to their position with respect to the cobalt atom is such that a 5° angular variation at a constant distance of 3 Å results in an 11 ppm change of the chemical shift, while a 0.1 Å distance change at a constant angle of 110° produces a 13 ppm shift. [15a] G. N. Lamar, J. P. Jesson, P. J. Meakin, *J. Am. Chem. Soc.* **1971**, *93*, 1286−1288. [15b] P. J. Domaille, *J. Am. Chem. Soc.* **1980**, *102*, 5392−5393.
[16] J. C. Calabrese, S. Trofimenko, *Inorg. Chem.* **1992**, *31*, 4810−4814.
[17] J. P. Jesson, S. Trofimenko, D. R. Eaton, *J. Am. Chem. Soc.* **1967**, *89*, 3148−3158.
[18] J. C. Calabrese, P. J. Domaille, S. Trofimenko, G. J. Long, *Inorg. Chem.* **1991**, *30*, 2795−2801.
[19] A. L. Rheingold, L. M. Liable-Sands, S. Trofimenko, *Inorg. Chem.* **2001**, *40*, 6509−6513.
[20] A. L. Rheingold, B. S. Haggerty, G. P. A. Yap, S. Trofimenko, *Inorg. Chem.* **1997**, *36*, 5097−5103.
[21] S. Trofimenko, A. L. Rheingold, unpublished work.
[22] N. Walker, D. Stuart, *Acta Crystallogr., Sect. A* **1983**, *39*, 158.
[23] Confronted with a difficult correction for absorption, a prudent crystallographer will sample the output of the many programs at his disposal, and then select the one that does the job best. In the realm of empirical and semi-empirical correction schemes, many programs have been written, some old and some new. Each analyzes the data in a somewhat different way, and each can produce different results. While DIFABS may be one of the older methods, it is, on occasion, the one that performs best, and because its routines are well known and some newer routines are undocumented "black boxes," its idiosyncrasies are also well known. We are unaware that anyone has declared DIFABS ineffective or fatally flawed, and until such time, it is a useful procedure that we intend to keep using.
[24] A. L. Rheingold, L. M. Liable-Sands, S. Trofimenko, *Inorg. Chem.* **2000**, *39*, 1333−1335.

Received February 27, 2002
[I02103]

Europium(II) Complexes With Benzo-18-Crown-6[‡]

Przemysław Starynowicz,*[a] Krystyna Bukietyńska,[a] Stanisław Gołąb,[b] Witold Ryba-Romanowski,[b] and Jerzy Sokolnicki[a]

Keywords: Europium / Lanthanides / Crown compounds / X-ray diffraction / Luminescence

Two compounds of Eu^{II} with benzo-18-crown-6, triaqua(benzo-18-crown-6)europium(II) diperchlorate (**1**) and triaqua(benzo-18-crown-6)europium(II) perchlorate hydrate benzo-18-crown-6 solvate (**2**), were synthesized by electrochemical reduction. The coordination environment of the metal cation in both cases contains six O atoms of the crown ligand and three water molecules. The first complex display strong blue luminescence with a maximum at 425 nm. The excitation spectra do not show any significant energy transfer from the benzo rings to europium.
(© Wiley-VCH Verlag GmbH, 69451 Weinheim, Germany, 2002)

Introduction

Crown ethers have attracted much attention owing to their specific and selective coordination of metal ions. Encapsulation of the metal by the ligand provides at least partial protection from the influence of other reagents that may be present in the system. Therefore crown ethers seem to be a promising class of ligands that may stabilize otherwise unstable entities such as divalent lanthanides. Compounds of divalent lanthanides (mainly Eu^{2+}) with crown ethers have therefore attracted much attention; the present state of the investigations on such complexes was excellently reviewed by Adachi et al.[1] The interest in these compounds arises both due to the luminescent properties of the Eu^{2+} cation in the macrocyclic coordination environment and by the ability of the ligand to stabilize the divalent oxidation state of the lanthanide. The encapsulation effected by the crown ethers leads to an increase of the luminescence quantum yield in comparison with noncyclic polyethers. The other interesting feature of the discussed complexes is their ability to shift the reduction potential of the Eu^{III}/Eu^{II} couple towards more positive values,[2] which may eventually open a way to the application of these compounds or their derivatives as redox-sensitive shift agents in MRI tomography. It is therefore important and very interesting to collect information about the structures and properties of macrocyclic complexes of Eu^{II} both in solution and in the solid state. In previous work[3] we have described the structure of bis(benzo-15-crown-5)europium(II) diperchlorate. This work, which is a continuation of our investigations on the structure and spectroscopy of Eu^{II} complexes with crown ethers in the solid state, deals with two other complexes: triaqua(benzo-18-crown-6)europium(II) diperchlorate (**1**) and triaqua(benzo-18-crown-6)europium(II) perchlorate hydrate benzo-18-crown-6 solvate (**2**).

[‡] Europium(II) Complexes With Benzo-18-Crown-6, Part 2. For part 1 see ref.[3]

[a] Wydział Chemii, Uniwersytet Wrocławski,
ul. F. Joliot-Curie 14, 50-383 Wrocław, Poland
Fax: (internat.) +48-71/328-2348
E-mail: psta@wchuwr.chem.uni.wroc.pl
[b] Instytut Niskich Temperatur i Badań Strukturalnych PAN,
ul. Okßlna 2, 50-422 Wrocław, Poland

Results and Discussion

Structures

Crystals of **1** are composed of complex trisaqua(benzo-18-crown-6)europium(II) cations and perchlorate anions, and they are isomorphic with the analogous compound of Sr.[4] Crystals of **2**, apart from the same constituents as in **1**, also contain other, uncoordinated, benzo-18-crown-6 molecules and water of crystallization. The coordination environment of europium is essentially the same in both crystals and consists of three water molecules and six oxygen atoms from the macrocycle ring. The coordination figure in either case is rather irregular. The roughly equatorial positions are occupied by the crown oxygen atoms, whereas two water molecules (OW2 and OW3) are located in axial positions on one side of the equatorial plane, and the third water molecule (OW1) is located in an axial position at the opposite side. A similar coordination geometry is also typical for nine-coordinate compounds of Ln^{III} with 18-crown-6 derivatives, for example triiodo(dibenzo-18-crown-6)samarium,[5] trichloro(18-crown-6)lanthanum(III),[6] and numerous dichloro(18-crown-6)lanthanide(III) solvates (e.g. water or an alcohol)[6–10] or chloro(18-crown-6)lanthanide(III) disolvates.[6,9,11–13] The Eu–O distances, presented

Table 1. The Eu−O distances (Å) for **1** and **2**

1		2	
Eu−OW1	2.584(3)	Eu−OW2	2.576(3)
Eu−OW2	2.592(3)	Eu−OW1	2.584(3)
Eu−OW3	2.596(3)	Eu−OW3	2.624(3)
Eu−O(4)	2.660(3)	Eu−O(3)	2.633(3)
Eu−O(2)	2.671(3)	Eu−O(2)	2.651(3)
Eu−O(3)	2.682(3)	Eu−O(5)	2.656(3)
Eu−O(6)	2.693(3)	Eu−O(6)	2.663(3)
Eu−O(5)	2.695(3)	Eu−O(4)	2.698(3)
Eu−O(1)	2.741(3)	Eu−O(1)	2.757(3)

in Table 1, are rather long in comparison with other Eu^{II}−O bond lengths. Their average values are the following: $Eu-O_{crown}$ = 2.690(29) Å for **1** and 2.676(45) Å for **2**, $Eu-O_{water}$ = 2.591(7) Å for **I** and 2.595(26) Å for **2**. These quantities compare well with the relevant values for the isomorphic Sr compound: $Sr-O_{crown}$ = 2.683(22) Å, and $Sr-O_{water}$ = 2.568(14) Å.[4] On the other hand it is interesting to see the difference between the analogous Eu^{II} and Eu^{III} complexes. For chlorodiaqua(18-crown-6)europium(III) cations[6,9] the overall mean $Eu-O_{crown}$ distance is 2.536(50) Å, and the $Eu-O_{water}$ distance is 2.424(35) Å. The differences between the values for our Eu^{II} compounds and the Eu^{III} complexes quoted above are in good agreement with the difference between the ionic radii of Eu^{2+} and Eu^{3+} for nine-coordinate compounds (0.18 Å).[14] It is noteworthy that in all the discussed complexes the water molecules are closer to the metal ion than the crown oxygen atoms. The cavity in the unligated crown molecule in **2** remains empty, although OW3 and the uncoordinated OW4 water molecule approach it somewhat (OW3 forms a hydrogen bond with O42, and OW4 interacts in the same way with O43). The coordination of Eu in **1** is shown in Figure 1, and a fragment of **2** is shown in Figure 2. Both crystals are held together by hydrogen bond networks, and electrostatic and Van der Waals interactions.

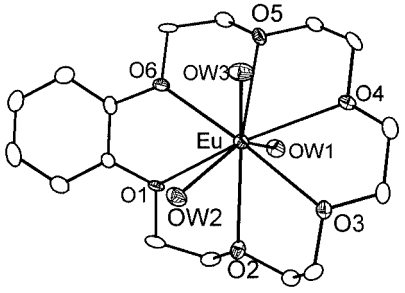

Figure 1. A view of the complex cation in **1**, together with labelling of the metal first coordination sphere

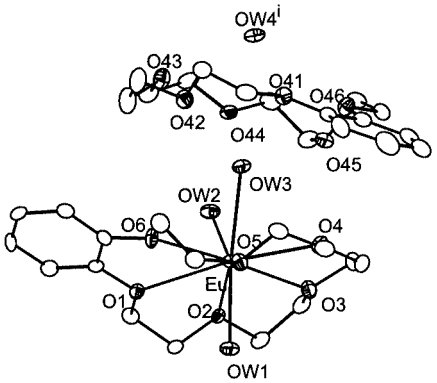

Figure 2. A view of a fragment of **2**; the labels are rendered for Eu and O atoms only for the sake of clarity; [i] represents the symmetry operation $-1/2 + x$, $1/2 - y$, $-1/2 + z$

Spectroscopy of 1

The compound displays bright blue luminescence with a maximum at 425 nm (23520 cm^{-1}) at room temperature, and at 430 nm (23260 cm^{-1}) at 77 K (see Figure 3). These values are similar to those reported for bis(benzo-15-crown-5)europium(II) diperchlorate[3] (422 and 426.5 nm, respectively) and remarkably different from the emission maximum observed for the complex formed from $EuCl_2$ and benzo-18-crown-6 in methanol (447 nm[1,15]). This difference may be due to several factors, such as: a) coordination of methanol instead of water, b) the possible coordination of Cl^-, and c) a different coordination number of the metal cation. The discrepancy between the present compound and the quoted complex in solution is manifested even more strikingly in the luminescence lifetimes of both systems. The luminescence lifetime of the $EuCl_2$/benzo-18-crown-6/methanol system was reported to be 0.028 μs. For the present compound the decay curves were measured at 293 and 77 K. At room temperature the decay is bi-exponential, with τ_1 = 8.34(6) μs and τ_2 = 137(11) μs; the decay equation may be expressed as: $I = I_0 \cdot \{0.890(3)\exp[-t/8.34(6)] + 0.110(3)\exp[-t/137(11)]\}$ the e.s.d.'s are given in parentheses. At 77 K the decay is a single exponential with a lifetime of 8.01(2) μs. The second, long lived component that appears at room temperature may be due to partial decomposition of the complex brought about by the laser flashes, and, accordingly, can be disregarded. The observed disparity between the τ values for the crystal and the solu-

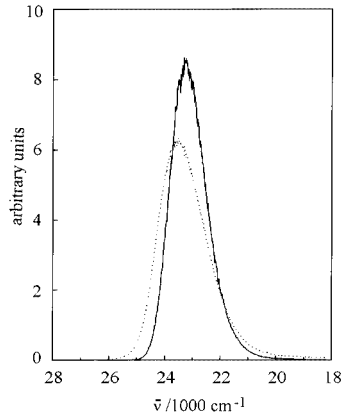

Figure 3. The emission spectrum of **1** at room temperature (dotted line) and at 77 K (solid line)

tion may be caused by several factors. We can safely eliminate the role of OH oscillators in the Eu first-coordination sphere, as they are present in both cases. Therefore the probable reasons for the discussed discrepancy are: a) internal rotations of the macrocycle ring, and b) the exchange dynamics of methanol molecules and possibly chloride anions. Finally, it is noteworthy that the luminescence lifetime for the present compound is an order of magnitude greater than that reported for the benzo-15-crown-5 complex (0.59 μs at 77 K).[3]

The excitation spectrum may be divided into two parts: one, larger, between 275 and 408 nm (24500−38900 cm^{-1}), and the other, smaller, between 230 and 275 nm (38900−43500 cm^{-1}). In the first part three maxima are discernible, at 392 nm (25510 cm^{-1}), 352 nm (28410 cm^{-1}) and 309 nm (32360 cm^{-1}). In the other part only one maximum can be identified at 248 nm (40320 cm^{-1}). The difference in wavenumbers between these and the lowest lying excited (emitting) level are 2250, 5150, 9100 and 17060 cm^{-1}, respectively. Using the simple approach of Johnson and Sandoe[16] we can interpret the first three maxima as being dominated mostly by $4f^6(^7F)5d$ states, whereas the last one, lying 17060 cm^{-1} above the emitting level, should include mainly the $4f^6(^5D)5d$ states, as the respective difference parallels that between the energies of the ^7F_J and ^5D_J levels in Eu^{3+}.

The excitation spectrum of **1**, juxtaposed with the absorption spectrum of the free ligand (Figure 4) shows no evidence for energy transfer from the benzo rings to the metal ion (the so called "antenna effect"), as no correspondence between the peaks in both spectra can be noticed.

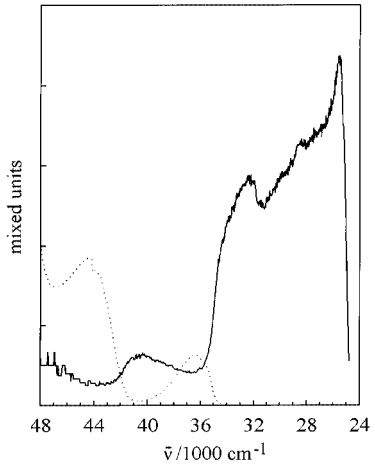

Figure 4. The excitation spectrum of **1** at 77 K (solid line), and the absorption spectrum of benzo-18-crown-6 in water/methanol solution (dotted line)

Conclusion

Two new complexes of Eu^{II} with benzo-18-crown-6 have been obtained in the crystalline state. In both complexes the metal ion is nine-coordinate and the coordination environment is composed of six O atoms belonging to the crown ligand and three water molecules. The spectroscopic properties are similar to those previously reported for a benzo-15-crown-5/Eu^{II} complex, with the exception of the luminescence lifetime, which is an order of magnitude larger in the present case. Both the emission maximum and luminescence lifetime are different from the analogous quantities reported for the $EuCl_2$/benzo-18-crown-6 complex in methanol solution.

Experimental Section

Preparation: a) Compound **1** was obtained by dissolving 0.5 g of Eu_2O_3 in $HClO_4$, evaporating the resulting solution until the evolution of white fumes, cooling down the resulting perchlorate, dissolving it in a 1:2 water/methanol mixture, and then adding 1 g of benzo-18-crown-6. The resulting solution was placed in the cathode compartment of an H-shaped electrolyzer with a sintered glass diaphragm and a pool Hg cathode. A dilute water/methanol (1:2) solution of $HClO_4$ was the anolyte. The reduction was performed at −1.2 V with respect to the saturated calomel electrode, and with a stream of N_2 passing slowly above the reduced solution. Colourless crystals of **1** formed after 1−2 days. The compound is unstable in air and begins to darken after ca. 10−15 min. $C_{16}H_{30}Cl_2EuO_{17}$ (717.26) calcd. C 26.8, H 4.2, Eu 21.2; found C 26.4, H 4.0, Eu 20.3. Compound **2** was the result of an unsuccessful attempt to prepare an acetate salt of the crown complex. The preparation was started from europium acetate, obtained by dissolving 0.5 g of Eu_2O_3 in concentrated acetic acid. The acetate was then dissolved in the water/methanol mixture and a few drops of moderately dilute $HClO_4$ were added to increase the solution conductivity. The synthesis continued similarly as in the case of **1**. The crystals of **2** were also colourless and unstable in air.

X-ray Crystallographic Study: Appropriate crystals were cut from larger ones and mounted on a Kuma KM4 diffractometer equipped with a CCD counter. The collected data were corrected for polarization, Lorentz and absorption effects; the latter were calculated from the crystal habits captured from photo scans. The positions of Eu were found from Patterson maps, and the rest of the non-H atoms from difference Fourier maps. The positions of the C-bonded hydrogen atoms were calculated geometrically. No attempt was made to localize the O-bonded H atoms The refinement was full-matrix with all non-H atoms anisotropic. The temperature factors of the H-atoms were constrained to 1.2 times the factors of the relevant C atoms. A peak with height of 2.0 e·$Å^{-3}$ (see Table 2) located 2.8 Å away from Eu and placed between OW2 and OW3, that appeared on the final residual difference Fourier map of **2**, was unrefinable, and therefore was not included in the model. The programs used were SHELXS-97[17] for the solution, SHELXL-97[18] for the refinement, and DIAMOND[19] for the molecular graphics. The data collection and refinement details are presented in Table 2.

Spectroscopy: The spectroscopic investigations for **1** only will be presented here. The luminescence and excitation spectra were taken on an SCL Aminco 500 spectrofluorimeter. The luminescence was excited with a lamp source with wavelength of 330 nm, and the excitation spectra were recorded for the emission at 425 nm. The luminescence decay curves were detected on a device equipped with a Hamamatsu photomultiplier and a Tektronix TDS-3052 digital oscilloscope. The sample was excited with the third harmonic of a neodymium laser (355 nm), and the registered output signal had

Table 2. Crystal data and structure refinement details

	1	**2**
Empirical formula	$C_{16}H_{30}Cl_2EuO_{17}$	$C_{32}H_{56}Cl_2EuO_{24}$
Molecular weight	717.26	1047.63
Temperature	100(2) K	100(2) K
Wave length	0.71073 Å	0.71073 Å
Crystal system, space group	monoclinic, $P2_1/n$	monoclinic, $P2_1/n$
Unit cell dimensions	a = 10.794(9) Å	a = 13.050(3) Å
	b = 21.397(16) Å	b = 17.633(3) Å
	c = 11.019(9) Å	c = 18.281(3) Å
	β = 94.74(6)°	β = 93.97(2)°
Volume	2536(4) Å^3	4196.6(14) Å^3
Z, calculated density	4, 1.878 Mg·m^{-3}	4, 1.658 Mg·m^{-3}
Absorption coefficient	2.762 mm^{-1}	1.710 mm^{-1}
F(000)	1436	2148
Crystal size	0.3 × 0.1 × 0.07 mm	0.3 × 0.15 × 0.1 mm
Theta range for data collection	3 to 28.5°	3 to 28°
Index ranges	$-14 \le h \le 12$, $-28 \le k \le 27$, $-14 \le l \le 13$	$-17 \le h \le 16$, $-20 \le k \le 23$, $-22 \le l \le 24$
Reflections collected/unique	16685/5885 (R_{int} = 0.0398)	27320/9774 (R_{int} = 0.0540)
Completeness to 2θ = 28.5°	89.2%	89.5%
Absorption correction		calculated from the crystal shape
Max. and min. transmission	0.804 and 0.550	0.874 and 0.674
Refinement method		full-matrix least-squares on F^2
Data/restraints/parameters	5885/ 0/ 325	9774/ 0/ 532
Goodness-of-fit on F^2	1.530	1.291
Final R indices [$I > 2\sigma(I)$]	$R(F)$ = 0.0451, $R_w(F^2)$ = 0.0534	$R(F)$ = 0.0595, $R_w(F^2)$ = 0.0570
R indices (all data)	$R(F)$ = 0.0637, $R_w(F^2)$ = 0.0552	$R(F)$ = 0.1015, $R_w(F^2)$ = 0.0628
Largest diff. peak and hole	1.091 and −0.666 e·Å^{-3}	2.178 and −2.000 e·Å^{-3}

23550 cm^{-1}. All the measurements (luminescence, excitation and life times) were recorded at room and 77 K temperatures. The absorption spectrum of a 2 × 10^{-4} M water/methanol (1:1) solution of the free ligand was recorded on a Cary 50 spectrophotometer.

CCDC-181112 (**1**) and CCDC-181113 (**2**) contain the supplementary crystallographic data for this paper. These data can be obtained free of charge at www.ccdc.cam.ac.uk/conts/retrieving.html [or from the Cambridge Crystallographic Data Centre, 12, Union Road, Cambridge CB2 1EZ, UK; Fax: (internat.) +44-1223/336-033; E-mail: deposit@ccdc.cam.ac.uk].

Acknowledgments

The authors thank D.Sci. Z. Ciunik for help in performing the X-ray measurements

[1] J. Jiang, N. Higashiyama, K. Machida, G.-y. Adachi, *Coord. Chem. Rev.* **1998**, *170*, 1−29.
[2] N. Higashiyama, K. Machida, G.-y. Adachi, *Chem. Express* **1992**, *7*, 113−116.
[3] P. Starynowicz, K. Bukietyńska, *Eur. J. Inorg. Chem.* **2002**, 1835−1838.
[4] D. L. Hughes, C. L. Mortimer, M. R. Truter, *Inorg. Chim. Acta* **1978**, *29*, 43−55.
[5] C. Runschke, G. Meyer, *Z. Anorg. Allg. Chem.* **1997**, *623*, 981−984.
[6] R. D. Rogers, A. N. Rollins, R. D. Etzenhouser, E. J. Voss, C. B. Bauer, *Inorg. Chem.* **1993**, *32*, 3451−3462.
[7] E. Forsellini, F. Benetollo, G. Bombieri, A. Cassol, G. De Paoli, *Inorg. Chim. Acta* **1985**, *109*, 167−171.
[8] G. R. Willey, P. R. Meehan, M. D. Rudd, H. J. Clase, N. W. Alcock, *Inorg. Chim. Acta* **1994**, *215*, 209−213.
[9] H. Hassaballa, J. W. Steed, P. C. Junk, M. R. J. Elsegood, *Inorg. Chem.* **1998**, *37*, 4666−4671.
[10] G. R. Willey, P. R. Meehan, P. A. Salter, M. G. B. Drew, *Polyhedron* **1996**, *15*, 4227−4232.
[11] R. D. Rogers, L. K. Kurihara, *Inorg. Chem.* **1987**, *26*, 1498−1502.
[12] R. D. Rogers, L. K. Kurihara, E. J. Voss, *Inorg. Chem.* **1987**, *26*, 2360−2365.
[13] R. D. Rogers, A. N. Rollins, R. F. Henry, J. S. Murdoch, R. D. Etzenhouser, S. E. Huggins, L. Nunez, *Inorg. Chem.* **1991**, *30*, 4946−4954.
[14] R. D. Shannon, *Acta Crystallogr., Sect. A* **1976**, *32*, 751−769.
[15] G. Adachi, K. Sorita (K. Sakai), K. Kawata, K. Tomiyoko, J. Shiokawa, *J. Less-Common Met.* **1983**, *93*, 81−87.
[16] K. E. Johnson, J.N. Sandoe, *J. Chem. Soc. (A)* **1969**, 1694−1697.
[17] G. M. Sheldrick, SHELXS-97. Program for structure solution. University of Göttingen, 1997.
[18] G. M. Sheldrick, SHELXL-97. Program for structure refinement. University of Göttingen, 1997.
[19] DIAMOND − Visual Crystal Structure Information System, CRYSTAL IMPACT, Postfach 1251, D-53002 Bonn, Germany.

Received March 15, 2002
[I02136]

Electrochemical Synthesis of Cobalt Complexes with 4-Methyl-*N*-(2-pyridylmethyl)benzenesulfonamide (HL) − Crystal Structures of HL, $[Co^{II}L_2]$ and $[Co^{III}L_2L^o]$ [L^o = {$HNC(CH_3)$}$_2C(CN)$]

María L. Durán,[a] Jose A. García-Vázquez,*[a] Cristina Gómez,[a] Antonio Sousa-Pedrares,[a] Jaime Romero,[a] and Antonio Sousa*[a]

Keywords: Cobalt / Electrochemistry / N ligands / X-ray crystal structures

Electrochemical oxidation of cobalt in a solution of 4-methyl-*N*-(2-pyridylmethyl)benzenesulfonamide (HL, **1**) in acetonitrile afforded the compounds $[Co^{II}L_2]$ (**2**) or $[Co^{III}L_2L^o]$ (**3**). When 2,2′-bipyridine (bipy) or 1,10-phenanthroline (phen) was added to the electrolytic phase, $[Co^{II}L_2bipy]$ (**4**) and $[Co^{II}L_2phen]$ (**5**) were obtained. The crystal structures of HL (**1**), $[Co^{II}L_2]$ (**2**) and $[Co^{III}L_2L^o]$ (**3**) were determined by X-ray diffraction techniques. The compound $[Co^{II}L_2]$ is mononuclear and has a distorted tetrahedral $[CoN_4]$ geometry, with each amide ligand acting as an anionic ($N_{amide}N_{py}$) bidentate ligand. In the monomeric complex $[Co^{III}L_2L^o]$ the cobalt atom is in a distorted octahedral $[CoN_6]$ environment defined by the amide and pyridyl nitrogen atoms of two L^- anionic ligands and the two nitrogen atoms of the NH groups of a new anionic ligand L^o, which is formed by trimerisation of three acetonitrile molecules in the electrolytic cell. The electronic, IR and FAB spectra of the compounds are discussed.

(© Wiley-VCH Verlag GmbH, 69451 Weinheim, Germany, 2002)

Introduction

Electrochemical procedures have been widely used for the synthesis of metal complexes, especially when the ligands have weakly acidic organic donor groups. It is well known that metal complex formation by substitution of the amide proton by a metal ion is not an easy process.[1] However, the presence of an additional donor atom in the molecule allows the formation of a stable five- or six-membered chelate ring with the metal ion[2] and this situation may facilitate the complexation process. In addition, the presence of a tosyl group in the amide increases the acidity of the amide hydrogen atom, making the formation of the anionic ligand easier.[3]

The work described here is a continuation of our previous studies on metal complexes with ligands containing a pyridyl ring and a tosylamide group.[4] This paper describes the preparation of the ligand [4-methyl-*N*-(2-pyridylmethyl)benzenesulfonamide] (HL, **1**) (Scheme 1), and the cobalt complexes $[Co^{II}L_2]$ (**2**), $[Co^{II}L_2L']$ [where L′ is 2,2′-bipyridine (bipy) (**4**), 1,10-phenanthroline (phen) (**5**) and $[Co^{III}L_2L^o]$ (**3**), where L^o (Scheme 1) represents the anionic form of an additional ligand formed during the electrochemical process by trimerisation of three molecules of acetonitrile.

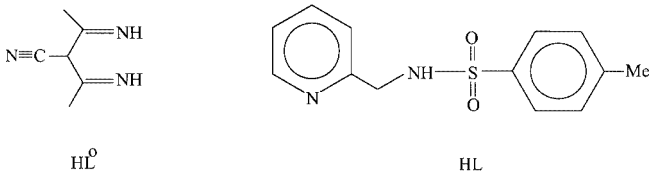

Scheme 1

Results and Discussion

The ligand [4-methyl-*N*-(2-pyridylmethyl)benzenesulfonamide] (HL) was prepared by a standard procedure, by treatment of 2-(aminomethyl)pyridine with *p*-toluenesulfonyl chloride in the presence of base. An interesting feature of the ^1H NMR spectrum of the ligand is the signal at δ = 11.6 ppm for the NH proton in $CDCl_3$; for simple sulfonamides of the form RSO_2NH-Ar this resonance normally appears at $\delta \approx 7$ ppm. The observed difference was probably due to the presence in solution of an intramolecular hydrogen bonding interaction between the NH group and the pyridine nitrogen atom. The same explanation can also be put forward to explain the very lowfield resonance of the OH proton in the case of the salicylaldimines.

Molecular Structure of the Ligand HL (1)

The molecular structure of [HL] is shown in Figure 1, together with the adopted atomic numbering scheme. Selected bond lengths and angles are given in Table 1.

[a] Departamento de Química Inorgánica, Universidad de Santiago de Compostela,
15782 Santiago de Compostela, Spain
E-mail: qiansoal@usc.es

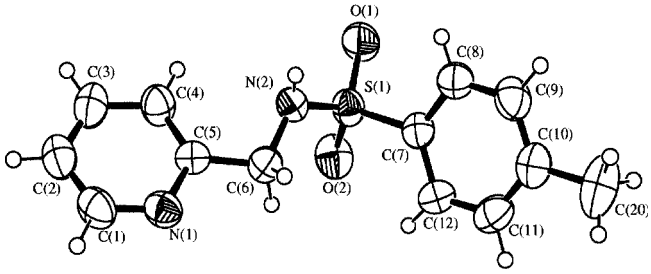

Figure 1. Perspective view of HL (50% probability displacement ellipsoids)

Table 1. Selected bond lengths [Å] and angles [°] for the ligand [HL]

S(1)−O(2)	1.419(4)	S(1)−O(1)	1.432(4)
S(1)−N(2)	1.603(5)	S(1)−C(7)	1.763(5)
N(1)−C(1)	1.341(7)	N(1)−C(5)	1.344(6)
N(2)−C(6)	1.447(7)	C(1)−C(2)	1.358(9)
C(2)−C(3)	1.357(10)	C(3)−C(4)	1.388(8)
C(4)−C(5)	1.372(8)	C(5)−C(6)	1.515(7)
C(7)−C(12)	1.389(8)	C(7)−C(8)	1.394(8)
C(8)−C(9)	1.377(9)	C(9)−C(10)	1.372(9)
C(10)−C(11)	1.387(9)	C(10)−C(20)	1.505(8)
C(11)−C(12)	1.3376(9)		
O(2)−S(1)−O(1)	119.7(3)	O(2)−S(1)−N(2)	107.5(3)
O(1)−S(1)−N(2)	106.1(3)	O(2)−S(1)−C(7)	108.1(3)
O(1)−S(1)−C(7)	107.5(3)	N(2)−S(1)−C(7)	107.4(3)
C(1)−N(1)−C(5)	117.3(5)	C(6)−N(2)−S(1)	122.5(4)
N(1)−C(1)−C(2)	124.5(6)	C(3)−C(2)−C(1)	117.7(6)
C(2)−C(3)−C(4)	120.0(7)	C(5)−C(4)−C(3)	118.9(7)
N(1)−C(5)−C(4)	121.6(5)	N(1)−C(5)−C(6)	115.1(5)
C(4)−C(5)−C(6)	123.3(5)	N(2)−C(6)−C(5)	111.4(5)
C(12)−C(7)−C(8)	120.7(6)	C(12)−C(7)−S(1)	120.9(5)
C(8)−C(7)−S(1)	118.4(5)	C(9)−C(8)−C(7)	118.7(7)
C(10)−C(9)−C(8)	122.1(7)	C(9)−C(10)−C(11)	117.9(6)
C(9)−C(10)−C(20)	121.5(7)	C(11)−C(10)−C(20)	120.7(7)
C(12)−C(11)−C(10)	122.2(7)	C(11)−C(12)−C(7)	118.4(6)

The bond lengths and bond angles of the phenyl and pyridine rings are similar to those found in other pyridylbenzenesulfonamide ligands.[5−9] The C(6)−N(2) and S(1)−N(2) distances [1.447(7) and 1.603(5) Å] are very close to those observed in *N*-(*p*-tolylsulfonyl)benzylamine [1.475(3) and 1.619(2) Å].[10]

The phenyl and pyridine rings are almost flat, with the maximum deviation of any atom from the best least-squares planes being 0.010(5) and 0.011(4) Å, respectively. The carbon atom C(20) and the sulfur atom S(1) lie approximately in the plane of the phenyl ring to which they are bound [deviation of 0.022(10) Å for C(20) and 0.019(7) Å for S(1)]. Atom C(6) is also out of the plane of the pyridine ring to which it is bound [0.102(10) Å]. The interplanar angle between the phenyl and pyridine rings is 55.7°.

The crystal structure is completed by half a water molecule, which is associated with the ligand molecules through intermolecular hydrogen bonds. Hydrogen bonds exist between the pyridine nitrogen atoms of two ligand molecules and the oxygen atom of the water molecule. In addition, the oxygen atom of the water molecule is involved in a hydrogen bond with the amide nitrogen atoms of two other neighbouring ligands. Therefore, infinite hydrogen bonded chains of ligand and water molecules are formed in this system (Table 2).

Table 2. Hydrogen bonds in the ligand

Atoms: A···HD	*d*(A···H)	*d*(H−D)	*d*(A···D)	< AHD
O3···H(20)−N(2)	2.168(5)	0.74(5)	2.880(7)	161.77(6)
N(1)#···H(31)−O(3)	1.824(7)	0.97(7)	2.775(6)	166.24(6)

Cobalt Complexes

The cobalt complex $[Co^{II}L_2]$ and its adducts with 2,2′-bipyridine (bipy) and 1,10-phenanthroline (phen) − $[Co^{II}L_2(bipy)]$ and $[Co^{II}L_2(phen)]$, respectively − were prepared in good yield by the simple one-step electrochemical method described below. In all cases, the product formed was separated by filtration as a crystalline product. In addition, all of the compounds were air-stable and moderately soluble in organic solvents such as ethanol or chloroform.

The values of the electrochemical efficiency, defined as the amount of metal dissolved per Faraday of charge, were all close to 0.5 mol·F^{-1}, irrespective of the presence or absence of additional ligands. This fact, in conjunction with the evolution of hydrogen at the cathode, is compatible with the following mechanism:

Cathode: $2\ HL + 2\ e^- \longrightarrow 2\ L^- + H_2$

Anode: $Co + 2\ L^- \longrightarrow [Co^{II}L_2] + 2\ e^-$

or, when an additional neutral ligand (L′ = bipy or phen) is added:

Anode: $Co + 2\ L^- + L' \longrightarrow [Co^{II}L_2L'] + 2\ e^-$

When the electrochemical oxidation of cobalt metal in an acetonitrile solution of the amide ligand was carried out at a much higher voltage than in the previous case, the compound $[Co^{III}L_2L^{\circ}]$ was formed. In this compound, besides the deprotonated amide ligands, a new ligand, formed by trimerisation of three acetonitrile molecules, appears in the coordination sphere of the metal ion.

The trimerisation of acetonitrile can be viewed as the result of a tandem reaction catalysed by the nucleophilic attack of a tosylamide anion, formed during the electrochemical reaction, on an acetonitrile molecule, as shown in Scheme 2.

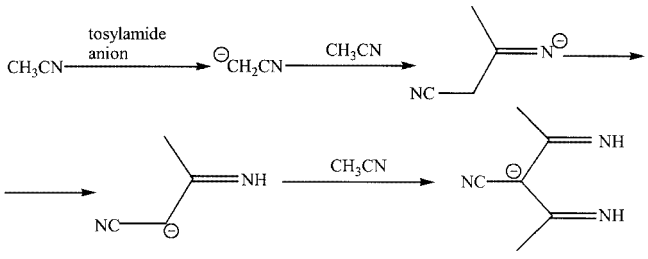

Scheme 2

It is most probable that these reactions occur in the coordination sphere of the metal ion, given the fact that they do not occur in its absence. The occurrence of this process may

be ascribed to the increased sensitivity of the acetonitrile molecule to nucleophilic attack as a result of coordination to the metal ion. This reaction can be considered as the intramolecular version of the Thorpe−Ziegler reaction.

The CH_3CN trimerisation process is not without precedent. It has previously been observed when MMe_3 (M = Al, Ga or In) was boiled for 24−72 h at 60−65 °C in acetonitrile in the presence of cesium halides ($X = F^-$, Cl^-, Br^-) to give $[CH_3M\{HNC(CH_3)\}_2C(CN)]$.[11,12]

Molecular Structure of $[Co^{II}L_2]$ (2)

The molecular structure of $[Co^{II}L_2]$ is shown in Figure 2, along with the adopted atomic numbering scheme. Selected bond lengths and angles are listed in Table 3. The structure of the complex consists of mononuclear units in which a tetracoordinated cobalt atom is bound to both nitrogen atoms of two bidentate monoanionic ligands in a distorted tetrahedral arrangement. Two different Co−N bond lengths are observed: the bonds involving amide nitrogen atoms [1.926(4), 1.946(4) Å] are significantly shorter than those involving pyridine nitrogen atoms [2.028(4), 2.040(4) Å]. These values are similar to those found in other cobalt compounds containing both anionic and neutral nitrogen donor atoms, such as in the tetrahedral complex [2-tosylamino(2′-pyridyl)anilinato]cobalt(II) [Co−N_{amide}, 1.959(13) Å][13] or in the cobalt(II) complex with the ligand obtained by the reaction between 2-(2-aminophenyl)pyridine with *p*-toluenesulfonyl chloride[3] [Co−N_{amide} 1.960(2), 1.967(2) Å; Co−$N_{pyridine}$ 2.041(2), 2.043(2) Å]. The tetrahedral environment of the cobalt atom is distorted due to the small bite required by N−Co−N = 81.37(16)−82.08(16)°, which also results in secondary deviation of the other perinuclear angles from the ideal values of 109°. Each five-membered chelate ring lies in a plane with the maximum deviation of any atom from this plane being 0.0004 and 0.0165 Å. The two planes are nearly perpendicular, with a dihedral angle of 82.11°. In each ligand the phenyl and pyridine rings are planar.

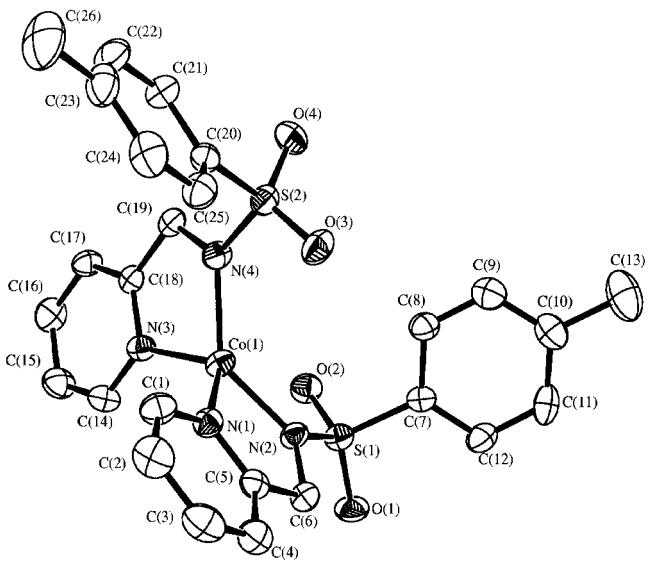

Figure 2. Perspective view of $[Co^{II}L_2]$ (50% probability displacement ellipsoids)

Table 3. Selected bond lengths [Å] and angles [°] for the complex $[Co^{II}L_2]$

Co(1)−N(2)	1.926(4)	Co(1)−N(4)	1.946(4)
Co(1)−N(3)	2.028(4)	Co(1)−N(1)	2.040(4)
S(1)−O(2)	1.449(3)	S(1)−O(1)	1.452(3)
S(1)−N(2)	1.577(4)	S(1)−C(7)	1.768(5)
S(2)−O(3)	1.437(3)	S(2)−O(4)	1.446(3)
S(2)−N(4)	1.586(4)	S(2)−C(20)	1.772(5)
N(1)−C(5)	1.335(6)	N(1)−C(1)	1.352(6)
N(2)−C(6)	1.476(5)	N(3)−C(18)	1.355(6)
N(3)−C(14)	1.355(6)	N(4)−C(19)	1.459(5)
C(1)−C(2)	1.372(7)	C(2)−C(3)	1.353(8)
C(3)−C(4)	1.377(7)	C(4)−C(5)	1.386(6)
C(5)−C(6)	1.497(6)	C(7)−C(12)	1.376(6)
C(7)−C(8)	1.382(6)	C(8)−C(9)	1.379(7)
N(2)−Co(1)−N(4)	134.84(17)	N(2)−Co(1)−N(3)	123.64(16)
N(4)−Co(1)−N(3)	81.37(16)	N(2)−Co(1)−N(1)	82.08(16)
N(4)−Co(1)−N(1)	117.84(16)	N(3)−Co(1)−N(1)	122.65(16)
O(2)−S(1)−O(1)	117.6(2)	O(2)−S(1)−N(2)	105.4(2)
O(1)−S(1)−N(2)	113.1(2)	O(2)−S(1)−C(7)	106.1(2)
O(1)−S(1)−C(7)	106.6(2)	N(2)−S(1)−C(7)	107.5(2)
O(3)−S(2)−O(4)	118.1(2)	O(3)−S(2)−N(4)	107.0(2)
O(4)−S(2)−N(4)	111.5(2)		

Molecular Structure of $[Co^{III}L_2L^o]$ (3)

The molecular structure of $[Co^{III}L_2L^o]$ is shown in Figure 3, together with the adopted atomic numbering scheme. The main bond lengths and angles are given in Table 4. The structure consists of monomer $[Co^{III}L_2L^o]$ units. The cobalt atom is in a $[CoN_6]$ environment produced by two amide and two pyridine nitrogen atoms of two bidentate monoanionic tosylamide ligands and two nitrogen atoms of the ligand L^o, formed by the trimerisation of three molecules of the acetonitrile used as the solvent in the electrochemical cell. Both amide nitrogen atoms are in a *trans* disposition.

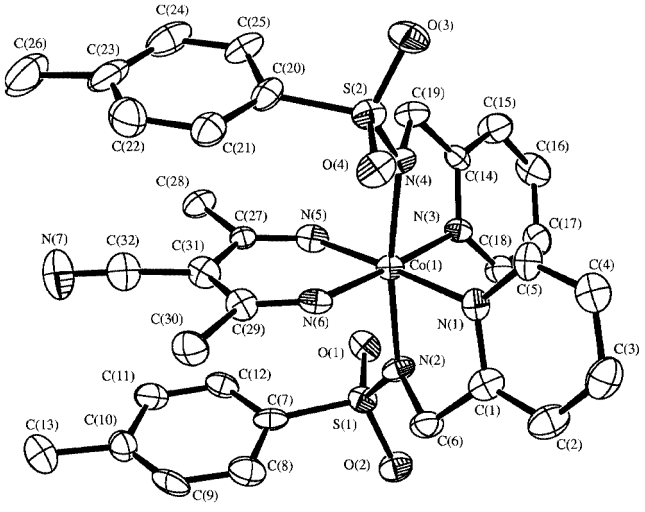

Figure 3. Perspective view of $[Co^{III}L_2L^o]$ (50% probability displacement ellipsoids)

Table 4. Selected bond lengths [Å] and angles [°] for the complex $[Co^{III}L_2L^o]$

Co(1)−N(6)	1.891(6)	Co(1)−N(5)	1.892(7)
Co(1)−N(3)	1.950(6)	Co(1)−N(4)	1.959(5)
Co(1)−N(2)	1.960(5)	Co(1)−N(1)	1.965(6)
S(1)−O(1)	1.422(5)	S(1)−O(2)	1.440(5)
S(2)−O(3)	1.433(5)	S(2)−O(4)	1.444(5)
S(1)−N(2)	1.591(5)	S(2)−N(4)	1.588(5)
S(1)−C(7)	1.775(9)	S(2)−C(20)	1.765(8)
N(1)−C(1)	1.368(9)	N(1)−C(5)	1.331(8)
N(2)−C(6)	1.458(8)	N(3)−C(14)	1.350(9)
N(3)−C(18)	1.321(8)	N(4)−C(19)	1.472(8)
N(5)−C(27)	1.275(10)	N(6)−C(29)	1.276(9)
N(7)−C(32)	1.155(6)	C(27)−C(28)	1.498(10)
C(29)−C(30)	1.552(10)	C(29)−C(31)	1.386(11)
N(6)−Co(1)−N(5)	88.8(3)	N(6)−Co(1)−N(3)	177.1(3)
N(5)−Co(1)−N(3)	89.2(3)	N(6)−Co(1)−N(4)	97.1(2)
N(5)−Co(1)−N(4)	89.7(3)	N(3)−Co(1)−N(4)	80.8(2)
N(6)−Co(1)−N(2)	90.2(2)	N(5)−Co(1)−N(2)	96.4(3)
N(3)−Co(1)−N(2)	92.1(2)	N(4)−Co(1)−N(2)	170.59(19)
N(6)−Co(1)−N(1)	90.6(2)	N(5)−Co(1)−N(1)	177.4(3)
N(3)−Co(1)−N(1)	91.5(18)	N(4)−Co(1)−N(1)	92.9(2)
N(2)−Co(1)−N(1)	81.0(2)		

The $Co-N_{amide}$ and $Co-N_{py}$ bond lengths have similar values. The average $Co-N_{py}$ bond length (1.957(5) Å) is longer than those found in other octahedral cobalt(III) complexes with pyridine nitrogen donor ligands, such as 1.882(5) Å in $[Co^{III}L^1]^+$ {HL^1 = 3,11-bis(methoxycarbonyl)-7-methyl-3,7,11,17-tetraazabicyclo[11.3.1]heptadeca-1(17),13,15-triene}[14] and 1.884(3) Å in $[Co^{III}L^3]$ [HL^3 = 3,7,11-tris(carboxymethyl)-3,7,11,17-tetraazabicyclo-[11.3.1]heptadeca-1(17),13,15-triene][14] or 1.911(3) and 1.915(3) Å in $[Co^{III}(dpkH)_2](MeO)(MeOH)$ [dpkh = bis(2-pyridyl) ketone hydrate],[15] but is only slightly longer than 1.934(2) Å found in the complex $[Co^{III}L(OH)](ClO_4)_2$ [L = 2,6-bis(1′,3′-diamino-2′-methylprop-2′-yl)pyridine].[16] The $Co-N_{amide}$ bond length, with an average value of 1.959(5) Å, is similar to those found in other cobalt(III) amide complexes, such as 1.97(2) Å in [Co(2-amino-4-imino-2-methylpentane)$_2$(methazolamidate)$(NH_3)](NO_3)_2$.[17]

Bond lengths and angles within the framework of the pyridinesulfonamide ligand fall within the range found for other related metal complexes with similar ligands.[9,18]

The Co−N bond lengths from the ligand L^o are equal [Co−N(5) = 1.892(7) and Co−N(6) = 1.891(6) Å] and similar to those found in other hexacoordinated cobalt complexes with ligands possessing the same chemical skeleton: 1.995(5) Å in [Co(*R*-ala)-(1,5*R*,7*R*,11-Me_4-2,3,2-tet)-Br_2·$3H_2O$[19] or 2.009(5) Å in *cis*-$[Co^{III}L^2Cl_2]Cl$, in which L^2 stands for (5*RS*,7*SR*)-dimethyl-1,4,8,11-tetraazacyclooctatetradecane.[20] The bond angles have normal values for a six-membered chelate ring and are 88.8°. The bond lengths N−C and C−C in the new ligand L^o are essentially identical to those found in the other complexes with this ligand.[11,12] The N(5)−C(27) [1.275(10) Å] and N(6)−C(29) [1.276(9) Å] bond lengths are in agreement with the value of 1.30 Å proposed for a C=N double bond,[21] and the C(32)−N(7) bond length of 1.155(6) Å is shorter than for C=N but not as short as for a C≡N triple bond.[22] The C−C bonds in the chelate ring and the C(31)−C(32) bond are shorter [1.386(11)−1.432(11) Å] than the other C−C bonds [1.498(10)−1.522(10) Å]. The C(31)−C(32)−N(7) angle is very close to the theoretical value for a linear disposition [176.9(5)°].

The crystal packing is such that the molecules and the Co−C(9)−C(8)−N(7) units of adjacent complex molecules appear to form chains parallel to the *b* axis. The distance from the N(7) atom of a given molecule to the Co atom of the neighbouring molecule is 4.615(5) Å.

Spectroscopic Studies

The IR spectra of the complexes are in accordance with the X-ray data discussed above. The ligand HL shows a broad band at around 3095 cm^{-1}, attributable to ν(N−H). This band is absent in the IR spectra of the complexes, a fact in agreement with the deprotonation of the N−H amide bond during the electrosynthesis. The stretching band of the pyridine ring, observed between 1600 and 1400 cm^{-1} and the ring deformation bands, which appear at about 600 and 400 cm^{-1}, are shifted to higher frequencies in the complexes. This behaviour has been proposed as evidence for the coordination of the pyridine nitrogen atom to the metal ion,[23] as confirmed by the structural data. In addition, the spectrum of the $[Co^{III}L_2L^o]$ complex also shows a sharp band at 3350 cm^{-1}, assigned to ν(N−H), as well as another band at 2190 cm^{-1} due to ν(C≡N) of the new ligand L^o.

The IR spectra of the mixed complexes containing 2,2′-bipyridine or 1,10-phenanthroline as additional ligands show the bands characteristic of these coordinated ligands[24,25] (bipy: ca. 770 and 720 cm^{-1}; phen: ca. 1520, 847 and 722 cm^{-1}).

The diffuse reflectance spectrum of $[Co^{II}L_2]$ in the NIR/Vis region shows two multicomponent bands, one at 7600, 8900 and 11200 cm^{-1} [assigned to $^4A_2 \rightarrow {}^4T_1(F)$ (ν_2)] and the other at 17100, 19455 and 20790 cm^{-1} [due to $^4A_2 \rightarrow {}^4T_1(F)$ (ν_3)], both of which are consistent with a distorted tetrahedral environment for the metal ion.[26] The $^4A_2 \rightarrow {}^4T_1$ (P) (ν_1) transition was not observed, but its position at ca. 5300 cm^{-1} was calculated by the method described by Lever. The presence of three closely spaced transitions in the spectrum of $[Co^{II}L_2]$ arises due to distortion from the regular tetrahedral symmetry, a situation resulting from the inequivalence of the pyridyl and sulfonamide donor atoms and the restrictive bite angle of the chelating ligands. At room temperature this complex has a magnetic moment of 4.0 B.M., which is well within the range expected for tetrahedral cobalt(II) compounds.

The solid-state electronic spectra of the mixed complexes $[Co^{II}L_2L']$ between 20000 and 5000 cm^{-1} are all very similar, but differ from those found for the $[Co^{II}L_2]$ and $[Co^{III}L_2L^o]$ complexes. The former complexes gave rise to three bands in the regions 7400−9500, 14600−15150 and 21800−23000 cm^{-1}, assigned to $^4T_{1g}(F) \rightarrow {}^4T_{2g}$ (ν_1), $^4T_{1g}(F) \rightarrow {}^4A_{2g}$ (ν_2) and $^3T_{1g}(F) \rightarrow {}^4T_{2g}(\nu_3)$ transitions, respectively, in a distorted octahedral field.[26] The magnetic moments of these complexes at room temperature are in the

range 4.60−4.80 B.M., and these values are on the low side of the range expected for octahedral cobalt(II) complexes, probably as a result of a reduced orbital contribution. The magnetic moment of the $[Co^{III}L_2L^o]$ complex shows that this compound is diamagnetic and which is consistent with a low-spin d^6 octahedral complex. The solid-state electronic spectrum shows two bands at 15200 and 21800 cm^{-1}, as would be expected for low-spin six-coordinated cobalt(III) complexes. The first band has been attributed to a $^1A_{1g} \rightarrow {}^1T_{1g}$ transition and the other band to a $^1A_{1g} \rightarrow {}^1T_{2g}$ transition.[26]

In the FAB mass spectra of $[Co^{II}L_2]$, $[Co^{III}L_2L^o]$, $[Co^{II}L_2bipy]$ and $[Co^{II}L_2phen]$, the molecular ion peaks are observed at m/z = 582, 703, 737 and 762, respectively, together with corresponding peaks at m/z = 426, 442, 476 and 500 formed by loss of one tosyl ligand from each complex. A peak is also observed at m/z = 580 in the spectrum of $[Co^{III}L_2L^o]$, and this corresponds to a fragment formed by loss of the ligand L^o.

Experimental Section

Materials and Instrumentation: Cobalt (Aldrich Chemie) was used as plates (ca. 2 × 2 cm). All other reagents, including 1,10-phenanthroline and 2,2′-bipyridine, were used as supplied. The C,H,N,S analyses of the compounds were performed with a Carlo−Erba EA 1108 microanalyzer. IR spectra were recorded as KBr mulls with a Bruker IFS-66V spectrophotometer. The ^1H NMR spectrum of the ligand was recorded with a Bruker AMX 300 MHz spectrometer, with $[D_6]$DMSO as solvent. The chemical shifts were recorded against TMS as an internal standard. FAB mass spectra were recorded with an Autospec-Micromass instrument, with 3-nitrobenzyl alcohol (3-NBA) as the matrix. Solid-state electronic spectra were recorded with a Shimadzu UV 3101 PC apparatus. Magnetic measurements were obtained with a DMS VSM 1160 instrument.

Synthesis of the Ligand HL (1): The ligand HL was prepared from equimolar amounts of 2-aminomethylpyridine (1.00 mL, 10.1 mmol) and tosyl chloride (1.93 g, 10.1 mmol) in dichloromethane (40 mL). Aqueous NaOH (10%) was added to the mixture until pH = 8 was reached, and a white product was obtained.[27] The solid was filtered off and dried in vacuo. Yield 78%. The purity of the product was assessed by microanalysis, IR and ^1H NMR spectroscopy. Crystals suitable for X-ray structure determination were obtained by crystallisation from dichloromethane. IR (KBr): $\tilde{\nu}$ = 3094 [ν(N−H)], 1598−1385 [ν(C=C, C=N)$_{py}$], 1328 [$\nu_{as}(SO_2)$], 1164 [$\nu_s(SO_2)$] cm^{-1}. ^1H NMR ($[D_6]$DMSO): δ = 11.6 (s, 1 H, N−H$_{tosyl}$), 8.5 (d, 1 H, 2-H$_{py}$), 2.1 (s, 3 H, Me$_{tosyl}$) ppm. $C_{13}H_{15}N_2O_{2.5}S$ (271.3): calcd. H 5.58, C 57.55, N 10.33, S 11.79; found H 5.38, C 57.52, N 10.10, S 12.22.

Preparation of the Complexes (General Procedure): The complexes were formed by an electrochemical procedure.[28] This method allows the preparation of different products simply by changing the conditions of the electrochemical reaction. The cell consisted of two electrodes submerged in a solution of the tosylated ligand and a small amount of tetraethylammonium perchlorate (ca. 15−20 mg) as a current carrier in acetonitrile. The cathode was a platinum wire and the anode a plate of the appropriate metal. For the synthesis of mixed complexes, the corresponding coligand − 1,10-phenanthroline or 2,2′-bipyridine − was also added to the solution. Applied voltages of 9−15 V allowed sufficient current flow for smooth dissolution of the metal. In all cases the electrochemical synthesis was carried out at room temperature. The cell can be summarised as Pt(−)/CH_3CN + HL/M(+).

Preparation of $[Co^{II}L_2]$ (2): Electrolysis of an acetonitrile solution containing HL (0.2932 g, 1.12 mmol) and a small amount of tetraethylammonium perchlorate (ca. 25 mg) at 10 mA and 9 V for 3 h dissolved 32 mg of cobalt (E_f = 0.49 mol·F^{-1}). At the end of the experiment, a purple solution had been obtained and was allowed to stand for a few days. Purple crystals suitable for X-ray diffraction formed, and these were collected and dried in vacuo. The compound was characterised as $[Co^{II}L_2]$. IR (KBr): $\tilde{\nu}$ = 1611−1439 [ν(C=C, C=N)$_{py}$], 1275 [$\nu_{as}(SO_2)$], 1147 [$\nu_s(SO_2)$] cm^{-1}. $C_{26}H_{26}CoN_4O_4S_2$ (581.5): calcd. H 4.51, C, 53.70, N 9.63, S 11.01; found H 4.47, C 53.52, N 9.62, S 9.76.

Preparation of $[Co^{III}L_2L^o]$ (3): Electrolysis of an acetonitrile solution containing HL (0.1947 g, 0.7432 mmol) and a small amount of tetraethylammonium perchlorate (ca. 20 mg) at 10 mA and 20.8 V for 2 h dissolved 20 mg of cobalt (E_f = 0.46 mol·F^{-1}). At the end of the experiment a brown solution had formed, with brown crystals at the bottom of the vessel. These crystals were filtered off and dried in vacuo and were suitable for X-ray crystallography. The compound was characterised as $[Co^{III}L_2L^o]$. IR (KBr): $\tilde{\nu}$ = 3354 [ν(NH)], 2189 [ν(C≡N)], 1604−1396 [ν(C=C, C=N)$_{py}$], 1280 [$\nu_{as}(SO_2)$], 1134 [$\nu_s(SO_2)$] cm^{-1}. $C_{32}H_{34}CoN_7O_4S_2$ (703.7): calcd. H 4.87, C 54.62, N 13.93, S 9.09; found H 4.88, C 54.45, N 13.41, S 9.75.

Preparation of $[Co^{II}L_2(bipy)]$ (4): Electrolysis of an acetonitrile solution containing HL (0.1947 g, 0.7432 mmol), 2,2′-bipyridine (0.0584 g, 0.3715 mmol) and a small amount of tetraethylammonium perchlorate (ca. 20 mg) at 10 mA and 20.3 V for 2 h dissolved 22 mg of cobalt (E_f = 0.51 mol·F^{-1}). At the end of the experiment a brown solid had formed, and this was filtered off, washed with acetonitrile and dried in vacuo. The compound was characterised as $[Co^{II}L_2(bipy)]$. IR (KBr): $\tilde{\nu}$ = 1628−1492 [ν(C=C, C=N)$_{py}$], 1283 [$\nu_{as}(SO_2)$], 1159 [$\nu_s(SO_2)$] cm^{-1}. $C_{36}H_{34}CoN_6O_4S_2$ (737.7): calcd. H 4.61, C 58.60, N 11.39, S 8.68; found H 4.57, C 59.39, N 12.07, S 7.92.

Preparation of $[Co^{II}L_2(phen)]$ (5): Electrolysis of an acetonitrile solution containing HL (0.1947 g, 0.7432 mmol) and a small amount of tetraethylammonium perchlorate (ca. 20 mg) at 10 mA and 24.6 V for 2 h dissolved 23 mg of cobalt (E_f = 0.53 mol·F^{-1}). At the end of the experiment a dark brown solid had formed, and this was filtered off, washed with acetonitrile and ether, and dried in vacuo. The compound was characterised as $[Co^{II}L_2(phen)]$. IR (KBr): $\tilde{\nu}$ = 1628−1429 [ν(C=C, C=N)$_{py}$], 1281 [$\nu_{as}(SO_2)$], 1160 [$\nu_s(SO_2)$] cm^{-1}. $C_{38}H_{34}CoN_6O_4S_2$ (761.8): calcd. H 4.46, C 59.90, N 11.03, S 8.40; found H 4.79, C 59.37, N 11.00, S 8.28.

Crystal Structure Determination: Crystals of HL (**1**) and $[Co^{III}L_2L^o]$ (**3**) were mounted on glass fibres and used for data collection with an Enraf Nonius CAD4 diffractometer, while a Siemens SMART CCD area detector diffractometer was used in the case of $[Co^{II}L_2]$ (**2**). Mo-K_α radiation (λ = 0.71073 Å, graphite monochromator) was used for the collection of the intensity data by a 2θ/ω-scan technique. Decomposition of the crystals did not occur during data collection. Corrections were applied for Lorentz and polarisation effects and for absorption.[29] The structures were solved by direct methods; missing atoms were located in the difference Fourier maps and included in subsequent refinement cycles. The structures were refined by full-matrix, least-squares refinement on F^2, with anisotropic displacement parameters used for all non-

Table 5. Summary of crystal data and structure refinement

	HL	$[Co^{II}L_2]$	$[Co^{III}L_2L^o]$
Empirical formula	$C_{13}H_{15}N_2O_{2.50}S$	$C_{26}H_{26}CoN_4O_4S_2$	$C_{32}H_{34}CoN_7O_4S_2$
Formula mass	271.33	581.56	703.71
Temperature [K]	293(2)	293(2)	293(2)
Wavelength [Å]	0.71073	0.71073	0.71073
Crystal system, space group	monoclinic, *C*2/*c*	monoclinic, $P2_1/n$	orthorhombic, *Pca*2(1)
a [Å]	27.145(11)	13.0552(3)	16.310(4)
b [Å]	6.0119(12)	7.8373(2)	10.4858(15)
c [Å]	16.690(7)	26.2839(2)	17.931(4)
β [°]	99.10(2)	95.1350(10)	90.00
Volume [Å^3]	2689(2)	2678.51(9)	3066.6(11)
Z	8	4	4
Density (calculated) [Mg/m^3]	1.340	1.442	1.524
Absorption coefficient [mm^{-1}]	0.241	0.836	0.747
F(000)	1144	1204	1464
Crystal size [mm], colour	0.35 × 0.15 × 0.10, colourless	0.15 × 0.10 × 0.05, purple	0.30 × 0.25 × 0.15, caramel
θ range for data collection [°]	3.04−30.01	1.56−28.27	1.94−24.97
Index ranges	$-37 \le h \le 37$, $0 \le k \le 8$, $0 \le l \le 22$	$-17 \le h \le 17$, $-10 \le k \le 5$, $-35 \le l \le 33$	$0 \le h \le 19$, $0 \le k \le 12$, $-21 \le l \le 21$
Reflections collected	4039	18454	2915
Independent reflections	3908 [R_{int} = 0.0384]	6573 [R_{int} = 0.1040]	2909 [R_{int} = 0.0159]
Reflections observed	1304	2752	2210
Criterion for observation	$> 2\sigma(I)$	$> 2\sigma(I)$	$> 2\sigma(I)$
Data/restraints/parameters	3908/0/218	6573/0/336	2909/1/427
Goodness-of-fit on F^2	1.027	1.046	1.039
Final *R* indices [$I > 2\sigma(I)$]	0.0840/0.1750	0.0780/0.1074	0.0401/0.0714
Absolute structure parameter			0.00(3)
Largest diff. peak and hole [e·Å^{-3}]	0.297 and −0.293	0.360 and −0.436	0.384 and −0.274

hydrogen atoms except those of the methyl group [C(20)] of the ligand HL, which were located in their calculated positions (C−H 0.96 Å). In all cases, hydrogen atoms were included by using a riding model with C−H distances of 0.93−0.97 Å and fixed isotropic thermal parameters. The weighting scheme of the form $\omega = 1/\sigma^2(F)$ was introduced, and the refinement proceeded smoothly to convergence with a maximum delta/σ of 0.001. The absolute configuration was determined for **3**.[30] The crystallographic programs used for the structure solutions and refinement were from SHELX97.[31] Atomic scattering factors and anomalous dispersion corrections for all atoms were taken from International Tables for X-ray Crystallography.[32] The crystal data and summary of data collection and structure refinement for these compounds are given in Table 5. Selected bond lengths and angles for **1**, **2** and **3** are given in Tables 1, 3 and 4. ORTEP3[33] drawings of the molecules with the numbering schemes used are shown in Figures 1−3. CCDC-171729 (**1**), -171730 (**2**) and -171731 (**3**) contain the supplementary crystallographic data for this paper. These data can be obtained free of charge at www.ccdc.cam.ac.uk/conts/retrieving.html or from the Cambridge Crystallographic Data Centre, 12, Union Road, Cambridge CB2 1EZ, UK [Fax: (internat.) + 44-1223/336-033; E-mail: deposit@ccdc.cam.ac.uk].

Acknowledgments

This work was supported by the Xunta de Galicia (XUGA20302B97 and PGIDT00PXI20910PR).

[1] L. Antolini, L. P. Battaglia, A. Bonamartini Corradi, G. Marcotrigliano, L. Menablue, G. C. Pellacani, *J. Am. Chem. Soc.* **1985**, *107*, 1369−1375.
[2] H. Siegel, R. B. Martin, *Chem. Rev.* **1982**, *82*, 385−426.
[3] C. A. Otter, S. M. Couchman, J. C. Jeffery, K. L. V. Mann, E. Psillakis, M. D. Ward, *Inorg. Chim. Acta* **1998**, *278*, 178−184.
[4] M. L. Durán, J. A. García-Vázquez, J. Romero, A. Castiñeiras, A. Sousa, A. D. Garnovskii, D. A. Garnovskii, *Polyhedron* **1997**, *16*, 1707−1711.
[5] E. Eliopoulos, B. Sheldrick, S. Hamodrakas, *Acta Crystallogr., Sect. C* **1983**, *39*, 1693−1695.
[6] A. K. Basak, S. Chaudhuri, S. K. Mazumdar, *Acta Crystallogr., Sect. C* **1984**, *40*, 1848−1851.
[7] I. Bar, J. Bernstein, *J. Pharm. Sci.* **1985**, *74*, 255−263 and references therein.
[8] J. Bernstein, *Acta Crystallogr., Sect. C* **1988**, *44*, 900−902.
[9] S. Cabaleiro, J. Castro, E. Vázquez-López, J. A. García-Vázquez, J. Romero, A. Sousa, *Polyhedron* **1999**, *18*, 1669−1674.
[10] T. S. Cameron, K. Prout, B. Denton, R. Spagna, E. White, *J. Chem. Soc., Perkin Trans. 2* **1975**, 176−185.
[11] M. R. Kopp, T. Krauter, A. Dashti-Mommertz, B. Neumuller, *Organometallics* **1998**, *17*, 4226−4231.
[12] M. R. Kopp, B. Neumuller, *Z. Anorg. Allg. Chem.* **1999**, *625*, 739−745; *Z. Anorg. Allg. Chem* 1246−1248.
[13] J. A. García-Vázquez, J. Romero, M. L. Durán, A. Sousa, A. D. Garnovskii, A. S. Burlov, D. A. Garnovskii, *Polyhedron* **1998**, *17*, 1547−1552.
[14] J. Costa, R. Delgado, M. G. B. Drew, V. Félix, R. T. Henriques, J. C. Waerenborgh, *J. Chem. Soc., Dalton Trans.* **1999**, 3253−3265.
[15] C. Hemmert, M. Renz, H. Gornitzka, S. Soulet, B. Meunier, *Chem. Eur. J.* **1999**, 1766−1774.
[16] T. Poth, H. Paulus, H. Elias, R. van Eldik, A. Grohmann, *Eur. J. Inorg. Chem.* **1999**, 643−650.
[17] G. Alzuet, S. Ferrer, J. Casanova, J. Borras, A. Castiñeiras, *Inorg. Chim. Acta* **1993**, *203*, 79−84.
[18] S. Cabaleiro, J. Castro, J. A. García-Vázquez, J. Romero, A. Sousa, *Polyhedron* **2000**, *19*, 1607−1614.
[19] M. Yashiro, M. Ajioka, S. Yano, K. Toriumi, T. Ito, S. Yoshikawa, *Bull. Chem. Soc. Jpn.* **1986**, *59*, 2255−2261.

[20] K. Mochizuki, K. Ikeuchi, T. Kondo, *Bull. Chem. Soc. Jpn.* **1998**, *71*, 2629−2634.
[21] J. N. Brown, R. L. Towns, L. M. Trefonas, *J. Am. Chem. Soc.* **1970**, *92*, 7436−7440.
[22] V. Chebolu, R. R. Whittle, A. Sen, *Inorg. Chem.* **1985**, *24*, 3082−3085, and references therein.
[23] A. Castiñeiras, J. A. Castro, M. L. Durán, J. A. García-Vázquez, A. Macías, J. Romero, A. Sousa, *Polyhedron* **1989**, *21*, 2543−2549 and references therein.
[24] R. G. Inskeep, *J. Inorg. Nucl. Chem.* **1962**, *24*, 763−776.
[25] A. A. Schilt, R. C. Taylor, *J. Inorg. Nucl. Chem.* **1959**, *9*, 211−211.
[26] A. B. P. Lever, *Inorganic Electronic Spectroscopy*, 2nd ed., Elsevier, Amsterdam, **1984**.
[27] *Vogel's Textbook of Practical Organic Chemistry*, 5th ed., Longman Scientific & Technical, New York, **1989**, p. 879.
[28] J. J. Habeeb, D. G. Tuck, F. H. Walters, *J. Coord. Chem.* **1978**, *8*, 27−32.
[29] N. Walker, D. Stuart, *Acta Crystallogr., Sect. A* **1983**, *39*, 158−166.
[30] H. D. Flack, *Acta Crystallogr., Sect. A* **1983**, *39*, 876−881.
[31] G. M. Sheldrick, *SHELX97* (includes SHELXS-97, SHELXL-97, CIFTAB) − *Programs for Crystal Structure Analysis* (Release 97-2), Institut für Anorganische Chemie der Universität, Tammanstrasse 4, 3400 Göttingen, Germany, **1998**.
[32] *International Tables for Crystallography* (Ed.: A. J. C. Wilson), Kluwer Academic Publishers, Dordrecht, The Netherlands, **1995**, vol. C.
[33] ORTEP3 for Windows: L. J. Farrugia, *J. Appl. Crystallogr.* **1997**, *30*, 565.

Received October 30, 2001
[I01427]

Structures of Complexes of Thallium(I) and Functionalized Benzoate Ligands with Pronounced Stereoactivity of the Lone Pair of Electrons and Metal−Phenyl π-Bonding

Olof Kristiansson[a]

Keywords: Thallium(I) / Stereoactive inert pair / Thallophilic interaction / Coordination polymer / Metal−phenyl π-bonding

Four complexes between thallium(I) and functionalized benzoate ligands, namely salicylate, *p*-aminosalicylate, 3,4-dimethoxybenzoate and 3,5-dimethoxybenzoate have been prepared and their structures determined by X-ray diffraction. They are all based on dimeric, centrosymmetric $Tl_2(RCOO)_2$ units with μ_2-bridging carboxylic groups resulting in Tl···Tl separations of 4.2–4.4 Å. These dimeric units are further linked to form infinite coordination polymers. In *catena*-[bis(μ_3-salicylato)dithallium(I)] (**1**) and *catena*-[bis(μ_3-4-aminosalicylato)dithallium(I)] (**2**) are adjacent units are held together by secondary Tl–O(hydroxy) interactions resulting in a crystal organization which can be described as stair-like, infinite one-dimensional polymers. In *catena*-[μ_4-(3,4-dimethoxybenzoato)thallium(I)] (**3**) bridges each carboxylic group four thallium(I) cations resulting in infinite two-dimensional, puckered sheets. Finally, in *catena*-[μ_3-(3,5-dimethoxybenzoato)thallium(I)] (**4**) each carboxylic unit acts as a μ_3-bridging ligand to give nearly planar, infinite double-stranded arrays of Tl^+ cations. Another characteristic structural motif is the tendency of the thallium ion to only use less than one hemisphere to coordinate ligands. This "half-nakedness" is due to the stereochemically active inert pair ($6s^2$), which thus plays a prominent role in controlling the structures of these compounds. The Tl^+ cations are in approximate pyramidal geometries, with four or five oxygen donor atoms in the basal plane and the stereoactive lone pair occupying the apex position of the pyramid. There are, on the naked side of the metal ions, relatively large spaces in non-polar environments provided by neighboring phenyl groups. The distances between the planes of the phenyl rings and the Tl^+ cation are in the range 3.3–3.5 Å, indicating that Tl^+–phenyl η^6-interactions are important in the crystal organization.

(© Wiley-VCH Verlag GmbH, 69451 Weinheim, Germany, 2002)

Introduction

The Tl^+ ion is nonspherical, with its inert pair ($6s^2$) partially hybridized leading to the formation of a local dipole that may strongly affect cation···ligand interactions. This "inert-pair effect" has, in a general way, been explained by Pitzer[1] and by Pykko and Desclaux[2] as a relativistic effect causing the outer s electrons to be more strongly attracted to the nucleus than normally expected. In p-block cations with an ns^2 np^0 electronic configuration, lone pairs of electrons may thus play a prominent role in controlling the structures and chemical behavior. In inorganic salts, the lone pair is manifested by a distortion of regular coordination geometries by a substantial elongation of certain bonds, as exemplified in, for example, TlF,[3] $Tl[CuAsO_4]$, $Tl[CuPO_4]$[4] or $TlZn(PO_3)_3$.[5] In several organometallic compounds, the stereoactive lone pair is manifested by a "half-naked" cation, with ligands only coordinating one hemisphere, as observed in the crystal structures of complexes between Tl^+ and tris(pyrazolyl)borate, where the lone pair occupies the fourth position of a tetrahedron bis(pyrazolyl)phosphinate,[6] with an obvious gap in the coordination sphere due to the lone pair, and also in [HB(3-*p*-tolylpyrazolyl)$_3$Tl].[7] In (malonohydroxamato)Tl, a square-pyramidal geometry of Tl^+ is observed, with the lone pair oriented in the axial direction.[8] In addition, in several organometallic thallium compounds the stereoactivity of the inert pair is apparent.[9]

There is a paucity of data on complexes between thallium(I) and arylcarboxylate ligands in the literature, the only known example being *catena*-[bis(μ_3-2-hydroxybenzoato)dithallium(I)].[10] In this paper we wish to present the crystal structures of four complexes between thallium(I) and functionalized benzoate ligands, namely salicylate (**1**), 4-aminosalicylate (**2**), 3,4-dimethoxybenzoate (**3**) and 3,5-dimethoxybenzoate (**4**) (Scheme 1). These ligands present a limited range of steric and electronic properties and are therefore useful for establishing basic patterns in thallium(I)−benzoate interactions. In following papers, we wish to extent these investigations to systems where steric requirements of the ligands impose restrictions on the thallium coordination geometries and also attempt the use of

[a] Department of Chemistry, SLU,
Box 7015, 75007 Uppsala, Sweden
E-mail: olof.kristiansson@kemi.slu.se

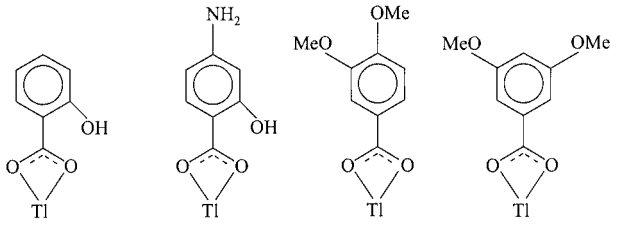

Scheme 1. Monomeric units of compound **1**−**4**

the inert lone pair as a Lewis base for the construction of extended solids.

Results and Discussion

catena-[Bis(μ$_3$-salicylato)dithallium(I)] (1) − Crystal Structure

The crystal structure is based on dimeric units as depicted in Figure 1. The carboxylate groups act as μ$_2$-bridging ligands. One oxygen atom is bound to two thallium ions and the other to one thallium ion. The doubly coordinated O1 bridges thallium ions unsymmetrically with Tl−O distances of 2.601(11) and 2.751(11) Å and a Tl−O−Tl angle of 103.8(4)°. The O1^i−Tl1−O1 and O1−Tl1−O2 angles equal 76.2(4) and 48.4(3)°, respectively. The singly coordinated O2 has a Tl−O distance of 2.778(11) Å. This geometry results in a Tl···Tl separation of 4.213(1) Å. Each Tl^+ ion is coordinated on one side to three oxygen atoms of two carboxylic groups and, at a longer distance, to one O3 atom of adjacent units. The other side is, however, completely "naked" due to the inert pair (6s^2) in an sp-hybridized orbital producing an electronic bulge on this side. Each Tl^+ cation is therefore in a distorted square-pyramidal geometry, with the four oxygen atoms in the basal plane and the stereoactive lone pair occupying the apex position of the pyramid (Figure 2). The Tl^+ ion is situated 1.64 Å from the least-squares plane defined by the oxygen atoms. There is, on the "naked" side of the metal ion, a relatively large space in a hydrophobic environment provided by two neighboring phenyl groups. The distance between the planes of the phenyl rings and the Tl^+ cation is 3.29 Å. This value is similar to that of 3.27 Å in [Tl(PhNNNPh)]$_2$ and 3.33 Å in [Tl(TolNNNNNTol)]$_2$[11] or to that in a complex between Tl^+ and Lasalocid A, an ionophore containing a salicylic group, where a distance of 3.22 Å is observed.[12] These values fall essentially within the range of van der Waals distances [the sum of the ionic radius of Tl^+ (1.47 Å)[13] and the van der Waals radius of the aromatic ring (1.77 Å)[14]], which is 3.24 Å, thus indicating Tl^+−phenyl η^6-interactions. The aromatic ring is nearly perpendicular (87.1°) to the vector joining the Tl^+ cation and the centroid of the phenyl group.

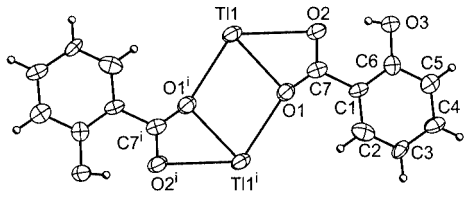

Figure 1. Molecular structure and atom numbering scheme for bis(salicylato)dithallium(I) (**1**); the displacement ellipsoids are drawn at the 50% probability level for non-H atoms; symmetry code: i: $-x$, $2-y$, $2-z$

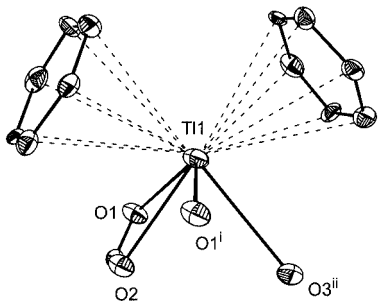

Figure 2. The coordination of the Tl^+ ion in **1** showing the stereoactivity of the lone pair; the geometry of the Tl^+ cation can be described as a distorted square-based pyramid, with the stereoactive lone pair occupying the apex position in a hydrophobic environment; the centroids of the phenyl rings are situated 3.29 Å from the Tl^+ cation; the displacement ellipsoids are drawn at the 50% probability level; bond lengths [Å]: Tl1−O1 2.601, Tl1−O2 2.778, Tl1−O1^i 2.751, Tl1−O3^{ii} 2.798; symmetry codes i: $-x$, $2-y$, $2-z$; ii: $x-1$, y, z

The $Tl_2(COO)_2$ unit is virtually planar with a mean deviation from the least-squares plane of 0.0128 Å. The phenyl rings form an angle of 11.1° with this plane, resulting in an average deviation from the plane defined by all atoms of the $Tl_2(C_7H_5O_3)_2$ molecule of 0.125 Å. The $Tl_2(COO)_2$ units are stacked into piles along the *c* axis. The units are tilted 47.9° versus the *c* axis giving a parallel displacement of 5.77 Å with a perpendicular distance of 3.23 Å between successive units. The displacement of successive planes makes aromatic π-interactions unfeasible in the crystal organization. Adjacent units are held together by secondary Tl−O3 interactions [*d*(Tl−O3) = 2.978(11) Å], resulting in stair-like, infinite one-dimensional polymers as schematically depicted in Figure 3. The packing in the unit cell is shown in Figure 4.

catena-[Bis(μ$_3$-*ortho*-aminosalicylato)dithallium(I)] (2) − Crystal Structure

The molecular structure of bis(2-aminosalicylato)dithallium(I) (**2**) is shown in Figure 5. In this case the carboxylate groups act also as μ$_2$-bridging ligands with one oxygen atom unsymmetrically bridging two thallium ions [*d*(Tl−O) = 2.614(12) and 2.713(11) Å] and the other one to one thallium ion [*d*(Tl−O) = 2.879(12) Å] which results in a Tl−Tl separation of 4.253(1) Å. The Tl^+ ion is in a distorted square-pyramidal geometry, with the four oxygen atoms in the basal plane and the stereoactive lone pair oc-

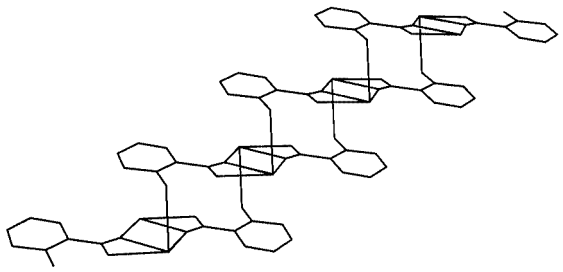

Figure 3. Schematic drawing of the crystal organization of **1**; each $Tl_2(C_6H_5OHCOO)_2$ unit is linked to adjacent units via two secondary Tl−O(hydroxy) interactions [*d*(Tl−O) = 2.97(1) Å]; successive units are parallel displaced by 5.77 Å producing a stair-like, infinite one-dimensional polymer

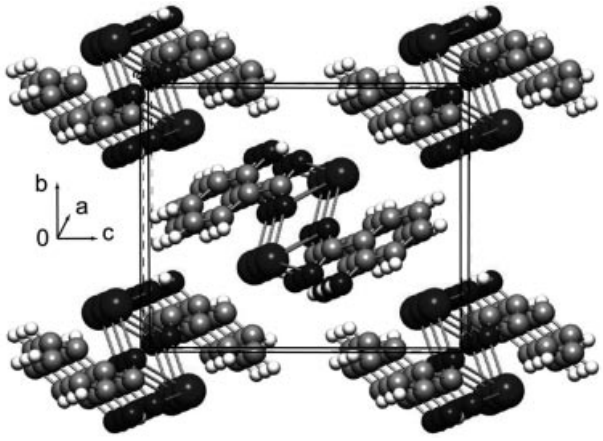

Figure 4. The unit cell content of **1** viewed along the crystallographic *a* axis

cupying the apex position of the pyramid, in a hydrophobic environment provided by two neighboring phenyl groups. The distance between the planes of the phenyl rings and the Tl^+ cation are 3.31 and 3.68 Å with angles of 87.2 and 62.7° between the aromatic plane and the vector joining the Tl^+ cation and the centroid of the phenyl group. In addition to the strong intramolecular hydrogen bond between O3 and O2 [*d*(O···O) = 2.53(2) Å] are also weak hydrogen bonds formed between the amino protons and O2 atoms of adjacent units [*d*(N···O) = 3.02(2) and 3.15(2) Å].

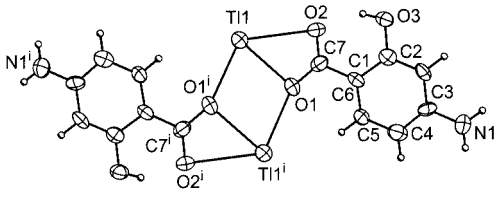

Figure 5. Molecular structure and atom numbering scheme for bis(2-aminosalicylate)dithallium(I) (**2**); the displacement ellipsoids are drawn at the 50% probability level for non-H atoms; symmetry code: i: $-x$, $2-y$, $2-z$

The crystal organization shows large similarities with that of compound **1**. The $Tl_2(COO)_2$ unit is slightly twisted with a mean deviation from the least-square plane of 0. 123 Å. The phenyl rings form an angle of 16.0° with this plane, resulting in an average deviation from the plane defined by all atoms of the $Tl_2(C_7H_5O_3)_2$ moiety of 0.217 Å. The $Tl_2(COO)_2$ units are stacked into piles along the *c* axis. The units are tilted 45.1° versus the *c* axis giving a parallel displacement of 6.00 Å. Adjacent units are held together by secondary Tl−O3 interactions [*d*(Tl−O3) = 2.923(11) Å]. The overall crystal organization can be described as stair-like, infinite one-dimensional polymers as depicted in Figure 3. The crystal structures of compounds **1** and **2** show certain similarities with that of a previous determination of *catena*-[bis(μ_3-2-hydroxybenzoato)dithallium(I)].[11] The dimeric unit in this compound shows a Tl−Tl separation of 4.129 Å and successive units are linked via Tl−O(hydroxy) interactions [*d*(Tl−O) = 2.727 Å] to give infinite polymers similar to those in Figure 3.

catena-[(3,4-Dimethoxybenzoato)thallium(I)] (3) − Crystal Structure

The crystal structure is based on dimeric $Tl_2(C_7H_6NO_3)_2$ units as shown in Figure 6. Each dimeric unit is extensively cross-linked to adjacent units to form an infinite two-dimensional network as schematically shown in Figure 7**.** One

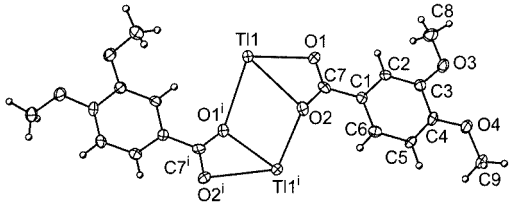

Figure 6. Molecular structure and atom numbering scheme for *catena*-[(3,4-dimethoxybenzoato)dithallium(I)] (**3**); the displacement ellipsoids are drawn at the 50% probability level for non-H atoms; symmetry code: i: $-x$, $-0.5+y$, $0.5-x$

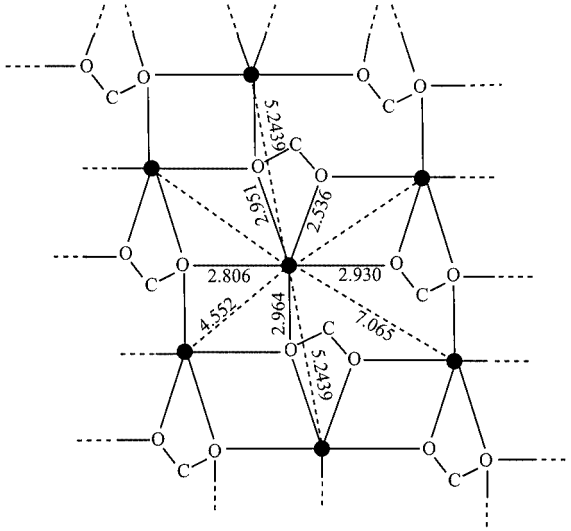

Figure 7. Schematic drawing of the crystal organization of **3**, which consists of infinite two-dimensional, puckered sheets of Tl^+ cations, linked by μ_4-bridging carboxylate groups

oxygen atom the carboxylate group is bound to three thallium ions and the other one to two thallium ions, with each carboxylate group acting as a μ_4-bridging ligand. The doubly coordinated oxygen atom O1 bridges two thallium ions unsymmetrically with Tl−O distances of 2.536(6) and 2.930(6) Å, while the triply coordinated O2 has a Tl−O distances of 2.806(7), 2.951(6) and 2.964(7) Å. As a result of this geometry each Tl^+ cation is surrounded by three other cations at comparatively short distances, two at 4.4111(8) Å and one at 4.552(1), and three cations at significantly longer distances, two at 5.244(1) and one at 7.065(1) Å. Each Tl^+ ion is coordinated on one side to five oxygen atoms of four carboxylic groups. In this case the other side is also completely naked due to the stereoactive lone pair. The geometry of the Tl^+ cation may be described as a distorted pyramid, with the five oxygen atoms in the basal plane and the stereoactive lone pair occupying the apex position of the pyramid, with the Tl^+ ion being situated 1.16 Å from the least-squares plane defined by the oxygen atoms. The phenyl rings form an angle of 46.0° with the Tl_2O_2 plane, resulting in an average deviation from the plane defined by all atoms of the $Tl_2(C_9H_9O_4)_2$ moiety of 0.692 Å. The crystal organization is shown in Figure 8. The infinite layers of Tl^+ cations extend perpendicular to the *a* axis, alternating with hydrophobic areas. The relatively large empty spaces, in hydrophobic environments, around one side of the Tl^+ cations are clearly seen.

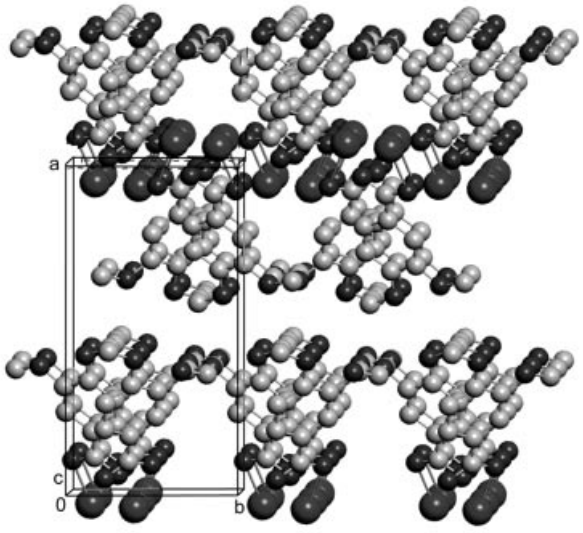

Figure 8. View parallel to the *c* axis of the packing of **3** in the unit cell; hydrogen atoms are omitted for clarity

catena-[(3,5-Dimethoxybenzoato)thallium(I)] (4) − Crystal Structure

The crystal structure is based on dimeric $Tl_2(C_9H_9O_4)_2$ units as shown in Figure 9. The Tl_2O_4 moiety is virtually planar, with a mean atomic displacement from the least-squares plane of 0.019 Å. This plane forms an angle of 7.5°

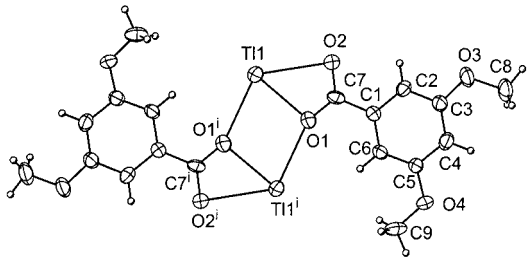

Figure 9. Molecular structure and atom numbering scheme for *catena*-[(3,5-dimethoxybenzoato)dithallium(I)] (**4**); the displacement ellipsoids are drawn at the 50% probability level for non-H atoms; symmetry code: i: $-x$, $1-y$, $-x$

with the aromatic planes which results in an average deviation from planarity for the entire $Tl_2(C_9H_9O_4)_2$ unit of 0.075 Å. The two Tl^+ ions are unsymmetrically bridged by the carboxylic oxygen atoms O1 and O1^i with Tl−O distances of 2.530(5) and 2.710(5) Å, respectively, and a Tl−O−Tl angle of 105.3(2) Å. The O2−Tl1 distance is 2.785(4) Å. This geometry results in a Tl−Tl separation of 4.1669(8) Å. Each Tl^+ ion is coordinated on one side to four oxygen atoms of three carboxylate groups. In this case the other side is also completely "naked" due to the inert pair ($6s^2$). The Tl^+ cation is therefore in a distorted square-pyramidal geometry, with the four oxygen atoms in the basal plane and the stereoactive lone pair occupying the apex position of the pyramid.

The dimeric $Tl_2(C_9H_9O_4)_2$ units are further linked to infinite one-dimensional chains as depicted in Figure 10. Each carboxylic unit acts as a μ_3-bridging ligand since the O2 oxygen atom links an adjacent unit with an O2−Tl1 distance of 2.720(6) Å. The result is a double-stranded, infinite linear one-dimensional polymeric array of Tl^+ cations with an average deviation from the plane defined by all Tl^+ cations within the chain of 0.014 Å. The chain forms an angle of 34.4° with the plane of the $Tl_2(C_9H_9O_4)_2$ unit. The closest separations between the Tl^+ cations within the chain are 4.1669(8) (within the basic unit), 4.2637(7) and 6.3813(9) Å (Figure 11). The chains run parallel to the *b* axis and the distance between adjacent chains is 5.55 Å. This arrangement results in the lamellar structure shown in Figure 12.

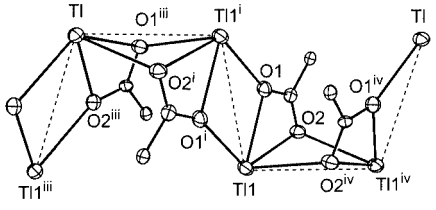

Figure 10. Part of one $[Tl_2(RCOO)_2]_n$ chain of **4** showing the μ_3-bridging mode of the carboxylate groups; phenyl groups are omitted for clarity; selected bond lengths [Å]: Tl1−O1 2.530(5), Tl1−O2 2.785(4), Tl−O1^i 2.710(5), Tl1−O2^{iv} 2.720(6); symmetry codes i: $-x$, $1-y$, $-z$; ii: $-x$, $2-y$, $-z$; iii: $-x$, y, $-z-0.5$; iv: $-x$, y, $-z+0.5$

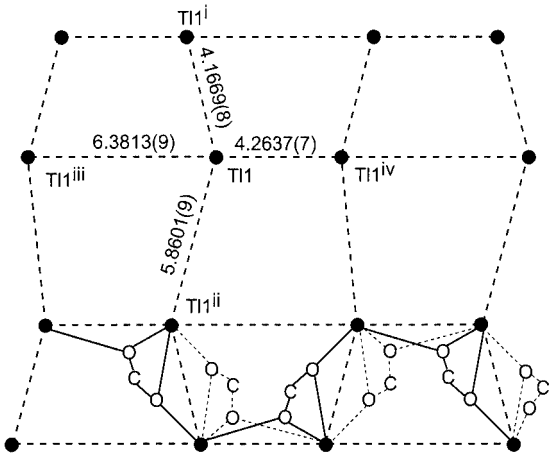

Figure 11. Schematic drawing of the crystal organization of **4** which consists of nearly planar, infinite arrays of Tl^+ cations linked by μ_3-bridging benzoate ligands; symmetry codes as in Figure 10

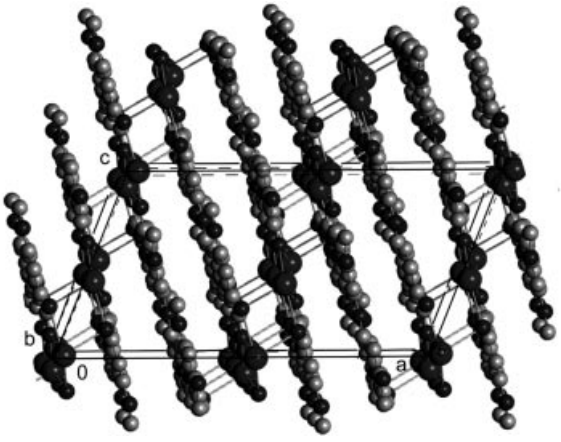

Figure 12. View of the extended lattice along the *c* axis of **4**; hydrogen atoms are omitted for clarity

Conclusions

The four complexes structurally determined in the present study, as well as (*o*-hydroxybenzoato)thallium(I) previously determined, are all based on centrosymmetric dimeric $Tl_2(RCOO)_2$ units. Geometrical parameters of this structural motif are summarized in Table 1. The carboxylate groups act as μ_2-bridging ligands within the unit. One oxygen atom is bound to two thallium ions and the other one to one thallium ion. The doubly coordinated oxygen atom bridges the thallium ions unsymmetrically with average Tl−O distances of 2.59(6) and 2.77(9) Å for the five thallium(I) benzoate compound so far structurally characterized. The singly coordinated oxygen atom has an average Tl−O distance of 2.79(6) Å. This geometry results in a Tl−Tl separation of 4.24(11) Å.

Another characteristic structural motif is the tendency of the thallium ion to only use less than one hemisphere to coordinate ligands. This "half-nakedness" is due to the stereochemically active inert pair ($6s^2$) in an sp-hybridized orbital producing an electronic bulge on one side. This lone pair of electrons thus plays a prominent role in controlling the structures of these compounds. The Tl^+ cations are therefore in pyramidal geometries, with four or five oxygen donor atoms in the basal plane and the stereoactive lone pair occupying the apex position of the pyramid. There are, on the "naked" side of the metal ions, relatively large spaces in a nonpolar environment provided by neighboring phenyl groups, with the nearest carbon atoms situated 3.2−3.4 Å from the Tl^+ ion. The aromatic rings are nearly perpendicular to the vector joining the Tl^+ cation and the centroid of the phenyl group, suggesting that Tl^+−phenyl η^6-interactions are of a certain importance for the crystal organization. Several other examples of structures with Tl^I−arene interactions have been presented, with comparable distances, as discussed by Janiak in his comprehensive review

Table 1. Geometry of the centrosymmetric $Tl_2(RCOO)_2$ moiety of five thallium(I)benzoate compounds

Compound:[a]		**1**	**2**	**3**	**4**	Ref.[11]	Average
Ligand:		Salicylate	4-Amino-salicylate	3,4-Dimethoxy-benzoate[b]	3,5-Dimethoxy-benzoate	3-Hydroxy-benzoate	
Tl1−O1	(Å)	2.601(11)	2.614(12)	2.536(6)	2.530(5)	2.663	2.59(6)
Tl1−O2	(Å)	2.778(11)	2.879(12)	2.806(7)	2.785(4)	2.775	2.79(6)
Tl1−O1^i	(Å)	2.751(11)	2.713(12)	2.930(6)	2.710(5)	2.727	2.86(9)
Tl···Tl	(Å)	4.213(1)	4.253(1)	4.4111(8)	4.1669(8)	4.129	4.23(11)
O1−Tl1−O2	(°)	48.4(3)	48.3(3)	47.2(1)	49.1(1)	48.4	48.3(7)
O1−Tl1−O1^i	(°)	76.2(4)	74.1(4)	68.0(1)	74.1(1)	79.2	74(4)
Tl1−O1−Tl1^i	(°)	103.8(4)	105.9(4)	100.0(2)	101.5(2)	100.8	102(2)
Tl1−Ph[c]	(Å)	3.276	3.312	3.417	3.474	3.265	–
Tl1−Ph[d]	(°)	87.1	87.2	84.0	79.2	89.3	–
Planarity[e]	(Å)	0.109	0.207	0.476	0.087	0.132	–
Twist[f]	(°)	11.0	16.0	45.4	9.5	12.8	–
Packing efficiency[g]	(%)	81.9	78.4	77.3	79.8	–	–

[a] Atomic numbering scheme as in Figures 1, 5 or 9. [b] Symmetry imposes a different numbering scheme as shown in Figure 6. [c] Distance between Tl1 and the centroid of the aromatic ring. [d] Angle between the plane of the aromatic ring and the vector joining Tl1 and the centroid of the aromatic ring. [e] Average atomic deviation from the least-squares plane defined by all atoms in the $Tl_2(C_6H_6COO)_2$ moiety. [f] Angle between the plane defined by the Tl1, Tl1^i, O1 and O2^i atoms and the plane defined by the benzoate ligands. [g] The fraction of the total cell volume occupied by atoms as determined by the Platon software.[19]

of thallium(I) chemistry.[15] The Tl−Tl distances observed in the present study, both within and between dimers, suggest a possible Tl···Tl metallophilic interaction, similar to the well-established aurophilic attraction.[16] Recent ab initio calculations on thallocene dimers suggests energy minima with Tl···Tl distances slightly under 4 Å and interaction strengths of the order of 10 kJ/mol.[17] This attractive interaction is due to dispersion mechanisms and can only be reproduced by ab initio calculations including explicit electron-electron correlation.

Despite the structural similarities, a large variation in crystal organization is observed. In *catena*-[bis(μ_3-salicylato)thallium(I)] (**1**), *catena*-[bis(μ_3-4-aminosalicylato)thallium(I)] (**2**) and *catena*-[bis(μ_3-2-hydroxybenzoato)thallium(I)][10] are adjacent units are held together by secondary Tl−O(hydroxy) interactions, with an average Tl−O distance of 2.96(3) Å, resulting in a crystal organizations which can be described as stair-like, infinite one-dimensional polymers as depicted in Figure 3. In *catena*-[μ_3-(3,4-dimethoxybenzoato)thallium(I)] (**3**), each carboxylic group acts as a μ_4-bridging ligand resulting in infinite two-dimensional, puckered sheets. Finally, in *catena*-[μ_3-(3,5-dimethoxybenzoato)thallium(I)] (**4**) bridges each carboxylic unit three Tl^+ cations to form double-stranded, nearly planar, infinite array of Tl^+ cations, resulting in the lamellar structure shown in Figure 12. The ligands used in this study present a rather limited range of steric and electronic properties and are therefore useful for establishing basic patterns in thallium(I)−benzoate interactions. In following papers, we wish to extent these investigations where steric requirements of the ligands impose restrictions on the thallium coordination geometries and also attempt the use of the inert lone pair as a Lewis base for the construction of extended solids.

Experimental Section

Materials and Methods: Chemicals were purchased from Aldrich Chemicals and used without further purification. IR spectra were recorded with a Perkin−Elmer 1720 X FT-IR spectrometer in the 4000−400-cm^{-1} region with 2 cm^{-1} resolution both as KBr pellets and as pure powders between NaCl windows.

Preparation: All compounds were prepared by adding 5.0 mM Tl_2CO_3 to 100 mL of H_2O and 10.0 mM salicylic acid, 4-aminosalicylic acid, 3,4-dimethoxybenzoic acid or 3,5-dimethoxybenzoic acid, respectively. The solutions were allowed to boil for 2 h while stirring which in all cases yielded clear solutions. The solutions were slowly concentrated which yielded crystals of X-ray quality. The crystals chosen for X-ray analysis and the bulk material were identical as shown by superimposable IR spectra. Total yield > 90%.

***catena*-[Bis(μ_3-salicylato)dithallium(I)] (1):** IR: $\tilde{\nu}$ = 3065 (w), 3049 (w), 1621 (m), 1584 (w), 1564 (s), 1478 (s), 1448 (s), 1406 (w), 1384 (s), 1333 (m), 1301 (m), 1289 (w), 1251 (w), 1137 (w), 1087 (w), 1023 (w), 982 (vw), 961 (vw), 862 (s), 810 (s), 770 (s), 698 (s), 666 (s), 565 (w), 537 (w), 528 (m), 452 (w) cm^{-1}.

***catena*-[Bis(μ_3-*o*-aminosalicylato)dithallium(I)] (2):** IR: $\tilde{\nu}$ = 3467 (w), 3341 (w), 1619 (m), 1573 (s), 1552 (m), 1503 (s), 1444 (s), 1372 (s), 1296 (s), 964 (w), 831 (m), 782 (m), 698 (m), 626 (s), 596 (w), 531 (w), 447 (m) cm^{-1}.

***catena*-[(3,4-Dimethoxybenzoato)thallium(I)] (3):** IR: $\tilde{\nu}$ = 3083 (w), 3010 (w), 2958 (w), 2932 (w), 2901 (w), 2828 (vw), 1598 (s), 1520 (s), 1511 (m), 1460 (m), 1444 (m), 1403 (m), 1374 (s), 1354 (m), 1268 (s), 1252 (m), 1231 (s), 1180 (m), 1133 (m), 1107 (s), 1021 (s), 947 (w), 923 (w), 875 (m), 835 (m), 789 (s), 778 (s), 766 (s), 726 (w), 624 (s), 612 (w), 523 (m) cm^{-1}.

catena-[(3,5-Dimethoxybenzoato)thallium(I)] (4): IR : $\tilde{\nu}$ = 3083 (w), 3010 (w), 2958 (w), 2932 (w), 2901 (w), 2836 (w), 1598 (s), 1520(vs), 1505 (s), 1460 (w), 1444 (w), 1403 (s), 1374 (s), 1354 (w), 1268 (s),

Table 2. Crystallographic data

	1	**2**	**3**	**4**
Empirical formula	$(C_7H_5O_3Tl)_2$	$(C_7H_6NO_3Tl)_2$	$C_9H_9O_4Tl$	$C_9H_9O_4Tl$
M [g·mol^{-1}]	682.96	713.00	385.53	385.53
T [K]	295	295	295	295
Crystal system	monoclinic	monoclinic	monoclinic	monoclinic
Space group	$P2_1/n$ (no. 11)	$P2_1/n$ (no. 11)	$P2_1/c$ (no. 14)	$C2/c$ (no. 15)
a [Å]	6.123(1)	7.039(1)	14.202(3)	19.850(3)
b [Å]	11.938(2)	11.904(2)	7.320(2)	9.793(1)
c [Å]	9.893(2)	9.463(1)	9.700(2)	10.645(1)
β [°]	93.354(4)	91.895(3)	103.427(4)	111.732(4)
V [Å^3]	721.9(2)	792.5(2)	980.8(4)	1922.2(4)
Z	2	2	4	8
Θ range [°]	2.68−25.99	2.75−26.49	3.15−28.00	2.21−28.00
Completeness to Θ_{max} (%)	99.8	95.2	96.9	97.4
μ [cm^{-1}]	22.319	20.341	16.452	16.788
Reflections measured	3894	3606	5295	5866
Unique reflections (R_{int})	1415 (0.0647)	1559 (0.0699)	2296 (0.0846)	2263 (0.0915)
Observed reflections [$I > 2\sigma(I)$]	985	955	1488	1440
R_1 (observed reflections)	0.0581	0.0627	0.0418	0.0380
wR_2 (all reflections)	0.1439	0.1487	0.0899	0.0676

1252 (w), 1231 (s), 1180 (w), 1156 (vw), 1133 (w), 1107 (s), 1033 (vw), 1021 (s), 947 (vw), 923 (vw), 875 (w), 835 (w), 789 (s), 778 (s), 766 (s), 726 (vw), 634 (s), 612 (w) cm^{-1}.

Single Crystal X-ray Crystallography: Single crystal diffraction data were collected at 298 K with a Bruker SMART platform equipped with a CCD area detector and a graphite monochromator using Mo-K_α radiation. Cell parameters were refined using 985, 955, 1488 and 1400 reflections for **1**, **2**, **3** and **4**, respectively. A hemisphere of data (1291 frames) was collected for each structure using the ω-scan method (0.3° frame width) with 40 s exposure time. The crystal−detector distance was 4.77 cm. The first 50 frames were re-measured at the end of the data collection to monitor instrument and crystal stability. Intensity decay was negligible for all compounds. Data reduction and empirical absorption correction were performed using the program packages Bruker SAINT and SADABS, respectively.[18] The structures were solved by the direct methods in SHELXTL and refined using full-matrix least-squares on F^2. Non-H atoms were treated anisotropically. Carbon-H atoms were generated in ideal positions riding on their respective carbon atom. Oxygen-H and nitrogen-H atoms were localized on difference Fourier maps but their distances were constrained to 0.82 and 0.86 Å, respectively. Crystal and experimental data are summarized in Table 2. CCDC-174558 (**1**), -174556 (**2**), -174555 (**3**) and -174557 (**4**) contain the supplementary crystallographic data for this paper. These data can be obtained free of charge at www.ccdc.cam.ac.uk/conts/retrieving.html or from the Cambridge Crystallographic Data Centre, 12, Union Road, Cambridge CB2 1EZ, UK [Fax: (internat.) + 44-1223/336-033; E-mail: deposit@ccdc.cam.ac.uk].

Acknowledgments

We are grateful to Dr. Ingmar Haglund for interesting discussions.

[1] K. S. Pitzer, *Acc. Chem. Res.* **1979**, *12*, 271−276.
[2] P. Pyykkö, J. P. Desclaux, *Acc. Chem. Res.* **1979**, *12*, 276−281.
[3] N. W. Alcock, H. D. B. Jenkins, *J. Chem. Soc., Dalton Trans.* **1974**, 1907−1911.
[4] P. Moser, H. M. Schwunck, W. Jung, *Z. Anorg. Allg. Chem.* **1998**, *624*, 1256−1261.
[5] A. El Abiad, B. Es-Sakhi, M. Mesnaoui, M. Maazaz, I. Belharouak, P. Graveraeau, C. Parant, G. Wallez, G. Le Flem, *J. Solid State Chem.* **2000**, *154*, 584−590.
[6] P. L. Jones, K. L. V. Mann, J. C. Jerrery, J. A. McCleverty, M. D. Ward, *Polyhedron* **1997**, 16−14), 2435−2440; D. A. Bardwell, J. C. Jerrery, J. A. McCleverty, M. D. Ward, *Inorg. Chim. Acta* **1998**, *267*, 232−328.
[7] E. Psillakis, J. C. Jerrery, J. A. McCleverty, M. D. Ward, *J. Chem. Soc., Dalton Trans.* **1997**, 1645−1651.
[8] G. Ferguson, M. C. Jennings, F. J. Taylor, *Acta Crystallogr., Sect. C* **1991**, *47*, 2079−2062.
[9] S.-H. Huang, R.-J. Wang, T. C. W. Mak, *J. Chem. Soc., Dalton Trans.* **1991**, 1379−1381.
[10] I. Haiduc, F. T. Edelmann, *Supramolecular Organometalic Chemistry*, Wiley-VCH Verlag, Weinheim, **1999**, p. 218−227.
[11] S. L. Rusakov, E. B. Chuklanova, A. I. Gusev, T. V. Lisyat, Yu. Ya. Kharitonov, I. S. Kolomnikov, *Koord. Khim.* **1987**, *13*, 1613.
[12] J. Beck, J. Strahle, *Z. Naturforsch., Teil B* **1986**, *41*, 1381−1386.
[13] K. Aoki, I. H. Suh, H. Nagashima, J. Uzawa, H. Yamazaki, *J. Am. Chem. Soc.* **1992**, *114*, 5722−5729.
[14] *CRC Handbook of Chemistry and Physics* (Ed.: R. C. Weast), The Chemical Rubber Co., Cleveland, OH, **1978**, p. F-213.
[15] A. Bondi, *J. Phys. Chem.* **1964**, *68*, 441−451.
[16] C. Janiak, *Coord. Chem. Rev.* **1997**, *163*, 107−216.
[17] P. Pyykkö, *Chem. Rev.* **1997**, *97*, 597−636.
[18] P. Pyykkö, M. Straka, T. Tamm, *Phys. Chem. Chem. Phys.* **1999**, *1*, 3441−3444.
[19] SMART v. 5.046, SAINT v. 5.01, SADABS, SHELXTL v. 5.1, Bruker Analytical X-ray Systems, Madison, Wisconsin, USA.
[20] P. van der Sluis, A. L. Spek, *Acta Crystallogr., Sect. A* **1990**, *46*, 194−201.

Received November 28, 2001
[I01485]

The Synthesis and Structure of Bis- and Tris(amino)-Functionalised Cyclopentadienylyttrium Derivatives

Marco M. Corradi,[a] Margaret A. D. McGowan,[a] Patrick C. McGowan,*[a] and Mark Thornton-Pett[a]

Keywords: N ligands / Cyclopentadienyl ligands / Yttrium

The reaction of YCl_3 with 2 or 3 equiv. of $NaC_5H_4CH([CH_2]_2)_2NMe$ in toluene affords $[\{Y[\eta\text{-}C_5H_4CH([CH_2]_2)_2NMe]_2(\mu\text{-}Cl)\}_2]$ (**1**) and $[Y\{\eta\text{-}C_5H_4CH([CH_2]_2)_2NMe\}_3]$ (**2**), respectively, in high yield; the three amino-functionalised cyclopentadienyl units of **2** are fluxional at room temperature, giving us a rare example of stabilisation of an yttrium centre without the use of extraneous ligands.

(© Wiley-VCH Verlag GmbH, 69451 Weinheim, Germany, 2002)

Introduction

Amino-functionalised cyclopentadienyl derivatives have been used to great effect in complexes of the d-block elements.[1,2] As part of our ongoing studies investigating the early transition metal systems for metal−dihydrogen bonding we decided, given previous successes, to concentrate on the (*N*-methylpiperid-4-yl)cyclopentadienyl ligand.[3−6] In this paper we present a number of new yttrium chloride complexes, one of which shows particularly interesting fluxional properties and provides a rare example of stabilisation of a cyclopentadienyl centre without the use of extraneous ligands.

Results and Discussion

As part of our ongoing work concerning the formation of new bis(cyclopentadienyl)yttrium hydride derivatives we report the synthesis and structure of $[\{Y[\eta\text{-}C_5H_4CH([CH_2]_2)_2NMe]_2(\mu\text{-}Cl)\}_2]$ (**1**) and $[Y\{\eta\text{-}C_5H_4CH([CH_2]_2)_2NMe\}_3]$ (**2**); the latter derivative is an intriguing fluxional tris(cyclopentadienyl) compound and provides the first example of a homoleptic base-stabilised tris(cyclopentadienyl)yttrium complex. The reaction of YCl_3 with 2 equiv. of $NaC_5H_4CH([CH_2]_2)_2NMe$ in THF at 45 °C afforded **1** in high yield (71%) (Scheme 1) which was characterised by ^1H, $^{13}C\{^1H\}$, and ^1H-^{13}C correlation NMR spectroscopy. The reaction of YCl_3 with 3 equiv. of $NaC_5H_4CH([CH_2]_2)_2NMe$ in THF at 50 °C similarly afforded **2** in high yield (85%) which was also formed when the reaction was carried out in toluene.

Crystallisation of **1** from a concentrated toluene solution at −30 °C afforded colourless prisms. The molecular structure, determined from a single-crystal X-ray diffraction study, revealed **1** to be dimeric with an inversion centre at the intersection of the Y(1)−Y(1′) and Cl(1)−Cl(1′) vectors and a *metallocene dichloride type* ligand geometry about the Y atoms (Figure 1) while the *N*-methylpiperid-4-yl moieties, in chair conformation, point to opposite sides of the *metallocene* geometry to minimise steric crowding. A similar bonding arrangement has been previously reported for $[\{Y(\eta\text{-}C_5H_4SiMe_3)_2(\mu\text{-}Cl)\}_2]$,[7,8] $[\{Y(\eta\text{-}C_5H_4[C_6H_9\text{-}2\text{-}i\text{Pr}\text{-}5\text{-}Me])_2(\mu\text{-}Cl)\}_2]$,[9] $[\{Y(\eta\text{-}C_5H_5)_2(\mu\text{-}Cl)\}_2]$,[10] and $[\{Y(\eta\text{-}C_5H_4PPh_2)_2(\mu\text{-}Cl)\}_2]$.[11] The Y(1)−Cl(1) and Y(1)−Cl(1′) bond lengths of 2.6850(7) and 2.6984(7) Å are similar to other reported chloro-bridged dimeric bis(cyclopentadienyl)-yttrium derivatives. The average cyclopentadienyl ring C−C bond lengths and angles are unexceptional [1.412(4) Å, 108.0(3)°].

Despite the relatively high coordination number, monomeric tris(cyclopentadienyl)Ln complexes are coordinatively unsaturated. In the absence of solvents, these molecules form oligomeric structures in the solid state.[12,13] With the addition of donor ligands or coordinating solvents molecules of the type $LnCp_3L$ can be formed, e.g., $[Y(\eta\text{-}C_5H_5)_3(THF)]$[14] and $[Y(\eta\text{-}C_5H_5)_2(\eta\text{-}C_5H_4CH_2CH_2OMe)]$.[15] Crystallisation of the extremely air- and moisture-sensitive compound **2** from a concentrated toluene solution at −30 °C afforded pale yellow prisms. The molecular structure was determined from a single-crystal X-ray diffraction study (Figure 2). The ligand geometry about the Y atom is slightly distorted from trigonal-planar, with

[a] Department of Chemistry, University of Leeds, Leeds LS2 9JT, United Kingdom

$$[\{Y(\eta\text{-}C_5H_4CH[CH_2]_4NMe)_2(\mu\text{-}Cl)\}_2] \xleftarrow{(i)} YCl_3 \xrightarrow{(ii)} [Y\{\eta\text{-}C_5H_4CH(CH_2)_4NMe\}_3]$$

1 **2**

Scheme 1. Reagents and conditions: (*i*) 2 $NaC_5H_4CH([CH_2]_2)_2NMe$, THF, 45 °C, 12 h; (*ii*) 3 $NaC_5H_4CH([CH_2]_2)_2NMe$, THF or toluene, 50 °C, 12 h

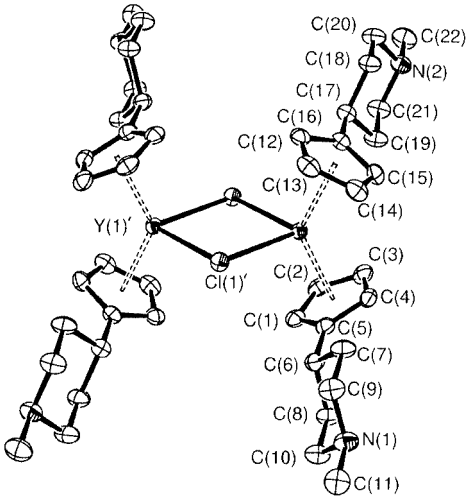

Figure 1. The molecular structure of **1** and atom numbering scheme with selected bond lengths [Å] and angles [°]; estimated standard deviations in parentheses: Y(1)−C(1) 2.652(3), Y(1)−C(12) 2.653(3), Y(1)−C(2) 2.612(3), Y(1)−C(13) 2.619(3), Y(1)−C(3) 2.589(3), Y(1)−C(14) 2.591(3), Y(1)−C(4) 2.618(3), Y(1)−C(15) 2.617(3), Y(1)−C(5) 2.667(3), Y(1)−C(16) 2.673(3), Y(1)−Cl(1) 2.6984(7), Y(1)−Cl(1)′ 2.6850(7); C(2)−Y(1)−C(1) 30.99(10), Y(1)−Cl(1)−Y(1)′ 96.30(2), C(4)−Y(1)−C(12) 132.04(10), C(10)−N(1)−C(11) 111.0(3), C(21)−N(2)−C(22) 110.0(3), C(9)−N(1)−C(11) 109.8(3)

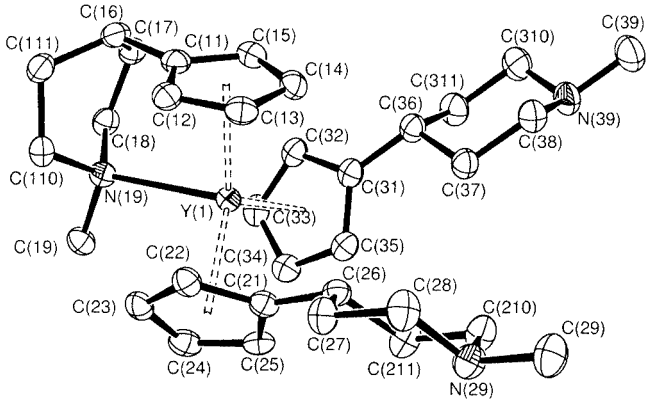

Figure 2. The molecular structure of **2** and atom numbering scheme with selected bond lengths [Å] and angles [°]; estimated standard deviations in parentheses: Y(1)−C(11) 2.723(2), Y(1)−C(14) 2.693(2), Y(1)−C(15) 2.680(2), Y(1)−C(34) 2.690(2), Y(1)−C(33) 2.712(2), Y(1)−C(35) 2.724(2), Y(1)−C(21) 2.732(2), Y(1)−C(22) 2.750(2), Y(1)−C(23) 2.738(2), Y(1)−C(24) 2.734(2), Y(1)−C(25) 2.743(2), Y(1)−N(19) 2.6954(19); C(11)−Y(1)−C(21) 122.32(7), C(26)−C(21)−Y(1) 119.12(15), C(19)−N(19)−Y(1) 107.14(14), C(19)−N(19)−C(18) 107.35(18), C(19)−N(19)−C(110) 107.27(19), C(18)−N(19)−C(110) 106.44(18), C(19)−N(19)−Y(1) 107.14(14), C(18)−N(19)−Y(1) 116.34(14), C(110)−N(19)−Y(1) 111.88(14)

the angles between the centroids of the cyclopentadienyl substituents, M−Y(1)−M, of ca. 116−118°.

Two of the *N*-methylpiperid-4-yl rings adopt a chair conformation and point away from the metal centre [Cp^A and

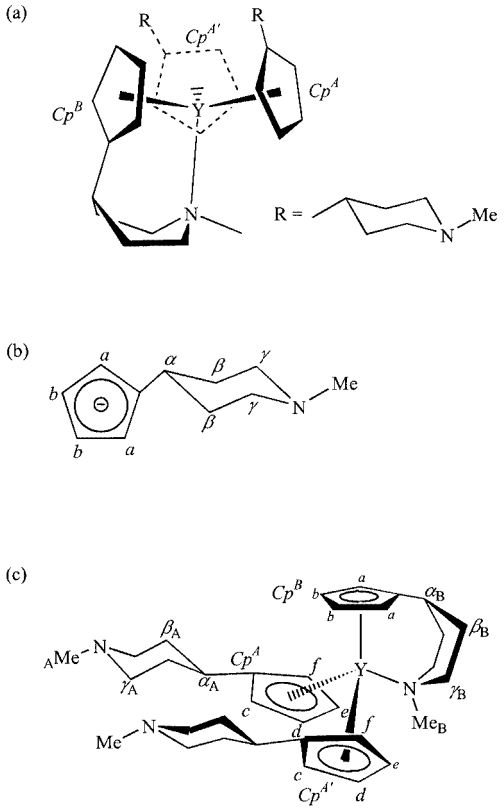

Figure 3. (a) Ligand geometry about the yttrium centre of **2**; (b) $C_5H_4CH([CH_2]_2)_2NMe$ ligand; (c) molecular structure of **2** at −60 °C

$Cp^{A'}$, see (a) in Figure 3], whereas the third *N*-methylpiperid-4-yl ring (Cp^B) is bound to the metal centre through the d_{z^2} metal orbital.[16] A similar bonding arrangement has been previously reported for [2-(dimethylamino)ethyl]cyclopentadienyl derivatives $[Ln(\eta\text{-}C_5H_4CH_2CH_2NMe_2)_3]$ (Ln = La, Nd).[17] The boat confomation of the Cp^B ring confirms the bound nature of the N moiety. The Y(1)−N(19) bond length of 2.6954(19) Å is somewhat longer than the distance of 2.501(4) Å reported for $[Y(\eta\text{-}C_5Me_5)(\eta\text{-}C_5H_4CHC_6H_4CH_2NMe_2)Cl]$[18] and **2** could be viewed as a strained 10-coordinate compound. The Y−C(Cp) bond lengths are similar to previously reported tris(cyclopentadienyl)Y derivatives.[12,14,15] The average cyclopentadienyl ring C−C bond lengths and angles are unexceptional [1.409(3) Å, 108.0(2)°].

Compound **2** was initially characterised by ^1H NMR spectroscopy; the room-temperature ^1H NMR spectrum (300.13 MHz, C_7D_8) displayed broad resonance signals, which sharpened upon warming to 80 °C to give the time-averaged ^1H NMR spectrum typical for the $C_5H_4CH([CH_2]_2)_2NMe$ ligand [see (b) in Figure 3]. Compound **2** was characterised at this elevated temperature by

^1H, $^{13}C\{^1H\}$, and ^1H-^{13}C correlation NMR spectroscopy. Cooling of **2** from room temperature to −60 °C afforded multiple resonance signals in the ^1H NMR spectrum, indicating the formation of a static structure with one of the pendant arms bound to the yttrium centre [see (c) in Figure 3]. This structural arrangement was also investigated by low-temperature $^{13}C\{^1H\}$, DEPT-135, INEPT (Figure 4), and ^1H-^{13}C correlation NMR spectroscopy. The $^{13}C\{^1H\}$ NMR resonance assignments for the *N*-methylpiperid-4-yl function at both 80 and −60 °C are summarised in Table 1.

The $^{13}C\{^1H\}$ NMR spectrum of **2** at −60 °C in the *N*-methylpiperid-4-yl region (δ ≈ 20−60 ppm) displays 9 distinct resonances due to slow structural isomer interconversion on the NMR time-scale. Two resonance signals are observed for the γ-CH_2 environment at δ = 56.5 and 53.1 ppm in the approximate ratio 2:1. Warming sees a gradual broadening and coalescence at ca. 20 °C eventually giving rise to one ^{13}C resonance at δ = 55.6 ppm. Two ^{13}C resonances are also observed for the Me environments (δ = 46.9 and 50.8 ppm coalescing at ca. 20 °C and giving one resonance at 50 °C at δ = 47.2 ppm) and the α-CH environment (δ = 25.1 and 36.7 ppm coalescing at ca. 30 °C giving one resonance at δ = 34.0 ppm). The β-CH_2 environments give rise at −60 °C, however, to three distinct resonances (δ = 25.0, 34.2, and 34.9 ppm), indicating a further decrease in the symmetry of the molecular fragment, due to close approach of the *N*-methylpiperid-4-yl arms at the β-position. A similar phenomenon has been previously observed in the

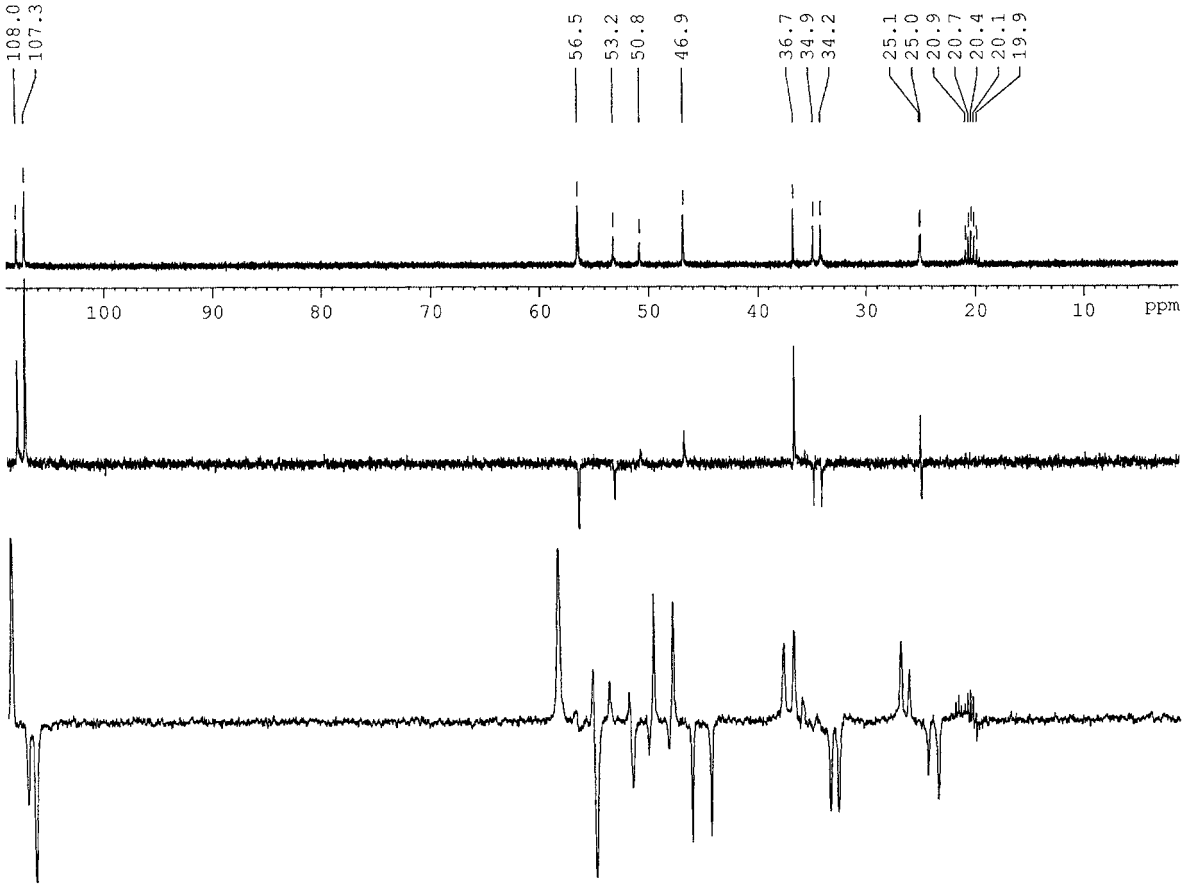

Figure 4. (a) $^{13}C\{^1H\}$, (b) DEPT 135, and (c) INEPT NMR spectra of **2** at −60 °C

Table 1. $^{13}C\{^1H\}$ NMR resonance assignments for the *N*-methylpiperid-4-yl function

Compound	Assignment			
	β-CH_2	α-CH	Me	γ-CH_2
$NaC_5H_4CH([CH_2]_2)_2NMe$ (C_4D_8O, room temp.)	36.7	38.4	47.4	58.3
1 (C_4D_8O, room temp.)	34.5	36.8	47.0	57.1
2 (C_7D_8, 80 °C)	32.0	34.0	47.2	55.6
2 (C_7D_8, −60 °C)	25.0 (β_B), 34.2 (β_A), 34.9 (β_A)	25.1 (α_B), 36.7 (α_A)	46.9 (Me_A), 50.8 (Me_B)	53.2 (γ_B), 56.5 (γ_A)

cyclohexyl derivative [Fe(η-C_5H_2-1,2,4-{$CH([CH_2]_2)_2$-CH_2}$_3$)$_2$].[19] The ^{1}H NMR spectrum of **1** at room temperature exhibits resonances typical for the $C_5H_4CH([CH_2]_2)_2NMe$ ligand. Comparison of the $^{13}C\{^1H\}$ resonance values of **2** with those of **1** at both −60 and 80 °C (Table 1) provides evidence for non-coordination of the *N*-methylpiperid-4-yl side arm to the Y^{3+} centre. Compound **1** was found to be only sparingly soluble in toluene, petroleum ether, and dichloromethane solvents. The ^{1}H and $^{13}C\{^1H\}$ NMR spectral assignments, obtained in C_4D_8O with resulting cleavage of the bridging Y−Cl bonds,[20] are thus of the THF adduct Y{η-$C_5H_4CH([CH_2]_2)_2$-NMe}$_2$Cl(THF).

In conclusion the following features of **1** and **2** are noteworthy. (*i*) The presence of the pendant arm functionality on **1** provides a Lewis base for protonation in close proximity to the metal centre. (*ii*) Compound **2** also reveals the potential advantage of the strained *N*-methylpiperid-4-yl-functionalised cyclopentadienyl ligand in the stabilisation and reaction of related yttrium hydride derivatives as it may point towards, yet only weakly bind to, the Y^{3+} metal centre. (*iii*) Compound **2** is the first example of a homoleptic base-stabilised tris(cyclopentadienyl)yttrium derivative.

Experimental Section

[{Y[η-$C_5H_4CH([CH_2]_2)_2NMe]_2(μ-Cl)$}$_2$] (1): To a Schlenk tube charged with a slurry of YCl_3 (0.61 g, 3.1 mmol) in THF (80 mL) was added a THF slurry (60 mL) of $NaC_5H_4CH([CH_2]_2)_2NMe$ (1.15 g, 6.2 mmol) at room temperature. The reaction mixture was warmed to 45 °C and stirred for 12 h to afford an off-white slurry. The THF was removed in vacuo and the resulting beige solid extracted with toluene (2 × 50 mL). The extracts were combined and the solvents were removed in vacuo to afford **1** as a white solid (0.99 g, 1.10 mmol, 71%). $C_{44}H_{64}Cl_2N_4Y_2$ (897.7): calcd. C 58.87, H 7.19, N 6.24; found C 55.0, H 7.2, N 3.7 (after many attempts, this was the best microanalysis found). ^{1}H NMR (300.13 MHz, C_4D_8O, room temp.): δ = 1.48 (m, 2 H, γ), 1.69 (br. s, THF), 1.87 (m, 4 H, β), 2.16 (s, 3 H, Me), 2.49 (tt, $J_{H,H}$ = 3.68, 11.76 Hz, 1 H, α), 2.76 (m, 2 H, γ), 3.53 (br. s, THF), 5.91 (br. s, 4 H, Cp) ppm. $^{13}C\{^1H\}$ NMR (75.47 MHz, C_4D_8O, room temp.): δ = 34.5 (β, $^1J_{CH}$ = 129 Hz), 36.8 (α, $^1J_{CH}$ = 131 Hz), 47.0 (Me, $^1J_{CH}$ = 132 Hz), 57.1 (γ, $^1J_{CH}$ = 132 Hz), 110.1 (Cp, $^1J_{CH}$ = 167 Hz), 110.2 (Cp, $^1J_{CH}$ = 167 Hz) ppm.

[Y{η-$C_5H_4CH([CH_2]_2)_2NMe$}$_3$] (2): To a Schlenk tube charged with a slurry of YCl_3 (0.99 g, 5.1 mmol) in THF (80 mL) was added a THF slurry (50 mL) of $NaC_5H_4CH([CH_2]_2)_2NMe$ (2.80 g, 15.2 mmol) dropwise at room temperature. An immediate colour change of white to pale yellow was observed. The reaction mixture was warmed to 50 °C and stirred for 12 h to afford a brown slurry. The THF was removed in vacuo and the resulting sticky brown solid extracted with toluene (3 × 30 mL). The toluene was removed in vacuo to afford **2** as a white solid (2.48 g, 4.3 mmol, 85%). $C_{33}H_{48}N_3Y$ (575.7): calcd. C 68.9, H 8.3, N 7.3; found C 68.45, H 8.2, N 6.9. ^{1}H NMR (300.13 MHz, C_7D_8, room temp.): δ = 1.98 (br. s, 6 H, β, γ), 2.21 (br. s, 3 H, Me), 2.82 (br. s, 1 H, α), 2.90 (br. s, 2 H, γ), 6.01 (br. s, 4 H, Cp) ppm; (300.13 MHz, C_7D_8, 80 °C): δ = 1.77 (m, 4 H, β), 1.90 (m, 2 H, γ), 2.15 (s, 3 H, Me), 2.56 (m, 1 H, α), 2.80 (m, 2 H, γ), 5.79 (m, 2 H, Cp), 5.82 (m, 2 H, Cp) ppm; (300.13 MHz, C_7D_8, −60 °C): δ = 1.27 (br. s, γ_B), 1.29 (br. s, β_B), 1.79 (s, Me_B, β_B), 1.84 (m, β_A), 1.95 (m, γ_A), 2.04 (m, β_A), 2.09 (m, β_A), 2.28 (s, Me_A), 2.49 (br. s, γ_B), 2.73 (br. s, α_A, α_B), 2.95 (bt, γ_A), 5.47 (s, Cp), 5.50 (s, Cp), 5.87 (s, Cp), 5.95 (s, Cp), 6.03 (s, Cp), 6.18 (s, Cp) ppm. $^{13}C\{^1H\}$ NMR (75.47 MHz, C_7D_8, −60 °C): δ = 25.0 (β_B, $^1J_{CH}$ = 130 Hz), 25.1 (α_B, $^1J_{CH}$ = 132 Hz), 34.2 (β_A, $^1J_{CH}$ = 127 Hz), 34.9 (β_A, $^1J_{CH}$ = 128 Hz), 36.7 (α_A, $^1J_{CH}$ = 135 Hz), 46.9 (Me_A, $^1J_{CH}$ = 132 Hz), 50.8 (Me_B, $^1J_{CH}$ = 137 Hz), 53.2 (γ_B, $^1J_{CH}$ = 139 Hz), 56.5 (γ_A, $^1J_{CH}$ = 132 Hz), 107.3 (Cp, $^1J_{CH}$ = 167 Hz), 108.0 (Cp, $^1J_{CH}$ = 167 Hz), 110.8 (Cp, $^1J_{CH}$ = 166 Hz), 111.6 (Cp, $^1J_{CH}$ = 164 Hz), 112.4 (Cp, $^1J_{CH}$ = 166 Hz) ppm; (75.47 MHz, C_7D_8, 80 °C): δ = 32.0 (β), 34.0 (α), 47.2 (Me), 55.6 (γ), 109.2 ($Cp_{a,b}$), 111.4 ($Cp_{a,b}$) 129.6 (Cp-C) ppm.

X-ray Structure Determination for 1 and 2

Crystal Data for [{Y[η-$C_5H_4CH([CH_2]_2)_2NMe]_2(μ-Cl)$}$_2$]·$C_7H_8$ (1·C_7H_8): Crystallographic measurements were made with a Nonius Kappa CCD area diffractometer using (Mo-K_α) radiation, λ = 0.71073 Å. The structure was solved by direct methods and refined on F^2 by the full-matrix least-squares procedure. T = 150(2) K. Specimen 0.53 × 0.46 × 0.22 mm, $C_{51}H_{72}Cl_2N_4Y_2$, M = 989.85, monoclinic, spacegroup $P2_1/c$, a = 16.1070(3), b = 21.8000(3), c = 7.02100(10) Å, β = 97.6950(10)°, V = 2443.10(7) Å^3, $D_{calcd.}$ = 1.346 Mg/m^3, Z = 2. For reflections with 0.998° ≤ θ ≤ 27.48°, $R(F)$ = 0.0442 for 4810 observed reflections [$I > 2\sigma(I)$] and $wR(F^2)$ = 0.1389 for 5576 independent reflections [R(int) = 0.0571]. A molecule of toluene was found which showed a symmetry-related disorder over 2 sites, which was modelled using a rigid body refinement.

Crystal Data for [Y{η-$C_5H_4CH([CH_2]_2)_2NMe$}$_3$] (2): Crystallographic measurements were made with a Nonius Kappa CCD area diffractometer using (Mo-K_α) radiation, λ = 0.71073 Å. The structure was solved by direct methods and refined on F^2 by the full-matrix least-squares procedure. T = 150(2) K. Specimen 0.36 × 0.28 × 0.22 mm, $C_{33}H_{48}N_3Y$, M = 575.65, monoclinic, spacegroup $C2/c$, a = 36.9061(6), b = 12.5796(2), c = 13.2611(2) Å, β = 108.9720(10)°, V = 5822.21(16) Å^3, $D_{calcd.}$ = 1.313 Mg/m^3, Z = 8. For reflections with 1.72° ≤ θ ≤ 26°, $R(F)$ = 0.0332 for 4803 observed reflections [$I > 2\sigma(I)$] and $wR(F^2)$ = 0.085 for 5701 independent reflections [R(int) = 0.0445].

Acknowledgments

We thank the EPSRC for funding.

[1] P. Jutzi, T. Redeker, *Eur. J. Inorg. Chem.* **1998**, 663−674.
[2] P. Jutzi, C. Müller, B. Neumann, H.-G. Stammler, *J. Organomet. Chem.* **2001**, *625*, 180−185.
[3] P. C. McGowan, C. E. Hart, B. Donnadieu, R. Poilblanc, *J. Organomet. Chem.* **1997**, *528*, 191−194.
[4] M. M. Abad, I. Atheaux, A. Maisonnat, B. Chaudret, *Chem. Commun.* **1999**, 381−382.
[5] S. Bradley, P. C. McGowan, K. A. Oughton, M. Thornton-Pett, M. E. Walsh, *Chem. Commun.* **1999**, 77−78.
[6] M. A. D. McGowan, P. C. McGowan, *Inorg. Chem. Commun.* **2000**, *3*, 337−340.
[7] R. D. Rogers, R. V. Bynum, J. L. Atwood, *J. Organomet. Chem.* **1980**, *192*, 65−73.

[8] W. J. Evans, M. S. Sollberger, J. L. Shreeve, J. M. Olofson, J. H. Hain, J. W. Ziller, *Inorg. Chem.* **1992**, *31*, 2492−2501.
[9] W.-P. Leung, F.-Q. Song, F. Xue, Z.-Y. Zhang, T. C. W. Mak, *J. Organomet. Chem.* **1999**, *582*, 292−300.
[10] E. B. Lobkovskii, G. L. Soloveichik, B. M. Bulichev, A. B. Erofeev, *Zh. Strukt. Khim.* **1984**, *25*, 170−171.
[11] R. Broussier, G. Delmas, P. Perron, B. Gautheron, J. L. Petersen, *J. Organomet. Chem.* **1996**, *511*, 185−192.
[12] M. Adam, U. Behrens, R. D. Fischer, *Acta Crystallogr., Sect. C* **1991**, *47*, 968−971.
[13] C. Qian, B. Wang, D. Deng, J. Sun, F. E. Hahn, J. Chen, P. Zheng, *J. Chem. Soc., Dalton Trans.* **1996**, 955−960.
[14] R. D. Rogers, J. L. Atwood, A. Emad, D. J. Sikora, M. D. Rausch, *J. Organomet. Chem.* **1981**, *216*, 383−392.
[15] C. Qian, B. Wang, D. Deng, X. Jin, *Polyhedron* **1993**, *12*, 2265−2269.
[16] W. W. Lukens, R. A. Andersen, *Organometallics* **1995**, *14*, 3435−3439.
[17] R. Anwander, W. A. Herrmann, W. Scherer, F. C. Munck, *J. Organomet. Chem.* **1993**, *462*, 163−174.
[18] H. Schumann, E. C. E. Rosenthal, J. Demtschuk, G. A. Molander, *Organometallics* **1998**, *17*, 5324−5333.
[19] J. A. Burman, M. L. Hays, D. J. Burkey, P. S. Tanner, T. P. Hanusa, *J. Organomet. Chem.* **1994**, *479*, 135−139.
[20] P. B. Hitchcock, M. F. Lappert, S. Tian, *Organometallics* **2000**, *19*, 3420−3428.

Received December 28, 2001
[I01529]

A Unique Dinuclear Cu^{II} Compound with Two Phase Transitions Clearly Visible from Thermal and Magnetic Behaviour; Synthesis, Magnetism and X-ray Structures at Three Temperatures of Bis(di-2-pyridylamine)bis-(μ-hydroxo)bis(μ-perchlorato-*O*,*O*)dicopper(II)

Sujittra Youngme,[a] Gerard A. van Albada,[c] Huub Kooijman,[d] Olivier Roubeau,[c] Wasit Somjitsripunya,[a] Anthony L. Spek,[d] Chaveng Pakawatchai,[b] and Jan Reedijk*[c]

Keywords: Copper / Bridging ligands / Magnetic properties / Phase transitions / X-ray structure

A new compound, $[Cu(dpyam)(OH)]_2(ClO_4)_2$ (dpyam = di-2-pyridylamine) is studied in detail and characterised by magnetic susceptibility and heat capacity measurements. This unique compound exhibits two phase transitions at 192 and 116 K. To obtain more insight into the origin of this transition, X-ray crystal structures at 3 different temperatures, below (**1A**, 110 K), between (**1B**, 150 K) and above (**1C**, 200 K) the transitions are measured. The structure consists of a dinuclear Cu^{II} unit with two bridging hydroxo groups and with two ligands bound to each copper atom via N, while the axial sites are occupied by oxygen atoms of bridging perchlorate anions, providing a distorted tetragonal environment with a Cu–Cu distance which varies from 2.9328(6) to 2.9633(6) Å, and a Cu–O–Cu angle which varies from 99.00(9) to 100.53(9)°. In all three structures, the $Cu_2O_2L_2$ unit does not change significantly. The only changes involve the position of the perchlorate anions and their H bonds with the bridging OH groups. These anions have slightly different positions at different temperatures and appear to be the major origin of the crystallographic phase-transitions. Fitting the magnetic susceptibility measurements revealed a singlet-triplet separation (J) of -37.2 cm^{-1} (antiferromagnetic), in the temperature ranges 275–190 K and 115–50 K. In the range 190–115 K a best fit, albeit inaccurate, of 29.3 cm^{-1} for J (ferromagnetic) is found. A small magnetic hysteresis of 0.5 K has been observed in the phase transition at 116 K. The heat capacity measurements have confirmed the transitions and the excess entropy (ΔS) and enthalpy (ΔH) have been calculated as 4.9 and 2.0 J K^{-1} mol^{-1} for ΔS (for 192.3 K and 116.4 K, respectively), and 0.96 and 0.25 kJ mol^{-1} for ΔH (for 192.3 K and 116.4 K, respectively).

(© Wiley-VCH Verlag GmbH, 69451 Weinheim, Germany, 2002)

Introduction

In the past decades a lot of work has been devoted to the magnetic and structural characterisation of square-planar dinuclear copper(II) complexes, formulated as $[LCu(OH)_2CuL]X(H_2O)_n$, where L = a didentate ligand and X = a variety of mono- and divalent anions.[1] Detailed analysis results in the linear correlation between the Cu−O−Cu angle and the singlet-triplet exchange parameter J established by Hodgson and Hatfield,[2] and is proposed as $J = -74.53 + 7270$ cm^{-1} (where is the Cu−O−Cu angle).[1b,2]

From this correlation it has been concluded that when the Cu−O−Cu angle is larger than 97.55°, i.e. in cases where the Cu_2L_2 chromophore is almost coplanar, the overall magnetic behaviour is antiferromagnetic, and for smaller values, a ferromagnetic coupling is observed. At a Cu−O−Cu angle of 97.55°, the singlet-triplet splitting energy would be zero.[2]

These earlier studies have also revealed that the nature of exchange coupling and the geometry of the copper environment is strongly influenced by the nature of the terminal ligands and the coordination of counterions and solvent molecules.[3] Copper(II) compounds with the ligand 2,2′-bipyridine have been investigated extensively, and it is postulated that they exhibit ferromagnetic interactions,[1b] where as for dpyam complexes (dpyam = di-2-pyridylamine), only three systems have been prepared and structurally characterised, both spectroscopically and magnetically, and indicated an antiferromagnetic interaction.[4]

[a] Department of Chemistry, Faculty of Science, Khon Kaen University,
Khon Kaen 40002, Thailand
[b] Department of Chemistry, Faculty of Science, Prince of Songkla University,
Hatyai 90112, Thailand
[c] Leiden Institute of Chemistry, Gorlaeus Laboratories, Leiden University,
P. O. Box 9502, 2300 RA Leiden, The Netherlands
[d] Bijvoet Center for Biomolecular Research, Crystal and Structural Chemistry, Utrecht, University,
Padualaan 8, 3584 CH Utrecht, The Netherlands

In the literature many dinuclear dihydroxo-bridged copper(II) compounds containing other terminal ligands with ClO_4^- as a counteranion were characterised.[3a,5] Three copper environments are commonly observed: rhombic coplanar, CuN_2O_2;[5a,5f] square-based pyramidal, CuN_2O_2X;[5c−5e,5g] and elongated rhombic octahedral, $CuN_2O_2X_2$.[3a,5b,5h]

In order to investigate the magnetic and structural correlation in the H bond donor cases, such as the dpyam system, the compound $[Cu(dpyam)(OH)_2Cu(dpyam)](ClO_4)_2$ has been synthesized and characterised.

By monitoring the temperature behaviour with respect to the magnetic properties, an abrupt change in the magnetism was noted at about 192 and about 116 K. Such an abrupt change is usually associated with a crystallographic phase transition. Reports on an abrupt variation in the magnetic interaction in coupled Cu^{II} systems are, however, very rare. In fact only a few reports on that phenomenon involving Cu^{II}, and which are fully magnetically and crystallographically investigated, are available.[6] $[[Cu(petdien)]_2(CO_3)](ClO_4)_2$ (petdien = *N*,*N*,*N*′,*N*′′,*N*"-pentaethyldiethylenetriamine)[6b] has a phase transition at 212−202 K, $[Cu(CH_3\text{-nso})NCS]$ {CH_3-nso = 2-[2-(dimethylamino)-ethylthio]ethanolato}[6a] has an abrupt phase transition at 240 and 180 K, while $[Cu(btaO)_2(MeOH)]_n$ [6c] (btaOH = 1-hydroxybenzotriazole) has a phase transition at 6.4 and 4.4 K. In this paper, $[Cu(dpyam)(OH)]_2(ClO_4)_2]$ is studied in detail and characterised by magnetic susceptibility and heat capacity measurements. The X-ray crystal structures at three different temperatures, above, between, and below the transitions are also studied in order to obtain an insight into the crystallographic changes of the compound.

Results and Discussion

Description of the Crystal Structures of $[Cu(dpyam)(OH)]_2(ClO_4)_2$ at 110 K (1A), 150 K (1B) and 200 K (1C)

According to the magnetic observations and heat capacity measurements (vide infra), two phase transitions are present, i.e. at about 192 and about 116 K. Therefore, it was decided to obtain the X-ray structures in all three temperature ranges. The X-ray data were collected at 110 K (structure **1A**), at 150 K (structure **1B**) and at 200 K (structure **1C**), all from the same single crystal. The structures of **1A** to **1C** all consist of a dinuclear $[Cu_2(OH)_2(dpyam)_2]^{2+}$ cation and two weakly coordinating, bridging ClO_4^- anions. The geometry of the cation is a distorted elongated octahedral with two bridging OH^- anions, two terminal bis-(chelating) dpyam ligands as equatorial ligands, and two weak axial $O_{(ClO4)}$ interactions.

The unit cell of **1A** contains two chemically identical, but crystallographically independent dinuclear units. The unit cell of **1B** contains two dinuclear units related to each other by an inversion centre. The unit cell of **1C** contains one dinuclear unit located on a crystallographic inversion centre. Atomic displacement plots, together with the numbering scheme of the three compounds are shown in Figure 1, Figure 2 and Figure 3, for structures **1A**, **1B** and **1C**, respectively, with selected distances and angles in Table 1.

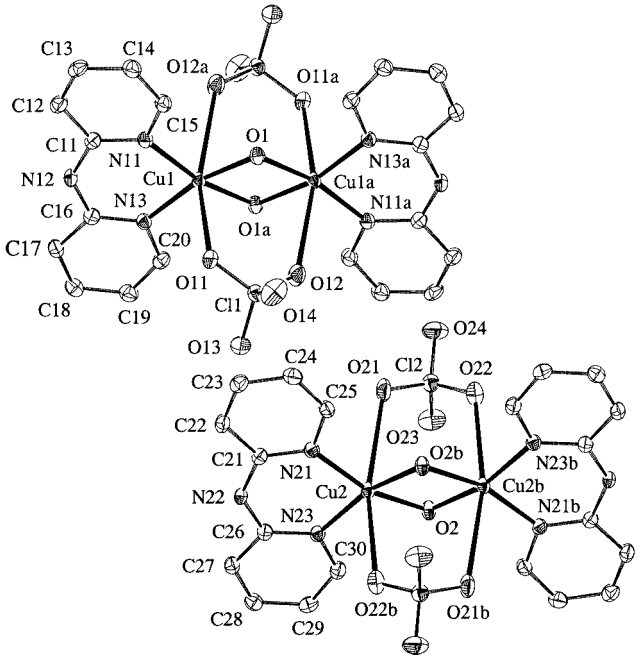

Figure 1. Atomic displacement plot (50% probability) of structure **1A** (110 K); both crystallographic dinuclear units are shown; atoms with suffix "a" are generated by symmetry operation $-x$, $-y$, $1-z$; atoms with suffix "b" are generated by symmetry operation $-x$, $1-y$, $-z$; hydrogen atoms are omitted for clarity

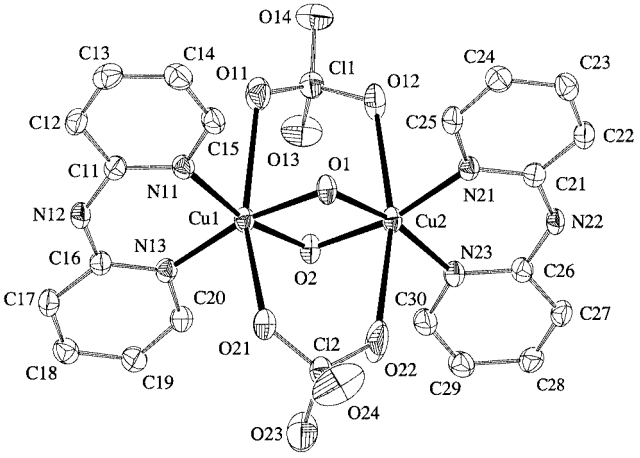

Figure 2. Atomic displacement plot (50% probability) of structure **1B** (150 K); hydrogen atoms are omitted for clarity

As seen from Table 1, the geometry of the $[Cu_2(OH)_2(dpyam)_2]^{2+}$ cation is basically the same in all three structures. Each copper atom has a distorted elongated octahedral geometry with two oxygen atoms of the bridging hydroxo groups and two nitrogen atoms of the dpyam ligand forming the basal plane; both axial sites of each copper atom are occupied by oxygen atoms of perchlorate anions at long (semi-coordinating) distances ($Cu-O_{(ClO4)}$ distances vary from 2.70 to 2.95 Å). The Cu−N distances vary from 1.975 to 2.004 Å, while the

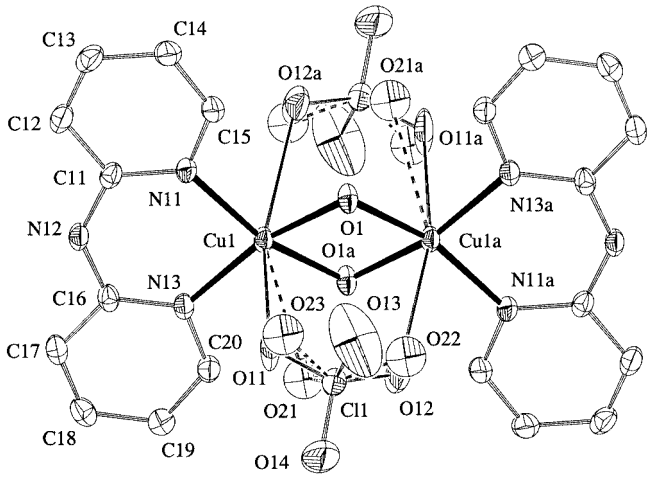

Figure 3. Atomic displacement plot (30% probability) of structure **1C** (200 K); atoms with suffix "a" are generated by symmetry operation $1 - x$, $1 - y$, $1 - z$; hydrogen atoms are omitted for clarity

$Cu-O_{(OH)}$ distances vary from 1.916 to 1.937 Å. These values are in accordance with earlier observations made for Cu^{II} dinuclear hydroxo-bridged compounds.[4,11b] The Cu−Cu distances in the three structures and the Cu−O−Cu angles are almost the same in all 3 structures with values of 2.933 and 2.963 Å for **1A**; 2.948 Å for **1B** and 2.941 Å for **1C**; and with Cu−O−Cu angles of 99.00 and 100.53° for **1A**; 99.76 and 99.54° for **1B**; and 99.53° for **1C**.

However, the main differences in the three structures are the orientation and distances of the perchlorate anions with respect to the CuN_2O_2 plane, as detailed below.

Due to the abrupt change in symmetry, the three structures are different with respect to the orientation of the perchlorate anion. This is shown in Figure 4, where the "canting" (tilting) of the perchlorate anions is projected in each case.

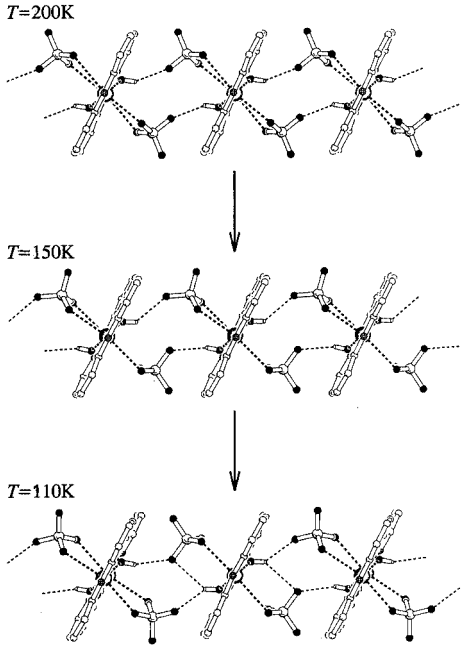

Figure 4. Plot showing the perchlorate orientations and the hydrogen bonds; projections are along the Cu···Cu axis

At 200 K (structure **1C**), the perchlorate is disordered along the Cl1−O14 axis and has to be refined in two positions. The ClO_4^- ions are centrosymmetrically located with respect to the $Cu(OH)_2Cu$ core. At 150 K (structure **1B**), this centrosymmetric arrangement is broken, and both ClO_4^- anions take their own position. In structure **1A** (110 K), after the second abrupt transition, the ClO_4^- anions are once again centrosymmetrically arranged around the dinuclear copper core, albeit that the unit cell now contains two different centrosymmetric units.

Since the planar CuO_2N_2 unit does not display significant differences (dihedral angles in the $Cu_2N_4O_2$ planes vary from 16 to 20°), the phase transitions must originate from

Table 1. Selected bond lengths [Å] and bond angles [°] for the crystal structure determinations of **1A** (110 K), **1B** (150 K) and **1C** (200 K); molecule 1 of structure **1A** refers to the complex containing Cu1; molecule 2 refers to the complex containing Cu2; part 1 of structure **1B** refers to the part containing Cu1; part 2 refers to the part containing Cu2

	1A Molecule 1	**1A** Molecule 2	**1B** Part 1	**1B** Part 2	**1C**
Cu−OH	1.934(2)	1.937(2)	1.934(2)	1.935(2)	1.930(3)
	1.9231(18)	1.9160(18)	1.926(2)	1.920(2)	1.923(3)
Cu−N	1.993(2)	1.975(2)	1.997(2)	1.989(2)	1.988(3)
	2.004(2)	2.001(2)	2.000(3)	2.003(3)	1.996(3)
$Cu-OClO_3$	2.822(2)	2.945(2)	2.908(2)	2.834(3)	2.942(5)
	2.760(2)	2.781(2)	2.705(2)	2.732(2)	2.709(6)
Cu···.Cu	2.9328(6)	2.9633(6)	2.9477(8)	2.9477(8)	2.9412(8)
HO-Cu−OH	81.00(8)	79.47(8)	80.28(9)	80.41(9)	80.47(11)
N−Cu−N	92.43(9)	92.55(9)	92.32(10)	92.35(10)	92.68(12)
N−Cu−OH *cis*	94.04(9)	95.24(9)	94.04(9)	94.31(9)	95.02(12)
	94.79(8)	96.33(9)	94.18(10)	95.62(10)	95.33(12)
N−Cu−OH *trans*	166.99(9)	163.27(9)	167.54(9)	165.48(10)	163.09(12)
	167.54(9)	165.15(9)	168.03(9)	166.76(9)	165.87(12)
Cu−OH−Cu	99.00(9)	100.53(9)	99.76(9)	99.54(10)	99.53(12)

Table 2. Hydrogen bond details (distances [Å] and angles [°])

1A (110 K) Donor−H···Acceptor [ARU]	D−H	H···A	D···A	D−H···A
O(1)−H(1)···O(23) [x, y, 1 + z]	0.74(3)	2.22(3)	2.931(3)	162(3)
O(2)−H(2)···O(14) [x, y, −1 + z]	0.78(3)	2.24(3)	2.890(3)	141(3)[a]
O(2)−H(2)···O(23) [x, y, z]	0.78(3)	2.59(3)	3.224(3)	139[a]
N(12)−H(12A)···O(22) [1 + x, y, 1 + z]	0.88	2.09	2.922(3)	157
N(22)−H(22A)···O(11) [1 − x, 1 − y, 1 − z]	0.88	2.07	2.940(3)	172
1B (150 K) Donor−H···Acceptor [ARU]	D−H	H···A	D···A	D−H···A
O(1)−H(1)···O(13) [−1 + x, y, z]	0.73(4)	2.21(4)	2.915(3)	164(4)
O(2)−H(2)···O(24) [1 + x, y, z]	0.77(4)	2.35(4)	2.959(3)	138(3)
N(12)−H(12A)···O(12) [x, 1 + y, z]	0.88	2.11	2.951(3)	160
N(22)−H(12B)···O(21) [x, −1 + y, z]	0.88	2.03	2.902(3)	168
1C (200 K) (major disordered component) Donor−H···Acceptor [ARU]	D−H	H···A	D···A	D−H···A
O(1)−H(1)···O(13) [−x, 1 − y, 1 − z]	0.77(4)	2.16(4)	2.844(8)	148(5)
N(12)−H(12A)···O(11) [1 − x, −y, 1 − z]	0.88	2.07	2.923(6)	162

[a] Bifurcated hydrogen bond; the sum of the angles involving H(2) is 359(4)°.

the tilting of the perchlorate anions, and their effect on the H bonds.

The lattice structures are stabilised by stacking between the pyridine groups, and by moderate to weak hydrogen bonding between the hydroxo atom and an oxygen atom of the perchlorate anion [D···A distances vary from 2.844(8) to 2.959(3) Å] and between the amine nitrogen atom and an oxygen atom of the perchlorate anion [distances vary from 2.902(3) to 2.951(3) Å]. Details of the hydrogen bonds are given in Table 2.

Spectroscopy

The most relevant features of the IR spectra are those involving the presence of hydroxo bridges and the perchlorate counteranion. The presence of the $Cu(OH)_2Cu$ unit is supported by the occurrence of a weak, but sharp peak of medium intensity at 3550 cm^{-1} (bridging OH stretching). The ν_3 mode of the ClO_4^- anion appears as a strong absorption, split into three broad components at about 1100, 1046 and 1015 cm^{-1}, consistent with its didentate and relatively long Cu−O bonding distance of 2.72 Å.[5h,7]

The electronic reflectance spectra of **1** measured as a powder at room temp. shows a broad band at 15430 cm^{-1} consistent with the distorted elongated octahedral geometry.[8] No spectroscopic data were recorded at low temperature.

EPR and Magnetic Properties

The X-band polycrystalline powder EPR spectra of this compound, up to 800 mT at 77 K, exhibits a typical triplet spectrum with four features at 150, 325, 590, 690 and 755 mT. The spectrum is qualitatively similar to that reported for other coupled copper(II) pairs with $D > h\nu$.[5c,9] The feature at 325 mT is most certainly from a mononuclear Cu^{II} impurity, which is often present in dinuclear species, and the weak absorption at low field (150 mT) comes from the $\Delta M_s = \pm 2$ transition. The presence of the other peaks at high field values is as expected for cases in which the value of the axial zero-field splitting parameter D is larger than the incident quantum (about 0.3 cm^{-1}). Although it is not the intention of this paper to perform a detailed EPR study, including variable frequencies, to determine the parameters D and E, an approximate analysis[10] yields a D value of about 0.5 cm^{-1}.

In a frozen solution (DMF/MeOH, 1:1), only a mononuclear $S = 1/2$ signal is observed with a $g_\perp$ value of 2.04, a $g_{//}$ of 2.28 and an $A_{//}$ value of about 15.8 mT, indicating that the compound dissociates in this solution.

The temperature dependence of the molar magnetic susceptibility χ_m^{-1} of **1** down to 5 K, measured on a powder sample, is shown in Figure 5. At 275 K, χ_M is equal to 2.87 $\times 10^{-3}$ cm^3 mol^{-1}, which is very close to what is expected for two noninteracting copper(II) ions ($g = 2$). When cooled to 50 K, χ_M slowly increases to 11.14 $\times 10^{-3}$ cm^3 mol^{-1}. The absence of any maximum indicates, at best, weakly antiferromagnetically coupled copper(II) ions within the dinuclear units. However, two discontinuities are observed at 192 K and 116 K. The magnetic data therefore point at the presence of two phase changes that are likely to have a consequence for the magnetic behaviour of compound **1**. The susceptibility increases at 192 K and decreases again at 116 K, but in an asymmetric manner, the decrease at 116 K being larger than the increase at 192 K. This indicates that a difference in g value cannot be the origin of these changes. Most likely, the interaction between the two copper ions changes quite drastically. Below 50 K χ_M increases more sharply, to reach 0.113 cm^3 mol^{-1} at 5 K. In the same range, the effective magnetic moment of **1** remains almost

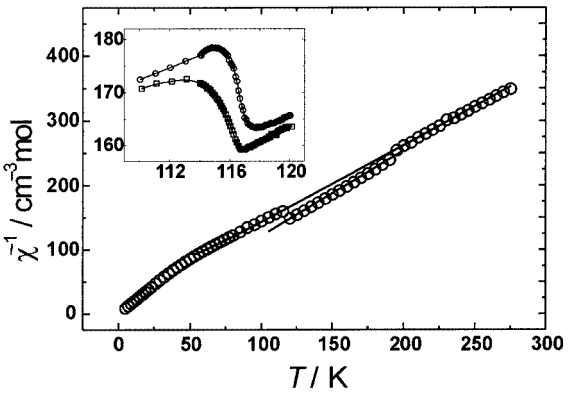

Figure 5. A plot of temperature dependence of χ_m^{-1} vs. T for compound **1**; the full lines correspond to fits of the different temperature ranges (see text); insert: variation of χ_M^{-1} in the 110−120 K temperature range on cooling (○) and warming (□)

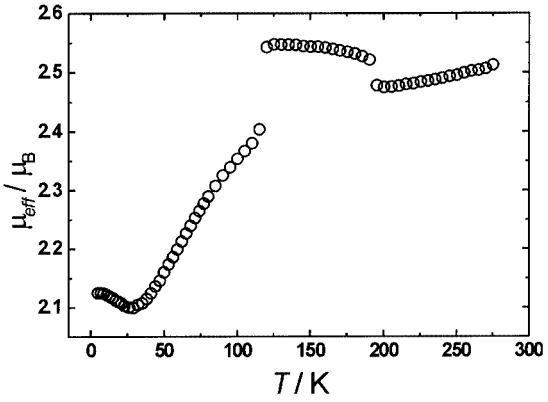

Figure 6. A plot of temperature dependence of μ_{eff} vs. T for compound **1**

constant at a value of 2.12 μ_B (Figure 6). This low-temperature behaviour cannot be attributed to a paramagnetic impurity, and is not understood yet, and therefore omitted from the present analysis. Full analysis would also require X-ray structures below 50 K. Subsequently, the fitting procedure was performed from 275 to 50 K (vide infra). The magnetic data above 50 K, and above and below the two discontinuities, can be reproduced (see Figure 5), with the theoretical expression of the magnetic susceptibility of a copper(II) pair given in the following equation, where J is the singlet-triplet energy gap (a positive or negative J value corresponds to a ferromagnetic or antiferromagnetic interaction, respectively) and the other parameters have their usual meaning.[1b]

$$\chi_M = \frac{2N_A\beta^2g^2}{k_BT}\left[3+\exp\left(\frac{-J}{k_BT}\right)\right]^{-1}$$

The minimisation of $R = \Sigma\,(\chi_M^{calcd.} - \chi_M^{obs.})^2/\Sigma(\chi_M^{obs})^2$ led to $J = -37.2$ cm^{-1} and $g = 2.09$, with $R = 3.37 \times 10^{-3}$. Applying the same expression to the data between the two discontinuities, yields $J = 29$ cm^{-1} and $g = 2.0$ with $R = 5.1 \times 10^{-3}$. Although the exact value of J may not be precisely defined because of the small number of data points fitted, a change in the sign of J is clearly observed. Indeed, the effective magnetic moment of **1** in that temperature range increases, whereas it decreases in the other fitted regions, also indicating a change in the sign of the exchange interaction. Such a drastic change of the magnetic interaction in a polynuclear compound upon a crystallographic phase transition is unprecedented. Sletten et al.[6b] have observed a change of 7 cm^{-1} in the strength of the antiferromagnetic interaction in $\{[Cu(petdien)]_2(CO_3)\}(ClO_4)_2$, but the perchlorate anions are not coordinated and the two copper ions are bridged by a carbonato anion. In that case, the change in the S-T energy gap has been related to a subtle change of the character of the magnetic orbital.

Here, the present phase transitions must mainly result from changes in the perchlorate anion orientation with respect to the $Cu_2(dpym)_2$ plane. Considering the Hatfield−Hodgson relationship[2] between J and the Cu−O−Cu angle for bis(μ-dihydroxo)copper dimers, the expected value for the S-T energy gap in **1** would range from −148 to −157 cm^{-1}. Such a discrepancy from the measured value was already observed in two of the rarely studied bis(μ-dihydroxo)copper dinuclear compounds having perchlorate anions coordinated, or semi-coordinated via two oxygen atoms.[11] It is thought[11a] that the perchlorate coordination greatly, but indirectly, affects the exchange interaction, and hence in two possible ways. The electronic perturbation due the additional coordination can affect the superexchange mechanism through the hydroxo oxygen atom, by altering the electron density available to it.

Alternatively, the very small changes in the Cu geometries (deviations from planarity) may be the origin.[11c,11d] None of these origins can be excluded in **1**. The abrupt change in behaviour from the ordering and change in orientation of the perchlorate anions only proves the strong influence of their coordination on the magnetic interaction. What is clear in this case is that the magnetic properties cannot be explained on the basis of Cu−Cu distances and Cu−OH−Cu angles alone.

The two ranges of temperature showing discontinuities were reinvestigated by cooling and heating at a much lower rate. A small hysteresis of 0.5 K is detected at the low-temperature transition, with $T^{\downarrow} = 116.2$ K and $T^{\uparrow} = 116.6$ K (see insert in Figure 5), which is in good agreement with the calorimetric measurements (see separate section). However, the step at high temperature occurs at $T = 5$ K on cooling and heating, which differs from the calorimetric measurements in which a hysteresis of 2 K was detected.

Heat Capacity Measurements

To understand more of these two phase transitions, calorimetric analyses have been performed on **1**. The sample was first rapidly cooled down to 250 K, measurements were then carried out on cooling to 85 K and warming back to 240 K. The temperature dependence of the molar heat ca-

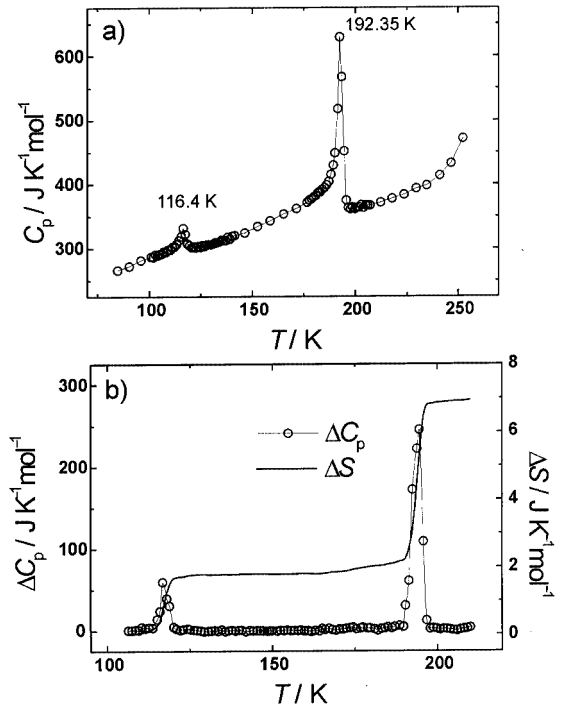

Figure 7. Temperature dependence of a) the heat capacity of compound **1** in the cooling mode and b) the excess heat capacity (empty circles) and the derived entropy gain (full line) in the warming mode

pacity of **1** in the cooling mode is shown in Figure 7a. Two thermal anomalies are found at 192.3 ($T_{c1}^{\downarrow}$) and 116.4 K ($T_{c2}^{\downarrow}$), and the same is observed in the warming mode at 116.8 ($T_{c2}^{\uparrow}$) and 194.4 K ($T_{c1}^{\uparrow}$). These values are in good agreement with the steps observed in the magnetic properties. The presence of hysteresis in the phase change at high temperature is also confirmed, with $T_{c1}^{\uparrow}$ and $T_{c1}^{\downarrow}$ differing by 2 K. The presence of hysteresis in the high-temperature transition, where no hysteresis could be detected by magnetic measurements, may indicate that the magnetic change does not occur while the structural phase transition takes place, but just after it has occurred. Since the hysteresis is so small, the magnetic change then appears at the same temperature on cooling and warming. The enthalpy gain ΔH and the entropy gain ΔS, associated with the excess heat capacities ΔC_p, were determined by integration of ΔC_p with respect to T and ln$T$, respectively, both in the cooling and warming mode. The temperature dependence of ΔC_p and the excess entropy in the warming mode are shown in Figure 7b. The ultimate value at high temperatures corresponds to $\Delta S = (6.9 \pm 0.7)$ J K^{-1} mol^{-1}, while the excess enthalpy was found to be $\Delta H = (1.2 \pm 0.1)$ kJ mol^{-1}. Similar calorimetric values were found in the cooling mode, the only marked difference being the temperatures. This confirms the reversibility of the phase changes in compound **1**. Large errors are due to the ambiguity in the determination of normal heat capacity curves, which were done by fitting the experimental data above, below and between the C_p anomalies, to a polynomial function. Since the two C_p anomalies are well separated, an approximation of the excess entropy and enthalpy associated with the two transitions is possible, e.g. $\Delta S(T_{c1}) = 4.9$ J K^{-1} mol^{-1}/$\Delta H(T_{c1}) = 0.96$ kJ mol^{-1} and $\Delta S(T_{c2}) = 2.0$ J K^{-1} mol^{-1}/ $\Delta H(T_{c2}) = 0.25$ kJ mol^{-1}. The entropy variation ΔS is usually[12] written as $\Delta S = \Delta S_{el} + \Delta S_{vib,intra} + \Delta S_{vib,inter}$.

In the present case, there is almost no variation in the metal−ligand bond lengths, and the intramolecular geometry is not modified, as shown by the very similar Cu−O−Cu angles. Therefore, $\Delta S_{vib,intra}$ is negligible. The observed change in magnetic interaction may result in a small contribution of the electronic entropy ΔS_{el}, while the dominant term is probably the lattice term $\Delta S_{vib,inter}$. The high-temperature transition entropy is approximated, within the error, in terms of Rln 2 (5.76), which agrees with an order-disorder phenomenon occurring between two positions. This is indeed in agreement with the structural data at 200 and 150 K. On the other hand, the phase change between the 150 and 110 K structures only involves changes in the crystal lattice. This is in agreement with the amount of entropy gain measured at T_{c2}, which can reasonably arise from lattice vibrations.

Conclusions

The results described above have shown a unique double phase transition for a dinuclear hydroxo-bridged Cu^{II} compound. X-ray structures were measured at three different temperatures (below, between and above the two phase transitions), and it can be concluded that the main reason for the crystallographic phase transition must originate from the abrupt change in the positions (canting or tilting) of the perchlorate anions, and therefore influencing the Cu−O$_{(ClO4)}$ bonds and Cu geometries. The abrupt change in behaviour from the ordering and change in orientation of the perchlorate anions confirms the influence of their coordination on the magnetic interaction.

More insight in the exact mechanism of the transition from more studies using other examples would be desirable. In fact, it is likely that such phase transitions, involving the movements of (semi)coordinated anions do occur, since many coordination compounds are studied only at one temperature and in many cases no magnetic susceptibility measurements are performed.

Experimental Section

General: All reagents were commercial-grade materials and were used without further purification. C,H,Cu,N determinations were performed by the Microanalytical Service of Science and Technological Research Equipment Centre, Chulalongkorn University. Infrared spectra were taken with a Biorad FTS-7/PC FTIR spectrophotometer as KBr pellets in the 4000−450 cm^{-1} region. Solid-state (diffuse reflectance) electronic spectra were recorded as polycrystalline samples with a Perkin−Elmer Lambda 2S spectrophotometer over the range 8000−18000 cm^{-1}. X-band EPR spectra were recorded on polycrystalline samples with a Jeol RE2X electron spin resonance spectrometer using DPPH ($g = 2.0036$) as a standard.

Table 3. Crystal and refinement data

Compound	**1A** (110 K)	**1B** (150 K)	**1C** (200 K)
Empirical formula	$C_{20}H_{20}Cu_2N_6O_2(ClO_4)_2$	$C_{20}H_{20}Cu_2N_6O_2(ClO_4)_2$	$C_{20}H_{20}Cu_2N_6O_2(ClO_4)_2$
T/K	110	150	200
Crystal system	triclinic	triclinic	triclinic
Space Group	$P\bar{1}$ (no. 2)	$P\bar{1}$ (no. 2)	$P\bar{1}$ (no. 2)
a/Å	10.0337(12)	7.4898(12)	7.4730(12)
b/Å	11.1292(14)	9.4322(16)	9.4614(18)
c/Å	13.1017(15)	18.700(4)	9.697(2)
α/°	104.334(10)	100.933(10)	73.092(10)
β/°	98.705(10)	91.431(10)	80.652(10)
γ/°	115.985(10)	108.268(10)	71.048(10)
V/Å^3	1216.2(3)	1226.7(4)	618.7(2)
Z	2	2	1
$D_{calcd.}$/g·cm^{-3}	1.918	1.902	1.885
μ/mm^{-1}	2.039	2.022	2.004
F(000)	708	708	354
Crystal size [mm]	0.05 × 0.10 × 0.35	0.05 × 0.10 × 0.35	0.05 × 0.10 × 0.35
Total refl.	23865	21228	12098
Indep.refl. (R_{int})	5515 (0.0793)	5445 (0.0721)	2789 (0.0644)
No. parameters used	367	367	194
GOF	1.027	1.032	1.042
Final *R*[a] indices	$R1 = 0.0383$	$R1 = 0.0414$	$R1 = 0.0450$
indices	[4308, $I > 2\sigma(I)$]	[4258, $I > 2\sigma(I)$]	[2306, $I > 2\sigma(I)$]
	$wR2 = 0.1041$	$wR2 = 0.1084$	$wR2 = 0.1247$
Min./max. resd.dens. [e Å^{-3}]	−0.90/0.57	−0.86/0.53	−0.68/0.71

[a] $R = \Sigma||F_o| - |F_c||/\Sigma|F_o|$, $R_w = \{\Sigma[w(F_o^2 - F_c^2)^2]/\Sigma[w(F_o^2)^2]\}^{1/2}$.

Magnetic susceptibility measurements (5−275 K) were carried out using a Quantum Design MPMS-5 5T SQUID magnetometer (measurements carried out at 0.1 and 1 T). Data were corrected for magnetisation of the sample holder and for diamagnetic contributions, which were estimated from Pascal constants. Heat-capacity measurements were carried out using the heat-capacity option of a Quantum Design PPMS model 6000. A few crystals (total mass = 2.3 mg) were mounted onto the sample platform of the heat capacity puck with a little Apiezon N grease, which was previously measured as an addendum (puck + grease). The heat-capacity option uses a relaxation technique, fitting the whole thermal response to a heating period followed by a cooling period with a model that accounts for both thermal relaxation from the sample platform to the bath and the relaxation between the platform and the sample.

Synthesis of the Title Compound: Solid sodium carbonate (0.052 g, 0.5 mmol) was slowly added under continuous stirring to an aqueous solution (60 mL) containing copper(II) perchlorate hexahydrate (0.370 g, 1.0 mmol) and di-2-pyridylamine (0.171 g, 1.0 mmol). The greenish-blue solution was allowed to concentrate at room temperature. After several days, purple-blue rod-shaped crystals were formed. They were filtered off, washed with the mother liquor and air-dried. Yield: ca. 0.32 g (45%). $C_{20}H_{20}Cl_2Cu_2N_6O_{10}$ (702.4): calcd. C 34.0, H 2.6, Cu 17.8, N 11.8; found C 34.2, H 2.9, Cu 18.1, N 12.0. ***Caution:*** Perchlorate salts are potentially explosive, caution is advised and handling of only small quantities is recommended.

X-ray Data Collection and Structure Determination: A crystal was mounted on top of a glass fibre (using the inert-oil technique) and transferred to a cold nitrogen stream of a Nonius Kappa-CCD diffractometer for data collection at 200, 150 and 110 K (rotating anode, graphite-monochromated Mo-K_α radiation, λ = 0.71073 Å). The unit-cell parameters were checked for the presence of higher lattice symmetry.[13c] No absorption correction was applied. The structure was solved by automated direct methods (SHELXS-86).[13a] Refinement on F^2 was carried out by full-matrix least-squares techniques (SHELXL-97).[13b] For the structure determination of **1C**, a two-site disorder model was adopted for the ClO_4^- ion. The occupancy of the major component was refined to 0.811(5). Mild distance restraints and a common displacement parameter were applied to the minor component. Anisotropic displacement parameters were used for all non-hydrogen atoms, except for those belonging to the minor disorder component. Hydroxo hydrogen atoms were located on a difference Fourier map and their positions were refined. All other hydrogen atoms were introduced at calculated positions and included in the refinement riding on their carrier atoms. Geometrical calculations, including the ORTEP illustrations were performed with the PLATON package.[13c] Crystallographic details are tabulated in Table 3. CCDC-173825, -173824 and CCDC-173823 for structures **1A**, **1B** and **1C** contain the supplementary crystallographic data for this paper. These data can be obtained free of charge at www.ccdc.cam.ac.uk/conts/retrieving.html or from the Cambridge Crystallographic Data Centre, 12, Union Road, Cambridge CB2 1EZ, UK [Fax: (internat.) + 44-1223/336-033; E-mail: deposit@ccdc.cam.ac.uk].

Acknowledgments

The Khon Kaen University, Thailand is thanked for their research grant and the Postgraduate Education and Research Program in Chemistry for their support (S. Y., W. S., C. P.). The work described in the present paper has been supported by the Leiden University Study group WFMO (Werkgroep Fundamenteel Materialen Onderzoek) and the Council for Chemical Sciences of the Netherlands Organisation for Scientific Research (CW-NWO). Part of the work has been supported financially by the Graduate Research School Combination "Catalysis".

[1] [1a] O. Kahn, Y. Pei, Y. Journaux, in *Inorganic Materials* (Eds.: Q. W. Bruce, D. O'Hare), John Wiley & Sons, Chichester, U.K., **1992**. [1b] O. Kahn, *Molecular Magnetism*, VCH Publishers, New York, **1993**. [1c] D. Gatteschi, O. Kahn, J. S. Miller, F. Palacio, *Magnetic Molecular Materials*, Kluwer Academic, Dordrecht, The Netherlands, **1991**. [1d] V. V. Volkov, Y. V. Rakitin, V. T. Kalinnikov, *Koord. Khim.* **1983**, *9*, 31−33.

[2] H. Crawford, H. W. Richardson, J. R. Wasson, D. J. Hodgson, W. E. Hatfield, *Inorg. Chem.* **1976**, *15*, 2107−2110.

[3] [3a] I. Castro, M. Julve, G. De Munno, G. Bruno, J. A. Real, F. Lloret, J. Faus, *J. Chem. Soc., Dalton Trans.* **1992**, 1739−1744. [3b] E. Ruiz, P. Alemany, S. Alvarez, J. Cano, *J. Am. Chem. Soc.* **1997**, *119*, 1297−1303. [3c] E. Ruiz, P. Alemany, S. Alvarez, J. Cano, *Inorg. Chem.* **1997**, *36*, 3683−3688.

[4] [4a] S. Youngme, W. Somjitsripunya, K. Chinnakali, S. Chantrapromma, H. K. Fun, *Polyhedron.* **1999**, *18*, 857−862. [4b] S. Youngme, G. A. van Albada, O. Roubeau, C. Pakawatchai, N. Chaichit, W. Somjitsripunya, J. Reedijk, *Inorg. Chim. Acta*, in press. [4c] L.-P. Wu, M. E. Keniry, B. J. Hathaway, *Acta Crystallogr., Sect. C* **1992**, *48*, 35−40.

[5] [5a] C. Arcus, K. P. Fivizzani, S. F. Pavkovic, *J. Inorg. Nucl. Chem.* **1977**, *39*, 285−287. [5b] M. Toofan, A. Boushehri, M. Ul-Haque, *J. Chem. Soc., Dalton Trans.* **1976**, 217−219. [5c] I. Castro, J. Faus, M. Julve, C. Bois, J. A. Real, F. Lloret, *J. Chem. Soc., Dalton Trans.* **1992**, 47−52. [5d] D. Y. Jetter, D. L. Lewis, J. C. Hempel, D. J. Hodgson, W. E. Hatfield, *Inorg. Chem.* **1972**, *11*, 1958−1960. [5e] D. L. Lewis, K. T. McGregor, W. E. Hatfield, D. J. Hodgson, *Inorg. Chem.* **1972**, *11*, 2216−2221. [5f] E. D. Estes, W. E. Hatfield, D. J. Hodgson, *Inorg. Chem.* **1974**, *13*, 1654−1657. [5g] D. L. Lewis, K. T. McGregor, W. E. Hatfield, D. J. Hodgson, *Inorg. Chem.* **1974**, *13*, 1013−1019. [5h] D. L. Lewis, W. E. Hatfield, D. J. Hodgson, *Inorg. Chem.* **1974**, *13*, 147−152.

[6] [6a] M. Mikuriya, H. Okawa, S. Kida, *Bull. Chem. Soc. Jpn.* **1981**, *54*, 2979−2982. [6b] J. Sletten, H. Hope, M. Julve, O. Kahn, M. Verdaguer, A. Dworkin, *Inorg. Chem.* **1988**, *27*, 542−549. [6c] V. Tangoulis, C. P. Raptopoulou, V. Psycharis, A. Terzis, K. Skorda, S. P. Perlepes, O. Cador, O. Kahn, E. G. Bakalbassis, *Inorg. Chem.* **2000**, *39*, 2522−2529.

[7] J. Foley, D. Kennefick, D. Phelan, S. Tyagi, B. J. Hathaway, *J. Chem. Soc., Dalton Trans.* **1983**, 2333−2338.

[8] [8a] B. J. Hathaway, in *Comprehensive Coordination Chemistry* (Eds.: G. Wilkinson, R. D. Gill, J. A. McCleverty), Pergamon Press, Oxford, **1987**, vol. 5. [8b] S. Amani Komaei, G. A. van Albada, I. Mutikainen, U. Turpeinen, J. Reedijk, *Polyhedron* **1999**, *18*, 1991−1997. [8c] G. A. van Albada, M. T. Lakin, N. Veldman, A. L. Spek, J. Reedijk, *Inorg. Chem.* **1995**, *34*, 4910−4917.

[9] [9a] G. De Munno, M. Julve, F. Lloret, J. Faus, M. Verdaguer, A. Caneschi, *Inorg. Chem.* **1995**, *34*, 157−165. [9b] J. M. Seco, U. Amador, M. J. González Garmendia, *Polyhedron* **1999**, *18*, 3605−3610. [9c] L. Banci, A. Bencini, D. Gatteschi, *J. Am. Chem. Soc.* **1983**, *105*, 761−764. [9d] G. A. van Albada, I. Mutikainen, W. J. J. Smeets, A. L. Spek, U. Turpeinen, J. Reedijk, *Inorg. Chim. Acta* **2001**, *327*, 134−139. [9e] G. A. van Albada, I. Mutikainen, U. Turpeinen, J. Reedijk, *Inorg. Chim. Acta* **2001**, *324*, 273−277.

[10] J. Reedijk, B. Nieuwenhuijse, *Recl. Trav. Chim.* **1972**, *91*, 533−551.

[11] [11a] K. T. McGregor, D. J. Hodgson, W. E. Hatfield, *Inorg. Chem.* **1976**, *15*, 421−425. [11b] S. Amani Komaei, G. A. van Albada, J. G. Haasnoot, H. Kooijman, A. L. Spek, J. Reedijk, *Inorg. Chim. Acta* **1999**, *286*, 24−29. [11c] D. G. Hodgson, *Inorg. Chem.* **1976**, *15*, 3174−3175. [11d] H. Astheimer, W. Haase, *J. Chem. Phys.* **1986**, *85*, 1427−1432.

[12] C. N. R. Rao, K. J. Rao *Phase transition in solids: an approach to the chemistry and physics of solids*, McGraw-Hill, New York, **1978**.

[13] [13a] G. M. Sheldrick, *SHELXS-86, Program for crystal structure solution*, University of Göttingen, Germany, **1986**. [13b] G. M. Sheldrick, *SHELXL-97, Program for crystal structure refinement*, University of Göttingen, Germany, **1997**. [13c] A. L. Spek, *PLATON, A multipurpose Crystallographic Tool*, Utrecht University, The Netherlands, **2000**; http://www.cryst.chem.uu.nl/platon

Received December 28, 2001
[I01530]

Oxa-aza Crown Ethers as Ligands for Mixed-Ligand Cisplatin Derivatives and Dinuclear Platinum Anticancer Drugs

Bart A. J. Jansen,[a] Peter Wielaard,[a] Hans den Dulk,[b] Jaap Brouwer,[b] and Jan Reedijk*[a]

Keywords: Anticancer drugs / Platinum / DNA binding / Crown ethers / A2780 human ovarian cancer

In the search for novel platinum anticancer drugs, cisplatin derivatives and dinuclear platinum complexes containing oxa-aza crown ether and oxa-diaza crown ether ligands have been prepared. The cisplatin derivatives *cis*-[$PtCl_2(NH_3)$(1,4,7,10,13-pentaoxa-16-azacyclooctadecane-*N*)] (**AO18**) and *cis*-[$PtCl_2(NH_3)$(1,4,7,10-tetraoxa-13-azacyclopentadecane-*N*)] (**AO15**), and the dinuclear cationic platinum complexes [{*trans*-$PtCl(NH_3)_2$}$_2$(μ-1,4,10,13-tetraoxa-7,16-diazacyclooctadecane-*N*,*N*′)]$(NO_3)_2$ (**DAO18**) and [{*trans*-$PtCl(NH_3)_2$}$_2$(μ-1,4,10-trioxa-7,13-diazacyclopentadecane-*N*,*N*′)]$(NO_3)_2$ (**DAO15**) were investigated for their cytotoxic properties, cellular uptake and intracellular DNA binding in A2780 human ovarian cancer. The cisplatin derivative **AO15** shows the highest cytotoxic activity, whereas the cationic dinuclear complexes **DAO18** and **DAO15** display a disappointing lack of biological activity at concentrations up to 100 μM. In the intracallular DNA platination experiments, the fifteen-membered rings were found to have a threefold higher intracellular DNA binding compared to their 1eight-membered analogues for the neutral cisplatin derivatives as well as for the cationic dinuclear complexes. The crown ether complex with the most effective binding to DNA, **AO15**, also shows the highest cytotoxicity against A2780 cancer cells. It is remarkable that, although **AO15** binds more effectively to DNA than cisplatin, its cytotoxic effect is much lower.

(© Wiley-VCH Verlag GmbH, 69451 Weinheim, Germany, 2002)

Introduction

The success of the anticancer drug cisplatin [*cis*-$PtCl_2(NH_3)_2$] has inspired the search for new platinum complexes with anticancer properties.[1−3] In the current paper, new platinum complexes based on aza crown ethers are described for their cytotoxic properties and binding to intracellular DNA. Binding to DNA is assumed to be a major mechanism of action,[4] leading to the death of cancer cells in platinum anticancer therapy.[5]

Although crown ethers are not known to possess medicinal properties themselves, they may improve drug uptake and transport properties.[6,7] Crown ethers are known to form cationic complexes with alkali metal ions and tertiary amines.[8] The special complexing properties of crown ethers have led to applications in drug delivery systems[9,10] and as targeting functionalities incorporated in drug derivatives and DNA-binding agents.[11−18] It was shown in DNA-binding studies that the positive charge of cation−crown ether complexes increases the affinity of crown ether linked compounds with the polyanionic phosphate backbone of DNA.[11,19] Thus, crown ether derivatized drugs may gain an increased interaction with DNA by the formation of cationic complexes with ions that are abundant in cells, such as sodium (5−15 mM) or potassium (140 mM).[20]

The groups of Keppler[21] and Sohn[22] have reported complexes where a crown ether is linked to a platinum atom through a functionalized bipyridine ligand. The bipyridine−crown ether compounds are biologically active and overcome cisplatin resistance. Sohn[22] also prepared carboplatin analogues of theses complexes by replacing the chloride leaving groups with 1,1-cyclobutanedicarboxylate. Similar to carboplatin, these complexes have a significantly lower cytotoxicity than the corresponding cisplatin (chloride) derivatives, probably due to their lower reactivity. A dinuclear platinum complex with a polycarboxylato crown ether as a bridging ligand has been reported by Fruhauf and Zeller.[23,24] The crown ether acts as a leaving group, releasing aquated species of cisplatin. The complex shows remarkable activity and DNA-binding properties in sensitive ovarian tumor cells as well as cisplatin-resistant cell lines.

In the platinum−crown ether complexes described above, the platinum atom is linked through a spacer or to pendant coordinating groups. In the current chapter, two types of platinum complexes are presented (Scheme 1), where the

[a] Leiden Institute of Chemistry, Gorlaeus Laboratories, Leiden University,
P. O. Box 9502, 2300 RA Leiden, Netherlands
Fax: (internat.) + 31-71/527-4671
E-mail: reedijk@chem.leidenuniv.nl
[b] Molecular Genetics, Leiden Institute of Chemistry, Gorlaeus Laboratories, Leiden University,
P. O. Box 9502, 2300 RA Leiden, Netherlands

platinum atom is directly coordinated to the nitrogen atom in an aza crown ether. The first type comprise mixed-amine cisplatin derivatives of the general formula *cis*-$[PtCl_2(NH_3)(L)]$, where L are azacrown ethers. The second type are cationic dinuclear *trans* complexes using diaza crown ethers as linkers, similar to the anticancer active cationic dinuclear *trans*-(diaminoalkyl)platinum complexes as developed by Farrell.[25–28] The cytotoxic properties of the complexes are investigated, and the results are related to the efficiency of DNA binding in A2780 human ovarian cancer cells.

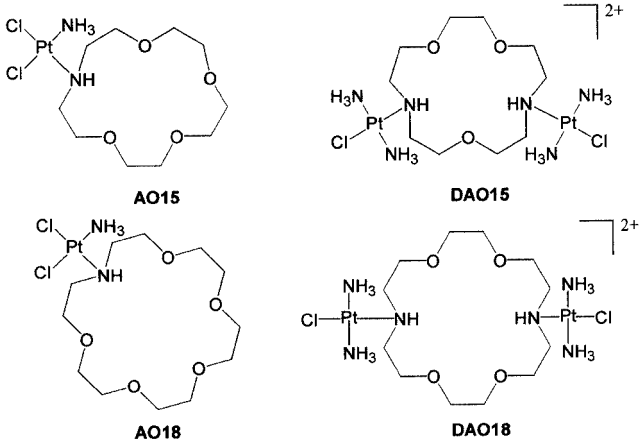

Scheme 1. Oxa-aza crown ether cisplatin derivatives **AO18** and **AO15** and the cationic oxa-diaza crown ether dinuclear platinum complexes **DAO18** and **DAO15**

Results and Discussion

Synthesis

Both cisplatin derivatives[29,30] and dinuclear oxa-aza crown ether platinum complexes[25] could be prepared employing standard synthesis methods.

The reactions of $Ph_4P[Pt(NH_3)Cl_3]$ with the appropriate oxa-aza crown ether produced the asymmetric cisplatin derivatives **AO18** and **AO15**. Yields after recrystallization from methanol were found to be 15% and 39%, respectively. The ^{195}Pt NMR shifts of **AO18** and **AO15** are at $\delta = -2222$ and -2231 ppm, respectively, both in the typical range for $PtCl_2N_2$ complexes.[31]

The dinuclear complexes **DAO18** and **DAO15** were obtained in 24% and 51% yield from the reaction of silver nitrate activated *trans*-$PtCl_2(NH_3)_2$ with the appropriate diamine linker. The oxa-diaza crown ether complexes have the platinum atom coordinated to a secondary amine group. The ^{195}Pt NMR chemical shifts of **DAO18** ($\delta = -2408$ ppm) and **DAO15** ($\delta = -2424$ ppm) are somewhat higher than those of related alkyldiamine complexes where the platinum atom coordinates to primary amines ($\delta \approx -2385$ ppm).[25,32]

The formation of all four platinum complexes is quantitative, as can be monitored by ^{195}Pt NMR, the final yields are relatively low. The solubility properties of the crown ether complexes resulted in losses in the purification steps. Elemental analysis results are not completely satisfactory for all complexes, apparently the samples still include some impurities that were not removed even with repeated recrystallization. Possibly, the impurities are related to degraded crown ether moieties, although these were not apparent from the ^1H NMR spectroscopic data. The ^{195}Pt NMR spectra showed only a single signal even after overnight measurements. The inclusion of considerable amounts of highly active platinum species like cisplatin, that could influence the outcome of the cytotoxicity assays, can be ruled out on basis of these data.

Cytotoxicity Assays

All complexes were tested for cytotoxicity by determination of the IC_{50} values in the human ovarian cancer cell line A2780 and the cisplatin-resistant A2780cisR line. Cytotoxicity results are summarized in Table 1. In the A2780 cell line, the neutral cisplatin derivative **AO15** is the most active oxa-aza crown ether platinum complex, followed by **AO18**. Interestingly, in a recently published series of crown ether analogues of actinomycin D, the 15-crown-5 derivatives were also found to be biologically more active than the 18-crown-6 compounds.[18] The dinuclear diazacrown ether complexes show a disappointing lack of cytotoxic effect. In the cisplatin-resistant cell line, all oxa-aza crown ether complexes failed to induce a cytotoxic effect at concentrations as high as 100 μM. When compared with the established platinum anticancer drug cisplatin, none of the oxa-aza crown ether complexes appears to be a potential anticancer drug.

Table 1. Cytotoxicity results in human ovarian cancer A2780 and the cisplatin-resistant derivative A2780cisR

Compound	IC_{50} (μM)	
	A2780	A2780cisR
cisplatin	0.37	2.4
AO18	66	> 100
AO15	21	> 100
DAO18	> 100	> 100
DAO15	> 100	> 100

Intracellular DNA Platination

A2780 cells were incubated for 1 h at drug concentrations of 200 μM. After the DNA was extracted from the cells, the drug-to-base pair ratio (r_b) was determined by UV and FAAS. The results are presented in Figure 1.

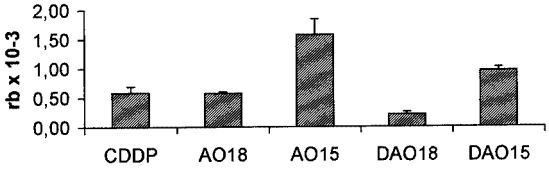

Figure 1. DNA binding (r_b = drug-to-basepair ratio) of cisplatin and aza crown ether platinum complexes in A2780 cells after a 1 h incubation at 200 μM

For both the mononuclear and dinuclear complexes, the 15-crown-5 derivatives show a higher binding to DNA than the corresponding 18-crown-6 compounds. The complex with the highest biological activity of the oxa-aza crown ether complexes studied, **AO15**, also shows the highest binding to DNA in the A2780 cells. The difference in lipophilicity may play an important role here, as it influences the permeation of the cell membrane. Interestingly, a comparable result was found for a series of crown ether derivatized phenoxazone drugs,[18] were the fifteen-membered compounds were also more effective in biological activity and intracellular DNA binding than the eighteen-membered derivatives.

It is remarkable that although **AO15** binds more effectively to DNA than cisplatin, its IC_{50} is much higher. Apparently, not only the amount of DNA damage is important for the cytotoxic effect, but also the type of molecule that binds DNA.

For the dinuclear cationic complexes, the fifteen-membered ring compound **DAO15** performs better in intracellular DNA binding than the eighteen-membered ring compound **DAO18**. Both show a reduced DNA binding compared to the corresponding neutral cisplatin derivatives. **DAO18** binds even less than cisplatin. This is remarkable, because in several cell studies related cationic polynuclear platinum complexes with alkyldiamine linkers were shown to have a much higher affinity for DNA than cisplatin.[28,33−35] Active uptake mechanisms,[32] that are thought to transport cationic polynuclear platinum complexes into cells, may not facilitate the transport of the crown ether compounds.

Conclusion

For both neutral cisplatin derivatives and the cationic dinuclear complexes, the fifteen-membered rings were found to have an increased binding to intracellular DNA compared to their eighteen-membered counterparts. The complex with the highest affinity for DNA, **AO15**, also showed the highest cytotoxicity of the series against A2780 cancer cells. Although **AO15** was found to bind more effectively to intracellular DNA than cisplatin, its cytotoxicity was found to be significantly lower. The effectivity of DNA binding appears not to be the determining factor for cytotoxicity. Apparently, the crown ether moiety plays a role here, but its interactions with for instance DNA repair systems would require further study.

Due to charge interactions, most cationic polynuclear platinum complexes show a significantly higher affinity for DNA than neutral platinum complexes, like cisplatin.[28,33−35] Surprisingly, the cationic dinuclear complexes with oxa-diaza crown ethers exhibit a lower DNA binding in the A2780 cells than cisplatin and its mono-aza crown ether derivatives. Although the efficiency of transport by diffusion probably depends on the lipophilicity of the linker, it has also been suggested that, due to their resemblance of natural polyamines like spermine and spermidine, cationic dinuclear complexes are taken up through active transport mechanisms.[34,35] The present results suggest that the linear shape of the linker is important for these molecules to enter the cell.

Experimental Section

General: Oxa-aza crownethers and oxa-diaza crown ethers were either a gift from Dr. L. G. A. van de Water (Leiden Institute of Chemistry), or obtained from Acros Chemicals, the Netherlands. K_2PtCl_4 was obtained as a loan from Johnson-Matthey. The complex $Ph_4P[PtCl_3(NH_3)]$ was prepared from *cis*-$[PtCl_2(NH_3)_2]$ using literature procedures.[29,30] Solvents and other chemicals were obtained from Acros and Aldrich. NMR spectra were recorded with a Bruker DPX 300 spectrometer with a 5-mm multi-nucleus probe. ^1H NMR spectra were determined with respect to external TMS. ^{195}Pt spectra were calibrated using K_2PtCl_4 as an external reference at $\delta = -1614$ ppm. Reaction mixtures could be monitored using ^{195}Pt NMR by adding 10% of a deuterated solvent (D_2O or $CDCl_3$) for the locking signal. C, H and N analyses were performed with a Perkin−Elmer 240B microanalyzer. Platinum concentrations were determined by using graphite-oven flameless atomic absorption spectroscopy (FAAS), based on a previously published method.[28] Measurements were carried out with a Perkin−Elmer 3100 AAS apparatus, equipped with a platinum hollow cathode lamp and an AS-60 graphite-oven autosampler. For each determination, 20 μL of sample was injected. The used furnace program was: drying 120 °C/90 s, ashing 1300 °C/60s, 20 °C/15s, atomization and measurement 2650 °C/5s, purging 2600 °C/5 s. The furnace was purged with argon gas.

Synthesis

***cis*-[$PtCl_2(NH_3)$(1,4,7,10,13-pentaoxa-16-azacyclooctadecane-*N*)] (AO18):** To a solution of 102 mg (0.155 mmol) of $Ph_4P[Pt(NH_3)Cl_3]$ in 5 mL of methanol a solution of 40 mg (0.152 mmol) of aza-18-crown-6 (1,4,7,10,13-pentaoxa-16-azacyclooctadecane) in 5 mL of methanol was added. The mixture was stirred for 48 h at room temperature. The intensity of the yellow/orange color of the solution gradually decreased. After 48 h, the volume was reduced to 5 mL by rotary evaporation and the mixture was allowed to stand overnight at −20 °C. A yellow precipitate was formed. The product was filtered off, washed with diethyl ether and dried in air. A second crop was obtained by reducing the volume further by rotary evaporation. The solution was allowed to stand overnight at −20 °C. The product was recrystallized from a minimum amount of methanol. Yield: 13 mg (15%). ^1H NMR (MeOD): $\delta = 2.5$ (m, 2 H), 2.83 (m, 2 H), 3.5 (m, 18 H), 3.78 (m, 2 H), 5.09 (m, 2 H), 5.23 (s, br, 1 H) ppm. ^{195}Pt NMR (MeOD): $\delta = -2222$ ppm. $C_{12}H_{28}Cl_2N_2O_5Pt$ (546.3): calcd. C 26.38, H 5.17, N 5.13; found C 25.37, H 5.28, N 5.04.

***cis*-[$PtCl_2(NH_3)$(1,4,7,10-tetraoxa-13-azacyclopentadecane-*N*)] (AO15):** Complex **AO15** was prepared according to the procedure as described for **AO18**, with 33.3 mg (0.15 mmol) of aza-15-crown-5 (1,4,7,10-tetraoxa-13-azacyclopentadecane). Yield: 29 mg (39%). ^1H NMR (D_2O): $\delta = 2.70$ (m, 2 H), 3.25 (m, 2 H), 3.70 (m, 16 H), 4.00 (br, 1 H), 5.10 (br, NH) ppm. ^{195}Pt NMR (D_2O): $\delta = -2231$ ppm. $C_{10}H_{24}Cl_2N_2O_4Pt$ (502.3): calcd. C 23.91, H 4.82, N 5.58; found C 23.70, H 4.56, N 5.77.

[{*trans*-$PtCl(NH_3)_2$}$_2$(μ-1,4,10,13-tetraoxa-7,16-diazacyclooctadecane-*N*,*N*′)]$(NO_3)_2$ (DAO18): To a solution of 302 mg (1.0 mmol) of *trans*-$[PtCl_2(NH_3)_2]$ in 5 mL of DMF a solution of 162 mg (0.95

mmol) of $AgNO_3$ in 5 mL of DMF was added. The solution was stirred in the dark overnight at room temperature. The precipitated AgCl was filtered off and a solution of 98 mg (0.37 mmol) of 1,4,10,13-tetraoxa-7,16-diazacyclooctadecane (diaza-18-crown-6) in 5 mL of DMF was added to the yellow filtrate. The solution was stirred for 72 h at 40 °C. Subsequently, diethyl ether (400 mL) was added to the solution and an off-white precipitate appeared immediately. The solution was allowed to stand overnight at 4 °C and the precipitate was filtered off. The product was suspended in methanol and stirred for 1 h at 40 °C. Insoluble material was filtered off. Diethyl ether (400 mL) was added to the filtrate, a white precipitate appeared immediately. The mixture was allowed to stand overnight at 4 °C. The white product was filtered off, washed with diethyl ether and dried under vacuum. Yield: 81 mg (24%). ^{1}H NMR (D_2O): δ = 3.06 (m, 6 H), 3.70 (m, 8 H), 3.94 (m, 8 H), 4.20 (m, 2 H), 5.1 (s, br, 2 H), 4.75 (m, 2 H) ppm. ^{195}Pt NMR (D_2O): δ = −2408 ppm. $C_{12}H_{38}Cl_2N_8O_{10}Pt_2$ (915.5): calcd. C 15.74, H 4.18, N 12.24; found C 15.57, H 4.44, N 11.95.

[{*trans*-PtCl(NH$_3$)$_2$}$_2$(μ-1,4,10-trioxa-7,13-diazacyclopentadecane-*N*,*N*′)](NO$_3$)$_2$ (DAO15): The complex was prepared according to the procedure for **DAO18**, using 66.8 mg (0.31 mmol) of 1,4,10-trioxa-7,13-diazacyclopentadecane (diaza-15-crown-5) as the linker. Yield: 136 mg (51%). ^{1}H NMR (D_2O): δ = 3.15 (m, 12 H), 3.8 (m, 4 H), 4.2 (br, 2 H), 4.4 (m, 4 H) ppm. ^{195}Pt NMR (D_2O): δ = −2424 ppm. $C_{10}H_{34}Cl_2N_8O_9Pt_2$ (895.5): calcd. C 13.78, H 3.93, N 12.86; found C 14.40, H 3.86, N 12.90.

Cytotoxic Studies: A2780 and A2780cisR human ovarium cell lines were a gift from Dr. J. M. Perez (Universidad Autónoma de Madrid, Spain). The cell lines were grown as monolayers in Dulbecco's modified Eagle's Medium (DMEM) supplemented with 10% fetal calf serum (Gibco, Paisley, Scotland), penicillin (100 units/ml: Duchefa, Netherlands) and streptomycin (100 μg/ml: Duchefa, Netherlands) in a humidified 6% CO_2, 94% air atmosphere. Cells were passed after trypsinization when the plates were 80−90% full. Growth inhibition by the platinum compounds was determined using an MTT-based assay.

Intracellular DNA Binding Studies: For the uptake/DNA binding experiment, A2780 cells were grown in 6-cm plates with 4 mL of DMEM medium, until a concentration of approximately 1×10^7 cells was reached. At this point, the medium was replaced by 4 mL of serum-free DMEM medium, as the binding of platinum complexes to proteins in the serum might influence the uptake efficiencies. Fresh stock solutions of the platinum complexes were added to a concentration of 200 μM. Each experiment was performed in duplicate. After 1 h of incubation (37 °C, 6% CO_2, dark), the medium was removed and the cells were washed twice with 1 mL of PBS (0.1 M phosphate buffer in 0.15 M NaCl). The cells were then trypsinized and centrifuged at 1000 G for 10 min. At this point, the cell pellets may be stored at −20 °C for future use. DNA was isolated from the cells by using the following procedure. Cell pellets were suspended in 300 μL of buffer (10 mM tris, pH = 8, 150 mM NaCl, 10 mM edta). 5 μL of proteinase K solution was added and mixed well with the cells. Finally, 50 μL of 10% SDS was added and the resulting mixture was heated at 50−55 °C for 1.5 h. The solutions were transferred to 2-mL Eppendorf Phaselock tubes, and extracted with 300 μL of chloroform/phenol/amyl alcohol (24:25:1), and subsequently with 300 μL of chloroform/amyl alcohol (24:1). DNA was precipitated by adding 600 μL of isopropyl alcohol to the water layer. The DNA pellet was washed once with cold 70% ethyl alcohol, and then dissolved in 1 mL of milli-Q water. The DNA concentration was determined by measuring the UV absorption at 260 nm. From this absorption, the concentration of base pairs was calculated, using an average molar extinction coefficient per base pair of ε_{260} = 16800 $M^{-1}cm^{-1}$. The platinum concentration was measured by FAAS. From the platinum concentration, the actual drug concentration was derived. Combining FAAS and UV results, the drug molecules per base pair ratio (r_b) was calculated.

Acknowledgments

The authors are indebted to the EU for a grant as Host Institute in the EU programme Human Capital and Mobility. Also support and sponsorship by COST Actions D8/0007/97 and D20/0003/00 is kindly acknowledged. The authors wish to thank Johnson & Matthey (Reading, UK) for their generous loan of K_2PtCl_4. This work has been performed under auspices of the joint BIOMAC Research Graduate School of Leiden University and Delft University of Technology.

[1] J. Reedijk, *Chem. Commun.* **1996**, 801−806.
[2] T. W. Hambley, *Coord. Chem. Rev.* **1997**, *166*, 181−223.
[3] E. Wong, C. M. Giandomenico, *Chem. Rev.* **1999**, *99*, 2451−2466.
[4] E. R. Jamieson, S. J. Lippard, *Chem. Rev.* **1999**, *99*, 2467−2498.
[5] V. M. Gonzalez, M. A. Fuertes, C. Alonso, J. M. Perez, *Mol. Pharmacol.* **2001**, *59*, 657−663.
[6] M. N. Borrel, M. Fiallo, I. Veress, A. Garnier-Suillerot, *Biochem. Pharmacol.* **1995**, *50*, 2069−2076.
[7] A. Garnier-Suillerot, C. Marbeuf-Gueye, M. Salerno, C. Loetchutinat, I. Fokt, M. Krawczyk, T. Kowalczyk, W. Priebe, *Curr. Med. Chem.* **2001**, *8*, 51−64.
[8] J. W. Steed, *Coord. Chem. Rev.* **2001**, *215*, 171−221.
[9] I. A. Darwish, I. F. Uchegbu, *Int. J. Pharm.* **1997**, *159*, 207−213.
[10] I. F. Uchegbu, S. P. Vyas, *Int. J. Pharm.* **1998**, *172*, 33−70.
[11] R. Fukuda, S. Takenaka, M. Takagi, *J. Chem. Soc., Chem. Commun.* **1990**, 1028−1030.
[12] B. Dumont, J. P. Joly, Y. Chapleur, A. Marsura, *Bioorg. Med. Chem. Lett.* **1994**, *4*, 1123−1126.
[13] S. M. Kerwin, *Tetrahedron Lett.* **1994**, *35*, 1023−1026.
[14] W. M. Dai, K. C. Fong, *Tetrahedron Lett.* **1995**, *36*, 5613−5616.
[15] E. N. Glibin, N. G. Plekhanova, D. V. Ovchinnikov, Z. I. Korshunova, *Zh. Org. Khim.* **1996**, *32*, 406−408.
[16] R. Ostaszewski, E. Wilczynska, M. Wolszczak, *Pol. J. Chem.* **1999**, *73*, 1725−1732.
[17] M. M. McPhee, J. T. Kern, B. C. Hoster, S. H. Kerwin, *Bioorg. Chem.* **2000**, *28*, 98−118.
[18] L. Karawajew, E. N. Glibin, V. Y. Maleev, G. Czerwony, B. Dorken, D. B. Davies, A. N. Veselkov, *Anti-Cancer Drug Des.* **2000**, *15*, 331−338.
[19] E. B. Moroshkina, N. V. Zagoruiko, E. N. Glibin, *Mol. Biol.* **2001**, *35*, 98−105.
[20] B. Alberts, D. Bray, J. Lewis, M. Raff, K. Roberts, J. D. Watson, *Molecular Biology of the Cell*, 3rd ed., Garland Publishing, New York, **1994**.
[21] A. Gund, B. K. Keppler, *Angew. Chem. Int. Ed. Engl.* **1994**, *33*, 186−188.
[22] J. S. Yoo, Y. S. Sohn, Y. K. Do, *J. Inorg. Biochem.* **1999**, *73*, 187−193.
[23] S. Fruhauf, W. J. Zeller, *Cancer Res.* **1991**, *51*, 2943−2948.
[24] S. Fruhauf, W. J. Zeller, *Cancer Chemother. Pharmacol.* **1991**, *27*, 301−307.
[25] H. Rauter, R. di Domenico, E. Menta, A. Oliva, Y. Qu, N. Farrell, *Inorg. Chem.* **1997**, *36*, 3919−3927.

[26] N. Farrell, Y. Qu, U. Bierbach, M. Valsecchi, E. Menta, in *Cisplatin, Chemistry and Biochemistry of a Leading Anticancer Drug* (Ed.: B. Lippert), Wiley VCH, Weinheim, **1999**, pp. 479−496.
[27] Y. Qu, H. Rauter, A. P. S. Fontes, R. Bandarage, L. R. Kelland, N. Farrell, *J. Med. Chem.* **2000**, *43*, 3189−3192.
[28] B. A. J. Jansen, J. van der Zwan, H. den Dulk, J. Brouwer, J. Reedijk, *J. Med. Chem.* **2001**, *44*, 245−249.
[29] M. J. Abrams, C. M. Giandomenico, J. F. Vollano, D. A. Schwartz, *Inorg. Chim. Acta* **1987**, *131*, 3−4.
[30] E. G. Talman, W. Brüning, J. Reedijk, A. L. Spek, N. Veldman, *Inorg. Chem.* **1997**, *36*, 854−861.
[31] D. P. Bancroft, C. A. Lepre, S. J. Lippard, *J. Am. Chem. Soc.* **1990**, *112*, 6860−6871.
[32] B. A. J. Jansen, J. van der Zwan, J. Reedijk, H. den Dulk, J. Brouwer, *Eur. J. Inorg. Chem.* **1999**, 1429−1433.
[33] P. di Blasi, A. Bernareggi, G. Beggiolin, L. Piazzoni, E. Menta, M. L. Formento, *Anticancer Res.* **1998**, *18*, 3113−3117.
[34] J. D. Roberts, G. Beggiolin, C. Manzotti, L. Piazzoni, N. Farrell, *J. Inorg. Biochem.* **1999**, *77*, 47−50.
[35] J. D. Roberts, J. Peroutka, N. Farrell, *J. Inorg. Biochem.* **1999**, *77*, 51−57.

Received March 19, 2002
[I02141]

Cucurbituril as a New Macrocyclic Ligand for Complexation of Lanthanide Cations in Aqueous Solutions

Denis G. Samsonenko,[a] Janusz Lipkowski,[b] Olga A. Gerasko,[a] Alexander V. Virovets,[a] Maxim N. Sokolov,[a] Vladimir P. Fedin,*[a] Javier G. Platas,[c] Rita Hernandez-Molina,[d] and Alfredo Mederos[d]

Dedicated to Professor F. A. Kuznetsov on the occasion of his 70th birthday

Keywords: Lanthanides / Solid-state structures / Supramolecular chemistry / Aqua complexes / Cucurbituril

(Aqua)lanthanide complexes with cucurbituril {[Gd(NO_3)(H_2O)$_4$]($C_{36}H_{36}N_{24}O_{12}$)}(NO_3)$_2$·7H_2O (**1**), {[Gd(NO_3)(C_2H_5OH)(H_2O)$_3$]($C_{36}H_{36}N_{24}O_{12}$)}(NO_3)$_2$·5.5H_2O (**2**), {[Ho(NO_3)(H_2O)$_4$]($C_{36}H_{36}N_{24}O_{12}$)}(NO_3)$_2$·7H_2O (**3**), {[Yb(NO_3)(H_2O)$_4$]($C_{36}H_{36}N_{24}O_{12}$)}(NO_3)$_2$·6H_2O (**4**), {[La(H_2O)$_6$(SO_4)]($C_{36}H_{36}N_{24}O_{12}$)}(NO_3)·12H_2O (**5**), {[Gd(H_2O)$_4$]$_2$($C_{36}H_{36}N_{24}O_{12}$)$_3$}Br_6·45H_2O (**6**), and {[Ce(H_2O)$_5$]$_2$($C_{36}H_{36}N_{24}O_{12}$)$_2$}Br_6·26H_2O (**7**) were obtained in high yield by reaction of cucurbituril with aqueous solutions of lanthanide(III) species. The crystal structures of the compounds show a packing of 1:1, 2:2, and 2:3 in the (cucurbituril)lanthanide complexes in which cucurbituril plays a bidentate ligand role, and water molecules of the (aqua)lanthanide complexes form hydrogen bonds with carbonyl groups of the cucurbituril molecule. The guest water molecule is situated in the cucurbituril molecule cavity of **2** and **5**. The crystal structure of **6** is a packing of three-deck sandwiches, built from alternating cucurbituril molecules and Gd(H_2O)$_4^{3+}$ ions. The largest distance between outermost oxygen atoms in the sandwiches is 30.04 Å.
(© Wiley-VCH Verlag GmbH, 69451 Weinheim, Germany, 2002)

Introduction

Lanthanide(III) species exhibit rich and unique spectroscopic and magnetic properties, and rare-earth compounds are used for numerous applications, as relaxation agents in nuclear magnetic resonance imaging,[1] as luminescent probes in biology and medicine,[2] or as catalysts for the cleavage of RNA and DNA.[3]

In aqueous solution, large f-element ions form high-coordination number aqua complexes with various, often unique, coordination environments. The extremely high rates of exchange of ligands at f-element centers make the isolation of their coordination complexes difficult, particularly from aqueous solutions. A successful method of overcoming this kinetic instability is to increase the thermodynamic stability of the complexes by exploring the chelate and macrocyclic effects.[4]

There is a considerable body of information concerning macrocyclic ligand complexes of the lanthanides, where a metal atom is coordinated in a multidentate manner with nitrogen- or oxygen-donor ligands: crown ethers, calixarenes, etc.[5,6] The coordination selectivity exhibited by these ligands towards rare-earth cations has been widely investigated, in particular because of its role in processes of separation of f-elements in acidic aqueous solution, which is an important step in strategies for management and storage of high-level radioactive waste and clean-up of decommissioned nuclear facilities.[7]

However, the scope of neutral macrocyclic ligand systems studied for f-elements is limited, as the complexation with most of them occurs in organic solvents and not in aqueous solutions, where water acts as a very strong competitor. Introduction of the sulfonate group in the *para* position to the phenolic group of calixarenes made it possible to prepare (calixarene)lanthanide complexes in aqueous solution, but the metal ion coordinates to the ligand through the sulfonate functionalities, and in no case was evidence obtained

[a] Institute of Inorganic Chemistry, Russian Academy of Sciences, pr. Lavrentjeva 3, Novosibirsk 630090, Russia
E-mail: cluster@che.nsk.su
[b] Institute of Physical Chemistry, Polish Academy of Sciences, ul. Kasprzaka 44/52, Warszawa 01224, Poland
E-mail: klatrat@ichf.edu.pl
[c] Universidad de La Laguna, Departamento de Fisica Fundamental II, 30204 La Laguna, Tenerife, Canary Islands, Spain
[d] Departamento de Quimica Inorganica, Universidad de La Laguna, 38200 La Laguna, Tenerife, Canary Islands, Spain
Supporting information for this article is available on the WWW under http://www.eurjic.com or from the author.

for a multidentate mode of lanthanide complexation by the calixarene involving the phenolic oxygen atoms.[6a−6d]

In the present work, we report the synthesis and crystallization of lanthanide (La, Ce, Gd, Ho, Yb) complexes in aqueous media with the macrocyclic ligand cucurbituril. Using lanthanide nitrates or bromides, the following compounds were obtained: {[Gd(NO$_3$)(H$_2$O)$_4$](C$_{36}$H$_{36}$N$_{24}$O$_{12}$)}(NO$_3$)$_2$·7H$_2$O (**1**), {[Gd(NO$_3$)(C$_2$H$_5$OH)(H$_2$O)$_3$](C$_{36}$H$_{36}$N$_{24}$O$_{12}$)}(NO$_3$)$_2$·5.5H$_2$O (**2**), {[Ho(NO$_3$)(H$_2$O)$_4$](C$_{36}$H$_{36}$N$_{24}$O$_{12}$)}(NO$_3$)$_2$·7H$_2$O (**3**), {[Yb(NO$_3$)(H$_2$O)$_4$](C$_{36}$H$_{36}$N$_{24}$O$_{12}$)}(NO$_3$)$_2$·6H$_2$O (**4**), {[La(H$_2$O)$_6$(SO$_4$)](C$_{36}$H$_{36}$N$_{24}$O$_{12}$)}(NO$_3$)·12H$_2$O (**5**), {[Gd(H$_2$O)$_4$]$_2$(C$_{36}$H$_{36}$N$_{24}$O$_{12}$)$_3$}Br$_6$·45H$_2$O (**6**), and {[Ce(H$_2$O)$_5$]$_2$(C$_{36}$H$_{36}$N$_{24}$O$_{12}$)$_2$}Br$_6$·26H$_2$O (**7**) and characterized by single-crystal X-ray analysis.

Results and Discussion

Cucurbituril (C$_{36}$H$_{36}$N$_{24}$O$_{12}$) is a barrel-shaped macrocyclic cavitand with an internal cavity having a ca. 5.5 Å diameter and two identical carbonyl-fringed portals on each side.[8] Each portal of this molecule has six carbonyl oxygen atoms located in a plane which can interact with metal cations in such a way that cucurbituril behaves like a macrocyclic ligand. These portal atoms have a higher electric charge compared with crown ether oxygen atoms and consequently stronger interactions between carbonyl groups and positively charged ions take place.[9] Its easy synthesis, rigid structure, and chemical and thermal stability make cucurbituril very attractive for complexation of cations in aqueous solution.

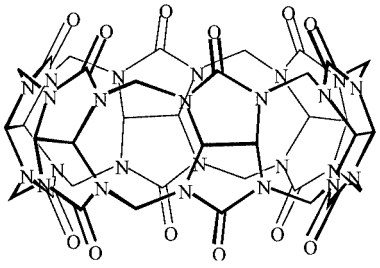

Scheme 1. Cucurbituril

A number of adducts of cucurbituril and s-metals (Na^+, K^+, Rb^+, Cs^+, Ca^{2+}) have been prepared with their quite unique structures and reactivities.[10] Due to the strong interactions of carbonyl oxygen donor atoms with cations, stable complexes are formed, and the metal ions and their coordinated water molecules cover each portal of cucurbituril like a "lid" on a "barrel". Also aliphatic and aromatic ammonium ions show a high affinity toward cucurbituril to form host−guest complexes.[11]

We have recently shown that the macrocyclic cavitand cucurbituril is by its geometry almost ideally suited for design of supramolecular adducts with triangular cluster aqua ions $[M_3Q_4(H_2O)_9]^{4+}$ (M = Mo, W; Q = S, Se), as well as their heterometal cuboidal derivatives.[12] Six water molecules, coordinated to the cluster core, form hydrogen bonds with the six carbonyl oxygen atoms of cucurbituril leading to the formation of nanosized molecules with the ratio of cluster/cucurbituril of 1:1 or 2:1. In the latter case the cavity in the cavitand molecule is effectively closed by cluster "lids" and small molecules or ions can be trapped inside. We have also shown that cucurbituril molecules are associated with (aqua)indium and -aluminum cations by hydrogen bonds with the portal oxygen atoms and also coordinate to the cluster water molecules.[13] An attractive point here is that, since cucurbituril usually belongs to the second coordination sphere, the aqua complexes will be much less perturbed by the adduct formation with cucurbituril than by introducing other ligands in the first coordination sphere. This enhances the relevance of the structural information obtained from cucurbituril adducts to the hydrolytic species actually present in solution. However, as we found in the present study cucurbituril can coordinate directly to Ln^{3+}.

The synthesis of the compounds **1**−**7** is straightforward. They were obtained by reaction of cucurbituril with aqueous solutions of lanthanide(III) species. Cucurbituril is not soluble in water, but it is well soluble in hot saturated aqueous solutions of Ln^{III} salts. Within a week or even overnight well-shaped colorless crystals suitable for X−ray studies separate in high yields. When taken out of the mother liquor, the crystals of compounds **6** and **7** lose water of crystallization and crystallinity. This fact explains the difference between the analytically deduced formulae and the stoichiometry found by X-ray analysis, performed at a low temperature with crystals sealed inside quartz capillaries.

The gadolinium complex **1** was obtained from solutions containing gadolinium nitrate and cucurbituril. The elemental analysis gives the formula {[Gd(NO$_3$)(H$_2$O)$_4$](C$_{36}$H$_{36}$N$_{24}$O$_{12}$)}(NO$_3$)$_2$·7H$_2$O (**1**). The crystals suitable for the X-ray experiment were obtained by diffusion of ethanol into the solution used to prepare **1**, and have the composition {[Gd(NO$_3$)(C$_2$H$_5$OH)(H$_2$O)$_3$](C$_{36}$H$_{36}$N$_{24}$O$_{12}$)}(NO$_3$)$_2$·5.5H$_2$O (**2**).

The crystal structure of compound **2** shows a 1:1 packing of (cucurbituril)gadolinium complexes in which cucurbituril plays the role of the bidentate ligand (Figure 1). One guest water molecule is situated inside the cucurbituril molecule cavity. In addition to the two oxygen atoms of the two cucurbituril carbonyl groups, the gadolinium cation has one ethanol molecule, one bidentate nitrate and three aqua ligands in its coordination environment. The coordination number of gadolinium is eight and its coordination polyhedron is a distorted triangulated dodecahedron in which the nitrate anion occupies the shortest edge.

Isostructural complexes of holmium, {[Ho(NO$_3$)(H$_2$O)$_4$](C$_{36}$H$_{36}$N$_{24}$O$_{12}$)}(NO$_3$)$_2$·7H$_2$O (**3**), and ytterbium, {[Yb(NO$_3$)(H$_2$O)$_4$](C$_{36}$H$_{36}$N$_{24}$O$_{12}$)}(NO$_3$)$_2$·6H$_2$O (**4**), were obtained under the same conditions, but in contrast to the gadolinium complex **2**, holmium and ytterbium cations have no ethanol molecules in their coordination environment (Figure 2). The space vacated by ethanol is occupied with water molecules forming hydrogen bonds with one another and the carbonyl groups of the cucurbituril molecule.

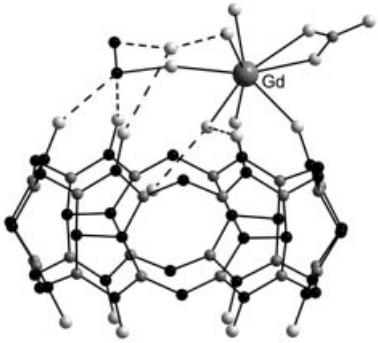

Figure 1. Structure of $\{[Gd(H_2O)_3(C_2H_5OH)(NO_3)](1/2\text{-}H_2O\subset C_{36}H_{36}N_{24}O_{12})\}^{2+}$ complex in **2**; dashed lines show hydrogen bonds

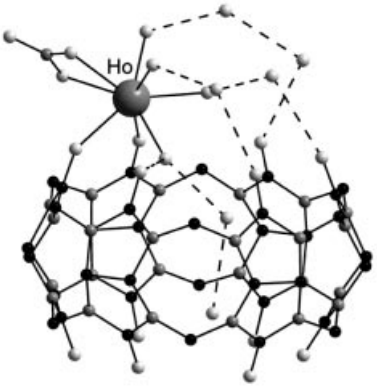

Figure 2. Structure of $\{[Ho(H_2O)_4(NO_3)](H_2O\subset C_{36}H_{36}N_{24}O_{12})\}^{2+}$ complex in **3**; dashed lines show hydrogen bonds

The crystal packing of compound **3** is shown in Figure 3. The cationic complexes form polar, i.e. having a preferential direction, hydrogen-bonded chains running along the *c* axis and the centers of the supermolecules form a body-centered motif. The chains are shifted from each other by one-half of a crystallographic translation along the axis of their expansion. The space between the polar chains is filled with solvate water molecules and nitrate anions. The ytterbium compound **4** has the same crystal structure, but complex **3** has one more solvate water molecule.

The comparison of calculated and experimental X-ray powder diffraction data for compounds **1** and **3** shows that complex **1** is isostructural with **3** (see figure in the Supporting Information).

Another example of 1:1 stoichiometry is given by an adduct with hexaaqualanthanum(III) sulfate, $\{[La(H_2O)_6(SO_4)](C_{36}H_{36}N_{24}O_{12})\}(NO_3)\cdot 12H_2O$ (**5**). It was isolated from an aqueous solution containing lanthanum nitrate, copper(II) sulfate and cucurbituril. The crystal structure of compound **5** is a packing of supermolecules, which consist of a cucurbituril molecule capped by a cationic (aqua)lanthanum complex on one side (Figure 4). Cucurbituril is bound to the lanthanum cation via two carbonyl groups and the coordination polyhedron of La^{3+}

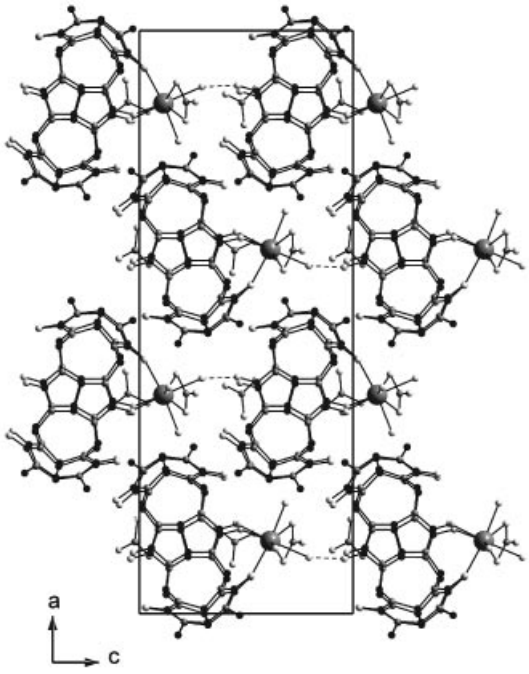

Figure 3. Crystal packing in **3** (projection on the *ac* plane); solvate water molecules and nitrate anions are omitted for clarity

(CN = 9, mono-capped square antiprism) is completed by six water molecules and one monodentate sulfate anion. The sulfate is disordered over two orientations around the S(1)−O(1S) bond with relative weights of 0.60 and 0.40 for O(2S1), O(3S1), O(4S1) and O(2S2), O(3S2), O(4S2), respectively. Three aqua ligands participate in hydrogen bonding with four carbonyl groups and another one does the same with a guest water molecule disordered over two positions (Figure 4). There is one water molecule in the open portal of the cucurbituril molecule, which is hydrogen-bound with the guest water molecule.

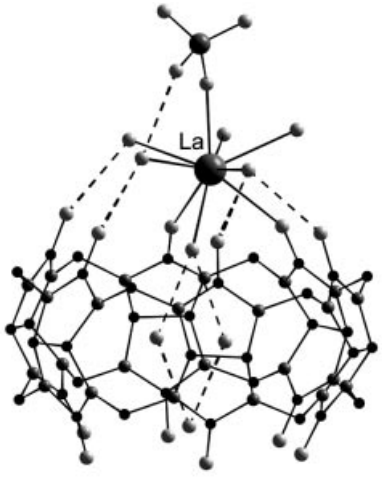

Figure 4. Structure of $\{[La(H_2O)_6(SO_4)](2H_2O\subset C_{36}H_{36}N_{24}O_{12})\}^{2+}$ complex in **5**; dashed lines show hydrogen bonds

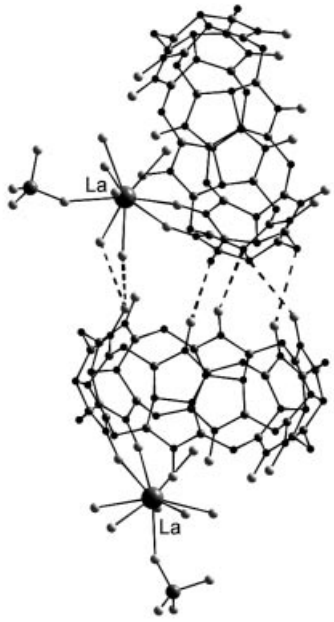

Figure 5. Two supermolecules in **5**; dashed lines show hydrogen bonds

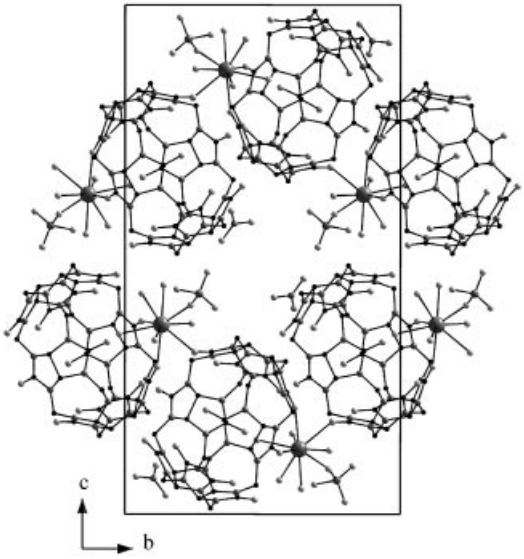

Figure 6. Crystal packing in **5** (projection on the *bc* plane); solvate water molecules and nitrate anions are omitted for clarity

Two neighboring supermolecules form hydrogen bonds between carbonyl groups of one supermolecule and aqua ligands (mean O···O distance: 2.861 Å) and the C−H groups (mean O···C distance: 3.050 Å) of another one (Figure 5). The supermolecules are stacked in columns shifted by one half of a crystallographic translation with regards to each other. The columns form corrugated layers parallel to the *ab* plane (Figure 6). There are channels between the layers filled with water of crystallization and nitrate anions. All the moieties of **5** are involved in a complicated network of hydrogen bonds.

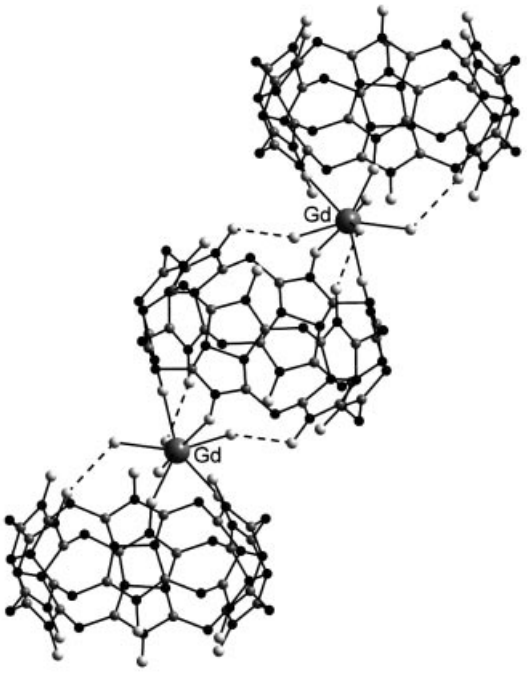

Figure 7. Three-deck sandwich $\{(C_{36}H_{36}N_{24}O_{12})[Gd(H_2O)_4](C_{36}H_{36}N_{24}O_{12})[Gd(H_2O)_4](C_{36}H_{36}N_{24}O_{12})\}^{6+}$ complex in **6**; dashed lines show hydrogen bonds

Compound **6**, $\{[Gd(H_2O)_4]_2(C_{36}H_{36}N_{24}O_{12})_3\}Br_6 \cdot 45H_2O$, was obtained from an aqueous solution containing gadolinium bromide and cucurbituril. The crystal structure of **6** reveals a packing of nanosized three-deck sandwiches, $\{(C_{36}H_{36}N_{24}O_{12})[Gd(H_2O)_4](C_{36}H_{36}N_{24}O_{12})[Gd(H_2O)_4](C_{36}H_{36}N_{24}O_{12})\}^{6+}$ (Figure 7), built from alternating cucurbituril molecules and Gd^{3+} cations. The shape of the sandwich complex can be approximated by an oblique cylinder with van der Waals dimensions about 15 × 28 Å. The largest distance between the oxygen atoms from the opposite sides is 30.04 Å.

Each Gd^{3+} is octacoordinated by two bidentate cucurbituril molecules, the mean Gd−O distance being 2.375 Å, and by four aqua ligands with a mean Gd−O distance of 2.397 Å. The coordination polyhedron of gadolinium is a slightly distorted square antiprism.

Crystal packing of sandwich complexes in **6** is shown in Figure 8. The centers of sandwiches coincide with centers of inversion in a body-centered motif (crystallographic position *2b* (1/2, 0, 0; 0, 1/2, 1/2) of $P2_1/n$ space group). The complexes are arranged in pillars oriented along the *a* axis. In each pillar, the sandwiches stack parallel to each other, being related by crystallographic translation. Each pillar has four other pillars as neighbors, oriented with respect to the former at angles of ca. 90°. The pillars are shifted by one-half of a crystallographic translation along the axis of their expansion and leaving quadrangular channels between them. The channels are filled with disordered solvate water molecules and bromide anions.

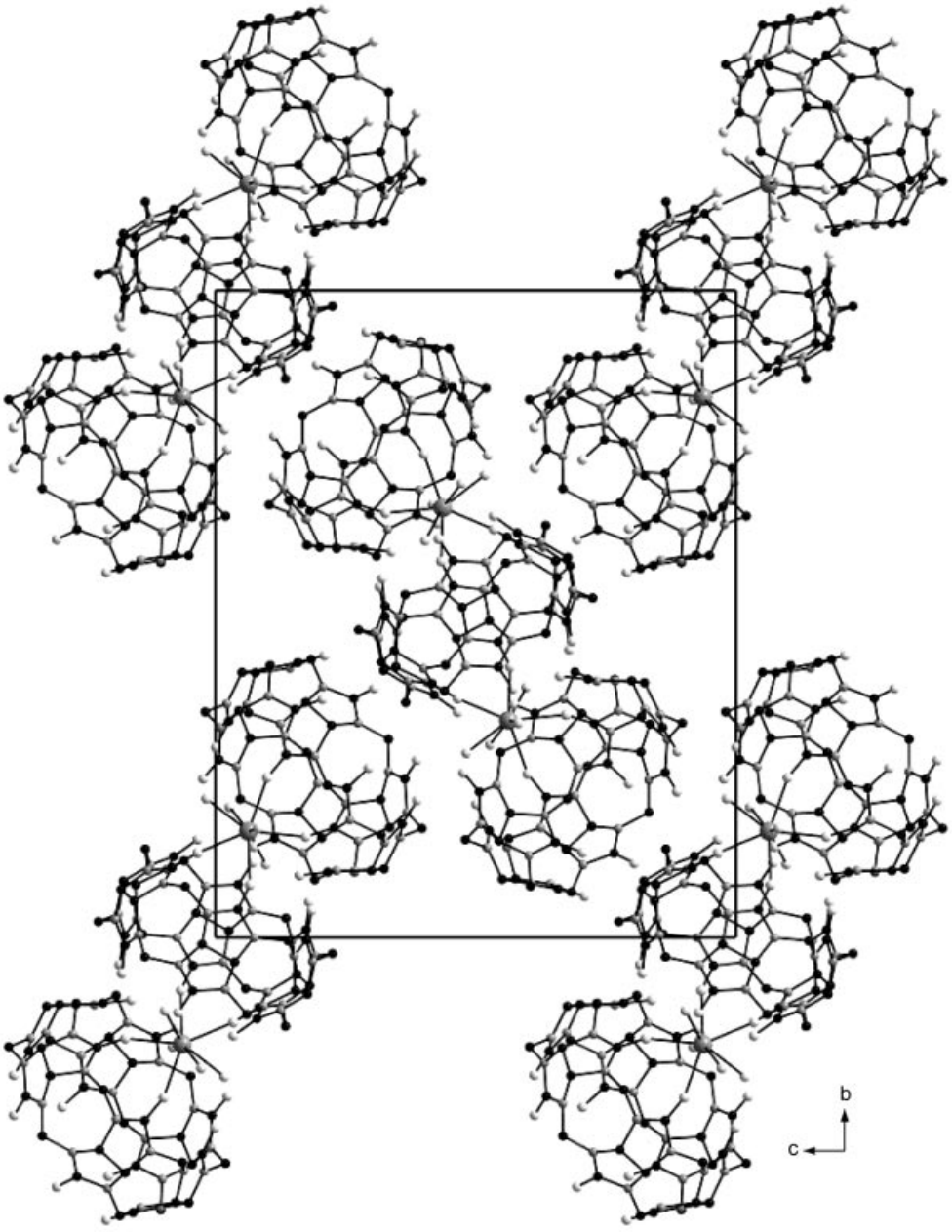

Figure 8. Crystal packing in **6** (projection on the *bc* plane); solvate water molecules and bromide anions are omitted for clarity

As a whole, the structure of **6** can be described as two interpenetrating networks, one of them being built of sandwich complexes and another representing a complicated network of hydrogen bonds formed by solvate water molecules and bromide anions.

Calculations carried out with the KPACK[14] program showed the sandwich complexes occupy 46.0% of the cell volume. The water molecules and bromide anions occupy another 18.0%. The packing coefficient in **6** is thus 0.64. Water molecules coat the sandwiches forming a bulky network of hydrogen bonds.

Another sandwich compound is a 2:2 (cucurbituril)cerium(III) complex, $\{[Ce(H_2O)_5]_2(C_{36}H_{36}N_{24}O_{12})_2\}Br_6 \cdot 26H_2O$ (**7**), crystallized from an aqueous solution containing cerium bromide and cucurbituril. The crystal structure of **7** represents a packing of supermolecules built from two cucurbituril molecules and two (aqua)cerium(III) ions sandwiched between them (Figure 9). Nonacoordinated Ce^{3+} has four oxygen atoms of cucurbituril carbonyl groups and five aqua ligands in its coordination environment. Two of the five aqua ligands of each cerium cation are disordered over two positions.

The trigonal crystal packing of sandwich complexes in **7** is shown in Figure 10. Large triangular channels with a van der Waals diameter of about 4.3 Å are filled with disordered water molecules and bromide anions.

To summarize, the cases when cucurbituril directly coordinates to a metal center, seem to be limited by

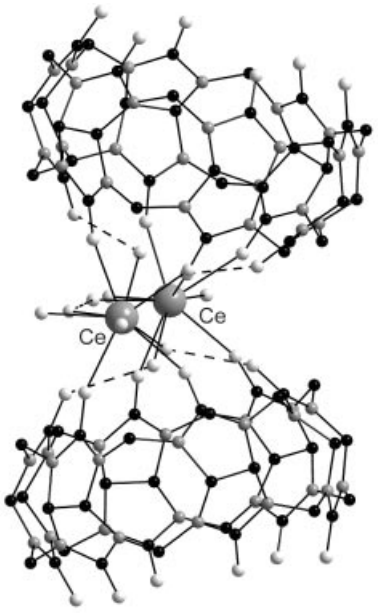

Figure 9. Structure of $\{[Ce(H_2O)_5]_2(C_{36}H_{36}N_{24}O_{12})_2\}^{6+}$ complex in **7**; dashed lines show hydrogen bonds

alkali,[10a−10c] alkali earth[10d,10e] and rare earth metal cations (groups 1−3). These are the most electropositive metals, forming hard and large (e.g., ionic radius of Na^+ 0.97 Å, Ca^{2+} 1.03 Å, Gd^{3+} 0.94 Å, Lu^{3+} 0.86 Å[12i]) ions, whose bonding to ligands can be accounted for in terms of electrostatic (ion−dipole) interactions. Only under these conditions can cucurbituril, being a weak donor, but possessing polar C=O groups, compete with other ligands for the first coordination sphere. Transition metals (and metals of group 13) form smaller ions (In^{3+} 0.76 Å, Al^{3+} 0.50 Å, Ni^{2+} 0.67 Å[12i]) which prefer covalent bonding. The higher charge and smaller size of the metal cation enhance the acidity of the coordinated water in the aqua-coordinated ions, so that, e.g., $[Al(H_2O)_6]^{3+}$ and $[In(H_2O)_6]^{3+}$ are by 4−5 orders of magnitude more acidic than any $[Ln(H_2O)_n]^{3+}$, (n = 8, 9).[15] This acidity allows for the formation of strong hydrogen bonds between the polar C=O groups of cucurbituril and the coordinated water molecules, thus increasing the energy gain of keeping cucurbituril in the second coordination sphere instead of substituting it for coordinated water.

Experimental Section

General: The lanthanide nitrates and bromides were of commercial quality and used without further purification. Cucurbituril was synthesized by published procedures.[8] Elemental analyses were carried out in the Laboratory of Microanalysis, Institute of Organic Chemistry SB RAS, Novosibirsk. The IR spectra were recorded on KBr pellets with an IFS-85 spectrometer (Bruker). X-ray powder patterns were recorded with a Philips APD diffractometer (Cu-K_α radiation).

X-ray Structure Determination: A summary of the crystallographic data, data collection and refinement parameters for compounds **2**−**7** is given in Table 1. For **2**, **4** and **5**, data were reduced in the usual way and absorption correction from ψ-scans was applied using the HELENA[16] program. For crystals **3**, **6** and **7**, data reduction and cell refinement were carried out using the Denzo,[17] Scalepak[17] and maXus[18] packages. The structures were solved by direct methods using SIR97[19] (for **2**) and SHELXS-97[20] (for **3**−**7**) programs and refined anisotropically for non-hydrogen atoms (except for some disordered atoms) by full-matrix least squares on F_o^2 using the SHELXL-97[20] program. In the case of **3**, **4** and **7** a racemic merohedral twinning was found with the twinning law of {−1, 0, 0, 0, −1, 0, 0, 0, −1} and relative component weights of 0.66(1)/0.34(1) for **3**, 0.53(5)/0.47(5) for **4** and 0.45(2)/0.55(2) for **7**. The hydrogen atoms of cucurbituril molecules were refined in the rigid-body approximation. The positions of hydrogen atoms of the coordinated water molecules in the structure of **2** were calculated using the CALC-OH[21] program. In the case of **7** only 15 bromide ions out of a total of 18 per unit cell could be found, but the chemical analysis confirmed the formula with 18 Br^-. Figures showing the coordination environment of lanthanide cations and tables with selected bond lengths and valence angles for compounds **2**−**7** are given in the Supporting Information. CCDC-177555 (**2**), -177556 (**3**), -177557 (**4**), -177558 (**5**), -177559 (**6**) and -177560 (**7**) contain the supplementary crystallographic data for this paper. These data can be obtained free of charge at www.ccdc.cam.ac.uk/conts/retrieving.html or from the Cambridge Crystallographic Data Centre, 12, Union Road, Cambridge CB2 1EZ, UK [Fax: (internat.) + 44-1223/336-033; E-mail: deposit@ccdc.cam.ac.uk].

Syntheses

$\{[Gd(NO_3)(H_2O)_4](C_{36}H_{36}N_{24}O_{12})\}(NO_3)_2\cdot 7H_2O$ (1): In a solution of $Gd(NO_3)_3\cdot 5H_2O$ (0.24 g, 0.54 mmol) in water (5 mL), cucurbituril (0.025 g, 0.021 mmol) was dissolved after heating for 15 min on a hot plate. The solution was filtered and the filtrate was left in an open beaker for 1 d. Colorless crystals of **1** were separated and dried on a filter paper. Yield: 0.028 g (86%). IR (KBr): $\tilde{\nu}$ = 634 (m), 676 (m), 757 (m), 801 (s), 966 (s), 1149 (s), 1191 (s), 1235 (s), 1326 (s), 1381 (s), 1487 (s), 1735 (s), 3362 cm^{-1} (s). μ_{eff} (298 K) = 7.81 μ_B. $C_{36}H_{58}GdN_{27}O_{32}$ (1538.27): calcd. C 28.11, H 3.80, N 24.58; found C 28.57, H 3.81, N 24.56. Crystals of $\{[Gd(NO_3)(C_2H_5OH)(H_2O)_3](C_{36}H_{36}N_{24}O_{12})\}(NO_3)_2\cdot 5.5H_2O$ (**2**) for X-ray experiments were obtained by diffusion of ethanol into an aqueous solution of **1**.

$\{[Ho(NO_3)(H_2O)_4](C_{36}H_{36}N_{24}O_{12})\}(NO_3)_2\cdot 7H_2O$ (3): In a solution of $Ho(NO_3)_3\cdot 5H_2O$ (0.23 g, 0.52 mmol) in water (5 mL), cucurbituril (0.022 g, 0.019 mmol) was dissolved after heating for 10 min on a hot plate. The solution was left in an open beaker for 1 d. Pale crystals of **3** were separated and dried on a filter paper. Yield: 0.022 g (76%). $C_{36}H_{58}HoN_{27}O_{32}$ (1545.95): calcd. C 27.97, H 3.78, N 24.46; found C 27.81, H 3.35, N 24.10.

$\{[Yb(NO_3)(H_2O)_4](C_{36}H_{36}N_{24}O_{12})\}(NO_3)_2\cdot 6H_2O$ (4): In a solution of $Yb(NO_3)_3\cdot 5H_2O$ (0.21 g, 0.47 mmol) in water (5 mL), cucurbituril (0.021 g, 0.018 mmol) was dissolved after heating for 10 min on a hot plate. The solution was left in an open beaker for 1 d. Colorless crystals of **4** were separated and dried on a filter paper. Yield: 0.020 g (73%). $C_{36}H_{56}N_{27}O_{31}Yb$ (1536.04): calcd. C 28.15, H 3.67, N 24.62; found C 28.13, H 3.70, N 24.51.

$\{[La(H_2O)_6(SO_4)](C_{36}H_{36}N_{24}O_{12})\}(NO_3)\cdot 12H_2O$ (5): In a solution of $La(NO_3)_3\cdot 5H_2O$ (0.13 g, 0.31 mmol) and $CuSO_4\cdot 5H_2O$ (0.18 g, 0.72 mmol) in water (10 mL), cucurbituril (0.030 g, 0.026 mmol) was dissolved after heating for 15 min on a hot plate. The solution was left in an open beaker for about 7 d. Colorless crystals of **5** were separated and dried on a filter paper. Yield: 0.027 g (68%).

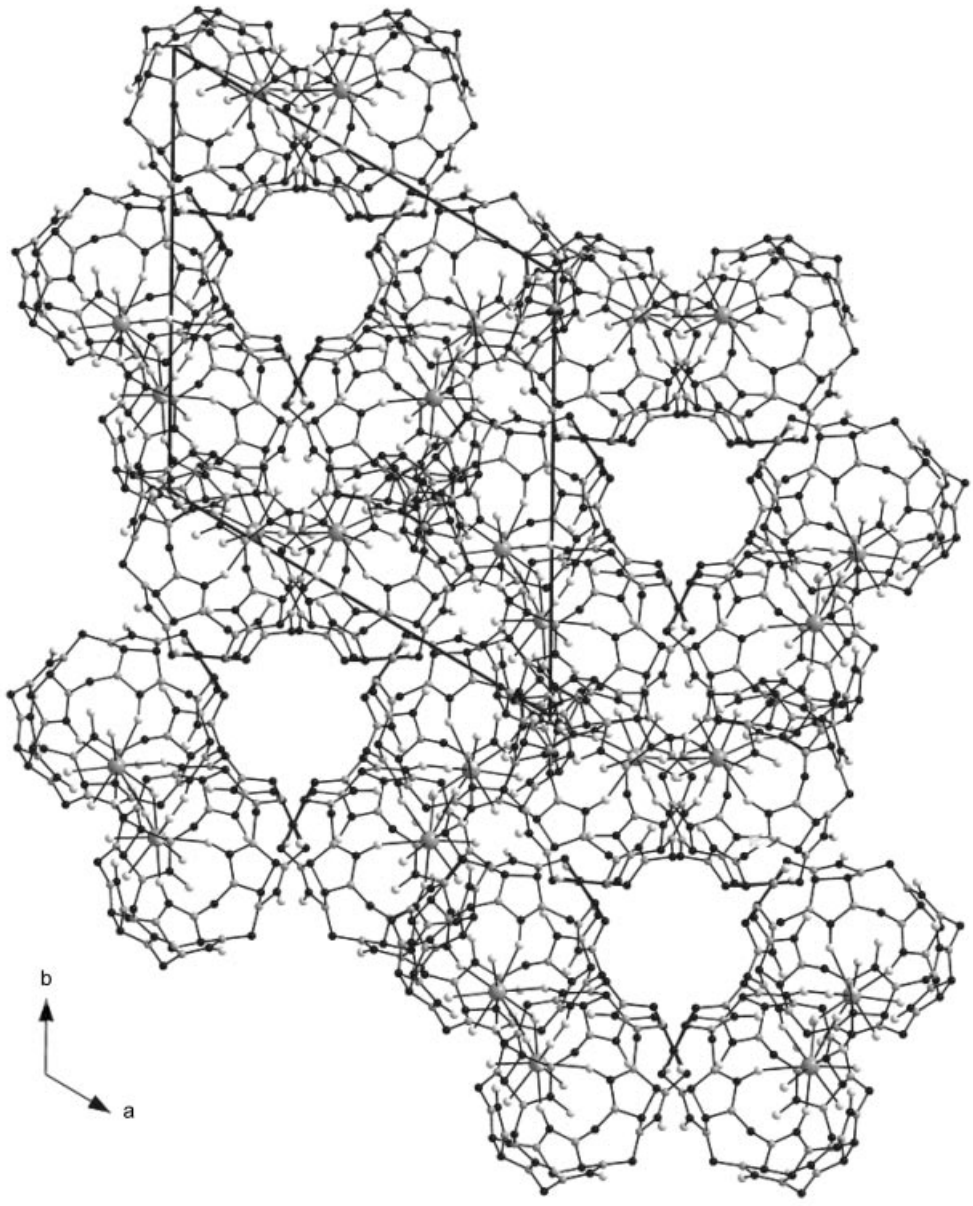

Figure 10. Crystal packing in **7** (projection on the *ab* plane); solvate water molecules and bromide anions are omitted for clarity

$C_{36}H_{72}LaN_{25}O_{37}S$ (1618.09): calcd. C 26.72, H 4.49, N 21.64, S 1.98; found C 27.01, H 4.56, N 21.78, S 2.02.

{[Gd(H$_2$O)$_4$]$_2$(C$_{36}$H$_{36}$N$_{24}$O$_{12}$)$_3$}Br$_6$·45H$_2$O (6): In a solution of $GdBr_3$ (0.15 g, 0.38 mmol) in water (13 mL), cucurbituril (0.052 g, 0.044 mmol) was dissolved after heating for 15 min on a hot plate. The solution was left in an open beaker for about 7 d. Colorless crystals of **6** were separated and dried on a filter paper. Yield: 0.050 g (77%). $C_{108}H_{180}Br_6Gd_2N_{72}O_{72}$ ({[Gd(H$_2$O)$_4$]$_2$-(C$_{36}$H$_{36}$N$_{24}$O$_{12}$)$_3$}Br$_6$·28H$_2$O) (4432.98): calcd. C 29.26, H 4.06, Br 10.81, N 22.75; found C 29.00, H 3.87, Br 10.86, N 23.25.

{[Ce(H$_2$O)$_5$]$_2$(C$_{36}$H$_{36}$N$_{24}$O$_{12}$)$_2$}Br$_6$·26H$_2$O (7): In a solution of $CeBr_3$ (0.11 g, 0.30 mmol) in water (5 mL), cucurbituril (0.022 g, 0.020 mmol) was dissolved after heating for 15 min on a hot plate. The solution was left in an open beaker for about 7 d. Colorless crystals of **7** were separated and dried on a filter paper. Yield: 0.020 g (63%). $C_{72}H_{144}Br_6Ce_2N_{48}O_{60}$ (3401.88): calcd. C 25.42, H 4.27, N 19.76; Br 14.09. found C 25.25, H 4.34, N 19.46, Br 14.29.

Acknowledgments

The Spanish team thanks the University of La Laguna for financial support. The Russian team is grateful to the Russian Foundation for Basic Research (grants 01-03-32789 and 01-03-06274) and INTAS (grant 2002-2346) for supporting this work. V. P. F. thanks the University of La Laguna for a Visiting Professor position.

Table 1. Crystal data and structure refinement for **2**−**7**

	2	**3**	**4**	**5**	**6**	**7**
Empirical formula	$C_{38}H_{59}GdN_{27}O_{30.50}$	$C_{36}H_{58}N_{27}O_{32}Ho$	$C_{36}H_{56}N_{27}O_{31}Yb$	$C_{36}H_{72}LaN_{25}O_{37}S$	$C_{108}H_{214}Br_6Gd_2N_{72}O_{89}$	$C_{72}H_{144}Br_6Ce_2N_{48}O_{60}$
Crystal system	orthorhombic	orthorhombic	orthorhombic	monoclinic	monoclinic	trigonal
Space group	$Pna2_1$	$Pna2_1$	$Pna2_1$	$P2_1/c$	$P2_1/n$	$P3_2$
Unit cell dimensions [Å, °]	a = 31.976(3), b = 14.727(2) c = 11.808(1)	a = 32.0840(1) b = 14.7160(1) c = 11.7250(1)	a = 31.946(5) b = 14.794(2) c = 11.8048(8)	a = 12.603(1) b = 16.225(2) c = 30.244(4) β = 97.047(8)	a = 16.5490(1) b = 26.9470(2) c = 21.9000(2) β = 100.3160(5)	a = 20.7418(2), c = 29.3987(3)
Volume [Å^3]	5560.5(10)	5535.94(15)	5579.1(12)	6137.7(12)	9608.34(13)	10953.46(19)
Z	4	4	4	4	2	3
$D_{calcd.}$ [Mg/m^3]	1.839	1.855	1.829	1.751	1.638	1.547
Temperature [K]	200(2)	150(2)	296(2)	293(2)	150(2)	150(2)
Diffractometer	Enraf−Nonius MACH-3	Nonius Kappa CCD	Enraf−Nonius CAD4	Bruker	Nonius Kappa CCD	Nonius Kappa CCD
Radiation [Å]	0.71073 (Mo-K_α)	0.71073 (Mo-K_α)	0.71073 (Mo-K_α)	0.71073 (Mo-K_α)	0.71073 (Mo-K_α)	0.71073 (Mo-K_α)
Data collection method	ω-scans	CCD technique	ω-scans	2θ/ω-scans	CCD technique	CCD technique
$2\theta_{max}$ [°]	59.94	54.88	59.88	50.00	66.04	43.92
Crystal size [mm]	0.27 × 0.15 × 0.10	0.18 × 0.15 × 0.12	0.75 × 0.43 × 0.35	0.48 × 0.43 × 0.30	0.44 × 0.36 × 0.28	0.28 × 0.25 × 0.18
μ(Mo-K_α) [mm^{-1}]	1.316	1.555	1.799	0.853	2.046	2.356
Absorption correction	ψ-scans	none	ψ-scans	ψ-scans	none	none
Reflns. collected	8461	48262	6445	11607	95034	26529
Unique reflns.	8461	12620	6445	10482	35921	17777
R_{int}	0	0.0721	0	0.0520	0.0695	0.0345
Observed reflns.	5890	10479	4719	6236	22384	15871
Final R indices [$F \geq 4\sigma(F)$][a]	$R1$ = 0.0478, $wR2$ = 0.1201	$R1$ = 0.0577, $wR2$ = 0.1366	$R1$ = 0.0576, $wR2$ = 0.1600	$R1$ = 0.0616, $wR2$ = 0.1487	$R1$ = 0.0697, $wR2$ = 0.2061	$R1$ = 0.0797, $wR2$ = 0.2113
R indices (all data)	$R1$ = 0.1055, $wR2$ = 0.1390	$R1$ = 0.0741, $wR2$ = 0.1435	$R1$ = 0.0730, $wR2$ = 0.1644	$R1$ = 0.1181, $wR2$ = 0.1780	$R1$ = 0.1240, $wR2$ = 0.2266	$R1$ = 0.0910, $wR2$ = 0.2183
GooF on F^2	1.070	1.032	1.014	1.021	1.096	1.078

[a] Definitions: $R1 = \Sigma||F_o| - |F_c||/\Sigma|F_o|$, $wR2 = \{\Sigma[w(F_o^2 - F_c^2)^2]/\Sigma[w(F_o^2)^2]\}^{1/2}$, $GooF = \{\Sigma[w(F_o^2 - F_c^2)^2]/(n - p)\}^{1/2}$.

[1] [1a] S. Aime, M. Botta, M. Fasano, E. Terreno, *Chem. Soc. Rev.* **1998**, *27*, 19. [1b] V. Comblin, D. Gilsoul, M. Hermann, V. Humblet, V. Jacques, M. Mesbahi, C. Sauvage, J.-F. Desreux, *Coord. Chem. Rev.* **1999**, *185*−*186*, 451.

[2] [2a] J.-C. G. Bunzli in *Lanthanide Probes in Life, Chemical and Earth Sciences* (Eds.: J.-C. G. Bunzli, G. R. Choppin), Elsevier, Amsterdam, **1989**, p. 219. [2b] M. Elhabiri, R. Scopelliti, J.-C. G. Bunzli, C. Piguet, *J. Am. Chem. Soc.* **1999**, *121*, 10747.

[3] [3a] T. C. Bruice, A. Tsubouchi, R. O. Dempcy, L. P. Olson, *J. Am. Chem. Soc.* **1996**, *118*, 9867. [3b] S. J. Oh, Y.-S. Choi, S. Hwangbo, S. C. Bae, J. K. Ku, J. W. Park, *Chem. Commun.* **1998**, 2189.

[4] N. Kaltsoyannis, P. Scott in *The f elements* (Eds.: S. G. Davies, R. G. Compton, J. Evans, L. F. Gladden), Oxford University Press, New York, **1999**, p. 56.

[5] [5a] J.-C. G. Bunzli, J. A. Harrowfield, "Lanthanide Ions and Calixarenes" in *Calixarenes: A Versatile Class of Macrocyclic Compounds* (Eds.: J. Vicens, V. Bohmer), Kluwer, Boston, **1991**. [5b] R. Rogers, C. Bauer, "Structural Chemistry of Metal-Crown Ether and Polyethylene Glycol Complexes Excluding Groups 1 and 2" in *Comprehensive Supramolecular Chemistry* (Eds.: J. Atwood, J. Davies, D. Macinol, Vogtle), Pergamon, New York, **1996**, vol. 1, p. 315. [5c] V. Alexander, *Chem. Rev.* **1995**, *95*, 273. [5d] P. Delange, C. Husson, C. Lebrun, J. Pecaut, P. J. A. Vottero, *Inorg. Chem.* **2001**, *40*, 2953. [5e] J. F. Malone, D. J. Marrs, M. A. McKervey, P. O'Hagan, N. Simon, *J. Chem. Soc., Chem. Commun.* **1995**, 2151. [5f] B. M. Furphy, J. M. Harrowfield, D. L. Kepert, B. W. Skelton, A. H. White, F. R. Wilner, *Inorg. Chem.* **1987**, *26*, 4231. [5g] M. F. Loncin, J.-F. Desreux, E. Merciny, *Inorg. Chem.* **1986**, *25*, 2646. [5h] K. K. Abid, D. E. Fenton, U. Casellato, P. A. Vigato, R. Graziani, *J. Chem. Soc., Dalton Trans.* **1984**, 351. [5i] K. K. Abid, D. E. Fenton, *Inorg. Chim. Acta* **1984**, *95*, 199. [5j] A. Navaza, F. Villain, P. Charpin, *Polyhedron* **1984**, *3*, 143. [5k] E. A. Cuellar, T. J. Marks, *Inorg. Chem.* **1981**, *20*, 3766. See also references cited within these papers.

[6] [6a] A. Drljaca, M. J. Hardie, J. A. Johnson, C. L. Raston, H. R. Webb, *Chem. Commun.* **1999**, 1135. [6b] J. L. Atwood, G. W. Orr, N. C. Means, F. Hamada, H. Zhang, S. G. Bott, K. D. Robinson, *Inorg. Chem.* **1992**, *31*, 603. [6c] G. W. Orr, L. J. Barbour, J. L. Atwood, *Science* **1999**, *285*, 1049. [6d] J. W. Steed, C. P. Johnson, C. L. Barnes, R. K. Juneja, J. L. Atwood, S. Reilly, R. L. Hollis, P. H. Smith, D. L. Clark, *J. Am. Chem. Soc.* **1995**, *117*, 11426. [6e] P. D. Beer, M. J. B. Drew, M. I. Ogden, *J. Chem. Soc., Dalton Trans.* **1997**, 1489. [6f] P. D. Beer, M. J. B. Drew, A. Greve, M. Kan, P. B. Leeson, G. Nicholson, M. I. Ogden, G. Williams, *Chem. Commun.* **1996**, 1117. [6g] P. D. Beer, M. J. B. Drew, M. Kan, P. B. Leeson, M. I. Ogden, G. Williams, *Inorg. Chem.* **1996**, *35*, 2202. [6h] J. Mao, Z. Jin, J. Ni, *Polyhedron* **1994**, *13*, 313.

[7] K. L. Nash, *Solvent Extr. Ion Exch.* **1993**, *11*, 729.

[8] [8a] R. Behrend, E. Meyer, F. Rusche, *Justus Liebigs Ann. Chem.* **1905**, *339*, 1. [8b] W. A. Freeman, W. L. Mock, N.-Y. Shih, *J. Am. Chem. Soc.* **1981**, *103*, 7367.

[9] H.-J. Buschmann, E. Cleve, E. Schollmeyer, *Inorg. Chim. Acta* **1992**, *193*, 93.

[10] [10a] K. Kim, J. Heo, S.-Y. Kim, D. Whang, *Angew. Chem. Int. Ed.* **1999**, *38*, 641. [10b] K. Kim, J. Heo, J. Kim, D. Whang, *Inorg. Chem. Acta* **2000**, *297*, 307. [10c] K. Kim, D. Whang, J. Heo, J. H. Park, *Angew. Chem. Int. Ed.* **1998**, *37*, 78. [10d] W. A. Freeman, *Acta Crystallogr., Sect. B* **1984**, *40*, 382. [10e] D. G. Samsonenko, A. A. Sharonova, M. N. Sokolov, A. V. Virovets, V. P. Fedin, *Russ. J. Coord. Chem.* **2001**, *27*, 10.

[11] [11a] S.-G. Roh, K.-M. Park, G.-J. Park, S. Sakamoto, K. Yamaguchi, K. Kim, *Angew. Chem. Int. Ed.* **1999**, *38*, 638. [11b] D. Whang, Y.-M. Jeon, J. Heo, K. Kim, *J. Am. Chem. Soc.* **1996**, *118*, 11333.
[12] [12a] V. P. Fedin, A. V. Virovets, M. N. Sokolov, D. N. Dybtsev, O. A. Gerasko, W. Clegg, *Inorg. Chem.* **2000**, *39*, 2227. [12b] M. N. Sokolov, A. V. Virovets, D. N. Dybtsev, O. A. Gerasko, V. P. Fedin, R. Hernandez-Molina, W. Clegg, A. G. Sykes, *Angew. Chem. Int. Ed.* **2000**, *39*, 1659. [12c] D. N. Dybtsev, O. A. Gerasko, A. V. Virovets, M. N. Sokolov, V. P. Fedin, *Inorg. Chem. Commun.* **2000**, *3*, 345. [12d] M. N. Sokolov, D. N. Dybtsev, A. V. Virovets, K. Hegetschweiler, V. P. Fedin, *Russ. Chem. Bull.* **2000**, *49*, 1877. [12e] O. A. Gerasko, A. V. Virovets, D. N. Dybtsev, W. Clegg, V. P. Fedin, *Koord. Khim.* **2000**, *7*, 512. [12f] M. N. Sokolov, D. N. Dybtsev, A. V. Virovets, W. Clegg, V. P. Fedin, *Russ. Chem. Bull.* **2001**, *50*, 1144. [12g] D. N. Dybtsev, O. A. Gerasko, A. V. Virovets, M. N. Sokolov, T. Weber, V. P. Fedin, *Zh. Neorg. Khim.* **2001**, *46*, 908. [12h] V. P. Fedin, V. Gramlich, M. Wörle, Th. Weber, *Inorg. Chem.* **2001**, *40*, 1074. [12i] S. S. Batsanov, *Zh. Neorg. Khim.* **1991**, *36*, 3015.
[13] D. G. Samsonenko, M. N. Sokolov, A. V. Virovets, N. V. Pervukhina, V. P. Fedin, *Eur. J. Inorg. Chem.* **2001**, 167.
[14] A. V. Virovets, N. V. Podberezskaya, *Kristallografia* **1992**, *37*, 1017.
[15] D. T. Richens, *The Chemistry of Aqua Ions*, John Wiley & Sons, **1997**.
[16] A. L. Spek, *HELENA, Program for Data Reduction*, Utrecht University, The Netherlands, **1997**.
[17] Z. Otowinowski, W. Minor, *Methods in Enzymology, Macromolecular Crystallography* **1997**, *A276*, 307 (Eds.: C. W. Carter, Jr., R. M. Sweet), Academic Press.
[18] S. Mackay, W. Dong, C. Edwards, A. Henderson, C. Gilmore, N. Stewart, K. Shankland, A. Donald, *maXus, Comprehensive crystallography software, version 4.0*, University of Glasgow, Glasgow, Scotland; MAC Science Co. Ltd., Japan; Nonius B. V., Netherlands, **1999**.
[19] A. Altomare, M. C. Burla, M. Camalli, G. L. Cascarano, C. Giacovazzo, A. Guagliardi, A. G. G. Moliterni, G. Polidori, R. Spagna, *J. Appl. Crystallogr.* **1999**, *32*, 115.
[20] G. M. Sheldrick, *SHELX-97 Release 97-2*, Göttingen University, Germany, **1998**.
[21] M. Nardelli, *J. Appl. Crystallogr.* **1999**, *32*, 563.

Received January 22, 2002
[I02036]

The First Crystal and Molecular Structure of a *syn*-Acetato-Bridged Dinuclear Cyclometallated Complex [Pd{2,3,4-$(MeO)_3C_6HC(H)=NCH_2CH_2OH$}-(μ-OAc)]$_2$

Alberto Fernández,*[a] Digna Vázquez-García,[a] Jesús J. Fernández,[a] Margarita López-Torres,[a] Antonio Suárez,[a] Samuel Castro-Juiz,[a] and José M. Vila*[b]

Keywords: C-H activation / Cyclometallation / P ligands / Schiff bases / Palladium

Treatment of the Schiff base ligands 2,3,4-$(MeO)_3C_6H_2C(H)=NR$ (R = CH_2CH_2OH, **1**; R = Me, **17**; R = Et, **18**; R = Pr, **19**; R = *t*Bu, **20**) with palladium(II) acetate in toluene gave the dinuclear cyclometallated complexes [Pd{2,3,4-$(MeO)_3C_6HC(H)=NR$}(μ-O_2CMe)]$_2$ (R = CH_2CH_2OH, **2**; R = Me, **21**; R = Et, **22**; R = Pr, **23**; R = *t*Bu, **24**), with the ligand bonded to the palladium atom through the imine nitrogen and the C6 carbon atoms. The ^1H and $^{13}C\{^1H\}$ NMR spectra of the complexes showed the presence of the *anti* and *syn* isomers in solution. The *anti*/*syn* ratio varies with the solvent and the nature of the imine nitrogen substituent R. Complex **24** with the bulky *t*Bu group showed a 28:1 ratio in chloroform whilst the less bulky substituted complexes showed lower ratios. The X-ray crystal structure of the *syn* isomer of complex **2** is described. Reaction of the acetato-bridged complex **2** with PPh_3 gave the mononuclear complex **4**, in a bridge-splitting reaction. Reaction of **2** with the diphosphanes dppm, dppp and dppb in a 1:1 molar ratio gave the dinuclear cyclometallated complexes **5**, **6** and **7**, respectively. Treatment of **2** with an aqueous solution of sodium chloride gave the chloro-bridged complex **3**. Treatment of the cyclometallated chloro-bridged complex **3** with PPh_3 in acetone yielded the mononuclear complex **8**, and reaction of **3** with silver triflate gave the cyclometallated complex **9**, with the palladium atom bonded to four different atoms C, N, O and P. Treatment of **3** with the tertiary diphosphanes dppp, dppb and dppf, in a 1:1 molar ratio gave the dinuclear complexes **10**, **11** and **12**, respectively, with terminal chloride ligands. However, reaction of **3** with the small "bite" diphosphane dppm gave **13**, with a bridging chloride ligand. Reaction of **11** with silver triflate in acetone gave the new dinuclear complex **14**, with the Schiff base ligand as [C,N,O] terdentate. Reaction of **3** with the diphosphane dppe in a 1:2 molar ratio, and silver perchlorate, gave the mononuclear complex **15**. Treatment of **3** with the triphosphane bis(2-diphenylphosphanylethyl)phenylphosphane in a 1:2 molar ratio, followed by treatment with sodium perchlorate, gave **16**, in which the palladium atom was bonded to the triphosphane through the three phosphorus atoms. The X-ray crystal structures of complexes **8**, **9**, **15** and **16** are also reported.

(© Wiley-VCH Verlag GmbH, 69451 Weinheim, Germany, 2002)

Introduction

Cyclometallated compounds have attracted much attention in recent years and abundant reports concerning them have appeared.[1−7] They are important not only because they show numerous applications in organic and organometallic synthesis[8] and in biologically active compounds,[9,10] among others, but also due to the new structural features they promote.[11,12] Lately, we have been interested in the study of Schiff base cyclometallated complexes prepared by direct reaction of the ligand with palladium(II) acetate, which gives dimeric acetato-bridged complexes with the characteristic open-book geometry;[13,14] these species are good starting materials for a great number of cyclometallated derivatives. Two different dispositions are possible for such compounds: the *syn* isomer with overall C_s symmetry, and the *anti* isomer with overall C_2 symmetry. The latter is by far the most common, and the known crystal structures of dinuclear acetato-bridged complexes correspond to the *anti* isomer.[10,15−27] We therefore sought to isolate and characterise the *syn* isomer in a pure form by modifying the steric requirements of the substituent at the imine nitrogen atom, i.e., substituents with small or negligible steric hindrance, which should allow the nitrogen atoms to lie above each other in the *syn* form without repulsions arising from the N-R groups, and in the present paper we report the crystal and molecular structure of a dinuclear acetato-bridged cyclometallated complex **2**, which, to the best of our knowledge, is the first example of a *syn* isomer. Compound **2** was obtained as an equilibrium mixture of the *anti* and *syn* isomers, and the features involved in the

[a] Departamento de Química Fundamental, Universidad de La Coruña,
15071 La Coruña, Spain
Fax: (internat.) +34-981/167-065
E-mail: qiluaafl@udc.es
[b] Departamento de Química Inorgánica, Universidad de Santiago de Compostela,
15782 Santiago de Compostela, Spain
Fax: (internat.) +34-981/595-012
E-mail: qideport@usc.es

equilibrium are also described. As we have observed before in related compounds with terdentate [C, N, X] (X = N, O, S] ligands,[28−31] the reactivity of the acetate dimeric compounds, and of their chloro-bridged derivatives, is fairly extensive, especially when they react with mono-, di- and triphosphanes, and herein we also report this chemistry, as well as the synthesis of [C, N, O] derivatives with Pd−O bond formation via halide abstraction by a silver(I) salt. The crystal structures of the cyclometallated compounds **8**, **9**, **15** and **16** are also given.

Results and Discussion

For the convenience of the reader the compounds and reactions are shown in Schemes 1, 2 and 3. The compounds described in this paper were characterised by elemental analysis (C, H, N), IR spectroscopy and by ^{1}H, ^{31}P{^{1}H} and, in part, ^{13}C{^{1}H} NMR spectroscopy and FAB mass spectrometry (data in the Exp. Sect.).

Reaction of the Schiff base ligand 2,3,4-$(MeO)_3C_6H_2C(H)=NCH_2CH_2OH$ (**1**) with palladium(II) acetate (Scheme 1) gave the dinuclear acetato-bridged complex $[Pd\{2,3,4\text{-}(MeO)_3C_6HC(H)=NCH_2CH_2OH\}(\mu\text{-}O_2CMe)]_2$ (**2**) as an orange air-stable solid which was fully characterised. *Syn* and *anti* isomers are possible for the folded arrangement of the acetato-bridged dimers: the *anti* isomer with C_2 symmetry and the *syn* isomer with C_s symmetry

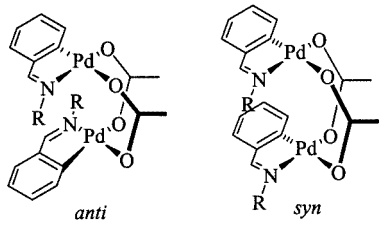

Figure 1. Isomers of compound **2**

(see Figure 1), with the *anti* disposition being by far the most frequent.[14]

If both isomers are present in the final product two resonances would be expected for the *H*C=N and aromatic protons and three for the *Me*COO protons in the ^{1}H NMR spectrum: one for the *anti* isomer and two for the *syn* isomer. Thus, the ^{1}H NMR spectrum of **2** shows two sets of signals, one for each isomer. The resonance corresponding to the HC=N proton appears as a singlet (δ = 7.57 and 7.81 ppm, for the *anti* and *syn* isomers, respectively) shifted to lower frequency due to the coordination of the imine group to the palladium atom through the lone pair of the nitrogen atom.[32] The H^5 resonance also appears as a singlet, confirming metallation of the C6 carbon. The ^{1}H NMR spectrum shows the signal of the *Me*COO protons as a singlet at δ = 2.07 ppm, for the *anti* isomer, and as two singlets at δ = 2.25 and 2.02 ppm for the *syn* isomer. The IR spectrum of **2** shows the ν(C=N) stretch at 1604 cm^{-1}, shifted

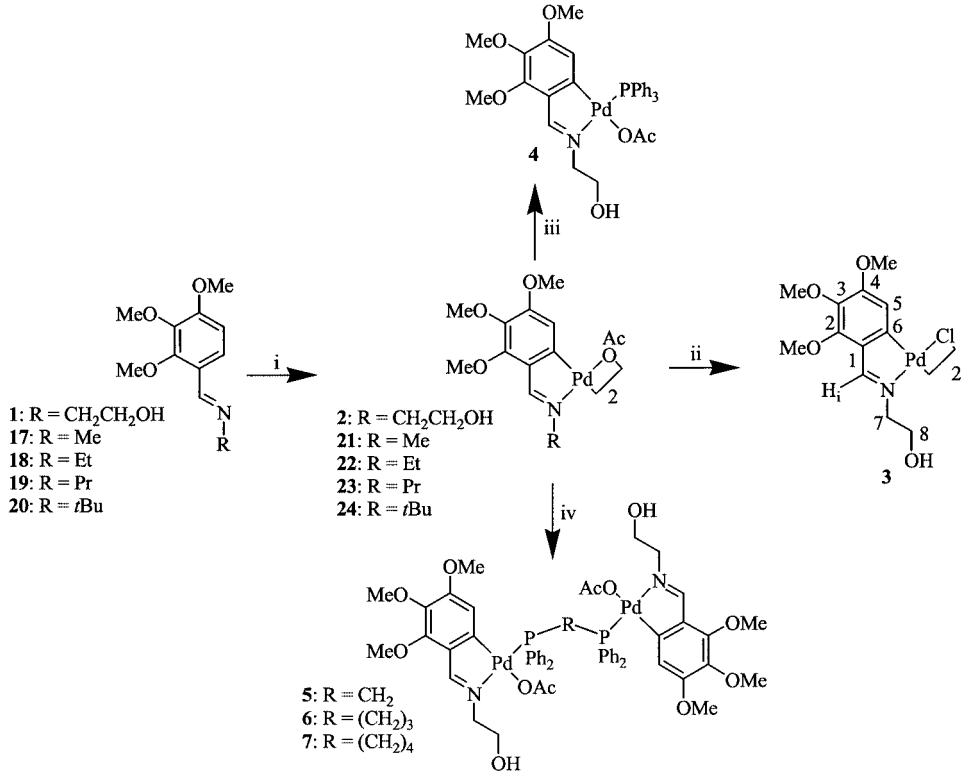

Scheme 1. (i) $Pd(ACO)_2$, (toluene), (ii) NaCl (acetone/water), (iii) PPh_3 (acetone), (iv) dppm, dppp or dppb (acetone, 1:1 molar ratio)

to lower wavenumbers (relative to the free ligand) due to N-coordination of the imine.[33,34] The IR spectrum also shows strong bands assigned to the symmetric and asymmetric ν(COO) vibrations, in agreement with bridging acetate ligands[35] (see Exp. Sect.). The ν(O−H) stretch appears at 3384 cm^{-1}, close to its position in the spectrum of the free ligand, in agreement with a noncoordinated hydroxyl group. From the integration of the peaks corresponding to both isomers in the ^1H NMR spectrum we concluded that the *anti*/*syn* ratio is ca. 5:1

The $^{13}C\{^1H\}$ NMR spectrum showed the presence of signals corresponding to both isomers, with the C=N, C6 and C1 resonances shifted toward higher frequency, thus confirming that metallation had occurred.[28] The mass FAB spectrum of **2** shows a cluster of peaks, centred at 808 amu, which correspond to $[M]^+$. The isotopic pattern is in good agreement with the expected dinuclear structure.

The synthesis of complex **2** was performed under different reaction conditions: toluene at 60 °C, chloroform at room temperature and boiling methanol. Irrespective of the method used the *anti*/*syn* ratio is ca. 5:1 in all cases, which seems to be the equilibrium ratio. Although we cannot ascertain completely that the solid state of **2** contains only crystals of the *syn* form, the ^1H NMR spectrum of the solid, freshly dissolved in $CDCl_3$, also shows the presence of both isomers in the resulting solution in a 5:1 ratio, and the relative amount of isomers does not vary perceptively with temperature: heating a chloroform solution does not change the ^1H NMR spectrum of **2**, nor its concentration. However, the solvent in which the spectra were recorded does have a noticeable effect on the isomer ratio. Thus, the ^1H NMR spectrum in $[D_3]$acetonitrile shows an *anti*/*syn* ratio of 3:1 and a solution in $[D_6]$acetone a ratio of ca. 4:1, whereas dissolution in $[D_6]$DMSO causes partial decomposition of the compound. Nevertheless, the ^1H NMR spectrum recorded after removal of $[D_6]$acetone from the NMR tube and dissolution of the product in $CDCl_3$, again shows the initial 5:1 ratio. Therefore, it seems that solubility factors could account for such an equilibrium. Furthermore, we also considered that steric factors should be regarded, i.e., the bulkiness of the -N−R group could also influence the *anti*/*syn* ratio. It is known that most of the acetato-bridged dimer complexes for which the existence of *syn* and *anti* isomers has been reported are phenylimidazole derivatives. The imidazole ligand, after [C,N] coordination to the palladium atom, adopts a *quasi* planar disposition,[36−39] and we therefore suppose that the small steric repulsion between the imidazole rings in the *syn* disposition should favour this geometry. However, Schiff base ligands with more or less bulky substituents at the imine nitrogen should favour a *trans* disposition in order to avoid the steric hindrance. In complex **2**, the CH_2CH_2OH moiety allows a *cis* disposition of the ligands. To confirm this we prepared analogues to **1**, ligands **17**−**20**, which, upon reaction with palladium(II) acetate in toluene (Scheme 1), gave the acetato-bridged complexes $[Pd\{2,3,4\text{-}(MeO)_3C_6HC(H)=NR\}(\mu\text{-}O_2CMe)]_2$, (**21**, R = Me; **22**, R = Et; **23**, R = Pr; **24**, R = *t*Bu). The resonances for the *anti* and *syn* isomers were ascribed accordingly (see Exp. Sect.).

The integration of the signals corresponding to both isomers showed that the *anti*/*syn* ratio is ca. 7.5:1 for complexes **21**, **22** and **23** in $CDCl_3$, whereas in $[D_6]$acetone a 5:1 ratio is observed (cf. compound **2**), and for complex **24**, with the bulky *t*Bu moiety bonded to the imine nitrogen a value of 28:1 is found.

Molecular Structure of $[Pd\{2,3,4\text{-}(MeO)_3C_6HC(H)=NCH_2CH_2OH\}(\mu\text{-}OAc)]_2$ (2)

Suitable crystals were grown by slowly evaporating a chloroform/*n*-hexane solution of the complex. The molecular structure is illustrated in Figure 2. Crystal data are given in Table 1 and selected bond lengths and angles with estimated standard deviations are shown in Table 2.

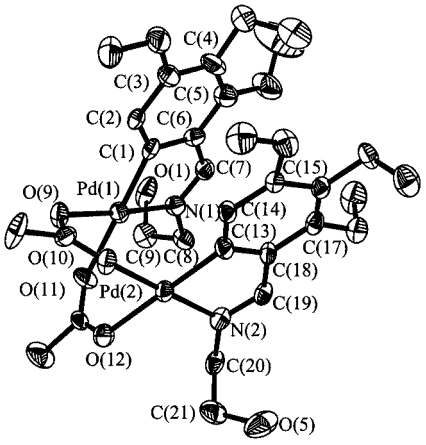

Figure 2. Molecular structure of $[Pd\{2,3,4\text{-}(MeO)_3C_6HC(H)=NCH_2CH_2OH\}(\mu\text{-}OAc)]_2$ (**2**), with labelling scheme; hydrogen atoms have been omitted for clarity

The structure consists of dimeric molecules at van der Waals distances. The molecular structure corresponds to the *syn* isomer, with the cyclometallated moieties in an open-book disposition and two acetate ligands bridging the palladium atoms. Although a large number of crystal structures of dinuclear acetato-bridged cyclometallated complexes have been reported, to the best of our knowledge this is the first example of a *syn* disposition of the metallated ligands.

The Pd(1)−Pd(2) bond length of 2.8514(13) Å is similar to values reported for related complexes [13] and can be regarded as nonbonding. Each palladium atom is bonded in a slightly distorted square-planar geometry to four atoms: a carbon atom of the phenyl ring and the imine nitrogen atom of the Schiff base ligand, and two oxygen atoms of the bridging acetate ligands.

The sum of the angles around the palladium atoms is approximately 360°. The angles between adjacent atoms in the coordination sphere are close to the expected value of 90°, with the most noticeable distortions corresponding to the C(1)−Pd(1)−N(1) and C(13)−Pd(2)−N(2) angles [81.9(4) and 82.1(4)°, respectively] due to chelation. The

Table 1. Crystallographic Data for complexes **2**, **8**, **9** and **16**

	2	**8**	**9**	**15**	**16**
Empirical formula	$C_{28}H_{42}N_2O_{14}Pd_2$	$C_{30}H_{31}NO_4ClPPd$	$C_{31}H_{31}NO_7F_3ClPPdS$	$C_{38}H_{40}NO_8ClP_2Pd$	$C_{46}H_{49}NO_8ClP_3Pd$
Formula mass	843.44	642.38	756.00	842.50	978.62
T [K]	293(2)	293(2)	293(2)	293(2)	293(2)
λ [Å]	0.71073	0.71073	0.71073	0.71073	0.71073
Crystal system	Monoclinic	Triclinic	Triclinic	Orthorhombic	Monoclinic
Space group	$P2_1/a$	$P\bar{1}$	$P\bar{1}$	Pbca	$P2_1/n$
a [Å]	10.552(1)	9.631(1)	9.280(1)	17.267(2)	11.397(2)
b [Å]	28.406(2)	10.174(1)	10.860(1)	18.250(2)	21.492(4)
c [Å]	12.173(1)	15.029(1)	17.512(1)	24.162(3)	19.189(4)
α [°]		96.623(1)	99.472(1)		
β [°]	109.814(2)	107.717(1)	104.640(1)		106.739(4)
γ [°]		95.514(1)	106.296(1)		
V [Å^3]	3432.7(5)	1386.9(1)	1585.4(1)	7614.0(1)	4501.0(1)
Z	4	2	2	8	4
μ [mm^{-1}]	1.114	0.860	0.767	0.693	0.632
Max., min. transmissions	0.81, 0.73	0.88, 0.75	0.70, 0.70	0.95, 0.75	0.96, 0.83
$\rho_{calc.}$ [gcm^{-3}]	1.632	1.538	1.584	1.470	1.444
θ range [°]	1.43 to 25.00	1.43 to 29.10	2.02 to 28.32	1.69 to 28.32	1.46 to 26.45
Reflections collected	18957	10056	11258	45948	9253
Independent reflections	6053 (R_{int} = 0.020)	6786 (R_{int} = 0.037)	7716 (R_{int} = 0.017)	9254 (R_{int} = 0.072)	9253 (R_{int} = 0.028)
R_1[a]	0.0776	0.0460	0.0294	0.0412	0.0466
wR_2[b]	0.1690	0.1992	0.0776	0.1137	0.0829

[a] $R_1 = \Sigma||F_0| - |F_c||/\Sigma|F_0|$, $[F > 4\sigma(F)]$. [b] $wR_2 = \Sigma[w(F_0^2 - F_c^2)^2/\Sigma w(F_0^2)^2]^{1/2}$, all data.

Table 2. Selected bond lengths (Å) and angles (°) for complex **2**

Pd(1)−Pd(2)	2.8514(13)		
Pd(1)−C(1)	1.973(11)	Pd(2)−C(13)	1.963(10)
Pd(1)−N(1)	2.018(9)	Pd(2)−N(2)	2.012(9)
Pd(1)−O(9)	2.084(7)	Pd(2)−O(10)	2.064(8)
Pd(1)−O(11)	2.131(7)	Pd(2)−O(12)	2.130(8)
C(1)−C(6)	1.396(15)	C(13)−C(18)	1.384(15)
C(6)−C(7)	1.434(15)	C(18)−C(19)	1.424(14)
N(1)−C(7)	1.276(13)	N(2)−C(19)	1.298(13)
C(1)−Pd(1)−N(1)	81.9(4)	C(13)−Pd(2)−N(2)	82.1(4)
C(1)−Pd(1)−O(9)	93.3(4)	C(13)−Pd(2)−O(10)	95.0(4)
N(1)−Pd(1)−O(9)	175.1(4)	N(2)−Pd(2)−O(10)	175.8(3)
C(1)−Pd(1)−O(11)	178.6(4)	C(13)−Pd(2)−O(12)	176.0(4)
N(1)−Pd(1)−O(11)	97.7(4)	N(2)−Pd(2)−O(12)	94.8(4)
O(9)−Pd(1)−O(11)	87.2(3)	O(10)−Pd(2)−O(12)	88.2(3)

Pd(1)−C(1) and Pd(2)−C(13) bond lengths of 1.973(11) and 1.963(10) Å, respectively, are somewhat shorter than the values predicted from their covalent radii[40] but similar to values found earlier.[13,14] However, the Pd(1)−N(1) and Pd(2)−N(2) bond lengths of 2.018(9) and 2.012(9) Å, respectively, are in agreement with the value based on the sum of the covalent radii for nitrogen and palladium,[40] and are similar to values reported previously.[13,14] The differing Pd(1)−O(9) and Pd(1)−O(11) [2.084(7) and 2.131(7) Å, respectively] and Pd(2)−O(10) and Pd(2)−O(11) [2.064(8) and 2.130(8) Å, respectively] bond lengths reflect the higher *trans* influence of the aryl carbon as compared to the imine nitrogen atom.

As a result of the palladium atoms being bridged by two mutually *cis* μ-acetate ligands the metallated Schiff bases are forced to lie above one another in the dimeric molecules. This leads to inter-ligand repulsions and results in the coordination planes of the palladium atoms (planes 1 and 2) being tilted at an angle of 25.0°. The disposition of the chelating C,N ligands is not completely eclipsed, probably as a consequence of these repulsions. This is shown by the dihedral angles C(1)−Pd(1)−Pd(2)−C(13), N(1)−Pd(1)−Pd(2)−N(2), O(9)−Pd(1)−Pd(2)−O(10) and O(11)−Pd(1)−Pd(2)-0(12) of 17.3(5), 17.6(4), 15.3(3) and 14.0(3)°, respectively. No intra- or intermolecular O−H···O−H bonding is observed.

Reactivity of the Acetato-Bridged Complex 2

The reaction of **2** with aqueous sodium chloride gave the chloro-bridged complex [Pd{2,3,4-$(MeO)_3C_6HC(H)$=NCH_2CH_2OH}(μ-Cl)]$_2$ (**3**; Scheme 2), which was fully characterised (see Exp. Sect.). The IR spectrum of this complex shows the absence of the ν(COO) bands. The ^{1}H NMR spectra of **3** shows the HC=N and H^5 resonances at δ = 8.08 and 7.51 ppm, respectively.

Reaction of **2** with PPh_3 gave the complex [Pd{2,3,4-$(MeO)_3C_6HC(H)$=NCH_2CH_2OH}$(O_2CMe)(PPh_3)$] (**4**) as an air-stable solid which was fully characterised (see Exp. Sect.). The IR spectrum of **4** shows strong bands at 1290 and 1570 cm^{-1} assigned to the symmetric and asymmetric ν(COO) vibrations, respectively, in agreement with those expected for monocoordinate acetate ligands.[35] The IR spectrum also shows the νC=N stretch at 1613 cm^{-1}. This absorption is shifted to lower wavenumbers relative to the free ligand due to N-coordination of the imine;[32] the ν(O−H) band at 3400 cm^{-1} (3402 cm^{-1} in the free ligand) is as ex-

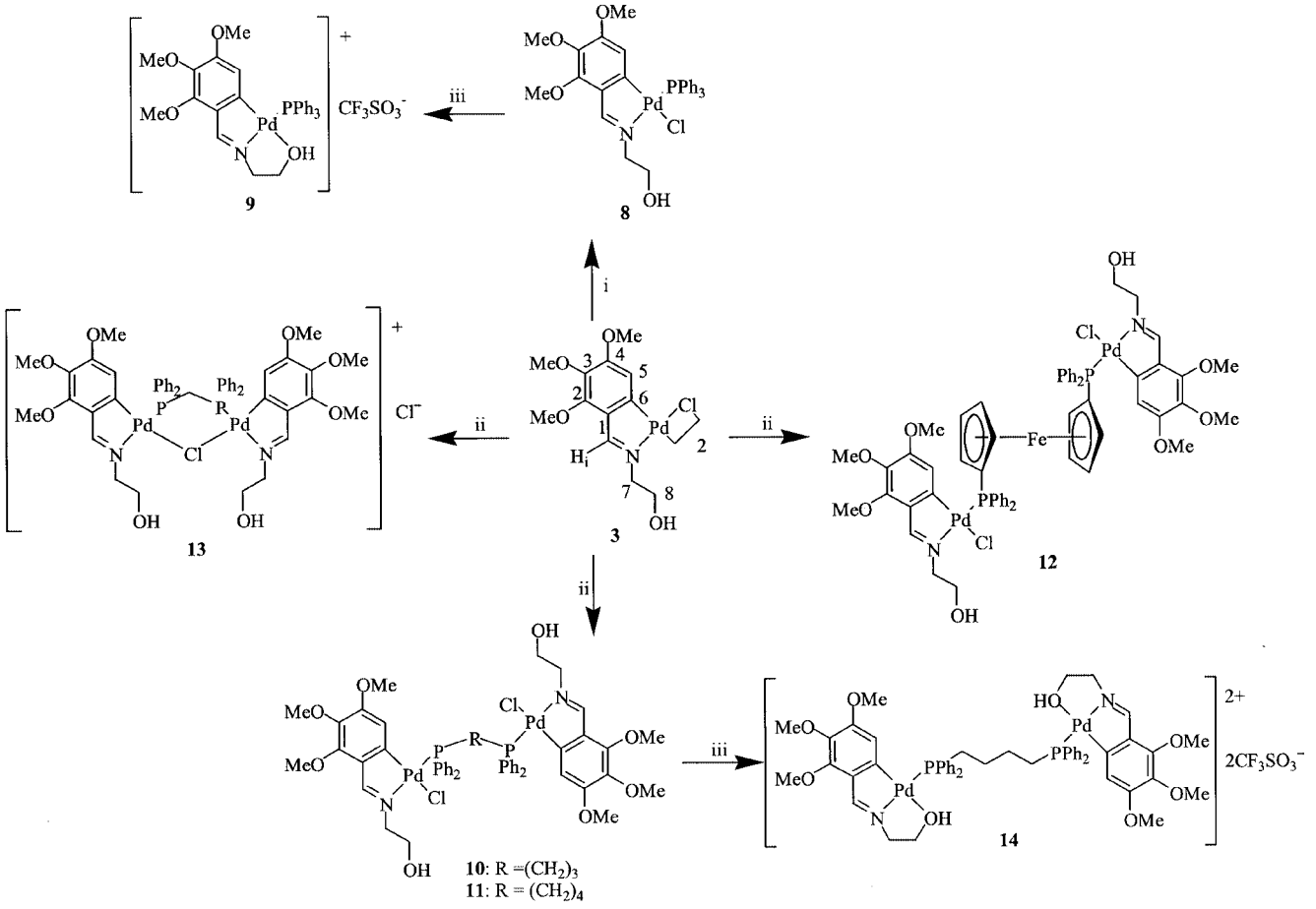

Scheme 2. (i) PPh_3 (acetone), (ii) dppm, dppp, dppb or dppf (acetone, 1:1 molar ratio), (iii) $AgCF_3SO_3$ (acetone)

pected for a noncoordinated OH group. The ^1H NMR spectrum shows the *H*C=N and H^5 resonances coupled to the phosphorus nucleus [δ = 8.31 ($J_{P,H}$ = 7.8) and δ = 5.70 ($J_{P,H}$ = 5.8 Hz), respectively], and the C(4)−O*C*H_3 resonance shifted towards lower frequency by ca. 0.8 ppm, relative to complex **2**, due to the shielding effects of the phosphane phenyl ring;[41] in the $^{31}P\{^1H\}$ spectrum the resonance of the coordinated phosphane appears as a singlet at δ = 40.8 ppm. These findings are in agreement with a phosphorus *trans* to nitrogen arrangement, as we and others have observed earlier, which seems to be the more common arrangement for the entering phosphane.[41−46] The novel term *transphobia* has been introduced by J. Vicente et al. to describe the restricted coordination of mutually *trans* phosphanes and phenyl carbon atoms.[44,45]

The FAB-mass spectrum shows peaks centred at 666 and 608 amu assigned to the $[MH]^+$ and $[M - OAc]^+$ fragments, respectively.

Reaction of complex **2** with $Ph_2PCH_2PPh_2$ (dppm), $Ph_2P(CH_2)_3PPh_2$ (dppp) or $Ph_2P(CH_2)_4PPh_2$ (dppb), in a 1:1 complex-to-phosphane molar ratio gave the dinuclear cyclometallated complexes [{Pd[2,3,4-$(MeO)_3C_6HC(H)$=NCH_2CH_2OH](O_2CMe)}$_2$(μ-$Ph_2P(CH_2)_nPPh_2$)] (**5**, *n* = 1; **6**, *n* = 3; **7**, *n* = 4). The IR spectra of these complexes are in agreement with monocoordinate acetate ligands and with noncoordinated hydroxyl groups (vide supra). The ^1H NMR spectra show the coupling of the *H*C=N and the H^5 resonances to the phosphorus nucleus, and in the $^{31}P\{^1H\}$ NMR spectra the resonance of the phosphorus nuclei appears as a singlet at ca. δ = 31 ppm in accordance with the centrosymmetric nature of the complexes. We tentatively propose this structure in accordance with the conductivity data for **5**, **6** and **7**, which show them to be nonelectrolytes.

Reaction of the cyclometallated chloro-bridged complex **3** with PPh_3 in acetone yielded the mononuclear complex [Pd{2,3,4-$(MeO)_3C_6HC(H)$=NCH_2CH_2OH}(Cl)(PPh_3)] (**8**) which was fully characterised (see Exp. Sect.). The IR and NMR spectra of **8** are similar to those for complex **4**; the most noticeable difference in the IR spectra is the absence of the ν(COO) bands.

The ^1H NMR spectrum shows doublets assigned to the *H*C=N and H^5 protons coupled to the ^{31}P nucleus [δ = 8.38 ppm ($J_{P,H}$ = 8.3) and δ = 5.74 ppm ($J_{P,H}$ = 6.3 Hz), respectively], and the $^{31}P\{^1H\}$ NMR spectrum shows a singlet resonance at δ = 40.3 ppm. The mass FAB spectrum shows peaks centred at 606 amu corresponding to the $[M - Cl]^+$ fragment.

Treatment of **3** with the tertiary diphosphanes $Ph_2P(CH_2)_3PPh_2$ (dppp), $Ph_2P(CH_2)_4PPh_2$ (dppb) and $Ph_2PC_5H_4FeC_5H_4PPh_2$ (dppf) in a 1:1 molar ratio gave the dinuclear complexes [{Pd[2,3,4-$(MeO)_3C_6HC(H)$=NCH_2CH_2OH](Cl)}$_2${μ-$Ph_2P(CH_2)_nPPh_2$}], (**10**, *n* = 3; **11**,

n = 4), and the trinuclear compound [{Pd[2,3,4-$(MeO)_3$-$C_6HC(H)=NCH_2CH_2OH$](Cl)}$_2${μ-$Ph_2PC_5H_4FeC_5H_4$-PPh_2}] (**12**), respectively. The IR and NMR spectra of these complexes show similar features to those described for the spectra of compound **8** suggesting a similar disposition around the palladium atoms. The $^{31}P\{^1H\}$ NMR spectrum shows a singlet resonance for the phosphorus nuclei indicating the symmetric nature of the complexes. Conductivity measurements in dry acetonitrile showed the complexes to be molecular nonelectrolytes.

However, when complex **3** was reacted with $Ph_2PCH_2PPh_2$ (dppm) the dinuclear complex [{Pd[2,3,4-$(MeO)_3C_6HC(H)=NCH_2CH_2OH$]}$_2$(μ-Cl)(μ-$Ph_2PCH_2$-$PPh_2$)][Cl] (**13**) was obtained (see Exp. Sect.). The ^1H NMR spectrum also shows coupling of the *H*C=N and H^5 protons to the phosphorus nucleus and the $^{31}P\{^1H\}$ NMR spectra shows a singlet resonance. The specific molar conductivity in dry acetonitrile (175.1 ohm^{-1} cm^2 mol^{-1}) is in agreement with the value expected for a 1:1 electrolyte.[47] This behaviour is in contrast to that observed for compound **5**, where a 1:1 electrolyte formulation with both palladium atoms bridged by the diphosphane and by one acetate ligand would be possible. However, the low conductivity values preclude this formulation for **5**.

In order to promote coordination of the hydroxyl oxygen, thus giving a coordinated [C,N,O] ligand, we treated the cyclometallated complexes **8** and **11** with silver triflate to remove the chloride moiety. Thus, treatment of **8** with silver triflate gave the complex [Pd{2,3,4-$(MeO)_3C_6HC(H)=NCH_2CH_2OH$}$(PPh_3)$][$CF_3SO_3$] (**9**) and an AgCl precipitate. The IR spectrum shows a band assigned to the ν(O−H) vibration at 3245 cm^{-1} shifted to lower wavenumber (3402 and 3365 cm^{-1} in the spectra of the free ligand and compound **8**, respectively) due to Pd−O bond formation.[48] The most noteworthy differences in the ^1H NMR spectrum of **9** from that of **8** are in the lowfield shift of the -O*H* hydroxyl proton resonance which appears as a triplet at δ = 7.02 ppm ($J_{H,H}$ = 5.6 Hz), (for complex **8** a broad resonance at ca. δ = 3.2 ppm was assigned to O*H*) and the resolution of the CH_2CH_2OH signals, which appear as a multiplet in the spectrum of **8** at δ = 4.03 ppm and as two broad resonances at δ = 4.13 and 3.89 ppm for **9**.

In the $^{13}C\{^1H\}$ NMR spectrum the resonances assigned to the CH_2CH_2OH carbon atoms appear at δ = 67.7 and 56.8 ppm shifted to high and low frequency, respectively, relative to compound **8** (δ = 62.9 and 61.8 ppm in the spectrum of **8**). We have observed a similar behaviour in the $^{13}C\{^1H\}$ NMR spectra of cyclometallated complexes derived from the Schiff base ligand 2-$ClC_6H_4C(H)=NCH_2CH_2NMe_2$ with formation of a new Pd−NMe_2 bond after treatment with a silver(I) salt.[29] Conductivity measurements carried out in dry acetonitrile gave a value for the molar conductivity of 116.2 ohm^{-1} cm^2 mol^{-1}, characteristic of 1:1 electrolytes.[47]

Similarly, when compound **11** was treated with silver triflate in acetone the new dinuclear complex [{Pd[2,3,4-$(MeO)_3C_6HC(H)=NCH_2CH_2OH$]}$_2${μ-$Ph_2P(CH_2)_4PPh_2$}]-[$CF_3SO_3$]$_2$ (**14**) was obtained with the Schiff base ligand as [C,N,O] terdentate. The IR spectrum of this complex shows a broad band due to the ν(O−H) stretch centred at ca. 3250 cm^{-1}. The ^1H NMR spectrum shows similar features to those observed for the spectrum of **9**. Similarly, the $^{13}C\{^1H\}$ NMR spectrum shows the signals assigned to the methylene carbon atoms at δ = 66.3 and 57.5 ppm. Conductivity measurements carried out in dry acetonitrile showed the complex to be a 1:2 electrolyte.

Reaction of complex **3** with the diphosphane $Ph_2P(CH_2)_2PPh_2$ (dppe) in a 1:2 molar ratio, followed by treatment with sodium perchlorate, gave the mononuclear complex [Pd{2,3,4-$(MeO)_3C_6HC(H)=NCH_2CH_2OH$}-{$PPh_2(CH_2)_2PPh_2$-*P,P*}][$ClO_4$] (**15**; Scheme 3) as an air-stable solid which was fully characterised (see Exp. Sect.). The ^1H NMR spectrum shows the signal corresponding to H^5 at δ = 5.93 ppm, coupled to both phosphorus atoms ($J_{H,P}$ = 8.8, 5.8 Hz). However, the *H*C=N resonance only shows coupling to the ^{31}P nucleus *trans* to nitrogen (δ = 8.50 ppm; $J_{H,P}$ = 8.3 Hz). The $^{31}P\{^1H\}$ NMR spectrum shows two doublets for the two nonequivalent phosphorus nuclei (δ = 61.0, 43.0 ppm; $J_{P,P}$ = 25.4 Hz). The resonance at lower frequency was assigned to the phosphorus nucleus *trans* to the phenyl carbon atom in accordance with the higher *trans* influence of the latter with respect to the C=N nitrogen atom.[49] The $^{13}C\{^1H\}$ spectrum shows coupling of the C6 resonance to the two phosphorus nuclei (δ = 156.0 ppm; $J_{P,C}$ = 12.0, 5.6 Hz). Conductivity measurements were in accordance with a 1:1 electrolyte formulation.

Treatment of **3** with the triphosphane bis(2-diphenylphosphanylethyl)phenylphosphane in a 1:2 molar ratio, followed by treatment with sodium perchlorate, gave [Pd{2,3,4-$(MeO)_3C_6HC(H)=NCH_2CH_2OH$}{$(PPh_2CH_2$-$CH_2)_2$PPh-*P,P,P*}][$ClO_4$] (**16**; Scheme 3). The phosphorus resonances in the $^{31}P\{^1H\}$ NMR spectrum of **16** are shifted downfield from their values in the free phosphane sug-

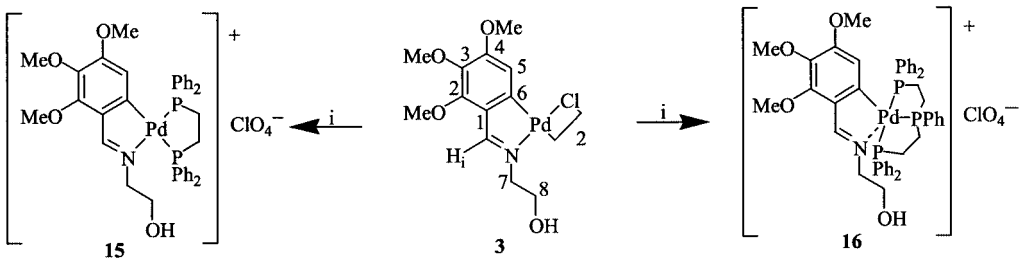

Scheme 3. (i) 1: dppe or triphos (acetone, 1:2 molar ratio), 2: $NaClO_4$

gesting coordination of the three phosphorus atoms to the metal centre. A triplet resonance at δ = 86.0 ppm was assigned to the central ^{31}P nucleus *trans* to the phenyl carbon atom, and a doublet at δ = 44.5 was assigned to the two equivalent mutually *trans* phosphorus nuclei. This latter signal appears at lower frequency due to the higher *trans* influence of the phosphane ligand.[49] The resonance of the proton in the *ortho* position to the metallated carbon atom appears as a doublet of triplets showing coupling to the central ^{31}P atom ($J_{P,H}$ = 8.8 Hz) and to the terminal phosphorus atoms ($J_{P,H}$ = 2.4 Hz). The shift of the ν(C=N) stretching vibration to lower wavenumber in the IR spectrum and the upfield shift of the HC=N proton resonance in the ^1H NMR spectra indicate the existence of a palladium-nitrogen interaction in solution. These results strongly agree with those previously obtained by us in related pentacoordinate palladium(II) species,[12] and although the proposed structure in Scheme 3 seems slightly different from the solid state structure (Figure 6), we suggest the former as the probable solution disposition; for a thorough discussion regarding this issue see ref.[12] The C=N signal in the $^{13}C\{^1H\}$ NMR spectrum at δ = 167.3 ppm coupled to the central phosphorus ($J_{P,C}$ = 5.7 Hz) is also indicative of a Pd-N interaction. Molar conductivity measurements showed that complex **16** is a 1:1 electrolyte. The FAB-mass spectrum shows a set of peaks centred at 979 and 877 amu assigned to the $[M]^+$ and the $[M - ClO_4]^+$ fragments, respectively.

Molecular Structure of Complexes 8, 9, 15 and 16

Suitable crystals were grown by slowly evaporating chloroform solutions of the complexes. Crystal data are given in Table 1 and selected bond lengths and angles with estimated standard deviations are shown in Table 3.

Table 3. Selected bond lengths (Å) and angles (°) for complexes **8**, **9**, **15** and **16**

	8	**9**	**15**	**16**
Pd(1)−C(1)	2.061(5)	1.997(2)	2.052(4)	2.064(4)
Pd(1)−P(1)	2.2443(13)	2.2751(5)	2.2557(10)	2.2893(12)
Pd(1)−N(1)	2.093(4)	2.028(2)	2.108(3)	2.480(3)
Pd(1)−Cl(1)	2.4263(15)			
Pd(1)−O(1)		2.208(1)		
Pd(1)−P(2)			2.33347(10)	2.2773(11)
Pd(1)−P(3)				2.3243(12)
C(1)−C(6)	1.407(7)	1.411(3)	1.409(5)	1.387(5)
C(6)−C(7)	1.482(8)	1.448(3)	1.447(5)	1.456(5)
N(1)−C(7)	1.285(7)	1.271(3)	1.279(5)	1.274(4)
C(1)−Pd(1)−N(1)	82.80(19)	82.31(7)	80.6(1)	76.0(1)
N(1)−Pd(1)−P(1)	171.37(12)	177.29(5)	175.22(9)	113.81(9)
C(1)−Pd(1)−P(1)	92.60(15)	99.85(5)	95.9(1)	95.9(1)
C(1)−Pd(1)−Cl(1)	171.38(14)			
P(1)−Pd(1)−Cl(1)	94.48(5)			
N(1)−Pd(1)−Cl(1)	90.78(13)			
N(1)−Pd(1)−O(1)		77.46(6)		
C(1)−Pd(1)−O(1)		159.33(7)		
P(1)−Pd(1)−O(1)		100.19(4)		
P(2)−Pd(1)−P(1)			84.52(4)	84.24(4)
P(2)−Pd(1)−N(1)			98.79(9)	109.69(9)
C(1)−Pd(1)−P(2)			176.8(1)	173.7(1)
N(1)−Pd(1)−P(3)				90.61(9)
P(1)−Pd(1)−P(3)				155.43(4)
P(2)−Pd(1)−P(3)				85.01(4)
C(1)−Pd(1)−P(3)				92.4(1)

[Pd{2,3,4-(MeO)$_3$C$_6$HC(H)=NCH$_2$CH$_2$OH}(Cl)(PPh$_3$)] (8)

The crystal structure of this complex (Figure 3) consists of discrete molecules separated by van der Waals distances. The palladium atom is bonded in a slightly distorted square-planar geometry to the C(1) carbon atom of the phenyl ring, to the imine N(1) atom of the Schiff base ligand, to the Cl(1) atom and to the P(1) phosphorus atom of the triphenylphosphane ligand. The angles between adjacent atoms in the coordination sphere of palladium are close to the expected value of 90° with the most noticeable distortions corresponding to the bite angle C(1)−Pd(1)−N(1) of 82.8(2)°. The sum of the angles about palladium is approximately 360°.

The geometry around palladium is planar [mean deviation from the least-square plane Pd(1), C(1), N(1), P(1), Cl(1), (plane 1), of 0.960 Å] and approximately co-planar with the metallated ring [Pd(1), C(1), C(6), C(7), N(1), mean deviation 0.0166 Å (plane 2)] and with the phenyl ring [plane 3, mean deviation of 0.0031 Å] (angles between planes are: plane 1:2, 6.0°; plane 1:3, 10.1°; 2:3, 5.0°). All bond lengths and angles are normal. The OH group, hydrogen H(1) and the Cl(1) atom are bonded by intramolecular H-bonding [O(1)−H(1)···Cl(1): 3.079(6) Å, 173.8°].

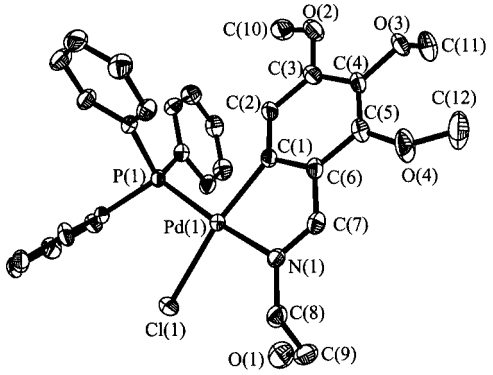

Figure 3. Molecular structure of complex [Pd{2,3,4-(MeO)$_3$C$_6$HC(H)=NCH$_2$CH$_2$OH}(Cl)(PPh$_3$)] (**8**), with labelling scheme; hydrogen atoms have been omitted for clarity

[Pd{2,3,4-(MeO)$_3$C$_6$HC(H)=NCH$_2$CH$_2$OH}(PPh$_3$)][CF$_3$SO$_3$] (9)

The crystal structure of this complex (Figure 4) contains one $[Pd\{2,3,4\text{-}(MeO)_3C_6HC(H)=NCH_2CH_2OH\}(PPh_3)]^+$ cation and one $CF_3SO_3^-$ anion per asymmetric unit.

The palladium atom is bonded in a slightly distorted square-planar geometry to the C(1) carbon atom of the phenyl ring, the imine N(1) nitrogen atom, the O(1) oxygen atom and to the phosphorus atom of the triphenylphos-

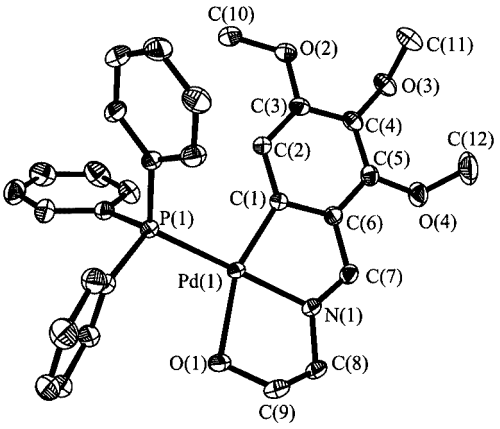

Figure 4. Perspective view of the cation of complex [Pd{2,3,4-(MeO)$_3$C$_6$HC(H)=NCH$_2$CH$_2$OH}(PPh$_3$)][CF$_3$SO$_3$] (**9**), with labelling scheme; hydrogen atoms have been omitted for clarity

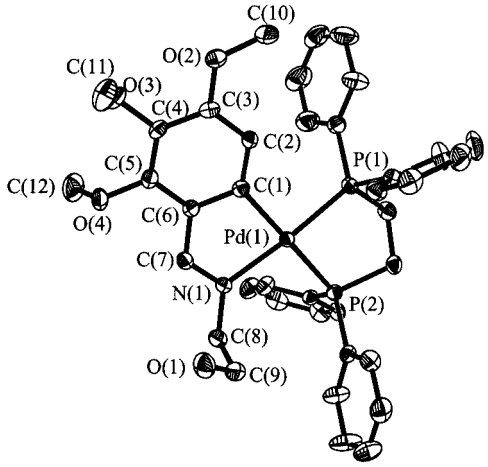

Figure 5. Perspective view of the cation of complex [Pd{2,3,4-(MeO)$_3$C$_6$HC(H)=NCH$_2$CH$_2$OH}{PPh$_2$(CH$_2$)$_2$PPh$_2$-*P,P*}][ClO$_4$] (**15**), with labelling scheme; hydrogen atoms have been omitted for clarity

phane ligand P(1). The angles between adjacent atoms in the coordination sphere of palladium are close to the expected value of 90°, with the most noticeable distortions corresponding to the C(1)−Pd(1)−N(1) and N(1)−Pd(1)−O(1) angles of 81.31(7)° and 78.46(6)°, respectively. The sum of the angles about palladium is approximately 360°.

The cation of **9** forms hydrogen bonds with the CF_3SO_3 anion [O(1)−H(1)···O(2s): 3.783(3) Å, 165(4)°].

The most noticeable differences between the structures of complexes **8** and **9** correspond to a shortening of the Pd−C and Pd−N bond lengths [2.061(5) and 2.093(4) Å, respectively, for complex **8** vs. 1.997(2) and 2.028(2) Å, also respectively, for complex **9**] and the greater C(1)−Pd(1)−P(1) angle [92.60(15)° for complex **8**; 99.85(5)° for complex **9**]. The latter is probably due to the steric repulsion between the large chlorine Cl(1) atom in complex **8**, as opposed to the smaller O(1) oxygen atom in complex **9**, and the bulky PPh_3 ligand. In complex **9**, the small "bite" of the NCH_2CH_2OH chelate [shown by the N(1)−Pd(1)−O(1) bond angle of 77.46(6)°], which forces the O(1) hydroxyl oxygen and the phosphorus P(1) atoms apart, also reduces repulsion.

[Pd{2,3,4-(MeO)$_3$C$_6$HC(H)=NCH$_2$CH$_2$OH}{PPh$_2$-(CH$_2$)$_2$PPh$_2$-P,P}][ClO$_4$] (15)

The crystal structure of this complex (Figure 5) contains one [Pd{2,3,4-(MeO)$_3$C$_6$HC(H)=NCH$_2$CH$_2$OH}{PPh$_2$-(CH$_2$)$_2$PPh$_2$-*P,P*}]$^+$ cation and one ClO_4^- anion per asymmetric unit. The palladium atom is bonded to four atoms: the adjacent C(1) carbon atom and the N(1) nitrogen of the Schiff base ligand **1**, and the phosphorus atoms P(1) and P(2) of the dppe ligand. The different *trans* influences of the C(1) carbon atom and the N(1) nitrogen atom are reflected in the somewhat enlarged Pd(1)−P(2) bond length of 2.3335(1) Å [Pd(1)−P(1): 2.256(1) Å]. These distances are in agreement with values previously reported.[28,48,50] Hydrogen bonding between the O−H(1) hydroxyl hydrogen and O(3s) oxygen atom of the perchlorate anion was found [O(1)−H(1)···O(3s): 3.021(6) Å, 156(11)°].

Pd{2,3,4-(MeO)$_3$C$_6$HC(H)=NCH$_2$CH$_2$OH}{(PPh$_2$-CH$_2$CH$_2$)$_2$PPh-P,P,P}][ClO$_4$] (16)

The crystal structure of this complex (Figure 6) contains one [Pd{2,3,4-(MeO)$_3$C$_6$HC(H)=NCH$_2$CH$_2$OH}{(PPh$_2$-CH$_2$CH$_2$)$_2$PPh-*P,P,P*}]$^+$ cation and one ClO_4^- anion per asymmetric unit. The palladium atom is bonded to the C(1) carbon atom of the metallated ring and to the three phosphorus atoms P(1), P(2) and P(3), of the triphos ligand. A fifth interaction with the imine nitrogen completes the coordination sphere about the palladium atom.

The Pd(1)−N(1) distance of 2.480(3) Å is somewhat longer than the values of 2.338(3) Å, reported recently by us in a similar complex with a triphos ligand[51] and 2.23(2)

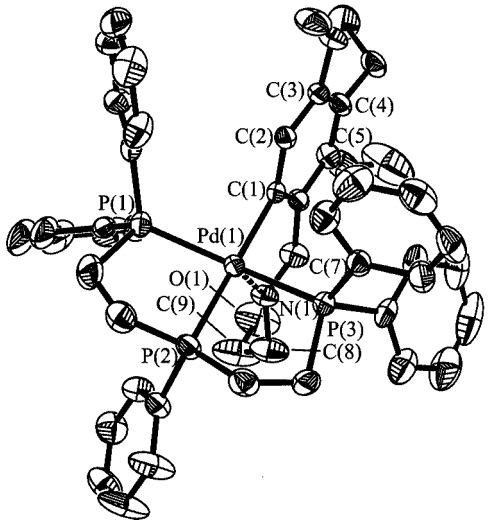

Figure 6. Perspective view of the cation of complex [Pd{2,3,4-(MeO)$_3$C$_6$HC(H)=NCH$_2$CH$_2$OH}{(PPh$_2$CH$_2$CH$_2$)$_2$PPh-*P,P,P*}]-[ClO$_4$] (**16**), with labelling scheme; hydrogen atoms have been omitted for clarity

Å found in an authentic pentacoordinate palladium(II) complex.[52] However, the Pd−N bond length is shorter than the weak interactions in the range 2.576(4)−2.805(5) found in other five-coordinate complexes of palladium.[44,53−58] The coordination around the palladium atom may be viewed as a trigonal bipyramid, with the Pd(1), N(1), P(1) and P(3) atoms in the equatorial plane (r.m.s. for the mean plane; 0.0158 Å); the metallated carbon atom and the central phosphorus atom are at the apical positions. However, the trigonal bipyramidal geometry is severely distorted as shown by the N(1)−Pd(1)−P(1) and N(1)−Pd(1)−P(3) bond angles of 113.81(9) and 91.61(9)°, respectively, which differ considerably from the ideal value of 120°. Nevertheless, the bond angle values at palladium preclude the geometry from being considered as square pyramidal.

The Pd(1)−C(1) bond length of 2.064(4) Å is similar to values reported for related five-coordinate complexes.[12,51] The Pd(1)−P(1), Pd(1)−P(2) and Pd(1)−P(3) bond lengths of 2.2893(12), 2.2773(11) and 2.3243(12) Å, respectively, are also similar to those found in related Pd^{II} complexes.[12,51]

Hydrogen bonding between the O−H(4) hydroxyl hydrogen and the O(7) oxygen atom of the disordered perchlorate anion was found [O(1)−H(4)···O(7a): 2.692(3) Å, 167.3(4)°; O(1)−H(4)···O(7b): 2.990(3) Å, 140.7(4)°].

Experimental Section

General Remarks: Solvents were purified by standard methods.[59] Chemicals were reagent grade. The phosphanes PPh_3, $Ph_2PCH_2PPh_2$ (dppm), $Ph_2P(CH_2)_2PPh_2$ (dppe), $Ph_2P(CH_2)_3PPh_2$ (dppp), $Ph_2P(CH_2)_4PPh_2$ (dppb), $Ph_2PC_5H_4FeC_5H_4PPh_2$ (dppf) and $(Ph_2PCH_2CH_2)_2PPh$ (triphos), were purchased from Aldrich. Microanalyses were carried out using a Carlo Erba Elemental Analyser, Model 1108. IR spectra were recorded as Nujol mulls or polythene discs on a Perkin−Elmer 1330 or on a Mattson spectrophotometer. NMR spectra were obtained as $CDCl_3$ solutions. They are referenced to $SiMe_4$ (^1H, $^{13}C\{^1H\}$) or 85% H_3PO_4 ($^{31}P\{^1H\}$) and were recorded on a Bruker AC-200F spectrometer. All chemical shifts are reported downfield from these standards. The FAB mass spectra were recorded using a VG Quatro mass spectrometer with a Cs ion gun; 3-nitrobenzyl alcohol was used as the matrix.

CAUTION: Perchlorate salts of metal complexes with organic ligands are potentially explosive. Only small amounts of these materials should be prepared and handled with great caution.

Preparation of 2,3,4-$(MeO)_3C_6H_2C(H)=NCH_2CH_2OH$ (1): 2,3,4-$(MeO)_3C_6H_2COH$ (3.21 g, 16.38 mmol) and $NH_2CH_2CH_2OH$ (1.01 g, 16.45 mmol) were added to 50 cm^3 of dry chloroform. The mixture was heated under reflux in a Dean−Stark apparatus for 4 h. After cooling to room temperature, the solvent was evaporated to give a yellow oil. Yield: 3.52 g (90%). IR (nujol mull): ν(O−H) = 3402m; ν(C=N) = 1642s cm^{-1}. ^1H NMR (200 MHz, $CDCl_3$): δ = 3.71, 3.68, 3.67 (s, 9 H, OMe), 3.54 (br. s, 2 H, -CH_2), 4.01 (br. s, 2 H, -CH_2), 6.50 (d, $J_{H5,H6}$ = 8.8 Hz,1 H, H^5), 7.47 (d, 1 H, H^6), 8.36 (s, 1 H, H_i) ppm. $^{13}C\{^1H\}$ NMR (50.28 MHz, $CDCl_3$): δ = 61.8, 60.8, 55.9 (O*C*H_3), 63.5, 62.3 (C8, C9), 107.7 (C5), 122.1 (C6), 122.4 (C1), 141.7 (C3), 155.9, 153.8 (C2, C4), 158.6 (C=N) ppm. FAB-MS: *m/z* = 240 $[MH]^+$.

The Schiff base ligands **19** and **20** were prepared similarly.

2,3,4-$(MeO)_3C_6H_2C(H)=NCH_2CH_2CH_3$ (19): Yield: 3.50 g (90%). IR (nujol mull): ν(C=N) = 1638s cm^{-1}. ^1H NMR (200 MHz, $CDCl_3$): δ = 0.90 (t, $J_{H,H}$ = 7.3 Hz, 3 H, $NCH_2CH_2CH_3$), 1.67 (m, 2 H, $NCH_2CH_2CH_3$), 3.51 (t, $J_{H,H}$ = 7.3 Hz, 2 H, NCH_2CH_2), 3.83, 3.88 (s, 9 H, OMe), 6.67 (d, $J_{H5,H6}$ = 8.8 Hz,1 H, H^5), 7.64 (d, 1 H, H^6), 8.47 (s, 1 H, H_i) ppm.

2,3,4-$(MeO)_3C_6H_2C(H)=NC(CH_3)_3$ (20): Yield: 3.91 g (95%). IR (nujol mull): ν(C=N) = 1636s cm^{-1}. ^1H NMR (200 MHz, $CDCl_3$): δ = 1.15 [s, 9 H, $NC(CH_3)_3$], 3.73, 3.79 (s, 9 H, OMe), 6.56 (d, $J_{H5,H6}$ = 8.8 Hz, 1 H, H^5), 7.56 (d, 1 H, H^6), 8.42 (s, 1 H, H_i) ppm.

Preparation of 2,3,4-$(MeO)_3C_6H_2C(H)=NCH_3$ (17): A pressure tube containing 2,3,4-$(MeO)_3C_6H_2COH$ (3.21 g, 16.38 mmol) and 40 cm^3 of dry chloroform was cooled to −20 °C and an excess of NH_2Me (1.53 g, 49.14 mmol; 200% excess), also cooled to −20 °C, was added. The tube was sealed and heated to 80 °C for 24 h. After cooling to room temperature, the solvent and the unreacted NH_2Me were removed under vacuum to give a yellow oil. Yield: 3.26 g (95%). IR (nujol mull): ν(C=N) = 1644s cm^{-1}. ^1H NMR (200 MHz, $CDCl_3$): δ = 3.50 (s, 3 H, N−CH_3), 3.87, 3.88, 3.92 (s, 9 H, OMe), 6.71 (d, $J_{H5,H6}$ = 8.8 Hz, 1 H, H^5), 7.63 (d, 1 H, H^6), 8.52 (s, 1 H, H_i) ppm.

Ligand **18** was prepared similarly.

2,3,4-$(MeO)_3C_6H_2C(H)=NCH_2CH_3$ (18): Yield: 3.51 g (96%). IR (nujol mull): ν(C=N) = 1638s cm^{-1}. ^1H NMR (200 MHz, $CDCl_3$): δ = 1.04 (t, 3 H, NCH_2CH_3), 3.37 (q, $J_{H,H}$ = 7.3 Hz, 2 H, NCH_2CH_3), 3.59, 3.60, 3.66 (s, 9 H, OMe), 6.44 (d, $J_{H5,H6}$ = 8.8 Hz, 1 H, H^5), 7.43 (d, 1 H, H^6), 8.29 (s, 1 H, H_i) ppm.

Preparation of $[Pd\{2,3,4\text{-}(MeO)_3C_6HC(H)=NCH_2CH_2OH\}(\mu\text{-}O_2CMe)]_2$ (2): A pressure tube was charged with 2,3,4-$(MeO)_3C_6H_2C(H)=NCH_2CH_2OH$ (**1**) (0.219 g, 0.92 mmol), palladium(II) acetate (0.206 g, 0.92 mmol) and 20 cm^3 of dry toluene was then sealed under argon. The mixture was heated for 24 h at 60 °C. After cooling to room temp. the solution was filtered through celite to remove the black palladium formed. The solvent was then removed under vacuum to give a brown oil, which was chromatographed on a column packed with silica gel. Elution with dichloromethane/ethanol (92:8) afforded the final product as a yellow oil after solvent removal. Yield: 0.30 g (40%). M.p. 111.3 °C. $C_{28}H_{38}N_2O_{12}Pd_2$ (807.4): calcd. C 41.6, H 4.7, N 3.5; found C 40.9, H 4.8, N 3.6. IR (polythene disc): ν(O−H) = 3384m cm^{-1}; ν(C=N) = 1604sh, m cm^{-1}; ν_{as}(COO) = 1563s cm^{-1}; ν_s(COO) = 1421s cm^{-1}. ^1H NMR (200 MHz, $CDCl_3$), *anti* isomer: δ = 2.07 (s, 3 H, OAc), 3.73, 3.80, 3.84 (s, 9 H, OMe), 2.23 (br. s, 2 H, -CH_2), 6.22 (s, 1 H, H^5), 7.57 (s, 1 H, H_i); *syn* isomer: δ = 2.25, 2.02 (s, 3 H, OAc), 3.20 (br. s, 1 H, OH), 3.68, 3.71, 3.82 (s, 9 H, OMe), 6.00 (s, 1 H, H^5), 7.81 (s, 1 H, H_i) ppm. $^{13}C\{^1H\}$ NMR (50.28 MHz, $CDCl_3$), *anti* isomer: δ = 24.4 (*C*H_3COO), 61.7, 61.3, 55.9 (O*C*H_3), 61.6 (C8, C9), 110.2 (C5), 130.7 (C1), 137.9 (C6), 154.4, 151.3, 151.0 (C2, C3, C4), 170.6 (C=N), 181.5 (CH_3*C*OO) ppm; *syn* isomer: δ = 24.4, 24.1 (*C*H_3COO), 61.6, 60.6, 55.5 (O*C*H_3), 110.6 (C5), 130.3 (C1), 137.3 (C6), 154.1, 151.3, 150.9 (C2, C3, C4), 171.2 (C=N), 182.2, 180.9 (CH_3*C*OO) ppm. FAB-MS: *m/z* = 808 $[M]^+$, 659 $[M - OAc - CH_2CH_2OH]^+$, 404 $[M - OAc - L - Pd]^+$, 344 $[M - 2OAc - L - Pd]^+$.

Compounds **21**, **22**, **23** and **24** were prepared similarly and isolated as yellow solids.

$[Pd\{2,3,4\text{-}(MeO)_3C_6HC(H)=NCH_3\}(\mu\text{-}O_2CMe)]_2$ (21): Yield: 0.39 g (50%). M.p. 120.3 °C. $C_{26}H_{34}N_2O_{10}Pd_2$ (747.4): calcd. C

41.8, H 4.6, N 3.7; found C 41.6, H 4.8, N 3.9. IR (polythene disc): ν(C=N) = 1610sh, m cm^{-1}; ν_{as}(COO) = 1572s cm^{-1}; ν_s(COO) = 1413s cm^{-1}. ^1H NMR (200 MHz, $CDCl_3$), *anti* isomer: δ = 2.13 (s, 3 H, OAc), 2.88 (s, 3 H, NCH_3), 3.73, 3.83, 3.86 (s, 9 H, OMe), 6.34 (s, 1 H, H^5), 7.27 (s, 1 H, H_i); *syn* isomer: δ = 2.05, 2.23 (s, 3 H, OAc), 3.28 (s, 3 H, NCH_3), 3.69, 3.69, 3.78 (s, 9 H, OMe), 5.99 (s, 1 H, H^5), 7.73 (s, 1 H, H_i) ppm.

[Pd{2,3,4-(MeO)$_3$C$_6$HC(H)=NCH$_2$CH$_3$}(μ-O$_2$CMe)]$_2$ (22): Yield: 0.38 g (50%). M.p. 125.7 °C (dec.). $C_{28}H_{38}N_2O_{10}Pd_2$ (775.4): calcd. C 43.4, H 4.9, N 3.6; found C 42.8, H 4.8, N 3.5. IR (polythene disc): ν(C=N) = 1604sh, m cm^{-1}; ν_{as}(COO) = 1566s cm^{-1}; ν_s(COO) = 1413s cm^{-1}. ^1H NMR (200 MHz, $CDCl_3$), *anti* isomer: δ = 1.10 (t, $J_{H,H}$ = 7.3 Hz, 3 H, NCH_2CH_3), 2.01 (s, 3 H, OAc), 2.77 (m, 1 H, NCH_2CH_3), 3.19 (m, 1 H, NCH_2CH_3), 3.74, 3.81, 3.84 (s, 9 H, OMe), 6.32 (s, 1 H, H^5), 7.44 (s, 1 H, H_i); *syn* isomer: δ = isomer: 0.85 (t, $J_{H,H}$ = 7.3 Hz, 3 H, NCH_2CH_3), 1.99, 2.21 (s, 3 H, OAc), 3.65, 3.68, 3.77 (s, 9 H, OMe), 5.99 (s, 1 H, H^5), 7.74 (s, 1 H, H_i) ppm.

[Pd{2,3,4-(MeO)$_3$C$_6$HC(H)=NCH$_2$CH$_2$CH$_3$}(μ-O$_2$CMe)]$_2$ (23): Yield: 0.37 g (50%). M.p. 141.3 °C. $C_{30}H_{42}N_2O_{10}Pd_2$: calcd. C 44.9, H 5.3, N 3.5; found C 45.4, H 4.9, N 3.7. IR (polythene disc): ν(C=N) = 1606sh, m cm^{-1}; ν_{as}(COO) = 1558s cm^{-1}; ν_s(COO) = 1415s cm^{-1}. ^1H NMR (200 MHz, $CDCl_3$), *anti* isomer: δ = 0.76 (t, $J_{H,H}$ = 7.3 Hz, 3 H, $NCH_2CH_2CH_3$), 1.60 (m, 2 H, NCH_2CH_2), 2.01 (s, 3 H, OAc), 2.55 (m, 1 H, NCH_2CH_2), 3.13 (m, 1 H, NCH_2CH_2), 3.75, 3.81, 3.84 (s, 9 H, OMe), 6.32 (s, 1 H, H^5), 7.41 (s, 1 H, H_i); *syn* isomer: δ = 0.90 (t, $J_{H,H}$ = 7.3 Hz, 3 H, $NCH_2CH_2CH_3$), 1.98, 2.20 (s, 3 H, OAc), 3.65, 3.67, 3.77 (s, 9 H, OMe), 5.98 (s, 1 H, H^5), 7.69 (s, 1 H, H_i) ppm.

[Pd{2,3,4-(MeO)$_3$C$_6$HC(H)=NC(CH$_3$)$_3$}(μ-O$_2$CMe)]$_2$ (24): Yield: 0.37 g (50%). M.p. 121.7 °C. $C_{32}H_{46}N_2O_{10}Pd_2$ (831.5): calcd. C 46.2, H 5.6, N 3.4; found C 46.6, H 5.3, N 3.5. IR (polythene disc): ν(C=N) = 1601sh, m cm^{-1}; ν_{as}(COO) = 1570s cm^{-1}; ν_s(COO) = 1413s cm^{-1}. ^1H NMR (200 MHz, $CDCl_3$), *anti* isomer: δ = 1.10 [s, 9 H, $NC(CH_3)_3$], 2.04 (s, 3 H, OAc), 3.66, 3.72, 3.86 (s, 9 H, OMe), 6.13 (s, 1 H, H^5), 7.79 (s, 1 H, H_i),; *syn* isomer: δ = 1.18 [s, 9 H, $NC(CH_3)_3$], 1.94, 1.98 (s, 3 H, OAc), 3.95, 3.67, 3.77 (s, 9 H, OMe), 6.02 (s, 1 H, H^5), 8.00 (s, 1 H, H_i) ppm.

Preparation of [Pd{2,3,4-(MeO)$_3$C$_6$HC(H)=NCH$_2$CH$_2$OH}(μ-Cl)]$_2$ (3): A solution of **2** (0.310 g, 0.384 mmol) in 15 cm^3 of acetone was treated with a saturated solution of NaCl in ca. 20 cm^3 of water. The yellow precipitate formed was filtered off, washed with water and dried under vacuum. Yield 0.24 g (84%). M.p. 215.1 °C (dec.). $C_{24}H_{32}Cl_2N_2O_8Pd_2$ (760.2): calcd. C 37.9, H 4.2, N 3.7; found C 37.7, H 4.8, N 3.6. IR (nujol mull): ν(O−H) = 3487m cm^{-1}; ν(C=N) = 1605s cm^{-1}. ^1H NMR (200 MHz, [D$_6$]DMSO): δ = 3.31, 3.62 (br. s, 4 H, $-CH_2$), 3.67, 3.76, 3.84 (s, 9 H, OMe), 4.71 (br. s, 1 H, OH), 7.51 (s, 1 H, H^5), 8.08 (s, 1 H, H_i). FAB-MS: *m*/*z* = 785 $[M + Na]^+$.

Preparation of [Pd{2,3,4-(MeO)$_3$C$_6$HC(H)=NCH$_2$CH$_2$OH}-(O$_2$CMe)(PPh$_3$)] (4): PPh_3 (0.014 g, 0.05 mmol) was added to a suspension of **2** (0.023 g, 0.03 mmol) in acetone (15 cm^3). The mixture was stirred for 12 h and the solvent was then removed to give a white solid which was recrystallised from dichloromethane/hexane. Yield: 0.029 g (83%). M.p. 182.5 °C. $C_{32}H_{34}NO_6PPd$ (666.0): calcd. C 57.7, H 5.1, N 2.1; found C 57.6, H 4.8, N 2.3. IR (polythene disc): ν(O−H) = 3400m cm^{-1}; ν(C=N) = 1613s cm^{-1}; ν_{as}(COO) = 1570s cm^{-1}; ν_s(COO) = 1290s cm^{-1}. ^1H NMR (200 MHz, $CDCl_3$): δ = 1.31 (s, 3 H, OAc), 2.88 [s, 3 H, C(4)−OMe], 3.92, 3.70 (s, 6 H, OMe), 3.74, 3.89 (br. s, 4 H, $-CH_2$), 5.70 (d, $J_{P,H}$ = 5.8 Hz, 1 H, H^5), 8.31 (d, $J_{P,H}$ = 7.8 Hz, 1 H, H_i) ppm. $^{31}P\{^1H\}$ NMR (80.9 MHz, $CDCl_3$): δ = 40.8 (s) ppm. FAB-MS: *m*/*z* = 666 $[MH]^+$, 608 $[M - OAc]^+$.

Compounds **5**, **6** and **7** were obtained following a similar procedure, using a cyclometallated complex/diphosphane molar ratio of 1:1, as yellow (**5** and **6**) or white (**7**) air stable solids.

[{Pd[2,3,4-(MeO)$_3$C$_6$HC(H)=NCH$_2$CH$_2$OH](O$_2$CMe)}$_2$(μ-Ph$_2$PCH$_2$PPh$_2$)] (5): Yield: 0.027 g (48%). M.p. 166.7 °C (dec.). $C_{53}H_{60}N_2O_{12}P_2Pd_2$ (1191.8): calcd. C 53.4, H 5.1, N 2.3; found C 54.0, H 4.9, N 2.4. IR (polythene disc): ν(O−H) = 3307m cm^{-1}; ν(C=N) = 1614m, sh cm^{-1}; ν_{as}(COO) = 1573s cm^{-1}; ν_s(COO) = 1286s cm^{-1}. ^1H NMR (200 MHz, $CDCl_3$): δ = 1.65 (s, 3 H, OAc), 2.91 [s, 3 H, C(4)−OMe], 3.10 (br. s, 1 H, OH), 3.63, 4.01 (s, 6 H, OMe), 3.75, 4.03 (br. s, 4 H, $-CH_2$), 5.45 (d, $J_{P,H}$ = 5.4 Hz, 1 H, H^5), 8.36 (d $J_{P,H}$ = 8.2 Hz, 1 H, H_i,) ppm. $^{31}P\{^1H\}$ NMR (80.9 MHz, $CDCl_3$): δ = 32.0 (s) ppm. FAB-MS: *m*/*z* = 1073 [M − 2OAc]$^+$; 728 [MH − 2OAc − L − Pd]$^+$.

[{Pd[2,3,4-(MeO)$_3$C$_6$HC(H)=NCH$_2$CH$_2$OH](O$_2$CMe)}$_2${μ-Ph$_2$P(CH$_2$)$_3$PPh$_2$}] (6): Yield: 0.032 g (49%). M.p. 217.3 °C (dec.). $C_{55}H_{64}N_2O_{12}P_2Pd_2$ (1219.9): calcd. C 54.1, H 5.3, N 2.3; found C 54.3, H 5.1, N 2.4. IR (polythene disc): ν(O−H) = 3345m cm^{-1}; ν(C=N) = 1612m, sh cm^{-1}; ν_{as}(COO) = 1573s cm^{-1}; ν_s(COO) = 1284s cm^{-1}. ^1H NMR (200 MHz, $CDCl_3$): 1.54 (s, 3 H, OAc), 2.99 [s, 3 H, C(4)−OMe], 3.69, 3.93 (s, 6 H, OMe), 3.66, 3.88 (br. s, 4 H, $-CH_2$), 5.73 (d, $J_{P,H}$ = 5.3 Hz, 1 H, H^5], 8.28 (d, $J_{P,H}$ = 7.3 Hz, 1 H, H_i) ppm. $^{31}P\{^1H\}$ NMR (80.9 MHz, $CDCl_3$) 32.3 (s) ppm. FAB-MS: *m*/*z* = 756 [M − 2OAc − L − Pd]$^+$.

[{Pd[2,3,4-(MeO)$_3$C$_6$HC(H)=NCH$_2$CH$_2$OH](O$_2$CMe)}$_2${μ-Ph$_2$P(CH$_2$)$_4$PPh$_2$}] (7): Yield: 0.030 g (76%). M.p. 187.6 °C (dec.). $C_{56}H_{66}N_2O_{12}P_2Pd_2$: calcd. C 54.5, H 5.4, N 2.3; found C 54.2, H 5.0, N 2.7. IR (polythene disc): ν(O−H) = 3399m cm^{-1}; ν(C=N) = 1614m, sh cm^{-1}; ν_{as}(COO) = 1573s cm^{-1}; ν_s(COO) = 1286s cm^{-1}. ^1H NMR (200 MHz, $CDCl_3$): δ = 1.61 (s, 3 H, OAc), 2.97 [s, 3 H, C(4)−OMe], 3.68, 3.88 (s, 6 H, OMe), 3.71, 3.92 (br. s, 4 H, $-CH_2$), 5.73 (d, $J_{P,H}$ = 5.8 Hz, 1 H, H^5), 8.25 (d, $J_{P,H}$ = 7.3 Hz, 1 H, H_i) ppm. $^{31}P\{^1H\}$ NMR (80.9 MHz, $CDCl_3$): δ = 32.8 (s) ppm. FAB-MS: *m*/*z* = 769 [M − 2OAc − L − Pd]$^+$.

Preparation of [Pd{2,3,4-(MeO)$_3$C$_6$HC(H)=NCH$_2$CH$_2$OH}-(Cl)(PPh$_3$)] (8): PPh_3 (0.074 g, 0.28 mmol) was added to a suspension of **3** (0.108 g, 0.14 mmol) in acetone (15 cm^3). The mixture was stirred for 12 h and the solvent was then removed to give a white solid which was recrystallised from dichloromethane/hexane. Yield: 0.12 g (66%). M.p. 199.8 °C (dec.). $C_{30}H_{31}ClNO_4PPd$ (642.4): calcd. C 56.1, H 4.9, N 2.2; found C 56.6, H 4.5, N 2.1. IR (nujol mull): ν(O−H) = 3365m cm^{-1}; ν(C=N) = 1619s cm^{-1}. ^1H NMR (200 MHz, $CDCl_3$): δ = 2.82 [s, 3 H, C(4)−OMe], 3.2 (br. s, 1 H, OH), 3.70, 3.95 (s, 6 H, OMe), 4.03 (m, 4 H, CH_2), 5.74 (d, $J_{P,H}$ = 6.3 Hz, 1 H, H^5), 8.38 (d, $J_{P,H}$ = 8.3 Hz, 1 H, H_i) ppm. $^{13}C\{^1H\}$ NMR: (50.28 MHz, $CDCl_3$): δ = 62.9, 61.8 (C8, C9), 61.8, 60.7, 55.2 (OCH_3), 118.0 (d, $J_{P,C}$ = 12.1 Hz, C5), 133.3 (C1), 154.4 (d, $J_{P,C}$ = 5.4 Hz, C6), 154.0, 152.0, 137.5 (C2, C3, C4), 173.1 (d, $J_{P,C}$ = 2.8 Hz, C=N). P-phenyl: δ = 128.1 (d, $J_{P,C}$ = 11.3 Hz, C_m), 130.1 (d, $J_{P,C}$ = 50.4 Hz, C_i), 135.4 (d, $J_{P,C}$ = 12.1 Hz, C_o), 130.8 (d, $J_{P,C}$ = 2.1 Hz, C_p) ppm. $^{31}P\{^1H\}$ NMR (80.9 MHz, $CDCl_3$): δ = 43.0 (s) ppm. FAB-MS: *m*/*z* = 606 $[M - Cl]^+$.

Compounds **10**, **11**, **12** and **13** were synthesised similarly, using a cyclometallated complex/diphosphane molar ratio of 1:1, as yellow solids.

[{Pd[2,3,4-(MeO)$_3$C$_6$HC(H)=NCH$_2$CH$_2$OH](Cl)}$_2${μ-Ph$_2$P-(CH$_2$)$_3$PPh$_2$}] (10): Yield: 2.7 mg (76%). M.p. 182.6 °C (dec.).

$C_{51}H_{58}Cl_2N_2O_8P_2Pd_2$ (1172.7): calcd. C 52.2, H 5.0, N 2.4; found C 52.4, H 4.9, N 2.5. IR (nujol mull): ν(O−H) = 3420m cm^{-1}; ν(C=N) = 1613s cm^{-1}. ^1H NMR (200 MHz, $CDCl_3$): δ = 2.88 [s, 3 H, C(4)−OMe], 3.67, 3.92 (s, 6 H, OMe), 3.96 (br. s, 4 H, -CH_2), 5.74 (d, $J_{P,H}$ = 6.3 Hz, 1 H, H^5), 8.26 (d, $J_{P,H}$ = 8.3 Hz, 1 H, H_i) ppm. $^{31}P\{^1H\}$ NMR (80.9 MHz, $CDCl_3$): δ = 33.4 (s) ppm. FAB-MS: *m/z* = 1136 [MH − Cl]$^+$, 1103 [MH − 2Cl]$^+$, 756 [MH − 2Cl − L − Pd]$^+$.

[{Pd[2,3,4-(MeO)$_3$C$_6$HC(H)=NCH$_2$CH$_2$OH](Cl)}$_2${μ-Ph$_2$P-(CH$_2$)$_4$PPh$_2$}] (11): Yield: 41 mg (79%). M.p. 148.9 °C (dec.). $C_{52}H_{60}Cl_2N_2O_8P_2Pd_2$ (1186.7): calcd. C 52.6, H 5.1, N 2.4; found C 52.7, H 5.3, N 2.1. IR (nujol mull): ν(O−H) = 3426m cm^{-1}; ν(C=N) = 1614s cm^{-1}. ^1H NMR (200 MHz, $CDCl_3$): δ = 2.88 [s, 3 H, C(4)−OMe], 3.70, 3.92 (s, 6 H, OMe), 4.01 (br. s, 4 H, -CH_2), 5.79 (d, $J_{P,H}$ = 5.8 Hz, 1 H, H^5), 8.32 (d, $J_{P,H}$ = 7.8 Hz, 1 H, H_i) ppm. $^{13}C\{^1H\}$ NMR (50.28 MHz, $CDCl_3$): δ = 62.6, 60.4 (C8, C9), 61.8, 60.7, 55.1 (O*C*H$_3$), 117.4 (d, $J_{P,C}$ = 12.1 Hz, C5), 133.2 (d, $J_{P,C}$ = 1.4 Hz, C1), 154.5 (d, $J_{P,C}$ = 6.5 Hz, C6), 153.7, 152.1, 137.5 (C2, C3, C4), 172.6 (d, $J_{P,C}$ = 4.2 Hz, C=N); P-phenyl: δ = 128.6 (d, $J_{P,C}$ = 10.1 Hz, C_m), 130.8 (C_p), 130.0 (d, $J_{P,C}$ = 46.8 Hz, C_i), 133.9 (d, $J_{P,C}$ = 12.1 Hz, C_o); P(*C*H$_2$)$_4$P: δ = 29.3 (d, $J_{P,C}$ = 33.3 Hz, P*C*H$_2$CH$_2$), 26.1 (d, $J_{P,C}$ = 16.3 Hz, PCH$_2$*C*H$_2$) ppm. $^{31}P\{^1H\}$ NMR (80.9 MHz, $CDCl_3$): δ = 33.9 (s) ppm. FAB-MS: *m/z* = 770 [MH − 2Cl − L − Pd]$^+$.

[{Pd[2,3,4-(MeO)$_3$C$_6$HC(H)=NCH$_2$CH$_2$OH](Cl)}$_2${μ-Ph$_2$PC$_5$H$_4$FeC$_5$H$_4$PPh$_2$}] (12): Yield: 74 mg (71%). M.p. 168.4 °C (dec.). $C_{58}H_{60}Cl_2FeN_2O_8P_2Pd_2$ (1314.6): calcd. C 53.0, H 4.6, N 2.1; found C 52.7, H 5.0, N 2.3. IR (nujol mull): ν(O−H) = 3399m cm^{-1}; ν(C=N) = 1614s cm^{-1}. ^1H NMR (200 MHz, $CDCl_3$): δ = 2.85 [s, 3 H, C(4)−OMe], 3.74, 3.96 (s, 6 H, OMe), 4.03 (br. s, 4 H, -CH_2), 5.22, 4.53 (br. s, 4 H, $H^{ferr.}$), 5.76 (d, $J_{P,H}$ = 6.3 Hz, 1 H, H^5), 8.36 (d, $J_{P,H}$ = 8.3 Hz, 1 H, H_i) ppm. $^{31}P\{^1H\}$ NMR (80.9 MHz, $CDCl_3$): δ = 31.7 (s) ppm. FAB-MS: *m/z* = 898 [M − 2Cl − L − Pd]$^+$.

[{Pd[2,3,4-(MeO)$_3$C$_6$HC(H)=NCH$_2$CH$_2$OH]}$_2$(μ-Cl)(μ-Ph$_2$PCH$_2$PPh$_2$)][Cl] (13): Yield: 7.9 mg (65%). M.p. 145.6 °C (dec.). $C_{49}H_{54}Cl_2N_2O_8P_2Pd_2$ (1144.6): calcd. C 51.4, H 4.8, N 2.4; found C 51.0, H 5.1, N 2.7. IR (nujol mull): ν(O−H) = 3514, 3441m cm^{-1}; ν(C=N) = 1613s cm^{-1}. ^1H NMR (200 MHz, $CDCl_3$): δ = 2.88 [s, 3 H, C(4)−OMe], 3.67, 3.91 (s, 6 H, OMe), 3.99 (br. s, 4 H, -CH_2), 4.70 (m, 2 H, PCH$_2$P), 5.50 (d, $J_{P,H}$ = 6.3 Hz, 1 H, H^5), 8.24 (d, $J_{P,H}$ = 8.3 Hz, 1 H, H_i) ppm. $^{31}P\{^1H\}$ NMR (80.9 MHz, $CDCl_3$): δ = 30.2 (s) ppm. FAB-MS: *m/z* = 1109 [M − Cl]$^+$, 728 [M − 2Cl − L − Pd]$^+$. Specific molar conductivity: Λ_m = 175.1 $ohm^{-1}{\cdot}cm^2{\cdot}mol^{-1}$ (in acetonitrile).

Preparation of [Pd{2,3,4-(MeO)$_3$C$_6$HC(H)=NCH$_2$CH$_2$OH}-(PPh$_3$)][F$_3$CSO$_3$] (9): A suspension of **4** (0.093 g, 0.14 mmol) in acetone (15 cm^3) was treated with silver triflate (0.037 g, 0.14 mmol) and stirred for 2 h. The solution was filtered through Celite to eliminate the AgCl precipitate and then the solvent was removed to give a yellow solid which was recrystallised from dichloromethane/hexane. Yield: 0.095 g (44%). M.p. 223.7 °C (dec.). $C_{31}H_{31}F_3NO_7PPdS$ (756.0): calcd. C 49.2, H 4.1, N 1.8; found C 49.6, H 4.0, N 1.9. IR (nujol mull): ν(O−H) = 3245m cm^{-1}; ν(C=N) = 1625s cm^{-1}. ^1H NMR (200 MHz, $CDCl_3$): δ = 2.91 [s, 3 H, C(4)−OMe], 3.73, 3.97 (s, 6 H, OMe), 3.89, 4.13 (br. s, 4 H, -CH_2), 5.62 (d, $J_{P,H}$ = 4.9 Hz, 1 H, H^5), 7.02 (t, J_{HO,CH_2} = 5.6 Hz, 1 H, OH,], 8.27 (d, $J_{P,H}$ = 9.8 Hz, 1 H, H_i) ppm. $^{13}C\{^1H\}$ NMR (50.28 MHz, $CDCl_3$): δ = 67.7, 56.8 (C8, C9), 61.9, 60.8, 55.5 (O*C*H$_3$), 117.6 (d, $J_{P,C}$ = 10.6 Hz, C5), 135.9 (C1), 144.4 (d, $J_{P,C}$ = 5.7 Hz, C6), 155.0, 155.1, 152.8 (C2, C3, C4), 169.3 (d, $J_{P,C}$ = 4.2 Hz, C=N); P-phenyl: δ = 129.1 (d, $J_{P,C}$ = 10.6 Hz, C_m), 131.8 (d, $J_{P,C}$ = 2.9 Hz, C_p), 134.5 (d, $J_{P,C}$ = 12.1 Hz, C_o) ppm. $^{31}P\{^1H\}$ NMR (80.9 MHz, $CDCl_3$): δ = 36.1 (s) ppm. FAB-MS: *m/z* = 606 [M − CF_3SO_3]$^+$. Specific molar conductivity: Λ_m = 116.2 $ohm^{-1}{\cdot}cm^2{\cdot}mol^{-1}$ (in acetonitrile).

Compound **14** was obtained following a similar procedure using complex **11** as starting material.

[{Pd[2,3,4-(MeO)$_3$C$_6$HC(H)=NCH$_2$CH$_2$OH]}$_2${μ-Ph$_2$P(CH$_2$)$_4$-PPh$_2$}][CF$_3$SO$_3$]$_2$ (14): Yield 0.024 g (63%). M.p. 173.5 °C (dec.). $C_{54}H_{60}F_6N_2O_{14}P_2Pd_2S_2$ (1413.9): calcd. C 45.9, H 4.3, N 2.0; found C 45.7, H 4.3, N 2.0. IR (nujol mull): ν(O−H) = 3250m cm^{-1}; ν(C=N) = 1619s cm^{-1}. ^1H NMR (200 MHz, $CDCl_3$): δ = 2.99 [s, 3 H, C(4)−OMe], 3.70, 3.94 (s, 6 H, OMe), 3.87, 4.19 (br. s, 4 H, -CH_2), 5.63 (d, $J_{P,H}$ = 5.4 Hz, 1 H, H^5), 6.89 (br. s, 1 H, OH), 8.24 (d, $J_{P,H}$ = 9.3 Hz, 1 H, H_i) ppm. $^{13}C\{^1H\}$ NMR (50.28 MHz, $CDCl_3$): δ = 66.3, 57.5 (C8, C9), 61.9, 60.7, 55.4 (O*C*H$_3$), 117.1 (d, $J_{P,C}$ = 11.3 Hz, C5), 138.2 (C1), 146.7 (d, $J_{P,C}$ = 2.8 Hz, C6), 155.1, 154.9, 156.6 (C2, C3, C4), 170.2 (d, $J_{P,C}$ = 2.8 Hz, C=N); P-phenyl: δ = 129.1 (d, $J_{P,C}$ = 10.6 Hz, C_m), 131.6 (d, $J_{P,C}$ = 2.1 Hz, C_p), 133.8 (d, $J_{P,C}$ = 12.1 Hz, C_o);. P(*C*H$_2$)$_4$P: δ = 27.4 (d, $J_{P,C}$ = 29.1 Hz, P*C*H$_2$CH$_2$), 26.2 (d, $J_{P,C}$ = 17.1 Hz, PCH$_2$*C*H$_2$) ppm. $^{31}P\{^1H\}$ NMR (80.9 MHz, $CDCl_3$): δ = 30.2 (s) ppm. FAB-MS: *m/z* = 1265 [M − CF_3SO_3]$^+$, 770 [MH − L − Pd − 2CF_3SO_3]$^+$. Specific molar conductivity: Λ_m = 237.1 $ohm^{-1}{\cdot}cm^2{\cdot}mol^{-1}$ (in acetonitrile).

Preparation of [Pd{2,3,4-(MeO)$_3$C$_6$HC(H)=NCH$_2$CH$_2$OH}-{PPh$_2$(CH$_2$)$_2$PPh$_2$-*P,P*}][ClO$_4$] (15): PPh$_2$(CH$_2$)$_2$PPh$_2$ (0.067 g, 0.17 mmol) was added to a suspension of **3** (0.064 g, 0.08 mmol) in acetone (20 cm^3). The mixture was stirred for 1 h, after which an excess of sodium perchlorate was added. The mixture was stirred for a further 4 h, and then the complex was precipitated out by addition of water, filtered off and dried in vacuo. Recrystallization from dichloromethane/hexane gave the final compound as a yellow solid. Yield: 0.11 g (80%). $C_{38}H_{40}ClNO_8P_2Pd$ (842.5): calcd. C 54.2, H 4.8, N 1.7; found C 53.9, H 4.6, N 1.7. IR (nujol mull): ν(O−H) = 3555, 3488m cm^{-1}; ν(C=N) = 1606s cm^{-1}. ^1H NMR (200 MHz, $CDCl_3$): δ = 2.97 [s, 3 H, C(4)−OMe], 3.73, 3.96 (s, 6 H, OMe), 2.91, 3.42 (br. s, 4 H, -CH_2), 5.93 (dd, $J_{P,H}$ = 8.8, 5.8 Hz, 1 H, H^5), 8.50 (d, $J_{P,H}$ = 8.3 Hz, 1 H, H_i) ppm. $^{13}C\{^1H\}$ NMR (50.28 MHz, $CDCl_3$): δ = 63.6, 59.3 (C8, C9), 62.1, 60.8, 55.5 (O*C*H$_3$), 117.5 (dd, $J_{P,C}$ = 12.1, 3.5 Hz, C5), 138.0 (d, $J_{P,C}$ = 1.4 Hz, C1), 156.0 (dd, $J_{P,C}$ = 12.0, 5.6 Hz, C6), 164.0, 164.6, 153.6 (C2, C3, C4), 179.4 (d, $J_{P,C}$ = 4.5 Hz, C=N); P-phenyl: δ = 127.3, 126.2 (d, $J_{P,C}$ = 36.9, 50.4 Hz, C_i), 129.9, 129.8 (d, $J_{P,C}$ = 10.6, 11.3 Hz, C_m), 132.5, 132.7 (d, $J_{P,C}$ = 2.8 Hz, C_p), 134.1, 133.4 (d, $J_{P,C}$ = 12.1, 12.7 Hz, C_o); P(*C*H$_2$)$_2$P: δ = 30.5 (dd, $J_{P,C}$ = 35.1, 18.0 Hz, P*C*H$_2$CH$_2$P), 26.1 (dd, $J_{P,C}$ = 29.8, 9.2 Hz, PCH$_2$*C*H$_2$P) ppm. $^{31}P\{^1H\}$ NMR (80.9 MHz, $CDCl_3$): δ = 43.0 (d, $J_{P,P}$ = 25.4 Hz), 61.0 (d) ppm. FAB-MS: *m/z* = 742 [M − ClO_4]$^+$. Specific molar conductivity: Λ_m = 142.8 $ohm^{-1}{\cdot}cm^2{\cdot}mol^{-1}$ (in acetonitrile).

Compound **16** was obtained following a similar procedure as a yellow, air stable, solid.

[Pd{2,3,4-(MeO)$_3$C$_6$HC(H)=NCH$_2$CH$_2$OH}{(PPh$_2$CH$_2$CH$_2$)$_2$-PPh-*P,P,P*}][ClO$_4$] (16): Yield: 7.8 mg (59%). $C_{46}H_{49}ClNO_8P_3Pd$ (978.7): calcd. C 56.4, H 5.0, N 1.4; found C 56.9, H 4.6, N 1.5. IR (nujol mull): ν(O−H) = 3501m cm^{-1}; ν(C=N) = 1614s cm^{-1}. ^1H NMR (200 MHz, $CDCl_3$): δ = 2.80 [s, 3 H, C(4)−OMe], 3.71, 3.88 (s, 6 H, OMe), 2.82, 3.36 (br. s, 4 H, -CH_2), 5.25 (dd, $J_{P,H}$ = 8.8, 2.4 Hz, 1 H, H^5), 8.40 (s, 1 H, H_i) ppm. $^{13}C\{^1H\}$ NMR (50.28 MHz, $CDCl_3$): δ = 167.3 (d, $J_{P,C}$ = 5.7 Hz, C=N), 163.3, 161.1, 154.1 (C2, C3, C4), 154.0 (m, C6), 116.3 (m, C5), 62.8, 61.6

(C8, C9), 62.1, 60.9, 54.8 (OCH_3); $P(CH_2)_2P$: δ = 32.3, 25.9 (m) ppm. $^{31}P\{^1H\}$ NMR (80.9 MHz, $CDCl_3$): δ = 44.5 (d, $J_{P,P}$ = 26.3), 86.0 (t) ppm. FAB-MS: *m/z* = 979 $[M]^+$, 877 $[M - ClO_4]^+$. Specific molar conductivity,: Λ_m = 125.9 ohm^{-1} cm^2 mol^{-1} (in acetonitrile).

X-ray Crystallographic Study: Three-dimensional, room temperature X-ray data were collected on a Siemens Smart CCD diffractometer by the ω scan method using graphite-monochromated Mo-K_α radiation. All the measured reflections were corrected for Lorentz and polarisation effects and for absorption by semi-empirical methods based on symmetry equivalent and repeated reflections. The structures were solved by direct methods and refined by full-matrix least-squares on F^2. Hydrogen atoms were included in calculated positions (except the -O*H* hydrogens which were located in a difference Fourier map) and refined in a riding mode. The O(6), O(7) and O(8) oxygen atoms of the perchlorate counterion in complex **16** were found to be disordered over two positions (with occupancies of approximately 50%). The refinement was carried out taking into account both components. Refinement converged at a final R = 0.0776, 0.0460, 0.0294, 0.0412 and 0.0466 (for complexes **2**, **8**, **9**, **15** and **16**, respectively, observed data, F) and wR_2 = 0.1690, 0.1992, 0.0776, 0.1137 and 0.0829 (for complexes **2**, **8**, **9**, **15** and **16**, respectively, unique data, F^2), with allowance for the thermal anisotropy of all non-hydrogen atoms. The structure solution and refinement were carried out using the program package SHELX-97.[60]

CCDC-178027 (**2**), -178028 (**8**), -178029 (**9**), -178030 (**15**) and -178031 (**16**) contain the supplementary crystallographic data for this paper. These data can be obtained free of charge at www.ccdc.cam.ac.uk/conts/retrieving.html [or from the Cambridge Crystallographic Data Centre, 12, Union Road, Cambridge CB2 1EZ, UK; Fax: (internat.) +44−1223/336−033; E-mail: deposit@ccdc.cam.ac.uk].

Acknowledgments

We thank the Ministerio de Educación y Cultura (Proyecto PB98-0638-C02-01/02), the Xunta de Galicia (Proyecto PGIDT99PXI20907B) and the Universidad de la Coruña for financial support.

[1] I. Omae, in *Organometallic Intramolecular-Coordination Compounds*, Elsevier Science, Amsterdam-New York, **1986**.
[2] V. V. Dunina, O. A. Zalevskaya, V. M. Potapov, *Russ. Chem. Rev.* **1984**, *571*, 250−269.
[3] G. R. Newkome, W. E. Puckett. W. K. Gupta, G. E. Kiefer, *Chem. Rev.* **1986**, *86*, 451−489.
[4] A. D. Ryabov, *Chem. Rev.* **1990**, *90*, 403−424.
[5] M. Pfeffer, *Recl. Trav. Chim. Pays-Bas* **1990**, *109*, 567−576.
[6] M. Albrecht, G. van Kotten, *Angew. Chem. Int. Ed.* **2001**, *40*, 3750−3781.
[7] J. Dupont, M. Pffefer, J. Spencer, *Eur. J. Inorg. Chem.* **2001**, 1917−1927.
[8] M. Pfeffer, J. P. Sutter, M. A. Rotteveel, A. de Cian, J. Fischer, *Tetrahedron* **1992**, *48*, 2427−2440.
[9] C. Navarro-Ranninger, I. López-Solera, J. Rodríguez, J. L. García-Ruano, P. R. Raithby, J. R. Masaguer, C. Alonso, *J. Med. Chem.* **1993**, *36*, 3795−3801.
[10] C. Navarro-Ranninger, I. López-Solera, V. M. Gonzalez, J. M. Pérez, A. Alvarez-Valdes, A. Martin, P. R. Raithby, J. R. Masaguer, C. Alonso, *Inorg. Chem.* **1996**, *35*, 5181−5187.
[11] M. López-Torres, A. Fernández, J. J. Fernández, S. Castro-Juiz, A. Suárez, J. M. Vila, M. T. Pereira, *Organometallics* **2001**, *20*, 1350−1353.
[12] J. M. Vila, M. T. Pereira, J. M. Ortigueira, J. J. Fernández, A. Fernández, M. López-Torres, H. Adams, *Organometallics* **1999**, *18*, 5484−5487.
[13] B. Teijido, A. Fernández, M. López-Torres, S. Castro-Juiz, A. Suárez, J. M. Ortigueira, J. M. Vila, J. J. Fernández, *J. Organomet. Chem.* **2000**, *598*, 71−79.
[14] M. Lousame, A. Fernández, M. López-Torres, D. Vázquez-García, J. M. Vila, A. Suárez, J. M. Ortigueira, J. J. Fernández, *Eur. J. Inorg. Chem.* **2000**, 2055−2062.
[15] G. J. Gainsford, R. Mason, *J. Organomet. Chem.* **1974**, *80*, 395−406.
[16] J. Selbin, K. Abboud, S. F. Watkins, M. A. Gutierrez, F. R. Fronczek, *J. Organomet. Chem.* **1983**, *241*, 259−268.
[17] A. Albinati, P. S. Pregosin, R. Ruedi, *Helv. Chim. Acta* **1985**, *68*, 2046−2061.
[18] R. Ruger, W. Rittner, P. G. Jones, W. Isenberg, G. M. Sheldrick, *Angew. Chem. Int. Ed. Engl.* **1981**, *93*, 389−390.
[19] E. Wehman, G. van Koten, J. T. B. H. Jastrzebski, H. Ossor, M. Pfeffer, *J. Chem. Soc., Dalton Trans.* **1988**, 2975−2981.
[20] G. Balavoine, J. C. Clinet, P. Zerbib, K. Boubekeur, *J. Organomet. Chem.* **1990**, *389*, 259−275.
[21] M. Ohff, A. Ohff, D. Milstein, *Chem. Commun.* **1999**, 357−358.
[22] J. L. Garcia-Ruano, I. Lopez-Solera, J. R. Masaguer, C. Navarro-Ranninger, J. H. Rodriguez, S. Martinez-Carrera, *Organometallics* **1992**, *11*, 3013−3018.
[23] A. Boehm, K. Polborn, K. Suenkel, W. Beck, *Z. Naturforsch., Teil B* **1998**, *53*, 448−458.
[24] M. R. Churchill, H. J. Wasserman, G. J. Young, *Inorg. Chem.* **1980**, *19*, 762−770.
[25] W. A. Herrmann, C. Brossmer, K. Ofele, C. P. Reisinger, T. Priermeier, M. Beller, H. Fischer, *Angew. Chem. Int. Ed. Engl.* **1995**, *34*, 1844−1847.
[26] W. A. Herrmann, V. P. W. Bohm, C. P. Reisinger, *J. Organomet. Chem.* **1999**, *576*, 23−41.
[27] D. Freiesleben, K. Polborn, C. Robl, K. Sunkel, W. Beck, *Can. J. Chem.* **1995**, *73*, 1164−1174.
[28] J. M. Vila, M. Gayoso, M. T. Pereira, M. López-Torres, J. J. Fernández, A. Fernández, J. M. Ortigueira, *J. Organomet. Chem.* **1997**, *532*, 171−180.
[29] A. Fernández, P. Uría, J. J. Fernández, M. López-Torres, A. Suárez, D. Vázquez-García, M. T. Pereira, J. M. Vila, *J. Organomet. Chem.* **2001**, *620*, 8−19.
[30] J. M. Vila, M. T. Pereira, J. M. Ortigueira, M. López-Torres, D. Lata, M. Graña, A. Suárez, J. J. Fernández, A. Fernández, *J. Chem. Soc., Dalton Trans.* **1999**, 4193−4201.
[31] D. Vázquez-García, A. Fernández, J. J. Fernández, M. López-Torres, A. Suárez, J. M. Ortigueira, J. M. Vila, H. Adams, *J. Organomet. Chem.* **2000**, *595*, 199−207.
[32] Y. Ustynyuk, V. A. Chertov, J. V. Barinov, *J. Organomet. Chem.* **1971**, *29*, C53.
[33] H. Onoue, I. Moritani, *J. Organomet. Chem.* **1972**, *43*, 431−436.
[34] H. Onoue, K. Minami, K. Nakagawa, *Bull. Chem. Soc. Jpn.* **1970**, *43*, 3480−3485.
[35] K. Nakamoto, *IR and Raman Spectra of Inorganic and Coordination Compounds*, 5th ed., Wiley & Sons, New York **1997**.
[36] F. Zamora, S. Laguna, P. Amo-Ochoa, L. A. Martínez-Cruz, A. Vegas, *J. Organomet. Chem.* **1996**, *522*, 97−103.
[37] C. Navarro-Ranninger, F. Zamora, L. A. Martínez-Cruz, R. Isea, J. R. Masaguer, *J. Organomet. Chem.* **1996**, *518*, 29−36.
[38] A. Suárez, J. M. Vila, M. T. Pereira, E. Gayoso, M. Gayoso, *Synth. React. Inorg. Met.-Org. Chem.* **1990**, *20*, 1425−1440.
[39] K. Hiraki, Y. Fuchita, H. Nakaya, S. Takakura, *Bull. Chem. Soc. Jpn.* **1979**, *52*, 2531−2534.
[40] L. Pauling, *The Nature of the Chemical Bond*, 3rd ed., Cornell University Press, New York, **1960**.
[41] J. M. Vila, M. Gayoso, M. T. Pereira, M. López-Torres, G. Alonso, J. J. Fernández, *J. Organomet. Chem.* **1993**, *445*, 287−294.

[42] R. Bosque, J. Granell, J. Sales, M. Font-Bardiá, X. Solans, *J. Organomet. Chem.* **1994**, *453*, 147−154.
[43] R. Bosque, J. Granell, J. Sales, M. Font-Bardiá, X. Solans, *Organometallics* **1995**, *14*, 1393−1404.
[44] J. Vicente, A. Arcas, D. Bautista, P. G. Jones, *Organometallics* **1997**, *16*, 2127−2138.
[45] J. Vicente, J. Abad, A. D. Frankland, M. C. Ramírez de Arellano, *Chem. Eur. J.* **1999**, *5*, 3066−3075.
[46] J. Albert, R. Bosque, J. M. Cadena, S. Delgado, J. Granell, *J. Organomet. Chem.* **2001**, *634*, 83−89.
[47] W. J. Geary, *Coord. Chem. Rev.* **1971**, *7*, 81−122.
[48] C. Cativiela, L. R. Falvello, J. C. Ginés, R. Navarro, E. P. Urriolabeitia, *New J. Chem.* **2001**, *25*, 344−352.
[49] P. S. Pregosin and R. W. Kuntz, *^{31}P and ^{13}C NMR of Transition Metal Phosphane Complexes* (Eds.: P. Diehl, E. Fluck and R. Kosfeld), Vol. 16, Springer, Berlin, **1979**.
[50] J. M. Vila, M. Gayoso, A. Fernández, H. Adams, N. A. Bailey, *J. Organomet. Chem.* **1993**, *448*, 233−239.
[51] M. López-Torres, A. Fernández, J. J. Fernández, A. Suárez, M. T. Pereira, J. M. Ortigueira, J. M. Vila, H. Adams, *Inorg. Chem.* **2001**, *40*, 4583−4587.
[52] F. Cecconi, C. A. Ghilardi, S. Midollini, S. Moneti, A. Orlandini, G. Scapacci, *J. Chem. Soc., Dalton Trans.* **1989**, 211−216.
[53] J. Granell, D. Sainz, J. Sales, X. Solans, M. Font-Altaba, *J. Chem. Soc., Dalton Trans.* **1986**, 1785−1790.
[54] J. Granell, J. Sales, J. Vilarrasa, J. P. Declercq, G. Germain, C. Miravilles, X. Solans, *J. Chem. Soc., Dalton Trans.* **1983**, 2441−2446.
[55] Z. Taira, S. Yamazaki, *Bull. Chem. Soc. Jpn.* **1986**, *59*, 649−650.
[56] L. A. Villanueva, K. Abboud, J. M. Boncella, *Organometallics* **1991**, *10*, 2969−2972.
[57] D. Onggo, D. C. Craig, A. D. Rae, H. A. Goodwin, *Aust. J. Chem.* **1991**, *44*, 219−231.
[58] O. Schlager, K. Wieghardt, B. Nuber, *Inorg. Chem.* **1995**, *34*, 6449−6455.
[59] D. D. Perrin, W. L. F. Armarego, *Purification of Laboratory Chemicals*, 4th ed., Butterwort-Heinemann, **1996**.
[60] G. M. Sheldrick, *SHELX-97, An integrated system for solving and refining crystal structures from diffraction data*, University of Gottingen, Germany **1997**.

Received January 29, 2002
[I02051]

New Mixed-Ligand Re^V Complexes with Bis(2-mercaptoethyl) Sulfide and Functionalized Thioimidazolyl Ligands

Elisa Palma,[a] João D. G. Correia,[a] Ângela Domingos,[a] and Isabel Santos*[a]

Keywords: S ligands / Rhenium / Peptides / N ligands

The preparation of the mixed-ligand Re^V complexes [Re(O)(κ^3-SSS)(κ^1-Simz)] (**1**), [Re(O)(κ^3-SSS)(κ^1-Simz)]·HCl (**2**) and [Re(O)(κ^3-SSS)(κ^1-SimzCOGlyGly)] (**3**) are described. These [3+1] type compounds are stabilized by tridentate bis(2-mercaptoethyl) sulfide (HSSSH) and by monodentate functionalized thioimidazolyl ligands. Complexes **1**, **2** and **3** were fully characterized by IR and ^{1}H NMR spectroscopy, and by X-ray diffraction analysis in the case of **1** and **2**. In complexes **1** and **2** the Re atom is five-coordinate, presenting a distorted square pyramidal coordination geometry. Based on the angular structural parameter, τ, this distortion lies towards a trigonal bipyramidal geometry (τ = 0.40, **1**; τ = 0.46, **2**).

(© Wiley-VCH Verlag GmbH, 69451 Weinheim, Germany, 2002)

Introduction

The development of mixed-ligand complexes of Re and Tc, of the so-called [3+1] type, has been thoroughly investigated for labeling biomolecules, namely CNS receptor ligands. For this purpose different tridentate ligands and mono thiol co-ligands have been used.[1−7] This approach can be considered to be greatly advantageous since the combination of different ligands has allowed the synthesis of complexes with a wide variety of chemical and biochemical properties. However, in spite of this versatility they show a remarkable *in vivo* reactivity against nucleophiles, namely SH-group containing compounds like glutathione. This instability arises not only from ligand-exchange reactions between the co-ligand and nucleophiles, but also from the presence of a vacant coordination site trans to the oxo group.[3,6] Both processes depend on the nature and the concentration of the tridentate and monodentate ligands. In order to overcome this problem we studied the chemistry of Re and Tc using the well-known tridentate ligand bis(2-mercaptoethyl) sulfide (HSSSH) and functionalized thioimidazolyl molecules as co-ligands. This type of co-ligands can coordinate through the nitrogen and sulfur atoms. This bidentate coordination mode could provide complexes with higher stability against substitution.[3,6] The functionalized thioimidazolyl molecules will also allow the labelling of small peptides with $[^{99m}Tc(O)]^{3+}$. In this paper, we report on the synthesis and characterization of the mixed-ligand Re^V complexes, stabilized with these co-ligands, including one bearing a dipeptide (GlyGly): [Re(O)(κ^3-SSS)(κ^1-Simz)] (**1**), [Re(O)(κ^3-SSS)(κ^1-Simz)]·HCl (**2**) and [Re(O)(κ^3-SSS)(κ^1-SimzCOGlyGly)] (**3**).

[a] Departamento de Química, ITN,
Estrada Nacional 10, 2686−953 Sacavém Codex, Portugal
Fax: (internat.) +351−219941455
E-mail address: isantos@itn1.itn.pt

Results and Discussion

Synthesis and Characterization of the Simz, SimzCOOH and SimzCOGlyGly Co-Ligands

Methyl (2-mercapto-3-methylimidazol-4-yl)methanoate (**Simz**) was obtained, in a fair yield (68%), by a slight modification of a previously reported method.[9] The synthetic pathway for its preparation involves the formation of *N*-formyl and *C*-formyl intermediates, followed by ring formation with KSCN (Scheme 1).

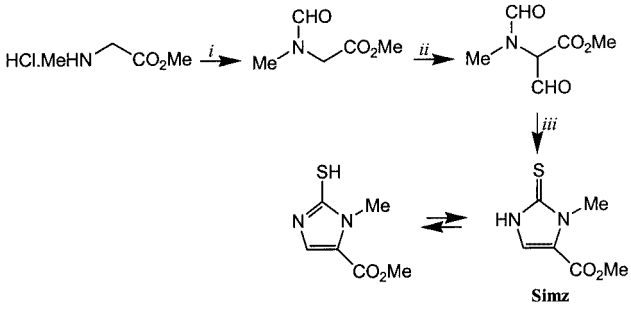

Scheme 1. Synthesis of the **Simz** co-ligand; (*i*) NEt_3, HCOOH, THF, reflux; (*ii*) $NaOCH_3$, CH_3OCHO, room temperature; (*iii*) HCl, KSCN, 65−70° C

2-(Mercapto-3-methylimidazol-4-yl)methanoic acid (**SImzCOOH**) was isolated as a white precipitate in an almost quantitative yield (97%) by classical hydrolysis of the **Simz** ester under basic conditions, followed by acidification of the reaction solution. The compound glycylglycine (2-

mercapto-3-methylimidazol-4-yl)methanamide (**SimzCOGlyGly**) was obtained by reacting [(2-mercapto-3-methylimidazol-4-yl)methyloxy]succinimide (**SimzCOSucc**)[10,11] with Glycylglycine (**GlyGly**) (Scheme 2). For the coupling reaction to proceed, it is necessary of the presence of a deprotonating agent such as triethylamine. The compound **SimzCOGlyGly** is poorly soluble in most organic solvents, and is readily soluble in aqueous alkaline solutions only (pH ≈ 12).

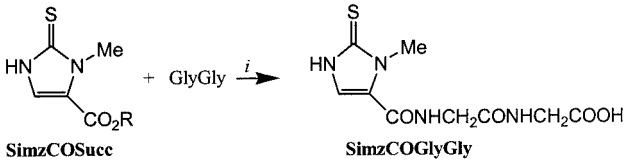

Scheme 2. Synthesis of **SimzCOGlyGly**; R = *N*-succinimido; (*i*) NEt_3, THF, DMF, H_2O, room temperature

The most important features in the IR spectra of **Simz** and derivatives is the existence of strong bands in the 1630−1765 cm^{-1} range, and medium intensity bands in the 735−760 cm^{-1} range, which are assigned to the ν(C=O) and ν(C=S) stretching vibrations, respectively.

The ^1H NMR spectra of **Simz**, **SimzCOOH** and **SimzCOSucc** in CD_3OD present one singlet at δ = 3.81, 3.81 and 3.78 ppm, respectively, assigned to the methyl group attached to one of the nitrogen atoms of the thioimidazolyl ring. **Simz** presents another singlet at δ = 3.83 ppm, which is assigned to the methyl group of the ester. In all spectra, one resonance assigned to the methylenic proton of the ring system can also be observed (**Simz**: δ = 7.61 ppm; **SimzCOOH**: δ = 7.57 ppm; **SimzCOsucc**: δ = 8.05 ppm). The NH proton of the thioimidazolyl ring is also observed when $CDCl_3$, CD_3CN or $[(CD_3)_2SO]$ is used as solvent. For instance, in the case of the **Simz** ligand, that signal appears as a broad singlet at δ = 12.08 ppm in $CDCl_3$ and at δ = 10.28 ppm in CD_3CN. In the IR spectrum, the (glygly)-functionalized thioimidazolyl ligand (**SimzCOGlyGly**) presents two strong bands at 1630 cm^{-1} and 1715 cm^{-1}, assigned to the ν(C=O) stretching vibrations of the amide functionalities and of the free carboxylic acid of the dipeptide. A characteristic medium band at 760 cm^{-1} also appears, which is assigned to the $\tilde{\nu}$(C=S) stretching vibration. The ^1H NMR spectrum in $[(CD_3)_2SO]$ of this ligand compares well with the above mentioned thioimidazolyl derivatives: a singlet at δ = 3.66 ppm assigned to the methyl group, a singlet at δ = 7.58 ppm assigned to the methylenic proton of the ring, and a broad singlet at δ = 12.55 ppm assigned to the NH group of the ring. The signals corresponding to the dipeptide are also clearly observed: two sets of doublets at δ = 3.75 and 3.83 ppm are assigned to the CH_2 groups, and two sets of triplets at δ = 8.23 and 8.60 ppm are assigned to the protons of the amide.

Synthesis and Characterization of the Complexes

Reactions of **Simz** and **SimzCOGlyGly** with the (chloro)oxorhenium(V) complex [ReO(SSS)Cl],[8] under different conditions, afforded the mixed-ligand complexes [Re(O)(κ³-SSS)(κ¹-Simz)] (**1**), [Re(O)(κ³-SSS)(κ¹-Simz)]·HCl (**2**) and [Re(O)(κ³-SSS)(κ¹-SimzCOGlyGly)] (**3**) (Scheme 3).

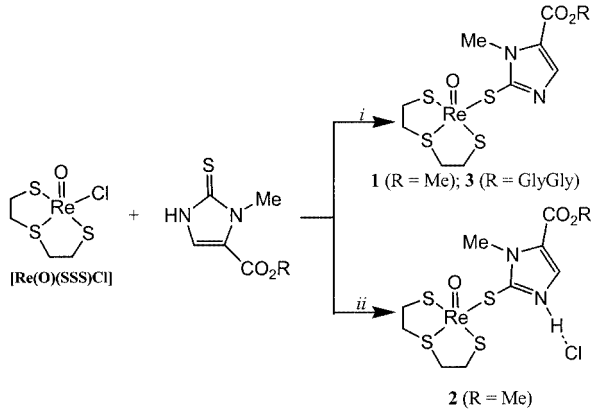

Scheme 3. Synthesis of complexes **1**, **2** and **3**; (*i*) NEt_3, CH_2Cl_2 (**1**), CH_3CN (**3**), reflux; (*ii*) CH_3CN, reflux

The neutral oxo complex **1** was obtained in a 68% yield, after appropriate workup, by refluxing [Re(O)(SSS)Cl] with **Simz** in CH_2Cl_2, with NEt_3 as the deprotonating agent. In this complex, the monodentate thioimidazolyl co-ligand is mononegative. When the reaction is run in CH_3CN, and in the absence of a base, the ^1H NMR spectrum of the product obtained, after workup, indicates a mixture of three species. Two of these species are unambiguously identified as [Re(O)(SSS)Cl] and free functionalized thioimidazolyl. The third species presented an ^1H NMR spectrum that is consistent with the presence of one tridentate SSS and one neutral **Simz** ligand (^1H NMR (δ, CD_3CN): 10.43 (1 H, s, br., NH), 7.84 (1 H, s, CH), 4.10−4.05 (2 H, m, CH_2), 3.88 (3 H, s, CH_3), 3.85 (3 H, s, CH_3), 3.13 (2 H, m, CH_2)). Recrystallization of the crude product of this reaction, from CH_3CN/hexane, led to the formation of violet crystals and to the precipitation of a blue solid. The blue solid was identified by ^1H NMR spectroscopy as [Re(O)(SSS)Cl]. The X-ray diffraction analysis of the violet crystals allowed the formulation of complex **2**, where the Simz is not deprotonated and is neutral. These crystals, after being washed with CH_3CN to remove any [Re(O)(SSS)Cl] present, were analyzed by NMR spectroscopy. The spectrum was identical to the one observed for the crude product. This result can only be explained by assuming that in solution **2** dissociates as indicated in Scheme 4.

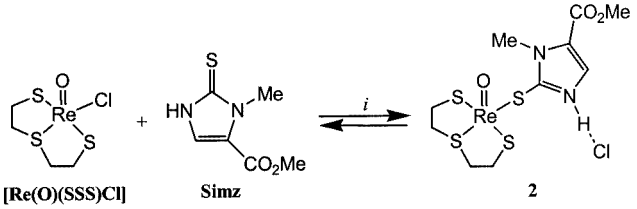

Scheme 4. (*i*) CH_3CN

The neutral oxo complex **3** was obtained in a 60% yield by refluxing [ReO(SSS)Cl] and **SimzCOGlyGly** in dry

CH_3CN in the presence of NEt_3. Complex **1** is soluble in chlorinated solvents and insoluble in methanol and water. Complex **3**, which bears a GlyGly moiety, is soluble in methanol, relatively soluble in water and insoluble in chlorinated solvents. Both complexes **1** and **3** are air- and moisture-stable.

Complexes **1**, **2** and **3** present strong bands in the IR spectra at 970 cm^{-1}, which are assigned to the ν(Re=O) stretching vibrations. This value compares well with those found in other compounds of the [3+1] type, previously described (930−980 cm^{-1}).[7] Strong bands at 1715, 1725, and at 1535 cm^{-1}/1645 cm^{-1} are assigned to the ν(C=O) stretching vibrations of complexes **1**, **2** and **3**, respectively.

In the ^1H NMR spectra of **1** and **3**, four sets of multiplets appear, which are assigned to the methylenic protons of the tridentate ligand HSSSH; most of these signals are shifted upfield relative to those of the corresponding free ligand. For complex **2**, the identification of all methylenic protons of the tridentate ligand was not possible since two of the resonances are superimposable with those of [ReO(SSS)Cl], which is also present due to the equilibrium depicted in Scheme 4.

The chemical shifts corresponding to the monodentate ligand of the complexes **1** (δ = 7.73, 3.85 and 3.82 ppm) and **2** (δ = 10.43, 7.84, 3.88 and 3.85 ppm) in CD_3CN are shifted downfield relative to those of the free ligand (δ = 10.28, 7.45, 3.78 and 3.73 ppm) in the same solvent. The same holds true for complex **3** in CD_3OD (**3**: δ = 7.76, 4.05, 3.94 and 3.89 ppm; **SimzCOGlyGly**: δ = 7.51, 4.00, 3.88 and 3.79).

Crystal Structures of [Re(O)(κ³-SSS)(κ¹-Simz)] (1) and [Re(O)(κ³-SSS)(κ¹-Simz)]·HCl (2): Suitable crystals for X-ray structural analysis were obtained for complexes **1** and **2**. ORTEP views are shown in Figure 1 and Figure 2, and selected bond lengths and angles for both complexes are presented in Table 1.

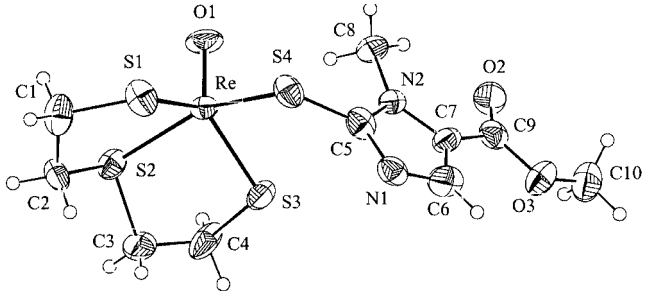

Figure 1. ORTEP drawing of complex **1** with the atom numbering scheme; thermal ellipsoids are drawn at the 40% probability level. Hydrogen atoms were introduced in calculated positions.

Complex **2** is monocationic with a chloride atom as the counterion, while complex **1** is neutral. In both compounds the coordination geometry around the five-coordinate Re^v atom is best described as distorted square-pyramidal, with the axial Re−O(1) bond length significantly shorter than the Re−L(basal) distances. The Re=O(1) bond lengths in **1** [1.683(8) Å] and **2** [1.673(5) Å] are comparable, and are in the range (1.67−1.70 Å) so far observed for this type of

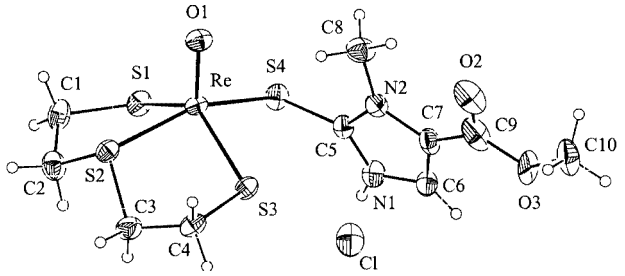

Figure 2. ORTEP drawing of complex **2** with the atom numbering scheme; thermal ellipsoids are drawn at the 30% probability level. Hydrogen atoms were introduced in calculated positions.

Table 1. Selected bond lengths (Å) and Angles (°) for [Re(O)(κ³-SSS)(κ¹-Simz)] (**1**), and [Re(O)(κ³-SSS)(κ¹-Simz)]·HCl (**2**)

	1	2
Re−O(1)	1.683(8)	1.673(5)
Re−S(1)	2.285(3)	2.290(2)
Re−S(2)	2.367(3)	2.364(2)
Re−S(3)	2.285(3)	2.282(2)
Re−S(4)	2.327(3)	2.345(2)
S(4)−C(5)	1.745(13)	1.734(7)
O(1)−Re−S(1)	114.5(3)	116.6(2)
O(1)−Re−S(2)	100.6(3)	99.3(2)
O(1)−Re−S(3)	115.1(3)	115.4(2)
O(1)−Re−S(4)	105.3(3)	105.1(2)
S(1)−Re−S(3)	130.35(14)	127.86(7)
S(3)−Re−S(4)	87.64(12)	88.29(7)
S(1)−Re−S(4)	82.38(12)	81.15(7)
S(3)−Re−S(2)	84.25(11)	84.44(7)
S(1)−Re−S(2)	84.18(11)	84.76(7)
S(4)−Re−S(2)	154.00(11)	155.29(7)
Re−S(4)−C(5)	110.7(4)	110.1(2)

3+1 compounds.[1−6,12−16] The C−S bond lengths [1.745(13) Å (**1**), 1.734(7) Å (**2**)] are comparable and are similar to those found previously,[17] which range from 1.68 to 1.73 Å. Additionally, provided that the values found for the best least-square planes through the atoms S(1)−S(2)−S(3)−S(4) (RMSD = 0.218 Å for **1**, RMSD = 0.253 Å for **2**) show significant deviations from planarity, we conclude that these atoms in both structures do not define a basal plane. The chloride ion is hydrogen bonded to N(1) and the distance between them [3.023(8) Å] allows for the presence of a hydrogen atom [N(1)−H(1): 0.86 Å, H(1)···Cl: 2.18 Å]. The angle N(1)−H(1)−Cl is 166.7°, which can be considered to be linear. Relative to the coordination positions, in both complexes (**1** and **2**), only one of the axial positions is occupied by the oxo group. The equatorial positions are defined by sulfur atoms, three from the tridentate and dianionic ligand $(SSS)^{2-}$, and a thione sulfur atom belonging to the monodentate thioimidazolyl co-ligand.

The Re−S(4) bond lengths in **1** [2.327(3) Å] and **2** [2.345(2) Å] are comparable and typical of a monothiolate. The Re−S bonds within the tridentate ligand in **1** [2.285(3), 2.367(3) and 2.285(3) Å] and **2** [2.290(2), 2.364(2) and 2.282(2) Å] compare with the values found for the same

Table 2. Crystallographic data for complexes **1** and **2**

	1	**2**
Empirical formula	$C_{10}H_{15}N_2O_3S_4Re{\cdot}CHCl_3$	$C_{10}H_{16}ClN_2O_3S_4Re$
Formula mass	645.05	578.14
Crystal size, mm	0.18 × 0.17 × 0.17	0.34 × 0.18 × 0.10
Temperature, K	293(2)	293(2)
Crystal system	Monoclinic	Triclinic
Space group	$P2_1/c$	$P\bar{1}$
a, Å	8.275(2)	8.069(2)
b, Å	17.287(2)	9.935(2)
c, Å	14.373(3)	12.664(2)
α, deg		96.830(10)
β, deg	98.37(2)	92.000(10)
γ, deg		109.80(2)
V, Å^3	2034.2(7)	945.3(3)
Z	4	2
Density (calcd.), g·cm^{-3}	2.106	2.031
Absorption coefficient, mm^{-1}	6.791	7.024
2θ Range, deg	3.7−56.00	3.24−54.00
Reflections collected	5082	4385
Independent reflections	4896 [*R*(int) = 0.0502]	4140 [*R*(int) = 0.0201]
Parameters	217	223
Observed reflections [$I>2\sigma(I)$]	2917	3539
Final *R* indices [$I>2\sigma(I)$]	$R1$[a] = 0.0637 $wR2$[b] = 0.0995	$R1$[a] = 0.0390 $wR2$[b] = 0.0869
Goodness-of-fit	1.087	1.052

[a] $R1 = \Sigma||F_o| - |F_c||/\Sigma|F_o|$. [b] $wR2 = \{\Sigma[w(F_o^2 - F_c^2)^2]/\Sigma[w(F_o^2)^2]\}^{1/2}$; $w = 1/[\sigma^2(F_o^2) + (aP)^2 + bP]$, where $P = (F_o^2 + 2F_c^2)/3$.

type of bond in complexes of the 3+1 type, stabilized by SSS chelates.[1,18]

The five-membered rings, formed by the atoms Re, S(1), C(1), C(2) and S(2) are in the twisted form in both complexes. Relative to the plane [Re−S(1)−S(2)], C(1) is 0.53 and 0.50 Å above the plane for **1** and **2**, respectively, and C(2) is −0.25 and −0.21 Å below the plane for **1** and **2**, respectively.

The five-membered rings, formed by the atoms Re, S(2), C(3), C(4) and S(3) are in the twisted form in both complexes. Relative to the plane [Re−S(2)−S(3)], C(3) and C(4) are equally far from the plane by 0.37 Å in complex **1,** and in **2** are 0.30 and −0.39 Å above and below the plane, respectively.

In terms of the trigonality index, τ, the values are 0.40 and 0.46 for **1** and **2**, respectively (τ = 0 for a regular square pyramid, τ = 1 for a regular trigonal bipyramid).[19] According to the results in this work and those obtained earlier for complexes with a SSS/S donor atom set,[1,18] the τ values remain between 0.253−0.473. This means that the majority of structures in this study may be classified as intermediate between the square pyramidal and trigonal bipyramidal limiting geometries, but in agreement with the structural index parameter (τ) adopted, all of the structures are described as distorted square pyramidal rather than distorted trigonal bipyramidal. The major distortions from the regular square pyramidal geometry arise from the chelate bite angles of the tridentate ligand (see Table 2).

We also note that one of the reasons that the thioimidazolyl co-ligand acts as a monodentate ligand may be due to the existence of a wide angle [Re−S(4)−C(5): 110.7(4)° (for **1**) and 110.1(2)° (for **2**)] that prevents N(1) from coordinating to the metal.

Concluding Remarks

Using the tridentate bis(2-mercaptoethyl) sulfide ligand and functionalized thioimidazolyl co−ligands, it was possible to isolate and characterize oxorhenium(V) complexes of the [3+1] type. The complexes are stable in solution when the monodentate thioimidazolyl co-ligands are monoanionic. The functionalization of the thioimidazolyl with a dipeptide leads to a water soluble complex, which is promising for biomedical applications.

Experimental Section

General Procedures: All chemicals were of reagent grade. Solvents were dried and distilled prior to use, according to described procedures. Methyl (2-mercapto-3-methylimidazol-4-yl) methanoate (**Simz**) was prepared by a modification of a reported method and [Re(O)(SSS)Cl] as described in the literature.[8,9] The reactions were run in air unless otherwise indicated. ^{1}H NMR spectra were recorded on a Varian Unit 300 MHz spectrometer. ^{1}H chemical shifts were referenced to the residual solvent resonance relative to tetramethylsilane. The NMR samples were prepared in $CDCl_3$, CD_3OD, $[(CD_3)_2SO]$ and CD_3CN. Infrared spectra were recorded in the range 4000−200 cm^{-1} on a Perkin−Elmer 577 spectrometer with KBr pellets. Elemental analyses were performed on a Perkin−Elmer automatic analyser.

Methyl (2-Mercapto-3-methylimidazol-4-yl)methanoate (Simz). i. Methyl *N*-Formylsarcosinate: Triethylamine (48 mL, 0.344 mol) and formic acid (4.8 mL, 0.127 mol) were added to a solution of sarcosine methyl ester hydrochloride (16.0 g, 0.115 mol) in THF (30 mL). The suspension was stirred at 125° C overnight, cooled to room temperature, filtered, and the obtained solid rinsed with THF. The filtrate was collected and the solvent evaporated to dryness. The obtained yellow oil was dissolved in water (20 mL) and a solution of NaOH (1 N) was added dropwise until pH = 7. After extracting with CH_2Cl_2 (3 × 20 mL), the solution was dried over magnesium sulfate, filtered and concentrated to dryness. A white solid was obtained. Yield: 8.53 g (57%). ^{1}H NMR (δ, $CDCl_3$) two rotamers: 2.62 (s, 3 H, NCH_3), 2.77 (s, 3 H, NCH_3), 3.46 (s, 2 H, CH_2), 3.49 (s, 2 H, CH_2), 3.79 (s, 1 H, OCH_3), 3.82 (s, 1 H, OCH_3), 7.76 (s, 1 H, CHO), 7.83 (s, 1 H, CHO).

ii. Methyl (2-Mercapto-3-methylimidazol-4-yl)methanoate (Simz): A solution of methyl *N*-formylsarcosinate (8.52 g, 65.0 mmol) in methyl formate (14 mL, 0.227 mol) was added dropwise to a solution of sodium methoxide (4.11 g, 76.1 mmol) in distilled THF (40 mL), at 10-15° C. The resulting mixture was stirred overnight at room temperature. The solvent was removed under vacuum and the residue diluted with 150 mL MeOH/H_2O (1:1). The solution was treated with activated carbon, filtered and cooled in ice. Hydrochloric acid (12 N, 13 mL) and a solution of potassium thiocyanate (7.92 g, 81.5 mmol) in a minimum amount of water were added, and the resulting solution heated at 65°-70° C for 24 hours. The precipitate formed was removed by filtration, and the solvent was evaporated to dryness affording a white solid that corresponds to the pure product. Yield: 7.57 g (68%). ^{1}H NMR ($CDCl_3$): δ = 3.84 (s, 3 H, CH_3), 3.87 (s, 3 H, CH_3), 7.42 (s, 1 H, CH), 12.08 (br. s, 1 H, NH) ppm. ^{1}H NMR (CD_3OD): δ = 3.81 (s, 3 H, CH_3), 3.83 (s, 3 H, CH_3), 7.61 (s, 1 H, CH) ppm. ^{1}H NMR (CD_3CN): δ = 3.73 (s, 3 H, CH_3), 3.78 (s, 3 H, CH_3), 7.45 (s, 1 H, CH), 10.28 (br. s, 1 H, NH) ppm. IR (KBr): $\tilde{\nu}$ = 1715 cm^{-1} (vs, C=O), 755 cm^{-1} (m, C=S).

(2-Mercapto-3-methylimidazol-4-yl)methanoic Acid (SImzCOOH): Methyl (2-mercapto-3-methylimidazol-4-yl)methanoate (Simz) (6.00 g, 34.8 mmol) was dissolved in a NaOH solution (50 mL, 2.1 M). After 3 hours at room temperature, whilst stirring, HCl (3 N) was added dropwise until pH = 1−2. A white solid precipitated that was collected by filtration, washed with water and dried. Yield: 5.33 g (97%). ^{1}H NMR (CD_3OD): δ = 3.81 (s, 3 H, CH_3), 7.57 (s, 1 H, CH) ppm. IR (KBr): $\tilde{\nu}$ = 1670 cm^{-1} (vs, C=O), 755 cm^{-1} (m, C=S). $C_5H_6N_2O_2S$ (158.2): calcd. C 37.97, H 3.82, N 17.71, S 20.27; found C 38.13, H 4.11, N 17.55, S 20.52.

[(2-Mercapto-3-methylimidazol-4-yl)methyloxy]succinimide (SimzCOSucc): *N*-hydroxysuccinimide (0.71 g; 6.2 mmol) was added to a suspension of SimzCOOH (0.89 g; 5.6 mmol) in CH_2Cl_2 (15 mL) in an ice bath, and the mixture was stirred for 15 minutes. On addition of *N*-(3-dimethylaminopropyl)-*N*′-ethylcarbodiimidehydrochloride (1.19 g; 6.2 mmol) and after stirring for 63 hours, the reaction was complete. The solvent was evaporated to dryness, and the urea formed and the excess *N*-hydroxysuccinimide were removed by washing the residue with water. The compound was then vacuum-dried for several hours and used without further purification. Yield: 1.35 g (95%). ^{1}H NMR (CD_3OD): δ = 2.88 (s, 4 H, C_2H_2), 3.78 (s, 3 H, CH_3), 8.05 (s, 1 H, CH) ppm. ^{1}H NMR [$(CD_3)_3SO$]: δ = 2.86 (s, 4 H, C_2H_2), 3.66 (s, 3 H, CH_3), 8.34 (s, 1 H, CH), 13.21 (br. s, 1 H, NH) ppm. IR (KBr): $\tilde{\nu}$ = 1725 cm^{-1}, 1765 cm^{-1} (vs, C=O), 735 cm^{-1} (m, C=S). $C_9H_9N_3O_4S{\cdot}H_2O$ (273.3): calcd. C 39.56, H 4.06, N 15.38, S 11.73; found C 40.02, H 3.92, N 15.52, S 12.03.

Glycylglycine (2-Mercapto-3-methylimidazol-4-yl)methanamide (SimzCOGlyGly): A mixture of glycylglycine (0.25 g; 1.9 mmol) and triethylamine (0.30 mL, 2.2 mmol) in THF/H_2O 3:4 (7 mL) was added dropwise, at room temperature, to a stirred solution of SimzCOSucc (0.25 g; 0.97 mmol) in THF/DMF 1:1 (4 mL). After 20 hours, whilst stirring at room temperature, the solvent was evaporated to dryness and the white solid obtained was washed with water. Yield: 0.053 g (20%). ^{1}H NMR (CD_3OD): δ = 3.79 (s, 3 H, CH_3), 3.88 (s, 2 H, CH_2), 4.00 (s, 2 H, CH_2), 7.51 (s, 1 H, CH). ^{1}H NMR [$(CD_3)_2SO$]: δ = 3.66 (s, 3 H, CH_3), 3.75 (d, 2 H, CH_2), 3.83 (d, 2 H, CH_2), 7.58 (s, 1 H, CH), 8.23 (t, 1 H, NH), 8.60 (t, 1 H, NH), 12.55 (br. s, 1 H, NH) ppm. IR (KBr): $\tilde{\nu}$ = 3060 cm^{-1}, 3220 cm^{-1}, 3320 cm^{-1}(m, N−H), 1630 cm^{-1}, 1715 cm^{-1} (vs, C=O), 760 cm^{-1} (m, C=S). $C_9H_{12}N_4O_4S$ (272.3): calcd. C 39.70, H 4.44, N 20.58, S 11.77; found C 38.97, H 4.32, N 20.01, S 11.18.

[Re(O)(κ^3-SSS)(κ^1-Simz)] (1): A solution of **Simz** (0.071 g; 0.41 mmol) and triethylamine (68 μL, 0.49 mmol) in dichloromethane (2 mL) was added dropwise, at room temperature, to a stirred solution of [Re(O)Cl(SSS)] (0.080 g; 0.21 mmol) in the same solvent (9 mL). After several minutes the color of the solution turned brown. The mixture was refluxed under a nitrogen atmosphere for 4 hours. A brown solid was obtained after evaporation of the solvent and washing with methanol. Brown crystals suitable for X-ray diffraction analysis were obtained by slow diffusion of hexane to a solution of the complex in chloroform. Yield: 0.072 g (67%). ^{1}H NMR (CD_3CN): δ = 2.28−2.18 (m, 2 H, CH_2), 3.14−3.04 (m, 2 H, CH_2), 3.82 (s, 3 H, CH_3), 3.85 (s, 3 H, CH_3), 4.07−4.02 (m, 2 H, CH_2), 4.24−4.18 (m, 2 H, CH_2), 7.73 (s, 1 H, CH) ppm. IR (KBr): $\tilde{\nu}$ = 1715 cm^{-1}, (vs, C=O), 970 cm^{-1} (s, Re=O), 740 cm^{-1}, 760 cm^{-1}, 770 cm^{-1}. $C_{10}H_{15}N_2O_3S_4Re{\cdot}3CHCl_3$ (883.8): calcd. C 17.67, H 2.05, N 3.17 S 14.51; found C 17.52 H 1.98, N 3.08, S 14.02.

[Re(O)(κ^3-SSS)(κ^1-Simz)]·HCl (2): A suspension of Simz (0.022 g, 0.13 mmol) in CH_3CN (2 mL) was added dropwise, at room temperature, to a blue solution of [Re(O)Cl(SSS)] (0.050 g, 0.13 mmol) in the same solvent (9 mL). The violet mixture was refluxed under a nitrogen atmosphere for 4 hours. The solvent was evaporated, the crude product was washed with CH_3CN and, after drying under vacuum, analyzed by ^{1}H NMR spectroscopy. The NMR spectrum indicates a mixture of three species, two of them identified as **Simz** and [Re(O)Cl(SSS)]. Recrystallization of the crude solid from CH_3CN/hexane led to violet crystals, which were formulated as complex **2** by X-ray diffraction analysis. IR (KBr): $\tilde{\nu}$ = 1725 cm^{-1} (vs, C=O), 965 cm^{-1}(s, Re=O), 750 cm^{-1}, 760 cm^{-1}.

[Re(O)(κ^3-SSS)(κ^1-SimzCOGlyGly)] (3): A mixture of **SimzCOGlyGly** (0.029 g, 0.11 mmol) and triethylamine (18 μL, 0.13 mmol) in acetonitrile (2 mL) and a few drops of dry dimethylformamide was added dropwise, at room temperature, to a stirred solution of [Re(O)Cl(SSS)] (0.050 g, 0.13 mmol) in acetonitrile (9 mL). After several minutes the color of the solution turned brown. The reaction mixture was refluxed under a nitrogen atmosphere overnight and the solvent evaporated to dryness. The residue obtained was extracted with methanol and a brown solid was obtained after evaporation of the solvent. This compound was then washed with acetonitrile and further purified by recrystallization from methanol/dichloromethane. Yield: 0.044 g (64%). ^{1}H NMR (CD_3OD): δ = 2.32−2.22 (m, 2 H, CH_2), 3.13−3.03 (m, 2 H, CH_2), 3.89 (s, 3 H, CH_3), 3.94 (s, 2 H, CH_2), 4.05 (s, 2 H, CH_2), 4.13−4.08 (m, 2 H, CH_2), 4.26−4.20 (m, 2 H, CH_2), 7.76 (s, 1 H, CH) ppm. IR (KBr): $\tilde{\nu}$ = 1645 cm^{-1}, 1535 cm^{-1} (vs, C=O), 970 cm^{-1} (s, Re=O). $C_{13}H_{19}N_4O_5S_4Re{\cdot}2CH_2Cl_2$ (795.6): calcd. C 22.64, H 2.91, N 7.04, S 16.12; found C 22.69, H 2.64, N 7.32, S 16.35.

X-ray Crystallographic Analysis: A brown crystal of **1** was obtained by recrystallization from $CHCl_3$/hexane, and a violet crystal of **2** was obtained from CH_3CN/hexane. Both were mounted in thin-walled glass capillaries. Data were collected at room temperature on an Enraf−Nonius CAD-4 diffractometer with graphite-monochromatized Mo-K_α radiation, using a ω-20 scan mode. The crystallographic data for both complexes are summarized in Table 2. Unit cell dimensions were obtained by least-squares refinement of the setting angles of 25 reflections with $14.85<2\theta<27.28°$ for **1** and $15.30<2\theta<26.87°$ for **2**. Data were corrected for Lorentz and polarization effects, for linear decay (for **1**) and for absorption by empirical corrections based on ψ scans.[20] The heavy atom positions were located by Patterson methods using SHELXS-86.[21] The remaining atoms were located by successive different Fourier maps and refined by least-squares refinements on F^2 using SHELXL-93.[22] One $CHCl_3$ molecule of crystallization was also located in the Fourier difference map for **1**. In **2**, the atoms O(2), C(3) and C(10) are disordered over two positions rotated about the C(7)−C(9) bond, which refined with site occupancy factors of 0.69 and 0.31, respectively (in the interests of clarity only one site is shown in Figure 2). In the residual electron density of **2**, the highest peak was assumed to be an oxygen atom of a water molecule, which presents a high thermal motion. All the non-hydrogen atoms were refined with anisotropic thermal motion parameters and the contribution of the hydrogen atoms was included in calculated positions, (except the hydrogens of the water molecule in **2**). The drawings were made with ORTEP-3 and the calculations were performed on a DEC α 3000 computer.[23] CCDC-178292 (**1**) and CCDC-178293 (**2**) contain the supplementary crystallographic data for this paper. These data can be obtained free of charge at www.ccdc.cam.ac.uk/conts/retrieving.html [or from the Cambridge Crystallographic Data Centre, 12, Union Road, Cambridge CB2 1EZ, UK; Fax: (internat.) +44−1223/336−033; E-mail: deposit@ccdc.cam.ac.uk].

Acknowledgments

This work has been partially supported by POCTI/35423/QUI/99 and by COST Action B12. Elisa Palma acknowledges FCT for a BIC grant.

[1] K. P. Maresca, F. J. Femia, G. H. Bonavia, J. W. Babich, J. Zubieta, *Inorg. Chim. Acta* **2000**, *297*, 98−105.
[2] H. Spies, T. Fietz, H. J. Pietsch, B. Johannsen, P. Leibnitz, G. Reck, D. Scheller, K. Klostermann, *J. Chem. Soc., Dalton Trans.* **1995**, 2277−2280.
[3] B. A. Nock, T. Maina, D. Yannoukakos, I. C. Pirmettis, M. S. Papadopoulos, E. Chiotellis, *J. Med. Chem.* **1999**, *42*, 1066−1075.
[4] M. Friebe, H. Spies, W. Seichter, P. Leibnitz, B. Johannsen, *J. Chem. Soc., Dalton Trans.* **2000**, 2471−2475.
[5] A. Rey, I. Pirmettis, M. Pelecanou, M. Papadopoulos, C. P. Raptopoulou, L. Mallo, C. I. Stassinopoulou, A. Terzis, E. Chiotellis, A. Léon, *Inorg. Chem.* **2000**, *39*, 4211−4218.
[6] B. Nock, T. Maina, A. Tsortos, M. Pelecanou, C. P. Raptopoulou, M. Papadopoulos, H. J. Pietzsch, C. I. Stassinopoulou, A. Terzis, H. Spies, G. Nounesis, E. Chiotellis, *Inorg. Chem.* **2000**, *39*, 4433−4441.
[7] J. D. G. Correia, Â. Domingos, I. Santos, H. Spies, *J. Chem. Soc., Dalton Trans.* **2001**, 2245−2250.
[8] T. Fietz, H. Spies, H.-J. Pietzsch, P. Leibnitz, *Inorg. Chim. Acta* **1995**, *231*, 233−236.
[9] M. P. HaY, W. R. Wilson, W. A. Denny, *Tetrahedron* **2000**, *56*, 645−657.
[10] M. Santimaria, T. Maina, U. Mazzi, M. Nicolini, *Inorg. Chim. Acta* **1995**, *240*, 291−297.
[11] A. Kramer, R. Alberto, A. Egli, I. Novak-Hofer, K. Hegetschweiler, U. Abram, P. V. Bernahardt, P. A. Schubiger, *Bioconjugate Chem.* **1998**, *9*, 691−702.
[12] K. P. Maresca, F. J. Femia, G. H. Bonavia, J. W. Babich, J. Zubieta, *Inorg. Chem. Commun.* **1998**, *1*, 209−212.
[13] F. Tisato, F. Refosco, U. Mazzi, G. Bandoli, M. Nicolini, *J. Chem. Soc., Dalton Trans.* **1987**, 1693−1699.
[14] M. Pelecanou, I. C. Pirmettis, M. S. Papadopoulos, C. P. Raptopoulou, A. Terzis, E. Chiotellis, C. I. Stassinopoulou, *Inorg. Chim. Acta* **1999**, *287*, 142−151.
[15] M. S. Papadopoulos, M. Pelecanou, I. C. Pirmettis, D. M. Spyriounis, C. P. Raptopoulou, A. Terzis, C. I. Stassinopoulou, E. Chiotellis, *Inorg. Chem.* **1996**, *35*, 4478−4483.
[16] R. Syhre, S. Seifert, H. Spies, A. Gupta, B. Johannsen, *Eur. J. Nucl. Med.* **1998**, *25*, 793−796.
[17] R. Garcia, A. Paulo, Â. Domingos, I. Santos, *J. Organomet. Chem.* **2001**, *632*, 41−48.
[18] K. P. Maresca, G. H. Bonavia, J. W. Babich, J. Zubieta, *Inorg. Chim. Acta* **1999**, *284*, 252−257.
[19] A.W. Addison, T. N. Rao, J. Reedijk, J. van Rijn, G. Verschoor, *J. Chem. Soc., Dalton Trans.* **1984**, 1349−1356.
[20] C. K. Fair, *MOLEN*, Enraf−Nonius, Delft, The Netherlands, **1990**.
[21] G. M. Sheldrick, *SHELXS-86*, *Program for the solution of Crystal Structure*s, University of Göttingen, Germany, **1986**.
[22] G. M. Sheldrick, *SHELXL-93*, *Program for the refinement of crystal structures*, University of Göttingen, Germany, **1993**.
[23] L. Farrugia, *J. Appl. Crystallogr.* **1997**, *32*, 837−838.

Received January 31, 2002
[I02053]

Synthesis and Late Transition Metal Complexes of the Heterofunctional Phosphane *o*-$Ph_2PNHC_6H_4P(S)Ph_2$

Stephen M. Aucott,[a] Alexandra M. Z. Slawin,[a] and J. Derek Woollins*[a]

Keywords: Phosphorus−sulfur ligands / Monodentate complexes / Chelate complexes

The difunctional ligand *o*-$Ph_2PNHC_6H_4P(S)Ph_2$ (PS) has been prepared by treatment of the lithium amide salt of 2-(diphenylthiophosphanyl)aniline {2-$[Ph_2P(S)]C_6H_4NH_2$} with Ph_2PCl. The new ligand was oxidised to give the mixed chalcogen species $Ph_2P(E)NHC_6H_4P(S)Ph_2$, by treatment with H_2O_2 (where E = O) or aerial oxidation by recrystallisation from MeOH, and by reaction with Se_8 (where E = Se) in warm toluene. The complexes [M(Cl)(η^3-C_3H_5)(PS)] (M = Pt or Pd), *cis*-[$PtCl_2$(PS)(PMe_2Ph)], [(AuCl)(PS)], *cis*-[$MCl_2(PS)_2$] (M = Pt or Pd), *cis*-[$PtMe_2(PS)_2$] and *trans*-[PtMeCl$(PS)_2$] have been synthesised by reaction of either [Pt(μ-Cl)(μ-η^2:η^1-C_3H_5)]$_4$, [Pd(μ-Cl)(η^3-C_3H_5)]$_2$, [{PtCl(μ-Cl)(PMe_2Ph)}$_2$], [AuCl(tht)] (tht = tetrahydrothiophene), [$PdCl_2$(cod)] or [PtX_2(cod)] (X = Me or Cl; cod = cycloocta-1,5-diene) with (PS). In all these complexes the ligand (PS) is monodentate *P*-bound. Chloride abstraction from [M(Cl)(η^3-C_3H_5)(PS)] (M = Pt or Pd), *cis*-[$PtCl_2$(PS)(PMe_2Ph)], *cis*-[$PtCl_2(PS)_2$] and *trans*-[PtMeCl$(PS)_2$], using Ag[ClO_4], gave the monocationic [M(η^3-C_3H_5)(PS)][ClO_4] (M = Pt or Pd), *cis*-[PtCl(PS)(PMe_2Ph)][ClO_4], *trans*-[PtMe$(PS)_2$][ClO_4] or dicationic [$Pt(PS)_2$][ClO_4]$_2$ compounds in which the ligand (PS) is κ^2-*P*,*S*-bound. All compounds described here have been characterised by a combination of $^{31}P\{^1H\}$ and ^1H NMR spectroscopy, microanalyses, FAB mass spectrometry and IR spectroscopy. The molecular structures of [AuCl($Ph_2PNHC_6H_4P$-$(S)Ph_2$-*P*)] in which there is an intramolecular hydrogen-bonding interaction between the amine proton and the sulfur atom of the thiophosphoryl group and *trans*-[$Pt(Ph_2PNHC_6H_4P(S)Ph_2$-κ^2-*P*,*S*)$_2$][ClO_4]$_2$·CH_2Cl_2·$2H_2O$ in which the perchlorate counterions are associated by hydrogen-bonding interactions to the amine protons of the κ^2-*P*,*S* ligands have been determined by single-crystal X-ray diffraction.

(© Wiley-VCH Verlag GmbH, 69451 Weinheim, Germany, 2002)

Introduction

There are numerous examples in the literature of ligands containing both phosphorus and sulfur donor atoms. Meek and co-workers described the preparation of [*o*-(methylthio)phenyl]diphenylphosphane[1] − a ligand with an aromatic backbone which chelates to form five-membered C_2PSM rings.[1,2] Rigo and Bressan prepared a series of P−S donor ligands ($Ph_2PCH_2CH_2SR$) (R = Me, Et and Ph) by the addition of the appropriate chloro derivative $RS(CH_2)_2Cl$ to sodium diphenylphosphide in liquid ammonia.[3] The methylene-bridged ligand Ph_2PCH_2SMe was found to exhibit both monodentate *P*-bound and bidentate bridging coordination modes.[4,5] Other phosphane−thioether-based ligands have also been explored[6−9] as have phosphane−thiolate,[10−13] phosphane−thioformamide,[14] phosphane−thiophene,[15−17] phosphane−sulfoxide,[18] phosphane−sulfide[19−21] and phosphane−aminophosphane−sulfide ligands including $Ph_2PNHP(S)Ph_2$,[22] $Ph_2PNPhP(S)Ph_2$,[23] in addition to the methylene-, ethylene-, and −$[CH_2]_3$−backboned bis(phosphane−monosulfides) $Ph_2PCH_2P(S)Ph_2$,[24,25] $Ph_2PCH_2CH_2P(S)Ph_2$,[25] and $Ph_2PCH_2CH_2CH_2P(S)Ph_2$,[26] respectively. A logical extension to investigations into the reactivity of $Ph_2PNHC_6H_4PPh_2$ [27,28] is the chemistry of the monochalcogens $Ph_2P(E)NHC_6H_4PPh_2$ or $Ph_2PNHC_6H_4P(E)Ph_2$ (E = O, S or Se). We anticipated that these molecules would exhibit a variety of coordination modes, notably as monodentate phosphorus donors and as bidentate phosphorus−chalcogen donor ligands resulting in the formation of seven-membered metallacycles. The nitrogen atom presents a further site to be explored if deprotonation is possible. To further understand the chemistry of these molecules we have synthesised $Ph_2PNHC_6H_4P(S)Ph_2$ and investigated its reactivity towards Au^I, Pt^{II}, and Pd^{II}. In addition, we have prepared the mixed chalcogen compounds $Ph_2P(O)NHC_6H_4P(S)Ph_2$ and $Ph_2P(Se)NHC_6H_4P(S)Ph_2$.

[a] School of Chemistry, University of St Andrews, St Andrews, Fife, Scotland KY16 9ST, UK
Fax: (internat.) + 44-1334/4633784
E-mail: jdw3@st-and.ac.uk

Results and Discussion

Preparation and Characterisation of $Ph_2PNHC_6H_4P(S)Ph_2$

Treatment of 2-[diphenyl(thio)phosphanyl]aniline with *n*BuLi, at −78 °C in diethyl ether, followed by reaction with Ph_2PCl, gave **1** in good to excellent yields (71−85%) [Equation (1)].

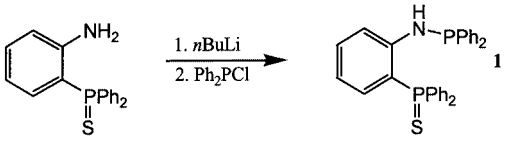

(1)

Attempted preparation of the oxo and seleno analogues $Ph_2PNHC_6H_4P(E)Ph_2$ (E = O, Se) under the same conditions resulted in re-isolation of the $Ph_2P(O)C_6H_4NH_2$ starting material and the formation of a complex mixture, respectively. Since the synthesis of the oxo and seleno ligands by the addition of Ph_2PCl to the lithium salt of the appropriate aniline proved unsuccessful, an alternative synthesis was sought. A second possible route to monochalcogen compounds of $Ph_2PNHC_6H_4PPh_2$ is by selective oxidation. This route has been applied to the synthesis of $Ph_2PNHP(E)Ph_2$ (E = O, S and Se).[22,29] A series of experiments involving the reaction of $Ph_2PNHC_6H_4PPh_2$ [27] with a slightly less than stoichiometric quantity of the appropriate chalcogen or aqueous H_2O_2 in various solvent systems at 0 °C gave poor results. These reactions usually resulted in the precipitation of the dichalcogen compounds $Ph_2P(E)NHC_6H_4P(E)Ph_2$,[28] while lesser amounts of starting material and both mixed P^{III},P^{V} species $Ph_2P(E)NHC_6H_4PPh_2$ and $Ph_2PNHC_6H_4P(E)Ph_2$ remain in solution. Separation of these mixtures was not attempted. $Ph_2PNHC_6H_4P(S)Ph_2$ (**1**) was isolated as a colourless solid and displays similar solubilities and the same sensitivity to air or light as $Ph_2PNHC_6H_4PPh_2$. The $^{31}P\{^1H\}$ NMR spectrum (in $CDCl_3$) of **1** displays two single resonances at $\delta(P_A) = 28.2$ ppm and $\delta(P_X) = 39.6$ ppm {the starting material 2-[diphenyl(thio)phosphanyl]aniline has $\delta(P) = 39.6$ ppm} for the $-NHPPh_2$ and $-P(S)Ph_2$ groups, respectively; the $^4J(^{31}P_A\text{-}^{31}P_X)$ coupling was not resolved. The ^1H NMR spectrum (in $CDCl_3$) showed the amine proton as a doublet at $\delta(H) = 5.68$ ppm [$^2J(^{31}P\text{-}^1H) = 9$ Hz]. From the IR spectrum we can identify ν(N−H), ν(P−N) and ν(P=S) at $\tilde{\nu} = 3223$, 896 and 634 cm^{-1}, respectively. Microanalytical data were within specified limits and the positive-ion FAB mass spectrum gave the expected parent-ion peak at $m/z = 494$ with appropriate isotope distribution and fragmentation patterns.

Synthesis of $Ph_2P(E)NHC_6H_4P(S)Ph_2$

The syntheses of the mixed chalcogen species are straightforward (Scheme 1). The mixed sulfur,oxygen species $Ph_2P(O)NHC_6H_4P(S)Ph_2$ (**2**) is prepared in 90% yield by the dropwise addition of aqueous hydrogen peroxide to a THF solution of **1**. The sulfur,oxygen species **2** was also isolated after recrystallisation in air of **1** from MeOH (59%) Warming **1** with a stoichiometric amount of elemental selenium in toluene at 60 °C followed by filtration of the warm solution, concentration and storage at below 0 °C gives the mixed S,Se species $Ph_2P(Se)NHC_6H_4P(S)Ph_2$ (**3**) in good yield (85%). Synthesis and characterisation of the disulfide has been reported elsewhere.[28] The mixed chalcogen species **2** and **3** are air- and moisture-tolerant colourless solids and in common with **1** display two sharp single resonances in their $^{31}P\{^1H\}$ NMR spectra (Table 1) with no observable $^4J(^{31}P_A\text{-}^{31}P_X)$ couplings in addition to amine proton resonances as broad doublets at $\delta(H) = 8.66$ ppm [$^2J(^{31}P\text{-}^1H) = 10$ Hz] (**2**) and $\delta(H) = 8.34$ ppm [$^2J(^{31}P\text{-}^1H) = 8$ Hz] (**3**). The infrared spectra of compounds **1** and **2** are consistent with the proposed structures and show bands attributable to ν(P=O) at $\tilde{\nu} = 1212$ cm^{-1} (**2**) and ν(P=Se) at $\tilde{\nu} = 548$ cm^{-1} (**3**) as well as the anticipated ν(N−H), ν(P−N) and ν(P=S) bands (see Exp. Sect.).

Monodentate Coordination Chemistry of $Ph_2PNHC_6H_4P(S)Ph_2$

Treatment of suspensions of the di- and tetranuclear species $[Pd(\mu\text{-}Cl)(\eta^3\text{-}C_3H_5)]_2$ and $[Pt(\mu\text{-}Cl)(\mu\text{-}\eta^2\text{:}\eta^1\text{-}C_3H_5)]_4$ (in toluene and THF, respectively) with **1**, results in bridge cleavage to give the mononuclear complexes $[MCl(\eta^3\text{-}C_3H_5)(Ph_2PNHC_6H_4P(S)Ph_2\text{-}P)]$ [where M = Pd (**4**) (83%) or Pt (**5**) (88%)] (Scheme 1). The $^{31}P\{^1H\}$ NMR ($CDCl_3$) spectra of **4** and **5** show the $-NHPPh_2$ resonances at $\delta(P) = 55.3$ (**4**) and 51.0 ppm [$^1J(^{195}Pt\text{-}^{31}P)$ 4946 Hz] (**5**) and the pendent $-P(S)Ph_2$ group resonances at $\delta(P) = 39.8$ (**4**) and 39.9 ppm (**5**) which are similar to that of the "free" ligand. The unsymmetrical mixed-ligand complex *cis*-$[PtCl_2\{Ph_2PNHC_6H_4P(S)Ph_2\text{-}P\}(PMe_2Ph)]$ (**6**) was prepared by chloride bridge cleavage of the platinum(II) dimer $[\{PtCl(\mu\text{-}Cl)(PMe_2Ph)\}_2]$ with **1** in CH_2Cl_2 (Scheme 1). The $^{31}P\{^1H\}$ NMR ($CDCl_3$) spectrum of **6** reveals a small phosphorus-phosphorus coupling constant (18 Hz), indicative of a structure with a *cis* arrangement of monodentate phosphane ligands. Two of the three unique phosphorus environments display large Pt-P couplings $\delta(P) = -16.3$ ppm [$^1J(^{195}Pt\text{-}^{31}P) = 3436$ Hz] assigned to the PMe_2Ph group and $\delta(P) = 32.6$ ppm [$^1J(^{195}Pt\text{-}^{31}P) = 4100$ Hz] to the $-NHPPh_2$ group of **1**. Furthermore, the chemical shift of the pendent $-P(S)Ph_2$ group [$\delta(P) = 39.4$ ppm] is similar to that observed for **1** and displays no platinum satellites indicating no interaction of the $-P(S)Ph_2$ moiety with the platinum centre. Evidence in support of the structural assignment of **6** is found in the IR spectrum showing two distinct ν(Pt−Cl) stretches at $\tilde{\nu} = 317$ and 291 cm^{-1} consistent with *cis*-$PtCl_2$ geometry. The reaction between $[\{PtCl(\mu\text{-}Cl)(PMe_2Ph)\}_2]$ and **1** was found to be somewhat sensitive to the reaction conditions as out of a total of five subsequent preparations of **6**, twice we found the isolated material to consist of an approximate 1:1 mixture of *cis* and *trans* isomers. Examination of the $^{31}P\{^1H\}$ NMR spectrum (in $CDCl_3$) of the isolated product showed the resonances of **6** and additional lines which display a large $^2J(^{31}P\text{-}^{31}P)$ coupling constant of 535 Hz indicative of a structure with a *trans* arrangement of phosphane ligands. As expected, two of the three distinct phosphorus environments display $^1J(^{195}Pt\text{-}^{31}P)$ couplings that are characteristically smaller than those previously observed for the *cis* isomer **6**. The doublet centred at $\delta(P) = -6.9$ ppm [$^1J(^{195}Pt\text{-}^{31}P) = 2531$ Hz] is assigned to the coordinated PMe_2Ph group and the doublet at $\delta(P) = 46.1$ ppm [$^1J(^{195}Pt\text{-}^{31}P) = 2715$ Hz]

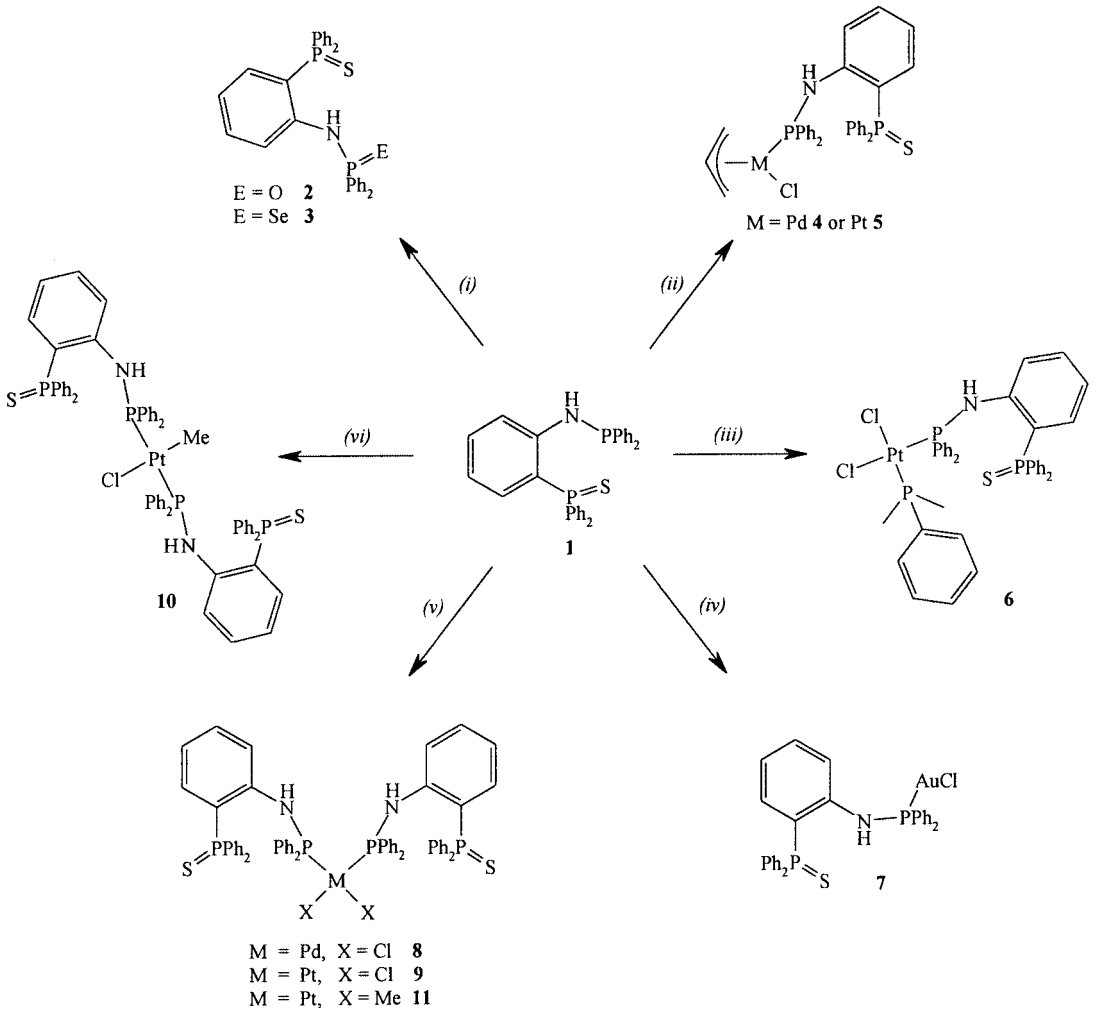

Scheme 1. *(i)* H_2O_2(aq), THF or Se_8, C_6H_5Me, 60 °C; *(ii)* $[Pd(\mu\text{-}Cl)(\eta^3\text{-}C_3H_5)]_2$, C_6H_5Me or $[Pt(\mu\text{-}Cl)(\mu\text{-}\eta^2\text{:}\eta^1\text{-}C_3H_5)]_4$, THF; *(iii)* $[\{PtCl(\mu\text{-}Cl)(PMe_2Ph)\}_2]$, CH_2Cl_2; *(iv)* [AuCl(tht)], CH_2Cl_2; *(v)* $[MX_2(cod)]$ (M = Pt, X = Cl or Me; M = Pd, X = Cl), CH_2Cl_2; *(vi)* [PtClMe(cod)], CH_2Cl_2

Table 1. Selected bond lengths [Å] and angles [°] for $[AuCl(Ph_2PNHC_6H_4P(S)Ph_2\text{-}P)]$ (**7**)

P(2)−S(2)	1.971(2)	P(2)−C(2)	1.826(5)
C(2)−C(1)	1.409(7)	C(1)−N(1)	1.408(6)
N(1)−P(1)	1.685(4)	P(1)−Au(1)	2.237(2)
Au(1)−Cl(1)	2.269(2)		
S(2)−P(2)−C(2)	114.20(2)	P(2)−C(2)−C(1)	120.00(4)
C(2)−C(1)−N(1)	120.00(4)	C(1)−N(1)−P(1)	126.30(4)
N(1)−P(1)−Au(1)	155.20(2)	P(1)−Au(1)−Cl(1)	177.40(7)

to the coordinated $-NHPPh_2$ group of **1**. The single resonance at δ(P) = 41.5 ppm is assigned to the pendent $-P(S)Ph_2$ group and, although at slightly higher frequency than those observed for either **1** or **6**, remains uncoordinated, as indicated by the absence of platinum satellites. A number of literature studies have focused upon the solution *cis*/*trans* isomerism of platinum complexes of the type $[PtX_2(PR_3)_2]$ (where X = Cl, Br, or I and R = alkyl or aryl groups) and showed, in the main, that the kinetic *cis* isomer was rapidly converted into the thermodynamic *trans* isomer by the addition of a catalytic amount of PR_3.[29−32] We found that the addition of a small quantity (ca. 3−5 mg) of **1** to a dichloromethane solution of the *cis*/*trans* mixture resulted in isomerisation of the *trans* species to give pure *cis* isomer **6** (by $^{31}P\{^1H\}$ NMR). We have previously employed this technique to convert *trans*-$[PtCl_2(HL)(PMe_2Ph)]$ to *cis*-$[PtCl_2(HL)(PMe_2Ph)]$ [where HL = $Ph_2PNHP(O)Ph_2$].[33] In the absence of added **1** the composition of a CD_2Cl_2 solution of the *cis*/*trans* mixture remained unchanged after storage for up to six weeks at ambient temperature. Preparation of the pure *trans* isomer was not pursued. Compound **1** reacts cleanly with [AuCl(tht)] in CH_2Cl_2 by displacement of the tht molecule to give $[AuCl\{Ph_2PNHC_6H_4P(S)Ph_2\text{-}P\}]$ (**7**) (Scheme 1) as a colourless solid in 83% yield. The complex is slightly sensitive to light when in solution and a grey solid was deposited, presumably gold metal, after only moderate exposure. The ^{31}P NMR spectrum (in $CDCl_3$) shows two single lines at δ(P) = 40.1 and 58.2 ppm assigned to the $-P(S)Ph_2$ group and the gold-coordinated $-NHPPh_2$ group, respectively. Upon coordination, the signal of the phosphorus(III) centre

is shifted to higher frequency by 30 ppm relative to the that of the "free" ligand. The IR spectrum (KBr) of **7** shows that the ν(N−H) band at $\tilde{\nu}$ = 3109 cm^{-1} has undergone a large shift to lower frequency compared to that of **1** [ν(N−H) at $\tilde{\nu}$ = 3223 cm^{-1}] which suggests that the amine proton may be involved in intra/intermolecular hydrogen bonding. Crystals of X-ray quality were grown by layering a CH_2Cl_2 solution of **7** with diethyl ether. The crystal structure of [AuCl{$Ph_2PNHC_6H_4P(S)Ph_2$-*P*}] (**7**) along with selected bond lengths and angles (Table 1) is shown in Figure 1 and reveals an intramolecular hydrogen-bonding interaction between the S(2) atom and the amine hydrogen atom H(1n) of N(1) [H(1n)···S(2) 2.36 Å, S(2)···N(1) 3.25 Å, N(1)−H(1n)···S(2) 158°], corroborating the IR evidence. The molecule has a near planar P(2)−C(2)−C(1)−N(1)−P(1) backbone [maximum deviation from the mean plane 0.1 Å for P(1)]. The P(1)−Au(1)−Cl(1) angle is approximately linear [177.40(7)°] and is "*anti*" with respect to the amine proton H(1n) which appears to be a consequence of the previously discussed hydrogen-bonding interaction. The addition of 2 equiv. of **1** to a CH_2Cl_2 solution of [$PdCl_2$(cod)] gave a pale-yellow precipitate after only 5 min of stirring. The product, characterised as *cis*-[$PdCl_2${$Ph_2PNHC_6H_4P(S)Ph_2$-*P*}$_2$] (**8**), was recovered in near quantitative yield (97%). The extreme insolubility of this material in all common organic solvents prevented measurement of its $^{31}P\{^1H\}$, ^1H NMR and mass spectra. Structural and geometrical assignments therefore, are based solely on microanalytical and IR data, the former was in excellent agreement with the proposed formulation, the latter showing two bands at $\tilde{\nu}$ = 318 and 298 cm^{-1} for ν(Pd−Cl), consistent with *cis*-$PdCl_2$ geometry. The ν(NH) stretch at $\tilde{\nu}$ = 3106 cm^{-1} like that of [AuCl{$Ph_2PNHC_6H_4P(S)Ph_2$-*P*}] (**7**) occurs at a much lower frequency than in the "free" ligand [ν(NH) at $\tilde{\nu}$ = 3223 cm^{-1}]. This suggests that the amine protons of *cis*-[$PdCl_2${$Ph_2PNHC_6H_4P(S)Ph_2$-*P*}$_2$] (**8**) are involved in hydrogen-bonding interactions similar to those observed in complex **7**, which may account for the insolubility of **8**. In contrast, the preparation of the platinum analogue *cis*-[$PtCl_2${$Ph_2PNHC_6H_4P(S)Ph_2$-*P*}$_2$] (**9**) under the same reaction conditions gave a pale-yellow solution that showed no sign of precipitation even after prolonged stirring. The product was precipitated by the addition of diethyl ether and isolated after recrystallisation from CH_2Cl_2/diethyl ether as a colourless solid in 88% yield (Scheme 1). Once dry, **9** displayed limited solubility in $CHCl_3$ but was readily soluble in CH_2Cl_2. The $^{31}P\{^1H\}$ NMR spectrum (in CD_2Cl_2) of *cis*-[$PtCl_2${$Ph_2PNHC_6H_4P(S)Ph_2$-*P*}$_2$] showed two distinct phosphorus environments at δ(P) = 37.6 ppm [$^1J(^{195}Pt\text{-}^{31}P)$ = 4103] and δ(P) = 40.6 ppm, corresponding to the coordinated phosphorus(III) centres and the "dangling" phosphorus(V) moieties, respectively. The large $^1J(^{195}Pt\text{-}^{31}P_A)$ coupling constant of 4103 Hz is in good agreement with a *cis* disposition of ligands (i.e. P *trans* to Cl). In addition, no platinum satellites were observed for the uncoordinated phosphorus(V) groups, also, the chemical shift of the pendent $-P(S)Ph_2$ group is similar to that found in **1** [δ(P) = 39.6 ppm] implying no interaction with the metal centre. The $^{31}P\{^1H\}$ NMR spectrum of **9** also showed that the isolated product (from three separate syntheses) was consistently contaminated with an impurity (ca. 4−5%) observed as two singlets at δ(P) = 40.2 and 40.8 ppm thought to be *trans*-[$PtCl_2${$Ph_2PNHC_6H_4P(S)Ph_2$-*P*}$_2$]; positive assignment of the impurity resonances to the appropriate phosphorus(III) and -(V) centres is impossible as no obvious platinum satellites were observed for either peak. Further evidence in support of the neutral nonchelating *cis* structure comes from the IR spectrum (KBr) which shows two ν(Pt−Cl) stretches at $\tilde{\nu}$ = 311 and 290 cm^{-1}, consistent with a *cis*-$PtCl_2$ geometry. The 2:1 molar ratio reaction of **1** with a CH_2Cl_2 solution of [PtClMe(cod)] results in the deposition of a colourless solid and near-quantitative recovery (98%) of the surprisingly insoluble complex *trans*-[PtClMe{$Ph_2PNHC_6H_4P(S)Ph_2$-*P*}$_2$] (**10**). As for **8**, the insolubility of **10** in common organic solvents prevents measurement of its NMR or mass spectra, hence only infrared and microanalytical data are available. Elemental analysis confirms that the isolated material has been correctly formulated as [PtMeCl{$Ph_2PNHC_6H_4P(S)Ph_2$}$_2$]. The assignment of *trans* geometry to complex **10** is based purely upon the product obtained, **15**, using **10** as starting material (see below). Reaction of 2 equiv. of **1** with [$PtMe_2$(cod)] in CH_2Cl_2 produces an off-white powder, characterised as the dimethyl derivative *cis*-[$PtMe_2${$Ph_2PNHC_6H_4P(S)Ph_2$-*P*}$_2$] (**11**), as is evident from the $^{31}P\{^1H\}$ NMR spectrum (in $CDCl_3$) where the much smaller $^1J(^{195}Pt\text{-}^{31}P)$ coupling constant of 2059 Hz is concordant with *cis* (P *trans* to CH_3) geometry. The coordinated $-NHPPh_2$ and "dangling" $-P(S)Ph_2$ group resonances occur at δ(P) = 55.3 and 39.6 ppm, respectively. The ^1H NMR ($CDCl_3$) spectrum displays the amine protons as a broad multiplet at δ(H) = 8.1 ppm and the $PtMe_2$ moiety at δ(H) = 0.20 ppm as a double doublet, flanked by ^{195}Pt satellites [$^2J(^{195}Pt\text{-}^1H)$ = 72 Hz]. In all of the above complexes (**4**−**11**) the IR spectra (KBr) provide additional evidence of coordination through P only showing strong ν(P=S) absorption at $\tilde{\nu} \approx$ 632−634 cm^{-1} ["free" ligand ν(P=S) at $\tilde{\nu}$ = 634 cm^{-1}] which is characteristic of no interaction between the $-P(S)Ph_2$ group and the metal centre.

Bidentate Coordination Chemistry of $Ph_2PNHC_6H_4P(S)Ph_2$

We have previously reported that chelation of the potentially bidentate mixed P^{III},P^V P,O ligand $Ph_2PNHP(O)Ph_2$[34] the P,N ligand Ph_2PNHpy,[35] and the unsymmetric P,P′ ligand $Ph_2PNHC_6H_4PPh_2$[27] can be induced by the use of halide abstractors such as $Ag[BF_4]$ and $Ag[ClO_4]$ in CH_2Cl_2. This preparative technique has been extended with good results to bring about the chelation of monodentate $Ph_2PNHC_6H_4P(S)Ph_2$ (**1**) resulting in the formation of cationic species containing seven-membered P−N−C−C−P−S−M rings. Smooth conversion of the neutral (allyl)Pd^{II} (**4**) and -Pt^{II} (**5**) complexes to the cationic "ring-closed" complexes [Pd(η^3-C_3H_5){$Ph_2PNHC_6H_4P(S)Ph_2$-κ^2-*P*,*S*}][ClO_4] (**12**) and [Pt(η^3-C_3H_5)-

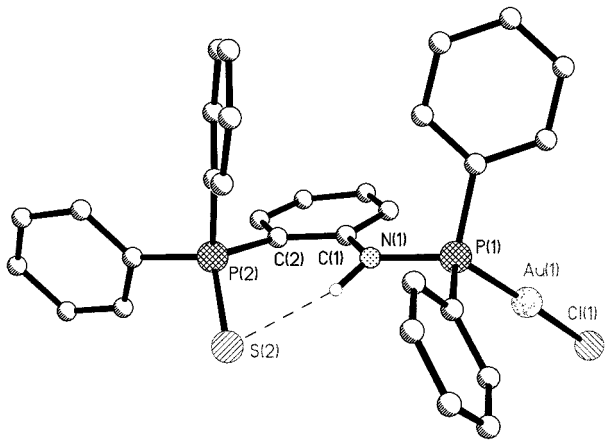

Figure 1. Crystal structure of [AuCl($Ph_2PNHC_6H_4P(S)Ph_2$-*P*)] (**7**)

{$Ph_2PNHC_6H_4P(S)Ph_2$-κ^2-*P*,*S*}][ClO_4] (**13**) [Equation (2)] was achieved by the addition of a small excess of Ag[ClO_4] to CH_2Cl_2 solutions of **3** and **4**.

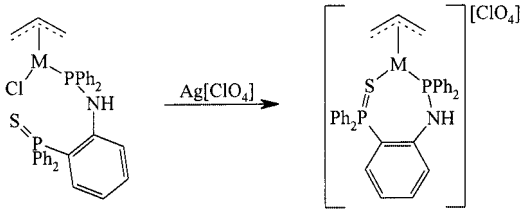

(2)

The products **12** and **13** were isolated in excellent yields (92 and 95%, respectively) as cream-coloured solids. The $^{31}P\{^1H\}$ NMR spectra for complexes **12** and **13** are of the AX type and show two sharp doublets at δ(P^{III}) = 69.5 ppm and δ(P^V) = 46.4 ppm for **12** and δ(P^{III}) = 58.3 ppm and δ(P^V) = 45.6 ppm for **13** which occur at higher frequency than their monodentate *P*-bound parent compounds. Indicative of chelating ligand behaviour are the small $^2J(P^{III}\text{-}P^V)$ couplings of 16 (**12**) and 13 Hz (**13**), the corresponding platinum satellites for compound **13** are particularly diagnostic and show a large $^1J(^{195}Pt\text{-}P^{III})$ coupling of 4720 Hz and a much smaller $^2J(^{195}Pt\text{-}P^V)$ coupling of 123 Hz. The complexes *cis*-[PtCl{$Ph_2PNHC_6H_4P(S)Ph_2$-κ^2-*P*,*S*}(PMe_2Ph)][ClO_4] (**14**) and *trans*-[PtMe{$Ph_2PNHC_6H_4P(S)Ph_2$-*P*}{$Ph_2PNHC_6H_4P(S)Ph_2$-κ^2-*P*,*S*}][ClO_4] (**15**) were prepared from *cis*-[$PtCl_2$\{$Ph_2PNHC_6H_4P(S)Ph_2$-*P*\}(PMe_2Ph)] (**6**) and *trans*-[PtMeCl{$Ph_2PNHC_6H_4P(S)Ph_2$-*P*}$_2$] (**10**) in an identical manner to complexes **12** and **13** [Equations (3) and (4), respectively).

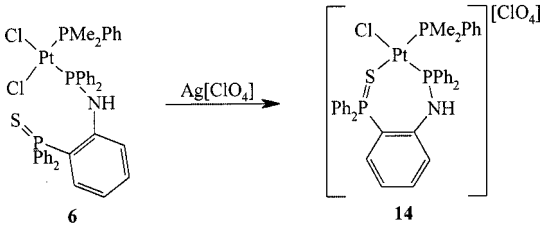

(3)

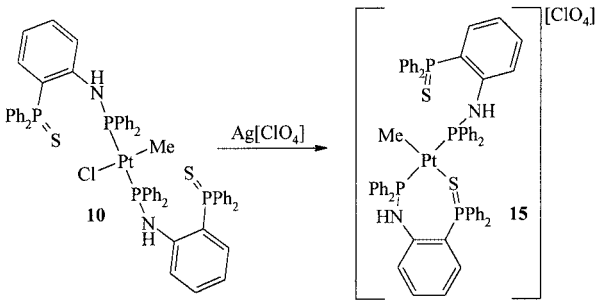

(4)

Both compounds were precipitated by the addition of diethyl ether and isolated as cream-coloured or colourless solids in 95 (**14**) and 82% (**15**) yields and are readily soluble in CH_2Cl_2 and MeOH but less so in $CHCl_3$. The $^{31}P\{^1H\}$ NMR spectrum of **14** reveals a small $^2J(^{31}P\text{-}^{31}P)$ coupling of 15 Hz, confirming that *cis* geometry was retained upon chelation. The low-frequency double doublet at δ(P) = −4.4 ppm [$^1J(^{195}Pt\text{-}^{31}P)$ = 3390 Hz] is assigned to the PMe_2Ph ligand and displays two P-P couplings, the previously mentioned $^2J(^{31}P\text{-}^{31}P)$ *cis* coupling and a $^3J(^{31}P\text{-}^{31}P)$ *trans* coupling of 9 Hz. The −$NHPPh_2$ group P resonance appears as a doublet at δ(P) = 40.5 ppm [$^1J(^{195}Pt\text{-}^{31}P)$ = 3821 Hz] and displays only the *cis* $^2J(^{31}P\text{-}^{31}P)$ coupling. The high-frequency resonance at δ(P) = 43.6 ppm appears as a doublet and is assigned to the coordinated −$P(S)Ph_2$ group by virtue of the small $^2J(^{195}Pt\text{-}^{31}P)$ coupling of 47 Hz. The $^{31}P\{^1H\}$ NMR spectrum (in CD_2Cl_2) of **15** shows four unique phosphorus environments. The first resonance at δ(P) = 43.1 ppm, assigned to the pendant −$P(S)Ph_2$ group, appears as a singlet with no platinum satellites which is consistent with noncoordinating behaviour. The double doublet resonance at δ(P) = 44.7 ppm, assigned to the coordinated −$P(S)Ph_2$ group of the chelating ligand, shows two distinct $^3J(^{31}P\text{-}^{31}P)$ couplings of 3 and 11 Hz in addition to platinum satellites with a small $^2J(^{195}Pt\text{-}^{31}P)$ coupling of 70 Hz. The doublet at δ(P) = 59.2 ppm, assigned to the −$NHPPh_2$ group of the nonchelating ligand, is coupled to the coordinated P^V centre [$^3J(^{31}P\text{-}^{31}P)$ = 11 Hz] and displays a small $^1J(^{195}Pt\text{-}^{31}P)$ coupling of 3192 Hz which is characteristic of mutual *trans* phosphane geometry. The high-frequency resonance at δ(P) = 64.4 ppm is assigned to the −$NHPPh_2$ group of the chelating ligand as chelation has previously been observed to cause a shift to higher frequency in both the P^{III} and P^V centres, cf. the conversions of [$MCl(\eta^3\text{-}C_3H_5)$\{$Ph_2PNHC_6H_4P(S)Ph_2$-*P*\}] [where M = Pd (**4**) or Pt (**5**)] to [$M(\eta^3\text{-}C_3H_5)$\{$Ph_2PNHC_6H_4P(S)Ph_2$-κ^2-*P*,*S*\}][ClO_4] [where M = Pd (**12**) or Pt (**13**)]. The phosphorus atom of this group is *cis*-coupled to the coordinated −$P(S)Ph_2$ group as suggested by the small $^3J(^{31}P\text{-}^{31}P)$ *cis* coupling of 3 Hz. The $^1J(^{195}Pt\text{-}^{31}P)$ coupling of 3225 Hz is also consistent with *trans* geometry as is the absence of any typically small (ca. 2000 Hz) phosphorus *trans* to methyl couplings. Contrary to expectation there is no resolvable *trans* $^2J(^{31}P\text{-}^{31}P)$ coupling, which we would expect to be of the order of ca. 500 Hz in magnitude. ($^{31}P\text{-}^{31}P$) COSY ex-

periments and re-recording of the spectrum at higher field do not shed any light on this anomaly. It is also worth noting the absence of $^2J(^{31}P\text{-}^{31}P)$ *trans* coupling between the two coordinated chemically inequivalent $-NHPPh_2$ groups. The ^1H NMR spectrum of **15** (in CD_2Cl_2) is consistent with the proposed structure and shows two multiplets at δ(H) = 8.62 ppm [$^3J(^{195}Pt\text{-}^1H)$ = 34 Hz] and δ(H) = 5.78 ppm [$^3J(^{195}Pt\text{-}^1H)$ = 54 Hz], assigned to the *P*-bound and the κ^2-*P*,*S*-bound ligand amine protons, respectively, with platinum satellites. The expected Pt−Me proton resonance appears as a broad pseudotriplet at δ(H) = −0.20 ppm with typical $^2J(^{195}Pt\text{-}^1H)$ and $^3J(^{31}P\text{-}^1H)$ couplings of 76 and 15 Hz, respectively. The IR spectrum is diagnostic and shows two ν(N−H) bands at $\tilde{\nu}$ = 3190 and 3144 cm^{-1} and two ν(P=S) bands at $\tilde{\nu}$ = 632 and 622 cm^{-1}, corresponding to pendant and coordinated $-P(S)Ph_2$ groups, respectively. In addition, the ν(P−N) band at $\tilde{\nu}$ = 916 cm^{-1} shows a prominent shoulder at $\tilde{\nu}$ = 925 cm^{-1} which is also compatible with two ligand environments. Treatment of *cis*-[$PtCl_2$\{$Ph_2PNHC_6H_4P(S)Ph_2$-*P*\}$_2$] (**9**) with 2 equiv. of $Ag[ClO_4]$ in CH_2Cl_2 resulted in abstraction of both chloride ligands and the formation of the dicationic bis(chelate) species *cis*-[Pt\{$Ph_2PNHC_6H_4P(S)Ph_2$-κ^2-*P*,*S*\}$_2$][ClO_4]$_2$ (**16**) isolated as an off-white microcrystalline solid in 88% yield. The isolated product, despite repeated recrystallisation, was consistently contaminated with an impurity (ca. 5%), observed as two triplets in the $^{31}P\{^1H\}$ NMR spectrum at δ(P) = 42.9 and 55.3 ppm [$^1J(^{195}Pt\text{-}^{31}P)$ = 2596 Hz], which was thought to be the *trans* isomer of **16**, formed from the suspected *trans*-[$PtCl_2$\{$Ph_2PNHC_6H_4P(S)Ph_2$-*P*\}$_2$] impurity in **9**. The complex is readily soluble in CH_2Cl_2 and MeOH but sparingly so in $CHCl_3$. The ^{31}P NMR spectrum (in CD_2Cl_2) of the platinum complex **16** shows two sets of resonances at δ(P) = 48.8 ppm [$^1J(^{195}Pt\text{-}^{31}P_X)$ = 3649 Hz] and δ(P) = 45.3 ppm [$^2J(^{195}Pt\text{-}^{31}P_A)$ = 38 Hz], corresponding to the coordinated phosphorus(III) and phosphorus(V) groups, respectively. Once again, chelation results in a shift of signals in both phosphorus environments to higher frequency relative to those of the neutral species *cis*-[$PtCl_2$\{$Ph_2PNHC_6H_4P(S)Ph_2$-*P*\}$_2$] (**9**) [$\delta(P^{III})$ = 37.6 ppm and $\delta(P^V)$ = 40.6ppm]. The $^1J(^{195}Pt\text{-}^{31}P^{III})$ coupling is decreased by over 450 Hz to 3649 Hz relative to that of **9** but is still consistent with the proposed *cis* geometry. Further evidence of ligand chelation is the now apparent small $J(^{31}P_A\text{-}^{31}P_X)$ coupling constant of 5 Hz. It is unclear whether the observed $J(^{31}P_A\text{-}^{31}P_X)$ coupling of 5 Hz is *cis* or *trans* in origin or a combination of both as the $^{31}P\{^1H\}$ NMR spectra of *cis*-[PtCl\{$Ph_2PNHC_6H_4P(S)Ph_2$-κ^2-*P*,*S*\}(PMe_2Ph)][ClO_4] (**14**) (see above), which has a single PtP_2C_2SN ring, and, as such, no *trans*-P−Pt−S−P grouping, contain no such coupling. However, the $^{31}P\{^1H\}$ NMR spectra of *trans*-[PtMe\{$Ph_2PNHC_6H_4P(S)Ph_2$-*P*\}\{$Ph_2PNHC_6H_4P(S)Ph_2$-*k*^{2}-*P*,*S*\}][ClO_4] (**15**) shows two distinct *cis* $^3J(^{31}P_A\text{-}^{31}P_X)$ couplings (see above). The IR spectrum supports the bis(chelate) structure, most notably by the observed shift to lower wavenumber of the ν(P=S) band [623 cm^{-1} vs. 634 cm^{-1} found in **9**] which is a trend also observed in all of the previously described k^2-*P*,*S* chelate complexes (**12**−**15**). An attempt to grow crystals of *cis*-[Pt\{$Ph_2PNHC_6H_4P(S)Ph_2$-*k*^{2}-*P*,*S*\}$_2$][ClO_4]$_2$ (**16**), suitable for X-ray crystallographic analysis by layering a CH_2Cl_2 solution with diethyl ether, resulted in crystallisation of the *trans* isomer. A $^{31}P\{^1H\}$ NMR study of CD_2Cl_2 and CD_2Cl_2/Et_2O solutions of **16** over a six week period showed that the *cis*/*trans* ratio of the compound, i.e. 95:5, remained constant and allowed us to discount the occurrence of slow *cis*-to-*trans* isomerism. The structure of *trans*-**16** (Figure 2) along with its core geometry (Figure 3) are displayed with selected bond lengths and angles (Table 2). The crystal structure of *trans*-[Pt\{$Ph_2PNHC_6H_4P(S)Ph_2$-κ^2-

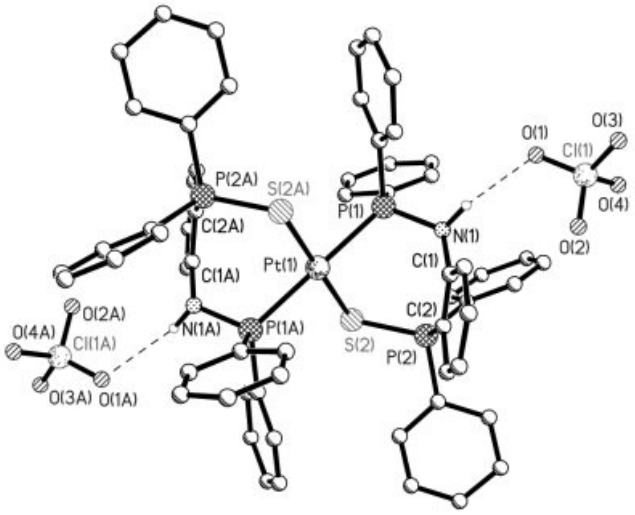

Figure 2. Crystal structure of *trans*-[Pt\{$Ph_2PNHC_6H_4P(S)Ph_2$-*P*,*S*\}$_2$][ClO_4]$_2$·CH_2Cl_2·$2H_2O$; the CH_2Cl_2 and water molecules are omitted for clarity

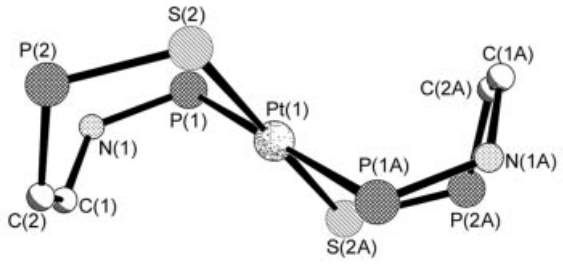

Figure 3. Core geometry of *trans*-[Pt\{$Ph_2PNHC_6H_4P(S)Ph_2$-*P*,*S*\}$_2$][ClO_4]$_2$

Table 2. Selected bond lengths [Å] and angles [°] for *trans*-[Pt\{$Ph_2PNHC_6H_4P(S)Ph_2$-*P*,*S*\}$_2$][ClO_4]$_2$·CH_2Cl_2·$2H_2O$

Pt(1)−S(2)	2.2432(14)	S(2)−P(2)	2.027(2)
P(2)−C(2)	1.794(6)	C(2)−C(1)	1.405(8)
C(1)−N(1)	1.428(7)	N(1)−P(1)	1.671(5)
P(1)−Pt(1)	2.3325(13)		
P(1)−Pt(1)−P(1A)	180.0	S(2)−Pt(1)−S(2A)	180.0
P(1)−Pt(1)−S(2)	90.71(5)	P(1)−Pt(1)−S(2A)	89.29(5)
S(2)−P(2)−C(2)	111.3(2)	Pt(1)−S(2)−P(2)	108.18(7)
C(2)−C(1)−N(1)	120.5(5)	P(2)−C(2)−C(1)	121.1(4)
N(1)−P(1)−Pt(1)	110.1(2)	C(1)−N(1)−P(1)	123.5(4)

$P,S\}_2][ClO_4]_2$ reveals that the molecule possesses a crystallographic centre of symmetry through the platinum atom and that one CH_2Cl_2 and two H_2O molecules (not shown for clarity) per molecule of complex are present. Near-perfect square-planar geometry at the metal centre is evident, presumably because of the lack of strain imposed at the platinum centre by the seven-membered rings. The two seven-membered PtP_2C_2NS metallacycles adopt a conformation best described as pseudo-boat form. Each ring consists of three distinct planes of atoms, [P(1), N(1), S(2), P(2)], [P(2)−C(2)−C(1)−N(1)] and [P(1)−Pt(1)−S(2)]. The angle between [P(1), N(1), S(2), P(2)] and [P(2)−C(2)−C(1)−N(1)] is approximately 119° whilst that between [P(1), N(1), S(2), P(2)] and [P(1)−Pt(1)−S(2)] is 56°. The dicationic nature of the complex is highlighted by the presence of two disordered $[ClO_4]^-$ counterions which are involved in hydrogen-bonding interactions with the two amine protons [H(1n)···O(2) 2.27(7) Å, O(1)···N(1) 3.03(1) Å, N(1)−H(1n)···O(1) 134(7)°]. Reaction of the near insoluble palladium complex **8** with $Ag[ClO_4]$ in a CH_2Cl_2/MeOH solvent mixture gave, after removal of the deposited AgCl and precipitation of the product with diethyl ether, a yellow solid. Examination of this material by $^{31}P\{^1H\}$ NMR (in CD_2Cl_2) showed that multiple products had been formed. No further attempt was made to prepare *cis*-$[Pd\{Ph_2PNHC_6H_4P(S)Ph_2$-$k^2$-$P,S\}_2][ClO_4]_2$.

Anionic Bidentate Coordination Chemistry of $Ph_2PNHC_6H_4P(S)Ph_2$

Previous work has demonstrated that metal complexes constructed using ligands bearing phosphanylamine groups can be easily deprotonated using a relatively mild base, e.g. Et_3N or the metal alkoxide *t*BuOK, to afford neutral chelate ring metallacycles.[29,30] Upon reaction of complexes **8** and **9** with *t*BuOK in MeOH a rapid change in colour is observed. Bright-yellow and bright-orange solids were isolated from the platinum and palladium reactions, respectively. Although the positive-ion FAB MS data gave promising results, i.e. showed isotope profiles at m/z = 1091/2 for palladium and 1180 for platinum corresponding to $[M\{Ph_2PNC_6H_4P(S)Ph_2$-κ^2-$P,S\}_2]^+$, supporting evidence was poor. In particular, $^{31}P\{^1H\}$ NMR evidence showed that multiple products had been formed. Attempts to isolate single products from the mixtures were not successful. Substitution of *t*BuOK for the milder base Et_3N failed as no reaction was observed even at reflux in MeOH.

Conclusion

We have shown that the mixed P^{III},P^V ligand $Ph_2PNHC_6H_4P(S)Ph_2$ (**1**) can be prepared by treating the lithium amide salt of $Ph_2P(S)C_6H_4NH_2$ with Ph_2PCl and that this ligand has the potential to ligate in a number of bonding modes. Apart from behaving as a typical unidentate *P*-bonded ligand, participation of the P=S function can be induced by removal from a metal complex of a chloride ligand using a halide abstractor. Further studies are currently in progress into additional coordination modes of this ligand.

Experimental Section

General: Unless otherwise stated, manipulations were performed under oxygen-free dinitrogen using predried solvents and standard Schlenk techniques. 2-[Diphenyl(thio)phosphanyl]aniline was prepared by the addition of a stoichiometric quantity of elemental sulfur to a toluene solution of 2-(diphenylphosphanyl)aniline. The complexes $[Pd(\mu\text{-}Cl)(\eta^3\text{-}C_3H_5)]_2$,[36] $[Pt(\mu\text{-}Cl)(\mu\text{-}\eta^2\text{:}\eta^1\text{-}C_3H_5)]_4$,[37] $[\{PtCl(\mu\text{-}Cl)(PMe_2Ph)\}_2]$,[38] [MX(Y)(cod)] (M = Pt or Pd; X, Y = Me, Cl, Br or I; cod = cycloocta-1,5-diene),[39−32] or $[AuCl(tht)]$[33] (tht = tetrahydrothiophene) were prepared according to literature procedures. *n*BuLi (Lancaster) was titrated against diphenylacetic acid just prior to use. Aqueous H_2O_2 (30% w/w, Fluka) and $Ag[ClO_4]$ (99% purity, Aldrich) were obtained commercially and used without further purification. Infrared spectra were recorded as KBr pellets in the range 4000−220 cm^{-1} with a Perkin−Elmer system 2000 Fourier transform spectrometer, ^1H NMR spectra (250 or 270 MHz) either with a Bruker AC250 FT or a JEOL GSX270 spectrometer with δ referenced to external $SiMe_4$ and $^{31}P\{^1H\}$ NMR spectra (36.2, 101.3 or 109.4 MHz) either with a JEOL FX90Q, a Bruker AC250 FT, or a JEOL GSX270 spectrometer with δ referenced to external H_3PO_4. Microanalyses were performed by the St Andrews University School of Chemistry Service. Precious metal salts were provided on loan by Johnson Matthey plc.

$Ph_2PNHC_6H_4P(S)Ph_2$ (1): A solution of 2.43 M *n*BuLi (4.0 mL, 9.72 mmol) in hexane was added dropwise over a period of 10 min to a cooled (−78 °C cardice/acetone), stirred suspension of 2-[diphenyl(thio)phosphanyl]aniline (3.00 g, 9.70 mmol) in dry, degassed diethyl ether (200 mL). The mixture was stirred at −78 °C for 1 h, warmed to room temperature and stirred for a further 3 h giving a white suspension in a dark orange solution. The reaction mixture was cooled once more to −78 °C (cardice/acetone) and neat chlorodiphenylphosphane (1.75 mL, 2.15 g, 9.74 mmol) was added dropwise over 5 min. The white suspension in a pale yellow solution was stirred at −78 °C for 30 min, warmed to room temperature, stirred for 3 h and then stripped of solvent in vacuo. The pale brown oily solid was then triturated with dry MeOH (30 mL) at 0 °C for 10 min. The colourless solid was collected by suction filtration, washed with ice-cold MeOH (2 × 10 mL) and dried overnight in vacuo. Yield: 4.07 g, 85%. ^1H NMR ($CDCl_3$): δ = 7.75−7.66 (m, 4 H, aromatics), 7.56−7.16 (m, 18 H, aromatics), 6.71−6.59 (m, 2 H, aromatics), 5.68 [br. d, $^2J(^{31}P\text{-}^1H)$ = 9 Hz, 1 H, NH] ppm. FAB^+ MS: m/z = 494 $[M]^+$. Selected IR data (KBr): $\tilde{\nu}$ = 3223 [br, ν(N−H)], 896 [vs, ν(P−N)], 634 [vs, ν(P=S)] cm^{-1}.

$Ph_2P(O)NHC_6H_4P(S)Ph_2$ (2). Method A: To a stirred THF (25 mL) solution of **1** (0.480 g, 0.973 mmol) was added aqueous hydrogen peroxide (30% w/w, 0.2 mL, 1.76 mmol) dropwise over a 10 min period. The mixture was stirred for 10 min, then concentrated to dryness, giving an off-white oily residue. The residue was taken up in CH_2Cl_2 and dried with anhydrous $MgSO_4$. Filtration to remove the drying agent, followed by concentration of the filtrate to dryness, and recrystallisation from a minimum of hot toluene gave **2** as a colourless crystalline solid. The product was collected by suction filtration, washed with toluene (2 × 5 mL) and dried in vacuo. Yield: 0.445 g, 90%. ^1H NMR ($CDCl_3$): δ = 8.66 [br. d, $^2J(^{31}P\text{-}^1H)$ = 10 Hz, 1 H, NH], 7.78−7.69 (m, 4 H, aromatics), 7.57−7.24 (m, 18 H, aromatics), 6.77−6.79 (m, 2 H, aromatics)

ppm. FAB^+ MS: *m*/*z* = 510 $[M]^+$. Selected IR data (KBr): $\tilde{\nu}$ = 3117 [w,ν(N−H)], 1212 [s, ν(P=O)], 924 [s, ν(P−N)], 632 [vs, ν(P=S)] cm^{-1}. **Method B:** $Ph_2PNHC_6H_4P(S)Ph_4$ (**1**) (0.536 g, 1.086 mmol) was dissolved in boiling MeOH (30 mL) and the hot solution was first cooled to room temperature and then stored at 4 °C overnight to give **2** as a colourless powder, which was collected by suction filtration, washed with ice-cold MeOH (2 × 10 mL), and dried overnight in vacuo. Yield: 0.324 g, 59%. $^{31}P\{^1H\}$ NMR ($CDCl_3$) and microanalytical data are similar to those of the material generated by Method A.

$Ph_2P(Se)NHC_6H_4P(S)Ph_2$ (3): Elemental selenium (0.085 g, 1.076 mmol) and **1** (0.534 g, 1.072 mmol) were stirred in warm (60 °C) toluene (20 mL) for 30 min. The solution was filtered through Celite while still warm to remove a trace amount of unchanged selenium. The Celite was washed with warm (60 °C) toluene (2 × 10 mL). The filtrate and washings were combined and reduced in volume to ca. 15 mL, and the resulting colourless solid was collected by suction filtration, washed with toluene (2 × 5 mL) and ice-cold diethyl ether (2 × 5 mL), and dried in vacuo. Yield: 0.524 g, 85%. ^1H NMR ($CDCl_3$): δ = 8.34 [br. d, $^2J(^{31}P\text{-}^1H)$ = 8 Hz, 1 H, NH], 7.79−7.68 (m, 4 H, aromatics), 7.63−7.24 (m, 18 H, aromatics), 6.85 (m, 1 H, aromatic), 6.77−6.67 (m, 1 H, aromatic) ppm. FAB^+ MS: *m*/*z* = 573 $[M]^+$. Selected IR data (KBr): $\tilde{\nu}$ = 3098 [s, ν(N−H)], 925 [vs, ν(P−N)], 631 [s, ν(P=S)], 548 [vs, ν(P=Se)] cm^{-1}.

[PdCl(η³-C_3H_5){$Ph_2PNHC_6H_4P(S)Ph_2$-*P*}] (4): To a stirred toluene (15 mL) suspension of [Pd(μ-Cl)(η³-C_3H_5)]$_2$ (0.115 g, 0.316 mmol) was added in one portion solid **1** (0.312 g, 0.632 mmol). The mixture was stirred for 3 h to give a light, cream-coloured precipitate. The solvent volume was reduced in vacuo to ca. 5 mL and light petroleum ether (40−60 °C) (20 mL) was added to further precipitate the product, which was collected by suction filtration, washed with light petroleum ether (40−60 °C) (2 × 15 mL), and dried in vacuo. Yield: 0.354 g, 83%. ^1H NMR ($CDCl_3$): δ = 8.02 (s, 1 H, NH), 7.81−7.24 (m, 22 H, aromatics), 6.82−6.73 (m, 2 H, aromatic), 5.36 (m, 1 H, allyl), 4.64 (m, 1 H, allyl), 3.59 (m, 1 H, allyl), 3.04 (m, 1 H, allyl), 2.39 (m, 1 H, allyl) ppm. FAB^+ MS: *m*/*z* = 676 $[M]^+$, 641 $[M - Cl]^+$, 600 $[M - Cl - C_3H_5]^{2+}$. Selected IR data (KBr): $\tilde{\nu}$ = 3144 [br, ν(N−H)], 912 [m, ν(P−N)], 632 [m, ν(P=S)] cm^{-1}.

[PtCl(η³-C_3H_5){$Ph_2PNHC_6H_4P(S)Ph_2$-*P*}] (5): To a stirred THF (20 mL) suspension of [Pt(μ-Cl)(μ-η²:η¹-C_3H_5)]$_4$ (0.153 g, 0.141 mmol) was added in one portion solid **1** (0.280 g, 0.568 mmol). The mixture was stirred for 6 h to give a dirty yellow solution that was filtered through a Celite plug to remove a small quantity of dark insoluble material. The resulting very pale yellow solution was reduced in vacuo to ca. 4−5 mL, and light petroleum ether (40−60 °C) (25 mL) was added to precipitate the product as a cream-coloured powder, which was collected by suction filtration, washed with light petroleum ether (40−60 °C) (2 × 10 mL), and dried in vacuo. Yield: 0.379 g, 88%. ^1H NMR ($CDCl_3$): δ = 8.07 [s, $^3J(^{195}Pt\text{-}^1H)$ = 47 Hz, 1 H, NH], 7.80−7.19 (m, 22 H, aromatics), 6.78−6.71 (m, 2 H, aromatic), 4.76 (m, 1 H, allyl), 4.28 (m, 1 H, allyl), 2.92 (m, 2 H, allyl) 1.87 [m, $^3J(^{195}Pt\text{-}^1H)$ = 78 Hz, 1 H, allyl] ppm. FAB^+ MS: *m*/*z* = 765 $[M]^+$, 730 $[M - Cl]^+$, 689 $[M - Cl - C_3H_5]^{2+}$. Selected IR data (KBr): $\tilde{\nu}$ = 3142 [br, ν(N−H)], 912 [s, ν(P−N)], 634 [s, ν(P=S)], 298 [w, ν(Pt−Cl)] cm^{-1}.

***cis*-[$PtCl_2${$Ph_2PNHC_6H_4P(S)Ph_2$-*P*}(PMe_2Ph)] (6):** To a stirred CH_2Cl_2 (25 mL) solution of [{PtCl(μ-Cl)(PMe_2Ph)}$_2$] (0.126 g, 0.156 mmol) was added dropwise over 10 min a CH_2Cl_2 (20 mL) solution of **1** (0.154 g, 0.312 mmol). The resulting pale yellow solution was stirred for 30 min and then concentrated under reduced pressure to ca. 1−2 mL, and addition of petroleum ether (60−80 °C) precipitated an off-white solid. The product was collected by suction filtration, washed with petroleum ether (60−80 °C) (3 × 10 mL) and dried in vacuo. Yield: 0.246 g, 88%. ^1H NMR ($CDCl_3$): δ = 8.47 (m, 1 H, NH), 7.90 (m, 1 H, aromatic), 7.83 (m, 22 H, aromatics), 6.82−6.68 (m, 2 H, aromatics) and 1.46 [d, $^2J(^{31}P\text{-}^1H)$ = 11, $^3J(^{195}Pt\text{-}^1H)$ = 35 Hz, 6 H, PMe] ppm. FAB^+ MS: *m*/*z* = 898 $[M]^+$, 862 $[M - Cl]^+$, 827 $[M - 2\ Cl]^{2+}$. Selected IR data (KBr): $\tilde{\nu}$ = 3143 [w, ν(N−H)], 912 [s, ν(P−N)], 634 [m, ν(P=S)], 317 (w) + 291 (w) [ν(PtCl)] cm^{-1}.

[AuCl{$Ph_2PNHC_6H_4P(S)Ph_2$-*P*}] (7): To a stirred solution of [AuCl(tht)] (0.045 g, 0.140 mmol) in CH_2Cl_2 (4 mL) was added **1** (0.070 g, 0.142 mmol) as a solid in one portion. The mixture was stirred for 1 h and filtered through a Celite plug to remove a small amount of grey insoluble material. Diethyl ether (35 mL) was added slowly until a white solid precipitated. The product was collected by suction filtration, washed with diethyl ether (2 × 10 mL), and dried in vacuo. Yield: 0.085 g, 83%. ^1H NMR ($CDCl_3$): δ = 8.00 [br. d, $^2J(^{31}P\text{-}^1H)$ = 3 Hz, 1 H, NH], 7.71−7.29 (m, 21 H, aromatics), 7.14 (m, 1 H, aromatic), 6.95 (m, 1 H, aromatic) and 6.71 (m, 1 H, aromatic) ppm. FAB^+ MS: *m*/*z* = 726 $[M]^+$, 691/692 $[M - Cl]^+$. Selected IR data (KBr): $\tilde{\nu}$ = 3109 [m, ν(N−H)], 927 [m, ν(P−N)], 632 [s, ν(P=S)], 339 [w, ν(Au−Cl)] cm^{-1}.

***cis*-[$PdCl_2${$Ph_2PNHC_6H_4P(S)Ph_2$-*P*}$_2$] (8):** To a stirred solution of [$PdCl_2$(cod)] (0.078 g, 0.273 mmol) in CH_2Cl_2 (2.5 mL) was added **1** (0.273 g, 0.553 mmol) as a solid in one portion. The resulting clear pale yellow solution was stirred for 10 min, and the pale yellow precipitate was collected by suction filtration, washed with CH_2Cl_2 (2 × 2 mL) and diethyl ether (3 × 10 mL), and dried in vacuo. Yield: 0.309 g, 97%. Selected IR data (KBr): $\tilde{\nu}$ = 3108 [br, ν(N−H)], 919 [vs, ν(P−N)], 632 [vs, ν(P=S)], 318 (w) + 298 (w) [ν(Pd−Cl)] cm^{-1}.

***cis*-[$PtCl_2${$Ph_2PNHC_6H_4P(S)Ph_2$-*P*}$_2$] (9):** This compound was prepared in the same way as **8** using [$PtCl_2$(cod)] (0.051 g, 0.136 mmol) in CH_2Cl_2 (2.5 mL) and **1** (0.138 g, 0.280 mmol). The resulting clear pale yellow solution was stirred for 2 h, and the product was precipitated by slow addition of diethyl ether (15 mL). The crude product was immediately redissolved in CH_2Cl_2 (5 mL) and reprecipitated by slow addition of diethyl ether (30 mL), washed with ice-cold CH_2Cl_2/diethyl ether (1:1) (4 mL) and diethyl ether (3 × 10 mL). The resulting white solid was collected by suction filtration and dried in vacuo. Yield: 0.150 g, 88%. ^1H NMR (CD_2Cl_2): δ = 7.90 [br. d, $^2J(^{31}P\text{-}^1H)$ = 7 Hz, 2 H, NH], 7.76−7.08 (m, 44 H, aromatics) and 6.71−6.58 (m, 4 H, aromatics) ppm. FAB^+ MS: *m*/*z* = 1217/8 $[M - Cl]^+$, 1182 $[M - 2\ Cl]^{2+}$. Selected IR data (KBr): $\tilde{\nu}$ = 3125 [m, ν(N−H)], 920 [s, ν(P−N)], 634 [s, ν(P=S)], 311 (w) + 290 (w) [ν(Pt−Cl)] cm^{-1}. The product was consistently contaminated with an impurity (ca. 4−5%) observed as two singlets in the $^{31}P\{^1H\}$ NMR at δ(P) = 40.2 and 40.8 ppm, thought to be *trans*-[$PtCl_2${$Ph_2PNHC_6H_4P(S)Ph_2$-*P*}$_2$].

***trans*-[PtClMe{$Ph_2PNHC_6H_4P(S)Ph_2$-*P*}$_2$] (10):** This was prepared in the same way as **8** using [PtClMe(cod)] (0.093 g, 0.263 mmol) in CH_2Cl_2 (4 mL) and **1** (0.270 g, 0.547 mmol). The white solid was collected by suction filtration, washed with CH_2Cl_2 (2 × 2 mL) and diethyl ether (3 × 10 mL) and dried in vacuo. Yield: 0.318 g, 98%. Selected IR data (KBr): $\tilde{\nu}$ = 3128 [br, ν(N−H)], 911 [vs, ν(P−N)], 633 [vs, ν(P=S)], 288 [w, ν(Pt−Cl)] cm^{-1}.

***cis*-[$PtMe_2${$Ph_2PNHC_6H_4P(S)Ph_2$-*P*}$_2$] (11):** This was prepared in the same way as **8** using [$PtMe_2$(cod)] (0.070 g, 0.210 mmol) in toluene (4 mL) and **1** (0.210 g, 0.43 mmol). The resulting clear pale

yellow solution was stirred for 2 h resulting in the deposition of a light precipitate. Petroleum ether (60−80 °C) (30 mL) was added with stirring to further precipitate the product. The off-white solid was collected by suction filtration, washed with petroleum ether (60−80 °C) (3 × 10 mL), and dried in vacuo. Yield: 0.215 g, 84%. ^{1}H NMR ($CDCl_3$): δ = 8.10 (m, 2 H, NH), 7.86−6.59 (m, 48 H, aromatics) and 0.20 [dd, $^2J(^{195}Pt\text{-}^1H)$ = 72 Hz, 6 H, PtMe] ppm. FAB$^+$ MS: *m*/*z* = 1235 [M + Na]$^+$, 1212 [M]$^+$ and 1196 [M − Me]$^+$. Selected IR data (KBr): $\tilde{\nu}$ = 3168 [br, ν(N−H)], 902 [s, ν(P−N)], 634 [s, ν(P=S)] cm^{-1}.

[Pd(η^3-C_3H_5){$Ph_2PNHC_6H_4P(S)Ph_2$-κ^2-*P*,*S*}][ClO_4] (12): To a stirred CH_2Cl_2 (15 mL) solution of **4** (0.171 g, 0.253 mmol) was added Ag[ClO_4] (0.055 g, 0.265 mmol) as a solid in one portion. The resulting mixture was stirred in the dark for 17 h and then filtered through Celite to remove the AgCl. The pale yellow filtrate was concentrated in vacuo to ca. 5−6 mL and upon addition of diethyl ether (25 mL) deposited a cream-coloured solid. The solid was collected by suction filtration, washed with diethyl ether (3 × 10 mL), and dried in vacuo. Yield: 0.172 g, 92%. ^{1}H NMR ($CDCl_3$): δ = 7.93−6.97 (m, 23 H, aromatics), 6.66 (m, 1 H, aromatics), 5.61 (m, 1 H, allyl), 5.21 [br. d, $^2J(^{31}P\text{-}^1H)$ = 11 Hz, 1 H, NH], 4.76 (m, 1 H, allyl), 3.76 (m, 1 H, allyl), 3.56 (m, 1 H, allyl), 2.87 [br. d, $J(^1H\text{-}^1H)$ = 13 Hz, 1 H, allyl] ppm. FAB$^+$ MS: *m*/*z* = 641 [M − ClO_4]$^+$, 600 [M − ClO_4 − C_3H_5]$^{2+}$. Selected IR data (KBr): $\tilde{\nu}$ = 3196 [br, ν(N−H)], 1099 [vs (br), ν(ClO_4)], 907 [s, ν(P−N)], 622 [s, ν(P=S)] cm^{-1}.

[Pt(η^3-C_3H_5){$Ph_2PNHC_6H_4P(S)Ph_2$-κ^2-*P*,*S*}][ClO_4] (13): This was prepared in the same way as **12** using **5** (0.183 g, 0.239 mmol) and Ag[ClO_4] (0.052 g, 0.251 mmol). The mixture was filtered through Celite and concentrated in vacuo to ca. 3 mL whereupon an off-white solid **13** was deposited. Further precipitation was induced by the addition of diethyl ether (35 mL). The resulting cream-coloured powder was collected by suction filtration, washed with diethyl ether (3 × 10 mL), and dried in vacuo. Yield: 0.188 g, 95%. ^{1}H NMR (CD_2Cl_2): δ = 7.88−6.95 (m, 23 H, aromatics), 6.63 (m, 1 H, aromatics), 5.81 [br. d, $^2J(^{31}P\text{-}^1H)$ = 8, $^3J(^{195}P\text{-}^1H)$ = 82 Hz, 1 H, NH], 4.97 [m, $^3J(^{195}P\text{-}^1H)$ = 64 Hz, 1 H, allyl], 4.39 (br. m, 1 H, allyl), 3.37 (m, 1 H, allyl), 2.94 (m, 1 H, allyl) and 2.27 [m, $^3J(^{195}P\text{-}^1H)$ = 71 Hz, 1 H, allyl] ppm. FAB$^+$ MS: *m*/*z* = 730 [M − ClO_4]$^+$, 689 [M − ClO_4 − C_3H_5]$^{2+}$. Selected IR data (KBr): $\tilde{\nu}$ = 3185 [br, ν(N−H)], 1098 [vs (br), ν(ClO_4)], 907 [m, ν(P−N)], 623 [m, ν(P=S)] cm^{-1}.

***cis*-[PtCl{$Ph_2PNHC_6H_4P(S)Ph_2$-κ^2-*P*,*S*}(PMe_2Ph)][ClO_4] (14):** This was prepared in the same way as **12** using **6** (0.142 g, 0.158 mmol) and Ag[ClO_4] (0.032 g, 0.154 mmol). The resulting cream-coloured powder was collected by suction filtration, washed with diethyl ether (3 × 10 mL), and dried in vacuo. Yield: 0.144 g, 95%. ^{1}H NMR ($CDCl_3$): δ = 7.93−7.77 (m, 2 H, aromatics), 7.64−7.00 (m, 21 H, aromatics and NH), 6.87 (m, 2 H, aromatics) and 1.38 [d, $^2J(^{31}P\text{-}^1H)$ = 11, $^3J(^{195}Pt\text{-}^1H)$ = 34 Hz, 6 H, PMe] ppm. FAB$^+$ MS: *m*/*z* = 862 [M − ClO_4]$^+$, 827 [M − ClO_4 − Cl]$^{2+}$. Selected IR data (KBr): $\tilde{\nu}$ = 3216 [br, ν(N−H)], 1100 [vs (br), ν(ClO_4)], 910 [s, ν(P−N)], 622 [m, *ν*(P=S)], 302 [w, *ν*(Pt-Cl)] cm^{-1}.

***trans*-[PtMe{$Ph_2PNHC_6H_4P(S)Ph_2$-*P*}{$Ph_2PNHC_6H_4P(S)Ph_2$-κ^2-*P*,*S*}][ClO_4] (15):** This was prepared in the same way as **12** using **10** (0.150 g, 0.122 mmol) and Ag[ClO_4] (0.026 g, 0.125 mmol). The white solid was collected by suction filtration, washed with diethyl ether (3 × 10 mL), and dried in vacuo. Yield: 0.129 g, 82%. ^{1}H NMR (CD_2Cl_2): δ = 8.62 [m, $^3J(^{195}Pt\text{-}^1H)$ = 34 Hz, 1 H, NH], 7.77−6.61 (m, 48 H, aromatics), 5.78 [m, $^3J(^{195}Pt\text{-}^1H)$ = 54 Hz, 1 H, NH], −0.20 [br. t, $^2J(^{195}Pt\text{-}^1H)$ = 76, $^3J(^{31}P\text{-}^1H)$ = 15 Hz, 3 H, PtMe] ppm. FAB$^+$ MS: *m*/*z* = 1197/1198 [M − ClO_4]$^+$, 1182 [M − ClO_4 − Me]$^+$. Selected IR data (KBr): $\tilde{\nu}$ = 3190 [w, ν(N−H)], 1100 [vs (br), ν(ClO_4)], 916 [m, *ν*(P−N)], 622 [s, ν(P=S)] cm^{-1}.

***cis*-[Pt{$Ph_2PNHC_6H_4P(S)Ph_2$-κ^2-*P*,*S*}$_2$][ClO_4]$_2$ (16):** This was prepared in the same way as **12** using **9** (0.200 g, 0.160 mmol) in CH_2Cl_2 (25 mL) and Ag[ClO_4] (0.068 g, 0.328 mmol). The filtered reaction mixture was concentrated to ca. 2−4 mL, and diethyl ether (20 mL) was added causing an off-white crystalline solid to precip-

Table 3. $^{31}P\{^1H\}$ NMR data for complexes of $Ph_2PNHC_6H_4P(S)Ph_2$. (where P_A = aminophosphane −NHPPh$_2$ and P_X = thiophosphoryl −P(S)Ph$_2$ moieties)

Compound	Chemical shifts/ppm		Coupling constants/Hz		
	δ(P_A)	δ(P_X)	^1J(Pt-P_A)	^2J(Pt-P_X)	^3J(P_A-P_X)
1[a]	28.2	39.6	−	−	−
2[a]	18.4	39.7	−	−	−
3[a]	47.0 (783)[b]	40.0	−	−	−
4[c]	55.3	39.8	−	−	−
5[c]	50.1	39.9	4946	−	−
6[a][d]	32.6	39.4	4100	−	−
7[a]	58.2	40.1	−	−	−
8	−	−	−	−	−
9[a]	37.6	40.6	4103	−	−
10	−	−	−	−	−
11[e]	55.3	39.6	2059	−	−
12[c]	69.5	46.4	−	−	16
13[f]	58.3	45.6	4720	123	13
14[a][g]	40.5	43.6	3821	47	n.o.[h]
15[e]	56.2, [69.4][i]	43.1, [44.7][i]	3192, [3225][i]	70	11, [3][i]
16[e]	48.8	45.3	3649	38	5

[a] Spectra (36.2 MHz) measured in $CDCl_3$. [b] Values in parentheses denote $^1J(^{77}Se\text{-}^{31}P)$/Hz. [c] Spectra (109.4 MHz) measured in $CDCl_3$. [d] Other $^{31}P\{^1H\}$ spectral parameters for **6** δ (PMe_2Ph) −16.3 [$^1J(^{195}Pt-PMe_2Ph)$ 3436 Hz], $^2J(PMe_2Ph\text{-}P_A)$ 18 Hz. [e] Spectra (101.3 MHz) measured in CD_2Cl_2. [f] Spectra (109.4 MHz) measured in $CDCl_3$/dmso. [g] Other $^{31}P\{^1H\}$ spectral parameters for **14** δ (PMe_2Ph) −4.4(dd) [$^1J(^{195}Pt-PMe_2Ph)$ 3390 Hz], $^2J(PMe_2Ph\text{-}P_A)$ 15, $^3J(PMe_2Ph\text{-}P_x)$ 9 Hz. [h] n.o. = Not observed. [i] Values in square brackets denote $^{31}P\text{-}\{^1M\}$ parameters for the chelating (PS) ligand of **15**.

Table 4. Microanalytical data for compounds **1**−**16** (calculated values in parentheses) where PS = *P*-bound and PS* = *PS*-bound $Ph_2PNHC_6H_4P(S)Ph_2$

Compound		C	H	N
1	(PS)	73.41 (73.01)	5.46 (5.11) /P'	3.04 (2.84)
2	[P(O)S]	71.69 (70.72)	5.25 (4.95)	2.47 (2.75)
3	[P(Se)S]	62.04 (62.94),	4.43 (4.40)	2.56 (2.45)
4	$[PdCl(C_3H_5)\{PS\}]$	58.14 (58.59)	3.98 (4.47)	2.01 (2.07)
5	$[PtCl(C_3H_5)\{PS\}]$	52.08 (51.80)	3.74 (3.95)	1.77 (1.83)
6	$[PtCl_2(PMe_2Ph)\{PS\}]$	50.95 (50.84)	3.86 (4.04)	2.27 (1.56)
7	$[AuCl\{PS\}]$	49.22 (49.63)	3.57 (3.47)	1.70 (1.93)
8	$[PdCl_2\{PS\}_2]$	61.69 (61.89)	4.54 (4.33)	2.37 (2.41)
9	$[PtCl_2\{PS\}_2]$	57.20 (57.51)	4.35 (4.02)	2.15 (2.24)
10	$[PtClMe\{PS\}_2]$	60.02 (59.44)	4.34 (4.33)	2.42 (2.27)
11	$[PtMe_2\{PS\}_2]$	61.03 (61.43)	4.71 (4.66)	2.14 (2.31)
12	$[Pd(C_3H_5)\{PS^*\}][ClO_4]$	53.25 (53.53)	3.69 (4.08)	1.87 (1.89)
13	$[Pt(C_3H_5)\{PS^*\}][ClO_4]$	47.71 (47.80)	3.26 (3.65)	1.61 (1.69)
14	$[PtCl(PMe_2Ph)\{PS^*\}][ClO_4]$	46.73 (47.46)	3.70 (3.77)	1.37 (1.46)
15	$[PtMe\{PS\}\{PS^*\}][ClO_4]$	55.87 (56.50)	4.16 (4.12)	2.24 (2.16)
16	$[Pt\{PS^*\}_2][ClO_4]_2$	51.70 (52.18)	3.53 (3.65)	1.78 (2.03)

itate. The cream-coloured microcrystalline product was collected by suction filtration, washed with diethyl ether (2 × 10 mL)and dried in vacuo. Yield: 0.194 g, 88%. ^1H NMR (CD_2Cl_2): δ = 7.96−7.85 (m, 8 H, aromatics), 7.69−6.88 (m, 36 H, aromatics) and 6.72−6.59 (m, 6 H, aromatics and NH) ppm. FAB$^+$ MS: *m*/*z* = 1281/1282 $[M - ClO_4]^+$ and 1182 $[M - 2\ ClO_4]^{2+}$. Selected IR data (KBr): $\tilde{\nu}$ = 3164 [br, ν(N−H)], 1099 [vs (br), ν(ClO_4)], 927 [m, ν(P−N)], 623 [s, ν(P=S)] cm^{-1}. The product was consistently contaminated with an impurity (ca. 5%) observed as two triplets in the $^{31}P\{^1H\}$ NMR spectrum at δ(P) = 42.9 and 55.3 ppm [$^1J(^{195}Pt-^{31}P)$ = 2596 Hz] thought to be *trans*-$[Pt\{Ph_2PNHC_6H_4P(S)Ph_2\text{-}P,S\}_2][ClO_4]_2$.

The $^{31}P\{^1H\}$ spectroscopic and microanalytical data for all new compounds are compiled in Tables 3 and 4, respectively.

X-ray Crystallography: X-ray diffraction measurements were made with graphite-monochromated Mo-K_α radiation (λ = 0.71073 Å) using a Siemens SMART diffractometer, intensity data were collected using 0.3° or 0.15° width ω steps accumulating area detector frames spanning a hemisphere of reciprocal space for all structures (data were integrated using the SAINT program) and for the Rigaku AFC7S data collections by ω scans over a single quadrant of reciprocal space. All data were corrected for Lorentz, polarisation and long-term intensity fluctuations. Absorption effects were corrected on the basis of multiple equivalent reflections (SADABS) or by semi-empirical methods.[44] Structures were solved by direct methods and refined by full-matrix least squares against F^2 (SHELXTL). All hydrogen atoms (except those on the water molecules of complex **16**, which we have not included in the refinement) were assigned isotropic displacement parameters and were constrained to idealised geometries. All calculations were made with SHELXTL.[44] $C_{30}H_{25}AuClNP_2S$ (**7**), *M* = 725.9, monoclinic, space group *C*2/*c*, *a* = 18.2461(2), *b* = 9.3531(2), *c* = 33.2678(3) Å, β = 92.23(1)°, *V* = 5673.1(1) Å^3, *T* = 293 K, *Z* = 8, μ(Mo-K_α) = 5.487 mm^{-1}, 16863 reflections measured, 6645 unique (R_{int} = 0.0475), observed independent reflections 4353, final *R*1[$I > 2\sigma(I)$] = 0.0459. $C_{60}H_{50}N_2P_4PtS_2[ClO_4]_2[CH_2Cl_2][H_2O]_2$ (**16**), *M* = 1502.0, monoclinic, space group $P2_1/n$, *a* = 12.4175(4), *b* = 20.5319(7), *c* = 13.8955(5) Å, β = 99.38(1)°, *V* = 5673.1(1) Å^3, *T* = 293 K, *Z* = 2, μ(Mo-K_α) = 2.364 mm^{-1}, 21230 reflections measured, 8178 unique (R_{int} = 0.0430), observed independent reflections 5041, final *R*1[$I > 2\sigma(I)$] = 0.0487. CCDC-164211 and -164212 contain the supplementary crystallographic data for for the structures **7** and **16** reported in this paper. These data can be obtained free of charge at www.ccdc.cam.ac.uk/conts/retrieving.html or from the Cambridge Crystallographic Data Centre, 12, Union Road, Cambridge CB2 1EZ, UK [Fax: (internat.) + 44-1223/336-033; E-mail: deposit@ccdc.cam.ac.uk].

Acknowledgments

We should like to thank the EPSRC for financial support and Johnson Matthey for the loan of precious metals. We would also like to thank the Joint Research Equipment Initiative for equipment grants.

[1] M. E. Workmann, G. Dyer, D. W. Meek, *Inorg. Chem.* **1967**, *6*, 1543−1548.
[2] A. Benefiel, D. M. Roundhill, W. C. Fultz, A. L. Rheingold, *Inorg. Chem.* **1984**, *23*, 3316−3324.
[3] P. Rigo, M. Bressan, *Inorg. Chem.* **1975**, *14*, 1491−1494.
[4] G. K. Anderson, R. Kumar, *Inorg. Chim. Acta* **1985**, 97, L21−L23.
[5] G. K. Anderson, R. Kumar, *J. Organomet. Chem.* **1988**, *342*, 263−268.
[6] E. W. Abel, J. C. Dormer, D. Ellis, K. G. Orrell, V. Sik, M. B. Hursthouse, M. A. Mazid, *J. Chem. Soc., Dalton Trans.* **1992**, 1073−1080.
[7] A. D. Zotto, P. Rigo, *Inorg. Chim. Acta* **1988**, *147*, 55−59.
[8] M. Bressan, C. Bonuzzi, F. Morandini, A. Morvillo, *Inorg. Chim. Acta* **1991**, *182*, 153−156.
[9] P. Di Bernardo, M. Tolazzi, P. Zanonato, *J. Chem. Soc., Dalton Trans.* **1995**, 1349−1355.
[10] K. Issleib, W. Gans, *Z. Anorg. Allg. Chem.* **1981**, *475*, 116−130.
[11] K. Issleib, W. Gans, *Z. Anorg. Allg. Chem.* **1982**, *491*, 163−174.
[12] P. H. Leung, A. C. Willis, S. B. Wild, *Inorg. Chem.* **1992**, *31*, 1406−1410.
[13] S. T. Liu, D. R. Hou, T. C. Lin, M. C. Cheng, S. M. Peng, *Organometallics* **1995**, *14*, 1529−1532.
[14] U. Kunze, H. Jawad, E. Boziaris, *J. Organomet. Chem.* **1986**, *312*, 67−80.
[15] M. Alvarez, N. Lugan, B. Donnadieu, R. Mathieu, *Organometallics* **1995**, *14*, 365−370.
[16] M. Alvarez, N. Lugan, B. Donnadieu, R. Mathieu, *Inorg. Chem.* **1993**, *32*, 5652−5657.

[17] O. Clot, M. O. Wolf, G. P. A. Yap, B. O. Patrick, *J. Chem. Soc., Dalton Trans.* **1995**, 2729−2737.
[18] S. Y. Siah, P. H. Leung, K. F. Mok, *Polyhedron* **1994**, *13*, 3253−3255.
[19] S. O. Grim, P. H. Smith, I. J. Colquhoun, W. McFarlane, *Inorg. Chem.* **1980**, *19*, 3195−3198.
[20] I. J. Colquhoun, S. O. Grim, W. McFarlane, J. D. Mitchell, P. H. Smith, *Inorg. Chem.* **1981**, *20*, 2516−2521.
[21] T. C. Blagborough, R. Davis, P. Ivison, *J. Organomet. Chem.* **1994**, *467*, 85−94.
[22] P. Bhattacharyya, A. M. Z. Slawin, D. J. Williams, J. D. Woollins, *J. Chem. Soc., Dalton Trans.* **1995**, 3189−3194.
[23] M. S. Balakrishna, R. Klien, S. Uhlenbrock, A. A. Pinkerton, R. G. Cavell, *Inorg. Chem.* **1993**, *32*, 5676−5681.
[24] M. J. Baker, M. F. Giles, A. G. Orpen, M. J. Taylor, R. J. Watt, *J. Chem. Soc., Chem. Commun.* **1995**, 197−198.
[25] G. P. Suranna, P. Mastrorilli, C. F. Nobile, W. Keim, *Inorg. Chim. Acta* **2000**, *305*, 151−156.
[26] I. M. Aladzheva, O. V. Bykhovskaya, D. I. Lobanov, P. V. Petrovskii, M. Y. Antipin, K. A. Lysenko, T. A. Mastryukova, M. I. Kabachnik, *Phosphorus, Sulfur, Silicon* **1996**, *111*, 116.
[27] S. M. Aucott, A. M. Z. Slawin, J. D. Woollins, *J. Organomet. Chem.* **1999**, *582*, 83−89.
[28] S. M. Aucott, A. M. Z. Slawin, J. D. Woollins, *J. Chem. Soc., Dalton Trans.* **2001**, 2279−2287.
[29] P. Haake, R. M. Pfeiffer, *J. Chem. Soc., Chem. Commun.* **1969**, 1330.
[30] P. Haake, R. M. Pfeiffer, *J. Am. Chem. Soc.* **1970**, *92*, 4996−4997.
[31] P. Haake, R. M. Pfeiffer, *J. Am. Chem. Soc.* **1970**, *92*, 5243.
[32] D. G. Cooper, J. Powell, *J. Am. Chem. Soc.* **1973**, *95*, 1102−1108.
[33] A. M. Z. Slawin, M. B. Smith, J. D. Woollins, *J. Chem. Soc., Dalton Trans.* **1996**, 4567−4573.
[34] P. Bhattacharyya, A. M. Z. Slawin, M. B. Smith, J. D. Woollins, *Inorg. Chem.* **1996**, *35*, 3675−3682.
[35] S. M. Aucott, A. M. Z. Slawin, J. D. Woollins, *J. Chem. Soc., Dalton Trans.* **2000**, 2559−2575.
[36] A. L. Balch, L. S. Benner, *Inorg. Synth.* **1990**, *28*, 340−342.
[37] J. Lukas, *Inorg. Synth.* **1974**, *15*, 75−81.
[38] W. Baratta, P. S. Pregosin, *Inorg. Chim. Acta* **1993**, *209*, 85−87.
[39] H. C. Clark, L. E. Manzer, *J. Organomet. Chem.* **1973**, *59*, 411−428.
[40] E. Costa, P. G. Pringle, M. Ravetz, *Inorg. Synth.* **1997**, *31*, 284−292.
[41] D. Drew, J. R. Doyle, *Inorg. Synth.* **1972**, *13*, 47−55.
[42] J. X. McDermott, J. F. White, G. M. Whitesides, *J. Am. Chem. Soc.* **1976**, *98*, 6521−6528.
[43] R. Uson, A. Laguna, M. Laguna, *Inorg. Synth.* **1989**, *26*, 85−91.
[44] *SHELXTL, Structure Solution and Determination Package*, Bruker AXS, Madison, WI, USA, **1999**.

Received February 4, 2002
[I02057]

Synthesis, Reactivity and Molecular Structures of Bis(diphenylphosphanyl)methane-Bridged Heterobimetallic Iron−Platinum Isocyanide Complexes: Breaking and Formation of Metal−Metal Bonds

Michael Knorr,*[a] Isabelle Jourdain,[a] Grégorio Crini,[a] Katja Frank,[b] Hermann Sachdev,[b] and Carsten Strohmann[c]

Keywords: Heterobimetallics / Isocyanide ligands / Metal−metal interactions / Iron / Platinum

When $[(OC)_3Fe(\mu\text{-}CO)(\mu\text{-}dppm)PtCl_2]$ (**1**) is allowed to react with stoichiometric amounts of various isocyanides, cleavage of the metal–metal bond occurs, yielding the heterodinuclear isocyanide complexes $[(OC)_4Fe\{\mu\text{-}dppm\}Pt(Cl)_2(CNR)]$ (**2a**: R = 2,6-xylyl; **2b**: R = *o*-anisyl; **2c**: R = benzyl; **2d**: R = cyclohexyl; **2e**: R = tosylmethyl). Reduction of **2a**–**2e** by $NaBH_4$ in the presence of PPh_3 affords the isocyanide-bridged complexes $[(OC)_3Fe(\mu\text{-}C{=}N\text{–}R)(\mu\text{-}dppm)Pt(PPh_3)]$ (**3a**: R = 2,6-xylyl; **3b**: R = *o*-anisyl; **3c**: R = benzyl; **3d**: R = cyclohexyl; **3e**: R = tosylmethyl). Metathesis of **2a**–**2d** with NaI rapidly results in the formation of $[(OC)_4Fe\{\mu\text{-}dppm\}PtI_2(CNR)]$ (**4a**–**4d**), which is slowly transformed under extrusion of CO giving $[(OC)_2IFe\{\mu\text{-}dppm\}(\mu\text{-}CO)PtI(CNR)]$ (**6a**: R = 2,6-xylyl; **6b**: R = *o*-anisyl; **6c**: R = benzyl; **6d**: R = cyclohexyl), bearing an iodine ligand at the iron center. Due to this intramolecular iodide migration from Pt to Fe, an Fe^I d^7 fragment interacts with a Pt^I d^9 fragment through a covalent bond. Alternatively, **6a**–**6d** are obtained by stoichiometric treatment of $[(CO)_3Fe(\mu\text{-}I)(\mu\text{-}dppm)PtI]$ (**5**) with CNR. Single-crystal X-ray diffraction studies are performed on **2d**, **2e** and **3c** as well as on **6d**. In the solid state, the two metal centers of **2e** remain in close contact (3.862 Å), whereas in the case of **2d** they are separated by 6.573 Å after cleavage of the metal–metal bond by CNR.

(© Wiley-VCH Verlag GmbH, 69451 Weinheim, Germany, 2002)

Introduction

The continuing interest in the preparation and reactivity of heterometallic complexes results from the possibility to investigate (i) cooperativity effects between the different metal centers, (ii) metallosite selectivity on reaction with substrate molecules, and comparison with the reactivity of related monometallic complexes and (iii) possible correlations between unusual bonding modes of coordinated ligands and their activation.[1−10] As part of our studies on the coordination and activation of isocyanide ligands on heterodimetallics,[11−16] we have recently shown that heterodinuclear isocyanide-bridged complexes $[(OC)_3Fe(\mu\text{-}C{=}N{-}R)(\mu\text{-}dppm)Pt(PPh_3)]$ with aromatic substituents R (R = 2,6-xylyl, *o*-anisyl, *p*-anisyl; *p*-$C_6H_4NH_2$) can be obtained by treatment of $[(OC)_3Fe\{Si(OMe)_3\}(\mu\text{-}dppm)Pt(H)(PPh_3)]$ with CNR.[15] Alternatively, some bis(diphenylphosphanyl)amine-bridged complexes $[(OC)_3Fe(\mu\text{-}C{=}N{-}R)(\mu\text{-}dppa)Pt(PPh_3)]$ were prepared by selective substitution of the bridging carbonyl ligand of $[(OC)_3Fe(\mu\text{-}C{=}O)(\mu\text{-}dppa)Pt(PPh_3)]$ by CNR.[13]

In contrast to the well-established μ-CNR bonding mode for homodimetallic systems,[17,18] this bonding mode is extremely rare for heterometallic systems,[19] therefore, we are interested in developing synthetic methods for [M(μ-C=N−R)M′] complexes. Here, we report on the reactivity of $[(CO)_3Fe(\mu\text{-}CO)(\mu\text{-}dppm)PtCl_2]$ (**1**) towards various isocyanides, intramolecular redox reactions due to migration of iodo ligands between two adjacent metal centers, and present the molecular structures of several Fe−Pt compounds ligated by terminal or bridging CNR ligands.

Results and Discussion

Reactivity of 1 towards Isocyanides

Since it is easy to substitute the bridging carbonyl ligand of $[(OC)_3Fe(\mu\text{-}C{=}O)(\mu\text{-}dppa)Pt(PPh_3)]$ by CNR (see above), it seemed promising to prepare $[(CO)_3Fe\{\mu\text{-}CNR\}(\mu\text{-}dppm)PtCl_2]$ using Shaw's compound $[(CO)_3Fe\{\mu\text{-}CO\}(\mu\text{-}dppm)PtCl_2]$ (**1**) as the starting material.[20] For the latter compound, the presence of a semi-bridging carbonyl ligand has been established both in solution and in the solid

[a] Laboratoire de Chimie des Matériaux et Interfaces, Université de Franche-Comté, Faculté des Sciences et des Techniques, 16, Route de Gray, 25030 Besançon Cedex, France
E-mail: michael.knorr@univ-fcomte.fr
[b] Institut für Anorganische Chemie der Universität des Saarlandes, Postfach 151150, 66041 Saarbrücken, Germany
[c] Institut für Anorganische Chemie der Universität Würzburg, Am Hubland, 97074 Würzburg, Germany

state. Instead of the anticipated CO substitution reaction, instantaneous opening of the dative iron→platinum bond occurred at ambient temperature on addition of stoichiometric amounts of RNC to a CH_2Cl_2 solution of **1**. The resulting complexes $[(OC)_4Fe\{\mu\text{-dppm}\}Pt(Cl)_2(CNR)]$ (**2a**: R = 2,6-xylyl; **2b**: R = *o*-anisyl; **2c**: R = benzyl; **2d**: R = cyclohexyl; **2e**: R = tosylmethyl) (Scheme 1) were isolated in high yields as yellow solids, which can be handled in air without significant decomposition. They show poor solubility in hexane or Et_2O, but are very soluble in THF or dichloromethane.

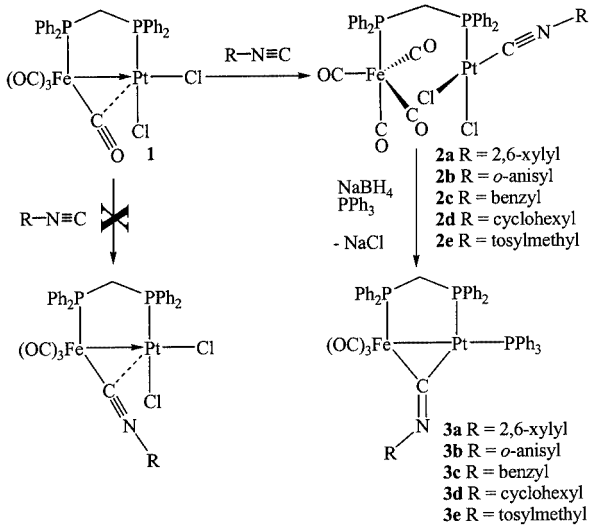

Scheme 1

The IR spectrum of **2a** indicates the breaking of the Fe−Pt bond**.** The pattern and position of the four ν(CO) stretching modes at 2051, 1978, 1942 and 1936 cm^{-1} in the IR spectrum is very similar to that of $[(OC)_4Fe(\eta^1\text{-dppm})]$.[21] The ν(C≡N) vibration at 2199 cm^{-1} is assigned to the terminally bound isocyanide ligand on Pt. Due to the absence of a metal−metal bond, the $^2J_{P,P}$ coupling of the two doublets found at δ = 64.5 (P_{Fe}) and 2.9 ppm (P_{Pt}) in the $^{31}P\{^1H\}$ NMR spectrum, is reduced to 26 Hz compared with 51 Hz reported for **1**. The data of all other derivatives are very similar and are listed in Table 1. The $^{195}Pt\{^1H\}$ NMR spectra of **2a**, **2b** and **2e** give rise to broadened doublets at δ ≈ −2400 ppm, whose $^3J_{Pt,P}$ coupling is not resolved. This is in contrast to the sharp resolved $^{31}P\{^1H\}$ NMR spectra that exhibit a $^3J_{Pt,P}$ coupling of ca. 90 Hz, in addition to an averaged $^1J_{Pt,P}$ coupling of 3300 Hz. The cleavage of the Fe−Pt bond of **2d** and **2e** was further corroborated by an X-ray diffraction study.

Crystal Structures of $[(OC)_4Fe\{\mu\text{-dppm}\}PtCl_2(CNCH_2SO_2C_6H_4Me)]\cdot 0.5CH_2Cl_2$ (2e) and $[(OC)_4Fe\{\mu\text{-dppm}\}PtCl_2(CNC_6H_{11})]$ (2d)

Suitable crystals of **2e**·$0.5CH_2Cl_2$ were grown from CH_2Cl_2/Et_2O. The molecular structure is shown in Figure 1 with selected bond lengths and angles. The cleavage of the metal−metal bond by the isocyanide ligand is shown by the separation of 3.862 Å between the iron center and the platinum center. The angle P(2)−C(17)−P(1) of 121.7(3)° is larger than in the case of $(CO)_3Fe\{\mu\text{-C=N-benzyl}\}(\mu\text{-dppm})Pt(PPh_3)]$ (**3c**), for which a P−C−P angle of 112.8(2)° is found (see below). The coordination sphere around Pt is square-planar, the root mean square deviation from the plane defined by Cl(1), Cl(2), P(2), C(30) and Pt is quite small (0.045 Å). The two chlorine atoms are in a *cis* arrangement [Cl(1)−Pt−Cl(2) = 90.64(10)°], the angles P(2)−Pt−Cl(1) and P(2)−Pt−Cl(2) are 84.93(8)° and 175.53(7)°, respectively. The two Pt−Cl bond lengths of 2.331(2) Å and 2.350(2) Å are very similar. The Pt−P(2) and Fe−P(1) distances of 2.253(2) Å and 2.256 Å are comparable to those found in **3c**. The Pt−C(30)−N−C(31) array of the terminally bound isocyanide ligand {*d*[C(30)]−N = 1.164(11) Å}, having angles of 178.2(7)° and 173.7(9)°, is almost linear. The geometry around the iron center can be described as a weakly deformed trigonal bipyramid, in which the angle C(2)−Fe−P(1) [171.7(4)°] of

Table 1. Selected $^{31}P\{^1H\}$ and $^{195}Pt\{^1H\}$ NMR data (δ in ppm and *J* in Hz)

Complex	$\delta(P_{Fe})$	$\delta(P_{Pt})$	$\delta(PPh_3)$	$^2J_{P,P}$, $^2J_{P,P}$; $^1J_{Pt,P}$, $^3J_{Pt,P}$	$\delta(^{195}Pt)$
2a	64.5 d	2.9 d		26; 3344, 82	−2387 d, br.
2b	64.9 d	3.0 d		26; 3336, 83	−2400 d, br.
2c	64.9 d	3.9 d		23; 3360, 95	
2d	64.3 d	4.0 d		25; 3392, 99	
2e	64.4 d	3.8 d		23; 3271, 96	−2431 d, br.
3a	73.6 dd	32.7 dd	42.0 dd	152, 5, 27; 4266, 2527, 75	−2586 ddd
3b	71.3 dd	30.7 ff	41.6 dd	152, 5, 28; 4188, 2549, 69	−2594 ddd
3c	71.1 dd	30.1 dd	40.8 dd	156, 4, 28; 4208, 2570, 64	−2608 ddd
3d[a]	72.7 d	30.7 dd	39.9 d	155, 31; 4247, 2541, 66	
3e	69.5 dd	28.7 dd	39.3 dd	144, 6, 25; 4129, 2516, 66	−2580 ddd
4b	66.5 d	−1.0 d		28; 3168, 73	
4c	66.7 d	0.6 d		27; 3185, 84	
4d	66.4 d	1.5 d		26; 3219, 96	
6b	49.1 d	6.4 d		75; 3163, 151	
6c	50.4 d	7.2 d		74; 3159, 152	
6d	50.4 d	7.5 d		75; 3175, 152	

[a] T = 243 K.

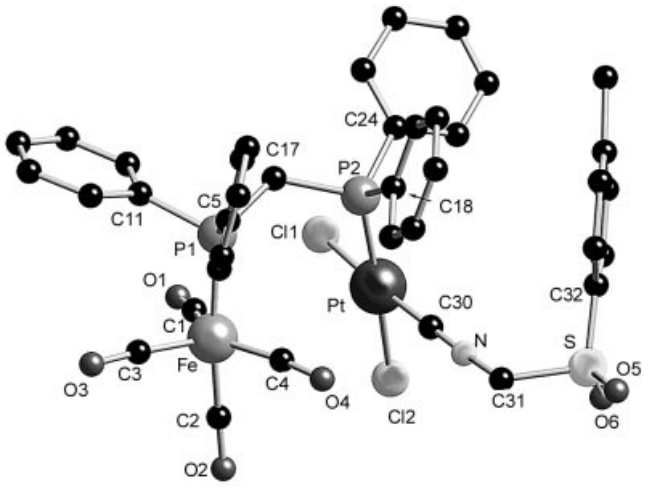

Figure 1. View of the crystal structure of **2e** ,showing the atom numbering scheme; selected bond lengths [Å] and angles [°]: Pt−C(30) 1.876(8), C(30)−N 1.164(11), C(31)−N 1.386(11), Pt−Cl(1) 2.331(2), Pt−Cl(2) 2.350(2), Pt−P(2) 2.253(2), P(2)−C(17) 1.832(6), P(1)−C(17) 1.844(7), Fe−P(1) 2.256(2), Fe−C(1) 1.791(10), Fe−C(2) 1.774(10), Fe−C(3) 1.801(9), Fe−C(4) 1.778(8), C(1)−O(1) 1.156(12), C(2)−O(2) 1.147(12), C(3)−O(3) 1.144(10), C(4)−O(4) 1.151(10); Cl(2)−Pt−Cl(1) 90.64(10), Cl(1)−Pt−P(2) 84.93(8), Pt−C(30)−N 178.2(7), C(30)−N−C(31) 173.7(9), N−C(31)−S 112.8(7), C(31)−S−C(32) 104.5(4), Cl(1)−Pt−C(30) 175.1(2), C(1)−Fe−C(3) 109.6(4), C(1)−Fe−C(2) 109.6(4), C(1)−Fe−C(4) 139.0(4), C(3)−Fe−C(4) 111.3(4), C(2)−Fe−C(4) 85.4(4), C(1)−Fe−P(1) 88.3(3), C(2)−Fe−P(1) 171.7(4), C(3)−Fe−P(1) 92.2(3), C(4)−Fe−P(1) 92.7(4), Fe−C(1)−0(1) 173.2(9), Fe−C(2)−0(2) 179.0(13), Fe−C(3)−0(3) 176.5(8), Fe−C(4)−0(4) 172.8(7), P(1)−C(17)−P(2) 121.7(3)

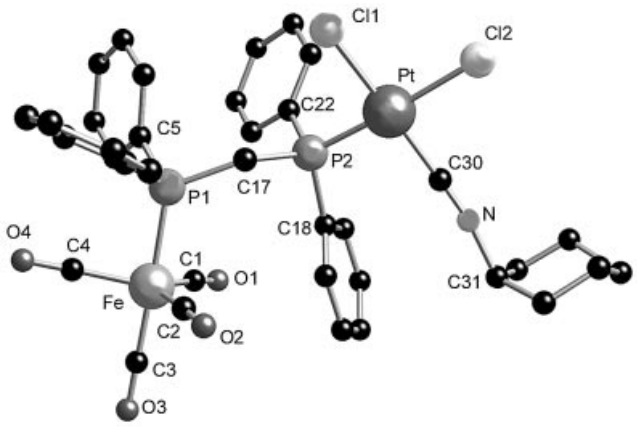

Figure 2. View of the crystal structure of **2d** ,showing the atom numbering scheme; selected bond lengths [Å] and angles [°]: Pt−C(30) 1.929(3), C(30)−N 1.136(6), C(31)−N 1.489(7), Pt−Cl(1) 2.3218(12), Pt−Cl(2) 2.3615(15), Pt−P(2) 2.2540(13), P(2)−C(17) 1.835(4), P(1)−C(17) 1.860(4), Fe−P(1) 2.2565(14), Fe−C(1) 1.784(5), Fe−C(2) 1.798(6), Fe−C(3) 1.787(5), Fe−C(4) 1.810(5), C(1)−O(1) 1.148(6), C(2)−O(2) 1.137(7), C(3)−O(3) 1.136(7), C(4)−O(4) 1.136(4); Cl(2)−Pt−Cl(1) 89.68(5), Cl(1)−Pt−P(2) 88.81(5), Pt−C(30)−N 178.0(5), C(30)−N−C(31) 171.4(5), Cl(1)−Pt−C(30) 176.9(2), C(1)−Fe−C(3) 88.2(2), C(1)−Fe−C(2) 123.1(2), C(1)−Fe−C(4) 119.8(2), C(3)−Fe−C(4) 90.2(2), C(2)−Fe−C(4) 117.1(3), C(1)−Fe−P(1) 92.45(14), C(2)−Fe−P(1) 89.4(2), C(3)−Fe−P(1) 178.2(2), C(4)−Fe−P(1) 88.0(2), Fe−C(1)−0(1) 175.4(4), Fe−C(2)−0(2) 177.2(5), Fe−C(3)−0(3) 178.6(6), Fe−C(4)−0(4) 178.6(4), P(1)−C(17)−P(2) 130.1(2)

the axial ligands deviates slightly from the ideal value. The angles of the equatorial carbonyl ligands deviate considerably from the ideal value of 120°; C(1)−Fe−C(4) and C(1)−Fe−C(3) are 139.0(4) and 109.6(4)°, respectively.

Surprisingly, despite the similarity of the spectroscopic data recorded in solution, the mutual arrangement of the two metal fragments of **2d** in the crystalline state is very different from that of **2e**. Although the geometry and ligand arrangement of each individual moiety remains unaltered (square-planar around Pt and trigonal-bipyramidal around Fe), the two metal centers are far apart from each other (6.573 Å) after cleavage of the metal−metal bond by cyclohexyl isocyanide (see Figure 2). The angle P(2)−C(17)−P(1) [130.1(2)°] is still larger than in the case of **2e**, for which a P−C−P angle of 121.7(3)° is found. Compared with **2e**, the distances Fe−P(1) and Pt−P(2) [2.2565(14) and 2.2540(13) Å, respectively] of **2d** remain almost identical. However, all interligand angles on the iron fragment are now much closer to the values expected for an ideal trigonal-bipyramidal polyhedron. Notably the angles between the equatorial carbonyl ligands C(1), C(2) and C(4) are 123.1(2), 119.8(2) and 117.1(3)°, which are much closer to 120°. Furthermore, the angle P(1)−Fe−C(3) [178.2(2)°] is much closer to 180° than the angle 171.7(4)° found for derivative **2e**.

A very similar important separation of the two dppm-spanned metal fragments has recently been encountered, after cleavage of the dative metal−metal bond of [MeCp-$(OC)_2$Mn(μ-CO)(μ-dppm)PdCl_2] by isocyanides.[22] In the case of [(η^5)-MeCp$(OC)_2$Mn(μ-dppm)Pd(CNxylyl)Cl_2], an X-ray diffraction study determined a separation of 6.31 Å between the square-planar palladium center and the three-legged piano-stool MeCp$(OC)_2$MnP fragment.

These findings outline the flexibility and the rotational degrees of freedom along the M−P−C−P−M′ chains. At present we cannot state whether the different arrangements of **2d** and **2e** are only due to *packing effects* in the crystalline state, or whether the different *electronic behavior* of the CNR ligands may account for this phenomenon. The C_6H_{11} group is known as electron-releasing, whereas the CH_2SO_2*p*-tolyl group should somewhat lower the electron density on Pt by the enhanced propensity of tosylmethyl isocyanide to act as a π-accepting ligand.[14] In the latter case, the proximity of the two adjacent metal centers and the widening of the angle C(1)−Fe−C(4) to 139.0(4)°, may tentatively be interpreted as *incipient dative metallic interaction* between the iron and platinum fragment. [The closest contacts between Pt and C(4) and C(1) are 3.499 Å and 3.819 Å, respectively.] Examples of heterodimetallic complexes with dative Fe→Pt bonds such as [$(OC)_3$Fe(μ-CO)(μ-dppm)PtBr_2] and [$(CO)_3$Fe(μ-I)(μ-dppm)PtI] (**5**) exhibit metal−metal separations of 2.647(4) and 2.523(4) Å, respectively.[20] For the cyclopentadienethiolato compound [$(C_5H_4S)_2$FePdPPh_3], which possesses a weak dative Fe→Pd interaction, a value of 2.878(1) Å has been reported.[23] A separation of 3.784 Å, which is quite close to that of **2e**, has been determined for the dppm-spanned complex [Cp(PPh_3)Ru(μ-dppm)(μ-Cl)PtCl_2].[24] However, in the

latter case a bridging chloro ligand additionally links the two moieties. Of course, further molecular structures of derivatives of **2** ligated by strongly π-accepting CNR ligands are necessary to corroborate (or exclude) this hypothesis.

Reduction of 2a−2e Yielding μ-Isocyanide Complexes

Due to the paucity of heterometallic M(μ-C=N−R)M′ systems, it is desirable to develop facile preparative routes to deepen the knowledge on the structural features and reactivity pattern of this class of compounds. We found that apart from the two strategies mentioned in the introduction, Fe(μ-C=N−R)Pt systems are also accessible using **2a−2e** as precursors. When **2a−2b** were reduced by $NaBH_4$ in the presence of 1 equiv. of PPh_3 using a CH_2Cl_2/MeOH mixture as the solvent, the recently described μ-isocyanide complexes $[(CO)_3Fe(\mu\text{-}C{=}N\text{-aryl})(\mu\text{-dppm})Pt(PPh_3)]$ **3a−3b** were isolated after workup in ca. 60% yield. In an analogous manner, the stable complexes **3c−3e**, possessing μ-CNR bridges with aliphatic groups R, have been obtained in moderate yields as yellow-orange solids. The ^{31}P and ^{195}Pt NMR spectroscopic data, which have already been discussed in detail,[15] are listed in Table 1. A comparison of the ν(C=N) vibration in the IR spectra reveals that the position of this absorption can roughly be correlated with the donor/acceptor properties of the group R. Thus, the CH_2SO_2*p*-tolyl substituent, which is the best π-acceptor in this series, gives rise to a ν(C=N) vibration at 1648 cm^{-1}. For R = xylyl and *o*-anisyl a ν(C=N) vibration at 1667 and 1668 cm^{-1}, respectively, has been reported,[15] and for the benzyl derivative a ν(C=N) vibration appears at 1679 cm^{-1}. Finally, in the case of **3d** with a strongly electron-donating C_6H_{11} group, this stretching mode is shifted to 1689 cm^{-1}.

Crystal Structure of $[(CO)_3Fe\{\mu\text{-}C{=}N\text{-}Bz\}(\mu\text{-dppm})Pt(PPh_3)]\cdot 0.5CH_2Cl_2$ (3c)

The molecular structure of the benzyl derivative is depicted in Figure 3 with selected bond lengths and angles. The Fe−Pt distance of 2.5575(10) Å confirms the existence of a metal−metal bond and is almost identical to those of $[(CO)_3Fe(\mu\text{-}C{=}N{-}R)(\mu\text{-dppm})Pt(PPh_3)]$ and $[(CO)_3Fe(\mu\text{-}C{=}O)(\mu\text{-dppm})Pt(PPh_3)]$ [2.579(4) Å].[21] On the whole, there are many parallels in the overall structure, therefore only the most salient structural features of **3c** will be mentioned. The bridging isocyanide ligand is again symmetrically ligated between the two metal centers, the Fe−C(1) and Pt−C(1) distances are 2.040(5) and 1.984(5) Å, respectively. The angle defined by the two planes Fe−P(1)−P(2)−Pt and Fe−C(1)−Pt is 6.02°. The length of the C(1)=N double bond [1.234(6) Å] compares with that of other dimetallic isocyanide-bridged systems. Distances of 1.239(7) and 1.23(3) Å have been reported for $[Ni_2(\mu\text{-dppm})_2\{\mu\text{-}C{=}NMe\}(CNMe)_2]$ and for $[Pd_2(\mu\text{-dppm})_2\{\mu\text{-}C{=}NMe\}(CNMe)_2][PF_6]_2$.[25,26] The C(1)−N−C(2) bending of 122.0(4)° is even more accentuated than in the above-mentioned homodimetallic Ni−Ni [129.9(6)°] and Pd−Pd systems [131.0(2)°], and parallels that of $[Fe_2(\mu\text{-}C{=}NEt)_3(CNEt)_6]$ [123.1(1)°].[27] Due to the bending of the organic

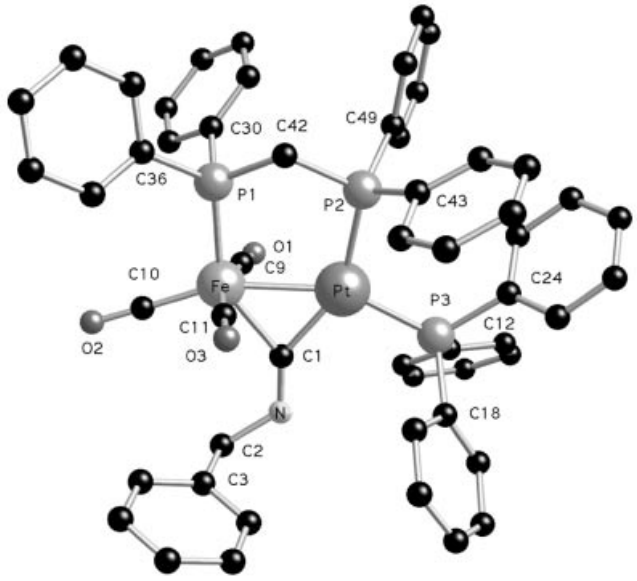

Figure 3. View of the crystal structure of **3c** showing the atom numbering scheme; selected bond lengths [Å] and angles [°]: Fe−Pt 2.5577(10), Fe−P(1) 2.240(2), Pt−P(2) 2.3087(13), Pt−P(3) 2.2632(13), Pt−C(1) 1.984(5), Fe−C(1) 2.040(5), Fe−C(9) 1.788(5), Fe−C(10) 1.762(5), Fe−C(11) 1.786(5), C(1)−N 1.234(6), C(2)−N 1.470(6), C(10)−O(2) 1.150(6), C(10)−O(2) 1.150(6), C(11)−O(3) 1.152(6), P(1)−C(42) 1.854(9), P(2)−C(42) 1.859(5); C(1)−N(1)−C(2) 122.0(4), Pt−C(1)−Fe 78.9(2), Fe−Pt−C(1) 51.51(14), C(1)−Fe−Pt 49.58(12), C(1)−Fe−P(1) 144.08(13), C(1)−Pt−P(2) 148.99(14), C(1)−Pt−P(3) 102.70(14), C(1)−Fe−C(9) 82.1(2), C(1)−Fe−C(10) 110.2(2), C(1)−Fe−C(11) 83.1(2), N−C(1)−Fe 140.0(3), N−C(1)−Pt 140.9(4), P(1)−Fe−Pt 93.63(8), P(2)−Pt−P(3) 107.17(5), Fe−Pt−P(3) 154.18(4), P(1)−C(42)−P(2) 112.8(2)

group R of the isocyanide bridge, two isomeric forms, with orientation towards Pt or Fe, are conceivable a priori. From Figure 3 it can be seen that from a steric point of view, an orientation of the benzyl group towards the carbonyliron fragment is imposed in order to avoid repulsion with the bulky PPh_3 ligand.

Iodide Migration from Pt to Fe

With the objective of obtaining additional information on the parameters influencing the structural features of **2,** we tried to prepare the iodo derivatives $[(OC)_4Fe(\mu\text{-dppm})PtI_2(CNR)]$ (**4**) in a metathesis reaction by addition of an excess of NaI to a CH_2Cl_2/THF solution of **2a−2d** according Scheme 2. Surprisingly, **4a** could not be isolated in a pure form. Instead, after 8 h at ambient temperature, and subsequent workup, red-brown crystals were isolated in a 60% yield. The spectroscopic data and elemental analysis were consistent with the formation of the heterodimetallic complex $[(OC)_2FeI(\mu\text{-dppm})(\mu\text{-CO})PtI(Xylyl\text{-}CN)]$ (**6a**). Compound **6a** can be described as a dinuclear complex, in which the Fe^I d^7 fragment interacts with the Pt^I d^9 fragment through a covalent Fe−Pt bond. This description, implying the formal oxidation of Fe and reduction of Pt, satisfies an 18-e configuration for Fe and a 16-e configuration for Pt. Mechanistically, this reaction can be rationalized as the migration of a *Pt*-bound iodide ligand to Fe,

initiated by the extrusion of a carbonyl ligand (due to the bigger diameter of iodide compared with a chloride ligand). Although an intermolecular ligand transfer cannot be excluded unambiguously, an intramolecular migration seems more probable. This hypothesis is corroborated by the observation that isolated **4c** or **4d** are converted within ca. 8 h quantitatively to **6c**, **6d** after dissolution in CH_2Cl_2. Halide transfer reactions are not unusual in heterodimetallic chemistry.[28−33] For example, the reaction of *cis*-[Pt(DMSO)$_2$Cl$_2$] with [CpRh(CO)(Ph$_2$Ppy)] yielded (via some intermediates) the $Rh^{II}-Pt^{I}$ compound [CpRhCl(μ-Ph$_2$Ppy)Pt(CO)Cl] by mutual CO/chloride exchange.[28]

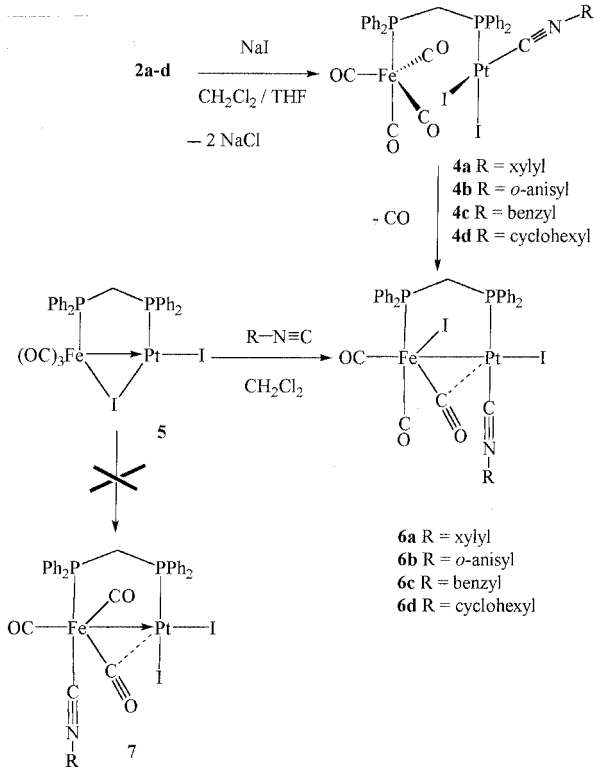

Scheme 2

Spectroscopic Data

^{31}P NMR spectroscopic monitoring of the metathesis reaction of **2b** in a $CDCl_3$/acetone solution revealed the formation of a new species whose chemical shifts [δ = 66.5 (P_{Fe}) and −1.0 (P_{Pt})] and coupling constants ($^2J_{P,P}$ = 28, $^1J_{P,Pt}$ = 3168, $^3J_{P,Pt}$ = 73 Hz) are very similar to those of **2b**, indicating the formation of **4b** as an intermediate. In the course of several hours, a new AX pattern due to **6b** emerged. It consists of two doublets at δ = 49.1 ppm ($^{2+3}J_{P,P}$ = 75 Hz), assigned to the *Fe*-bound phosphorus nucleus, and at δ = 6.4 ppm for the *Pt*-bound phosphorus nucleus. All resonance signals are flanked by ^{195}Pt satellites, the Pt−P couplings are 152 and 3159 Hz. After 7 h, **4b** was completely converted to **6b**. The IR spectrum of **4b** (recorded in CH_2Cl_2) exhibits 4 vibrations due to the Fe(CO)$_4$ fragment, whose positions are, as expected, very close to that of **2b**. However, the ν(C≡N) absorption at 2093 cm^{-1} shifts to a lower frequency by 11 cm^{-1}, relative to the chloro precursor **2b**. The IR spectrum of **6b** exhibits two terminal ν(CO) stretching modes at 2013 and 1947 cm^{-1}, a vibration due to a semi-bridging carbonyl ligand is found at 1840 cm^{-1}. The strong absorption at 2189 cm^{-1} is assigned to the ν(CN) stretching mode of the terminally bound isocyanide ligand on Pt.

We were further interested in examining the reactivity of the iodide-bridged complex **5** towards the addition of stoichiometric amounts of isocyanide. This reaction could also a priori lead to **6** by the coordination of CNR on Pt and the formation of a terminal iron−iodine bond. Alternatively, the formation of an isomeric complex of type **7**, bearing a terminal CNR ligand on a formally Fe^0 center and two iodine ligands on a Pt^{II} center (the two metal atoms connected by a dative metal−metal bond), could be envisaged. However, performing this experiment in dichloromethane at ambient temperature with xylyl-, benzyl- or cyclohexyl isocyanide exclusively afforded **6a**−**6d**, with excellent yields.

It is interesting to compare this reactivity pattern of **5** towards the CNR donor ligand, with the results of Shaw's group who used PPh_3. In the latter case, the iodide bridge between the two metal atoms remained intact and the formation of [(CO)$_3$Fe(μ-I)(μ-dppm)Pt(PPh$_3$)I] was observed.[20]

Crystal Structure of [(OC)$_2$FeI(μ-CO)(μ-dppm)PtI-(CNC$_6$H$_{11}$)]·CH$_2$Cl$_2$ (6d)

Suitable red-violet crystals were obtained by slow diffusion of heptane into a saturated dichloromethane solution of **6d**. The molecular structure of the cyclohexyl derivative, including the atom numbering scheme is shown in Figure 4 with selected bond lengths and angles. The iron and platinum moieties are linked by a dppm bridge giving a five-membered Fe−P−C−P−Pt ring. The Fe−Pt distance of 2.6981(8) Å confirms the existence of a metal−metal bond, and is close to that of [(OC)$_3$Fe{Si(OMe)$_3$}(μ-dppa)Pt(H)(PPh$_3$)] [2.670(2) Å],[15] but appreciably longer than that of **3c**. The Pt−C(3) distance of 2.250(5) Å and the angles Fe−C(3)−O(3) [158.5(4)°] and Pt−C(3)−O(3) [118.6(3)°] indicate the presence of a semi-bridging carbonyl ligand, as suggested by the IR spectra. The Fe atom is located in a distorted octahedral environment due to the semi-bridging C(3)O(3) group [C(2)−Fe−I(1) 114.7(2)°, C(2)−Fe−C(3) 104.1(2)°]; the P(1) and I(1) atoms are in a mutual *cis* arrangement [I(1)−Fe−P(1) 87.42(4)°], whereas the remaining coordination sites are occupied by the Pt atom and three carbonyl groups. The square-planar geometry around Pt [neglecting the weak Pt−C(3) interaction] is achieved by bonding with Fe, P(2), C(29) and I(2). The latter I atom is *cis* to P(2) [I(2)−Pt−P(2) 90.50(4)°] and *trans* to the Fe−Pt bond [I(2)−Pt−Fe 168.95(2)°], forming a torsion angle I(1)−Fe−Pt−I(2) of 15.44°.

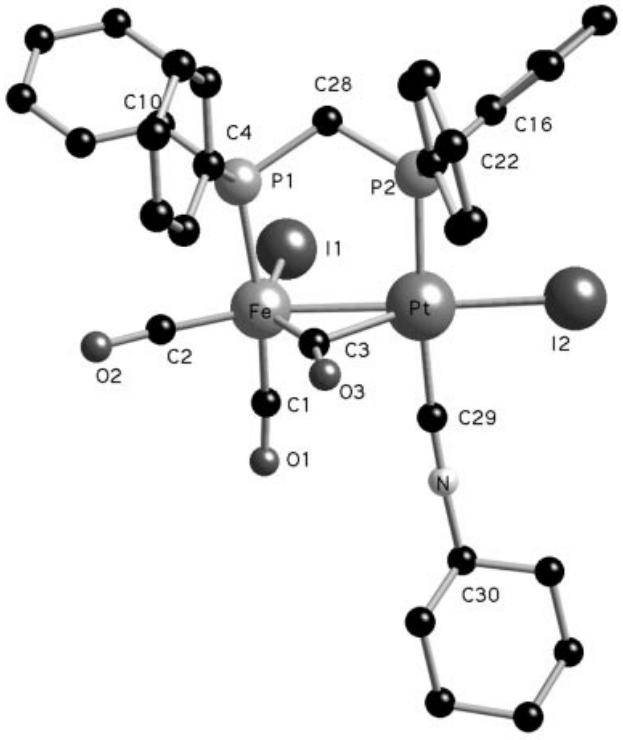

Figure 4. View of the crystal structure of **6d** showing the atom numbering scheme; selected bond lengths [Å] and angles [°]: Fe−Pt 2.6981(8), Fe−I(1) 2.660(5), Fe−P(1) 2.2712(13), Pt−P(2) 2.2891(12), Pt−I(2) 2.6553(6), Pt−C(29) 1.980(5), Pt−C(3) 2.250(5), Fe−C(1) 1.813(6), Fe−C(2) 1.755(6), Fe−C(3) 1.800(4), C(29)−N 1.146(6), C(1)−O(1) 1.130(7), C(2)−O(2) 1.157(7), C(3)−O(3) 1.174(6), P(1)−C(28) 1.822(5), P(2)−C(28) 1.832(4); N−C(29)−Pt 175.6(5), C(29)−N−C(30) 177.4(6), Pt−C(3)−Fe 82.7(2), Fe−Pt−C(29) 93.59(14), I(1)−Fe−Pt 85.40(3), I(2)−Pt−Fe 168.95(2), I(1)−Fe−P(1) 87.42(4), I(2)−Pt−P(2) 90.50(4), C(29)−Pt−P(2) 174.74(13), C(29)−Pt−Fe 93.59(14), C(1)−Fe−C(2) 87.4(2), C(1)−Fe−C(3) 94.2(2), C(2)−Fe−C(3) 104.1(2), O(3)−C(3)−Fe 158.5(4), O(3)−C(3)−Pt 118.6(3), P(1)−Fe−Pt 96.63(4), Fe−Pt−P(2) 91.44(4), P(1)−C(28)−P(2) 111.5(2)

Conclusion

These investigations have shown that **1** is a very useful precursor for the synthesis of heterodimetallic complexes ligated by aliphatic and aromatic isocyanide ligands in a terminal or bridging bonding mode. This study has shown that complexes **2**, resulting from the rupture of the dative Fe→Pt bond of **1**, possess diverging conformations in the crystalline state, depending on the nature of R of the CNR ligand. By varying (i) the steric and electronic properties of R, (ii) the spanning diphosphane ligand and (iii) the substitution of the two *Pt*-bound chloro ligands by other ligands, future studies may elucidate the origin of the different conformations of the Fe−P−C−P−Pt arrays encountered for **2d**, **2e**. Furthermore, the iodo complexes [$(OC)_2$FeI(μ-dppm)(μ-CO)PtI(RCN)] (**6**), obtained by intramolecular halide transfer, seem to be promising starting materials for reactivity studies towards unsaturated small molecules, for the transformation of the reactive CN triple bond to other organic functional groups, such as aminocarbenes, as well as for C−C coupling reactions.[17,34−38]

Experimental Section

General: All reactions were performed in Schlenk-tube flasks under purified nitrogen. Solvents were dried and distilled under nitrogen before use, toluene and hexane from sodium, dichloromethane from P_4O_{10}. Nitrogen was passed through BASF R3-11 catalyst and molecular sieve columns to remove residual oxygen and water. IR spectra were recorded with a Nicolet Nexus 470 spectrometer. Elemental C, H, N analyses were performed with a Leco Elemental Analyser CHN 900. The ^{1}H, ^{31}P{^{1}H}, and ^{13}C{^{1}H} NMR spectra were recorded at 200.13, 81.01 and 50.32 MHz, respectively, with a Bruker ACP 200 instrument and a Bruker Avance 300 MHz (300.13 and 121.49 MHz for ^{1}H and ^{31}P, respectively). ^{31}P chemical shifts were referenced to 85% H_3PO_4 in H_2O, with downfield shifts reported as positive. ^{195}Pt chemical shifts were measured with a Bruker ACP 200 instrument (42.95 MHz) and externally referenced to K_2PtCl_4 in water, with downfield chemical shifts reported as positive. NMR spectra were recorded in pure $CDCl_3$, unless otherwise stated. The presence and amount of CH_2Cl_2 retained in **2a**−**2c**, **2e**, **3c**, **3e** and **6** were determined from the ^{1}H NMR spectra. The reactions were generally monitored by IR spectroscopy in the ν(CO) region. The isocyanides were obtained from Aldrich and Fluka and were used as received.

Preparation of [$(OC)_4$Fe(μ-dppm)$PtCl_2$(CNR)] (2): To a suspension of **1** (409 mg, 0.5 mmol) in CH_2Cl_2) (10 mL), the equivalent amount of CNR was added (over 5 min) in several portions as a solid, or dropwise via a syringe in the case of liquid isocyanides. The resulting clear yellow solution was stirred for a further 10 min, then the solvent was removed affording yellow **2**, in quantitative yields, in sufficient purity for further reactions. If required, **2** can be recrystallized in a refrigerator from a saturated CH_2Cl_2 solution layered with Et_2O or hexane.

2a: Yield: 474 mg. IR (CH_2Cl_2): $\tilde{\nu}$ = 2199 (s) ν(C≡N); 2051 (s), 1978 (m), 1942 (vs), 1936 (sh) ν(CO). ^{1}H NMR: δ = 1.93 (s, 6 H, xylyl−CH_3), 4.52 (t, 2 H, CH_2, $^3J_{P,H}$ = 11.0 Hz), 6.94−7.92 (m, 23 H, phenyl). $C_{58}H_{31}Cl_2FeNO_4P_2Pt{\cdot}CH_2Cl_2$ (949.45 + 84.93): calcd. C 45.298, H 3.22, N 1.35; found C 44.89, H 3.02, N 1.20.

2b: Yield: 475 mg. IR (CH_2Cl_2): $\tilde{\nu}$ = 2205 (s) ν(C≡N); 2050 (s), 1971 (m), 1938 (vs), 1928 (sh) ν(CO). ^{1}H NMR: δ = 3.73 (s, 3 H, OCH_3), 4.53 (t, 2 H, CH_2, $^2J_{P,H}$ = 12.0 Hz), 6.54−7.98 (m, 24 H, phenyl). $C_{37}H_{29}Cl_2FeNO_5P_2Pt{\cdot}CH_2Cl_2$ (951.42 + 84.93): calcd. C 44.04, H 3.01, N 1.35; found C 44.81, H 3.24, N 1.57.

2c: Yield: 467 mg. IR (CH_2Cl_2): $\tilde{\nu}$ = 2238 (s) ν(C≡N); 2051 (s), 1977 (m), 1938 (vs), 1928 (sh) ν(CO). ^{1}H NMR: δ = 4.50 (t, 2 H, CH_2, $^2J_{P,H}$ = 11.0 Hz), 4.26 (s, 2 H, NCH_2), 6.99−7.57 (m, 25 H, phenyl). $C_{37}H_{29}Cl_2FeNO_4P_2Pt{\cdot}CH_2Cl_2$ (935.43 + 84.93): calcd. C 44.73, H 3.06, N 1.37; found C 44.89, H 3.08, N 1.20.

2d: Yield: 463 mg. IR (CH_2Cl_2): $\tilde{\nu}$ = 2205 (s) ν(C≡N); 2050 (s), 1971 (m), 1938 (vs), 1928 (sh) ν(CO). ^{1}H NMR: δ = 3.73 (s, 3 H, OCH_3), 4.53 (t, 2 H, CH_2, $^2J_{P,H}$ = 12.0 Hz), 6.54−7.98 (m, 24 H, phenyl). $C_{36}H_{33}Cl_2FeNO_4P_2Pt$ (927.44): calcd. C 46.62, H 3.59, N 1.51; found C 46.23, H 3.22, N 1.40.

2e: Yield: 506 mg. IR (CH_2Cl_2): $\tilde{\nu}$ = 2223 (s) ν(C≡N); 2052 (s), 1978 (m), 1943 (vs), 1932 (sh) ν(CO). ^{1}H NMR: δ = 2.35 (s, 3 H, CH_3), 3.99 (s, 2 H, NCH_2), 4.40 (t, 2 H, CH_2, $^2J_{P,H}$ = 11.2 Hz), 7.21−7.73 (m, 24 H, phenyl). $C_{38}H_{31}Cl_2FeNO_6P_2PtS{\cdot}0.5\ CH_2Cl_2$

(1013.53 + 42.47): calcd. C 44.13, H 3.06, N 1.33; found C 44.89, H 3.40, N 1.32.

Preparation of [(OC)$_3$Fe(μ-C=N−R)(μ-dppm)Pt(PPh$_3$)] (3): A solution of an excess of $NaBH_4$ (106 mg, 2.8 mmol) in MeOH (5 mL) was added dropwise to a solution of **2** (0.5 mmol) and PPh_3 (131 mg, 0.5 mmol) in CH_2Cl_2 (15 mL). The orange solution was stirred for 1 h, and the solvents were then removed under reduced pressure. Extraction with CH_2Cl_2 afforded **3** as yellow-orange solids in moderate yields (50−60%). Analytically pure **3** was obtained by recrystallization in a refrigerator from a saturated CH_2Cl_2 solution, layered with Et_2O or hexane.

3c: Yield: 282 mg, 52%. IR (CH_2Cl_2): $\tilde{\nu}$ = 1992 (m), 1924 (vs) ν(CO); 1679 (m, br.) ν(C=N). ^{1}H NMR: δ = 3.75 (dt, 2 H, CH_2, $^2J_{P,H}$ = 1.5, 10.0, $^3J_{Pt,H}$ = 39.8 Hz), 4.90 (s, br., 2 H, NCH_2), 6.82−7.55 (m, 40 H, phenyl). $C_{54}H_{44}FeNO_3P_3Pt$·0.5 CH_2Cl_2 (1098.80 + 42.47): calcd. C 57.36, H 3.97, N 1.23; found C 57.34, H 3.94, N 1.27.

3d: Yield: 305 mg, 56%. IR (CH_2Cl_2): $\tilde{\nu}$ = 1988 (m), 1921 (vs) ν(CO); 1689 (m, br.) ν(C=N). ^{1}H NMR: δ = 0.82−1.84 (m, 11 H, C_6H_{11}), 3.71 (t, 2 H, CH_2, $^2J_{P,H}$ = 10.0, $^3J_{Pt,H}$ = 40.0 Hz), 6.89−7.74 (m, 35 H, phenyl). $C_{53}H_{48}FeNO_3P_3Pt$ (1090.82): calcd. C 58.36, H 4.43, N 1.28; found C 58.58, H 4.68, N 1.28.

3e: Yield: 300 mg, 51%. IR (CH_2Cl_2): $\tilde{\nu}$ = 1996 (m), 1928 (vs) ν(CO); 1648 (m, br.) ν(C=N). ^{1}H NMR: δ = 2.17 (s, 2 H, CH_3), 3.75 (t, 2 H, CH_2, $^2J_{P,H}$ =10.0, $^3J_{Pt,H}$ = 40.3 Hz), 4.88 (s, br., 2 H, NCH_2), 6.89−7.55 (m, 40 H, phenyl). $C_{55}H_{46}FeNO_5P_3PtS$·1.5 CH_2Cl_2 (1176.93 + 127.39): calcd. C 52.03, H 3.79, N 1.07; found C 52.04, H 3.98, N 1.26.

Preparation of [(OC)$_2$FeI(μ-dppm)(μ-CO)PtI(CNR)] (6). Method A: NaI, in a 5-fold excess, was added to a solution of **2** (0.2 mmol) in a mixture of THF/CH_2Cl_2 (50:50, 10 mL). The initially orange-yellow solution gradually changed to red-violet. After 8 h, all volatiles were removed under reduced pressure. The residue was redissolved in CH_2Cl_2, NaI and NaCl were filtered off, and the solution concentrated to ca. 5 mL. After layering with heptane, **6** was obtained in the form of air-stable red-violet crystals in yields varying between 50 and 60%. When the reaction was stopped after ca. 1 h by removing all volatiles, the intermediates [(OC)$_4$Fe(μ-dppm)PtI$_2$(CNR)] (**4**) (contaminated by small quantities of **6**) could be isolated after extraction with CH_2Cl_2, as yellow-orange solids. Selected spectroscopic data for **4c**: IR (ATR): $\tilde{\nu}$ = 2224 (m) ν(C≡N); 2048 (s), 1970 (m), 1940 (vs), 1926 (vs) ν(CO). ^{1}H NMR: δ = 4.71 (t, 2 H, CH_2, $^2J_{P,H}$ = 11.0 Hz), 4.21 (s, 2 H, NCH_2), 6.99−7.57 (m, 25 H, phenyl). **4d**: IR (ATR): $\tilde{\nu}$ = 2217 (m) ν(C≡N); 2047 (s), 1968 (m), 1940 (vs), 1927 (vs) ν(CO). **Method B:** An equimolar amount of CNR was added to a solution of **5** (543 mg, 0.5 mmol) in CH_2Cl_2 (15 mL). The red-violet solution was stirred for 15 min after which all volatiles were removed under reduced pressure affording almost quantitatively pure **6**. If required, **6** can be recrystallized in a refrigerator from a saturated CH_2Cl_2 solution, layered with heptane.

6a: Yield: 134 mg, 61%. IR (ATR): $\tilde{\nu}$ = 2183 (s) ν(C≡N); 2011 (vs), 1946 (vs), 1844 (m) ν(CO). ^{1}H NMR: δ = 2.50 (s, 6 H, xylyl−CH_3), 4.55 (t, 2 H, CH_2, $^3J_{P,H}$ = 12.0 Hz), 6.95−7.86 (m, 23 H, phenyl). $C_{37}H_{31}FeI_2NO_3P_2Pt$·$CH_2Cl_2$ (1104.34 + 84.93): calcd. C 38.38, H 2.80, N 1.18; found C 38.53, H 2.70, N 1.17.

6b: Yield: 128 mg, 58%. IR (ATR): $\tilde{\nu}$ = 2188 (s) ν(C≡N); 2012 (vs), 1947 (vs), 1840 (m) ν(CO). ^{1}H NMR: δ = 3.85 (s, 3 H, OCH_3), 4.64 (t, 2 H, CH_2, $^3J_{P,H}$ = 12.0 Hz), 6.64−7.95 (m, 24 H, phenyl). $C_{36}H_{29}FeI_2NO_5P_2Pt$·$CH_2Cl_2$ (1105.87 + 84.93): calcd. C 37.31, H 2.62, N 1.18; found C 37.82, H 3.02, N 1.20.

6c: Yield: 133 mg, 61%. IR (ATR): $\tilde{\nu}$ = 2224 (s) ν(C≡N); 2015 (vs), 1944 (vs), 1837 (m) ν(CO). ^{1}H NMR: δ = 4.57 (m, not resolved, 2 H, CH_2), 5.07 (s, 2 H, NCH_2), 7.08−7.95 (m, 25 H, phenyl). $C_{36}H_{29}FeI_2NO_3P_2Pt$·$CH_2Cl_2$ (1090.32 + 84.93): calcd. C 37.81, H 2.66, N 1.19; found C 37.94, H 3.04, N 1.25.

6d: Yield: 121 mg, 56%. IR (ATR): $\tilde{\nu}$ = 2213 (s) ν(C≡N); 2008 (vs), 1952 (vs), 1851 (m) ν(CO). ^{1}H NMR: δ = 1.33−2.10 (m, 11 H, C_6H_{11}), 4.57 (t, 2 H, CH_2, $^3J_{P,H}$ = 11.5 Hz), 7.06−7.87 (m, 20 H, phenyl). $C_{36}H_{33}FeI_2NO_3P_2Pt$·$CH_2Cl_2$ (1082.35 + 84.93): calcd. C 37.04, H 3.02, N 1.20; found C 37.54, H 3.42, N 1.28.

Collection of the X-ray Data and Structure Determination: Data were collected with a Siemens Stoe AED2 four-circle diffractometer (**3c**) or a Siemens Stoe IPDS (**2d**, **2e**, **6d**) using graphite-monochromated Mo-K_α radiation (λ = 0.71073 Å). The final unit cell parameters were obtained by least squares on the setting angles for 20 reflections with 2Θ = 20−23°. Data were corrected by semi-empirical methods for the absorption correction, using Ψ scans. SHELXS-97 and SHELXL-97 computer programs were used.[39] CCDC-179020 to -179023 contain the supplementary crystallographic data for this paper. These data can be obtained free of charge at www.ccdc.cam.ac.uk/conts/retrieving.html or from the Cambridge Crystallographic Data Centre, 12, Union Road, Cambridge CB2 1EZ, UK [Fax: (internat.) + 44-1223/336-033; E-mail: deposit@ccdc.cam.ac.uk].

Crystal Structure Determination of 2d: Collection of crystallographic data: intensity data were collected using the Ω/2Θ scan mode at 173 K. $C_{36}H_{33}Cl_2FeNO_4P_2Pt$ (927.41): yellow crystals with approximate dimensions 0.4 × 0.3 × 0.2 mm, triclinic, space group $P\bar{1}$; a = 9.713(2), b = 11.393(3), c = 17.435(6) Å, α = 79.91(4), β = 86.45(3), γ = 70.11(13)°, V = 1786.3(8) Å^3, Z = 2, $\rho_{calcd.}$ = 1.724 g cm^{-3}, $F(000)$ = 912; 7273 independent reflections in the scan range 4.74° < 2θ < 54°, of which 6567 with $I > 2\sigma(I)$ were used in the structure solution and refinement for 424 parameters; $R1 = \Sigma|F_o - F_c|/\Sigma|F_o|$ = 0.0330 [$I > 2\sigma(I)$], $wR2 = [\Sigma w(F_o^2 - F_c^2)^2/\Sigma wF_o^4]^{1/2}$ = 0.0896 (all data), GoF = 1.052; anisotropic refinement for non-hydrogen atoms; hydrogen atoms in idealized geometries, except for H(1) and H(2), which were refined isotropically. Highest residual electron density 1.764 e·Å^{-3}.

Crystal Structure Determination of 2e: Collection of crystallographic data: intensity data were collected at 293 K. $C_{38.5}H_{32}Cl_3FeNO_6P_2PtS$ (1055.94): yellow crystals with approximate dimensions 0.2 × 0.3 × 0.4 mm, triclinic, space group $P\bar{1}$; a = 11.178(2), b = 11.245(2), c = 19.578(3) Å, α = 85.392(11), β = 80.148(11), γ = 63.417(10)°, V = 2168.2(5) Å^3, Z = 2, $\rho_{calcd.}$ = 1.617 g cm^{-3}, $F(000)$ = 1038; 6487 independent reflections in the scan range 4.2° < 2θ < 48.5°, of which 6086 with $I > 2\sigma(I)$ were used in the structure solution and refinement for 488 parameters; $R1 = \Sigma|F_o - F_c|/\Sigma|F_o|$ = 0.0628 [$I > 2\sigma(I)$], $wR2 = [\Sigma w(F_o^2 - F_c^2)^2/\Sigma wF_o^4]^{1/2}$ = 0.1615 (all data), GoF = 1.091; anisotropic refinement for non-hydrogen atoms; hydrogen atoms in idealized geometries. Highest residual electron density 2.278 e·Å^{-3}.

Crystal Structure Determination of 3c: Collection of crystallographic data: intensity data were collected at 293 K. $C_{54.5}H_{45}ClFeNO_3P_3Pt$ (1141.21): orange crystals with approximate dimensions 0.2 × 0.3 × 0.35 mm, triclinic, space group $P\bar{1}$; a = 11.713(2), b = 12.779(3), c = 18.798(4) Å, α = 107.03(3), β = 92.26(3), γ = 113.18(3)°, V = 2434(9) Å^3, Z = 2, $\rho_{calcd.}$ = 1.557 g cm^{-3}, $F(000)$ = 1138; 8562 independent reflections in the scan

range $3.62° < 2\theta < 50.0°$, of which 7871 with $I > 2\sigma(I)$ were used in the structure solution and refinement for 594 parameters; $R1 = \Sigma|F_o - F_c|/\Sigma|F_o| = 0.0323$ [$I > 2\sigma(I)$], $wR2 = [\Sigma w(F_o^2 - F_c^2)^2/\Sigma wF_o^4]^{1/2} = 0.0861$ (all data), $GoF = 1.009$; anisotropic refinement for non-hydrogen atoms; hydrogen atoms in idealized geometries. Highest residual electron density 1.452 e·Å^{-3}.

Crystal Structure Determination of 6d: Collection of crystallographic data: intensity data were collected at 173 K. $C_{36}H_{35}Cl_2FeI_2NO_3P_2Pt$ (1167.23): red violet crystals with approximate dimensions 0.3 × 0.2 × 0.2 mm, monoclinic, space group $P2_1/c$; $a = 15.236(3)$, $b = 11.781(2)$, $b = 22.430(5)$ Å, $\beta = 98.17(3)°$, $V = 3985.4(14)$ Å^3, $Z = 4$, $\rho_{calcd.} = 1.945$ g cm^{-3}, $F(000) = 2224$; 6815 independent reflections in the scan range $4.38° < 2\theta < 50.0°$, of which 5560 with $I > 2\sigma(I)$ were used in the structure solution and refinement for 433 parameters; $R1 = \Sigma|F_o - F_c|/\Sigma|F_o| = 0.0289$ [$I > 2\sigma(I)$], $wR2 = [\Sigma w(F_o^2 - F_c^2)^2/\Sigma wF_o^4]^{1/2} = 0.0642$ (all data), $GoF = 0.931$; anisotropic refinement for non-hydrogen atoms; hydrogen atoms in idealized geometries. Highest residual electron density 0.994 e·Å^{-3}.

Acknowledgments

The Deutsche Forschungsgemeinschafte, the Ministère de la Recherche et de la Technologie and the Région de Franche-Comté are gratefully thanked for financial support to M. K., H. S. and C. S.

[1] D. Sonnenberger, J. D. Atwood, *J. Am. Chem. Soc.* **1980**, *102*, 3484−3489.
[2] W. L. Ingham, N. J. Coville, *Inorg. Chem.* **1992**, *31*, 4084−4090.
[3] R. J. Puddephatt, *Chem. Soc. Rev.* **1983**, *12*, 99−127.
[4] B. Chaudret, B. Delavaux, R. Poilblanc, *Coord. Chem. Rev.* **1988**, *86*, 191−243.
[5] J. T. Mague, *J. Cluster Sci.* **1995**, *6*, 217−269.
[6] *Metal Clusters in Chemisty* (Eds.: P. Braunstein, L. A. Oro, P. R. Raithby), Wiley-VCH, Weinheim, **1999**.
[7] P. Braunstein, J. Rosé, "Catalysis and related reactions with compounds containing heteronuclear metal-metal bonds", in *Comprehensive Organometallic Chemistry II* (Eds.: E. W. Abel, F. G. A. Stone, G. Wilkinson), Elsevier, Oxford, **1995**, p. 351−385.
[8] P. Braunstein, M. Knorr, C. Stern, *Coord. Chem. Rev.* **1998**, *178−180*, 903−965.
[9] N. Wheatley, P. Kalck, *Chem. Rev.* **1999**, *99*, 3379−3420.
[10] L. H. Gade, *Angew. Chem.* **2000**, *112*, 2768−2789; *Angew. Chem. Int. Ed.* **2000**, *39*, 2658−2678.
[11] M. Knorr, C. Strohmann, P. Braunstein, *Organometallics* **1996**, *15*, 5653−5663.
[12] M. Knorr, P. Braunstein, A. Tiripicchio, F. Ugozzoli, *J. Organomet. Chem.* **1996**, *526*, 105−116.
[13] M. Knorr, C. Strohmann, *Eur. J. Inorg. Chem.* **1998**, 495−499.
[14] M. Knorr, C. Strohmann, *Organometallics* **1999**, *18*, 248−257.
[15] M. Knorr, C. Strohmann, *Eur. J. Inorg. Chem.* **2000**, 241−252.
[16] P. Braunstein, M. Knorr, G. Reinhard, U. Schubert, T. Stährfeldt, *Chem. Eur. J.* **2000**, *6*, 4265−4278.
[17] E. Singleton, H. E. Oosthuizen, *Adv. Organomet. Chem.* **1983**, *22*, 209−310.
[18] D. Lentz, *Angew. Chem.* **1994**, *106*, 1377−1393; *Angew. Chem. Int. Ed. Engl.* **1994**, *33*, 1315−1331.
[19] K. S. Ratliff, P. E. Fanwick, C. P. Kubiak, *Polyhedron* **1990**, *9*, 2651−2653.
[20] G. B. Jacobsen, B. L. Shaw, M. Thornton-Pett, *J. Chem. Soc., Dalton Trans.* **1987**, 3079−3083.
[21] X. L. R. Fontaine, G. B. Jacobsen, B. L. Shaw, M. Thornton-Pett, *J. Chem. Soc., Dalton Trans.* **1988**, 741−750.
[22] P. Braunstein, M. Knorr, M. Strampfer, Y. Dusausoy, D. Bayeul, A. DeCian, J. Fischer, P. Zanello, *J. Chem. Soc., Dalton Trans.* **1994**, 1533−1547.
[23] M. Cowie, R. Dickson, *J. Organomet. Chem.* **1987**, *326*, 269−280.
[24] M. E. Tess, P. L. Hill, K. E. Torraca, M. E. Kerr, K. A. Abboud, L. McElwee-White, *Inorg. Chem.* **2000**, *39*, 3942−3944.
[25] D. L. DeLaet, P. E. Fanwick, C. P. Kubiak, *Organometallics* **1986**, *5*, 1807−1811.
[26] M. M. Olmstead, H. Hope, L. S. Benner, A. L. Balch, *J. Am. Chem. Soc.* **1977**, *99*, 5502−5503
[27] J. M. Basset, G. K. Barker, M. Green, J. A. K. Howard, F. G. A. Stone, W. C. Wolsey, *J. Chem. Soc., Dalton Trans.* **1981**, 219−227.
[28] S. L. Schiavo, E. Rotondo, G. Bruno, F. Faraone, *Organometallics* **1991**, *10*, 1613−1620.
[29] B. F. Hoskins, R. J. Steen, T. W. Turney, *J. Chem. Soc., Dalton Trans.* **1984**, 1831−1836.
[30] J. T. Mague, *Inorg. Chem.* **1994**, *13*, 4261−4270.
[31] M. P. Brown, D. Burns, R. Das, P. A. Dolby, M. M. Harding, R. W. Jones, E. J. Robinson, A. K. Smith, *J. Chem. Soc., Dalton Trans.* **1991**, 351−354.
[32] G. K. Anderson, *J. Organomet. Chem.* **1989**, *368*, 385−390.
[33] J. P. Farr, M. M. Olmstead, N. M. Rutherford, F. E. Wood, A. L. Balch, *Organometallics* **1983**, *2*, 1758−1762.
[34] M. E. M. Badley, J. Chatt, R. L. Richards, *J. Chem. Soc. A* **1971**, 21.
[35] R. Bertani, M. Mozzon, F. Benetollo, G. BombierI, R. A. Michelin, *J. Chem. Soc., Dalton Trans.* **1990**, 1197−1205.
[36] K. L. Lu, C. J. Chen, Y. W. Lin, H. W. Gau, F. E. Hong, Y. S. Wen, *Organometallics* **1993**, *12*, 2188−2196.
[37] F. E. Hahn, L. Imhoff, *Organometallics* **1997**, *16*, 763−769.
[38] C. Collazoi, D. Rodewald, H. Schmidt, D. Rheder, *Organometallics* **1996**, *15*, 4884−4887.
[39] G. M. Sheldrick, *SHELXL-97, SHELXS-97*, Universität Göttingen, Germany, **1997**.

Received February 11, 2002
[I02070]

The Case of (2,3,9,10-Tetramethyl-1,4,8,11-tetraazacyclotetradeca-1,3,8,10-tetraene)(H_2O)$Co^{III}-OOR^{2+}$ (R = CH_2OH, CH_2CN, CCl_3) and Reactions with the Methylperoxyl Radical[‡]

Ela Solomon-Rapaport,[a] Alexandra Masarwa,*[a] Haim Cohen,[a,b] Joan S. Valentine,[c] and Dan Meyerstein[a,d]

Keywords: Cobalt / Peroxides / Radicals / Radiation chemistry

The long-lived transient complexes (2,3,9,10-tetramethyl-1,4,8,11-tetraazacyclo-tetradeca-1,3,8,10-tetraene)(H_2O)-Co^{III}–OOR^{2+}, [(tim)(H_2O)Co^{III}–O_2R]$^{2+}$ (R = CH_2OH, CH_2CN, CCl_3) were prepared from the reaction of [Co^{II}(tim)(H_2O)$_2$]$^{2+}$ with the corresponding peroxyl radicals, applying radiation chemistry techniques. The resultant transient complexes, which are relatively stable (lifetime of days), were subsequently treated with methylperoxyl ($CH_3O_2^{\cdot}$) radicals to form [Co^{III}(tim)(H_2O)$_2$]$^{3+}$ and formaldehyde. The results point out that the $CH_3O_2^{\cdot}$ radicals rapidly oxidize MOOR peroxides.

(© Wiley-VCH Verlag GmbH, 69451 Weinheim, Germany, 2002)

Introduction

Peroxyl radicals are key intermediates in a large variety of oxidation processes that include, amongst others, catalytic oxidations by peroxides, which proceed via radical mechanisms[1] (for example processes which involve the Fenton reaction[2]), catalytic oxidations by dioxygen,[3] and radical processes, involving organic radicals, in oxygenated solutions.[4] Of special importance here are deleterious radical processes in biological systems.[5] It is therefore not surprising that the properties of peroxyl radicals have been studied by many research teams and summarized in several comprehensive reviews.[6]

Surprisingly enough the kinetics and reaction mechanisms of peroxyl radicals with different types of peroxides have not been studied — no rates of such reactions are reported in the compilation of the rates of reaction of peroxyl radicals.[4] This is surprising as peroxides are formed in many of the reactions of peroxyl radicals and might therefore participate in the processes studied and thus affect the nature of the final products in a variety of catalytic oxidations and biological processes. Of special importance are systems where one of the reactants is a transition metal peroxo complex, as intermediates of this type are formed in most catalytic — including enzymatic — processes.[1–3]

Recently, while studying the properties of the relatively long lived peroxide [L^1(H_2O)$Co^{III}-OOCH_3$]$^{2+}$ (L^1 = tim = 2,3,9,10-tetramethyl-1,4,8,11-tetraazacyclotetradeca-1,3,8,10-tetraene) it was noted that the $CH_3OO^{\cdot}$ radical reacts with it via reaction (1):[7]

$$[L^1(H_2O)Co^{III}-OOCH_3]^{2+} + CH_3OO^{\cdot} \rightarrow [L^1Co^{II}(H_2O)_2]^{2+} + CH_2O + CH_3OH + O_2 \quad (1)$$

$k = 1.5 \times 10^9$ M^{-1}s^{-1} [7]

i.e. via a mechanism which yields the same products as one of the possible mechanisms for the decomposition of $CH_3OOOOCH_3$,[8] and thus results in the same products as the dimerization of the peroxyl radical. However, the formation of the dimer $CH_3OOOOCH_3$ in this reaction seems unlikely. It is therefore of interest to note that the same products would also be expected if the peroxyl radical acts as a reducing agent towards the [L^1(H_2O)$Co^{III}-OOCH_3$]$^{2+}$ peroxide. {The CH_3OO^+ formed will decompose in aqueous solutions, maybe synchronously, into dioxygen and methanol and the [L^1(H_2O)$Co^{II}-OOCH_3$]$^+$ into [L^1Co^{II}(H_2O)$_2$]$^{2+}$ and CH_3OOH which yields CH_2O}. In principle, the same products will also be formed if the peroxyl radicals oxidize the [L^1(H_2O)$Co^{III}-OOCH_3$]$^{2+}$ peroxide forming [L^1(H_2O)$Co^{IV}-OOCH_3$]$^{3+}$ and CH_3OO^-. {[L^1(H_2O)-

[‡] On the Chemical Properties of the Transient Complexes L_mM^{n+1}-OOR, Part 2. Part 1: Ref.[7]

[a] Chemistry Department Ben-Gurion University of the Negev, Beer-Sheva, Israel
[a,b] Nuclear Research Centre Negev, Beer-Sheva, Israel
[c] Dept. Chem. & Biochem., University of California at Los Angeles, CA 90095 USA
[a,d] The College of Judea and Samaria, Ariel, Israel
E-mail: massarwa@bgumail.bgu.ac.il

$Co^{IV}-OOCH_3]^{3+}$ has then to decompose into $[L^1Co^{II}(H_2O)_2]^{2+} + CH_3^+ + O_2$ in order to form the observed products.} However, as L^1 stabilizes low-valent complexes due to the four imine ligating groups, the formation of a Co^{IV} transient complex seems unlikely. However, the results of this study point out that the peroxyl radicals oxidize the peroxide bound to the central cation.

The reaction of the peroxyl radical with $[L^1(H_2O)Co^{III}-OOCH_3]^{2+}$ is extremely fast,[7] even faster than the dimerization reaction of the radical ($CH_3OO^{\cdot} + CH_3OO^{\cdot}$ = products, $k = 4 \times 10^8$ M^{-1}s^{-1}).[9] This observation is of special interest as the reactions of peroxyl radicals with many transition metal complexes yield transient complexes of the type $L_mM^{n+1}-OOR$,[5b] and complexes of this type are also formed in a variety of biological and catalytic processes involving oxidation by peroxides or dioxygen.[1−3] Recent reports suggest that these transient complexes are relatively stable in some systems.[10] In some cases for transient complexes of the type $L_mM^{n+1}-OOH$ the reversible, pH dependent, switching of the hydro-peroxide complex and the peroxide complex has been demonstrated.[11] Reactions of the $L_mM^{n+1}-OOR$ complexes with peroxyls are therefore mechanistically of similar importance to the reaction of high-valent iron-oxenes with peroxides.[12]

It therefore seemed of crucial importance to study the mechanisms and rates of reactions of a variety of peroxyl radicals with a variety of peroxides in order to elucidate the detailed mechanisms of these reactions and the factors that affect them and their rates. For the present study radiation chemistry techniques were chosen.[13,14] In order to obtain a better understanding of the mechanisms of the reactions studied it was decided to prepare relatively stable $[L(H_2O)Co^{III}-OOR]^{2+}$ ($R \neq CH_3$) complexes and react them with $CH_3O_2^{\cdot}$ radicals. Such a study was expected to yield different final products depending on whether the $CH_3O_2^{\cdot}$ radical reacted as an oxidizing or as a reducing agent. The results demonstrate that the complexes with R = CH_2OH, CH_2CN, CCl_3 are indeed stable enough.

Results

Formation of the Transients $[(tim)(H_2O)Co^{III}-OOR]$

The following solutions were irradiated by a short electron pulse from the linear accelerator. *MeOH/CH₃CN system:* 70% N_2O and 30% O_2 saturated solutions containing 0.3 M MeOH or CH_3CN and $[Co(tim)(H_2O)_2]^{2+}$ $(0.5-2.0) \times 10^{-4}$ M at pH = 3.0.

CCl_4 system: 70% Helium or Argon and 30% O_2 saturated solutions containing 0.1% CCl_4, 10% 2-propanol and $[Co(tim)(H_2O)_2]^{2+}$ $(0.5-2.0) \times 10^{-4}$ M at pH = 3.0.

Under these conditions more than 90% of the primary radicals are converted into the desired $^{\cdot}OOR$ (R = CH_2OH, CH_2CN, CCl_3) radicals during the pulse (see Exp. Sect.). In all the systems studied a formation reaction was observed after conversion of the initially formed radicals into the peroxyl radicals. A typical reaction is shown in Figure 1. The formation of the transients obey pseudo first order rate laws, under conditions of excess $[Co(tim)(H_2O)_2]^{2+}$, and the observed rates are proportional to the initial $[Co(tim)(H_2O)_2]^{2+}$ concentration (see Figure 2). The rates are independent of the concentration of all other components of the solution, pH, pulse intensity and wavelength of observation. The kinetics of the formation of the transient complexes indicate that they are produced from a reaction between $[Co(tim)(H_2O)_2]^{2+}$ and the specific peroxyl radical formed by the radiation, as in the reaction of $[Co(tim)(H_2O)_2]^{2+}$with methylperoxyl radicals.[7] Thus it is proposed that the reaction observed is:

$$[Co(tim)(H_2O)_2]^{2+} + RO_2^{\cdot} \rightarrow [(tim)(H_2O)Co^{III}-OOR]^{2+} \quad (2)$$

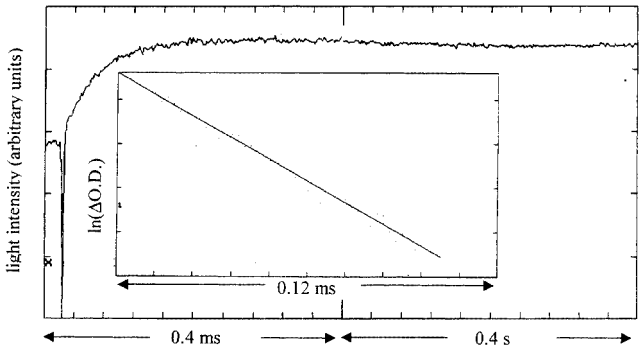

Figure 1. Increase of the absorption (at 314 nm) due to the formation of $[(tim)(H_2O)Co^{III}-OOCH_2CN]^{2+}$ in the presence of oxygen (30% O_2, 70% N_2O) and first order plot (insert); conditions: 0.3 M CH_3CN, 5×10^{-5} M $[Co(tim)(H_2O)_2]^{2+}$

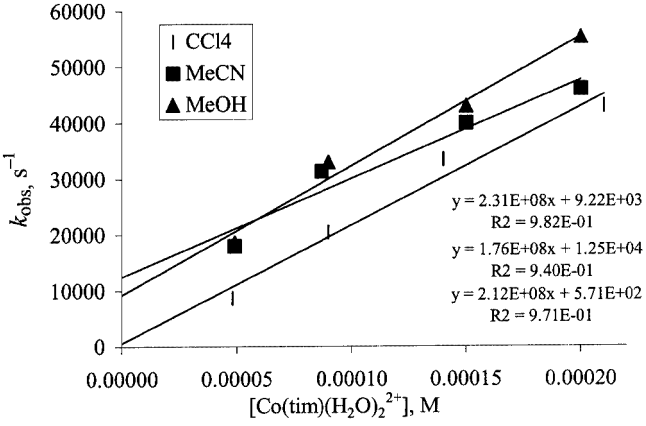

Figure 2. Dependence of k_{obs} for the transients formation on $[Co(tim)(H_2O)_2]^{2+}$

The derived second order rate constants, i.e. the specific rate constants of the cobalt peroxo complex formation, are calculated as $(1.8-2.3) \times 10^8$ M^{-1}s^{-1}, in good agreement with the value measured for the formation of the methylperoxo complex,[7] see Table 1.

Table 1. Formation rate constants of the complexes $[(tim)(H_2O)Co^{III}-OOR]$

R	$k_f \times 10^{-8}$ M^{-1}s^{-1} ± 0.3
CH_2OH	2.3
CH_2CN	1.8
CCl_3	2.1
CH_3	1.8 [7]

Decomposition of the Transients $[(tim)(H_2O)Co^{III}-OOR]$

The transient complexes are relatively long lived. The transient complexes absorb in the UV region similar to $[(tim)(H_2O)Co^{III}-O_2CH_3]^{2+}$,[7] and they do not absorb around 520 nm where the absorption spectrum of $[Co(tim)(H_2O)_2]^{2+}$ has a maximum. The complex with R = CH_2CN is the longest lived one — it decomposes within about eight days — followed by R = CH_2OH, decomposing within 2.5 days, and R = CCl_3, decomposing within 1.5 days under the experimental conditions. Figure 3 shows a typical decomposition sequence. In comparison to these $[(tim)(H_2O)Co^{III}-O_2CH_3]^{2+}$ has a half life time of only approximately ten minutes at pH = 3.0 under the experimental conditions.[7] The final product of the decomposition in all cases is $[(tim)Co(H_2O)_2]^{3+}$ as verified by comparison of its spectrum with the spectra obtained after several days (see Figure 3).

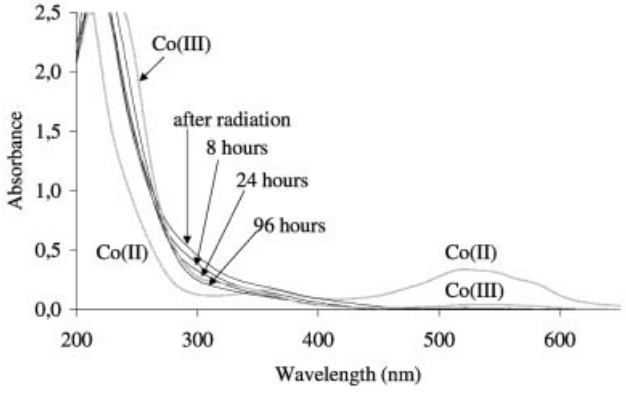

Figure 3. Decomposition sequence of the transient $[tim(H_2O)Co^{III}-OOR]$ (R = CH_2OH) over a period of four days after irradiation of an aqueous solution (70% N_2O and 30% O_2 saturated) containing $[Co(tim)(H_2O)_2]^{2+}$ (9.6×10^{-5} M) and CH_3OH (0.3 M) for 45 min in a ^{60}Co γ-source

Reaction of the Transients $[(tim)(H_2O)Co^{III}-OOR]$ (R = CH_2CN, CH_2OH) with the $^{\cdot}OOCH_3$ Radical

As the resulting peroxo complexes proved to be so stable, although experiments to purify them by ion exchange failed, these complexes were considered ideal candidates to investigate their reaction with a different peroxyl radical (reaction 3).

$$[(tim)(H_2O)Co^{III}-OOR]^{2+} + R'O_2^{\cdot} \rightarrow \text{products} \quad (3)$$

Initially, the simplest peroxyl radical, methylperoxyl, was chosen as we had previously investigated its reaction with the $[Co(tim)(H_2O)_2]^{2+}$ complex.[7] For these experiments the solutions were irradiated twice: during the first irradiation the relatively stable peroxo cobalt complex was formed and in the second irradiation the methylperoxyl radical was formed in the presence of the long-lived metal peroxy complex. The reaction of the peroxo cobalt complex with the methylperoxyl radical was monitored by recording UV/Vis spectra and measuring the amount of formaldehyde produced in the systems.

Solutions prepared as above to yield the peroxo cobalt complexes, for two different cobalt complex concentrations for each system (7.5×10^{-5} and 9.6×10^{-5} M for R = CH_2CN and 9.7×10^{-5} and 1.2×10^{-4} M for R = CH_2OH), were irradiated in the ^{60}Co γ-source for 35 and 45 minutes for R = CH_2CN and 40 and 55 minutes for R = CH_2OH. These times were calculated to yield a slight excess of the peroxyl radical over the $[(tim)Co(H_2O)_2]^{2+}$ complex and thus a radiation dose sufficient to convert all the $[(tim)Co(H_2O)_2]^{2+}$ complex into the specific peroxo cobalt complex, as verified by the absence of the specific absorbance of $[(tim)Co(H_2O)_2]^{2+}$ at 520 nm. The yield of the peroxo cobalt complex was calculated accordingly by the disappearance of the absorbance at 520 nm. Before the second radiation two thirds (8 mL) of the derived solution had N_2O bubbled through it; DMSO was then added to achieve a final concentration of 1 M, and distilled water saturated with O_2 added to give a final volume of 12 mL and a final concentration of 30% dioxygen and 70% N_2O. These solutions were then irradiated in the ^{60}Co γ-source by an additional dose producing $CH_3O_2^{\cdot}$ radicals so that

Table 2. Formaldehyde produced during the reaction of the complexes $[(tim)(H_2O)Co^{III}-OOR]^{2+}$ with the methylperoxyl radical

R	$[(tim)Co(H_2O)_2{}^{2+}]_{init}$ M	$[(tim)(H_2O)Co^{III}-OOR]$[a] M	$[H_2CO]$ M
CH_2CN	7.5×10^{-5}	5.0×10^{-5}	5.1×10^{-5}
CH_2CN	9.6×10^{-5}	6.4×10^{-5}	5.9×10^{-5}
CH_2OH	9.7×10^{-5}	6.1×10^{-5}	5.8×10^{-5}[b]
CH_2OH	1.2×10^{-4}	8.2×10^{-5}	7.4×10^{-5} [b]

[a] Approximately 2/3 of the derived concentration after the first irradiation as measured by the disappearance of the UV/Vis band due to $[(tim)Co(H_2O)_2]^{2+}$. [b] These values were corrected for those derived in blank solutions.

$[CH_3O_2^{\cdot}] = 1.1[(tim)(H_2O)Co^{III}-OOR^{2+}]$. The UV/Vis spectra of these solutions were recorded. The spectra demonstrated that the $[(tim)(H_2O)Co^{III}-OOR]^{2+}$ complexes were consumed during the second irradiation and transformed into $[Co^{III}(tim)(H_2O)_2]^{3+}$; no $[Co^{II}(tim)(H_2O)_2]^{2+}$ was formed during the second irradiation.

The yields of formaldehyde found in the two systems after the second irradiations are tabulated in Table 2. It should be noted that no formaldehyde was produced for R = CH_2CN after the first irradiation, i.e. during the formation of the $[(tim)(H_2O)Co^{III}-OOCH_2CN]^{2+}$ complex. For R = CH_2OH a slight amount of formaldehyde, similar to a blank solution containing only methanol, was produced after the first irradiation, probably due to the reaction of $^{\cdot}O_2CH_2OH$ radicals with each other.

Discussion

Formation of the Transients $[(tim)(H_2O)Co^{III}-OOR]^{2+}$

The rate constants of the reactions of $[Co(tim)(H_2O)_2]^{2+}$ with the peroxyl radicals $^{\cdot}OOR$ (R = CH_2OH, CH_2CN, CCl_3) to form $[(tim)(H_2O)Co^{III}-OOR]^{2+}$ obtained in this work, $k = (1.8-2.3) \times 10^8$ M^{-1}s^{-1} agree well with the value of $k = (1.8 \pm 0.3) \times 10^8$ M^{-1}s^{-1} reported earlier for R = CH_3 [7] (see Table 1). These rates are in agreement with the known rates of ligand exchange of cobalt(II) in such complexes,[15] and indicate that the rate-determining step in these reactions is the ligand exchange, in agreement with reports for a variety of radical reactions with transition metal complexes.[15b]

The very long lifetime of the $[(tim)(H_2O)Co^{III}-OOR]^{2+}$ transient complexes suggests that k_{-2} is very low, otherwise the transient complexes would decompose much faster via 2 $RO_2^{\cdot} \rightarrow$ products or via $RO_2^{\cdot}$ + $[(tim)(H_2O)Co^{III}-OOR]^{2+}$.

$$[Co(tim)(H_2O)_2]^{2+} + RO_2^{\cdot} \underset{k_{-2}}{\rightleftharpoons} [(tim)(H_2O)Co^{III}-OOR]^{2+} \quad (2)$$

The lifetimes of the transient complexes are relatively long, in the range of days at pH = 3.0 under the experimental conditions. As the transient complexes are strong oxidizing agents, such long lifetimes suggest that reactions of transients of this type with different substrates might play a crucial role both in catalytic systems and in deleterious biological processes.

Reaction of the Transients $[(tim)(H_2O)Co^{III}-OOR]^{2+}$ (R = CH_2CN, CH_2OH) with the $^{\cdot}OOCH_3$ Radical

The reaction of $[(tim)(H_2O)Co^{III}-OOR]^{2+}$ (R = CH_2CN, CH_2OH) with $^{\cdot}OOCH_3$ radicals was followed and shown to produce formaldehyde and $[Co^{III}(tim)(H_2O)_2]^{3+}$ in all cases. The amount of formaldehyde produced is equal to the concentration of the peroxometal complex reacted with the methylperoxyl radical.

The observation that all the transient complexes $[(tim)(H_2O)Co^{III}-OOR]^{2+}$ decomposed during the second irradiation suggests that under the experimental conditions the rate of reaction (4) is relatively fast, competing with reaction (5).

$$[(tim)(H_2O)Co^{III}-OOR]^{2+} + CH_3O_2^{\cdot} \rightarrow \text{products} \quad (4)$$

$$2CH_3O_2^{\cdot} \rightarrow \text{products} \ (k_5 = 4 \times 10^8 \text{ M}^{-1}\text{s}^{-1}) \quad (5)$$

From the dose rate of the ^{60}Co source and k_5 one can calculate (see Exp. Sect.) that $k_4 \geq 2 \times 10^5$ M^{-1}s^{-1}.

The fact that CH_2O is quantitatively formed in reaction (4), and no CH_2O is formed when the solutions are irradiated without the addition of DMSO, proves that the $CH_3O_2^{\cdot}$ radicals react as an oxidizing agent in this reaction. As the redox potential of the $CH_3O_2^{\cdot}$ radicals, 0.77 V vs. NHE,[8] is probably too low to oxidize the central Co^{III} cation, it is proposed that the reaction observed is:

$$[(tim)(H_2O)Co^{III}-OOR]^{2+} + CH_3O_2^{\cdot} \rightarrow [(tim)(H_2O)Co^{III}-OOR]^{3+} + CH_3O_2^{-} \quad (6)$$

followed by

$$CH_3O_2^{-} + H_3O^{+}/H_2O \rightarrow CH_3OOH + H_2O/OH^{-} \quad (7)$$

$$CH_3OOH \rightarrow CH_2O + H_2O \quad (8)$$

and as the other final product is $[Co^{III}(tim)(H_2O)_2]^{3+}$ by

$$[(tim)(H_2O)Co^{III}-(^{\cdot}OOR)]^{3+} \rightarrow [Co^{III}(tim)(H_2O)_2]^{3+} + {}^{\cdot}OOR \rightarrow \text{products} \quad (9)$$

It is of interest to note that the final product of reaction (1), which is analogous to reaction (6), is $[Co^{III}(tim)(H_2O)_2]^{2+}$ and not $[Co^{II}(tim)(H_2O)_2]^{3+}$. If reaction (1) proceeds via an analogous mechanism to reaction (6) one has to conclude that the mechanism of decomposition of the transient complexes $[(tim)(H_2O)Co^{III}-(^{\cdot}OOR)]^{3+}$ depends on the redox potentials of the $ROO^{+}/ROO^{\cdot}$ couples. Electron-withdrawing substituents such as -CN and -OH are expected to shift this potential anodically and therefore these transient complexes decompose via the right pathway in the scheme whereas the transient with R = CH_3 decomposes via the left pathway.

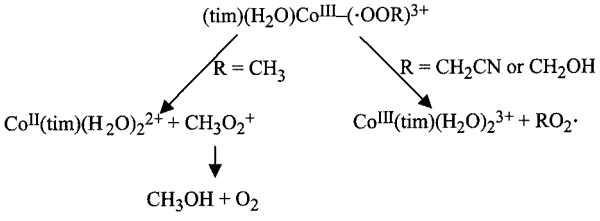

In order to verify this hypothesis other stable complexes of the type $[(L)(H_2O)Co^{III}-OOR]$ have to be found where R is an electron-donating substituent.

Concluding Remarks

The results obtained in this study suggest that transient complexes of the type $L_mM^{n+1}-OOR$ might be relatively stable, at least for $M^{n+1} = Co^{III}$, even in aqueous solutions.

The results demonstrate that $RO_2^{\cdot}$ radicals react by fast reactions with complexes of the type $L_mM^{n+1}-OOR$. It is suggested that these reactions proceed via $R'O_2^{\cdot} + LM^{n+1}-(^{-}OOR) \rightarrow R'O_2^{-} + LM^{n+1}-(^{\cdot}OOR)$.

These reactions might be of crucial importance in a variety of catalytic and biological processes.

Experimental Section

Materials: All solutions were prepared from A.R. grade chemicals and from distilled water further purified by passing through a Milli Q Millipore setup, final resistivity >10 MΩ/cm.

$[Co(tim)Cl_2]PF_6$ was prepared according to literature methods[16] and characterized by NMR spectroscopy and UV/Vis spectrophotometry. Solutions of $[Co(tim)Cl_2]^+$ at pH = 2 were reduced by the introduction of the Adams catalyst, PtO_2, and bubbling dihydrogen for ca. 1 h. The spectrum of $[Co(tim)(H_2O)_2]^{2+}$ thus obtained is identical to that reported in the literature.[16]

Techniques: Solutions were handled by syringe techniques. pH values were measured with a Hanna HI 9017 pH meter and adjusted with $HClO_4$ and/or NaOH.

Irradiations: Pulse-radiolysis experiments were carried out with the Varian 7715 linear electron accelerator of the Hebrew University of Jerusalem. The pulse duration was 0.1−1.5 μs with a 200 mA current of 5 MeV electrons. The dose per pulse was 3−30 Gray. Irradiations were carried out in a 4 cm spectrosil optical cell, the analyzing light passing three times through the cell. A 150-W Xenon arc provided the analyzing light. The experimental setup was identical to that described earlier in detail.[17a]

For dosimetry, an N_2O-saturated solution containing 1×10^{-3} M KSCN was used. The yield of $(SCN)_2^{\cdot-}$ was measured by using $\varepsilon_{475} = 7600\ M^{-1}cm^{-1}$ and the dose per pulse was calculated assuming $G(SCN)_2^{\cdot-} = 6.0$[17] (the G value is defined as the number of molecules of each product/100 eV radiation absorbed by the solution) and an optical path of 12.3 cm. The dose per pulse was set so that the initial radical concentration was 2−20 μM. The value of the molar extinction coefficients calculated from the dosimetry measurements carry an error limit of 15% due to the scatter of the pulse intensity and uncertainties in G values.

A ^{60}Co source, Noratom, with a dose rate of 4 Gray/min was used for low dose-rate experiments and product analysis.

Simulation of k_4: The rate constant was estimated with the help of the Pro-K global analysis/simulation software by Applied Photophysics. The γ-source irradiation was mimicked by formally adding a reaction forming the radicals at the appropriate rate over the course of the reaction.

Production of Radicals: The radiolysis of water in dilute aqueous solutions can be summarized by:[17]

$$H_2O \xrightarrow{e^-,\gamma} e^-aq\ (2.65),\ \ldots \quad (10)$$

$$\ldots\ OH^{\cdot}\ (2.65),\ H^{\cdot}\ (0.60),\ H_2\ (0.45),\ H_2O_2\ (0.75)$$

(G value in parentheses). In concentrated solutions, the yields of the primary radicals are somewhat higher and those of H_2O_2 and H_2 are somewhat lower.[17]

In neutral N_2O-saturated solutions ($[N_2O] = 0.022$ M) the hydrated electron is converted into the hydroxyl radical via:

$$e^-aq + N_2O \xrightarrow{H_2O} N_2 + OH^- + {}^{\cdot}OH \quad (11)$$

$$k_{11} = 8.7 \cdot 10^9\ M^{-1}\ s^{-1}\ [18]$$

In acidic solutions the reaction of e^-_{aq} with H^+, which produces $H^{\cdot}$ atoms, becomes important:

$$e^-_{aq} + H^+ \rightarrow H^{\cdot}\ (k_{12} = 2.2 \times 10^{10}\ M^{-1}s^{-1}) \quad (12)\ [18]$$

however at pH > 3 the contribution of $H^{\cdot}$ atoms to the total radical yield is less than 10%.

Methyl radicals were prepared by the reaction of $^{\cdot}OH$ radicals with $(CH_3)_2SO$:

$$(CH_3)_2SO + {}^{\cdot}OH \rightarrow (CH_3)_2{}^{\cdot}S(O)OH \quad (k_{13} = 7.0 \times 10^9\ M^{-1}s^{-1}) \quad (13)[19]$$

$$(CH_3)_2{}^{\cdot}S(O)OH \rightarrow {}^{\cdot}CH_3 + CH_3S(O)OH \quad (k_{14} = 1.5 \times 10^7\ M^{-1}s^{-1}) \quad (14)[19]$$

$^{\cdot}CH_2OH$ and $^{\cdot}CH_2CN$ radicals were formed by hydrogen abstraction:

$$CH_3OH + {}^{\cdot}OH \rightarrow {}^{\cdot}CH_2OH + H_2O \quad (k_{15} = 9.7 \times 10^8\ M^{-1}s^{-1}) \quad (15)\ [18]$$

$$CH_3OH + {}^{\cdot}H \rightarrow {}^{\cdot}CH_2OH + H_2 \quad (k_{16} = 2.6 \times 10^6\ M^{-1}s^{-1}) \quad (16)\ [18]$$

$$CH_3CN + {}^{\cdot}OH \rightarrow {}^{\cdot}CH_2CN + H_2O \quad (k_{17} = 2.2 \times 10^7\ M^{-1}s^{-1}) \quad (17)\ [20a]$$

$$CH_3CN + {}^{\cdot}H \rightarrow {}^{\cdot}CH_2CN + H_2\ (k_{18} = 3.6 \times 10^6\ M^{-1}s^{-1}) \quad (18)\ [20b]$$

$^{\cdot}CCl_3$ radicals were prepared from solutions containing 2-propanol and CCl_4 via the reactions below (these reactions were performed in solutions containing argon or helium instead of N_2O):

$$CCl_4 + e^-_{aq} \rightarrow {}^{\cdot}CCl_3 + Cl^-\ (k_{19} = 1.3 \times 10^{10}\ M^{-1}s^{-1}) \quad (19)\ [21]$$

$$(CH_3)_2CHOH + {}^{\cdot}OH/{}^{\cdot}H \rightarrow {}^{\cdot}C(CH_3)_2OH + H_2O/H_2 \quad (k_{20} = 1.9 \times 10^9/7.4 \times 10^7\ M^{-1}s^{-1}) \quad (20)\ [18]$$

$$^{\cdot}C(CH_3)_2OH + CCl_4 \rightarrow CH_3COCH_3 + {}^{\cdot}CCl_3 + Cl^- + H^+ \quad (k_{21} = 1 \times 10^8\ M^{-1}s^{-1}) \quad (21)\ [22]$$

For experiments performed in this work the N_2O or Ar/He saturated solutions were mixed with identical O_2 saturated solutions in the ratio 70:30 prior to irradiation. Under these conditions the $^{\cdot}R$ radicals react with dioxygen to form the desired peroxyl radicals:

$$^{\cdot}R + O_2 \rightarrow RO_2^{\cdot} \quad (22)$$

These reactions are very fast and approach the diffusion controlled limit, e.g.: $k_{22} = 4.7 \times 10^9\ M^{-1}s^{-1}$ for $R = CH_3^{\cdot}$.[4,23]

Product Analysis: UV/Vis spectra were recorded on a Hewlett-Packard 8452A diode array spectrophotometer.

Analysis of formaldehyde was performed according to a literature procedure.[24] Formaldehyde reacts with a reagent containing 0.05 M acetylacetone, 1 M ammonium acetate and 0.033 M acetic acid, to form a yellow complex. The concentration of formaldehyde was determined colorimetrically at the wavelength of maximum absorption (412 nm).

Acknowledgments

This study was supported in part by grants from the Israel Science Foundation and from the Budgeting and Planning Committee of The Council of Higher Education and the Israel Atomic Energy Commission. D. M. wishes to express his thanks to Mrs. Irene Evens for her ongoing interest and support.

[1] [1a] *Catalytic Oxidations with Hydrogen Peroxide as Oxidant* (Ed.: G. Strukul), Kluwer Academic Publishers, Dordrecht, **1992**. [1b] *Applied Homogeneous Catalysis with Organometallic Compounds* (Eds.: B. Cornils, W. A. Herrmann), VCH Verlagsgesellschaft, Weinheim, **1996**.

[2] [2a] S. Goldstein, G. Czapski, D. Meyerstein, *Free Radicals in Biol. Med.* **1993**, *15*, 435−445. [2b] S. Goldstein, D. Meyerstein, *Acc. Chem. Res.* **1999**, *32*, 547−550.

[3] [3a] L. I. Simandi, *Catalytic Activation of Dioxygen by Metal Complexes*, Kluwer Academic publishers, Dordrecht, **1992**. [3b] *Active Oxygen in Biochemistry* (Eds.: J. S. Valentine, C. S. Foote, A. Greenberg, J. F. Liebman), Search Series Vol. 3, Blackie Academic & Professional, London, **1995**.

[4] P. Neta, R. E. Huie, A. B. Ross, *J. Phys. Chem. ref. Data* **1990**, *19*, 413−513.

[5] [5a] *Free Radical Damage and its Control* (Eds.: C. A. Rice-Evans, R. H. Burdon), in *New Comprehensive Biochemistry*, A. Neuberger, L. L. M. van Deenen, Vol. 28, Elsevier, **1994**. [5b] D. Meyerstein, *Metal Ions in Biological Systems*, **1999**, 36, 41−77.

[6] *Peroxyl Radicals in the Chemistry of Free Radicals* (Ed.: Z. B. Alfassi), Wiley, Chichester, **1997**.

[7] E. Solomon-Rapaport, A. Masarwa, H. Cohen, D. Meyerstein, *Inorg. Chim. Acta* **2000**, *299*, 41−46.

[8] C. von Sonntag, H. P. Schumann, in *Peroxyl Radicals in the Chemistry of Free Radicals* (Ed.: Z. Alfassi), Wiley, Chichester, p.173, **1997**.

[9] A. I. Nikolaev, R. L. Safiullin, L. R. Enikeeva, V. D. Komissarov, *Khim. Fiz.* **1992**, *11*, 69−72; *Chem. Abstr.* **1993**, *119*, 237727.

[10] [10a] A. Wada, S. Ogo, M. Mukai, T. Kitagawa, K. Jitsukawa, H. Masuda, H. Einaga, *Inorg. Chem.* **1999**, *38*, 3592−3593. [10b] G. Roelfes, M. Lubben, K. Chen, R. Y. N. Ho, A. Meetsma, S. Genseberger, R. M. Hermant, R. Hage, S. K. Mandal, V. G. Young Jr., Y. Zang, H. Koojiman, A. L. Spek, L. Que, Jr., B. L. Feringa, *Inorg. Chem.* **1999**, *38*, 1929−1936. [10c] L. Que, R. Ho, *Chem. Rev.* **1996**, *96*, 2607−2624.

[11] [11a] K. B. Jensen, C. J. McKenzie, L. P. Nielsen, J. Z. Pedersen, H. M. Svendsen, *Chem. Commun.* **1999**, 1313−1314. [11b] M. Selke, J. S. Valentine, *J. Am. Chem. Soc.* **1998**, *120*, 2652−2653.

[12] T. G. Traylor, C. Kim, W. P. Fann, C. L. Perrin, *Tetrahedron* **1998**, *54*, 7977−7986.

[13] Y. Tabata, Pulse Radiolysis, CRC Press, Boca-Raton; Ann-Arbor; Boston, **1990**.

[14] D. Meyerstein, *Acc. Chem. Res.* **1978**, *11*, 43−48.

[15] [15a] A. Bakac, J. Espenson, *Inorg. Chem.* **1989**, *28*, 4319−4322. [15b] R. van Eldik, H. Cohen, D. Meyerstein, *Inorg. Chem.* **1994**, *33*, 1566−1568.

[16] [16a] S. C. Jackels, K. Farmery, E. K. Barefield, N. J. Rose, D. H. Busch, *Inorg. Chem.* **1972**, *11*, 2893−2901. [16b] A. M. Tait, M. Z. Hoffman, E. Hayon, *J. Am. Chem. Soc.* **1976**, *98*, 86−93. [16c] A. Marchaj, A. Bakac, J. H. Espenson, *Inorg. Chem.* **1992**, *31*, 4860−4863.

[17] [17a] S. Goldstein, G. Czapski, H. Cohen, D. Meyerstein, *Inorg. Chem.* **1992**, *31*, 2439−2444. [17b] M. S. Matheson, M. L. Dorfman, *Pulse Radiolysis*, MIT Press, Cambridge, MA, **1969**.

[18] G. V. Buxton, C. L. Greenstock, W. P. Helman, A. B. Ross, *J. Phys. Chem. ref. Data* **1988**, *17*, 513−886.

[19] D. Veltwisch, E. Janata, K. D. Asmus, *J. Chem. Soc., Perkin Trans.* **1980**, 146−153.

[20] [20a] P. Neta, R. H. Schuler, *J. Phys. Chem.* **1975**, *79*, 1−6. [20b] I. Draganic, Z. Draganic, L. Petkovic, A. Nikolic, *J. Am. Chem. Soc.* **1973**, *95*, 7193−7199.

[21] A. M. Afanassiev, K. Okazaki, G. R. Freeman, *J. Phys. Chem.* **1979**, *83*, 1244−1249.

[22] R. Koester, K. D. Asmus, *Z. Naturforsch., Teil B* **1971**, *26*, 1104−1108.

[23] J. K. Thomas, *J. Phys. Chem.* **1967**, *71*, 1919−1925.

[24] T. Nash, *Nature* **1952**, *170*, 976.

Received February 28, 2002
[I02104]

Selective Self-Assembly of a Sequential Bipyridine–Bipyrazine Ligand Strand into a Double-Stranded Cu^{I} Helicate

Julien Mathieu,[a] Alain Marsura,*[a] Nouzha Bouhmaida,[b] and Noureddine Ghermani[c]

Keywords: Helicates / Self-assembly / Copper / NMR spectroscopy / N ligands

In this paper new aspects on the self-assembly processes of didentate coordinating ligands leading to a double-stranded helicate are described. It was reported, that directionality in the self-recognition of Cu^{I} ions could be driven by factors relating to the electronic configuration of heterocycles in carefully designed heterotopic ligands. If the sequential bipyrazine–bipyridine ligand strand **4** reacts with 1 equiv. of Cu^{I} the dimetallic complex $[Cu_2(\mathbf{L4})_2][PF_6]_2$ is formed in a cooperative process. In this coordination compound the two strands are oriented in opposite directions (HT) as illustrated by the X-ray structure of $[Cu_2(\mathbf{L4})_2][PF_6]_2$.

(© Wiley-VCH Verlag GmbH, 69451 Weinheim, Germany, 2002)

Introduction

In recent years, intensive research on self-assembling processes has been derived. Among numerous structures published in the literature[1] the spontaneous formation of double-stranded or more complex organometallic helical complexes was extensively studied. The formation of a helicate depends on the nature of the metal and ligands, and sometimes on additional information introduced by appropriate templating.[2]

Some years ago, papers dealt with the self-assembly of a class of directional ligands, which led to saturated double-stranded heterotopic helicates with Cu^{I} [3] or Pd^{II}.[4] In the latter case the two strands selectively adopt a head-to-tail arrangement which leads to a C_2-symmetrically saturated heterotopic double-stranded helicate, with each Pd^{II} lying in a distorted five-coordinated environment, produced by the coordination of one bipyridine and one terpyridine subunit in each strand. In the former case introduction of bulky substituents in the basic quaterpyridine by Constable and co-workers[5,5a] was shown to induce a distinction between head-to-head (HH) and head-to-tail (HT) conformers leading to the exclusive formation of an (HH) C_2-symmetrical double-stranded Cu^{I} helicate in solution and in the solid state. In a previous study, Albrecht and Fröhlich synthesized a sequential ligand which contains one catecholate and one aminophenolate unit, in which the ability of the two nucleophilic sites to control the metal-directed self-assembly of chelates was reported.[6]

The aim of this work was to pursue the research to resolve unknown features on the Cu^{I} complexing behavior, concerning saturated heterotopic ligands, which here provide an original example, since they may be separated into one didentate "bipyridine" segment and one didentate "bipyrazine" segment upon complexation to metal ions. This means that only the same number of four inner nitrogen atoms could be engaged in the coordination with Cu^{I} to form a helicate, which is a coordination complex and not a chelate. Thus, a potentially induced directionality cannot come from outside modifications on the strand as reported for quaterpyridine examples[5] or from different nucleophilic centers as in the case of catecholate vs. aminophenolate,[6] but probably from the different electronic configuration of the bipyrazine nucleus[7] vs. bipyridine.

Results and Discussion

Because of a poor reproducibility of reactions leading to the rather difficult functionalization of 6,6′-dimethyl-2,2′-bipyrazine (**1**) into the 6-(hydroxymethyl)-6′-methyl-2,2′-bipyrazine (**3**), our concern was first to improve the synthesis of **4**. Using an unusual reagent like the tetrachloro-diphenylglycouril (Scheme 1) in the radical chlorination limiting step, we selectively obtained the 6-(chloromethyl)-6′-methyl-2,2′-bipyrazine in good yield (58%). Compared with

[a] GEVSM Unité Mixte de Recherche CNRS, Structure et Réactivité des Systèmes Moléculaires Complexes
5 rue A. Lebrun BP 403, 54250 Nancy Cedex, France
Fax: (internat.) + 33-3/83178845
E-mail: Alain.Marsura@pharma.u-nancy.fr
[b] Laboratoire des Sciences des Matériaux, LSM, Université Cadi Ayyad, Faculté des Sciences Semlalia
Boulevard Prince Moulay Abdallah BP 2390, 4000 Marrakech, Morocco
E-mail: nouzha@ucam.ac.ma
[c] Laboratoire de Physique Pharmaceutique UMR 8612 Université Paris XI, Faculté de Pharmacie,
5 rue J. B. Clément, 92296 Châtenay-Malabry, France
E-mail: noureddine.ghermani@cep.u-psud.fr

our previously reported synthesis[7a] the changes in the synthetic pathway led to a better yield (70%) of **4**. An equimolar amount of $[Cu(CH_3CN)_4][PF_6]$ added to **4** in anhydrous CH_3CN spontaneously led to a deep-red solution which confirmed the occurrence of the Cu^I coordination process. A thin layer chromatographic control showed that the ligand was totally consumed in the reaction. The crude material was recrystallized by slow diffusion of ether through an acetonitrile solution of the copper complex giving deep-red crystals that were stable in air.

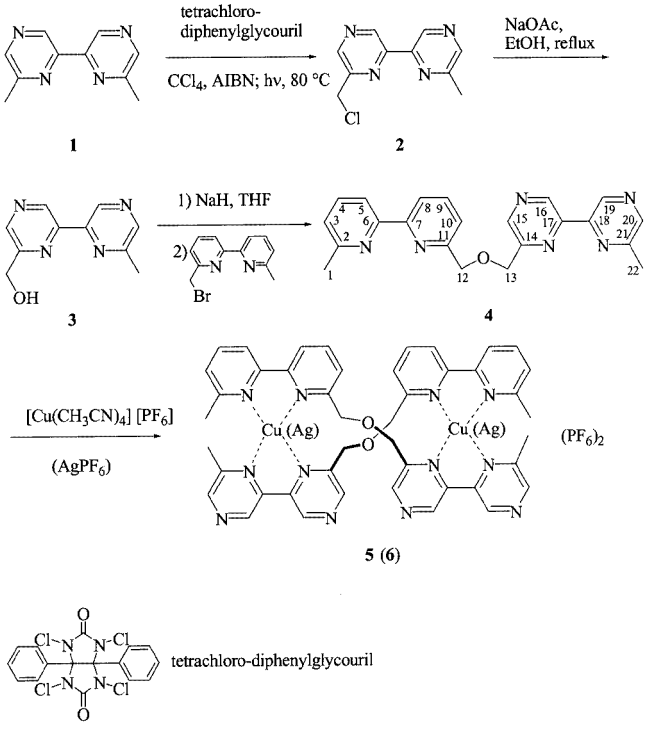

Scheme 1

The ligand **4** (or **L4**) spontaneously forms the desired $[L_2Cu_2][PF_6]_2$ dinuclear double-stranded helical structure (see Exp. Sect.) as indicated by X-ray diffraction in the solid state. This structure persists in the dissolved state as established by various spectroscopic techniques (UV/Vis, ^1H NMR, ^{13}C NMR, and ES MS). An UV/Vis spectrophotometric titration of the ligand **4** by $[Cu(CH_3CN)_4][PF_6]$ in CH_3CN solution (see B in Figure 1) exhibits a clear isosbestic point indicating that a single species was formed and the appearance of an MLCT at 450 nm indicates the effective coordination of the Cu^I atoms. The titration plots (see A in Figure 1) assess that this species has a composition of ca. 1 Cu atom for 1 equiv. of **4** in agreement with the stoichiometry expected for the dihelicate $[Cu_2(\mathbf{L4})_2]^{2+}$.[8] The formation of the dinuclear helicate proceeds with a positive cooperativity as indicated by the increasing values of the calculated binding constants $\log\beta_{metal-ligand}$:[9] $\log\beta_{11} = 5.93$·for $[Cu(\mathbf{L4})]^+$; $\log\beta_{12} = 9.35$·for $[Cu(\mathbf{L4})_2]^+$; $\log\beta_{22} = 15.29$·for $[Cu_2(\mathbf{L4})_2]^{2+}$. This means that the formation of the final helicate is highly favored. In addition, preliminary results with other metal ions like Ag^I giving the $[Ag_2(\mathbf{L4})_2]$ complex **6** (Figure 2) show that the double-stranded

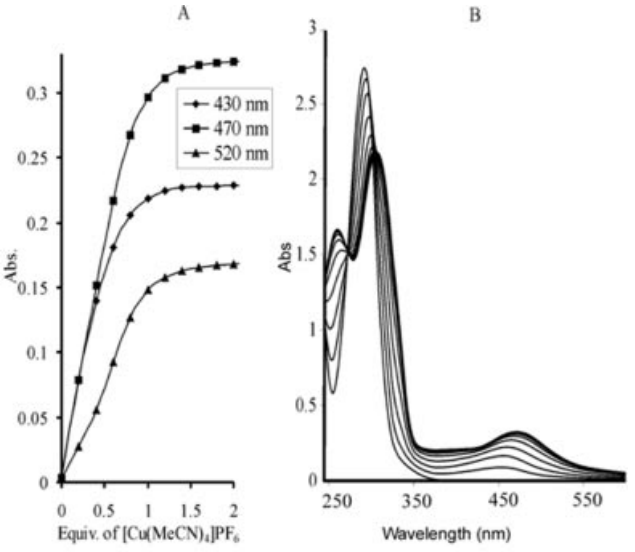

Figure 1. Spectrophotometric titration of the ligand **4** with $[Cu(MeCN)_4]PF_6$ (0.2−2.0 equiv.) in MeCN: A) plots of absorbance vs. added salt at three wavelengths and B) UV/Vis absorption spectra

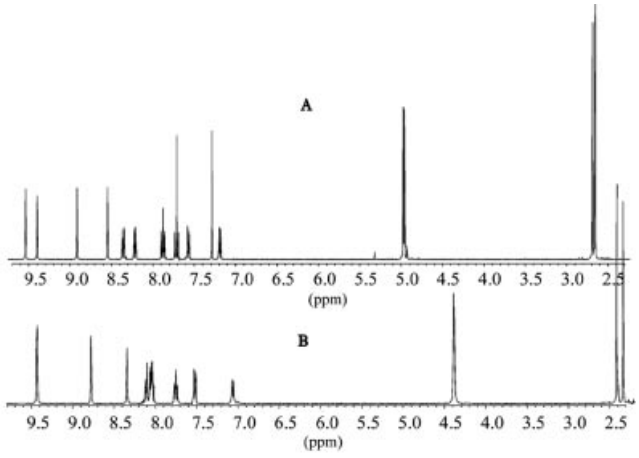

Figure 2. ^1H NMR spectra (400 MHz) of the free ligand **4** (A) and $[Ag_2(\mathbf{L4})_2][PF_6]_2$ in CD_3CN (B)

helix formation with **4** is probably a more extended phenomenon.

As previously established by Lehn and co-workers,[10] the ^1H NMR spectra of ligand **4** and its Cu^I complex (Figure 3) show the splitting of the enantiotopic methylene protons of the oxopropylene bridges in **4** (A_2 spin systems) to diastereotopic protons and doublets (AB spin systems) in the copper complex, on lowering the temperature. Methylene protons are also very useful for the estimation of the dynamic interconversion between dinuclear right-handed (*P*) and left-handed (*M*) enantiomeric helicates.[11] An investigation of the helical interconversion of complex **5** in a CD_3CN solution was realized using variable-temperature ^1H NMR experiments with analysis of the lateral methylene proton pattern between $\delta = 4.2$ and 3.4 ppm (Figure 3). The free energy for the (*P*)/(*M*) interconversion in solution was estimated by the Eyring equation as $\Delta G^{\ddagger} = 66.9$ kJ·mol^{-1}, this value is close to those found for analogous copper helicates.[12]

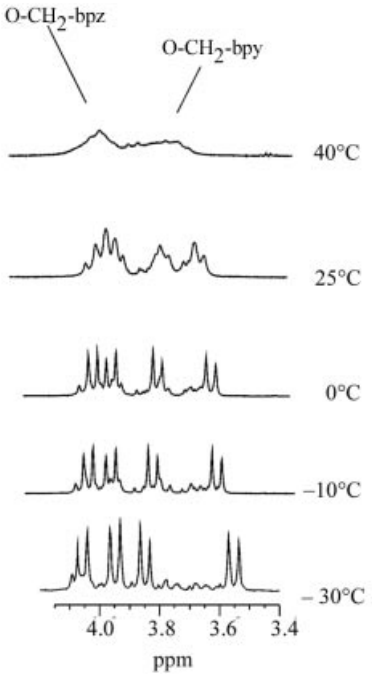

Figure 3. Variable-temperature ^{1}H NMR spectra of $[Cu_2(\mathbf{L4})_2][PF_6]_2$ in CD_3CN; selected region of methylene proton signals; each group of methylene protons is split into two distinct AB systems

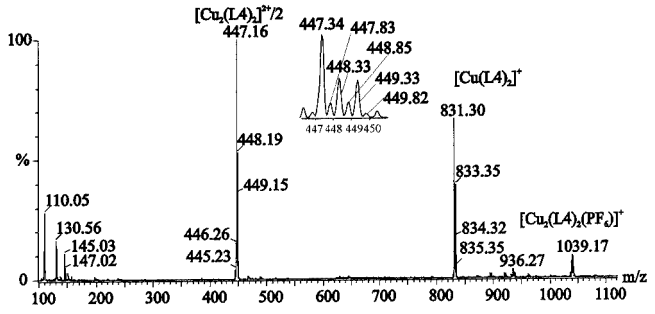

Figure 4. ES mass spectrum of the dinuclear double-stranded helical complex $[Cu_2(\mathbf{L4})_2][PF_6]_2$ (**5**) in acetonitrile

Finally, ES mass spectra (Figure 4) of **5** led to the observation of the $[Cu_2(\mathbf{L4})_2]^{2+}$ doubly charged ion (m/z = 447 a.m.u.) and the $[Cu_2(\mathbf{L4})_2(PF_6^-)]^+$ singly charged ion (m/z = 1040 a.m.u.). The isotopic distribution of the m/z = 447 ion shows peaks separated by 0.5 Da which is only compatible with a doubly charged species and the formation of the double-stranded helicate.[13] Similar results were obtained with the silver complex **6**. ES mass spectra exhibit the $[Ag_2(\mathbf{L4})_2]^{2+}$ doubly charged ion (m/z = 491 a.m.u.) and the $[Ag_2(\mathbf{L4})_2(PF_6^-)]^+$ singly charged ion (m/z = 1128 a.m.u.) with an isotopic distribution of the m/z = 491 ion showing peaks separated by 1.0 Da compatible with a doubly charged species.

X-ray diffraction analysis of a single crystal of the salt of the copper complex shows the presence of a double-stranded head-to-tail heterotopic helicate (Figure 5) which could be obtained by slow diffusion of diethyl ether into an acetonitrile solution containing **L4** and $[Cu(CH_3CN)_4][PF_6]$ in a 1:1 molar ratio. This structure represents the first example of such a helicate, having a strong directionality in self-assembly without external steric induction. The compound crystallizes in the triclinic $P\bar{1}$ space group with two dinuclear Cu^I complexes (a and b) and four PF_6^- disordered counterions in the asymmetric unit. Figure 5 depicts an ORTEP[14] view of the Cu^I complex structures displaying left- and right-handed helices. The Cu−Cu distances are 6.45 and 6.20 Å in the a and b complexes, respectively. The angle between the two corresponding Cu−Cu axes is 21°. Each Cu^I cation is in a distorted tetrahedral coordination and is attached to two pairs of N atoms belonging to one bipyridine and one bipyrazine molecule, respectively. All Cu−N bond lengths are equal to 2 Å within a narrow deviation interval (caption of Figure 5). The N−Cu−N angle values range from 80 to 135°, the most distorted helicate complex being the b one. All the bond lengths and angles are in good agreement with those obtained for (4,4′-bipyrimidine)- and (2,2′-bipyrazine)copper complexes.[15] In the present study, bipyrazine and bipyridine molecules are not ideally planar, the corresponding torsion angle between the two connected rings varies by up to 10° in order to accommodate the copper coordination on one hand and the outer interactions on the other. However, in each dinuclear complex, the bipyridine molecule mean planes are almost parallel. This is not true for the bipyrazine molecules which are attracted to each other in both the a and b complexes enhancing the metal tetrahedron distortions. Such an attraction of heterocycle molecules has been reported in our pre-

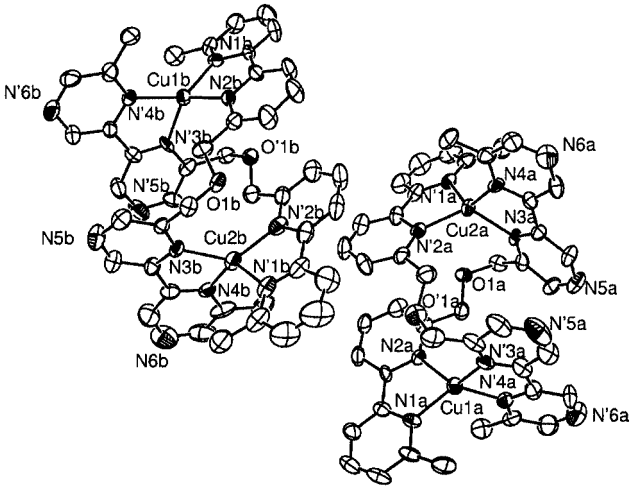

Figure 5. Structure (ORTEP view) of the two helicates in the asymmetric unit; the hexafluorophosphate anions and hydrogen atoms have been omitted for clarity; selected distances [Å] and angles [°]: Cu1a−N′3a 1.99 (1), Cu2a−N′2a 2.00(1), Cu1a−N1a 2.01(1), Cu2a−N3a 2.02(1), Cu1a−N2a 2.04(1), Cu2a−N4a 2.03(1), Cu1a−N′4a 2.06(1), Cu2a−N′1a 2.03(1), N′3a−Cu1a−N2a 123.7(5), N′2a−Cu2a−N3a 123.2(5), N1a−Cu1a−N′4a 124.7(5), N4a−Cu2a−N′1a 127.9(5), N′3a−Cu1a−N′4a 82.6(6), N3a−Cu2a−N4a 81.8(5), N1a−Cu1a−N2a 81.6(5), N′2a−Cu2a−N′1a 82.6(5); Cu1b−N′3b 2.01(1), Cu2b−N′2b 2.01(1), Cu1b−N1b 2.00(1), Cu2b−N3b 2.05(1), Cu1b−N2b 2.03(1), Cu2b−N4b 2.04(1), Cu1b−N′4b 2.01(1), Cu2b−N′1b 2.03(1), N′4b−Cu1b−N1b 134.6(5), N′1b−Cu2b−N4b 122.8(5), N′3b−Cu1b−N′4b 81.2(5), N3b−Cu2b−N4b 80.9(5), N2b−Cu1b−N1b 82.0(5), N′2b−Cu2b−N′1b 80.7(6), N2b−Cu1b−N′3b 120.8(5), N′2b−Cu2b−N3b 129.6(5)

vious work.[15] The crystal packing (see CCDC supplementary material) shows how the disordered PF_6^- counterions are distributed in the interstices.

In addition to the high atomic thermal vibration (room-temperature data in this study), the PF_6^- anion disorder probably breaks down a symmetry operation (center of inversion) which can hypothetically relate the two heterotopic helicates of the asymmetric unit. Furthermore, PF_6^- anions interact with the dinuclear complexes as revealed by the close F···H contacts ranging from 2.3 to 2.6 Å. Therefore, in the solid state, the PF_6^- counterion found close to the two bipyrazine heterocycles, belonging to the same helicate, can explain the non-parallelism of the corresponding molecular mean planes. The other counterions are found approximately in the same plane as the bipyridine molecule of one complex and are connected to the methyl group attached to the bipyrazine heterocycle of the second helicate.

Conclusions

In contrast to other helicates previously described, a directional selective double-stranded head-to-tail spontaneous assembly has been obtained from a heterotopic ligand without the help of external hindered factors, stereochemical requirements or the electronic nature of a chelating center[6] belonging to the coordination preference of the metal ions. In the asymmetric unit Cu−N bond lengths (2 Å) of the same distance were found whatever the nature of the biheterocycle involved in the coordination with the copper atom. The PF_6 disorder in the solid state induces a geometrical distinction of two double-stranded dinuclear complexes in the asymmetric unit. Furthermore, particular interactions between the PF_6 counteranions and biheterocycle protons of the ligand **4** through F−H hydrogen bonds were observed. In this study, it was reported that a careful design of the ligands can lead to a new class of helicates, which appear to be driven in their assembling process by the electronic configuration of the biheterocyclic units. Previous results of the experimental electron density,[7] which clearly pointed to the greater non-aromatic character of the 2,2′-bipyrazine compared to other diazines or monoazines, corroborate this hypothesis. Further work is in progress to analyze the general character of these results with other sequential heterotopic ligands.[16]

Experimental Section

General Remarks: ^1H and ^{13}C NMR spectra were recorded with a Bruker DRX 400 spectrometer. UV/Vis spectra were recorded with a UVmC^2 Safas spectrometer. Mass spectra (ES) were taken with a Micromass Platform spectrometer. Elemental analyses were obtained with a Perkin−Elmer 240C CHN-O-S analyzer. The solvents were purified by standard methods.

6-Chloromethyl-6′-methyl-2,2′-bipyrazine (2): To a solution of 6,6′-dimethyl-2,2′-bipyrazine (1 g, 5.38 mmol) in CCl_4 (100 mL) under Ar, tetrachloro-diphenylglycouril {1,3,4,6-tetrachloro-3a,6a-diphenyltetrahydroimidazo[4,5-*d*]imidazole-2,5(1*H*,3*H*)-dione} (1 g, 2.32 mmol) and AIBN were added. The mixture was refluxed and irradiated by a tungsten lamp (100 W) for 24 h. The resulting precipitate was filtered, washed with CH_2Cl_2, and the solvent was removed in vacuo. The crude product was purified by chromatography on silica gel (elution: CH_2Cl_2/Et_2O, 95:5) to give two fractions. Fraction 1: **2:** Yield 683 mg (58%). ^1H NMR ($CDCl_3$, 25 °C): δ = 9.54 (s, 1 H), 9.38 (s, 1 H), 8.81 (s, 1 H), 8.53 (s, 1 H), 4.78 (s, 2 H), 2.66 (s, 3 H) ppm. ^{13}C NMR ($CDCl_3$, 25 °C): δ = 153.1, 151.0, 148.5, 147.7, 145.2, 144.4, 143.1, 142.4, 43.9, 21.6 ppm. Fraction 2: **6,6′-Bis(chloromethyl)-2,2′-bipyrazine:** Yield 257 mg (19%). ^1H NMR ($CDCl_3$, 25 °C): δ = 9.57 (s, 2 H), 8.84 (s, 2 H), 4.80 (s, 4 H) ppm. ^{13}C NMR ($CDCl_3$, 25 °C): δ = 151.1, 147.8, 144.8, 142.6, 43.8 ppm.

6-(Hydroxymethyl)-6′-methyl-2,2′-bipyrazine (3): To a solution of **2** (477 mg, 2.16 mmol) in anhydrous EtOH (20 mL), NaOAc (1.77 g, 21.60 mmol) was added. The mixture was refluxed for 24 h. The resulting precipitate was filtered and the solvent was removed in vacuo. The crude product was purified by chromatography on silica gel (elution: CH_2Cl_2/MeOH, 95:5) to give two fractions. Fraction 1: **3:** Yield 250 mg (57%). ^1H NMR ($CDCl_3$, 25 °C): δ = 9.50 (s, 1 H), 9.36 (s, 1 H), 8.73 (s, 1 H), 8.52 (s, 1 H) 4.95 (d, *J* = 4.2 Hz, 2 H), 3.66 (s, 1 H), 2.67 (s, 3 H) ppm. ^{13}C NMR ($CDCl_3$, 25 °C): δ = 153.9, 153.3, 148.1, 148.0, 145.0, 143.0, 141.8, 140.0, 63.0, 21.6 ppm. Fraction 2: **6-(Acetoxymethyl)-6′-methyl-2,2′-bipyrazine:** Yield 102 mg (19%). ^1H NMR ($CDCl_3$, 25 °C): δ = 9.50 (s, 1 H), 9.34 (s, 1 H), 8.68 (s, 1 H), 8.51 (s, 1 H), 5.34 (s, 2 H), 2.64 (s, 3 H), 2.19 (s, 3 H) ppm, ^{13}C NMR ($CDCl_3$, 25 °C): δ = 170.3, 153.0, 150.1, 148.5, 147.8, 145.0, 143.4, 142.3, 140.2, 64.6, 21.5, 20.7 ppm.

6-Methyl-6′-[(6′-methyl-2,2′-bipyridin-6-yl)methoxymethyl]-2,2′-bipyrazine (4): To NaH (54 mg, 2.24 mmol) in anhydrous THF (5 mL) under Ar at 0 °C **3** (268 mg, 1.32 mmol) in THF (10 mL) was added. The mixture was stirred at 0 °C for 1 h. 6-(Bromomethyl)-6′-methyl-2,2′-bipyridine (348 mg, 1.32 mmol) in THF (10 mL) was then added, and the mixture was allowed to warm to room temp. The mixture was stirred at 40 °C for 24 h. After cooling to room temp., H_2O (10 mL) was added to the mixture and the phases were separated. The aqueous layer was extracted with CH_2Cl_2 (3×30 mL). The combined organic phases were dried with $MgSO_4$, and the solvent was removed in vacuo. The crude product was purified by chromatography on alumina gel (elution: CH_2Cl_2) to give a white powder. Yield 353 mg (70%); m.p 142 °C. ^1H NMR ($CDCl_3$, 25 °C): δ = 9.52 (s, 1 H, bpz), 9.39 (s, 1 H, bpz), 8.90 (s, 1 H, bpz), 8.53 (s, 1 H, bpy), 8.35 (d, $^3J_{8,9}$ = 7.8 Hz, 1 H, bpy), 8.20 (d, $^3J_{5,4}$ = 7.8 Hz, 1 H, bpy), 7.86 (t, $^3J_{9,10}$ = 7.8 Hz, 1 H, bpy), 7.70 (t, $^3J_{4,3}$ = 7.8 Hz, 1 H, bpy), 7.55 (d, $^3J_{10,9}$ = 7.6 Hz, 1 H, bpy), 7.17 (d, $^3J_{3,4}$ = 7.6 Hz, 1 H, bpy), 4.96 (s, 2 H), 4.94 (s, 2 H), 2.67 (s, 3 H), 2.64 (s, 3 H) ppm. ^{13}C NMR ($CDCl_3$, 25 °C): δ = 157.9 (C^{21}), 157.1 (C^{14}), 155.9 (C^{18}), 155.3 (C^{17}), 153.0 (C^2), 152.5 (C^{11}), 148.3 (C^6), 148.1 (C^7), 145.0 (C^{19}), 143.7 (C^{20}), 142.0 (C^{15}), 140.2 (C^{16}), 137.5 (C^9), 137.0 (C^4), 123.2 (C^3), 121.2 (C^{10}), 120.0 (C^8), 118.2 (C^5), 74.2 (C^{13}), 71.8 (C^{12}), 24.6 (C^1), 21.6 (C^{22}) ppm. UV/Vis (CH_3CN): λ_{max} (ε)$_{max}$ = 292 nm (27339). $C_{22}H_{20}N_6O$ (384.4): calcd. C 68.72, H 5.24, N 21.86; found C 68.64, H 5.22, N 21.73.

$[Cu_2(L4)_2][PF_6]_2$ (5): $[Cu(CH_3CN)_4][PF_6]$ (194 mg, 0.52 mmol) was added to the ligand **4** (200 mg, 0.52 mmol) in anhydrous CH_3CN (50 mL) solution under Ar. The mixture was stirred at room temp. and spontaneously led to a deep-red solution. After evaporation of the solvent, the solid residue was crystallized by slow diffusion of diethyl ether into an acetonitrile solution, which gave deep-red crystals. ^1H NMR (CD_3CN, −30 °C): δ = 9.68 (s, 4 H, bpz), 8.91 (s, 2 H, bpz), 8.34−8.32 (m, 4 H, 2 H-bpz, 2 H-bpy), 8.19−7.96 (m, 6 H, bpy), 7.57 (d, $^3J_{10,9}$ = 7.5 Hz, 2 H, bpy), 7.01 (d, $^3J_{3,4}$ = 7.4 Hz, 2 H. 1 H-bpy and 1 H-bpy′), 4.09−3.54 (m, 8 H, 4 CH_2), 2.42 (s, 3 H, CH_3), 2.26 (s, 3 H, CH_3), 2.15 (t, ^2J = 8.8 Hz; CH_3), 2.05 (s, 3 H,CH_3)

ppm. ^{13}C NMR (CD_3CN, −30 °C): δ = 158.4 (q), 154.8 (q), 152.4 (2 q), 150.6 (2 q), 149.3 (2 q), 149.0 (C^{19}), 145.5 (C^{20}), 143.6 (C^{15}), 142.0 (C^{16}), 139.9 (C^9), 139.6 (C^4), 127.0 (C^3), 126.1 (C^{10}), 122.5 (C^8), 120.5 (C^5), 71.7 (C^{13}), 68.4 (C^{12}), 24.1 (C^1), 21.5 (C^{22}) ppm. ^{13}C CPMAS NMR (75 MHz, 7 kHz, 20 °C): δ = 156.0 (q), 149.0 (q), 142.0 (C^{15}, C^{16}), 139.0 (C^9, C^4), 128.0 (C^3, C^{10}), 122.0−120.0 (C^8, C^5), 70.0 (C^{13}, C^{12}), 25.0 (C^1), 22.0 (C^{22}) ppm. UV/Vis (CH_3CN): λ_{max} $(\varepsilon)_{max}$ = 306 nm (21680). ES MS: *m*/*z* (%) = 1040.2 (20) $[Cu_2(\mathbf{L4})_2(PF_6^-)]^+$, 831.3 (90) $[Cu_2(\mathbf{L4})]^+$, 447.3 (100) $[Cu_2(\mathbf{L4})_2]^{2+}$/2. $C_{44}H_{40}Cu_2F_{12}N_{12}O_2P_2$ (1185.9): calcd. C 44.56, H 3.40, N 14.17; found C 44.52, H 3.37, N 13.95.

$[Ag_2(L4)_2][PF_6]_2$ (6): $AgPF_6$ (65.84 mg, 0.26 mmol) was added to the ligand **4** (100 mg, 0.26 mmol) in anhydrous CH_3CN (20 mL) solution under Ar. The mixture was stirred at room temp. and after evaporation of the solvent, the solid residue was crystallized by slow diffusion of diethyl ether into an acetonitrile solution, which gave white crystals. ^{1}H NMR (CD_3CN, 25 °C): δ = 9.43 (s, 1 H, bpz), 9.42 (s, 1 H, bpz), 8.77 (s, 1 H, bpz), 8.34 (s, 1 H, bpz), 8.11 (m, 3 H, bpy), 7.75 (t, ^3J = 7.8 Hz, 1 H, bpy), 7.52 (d, ^3J = 7.8 Hz, 1 H, bpy), 7.06 (d, ^3J = 7.6 Hz, 1 H, bpy), 4.39 (s, 2 H, CH_2), 4.38 (s, 2 H, CH_2), 2.41 (s, 3 H, CH_3), 2.33 (s, 3 H, CH_3) ppm. ^{13}C NMR (CD_3CN, 25 °C): δ = 158.8 (q), 156.0 (q), 154.8 (q), 151.3 (q), 150.8 (q), 147.9, 145.7, 143.6, 141.7, 140.2, 140.0 (CH bpy), 126.1, 124.6, 122.5, 120.8 (CH bpz), 74.0 (CH_2 bpz), 70.5 (CH_2 bpy), 26.2 (CH_3 bpz), 22.4 (CH_3 bpy) ppm. UV/Vis (CH_3CN): λ_{max} $(\varepsilon)_{max}$ = 298 nm (25379). ES MS: *m*/*z* (%) = 1128.9 (10) $[Ag_2(\mathbf{L4})_2(PF_6^-)]^+$, 491.2 (100) $[Ag_2(\mathbf{L4})_2]^{2+}$/2.

X-ray Structural Analysis of $[Cu(C_{22}H_{20}N_6O)]_2[PF_6]_2$: The crystal structure of $[Cu(C_{22}H_{20}N_6O)]_2[PF_6]_2$, $\rho_{calcd.}$ = 1.61 Mg·m^{-3}, μ(Mo-K_α) = 1.036 mm^{-1}, was determined from a single-crystal X-ray diffraction experiment. The deep-red crystals obtained are plate-like and very fragile. A crystalline fragment sample was mounted on an Enraf−Nonius CAD-4F diffractometer. Several attempts were made because of the diffraction-limited power of the samples. Therefore, data collection was performed at room temp. on a large crystal fragment (approximately 0.5 × 0.9 × 0.2 mm) with Mo-K_α X-ray radiation (λ = 0.71073 Å). $[Cu(\mathbf{L4})]_2[PF_6]_2$ crystallizes in the triclinic $P\bar{1}$ space group, Z = 4 (two dinuclear complexes in the asymmetric unit). The unit cell parameters were obtained by least-squares fit to setting angles of 25 reflections in the range 12° < 2θ < 26°. The cell parameters are a = 13.912(2), b = 19.903(4), c = 20.062(3) Å, α = 97.67(2), β = 105.49(1), γ = 109.89(2)°, V = 4877.2(17) Å^3. The ω-2θ scan mode was used to record the diffracted intensities. Three standard reflections (−5 −1 2), (−5 0 0) and (−3 1 −1) were monitored every 2 h in order to control the intensity decay, which is not significant. 25304 reflections were collected up to $2\theta_{max}$ = 55.9°. Lorentz polarization corrections and data reduction was performed by using the WINGX package[17] for CAD4-collected intensities. The structure was solved by direct methods by using the SIR92 program.[18] Due to a large amount of weak intensities, only 22843 observed reflections were taken into account in order to refine the structure by full-matrix least squares based on $|F^2|$ by using the SHELX97[19] program. Thermal displacements of non-hydrogen atoms were refined anisotropically. Hydrogen atoms were included at their idealized positions but not refined. Three of the four PF_6^- counterions in the asymmetric unit are disordered. Two atomic positions were assigned to one phosphorus and 16 fluorine atoms, respectively. The site occupancy factors of these disordered atomic positions were refined. During the last cycles of refinement, an empirical absorption correction was applied (T_{min} = 0.040, T_{max} = 0.441) using the DIFABS program in the WINGX package.[17] The final statistical factors are $R1$(all observed data) = 0.319, $wR2$ = 0.387 for 22843 data and 1495 parameters, $R1$ [$I > 2\sigma(I)$] = 0.127 for 6758 data with $I > 2\sigma(I)$. The weak ratio N_{obs}/N_{par} is assigned to the high disorder of the PF_6^- counterions in the solid state. The final residual densities in the unit cell are +0.85 and −0.80 e·Å^{-3}. CCDC-176336 contains the supplementary crystallographic data for this paper. These data can be obtained free of charge at www.ccdc.cam.ac.uk/conts/retrieving.html or from the Cambridge Crystallographic Data Centre, 12, Union Road, Cambridge CB2 1EZ, UK [Fax: (internat.) +b 44-1223/336-033; E-mail: deposit@ccdc.cam.ac.uk].

Acknowledgments

This work was supported by the CNRS and the MESR. We thank Dr. A. Lambert for the logβ determination, J. M. Ziegler for recording ES mass spectra, Mrs. E. Eppiger for recording NMR spectra, and Mrs. N. Marshall for correcting the manuscript.

[1] M. Albrecht, *Chem. Rev.* **2001**, *101*, 3457−3497.
[2] C. Piguet, G. Bernardinelli, G. Hopfgartner, *Chem. Rev.* **1997**, *97*, 2005−2062.
[3] C. Piguet, G. Bernardinelli, B. Bocquet, A. Quattropani, A. F. Williams, *J. Am. Chem. Soc.* **1992**, *114*, 7440−7451.
[4] E. C. Constable, S. M. Elder, J. Healy, M. D. Ward, *J. Am. Chem. Soc.* **1990**, *112*, 4590−4592.
[5] [5a] E. C. Constable, F. R. Heirtzler, M. Neuburger, M. Zhender, *Supramol. Chem.* **1995**, *5*, 197−200. [5b] E. C. Constable, F. R. Heirtzler, M. Neuburger, M. Zhender, *Chem. Commun.* **1996**, 933.
[6] M. Albrecht, R. Fröhlich, *J. Am. Chem. Soc.* **1997**, *119*, 1656−1661.
[7] [7a] F. Bodar-Houillon, Y. Elissami, A. Marsura, N. Ghermani, E. Espinosa, N. Bouhmaida, A. Thalal, *Eur. J. Org. Chem.* **1999**, 1427−1440. [7b] F. Bodar-Houillon, A. Marsura, *Supramol. Chem.* **1998**, *9*, 191−198.
[8] The behavior of the titration curve at 520 nm could indicate the presence (at ca. 0.5 equiv. of Cu^I) of traces of another species. Knowing that both (HH) and (HT) conformers belong to the same C_2 point group, the collected NMR data in solution cannot distinguish between the two possibilities. Nevertheless, the ^{107}Ag NMR spectrum of complex **6** (not shown) exhibits a single resonance, indicating the same environment for silver atoms in the helicate. This situation is in agreement with an (HT) orientation of the sequential ligand **4** in solution.
[9] logβ values were calculated using the SPECFIT® program v. 3.0 (Ed.: R. A. Binstead), Spectrum Software Associates, **1993−2001**.
[10] J.-M. Lehn, A. Rigault, *Angew. Chem. Int. Ed. Engl.* **1988**, *27*, 1095−1097; *Angew. Chem.* **1988**, *100*, 1121−1122.
[11] A. F. Williams, C. Carina, L. Charbonnière, P. Desmartin, C. Piguet, *Thermodynamic and Kinetic Stability of Polynuclear Complexes in Physical Supramolecular Chemistry* (Eds.: L. Echegoyen, A. E. Kaifer), NATO AST Series, Kluwer, Dordrecht, The Netherlands, **1996**, p. 379.
[12] R. F. Carina, A. F. Williams, C. Piguet, *Helv. Chim. Acta* **1998**, *81*, 548−557.
[13] G. Hopfgartner, C. Piguet, J.D. Henion, A. F. Williams, *Helv. Chim. Acta* **1993**, *32*, 1759−1766.
[14] L. J. Farrugia, *J. Appl. Crystallogr.* **1997**, *30*, 565.
[15] F. Bodar-Houillon, T. Humbert, A. Marsura, J. B. Regnouf de Vains, O. Dusausoy, N. Bouhmaida, N.E. Ghermani, Y. Dusausoy, *Inorg. Chem.* **1995**, *34*, 5205−5209.
[16] J. Mathieu, A. Marsura, N. Bouhmaida, N. E. Ghermani, *Chem. Eur. J.*, to be submitted.
[17] L. J. Farrugia, *J. Appl. Crystallogr.* **1999**, *32*, 837−838.
[18] A. Altomare, G. Cascarano, C. Giacovazzo, A. Guagliardi, *J. Appl. Crystallogr.* **1993**, *26*, 343−350.
[19] G. M. Sheldrick, *SHELX97 − Programs for Crystal Structure Analysis*, release 97-2.

Received March 4, 2002
[I02113]

Chiral 2,3-Dihydro-1*H*-1,3,2-diazaboroles

Lothar Weber,*[a] Andreas Rausch,[a] Henning B. Wartig,[a] Hans-Georg Stammler,[a] and Beate Neumann[a]

Keywords: Boron / Chirality / Diazaboroles / Heterocycles / Crystal structure

A series of differently substituted chiral 2,3-dihydro-1*H*-1,3,2-diazaboroles has been prepared by various methods. 2-Bromo-1-*tert*-butyl-3-[(*S*)-1-phenylethyl]-2,3-dihydro-1*H*-1,3,2-diazaborole (**3a**), 2-bromo-1,3-di[(*S*)-1-phenylethyl]-2,3-dihydro-1*H*-1,3,2-diazaborole (**3b**) and 2-bromo-1,3-di[(*S*)-1-cyclohexylethyl]-2,3-dihydro-1*H*-1,3,2-diazaborole (**3c**) were formed from the reaction of the corresponding 1,4-diazabutadienes and boron tribromide and the subsequent reduction of the resulting borolium salts [R^1N^a = CH–CH=$N^b(R^2)BBr_2$]Br(N^a–*B*) [**2a**: R^1 = *t*Bu, R^2 = CH(Me)Ph; **2b**: R^1 = R^2 = CH(Me)Ph; **2c**: R^1 = R^2 = CH(Me)(*c*C_6H_{11})] with sodium amalgam. Treatment of (*S*)-**3a** with $LiAlH_4$ or methyllithium afforded 1-*tert*-butyl-2-hydro-3-[(*S*)-1-phenylethyl]-2,3-dihydro-1*H*-1,3,2-diazaborole [(*S*)-**6**] and 1-*tert*-butyl-2-methyl-3-[(*S*)-1-phenylethyl]-2,3-dihydro-1*H*-1,3,2-diazaborole [(*S*)-**7**], respectively. Aminolysis of the BBr bond of (*S*)-**3a** by *tert*-butylamine or (*S*)-1-phenylethylamine gave the corresponding 2-*tert*-butylamino- and 2-[1-phenylethylamino]-2,3-dihydro-1*H*-1,3,2-diazaboroles (*S*)-**8** and (*S,S*)-**9**, respectively. Similarly, (*S,S*)-**3b** and (*S,S*)-**3c** were reacted with *tert*-butylamine to furnish the 2-*tert*-butylamino-2,3-dihydro-1*H*-1,3,2-diazaborole derivatives (*S,S*)-**11** and (*S,S*)-**12**, respectively. The 2-trimethylstannyl-2,3-dihydro-1*H*-1,3,2-diazaboroles (*S,S*)-**10** and (*S,S*)-**14** were accessible from **3b** or **3c** and trimethylstannyllithium. The transformation of achiral 2-bromo-1,3-di-*tert*-butyl-2,3-dihydro-1*H*-1,3,2-diazaborole into the chiral (*S*)-2-[1-phenylethylamino]- and (*S*)-2-[1-cyclohexyl-ethylamino] derivatives (*S*)-**15** and (*S*)-**16** was effected by aminolysis with enantiomerically pure (*S*)-1-phenylethylamine or (*S*)-1-cyclohexylethylamine. The novel compounds were characterized by ^1H, ^{11}B, ^{13}C, and ^{119}Sn NMR spectroscopy as well as mass spectrometry and determination of the optical rotation. The molecular structure of compound **3c** was confirmed by X-ray structural analysis.
(© Wiley-VCH Verlag GmbH, 69451 Weinheim, Germany, 2002)

Introduction

The synthesis of the first 2,3-dihydro-1*H*-1,3,2-diazaboroles **I** dates back to the early 1970s,[1,2] and since then a series of contributions concerning the synthesis, structure, and bonding of such heterocycles has been published.[3–6]

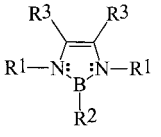

I

I	R1	R2	R3
a	Me	Ph	H
b	Ph	Me	Me
c	Me	*t*Bu	H
d	H/Me	Ph	H

Recently, we started a program investigating the synthesis of 2-halo-2,3-dihydro-1*H*-1,3,2-diazaboroles **II** as starting materials for further chemical transformations.[7,8] Treatment of **II** with organolithium compounds,[9] $LiSnMe_3$,[9] $LiAlH_4$,[9] imidazol-2-ylidenes,[7] amines[10] and silver salts[8] afforded a series of novel 1,3,2-diazaboroles **III**–**VIII** (Scheme 1).

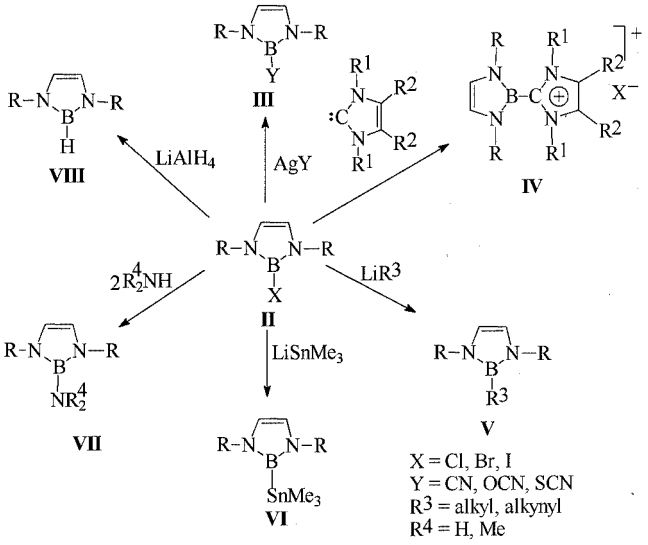

Scheme 1. Chemical transformations of **II**

Terminal as well as internal alkynes are inserted regioselectively into the B–Sn bond of **VI** in a reaction catalyzed by low-valent Pd species (Scheme 2).[11]

[a] Fakultät für Chemie der Universität Bielefeld
Universitätsstraße 25, 33615 Bielefeld, Germany
Fax: (internat.) + 49-(0)5201/106-6146
E-mail: lothar.weber@uni-bielefeld.de

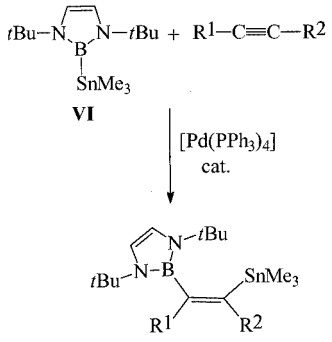

Scheme 2. Insertion of alkynes into the B−Sn bond of **VI**

Moreover, it was demonstrated that 1,3,2-diazaboroles are smoothly converted into 1,3,2-oxazaborolidines **IX** upon reaction with an equimolar amount of diphenylketene (Scheme 3).[12]

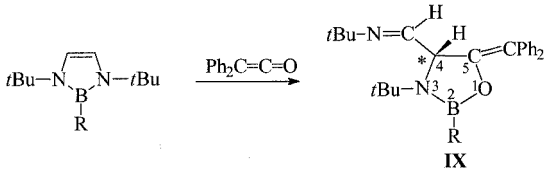

Scheme 3. Conversion of 2,3-dihydro-1*H*-diazaboroles into 1,3,2-oxazaborolidines by treatment with diphenylketene

Here a stereogenic center was created at C(4), and it was challenging to elaborate conditions that would allow the stereoselective synthesis of these compounds.

Results and Discussion

The intention of the work described herein is to provide efficient syntheses of chiral 2,3-dihydro-1*H*-1,3,2-diazaboroles as the required precursors for such transformations. The most obvious way to introduce chirality into 1,3,2-diazaboroles is the use of chiral substituents at the heteroatoms of the ring. This target may be achieved by the employment of chiral 1,4-diazabutadienes as starting materials. The latter are available from the condensation of glyoxal and chiral primary amines such as (*S*)-1-phenylethylamine or (*S*)-1-cyclohexylethylamine. The combined condensation of glyoxal with *tert*-butylamine and (*S*)-phenylethylamine in a molar ratio of 4:7:1 leads to the formation of a 3:1 mixture of 1,4-di-*tert*-butyl-1,4-diazabutadiene and Ph(Me)CHN=CH−CH=N*t*Bu (**1a**). The former product is easily removed in vacuo at ambient temperature. The residue of crude **1a** was purified by distillation to give a light yellow oil (43% yield). This compound is thermolabile and has to be stored at −30 °C. According to NMR spectroscopic data **1a** is a 1:2 mixture of two isomers.

The diazabutadienes (*S*,*S*)-Ph(Me)CHN=CH−CH=NCH(Me)Ph (**1b**)[13] and (*S*,*S*)-*c*-C_6H_{11}(Me)CHN=CH−CH=N−CH(Me)(*c*-C_6H_{11}) (**1c**) were prepared from an aqueous glyoxal solution and the respective amines in a molar ratio of 1:2. Compound **1c** was isolated as colorless crystals in 82% yield, whereas **1b** was obtained as a colorless oil as described previously.

Combination of equimolar amounts of **1a** and BBr_3 in hexane at 20 °C led to the precipitation of the orange borolium salt **2a**. Its moisture sensitivity and low volatility precluded reliable elemental analyses and useful mass spectra. The reduction of compound **2a** with sodium amalgam in hexane afforded 1,3,2-diazaborole **3a** as a yellow oil in 66% yield after distillation (Scheme 4).

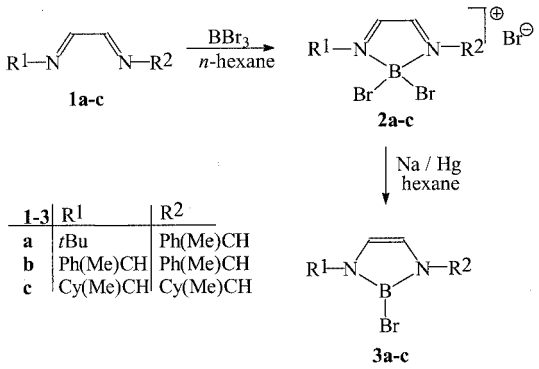

Scheme 4. Preparation of 1,3,2-diazaboroles **3a**−**c** (Cy = cyclohexyl)

Neat **3a** decomposes to a brown oil after 24 h at 20 °C, therefore it is recommended to store the reaction mixture and to isolate the compound only prior to use.

The preparation of the yellow borolium salt **2b** was achieved by reaction of diazabutadiene (**1b**) and boron tribromide under similar conditions. Sodium amalgam reduction of **2b** over a period of two days led to a 32% yield of crude oily **3b**. Like **3a**, compound **3b** should only be isolated immediately before subsequent transformations.

In contrast to this, the reduction of analogously prepared orange moisture-sensitive **2c** with sodium amalgam led to the formation of colorless crystalline **3c** (60.5%), which separated upon concentrating the hexane reaction solution. Further purification of the thermostable product was achieved by sublimation at 80 °C and 5×10^{-6} bar.

In the $^{11}B\{^1H\}$ NMR spectra the 2-bromo-1,3,2-diazaboroles **3a**−**c** show singlets at δ = 17.3 (**3a**), 19.0 (**3b**) and 18.2 ppm (**3c**), which are very similar to the ^{11}B resonance in *t*BuN^{a}CH=CHN^b(*t*Bu)BBr(N^a−*B*) (δ = 16.2 ppm).[7] The ^1H and ^{13}C NMR resonances of the CH=CH building block (δ_H = 6.13−6.41 ppm and δ_C = 111.9−114.9 ppm are also very similar to the corresponding data for *t*BuN^a-CH=CHN^b(*t*Bu)BBr (δ_H = 6.27 ppm, δ_C = 113.6 ppm).

A series of chiral 1,3,2-diazaboroles were derived from **3a** by nucleophilic substitution at the boron center. Reaction of **3a** with silver cyanide in acetonitrile for 1 h furnished a liquid mixture of 2-isocyano-1,3,2-diazaborole (**4**) and 2-cyano-1,3,2-diazaborole (**5**) (Scheme 5)

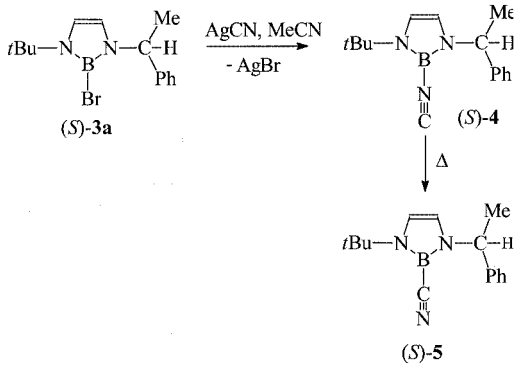

Scheme 5. Reaction of (*S*)-**3a** with AgCN

The presence of both isomers was confirmed by the ^{1}H, ^{13}C NMR and IR spectra of a freshly prepared sample. Particularly informative is the IR spectrum where sharp bands at $\tilde{\nu}$ = 2113 and 2206 cm^{-1} are attributed to the ν(CN) vibrations of the isocyano function in **4** and the cyano group in **5**, respectively. Storing the product mixture at −30 °C for two weeks or vacuum distillation at 200 °C led to the complete disappearance of the band at 2113 cm^{-1}. After the rearrangement **4** → **5** the pure cyano derivative was obtained as a colorless solid (57% yield). In contrast to precursor **3a**, compound **5** is stable at room temperature. A similar rearrangement was not observed during the preparation of *t*BuN^{a}−CH=CH−N^{b}(*t*Bu)BCN(*N^{a}*−*B*) from the corresponding 2-bromo-1,3,2-diazaborole and AgCN. To the best of our knowledge stable boryl isocyanides are still undocumented. The $^{11}B\{^{1}H\}$ NMR spectrum of **5** is characterized by a singlet at δ = 11.6 ppm. In the ^{1}H and $^{13}C\{^{1}H\}$ NMR spectra the HC=CH unit gives rise to two doublets at δ = 6.25 and 6.40 ppm ($^{3}J_{H,H}$ = 2.3 Hz) and two singlets at δ = 114.8 and 116.1 ppm, respectively. In *t*BuN^{a}−CH=CH−N^{b}(*t*Bu)BCN(*N^{a}*−*B*) the corresponding resonances were observed at δ_B = 12.0 ppm (s), δ_H = 6.14 ppm (s) and δ_C = 114.6 ppm (s).

Reduction of (*S*)-**3a** with lithium aluminium hydride in a THF/hexane mixture (Scheme 6) afforded the 2-hydro-1,3,2-diazaborole (*S*)-**6** as a yellow oil (95%). Purification by vacuum distillation to give (*S*)-**6** as a colorless liquid was accompanied by considerable loss of product (47%). At room temperature decomposition of a pure sample to a brown oil was complete within 24 h. In the IR spectrum a strong band at $\tilde{\nu}$ = 2621 cm^{-1} is due to the ^{11}B-H stretching mode. In the proton-coupled ^{11}B NMR spectrum ($CDCl_3$ solution) compound (*S*)-**6** exhibits a doublet at δ = 19.4 ppm ($^{1}J_{B,H}$ = 146 Hz). These values compare well with the result given for *t*BuN^{a}CH=CH−N^{b}(*t*Bu)BH(*N^{a}*−*B*) [δ_B = 18.9 ppm (d, $^{1}J_{B,H}$ = 149 Hz)].[9] In contrast to the latter compound, where the boron-ligated hydrogen atom appears in the ^{1}H NMR spectrum as a quadruplet resonance (δ = 4.78 ppm, $^{1}J_{B,H}$ = 150 Hz) no such signal was detected in the ^{1}H NMR spectrum of (*S*)-**6**.

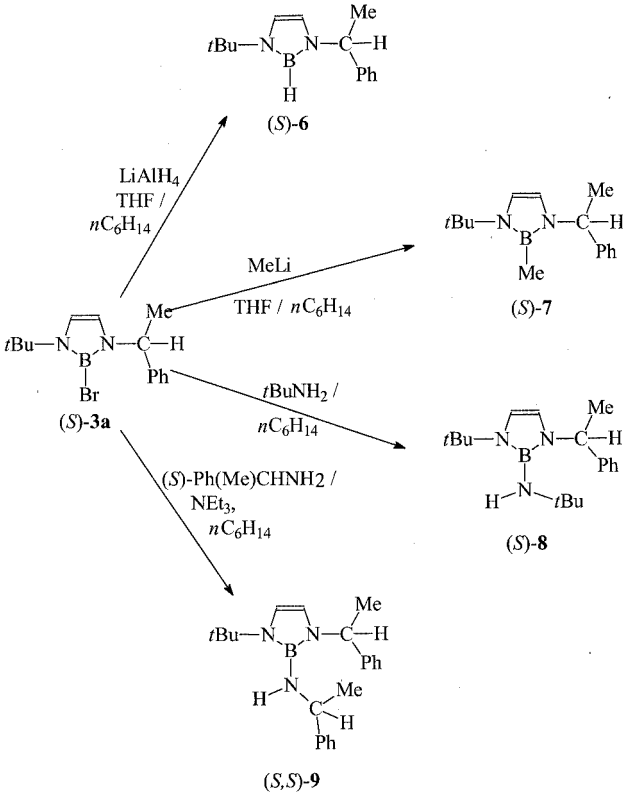

Scheme 6. Reaction of (*S*)-**3a** with $LiAlH_4$, MeLi, *t*$BuNH_2$ and (*S*)-Ph(Me)CH−NH_2

The reaction of 2-bromo-1,3,2-diazaborole (*S*)-**3a** with methyllithium in a mixture of hexane and THF (Scheme 6) cleanly afforded (*S*)-**7** as a colorless oil after distillation at 200 °C and 10^{-5} bar (51%). The $^{11}B\{^{1}H\}$ NMR spectrum of (*S*)-**7** shows a singlet at δ = 26.2 ppm, which is identical with that of *t*BuN^{a}CH=CHN^{b}(*t*Bu)BCH$_3$(*N^{a}*−*B*).[3] The CH=CH unit appears as two doublets at δ = 6.32 and 6.48 ppm ($^{3}J_{H,H}$ = 2.5 Hz) in the ^{1}H NMR spectrum and two singlets at δ = 111.1 and 113.5 ppm in the $^{13}C\{^{1}H\}$ NMR spectrum of the compound.

To increase the steric demand of chiral 1,3,2-diazaboroles we introduced bulky amino substituents at the boron atom of the ring. Reaction of (*S*)-**3a** with an excess of *tert*-butylamine in hexane gave (*S*)-**8** (Scheme 6), which was isolated as a yellow oil by vacuum distillation (300 °C, 10^{-5} bar, 74%). Compound (*S*,*S*-**9**) resulted from the treatment of (*S*)-**3a** with an equimolar amount of (*S*)-1-phenylethylamine in the presence of triethylamine. The heterocycle was isolated as a colorless liquid in 48% yield by vacuum distillation. The ^{11}B NMR signals of (*S*)-**8** (δ = 22.3 ppm) and (*S*,*S*)-**9** (δ = 21.6 ppm) are similar to those of the amino-functionalized 1,3,2-diazaboroles *t*BuN^{a}CH=CHN^{b}(*t*Bu)BN(H)*t*Bu(N^{a}−B) (δ = 22.9 ppm) and *t*BuN^{a}-CH=CHN^{b}(*t*Bu)BNH(2,6-$Me_2C_6H_3$)(*N^{a}*−*B*) (δ = 21.6 ppm).[10]

It was also intended to convert the chiral 1,3,2-diazaborole (*S*,*S*)-**3b** into more stable and sterically more congested

derivatives. A hexane solution of (*S*,*S*)-**3b** was combined with a solution of a slight excess of $LiSnMe_3$ in THF at room temperature, whereupon the stannylated heterocycle (*S*,*S*)-**10** was generated. Analytically pure colorless (*S*,*S*)-**10** was obtained by crystallizing the crude material from toluene (67% yield). (Scheme 7)

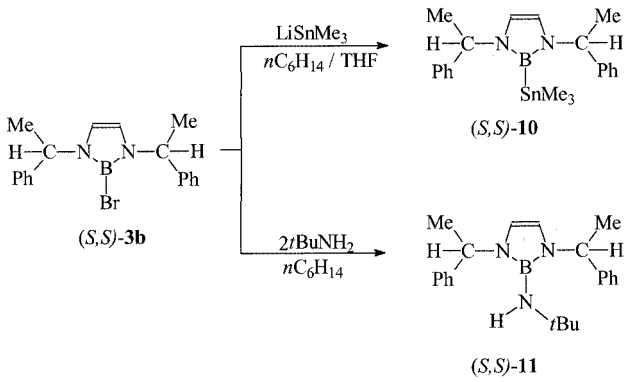

Scheme 7. Conversion of (*S*,*S*-**3b**) into (*S*,*S*-**10**) and (*S*,*S*-**11**)

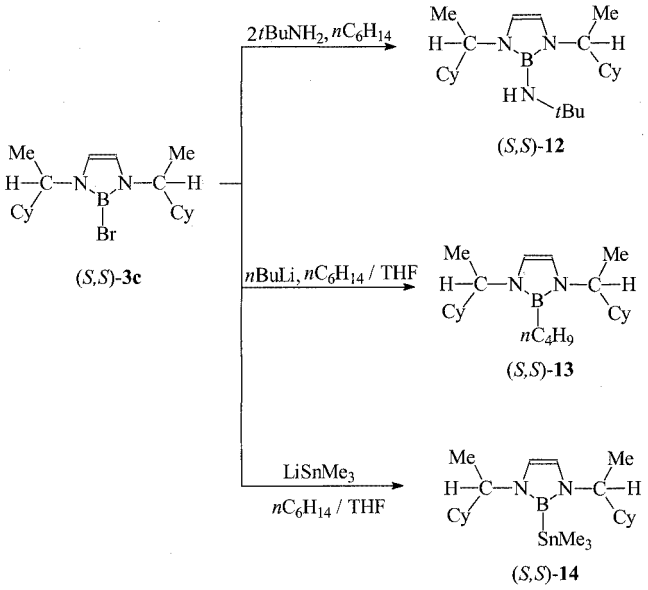

Scheme 8. Synthesis of (*S*,*S*)-**12**, (*S*,*S*)-**13** and (*S*,*S*)-**14** from (*S*,*S*)-**3c**

Compound **10** can be stored at room temperature under an inert atmosphere without discernible decomposition. The singlet at δ = 28.2 ppm in the $^{11}B\{^1H\}$ NMR spectrum is accompanied by ^{119}Sn satellites ($^1J_{Sn,B}$ = 994 Hz). Similarly, the $^{119}Sn\{^1H\}$ NMR spectrum of **10** features a quadruplet at δ = 150.0 ppm ($^1J_{Sn,B}$ = 994 Hz). The $^{11}B\{^1H\}$ NMR spectrum of 2,6-$Me_2C_6H_3N^aCH{=}CHN^b$(2,6-$Me_2C_6H_3$)$BSnMe_3$(*N*^{a}−*B*) is characterized by a singlet at δ = 28.2 ppm with ^{119}Sn satellites ($^1J_{Sn,B}$ = 960 Hz). The $^{119}Sn\{^1H\}$ NMR resonance of this molecule appears as a quadruplet at δ = 146 ppm with $^1J_{Sn,B}$ = 960 Hz.

The stable amino-functionalized 1,3,2-diazaborole (*S*,*S*)-**11** was isolated as a yellow liquid from the reaction of **3b** with a twofold equimolar amount of *tert*-butylamine in hexane at 20 °C (50%). Similarly, the colorless liquid diazaborole (*S*,*S*)-**12** was synthesized from (*S*,*S*)-**3c** and *tert*-butylamine (58% after distillation at 300 °C, 4 × 10^{-6} bar; Scheme 8). Preparation of the 2-butyl-1,3,2-diazaborole (*S*,*S*)-**13** was accomplished by reaction of **3c** with an excess of *n*-butyllithium in a hexane/THF mixture at −15 to 20 °C. Pure colorless oily **13** was obtained by distillation (250 °C, 5 × 10^{-6} bar, 47%).

Analogously to the preparation of (*S*,*S*)-**10** the stannylated diazaborole (*S*,*S*)-**14** was synthesized as a colorless liquid from **3c** and $LiSnMe_3$ in a THF/hexane mixture (58% yield).

A different approach to chiral 1,3,2-diazaboroles was based upon the reaction of achiral *t*$BuN^aCH{=}CHN^b$(*t*Bu)BBr(*N*^{a}−*B*) with the chiral auxiliaries (*S*)-Ph(Me)$CHNH_2$ and (*S*)-Cy(Me)$CHNH_2$ in the presence of triethylamine (Scheme 9). Heterocycle **15** was isolated as a pale yellow oil in 74% yield by distillation (200 °C, 10^{-5} bar). The same holds for **16**, which was isolated as a colorless oil after distillation (150 °C, 2 × 10^{-6} bar, 72%). The $^{11}B\{^1H\}$ spectra of the 2-amino-1,3,2-diazaboroles (*S*,*S*)-**11** [δ = 22.5 (s)], (*S*,*S*)-**12** [δ = 22.1 (s)], (*S*)-**15** [δ = 22.3 (s)] and (*S*)-**16** [δ = 22.0 (s)] resemble those of **8** and **9** and do not show any marked influence of the substituent at the nitrogen atom.

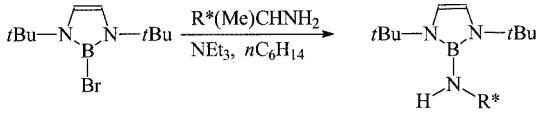

Scheme 9. Preparation of (*S*)-**15** and (*S*)-**16**

X-ray Structural Analysis of (*S*,*S*)-3c

The molecular structure of (*S*,*S*)-**3c** (Figure 1) features a planar 1,3,2-diazaborole ring with two nearly orthogonally oriented 1-cyclohexylethyl substituents at the nitrogen atoms. A C_2 axis bisects the molecule along the B(1)−Br(1) vector. The bond length B(1)−Br(1) [1.930(2) Å] is close to the sum of the covalent radii of boron (0.81 Å) and bromine (1.14)[14] and compares well with the B−Br distances in [(2,4,6-$Me_3C_6H_2$)(Br)B]$_2$ [1.928(4) and 1.932(4) Å].[15] B−Br bond lengths involving sp^2-hybridized boron atoms range from 1.87(1) Å in [*i*$Pr_3P{=}N^a{-}B^a$(Br)N^b-(=P*i*Pr$_3$)B^bBr_2]Br(*N*^{a}−*B*^{b})[16] or 1.902(5) Å in 2,6-$Mes_2C_6H_3BBr_2$ (Mes = 2,4,6-$Me_3C_6H_2$)[17] to 2.00(1) Å in the triborane [(Me_2N)(Br)B]$_2$$BNMe_2$.[18] Atomic distances and valence angles within the diazaborole ring are in good agreement with the corresponding data for (2,6-$Me_2C_6H_3$)$N^a{-}CH{=}CH{-}N^b$(2,6-$Me_2C_6H_3$)BI(*N*^{a}−*B*).[18] In (*S*,*S*)-**3c** the B−N bond length [1.417(1) Å] indicates multiple bond character. In a series of diazaboroles the B−N bond lengths range from 1.407(5) to 1.450(2) Å. The atomic distance C(1)−C(1A) [1.350(3) Å] and the

N−C(sp^2) bond length [1.403(2) Å] also indicate multiple bonding. For the N(sp^2)−C(sp^3) single bond N(1)−C(2) a length of 1.471(2) Å was determined. The endocyclic angles in (*S*)-**3c** — N(1)−B(1)−N(1A) [107.7(1)°] B(1)−N(1)−C(1) [106.6(1)°], and N(1)−C(1)−C(1A) [109.5(1)°] — are similar to those in 2,6-$Me_2C_6H_3N^aCH$=CHN^b(2,6-$Me_2C_6H_3$)BI(*N*^{a}−*B*) [106.9(4)°, 107.5(3)°, and 109.1(2)°, respectively].[8] This also applies to the exocyclic angle N(1)−B(1)−Br(1) [126.1(1)°] in (*S*)-**3c** and the N(1)−B(1)−I(1) angle [126.6(2)°] in 2,6-$Me_2C_6H_3N^a$−CH=CHN^b(2,6-$Me_2C_6H_3$)BI(*N*^{a}−*B*).

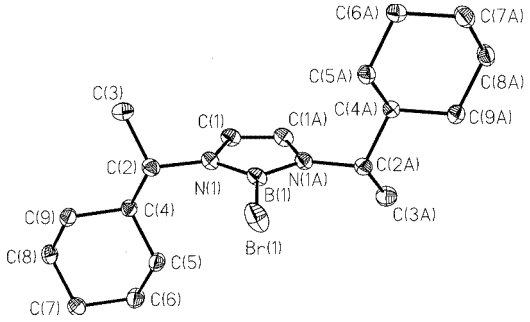

Figure 1. Molecular structure of (*S*,*S*)-**3c** in the crystal; selected bond lengths [Å] and bond angles [°]: B(1)−Br(1) 1.930(2), B(1)−N(1) 1.417(1), N(1)−C(1) 1.403(2), N(1)−C(2) 1.471(2), C(1)−C(1A) 1.350(3); N(1)−B(1)−N(1A) 107.7(1), Br(1)−B(1)−N(1) 126.1(1), B(1)−N(1)−C(1) 106.6(1), B(1)−N(1)−C(2) 131.0(1), N(1)−C(1)−C(1A) 109.5(1); B(1)−N(1)−C(2)−C(3) 124.3, B(1)−N(1)−C(2)−C(4) −110.0

Experimental Section

General: All manipulations were performed under dry argon. Solvents were rigorously dried with an appropriate drying agent and freshly distilled before use. The following compounds were prepared as described in the literature: (*S*,*S*)-Ph(Me)CHN=CH−CH=NCH(Me)Ph (**1b**),[13] *t*BuN^aCH=CHN^b(*t*Bu)BBr(*N*^{a}−*B*).[7]

An aqueous glyoxal solution (40%) of *tert*-butylamine, boron tribromide, silver cyanide, trimethyltin chloride, *n*-butyllithium, methyllithium, triethylamine, (*S*)-1-phenylethylamine and (*S*)-1-cyclohexylethylamine were purchased commercially. IR spectra Bruker FTIR Vector 22, Bruker FTIR IFS66. ^{1}H, ^{11}B, ^{13}C NMR spectra: Bruker AC 100 (^{1}H, 100.13 MHz, ^{11}B (32.13 MHz); Bruker Avance DRX 500 (^{1}H, 500.13 MHz, ^{11}B, 160.46 MHz, ^{13}C, 125.75 MHz); references: $SiMe_4$ (^{1}H, ^{13}C), BF_3·OEt_2 (^{11}B). Mass spectra EI (70 eV), CI (NH_3): Autospec sector-field mass spectrometer (Micromass). Optical rotations were measured with a Jasco DIP-360 in CH_2Cl_2 solution [c = 0.01 g·mL^{-1}, d = 1 dm].

Preparation of the 1,4-Diazabutadienes. (*S*)-*t*BuN=CH−CH=N−CH(Me)Ph (1a): Solutions of (*S*)-1-phenylethylamine (28.8 g, 0.24 mol) in hexane (200 mL) and *tert*-butylamine (121.7 g, 1.90 mol) in hexane (200 mL) were simultaneously added dropwise to a well-stirred chilled mixture of an aqueous solution of glyoxal 114.3 mL (114.2 mL, 1.0 mol, 0 °C) and 400 mL of hexane. Then stirring was continued at room temp. for 30 min. The liquid content of the flask separated into two phases. The aqueous phase was extracted with hexane (30 mL) and then discarded. The combined hexane phases were dried (Na_2SO_4) and then freed from solvent. The remaining yellow oil was kept at 5 × 10^{-6} bar and 20 °C to remove *t*BuN=CH−CH=N*t*Bu (49.0 g crude **1a**). The brown oily residue (10.0 g) was distilled at (5 × 10^{-6} bar, and 70 °C) to give 4.5 g (43%) of **1a** as a light-yellow liquid. This purification step could not be scaled up because of serious loss of product. IR (film): $\tilde{\nu}$ = 3062 cm^{-1} w, 3029 m, 2981 s, 2864 s, 1629 s [ν(C=N)], 1493 m, 1451 m, 1361 s, 1213 s, 759 s, 699 s. ^{1}H NMR ($CDCl_3$): δ = 1.21 and 1.23 (2s, 9 H, *t*Bu), 1.55 and 1.56 (2d, $^3J_{H,H}$ = 6.4, 6.8 Hz, 3 H, CH_3), 4.48 [q, $^3J_{H,H}$ = 6.8 Hz, 1 H, C*H*Me], 7.23−7.33 (m, 5 H, *H*−Ph), 7.92−8.02 (m, 2 H, N=CH) ppm. ^{13}C{^{1}H} NMR ($CDCl_3$): δ = 23.9 (s, CH*C*H$_3$), 29.27 and 29.34 [2s, C(*C*H$_3$)], 58.2 and 58.3 [2s, *C*(CH$_3$)$_3$], 69.66 and 69.71 (2s, *C*HCH$_3$), 126.6, 126.7, 127.2, 128.5, 128.6, 143.6, 143.7 (7s, *C*−Ph), 157.0, 157.8, 160.7, 161.5 (4s, H*C*=N) ppm. MS/EI: *m*/*z* (%) = 216 (6) [M$^+$], 201 (36) [M$^+$ − CH_3], 159 (33) [M$^+$ − *t*Bu], 145 (100) [M$^+$ − CH_3 − CH_2=CMe_2]. [α]$_D^{24}$ = −97. $C_{14}H_{20}N_2$ (216.33): calcd. C 77.73, H 9.32, N 12.95; found C 77.40, H 9.56, N 12.86.

(*S*,*S*)-Cy(Me)CH−N=CH−CH=N−CH(Me)Cy (1c): A solution of (*S*)-1-cyclohexylethylamine (17.8 g, 140 mmol) in 80 mL of hexane was added during 30 min to a vigorously stirred mixture of 8 mL of aqueous glyoxal (70 mmol) and 50 mL of hexane. Both phases were separated and the aqueous layer was extracted with 50 mL of hexane. The combined organic phases were dried twice with Na_2SO_4. Solvent was removed in vacuo to afford 16.1 g (82%) of **1c** as colorless crystals. ^{1}H NMR ($CDCl_3$): δ = 0.85 (m, 2 H, Cy), 0.93 (m, 2 H, Cy), 1.15 (m, 8 H, Cy), 1.23 (m, 4 H, Cy), 1.42 (m, 2 H, Cy), 1.63 (m, 4 H, Cy), 1.75 (m, 6 H, CH_3), 2.97 (q, $^3J_{H,H}$ = 6.6 Hz, 2 H, C*H*CH$_3$), 7.85 (s, 2 H, N=CH) ppm. ^{13}C{^{1}H} NMR ($CDCl_3$): δ = 19.6 (s, CH_3), 26.2, 26.3, 26.5, 29.5, 29.8, 43.4 (6s, Cy), 71.6 (s, *C*HCH$_3$), 160.2 (s, CH=N) ppm. MS/EI: *m*/*z* (%) = 276 (7) [M$^+$], 193 (100) [M$^+$ − Cy]. [α]$_D^{24}$ = +34. $C_{18}H_{32}N_2$ (276.47): calcd. C 78.20, H 11.67, N 10.13; found C 77.40, H 11.94, N 10.30.

Preparation of the 2,3-Dihydro-1*H*-1,3,2-diazaboroles. (*S*)-*t*BuN^a-CH=CHN^b {CH(Ph)Me}BBr(*N*^{a}−*B*) (3a): A solution of 1,4-diazabutadiene **1a** (3.3 g, 15.3 mmol) in 50 mL of hexane and a solution of boron tribromide (3.85 g, 15.5 mmol) in 50 mL of hexane were added dropwise and simultaneously at 20 °C to a volume of 100 mL of hexane. The resulting orange slurry was stirred for another 30 min and filtered. The filter cake was washed with pentane (50 mL) and dried at 5 × 10^{-3} bar. The borolium salt (*S*)-*t*BuN^a=CH−CH=N^b {CH(Ph)Me}BBr$_2$]Br(*N*^{a}−*B*) **2a** was obtained as an orange powder (6.4 g, 90%). ^{1}H NMR ($CDCl_3$): δ = 1.75 (s, 9 H, *t*Bu), 2.02 (d, $^3J_{H,H}$ = 6.9 Hz, 3 H, CHC*H*$_3$), 5.35 (q, $^3J_{H,H}$ = 6.9 Hz, 1 H, C*H*CH$_3$), 7.40 (m, 3 H, Ph), 7.57 (m, 2 H, Ph), 8.40 (d, $^3J_{H,H}$ = 7.9 Hz, 1 H, *C*H=N−CH), 8.68 (d, $^3J_{H,H}$ = 7.9 Hz, 1 H, *C*H=N*t*Bu) ppm. ^{11}B{^{1}H} NMR ($CDCl_3$): δ = −1.2 (s) ppm. Compound **2a** (11.5 g, 24.6 mmol) was added to a mixture of sodium amalgam (from 2.5 g, 108 mmol Na and 240 g Hg) and hexane (200 mL) and vigorously stirred for two days. The yellow hexane solution was then decanted and the solvent evaporated. The remaining brown oil was distilled by means of a hot air gun to afford **3a** as a yellow oil (5.1 g, 66%). As pure diazaborole **3a** decomposes markedly at ambient temp. within one day, it is recommended to store the compound in the hexane solution over sodium amalgam and to use the freshly isolated material. IR (film): $\tilde{\nu}$ = 3030 cm^{-1} m, 2985 s, 2873 s, 1603 w, 1495 m, 1450 s, 1147 m, 962 m, 755 m, 700 s, 610 m. ^{1}H NMR ($CDCl_3$): δ = 1.51 (s, 9 H, *t*Bu), 1.66 (d, $^3J_{H,H}$ = 7.1 Hz, 3 H, CH_3), 5.19 (q, $^3J_{H,H}$ = 7.1 Hz, 1 H, C*H*CH$_3$), 6.19 (d, $^3J_{H,H}$ = 2.4 Hz, 1 H, *H*C=NCHMe), 6.41 (d, $^3J_{H,H}$ = 2.4 Hz, 1 H, *H*C=N*t*Bu), 7.26 (m, 3 H, Ph), 7.3 (m, 2 H,

Ph) ppm. $^{13}C\{^1H\}$ NMR ($CDCl_3$): δ = 21.4 (s, CH*C*H_3), 31.2 [s, C(*C*H_3)$_3$], 52.8 [s, *C*(CH$_3$)$_3$], 58.3 (s, *C*HCH$_3$), 111.9 (s, H*C*=NCHMe), 114.9 (s, H*C*=N*t*Bu), 126.5, 126.8, 128.3, 144.0 (4s, Ph) ppm. $^{11}B\{^1H\}$ NMR ($CDCl_3$): δ = 17.3 s ppm. MS/EI: *m*/*z* (%) = 308 (6) [M^+ with ^{81}Br], 306 (7). [M^+ with ^{79}Br]. $[\alpha]_D^{24}$ = −104. $C_{14}H_{20}BBrN_2$ (307.04): calcd. C 54.77, H 6.57, N 9.12; found C 55.40, H 6.89, N 8.62.

(*S*,*S*)-Me(Ph)HCN^a−CH=CH−N^b\|CH(Ph)Me\|BBr(*N*^{a}−*B*) (3b): A solution of (*S*,*S*)−Me(Ph)HC−N=CH−CH=N−CH(Ph)Me (**1b**) (7.04 g, 27.0 mmol) in 50 mL of hexane and a solution of BBr_3 (6.67 g, 27.0 mmol) in 50 mL of hexane were added slowly at 20 °C to 300 mL of hexane, whereupon a yellow precipitate separated. Stirring was continued for two days. The mixture was then filtered, the filter cake was washed with hexane (50 mL) and then dried in vacuo. Yield: 11.2 g (81.4%) [(*S*,*S*)−Me(Ph)HC−N^a=CH−CH=N^b−CH(Ph)MeBBr$_2$]Br(*N*^{a}−*B*) (**2b**).

A slurry of **2b** (8.0 g, 18.4 mmol) and sodium amalgam (from 230 g Hg and 2.4 g Na) in 200 mL of hexane was stirred vigorously for two days. The yellow organic phase was decanted and the solvents evaporated to dryness to afford 2.1 g (32%) of crude **3b**. The marked thermolability of this compound thwarted reliable elemental analyses. As in the case of **3a** it is recommended to store the reaction mixture and to isolate the required amount of compound prior to use. ^1H NMR (C_6D_6): δ = 1.38 (d, $^3J_{H,H}$ = 7.1 Hz, 6 H, CH$_3$), 5.13 (q, $^3J_{H,H}$ = 7.1 Hz, 2 H, C*H*CH$_3$), 6.13 (s, 2 H, CH=N), 7.01−7.17 (m, 10 H, Ph) ppm. $^{13}C\{^1H\}$ NMR (C_6D_6): δ = 21.5 (s, CH*C*H$_3$), 53.9 (s, *C*HCH$_3$), 114.6 (s, CH=N), 126.7, 127.1, 128.5, 144.3 (4s, Ph). $^{11}B\{^1H\}$ NMR (C_6D_6): δ = 19.0 (s) ppm.

(*S*,*S*)-Me(Cy)HC−N^{a}CH=CH−N^b\|CH(Cy)Me\|BBr(*N*^{a}−*B*) (3c): A solution of 1,4-diazabutadiene **1c** (8.0 g, 29.0 mmol) in 100 mL of hexane and a solution of BBr_3 (7.52 g, 30.0 mmol) in 100 mL of hexane were added simultaneously at 0 °C to 100 mL of hexane. The resulting slurry was allowed to stir for 1 h at 20 °C and was then filtered. The filter cake was washed with 100 mL of pentane and dried in vacuo. The borolium salt (*S*,*S*)-[Me(Cy)CH−N^a=CH−CH=N^b{CH(Cy)Me}BBr$_2$]Br(*N*^{a}−*Br*) (**2c**) was obtained as an orange solid (14.5 g, 93%). ^1H NMR (C_6D_6): δ = 0.69−2.00 (m, 22 H, C_6H_{11}), 1.41 (d, $^3J_{H,H}$ = 6.8 Hz, 6 H, CH$_3$), 3.76 (m, 2 H, C*H*CH$_3$), 9.12 (s, 2 H, HC=CH) ppm. $^{13}C\{^1H\}$ NMR (C_6D_6): δ = 18.4 (s, CH$_3$), 26.2, 26.3 (2s, 3,5-*C*−Cy), 29.0, 31.5 (2s, 2,6-*C*−Cy), 42.2 (s, 1-*C*−Cy), 60.9 (s, *C*HCH$_3$), 146.7 (s, HC=CH) ppm. $^{11}B\{^1H\}$ NMR (C_6D_6): δ = 0.6 (s, BBr_2), −23.8 (s, BBr_4^-) ppm.

Solid borolium salt **2c** (9.5 g, 18.0 mmol) was combined with sodium amalgam [from Na (1.3 g, 55.0 mmol) and 130 g of Hg]. After the addition of 200 mL of hexane the resulting slurry was stirred at room temp. for three days. The yellow hexane phase was decanted and concentrated to ca 10 mL, whereby crystalline colorless **3c** precipitated (4.0 g, 60.5%). The purity of the sample was satisfactory for most chemical transformations. Analytically pure **3c** was obtained by sublimation at 80 °C and 5 × 10^{-6} bar. ^1H NMR ($CDCl_3$): δ = 0.79−1.81 (m, 22 H, C_6H_{11}), 1.25 (d, $^3J_{H,H}$ = 6.8 Hz, 6 H, CH$_3$), 3.46 (m, 2 H, C*H*CH$_3$), 6.17 (s, 2 H, HC=CH) ppm. $^{13}C\{^1H\}$ NMR ($CDCl_3$): δ = 19.6 (s, CH$_3$), 26.15, 26.22 (2s, 3,5-*C*−Cy), 26.3 (s, 4-*C*−Cy), 29.9, 30.3 (2s, 2,6-*C*−Cy), 44.1 (s, 1-*C*−Cy), 55.6 (s, *C*HCH$_3$), 113.5 (s, HC=CH) ppm. $^{11}B\{^1H\}$ NMR: δ = 18.2 (s) ppm. MS/CI (toluene): *m*/*z* (%) = 367 (9) [MH^+]. $[\alpha]_D^{24}$ = −29. $C_{18}H_{32}BBrN_2$ (367.18): calcd. C 58.88, H 8.78, N 7.63; found C 58.44, H 9.17, N 7.48.

(*S*)-*t*BuN^{a}CH=CHN^b\|CH(Ph)Me\|B−NC(*N*^{a}−*B*) (4) and (*S*)-*t*BuN^{a}CH=CHN^b\|CH(Ph)Me\|BCN(*N*^{a}−*B*) (5): A solution of **3a** (0.65 g, 2.1 mmol) in 5 mL of acetonitrile was added to a slurry of silver cyanide (0.3 g, 2.2 mmol) in hexane (70 mL) and the mixture was stirred for 1 h. The supernatant yellow solution was decanted, and the residue was extracted with pentane (2 × 20 mL). The combined organic phases were evaporated to dryness to afford a mixture of isocyanide **4** and cyanide **5** as a yellow oil (0.41 g). This mixture was dissolved in hexane (30 mL) and stored at −30 °C for two weeks. The solvent was then removed and the solid brown residue was distilled by means of a hot air gun (200 °C, 5 × 10^{-3} bar) to give 0.3 g (57%) of the 2-cyano derivative **5** as a colorless solid. IR (KBr): $\tilde{\nu}$ = 2976 cm^{-1} (s), 2206 w [ν(C≡N)], 1455 s, 1414 m, 1372 w, 1336 w, 1259 w, 1228 m, 1156 m, 704 s, 647 m. ^1H NMR ($CDCl_3$): δ = 1.49 (s, 9 H, *t*Bu), 1.74 (d, $^3J_{H,H}$ = 7.1 Hz, 3 H, CH$_3$), 5.19 (q, $^3J_{H,H}$ = 7.1 Hz, 1 H, C*H*CH$_3$), 6.25 (d, $^3J_{H,H}$ = 2.3 Hz, 1 H, =C*H*−NCH), 6.40 (d, $^3J_{H,H}$ = 2.3 Hz, 1 H, =C*H*N*t*Bu), 7.27 (m, 3 H, Ph), 7.31 (m, 2 H, Ph) ppm. $^{13}C\{^1H\}$ NMR ($CDCl_3$): δ = 22.1 (s, CH*C*H$_3$), 31.6 [s, C(*C*H$_3$)$_3$], 53.6 [s, *C*(CH$_3$)$_3$], 55.1 (s, *C*HCH$_3$), 114.8 (s, =*C*NCH), 116.1 (s, =*C*N*t*Bu), 126.3 (s, C≡N), 126.4, 127.3, 128.5, 143.4 (4s, Ph) ppm. $^{11}B\{^1H\}$ NMR ($CDCl_3$): δ = 11.6 (s) ppm. MS/EI: *m*/*z* (%) = 253 (40) [M^+], 252 (10) [M^+ with ^{10}B]. $[\alpha]_D^{24}$ = −140. $C_{15}H_{20}BN_3$ (253.16): calcd. C 71.17, H 7.96, N 16.60; found C 71.16, H 7.93, N 16.41.

4: IR (KBr): $\tilde{\nu}$ = 2113 cm^{-1} w [ν(B−N≡C)]. ^1H NMR ($CDCl_3$): δ = 1.51 (s, 9 H, *t*Bu), 1.78 (d, $^3J_{H,H}$ = 7.0 Hz, 3 H, CH$_3$), 5.10 (q, $^3J_{H,H}$ = 7.0 Hz, 1 H, C*H*CH$_3$), 6.22 (d, $^3J_{H,H}$ = 2.3 Hz, 1 H, =C*H*NCH), 6.37 (d, $^3J_{H,H}$ = 2.3 Hz, 1 H, =C*H*N*t*Bu) ppm. $^{13}C\{^1H\}$ NMR ($CDCl_3$): δ = 22.5 (s, CH$_3$), 31.6 [s, C(*C*H$_3$)$_3$], 53.7 [s, *C*(CH$_3$)$_3$], 55.7 (s, *C*HCH$_3$], 114.7 (s, =*C*N*t*Bu), 116.0 (s, =*C*N−CH), 126.3, 127.2, 128.4, 143.3 (4s, Ph).

(*S*)-*t*BuN^{a}CH=CHN^b\|CH(Ph)Me\|BH(*N*^{a}−*B*) (6): At 0 °C a quantity of $LiAlH_4$ (0.05 g, 1.3 mmol) was added to a slurry of **3a** (0.4 g, 1.3 mmol) in a mixture of 20 mL of hexane and 5 mL of THF. After a few minutes of stirring the reaction mixture became clear. It was then filtered, and the filtrate was evaporated to dryness. The residue was triturated with pentane (6 mL), and filtered again. Removal of pentane afforded 0.28 g (95%) of crude **6** as a yellow oil. Distillation with a hot air gun at 150 °C and 2 × 10^{-5} bar afforded pure **6** as a colorless liquid (0.14 g, 47%). This product is temperature-sensitive at room temp.; decomposition to a brown oil was complete after 24 h (NMR control). IR (film): $\tilde{\nu}$ = 3086 m, 3063 m, 3027 m, 2973 s, 2868 s, 2621 s [ν(BH)], 1603 m, 1494 m, 1151 m, 920 m, 753 m, 664 s. ^1H NMR ($CDCl_3$): δ = 1.44 (s, 9 H, *t*Bu), 1.71 (d, $^3J_{H,H}$ = 7.0 Hz, 3 H, CH$_3$), 4.88 (q, $^3J_{H,H}$ = 7.0 Hz, 1 H, C*H*CH$_3$), 6.15 (d, $^3J_{H,H}$ = 2.0 Hz, 1 H, =C*H*NCH), 6.40 (d, $^3J_{H,H}$ = 2.0 Hz, 1 H, =C*H*N*t*Bu), 7.27 (m, 3 H, Ph), 7.30 (m, 2 H, Ph) ppm. $^{13}C\{^1H\}$ NMR ($CDCl_3$): δ = 24.0 (s, CH$_3$), 31.8 [s, C(*C*H$_3$)$_3$], 51.5 [s, *C*(CH$_3$)$_3$], 56.5 (s, *C*HCH$_3$), 114.4 (s, =*C*NCH), 116.2 (s, =*C*N*t*Bu), 126.1, 126.7, 128.3, 146.1 (4s, Ph) ppm. ^{11}B NMR ($CDCl_3$): δ = 19.4 (d, $^1J_{B,H}$ = 146 Hz) ppm. MS/EI: *m*/*z* (%) = 228 (7) [M^+], 213 (7) [$M^+ - CH_3$]. $[\alpha]_D^{24}$ = +94. $C_{14}H_{21}BN_2$ (228.15): calcd. C 73.70, H 9.28, N 12.28; found C 73.44, H 9.39, N 12.21.

(*S*)-*t*BuN^{a}CH=CHN^b\|CH(Ph)Me\|BCH$_3$(*N*^{a}−*B*) (7): A sample of **3a** (0.57 g, 1.8 mmol) was suspended in a mixture of hexane (40 mL) and THF (2.5 mL). An ethereal solution of methyllithium was then added (2 mL, 1.6 M), and the resulting mixture was stirred at 20 °C for two days. The volatile components were removed in vacuo, and the residue was extracted twice with 2.5 mL of hexane.

After filtration it was evaporated to dryness to give crude **7** (0.4 g, 92%) as a red oil. Purification was achieved by hot air distillation (200 °C, 1.5×10^{-5} bar) to yield 0.23 g (51%) of **7** as a colorless liquid. IR (film): $\tilde{\nu}$ = 3027 s, 2972 s, 1602 m, 1401 s, 1253 s, 1152 m, 1029 m, 758 m, 700 s, 665 m. ^{1}H NMR ($CDCl_3$): δ = 0.75 (s, 3 H, BCH_3), 1.56 (s, 9 H, *t*Bu), 1.80 (d, $^3J_{H,H}$ = 7.1 Hz, 3 H, $CHCH_3$), 5.12 (q, $^3J_{H,H}$ = 7.1 Hz, 1 H, $CHCH_3$), 6.32 (d, $^3J_{H,H}$ = 2.5 Hz, 1 H, =C*H*−NCH), 6.48 (d, $^3J_{H,H}$ = 2.5 Hz, 1 H, =C*H*N*t*Bu), 7.34 (m, 3 H, Ph), 7.41 (m, 2 H, Ph) ppm. ^{13}C{^{1}H} NMR ($CDCl_3$): δ = 22.2 ($CHCH_3$), 31.6 [s, $C(CH_3)_3$], 52.4 [s, $C(CH_3)_3$], 55.7 (s, $CHCH_3$), 111.1 (s, =*C*HNCH), 113.5 (s, =*C*HN*t*Bu), 126.2, 126.3, 128.4, 145.7, (4 s, Ph) ppm. ^{11}B{^{1}H} NMR ($CDCl_3$): δ = 26.2 (s) ppm. MS/EI: *m*/*z* (%) = 242 (75) [M^+], 241 (19) [M^+ with ^{10}B], 227 (54) [$M^+ - CH_3$]. $[\alpha]_D^{24}$ = −111. $C_{15}H_{23}BN$ (242.17): calcd. C 73.06, H 10.07, N 12.17; found C 73.28, H 9.85, N 12.19.

(*S*)-*t*BuN^{a}CH=CHN^b[CH(Ph)Me]BNH*t*Bu(*N^a*−*B*) (8): *tert*-Butylamine (1 mL, 0.66 g, 9.0 mmol) was added at room temp. to a well stirred slurry of **3a** (1.3 g, 4.2 mmol) in hexane (10 mL). A colorless precipitate was formed immediately. After filtration the filtrate was freed from solvent to yield 1.17 g of a brown oil, which was subsequently purified by distillation with a hot air gun (300 °C, 10^{-5} bar). Compound **8** was obtained as a yellow oil (yield 0.93 g, 74%). IR (film): $\tilde{\nu}$ = 3443 cm^{-1} w [ν(NH)], 3061 m, 3027 m, 2986 s, 2865 s, 1602 w, 1494 s, 1135 m, 1028 m, 817 m, 789 m, 753 m, 699 s, 647 m. ^{1}H NMR ($CDCl_3$): δ = 1.28 (s, 9 H, NH*t*Bu), 1.47 (s, 9 H, =CHN−*t*Bu), 1.69 (d, $^3J_{H,H}$ = 7.0 Hz, 3 H, CH_3), 5.22 (q, $^3J_{H,H}$ = 7.0 Hz, 1 H, $CHCH_3$), 5.93 (d, $^3J_{H,H}$ = 2.8 Hz, 1 H, =C*H*−NCH), 6.24 (d, $^3J_{H,H}$ = 2.8 Hz, 1 H, =C*H*−N*t*Bu), 7.21 (m, 1 H, Ph), 7.29 (m, 4 H, Ph) ppm. ^{13}C{^{1}H} NMR ($CDCl_3$): δ = 21.9 (s, CH_3), 31.6 [s, $NC(CH_3)_3$], 33.6 [s, $NHC(CH_3)_3$], 49.2 [s, $NHC(CH_3)_3$], 51.8 [s, =CH−N$C(CH_3)_3$], 52.2 (s, $CHCH_3$), 109.6 (s, =H*C*N−CH), 113.0 (s, =*C*HN*t*Bu), 126.1, 126.4, 128.3, 144.0 (4s, Ph) ppm. ^{11}B{^{1}H} NMR ($CDCl_3$): δ = 22.3 (s) ppm. $[\alpha]_D^{24}$ = −125. $C_{18}H_{30}BN_3$ (299.27): calcd. C 72.24, H 10.10, N 14.04; found C 71.91, H 10.20, N 13.87.

(*S*,*S*)−*t*BuN^a−CH=CHN^b−[CH(Ph)Me]BNH[CH(Ph)Me]-(*N^a*−*B*) (9): Triethylamine (0.12 g, 1.2 mmol) was added to a slurry of (*S*)-**3a** (0.38 g, 1.2 mmol) in hexane (15 mL) at ambient temp. followed by the addition of (*S*)-1-phenylethylamine (0.16 g, 1.3 mmol). The reaction mixture spontaneously turned cloudy with separation of a colorless precipitate. The mixture was stirred for 15 min and then filtered. The filtrate was evaporated to dryness to yield (*S*,*S*)-**9** as a red-brown oil (yield 0.38 g, 92%). Distillation of the product (hot air gun, 150 °C, 2×10^{-6} bar) gave 0.2 g (48%) of **9** as a colorless liquid. IR (film): $\tilde{\nu}$ = 3463 cm^{-1} w [ν(NH)], 3061 m, 3026 m, 2961 s, 2865 s, 1601 w, 1478 w, 1332 s, 1137 m, 1028 m, 908 w, 758 m, 700 s, 636 m. ^{1}H NMR ($CDCl_3$): δ = 1.24 (d, $^3J_{H,H}$ = 6.9 Hz, 3 H, BNHCC*H*$_3$), 1.33 (d, $^3J_{H,H}$ = 6.7 Hz, = HC−NCHC*H*$_3$), 1.46 (s, 9 H, *t*Bu), 2.27 (d, $^3J_{H,H}$ = 8.8 Hz, 1 H, *NH*), 4.37 [m, 1 H, N(H)C*H*CH_3], 4.72 (q, $^3J_{H,H}$ = 7.0 Hz, 1 H, CH=NC*H*CH_3), 5.86 (d, $^3J_{H,H}$ = 2.6 Hz, 1 H, =C*H*NCH), 6.13 (d, $^3J_{H,H}$ = 2.6 Hz, 1 H, =C*H*N*t*Bu), 7.20 (m, 4 H, Ph), 7.34 (m, 6 H, Ph) ppm. ^{13}C{^{1}H} NMR ($CDCl_3$): δ = 22.1 (s, CNCH*C*H_3), 28.2 (s, HNCH*C*H_3), 31.1 [s, $C(CH_3)_3$], 51.5 [s, $C(CH_3)_3$], 51.9 (s, $CHCH_3$), 52.0 (s, $CHCH_3$), 109.2 (s, =*C*HNCH), 111.9 (s, =*C*HN*t*Bu), 125.3, 125.9, 126.1, 126.15, 128.1, 128.2, 146.5, 148.8 (8s, Ph) ppm. ^{11}B{^{1}H} NMR ($CDCl_3$): δ = 21.6 (s) ppm. MS/EI: *m*/*z* (%) = 347 (37) [M^+], 346 (9) [M^+ with ^{10}B]. $[\alpha]_D^{24}$ = −99. $C_{22}H_{30}BN_3$ (347.31): calcd. C 76.08, H 8.71, N 12.10; found C 76.10, H 8.77, N 11.86.

(*S*)-Me(Ph)CH−N^a−CH=CH−N^b[CH(Ph)Me]BSnMe$_3$(*N^a*−*B*) (10): Trimethyltin chloride (1.68 g, 8.45 mmol) was added to a slurry of lithium sand (0.13 g, 18.6 mmol) in THF (80 mL) and stirred at 20 °C until a green solution was formed (ca. 2 h). A solution of **3b** (1.31 g, 5.6 mmol) in hexane (30 mL) was then added dropwise to this mixture and stirring was continued for another 2 h. The volatile components were removed in vacuo and the residue was extracted with pentane (3 × 10 mL). The filtrate was evaporated to dryness. Recrystallization of the residue from toluene gave 1.66 g (67%) of **10** as colorless crystals. ^{1}H NMR (C_6D_6): δ = 0.22 (t, $^2J_{Sn,H}$ = 47.3 Hz, 9 H, $SnMe_3$), 1.51 (d, $^3J_{H,H}$ = 7.1 Hz, 6 H, $CHCH_3$), 5.15 (q, $^3J_{H,H}$ = 7.1 Hz, 2 H, $CHCH_3$), 6.38 (s, 2 H, HC=CH), 7.01 (t, $^3J_{H,H}$ = 7.3 Hz, 2 H, *p*-H−Ph), 7.09 (m, 4 H, Ph), 7.16 (m, 4 H, Ph) ppm. ^{13}C{^{1}H} NMR (C_6D_6): δ = −9.4 [t, $^1J_{Sn,C}$ = 298.9 Hz, $Sn(CH_3)_3$], 23.0 (s, $CHCH_3$), 55.9 (s, $CHCH_3$), 116.4 (s, HC=CH), 126.5, 126.7, 128.6, 145.5 (4s, Ph) ppm. ^{11}B{^{1}H} NMR (C_6D_6): δ = 28.2 (t, $^1J_{Sn,B}$ = 994 Hz). ^{119}Sn{^{1}H} NMR (C_6D_6): δ = −150.0 (q, $^1J_{Sn,B}$ = 994 Hz) ppm. MS/EI: *m*/*z* (%) = 440 (2) [M^+]. $[\alpha]_D^{24}$ = −119. $C_{21}H_{29}BN_2Sn$ (439.00): calcd. C 56.62, H 6.58, N 6.28; found C 57.46, H 6.66, N 6.38.

(*S*,*S*)-Me(Ph)CH−N^a−CH=CH−N^b[CH(Ph)Me]B(NH*t*Bu)-(*N^a*−*B*) (11): A slurry of **3b** (1.80 g, 5.0 mmol) in hexane (50 mL) was treated with *tert*-butylamine (0.74 g, 1.1 mL, 10 mmol) and stirred for 5 min at room temperature. The mixture was then filtered. The filtrate was evaporated to dryness to give a red oil (1.75 g), which was distilled at 200 °C (hot air gun) and 2×10^{-6} bar to afford **11** as a pale yellow liquid (0.86 g, 50%). IR (film): $\tilde{\nu}$ = 3414 cm^{-1} w [ν(NH)], 3060 m, 3026 m, 2969 s, 2871 m, 1946 w, 1602 m, 1493 s, 1243 m, 1167 m, 1027 m, 757 m, 699 s. ^{1}H NMR ($CDCl_3$): δ = 1.15 (s, 9 H, *t*Bu), 1.70 (d, $^3J_{H,H}$ = 7.0 Hz, 6 H, CH_3), 5.04 (q, $^3J_{H,H}$ = 7.0 Hz, 2 H, $CHCH_3$), 6.12 (s, 2 H, CH=CH), 7.30 (m, 4 H, Ph), 7.34 (m, 6 H, Ph) ppm. ^{13}C{^{1}H} NMR ($CDCl_3$): δ = 22.4 (s, CH_3), 33.2 [s, $C(CH_3)_3$], 49.1 [s, $C(CH_3)_3$], 111.9 (s, H*C*=*C*H), 126.1, 126.4, 128.2, 145.7, (4s, Ph) ppm. ^{11}B{^{1}H} NMR ($CDCl_3$): δ = 22.5 (s) ppm. $[\alpha]_D^{24}$ = −165. $C_{22}H_{30}BN_3$ (347.31): calcd. C 76.08, H 8.71, N 12.10; found C 75.90, H 8.93, N 11.66.

(*S*,*S*)-Me(Cy)CHN^a−CH=CH−N^b[CH(Cy)Me]BN(H)*t*Bu (12): A solution of **3c** (0.70 g, 1.9 mmol) in hexane (25 mL) was treated at 20 °C with *tert*-butylamine (0.29 g, 4.0 mmol). After stirring for 10 min this mixture was filtered, and the filtrate was evaporated to dryness. The residual yellow oil was distilled by means of a hot air gun (300 °C, 4×10^{-6} bar) to afford 0.40 g (58%) of **12** as a colorless oil. IR (film): $\tilde{\nu}$ = 3419 cm^{-1} w [ν(NH)], 2923 s, 2843 s, 2658 w, 1446 s, 1229 s, 890 s, 657 s. ^{1}H NMR ($CDCl_3$): δ = 0.87−1.80 (m, 22 H, C_6H_{11}), 1.20 (d, $^3J_{H,H}$ = 6.8 Hz, 6 H, $CHCH_3$), 1.21 (s, 9 H, *t*Bu), 3.25 (m, 2 H, $CHCH_3$), 5.95 (s, 2 H, HC=CH) ppm. ^{13}C{^{1}H} NMR ($CDCl_3$): δ = 22.7 (s, $CHCH_3$), 26.4 (s, 3,5-*C*−Cy), 26.5 (s, 4-*C*−Cy), 30.4, 30.8 (2s, 2,6-*C*−Cy), 31.6 [s, $C(CH_3)_3$], 33.6 [s, $C(CH_3)_3$], 44.5 (s, 1-*C*−Cy), 54.4 (s, $CHCH_3$), 110.6 (s, HC=CH) ppm. ^{11}B{^{1}H} NMR ($CDCl_3$): δ = 22.1 (s) ppm. MS/CI (NH_3): *m*/*z* (%) = 360 (87) [MH^+], 359 (100) [MH^+ with ^{10}B and M^+ with ^{11}B], 358 (22) [M^+, ^{10}B]. $[\alpha]_D^{24}$ = −55. $C_{22}H_{42}BN_3$ (359.41): calcd. C 73.52, H 11.78, N 11.69; found C 73.23, H 12.06, N 11.40.

(*S*,*S*)−Me(Cy)CHN^a−CH=CH−N^b[CH(Cy)Me]B−*n*C$_4$H$_9$(*N^a*-*B*) (13): A hexane solution of *n*-butyllithium (12%, 2.0 g, 3.8 mmol) was added dropwise at −15 °C to a solution of **3c** (0.76 g, 2.1 mmol) in a mixture of 50 mL of hexane and 10 mL of THF. After stirring for one day at 20 °C the solvent and volatile components were removed in vacuo. The residue was extracted with 30 mL of pentane. Removal of solvent gave a yellow oil (0.75 g) which was

distilled at 250 °C and 5×10^{-6} bar to give 0.32 g (47%) of **13** as a colorless oil. ^{1}H NMR (C_6D_6): δ = 0.80−1.70 (m, 31 H, C_6H_{11} and C_4H_9), 1.24 (d, $^3J_{H,H}$ = 6.8 Hz, 6 H, CHCH_3), 3.37 (m, 2 H, CHCH$_3$), 6.19 (s, 2 H, HC=CH) ppm. ^{13}C{^{1}H} NMR (C_6D_6): δ = 14.4 (s, CH_2CH_3), 20.9 (s, CHCH$_3$), 26.5 (s, CH_2CH_3), 26.7 (s, 3,5-C−Cy), 26.8 (s, 4-C−Cy), 30.3 (s, $CH_2CH_2CH_3$), 30.7, 30.9 (2s, 2,6-C−Cy), 44.5 (s, 1-C−Cy), 55.6 (s, CHCH$_3$), 112.4 (s, HC=CH) ppm. ^{11}B{^{1}H} NMR (C_6D_6): δ = 26.4 (s) ppm. MS/EI: *m*/*z* (%) = 344 (50) [M$^+$, ^{11}B], 343 (14) [M$^+$, ^{10}B], 262 (20) [M$^+$ − C_6H_{10}], 261 (100) [M$^+$ − C_6H_{11}]. $[\alpha]_D^{24}$ = −18. $C_{22}H_{41}BN_2$ (344.39): calcd. C 76.73, H 12.00, N 8.13; found C 76.47, H 12.12, N 7.88.

(*S*,*S*)-Me(Cy)CHN^a−CH=CH−N^b\|CH(Cy)Me\|BSnMe$_3$(*N*^{a}−*B*) (14): Lithium sand (0.14 g, 20 mmol) was added to a solution of trimethyltin chloride (0.77 g, 3.9 mmol) in 40 mL of THF and the slurry was stirred at ambient temp. with sonification. The resulting mixture was combined with a solution of (*S*,*S*)-**3c** (1.45 g, 3.95 mmol) in hexane (20 mL). Stirring was continued for 1 h. The mixture was then evaporated to dryness, and 30 mL of hexane was added to the residue. It was filtered, and the filtrate was freed from solvent to give crude (*S*,*S*)-**14** as a cloudy yellow oil (1.7 g). Distillation (250 °C, 1×10^{-5} bar) gave 1.02 g (58%) of pure (*S*,*S*)-**14** as colorless liquid. IR (film): $\tilde{\nu}$ = 2979 cm^{-1} m, 2924 s, 2853 s, 2651 w, 2348 w, 1643 s, 1449 s, 1398 s, 1225 m [δ(SnMe$_3$)], 891 w, 764 s, [(SnMe$_3$)], 513 s. ^{1}H NMR (C_6D_6): δ = 0.4 (s, $^2J_{Sn,H}$ = 45.2 Hz, 9 H, SnMe$_3$), 0.78−1.74 (m, 22 H, C_6H_{11}), 1.22 (d, $^3J_{H,H}$ = 6.3 Hz, 6 H, CHCH_3), 3.49 (m, 2 H, CHCH$_3$), 6.37 (s, $^4J_{Sn,H}$ = 12.6 Hz, 2 H, CH=CH) ppm. ^{13}C{^{1}H} NMR (C_6D_6): δ = −9.7 (s, $^1J_{Sn,C}$ = 269 Hz, $SnCH_3$), 20.9 (s, CHCH$_3$), 26.6 (s, 4-C−Cy), 26.6, 26.7 (2s, 3,5-C−Cy), 30.68/31.72 (2s, 2,6-C−Cy), 44.7 (s, 1-C−Cy), 58.4 (s, CHCH$_3$), 115.4 (s, $^3J_{Sn,C}$ = 37.9 Hz, HC=CH) ppm. ^{11}B{^{1}H} NMR (C_6D_6): δ = 30.8 (s, $^1J_{Sn,B}$ = 986 Hz) ppm. ^{119}Sn{^{1}H} NMR (C_6D_6): δ = −149.1 (q, $^1J_{Sn,B}$ = 986 Hz) ppm. MS/CI (NH_3): *m*/*z* = 453 (100) [M$^+$ + H]. $[\alpha]_D^{24}$ = −44. $C_{21}H_{41}BN_2Sn$ (451.08): calcd. C 55.92, H 9.16, N 6.21; found C 56.11, H 9.05, N 6.21.

(*S*)-*t*BuN^a−CH=CH−N^b(*t*Bu)B−N(H)CH(Ph)Me(*N*^{a}−*B*) (15): Equimolar amounts of 1,3,2-diazaborole *t*BuN^{a}CH=CHN^b(*t*Bu)BBr(*N*^{a}−*B*) (2.33 g, 9.0 mmol) and triethylamine (1.25 mL, 9.0 mmol) were dissolved in hexane (70 mL). At room temperature (*S*)-1-phenylethylamine (1.1 g, 9.0 mmol) was then added. After 15 min of stirring the mixture was filtered, and the filtrate was freed from solvent and volatile components to afford a cloudy oil (2.27 g). Pure compound **14** (2.02 g, 74%) was obtained as a pale yellow oil by distillation (200 °C, hot air gun, 10^{-5} bar). IR (film): $\tilde{\nu}$ = 3443 cm^{-1} w [ν(NH)], 2971 s, 2930 m, 2862 m, 1601 s, 1395 s, 1365 s, 1233 s, 1133 m, 1021 w, 821 w, 699 m, 631 m. ^{1}H NMR (C_6D_6): δ = 1.31 (s, 18 H, *t*Bu), 1.47 (d, $^3J_{H,H}$ = 6.7 Hz, 3 H, CHCH_3), 1.90 (d, $^3J_{H,H}$ = 11.3 Hz, 1 H, NH), 4.64 (m, 1 H, CHCH$_3$), 6.19 (s, 2 H, CH=CH), 7.01 (m, 1 H, *p*-*H*−Ph), 7.18 (m, 2 H, *m*-*H*−Ph), 7.36 (d, $^3J_{H,H}$ = 7.2 Hz, 2 H, *o*-*H*−Ph) ppm. ^{13}C{^{1}H} NMR (C_6D_6): δ = 26.4 (s, CHCH$_3$), 31.8 [s, C(CH$_3$)$_3$], 51.9 [s, C(CH$_3$)$_3$], 54.6 (s, CHCH$_3$), 111.3 (s, HC=CH), 126.3, 128.6, 148.3 (3s, Ph) ppm. ^{11}B{^{1}H} NMR (C_6D_6): δ = 22.3 (s) ppm. MS/CI (NH_3): *m*/*z* (%) = 300 (100) [MH$^+$], 299 (45) [M$^+$]. $[\alpha]_D^{24}$ = −29. $C_{18}H_{30}BN_3$ (299.27): calcd. C 72.24, H 10.10, N 10.04; found C 71.88, H 10.18, N 13.85.

(*S*)-*t*BuN^a−CH=CH−N^b(*t*Bu)BN(H)CH(Cy)Me(*N*^{a}−*B*) (16): Analogously 1.1 g of crude **16** were prepared from *t*BuN^{a}CH=CHN^b(*t*Bu)BBr(*N*^{a}−*B*) (0.93 g, 3.6 mmol), triethylamine (0.37 g, 5.0 mmol) and (*S*)-1-cyclohexylethylamine (0.46 g, 3.6 mmol). Purification to afford a colorless oil (0.23 g, 72%) was achieved by vacuum distillation (150 °C, hot air gun, 2×10^{-6} bar). IR (film): $\tilde{\nu}$ = 3450 cm^{-1} w [ν(NH)], 2925 s, 2853 m, 1396 s, 1365 s, 1233 s, 1133 m, 821 w, 625 m. ^{1}H NMR ($CDCl_3$): δ = 0.85−1.84 (m, 11 H, C_6H_{11}), 1.04 (d, $^3J_{H,H}$ = 6.6 Hz, 3 H, CHCH_3), 1.40 (s, 18 H, *t*Bu), 3.29 (m, 1 H, CHCH$_3$), 6.06 (s, 2 H, HC=CH) ppm. ^{13}C{^{1}H} NMR ($CDCl_3$): δ = 21.5 (s, CHCH$_3$), 26.6, 26.7 (2s, 3,5-C−Cy), 28.6 (s, 4-C−Cy), 30.1 (s, 2,6-C−Cy), 31.4 [s, C(CH$_3$)], 46.5 (s, 1-C−Cy), 51.7 [s, C(CH$_3$)$_3$], 110.0 (s, CH=CH) ppm. ^{11}B{^{1}H} NMR ($CDCl_3$): δ = 22.0 (s) ppm. MS/EI: *m*/*z* (%) = 305 (62) [M$^+$]. $[\alpha]_D^{24}$ = −6. $C_{18}H_{36}BN_3$ (305.32): calcd. C 70.81, H 11.89, N 13.76; found C 70.75, H 12.04, N 13.73.

X-ray Structural Analysis of (*S*,*S*)-3c: Colorless single crystals were grown from *n*-hexane; 0.27 × 0.24 × 0.15 mm, T = 100 K; Nonius Kappa CCD Mo-K_α (graphite monochromator, λ = 0.71073 Å) empirical formula $C_{18}H_{30}BBrN_2$, tetragonal space group $P4_12_12$; unit cell dimensions: $a = b$ = 10.8870(1), c = 16.0510(1) Å; V = 1902.47(3) Å^3, $d_{calcd.}$ = 1.275 g·cm^{-3}, Z = 4; μ = 2.16 mm^{-1}; range for data collection: 2.9 < θ < 30.0°; index ranges −15 < h < 15, −10 < k < 10, −22 < l < 22; reflection collected 56253; unique reflections 2761 (R_{int} = 0.049); parameters 102; absorption correction multi-scan, min/max transmission 0.738/0.593: Program used: SHELXL-97; structure refinement: full-matrix least-squares on F^2, wR_{F^2} = 0.064 (all data) R_F = 0.024, wR_F = 0.063 based on 2651 unique reflections with $I > 2\sigma(I)$, GOOF (F^2) = 1.057, maximum residual electron density 0.561 e Å^{-3}; hydrogen atoms treated as riding group.

CCDC-180671 [(*S*,*S*)-**3c**] contains the supplementary crystallographic data for this paper. These data can be obtained free of charge at www.ccdc.cam.ac.uk/conts/retrieving.html [or from the Cambridge Crystallographic Data Center, 12, Union Road, Cambridge CB2 1EZ, UK; Fax: (internat.) +44-1223/336-033; E-mail: deposit@ccdc.cam.ac.uk].

Acknowledgments

This work was generously supported by the Deutsche Forschungsgemeinschaft and the Fonds der Chemischen Industrie.

[1] [1a] K. Niedenzu, J. S. Merriam, *J. Organomet. Chem.* **1973**, *51*, C1−C2. [1b] K. Niedenzu, J. S. Merriam, *Z. Anorg. Allg. Chem.* **1974**, *406*, 251−259.
[2] L. Weber, G. Schmid, *Angew. Chem.* **1974**, *86*, 519; *Angew. Chem. Int. Ed. Engl.* **1974**, *13*, 467.
[3] G. Schmid, J. Schulze, *Chem. Ber.* **1977**, *110*, 2744−2750.
[4] [4a] G. Schmid, J. Schulze, *Angew. Chem.* **1977**, *89*, 258−259; *Angew. Chem. Int. Ed. Engl.* **1977**, *16*, 249. [4b] G. Schmid, J. Schulze, *Chem. Ber.* **1981**, *114*, 495−504.
[5] G. Schmid, M. Polk, R. Boese, *Inorg. Chem.* **1990**, *29*, 4421−4429.
[6] G. Schmid, J. Lehr, M. Polk, R. Boese, *Angew. Chem.* **1991**, *103*, 1029−1031; *Angew. Chem. Int. Ed. Engl.* **1991**, *30*, 1015.
[7] L. Weber, E. Dobbert, H.-G. Stammler, B. Neumann, R. Boese, D. Bläser, *Chem. Ber./Recueil* **1997**, *130*, 705−710.
[8] L. Weber, E. Dobbert, R. Boese, M. T. Kirchner, D. Bläser, *Eur. J. Inorg. Chem.* **1998**, 1145−1152.
[9] L. Weber, E. Dobbert, H.-G. Stammler, B. Neumann, R. Boese, D. Bläser, *Eur. J. Inorg. Chem.* **1999**, 491−497.
[10] L. Weber, E. Dobbert, A. Rausch, H.-G. Stammler, B. Neumann, *Z. Naturforsch., Teil B* **1999**, *54*, 363−371.
[11] L. Weber, H. B. Wartig, H.-G. Stammler, A. Stammler, B. Neumann, *Organometallics* **2000**, *19*, 2891−2895.

[12] L. Weber, M. Schnieder, T. C. Maciel, H. Wartig, M. Schimmel, R. Boese, D. Bläser, *Organometallics* **2000**, *19*, 5791−5794.
[13] H. tom Dieck, J. Dietrich, *Chem. Ber.* **1984**, *117*, 694−701.
[14] A. F. Holleman, E. Wiberg, *Lehrbuch der Anorganischen Chemie*, 91−100th ed., Walter de Gruyter Publ., Berlin, New York, **1985**, p. 133.
[15] H. Hommer, H. Nöth, J. Knizek, W. Ponikwar, H. Schwenk-Kirchner, *Eur. J. Inorg. Chem.* **1998**, 1519−1527.
[16] M. Möhlen, B. Neumüller, N. Faza, C. Müller, W. Massa, K. Dehnicke, *Z. Anorg. Allg. Chem.* **1997**, *623*, 1567−1576.
[17] W. J. Grigsby, P. P. Power, *J. Am. Chem. Soc.* **1996**, *118*, 7981−7988.
[18] G. Linti, D. Loderer, H. Nöth, K. Polborn, W. Rattay, *Chem. Ber.* **1994**, *127*, 1909−1922.

Received March 5, 2002
[I02114]

Unprecedented Formation of Dinuclear Macrocyclic Complexes by Insertion of 2,3,5,6-Tetrafluoro-7,7,8,8-tetracyanoquinodimethane (F4-Tcnq) into a C−H Bond and Subsequent Coordination to Metal Atoms

Yasuhiro Yamamoto,*[a] Hitoshi Settu,[a] Kazunori Nishiyama,[a] Katsuaki Kuge,[b] and Kazuyuki Tatsumi[b]

Keywords: Cyclopentadienyl ligands / Rhodium / Iridium / Lithium / Macrocyclic ligands

The complexes [Cp*RhCl{PPh[C_6H_3-2,6-$(MeO)_2$](C_6H_3-2-O-6-OMe)-*P,O*}] (**1a**) and [Cp*MCl{PPh_2(C_6H_3-2-O-6-MeO)-*P,O*}] (**1b**: M = Rh; **3b**: M = Ir) with P,O chelating coordination react readily with lithium 2,3,5,6-tetrafluoro-7,7,8,8-tetracyanoquinodimethane [Li(F_4-tcnq)] to form the dimeric complexes **2a**, **2b** and **4b** by substitution of the H atom adjacent to the metal-O bond with F_4-tcnq and coordination through the nitrogen atom of a cyano group to another metal. The X-ray crystal structure of **2a** is described. Reaction of **1b** with F_4-tcne proceeds by an insertion into the C–H bond adjacent to the Rh–O bond.

(© Wiley-VCH Verlag GmbH, 69451 Weinheim, Germany, 2002)

Introduction

Aromatic phosphanes bearing the two methoxy groups at the *ortho* positions have extreme nucleophilicity and large cone angles.[1,2] Previously we reported that one of the *ortho*-methoxy groups in (2,6-dimethoxyphenyl)diphenylphosphane and bis(2,6-dimethoxyphenyl)phenylphosphane were demethylated upon treatment with bis[dichloro(η^6-arene)ruthenium(II)] or bis[dichloro(η^5-pentamethylcyclopentadienyl)rhodium(III) (or iridium(III))] to give ruthenium(II),[3,4] rhodium(III)[5] and iridium(III)[6] complexes with P,O chelating phosphane ligands, as shown in Scheme 1. The rhodium and iridium complexes (**1a**: M = Rh, R = C_6H_3-2,6-$(MeO)_2$; **1b**: M = Rh, R = Ph; **3b**: M = Ir, R = Ph) reacted with mono- or disubstituted alkyne in the presence of KPF_6 or $NaPF_6$ to give novel six- or seven-membered metallacycles arising from a single or double insertion of alkyne into the Rh−O or P−C bond.[7−9] When complexes **1b** and **3b** were treated with electron-deficient olefins such as tetracyanoethylene (tcne) or 7,7,8,8-tetracyano-*p*-quinodimethane (tcnq), the olefin inserted into weakly activated C−H bond on the phenyl ring of the phosphane ligand (Scheme 1).[10,11]

A similar insertion of an electron-deficient olefin into the C−H bond has been documented for 2-furanyl- and 2-thienylplatinum complexes.[12] We also reported that the reaction of [Cp*IrCl{PPh_2(C_6H_3-2-*O*-6-MeO)}] (**3b**) with Li(tcnq) afforded the green charge-transfer complex [Cp*Ir{PPh_2(C_6H_3-2-*O*-6-MeO)}(tcnq)].[11]

During our research on interactions of the aforementioned complexes with lithium 2,3,5,6-tetrafluoro-7,7,8,8-tetracyanoquinodimethane [Li(F_4-tcnq)], we found that the F_4-tcnq molecule underwent a substitution reaction at the position adjacent to the M−O bond and coordination to another metal atom of a cyano group, forming a dinuclear macrocyclic complex. This type of compounds provides a new entry into the family of inorganic macrocycles.

Results and Discussion

When compound **1a** was treated with Li(F_4-tcnq) at room temperature (Scheme 2), the orange yellow complex **2a** was formed. Its FAB mass spectrum shows peaks at *m*/*z* = 1761 (26.5%) and *m*/*z* = 881 (100%). The former is the molecular peak with a mass corresponding to a dimer [Cp*Rh{PPh[C_6H_2-2,6-$(MeO)_2$](C_6H_3-2-O-6-MeO)-*P,O*}-(F_4-tcnq)]$_2$ (mol. wt. = 1761.3). The base peak of the spectrum corresponds to half of the molecular peak value ([M/2] = 880.6). This result suggested that **2a** has a dimeric structure. The electronic spectrum shows a strong absorption band at 332 nm (Figure 1a). The IR spectrum has absorptions at 2194 and 2164 cm^{-1} due to a C-N triple bond. The ^1H NMR spectrum shows broad resonances at δ = 1.59, 3.20 and 3.46 ppm, the former being assignable to Cp*

[a] Department of Chemistry, Faculty of Science, Toho University, Miyama, Funabashi, Chiba 274-8510, Japan
Fax: (internat.) +81-47/475-1855
E-mail: yamamoto@chem.sci.toho-u.ac.jp
[b] Research Center for Materials Science and Department of Chemistry, Graduate School of Science, Nagoya University, Furo-cho, Chikusa-ku, Nagoya 454-8602, Japan
Fax: (internat.) +81-52/789-2943
E-mail: i45100a@nucc.cc.nagoya-u.ac.jp

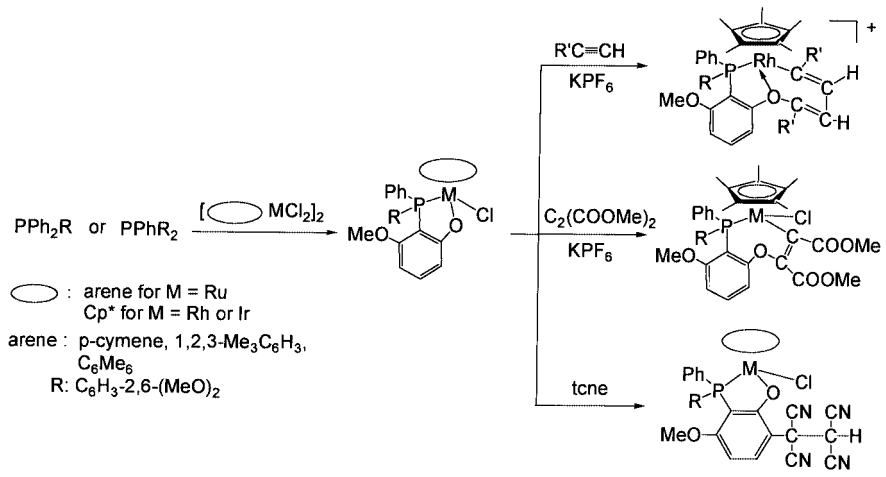

Scheme 1

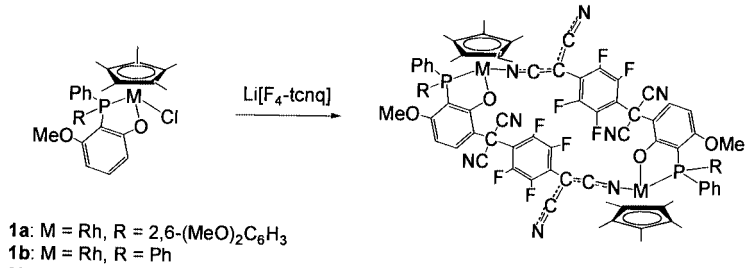

Scheme 2

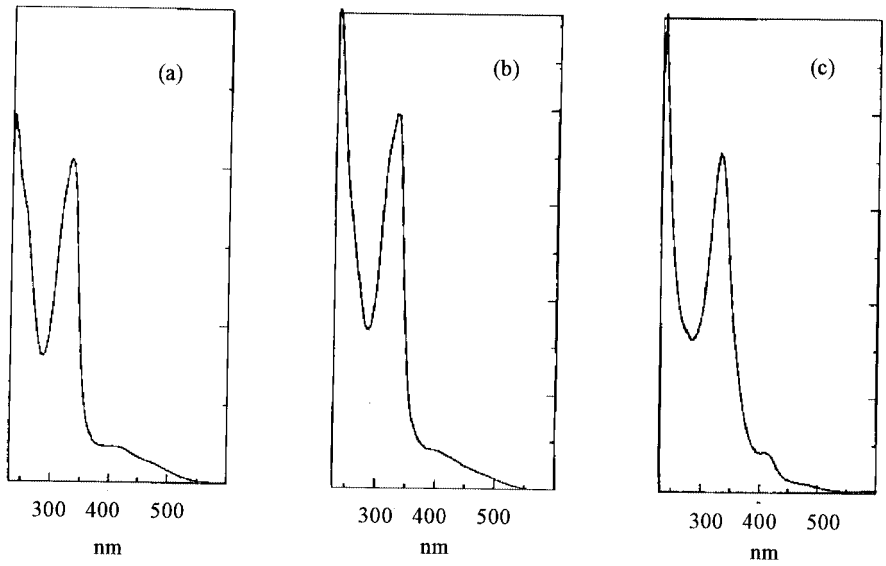

Figure 1. Electronic spectra of: (a) **2a**, (b) **2b** and (c) **4b**

protons and the others to methoxy protons, indicating that the molecule has a symmetric structure.

The detailed structure was confirmed by X-ray analysis (Figure 2 and Table 1). The molecule constructs of a macrocyclic structure with two Cp*Rh{PPh[C_6H_3-2,6-$(MeO)_2$](C_6H_2-2-*O*-6-MeO)-*P*,*O*} moieties connected by two F_4-tcnq molecules. Each F_4-tcnq molecule has undergone the aromatization of a quinone ring to a benzene one by the substitution of an H atom adjacent to an ether-O coordination, and one of the C-N triple bonds is coordinated to another Rh center. The dihedral angles between the benzene rings bearing F atoms (C35-C36-C37-C38-C39-

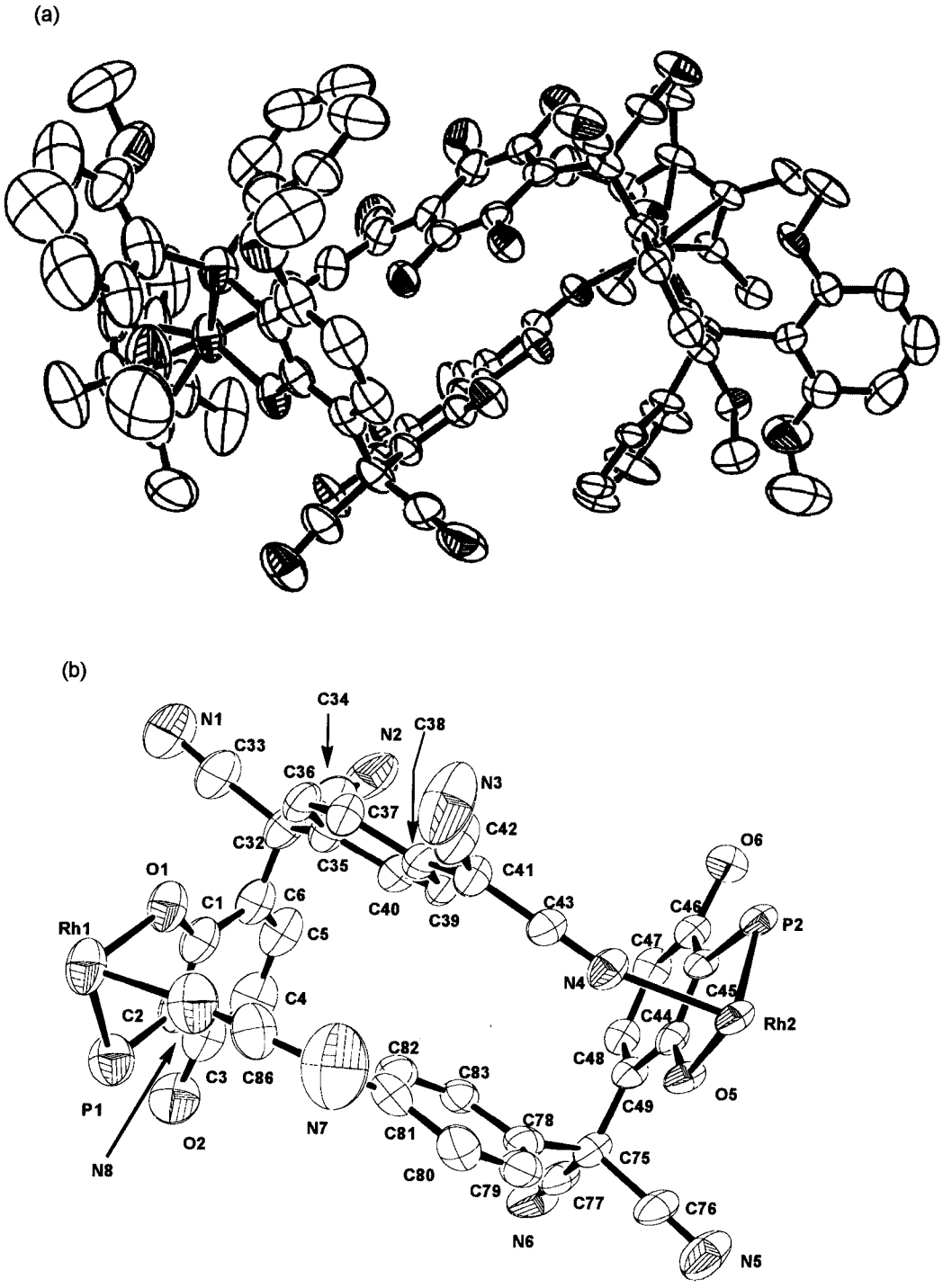

Figure 2. (a) Molecular structure of **2a**; the C84 and C85 atoms sit behind the N7 atom; displacement ellipsoids are shown at the 30% probability level; (b) framework for a core of **2a**; the Cp*, PF_6 anions, F and some other atoms have been omitted for clarity

C40 and C78-C79-C80-C81-C82-C83) and the six-membered rings (C1-C2-C3-C4-C5-C6 and C44-C45-C46-C47-C48-C49) containing the P,O coordination are nearly perpendicular in the range 81−99°. The dihedral angles between two opposite benzene rings are 142.5° and 20.1°, respectively, forming a distorted-rectangular cavity with the dimensions of about 3.5 × 7.0 Å.

The average angles around the C41 and C84 atoms are 120.0°, compared to the more normal bond angles of 109.4° and 109.5° around the C32 and C75 atoms, respectively. These data suggest that the C41 and C84 atoms are sp^2 hybridized. The average C−C and C≡N bond lengths in the inner C-C≡N groups containing the C32 and C75 atoms are 1.49 and 1.13 Å, respectively, and are therefore

Table 1. Selected bond lengths (Å) and angles (°) for **2a**

Rh(1)−P(1)	2.322(3)	Rh(1)−O(1)	2.081(6)	Rh(1)−N(8)	2.076(9)
Rh(2)−P(2)	2.325(2)	Rh(2)−O(5)	2.079(4)	Rh(2)−N(4)	2.078(6)
N(1)−C(33)	1.14(1)	C(33)−C(32)	1.49(1)	N(2)−C(34)	1.15(1)
C(34)−C(32)	1.47(1)	N(3)−C(42)	1.17(1)	C(41)−C(42)	1.39(1)
N(4)−C(43)	1.147(8)	C(43)−C(41)	1.388(9)	N(5)−C(76)	1.122(9)
C(75)−C(76)	1.497(10)	N(6)−C(77)	1.134(9)	C(75)−C(77)	1.492(10)
N(7)−C(85)	1.16(1)	C(84)−C(85)	1.39(1)	N(8)−C(86)	1.16(1)
C(84)−C(86)	1.37(1)				
P(1)−Rh(1)−O(1)	82.1(2)	P(1)−Rh(1)−N(8)	90.6(2)	O(1)−Rh(1)−N(8)	86.3(3)
P(2)−Rh(2)−O(5)	81.5(1)	P(2)−Rh(2)−N(4)	87.9(2)	O(5)−Rh(2)−N(4)	85.2(2)
Rh(1)−P(1)−C(2)	100.2(3)	Rh(1)−O(1)−C(1)	120.8(6)	P(1)−C(2)−C(1)	114.4(6)
O(1)−C(1)−C(2)	122.0(8)	Rh(2)−P(2)−C(45)	100.2(2)	Rh(2)−O(5)−C(44)	120.1(4)
P(2)−C(45)−C(44)	114.0(4)	O(5)−C(44)−C(45)	122.5(5)	Rh(1)−N(8)−C(86)	174.1(9)
N(8)−C(86)−C(84)	179(1)	C(85)−C(84)−C(86)	117.0(8)	C(81)−C(84)−C(85)	117.0(8)
C(81)−C(84)−C(86)	119.7(8)	Rh(2)−N(4)−C(43)	166.2(6)	N(4)−C(43)−C(41)	177.4(7)
C(43)−C(41)−C(38)	122.7(6)	C(42)−C(41)−C(43)	113.5(6)	C(38)−C(41)−C(42)	123.7(6)

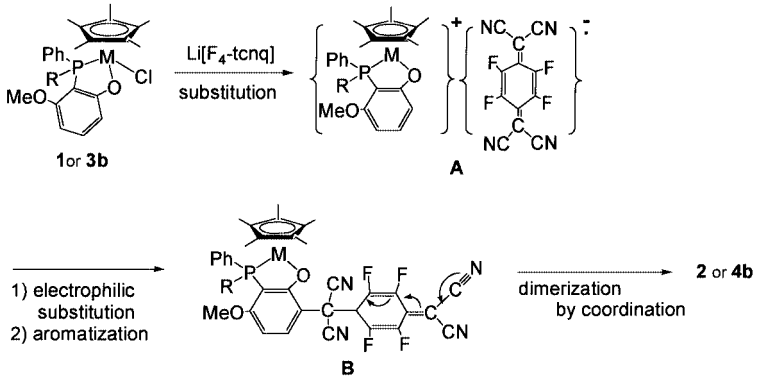

Scheme 3

similar to normal C-C single and C-N triple bonds. However, the average C−C bond length of 1.39 Å in the C-C≡N groups containing the C81 and C84 atoms is shorter by 0.1 Å than that in the inner C-C≡N groups, falling in the region of a C-C double bond, and the N7−C85 bond length of 1.16 Å is slightly long than those in the inner C-C≡N groups. These bond lengths suggest the presence of electron delocalization through the N3−C42−C41−C43−N4 and N7−C85−C84−C86−N8 bonds. The average Rh−P and Rh−O bond lengths are 2.323 Å and 2.080 Å, respectively [those found in the parent complex **1a** are 2.323(2) Å and 2.050(5) Å].[9] The average Rh−N bond length of 2.077 Å is normal for a Rh−N bond.

A similar reaction occurred for **1b** to give the dimeric complex **2b** as yellow crystals, which showed an electronic spectrum very similar to that of **2a** (Figure 1b).

The iridium complex **3b** reacts readily with Li(F_4-tcnq) to generate a brown complex **4b**, which has a molecular peak of m/z = 1819, corresponding to a binuclear complex. The IR spectrum of **4b** has absorptions at 2218 and 2170 cm^{-1} due to C-N triple bonds and at 1640 cm^{-1} due to C-N or C-C double bonds. The UV/Vis spectrum shows a sharp absorption band at 330 nm and has a similar pattern to those of **2a** and **2b** (Figure 1c). These results suggested that **4b** has a macrocyclic structure similar to **2**.

Previously, we have reported that a similar reaction of **3b** with Li(tcnq) affords the green charge-transfer complex [Cp*Ir{PPh_2(C_6H_3-2-O-6-MeO)-*P*,*O*}(tcnq)] (a tcnq analogy of intermediate A in Scheme 3) without generating the corresponding dinuclear complex.[11] The difference in electrophilicity between F_4-tcnq and tcnq is assumed to be the driving force leading to the formation of the dinuclear complex.

This reaction consists of the initial formation of a charge-transfer complex A, followed by an electrophilic substitution of a F_4-tcnq radical to the carbon atom adjacent to the ether-O atom, forming an intermediate species B. In the reaction with Li(tcnq), a tcnq analog of the charge transfer complex A was isolated. In the case of Li(F_4-tcnq), the reaction proceeds further and completes by aromatization of the quinone ring and coordination to the metal atom of another molecule to generate the dimeric complex **2** or **4** (Scheme 3).

Finally, the reaction of **1b** with F_4-tcnq led to insertion of F_4-tcnq into a C−H bond adjacent to the ether-O rhodium bond to generate the mononuclear complex **5**

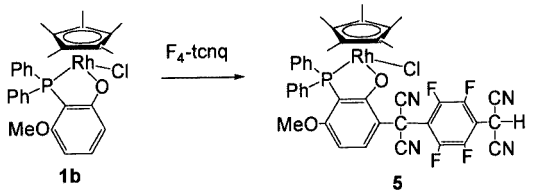

Scheme 4

(Scheme 4). This type of insertion has already been reported.[10,11]

Experimental Section

All reactions were carried out under a nitrogen atmosphere. Dichloromethane was distilled from over CaH_2 and diethyl ether was distilled from over $LiAlH_4$. The pentamethylcyclopentadienyl complexes of rhodium and iridium [Cp*MCl{PPh_2(C_6H_3-2-O-6-MeO)-*P*,*O*}] (**1b**: M = Rh;[5] **3b**: M = Ir[6]) and [Cp*RhCl{$PPh(C_6H_3$-2,6-$(MeO)_2$](C_6H_3-2-O-6-MeO)-*P*,*O*}}][5] (**1a**) were prepared according to literature procedures. Lithium 2,3,5,6-tetracyanotetrafluoroquinodimethane [Li(F_4-tcnq)] was prepared by modification of a literature method.[13] The infrared and electronic absorption spectra were measured on FT/IR-5300 and U-best 30 instruments, respectively. The ^1H NMR spectra were measured on a Bruker AC250 instrument at 250 MHz, and $^{31}P\{^1H\}$ NMR spectra were measured at 101 MHz using 85% H_3PO_4 as an external reference. Elementary analyses were preformed by the Analytical Center, School of Pharmaceutical Science, Toho University.

Reaction of 1a with Li(F_4-tcnq): Li(F_4-tcnq) (33.8 mg, 0.123 mmol) was added at room temperature to a solution of **1a** (65 mg, 0.101 mmol) in CH_2Cl_2 (20 mL). After 5 h, the solvent was removed. The residue was washed with diethyl ether and recrystallized from CH_2Cl_2 and diethyl ether, giving **2a** as an orange solid (13.2 mg, 14.8%). FAB MS: *m*/*z* (%) = 1761 (26) $[M]^+$, 881 $[M/2]^+$. IR (Nujol): $\tilde{\nu}$ = 2194, 2164 (C≡N), 1647 (C=N) cm^{-1}. UV/Vis (CH_2Cl_2): λ_{max} = 400 (sh), 331 nm. ^1H NMR ($CDCl_3$): δ = 1.59 (br. s, Cp*, 30 H), 3.20 (s, MeO, 3 H), 3.45 (s, MeO, 3 H), 5.27 (s, CH_2Cl_2), 6.9−7.9 (m, Ph, 11 H) ppm. $^{31}P\{^1H\}$ NMR ($CDCl_3$): δ = 69.5 (s) ppm. $C_{86}H_{68}F_8N_8O_8P_2Rh_2 \cdot CH_2Cl_2$ (1864.2): calcd. C 56.60, H 3.82, N 6.07; found C 56.32, H 4.01, N 5.92.

Reaction of 1b with Li(F_4-tcnq): According to the above-mentioned procedure, the binuclear macrocycle **2b** (yellow, 40.5 mg, 38.0%) was obtained from **1b** (75.5 mg, 0.130 mmol) and Li(F_4-tcnq) (37.0 mg, 0.131 mmol). FAB MS: *m*/*z* (%) = 1641 $[M]^+$. IR (Nujol): $\tilde{\nu}$ = 2202, 2156 (C≡N), 1643 (C=N) cm^{-1}. UV/Vis (CH_2Cl_2): λ_{max} = 410 (sh), 330 nm. $C_{82}H_{60}F_8N_8O_4P_2Rh_2$ (1641.5): calcd. C 60.01, H 3.68, N 6.82; found C 59.31, H 3.80, N 6.74.

Reaction of 1b with F_4-tcnq: A mixture of **1b** (71.7 mg, 0.123 mmol) and F-tcnq (34.7 mg, 0.126 mol) was stirred in CH_2Cl_2 (15 mL) at room temperature. After 5 h, the solvent was removed in vacuo. The residue was washed with diethyl ether and recrystallized from CH_2Cl_2 and diethyl ether to afford reddish brown crystals of **5** (38.4 mg, 36.3%). FAB MS: *m*/*z* = 857 $[M]^+$. IR (Nujol): $\tilde{\nu}$ = 2156 (C≡N) cm^{-1}. UV/Vis (CH_2Cl_2): λ_{max} = 333, 260 nm. $C_{41}H_{31}ClN_4O_2F_4PRh$ (857.0): calcd. C 57.46, H 3.65, N 6.54; found C 57.18, H 3.85, N 6.44.

Reaction of 3b with Li(F_4-tcnq): According to the above-mentioned procedure, the iridium macrocycle **4b** (yellow, 39.1 mg, 40.2%) was obtained from **3b** (71.6 mg, 0.107 mmol) and Li(F_4-tcnq) (31.03 mg, 0.111 mmol). IR (Nujol): $\tilde{\nu}$ = 2189, 2137 (C≡N), 1641 (C=N) cm^{-1}. UV/Vis (CH_2Cl_2): λ_{max} = 410(h), 330 nm. $C_{82}H_{60}F_8Ir_2N_8O_4P_2$ (1819.8): calcd. C 54.12, H 3.32, N 6.15; found C 52.10, H 3.44, N 5.91.

X-ray Crystallography: Complex **2a** was recrystallized from CH_2Cl_2/diethyl ether. A crystal was mounted at the top of a quartz fiber using perfluoro(polyoxopropylene ethyl ether), which was set on a MSC/ADSC Quantum CCD/Rigaku AFC8(ultraX 18) diffractometer. The measurement was made using Mo-K_α radiation at 0 °C under a cold nitrogen stream. Four preliminary data frames were measured at 0.5° increments of ω, in order to assess the crystal quality, and preliminary unit cell parameters were calculated. The cell parameters were refined using all the reflections measured in the range $2.8° < 2\theta < 40°$. The intensity images were measured at 0.5° intervals of ω for a duration of 20 s. The frame data were integrated using the d*TREK program package, and the data sets were corrected for absorption with the REQAB program. The crystal parameters along with data collection are summarized in Table 2. The data were corrected for Lorentz and polarization effects. Atomic scattering factors were taken from Cromer and Waber with the usual tabulation.[14] Anomalous dispersion effects were included in F_c;[15] the values of Δf′ and Δf″ were those of Creagh and McAuley.[16] All calculations were performed using the teXsan crystallographic software package.[17] The structure was solved by direct methods (SIR92). The positions of all non-hydrogen atoms were refined with anisotropic thermal parameters by using full-matrix least-squares methods. All hydrogen atoms were calculated at the ideal positions with a C−H distance of 0.97 Å.

Table 2. Crystal data for **2a**

Formula	$C_{86}H_{68}O_8P_2N_8F_8Rh_2$
Molecular weight	1761.26
Crystal system	monoclinic
Space group	$P2_1/c$ (No14)
a Å	22.755(1)
b Å	16.109(1)
c Å	25.0019(4)
β °	113.3895(6)
V Å^3	8412.0(6)
Z	4
D_{calc} g/cm^3#1.419	
μ (Mo-K_α) cm^{-1}	5.38
Reflections (< 2θ°)	80.0
Reflections observed ($I > 2\sigma(I)$]	10276
Parameters	1027
R/*Rw* [a]	0.070/0.102
*R*1	0.070 (for 10276 reflections)
GOF [b]	3.23

[a] $R = \Sigma||F_0| - |F_c||/\Sigma|F_0|$, $Rw = (\Sigma\omega(|F_0| - |F_c|)^2/\Sigma\omega F_0^2)^{1/2}$. [b] GOF = $(\Sigma\omega(|F_0| - |F_c|)^2 /(N_o - N_v)]^{1/2}$, where N_o = number of observations and N_v = number of variables.

CCDC-182949 contains the supplementary crystallographic data for this paper. These data can be obtained free of charge at www.ccdc.cam.ac.uk/conts/retrieving.html [or from the Cambridge Crystallographic Data Centre, 12, Union Road, Cambridge CB2 1EZ, UK; Fax: (internat.) +44-1223/336-033; E-mail: deposit@ccdc.cam.ac.uk].

Acknowledgments

We thank Professor Shigetoshi Takahashi and Dr. Fumie Takei for measurements of FAB mass spectra. This work was partially supported by a Grant-in-Aid for Scientific Research from the Ministry of Education, Science, Culture, and Sports, Japan (12640545).

[1] M. Wada, S. Higashizaki, A. Tsuboi, *J. Chem. Soc. Synp.* **1985**, 38−43; *J. Chem. Res. Miniprint* **1985**, 0467.
[2] Y. Yamashoji, T. Matsushita, M. Wada, T. Shono, *Chem. Lett.* **1988**, 43−44.
[3] Y. Yamamoto, R. Satoh, M. Ohshima, F. Matsuo, C. Sudoh, *J. Organomet. Chem.* **1995**, *489*, C68−C70.
[4] Y. Yamamoto, R. Satoh, F. Matsuo, C. Sudoh, T. Igoshi, *Inorg. Chem.* **1996**, *35*, 2329−2336.
[5] X.-H. Han, Y. Yamamoto, *J. Organomet. Chem.* **1998**, *561*, 154−165.
[6] Y. Yamamoto, K. Kawasaki, S. Nishimura, *J. Organomet. Chem.* **1999**, *587*, 49−57.
[7] Y. Yamamoto, X.-H. Han, J.-F. Ma, *Angew. Chem. Int. Ed.* **2000**, *39*, 1965−1968.
[8] Y. Yamamoto, K. Sugawara, *J. Chem. Soc., Dalton Trans.* **2000**, 2896−2897.
[9] Y. Yamamoto, K. Sugawara, X-H. Han, *J. Chem. Soc., Dalton Trans.* **2002**, 195−211.
[10] Y. Yamamoto, X.-H. Han, K. Sugawara, S. Nishimura, *Angew. Chem. Int. Ed.* **1999**, *38*, 1242−1244.
[11] Y. Yamamoto, X.-H. Han, S. Nishimura, N. Nezu, T. Tanase, *Organometallics* **2000**, *20*, 266−272.
[12] K. Onitsuka, H. Urayama, K. Sonogashira, F. Ozawa, *Chem. Lett.* **1995**, 1019−1020.
[13] L. R. Melby, R. J. Harder, W. R. Hertler, W. Mahler, R. E. Benson, W. E. Mochel, *J. Am. Chem. Soc.* **1962**, *84*, 3374.
[14] D. T. Cromer, J. T. Waber, *International Tables for X-ray Crystallography*, Kynoch, Birmingham (England), **1974**, Table 2.2A.
[15] J. A. Ibers, W. C. Hamilton, *Acta Crystallogr.* **1964**, *17*, 718−785.
[16] D. C. Creagh, W. J. McAulley, *International Tables for Crystallography, Vol.* C, Kluwer, Boston, **1992** Table 4.2.6.8, pp 219−222.
[17] teXsan: Crystal Structure Analysis Package, Molecular Structure Corporation Houston, TX, **1985** and **1992**.

Received April 8, 2002
[I02180]

Serendipity and Rational Design of One-Dimensional Doubly Stranded Chains with Nanometric Cavities Based on Ag^I Coordination Chemistry

Lamia Mimassi,[a] Carine Guyard-Duhayon,[a] Laurence Raehm,[a] and Hani Amouri*[a]

Keywords: Coordination chemistry / Polymers / Silver / Self-assembly / Supramolecular chemistry

Spontaneous and cooperative self-assembly processes allowed the preparation of two complexes $\{[AgL^1_2][X]\}_n$ [X = CF_3SO_3, (**3a**); X = BF_4, (**3b**)] in quantitative yields, identified as 1-D doubly stranded chains. The X-ray molecular structures of **3a,b** are reported. Complexes **3a,b** are isostructural and crystallize in the triclinic unit cell. The structures of **3a** and **3b** show the formation of a one-dimensional coordination polymer exhibiting as an outstanding feature the presence of infinite chained metallomacrocycles with nanometric cavities. Interestingly, NMR spectroscopy and electrospray mass spectrometry suggest that the identified elemental sub-unit $[AgL^1_2]^+$ is the key building block which self-assembles to provide the inorganic polymers **3a,b**. The effect of weakly coordinating counteranions and the assembling ligand L^1 on the supermolecule design are presented and discussed.

(© Wiley-VCH Verlag GmbH, 69451 Weinheim, Germany, 2002)

Introduction

The design of mono- and double-stranded chains is a great challenge for supramolecular chemists.[1] These supramolecular architectures are aesthetically appealing and exhibit potential applications as molecular wires,[2] electrical conductors,[3] molecular magnets,[4] in host-guest chemistry[5] and in catalysis.[6] Particular interest has been devoted to the construction of helical chains. For instance, polymetallic double helices have been elegantly self-assembled from poly-2,2′-bipyridine ligand strands with ether linkages and tetrahedral Ag^I ions.[7] More recently, efforts have been directed to the preparation of infinite coordination helices. Such infinite chains have been reported by Jung and co-workers,[8] von Zelewsky and co-workers,[9] Ciani and co-workers[10] and Erxleben[10] using tectonic bridging ligands[11] and taking advantage of the tetrahedral nature of Ag^I ions. Although this process sounds relatively straightforward, the rational design of these materials is complicated by the uncertain coordination propensity of the metal ion, which is influenced by such factors as the counteranion,[12] the solvent and the ligand geometry. Thus, controlling these elements is at the heart of controlling supramolecular coordination chemistry.

Pursuing our research in the area of supramolecular chemistry, in particular the design of metallomacrocyles, metallocryptands, and metallocryptates as anion hosts,[13] we extended our investigations to the construction of 1-D chains with appropriate cavities that would host anionic guests. In this work we report novel and rare infinite doubly stranded chains with a propeller arrangement around each metal center, using the tectonic ligand L^1 (Scheme 1) and Ag^I ions. Initially this assembly was discovered by serendipity, as are most assemblies in the area of supramolecular chemistry, but later it was rationally reproduced with $AgCF_3SO_3$ (**1a**) and $AgBF_4$ (**1b**).

Results and Discussion

Self-Assembly of the Doubly Stranded Chain Complexes $\{[AgL^1_2][X]\}_n$ [X = CF_3SO_3, (3a); X = BF_4, (3b)]

To demonstrate the viability of our strategy we prepared the bidentate ligand 1,3-bis(benzimidazol-1-ylmethyl)-2,5-dimethoxy-4,6-dimethylbenzene (L^1, **2a**). It was synthesized by allowing the corresponding bis(chloromethyl) derivative to react with two equivalents of benzimidazole in the presence of K_2CO_3 in CH_3CN (overall yield: 90%). Its spectroscopic data are consistent with the proposed structure.

Significantly, treatment of $AgCF_3SO_3$ (**1a**) with two equivalents of L^1 in CH_3CN/CH_2Cl_2 solution gave a white precipitate after five minutes of stirring. The reaction was allowed to proceed for several hours without any further change being observed. The white precipitate was isolated in quantitative yield and identified as 1-D doubly stranded chains of $\{[AgL^1_2][CF_3SO_3]\}_n$ (**3a**). Complex **3a** was found to be soluble in polar solvents such as methanol, acetonitrile and dimethyl sulfoxide, hence the ^1H NMR spectrum was recorded in CD_3CN (Figure 1). The ^1H and ^{13}C NMR spectroscopic data are consistent with the proposed formulae and show that the coordinated ligand L^1 displays a sym-

[a] Laboratoire de Chimie Inorganique et Matériaux, Moléculaires UMR CNRS 7071, Université Pierre et Marie Curie
4, place Jussieu, case 42, 75252 Paris cedex 05, France
Fax (internat.) +33-1/4427-3841
E-mail: amouri@ccr.jussieu.fr

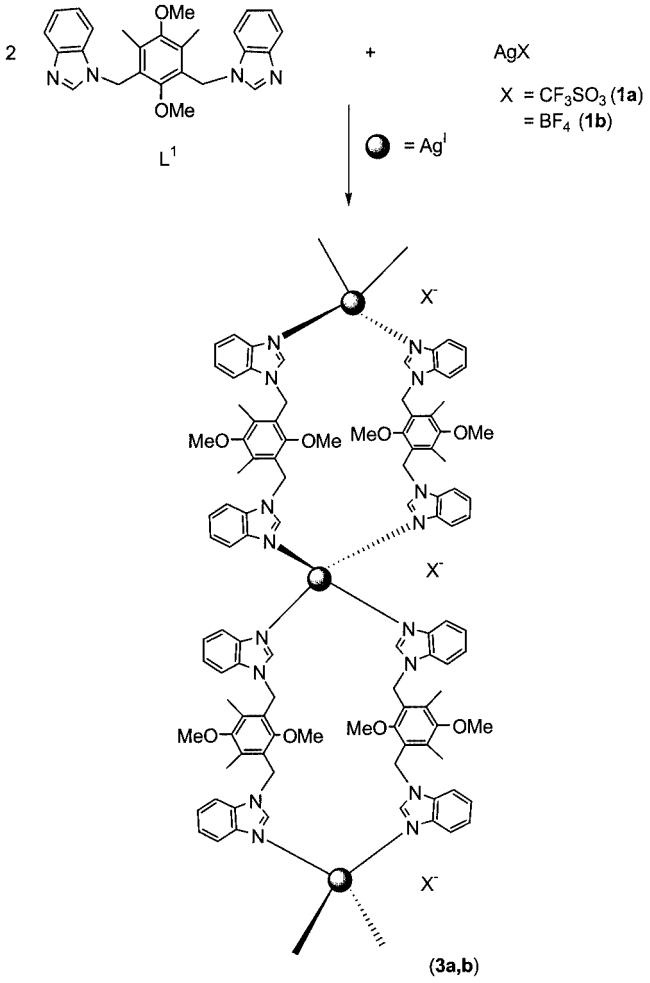

Scheme 1. General synthetic strategy for 1-D chains (**3a,b**)

metric pattern close to that of the free ligand L^1. Most remarkably, the resonances ascribed to the protons of the benzimidazole group appear at δ = 7.92 (s, 2 H), 7.71 (m, 4 Hz, 4 H), 7.55 (m, 4 H) and 7.29 ppm (m, 8 H) (see Figure 1). The NMR symmetry is probably due to the fragmentation of the polymer and formation of oligomeric species during the dissolution process. The electrospray (ES) mass spectrum shows a peak at m/z = 961.19 which corresponds to the formation of $[Ag(L^1)_2]^+$ species in solution. This suggests that the $[Ag(L^1)_2]^+$ sub-unit is the key building block which leads to the formation of the doubly stranded chains $\{[AgL^1_2][CF_3SO_3]\}_n$ (**3a**) through self-assembly. Variable temperature ^{1}H NMR spectra recorded for **3a** in CD_3CN show no signal broadening, suggesting that the exchange phenomenon may be fast on the NMR time scale. It is worth noting that von Zelewsky and co-workers have reported that a polymeric double-helix silver complex breaks down in solution to produce circular helicates or oligomers which are in rapid dynamic equilibrium.[9]

Suitable crystals of **3a** were obtained by slow evaporation of Et_2O into a CH_3CN solution. The complex crystallizes in the triclinic unit cell space group $P\bar{1}$. Crystallographic data for **3a** are shown in Table 1. Selected bond lengths and angles are shown in Table 2. The structure shows that complex **3a** consists of one-dimensional doubly stranded chains (Figure 2a). Four L^1 ligands wrap around the Ag^I ion to give a tetrahedral coordination geometry and are disposed in a propeller arrangement with a dihedral angle θ of 80.3°. Each ligand L^1 connects another Ag^I center through the other benzimidazole arm generating a 1D-doubly stranded chain. Further we note the presence of a center of symmetry lying half way between two parallel phenyl rings within the double stranded chain (Figure 2b). Interestingly, the phenyl rings of two close doubly stranded chains show an offset π-stacking phenomenon, with a plane-to-plane

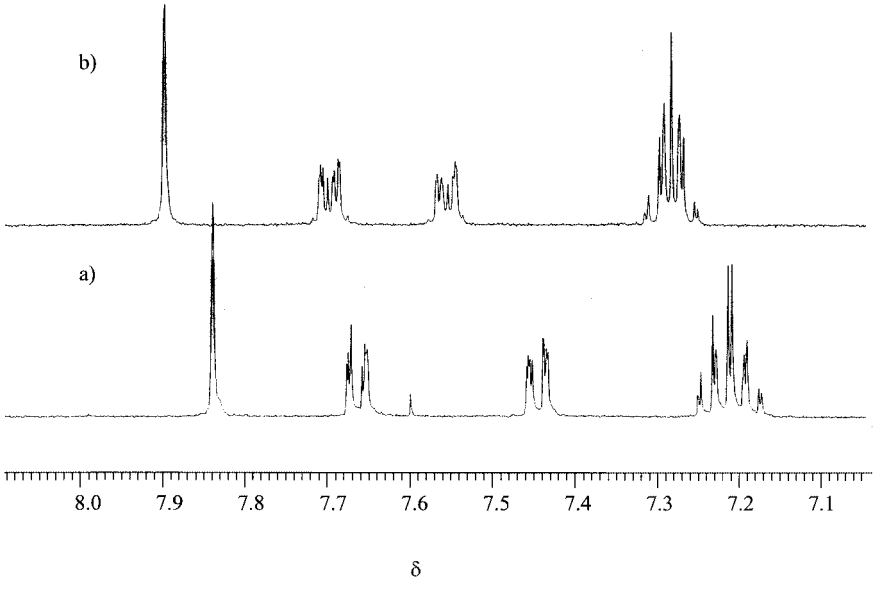

Figure 1. Section of the ^{1}H NMR spectra (400 MHz) showing the aromatic region for: a) the free ligand L^1 recorded in CD_3CN, and b) **3a** recorded in CD_3CN

Table 1. Crystal data and structures refinement for **3a**

	3a
Formula	$Ag(N_4C_{26}O_2H_{26})_2{\cdot}(CF_3SO_3){\cdot}H_2O$
M_r	1127.99
Crystal size	0.2 × 0.2 × 0.4
Crystal system	triclinic
Space group	$P\bar{1}$
a (Å)	11.752 (1)
b (Å)	12.689 (2)
c (Å)	20.672 (3)
α (deg)	95.78 (1)
β (deg)	100.71 (1)
γ (deg)	116.87 (1)
V (Å^3)	2641.2 (7)
Z	2
$\rho_{calcd.}$ (g·cm^{-3})	1.42
Temp (°C)	27
λ (Mo-K_α) (Å)	0.71069
μ (cm^{-1})	4.93
$R(F_o)$[a]	0.056
$R_w(F_o)$[b]	0.061

[a] $R = \Sigma(|F_o| - |F_c|)/\Sigma F_o$. [b] $Rw = [\Sigma w(|F_o| - |F_c|)^2/\Sigma w F_o^2]^{1/2}$.

Table 2. Selected interatomic distances [Å] and angles for **3a**

Ag(1)−N(1)	2.246 (3)
Ag(1)−N(101)	2.266(3)
N(1)−Ag(1)−N(4)	99.02(13)
N(1)−Ag(1)−N(101)	132.97(15)
N(4)−Ag(1)−N(104)	112.50(14)
Ag(1)−N(4)	2.357(4)
Ag(1)−N(104)	2.455 (4)
N(1)−Ag(1)−N(104)	105.79(13)
N(4)−Ag(1)−N(101)	110.70 (14)
N(101)−Ag(1)−N(104)	95.69 (13)

distance of 3.8 Å. This weak π-interaction is observed throughout the infinite chain and only between alternate metallomacrocycles (Figure 2c).[14] In a well-documented paper, Janiak reported on π-π stacking in metal complexes with aromatic ligands. He showed that strong interactions exist when plane-to plane-distances are around 3.3 Å. These interactions are weaker when the distance is above 3.6 Å with 3.8 Å being approximately the maximum for which π-π interactions are accepted.[14d] It is clear that the two L^1 ligands and the two Ag^I centers describe a 25-membered ring with a nanometric cavity where both extremities are capped by the silver centers (Figure 2b). The average Ag−Ag distance in **3a** is 12.7 Å (1.27 nm), while the average distance between the two phenyl rings is 8.4 Å (0.84 nm). Perhaps due to the steric hindrance presented by the internal methoxy groups, all the $CF_3SO_3^-$ anions are located outside the metallomacrocyclic cavity and in between two doubly stranded chains (Figure 2c). The average Ag−Ag distance between two close doubly stranded chains is 11.3 Å. Taken together, this is a rare one-dimensional structure for Ag^I ions connected by benzimidazole ligands. Related complexes of this family are often obtained as classical mono-helix or doubly stranded helical chains.[8−10]

It is interesting to speculate as to the extent to which this π-π stacking interaction is responsible for the self-assembly and stability of these doubly stranded chains. In this context we note that Lehn and co-workers have elegantly shown that a pre-organized helical conformation of discrete encoded oligoheterocyclic strand can be envisaged through π-π interactions between parallel aromatic heterocycles of neighboring molecules.[15a] Furthermore, Stoddart and co-workers have beautifully shown that an infinite two-dimensional polymeric supramolecular network is generated as a result of extended π-π stacking interactions.[15b]

We then examined the role of the anion on the formation of this one-dimensional chain. Thus we repeated the above experiment but using $AgBF_4$ (**1b**) instead of $AgCF_3SO_3$ (**1a**). A white precipitate was similarly obtained in quantitative yield and was identified as 1D-doubly stranded chains of $\{[AgL^1_2][BF_4]\}_n$ (**3b**) analogous to **3a**. The spectroscopic data were identical to those obtained for **3a**. To confirm the solid-state structure of **3b** an X-ray structural determination was carried out on a single crystal of **3b**. Although complete refinement could not be achieved due to the small size of the crystals, we were able to obtain valuable information about complex **3b**.

The structure shows indeed that **3b** consists of doubly stranded chains, and that the BF_4 anions are located outside the metallomacrocyles and in between the two doubly stranded chains. The average Ag−Ag distance in **3b** is 12.3 Å (1.23 nm), while the average distance between the two phenyl rings is 8.5 Å (0.85 nm). The Ag−Ag distance between two close doubly stranded chains is 12.1 Å (1.21 nm). These results are similar to those obtained for **3a** and they show that the size of the weakly coordinating counterion does not affect the overall structure.

It is noteworthy, however, that it has been reported recently that treatment of $AgCF_3SO_3$ or $Cu(ClO_4)_2$ with the analogous bidentate ligands L^2 and L^3 possessing two benzimidazole arms in the 1,3- and 1,4-positions of a phenyl ring, respectively, afforded the binuclear boxes M_2L_3 and M'_2L_4 (M = Ag, M′ = Cu) in which an anion guest is encapsulated.[16] Our results contrast sharply with those reported and this is no doubt related to the steric factors displayed by our ligand L^1.

Conclusion

In conclusion, using the tetrahedral coordination chemistry of Ag^I ions and the tectonic ligand L^1, we have reported a rational synthetic strategy for the formation of rare doubly stranded chains (**3a,b**). The cavity size in these 1D-chains is of nanometric size and we expect that it can be modulated, depending on the bridging di-benzimidazole ligands used. These surprising results address once again the important role of assembling tectonic ligands, metal and ligand geometries, coordination sites, π-π interactions and steric effects which determine the final structure of the supramolecular species obtained. Thus, ligand tailoring is at the heart of the art and science of inorganic supramolecular construction.

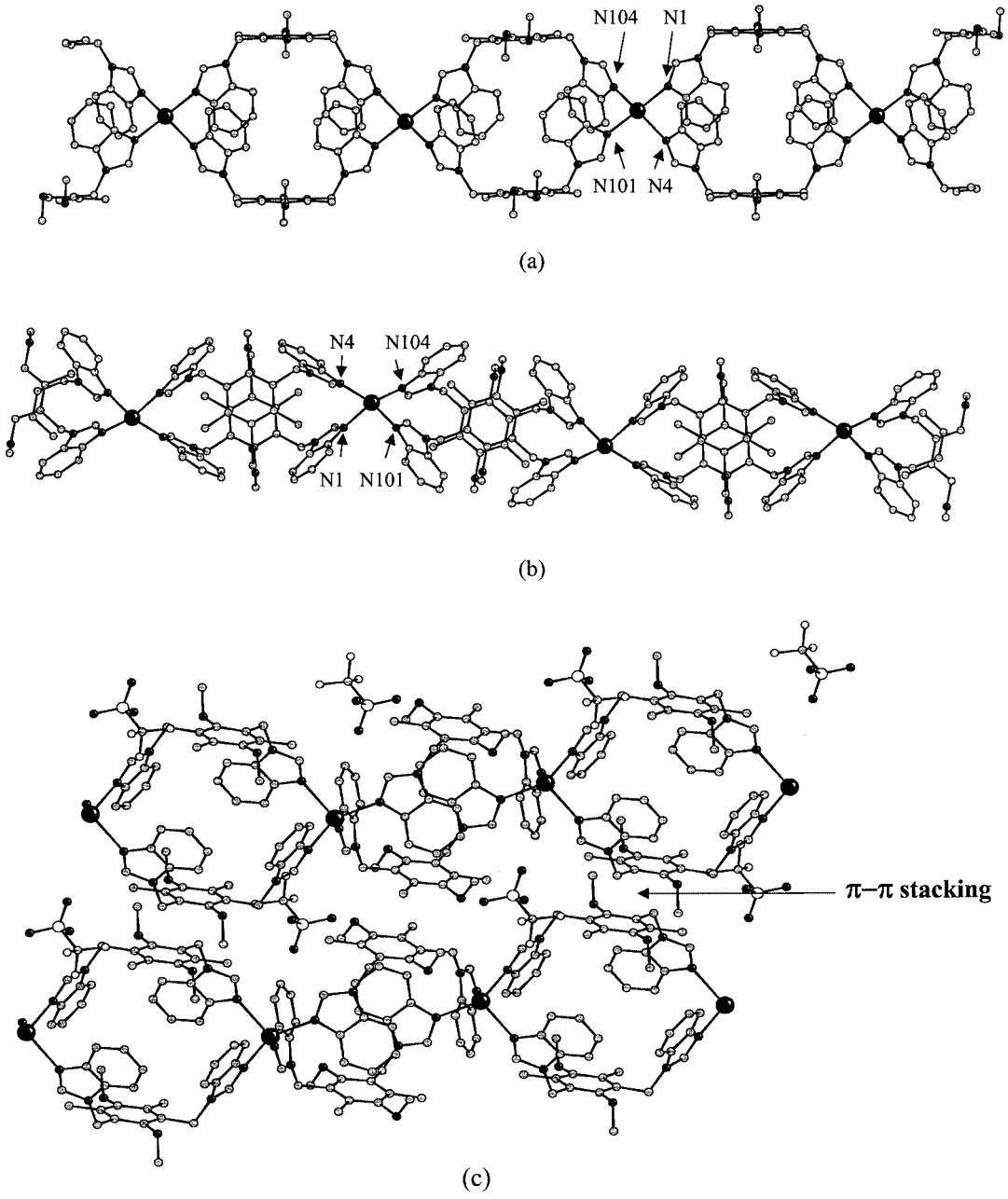

Figure 2. a) Crystallographic structure of the cationic part of the doubly stranded infinite chains **3a** perpendicular to the *b* axis with atom numbering system; hydrogens have been omitted for clarity; b) crystallographic structure of the cationic part of **3a** showing the two coplanar phenyl rings within each metallomacrocyle of the infinite chain; note the alternate arrangement of the metallomacrocycles; c) view of the infinite 1D-chain of $\{[AgL_2][CF_3SO_3]\}_n$ (**3a**) showing the triflate anions lying in between two doubly stranded chains as well as the offset π-π stacking phenomenon between the phenyl rings of two neighboring doubly stranded chains

Further investigations are ongoing on this and related 1-D and 2-D supramolecular assemblies with the aim of obtaining selective hosts for a variety of anionic guests.

Experimental Section

All experimental manipulations were carried out under argon using Schlenk tube techniques.

Synthesis of L[1]: This bidentate ligand was prepared by addition of 1,3-di(chloromethyl)-2,5-dimethoxy-4,6-dimethylbenzene (1.09 g, 4.41 mmol) in CH_3CN to benzimidazole (0.98 g, 8.3 mmol) in the presence of K_2CO_3 (1.14 g, 8.24 mmol). The reaction was stirred for 30 minutes before being refluxed for 12 hours. The resulting precipitate was filtered and extracted with $CHCl_3$. After being washed with distilled water the organic phase was isolated before being dried over $MgSO_4$. The solvent was removed on a rotary evaporator to yield an off-white microcrystalline solid. Yield: 1.58 g (90%). $C_{26}H_{26}N_4O_2{\cdot}H_2O$ (444): calcd. C 70.27, H 6.30, N 12.61; found C 70.64, H 6.10, N 12.57. ^{1}H NMR (400 MHz, [D$_6$]DMSO): δ = 8.10 (s, 2 H, =CH), 7.63 (d, 2 H, =CH), 7.47 (d, 2 H, =CH), 7.16 (m, 4 H, H-aromatic), 5.49 (s, 4 H, -CH_2-), 3.70 (s, 3 H, MeO), 3.50 (s, 3 H, MeO), 2.12 (s, 6 H, CH_3).

Synthesis of 3a: A solution of L^1 (**2a**) (438 mg, 1.02 mmol) in $CHCl_3$ (10 mL) was added to a solution of $AgCF_3SO_3$ (**1a**; 126 mg, 0.5 mmol) in CH_3CN (10 mL). After 5 minutes stirring, a white precipitate was formed. The reaction was allowed to proceed for several hours without any further changes. The precipitate was filtered and washed several times with CH_2Cl_2 then dried under vacuum. Yield: 550 mg (quantitative). ^1H NMR (400 MHz, [D$_6$]DMSO): δ = 8.25 (s, 2 H, =CH), 7.74 (dd, 4 H, H-aromatic), 7.58 (dd, 4 H, H-aromatic), 7.23 (m, 8 H, H-aromatic), 5.56 (s, 8 H, -CH$_2$-N), 3.70 (s, 6 H, -OCH$_3$), 3.53 (s, 6 H, -OCH$_3$), 2.16 (s, 12 H, -CH$_3$) ppm. ^{13}C NMR (100.62 MHz, [D$_6$]DMSO): δ = 154.4, 153.8, 144.5, 142.4, 133.5, 133.1, 125.9, 123.3, 122.6, 119.5, 111.2, 63.5, 60.2, 41.3, 12.5 ppm. ^{19}F NMR (376.49 MHz, [D$_6$]DMSO): δ = −78.18 (s, free CF_3SO_3) ppm. IR (KBr): $\tilde{\nu}$=1267 s (ν_{C-F}) cm^{-1}.

Synthesis of 3b: Compound **3b** was prepared in a similar way to **3a** but using $AgBF_4$ instead of $AgCF_3SO_3$. It was obtained quantitatively. $C_{52}H_{52}AgBF_4N_8O_4$ (1047.8): calcd. C 59.61, H 5.00, N 10.70; found C 59.38, H 5.01, N 11.60. ^1H NMR (400 MHz, [D$_6$]DMSO): δ = 8.26 (s, 2 H, =CH), 7.76 (dd, 4 H, H-arom.), 7.62 (dd, 4 H, H-arom.), 7.26 (m, 8 H, H-arom.), 5.57 (s, 8 H, -CH$_2$-N), 3.69 (s, 6 H, -OCH$_3$), 3.55 (s, 6 H, -OCH$_3$), 2.17 (s, 12 H, -CH$_3$) ppm. ^{13}C NMR (100.62 MHz, [D$_6$]DMSO): δ = 154.5, 153.8, 144.6, 142.1, 133.4, 133.2, 125.8, 123.5, 122.8, 119.5, 111.3, 63.5, 60.2, 41.3, 12.5 ppm. ^{19}F NMR (376.49 MHz, [D$_6$]DMSO): δ = −148.70 (s, free BF_4) ppm. IR (KBr): $\tilde{\nu}$ = 1068 s (ν_{B-F}) cm^{-1}.

X-ray Structure Determination: A colorless needle-shaped crystal of **3a** was mounted on a glass fiber. All measurements were made on a Enraf−Nonius Mach-3 diffractometer, Mo-K_α radiation (λ = 0.71069 Å), collection range 2θ = 2−50°. The Ψ-scan curve of **3a** was flat, hence no absorption correction was applied. The structure was determined by direct methods and subsequent difference-Fourier syntheses, and refined by full-matrix least-squares on *F* using the programs of the PC version of CRYSTALS. All non-hydrogen atoms were refined anisotropically. Hydrogen atoms were located on a difference-Fourier map and their coordinates were refined with an overall isotropic thermal parameter.

CCDC-166133 (**3a**) contains the supplementary crystallographic data for this paper. These data can be obtained free of charge at www.ccdc.cam.ac.uk/conts/retrieving.html [or from the Cambridge Crystallographic Data Centre, 12, Union Road, Cambridge CB2 1EZ, UK; Fax: (internat.) +44-1223/336-033; E-mail: deposit@ccdc.cam.ac.uk].

Acknowledgments

The CNRS and UPMC are gratefully acknowledged for supporting this work. We would like to thank M. N. Rager for NMR analysis, and Professor Y. Jeanin for structural analysis.

[1] J.-M. Lehn, *Supramolecular Chemistry, Concepts and Perspectives*, VCH, Weinheim, **1995**.

[2] [2a] K.-T. Wong, J.-M. Lehn, S.-M. Peng, G.-H. Lee, *Chem. Commun.* **2000**, 2259−2260. [2b] J. A. Ramsden, W. Weng, A. M. Arif, J. A. Gladysz, *J. Am. Chem. Soc.* **1992**, *114*, 5890−5891. [2c] W. Weng, J. A. Ramsden, A. M. Arif, *J. Am. Chem. Soc.* **1993**, *115*, 3824−3825. [2d] T. Bartik, W. Weng, J. A. Ramsden, S. Szafert, S. B. Falloon, A. M. Arif, J. A. Gladysz, *J. Am. Chem. Soc.* **1998**, *120*, 11071−11081. [2e] R. Dembinski, T. Bartik, B. Bartik, M. Jaeger, J. A. Gladysz, *J. Am. Chem. Soc.* **2000**, *122*, 810−822. [2f] W. Mohr, J. Stahl, F. Hampel, J. A. Gladysz, *Inorg. Chem.* **2001**, *40*, 3263−3264. [2g] N. Le Narvor, L. Toupet, C. Lapinte, *J. Am. Chem. Soc.* **1995**, *117*, 7129−7138. [2h] M. I. Bruce, P. J. Low, K. Costuas, J.-F. Halet, S. P. Best, G. A. Heath, *J. Am. Chem. Soc.* **2000**, *122*, 1949−1962.

[3] [3a] *Extended Linear Chain Compounds* (Ed.: J. S. Miller), Plenum Press: New York, 1982, Vol. 1. [3b] A. Aumuller, P. Erk, G. Klebe, S. Hunig, J.U. von Schutz, H.-P. Werner, *Angew. Chem.* **1986**, *98*, 759−760; *Angew. Chem. Int. Ed. Engl.* **1986**, *25*, 740−741. [3c] A. G. Bunn, P. J. Carroll, B. B. Wayland, *Inorg. Chem.* **1992**, *31*, 1297−1299.

[4] [4a] M. A. M. Abu-Youssef, A. Escuer, D. Gatteschi, M. A. S. Goher, F. A. Mautner, R. Vicente, *Inorg. Chem.* **1999**, *38*, 5716−5723 and references therein. [4b] A. Caneschi, D. Gatteschi, N. Lalioti, C. Sangregorio, R. Sessoli, G. Venturi, A. Vindigni, A. Rettori, M. G. Pini, M. A. Novak, *Angew. Chem. Int. Ed.* **2001**, *40*, 1760−1763.

[5] [5a] M. Aoyagi, K. Biradha, M. Fujita, *J. Am. Chem. Soc.* **1999**, *121*, 7457−7458. [5b] A. Tanatani, M. J. Moi, J. S. Moore, *J. Am. Chem. Soc.* **2001**, *123*, 1792−1793. [5c] K. Biradha, C. Seward, M. J. Zaworotko, *Angew. Chem.* **1999**, *111*, 584−587; *Angew. Chem. Int. Ed.* **1999**, *38*, 492−495.

[6] M. Fujita, Y. J. Kwon, S. Washizu, K. J. Ogura, *J. Am. Chem. Soc.* **1994**, *116*, 1151−1152.

[7] T. M. Garret, U. Koert, J.-M. Lehn, A. Rigault, D. Meyer, J. Fischer, *Chem. Commun.* **1990**, 557−558.

[8] [8a] O.-S. Jung, S. H. Park, D. C. Kim, K. M. Kim, *Inorg. Chem.* **1998**, *37*, 610−611. [8b] O.-S. Jung, Y. J. Kim, Y.-A. Lee, J. K. Park, H. K. Chae, *J. Am. Chem. Soc.* **2000**, *122*, 9921−9925. [8c] O.-S. Jung, Y. J. Kim, Y.-A. Lee, H. K. Chae, H. G. Jang, J. Hong, *Inorg. Chem.* **2001**, *40*, 2105−2110.

[9] O. Mamula, A. von Zelewsky, T. Bark, G. Bernardinelli, *Angew. Chem.* **1999**, *111*, 3129; *Angew. Chem. Int. Ed.* **1999**, *38*, 2945−2948.

[10] [10a] L. Carlucci, G. Ciani, D. W. v. Gudenberg, D. M. Proserpio, *Inorg. Chem.* **1997**, *36*, 3812−3813. [10b] L. Carlucci, G. Ciani, D. M. Proserpio, A. Sironi, *Inorg. Chem.* **1998**, *37*, 5941−5943. [10c] A. Erxleben, *Inorg. Chem.* **2001**, *40*, 2928−2931.

[11] Tectons are molecules whose specific interactions induce the assembly of aggregates with controlled geometries see P. Brunet, M. Simard, J. D. Wuest, *J. Am. Chem. Soc.* **1997**, *119*, 2737−2738 and references therein.

[12] [12a] K. A. Hirsch, D. Venkataraman, S. R. Wilson, J. S. Moore, S. Lee, *J. Chem. Soc., Chem. Commun.* **1995**, 2199−2200. [12b] K. A. Hirsch, S. R. Wilson, J. S. Moore, *Inorg. Chem.* **1997**, *36*, 2960−2963. [12c] M. A. Withersby, A. J. Blake, N. R. Champness, P. A. Cooke, P. Hubberstey, W.-S. Li, M. Schroder, *Inorg. Chem.* **1999**, *38*, 2259−2266.

[13] [13a] H. Amouri, M. N. Rager, F. Cagnol, J. Vaissermann, *Angew. Chem.* **2001**, *113*, 3748−3750; *Angew. Chem. Int. Ed.* **2001**, *40*, 3636−3638. [13b] H. Amouri, Y. Besace, M. N. Rager, J. Vaissermann, *Inorg. Chem.* **1999**, *38*, 1211−1216. [13c] H. Amouri, C. Guyard-Duhayon, J. Vaissermann, M. N. Rager, *Inorg. Chem.* **2002**, *41*, 1397−1403.

[14] [14a] C. M. Hartshorn, P. J. Steel, *Inorg. Chem.* **1996**, *35*, 6902−6903. [14b] K. S. Mandal, L. K. Thompson, M. J. Newlands, E. J. Gabe, F. L. Lee, *Chem. Commun.* **1989**, 744−746. [14c] K. S. Mandal, L. K. Thompson, M. J. Newlands, E. J. Gabe, F. L. Lee, *Inorg. Chem.* **1990**, *29*, 3556−3561. [14d] C. Janiak, *J. Chem. Soc., Dalton Trans.* **2000**, 3885−3896.

[15] [15a] L. A. Cuccia, J.-M. Lehn, J.-C. Homo, M. Schmutz, *Angew. Chem. Int. Ed.* **2000**, *39*, 233−237. [15b] M. C. T. Fyee, J. F. Stoddart, *Acc. Chem. Res.* **1997**, *30*, 393−401 and references therein. [15c] D. Philp, J. F. Stoddart, *Angew. Chem. Int. Ed. Engl.* **1996**, *35*, 1154−1196.

[16] C.-Y. Su, Y.-P. Cai, C.-L. Chen, H.-X. Zhang, B.-S. Kang, *J. Chem. Soc., Dalton Trans.* **2001**, 359−361.

Received March 4, 2002
[I02108]

Zinc Complexes of a Helical 22-mer Peptide with Two Histidine Donors[‡]

Michael Gelinsky[a] and Heinrich Vahrenkamp*[a]

Dedicated to Professor Karl Wieghardt on the occasion of his 60th birthday

Keywords: Zinc / Peptides / Bioinorganic chemistry / Enzyme mimics

A new 22-mer model peptide **P22** was designed for maximal α-helicity in nonpolar media, synthesized by solid-phase methods, and isolated in an analytically pure state. It contains histidine at positions 10 and 14 representing the *i*, *i* + 4 motif which is typical for metal ion binding. Treatment with zinc halides yielded the uncharged molecular complexes (**P22**)$ZnCl_2$ and (**P22**)ZnI_2 which are the first metal complexes of medium-sized peptides to be isolated in an analytically pure state and identified by mass spectrometry. The helicity of both the free peptide and its complexes was confirmed by IR and CD spectroscopy as well as by molecular mechanics calculations. This has allowed us to propose a molecular structure which shows that the complexes are viable models for zinc-binding sections in zinc finger proteins.
(© Wiley-VCH Verlag GmbH, 69451 Weinheim, Germany, 2002)

Introduction

Of the two functions of zinc in biology — structural and catalytic[2] — the latter has found much more attention in the literature even though the structural function may be the more important. It is essential for many enzymes,[3] and the ubiquity of zinc finger motifs[4] is underlined by the fact that about 1% of the human genome seem to encode zinc finger proteins.[5]

The classical zinc finger sequence is X_3-Cys-X_{2-4}-Cys-X_{12}-His-X_3-His-X_4 with X being any amino acid.[6] Its most well preserved feature is the location of two histidines in the *i* and *i* + 4 positions on a helical peptide chain. This has been found in the two X-ray structure determinations of zinc finger fragments,[7] and confirmed by chemical modifications of truncated zinc finger peptides.[8]

Based on this information the methods of chemical peptide synthesis were applied to the design of some medium-sized peptides containing pairs of cysteine and/or histidine residues at appriopriately spaced positions on the peptide chain.[9] It was found that such peptides form stable zinc complexes when the donor residues are placed at the *i* and *i* + 4 positions.[9−17] In some cases the addition of zinc and other metal ions enhanced the helicity of these peptides.[10−12,15] This proves the metal binding by the two His or Cys donors, which in the *i* and *i* + 4 positions on the α-helix point in the same direction. So far the identification of such metal-peptide complexes has rested only on spectroscopic methods, and none of them has been isolated in a pure state or subjected to mass spectrometry.

Our own contributions to the chemistry of zinc-peptide complexes[1] have focused so far on small peptides, as exemplified by the role of structural zinc in bis(cysteinyl) protein sequences[18] or in β-turn motifs,[19] and the parameterization of the donor qualities of histidine and cysteine in peptides toward zinc.[20] In continuation of this we have now turned to the complexation of zinc by histidine and cysteine donors which are constituents of helical peptides. This calls for the synthesis of medium-sized peptides and the use of amino acids which favor helix formation. This paper reports our first results in this area in the form of the preparation, isolation in the pure state, and the full characterization of a zinc complex of a 22-mer peptide with histidine in the *i* and *i* + 4 positions.

Results and Discussion

In order to enable the isolation and full characterization of both the peptide and its zinc complexes a strategy was chosen which differs from that in the previous investigations. The peptide was chosen to be hydrophobic and to contain no donor functions other than two histidine constituents. This should allow us to work in non-aqueous media and facilitate isolations. For the same reason both termini of the peptide were derivatized: the N-terminus was chosen to be *N*-acetyl glycine as the simplest terminator of a capping box,[21] and the C-terminus was protected as the

[‡] Zinc Complexes of Amino Acids and Peptides, 17. Part 16: Ref.[1]

[a] Institut für Anorganische und Analytische Chemie der Universität Freiburg,
Albertstr. 21, 79104 Freiburg, Germany
Fax: (internat.) +49-(0)761/203-6001
E-mail: vahrenka@uni-freiburg.de

amide. Only amino acids that are predominantly hydrophobic were considered, and among these those with the highest tendency for helix formation. This limited the choice of the amino acids for the peptide backbone to alanine, leucine, methionine and phenylalanine, which hold the top positions in the various rankings of helix formation propensity.[22−25]

The length of the peptide was chosen to be above the minimum length for helix formation (16−18)[26] but below the maximum length for clean chromatographic separation (25−30). It was decided to use a 22-mer peptide with histidine at positions 10 and 14. The amino acid sequence was optimized with the AGADIR algorithm[27] for a maximum degree of α-helicity. Among 100 randomly chosen sequences made up from the four amino acids the computation selected the one given below in the peptide **P22** as the best choice, with a computed helicity of 88%.

NAc-Gly-Phe-Leu-Met-Ala-Phe-Leu-Met-Ala-His-Phe-Leu-Met-His-Phe-Leu-Met-Ala-Phe-Leu-Met-Ala-NH_2

P22

P22 was prepared on a solid-phase synthesizer using Fmoc-protected amino acids and purified by reversed-phase HPLC. Its purity was confirmed by elemental analysis, and its identity was verified by an ESI mass spectrum which reproduced the calculated isotope pattern for $C_{128}H_{187}N_{27}O_{23}S_5$. As expected, **P22** was found to have a very low solubility in water but to be quite soluble in acetonitrile and THF. This was the first indication of the helical structure of **P22**, based on the experience that hydrophobic oligopeptides which are not helical (i.e. which don't have their hydrogen bonds in their interior) have a very low solubility in these solvents.[28]

Further support for the helical nature of **P22** was obtained by FTIR and CD spectroscopy. The intense amide-I band in the IR spectrum was observed at 1654 cm^{-1} in THF solution and at 1658 cm^{-1} in a KBr matrix, as expected for α-helices.[29] The CD spectra of **P22** and its $ZnCl_2$ complex are shown in Figure 1. The CD spectrum in acetonitrile displays a molar ellipticity Θ at 222 nm of −497000 deg·cm^2·$dmol^{-1}$. This converts to an average ellipticity per peptide function (n = 21) of −24000 deg·cm^2·$dmol^{-1}$. According to the equation

helicity [%] = $100 \cdot \Theta_{222}/[-39500 \cdot (1 - 2.57/n)]$[30]

the helicity of **P22** is thus 69%. Considering that five of the 22 amino acids in **P22** are phenylalanine, which at 222 nm has a positive ellipticity, it can be concluded that the 69% value is a lower limit and the actual helicity is considerably higher. This is confirmed by the CD spectrum in 2,2,2-trifluoroethanol, a solvent which strongly favors the formation of α-helices.[31] In this solvent the Θ_{222} value of **P22** is even slightly lower than in acetonitrile, i.e. the helicity of **P22** cannot be raised, supporting the notion that **P22** is nearly perfectly helical even in the absence of 2,2,2-trifluoroethanol.[32]

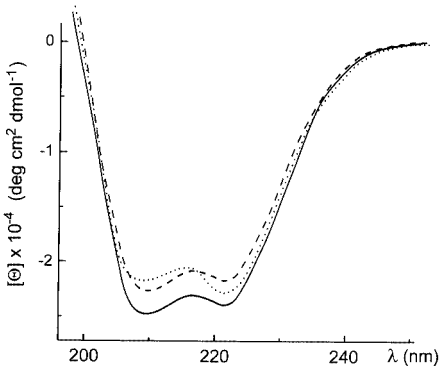

Figure 1. CD spectra of **P22** in acetonitrile (solid line) and in 2,2,2-trifluoroethanol (dashed line) and of **P22**·$ZnCl_2$ (**1**) in acetonitrile (dotted line); concentrations 0.4−0.5 mM

The NMR spectroscopic data of **P22** were not as informative as expected. As is typical for α-helical peptides,[33] the ^{1}H NMR resonances of the amide protons are spread over a range of several ppm, and the resonances of the mobile side-chains are sharper than those of the α-CH and amide groups in the peptide backbone. Unfortunately the side-chain interactions, which are very diagnostic for α-helical peptides,[34] could not be extracted from NOESY and ROESY spectra, even when taken at 500 MHz, as neither intensive NOE effects with a positive nor those with a negative phase occurred. For the same reason the resonances for the individual amino acids (alanine, phenylalanine, leucine and methionine occur 4 or 5 times each) could not be assigned. The failure to obtain structural information from NMR spectroscopic data, albeit not unprecedented for medium-sized peptides or their zinc complexes,[16,35] is a drawback of this work. It calls for a more detailed NMR study which is beyond the scope of this investigation.

As isolated by HPLC, peptide **P22** contained about five equivalents of trifluoroacetic acid. In order to remove these before the reaction with zinc salts, **P22** was treated with gaseous ammonia in THF solution. Filtration and prolonged pumping left **P22** in a water-, acid- and base-free form. In this form **P22** as an uncharged hydrophobic molecule is soluble only in nonpolar media. As such it is a chelating organic bis-nitrogen ligand, and in terms of zinc coordination chemistry it is well suited to form molecular L·ZnX_2 complexes. In contrast, we have experienced repeatedly that small bis-histidine peptides form insoluble coordination polymers with ionic zinc species such as $Zn(ClO_4)_2$.[36] For this reason we reacted **P22** with zinc salts which are themselves molecular in nonpolar media, i.e. the zinc halides.

Treatment of THF solutions of **P22** with equimolar amounts of anhydrous $ZnCl_2$ or ZnI_2 resulted in clear solutions of complexes **1** and **2**, respectively. After workup both complexes were isolated as yellow or brown powders which are analytically pure. Both **1** and **2** are quite soluble in nonpolar solvents but insoluble in water. Many attempts to obtain them as X-ray quality crystals were unsuccessful.

(**P22**)$ZnCl_2$ (**P22**)ZnI_2

1 **2**

The fact that **1** and **2** are molecular entities and not constituents of equilibrium mixtures containing **P22**, Zn^{2+} and Hal^- is not only evident from their insolubility in water, but could also be proved by their ESI mass spectra taken from acetonitrile solutions (see Exp. Sect.), which show the complex constituents but neither the free peptide nor the free zinc halide. The conservation of the peptide structure in the complexes is indicated by the amide-I IR bands which, for both **1** and **2**, are observed at 1655 cm^{-1}, i.e. almost at the same position as that of the free peptide. The CD spectra, displaying the 222 nm maxima with about the same intensities as that of free **P22** (see Figure 1), lead to the same conclusion.

The attachment of the $ZnHal_2$ units to the peptide could clearly be identified by ^1H NMR spectroscopy. While most of the proton resonances remained in place both after deprotonation with ammonia and after addition of the zinc halide (which means that the helical secondary structure is not affected), significant shifts of the histidine imidazole CH resonances were observed. Table 1 lists the four imidazole CH signals for the three states of the peptide. They were assigned by H,H-COSY NMR spectra taken in CD_3CN. Under these conditions the NH resonances could not be observed. Upon deprotonation all four CH signals move to higher field, the successive zinc complexation moves two of them further up but the two others down again. The shifts for the protonation of the uncharged peptide are larger than those for zinc binding. Altogether the NMR spectroscopic data are the clearest indication for the attachment of the $ZnHal_2$ units to both imidazole side chains of the histidine constituents in the 10 and 14 positions. In the absence of X-ray structure data they also provide the main basis for a structural assignment of the complexes.

Table 1. ^1H NMR spectroscopic data for the imidazole CH protons in Peptide **P22**

	CH^2	$CH^{2'}$	CH^4	$CH^{4'}$
protonated	8.02	8.45	7.14	7.21
deprotonated	7.64	7.89	6.58	6.70
$ZnCl_2$ complex	7.85	7.86	6.51	6.77
ZnI_2 complex	7.83	7.86	6.49	6.75

Conclusions

The approach and outcome of this work represent a conceptual difference from previous work on medium-sized peptides and their metal complexes. Both the peptide **P22** and its zinc complexes were designed to be nonpolar molecular entities. This has not only simplified their synthesis and isolation but also made them susceptible to the rules of molecular zinc chemistry. This means that **1** and **2** could be predicted to be stable and inert toward dissociation and that the chelate ligand **P22** and the halide ligands would be an ideal combination for a tetrahedral ZnN_2Hal_2 coordination. The accumulated evidence supports these predictions.

As expected and designed, the peptide **P22** was found to exist in the α-helical form. The usual criteria applied to this − solubility, IR and CD spectra − have confirmed it both for the free peptide and for its complexes with $ZnCl_2$ and ZnI_2. Although NMR spectroscopy has failed to assist in the structural assignment of the peptide, it has shown unambiguously that the $ZnHal_2$ units are attached to the two imidazole side chains of the histidines. As these are placed in the 10 and 14 positions of the peptide they are located one above the other and are separated by one turn of the helix. The identity of both the peptide and its zinc complexes was certified by mass spectra. To the best of our knowledge this is the first time that metal complexes of a medium-sized peptide have been isolated in an analytically pure form and fully characterized.

The available data allowed us to assign the peptide and complex structures with confidence by molecular modelling software. This was done by applying the force field method MM+ of the HYPERCHEM program package.[37] Figure 2 shows the energy-minimized structures of the uncharged peptide and its $ZnCl_2$ complex. It is obvious that only minimal conformational changes are necessary to convert the peptide to the complex. Thus the aims of this investigation − the design of a highly helical peptide with two preorganized binding sites for zinc − have been achieved.

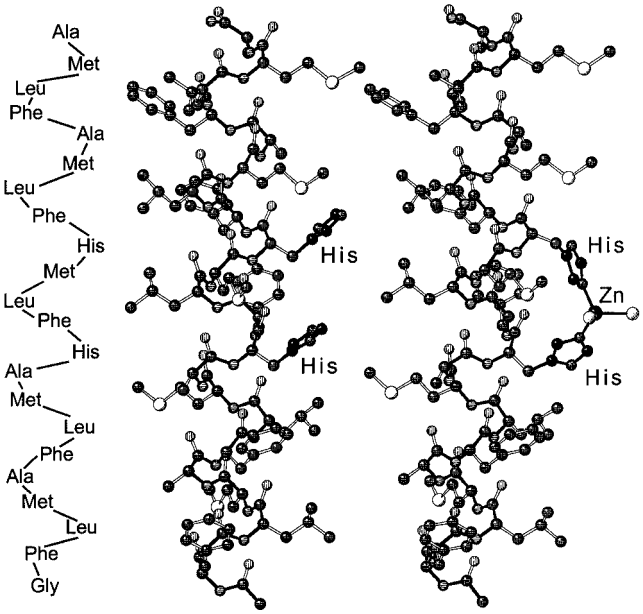

Figure 2. Computed structures[37] of peptide **P22** (left) and its $ZnCl_2$ complex (right); hydrogen atoms omitted, N-terminus at the bottom

Experimental Section

General: All manipulations were performed under an inert gas atmosphere. Starting materials were obtained commercially. IR: Bruker IFS-25 FTIR. NMR: Varian Unity 300 and Bruker Avance DPX 500. CD: Jobin-Yvon CD6. MS: Finnigan TSQ 700. Peptide synthesis: Milligan 9050 Synthesizer, PAL-PEG-PS resin, Fmoc protected L-amino acids, coupling reagent TBTU, for further details see ref.[38] Chromatography: Waters Model 4000, Waters DeltaPak C18 PrepPak reversed phase column. The figure was produced with SCHAKAL.[39]

Peptide P22: This peptide was prepared to order by the Merrifield method at the Institut für Biologie II of Freiburg University. The details of preparation and workup corresponded to the published procedures.[38] The raw product was dissolved in acetonitrile and purified by HPLC using a gradient of acetonitrile/water (75:25 → 100:0) containing 0.1% of HTFA. Retention time: 35 min. After freeze-drying 194 mg (28%) of **P22**·4.8HTFA were obtained as a colorless powder, m.p. 135 °C (dec.) whose HTFA content was determined by potentiometric titration.[16] $C_{128}H_{187}N_{27}O_{23}S_5$·$4.8C_2HF_3O_2$ (2632.38 + 547.31): calcd. C 51.98, H 6.08, N 11.89; found C 51.88, H 6.08, N 11.69. ESI-MS: correct isotope pattern for M^+ from 2630.3 to 2637.3. IR (KBr): $\tilde{\nu}$ = 3299s, 2959w, 2922w, 1658vs, 1543s, 1454w, 1203m (CF), 1174m, 833w, 800w, 701w, 628w cm^{-1}. ^1H NMR (signal ranges) in CD_3CN: δ = 0.74−2.80 (95 H, aliphatic protons), 2.80−3.40 (14 H, β-protons of Phe and His), 3.71 (t, 2 H, CH_2-Gly), 3.78−4.37 (21 H, α-protons), 7.13−7.33 (25 H, Phe-aromatic), 7.20−8.68 (26 H, NH and imidazole-CH).

Complex 1: Ammonia was bubbled for 3 min through a solution of **P22**·4.8HTFA (25 mg, 7.77 μmol) in 15 mL of dry THF. After pumping to remove excessive NH_3 and to reduce the volume to 10 mL, the mixture was filtered through a fine-porosity frit. A 0.01 M solution of anhydrous $ZnCl_2$ in THF (0.78 mL, 7.8 μmol) was then added. Slow evaporation of the solvent left a yellow oil. This was treated several times with a few millilitres of water to remove the remaining ammonia and ammonium salts. After prolonged pumping 21 mg (96%) of **1** remained as a pale yellow powder, m.p. 142 °C (dec.). $C_{128}H_{187}Cl_2N_{27}O_{23}S_5Zn$ (2768.68): calcd. C 54.53, H 6.81, N 13.66, Zn 2.36; found C 54.65, H 6.89, N 12.12, Zn 1.94. ESI-MS: *m*/*z* = 2733 (11) [M − Cl], 2698 (13) [M − 2Cl], 1349 (7) [M − 2Cl]$^{2+}$. IR (KBr): $\tilde{\nu}$ = 3300m, br, 2958w, 2924w, 1655vs, 1541s, 1453w, 1297w, 1129w, 802w, 700w cm^{-1}. ^1H NMR (CD_3CN): identical to **P22** except for the data in Table 1.

Complex 2: Prepared in a similar manner to complex **1** from 25 mg (7.77 μmol) of **P22**·4.8 HTFA and 0.78 mL (7.8 μmol) of a 0.01 M ZnI_2 solution. Yield 22 mg (96%), light brown powder, m.p. 179 °C (dec.). $C_{128}H_{187}I_2N_{27}O_{23}S_5Zn$ (2951.58): calcd. C 52.09, H 6.39, N 11.81, Zn 2.22; found C 49.58, H 6.29, N 11.72, Zn 2.66. ESI-MS: *m*/*z* = 2825 (59) [M − I], 2698 (20) [M − 2I], 1349 (45) [M − 2I]$^{2+}$. IR (KBr): $\tilde{\nu}$ = 3301m, br, 2957w, 2922w, 1655vs, 1540s, 1453w, 1296w, 1114w, 700w cm^{-1}.

Acknowledgments

This work was supported by the Fonds der Chemischen Industrie. We are indebted to Prof. W. Haehnel, Prof. G. Schulz and his group, Drs. R. Vogler, W. Deck, A. Meißner and J. Wörth as well as to Mr. J. Seebacher, Mrs. R. Loyal and Mrs. M. Wagner for help with the preparations and measurements, as well as with interpretations and software applications.

[1] M. Gelinsky, R. Vogler, H. Vahrenkamp, *Inorg. Chem.* **2002**, *41*, 2560−2564.
[2] *Zinc and its Role in Biology and Nutrition* (Ed.: H. Sigel), Marcel Dekker, New York, **1983**. *Zinc Enzymes* (Eds.: I. Bertini, C. Luchinat, W. Maret, M. Zeppezauer), Birkhäuser, Boston, **1986**.
[3] D. W. Christianson, *Adv. Protein Chem.* **1991**, *42*, 281−355. B. L. Valle, D. S. Auld, *Acc. Chem. Res.* **1993**, *26*, 543−551.
[4] G. H. Jacobs, *EMBO J.* **1992**, *11*, 4507−4517.
[5] P. Rhodes, A. Klug, *Sci. Am.* **1993**, *268*, 56−65.
[6] G. Jacobs, G. Michaels, *New Biol.* **1990**, *2*, 583−589.
[7] N. P. Pavletich, C. O. Pabo, *Science* **1991**, *252*, 809−817. N. P. Pavletich, C. O. Pabo, *Science* **1993**, *261*, 1701−1707.
[8] B. A. Krizek, B. T. Amann, V. J. Kilfoil, D. L. Merkle, J. M. Berg, *J. Am. Chem. Soc.* **1991**, *113*, 4518−4523. D. L. Merkle, M. H. Schmidt, J. M. Berg, *J. Am. Chem. Soc.* **1991**, *113*, 5450−5451. B. A. Krizek, J. M. Berg, *Inorg. Chem.* **1992**, *31*, 2984−2986. B. A. Krizek, D. L. Merkle, J. M. Berg, *Inorg. Chem.* **1993**, *32*, 937−940. P. C. Roehm, J. M. Berg, *J. Am. Chem. Soc.* **1998**, *120*, 13083−13087.
[9] J. P. Schneider, J. W. Kelly, *Chem. Rev.* **1995**, *95*, 2169−2187. R. B. Hill, D. P. Raleigh, A. Lombardi, W. F. DeGrado, *Acc. Chem. Res.* **2000**, *33*, 745−754.
[10] M. R. Ghadiri, C. Choi, *J. Am. Chem. Soc.* **1990**, *112*, 1630−1632.
[11] T. Handel, W. F. DeGrado, *J. Am. Chem. Soc.* **1990**, *112*, 6710−6711.
[12] F. Ruan, Y. Chen, P. B. Hopkins, *J. Am. Chem. Soc.* **1990**, *112*, 9403−9404.
[13] L. Regan, N. D. Clarke, *Biochemistry* **1990**, *29*, 10878−10883. M. Klemba, L. Regan, *Biochemistry* **1995**, *34*, 10094−10100.
[14] M. Klemba, K. H. Gardner, S. Marino, N. D. Clarke, L. Regan, *Nature Struct. Biol.* **1995**, *2*, 368−373.
[15] G. Impellizeri, G. Pappalardo, R. Purrello, E. Rizzarelli, *Chem. Eur. J.* **1998**, *4*, 1791−1798.
[16] C. A. Blasie, J. M. Berg, *Inorg. Chem.* **2000**, *39*, 348−351.
[17] G. Platt, C. W. Chung, M. S. Searle, *Chem. Commun.* **2001**, 1162−1163.
[18] A. Meißner, W. Haehnel, H. Vahrenkamp, *Chem. Eur. J.* **1997**, *3*, 261−267.
[19] P. Gockel, M. Gelinsky, R. Vogler, H. Vahrenkamp, *Inorg. Chim. Acta* **1998**, *272*, 115−124.
[20] R. Vogler, H. Vahrenkamp, *Eur. J. Inorg. Chem.* **2002**, 761−766.
[21] A. J. Doig, R. L. Baldwin, *Protein Sci.* **1995**, *4*, 1325−1336.
[22] P. Y. Chou, G. D. Fasman, *Biopolymers* **1974**, *13*, 211−222.
[23] P. C. Lyu, M. I. Liff, L. A. Marky, N. R. Kallenbach, *Science* **1990**, *250*, 669−673.
[24] S. Padmanabhan, S. Marquesee, T. Ridgeway, T. M. Laue, R. L. Baldwin, *Nature* **1990**, *344*, 268−270.
[25] K. T. O'Neil, F. W. DeGrado, *Science* **1990**, *250*, 646−650.
[26] C. A. Rohl, J. M. Scholtz, E. J. York, J. M. Stewart, R. L. Baldwin, *Biochemistry* **1992**, *31*, 1263−1269.
[27] V. Muñoz, L. Serrano, *Biopolymers* **1997**, *41*, 495−509. Computations were performed via the Internet at www.embl.heidelberg.de/services/serrano/agadir/agadir-start-html.
[28] R. Katakai, *Biopolymers* **1986**, *25*, 1−4.
[29] P. I. Harris, D. Chapman, *Biopolymers* **1995**, *37*, 251−263.
[30] Y. H. Chen, J. T. Yang, K. H. Chau, *Biochemistry* **1974**, *13*, 3350−3359.
[31] T. Sugihara, E. R. Blout, B. A. Wallace, *Biochemistry* **1982**, *21*, 3444−3452. J. W. Nelson, N. R. Kallenbach, *Biochemistry* **1989**, *28*, 5256−5261.
[32] J. S. Johannson, B. R. Gibney, J. J. Skalicky, A. J. Wand, P. L. Dutton, *J. Am. Chem. Soc.* **1998**, *120*, 3881−3886.
[33] T. Asakura, K. Taoka, M. Demura, M. P. Williamson, *J. Biomol. NMR* **1995**, *6*, 227−236. D. S. Wishart, C. G. Brigham, A. Holm, R. S. Hodges, B. D. Sykes, *J. Biomol. NMR* **1995**, *5*, 67−81.

[34] A. A. Vinogradov, F. Mari, R. E. Humphreys, G. E. Wright, *Int. J. Pept. Protein Res.* **1996**, *47*, 467−476. J. Kemmink, R. M. Shreek, *J. Biomol. NMR* **1995**, *6*, 33−40.
[35] L. Harper, B. T. Aman, V. K. Wilson, J. M. Berg, *J. Am. Chem. Soc.* **1993**, *115*, 2577−2580.
[36] M. Förster, H. Vahrenkamp, *Chem. Ber.* **1995**, *128*, 541−550. M. Förster, I. Brasack, A. K. Duhme, H. F. Nolting, H. Vahrenkamp, *Chem. Ber.* **1996**, *129*, 347−353.
[37] HYPERCHEM™ Release 4.0 for Windows, Hypercube Inc., **1994**.
[38] H. K. Rau, W. Haehnel, *J. Am. Chem. Soc.* **1998**, *120*, 468−476.
[39] E. Keller, SCHAKAL for Windows, Universität Freiburg, **1998**.

Received February 7, 2002
[I02067]

Preparation, Crystal and Magnetic Structure of the Double Perovskites Ba_2CoBO_6 (B = Mo, W)

María J. Martínez-Lope,[a] José A. Alonso,*[a] María T. Casais,[a] and María T. Fernández-Díaz[b]

Keywords: Perovskite structure / Neutron diffraction / Magnetic properties / Antiferromagnetic ordering / Cobalt

Ba_2CoBO_6 (B = Mo, W) perovskites have been prepared in polycrystalline form by thermal treatment, in air, of previously decomposed citrate precursors. These materials have been characterized by X-ray (XRD) and neutron powder diffraction (NPD) data and magnetization measurements. At room temperature, the crystal structure is cubic, space group $Fm\bar{3}m$, with a = 8.08623(3) and 8.10799(3) Å for the Mo and W compounds, respectively. The crystal contains alternating CoO_6 and $Mo(W)O_6$ octahedra, with an almost negligible anti-site disordering. The low temperature antiferromagnetic ordering has been followed from sequential neutron diffraction data. Peaks of magnetic origin appear at the NPD patterns below temperatures of T_N = 27 K and T_N = 19 K for the Mo and W compounds, respectively. The magnetic structures are both defined by a propagation vector k = (1/2, 1/2, 1/2). They can be described as an array of ferromagnetic layers of Co moments, perpendicular to the [111] directions, coupled antiferromagnetically. The refined magnitude of the Co^{2+} magnetic moments suggests a high-spin electronic configuration (S = 3/2); covalence effects account for the slight reduction in the low-temperature ordered moments, although this effect is minimized for the W compound. Structural and magnetic features are discussed in relation to the chemical nature of the species present in the solids.
(© Wiley-VCH Verlag GmbH, 69451 Weinheim, Germany, 2002)

Introduction

The description of colossal magnetoresistance (CMR) properties in perovskite-related materials has triggered a revival of interest in transition metal oxides in an effort to optimize the observed CMR properties and to understand the involved mechanisms. CMR materials undergo a large change in electrical resistance in response to an external magnetic field. In these compounds, the applied field tends to align the local spins and hence leads to a rapid drop of the measured resistivity by suppressing spin fluctuations and enhancing electronic transfer. CMR was first reported in $LaMnO_3$ perovskite derivatives; further research demonstrated that it is also present in a range of compounds, most of them exhibiting ferromagnetic and semimetallic characteristics simultaneously.[1,2] It is well established now that the ferromagnetic Curie temperature of mixed-valence manganites (based upon $LaMnO_3$) cannot be increased above 400 K by any chemical substitution. Materials with a substantially higher T_c must be developed to operate in a useful temperature range around room temperature.

Recently, the double perovskite Sr_2FeMoO_6 has been proposed as a half-metallic ferromagnet and an alternative to perovskite manganites.[3−7] Further studies on other double perovskites seem to indicate that the occurrence of MR properties is a common feature in some of them. The A = Ca, Ba analogues of the A_2FeMoO_6 family were also found to exhibit semimetallic and ferromagnetic properties.[8,9] Furthermore, Sr_2FeReO_6 has[10] an electronic structure similar to that of Sr_2FeMoO_6: these results have expanded the options for optimizing CMR properties for specific technological applications, searching in other members of the wide family of perovskites of composition $A_2B'B''O_6$ (A: alkaline earth metal; B′, B″: transition metals).

We have become interested in revisiting other transition metal double perovskites, prepared in the Sixties and forgotten for more than 30 years. We have chosen the Co derivatives in the series A_2CoBO_6 (A = Ba, Sr; B = Mo, W). Recently, we described CMR properties in conveniently reduced $Sr_2CoMoO_{6-\delta}$;[11] we have now focused our attention on the Ba derivatives. There is very little literature concerning these phases. Ba_2CoBO_6 (B = Mo, W) perovskites were first studied in the sixties.[12−15] The crystal structure of the Mo phase was described as cubic (with a = 4.043 Å) assuming a random distribution of Co and Mo cations. The W compound was also reported to be cubic, with a = 8.098 Å, exhibiting an ordered $(NH_4)_3FeF_6$ crystal structure. There are a few studies on their magnetic properties;[16−18] Ba_2CoWO_6 was reported to be an antiferromagnet with T_N = 17 K.[16] Its magnetic structure was also studied by

[a] Instituto de Ciencia de Materiales de Madrid, C.S.I.C., Cantoblanco, 28049 Madrid, Spain
[b] Institut Laue-Langevin, B. P. 156, 38042 Grenoble Cedex 9, France

neutron diffraction at 4.2 K,[19] and described as ferromagnetic [111] Co layers coupled antiparallel to adjacent Co layers. There are no reports on the magnetic structure of the Mo compound.

In the present work we describe the synthesis of Ba_2CoBO_6 (B = Mo, W), prepared by soft chemistry procedures, and the results of a neutron diffraction (NPD) study on well-crystallized samples. The crystal structure has been revisited; we report complete structural data for these perovskites. The magnetic data suggest the presence of an unquenched orbital contribution to the effective magnetic moment. Low temperature NPD data allowed us to probe the microscopic origin of the antiferromagnetic ordering, and the evolution of the ordered Co^{2+} magnetic moments.

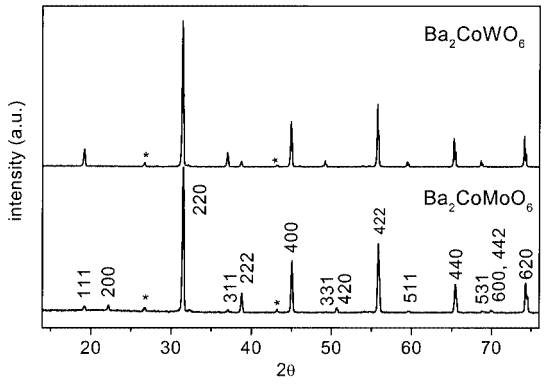

Figure 1. XRD patterns for Ba_2CoBO_6 (B = Mo, W), indexed in a cubic unit cell with $a = 2a_0$, $a_0 \approx 4$ Å; the asterisks indicate the main reflections of the $BaBO_4$ impurity phases

Results

The perovskites Ba_2CoBO_6 (B = Mo, W) were obtained as well crystallized powders; the XRD diagrams are shown in Figure 1. The patterns are characteristic of perovskite structures, showing superstructure peaks (with odd indices) corresponding to the Co/B (B = Mo, W) ordering. The superstructure peaks are more intense in the W compound, due to the higher difference in scattering power with respect to Co. Minor amounts of $BaBO_4$ (B = Mo, W) were detected from both XRD and NPD data; the main reflections of the impurities are indicated with a star in Figure 1.

Magnetic Data

The magnetic susceptibility vs. temperature data for Ba_2CoBO_6 (B = Mo, W) are displayed in Figure 2. The susceptibility exhibits, in both cases, a low temperature maximum, at $T_N = 20$ K and 17 K for B = Mo, W, respectively.

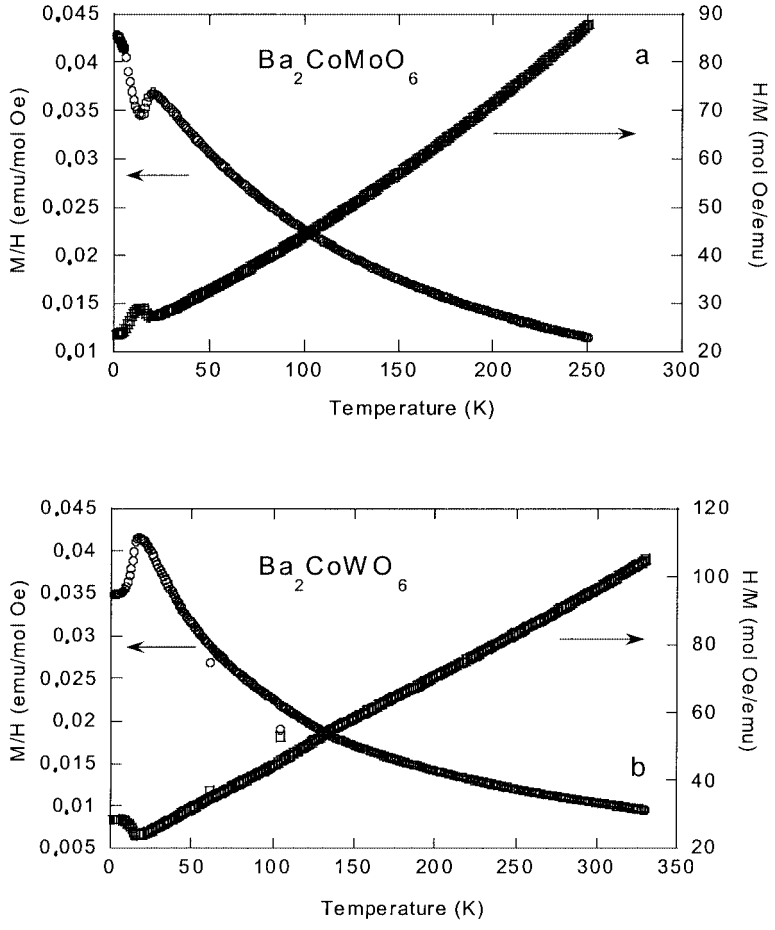

Figure 2. Thermal evolution of the magnetic susceptibility (left axes) and the reciprocal susceptibility (right axes) for (a) Ba_2CoMoO_6 and (b) Ba_2CoWO_6

These maxima correspond to the transition from the high-temperature paramagnetic state to a low-temperature antiferromagnetically ordered phase. A similar Néel temperature (17 K) has been reported for the B = W compound.[17] The reciprocal susceptibility data above T_N (right axes of Figure 2) show a slight curvature, probably due to crystal field effects or a progressive change in the population of the low-spin vs. high-spin electronic configurations for Co cations. A tentative Curie−Weiss fit above 100 K gives paramagnetic moments of 5.24 μ_B/f.u. (f.u. = formula unit) and 5.58 μ_B/f.u. for B = Mo and W, respectively. These values are much larger than expected for spin only Co^{2+}/Mo^{6+} (in any spin configuration for Co^{2+}). This point will be discussed in detail later. The Weiss temperatures of −47.1 K and −75.2 K for B = Mo, W, respectively, confirm the presence of antiferromagnetic interactions in the paramagnetic region. The magnetization vs. field data displayed in Figure 3 are also characteristic of antiferromagnetically ordered systems. The field evolution of the magnetization at 5 K is perfectly linear, excluding the presence of any weak ferromagnetic effect.

Structural Refinement

The structural refinement from room temp. high resolution NPD data was performed in the $Fm\bar{3}m$ space group (No. 225), $Z = 4$, with unit-cell parameters related to a_0 (ideal cubic perovskite, $a_0 \approx 4$ Å) as $a = b = c = 2a_0$. The Ba atoms were located at *8c* positions, Co at *4a*, Mo or W at *4b* sites, and oxygen atoms at *24e* positions. Minor impurities of $BaBO_4$ (B = Mo, W) were included in the refinement as second phases, defined in the space group $I4_1/a$. From the scale factors, the amount of impurity phase is 4.5% and 5.2% for Mo and W, respectively. An excellent fit was obtained for this model, as shown in Figure 4. In the final refinement, the possibility of anti-site disordering was checked by assuming that some Co atoms could occupy Mo or W sites, and vice versa: the refinement of the inversion degree led to less than 1% of anti-site disordering. The oxygen stoichiometry was also checked by refining its occupancy factors; no deficiency was detected within the standard deviations. The most important structural parameters of the crystallographic

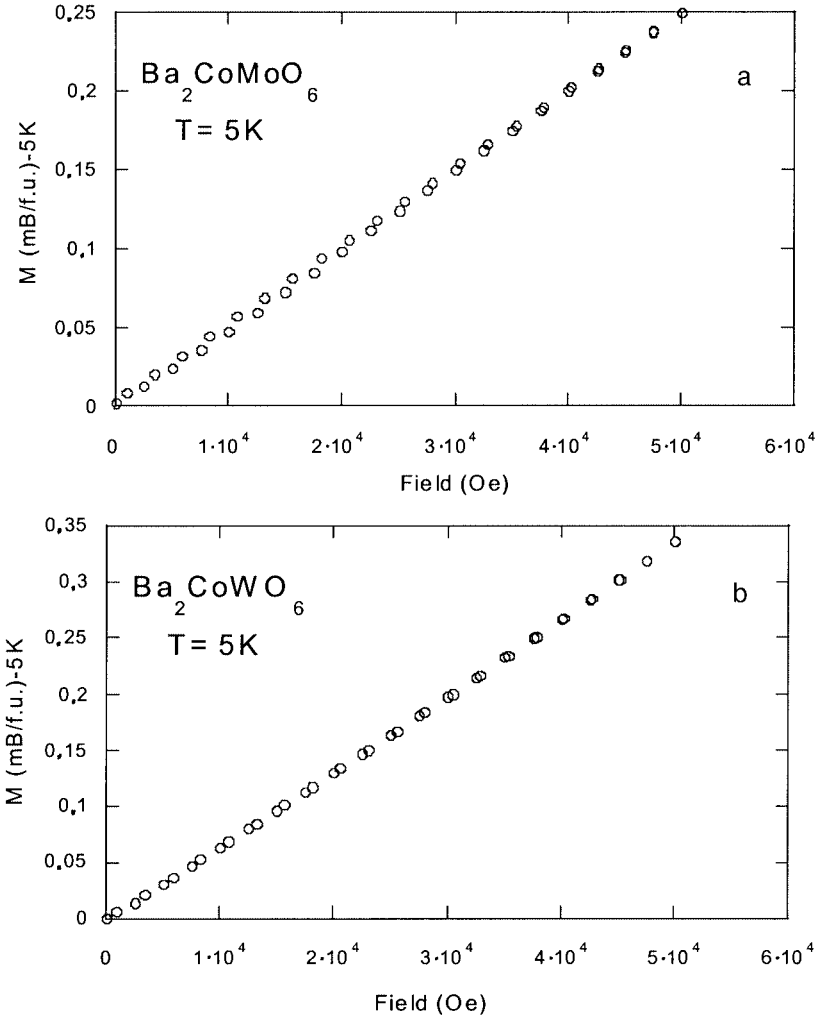

Figure 3. Magnetization vs. field plots for (a) Ba_2CoMoO_6 and (b) Ba_2CoWO_6

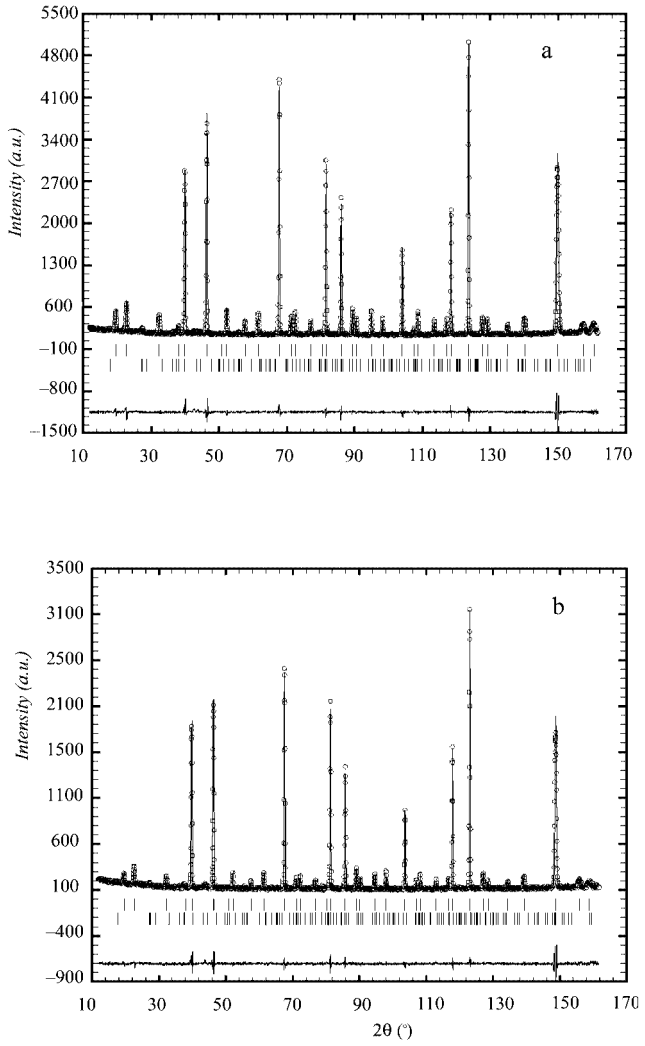

Figure 4. Observed (crosses), calculated (full line) and difference (bottom) high resolution NPD Rietveld profiles for Ba_2CoBO_6 at 295 K for (a) B = Mo, (b) B = W; the second series of tick marks correspond to the Bragg reflections of the $BaBO_4$ impurity phase

structure at room temp. and the discrepancy factors after the refinements are listed in Table 1. The main interatomic distances and angles are included in Table 2. A view of the crystal structure is shown in Figure 5.

The cubic unit cell of Ba_2CoWO_6 is slightly larger than that of Ba_2CoMoO_6, as expected for the larger ionic radius of W^{6+} (0.60 Å) versus Mo^{6+} (0.59 Å) in octahedral coordination.[20] It is interesting to note the significant expansion of the Co−O interatomic distances (Table 2) from the Mo compound [Co−O: 2.114(1) Å] to the W perovskite [Co−O: 2.129(1) Å]. This expansion of Co−O bond lengths is a result of the competing interactions of Co−O and B−O (B = Mo, W) bonds through common oxygens; the higher electronegativity of W than Mo accounts for a more covalent (or less ionic) W−O bond and a weakening of the Co−O chemical bonding in Ba_2CoWO_6.

Magnetic Structure

The magnetic structure of Ba_2CoMoO_6 and its thermal evolution was analyzed by considering a set of NPD patterns collected in the range $2 < T < 72$ K with $\lambda = 2.42$ Å. On decreasing the temperature below 27 K, new reflections appear at positions forbidden for the Bragg reflections in the space group $Fm\bar{3}m$. These new peaks correspond to magnetic satellites defined by the propagation vector $k = (1/2, 1/2, 1/2)$. An antiferromagnetic structure was modeled with magnetic moments at the Co positions; after the full refinement of the profile, including the magnetic moment

Table 1. Unit cell, positional and thermal parameters for Ba_2CoBO_6 (B = Mo, W) in the cubic $Fm\bar{3}m$ space group, from NPD data at 295 K

	B = Mo	B = W
$a = b = c$ (Å)	8.08623(3)	8.10799(3)
V (Å^3)	528.734(3)	533.015(4)
Ba *8c* (1/4, 1/4, 1/4)		
B (Å^2)	0.40(2)	0.37(2)
Co *4a* (0, 0, 0)		
B (Å^2)	0.68(7)	0.54(8)
B *4b* (1/2, 0, 0)		
B (Å^2)	0.24(2)	0.22(4)
O *24e* (x, 0, 0)		
x	0.2614(1)	0.2625(1)
B (Å^2)	0.59(1)	0.52(1)
Reliability factors		
R_p (%)	4.26	4.54
R_{wp} (%)	5.76	6.03
R_{exp} (%)	3.69	4.41
χ^2	2.43	1.87
R_I (%)	2.08	2.04

Table 2. Main bond lengths (Å) and selected angles (°) for cubic Ba_2CoBO_6 (B = Mo, W) determined from NPD data at 295 K

	B = Mo	B = W
Ba−O1 (×12)	2.8604(7)	2.8684(6)
Co−O1 (×6)	2.114(1)	2.1288(8)
B−O1 (×6)	1.930(1)	1.9252(8)
Co−O1−B	180.0	180.0
O1−Co−O1	90.0	90.0
O1−B−O1	90.0	90.0

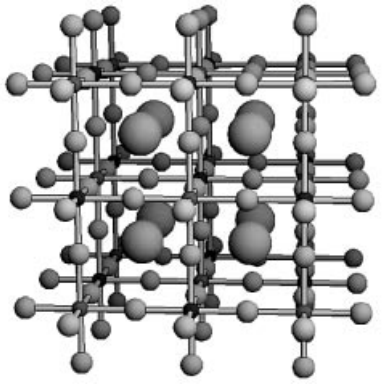

Figure 5. A view of the crystal structure of the Ba_2CoMoO_6 double perovskite; each CoO_6 octahedron is linked to six MoO_6 octahedra

magnitude, a discrepancy factor R_{mag} of 10.6% was reached for the 2 K diagram, collected with a longer counting time. The determination of the orientation of the moments is not possible in a cubic structure from powder data. We supposed that the moments are lying along the [001] direction. The magnetic structure is stable from 2 K to T_N, as demonstrated in a sequential refinement in all the available temperature range. The thermal evolution of the magnetic moments at the Co positions and the lattice parameter are shown in Figure 6 and 7. The good agreement between the observed and calculated pattern at $T = 2$ K is illustrated in Figure 8a. For Ba_2CoWoO_6, the magnetic reflections appear at temperatures below $T_N = 19$ K; these reflections can be indexed with the same propagation vector $k = (1/2, 1/2, 1/2)$. After the refinement of the antiferromagnetic structure, a discrepancy factor of $R_{mag} = 13.6\%$ was obtained. The evolution of the magnetic moments and a unit-cell parameter with temperature are displayed in Figure 6b and 7b; the goodness of the fit at 2 K, including the magnetic structure, is depicted in Figure 8b. A view of the magnetic structure for both materials is shown in Figure 9. It consists of ferromagnetic layers of Co moments, perpendicular to the [111] directions, coupled antiferromagnetically. This magnetic structure compares well with that determined by Cox et al. for Ba_2CoWO_6.[19]

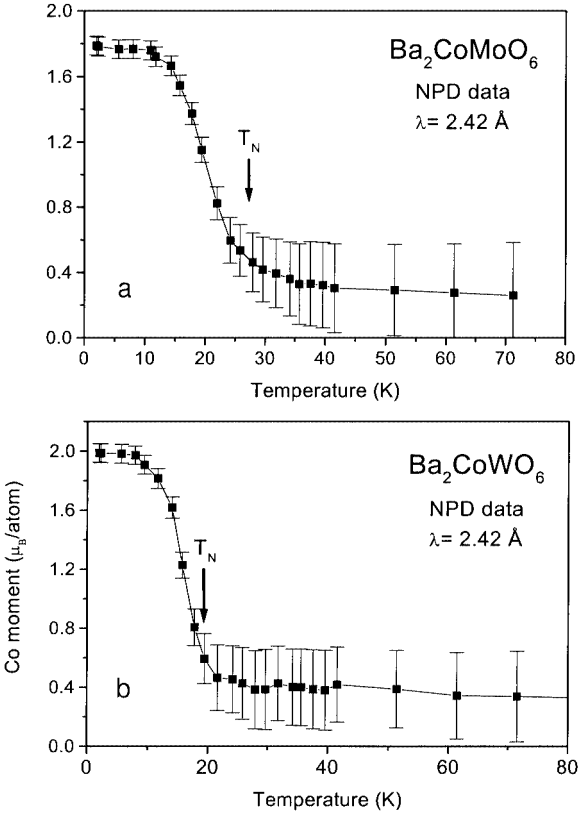

Figure 6. Thermal variation of the ordered Co magnetic moment for the antiferromagnetic structure of Ba_2CoBO_6: (a) B = Mo (b) B = W

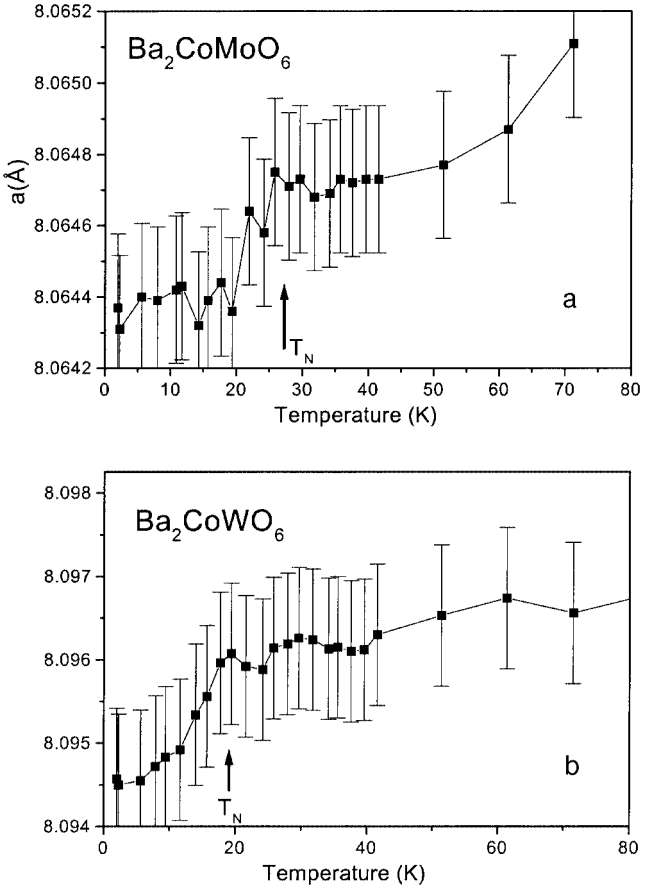

Figure 7. Thermal variation of the a unit-cell parameter for Ba_2CoBO_6: (a) B = Mo (b) B = W

Discussion

Ba_2CoMoO_6 and Ba_2CoWO_6 adopt the well-known $(NH_4)_3FeF_6$ structure, corresponding to a perfect 1:1 B-site ordering, due to the large differences in charge existing between Co^{2+} and $Mo(W)^{6+}$ cations. The refinement of a possible inversion or anti-site disordering confirms an almost complete ordering degree between both cations. A bond valence calculation[21] from the observed bond lengths can give some insight into the actual oxidation states of the different cations present in the crystal structures. In Ba_2CoMoO_6, the calculated valences for Ba, Co and Mo are 2.57, 1.93 and 5.61, respectively; in Ba_2CoWO_6 the calculated valences for Ba, Co and W are 2.51, 1.85 and 5.85, respectively. In both compounds the Ba cations seem to be significantly overbonded, exhibiting valences much higher than the expected 2+ value. In fact, the observed Ba−O distances are much shorter (Table 2) than expected from the sum of the ionic radii (2.95 Å). It seems that the much more covalent network determined by CoO_6 octahedra and BO_6 octahedra (B = Mo, W) mainly determines the size of the unit cell; the low degree of freedom of this cubic crystallographic structure constrains the Ba−O bond lengths outside of the

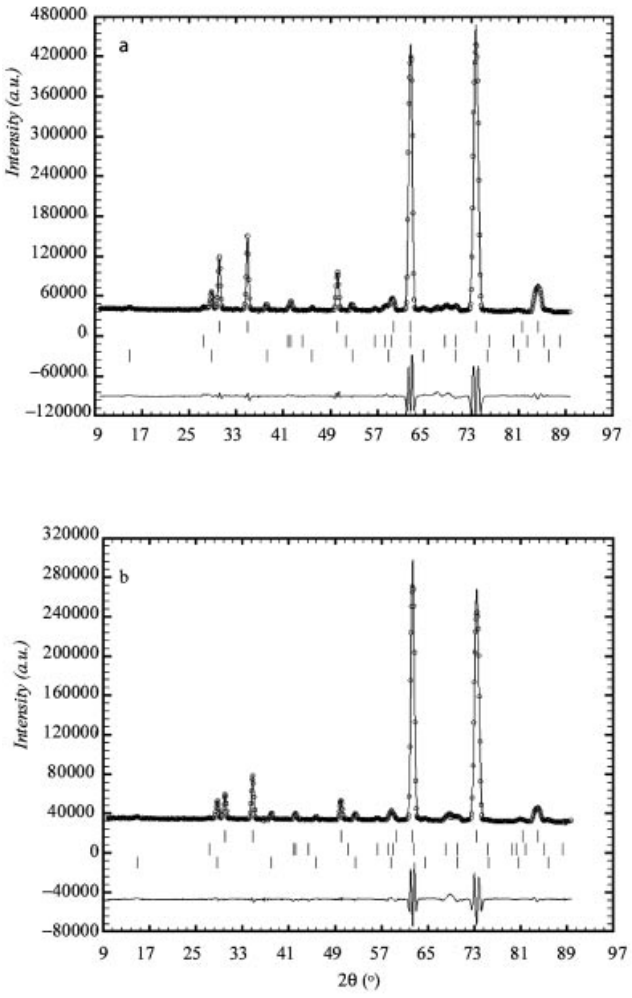

Figure 8. Observed (solid circles), calculated (solid line) and difference (bottom line) NPD patterns collected at 2 K with λ = 2.42 Å; the two series of tick marks correspond to the crystallographic and magnetic Bragg reflections: (a) Ba_2CoMoO_6 (b) Ba_2CoWO_6

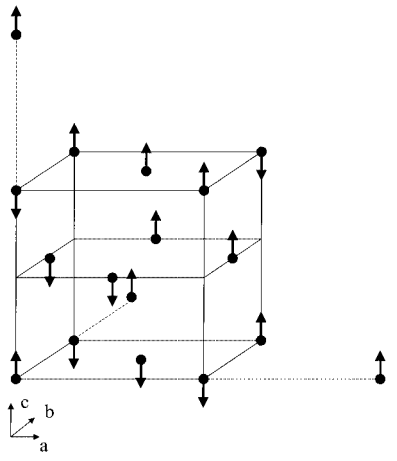

Figure 9. A sketch of the magnetic structure for k = (1/2, 1/2, 1/2); for the sake of clarity, the figure shows the chemical cell ($a \approx 8$ Å) and a part of three adjacent cells

optimal values. This is not an isolated behavior; in many other double perovskites, the Ba−O bond lengths exhibit values within a wide range: for instance, the Ba−O distances range from 2. 85 Å for Ba_2NiWO_6 to 2.96 Å for Ba_2CdWO_6. The valences for Co and Mo(W), although slightly lower than expected, suggest the divalent and hexavalent oxidation states for both cations, respectively.

In relation to the electronic configurations of the B cations, the comparison with Sr_2FeMoO_6 (prepared under reducing conditions and showing half-metallic and ferromagnetic properties) is enlightening: although the actual electronic configurations $Fe^{3+}(3d^5)$-$Mo^{5+}(4d^1)$ vs. $Fe^{2+}(3d^6)$-$Mo^{6+}(4d^0)$ have been considered as possible, the average valence for Fe has been found to be intermediate between high-spin configuration values of Fe^{2+} and Fe^{3+} from Mössbauer spectroscopy studies.[22] The case of $Ba_2Co(Mo,W)O_6$ is rather different: from the chemical point of view, the preparation in air suggests a hexavalent oxidation state for Mo cations, with the Co cations being divalent. From this chemical point of view, the electronic configuration $Co^{2+}(3d^7)$-$Mo(W)^{6+}(4d^0)$ seems to be more probable than $Co^{3+}(3d^6)$-$Mo(W)^{5+}(4d^1)$, although a slight degree of dynamic electron transfer between Co and Mo cations should not be excluded in view of the bond valence results.

To account for the results from the magnetic susceptibility data, the electronic configuration $Co^{2+}(3d^7)$-$Mo^{6+}(4d^0)$ requires a completely unquenched orbital contribution for the high-spin Co^{2+} cation, which would explain the large effective moment obtained in the paramagnetic region, well above T_N, of 5.24 μ_B/f.u. and 5.58 μ_B/f.u for B = Mo, W. Recently, Primo-Martín et al.[23] studied the $Sr_3CoSb_2O_9$ double perovskite, with an effective moment of 5.39 μ_B and also proposed a high-spin Co^{2+} configuration with a completely unquenched orbital contribution ($^4T_{1g}$ term). This is not an isolated observation; many Co^{2+} compounds show effective moments between 3.87 μ_B (spin only) and 5.20 μ_B (spin plus completely unquenched orbital contribution);[24,25] some examples are CoF_2 (μ_{eff} = 5.15 μ_B) or CoO (μ_{eff} = 5.1 μ_B).

In relation to the ordered magnetic moment obtained for Co cations from the refinement of the magnetic structure at 2 K, it seems to saturate at a value close to 2 μ_B, for both compounds with B = Mo, W. Again, this suggests a high spin configuration for the Co^{2+} cations ($t_{2g}^5\ e_g^2$, S = 3/2) as a low-spin configuration would imply S = 1/2. The reduction of the saturation moment with respect to the expected value of 3 μ_B is believed to be due to covalence effects. In fact, the ordered moment is slightly higher for the W compound (Figure 6): this is related to the increase in Co−O atomic distances (as commented above) and a decrease of the orbital overlapping and covalence effects.

Finally, the thermal evolution of the unit cell parameters (Figure 7) seems to indicate a contraction of the unit-cell size at the onset of the antiferromagnetic ordering for both compounds; this effect suggests the possibility of a magneto-elastic coupling, which has not been described before for antiferromagnetic double perovskites. This effect is not common in magnetic oxides, unless the magnetic transition is associated with an electronic fluctuation which is responsible for the change in bonding strength between the metallic element and oxygen; a paradigmatic example is

that of the $RNiO_3$ perovskites,[26] where the AFM transition is coupled with a metal-insulator transition and a dramatic contraction in unit-cell volume is observed upon electron delocalization. The present magneto-volume effect suggests a subtle change in the electron localization concomitant with the AFM transition in the Ba_2CoBO_6 double perovskites.

Conclusions

The study of the crystallographic structure of the double perovskites Ba_2CoMoO_6 and Ba_2CoWO_6 from neutron powder diffraction data allowed us to determine subtle structural features relating the Co−O bond lengths and ordered magnetic moments with the chemical environment in the crystals; the larger electronegativity for W in front of Mo accounts for a more ionic, weaker Co−O bond with a larger magnetic moment for Co in Ba_2CoWO_6. These compounds experience a low-temperature antiferromagnetic ordering characterized by an isotropic propagation vector k = (1/2, 1/2, 1/2), giving rise to antiferromagnetic couplings between each Co moment and the six nearest neighbors. It seems clear that the Co ions adopt a divalent oxidation state, in a high-spin configuration. A completely unquenched orbital contribution for the Co^{2+} cation is necessary to account for the large effective moment obtained in the paramagnetic region A magneto-elastic effect observed at the onset of the antiferromagnetic ordering is unusual in completely localized oxides, suggesting a certain degree of electron itinerancy in these compounds.

Experimental Section

Ba_2CoBO_6 (B = Mo, W) perovskites were prepared as black (B = Mo) or brown (B = W) polycrystalline powders from citrate precursors obtained by soft chemistry procedures. Stoichiometric amounts of analytical grade $Ba(NO_3)_2$, $Co(NO_3)_2{\cdot}6H_2O$, $(NH_4)_6Mo_7O_{24}{\cdot}4H_2O$ or $H_{26}N_6O_{41}W_{12}{\cdot}18H_2O$ were dissolved in citric acid. The citrate + nitrate solutions were slowly evaporated, leading to organic resins containing a random distribution of the involved cations at an atomic level. These resins were first dried at 120 °C and then slowly decomposed at temperatures up to 600 °C. All the organic materials and nitrates were eliminated in a subsequent treatment at 800 °C in air, for 2 hours. This treatment gave rise to highly reactive precursor materials. Afterwards, the resulting black or brown powders were treated at 1100 °C in air for 12 hours.

The initial characterization of the products was carried out by laboratory X-ray diffraction (XRD) (Cu-K_α, λ = 1.5406 Å). Neutron powder diffraction (NPD) diagrams were collected at the Institut Laue-Langevin (ILL) in Grenoble (France). The crystallographic structures were refined from the high resolution NPD patterns, acquired at room temperature at the D2B diffractometer with λ = 1.594 Å. For the determination of the magnetic structures and the study of their thermal variation, a series of NPD patterns were obtained at the D20 high-flux diffractometer (ILL, Grenoble) with a wavelength of 2.42 Å, in the temperature range from 2 to 72 K for B = Mo and 2 to 99 K for B = W. The refinements of both crystal and magnetic structures were performed by the Rietveld method, using the FULLPROF refinement program.[27] A pseudo-Voigt function was chosen to generate the line shape of the diffraction peaks. The coherent scattering lengths for Ba, Co, Mo, W and O were 5.07, 2.49, 6.72, 4.86 and 5.803 fm, respectively. The magnetic form factor considered for the Co^{2+} cation was determined with the coefficients taken from the International Tables of Crystallography. The *dc* magnetic susceptibility was measured with a commercial SQUID magnetometer on powdered samples, in the temperature range 1.5 to 250 K (B = Mo) and 330 K (B = W).

Acknowledgments

We thank the financial support of CICyT to the project MAT2001-0539, and we are grateful to ILL for making all facilities available.

[1] A. P. Ramirez, *J. Phys.: Condens. Matter* **1997**, *9*, 8171.
[2] *Colossal Magnetoresistance and Other Related Properties in 3d Oxides* (Eds.: C. N. R. Rao, B. Raveau), World Scientific: Singapore, **1998**.
[3] K.-I. Kobayashi, T. Kimura, H. Sawada, K. Terakura, Y. Tokura, *Nature* **1998**, *395*, 677.
[4] B. García-Landa, C. Ritter, M. R. Ibarra, J. Blasco, P. A. Algarabel, R. Mahendiran, J. García, *Solid State Commun.* **1999**, *110*, 435.
[5] A. Maignan, B. Raveau, C. Martin, M. Hervieu, *J. Solid State Chem.* **1999**, *144*, 224.
[6] K.-I. Kobayashi, T. Kimura, Y. Tomioka, H. Sawada, K. Terakura, Y. Tokura, *Phys. Rev. B* **1999**, *59*, 11159.
[7] T. H. Kim, M. Uehara, S-W. Cheong, S. Lee, *Appl. Phys. Lett.* **1999**, *74*, 1737.
[8] J. A. Alonso, M. T. Casais, M. J. Martínez-Lope, J. L. Martínez, P. Velasco, A. Muñoz, M. T. Fernández-Díaz, *Chem. Mat.* **2000**, *12*, 161.
[9] C. Ritter, M. R. Ibarra, L. Morellón, J. García, J. M. De Teresa, *J. Phys.: Condens. Matter* **2000**, *12*, 8295.
[10] W. Prellier, W. Smolyaninova, A. Bisbas, C. Galley, R. L. Greene, K. Ramesha, J. Golapakrishnan, *J. Phys.: Condens. Matter* **2000**, *12*, 965.
[11] M. C. Viola, M. J. Martínez-Lope, J. A. Alonso, P. Velasco, J. L. Martínez, J. C. Pedregosa, R. E. Carbonio, M. T. Fernández-Díaz, *Chem. Mat.* **2002**, *14*, 812−818.
[12] F. Galasso, *Structure, Properties and Preparation of Perovskite-Type Compounds*, Pergamon Press, Oxford **1969**.
[13] F. J. Fresia, L. Katz, R. Ward, *J. Am. Chem. Soc.* **1959**, *81*, 4783.
[14] L. J. Brixner, *Phys. Chem.* **1960**, *64*, 165.
[15] Landolt-Bornstein, *Zahlenwerte und Funktionen aus Naturwissenschaften und Technik*, Neue Serie, Band 4, Teil a, Springer-Verlag, Berlin **1970**.
[16] G. Blasse, *Proc. Int. Conf. Mag. Nottingham* 1964, p. 350, Inst. Phys. London **1965**.
[17] A. Bokov, *Soviet Phys.-Solid State (English Trans.)* **1972**, *15*, 400.
[18] B. Khattak, *Mater. Res. Bull.* **1975**, *10*, 1343.
[19] D. E. Cox, G. Shirane, B. C. Frazer, *J. Appl. Phys.* **1967**, *38*, 1459.
[20] R. D. Shannon, *Acta Crystallogr., Sect. A* **1976**, *32,* 751.
[21] N. E. Brese, M. O'Keefe, *Acta Crystallogr., Sect. B* **1991**, *47*, 192.
[22] J. Linden, T. Yamamoto, M. Karppinen, H. Yamauchi, T. Pietari, *Appl. Phys. Lett.* **2000**, *76*, 2925.
[23] V. Primo-Martín, M. Jansen, *J. Solid State Chem.* **2001**, *157*, 76.
[24] R. J. Radwanski, Z. Ropka, *Physica B* **2000**, 281&282, 507.
[25] A. Mahendra, D. C. Khan, *Phys. Rev. B* **1971**, *4*, 3901.
[26] J. L. García-Muñoz, J. Rodríguez-Carvajal, P. Lacorre, J. B. Torrance, *Phys. Rev. B* **1992**, *46*, 4414.
[27] J. Rodríguez-Carvajal, *Physica B* (Amsterdam) **1993**, *192*, 55.

Received January 29, 2002
[I02047]

New Group 4 Metallocene and Niobocene Complexes Containing Phosphane-Functionalized *ansa*-Ligands

Antonio Antiñolo,[a] Rafael Fernández-Galán,[a] Irache Orive,[a] Antonio Otero,*[a] and Sanjiv Prashar[b]

Keywords: Metallocenes / Niobium / Phosphane ligands / Homogeneous catalysis / Insertion

The asymmetric *ansa*-ligand precursors $Me_2Si(C_5Me_4H)(C_5H_4R)$ [R = $CH_2CH_2PPh_2$ (**1**), PPh_2 (**2**)] and their lithium derivatives $Li_2\{Me_2Si(C_5Me_4)(C_5H_3R)\}$ [R = $CH_2CH_2PPh_2$ (**3**), PPh_2 (**4**)] have been prepared. The group 4 metal *ansa* complexes $[M\{Me_2Si(\eta^5\text{-}C_5Me_4)(\eta^5\text{-}C_5H_3R)\}Cl_2]$ [M = Ti, R = $CH_2CH_2PPh_2$ (**5**), PPh_2 (**6**); M = Zr, R = $CH_2CH_2PPh_2$ (**7**), PPh_2 (**8**); M = Hf, R = $CH_2CH_2PPh_2$ (**9**), PPh_2 (**10**)] were obtained by the reaction of $[TiCl_4(THF)_2]$ or MCl_4 (M = Zr or Hf) and the corresponding lithiated *ansa* derivative. The reaction of complexes **7** and **8** with two equivalents of MgMeCl led to the formation of the alkyl complexes $[Zr\{Me_2Si(\eta^5\text{-}C_5Me_4)(\eta^5\text{-}C_5H_3R)\}Me_2]$ [R = $CH_2CH_2PPh_2$ (**11**), PPh_2 (**12**)]. Methyl abstraction from **11** and **12** with $B(C_5F_6)_3$ gave the cationic species $[Zr\{Me_2Si(\eta^5\text{-}C_5Me_4)(\eta^5\text{-}C_5H_3R)\}Me]^+$ [R = $CH_2CH_2PPh_2$ (**13**), PPh_2 (**14**)]. The insertion reaction of the isocyanide reagent $CNC_6H_3Me_2$-2,6 into the Zr–Me bond of complex **12** giving the corresponding η^2-iminoacyl compound $[Zr\{Me_2Si(\eta^5\text{-}C_5Me_4)(\eta^5\text{-}C_5H_3PPh_2)\}\{\eta^2\text{-}MeC{=}N(C_6H_3Me_2\text{-}2,6)\}(Me)]$ (**15**) is described. The *ansa*-niobocene imide $[Nb(=N\mathit{t}Bu)\{Me_2Si(\eta^5\text{-}C_5Me_4)(\eta^5\text{-}C_5H_3PPh_2)\}Cl]$ (**16**) and the niobocene imide complexes $[Nb(=N\mathit{t}Bu)(\eta^5\text{-}C_5H_4PPh_2)_2Cl]$ (**17**) were synthesised by the reaction of $[Nb(=N\mathit{t}Bu)Cl_3(py)_2]$ with $Li_2\{Me_2Si(C_5Me_4)(C_5H_3PPh_2)\}$ (**4**) or two equivalents of $Li(C_5H_4PPh_2)$, respectively. Preliminary results for the catalytic activity of **7** and **8** in the polymerization of ethylene are presented.

(© Wiley-VCH Verlag GmbH, 69451 Weinheim, Germany, 2002)

Introduction

The use of *ansa*-cyclopentadienyl ligands has received wide attention in the chemistry of group 4 metals,[1] due mainly to their ability to impart to their complexes a selective degree of catalytic activity.[2] Recent studies have demonstrated that the incorporation of an *ansa* bridge may have a profound influence on the chemistry of the metallocene system.[3]

In 1996 we reported the first *ansa*-niobocene complexes, in which both cyclopentadienyl rings are bound only in an η^5 mode to niobium,[4] and since then several complexes of this type have been described.[5]

Furthermore the use of substituted *ansa*-cyclopentadienyl ligands in the synthesis of group 4 metal complexes and their importance in catalysis is receiving special attention,[6] but there are only a few examples for group 5.[3b,5d,6–8] Some examples of asymmetric *ansa*-zirconocene complexes have been described,[8–10] although the vast majority contain indenyl or fluorenyl systems.[11]

Chiral group 4 *ansa*-metallocene complexes are important stereoselective olefin polymerization catalysts, and have also been used as catalysts or reagents in stereoselective olefin and imine hydrogenation, Diels–Alder reactions, and cyclopolymerization.[12] We are investigating the stereoselective synthesis of *ansa*-metallocene complexes and the application of these compounds as catalysts. For example, we recently developed a general synthesis of some $SiMe_2$-bridged asymmetric *ansa*-zirconocene complexes[8,9] and this series of highly active C_1 symmetric olefin polymerization catalysts polymerize propylene with a high level of stereospecificity.[9] Our research in this area is now focused on the elucidation of the mechanism of olefin polymerization as well as on the use of new types of metallocene complexes in stereoselective catalysis.

The role of cyclopentadienyl ligands with attached tertiary phosphane groups in the chemistry of metallocene complexes has been well documented.[13] In the chemistry of group 4 elements several examples of this type of complex have been described. These include $[Ti(\eta\text{-}C_5H_4CH_2CH_2PPh_2)_2Cl_2]$[14] and $[Zr(\eta\text{-}C_5H_4CMe_2\text{-}PPh_2)_2X_2]$ (X = Cl, Me).[15] Special interest in this chemistry has been placed in the ability of the phosphane moiety to join two different metallic centres[16] and to stabilize cat-

[a] Departamento de Química Inorgánica, Orgánica y Bioquímica, Universidad de Castilla-La Mancha, Facultad de Químicas, Campus Universitario, 13071-Ciudad Real, Spain
Fax: (internat.) +34-926/295-318
E-mail: Antonio.Otero@uclm.es
[b] Departamento de Ciencias Experimentales e Ingeniería, E.S.C.E.T., Universidad Rey Juan Carlos, 28933 Móstoles (Madrid), Spain

ionic species by intramolecular bonding to the metal centre.[15] However, despite the large number of related complexes reported there has been only one publication on the use of phosphane-substituted cyclopentadienyl ligands in the chemistry of the group 5 elements, in which the synthesis and reactivity of the tantalum complex, [Ta(η-C_5Me_5)(η-$C_5H_4PPh_2$)Cl_2] is described.[17] To the best of our knowledge the incorporation of such precursors in *ansa*-metallocene systems has not been reported previously.

As an extension of our previous work related to *ansa*-metallocene complexes of zirconium and niobium[4,5d,8,9] we now report the synthesis and characterization of the first phosphane-substituted *ansa*-cyclopentadienyl ligands and their incorporation in new metallocene complexes of the group 4 and 5 elements.

Results and Discussion

We have previously reported the synthesis of asymmetrically substituted cyclopentadienyl *ansa* ligands such as $Me_2Si(C_5Me_4H)(C_5H_4R)$ (R = H, Me, Et, *i*Pr, *t*Bu, $SiMe_3$)[8,9] and using the same methodology the *ansa* ligands $Me_2Si(C_5Me_4H)(C_5H_4CH_2CH_2PPh_2)$ (**1**) and $Me_2Si(C_5Me_4H)(C_5H_4PPh_2)$ (**2**) and their lithium derivatives $Li_2\{Me_2Si(C_5Me_4)(C_5H_3CH_2CH_2PPh_2)\}$ (**3**) and $Li_2\{Me_2Si(C_5Me_4)(C_5H_3PPh_2)\}$ (**4**) were prepared [Equation (1)].

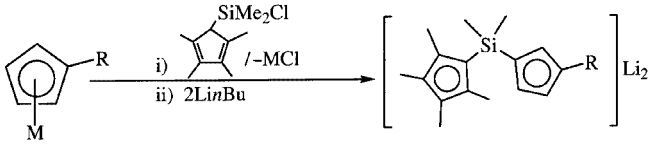

R = $CH_2CH_2PPh_2$ or PPh_2; M = K or Li

R = $CH_2CH_2PPh_2$ (**3**) Yield 96%
R = PPh_2 (**4**) Yield 93%

(1)

The possibility of various isomers for the *ansa* ligands **1** and **2** was confirmed by ^{1}H NMR spectroscopy. In addition **1** and **2** were characterised by electron impact mass spectrometry (see Exp. Sect.).

The reaction of the di-lithium derivatives of the phosphane-substituted *ansa* ligands **3** and **4** with $[TiCl_4(THF)_2]$ gave the *ansa*-titanocene(IV) complexes [Ti{Me_2Si(η^5-C_5Me_4)(η^5-$C_5H_3CH_2CH_2PPh_2$)}Cl_2] (**5**) and [Ti{Me_2Si(η^5-C_5Me_4)(η^5-$C_5H_3PPh_2$)}Cl_2] (**6**) [see Equation (2)].

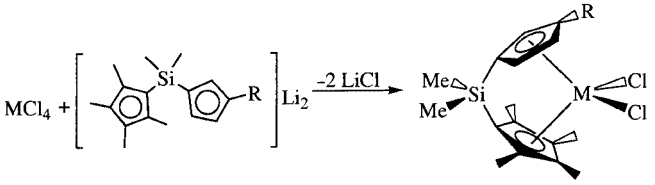

M = Ti; R = $CH_2CH_2PPh_2$ (**5**) Yield 64%; PPh_2 (**6**) Yield 58%
M = Zr; R = $CH_2CH_2PPh_2$ (**7**) Yield 52%; PPh_2 (**8**) Yield 55%
M = Hf; R = $CH_2CH_2PPh_2$ (**9**) Yield 61%; PPh_2 (**10**) Yield 59%

(2)

Complexes **5** and **6** were isolated as crystalline solids and characterised spectroscopically. Their ^{1}H NMR spectra show the lack of symmetry in these chiral C_1 symmetric complexes. Observed signals were assigned to the four inequivalent methyl groups attached to one of the cyclopentadienyl rings, the two distinct methyl groups of the $SiMe_2$ bridge and the three protons of the functionalized cyclopentadienyl moiety (see Exp. Sect.). In addition, in the ^{1}H NMR spectrum of **5** the expected signals for the alkyl chain and phenyl groups were observed. The ^{31}P NMR spectrum of **5** and **6** gave unique signals at δ = −42.8 and δ = −44.0 ppm, respectively indicating that the phosphorus atom is not interacting directly with the metal centre.[13b]

The *ansa*-metallocene complexes [M{Me_2Si(η^5-C_5Me_4)(η^5-C_5H_3R)}Cl_2] [M = Zr, R = $CH_2CH_2PPh_2$ (**7**), PPh_2 (**8**); M = Hf, R = $CH_2CH_2PPh_2$ (**9**), PPh_2 (**10**)] were prepared by the reaction of **3** or **4** with $ZrCl_4$ or $HfCl_4$ [see Equation (2)].

The ^{1}H NMR spectra for **7**−**10** concurred with those recorded for their titanocene analogues **5** and **6** (see Exp. Sect.). Complexes **5**−**10** represent, to the best of our knowledge, the first examples of group 4 *ansa*-metallocene complexes containing phosphane-substituted cyclopentadienyl moieties.

Compounds **7** and **8** were tested as catalysts in the polymerization of ethylene. The experiments were conducted at 25 °C and 1.5 bar with a zirconocene/MAO ratio of 1:500. Compared with [Zr(η^5-$C_5H_5)_2Cl_2$] [5000 kg polymer (mol Zr·h)$^{-1}$], complex **8** has a somewhat lower catalytic activity [3110 kg polymer (mol Zr·h)$^{-1}$]. Complex **7** was found to be a very poor catalyst [600 kg polymer (mol Zr·h)$^{-1}$]. The interaction of MAO with the phosphane group and the consequent steric effects exerted by the bulky Ph_2P-MAO unit may be responsible for the low catalytic activities observed.

The alkylzirconocene derivatives [Zr{Me_2Si(η^5-C_5Me_4)(η^5-C_5H_3R)}Me_2] [R = $CH_2CH_2PPh_2$ (**11**), PPh_2 (**12**)] were prepared by the reaction of two equivalents of the Grignard reagent MgMeCl with the corresponding *ansa*-metallocene dichloride complex **5** or **6**, respectively [see Equation (3)].

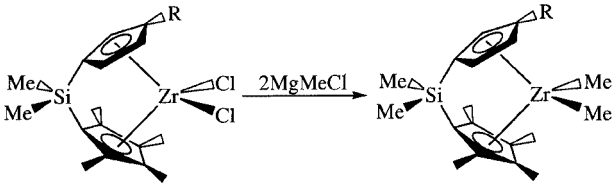

R = $CH_2CH_2PPh_2$ (**11**) Yield 81%
R = PPh_2 (**12**) Yield 80%

(3)

Compounds **11** and **12** were characterised by spectroscopic methods (see Exp. Sect.). ^{1}H NMR spectroscopy showed the expected signals for the C_1 symmetric complexes **11** and **12**. For the metal-bonded methyl groups two singlets at δ = −0.48 and −0.35 ppm were observed for **11**. In **12** these signals overlap to give one peak at δ = −0.49 ppm. However, the ^{13}C NMR spectrum of **12** gave the ex-

pected two distinct signals for the metal-bonded methyl groups. The ^{31}P NMR spectrum of **11** and **12** showed no significant changes with respect to their parent compounds **7** and **8** and therefore it can be proposed that there is no alteration in the coordination mode of the phosphorous atom.

The reaction of **11** and **12** with one molar equivalent of $B(C_6F_5)_3$ gave the cationic species $[Zr\{Me_2Si(\eta^5\text{-}C_5Me_4)(\eta^5\text{-}C_5H_3R)\}Me]^+$ [R = $CH_2CH_2PPh_2$ (**13**), PPh_2 (**14**)] with $MeB(C_6F_5)_3$ as the counteranion. The borane reagent reacts preferentially at the more nucleophilic methyl group rather than the phosphane substituent. Complexes **13** and **14** were characterised by ^{1}H, ^{11}B and ^{31}P NMR spectroscopy. The ^{1}H NMR spectra of **13** and **14** revealed the disappearance of one methyl peak and a shifting of the remaining peaks. In addition the Me-B proton resonance was observed as a broad signal at $\delta = 0.31$ ppm.

Initially there exists two possibilities for the methyl abstraction of **11** and **12**. The borane derivative can interact with either the methyl group positioned below or that orientated away from the phosphane substituent of the cyclopentadienyl moiety. ^{1}H NMR spectroscopy revealed in all cases the presence of only one compound and it appears likely on the grounds of steric effects that this corresponds to the product of the alkyl abstraction at the less hindered metal-methyl group. Nevertheless we cannot rule out the rapid exchange of coordination positions between the metal-methyl and boron-coordinated methyl groups; for a similar C_s symmetric *ansa*-system, $[Zr\{Me_2Si(\eta^5\text{-}C_5Me_4)(\eta^5\text{-}C_5H_4)\}Me]^+$,[9] however, such a phenomenon was not observed. An extensive study into the behaviour of alkyl-zirconocene borate ion pairs has been published recently.[18]

^{31}P NMR spectroscopy revealed that the phosphane groups in **13** and **14** behave in different ways. For **13** a signal at $\delta = -4.3$ ppm (compared with $\delta = -40.0$ ppm for the parent compound **11**) was observed in the ^{31}P NMR spectrum. This is indicative of a change in the coordination mode of the phosphorous atom.[13b] This shift can be explained by the fact that the abstraction of a methyl group by $B(C_6F_5)_3$ creates a vacant coordination site at the metal centre which is occupied by the phosphorous atom of the pendant phosphane ligand (see Figure 1). However, in **14** the geometric restrictions of the phosphane group which is directly attached to the cyclopentadienyl moiety inhibit its coordination to the metal centre in the cationic species and thus ^{31}P NMR spectroscopy gives a signal at $\delta = -41.4$ ppm similar to that observed for the parent complex **12** (see Figure 2).

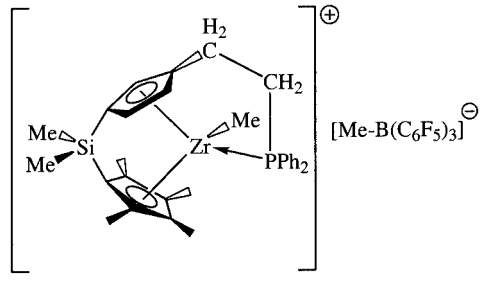

Figure 1. Proposed structure for $[Zr\{Me_2Si(\eta^5\text{-}C_5Me_4)(\eta^5\text{-}C_5H_3CH_2CH_2PPh_2)\}Me][MeB(C_6F_5)_3]$ (**13**)

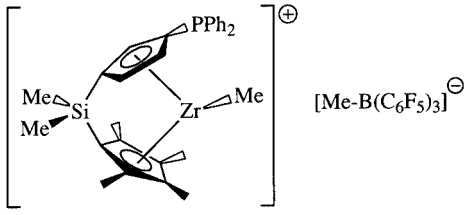

Figure 2. Proposed structure for $[Zr\{Me_2Si(\eta^5\text{-}C_5Me_4)(\eta^5\text{-}C_5H_3PPh_2)\}Me][MeB(C_6F_5)_3]$ (**14**)

The reaction of the isocyanide reagent $CNC_6H_3Me_2$-2,6 with **12** has also been studied [Equation (4)]. The product of the insertion reaction $[Zr\{Me_2Si(\eta^5\text{-}C_5Me_4)(\eta^5\text{-}C_5H_3PPh_2)\}\{\eta^2\text{-}MeC{=}N(C_6H_3Me_2\text{-}2,6)\}(Me)]$ (**15**) was characterised by ^{1}H, ^{13}C and ^{31}P NMR spectroscopy.

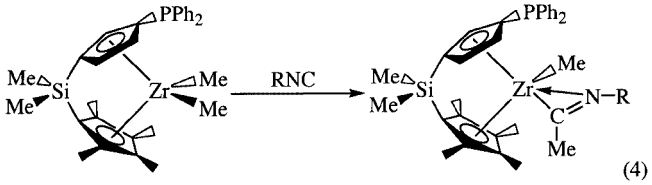

(4)

15
Yield 60%

The migratory insertion of alkyl groups towards isocyanide ligands allows the introduction of iminoacyl groups, which are present in different coordination modes. In fact, for high-valent oxophilic early transition metals, the iminoacyl group typically adopts an η^2-coordination mode through both the nitrogen and carbon atoms.[19] Similarly, an η^2-coordination mode is proposed for the iminoacyl ligand in **15** on the basis of IR and ^{13}C NMR spectroscopy, which show the characteristic ν(C=N) stretching vibration at 1584 cm^{-1} and the iminoacyl quaternary carbon atom signal at $\delta = 246.8$ ppm, respectively.

The ^{1}H NMR spectrum of **15**, in addition to the expected signals for the *ansa*-metallocene protons, gave signals for the metal-bonded methyl group at $\delta = 0.28$ ppm and for the iminoacyl methyl group at $\delta = 2.19$ ppm. The chemical shift observed for the only signal in the ^{31}P NMR spectrum ($\delta = -43.5$ ppm) showed that the chemical properties of the phosphorous atom remained unaltered with respect to the parent complex.

In **12** the two methyl groups are not equivalent and the insertion of the isocyanide probably occurs preferentially into one of the metal-methyl bonds. This was confirmed by NMR spectroscopy, which showed the presence of only one of the possible isomers. For steric reasons we propose that the insertion takes place at the metal-methyl group that is

orientated away from the bulky phosphane moiety (Figure 3).

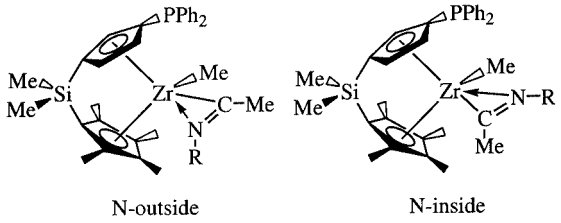

Figure 3. Two possible conformations for the metal-iminoacyl complex **15**

In addition the iminoacyl group can position itself in two distinct conformations, the "proximal" or "N-outside" and the "distal" or "N-inside" configurations (see Figure 3). ^{1}H and ^{13}C NMR spectroscopic data indicated the presence of only one of the two possible conformations. Although it has been demonstrated that the N-outside isomer is the resulting initial kinetic iminoacyl product of the insertion reaction, most group 4 metal derivatives show the structure of the N-inside isomer which results from thermodynamic control.[20] For **15** the isolated product was observed not to evolve over time and, in addition, the NOE experiment showed a negligible effect between the metal-methyl and iminoacyl-methyl groups. Therefore we propose that **15** is the product resulting from thermodynamic control and adopts the N-inside conformation.

A second insertion into the remaining methyl group was not observed even when stoichiometries greater than 1:1 were tested.

The use of phosphane-substituted cyclopentadienyl ligands in the chemistry of group 5 elements has been restricted to one reference concerning the tantalum complex $[Ta(\eta\text{-}C_5Me_5)(\eta\text{-}C_5H_4PPh_2)Cl_2]$ and its reactivity.[17] To the best of our knowledge there have been no reports of this type of compounds in the chemistry of niobium.

By the reaction of the lithium derivative $Li_2\{Me_2Si(C_5Me_4)(C_5H_3PPh_2)\}$ (**4**) with $[Nb(=N\textit{t}Bu)Cl_3(py)_2]$ we have also prepared the *ansa*-phosphane niobocene imido complex $[Nb(=N\textit{t}Bu)\{Me_2Si(\eta^5\text{-}C_5Me_4)(\eta^5\text{-}C_5H_3PPh_2)\}Cl]$ (**16**) [Equation (5)]. The complex $[Nb(=N\textit{t}Bu)(\eta^5\text{-}C_5H_4PPh_2)_2Cl]$ (**17**), was prepared in a similar manner by reaction of two equivalents of $Li(C_5H_4PPh_2)$ with $[Nb(=N\textit{t}Bu)Cl_3(py)_2]$.

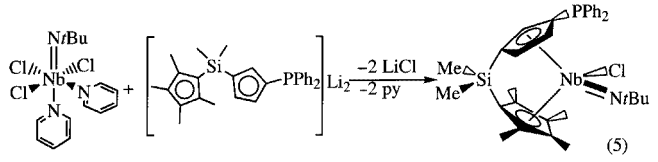

16
Yield 63%

By comparison with our previous work in imidoniobocene chemistry[5d,8,21] we can assume that the imido group acts as a four-electron donor. Complexes **16** and **17** can therefore be considered as "20-electron" complexes. However the two excess electrons are most probably located in a ligand-based orbital as has previously been reported for similar compounds.[22]

Both **16** and **17** were characterised spectroscopically. The ^{1}H NMR spectrum of **16** showed the lack of symmetry in this chiral complex. The four methyl groups attached to the cyclopentadienyl ring are inequivalent as are the methyl groups of the $SiMe_2$ bridge. In addition signals were observed for the alkyl-imido and phenyl groups and the three protons of the phosphane-substituted cyclopentadienyl moiety (see Exp. Sect.). In the case of **17** an ABCD system was observed in the ^{1}H NMR spectrum due to the inequivalency of the cyclopentadienyl ring protons, although a plane of symmetry makes the two cyclopentadienyl rings equivalent, thus giving four multiplets for the eight ring protons. The expected signals for the alkyl-imido and phenyl groups were also observed (see Exp. Sect.).

Complex **16** has the possibility to form two isomers depending on the position of the phosphane group, which can either be orientated towards or away from the imido group (see Figure 4). ^{1}H NMR spectroscopy revealed that only one isomer was present. For other alkyl-substituted *ansa*-niobium complexes this same phenomenon was observed,[8] and all the molecular structures reported for related complexes revealed that the substituent was situated pointing away from the bulky imido group. It is logical to assume the same is true for **16** and therefore the proposed structure (a) is that illustrated in Figure 4.

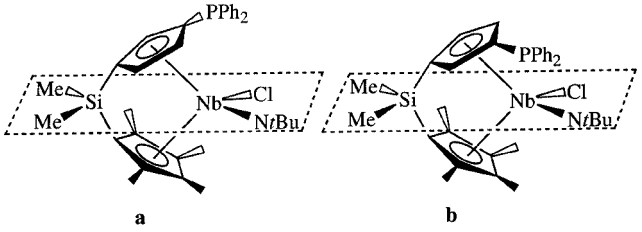

Figure 4. Possible isomers for $[Nb(=N\textit{t}Bu)\{Me_2Si(\eta^5\text{-}C_5Me_4)(\eta^5\text{-}C_5H_3PPh_2)\}Cl]$ (**16**)

In conclusion we have reported the synthesis of new phosphane-containing *ansa*-cyclopentadienyl ligands and their lithium derivatives. We have prepared the first phosphane-substituted *ansa*-metallocene complexes with group 4 and group 5 elements. The catalytic activity of the zirconocene complexes has been tested in olefin polymerization and discussed as a function of the phosphane group attached to the cyclopentadienyl ring. The reactivity of some of these compounds has been described.

Experimental Section

General Remarks: All reactions were performed using standard Schlenk-tube techniques under an atmosphere of dry nitrogen. Solvents were distilled from appropriate drying agents and degassed before use. $K(C_5H_4CH_2CH_2PPh_2)$,[23] $Li(C_5H_4PPh_2)$[24] and $[Nb(=N\textit{t}Bu)Cl_3(py)_2]$[25] were prepared as described earlier. $[TiCl_4(THF)_2]$, $ZrCl_4$, $HfCl_4$, $Me_2Si(C_5Me_4H)Cl$, MgMeCl, $B(C_6F_5)_3$ and (2,6-dimethylphenyl)isocyanide were purchased from

Aldrich and used directly. IR spectra were recorded on a Perkin−Elmer PE 883 IR spectrophotometer. ^{1}H and ^{13}C spectra were recorded on Varian FT-300 and Varian Gemini FT-200 spectrometers and referenced to the residual deuterated solvent. Microanalyses were carried out with a Perkin−Elmer 2400 micro analyzer. Mass spectroscopic analyses were performed on a Hewlett−Packard 5988A (*m*/*z* = 50−1000) instrument (electron impact).

Preparation of $Me_2Si(C_5Me_4H)(C_5H_4CH_2CH_2PPh_2)$ (1): $Me_2Si(C_5Me_4H)Cl$ (1.36 g, 6.32 mmol) in THF (50 mL) was added to a solution of $K(C_5H_4CH_2CH_2PPh_2)$ (2.00 g, 6.32 mmol) in THF (50 mL) at −78 °C. The reaction mixture was allowed to warm to room temperature and stirred for 18 h. Solvent was removed in vacuo and hexane (150 mL) was added to the resulting orange oil. The mixture was filtered and solvent removed from the filtrate under reduced pressure to yield the title compound as a yellow oil (2.78 g, 96%). ^{1}H NMR (200 MHz, C_6D_6, 25 °C) (for the predominant isomer, 60%): δ = 0.10 (s, 6 H, Si*Me*$_2$), 1.75 and 1.85 (2s, each 6 H, C_5Me_4), 2.20−2.60 and 3.00−3.30 (2m, each 2 H, -CH_2CH_2-), 2.80 and 3.47 (2m, each 1 H, *H*C$_5$), 6.35, 6.37 and 6.56 (3m, each 1 H, C_5H_3), 7.00−7.60 (m, 10, P*Ph*$_2$) ppm. EI-MS: *m*/*z* (%) = 456 (25) [M$^+$], 335 (30) [M$^+$ − C_5Me_4H], 179 (100) [M$^+$ − $C_5H_4CH_2CH_2PPh_2$], 123(65) [M$^+$ − C_5Me_4H − $CH_2CH_2PPh_2$].

Preparation of $Me_2Si(C_5Me_4H)(C_5H_4PPh_2)$ (2): The synthesis of **2** was carried out in an identical manner to **1**. $Me_2Si(C_5Me_4H)Cl$ (1.10 g, 5.12 mmol) and $Li(C_5H_4PPh_2)$ (1.31 g, 5.12 mmol). Yield 2.05 g, 94%. ^{1}H NMR (200 MHz, C_6D_6, 25 °C) (for the predominant isomer, 60%): δ = 0.05 (s, 6 H, Si*Me*$_2$), 1.70 and 1.80 (2s, each 6 H, C_5Me_4), 3.05 and 3.35 (2m, each 1 H, *H*C$_5$), 6.28, 6.32 and 6.52 (3m, each 1 H, C_5H_3), 7.00−7.60 (m, 10, P*Ph*$_2$) ppm. EI-MS: *m*/*z* (%) = 428 (20) [M$^+$], 307 (25) [M$^+$ − C_5Me_4H], 179 (100) [M$^+$ − $C_5H_4PPh_2$], 123(70) [M$^+$ − C_5Me_4H − PPh_2].

Preparation of $Li_2\{Me_2Si(C_5Me_4)(C_5H_3CH_2CH_2PPh_2)\}$ (3): *n*BuLi (1.6 M in hexane) (7.6 mL, 12.18 mmol) was added via syringe to a solution of **1** (2.78 g, 6.09 mmol) in Et_2O (75 mL) at −78 °C. The mixture was allowed to warm to 10 °C and stirred for 15 h. Solvent was removed in vacuo to give a white solid which was washed with hexane (2 × 50 mL) and dried under vacuum to yield a white solid of the title complex (2.74 g, 96%). $C_{30}H_{35}Li_2PSi$ (468.5): calcd. C 76.90, H 7.53; found C 76.62, H 7.43.

Preparation of $Li_2\{Me_2Si(C_5Me_4)(C_5H_3PPh_2)\}$ (4): The synthesis of **4** was carried out in an identical manner to **3** from **2** (2.19 g, 5.11 mmol) and *n*BuLi (1.6 M in hexane) (6.39 mL, 10.22 mmol). Yield 2.09 g, 93%. $C_{28}H_{31}Li_2PSi$ (440.5): calcd. C 76.35, H 7.09; found C 76.19, H 7.00.

Preparation of $[Ti\{Me_2Si(\eta^5\text{-}C_5Me_4)(\eta^5\text{-}C_5H_3CH_2CH_2PPh_2)\}Cl_2]$ (5): Compound **3** (1.50 g, 3.20 mmol) in THF (50 mL) was added to a solution of $[TiCl_4(THF)_2]$ (1.07 g, 0.64 mmol) in THF (50 mL). The resulting dark red solution was stirred for 18 h. Solvent was removed in vacuo and toluene (75 mL) was added. The suspension was filtered and the filtrate was concentrated (10 mL) and cooled (−30 °C) to yield the title complex as a red crystalline solid (1.17 g, 64%). ^{1}H NMR (200 MHz, C_6D_6, 25 °C): δ = −0.01 and 0.34 (2s, each 3 H, Si*Me*$_2$), 1.45, 1.60, 2.07 and 2.09 (4s, each 3 H, C_5Me_4), 2.04−2.61 and 2.98−3.35 (2m, each 2 H, -CH_2CH_2-), 4.88, 5.31 and 6.93 (3m, each 1 H, C_5H_3), 7.06−7.12, 7.32−7.55 (m, 10 H, P*Ph*$_2$) ppm. ^{13}C{^{1}H} NMR (300 MHz, C_6D_6, 25 °C): δ = −0.7, −0.6 (Si*Me*$_2$), 12.1, 12.2, 14.5, 14.7 (C_5Me_4), 27.0 (d, $^1J_{C,P}$ = 19.7 Hz), 28.6 (d, $^2J_{C,P}$ = 13.8 Hz) (-*C*H_2CH_2-), 110.0, 110.7, 112.6 125.0, 126.10 (*C*$_5$H$_3$), 128.0−141.0 (various signals assigned to P*Ph*$_2$ and *C*$_5$Me$_4$) ppm. ^{31}P{^{1}H} NMR (300 MHz, C_6D_6, 25 °C): δ = −42.8 ppm. $C_{30}H_{35}Cl_2PSiTi$ (573.5): calcd. C 62.84, H 6.15; found C 62.56, H 6.09.

The syntheses of **6**−**10** were carried out in an identical manner to **5**.

$[Ti\{Me_2Si(\eta^5\text{-}C_5Me_4)(\eta^5\text{-}C_5H_3PPh_2)\}Cl_2]$ (6): From $[TiCl_4(THF)_2]$ (1.18 g, 0.89 mmol) and **4** (1.56 g, 3.54 mmol). Yield 1.12 g, 58%. ^{1}H NMR (200 MHz, C_6D_6, 25 °C): δ = 0.08 and 0.16 (2s, each 3 H, Si*Me*$_2$), 1.39, 1.54, 1.96 and 2.04 (4s, each 3 H, C_5Me_4), 5.34, 5.45 and 6.32 (3m, each 1 H, C_5H_3), 7.37−7.74 (m, 10 H, P*Ph*$_2$) ppm. ^{13}C{^{1}H} NMR (300 MHz, C_6D_6, 25 °C): δ = −1.1, −0.2 (Si*Me*$_2$), 11.3, 12.9, 13.6, 13.9 (C_5Me_4), 110.4, 112.6, 117.4, 118.4 (d, $^1J_{C,P}$ = 32.4 Hz), 125.6 (*C*$_5$H$_3$), 128.0−138.0 (various signals assigned to P*Ph*$_2$ and *C*$_5$Me$_4$) ppm. ^{31}P{^{1}H} NMR (300 MHz, C_6D_6, 25 °C): δ = −42.2 ppm. $C_{28}H_{31}Cl_2PSiTi$ (545.4): calcd. C 61.66, H 5.73; found C 61.47, H 5.66.

$[Zr\{Me_2Si(\eta^5\text{-}C_5Me_4)(\eta^5\text{-}C_5H_3CH_2CH_2PPh_2)\}Cl_2]$ (7): From $ZrCl_4$ (0.99 g, 4.27 mmol) and **3** (2.00 g, 4.27 mmol). Yield 1.37 g, 52%. ^{1}H NMR (200 MHz, C_6D_6, 25 °C): δ = 0.33 and 0.37 (2s, each 3 H, Si*Me*$_2$), 1.58, 1.69, 1.98 and 1.99 (4s, each 3 H, C_5Me_4), 2.28−2.57 and 2.95−3.26 (2m, each 2 H, -CH_2CH_2-), 5.04, 5.37 and 6.72 (3m, each 1 H, C_5H_3), 7.01−7.10, 7.43−7.53 (m, 10 H, P*Ph*$_2$) ppm. ^{13}C{^{1}H} NMR (300 MHz, C_6D_6, 25 °C): δ = −0.7, −0.6 (Si*Me*$_2$), 12.3, 12.4, 14.8, 15.0 (C_5Me_4), 27.0 (d, $^1J_{C,P}$ = 19.8 Hz), 28.6 (d, $^2J_{C,P}$ = 13.5 Hz) (-*C*H_2CH_2-), 112.3, 113.1, 125.0, 125.1, 126.1 (*C*$_5$H$_3$), 128.0−141.0 (various signals assigned to P*Ph*$_2$ and *C*$_5$Me$_4$) ppm. ^{31}P{^{1}H} NMR (300 MHz, C_6D_6, 25 °C): δ = −39.5 ppm. $C_{30}H_{35}Cl_2PSiZr$ (616.8): calcd. C 58.42, H 5.72; found C 58.33, H 5.68.

$[Zr\{Me_2Si(\eta^5\text{-}C_5Me_4)(\eta^5\text{-}C_5H_3PPh_2)\}Cl_2]$ (8): From $ZrCl_4$ (0.80 g, 3.41 mmol) and **4** (1.50 g, 3.41 mmol). Yield 1.12 g, 55%. ^{1}H NMR (200 MHz, C_6D_6, 25 °C): δ = 0.18 and 0.30 (2s, each 3 H, Si*Me*$_2$), 1.56, 1.64, 1.95 and 2.00 (4s, each 3 H, C_5Me_4), 5.54 (2 H), 6.75 (1 H) (m, C_5H_3), 6.97−7.13, 7.38−7.73 (m, 10 H, P*Ph*$_2$) ppm. ^{13}C{^{1}H} NMR (300 MHz, C_6D_6, 25 °C): δ = −1.0, −0.7 (Si*Me*$_2$), 12.4, 12.5, 14.8, 15.0 (C_5Me_4), 110.7, 114.4, 116.5, 120.4, 125.4 (d, $^1J_{C,P}$ = 33.6 Hz) (*C*$_5$H$_3$), 128.0−138.0 (various signals assigned to P*Ph*$_2$ and *C*$_5$Me$_4$) ppm. ^{31}P{^{1}H} NMR (300 MHz, C_6D_6, 25 °C): δ = −43.8 ppm. $C_{28}H_{31}Cl_2PSiZr$ (588.7): calcd. C 57.12, H 5.31; found C 56.99, H 5.25.

$[Hf\{Me_2Si(\eta^5\text{-}C_5Me_4)(\eta^5\text{-}C_5H_3CH_2CH_2PPh_2)\}Cl_2]$ (9): From $HfCl_4$ (1.08 g, 3.37 mmol) and **3** (1.58 g, 3.37 mmol). Yield 1.45 g, 61%. ^{1}H NMR (200 MHz, C_6D_6, 25 °C): δ = 0.31 and 0.35 (2s, each 3 H, Si*Me*$_2$), 1.63, 1.75, 1.99 and 2.00 (4s, each 3 H, C_5Me_4), 2.24−2.59 and 2.98−3.24 (2m, each 2 H, -CH_2CH_2-), 4.98, 5.31 and 6.62 (3m, each 1 H, C_5H_3), 7.01−7.10, 7.40−7.51 (m, 10 H, P*Ph*$_2$) ppm. ^{13}C{^{1}H} NMR (300 MHz, C_6D_6, 25 °C): δ = −0.7, −0.6 (Si*Me*$_2$), 12.1, 12.2, 14.5, 14.7 (C_5Me_4), 27.0 (d, $^1J_{C,P}$ = 19.7 Hz), 28.6 (d, $^2J_{C,P}$ = 13.8 Hz) (−*C*H_2CH_2-), 110.0, 110.7, 112.61 125.0, 126.1 (*C*$_5$H$_3$), 128.0−141.0 (various signals assigned to P*Ph*$_2$ and *C*$_5$Me$_4$) ppm. ^{31}P{^{1}H} NMR (300 MHz, C_6D_6, 25 °C): δ = −39.8 ppm. $C_{30}H_{35}Cl_2HfPSi$ (704.1): calcd. C 51.18, H 5.01; found C 50.91, H 4.90.

$[Hf\{Me_2Si(\eta^5\text{-}C_5Me_4)(\eta^5\text{-}C_5H_3PPh_2)\}Cl_2]$ (10): From $HfCl_4$ (1.10 g, 3.43 mmol) and **4** (1.51 g, 3.43 mmol). Yield 1.37 g, 59%. ^{1}H NMR (200 MHz, C_6D_6, 25 °C): δ = 0.20 and 0.32 (2s, each 3 H, Si*Me*$_2$), 1.65, 1.73, 1.99, 2.05 (4s, each 3 H, C_5Me_4), 5.52, 5.54 and 6.72 (3m, each 1 H, C_5H_3), 6.99−7.14, 7.37−7.71 (m, 10 H, P*Ph*$_2$) ppm. ^{13}C{^{1}H} NMR (300 MHz, C_6D_6, 25 °C): δ = −1.0, −0.7 (Si*Me*$_2$), 12.2, 12.3, 14.5, 14.7 (C_5Me_4), 112.1, 114.3, 116.5, 120.1, 125.4 (d, $^1J_{C,P}$ = 33.6 Hz) (*C*$_5$H$_3$), 128.0−138.0 (various signals assigned to P*Ph*$_2$ and *C*$_5$Me$_4$) ppm. ^{31}P{^{1}H} NMR (300 MHz,

C_6D_6, 25 °C): δ = −41.0 ppm. $C_{28}H_{31}Cl_2HfPSi$ (676.0): calcd. C 49.75, H 4.62; found C 49.63, H 4.55.

Preparation of [Zr{Me$_2$Si(η^5-C$_5$Me$_4$)(η^5-C$_5$H$_3$CH$_2$CH$_2$PPh$_2$)}Me$_2$] (11): A 3 M solution of MgMeCl in THF (0.43 mL, 1.30 mmol) was added to a stirred solution of **7** (0.40 g, 0.65 mmol) in THF (50 mL) at −78 °C. The solution was allowed to warm to room temperature and stirred for 4 h. Solvent was removed in vacuo and the remaining solid extracted with hexane (30 mL). A white crystalline solid was obtained by concentrating (5 mL) and cooling (−30 °C) the solution (0.30 g, 81%). ^{1}H NMR (200 MHz, C_6D_6, 25 °C): δ = −0.48 and −0.35 (2s, each 3 H, Zr-C*H*$_3$), 0.34 and 0.37 (2s, each 3 H, Si*Me*$_2$), 1.54, 1.65, 1.91 and 1.92 (4s, each 3 H, C$_5$*Me*$_4$), 2.38−3.05 (m, 4 H, -C*H*$_2$C*H*$_2$-), 5.05, 5.28 and 6.58 (3m, each 1 H, C$_5$*H*$_3$), 7.01−7.14, 7.42−7.52 (m, 10 H, P*Ph*$_2$) ppm. ^{13}C{^{1}H} NMR (300 MHz, C_6D_6, 25 °C): δ = −0.3, 1.4 (Si*Me*$_2$), 11.6, 11.7, 14.3, 14.5 (C$_5$*Me*$_4$), 26.9 (d, $^1J_{C,P}$ = 19.6 Hz), 30.5 (d, $^2J_{C,P}$ = 8.6 Hz) (−*C*H$_2$*C*H$_2$-), 31.4, 35.2 (Zr-*C*H$_3$), 111.4, 112.2, 125.0, 125.1, 126.1 (*C*$_5$H$_3$), 128.0−140.0 (various signals assigned to P*Ph*$_2$ and *C*$_5$Me$_4$) ppm. ^{31}P{^{1}H} NMR (300 MHz, C_6D_6, 25 °C): δ = −40.0 ppm. $C_{32}H_{41}PSiZr$ (576.0): calcd. C 66.73, H 7.18; found C 66.51, H 7.12.

Preparation of [Zr{Me$_2$Si(η^5-C$_5$Me$_4$)(η^5-C$_5$H$_3$PPh$_2$)}Me$_2$] (12): The synthesis of **12** was carried out in an identical manner to that of **11**, with a 3 M solution of MgMeCl in THF (0.51 mL, 1.52 mmol) and **8** (0.45 g, 0.76 mmol). Yield 0.34 g, 80%. ^{1}H NMR (200 MHz, C_6D_6): δ = −0.49 (s, 6 H, Zr-C*H*$_3$), 0.26 and 0.37 (2s, each 3 H, Si*Me*$_2$), 1.56, 1.63, 1.89 and 1.97 (4s, each 3 H, C$_5$*Me*$_4$), 5.47, 5.57 and 6.74 (3m, each 1 H, C$_5$*H*$_3$), 7.07−7.17, 7.52−7.74 (m, 10 H, P*Ph*$_2$) ppm. ^{13}C{^{1}H} NMR (300 MHz, C_6D_6, 25 °C): δ = −0.7, 0.1 (Si*Me*$_2$), 11.6, 11.7, 14.4, 14.5 (C$_5$*Me*$_4$), 37.3, 37.7 (Zr-*C*H$_3$), 110.4, 115.6, 116.5, 125.5, 127.4 (*C*$_5$H$_3$), 128.0−140.0 (various signals assigned to P*Ph*$_2$ and *C*$_5$Me$_4$) ppm. ^{31}P{^{1}H} NMR (300 MHz, C_6D_6, 25 °C): δ = −44.1 ppm. $C_{30}H_{37}PSiZr$ (547.9): calcd. C 65.76, H 6.81; found C 65.49, H 6.71.

Preparation of [Zr{Me$_2$Si(η^5-C$_5$Me$_4$)(η^5-C$_5$H$_3$CH$_2$CH$_2$PPh$_2$)}Me][MeB(C$_6$F$_5$)] (13): A solution of B(C$_6$F$_5$)$_3$ (0.25 g, 0.49 mmol) in toluene (25 mL) was added to a stirred solution of **11** (0.28 g, 0.49 mmol) in toluene (25 mL) at −78 °C. The mixture was allowed to warm to room temperature and stirred for 30 min. Solvent was removed in vacuo to give the title complex as an orange oil. ^{1}H NMR (300 MHz, [D$_8$]toluene, 25 °C): δ = −0.11 (s, 3 H, Zr-C*H*$_3$), 0.31 (br, 3 H, B-C*H*$_3$), 0.50 and 1.17 (2s, each 3 H, Si*Me*$_2$), 1.29, 1.34, 1.40 and 1.96 (4s, each 3 H, C$_5$*Me*$_4$), 2.20−2.80 (m, 4 H, -C*H*$_2$C*H*$_2$-), 4.84, 5.01 and 6.58 (3m, each 1 H, C$_5$*H*$_3$), 7.01−7.42 (m, 10 H, P*Ph*$_2$) ppm. ^{11}B{^{1}H} NMR (300 MHz, [D$_8$]toluene, 25 °C): δ = 15 ppm. ^{31}P{^{1}H} NMR (300 MHz, [D$_8$]toluene, 25 °C): δ = −4.29 ppm.

Preparation of [Zr{Me$_2$Si(η^5-C$_5$Me$_4$)(η^5-C$_5$H$_3$PPh$_2$)}Me][MeB(C$_6$F$_5$)] (14): The synthesis of **14** was carried out in an identical manner to that of **13**, from B(C$_6$F$_5$)$_3$ (0.25 g, 0.49 mmol) and **12** (0.27 g, 0.49 mmol). ^{1}H NMR (300 MHz, [D$_8$]toluene, 25 °C): δ = −0.49 (s, 3 H, Zr-C*H*$_3$), 0.18 and 0.30 (2s, each 3 H, Si*Me*$_2$), 0.31 (br, 3 H, B-C*H*$_3$), 1.56, 1.63, 1.89 and 1.97 (4s, each 3 H, C$_5$*Me*$_4$), 4.98, 5.64 and 6.22 (3m, each 1 H, C$_5$*H*$_3$), 7.01−7.34 (m, 10 H, P*Ph*$_2$) ppm. ^{11}B{^{1}H} NMR (300 MHz, [D$_8$]toluene, 25 °C): δ = 15 ppm. ^{31}P{^{1}H} NMR (300 MHz, [D$_8$]toluene, 25 °C): δ = −44.6 ppm.

Preparation of [Zr{Me$_2$Si(η^5-C$_5$Me$_4$)(η^5-C$_5$H$_3$PPh$_2$)}{η^2-MeC=N(C$_6$H$_3$Me$_2$-2,6)}(Me)] (15): (2,6-dimethylphenyl)isocyanide (0.12 g, 0.91 mmol) and **12** (0.50 g, 0.91 mmol) were dissolved in THF (100 mL). The resulting orange solution was stirred at room temperature for 18 h. Solvent was removed in vacuo and the remaining solid extracted with toluene (30 mL). An orange solid was obtained by concentrating (5 mL) and cooling (−30 °C) the solution (0.37 g, 60%). IR (Nujol): ν$_{C=N}$ 1584 cm^{-1}. ^{1}H NMR (200 MHz, C_6D_6, 25 °C): δ = 0.25 (s, 3 H, Zr-C*H*$_3$), 0.36 and 0.58 (2s, each 3 H, Si*Me*$_2$), 1.28 and 1.50 (2s, each 3 H, C$_6$H$_3$*Me*$_2$), 1.75, 1.82, 1.90 and 1.95 (4s, each 3 H, C$_5$*Me*$_4$), 2.19 (s, 3 H, C-C*H*$_3$ iminoacyl) 5.54, 5.65 and 5.88 (3m, each 1 H, C$_5$*H*$_3$), 6.82−7.07, 7.32−7.53 (m, P*Ph*$_2$ and C$_6$*H*$_3$Me$_2$) ppm. ^{13}C{^{1}H} NMR (300 MHz, C_6D_6, 25 °C): δ = −0.7, 0.1 (Si*Me*$_2$), 11.6, 11.7, 14.4, 14.5 (C$_5$*Me*$_4$), 19.8 (C*C*H$_3$ iminoacyl), 25.8 (Zr-*C*H$_3$), 110.7, 113.4, 120.9, 125.5, 127.4 (*C*$_5$H$_3$), 128.0−140.0 (various signals assigned to P*Ph*$_2$, *C*$_6$H$_3$Me$_2$, and *C*$_5$Me$_4$), 246.8 (*C*CH$_3$ iminoacyl) ppm. ^{31}P{^{1}H} NMR (300 MHz, C_6D_6, 25 °C): δ = −43.5 ppm. $C_{39}H_{46}NPSiZr$ (679.1): calcd. C 68.98, H 6.83, N 2.06; found C 68.75, H 6.77, N 2.00.

Preparation of [Nb(=N*t*Bu){Me$_2$Si(η^5-C$_5$Me$_4$)(η^5-C$_5$H$_3$PPh$_2$)}Cl] (16): THF (50 mL) was added to a solid mixture of [Nb(=N*t*Bu)Cl$_3$(py)$_2$] (0.78 g, 1.82 mmol) and **4** (0.80 g, 1.82 mmol). The resulting brown solution was stirred for 12 h. Solvent was removed in vacuo and hexane added (75 mL) to the resulting solid. The mixture was filtered and the filtrate concentrated (10 mL) and cooled to −30 °C. The resulting yellow solid that precipitated from the solution was isolated by filtration (0.67 g, 63%). IR (Nujol): ν$_{Nb=N}$ = 1255 cm^{-1}. ^{1}H NMR (200 MHz, C_6D_6, 25 °C): δ = 0.10 and 0.45 (2s, each 3 H, Si*Me*$_2$), 0.87 (s, 9 H, C*Me*$_3$), 1.65, 1.71, 2.03 and 2.25 (4s, each 3 H, C$_5$*Me*$_4$), 5.61, 6.27 and 6.42 (3m, each 1 H, C$_5$*H*$_3$), 6.91−7.80 (m, P*Ph*$_2$) ppm. ^{13}C{^{1}H} NMR (300 MHz, C_6D_6, 25 °C): δ = −1.5, −0.8 (Si*Me*$_2$), 12.6, 13.3, 13.4, 16.4 (C$_5$*Me*$_4$), 31.2 (C*Me*$_3$), 71.3 (*C*Me$_3$), 102.0, 104.7, 114.5, 114.9, 115.0 (*C*$_5$H$_3$), 128.0−135.0 (various signals assigned to P*Ph*$_2$ and *C*$_5$Me$_4$) ppm. ^{31}P{^{1}H} NMR (300 MHz, C_6D_6, 25 °C): δ = −43.49 ppm. $C_{32}H_{40}ClNNbPSi$ (626.1): calcd. C 61.39, H 6.44, N 2.24; found C 61.17, H 6.36, N 2.25.

Preparation of [Nb(=N*t*Bu)(η^5-C$_5$H$_4$PPh$_2$)$_2$Cl] (17): The synthesis of **17** was carried out in an identical manner to **16**, from [Nb(=N*t*Bu)Cl$_3$(py)$_2$] (0.50 g, 1.16 mmol) and Li(C$_5$H$_4$PPh$_2$) (0.60 g, 2.34 mmol). Yield 0.58 g, 72%. IR (Nujol): ν$_{Nb=N}$ = 1240 cm^{-1}. ^{1}H NMR (200 MHz, C_6D_6, 25 °C): δ = 0.96 (s, 9 H, C*Me*$_3$), 5.89, 6.05, 6.12 and 6.18 (4m, each 2 H, 2 × C$_5$*H*$_4$), 6.91−7.50 (10 H) (m, P*Ph*$_2$) ppm. ^{13}C{^{1}H} NMR (300 MHz, C_6D_6, 25 °C): δ = 29.9 (C*Me*$_3$), 70.6 (*C*Me$_3$), 111.8, 112.7, 120.6, 120.7 124.7 (*C*$_5$H$_4$), 128.0−134 (various signals assigned to P*Ph*$_2$) ppm. ^{31}P{^{1}H} NMR (300 MHz, C_6D_6, 25 °C). δ = −40.10 ppm. $C_{38}H_{37}ClNNbP_2$ (698.0): calcd. C 65.39, H 5.34, N 2.01; found C 65.17, H 5.23, N 1.99.

Polymerization Experiments: The *ansa*-zirconocene catalyst (**7** or **8**; 6 μmol), MAO (10% in toluene) (3000 μmol) and toluene (150 mL) were mixed together in a Schlenk tube. The N_2 pressure inside the Schlenk tube was reduced by applying vacuum. An ethylene pressure of 1.5 bar was then applied to the Schlenk tube and stirring of the mixture commenced. After exactly 30 min, stirring was halted and the ethylene pressure was released. Excess MAO was then destroyed by adding a mixture of methanol/HCl (90:10) cautiously. The polymer formed was isolated by filtration, washed with ethanol and dried under vacuum at 60 °C for 12 h.

Acknowledgments

We gratefully acknowledge financial support from the Dirección General de Enseñanza Superior e Investigación Científica, Spain (Grants. No. PB 98-0159-C02-01-02 and No. BQU2000-0463) and

funding for S. P. from the FEDER project 1FD97-1375. We would also like to thank Dr. M. Laguna for providing mass spectrometry data.

[1] *Comprehensive Organometallic Chemistry II* (Eds.: E. W. Abel, F. G. A. Stone, G. Wilkinson), Pergamon Press, Oxford, **1995**, vol. 4.
[2] B. Rieger, G. Jany, R. Fawzi, M. Steimann, *Organometallics* **1994**, *13*, 647−653.
[3] [3a] S. L. J. Conway, T. Dijkstra, L. H. Doerrer, J. C. Green, M. L. H. Green, A. H. H. Stephens, *J. Chem. Soc., Dalton Trans.* **1998**, 2689−2695. [3b] J. H. Shin, G. Parkin, *Chem. Commun.* **1999**, 887−888.
[4] A. Antiñolo, M. Martínez-Ripoll, Y. Mugnier, A. Otero, S. Prashar, A. M. Rodriguez, *Organometallics* **1996**, *15*, 3241−3243.
[5] [5a] N. J. Bailey, J. A. Cooper, H. Gailus, M. L. H. Green, J. T. James, M. A. Leech, *J. Chem. Soc., Dalton Trans.* **1997**, 3579−3584. [5b] N. J. Bailey, M. L. H. Green, M. A. Leech, J. F. Saunders, H. M. Tidswell, *J. Organomet. Chem.* **1997**, *538*, 111−118. [5c] W. A. Herrmann, W. Baratta, E. Herdtweck, *J. Organomet. Chem.* **1997**, *541*, 445−460. [5d] A. Antiñolo, A. Otero, S. Prashar, A. M. Rodriguez, *Organometallics* **1998**, *17*, 5454−5459.
[6] M. E. Huttenloch, B. Dorer, U. Rief, M.-H. Prosenc, K. Schmidt, H. H. Brintzinger, *J. Organomet. Chem.* **1997**, *541*, 219−232.
[7] S. L. J. Conway, L. H. Doerrer, M. L. H. Green, M. A. Leech, *Organometallics* **2000**, *19*, 630−637.
[8] A. Antiñolo, I. López-Solera, I. Orive, A. Otero, S. Prashar, A. M. Rodríguez, E. Villaseñor, *Organometallics* **2001**, *20*, 71−78.
[9] A. Antiñolo, I. López-Solera, A. Otero, S. Prashar, A. M. Rodríguez, E. Villaseñor, *Organometallics* **2002**, *21*, 2460−2467.
[10] [10a] Y. Obora, C. L. Stern, T. J. Marks, P. N. Nickias, *Organometallics* **1997**, *16*, 2503−2505. [10b] M. A. Giardello, M. S. Eisen, C. L. Stern, T. J. Marks, *J. Am. Chem. Soc.* **1993**, *115*, 3326−3327. [10c] M. A. Giardello, M. S. Eisen, C. L. Stern, T. J. Marks, *J. Am. Chem. Soc.* **1995**, *117*, 12114−12129. [10d] H. Schumann, K. Zietzke, R. Weimann, J. Demtschuk, W. Kaminsky, A.-M. Schauwienold, *J. Organomet. Chem.* **1999**, *574*, 228−240. [10e] C. Müller, D. Lilge, M. O. Kristen, P. Jutzi, *Angew. Chem.* **2000**, *112*, 800−803; *Angew. Chem. Int. Ed.* **2000**, *39*, 789−792. [10f] N. Suzuki, T. Mise, Y. Yamaguchi, T. Chihara, Y. Ikegami, H. Ohmori, A. Matsumoto, Y. Wakatsuki, *J. Organomet. Chem.* **1998**, *560*, 47−54. [10g] T. A. Herzog, D. L. Zubris, J. E. Bercaw, *J. Am. Chem. Soc.* **1996**, *118*, 11988−11989.
[11] [11a] R. W. Baker, M. A. Foulkes, P. Turner, *J. Chem. Soc., Dalton Trans.* **2000**, 431−433. [11b] A. Razavi, J. Ferrara, *J. Organomet. Chem.* **1992**, *435*, 299−310. [11c] A. Razavi, J. L. Atwood, *J. Organomet. Chem.* **1993**, *459*, 117−123. [11d] J. A. Ewen, J. L. Jones, A. Razavi, J. Ferrara, *J. Am. Chem. Soc.* **1988**, *110*, 6255−6256. [11e] G. H. Llinas, R. O. Day, M. D. Rausch, J. C. W. Chien, *Organometallics* **1993**, *12*, 1283−1288. [11f] B. Rieger, G. Jany, R. Fawzi, M. Steimann, *Organometallics* **1994**, *13*, 647−653. [11g] M. L. H. Green, N. Ishihara, *J. Chem. Soc., Dalton Trans.* **1994**, 657−665. [11h] A. Razavi, J. L. Atwood, *J. Organomet. Chem.* **1995**, *497*, 105−111. [11i] Y.-X. Chen, M. D. Rausch, J. C. W. Chien, *J. Organomet. Chem.* **1995**, *497*, 1−9. [11j] T. Bürgi, H. Berke, D. Wingbermühle, C. Psiorz, R. Noe, T. Fox, M. Knickmeier, M. Berlekamp, R. Fröhlich, G. Erker, *J. Organomet. Chem.* **1995**, *497*, 149−159. [11k] W. Kaminsky, O. Rabe, A.-M. Schauwienold, G. U. Schupfner, J. Hanss, J. Kopf, D. Veghini, L. M. Henling, T. J. Burkhardt, J. E. Bercaw, *J. Am. Chem. Soc.* **1999**, *121*, 564−573. [11l] J. A. Ewen, R. L. Jones, M. J. Elder, *J. Am. Chem. Soc.* **1998**, *120*, 10786−10787. [11m] K. Patsidis, H. G. Alt, W. Milius, S. J. Palackal, *J. Organomet. Chem.* **1996**, *509*, 63−71. [11n] U. Dietrich, M. Hackmann, B. Rieger, M. Klinga, M. Leskelä, *J. Am. Chem. Soc.* **1999**, *121*, 4348−4355. [11o] E. J. Thomas, J. C. W. Chien, M. D. Rausch, *Organometallics* **1999**, *18*, 1439−1443. [11p] S. C. Yoon, T. K. Han, B. W. Woo, H. Song, S. I. Woo, J. T. Park, *J. Organomet. Chem.* **1997**, *534*, 81−87.
[12] A. H. Hoveyda, J. P. Morken, *Angew. Chem.* **1996**, *108*, 1378−1399; *Angew. Chem. Int. Ed. Engl.* **1996**, *35*, 1262−1284.
[13] [13a] H. Butenschön, *Chem. Rev.* **2000**, *100*, 1527−1564. [13b] R. M. Bellabarba, G. P. Clancy, P. T. Gomes, A. M. Martins, L. H. Rees, M. L. H. Green, *J. Organomet. Chem.* **2001**, *640*, 93−112 and cited references.
[14] J. C. Leblanc, C. Moise, A. Maisonnat, R. Poilblanc, C. Charrier, F. Mathey, *J. Organomet. Chem.* **1982**, *231*, C43−C48.
[15] [15a] B. E. Bosch, G. Erker, R. Fröhlich, O. Meyer, *Organometallics* **1997**, *16*, 5449−5456. [15b] I. Ara, E. Delgado, J. Fornies, E. Hernandez, E. Lalinde, N. Mansilla, M. T. Moreno, *J. Chem. Soc., Dalton Trans.* **1996**, 3201−3207.
[16] [16a] X.-D. He, A. Maisonnat, F. Dahan, R. Poilblanc, *Organometallics* **1989**, *8*, 2618−2626. [16b] W. Tikkanen, Y. Fujita, J. L. Petersen, *Organometallics* **1986**, *5*, 888−894. [16c] R. M. Bullock, C. P. Casey, *Acc. Chem. Res.* **1987**, *20*, 167−173. [16d] F. T. Ladipo, G. K. Anderson, N. P. Rath, *Organometallics* **1994**, *13*, 4741−4745. [16e] J. Szymoniak, M. M. Kubicki, J. Besançon, C. Moïse, *Inorg. Chim. Acta* **1991**, *180*, 153−160.
[17] C. Poulard, G. Boni, P. Richard, C. Moïse, *J. Chem. Soc., Dalton Trans.* **1999**, 2725−2730.
[18] S. Beck, S. Lieber, F. Schaper, A. Geyer, H.-H. Brintzinger, *J. Am. Chem. Soc.* **2001**, *123*, 1483−1489.
[19] L. D. Durfee, I. P. Rothwell, *Chem. Rev.* **1988**, *88*, 1059−1079.
[20] G. Erker, *Acc. Chem. Res.* **1984**, *17*, 103−109.
[21] [21a] A. Antiñolo, M. Fajardo, C. López-Mardomingo, I. López-Solera, A. Otero, Y. Pérez, S. Prashar, *Organometallics* **2001**, *20*, 3132−3138. [21b] A. Antiñolo, M. Fajardo, C. Huertas, A. Otero, S. Prashar, A. M. Rodriguez, *J. Organomet. Chem.* **1999**, *585*, 154−161. [21c] A. Antiñolo, P. Espinosa, M. Fajardo, P. Gómez-Sal, C. López-Mardomingo, A. Martin-Alonso, A. Otero, *J. Chem. Soc., Dalton Trans.* **1995**, 1007−1013. [21d] A. Antiñolo, F. Carrillo-Hermosilla, A. Otero, M. Fajardo, A. Garcés, P. Gómez-Sal, C. López-Mardomingo, A. Martín, C. Miranda, *J. Chem. Soc., Dalton Trans.* **1998**, 59−65.
[22] [22a] A. J. Bridgeman, L. Davis, S. J. Dixon, J. C. Green, I. N. Wright, *J. Chem. Soc., Dalton Trans.* **1995**, 1023−1027. [22b] J. C. Green, M. L. H. Green, J. T. James, P. C. Konidaris, G. H. Maunder, P. Mountford, *J. Chem. Soc., Chem. Commun.* **1992**, 1361−1364. [22c] M. H. Schofield, T. P. Kee, J. T. Anhaus, R. R. Schrock, K. H. Johnson, W. M. Davis, *Inorg. Chem.* **1991**, *30*, 3595−3604. [22d] J. T. Anhaus, T. P. Kee, M. H. Schofield, R. R. Schrock, *J. Am. Chem. Soc.* **1990**, *112*, 1642−1643.
[23] T. W. Graham, A. Llamazares, R. McDonald, M. Cowie, *Organometallics* **1999**, *18*, 3490−3501.
[24] L. P. Casey, R. M. Bullock, W. C. Fultz, A. L. Rheingold, *Organometallics* **1982**, *1*, 1591−1596.
[25] J. Sundermeyer, J. Putterlik, M. Foth, J. S. Field, N. Ramesar, *Chem. Ber.* **1994**, *127*, 1201−1212.

Received March 19, 2002
[I02140]

Palladium and Platinum Units Grafted on the Periphery of Carbosilane Dendrimers

Mónica Benito,[a] Oriol Rossell,*[a] Miquel Seco,[a] Guillermo Muller,[a] Juan I. Ordinas,[a] Mercè Font-Bardia,[b] and Xavier Solans[b]

Keywords: Dendrimers / Alkynes / Homogeneous catalysis / Palladium / Platinum

The reaction of a series of phosphanyl-terminated carbosilane dendrimers with palladium and platinum complexes was carried out. The new metallodendrimers containing $PdCl(\eta^3\text{-}2\text{-}MeC_3H_4)$ and $PtCl_2$ or $Pt(C{\equiv}CPh)_2$ as peripheral groups were characterized by ^1H, ^{13}C, ^{29}Si, ^{31}P, and ^{195}Pt NMR spectroscopy, and, in some cases, by mass spectrometry. The $PtCl_2$-containing species of the second-generation carbosilane dendrimer displays only one of the two possible stereoisomers. By comparison with the ^{31}P NMR spectra of the model compounds *cis*-$[PtCl_2(PPh_2CH_2SiMe_3)_2]$ (**4**) and *cis*-$[PtCl_2\{Me_2Si(CH_2PPh_2)_2\}]$ (**5**), it was deduced that the $PtCl_2$ units are bound on the surface of the dendrimer through two phosphorus atoms belonging to the same branch. The palladium dendrimers were tested as catalysts in the hydrovinylation of styrene, and their activity was compared with that of the model catalyst $[PdCl(\eta^3\text{-}2\text{-}MeC_3H_4)(PPh_2CH_2SiMe_3)]$. The crystal structures of **4**, **5**, and $[Pt(C{\equiv}CPh)_2\{Me_2Si(CH_2PPh_2)_2\}]$ (**6**) were solved by X-ray diffraction analysis.
(© Wiley-VCH Verlag GmbH, 69451 Weinheim, Germany, 2002)

Introduction

There is currently an interest in the synthesis of dendrimers and in the development of their chemistry.[1] Carbosilane dendrimers have been widely used in recent years because they are very stable, both kinetically and thermodynamically.[2] Moreover, peripheral groups, such as Si−Cl offer the opportunity of introducing other functions through the appropriate chemistry; such as the synthesis of carbosilane dendrimers containing diphenylphosphane-terminated groups.[3] Recently, we used these species as "dendrimer ligands" to coordinate a number of metal units (e.g., AuCl).[4] These units reacted, in turn, with metal anions to give dendrimers decorated on the surface by transition metal clusters.[5] We now report an extension of our previous efforts to graft palladium and platinum fragments on the periphery of the dendrimers and the study of the reactivity of such types of species, including the use of palladium compounds as catalytic precursors in the hydrovinylation of styrene.

Results and Discussion

The carbosilane dendrimers chosen for this study are listed in Scheme 1. They display different numbers of terminal phosphanyl groups on the surface (**1** and **2**), and the surface congestion on **3** is lower due to the presence of $CH_2-CH_2-SiMe_2$ spacers in the arms. The dendrimers were obtained by a repetitive stepwise synthetic route of hydrosilylation of the vinylic end groups of the dendrimer with chlorosilanes followed by alkenylation with vinylmagnesium chloride.[3] Next, reaction with the tetramethylethylenediamine complex of [(diphenylphosphanyl)methyl]lithium permitted the incorporation of terminal CH_2PPh_2 groups.

Platinum Dendrimers

Generally, the functionalization of the peripheral *P*-branched dendrimers with transition metals is simply achieved by taking advantage of the complexation ability of these species.[6] For example, they have been treated with complexes such as [Rh(acac)(COD)][7] or $[Pd(\mu\text{-}Cl)(\eta^3\text{-}2\text{-}MeC_3H_4)]_2$.[8] Several reports describe peripheral platinum-containing dendrimers, but only one example shows platinum centers bonded to phosphorus atoms.[7]

In this paper we have functionalized the surface of our *P*-branched dendrimers with platinum by reaction with [$PtCl_2$(COD)]. We also synthesised the model compounds $[PtCl_2(PPh_2CH_2SiMe_3)_2]$ (**4**) and $[PtCl_2\{Me_2Si(CH_2PPh_2)_2\}]$ (**5**). Compound **4** was synthesised from $PPh_2CH_2SiMe_3$ (2 equiv.) and [$PtCl_2$(COD)] (1 equiv.), and **5** from [$PtCl_2$(COD)] (1 equiv.) and $Me_2Si(CH_2PPh_2)_2$ (1 equiv) (Scheme 2). Details of spectroscopy data of these compounds are given in the Exp. Sect.

[a] Departament de Química Inorgànica, Universitat de Barcelona, Martí i Franquès 1−11, 08028 Barcelona, Spain
Fax: (internat.) + 34-93/490-7725
E-mail: oriol.rossell@qi.ub.es
[b] Departament de Cristal·lografia, Mineralogia i Dipòsits Minerals, Universitat de Barcelona, Martí i Franquès s/n, 08028 Barcelona, Spain

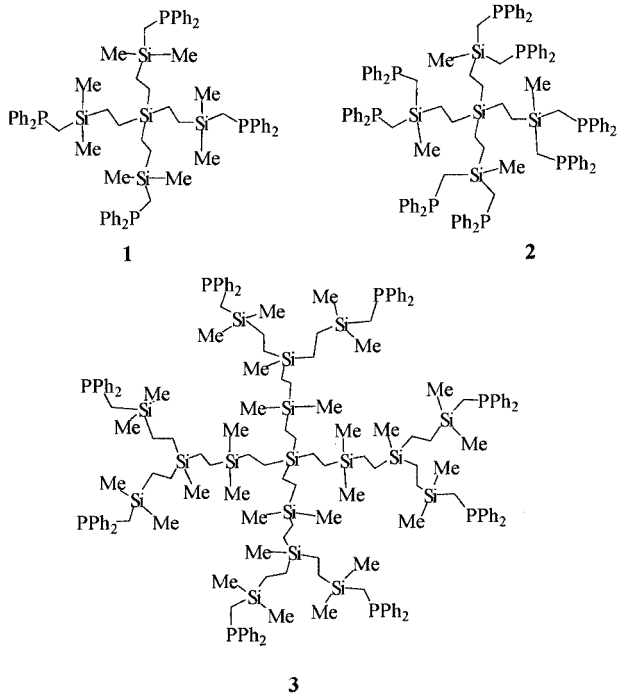

Scheme 1

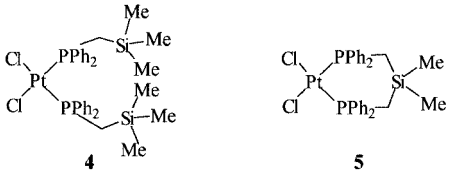

Scheme 2

X-ray Crystal Structures of 4 and 5

A view of the compound *cis*-[$PtCl_2(PPh_2CH_2SiMe_3)_2$] (**4**) appears in Figure 1, and selected bond lengths and angles are given in Table 1. The platinum atom has a planar coordination with the slight tetrahedral distortion frequently observed for d^8 metal ions with bulky ligands.

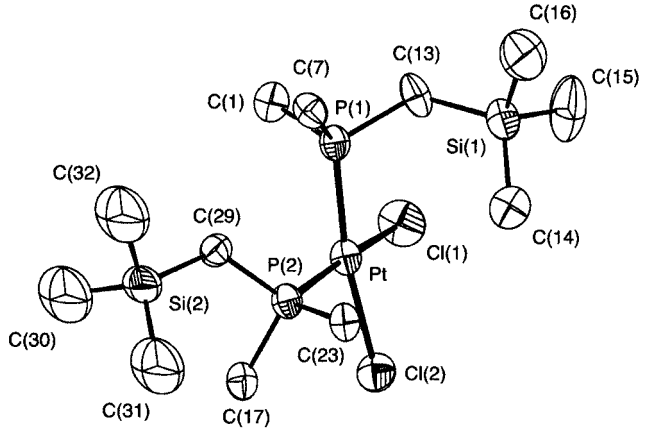

Figure 1. ORTEP drawing of the molecular structure and numbering scheme of **4**

Table 1. Selected bond lengths [Å] and angles [°] for **4**

Pt−P(1)	2.2401(9)	P(2)−C(29)	1.813(3)
Pt−P(2)	2.2545(8)	Si(1)−C(13)	1.892(4)
Pt−Cl(1)	2.3563(8)	Si(2)−C(29)	1.901(3)
Pt−Cl(2)	2.3506(9)	P(1)−C(13)	1.825(3)
P(1)−Pt−P(2)	100.90(3)	P(2)−C(29)−Si(2)	126.43(17)
P(1)−Pt−Cl(2)	169.85(3)	C(17)−P(2)−Pt	110.46(11)
P(2)−Pt−Cl(2)	87.89(3)	C(23)−P(2)−Pt	111.47(10)
P(1)−Pt−Cl(1)	84.92(3)	Cl(2)−Pt−Cl(1)	86.70(3)
P(2)−Pt−Cl(1)	172.88(3)	C(7)−P(1)−Pt	120.23(11)
C(13)−P(1)−Pt	112.61(14)	C(1)−P(1)−Pt	112.43(12)
C(29)−P(2)−Pt	118.06(10)		

The phosphane ligands adopt a *cis* configuration, in spite of the known fact that the bulky phosphane favors the formation of *trans* isomers to minimize ligand interactions. The Pt−Cl bond lengths are in the expected range, and the Pt−P distances are not elongated to any significant extent. The angles around the platinum atom are in the range 84.92(3)° [P(1)−Pt−Cl(1)] to 100.90(3)° [P(1)−Pt−P(2)]. The latter is intermediate between that found for [$PtCl_2(PPh_3)_2$] (97.8°)[9] and [$PtCl_2(PCy_3)_2$] (107.6°).[10] There is a steric tension between C(31) and the phenyl group C(17), which implies an increase in the Si(2)−C(29)−P(2) angle to 126.4°.

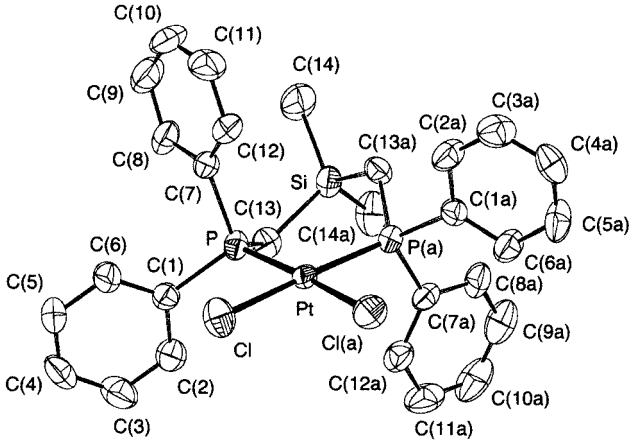

Figure 2. View of the molecular structure of **5** together with the atomic numbering scheme

The molecular structure of **5** is shown in Figure 2. Selected bond lengths and angles are listed in Table 2. Com-

Table 2. Selected bond lengths [Å] and angles [°] for **5**

Pt−P(1)	2.2456(16)	Si(1)−C(14)	1.845(7)
Pt−Cl(1)	2.3440(17)	Si(1)−C(13)	1.872(7)
P(1)−C(1)	1.822(6)	P(1)−C(13)	1.806(7)
P(1)−C(7)	1.810(6)		
P(1)−Pt−Cl(1)	88.59(7)	P(1)−Pt−Cl(1′)	175.98(6)
Cl(1)−Pt−Cl(1′)	87.40(10)	C(14′)−Si−C(13)	105.9(4)
C(14′)−Si−C(14)	109.3(6)	C(13)−Si−C(13′)	107.5(4)
C(14)−Si−C(13)	114.3(4)	C(13)−P−Pt	115.5(2)
C(7)−P−C(1)	105.4(3)	C(7)−P−Pt	113.9(2)
P−C(13)−Si	118.1(4)	C(1)−P−Pt	114.9(2)
P−Pt−P′	95.43(8)		

plex **5** contains a four-coordinate distorted square-planar platinum center, with the chlorine ligands displaced by −0.0052(1) Å (Cl) and 0.0052(1) Å [Cl(a)] from the Pt−P−P(a) plane. The ligand PP is bound in a bidentate fashion.

It should be noted that the ligand 2,2-dimethyl-1,3-bis(diphenylphosphanyl)-2-silapropane is an analogue of dppp, although the substitution of the CH_2 unit for $SiMe_2$ in the backbone not only increases complex solubility but also provides an excellent NMR spectroscopic handle. The Pt−P distances compare well with values reported in the compound $[PtCl_2(dppp)]$.[11] The shorter Pt−P bond lengths also suggest that a stronger bond than normal results from the chelate ring formation.

The six-membered chelate ring comprising Pt−P−C−Si−C−P adopts a twisted boat conformation, as found, for example, in $[Ni(NO_3)_2\{Ph_2PCH_2Si(CH_3)_2CH_2PPh_2\}]$.[12] It is noteworthy that the equivalent chelate ring in $[CoBr_2\{Me_2Si(CH_2PPh_2)_2\}]$[13] adopts a chair conformation, presumably due to the tetrahedral metal center. The chelate bite angle in **5** is 95.43(8)° (P1−Pt−P1′), somewhat shorter than that found for **4** and for the tetrahedral metal compounds $[CdCl_2(PP)]$,[14] $[CoCl_2(PP)]$,[13] and $[HgI_2(PP)]$[15] [PP = $Me_2Si(CH_2PPh_2)_2$].

Synthesis

Dendrimers **1** and **2** reacted with $[PtCl_2(COD)]$ in CH_2Cl_2 at room temperature to give, after COD displacement, the soluble, yellow, platinum-containing dendrimers **1a** and **2a**, respectively, within a few minutes (Scheme 3).

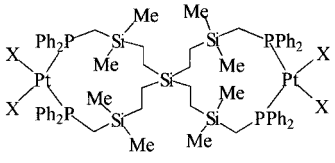

1a

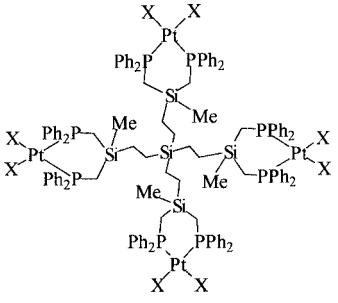

2a X= Cl
2b X= C≡CPh
2c X= $Co_2(CO)_6(C_2Ph)$

Scheme 3

The unique signal in the ^{31}P NMR spectra of their solutions clearly indicate that no mixture of compounds was formed, and reveal the complexation of platinum by the presence of platinum satellites (J_{Pt-P} = 3686 Hz for **1a** and 3558 Hz for **2a**). Two silicon signals are observed for both compounds, namely δ = 8.98 ppm (Si_0) and δ = 4.04 ppm (Si_1) ($CDCl_3$) for **1a**, and δ = 9.54 ppm (Si_0) and δ = 0.49 ppm (Si_1) ($[D_6]$DMSO) for **2a**. The ^{195}Pt NMR spectra showed a triplet at δ = −4320 ppm for **1a** and at δ = −4482 ppm for **2a** indicating the equivalence of the platinum atoms.

It is worth noting that the $PtCl_2$ units can be bound on the surface of the dendrimer through two P atoms belonging to the same branch, or alternatively, to different branches. Accordingly, **2a** can exhibit another stereoisomer, **2a′** (Scheme 4). A third possibility would be the simultaneous interaction of the platinum fragment with two molecules of dendrimer. However, in this case, the solubility of the resulting polymer species would probably be very low.

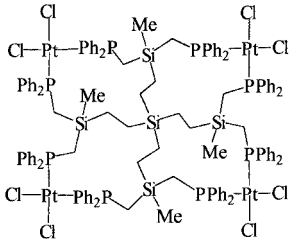

2a'

Scheme 4

As mentioned earlier, the unique resonance in the ^{31}P NMR spectrum indicates that only one isomer is formed. In order to assign it to **2a** or **2a′**, model compounds **4** and **5** are useful. Thus, for **4**, the angle P−Pt−P is 100.9° and J_{P-Pt} = 3673 Hz (δ = 4.2 ppm), while for **5**, the P−Pt−P angle is 95.43° and J_{P-Pt} = 3560 Hz (δ = 3.48 ppm). Although both values are close, we tentatively propose that the stereoisomer formed is **2a** (J_{P-Pt} = 3558 Hz; δ = 3.23 ppm), based on these data.

The FAB mass spectrum of **1a** contains two ion peaks at 1665.0 (calcd. 1666) and 815.0 (calcd. 815.4) corresponding to $[M - Cl]^+$ and $[M - 2\ Cl]^{2+}$, respectively. For **2a**, ion peaks at 1450, 954, and 707 were assigned to fragments $[M - 2\ Cl]^{2+}$, $[M - 3\ Cl]^{3+}$, and $[M - 4\ Cl]^{4+}$, respectively.

In contrast with the reported results for **1a** and **2a**, the ^{31}P NMR spectrum of the reaction of **3** with $[PtCl_2(COD)]$ to afford **3a**, shows, along with a sharp signal at δ = 4.4 ppm (t, J_{P-Pt} = 3683 Hz), another broad resonance at δ = 3.7 ppm (J_{P-Pt} = 3545 Hz). This spectrum indicates the presence of a mixture of stereoisomers, which was confirmed by the ^{195}Pt NMR spectrum. However, attempts to separate these isomers were unsuccessful. Electrospray spectrometry showed peaks corresponding to $[M - n\ Cl]^{n+}$ (n = 2, 3, 4, 6).

Following the same methodology for **1a**, **2a**, and **3a**, novel organometallic dendrimers containing platinum acetylide units were prepared. This class of derivatives has been actively investigated in the design of polymeric transition-metal complexes containing σ-bonded acetylide units because of their potential use in catalytic processes and as

precursors to cluster-containing dendrimers.[16] Two examples of organometallic dendrimers with a backbone composed of platinum acetylide units have been recently reported.[17]

We grafted $Pt(C{\equiv}CPh)_2$ fragments onto the surface of dendrimers **1** and **2** by treating them with $[Pt(C{\equiv}CPh)_2(COD)]$. According to the methodology followed in this paper, the model compound **6** was firstly synthesised from $Me_2Si(CH_2PPh_2)_2$ and $[Pt(C{\equiv}CPh)_2(COD)]$. (Scheme 5).

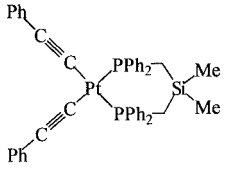

6

Scheme 5

The $^{195}Pt\{^1H\}$ NMR spectrum of **6** shows a resonance at $\delta = -3813$ ppm ($J_{P-Pt} = 2266$ Hz) and the ^1H NMR spectrum reveales the coupling of the CH_2 protons of the CH_2P fragment with the P and Pt nucleus ($J_{H-P} = 11.2$ Hz and $^3J_{H-Pt} = 32.95$ Hz). In accordance with its structure, the C_α acetylene carbon resonances appear in the $^{13}C\{^1H\}$ NMR spectrum at $\delta = 104.9$ ppm as a first-order doublet of doublets ($^2J_{C\alpha-Pcis} = 20.1$ Hz; $^2J_{C\alpha-Ptrans} = 150.2$ Hz), while the C_β signal is found at $\delta = 109.67$ ppm as the typical A part of a second-order AXX′ system [$^3J_{C\beta-Pcis} + {}^3J_{C\beta-Ptrans} = 35.5$ Hz)]. These values are very close to those reported by Forniés et al. in a series of *cis*-bis(alkynyl)platinum complexes.[18]

Crystal Structure of 6

The molecular structure of **6** was determined by X-ray structure analysis (Figure 3). Selected bond lengths and angles are collected in Table 3. Compound **6** is a nearly square-planar 16e$^-$ platinum complex formed by a diphosphane ligand and two mutually *cis*-oriented acetylide groups. The six atoms that form the chelate ring adopt a boat conformation with no appreciable twist distortion compared with that of **5**. The Pt−C and Pt−P distances are within the range of values quoted in the literature for *cis*-acetylide complexes. Bond lengths and angles in the two independent acetylide ligands are normal and the Pt−C≡C−C systems do not deviate significantly from linearity (see Table 3).[18,19]

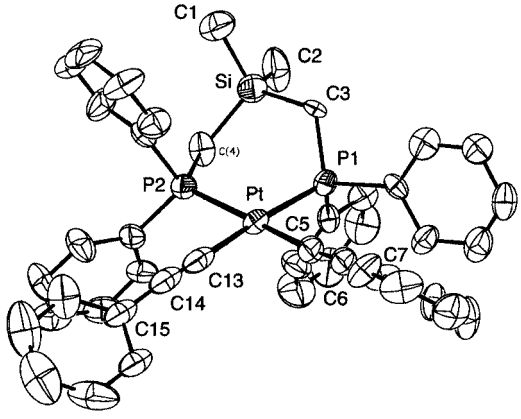

Figure 3. ORTEP drawing of the molecular structure and numbering scheme of **6**

Table 3. Selected bond lengths [Å] and angles [°] for **6**

Pt−C(13)	1.945(9)	Pt−P(1)	2.294(2)
Pt−C(5)	1.993(8)	Pt−P(2)	2.299(2)
P(1)−C(3)	1.799(6)	P(2)−C(4)	1.819(6)
Si−C(2)	1.859(7)	Si−C(4)	1.867(7)
Si−C(1)	1.870(8)	Si−C(3)	1.916(7)
C(5)−C(6)	1.209(9)	C(6)−C(7)	1.461(10)
C(13)−C(14)	1.148(10)	C(14)−C(15)	1.530(11)
C(13)−Pt−C(5)	87.3(3)	C(13)−Pt−P(1)	175.8(2)
C(5)−Pt−P(1)	91.7(2)	C(13)−Pt−P(2)	86.2(2)
C(5)−Pt−P(2)	171.2(2)	P(1)−Pt−P(2)	95.21(8)
C(3)−P(1)−Pt	112.9(2)	C(4)−P(2)−Pt	117.4(2)
C(4)−Si−C(3)	110.0(3)	P(1)−C(3)−Si	117.4(3)
P(2)−C(4)−Si	118.5(4)	C(6)−C(5)−Pt	173.1(7)
C(5)−C(6)−C(7)	177.7(8)	C(14)−C(13)−Pt	175.2(8)
C(13)−C(14)−C(15)	172.1(9)		

The reaction of **2** with the platinum acetylide complex in a 1:4 molar ratio gave **2b** in a high yield. The analytical and spectroscopic (IR and ^1H, ^{13}C, ^{31}P, ^{29}Si, ^{195}Pt NMR) data are in agreement with the formula proposed for the new complex. The most remarkable feature of the IR spectrum is the presence of an absorption at 2117 cm^{-1} attributed to the $\nu_{C\equiv C}$ stretching vibration, which is considerably shifted to lower wavenumbers compared to that of the σ-alkynyl precursor. The C_α alkynyl carbon resonance in the $^{13}C\{^1H\}$ NMR spectrum appears at $\delta = 104.4$ ppm ($^2J_{C\alpha-Pcis} = 20.0$ Hz; $^2J_{C\alpha-Ptrans} = 150.3$ Hz); that of C_β appears at $\delta = 109.97$ ppm [$^3J_{C\beta-Pcis} + {}^3J_{C\beta-Ptrans} = 32.0$ Hz)]. The ^{195}Pt NMR spectrum shows a triplet with a coupling constant ($J_{Pt-P} = 2255$ Hz), very similar to that found for **6**, which, along with the NMR spectroscopic data discussed above, confirms the proposed structure for **2b**.

As expected, the attachment of the acetylide group increased its solubility considerably compared with that of **2a**. In contrast, the reaction of the platinum acetylide compound with **1** gave a mixture of species. These species were not analyzed because of their complexity. It seems that the bite angle P−Pt−P displayed in **1**, as compared with **2**, is higher than that required for the complexation of the $Pt(C{\equiv}CPh)_2$ fragment.

Reaction with $Co_2(CO)_8$

Alkyne systems easily react with $Co_2(CO)_8$ to afford $C_2[Co(CO)_3]_2$ tetrahedrane clusters that can be used as a part of the backbone dendritic connectivity or as peripheral groups. This is a facile method for the introduction of mul-

tiple metal clusters, but it has found little use in metallodendrimer chemistry,[20] although it is well known in the area of heterometallic stars.[21]

This strategy was thus applied to our dendrimers, in an attempt to form multiple $\{C_2Co_2(CO)_6\}$ cluster sites. A previous reaction between the model compound **6** and $Co_2(CO)_8$ gave $[Pt\{C_2PhCo_2(CO)_6\}_2\{Me_2Si(CH_2PPh_2)_2\}]$ (**7**) (Scheme 6), the spectroscopic data of which are listed in the Exp. Sect., thus permitting optimization of the reaction conditions.

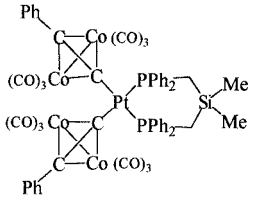

7

Scheme 6

Compound **2b** was treated in dichloromethane at room temperature with the octacarbonyldicobalt compound, and the new species **2c** was obtained in moderate yields after 2 h.

The incorporation of the carbonylmetal units was confirmed by the appearance of strong absorptions in the IR spectrum at 2081, 2060, and 2016 cm^{-1}, typical of $[Co_2(CO)_6(RCCR)]$ clusters. Strong evidence of cluster formation could not be inferred from the ^{13}C NMR spectrum, given the poor solubility of **2c**. A single signal at $\delta = 210$ ppm was assigned to the carbonyl carbon atoms. In the ^1H NMR spectrum the broad signal at $\delta = 1.65$ ppm is in agreement with the diastereotopic and therefore nonequivalent nature of the CH_2−P protons. This fact was observed analogously in the spectra of **2a** and **2b**. The ^{31}P NMR spectrum shows only one signal at $\delta = 12.6$ ppm flanked by platinum satellites. The $Co_2(CO)_6$ coordination caused an increase of the coupling constant J_{P-Pt} from 2254 Hz of **2b** to 3496 Hz. We are currently extending the chemical and structural aspects of these novel high-nuclearity species.

Palladium Dendrimers

Before the synthesis of the Pd-containing dendrimers, we prepared the model compound $[PdCl(\eta^3\text{-}2\text{-}MeC_3H_4)(PPh_2CH_2SiMe_3)]$ (**8**) by treating $[Pd(\mu\text{-}Cl)(\eta^3\text{-}2\text{-}MeC_3H_4)]_2$ with $PPh_2CH_2SiMe_3$ (Scheme 7).

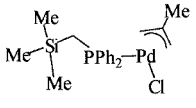

8

Scheme 7

The ^{31}P NMR spectrum of **8** shows only one signal at $\delta = 17.8$ ppm and the ^{29}Si NMR spectrum, another one at $\delta = 0.8$ ppm. The ^1H and ^{13}C NMR spectra evidence the presence of the allyl and the dendrimer ligands.

The grafting of the palladium fragments $Pd(\eta^3\text{-}2\text{-}MeC_3H_4)Cl$ on the surface of our dendrimers was achieved in good yields by treating **1** and **3** with the dinuclear allyl complex $[Pd(\mu\text{-}Cl)(\eta^3\text{-}2\text{-}MeC_3H_4)]_2$ in THF at room temperature (Scheme 8).

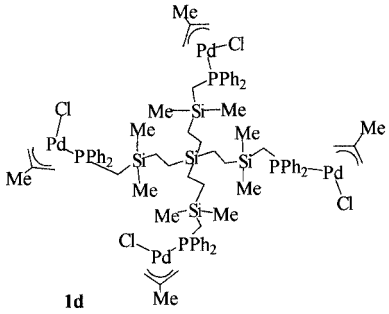

1d

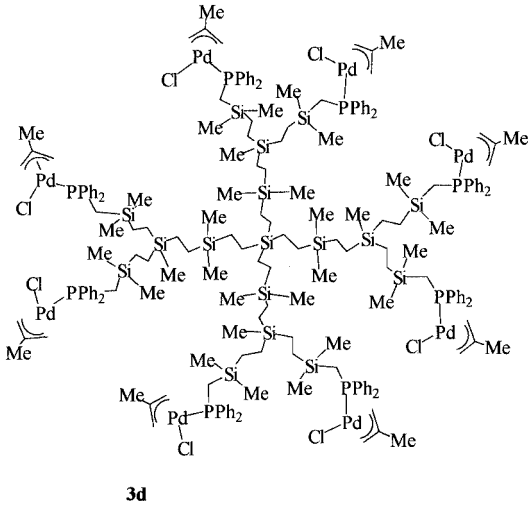

3d

Scheme 8

The synthesis of the new palladodendrimers **1d** and **3d** was monitored by ^{31}P NMR spectroscopy. In both cases, the complete disappearance of the signal at $\delta = -23$ ppm along with the emergence of a new one at $\delta \approx 17$ ppm confirmed that the reaction occurred quantitatively. The yellow compounds obtained were pure within the limits of the NMR spectroscopic detection. They were soluble in the most common organic solvents, and were characterized by elemental analyses, ^1H, ^{13}C, ^{31}P, and ^{29}Si NMR, as well as by fast atom bombardment (FAB) or electrospray mass spectrometry.

The ^1H NMR spectra for **1d** and **3d** showed the resonances for the methyl, methylene, and ethylene protons with chemical shifts in the corresponding regions of the spectrum in the expected integrated ratio. The coordination of the palladium fragment to the dendrimer gives rise to the coupling of the H^1 and H^2 with the phosphorus nucleus

($^3J_{H-P}$ = 6.5 and 10 Hz) and the high-field shifts of the H^3 and H^4 resonances (Scheme 9).

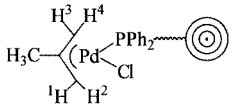

Scheme 9

The ^{13}C NMR spectra confirmed the presence of the above-mentioned groups. The ^{29}Si NMR spectra display clearly separated signals (two for **1d** and four for **3d**) for the different types of silicon atoms in the molecules. These signals can be easily assigned on the basis of the chemical shifts and the peak intensities. The presence of only one signal in the ^{31}P NMR spectra indicates that no mixture of products is formed in the reaction.A solution of sodium chloride in THF was added to the samples **1d** and **3d** in order to improve the peak resolution in mass spectrometry. Thus, FABMS showed the $[M - Cl]^+$ peak at m/z = 1923.6 for **1d** (calcd. 1920.5), and the MS/ES, the peak $[M - 3\{Pd(2\text{-}CH_3\text{-}C_3H_4)Cl\} - 3\ Cl]^{3+}$ at m/z = 1272.2 for **3d** (calcd. 1273.1) in accordance with the proposed formula. Other fragments were also assigned (see Exp. Sect.).

Catalytic Studies

One of the main applications of dendrimers is in catalysis. The well-defined structure and the possibility of attaching a large number of active sites makes them especially interesting for catalyst immobilization and catalyst recycling.[22] Recently, some palladium-containing carbosilane dendrimers have been used as catalysts in allylic alkylation reactions[8] and in the selective hydrovinylation of styrene performed in a continuous flow membrane reactor.[23] Here, the palladium dendrimers **1d** and **3d** were tested as catalysts in the hydrovinylation of styrene (Scheme 10), and their activity was compared with that of the mononuclear model complex $[PdCl(\eta^3\text{-}2\text{-}MeC_3H_4)(PPh_2CH_2SiMe_3)]$ (**8**). Interestingly, hydrovinylation of styrene produced 3-phenyl-1-butene as a main product, this process being a model reaction for the synthesis of compounds with pharmacological activity.

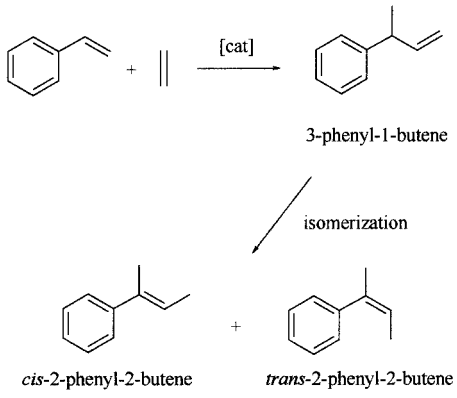

Scheme 10

The fact that **8**, **1d**, and **3d** have an $RCH_2Si(CH_3)_2\text{-}CH_2PPh_2$ moiety in common permits the evaluation of the steric effects caused only by changes in the dendrimeric structure.

It is well known that active catalysts in hydrovinylation reactions are cationic species, so we synthesised the cationic species of our dendrimers in situ by adding $Ag[BF_4]$ to their dichloromethane solutions and removing the silver chloride by filtration. Otherwise, the cationic complexes stabilized with CH_3CN ligands were isolated as solids and their activity compared with that exhibited by the species prepared in situ. In order to differentiate between the two types of species, we will refer to the cationic dendrimers obtained in situ as **1d**$^+$, **3d**$^+$, and **8**$^+$, and the salts stabilized with CH_3CN as **1d***, **3d***, and **8***.

The catalytic data obtained in the hydrovinylation of styrene using the described compounds are shown in Table 4.

Table 4. Hydrovinylation of styrene by palladium compounds

Entry[a]	Precursor	T [°C]	t [h]	Conversion[b]	Selectivity[c]	TOF/h[d]
1	**8**$^+$	15	2	94.2	80.3	465
2	**8**$^+$	25	0.5	86.8	85.7	1710
3	**8**$^+$	25	0.33	57.5	95.9	1695
4	**1d**$^+$	25	2	88.6	85.9	440
5	**1d**$^+$	25	1	55.4	96.0	550
6	**3d**$^+$	25	1	63.0	94.4	620
7	**8***	25	0.75	78.5	91.6	1040
8	**8***	15	2	71.5	94.4	355
9	**1d***	15	2	29.6	100	145
10	**1d***	25	2	74.2	92.1	368
11[e]	**1d***	25	2	3.5	100	18
12	**3d***	25	1	43.0	97.6	425
13	**3d***	25	1.5	57.4	94.9	380

[a] Initial ethylene pressure, 15 bar; solvent: CH_2Cl_2; ratio styrene/Pd 1000:1. [b] Conversion of starting styrene. [c] Selectivity:% of 3-phenyl-1-butene respect to the total amount of arylbutenes formed. [d] TOF/h calculated as the total amount of arylbutenes formed. [e] In THF.

As can be seen from Table 4, activity is lower for the cationic dendritic precursors **1d**$^+$ (or **1d***) and **3d**$^+$ (or **3d***), compared with the mononuclear precursor **8**. The same effect was observed by Vogt and van Koten in similar hemilabile PO-stabilized dendritic precursors.[24] Probably, the dendrimers block some of the space that olefins can use in their approach to the palladium atoms, the active sites. However, it is remarkable that the activity of the biggest system **3d** is higher or similar to that of **1d** (Entries 5 and 6) in spite of the fact that the first shows 8 PPh_2 groups in comparison with the 4 PPh_2 ligands displayed by the second. This interesting effect can be explained by the fact that **3d** has one methyl group over the neighboring Si while bulkier ligands are attached to the neighboring Si in **1d**. This can be seen by comparing Entries 2, 5, 6, with 7, 10, 13. Moreover, Table 4 shows that the catalysts obtained in situ in dichloromethane are better than those previously isolated, due to the ineffective coordinating ability of the

solvent. When a solvent of greater coordination ability, like THF, was used, an impressive decrease in activity was observed (Entries 10 and 11). Formation of oligomers or higher co-oligomers is not significant. In conclusion, it is clear from our data that the catalytic activity is affected by "surface congestion".

The isomerization of the chiral product 3-phenyl-1-butene to achiral (*E*) and (*Z*) internal olefins (Scheme 10) is related to the conversion of the process. Thus, at high conversions the consecutive isomerization reaction becomes important and consequently an increase of the internal olefins is obtained (Table 4). It is well known that the isomerization occurs through the previous coordination of the 3-phenyl-1-butene to the catalyst. Thus, the coordination ability of other molecules present in the reaction media determines the selectivity. Obviously, in our case, the solvent can compete with the 3-phenyl-1-butene. For example, Entries 1−3 and 8 indicate that the presence of stoichiometric amounts of acetonitrile competes successfully with 3-phenyl-1-butene and avoids its attachment to the catalyst, thus improving the selectivity of the process. In conclusion, in order to improve the selectivity of the process, a major goal would be to find a ligand or a hemilabile bidentate ligand with a coordinating ability towards the metallic system intermediate between styrene and 3-phenyl-1-butene.

From Table 4 we can observe in all cases a decrease of the activity in increasing the reaction times, as a consequence of the deactivation of the catalytic species. This effect is more important for the dendrimers. The deactivation of the catalyst is clearly observed when runs at different reaction times are compared − Entries 4 and 5 or 12 and 13. This is evidenced by a decrease in the TOF number upon increasing the reaction time, in the significant range of conversions. The model compound **8** showed higher stability, but shorter reaction times − Entries 2 and 3. Our preliminary results showed similar loss of activity of **1d** and **3d** precursors. Interestingly, no precipitation of palladium black was observed before total conversion. In order to obtain more conclusive results about the relative stability of these dendritic systems as a function of their size we would need to test the activity of catalyst based on higher generations.

In summary, the dendrimers studied in this paper are active for the hydrovinylation of styrene, but their activity is lower than that shown by the mononuclear model **8** and other related palladium complexes containing different phosphane ligands.[25] However, polynuclear complexes **1d** and **3d** are more active compared with other dendritic catalysts containing 8 and 12 terminal bidentate PO coordinating atoms on the surface.[24] Moreover, the good selectivity of our dendrimers towards 3-phenyl-1-butene is remarkable.

Experimental Section

General: All reactions were carried out under dry nitrogen using standard Schlenk techniques. Solvents were distilled from sodium/benzophenone ketyl (THF and Et_2O), $CaCl_2$ and stored over molecular sieves (acetone) or dried with $CaCl_2$ and distilled from CaH_2 (CH_2Cl_2) under N_2 prior to use. Elemental analyses (C, H) were performed at the Servicio de Microanálisis del Centro de Investigación y Desarrollo del Consejo Superior de Investigaciones Científicas (CSIC). ^1H, $^{13}C\{^1H\}$, $^{29}Si\{^1H\}$, $^{31}P\{^1H\}$, and $^{195}Pt\{^1H\}$ NMR spectra were recorded at 25 °C with a Bruker 250 spectrometer. Chemical shifts are reported in ppm relative to external standards ($SiMe_4$ for ^1H, ^{13}C and ^{29}Si, 85% H_3PO_4 for ^{31}P and H_2PtCl_6 for ^{195}Pt) and coupling constants are given in Hz. Infrared spectra were recorded with FT-IR 520 Nicolet or Impact 400 Nicolet spectrometers in the 4000−400 cm^{-1} range as KBr pellets. MS (FAB and ES) spectra were recorded with a Fisons VGQuattro spectrometer using NBA (3-nitrobenzyl alcohol) as a matrix for FAB spectra. MALDI-TOF spectra were recorded with a Voyager DE-RP (Perspective Biosystems) spectrometer using DHB (2,5-dihydrobenzoic acid) as a matrix. The starting materials $Me_2Si(CH_2PPh_2)_2$,[26] $[Pd(\mu\text{-}Cl)(\eta^3\text{-}2\text{-}Me\text{-}C_3H_4)]_2$,[27] $[PtCl_2(COD)]$,[28] and $[Pt(C{\equiv}CPh)_2(COD)]$[29] were prepared according to published procedures. Other reagents were purchased from commercial suppliers and used as received.

Synthesis of Diphenyl[(trimethylsilyl)methyl]phosphane ($PPh_2CH_2SiMe_3$): This phosphane, described in the literature,[30] was synthesised by a different method here. To a suspension of the Grignard reagent (slight excess) of (chloromethyl)trimethylsilane, prepared from 1.77 g (14.4 mmol) of (chloromethyl)trimethylsilane and 0.45 g (18.5 mmol) of magnesium in THF (50 mL), was slowly added chlorodiphenylphosphane (2.95 g, 13.4 mmol); the resulting mixture was stirred at room temperature for 30 min and hydrolysed with an aqueous solution of NH_4Cl (10%). The organic layer was washed twice with water and dried with Na_2SO_4. Concentration of this solution to dryness gave the desired phosphane as a colorless oil (2.92 g, yield 80%). ^1H NMR (250 MHz, $CDCl_3$, 25 °C): δ = −0.25 (s, 9 H, CH_3), 1.34 (s, 2 H, CH_2), 7.28−7.34 (m, 6 H, C_6H_5), 7.45−7.50 (m, 4 H, C_6H_5) ppm. ^{31}P NMR (101.26 MHz, $CDCl_3$, 25 °C): δ = −22.05 (s) ppm. ^{29}Si NMR (49.66 MHz, $CDCl_3$, 25 °C): δ = 1.26 (d, J = 14.7 Hz) ppm. ^{13}C NMR (75.4 MHz, $CDCl_3$, 25 °C): δ = −0.2 (d, J = 4.7 Hz, CH_3), 14.6 (d, J = 29.0 Hz, CH_2), 128.1−141.2 (m, C_6H_5) ppm.

Synthesis of $[PtCl_2(Me_3SiCH_2PPh_2)_2]$ (4): $[PtCl_2(COD)]$ (0.08 g, 0.21 mmol) was dissolved in CH_2Cl_2 (10 mL) and a solution of $PPh_2CH_2Si(Me_2)CH_2PPh_2$ (0.12 g, 0.43 mmol) in CH_2Cl_2 (10 mL) was added. The solution was stirred overnight and then concentrated to dryness. The solid was recrystallized from CH_2Cl_2/Et_2O and dried under vacuum. Yield: 172 mg, 50%. ^1H NMR (250 MHz, $CDCl_3$, 25 °C): δ = −0.18 (s, 18 H, CH_3), 1.72 (d, $^2J_{H-P}$ = 15.7, $^3J_{H-Pt}$ = 32 Hz, 4 H, CH_2P), 7.24−7.57 (m, 20 H, C_6H_5) ppm. $^{13}C\{^1H\}$ NMR (62.86 MHz, $CDCl_3$, 25 °C): δ = 0.9 (s, CH_3), 18.3 (m, CH_2P), 128.1−133.2 (m, C_6H_5) ppm. $^{29}Si\{^1H\}$ NMR (49.66 Hz, $CDCl_3$, 25 °C): δ = 0.11 ppm. $^{31}P\{^1H\}$ NMR (101.26 MHz, $CDCl_3$, 25 °C): δ = 4.2 (s, $^1J_{P-Pt}$ = 3673.2 Hz) ppm. $^{195}Pt\{^1H\}$ NMR (53.54 MHz, $CDCl_3$, 25 °C): δ = −4318.0 (t) ppm. $ESMS^+$ (CH_2Cl_2): m/z = 775.7 $[M - Cl]^+$. $MSFAB^+$ (THF): m/z = 810.2 $[M]^+$, 775.3 $[M - Cl]^+$. $C_{32}H_{42}Cl_2P_2PtSi_2$ (810.80): calcd. C 47.36, H 5.22; found C 48.26, H 5.43.

Synthesis of $[PtCl_2\{Me_2Si(CH_2PPh_2)_2\}]$ (5): Experimental conditions and workup were identical to those for the preparation of **4**. Yield: 218 mg, 90%. ^1H NMR (250 MHz, CD_2Cl_2, 25 °C): δ = −0.34 (s, 6 H, CH_3), 1.77 (d, 4 H, $^2J_{P-H}$ = 12.3, $^3J_{H-Pt}$ = 62.3 Hz, CH_2P), 7.4−7.8 (m, 20 H, C_6H_5) ppm. $^{13}C\{^1H\}$ NMR (62.86 MHz, CD_2Cl_2, 25 °C): δ = −0.1 (t, $^3J_{C-P}$ = 3.4 Hz, CH_3), 12.2 (m, CH_2P), 128.2−133.5 (m, C_6H_5) ppm. $^{29}Si\{^1H\}$ NMR (49.66 MHz, CD_2Cl_2, 25 °C): δ = −0.96 ppm. $^{31}P\{^1H\}$ NMR (101.26 MHz, CD_2Cl_2, 25 °C): δ = 3.5 (s, $^1J_{P-Pt}$ = 3559.8 Hz,

PPh_2) ppm. $^{195}Pt\{^1H\}$ NMR (53.54 MHz, CD_2Cl_2, 25 °C): δ = −4491.7 (t) ppm. MSFAB$^+$ (CH_2Cl_2): *m/z* = 687.2 [M − Cl]$^+$. $C_{28}H_{30}Cl_2P_2PtSi$ (722.58): calcd. C 46.54, H 4.19; found C 45.60, H 4.23.

Synthesis of 1a: Experimental conditions and workup were identical to those for the preparation of **4**. Yield: 145 mg, 71%. ^1H NMR (250 MHz, $CDCl_3$, 25 °C): δ = −0.06 (br. s, 24 H, CH_3), 0.75−1.44 (br. s, 16 H, CH_2), 1.92 (d, $^2J_{H-P}$ = 15.8 Hz, 8 H, CH_2P), 7.00−7.70 (m, 40 H, C_6H_5) ppm. $^{13}C\{^1H\}$ NMR (62.86 MHz, $CDCl_3$, 25 °C): δ = −0.6 (s, C^1H_3), 4.7 (s, $-CH_2-$), 10.3 (s, $-CH_2-$), 16.2 (m, CH_2P), 127.7−132.4, (m, C_6H_5) ppm. $^{29}Si\{^1H\}$ NMR (49.66 MHz, $CDCl_3$, 25 °C): δ = 4.04 (s, Si_1), 8.98 (s, Si_0) ppm. $^{31}P\{^1H\}$ NMR (101.26 MHz, $CDCl_3$, 25 °C): δ = 4.4 (s, $^1J_{P-Pt}$ = 3686.4 Hz, PPh_2) ppm. $^{195}Pt\{^1H\}$ NMR (53.54 MHz, $CDCl_3$, 25 °C): δ = −4322.0 (t) ppm. ESMS$^+$ (THF): *m/z* = 1665.0 [M − Cl]$^+$, 815.0 [M − 2 Cl]$^{2+}$. $C_{68}H_{88}Cl_4P_4Pt_2Si_5$ (1701.77): calcd. C 47.99, H 5.21; found C 47.70, H 5.27.

Synthesis of 2a: Experimental conditions and workup were identical to those for the preparation of **4** Yield: 170 mg, 50%. ^1H NMR (250 MHz, [D$_6$]DMSO, 25 °C): δ = −(0.64−0.52) (s, 12 H + 16 H, $-CH_3$; $-CH_2-$), 1.66−1.93 (m, 16 H, CH_2P); 7.30−7.76 (m, 40 H, C_6H_5) ppm. $^{13}C\{^1H\}$ NMR (62.86 MHz, [D$_6$]DMSO, 25 °C): δ = −2.8 (s, CH_3-), 0.6 (s, $-CH_2-$), 7.6 (s, $-CH_2-$), 10.2 (m, CH_2P), 128.3−133.8 (m, C_6H_5) ppm. $^{29}Si\{^1H\}$ NMR (49.66 MHz, [D$_6$]DMSO, 25 °C): δ = 0.49 (s, Si_1), 9.54 (s, Si_0) ppm. $^{31}P\{^1H\}$ NMR (101.26 MHz, [D$_6$]DMSO, 25 °C): δ = 4.1 (s, $^1J_{P-Pt}$ = 3558.4 Hz, PPh_2) ppm. $^{195}Pt\{^1H\}$ NMR (53.54 Hz, [D$_6$]DMSO, 25 °C): δ = −4482.0 (s). ESMS$^+$ (CH_2Cl_2): *m/z* = 1450.0 [M − 2 Cl]$^{2+}$, 954.0 [M − 3 Cl]$^{3+}$, 707.0 [M − 4 Cl]$^{4+}$. $C_{116}H_{124}Cl_8P_8Pt_4Si_5$ (2970.47): calcd. C 46.90, H 4.21; found C 46.60, H 4.27.

Synthesis of 3a: Experimental conditions and workup were identical to those for the preparation of **4**. Yield: 220 mg, 65%. ^1H NMR (250 MHz, $CDCl_3$, 25 °C): δ = −0.22−0.00 (m, 84 H, CH_3), 0.29 (br. s, 64 H, $-CH_2-$), 1.59−1.64 (m, 16 H, CH_2P), 7.29−7.59 (m, 80 H, C_6H_5) ppm. $^{13}C\{^1H\}$ NMR (62.86 MHz, $CDCl_3$, 25 °C): δ = −6.6 (s, CH_3), −4.2 (s, CH_3), −1.6 (s, CH_3), 2.8 (s, $-CH_2-$), 4.5 (s, $-CH_2-$), 6.7 (s, $-CH_2-$), 9.4 (s, $-CH_2-$), 10.3 (s, $-CH_2-$), 16.3 (sbr, CH_2P), 128.0−133.0 (m, C_6H_5) ppm. $^{29}Si\{^1H\}$ NMR (49.66 MHz, $CDCl_3$, 25 °C): δ = 3.80 (s, Si_3), 5.71 (s, Si_1), 7.84 (s, Si_2), 9.32 (s, Si_0) ppm. $^{31}P\{^1H\}$ NMR (101.26 MHz, $CDCl_3$, 25 °C): δ = 3.7 (s, $^1J_{P-Pt}$ = 3545 Hz, PPh_2), 4.4 (s, $^1J_{P-Pt}$ = 3683 Hz, PPh_2) ppm. $^{195}Pt\{^1H\}$ NMR (53.54 MHz, $CDCl_3$, 25 °C): δ = −4311.0 (t, major isomer), −4325.2 (t, minor isomer). ESMS$^+$ (CH_2Cl_2): *m/z* = 1968.3 [M − 2 Cl]$^{2+}$, 1298.6 [M − 3 Cl]$^{3+}$, 965.6 [M − 4 Cl]$^{4+}$, 631.0 [M − 6 Cl]$^{6+}$. $C_{164}H_{244}Cl_8P_8Pt_4Si_{17}$ (4004.99): calcd. C 49.18, H 6.14; found C 48.89, H 6.25.

Synthesis of [Pt(C≡CPh)$_2${Me$_2$Si(CH$_2$PPh$_2$)$_2$}] (6): [Pt(C≡CPh)$_2$(COD)] (0.16 g, 0.31 mmol) was suspended in acetone (10 mL) and a solution of $Me_2Si(CH_2PPh_2)_2$ (0.14 g, 0.31 mmol) in acetone (10 mL) was added; resulting in a quick dissolution. The resulting yellow solution was stirred at room temperature for 2 h and then concentrated to dryness, washed with diethyl ether and dried under vacuum. Crystals suitable for X-ray analysis were collected from a CH_2Cl_2/Et_2O mixture at −20 °C. Yield: 194 mg, 73%. ^1H NMR (250 MHz, $CDCl_3$, 25 °C): δ = −0.30 (s, 6 H, CH_3), 1.70 (d, $^2J_{H-P}$ = 11.2, $^3J_{H-Pt}$ = 32.95 Hz, 4 H, CH_2P), 6.80−7.70 (m, 30 H, C_6H_5) ppm. $^{13}C\{^1H\}$ NMR (62.86 MHz, $CDCl_3$, 25 °C): δ = 0.8 (t, $^3J_{C-P}$ = 3.4 Hz, CH_3), 11.7 (m, CH_2P), 105.0 (dd, $^2J_{C\alpha-Pcis}$ = 20.1, $^2J_{C\alpha-Ptrans}$ = 150.2 Hz, C_α), 109.7 (AXX′, $^3J_{C\beta-Pcis}$ + $^3J_{C\beta-Ptrans}$ = 35.5 Hz, C_β), 124.7−133.6 (m, C_6H_5) ppm. $^{29}Si\{^1H\}$ NMR (49.66 MHz, $CDCl_3$, 25 °C): δ = 0.0 ppm. $^{31}P\{^1H\}$ NMR (101.26 MHz, $CDCl_3$, 25 °C): δ = 1.6 (s, $^1J_{P-Pt}$ = 2258.1 Hz, CH_2P) ppm. $^{195}Pt\{^1H\}$ NMR (53.54 MHz, $CDCl_3$, 25 °C): δ = −3813.0 (t) ppm. IR (KBr, cm^{-1}): ν(C≡C) = 2120. ESMS$^+$ (CH_2Cl_2): *m/z* = 854.1 [M]$^+$. $C_{44}H_{40}P_2PtSi$ (853.93): calcd. C 61.89, H 4.72; found C 61.75, H 4.67.

Synthesis of 2b: Experimental conditions and workup were identical to those for the preparation of **6**. Yield: 222 mg, 84%. ^1H NMR (250 MHz, $CDCl_3$, 25 °C): δ = −(0.38−0.16) (m, 12 H + 16 H, CH_3, $-CH_2-$), 1.60 (m, 16 H, $-CH_2P$), 6.8−7.8 (m, 120 H, C_6H_5) ppm. $^{13}C\{^1H\}$ NMR (62.86 MHz, $CDCl_3$, 25 °C): δ = −1.7 (s, CH_3-), 1.1 (s, $-CH_2-$), 8.4 (s, $-CH_2-$), 10.1 (m, $-CH_2P$), 104.4 (dd, $^2J_{C\alpha-Pcis}$ = 20, $^2J_{C\alpha-Ptrans}$ = 150.3 Hz, C_α), 109.97 (AXX′, $^3J_{C\beta-Ptrans}$ + $^3J_{C\beta-Pcis}$ = 32.0 Hz, C_β), 124.8−135.7 (m, C_6H_5). $^{29}Si\{^1H\}$ NMR (49.66 MHz, $CDCl_3$, 25 °C): δ = 2.85 (s, Si_1), 9.66 (s, Si_0) ppm. $^{31}P\{^1H\}$ NMR (101.26 MHz, $CDCl_3$, 25 °C): δ = 1.4 (s, $^1J_{P-Pt}$ = 2254.4 Hz, PPh_2) ppm. $^{195}Pt\{^1H\}$ NMR (53.54 MHz, $CDCl_3$, 25 °C): δ = −4802.4 (t) ppm. IR (KBr, cm^{-1}): ν(C≡C) 2117. $C_{180}H_{164}P_8Pt_4Si_5$ (3495.87): calcd. C 61.84, H 4.73; found C 60.14, H 4.81.

Synthesis of [Pt{C$_2$PhCo$_2$(CO)$_6$}$_2${Me$_2$Si(CH$_2$PPh$_2$)$_2$}] (7): Compound **6** (0.09 g, 0.10 mmol) was dissolved in CH_2Cl_2 (10 mL) and $Co_2(CO)_8$ (0.10 g, 0.29 mmol) was added as a solid. The mixture was stirred at room temperature for 2 h. The resulting brown solution was concentrated to half the original volume and filtered through a small column of alumina. The solution obtained was concentrated to dryness. Yield: 74 mg, 49%. ^1H NMR (250 MHz, $CDCl_3$, 25 °C): δ = −0.61 (s, 6 H, CH_3), 1.73 (d, $^2J_{H-P}$ = 10.6, $^3J_{H-Pt}$ = 48.8 Hz, 4 H, CH_2P), 7.46−7.81 (m, 30 H, C_6H_5) ppm. $^{13}C\{^1H\}$ NMR (62.86 MHz, $CDCl_3$, 25 °C): δ = 0.2 (s, CH_3), 14.1 (m, CH_2P), 128.2−137.6 (m, C_6H_5), 209.7 (s, CO) ppm. $^{31}P\{^1H\}$ NMR (101.26 MHz, $CDCl_3$, 25 °C): δ = 13.2 (s, $^1J_{P-Pt}$ = 3498.9 Hz, CH_2P) ppm. IR (CH_2Cl_2, cm^{-1}): ν(CO) = 2095 w, 2081 w, 2055 vs, 2014 vs, 1950 s. ESMS$^+$ (CH_2Cl_2): *m/z* = 994.4 [M − $Co_3(CO)_9$]$^+$, 967.5 [M − $Co_3(CO)_{10}$]$^+$, 853.4 [M − $Co_4(CO)_{12}$]$^+$. $C_{56}H_{40}Co_4O_{12}P_2PtSi$ (1425.78): calcd. C 47.18, H 2.83; found C 47.01, H 2.85.

Synthesis of 2c: Experimental conditions and workup were identical to those for the preparation of **7**. Yield: 194 mg, 79%. ^1H NMR (250 MHz, $CDCl_3$, 25 °C): δ = −(0.74−0.32) (s, 12 H + 16 H, CH_3-, $-CH_2-$), 1.65 (br. m, 16 H, CH_2P), 6.8−7.6 (m, C_6H_5) ppm. ^{31}P NMR (101.26 MHz, CD_2Cl_2, 25 °C): δ = 12.68 (s, $^1J_{P-Pt}$ = 3496.0 Hz, PPh_2) ppm. IR (CH_2Cl_2, cm^{-1}): ν(CO) = 2100 w, 2081 s, 2060 vs, 2016 vs, 1989 ssh, 1890 w. $C_{228}H_{164}Co_{16}O_{48}P_8Pt_4Si_5$ (5783.28): calcd. C 47.35, H 2.86; found C 47.09, H 2.94.

Synthesis of [PdCl(η^3-2-MeC$_3$H$_4$)(PPh$_2$CH$_2$SiMe$_3$)] (8): To a solution of [Pd(η^3-C_4H_7)(μ-Cl)]$_2$ (0.62 g, 1.57 mmol) in CH_2Cl_2 (30 mL), was added $Me_3SiCH_2PPh_2$ (0.86 g, 3.14 mmol) and the reaction mixture stirred for 30 min at room temperature. The solvent was evaporated to dryness and the solid was washed with diethyl ether and dried under vacuum. Yield: 1.18 g (80%). ^1H NMR (250 MHz, $CDCl_3$, 25 °C): δ = −0.04 (s, 9 H, CH_3), 1.90 (s, 3 H, CH_3), 1.97 (d, $^2J_{H-P}$ = 14.3 Hz, 2 H, CH_2P), 2.63 (s, 1 H, H^4), 3.33 (br. s, 1 H, H^3), 3.46 (d, $^3J_{H-P}$ = 10.1 Hz, 1 H, H^2), 4.44 (dd, $^3J_{H-P}$ = 6.9 Hz, J_{H-H} = 2.8 Hz, 1 H, H^1), 7.30−7.65 (m, 10 H, C_6H_5) ppm. $^{13}C\{^1H\}$ NMR (75.4 MHz, $CDCl_3$, 25 °C): δ = 0.4 (d, $^3J_{C-P}$ = 3.8 Hz, CH_3), 14.4 (d, $^1J_{C-P}$ = 11.4 Hz, CH_2P), 23.2 (s, CH_3), 57.8 (s, C_{cis}), 76.9 (d, $^2J_{C-P}$ = 33.2 Hz, C_{trans}), 128.3−136.2 (m, C_6H_5) ppm. $^{29}Si\{^1H\}$ NMR (49.66 MHz, $CDCl_3$, 25 °C): δ = 0.82 (s) ppm. $^{31}P\{^1H\}$ NMR (101.26 MHz, $CDCl_3$, 25 °C): δ = 17.8 (s). $C_{20}H_{28}ClPPdSi$ (469.36): C 51.18, H 6.01; found C 51.13, H 6.11.

Synthesis of 1d: Experimental conditions and workup were identical to those for the preparation of **8**. Yield 380 mg, 85%. ^{1}H NMR (250 MHz, $CDCl_3$, 25 °C): δ = −0.03, −0.07 (s, 24 H, CH_3), 0.15 (s, 16 H, $-CH_2-$), 1.96 (s, 12 H, CH_3), 2.05 (d, $^2J_{H-P}$ = 15.0 Hz, 8 H, CH_2P), 2.70 (s, 4 H, H^4), 3.31 (s, 4 H, H^3), 3.42 (d, $^3J_{H-P}$ = 9.8 Hz, 4 H, H^2), 4.39 (d, $^3J_{H-P}$ = 6.2 Hz, 4 H, H^1), 7.44−7.66 (m, 40 H, C_6H_5) ppm. $^{13}C\{^1H\}$ NMR (62.86 MHz, $CDCl_3$, 25 °C): δ = − 2.0 (s, CH_3), 2.5 (s, $-CH_2-$), 9.1 (d, $^3J_{C-P}$ = 4.8 Hz, $-CH_2-$), 12.8 (d, $^1J_{C-P}$ = 11.0 Hz, CH_2P), 23.3 (s, CH_3), 58.0 (s, C_{cis}), 76.7 (d, $^2J_{C-P}$ = 32.0 Hz, C_{trans}), 128.3−136.3 (m, C_6H_5) ppm. $^{29}Si\{^1H\}$ NMR (49.66 MHz, $CDCl_3$, 25 °C): δ = 3.0 (s, Si_1), 18.5 (s, Si_0) ppm. $^{31}P\{^1H\}$ NMR (101.26 MHz, $CDCl_3$, 25 °C): δ = 17.4 (s, PPh_2) ppm. MSFAB$^+$: *m/z*: 1923.6 [M$^+$ − Cl]. $C_{84}H_{116}Cl_4P_4Pd_4Si_5$ (1956.03): calcd. C 51.53, H 5.93; found C 52.07, H 6.17.

Synthesis of 3d: Experimental conditions and workup were identical to those for the preparation of **8**. Yield: 430 mg, 82%. ^{1}H NMR (500 MHz, $CDCl_3$, 25 °C): δ = −0.26 (s, 12 H, C^2H_3), −0.13 (s, 24 H, C^1H_3), −0.09, −0.05 (s, 48 H, C^3H_3, $C^{3'}H_3$), 0.16−0.20 (m, 64 H, $-CH_2-$), 1.86 (s, 24 H, C^4H_3), 1.90 (d, $^2J_{H-P}$ = 11.0 Hz, CH_2P), 1.90 (d, $^2J_{H-P}$ = 10.5 Hz, CH'_2P), 2.61 (s, 8 H, H^4), 3.30 (s, 8 H, H^3), 3.41 (d, $^3J_{H-P}$ = 10.0 Hz, 8 H, H^2), 4.37 (d, $^3J_{H-P}$ = 4.6 Hz, 8 H, H^1), 7.32−7.55 (m, 80 H, C_6H_5) ppm. $^{13}C\{^1H\}$ NMR (62.86 MHz, $CDCl_3$, 25 °C): δ = −6.7 (s, C^2H_3), −4.5 (C^1H_3), −2.1 (s, C^3H_3, $C^{3'}H_3$), 4.2 (s, $-C^1H_2-$, $-C^2H_2-$), 4.5 (s, $-C^3H_2-$), 6.5 (d, $-C^5H_2-$), 8.9 (d, $^3J_{C-P}$ = 3.7 Hz, $-C^6H_2-$), 12.6 (d, $^1J_{C-P}$ = 11.0 Hz, CH_2P), 23.1 (s, C^4H_3), 57.8 (s, C_{cis}), 76.4 (d, $^2J_{C-P}$ = 32.9 Hz, C_{trans}), 128.2−136.1 (m, C_6H_5) ppm. $^{29}Si\{^1H\}$ NMR (49.66 MHz, $CDCl_3$, 25 °C): δ = 3.14 (s, Si_3), 5.72 (s, Si_1), 8.04 (s, Si_2), 9.43 (s, Si_0) ppm. $^{31}P\{^1H\}$ NMR (101.26 MHz, $CDCl_3$, 25 °C): δ = 17.7 (s, PPh_2). ESMS$^+$ (acetonitrile): *m/z* = 2122.8 [M − {Pd(2-CH_3−C_3H_4)Cl} − 2 Cl]$^{2+}$, 2026.2 [M − 2 {Pd(2-CH_3-C_3H_4)Cl} − 2 Cl]$^{2+}$, 1339.4 [M − 2 {Pd(2-CH_3-C_3H_4)Cl} − 3 Cl]$^{3+}$, 1274.1 [M − 3 {Pd(2-CH_3-C_3H_4)Cl} − 3 Cl]$^{3+}$. $C_{196}H_{300}Cl_8P_8Pd_8Si_{17}$ (4516.62): calcd. C 52.12, H 6.70; found C 52.34, H 7.13.

Synthesis of the Cationic Complexes 1d*, 3d* and 8*: To a solution of **1d**, **3d**, or **8** (2.24 mmol) in CH_2Cl_2 (40 mL) were added a few drops of acetonitrile and $AgBF_4$ (0.45 g, 2.78 mmol). The mixture was stirred for 1 h in the dark, and the AgCl formed was removed by filtration through Celite. The resulting solution was concentrated and the addition of ether caused the precipitation of a white solid as a resin, which was washed twice with ether and dried. Yield: 60−70%. **1d***: ^{1}H NMR (500 MHz, $CDCl_3$, 25 °C): δ = −0.132 (s, 24 H, Me), 0.352 (s, 16 H, CH_2), 1.914 (s, 12 H, Me), 2.310 (s, 12 H, $NCCH_3$), 2.739 (s, 4 H, H^4), 3.335 (s, 4 H, H^3), 3.617 (s, 4 H, H^2), 4.764 (s, 4 H, H^1), 7.20−7.60 (m, 40 H, C_6H_5) ppm. ^{13}C NMR (62.90 MHz, $CDCl_3$, 25 °C): δ = −2.4 (s, 8 C, Me), 1.0 (s, 8 C, CH_2), 3.0 (s, $NCCH_3$), 12.9 (s, 4 C, CH_2P), 23.1 (s, 4 C, Me), 58.9 (s, 4 C, C_{cis}), 79.8 (d, *J* = 27.12 Hz, 4 C, C_{trans}), 129.0−136.6 (m, C_6H_5) ppm. ^{29}Si NMR (49.66 MHz, $CDCl_3$, 25 °C): δ = 3.35 (s, 4Si) ppm, the core signal was not observed. ^{31}P NMR (101.26 MHz, $CDCl_3$, 25 °C): δ = 15.76 (s) ppm. **3d***: ^{1}H NMR (500 MHz, $CDCl_3$, 25 °C): Spectrum similar to that of **1d*** but with very broad signals. ^{31}P NMR (101.26 MHz, $CDCl_3$, 25 °C): δ = 14.5 (br. s) ppm. **8***: ^{31}P NMR (101.26 MHz, $CDCl_3$, 25 °C): δ = 14.26 (s) ppm. ^{29}Si NMR (49.66 MHz, $CDCl_3$, 25 °C): δ = 1.31 (s) ppm. ^{1}H NMR (500 MHz, $CDCl_3$, 25 °C): δ = −0.01 (s, 9 H, CH_3), 1.85 (d, *J* = 14.39 Hz, 2 H, CH_2), 1.97 (s, 3 H, CH_3), 2.32 (s, 3 H, $NCCH_3$), 2.72 (s, 1 H, H^4), 3.28 (s, 1 H, H^3), 3.70 (d, *J* = 9.24 Hz, 1 H, H^2), 4.93 (br. s, 1 H, H^1), 7.30−7.60 (m, 10 H, C_6H_5) ppm. ^{13}C NMR (75.4 MHz, $CDCl_3$, 25 °C): δ = 0.3 (d, *J* = 3.5 Hz, CH_3), 2.8 (s, $NCCH_3$), 14.9 (d, *J* = 11.4 Hz, CH_2), 23.1 (s, CH_3), 58.6 (s, $CH_{2,cis}$), 80.7 (d, *J* = 26.7 Hz, $CH_{2,trans}$).

Catalytic Reactions: Hydrovinylation reactions were performed in a stainless-steel autoclave fitted with an external jacket connected to a thermostatically controlled isobutyl alcohol bath maintained

Table 5. Crystal data and structure refinement for **4**, **5**, and **6**

Compound	**4**	**5**	**6**
Empirical formula	$C_{32}H_{42}Cl_2P_2PtSi_2{\cdot}0.5H_2O$	$C_{28}H_{30}Cl_2P_2PtSi$	$C_{44}H_{40}P_2PtSi$
Formula mass	819.77	722.54	853.88
Temperature	293(2) K	293(2) K	293(2) K
Wavelength	0.71069 Å	0.71069 Å	0.71069 Å
Crystal system, space group	monoclinic, $P2_1/n$	orthorhombic, *Pcnb*	monoclinic, $P2_1/c$
Unit cell dimensions	*a* = 9.9960(10) Å *b* = 18.9050(10) Å, β = 91.2250(10)° *c* = 19.5690(10) Å	*a* = 11.2090(10) Å *b* = 14.7280(10) Å *c* = 16.6540(10) Å	*a* = 18.108(5) Å *b* = 10.773(12) Å, β = 90.60(3)° *c* = 19.687(11) Å
Volume	3697.2(5) Å^3	2749.3(3) Å^3	3840(5) Å^3
Z	4	4	4
Calculated density	1.473 Mg/m^3	1.746 Mg/m^3	1.477 Mg/m^3
Absorption coefficient	4.112 mm^{-1}	5.474 mm^{-1}	3.798 mm^{-1}
F(000)	1636	1416	1704
Crystal size	0.1 × 0.1 × 0.2 mm	0.1 × 0.1 × 0.2 mm	0.1 × 0.1 × 0.3 mm
Θ range for data collection	2.27−28.89°	2.81−24.96°	2.34−29.95°
Index ranges	$-11 \le h \le 10$, $0 \le k \le 25$, $0 \le l \le 26$	$0 \le h \le 12$, $0 \le k \le 16$, $0 \le l \le 19$	$-25 \le h \le 25$, $0 \le k \le 15$, $0 \le l \le 27$
Reflections collected/unique	22007/8165 [*R*(int) = 0.0462]	11504/2402 [*R*(int) = 0.00309]	11092/11092 [*R*(int) = 0.0926]
Refinement method	Full-matrix least squares on F^2	Full-matrix least squares on F^2	Full-matrix least squares on F^2
Data/parameters	8165/364	2402/206	11092/433
Goodness-of-fit on F^2	0.899	1.101	0.756
Final *R* indices [$I > 2\sigma(I)$]	*R*1 = 0.0261, *wR*2 = 0.0518	*R*1 = 0.0329, *wR*2 = 0.0728	*R*1 = 0.0431, *wR*2 = 0.0568
R indices (all data)	*R*1 = 0.0608, *wR*2 = 0.0557	*R*1 = 0.0480, *wR*2 = 0.0789	*R*1 = 0.2656, *wR*2 = 0.0899
Largest diff. peak and hole (e Å^{-3})	0.619 and −0.600	0.551 and −0.470	0.420 and −0.365

to ± 0.5 °C. The internal temperature was monitored by means of a thermocouple. Internal temperature and pressure as a function of time were registered with a Linseis L-200 Recorder. Gas chromatography was run using an HP 5890 series two chromatograph.

Hydrovinylation Reactions

a) 1d$^+$, 3d$^+$, and 8$^+$ as Catalysts: A mixture of 4.0×10^{-5} mol of the neutral palladium complex, **1d**, **3d**, or **8**, $AgBF_4$ (in a 1:4, 1:8, and 1:1 molar ratio, respectively) and styrene (0.04 mol) in 10 mL of freshly distilled CH_2Cl_2 was stirred for 5 min in the dark under nitrogen. After filtering off the AgCl formed, the solution was placed in a thermostatically controlled autoclave, which had previously been purged with successive applications of vacuum and argon. The autoclave was then pressurized with ethylene to 15 bar. After the desired time, the autoclave was slowly depressurized and 10% HCl (10 mL) was added. The mixture was stirred for 10 min in order to quench the catalyst. The CH_2Cl_2 layer was decanted and dried with Na_2SO_4. The quantitative distribution of products fractions was determined by GC analysis.

b) 1d*, 3d*, and 8* as Catalysts: A solution of 4.0×10^{-5} mol of the cationic palladium complexes, **1***, **3***, or **8***, and styrene (0.0400 mol) in freshly distilled CH_2Cl_2 (10 mL) was prepared under an inert gas. The solution was transferred via syringe under argon into the autoclave, which had previously been purged with successive applications of vacuum and argon. Ethylene was admitted until the initial pressure of 15 bar was reached. The workup procedure was as already described.

X-ray Structure Determination of 4, 5 and 6: Block crystals of compounds **4** and **5** were selected and mounted on a MAR345 diffractometer with image plate detector. A crystal of **6** was mounted on an Enraf−Nonius CAD4 four-circle diffractometer. Crystallographic and experimental details of both compounds are summarized in Table 5. Data were collected at room temperature. Intensities were corrected for Lorentz and polarization effects in the usual manner. The structures were solved by Direct Methods, using SHELXS computer program and refined by full-matrix least-squares methods with SHELX97 computer program.[31] The function minimized was $\Sigma w||F_o|^2 - |F_c|^2|^2$, where $w = [\sigma^2(I) + (0.0774 P)^2]^{-1}$, and $P = (|F_o|^2 + 2|F_c|^2)/3$; f, f' and f'' were taken from International Tables of X-ray Crystallography .[32] All H atoms were computed and refined with an overall isotropic temperature factor equal to 1.2 times the equivalent isotropic temperature factor of the atoms, which were linked using a riding model. The supplementary crystallographic data for this paper can be found in publications CCDC-181768 (**4**), -181770 (**5**), and -181769 (**6**.) These data can be obtained free of charge at www.ccdc.cam.ac.uk/conts/retrieving.html or from the Cambridge Crystallographic Data Centre, 12, Union Road, Cambridge CB2 1EZ, UK [Fax: (internat.) + 44-1223/336-033; E-mail: deposit@ccdc.cam.ac.uk].

Acknowledgments

This work was supported by the DGICYT (Projects BQU2000-0644 and PB97-0407-C05-04) and the CIRIT (Project 1999 SGR 00045). M. B. is indebted to the Ministerio de Ciencia y Tecnologia for a scholarship.

[1] For reviews, see [1a] D. A. Tomalia, A. M. Naylor, W. A. Goddard III, *Angew. Chem. Int., Ed. Engl.* **1990**, *29*, 138−175; *Angew. Chem.* **1990**, *102*, 119−157. [1b] A. W. Bosman, H. M. Jansen, E. W. Meijer, *Chem. Rev.* **1999**, *99*, 1665−1688.

[2] [2a] H. Frey, C. Lach, K. Lorenz, *Adv. Mater.* **1998**, *10*, 279−293. [2b] I. Cuadrado, M. Morán, J. Losada, C. M. Casado, C. Pascual, B. Alonso, F. Lobete in: G. R. Newkome, *Advances in Dendritic Macromolecules*, JAI Press, Greenwich, CT, **1996**, vol. 3. [2c] S. Arévalo, E. de Jesús, F. J. de la Mata, J. C. Flores, R. Gómez, *Organometallics* **2001**, *20*, 2583−2592.

[3] M. Benito, O. Rossell, M. Seco, G. Segalés, *Inorg. Chim. Acta* **1999**, *291*, 247−251.

[4] O. Rossell, M. Seco, A. M. Caminade, J. P. Majoral, *Gold Bull.* **2001**, *34*, 88−94.

[5] [5a] M. Benito, O. Rossell, M. Seco, G. Segalés, *Organometallics* **1999**, *18*, 5191−5193. [5b] M. Benito, O. Rossell, M. Seco, G. Segalés, *J. Organomet. Chem.* **2001**, *619*, 245−251.

[6] [6a] G. R. Newkome, E. He, C. N. Moorefield, *Chem. Rev.* **1999**, *99*, 1689−1746. [6b] J. P. Majoral, A. M. Caminade, *Chem. Rev.* **1999**, *99*, 845−880.

[7] M. Bardají, M. Kustos, A. M. Caminade, J. P. Majoral, B. Chaudret, *Organometallics* **1997**, *16*, 403−410.

[8] D. de Groot, J. C. de Wilde, R. J. van Haaren, J. N. H. Reek, P. C. J. Kamer, P. W. N. M. van Leeuwen, E. B. Eggeling, D. Vogt, H. Kooijman, A. L. Speek, A. W. van der Made, *Chem. Commun.* **1999**, 1623−1624.

[9] G. K. Anderson, H. C. Clark, J. A. Davies, G. Ferguson, M. Parvez, *J. Crystallogr. Spectrosc. Res.* **1982**, *12*, 449−458.

[10] T. S. Cameron, H. C. Clark, A. Linden, A. M. Nicholas, M. J. Hampden-Smith, *Inorg. Chim. Acta* **1989**, *162*, 9−10.

[11] G. B. Robertson, W. A. Wickramasinghe, *Acta Crystallogr., Sect. C* **1987**, *43*, 1694−1697.

[12] E. C. Alyea, G. Ferguson, B. L. Ruhl, R. Shakya, *Polyhedron* **1987**, *6*, 1223−1227.

[13] P. R. Meehan, E. C. Alyea, R. P. Shakya, G. Ferguson, *Polyhedron* **1997**, *17*, 11−16.

[14] P. R. Meehan, G. Ferguson, R. P. Shakya, E. C. Alyea, *J. Chem. Soc., Dalton Trans.* **1997**, 3487−3491.

[15] E. C. Alyea, G. Ferguson, R. P. Shakya, P. R. Meehan, *Inorg. Chem.* **1997**, *36*, 4749−4752.

[16] J. Forniés, E. Lalinde, *J. Chem. Soc., Dalton Trans.* **1996**, 2587−2599 and references therein.

[17] N. Ohshire, F. Takei, K. Onitsuka, S. Takahashi, *J. Organomet. Chem.* **1998**, *569*, 195−202.

[18] L. R. Falvello, J. Forniés, J. Gómez, E. Lalinde, A. Martin, M. T. Moreno, J. Sacristan, *Chem. Eur. J.* **1999**, *5*, 474−491.

[19] [19a] R. A. Mariezcurrena, S. E. Rasmusssen, *Acta Chem. Scand.* **1973**, *27*, 2678−2680. [19b] A. Furlani, S. Licoccia, M. V. Russo, A. C. Villa, C. Guastini, *J. Chem. Soc., Dalton Trans.* **1984**, 2197−2206. [19c] W. Weigand, C. Robl, *Chem. Ber.* **1993**, *126*, 1807−1809. [19d] J. D. Bradshaw, L. Guo, C. A. Tessier, W. J. Youngs, *Organometallics* **1996**, *15*, 2582−2584. [19e] J. A. Whiteford, C. V. Lu, P. J. Stang, *J. Am. Chem. Soc.* **1997**, *119*, 2524−2533. [19f] M. I. Bruce, B. C. Hall, P. J. Low, M. E. Smith, B. W. Skelton, A. H. White, *Inorg. Chim. Acta* **2000**, *300−302*, 633−644.

[20] [20a] D. Seyferth, T. Kugita, A. L. Rheingold, G. A. P. Yap, *Organometallics* **1995**, *14*, 5362−5366. [20b] G. R. Newkome, C. N. Moorefield, G. R. Baker, A. L. Johnson, R. K. Behera, *Angew. Chem. Int. Eng. Ed.* **1991**, *30*, 1176−1178; *Angew. Chem.* **1991**, *103*, 1205−1207. [20c] C. Kim, I. Jung, *J. Organomet. Chem.* **1999**, *588*, 9−19.

[21] E. C. Constable, O. Eich, D. Fenske, C. E. Housecroft, L. Johnston, *Chem. Eur. J.* **2000**, *6*, 4364−4370.

[22] [22a] J. W. J. Knappen, A. W. van der Made, J. C. de Wilde, P. W. N. M. van Leeuwen, P. Wijkens, D. M. Grove, G. van Koten, *Nature* **1994**, *372*, 659−663. [22b] A. W. Kleij, R. A. Gossage, J. T. B. M. Jastrzebski, J. Boersma, G. van Koten, *Angew. Chem. Int. Eng. Ed.* **2000**, *39*, 176−178; *Angew. Chem.* **2000**, *112*, 179−181 [22c] G. E. Oosterom, J. N. H. Reek, P. C. J. Kamer, P. W. N. M. van Leeuwen, *Angew. Chem. Int. Eng. Ed.*

2001, *40*, 1828−1849; *Angew. Chem.* **2001**, *113*, 1878−1901.
[22d] D. Astruc, F. Chardac, *Chem. Rev.* **2001**, *101*, 2991−3023.
[22e] V. Maraval, R. Laurent, A. M. Caminade, J. P. Majoral, *Organometallics* **2000**, *19*, 4025−4029.
[23] N. J. Hovestad, E. B. Eggeling, H. J. Heidbüchel, J. T. B. H. Jastrzebski, U. Kragl, W. Keim, D. Vogt, G. van Koten, *Angew. Chem. Int. Ed.* **1999**, *38*, 1655−1658; *Angew. Chem.* **1999**, *111*, 1763−1765.
[24] E. V. Eggeling, N. J. Hovestad, J. T. B. H. Jastrzebski, D. Vogt, G. van Koten, *J. Org. Chem.* **2000**, *65*, 8857−8865.
[25] G. Muller, J. I. Ordinas, *J. Mol. Cat. A* **1997**, *125*, 97−108.
[26] E. C. Alyea, K. J. Fisher, T. P. Shakya, A. E. Vogioukas, *Synth. React. Inorg. Met. Org. Chem.* **1988**, *18*, 163−178.
[27] Y. Tatsuno, T. Yoshiba, S. Otsuka, *Inorg. Synth.* **1990**, *28*, 342−345.
[28] J. X. McDermott, J. F. White, G. M. Whitesides, *J. Am. Chem. Soc.* **1976**, *98*, 6521−6528.
[29] R. J. Cross, M. F. Davidson, *J. Chem. Soc., Dalton Trans.* **1986**, 1987−1992.
[30] B. E. Cooper, W. J. Owen, *J. Organomet. Chem.* **1970**, *21*, 329−332.
[31] G. M. Sheldrick, *SHELXL-97*, Universität Göttingen, **1997**.
[32] *International Tables of X-ray Crystallography*, Kynoch Press, **1974**, vol. IV, p. 99−100 and 149.

Received March 21, 2002
[I02147]

A One-Dimensional Manganese(II) Coordination Polymer Derived from Zerovalent Manganese and 1-Hydroxybenzotriazole − Synthesis, Characterization, Crystal Structure and Magnetic Properties

Giannis S. Papaefstathiou,[a] Ramon Vicente,[b] Catherine P. Raptopoulou,[c] Aris Terzis,[c] Albert Escuer,*[b] and Spyros P. Perlepes*[a]

Keywords: Coordination polymers / Nitrogen heterocycles / Magnetic properties / Manganese / X-ray crystal structure

The reaction of zerovalent manganese with 1-hydroxybenzotriazole, btaOH, and NH_4SCN in DMF in the presence of dioxygen allows isolation of the one-dimensional coordination polymer $[Mn_3(btaO)_2(NCS)_4(DMF)_8]_n$ (**3**). X-ray diffraction analysis reveals that the chain is best described as $[Mn_2(btaO)_2(NCS)_2(DMF)_6]$ dimers linked by $Mn(NCS)_2(DMF)_2$ bridges. Molar magnetic susceptibility measurements of **3** in the 5–300 K range indicate weak antiferromagnetic coupling between the Mn^{II} atoms within the dinuclear subunits of the chain.
(© Wiley-VCH Verlag GmbH, 69451 Weinheim, Germany, 2002)

Introduction

Over the last twenty years, we[1] and others[2] have been exploring the coordination chemistry of benzotriazole (btaH, Scheme 1) and its derivatives. The first reason for this is the anticorrosion properties of btaH and benzene ring-substituted benzotriazoles toward certain metals, particularly copper and its alloys.[3] The second reason is the observation that reactions between metal β-diketonates or carboxylates and btaH or its ring-substituted (with non-donor groups) derivatives lead to incomplete replacement of β-diketonato or carboxylato ligands by the deprotonated benzotriazoles and the formation of large heteroleptic 3d-metal cages with unique structural motifs and exciting magnetic properties.[1a,2b,2c] Thus, benzotriazolato ligands are amongst the most important in the field of high-nuclearity transition metal chemistry.

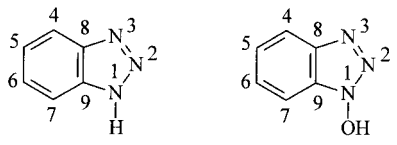

btaH btaOH

Scheme 1

More recently,[4,5] our efforts have turned towards the use of benzotriazoles, substituted on the azole ring with donor groups, to see how incorporation of this ligand type might affect the structures and physical properties of the products. The first ligand employed was 1-hydroxybenzotriazole (btaOH, Scheme 1). The synthetic investigation of the $[Cu_2(O_2CMe)_4(H_2O)_2]$/btaOH reaction system in MeOH resulted in the isolation of the three-dimensional (3D), diamond-like polymeric complex $[Cu(btaO)_2(MeOH)]_n$ (**1**), which is a soft magnet exhibiting two critical temperatures at 6.4 and 4.4 K.[4] Reaction of $[Ni(NO_3)_2]\cdot 6H_2O$ with btaOH in DMF/aqueous NH_3 has recently yielded the trinuclear complex $[Ni_3(btaO)_6(NH_3)_6]$ (**2**).[5]

In the present work, reactions of btaOH with zero-valent manganese were investigated. Zero-valent transition metals as starting materials are a good source for the construction of unusual polymeric and/or discrete metal complexes, which exhibit interesting magnetic properties and cannot be synthesised starting from conventional metal salts.[6] The subject of the present paper is the 1D coordination polymer $[Mn_3(btaO)_2(NCS)_4(DMF)_8]_n$ (**3**) which is the product of the reaction between Mn^0, btaOH and NH_4SCN in DMF under aerobic conditions.

Transition metal coordination polymers are of considerable interest as magnetic, electronic and photooptical materials.[7] Compounds with fascinating topologies and intricate interweaving of multiple networks have been discovered. Restricting further discussion to magnetic coordination polymers, we should mention that these molecular compounds may contain the same metal ion, two kinds of spin carriers (either two different metal ions or a metal ion and an organic radical) and, in a very limited number of cases,

[a] Department of Chemistry, University of Patras, 265 00 Patras, Greece
[b] Departament de Química Inorgànica, Universitat de Barcelona, Diagonal 647, 08028 Barcelona, Spain
[c] Institute of Materials Science, NCSR "Demokritos", 153 10 Aghia Paraskevi Attikis, Greece

three spin carriers. The attainment of magnetic ordering generally requires[8] the organisation of transition metal centres into 3D networks. However, to better interpret magnetic properties of 3D coordination polymers, reduced dimensionalities (i.e. 1D and 2D) are preferred to develop the necessary theoretical models.[9,10] In this context, 1D magnetic systems are being thoroughly investigated from both experimental and theoretical viewpoints.[11]

Results and Discussion

Synthesis

The preparation of complex **3** can be achieved by the reaction of zero-valent manganese with btaOH and NH_4SCN in DMF under reflux in air for 2 h. This preparation is summarised in Equation (1).

$$3n\text{Mn} + 2n\text{btaOH} + 4n\text{NH}_4\text{SCN} + 8n\text{DMF} + 3/2n\text{O}_2 \xrightarrow[\text{reflux}]{\text{DMF}} [\text{Mn}_3(\text{btaO})_2(\text{NCS})_4(\text{DMF})_8]_n + 4n\text{NH}_3 + 3n\text{H}_2\text{O} \quad (1)$$

3

In this reaction dioxygen is reduced to give H_2O and Mn is oxidized to Mn^{II}. The same product can be isolated from the 2:1:1, 1:1:1, 1:2:2, 1:2:3, 1:3:4, 1:4:4, 1:3:5, 1:4:5 and 1:5:5 Mn/btaOH/NH_4SCN reaction systems in DMF. When btaOH and/or SCN^- are in excess the reaction proceeds faster (in less than 2 h) giving the same product in almost the same yield, while, when the quantities of btaOH and/or SCN^- are less than the stoichiometric ones, the reaction proceeds more slowly and we do not observe complete dissolution of the Mn powder.

IR Spectra

The IR spectrum of **3** exhibits the ν(CN), ν(CS) and δ(NCS) modes at 2078, 787 and 478 cm^{-1}, respectively; these frequencies are typical of terminal isothiocyanato groups.[12] The presence of coordinated DMF in **3** is manifested by a strong band at 1650 cm^{-1} and a medium intensity band at 1496 cm^{-1}, assigned to ν(C=O) and ν(C−N), respectively.[13] The spectra of the sodium and potassium salts of 1-hydroxybenzotriazole (btaONa, btaOK) exhibit bands at 1178 and 1102 cm^{-1}, associated with the ν(N=N) and ν(N−N) vibrational modes, respectively.[4] These bands are shifted to 1213 and 1128 cm^{-1}, respectively, in the spectrum of the complex; these shifts to higher frequencies are compatible with N(3) (Scheme 1) being the N-donor atom of $btaO^-$.[1b] The band assignable to the N−O stretching vibration appears at 1224 cm^{-1} in the IR spectrum of btaOK.[5] This band is shifted to 1155 cm^{-1} in the spectrum of **3** due to the coordination of the oxygen atom to the metal.[4]

X-ray Crystal Structure

A labelled ORTEP[14] drawing of the structure is shown in Figure 1. Selected distances and angles are listed in Table 1. The asymmetric unit of the one-dimensional (1D) polymer consists of three independent Mn^{II} atoms, Mn(2), Mn(1) and Mn(3). If we name the Mn(2), Mn(1) and Mn(3) ions as A, B and C, respectively, then a satisfactory way to describe this structure is to consider it as a chain of the alternating dimers CC and AA, which are connected via the Mn(1) ion (B) (Figure 2). Each dinuclear subunit (AA or CC) consists of two Mn^{II} atoms which are bridged by two μ_2-O atoms of two symmetry-related $btaO^-$ ligands, forming a planar four-membered ring (Mn_2O_2), in the centre

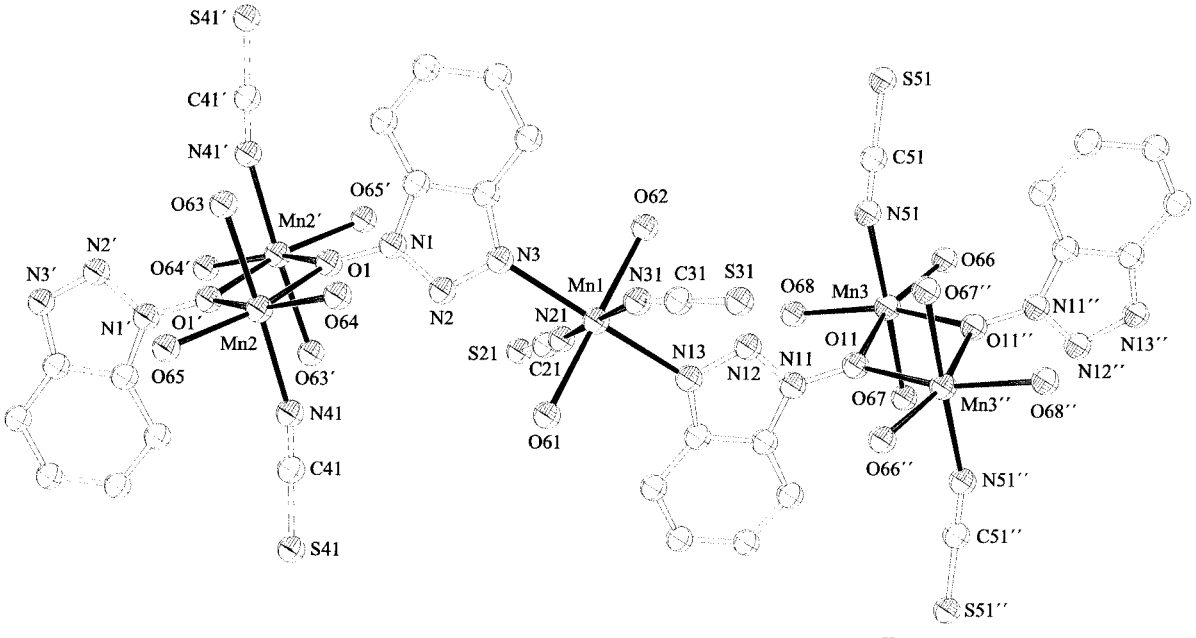

Figure 1. ORTEP plot of $[Mn_3(btaO)_2(NCS)_4(DMF)_8]_n$ (**3**) at the 30% probability level; five Mn^{II} atoms are shown; all the carbon and nitrogen atoms of the DMF molecules, as well as all H atoms, have been omitted for clarity; the symbols ′ and ′′ denote atoms related by symmetry (see Table 1)

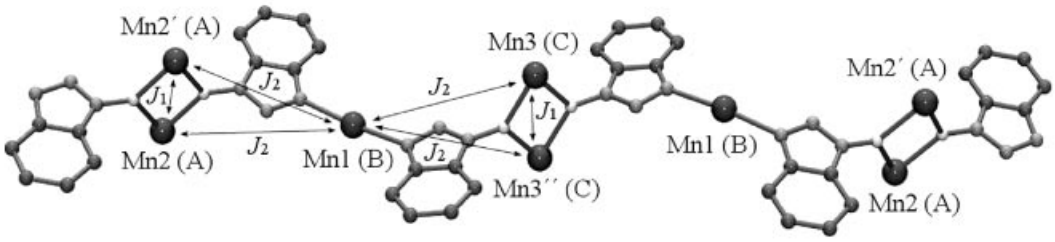

Figure 2. Ball and stick drawing of $[Mn_3(btaO)_2(NCS)_4(DMF)_8]_n$ (**3**), where the ...AA-B-CC-B-AA... view of the chain is emphasized; only the Mn^{II} atoms and the bridging $btaO^-$ ligands have been drawn; the magnetic exchange pathways between the metal ions are also shown

Table 1. Selected bond lengths (Å) and angles (°) for $[Mn_3(btaO)_2(NCS)_4(DMF)_8]_n$ (**3**); symmetry transformations used to generate equivalent atoms: (′): $-x+2, -y, -z+1$; (′′): $-x+1, -y+1, -z$

Mn(1)−N(31)	2.199(6)	Mn(3)−O(11′′)	2.194(4)
Mn(1)−N(21)	2.218(6)	Mn(3)−O(67)	2.226(5)
Mn(1)−O(61)	2.219(4)	O(1)−N(1)	1.336(5)
Mn(1)−O(62)	2.221(4)	O(11)−N(11)	1.334(5)
Mn(1)−N(13)	2.262(4)	N(1)−N(2)	1.335(6)
Mn(1)−N(3)	2.277(4)	N(3)−N(2)	1.326(6)
Mn(2)−O(65)	2.155(5)	N(11)−N(12)	1.325(6)
Mn(2)−N(41)	2.162(6)	N(13)−N(12)	1.338(6)
Mn(2)−O(64)	2.176(4)	N(21)−C(21)	1.158(8)
Mn(2)−O(1)	2.186(4)	N(31)−C(31)	1.152(8)
Mn(2)−O(1′)	2.206(4)	N(41)−C(41)	1.147(7)
Mn(2)−O(63)	2.217(4)	N(51)−C(51)	1.152(8)
Mn(3)−N(51)	2.155(6)	C(21)−S(21)	1.626(8)
Mn(3)−O(66)	2.169(5)	C(31)−S(31)	1.630(7)
Mn(3)−O(68)	2.176(5)	C(41)−S(41)	1.627(7)
Mn(3)−O(11)	2.184(4)	C(51)−S(51)	1.636(7)
N(21)−Mn(1)−O(61)	91.5(2)	O(64)−Mn(2)−O(1)	90.4(1)
N(31)−Mn(1)−O(62)	88.6(2)	O(65)−Mn(2)−O(1′)	93.6(2)
N(21)−Mn(1)−O(62)	89.8(2)	N(41)−Mn(2)−O(1′)	94.7(2)
O(61)−Mn(1)−O(62)	178.7(2)	O(64)−Mn(2)−O(1′)	160.4(1)
N(31)−Mn(1)−N(13)	91.5(2)	Mn(2)−O(1)−Mn(2′)	109.6(1)
N(21)−Mn(1)−N(13)	86.1(2)	N(51)−Mn(3)−O(67)	173.8(2)
O(61)−Mn(1)−N(13)	90.1(2)	O(66)−Mn(3)−O(67)	88.0(2)
N(31)−Mn(1)−N(21)	177.1(2)	O(68)−Mn(3)−O(67)	82.8(2)
N(31)−Mn(1)−O(61)	90.1(2)	O(11)−Mn(3)−O(67)	88.5(2)
O(62)−Mn(1)−N(13)	90.1(2)	O(11′′)−Mn(3)−O(67)	90.7(2)
N(31)−Mn(1)−N(3)	93.9(2)	N(51)−Mn(3)−O(66)	88.1(2)
N(21)−Mn(1)−N(3)	88.4(2)	N(51)−Mn(3)−O(68)	93.4(2)
O(61)−Mn(1)−N(3)	92.4(2)	O(66)−Mn(3)−O(68)	102.8(2)
O(62)−Mn(1)−N(3)	87.6(2)	N(51)−Mn(3)−O(11)	96.6(2)
N(13)−Mn(1)−N(3)	174.0(2)	O(66)−Mn(3)−O(11)	163.7(2)
O(65)−Mn(2)−N(41)	87.8(2)	O(68)−Mn(3)−O(11)	92.5(2)
O(65)−Mn(2)−O(64)	105.1(2)	N(51)−Mn(3)−O(11′′)	94.3(2)
N(41)−Mn(2)−O(64)	91.7(2)	O(66)−Mn(3)−O(11′′)	93.4(2)
O(65)−Mn(2)−O(1)	163.5(2)	O(68)−Mn(3)−O(11′′)	162.2(2)
N(41)−Mn(2)−O(1)	97.5(2)	O(11)−Mn(3)−O(11′′)	70.7(1)
O(1)−Mn(2)−O(1′)	70.4(1)	Mn(3)−O(11)−Mn(3′′)	109.3(1)
O(65)−Mn(2)−O(63)	86.9(2)	N(21)−C(21)−S(21)	176.5(7)
N(41)−Mn(2)−O(63)	172.8(2)	N(31)−C(31)−S(31)	178.7(6)
O(64)−Mn(2)−O(63)	84.9(2)	N(41)−C(41)−S(41)	178.7(6)
O(1)−Mn(2)−O(63)	88.9(2)	N(51)−C(51)−S(51)	179.0(6)
O(1′)−Mn(2)−O(63)	90.6(2)		

of which there is an inversion centre. The Mn···Mn distances are 3.588(1) and 3.570(1) Å for the AA [Mn(2)···Mn(2′)] and CC [Mn(3)···Mn(3′′)] subunits, respectively. The octahedral coordination at each Mn^{II} atom, which is part of a dinuclear subunit, is completed by three oxygen atoms of three DMF molecules at *fac* positions and one nitrogen atom of a linear, terminal SCN^- anion. Thus, the empirical formula of each dinuclear subunit is $Mn_2(btaO)_2(NCS)_2(DMF)_6$. The two dinuclear subunits AA and CC are connected via a mononuclear subunit containing the Mn(1) (B) ion, through the nitrogen atom at the 3-position of the 1-hydroxybenzotriazolato(−1) ligands. The octahedral coordination at Mn(1) is completed by the oxygen atoms [O(61), O(62)] of two *trans* DMF molecules and the nitrogen atoms [N(21), N(31)] of two *trans* isothiocyanato ligands. The Mn···Mn distances between the isolated Mn(1) ion (B) and the Mn^{II} atoms of the dinuclear subunits (AA and CC) are 6.687(1) and 6.875(1) Å for the Mn(1)···Mn(2) and Mn(1)···Mn(2′) pairs, and 6.601(1) and 6.965(1) Å for the Mn(1)···Mn(3) and Mn(1)···Mn(3′′) pairs, respectively.

The $Mn-N_{isothiocyanato}$ bond lengths are in the range 2.155(6)−2.218(6) Å; this range is typical for octahedral manganese(II) complexes containing terminal isothiocyanato ligands.[15a] The SCN^- ions are not perfectly linear, the N−C−S bond angles being in the range 176.5(7)−179.0(6)°. The terminal isothiocyanate anions involving N(31), N(41) and N(51) as donor atoms are coordinated in a slightly bent fashion, as indicated by the Mn−N≡C angles [157.7(5)−164.6(5)°]; the fourth SCN^- ion is coordinated in an almost linear fashion [Mn(1)−N(21)−C(21) = 176.8(6)°]. The average $Mn(1,2,3)-O_{DMF}$ bond length is 2.194(5) Å, as in other high-spin octahedral manganese(II) complexes with O-donors.[15b] The Mn(2)−O(1)−Mn(2′) and Mn(3)−O(11)−Mn(3′′) angles are 109.6(1) and 109.3(1)°, respectively. The angles around the Mn^{II} atoms show that the $Mn(1)N_4O_2$, $Mn(2)NO_5$ and $Mn(3)NO_5$ coordination octahedra are distorted, with the Mn(1) polyhedron being less distorted.

Complex **3** joins a small family of structurally characterised, neutral, 1D coordination polymers containing six-coordinate Mn^{II} sites; representative examples have been described previously.[16−18] This compound also extends to three the number of structurally characterised coordination complexes of any metal with $btaO^-$ ion as ligand; the other two examples are complexes **1** and **2**.

Magnetic Properties

Complex **3** shows a $\chi_M T$ value of 12.98 $cm^3 \cdot K \cdot mol^{-1}$ at room temperature for each Mn_3 unit, which is slightly lower than the expected value for three isolated Mn^{II} centres.

Upon cooling, $\chi_M T$ decreases continuously down to 6.07 $cm^3 \cdot K \cdot mol^{-1}$ at 5 K, indicating an overall antiferromagnetic coupling. The molar susceptibility χ_M increases continuously upon decreasing the temperature. The EPR spectrum at room temperature (Figure 3) consists of an isotropic signal (ΔH_{pp} = 210 G) centred at g = 2.01, and one weak half-field signal centred at g = 3.97 (ΔH_{pp} = 180 G), which arises from the dipolar interaction in the Mn_2O_2 rings, in which the average Mn···Mn distance is only 3.579(1) Å.

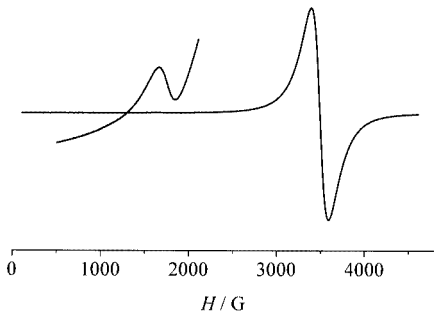

Figure 3. Room-temperature X-band EPR spectrum of a powdered sample of complex $[Mn_3(btaO)_2(NCS)_4(DMF)_8]_n$ (**3**), showing an isotropic signal centred at g = 2.01 and a weak half-field signal centred at g = 3.97

From the structural data we can assume that the magnetic interactions between the isolated Mn(1) ion (B) and the four surrounding Mn(2) (A), Mn(2′) (A), Mn(3) (C) and Mn(3′′) (C) ions are the same, and that the magnetic interactions within the Mn(2), Mn(2′) [AA] and Mn(3), Mn(3′′) [CC] dinuclear subunits are also equal because the Mn−O−Mn bond angles differ by only 0.3°. Thus we can describe the chain as an alternating system with a J_1-$(J_2)_2$-$(J_2)_2$-J_1 interaction sequence, where J_1 describes the magnetic interaction between the Mn^{II} atoms within each dinuclear subunit and J_2 describes the magnetic interaction between the central Mn(1) ion and each one of the Mn^{II} atoms of the neighbouring dinuclear subunits (Figure 2).

Analytical expressions to calculate the interaction parameters for systems of this kind are not available, but a simplified analysis of this system can be done assuming that the value of the J_2 coupling parameter is close to zero. This assumption is fully justified on the basis of the large distances (6.601−6.965 Å) between Mn(1) and Mn(2,2′,3,3′′) ions bridged by a four-atom ligand, and the reported magnetic properties of complex **1**,[20] which shows a very weak coupling for a similar bridge. Additionally, in **3**, the quasi-orthogonal arrangement of the Mn_2O_2 plane with respect to the $btaO^-$ plane reduces the possibility of any coupling between the isolated Mn(1) atom and each of the Mn^{II} atoms of the dinuclear subunits. Assuming that J_2 = 0, compound **3**, which is a one-dimensional system from the structural viewpoint, may be adequately described from the magnetic viewpoint as an ordered sequence of dinuclear units and isolated Mn^{II} paramagnetic centres.

The molar susceptibility for this system can be treated as the sum of two contributions: a contribution from one dimeric entity for which the Hamiltonian $H = -J_1 S_1 \cdot S_2$ can be applied,[19] and a second Curie-law contribution corresponding to one isolated isotropic Mn^{II} atom. The analytical expression used to fit the experimental data was therefore the conventional equation for a pair of interacting S = 5/2 centres plus a constant S = 5/2 Curie contribution with g = 2.00. The best-fit parameters for the dimeric unit were J_1 = −2.45(4) cm^{-1} and g = 2.024(4), with $R = 2.2 \times 10^{-4}$ [agreement factor $R = \Sigma(\chi_M^{calc} - \chi_M^{obs})^2/(\chi_M^{obs})^2$]. The fit is in very good agreement with the experimental data, confirming the validity of the J_2 = 0 approach. Figure 4 shows the best-fit plot, together with the isolated contributions of the single Mn(1) atoms (a typical exponential Curie−Weiss plot) and the dimeric Mn(2), Mn(2′) and Mn(3), Mn(3′′) subunits, for which the plot exhibits a susceptibility maximum at 10 K. It has recently been pointed out that a weak antiferromagnetic coupling should be expected between O-bridged Mn^{II} atoms when the Mn−O−Mn bond angles are large.[20] The low J value in **3** is in good agreement with the low J values (−1 to −5 cm^{-1}) found for other RO^- bridges between Mn^{II} atoms with Mn−O−Mn bond angles larger than 105°.[21]

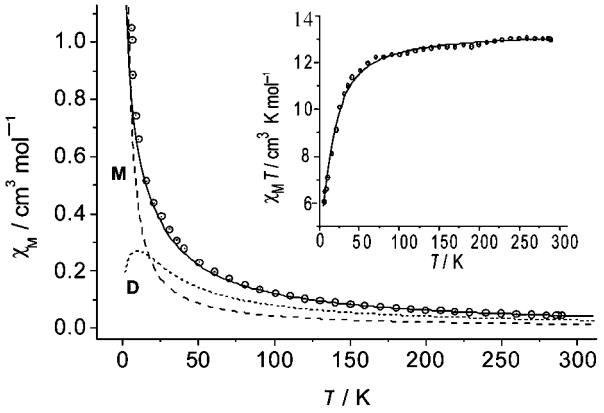

Figure 4. Susceptibility plot versus temperature for $[Mn_3(btaO)_2(NCS)_4(DMF)_8]_n$ (**3**); dot-centred circles correspond to the experimental data and the solid line is the best fit, the solid line can be considered the addition of a antiferromagnetically coupled dinuclear subunit (plot D) and one isolated Mn^{II} atom (plot M); inset: the $\chi_M T$ versus T plot is presented showing the best overall fit

Conclusions

The initial use of btaOH in manganese chemistry has provided access to an 1D manganese(II) complex with interesting structural and magnetic characteristics. The use of zero-valent Mn has also fulfilled its promise as a source of unusual products. Compound **3** is the third structurally characterised coordination complex of any metal containing $btaO^-$ ions as ligands, the other two complexes being **1** and **2**. The ligand adopts completely different coordination modes in the three complexes (Scheme 2). Al-

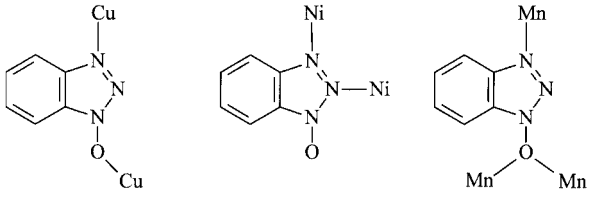

Scheme 2

though the outcome of the reaction system described by Equation (1) was unpredictable, the btaO$^-$ ion in **3** exhibits a novel μ_3-coordination mode binding through N(3) to an Mn^{II} atom and bridging two other Mn^{II} atoms through the deprotonated oxygen. The 1-hydroxybenzotriazolate ligand is also present[22] in the organometallic compounds $[Os_3(\mu\text{-}H)(CO)_{10}(btaO)]$, $[Os_3(CO)_{10}(btaO)(C{=}NHnPr)]$ and $[Os_3(CO)_{10}(btaO)(C{=}NHCH_2Ph)]$, where it adopts the μ_2-coordination mode observed in the Ni^{II} complex **2**. The flexibility of btaO$^-$ observed in the structures of **1**, **2**, **3** and some new complexes (recently isolated by us) makes this ion a versatile new ligand for a variety of objectives, including variable denticity levels, high-nuclearity cluster formation, linking of clusters into 1D, 2D and 3D polymeric arrays, 3d-4f mixed-metal chemistry and ferromagnetic exchange interactions.

As far as the magnetic properties of **3** are concerned, the system can be described as a summation of antiferromagnetically coupled dinuclear subunits and isolated mononuclear subunits.

Experimental Section

Physical Methods: Elemental analyses (C, H N) were performed by the University of Ioannina (Greece) Microanalytical Laboratory using an EA 1108 Carlo Erba analyzer. Magnetic susceptibility measurements were carried out on a polycrystalline sample of **3** with a DSM8 pendulum-type susceptometer working in the range 5−300 K at magnetic fields of approximately 1 T. Diamagnetic corrections were estimated from Pascal tables. EPR spectra were recorded on a Bruker ES200 spectrometer at X-band frequency. Infrared spectra (4400−450 cm^{-1}) were recorded from KBr pellets on a Perkin−Elmer PC 16 FTIR spectrometer.

Preparation of $[Mn_3(btaO)_2(NCS)_4(DMF)_8]_n$ (3): Solid btaOH (0.08 g, 0.6 mmol) and NH_4SCN (0.09 g, 1.2 mmol) were dissolved with stirring in DMF (25 cm^3). Manganese powder (0.05 g, 0.9 mmol) was then added and the mixture was refluxed for approximately 2 h until all the powder had disappeared and the solution had turned yellow. The yellow solution was cooled and layered with Et_2O (50 cm^3). Yellow, X-ray quality crystals of the product formed over a period of three weeks. The needles were collected by filtration, washed with Et_2O and dried in air. Yield 0.28 g, 74%. $C_{40}H_{64}Mn_3N_{18}O_{10}S_4$ (1250.2): calcd. C 38.43, H 5.16, N 20.16; found C 38.40, H 5.10, N 20.18.

Crystal Structure Determination and Refinement of the Structure: A crystal of **3** with approximate dimensions of 0.10 × 0.10 × 0.50 mm was mounted in a capillary filled with drops of mother liquor. Diffraction measurements were made on a Crystal Logic Dual Goniometer diffractometer using graphite monochromated Mo-K_α radiation. Complete crystal data and parameters for data collection and refinement are listed in Table 2. Unit cell dimensions were determined and refined by using the angular settings of 25 automatically centred reflections in the range $11 < 2\theta < 23°$. Intensity data were recorded using a θ-2θ scan with a scan speed of 2°·min^{-1} and a scan range of 2° plus $\alpha_1\alpha_2$ separation. Three standard reflections monitored every 97 reflections showed less than 3% variation and no decay. Lorentz polarisation corrections were applied using the Crystal Logic software package.

Table 2. Crystal data and structure refinement for $[Mn_3(btaO)_2(NCS)_4(DMF)_8]_n$ (**3**)

Empirical formula	$C_{40}H_{64}Mn_3N_{18}O_{10}S_4$
Mol. wt.	1250.15
Colour and habit	Yellow prisms
Crystal size [mm]	0.10 × 0.10 × 0.50
Crystal system	Triclinic
Space group	$P\bar{1}$
a [Å]	13.582(7)
b [Å]	11.313(5)
c [Å]	20.474(9)
α [°]	89.67(2)
β [°]	86.65(2)
γ [°]	73.98(2)
V [Å^3]	3019(1)
Z	2
ρ [Mg·m^{-3}]	1.375
T [°C]	25
λ (Mo-K_α) [Å]	0.71073
μ [mm^{-1}]	0.819
F(000)	1298
$2\theta_{max}$ [°]	48
Index ranges [°]	$-15 \le h \le 15$
	$-12 \le k \le 12$
	$0 \le l \le 23$
No. of reflections collected	9778
No. of indep. refls./R_{int}	9468/0.0377
Data with $I > 2\sigma(I)$	6209
Parameters refined	864
$[\Delta/\sigma]_{max}$	0.146
GOF (on F^2)	1.118
$R1$[a]	0.0615
$wR2$[b]	0.1333
Residuals [e Å^{-3}]	0.909/−0.606

[a] $R1 = \Sigma||F_0| - |F_c||/\Sigma|F_0|$. [b] $wR2 = \{\Sigma[w(F_0^2 - F_c^2)^2]/\Sigma[w(F_0^2)^2]\}^{1/2}$.

The structure was solved by direct methods using SHELXS-86[23a] and refined by full-matrix least-squares techniques on F^2 with SHELXL-93.[23b] All hydrogen atoms [except those on C(66), C(69), C(77) and C(78), which were introduced at calculated positions as riding on their parent atoms] were located by difference maps and refined isotropically. All non-hydrogen atoms were refined anisotropically.

CCDC-179198 contains the supplementary crystallographic data for this paper. These data can be obtained free of charge at www.ccdc.cam.ac.uk/conts/retrieving.html [or from the Cambridge Crystallographic Data Centre, 12 Union Road, Cambridge CB2 1EZ, UK; Fax: (internat.) +44-1223/336-033; E-mail: deposit@ccdc.cam.ac.uk].

Acknowledgments

This work was supported by the Greek General Secretariat of Research and Technology (Grant 99ED139 to S.P.P.) and the CICYT (Grant BQU2000/0791 to A.E. and R.V.).

[1] [1a] V. Tangoulis, C. P. Raptopoulou, A. Terzis, E. G. Bakalbassis, E. Diamantopoulou, S. P. Perlepes, *Inorg. Chem.* **1998**, *37*, 3145. [1b] K. Skorda, R. Keuleers, A. Terzis, C. P. Raptopoulou, S. P. Perlepes, J. C. Plakatouras, *Polyhedron* **1999**, *18*, 3067, and references cited therein.

[2] [2a] J. Reedijk, G. Roelofsen, A. R. Siedle, A. L. Spek, *Inorg. Chem.* **1979**, *18*, 1947. [2b] J. Handley, D. Collison, C. D.

Garner, M. Helliwell, R. Docherty, J. R. Lawson, P. A. Tasker, *Angew. Chem. Int. Ed. Engl.* **1993**, *32*, 1036. [2c] M. Murrie, D. Collison, C. D. Garner, M. Helliwell, P. A. Tasker, S. S. Turner, *Polyhedron* **1998**, *17*, 3031.
[3] [3a] B.-S. Fang, C. G. Olson, D. W. Lynch, *Surf. Sci.* **1986**, *176*, 476, and references cited therein. [3b] W. Qafsaoui, Ch. Blanc, J. Roques, N. Pebere, A. Srhiri, C. Mijoule, G. Mankowski, *J. Appl. Electrochem.* **2001**, *31*, 223.
[4] V. Tangoulis, C. P. Raptopoulou, V. Psycharis, A. Terzis, K. Skorda, S. P. Perlepes, O. Cador, O. Kahn, E. G. Bakalbassis, *Inorg. Chem.* **2000**, *39*, 2522.
[5] E. Diamantopoulou, S. P. Perlepes, D. Raptis, C. P. Raptopoulou, *Trans. Met. Chem.* **2002**, *27*, 377.
[6] [6a] V. N. Kokozay, O. Y. Vassilyeva, P. Weinberger, M. Wasinger, W. Linert, *Rev. Inorg. Chem.* **2000**, *20*, 255. [6b] E. A. Vinogradova, O. Y. Vassilyeva, V. N. Kokozay, P. J. Squattrito, J. Reedijk, G. A. Van Albada, W. Linert, S. K. Tiwary, P. R. Raithby, *New J. Chem.* **2001**, *25*, 949.
[7] [7a] O. Kahn, *Acc. Chem. Res.* **2000**, *33*, 647. [7b] S. R. Batten, *Curr. Opin. Solid State Mater. Sci.* **2001**, *5*, 107, and references cited therein.
[8] H. O. Stumpf, L. Quahab, Y. Pei, P. Bergerat, O. Kahn, *J. Am. Chem. Soc.* **1994**, *116*, 3866.
[9] J. L. Manson, A. M. Arif, J. S. Miller, *Chem. Commun.* **1999**, 1479.
[10] K. Skorda, G. S. Papaefstathiou, A. Vafiadis, A. Lithoxoidou, C. P. Raptopoulou, A. Terzis, V. Psycharis, E. Bakalbassis, V. Tangoulis, S. P. Perlepes, *Inorg. Chim. Acta* **2001**, *326*, 53.
[11] [11a] G. De Munno, M. Julve, F. Lloret, J. Faus, M. Verdaguer, A. Caneschi, *Inorg. Chem.* **1995**, *34*, 157, and references cited therein. [11b] J. J. Borràs-Almenar, E. Coronado, J. Curely, R. Georges, J. C. Gianduzzo, *Inorg. Chem.* **1994**, *33*, 5171, and references cited therein. [11c] *Magnetic Molecular Materials* (Eds.: D. Gatteschi, O. Kahn, J. C. Miller, F. Palacio), NATO ASI Series E, Vol. 198, Kluwer Academic Publishers, Dordrecht, The Netherlands, **1991**.
[12] K. Nakamoto, *Infrared and Raman Spectra of Inorganic and Coordination Compounds*, 4th ed., Wiley, New York, **1986**, pp. 283−287.
[13] E. Manessi-Zoupa, S. P. Perlepes, V. Hondrellis, J. M. Tsangaris, *J. Inorg. Biochem.* **1994**, *55*, 217.
[14] L. J. Farrugia, *J. Appl. Cryst.* **1997**, *30*, 565.
[15] [15a] P. Lumme, I. Mutikainen, E. Lindell, *Inorg. Chim. Acta* **1983**, *71*, 217. [15b] R. Keuleers, G. S. Papaefstathiou, C. P. Raptopoulou, S. P. Perlepes, H. O. Desseyn, *J. Mol. Struct.* **2000**, *525*, 173.
[16] R. Cortés, M. Drillon, X. Solans, L. Lezama, T. Rojo, *Inorg. Chem.* **1997**, *36*, 677.
[17] B. Albela, M. Corbella, J. Ribas, I. Castro, J. Sletten, H. Stoeckli-Evans, *Inorg. Chem.* **1998**, *37*, 788.
[18] M. Lubben, A. Meetsma, B. L. Feringa, *Inorg. Chim. Acta* **1995**, *230*, 169.
[19] O. Kahn, *Molecular Magnetism*, VCH Publishers, New York, **1993**.
[20] E. Ruiz, S. Alvarez, P. Alemany, *Chem. Commun.* **2000**, 2767.
[21] [21a] A. Caneschi, D. Gatteschi, L. Laugier, P. Rey, C. Zanchini, *Inorg. Chem.* **1989**, *28*, 1969. [21b] M. D. Carducci, R. J. Doedens, *Inorg. Chem.* **1989**, *28*, 2492. [21c] G. Aromi, P. C. Berzal, P. Gamez, O. Roubeau, H. Kooijman, A. L. Spek, W. L. Driessen, J. Reedijk, *Angew. Chem. Int. Ed.* **2001**, *40*, 3444.
[22] K.-L. Lu, S. Kumaresan, Y.-S. Wen, J. R. Hwu, *Organometallics* **1994**, *13*, 3170.
[23] [23a] G. M. Sheldrick, *SHELXS-86, Program for the Solution of Crystal Structures*, University of Gottingen, Germany, **1986**. [23b] G. M. Sheldrick, *SHELXL-93, Program for the Refinement of Crystal Structures*, University of Gottingen, Germany, **1993**.

Received February 26, 2002
[I02101]

Synthesis, Stereochemistry and Molecular Structures of Chiral-at-Metal (Cycloheptatrienyl)molybdenum Complexes Containing the Diphosphane Prophos[‡]

Henri Brunner,*[a] Jürgen Klankermayer,[a] and Manfred Zabel[a][‡]

Keywords: Chirality / Molybdenum / Half-sandwich complexes / Configuration determination

The synthesis of a series of 18-electron chiral-at-metal (cycloheptatrienyl)molybdenum complexes [(η^7-C_7H_7)Mo(prophos)X] [prophos = (*R*)-1,2-bis(diphenylphosphanyl)propane; X = $NCMeBF_4$, Cl, I, CN, H, Me] is reported, which consist of diastereomers differing only in the metal configuration. Diastereomer enrichments have been achieved and the configurational stability of the compounds [(η^7-C_7H_7)Mo(prophos)X] has been studied and compared with the isoelectronic ruthenium complexes [(η^5-C_5H_5)Ru(prophos)X]. The stereochemistry of the substitution reactions has been investigated, and X-ray analysis and NMR spectroscopy were used to determine the absolute configuration of the complexes.
(© Wiley-VCH Verlag GmbH, 69451 Weinheim, Germany, 2002)

Introduction

Cyclopentadienyl (η^5-C_5H_5) and benzene (η^6-C_6H_6) are among the most common ligands encountered in organotransition metal chemistry. Although transition metal complexes of the cycloheptatrienyl ligand η^7-C_7H_7 have been known for more than four decades, the chemistry of this ligand has not been studied much in comparison.[1] Until now, there is only one example of a chiral-at-metal cycloheptatrienyl complex.[2]

Whereas the neutral η^5-C_5H_5 ligand contributes 5 electrons to a metal centre, the (η^7-C_7H_7) ligand is a 7-electron ligand. As Ru has two electrons more than Mo, the isoelectronic fragments (η^5-C_5H_5)Ru and (η^7-C_7H_7)Mo should be intimately related (Scheme 1). The similarity of their chemistry will be corroborated in the present paper and in subsequent publications.[3,4]

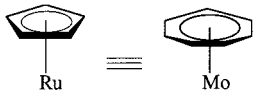

Scheme 1

Three-legged "piano stool" complexes [(η^n-C_nH_n)MLL′L′′] are prominent examples of chiral-at-metal compounds.[5–7] Frequently, in these complexes the metal atom is the unique centre of chirality, with the compounds forming racemates. If one of the ligands is enantiomerically pure, a pair of diastereomers arises, differing only in the metal configuration. Usually, such diastereomers can be distinguished on the basis of their NMR spectra. Therefore, the diastereomer ratio and enrichment can be determined by the integration of suitable signals.

In solution some of the chiral-at-metal complexes are configurationally stable even at higher temperatures, whereas others are labile with respect to the metal configuration. Mostly, changes in the metal configuration are initiated by ligand dissociation, which converts an 18-electron species into an unsaturated 16-electron intermediate. Theoretical studies claim that for a series of isoelectronic 16-electron fragments [(η^n-C_nH_n)M(CO)$_2$] the ring size of the polyenyl ligand and the location of the metal in the periodic table have a distinct influence on the barrier of the pyramidal inversion at the metal centre.[8,9] The calculations showed that [(η^5-C_5H_5)Mn(CO)$_2$] and [(η^6-C_6H_6)Cr(CO)$_2$] have a pyramidal ground state and high inversion barriers. Interestingly, the situation changes upon going to either [(η^4-C_4H_4)Fe(CO)$_2$] or [(η^7-C_7H_7)V(CO)$_2$]. In both cases extremely shallow, only weakly pyramidal minima were found. As a consequence, [(η^5-C_5H_5)RuLL′L′′] and [(η^7-C_7H_7)MoLL′L′′] complexes should differ in their configurational stability, provided the change in the metal configuration includes a ligand dissociation.

In the present paper we compare the stereochemistry of the ruthenium complexes [(η^5-C_5H_5)Ru(prophos)X], studied by Consiglio et al.,[10] with the corresponding molybdenum compounds [(η^7-C_7H_7)Mo(prophos)X] (X = $NCMeBF_4$, Cl, I, CN, H, Me) (Scheme 2).[11]

[‡] Optically Active Transition Metal Complexes, 127. Part 126: H. Brunner, T. Zwack, *Organometallics* **2000**, *19*, 2423.

[a] Institut für Anorganische Chemie der Universität, 93040 Regensburg, Germany
Fax: (internat.) + 49-(0)941/943-4439
E-mail: henri.brunner@chemie.uni-regensburg.de

[‡‡] X-ray structure analyses.

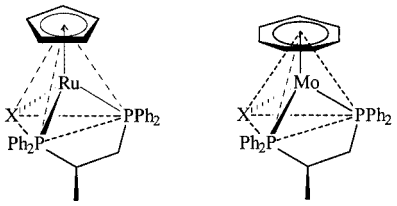

Scheme 2

Results and Discussion

1. Synthesis and Characterisation of Complexes 1a/1b

Reaction of the reactive complex $[(\eta^7\text{-}C_7H_7)Mo(\eta^6\text{-}C_6H_5CH_3)]BF_4$ [12] with the chiral diphosphane (*R*)-1,2-bis(diphenylphosphanyl)propane, (*R*)-prophos,[13] in CH_3CN resulted in the formation of a diastereomeric mixture $[(\eta^7\text{-}C_7H_7)Mo(prophos)(NCMe)]BF_4$ **1a/1b** (Scheme 3). The ratio of diastereomers could be determined by ^1H NMR spectroscopy as **1a/1b** = 93:7 in [D_6]acetone. It remained unchanged after 1 d in acetone solution. In the major diastereomer **1a**, the $\eta^7\text{-}C_7H_7$ signal was shifted to lower field compared to that of the minor diastereomer **1b**. Besides the C_7H_7 and the phenyl resonances, the ^1H NMR spectra of both diastereomers showed three signals due to the CH_2 and CH protons and a signal due to the methyl group of the diphosphane ligand, characterised by the expected coupling constants. The $^{31}P\{^1H\}$ NMR spectrum of the major diastereomer **1a** consisted of two doublets at δ = 71.7 and 56.1 ppm. The resonances of the minor diastereomer **1b** were shifted to δ = 76.1 and 62.7 ppm.

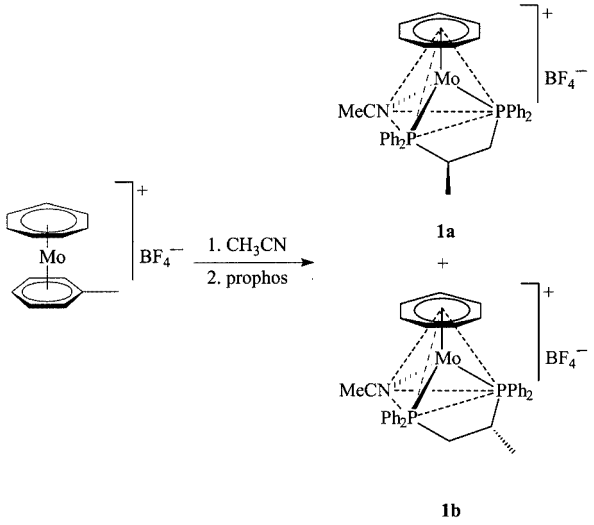

Scheme 3

Consiglio et al. had reported that in compounds of the type $[(\eta^5\text{-}C_5H_5)Ru(prophos)X]$ the major diastereomers having an (S_{Ru},R_C) configuration exhibited differences in the ^{31}P chemical shifts of the two phosphorus atoms P_A and P_B which were always larger than those of $P_{A'}$ and $P_{B'}$ of the (R_{Ru},R_C) diastereomers. Furthermore, the chemical shifts of the (R_{Ru},R_C) diastereomers usually fell between those of the (S_{Ru},R_C) diastereomers.[11] In keeping with such an empirical correlation, the absolute configuration of **1a/1b** was assigned on the basis of the ^{31}P chemical shifts of the molybdenum complexes **2**, **4**−**6** shown in Table 1. The absolute configurations of **2** and **4** are known from their X-ray structure determinations (see below), and those of **5** and **6** from NOE spectroscopy (see below). All 5 diastereomer pairs exhibit the same ^{31}P NMR pattern. Since the ^{31}P chemical shifts of the $P_{A'}$ and $P_{B'}$ signals of the minor (R_{Mo},R_C) diastereomers of **2b**, **4b**, **5b** and **6b** are larger than than those of P_A and P_B of the major (S_{Mo},R_C) diastereomers **2a**, **4a**, **5a** and **6a**, we assign an (R_{Mo},R_C) configuration to **1b** and an (S_{Mo},R_C) configuration to **1a**.

Table 1. ^{31}P chemical shifts for the two phosphorus atoms in the molybdenum complexes **1**, **2**, **4**, **5**, **6**

Complex (solvent)	P_A [ppm]	$P_{A'}$ [ppm]	P_B [ppm]	$P_{B'}$ [ppm]
1 ([D_6]acetone)	71.7	76.1	56.1	62.7
2 (C_6D_6)	65.5	65.8	51.1	56.1
4 (C_6D_6)	69.7	74.3	53.9	61.8
5 (C_6D_6)	81.1	86.3	64.1	68.3
6 (C_6D_6)	77.6	77.4	60.0	64.0

The CH_3CN ligand in $[(\eta^7\text{-}C_7H_7)Mo(prophos)(NCMe)]BF_4$ (**1**) proved to be substitutionally labile. It could be replaced by CD_3CN (20 equiv.) in a solution of **1** in [D_6]acetone at room temperature [Equation (1)].

$$[(\eta^7\text{-}C_7H_7)Mo(prophos)(CH_3CN)]BF_4 + CD_3CN \rightarrow [(\eta^7\text{-}C_7H_7)Mo(prophos)(CD_3CN)]BF_4 + CH_3CN \quad (1)$$

The kinetics of this process was studied by ^1H NMR spectroscopy and analysed for pseudo-first-order conditions. The first-order rate constant obtained was $1.86 \cdot 10^{-3}$ min^{-1} at 21.8 °C (half-life 373 min). During the exchange no significant change in the diastereomeric ratio was observed. In comparison to the related ruthenium complex $[(\eta^5\text{-}C_5H_5)Ru(ppfa)(NCMe)]PF_6$ {ppfa = 2-[1-(dimethylamino)ethyl]-1-(diphenylphosphanyl)ferrocene}, the CH_3CN exchange in **1** was considerably slower.[14]

2. Synthesis and Characterisation of Complexes 2a/2b

Treatment of $[(\eta^7\text{-}C_7H_7)Mo(\eta^6\text{-}C_6H_5CH_3)]BF_4$ in acetone with 1 equiv. of (*R*)-prophos caused displacement of the $(\eta^6\text{-}C_6H_5CH_3)$ ligand. Reaction with an excess of anhydrous LiCl afforded the 17-electron cation $[(\eta^7\text{-}C_7H_7)Mo(prophos)Cl]^+$. The synthesis of the neutral 18-electron diastereomers $[(\eta^7\text{-}C_7H_7)Mo(prophos)Cl]$ (**2a/2b**) from the radical cation in $[(\eta^7\text{-}C_7H_7)Mo(prophos)Cl]BF_4$ was achieved by reduction with $CoCp_2$ in toluene (Scheme 4).[15−17] The complexes **2a/2b** initially failed to give satisfactory NMR spectra, probably due to trace oxidation. However, good NMR spectroscopic data for **2a/2b** were obtained on addition of a small quantity of $CoCp_2$ to the sample.[18] The diastereomer ratio could be determined

by ^{1}H NMR spectroscopy as **2a/2b** = 82:18 in C_6D_6. It remained unchanged after 1 d in benzene solution. In the major diastereomer **2a**, the η^7-C_7H_7 signal was shifted to

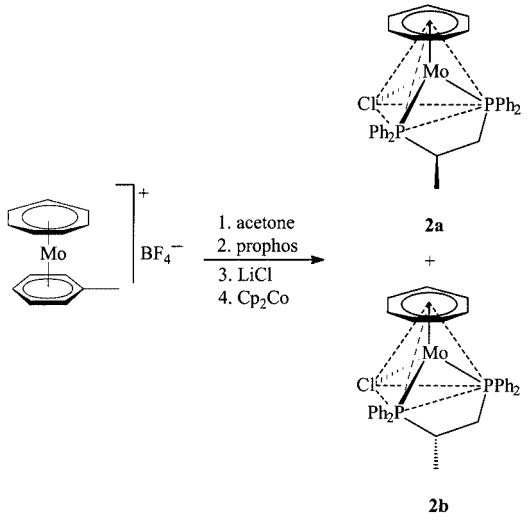

Scheme 4

lower field compared to that of the minor diastereomer **2b**.

Consiglio et al. had found in their studies, that the chiral-at-metal complex [(η^5-C_5H_5)Ru(prophos)Cl] was configurationally stable at room temperature and even did not epimerise in benzene at 80 °C.[19] In contrast, the analogous molybdenum complex [(η^7-C_7H_7)Mo(prophos)Cl] (**2**) epimerised at higher temperatures at the metal centre with no apparent decomposition. Thus, an 82:18 mixture of **2a/2b** changed to 90:10 after 18 h and to 93:7 after 42 h at 60 °C in C_6D_6. This result confirms the theoretical studies[8,9] that had predicted a lower barrier of the pyramidal inversion for (η^7-C_7H_7)MoLL systems compared to (η^5-C_5H_5)RuLL systems.

3. Molecular Structure of Diastereomer 2a

To determine the absolute configuration of the major diastereomer [(η^7-C_7H_7)Mo(prophos)Cl] (**2a**) by X-ray analysis, single crystals were grown in CH_2Cl_2/hexane from a 93:7 mixture of **2a/2b**. The molecular structure of **2a** is depicted in Figure 1 and selected structural parameters are listed in Table 2.

The η^7-C_7H_7 ring occupies three *fac* positions of an octahedral metal environment, which is completed by the chelate phosphane group and a terminal chlorine atom. The absolute configuration of the metal centre is (S_{Mo}) in agreement with the ligand priority sequence[20,21] η^7-C_7H_7 > Cl > P1(CH_3) > P2. Thus, the thermodynamically more stable diastereomer **2a** has (S_{Mo},R_C) configuration.

The cycloheptatrienyl ring is almost planar. The molybdenum atom lies 1.612 Å apart from the least-squares plane through the carbocyclic ring. The two Mo−P bond lengths are slightly different from each other. The sequence of the angles around the molybdenum atom is P1−Mo1−P2 < P1−Mo1−Cl1 < P2−Mo1−Cl1, with the chlorine ligand displaced towards P1.

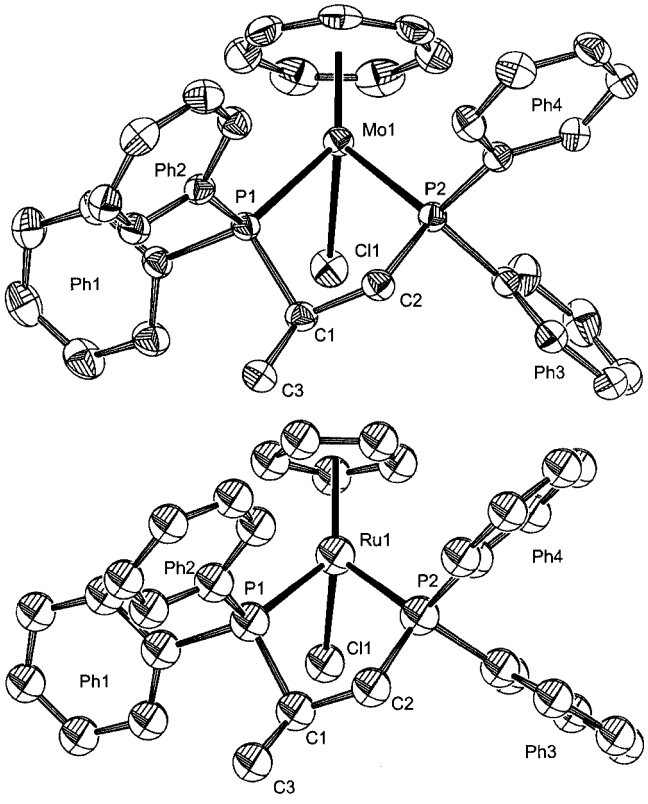

Figure 1. Molecular structures of (S_{Mo},R_C)-[(η^7-C_7H_7)Mo(prophos)Cl] (**2a**) (top) and (S_{Ru},R_C)-[(η^5-C_5H_5)Ru(prophos)Cl][20] (bottom); hydrogen atoms have been omitted for clarity

As compound (S_{Mo},R_C)-[(η^7-C_7H_7)Mo(prophos)Cl] (**2a**) resembles the complex (S_{Ru},R_C)-[(η^5-C_5H_5)Ru(prophos)Cl],[19] it was interesting to compare their molecular structures (Figure 1). The similarity is striking. In both complexes even the phenyl rings (except Ph4) of the prophos ligand are orientated in the same way. As a consequence of the smaller polyenyl ligand, the bond C(g)−Ru (1.851 Å) in [(η^5-C_5H_5)Ru(prophos)Cl] is longer than the bond C(g)−Mo (1.612 Å) in **2a** [C(g) = ring centroid]. Due to the different metal radii, the M−P bonds are about 0.2 Å shorter in the ruthenium complex.

The Mo(prophos) metallacycle in [(η^7-C_7H_7)Mo(prophos)Cl] (**2a**) has λ conformation allowing an equatorial disposition of the methyl group C3 of the (*R*)-prophos ligand. The two carbon atoms C1 and C2 of the five-membered ring are both on the same side of the P1−Mo1−P2 plane, a frequently found conformation (distorted envelope conformation).[22] The Ru(prophos) metallacycle in [(η^5-C_5H_5)Ru(prophos)Cl] also has λ conformation with a torsion angle P2−C2−C1−P1 of −43.77°, which is smaller than the analogous angle in **2a** of −53.21° (Figure 2).

4. Synthesis and Characterization of Complexes 3a/b and 4a/b

Reaction of [(η^7-C_7H_7)Mo(prophos)(NCMe)]BF_4 (**1**) with an excess of NaI in acetone afforded the 18-electron complex [(η^7-C_7H_7)Mo(prophos)I] (**3**) (Scheme 5). The dia-

Table 2. Selected bond lengths [Å] and angles [°] for compounds [(η^n-C_nH_n)M(prophos)X]: [(η^5-C_5H_5)Ru(prophos)Cl],[19] [(η^7-C_7H_7)Mo(prophos)Cl] (**2a**), -[(η^7-C_7H_7)Mo(prophos)I] (**3a**) and [(η^7-C_7H_7)Mo(prophos)CN] (**4a**)

Complex	[CpRu(prophos)Cl]	**2a**	**3a**	**4a**
Stereochemistry	(S_{Ru},R_C)	(S_{Mo},R_C)	(R_{Mo},R_C)	(S_{Mo},R_C)
X	Cl	Cl	I	CN
M−P1	2.278(2)	2.4898(5)	2.5152(7)	2.4740(18)
M−P2	2.276(2)	2.4692(6)	2.4801(7)	2.4551(17)
M−X	2.444(2)	2.5355(5)	2.8774(3)	2.116(9)
M−C(g)[a]	1.851	1.612	1.621	1.626
P1−M−P2	82.9(1)	78.14(2)	78.04(2)	78.79(5)
P1−M−X	84.0(1)	78.86(2)	80.72(2)	78.61(19)
P2−M−X	92.9(1)	86.77(2)	89.62(2)	85.36(19)
P2−C2−C1−P1	−43.77	−53.21(15)	−52.75(19)	−51.5(5)
P1−M−P2−C2	10.8	−0.67(6)	−0.70(9)	−0.5(2)
P2−M−P1−C1	−29.9	−24.68(7)	−24.35(8)	−24.1(2)

[a] C(g) indicates the centre of the polyenyl ligand.

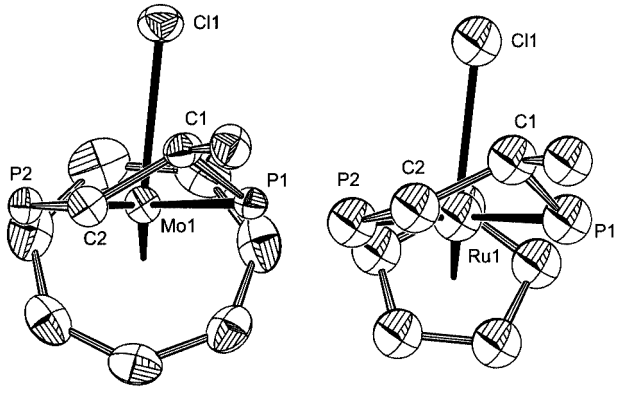

Figure 2. (S_{Mo},R_C)-[(η^7-C_7H_7)Mo(prophos)Cl] (**2a**) (left) and (S_{Ru},R_C)-[(η^5-C_5H_5)Ru(prophos)Cl] (right); view along the plane P1−M−P2 that is normal to the plane of the drawing, showing the λ conformation of the M(prophos) ring and the equatorial arrangement of the methyl group of prophos

stereomer ratio could be determined by ^{1}H NMR spectroscopy as **3a/3b** = 94:6 in C_6D_6. It remained unchanged after 1 d in benzene solution. By fractional crystallisation it was possible to increase the diastereomer ratio to 98:2. After 3 h at 70 °C in benzene solution, the diastereomer ratio changed to 94:6. Thus, analogous to complex **2**, compound [(η^7-C_7H_7)Mo(prophos)I] (**3**) epimerised at higher temperatures in solution. Interestingly, the variation of the halogen had no considerable influence on the equilibrium ratio.

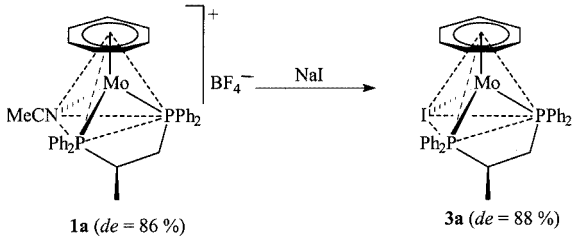

Scheme 5

The cyano complex [(η^7-C_7H_7)Mo(prophos)(CN)] (**4a/4b**) was obtained from the reaction of [(η^7-C_7H_7)Mo(prophos)($OCMe_2$)]BF_4 with KCN in acetone/methanol (Scheme 6). It was isolated as a red solid after purification by column chromatography. The diastereomer ratio could be determined by ^{1}H NMR spectroscopy as **4a/4b** = 93:7 in $CDCl_3$. This ratio remained unchanged after 1 d in $CDCl_3$ solution.

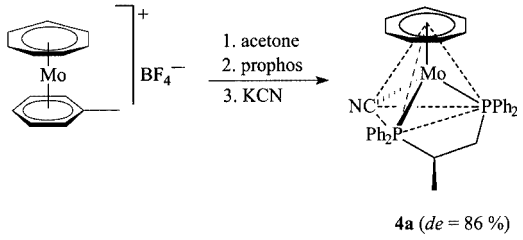

Scheme 6

5. Molecular Structures of Complexes 3a and 4a

Single crystals of [(η^7-C_7H_7)Mo(prophos)I] (**3a**) were grown at room temp. from toluene/pentane using a **3a/3b** = 98:2 mixture. An ORTEP view of **3a** is shown in Figure 3. The structure determination confirmed the (R_C) configuration of the stereogenic carbon centre. The configuration of the molybdenum centre was specified as (R_{Mo}) using the priority sequence I > η^7-C_7H_7 > P1(CH_3) > P2.

There is a change in the priority sequence of the ligands in **3a** and **2a**. Thus, (R_{Mo},R_C)-[(η^7-C_7H_7)Mo(prophos)I] (**3a**) and (S_{Mo},R_C)-[(η^7-C_7H_7)Mo(prophos)Cl] (**2a**) have opposite descriptors for the chiral metal atoms, although they have the same relative configuration (Figure 1 and Figure 3). The structural parameters of **3a** are very similar to those of **2a** except for the Mo−Hal part (Table 2). The cycloheptatrienyl ligand in **3a** is roughly planar with slightly different C−C [range 1.398(5)−1.417(4) Å] and Mo−C bond lengths, a consequence of the asymmetry of the coordination around the metal centre.

To determine the absolute configuration of the major diastereomer [(η^7-C_7H_7)Mo(prophos)CN] (**4a**) by X-ray analysis, single crystals were grown in $CHCl_3$/pentane from a

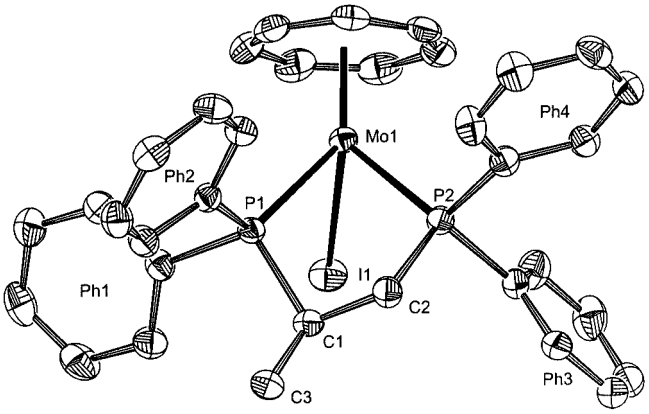

Figure 3. Molecular structure of (R_{Mo},R_C)-[(η^7-C_7H_7)Mo(prophos)I] (**3a**) (hydrogen atoms omitted for clarity)

93:7 mixture of **4a/4b**. The molecular structure of **4a** is shown in Figure 4. It has an (S_{Mo},R_C) configuration which relates it to the relative configuration of **2a** and **3a**.

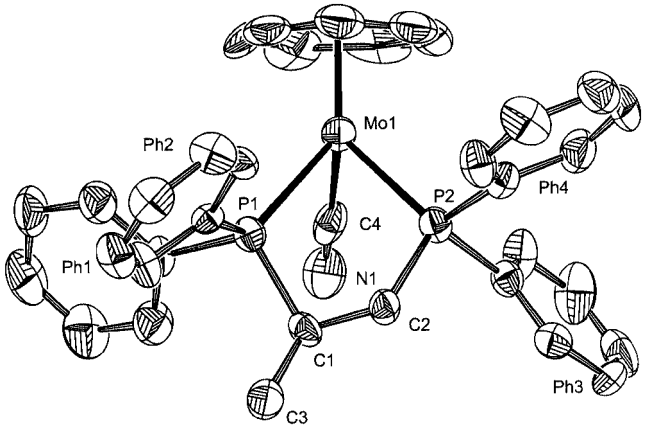

Figure 4. Molecular structure of (S_{Mo},R_C)-[(η^7-C_7H_7)Mo(prophos)CN] (**4a**) (hydrogen atoms omitted for clarity)

6. Formation of the Complexes 5a/b and 6a/b

Starting from [(η^7-C_7H_7)Mo(prophos)I] with a diastereomer ratio of **3a/3b** = 98:2 the reduction with sodium dihydrobis(2-methoxyethoxy)aluminate gave the hydrido compound [(η^7-C_7H_7)Mo(prophos)H] (**5a/5b**) (Scheme 7). The diastereomer ratio of the product could be determined by ^{1}H NMR spectroscopy as **5a/5b** = 67:33 in C_6D_6. The same ratio was obtained starting from [(η^7-C_7H_7)Mo(prophos)Cl] with a diastereomer ratio of **2a/2b** = 82:18. These results indicate that the metal centre in [(η^7-C_7H_7)Mo(prophos)H] **5a/5b** is configurationally labile. Obviously, the 67:33 mixture is the equilibrium ratio for **5a/5b**.

Complex [(η^7-C_7H_7)Mo(prophos)Me] (**6a/6b**) was prepared by reaction of [(η^7-C_7H_7)Mo(prophos)I] with MeLi in THF at 30 °C. The diastereomer ratio of the product could be determined as **6a**:**6b** = 87:13 in C_6D_6. This ratio remained unchanged after 1 d at 21 °C in solution. At higher temperatures decomposition occurred. By contrast,

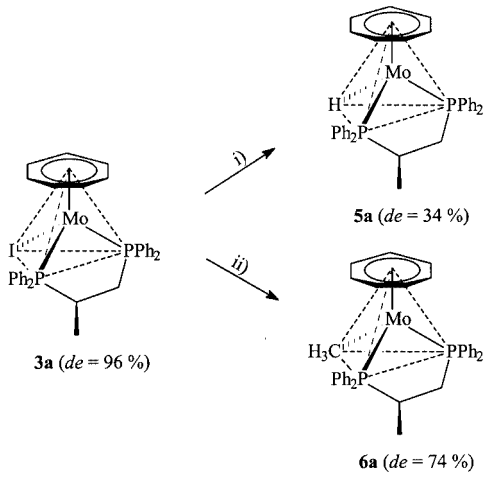

Scheme 7. i) $Na[AlH_2(OCH_2CH_2OCH_3)_2]$ in toluene; ii) MeLi in THF

reaction of [(η^5-C_5H_5)Ru(prophos)Cl] at room temperature in toluene with an ether solution of CH_3MgBr stereospecifically had given the corresponding methyl derivative [(η^5-C_5H_5)Ru(prophos)Me] and reaction of [(η^5-C_5H_5)Ru(prophos)Cl] with methanolic CH_3ONa leading to the hydride [(η^5-C_5H_5)Ru(prophos)H] took place with retention of configuration at the ruthenium atom.[23]

As it was not possible to obtain single crystals of **5** and **6** for an X-ray analysis, the stereochemical assignment of **5** and **6** was accomplished by NOE experiments.[11] The thermodynamically more stable diastereomers were the (S_{Mo},R_C) epimers **5a** and **6a**. The determination of the absolute configuration at the chiral molybdenum atom was based on the NOEs between R (**5a**, R = H; **6a**, R = Me) and the hydrogen atom H_g bound to the chiral carbon atom of the diphosphane. The assignment of the *ortho* proton resonances for the four phenyl groups was made by inspection of their NOEs with R, H_g, H_c, H_t and the Me group of the diphosphane ligand. These NOEs supported an equatorial disposition of the methyl group in **5a** and **6a** with a λ conformation of the Mo(prophos) metallacycle (Figure 5).

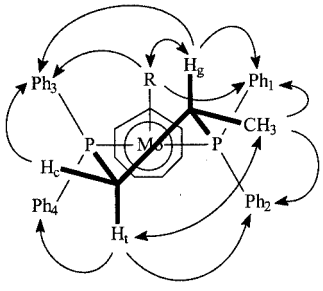

Figure 5. Schematic view of the prophos ligand in (S_{Mo},R_C)-[(η^7-C_7H_7)Mo(prophos)H] (**5a**) (R = H) and (S_{Mo},R_C)-[(η^7-C_7H_7)Mo(prophos)Me] (**6a**) (R = Me) projected onto the C_7H_7 ring; some selected NOEs are shown

Conclusions

The new (η^7-C_7H_7)Mo complexes described in this paper are isolobal with the corresponding (η^5-C_5H_5)Ru complexes investigated by Consiglio et al.[10,19,23] Whereas [(η^7-C_7H_7)Mo(prophos)Cl] undergoes epimerization in solution at temperatures around 60 °C, [(η^5-C_5H_5)Ru(prophos)Cl] is configurationally stable at this temperature. In contrast to the analogous ruthenium complexes, the formation of [(η^7-C_7H_7)Mo(prophos)H] and [(η^7-C_7H_7)Mo(prophos)Me] was not stereospecific. Thus, our investigations demonstrate that the new (η^7-C_7H_7)Mo complexes are configurationally more labile at the metal centre than their (η^5-C_5H_5)Ru counterparts.

Experimental Section

General Remarks: All manipulations were carried out under dry nitrogen using standard Schlenk techniques. Most of the commercially available reagents were used without further purification. Solvents were dried by standard methods and distilled prior to use. Melting points (not corrected): Büchi SMP 20. IR spectra: BioRad FT-IR (KBr pellets). Mass spectra: Finnigan Mat 311 A, Finnigan Mat 95 and ThermoQuest TSQ 7000. Optical rotations: Perkin−Elmer 241 polarimeter at room temperature. ^{1}H NMR spectra: Bruker ARX 400 spectrometer (400 MHz). ^{31}P NMR spectra: Bruker ARX 400 spectrometer (162 MHz). Elemental analyses: Heraeus Elementar Vario El III. The diphosphane (*R*)-prophos[13] and the complex [(η^7-C_7H_7)Mo(η^6-$C_6H_5CH_3$)]BF_4 [12] were prepared according to the literature.

[(η^7-C_7H_7)Mo(prophos)(NCMe)]BF_4 (1): A solution of [(η^7-C_7H_7)Mo(η^6-$C_6H_5CH_3$)]BF_4 (0.190 g, 0.47 mmol) was refluxed in CH_3CN for 1 h. The red solution was cooled to 0 °C, treated with prophos (0.185 g, 0.45 mmol) and refluxed for 3 h. The resulting solution was filtered and the volume was reduced to ca. 5 mL. Addition of diethyl ether precipitated **1** as a pink solid. Yield 298 mg (91%). M.p. 209 °C. IR (KBr): $\tilde{\nu}$ = 3060 w, 2990 w, 2970 w, 1490 m, 1440 s, 1070 s, 830 m, 750 m, 710 m cm^{-1}. ^{1}H NMR (400 MHz, [D$_6$]acetone; signal of the minor diastereomer in parentheses): δ = 7.73−7.13 (m, 20 H, Ph-*H*), 5.09 (4.88) (dd, J_{HP} = 2.2 Hz, J_{HP} = 2.1 Hz, 7 H, η^7-C_7H_7), 2.99 (dddd, J_{HP} = 48.9, $^2J_{H,H}$ = 14.9 Hz, J_{HP} = 12.6, $^3J_{H,H}$ = 4.3 Hz, 1 H, CH_AH$_B$), 2.15 (m, 1 H, C*H*CH$_3$), 1.87 (dddd, $^2J_{H,H}$ = 14.9, $^3J_{H,H}$ = 14.9 Hz, J_{HP} = 6.4 Hz, J_{HP} = 2.5 Hz, 1 H, CH$_A$*H*$_B$), 1.63 (dd, J_{HP} = 1.6 Hz, J_{HP} = 1.6 Hz, 3 H, NCC*H*$_3$), 0.97 (ddd, J_{HP} = 10.4, $^3J_{H,H}$ = 6.6 Hz, J_{HP} = 1.2 Hz, 3 H, CHC*H*$_3$) ppm. ^{31}P{^{1}H} NMR (162 MHz, [D$_6$]acetone; signal of the minor diastereomer in parentheses): δ = 71.7 (76.1) (d, J_{PP} = 23.7 Hz), 56.1 (62.7) (d) ppm. MS (FAB-MS): *m*/*z* (%) = 642 (15) [cation], 601 (100) [cation − NCMe]. [α]$_D$ = +10, [α]$_{578}$ = −20, [α]$_{546}$ = −170, [α]$_{436}$ = −600 (*c* = 0.16, acetone). $C_{36}H_{36}BF_4MoNP_2$ (727.38): calcd. C 59.45, H 4.99, N 1.93; found C 58.42, H 4.97, N 1.94.

[(η^7-C_7H_7)Mo(prophos)Cl] (2): A solution of [(η^7-C_7H_7)Mo(η^6-$C_6H_5CH_3$)]BF_4 (0.150 g, 0.41 mmol) and prophos (0.170 g, 0.41 mmol) was stirred in acetone for 20 h. Then the solution was treated with LiCl (0.250 g, 5.9 mmol) and stirred for 20 h. The solvent was removed and the residue was washed with toluene and dried; 0.180 g of the green solid was suspended in toluene and treated with Cp_2Co (0.047 g, 0.25 mmol). The mixture was stirred at 35 °C. After 3 h, the solution was filtered and the solvent was removed. Recrystallisation of the crude product from CH_2Cl_2/hexane gave **2** as a green solid. Yield 80 mg (30%). M.p. > 250 °C. IR (KBr): $\tilde{\nu}$ = 3060 w, 2990 w, 2970 w, 1490 m, 1440 s, 1100 m, 820 m, 740 m, 690 m cm^{-1}. ^{1}H NMR (400 MHz, C_6D_6; signal of the minor diastereomer in parentheses): δ = 8.01−7.90 (m, 2 H, Ph-*H*), 7.65−7.47 (m, 2 H, Ph-*H*), 7.37−6.92 (m, 16 H, Ph-*H*), 4.86 (4.79) (dd, J_{HP} = 1.9 Hz, J_{HP} = 1.9 Hz, 7 H, η^7-C_7H_7), 2.62 (m, 1 H, C*H*CH$_3$), 2.09 (dddd, J_{HP} = 46.7, $^2J_{H,H}$ = 14.7 Hz, J_{HP} = 10.9, $^3J_{H,H}$ = 5.2 Hz, 1 H, CH_AH$_B$), 1.38 (dddd, $^2J_{H,H}$ = 14.7, $^3J_{H,H}$ = 14.5 Hz, J_{HP} = 6.4 Hz, J_{HP} = 2.5 Hz, 1 H, CH$_A$*H*$_B$), 0.62 (0.76) (ddd, J_{HP} = 9.4, $^3J_{H,H}$ = 6.8 Hz, J_{HP} = 1.1 Hz, 3 H, CHC*H*$_3$) ppm. ^{31}P{^{1}H} NMR (162 MHz, C_6D_6; signal of the minor diastereomer in parentheses): δ = 65.5 (65.8) (d, J_{PP} = 16.0 Hz), 51.1 (56.1) (d) ppm. MS (FD-MS, CH_2Cl_2): *m*/*z* (%) = 636 (100) [M$^+$]. [α]$_D$ = −860, [α]$_{578}$ = −890, [α]$_{546}$ = −660 (*c* = 0.12, CH_2Cl_2). $C_{34}H_{33}ClMoP_2$ (634.98): calcd. C 64.31, H 5.24; found C 63.87, H 5.35.

[(η^7-C_7H_7)Mo(prophos)I] (3): Compound **1** (0.235 g, 0.32 mmol) in 30 mL of acetone was treated with NaI (0.200 g, 1.33 mmol). The reaction mixture was stirred for 20 h at room temp. and 3 h at 40 °C. The solvent was then removed and the residue was extracted with toluene (60 mL). The solution was filtered and reduced in volume. Addition of pentane gave green needles of **3**, which were dried in vacuo. Yield 181 mg (78%). M.p. > 250 °C. IR (KBr): $\tilde{\nu}$ = 3048 w, 2978 w, 2923 w, 2869 w, 1482 m, 1434 s, 1093 m, 814 s, 742 s, 696 s, 518 s cm^{-1}. ^{1}H NMR (400 MHz, C_6D_6; signal of the minor diastereomer in parentheses): δ = 7.97−7.90 (m, 2 H, Ph-*H*), 7.63−7.57 (m, 2 H, Ph-*H*), 7.48−7.42 (m, 2 H, Ph-*H*), 7.33−7.21 (m, 5 H, Ph-*H*), 7.20−7.02 (m, 9 H, Ph-*H*), 4.88 (4.82) (dd, J_{HP} = 1.9 Hz, J_{HP} = 1.9 Hz, 7 H, η^7-C_7H_7), 2.99 (m, 1 H, C*H*CH$_3$), 2.23 (dddd, J_{HP} = 46.4, $^2J_{H,H}$ = 14.7 Hz, J_{HP} = 10.7, $^3J_{H,H}$ = 5.5 Hz, 1 H, CH_AH$_B$), 1.32 (dddd, $^2J_{H,H}$ = 14.7, $^3J_{H,H}$ = 14.5 Hz, J_{HP} = 5.2 Hz, J_{HP} = 4.9 Hz, 1 H, CH$_A$*H*$_B$), 0.65 (0.97) (ddd, J_{HP} = 9.6, $^3J_{H,H}$ = 6.8 Hz, J_{HP} = 1.4 Hz, 3 H, CHC*H*$_3$) ppm. MS (FD-MS, CH_2Cl_2): *m*/*z* (%) = 728 (100) [M$^+$]. [α]$_D$ = −750, [α]$_{578}$ = −790, [α]$_{546}$ = −670, [α]$_{436}$ = −1500 (*c* = 0.16, CH_2Cl_2). $C_{34}H_{33}IMoP_2$ (726.43): calcd. C 56.22, H 4.58; found C 55.84, H 4.70.

[(η^7-C_7H_7)Mo(prophos)CN] (4): A solution of [(η^7-C_7H_7)Mo(η^6-$C_6H_5CH_3$)]BF_4 (0.364 g, 1.00 mmol) and prophos (0.412 g, 1.00 mmol) in 40 mL of acetone was refluxed for 18 h. The solution was reduced in volume to 10 mL and methanol (30 mL) was added. The resulting solution was treated with KCN and stirred for 30 min at 50 °C. The solvent was removed and the residue was extracted with CH_2Cl_2 (20 mL). The mixture was filtered through a plug of Al_2O_3 and the solvents were evaporated to dryness. The resulting solid was dissolved in CH_2Cl_2 and transferred to an Al_2O_3/hexane chromatography column cooled to 10 °C. Elution with acetone/hexane gave a red band, which was collected and the solvents were evaporated to dryness. Crystallisation of the crude product from $CHCl_3$/pentane gave **4** as red plates. Yield 199 mg (32%). M.p. > 250 °C. IR (KBr): $\tilde{\nu}$ = 3050 w, 2980 w, 2920 w, 2860 w, 2070 s, 1440 s, 1100 m, 820 m, 740 m, 690 m cm^{-1}. ^{1}H NMR (400 MHz, $CDCl_3$; signal of the minor diastereomer in parentheses): δ = 7.83−6.95 (m, 20 H, Ph-*H*), 4.70 (4.54) (dd, J_{HP} = 2.2 Hz, J_{HP} = 2.2 Hz, 7 H, η^7-C_7H_7), 2.68−2.54 (m, 1 H, C*H*CH$_3$), 2.40 (dddd, J_{HP} = 48.1, $^2J_{H,H}$ = 14.7 Hz, J_{HP} = 11.7, $^3J_{H,H}$ = 5.1 Hz, 1 H, CH_AH$_B$), 1.52 (dddd, $^2J_{H,H}$ = 14.7, $^3J_{H,H}$ = 14.5 Hz, J_{HP} = 6.4 Hz, J_{HP} = 4.3 Hz, 1 H, CH$_A$*H*$_B$), 0.84 (0.75) (ddd, J_{HP} = 8.8, $^3J_{H,H}$ = 7.8 Hz, J_{HP} = 1.3 Hz, 3 H, CHC*H*$_3$) ppm. ^{31}P{^{1}H} NMR (162 MHz, C_6D_6; signal of the minor diastereomer in parentheses): δ = 69.7 (74.3) (d, J_{PP} = 26.7 Hz), 53.9 (61.8) (d) ppm. MS (FD-MS, CH_2Cl_2): *m*/*z* (%) = 627 (100) [M$^+$]. $C_{35}H_{33}MoNP_2$ (625.54): calcd. C 67.20, H 5.32, N 2.24; found C 66.12, H 5.95, N 1.84.

[(η⁷-C_7H_7)Mo(prophos)H] (5): Compound [(η⁷-C_7H_7)Mo(prophos)I] (**3**) (60.0 mg, 0.83 μmol) was dissolved in 15 mL of toluene. To this solution was added RedAl© (80 μL of a 70% solution in toluene) at −20 °C. The mixture was stirred for 16 h at room temp. and then for 10 h at 30 °C. After cooling to 0 °C, water (0.1 mL) was added and the solvent was removed. The residue was extracted with toluene (5 mL). The mixture was filtered and the solvents were evaporated to dryness. Yield 32 mg (68%). ^{1}H NMR (400 MHz, C_6D_6; signal of the minor diastereomer in parentheses): δ = 8.07−6.90 (m, 20 H, Ph-*H*), 4.78 (4.72) (ddd, J_{HP} = 1.9 Hz, J_{HP} = 1.9 Hz, $J_{H,H}$ = 1.3 Hz, 7 H, η⁷-C_7H_7), 2.11 (dddd, J_{HP} = 50.1, $^2J_{H,H}$ = 13.7 Hz, J_{HP} = 10.0, $^3J_{H,H}$ = 4.4 Hz, 1 H, CH_AH$_B$), 2.03−1.87 (m, 1 H, C*H*CH$_3$), 1.60 (dddd, $^3J_{H,H}$ = 13.8, $^2J_{H,H}$ = 13.7 Hz, J_{HP} = 6.7 Hz, J_{HP} = 3.1 Hz, 1 H, CH$_A$$H_B$), 0.72 (0.66) (dd, J_{HP} = 9.4, $^3J_{H,H}$ = 6.8 Hz, 3 H, CHCH_3), −4.07 (−3.58) (dd, J_{HP} = 59.1 Hz, J_{HP} = 41.7 Hz, 1 H, Mo-*H*) ppm. ^{31}P{^{1}H} NMR (162 MHz, C_6D_6; signal of the minor diastereomer in parentheses): δ = 81.1 (86.3) (d, J_{PP} = 25.2 Hz), 64.1 (68.3) (d).

[(η⁷-C_7H_7)Mo(prophos)Me] (6): Methyllithium (0.8 mL of a 1.6 M solution in diethyl ether) was added to [(η⁷-C_7H_7)Mo(prophos)I] (**3**) (60.0 mg, 83 μmol) in THF (16 mL) at −78 °C. The solution was warmed to 0 °C and stirred for 3 h at this temperature. After 30 min at room temp., the solvent was removed. The residue was filtered through a plug of Celite® and the solvents were evaporated. The resulting solid was dissolved in hexane and transferred to a cooled Al_2O_3/hexane chromatography column maintained at −78 °C. Elution with hexane gave a red band, which was collected and the solvents were evaporated to dryness. Yield 49 mg (78%). ^{1}H NMR (400 MHz, C_6D_6; signal of the minor diastereomer in parentheses): δ = 7.79−6.94 (m, 20 H, Ph-*H*), 4.67 (4.66) (dd, J_{HP} = 1.9 Hz, J_{HP} = 1.9 Hz, 7 H, η⁷-C_7H_7), 2.28 (dddd, J_{HP} = 48.0, $^2J_{H,H}$ = 14.5 Hz, J_{HP} = 10.9, $^3J_{H,H}$ = 4.8 Hz, 1 H, CH_AH$_B$), 2.04−1.89 (m, 1 H, C*H*CH$_3$), 1.56 (dddd, $^3J_{H,H}$ = 14.7, $^2J_{H,H}$ = 14.5 Hz, J_{HP} = 6.0 Hz, J_{HP} = 3.3 Hz, 1 H, CH$_A$$H_B$), 0.66 (0.88) (ddd, J_{HP} = 9.0, $^3J_{H,H}$ = 6.7 Hz, J_{HP} = 1.0 Hz, 3 H, CHCH_3), −0.66 (−0.42) (dd, J_{HP} = 8.6 Hz, J_{HP} = 6.8 Hz, 3 H, CH_3) ppm. ^{31}P{^{1}H} NMR (162 MHz, C_6D_6; signal of the minor diastereomer in parentheses): δ = 77.6 (77.4) (d, J_{PP} = 17.2 Hz), 60.0 (64.0) (d).

Acetonitrile Exchange Kinetics with 1 in [D$_6$]Acetone: The CH_3CN exchange in **1** was studied by monitoring the decrease in intensity of the ^{1}H NMR signal of the coordinated [CH_3CN]$_c$ (at δ = 1.63 ppm) and the increase of the free [CH_3CN]$_f$ (at δ = 2.05 ppm) after injection of CD_3CN. After adjusting to the selected temperature, the deuterated acetonitrile was added and spectra were taken at regular intervals. The time dependence of the mol fraction x = [CH_3CN]$_c$/([CH_3CN]$_c$ + [CH_3CN]$_f$), obtained by integration of the corresponding signals, was fitted to Equation (2),[14,24] in which x_0 and x_∞ are the values of x at t = 0 and ∞, and k is the observed first-order rate constant for the exchange.

$$x = x_\infty + (x_0 - x_\infty)\exp[-kt/(1 - x_\infty)] \quad (2)$$

Table 3. Crystal data, data collection and structure refinement for [(η⁷-C_7H_7)Mo(prophos)Cl] (**2a**), [(η⁷-C_7H_7)Mo(prophos)I] (**3a**), and [(η⁷-C_7H_7)Mo(prophos)CN] (**4a**)

	2a	**3a**	**4a**
Empirical formula	$C_{34}H_{33}ClMoP_2$	$C_{34}H_{33}IMoP_2$	$C_{35}H_{33}MoNP_2$
Formula mass	634.98	726.43	625.54
Crystal system	orthorhombic	orthorhombic	orthorhombic
Space group	$P2_12_12_1$	$P2_12_12_1$	$P2_12_12_1$
Radiation	Mo-K_α	Mo-K_α	Cu-K_α
Z	4	4	4
Unit cell dimensions	a = 11.4591(8) Å	a = 11.7172(6) Å	a = 11.5122(8) Å
	b = 15.5525(10) Å	b = 15.6560(8) Å	b = 15.6901(15) Å
	c = 16.5821(15) Å	c = 16.4373(11) Å	c = 16.6296 (19) Å
Cell volume	2955.2(4) Å^3	3015.3(3) Å^3	3003.8(5) Å^3
Density (calculated)	1.427 g/cm^3	1.600 g/cm^3	1.383 g/cm^3
Absorption coefficient	0.66 mm^{-1}	1.587 mm^{-1}	4.75 mm^{-1}
F(000)	1304	1448	1288
Crystal size	0.48 × 0.18 × 0.18 mm	0.34 × 0.12 × 0.10 mm	0.16 × 0.04 × 0.04 mm
Crystal shape	prismatic	prismatic	rod
Crystal colour	brown	green-brown	red
θ range for data collection	2.21−25.80°	2.17−25.81°	3.87−39.93°
Temperature	173 K	173 K	297 K
Limiting indices	$-14 \le h \le 14$	$-14 \le h \le 14$	$-9 \le h \le 9$
	$-18 \le k \le 18$	$-19 \le k \le 19$	$-13 \le k \le 13$
	$-20 \le l \le 20$	$-20 \le l \le 20$	$-13 \le l \le 13$
Reflections collected	26619	24164	7211
Independent reflections (R_{int})	5619 (0.0654)	5767 (0.0467)	1811 (0.0721)
Reflections [$I > 2\sigma(I)$]	5325	5472	1695
Data/restraints/parameters	5619/0/343	5767/0/343	1811/0/352
Goodness-of-fit on F^2	1.047	1.034	1.096
Final R indices [$I > 2\sigma(I)$]	R_1 = 0.0204	R_1 = 0.0207	R_1 = 0.0218
	wR_2 = 0.0498	wR_2 = 0.0473	wR_2 = 0.0451
R indices (all data)	R_1 = 0.0220	R_1 = 0.0224	R_1 = 0.0254
	wR_2 = 0.0502	wR_2 = 0.0477	wR_2 = 0.0463
Absolute structure parameter	−0.02(2)	−0.03(1)	−0.02(1)
Largest diff. peak/hole	0.411/−0.195 e Å^{-3}	0.831/−0.286 e Å^{-3}	0.197/−0.224 e Å^{-3}
CCDC	178662	178663	178661

X-ray Crystallographic Studies: The data were collected with a STOE-IPDS (Mo-K_α radiation) and an Enraf−Nonius CAD-4 diffractometer (Cu-K_α radiation). Crystal data, data collection, structure refinement and CCDC numbers are given in Table 3. The structures were solved by direct methods (SIR97).[25] Refinement was done by full-matrix least-squares on F^2 (SHELXL-97).[26] CCDC-178662, -178661 and -178663 contain the supplementary crystallographic data for this paper. These data can be obtained free of charge at www.ccdc.cam.ac.uk/conts/retrieving.html or from the Cambridge Crystallographic Data Centre, 12, Union Road, Cambridge CB2 1EZ, UK [Fax: (internat.) + 44-1223/336-033; E-mail: deposit@ccdc.cam.ac.uk].

[1] M. L. H. Green, D. K. P. Ng, *Chem. Rev.* **1995**, *95*, 439.
[2] H. Brunner, M. Muschiol, I. Bernal, G. M. Reisner, *J. Organomet. Chem.* **1980**, *198*, 169.
[3] H. Brunner, J. Klankermayer, *Organometallics*, submitted.
[4] H. Brunner, J. Klankermayer, *Z. Anorg. Allg. Chem.*, in press.
[5] H. Brunner, *Adv. Organomet. Chem.* **1980**, *18*, 151.
[6] H. Brunner, *Angew. Chem.* **1999**, *111*, 1248; *Angew. Chem. Int. Ed.* **1999**, *38*, 1194.
[7] H. Brunner, *Eur. J. Inorg. Chem.* **2001**, 905.
[8] P. Hofmann, *Angew. Chem.* **1977**, *89*, 551; *Angew. Chem. Int. Ed. Engl.* **1977**, *16*, 536.
[9] T. R. Ward, O. Schafer, C. Daul, P. Hofmann, *Organometallics* **1997**, *16*, 3207.
[10] G. Consiglio, F. Morandini, *Chem. Rev.* **1987**, *87*, 761.
[11] J. Klankermayer, PhD Thesis, Univ. Regensburg, **2001**.
[12] M. Bochmann, M. Cooke, M. Green, H. P. Kirsch, F. G. A. Stone, A. J. Welch, *J. Chem. Soc., Chem. Commun.* **1976**, 381.
[13] M. D. Fryzuk, B. Bosnich, *J. Am. Chem. Soc.* **1978**, *100*, 5491.
[14] C. Slugovc, W. Simanko, K. Mereiter, R. Schmid, K. Kirchner, L. Xiao, W. Weissensteiner, *Organometallics* **1999**, *18*, 3865.
[15] M. L. H. Green, R. B. A. Pardy, *Polyhedron* **1985**, *4*, 1035.
[16] C. Bitcon, R. Breeze, P. F. Miller, M. W. Whiteley, *J. Organomet. Chem.* **1989**, *364*, 181.
[17] G. M. Aston, S. Badriya, R. D. Farley, R. W. Grime, S. J. Ledger, F. E. Mabbs, E. J. L. McInnes, H. W. Morris, A. Ricalton, C. C. Rowlands, K. Wagner, M. W. Whiteley, *J. Chem. Soc., Dalton Trans.* **1999**, 4379.
[18] S. P. M. Disley, R. W. Grime, E. J. L. McInnes, D. M. Spencer, N. Swainston, M. W. Whiteley, *J. Organomet. Chem.* **1998**, *566*, 151.
[19] F. Morandini, G. Consiglio, B. Straub, G. Ciani, A. Sironi, *J. Chem. Soc., Dalton Trans.* **1983**, 2293.
[20] C. Lecomte, Y. Dusausoy, J. Protas, J. Tirouflet, A. Dormond, *J. Organomet. Chem.* **1974**, *73*, 67.
[21] H. Brunner, *Enantiomer* **1997**, *2*, 133.
[22] H. Brunner, A. Winter, J. Breu, *J. Organomet. Chem.* **1998**, *553*, 285.
[23] F. Morandini, G. Consiglio, V. Lucchini, *Organometallics* **1985**, *4*, 1202.
[24] L. Helm, L. Elding, A. E. Merbach, *Inorg. Chem.* **1985**, *24*, 1719.
[25] A. Altomare, G. Cascarano, C. Ciacovazzo, A. Guagliardi, *J. Appl. Crystallogr.* **1993**, *26*, 343.
[26] G. M. Sheldrick, *SHELXL-97*, University of Göttingen, **1997**.

Received February 7, 2002
[I02063]

Polynuclear Mn^{II} Complexes with Chloroacetate Bridge − Syntheses, Structure, and Magnetic Properties

Gema Fernández,[a] Montserrat Corbella,*[a] José Mahía,[b] and Miguel A. Maestro[b]

Keywords: Manganese / Crystal structures / Magnetic properties / EPR spectroscopy / Bridging ligands

Three new polynuclear Mn^{II} complexes with chloroacetate bridges were obtained and characterized by X-ray diffraction: $[Mn_3(\mu\text{-}ClCH_2COO)_6(bpy)_2]$ (**1**), $[Mn_2(\mu\text{-}ClCH_2COO)_2(phen)_4](ClO_4)_2$ (**2**), and $[Mn(\mu\text{-}ClCH_2COO)_2(phen)]_n$ (**3**). The Mn···Mn distance for **1** (3.624 Å) is smaller than for **2** (4.613 Å) and **3** (4.530 Å); this is in agreement with the number of carboxylate bridges. The three compounds show a weak antiferromagnetic coupling. The J values are –3.82 cm^{-1} for **1**, –0.85 cm^{-1} for **3**, and no coupling was observed for **2**. Each compound showed a characteristic EPR spectrum at 4 K. Simulation of these spectra could be obtained with D = –0.16 cm^{-1} and E = –0.015 cm^{-1} for compound **1**, and D = –0.045 cm^{-1} and E = –0.004 cm^{-1} for compound **2**.

(© Wiley-VCH Verlag GmbH, 69451 Weinheim, Germany, 2002)

Introduction

Manganese is found in several metalloproteins. Usually, the manganese ion binds the protein through the carboxylate groups of aspartate or glutamate. In coordination chemistry, this sort of ligand is often found bridging two metal ions, which helps polymerization. This fact is also observed in biological systems, where the reaction centers have between 1 and 4 Mn ions.

The Mn^{II} ion usually plays a structural and/or hydrolytic role; however, it is also found in the reduced form in manganese redox enzymes. There are some dinuclear Mn−carboxylate active sites, e.g. catalase,[1] aminopeptidase,[2] arginase.[3] Recently, it has been shown that one pyrophosphatase needs 3 Mn^{II} ions for catalytic activity.[4] Further, interest in Mn^{II}−carboxylate chemistry has arisen due to the fact that the spectroscopic properties of Mn^{II} have been used as a probe for the sites that normally bind other metal ions. Understanding the structural and magnetic properties of different Mn^{II}−carboxylate complexes will therefore be useful in gaining insight into the structural details of the active site(s) that may influence the chemical mechanisms of catalysis.

Some dinuclear complexes with carboxylate bridges are reported in the literature, with $[Mn_2(\mu\text{-}H_2O)(\mu\text{-}RCOO)_2]^{2+}$,[5−7] $[Mn_2(\mu\text{-}OH)(\mu\text{-}RCOO)_2]^{+}$,[8,9] and $[Mn_2(\mu\text{-}OR)(\mu\text{-}RCOO)_2]^{+}$ cores.[10−14] There are also some dinuclear compounds which only have carboxylate bridges, e.g. three,[9,15−18] two,[19−29] or one.[30,31]

On the other hand, the number of trinuclear Mn^{II} complexes with bridging carboxylate groups is limited.[32−37] Finally, the number of one-dimensional Mn^{II} polymers is increasing,[28,29,39−44] but very few have two carboxylate bridges.[19,45−47]

In this paper we report the isolation and characterization of three new Mn^{II} compounds, with the same carboxylate ligand, $ClCH_2COO^-$. The nuclearity of these compounds differs; $[Mn_3(\mu\text{-}ClCH_2COO)_6(bpy)_2]$ (**1**) is trinuclear, $[Mn_2(\mu\text{-}ClCH_2COO)_2(phen)_4](ClO_4)_2$ (**2**) is dinuclear, and $[Mn(\mu\text{-}ClCH_2COO)_2(phen)]_n$ (**3**) is a one-dimensional compound. The structural characterization of these compounds was achieved by X-ray diffraction, and both their magnetic behavior and their EPR spectra were studied.

Results and Discussion

Syntheses

In a previous paper we studied the reactivity of $Mn(RCOO)_2{\cdot}nH_2O$ (R = 2-ClC_6H_4, 3-ClC_6H_4, and 4-ClC_6H_4) with 2,2′-bipyridine.[19] Mn^{II}/bpy ratios of 1:$^2/_3$ and 1:1 were considered, but each carboxylate had a preferred nuclearity (trinuclear complex or chain). In the present work we studied the analogous reaction of $Mn(ClCH_2COO)_2{\cdot}2H_2O$ with various bidentate amines, 2,2′-bipyridine, and 1,10-phenanthroline. Independent of the Mn^{II}/amine ratio, two different compounds were found for the same carboxylate. The 2,2′-bipyridine ligand gave a trinuclear complex $[Mn_3(\mu\text{-}ClCH_2COO)_6(bpy)_2]$ (**1**), while the 1,10-phenanthroline ligand gave a chain $[Mn(\mu\text{-}ClCH_2COO)_2(phen)]_n$ (**3**).

[a] Departament de Química Inorgànica, Universitat de Barcelona, Martí i Franquès 1−11, 08028 Barcelona, Spain
E-mail: montse.corbella@qi.ub.es
[b] Servicios Xerais de Apoio á Investigación, Universidade da Coruña, Edificio Anexo Facultade de Ciencias
15071 A Coruña, Spain

In the synthesis of the dinuclear compound $[Mn_2(\mu\text{-}ClCH_2COO)_2(phen)_4](ClO_4)_2$ (**2**), a 1:2:1 ratio of Mn^{II}/phen/ClO_4^- was considered. Attempts to obtain the analogous compound with bpy led to the formation of the more stable mononuclear compound $[Mn(bpy)_3](ClO_4)_2$.

Crystal Structures

$[Mn_3(\mu\text{-}ClCH_2COO)_6(bpy)_2]$ (1)

The structure of compound **1** is depicted in Figure 1; selected bond lengths and angles are collected in Table 1; **1** consists of a linear array of three Mn^{II} ions with an Mn(2)−Mn(1)−Mn(2_2) angle of 179.98°. Each Mn(2)···Mn(1) pair is separated by 3.624 Å, a similar distance to that reported for the analogous complex with acetate bridges $[Mn_3(\mu\text{-}CH_3COO)_6(bpy)_2]$ (3.614 Å).[32] For the complex with benzoate ligands $[Mn_3(\mu\text{-}PhCOO)_6(bpy)_2]$,[34] this distance is a bit shorter (3.588 Å). Mn(1) is located on a crystallographic inversion center, and it is bridged to both Mn(2) by three chloroacetate ligands. Two of these ligands coordinate through the two oxygen atoms ($\mu_{1,3}$-$ClCH_2COO$), while the third carboxylate group coordinates through just one oxygen atom ($\mu_{1,1}$-$ClCH_2COO$). In this case, the other oxygen atom chelates through a weak bond the terminal Mn(2) ion. This unusual coordination mode of the carboxylate group provokes a great distortion around Mn(2). The two $\mu_{1,3}$-carboxylate groups are similar, with greater $Mn(1)-O_{carb}$ distances (av. 2.174 Å) than $Mn(2)-O_{carb}$ distances (av. 2.095 Å). The same is observed for the $\mu_{1,1}$-carboxylate, the $Mn(1)-O_{bridge}$ distance is 2.217 Å, while the $Mn(2)-O_{bridge}$ distance is 2.151 Å. For the acetate complex,[32] these distances are very similar (2.201 and 2.155 Å), however, for the benzoate complex,[34] the $Mn_{central}-O_{bridge}$ distance is 2.239 Å, while the $Mn_{terminal}-O_{bridge}$ distance is 2.286 Å. A similar difference is found for the Mn(2)−O(5)−Mn(1) angle. This angle is 112.12° for complex **1**, 112.2° for the acetate complex, and 104.94° for the benzoate complex. Another important difference between complexes with aliphatic and aromatic carboxylate groups is the $Mn_{terminal}-O_{terminal}$ distance. For the $\mu_{1,1}$-carboxylate, this distance is 2.611 Å with $ClCH_2COO^-$, 2.605 Å with CH_3COO^-; however, this distance is shorter with $PhCOO^-$ (2.274 Å) and quite similar to the $Mn_{terminal}-O_{bridge}$ distance. Therefore, the carboxylate is important for the localization or delocalization of the π-system−COO^-. The benzoate favors delocalization, while the aliphatic carboxylate, with or without a chloro substituent, favors the asymmetry of the $-COO^-$ group.

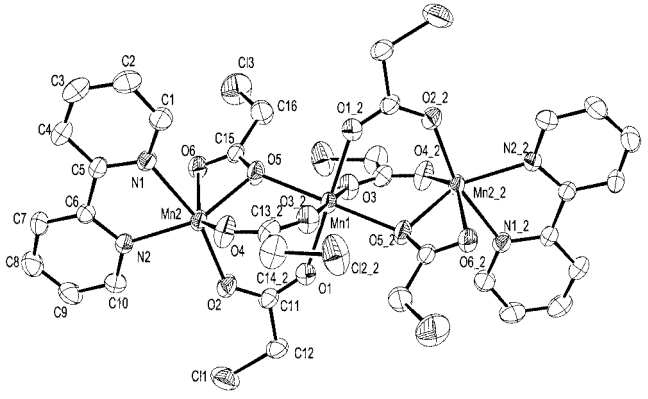

Figure 1. ORTEP drawing of complex **1**

The six-coordination of Mn(2) is completed by a 2,2′-bipyridine ligand. The acute angles O(5)−Mn(2)−O(6) (53.81°) and N(1)−Mn(2)−N(2) (73.19°) and the difference between the bond lengths Mn(2)−N and Mn(2)−O lead to

Table 1. Selected bond lengths [Å] and angles [°] with estimated standard deviations (e.s.d.s) in parentheses for $[Mn_3(\mu\text{-}ClCH_2COO)_6(bpy)_2]$ (**1**)

Mn(1)−O(1)	2.155(3)	Mn(2)−O(2)	2.090(3)
Mn(1)−O(1_2)	2.155(3)	Mn(2)−O(4)	2.099(3)
Mn(1)−O(3_2)	2.194(2)	Mn(2)−O(5)	2.151(2)
Mn(1)−O(3)	2.194(2)	Mn(2)−O(6)	2.611(3)
Mn(1)−O(5)	2.217(2)	Mn(2)−N(2)	2.219(3)
Mn(1)−O(5_2)	2.217(2)	Mn(2)−N(1)	2.246(3)
Mn(1)···Mn(2)	3.624(1)	Mn(1)−O(5)−Mn(2)	112.13(11)
O(1)−Mn(1)−O(1_2)	180.00(14)	O(2)−Mn(2)−O(4)	93.95(13)
O(1)−Mn(1)−O(3_2)	89.48(11)	O(2)−Mn(2)−O(5)	98.50(11)
O(1_2)−Mn(1)−O(3_2)	90.52(11)	O(4)−Mn(2)−O(5)	97.34(11)
O(1)−Mn(1)−O(3)	90.52(11)	O(2)−Mn(2)−N(2)	90.66(11)
O(1_2)−Mn(1)−O(3)	89.48(11)	O(4)−Mn(2)−N(2)	120.38(11)
O(3_2)−Mn(1)−O(3)	180.0(2)	O(5)−Mn(2)−N(2)	140.51(10)
O(1)−Mn(1)−O(5)	91.35(10)	O(2)−Mn(2)−N(1)	163.14(11)
O(1_2)−Mn(1)−O(5)	88.65(10)	O(4)−Mn(2)−N(1)	90.23(11)
O(3_2)−Mn(1)−O(5)	89.12(9)	O(5)−Mn(2)−N(1)	97.16(11)
O(3)−Mn(1)−O(5)	90.88(9)	N(2)−Mn(2)−N(1)	73.19(10)
O(1)−Mn(1)−O(5_2)	88.65(10)	O(2)−Mn(2)−O(6)	103.08(11)
O(1_2)−Mn(1)−O(5_2)	91.35(10)	O(4)−Mn(2)−O(6)	148.00(11)
O(3_2)−Mn(1)−O(5_2)	90.88(9)	O(5)−Mn(2)−O(6)	53.81(8)
O(3)−Mn(1)−O(5_2)	89.12(9)	N(1)−Mn(2)−O(6)	81.28(10)
O(5)−Mn(1)−O(5_2)	180.0(2)	N(2)−Mn(2)−O(6)	86.70(9)

a distorted octahedral geometry around the terminal Mn ions. On the other hand, the central Mn atom linked to six oxygen atoms has a more regular octahedral environment (Mn−O distances from 2.155 to 2.217 Å and O−Mn−O angles from 88.65 to 91.35°).

$[Mn_2(\mu\text{-}ClCH_2COO)_2(phen)_4](ClO_4)_2\cdot 2CH_2Cl_2$ (2)

The structure of the cationic complex of compound **2** is depicted in Figure 2. Selected bond lengths and angles are listed in Table 2. The molecule contains a crystallographic inversion center, relating both halves of the dinuclear unit. There are two perchlorate anions, and two molecules of solvent (CH_2Cl_2) captured in the crystal lattice for each dinuclear unit.

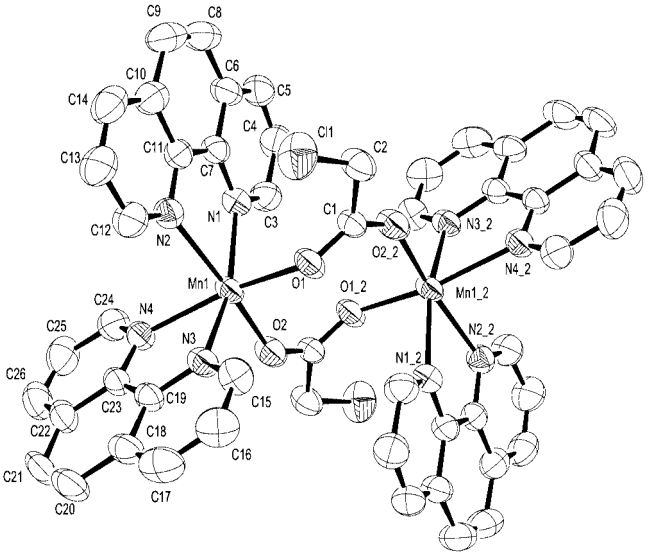

Figure 2. ORTEP drawing of the cation $[Mn_2(\mu\text{-}ClCH_2COO)_2(phen)_4]^{2+}$ in complex **2** showing the *syn-anti* conformation of the carboxylate bridges

Table 2. Selected bond lengths [Å] and angles [°] with estimated standard deviations (e.s.d.s) in parentheses for $[Mn_2(\mu\text{-}ClCH_2COO)_2(phen)_4](ClO_4)_2\cdot 2CH_2Cl_2$ (**2**)

Mn(1)−O(1)[a]	2.129(3)	Mn(1)−N(4)	2.271(4)
Mn(1)−O(2)	2.150(3)	Mn(1)−N(2)	2.327(4)
Mn(1)−N(1)	2.275(4)	Mn(1)−N(3)	2.278(4)
Mn(1)···Mn(1_2)	4.613(2)	O(1)−Mn(1)−O(2)	99.92(13)
O(1)−Mn(1)−N(4)	161.83(13)	N(4)−Mn(1)−N(3)	73.61(13)
O(2)−Mn(1)−N(4)	84.62(12)	N(1)−Mn(1)−N(3)	161.15(14)
O(1)−Mn(1)−N(1)	90.48(12)	O(1)−Mn(1)−N(2)	90.03(13)
O(2)−Mn(1)−N(1)	100.25(13)	O(2)−Mn(1)−N(2)	167.79(13)
N(4)−Mn(1)−N(1)	106.13(13)	N(4)−Mn(1)−N(2)	88.10(13)
O(1)−Mn(1)−N(3)	88.28(12)	N(1)−Mn(1)−N(2)	72.40(13)
O(2)−Mn(1)−N(3)	98.49(13)	N(3)−Mn(1)−N(2)	88.79(13)

[a] Symmetry codes: a: $-x + 2, -y + 1, -z + 1$.

The manganese ions are bridged by two chloroacetate ligands, in a *syn-anti* fashion. Six-coordination on each manganese ion is completed by two chelating 1,10-phenanthroline groups. The interatomic Mn···Mn distance of 4.613 Å is a bit longer than Mn···Mn distances found in analogous complexes with only two bridging *syn-anti* carboxylates; $[Mn_2(\mu\text{-}CH_3COO)_2(bpy)_4](ClO_4)_2$ (4.583 Å),[20] $[Mn_2(\mu\text{-}PhCOO)_2(bpy)_4](ClO_4)_2$ (4.509 Å).[19] When a third bridging ligand is present, e.g. another carboxylate,[9,16−18] aqua,[5−7] hydroxo,[8,9] or phenoxo[10−13] group, the Mn···Mn distance becomes smaller (4.03−3.35 Å).

The Mn−O distances are 2.129 Å ($Mn-O_{anti}$) and 2.151 Å ($Mn-O_{syn}$), which are shorter than the Mn−N distances (2.271−2.327 Å). Moreover, the N(1)−Mn(1)−N(2) angle (72.4°) and N(3)−Mn(1)−N(4) angle (73.6°) are far from 90°, due to the restricted geometry of the phenanthroline ligands. Both factors contribute to the distortion of the octahedral geometry around the manganese ions.

For this compound, $d(Mn-O_{anti}) < d(Mn-O_{syn})$, while for the acetate[20] and the benzoate[19] complexes $d(Mn-O_{anti}) > d(Mn-O_{syn})$.

$[Mn(\mu\text{-}ClCH_2COO)_2(phen)]_n$ (3)

The structure consists of an infinite zigzag chain, as shown in Figure 3. Selected bond lengths and angles are presented in Table 3. The manganese atoms in the chain are bridged by two chloroacetate ligands coordinated in a *syn-anti* fashion. The six-coordination of each metal center is completed by one phenanthroline ligand. Surprisingly, the interatomic Mn···Mn distance (4.530 Å) is shorter than the distance found for complex **2** (4.613 Å). Both compounds have the same bridging ligands, and the same terminal amine. The Mn···Mn distance for $[Mn(\mu\text{-}3\text{-}ClC_6H_4COO)_2(bpy)]_n$,[19] where the carboxylate bridge is also coordinated in a *syn-anti* fashion, is 4.515 Å. However, for $[Mn_2(\mu\text{-phth})(phen)_4]_n(ClO_4)_{2n}$ (phth= isophthalate),[47] where both manganese ions are bridged by two carboxylate groups coordinated in a *syn-syn* mode, the Mn···Mn distance is longer (4.86 and 4.66 Å).

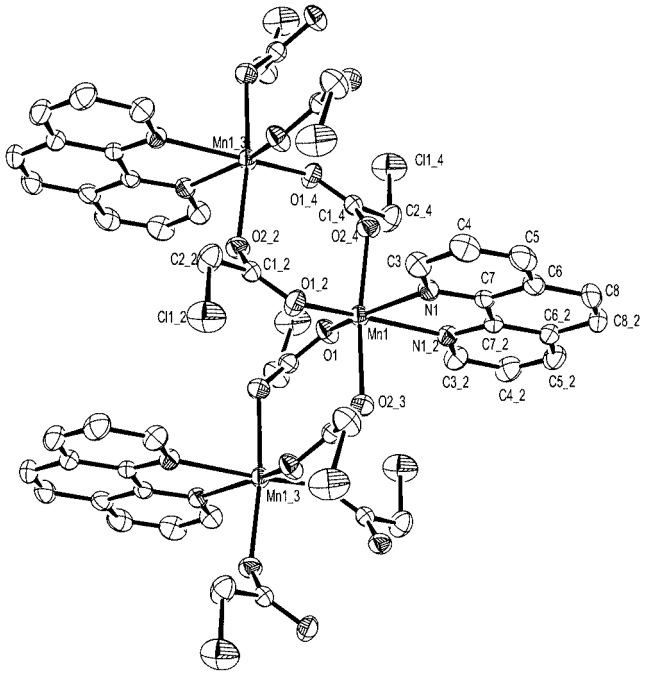

Figure 3. Plot of the one-dimensional complex **3**

Table 3. Selected bond lengths [Å] and angles [°] with estimated standard deviations (e.s.d.s) in parentheses for $[Mn(\mu\text{-}ClCH_2COO)_2(phen)]_n$ (**3**)

Mn(1)−O(1)[a]	2.1341(14)	Mn(1)−O(1_2)	2.1341(14)
Mn(1)−O(2_3)	2.1829(18)	Mn(1)−O(2_4)	2.1829(18)
Mn(1)−N(1)	2.3057(17)	Mn(1)−N(1_2)	2.3057(17)
Mn(1)···Mn(1_3)	4.530(2)	O(1)−Mn(1)−N(1)	156.96(6)
O(1)−Mn(1)−O(1_2)	114.51(9)	O(1_2)−Mn(1)−N(1_2)	156.96(6)
O(1)−Mn(1)−O(2_3)	97.95(6)	O(2_3)−Mn(1)−O(2_4)	172.73(7)
O(1)−Mn(1)−O(2_4)	86.00(6)	O(1_2)−Mn(1)−O(2_4)	97.95(6)
O(1)−Mn(1)−N(1_2)	87.46(6)	O(1_2)−Mn(1)−O(2_3)	86.00(6)
O(2_3)−Mn(1)−N(1)	90.11(6)	O(1_2)−Mn(1)−N(1)	87.46(6)
O(2_3)−Mn(1)−N(1_2)	84.00(5)	O(2_4)−Mn(1)−N(1)	84.00(5)
N(1)−Mn(1)−N(1_2)	71.88(8)	O(2_4)−Mn(1)−N(1_2)	90.11(6)

[a] Symmetry codes: a: $-x + 2, y, -z + 3/2$; b: $-x + 2, -y, -z + 1$; c: $x, -y, z + 1/2$.

There are two equivalent Mn−N distances (2.306 Å), and the Mn−O distance is slightly shorter for the carboxylate oxygen atom *trans* to the phenanthroline nitrogen atom [$d(Mn-O_{transN}) = 2.134$ Å] than for the two carboxylate oxygen atoms *trans* to each other [$d(Mn-O_{transO}) = 2.183$ Å]. The O_{transN} are O_{syn}, while the O_{transO} atoms are O_{anti}, therefore $d(Mn-O_{anti}) > d(Mn-O_{syn})$. This is observed for the analogous chain $[Mn(\mu\text{-}3\text{-}ClC_6H_4COO)_2(bpy)]_n$,[19] but differs from the behavior shown by compound **2**. Moreover, the Mn−O distances are longer for the one-dimensional compound **3** than for the dinuclear complex **2**. The N−Mn−N angle (71.88°) is similar to the values found for the same amine group in compound **2**. Thus, the geometry around each manganese atom is distorted octahedral.

The chain runs parallel to the *c* axis, of the *C*2/*c* space group, in a helix-type conformation, and the phenanthroline ligands are stacked, with a phen···phen distance of 7.491 Å. The smallest interchain metal separation is 9.598 Å.

Magnetic Properties

Magnetic susceptibility data were recorded for the three complexes, from room temperature to 4 K. The $\chi_M T$ vs. T plots for compounds **1**−**3** are shown in Figure 4. For the dinuclear complex **2**, the $\chi_M T$ value is ca. 8.8 $cm^3mol^{-1}K$ in the range room temperature to 18 K. This value is very close to that expected for two uncoupled Mn^{II} ions. The decrease in $\chi_M T$ below this temperature may be a result of the antiferromagnetic interactions (intra- or intermolecular), or of the ZFS (Zero Field Splitting), which is usually small for Mn^{II} ions.

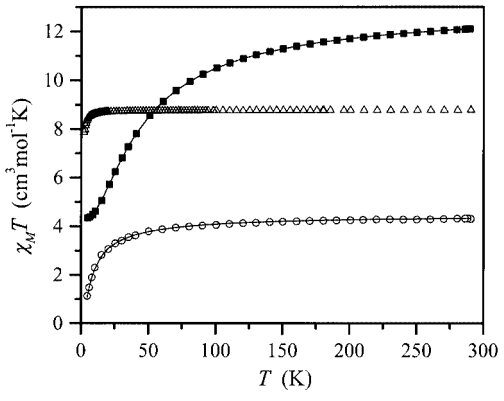

Figure 4. $\chi_M T$ vs. T plot for $[Mn_3(\mu\text{-}ClCH_2COO)_6(bpy)_2]$ (**1**) (■), $[Mn_2(\mu\text{-}ClCH_2COO)_2(phen)_4](ClO_4)_2$ (**2**) (Δ), and $[Mn(\mu\text{-}ClCH_2COO)_2(phen)]_n$ (**3**) (O); the solid line is the best fit to the experimental data

For the trinuclear complex **1**, $\chi_M T$ decreases from 12.10 $cm^3mol^{-1}K$ at 290 K to 4.34 $cm^3mol^{-1}K$ at 4.8 K. The $\chi_M T$ value at room temperature, is smaller than the expected value for three uncoupled Mn^{II} ions (13.125 $cm^3mol^{-1}K$). This is indicative of an antiferromagnetic coupling, as confirmed by the decrease in $\chi_M T$ when T decreases. At low temperature, the $\chi_M T$ value is indicative of an $S = 5/2$ spin state.

Taking into account the structure of this compound, the spin Hamiltonian considered would be $\boldsymbol{H}_S = -J(\boldsymbol{S}_1\cdot\boldsymbol{S}_2+\boldsymbol{S}_2\cdot\boldsymbol{S}_1) - J'(\boldsymbol{S}_2\cdot\boldsymbol{S}_2)$. However, the magnetic interaction between the terminal manganese ions ($Mn_2\cdots Mn_2$) in a linear complex is negligible ($J' \approx 0$),[19,32] and only the $Mn_1\cdots Mn_2$ interaction (J) is considered. The best fit corresponds to $J = -3.82$ cm^{-1}, $g = 2.01$ and $R = 1.9\ 10^{-7}$.

For the one-dimensional compound **3**, $\chi_M T$ values decrease monotonically from 4.18 $cm^3mol^{-1}K$ at 298 K to 1.10 $cm^3mol^{-1}K$ at 5 K. The magnetic susceptibility data were analyzed by the analytical expression derived by Fisher[48] for an infinite chain of classical spins based on the Hamiltonian $\boldsymbol{H} = -J\Sigma\boldsymbol{S}_i\cdot\boldsymbol{S}_{i+1}$, for local spin values of $S = 5/2$. The best fit corresponds to $J = -0.89$ cm^{-1}, $g = 2.01$ and $R = 2.6\ 10^{-4}$.

The three compounds reported here have the same bridging ligands, through which the magnetic interaction arises. In spite of this fact, a certain difference in the coupling constant could be appreciated. The trinuclear complex **1** presents a major Mn···Mn interaction. It differs from the other two compounds in the coordination mode of the bridge; there are two $ClCH_2COO$ ligands coordinated in a *syn-syn* fashion, and a third carboxylate ligand, $\mu_{1,1}$-$ClCH_2COO$, which provides a new interaction pathway, through only one oxygen atom. Unfortunately, the number of compounds described in the literature with this kind of structure it is limited,[32−36] and to the best of our knowledge, a magnetic study was reported for only three of them.[32,33,35] The compound $[Mn_3(\mu\text{-}AcO)_6(BiC_6H_4$-

Table 4. Comparison of the structural parameters (distances [Å] and angles [°]) and magnetic interaction (J [cm^{-1}]) for the Mn^{II} polynuclear complexes

3 carboxylate bridges	$d(Mn_t-O_b)$[a]	$d(Mn_c-O_b)$[a]	$d(Mn_t-O_t)$[a]	α[a]		J[b]	Ref.
$[Mn_3(\mu\text{-}ClCH_2COO)_6(bpy)_2]$ (**1**)	2.151	2.217	2.611			−3.81	*
$[Mn_3(\mu\text{-}AcO)_6(bpy)_2]$	2.155	2.201	2.605	112.2		−4.40	[32]
$[Mn_3(\mu\text{-}AcO)_6(pybim)_2]$[c]	2.132	2.235	2.823	109.1		−3.80	[35]
$[Mn_3(\mu\text{-}AcO)_6(BiPhMe)_2]$[d]	2.17−2.27	2.18−2.24	2.31−2.79	112.3		−4.8	[33]
2 carboxylate bridges	d_{anti}[e]	d_{syn}[e]	α[e]	β[e]	γ[e]	J	Ref.
$[Mn_2(\mu\text{-}ClCH_2COO)_2(phen)_4]^{2+}$ (**2**)	2.129	2.150	99.92	138.2	135.31	ca. 0	*
$[Mn_2(\mu\text{-}PhCOO)_2(bpy)_4]^{2+}$	2.139	2.118	103.55	151.9	126.38	−1.76	[19]
$[Mn_2(\mu\text{-}AcO)_2(tpa)_2]^{2+}$ [f]	2.160	2.060	107.6	133.5	128.0	−1.94	[22]
$[Mn(\mu\text{-}ClCH_2COO)_2(phen)]_n$ (**3**)	2.183	2.134	97.95	123.9	130.91	−0.89	*
$[Mn(\mu\text{-}3\text{-}ClC_6H_4COO)_2(bpy)]_n$	2.196	2.104	100.50	134.4	131.92	−1.72	[19]

[a] Mn_t = Mn terminal; O_b = O_1 of the $\mu_{1,1}$-carboxylate; Mn_c = Mn central; O_t = the other O of the $\mu_{1,1}$-carboxylate; α = $Mn_tO_bMn_c$ angle. [b] With the same Hamiltonian and J_{13} = 0; *: this work. [c] pybim = *N*-[2-(2-pyridylmethyleneamino)phenyl]pyridine-2-carboxamide. [d] BiPhMe = 2-[methoxy(1-methyl-1*H*-imidazol-2-yl)phenylmethyl]-1-methyl-1*H*-imidazole. [e] d_{anti} = $d(Mn-O_{anti})$; d_{syn} = $d(Mn-O_{syn})$; α = $O_{anti}MnO_{syn}$ angle; β = $MnO_{syn}C$ angle; γ = $MnO_{anti}C$ angle. [f] tpa = tris(2-pyridylmethyl)amine.

$Me)_2]$[33] presents different isomeric forms with different Mn−O distances; in general $d(Mn_t-O_b) \approx d(Mn_c-O_b)$. For **1**, $[Mn_3(\mu\text{-}AcO)_6(pybim)_2]$[35] and $[Mn_3(\mu\text{-}AcO)_6(bpy)_2]$[32] (Table 4), $d(Mn_t-O_b) < d(Mn_c-O_b)$ and is markedly different from $d(Mn_t-O_t)$. The magnetic interaction for all of these compounds is of the same order. Normally, a carboxylate group that is coordinated in a *syn-syn* fashion gives a moderate antiferromagnetic coupling.

Compounds **2** and **3** have the same kind of bridge, two $ClCH_2COO$ groups coordinated in a *syn-anti* fashion; however, while the one-dimensional compound shows a certain antiferromagnetic interaction, in the dinuclear complex this interaction is practically zero. The magnetic interaction through a *syn-anti* carboxylate bridge should be very sensitive to small structural changes. Figure 5 shows a schematic representation of the relative orientations of two magnetic orbitals for these compounds. The Mn···Mn interaction could be affected by several factors: the Mn−O distance, the $O_{anti}-Mn-O_{syn}$ angle (α), the $Mn-O_{syn}-C$ angle (β), the $Mn-O_{anti}-C$ angle (γ) and also by the non-planarity of the bridge (τ). Small changes in these parameters could change the overlap through the carboxylate group. Table 4 shows some structural parameters for these compounds in comparison with analogous compounds described in the literature. For the one-dimensional compound **3**, a major difference between d_{anti} and d_{syn} can be observed, probably due to the fact that *trans* to O_{anti} there is another O_{anti} of the chain. The same trend could be observed in the analogous compound with $3\text{-}ClC_6H_4COO$,[19] but the angle around O_{syn} is large, and a greater antiferromagnetic interaction was found.

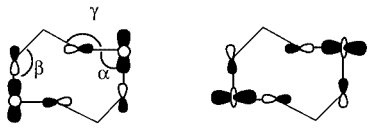

Figure 5. Relative orientation of two manganese(II) magnetic orbitals and their interaction through the carboxylate bridges with a *syn-anti* conformation in the $[Mn_2(\mu\text{-}ClCH_2COO)_2]^{2+}$ core (dinuclear compound **2** and one-dimensional compound **3**)

Compounds **2** and **3** have similar α angles, but they show some differences in the β and γ angles. The dinuclear compound presents a set of larger angles (α, β, γ) than the chain, in spite of the fact that the O−C−O angles are similar. For the dinuclear complex **2**, where d_{syn} is similar to d_{anti}, the angles around O_{syn} (β) and O_{anti} (γ) are also similar, while for $[Mn_2(\mu\text{-}PhCOO)_2(bpy)_4]^{2+}$ [19] β > γ, and for $[Mn_2(\mu\text{-}AcO)_2(tpa)_2]^{2+}$ [22] β is only slightly greater than γ, and d_{anti} and d_{syn} are markedly different. Both compounds show an antiferromagnetic interaction, in contrast to that found in compound **2** where no magnetic coupling is observed. The major asymmetry could contribute to a major overlap through the bridge.

EPR Spectra

The three compounds studied here show weak Mn···Mn interactions, so even at low temperatures several spin states may be populated. This may lead to many possible transitions, and thus to a complicated EPR spectrum.[30] At room temperature all the complexes show a broad signal centered at $g \approx 2$. However, at 4 K, the spectrum of each compound is quite different (Figure 6, solid line).

The spectrum at room temperature for the trinuclear complex (compound **1**) presents a broad signal (ΔH_{pp} = 1055 G) centered at $g \approx 2$. The intensity of this signal decreases with temperature. At 60 K, the shape of the spectrum is the same as the shape of the spectrum at room temperature. Variable-temperature EPR spectra are shown in Figure 7. At 17 K, the spectrum shows a new intense and broad band at $g \approx 3.3$, and another less intense feature at $g \approx 8$, which is already present at 40 K. At 4 K, the spectrum becomes complicated; the signal at $g \approx 2$ almost disappears, while many signals at high field and the more intense signals at low field ($g \approx 6.7$ and $g \approx 4$) remain. This spectrum is similar to that reported for the acetate[32] and chlorobenzoate[19] analogues. Considering the J value of

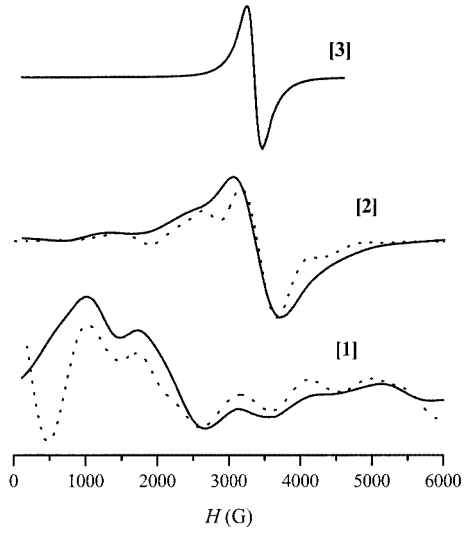

Figure 6. Comparative X-band EPR spectra of a microcrystalline sample at 4 K of complexes $[Mn(\mu\text{-}ClCH_2COO)_2(phen)]_n$ (**3**), $[Mn_2(\mu\text{-}ClCH_2COO)_2(phen)_4](ClO_4)_2$ (**2**), and $[Mn_3(\mu\text{-}ClCH_2COO)_6(bpy)_2]$ (**1**) (solid line); simulated spectra of complexes **2** and **1** (dashed line)

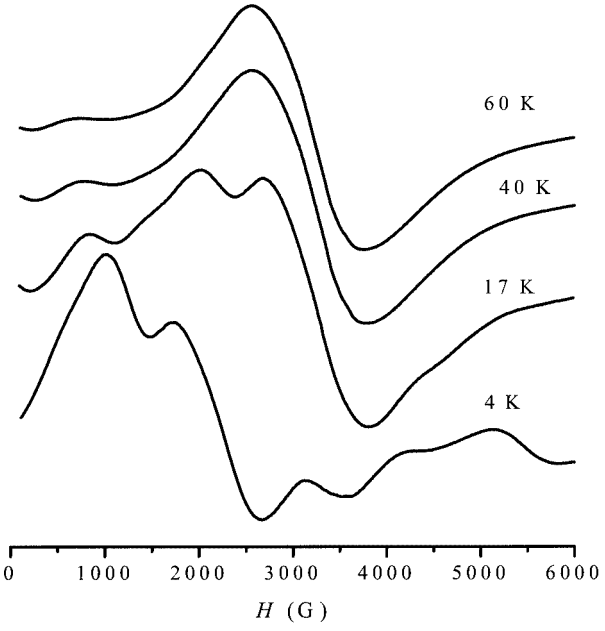

Figure 7. Variable-temperature X-band EPR spectra of $[Mn_3(\mu\text{-}ClCH_2COO)_6(bpy)_2]$ (**1**)

-3.82 cm^{-1}, at 4 K only the ground state ($S_T = 5/2$) may be populated. For the simulation of the experimental spectrum only the ground state was considered, and therefore, the possible transitions between the ground state and the excited states were not considered for the simulation. In spite of this approach, a quite good simulation has been obtained with $D = -0.16$ cm^{-1}, $E = -0.015$ cm^{-1}, $g_x = 2.20$, $g_y = 1.98$, $g_z = 1.95$ and a bandwidth of 270 G. (Figure 6, dashed line).

The EPR spectra at different temperatures for the dinuclear complex (compound **2**) show a broad signal centered at $g \approx 2$. Variable-temperature EPR spectra are shown in

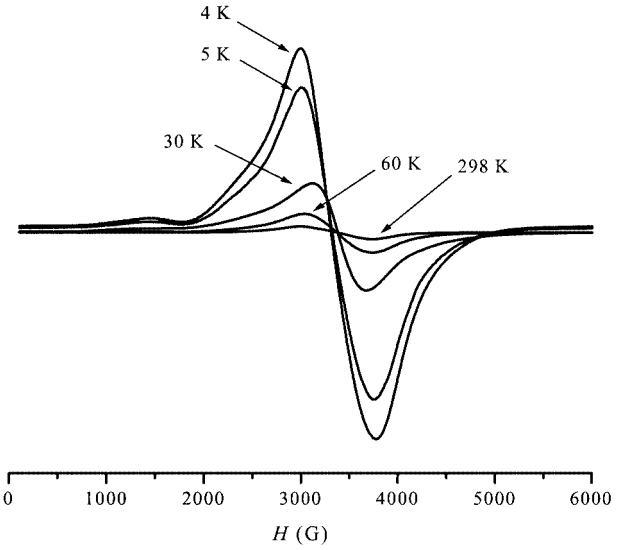

Figure 8. Variable-temperature X-band EPR spectra of $[Mn_2(\mu\text{-}ClCH_2COO)_2(phen)_4](ClO_4)_2$ (**2**)

Figure 8. The intensity of the signal increases when the temperature decreases. At 4 K, the broad signal centered at $g \approx 2$, with a $\Delta H_{pp} = 650$ G, is flanked by one feature at $g \approx 2.8$ and another at $g \approx 5.2$. Considering the fact that the Mn···Mn interaction is negligible, the spectrum can be considered to be that of an isolated Mn^{2+} ion. A good simulation could be obtained with $D = -0.045$ cm^{-1}, $E = -0.004$ cm^{-1}, and an isotropic $g = 2.06$ (Figure 6, dashed line). For the simulation of the spectrum, a bandwidth of 200 G was considered. With a bandwidth of 300 G a superimposable spectrum could be obtained. The variation in the intensity of the spectrum with temperature is due to the ZFS. For both simulations (for compounds **1** and **2**), a spin state of $S = 5/2$ was considered. For compound **2**, with no coupling between the Mn^{2+} ions, the ZFS parameters correspond to each Mn center of the dinuclear complex. The distortion around the metal ion is small, and the D and E values are also small. For compound **1**, the spin state of $S = 5/2$ is as a result of the Mn···Mn interaction in the trinuclear complex. This system shows a central Mn^{2+} ion, with a regular octahedral geometry, and two terminal Mn^{2+} ions with a greatly distorted geometry. The ZFS parameters include the single-ion ZFS for each manganese center, and the ZFS arising from spin-coupling. In this case, the values for D and E are greater than for the dinuclear complex where the distortion is smaller.

The spectrum of the chain (complex **3**) presents a single band centered at $g \approx 2$ at room temperature, with a peak-to-peak line width of 147 G. The broadness of the band increases at 4 K ($\Delta H_{pp} = 220$ G), and no change in position is observed (Figure 6). This behavior was also observed for the similar compound $[Mn(\mu\text{-}3\text{-}ClC_6H_4COO)_2(bpy)]_n$.[19]

Conclusion

With the same carboxylate bridging (chloroacetate) it was possible to obtain complexes of different nuclearity; dinuc-

lear, trinuclear and one-dimensional compounds. There are two factors that influence these results: the bidentate blocking ligand (phenanthroline or bipyridine), and the presence of perchlorate anions in the solution. The trinuclear complex was only obtained with the less rigid ligand, bipyridine, and surprisingly, it was not possible to obtain the ionic dinuclear complex with this amine. With the phenanthroline ligand, a neutral one-dimensional compound and the ionic dinuclear compound were obtained. The trinuclear complex **1** shows two *syn-syn* $ClCH_2COO$ bridges and one $\mu_{1,1}$-$ClCH_2COO$ bridge; this kind of bridge was also found in the arginase.[3] The observed Mn···Mn distance for **1** (3.624 Å) is slightly greater than for the arginase (3.3 Å), and very close to the Mn···Mn distance of the manganese-substituted ribonucleotide reductase (ca. 3.6 Å).[49] On the other hand, the dinuclear complex **2** and the one-dimensional compound **3** show greater values for the Mn···Mn distances (ca. 4.6 Å).

The magnetic measurement showed an antiferromagnetic Mn···Mn interaction. This antiferromagnetism is very small due to the presence of only carboxylate bridges, and the *J* value depends on the number and the coordination mode of the carboxylate bridges: $|J|_{trinuclear} > |J|_{chain} > |J|_{dinuclear}$. For compound **2**, with $J \approx 0$, the set of *d*(Mn−O), α, β, γ, and τ can probably give a small overlap through the bridge, then $J_{AF} \approx J_F$.

It is possible to differentiate the trinuclear complex **1** from the other two complexes **2** and **3** from their EPR spectrum at 4 K. The simulation of the EPR spectrum at this temperature for both compounds **1** and **2** give a *E*/*D* ratio of ca. 0.09. However, for the trinuclear complex **1**, the ZFS parameters *D* and *E* are bigger than for the dinuclear complex **2**.

Experimental Section

Syntheses: All manipulations were performed under aerobic conditions. Reagent grade solvents were used without further purification and organic reagents were used as received. $Mn(ClCH_2COO)_2{\cdot}2H_2O$ was synthesized by the reaction of $MnCO_3$ and $ClCH_2COOH$ in hot water. After several hours, the solution was filtered and the solvent was removed by evaporation giving a pale pink precipitate of the desired product. Yield ca. 70%. $C_4H_8Cl_2MnO_6$ (277.95): calcd. C 17.28, H 2.90; found C 17.5, H 2.9. ***Caution:*** Perchlorate salts of metal complexes with organic ligands are potentially explosive. Only a small amount of material should be prepared, and it should be handled with caution.

$[Mn_3(\mu\text{-}ClCH_2COO)_6(bpy)_2]$ (1): This compound was synthesized by adding an ethanolic solution of 2,2′-bipyridine (0.18 g, 1.2 mmol) to a solution of $Mn(ClCH_2COO)_2{\cdot}2H_2O$ (0.50 g, 1.8 mmol) in EtOH (30 mL) and H_2O (1 mL). The resulting mixture was left undisturbed at room temperature for several days. Yellow crystals suitable for X-ray determination were formed. Yield 0.36 g (ca. 58%). $C_{32}H_{28}Cl_6Mn_3N_4O_{12}$ (1038.11): calcd. C 37.02, H 2.72, N 5.40; found C 37.5, H 2.8, N 5.5. IR (cm^{-1}): $\tilde{\nu}$ = 1631 (vs), 1446 (m), 1407 (s), 1249 (m), 1242 (m), 795 (m), 769 (m).

$[Mn_2(\mu\text{-}ClCH_2COO)_2(phen)_4](ClO_4)_2$ (2): $Mn(ClCH_2COO)_2{\cdot}2H_2O$ (0.42 g, 1.5 mmol) and sodium perchlorate monohydrate (0.21 g, 1.5 mmol) were mixed in $EtOH/CH_2Cl_2$ (1:1, 50 mL). 1,10-Phenanthroline (0.54 g, 3.0 mmol), dissolved in the same solvent mixture, was then added to the solution, which immediately turned yellow. The solution was left undisturbed in a refrigerator for several days. Yellow crystals, stable only at low temperatures, were formed. Yield 0.73 g (ca. 80%). $C_{52}H_{36}Cl_4Mn_2N_8O_{12}$ (1216.58): calcd. C 51.34, H 2.98, N 9.21; found C 50.6, H 3.1, N 9.0 . IR (cm^{-1}): $\tilde{\nu}$ = 1650 (vs), 1624 (vs), 1520 (s), 1430 (vs), 1150 (vs), 1130 (vs), 1095 (vs), 854 (vs), 736 (vs), 643 (s).

$[Mn(\mu\text{-}ClCH_2COO)_2(phen)]_n$ (3): This compound was synthesized by mixing ethanolic solutions (total volume: 60 mL) of $Mn(ClCH_2COO)_2{\cdot}2H_2O$ (0.50 g, 1.8 mmol) and 1,10-phenanthroline (0.32 g, 1.8 mmol). The pale yellow precipitate formed was filtered and washed in ether. Recrystallization from $EtOH/H_2O$ (9:1) yielded pale yellow crystals suitable for X-ray determination. Yield 0.64 g (ca. 84%). $C_{16}H_{12}Cl_2MnN_2O_4$ (422.12): calcd. C 45.53, H 2.87, Cl 16.80, N 6.64; found C 44.9, H 2.8, Cl 16.5, N 6.5. IR (cm^{-1}): $\tilde{\nu}$ = 1657 (vs), 1614 (vs), 1524 (m), 1413 (s), 1250 (m), 848 (m), 775 (m), 735 (m), 700 (m).

Spectral and Magnetic Measurements: Infrared spectra (4000−400 cm^{-1}) were recorded from KBr pellets with a Perkin−Elmer 380-B spectrophotometer. Magnetic susceptibility measurements were carried out using a Faraday-type magnetometer (MANICS DSM8) equipped with an Oxford CF 1200 S helium continuous-flow cryostat working in the temperature range 4−300 K. Diamagnetic corrections were estimated from Pascal Tables. The agreement factor considered to fit the experimental data to the corresponding equation is defined as $R = \Sigma(Y_i^{exp} - Y_i^{cal})^2/\Sigma(Y_i^{exp})^2$. The best fit corresponds to the minimum value of *R*. EPR spectra were recorded at X-band (9.4 GHz) frequencies using a Bruker ESP-300E spectrometer, from room temperature to 4 K.

EPR Simulation: A program written by H. Weihe[50] was used to simulate powder EPR spectra. The simulation was performed by generating the energy matrix for each orientation of the molecule relative to the magnetic field. The resonance condition for each transition was then found by successive diagonalizations and iterations of the energy matrix, and the relative intensities were calculated from the eigenvectors multiplied by the appropriate Boltzmann factor at 4 K. Summation of all the transitions over the whole space, where each transition is represented by a differentiated Gaussian curve, gives the simulated spectrum. The spin Hamiltonian used for the simulation include the ZFS parameters *D* and *E*.

Crystallographic Data Collection and Refinement: Suitable single crystals of $[Mn_3(\mu\text{-}ClCH_2COO)_6(bpy)_2]$ (**1**, needle, yellow, dimensions 0.50 × 0.10 × 0.10 mm), $[Mn_2(\mu\text{-}ClCH_2COO)_2(phen)_4](ClO_4)_2{\cdot}2CH_2Cl_2$ (**2**, prism, yellow, dimensions 0.50 × 0.30 × 0.25 mm) and $[Mn(\mu\text{-}ClCH_2COO)_2(phen)]_n$ (**3**, prism, yellow, dimensions 0.50 × 0.30 × 0.20 mm) were used for the structure determination. X-ray data were collected using a Bruker SMART CCD area detector single-crystal diffractometer, with graphite-monochromatized Mo-K_α radiation (λ = 0.71073 Å), using the -ω scan method. A total of 1271 frames of intensity data were collected for each compound. The first 50 frames were recollected at the end of data collection to monitor for decay. The integration process yielded a total of 6812 reflections for **1**, 8061 for **2**, and 4543 for **3**, of which 4855 [*R*(int) = 0.0287], 5123 [*R*(int) = 0.0195], and 2059 [*R*(int) = 0.0191], respectively, were independent. Absorption corrections were applied using the SADABS[51] program (maximum and minimum transmission coefficients, 0.875 and 0.548 for **1**; 0.814 and 0.674 for **2**; and 0.765 and 0.602 for **3**). The structures were solved using the Bruker SHELXTL-PC[52] software by direct

Table 5. Crystallographic details for compounds **1**, **2**·2CH_2Cl_2, and **3**

	1	**2**	**3**
Empirical formula	$C_{32}H_{28}Cl_6Mn_3N_4O_{12}$	$C_{54}H_{40}Cl_8Mn_2N_8O_{12}$	$C_{16}H_{12}Cl_2MnN_2O_4$
M	1038.10	1386.42	422.12
Space group	$P\bar{1}$	$P\bar{1}$	$C2/c$
cryst system	triclinic	triclinic	monoclinic
Z	1	1	4
a [Å]	8.247(1)	11.506(3)	19.702(5)
b [Å]	10.298(1)	12.198(4)	11.386(5)
c [Å]	13.560(1)	12.215(2)	7.491(5)
α [°]	69.170(2)	87.660(2)	90
β [°]	79.242(1)	63.963(1)	93.892(5)
γ [°]	72.340(2)	74.40(2)	90
V [Å^3]	1021.6(1)	1477.8(7)	1676.6(1)
ρ(calcd.) [g/cm^3]	1.687	1.558	1.672
$\mu_{calcd.}$ [mm^{-1}]	1.369	0.856	1.130
Radiation (Mo-K_α) [Å]	0.70173	0.70173	0.70173
T [K]	298(2)	298(2)	298(2)
θ range for data collection	1.6−28.3	1.7−25.0	2.1−28.2
Final R indices[a]	$R1 = 0.0593$	$R1 = 0.0650$	$R1 = 0.0375$
[$I > 2\sigma(I)$]	$wR2 = 0.1506$	$wR2 = 0.1951$	$wR2 = 0.0996$
Final R indices	$R1 = 0.0845$	$R1 = 0.0803$	$R1 = 0.0420$
[for all data]	$wR2 = 0.1689$	$wR2 = 0.2125$	$wR2 = 0.1027$

[a] $R1 = \Sigma||F_o| - |F_c||/\Sigma|F_o|$ and $wR2 = \{\Sigma[w(F_o^2 - F_c^2)^2]/\Sigma[w(F_o^2)^2]\}^{1/2}$.

methods and refined by full-matrix least-squares methods on F^2. Hydrogen atoms were included in calculated positions and refined in the riding mode. The Cl(2) atom in compound **1** was refined in two different positions with partial occupation factors of 0.63 and 0.37. For **1**, convergence was reached at a final $R1 = 0.0593$ [for $I > 2\sigma(I)$], $wR2 = 0.1689$ [for all data], 269 parameters, with allowance for the thermal anisotropy for all non-hydrogen atoms. The weighting scheme employed was $w = [\sigma^2(F_o^2) + (0.1032 \cdot P)^2]$, $P = (|F_o|^2 + 2|F_c|^2)/3$; and the goodness of fit on F^2 was 1.001 for all observed reflections. For **2**, convergence was reached at a final $R1 = 0.0650$ [for $I > 2\sigma(I)$], $wR2 = 0.2125$ [for all data], 379 parameters, with allowance for the thermal anisotropy for all non-hydrogen atoms. The weighting scheme employed was $w = [\sigma^2(F_o^2) + (0.1377 \cdot P)^2 + (0.9991 \cdot P)]$, $P = (|F_o|^2 + 2|F_c|^2)/3$; and the goodness of fit on F^2 was 1.043 for all observed reflections. For **3**, convergence was reached at a final $R1 = 0.0375$ [for $I > 2\sigma(I)$], $wR2 = 0.1027$ [for all data], 114 parameters, with allowance for the thermal anisotropy for all non-hydrogen atoms. The weighting scheme employed was $w = [\sigma^2(F_o^2) + (0.0562 \cdot P)^2 + (1.2574 \cdot P)]$, $P = (|F_o|^2 + 2|F_c|^2)/3$; and the goodness of fit on F^2 was 1.065 for all observed reflections. Crystal data and details on the data collection and refinement are summarized in Table 5. CCDC-156272 for **1**, -156273 for **2**, and -156274 for **3** contain the supplementary crystallographic data for this paper. These data can be obtained free of charge at www.ccdc.cam.ac.uk/conts/retrieving.html or from the Cambridge Crystallographic Data Centre, 12 Union Road, Cambridge CB2 1EZ, UK [Fax: (internat.) + 44-1223/336-033; E-mail: deposit@ccdc.cam.ac.uk].

Acknowledgments

This research was supported by Dirección General de Investigación Científica y Técnica (Grant BQ2000/0791), G. F. received a PhD Grant from Universitat de Barcelona.

[1] S. V. Antonyuk, V. R. Melikadamyan, A. N. Popov, V. S. Lamzin, P. D. Hempstead, P. M. Harrison, P. J. Artymyuk, V. V. Barynin, *Crystallogr. Rep.* **2000**, *45*, 105−116.
[2] M. C. J. Wilce, C. S. Bond, N. E. Dixon, H. C. Freeman, J. M. Guss, P. E. Lilley, J. A. Wilce, *Proc. Nat. Acad. Sci. Usa* **1998**, *95*, 3472−3477.
[3] M. C. Bewley, P. D. Jeffrey, M. L. Patchett, Z. F. Kanyo, E. N. Baker, *Struct. Fold. Des.* **1999**, *7*, 435−448.
[4] G. B. Conyers, G. Wu, M. J. Bessman, A. S. Mildvan, *Biochemistry* **2000**, *39*, 2347−2354.
[5] S.-B. Yu, A. Bino, I. Shweky, S. J. Lippard, *Inorg. Chem.* **1992**, *31*, 3502−3504.
[6] A. Caneschi, F. Ferraro, D. Gatteschi, M. Ch. Melandri, P. Rey, R. Sessoli, *Angew. Chem. Int. Ed. Engl.* **1989**, *28*, 1365−1367.
[7] B. H. Ye, T. Mak, I. D. Williams, X. Y. Li, *Chem. Commun.* **1997**, 1813−1814.
[8] U. Bossek, K. Wieghardt, B. Nuber, J. Weiss, *Inorg. Chim. Acta* **1989**, *165*, 123−129.
[9] K. Wieghardt, U. Bossek, B. Nuber, J. Weiss, J. Bonvoisin, M. Corbella, S. E. Vitols, J.-J. Girerd, *J. Am. Chem. Soc.* **1988**, *110*, 7398−7411.
[10] M. Mikuriya, T. Fujii, T. Tokii, A. Kawamori, *Bull. Chem. Soc. Jpn.* **1993**, *66*, 1675−1686.
[11] Y. Gultneh, A. Farooq, S. Liu, K. D. Karlin, J. Zubieta, *Inorg. Chem.* **1992**, *31*, 3607−3611.
[12] H. Sakiyama, H. Tamaki, M. Kodera, N. Matsumoto, H. Okawa, *J. Chem. Soc., Dalton Trans.* **1993**, 591−595.
[13] C. Higuchi, H. Sakiyama, H. Okawa, R. Isobe, D. E. Fenton, *J. Chem. Soc., Dalton Trans.* **1994**, 1097−1103.
[14] C. Higuchi, H. Sakiyama, H. Okawa, D. E. Fenton, *J. Chem. Soc., Dalton Trans.* **1995**, 4015−4020.
[15] U. P. Singh, R. Singh, S. Hikichi, M. Akita, Y. Moro-oka, *Inorg. Chim. Acta* **2000**, *310*, 273−278.
[16] H. Matsushima, E. Ishiwa, M. Koikawa, M. Nakashima, T. Tokii, *Chem. Lett.* **1995**, 129−130.
[17] M. Yamami, M. Tanaka, H. Sakiyama, T. Koga, K. Kobaya-

shi, H. Miyasaka, M. Ohba, H. Okawa, *J. Chem. Soc., Dalton Trans.* **1997**, 4595−4601.
[18] M. Osawa, U. P. Singh, M. Tanaka, Y. Morooka, N. Kitajima, *J. Chem. Soc., Chem. Commun.* **1993**, 310−311.
[19] B. Albela, M. Corbella, J. Ribas, I. Castro, J. Sletten, H. Stoeckli-Evans, *Inorg. Chem.* **1998**, *37*, 788−798.
[20] R. L. Rardin, W. B. Tolman, S. J. Lippard, *New J. Chem.* **1991**, *15*, 417−430.
[21] C.-M. Che, W.-T. Tang, K.-T. Wong, W.-T. Wong, T.-F. Lai, *J. Chem. Research (S)* **1991**, 30.
[22] H. Oshio, E. Ino, I. Mogi, T. Ito, *Inorg. Chem.* **1993**, *32*, 5697−5703.
[23] B. Albela, M. Corbella, J. Ribas, *Polyhedron* **1996**, *15*, 91−96.
[24] T. Tanase, S. J. Lippard, *Inorg. Chem.* **1995**, *34*, 4682−4690.
[25] C. H. Kennard, G. Smith, E. O′Reilly, W. Chiangjin, *Inorg. Chim. Acta* **1983**, *69*, 53−59.
[26] T. Glowiak, H. Kozlowski, L. S. Erre, G. Micera, *Inorg. Chim. Acta* **1995**, *236*, 149−154.
[27] H. Iikura, T. Nagata, *Inorg. Chem.* **1998**, *37*, 4702−4711.
[28] M. McCann, M. T. Casey, M. Devereux, M. Curran, G. Ferguson, *Polyhedron* **1997**, *16*, 2547−2552.
[29] J. Kim, J. M. Lim, M. C. Suh, H. Yun, *Polyhedron* **2001**, *20*, 1947−1951.
[30] H. Adams, N. A. Bailey, N. Debaecker, D. E. Fenton, W. Kanda, J. M. Latour, H. Okawa, H. Sakiyama, *Angew. Chem. Int. Ed. Engl.* **1995**, *34*, 2535−2537.
[31] X.-M. Chen, Y.-X. Tong, Z.-T. Xu, T. C. W. Mak, *J. Chem. Soc., Dalton Trans.* **1995**, 4001−4004.
[32] S. Ménage, S. E. Vitols, P. Bergerat, E. Codjovi, O. Kahn, J.-J. Girerd, M. Guillot, X. Solans, T. Calvet, *Inorg. Chem.* **1991**, *30*, 2666−2671.
[33] R. L. Rardin, P. Poganiuch, A. Bino, D. P. Goldberg, W. B. Tolman, S. Liu, S. J. Lippard, *J. Am. Chem. Soc.* **1992**, *114*, 5240−5249.
[34] G. Christou, *Acc. Chem. Res.* **1989**, *22*, 328−335.
[35] V. Tangoulis, D. A. Malamatari, K. Soulti, V. Stergiou, C. P. Raptopoulou, A. Terzis, T. A. Kabanos, D. P. Kessissoglou, *Inorg. Chem.* **1996**, *35*, 4974−4983.
[36] R. L. Rardin, A. Bino, P. Poganiuch, W. B. Tolman, S. Liu, S. J. Lippard, *Angew. Chem. Int. Ed. Engl.* **1990**, *29*, 812−814.
[37] Z. J. Zhong, X. Z. You, *Polyhedron* **1994**, *13*, 2157−2161.
[38] M. J. Baldwin, J. W. Kampf, V. L. Pecoraro, *J. Chem. Soc., Chem. Commun.* **1993**, 1741−1743.
[39] Z. Sun, P. K. Gantzel, D. N. Hendrickson, *Polyhedron* **1998**, *17*, 1511−1516.
[40] M. J. Baldwin, J. W. Kampf, M. L. Kirk, V. L. Pecoraro, *Inorg. Chem.* **1995**, *34*, 5252−5260.
[41] E. Colacio, J. M. Dominguezvera, M. Ghazi, R. Kivekas, M. Klinga, J. M. Moreno, *Eur. J. Inorg. Chem.* **1999**, 441−445.
[42] C. Policar, F. Lambert, M. Cesario, I. Morgenstern-Badarau, *Eur. J. Inorg. Chem.* **1999**, 2201−2207.
[43] Z. Sun, P. K. Gantzel, D. N. Hendrickson, *Polyhedron* **1997**, *16*, 3267−3271.
[44] X. S. Tan, D. F. Xiang, W. X. Tang, K. B. Yu, *Polyhedron* **1997**, *16*, 1411−1415.
[45] M. Devereux, M. Curran, M. McCann, M. T. Casey, V. McKee, *Polyhedron* **1996**, *15*, 2029−2033.
[46] J. Cano, G. Demunno, J. Sanz, R. Ruiz, F. Lloret, J. Faus, M. Julve, *J. Chem. Soc., Dalton Trans.* **1994**, 3465−3469.
[47] X. S. Tan, J. Sun, D. F. Xiang, W. X. Tang, *Inorg. Chim. Acta* **1997**, *255*, 157−161.
[48] M. E. Fisher, *Am. J. Phys.* **1964**, *32*, 343.
[49] T. L. Stemmler, T. M. Sossong, Jr., J. I. Goldstein, D. E. Ash, T. E. Elgren, D. M. Kurtz Jr, J. E. Penner-Hahn, *Biochemistry* **1997**, *36*, 9847−9858.
[50] The simulation software package is freely distributed by Dr. H. Weihe; for more information see the www page: http://sophus.kiku.dk/software/epr/epr.html
[51] G. M. Sheldrick, *SADABS, Program for absorption corrections using Bruker CCD data*, University of Göttingen, Germany, **1996**.
[52] G. M. Sheldrick, *Bruker SHELXTL-PC*, University of Göttingen, Germany, **1997**.

Received April 16, 2002
[I02198]

Mixed Chloride/Azide Complexes of Arsenic and Antimony

Thomas M. Klapötke,*[a] Heinrich Nöth,[a][‡] Thomas Schütt,[a] and Max Suter[a][‡]

Keywords: Azides / Antimony / Arsenic / Lewis acids / Lewis bases / Density functional calculations

The Lewis acid base complexes $AsCl(N_3)_2$·pyridine and $SbCl_2N_3$·2 pyridine were prepared. The products formed were characterised by Raman, IR and NMR spectroscopy. Density functional theory (B3LYP) was applied to calculate structural and vibrational data. Vibrational assignments of the normal modes for the isolated compounds were made on the basis of their vibrational spectra in comparison with computational results. The molecular structures of both complexes were determined by X-ray diffraction. The bonding situation of these Lewis acid base complexes is discussed on the basis of NBO analyses, which were performed, on the crystallographic data.
(© Wiley-VCH Verlag GmbH, 69451 Weinheim, Germany, 2002)

Introduction

Mixed halogen compounds of arsenic and antimony are known few in number. A compound does exist in the +5 oxidation state with the empirical formula $AsCl_2F_3$, which has an ionic structure with the composition $[AsCl_4][AsF_6]$ in the solid state.[1] This salt is a synthon for the preparation of chlorofluoroarsoranes. The mixed chlorofluoroarsorane $AsCl_4F$ was synthesised by vacuum thermolysis of $[AsCl_4][AsF_6]$.[2] $AsCl_2F_3$ [3] and $AsClF_4$ [4] were formed by intermolecular ligand exchange in the gas phase at 173 K. These compounds are extremely unstable due to dismutation under halogen exchange in the respective halides.[5] $AsCl_2F_3$ is the only structurally characterised mixed halogen compound of arsenic. The gas-phase structure of $AsCl_2F_3$ has been determined experimentally by electron diffraction.[5]

$AsCl_2Br$ and $AsClBr_2$ are the only reported mixed halogen compounds of arsenic in the +3 oxidation state. Müller et al. reported on the vibrational spectroscopic investigations of these mixed bromochloroarsanes.[6,7] The isolation of these compounds as pure substances was not possible due to fast dismutation into the respective trihalides.[6,8]

Mixed halogen/azide compounds in the +3 oxidation state are only reported for phosphorus. Dillon et al. characterised PX_2N_3 and $PX(N_3)_2$ (X = Cl, Br) by ^{31}P NMR spectroscopy.[9] The corresponding fluoro compound (PF_2N_3) could be synthesised by the reaction of PF_2X (X = I, Br) with MN_3 (M = Na, Li)[10] or PF_2Cl with NaN_3.[11]

$SbCl_4N_3$ is the only ternary synthesised[12] and structurally characterised antimony(V) azide species. X-ray diffraction revealed that this compound shows a dimeric structure in the solid state.[13]

Recently, we reported on the first structurally characterised ternary halogen/azide compound of antimony, $SbCl(N_3)_2$.[14] In this paper we report about the synthesis, the spectroscopic properties, the crystal structures and NBO (Natural Bond Orbital) analyses of the first mixed halide pseudohalide arsenic(III) species as its pyridine adduct, $AsCl(N_3)_2$·pyridine, as well as the monoazido-substituted antimony(III) species as its pyridine adduct, $SbCl_2N_3$·2pyridine.

Results and Discussion

Syntheses and Properties

The synthesis and characterisation of mixed halogen azide compounds of arsenic and antimony in the +3 oxidation state proved to be very difficult. On the one hand the compounds tend to dismutate easily,[6,8] on the other hand there is no suitable means of characterising such compounds. Neither the ^{75}As nor the ^{121}Sb nuclei can be detected by NMR spectroscopy in the +3 oxidation state due to the large quadrupole moment of these nuclei.[15]

Reactions of MF_3 (M = As, Sb) with stoichiometric amounts of AgN_3, NaN_3 or $TMS-N_3$ seemed to be especially suited for the synthesis of mixed halogen azide species of arsenic and antimony. These reactions were monitored by ^{14}N and ^{19}F NMR spectroscopy. It was shown, that in the ^{14}N NMR spectra resonances occurred, which could be assigned to covalently bound azide species. The ^{19}F NMR spectra, however, showed resonances, which could be assigned to AsF_3 and SbF_3. It thus follows that intermediary formed mixed fluoride/azide species dismutate easily into the trifluorides and triazides, respectively.

[a] Department of Chemistry,
Ludwig-Maximilians-Universität München,
Butenandtstr. 5−13, 81377 München, Germany
Fax: (internat.) + 49-(0)89/2180-7492
E-mail: Thomas.M.Klapoetke@cup.uni-muenchen.de
[‡] X-ray structure determination

Raman spectroscopy also shows that the reactions of MX_3 (M = As, Sb; X = Br, I) with AgN_3, NaN_3 or $TMS-N_3$ dismutate in the respective trihalides and triazides.

Reactions of arsenic(III) and antimony(III) chloride with $TMS-N_3$ yielded the expected compounds. Admittedly, the compounds could only be crystallised as Lewis acid base adducts with pyridine. The compounds were synthesised according to Equations (1) and (2).

$$AsCl_3 + 2\ TMS\text{-}N_3 + py \xrightarrow{CH_2Cl_2} AsCl(N_3)_2 \cdot py + 2\ TMS\text{-}Cl \quad (1)$$

$$SbCl_3 + TMS\text{-}N_3 + 2\,py \xrightarrow{CH_2Cl_2} SbCl_2N_3 \cdot 2py + TMS\text{-}Cl \quad (2)$$

NMR Properties

$AsCl(N_3)_2$·pyridine and $SbCl_2N_3$·2pyridine have been characterised by ^1H, ^{13}C and ^{14}N NMR spectroscopy. The most useful method for the characterisation of covalently bonded azides is undoubtedly ^{14}N NMR spectroscopy. For covalently bound azide species three well-resolved resonances can be found in the ^{14}N NMR spectra and assignment of the individual resonances to N_α, N_β and N_γ (connectivity: $M-N_\alpha-N_\beta-N_\gamma$) was made on the basis of arguments given in the literature.[16−18] The N_β atom of $AsCl(N_3)_2$·pyridine shows a very sharp resonance at δ = −139 ppm, the N_γ atom at δ = −181 ppm and the N_α atom a very broad resonance at δ = −269 ppm; $SbCl_2N_3$·2pyridine shows the analogous resonances at δ = −143 (N_β), −172 (N_γ) and −275 ppm (N_α). In addition to these resonances, the spectra show resonances at δ = −164 ppm [$AsCl(N_3)_2$·pyridine] and δ = −157 ppm ($SbCl_2N_3$·2pyridine). These resonances can be assigned to the nitrogen atoms of the pyridine rings. The resonances are shifted significantly towards higher field compared to free pyridine (pyridine: δ = −64 ppm).[19] Not only do the compounds form stable adducts in the solid state but also in solution. The ^1H and ^{13}C NMR spectra show the expected resonances for pyridine (see Exp. Sect.).

Vibrational Spectra

Table 1 summarises selected computed and experimentally observed IR and Raman frequencies for $AsCl(N_3)_2$·pyridine and $SbCl_2N_3$·2pyridine. The recorded vibrational data agree well enough with our theoretical calculations (B3LYP) to allow assignment. It should be kept in mind that the computations were carried out for single, isolated (gas-phase) molecules. There may well be significant differences between gas-phase and solid-state spectra.

The measured IR and Raman spectra clearly show the presence of azide ligands bonded covalently to arsenic or antimony, as demonstrated by the simultaneous appearance of the antisymmetric (ca. 2100 cm^{-1}) and the symmetric (1250 cm^{-1}) azide stretching mode in both spectra (IR and Raman) and the presence of strong As−N and Sb−N stretching bands at ca. 386 cm^{-1} up to 452 cm^{-1} again in the IR and the Raman spectra. Based on our calculations the deformation vibration of the azide group should be split into four signals due to "in phase" and "out of phase" coupling of the "in plane" (637−670 cm^{-1}) and "out of plane" (567−595 cm^{-1}) deformation. The δN_3 "in phase" vibration appears at higher frequencies compared to the δN_3 "out of phase" vibration.

The symmetric Sb−Cl stretching vibration of $SbCl_2N_3$·2pyridine shows a signal at 326 cm^{-1} in the Raman spectrum and the antisymmetric stretching vibration shows a signal at 285 cm^{-1}. Both vibration modes are therefore shifted significantly to lower frequencies compared to the symmetric and antisymmetric Sb−Cl stretching modes of the parent $SbCl_3$ (ν_{as}: Sb−Cl 381 cm^{-1}; ν_s: Sb−Cl 359 cm^{-1}).[20] The Sb−Cl stretching modes of $SbCl(N_3)_2$ appear at 347 cm^{-1}.[14] These signals are less shifted towards

Table 1. Selected calculated (B3LYP) and observed vibrational frequencies [cm^{-1}] for $AsCl(N_3)_2$·pyridine and $SbCl_2N_3$·2pyridine

$AsCl(N_3)_2$·pyridine calcd.[a][b]	Raman[c]	IR	$SbCl_2N_3$·2pyridine calcd.[a][b]	Raman[c]	IR	Assignment
2267 (500)	2118 (2.5)	2113 vs	2254 (646)	2091 (0.5)	2136 m	$\nu_{as}N_3$ "in phase"[d]
2244 (506)	2085 (1.5)				2079 vs	$\nu_{as}N_3$ "out of phase"[d]
1327 (146)	1268 (1)		1343 (153)	1210 (2)	1251 s	ν_sN_3 "in phase"[d]
1312 (174)	1258 (0.5)	1257 vs				ν_sN_3 "out of phase"[d]
662 (20)	670 (1.5)	670 sh	658 (10)	650 (1.5)	648 w	δN_3 "in phase"[d]
651 (17)	647 (1)	637 s				δN_3 "out of phase"[d]
585 (11)			595 (11)		594 s	δN_3 "in phase/90°"[d]
581 (7)		567 m				δN_3 "out of phase/90°"[d]
444 (25)	452 (10)		404 (28)	386 (2)		ν_sMN_{azide}[e]
407 (89)	433 (1)	431 m				$\nu_{as}MN_{azide}$[e]
275 (15)	265 (2.5)		238 (13)	241 (4)		δMN_{azide}
321 (173)	287 (2)		306 (109)	326 (10)		ν_sMCl
			293 (135)	285 (9)		$\nu_{as}MCl$
232 (9)	216 (2)		157 (9)	166 (1.5)		$\nu MN_{pyridine}$
135 (1)	139 (1.5)		108 (1)	108 (3)		$\delta MN_{pyridine}$

[a] In parentheses: IR intensity [in km mol^{-1}]. [b] In parentheses: rel. Raman intensity. [c] The distinction "*in/out of phase*" is not applicable for $SbCl_2N_3$·2pyridine. [d] The distinction "*symmetric/antisymmetric*" is not applicable for $SbCl_2N_3$·2pyridine. [e] All calculated frequencies are unscaled.

lower frequencies. Therefore, the Sb−Cl bond lengths should decrease in the following order: $SbCl_2N_3$·2pyridine > $SbCl(N_3)_2$ > $SbCl_3$. Increasing Sb−Cl bond lengths should cause decreasing Sb−Cl stretching modes towards lower frequencies. A similar shift of the As−Cl stretching mode could be observed for $AsCl(N_3)_2$·pyridine in the Raman spectrum. The As−Cl stretching mode shows a band at 287 cm^{-1} and is therefore significantly shifted to lower frequencies, by about 120 cm^{-1}, compared to the symmetric and antisymmetric As−Cl stretching modes of the parent $AsCl_3$ [20] For this, the As−Cl bond lengths should be longer compared with the parent, $AsCl_3$. This presumption could be verified by X-ray determination in both cases [see crystal structure of $AsCl(N_3)_2$·pyridine].

The covalent donor−acceptor properties of $AsCl(N_3)_2$·pyridine and $SbCl_2N_3$·2pyridine can be obtained by signals assigned to the As− and Sb−N_{py} stretching and deformation vibrations. $AsCl(N_3)_2$·pyridine shows a band at 216 cm^{-1} assigned to the As−N_{py} stretching mode. The deformation mode appears at 139 cm^{-1}; $SbCl_2N_3$·2pyridine shows the analogous stretching mode at 166 cm^{-1} and the analogous deformation mode at 108 cm^{-1} in the Raman spectrum.

Crystal Structure of $AsCl(N_3)_2$·pyridine

$AsCl(N_3)_2$·pyridine crystallises in the triclinic space group $P\bar{1}$ with two molecules in the unit cell (Figure 1). The crystallographic data and refinement details for this compound are summarised in the Exp. Sect. The experimentally observed and calculated bond lengths and bond angles are compiled in Table 2.

The arsenic atom is surrounded in a Ψ-trigonal-bipyramidal fashion by three nitrogen atoms and one chlorine atom. Both azide ligands (N2−N3−N3 and N4−N5−N6) are in an equatorial position. The axial positions are occupied by the coordinating pyridine molecule and the chlorine atom. The free lone pair of the arsenic atom occupies, in accordance with the predictions of the VSEPR model,[21] the third equatorial position, due to the fact that the lone pair requires more space compared to the pyridine molecule and the chlorine atom. The experimentally observed and calculated (B3LYP) bonding parameters agree with this predicted Ψ-trigonal-bipyramidal arrangement of the ligands (Table 2).

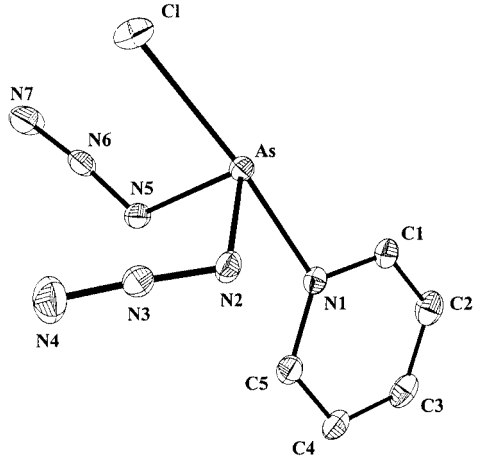

Figure 1. Molecular structure of $AsCl(N_3)_2$·pyridine (hydrogen atoms are omitted for clarity); the thermal ellipsoids represent a 25% probability

Table 2. Selected calculated (B3LYP) and observed bond lengths [Å] and bond angles [°] for $AsCl(N_3)_2$·pyridine

	X-ray determination	B3LYP calculation
As−N(1)	2.158(3)	2.459
As−Cl	2.4848(9)	2.296
As−N(2)	1.897(2)	1.914
As−N(5)	1.916(3)	1.914
N(2)−N(3)	1.210(4)	1.235
N(3)−N(4)	1.138(4)	1.140
N(5)−N(6)	1.185(4)	1.235
N(6)−N(7)	1.149(4)	1.140
N(1)−As−N(2)	84.1(1)	79.9
N(1)−As−N(5)	85.9(1)	79.9
Cl−As−N(2)	91.35(8)	97.2
Cl−As−N(5)	91.56(9)	97.2
N(2)−As−N(5)	94.9(1)	99.8
Cl−As−N(1)	174.51(6)	175.4
As−N(2)−N(3)	117.6(2)	119.7
As−N(5)−N(6)	118.0(2)	119.7
N(2)−N(3)−N(4)	175.7(3)	175.0
N(5)−N(6-N(7)	174.2(3)	175.0

The molecule does not show any special symmetry within the crystal. The calculations at the B3LYP level of theory predict an ideal C_s symmetry for this molecule in the gas phase. The predicted mirror plane can also almost be found in the crystal structure. The shape of this molecule agrees very well with the shape of the Lewis acid base adduct $AsCl_3$·NMe_3.[22]

The calculated bonding parameters of the azide ligands are in good agreement with the experimentally observed As−N and N−N bond lengths as well as with the As−N−N and N−N−N bond angles (Table 2). The molecule shows a relatively long bond between the arsenic and chlorine atom [2.4848(9) Å], whereas the coordinative bond between the arsenic atom and the nitrogen molecule of the pyridine ring is very short [As−N1 2.158(3) Å]. The strong coordination of the very strong Lewis base pyridine at the arsenic centre weakens the As−Cl bond. This lengthens the As−Cl bond, which is significantly longer than it is in the cationic species $AsCl_4^+$ [2.042(3)−2.0545(9) Å][1,23] or binary $AsCl_3$ [2.17(2) Å].[24]

The calculations show a coordinative bond (2.459 Å) between the arsenic atom and the nitrogen atom of the pyridine ring, which is weaker in the gas phase compared to the solid state [2.158(3) Å]. Due to the weaker interaction between the Lewis acid $AsCl(N_3)_2$ and the Lewis base in the gas phase, the calculated As−Cl bond shows a normal bond length (2.296 Å).

It should be noted, that structures of such weakly bound systems may differ considerably between the gas phase and the solid state.[25,26]

Crystal Structure of $SbCl_2N_3$·2pyridine

$SbCl_2N_3$·2pyridine crystallises in the orthorhombic space group *Pbca* with eight molecules in the unit cell and the lattice parameters a = 6.5566(5), b = 13.635(1) and c = 30.901(2) (Figure 2). The experimentally observed and calculated (B3LYP) bond parameters are summarized in Table 3.

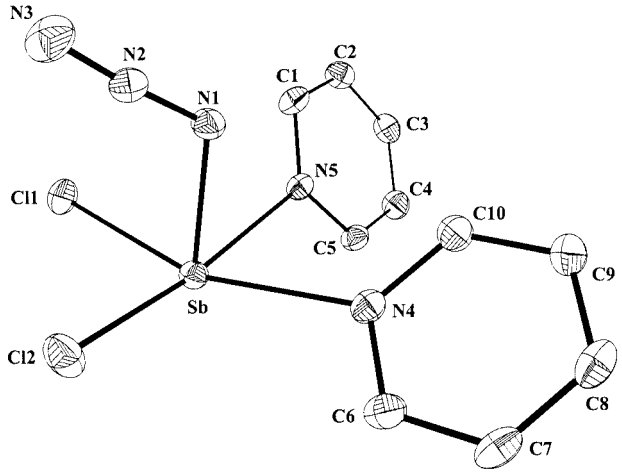

Figure 2. Molecular structure of $SbCl_2N_3$·2pyridine (hydrogen atoms are omitted for clarity); the thermal ellipsoids represent a 25% probability

Table 3. Selected calculated (B3LYP) and observed bond lengths [Å] and bond angles [°] for $SbCl_2N_3$·2pyridine

	X-ray determination	B3LYP calculation
Sb−N(1)	2.084(2)	2.101
Sb−Cl(1)	2.4995(8)	2.451
Sb−Cl(2)	2.5352(8)	2.461
Sb−N(4)	2.466(2)	2.790
Sb−N(5)	2.392(2)	2.687
N(1)−N(2)	1.210(3)	1.230
N(2)−N(3)	1.141(3)	1.143
N(1)−Sb−Cl(1)	86.40(7)	93.1
N(1)−Sb−Cl(2)	87.91(7)	95.1
Cl(1)−Sb−Cl(2)	95.96(3)	95.0
N(1)−Sb−N(4)	78.14(9)	77.6
N(1)−Sb−N(5)	78.30(8)	75.2
N(4)−Sb−N(5)	82.24(8)	95.4
N(4)−Sb−Cl(1)	162.90(6)	170.2
N(5)−Sb−Cl(2)	165.55(6)	170.2
Sb−N(1)−N(2)	119.1(2)	120.1
N(1)−N(2)−N(3)	175.9(3)	175.3

The crystal structure reveals that $SbCl_2N_3$·2pyridine forms isolated molecules without intermolecular contacts, in which the antimony atom is surrounded, in an Ψ-octahedral or square-pyramidal fashion by three nitrogen atoms, two chlorine atoms and a free lone pair. The pyridine molecules and the chlorine atoms occupy the edges of an almost ideal planar plane. The N1 atom of the azide ligand occupies the top of the square pyramid. The experimentally observed and calculated bond parameters prove that the arrangement of the ligands is Ψ-octahedral (ca. 90°, Table 3).

The structural parameters obtained for the azide unit compares well with the calculated parameters. The Sb−N1 bond that is 2.084(2) Å, along with the N−N bond lengths within the azide unit, are in agreement with Sb−N and N−N bond lengths of other antimony azide compounds.[13,27−30]

The average Sb−Cl bond lengths are 2.5174 Å. Compared to the Sb−Cl bond lengths of $SbCl_3$ (2.36 Å)[31] these bond lengths are noticeably longer. Similar Sb−Cl bond lengths could only be observed in the bridging $Sb_2Cl_8^{2-}$ anions[32,33] or the Lewis acid base adduct $SbCl_3$·NH_2Ph[34] (2.52 Å).

The average Sb−N bond lengths between the antimony atom and the nitrogen atom of the coordinating pyridine molecule are 2.429 Å, leading to a relatively weak coordination of the pyridine molecules.

NBO Analyses

The molecular adduct complexes of arsenic and antimony trihalides or pseudohalides with pyridine are typical Lewis acid−base complexes. One of the major characteristics of these adducts is the total charge transfer q_{ct} between the donor molecule (pyridine) and the acceptor molecules [$AsCl(N_3)_2$ and $SbCl_2N_3$]. To obtain further insight into the donor−acceptor interaction we carried out NBO analyses on the data of the crystal structures of the two complexes.[35,36]

The NBO analyses of the adduct complexes $AsCl(N_3)_2$·pyridine and $SbCl_2N_3$·2pyridine show fairly polarised molecules. Table 4 summarises the NPA (Natural Population Analysis) partial charges and the total amount of transferred charge in both adducts.

Table 4. NPA partial charges (e) for $AsCl(N_3)_2$·pyridine and $SbCl_2N_3$·2pyridine

	$AsCl(N_3)_2$·pyridine	$SbCl_2N_3$·2 pyridine
M (M = As, Sb)	1.35	1.46
Cl[a]	−0.55	−0.56
N_{Py}[b]	−0.53	−0.53
N_α[c]	−0.68	−0.75
N_β[c]	0.24	0.24
N_γ[c]	−0.07	−0.09
q_{ct}	0.20	0.27

[a] Average of two chlorine atoms in $SbCl_2N_3$·2pyridine. [b] Average of two nitrogen atoms of the pyridine rings in $SbCl_2N_3$·2pyridine. [c] Average of the equivalent azide nitrogen atoms in $AsCl(N_3)_2$·pyridine.

The total amount for the charge transfer q_{ct} in these donor−acceptor complexes from the pyridine molecules to the Lewis acids [$AsCl(N_3)_2$ and $SbCl_2N_3$] was found to be 0.20 electrons for $AsCl(N_3)_2$·pyridine and 0.27 electrons for $SbCl_2N_3$·2pyridine. This result is in good agreement with the concept of +I and −I effects.

In $SbCl_2N_3$·2pyridine 0.13 electrons are transferred from one pyridine molecule and 0.14 electrons are transferred from the other pyridine molecule to the antimony centre. Therefore, the donor−acceptor interaction of $SbCl_2N_3$·2pyridine is much weaker than in $AsCl(N_3)_2$·pyridine. This is in good agreement with the experimentally obtained $As-N_{py}$ and $Sb-N_{py}$ bond lengths. The $As-N_{py}$ bond is extremely short [2.158(3) Å] and leads to a very strong interaction between the pyridine molecule and the $AsCl(N_3)_2$ unit. The average $Sb-N_{Py}$ bond lengths are noticeably longer (2.429 Å), pointing to a weaker interaction.

In addition, the NBO analyses at the B3LYP level of theory show that within the azide units, the charge distribution is fairly polarised. The N_α atoms of the azide unit have an average charge of −0.72 electron, the N_β atoms have an average charge of +0.24 electrons and the terminal N_γ atoms 0.08 electrons (connectivity: $M-N_\alpha-N_\beta-N_\gamma$).

Conclusion

Mixed chloride/azide compounds of arsenic and antimony in the +3 oxidation state could be synthesised. $AsCl(N_3)_2$ and $SbCl_2N_3$ were crystallised as pyridine adducts.

These adducts were characterised by Raman, IR and multinuclear NMR spectroscopy. The structures and normal modes were calculated at the B3LYP level of theory, and compared with experimentally observed data. The agreement between theory and experiment is good. The vibrational spectra of $AsCl(N_3)_2$·pyridine and $SbCl_2N_3$·2pyridine show bands, which can be assigned to the stretching vibrations as well as the deformation vibrations of the $M-N_{py}$ bonds (M = As, Sb).

Both adducts have been characterised by ^{14}N NMR spectroscopy. The ^{14}N NMR spectra show, in addition to three signals which can be assigned to the three different nitrogen atoms of the azide units, signals which can be assigned to the nitrogen atoms of the coordinated pyridine molecules. These resonances are significantly shifted compared to free pyridine.

Adduct structures which represent true minima structures (*NIMAG* = 0) were found for both adducts. The agreement between the calculated and experimentally observed bonding parameters is exceedingly good. The central atoms in $AsCl(N_3)_2$·pyridine are surrounded in a Ψ-trigonal-bipyramidal fashion, those in $SbCl_2N_3$·2pyridine are Ψ-octahedral.

On the basis of the experimentally observed atom coordinates, NBO analyses (B3LYP) have been performed to obtain more insight into the bonding situation of those weakly bonded Lewis acid base adducts. In $AsCl(N_3)_2$·pyridine 0.20 electrons are transferred from the pyridine molecule to $AsCl(N_3)_2$ and in $SbCl_2N_3$·2pyridine 0.27 electrons of both pyridine molecules are transferred to $SbCl_2N_3$. The average interaction of each pyridine molecule is much weaker than that of $AsCl(N_3)_2$·pyridine. This result is reflected in the experimentally observed $M-N_{py}$ bond lengths.

Experimental Section

General Remarks: ***CAUTION:*** Arsenic and antimony azide compounds are toxic and potentially explosive! They may explode violently under various conditions and should be handled only in small amounts with extreme care. The use of safety equipment like leather gloves, leather coat and face-shield is strongly recommended. $AsCl_3$[37] was prepared by literature methods and freshly distilled prior to use. Commercially available $SbCl_3$ (Fluka) was sublimed twice prior to use. Pyridine (Aldrich) and $(CH_3)_3SiN_3$ (Aldrich) were used as received. CH_2Cl_2 was dried by standard methods and freshly distilled prior to use. All the compounds reported here are moisture sensitive. Consequently, all manipulations were carried out under dinitrogen using Schlenk-techniques. NMR: Jeol EX 400, ^1H (400.0 MHz), ^{13}C (100.0 MHz): chemical shifts refer to δ(TMS) = 0.00 ppm; ^{14}N (28.6 MHz): shifts refer to CH_3NO_2. IR: Nicolet 520 FT-IR (KBr pellets). Raman: Perkin−Elmer FTIR-2000 spectrometer (Nd-Yag Laser: 1064 nm).

[Arsenic(iii) Diazide·Chloride]−Pyridine: $(CH_3)_3SiN_3$ (0.53 mL, 4.0 mmol) was added to a solution of $AsCl_3$ (0.17 mL, 2.0 mmol) in 25 mL of CH_2Cl_2 at 25 °C. After 1 h of stirring at room temperature, pyridine (0.32 mL, 4.00 mmol) was added. The solvent and the resulting $(CH_3)_3SiCl$ were removed in a dynamic vacuum. After recrystallisation from CH_2Cl_2 at −25 °C, colourless crystals were obtained. Yield 0.39 g (71%). IR (KBr): $\tilde{\nu}$ = 3066 (m), 2113 (vs, $\nu_{as}N_3$), 1635 (w), 1600 (s), 1537 (s), 1486 (s), 1447 (vs), 1339 (m), 1257 (vs, ν_sN_3), 1158 (m), 1065 (s), 1036 (s), 1008 (s), 946 (m), 755 (s), 670 (sh, δN_3), 637 (s, δN_3), 567 (m, δN_3), 431 (m, νAsN) cm^{-1}. Raman (66 scans, 150 mW, 180°, 20 °C): $\tilde{\nu}$ = 3073 (3), 2118 (2.5, $\nu_{as}N_3$), 2085 (1.5, $\nu_{as}N_3$), 1606 (1), 1575 (1), 1268 (1, ν_sN_3), 1258 (0.5, ν_sN_3), 1038 (3), 1013 (4), 670 (1.5, δN_3), 647 (1, δN_3), 452 (10, νAsN), 433 (1, νAsN), 287 (2, νAsCl), 265 (2.5, δAsN), 216 (2, νAsN_{py}), 180 (3), 139 (1.5, δAsN_{py}) cm^{-1}. ^1H NMR (CD_2Cl_2, 25 °C): δ = 6.33 (m, 2-H), 7.12 (m, 3-H), 8.22 (d, 1-H) ppm. ^{13}C NMR (CD_2Cl_2, 25 °C): δ = 124.0 (s, C-2), 127.7 (m, C-3), 141.1 (d, C-1) ppm. ^{14}N NMR (CH_2Cl_2, 25 °C): δ = −139 (s, N_β), −164 (s, N_{py}), −181 (s, N_γ), −269 (s, N_α) ppm.

[Antimony(iii) Azide Dichloride]−2Pyridine (2): $(CH_3)_3SiN_3$ (0.26 mL, 2.0 mmol) was added to a solution of $SbCl_3$ (0.456 g, 2.0 mmol) in 25 mL of CH_2Cl_2 at 25 °C. After 1 h of stirring at room temperature, pyridine (0.32 mL, 4.00 mmol) was added. The solvent and the resulting $(CH_3)_3SiCl$ were removed in a dynamic vacuum. After recrystallisation from CH_2Cl_2 at −25 °C, colourless crystals were obtained. Yield 0.52 g (66%). IR (KBr): $\tilde{\nu}$ = 3063 (m), 2136 (m, $\nu_{as}N_3$), 2079 (vs, $\nu_{as}N_3$), 1634 (s), 1608 (s), 1538 (s), 1485 (s), 1389 (w), 1331 (m), 1251 (s, ν_sN_3), 1179 (s, 1054 (s), 1004 (s), 936 (m), 750 (s), 648 (w, δN_3), 594 (s, δN_3), 509 (m) cm^{-1}. Raman (196 scans, 150 mW, 180°, 20 °C): $\tilde{\nu}$ = 3075 (3.5), 2091 (0.5,

$\nu_{as}N_3$), 1602 (2), 1572 (1.5), 1210 (2, ν_sN_3), 1035 (5), 1014 (5), 650 (1.5, δN_3), 386 (2, νSbN), 326 (10, νSbCl), 285 (9, νSbCl), 241 (4, δSbN), 166 (1.5, νSbN_{py}), 108 (3, δSbN_{py}) cm^{-1}. ^1H NMR (CD_2Cl_2, 25 °C): δ = 6.52 (m, 2-H), 7.42 (m, 3-H), 8.32 (d, 1-H) ppm. ^{13}C NMR (CD_2Cl_2, 25 °C): δ = 124.9 (s, C-2), 126.7 (m, C-3), 143.2 (d, C-1) ppm. ^{14}N NMR (CH_2Cl_2, 25 °C): δ = −143 (s, N_β), −157 (s, N_{py}), −172 (s, N_γ), −275 (s, N_α) ppm.

X-ray Crystallographic Study: $AsCl(N_3)_2$·pyridine: $C_5H_5AsClN_7$, M = 273.53, crystal size: 0.30 × 0.30 × 0.30 mm, colourless prism, triclinic, space group $P\bar{1}$, a = 7.3826(8), b = 8.0314(9), c = 9.621(1) Å, α = 108.497(2), β = 103.881(2), γ = 101.632(2)°, V = 500.22(9) $Å^3$, Z = 2, $d_{calcd.}$ = 1.816 Mg/m^3, μ = 3.637 mm^{-1}, $F(000)$ = 268. Siemens SMART Area detector, Mo-K_α, λ = 0.71073 Å, T = 193(2) K, θ range = 2.36−28.73° in $-9 \le h \le 8$, $-10 \le k \le 10$, $-11 \le l \le 10$, reflections collected: 2847, independent reflections: 1494 (R_{int} = 0.0171), observed reflections: 1376 [$F>4\sigma(F)$]. Structure solution program: SHELXS-97,[38] full-matrix least-squares methods, parameter/restraints ratio: 127:0, final R indices [$F > 4\sigma(F)$]: $R1$ = 0.0248, $wR1$ = 0.0652; $R2$ = 0.0278, $wR2$ = 0.0668 (all data), GOF on F^2 = 1.042, largest difference peak/hole: 0.493/−0.419 e $Å^{-3}$, program used: SHELXL-97.[39] $SbCl_2N_3$·2pyridine: $C_{10}H_{10}Cl_2N_5Sb$, M = 392.88, crystal size: 0.30 × 0.30 × 0.30 mm, colourless prism, orthorhombic, space group $Pbca$, a = 6.5566(5), b = 13.635(1), c = 30.901(2) Å, V = 2762.4(4) $Å^3$, Z = 8, $d_{calcd.}$ = 1.889 Mg/m^3, μ = 2.373 mm^{-1}, $F(000)$ = 1520. Siemens SMART Area detector, Mo-K_α, λ = 0.71073 Å, T = 193(2) K, θ range = 2.64−29.07° in $-8 \le h \le 8$, $-17 \le k \le 17$, $-30 \le l \le 41$, reflections collected: 14636, independent reflections: 2796 (R_{int} = 0.0285), observed reflections: 2369 [$F > 4\sigma(F)$]. Structure solution program: SHELXS-97,[38] full-matrix least-squares methods, parameter/restraints ratio: 163:0, final R indices [$F > 4\sigma(F)$]: $R1$ = 0.0243, $wR1$ = 0.0530; $R2$ = 0.0326, $wR2$ = 0.0551 (all data), GOF on F^2 = 1.116, largest difference peak/hole: 0.267/−0.494 e $Å^{-3}$, program used: SHELXL-97.[39] CCDC-181324 and -181325 contain the supplementary crystallographic data for this paper. These data can be obtained free of charge at www.ccdc.cam.ac.uk/conts/retrieving.html or from the Cambridge Crystallographic Data Centre, 12, Union Road, Cambridge CB2 1EZ, UK [Fax: (internat.) + 44-1223/336-033; E-mail: deposit@ccdc.cam.ac.uk].

Computational Methods: The structures and vibrational data for the reported compounds were calculated using the density functional theory with the program package Gaussian 98.[40] The calculations were carried out at the electron-correlated B3LYP level of theory[41] which includes a mixture of Hartree−Fock exchange with DFT exchange correlation. For C, H, N and Cl a standard 6-31G(d,p) double-zeta basis set was used and for As and Sb a quasi-relativistic pseudopotential (As: ECP28MWB; Sb: ECP46MWB)[42] and a (5s5p1d)/[3s3p1d]-DZ+P basis set.[43] Becke's 3-parameter functional, where the nonlocal correlation is provided by the LYP expression (Lee, Yang, Parr correlation functional), was used which is implemented in Gaussian 98.[40]

Acknowledgments

We are indebted to and thank Dr. M.-J. Crawford for stimulating ideas to start this research. Financial support of this work by the University of Munich and the Fonds der Chemischen Industrie is gratefully acknowledged.

[1] R. Minkwitz, J. Nowicki, *Z. Anorg. Allg. Chem.* **1991**, *596*, 93.
[2] R. Minkwitz, H. Prenzel, *Z. Anorg. Allg. Chem.* **1986**, *534*, 150.
[3] R. Minkwitz, F. Claus, M. Glaser, *Z. Anorg. Allg. Chem.* **1983**, *506*, 178.
[4] F. Claus, R. Minkwitz, *Z. Anorg. Allg. Chem.* **1983**, *501*, 19.
[5] R. Minkwitz, H. Prenzel, A. Schardey, H. Oberhammer, *Inorg. Chem.* **1987**, *26*, 2730.
[6] A. Müller, E. Niecke, B. Krebs, O. Glemser, *Z. Naturforsch., Teil B* **1968**, *23*, 588.
[7] A. Müller, B. Krebs, *J. Mol. Structure* **1968**, *2*, 149.
[8] H. Preiss, E. Alsdorf, A. Lehmann, *Carbon* **1987**, *25*, 727.
[9] K. B. Dillon, A. W. G. Platt, T. C. Waddington, *Inorg. Nucl. Chem. Lett.* **1978**, *14*, 511.
[10] E. L. Lines, L. F. Centofanti, *Inorg. Chem.* **1972**, *11*, 2269.
[11] S. R. O'Neill, J. M. Shreeve, *Inorg. Chem.* **1972**, *11*, 1630.
[12] [12a] U. Müller, K. Dehnicke, *Z. Anorg. Allg. Chem.* **1967**, *350*, 113. [12b] A. Schmidt, *Chem. Ber.* **1971**, *104*, 31.
[13] U. Müller, *Z. Anorg. Allg. Chem.* **1972**, *388*, 207.
[14] T. M. Klapötke, H. Nöth, T. Schütt, M. Warchold, *Z. Anorg. Allg. Chem.* **2001**, *627*, 81.
[15] [15a] G. Baliman, P. S. Pregosin, *J. Magn. Reson.* **1977**, *26*, 283. [15b] C. Brevard, P. Granger, *Handbook of High Resolution Multinuclear NMR*, J. Wiley, New York, Chichester, **1981**, p. 136−137. [15c] H. P. A. Mercier, J. C. P. Sanders, G. J. Schrobilgen, *J. Am. Chem. Soc.* **1994**, *116*, 2921. [15d] M. F. A. Dove, J. C. P. Sanders, E. L. Jones, M. J. Parkin, *J. Chem. Soc., Chem. Commun.* **1984**, 1578.
[16] T. M. Klapötke, H. Nöth, T. Schütt, M. Warchold, *Angew. Chem.* **2000**, *112*, 2197; *Angew. Chem. Int. Ed.* **2000**, *39*, 2108.
[17] W. Beck, W. Becker, K. F. Chew, W. Derbyshire, N. Logan, D. M. Revitt, D. B. Sowerby, *J. Chem. Soc., Dalton Trans.* **1972**, 245.
[18] M. Witanowski, *J. Am. Chem. Soc.* **1968**, *90*, 5683.
[19] G. A. Webb, *Annual Reports on NMR Spectroscopy*, Academic Press, Inc., London, **1986**, vol. 18.
[20] K. Nakamoto, *Infrared and Raman Spectra of Inorganic and Coordination Compounds*, J. Wiley, New York, **1986**.
[21] [21a] R. J. Gillespie, *Molecular Geometry*, Van Nostrand Reinhold, London, **1972**. [21b] R. J. Gillespie, I. Hargittai, *The VSEPR Model of Molecular Geometry*, Prentice-Hall, New-Jersey, **1991**. [21c] R. J. Gillespie, *Chem. Soc. Rev.* **1991**, *21*, 59.
[22] M. Webster, S. Keats, *J. Chem. Soc. A* **1971**, 837.
[23] M. Gerken, P. Kolb, A. Wegner, H. P. A. Mercier, H. Borrmann, D. A. Dixon, G. J. Schrobilgen, *Inorg. Chem.* **2000**, *39*, 2813.
[24] P. W. Allen, L. E. Sutton, *Acta Crystallogr.* **1950**, *3*, 46.
[25] R. Jürgens, J. Almöf, *Chem. Phys. Lett.* **1991**, *276*, 263.
[26] R. Ahlrichs, M. R. Bär, M. Häser, E. Sattler, *Chem. Phys. Lett.* **1991**, *184*, 353.
[27] D. F. Moser, I. Schranz, M. C. Gerrety, L. Stahl, R. J. Staples, *J. Chem. Soc., Dalton Trans.* **1999**, 751.
[28] G. Ferguson, F. C. March, D. R. Ridley, *Acta Crystallogr., Sect. B* **1975**, *31*, 1260.
[29] J. Müller, U. Müller, A. Loss, J. Lorberth, H. Donath, W. Massa, *Z. Naturforsch., Teil B* **1985**, *40*, 1320.
[30] G. Ferguson, D. R. Ridley, *Acta Crystallogr., Sect. B* **1973**, *29*, 2221.
[31] N. N. Greenwood, A. Earnshaw, *Chemie der Elemente*, VCH, Weinheim, **1988**.
[32] [32a] W. S. Sheldrick, H.-J. Häusler, J. Kaub, *Z. Naturforsch., Teil B* **1988**, *43*, 789. [32b] A. T. Mohammed, U. Müller, *Acta Crystallogr., Sect. C* **1985**, *41*, 329. [32c] W. Czado, S. Rabe, U. Müller, *Z. Naturforsch., Teil B* **1998**, *54*, 288.
[33] U. Ensinger, W. Schwarz, A. Schmidt, *Z. Naturforsch., Teil B* **1982**, *37*, 1584.
[34] R. Hulme, J. C. Scruton, *J. Chem. Soc. A* **1968**, 2448.
[35] A. E. Reed, L. A. Curtiss, F. Weinhold, *Chem. Rev.* **1988**, *88*, 899.

[36] A. E. Reed, R. B. Weinstock, F. Weinhold, *J. Chem. Phys.* **1985**, *83*, 735.
[37] G. Brauer, *Handbuch der präparativen anorganischen Chemie.* 2nd ed., F. Enke, Stuttgart, **1975**.
[38] G. M. Sheldrick, *SHELXS-97, Program for Crystal Structure Solution*, Universität Göttingen, **1997**.
[39] G. M. Sheldrick, *SHELXL-97, Program for Crystal Structure Refinement*, Universität Göttingen, **1997**.
[40] M. J. Frisch, G. W. Trucks, H. B. Schlegel, G. E. Scuseria, M. A. Robb, J. R. Cheeseman, V. G. Zakrzewski, J. A. Montgomery, R. E. Stratmann, J. C. Burant, S. Dapprich, J. M. Millam, A. D. Daniels, K. N. Kudin, M. C. Strain, O. Farkas, J. Tomasi, V. Barone, M. Cossi, R. Cammi, B. Mennucci, C. Pomelli, C. Adamo, S. Clifford, J. Ochterski, G. A. Petersson, P. Y. Ayala, Q. Cui, K. Morokuma, D. K. Malick, A. D. Rabuck, K. Raghavachari, J. B. Foresman, J. Cioslowski, J. V. Ortiz, B. B. Stefanov, G. Liu, A. Liashenko, P. Piskorz, I. Komaromi, R. Gomperts, R. L. Martin, D. J. Fox, T. Keith, M. A. Al-Laham, C. Y. Peng, A. Nanayakkara, C. Gonzalez, M. Challacombe, P. M. W. Gill, B. Johnson, W. Chen, M. W. Wong, J. L. Andres, C. Gonzalez, M. Head-Gordon, E. S. Replogle, J. A. Pople, *Gaussian 98*, revision A.3, Gaussian, Inc., Pittsburgh PA, **1998**.
[41] [41a] C. Lee, W. Yang, R. G. Parr, *Phys. Rev.* **1988**, *B37*, 785. [41b] A. D. Becke, *Phys. Rev.* **1988**, *A38*, 3098. [41c] B. Miehlich, A. Savin, H. Stoll, H. Preuss, *Chem. Phys. Lett.* **1989**, *157*, 200. [41d] A. D. Becke, *J. Chem. Phys.* **1993**, *98*, 5648.
[42] A. Bergner, M. Dolg, W. Kuechle, H. Preuss, *Mol. Phys.* **1993**, *80*, 1431.
[43] M. Kaupp, R. v. R. Schleyer, H. Stoll, H. Preuss, *J. Am. Chem. Soc.* **1991**, *113*, 1602.

Received March 15, 2002
[I02130]

EurJIC
European Journal of Inorganic Chemistry

October 2002
Issue 10
Pages 2519–2744

Papers available ahead of print in Early View at www.interscience.wiley.com

Earliest available Table of Contents:
Automatically, free of charge by e-mail through
www.interscience.wiley.com/alerts

COVER PICTURE

The cover picture shows the [2×2] grid, $[Cu^{1}_{4}(2+2)_{2}]^{4+}$, of four copper(I) ions and two (2+2) Schiff-base macrocycles, which self-assembles when copper(I) ions are used to template the reaction of 3,6-diformylpyridazine with 1,3-diaminopropane. In each case the two parallel strands of the [2×2] grid are linked together in a single (2+2) Schiff-base macrocycle, and the two macrocycles approach each other at right angles to give rise to the perpendicular strands of the grid structure. Thus, the copper(I) ions have distorted tetrahedral geometries, with each macrocycle providing a bidentate donor set at right angles to that supplied by the other macrocycle. Details are discussed in the Microreview by S. Brooker on p. 2535 ff. The cover image was generated by M. Crawford (University of Otago) with Strata Studio Pro (Strata).

MICROREVIEW

Contents

2535 **S. Brooker**

Some Copper and Cobalt Complexes of Schiff-Base Macrocycles Containing Pyridazine Head Units

Keywords: N ligands / Schiff bases / Macrocyclic ligands / Electrochemistry / Magnetic properties

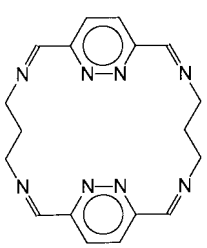

L14, a (2+2) macrocycle

 © WILEY-VCH Verlag GmbH, 69451 Weinheim, Germany, 2002 1434–1948/02/1010–2523 $ 20.00+.50/0

SHORT COMMUNICATIONS

2549 **M. I. J. Polson, J. A. Lotoski, K. O. Johansson, N. J. Taylor, G. S. Hanan,* B. Hasenknopf, R. Thouvenot,* F. Loiseau, R. Passalaqua, S. Campagna***

Symmetric and Asymmetric Coupling of Pyridylpyrimidine for the Synthesis of Polynucleating Ligands

Keywords: Heterocycles / Ruthenium / N ligands / Radical reactions / Addition reactions

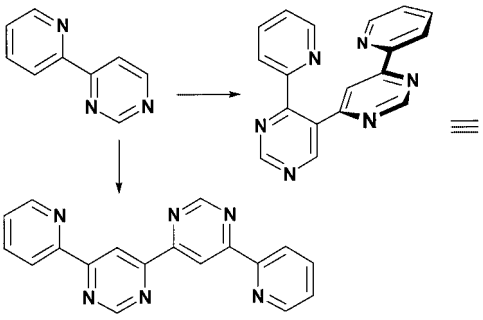

2553 **J. Weng, M. Hong,* Q. Shi, R. Cao, A. S. C. Chan**

Chiral Supramolecular Assemblies Derived from the Insertion of a Segmental Ligand into a Copper-Tyrosine Framework

Keywords: Amino acids / Copper / Self-assembly / Polymers

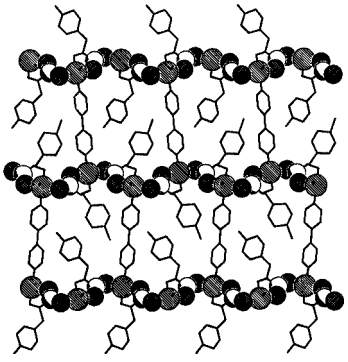

2557 **R. Steudel,* Y. Steudel, D. Lentz**

Tetraamidosulfurane and its Decomposition Products − an ab initio MO Study

Keywords: Sulfur / Hypervalent compounds / Reaction mechanisms / Ab initio calculations

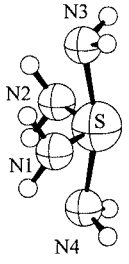

5

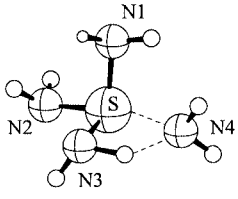

TS

2561 **J. A. Cabeza,* I. del Río, S. García-Granda, V. Riera, M. G. Sánchez-Vega**

Facile C−S Bond Activation of Levamisole Hydrochloride on a Triruthenium Cluster Core

Keywords: Ruthenium / Metal clusters / Levamisole / S ligands / C−S bond activation

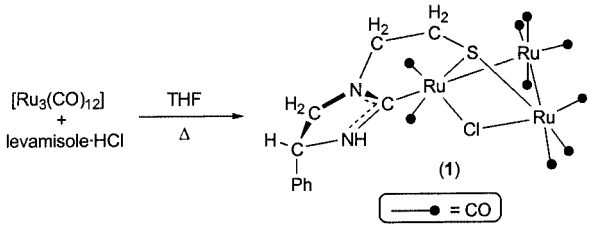

2565 **A. V. Usatov,* E. V. Martynova, F. M. Dolgushin, A. S. Peregudov, M. Yu. Antipin, Yu. N. Novikov**

Fullerene and Carborane in One Coordination Sphere: Synthesis and Structure of a Mixed η^2-C_{60} and σ-Carboranyl Complex of Iridium

Keywords: Fullerenes / Boranes / Iridium / Complexes / X-ray analysis

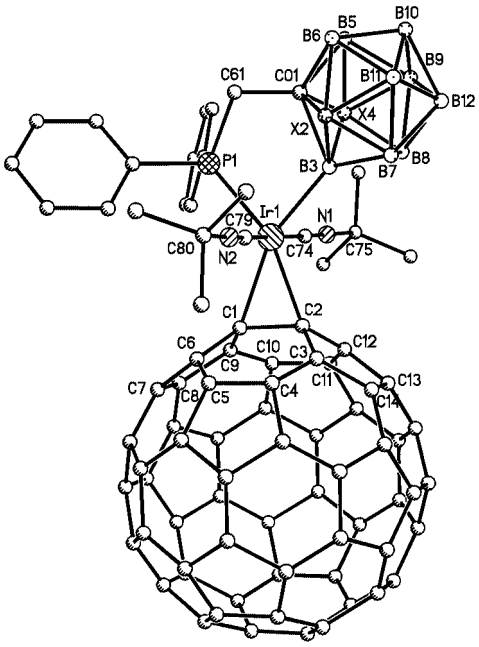

FULL PAPERS

2569 **B. Bartels, C. García-Yebra, F. Rominger, G. Helmchen***

Iridium-Catalysed Allylic Substitution: Stereochemical Aspects and Isolation of Ir^{III} Complexes Related to the Catalytic Cycle

Keywords: Iridium / Allyl complexes / NMR spectroscopy / Allylic substitution / Asymmetric catalysis

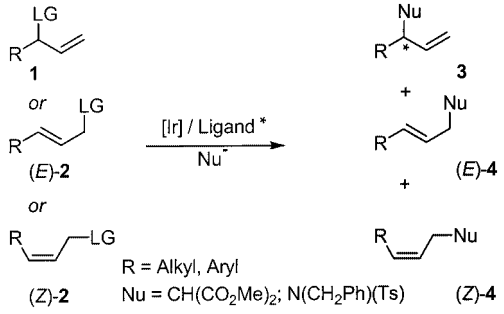

2587 **R. Contant, M. Richet, Y. W. Lu, B. Keita, L. Nadjo***

Isomerically Pure α_1-Monosubstituted Tungstodiphosphates: Synthesis, Characterization and Stability in Aqueous Solutions

Keywords: Polyanions / Phosphates / Tungsten

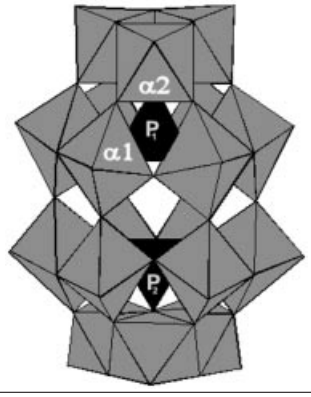

2594 **H. Brunner,* S. Dormeier, M. Zabel**

Stereochemical Exploitation of the Chiral (+)-9-Phenyldeltacyclanyl Substituent in Diphosphanes and Their Ni, Pd and Pt Complexes

Keywords: Deltacyclenes / Chiral ligands / Phosphanes / Nickel / Palladium / Platinum

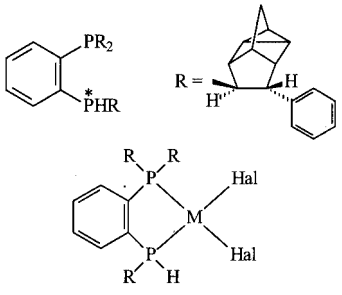

2603 **H. Brunner,* S. Dormeier, I. Grau, M. Zabel**

Dinuclear and Trinuclear Ni−, Pd−, and Pt−Halide Complexes of the Easily Accessible Chiral Ligand *P,P,P′*-Tris[(+)-9-phenyldeltacyclan-8-yl]-1,2-bis(phosphanyl)benzene

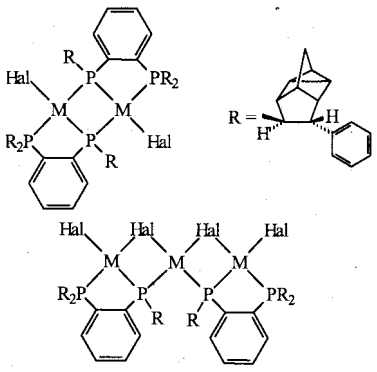

Keywords: Nickel complexes / Palladium complexes / Platinum complexes / Phosphido bridges / Phosphorus configuration

2614 **A. Bayer, P. Murszat, U. Thewalt, B. Rieger***

Chiral Mono- and Bidentate Ligands Derived from D-Mannitol and Their Application in Rhodium(I)-Catalyzed Asymmetric Hydrogenation Reactions

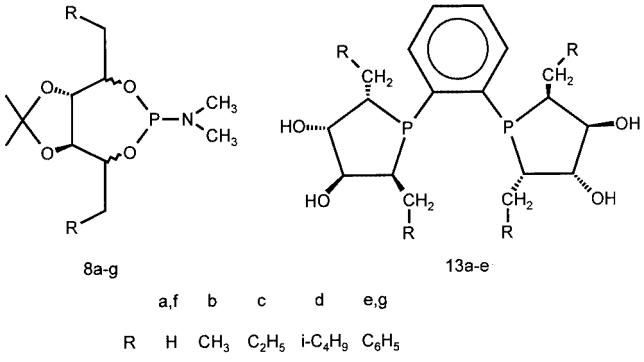

Keywords: Chiral pool / P ligands / Rhodium / Asymmetric catalysis / Hydrogenation

2625 **G. Müller, M. Klinga, M. Leskelä, B. Rieger***

Metal Complexes of the Tetradentate Ligands *rac*- and *meso*-N,P,P,N: Synthesis, Separation and Structural Characterization

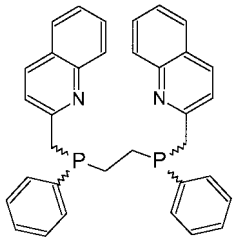

***rac*- and *meso*-N,P,P,N**

Keywords: N ligands / P ligands / Iron / Palladium / Cobalt

2633 **D. Hüerländer, N. Kleigrewe, G. Kehr, G. Erker,* R. Fröhlich**

Synthesis, Structural and Chemical Characterization of Unsaturated C_4- and C_{10}-Bridged Group-4 *ansa*-Metallocenes Obtained Through a Ring-Closing Olefin Metathesis Reaction

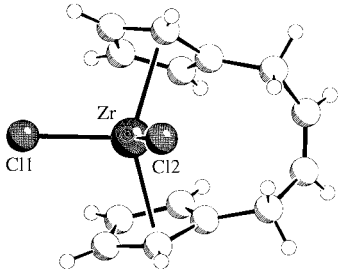

Keywords: Carbenes / Metallocenes / Metathesis / Olefins / Ruthenium / Zirconium

2643 G. Linti,* W. Köstler, H. Pritzkow

Bismuthanides and Bismuthanediides − Synthesis and Structural Characterization of $[R_2Bi]^-$ and $[(RBi)_{12}Na_{21}]^{3-}$ Salts with Bulky Silyl Substituents

Keywords: Bismuth / Lithium / Sodium / Silicon / Cluster compounds

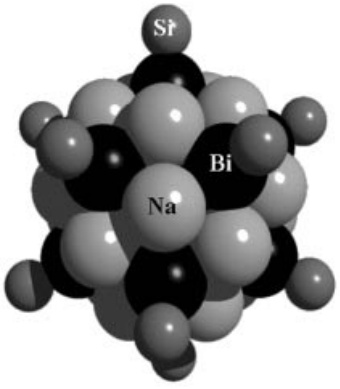

2648 V. B. Di Marco, R. A. Yokel, M. G. Ferlin, A. Tapparo, G. G. Bombi*

Evaluation of 3,4-Hydroxypyridinecarboxylic Acids as Possible Bidentate Chelating Agents for Aluminium(III): Synthesis and Metal−Ligand Solution Chemistry

Keywords: Aluminium / Carboxylate ligands / Potentiometry / Chelation therapy

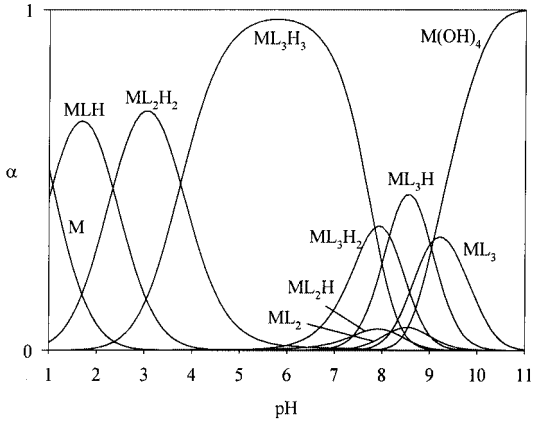

2656 M. V. Butovskii, U. Englert, A. A. Fil'chikov, G. E. Herberich,* U. Koelle, A. R. Kudinov*

(Tetramethylcyclobutadiene)cobalt Complexes − Syntheses of Tris(ligand) Derivatives and Structures of $[(C_4Me_4)Co(CO)_3]BF_4$ and $[(C_4Me_4)Co(NCMe)_3]PF_6$

Keywords: Cobalt / Cyclobutadiene complexes / Metallo-electrophiles

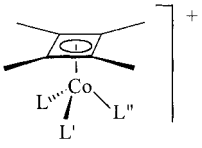

2664 W. Chen, K. Matsumoto*

Synthesis and Structural Characterization of Trinuclear, Amidate-Bridged Heterobimetallic Complexes $[\{Pt(NH_3)_2(NHCOtBu)_2\}_2M]X_n$ (M = Mn, Fe, Co, Ni, Cu; X = BF_4^-, ClO_4^-; n = 2 or 3)

Keywords: N ligands / Bridging ligands / Platinum / Manganese / Iron / Cobalt / Nickel / Copper

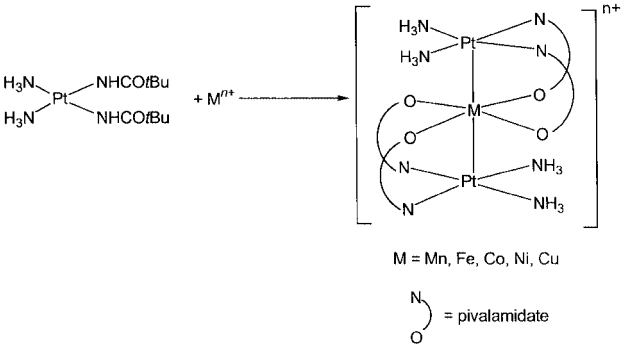

2671 **B. de Bruin,* T. P. J. Peters, J. B. M. Wilting, S. Thewissen, J. M. M. Smits, A. W. Gal***

Dioxygenation of Sterically Hindered (Ethene)-Rh^{I} and -Ir^{I} Complexes to (Peroxo)Rh^{III} and (Ethene)(peroxo)Ir^{III} Complexes

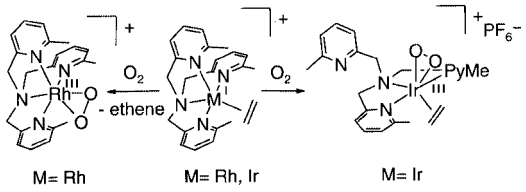

Keywords: Alkene ligands / Iridium / O−O activation / Oxidations / Peroxo ligands

2681 **H. Sachdev**

New Aspects in the Coordination Chemistry of Magnesium Hydrazides

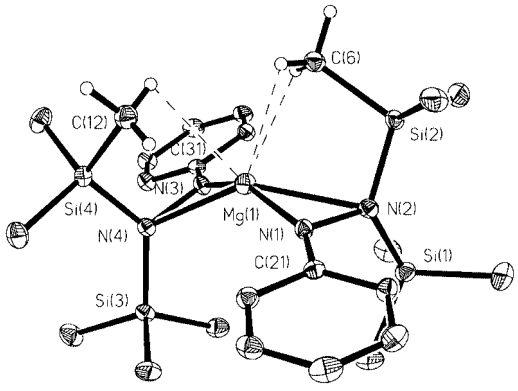

Keywords: Hydrazides / Coordination chemistry / Magnesium / N ligands

2686 **F. Botteman, G. M. Nicolle, L. Vander Elst, S. Laurent, A. E. Merbach, R. N. Muller***

Synthesis, Variable Temperature and Pressure ^{17}O NMR Study of Bis(alkylamide) Derivatives of $[(Gd\text{-}DTPA)(H_2O)]^{2-}$ − An Assessment of the Substitution Effect on Water Exchange Kinetics

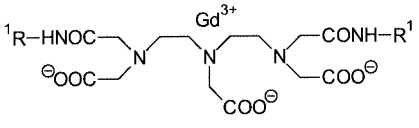

Keywords: Water exchange / MRI contrast agents / DTPA-bis(amide) derivatives / Substituent effects / ^{17}O

2694 **B. Julián, H. Beltrán, E. Cordnoncillo, P. Escribano,* J. V. Folgado, M. Vallet-Regí, R. P. del Real**

A Study of the Method of Synthesis and Chromatic Properties of the Cr-SnO_2 Pigment

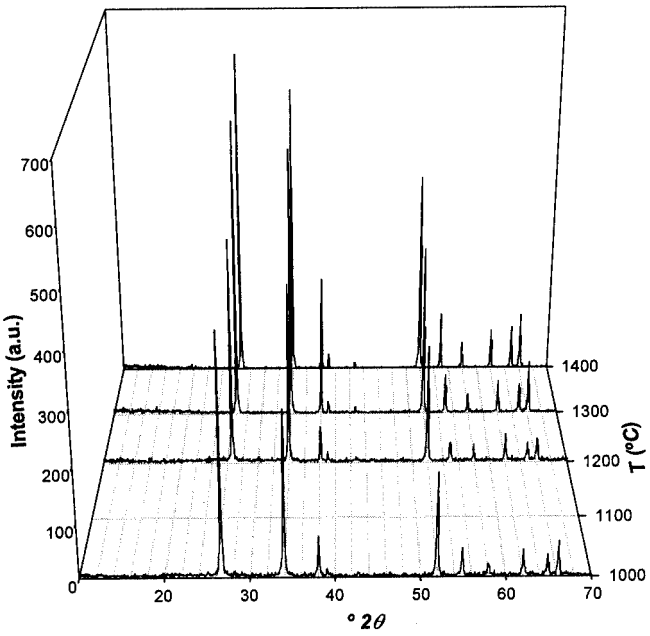

Keywords: Ceramics / Chromium / Chromium-tin pigment / Solid-state reactions

2701 **T. M. Klapötke,* B. Krumm, P. Mayer, H. Piotrowski, I. Schwab, M. Vogt**

Synthesis and Structures of Triorganotelluronium Pseudohalides

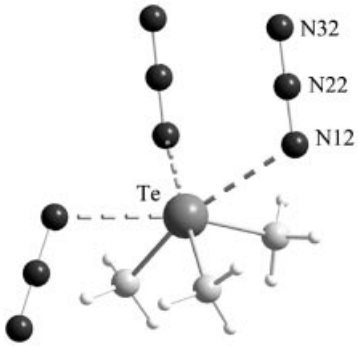

Keywords: Tellurium / Azides / NMR spectroscopy / Noncovalent interactions

2710 **C. Hureau, E. Anxolabéhère-Mallart, M. Nierlich, F. Gonnet, E. Rivière, G. Blondin***

Synthesis, Structure and Characterisation of New Phenolato-Bridged Manganese Complexes $[L_2Mn_2]^{2+}$ − Formation by Ligand Oxidation in L_aH [L_aH = *N*-(2-hydroxybenzyl)-*N*,*N*′-bis(2-pyridylmethyl)ethane-1,2-diamine]

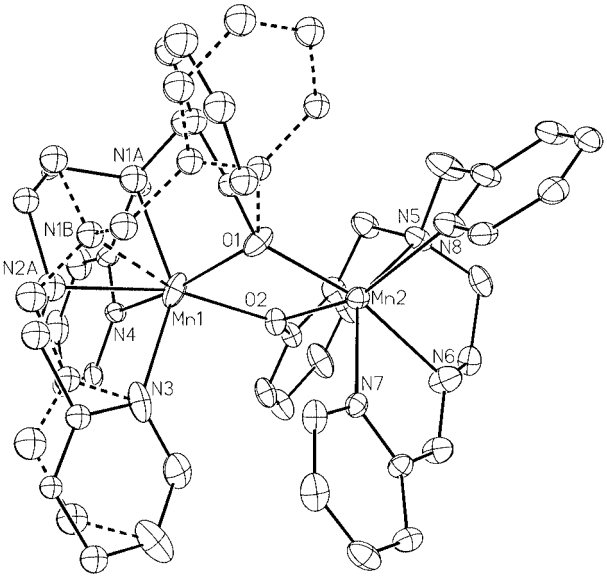

Keywords: Manganese / N,O ligands / Electrochemistry / EPR spectroscopy

2720 **A. M. Thomas, G. Neelakanta, S. Mahadevan, M. Nethaji, A. R. Chakravarty***

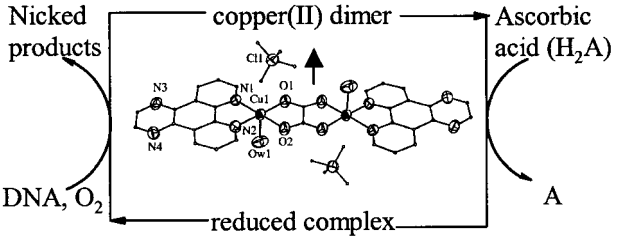

Syntheses, Crystal Structure, and Nuclease Activity of Oxalato-Bridged Dicopper(II) Complexes with Planar N-Donor Heterocyclic Bases

Keywords: Catalysis / Copper / Crystal structure / Magnetic properties / Nuclease activity

2727 **E. Sutra, L. Lamandé, H. Gornitzka, J. Bellan***

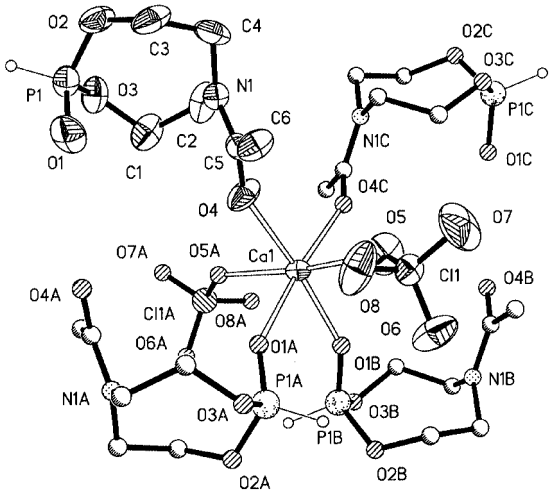

A New Oligomeric Complex of Cyclic Hydrogenphosphonates with Calcium Perchlorate

Keywords: Phosphorus heterocycles / Calcium / P ligands / Self-assembly / Noncovalent interactions

2730 **Z.-Y. Fu, X.-T. Wu,* J.-C. Dai, S.-M. Hu, W.-X. Du, H.-H. Zhang, R.-Q. Sun**

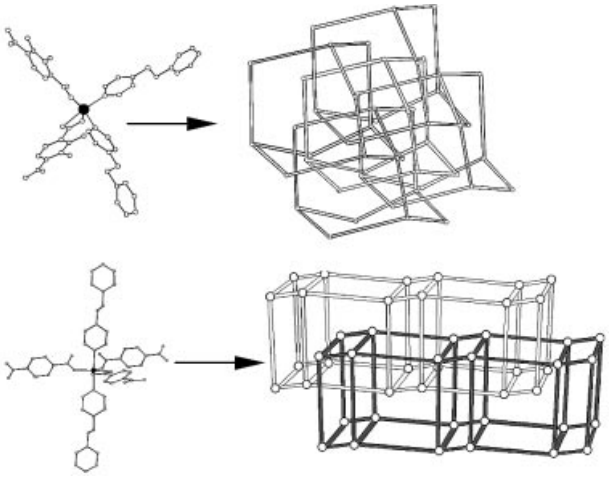

The Structure and Fluorescence Properties of Two Novel Mixed-Ligand Supramolecular Frameworks with Different Structural Motifs

Keywords: Crystal engineering / Cobalt / Fluorescence / Supramolecular chemistry

2736 **J. Ruiz,* F. Florenciano, V. Rodríguez, C. de Haro, G. López, J. Pérez**

New Dimetallic Palladium and Platinum Complexes Containing the Tetrakis(1-pyrazolyl)-borate Ligand − Crystal Structures of $[\{(C_6F_5)_2Pd\}_2(\mu\text{-pz})_2B(\mu\text{-pz})_2]^-$, $[\{(C_6F_5)(t\text{BuNC})\text{-}Pd\}_2(\mu\text{-pz})_2B(\mu\text{-pz})_2]^+$ and $[(C_6F_5)_2Pd(\mu\text{-pz})_2B(\mu\text{-pz})_2Pd(\eta^3\text{-}C_4H_7)]$

Keywords: Palladium / Platinum / N ligands / Bridging ligands / Structure elucidation

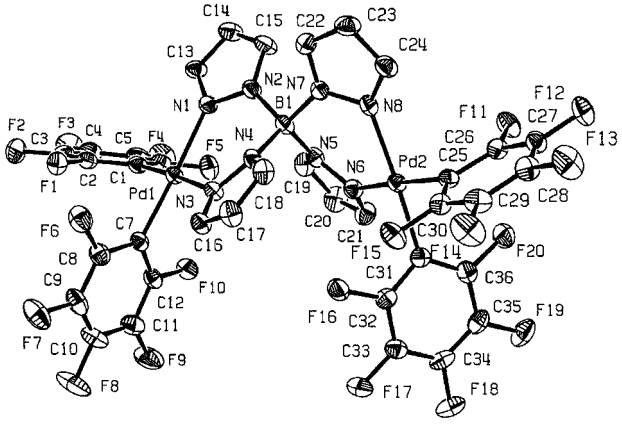

Some Copper and Cobalt Complexes of Schiff-Base Macrocycles Containing Pyridazine Head Units[‡]

Sally Brooker[a]

Keywords: N ligands / Schiff bases / Macrocyclic ligands / Electrochemistry / Magnetic properties

The Schiff-base macrocycle L14, formed by the [2+2] condensation of 3,6-diformylpyridazine and 1,3-diaminopropane, has facilitated the preparation of the first extensive family of pyridazine-bridged macrocyclic complexes. The structural, magnetic and electrochemical behaviour of these complexes is of considerable interest. This microreview provides an overview of prior relevant studies and then describes some of the recent copper and cobalt chemistry of the macrocyclic ligand L14.

(© Wiley-VCH Verlag GmbH, 69451 Weinheim, Germany, 2002)

Contents

1. Scope
2. Background
2.1 Acyclic Pyridazine and Phthalazine Ligands
2.1.1 Copper Complexes of Acyclic Pyridazine and Phthalazine Ligands
2.1.2 Cobalt Complexes of Acyclic Pyridazine and Phthalazine Ligands
2.2 Macrocyclic Pyridazine and Phthalazine Ligands
3. Macrocycles Built from 3,6-Diformylpyridazine
3.1 Macrocycles L14 and L14′ from 3,6-Diformylpyridazine and 1,3-Diaminopropane
3.1.1 Copper Complexes of the L14 Schiff-Base Macrocycle
3.1.2 Cobalt Complexes of the L14 Schiff-Base Macrocycle
4. Conclusions and Outlook

[‡] The advice, enthusiasm and encouragement of Professor Karl Wieghardt (MPI für Strahlenchemie) is gratefully acknowledged on the occasion of his 60th birthday

[a] Department of Chemistry, University of Otago
P. O. Box 56, Dunedin, New Zealand
E-mail: sbrooker@alkali.otago.ac.nz

1. Scope

This microreview covers some aspects of the recent introduction of a new head unit, 3,6-diformylpyridazine (Figure 1), into Schiff-base macrocyclic chemistry,[1,2] focussing on the interesting copper and cobalt chemistry that it has generated to date.[3−11] The reader is referred to earlier reviews on Schiff-base macrocycles for excellent introductions to this general area and in-depth reviews of Schiff-base macrocycles incorporating pyridine- and phenol-based head units (e.g. $L2^{2-}$, Figure 2).[12−17] Recently, an overview of

Sally Brooker was born in Waikari, North Canterbury, New Zealand and educated at Hawarden Area School (1970−1982). She then studied at the University of Canterbury (NZ) and obtained her BSc(Hons) with first class honours in Chemistry in 1986, followed by her PhD with Dr Vickie McKee (now Professor and Head of Inorganic Chemistry at Loughborough University, UK) in 1989. After postdoctoral research, 1990−1991, at Georg-August-Universität Göttingen (Germany) with Professor George M. Sheldrick, she took up a Lectureship at the University of Otago (NZ) where she is now an Associate Professor (Reader). She has taken two periods of sabbatical leave, the first as an Alexander von Humboldt Fellow in Professor Karl Wieghardt's laboratory (MPI für Strahlenchemie) and the second as a Visiting Professor at Queens University of Belfast with Professor Jane Nelson followed by time on a Royal Society of Chemistry Journals Grant with Professors Mike D. Ward and Jon McCleverty and Dr John C. Jeffery at the University of Bristol. Sally was recently awarded the Easterfield Medal by the Royal Society of Chemistry and New Zealand Institute of Chemistry. Her research interests concern the design, synthesis and full characterisation of, primarily paramagnetic, di- and polymetallic complexes of communicating transition metal ions with new polydentate and macrocyclic ligands (http://neon.otago.ac.nz/chemistry/research/sab/sab-res.htm).

MICROREVIEWS: This feature introduces the readers to the author's research through a concise overview of the selected topic. Reference to important work from others in the field is included.

those which incorporate thiophenolate-based head units has been published (e.g. $L3^{2-}$, Figure 2),[18] and macrobicycles, or cryptands, have been comprehensively reviewed.[19]

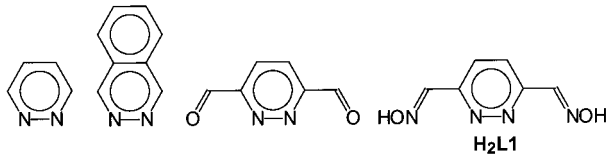

Figure 1. From left to right: pyridazine, phthalazine, 3,6-diformylpyridazine, H_2L1

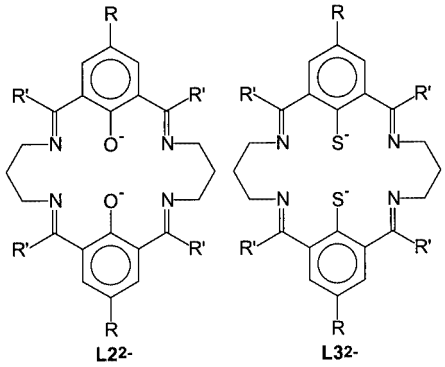

Figure 2. Phenolate macrocycles $L2^{2-}$ (e.g. R = CH_3, *tert*-butyl, CF_3; R′ = H, CH_3, phenyl) and thiophenolate macrocycles $L3^{2-}$ (R = CH_3, *tert*-butyl; R′ = H)

2. Background

2.1 Acyclic Pyridazine and Phthalazine Ligands

Aromatic nitrogen heterocycles such as diazines have been extensively and effectively employed as bridging ligands.[20] In keeping with this, pyridazine- and phthalazine-based acyclic ligands and their complexes are numerous and well-known. The earliest studies relevant to our work are those by Blake and co-workers[21–24] and Lever and co-workers,[25,26] concerning structural and magnetic studies of acyclic pyridazine- and phthalazine-bridged dimetallic complexes of first row transition metal ions. Since the 1980's Thompson and co-workers have been the key players in the development of, in particular, magnetostructural data on pyridazine- and phthalazine-bridged acyclic dicopper(II) complexes.[27–75]

However, of all the acyclic studies reported in the literature, the paper that most caught our attention was one by Bremard and co-workers, in 1991, in which the observation of antiferromagnetic coupling in the dicopper(II) complex of the acyclic dioxime ligand H_2L1 derived from 3,6-diformylpyridazine was reported (Figure 1).[76] As coordination chemists with a strong background in Schiff-base ligand chemistry, the possibility of incorporating the interesting pyridazine bridging unit into Schiff-base macrocycles, using 3,6-diformylpyridazine as a head unit (see Section 3), was a natural extension of the chemistry reported by Bremard and co-workers. Before focussing on studies of pyridazine- and phthalazine-containing macrocycles, a short overview is presented of the — more numerous — copper and cobalt complexes of acyclic pyridazine- and phthalazine-containing ligands.

2.1.1 Copper Complexes of Acyclic Pyridazine and Phthalazine Ligands

There are many reports of copper complexes containing a Cu–N(pyridazine moiety) bond (SciFinder Scholar[77] indicates that there are 943 such complexes in 218 papers, as of 12.2.02). Many of these complexes have been structurally characterised, as a search of the Cambridge Crystallographic Database[78] (CSD version 5.22 October 2001) shows: there are 130 entries for crystallographically characterised copper complexes containing a Cu–N(pyridazine moiety) bond. Of these, other than the structures of our pyridazine-bridged copper complexes (only three of which are in the CSD[78] version 5.22 October 2001 as the others were published after this version was released),[3,6,7] there are 93 entries which contain copper ions bridged by a pyridazine or phthalazine moiety: the majority of these structures are of di- or polycopper(II) complexes (69 entries), with a smaller number of di- or polycopper(I) complexes (26 entries), and no examples of mixed-valent complexes other than one of ours[6] (Table 1). Narrowing the field still further, relatively few of these complexes contain copper ions doubly or triply bridged by pyridazine or phthalazine, with only seven dicopper(II) examples (none of these involve triple pyridazine or phthalazine bridges) and 17 di- or polycopper(I) compounds (Table 1).

Studies on acyclic pyridazine- and phthalazine-bridged dicopper(II) complexes have clearly shown that these moieties are capable of mediating moderate to strong antiferromagnetic coupling, although it should be remembered that, with only one structurally characterised exception,[76] hydroxide, halide, azide, alkoxide, nitrate or sulfate exogenous bridges are always present in addition to the diazine bridge(s) in these acyclic copper complexes.[30–34,36–39,41,42,44,45,47,48,50,52,53,57,60–62,67,68,70–73,79,80] Another point to note in this regard is that on coordination of two metal ions these acyclic ligands form either two five-membered chelate rings (as in the case of complexes of H_2L1) or two six-membered chelate rings, and this affects the planarity of the ligand in the complex, the number and type of exogenous bridging groups bound to the copper atoms, and hence the magnetic properties of the complexes.

As expected, the bridging π-acceptor pyridazine moiety has been shown to be able to stabilise copper ions in the +1 oxidation state, with Cu^I/Cu^{II} couples commonly observed at positive potentials relative to SCE,[37,39,42,44–46,60–62,73] with very few exceptions.[41] Generally pyridazine- and phthalazine-bridged dicopper complexes undergo a single — albeit sometimes quite broad — two-electron process $Cu_2^{II} \rightleftarrows Cu_2^{I}$.[37,42,44,45,60–62,73] There are very few examples of two well-separated one-electron waves being observed,[39,46,81] which is in stark contrast to the dicopper(II) complexes of related phenolate ligands,

Table 1. Entries (given as Refcodes with the associated literature reference) from the Cambridge Crystallographic Database[78] (CSD version 5.22 October 2001) which contain pyridazine- or phthalazine-bridged copper ions; $x \geq 2$

Cu_x^{II}	Single pyridazine (or related) bridge (30 entries)	BEGNOQ;[122] BITQEA;[123] BITQIE;[123] BUKXIO;[124] CAPJUY;[125] CERCUX;[126] CICPIN;[127] COTCET;[128] DIMQIZ;[75] DOGLUG;[38] DOGMAN;[38] FAGXOA;[43] FEKZAW;[44] FEKZEA;[44] FODHOV;[45] GALBUQ;[47] HENTOJ;[129] NIHWUW;[72] NIHXAD;[72] NOWVAW;[80] NOWVEA;[80] PAHGUA;[58] PECJEM;[130] PECJOW;[130] TAZWUM;[73] VEHKAU;[131] YETZIG;[67] YETZOM;[67] YETZUS;[67] YUBKUB[68]
	Single phthalazine (or related) bridge (32 entries)	BAYZOQ;[132] BITQOK;[123] BUCJOY;[31] COLDOW;[34] COLDUC;[34] DEKWIZ;[37] DETCUA;[32] DURXET;[39] DUTCIE;[41] DUTCIE10;[52] FAGXEQ;[43] FEKZIE;[44] FURSAM;[50] HAHNEJ;[62] HAHNIN;[62] HAHNOT;[62] HODXED;[74] JODNIZ;[54] JODNIZ10;[58] LASZUA;[60] LASZUA10;[70] NIHWOQ;[72] YETZAY;[67] YETZEC;[67] YEVBAC;[67] YUBKAH;[68] YUBKEL;[68] YUBKIP;[68] YUBKOV;[68] ZIGQEL;[69] ZIMWOH;[70] ZOFVOF[61]
	Double pyridazine (or related) bridge (6 entries)	GAGMUW;[51] HENTUP;[79] HENTUP01;[114] RAPCAM;[3] [a] VIVHOX;[76] VIVHOZ[76]
	Double phthalazine (or related) bridge (1 entry)	PAGWOJ[57]
	Triple pyridazine or phthalazine (or related) bridge (0 entries)	No examples
Cu_x^{I}	Single pyridazine (or related) bridge (9 entries)	CAQXIB;[115] FEDBIZ;[119] JUGBES;[110] KIKBEL;[113] MEHJUE;[6] [a] RETPOV;[116] RIXHOV;[117] RIXHUB;[117] YOYFOH[118]
	Single phthalazine (or related) bridge (0 entries)	No examples
	Double pyridazine (or related) bridge (10 entries)	CAQXAT;[115] CAQXEX;[115] CAQXOH;[115] FUPREN;[133] GABYIR;[46] GONSAD;[134] [b] LIFKIU;[135] PILTOT;[136] PYAZCU10;[137] SOJGUT[81]
	Double phthalazine (or related) bridge (1 entry)	ZOFVUL[61]
	Triple pyridazine (or related) bridge (6 entries)	COCQEQ;[111] COCQIU;[111] COCQOA;[111] COCROB;[111] LIFKOA;[135] PILTIN[136]
	Triple phthalazine (or related) bridge (0 entries)	No examples
$Cu^{I}Cu^{II}$	Double pyridazine (or related) bridge (1 entry)	MEHJOY[6] [a][c]

[a] Macrocyclic-pyridazine bridging (our work). [b] Valence sum calculations indicate that the average oxidation state of copper is +1 in this mixed metal complex. [c] The only pyridazine- or phthalazine-bridged mixed-valent copper complex of any kind reported to date.

such as $L2^{2-}$ (Figure 2), in which this is commonly observed (albeit at negative potentials vs. SCE).[82] Consistent with these observations, there are some examples of di- and polycopper(I) complexes of bridging pyridazine and phthalazine acyclic ligands which have been isolated and fully characterised (including single crystal X-ray structure determination, Table 1), but, prior to our work, no example of a pyridazine- or phthalazine-bridged copper(I)/copper(II) mixed-valent complex.

2.1.2 Cobalt Complexes of Acyclic Pyridazine and Phthalazine Ligands

Whilst less common than copper pyridazine and phthalazine complexes, there are still numerous reports of cobalt complexes containing a Co−N(pyridazine moiety) bond (SciFinder Scholar[77] indicates that there are 192 such complexes, with a variety of oxidation states of cobalt, in 77 papers, as of 12.2.02). Of these, those concerned with cobalt(II) complexes are of some relevance to the studies described herein,[21,24,26,35,40,48,49,83−89] with those di- or polycobalt(II) complexes in which pyridazine[21,24,40,84,85] or phthalazine[21,24,26,35,49,89] bridging is observed being of most relevance. Focussing in on these pyridazine- or phthalazine-bridged cobalt(II) complexes: (a) for all cases in which magnetic data are reported the cobalt(II) ions are in the high-spin state and are only weakly antiferromagnetically coupled;[21,24,26,40,49,84] (b) only two of the complexes contain macrocyclic ligands and neither of these complexes are fully characterised;[88,89] (c) whilst aerobic oxidation leads to the production of dicobalt(III) complexes in some cases,[28] no electrochemical studies have been reported, other than a brief mention of the interesting fact that a macrocyclic dicobalt complex with double phthalazine bridges catalyses the four-electron reduction of O_2 in alkaline solutions when absorbed onto graphite.[89,90]

Very few such complexes have been structurally characterised, as a search of the Cambridge Crystallographic Database[78] (CSD version 5.22 October 2001) shows. There

are still — other than our own cobalt pyridazine complexes[4,5,8,9,11] — only four other crystallographically characterised cobalt complexes containing a Co−N(pyridazine moiety) bond.[49,83,91,92] The first structurally characterised example was a red-brown high-spin phthalazine-bridged dicobalt(II) complex $[Co_2^{II}\{1,4\text{-bis}[(6\text{-methylpyridine-2-carboxaldimino})\text{amino}]\text{phthalazine}\}Cl](H_2O)_4Cl_3$ [av. Co−N(phthalazine ligand) 2.151(5) Å].[49] Haupt and co-workers then reported two structurally characterised complexes, a dicobalt(I) complex $[Co_2^{I}\{\mu_2\text{-benzo}[c]\text{cinnoline-}N,N'\}\text{-bis}(\eta^5\text{-cyclopentadienyl})\text{trimethylphosphane}]$,[91] and a monocobalt(0) complex, $[Co^{0}\{\eta^2\text{-benzo}[c]\text{cinnoline-}N,N'\}\text{tris(trimethylphosphane)}]$.[92] Finally, an orange high-spin monocobalt(II) complex $[Co^{II}(\text{pyridazine})_4(NCS)_2]$ was reported in 1998 [Co−N(NCS) 2.057(2), av. Co−N(monodentate pyridazine) 2.204(2) Å].[83]

2.2 Macrocyclic Pyridazine and Phthalazine Ligands

Prior to our studies,[1−11] very little pyridazine- or phthalazine-based macrocyclic chemistry had been reported in the literature, despite an isolated but interesting example described early on by Rosen.[93] This 1971 publication described one of the earliest macrocycles to completely encircle *two* metal ions (following on from the independent breakthroughs in 1970 by Robson and co-workers[94] and by Busch and co-workers[95] in encircling two metal ions with a macrocycle), in this case two nickel(II) ions.[93] The macrocycle synthesis is reminiscent of the Curtis macrocycles,[96] being prepared from 1,4-dihydrazinophthalazine (expensive but commercially available as the dihydrochloride salt) and 2,2-dimethoxypropane in the presence of an acid and the metal salt. It was, quite reasonably, proposed that the phthalazine groups of L4 (Figure 3) bridge the nickel ions, but this was not confirmed by a single crystal X-ray structure determination.

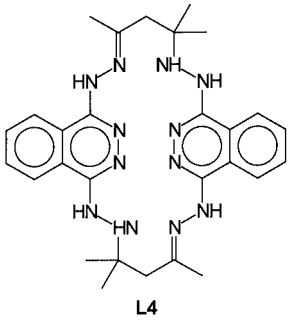

Figure 3. Phthalazine-containing macrocyclic ligand L4

A dicobalt complex of the Rosen phthalazine-containing macrocycle L4 is also mentioned in the literature, in the context that it catalyses the four-electron reduction of O_2 in alkaline solutions when absorbed onto graphite.[89][90] No synthetic detail or further characterisation information was provided for this complex.

There is one further isolated case of a phthalazine-containing macrocycle, H_2L5 (Figure 4), being prepared. In this case it is proposed by Okur that the macrocyclic cavity only incorporates a single metal ion (paramagnetic Co^{II} or diamagnetic Ni^{II}); again no structural information is available for either of these complexes.[88]

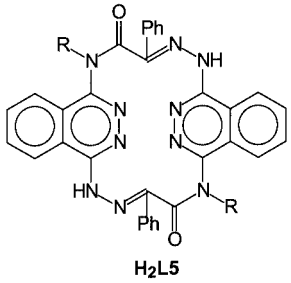

Figure 4. Phthalazine-containing macrocyclic ligand H_2L5

In addition to their extensive studies of complexes of acyclic pyridazine- and phthalazine- containing ligands (Section 2.1), Thompson and co-workers have also prepared a range of pyridazine- and phthalazine-containing macrocyclic thioether ligands, by reacting commercially available 3,6-dichloropyridazine (affordable) and 1,4-dichlorophthalazine (relatively expensive) with appropriate dithiolate reagents (e.g. L6 to H_2L12, Figure 5).[55,56,59,64−66]

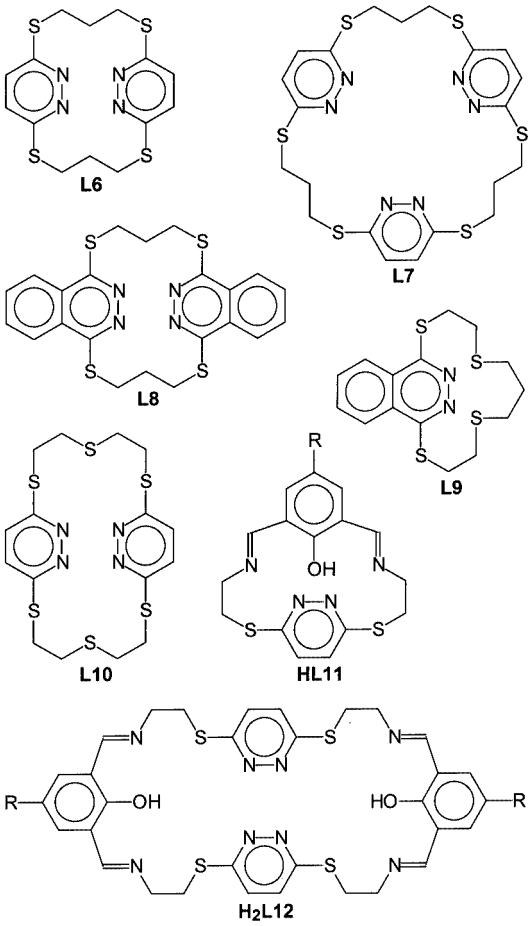

Figure 5. A selection of thioether pyridazine- and phthalazine-containing macrocycles

Initially both [2+2] and [3+3] thioether macrocycles were obtained from the reaction of 3,6-dichloropyridazine and 1,3-propanedithiol (L6 and L7, Figure 5): these macrocycles were separated from one another readily on the basis of solubility.[56] Other dithiols employed in the cyclisation with 3,6-dichloropyridazine included 3,7-dithianonane-1,9-dithiol,[55] 2,2′-thiodiethanethiol (L10, Figure 5),[64,65] and 1,4,7,10-tetrathiadecane.[65] Some [2+2] phthalazine analogues were prepared by reaction of 1,4-dichlorophthalazine with 1,3-propanedithiol (L8, Figure 5), 3,7-dithianonane-1,9-dithiol (L9, Figure 5) or 2,2′-thiodiethanethiol.[65] A series of copper(II), copper(I) and silver(I) complexes were characterised,[55,56,64,65] including an example of a mixed-valent copper(I)/copper(II) complex [Cu_2(L10)Br_3], which was not structurally characterised, but which was proposed to have a polymeric structure with the copper(II) ion bound within the macrocycle and the copper(I) ion, involved in bridging the macrocyclic rings, bound in an exocyclic manner.[64] In none of these complexes did the pyridazine rings bridge the metal ions.

The next development was the preparation of a "two armed pyridazine diamine", 3,6-bis[(2-aminoethyl)thio]pyridazine, from 3,6-dichloropyridazine, in 87% yield, which opened up the possibility of using metal ions to template the formation of Schiff base macrocycles.[66] Copper(II) template ions were employed in the reactions of this diamine with 2,6-diformyl-4-methylphenol or with 2,6-diformyl-4-*tert*-butylphenol (e.g. HL11 and H_2L12, Figure 5) and this resulted in a range of mono-, di- and tetranuclear copper complexes,[59,66] including examples of mixed valent copper(II)/copper(I) complexes.[66] However, once again, pyridazine bridging is not a feature of these complexes.[59,66] Rather, they contain phenolate bridge(s) so they are actually more closely related to the dicopper complexes of phenolate-containing macrocycles such as $L2^{2-}$ (Figure 2).[82]

More recently, Lehn and co-workers have reported a pyridazine-containing cryptand ligand, L13 (Figure 6), that can accommodate two sodium ions which are believed to be triply bridged by the pyridazine moieties, although no details are provided.[97]

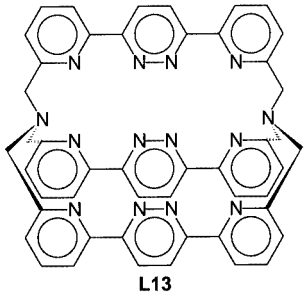

Figure 6. Pyridazine-containing cryptand ligand L13

To summarise, despite the construction of some pyridazine- and phthalazine-containing macrocycles,[55,56,59,64−66,88−90,93,97] in only three isolated cases was bridging of the incorporated metal ions by these moieties proposed (for L4 and L13, Figure 3 and 6 respectively).[89,90,93,97] Therefore we set out to carefully design and construct pyridazine-containing macrocycles in which bridging by this 1,2-diazine moiety was facilitated, and to subsequently thoroughly examine the resulting families of complexes to determine whether or not special features had resulted from incorporating this interesting diazine bridging unit into a macrocyclic framework.

3. Macrocycles Built from 3,6-Diformylpyridazine

3,6-Diformylpyridazine was targeted (Section 2.1, Figure 1) as a suitable macrocycle precursor to achieve the initial aim of producing a family of macrocycles capable of binding two metal ions and providing two pyridazine bridges. Initially this dialdehyde was prepared from 3,6-bis(hydroxymethyl)furan by the four-step method reported by Bremard and co-workers [Figure 7, steps (i)−(iv)],[76] modifying the final step from the reported Swern oxidation to an MnO_2 oxidation[98] in order to readily isolate the dialdehyde.[2] However this route[99,100] was less than satisfactory because: (a) the starting material, whilst not particularly expensive, was not cheap, (b) step (ii) was found to be unreliable, and (c) it was found that an extra step was necessary [step (iii) was replaced with steps (v) and (vi)] making it a five-step synthesis.[2] Hence a more convenient synthesis was sought. Wiley[101] has described a three step synthesis [Figure 7, steps (1)−(3)], starting from cheap starting materials, and this was found to be a good alternative route to 3,6-diformylpyridazine. The first two steps are reported as moderately large scale reactions which is advantageous, whilst the third and final step, being an ozonolysis reaction, must be done on a small scale for safety reasons.[2,101]

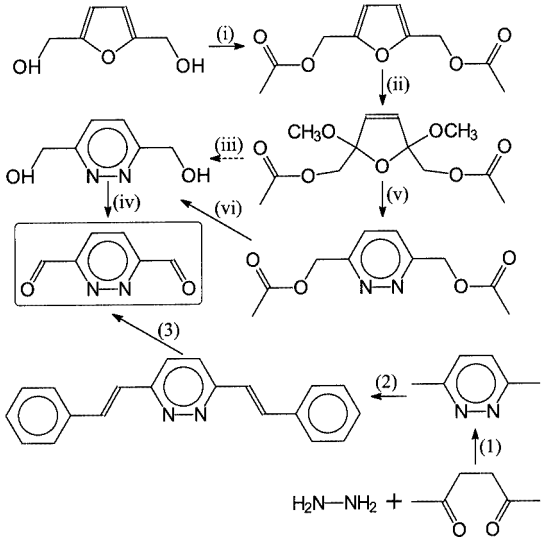

Figure 7. Syntheses of 3,6-diformylpyridazine from 2,5-bis(hydroxymethyl)furan [steps (i)−(v)] or from acetonylacetone and hydrazine hydrate [steps (1)−(3)]; reagents and conditions: (i) acetic anhydride/pyridine; (ii) Br_2/CH_3OH; (iii) 1% acetic acid/CH_3OH/$H_2NNH_2{\cdot}H_2O$; (iv) activated Amberlite IRA400 resin/CH_3OH; (v) oxalyl chloride/dmso or MnO_2/dioxane; (1) Pd/C-benzene; (2) $ZnCl_2$; (3) O_3/MeOH

With a good synthesis of 3,6-diformylpyridazine in hand, attention turned to preparing Schiff-base macrocyclic, and related acyclic, ligands and complexes from them. Whilst the condensation of this dialdehyde head unit is being explored with a wide range of amines,[11] this microreview will focus entirely on the results obtained using 1,3-diaminopropane.

3.1. Macrocycles L14 and L14′ from 3,6-Diformylpyridazine and 1,3-Diaminopropane

Models indicated that a [2+2] condensation of 1,3-diaminopropane with 3,6-diformylpyridazine would produce a macrocycle which would bind two first row transition metal ions well. Hence this was the diamine used initially, and the resulting [2+2] and [4+4] macrocycles, L14 and L14′ (Figure 8), are the focus of this section.

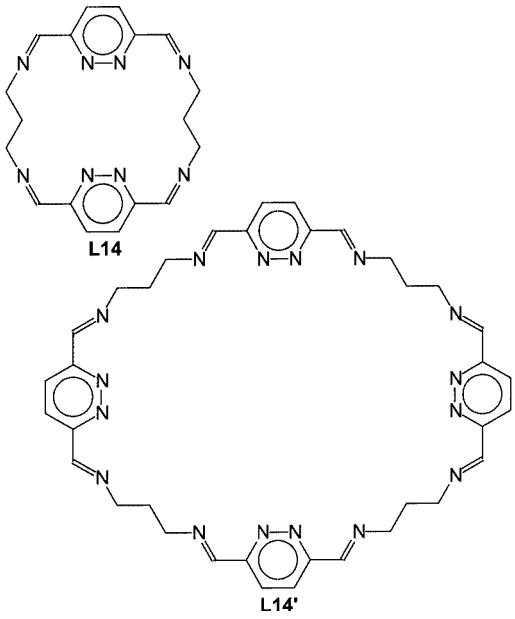

Figure 8. Pyridazine-containing [2+2] and [4+4] Schiff-base macrocycles L14 and L14′

It is relevant to note that many interesting complexes have been prepared from the [2+2] macrocycles formed by condensing 1,3-diaminopropane with either 2,6-diformylphenols[82,102] or 2,6-diformylthiophenols[18] (the $L2^{2-}$ and $L3^{2-}$ families of macrocycles, Figure 2). There are clearly both similarities and differences between phenolate and pyridazine moieties. Features they share include the well-established ability to bridge metal ions and to mediate magnetic exchange. However, they are also very different in that phenolate has a negative charge whilst pyridazine is neutral and is a π-acceptor ligand. Another key difference is that phenolate provides a one-atom bridge whereas pyridazine provides a two-atom bridge. These differences are significant and should impact on the properties of the complexes, in particular on the magnetic and redox chemistry, hence the interest in incorporating bridging pyridazines into Schiff base macrocycles for the first time.

Success came with a lead(II) templated cyclisation reaction of 3,6-diformylpyridazine and 1,3-diaminopropane, the results of which were published as a communication in 1994.[1] An unexpected [4+4] cyclisation occurred (confirmed by single crystal X-ray structural analysis, Figure 9) producing what was at the time only the second example of a [4+4] Schiff-base macrocycle.[103,104] Subsequently it was found that, depending on the reaction stoichiometry, one could produce either the [4+4] or the [2+2] macrocycle, as $[Pb_2L14'](ClO_4)_4$ or $[Pb_2L14](ClO_4)_4$ respectively, in good yields (Figure 8).[2] This ability to control the ring size of the product macrocycle by stoichiometry alone is unique to the best of our knowledge.

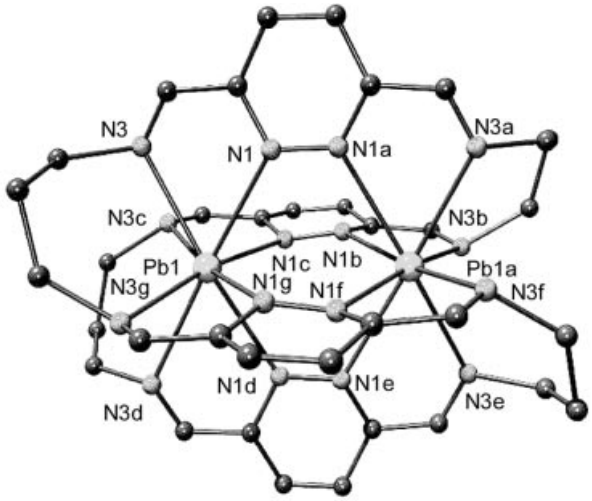

Figure 9. Perspective view of the cation of $[Pb_2L14']^{4+}$

Transmetallation reactions, starting from either $[Pb_2L14'](ClO_4)_4$ or $[Pb_2L14](ClO_4)_4$, allowed the preparation of the first row transition metal complexes of interest. Alternatively, these complexes could, in principle, have been prepared by using the transition metal ions as template ions, but in practice this was unsuccessful for most of the metal ions studied, including copper(II) and cobalt(II) ions. One of the key exceptions to this generalisation is that copper(I) ions could be used as template ions for the formation of L14 (see below).

Usually, for reasons of ease of synthesis of clean samples, $[Pb_2L14'](ClO_4)_4$ was the preferred precursor complex for the transmetallation reactions. The use of this precursor complex immediately raised the question as to whether the transition metal complexes would be of the [4+4] macrocycle L14′ or of the [2+2] macrocycle L14. The answer to this question is that, to date, all of the products obtained have been of the [2+2] macrocycle L14.[11] Hence the [4+4] Schiff-base macrocycle L14′ rearranges during the transmetallation reaction to form the [2+2] macrocycles L14, in contrast to the first known example of a [4+4] Schiff-base macrocycle in which the reverse was believed to be occurring (the [4+4] macrocycle was proposed to form from two [2+2] macrocycles coming together).[104] Interestingly, this substantial ring-size change from L14′ to L14 occurs suc-

cessfully even when inserting transition metal ions which cannot be used to template the macrocycle formation from 3,6-diformylpyridazine and 1,3-diaminopropane. Relatively minor changes to the size of Schiff-base macrocycles can occur during transmetallation reactions by the nucleophilic addition of solvent alcohol[105] to the imine bond(s) or by intramolecular attack of an alcohol[106] or amine[107] moiety on the imine bond(s), but a change in the actual number of head and lateral units making up the macrocyclic framework, such as is occurring here, is very uncommon.[104][108]

The metal ions incorporated into L14 to date include manganese, iron, cobalt, nickel, copper and zinc: here we will focus on the results obtained with copper and cobalt.

3.1.1 Copper Complexes of the L14 Schiff-Base Macrocycle

Direct reactions, employing copper(II) as a template ion for the cyclisation, were unsuccessful, presumably due to the tendency of the copper(II) ions to participate to some extent in redox chemistry in the presence of the ligand components.[3,7] Rather, the transmetallation route from $[Pb_2L14'](ClO_4)_4$ was followed and this yielded single crystals of an emerald green complex, $[Cu^{II}_2L14(CH_3CN)_4](ClO_4)_4$, in good yield.[3,7] The single crystal structure determination (Figure 10) shows that the macrocycle conformation is somewhat bent, with an angle of 29.67(7) ° between the planes of the two pyridazine rings. The copper(II) ions are square pyramidal with a weak interaction to a perchlorate ion in the otherwise vacant sixth site of the distorted octahedron. As expected (Section 2.1.1), strong antiferromagnetic coupling was observed between the doubly pyridazine-bridged copper(II) ions, with $-2J = 482\ cm^{-1}$. This value is similar to the $-2J$ values of 536 cm^{-1} and 489 cm^{-1} obtained for the only two closely related acyclic complexes known: orange-red $[Cu^{II}_2(HL1)_2(H_2O)_2(ClO_4)_2]$ and olive-green $[Cu^{II}(DHPH)_2(H_2O)_2](ClO_4)_2$ (where DHPH = 1,4-dihydrazinophthalazine), in which the copper(II) ions are doubly bridged by pyridazine[76] and phthalazine[57] moieties, respectively, and there are no other bridging moieties present.

Electrochemical experiments revealed the presence of two well-separated reversible one electron processes at positive potentials vs. SCE, which correspond to $Cu^{II}_2 \rightleftarrows Cu^{II}Cu^{I} \rightleftarrows Cu^{I}_2$. This result contrasts with the previous studies on acyclic pyridazine complexes in which the norm was the observation of a single two-electron process of varying reversibility (Section 2.1.1). The observation of two well-separated reversible processes is more reminiscent of the analogous doubly phenolate-bridged dicopper(II) macrocyclic complexes (e.g. $L2^{2-}$, Figure 2), however, in that case, the processes occur at negative potentials (Section 2.1.1), in contrast to the positive potentials observed in the case of dicopper(II) complexes of the pyridazine macrocycle L14. These redox properties opened up a unique opportunity to access not only the mixed valent copper(I)/copper(II) complex but also the dicopper(I) complex.

As a first attempt to prepare the dicopper(I) complex a transmetallation reaction was carried out with

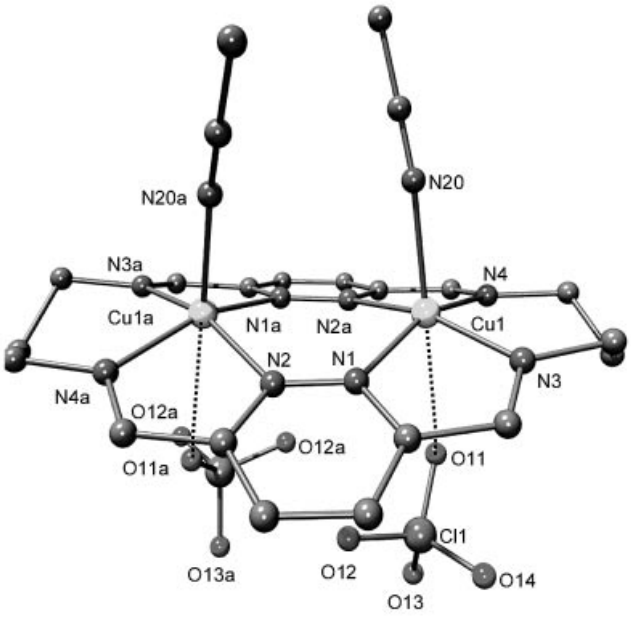

Figure 10. Perspective view of the cation of $[Cu^{II}_2L14(CH_3CN)_2(ClO_4)_2]^{2+}$

$[Cu^{I}(CH_3CN)_4](PF_6)$ in acetonitrile under argon. For ease of workup, vapour diffusion of diethyl ether into the resulting red-brown solution was carried out in air. This resulted in the isolation of red-brown single crystals of the mixed valent complex, $[Cu^{I}Cu^{II}L14(CH_3CN)_2](ClO_4)_2(PF_6)$, in 41% yield, due to the in situ air oxidation of the dicopper(I) complex, which was presumably the initial product of the transmetallation reaction.[6] A structure determination carried out on one of these crystals at low temperature clearly showed that this is a valence-localised compound: longer bond lengths are observed to the copper(I) atom and it is further out of the N_4 plane (Figure 11; Cu1 0.72 Å out-of-plane, Cu2 0.26 Å out-of-plane). The observation of a four-line EPR spectrum is consistent with this

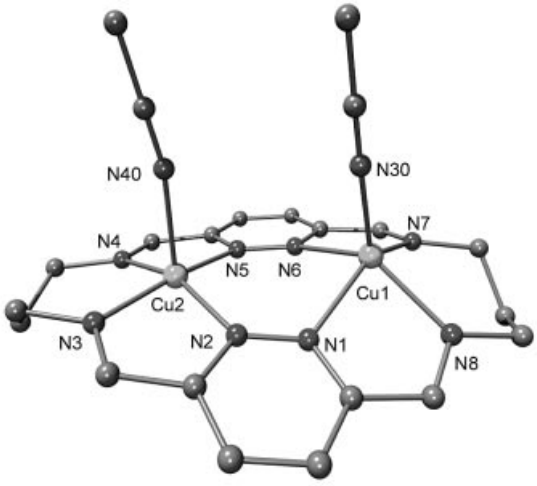

Figure 11. Perspective view of the cation of $[Cu^{I}Cu^{II}L14(CH_3CN)_2]^{3+}$

assignment.[7] It is also interesting to note that this is a relatively rare example of five coordinate copper(I).[109]

The use of copper(I) ions as template ions seemed an improbable route to clean L14 macrocycle formation given the preference of copper(I) for a tetrahedral (not square-based) geometry and the demands of L14 macrocycle formation. However, this experiment was attempted because related acyclic ligands have, in this laboratory[11] and elsewhere,[110] given grid complexes with tetrahedral copper(I) ions. Therefore an interesting and unusual result was possible, providing the propylene lateral units were capable of linking up the pyridazine head units which would be expected to be held perpendicular to one another by the copper(I) template ions. Fortunately this was the case, and brown single crystals of $[Cu^{I}_{4}(L14)_2](PF_6)_4$ were formed, in 61% yield, on diffusing diethyl ether vapour into the acetonitrile reaction solution, in air. The complex does have a grid structure, where each of the two parallel strands are linked together in a single macrocycle, and the two macrocycles approach each other at right angles to give rise to the perpendicular strands of the grid structure (Figure 12).[6] Thus the copper(I) atoms have distorted tetrahedral geometries, with each macrocycle providing a bidentate donor set at right angles to that supplied by the other macrocycle.

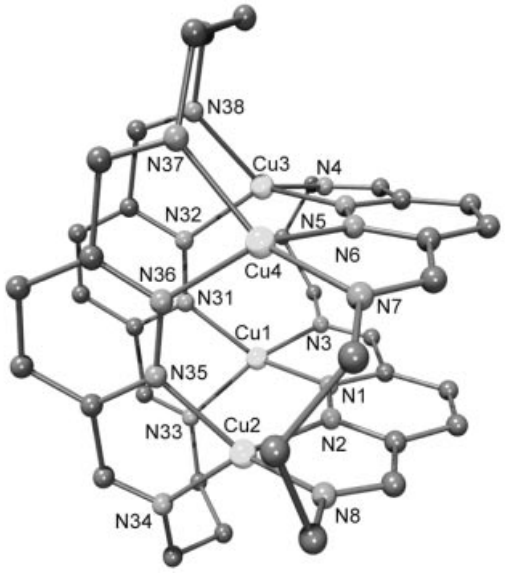

Figure 12. Perspective view of the cation of $[Cu^{I}_{4}(L14)_2]^{4+}$

In noncoordinating solvents, for example nitromethane and acetone, this tetracopper complex is stable in air. However, there is evidence, from both NMR spectroscopy and cyclic voltammetry, that when this complex is dissolved in coordinating solvents, such as acetonitrile, that it is then in equilibrium with an open form that looks like the dicopper(II) and mixed valent forms (Figure 10, 11 and 13).[7] In this "open" form (Figure 13) it is expected to be air sensitive, as it has already been observed that the transmetallation of the lead complex with copper(I), on air workup, yielded the mixed valent complex $[Cu^{I}Cu^{II}L14(CH_3CN)_2](ClO_4)_2(PF_6)$. Therefore, in order to improve the 61% yield one should presumably carry out the template synthesis completely under argon or in a noncoordinating solvent (but not acetone,[96] or nitromethane which makes explosive mixtures with amines). More importantly though, the presence of this equilibrium mixture in acetonitrile solution provides an easy route to cleanly isolate the dicopper(I) complex.

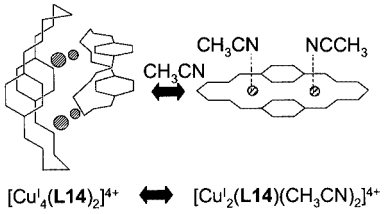

Figure 13. Proposed equilibrium formed between $[Cu^{I}_{4}(L14)_2]^{4+}$ and $[Cu^{I}_{2}L14(CH_3CN)_2]^{2+}$ in acetonitrile solution; reprinted from *Coord. Chem. Rev.* **2001**, *216–217*, 3–30, S. Brooker *et al.*, Doubly pyridazine-bridged macrocyclic complexes of copper in +1, +2 and mixed valent oxidation states, with permission from Elsevier Science

The reaction of $[Cu^{I}_{4}(L14)_2](PF_6)_4$ in acetonitrile with two equivalents of PPh_3 yields brown single crystals of $[Cu^{I}_{2}L14(PPh_3)_2](PF_6)_2$ in 51% yield.[7] PPh_3 was used in order to provide a donor that was better able to stabilise copper(I) than acetonitrile.[111–113] As expected, the steric bulk of the triphenylphosphane groups leads to the observation of a trans arrangement of the two PPh_3 groups relative to the macrocycle plane (Figure 14).[7] The five-coordinate copper(I) atoms are even further displaced from the N_4 plane [0.822(1) Å] than in the previous complexes. Despite the unusual five coordination of the copper(I) atoms the Cu–PPh_3 bond length [2.2239(8) Å] is at the lower end of

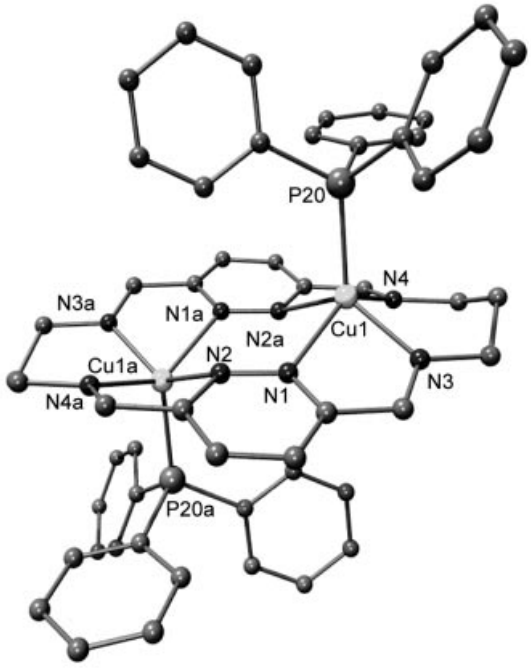

Figure 14. Perspective view of the cation of $[Cu^{I}_{2}L14(PPh_3)_2]^{2+}$

the range observed for the four copper(I) pyridazine phosphane complexes which have been structurally characterised to date, all of which contain copper(I) atoms in a distorted tetrahedral geometry [two monocopper(I) complexes $Cu^{I}-PPh_3$ 2.244−2.293 Å;[111,112] one singly pyridazine-bridged dicopper(I) complex with double bis(diphenylphosphanyl)methane bridging $Cu^{I}-P$ 2.23−2.29 Å;[113] one triply-pyridazine-bridged dicopper(I) complex $Cu^{I}-PPh_3$ 2.217 and 2.208 Å;[111]].

An expected difference between these doubly pyridazine-bridged macrocyclic complexes and those of the doubly phenolate-bridged macrocyclic complexes of $L2^{2-}$ was the metal ion separation (Section 3.1, Figure 2). The Cu···Cu separation in the dicopper(II) complexes of $L2^{2-}$ is typically 3.06−3.22 Å[82] whereas in the dicopper(II) complexes of L14 it is 3.805(3) Å in $[Cu_2^{II}L14(CH_3CN)_4](ClO_4)_4$ [3] and 3.888(3) Å in $[Cu_2^{II}L14(H_2O)_2](ClO_4)_4$.[7] The impact of the two-atom pyridazine bridge, as opposed to the one-atom phenolate bridge, is therefore clear. These Cu···Cu separations can also be usefully compared with the six acyclic structurally characterised doubly pyridazine- or phthalazine-bridged copper(II) complexes (Table 1). In three out of the six entries only double pyridazine/phthalazine bridging is present and the Cu···Cu separations are somewhat shorter than those observed in the macrocyclic complexes, at 3.760 Å (VIVHOX)[76] and 3.729 Å (PAGWOJ);[57] no detailed information is available for VIVHOZ.[76] In the other three entries an additional one-atom exogenous bridge is present (chloride or nitrate) and this results in a significant shortening of the Cu···Cu separation, to 3.269−3.406 Å.[51,79,114]

In the mixed-valent complexes the $Cu^{I}\cdots Cu^{II}$ separations are 3.8986(9) Å in $[Cu^{I}Cu^{II}L14(NCS)_4Cu^{I}]$[7] and 3.9599(4) Å in $[Cu^{I}Cu^{II}L14(CH_3CN)_2](ClO_4)_2(PF_6)$.[6] The Cu···Cu separation is a large 4.4316(12) Å for the dicopper(I) triphenylphosphane complex $[Cu_2^{I}L14(PPh_3)_2](PF_6)_2$, due primarily to the fact that the copper ions are displaced from the macrocyclic plane in opposite directions.[7] Double pyridazine or phthalazine bridging of copper(I) ions (Table 1) by acyclic ligands usually results in Cu···Cu separations in the range 2.970−3.679 Å, with a mean value of 3.261 Å which is significantly lower than the 4.4316(12) Å observed here.

Interestingly the shortest Cu···Cu separations observed in this series of macrocyclic pyridazine-bridged copper complexes are found in the tetracopper(I) complex $[Cu_4^{I}(L14)_2](PF_6)_4$, in which only one pyridazine bridge, not two, is observed between neighbouring copper atoms. In this case the nearest copper(I) atoms are separated by just 3.711(3)−3.738(3) Å.[6] The other eight entries of singly pyridazine- or phthalazine-bridged copper(I) complexes (Table 1) have shorter Cu···Cu separations, in the range 3.438−3.688 Å,[110,113,115−118] with the exception of FEDBIZ in which the separation is even shorter (2.788 Å).[119] The structure of the $[Cu_4^{I}(dppn)_4]^{4+}$ complex [dppn = 3,6-bis(2′-pyridyl)pyridazine], described by Youinou and co-workers,[110] is particularly closely related to that of $[Cu_4^{I}(L14)_2](PF_6)_4$ so the difference in Cu···Cu separations [3.566(1) and 3.582(1) Å vs. 3.711(3)−3.738(3) Å] is presumably due to the restrictions imposed by the macrocyclic nature of the two coordinated L14 ligands as opposed to the relative freedom of the four coordinated acyclic ligands in that study.

3.1.2 Cobalt Complexes of the L14 Schiff-Base Macrocycle

Direct reactions, employing cobalt(II) as a template ion for the cyclisation, were unsuccessful.[9] Instead, the transmetallation route was followed and this gave single crystals of a deep red complex, $[Co_2^{II}L14(CH_3CN)_4](ClO_4)_4$, in good yield.[4] This dicobalt(II) complex was prepared in air so clearly it does not react spontaneously with oxygen, unlike the cobalt complexes of the large unsymmetrical phenolate macrocycles described by Okawa and co-workers which must be prepared carefully under an inert atmosphere.[120] In this sense, $[Co_2^{II}L14(CH_3CN)_4](ClO_4)_4$ is more similar to the dicobalt(II) complexes of the phenolate macrocycle $L2^{2-}$, $[Co_2^{II}L2X_2]\cdot yCH_3OH$ (where X = Cl^- and y = 2; or X = Br^- and y = 1), which are air stable even in solution.[121]

The deep red colour indicates that $[Co_2^{II}L14(CH_3CN)_4](ClO_4)_4$ is a low-spin cobalt(II) complex and a careful analysis of the parameters obtained from the low temperature single crystal structure analysis (Figure 15)[4] was consistent with this prediction. For example, the average Co−N(macrocycle) bond length is 1.983(4) Å, which strongly indicates that the cobalt(II) ion is low spin as the bond lengths are typically ca. 0.15 Å shorter for low-spin complexes than they are for high-spin complexes (Section 2.1.2).[9,120] The cobalt ions are in distorted octahedral environments and the macrocycle adopts a remarkably flat conformation. Detailed magnetic studies have subsequently confirmed the low-spin state of this complex at the temperature of the X-ray data collection.[9]

This complex, $[Co_2^{II}L14(CH_3CN)_4](ClO_4)_4$, was the first pyridazine-bridged cobalt complex[21,24,40,84] established to

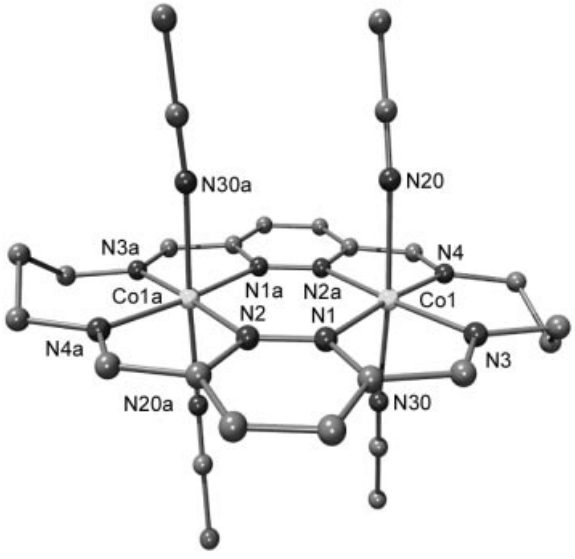

Figure 15. Perspective view of the cation of $[Co_2^{II}L14(CH_3CN)_4]^{4+}$

be low spin (Section 2.1.2). This implies that building the pyridazine moiety into a macrocyclic ligand has resulted in a unique and rather special environment for the encircled cobalt ions. Four reversible one-electron processes are a feature of the electrochemistry of this complex,[4] however, the magnetic properties have been the focus of attention to date. Given that the macrocycle encircles the two cobalt ions, providing each with a planar N_4 donor set, this leaves two axial sites on each cobalt ion available to be occupied by exogenous ligands. In the $[Co_2^{II}L14(CH_3CN)_4](ClO_4)_4$ complex the axial sites are occupied by solvent acetonitrile molecules. The next question was therefore: can the spin state be tuned by altering the group occupying the axial sites?

The first clue to the answer of this question was provided by the observation that on adding water to the deep red residues left on the glassware used to make $[Co_2^{II}L14(CH_3CN)_4](ClO_4)_4$ (i.e. washing up), an orange solution, indicative of high spin cobalt(II), was obtained. When this was repeated and optimised in a scientific manner it was found that the recrystallisation of $[Co_2^{II}L14(CH_3CN)_4](ClO_4)_4$ from 9% water (by volume) in acetonitrile by vapour diffusion of diethyl ether, yielded orange single crystals of the tetra-aquo adduct $[Co_2^{II}L14(H_2O)_4](ClO_4)_4$.[9] The low temperature crystal structure determination reveals a very similar overall structure (Figure 16) to that of the tetra-acetonitrile adduct, however the bond lengths are, as expected for this high-spin complex, significantly longer [av. $Co-N_{macro}$ 2.104(4) Å] than those in the low-spin tetra-acetonitrile adduct [av. $Co-N_{macro}$ 1.992(4) Å] and the bond angles are somewhat more distorted from those expected for an octahedron [tetra-aquo adduct 76.6−110.6°; vs. tetra-acetonitrile adduct 80.8−103.7°].[9]

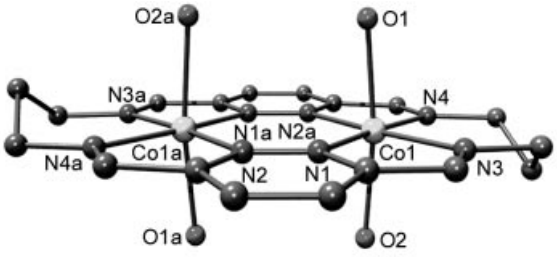

Figure 16. Perspective view of the cation of $[Co_2^{II}L14(H_2O)_4]^{4+}$

Sodium thiocyanate is often found to be useful when exogenous ligands are required in macrocyclic chemistry so this was the next reagent used in attempts to vary the nature of the axial ligands. In this case dark red-black single crystals of $[Co_2^{II}L14(NCS)_2(SCN)_2]$ formed when acetonitrile solutions of $[Co_2^{II}L14(CH_3CN)_4](ClO_4)_4$ and NaSCN were slowly diffused together. The colour indicated that the complex was low spin.[5] The low temperature single crystal structure determination revealed the same very flat macrocycle conformation seen in the previous two structures, and once again the presence of octahedral cobalt ions (Figure 17). Of note in this structure is that each cobalt ion has one N-bound and one S-bound thiocyanate ion, the latter being a first for cobalt(II). The bond lengths are consistent with the low spin configuration [av. $Co-N_{macro}$ 1.951(3) Å], and the angles at cobalt approach 90° more closely [86.8−92.8°] than they do in the high-spin complexes. The magnetic behaviour of this complex is even more interesting than the previous two complexes as it turns out that it is

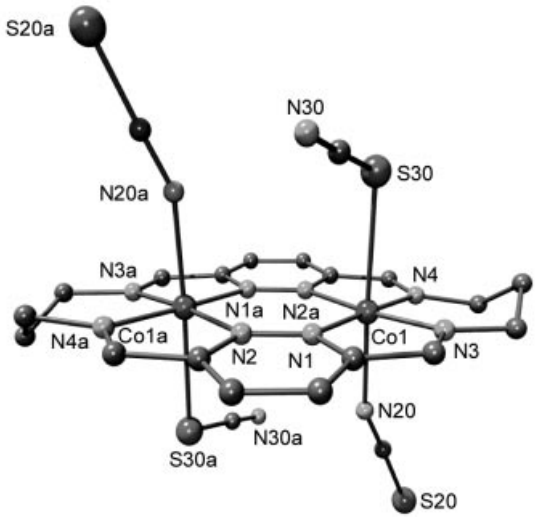

Figure 17. Perspective view of $[Co_2^{II}L14(NCS)_2(SCN)_2]$

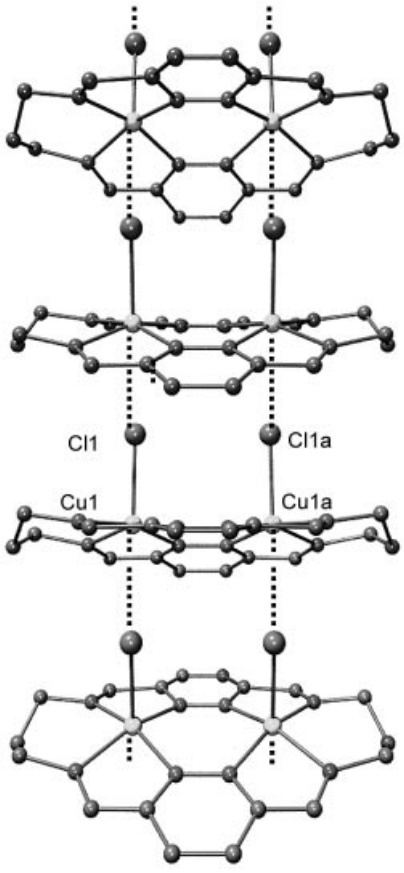

Figure 18. Perspective view of the cation of $[Cu_2^{II}L14(Cl)_2]^{2+}$

the first cobalt complex to exhibit both exchange coupling and spin-crossover effects.

Further variations have been made to the groups occupying the axial sites.[9] Attempts, unsuccessful to date, have also been made to insert bridging ligands in these sites in order to stack these complexes,[9] as has been seen before in the case of the "ladder" complex observed for copper(II), $[Cu_2^{II}L14Cl_2]_\infty^{2+}$ (Figure 18).[7]

4. Conclusions and Outlook

The incorporation of 3,6-diformylpyridazine into Schiff-base macrocycles has resulted in a novel coordination chemistry and a rich structural diversity. The first examples of complexes in which Schiff-base macrocyclic pyridazine bridging of encapsulated metal ions is observed have been isolated and fully characterised. A rare example of a [4+4] macrocycle, L14′, has been prepared and structurally characterised as a dilead(II) complex: in all cases transmetallation of this complex with first row transition metal ions has resulted in ring-size alteration to form complexes of the [2+2] macrocycle L14. Both $[M_2\{2+2\}]^{x+}$ and $[M_4\{2+2\}_2]^{y+}$ complexes have been formed and both flat and folded macrocycle conformations have been observed. Coordination numbers for metal ions encapsulated in either the [2+2] or [4+4] macrocycle range from 4−8 (examples of seven coordination are not discussed here[2]).

A rich and reversible electrochemistry is a feature of these complexes of L14. The macrocyclic framework has led to increased stability of the redox products over that generally observed for related acyclic complexes. This also led to the isolation of the first mixed-valent pyridazine-bridged complex (of copper), due to significant stabilisation of the mixed-valent oxidation state, in marked contrast to the acyclic analogues.

Exciting magnetochemistry is a feature of the cobalt(II) complexes. Incorporation of the bridging pyridazine moiety into this macrocyclic framework has resulted in the first examples of low-spin and spin-crossover cobalt(II) for pyridazine-bridged complexes of any type.

Many new and interesting avenues remain to be explored. These include the condensation of 3,6-diformylpyridazine with other mono-, di- and triamines.[11] For example, the reaction of this head unit with tris(2-aminoethyl)amine (tren) has provided ready access to a new cryptand and the coordination chemistry of this cryptand, and the amine analogue, is well underway.[8,10,11] The incorporation of related heterocycles into macrocyclic frameworks,[11] and the design and synthesis of polydentate acyclic ligands for use in extending and developing the grid-like behaviour observed in some of the macrocyclic complexes described above (e.g. Figure 12)[6,7] are other areas of considerable and ongoing interest to us.[11]

Acknowledgments

I am extremely grateful to the following research students and assistants, postdoctoral and research fellows, and collaborators who have "made things happen": Dr. Robert J. Kelly (research assistant and PhD student), Dr. Paul G. Plieger (PhD student), Janna D. Ewing [BSc(Hons) student], Dr. Duncan J. de Geest, Dr. Dietmar K. Kennepohl, Dr. David S. Larsen (organic synthesis advice), Dr. Eckhard Bill (EPR, MPI für Strahlenchemie), Dr. Eberhard Bothe (electrochemistry, MPI für Strahlenchemie), Dr. Boujemaa Moubaraki (magnetism, Monash University), Professor Keith S. Murray (magnetism, Monash University) and Professor Jane Nelson (pyridazine cryptates, Queens University of Belfast). This research program gained momentum thanks in large part to a small grant from the Public Good Science Fund (Foundation for Research, Science and Technology, NZ) in 1993 which meant I could employ RJK (research assistant) full time for seven months. Support from a variety of grants from the University of Otago has been vital throughout, and we are very fortunate that we currently have a three year grant from the Marsden Fund (Royal Society of New Zealand).

[1] S. Brooker, R. J. Kelly, G. M. Sheldrick, *J. Chem. Soc., Chem. Commun.* **1994**, 487.
[2] S. Brooker, R. J. Kelly, *J. Chem. Soc., Dalton Trans.* **1996**, 2117.
[3] S. Brooker, R. J. Kelly, B. Moubaraki, K. S. Murray, *Chem. Commun.* **1996**, 2579.
[4] S. Brooker, R. J. Kelly, P. G. Plieger, *Chem. Commun.* **1998**, 1079.
[5] S. Brooker, P. G. Plieger, B. Moubaraki, K. S. Murray, *Angew. Chem. Int. Ed.* **1999**, *38*, 408.
[6] S. Brooker, S. J. Hay, P. G. Plieger, *Angew. Chem. Int. Ed.* **2000**, *39*, 1968.
[7] S. Brooker, T. C. Davidson, S. J. Hay, R. J. Kelly, D. K. Kennepohl, P. G. Plieger, B. Moubaraki, K. S. Murray, E. Bill, E. Bothe, *Coord. Chem. Rev.* **2001**, *216−217*, 3.
[8] S. Brooker, J. D. Ewing, J. Nelson, *Inorg. Chim. Acta* **2001**, *317*, 53.
[9] S. Brooker, D. J. de Geest, R. J. Kelly, P. G. Plieger, B. Moubaraki, K. S. Murray, G. B. Jameson, *J. Chem. Soc., Dalton Trans.* **2002**, 2080.
[10] S. Brooker, J. D. Ewing, J. Nelson, J. C. Jeffery, *Inorg. Chim. Acta* **2002**, *337*, in press.
[11] S. Brooker and co-workers, unpublished results.
[12] S. M. Nelson, *Pure & Appl. Chem.* **1980**, *52*, 2461.
[13] D. E. Fenton, *Pure & Appl. Chem.* **1986**, *58*, 1437.
[14] L. F. Lindoy, *The Chemistry of Macrocyclic Ligand Complexes*, Cambridge University Press, Cambridge 1990.
[15] V. Alexander, *Chem. Rev.* **1995**, *95*, 273.
[16] S. R. Collinson, D. E. Fenton, *Coord. Chem. Rev.* **1996**, *148*, 19.
[17] N. V. Gerbeleu, V. B. Arion, J. Burgess, *Template Synthesis of Macrocyclic Compounds*, Wiley-VCH, Weinheim 1999.
[18] S. Brooker, *Coord. Chem. Rev.* **2001**, *222*, 33.
[19] J. Nelson, V. McKee, G. Morgan, *Prog. Inorg. Chem.* **1998**, *47*, 167.
[20] P. J. Steel, *Coord. Chem. Rev.* **1990**, *106*, 227.
[21] J. E. Andrew, P. W. Ball, A. B. Blake, *J. Chem. Soc., Chem. Commun.* **1969**, 143.
[22] J. E. Andrew, A. B. Blake, *J. Chem. Soc. (A)* **1969**, 1408.
[23] P. W. Ball, A. B. Blake, *J. Chem. Soc. (A)* **1969**, 1415.
[24] P. W. Ball, A. B. Blake, *J. Chem. Soc., Dalton Trans.* **1974**, 852.
[25] L. K. Thompson, V. T. Chacko, J. A. Elvidge, A. B. P. Lever, R. V. Parish, *Can. J. Chem.* **1969**, *47*, 4141.
[26] A. B. P. Lever, L. K. Thompson, W. M. Reiff, *Inorg. Chem.* **1972**, *11*, 104.
[27] J. A. Doull, L. K. Thompson, *Can. J. Chem.* **1980**, *58*, 221.
[28] J. C. Dewan, L. K. Thompson, *Can. J. Chem.* **1982**, *60*, 121.
[29] F. W. Hartstock, L. K. Thompson, *Inorg. Chim. Acta* **1983**, *72*, 227.

[30] G. Bullock, F. W. Hartstock, L. K. Thompson, *Can. J. Chem.* **1983**, *61*, 57.
[31] L. K. Thompson, *Can. J. Chem.* **1983**, *61*, 579.
[32] L. K. Thompson, F. W. Hartstock, P. Robichaud, A. W. Hanson, *Can. J. Chem.* **1984**, *62*, 2755.
[33] P. Robichaud, L. K. Thompson, *Inorg. Chim. Acta* **1984**, *85*, 137.
[34] L. K. Thompson, A. W. Hanson, B. S. Ramaswamy, *Inorg. Chem.* **1984**, *23*, 2459.
[35] G. Bullock, A. Cook, A. Foster, L. Rosenberg, L. K. Thompson, *Inorg. Chim. Acta* **1985**, *103*, 207.
[36] L. K. Thompson, F. W. Hartstock, L. Rosenberg, T. C. Woon, *Inorg. Chim. Acta* **1985**, *97*, 1.
[37] S. K. Mandal, L. K. Thompson, A. W. Hanson, *J. Chem. Soc., Chem. Commun.* **1985**, 1709.
[38] L. K. Thompson, T. C. Woon, D. B. Murphy, E. J. Gabe, F. L. Lee, Y. L. Page, *Inorg. Chem.* **1985**, *24*, 4719.
[39] S. K. Mandal, T. C. Woon, L. K. Thompson, M. J. Newlands, E. J. Gabe, *Aust. J. Chem.* **1986**, *39*, 1007.
[40] L. Rosenberg, L. K. Thompson, E. J. Gabe, F. L. Lee, *J. Chem. Soc., Dalton Trans.* **1986**, 625.
[41] L. K. Thompson, S. K. Mandal, E. J. Gabe, J.-P. Charland, *J. Chem. Soc., Chem. Commun.* **1986**, 1537.
[42] T. C. Woon, R. McDonald, S. K. Mandal, L. K. Thompson, S. P. Connors, A. W. Addison, *J. Chem. Soc., Dalton Trans.* **1986**, 2381.
[43] S. K. Mandal, L. K. Thompson, M. J. Newlands, F. L. Lee, Y. Lepage, J.-P. Charland, E. J. Gabe, *Inorg. Chim. Acta* **1986**, *122*, 199.
[44] L. K. Thompson, S. K. Mandal, E. J. Gabe, F. L. Lee, A. W. Addison, *Inorg. Chem.* **1987**, *26*, 657.
[45] L. K. Thompson, S. K. Mandal, L. Rosenberg, F. Lee, E. J. Gabe, *Inorg. Chim. Acta* **1987**, *133*, 81.
[46] S. K. Mandal, L. K. Thompson, E. J. Gabe, F. L. Lee, J.-P. Charland, *Inorg. Chem.* **1987**, *26*, 2384.
[47] L. K. Thompson, S. K. Mandel, J.-P. Charland, E. J. Gabe, *Can. J. Chem.* **1988**, *66*, 348.
[48] S. K. Mandal, L. K. Thompson, E. J. Gabe, J.-P. Charland, F. L. Lee, *Inorg. Chem.* **1988**, *27*, 855.
[49] T. Wen, L. K. Thompson, F. L. Lee, E. J. Gabe, *Inorg. Chem.* **1988**, *27*, 4190.
[50] L. K. Thompson, F. L. Lee, E. J. Gabe, *Inorg. Chem.* **1988**, *27*, 39.
[51] S. K. Mandal, L. K. Thompson, E. J. Gabe, J.-P. Charland, F. L. Lee, *Inorg. Chem.* **1988**, *27*, 855.
[52] S. K. Mandal, L. K. Thompson, M. J. Newlands, J.-P. Charland, E. J. Gabe, *Inorg. Chim. Acta* **1990**, *178*, 169.
[53] S. S. Tandon, S. K. Mandal, L. K. Thompson, R. C. Hynes, *J. Chem. Soc., Chem. Commun.* **1991**, 5072.
[54] S. S. Tandon, S. K. Mandal, L. K. Thompson, R. C. Hynes, *J. Chem. Soc., Chem. Commun.* **1991**, 1572.
[55] L. Chen, L. K. Thompson, J. N. Bridson, *Can. J. Chem.* **1992**, *70*, 2709.
[56] L. Chen, L. K. Thompson, J. N. Bridson, *Can. J. Chem.* **1992**, *70*, 1886.
[57] S. S. Tandon, L. K. Thompson, R. C. Hynes, *Inorg. Chem.* **1992**, *31*, 2210.
[58] S. S. Tandon, S. K. Mandal, L. K. Thompson, R. C. Hynes, *Inorg. Chem.* **1992**, *31*, 2215.
[59] S. S. Tandon, L. K. Thompson, J. N. Bridson, M. Bubenik, *Inorg. Chem.* **1993**, *32*, 4621.
[60] Y. Zhang, L. K. Thompson, M. Bubenik, J. N. Bridson, *J. Chem. Soc., Chem. Commun.* **1993**, 1375.
[61] L. Chen, L. K. Thompson, J. N. Bridson, *Inorg. Chim. Acta* **1993**, *214*, 67.
[62] L. Chen, L. K. Thompson, J. N. Bridson, *Inorg. Chem.* **1993**, *32*, 2938.
[63] S. S. Tandon, L. Chen, L. K. Thompson, S. P. Connors, J. N. Bridson, *Inorg. Chim. Acta* **1993**, *213*, 289.
[64] L. Chen, L. K. Thompson, J. N. Bridson, *Can. J. Chem.* **1993**, *71*, 1086.
[65] L. Chen, L. K. Thompson, S. S. Tandon, J. N. Bridson, *Inorg. Chem.* **1993**, *32*, 4063.
[66] S. S. Tandon, L. K. Thompson, J. N. Bridson, *Inorg. Chem.* **1993**, *32*, 32.
[67] S. S. Tandon, L. K. Thompson, M. E. Manuel, J. N. Bridson, *Inorg. Chem.* **1994**, *33*, 5555.
[68] L. K. Thompson, S. S. Tandon, M. E. Manuel, *Inorg. Chem.* **1995**, *34*, 2356.
[69] S. S. Tandon, L. K. Thompson, D. O. Miller, *J. Chem. Soc., Chem. Commun.* **1995**, 1907.
[70] Y. Zhang, L. K. Thompson, J. N. Bridson, M. Bubenik, *Inorg. Chem.* **1995**, *34*, 5870.
[71] L. K. Thompson, S. S. Tandon, *Comments Inorg. Chem.* **1996**, *18*, 125.
[72] C. L. Sheppard, S. S. Tandon, L. K. Thompson, J. N. Bridson, D. O. Miller, M. Handa, F. Lloret, *Inorg. Chim. Acta* **1996**, *250*, 227.
[73] L. Chen, L. K. Thompson, J. N. Bridson, *Inorg. Chim. Acta* **1996**, *244*, 87.
[74] A. E. Goeta, L. K. Thompson, C. L. Sheppard, S. S. Tandon, C. W. Lehmann, J. Cosier, C. Webster, J. A. K. Howard, *Acta Crystallogr., Sect. C* **1999**, *55*, 1243.
[75] Z. Xu, L. K. Thompson, C. J. Matthews, D. O. Miller, A. E. Goeta, C. Wilson, J. A. K. Howard, M. Ohba, H. Okawa, *J. Chem. Soc., Dalton Trans.* **2000**, 69.
[76] F. Abraham, M. Lagrenee, S. Sueur, B. Mernari, C. Bremard, *J. Chem. Soc., Dalton Trans.* **1991**, 1443.
[77] SciFinder Scholar 2001; American Chemical Society, Chemical Abstracts Service: Columbus Ohio (accessed 12 February 2002).
[78] F. H. Allen, S. A. Bellard, M. D. Brice, B. A. Cartwright, A. Doubleday, H. Higgs, T. Hummelink, B. G. Hummelink-Peters, O. Kennard, W. D. S. Motherwell, J. R. Rodgers, D. G. Watson, *Acta Crystallogr., Sect. B* **1979**, *35*, 2331.
[79] L. Carlucci, G. Ciani, M. Moret, A. Sironi, *J. Chem. Soc., Dalton Trans.* **1994**, 2397.
[80] E. Spodine, A. M. Atria, J. Manzur, A. M. García, M. T. Garland, A. Hocquet, E. Sanhueza, R. Baggio, O. Peña, J.-Y. Saillard, *J. Chem. Soc., Dalton Trans.* **1997**, 3683.
[81] S. Kitagawa, M. Munakata, T. Tanimura, *Chem. Lett.* **1991**, 623.
[82] See for example: [82a] A. W. Addison, *Inorg. Nucl. Lett.* **1976**, *12*, 899. [82b] R. R. Gagné, C. A. Koval, T. J. Smith, *J. Am. Chem. Soc.* **1977**, *99*, 8367. [82c] R. R. Gagné, C. A. Koval, T. J. Smith, M. C. Cimolino, *J. Am. Chem. Soc.* **1979**, *101*, 4571. [82d] R. R. Gagné, L. M. Henling, T. J. Kistenmacher, *Inorg. Chem.* **1980**, *19*, 1226. [82e] R. C. Long, D. N. Hendrickson, *J. Am. Chem. Soc.* **1983**, *105*, 1513. [82f] S. K. Mandal, K. Nag, *J. Chem. Soc., Dalton Trans.* **1983**, 2429. [82g] P. Lacroix, O. Kahn, A. Gleizes, L. Valade, P. Cassoux, *New J. Chem.* **1984**, *8*, 643. [82h] S. K. Mandal, B. Adhikary, K. Nag, *J. Chem. Soc., Dalton Trans.* **1986**, 1175. [82i] P. Lacroix, O. Kahn, F. Theobald, J. Leroy, C. Wakselman, *Inorg. Chim. Acta* **1988**, *142*, 129. [82j] S. K. Mandal, L. K. Thompson, M. J. Newlands, E. J. Gabe, *Inorg. Chem.* **1989**, *28*, 3707. [82k] S. K. Mandal, L. K. Thompson, M. J. Newlands, E. J. Gabe, K. Nag, *Inorg. Chem.* **1990**, *29*, 1324. [82l] S. S. Tandon, L. K. Thompson, J. N. Bridson, V. McKee, A. J. Downard, *Inorg. Chem.* **1992**, *31*, 4635.
[83] F. Lloret, G. De Munno, M. Julve, J. Cano, R. Ruiz, A. Caneschi, *Angew. Chem. Int. Ed.* **1998**, *37*, 135.
[84] A. Escuer, R. Vicente, B. Mernari, A. E. Gueddi, M. Pierrot, *Inorg. Chem.* **1997**, *36*, 2511.
[85] N. Masciocchi, P. Cairati, L. Carlucci, G. Ciani, G. Mezza, A. Sironi, *J. Chem. Soc., Dalton Trans.* **1994**, 3009.
[86] D. Onggo, A. D. Rae, H. A. Goodwin, *Inorg. Chim. Acta* **1990**, *178*, 151.

[87] E. S. Ardiwinata, D. C. Craig, D. J. Phillips, *Inorg. Chim. Acta* **1989**, *166*, 233.
[88] A. I. Okur, *J. Chem. Soc., Dalton Trans.* **1988**, 2293.
[89] E. Yeager, *Electrochim. Acta* **1984**, *29*, 1527.
[90] A. van der Putten, A. Elzing, W. Visscher, E. Barendrecht, *J. Chem. Soc., Chem. Commun.* **1986**, 477.
[91] H.-F. Klein, M. Helwig, U. Koch, U. Florke, H.-J. Haupt, *Z. Naturforsch., Teil B* **1993**, *48*, 778.
[92] H.-F. Klein, M. Helwig, M. Karnop, H. Konig, B. Hammerschmitt, G. Cordier, U. Florke, H.-J. Haupt, *Z. Naturforsch., Teil B* **1993**, *48*, 785.
[93] W. Rosen, *Inorg. Chem.* **1971**, *10*, 1832.
[94] N. H. Pilkington, R. Robson, *Aust. J. Chem.* **1970**, *23*, 2225.
[95] K. Travis, D. H. Busch, *J. Chem. Soc., Chem. Commun.* **1970**, 1041.
[96] See for example: [96a] N. F. Curtis, *J. Chem. Soc.* **1960**, 4409. [96b] N. F. Curtis, D. A. House, *Chem. and Ind.* **1961**, 1708. [96c] M. M. Blight, N. F. Curtis, *J. Chem. Soc.* **1962**, 1204. [96d] M. M. Blight, N. F. Curtis, *J. Chem. Soc.* **1962**, 3016, and subsequent papers.
[97] J.-M. Lehn, *Supramolecular Chemistry*, VCH 1995.
[98] E. P. Papadopoulos, A. Jarrar, C. H. Issidorides, *J. Org. Chem.* **1966**, *31*, 615.
[99] N. Clauson-Kaas, F. Limborg, *Acta Chem. Scand.* **1947**, 619.
[100] J. Levisalles, *Bull. Soc. Chim. France* **1957**, 997.
[101] R. H. Wiley, *J. Macromol. Sci. Chem.* **1987**, *A24*, 1183.
[102] See for example: reference 94. [102a] H. Okawa, S. Kida, *Bull. Chem. Soc. Jpn.* **1972**, *45*, 1759. [102b] R. R. Gagné, C. L. Spiro, T. J. Smith, C. A. Hamann, W. R. Thies, A. K. Shiemke, *J. Am. Chem. Soc.* **1981**, *103*, 4073. [102c] H. Adams, N. A. Bailey, P. Bertrand, C. O. R. de Barbarin, D. E. Fenton, S. Gou, *J. Chem. Soc., Dalton Trans.* **1995**, 275. [102d] L. K. Thompson, S. K. Mandal, S. S. Tandon, J. N. Bridson, M. K. Park, *Inorg. Chem.* **1996**, *35*, 3117. [102e] T. Aono, H. Wada, M. Yonemura, H. Furutachi, M. Ohba, H. Okawa, *J. Chem. Soc., Dalton Trans.* **1997**, 3029. [102f] S. K. Dutta, J. Ensling, R. Werner, U. Florke, W. Haase, P. Gutlich, K. Nag, *Angew. Chem. Int. Ed. Engl.* **1997**, *36*, 152.
[103] V. McKee, W. B. Shepard, *J. Chem. Soc., Chem. Commun.* **1985**, 158.
[104] S. Brooker, V. McKee, W. Shepard, L. Pannell, *J. Chem. Soc., Dalton Trans.* **1987**, 2555.
[105] See for example: M. G. B. Drew, J. Nelson, S. M. Nelson, *J. Chem. Soc., Dalton Trans.* **1981**, 1691.
[106] See for example: H. Adams, N. A. Bailey, D. E. Fenton, R. J. Good, R. Moody, C. O. R. de Barbarin, *J. Chem. Soc., Dalton Trans.* **1987**, 207.
[107] See for example: M. G. B. Drew, J. Nelson, S. M. Nelson, *J. Chem. Soc., Dalton Trans.* **1981**, 1678.
[108] S. R. Korupoju, N. Mangayarkarasi, S. Ameerunisha, E. J. Valente, P. S. Zacharias, *J. Chem. Soc., Dalton Trans.* **2000**, 2845.
[109] F. A. Cotton, G. Wilkinson, C. A. Murillo, M. Bochmann, *Advanced Inorganic Chemistry*, John Wiley & Sons, Inc., New York 1999.
[110] M.-T. Youinou, N. Rahmouni, J. Fischer, J. A. Osborn, *Angew. Chem. Int. Ed. Engl.* **1992**, *31*, 733.
[111] A. S. Batsanov, M. J. Begley, M. W. George, P. Hubberstey, M. Munakata, C. E. Russell, P. H. Walton, *J. Chem. Soc., Dalton Trans.* **1999**, 4251.
[112] M. Belicchi Ferrari, G. Gasparri Fava, G. Pelosi, G. Denti, *J. Chem. Cryst.* **1997**, *27*, 257.
[113] M. P. Gamasa, J. Gimeno, E. Lastra, J. M. R. Gonzalez, S. Garcia-Granda, *Polyhedron* **1990**, *9*, 2603.
[114] T. Otieno, S. J. Rettig, R. C. Thompson, J. Trotter, *Inorg. Chem.* **1995**, *34*, 1718.
[115] T. Kromp, W. S. Sheldrick, *Z. Naturforsch., Teil B* **1999**, *54*, 1175.
[116] P. N. W. Baxter, H. Sleiman, J. M. Lehn, K. Rissanen, *Angew. Chem. Int. Ed. Engl.* **1997**, *36*, 1294.
[117] H. Sleiman, P. N. W. Baxter, J. M. Lehn, K. Airola, K. Rissanen, *Inorg. Chem.* **1997**, *36*, 4734.
[118] P. Hubberstey, C. E. Russell, *J. Chem. Soc., Chem. Commun.* **1995**, 959.
[119] A. Toth, C. Floriani, A. Chiesi-Villa, C. Guastini, *Inorg. Chem.* **1987**, *26*, 236.
[120] See for example: [120a] S. Kita, H. Furutachi, H. Okawa, *Inorg. Chem.* **1999**, *38*, 4038. [120b] H. Furutachi, S. Fujinami, M. Suzuki, H. Okawa, *J. Chem. Soc., Dalton Trans.* **1999**, 2197. [120c] H. Furutachi, H. Okawa, *Inorg. Chem.* **1997**, *36*, 3911. [120d] H. Furutachi, S. Fujinami, M. Suzuki, H. Okawa, *Chem. Lett.* **1998**, 779.
[121] See for example: reference 94. [121a]B. F. Hoskins, G. A. Williams, *Aust. J. Chem.* **1975**, *28*, 2607. [121b] B. F. Hoskins, G. A. Williams, *Aust. J. Chem.* **1975**, *28*, 2593. [121c] B. F. Hoskins, R. Robson, G. A. Williams, *Inorg. Chim. Acta* **1976**, *16*, 121. [121d] G. A. Williams, R. Robson, *Aust. J. Chem.* **1981**, *34*, 65.
[122] M. Ghedini, G. De Munno, G. Denti, A. M. M. Lanfredi, A. Tiripicchio, *Inorg. Chim. Acta* **1982**, *57*, 87.
[123] C. Li, N. Kanehisa, Y. Miyagi, Y. Nakao, *Bull. Chem. Soc. Jpn.* **1997**, *70*, 2429.
[124] P. Dapporto, G. De Munno, G. Bruno, M. Romeo, *Acta Crystallogr., Sect. C* **1983**, *39*, 718.
[125] G. De Munno, G. Denti, P. Dapporto, *Inorg. Chim. Acta* **1983**, *74*, 199.
[126] G. De Munno, G. Denti, *Acta Crystallogr., Sect. C* **1984**, *40*, 616.
[127] P. Dapporto, G. De Munno, A. Sega, C. Mealli, *Inorg. Chim. Acta* **1984**, *83*, 171.
[128] G. De Munno, G. Brunno, *Acta Crystallogr., Sect. C* **1984**, *40*, 2022.
[129] L. Carlucci, G. Ciani, M. Moret, A. Sironi, *J. Chem. Soc., Dalton Trans.* **1994**, 2397.
[130] J. Manzur, A. M. Garcia, R. Letelier, E. Spodine, O. Pena, D. Grandjean, M. M. Olmstead, B. C. Noll, *J. Chem. Soc., Dalton Trans.* **1993**, 905.
[131] T. Fetzer, A. Lentz, T. Debaerdemaeker, O. Abou-El-Wafa, *Z. Naturforsch., Teil B* **1990**, *45*, 199.
[132] G. Marongiu, E. C. Lingafelter, *Acta Crystallogr., Sect. B* **1982**, *38*, 620.
[133] M. G. B. Drew, P. C. Yates, J. Trocha-Grimshaw, A. Lavery, K. P. McKillop, S. M. Nelson, J. Nelson, *J. Chem. Soc., Dalton Trans.* **1988**, 347.
[134] D. Hagman, C. Sangregorio, C. J. O'Connor, J. Zubieta, *J. Chem. Soc., Dalton Trans.* **1998**, 3707.
[135] M. J. Begley, P. Hubberstey, C. E. Russell, P. H. Walton, *J. Chem. Soc., Dalton Trans.* **1994**, 2483.
[136] M. Maekawa, M. Munakata, T. Kuroda-Sowa, Y. Nozaka, *J. Chem. Soc., Dalton Trans.* **1994**, 603.
[137] D. J. Cromer, A. C. Larson, *Acta Crystallogr., Sect. B* **1972**, *28*, 1052.

Received March 17, 2002
[I02137]

Symmetric and Asymmetric Coupling of Pyridylpyrimidine for the Synthesis of Polynucleating Ligands

Matthew I. J. Polson,[a] John A. Lotoski,[a] K. Olof Johansson,[a] Nicholas J. Taylor,[a] Garry S. Hanan,*[a] Bernold Hasenknopf,[b] René Thouvenot,*[b] Frédérique Loiseau,[c] Rosalba Passalaqua,[c] and Sebastiano Campagna*[c]

Keywords: Heterocycles / Ruthenium / N ligands / Radical reactions / Addition reactions

A convenient synthetic approach to build up new polynucleating ligands is presented. Symmetric and asymmetric pyridylpyrimidine dimers are produced by radical anion coupling and nucleophilic addition, respectively. A diruthenium complex of the asymmetric ligand was synthesised and characterised by cyclic voltammetry, luminescence and ^{99}Ru NMR spectroscopy.

(© Wiley-VCH Verlag GmbH, 69451 Weinheim, Germany, 2002)

Introduction

Oligo(azaheterocyclic) compounds are highly regarded by coordination chemists for their use in building up large polymetallic complexes.[1,2] This appreciation stems from their stability in a wide range of reaction conditions and their ability to form stable complexes with most transition metal ions. They are synthesised in a variety of ways: ring-forming reactions (e.g., Kröhnke synthesis), ring-coupling reactions (e.g., Stille reaction), or a combination of the two. However, these reactions have the drawback of usually requiring substituted heterocycles in order to bring two moieties together. We report herein on a rapid and convenient synthesis of isomeric oligo(azaheterocyclic) ligands for incorporation into metallodendrimers starting from unsubstituted heterocycles. In addition, the diruthenium complex of one dinucleating ligand has been prepared and fully characterised.

[a] Department of Chemistry, University of Waterloo,
200 University Ave., Waterloo, Ontario N2L 3G1, Canada
Fax: (internat.) + 1-519/746-0435
E-mail: ghanan@uwaterloo.ca
[b] Université Pierre et Marie Curie, Chimie Inorganique et Matériaux Moléculaires, UMR 7071
Case Courrier 42, 4, place Jussieu, 75252 Paris cedex 05, France
Fax: (internat.) + 33-1/44273841
E-mail: rth@ccr.jussieu.fr
[c] Dipartimento di Chimica Inorganica, Chimica Analitica, e Chimica Fisica, Universita di Messina,
98166 Messina, Italy
Fax: (internat.) + 39-090/393756
E-mail: photochem@chem.unime.it

Supporting information for this article is available on the WWW under http://www.eurjic.org or from the author.

Results and Discussion

We previously demonstrated that an Ni-catalysed coupling reaction could be used to increase the metal ion content in metallodendrimers and proposed a general method to create new binding sites in metal complexes (Scheme 1).[3,4] Although dimetallic complex **2b** was readily synthesised by an Ni-catalysed coupling of monometallic complex **1b**, metal-free ligand **2a** was required to fully interpret the electrochemical and spectroscopic properties of its complexes.

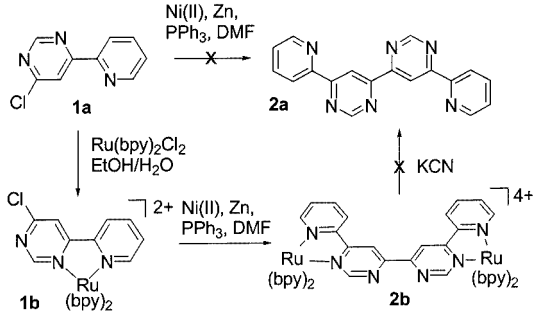

Scheme 1. The attempted synthesis of ligand **2a**

Our initial attempt to synthesise **2a** by the nickel-catalysed coupling of **1a** failed to afford significant quantities of **2a** (Scheme 1), presumably due to the sequestering of the nickel catalyst by the free chelating site in **1a** or to its deactivation toward coupling as was previously shown for carbonylmetal compounds of chlorophenanthrolines.[5] In another attempt, dimetallic complex **2b** could not be demetallated using CN^-. Thus, a synthesis of **2a** without transition metals was required, and direct lithiation/addition appeared to be the best route.

Direct metallation of azaheterocycles is usually aided by directing metallation groups (DMGs),[6,7] such as those used for aromatic hydrocarbons.[8,9] The functional group serves to direct the lithiation either electronically or by coordination. However, there are a few reported cases of direct lithiation of unsubstituted electron-deficient heterocycles.[10,11] Pyrimidine can be lithiated directly in the 4-position using lithium 2,2,6,6-tetramethylpiperidide (LTMP), and its addition to pyrimidine gives 4,4′-bipyrimidine (bpym) in modest yield.[11] This suggested that lithiation of 4-(2-pyridyl)pyrimidine (**3**)[12] in the 6-position, followed by addition to another ligand **3**, would give **2a**. However, as the pyridine in **3** could also serve as a DMG,[13] an asymmetric coupling reaction could also occur (Scheme 2, route a).

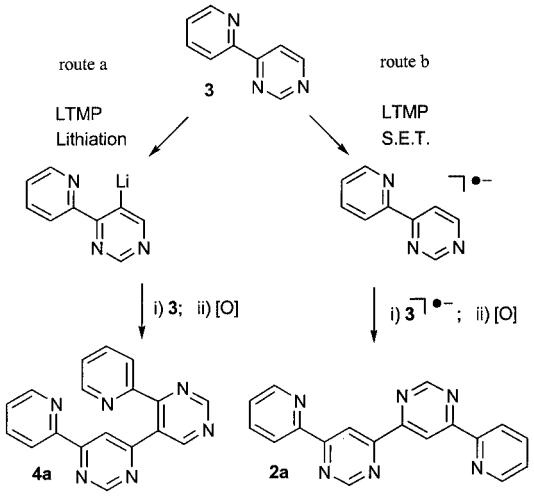

Scheme 2. Synthetic routes to symmetric ligand **2a** and asymmetric ligand **4a** using LTMP with **3**

Direct lithiation/addition routes were attempted as outlined in Scheme 2 and Table 1. Thus, **3** was treated with LTMP at −78 °C in an effort to lithiate the 6-position, followed by its addition to **3**. Subsequent warming and air oxidation afforded the symmetric dimer **2a** and the asymmetric dimer **4a** in 16% and 22% yield, respectively (Table 1, Entry 1).

LTMP and **3** were recombined at −78 °C in order to verify the positions of lithiation and their relative ratios (Table 1).[14] The lithio intermediates were trapped by the addition of TMSCl at timed intervals after LTMP addition (Entries 2−4). The expected 6-lithio species was not formed in any appreciable amount after the first minute, instead only the 5-TMS adduct formed. After 5 min, **2a** had formed, even though no 6-TMS adduct could be trapped. This suggested that some other route may be operative as heterocyclic carbanions are usually trapped by TMSCl when competing with addition reactions to other heterocycles.[15] After 10 min, **4a** was formed by the addition of the 5-lithio species to the 6-position of **3**. The phenylation of **3** in the 6-position in 32% yield confirmed the site of addition (Entry 5). Interestingly, lithium diisopropylamide (LDA, Entry 6) gave only a minute quantity of **4a** via the 5-lithio species, with no sign of **2a**. LDA was previously shown to dimerize 2,2′-bipyridine and give its 3,6′-coupled dimer.[16,17]

Table 1. Lithiation/addition and radical anion coupling reactions for **3**

Entry	Ligand[a]	Alkali	Product[b]	Yield (%)
1	TMP	*n*BuLi	**2a**	16
			4a	22
2[c]	TMP	*n*BuLi	**2a**	0
			5-TMS-py-pm	30
3[d]	TMP	*n*BuLi	**2a**	11
			5-TMS-py-pm	58
4[e]	TMP	*n*BuLi	**2a**	17
			5-TMS-py-pm	28
			4a	10
5	−	PhLi	6-Ph-4-py-pm	32
6	−	LDA	**4a**	< 5
7[f]	−	$Na_{(s)}$	**2a**	95[g]
8[h]	TMP	*n* BuLi	**2a**	10
		+ $CuCl_2$	**4a**	22

[a] TMP = 2,2,6,6-tetramethylpiperidine. [b] 5-TMS-py-pm = 4-(2-pyridyl)-5-(trimethylsilyl)pyrimidine, 6-Ph-4-py-pm = 6-phenyl-4-(2-pyridyl)pyrimidine. [c] The reaction was quenched after 1 min with excess trimethylsilyl chloride. [d] The reaction was quenched after 5 min with excess trimethylsilyl chloride. [e] The reaction was quenched after 10 min with excess trimethylsilyl chloride. [f] No oxidation occurred with air. The residue was dissolved in acetone and an excess of $KMnO_4$ was added. The solution was stirred for 1 h before usual workup. [g] Based on recovered **3**, 40% conversion. [h] Reaction conducted in THF.[11]

As pyridine is well known to dimerize by way of its radical anion upon treatment with alkali metals[18,19] and LDA,[20] a radical pathway for the formation of **2a** with LTMP was still possible, especially considering the lower reduction potential of pyrimidine compared to pyridine.[21] A radical anion mechanism was indeed supported by the reduction of **3** with sodium (Entry 7), which afforded **2a** in 95% yield based on recovered **3**, with no sign of **4a** (Scheme 2b). Increasing the amount of sodium and the reaction time had no effect on the ratio **2a**/**3**.

The addition of a catalytic amount of the known radical quencher $CuCl_2$[11] to the reaction mixture (Entry 8, Table 1) resulted in a decrease in the yield of **2a**, but not its complete elimination. Increasing the amount of $CuCl_2$ leads to a lower yield of both isomers. Thus, we propose that the reaction in Entry 1 is a balance between a single electron transfer mechanism resulting in **2a** and an *ortho*-directed metallation at the pyrimidine 5-position followed by attack at the 6-position of the second ligand **3**, giving **4a** after oxidation. In the case of the reaction with Na(s), the lower reduction potential of the pyrimidine ring affords a direct route to homocoupled ligands through radical anion coupling.

Asymmetric ligands such as **4a** are generally more difficult to obtain than their symmetric counterparts,[16,17] but they can give valuable information on the interaction between metals in different binding sites. We therefore analysed the structure of **4a** and prepared its diruthenium complex. In this case, the steric hindrance about the C−C bond

joining the two pyrimidine rings may preclude metal−metal interaction in its dimetallic complex. An X-ray crystal structure determination allowed the bond connectivity in **4a** to be verified and the steric hindrance at both coordination sites to be compared. Thus, the bond between the two pyrimidine rings in **4a** (C13 to C9) is unequivocally assigned by X-ray crystallography (Figure 1).[22] The dihedral angle of 38.1° between the two pyrimidine rings clearly demonstrates the steric congestion about this bond. This is also seen in the 38.2° dihedral angle to the adjacent pyridine ring (C14 to C19), compared to the 2.7° dihedral angle at the other less encumbered pyridine ring (C1 to C7). The bond lengths and angles in **4a** are consistent with other pyridine- and pyrimidine-containing ligands.[23,24]

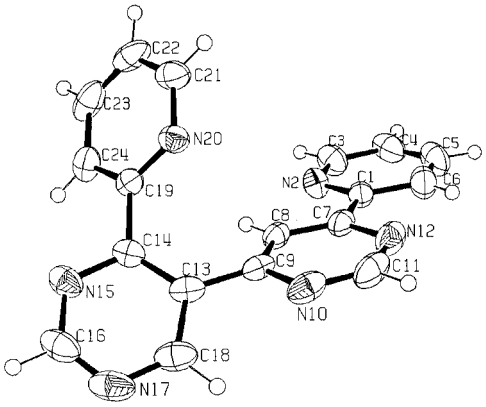

Figure 1. The crystal structure of **4a**

Diruthenium complex **4b** was readily prepared in 52% yield by allowing an excess (3 equiv.) of $Ru(bpy)_2Cl_2$ to react with **4a** in refluxing ethanol (Scheme 3). The complex was purified by chromatography on silica gel using a MeCN/water/KNO_3 (sat. aq.) (5:4:1) solution as eluent followed by anion exchange to its PF_6 salt. ^1H and ^{13}C NMR spectroscopic and mass spectrometric analyses confirm the dinuclear nature of **4b**. Cyclic and differential pulse voltammograms of **4b** in acetonitrile vs. SCE (in V, anodic and cathodic peak separation in mV) showed a single oxidation process which is assigned to two simultaneous, metal-based, one-electron oxidation processes [+1.40 V (100 mV)] and two reversible one-electron reduction processes [−0.70 V (62 mV), −1.00 V (63 mV)], which are assigned to successive one-electron reductions of the coordinated bridging ligand **4a**. No other reversible reductions were found out to −2.00 V. The coincidence of the two metal-centred oxidation processes indicates that the two metal centres are only weakly interacting with one another, as expected since the two chelating sites in **4b** cannot lie co-planar to afford orbital overlap (cf. Figure 1). The ligand-based reduction potentials are considerably less negative than bpy-centred reductions in $Ru(bpy)_3^{2+}$ (−1.28 V)[25] due to the electron-deficient nature of the pyrimidine rings.

The absorption and photophysical properties of **4b** are also in line with those of other dinuclear (polypyridine)Ru^{II} complexes containing relatively easy-to-reduce bridging ligands.[25] The electronic absorption spectrum of **4b** in acetonitrile shows the same general profile, with ligand-based absorptions predominating in the UV region: λ_{max} (ε [$M^{-1}cm^{-1}$]) = 247 (44,400), 286 nm (114,300)] and spin-allowed MLCT bands in the visible region: λ_{max} (ε [$M^{-1}cm^{-1}$]) = 429 (17,000), 518 nm (14,300)]. Complex **4b** is luminescent at room temperature, emitting at 784 nm with a lifetime of 34 ns. At 77 K, the emission shifts to shorter wavelength, 695 nm, and its lifetime extends to 126 ns.

Complex **4b** was further characterised using ^{99}Ru NMR.[26] At 343 K, the ^{99}Ru NMR spectrum of an acetonitrile solution of **4b** presents two baseline-resolved resonances of equal intensity at δ = 4660 and 4677 ppm (Figure 2). This agrees with the two inequivalent Ru sites in **4b**. The line width at half height ($W_{1/2}$), similar for both resonances (ca. 100 Hz, i.e. 4 ppm), is hardly larger than for the highly symmetrical analogue $Ru(bpy)_3^{2+}$ (65 Hz in CD_3CN at 22 °C).[27] This reflects the fact that the local symmetry at each Ru site is relatively higher than expected from the low symmetry of the whole complex **4b**. Attribution of the two signals to the ruthenium ions is virtually impossible, as there is no general correlation with other experimental data. It is nevertheless noteworthy that the very subtle differences of the two binding sites of asymmetric ligand **4a** are clearly reflected in different chemical shifts for the ruthenium atom. The observed difference in chemical shift between the two Ru nuclei (17 ppm) is very small when compared to the huge chemical shift range of ^{99}Ru (ca. 18,000 ppm) as well as to the various "medium" effects, such as the dependence of the ruthenium chemical shift on temperature, solvent and concentration. This confirms the

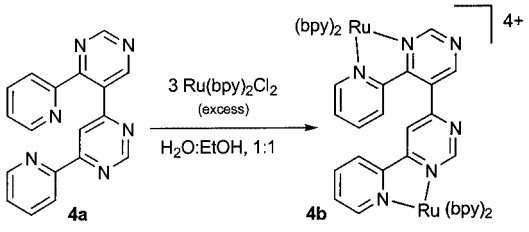

Scheme 3. Synthesis of diruthenium complex **4b**

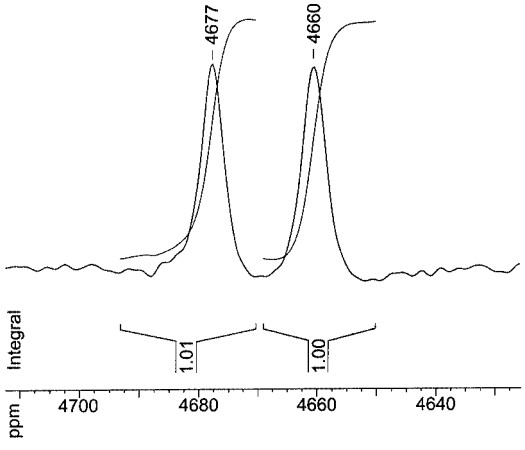

Figure 2. ^{99}Ru NMR of complex **4b** in acetonitrile at 343 K

high potential of ^{99}Ru NMR to characterise polynuclear ruthenium complexes.[27] We are currently working on other (azaheterocycle)di- and -triruthenium complexes and making use of ^{99}Ru NMR to probe ruthenium-containing dendrimers.

Conclusion

The combination of **3** and LTMP gives both radical anion coupling and lithiation/addition reactions, which were found to produce symmetric and asymmetric ligands **2a** and **4a**, respectively. Controlled radical anion coupling of the electron-deficient pyrimidine ring of **3** using Na has allowed a facile entry into the synthesis of trinucleating ligand **2a**. Thus, the judicious choice of reaction conditions is an easy way to produce different multinucleating ligands for coordination chemistry from unsubstituted azaheterocycles.

The diruthenium complex of asymmetric ligand **4a** has been fully characterised, including its ^{99}Ru NMR. It is noteworthy that although electrochemical studies could not clearly distinguish between the two metal centres in **4b**, this was readily accomplished using ^{99}Ru NMR. We are investigating methods to increase the overall yield of this reaction and to expand this approach to poly(azaheterocyclic) ligands.[28]

Acknowledgments

G. S. H. thanks the NSERC of Canada, the Province of Ontario, the Research Corporation, and Le Ministère de la Recherche, France for financial support. R. T. and B. H. thank the University Pierre et Marie Curie and the CNRS for support. S. C. thanks MIUR and CNR. F. L. thanks the EU for a Marie Curie fellowship grant. The EC-TMR Research Network and NSERC CRO Program for Nanometer-sized Metal Complexes are also thanked.

[1] G. R. Newkome, E. F. He, C. N. Moorefield, *Chem. Rev.* **1999**, *99*, 1689.
[2] G. F. Swiegers, T. J. Malefetse, *Chem. Rev.* **2000**, *100*, 3483.
[3] K. O. Johansson, J. A. Lotoski, C. C. Tong, G. S. Hanan, *Chem. Commun.* **2000**, 819.
[4] Other examples of this methodology: Y. Tomohiro, A. Satake, Y. Kobuke, *J. Org. Chem.* **2001**, *66*, 8442.
[5] P. M. Griffiths, F. Loiseau, F. Puntoriero, S. Serroni, S. Campagna, *Chem. Commun.* **2000**, 2297.
[6] A. Turck, N. Plé, F. Mongin, G. Quéguiner, *Tetrahedron* **2001**, *57*, 4489.
[7] F. Mongin, G. Quéguiner, *Tetrahedron* **2001**, *57*, 4059.
[8] B. Chauder, L. Green, V. Snieckus, *Pure Appl. Chem.* **1999**, *71*, 1521.
[9] V. Snieckus, *Chem. Rev.* **1990**, *90*, 879.
[10] J. Verbeek, A. V. E. George, R. L. P. de Jong, L. Brandsma, *J. Chem. Soc., Chem. Commun.* **1983**, 257.
[11] N. Plé, A. Turck, K. Couture, G. Quéguiner, *J. Org. Chem.* **1995**, *60*, 3781.
[12] E. Bejan, H. Ait-Haddou, J. C. Daran, G. G. A. Balavoine, *Synthesis* **1996**, 1012.
[13] J. A. Zoltewicz, C. D. Dill, *Tetrahedron* **1996**, *52*, 14469.
[14] BuLi (1.6 M in hexane, 200 μL, 0.32 mmol) and ligand (0.32 mmol) were added to 5 mL of THF at −78 °C and stirred for 15 min before being warmed to room temp. over 30 min. The solution was then returned to −78 °C and **3** (100 mg, 0.64 mmol) was dissolved in THF (5 mL) and added to the lithium solution by cannula. After stirring for 1 h at −78 °C, the solution was rapidly warmed to room temp. and quenched with ethanol (5 mL) and triethylamine (400 μL). Air was bubbled through the solution for 1 h. The solution was concentrated to dryness, dissolved in dichloromethane (20 mL) and extracted with water (2 × 20 mL). NMR was used to determine ratio of products to remaining starting material. The residue was then sublimed to remove the starting material (< 80 °C) and to collect the products (90−160 °C).
[15] R. Ribéreau, G. Quéguiner, *Tetrahedron* **1983**, *39*, 3593.
[16] M. D. Ward, *J. Chem. Soc., Dalton Trans.* **1994**, 3095.
[17] M. D. Ward, F. Barigelletti, *Coord. Chem. Rev.* **2001**, *216*, 127.
[18] J. Chaudhuri, S. Kume, J. Jagur-Grodzinski, M. Szwarc, *J. Am. Chem. Soc.* **1968**, *90* 6421.
[19] C. Desmarets, R. Schneider, Y. Fort, *Tetrahedron Lett.* **2000**, *41*, 2875.
[20] G. R. Newkome, D. C. Hager, *J. Org. Chem.* **1982**, *47*, 599.
[21] P. Ford, D. F. P. Rudd, R. Gaunder, H. Taube, *J. Am. Chem. Soc.* **1968**, *90*, 1187.
[22] Crystal data: **2a**, monoclinic, space group *P*21/*c*, a = 7.4707(9), b = 20.1567(19), c = 10.3384(11) Å, β =107.157(8)°, V = 1487.5(3) Å^3, Z =1, D_c = 1.395 g/cm^3, R_1 = 0.0403. CCDC-179442 contains the supplementary crystallographic data for this paper. These data can be obtained free of charge at www.ccdc.cam.ac.uk/conts/retrieving.html or from the Cambridge Crystallographic Data Centre, 12, Union Road, Cambridge CB2 1EZ, UK [Fax: (internat.) + 44-1223/336-033; E-mail: deposit@ccdc.cam.ac.uk].
[23] R. Krämer, I. O. Fritsky, *Eur. J. Org. Chem.* **2000**, 3505.
[24] L. Kovbasyuk, M. Hoppe, H. Pritzkow, R. Krämer, *Eur. J. Inorg. Chem.* **2001**, 1353.
[25] V. Balzani, A. Juris, M. Venturi, S. Campagna, S. Serroni, *Chem. Rev.* **1996**, *96*, 958.
[26] The ^{99}Ru NMR spectra have been recorded with a Bruker DRX 500 spectrometer tuned at 23.142 MHz and equipped with a 10-mm broad-band probehead. Complex **4b** (30 mg) was dissolved in acetonitrile (3 mL). The spectra were recorded without lock and the chemical shifts were referenced with respect to a saturated aqueous solution of $K_4Ru(CN)_6$ (δ = 0 ppm at 300 K). A preliminary spectrum obtained at 300 K showed a broad signal ($W_{1/2}$ ≈ 400 Hz, 16 ppm) at δ ≈ 4580 ppm with two distinct maxima. Raising the temperature to 343 K, in order to increase the relaxation time of the quadrupolar ^{99}Ru nucleus, resulted in a clean separation of the two resonances. In addition, there is a strong deshielding by nearly 100 ppm, with respect to the 300 K resonance. The spectrum in Figure 2 required a total of 4 × 10^6 scans with an acquisition time of 16 ms, a pre-acquisition delay of 11.4 μs and a spectral width of 62 kHz. Exponential multiplication with a line-broadening factor of 10 Hz was applied prior to Fourier transformation.
[27] G. Orellana, A. Kirsch-De Mesmaeker, N. J. Turro, *Inorg. Chem.* **1990**, *29*, 882.
[28] Supporting information for this article (synthesis of ligands **2a** and **4a**, and complex **4b**) is available, see footnote on the first page of this article.

Received May 13, 2002
[I02255]

Chiral Supramolecular Assemblies Derived from the Insertion of a Segmental Ligand into a Copper-Tyrosine Framework

Jiabao Weng,[a,b] Maochun Hong,*[a] Qian Shi,[a] Rong Cao,[a] and Albert S. C. Chan[c]

Keywords: Amino acids / Copper / Self-assembly / Polymers

The use of a predisposed 4,4-bipyridine segmental ligand in copper-tyrosine chiral complex self-assembly processes allows the preparation of a new type of complex $\{[Cu_2(tyrosine)_2(4,4\text{-bipyridine})\cdot 2H_2O]\cdot 2ClO_4\}_n$, which results in the fine tuning of network structure and stereo conformation.
(© Wiley-VCH Verlag GmbH, 69451 Weinheim, Germany, 2002)

The construction of metal-organic molecular coordination frameworks by metal coordination-directed self-assembly processes has become an area of intense research in recent years.[1−4] The network structures and properties of these coordination supramolecules can be fine-tuned by a systematic change of the organic linking ligands.[5−7] However, the study of metal-amino acid chiral supramolecular assemblies is less popular and the synthesis of these assemblies with a mixture of organic ligands is a significant challenge.

Among the natural amino acids, phenylalanine with hydroxyl group(s) plays an important role in biological systems.[8] Tyrosine has also been known to be located at the active sites of a series of metal proteins and to act as an important part in the protein factors.[9−13] On the other hand, copper is a bioelement and an active site in several metalloenzymes and proteins.[14] The blue copper proteins have received considerable interest because of their unusual spectral and structural properties. The geometry around copper in blue proteins is intermediate between tetrahedral and square planar and several model systems have been developed to study the molecular structure with the electronic group state of those complexes.[15−17] Hence, copper-amino acid complexes, especially aromatic amino acid ones, are of great interest, not only due to their importance in biological systems but also because of their remarkable properties derived from stacking, hydrogen bonding, and metal-aromatic ring interactions.[18] In the course of our studies on this structure-function relationship, we report here the synthesis and crystal structures of two copper(II) coordination polymers with tyrosine as ligand $[Cu(Tyr)_2]_n$ (**1**) and $\{[Cu_2(Tyr)_2(4,4\text{-bipy})\cdot 2H_2O]\cdot 2ClO_4\}_n$ (**2**) (Tyr = tyrosine; 4,4-bipy = 4,4-bipyridine), where 4,4-bipy acts as an inserting component that has a subtle effect on the structural characteristics of the copper-tyrosine complex by self-assembled control. The synthesis and the structures of the polymers provide a new insight into understanding the mode of action of copper(II)-tyrosine complexes and are important not only for coordination chemistry but also for biochemistry.

Complex **1** was obtained by slow evaporation of solutions prepared by mixing tyrosine and Cu^{II} perchlorate in methanol/water with a metal-to-ligand molar ratio of 1:1. Figure 1 shows the crystal structure of the biologically relevant complex **1** formed between Cu^{II} and tyrosine. The geometry around the Cu^{II} ion can be described as square pyramidal. Two tyrosine molecules chelate the Cu^{II} ion through the nitrogen and oxygen atoms forming two five-membered rings with the Cu^{II} ion located in the center of the N_2O_2 square plane. There are two kinds of coordination modes of tyrosine molecule in complex **1**: chelating, which leaves one oxygen atom of the carboxyl group free, and exobidentate bridging, with a μ-carboxyl group linking adjacent Cu^{II} ions through the oxygen atom at the vertex of the square pyramid giving rise to a one-dimensional right-handed chiral chain structure generated by a 2_1 operation (Figure 2). The angles between the axial Cu−O bond and the four equatorial bonds in the square plane lie in the range of 85.3−95.7°. All Cu−N and Cu−O bond lengths are normal (1.92 Å to 2.00 Å) except for the axial Cu−O bond (2.36 Å). The phenyl-bound hydroxyl group of the bridging tyrosine hydrogen-bonds with that of the non-bridging tyrosine and the free oxygen atom of the carboxyl

[a] State Key Laboratory of Structural Chemistry, Fujian Institute of Research on the Structure of Matter, Chinese Academy of Sciences,
Fuzhou, Fujian 350002, P. R. China
[b] Department of Chemistry, Fujian Teachers University,
Fuzhou, Fujian 350007, P. R. China
[c] Open Laboratory of Chirotechnology, Department of Applied Biology and Chemical Technology, the Hong Kong Polytechnic University,
Hong Hum, Hong Kong, China

group, which connects the adjacent chiral chains to form a three-dimensional supramolecular assembly.

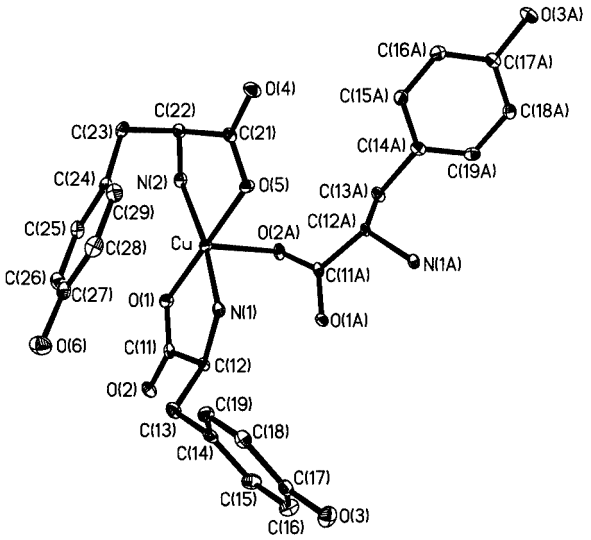

Figure 1. Coordination environment of **1**; the asymmetric unit is shown with ellipsoids at 30% probability; hydrogen atoms have been omitted for clarity

In order to insert an organic ligand into the chiral chains of the copper(II)-tyrosine assembly, 4,4-bipy was added to the reaction mixture of copper(II) and tyrosine; complex **2** was obtained. The structural subunit of complex **2** contains two copper ions(Figure 3), each of which is coordinated to one tyrosine molecule, one water molecule of crystallization and one 4,4-bipy molecule. The coordination geometry of Cu^{II} in **2** is also square pyramidal: the oxygen atom of the water molecule lies at the vertex of the square pyramid and four donor atoms — a nitrogen atom from 4,4-bipy, an oxy-

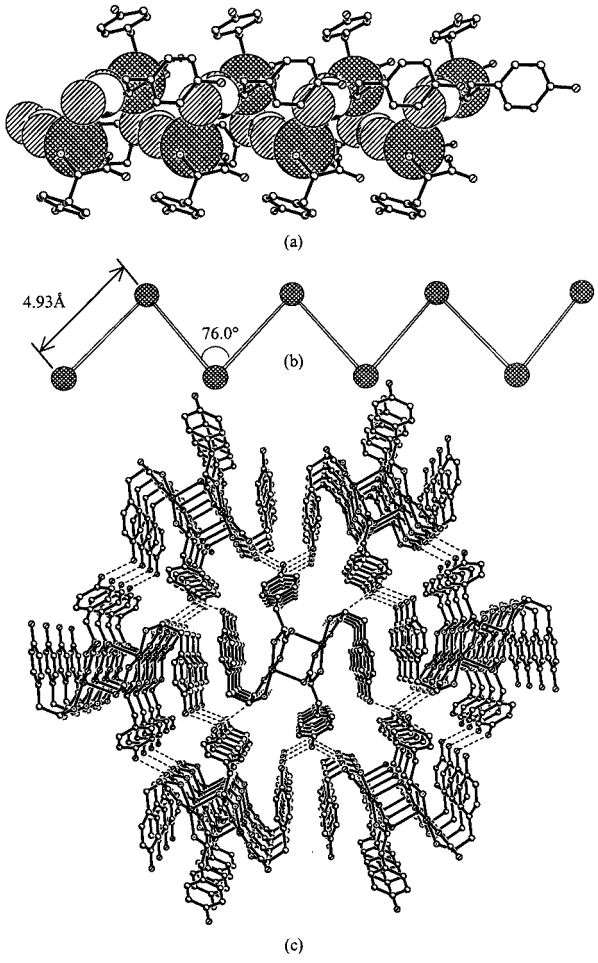

Figure 2. (a) Perspective view of the chiral chain structure of **1**; the Cu^{II} and bridging carboxyl are represented by larger circles; (b) 1-D chiral chain connectivity in **1**; the circles represent the $Cu(Tyr)_2$ unit; (c) stacking of the chiral chains of **1** viewed down the *a* axis

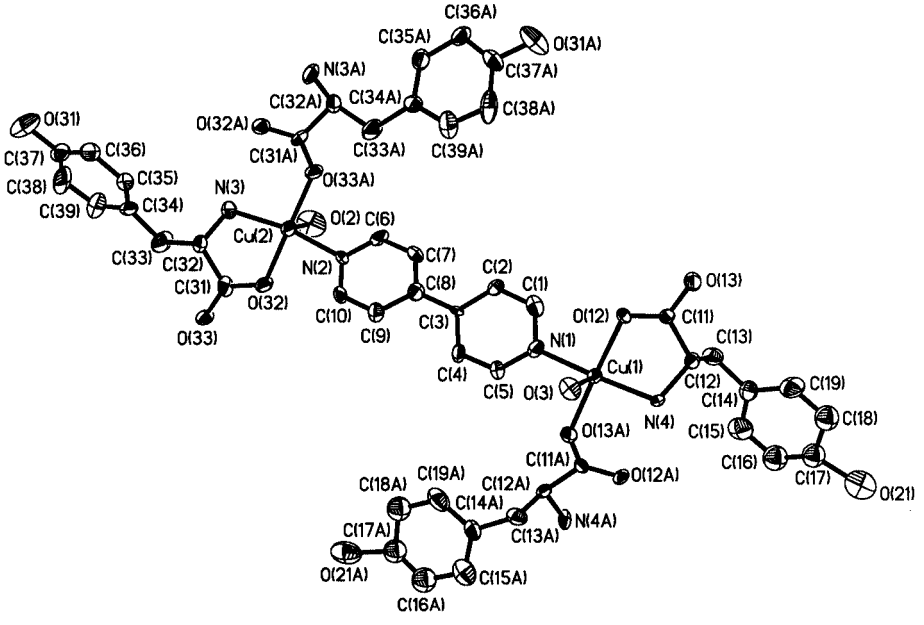

Figure 3. Coordination environment of **2**; the asymmetric unit is shown with ellipsoids at 30% probability; hydrogen atoms and the perchlorate anion have been omitted for clarity

gen atom from the μ-carboxyl group and the chelated N and O atoms — form the N_2O_2 square plane. The angles between the bond of the axial oxygen with Cu^{II} and the equatorial bonds ranges from 87.6 to 97.3°, while the bond lengths are similar to those in complex **1**. Similar to complex **1**, the tyrosine in complex **2** coordinates to Cu^{II} ion in a bidentate fashion through N and O donor atoms and a μ-carboxyl group links adjacent Cu^{II} ions (Figure 4). The adjacent subunits are related by a 2_1 operation to form an infinite chiral chain structure similar to complex **1**. The N(1) and O(1) atoms in complex **1** are replaced by a nitrogen atom from 4,4-bipy and an oxygen atom from the bridging carboxyl group in complex **2**, respectively, and the 4,4-bipy ligand bridges the adjacent chiral Cu-Tyr chains to form the extended two-dimensional plane. These 2-D sheets are stacked through hydrogen bonding between the ClO_4^- counterion and the free phenol hydroxyl groups and between the counterion and crystal water. Although both chiral chain structures in **1** and **2** are similar topologically, the Cu−Cu−Cu angle and the distance between adjacent Cu atoms in the same chain are different, as shown in Figure 2 and Figure 4 (76.0° and 4.93 Å in **1**, 141.6° and 5.35 Å in **2**) due to the different coordination position of the oxygen atom of the bridging carboxyl of tyrosine (it is axial in complex **1** and equatorial in complex **2**). We believe that the presence of the 4,4-bipy ligand in **2** is responsible for the subtle tuning of the chiral chain structure, forming a square-planar geometry in the self-assembly process with amino acids.[15,19] The Cu^{II} ion acts as a kind of Lewis acid[20] and can therefore bind Lewis bases, such as the oxygen atom of the bridging carboxyl group in complex **1** and a water molecule of crystallization in complex **2**, in its free axial coordination site.

In conclusion, the use of a 4,4-bipy segmental ligand in Cu-Tyr complex self-assembly processes allows the preparation of a new type of complex $\{[Cu_2(Tyr)_2(4,4\text{-bipy})\cdot 2H_2O]\cdot 2ClO_4\}_n$. This modification of the ligand environment has a considerable effect on the solid-state structure

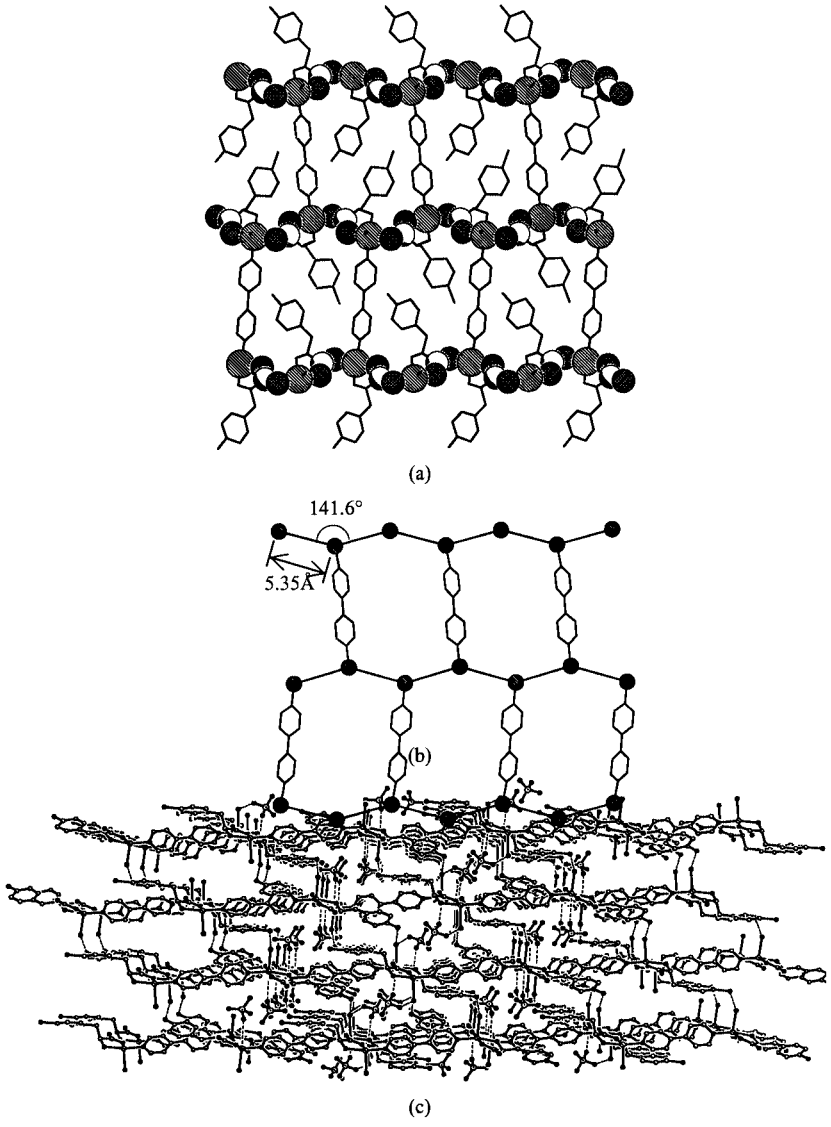

Figure 4. (a) perspective view of the 2-D sheet of **2**; the Cu^{II} and bridging carboxyl are represented by larger circles; (b) 2-D network connectivity in **2**; the filled circles represent the $Cu(Tyr)\cdot H_2O$ unit; (c) stacking of 2-D sheets of **2**

of Cu-Tyr complexes, thus leading to the fine tuning of the structural and stereo conformation.

Experimental Section

Synthesis of $[Cu(Tyr)_2]_n$ (1): A 1.0 M aqueous solution of NaOH was carefully added dropwise to a suspension of L-tyrosine (181 mg, 1.0 mmol) in 10 mL water, with vigorous stirring, until ligand dissolved. The solution was then mixed with a solution of copper perchlorate (576 mg, 1.0 mmol) in 10 mL methanol. The reaction mixture was stirred overnight to give a blue solution, which was then filtered. Blue needle-shaped crystals of $[Cu(Tyr)_2]_n$ (**1**) suitable for X-ray diffraction analysis were obtained after several days' evaporation at room temperature. Yield: 136 mg (64% for tyrosine). $C_{18}H_{20}CuN_2O_6$ (423.9): calcd. C 50.96, H 4.75, N 6.61; found C 50.47, H 4.66, N 6.82.

Synthesis of $\{[Cu_2(Tyr)_2(4,4\text{-bipy})\cdot 2H_2O]\cdot 2ClO_4\}_n$ (2): This complex was synthesized as for complex **1**. 4,4-Bipyridine (156 mg, 1.0 mmol) was added after the overnight reaction step and the mixture was stirred for another 4 h. Single crystals of complex **2** suitable for X-ray diffraction analysis were obtained by evaporation of the filtered mixture at room temperature after two weeks. Yield: 190 mg (43% for tyrosine). $C_{23}H_{32}Cl_2Cu_2N_4O_{16}$ (818.5): calcd. C 38.24, H 3.67, N 6.37; found C 38.86, H 3.68, N 6.62.

X-ray crystallography: The intensity data were collected on a Bruker CCD diffractometer with graphite-monochromated Mo-K_α radiation ($\lambda = 0.71073$ Å) at room temperature. All of the calculations were performed on an HP computer by using the SHELXTL-PL version 5.10 package. The structures were solved by direct methods and refined by full-matrix least-squares (Table 1).[21]

Crystal Data for 1: Blue needle, dimensions 0.25 × 0.20 × 0.10 mm, $C_{18}H_{20}CuN_2O_6$, M_r = 423.90, orthorhombic, space group $P2_12_12_1$; a = 6.0753(12) Å, b = 12.948(3) Å, c = 22.037(4) Å, V = 1733.4(6) Å^3; $\rho_{calc.}$ = 1.624 g/cm^3, Z = 4; $F(000)$ = 876; μ(Mo-K_α) = 1.300 mm^{-1}; 2340 reflections collected, 2340 reflections observed ($|F_0| \geq 2\sigma|F_0|$); R_1 = 0.0397; wR_2 = 0.1004.

Table 1. Crystallographic data for complexes **1** and **2**

	1	**2**
Mol. formula	$C_{18}H_{20}N_2O_6Cu$	$C_{28}H_{32}N_4O_{16}Cu_2Cl_2$
Mol. wt.	423.90	878.56
Crystal system	Orthorhombic	Monoclinic
Space group	$P2_12_12_1$	$P2_1$
a (Å)	6.0753(12)	8.4341(6)
b (Å)	12.948(3)	10.1027(8)
c (Å)	22.037(4)	20.9444(15)
β (deg)	90.00	97.449(2)
V (Å^3)	1733.4(6)	1769.6(2)
Z	4	2
D_c (g·cm^{-3})	1.624	1.649
μ (mm^{-1})	1.300	1.430
R_1 [$I < 2\sigma(I)$][a]	0.0397	0.0782
wR_2 (all data)[b]	0.1107	0.2308

[a] $R_1 = \|\|F_0| - |F_c\|/|F_0|$. [b] $wR_2 = [w(F_0^2 - F_c^2)^2/w(F_0^2)^2]^{1/2}$.

Crystal Data for 2: Blue plate, dimensions 0.30 × 0.30 × 0.20 mm, $C_{28}H_{32}Cl_2Cu_2N_4O_{16}$, M_r = 878.56, monoclinic, space group $P2_1$; a = 8.4341(6) Å, b = 10.1027(8) Å, c = 20.9444(15) Å, β = 97.449(2)°, V = 1769.6(2) Å^3; $\rho_{calc.}$ = 1.649 g/cm^3, Z = 2; $F(000)$ = 896; μ(Mo-K_α) = 1.430 mm^{-1}; 5643 reflections collected, 4318 reflections observed ($|F_o| \geq 2\sigma(|F_o|)$); R_1 = 0.0782; wR_2 = 0.1840. CCDC-176587 and CCDC-176588 contain the supplementary crystallographic data for this paper. These data can be obtained free of charge at www.ccdc.cam.ac.uk/conts/retrieving.html [or from the Cambridge Crystallographic Data Centre, 12, Union Road, Cambridge CB2 1EZ, UK; Fax: (internat.) +44-1223/336-033; E-mail: deposit@ccdc.cam.ac.uk].

Acknowledgments

This work was supported by grants from the National Nature Science Foundation of China, the Chinese Academy of Science and Hong Kong Polytechnic University.

[1] B. Moulton, M. J. Zaworotko, *Chem. Rev.* **2001**, *101*, 1629−1658.
[2] C. Janick, *Angew. Chem. Int. Ed. Engl.* **1997**, *36*, 1431−1438.
[3] O. M. Yaghi, H. Li, H. C. Davis, D. Richardson, T. L. Grog, *Acc. Chem. Res.* **1998**, *31*, 474−484.
[4] S. R. Batten, R. Robson, *Angew. Chem. Int. Ed.* **1998**, *37*, 1460−1494.
[5] Y.-H. Kiang, G. B. Gardner, S. Lee, Z. Xu, E. B. Lobkovsky, *J. Am. Chem. Soc.* **1999**, *121*, 8204−8215.
[6] G. K. M. Shimizu, G. D. Enright, C. I. Ratcliffe, J. A. Ripmeester, *Chem. Commun.* **1999**, 461−462.
[7] M. Kondo, T. Toshitomi, K. Seki, H. Matsuzaka, S. Kitagawa, *Angew. Chem. Int. Ed. Engl.* **1997**, *36*, 1725−1727.
[8] S. Suzuki, K. Yamaguchi, N. Nakamura, Y. Tagawa, H. Kuma, T. Kawamoto, *Inorg. Chim. Acta* **1998**, *283*, 260−267.
[9] C. E. Ruggiero, J. A. Smith, K. Tamizawa, D. M. Dooly, *Biochemistry* **1997**, *36*, 1953−1959.
[10] N. Ito, S. E. V. Phillips, K. D. S. Yadav, P. F. Knowles, *J. Mol. Biol.* **1994**, *238*, 794−801.
[11] N. Strater, T. Klabunde, P. Tucker, H. Witzel, B. Krebs, *Science* **1995**, *268*, 1489−1492.
[12] B. Kauppi, B. B. Nielsen, S. Ramaswamy, I. K. Larsen, M. Thelander, L. Thelander, H. Eklund, *J. Mol. Biol.* **1996**, *262*, 706−720.
[13] A. M. Orville, J. P. Lipscomb, D. H. Ohlendorf, *Biochemistry* **1997**, *36*, 10052−10066.
[14] K. W. Penfield, R. R. Gay, R. S. Himmelwright, N. C. Eickman, V. A. Norris, H. C. Freeman, E. I. Solomon, *J. Am. Chem. Soc.* **1981**, *103*, 4382−4388.
[15] I. Bertini, G. Canti, R. Grassi, *Inorg. Chem.* **1980**, *19*, 2198−2130.
[16] H. Yokoi, A. W. Addison, *Inorg. Chem.* **1997**, *16*, 1341−1349.
[17] H. Yokoi, *Bull. Chem. Soc. Jpn.* **1974**, *47*, 3037−3040.
[18] T. Sugimori, H. Hasuda, N. Ohata, K. Koikawa, A. Odami, O. Yamauchi, *Inorg. Chem.* **1997**, *36*, 576−583.
[19] N. Ito, S. E. V. Phillips, C. Stevens, Z. B. Ogel, M. J. McPherson, J. N. Kean, K. D. Yadav, P. F. Knowles, *Nature* **1991**, *350*, 87−90.
[20] K. Schuhmann, E.-G. Jägen, *Eur. J. Inorg. Chem.* **1998**, 2051−2054.
[21] G. M. Sheldrick, SHELXTL, An integrated system for solving, refining and displaying crystal structures from diffraction data (Version 5.1), University of Göttingen, Germany, 1997.

Received April 23, 2002
[I02209]

Tetraamidosulfurane and its Decomposition Products — an ab initio MO Study[‡]

Ralf Steudel,*[a] Yana Steudel,[a] and Dieter Lentz[b]

Keywords: Sulfur / Hypervalent compounds / Reaction mechanisms / Ab initio calculations

Ab initio MO calculations at the G3(MP2) level of theory show that sulfur tetraamide $S(NH_2)_4$ is a local minimum energy structure but thermodynamically unstable with respect to both sulfur diamide $S(NH_2)_2$ plus hydrazine and sulfurimidediamide $S(NH)(NH_2)_2$ plus ammonia. The activation enthalpy of the latter reaction is 63 kJ·mol^{-1} at 298 K.
(© Wiley-VCH Verlag GmbH, 69451 Weinheim, Germany, 2002)

Introduction

The hypercoordinate compounds of sulfur — also termed as hypervalent — have attracted much attention owing to their unusual bonding situation with formal violation of the octet rule. In particular, sulfur hexafluoride has been investigated theoretically many times. It is now generally accepted that the covalent bonds in this species can be understood on the basis of multi-center interactions of the 3s and 3p atomic orbitals of sulfur with the 2p orbitals of the fluorine atoms, while the high-energy sulfur 3d valence orbitals play a minor role and, to a first approximation, can be neglected, although d and f functions serve as polarization functions in the basis sets used.[1] Compounds of this type are, however, thermodynamically stable only with highly electronegative substituents. The same holds for sulfuranes of the type SX_4, of which many derivatives have been prepared. Examples are SF_4,[2] $SClF_3$,[3] SCl_2F_2,[3] SCl_3F[3] and a large number of tetraoxosulfuranes with bidentate ligands.[4] Tetrachlorosulfurane (SCl_4) is thermodynamically unstable with respect to SCl_2 and Cl_2.[2] Therefore, SCl_4 is still unknown and the same holds for SMe_4,[5] $S(SH)_4$ [6] and SH_4.[7] However, in favorable cases, sulfuranes with substituents of low electronegativity can be prepared, as the successful synthesis of bis(2,2′-biphenylylene)sulfurane has demonstrated.[8]

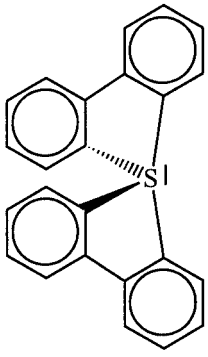

If there is a high enough barrier for the decomposition of SX_4 to the corresponding sulfane (SX_2) and X_2 the molecule SX_4 should be accessible experimentally even if unstable in a thermodynamic sense.

The missing sulfuranes with four identical first-row atoms attached to sulfur are the tetraamidosulfurane $S(NH_2)_4$ and substituted organic derivatives thereof. The electronegativity of nitrogen is slightly higher than that of chlorine on the scales published by Allred[9] and by Allen[10] and should sufficiently stabilize such a structure. Therefore, we have explored for the first time the structure and stability of $S(NH_2)_4$ which represents one of the most basic structures in the very rich chemistry of sulfur-nitrogen compounds.[11] In this context we have also studied the related imidodiamide $S(NH)(NH_2)_2$ and the diamide $S(NH_2)_2$, which are both hypothetical compounds but probable decomposition products of $S(NH_2)_4$. So far, only the sulfurdiamide has been studied by theoretical methods: Leroy et al. reported calculations at the MP2(full)/6-31G(d,p) level of theory resulting in a C_{2v} symmetry for $S(NH_2)_2$, although they did not publish any geometrical details.[12] Kontopoulos and Sigalas[13] optimized the geometry of $S(NH_2)_2$

[‡] Sulfur compounds, 224. Part 223: R. Steudel, K. Hassenberg, J. Pickardt, E. Grigiotto, P. Zanello, *Organometallics* **2002**, *21*, 2604−2608.

[a] Institut für Chemie, Technische Universität Berlin, Sekr. C2, Strasse d. 17. Juni 135, 10623 Berlin, Germany
[b] Institut für Chemie, Freie Universität Berlin, Fabeckstrasse 34−36, 14195 Berlin, Germany

at the MP2/3-21+G(d,p) level and reported two bond lengths and three bond angles but neither the molecular symmetry nor any torsion angles were published. It seems that the latter authors either assumed or obtained the molecular symmetry C_{2v} but the exact geometry remains unknown since two conformations of this symmetry are possible (see below). Partly and fully organyl-substituted derivatives of **1** are known.[11]

Calculations

Standard ab initio MO calculations were performed using the Gaussian 98[14] series of programs. The energies of various equilibrium structures and transition states were examined at the G3(MP2) level of theory.[15] In brief, the G3(MP2) method is a composite procedure which provides an accurate approximation to the high level of theory at QCISD(T)/GTMP2LARGE//MP2(full)/6-31G(d), with the incorporation of zero-point energy [calculated from HF/6-31G(d) vibrational wavenumbers, scaled by 0.8929] and higher level corrections. This level of theory is usually accurate to within 6 kJ·mol^{-1} of experimental values.[15] A charge density analysis, at the MP2(full)/6-31G* level, was performed using the natural bond orbital (NBO) approach.[16] Unless otherwise noted, all relative energies reported in this publication are given as $\Delta H°_{298}$ and correspond to the G3(MP2) level, while structural parameters were obtained at the MP2(full)/6-31G* level. The harmonic vibrational wavenumbers of $S(NH_2)_2$, $S(NH)(NH_2)_2$ and $S(NH_2)_4$ were calculated at the same level.

Results and Discussion

The structures of $S(NH_2)_2$, $S(NH)(NH_2)_2$ and $S(NH_2)_4$ are shown in Figure 1; selected geometrical parameters are given in Table 1. At the global minimum the diamide has C_{2v} symmetry (**1**), although two rotational isomers **2** (C_s) and **3** (C_{2v}) also exist. While **1** and **2** are almost degenerate ($\Delta H°_{298}$ = 1 kJ·mol^{-1}), isomer **3** is less stable than **1** by 9 kJ·mol^{-1} (Table 2), probably as the result of the repulsion between the nitrogen lone pairs which are directed towards each other. In all three conformers the nitrogen lone pairs are orthogonal to the sulfur 3p lone pair, which is expected to occupy the HOMO of these molecules. In the most stable isomer **1** the NBO atomic charges on sulfur, nitrogen and hydrogen are +0.61, −1.03 and +0.36, respectively. The geometrical parameters all have normal values.

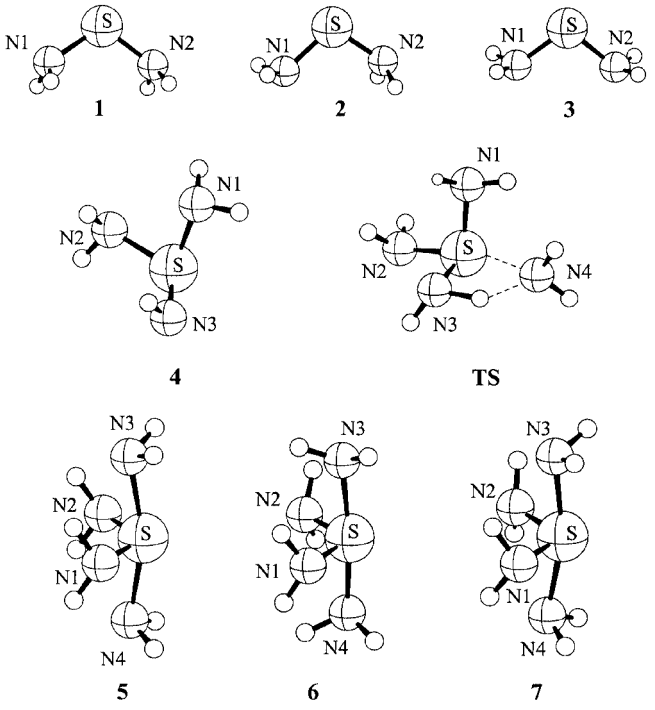

Figure 1. Structures of various rotamers of $S(NH_2)_2$ (**1**−**3**) and $S(NH_2)_4$ (**5**−**7**) as well as structure as $S(NH)(NH_2)_2$ (**4**) and of the transition state **TS** for the formation of **4** from **5**, calculated at the MP2(full)/6-31G* level

The imidodiamide **4** has no symmetry at all (C_1). The S=N bond length of 155.0 pm is considerably shorter than the two formal S−N single bonds of length 173.4 and 174.5 pm. The orientation of the two amido groups seems to be influenced by weak N−H···N hydrogen bonds between N1 and a hydrogen on N2 (250.2 pm) and between N2 and a

Table 1. Selected geometrical parameters of the most stable isomers of $S(NH_2)_2$, $S(NH)(NH_2)_2$ and $S(NH_2)_4$ and of the transition state **TS** for the ammonia extrusion reaction (bond lengths in pm, bond angles and torsion angles in degree); for numbering of atoms see Figure 1

	$S(NH_2)_2$ **1** (C_{2v})	$S(NH)(NH_2)_2$ **4** (C_1)	$S(NH_2)_4$ **5** (C_{2v})	**TS** (C_1)
S−N1	169.6	174.5	169.8	169.6
S−N2	169.6	173.4	169.8	172.3
S−N3		155.0	191.4	166.9
S−N4			191.4	234.9
N−H	101.6	102.1−102.9	102.0(eq)/102.6(ax)	102.0−102.6
N1−S−N2	110.5	87.9	116.9	98.4
N1−S−N3		118.7	85.5	105.5
N1−S−N4			85.5	87.6
N2−S−N3		106.4	85.5	94.3
H−N−H	111.4	109.1±0.2	103.9(ax)/111.4(eq)	
S−N−H	115.0	112.3(S=NH)		108.9(S=NH)

Table 2. Relative energies and enthalpies (kJ·mol^{-1}) of $S(NH_2)_2$ and $S(NH_2)_4$; the absolute energies of **1** and **5** are −509.47982 and −621.15958 hartree, respectively

G3(MP2)	ΔE_0°	ΔH°_{298}	ΔG°_{298}
$S(NH_2)_2$ **1**	0	0	0
$S(NH_2)_2$ **2**	1	1	1
$S(NH_2)_2$ **3**	8	9	8
$S(NH_2)_4$ **5**	0	0	0
$S(NH_2)_4$ **6**	12	12	11
$S(NH_2)_4$ **7**	14	15	13

hydrogen on N1 (249.4 pm); the N···H bond lengths given in parentheses are slightly shorter than the sum of the van der Waals radii (270 pm). The NBO atomic charges are +1.52 on sulfur, −1.14 on the amido nitrogens and −1.22 on the imido nitrogen. The four amido hydrogen atoms (+0.40) are slightly more positive than the imido hydrogen (+0.36). Salts containing the anion $S(NR)_3^{2-}$ — formally the substituted dianion of **4** — have been prepared recently.[17]

The tetraamide exists as three conformers: the most stable one is of C_{2v} symmetry (**5**) while the other two are of C_s symmetry (**6** and **7**). Their structures are in agreement with the expectations from VSEPR theory placing the lone pair at sulfur in an equatorial position of the trigonal bipyramids. The two axial substituents are bent towards the equatorial ones with $N_{ax}-S-N_{ax}$ bond angles of 162.7° (**5**), 165.4° (**7**) and 171.1° (**6**). The most symmetrical structure **5** seems to be stabilized by four N···H hydrogen bonds of length 215.8 pm between the axial nitrogens and the hydrogen atoms of the equatorial amido groups. However, since these bridges are bent by 94.4° and not aligned with the axes of the lone pair orbitals on the nitrogen atoms the hydrogen bonds will be weak. Interestingly, the two equatorial amido groups together with the sulfur atom have the same conformation as the most stable conformer of $S(NH_2)_2$ **1**. There are no indications for hydrogen bonds in rotational isomer **6**; however, four short N···H contacts of 216 pm (two) and 227 pm (two) can be recognized in **7**. However, for these interactions the same geometrical restrictions hold true as mentioned above in the case of isomer **5**. The absolute and relative energies of the di- and tetraamides are given in Table 2.

Table 3. Reaction energies and enthalpies (kJ·mol^{-1}) for the decomposition of $S(NH_2)_4$ **5**. The absolute energies of **TS**, $S(NH)(NH_2)_2$, N_2H_4 and NH_3 are −621.13591, −564.72321, −111.69962, and −56.47014 hartree, respectively

G3(MP2):	ΔE_0°	ΔH°_{298}	ΔG°_{298}
$S(NH_2)_4 \rightarrow S(NH_2)_2$ **1** + N_2H_4	−52	−48	−102
$S(NH_2)_4 \rightarrow$ **TS**	62	63	62
$S(NH_2)_4 \rightarrow S(NH)(NH_2)_2 + NH_3$	−87	−83	−134

The data presented in Table 3 demonstrate that tetraamidosulfurane is thermodynamically unstable with respect to a decomposition both to the diamide plus hydrazine and to the imidodiamide plus ammonia. The latter reaction is clearly favored with a reaction enthalpy of −83 kJ·mol^{-1} compared to only −48 kJ·mol^{-1} for the hydrazine extrusion.

The transition state (**TS**) for the ammonia elimination has been located; its structure is shown in Figure 1. The reaction begins with a transformation of **5** into **7**. Then, one of the axial S−N bonds increases from 191.3 pm in the sulfurane **7** to 243.9 pm in **TS** while one hydrogen atom of an equatorial amido group forms a bridge to the leaving axial NH_2 group with N···H distances of 117.2 (to N3) and 145.6 pm (to N4). The angle N3−H−N4 is 133.6°. Thus, the formation of NH_3 can clearly be recognized in the structure of **TS**, which is of C_1 symmetry. Simultaneously, the other axial S−N bond decreases in length from 191.3 pm in **7** to 172.3 pm in **TS**. The activation enthalpy at 298 K with respect to the most stable conformer **5** is 63 kJ·mol^{-1}. Thus, it is surprising that $S(NH_2)_4$ has not been prepared yet.

Unexpectedly, the decomposition of **5** to hydrazine and sulfurdiamide is also strongly exothermic despite the weak N−N bond in hydrazine. Despite numerous attempts, at various levels of theory, we did not succeed in locating a transition state for this reaction on the potential energy hypersurface. Instead, the formation of ammonia was always the preferred reaction. If the NH distances were kept con-

Table 4. Calculated harmonic fundamental modes (cm^{-1}) of the most stable conformers of $S(NH_2)_2$, $S(NH)(NH_2)_2$ and $S(NH_2)_4$ [unscaled; MP2(full)/6-31G* level]; infrared intensities in parentheses (km mol^{-1})

$S(NH_2)_2$ **1** (C_{2v})	$S(NH)(NH_2)_2$ **4** (C_1)	$S(NH_2)_4$ **5** (C_{2v})
symm.: 3544(1), 3540(3), 1690(27), 1676(2), 921(86), 868(5), 640(30), 564(547), 330(1)	3616(16), 3604(17), 3496(16), 3474(10), 3438(2), 1652(13), 1645(96), 1224(19), 1167(41), 1087(30), 1067(200), 921(145), 905(103), 716(99), 712(123), 660(306), 461(14), 404(23), 389(23), 303(23), 276(1)	symm.: 3547(1), 3500(29), 3495(2), 3439(1), 1680(3), 1646(163), 1636(8), 1026(28), 1005(31), 972(93), 920(125), 769(448), 740(0), 475(1), 412(4), 372(38), 313(25), 234(0)
asymm.: 3666(0), 3660(28), 1123(6), 1118(0), 527(78), 451(0)		asymm.: 3622(89), 3621(0), 3546(0), 3440(9), 1667(39), 1239(67), 1175(0), 973(0), 925(230), 601(354), 522(0), 466(73), 404(10), 397(0), 273(0)

stant to suppress the NH_3 formation the only transition states found were those for the pyramidal inversion at the nitrogen atoms. Furthermore, the transition states for the decomposition of SF_4, SCl_4 and $S(SMe)_4$ were used to design the starting geometries for the wanted transition state,but these attempts also failed.

The thermodynamic instability of $S(NH_2)_4$ may be explained by the weakness of the two axial S−N bonds, which can be estimated from their rather long bond lengths (191.4 pm in **5**) compared to those of the equatorial bonds (169.8 pm) and to the S−N bonds in $S(NH_2)_2$ (169.6 pm in **1**). The gain in entropy also favors the two decomposition reactions.

To support future preparative work on these compounds the knowledge of the fundamental harmonic vibrational modes may be helpful. These data are given in Table 4.

Acknowledgments

We are grateful to Prof. Richard Wong, Singapore, for his invaluable advice. This work has been supported by the Deutsche Forschungsgemeinschaft, the Verband der Chemischen Industrie and the Konrad-Zuse-Zentrum für Informationstechnik Berlin.

[1] A. E. Reed, F. Weinhold, *J. Am. Chem. Soc.* **1986**, *108*, 3586−3593; A. E. Reed, P. von R. Schleyer, *J. Am. Chem. Soc.* **1990**, *112*, 1434−1445; D. L. Cooper, T. P. Cunningham, J. Gerrat, P. B. Karadakov, M. Raimondi, *J. Am. Chem. Soc.* **1994**, *116*, 4414−4426.
[2] Y. Drozdova, R. Steudel, W. Koch, K. Miaskiewicz, I. A. Topol, *Chem. Eur. J.* **1999**, *5*, 1936−1943.
[3] R. Minkwitz, U. Nass, J. Sawatzki, *J. Fluorine Chem.* **1986**, *31*, 175−182.
[4] J. Drabowicz, in *Chemistry of Hypervalent Compounds* (Ed.: K. Akiba), Chapter 7, Wiley-VCH, New York, **1999**, pp. 211−240.
[5] C. J. Marsden, B. A. Smart, *Organometallics* **1995**, *14*, 5399−5409.
[6] R. Steudel, Y. Steudel, K. Miaskiewicz, *Chem. Eur. J.* **2001**, *7*, 3281−3290.
[7] Y. Yoshioka, J. D. Goddard, H. F. Schaefer, *J. Chem. Phys.* **1981**, *74*, 1855−1863; C. S. Ewig, J. R. Van Wazer, *J. Am. Chem. Soc.* **1989**, *111*, 1552−1558; J. Moc, A. E. Dorigo, K. Morokuma, *Chem. Phys. Lett.* **1993**, *204*, 65−72; C. S. Marsden, B. A. Smart, *Aust. J. Chem.* **1994**, *47*, 1431−1440.
[8] S. Ogawa, Y. Matsunaga, S. Sato, I. Iida, N. Furukawa, *J. Chem. Soc., Chem. Commun.* **1992**, 1141−1142.
[9] A. L. Allred, *J. Inorg. Nucl. Chem.* **1961**, *17*, 215−221; D. Quane, *J. Inorg. Nucl. Chem.* **1971**, *33*, 2722−2726.
[10] L. C. Allen, *J. Am. Chem. Soc.* **1989**, *111*, 9003−9014.
[11] *Gmelin Handbook of Inorganic and Organometallic Chemistry*, 8th ed., *Sulfur-Nitrogen Compounds*, Parts 1−10b, Springer, Berlin, **1977−1994**.
[12] G. Leroy, J.-P. Dewispelaere, H. Benkadour, D. Riffi Temsamani, C. Wilante, *J. Mol. Struct. (Theochem)* **1995**, *334*, 137−143.
[13] C. Kontopoulos, M. P. Sigalas, *J. Mol. Struct. (Theochem)* **1999**, *490*, 125−131.
[14] Gaussian 98 (Revision A.7), M. J. Frisch, G. W. Trucks, H. B. Schlegel, G. E. Scuseria, M. A. Robb, J. R. Cheeseman, V. G. Zakrzewski, J. A. Montgomery, R. E. Stratmann, J. C. Burant, S. Dapprich, J. M. Millam, A. D. Daniels, K. N. Kudin, M. C. Strain, O. Farkas, J. Tomasi, V. Barone, M. Cossi, R. Cammi, B. Mennucci, C. Pomelli, C. Adamo, S. Clifford, J. Ochterski, G. A. Petersson, P. Y. Ayala, Q. Cui, K. Morokuma, D. K. Malick, A. D. Rabuck, K. Raghavachari, J. B. Foresman, J. Cioslowski, J. V. Ortiz, B. B. Stefanov, G. Liu, A. Liashenko, P. Piskorz, I. Komaromi, R. Gomperts, R. L. Martin, D. J. Fox, T. Keith, M. A. Al-Laham, C. Y. Peng, A. Nanayakkara, C. Gonzalez, M. Challacombe, P. M. W. Gill, B. G. Johnson, W. Chen, M. W. Wong, J. L. Andres, M. Head-Gordon, E. S. Replogle, J. A. Pople, Gaussian, Inc., Pittsburgh, PA, **1998**.
[15] L. A. Curtiss, P. C. Redfern, K. Raghavachari, V. Rassolov, J. A. Pople, *J. Chem. Phys.* **1999**, *110*, 4703−4709.
[16] A. E. Reed, L. A. Curtiss, F. Weinhold, *Chem. Rev.* **1988**, *88*, 899−926.
[17] R. Fleischer, D. Stalke, *Coord. Chem. Rev.* **1998**, *176*, 431−450.

Received March 28, 2002
[I02165]

Facile C−S Bond Activation of Levamisole Hydrochloride on a Triruthenium Cluster Core

Javier A. Cabeza,*[a] Ignacio del Río,[a] Santiago García-Granda,[b] Víctor Riera,[a] and M. Gabriela Sánchez-Vega[c]

Keywords: Ruthenium / Metal clusters / Levamisole / S ligands / C−S bond activation

The reaction of $[Ru_3(CO)_{12}]$ with levamisole hydrochloride ([Hlvms]Cl) leads to $[Ru_3(\mu\text{-}Cl)(\mu\text{-}\eta^2\text{-}C_{11}H_{13}N_2S\text{-}C,S)(CO)_9]$ (**1**). This complex contains a new ligand that arises from an unprecedented oxidative addition of an S–C bond of protonated levamisole to a metal atom, and is the first example of a non-mononuclear complex derivative of levamisole. The mechanism of this reaction has been partially elucidated by studying the reaction of $[Ru_3(MeCN)_2(CO)_{10}]$ with [Hlvms]Cl and $[Ru_3(\mu\text{-}Cl)(CO)_{10}]^-$ with [Hlvms][BF_4]. It is concluded that upon treatment with levamisole hydrochloride, $[Ru_3(CO)_{12}]$ is attacked by the chloride anion to give $[Ru_3(\mu\text{-}Cl)(CO)_{10}]^-$; a subsequent coupling of this cluster anion with the $[Hlvms]^+$ cation leads to an uncharacterized neutral derivative which has an intact [Hlvms] group attached to a ruthenium atom through the sulfur atom. This neutral derivative readily undergoes an S–C bond activation process to give compound **1**. (© Wiley-VCH Verlag GmbH, 69451 Weinheim, Germany, 2002)

Introduction

Levamisole (lvms), (−)-2,3,5,6-tetrahydro-6-phenylimidazo[2,1-*b*]thiazole, and levamisole hydrochloride ([Hlvms]Cl) are well-known anthelmintic drugs with immunomodulatory[1] and anticancer[2] activities.

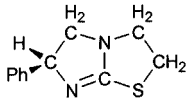

levamisole

From the point of view of coordination chemistry, levamisole is an attractive ligand because (a) it possesses three heteroatoms liable to attach metal atoms, (b) it has several C-heteroatom bonds that can be activated or modified by reaction with metal complexes, and (c) due to the presence of a stereogenic carbon atom, it may lead to optically active metal-containing products.

Very few inorganic derivatives of levamisole have been reported so far, the only examples being the complexes $[MCl_2(lvms)_2]$ (M = Co,[3] Ni,[3] Pd,[4] Cu,[3] Zn[3]), [Pd(η^2-amino acidato)$(lvms)_2$]Cl[4] and [PtCl(en)(lvms)]Cl.[5] Interestingly, the zinc complex $[ZnCl_2(lvms)_2]$ is less toxic and has a higher immunomodulating activity than uncomplexed levamisole.[3] In all these coordination compounds, levamisole behaves as a monodentate ligand which binds the metal through the N^7 atom. It is noteworthy that no complexes derived from levamisole hydrochloride and no complexes of nuclearity higher than one derived from any form of levamisole have been reported previously.

The molecular activation of C−S bonds by metal cluster complexes is currently receiving a great deal of attention in relation to hydrodesulfurization processes.[6] In particular, the use of transition metal carbonyl clusters as models for catalyst surfaces is based on the cluster-surface analogy proposed by Muetterties,[7] in which the cluster is viewed as a small fragment of the surface. Although it is realized that the metal atoms of molecular clusters are chemically very different from those of bulk metals, it is believed that the coordination of molecules to clusters and surfaces is similar because they are essentially localized phenomena.[6]

We now report the reactions of some triruthenium carbonyl cluster complexes with levamisole and levamisole hydrochloride, in which a facile C−S bond activation process has been recognized as a key reaction step.

Results and Discussion

The reactions of $[Ru_3(CO)_{12}]$ and $[Ru_3(MeCN)_2(CO)_{10}]$ with levamisole at different temperatures (10−80 °C) led to mixtures of many compounds which could not be satisfact-

[a] Departamento de Química Orgánica e Inorgánica, Instituto de Química Organometálica "Enrique Moles", Universidad de Oviedo-CSIC,
33071 Oviedo, Spain
Fax: (internat.) +34-985/103-446
E-mail: jac@sauron.quimica.uniovi.es
[b] Departamento de Química Física y Analítica, Universidad de Oviedo,
33071 Oviedo, Spain
[c] Departamento de Química, Universidad de Carabobo, Ciudad Universitaria,
Bárbula, Venezuela

orily separated and identified. However, levamisole hydrochloride reacted smoothly with $[Ru_3(CO)_{12}]$ in THF at reflux temperature to give $[Ru_3(\mu\text{-}Cl)(\mu\text{-}\eta^2\text{-}C_{11}H_{13}N_2S\text{-}C,S)(CO)_9]$ (**1**) in high yield (Scheme 1).

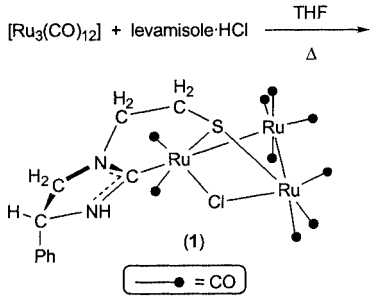

Scheme 1. Synthesis of compound **1**

An X-ray diffraction study on $\mathbf{1}\cdot C_6H_6$ (Figure 1, Table 1) revealed that this compound is a 50-electron cluster with an open edge which is doubly bridged by the chloride ligand and by the sulfur atom of a 1-ethylenethiolate-3,4,5-trihydro-4-phenylimidazol-2-yl ligand. The C^2 atom of the imidazole ring is also attached to one of the ruthenium atoms of the open edge. The original N-*H* proton and the original chirality of levamisole hydrochloride are maintained in compound **1**.

Interestingly, the new organic ligand of complex **1** arises from an unprecedented oxidative addition of an S−C bond of protonated levamisole to a metal atom. Complex **1** is also the first example of a non-mononuclear derivative of levamisole.

In an attempt to shed light on the reaction pathway that leads to compound **1** from $[Ru_3(CO)_{12}]$, we treated the activated complex $[Ru_3(MeCN)_2(CO)_{10}]$[8] with levamisole hydrochloride in dichloromethane, expecting the observation of intermediates that are stable at room temperature. The anionic complex $[Ru_3(\mu\text{-}Cl)(CO)_{10}]^-$ was observed immediately by IR spectroscopy.[9] A spot TLC analysis of the solution also indicated the presence of small amounts of **1**, $[Ru_3(CO)_{12}]$ and a yellow compound that decomposed on the TLC plate after a couple of minutes. Heating this solution to reflux temperature led to compound **1** as the major product. In a subsequent experiment, we treated $[Ru_3(\mu\text{-}Cl)(CO)_{10}]^-$ (formed in situ from $[Ru_3(CO)_{12}]$ and [PPN]Cl)[9] with $[Hlvms][BF_4]$ (made from levamisole and $[HOEt_2][BF_4]$). Again, a mixture of $[Ru_3(CO)_{12}]$, the unknown yellow product and compound **1** was observed *at room temperature*. Unfortunately, all attempts to isolate the yellow compound were unsuccessful, since chromatographic supports promoted its transformation into complex **1**.

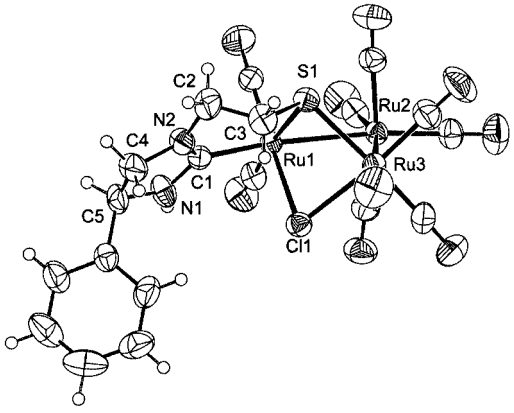

Figure 1. Molecular structure of compound **1**; thermal ellipsoids are drawn at the 50% probability level

Table 1. Selected interatomic distances and angles in $\mathbf{1}\cdot C_6H_6$

Distances (Å)		Angles (°)	
Ru(1)−Ru(2)	2.8788(9)	Ru(1)−Ru(2)−Ru(3)	68.87(3)
Ru(1)−Ru(3)	3.2431(8)	Ru(1)−S(1)−Ru(3)	84.58(6)
Ru(2)−Ru(3)	2.8568(8)	Ru(1)−Cl(1)−Ru(3)	80.91(5)
Ru(1)−S(1)	2.408(1)	Ru(1)−S(1)−C(3)	104.4(2)
Ru(1)−Cl(1)	2.506(1)	Ru(3)−S(1)−C(3)	107.9(2)
Ru(1)−C(1)	2.084(6)	Ru(1)−C(1)−N(1)	121.8(5)
Ru(3)−S(1)	2.411(1)	Ru(1)−C(1)−N(2)	130.3(5)
Ru(3)−Cl(1)	2.493(1)	S(1)−C(3)−C(2)	111.1(5)
S(1)−C(3)	1.826(6)	N(2)−C(2)−C(3)	112.1(6)
N(1)−C(1)	1.351(8)	C(1)−N(2)−C(2)	126.8(5)
N(1)−C(5)	1.460(7)	N(1)−C(1)−N(2)	107.8(5)
N(2)−C(1)	1.304(8)	C(1)−N(1)−C(5)	113.5(5)
N(2)−C(2)	1.464(9)	N(1)−C(5)−C(4)	101.6(5)
N(2)−C(4)	1.463(7)	C(1)−N(2)−C(4)	114.2(5)
C(2)−C(3)	1.49(1)	N(2)−C(2)−C(3)	112.1(6)
C(4)−C(5)	1.53(1)	N(2)−C(4)−C(5)	102.3(5)

The above data suggest that upon treatment with levamisole hydrochloride, $[Ru_3(CO)_{12}]$ is attacked by the chloride anion to give $[Ru_3(\mu\text{-}Cl)(CO)_{10}]^-$. A subsequent coupling of this anion with the $[Hlvms]^+$ cation would lead to a neutral derivative which probably has an intact [Hlvms] group attached to a ruthenium atom through the sulfur atom, but which readily undergoes an S−C bond activation process to give compound **1**. The low solubility of levamisole hydrochloride in THF at room temperature made it necessary to carry out the reaction at reflux temperature and this prevented the observation of intermediates.

Metal cluster-mediated S−C bond activation processes have often been achieved when working with organic sulfur-containing compounds at elevated temperatures.[6] However, such processes have never been observed at room temperature in ruthenium cluster chemistry.[10−14] For comparison purposes, it should be noted that the reaction of $[Ru_3(CO)_{12}]$ with thiophene proceeds via C−S bond cleavage to yield the sulfur-free ferrole-type complex $[Ru_2(\mu\text{-}C_4H_4)(CO)_6]$ and the tetranuclear cluster $[Ru_4(\mu_3\text{-}S)(\mu\text{-}C_4H_4)(CO)_{11}]$.[10] Analogous products were obtained from the reactions with 2-methylthiophene.[10] In the reaction of $[Ru_3(CO)_{12}]$ with benzothiophene, the insertion of a metal atom into the less hindered C−S bond occurs to give the ruthenium analogs of benzoferrole and benzothiaferrole, in addition to the desulfurized ruthenaindenyl complex $[Ru_3(\mu_3\text{-}C_8H_6)(CO)_6]$.[11] Similarly, regiospecific insertion into the less hindered C−S bond occurs in the reaction of $[Ru_3(CO)_{12}]$ with 2,2′-bithiophene, which leads to $[Ru_2(\mu\text{-}C_8H_6S)(CO)_6]$.[12] The sulfide derivatives $[Ru_3(\mu_3\text{-}S)(CO)_{10}]$, $[Ru_3(\mu_3\text{-}S)(\mu\text{-}H)_2(CO)_9]$ and $[Ru_4(\mu_4\text{-}S)(CO)_{11}]$ have been

prepared from $[Ru_3(CO)_{12}]$ and thiophenol.[13] The reaction of $[Ru_3(CO)_{12}]$ with 2-(diphenylphosphanyl)thiophenol gives the phenyl derivative $[Ru_3(\mu_3\text{-}S)(\mu\text{-}C_6H_5)(\mu\text{-}PPh_2)(PPh_3)(CO)_6]$, in which both C−S and C−P bonds have been activated.[14]

Further studies on the synthesis of levamisole-derived metal complexes are underway.

Concluding Remarks

From the above results, the following conclusions can be drawn:

(a) The synthesis of the first non-mononuclear metal complex derivative of levamisole is described (compound **1**). Only a few inorganic derivatives of levamisole have been reported previously,[3−5] some of which have important biological activity as immunomodulatory drugs.[3]

(b) Compound **1** is the first metal complex derivative of levamisole hydrochloride. The chirality of the free ligand is maintained in the metal complex.

(c) Compound **1** arises from a facile S−C bond activation process which opens the thiazolic ring. Such a process is unprecedented for levamisole and its derivatives.

(d) Chemical evidence has been presented that sheds light on the mechanism of the formation of compound **1** from $[Ru_3(CO)_{12}]$ and levamisole hydrochloride. It reveals that the S−C bond activation process also takes place at room temperature. The activation of S−C bonds by ruthenium clusters has never been observed previously at room temperature.

Experimental Section

General Remarks: Solvents were dried over sodium diphenyl ketyl (THF, hydrocarbons) and distilled under nitrogen prior to use. The reactions were carried out under nitrogen, using Schlenk-vacuum line techniques, and were routinely monitored by solution IR spectroscopy (carbonyl stretching region). IR: Perkin−Elmer Paragon 1000 FT. NMR: Bruker DPX-300, room temperature, $SiMe_4$ as internal standard. Microanalyses were obtained from the University of Oviedo Analytical Service. FAB-MS were obtained from the University of Santiago de Compostela Mass Spectroscopic Service; data given refer to the most abundant molecular ion isotopomer.

Compound 1: A mixture of $[Ru_3(CO)_{12}]$ (100 mg, 0.158 mmol) and levamisole hydrochloride (42 mg, 0.173 mmol) in THF (25 mL) was stirred at reflux temperature for 40 min. After cooling down to room temperature, the insoluble excess of levamisole hydrochloride was filtered off. Concentration to ca. 5 mL and addition of hexane (15 mL) led to precipitation of compound **1** as an orange solid (105 mg, 93%). $C_{20}H_{13}ClN_2O_9Ru_3S$ (796.09): calcd. C 30.18, H 1.65, N 3.52; found C 30.26, H 1.71, N 3.42. FAB-MS: *m/z* = 797 [M^+]. IR (CH_2Cl_2): ν(CO) = 2085 (m), 2048 (s), 2003 (vs), 1993 (sh), 1948 (w) cm^{-1}. ^1H NMR (CD_2Cl_2): δ = 7.6−7.2 (m, 5 H), 6.44 (br. s, 1 H), 5.05 (m, 1 H), 4.4−2.9 (m, 6 H) ppm.

X-ray Crystallographic Study: A single crystal of **1**·C_6H_6 was measured on a Nonius CAD4 diffractometer, equipped with a graphite crystal monochromator, using the ω-2θ scan technique with a variable scan rate and a maximum scan time of 60 s per reflection (Table 2). 2648 Friedel pairs were measured. An empirical absorption correction was applied using XABS2,[15] maximum and minimum transmission factors 0.683 and 0.571. Lorentz and polarization corrections were applied and data reduced to F_0^2 values. The structure was solved by Patterson interpretation using DIRDIF-96.[16] Isotropic and full-matrix anisotropic least-squares refinements were carried out using SHELXL-97.[17] All non H-atoms were refined anisotropically. Hydrogen atom positions were geometrically calculated and refined riding on their parent atoms, except for the N-*H* proton, which was observed and freely refined. The molecular plot was made with the EUCLID program package.[18] The WINGX program system[19] was used throughout the structure determination.

Table 2. Crystallographic and refinement data for **1**·C_6H_6

Formula	$C_{20}H_{13}ClN_2O_9Ru_3S{\cdot}C_6H_6$
Molecular weight	874.15
Crystal system	orthorhombic
Space group	$P2_12_12_1$
a [Å]	12.752(6)
b [Å]	13.174(4)
c [Å]	18.334(9)
V [Å^3]	3080.1(19)
Z	4
F(000)	1704
$D_{calcd.}$ [g cm^{-3}]	1.659
λ (radiation) [Å]	0.71073 (Mo-K_α)
Crystal size [mm^3]	0.33 × 0.26 × 0.23
T [K]	293(2)
μ [mm^{-1}]	1.659
Min./max. *h, k, l*	−15/15, −16/16, −22/22
Measured reflns	6776
Unique reflns	6035
Reflns with [$I > 2\sigma(I)$]	5109
Parameters	367
GoF on F^2	1.081
R_1 (on *F*, $I > 2\sigma(I)$]	0.0336
wR_2 (on F^2, all data)	0.0871
Min., max Δρ, [e Å^{-3}]	−0.631, 0.486
Flack parameter	−0.04(5)

CCDC-178931 contains the supplementary crystallographic data for this paper. These data can be obtained free of charge at www.ccdc.cam.ac.uk/conts/retrieving.html [or from the Cambridge Crystallographic Data Centre, 12, Union Road, Cambridge CB2 1EZ, UK; Fax: (internat.) +44-1223/336-033; E-mail: deposit@ccdc.cam.ac.uk].

Acknowledgments

This work was supported by the Spanish DGESIC (grant PB98-1555 to J.A.C.). M.G.S.-V. thanks the Universities of Oviedo and Carabobo for granting her a research stay in Oviedo.

[1] W. K. P. Amery, J. P. J. M. Bruynseels, *Int. J. Immunopharmacol.* **1992**, *14*, 481−486 and refs. cited therein.
[2] J. S. Kovach, P. A. Svingen, D. J. Schaid, *J. Natl. Cancer Inst.* **1992**, *84*, 515−519 and refs. cited therein.
[3] T. B. Kovachev, P. N. Stamberov, D. S. Ivanov, M. K. Mitcheva, S. P. Marinova, H. A. Astroug, J. N. Stoychkov, *Pharmazie* **1994**, *49*, 25−27.
[4] A. M. Nijasure, V. N. Joshi, A. D. Savant, *J. Inorg. Biochem.* **1999**, *73*, 109−115.

[5] G. M. Arvanitis, M. E. Bernardini, G. N. Parkinson, B. S. Schneider, *Acta Crystallogr., Sect. C* **1993**, *49*, 1246−1248.
[6] For a recent review on metal clusters as models for hydrodesulfurization catalysts, see: M. Brorson, J. D. King, K. Kiriakidou, F. Prestopino, E. Nordlander, in *Metal Clusters in Chemistry* (Eds.: P. Braunstein, L. A. Oro, P. R. Raithby), Wiley-VCH, Weinheim, **1999**, p.741.
[7] [7a] E. L. Muetterties, *Bull. Soc. Chim. Belg.* **1975**, *84*, 959−972. [7b] E. L. Muetterties, T. N. Rhodin, E. Band, C. F. Bruker, W. R. Pretzer, *Chem. Rev.* **1979**, *79*, 91−137.
[8] G. A. Foulds, B. F. G. Johnson, J. Lewis, *J. Organomet. Chem.* **1985**, *296*, 147−153.
[9] G. Lavigne, H. D. Kaesz, *J. Am. Chem. Soc.* **1984**, *106*, 4647−4648.
[10] A. J. Arce, P. Arrojo, A. J. Deeming, Y. de Sanctis, *J. Chem. Soc., Dalton Trans.* **1992**, 2423−2424.
[11] A. J. Arce, Y. de Sanctis, A. Karam, A. J. Deeming, *Angew. Chem. Int. Ed. Engl.* **1994**, *33*, 1381−1383.
[12] A. J. Arce, P. Arrojo, Y. de Sanctis, M. Márquez, A. J. Deeming, *J. Organomet. Chem.* **1994**, *479*, 159−164.
[13] R. D. Adams, J. E. Babin, M. Tasi, *Inorg. Chem.* **1986**, *25*, 4514−4519.
[14] J. A. Cabeza, M. A. Martínez-García, V. Riera, D. Ardura, S. García-Granda, *Eur. J. Inorg. Chem.* **2000**, 499−503.
[15] S. Parkin, B. Moezzi, H. Hope, *J. Appl. Crystallogr.* **1995**, *28*, 53−56.
[16] P. T. Beurskens, G. Beurskens, W. P. Bosman, R. de Gelder, S. García-Granda, R. O. Gould, R. Israël, J. M. M. Smits, *The DIRDIF-96 Program System*, Crystallography Laboratory, University of Nijmegen, The Netherlands, **1996**.
[17] G. M. Sheldrick, *SHELXL-97, version 97−2*, University of Göttingen, Germany, **1997**.
[18] A. L. Spek, *The EUCLID Package*, in *Computational Crystallography* (Ed.: D. Sayre), Clarendon Press, London, **1982**, p. 528.
[19] L. J. Farrugia, *J. Appl. Cryst.* **1999**, *32*, 837−838.

Received March 4, 2002
[I02111]

Fullerene and Carborane in One Coordination Sphere: Synthesis and Structure of a Mixed η^2-C_{60} and σ-Carboranyl Complex of Iridium

Alexander V. Usatov,*[a] Ekaterina V. Martynova,[a] Fedor M. Dolgushin,[a] Alexander S. Peregudov,[a] Mikhail Yu. Antipin,[a] and Yurii N. Novikov[a]

Keywords: Fullerenes / Boranes / Iridium / Complexes / X-ray analysis

The first representative of metal complexes containing two different polyhedral clusters (namely, a fullerene and a carborane) as ligands in the same coordination sphere of the metal atom, [(η^2-C_{60})Ir(*o*-$HCB_{10}H_9CCH_2PPh_2$-*B*,*P*)(*t*BuNC)$_2$] (**II**), was synthesized in the reaction of C_{60} with the metallacyclic carboranyliridium dihydride complex [Ir(H)$_2$(*o*-$HCB_{10}H_9CCH_2PPh_2$-*B*,*P*)(PPh_3)(L)] (L = CO or PPh_3) by reflux in toluene in the presence of 2 equiv. of *t*BuNC. The compound obtained was characterized by analytical and spectroscopic (UV, IR, ^{1}H and ^{31}P NMR) data. The molecular structure of complex **II** was determined by single-crystal X-ray diffraction analysis, which showed that the most interesting structural feature of **II** is the distortion of the iridacyclopropane moiety due to the strong *trans* influence of the B-σ-carboranyl fragment.

(© Wiley-VCH Verlag GmbH, 69451 Weinheim, Germany, 2002

Most of the currently obtained metal complexes of fullerenes are known to possess η^2-coordination due to both electron-acceptor properties and the weakly conjugated polyene character of the fullerene molecule. However, all the complexes known to date exhibit a "symmetrical" η^2-coordination, where the metal atom is equidistant from the carbon atoms of the double bond because of the *trans* arrangement of either identical ligands or ligands having similar *trans* influence with respect to these carbon atoms.[1,2] With the ligands substantially different in there *trans* influence, one would, however, expect the formation of metal complexes of fullerene with "nonsymmetric" or slip-distorted η^2-coordination. The aim of this work was to attempt the synthesis of the first representatives of slip-distorted metal η^2-complexes of fullerene.

The initial metal complexes were *cis*-dihydridoiridium complexes [Ir(H)$_2$(*o*-$HCB_{10}H_9CCH_2PPh_2$-*B*,*P*)(PPh_3)(L)] (**Ia**, L = PPh_3; **Ib**, L = CO) chelated to the B-σ-carboranylphosphane fragment recently obtained by us.[3] Reductive elimination of a dihydrogen molecule from these complexes can result in an unsaturated Ir^+ intermediate capable of forming corresponding adducts with the electron-acceptor fullerene molecule. In addition, the bulky B-σ-carboranyl fragment should occupy a *trans* position with respect to the fullerene ligand that has a much stronger *trans* influence compared to phosphane.

We found that dihydrides chosen by us do not react with fullerene upon heating in toluene or chlorobenzene. This seems to be due to their unusual thermal stability, since these compounds do not undergo reductive elimination of dihydrogen, even upon heating in toluene or decane. It is well known that the presence of electron-acceptor ligands in the coordination sphere of a metal atom promotes the reductive elimination. To this end, we used the *t*BuNC ligand that combines the strong π-acceptor and σ-donor properties and can stabilize the complexes of transition metals both in low and high oxidation states. Such stabilisation is of great importance both for the reductive elimination and, especially, for the coordination of the intermediate metal complex to the electron-accepting fullerene molecule in the next stage of reaction. Indeed, in the presence of 2 equiv. of *t*BuNC, the dihydrido complexes **Ia** or **Ib** react smoothly with fullerene C_{60} in refluxing toluene by replacement of the triphenylphosphane or carbonyl ligand, respectively, by isocyanide with elimination of an H_2 molecule. The novel (η^2-C_{60})Ir complex containing the B-σ-carboranyl group incorporated into the chelate metallacycle, viz. [(η^2-C_{60})Ir(*o*-$HCB_{10}H_9CCH_2PPh_2$-*B*,*P*)(*t*BuNC)$_2$] (**II**), was obtained in a high yield as shown in Scheme 1.

The complex obtained was characterized by elemental analysis as well as UV, IR, and ^{1}H and ^{31}P{^{1}H} NMR spectroscopy. Since the molecule contains no other chromophore groups, the UV/Vis spectrum of **II** is typical for η^2-complexes of C_{60} fullerene with transition metals[4,5] exhibiting characteristic bands at 258, 329, 400, 453, and 717 nm. The IR spectrum contains stretching vibration bands of the B−H bonds of the carborane moiety (at 2576 cm^{-1}), the C−C bonds of the fullerene cage (at 1432 and 1184 cm^{-1}),

[a] A. N. Nesmeyanov Institute of Organoelement Compounds, Russian Academy of Sciences
Vavilov St. 28, Moscow 119991, Russia
Fax: (internat.) + 7-095/135-5085
E-mail: usa@ineos.ac.ru

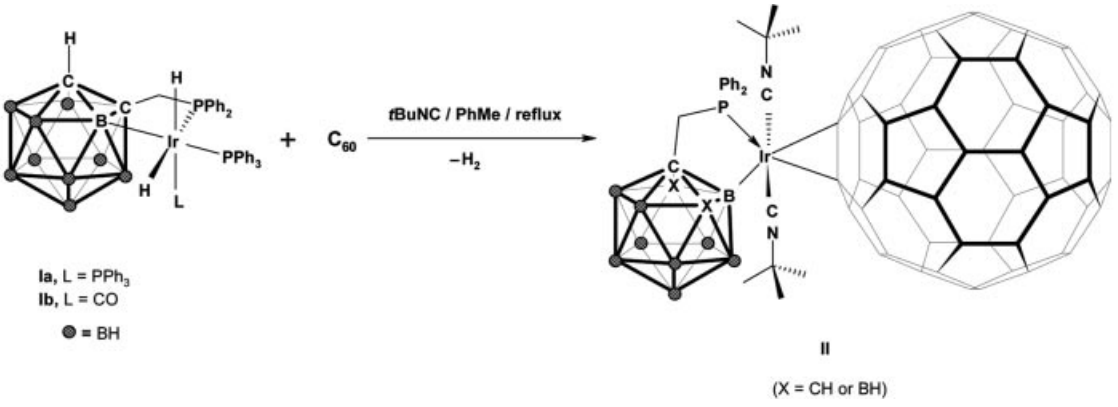

Scheme 1

and one strong, narrow absorption band of the isocyanide ligands [ν(NC)] at 2168 cm^{-1} corresponding to their mutual *trans* positions (*cis* arrangement of the ligands would require two IR-active stretching vibration bands) that completely determines the arrangement of all the ligands around the metal atom. The $^{31}P\{^1H\}$ NMR spectrum exhibits a singlet at δ_P = 37.8 ppm, which points to the existence of only one isomer with η^2-coordination of the fullerene fragment at the 1−2 bond. Otherwise (coordination at the 1−9 bond), we would observe the formation of two geometric isomers (for discussion, see, for example, refs.[5,6]). As in the initial dihydride complexes **Ia** and **Ib**, the molecular chirality of the carborane polyhedron is responsible for inequivalence of two *tert*-butyl isocyanide ligands, which manifests itself as two singlets from protons of the corresponding *tert*-butyl groups in the ^1H NMR spectrum. Similarly, protons of the methylene group in the five-membered metallacycle are inequivalent and their signals appear as an ABX system with the coupling constants ^2J(HH) = 16.2 Hz and ^2J(HP) = 6.6 and 9.6 Hz. These results are consistent with the proposed structure of compound **II** when taken together.

The molecular structure of this complex, determined by single-crystal X-ray diffraction, is presented in Figure 1. Selected bond lengths and bond angles are listed in Table 1. There are four solvate toluene molecules for each of the complex molecules in the crystal of the **II**·$4C_6H_5Me$ solvate whose crystal packing is characterized by the absence of specific interactions. All intermolecular distances correspond to the conventional van der Waals contacts. The carborane moiety involved in the five-membered metallacycle Ir(1)P(1)C(61)C(01)B(3) is bound to the iridium atom by a σ-bond through the boron atom in position 3(6) [Ir(1)−B(3) 2.101(5) Å]. The metallacycle adopts a flattened envelope conformation, with the P(1) atom deviating by 0.43 Å from the plane of the other four atoms in the cycle. A feature of the carborane ligand in complex **II** is disordering of the boron and carbon atoms in positions 2 and 4 of the carborane polyhedron (these positions are equally occupied and are denoted X2 and X4 in Figure 1). The disordering observed originates from the molecular chirality of the carborane moiety and points to the coexistence of both enantiomers in the crystal, differing in the mutual arrangement of these boron and carbon atoms with respect to the plane passing through the P(1), B(3), C(1), and C(2) atoms.

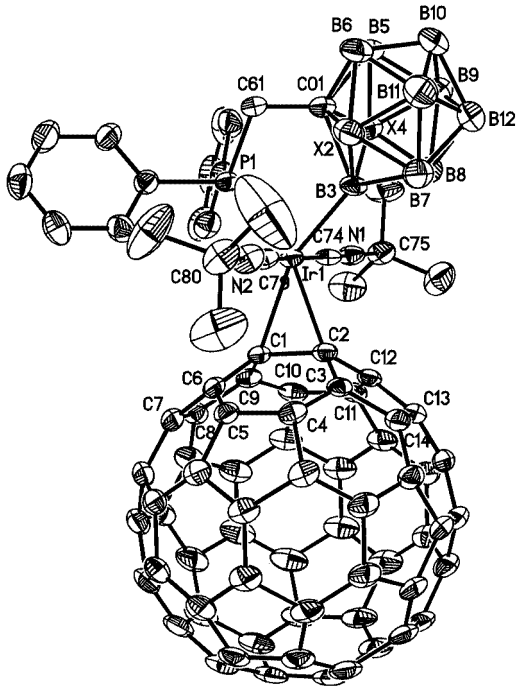

Figure 1. Molecular structure of **II** with numbering of key atoms (see text); hydrogen atoms are not shown

The iridium atom in **II** is coordinated to fullerene at the 6:6 bond C(1)−C(2), which is typical for η^2 complexes of fullerene with transition metals. As a result, the C(1)−C(2) coordination bond is appreciably lengthened as compared to the 6:6 bonds that are not involved in the coordination [cf. 1.525(6) and 1.394 Å, respectively) and is also very close to the corresponding bond length in the fullerene complex (η^2-C_{60})Ir(CO)Cl(PPh_3)$_2$ (**III**) (1.53 Å).[7] Distortion of the fullerene cage due to its coordination to the transition metal atom is also typical of this type of complex.[7,8] An important structural feature of complex **II** is strong distortion of the metallacyclopropane fragment C(1)−Ir(1)−C(2) due to

Table 1. Selected geometrical parameters for **II**

Bond lengths [Å]			
Ir(1)−C(1)	2.228(4)	C(01)−X(2)	1.656(8)
Ir(1)−C(2)	2.162(4)	C(01)−X(4)	1.653(8)
Ir(1)−P(1)	2.294(2)	C(01)−B(3)	1.814(7)
Ir(1)−B(3)	2.101(5)	C(1)−C(2)	1.525(6)
Ir(1)−C(79)	1.966(5)	C(1)−C(6)	1.480(6)
Ir(1)−C(74)	1.979(5)	C(1)−C(9)	1.454(6)
P(1)−C(61)	1.852(5)	C(2)−C(3)	1.477(6)
C(01)−C(61)	1.511(7)	C(2)−C(12)	1.482(6)
Bond angles [°]			
C(79)−Ir(1)−C(74)	172.3(2)	C(61)−P(1)−Ir(1)	109.0(2)
B(3)−Ir(1)−P(1)	84.5(2)	C(61)−C(01)−B(3)	112.9(4)
C(2)−Ir(1)−C(1)	40.6(2)	C(01)−B(3)−Ir(1)	116.8(3)
B(3)−Ir(1)−C(1)	158.0(2)	C(2)−C(1)−Ir(1)	67.4(2)
C(2)−Ir(1)−P(1)	157.9(1)	C(1)−C(2)−Ir(1)	72.0(2)

appreciable lengthening of the Ir(1)−C(1) bond compared to the Ir(1)−C(2) bond [2.228(4) vs. 2.162(4) Å, respectively] because of the strong *trans* influence of the other polyhedral ligand, i.e. the B-σ-carboranyl fragment. It should be mentioned that in the case of the symmetric ligand environment (e.g., in **III)** these bonds have the same length (2.19 Å).[7]

Thus, complex **II** is not only the first representative of metal complexes characterized by the simultaneous presence of two different polyhedral ligands in the coordination sphere of the metal atom, but also the first example of exohedral metallofullerenes with distorted η^2-coordination of fullerene to the transition metal atom. This can be both theoretically and practically valuable because of the possibility for selective insertion of various unsaturated substrates into the longer (and, correspondingly, more reactive) Ir−C bond.

Experimental Section

General: All experiments were carried out under dry, oxygen-free argon in deoxygenated solutions. IR spectra were obtained with a Specord M80 spectrometer. ^{1}H NMR spectra (400.3 MHz) and ^{31}P{^{1}H} NMR spectra (160.02 MHz) were recorded with a Bruker AMX-400 spectrometer relative to residual signals of the solvent (internal standard) and 85% H_3PO_4 (external standard), respectively.

Synthesis of [(η^2-C_{60})Ir(*o*-$HCB_{10}H_9CCH_2PPh_2$-*B,P*)(*t*BuNC)$_2$] (II): To a solution of C_{60} (0.0654 g, 0.09 mmol) in toluene (50 mL), dihydride complex **Ia** (0.0954 g, 0.09 mmol) and *t*BuNC (22 μL, 0.198 mmol) were added while stirring and the reaction mixture was refluxed for 3 h. After cooling, the reaction mixture was filtered, concentrated to 5 mL, and diluted with pentane. The precipitate formed was filtered off, washed successively with methanol and pentane, and dried in vacuo at 60°C to give 95.9 mg (70.5%) of complex **II** as 1:1 solvate with toluene. $C_{85}H_{40}B_{10}N_2PIr\cdot C_7H_8$ (1512.7): calcd. C 73.05, H 3.20, B 7.15; found C 72.53, H 3.34, B 7.15. UV/Vis (THF): λ = 258, 329, 400 (sh), 453, 717 nm. IR (KBr disc), $\tilde{\nu}$ = 2576 (BH), 2168 (NC) cm^{-1}. ^{31}P{^{1}H} NMR ($CDCl_3$): δ = 37.8 ppm. ^{1}H NMR ($CDCl_3$): δ = 1.22 (s, 9 H, *t*Bu), 1.24 (s, 9 H, *t*Bu), 2.35 (s, 3 H, Ph*CH*$_3$), 3.31 [dd, ^2J(HP) = 6.5, ^2J(HH) = 16.0 Hz, 1 H, CH_2], 3.60 (s, 1 H, CH^{carb}), 4.07 [dd, ^2J(HP) = 9.8, ^2J(HH) = 16.0 Hz, 1 H, CH_2], 7.17 (m, 3 H, *Ph*CH_3), 7.24 (m, 2 H, *Ph*CH_3), 7.44 (m, 6 H, Ph), 7.84 (m, 6 H, Ph) ppm.

X-ray Structure Determination of II: Single crystals of **II**·4$C_6H_5CH_3$ were grown from a toluene solution of complex **II** at room temperature. The crystals were triclinic with the space group $P\bar{1}$, a = 15.317(8), b = 16.751(8), c = 19.317(10) Å, α = 88.10(3), β = 72.48(3), γ = 60.87(2)°, V = 4090(3) Å^3, Z = 2, $d_{calcd.}$ = 1.453 g/cm^3, μ(Mo-K_α) = 17.09 cm^{-1}. The intensities of 14417 independent reflections (R_{int} = 0.0687) were measured at 193(2) K with a Syntex $P2_1$ diffractometer (graphite-monochromated Mo-K_α radiation, λ = 0.71073 Å, ω-scan technique, θ ≤ 25°). The structure was solved by the direct methods and refined by the full-matrix least-squares method against F^2 in the anisotropic (isotropic for H atoms) approximation. All hydrogen atoms of the carborane cage were located from the electron density difference synthesis, while the other H atoms were placed geometrically and included in the refinement using the rigid motion model. The refinement converged to wR_2 = 0.1253 and GOF = 1.068 for all independent reflections [R_1 = 0.0446 was calculated against F for 13363 observed reflections with $I > 2\sigma(I)$]; the number of refined parameters was 1184. All calculations were performed using the SHELXTL-97 software[9] with an IBM PC/AT. CCDC-185865 contains the supplementary crystallographic data for this paper. These data can be obtained free of charge at www.ccdc.cam.ac.uk/conts/retrieving.html or from the Cambridge Crystallographic Data Centre, 12, Union Road, Cambridge CB2 1EZ, UK [Fax: (internat.) + 44-1223/336-033; E-mail: deposit@ccdc.cam.ac.uk]

Acknowledgments

This work was supported by the Russian Foundation for Basic Research (grant nos. 00-03-32807 and 99-03-32893), the Russian Federation State Research Program "Fullerenes and atomic clusters" [contr. no. 107-14 (00)-II], and the Ministry of Industry, Science and Technology of the Russian Sub-Program "Fundamental Problems of Modern Chemistry" [contr. no. 402-19.6/22.3/23.1 (00)-II].

[1] P. J. Fagan, J. C. Calabrese, B. Malone, *Acc. Chem. Res.* **1992**, *25*, 134−142.
[2] A. L. Balch, M. M. Olmstead, *Chem. Rev.* **1998**, *98*, 2123−2165.
[3] A. V. Usatov, M. V. Martynova, F. M. Dolgushin, Yu. N. Novikov, Abstracts of School-Conference for Young Scientists "*Organometallic Chemistry towards the 21st Century*", Moscow, **1999**, PY 27.
[4] F. J. Brady, D. J. Cardin, M. Domin, *J. Organomet. Chem.* **1995**, *491*, 169−172.
[5] A. V. Usatov, K. N. Kudin, E. V. Vorontsov, L. E. Vinogradova, Yu. N. Novikov, *J. Organomet. Chem.* **1996**, *522*, 147−153.
[6] A. V. Usatov, S. M. Peregudova, L. I. Denisovich, E. V. Vorontsov, L. E. Vinogradova, Yu. N. Novikov, *J. Organomet. Chem.* **2000**, *599*, 87−96.
[7] A. L. Balch, J. W. Lee, *Inorg. Chem.* **1991**, *30*, 3980−3981.
[8] V. V. Burlakov, A. V. Usatov, K. A. Lyssenko, M. Yu. Antipin, Yu. N. Novikov, V. B. Shur, *Eur. J. Inorg. Chem.* **1999**, 1855−1857.
[9] G. M. Sheldrick, *SHELXTL-97*, V5.10, Bruker AXS, Inc., Madison, WI 53719, USA, **1997**.

Received May 28, 2002
[I02276]

Iridium-Catalysed Allylic Substitution: Stereochemical Aspects and Isolation of Ir^{III} Complexes Related to the Catalytic Cycle

Björn Bartels,[a] Cristina García-Yebra,[a] Frank Rominger,[a] and Günter Helmchen*[a]

Dedicated to Professor Gottfried Huttner on the occasion of his 65th birthday

Keywords: Iridium / Allyl complexes / NMR spectroscopy / Allylic substitution / Asymmetric catalysis

Ir-catalysed allylic alkylations of enantiomerically enriched monosubstituted allylic acetates proceed with up to 87% retention of configuration using $P(OPh)_3$ as ligand. High regio- and enantioselectivity of up to 86% *ee* in asymmetric allylic alkylations of achiral or racemic substrates is achieved with monodentate phosphorus amidites as ligands. Lithium *N*-tosylbenzylamide was identified as a suitable nucleophile for allylic aminations. Of particular importance is the use of lithium chloride as an additive, generally leading to increased enantioselectivities. Two (π-allyl)Ir^{III} complexes were characterised by X-ray crystal structure analysis and spectroscopic data.

Introduction

Asymmetric transition-metal-catalysed allylic substitution is a useful reaction in organic synthesis.[1] The selectivity of this reaction is a function of many factors, for example the metal ion, ligands, nucleophile and substituents of the allyl system. Over the last few years, work has been directed at finding catalysts that favour the formation of branched, chiral products **3** in the substitution of monosubstituted allylic substrates **1** and (*E*)-**2** (Scheme 1). With palladium complexes this is so far only possible for special cases.[2] With Mo- or W-based catalysts, branched products are generally preferred, with higher levels of both regio- and enantioselectivity reported for substrates with R = aryl.[3] It is assumed that in these cases the reactions proceed via π-allyl complexes, which can isomerize[3d] via π−σ−π rearrangement or related processes in such a way that memory of the chiral sense of the stereogenic centre in the branched substrate **1** is lost during the reaction.

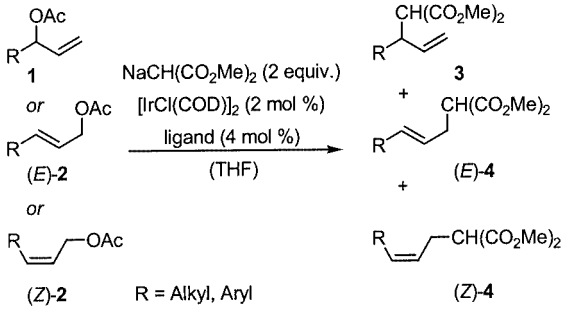

Scheme 1. General scheme for the Ir^{I}-catalysed allylic alkylation of monosubstituted allylic acetates

Substitutions catalysed by Rh, Fe or Ru complexes differ from the above as they generally proceed for branched substrates **1** with a high degree of conservation of enantiomeric excess (*cee*). It has been proposed that these reactions proceed via σ-allyl or π-allyl complexes, which isomerize slowly.[4] As a consequence, from enantiomerically enriched substrates **1**, even with achiral ligands enantiomerically enriched products **3** are obtained via reactions proceeding with double inversion.

Not many examples of Ir^{I}-catalysed allylic substitutions have been published so far. In the last few years, it has been shown that catalysts prepared by combining $[IrCl(COD)]_2$ with a strong π-acceptor ligand — for example triphenylphosphite — in situ give rise to excellent regioselectivities in favour of the branched product **3** for both aryl- and alkyl-substituted allylic substrates.[5] In 1997, we described the first enantioselective Ir^{I}-catalysed allylic alkylations of aryl-allyl acetates (*E*)-**2**, which gave high levels of regio- and enantioselectivity in favour of product **3** when the bidentate phosphinooxazoline **L1** (Figure 1) was used as the chiral ligand.[6] Better results were later achieved with monodentate chiral strong π-acceptor ligands.[7] Thus, branched products **3** are obtained in Ir^{I}-catalysed allylic alkylations of both monoaryl- and monoalkylallyl acetates, (*rac*)-**1** and (*E*)-**2**, with ligands such as phosphites and phosphorus amidites [(*R*)-**L2**]. It was also found that Ir^{I}-catalysed allylic alkylations of enantiomerically enriched acetates **1** with achiral ligands occurred with a noticeable "memory effect", i.e. partial conservation of the enantiomeric purity of the starting substrates. For example, a sample of (*R*)-**1** with 91% *ee* furnished (*R*)-**3** with 51% *ee* [R = $(CH_2)_2Ph$].[7a]

[a] Organisch-chemisches Institut der Universität Heidelberg, Im Neuenheimer Feld 270, 69120 Heidelberg, Germany
Fax: (internat.) +49-6221/544-205
E-mail: en4@popix.urz.uni-heidelberg.de

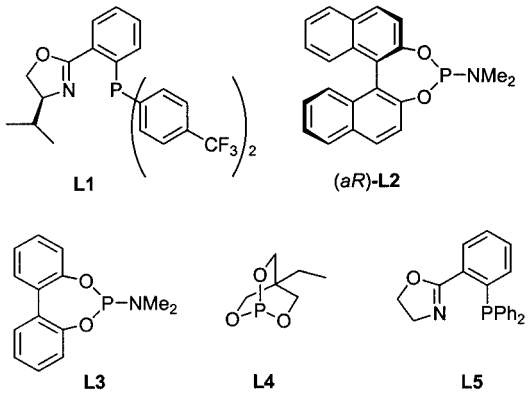

Figure 1. Ligands used in Ir^{I}-catalysed substitutions

This observation led us to consider the formation of π- as well as (σ-allyl)Ir^{III} complexes as intermediates, which undergo slow isomerization.[4d,8]

Herein we present a full account of our studies concerning the various factors affecting the course of the Ir^{I}-catalysed allylic alkylation and amination as well as the isolation and full characterization of Ir^{III} complexes related to the proposed intermediate species, in order to contribute to the elucidation of the still unclear mechanisms of these processes.

Results and Discussion

Synthesis of Allylic Substrates

The branched substrates **1** were prepared by reaction of aldehydes **5** with vinylmagnesium bromide and esterification of the resulting alcohols **6**. The linear substrates (*E*)-**2** were obtained by Wittig−Horner−Emmons olefination to give the (*E*)-α,β-unsaturated ester **7** which, after reduction to alcohols **8** and esterification, gave the acetates (*E*)-**2** (Scheme 2).

Substrates **1e**,**f** and (*E*)-**2f** were prepared in a similar way; the requisite aldehydes[9] were not commercially available and were prepared according to the procedure described in Scheme 3, involving formation of the orthoester **10** by reaction of diol **9** with trimethyl orthoformate, reduction of the orthoester with DIBAL-H[10] and, finally, oxidation of the resulting alcohol **11** with NMO/TPAP.[11]

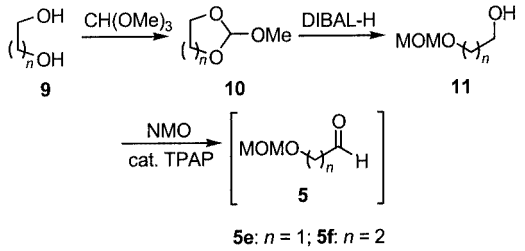

Scheme 3. Synthesis of aldehydes **5**; TPAP: (nPr_4N)[RuO_4]; MOM: methoxymethyl; DMAP: 4-dimethylaminopyridine; NMO: *N*-methylmorpholine *N*-oxide

Enantiomerically pure substrates **1a−c** were prepared either by esterification of commercially available enantiomerically pure alcohols (**6a** and **6c**) or by enzyme (Novozym 435®) catalysed kinetic resolution of *rac*-**6b** with vinyl acetate (**1b**) (Scheme 4).[12] The absolute configuration of (*R*)-**6b** was confirmed by X-ray crystal analysis of the corresponding ester **12** of (1*S*)-camphanic acid (Figure 2).

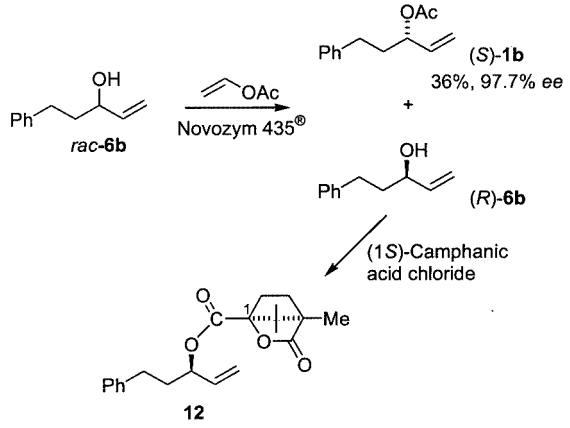

Scheme 4. Kinetic resolution of the alcohol **6b** by enzyme-catalysed esterification and confirmation of the absolute configuration of the products

Substrates (*Z*)-**2** were prepared as described in Scheme 5. (*Z*)-**2e** was obtained from the commercially available (*Z*)-2-buten-1,4-diol (**13**) via reaction with trimethyl orthoformate, reduction of the resulting orthoester **14**, and subsequent esterification.[10] The synthesis of the homologous alkene (*Z*)-**2f** was performed starting from 3-butyn-1-ol (**16**)

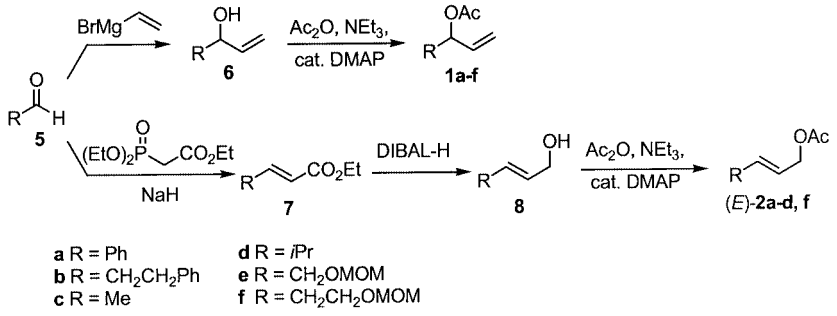

Scheme 2. Synthesis of substrates **1** and (*E*)-**2**; DIBAL-H: Diisobutylaluminium hydride; DMAP: 4-dimethylaminopyridine

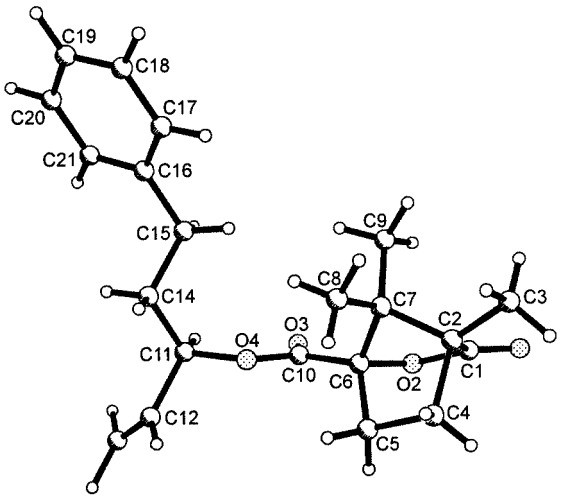

Figure 2. Crystal structure of ester **12** prepared by reaction of the enantiomerically pure alcohol (*R*)-**6b** with (1*S*)-camphanic acid chloride

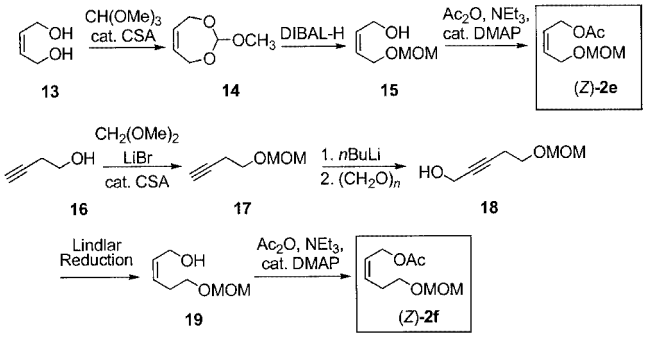

Scheme 5. Synthesis of substrates (*Z*)-**2e** and (*Z*)-**2f** (CSA: camphorsulfonic acid)

which, after a three-step sequence, afforded the (*Z*)-alkene **19**, which was then esterified to give acetate (*Z*)-**2f**.[13]

Factors Affecting the Rate and Regioselectivity of Ir^I-Catalysed Allylic Alkylation

Allylic alkylations of aryl- and alkyl-substituted allyl acetates **1** and (*E*)-**2** catalysed by $[IrCl(COD)]_2$ and combinations of this complex with PPh_3 or the strong π-acceptor ligand $P(OPh)_3$ were initially investigated. The results are summarized in Table 1.

Concerning the rate of the reaction, the allylic alkylation of linear substrate (*E*)-**2a** was slightly slower than that of the isomeric branched substrate **1a** when $[IrCl(COD)]_2$ without additional ligand was used as catalyst (Table 1, entries 2 and 5). Differences in reaction rates between branched and linear substrates have been observed for the Rh^I-catalysed reaction and they have been attributed to a S_N2' mechanism operating in the oxidative addition step.[4d]

While the combination of $[IrCl(COD)]_2$ with PPh_3 led to slow reactions and low degrees of regioselectivity (entries 6, 9 and 13), the π-acceptor ligand $P(OPh)_3$ gave rise to the shortest reaction times along with optimal yields and regioselectivities in favour of the branched product **3** (entries 1, 4, 7 and 11).[5a][5b] Furthermore, a 1:1 ratio of $P(OPh)_3$ and

Table 1. Allylic alkylation of acetates **1** and (*E*)-**2** catalysed by Ir^I complexes according to Scheme 1[a]

Entry	Substrate	Ligand	L/Ir	*T* [°C]	Time [h]	Yield [%][b] **3** and (*E*)-**4**	Ratio[c] **3**:(*E*)-**4**
1	**1a**	$P(OPh)_3$	1:1	25	3	99	98:2
2	**1a**	–	0	25	3	98	98:2
3	**1a**	PPh_3	1:1	25	3	15	98:2
4	(*E*)-**2a**	$P(OPh)_3$	1:1	25	3	98	98:2
5	(*E*)-**2a**	–	0	65	24	89	32:68
6	(*E*)-**2a**	PPh_3	1:1	65	24	58	64:36
7	**1b**	$P(OPh)_3$	1:1	25	3	99	95:5
8	**1b**	–	0	25	3	66	89:11
9	**1b**	PPh_3	1:1	25	3	0	–
10	**1b**	PPh_3	1:1	55	22	60	83:17
11	(*E*)-**2b**	$P(OPh)_3$	1:1	25	3	99	95:5
12	(*E*)-**2b**	–	0	25	3	0	–
13	(*E*)-**2b**	PPh_3	1:1	25	3	0	–
14	**1b**	$P(OPh)_3$	2:1	25	18	90	95:5

[a] All reactions were carried out in THF on a 0.5 mmol scale (0.125 M) with 2 equiv. of $NaCH(CO_2Me)_2$ and 2 mol % of $[IrCl(COD)]_2$. [b] Isolated yields are given. [c] Determined by GC/MS.

Ir^I gave the best results (compare entries 7 and 14). In this respect, it is significant that only one complex is formed by reaction of $[IrCl(COD)]_2$ with two equivalents ($L/Ir^I = 1:1$) of $P(OPh)_3$ (^{31}P NMR: $\delta = 86.77$ ppm),[14] while an excess of ligand gives rise to the formation of additional species.[5b]

It is also remarkable that while the regioselectivities obtained from the reaction of the branched substrates are generally high, the linear substrates give rise to lower degrees of regioselectivity, with PPh_3 showing a particularly strong "memory effect" (entries 6 and 10).

It has been reported that the geometry of the double bond of the linear substrates is also a factor determining the regioselectivity of Ir^I-catalysed allylic substitutions.[15] Using substrates **1e**, **1f** and **2f** (Scheme 1), the dependence on the geometry of the double bond in combination with the influence of σ-acceptor substituents in the substrate was studied. The results (Table 2) clearly show that the allylic alkylations of (*Z*)-**2e** and (*Z*)-**2f** preferentially yield (*Z*)-**4e** and (*Z*)-**4f** as products, respectively. It is also remarkable that the (*Z*)-substrates react distinctly faster than the (*E*)-substrates. Furthermore, it is apparent from Table 1 and 2 that regioselectivity (**3**:**4**) is a function of the substituent at the allylic moiety, giving rise to the order Ph > $(CH_2)_2$Ph > $(CH_2)_2$OMOM > CH_2OMOM, reflecting the ability of the substituent to stabilize a positive charge.

Some of the results described above contribute to the understanding of the mechanism of the Ir^I-catalysed allylic alkylation. Generally, the following steps are to be considered: a) oxidative addition of the substrate to the metal centre and formation of π- and/or σ-allyl complexes, b) isomerization of the intermediates via π–σ–π rearrangement or similar processes, and c) attack of a nucleophile (Scheme 6). If π-allyl complexes are the product determining intermediates, it is expected that cationic character favours attack at the substituted allylic terminus. It is, therefore, clear that the rate and regioselectivity of the nucleo-

Table 2. Influence of the configuration of the double bond of the substrates on the regioselectivity of the substitution[a]

Entry	Substrate	R	*T* [°C]	Time [h]	Yield [%]	Ratio[b] **3**:**4**	*E*/*Z* in **4**[b]
1	**1e**	CH_2OMOM	25	18	91	77:23	99:1
2	(*Z*)-**2e**	CH_2OMOM	24	4	65	0:100	8:92
3	**1f**	CH_2CH_2OMOM	25	18	94	93:7	99:1
4	(*E*)-**2f**	CH_2CH_2OMOM	25	18	95	97:3	99:1
5	(*Z*)-**2f**	CH_2CH_2OMOM	25	4	80	12:88	1:99

[a] All reactions were carried out in THF on a 0.5 mmol scale (0.125 M) with 2 equiv. of $NaCH(CO_2Me)_2$, 2 mol % $[IrCl(COD)]_2$ and 4 mol % $P(OPh)_3$. [b] Determined by GC/MS.

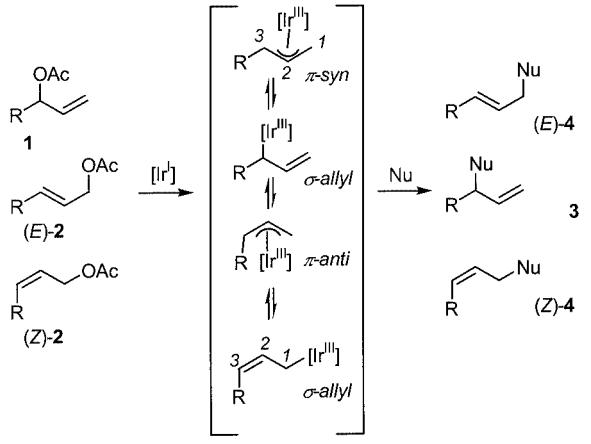

Scheme 6. Ir^I-catalysed allylic substitution of substrates **1** and **2** via σ- and π-allyl intermediates

philic attack would be higher with π-acceptor ligands such as $P(OPh)_3$ and olefins (such as COD) than with σ-donor ligands such as PPh_3.[16] It has been argued that nucleophilic attack on analogous Rh^{III} complexes is determined by the location of the acceptor ligand in the *trans* position to the higher substituted allyl terminus.[17] This argument neglects the fact that due to the strong *trans* influence of both an allyl and a phosphorus-based ligand, these ligands strongly prefer a mutual *cis* disposition. Furthermore, there is no marked influence of the steric bulk of the phosphorus ligand on the regioselectivity.[5b]

The fact that no (*Z*)-products were obtained from (*E*)-substrates while these are the major products in the allylic alkylation of (*Z*)-substrates is highly significant and is also found in the reaction catalysed by Fe complexes.[4b] As (*E*)-substrates would form *syn* π-allyl intermediates and (*Z*)-substrates *anti* π-allyl intermediates, these results clearly show that the *syn*-*anti* isomerization between these species is a slow process (Scheme 6). Considering a generally close analogy of Ir^I- and Rh^I-catalysed allylic substitutions, it is of interest to note that reactions of isolated *anti* (π-allyl)Rh^{III} complexes with carbon nucleophiles occur at the less substituted terminus of the allylic moiety, giving rise exclusively to the formation of (*Z*)-olefin complexes.[18] On the other hand, there are no facts which would rule out a reaction course via σ-complexes.

Steric Course of the Substitution and Memory Effects

It has already been reported that Rh^I- and Ir^I-catalysed allylic substitutions show a noticeable "memory effect",[4d,7a,19] i.e. enantiomerically enriched branched substrates **1** yield substitution products with retention of configuration and partial conservation of enantiomeric purity. Rather than aiming at high degrees of conservation we were interested in finding conditions that would maximally erode enantiomeric purity in order to achieve asymmetric induction via dynamic kinetic resolution. To this end, the influence of reaction conditions, such as concentration of the nucleophile, temperature, influence of additives and ligand, were studied in allylic alkylations of enantiomerically enriched acetates **1** using $[IrCl(COD)]_2$ combined in situ with achiral ligands $P(OPh)_3$ and **L3**−**L5** as catalysts. The results are summarized in Table 3.

The results allow the following conclusions: (a) phosphorus amidite **L3** gives rise to maximal erosion of enantiomeric purity (entries 7 and 8); (b) the highest degree of conservation of enantiomeric purity is induced by $[IrCl(COD)]_2$ without additional ligand (entry 11); (c) surprisingly, there is almost no influence of the concentration of the nucleophile (cf. entries 1 and 2). It was expected that an increase would lead to a higher degree of conservation of enantiomeric purity because of acceleration of the nucleophilic attack relative to isomerization of allyl complexes; (d) halide ions are known to accelerate the isomerization of allyl complexes via σ-allyl complexes.[20] Indeed, addition of LiCl induces an enhanced degree of racemisation (entries 5, 6 and 8), (e) finally, increase of the reaction temperature also favours racemisation (entry 6).

Concerning the steric course of the process, it was of interest to establish whether the Ir^I-catalysed reactions proceed with double inversion or retention. To this end, reactions with substrates **20** and **21** were investigated (Scheme 7).[21] These substrates do not allow a double inversion process because in **20** oxidative addition to Ir^I and in **21** nucleophilic attack at the (allyl)Ir^{III} intermediate are both prevented by steric hindrance. Indeed, no reaction occurred under reaction conditions typical for allylic alkylations.[22] Control experiments showed that under the same conditions the reaction of $NaCH(CO_2Me)_2$ with cyclopentenyl acetate proceeds to completion. These results demonstrate that the Ir^I-catalysed allylic alkylation proceeds via a double inversion process.

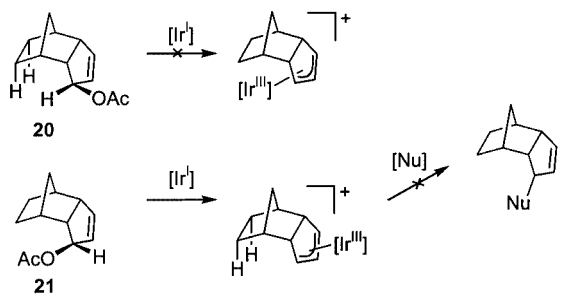

Scheme 7. Ir^I-catalysed allylic substitutions

Table 3. Influence of ligand, reaction conditions and addition of lithium chloride on allylic substitutions of substrates **1a**−**1c**[a]

Entry	Substrate	*ee* [%] of **1** (*conf.*)	Ligand	Time [h]	c_{Nu} [M]	Additive (equiv.)	Yield [%]	Ratio **3**:(*E*)-**4**[b]	*ee* [%][b] (*conf.*)	*cee* [%][c]
1	**1b**	95 (*R*)	$P(OPh)_3$	3	0.250	–	95	95:5	54 (*R*)	57
2[d]	**1b**	95 (*R*)	$P(OPh)_3$	3	0.125	–	79	96:4	60 (*R*)	63
3[d]	**1b**	98 (*S*)	$P(OPh)_3$	3	0.125	–	98	96:4	65 (*S*)	66
4	**1b**	91 (*R*)	$P(OPh)_3$	3	0.250	–	97	95:5	51 (*R*)	56
5	**1b**	91 (*R*)	$P(OPh)_3$	3	0.250	LiCl (1.0)	71	93:7	49 (*R*)	54
6[e]	**1b**	98 (*S*)	$P(OPh)_3$	3	0.250	LiCl (1.0)	91	91:9	38 (*S*)	39
7	**1b**	91 (*R*)	**L3**	3	0.250	–	98	99:1	39 (*R*)	43
8	**1b**	91 (*R*)	**L3**	3	0.250	LiCl (1.0)	61	79:21	34 (*R*)	37
9	**1b**	98 (*S*)	**L4**	18	0.250	–	99	84:16	70 (*S*)	71
10	**1b**	91 (*R*)	**L5**	3	0.250	–	93	53:47	66 (*R*)	73
11	**1b**	98 (*S*)	–	18	0.250	–	67	91:9	85 (*S*)	87
12	**1a**	94 (*R*)	$P(OPh)_3$	3	0.250	–	98	95:5	56 (*S*)	60
13	**1c**	99.8 (*R*)	$P(OPh)_3$	3	0.250	–	91	95:5	85 (*R*)	85

[a] All reactions were carried out in THF at a 0.5 mmol scale (0.125 M) with 2 mol % $[IrCl(COD)]_2$ and 4 mol % ligand, at room temperature. [b] Determined by HPLC (entries 1−12) or GC (entry 13). [c] Retention or *cee* (conservation of enantiomeric excess) is defined as [*ee*(product)/*ee*(substrate)]×100. [d] Ratio substrate/nucleophile 1:1. [e] Temperature: 50 °C.

To gain further insight, the alkylation of the symmetrically substituted acetate **22** was studied (Scheme 8).[7a] In this reaction enantiomerically pure (*R*)-**22** gave the product (*R*)-**23** with 71% *ee*.

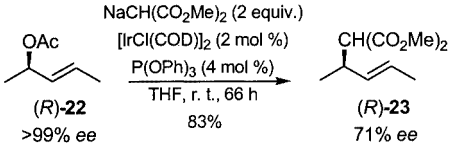

Scheme 8. Allylic substitution using a substrate with a potentially symmetric (π-allyl)Ir^{III} intermediate

This result rules out the intermediacy of a symmetric (π-allyl)Ir^{III} complex or a fast dynamic equilibrium between isomeric complexes, as is typical in palladium chemistry. Possible intermediates (Figure 3) are a σ-complex **A**, formed by direct oxidative addition with inversion, or a corresponding π-complex **B** with a nonsymmetric ligand sphere. A third type of intermediate conceivable is a *nondynamic* (σ+π)-allyl complex **C** formed by S_N2' attack of an Ir^I species. Complexes of this type have been proposed for Rh^I-catalysed allylic substitutions which proceed with almost complete conservation of enantiomeric purity.[4d] In principle, proposals **B** and **C** are identical as they are simply different ways of describing a nonsymmetric π-allyl complex. Assessing such intermediates is fairly straightforward

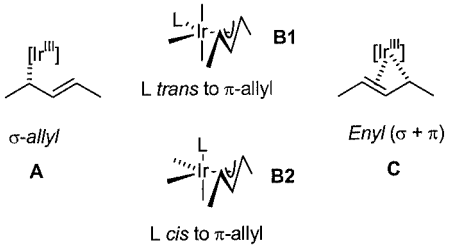

Figure 3. Possible intermediates in the allylic substitution of acetate (*R*)-**22**

for tetracoordinate planar Pd complexes.[23] However, for octahedral Ir^{III} or Rh^{III} complexes the *trans* disposition of an allyl and a phosphorus ligand, i.e. **B1**, is destabilised by their strong *trans* influence.[24] A complex **B2** with *cis* disposition of these ligands is expected to be more stable. Rescue of the argument, i.e. control of the substitution via the trans effect operating in **B1**, would require further assumption of a dynamic system with strong *kinetic* preference for attack of a nucleophile at the *trans* complex **B1**.

Also conceivable is a reaction via a (π-allyl)metal complex with *syn-anti* configuration of the allyl ligand. According to precedents in Pd-catalysed allylic substitutions, such a complex might react preferentially at the terminus carrying the *anti* substituent.[25] In view of the results for the Ir^I-catalysed allylic substitution of monosubstituted (*Z*)-substrates (vide infra), i.e. preferential formation of linear product, this possibility appears unlikely.[15]

Asymmetric Catalysis

The results in Table 3 show that isomerization among the various intermediate species is fastest with phosphorus amidites as ligands and, therefore, these appeared particularly suited for asymmetric Ir^I-catalysed allylic substitutions. In preliminary experiments we found that branched substrates yield higher degrees of enantio- as well as regioselectivity than linear substrates. Accordingly, reactions with branched substrates were studied preferentially. Using (*R*)-**L2** as the chiral ligand, the dependence of the enantioselectivity on the reaction conditions and substrate structure were investigated. These results are displayed in Table 4.

The ratio of ligand to iridium is an important parameter. In analogy to the earlier finding (Table 1), a 1:1 ratio was optimal (compare entries 2−4). In view of the previous discussion concerning allylic intermediates it is significant that a decrease of temperature leads to a lowering of enantioselectivity (cf. entries 2, 5 and 6). This is probably caused by a slow isomerization of intermediary allyl complexes. A further aspect to take into account is the influence of the

Table 4. Variation of reaction parameters in asymmetric allylic alkylations using (*R*)-**L2** as chiral ligand[a]

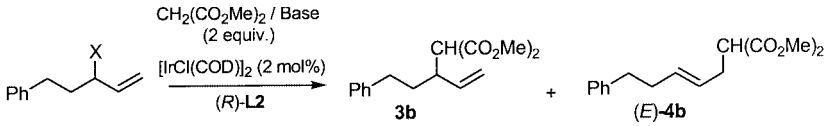

1b, X = OAc
24b, X = Cl
25b, X = OCO_2Et
26b, X = $PO(OEt)_2$

Entry	X	Solvent	Base	Ratio P/Ir	Additive[b]	*T*	Time	Yield [%][c]	**3**:(*E*)-**4**[d]	*ee* of **3** [%] (*R*)[e]
1	OAc	THF	NaH	0	–	room temp.	3 h	66	89:11	–
2	OAc	THF	NaH	1	–	room temp.	3 h	92	99:1	69
3	OAc	THF	NaH	2	–	room temp.	3 h	66	99:1	68
4	OAc	THF	NaH	4	–	room temp.	3 h	5	–[f]	–[f]
5	OAc	THF	NaH	1	–	0 °C	6 h	74	99:1	47
6	OAc	THF	NaH	1	–	65 °C	1 h	98	98:2	68
7	Cl	THF	NaH	1	–	room temp.	3 h	88	60:40	0
8	OCO_2Et	THF	NaH	1	–	room temp.	3 h	47	85:15	25
9	$OPO(OEt)_2$	THF	NaH	1	–	room temp.	3 h	41	82:18	0
10	OAc	ether	NaH	1	–	room temp.	3 d	65	99:1	25
11	OAc	toluene	NaH	1	–	room temp.	3 d	91	98:2	0
12	OAc	CH_2Cl_2	NaH	1	–	room temp.	3 d	10	99:1	53
13	OAc	THF	*n*BuLi[g]	1	–	room temp.	3 h	30	98:2	60
14	OAc	THF	*n*BuLi	1	$ZnCl_2$	room temp.	7 d	91	86:14	3
15	OAc	THF	Cs_2CO_3[h]	1	–	room temp.	3 h	76	99:1	29
16	OAc	THF	BSA[i]	1	–	room temp.	5 d	13	–[f]	20
17	OAc	THF	NaH	1	NMe_4Br	room temp.	3 h	95	99:1	49
18	OAc	THF	NaH	1	$N(nBu)_4Cl$	room temp.	3 h	15	99:1	25
19	OAc	THF	NaH	1	LiF	room temp.	3 h	99	99:1	58
20	OAc	THF	NaH	1	LiCl	room temp.	3 h	83	99:1	86
21	OAc	THF	NaH	1	LiCl	50 °C	3 h	97	99:1	80
22	OAc	THF	NaH	1	LiBr	room temp.	3 h	69	98:2	83

[a] Nucleophiles were prepared by treatment of $CH_2(CO_2Me)_2$ with base over a period of 30 min at room temperature in THF. [b] One equivalent (relative to substrate) of additive was added before the nucleophile. [c] Isolated yields. [d] Determined by GC/MS. [e] Determined by HPLC. [f] Not determined. [g] The nucleophile was generated by addition of *n*BuLi at −78 °C and keeping the reaction mixture at room temperature for 30 min. [h] The nucleophile was generated by reacting the base with dimethyl malonate in THF for 30 min at reflux temperature. [i] BSA = *N*,*O*-bis(trimethylsilyl)acetamide; KOAc (catalytic quantity) was added to start the reaction.

leaving group on rate, regio- and enantioselectivity (cf. entries 2, 7−9). Substrates with better leaving groups than acetate give rise to very low selectivities. As of now, the best results are obtained with acetates. Of the solvents used, tetrahydrofuran was found to be the most suitable (entries 2, 10−12).

Variation of the cation (entries 13−17) did not lead to an improvement of the enantioselectivity. This was surprising because an improvement had been achieved previously with zinc derivatives in a closely related reaction.[7b] In contrast, addition of *anhydrous* lithium bromide or lithium chloride resulted in an improved regio- and enantioselectivity (up to 86% *ee*) (entries 20−22).

Using the reaction conditions optimized for **1b**, allylic substitutions with a set of systematically varied substrates were investigated (Table 5). In every case addition of LiCl led to markedly improved enantioselectivities; this is probably due to an acceleration of the isomerization of the intermediary allyl complexes. A most surprising result was the low enantioselectivity obtained with the phenyl derivative **1a**. It is quite clear that further progress in this area will depend on establishing conditions for further enhanced rates of isomerization of allylic intermediates.

Ir^I-Catalysed Allylic Amination

Ir^I-Catalysed allylic aminations have so far only been described for amines as nucleophiles.[15] These reactions require polar solvents and/or high concentration and relatively high temperature. We have now found that lithium *N*-tosylbenzyl amide, already successfully employed in Rh^I-catalysed allylic aminations,[19a,26] reacts under the conditions typical for malonates (Scheme 9). Some preliminary results obtained in allylic aminations of both branched and linear substrates with this nucleophile are presented here (Table 6). With triphenylphosphite as ligand, only moderate yields and regioselectivities were obtained in the amination of substrate **1b** (entry 1). With the chiral phosphorus amidite (*R*)-**L2** as ligand (entries 2−3) yield (up to 97%) and regioselectivity (up to 99:1) were improved for the branched

Table 5. Asymmetric allylic substitutions with substrates **1a**−**f** using (*aR*)-**L2** as chiral ligand[a]

Entry	Substrate	R	Additive[b]	Time [h]	Yield [%]	Ratio[c] **3**:(*E*)-**4**	*ee* [%][d] (*config.*)
1	**1c**	Me	−	3	99	95:5	31 (*R*)
2	**1c**	Me	LiCl	3	99	94:6	57 (*R*)
3	**1a**	Ph	−	3	98	98:2	8 (*S*)
4	**1a**	Ph	LiCl	3	97	98:2	4 (*R*)
5	**1b**	CH_2CH_2Ph	−	3	92	98:2	69 (*R*)
6	**1b**	CH_2CH_2Ph	LiCl	3	83	99:1	86 (*R*)
7	**1d**	*i*Pr	−	48	41	99:1	66 (*R*)
8	**1d**	*i*Pr	LiCl	48	31	99:1	74 (*R*)
9	**1e**	CH_2OMOM	−	3	93	94:6	49 (*R*)
10	**1e**	CH_2OMOM	LiCl	3	90	95:5	78 (*R*)
11	**1f**	CH_2CH_2OMOM	−	3	94	99:1	31 (*R*)
12	**1f**	CH_2CH_2OMOM	LiCl	3	78	98:2	70 (*R*)

[a] All reactions were carried out in THF at 25 °C on a 0.5 mmol scale [0.125 M] with 2 equiv. $NaCH(CO_2Me)_2$, 2 mol % $[IrCl(COD)]_2$ and 4 mol % (*R*)-**L2**; a general procedure (II) for the Ir^I-catalysed allylic alkylation is described in the Exp. Sect. (see below). [b] One equivalent (relative to substrate) of additive was added before addition of the nucleophile. [c] Determined by GC/MS. [d] Determined by HPLC or GC (for details see Exp. Sect.).

product **27b**. Further work is required in order to improve the enantioselectivity of this reaction.

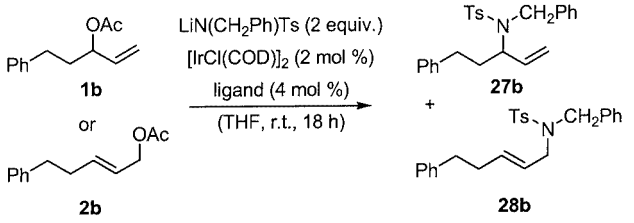

Scheme 9. Ir^I-catalysed allylic amination of (*rac*)-**1b** and (*E*)-**2b**

Table 6. Ir-catalysed allylic amination of acetates **1b** and (*E*)-**2b**[a]

Entry	Substrate	Ligand	Yield [%]	Ratio **27**:**28**[b]	*ee* [%][b] (*config.*)
1	**1b**	$P(OPh)_3$	47	77:23	−
2	**1b**	(*R*)-**L2**	97	99:1	11 (*S*)
3	(*E*)-**2b**	(*R*)-**L2**	47	85:15	13 (*S*)

[a] The reaction was carried out on a 0.5 mmol scale in THF (0.1 M) (18 h, room temp.), with 2 equiv. of $LiN(CH_2Ph)Ts$, 2 mol % $[IrCl(COD)]_2$ and 4 mol % ligand. [b] Determined by HPLC.

Characterization of Ir^I and Ir^{III} Complexes Related to the Catalytic Cycle

Both Ir^I- and σ- or (π-allyl)Ir^{III} complexes are expected to participate in the catalytic process. Therefore, the isolation and structural characterization of such complexes is of great interest. We have prepared a variety of these compounds by stoichiometric reactions of the type comprising the catalytic cycle.

A Chiral Ir^I Complex Containing a Chiral Phosphorus Amidite

Reaction of ligand **L** with complex $[IrCl(COD)]_2$ proceeds with cleavage of the chloride bridges to give monomeric complexes of the type [IrCl(COD)L].[27] Thus, with the chiral ligand (*R*)-**L2**, the complex [IrCl(COD){(*R*)-**L2**}] (**29**) was prepared and fully characterised by NMR spectroscopy and X-ray diffraction. The crystal structure of **29** together with a selection of bond lengths is shown in Figure 4.

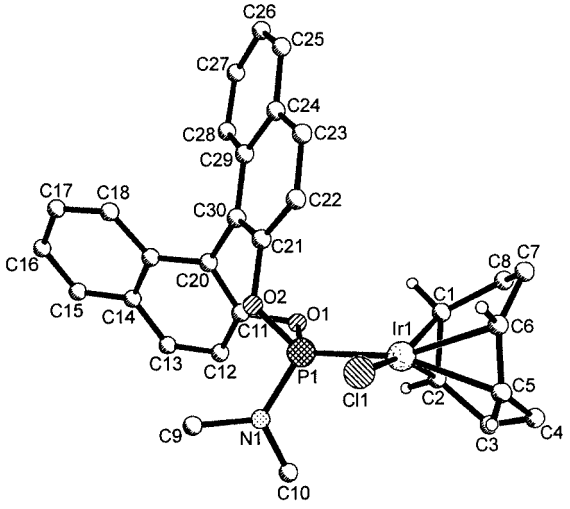

Figure 4. X-ray structure of complex **29**; selected bond lengths (Å): Ir(1)−C(1) 2.114(6), Ir(1)−C(2) 2.118(6), Ir(1)−C(5) 2.222(5), Ir(1)−C(6) 2.222(5), Ir(1)−P(1) 2.2363(13), Ir(1)−Cl(1) 2.358(1), C(1)−C(2) 1.434(8), C(5)−C(6) 1.371(8)

As expected, the coordinated double bond [C(1)-C(2)] *trans* to the chloro ligand is noticeably longer than that [C(5)-C(6)] *trans* to the phosphorus due to the greater *trans* influence of the phosphorus ligand, which is translated into a weakening of the Ir−C(5,6) bonds and a stronger C(5)-C(6) double bond character.

Preparation of (π-Allyl)Ir^{III} Complexes

Oxidative addition is a necessary step in the catalytic process. Therefore, we attempted to generate the corresponding (allyl)Ir^{III} intermediates by direct reaction of al-

lyl acetates with the Ir^I precursors $[IrCl(COD)]_2$ or complexes [IrCl(COD)(L)]. Surprisingly, despite long reaction times and a large excess of the allyl acetate, the expected oxidative addition reaction, which proceeds readily in palladium chemistry,[1c] did not take place here.

We observed that addition of the nucleophile $NaCH(CO_2Me)_2$ to a solution of the catalyst generally produced a change of colour from pale orange to pale yellow. This seemed to indicate that the true catalyst is produced by reaction with the nucleophile. Accordingly, the stoichiometric reaction of $[IrCl(COD)P(OPh)_3]$,[14] formed by treatment of $[IrCl(COD)]_2$ with triphenylphosphite (1:2), with $NaCH(CO_2Me)_2$ (1 equiv.) was explored. The $^{31}P\{^1H\}$ NMR spectrum of the mixture, recorded in $[D_8]$THF after one hour at room temperature, showed a singlet (δ = 86.3 ppm), corresponding to the initial complex, and two sets of doublets of which one (δ = 124.5 and 81.4 ppm, $^3J_{P,P}$ = 74 Hz) was identified as belonging to the previously reported orthometallation product $[Ir\{\eta^2\text{-}(P,C)\text{-}P(OC_6H_4)(OPh)_2\}(COD)\{P(OPh)_3\}]$.[14] The second set of doublets (δ = 104.3 and 85.1 ppm, $^3J_{P,P}$ = 43 Hz) indicates coordination of two equivalents of ligand per metal centre. Attempts to isolate and characterise this complex were unsuccessful.

Next, the oxidative addition of allyl halides to $[IrCl(COD)]_2$ was studied. The reaction of (*E*)-cinnamyl chloride with $[IrCl(COD)]_2$ and allyl bromide with $[IrBr(COD)]_2$ gave complexes **30** and **31**, respectively, in up to 80% yield (Scheme 10).[28] In the presence of phosphorus-derived ligands such as $P(OPh)_3$ or $P(C_6F_5)_3$ the same compounds were formed, which demonstrates the very strong coordination of COD. Complexes **30** and **31** were fully characterised by spectroscopic methods and X-ray diffraction.

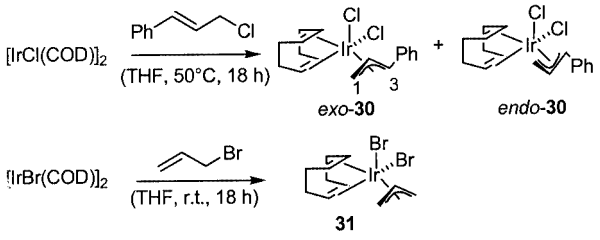

Scheme 10. Oxidative addition of allyl halides to Ir^I complexes

X-ray Crystal Structures of (π-Allyl)Ir^{III} Complexes 30 and 31

Complexes **30** and **31** gave yellow single crystals from dichloromethane/diethyl ether solutions.

The crystal of complex **30** (Figure 5) contains a ca. 1:1 mixture of *endo* and *exo* isomers.[29] As a consequence, the structural data of the allyl moieties are of low precision. The configuration of the complex is as expected on the basis of *trans* influences of the ligands. The *syn* configuration of the allyl ligands is typical for aryl-allyl ligands.

The allyl ligand of complex **31** was found to be in the *exo* disposition. The Ir(1)−C(10) bond [2.321(8) Å] is longer than the Ir(1)−C(12) bond [2.176(8) Å] due to the *trans* influence of the COD double bond C(1)−C(2) (Figure 6). Concerning the bond lengths within the allyl moiety, it is remarkable that the C(10)−C(11) bond [1.36(1) Å] is considerably shorter than the C(11)−C(12) bond [1.46(1) Å], i.e. the allyl ligand is highly unsymmetrical and distorted towards a σ-complex.

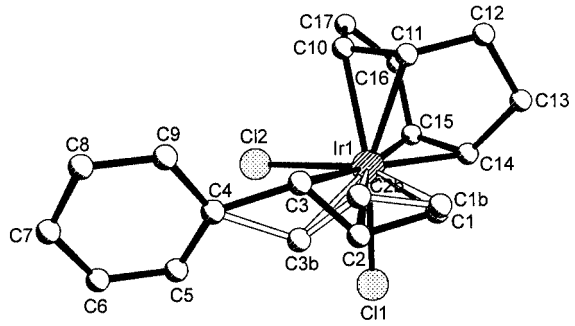

Figure 5. Crystal structure of complex **30**; selected bond lengths (Å) with estimated standard deviations: Ir(1)−C(1)/C(1B) 2.11(3)/2.31(5), Ir(1)−C(2)/C(2B) 2.24(2)/2.31(2), Ir(1)−C(3)/C(3B) 2.45(1)/2.48(1), C(1)−C(2) = 1.44(1), C(1B)−C(2B) 1.44(2), C(2)−C(3) 1.35(1), C(2B)−C(3B) 1.34(2)

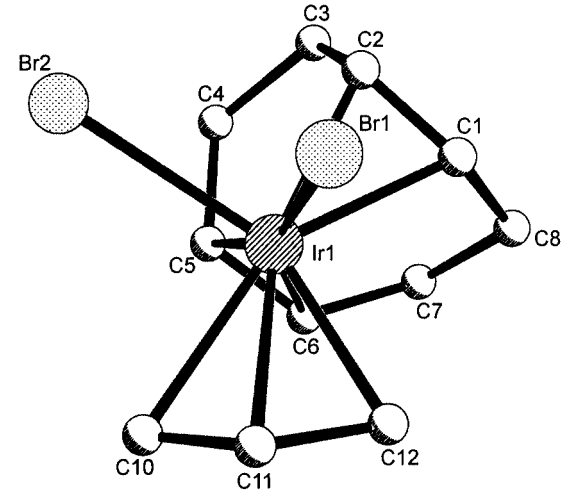

Figure 6. Crystal structure of complex **31**; selected bond lengths (Å) with estimated standard deviations: Ir(1)−C(10) 2.321(8), Ir(1)−C(11) 2.241(9), Ir(1)−C(12) 2.176(8), C(10)−C(11) 1.36(1), C(11)−C(12) 1.46(1), C(1)−C(2) 1.39(1), C(3)−C(4) 1.53(1), C(5)−C(6) 1.38(1), C(7)−C(8) 1.53(1)

Asymmetry in π-allyl systems as a consequence of either an asymmetric set of ligands or an asymmetric substitution pattern of the allyl group is quite common for Ir[30] or Mo[31] complexes and distinctly more pronounced than in Pd complexes.[32] For example, Fryzuk et al. have found a situation similar to that of **30** for the (π-allyl)Ir^{III} complexes $[Ir(\eta^3\text{-}CH_2CHCHMe)(H)\{N(SiMe_2CH_2PPh_2)_2\}]$ and $[Ir(\eta^3\text{-}CH_2CHCHCN)(H)\{N(SiMe_2CH_2PPh_2)_2\}]$, which display σ-character for the substituted allylic carbon and double bond character for the $CHCH_2$ moiety. The authors describe this situation as a $\sigma\text{-}\pi^2$-type allyl ligand.[30d] Many additional examples of such ligands have been

reported.[8e,30b−30d,31] Obviously, the previously discussed "enyl (σ+π)" species proposed as intermediates in Rh^{I}-catalysed allylic substitutions (cf. Scheme 8) belong to this type.[4d]

NMR Spectroscopic Study of (π-Allyl)Ir^{III} Complexes

(π-Allyl)Ir^{III} complexes generally show slow isomerisation compared to π-allyl complexes of the first and second row late transition metals such as Ni, Pd, Fe, Ru and Co.[8,30] In contrast, complexes **30** and **31** display broad peaks in their ^{1}H NMR spectra at room temperature, indicating that dynamic processes are taking place.

The ^{1}H and ^{13}C{^{1}H} NMR spectra of **30** at temperatures in the range −60 to −40 °C show a 2:1 ratio of two species which, on the basis of the proton coupling constants, are the *syn*-π-allyl complexes found in the crystal structure (cf. Scheme 10). The ^{1}H NMR spectrum of **30** at 50 °C shows one set of signals as a consequence of fast equilibration; coalescence was found at ca. 0 °C.

For both isomers of complex **30**, the resonances of the allylic protons appear in the range δ = 4−6.5 ppm (^{1}H NMR spectrum at −60 °C). The *syn*-configuration of the allyl ligand is apparent from the values of the coupling constant ($^3J_{2,3}$ = 14 Hz) for both isomers, indicating the *anti*-disposition of 3-H (for numbering see Scheme 10). An unusual feature is a marked downfield shift of 3-H for the minor (δ = 6.33 ppm) relative to the major isomer (δ = 4.93 ppm).

The ^{13}C{^{1}H} NMR spectroscopic data (recorded at −60 °C) were analysed with the help of HMQC and HMBC experiments. Resonances at δ = 40.9 and 42.6 ppm for the methylene carbon atoms (C-1) of the major and minor isomer, respectively, are characteristic of the CH_2 group of (π-allyl)Ir^{III} systems; σ-bound allylic CH_2 groups typically appear in the range δ = 0−25 ppm. Resonances at δ = 110.6 and 102.2 ppm for C-2 of the major and minor isomer, respectively, are also in the range typical for π systems; σ systems display values greater than δ = 130 ppm. The resonances for the substituted carbon (-*C*HPh) appear at δ = 111 and 123 ppm for the major and minor isomers, respectively. The latter value is unusually low compared to other (η^3-$CH_2CHCHPh$)Ir^{III} or (η^3-$CH_2CHCHPh$)Pd complexes.[8d,33]

The rate of interconversion of the isomers of **30** was determined as follows. By recording ^{1}H-^{1}H EXSY spectra at varied mixing times (t_m) at −40 °C, the magnetisation transfer between chosen atoms present in both isomers, denoted as **A** (minor isomer) and **B**, was measured (Figure 7).[34] From the 2D NMR spectra a correlation between the allylic protons in the isomers was chosen to perform the calculations. Applying Equation (1) (I_{ii}, I_{ij} integral values of diagonal and cross-peaks, respectively, X_i molar fraction)[35] to the data summarised in Table 7 a value of k = 4 Hz at −40 °C was determined for the rate constant.

The ^{1}H and ^{13}C{^{1}H} NMR spectra of complex **31** measured at −60 °C show two isomeric species in a 9:1 ratio; these are probably the *endo* and *exo* isomers in analogy to

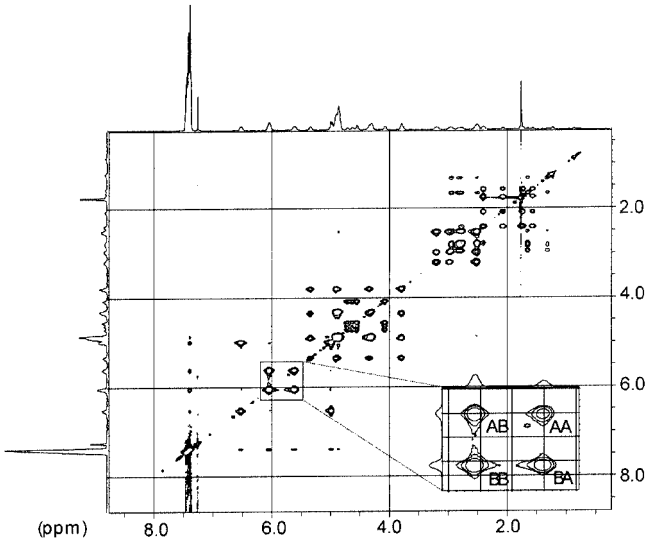

Figure 7. ^{1}H,^{1}H EXSY spectrum of complex **30** recorded at −40 °C ($CDCl_3$, 500.13 MHz); cross peaks chosen for the calculations are enlarged; A and B denote the minor and major isomer, respectively

Table 7. ^{1}H,^{1}H EXSY data for the determination of the isomerisation rate constant k [a]

t_m [ms]	X_A [b]	X_B [b]	I_{AA}	I_{BB}	I_{AB}	I_{BA}	r	k [s^{-1}]
25	0.43	0.57	1.00	1.77	0.065	0.069	23.74	3.37
50	0.42	0.58	1.00	1.88	0.150	0.147	10.32	3.89
100	0.41	0.59	1.00	2.08	0.309	0.302	5.16	3.92

[a] Measured at −40 °C in $CDCl_3$. [b] The molar fraction X_i is given by the formula $X_A = \sqrt{I_{AA}} / \left(\sqrt{I_{AA}} + \sqrt{I_{BB}}\right)$

complex **30**. Coalescence was found at ca. 50 °C. The ^{1}H NMR resonances are found in the expected range. In the ^{13}C{^{1}H} NMR spectrum (−60 °C), one of the CH_2 groups shows resonances in the expected range (δ = 44.6 and 44.9 ppm) while the other appears at unusually low field (δ = 79.7 and 89.6 ppm), for the major and minor isomer, respectively. The latter values are very unusual for (π-allyl)Ir^{III} complexes,[8a−8d,30c,36] although values at similarly low field are known for (π-allyl)Pd complexes.[33] Similar to complex **30**, the resonances of C-2 appear at fairly low field, δ = 114.5 and 107.9 ppm for the minor and major isomer, respectively.

$$k = \frac{1}{t_m} \cdot \ln\frac{r+1}{r-1} \qquad r = \frac{4X_A X_B \cdot \left(I_{AA} + I_{BB}\right)}{\left(I_{AB} + I_{BA}\right) - \left(X_A - X_B\right)^2} \tag{1}$$

Activity of Complex 30 in Stoichiometric Reactions with Nucleophiles and in Catalysis

The low-temperature stoichiometric reaction of complex **30** with dimethyl 2-sodiomalonate as nucleophile in the presence of chiral ligand (*R*)-**L2** was investigated. The ^{1}H and ^{31}P NMR spectra of the reaction mixture, recorded at −60 °C, show fast formation of the branched substitution

product **3a** and the complex {IrCl(COD)[(*R*)-**L2**]} (**29**) in a 1:1 ratio. After workup compound **29** was isolated in 32% yield and **3a** in 64% yield. A GC and HPLC investigation revealed that **3a** had been formed with 99% regioselectivity and 0% *ee*. The lack of enantioselectivity shows that nucleophilic attack at the allyl ligand is faster than coordination of the chiral ligand by displacement of a COD double bond.

Complexes **30** and **31** were found to possess catalytic activity. For example, allylic alkylations of substrates **1** and (*E*)-**2** with $NaCH(CO_2Me)_2$ gave very similar results with catalyst **30**/(*R*)-**L2** (4 mol %) and catalyst $[IrCl(COD)]_2$/(*R*)-**L2** (see Table 8). In agreement with the results obtained in the stoichiometric reaction described above, small amounts of racemic **3a** (HPLC) were formed in allylic alkylations of substrates **1b** and (*E*)-**2b** upon catalysis with **30**/(*R*)-**L2** as a consequence of attack of the nucleophile at the allyl ligand present in complex **30**. In this reaction, complex **29** is also formed, which acts as the catalyst of the process.

Table 8. Allylic alkylations of substrates **1** and (*E*)-**2** catalysed by mixtures of **30** and **L2** or [IrCl(COD)**L2**] (**29**)[a]

Entry	Substrate	Catalyst[b]	Time [h]	Yield [%] **3** and **4**	Ratio **3**:**4**	*ee* [%] of **3** (config.)[c]
1	**1a**	**30/L2** [1:1]	18	85	98:2	9 (*S*)
2	**1a**	[IrCl(COD)**L2**]	3	98	92:8	8 (*S*)
3	(*E*)-**2a**	**30/L2** [1:1]	18	38	95:5	34 (*R*)
4	(*E*)-**2a**	[IrCl(COD)**L2**]	3	99	98:2	37 (*R*)
5[d]	**1b**	**30/L2** [1:1]	3	80	99:1	67 (*R*)
6	**1b**	[IrCl(COD)**L2**]	3	92	98:2	69 (*R*)
7[d]	(*E*)-**2b**	**30/L2** [1:1]	18	12	50:50	40 (*R*)
8	(*E*)-**2b**	[IrCl(COD)**L2**]	3	54	95:5	43 (*R*)

All the reactions were performed at 25 °C in THF with 0.5 mmol of allyl substrate [0.125 M], 1 mmol of $NaCH(CO_2Me)_2$ and 4 mol % of [Ir]. [b] When catalyst [IrCl(COD)**L2**] was used, this was formed in situ by reaction of $[IrCl(COD)]_2$ (2 mol %) with (*R*)-**L2** (4 mol %). [c] Determined by HPLC. [d] Small quantities of **3a** were also formed.

Conclusions

Our results demonstrate that it is possible to achieve modest to high levels of enantioselectivity in Ir^I-catalysed asymmetric alkylations of monoalkylallyl acetates. Presently it is necessary to use racemic, branched allylic derivatives as substrates. Further progress will probably be achieved on the basis of more detailed mechanistic investigations. In particular, further investigations of the structure and dynamic properties of (allyl)Ir^{III} complexes are required.

Experimental Section

General: All reactions were carried out using dry solvents under an argon atmosphere. TLC: Macherey & Nagel Polygram Sil G/UV precoated sheets, treatment with I_2 or aqueous $KMnO_4$ solution for visualization of spots. Column chromatography: Fluka silica gel, grade 60 (0.04−0.063 mm). ^1H, ^{13}C and ^{31}P NMR spectra were recorded on Bruker DRX 200, DRX 300 or DRX 500 instruments. ^1H NMR chemical shifts are relative to residual non-deuterated solvent in $CDCl_3$ (δ = 7.26 ppm) or CD_2Cl_2 (δ = 5.32 ppm). ^{13}C NMR shifts are given relative to the solvents $CDCl_3$ (δ = 77.0 ppm) and CD_2Cl_2 (δ = 53.8 ppm) and ^{31}P NMR shifts are relative to 85% H_3PO_4 (δ = 0.00 ppm). MS: JEOL, JMS-700. FAB: JEOL, JMS-700; matrix: 4-nitrobenzyl alcohol (NBA) or 4-nitrophenyl octyl ether (NPOE). Optical rotation: Perkin−Elmer P 241. GC: Hewlett Packard HP 5890 with Chiraldex γ-CD TA column (30 m × 0.25 mm). GC/MS: Hewlett Packard HP 5890/7972 instrument with a HP 5 column (crosslinked methylsilicon, 25 m × 0.2 mm, helium). HPLC: Hewlett Packard HP 1090 with DAICEL Chiralcel ODH column (25 cm × 0.46 cm) in combination with DAICEL Chiralcel ODH precolumn (5 cm × 0.46 cm). Elemental analyses: Microanalytical laboratory of the Organisch-Chemisches Institut, Universität Heidelberg. The compounds (*aR*)-**L2**,[37] **L5**[38] and $[IrCl(COD)]_2$,[39] were prepared according to published procedures. The allylic esters were prepared by reaction of the corresponding alcohols with acetic anhydride [**1a**,[40] **1b**,[41] **1c**,[42] **1d**,[43] (*E*)-**2a**,[40] (*E*)-**2b**,[44] (*E*)-**2c**,[42]], methyl chloroformate (**25b**)[45] or diethyl chlorophosphate (**26b**). Compounds **3a**,[40] **3c**,[4d,42] **6b**,[12a] **7b**−**8b**,[46] **8d**,[47] **7a**,[48] **7c**−**7f**,[48] **20**−**21**,[21a] and **23**[4d] have been described and characterised previously. The enantiomerically pure allylic acetates (*S*)-**1b**,[12a] (*R*)-**1b**,[12a,49] and **22**[50] were obtained by enzyme-catalysed partial esterification of the corresponding racemic alcohols. Compounds **14** and **15**,[10] and **18**[13] were prepared according to previously published methods. 1-(*S*)-Phenylpropen-2-ol [(*S*)-**6a**], (*R*)-buten-2-ol [(*R*)-**6c**], tetra(*n*-propyl)ammonium perruthenate (TPAP), $[P(NMe_2)_3]$ and **L4** are commercially available.

General Procedure I. Acetylation of the Alcohols: A solution of the alcohol (10 mmol), DMAP (12 mg, 0.10 mmol) and NEt_3 (4.2 mL, 30 mmol) in CH_2Cl_2 (10 mL) was cooled to 0 °C. Freshly distilled Ac_2O (1.9 mL, 20 mmol) was added dropwise and the mixture was stirred for 18 h at room temperature. Water (20 mL) was then added and the aqueous layer extracted with CH_2Cl_2 (3 × 5 mL). The combined organic layers were washed with satd. NH_4Cl solution (20 mL), dried (Na_2SO_4) and concentrated in vacuo. Products were purified by flash chromatography.

1-Methoxymethoxymethylallyl Acetate (1e): Crude **1e** was prepared according to general procedure I from alcohol **6e** (740 mg, 5.6 mmol) and was purified by flash column chromatography (silica gel, petroleum ether/ethyl acetate 8:1). Yield: 58% (570 mg). ^1H NMR (300.13 MHz, $CDCl_3$, 25 °C): δ = 2.10 (s, 3 H, $COCH_3$), 3.36 (s, 3 H, CH_3OCH_2), 3.63−3.67 [m, 2 H, $CH_2CH(OAc)$], 4.63 (s, 2 H, OCH_2O), 5.26 [ddd, $^2J_{H,H}$ = 1.1, $^4J_{H,H}$ = 1.1, $^3J_{H,H}$ = 10.7 Hz, 1 H, *syn*-(=CH_2)], 5.34 [ddd, $^2J_{H,H}$ = 1.1, $^4J_{H,H}$ = 1.1, $^3J_{H,H}$ = 17.3 Hz, 1 H, *anti*-(=CH_2)], 5.44−5.48 [m, 1 H, CH(OAc)], 5.83 (ddd, $^3J_{H,H}$ = 6.3, $^3J_{H,H}$ = 10.7, $^3J_{H,H}$ = 17.3 Hz, 1 H, =CH) ppm. $^{13}C\{^1H\}$ NMR (75.47 MHz, $CDCl_3$, 25 °C): δ = 20.9 ($COCH_3$), 55.1 (CH_3OCH_2), 68.4 [CH_2CH(OAc)], 73.0 [CH(OAc)], 96.2 (OCH_2O), 117.9 (=CH_2), 133.0 (=CH), 170.0 (C=O) ppm. MS (CI, isobutane): *m*/*z* (%) = 175 (10) [M^+ + 1], 143 (90) [M^+ − OCH_3], 113 (100) [M^+ − OMOM]. HRMS (EI) for $C_7H_{11}O_3$ [M^+ − OCH_3]: calcd. 143.0708; found 143.0685.

1-(2-Methoxymethoxyethyl)allyl Acetate (1f): Crude **1f** was prepared according to general procedure I from alcohol **6f** (1.5 g, 10.3 mmol) and purified by flash chromatography (silica gel, petroleum ether/ethyl acetate 6:1). Yield: 86% (1.7 g). ^1H NMR (300.13 MHz, $CDCl_3$, 25 °C): δ = 1.85−1.99 [m, 2 H, CH_2CH(OAc)], 2.07 (s, 3 H, CH_3CO), 3.35 (s, 3 H, CH_3OCH_2), 3.56 (t, $^3J_{H,H}$ = 6.4 Hz, 2 H, MOMOCH_2), 4.60 (s, 2 H,

CH_3OCH_2), 5.19 [ddd, $^2J_{H,H}$ = 1.1, $^4J_{H,H}$ = 1.1, $^3J_{H,H}$ = 10.5 Hz, 1 H, *syn*−(=CH_2)], 5.27 [ddd, $^2J_{H,H}$ = 1.1, $^4J_{H,H}$ = 1.1, $^3J_{H,H}$ = 17.2 Hz, 1 H, *anti*−(=CH_2)], 5.80 (ddd, $^3J_{H,H}$ = 6.5, $^3J_{H,H}$ = 10.5, $^3J_{H,H}$ = 17.2 Hz, 1 H, =CH) ppm. $^{13}C\{^1H\}$ NMR (75.47 MHz, $CDCl_3$, 25 °C): δ = 21.0 (COCH_3), 34.1 [CH_2CH(OAc)], 55.0 (CH_3OCH_2), 63.4 (MOMOCH_2), 71.8 [CH(OAc)], 96.3 ($CH_3OCH_2OCH_2$), 116.7 (=CH_2), 136.0 (=CH), 170.0 (C=O) ppm. $C_9H_{16}O_4$ (188.22): calcd. C 57.43, H 8.57; found C 57.23, H 8.58.

5-Phenylpent-2-enyl Acetate [(*E*)-2b]: Crude **2b** was prepared according to general procedure I from alcohol **8b** (6.0 g, 37.0 mmol) and purified by flash chromatography (silica gel, petroleum ether/ethyl acetate 97:3). Yield: 83% (6.3 g). ^1H NMR (300.13 MHz, $CDCl_3$, 25 °C): δ = 2.08 (s, 3 H, $COCH_3$), 2.41 (dt, $^3J_{H,H}$ = 6.7, $^3J_{H,H}$ = 8.1 Hz, 2 H, $PhCH_2CH_2$), 2.74 (br. t, $^3J_{H,H}$ = 7.4 Hz, 2 H, $PhCH_2$), 4.54 (dd, $^4J_{H,H}$ = 0.9, $^3J_{H,H}$ = 6.4 Hz, 2 H, CH_2OAc), 5.58−5.89 (m, 2 H, =CH), 7.19−7.34 (m, 5 H, Ph) ppm. $^{13}C\{^1H\}$ NMR (75.47 MHz, $CDCl_3$, 25 °C): δ = 20.8 (COCH_3), 33.9 (CH_2), 35.2 (CH_2), 64.1 (CH_2OAc), 124.4 (=$CHCH_2OAc$), 126.1 (Ph), 128.2 (Ph), 128.3 (Ph), 135.2 (CH=$CHCH_2OAc$), 141.4 (Ph), 170.6 (C=O) ppm. $C_{13}H_{16}O_2$ (204.27): calcd. C 76.44, H 7.90; found C 76.26, H 7.85.

4-Methylpent-2-enyl Acetate [(*E*)-2d]: Crude **2d** was prepared according to general procedure I from alcohol **8d** (4.6 g, 46.5 mmol) and purified by flash chromatography (silica gel, petroleum ether/diethyl ether 95:5). Yield: 89% (5.9 g). ^1H NMR (300.13 MHz, $CDCl_3$, 25 °C): δ = 1.00 (d, $^3J_{H,H}$ = 7.0 Hz, 6 H, CH_3), 2.06 (s, 3 H, $COCH_3$), 2.31 [br. sext., $^3J_{H,H}$ = 7.0 Hz, 1 H, $CH(CH_3)_2$], 4.50 (d, $^3J_{H,H}$ = 6.6 Hz, 2 H, CH_2OAc), 5.50 (ddt, $^4J_{H,H}$ = 1.1, $^3J_{H,H}$ = 6.6, $^3J_{H,H}$ = 15.5 Hz, 1 H, =$CHCH_2OAc$), 5.74 (ddt, $^4J_{H,H}$ = 1.1, $^3J_{H,H}$ = 6.2, $^3J_{H,H}$ = 15.5 Hz, 1 H, CH=$CHCH_2OAc$) ppm. $^{13}C\{^1H\}$ NMR (75.47 MHz, $CDCl_3$, 25 °C): δ = 21.0 (COCH_3), 22.0 (two CH_3), 30.7 [$CH(CH_3)_2$], 65.4 (CH_2OAc), 120.9 ($CHCH_2OAc$), 143.2 (CH=$CHCH_2OAc$), 170.9 (C=O) ppm. $C_8H_{14}O_2$ (142.20): calcd. C 67.57, H 9.92; found C 67.69, H 10.07.

(*E*)-5-Methoxymethoxypent-2-enyl Acetate [(*E*)-2f]: Crude (*E*)-**2f** was prepared according to general procedure I from alcohol **8f** (1.2 g, 8.2 mmol) and purified by flash column chromatography (silica gel, petroleum ether/diethyl ether 5:1). Colourless oil. Yield: 97% (1.5 g). ^1H NMR (300.13 MHz, $CDCl_3$, 25 °C): δ = 2.06 (s, 3 H, $COCH_3$), 2.37 (dt, $^3J_{H,H}$ = 6.6, $^3J_{H,H}$ = 12.1 Hz, 2 H, MOMOCH_2CH_2), 3.35 (s, 3 H, CH_3O), 3.58 (t, $^3J_{H,H}$ = 6.6 Hz, 2 H, $MOMOCH_2$), 4.51 (dd, $^4J_{H,H}$ = 1.1, $^3J_{H,H}$ = 6.2 Hz, 2 H, CH_2OAc), 4.62 (s, 2 H, CH_3OCH_2), 5.61−5.72 (m, 1 H, CH), 5.74−5.85 (m, 1 H, CH) ppm. $^{13}C\{^1H\}$ NMR (75.47 MHz, $CDCl_3$, 25 °C): δ = 20.8 (COCH_3), 32.5 ($MOMOCH_2CH_2$), 55.0 (CH_3O), 64.8 (MOMOCH_2 or CH_2OAc), 66.6 (MOMOCH_2 or CH_2OAc), 96.2 (CH_3OCH_2), 125.7 (CH), 132.2 (CH), 170.6 (C=O) ppm. $C_9H_{16}O_4$ (188.22): calcd. C 57.43, H 8.57; found C 57.21, H 8.56.

(*Z*)-4-Methoxymethoxybut-2-enyl Acetate [(*Z*)-2e]: Crude (*Z*)-**2e** was prepared from alcohol **15** (6.8 g, 51.8 mmol) according to general procedure I and purified by flash column chromatography (silica gel, petroleum ether/ethyl acetate 6:1). Colourless oil. Yield: 69% (6.2 g). ^1H NMR (300.13 MHz, $CDCl_3$, 25 °C): δ = 2.03 (s, 3 H, CH_3CO), 3.30 (s, 3 H, OCH_3), 4.14 (d, $^3J_{H,H}$ = 5.7 Hz, 2 H, MOMOCH_2), 4.60 (s, 2 H, CH_3OCH_2), 4.63 (d, $^3J_{H,H}$ = 6.0 Hz, 2 H, CH_2OAc), 5.62−5.80 (m, 2 H, =CH) ppm. $^{13}C\{^1H\}$ NMR (75.47 MHz, $CDCl_3$, 25 °C): δ = 20.7 (CH_3CO), 55.2 (OCH_3), 60.1 (CH_2OAc), 62.6 (MOMOCH_2), 95.6 (CH_3OCH_2), 126.7, 130.2 (=CH), 170.7 (C=O) ppm. MS (EI): *m*/*z* (%) = 174 (1) [M^+], 129 (8) [$M^+ - CH_2OCH_3$], 99 (6) [$M^+ - CH_2OCH_3 - CH_2O$], 85 (32) [$M^+ - CH_2OCH_3 - CO_2$], 45 (100) [$CH_2OCH_3^+$]. HRMS (EI) - for $C_6H_9O_3$ [$M^+ - CH_2OCH_3$]: calcd. 129.0552; found 129.0557.

(*Z*)-5-Methoxymethoxypent-2-enyl Acetate [(*Z*)-2f]: Crude (*Z*)-**2f** was prepared from alcohol **19** (5.0 g, 34.2 mmol) according to general procedure I and purified by flash column chromatography (silica gel, petroleum ether/ethyl acetate 9:1). Colourless oil. Yield: 77% (4.9 g). ^1H NMR (300.13 MHz, $CDCl_3$, 25 °C): δ = 2.03 (s, 3 H, CH_3CO), 2.38 (dt, $^3J_{H,H}$ = 6.6, $^3J_{H,H}$ = 6.6 Hz, 2 H, MOMOCH_2CH_2), 3.32 (s, 3 H, OCH_3), 3.53 (t, $^3J_{H,H}$ = 6.6 Hz, 2 H, MOMOCH_2), 4.58 (s, 2 H, CH_3OCH_2), 4.60 (d, $^3J_{H,H}$ = 5.6 Hz, 2 H, CH_2OAc), 5.52−5.76 (m, 2 H, =CH) ppm. $^{13}C\{^1H\}$ NMR (75.47 MHz, $CDCl_3$, 25 °C): δ = 20.9 (CH_3CO), 28.1 (MOMOCH_2CH_2), 55.1 (OCH_3), 60.2 (CH_2OAc), 66.8 (MOMOCH_2), 96.3 (CH_3OCH_2), 125.4, 131.1 (=CH), 170.8 (C=O) ppm. $C_9H_{16}O_4$ (188.22): calcd. C 57.43, H 8.57; found C 57.27, H 8.72.

General Procedure II. Ir^I-Catalysed Allylic Alkylation: A solution of $[IrCl(COD)]_2$ (6.7 mg, 0.01 mmol) in THF (2 mL) was treated with substrate (0.5 mmol) and then ligand (0.02 mmol). The resulting solution was stirred for 5 min. If the reaction was run with additive, this was added now (0.5 mmol) and the solution stirred for a further 5 min. After that, a freshly prepared solution of dimethyl 2-sodiomalonate, prepared by suspending sodium hydride (24 mg, 1.0 mmol) in THF (2 mL) and dropwise addition of dimethyl malonate (115 μL, 1.0 mmol), was added. The mixture was stirred under the stated reaction conditions, then water (4 mL) was added and the mixture extracted with diethyl ether (3 × 5 mL). The combined organic layers were washed with a satd. NH_4Cl solution (10 mL), dried (Na_2SO_4) and concentrated in vacuo. The crude product was purified by flash column chromatography to give substitution products **3** and **4** as colourless oils.

2-(1-Phenethylallyl) Dimethylmalonate (3b): Compound **3b** was obtained by allylic alkylation of substrate **1b** (535 mg, 2.6 mmol) according to general procedure II [ligand: $P(OPh)_3$, reaction time: 3 h, room temperature]. After purification (silica gel, petroleum ether/ethyl acetate 97:3), a 95:5 mixture of **3b** and **4b** was obtained. Yield: 91% (650 mg). $[\alpha]_D^{20}$ = 11.4 (*c* = 0.63, $CHCl_3$) for **3b** with 93% *ee* (*R*). HPLC: DAICEL Chiralcel ODH column, length: 25 cm + 5 cm precolumn, flow: 0.5 mL·min^{-1}, eluent: *n*-hexane/*i*PrOH (99.5:0.5); **3b**: t_R(*R*) = 32.2 min, t_R(*S*) = 34.3 min; (*E*)-**4b**: t_R = 49.6 min. ^1H NMR (300.13 MHz, $CDCl_3$, 25 °C): δ = 1.57−1.88 (m, 2 H, $PhCH_2CH_2$), 2.46−2.77 (m, 2 H, $PhCH_2$), 2.84 (dddd, $^4J_{H,H}$ = 3.7, $^3J_{H,H}$ = 9.0, $^3J_{H,H}$ = 9.5, $^3J_{H,H}$ = 9.3 Hz, 1 H, $CHCH$=CH_2), 3.44 [d, $^3J_{H,H}$ = 9.0 Hz, 1 H, $CH(CO_2CH_3)_2$], 3.69 (s, 3 H, OCH_3), 3.71 (s, 3 H, OCH_3), 5.11−5.20 (m, 2 H, =CH_2), 5.73 (ddd, $^3J_{H,H}$ = 9.3, $^3J_{H,H}$ = 10.7, $^3J_{H,H}$ = 16.6 Hz, 1 H, CH=CH_2), 7.13−7.31 (m, 5 H, Ph) ppm. $^{13}C\{^1H\}$ NMR (75.47 MHz, $CDCl_3$, 25 °C): δ = 33.2 ($PhCH_2CH_2$), 33.9 ($PhCH_2$), 43.7 ($CHCH$=CH_2), 52.1 (CH_3), 52.2 (CH_3), 56.7 [$CH(CO_2CH_3)_2$], 117.9 (=CH_2), 125.8 (Ph), 128.2 (Ph), 128.3 (Ph), 137.6 (CH=CH_2), 141.6 (Ph), 168.3 (C=O), 168.5 (C=O) ppm. $C_{16}H_{20}O_4$ (276.33): calcd. C 69.55, H 7.30; found C 69.34, H 7.33.

2-(1-Isopropylallyl) Dimethylmalonate (3d): Ester **3d** was prepared by allylic alkylation of substrate **1d** (850 mg, 6.0 mmol) according to general procedure II [ligand: $P(OPh)_3$, reaction time: 5 days, room temperature]. After purification by flash chromatography (silica gel, petroleum ether/ethyl acetate 98:2), a 93:7 mixture of **3d** and **4d** was obtained. Yield: 69% (890 mg). $[\alpha]_D^{20}$ = 0.07 (*c* = 0.54, $CHCl_3$) for **3d** with 66% *ee* (*R*). GC: Chiraldex γ-CD TA column, length: 30 m, 100 kPa helium, 50→100 °C at 1 °C·min^{-1}, then 20 min at 100 °C; **3d**: t_R(*R*) = 44.8 min, t_R(*S*) = 46.3 min; (*E*)-**4d**: t_R = 56.7 min. ^1H NMR (300.13 MHz, $CDCl_3$, 25 °C): δ = 0.82

(d, $^3J_{H,H}$ = 7.0 Hz, 3 H, CH_3), 0.89 (d, $^3J_{H,H}$ = 7.0 Hz, 3 H, CH_3), 1.71 [dqq, $^3J_{H,H}$ = 5.2, $^3J_{H,H}$ = 7.0, $^3J_{H,H}$ = 7.0 Hz, 1 H, C*H*(CH_3)$_2$], 2.64 (ddd, $^3J_{H,H}$ = 5.2, $^3J_{H,H}$ = 9.6, $^3J_{H,H}$ = 9.9 Hz, 1 H, C*H*CH=CH_2), 3.56 [d, $^3J_{H,H}$ = 9.6 Hz, 1 H, C*H*(CO_2CH_3)$_2$], 3.67 (s, 3 H, OCH_3), 3.71 (s, 3 H, OCH_3), 5.05 [dd, $^2J_{H,H}$ = 1.8, $^3J_{H,H}$ = 16.9 Hz, 1 H, *anti*-(=CH_2)], 5.10 [dd, $^2J_{H,H}$ = 1.8, $^3J_{H,H}$ = 10.1 Hz, 1 H, *syn*-(=CH_2)], 5.67 (ddd, $^3J_{H,H}$ = 9.9, $^3J_{H,H}$ = 10.1, $^3J_{H,H}$ = 16.9 Hz, 1 H, C*H*=CH_2) ppm. $^{13}C\{^1H\}$ NMR (75.47 MHz, $CDCl_3$, 25 °C): δ = 17.5 (CH_3), 21.2 (CH_3), 29.0 [*C*H(CH_3)$_2$], 50.3 (*C*HCH=CH_2), 52.2 (OCH_3), 52.4 (OCH_3), 54.9 [*C*H(CO_2CH_3)$_2$], 118.6 (=CH_2), 134.8 (*C*H=CH_2), 168.7 (C=O), 169.0 (C=O) ppm. $C_{11}H_{18}O_4$ (214.26): calcd. C 61.66, H 8.47; found C 61.47, H 8.43.

2-[1-Methoxymethoxymethylallyl] Dimethylmalonate (3e): Ester **3e** was obtained by allylic alkylation of substrate **1e** (43 mg, 0.25 mmol) according to general procedure II [ligand: $P(OPh)_3$, reaction time: 18 h, room temperature]. After purification by flash chromatography (silica gel, petroleum ether/ethyl acetate 9:1), a 77:23 mixture of **3e** and **4e** was obtained. Yield: 91% (56 mg). $[\alpha]_D^{24}$ = 23.3 (*c* = 0.69, $CHCl_3$) for **3e** with 78% *ee* (*R*). GC: Chiraldex γ-CD TA column, length: 30 m, 100 kPa helium, 50→100 °C at 10 °C·min^{-1}, then 60 min at 100 °C; **3e**: t_R(*R*) = 54.1 min, t_R(*S*) = 55.8 min; (*E*)-**4e**: t_R = 63.5 min. ^1H NMR (300.13 MHz, $CDCl_3$, 25 °C): δ = 3.06−3.23 [m, 1 H, C*H*(CH=CH_2)] 3.32 (s, 3 H, C*H*$_3$OCH$_2$), 3.59 (d, $^3J_{H,H}$ = 6.3 Hz, 1 H, MOMOC*H*$_2$), 3.61 (d, $^3J_{H,H}$ = 5.5 Hz, 1 H, MOMOC*H*$_2$), 3.68 [d, $^3J_{H,H}$ = 8.1 Hz, 1 H, C*H*(CO_2Me)$_2$], 3.70 (s, 3 H, Me), 3.73 (s, 3 H, Me), 4.57 (s, 2 H, CH_3OCH_2), 5.11−5.21 (m, 2 H, =CH_2), 5.84 (ddd, $^3J_{H,H}$ = 8.8, $^3J_{H,H}$ = 10.3, $^3J_{H,H}$ = 17.3 Hz, 1 H, =CH) ppm. $^{13}C\{^1H\}$ NMR (75.47 MHz, $CDCl_3$, 25 °C): δ = 43.8 [*C*H(CH=CH_2)], 52.3 (Me), 52.5 (Me), 53.1 [*C*H(CO_2Me)$_2$], 55.3 (*C*H$_3$OCH$_2$), 68.4 (MOMO*C*H$_2$), 96.5 (CH_3OCH_2), 118.2 (=CH_2), 135.3 (=CH), 166.9 (C=O), 168.7 (C=O) ppm. $C_{11}H_{18}O_6$ (246.26): calcd. C 53.65, H 7.37; found C 53.37, H 7.23.

2-[1-(2-Methoxymethoxyethyl)allyl] Dimethylmalonate (3f): Ester **3f** was obtained by allylic alkylation of substrate **1f** (94 mg, 0.5 mmol) according to general procedure II [ligand: $P(OPh)_3$, reaction time: 18 h, room temperature]. After purification by flash chromatography (silica gel, petroleum ether/ethyl acetate 9:1), a 93:7 mixture of **3f** and **4f** was obtained. Yield: 94% (122 mg). $[\alpha]_D^{24}$ = −1.4 (*c* = 0.76, $CHCl_3$) for **3f** with 70% *ee* (*R*). HPLC: DAICEL Chiralcel ODH column, length: 25 cm + 5 cm precolumn, flow: 0.5 mL·min^{-1}, eluent: *n*-hexane/*i*PrOH (95:5); **3f**: t_R(*R*) = 23.2 min, t_R(*S*) = 24.6 min; (*E*)-**4f**: t_R = 28.9 min. ^1H NMR (300.13 MHz, $CDCl_3$, 25 °C): δ = 1.54−1.66 (m, 1 H, MOMOCH$_2$C*H*$_2$), 1.76−1.87 (m, 1 H, MOMOCH$_2$C*H*$_2$), 2.94−2.97 [m, 1 H, C*H*(CH=CH_2)], 3.45 [d, $^3J_{H,H}$ = 8.4 Hz, 1 H, C*H*(CO_2Me)$_2$], 3.39−3.58 (m, 2 H, MOMOC*H*$_2$), 3.70 (s, 3 H, Me), 3.75 (s, 3 H, Me), 4.56−4.61 (m, 2 H, =CH_2), 5.69 (ddd, $^3J_{H,H}$ = 9.6, $^3J_{H,H}$ = 9.6, $^3J_{H,H}$ = 16.9 Hz, 1 H, =CH), 3.34 (s, 3 H, C*H*$_3$OCH$_2$) ppm. $^{13}C\{^1H\}$ NMR (75.47 MHz, $CDCl_3$, 25 °C): δ = 32.1 (MOMOCH$_2$*C*H$_2$), 41.1 [*C*H(CH=CH_2)], 52.4 (Me), 52.6 (Me), 55.2 (*C*H$_3$OCH$_2$), 56.6 [*C*H(CO_2Me)$_2$], 65.1 (MOMO*C*H$_2$), 96.4 (CH_3OCH_2), 118.0 (=CH_2), 137.3 (=CH), 168.4 (C=O), 168.6 (C=O) ppm. $C_{12}H_{20}O_6$ (260.29): calcd. C 55.37, H 7.74; found C 55.28, H 7.63.

(*Z*)-[2-(4-Methoxymethoxybut-2-enyl)] Dimethylmalonate [(*Z*)-4e]: Ester (*Z*)-**4e** was obtained by allylic alkylation of substrate (*Z*)-**2e** (87 mg, 0.5 mmol) according to general procedure II [ligand: $P(OPh)_3$, reaction time: 4 h, room temperature]. After purification by flash chromatography (silica gel, petroleum ether/ethyl acetate 9:1) an 8:92 mixture of (*E*)-**4e** and (*Z*)-**4e** was obtained. Yield: 65% (80 mg). GC/MS (*Z*)-**4e**: t_R = 12.79 min; (*E*)-**4e**: t_R = 12.85 min. **(*Z*)-4:** ^1H NMR (300.13 MHz, $CDCl_3$, 25 °C): δ = 2.65 [dd, $^3J_{H,H}$ = 7.4, $^3J_{H,H}$ = 7.4 Hz, 2 H, C*H*$_2$CH(CO_2Me)$_2$], 3.34 (s, 3 H, C*H*$_3$OCH$_2$), 3.40 [t, $^3J_{H,H}$ = 7.4 Hz, 1 H, C*H*(CO_2Me)$_2$], 3.70 (s, 6 H, CO_2CH_3), 4.11 (d, $^3J_{H,H}$ = 6.2 Hz, 2 H, MOMOC*H*$_2$), 4.59 (s, 2 H, CH_3OCH_2), 5.40−5.72 (m, 2 H, C*H*=C*H*) ppm. $^{13}C\{^1H\}$ NMR (50.32 MHz, $CDCl_3$, 25 °C): δ = 26.4 [*C*H$_2$CH(CO_2Me)$_2$], 51.3 [*C*H(CO_2Me)$_2$], 52.5 (CO_2CH_3), 55.1 (*C*H$_3$OCH$_2$), 62.6 (MOMO*C*H$_2$), 95.7 (CH_3OCH_2), 128.2 (=CH), 129.0 (=CH), 169.1 (2s, C=O) ppm. HRMS (EI) for $C_{10}H_{15}O_5$ [M^+ − OCH_3]: calcd. 215.0919; found 215.0892.

(*Z*)-[2-(5-Methoxymethoxypent-2-enyl)] Dimethylmalonate [(*Z*)-4f]. Ester (*Z*)-**4f** was obtained by allylic alkylation of substrate (*Z*)-**2f** (752 mg, 4.0 mmol) according to the general method II [ligand: $P(OPh)_3$, reaction time: 4 h, room temperature]. After purification (silica gel, petroleum ether/ethyl acetate 9:1), a 6:1 mixture of (*Z*)-**4f** and **3f** was obtained. Yield: 80% (830 mg). GC/MS (*Z*)-**4f**: t_R = 13.33 min. ^1H NMR (200.13 MHz, $CDCl_3$, 25 °C): δ = 2.31 (dt, $^3J_{H,H}$ = 6.6, $^3J_{H,H}$ = 6.6 Hz, 2 H, MOMOCH$_2$C*H*$_2$), 2.61 [dd, $^3J_{H,H}$ = 6.6, $^3J_{H,H}$ = 6.6 Hz, 2 H, C*H*$_2$CH(CO_2Me)$_2$], 3.29 (s, 3 H, C*H*$_3$OCH$_2$), 3.32−3.39 [m, 1 H, C*H*(CO_2Me)$_2$], 3.48 (t, $^3J_{H,H}$ = 6.6 Hz, 2 H, MOMOC*H*$_2$), 3.68 (s, 6 H, CH_3), 4.56 (s, 2 H, CH_3OCH_2), 5.27−5.53 (m, 2 H, C*H*=C*H*) ppm. $^{13}C\{^1H\}$ NMR (50.32 MHz, $CDCl_3$, 25 °C): δ = 26.7 [*C*H$_2$CH(CO_2Me)$_2$], 27.7 (MOMOCH$_2$*C*H$_2$), 51.5 [*C*H(CO_2Me)$_2$], 52.3 (CH_3), 56.4 (*C*H$_3$OCH$_2$), 66.9 (MOMO*C*H$_2$), 96.2 (CH_3OCH_2), 126.5 (=CH), 129.1 (=CH), 169.2 (C=O) ppm. $C_{12}H_{20}O_6$ (260.29): calcd. C 55.37, H 7.74; found C 55.22, H 7.85.

1-Methoxymethoxybut-3-en-2-ol (6e): This compound was prepared via intermediates (see Schemes 2 and 3) that were not fully characterised.

11e: A solution of 2-methoxy-1,3-dioxolane (**10e**) (30.0 g, 0.288 mol) in 250 mL of dichloromethane was cooled to −70 °C. Then, a pre-cooled (−70 °C) solution of DIBAL-H in hexane (346 mL, 0.346 mol) was added dropwise and the reaction mixture was stirred for 90 min at −70 °C. Thereafter, the temperature was allowed to rise slowly to 0 °C and water (20 mL) was added. The resulting precipitate was dissolved by addition of aqueous NaOH (20%, 300 mL) and the resulting solution was extracted with dichloromethane (4 × 50 mL). The combined organic layers were washed with satd. NaCl solution (2 × 80 mL), dried (Na_2SO_4) and concentrated in vacuo to give an oil which was distilled [65 °C (10 Torr)] to give **11e**. Yield: 51% (15.2 g).[51] ^1H NMR (300.13 MHz, $CDCl_3$, 25 °C): δ = 2.44 (s, 1 H, OH), 3.38 (s, 3 H, C*H*$_3$OCH$_2$), 3.67 (m, 2 H, C*H*$_2$OH or MOMOC*H*$_2$), 3.73 (m, 2 H, C*H*$_2$OH or MOMOC*H*$_2$), 4.66 (s, 2 H, CH_3OCH_2) ppm. $^{13}C\{^1H\}$ NMR (75.47 MHz, $CDCl_3$, 25 °C): δ = 55.1 (*C*H$_3$OCH$_2$), 61.9, 70.1 (*C*H$_2$OH and MOMO*C*H$_2$), 96.3 (CH_3OCH_2) ppm.

6e: A mixture of **11e** (4.00 g, 37.7 mmol), NMO (6.63 g, 56.6 mmol), activated molecular sieves (4 Å) (18.86 g) and dichloromethane (75 mL) was cooled to 0 °C, then TPAP (0.132 g, 0.38 mmol) was added slowly and the mixture stirred for 30 min. After stirring for a further 2 h at room temperature the mixture was filtered through a short silica column. The filtrate containing the aldehyde **5e**,[52] was concentrated in vacuo and the residue was used immediately for the next step.

A solution of aldehyde **5e** (8 mL, 37.7 mmol) in THF (50 mL) was added dropwise to a pre-cooled (0 °C) solution of vinylmagnesium bromide in THF (1.0 M, 41.5 mL, 41.5 mmol). The resulting mixture was stirred for 1 h at 0 °C and 18 h at room temperature. Then,

water (ca. 50 mL) was added dropwise and the resulting precipitate was dissolved by addition of 2 N HCl. The solution was extracted with diethyl ether (4 × 20 mL) and the combined organic layers were washed with brine (30 mL), dried (Na_2SO_4) and concentrated in vacuo to give a yellow oil which was subjected to flash column chromatography (silica gel, petroleum ether/ethyl acetate 1:1). Yield: 10% (500 mg over 2 steps). ^{1}H NMR (300.13 MHz, $CDCl_3$, 25 °C): δ = 1.85 (s, 1 H, OH), 3.39 (s, 3 H, CH_3O), 3.47 [dd, $^3J_{H,H}$ = 7.4, $^2J_{H,H}$ = 10.6 Hz, 1 H, CH_2CH(OH)], 3.67 (dd, $^3J_{H,H}$ = 3.2, $^2J_{H,H}$ = 10.6 Hz, 1 H, CH_2CH(OH)], 4.29−4.34 [m, 1 H, CH(OH)], 4.67 (s, 2 H, CH_3OCH_2), 5.22 [d, $^3J_{H,H}$ = 10.6 Hz, 1 H, *syn*−(=CH_2)], 5.29 (d, $^3J_{H,H}$ = 17.3 Hz, 1 H, *anti*−(=CH_2)], 5.86 (ddd, $^3J_{H,H}$ = 5.5, $^3J_{H,H}$ = 10.6, $^3J_{H,H}$ = 17.3 Hz, 1 H, =CH) ppm. ^{13}C{^{1}H} NMR (75.47 MHz, $CDCl_3$, 25 °C): δ = 55.3 (CH_3O), 71.4 [CH(OH)], 72.5 [CH_2CH(OH)], 96.8 [CH_3OCH_2)], 116.3 (=CH), 136.4 (=CH_2) ppm. MS (CI, isobutane): *m*/*z* (%) = 133 (15) [M^+ + 1].

5-Methoxymethoxypent-1-en-3-ol (6f): This compound was prepared via intermediates (see Schemes 2 and 3) that were not fully characterised.

10f: Trimethyl orthoformate (151 mL, 1.38 mol) was dropwise added to a stirred solution of diol **9f** (50.0 mL, 0.69 mol) and camphorsulfonic acid monohydrate (1.73 g, 6.91 mmol) in dichloromethane (300 mL), and the mixture was stirred for 20 h at room temperature. The solvent was then removed under reduced pressure and the residue distilled to give **10f** (b.p. 148−152 °C) as a colourless oil.[53] Yield: 45% (37.02 g). ^{1}H NMR (300.13 MHz, $CDCl_3$, 25 °C): δ = 1.71−1.73 (m, 2 H, CH_2CH$_2$O), 3.36 (s, 3 H, CH_3O), 3.74−3.77 (m, 2 H, CH_2CH_2O), 4.13−4.15 (m, 2 H, CH_2CH_2O), 5.18 [s, 1 H, CH(OCH$_3$)] ppm. ^{13}C{^{1}H} NMR (75.48 MHz, $CDCl_3$, 25 °C): δ = 24.7 (CH_2CH_2O), 52.5 (CH_3), 61.7 (CH_2CH_2O), 110.2 (OCHO) ppm

11f: Treatment of **10f** (15 g, 0.127 mol) with DIBAL-H (153 mL, 1 M in hexane, 0.153 mol) in 200 mL dichloromethane, according to the procedure described above for **11e**, gave crude monoester **11f**, which was purified by distillation (85−87 °C, 10 Torr) as a colourless oil.[54] Yield: 40% (6.16 g). ^{1}H NMR (200.13 MHz, $CDCl_3$, 25 °C): δ = 1.83 (tt, $^3J_{H,H}$ = 6.0, $^3J_{H,H}$ = 6.0 Hz, 2 H, CH_2CH$_2$OH), 2.41 (s, 1 H, OH), 3.34 (s, 3 H, CH_3O), 3.70 (t, $^3J_{H,H}$ = 6.0 Hz, 2 H, MOMOCH_2 or CH_2OH), 3.74 (t, $^3J_{H,H}$ = 5.9 Hz, 2 H, MOMOCH_2 or CH_2OH), 4.60 (s, 2 H, OCH_2O) ppm. ^{13}C{^{1}H} NMR (50.32 MHz, $CDCl_3$, 25 °C): δ = 32.1 (CH_2CH_2OH), 55.2 (CH_3O), 61.0, 66.1 (CH_2OH and MOMOCH$_2$), 96.4 (OCH$_2$O) ppm

6f: Monoester **11f** (4.9 g, 41.37 mmol) was transformed into aldehyde **5f** and this reacted in situ with vinylmagnesium bromide (1 M in THF, 45.8 mmol), by following an analogous procedure to the one described above for the preparation of **6e**.[55] After purification by flash column chromatography (silica gel, petroleum ether/ethyl acetate 2:1) **6f** was obtained as an oil. Yield: 29% over 2 steps (17.5 g). ^{1}H NMR (300.13 MHz, $CDCl_3$, 25 °C): δ = 1.74−1.91 [m, 2 H, CH_2CH(OH)], 2.32 (s, 1 H, OH), 3.37 (s, 3 H, CH_3O), 3.60−3.80 (m, 2 H, MOMOCH_2), 4.31−4.36 [m, 1 H, CH(OH)], 4.62 (s, 2 H, CH_3OCH_2), 5.13 [ddd, $^2J_{H,H}$ = 1.4, $^4J_{H,H}$ = 1.4, $^3J_{H,H}$ = 10.5 Hz, 1 H, *syn*-(=CH_2)], 5.28 [ddd, $^2J_{H,H}$ = 1.4, $^4J_{H,H}$ = 1.4, $^3J_{H,H}$ = 17.2 Hz, 1 H, *anti*-(=CH_2)], 5.89 (ddd, $^3J_{H,H}$ = 5.6, $^3J_{H,H}$ = 10.5, $^3J_{H,H}$ = 17.2 Hz, 1 H, =CH) ppm. ^{13}C{^{1}H} NMR ($CDCl_3$, 75.47 MHz, 25 °C): δ = 36.3 [CH_2CH(OH)], 55.4 (CH_3O), 65.5 (MOMOCH$_2$), 71.6 [CH(OH)], 96.5 (CH_3OCH_2), 114.6 (=CH_2), 140.5 (=CH) ppm. MS (CI, isobutane): *m*/*z* (%) = 147 (100) [M^+ + 1], 129 (40) [M^+ + 1 − H_2O].

(*E*)-5-Methoxymethoxypent-2-en-1-ol (8f): A solution of ester **7f** (2.7 g, 14.4 mmol) in diethyl ether (50 mL) was cooled to −70 °C and DIBAL-H (31.6 mL of 1.0 M solution in hexane, 31.6 mmol) was slowly added via a dropping funnel. After stirring for 3.5 h at −70 °C, water (10 mL) was added dropwise and the solution was allowed to warm to room temperature. Additional water (10 mL) was added and the resulting precipitate was dissolved with 2 N HCl solution (ca. 90 mL). The mixture was extracted with diethyl ether (4 × 20 mL), the combined organic layers washed (2 × 30 mL satd. NH_4Cl solution), dried (Na_2SO_4) and concentrated in vacuo to give a colourless oil which was subjected to flash column chromatography (silica gel, diethyl ether/petroleum ether) to give **8f** with >95% purity (GC/MS). Yield: 66% (1.4 g, 9.5 mmol). ^{1}H NMR (300.13 MHz, $CDCl_3$, 25 °C): δ = 1.56 (s, 1 H, OH), 2.31−2.42 (m, 2 H, MOMOCH_2CH_2), 3.36 (s, 3 H, CH_3O), 3.59 (t, $^3J_{H,H}$ = 6.6 Hz, 2 H, MOMOCH_2), 4.02−4.13 (m, 2 H, CH_2OH), 4.63 (s, 2 H, CH_3OCH_2), 5.71−5.77 (m, 2 H, =CH) ppm. ^{13}C{^{1}H} NMR (75.47 MHz, $CDCl_3$, 25 °C): δ = 32.6 (MOMOCH_2CH_2), 55.2 (CH_3O), 63.7, 67.1 (CH_2OH and MOMOCH$_2$), 96.4 (CH_3OCH_2), 129.3, 131.1 (both =CH) ppm. MS (EI): *m*/*z* (%) = 145 (1) [M^+ − H], 129 (1) [M^+ − OH], 115 (10) [M^+ − OCH_3], 45 (100) [$H_3COCH_2^+$]. HRMS (EI) for $C_8H_{14}O_2$ [M^+ − (O=CH_2)]: calcd. 116.0837; found 116.0837.

(*R*)-5-Phenyl-1-penten-3-yl (1*S*,4*R*)-4,7,7-Trimethyl-3-oxo-2-oxabicyclo[2.2.1]heptane-1-carboxylate (12): (*R*)-5-phenyl-1-penten-3-ol [(*R*)-**6b**)] (0.50 g, 3.1 mmol) (prepared by enzyme-catalysed kinetic resolution of *rac*-**6b**)[12a] followed by 864 μL (6.2 mmol) of triethylamine were added dropwise to a cooled (0 °C) solution of (1*S*)-camphanic acid chloride (671 mg, 3.1 mmol) in anhydrous dichloromethane (10 mL). The solution was stirred at room temperature for 18 h and left to stand for 7 days. Colourless crystals precipitated from the mixture, were filtered off and washed with diethyl ether. The combined filtrates were concentrated in vacuo to give crude **12**. Crystals suitable for X-ray diffraction were obtained by recrystallization from ethyl acetate. Yield: 84% (890 mg). M. p. 55−58 °C.

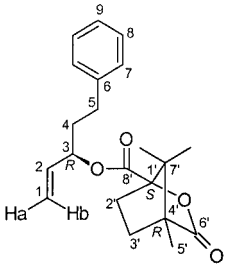

12

^{1}H NMR (300.13 MHz, $CDCl_3$, 25 °C): δ = 0.98 (s, 3 H, 7′-CH_3), 1.07 (s, 3 H, 7′-CH_3), 1.12 (s, 3 H, 5′-H), 1.71 (ddd, $^3J_{3'a,2'a}$ = 4.4, $^2J_{3'a,3'b}$ = 9.6, $^3J_{3'a,2'b}$ = 13.6 Hz, 1 H, 3′-Ha), 1.87−2.15 (m, 4 H, 4-H, 3′-Hb, 2′-Ha), 2.44 (ddd, $^3J_{2'b,3'b}$ = 4.4, $^2J_{2'b,2'a}$ = 10.7, $^3J_{2'b,3'a}$ = 13.6 Hz, 1 H, 2′-Hb), 2.67 (ddd, $^3J_{5,4a}$ = 3.3, $^3J_{5,3}$ = 6.6, $^3J_{5,4b}$ = 9.6 Hz, 2 H, 5-H), 5.25 (ddd, $^2J_{1a,1b}$ = 1.1, $^4J_{1a,3}$ = 1.1, $^3J_{1a,2}$ = 10.5 Hz, 1 H, 1-Ha), 5.32 (ddd, $^2J_{1b,1a}$ = 1.1, $^4J_{1b,3}$ = 1.1, $^3J_{1b,2}$ = 17.1 Hz, 1 H, 1-Hb), 5.36−5.45 (m, 1 H, 3-H), 5.83 (ddd, $^3J_{2,3}$ = 6.6, $^3J_{2,1a}$ = 10.5, $^3J_{2,1b}$ = 17.1 Hz, 1 H, 2-H), 7.13−7.32 (m, 5 H, *arom.* H) ppm. ^{13}C{^{1}H} NMR (75.47 MHz, $CDCl_3$, 25 °C): δ = 9.66 (C-5′), 16.80 (7′-CH_3), 28.95 (C-3′), 30.73 (C-4′), 31.31 (C-5), 35.75 (C-4), 54.19, 54.82 (C-4′ and C-7′), 75.82 (C-3), 91.05 (C-1′), 118.16 (C-2), 126.11 (C-9), 128.32, 128.49 (C-7 and C-8), 135.51 (C-1), 140.87 (C-6), 166.81 (C-8′), 178.21 (C-6′) ppm. MS (FAB): *m*/*z* (%) = 343 (42) [M^+ + 1], 199 (46) [{M^+ + 1} −

($PhCH_2CH_2$) − (CH-CH=CH_2)], 181 (36) [{M^+ + 1} − ($PhCH_2CH_2$) − (CHO)-CH=CH_2)], 153 (60) [{M^+ + 1} − ($PhCH_2CH_2$) − CH(OCO) − ($CHCH_2$)]. $C_{21}H_{26}O_4$ (342.44): calcd. C 73.66, H 7.65; found C 73.49, H 7.64.

(*Z*)-5-Methoxymethoxypent-2-en-1-ol (19): A mixture of Lindlar catalyst (1.2 g), quinoline (0.33 mL, 357 mg, 2.77 mmol), alcohol **18** (5.9 g, 40.1 mmol) and methanol (340 mL) was stirred under a H_2 atmosphere for 15 hours at room temperature. The catalyst was removed by filtration through celite and the brown filtrate was concentrated in vacuo. The residue was purified by flash column chromatography (silica gel, petroleum ether/ethyl acetate 2:1) to afford a colourless oil. Yield: 69% (4.1 g). ^{1}H NMR (300.13 MHz, $CDCl_3$, 25 °C): δ = 2.32 (ddt, $^4J_{H,H}$ = 1.5, $^3J_{H,H}$ = 6.2, $^3J_{H,H}$ = 6.2 Hz, 2 H, MOMOCH$_2$CH_2), 2.68 (br. s, 1 H, OH), 3.29 (s, 3 H, OCH_3), 3.50 (t, $^3J_{H,H}$ = 6.2 Hz, 2 H, MOMOCH_2), 4.09 (d, $^3J_{H,H}$ = 6.6 Hz, 2 H, CH_2OH), 4.55 (s, 2 H, CH_3OCH_2), 5.46−5.57 (m, 1 H, =CH), 5.62−5.77 (m, 1 H, =CH) ppm. ^{13}C{^{1}H} NMR (75.47 MHz, $CDCl_3$, 25 °C): δ = 27.8 (MOMOCH$_2$CH_2), 55.1 (OCH_3), 57.8 (CH_2OH), 66.5 (MOMOCH_2), 96.2 (CH_3OCH_2), 128.8, 130.9 (= CH) ppm.

5-Phenyl-1-penten-3-yl Diethylphosphonate (26b): A solution of alcohol **6b** (2.0 g, 12.3 mmol) in THF (40 mL) was cooled to −78 °C and *n*BuLi (13 mL, 1.6 M in hexane, 20.9 mmol) was added slowly with a syringe. After stirring for 30 min at −78 °C, diethyl chlorophosphate (5.35 mL, 6.36 g, 36.9 mmol) was added. The mixture was stirred for 18 h, while the temperature was allowed to slowly rise from −78 °C to 25 °C. Then, water (40 mL) was added and the mixture was extracted with diethyl ether (3 × 20 mL). The combined organic layers were washed with satd. NaCl solution (50 mL), dried (Na_2SO_4) and concentrated in vacuo. The crude product was purified by flash column chromatography (silica gel, petroleum ether/ethyl acetate 2:1) to give **26b** as a yellow oil. Yield: 64% (2.3 g). ^{1}H NMR (300.13 MHz, $CDCl_3$, 25 °C): δ = 1.32 (t, $^3J_{H,H}$ = 7.0 Hz, 3 H, CH_3), 1.33 (t, $^3J_{H,H}$ = 7.0 Hz, 3 H, CH_3), 1.87−2.14 (m, 2 H, CH_2CH), 2.65−2.74 (m, 2 H, PhCH_2), 4.10 (br. q, $^3J_{H,H}$ = 6.6 Hz, 4 H, OCH_2), 4.74−4.85 [m, 1 H, CHO-P(O)(OEt)$_2$], 5.25 (d, $^3J_{H,H}$ = 10.3 Hz, 1 H, =CH_2), 5.34 (d, $^3J_{H,H}$ = 17.3 Hz, 1 H, =CH_2), 5.88 (ddd, $^3J_{H,H}$ = 6.6, $^3J_{H,H}$ = 10.3, $^3J_{H,H}$ = 17.3 Hz, 1 H, =CH), 7.15−7.35 (m, 5 H, Ph) ppm. ^{13}C{^{1}H} NMR (75.47 MHz, $CDCl_3$, 25 °C): δ = 16.1 (2 CH_3), 31.0 (CH_2CHOR), 37.5 (PhCH_2), 63.7 (2 OCH_2), 79.2 (CHOR), 117.5 (=CH_2), 126.0 (Ph), 128.4 (Ph), 128.4 (Ph), 136.7 (=CH), 141.3 (Ph) ppm. ^{31}P NMR (121.49 MHz, $CDCl_3$, 25 °C): δ = −1.40 ppm. HRMS (FAB) for $C_{14}H_{24}O_4P$ [M^+ + 1]: calcd. 299.1412; found 299.1440.

***N*-Benzyl-4-methyl-*N*-(1-phenethylallyl) Benzenesulfonamide (27b):** An LHMDS solution (4.0 mL, 1.0 M in THF, 4.0 mmol) was added to a solution of *N*-tosylbenzylamine (1.1 g, 4.2 mmol) in THF (12 mL). The mixture was stirred for 30 min at room temperature and then added to a substrate/catalyst solution prepared as follows: $[IrCl(COD)]_2$ (26.8 mg, 0.04 mmol) was dissolved in THF (4 mL) and substrate **1b** (2.0 mmol) and then triphenylphosphite (21.7 μL, 0.08 mmol) were added. The reaction mixture was stirred for 18 h at room temperature and then, treated with water (20 mL) and extracted with diethyl ether (3 × 20 mL). The combined organic layers were washed with satd. $NaHCO_3$ (1 × 50 mL) and satd. NaCl solutions (1 × 50 mL) and dried over Na_2SO_4. After removal of the solvent in vacuo a yellow oil was obtained which was subjected to flash column chromatography (silica gel, petroleum ether/ethyl acetate 97:3) to give a 79:21 mixture of **27b** and **28b**. Yield: 47% (382 mg), colourless oil. $[\alpha]_D^{24}$ = 7.55 (*c* = 0.58, $CHCl_3$) for **27b** with 11% *ee* (*S*). HPLC: DAICEL Chiralcel ODH column, length: 25 cm + 5 cm precolumn, flow: 0.5 mL min^{-1}, eluent: *n*-hexane/*i*PrOH (95:5); **27b**: t_R(*S*) = 23.8 min, t_R(*R*) = 27.9 min; (*E*)-**28b**: t_R = 38.2 min.

27b: ^{1}H NMR (300.13 MHz, $CDCl_3$, 25 °C): δ = 1.53−1.75 (m, 2 H, PhCH$_2$CH_2), 2.44 (s, 3 H, CH_3), 2.43−2.53 (m, 2 H, PhCH_2), 4.10 (d, $^2J_{H,H}$ = 15.4 Hz, 1 H, PhCH_2N), 4.37 (ddd, $^3J_{H,H}$ = 6.6, $^3J_{H,H}$ = 6.6, $^3J_{H,H}$ = 7.7 Hz, 1 H, CHN), 4.60 (d, $^2J_{H,H}$ = 15.4 Hz, 1 H, PhCH_2N), 4.99 [ddd, $^4J_{H,H}$ = 1.1, $^2J_{H,H}$ = 1.5, $^3J_{H,H}$ = 17.3 Hz, 1 H, *anti*-(=CH_2)], 5.10 [ddd, $^4J_{H,H}$ = 1.1, $^2J_{H,H}$ = 1.5, $^3J_{H,H}$ = 10.7 Hz, 1 H, *syn*-(=CH_2)], 5.47 (ddd, $^3J_{H,H}$ = 6.6, $^3J_{H,H}$ = 10.7, $^3J_{H,H}$ = 17.3 Hz, 1 H, CH= CH_2), 6.78−6.84 (m, 2 H, *arom.* H), 7.08−7.21 (m, 3 H, *arom.* H), 7.24−7.35 (m, 5 H, *arom.* H), 7.38−7.45 (m, 2 H, *arom.* H), 7.70 [d, $^3J_{H,H}$ = 8.7 Hz, 2 H, *m*-(1-SO_2-4-Me-C_6H_4)] ppm. ^{13}C{^{1}H} NMR (75.48 MHz, $CDCl_3$, 25 °C): δ = 21.5 (CH_3), 32.6 (Ph*C*H$_2$), 34.1 (PhCH$_2$*C*H$_2$), 48.2 (Ph*C*H$_2$N), 60.3 [*C*H(NTs)(Bzl)], 118.6 (=CH_2), 125.7, 127.3, 127.5, 128.2, 128.3, 128.5, 128.6, 129.6 (all CH *arom.*), 135.8 (*C*H=CH_2), 138.1, 138.1, 141.6, 143.1 (s, all C *arom.*) ppm. MS (FAB): *m*/*z* (%) = 406 (60) [M^+ + H], 300 (100) [M^+ − PhCH$_2$CH$_2$], 262 (99) [M^+ − Ts]. $C_{25}H_{27}NO_2S$ (405.55): calcd. C 74.04, H 6.71, N 3.45, S 7.91; found C 74.03, H 6.74, N 3.51, S 7.76.

(5,7-Dioxa-6-phosphadibenzo[a,c]cyclohepten-6-yl)dimethylamine (L3): A mixture of 2,2′-dihydroxybiphenyl (1.00 g, 5.4 mmol), NH_4Cl (8.0 mg, 0.1 mmol) and [P(NMe_2)$_3$] (976 μL, 5.4 mmol) and toluene (15 mL) was stirred for 18 h at 80 °C and then concentrated in vacuo to give a yellow oil which was purified by flash column chromatography (silica gel, petroleum ether/ethyl acetate 98:2). Colourless oil. Yield: 29% (400 mg). ^{1}H NMR (500.13 MHz, $CDCl_3$, 25 °C): δ = 2.66 (d, $^3J_{H,P}$ = 9.4 Hz, 6 H, CH_3), 7.18 (d, $^3J_{H,H}$ = 8.0 Hz, 2 H, *arom.* H), 7.22−7.26 (m, 2 H, *arom.* H), 7.32−7.37 (m, 2 H, *arom.* H), 7.46 (br. d, $^3J_{H,H}$ = 8.0 Hz, 2 H, *arom.* H) ppm. ^{13}C{^{1}H} NMR (125.76 MHz, $CDCl_3$, 25 °C): δ = 35.9 (d, $^2J_{P,C}$ = 10.7 Hz, CH_3), 121.9 (*arom.* C), 124.5 (*arom.* C), 129.2 (*arom.* C), 129.6 (*arom.* C), 131.1 (d, $^2J_{P,C}$ = 2.8 Hz, *arom.* C), 151.5 (*arom.* C) ppm. ^{31}P NMR (202.46 MHz, $CDCl_3$, 25 °C): δ = 149.74 (s) ppm. $C_{14}H_{14}NO_2P$ (259.24): calcd. C 64.86, H 5.44, N 5.40, P 11.95; found C 64.95, H 5.37, N 5.45, P 11.91.

[IrCl(η^4-1,5-COD){(a*R*)-L2}] (29): THF (4 mL) was added to a mixture of $[IrCl(COD)]_2$ (20 mg, 0.03 mmol) and phosphorus amidite (*R*)-**L2** (21.3 mg, 0.06 mmol) at room temperature. Formation of complex **29** was observed by ^{1}H and ^{31}P NMR spectroscopy within 10 min. Recrystallization from diethyl ether furnished orange crystals of **29**. Yield: 90% (37.5 mg). ^{1}H NMR (500.13 MHz, $CDCl_3$, 25 °C): δ = 1.22−1.44 (m, 2 H, CH_2-COD), 1.74−1.84 (m, 2 H, CH_2-COD), 1.81−1.91 (m, 2 H, CH_2-COD), 1.93−2.04 (m, 1 H, CH_2-COD) 2.09−2.19 (m, 1 H, CH_2-COD), 2.20−2.30 (m, 1 H, CH-COD), 2.45−2.52 (m, 1 H, CH-COD), 2.79 (d, $^3J_{P,H}$ = 10.7 Hz, 6 H, CH_3), 3.35−3.42 (m, 1 H, CH-COD), 5.30−5.45 (m, 1 H, CH-COD), 7.27 (dd, $^3J_{H,H}$ = 8.4, $^3J_{H,H}$ = 8.7 Hz, 2 H, CH *arom.*), 7.30 (d, $^3J_{H,H}$ = 8.7 Hz, 1 H, CH *arom.*), 7.32 (d, $^3J_{H,H}$ = 8.4 Hz, 1 H, CH *arom.*) 7.42 (d, $^3J_{H,H}$ = 8.4 Hz, 1 H, CH *arom.*), 7.39−7.47 (m, 2 H, CH *arom.*), 7.89 (d, $^3J_{H,H}$ = 7.4 Hz, 1 H, CH *arom.*), 7.91 (d, $^3J_{H,H}$ = 8.7 Hz, 1 H, CH *arom.*) 7.95 (d, $^3J_{H,H}$ = 8.35 Hz, 2 H, CH *arom.*), 8.01 (d, $^3J_{H,H}$ = 9.0 Hz, 1 H, CH *arom.*) ppm. ^{13}C{^{1}H} NMR (125.77 MHz, $CDCl_3$, 25 °C): δ = 29.7 (d, $^4J_{P,C}$ = 1.9 Hz, CH_2-COD), 29.0 (d, $^4J_{P,C}$ = 2.8 Hz, CH_2-COD), 32.5 (d, $^4J_{P,C}$ = 2.8 Hz, CH_2-COD), 34.2 (d, $^4J_{P,C}$ = 3.8 Hz, CH_2-COD), 38.2 (d, $^3J_{P,C}$ = 10.36 Hz, CH_3), 52.2 (d, $^3J_{P,C}$ = 1.9 Hz, CH-COD), 55.3 (d, $^3J_{P,C}$ = 1.88 Hz, CH-COD), 102.7 (d, $^3J_{P,C}$ = 17.9 Hz, CH-COD), 103.22 (d, $^3J_{P,C}$ = 19.1 Hz, CH-COD), 121.1 (*C*H *arom.*), 122.1 (d, $^4J_{C,P}$ = 1.88 Hz, *C*-*arom.*), 122.9 (d, $^4J_{C,P}$ = 2.86 Hz, *C*-*arom.*), 123.9 (d, $^4J_{C,P}$ = 2.83 Hz, *C*H-*arom.*), 125.2,

126.1, 126.5, 126.8, 127.1, 128.3, 128.4, 129.9, 130.3 (s, all CH *arom.*), 131.0, 131.6 (both s, *C-arom.*), 132.2 (d, $^3J_{C,P}$ = 1.88 Hz, *C-arom.*), 132.5 (s, *C-arom.*), 148.4 (d, $^2J_{C,P}$ = 4.7 Hz, O*C-arom.*), 149.5 (d, $^2J_{C,P}$ = 12.9 Hz, O*C-arom.*) ppm. ^{31}P NMR (202.46 MHz, $CDCl_3$, 25 °C): δ = 116.3 (s) ppm. $C_{30}H_{30}ClIrNO_2P$ (694.4): calcd. C 51.79, H 4.35, N 2.01, P 4.46; found C 52.01, H 4.47, N 2.06, P 4.40.

[Ir(η^3-CH$_2$CHCHPh)(Cl)$_2$(η^4-1,5-COD)] (30): Cinnamyl chloride (83 μL, 91 mg, 0.596 mmol) was added to a solution of $[IrCl(COD)]_2$ (100 mg, 0.149 mmol) in THF (2 mL) and the mixture stirred for 18 h at 50 °C. A yellow precipitate of **30** was formed, which was isolated by filtration, washed with hexane and dried in vacuo. Yield: 82% (119.3 mg). A 2:1 mixture of two isomers was observed in solution at between −60 and −40 °C.

Major isomer: ^{1}H NMR (300.13 MHz, CD_2Cl_2, −60 °C): δ = 1.45−1.65 (m, 1 H, CH_2-COD), 1.65−1.83 (m, 1 H, CH_2-COD), 2.25−2.55 (m, 3 H, CH_2-COD), 2.60−3.00 (m, 2 H, CH_2-COD), 2.95−3.15 (m, 1 H, CH_2-COD), 3.72 3.87 (m, 1 H, CH-COD), 4.07 [d, $^3J_{H,H}$ = 8.8 Hz, 1 H, *anti*-(*allyl* CH_2)], 4.45 [d, $^3J_{H,H}$ = 6.8 Hz, 1 H, *syn*-(*allyl* CH_2)], 4.59−4.86 (m, 3 H, CH-COD), 4.93 [d, $^3J_{H,H}$ = 14.0 Hz, 1 H, *anti*-(*allyl* C*H*Ph)], 6.06 (ddd, $^3J_{H,H}$ = 6.8, $^3J_{H,H}$ = 8.8, $^3J_{H,H}$ = 14.0 Hz, 1 H, *allyl* CH), 7.20−7.90 (m, 5 H, -C_6H_5) ppm. ^{13}C{^{1}H} NMR (75 MHz, CD_2Cl_2, −60 °C): δ = 26.6 (CH_2-COD), 28.6 (CH_2-COD), 35.5 (CH_2-COD), 37.6 (CH_2-COD), 40.9 (*allyl* CH_2), 81.9 (CH-COD), 83.0 (CH-COD), 92.7 (CH-COD), 93.3 (CH-COD), 110.6 (*allyl* CH), 111.1 (*allyl C*HPh), 129.0, 130.3, (C_6H_5), 134.8 (C_{ipso}-C_6H_5) ppm.

Minor isomer: ^{1}H NMR (300.13 MHz, CD_2Cl_2, −60 °C): δ = 1.26−1.36 (m, 1 H, CH_2-COD), 1.45−1.65 (m, 1 H, CH_2-COD), 1.93−2.10 (m, 1 H, CH_2-COD), 2.25−2.55 (m, 2 H, CH_2-COD), 2.60−3.00 (m, 3 H, CH_2-COD), 4.13−4.26 (m, 1 H, CH-COD), 4.31−4.55 (m, 2 H, CH-COD and *allyl* CH_2), 4.59−4.86 (m, 2 H, CH-COD and *allyl* CH_2), 5.22−5.32 (m, 1 H, CH-COD), 5.55−5.74 (m, 1 H, *allyl* CH), 6.33 [d, $^3J_{H,H}$ = 14.1 Hz, 1 H, *anti*-(*allyl* C*H*Ph)], 7.20−7.90 (m, 5 H, -C_6H_5) ppm. ^{13}C{^{1}H} NMR (75 MHz, CD_2Cl_2, −60 °C): δ = 27.0 (CH_2-COD), 28.8 (CH_2-COD), 33.6 (CH_2-COD), 37.9 (CH_2-COD), 42.6 (*allyl* CH_2), 80.8 (CH-COD), 81.7(CH-COD) 89.4 (CH-COD), 92.6 (CH- COD), 102.2 (*allyl* CH), 123.0 (*allyl C*HPh), 128.5, 128.9, 130.8 (C_6H_5), 147.6 (C_{ipso}-C_6H_5) ppm. $C_{17}H_{21}Cl_2Ir$ (488.52): calcd. C 41.80, H 4.34; found C 41.84, H 4.37.

[Ir(Br)$_2$(η^3-C$_3$H$_5$)(η^4-1,5-COD)] (31). Method A: A solution of $[IrCl(COD)]_2$ (50 mg, 0.07 mmol) and allyl bromide (28.6 μL, 36.0 mg, 0.3 mmol) in THF (1 mL) was stirred for 18 h at 50 °C. A yellow precipitate of **31** formed which was washed with diethyl ether and recrystallised from dichloromethane/pentane. Yield: 81% (60 mg).

Method B: $[IrCl(COD)]_2$ (150 mg, 0.2 mmol) was treated with an excess of *anhydrous* LiBr (155.1 mg, 1.8 mmol) in acetone (15 mL). After stirring for 18 h, the solvent was removed under vacuum and the product $[IrBr(COD)]_2$ extracted three times with dichloromethane. Removal of the solvent gave an orange oil which was further treated with allyl bromide (57 μL, 79.8 mg, 0.7 mmol). After 18 h, a crystalline yellow precipitate had formed, which was isolated by filtration and washed with diethyl ether. Yield: 66% (145 mg). NMR spectroscopy at −60 °C showed a 9:1 mixture of two isomers.

Major isomer: ^{1}H NMR (500.13 MHz, CD_2Cl_2, −60 °C): δ = 1.46−1.59 (m, 1 H, CH_2-COD), 1.75−1.88 (m, 1 H, CH_2-COD), 2.23−2.35 (m, 1 H, CH_2-COD), 2.40−2.50 (m, 1 H, CH_2-COD), 2.50−2.61 (m, 1 H, CH_2-COD), 2.60−2.72 (m, 1 H, CH_2-COD), 3.00−3.10 (m, 1 H, CH_2-COD), 3.12 [d, $^3J_{H,H}$ = 13.3 Hz, 1 H, *anti*-(*allyl* CH_2)], 3.22−3.34 (m, 1 H, CH_2-COD), 3.33−3.41 (m, 1 H, CH-COD), 3.83 [d, $^3J_{H,H}$ = 10.0 Hz, 1 H, *anti*-(*allyl* CH_2)], 4.48 [d, $^3J_{H,H}$ = 6.7 Hz, 1 H, *syn*-(*allyl* CH_2)], 4.75−4.84 (m, 1 H, CH-COD), 4.93 [d, $^3J_{H,H}$ = 8.7 Hz, 1 H, *syn*-(*allyl* CH_2)], 4.95−5.03 (m, 1 H, CH-COD), 5.10−5.17 (m, 1 H, CH-COD), 5.74−5.87 (m, 1H. *allyl* CH) ppm. ^{13}C{^{1}H} NMR (125.76 MHz, CD_2Cl_2, −60 °C): δ = 26.4, 27.2, 36.4, 37.1 (all CH_2-COD), 44.6 (*allyl* CH_2), 83.2, 85.5 (both CH-COD), 79.7 (*allyl* CH_2), 91.8, 92.7 (both CH-COD), 114.5 (*allyl* CH) ppm.

Table 9. Crystal data and details of the structure refinement for compounds **12**, **29**, **30**, and **31**

Compound	**12**	**29**	**30**	**31**
Empirical formula	$C_{21}H_{26}O_4$	$C_{30}H_{30}ClIrNO_2P$	$C_{17}H_{21}Cl_2Ir$	$C_{11}H_{17}Br_2Ir$
Molecular weight [g·mol^{-1}]	342.42	695.17	488.44	501.27
Crystal system	Monoclinic	Orthorhombic	Monoclinic	Orthorhombic
Space group	$P2_1$	$P2_12_12_1$	$P2_1/n$	$Pna2_1$
Z	2	4	4	4
a [Å]	7.6989(3)	11.9440(1)	6.8597(1)	15.6809(3)
b [Å]	12.4705(5)	14.2192(1)	20.9350(3)	7.4221(1)
c [Å]	10.0936(4)	15.2164(2)	11.1414(2)	10.5656(2)
β [deg.]	99.888(1)	−	97.724(1)	−
Volume [Å^3]	954.68(7)	2584.26(4)	1585.48(4)	1229.68(4)
Absorption coefficient [mm^{-1}]	0.08	5.36	8.75	17.32
Max. and min. transmission	1.07 and 0.80	0.80 and 0.46	0.67 and 0.58	0.77 and 0.41
Crystal size [mm^3]	.64 × .13 × .13	.22 × .12 × .05	.14 × .08 × .06	.50 × .04 × .02
Theta range [deg.]	2.0 to 25.0	2.0 to 27.5	2.0 to 25.6	2.6 to 27.5
Reflections collected	8026	27013	11653	11961
Independent reflections	3350 (R_{int} = 0.052)	5926 (R_{int} = 0.075)	2761 (R_{int} = 0.034)	2816 (R_{int} = 0.066)
Observed reflections [$I > 2\sigma(I)$]	2568	5087	2301	2494
Refined parameters	330	343	209	154
Goodness-of-fit on F^2	1.06	0.99	1.09	1.00
Final $R1$ index [$I > 2\sigma(I)$]	0.043	0.030	0.023	0.027
Final $wR2$ index [$I > 2\sigma(I)$]	0.086	0.050	0.048	0.058
Absolute structure parameter	−1.4(12)	−0.018(6)	−	0.015(15)
Largest diff. peak/hole [e Å^{-3}]	0.15/−0.17	0.93/−0.72	0.60/−0.74	1.03/−1.23

Minor isomer: ^{1}H NMR (500.13 MHz, CD_2Cl_2, −60 °C): δ = 1.09−1.20 (m, 1 H, CH_2-COD), 1.57−1.67 (m, 1 H, CH_2-COD), 2.11−2.20 (m, 1 H, CH_2-COD), 2.24−2.35 (m, 1 H, CH_2-COD), 2.40−2.50 (m, 1 H, CH_2-COD), 2.69−2.79 (m, 1 H, CH_2-COD), 2.93−3.00 (m, 1 H, CH_2-COD), 3.00−3.10 (m, 1 H, CH_2-COD), 4.23−4.30 (m, 1 H, CH-COD), 4.62−4.70 (m, 3 H, CH-COD and *allyl* CH_2), 4.75−4.84 (m, 1 H, CH-COD), 4.90−4.97 (m, 1 H, *allyl* CH), 5.20−5.30 (m, 2 H, *allyl* CH_2), 5.58−5.63 (m, 1 H, CH-COD) ppm. $^{13}C\{^1H\}$ NMR (125.76 MHz, CD_2Cl_2, −60 °C): δ = 26.7, 27.2, 35.3, 37.7 (all CH_2-COD), 44.9 (*allyl* CH_2), 83.6, 85.4, 87.1 (all CH-COD), 89.6 (*allyl* CH_2), 93.9 (both CH-COD), 107.9 (*allyl* CH) ppm. $C_{11}H_{17}Br_2Ir$ (501.28): calcd. C 26.36, H 3.42; found C 26.30, H 3.56.

Stoichiometric Reaction of Complex 30 with Dimethyl 2-Sodiomalonate in the Presence of (*R*)-L2: A 0.24 M solution of $NaCH(CO_2Me)_2$ (0.4 mL, 0.1 mmol) in THF was syringed into a Schlenk tube and the solvent was removed under vacuum. To the residual white solid were added complex **30** (49.9 mg, 0.1 mmol) and the stoichiometric quantity of ligand (*R*)-**L2** (36.2 mg, 0.1 mmol), then $[D_8]THF/CD_2Cl_2$ (2:1; 1.5 mL) was added at −78 °C. The mixture was stirred for a few minutes at this temperature to give a clear light yellow solution that was transferred into a pre-cooled (−60 °C) NMR tube. The ^{1}H and ^{31}P NMR spectra of this solution, recorded at −60 °C, showed complete reaction to give exclusively a 1:1 mixture of *rac*-**3a** and complex **29** which were separated by flash column chromatography (silica gel, hexane/diethyl ether 9:1). Yield: 64% (16 mg) of **3a** (purity > 99% by GCMS) and 32% (22.6 mg) of **29** as orange crystals.

X-ray Crystallographic Studies: Crystals of compound **12** were obtained as needles by slow evaporation of solvent from a saturated solution in ethyl acetate. Single crystals of complex **29** were grown as orange needles by slow concentration of a saturated solution in diethyl ether. Single crystals of complexes **30** and **31** were grown, both as yellow needles, by slow diffusion of diethyl ether into a saturated solution in dichloromethane.

The measurements were made on a Bruker SMART-CCD diffractometer with graphite monochromated Mo-K_α radiation (0.71073 Å) at 200 K. Frames corresponding to a sphere of data were collected. 20 s exposures of 0.3 degree scans in omega were taken. An absorption correction was applied using SADABS (G. M. Sheldrick, SADABS, Bruker AXS, Inc.: Madison, WI, 1996) based on the laue symmetry of the reciprocal space. The structures were solved by direct methods and expanded using Fourier techniques. All non-hydrogen atoms were refined with anisotropic displacement parameters, most hydrogen atoms could be located in the Fourier map, in **12** all hydrogens were refined isotropically, in **29** and **30** only the allylic hydrogens and the olefinic hydrogens of the COD were refined isotropically, in **30** the allylic hydrogens were not included in the structure model due to the disorder, all the rest of the hydrogen atoms was taken into account at calculated positions. The full-matrix least-squares refinement against F^2 converged. All calculations were performed using the SHELXTL crystallographic software package of Bruker (G. M. Sheldrick, SHELXTL V5.10, Bruker AXS, Inc.: Madison, WI, 1997). For details and crystal data see Table 9.
CCDC-181254 (**12**), -181255 (**29**), -181256 (**30**) and -181257 (**31**) contain the supplementary crystallographic data for this paper. These data can be obtained free of charge via www.ccdc.cam.ac.uk/conts/retrieving.html (or from the CCDC, 12 Union Road, Cambridge CB2 1EZ, UK; Fax: (internat.) +44-1223/336-033; E-mail: deposit@ccdc.cam.ac.uk)

Acknowledgments

This work was supported by the Deutsche Forschungsgemeinschaft and the Fonds der Chemischen Industrie. C. G.-Y. thanks the Alexander von Humboldt Foundation for a Postdoctoral Fellowship and the European Community for a Marie Curie Fellowship, program "*Improving Human Research Potential and the Socio-economic Knowledge Base*" under contract number HPMF-CT-2000-00905. We thank T. D. Weiβ for NMR measurements, Prof. M. Reggelin, Darmstadt, for advice concerning EXSY spectroscopy, T. Leβmann and A. Spieβ for preparation of substrates, and Degussa AG for iridium salts.

[1] [1a] B. M. Trost, D. L. Van Vranken, *Chem. Rev.* **1996**, *96*, 395−422. [1b] T. Hayashi, *Catalytic Asymmetric Synthesis* (Ed.: I. Ojima), VCH, New York **1993**, p. 325. [1c] B. M. Trost, C. Lee, *Catalytic Asymmetric Synthesis* (Ed.: I. Ojima), 2nd ed., Wiley-VCH, Weinheim, Germany, **2000**. [1d]A. Pfaltz, M. Lautens, *Comprehensive Asymmetric Catalysis I−III* **1999**, *2*, 833−884.

[2] [2a] S.-L. You, X.-Z. Zhu, Y.-M. Luo, X.-L. Hou, L.-X. Dai, *J. Am. Chem. Soc.* **2001**, *123*, 7471−7472. [2b] R. Prêtôt, A. Pfaltz, *Angew. Chem.* **1998**, *110*, 337−339; *Angew. Chem. Int. Ed.* **1998**, *37*, 323−325. [2c] B. M. Trost, F. D. Toste, *J. Am. Chem. Soc.* **1998**, *120*, 9074−9075. [2d] T. Hayashi, M. Kawatsura, Y. Uozumi, *Chem. Commun.* **1997**, 561−562. [2e] T. Hayashi, A. Ohno, S.-J. Lu, Y. Matsumoto, E. Fukuyo, K. Yanagi, *J. Am. Chem. Soc.* **1994**, *116*, 4221−4226. [2f] T. Hayashi, K. Kishi, A. Yamamoto, V. Ito, *Tetrahedron Lett.* **1990**, *31*, 1743−1746.

[3] Mo: [3a] B. M. Trost, K. Droga, I. Hachiya, T. Emura, D. L. Hughes, S. Krska, R. A. Reamer, M. Palucki, N. Yasuda, P. J. Reider, *Angew. Chem.* **2002**, *114*, 2009−2012; *Angew. Chem. Int. Ed.* **2002**, *41*, 1929−1932. [3b] B. M. Trost, I. Hachiya, *J. Am. Chem. Soc.* **1998**, *120*, 1104−1105. [3c] F. Glorius, A. Pfaltz, *Org. Lett.* **1999**, *1*, 141−144. W: [3d] G. C. Lloyd-Jones, A. Pfaltz, *Angew. Chem.* **1995**, *107*, 534−536; *Angew. Chem. Int. Ed. Engl.* **1995**, *34*, 462−464. Isomerization is slow for W complexes.

[4] Fe: [4a] Y. Xu, B. Zhou, *J. Org. Chem.* **1987**, *52*, 974−977. [4b] U. Eberhardt, G. Mattern, *Chem. Ber.* **1988**, *121*, 1531−1534. [4c] D. Enders, B. Jandeleit, S. von Berg, G. Raabe, J. Runsink, *Organometallics* **2001**, *20*, 4312−4332. Rh: [4d] P. A. Evans, J. D. Nelson, *J. Am. Chem. Soc.* **1998**, *120*, 5581−5582. Ru: [4e] Y. Morisaki, T. Kondo, T.-A. Mitsudo, Y. Watanabe, *Organometallics* **1999**, *18*, 4742−4746. [4f] B. M. Trost, P. L. Fraisse, Z. T. Ball, *Angew. Chem.* **2002**, *114*, 1101−1103; *Angew. Chem. Int. Ed.* **2002**, *41*, 1059−1061.

[5] [5a] R. Takeuchi, M. Kashio, *Angew. Chem.* **1997**, *109*, 268−270; *Angew. Chem. Int. Ed. Engl.* **1997**, *36*, 263−265. [5b] R. Takeuchi, M. Kashio, *J. Am. Chem. Soc.* **1998**, *120*, 8647−8655. [5c] R. Takeuchi, *Polyhedron* **2000**, *19*, 557−561. [5d] R. Takeuchi, K. Tanabe, *Angew. Chem.* **2000**, *112*, 2051−2054; *Angew. Chem. Int. Ed.* **2000**, *39*, 1975−1978.

[6] J. P. Janssen, G. Helmchen, *Tetrahedron Lett.* **1997**, *38*, 8025−8026.

[7] [7a] B. Bartels, G. Helmchen, *Chem. Commun.* **1999**, 741−742. [7b] K. Fuji, N. Kinoshita, K. Tanaka, T. Kawabata, *Chem. Commun.* **1999**, 2289−2290.

[8] For characterised σ- and π-allyl complexes see: [8a] K. D. John, K. V. Salazar, B. L. Scott, R. T. Baker, A. P. Sattelberger, *Chem. Commun.* **2000**, 581−582. [8b] K. D. John, K. V. Salazar, B. L. Scott, R. T. Baker, A. P. Sattelberger, *Organometallics* **2001**, *2*, 296−304. [8c] J. B. Wakefield, J. M. Stryker, *Organometallics* **1990**, *9*, 2428−2430. [8d] C. S. Chin, D. Chong, S. Lee, Y. J. Park, *Organometallics* **2000**, *19*, 4043−4050. [8e] T. H. Tulip, J. A. Ibers, *J. Am. Chem. Soc.* **1979**, *101*, 4201−4212. [8f] E. L. Muetterties, K. D. Tau, J. F. Kirner, T. V. Harris, J. Stark, M.

R. Thompson, V. W. Day, *Organometallics* **1982**, *1*, 1562−1567. [8g] J. Müller, B. Passon, J. A. Pickardt, *J. Organomet. Chem.* **1982**, *236*, C11−C14. [8h] P. Powell, *J. Organomet. Chem.* **1983**, *252*, 205−208.[8i] O. Boutry, E. Gutiérrez, A. Monge, M. C. Nicasio, P. J. Pérez, E. Carmona, *J. Am. Chem. Soc.* **1992**, *114*, 7288−7290.

[9] Fast polymerization of aldehyde **5e** prevented the preparation of acetate (*E*)-**2e**.

[10] M. Takasu, Y. Naruse, H. Yamamoto, *Tetrahedron Lett.* **1988**, *29*, 1947−1950.

[11] S. V. Ley, J. Norma, W. Griffith, P. Marsden, *Synthesis* **1994**, 639−666.

[12] [12a] T. Itoh, E. Akasaki, K. Kudo, S. Shirakami, *Chem. Lett.* **2001**, 262−263. [12b] A Sharpless kinetic resolution of the alcohol **6b** has also been published: R. P. Discordia, D. C. Dittmer, *J. Org. Chem.* **1990**, *55*, 1414−1415.

[13] L. E. Overman, D. Lesuisse, M. Hashimoto, *J. Am. Chem. Soc.* **1983**, *105*, 5373−5379.

[14] R. B. Bedford, S. Castillón, P. A. Chaloner, C. Claver, E. Fernández, P. B. Hitchcock, A. Ruiz, *Organometallics* **1996**, *15*, 3990−3997.

[15] [15a] R. Takeuchi, N. Shiga, *Org. Lett.* **1999**, *2*, 265−267. [15b] R. Takeuchi, N. Ue, K. Tanabe, K. Yamashita, N. Shiga, *J. Am. Chem. Soc.* **2001**, *123*, 9525−9534.

[16] For a study of the influence of donor capacity of ligands on the stability of (allyl)Rh complexes see: [16a] H. C. Volger, K. Vrieze, *J. Organomet. Chem.* **1967**, *9*, 527−536. [16b] H. C. Volger, K. Vrieze, *J. Organomet. Chem.* **1967**, *9*, 537−548.

[17] G. Poli, G. Giambastiani, *Chemtracts: Org. Chem.* **2001**, *14*, 204−216.

[18] [18a] J. Wolf, H. Werner, *Organometallics* **1987**, *6*, 1164−1169. [18b] E. B. Tjaden, J. M. Stryker, *Organometallics* **1992**, *11*, 16−18.

[19] [19a] P. A. Evans, J. E. Robinson, J. D. Nelson, *J. Am. Chem. Soc.* **1999**, *121*, 6761−6762. [19b] P. A. Evans, D. K. Leahy, *J. Am. Chem. Soc.* **2000**, *122*, 5012−5013. [19c] P. A. Evans, J. E. Robinson, K. K Moffett, *Org. Lett.* **2001**, *3*, 3269−3271.

[20] [20a] T. A. Mobley, C. Shade, R. G. Bergman, *Organometallics* **1998**, *17*, 3574−3587. [20b] G. C. Lloyd-Jones, S. C. Stephen, *Chem. Commun.* **1998**, 2321−2322. [20c] U. Bruckhardt, M. Baumann, A. Togni, *Tetrahedron: Asymmetry* **1997**, *8*, 155−159. [20d] M. Kawatsura, Y. Uozumi, T. Hayashi, *Chem. Commun.* **1998**, 217−218. [20e] For a recent review see K. Fagnou, M. Lautens, *Angew. Chem. Int. Ed.* **2002**, *41*, 26−47.

[21] [21a] J.-C. Fiaud, J.-Y. Legros, *J. Org. Chem.* **1987**, *52*, 1907−1911. [21b] D. Dvorák, I. Starý, P. Kocovský, *J. Am. Chem. Soc.* **1995**, *117*, 6130−6131.

[22] 0.5 mmol of the corresponding substrate (**20, 21** or cyclopentenyl acetate) was treated with 1 mmol of $NaCH(CO_2Me)_2$ in the presence of $[IrCl(COD)]_2$ (0.01 mmol) and $P(OPh)_3$ (0.02 mmol) in THF (4 mL). After 3 h at room temperature and a further 15 h under reflux, the reaction mixture was worked up.

[23] B. Goldfuss, U. Kazmaier, *Tetrahedron* **2000**, *56*, 6493−6496.

[24] Trans influence or "*transphobia*" can strongly affect the stability and reactivity of organometallic compounds. See for example: J. Vicente, J. A. Abad, A. D. Frankland, M. C. Ramírez de Arellano, *Chem. Eur. J.* **1999**, *5*, 3066−3075 and references therein.

[25] [25a] B. Åkermark, S. Hansson, A. Vitagliano, *J. Am. Chem. Soc.* **1990**, *112*, 4587−4588. [25b] M. Sjögren, S. Hansson, P.-O. Norrby, B. Åkermark, M. E. Cucciolito, A. Vitagliano, *Organometallics* **1992**, *11*, 3954−3964. [25c] U. Kazmeier, F. L. Zumpe, *Angew. Chem.* **2000**, *112*, 805−807; *Angew. Chem. Int. Ed.* **2000**, *39*, 802−804.

[26] P. A. Evans, J. E. Robinson, *Org. Lett.* **1999**, *1*, 1929−1931.

[27] Survey on Ir complexes: G. J. Leigh, R. L Richards, *Comprehensive Organometallic Chemistry, Vol. 5*, Pergamon, Oxford, **1982**.

[28] The oxidative addition of allyl halides to Ir^{I} compounds is a general method for the synthesis of (allyl)Ir^{III} complexes, see: J. M. O′Connor, in *Science of Synthesis, vol. 1* (Ed.: M. Lautens), Thieme, Stuttgart, **2001**, p. 717.

[29] The terms *endo* and *exo* are defined in Scheme 10.

[30] See for example: [30a] J. A. Kaduk, A. T. Poulos, J. A. Ibers, *J. Organomet. Chem.* **1977**, *127*, 245−260 and references therein. [30b] J. S. Merola, *Organometallics* **1989**, *8*, 2975−2977. [30c] M. D. Fryzuk, L. Huang, N. T. McManus, P. Paglia, S. L. Rettig, G. S. White, *Organometallics* **1992**, *11*, 2979−2990. [30d] M. D. Fryzuk, X. Gao, S. J. Rettig, *J. Am. Chem. Soc.* **1995**, *117*, 3106−3117.

[31] A very similar bonding situation as in **31** has been reported for the complex $[(\eta^5\text{-}C_5H_5)Mo(\eta^3\text{-}C_3H_5)(NO)(I)]$: J. W. Faller, D. F. Chodosh, D. Katahira, *J. Organomet. Chem.* **1980**, 227−231.

[32] M. Kollmar, B. Goldfuss, M. Reggelin, F. Rominger, G. Helmchen, *Chem. Eur. J.* **2001**, *7*, 4913−4927.

[33] M. Kollmar, H. Steinhagen, J. Janssen, B. Goldfuss, S. Malinovskaya, F. Rominger, G. Helmchen, *Chem. Eur. J. in press.*

[34] H. Friebolin, *Basic One- and Two-Dimensional NMR Spectroscopy*, Wiley-VCH, Weinheim, **1998**.

[35] [35a] J. Jelner, B. H. Meier, P. Bachmann, R. R. Ernst, *J. Chem. Phys.* **1979**, *71*, 4546−4553. [35b] C. L. Perrin, T. J. Dwyer, *Chem. Rev.* **1990**, *90*, 935−967.

[36] [36a] K. E. Schwiebert, J. M. Stryker, *Organometallics* **1993**, *12*, 600−602. [36b] C. Tejel, M. A. Ciriano, A. J. Edwards, F. J. Lahoz, L. A. Oro, *Organometallics* **2000**, *19*, 4968−4976.

[37] R. Hulst, N. K. de Vries, B. L. Feringa, *Tetrahedron: Asymmetry* **1994**, *5*, 699−708.

[38] M. Peer, J. C. de Jong, M. Kiefer, T. Langer, H. Rieck, H. Schell, P. Sennhenn, J. Sprinz, H. Steinhagen, B. Wiese, G. Helmchen, *Tetrahedron* **1996**, *52*, 7547−7583.

[39] J. L. Herde, J. C. Lambert, C. V. Senoff, *Inorg. Synth.* **1974**, *15*, 18−20.

[40] J. L. Lehmann, G. C. Lloyd-Jones, *Tetrahedron* **1995**, *51*, 8863−8874; resolution of enantiomers of **3a** by HPLC: Chiracel ODH column, length: 25 cm + 5 cm precolumn, flow: 0.5 mL·min^{-1}, eluent: *n*-hexane/*i*PrOH (99.5:0.5); **3a**: $t_R(R)$ = 28.9 min, $t_R(S)$ = 31.6 min; (*E*)-**4a**: t_R = 45.1 min. $[\alpha]_D^{24}$ = 27.2 (c = 0.85, $CHCl_3$) for **3a** with 86 % ee (*R*).

[41] E. Keinan, E. Bosh, *J. Org. Chem.* **1986**, *51*, 4006−4016.

[42] A. L. J. Beckwith, A. A. Zavitas, *J. Am. Chem. Soc.* **1986**, *108*, 8230−8234; analysis of enantiomers of **3c** by GC: Chiraldex γ-CD TA column, length: 30 m, 100 kPa helium, flow 80 mL·min^{-1}, 50→100 °C at 1 °C·min^{-1}, then 20 min at 100 °C; **3c**: $t_R(R)$ = 35.7 min, $t_R(S)$ = 36.7 min; (*E*)-**4c**: t_R = 43.8 min. $[\alpha]_D^{27}$ = 12.1 (c = 1.23, CH_2Cl_2) for **3c** with 85 % ee (*R*).

[43] Y. D. Ward, L. A. Villanueva, G. D. Alfred, S. C. Payne, M. A. Semones, L. S. Liebeskind, *Organometallics* **1995**, *14*, 4132−4156.

[44] (*E*)-**2b** has been prepared previously by a different route: Z. Rappoport, S. Winstein, W. G. Young, *J. Am. Chem. Soc.* **1972**, *94*, 2320−2329.

[45] H. Matsuhashi, S. Asai, K. Hirabayashi, Y. Hatanaka, A. Mori, T. Hiyama, *Bull. Chem. Soc. Jpn.* **1997**, *70*, 1943−1952.

[46] M. T. Nunez, V. S. Martín, *J. Org. Chem.* **1990**, *55*, 1928−1932.

[47] L. A. Gorthey, M. Vairamani, C. Djerassi, *J. Org. Chem.* **1984**, *49*, 1511−17.

[48] S. W. Baldwin, J. Aubé, P. M. Gross, *Tetrahedron Lett.* **1987**, *28*, 179−182.

[49] For the preparation of (*R*)-**1b** the reaction was stopped at a conversion of 60%, the unconverted alcohol isolated by flash column chromatography and acetylated. (*S*)-**1b**: 36%, 97.7% *ee*; (*R*)-**1b**: 40%, 94.8% *ee*. $[\alpha]_D^{20}$ = −1.5 (*c* = 1.17, $CHCl_3$) for **1b** with 95.5% *ee* (*R*). HPLC: DAICEL Chiralcel ODH column, length: 25 cm + 5 cm precolumn, flow: 0.5 mL·min^{-1}, eluent: *n*-hexane/*i*PrOH (99.5:0.5); **1b**: $t_R(R)$ = 20.1 min, $t_R(S)$ = 22.6 min.

[50] T. E. Wessel, J. A. Berson, *J. Am. Chem. Soc.* **1994**, *116*, 495−505.
[51] Compound **11e** was prepared previously by another route: M. F. Shostakovskii, N. V. Kuznetsov; Y. B. Zaretskaya, *Bull. Acad. Sci. USSR Div. Chem. Sci. (Engl. Trans.)* **1963**, 830−831; *Izv. Akad. Nauk SSSR, Otd. Khim. Nauk* **1963**, 922−923.
[52] Compound **5e** was prepared previously by another route: J. Roos, F. Effenberger, *Tetrahedron: Asymmetry* **1999**, *10*, 2817−2828.
[53] A different synthesis for compound **10f** was first described by: E. Eliel, L. Giza, A. Chester, *J. Org. Chem.* **1968**, *33*, 3754−3758.
[54] Compound **11f** has been prepared previously by a different route: V. Bertine, F. Lucchesini, M. Pocci, A. de Munno, *Heterocycles* **1995**, *41*, 675−688.
[55] Compound **5f** has been prepared previously by a different route: A. B. Reitz, S. O. Nortey, B. E. Maryanoff, *J. Org. Chem.* **1987**, *52*, 4191−4202.

Received April 2, 2002
[I02168]

Isomerically Pure α_1-Monosubstituted Tungstodiphosphates: Synthesis, Characterization and Stability in Aqueous Solutions

Roland Contant,[b] Martine Richet,[b] Yu Wei Lu,[a] Bineta Keita,[a] and Louis Nadjo*[a]

Keywords: Polyanions / Phosphates / Tungsten

Isomerically pure samples of α_1-$P_2W_{17}O_{61}M$ were prepared, in which M represents Ca^{II} and mainly the first-row transition metal cations: Mn^{II}, Fe^{III}, Co^{II}, Ni^{II}, Cu^{II}, Zn^{II}. The formula is α_1-$P_2W_{17}O_{62}M$ for V^{V} and Mo^{VI}. The compounds were characterised by elemental analysis, IR, UV/Vis and ^{31}P NMR spectroscopy. The stability of these complexes was monitored by cyclic voltammetry and/or UV/Vis spectroscopy. All the compounds proved to be stable for at least 24 h in a pH = 3 medium, even in the presence of 0.2 M Na^+, except for the precursor lacunary species itself and the Ca^{II}-substituted derivative. In this medium, the transformation of the lacunary heteropolyanion yielded a mixture of α-$[P_2W_{18}O_{62}]^{6-}$ and $[H_2P_2W_{12}]^{12-}$. The same species were obtained, but at a much slower rate, through the decomposition of α_1-$P_2W_{17}O_{61}Ca$. This difference in stability between the lacunary and the Ca^{II}-substituted derivatives might be ascribed to size and charge effects, along with the rigidity of the vacant site. At pH = 5, the final product of the transformation of α_1-$[P_2W_{17}O_{61}]^{10-}$ is α_2-$[P_2W_{17}O_{61}]^{10-}$. The presence of Li^+ appears to be more favourable than Na^+ for the stability of these complexes.

(© Wiley-VCH Verlag GmbH, 69451 Weinheim, Germany, 2002)

Introduction

It is well established that numerous electrocatalytic processes can be triggered by heteropolyanions (HPA).[1] Specifically, sustained catalytic several-electron reduction processes demand that the necessary number of electrons be accumulated in the framework of the HPA and then delivered to the substrate in potential regions where neither structure change of the HPA nor derivatisation of the electrode might occur.[1d,2] In our continuing efforts to systematically examine the parameters and combinations of parameters that could favour or counteract the merging of the first several waves in the electrochemical study of heteropolyanions, two main parameters were identified. The pH of the solution is one obvious parameter, which can be combined successfully with the second parameter, namely substitution effects, to reveal the rich redox behaviour of HPAs.[3−5] This last parameter is particularly important because it will determine, at least in part, the stability domain of the substituted HPA. Furthermore, the location of the heterometal in the framework and the nature and the number of the substituents are likely to influence the interactions between the electroactive centres in the molecule. In this context, our present efforts are aimed at illustrating such ideas with compounds of the Dawson series. It can be recalled that the Dawson structure is an elongated ellipsoid that consists of six addenda atoms of one kind and twelve of another. The six metal atoms are assembled in two groups of edge-shared M_3O_{13} octahedra that occupy the two "polar" positions of the ellipsoid; the remaining twelve metal atoms form two rings of six alternately edge- and corner-shared MO_6 octahedra in what is usually termed the equatorial position. The metal atoms in the "cap" occupy what is termed α_2-positions and those in the "belt" α_1-positions. With regard to the α_2-series, the synthesis involved first-row transition metal ion substituted complexes[4] derived from $[(1,)2,3\text{-}P_2Mo_2W_{15}O_{61}]^{10-}$. Among other remarkable results, the electrochemistry of this series of compounds shows that the interplay of the pH effect facilitates the build-up of an overall three-electron process on the first wave of the Fe^{III}-substituted complex.[4a,6] Another, possibly complementary direction involves positional isomerism. Perusal of the literature on simple Dawson-type tungstodiphosphates reveals that the α_2-isomer and its substituted derivatives were the preferred,[5] owing presumably to the instability of lacunary α_1-$[P_2W_{17}O_{61}]^{10-}$ which isomerises easily to the α_2-form[7] and reconstitutes the parent $[P_2W_{18}O_{62}]^{6-}$. However, we have succeeded in obtaining previously pure samples of several compounds of the α_1-series.[6]

The aim of the present paper is to describe the synthesis and characterisation of pure samples of the lacunary and

[a] Laboratoire de Chimie Physique, UMR 8000, CNRS, Electrochimie et Photoélectrochimie, Université Paris-Sud, Bâtiment 420, 91405 Orsay Cedex, France
Fax: (internat.) + 33-1/69154328
E-mail: louis.nadjo@lcp.u-psud.fr
[b] Laboratoire de Chimie des Métaux de Transition, UMR 7071, CNRS, Université Paris VI, 4, place Jussieu, 75252 Paris Cedex 05, France

first-row transition metal ion substituted compounds of the α_1-series. In particular, their transformation in solution as a function of pH and time were monitored by cyclic voltammetry and/or UV/Vis spectroscopy. The interplay of ion-pairing remains a subject of interest,[8] and is obvious in several instances below. In a preceding paper[6c] devoted to the electrochemistry of these compounds and based on the present syntheses, we have demonstrated, by cyclic voltammetry, the successful synthesis of these metal ion substituted derivatives from the α_1-lacunary species. Thus, the conditions under which α_1-$[P_2W_{17}O_{61}]^{10-}$ is fairly stable could be determined. The metal cation substituted derivatives of α_1-$[P_2W_{17}O_{61}]^{10-}$ could then be obtained and studied. Further, in a pH = 3 medium, a characteristic fingerprint for the α_2-series has been found that allows us to distinguish them unequivocally from the corresponding α_1-isomers.[6c] Here, the details of the syntheses are given, with a full characterisation by elemental analysis, ^{31}P NMR, UV/Vis and IR spectroscopy. A further incentive for this work stems from the desire to study the influence of positional isomerism on the redox properties. It has been proposed,[9a][9b] and experimental evidence supports [8c] the fact that α-P_2W_{18} is initially reduced at one of the twelve equivalent tungsten atoms. Substitution in the α_1-position should then markedly influence electron transfer processes relative to the α_2-series.

^{31}P NMR Spectroscopy

In the following, the oxygen atoms and the negative charges are omitted when no confusion is possible.The following species, α-$[P_2W_{18}O_{62}]^{6-}$, α_1-$[P_2W_{17}O_{61}]^{10-}$, and α_2-$[P_2W_{17}O_{61}]^{10-}$, will be abbreviated as α-P_2W_{18}, α_1-P_2W_{17}, and α_2-P_2W_{17}, respectively.

Table 1 presents the ^{31}P NMR spectroscopic features obtained in the present work for α_1- and α_2-derivatives. Jorris et al.[10] have published ^{31}P NMR spectroscopic data on some compounds of the same families. Their results were confirmed, under slightly different experimental conditions, by Finke et al.[5b] on derivatives of the α_2-series. More recently, Francesconi et al.[7a] have published the data pertaining to the lithium salt of α_1-P_2W_{17} and to several other lanthanide complexes of this lacunary species. To the best of our knowledge, Jorris et al.[10] were the first to study the NMR spectroscopic behaviour of paramagnetic element containing HPAs of P_2W_{17} derivatives. Even though their syntheses resulted in mixtures of α_1- and α_2-isomers, their pioneering work constitutes a valuable basis for the interpretation of the present observations. In these complexes, it is convenient to designate the phosphorus atom nearer the substituent (eventually paramagnetic ion) as P(1), and the phosphorus atom further away from this element as P(2). From the ^{31}P NMR spectra of several Dawson structures substituted in the α_2-position, it can be seen that the chemical shift assigned to P(2) is practically unaffected by the nature of the substituent element. The only exception is when Co^{II} is the substituent. Such an observation is confirmed in Table 1. Provisionally, it is worth mentioning that the same observation (with the same exception) was also made for compounds of the $K_8P_2W_{15}Mo_2MO_{61}$ series, where M represents the divalent substituent cation.[4b] Table 1 shows that the same conclusions remain true for the chemical shifts assigned to P(2) in the α_1-$P_2W_{17}M$ derivatives, with the exceptions also extended to cases where M is Ni^{II} and Mn^{II}. As expected, the signal assigned to the P atom closest to the substitution site is shifted downfield considerably in the presence of paramagnetic cations. The shift is larger for α_1-derivatives. The ^{31}P NMR line widths depend on the nature of the particular substituent atom, and especially on its electronic ground state configuration. Usually, as can be seen in Table 1, very narrow or relatively narrow signals are observed for P(2), in contrast to that observed for the P(1) signal, which becomes exceedingly broadened in the case of the Mn^{II} derivative, whose ground state is orbitally nondegenerate. As a whole, it can be considered that satisfactory agreement with the observations of Jorris et al.,[9] and other literature results, [5b][7a] is obtained in the present work, provided the difference in medium composition is taken into account. The same reasoning is also applied to the interpretation of the spectra of the Mg^{II}-, Ca^{II}- and Cu^{II}-substituted derivatives. From the electronic configurations of Mg^{II} and Ca^{II}, no dramatic chemical shifts are expected for either P(2) or P(1) compared with those observed in the diamagnetic Zn^{II} isomorphs. The results in Table 1 validate this reasoning. In contrast, Cu^{II} is a paramagnetic d^9 ion that has a dramatic effect on the observed chemical shift, as expected.

IR Spectroscopy

The characteristic IR peaks were recorded. The assignments were made by taking into account those established in the literature.[11] As in related studies,[6a] introduction of a substituent metal cation in the vacancy basically restores the symmetry of the PO_4 tetrahedron, at least as far as the IR spectra are concerned. Consequently, the IR spectra are very similar from one complex to the next, thus preventing any reliable identification of a given anion. However, it is worth noting that the peak assigned to the $P-O_a-W$ vibration, where W is one of the "belt" atoms, is not observed in the Co^{II} and Ni^{II} derivatives.

Stability of α_1-P_2W_{17} and Its Substituted Derivatives: Electrochemistry and UV/Vis Spectroscopy

A constant observation in the transformation of α-P_2W_{18} as a function of pH and time, is that the nature of the resulting species depends strongly on the pH of the solution and on the identity and concentrations of the cations present in the solution.[9] Such a dependence is also expected in the cases of interest here. The evolution of α_1-P_2W_{17} is monitored by cyclic voltammetry at pH = 3 and 5. The

Table 1. ^{31}P NMR shifts (from 85% H_3PO_4) and line widths of α_1- and α_2-monometalloheptadecatungstodiphosphates at 298 K (0.01 M solutions of K^+ salts in LiCl 0.5 M, in 50% D_2O)

Compound	δ(P1) [ppm]	Δν(P1) [Hz]	δ(P2) [ppm]	Δν(P2) [Hz]
$\alpha_1K_9LiP_2W_{17}O_{61}$, 18 H_2O	−8.53 (−9.16)[a]		−12.86 (−13.48)[a]	
$\alpha_1K_8P_2W_{17}CaO_{61}$, 19 H_2O	−9.35	12	−13.04	5
$\alpha_1K_7P_2W_{17}VO_{62}$, 18 H_2O	−11.45	6	−12.52	7
$\alpha_1K_8P_2W_{17}MnO_{61}$, 15 H_2O	not observed	−	−2.55	700
$\alpha_1K_7P_2W_{17}FeO_{61}$, 16 H_2O	not observed	−	−4.6	700
$\alpha_1K_8P_2W_{17}CoO_{61}$, 16 H_2O	1129	150	−34	4
$\alpha_1K_8P_2W_{17}NiO_{61}$, 16 H_2O	895[b]	5700[b]	−16.47	60
$\alpha_1K_8P_2W_{17}CuO_{61}$, 19 H_2O	−1.30	800	−12.00	70
$\alpha_1K_8P_2W_{17}ZnO_{61}$, 16 H_2O	−7.96	2	−12.84	3
$\alpha_1K_6P_2W_{17}MoO_{62}$, 18 H_2O	−11.15	8	−12.08	11
$\alpha_1K_8P_2W_{17}MgO_{61}$, 17 H_2O	−7.44	3	−12.81	4
$\alpha_2K_{10}P_2W_{17}O_{61}$, 18 H_2O	−7.33	3	−13.48	4
$\alpha_2K_8P_2W_{17}CaO_{61}$, 19 H_2O	−7.13	2	−13.66	2
$\alpha_2K_7P_2W_{17}VO_{62}$, 18 H_2O	−10.84		−12.92	
$\alpha_2K_8P_2W_{17}MnO_{61}$, 15 H_2O	600[b]	40000[b]	−12.42	140
$\alpha_2K_7P_2W_{17}FeO_{61}$, 16 H_2O	not observed	−	−12.6	160
$\alpha_2K_8P_2W_{17}CoO_{61}$, 16 H_2O	245	25	−22.71	5
$\alpha_2K_8P_2W_{17}NiO_{61}$, 16 H_2O	226.2	750	−13.46	19
$\alpha_2K_8P_2W_{17}ZnO_{61}$, 16 H_2O	−8.06	15	−13.54	2
$\alpha_2K_8P_2W_{17}MgO_{61}$, 17 H_2O	−7.52	2	−13.53	2
$\alpha_2K_8P_2W_{17}CuO_{61}$, 19 H_2O	−33	1250	−12.58	21

[a] From ref.[7a] [b] From ref.[10]

voltammograms are limited to the first several waves spanning the potential region in which no derivatisation of the electrode surface is encountered.[3n] These waves appear to serve as sufficiently clear fingerprints for the various compounds. The stability of the substituted derivatives was studied by UV/Vis spectroscopy, complemented by cyclic voltammetry when necessary. A sodium medium was selected for a detailed study, since the presence of this cation gives an intermediate rate of transformation, suitable for correct monitoring by cyclic voltammetry.

Cyclic Voltammetric Monitoring of α_1-P_2W_{17} at pH = 3 and 5 in an Na^+ Medium

Table 2 summarises the evolution of the main observed cathodic peak potentials as a function of time. The significance of these values is indicated below.

Table 2. Evolution of the reduction peak potentials of the first three waves of $\alpha_1P_2W_{17}$ as a function of pH and time; for the compositions of the electrolytes and other details, see text

Duration/h	$-E_{p1}$/mV	pH = 3 $-E_{p2}$/mV	$-E_{p3}$/mV
0	310	580	925
168	30 and 210	635	902
		pH = 5	
0	500	656	1042
72	530	658	922

At pH = 3, the first three waves, run on a freshly prepared solution of α_1-P_2W_{17}, are initially considered. After a period of 2 h, transformation is already significant: the cathodic peak current intensity of the first wave decreases to 75% of its initial value; concomitantly, two new waves appear and begin to grow at a more positive potential than that observed for the former initial first wave. The initial first wave completely disappears after 26 h, after which the cyclic voltammogram remains practically the same and is composed of a four-wave system. The transformation scheme, as a function of pH, established previously for α-P_2W_{18} by Contant and Ciabrini[5k,12] and sketched in Scheme 1, is very helpful for identifying the possible species responsible for the observed voltammogram and for their quantitative determination.

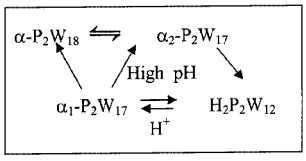

Scheme 1. Decomposition pathways of α_1-P_2W_{17}

The cyclic voltammograms of authentic samples of α-P_2W_{18} and P_2W_{12} are superimposed in Figure 1 (A). Key to the identification of the decomposition products is the observation that the single wave of P_2W_{12} in the explored potential region appears to be very close to the third wave of α-P_2W_{18} in Figure 1 (A). As a result, when a cyclic voltammogram is run on a sample of a mixture of the two species, the third wave is broad and composite, and is clearly different to the third wave observed in the voltammogram of α-P_2W_{18} alone.

Based on the cyclic voltammograms of these authentic samples of α-P_2W_{18} and P_2W_{12}, the decomposition pathways of α_1-P_2W_{17} could be described quantitatively in Figure 1 (B and C), which also shows a representative selection of the cyclic voltammograms of the mixture. It is assumed when calculating the percentages of the various species that

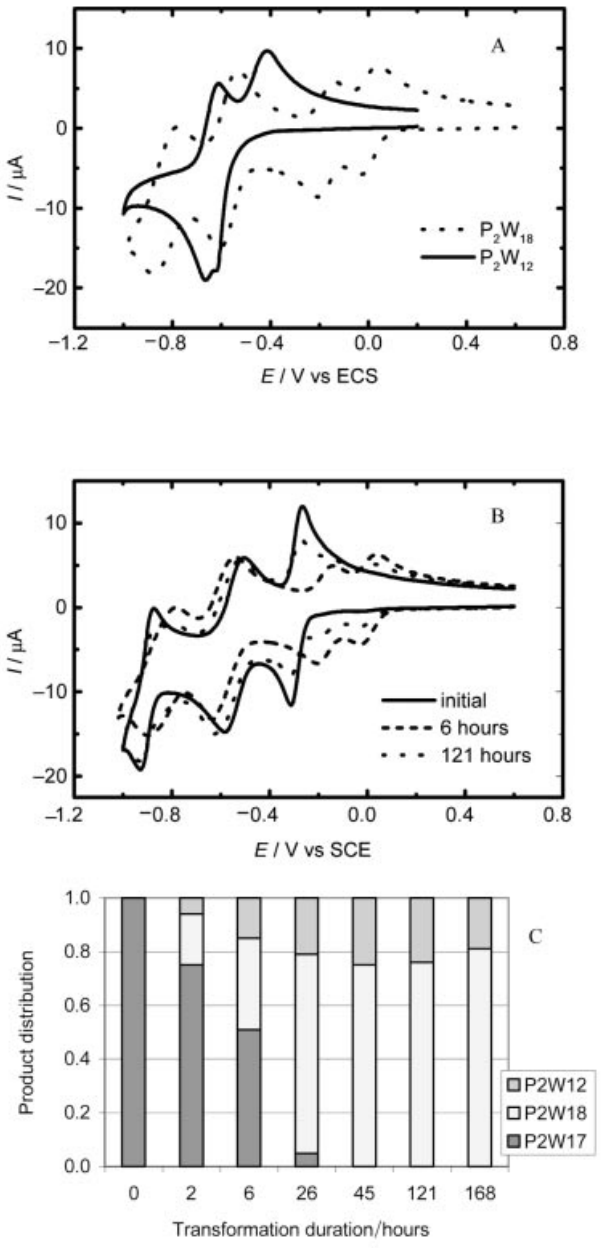

Figure 1. Identification of the decomposition pathway of α_1-P_2W_{17} in a pH = 3 medium (0.2 M Na_2SO_4 + H_2SO_4); (A) Cyclic voltammograms of authentic samples of α-P_2W_{18} and P_2W_{12}; (B) selection of representative cyclic voltammograms of α_1-P_2W_{17}, as a function of time; (C) electroactive products distribution, as a function of transformation duration; for further details, see text

only negligibly small amounts of possible non-electroactive species might exist in the mixture. Finally, the solution obtained after completion of the transformation of α_1-P_2W_{17} at pH = 3 contains α-P_2W_{18} and P_2W_{12}. This is in agreement with previous work.

Parallel experiments were performed at pH = 5 in sodium acetate buffer. The initial cyclic voltammogram is restricted to the three redox peaks observed between +0.6 and −1.1 V; the last two waves are composite. The initial and final reduction peak potential values are presented in Table 2. Cyclic voltammetry reveals that after only a few minutes the formation of the first two waves of α-P_2W_{18} can be seen, while the initial wave system is only slightly different, except for current intensities. However, after standing for 72 h, the waves of α-P_2W_{18} have completely disappeared and a new voltammetric pattern is observed, which can be ascribed to a pure electroactive product. Comparison of the cyclic voltammogram of α_2-P_2W_{17} with that obtained after completion of the transformation of α_1-P_2W_{17} at pH = 5, indicates unambiguously that α_1-P_2W_{17} is initially converted into a mixture of α_2-P_2W_{17} and α-P_2W_{18}, and that the final product at pH = 5 is pure α_2-P_2W_{17}.

The cyclic voltammetric monitoring of the species appearing in solution has allowed for the clarification of the transformation pathways of α_1-P_2W_{17} at pH = 3 and 5, as sketched in Scheme 1. Qualitatively, it is worth noting that the transformations are much slower at pH = 3 than at pH = 5.

Study of the Stability of α_1-$P_2W_{17}M$ Complexes (M = Ca^{II}, V^{V}, Mn^{II}, Fe^{II}, Co^{II}, Ni^{II}, Cu^{II}, Zn^{II} and Mo^{VI})

A sodium sulfate solution at pH = 3 was selected as the medium for this study. For each complex, the concentration in solution was approximately 2×10^{-5} M, and two spectra were run with the same sample with a time interval of 24 h. All the spectra are relatively featureless, almost identical to each other, and show a shoulder. The characteristic features are presented in Table 3. Not unexpectedly, large magnification of the absorbance scale indicates differences in the onsets of the absorption spectra.

On careful comparison of the spectra, only two complexes are not completely stable after 24 h in the pH = 3 medium: α_1-P_2W_{17} and α_1-$P_2W_{17}Ca$. The corresponding spectra can be seen in Figures 2 and 3. For the lacunary species, this observation is in agreement with the results of the cyclic voltammetric study. Provisionally, we note the close similarity between the spectra of the two complexes after 24 h at pH = 3, which could suggest similar transformation pathways for them. Therefore, a complementary voltammetric examination of α_1-$P_2W_{17}Ca$ as a function of time was carried out. In the sodium sulfate medium at pH = 3, and as observed for other complexes in the previous section, the relevant cyclic voltammogram consists of

Table 3. Characteristic wavelength and optical density measured for approximately 2×10^{-5} M of the relevant heteropolyanion in a pH = 3 medium

Compound	λ [nm] shoulder	O.D. [a.u.]
$\alpha_1K_9LiP_2W_{17}O_{61}$, 18 H_2O	249	1.15
$\alpha_1K_8P_2W_{17}CaO_{61}$, 19 H_2O	249	1.15
$\alpha_1K_7P_2W_{17}VO_{62}$, 18 H_2O	240	1.46
$\alpha_1K_8P_2W_{17}MnO_{61}$, 15 H_2O	248	1.26
$\alpha_1K_7P_2W_{17}FeO_{61}$, 16 H_2O	245	1.29
$\alpha_1K_8P_2W_{17}CoO_{61}$, 16 H_2O	251	1.15
$\alpha_1K_8P_2W_{17}NiO_{61}$, 16 H_2O	250	1.12
$\alpha_1K_8P_2W_{17}CuO_{61}$, 19 H_2O	253	1.10
$\alpha_1K_8P_2W_{17}ZnO_{61}$, 16 H_2O	260	1.07

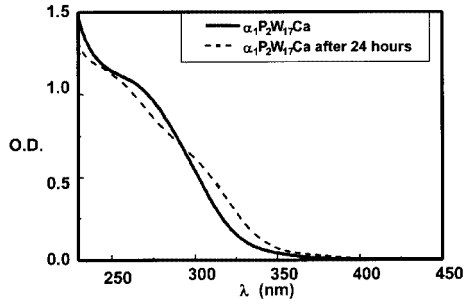

Figure 2. Evolution over 24 h of the UV/Vis spectra of α_1-$P_2W_{17}Ca$

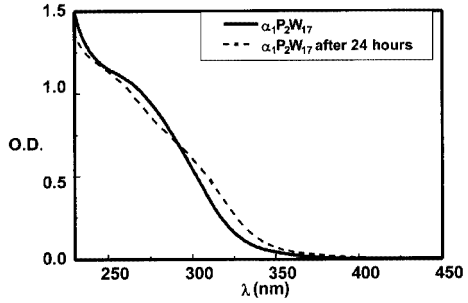

Figure 3. Evolution over 24 h of the UV/Vis spectra of α_1-P_2W_{17}

three chemically reversible waves. Their cathodic peak potentials are at − 0.320, − 0.570 and − 0.916 V. Figure 4 shows the cyclic voltammograms of α_1-$P_2W_{17}Ca$. Comparison of the voltammograms obtained after 15 d with that of α_1-P_2W_{17} after 7 d indicates that α-P_2W_{18} and P_2W_{12} are indeed the transformation products of α_1-$P_2W_{17}Ca$. However, the transformation is distinctly slower in the case of the latter complex; for instance, the transformation of α_1-P_2W_{17} gives 73% α-P_2W_{18} after 26 h, while the percentage obtained from α_1-$P_2W_{17}Ca$ after 15 d is only 67%. These observations agree with the previously discussed trends[4,6b] involving the cyclic voltammograms associated with the tungsten framework in monosubstituted Dawson heteropolyanions. It has been demonstrated that appropriate comparisons among cyclic voltammograms involve those of

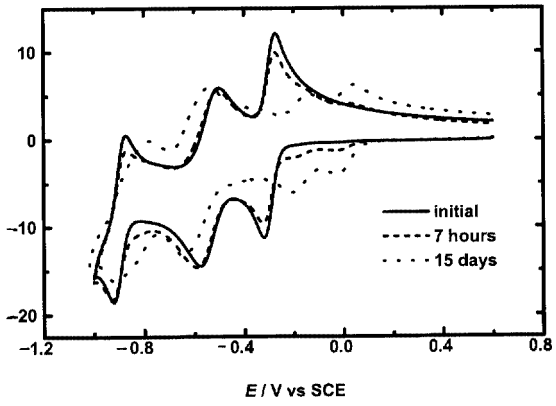

Figure 4. Selection of representative cyclic voltammograms observed during the transformation of α_1-$P_2W_{17}Ca$ in a pH = 3 medium (0.2 M Na_2SO_4 + H_2SO_4); for further details, see text

the monosubstituted species with that of the precursor lacunary complex, except for the cases of substitution by $Mo^{6+/5+}$ and $V^{5+/4+}$. Looking at the present example which is particularly remarkable, it can readily be seen that the reduction peak potentials of the Ca^{II}-substituted complex are very similar to the corresponding ones of the lacunary species. The following rationale, based on the respective charges of Na^+ and Ca^{2+}, can also be used to explain the greater stability of α_1-$P_2W_{17}Ca$ than α_1-P_2W_{17}. On dissolution of α_1-P_2W_{17} (α_1-$LiK_9P_2W_{17}O_{61}$) in 0.2 M Na_2SO_4 + H_2SO_4 (pH = 3), the relatively fast replacement of Li^+ by Na^+ might be favoured by the large concentration of the latter, which is known to be deleterious to the stability of the complex. Owing to the difference in charge, the corresponding replacement of Ca^{2+} by Na^+ is much slower for α_1-$P_2W_{17}Ca$, even though the two cations have approximately the same radius. In other words, the local negative charge of the vacancy is better compensated by Ca^{2+} which is therefore, more difficult to displace than Li^+.

A study was also carried out to compare the stability of α_1-$P_2W_{17}Ca$ in Li^+ (0.2 M Li_2SO_4/H^+, pH = 3) and Na^+ media. The transformation is slower in the presence of lithium, quantified by a percentage of 43% decomposition in Li^+ medium compared with 63% in Na^+ medium after 2 d. Thus, it appears that the relative stability of α_2-$P_2W_{17}Ca$ and α_1-$P_2W_{17}Ca$ might be explained in terms of steric reasons,[5k,6,13] but in combination with the effect of the charge of the substituent cation. It should be noted that the ideal size for a cation to fit in the vacancy should be very similar to the usually accepted size of W^{6+} ion (0.74 Å). The radii of Ca^{2+} (1.14 Å) and Na^+ (1.16 Å) collected from the literature[14] are similar, but are larger than that of W^{6+} (0.74 Å); hence the relative order of the stabilities of the corresponding species. However, the charge of the substituent cation also plays a part as discussed previously. For a further confirmation of this size hypothesis, Mg^{2+} (0.86 Å), which has the same charge but a smaller radius than Ca^{2+}, was selected for comparison with the latter. In the sodium solution at pH = 3, α_1-$P_2W_{17}Mg$ is remarkably more stable than α_1-$P_2W_{17}Ca$. This observation gives further support to the preceding assumptions. Another aspect of the steric effect must be traced to the location of the vacancy in the α_1- or α_2-position in the tungsten framework.[5k,6,13] The vacancy is distinctly more rigid in the α_1- than in the α_2-position. Therefore, the deformability of the latter vacancy makes it larger and favours the accommodation of a large cation. As a result, it is expected that α_2-$P_2W_{17}Ca$ is more stable than α_1-$P_2W_{17}Ca$. The test in the sodium medium at pH = 3 confirms the hypothesis. The decomposition of α_2-$P_2W_{17}Ca$ begins after 4 d compared with 7 h for α_1-$P_2W_{17}Ca$. After a period of 15 d, the percentage of α-P_2W_{18} formed from α_2-$P_2W_{17}Ca$ is only 20%.

Concluding Remarks

One of the aims of this work is to further investigate the parameters that could influence electron transfer processes

involving the first wave of heteropolyanions and, eventually, favour the apparently simultaneous uptake of several electrons. Positional isomerism is likely to be one of these parameters. It has been proposed, and experimental evidence supports the fact that α-P_2W_{18} is initially reduced at one of the twelve equivalent tungsten atoms. With the assumption that this behaviour remains valid in substituted compounds, substitution in the α_1-position should markedly influence electron transfer processes compared with the α_2-series. Conditions were found in which the lacunary ligand α_1-$[P_2W_{17}O_{61}]^{10-}$ is fairly stable. This result was achieved through the use of AcOLi for the dissolution of the complex, or by taking advantage of the favourable kinetics of addition vs. degradation when the solid lacunary HPA was added to a solution of the salt of the substituent cation. Its metal cation-substituted derivatives could then be obtained and studied. To the best of our knowledge, this work constitutes the first systematic synthesis and study of first-row transition metal cation monosubstituted complexes of the α_1-lacunary ligand. ^{31}P NMR spectroscopy and cyclic voltammetry were used to demonstrate the successful synthesis of these species. Their stability was monitored in pH = 3 and 5 media by cyclic voltammetry and UV/Vis spectroscopy. It is worth noting that even the relatively labile α_1-P_2W_{17} and α_1-$P_2W_{17}Ca$ are sufficiently stable to permit NMR spectroscopic and electrochemical characterisations. Relevant comparisons with the same derivatives in the α_2-series were carried out.

Experimental Section

Preparation: The potassium salts of α-$[P_2W_{18}O_{62}]^{6-}$, α_1-$[P_2W_{17}O_{61}]^{10-}$ and α_2-$[P_2W_{17}O_{61}]^{10-}$ were prepared by published methods.[5a] The compounds of the α_2-series have received extensive attention and their syntheses will not be described further.[5] In the α_1-series, the synthesis of Fe^{III}-substituted derivatives was described in detail previously.[6a] The synthesis of Mo- and V-substituted compounds were also described previously by one of the present authors.[5k−5m,7b,8c] The water contents were measured by gravimetric methods. Elemental analyses were performed by the Laboratoire Central d'Analyse of CNRS (Vernaison, France) and checked, except for the metallic cations, by standard methods.[6a] The precision of these analyses is not excellent, as is not unusual in the literature on polyoxometalates.

$\alpha_1K_8P_2W_{17}ZnO_{61}$, 16 H_2O: A sample of $\alpha_1K_9LiP_2W_{17}O_{61}$, 18 H_2O (10 g) was dissolved in 100 mL of acetate buffer at pH = 4.7, 0.5 M in lithium acetate AcOLi. The solution was not perfectly clear. $Zn(NO_3)_2$ (3 mL of a 1 M solution) was added whilst stirring. The solution was filtered through an ashless pleated filter and left to settle. The clear part of the solution (70 mL) was collected and treated with KCl (7 g). The precipitate was filtered, washed with ethanol and diethyl ether and air-dried; recovered: 7.5 g; yield: 75%. $\alpha_1K_8P_2W_{17}ZnO_{61}$, 16 H_2O (4830): calcd. K 6.48, P 1.28, Zn 1.35, W 64.71, H_2O 5.60; found K 6.70, P 1.24, Zn 1.25, W 62.60, H_2O 5.55.

$\alpha_1K_8P_2W_{17}MgO_{61}$, 17 H_2O: $Mg(NO_3)_2$ (5 mL of a 1 M solution) was added to 100 mL of water. $\alpha_1K_9LiP_2W_{17}O_{61}$, 18 H_2O (10 g) was then added whilst stirring, and the solution was filtered if necessary. The clear solution was treated with KCl (10 g) to obtain a white precipitate. The precipitate was filtered, washed with ethanol and diethyl ether and air-dried. Note that the same result could be obtained by starting with $MgCl_2$ instead of the nitrate; recovered: 7.9 g; yield: 80%. $\alpha_1K_8P_2W_{17}MgO_{61}$, 17 H_2O (4807): calcd. K 6.51, P 1.29, Mg 0.51, W 65.02, H_2O 6.00; found K 6.68, P 1.28, Mg 0.48, W 64.20, H_2O 6.02.

$\alpha_1K_8P_2W_{17}CaO_{61}$, 19 H_2O: The synthesis is the same as that of the Mg^{2+} derivative. The magnesium salt is replaced by $Ca(NO_3)_2$; recovered: 8.0 g; yield: 80%. $\alpha_1K_8P_2W_{17}CaO_{61}$, 19 H_2O (4877): calcd. K 6.41, P 1.27, Ca 0.82, W 64.09, H_2O 7.02; found K 6.60, P 1.24, Ca 0.79, W 62.67, H_2O 6.98.

$\alpha_1K_8P_2W_{17}NiO_{61}$, 16 H_2O: Ni^{2+} (2 mL of a 1 M $Ni(NO_3)_2$ solution) was added to LiCl (50 mL of a 0.2 M solution). $\alpha_1K_9LiP_2W_{17}O_{61}$, 18 H_2O (5 g) was then added whilst stirring, and the solution was filtered if necessary. The clear solution was treated with 30 mL of a saturated KCl solution. The precipitate was filtered, washed with ethanol and diethyl ether and air-dried. The same synthesis could be carried out in an acetate buffer containing 0.5 M AcOLi; recovered: 3.7 g; yield: 75%. $\alpha_1K_8P_2W_{17}NiO_{61}$, 16 H_2O (4823): calcd. K 6.49, P 1.28, Ni 1.22, W 64.80, H_2O 5.60; found K 6.74, P 1.25, Ni 1.25, W 62.42, H_2O 5.75.

$\alpha_1K_8P_2W_{17}CoO_{61}$, 16 H_2O: The synthesis is the same as that of the Zn^{2+} derivative; recovered: 7.5 g; yield: 75%. $\alpha_1K_8P_2W_{17}CoO_{61}$, 16 H_2O (4823): calcd. K 6.48, P 1.28, Co 1.22, W 64.80, H_2O 5.60; found K 6.75, P 1.24, Co 1.13, W 63.83, H_2O 5.71.

$\alpha_1K_8P_2W_{17}MnO_{61}$, 15 H_2O: A sample of $\alpha_1K_9LiP_2W_{17}O_{61}$, 18 H_2O (10 g) was dissolved in 100 mL of acetate buffer pH = 4.7, 0.5 M in lithium acetate AcOLi. The solution was not perfectly clear. Mn^{2+} (1.87 mL of a 1.6 M solution) was then added whilst stirring. The solution was filtered through an ashless pleated filter and left to settle. The clear part of the solution was collected and treated with KCl (10 g). The precipitate was filtered, washed with ethanol and diethyl ether and air-dried; recovered: 8.0 g; yield: 85%. $\alpha_1K_8P_2W_{17}MnO_{61}$, 15 H_2O (4819): calcd. K 6.51, P 1.29, Mn 1.14, W 65.09, H_2O 5.25; found K 6.53, P 1.24, Mn 1.13, W 64.01, H_2O 5.44.

$\alpha_1K_8P_2W_{17}CuO_{61}$, 19 H_2O: The synthesis is the same as that of the Zn^{2+} derivative; recovered: 7.5 g; yield: 75%. $\alpha_1K_8P_2W_{17}CuO_{61}$, 19 H_2O (4882): calcd. K 5.41, P 1.27, Cu 1.30, W 64.02, H_2O 6.64; found K 6.50, P 1.21, Cu 1.36, W 61.14, H_2O 6.65.

NMR, IR and UV/Vis Measurements: ^{31}P NMR spectra were recorded using a Bruker VM 250 apparatus operating at 101.2 MHz, in the Fourier transform mode. The ^{31}P chemical shifts were measured on 0.02 M solutions of the polyanions in aqueous 0.5 M LiCl (50% D_2O) solutions, and were referenced to external 85% H_3PO_4 by the substitution method. IR spectra were recorded with a Bio-Rad FTS 165 FTIR spectrophotometer. UV/Vis spectra were recorded with a Perkin−Elmer Lambda 19 spectrophotometer.

Electrochemical Experiments. Chemicals, Equipment and Apparatus: Pure water was used throughout. It was obtained by passing it through a Milli-RO_4 unit and subsequently through a Millipore Q water purification set. All the chemicals were of high-purity grade and were used as received. H_2SO_4 and Na_2SO_4 were commercial products (Prolabo). The pH = 3 electrolyte was usually made up of 0.2 M Na_2SO_4 + H_2SO_4, and will be abbreviated as Na_2SO_4/H^+ (pH = 3), except for the case where sodium is replaced by lithium, i.e. Li_2SO_4/H^+ (pH = 3). The pH = 5 medium was prepared with 0.4 M CH_3COONa + CH_3COOH and abbreviated CH_3COONa/

H^+ (pH = 5). The solutions were deaerated thoroughly for a least 30 min with pure argon and kept under a positive pressure of this gas during the experiments. The source, mounting and polishing of the glassy carbon (GC, Le Carbone Lorraine, France or Tokai, Japan) electrodes have been described.[3p] The glassy carbon samples had a diameter of 3 mm. The electrochemical set-up was an EG & G 273 A driven by a PC with the 270 software. The data were recorded using the computer, and then printed, when necessary to an HP DeskJet 560 C printer. Potentials are quoted against a saturated calomel electrode (SCE). The counter electrode was a platinum gauze of large surface area. Experiments were performed at laboratory temperature.

Acknowledgments

This work was supported by the CNRS (UMR 8000 and UMR 7071) and the Universities Paris XI and Paris VI. The help of B. Avisse is thankfully acknowledged. ***((AUTHOR: In future papers please quote also the last pages in the references!))***

[1] [1a] B. Keita, L. Nadjo, R. Contant, M. Fournier, G. Hervé, French Patent (CNRS) 89/1,728, February 10, **1989**. [1b] B. Keita, L. Nadjo, R. Contant, M. Fournier, G. Hervé, Eur. Patent (CNRS), Appl. EP 382,644; *Chem. Abstr.* **1991**, *114*, 191882u. [1c] B. Keita, A. Belhouari, L. Nadjo, R. Contant, *J. Electroanal. Chem.* **1995**, *181*, 243. [1d] J. E. Toth, F. C. Anson, *J. Am. Chem. Soc.* **1989**, *111*, 2444. [1e] J. E. Toth, F. C. Anson, *J. Electroanal. Chem.* **1989**, *256*, 361. [1f] J. E. Toth, J. D. Melton, D. Cabelli, B. H. J. Bielski, F. C. Anson, *Inorg. Chem.* **1990**, *29*, 1952. [1g] S. Dong, M. Liu, *J. Electroanal. Chem.* **1994**, *372*, 95. [1h] B. Keita, K. Essaadi, L. Nadjo, R. Contant, Y. Justum, *J. Electroanal. Chem.* **1996**, *404*, 271.

[2] B. Keita, L. Nadjo, *Mater. Chem. Phys.* **1989**, *22*, 77.

[3] [3a] B. Keita, L. Nadjo, *J. Electroanal. Chem. Interfacial Electrochem.* **1988**, *247*, 157. [3b] B. Keita, L. Nadjo, J. M. Saveant, *J. Electroanal. Chem. Interfacial Electrochem.* **1988**, *243*, 105. [3c] B. Keita, L. Nadjo, *J. Electroanal. Chem. Interfacial Electrochem.* **1988**, *243*, 87. [3d] B. Keita, L. Nadjo, *J. Electroanal. Chem. Interfacial Electrochem.* **1988**, *240*, 325. [3e] B. Keita, L. Nadjo, J. P. Haeussler, *J. Electroanal. Chem. Interfacial Electrochem.* **1987**, *230*, 85. [3f] B. Keita, L. Nadjo, *J. Electroanal. B. Chem.* **1987**, *227*, 265. [3g] Keita, L. Nadjo, *J. Electroanal. Chem. Interfacial Electrochem.* **1986**, *199*, 229. [3h] B. Keita, L. Nadjo, *J. Electroanal. Chem.* **1985**, *191*, 441. [3i] B. Keita, L. Nadjo, *J. Electroanal. Chem. Interfacial Electrochem.* **1987**, *230*, 267. [3j] B. Keita, L. Nadjo, *J. Electroanal. Chem. Interfacial Electrochem.* **1987**, *227*, 77. [3k] B. Keita, L. Nadjo, *J. Electroanal. Chem. Interfacial Electrochem.* **1987**, *219*, 355. [3l] B. Keita, L. Nadjo, *J. Electroanal. Chem. Interfacial Electrochem.* **1987**, *217*, 287. [3m] B. Keita, T. Lucas, L. Nadjo, *J. Electroanal. Chem. Interfacial Electrochem.* **1986**, *208*, 343. [3n] B. Keita, L. Nadjo, *Mater. Chem. Phys.* **1989**, *22*, 77. [3o] B. Keita, L. Nadjo, *Top. Curr. Electrochem.* **1993**, *2*, 77. [3p] B. Keita, K. Essaadi, L. Nadjo, *Electroanal. Chem. Interfacial Electrochem.* **1989**, *259*, 127.

[4] [4a] B. Keita, Y. W. Lu, L. Nadjo, R. Contant, M. Abbessi, J. Canny, M. Richet, *J. Electroanal. Chem. Interfacial Electrochem.* **1999**, *477*, 146. [4b] R. Contant, M. Abbessi, J. Canny, M. Richet, B. Keita, A. Belhouari, L. Nadjo, *Eur. J. Inorg. Chem.* **2000**, 567.

[5] [5a] R. Contant, *Inorg. Synth.* **1990**, *27*, 107. [5b] D. K. Lyon, W. K. Miller, T. Novet, P. J. Domaille, E. E. Evitt, D. C. Johnson, R. G. Finke, *J. Am. Chem. Soc.* **1991**, *113*, 7209. [5c] L. C. W. Baker, V. E. S. Baker, K. K. Eriks, M. T. Pope, M. Shibata, O. W. O. W. Rollins, J. H. Fang, L. L. Koh, *J. Am. Chem. Soc.* **1966**, *88*, 2329. [5d] F. Zonnevijlle, C. M. Tourné, G. F. Tourné, *Inorg. Chem.* **1982**, *21*, 2751. [5e] C. M. Tourné, G. F. Tourné, J. A. Malik, T. J. R. Weakly, *J. Inorg. Nucl. Chem.* **1970**, *32*, 3875. [5f] J. A. Malik, T. J. R. Weakley, *J. Chem. Soc. A* **1968**, 2647 [5g] C. Rong, M. T. Pope, *J. Am. Chem. Soc.* **1992**, *114*, 2932. [5h] C. Rong, F. C. Anson, *Inorg. Chem.* **1994**, *33*, 1064. [5i] T. McCormac, B. Fabre, G. Bidan, *J. Electroanal. Chem.* **1997**, *425*, 49. [5j] X. Zhang, M. T. Pope, M. R. Chance, G. B. Jameson, *Polyhedron* **1995**, *14*, 1381. [5k] J. P. Ciabrini, Thesis, Université Paris VI, **1982**. [5l] R. Contant, J. P. Ciabrini, *J. Chem. Res., Synop.* **1977**, 222; *J. Chem. Res., Miniprint* **1977**, 2601. [5m] R. Massart, R. Contant, J. P. Ciabrini, M. Fruchart, J-M. Fournier, *Inorg. Chem.* **1977**, *16*, 2916.

[6] [6a] R. Contant, M. Abbessi, J. Canny, A. Belhouari, B. Keita, L. Nadjo, *Inorg. Chem.* **1997**, *36*, 4961. [6b] B. Keita, A. Belhouari, L. Nadjo, R. Contant, *J. Electroanal. Chem.* **1998**, *442*, 49. [6c] B. Keita, F. Girard, L. Nadjo, R. Contant, J. Canny, M. Richet, *J. Electroanal. Chem.* **1999**, *478*, 76.

[7] [7a] J. Bartis, M. Dankova, J. J. Lessmann, Q. H. Luo, W. de W. Horrocks, Jr., L. C. Francesconi, *Inorg. Chem.* **1999**, *38*, 1042. [7b] R. Contant, J. P. Ciabrini, *J. Inorg. Nucl. Chem.* **1981**, *43*, 1525.

[8] [8a] B. Keita, Y. W. Lu, L. Nadjo, R. Contant, *Eur. J. Inorg. Chem.* **2000**, 2463. [8b] J. F. Kirby, L. C. W. Baker, *Inorg. Chem.* **1998**, *37*, 5537. [8c] V. A. Grigoriev, C. L. Hill, I. Weinstock, *J. Am. Chem. Soc.* **2000**, *122*, 3544. [8d] V. A. Grigoriev, D. Cheng, C. L. Hill, I. Weinstock, *J. Am. Chem. Soc.* **2001**, *123*, 5292.

[9] [9a] G. M. Varga, E. Papaconstantinou, M. T. Pope, *Inorg. Chem.* **1970**, *9*, 662. [9b] R. Acerete, S. Harmalker, C. F. Hammer, M. T. Pope, L. C. W. Baker, *J. Chem. Soc., Chem. Commun.* **1979**, 777. [9c] J. P. Ciabrini, R. Contant, J.-M. Fruchart, *Polyhedron* **1983**, *2*, 1229.

[10] T. L. Jorris, M. Kozik, N. Casan-Pastor, P. J. Domaille, R. G. Finke, W. K. Miller, L. C. Baker, *J. Am. Chem. Soc.* **1987**, *109*, 7402.

[11] [11a] C. Rocchiccioli-Deltcheff, R. Thouvenot, *Spectrosc. Lett.* **1979**, *12*, 127. [11b] R. Thouvenot, M. Fournier, R. Franck, C. Rocchiccioli-Deltcheff, *Inorg. Chem.* **1984**, *23*, 598.

[12] R. Contant, A. Teze, *Inorg. Chem.* **1985**, *24*, 4610.

[13] [13a] R. Contant, J. P. Ciabrini, *J. Chem. Res., Synop.* **1982**, 50−51; *J. Chem. Res., Miniprint* **1982**, 641. [13b] R. Contant, *J. Chem. Res., Synop.* **1984**, 120−121; *J. Chem. Res., Miniprint* **1984**, 1063.

[14] R. D. Shannon, *Acta Crystallogr., Sect. A* **1976**, *32*, 751.

Received February 21, 2002
[I02093]

Stereochemical Exploitation of the Chiral (+)-9-Phenyldeltacyclanyl Substituent in Diphosphanes and Their Ni, Pd and Pt Complexes[‡]

Henri Brunner,*[a] Stephan Dormeier,[a] and Manfred Zabel[a]

Dedicated to Professor Dr. Gottfried Huttner on the occasion of his 65th birthday

Keywords: Deltacyclenes / Chiral ligands / Phosphanes / Nickel / Palladium / Platinum

The (+)-9-phenyldeltacyclanyl moiety as a chiral phosphorus substituent contains eight configurationally fixed asymmetric carbon atoms. It is easily obtained from the reaction of norbornadiene and phenylacetylene via a Co-catalyzed enantioselective homo-Diels–Alder reaction, to give (+)-8-phenyldeltacyclene. In the reaction of (+)-8-phenyldeltacyclene with 1,2-$(H_2P)_2C_6H_4$ the trisubstitution product *P,P,P′*-tris[(+)-9-phenyldeltacyclan-8-yl)-1,2-bis(phosphanyl)benzene, **(+)$_\delta$-LH**, is obtained, in which a single P–H bond at the stereogenic phosphorus atom is left. **(+)$_\delta$-LH** crystallizes as a pure diastereomer, which isomerizes in solution with respect to the secondary phosphorus atom at –20 °C resulting in a 64:36 diastereomer mixture. Substitution of the P–H hydrogen atom in **(+)$_\delta$-LH** by benzyl, 3-bromobenzyl, 6-bromo-*n*-hexyl and 3-(diphenylphosphanyl)phenyl gave the bis(tertiary) diphosphanes **(+)$_\delta$-LR^1**–**(+)$_\delta$-LR^4**. $NiBr_2$, $PdHal_2$ (Hal = Cl, Br, I) and $PtHal_2$ (Hal = Cl, Br) complexes of **(+)$_\delta$-LH** and **(+)$_\delta$-LR^1**–**(+)$_\delta$-LR^4** have been synthesized. The complexes form two diastereomers differing in the configuration of the chiral P atom. X-ray structure analyses have been carried out with **(+)$_\delta$-LH**, **[(+)$_\delta$-LR^2]NiBr$_2$**, **[(+)$_\delta$-LH]PdI$_2$** and **[(+)$_\delta$-LCl]PdI$_2$**. Interestingly, for **[(+)$_\delta$-LH]PdI$_2$** both diastereomers are found in the same crystal lattice in a 1:1 ratio. In **[(+)$_\delta$-LH]PdI$_2$** and **[(+)$_\delta$-LCl]PdI$_2$** the configuration at the secondary phosphorus atom is stable in solution at room temperature, whereas in the free ligand **(+)$_\delta$-LH** it is configurationally labile.

(© Wiley-VCH Verlag GmbH, 69451 Weinheim, Germany, 2002)

Introduction

2,5-Norbornadiene undergoes thermal [2+2+2] homo-Diels−Alder reactions with acetylenes to give deltacyclenes, provided the acetylene carries strongly electron-withdrawing groups such as NO_2.[2] Non-reactive acetylenes form deltacyclenes with 2,5-norbornadiene only in the presence of transition metal catalysts, although other products may also be formed.[3] In 1978, a procedure was published to transform terminal acetylenes into deltacyclenes in high yield using a combination of $Co(acac)_3$, triphenylphosphane and a reducing agent.[4] This reaction was rendered chiral by replacing the achiral triphenylphosphane by optically active phosphanes.[5,6] Further investigations showed that the catalyst $Co(acac)_3$ together with norphos and the reducing agent Et_2AlCl in the solvent THF gave nearly enantiopure deltacyclenes.[7] (+)-8-Phenyldeltacyclene, used in the present work, can be prepared in this way from 2,5-norbornadiene and phenylacetylene in a reliable enantiomeric excess of *ee* > 97.5%. Subsequently, other catalytic systems, allowing the extension to substituted acetylenes, and other enantioselective studies have appeared.[8−15]

The double bond of (+)-8-phenyldeltacyclene enables further derivatization by addition reactions, e.g. of P−H bonds. Ph_2PH has been added to give a monodentate chiral phosphane.[13] The aim of the reaction of 1,2-bis(phosphanyl)benzene with a fourfold excess of (+)-8-phenyldeltacyclene was to synthesize a chelate ligand with four deltacyclanyl substituents at the two phosphorus atoms. However, the tetrasubstituted product, albeit detected in the mass spectrum, could not be obtained.[13] Obviously, the reaction of 1,2-$(H_2P)_2C_6H_4$ with (+)-8-phenyldeltacyclene stops after 3 P−H additions. Due to steric hindrance the fourth P−H bond does not add to another (+)-8-phenyldeltacyclene. The resulting trisubstitution product **(+)$_\delta$-LH** is a tertiary/secondary diphosphane open to further derivatization reactions at the chiral phosphorus atom. **(+)$_\delta$-LH** is the starting material for the studies described in the present and succeeding paper.[16]

[‡] Enantioselective Catalysis, 144. Part 143: Ref.[1]

[a] Institut für Anorganische Chemie, Universität Regensburg, 93040 Regensburg, Germany
Fax: (internat.) + 49-941/943-4439
E-mail: henri.brunner@chemie.uni-regensburg.de

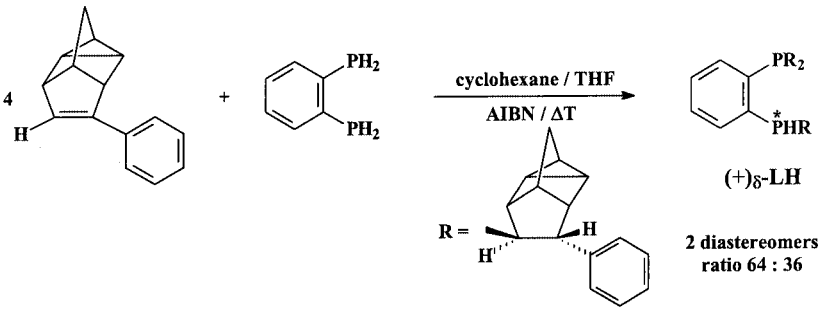

Scheme 1. Reaction of (+)-8-phenyldeltacyclene and 1,2-bis(phosphanyl)benzene to give *P,P,P′*-tris[(+)-9-phenyldeltacyclan-8-yl]-1,2-bis(phosphanyl)benzene, **(+)$_\delta$-LH**

Results and Discussion

P,P,P′-Tris[(+)-9-phenyldeltacyclan-8-yl]-1,2-bis(phosphanyl)benzene, (+)$_\delta$-LH

The tertiary/secondary diphosphane **(+)$_\delta$-LH** was obtained under radical conditions from (+)-8-phenyldeltacyclene and 1,2-bis(phosphanyl)benzene in boiling THF/cyclohexane in the presence of AIBN (Scheme 1).

After recrystallization from ethanol, **(+)$_\delta$-LH** was isolated as fine colorless needles in 45% yield. The ^{31}P NMR spectrum, in $CDCl_3$ at room temperature, showed that **(+)$_\delta$-LH** consists of two diastereomers with respect to the chiral P atom in a ratio of 64:36 (*de* = 28%). Interestingly, the needles obtained in the crystallization from ethanol contained only one of the two possible diastereomers of **(+)$_\delta$-LH**, as shown by low-temperature ^{31}P NMR spectroscopy (Figure 1). The cooled solution (−80 °C) of **(+)$_\delta$-LH** in [D_8]THF afforded only two doublets at δ = −15.0 and −29.9 ppm, the signals of the major isomer in the equilibrium mixture. The formation of the second diastereomer (δ = −10.8 and −31.7 ppm) was observed by warming up to temperatures around −20 °C. At room temperature the diastereomer ratio of 64:36 was obtained. The fast epimerization is in agreement with the known configurational lability of secondary phosphanes.[17−20]

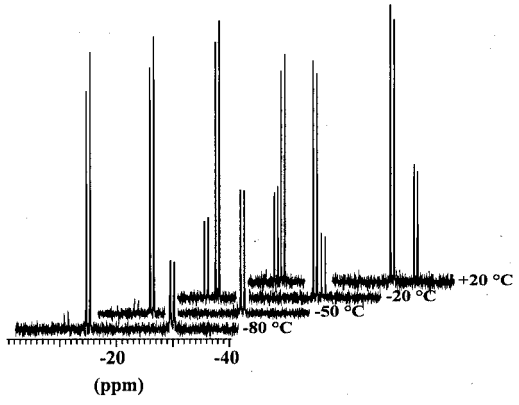

Figure 1. ^{31}P NMR spectrum of crystallized **(+)$_\delta$-LH** at −80 °C in [D_8]THF and equilibration of the diastereomers of **(+)$_\delta$-LH** on warming

A structural study performed with the needles of **(+)$_\delta$-LH** confirmed the presence of only one diastereomer (Figure 2). The phosphorus atom is *exo*-bonded to the 9-phenyldeltacyclan-8-yl substituent, pointing away from the deltacyclane cage, whereas the 9-phenyl group is *endo*-arranged beneath the deltacyclane cage. In principle, there are six alternatives to the addition of a P−H bond to (+)-8-phenyldeltacyclene.[13] However, in the structure of **(+)$_\delta$-LH** and the structures reported subsequently only one of them, 9-*exo*-P and 8-*endo*-Ph, is found, confirming former ^{1}H NMR assignments and calculations.[13] Note that in the P−H addition carbon atoms 8 and 9 of the deltacyclene skeleton change priorities. Thus, (+)-8-phenyldeltacyclene becomes the 9-phenyldeltacyclan-8-yl substituent. The symbol **(+)$_\delta$** in the ligand **(+)$_\delta$-LH** (and in its complexes) indicates that the 9-phenyldeltacyclan-8-yl substituents derived from (+)-8-phenyldeltacyclane are formed in a highly enantioselective homo-Diels−Alder reaction. The configuration of the chiral phosphorus atom could not be determined since the hydrogen atom at the secondary phosphorus atom was not localized in the X-ray structure analysis. As it is also labile in solution at room temperature, no configura-

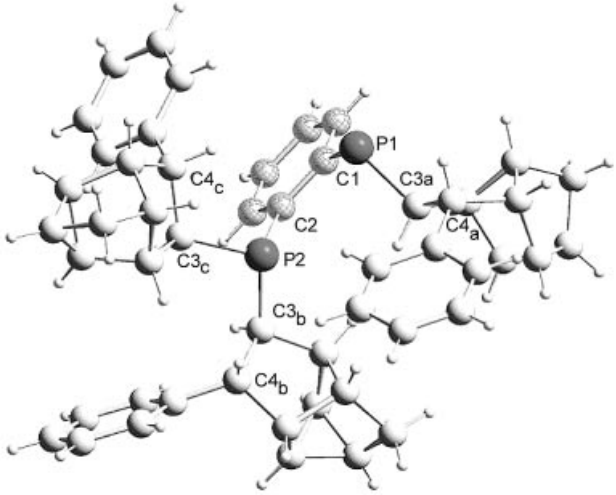

Figure 2. Molecular structure of **(+)$_\delta$-LH**, crystallized from ethanol; selected bond lengths [Å] and angles [°]: P1···P2 3.197(6), P1−C1 1.827(5), P2−C2 1.847(4), P1−$C3_a$ 1.853(5), P2−$C3_b$ 1.858(4), P2−$C3_c$ 1.842(3); C1−P1−$C3_a$ 102.01(16), C2−P2−$C3_b$ 100.14(19), C2−P2−$C3_c$ 98.85(18), $C3_b$−P2−$C3_c$ 102.80(14)

tional symbol for the secondary phosphorus atom in the ligand **(+)$_\delta$-LH** is used. However, in the complexes of **(+)$_\delta$-LH** the configuration of the secondary phosphorus atom is stabilized. Therefore, it is added for all the compounds that could be characterized by X-ray crystallography. The torsion angle P2−C2−C1−P1 of 2.41(44)° shows that the chelate ligand **(+)$_\delta$-LH** is nearly planar.

The synthesis of chiral building blocks frequently starts from amino acids and carbohydrates of the natural pool. Due to its easy accessibility from norbornadiene and phenylacetylene, (+)-8-phenyldeltacyclene is a promising artificial chiral building block. It contains six chiral carbon atoms, which are stereospecifically built up in the deltacyclene formation. After P−H addition to the double bond of (+)-8-phenyldeltacyclene, the number of asymmetric carbon atoms increases to eight in the (+)-9-phenyldeltacyclan-8-yl substituent. The trisubstitution product **(+)$_\delta$-LH** comprises 24 chiral centers (8 × 3) in the three deltacyclanyl substituents. The 25th stereogenic center in **(+)$_\delta$-LH** is the secondary phosphorus atom. In the present paper, **(+)$_\delta$-LH** is exploited for the synthesis of unsymmetrical bis(tertiary) phosphanes and mononuclear complexes with transition metal halides.[16] Di- and trinuclear complexes of **(+)$_\delta$-LH** will be described in the succeeding paper.

The Unsymmetrical Bis(tertiary) Diphosphanes (+)$_\delta$-LR^1 to (+)$_\delta$-LR^4

As the P−H bond of the trisubstitution product **(+)$_\delta$-LH** did not add to another (+)-8-phenyldeltacyclene due to steric reasons, sterically less demanding groups, to be used as the fourth substituent, were taken into consideration. Deprotonation of the P−H bond and reaction with the bromo derivative of the desired substituent seemed to be a suitable methodology.[12−14] Deprotonation of **(+)$_\delta$-LH** with *n*BuLi provides an achiral phosphide anion. Therefore, the diastereomeric excess obtained in consecutive reactions is independent of the diastereomer ratio of the secondary phosphane **(+)$_\delta$-LH**. However, the new phosphorus configuration will be influenced by the chirality of the 24 asymmetric centers of the three deltacyclane substituents.

Benzyl bromide is a reactive bromo derivative having only one coupling site. Treatment of a THF solution of **(+)$_\delta$-LH** with *n*BuLi at −78 °C followed by addition of benzyl bromide afforded the bis(tertiary) diphosphane **(+)$_\delta$-LR^1** in nearly 40% yield (Scheme 2). The ^{31}P NMR spectrum of **(+)$_\delta$-LR^1** in $CDCl_3$ displayed an AB system for each of the two diastereomers, the diastereomer ratio being 93:7 (*de* = 86%). Ligand **(+)$_\delta$-LR^2** is formed in 42% yield with a diastereomeric excess of *de* = 72% by using 1-bromo-3-(bromomethyl)benzene, which has an extra less reactive bromo substituent in the *meta* position of the benzyl group (Scheme 2). The best diastereomeric excess (*de* = 90%) was achieved with 1,6-dibromohexane. Ligand **(+)$_\delta$-LR^3** was isolated in 45% yield (Scheme 2). Formation of the disubstituted product was not observed.[16]

Halogen/metal exchange in **(+)$_\delta$-LR^2** with *n*BuLi, followed by reaction with chlorodiphenylphosphane, provided **(+)$_\delta$-LR^4** as a diastereomeric mixture with *de* = 56%

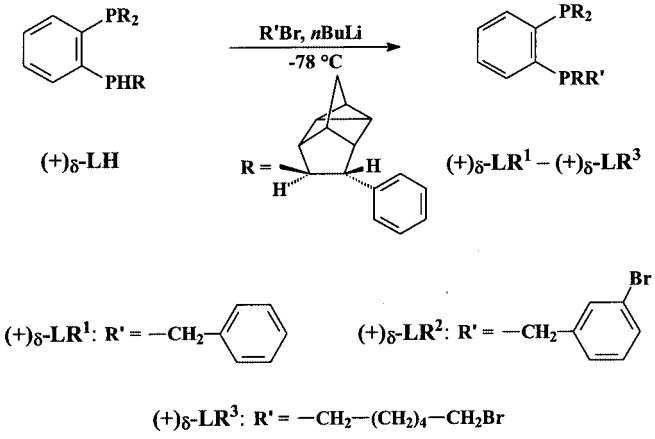

Scheme 2. Formation of the unsymmetrical bis(tertiary) diphosphanes **(+)$_\delta$-LR^1** to **(+)$_\delta$-LR^3**

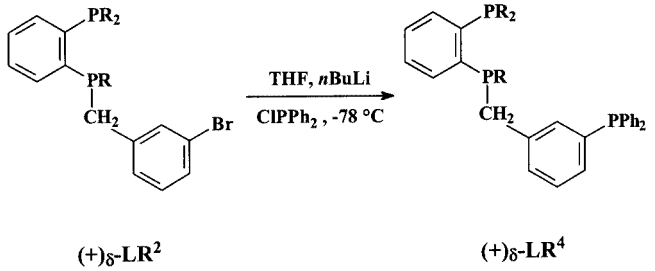

Scheme 3. Synthesis of **(+)$_\delta$-LR^4**

(Scheme 3). In addition to the signals of the AB system of the chelating unit, the ^{31}P NMR spectrum of **(+)$_\delta$-LR^4** showed singlets at δ = −4.73 and −5.09 ppm belonging to the phosphorus atoms of the PPh_2 group of the two diastereomers.

The $NiBr_2$ Complexes of the Diphosphanes (+)$_\delta$-LH and (+)$_\delta$-LR^1 to (+)$_\delta$-LR^3

Reaction of anhydrous $NiBr_2$ with **(+)$_\delta$-LH** in boiling ethanol provided the expected square-planar mononuclear dibromo(diphosphane)nickel(II) complex **[(+)$_\delta$-LH]$NiBr_2$** (Scheme 4). Crystallization of **[(+)$_\delta$-LH]$NiBr_2$** from a mixture of acetone, CH_2Cl_2, toluene and pentane gave fine red needles, which were amorphous in the X-ray structure analysis. The ^{31}P NMR spectrum showed two AB systems (δ = 72.34/43.27 and 74.70/49.76 ppm) resulting from the two diastereomers differing in the configuration of the secondary phosphorus atom in a ratio of 84:16. The splitting of the PHR signals at δ = 43.27 ppm (400.5 Hz) and δ = 49.76 ppm (408.2 Hz) in the proton-coupled ^{31}P NMR spectrum clearly proves that the hydrogen atom is still bonded to the secondary phosphorus atom. The tendency of **[(+)$_\delta$-LH]$NiBr_2$** to HBr elimination and the formation of dinuclear complexes will be discussed in the succeeding paper.

In the reaction of anhydrous $NiBr_2$ with the bis(tertiary) diphosphanes **(+)$_\delta$-LR^1** to **(+)$_\delta$-LR^3** mononuclear complexes are expected and found (Scheme 4). The ^{31}P NMR spectrum of **[(+)$_\delta$-LR^1]$NiBr_2$** showed two AB systems (δ =

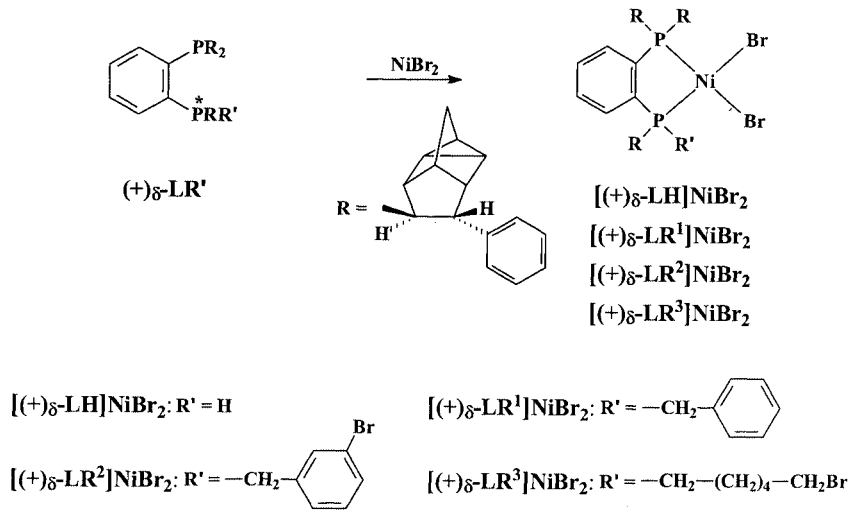

Scheme 4. Synthesis of the dibromonickel(II)-diphosphane complexes **[(+)$_\delta$-LH]NiBr$_2$**, **[(+)$_\delta$-LR^1]NiBr$_2$**, **[(+)$_\delta$-LR^2]NiBr$_2$** and **[(+)$_\delta$-LR^3]NiBr$_2$**

82.37/66.39 and 74.99/72.13 ppm, ratio 8:92) caused by the two possible diastereomers in a ratio which is similar to that of the free ligand **(+)$_\delta$-LR^1**. Compared to the ^{31}P NMR spectrum of **(+)$_\delta$-LR^1** the signals of the diamagnetic square-planar complex **[(+)$_\delta$-LR^1]NiBr$_2$** are shifted to higher ppm (coordination shift).

Using ligand **(+)$_\delta$-LR^2**, the corresponding mononuclear dibromonickel(II) complex **[(+)$_\delta$-LR^2]NiBr$_2$** could also be isolated as a mixture of two diastereomers. Evaluation of the ^{31}P NMR spectrum of **[(+)$_\delta$-LR^2]NiBr$_2$** provided two AB systems (δ = 82.79/67.02 and 74.77/72.57 ppm) with a 16:84 ratio of the two diastereomeric forms. From a mixture of CH_2Cl_2 and ethanol, fine orange plates of **[(+)$_\delta$-LR^2]NiBr$_2$**, suitable for X-ray structure analysis, were obtained.

The structural study confirmed the mononuclear character of the complex (Figure 3) and proved the presence of only one of the two possible diastereomeric forms. The configuration of the chiral phosphorus atom was determined as (*R*). The ^{31}P NMR spectrum of a solution of these crystals showed that only one diastereomer was present, indicating configurational stability of the chiral phosphorus atom in the complex, whereas the free ligand **(+)$_\delta$-LH** already isomerized at −20 °C. The diastereomer in the isolated crystals corresponded to the major diastereomer formed in the synthesis described above. The dihedral angles P1−C1−C2−P2 [2.66(60)°] and P1−P2−Br2−Br1 [2.82(4)°] showed that in **[(+)$_\delta$-LR^2]NiBr$_2$** the chelate ring and the nickel square were only slightly deformed. In the crystal of **[(+)$_\delta$-LR^2]NiBr$_2$** the bromobenzyl substituent was disordered. The conformation shown in Figure 3 had 92.3% probability. In the conformation with 7.7% probability, the benzyl substituent was rotated by 180° with respect to the C5−C$_{ipso}$ bond.

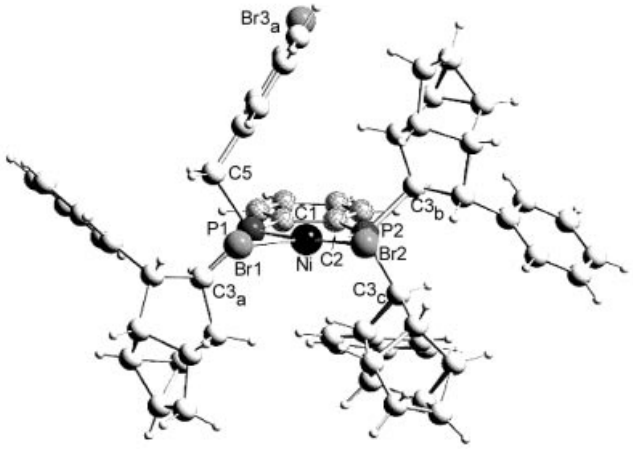

Figure 3. Molecular structure of **[(+)$_\delta$-LR^2]NiBr$_2$**, crystallized from CH_2Cl_2/ethanol; selected bond lengths [Å] and angles [°]: Ni−Br1 2.342(1), Ni−Br2 2.334(2), Ni−P1 2.151(2), Ni−P2 2.172(2), P1−C1 1.817(6), P2−C2 1.841(6), P1−C3$_a$ 1.858(7), P1−C5 1.839(7), P2−C3$_b$ 1.844(7), P2−C3$_c$ 1.842(7); C1−P1−C3$_a$ 103.20(23), C1−P1−C5 102.24(29), C5−P1−C3$_a$ 101.66(29), C3$_b$−P2−C3$_c$ 104.95(28), C2−P2−C3$_b$ 100.52(22), C2−P2−C3$_c$ 100.61(26), P1−Ni−Br1 86.13(5), P1−Ni−P2 89.24(6), P2−Ni−Br2 92.21(4), Br2−Ni−Br1 92.44(3)

In the complex **[(+)$_\delta$-LR^3]NiBr$_2$**, the ligand of which carried an aliphatic chain as the fourth substituent, there were two diastereomers (^{31}P NMR: δ = 78.14/68.92 (minor) and 73.82/71.85 ppm (major), ratio 4:96).

Palladium and Platinum Complexes of the Secondary Diphosphane (+)$_\delta$-LH

The first products of the reaction of **(+)$_\delta$-LH** with palladium and platinum dihalides were the corresponding mononuclear square-planar complexes (Scheme 5). Their

HHal elimination to afford di- and trinuclear complexes will be discussed in the succeeding paper.

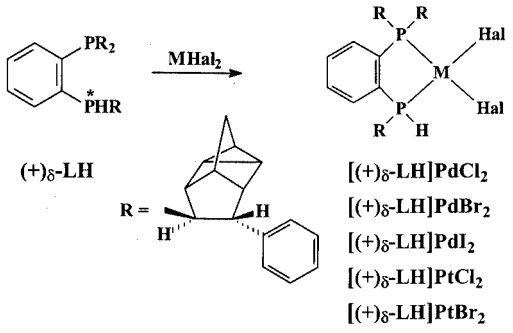

Scheme 5. Preparation of palladium and platinum dihalide complexes of **(+)$_\delta$-LH**

The diastereomeric excess in the preparation of **[(+)$_\delta$-LH]PdCl$_2$** depended on the reactants and the reaction conditions. Heating of **(+)$_\delta$-LH** and $PdCl_2$ in toluene in the presence of a small amount of concentrated HCl provided **[(+)$_\delta$-LH]PdCl$_2$**, the ^{31}P NMR spectrum of which showed two diastereomers in a ratio of 55:45. Using Na_2PdCl_4 in boiling ethanol, the diastereomer present in excess (δ = 76.75/41.10 ppm) was enriched to *de* = 84% (minor diastereomer: δ = 74.83/38.82 ppm). If the reaction was started in THF at −78 °C with $(PhCN)_2PdCl_2$ and diastereomerically pure **(+)$_\delta$-LH** as the starting material, the ^{31}P NMR spectrum of the product also showed the signals of the two diastereomers. However, in this case the diastereomer, which was the minor before, dominated with a ratio of 91:9. In **[(+)$_\delta$-LH]PdCl$_2$** the P−P couplings were typical for (diphosphane)palladium chelate complexes ($^2J_{PP}$ = 9.0 and 11.8 Hz), the P−H couplings were 405 and 410 Hz.

The syntheses of **[(+)$_\delta$-LH]PdBr$_2$** was succeeded by stirring a suspension of $PdBr_2$ and **(+)$_\delta$-LH** in CH_2Cl_2 for 4 d. The ^{31}P NMR spectrum of **[(+)$_\delta$-LH]PdBr$_2$** showed two isomers (major: δ = 79.10/43.96; minor: δ = 76.52/39.45 ppm; ratio 55:45). For **[(+)$_\delta$-LH]PdBr$_2$** the P−P couplings (14.5 and 17.6 Hz) and the P−H couplings (409 and 414 Hz) were larger than for **[(+)$_\delta$-LH]PdCl$_2$**.

A suspension of **(+)$_\delta$-LH** and PdI_2 was refluxed in benzene. After 4 h, all the PdI_2 had reacted and a dark red powder was isolated in nearly quantitative yield. The ^{31}P NMR spectrum of **[(+)$_\delta$-LH]PdI$_2$** showed two diastereomers, δ = 80.09/45.29 and 75.77/38.02 ppm in a ratio of 58:42 with P−P couplings (13.5 and 16.5 Hz) and P−H couplings (407 and 405 Hz). After putting a layer of methanol over a solution of **[(+)$_\delta$-LH]PdI$_2$** in CH_2Cl_2, red crystals of X-ray quality were obtained (Figure 4).

In the structural study the hydrogen atoms of the secondary phosphorus atoms could be localized. To our surprise from a solution of the two diastereomers of **[(+)$_\delta$-LH]PdI$_2$**, differing in the configuration at the secondary phosphorus atom in the ratio 58:42, single crystals could be obtained which contained both diastereomers exactly in a 1:1 ratio. This is extremely unusual, because normally each diastereomer crystallizes in its own lattice. In the case of **[(+)$_\delta$-LH]PdI$_2$** the (S_P) diastereomer and the (R_P) diastereomer

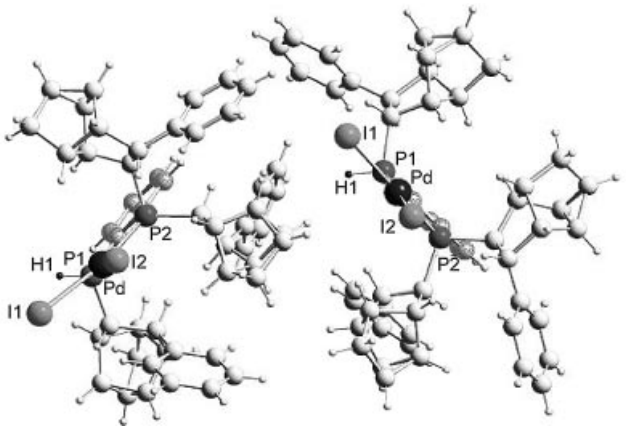

Figure 4. Molecular structures of the two diastereomers of **[(+)$_\delta$-LH]PdI$_2$**, crystallized from CH_2Cl_2/methanol; (R_P) diastereomer on the right, (S_P) diastereomer on the left; selected bond lengths [Å] and angles [°] of the (S_P) diastereomer of **[(+)$_\delta$-LH]PdI$_2$**: Pd−I1 2.659(1), Pd−I2 2.646(1), Pd−P1 2.244(1), Pd−P2 2.269(2), P1−C1 1.818(5), P2−C2 1.835(5), P1−C3$_a$ 1.842(3), P1−H1 1.219(47), P2−C3$_b$ 1.842(6), P2−C3$_c$ 1.844(3); H1−P1−C3$_a$ 99.87(202), C1−P1−C3$_a$ 112.15(15), C1−P1−H1 105.52(234), C3$_c$−P2−C3$_b$ 104.89(15), C2−P2−C3$_c$ 99.57(15), C2−P2−C3$_b$ 101.26(16), P1−Pd−P2 86.15(3), P2−Pd−I2 95.73(3), I2−Pd−I1 90.66(1), I1−Pd−P1 87.47(2)

formed a pair that was repeated in the lattice (Figure 4), a rare case of molecular recognition and supramolecular chemistry.[21] The ^{31}P NMR spectrum of the solution of the crystals showed the two diastereomers in a 50:50 ratio. Thus, the configuration at the secondary P atoms in the diastereomeric complexes was stable. In this specific case diastereomer enrichment on crystallization did not occur in the crystals but in the supernatant mother liquor. Whereas in **[(+)$_\delta$-LH]PdCl$_2$** the palladium square was only slightly deformed [dihedral angle P1−P2−I2−I1 1.28(2)°], the chelate ring was appreciably puckered [dihedral angle P1−C1−C2−P2 11.11(41)°].

In addition to the signals of **[(+)$_\delta$-LH]PdI$_2$** the ^{31}P NMR spectrum of the reaction mixture of PdI_2 and **(+)$_\delta$-LH** in CH_2Cl_2 exhibited many signals of other compounds. Within 12 h dark red crystals of **[(+)$_\delta$-LCl]PdI$_2$** of X-ray quality crystallized from a CH_2Cl_2/Et_2O solution. The X-ray structure analysis of **[(+)$_\delta$-LCl]PdI$_2$** (Figure 5) showed that the hydrogen atom, bonded to the secondary phosphorus atom in the ligand **(+)$_\delta$-LH**, had been replaced by a chlorine atom which must have come from the solvent CH_2Cl_2. The configuration of the chiral phosphorus atom was determined as (*S*). The ^{31}P NMR spectrum of the dissolved crystals exhibited only signals of one diastereomer at δ = 123.29 and 68.87 ppm. With the torsion angle P1−C1−C2−P2 [4.15(89)°] there was a slight puckering of the chelate ring. On the other hand the square-planar arrangement of the four atoms bonded to the palladium atom in **[(+)$_\delta$-LCl]PdI$_2$** was heavily distorted [dihedral angle P1−P2−I2−I1 13.78(5)°].

To synthesize the mononuclear platinum complex **[(+)$_\delta$-LH]PtCl$_2$**, K_2PtCl_4 was dissolved in a small amount of concentrated HCl. The dark brown solution was diluted with ethanol and heated to reflux. After dropwise addition of a

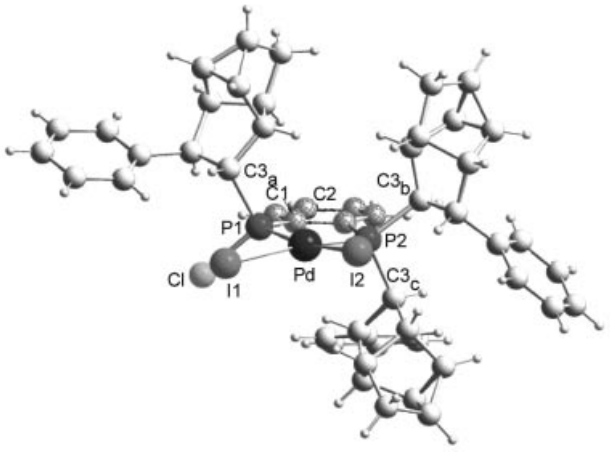

Figure 5. Molecular structure of **[(+)$_\delta$-LC]$_2$PdI$_2$**, crystallized from CH_2Cl_2/methanol; selected bond lengths [Å] and angles [°]: Pd−I1 2.647(2), Pd−I2 2.653(2), Pd−P1 2.228(2), Pd−P2 2.275(3), I1···Cl 3.901(4), P1−C1 1.818(10), P2−C2 1.836(9), P1−$C3_a$ 1.815(8), P1−Cl 2.231(14), P2−$C3_b$ 1.838(13), P2−$C3_c$ 1.828(8); Cl−P1−$C3_a$ 103.70(29), C1−P1−$C3_a$ 110.10(38), C1−P1−Cl 100.16(28), $C3_c$−P2−$C3_b$ 103.79(37), C2−P2−$C3_c$ 102.67(37), C2−P2−$C3_b$ 101.46(38), P1−Pd−P2 85.84(8), P2−Pd−I2 97.66(6), I2−Pd−I1 90.07(2), I1−Pd−P1 88.19(6)

toluene solution of **(+)$_\delta$-LH**, the complex **[(+)$_\delta$-LH]PtCl$_2$** could be isolated. The ^{31}P NMR spectrum of **[(+)$_\delta$-LH]PtCl$_2$** showed the signals of two different isomers. The diastereomer present in excess (δ = 48.67/15.90 ppm) was enriched to 80% (minor diastereomer: δ = 47.20/15.23 ppm). The P−P couplings (2.5 and 3.1 Hz) were much smaller for **[(+)$_\delta$-LH]PtCl$_2$** than for **[(+)$_\delta$-LH]PdCl$_2$**. In addition to P−H couplings (414 and 416 Hz) Pt−P couplings were observed (3508 and 3531 Hz), typical for mononuclear (diphosphane)platinum complexes.

The corresponding platinum bromide complex **[(+)$_\delta$-LH]PtBr$_2$** was obtained from Pt(cod)Br$_2$ and **(+)$_\delta$-LH** in benzene at room temperature. The ^{31}P NMR spectrum showed two diastereomers, the major diastereomer (δ = 49.77/18.19 ppm) being enriched to nearly 70% (minor diastereomer: δ = 51.81/21.49 ppm). The P−P couplings were smaller (2.2/2.4) and the P−H couplings larger (417/419) than those of the platinum chloride complex **[(+)$_\delta$-LH]PtCl$_2$** with the Pt−P couplings (3322/3504) in the expected range.

Experimental Section

General Remarks: All reactions were performed under dry nitrogen using standard Schlenk techniques. Solvents were purified and dried by standard procedures. (+)-8-Phenyldeltacyclene[7] and 1,2-bis(phosphanyl)benzene[22−24] were prepared as described in the literature. Mass spectra: Finnigan Mat 95 for field desorption (FD) and fast atom bombardment (FAB), Thermo Quest TSQ 7000 for electron spray injection (ESI), M^+ = the most intense peak of the isotope cluster of M. ^{1}H NMR spectra: Bruker ARX 400 spectrometer (400 MHz). ^{31}P NMR spectra: Bruker ARX 400 spectrometer (162 MHz). Melting points: Büchi SMP 20. Elemental analyses: Heraeus Elementar Vario EL III.

***P,P,P′*-Tris[(+)-9-phenyldeltacyclan-8-yl]-1,2-bis(phosphanyl)-benzene, (+)$_\delta$-LH:** To the boiling solution of (+)-8-phenyldeltacyclene (4.90 g, 25.0 mmol) in 20 mL of cyclohexane, 1,2-bis(phosphanyl)benzene (1.00 g, 7.0 mmol), AIBN (0.16 g, 1.0 mmol) in 20 mL of cyclohexane and 20 mL of THF was added dropwise. After heating for 16 h, the solvents were evaporated and the residue was suspended in 50 mL of pentane. The mixture was cooled to −20 °C for 1 h. Filtration gave the crude product. Recrystallization from hot ethanol provided **(+)$_\delta$-LH** (3.05 g) as thin colorless needles in 45% yield, m.p. 105−110 °C. Crystals of **(+)$_\delta$-LH**·0.75C_2H_5OH (colorless needles) were obtained from ethanol at −40 °C. $[\alpha]_D^{20}$ = +85 (*c* = 1; CH_2Cl_2). ^{1}H NMR ($CDCl_3$): δ = 3.76−0.39 (m, 30 H, aliph. H), 4.27 (m, $^1J_{PH}$ = 213.8 Hz, 1 H, PH), 7.63−6.43 (m, 19 H, arom. H) ppm. ^{31}P NMR ($CDCl_3$): δ = −11.3 (d, $^3J_{PP}$ = 116.8 Hz, 36% PR_2), −12.3 (d, $^3J_{PP}$ = 105.9 Hz, 64% PR_2), −32.3 (d, $^3J_{PP}$ = 105.9, $^1J_{PH}$ = 213.8 Hz, 64% PHR), −38.8 (d, $^3J_{PP}$ = 116.8, $^1J_{PH}$ = 213.8 Hz, 36% PHR) ppm. MS-FD (CH_2Cl_2): *m*/*z* = 724.3 [M^+]. $C_{51}H_{50}P_2$ (724.9): calcd. C 84.50, H 6.95; found C 84.19, H 7.25.

Preparation of the Tertiary Diphosphanes (+)$_\delta$-LR^1 to (+)$_\delta$-LR^3: A solution of **(+)$_\delta$-LH** in abs. THF (20 mL) was treated with a small excess of a 1.6 M solution of *n*BuLi in *n*-hexane. After stirring at room temperature for 1 h, the deep red solution was cooled to −78 °C. The appropriate bromo compound [1 equiv. relative to **(+)$_\delta$-LH**] was then dissolved in THF (5 mL) and added dropwise to the solution of the deprotonated phosphane. The solution was allowed to warm up to room temperature and stirred for 16 h. Removal of the solvent and purification by crystallization or chromatography provided the pure product.

***P′*-Benzyl-*P,P,P′*-tris[(+)-9-phenyldeltacyclan-8-yl]-1,2-bis(phosphanyl)benzene, (+)$_\delta$-LR^1: (+)$_\delta$-LH** (1.30 g, 1.7 mmol) was treated with *n*BuLi (1.26 mL, 1.8 mmol, 1.6 M solution in hexane) and (bromomethyl)benzene (0.30 g, 1.7 mmol) as described above. Recrystallization from petroleum ether/toluene provided **(+)$_\delta$-LR^1** (0.53 g) as a colorless powder in 38% yield, m.p. 129−132 °C. ^{1}H NMR ($CDCl_3$): δ = 4.07−0.34 (m, 32 H, aliph. H), 7.54−5.95 (m, 24 H, arom. H) ppm. ^{31}P NMR ($CDCl_3$): δ = −12.65 (d, $^3J_{PP}$ = 178.1 Hz, 7% PR_2), −13.37 (d, $^3J_{PP}$ = 170.0 Hz, 93% PR_2), −16.56 (d, $^3J_{PP}$ = 170.0 Hz, 93% PRR′), −19.93 (d, $^3J_{PP}$ = 178.1 Hz, 7% PRR′) ppm. MS-FD (CH_2Cl_2): *m*/*z* = 814.1 [M^+]. $C_{58}H_{56}P_2$ (815.0): calcd. C 85.47, H 6.93; found C 84.73, H 7.67.

***P′*-(3-Bromobenzyl)-*P,P,P′*-tris[(+)-9-phenyldeltacyclan-8-yl]-1,2-bis(phosphanyl)benzene, (+)$_\delta$-LR^2: (+)$_\delta$-LH** (3.30 g, 4.6 mmol) was treated with *n*BuLi (3.55 mL, 5.1 mmol, 1.6 M solution in hexane) and 1-bromo-3-(bromomethyl)benzene (1.17 g, 4.6 mmol). Recrystallization from petroleum ether/toluene provided **(+)$_\delta$-LR^2** (1.63 g) as a colorless powder in 42% yield, m.p. 121−127 °C. ^{1}H NMR ($CDCl_3$): δ = 3.67−0.43 (m, 32 H, aliph. H), 7.54−5.95 (m, 23 H, arom. H) ppm. ^{31}P NMR ($CDCl_3$): δ = −12.59 (d, $^3J_{PP}$ = 179.8 Hz, 14% PR_2), −12.89 (d, $^3J_{PP}$ = 167.5 Hz, 86% PR_2), −16.21 (d, $^3J_{PP}$ = 167.5 Hz, 86% PRR′), −19.48 (d, $^3J_{PP}$ = 179.8 Hz, 14% PRR′) ppm. MS-FD (CH_2Cl_2): *m*/*z* = 892.3 [M^+]. $C_{58}H_{55}BrP_2$ (893.9): calcd. C 77.93, H 6.20; found C 77.88, H 6.80.

***P′*-(6-Bromohexyl)-*P,P,P′*-tris[(+)-9-phenyldeltacyclan-8-yl]-1,2-bis(phosphanyl)benzene, (+)$_\delta$-LR^3: (+)$_\delta$-LH** (1.70 g, 2.3 mmol) was treated with *n*BuLi (1.7 mL, 2.4 mmol, 1.6 M solution in hexane) and 1,6-dibromohexane (0.53 g, 2.3 mmol). Chromatography with petroleum ether/toluene provided **(+)$_\delta$-LR^3** (0.90 g) as a colorless powder in 45% yield, m.p. 205−210 °C. ^{1}H NMR ($CDCl_3$): δ = 3.72−0.38 (m, 42 H, aliphat. H), 7.46−6.47 (m, 19 H, arom. H) ppm. ^{31}P NMR ($CDCl_3$): δ = −12.90 (d, $^3J_{PP}$ = 164.5 Hz, 5%

PR_2), −15.00 (d, $^3J_{PP}$ = 158.6 Hz, 95% PR_2), −22.57 (d, $^3J_{PP}$ = 158.6 Hz, 95% PRR′), −25.80 (d, $^3J_{PP}$ = 164.5 Hz, 5% PRR′) ppm. MS-FD (CH_2Cl_2): *m/z* = 887.3 [M^+]. $C_{57}H_{61}BrP_2$ (888.0): calcd. C 77.10, H 6.92; found C 77.15, H 6.91.

***P′*-[3-(Diphenylphosphanyl)benzyl]-*P,P,P′*-tris[(+)-9-phenyldeltacyclan-8-yl]-1,2-bis(phosphanyl)benzene, $(+)_\delta$-LR⁴: $(+)_\delta$-LR²** (0.22 g, 0.25 mmol) was treated with *n*BuLi (1.8 mL, 2.6 mmol, 1.6 M solution in hexane) and chlorodiphenylphosphane (0.06 g, 0.25 mmol). Recrystallization from ethanol provided **$(+)_\delta$-LR⁴** (0.15 g) as a fine colorless powder in 42% yield, m.p. 110−113 °C. ^{1}H NMR ($CDCl_3$): δ = 4.63−0.37 (m, 32 H, aliph. H), 7.85−5.59 (m, 33 H, arom. H) ppm. ^{31}P NMR ($CDCl_3$): δ = −4.73 (s, 22% PPh_2), −5.09 (s, 78% PPh_2), −12.65 (d, $^3J_{PP}$ = 171.8 Hz, 22% PR_2), −12.90 (d, $^3J_{PP}$ = 168.5 Hz, 78% PR_2), −16.56 (d, $^3J_{PP}$ = 168.5 Hz, 78% PRR′), −19.48 (d, $^3J_{PP}$ = 171.8 Hz, 22% PRR′) ppm. MS-FD (CH_2Cl_2): *m/z* = 998.6 [M^+]. $C_{70}H_{65}P_3$ (999.2): calcd. C 84.14, H 6.56; found C 83.31, H 6.95.

Dibromo{*P,P,P′*-tris[(+)-9-phenyldeltacyclan-8-yl]-1,2-bisphosphanylbenzene}nickel(II), $[(+)_\delta$-LH]$NiBr_2$: A suspension of **$(+)_\delta$-LH** (0.15 g, 0.21 mmol) and anhydrous $NiBr_2$ (0.05 g, 0.21 mmol) was heated in ethanol (20 mL). After cooling to room temperature, the red solution was filtered through silica gel and the solvents were evaporated to provide **$[(+)_\delta$-LH]$NiBr_2$** (0.16 g) as a dark red powder in 83% yield, m.p. 153−155 °C. ^{1}H NMR ($CDCl_3$): δ = 3.54−0.64 (m, 30 H, aliph. H), 7.72−6.34 (m, 19 H, arom. H) ppm. ^{31}P NMR ($CDCl_3$): δ = 43.27 (d, $^2J_{PP}$ = 50.9, $^1J_{PH}$ = 400.5 Hz, 84% PHR), 49.76 (d, $^2J_{PP}$ = 51.5, $^1J_{PH}$ = 408.2 Hz, 16% PHR), 72.34 (d, $^2J_{PP}$ = 50.9 Hz, 84% PR_2), 74.70 (d, $^2J_{PP}$ = 51.5 Hz, 16% PR_2) ppm. MS-FAB (CH_2Cl_2): *m/z* = 942.3 [M^+]. $C_{51}H_{50}Br_2NiP_2$ (943.4): calcd. C 64.93, H 5.34; found C 64.72, H 5.61.

{*P′*-Benzyl-*P,P,P′*-tris[(+)-9-phenyldeltacyclan-8-yl]-1,2-bisphosphanylbenzene}dibromonickel(II), $[(+)_\delta$-LR¹]$NiBr_2$: A suspension of **$(+)_\delta$-LR¹** (0.17 g, 0.21 mmol) and anhydrous $NiBr_2$ (0.05 g, 0.21 mmol) was heated in ethanol (20 mL). After cooling to room temperature, the red solution was filtered through silica gel and the solvents were evaporated to provide **$[(+)_\delta$-LR¹]$NiBr_2$** (0.21 g) as a red powder in 97% yield, m.p. 170−172 °C. ^{1}H NMR ($CDCl_3$): δ = 3.34−0.12 (m, 32 H, aliph.-H), 7.84−6.23 (m, 24 H, arom.-H) ppm. ^{31}P NMR ($CDCl_3$): δ = 66.39 (d, $^2J_{PP}$ = 50.2 Hz, 8% PRR′), 72.13 (d, $^2J_{PP}$ = 48.3 Hz, 92% PRR′), 74.99 (d, $^2J_{PP}$ = 48.3 Hz, 92% PR_2), 82.37 (d, $^2J_{PP}$ = 50.2 Hz, 8% PR_2) ppm. MS-FD (CH_2Cl_2): *m/z* = 1032.3 [M^+]. $C_{58}H_{56}Br_2NiP_2$ (1033.5): calcd. C 67.40, H 5.46; found C 67.96, H 6.98.

Dibromo{*P′*-(3-bromobenzyl)-*P,P,P′*-tris[(+)-9-phenyldeltacyclan-8-yl]-1,2-bis(phosphanyl)benzene}nickel(II), $[(+)_\delta$-LR²]$NiBr_2$: $(+)_\delta$-LR² (0.39 g, 0.44 mmol) and anhydrous $NiBr_2$ (0.1 g, 0.44 mmol) were stirred in dichloromethane (10 mL). After 2 h, the red solution was filtered through silica gel and the solvents were evaporated to provide **$[(+)_\delta$-LR²]$NiBr_2$** (0.46 g) as a red powder in 93% yield, m.p. 162−165 °C. Crystals of **$[(+)_\delta$-LR²]$NiBr_2$** (orange plates) were obtained from a mixture of CH_2Cl_2 and ethanol at room temperature. ^{1}H NMR ($CDCl_3$): δ = 3.91−0.28 (m, 32 H, aliph. H), 8.18−5.57 (m, 23 H, arom. H) ppm. ^{31}P NMR ($CDCl_3$): δ = 67.02 (d, $^2J_{PP}$ = 49.6 Hz, 16% PRR′), 72.57 (d, $^2J_{PP}$ = 47.9 Hz, 84% PRR′), 74.77 (d, $^2J_{PP}$ = 47.9 Hz, 84% PR_2), 82.79 (d, $^2J_{PP}$ = 49.6 Hz, 16% PR_2) ppm. MS-FD (CH_2Cl_2): *m/z* = 1112.3 [M^+]. $C_{58}H_{55}Br_3NiP_2$ (1112.4): calcd. C 62.62, H 4.98; found C 62.27, H 4.91.

Dibromo{*P′*-(6-bromohexyl)-*P,P,P′*-tris[(+)-9-phenyldeltacyclan-8-yl]-1,2-bisphosphanylbenzene}nickel(II), $[(+)_\delta$-LR³]$NiBr_2$: A suspension of **$(+)_\delta$-LR³** (0.18 g, 0.20 mmol) and anhydrous $NiBr_2$ (0.044 g, 0.2 mmol) was heated in ethanol (20 mL) for 1 h. After cooling to room temperature and evaporating the solvent, the red residue was dissolved in CH_2Cl_2 and filtered through silica gel. Concentration provided **$[(+)_\delta$-LR³]$NiBr_2$** (0.19 g) as a dark red powder in 84% yield, m.p. 160−163 °C. ^{1}H NMR ($CDCl_3$): δ = 3.21−0.60 (m, 40 H, aliph. H), 3.14 (t, ^1J = 6.7 Hz, 2 H, CH_2Br), 7.51−6.53 (m, 19 H, arom. H) ppm. ^{31}P NMR ($CDCl_3$): δ = 68.92 (d, $^2J_{PP}$ = 50.1 Hz, 4% PRR′), 71.85 (d, $^2J_{PP}$ = 48.5 Hz, 96% PRR′), 73.82 (d, $^2J_{PP}$ = 48.5 Hz, 96% PR_2), 78.14 (d, $^2J_{PP}$ = 50.1 Hz, 4% PR_2) ppm. MS-FD (CH_2Cl_2): *m/z* = 1106.3 [M^+]. $C_{57}H_{61}Br_3NiP_2$ (1106.5): calcd. C 61.87, H 5.56; found C 61.76, H 5.66.

Dichloro{*P,P,P′*-tris[(+)-9-phenyldeltacyclan-8-yl]-1,2-bis(phosphanyl)benzene}palladium(II), $[(+)_\delta$-LH]$PdCl_2$: $(+)_\delta$-LH (0.50 g, 0.70 mmol) was dissolved in THF at −78 °C. $Pd(NCPh)_2Cl_2$ (0.27 g, 0.70 mmol), dissolved in THF and cooled down to −78 °C, was added dropwise to the solution of the phosphane. The pale yellow solution was stirred while warming to room temperature. Washing several times with *n*-hexane and subsequent drying gave **$[(+)_\delta$-LH]$PdCl_2$** (0.62 g) as a yellow powder in 98% yield, m.p. 169 °C. ^{1}H NMR ($CDCl_3$): δ = 3.62−0.05 (m, 30 H, aliph. H), 7.67−5.33 (m, 19 H, arom. H) ppm. ^{31}P NMR ($CDCl_3$): δ = 38.82 (d, $^2J_{PP}$ = 11.8, $^1J_{PH}$ = 406.5 Hz, 91% PHR), 41.10 (d, $^2J_{PP}$ = 9.0, $^1J_{PH}$ = 410.6 Hz, 9% PHR), 74.83 (d, $^2J_{PP}$ = 11.8 Hz, 91% PR_2), 76.75 (d, $^2J_{PP}$ = 9.0 Hz, 9% PR_2) ppm. MS-FAB (CH_2Cl_2): *m/z* = 900.8 [M^+]. $C_{51}H_{50}Cl_2P_2Pd$ (902.2): calcd. C 67.89, H 5.59; found C 68.11, H 5.62.

Dibromo{*P,P,P′*-tris[(+)-9-phenyldeltacyclan-8-yl]-1,2-bis(phosphanyl)benzene}palladium(II), $[(+)_\delta$-LH]$PdBr_2$: $(+)_\delta$-LH (0.37 g, 0.51 mmol) and $PdBr_2$ (0.14 g, 0.51 mmol) were stirred in CH_2Cl_2 for 4 d at room temperature. Filtration and concentration provided **$[(+)_\delta$-LH]$PdBr_2$** (0.49 g) as an orange powder in 97% yield, m.p. 175 °C. ^{1}H NMR ($CDCl_3$): δ = 3.70−0.19 (m, 30 H, aliph. H), 7.53−5.19 (m, 19 H, arom. H) ppm. ^{31}P NMR ($CDCl_3$): δ = 39.45 (d, $^2J_{PP}$ = 17.6, $^1J_{PH}$ = 410.6 Hz, 45% PHR), 43.96 (d, $^2J_{PP}$ = 14.5, $^1J_{PH}$ = 419.0 Hz, 55% PHR), 76.52 (d, $^2J_{PP}$ = 17.6 Hz, 45% PR_2), 79.10 (d, $^2J_{PP}$ = 14.5 Hz, 55% PR_2) ppm. MS-FAB (CH_2Cl_2): *m/z* = 990.4 [M^+]. $C_{51}H_{50}Br_2P_2Pd$ (991.1): calcd. C 61.80, H 5.08; found C 61.16, H 5.72.

Diiodo{*P,P,P′*-tris[(+)-9-phenyldeltacyclan-8-yl]-1,2-bis(phosphanyl)benzene}palladium(II), $[(+)_\delta$-LH]PdI_2: $(+)_\delta$-LH (0.50 g, 0.70 mmol) and PdI_2 (0.25 g, 0.70 mmol) were suspended in benzene and refluxed for 4 h. After cooling to room temperature the solution was filtered and the solvent evaporated. **$[(+)_\delta$-LH]PdI_2** (0.49 g) remained as a red powder in 99% yield, m.p. 183 °C. Crystals of **$[(+)_\delta$-LH]PdI_2**·CH_2Cl_2 (orange plates) were obtained from a mixture of CH_2Cl_2 and methanol at room temperature. ^{1}H NMR ($CDCl_3$): δ = 3.35−0.08 (m, 30 H, aliph. H), 4.45 (m, 1 H, $^1J_{PH}$ = 404.9 Hz, 1 H, PH, 42%), 7.63−6.29 (m, 19 H, arom. H) ppm. ^{31}P NMR ($CDCl_3$): δ = 38.02 (d, $^2J_{PP}$ = 16.5, $^1J_{PH}$ = 404.9 Hz, 42% PHR), 45.29 (d, $^2J_{PP}$ = 13.5, $^1J_{PH}$ = 413.8 Hz, 58% PHR), 75.77 (d, $^2J_{PP}$ = 16.5 Hz, 42% PR_2), 80.09 (d, $^2J_{PP}$ = 13.5 Hz, 58% PR_2) ppm. MS-FAB (CH_2Cl_2): *m/z* = 1084.5 [M^+]. $C_{51}H_{50}I_2P_2Pd$ (1085.1): calcd. C 56.45, H 4.64; found C 56.43, H 4.86.

{*P′*-Chloro-*P,P,P′*-tris[(+)-9-phenyldeltacyclan-8-yl)-1,2-bis(phosphanyl)benzene}diiodopalladium(II), $[(+)_\delta$-LCl]PdI_2: $(+)_\delta$-LH (0.59 g, 0.81 mmol) and PdI_2 (0.29 g, 0.81 mmol) were suspended in CH_2Cl_2 and stirred for 3 d followed by filtration and evaporation of the solvent. Crystallization from a 1:2 mixture of CH_2Cl_2/diethyl ether gave **$[(+)_\delta$-LCl]PdI_2** (0.08 g) as dark red-brown crystals in nearly 10% yield, m.p. 188 °C. ^{1}H NMR ($CDCl_3$): δ = 3.50−0.08 (m, 30 H, aliph. H), 7.65−6.38 (m, 19 H, arom. H) ppm. ^{31}P NMR

Table 1. Crystal data, data collection, structure refinement and CCDC numbers

	$(+)_\delta$-LH	**$[(+)_\delta$-LR^2]NiBr$_2$**	**$[(+)_\delta$-LH]PdI$_2$**	**$[(+)_\delta$-LCl]PdI$_2$**
Empirical formula	$C_{51}H_{49}P_2 \cdot 0.75C_2H_5OH$	$C_{58}H_{55}Br_3NiP_2$	$C_{51}H_{50}I_2P_2Pd \cdot CH_2Cl_2$	$C_{51}H_{49}ClI_2P_2Pd$
M_r	758.40	1112.32	1170.00	1119.52
Crystal system	monoclinic	monoclinic	monoclinic	monoclinic
Space group	$P2_1$	$P2_1$	$P2_1$	$P2_1$
Z	4	2	4	4
Unit cell dimensions	a = 14.032(5) Å b = 10.574(5) Å c = 28.351(5) Å β = 91.79(0)°	a = 10.2507(5) Å b = 21.4953(14) Å c = 11.2945(5) Å β = 92.277(6)°	a = 17.4832(10) Å b = 25.0485(16) Å c = 10.8323(6) Å β = 81.189(6)°	a = 11.1979(8) Å b = 26.5169(13) Å c = 17.2105(13) Å β = 107.596(9)°
Volume	4205(3) Å^3	2486.7(2) Å^3	4687.8(5) Å^3	4871.3(6) Å^3
$D_{calcd.}$	1.198 g/cm^3	1.486 g/cm^3	1.658 g/cm^3	1.526 g/cm^3
Absorption coefficient	0.14 mm^{-1}	2.902 mm^{-1}	1.931 mm^{-1}	1.80 mm^{-1}
F(000)	1618	1132	2320	2216
Crystal size	0.24 × 0.10 × 0.06 mm	0.18 × 0.08 × 0.03 mm	0.70 × 0.68 × 0.09 mm	0.30 × 0.26 × 0.04 mm
Crystal description	prism	plates	plates	plates
Crystal color	colorless	orange	orange	red-brown
θ range for data collection	2.01−25.25°	1.89−25.81°	1.90−25.75°	1.94−25.23°
Limiting indices	$-16 \le h \le 16$ $-12 \le k \le 12$ $-33 \le l \le 33$	$-12 \le h \le 12$ $-26 \le k \le 26$ $-13 \le l \le 13$	$-21 \le h \le 21$ $-30 \le k \le 30$ $-13 \le l \le 13$	$-13 \le h \le 13$ $-31 \le k \le 31$ $-20 \le l \le 20$
Reflections collected	52421	23851	65722	42020
Independent reflections (R_{int})	15114 (0.0947)	9505 (0.0691)	16715 (0.0361)	16817 (0.0711)
Reflections $I > 2\sigma(I)$	7489	6391	16267	13587
Data/restraints/parameters	15114/1/955	9505/1/587	16715/1/1069	16817/1/1027
Absorption correction	none	numerical	numerical	numerical
Transmission (min/max)	−/−	0.8790/0.6667	0.8231/0.2928	0.8978/0.6379
Goodness-of-fit on F^2	0.686	0.848	1.067	0.902
Final R indices [$I > 2\sigma(I)$]	R_1 = 0.0436 wR_2 = 0.0611	R_1 = 0.0452 wR_2 = 0.0763	R_1 = 0.0259 wR_2 = 0.0680	R_1 = 0.0420 wR_2 = 0.0914
R indices (all data)	R_1 = 0.0984 wR_2 = 0.0719	R_1 = 0.0783 wR_2 = 0.0833	R_1 = 0.0269 wR_2 = 0.0716	R_1 = 0.0534 wR_2 = 0.0949
Absolute structure parameter	−0.03(6)	0.00(1)	−0.02(1)	−0.02(2)
Largest diff. peak/hole	0.318/−0.167 e Å^{-3}	0.749/−0.282 e Å^{-3}	0.949/−0.839 e Å^{-3}	1.489/−0.476 e Å^{-3}
CCDC-	178668	178669	178670	178667

($CDCl_3$): δ = 62.68 (d, $^2J_{PP}$ = 13.2 Hz, 15% PR_2), 68.87 (d, $^2J_{PP}$ = 8.8 Hz, 85% PR_2), 123.29 (d, $^2J_{PP}$ = 8.8 Hz, 85% PClR), 126.46 (d, $^2J_{PP}$ = 13.2 Hz, 15% PClR). MS-ESI (CH_3OH): m/z = 1151.3 [M + MeOH]$^+$. $C_{51}H_{49}ClI_2P_2Pd$ (1119.6): calcd. C 54.71, H 4.41; found C 55.46, H 4.99.

Dichloro{*P,P,P′*-tris[(+)-9-phenyldeltacyclan-8-yl]-1,2-bis(phosphanyl)benzene]platinum(II), $[(+)_\delta$-LH]PtCl$_2$: K_2PtCl_4 (0.16 g, 0.37 mmol) was dissolved in a small amount of concd. HCl, diluted with 40 mL of ethanol and heated to reflux. **$(+)_\delta$-LH** (0.27 g, 0.37 mmol), dissolved in 10 mL of toluene, was added dropwise to the dark brown solution and stirred for 3 h. After cooling to room temperature, the solution was filtered and the solvents were evaporated. **$[(+)_\delta$-LH]PtCl$_2$** (0.30 g) remained as a cream-colored powder in 83% yield, m.p. 225 °C. ^{1}H NMR ($CDCl_3$): δ = 5.03−0.15 (m, 30 H, aliph. H), 7.87−6.39 (m, 19 H, arom. H) ppm. ^{31}P NMR ($CDCl_3$): δ = 15.23 (d, $^2J_{PP}$ = 2.5, $^1J_{PH}$ = 416, $^1J_{PtP}$ = 3531 Hz, 20% PHR), 15.90 (d, $^2J_{PP}$ = 3.1, $^1J_{PH}$ = 414, $^1J_{PtP}$ = 3508 Hz, 80% PHR), 47.20 (d, $^2J_{PP}$ = 2.5, $^1J_{PtP}$ = 3531 Hz, 20% PR_2), 48.67 (d, $^2J_{PP}$ = 3.1, $^1J_{PtP}$ = 3508 Hz, 80% PR_2) ppm. MS-ESI (CH_2Cl_2): m/z = 987.5 [M$^+$]. $C_{51}H_{50}Cl_2P_2Pt$ (990.9): calcd. C 61.82, H 5.09; found C 62.24, H 5.02.

Dibromo{*P,P,P′*-tris[(+)-9-phenyldeltacyclan-8-yl]-1,2-bis(phosphanyl)benzene}platinum(II), $[(+)_\delta$-LH]PtBr$_2$: A solution of Pt(cod)Br_2 (0.11 g, 0.24 mmol) and **$(+)_\delta$-LH** (0.18 g, 0.24 mmol) in 20 mL of benzene was stirred for 20 h at room temperature. After filtration, the solvent was removed. The residue was washed with pentane to afford **$[(+)_\delta$-LH]PtBr$_2$** (0.19 g) as a pale yellow powder in 75% yield, m.p. > 250 °C. ^{1}H NMR ($CDCl_3$): δ = 3.75 (m, 30 H, aliph. H), 7.61−6.33 (m, 19 H, arom. H) ppm. ^{31}P NMR ($CDCl_3$): δ = 51.81 (s, $^2J_{PP}$ = 2.2, $^1J_{PtP}$ = 3484 Hz, 31% PR_2), 49.77 (s, $^2J_{PP}$ = 2.2, $^1J_{PtP}$ = 3504 Hz, 69% PR_2), 21.49 (s, $^2J_{PP}$ = 2.4, $^1J_{PH}$ = 419, $^1J_{PtP}$ = 3305 Hz, 31% PHR), 18.19 (s, $^2J_{PP}$ = 2.2, $^1J_{PH}$ = 417, $^1J_{PtP}$ = 3322 Hz, 69% PHR) ppm. MS-ESI (CH_2Cl_2/MeOH): m/z = 1079.2 [M − H]$^+$. $C_{51}H_{50}Br_2P_2Pt$ (1079.8): calcd. C 56.73, H 4.67; found C 56.63, H 4.85.

X-ray Crystallographic Studies: The data were collected with a STOE-IPDS diffractometer with Mo-K_α radiation and graphite monochromator at a temperature of 173(1) K. Crystal data, data collection, structure refinement and CCDC numbers for **$(+)_\delta$-LH**, **$[(+)_\delta$-LR^2]NiBr$_2$**, **$[(+)_\delta$-LH]PdI$_2$** and **$[(+)_\delta$-LCl]PdI$_2$** are given in Table 1. The structures were solved by direct methods (SIR-97) and refined by full-matrix least squares on F^2 (SHELXL-97). The H atoms were calculated geometrically and a riding model was applied during the refinement process. Absorption corrections, when necessary, were carried out numerically from the crystal shape (x-RED).[25] CCDC numbers given in Table 1 contain the supplementary crystallographic data for this paper. These data can be obtained free of charge at www.ccdc.cam.ac.uk/conts/retrieving.html or from the Cambridge Crystallographic Data Centre, 12, Union Road, Cambridge CB2 1EZ, UK [Fax: (internat.) + 44-1223/336-033; E-mail: deposit@ccdc.cam.ac.uk].

[1] H. Brunner, F. Henning, M. Weber, *Tetrahedron: Asymmetry* **2002**, *13*, 37.
[2] M. Lautens, W. Tam, J. C. Lautens, L. G. Edwards, C. M. Crudden, A. C. Smith, *J. Am. Chem. Soc.* **1995**, *117*, 6863.
[3] M. Lautens, W. Klute, W. Tam, *Chem. Rev.* **1996**, *96*, 49.
[4] J. E. Lyons, H. K. Myers, A. Schneider, *J. Chem. Soc., Chem. Commun.* **1978**, 636.
[5] H. Brunner, M. Muschiol, F. Prester, *Angew. Chem.* **1990**, *102*, 680; *Angew. Chem. Int. Ed. Engl.* **1990**, *29*, 653.
[6] M. Lautens, J. C. Lautens, A. C. Smith, *J. Am. Chem. Soc.* **1990**, *112*, 5627.
[7] H. Brunner, F. Prester, *J. Organomet. Chem.* **1991**, *414*, 401.
[8] I. F. Duan, C. H. Cheng, J. S. Shaw, S. S. Cheng, K. F. Lion, *J. Chem. Soc., Chem. Commun.* **199**1, 1347.
[9] P. Binger, S. Albus, *J. Organomet. Chem.* **1995**, *493*, C6.
[10] O. Pardigon, G. Buono, *Tetrahedron: Asymmetry* **1993**, *4*, 1977.
[11] O. Pardigon, T. Alphonse, G. Buono, *J. Org. Chem.* **1995**, *60*, 1868.
[12] H. Brunner, A. Reimer, *Bull. Soc. Chim. Fr.* **1997**, *134*, 307.
[13] H. Brunner, A. Reimer, *Chem. Ber./Recueil* **1997**, *130*, 1495.
[14] H. Brunner, A. Reimer, *Bull. Soc. Chim. Belg.* **1997**, *106*, 267.
[15] O. Pardigon, T. Alphonse, G. Buono, *Tetrahedron Lett.* **2000**, *41*, 4089.
[16] S. Dormeier, Dissertation, Universität Regensburg, **2001**.
[17] A. Bader, M. Pabel, S. B. Wild, *J. Chem. Soc., Chem. Commun.* **1994**, 1405.
[18] A. Bader, T. Nullmeyers, M. Pabel, G. Salem, A. C. Willis, S. B. Wild, *Inorg. Chem.* **1995**, *34*, 384.
[19] A. Bader, M. Pabel, A. C. Willis, S. B. Wild, *Inorg. Chem.* **1995**, *35*, 3874.
[20] J. Albert, J. M. Cadena, J. Granell, G. Muller, D. Panyella, C. Snudo, *Eur. J. Inorg. Chem.* **2000**, 1283.
[21] The phenomenon that two diastereomers crystallize together in one lattice, will be discussed in a review in *Coord. Chem. Rev.*
[22] E. P. Kyba, S.-T. Liu, R. L. Harris, *Organometallics* **1983**, *2*, 1877.
[23] L. Maier in *Organic Phosphorus Compounds*, vol. 1 (Eds.: G. M. Kosolapoff, L. Maier), Wiley, New York, **1972**.
[24] H. Fritzsche, U. Hasseroth, F. Korte, *Chem. Ber.* **1965**, *98*, 1681.
[25] *x-RED, Program for reduction of IPDS-data*, version 1.10, STOE & Cie GmbH, Darmstadt, **1998**.

Received February 20, 2002
[I02096]

Dinuclear and Trinuclear Ni−, Pd−, and Pt−Halide Complexes of the Easily Accessible Chiral Ligand *P,P,P′*-Tris[(+)-9-phenyldeltacyclan-8-yl]-1,2-bis(phosphanyl)benzene[‡]

Henri Brunner,*[a] Stephan Dormeier,[a] Ilias Grau,[a] and Manfred Zabel[a]

Dedicated to Professor Dr. Gottfried Huttner on the occasion of his 65th birthday

Keywords: Nickel complexes / Palladium complexes / Platinum complexes / Phosphido bridges / Phosphorus configuration

The synthesis of seven dinuclear complexes **[(+)$_\delta$-LMHal]$_2$** (M = Ni, Pd, Pt; Hal = Cl, Br, I) is described, in which **(+)$_\delta$-L$^-$** represents the deprotonated chiral chelate ligand *P,P,P′*-tris[(+)-9-phenyldeltacyclan-8-yl]-1,2-bis(phosphanyl)-benzene, easily accessible in a highly enantioselective homo-Diels–Alder reaction. All the dinuclear complexes are bent at the phosphido bridges which connect the two square-planar halves of the molecules. The phosphorus atoms of the phosphido bridges are stereogenic centers. For **[(+)$_\delta$-LNiBr]$_2$** and **[(+)$_\delta$-LPdCl]$_2$** both diastereomers with (S_P,S_P) and (R_P,R_P) configuration were observed, whereas for **[(+)$_\delta$-LPdBr]$_2$**, **[(+)$_\delta$-LPdI]$_2$**, and **[(+)$_\delta$-LPtCl]$_2$** only the (S_P,S_P) isomers could be obtained. Furthermore, the synthesis of eight trinuclear complexes **[(+)$_\delta$-L$_2$M$_3$Hal$_4$]** (M = Pd, Pt; Hal = Cl, Br) is reported, which contain unusual three-square arrays. In the trinuclear complexes all the halogens are oriented to one side. Halogeno and phosphido bridges connect the three squares leading to chair configurations (opposite scaffold chirality possible) and boat configurations. For **[(+)$_\delta$-L$_2$Pd$_3$Cl$_4$]**, **[(+)$_\delta$-L$_2$Pd$_3$Br$_4$]**, and **[(+)$_\delta$-L$_2$Pt$_3$Cl$_4$]** the two diastereomers with (S_P,S_P) and (R_P,R_P) configuration and for **[(+)$_\delta$-L$_2$Pt$_3$Br$_4$]** the diastereomers with (S_P,S_P) and (S_P,R_P) configuration could be isolated. In addition, the dinuclear complex **[(+)$_\delta$-LPt$_2$Br$_3$(cod)]** (cod = 1,5-cyclooctadiene) containing a single phosphido bridge was obtained.

(© Wiley-VCH Verlag GmbH, 69451 Weinheim, Germany, 2002)

Introduction

In the previous paper the synthesis of the chiral ligand *P,P,P′*-tris[(+)-9-phenyldeltacyclan-8-yl)-1,2-bis(phosphanyl)benzene **(+)$_\delta$-LH** and its mononuclear complexes was reported. **(+)$_\delta$-LH** is formed in the enantioselective homo-Diels−Alder reaction of norbornadiene with phenylacetylene[2,3] and the subsequent addition of 3 PH bonds of 1,2-bis(phosphanyl)benzene to the double bonds of (+)-8-phenyldeltacyclene.[1,4] **(+)$_\delta$-LH** contains 3 × 8 = 24 asymmetric carbon atoms in its three deltacyclanyl substituents and a stereogenic secondary phosphorus atom which is configurationally labile in the free ligand but stabilized in its mononuclear complexes **[(+)$_\delta$-LH]MHal$_2$**, M = Ni, Pd, Pt.[1] The symbol **(+)$_\delta$** in the ligand **(+)$_\delta$-LH** and in its complexes indicates the 24 asymmetric carbon atoms of a given configuration in the deltacyclane substituents built up in the highly enantioselective homo-Diels−Alder reaction. Here, the dinuclear and trinuclear compounds will be described, which form on HHal elimination from the complexes **[(+)$_\delta$-LH]MHal$_2$**.[5] The dinuclear complexes have roof-shaped structures with bridging phosphorus atoms. In the trinuclear compounds three square-planar units are connected in an uncommon way. In addition to the 48 asymmetric carbon atoms of fixed configuration both dinuclear and trinuclear complexes contain two stereogenic phosphorus atoms of the phosphido bridges. As the phosphorus atoms may occur in (S_P,S_P) as well as (R_P,R_P) in one case even (S_P,R_P) configuration series of diastereomers could be isolated and characterized differing only in the configuration of the phosphido bridges. Thus, the dinuclear compounds **(S_P,S_P)-** and **(R_P,R_P)-[(+)$_\delta$-MHal]$_2$** and the trinuclear compounds **(S_P,S_P)-**, **(R_P,R_P)-** and **(S_P,R_P)-[(+)$_\delta$-L$_2$M$_3$Hal$_4$]** are not enantiomers but diastereomers.

All the molecules shown in Schemes 1 and 2 and discussed in Tables 1−6 {except **(R_P)-[(+)$_\delta$-L$_2$Pt$_3$Br$_3$(cod)]**} are C_2-symmetric. However, only for **(S_P,S_P)-[(+)$_\delta$-L$_2$Pd$_3$Br$_4$]**, **(R_P,R_P)-[(+)$_\delta$-L$_2$Pd$_3$Br$_4$]**, and **(S_P,S_P)-[(+)$_\delta$-L$_2$Pt$_3$Br$_4$]** the C_2 axis of the molecule is also a symmetry element of the unit cell. Consequently, in all the other cases the two halves of the molecules are different. Nevertheless, throughout the paper only one half of each molecule is described and discussed (the left halves in Figures 1−5).

[‡] Enantioselective Catalysis, 145. Part 144: Ref.[1]

[a] Institut für Anorganische Chemie, Universität Regensburg, 93040 Regensburg, Germany
Fax: (internat.) + 49-941/943-4439
E-mail: henri.brunner@chemie.uni-regensburg.de

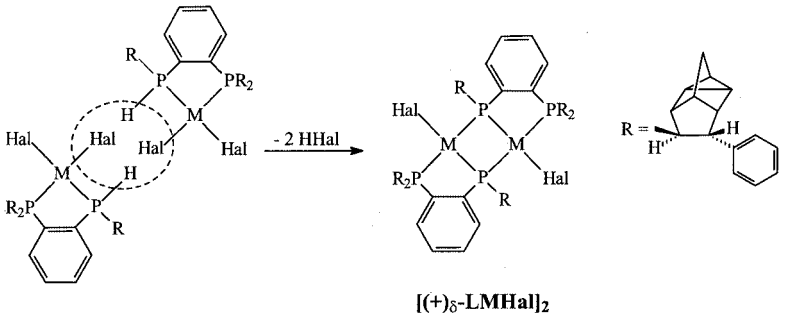

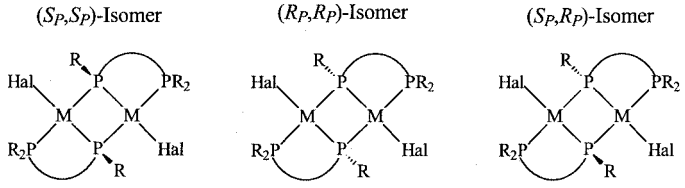

[(+)δ-LNiBr]2 [(+)δ-LNiBr]2
[(+)δ-LPdCl]2 [(+)δ-LPdCl]2
[(+)δ-LPdBr]2
[(+)δ-LPdI]2
[(+)δ-LPtCl]2

Scheme 1. Reaction of two mononuclear complexes **[(+)$_\delta$-LH]MHal$_2$** to give the dinuclear phosphido-bridged compounds **[(+)$_\delta$-LMHal]$_2$** (top) and the three possible isomers **(S_P,S_P)-**, **(R_P,R_P)-**, and **(S_P,R_P)-[(+)$_\delta$-LMHal]$_2$** (bottom)

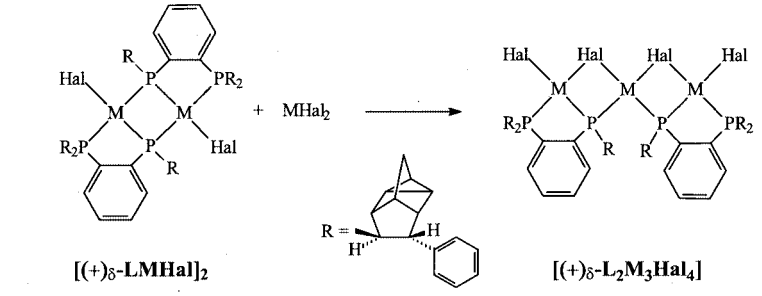

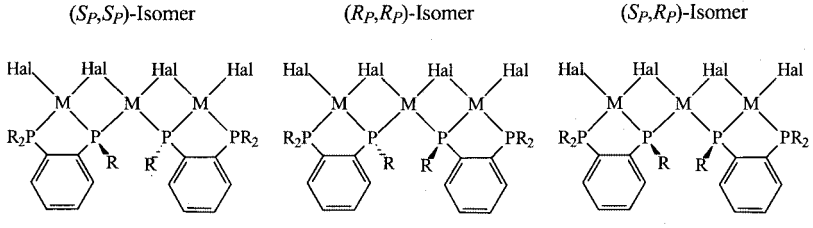

[(+)δ-L2Pd3Cl4] [(+)δ-L2Pd3Cl4]
[(+)δ-L2Pd3Br4] [(+)δ-L2Pd3Br4]
[(+)δ-L2Pt3Cl4] [(+)δ-L2Pt3Cl4]
[(+)δ-L2Pt3Br4] [(+)δ-L2Pt3Br4]

Scheme 2. Reaction of a dinuclear complex **[(+)$_\delta$-LMHal]$_2$** and $MHal_2$ to give trinuclear compounds **[(+)$_\delta$-L$_2$M$_3$Hal$_4$]** (top) and the three possible isomers **(S_P,S_P)-**, **(R_P,R_P)-**, and **(S_P,R_P)-[(+)$_\delta$-L$_2$M$_3$Hal$_4$]** of the trinuclear phosphido- and halo-bridged complexes having all the halides on one side (bottom)

The Dinuclear Phosphido-Bridged Complexes [(+)$_\delta$-LMHal]$_2$

Although most of the syntheses of the dinuclear complexes **[(+)$_\delta$-LMHal]$_2$** given in the Exp. Sect. started from the ligand **(+)$_\delta$-LH** and suitable metal precursors, the intermediacy of the corresponding mononuclear complexes **[(+)$_\delta$-LH]MHal$_2$** must be assumed.[1] As indicated in Scheme 1 two mononuclear complexes give the dinuclear phosphido-bridged compounds by twofold HHal elimination. Some of the dinuclear complexes were obtained in attempts to recrystallize the mononuclear compounds **[(+)$_\delta$-LH]MHal$_2$** demonstrating their tendency to loose HHal.

In the dinuclear complexes **[(+)$_\delta$-LMHal]$_2$** two square-planar units are connected by bridging phosphorus atoms. The phosphorus atoms of these phosphido bridges are stereogenic centers, as they have four different substituents: the palladium atom which is part of the chelate ring, the palladium atom which is not part of the chelate ring, the chelate ring, and the (+)-9-phenyldeltacyclanyl substituent. This priority sequence is the basis for the assignment of (*R*) and (*S*) configuration to these stereogenic phosphido phosphorus atoms. In all the dinuclear complexes **[(+)$_\delta$-LMHal]$_2$** the (+)-9-phenyldeltacyclanyl substituents have the same stereochemistry. It is the configuration of the bridging phosphorus atoms which differentiates the diastereomers.

At the bottom of Scheme 1 the three possible isomers for the dinuclear complexes are shown. In combination with the enantiomerically pure deltacyclane substituents abbreviated by **(+)$_\delta$** the configuration of the bridging phosphorus atoms can be (S_P,S_P), (R_P,R_P), or (S_P,R_P) giving rise to three diastereomers. Obviously, the **(S_P,S_P)-[(+)$_\delta$-LMHal]$_2$** diastereomers are highly favored. However, for the fragments NiBr and PdCl both diastereomers **(S_P,S_P)-** and **(R_P,R_P)-[(+)$_\delta$-LMHal]$_2$** could be isolated and characterized. The **(S_P,R_P)-[(+)$_\delta$-LMHal]$_2$** isomer, *meso*-configurated with respect to the central core (excluding the deltacyclanyl substituents), was never observed.

Dinuclear complexes in which two square-planar units are connected by bridges can be coplanar or bent.[6,7] Diphenylphosphido-bridged complexes usually are planar, e.g. [Hal(PPh$_2$H)M(μ-PPh$_2$)$_2$M(PPh$_2$H)Hal] (M = Pd, Pt; Hal = Cl, I).[8−10] On the other hand complexes containing unsymmetrically substituted phosphido bridges PRR′ are bent.[6] Consequently, the bridging phosphido groups discussed here, in which the phosphorus atoms have a phenylene and a deltacyclanyl substituent, are expected to be bent, the roof angle depending on the type of diastereomer.

Reaction of anhydrous NiBr$_2$ with **(+)$_\delta$-HL** and Na$_2$CO$_3$ in boiling ethanol provided a crude product, the ^{31}P NMR spectrum of which showed the signals of several compounds including those of the dinuclear complexes **(S_P,S_P)-[(+)$_\delta$-LNiBr]$_2$** (main product) and **(R_P,R_P)-[(+)$_\delta$-LNiBr]$_2$** (see below). Crystallization from CH$_2$Cl$_2$ gave red needles suitable for X-ray structure analysis. The ^{31}P NMR spectrum exhibited the AA′XX′ system of only one of the possible diastereomers. The structural study confirmed the dinuclear character of the complex (Figure 1) proving the presence of only one of the possible isomers.

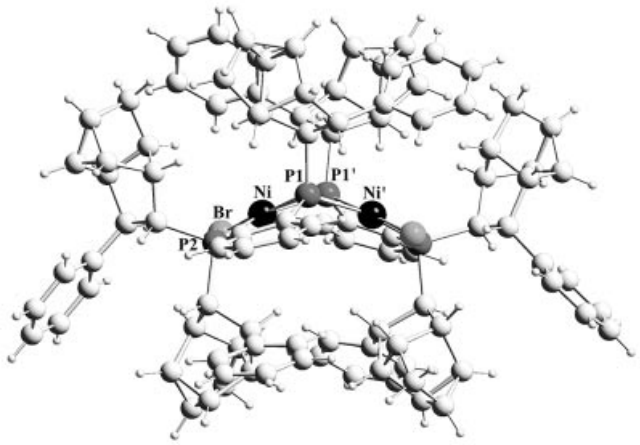

Figure 1. Molecular structure of **(S_P,S_P)-[(+)$_\delta$-LNiBr]$_2$**, crystallized from CH$_2$Cl$_2$; selected bond lengths [A], bond angles [°], and dihedral angles [°]: Ni···Ni′ = 3.277(12), P1···P1′ = 2.689(8), Ni−Br = 2.349(1), Ni−P1 = 2.181(3), Ni−P1′ = 2.217(1), Ni−P2 = 2.207(3); Br−Ni−P1′ = 97.60(3), P1′−Ni−P1 = 75.39(4), P1−Ni−P2 = 88.39(4), P2−Ni−Br = 98.30(3), P1−Ni−Br = 172.95(3), P1′−Ni−P2 = 160.29(4); Ni−P1′−P1−Br = 0.53(2), Ni−P1′−P1−P2 = 8.24(3), P2−P1−P1′−Br = 7.71(3), Ni−P1−P1′−Ni′ = 140.84(4), Ni−P1−P2/C1−C2 = 10.5(2): δ

The configuration of the two bridging chiral phosphorus atoms was determined as (S_P,S_P). **(S_P,S_P)-[(+)$_\delta$-LNiBr]$_2$** is bent at the phosphido bridges. The "roof angle" between the two square-planar units is 140.84°. The dihedral angle of the metal substituents P2−P1−P1′−Br (of the left half of the molecule) shows that there is a small deformation of the square-planar arrangement of 7.71°. The chelate ring Ni−P1−C1−C2−P2 is slightly puckered indicated by the inclination of the bond C1−C2 of the benzene ring with respect to the plane Ni−P1−P2. The angle of this inclination is a measure of the chirality of the helix defined by the two skew lines C1−C2 and P1−P2 (which is part of the plane Ni−P1−P2). The chirality of the chelate ring Ni−P1−C1−C2−P2 is induced by the given chirality of the deltacyclanyl substituents and the configuration of the bridging phosphorus atoms. In **(S_P,S_P)-[(+)$_\delta$-LNiBr]$_2$** the inclination angle of C1−C2 with respect to the plane Ni−P1−P2 is 10.5°, defining δ helicity. The parameters discussed for **(S_P,S_P)-[(+)$_\delta$-LNiBr]$_2$** are typical for the (S_P,S_P) diastereomers. They differ for the (R_P,R_P) diastereomers (Table 1).

Reaction of anhydrous NiBr$_2$ with **(+)$_\delta$-HL** and *n*BuLi in CH$_2$Cl$_2$, followed by crystallization from acetone, afforded brown crystals of **(R_P,R_P)-[(+)$_\delta$-LNiBr]$_2$** suitable for X-ray structure analysis (Figure 2).

The diastereomer **(R_P,R_P)-[(+)$_\delta$-LNiBr]$_2$** is also bent at the phosphido bridges. However, the roof angle of 156.53° shows a flattening compared to **(S_P,S_P)-[(+)$_\delta$-LNiBr]$_2$**, which is also obvious from the lengthening of the nonbonding Ni−Ni distance from 3.28 to 3.45 Å (Table 1). In **(R_P,R_P)-[(+)$_\delta$-LNiBr]$_2$** the plane of the metal substituents P2−P1−P1′−Br is heavily deformed by 25.97°. This strong deformation, which is typical for all (R_P,R_P) isomers

Table 1. Roof-angles, M···M distances, square deformations, chelate angles, and helicity of the dinuclear complexes **(S_P,S_P)-** and **(R_P,R_P)-[(+)$_\delta$-LMHal]$_2$**

	(S_P,S_P)-[(+)$_\delta$-LPdCl]$_2$		(R_P,R_P)-[(+)$_\delta$-LPdCl]$_2$
Complex	(S_P,S_P)	Data	(R_P,R_P)
[(+)$_\delta$-LNiBr]$_2$	140.84	roof angle [°] Ni−P1−P1′−Ni′	156.53
	3.277	distance [Å] Ni···Ni′	3.454
	7.71	square deformation [°] P2−P1−P1′−Br[a]	25.97
	10.5, δ	angle [°] Ni−P1−P2/C1−C2, helicity[b]	0.9, λ
[(+)$_\delta$-LPdCl]$_2$	141.31	roof angle [°] Pd−P1−P1′−Pd′	156.40
	3.422	distance [Å] Pd···Pd′	3.580
	7.33	square deformation [°] P2−P1−P1′−Cl[a]	22.92
	9.8, δ	angle [°] Pd−P1−P2/C1−C2, helicity[b]	2.6, λ
[(+)$_\delta$-LPdBr]$_2$	140.59	roof angle [°] Pd−P1−P1′−Pd′	
	3.419	distance [Å] Pd···Pd′	
	7.72	square deformation [°] P2−P1−P1′−Br[a]	
	10.7, δ	angle [°] Pd−P1−P2/C1−C2, helicity[b]	
[(+)$_\delta$-LPdI]$_2$	139.35	roof angle [°] Pd−P1−P1′−Pd′	
	3.410	distance [Å] Pd···Pd′	
	7.92	square deformation [°] P2−P1−P1′−I[a]	
	9.3, δ	angle [°] Pd−P1−P2/C1−C2, helicity[b]	
[(+)$_\delta$-LPtCl]$_2$	144.49	roof angle [°] Pt−P1−P1′−Pt′	
	3.477	distance [Å] Pt···Pt′	
	11.89	square deformation [°] P2−P1−P1′−Cl[a]	
	6.7, δ	angle [°] Pt−P1−P2/C1−C2, helicity[b]	

[a] Left square. [b] Chelate ring of left square.

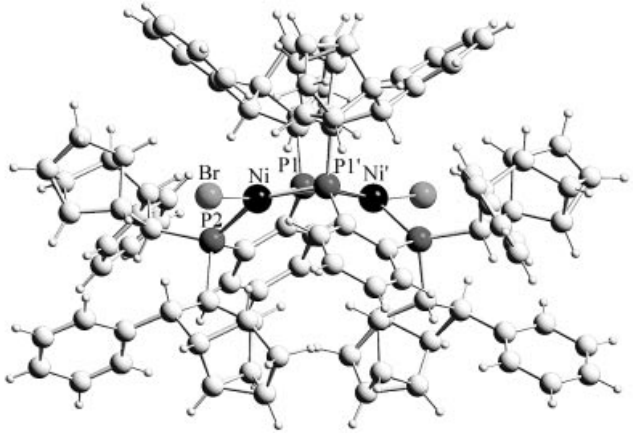

Figure 2. Molecular structure of **(R_P,R_P)-[(+)$_\delta$-LNiBr]$_2$**, crystallized from acetone; selected bond lengths [Å], bond angles [°], and dihedral angles [°]: Ni···Ni′ = 3.454(21), P1···P1′ = 2.650(11), Ni−Br = 2.344(4), Ni−P1 = 2.181(4), Ni−P1′ = 2.223(10), Ni−P2 = 2.201(4); Br−Ni−P1′ = 102.93(10), P1′−Ni−P1 = 73.96(1), P1−Ni−P2 = 90.19(2), P2−Ni−Br = 97.36(10), P1−Ni−Br = 168.28(11), P1′−Ni−P2 = 149.42(11); Ni−P1′−P1−Br = 7.43(7), Ni−P1′−P1−P2 = −18.54(9), P2−P1−P1′−Br = −25.97(10), Ni−P1−P1′−Ni′ = 156.53(15), Ni−P1−P2/C1−C2 = 0.9(6): λ

(Table 1), may be the reason for their discrimination compared to the (S_P,S_P) isomers. On the other hand, the chelate rings are almost planar in the (R_P,R_P) diastereomers. In **(R_P,R_P)-[(+)$_\delta$-LNiBr]$_2$** the inclination angle is only 0.9° with λ helicity (Table 1).

Similar to the NiBr series, it was possible in the PdCl series to isolate and characterize both diastereomers **(S_P,S_P)-** and **(R_P,R_P)-[(+)$_\delta$-LPdCl]$_2$** (Tables 1 and 3). The structural parameters (roof angle, nonbonding M−M distance, square deformation, inclination angle, and helicity) for the diastereomers **(S_P,S_P)-** and **(R_P,R_P)-[(+)$_\delta$-LPdCl]$_2$** link up with those of the diastereomers **(S_P,S_P)-** and **(R_P,R_P)-[(+)$_\delta$-LNiBr]$_2$**. Similar to the NiBr system, the two diastereomers of the PdCl system do not interconvert in solution, because their ^{31}P NMR spectra are different and stay different.

Using Na_2PdCl_4/LiBr, PdI_2, and **[(+)$_\delta$-LH)PtCl$_2$** as starting materials the dinuclear complexes **(S_P,S_P)-[(+)$_\delta$-LPdBr]$_2$**, **(S_P,S_P)-[(+)$_\delta$-LPdI]$_2$**, and **(S_P,S_P)-[(+)$_\delta$-LPtCl]$_2$** (Table 4) were isolated and characterized. They all belong to the (S_P,S_P) diastereomer series and resemble the (S_P,S_P) diastereomers described above in having roof angles

about 140°, dihedral angels of the metal substituents between 7 and 12° and δ helicity in the slightly puckered chelate rings (Table 1).

The complex **(R_P)-[(+)$_δ$-LPt$_2$Br$_3$(cod)]** was obtained during crystallization of **[(+)$_δ$-LH)PtBr$_2$** which had been prepared from Pt(cod)Br$_2$ (Figure 3). The compound has only one **(+)$_δ$-L$^-$** substituent which connects two platinum atoms by a single phosphido bridge. The configuration of this phosphorus atom was determined as (R_P). To one of the platinum atoms a cod molecule is coordinated, left over from the starting material Pt(cod)Br$_2$.

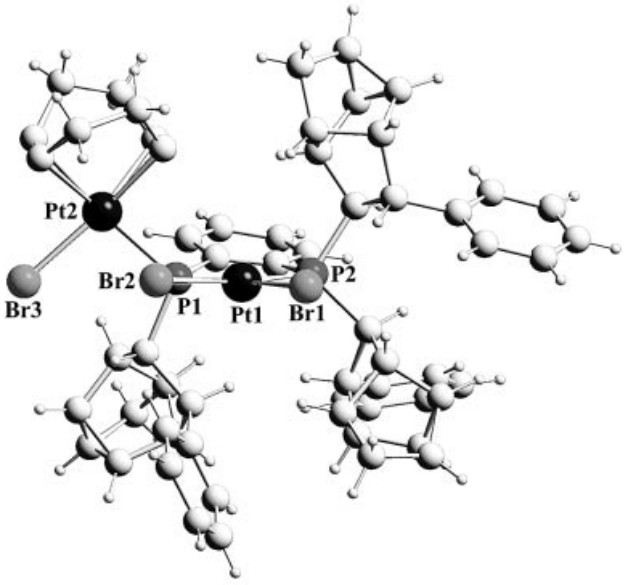

Figure 3. Molecular structure of **(R_P)-[(+)$_δ$-LPt$_2$Br$_3$(cod)]**, crystallized from CH_2Cl_2/methanol; selected bond lengths [Å], bond angles [°], and dihedral angles [°]: Pt1···Pt2 = 3.832(2), Pt1−Br1 = 2.449(1), Pt1−Br2 = 2.507(1), Pt1−P1 = 2.249(2), Pt1−P2 = 2.239(2), Pt2−Br3 = 2.430(1), Pt2−P1 = 2.339(2); P1−Pt1−Br2 = 85.89(5), Br2−Pt1−Br1 = 88.98(3), Br1−Pt1−P2 = 97.11(5), P2−Pt1−P1 = 88.30(6), P1−Pt1−Br1 = 174.36(5), P2−Pt1−Br2 = 170.18(5), Pt1−P1−Pt2 = 113.27(7), P1−Pt2−Br3 = 94.98(4); Pt1−P1−Br2−P2 = 5.69(4), Pt1−P1−Br2−Br1 = −1.66(4), P1−Br2−Br1−P2 = 6.46(5), Pt1−P1−Br2−Pt2 = 140.28(7), Pt1−P1−Br2/Pt2−P1−Br3 = 78.18(8), Pt1−P1−P2/C1−C2 = 6.0(4): λ

The Unusual Trinuclear Phosphido-Bridged Complexes [(+)$_δ$-L$_2$M$_3$Hal$_4$]

The dinuclear compounds **[(+)$_δ$-LMHal]$_2$** discussed above are ubiquitous in the chemistry of palladium(II) and platinum(II). However, the trinuclear compounds **[(+)$_δ$-L$_2$M$_3$Hal$_4$]** discussed here are extremely rare. Formally MX_2 is inserted into the dinuclear compounds **[(+)$_δ$-LMHal]$_2$** as shown in Scheme 2.

Seven of the eight characterized trinuclear complexes were isolated during crystallization attempts of the mononuclear complexes **[(+)$_δ$-LH]MHal$_2$**. Only the (R_P,R_P) isomer of the palladium chloride series was obtained by heating **(+)$_δ$-LH** and $PdCl_2$ in toluene. As indicated in Scheme 2 (top) two mononuclear complexes in combination with $MHal_2$ give the trinuclear phosphido- and halide-bridged compounds by twofold HHal elimination.

Many isomers are possible for trinuclear compounds of the type **[(+)$_δ$-L$_2$M$_3$Hal$_4$]**. All halogens can be oriented to one side and the two stereogenic phosphido phosphorus atoms may have the configurations (S_P,S_P), (R_P,R_P), and also (S_P,R_P). All three isomers have been isolated. In addi-

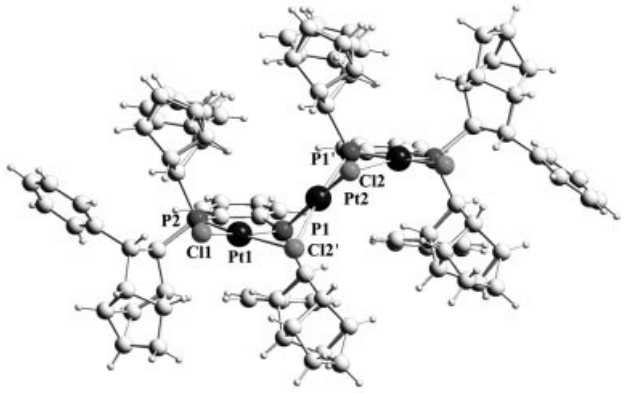

Figure 4. Molecular structure of **(S_P,S_P)-[(+)$_δ$-L$_2$Pt$_3$Cl$_4$]** crystallized from CH_2Cl_2/methanol; selected bond lengths [Å] bond angles [°], and dihedral angles [°]: Pt1···Pt2 = 3.135(1), P1···Cl2 = 3.172(4), Pt1−P1 = 2.237(3), Pt1−Cl1 = 2.384(3), Pt1−Cl2 = 2.531(2), Pt1−P2 = 2.209(3), Pt2−P1 = 2.262(3), Pt2−Cl2 = 2.585(2); P2−Pt1−P1 = 88.54(10), P1−Pt1−Cl2 = 83.17(8), Cl2−Pt1−Cl1 = 88.37(8), Cl1−Pt1−P2 = 99.65(10), P2−Pt1−Cl2 = 171.49(8), P1−Pt1−Cl1 = 169.45(10), P1−Pt2−P1′ = 112.83(9), Cl2−Pt2−Cl2′ = 84.46(7), P1−Pt2−Cl2 = 81.47(8), P1−Pt2−Cl2′ = 165.51(8); Pt1−P1−Cl2−P2 = −1.40(6), Pt1−P1−Cl2−Cl1 = −4.38(7), P1−Cl2−Cl1−P2 = 2.62(9), Pt2−P1−Cl2−Cl2′ = 2.55(6), Pt2−P1−Cl2−P1′= −2.37(5), P1−P1′−Cl2′−Cl2 = 4.96(7), Pt1−P1−Cl2−Pt2 = 121.42(10), Pt1−P1−P2/C1−C2 = 4.0(6): δ

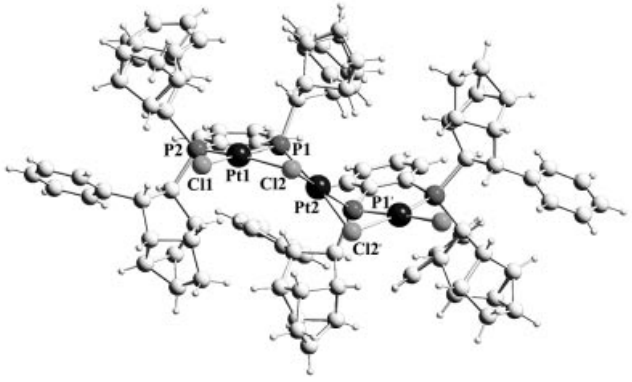

Figure 5. Molecular structure of **(R_P,R_P)-[(+)$_δ$-L$_2$Pt$_3$Cl$_4$]**, crystallized from CH_2Cl_2/ethanol; selected bond lengths [Å], bond angles [°], and dihedral angles [°]: Pt1···Pt2 = 3.206(32), P1···Cl2 = 3.050(4), Pt1−P1 = 2.236(24), Pt1−Cl1 = 2.385(21), Pt1−Cl2 = 2.434(8), Pt1−P2 = 2.215(4), Pt2−P1 = 2.254(2), Pt2−Cl2 = 2.450(11); P2−Pt1−P1 = 88.61(7), P1−Pt1−Cl2 = 81.41(6), Cl2−Pt1−Cl1 = 89.29(7), Cl1−Pt1−P2 = 100.63(8), P2−Pt1−Cl2 = 169.54(7), Cl1−Pt1−P1 = 170.67(8), P1−Pt2−P1′ = 112.44(7), Cl2′−Pt2−Cl2 = 85.90(6), Cl2−Pt2−P1 = 80.71(6), P1−Pt2−Cl2′ = 165.95(6); Pt1−P1−Cl2−Cl1 = 0.55(5), Pt1−P1−Cl2−P2 = 2.27(5), P1−Cl2−Cl1−P2 = 1.50(7), Pt2−P1−Cl2−Cl2′ = −3.15(5), Pt2−P1−Cl2−P1′ = 1.37(4), P1−P1′−Cl2′−Cl2 = −4.50(6), Pt1−P1−Cl2−Pt2 = 128.96(7), Pt1−P1−P2/C1−C2 = 3.9(4): δ

Table 2. Roof angles, M···M distances, square deformations, chelate angles, and helicity of the trinuclear complexes **(S_P,S_P)-**, **(R_P,R_P)-**, and **(S_P,R_P)-[(+)$_\delta$-L$_2$M$_3$Hal$_4$]**

	(S_P,S_P)-[(+)$_\delta$-L$_2$Pd$_3$Br$_4$]		**(R_P,R_P)-[(+)$_\delta$-L$_2$Pd$_3$Br$_4$]**
			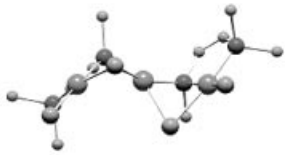
Complex	(S_P,S_P)	Data	(R_P,R_P)
[(+)$_\delta$-L$_2$Pd$_3$Cl$_4$]	132.02	roof angle [°] Pd1−P1−Cl2−Pd2	128.69
	3.223	distance [Å] Pd1···Pd2	3.157
	4.29, 0.68	square deformation [°][a]	6.02, 6.31
	5.8, δ	angle [°] Pd1−P1−P2/C1−C2, helicity[b]	1.83, δ
[(+)$_\delta$-L$_2$Pd$_3$Br$_4$]	124.02	roof angle [°] Pd1−P1−Br2−Pd2	156.40
	3.156	distance [Å] Pd1···Pd2	2.934
	12.41, 17.44	square deformation [°][a]	3.73, 29.29
	1.8, δ	angle [°] Pd1−P1−P2/C1−C2, helicity[b]	1.3, λ
[(+)$_\delta$-L$_2$Pt$_3$Cl$_4$]	121.42	roof angle [°] Pt1−P1−Cl2−Pt2	128.96
	3.135	distance [Å] Pt1···Pt2	3.206
	2.62, 4.96	square deformation [°][a]	1.50, 4.50
	4.0, δ	angle [°] Pt1−P1−P2/C1−C2, helicity[b]	3.9, δ
[(+)$_\delta$-L$_2$Pt$_3$Br$_4$]	127.16	roof angle [°] Pt1−P1−Br2−Pt2	132.77
	3.216	distance [Å] Pt1···Pt2	3.258
	12.47, 15.30	square deformation [°][a]	0.60, 12.09
	2.7, δ	angle [°] Pt1−P1−P2/C1−C2, helicity[b]	1.5, δ

(S_P,R_P)-[(+)$_\delta$-L$_2$Pt$_3$Br$_4$]

[a] First entry left peripheral square P2−P1−Hal2−Hal1, second entry central square P1−P1′−Hal2′−Hal2. [b] Chelate ring of left peripheral square.

tion, there should be isomers having the halogens on different sides. Such isomers have not been observed up to now. The (+)-9-phenyldeltacyclanyl substituents in the trinuclear compounds have the same stereochemistry. It is the configuration of the two stereogenic phosphorus atoms which gives rise to the differences between the diastereomers.

The three isomers for the trinuclear complexes having all the halides on one side are shown at the bottom of Scheme 2. In the PdCl, PdBr, and PtCl series the diastereomers **(S_P,S_P)-** and **(R_P,R_P)-[(+)$_\delta$-L$_2$M$_3$Hal$_4$]** could be isolated and characterized. In the PtBr series the diastereomers **(S_P,S_P)-** and **(S_P,R_P)-[(+)$_\delta$-L$_2$M$_3$Hal$_4$]** were obtained.

All the new complexes are bent at the phosphido and halo bridges. This bending leads to chair and boat configurations for the three-square arrays in the trinuclear complexes **(S_P,S_P)-**, **(R_P,R_P)-**, and **(S_P,R_P)-[(+)$_\delta$-L$_2$M$_3$Hal$_4$]**. The chair configurations contain a C_2 axis passing through the central metal atoms. They subdivide into the diastereomers **(S_P,S_P)-** and **(R_P,R_P)-[(+)$_\delta$-L$_2$M$_3$Hal$_4$]** differing only in the phosphorus configuration. The isomer **(S_P,R_P)-[(+)$_\delta$-L$_2$Pt$_3$Br$_4$]** has a symmetry plane passing through the central Pt atom (without consideration of the chiral deltacyclanyl substituents). It is *meso*-configurated with respect to its central core.

Trinuclear compounds consisting of an array of three square-planar units connected by bridges are peculiar and rare. Whereas mononuclear compounds, such as $(PPh_3)_2PdCl_2$, and their chloro-bridged dinuclear pendants, e.g. $(PPh_3)ClPd(\mu\text{-}Cl)_2PdCl(PPh_3)$, are common, the corresponding trinuclear compound $(PPh_3)ClPd(\mu\text{-}Cl)_2Pd(\mu\text{-}Cl)_2PdCl(PPh_3)$ is unknown. For trinuclear phosphido-bridged complexes there is precedent in the literature.[11] In 2001 a series of new trinuclear complexes was described, which in contrast to our compounds (two phosphido and

two halide bridges) contained four diphenylphosphido bridges.[12] An X-ray structural analysis of one of the trinuclear complexes showed a chair configuration with regard to the three-square array. The roof angles between the squares were 152.7° in agreement with our results.

The trinuclear compounds **(S_P,S_P)-** and **(R_P,R_P)-[(+)$_\delta$-$L_2Pt_3Cl_4$]** were isolated in attempts to crystallize **[(+)$_\delta$-LH)PtCl$_2$]** from CH_2Cl_2 and CH_2Cl_2/EtOH, respectively. Both compounds were characterized by X-ray crystallography. A comparison of the structural parameters of the diastereomeric platinum chloride complexes **(S_P,S_P)-** and **(R_P,R_P)-[(+)$_\delta$-$L_2Pt_3Cl_4$]** shows that there are no large differences (Figures 4 and 5). The roof angles are very similar (121.42 and 128.96°, respectively) and the deformations of the peripheral and central squares P2−P1−Cl2−Cl1 and P1−P1′−Cl2′−Cl2 are insignificant (Table 2). The chelate rings Pt1−P1−C1−C2−P2 of the diastereomeric complexes are only slightly disturbed (2.7 and 1.5° respectively) both having δ chirality. Obviously, four chloride ligands on one side and four phosphorus atoms on the other side do not result in distinct distortions of the two diastereomers with opposite chair chirality.

With respect to structural aspects palladium compounds are similar to their platinum analogues. Accordingly, the palladium chloride diastereomers **(S_P,S_P)-** and **(R_P,R_P)-[(+)$_\delta$-$L_2Pd_3Cl_4$]** closely resemble their platinum congeners (Tables 2, 5 and 6).

In contrast to the platinum chloride and palladium chloride series, the two (S_P,S_P) and (R_P,R_P) diastereomers in the palladium bromide system show large differences (Tables 2 and 5). The roof angle of **(S_P,S_P)-[(+)$_\delta$-$L_2Pd_3Br_4$]** is more than 30° smaller than the roof angle of **(R_P,R_P)-[(+)$_\delta$-$L_2Pd_3Br_4$]**, which inversely affects the Pd−Pd distances. With 12.41 and 17.44°, respectively, the deformations of the peripheral and central squares P2−P1−Br2−Br1 and P1−P1′−Br2′−Br2 of the (S_P,S_P) diastereomer are strong but similar. In the (R_P,R_P) diastereomer, however, the peripheral squares are nearly undisturbed (3.73°), whilst the central square P1−P1′−Br2′−Br2 is extremely distorted (29.29°) as obvious from the formula in the upper right-hand corner of Table 2. The chelate rings in **(S_P,S_P)-** and **(R_P,R_P)-[(+)$_\delta$-$L_2Pd_3Br_4$]** are almost planar having opposite helicity (Table 2).

Similar to the trinuclear palladium bromide compounds the trinuclear platinum bromide complexes exhibited strong distortions. Table 2 shows that **(S_P,S_P)-[(+)$_\delta$-$L_2Pt_3Br_4$]** closely resembles the corresponding palladium derivative (Table 6) but the diastereomer **(R_P,R_P)-[(+)$_\delta$-$L_2Pt_3Br_4$]**, which would have been expected to be heavily distorted, could not be obtained at all. Instead, the only boat isomer **(S_P,R_P)-[(+)$_\delta$-$L_2Pt_3Br_4$]** was isolated (Figure 6, Table 2 bottom right).

In the boat isomer **(S_P,R_P)-[(+)$_\delta$-$L_2Pt_3Br_4$]** the left side (Table 2) and the right side of the molecule were appreciably different. Whereas the peripheral square on the right side was nearly planar (0.60°), the left and the central squares were distorted (13.90 and 11.97°, respectively). The boat isomer also had two unequal roof angles (left side 144.01°, right side 132.77°) resulting in a difference of the metal−metal distances of approximately 0.2 Å. The chelate rings Pt1−P1−C1−C2−P2 and Pt1′−P1′−C1′−C2′−P2′ on the two sides are only slightly disturbed (1.5 and 5.9°, respectively) both having δ chirality.

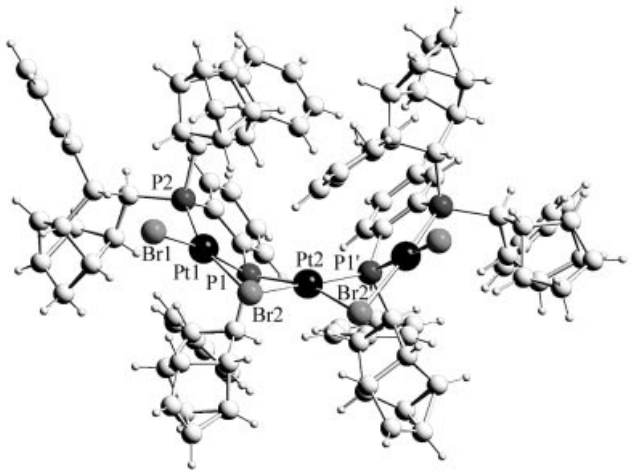

Figure 6. Molecular structure of **(R_P,S_P)-[(+)$_\delta$-$L_2Pt_3Br_4$]**, crystallized from benzene; selected bond lengths [Å], bond angles [°], and dihedral angles [°]: Pt1···Pt2 = 3.258(1), P1···Cl2 = 3.258(1), Pt1−P1 = 2.213(2), Pt1−Br1 = 2.483(2), Pt1−Br2 = 2.528(2), Pt1−P2 = 2.200(3), Pt2−P1 = 2.253(3), Pt2−Br2 = 2.575(2); P2−Pt1−P1 = 89.64(11), P1−Pt1−Br2 = 84.02(8), Br2−Pt1−Br1 = 89.82(5), Br1−Pt1−P2 = 96.41(9), P2−Pt1−Br2 = 173.37(9), P1−Pt1−Br1 = 173.19(9), P1−Pt2−Br2 = 82.15(8), P1−Pt2−P1′ = 113.87(11), Br2−Pt2−Br2′ = 84.68(5), P1−Pt2−Br2′ = 160.80(9); Pt1−P1−Br2−P2 = 1.37(6), Pt1−P1−Br2−Br1 = 2.05(6), P1−Br2−Br1−P2 = −0.60(8), Pt2−P1−Br2−Br2′ = −5.96(6), Pt2−P1−Br2−P1′ = 6.01(6), P1−P1′−Br2′−Br2 = −12.09(8), Pt1−P1−Br2−Pt2 = 132.77(11), Pt1−P1−P2/C1−C2 = 1.5(8): δ; Pt1′−P1′−P2′/C1′−C2′ = 5.9(7): δ

Experimental Section

General Remarks: All reactions were performed under dry nitrogen using standard Schlenk techniques. Solvents were purified and dried by standard procedures. *P,P,P′*-Tris[(+)-9-phenyldeltacyclan-8-yl)-1,2-bis(phosphanyl)benzene **[(+)$_\delta$-LH]** was prepared as described in the previous paper. Spectroscopy and analyses as in the previous paper. For the AA′XX′ systems in the ^{31}P NMR spectra the chemical shifts of the signals are given.

(S_P,S_P)-[(+)$_\delta$-LNiBr]$_2$: A suspension of **(+)$_\delta$-LH** (0.57 g, 0.77 mmol) and anhydrous $NiBr_2$ (0.18 g, 0.77 mmol) was heated for 30 min in ethanol (150 mL) in the presence of 2 g of Na_2CO_3. After cooling to room temperature, the red solution was concentrated, the residue dissolved in acetone and filtered through silica gel. Evaporation of the solvent and crystallization of the residue from CH_2Cl_2 provided **(S_P,S_P)-[(+)$_\delta$-LNiBr]$_2$** (0.20 g) as red crystals in 30% yield, m.p. > 250 °C. ^{1}H NMR ($CDCl_3$): δ = 3.48−0.38 (m, 60 H, aliph. H), 7.91−6.34 (m, 38 H, arom. H) ppm. ^{31}P NMR ($CDCl_3$): δ = 45.42, 44.99, 44.36, 43.93 (PR_2); −52.73, −53.17, −53.80, −54.23 (PR) ppm. MS (FD, CH_2Cl_2): *m*/*z* = 1724.6 [M^+].

(R_P,R_P)-[(+)$_\delta$-LNiBr]$_2$: A suspension of **(+)$_\delta$-LH** (0.32 g, 0.44 mmol) and anhydrous $NiBr_2$ (0.10 g, 0.44 mmol) was heated in CH_2Cl_2 (50 mL) for 1 h. After the addition of *n*BuLi (0.5 mL, 0.74 mmol, 1.6 M solution in hexane), the solution was heated for

another 30 min, cooled to room temperature, filtered through silica gel, and concentrated. Crystallization from acetone provided **(R_P,R_P)-[(+)$_\delta$-LNiBr]$_2$** (0.20 g) as brown crystals in 54% yield, m.p. > 250 °C. ^{1}H NMR ($CDCl_3$): δ = 3.73−0.64 (m, 60 H, aliph. H), 7.90−5.90 (m, 38 H, arom. H) ppm. ^{31}P NMR ($CDCl_3$): δ = 44.78, 44.22, 43.68, 43.11, (PR_2); −69.86, −70.43, −70.98, −71.53 (PR) ppm. MS (FD, CH_2Cl_2): *m*/*z* = 1724.3 [M^+].

(S_P,S_P)-[(+)$_\delta$-LPdCl]$_2$: A suspension of **(+)$_\delta$-LH** (0.34 g, 0.47 mmol) and Na_2PdCl_4 (0.14 g, 0.47 mmol) in ethanol was stirred at room temperature for 36 h, followed by filtration through silica gel and concentration. Crystallization from CH_2Cl_2/Et_2O gave **(S_P,S_P)-[(+)$_\delta$-LPdCl]$_2$** (0.39 g) as pale yellow crystals in 95% yield, m.p. > 250 °C. $C_{102}H_{98}Cl_2P_4Pd_2$ (1731.5): calcd. C 70.75, H 5.70; found C 70.57, H 5.88. ^{1}H NMR ($CDCl_3$): δ = 4.95−0.20 (m, 60 H, aliph. H), 7.87−6.39 (m, 38 H, arom. H) ppm. ^{31}P NMR ($CDCl_3$): δ = 54.72, 54.00, 53.44, 51.96, 51.40, 50.71 (PR_2); −49.35, −50.07, −50.63, −52.11, −52.67, −53.37, (PR) ppm. MS (FAB, CH_2Cl_2): *m*/*z* = 1731.3 [M^+].

(R_P,R_P)-[(+)$_\delta$-LPdCl]$_2$: Compound **(+)$_\delta$-LH** (0.18 g, 0.25 mmol) and KO*t*Bu (0.028 g, 0.25 mmol) were stirred in THF. After 1 h, $(PhCN)_2PdCl_2$ (0.095 g, 0.25 mmol) was added to the pale yellow solution which was then stirred at room temperature for another 16 h. Evaporation of the solvent provided **(R_P,R_P)-[(+)$_\delta$-LPdCl]$_2$** (0.20 g) as a dark orange powder in 93% yield, m.p. > 250 °C. $C_{102}H_{98}Cl_2P_4Pd_2$ (1731.5): calcd. C 70.75, H 5.70; found C 70.52, H 5.93. ^{1}H NMR ($CDCl_3$): δ = 5.06−0.34 (m, 60 H, aliph. H), 7.94−6.28 (m, 38 H, arom. H) ppm. ^{31}P NMR ($CDCl_3$): δ = 60.73, 60.01, 56.31, 57.92, 57.22, 56.49 (PR_2); −72.25, −72.97, −73.66, −75.06, −75.75, −76.47, (PR) ppm. MS (FAB, CH_2Cl_2): *m*/*z* = 1731.3 [M^+].

(S_P,S_P)-[(+)$_\delta$-LPdBr]$_2$: Na_2PdCl_4 (0.094 g, 0.32 mmol) and a twelvefold excess of LiBr (0.34 g) were suspended at room temperature in 20 mL of ethanol. After 30 min, **(+)$_\delta$-LH** (0.23 g, 0.32 mmol) was added to the dark red solution, which was stirred for another 16 h. Filtration through silica gel and evaporation of the solvent gave **(S_P,S_P)-[(+)$_\delta$-LPdBr]$_2$** (0.27 g) as an orange powder in 94% yield, m.p. > 250 °C. $C_{102}H_{98}Br_2P_4Pd_2$ (1820.4): calcd. C 67.30, H 5.43; found C 67.05, H 5.59. ^{1}H NMR ($CDCl_3$): δ = 5.05−0.15 (m, 60 H, aliph. H), 7.86−6.36 (m, 38 H, arom. H) ppm. ^{31}P NMR ($CDCl_3$): δ = 55.11, 54.45, 53.90, 52.41, 51.86, 51.21 (PR_2); −51.73, −52.40, −52.95, −54.44, −54.99, −55.66 (PR) ppm. MS (ESI, CH_3OH): *m*/*z* = 1820.2 [M^+].

(S_P,S_P)-[(+)$_\delta$-LPdI]$_2$: Compound **(+)$_\delta$-LH** (0.24 g, 0.33 mmol) and PdI_2 (0.12 g, 0.33 mmol) were suspended in toluene and stirred at

Table 3. Crystal data, data collection, structure refinement, and CCDC numbers

	(S_P,S_P)-[(+)$_\delta$-LNiBr]$_2$	**(R_P,R_P)-[(+)$_\delta$-LNiBr]$_2$**	**(S_P,S_P)-[(+)$_\delta$-LPdCl]$_2$**	**(R_P,R_P)-[(+)$_\delta$-LPdCl]$_2$**
Empirical formula	$C_{102}H_{98}Br_2Ni_2P_4{\cdot}2CH_2Cl_2$	$C_{102}H_{98}Br_2Ni_2P_4$	$C_{102}H_{98}Cl_2P_4Pd_2$	$C_{102}H_{98}Cl_2P_4Pd_2{\cdot}1.5C_3H_6O$
M_r	1894.72	1724.87	1731.43	1818.50
Crystal system	monoclinic	triclinic	monoclinic	monoclinic
Space group	$P2_1$	$P1$	$P2_1$	$P2_1$
Z	2	1	2	2
Unit cell dimensions	a = 11.1744(7) Å b = 25.1435(11) Å c = 15.5240(9) Å β = 94.157(7) °	a = 10.3853(6) Å b = 14.1556(8) Å c = 16.8320(11) Å α = 107.957(7)° β = 95.405(7)° γ = 104.448(7)°	a = 11.2145(9) Å b = 25.2275(12) Å c = 15.6089(10) Å β = 93.020(8)°	a = 10.3483(7) Å b = 26.2025(12) Å c = 18.0479(12) Å β = 91.314(8)°
Volume	4350.2(4) Å^3	2239.8(3) Å^3	4409.8(5) Å^3	4892.4(5) Å^3
$D_{calcd.}$	1.446 g/cm^3	1.279 g/cm^3	1.304 g/cm^3	1.234 g/cm^3
Absorption coefficient	1.60 mm^{-1}	1.43 mm^{-1}	0.59 mm^{-1}	0.534 mm^{-1}
F(000)	1960	896	1792	1888
Crystal size	0.30 × 0.26 × 0.18 mm	0.24 × 0.16 × 0.04 mm	0.30 × 0.15 × 0.06 mm	0.40 × 0.30 × 0.25 mm
Crystal shape	prism	plate	plate	prism
Crystal color	red	brown	colorless	yellow
θ range for data collection	1.83−25.78°	2.22−25.17°	1.99−25.78°	1.92−25.19°
Limiting indices	$-13 \le h \le 13$ $-30 \le k \le 30$ $-18 \le l \le 18$	$-10 \le h \le 12$ $-15 \le k \le 16$ $-20 \le l \le 19$	$-13 \le h \le 13$ $-30 \le k \le 30$ $-28 \le l \le 18$	$-12 \le h \le 12$ $-31 \le k \le 31$ $-21 \le l \le 21$
Reflections collected	39823	12586	39695	52100
Independent reflections (R_{int})	16334 (0.0503)	11690 (0.0903)	16357 (0.0695)	17488 (0.0387)
Reflections $I > 2\sigma(I)$	14147	6183	13803	14440
Data/restraints/parameters	16334/1/1045	11690/3/991	16357/1/991	17488/1/1002
Absorption correction	numerical	numerical	none	none
Transmission (min/max)	0.8087/0.7268	0.9357/0.7861	−/−	−/−
Goodness-of-fit on F^2	1.412	0.807	0.983	0.966
Final R indices [$I > 2\sigma(I)$]	R_1 =0.0323 wR_2 = 0.0618	R_1 =0.0605 wR_2 = 0.1301	R_1 = 0.0458 wR_2 = 0.1035	R_1 = 0.0362 wR_2 = 0.0904
R indices (all data)	R_1 =0.0404 wR_2 = 0.0626	R_1 =0.1023 wR_2 = 0.1434	R_1 = 0.0534 wR_2 = 0.1062	R_1 = 0.0446 wR_2 = 0.0935
Absolute structure parameter	0.01(1)	0.02(1)	−0.03(2)	−0.01(1)
Largest diff. peak/hole	1.028/−0.383 e Å^{-3}	0.582/−0.656 e Å^{-3}	1.865/−0.627 e Å^{-3}	2.459/−0.474 e Å^{-3}
CCDC-	179308	179311	179309	179312

Table 4. Crystal data, data collection, structure refinement, and CCDC numbers

	(S_P,S_P)-[(+)$_\delta$-LPdBr]$_2$	**(S_P,S_P)-[(+)$_\delta$-LPdI]$_2$**	**(S_P,S_P)-[(+)$_\delta$-LPtCl]$_2$**	**(R_P)-[(+)$_\delta$-LPt$_2$Br$_3$(cod)]**
Empirical formula	$C_{102}H_{98}Br_2P_4Pd_2{\cdot}2CH_2Cl_2$	$C_{102}H_{98}I_2P_4Pd_2{\cdot}2CH_2Cl_2$	$C_{102}H_{98}Cl_2P_4Pt_2{\cdot}CH_2Cl_2$	$C_{59}H_{57}Br_3P_2Pt_2{\cdot}C_6H_6$
M_r	1990.18	2084.18	1993.68	1535.96
Crystal system	monoclinic	monoclinic	monoclinic	monoclinic
Space group	$P2_1$	$P2_1$	$P2_1$	$P2_1$
Z	2	2	2	4
Unit cell dimensions	a = 11.2099(7) Å b = 25.1732(11) Å c = 15.6498(10) Å β = 93.853(8)°	a = 11.2685(4) Å b = 25.1820(13) Å c = 15.6705(5) Å β = 93.332(4)°	a = 10.8345(5) Å b = 15.8537(8) Å c = 25.3733(15) Å β = 97.999(7)°	a = 23.3980(15) Å b = 10.6649(7) Å c = 24.8351(17) Å β = 109.9660(7)°
Volume	4406.2(4) Å^3	4439.2(3) Å^3	4315.9(4) Å^3	5824.8(7) Å^3
$D_{calcd.}$	1.500 g/cm^3	1.559 g/cm^3	1.534 g/cm^3	1.752 g/cm^3
Absorption coefficient	1.56 mm^{-1}	1.34 mm^{-1}	3.485 mm^{-1}	6.950 mm^{-1}
F(000)	2032	2104	2004	2976
Crystal size	0.65 × 0.40 × 0.12 mm	0.12 × 0.08 × 0.04 mm	0.40 × 0.10 × 0.10 mm	0.32 × 0.20 × 0.08 mm
Crystal shape	prism	prism	prism	plate
Crystal color	yellow	yellow	colorless	colorless
θ range for data collection	2.08−25.81°	1.98−25.78°	2.07−25.89°	1.85−25.80°
Limiting indices	$-13 \le h \le 13$ $-30 \le k \le 30$ $-19 \le l \le 19$	$-13 \le h \le 10$ $-30 \le k \le 30$ $-18 \le l \le 17$	$-13 \le h \le 12$ $-19 \le k \le 19$ $-31 \le l \le 30$	$-28 \le h \le 28$ $-13 \le k \le 13$ $-30 \le l \le 30$
Reflections collected	62739	23846	32914	61516
Independent reflections (R_{int})	16897 (0.0390)	15618 (0.0619)	16160 (0.0558)	22238 (0.0521)
Reflections $I > 2\sigma(I)$	15985	9593	13960	16785
Data/restraints/parameters	16897/1/1045	15618/1/1045	16160/1/1018	22238/1/1297
Absorption correction	numerical	empirical	numerical	numerical
Transmission (min/max)	0.8416/0.5277	0.823/0.459	0.7326/0.5938	0.6144/0.2603
Goodness-of-fit on F^2	0.996	0.631	0.970	0.872
Final R indices [$I > 2\sigma(I)$]	R_1 = 0.0221 wR_2 = 0.0520	R_1 = 0.039 wR_2 0.0593	R_1 = 0.0379 wR_2 = 0.0880	R_1 = 0.0305 wR_2 = 0.0673
R indices (all data)	R_1 = 0.0241 wR_2 = 0.0526	R_1 = 0.0814 wR_2 = 0.0710	R_1 = 0.0444 wR_2 = 0.0896	R_1 = 0.0423 wR_2 = 0.0696
Absolute structure parameter	0.00(1)	−0.04(2)	−0.01(1)	−0.03(1)
Largest diff. peak/hole	0.644/−0.389 e Å^{-3}	0.593/−0.786 e Å^{-3}	2.618/−0.702 e Å^{-3}	2.649/−0.913 e Å^{-3}
CCDC-	179315	179316	179322	179319

room temperature for 16 h. Filtration through silica gel, evaporation of the solvent and crystallization from CH_2Cl_2/Et_2O provided **(S_P,S_P)-[(+)$_\delta$-LPdI]$_2$** (0.25 g) as red crystals in 78% yield, m.p. > 250 °C. $C_{102}H_{98}I_2P_4Pd_2$ (1914.4): calcd. C 63.90, H 5.30; found C 64.04, H 5.17. ^{1}H NMR ($CDCl_3$): δ = 5.25−0.14 (m, 60 H, aliph. H), 7.84−6.42 (m, 38 H, arom. H) ppm. ^{31}P NMR ($CDCl_3$): δ = 56.63, 56.01, 55.48, 53.99, 53.47, 52.84 (PR_2); −61.50, −62.12, −62.64, −64.14, −64.66, −65.29 (PR) ppm. MS (ESI, CH_2Cl_2): m/z = 1914.9 [M^+].

(S_P,S_P)-[(+)$_\delta$-LPtCl]$_2$: Compound **(S_P,S_P)-[(+)$_\delta$-LPtCl]$_2$** was isolated as colorless crystals during crystallization of **[(+)$_\delta$-LH]PtCl$_2$** (described in the previous paper) in CH_2Cl_2/MeOH, m.p. > 250 °C. ^{1}H NMR ($CDCl_3$): δ = 5.07−0.20 (m, 60 H, aliph. H), 7.83−6.38 (m, 38 H, arom. H) ppm. ^{31}P NMR ($CDCl_3$): δ = 49.94, 49.53, 49.23, 47.52, 47.23, 46.76 (PR_2); −67.53, −67.99, −68.26, −70.02, −70.30, −70.76 (PR, $^1J_{PtP}$ = 2009 Hz) ppm. MS (ESI, CH_2Cl_2/MeOH): m/z = 1873.2 [(M − Cl)$^+$].

(R_P)-[(+)$_\delta$-LPt$_2$Br$_3$(cod)]: Compound **(R_P)-[(+)$_\delta$-LPt$_2$Br$_3$(cod)]** was isolated during crystallization of **[(+)$_\delta$-LH)PtBr$_2$** [described in the previous paper and prepared from Pt(cod)Br$_2$] in benzene.

(S_P,S_P)-[(+)$_\delta$-L$_2$Pd$_3$Cl$_4$]: Compound **(S_P,S_P)-[(+)$_\delta$-L$_2$Pd$_3$Cl$_4$]** was isolated as orange crystals during crystallization of **[(+)$_\delta$-LH]PdCl$_2$** (described in the previous paper) in CH_2Cl_2/Et_2O, m.p. > 250 °C. ^{1}H NMR ($CDCl_3$): δ = 4.93−0.23 (m, 60 H, aliph. H), 7.88−6.42 (m, 38 H, arom. H) ppm. ^{31}P NMR ($CDCl_3$): δ = 101.24, 101.21 (PR); 71.17, 71.14, 71.10, 71.06 (PR_2) ppm. MS (FAB, CH_2Cl_2): m/z = 1908.3 [M^+].

(R_P,R_P)-[(+)$_\delta$-L$_2$Pd$_3$Cl$_4$]: Compound **(+)$_\delta$-LH** (0.20 g, 0.28 mmol) and $PdCl_2$ (0.05 g, 0.28 mmol) were heated in toluene (50 mL) for 16 h. After cooling to room temperature, the dark red solution was filtered through silica gel and concentrated. Crystallization from CH_2Cl_2/Et_2O provided **(R_P,R_P)-[(+)$_\delta$-L$_2$Pd$_3$Cl$_4$]** (0.18 g) as orange crystals in 52% yield, m.p. > 250 °C. $C_{102}H_{98}Cl_4P_4Pd_3$ (1908.8): calcd. C 64.18, H 5.17; found C 64.05, H 5.30. ^{1}H NMR ($CDCl_3$): δ = 4.95−0.20 (m, 60 H, aliph. H), 7.89−6.39 (m, 38 H, arom. H) ppm. ^{31}P NMR ($CDCl_3$): δ = 95.71, 95.58, 95.56, 95.50, 95.47, 95.35 (PR); 74.01, 73.88, 73.85, 73.80, 73.77, 73.65 (PR_2) ppm. MS (FAB, CH_2Cl_2): m/z = 1908.5 [M^+].

(S_P,S_P)-[(+)$_\delta$-L$_2$Pd$_3$Br$_4$]: Compound **(S_P,S_P)-[(+)$_\delta$-L$_2$Pd$_3$Br$_4$]** was isolated as red crystals during crystallization of **[(+)$_\delta$-LH]PdBr$_2$** (described in the previous paper) in CH_2Cl_2/Et_2O, m.p. > 250 °C. $C_{102}H_{98}Br_4P_4Pd_3$ (2086.6): calcd. C 58.71, H 4.73; found C 58.22, H 5.10. ^{1}H NMR ($CDCl_3$): δ = 4.95−0.20 (m, 60 H, aliph. H), 7.89−6.39 (m, 38 H, arom. H) ppm. ^{31}P NMR ($CDCl_3$): δ =

Table 5. Crystal data, data collection, structure refinement, and CCDC numbers

	(S_P,S_P)-[(+)$_\delta$-$L_2Pd_3Cl_4$]	**(R_P,R_P)-[(+)$_\delta$-$L_2Pd_3Cl_4$]**	**(S_P,S_P)-[(+)$_\delta$-$L_2Pd_3Br_4$]**	**(R_P,R_P)-[(+)$_\delta$-$L_2Pd_3Br_4$]**
Empirical formula	$C_{102}H_{98}Cl_4P_4Pd_3$	$C_{102}H_{98}Cl_4P_4Pd_3 \cdot 3.25C_3H_6O$	$C_{102}H_{98}Br_4P_4Pd_3 \cdot 4C_6H_6 \cdot CH_2Cl_2$	$C_{102}H_{98}Br_4P_4Pd_3 \cdot 3C_4H_{10}O$
M_r	1908.68	2097.44	2483.91	2308.88
Crystal system	orthorhombic	orthorhombic	orthorhombic	orthorhombic
Space group	$P2_12_12$	$C222_1$	$P22_12_1$	$P2_12_12_1$
Z	4	4	2	4
Unit cell dimensions	a = 16.1149(15) Å	a = 15.1572(7) Å	a = 10.8826(4) Å	a = 10.5228(6) Å
	b = 23.404(4) Å	b = 19.8262(8) Å	b = 16.8315(10) Å	b = 29.3284(14) Å
	c = 26.315(3) Å	c = 37.3399(19) Å	c = 29.5292(12) Å	c = 32.6634(17) Å
Volume	9925(2) Å^3	11221.0(9) Å^3	5408.9(4) Å^3	10080.5(9) Å^3
$D_{calcd.}$	1.277 g/cm^3	1.242 g/cm^3	1.525 g/cm^3	1.472 g/cm^3
Absorption coefficient	0.752 mm^{-1}	0.674 mm^{-1}	2.130 mm^{-1}	2.23 mm^{-1}
F(000)	3904	4320	2516	4528
Crystal size	0.34 × 0.20 × 0.12 mm	0.40 × 0.24 × 0.20 mm	0.20 × 0.10 × 0.08 mm	0.26 × 0.10 × 0.03 mm
Crystal shape	plate	prism	prism	plate
Crystal color	red	red	orange	red
θ range for data collection	2.00−25.99°	2.01−25.14°	1.83−25.26°	1.87−24.78°
Limiting indices	$-19 \le h \le 18$	$-18 \le h \le 18$	$-12 \le h \le 12$	$-12 \le h \le 12$
	$-28 \le k \le 28$	$-23 \le k \le 23$	$-20 \le k \le 20$	$-34 \le k \le 34$
	$-32 \le l \le 30$	$-44 \le l \le 44$	$-35 \le l \le 34$	$-38 \le l \le 38$
Reflections collected	69751	35924	40151	69645
Independent reflections (R_{int})	18994 (0.1856)	9999 (0.0329)	9693 (0.0392)	17170 (0.1024)
Reflections $I > 2\sigma(I)$	13910	9690	8775	11165
Data/restraints/parameters	18994/0/497	9999/0/518	9693/0/632	17170/0/1058
Absorption correction	none	none	numerical	numerical
Transmission (min/max)	−/−	−/−	0.8008/0.7209	0.8816/0.6554
Goodness-of-fit on F^2	1.051	1.095	0.988	0.893
Final R indices [$I > 2\sigma(I)$]	R_1 = 0.1171	R_1 = 0.0278	R_1 = 0.0261	R_1 = 0.0567
	wR_2 = 0.2913	wR_2 = 0.0831	wR_2 = 0.0601	wR_2 = 0.1029
R indices (all data)	R_1 = 0.1349	R_1 = 0.0294	R_1 = 0.0305	R_1 = 0.0964
	wR_2 = 0.3065	wR_2 = 0.0837	wR_2 = 0.0612	wR_2 = 0.1135
Absolute structure parameter	0.18(6)	−0.02(2)	0.00(1)	0.02(1)
Largest diff. peak/hole	6.233/−1.097 e Å^{-3}	0.792/−0.675 e Å^{-3}	0.487/−0.650 e Å^{-3}	1.272/−0.639 e Å^{-3}
CCDC-	179313	179310	179317	179314

104.65, 104.60, 104.40, 104.29 (PR); 73.81, 73.75, 73.71, 73.66 (PR_2) ppm. MS (ESI, CH_3OH): m/z = 2086.2 [M^+].

(R_P,R_P)-[(+)$_\delta$-$L_2Pd_3Br_4$]: Compound **(R_P,R_P)-[(+)$_\delta$-$L_2Pd_3Br_4$]** was isolated as red crystals during crystallization of **[(+)$_\delta$-LH]PdBr$_2$** (described in the previous paper) in acetone m.p. > 250 °C.

(S_P,S_P)-[(+)$_\delta$-$L_2Pt_3Cl_4$]: Compound **(S_P,S_P)-[(+)$_\delta$-$L_2Pt_3Cl_4$]** was isolated as yellow crystals during crystallization of **[(+)$_\delta$-LH]PtCl$_2$** (described in the previous paper) in CH_2Cl_2.

(R_P,R_P)-[(+)$_\delta$-$L_2Pt_3Cl_4$]: Compound **(R_P,R_P)-[(+)$_\delta$-$L_2Pt_3Cl_4$]** was isolated as yellow crystals during crystallization of **[(+)$_\delta$-LH]PtCl$_2$** (described in the previous paper) in CH_2Cl_2/ethanol, m.p. > 250 °C. $C_{102}H_{98}Cl_4P_4Pt_3$ (2174.8). ^{1}H NMR ($CDCl_3$): δ = 4.95−0.23 (m, 60 H, aliph. H), 7.86−6.16 (m, 38 H, arom. H) ppm. ^{31}P NMR ($CDCl_3$): δ = 43.81 (PR); 18.21 (PR_2) ppm. MS (ESI, CH_2Cl_2/CH_3OH): m/z = 2139.1 [(M − Cl)$^+$].

(S_P,S_P)-[(+)$_\delta$-$L_2Pt_3Br_4$]: Compound **(S_P,S_P)-[(+)$_\delta$-$L_2Pt_3Br_4$]** was isolated as yellow crystals during crystallization of **[(+)$_\delta$-LH]PtBr$_2$** (described in the previous paper) in benzene and in CH_2Cl_2/EtOH, m.p. > 250 °C. $C_{102}H_{98}Br_3P_4Pt_3$ (2352.6): calcd. C 52.07, H 4.20, Br 13.59; found C 53.26, H 4.85, Br 13.12. ^{1}H NMR ($CDCl_3$): δ = 5.16−0.20 (m, 60 H, aliph. H), 7.66−6.09 (m, 38 H, arom. H) ppm. ^{31}P NMR ($CDCl_3$): δ = 49.32 (PR); 10.74 (PR_2, $^1J_{PtP}$ = 4374 Hz) ppm. MS (ESI, CH_2Cl_2/MeOH): m/z = 2272.6 [(M − Br)$^+$].

(R_P,S_P)-[(+)$_\delta$-$L_2Pt_3Br_4$]: Compound **(R_P,S_P)-[(+)$_\delta$-$L_2Pt_3Br_4$]** was isolated as yellow crystals during crystallization of **[(+)$_\delta$-LH]PtBr$_2$** (described in the previous paper) in CH_2Cl_2/ethanol m.p. > 250 °C. MS (ESI CH_2Cl_2/MeOH): m/z = 2272.6 [(M − Br)$^+$].

X-ray Crystallographic Studies: The data were collected with a STOE-IPDS diffractometer with Mo-K_α radiation and graphite monochromator at a temperature of 173(1) K. Crystal data, data collection, structure refinement, and CCDC numbers for all complexes are given in Tables 3−6. The structures were solved by direct methods (SIR-97) and refined by full-matrix least squares on F^2 (SHELXL-97). The H atoms were calculated geometrically and a riding model was applied during the refinement process. Absorption corrections, when necessary, were carried out numerically from crystal shape (x-RED)[13] or emperical (PLATON)[14]. CCDC numbers given in Tables 3−6 contain the supplementary crystallographic data for this paper. These data can be obtained free of charge at www.ccdc.cam.ac.uk/conts/retrieving.html or from the Cambridge Crystallographic Data Centre 12 Union Road Cambridge CB2 1EZ, UK [Fax: (internat.) + 44-1223/336-033; E-mail: deposit@ccdc.cam.ac.uk].

Table 6. Crystal data, data collection, structure refinement, and CCDC numbers

	(S_P,S_P)-[(+)$_\delta$-$L_2Pt_3Cl_4$]	(R_P,R_P)-[(+)$_\delta$-$L_2Pt_3Cl_4$]	(S_P,S_P)-[(+)$_\delta$-$L_2Pt_3Br_4$]	(S_P,R_P)-[(+)$_\delta$-$L_2Pt_3Br_4$]
Empirical formula	$C_{102}H_{98}Cl_4P_4Pt_3{\cdot}CH_3OH$	$C_{102}H_{98}Cl_4P_4Pt_3{\cdot}CH_2Cl_2$	$C_{102}H_{98}Br_4P_4Pt_3{\cdot}4C_6H_6$	$C_{102}H_{98}Br_4P_4Pt_3$
M_r	2206.77	2259.66	2662.95	2352.53
Crystal system	orthorhombic	monoclinic	orthorhombic	orthorhombic
Space group	$P22_12_1$	$P2_1$	$P22_12_1$	$P2_12_12_1$
Z	4	2	4	4
Unit cell dimensions	a = 16.6511(9) Å b = 21.5999(14) Å c = 26.1655(17) Å β = 90°	a = 14.554(3) Å b = 21.655(4) Å c = 16.011(3) Å β = 103.54(2)°	a = 10.8380(4) Å b = 16.7888(7) Å c = 29.7005(15) Å β = 90°	a = 10.6592(6) Å b = 25.4143(13) Å c = 37.398(2) Å β = 90°
Volume	9410.7(10) Å^3	4905.9(17) Å^3	5404.2(4) Å^3	10131.0(9) Å^3
$D_{calcd.}$	1.558 g/cm^3	1.530 g/cm^3	1.637 g/cm^3	1.542 g/cm^3
Absorption coefficient	4.677 mm^{-1}	4.540 mm^{-1}	5.461 mm^{-1}	5.815 mm^{-1}
F(000)	4360	2228	2620	4576
Crystal size	0.26 × 0.16 × 0.06 mm	0.69 × 0.52 × 0.10 mm	0.52 × 0.20 × 0.12 mm	0.18 × 0.17 × 0.17 mm
Crystal shape	plate	plate	plate	prism
Crystal color	yellow	yellow	yellow	yellow
θ range for data collection	1.73−25.14°	1.95−25.07°	1.83−25.25°	1.69−23.85°
Limiting indices	$-19 \le h \le 19$ $-25 \le k \le 25$ $-31 \le l \le 31$	$-17 \le h \le 17$ $-25 \le k \le 25$ $-19 \le l \le 19$	$-12 \le h \le 12$ $-20 \le k \le 20$ $-35 \le l \le 35$	$-12 \le h \le 12$ $-28 \le k \le 28$ $-42 \le l \le 42$
Reflections collected	57178	63890	57351	66093
Independent reflections (R_{int})	16522 (0.0828)	17287 (0.0647)	9732 (0.0851)	14904 (0.0868)
Reflections $I > 2\sigma(I)$	12317	16162	8984	12959
Data/restraints/parameters	16522/0/1031	17287/1/1045	9732/0/558	14904/0/998
Absorption correction	numerical	numerical	numerical	numerical
Transmission (min/max)	0.7474/0.4094	0.6125/0.0900	0.6035/0.3017	0.5512/0.3228
Goodness-of-fit on F^2	0.926	1.034	1.026	1.036
Final R indices [$I > 2\sigma(I)$]	R_1 = 0.0427 wR_2 = 0.0923	R_1 = 0.0351 wR_2 = 0.086	R_1 = 0.0298 wR_2 = 0.0732	R_1 = 0.0542 wR_2 = 0.1277
R indices (all data)	R_1 = 0.0657 wR_2 = 0.0978	R_1 = 0.0380 wR_2 = 0.0875	R_1 = 0.0334 wR_2 = 0.0747	R_1 = 0.0629 wR_2 = 0.1314
Absolute structure parameter	−0.01(1)	0.01(1)	−0.03(1)	0.02(1)
Largest diff. peak/hole	2.670/−0.728 e Å^{-3}	1.646/−1.315 e Å^{-3}	1.489/−0.476 e Å^{-3}	2.964/−1.065 e Å^{-3}
CCDC-	179323	179321	179320	179318

[1] H. Brunner, S. Dormeier, M. Zabel, *Eur. J. Inorg. Chem.*, **2002**, 2594−2602.
[2] H. Brunner, M. Muschiol, F. Prester, *Angew. Chem.* **1990**, *102*, 680; *Angew. Chem. Int. Ed. Engl.* **1990**, *29*, 653.
[3] H. Brunner, F. Prester, *J. Organomet. Chem.* **1991**, *414*, 401.
[4] H. Brunner, A. Reimer, *Chem. Ber./Recueil* **1997**, *130*, 1495.
[5] S. Dormeier, Dissertation, Universität Regensburg, **2001**.
[6] G. Aullón, G. Ujaque, A. Lledós, S. Alvarez, P. Alemany, *Inorg. Chem.* **1998**, *37*, 804.
[7] G. Aullón, A. Lledós, S. Alvarez, *Inorg. Chem.* **2000**, *39*, 906.
[8] A. J. Carty, F. Hartstock, N. J. Taylor, *Inorg. Chem.* **1982**, *21*, 1349.
[9] T. Gebauer, G. Frenzen, K. Dehnicke, *Z. Naturforsch., Teil B* **1992**, *47*, 1505.
[10] M. A. Zhuravel, J. R. Moncarz, D. S. Glueck, *Organometallics* **2000**, *19*, 3447.
[11] R. Glaser, D. J. Kountz, R. D. Waid, J. C. Gallucci, D. W. Meek, *J. Am. Chem. Soc.* **1984**, *106*, 6324.
[12] E. Alonso, J. M. Casas, J. Forniés, C. Fortuno, A. Martin, A. G. Orpen, C. A. Tsipis, A. C. Tsipis, *Organometallics* **2001**, *20*, 5571.
[13] x-RED: Program for reduction of IPDS-data, version 1.10, STOE & Cie GmbH, Darmstadt, **1998**.
[14] A. L. Spek, *Acta Crystallogr., Sect. A* **1990**, *46*, C-34.

Received February 20, 2002
[I02097]

Chiral Mono- and Bidentate Ligands Derived from D-Mannitol and Their Application in Rhodium(I)-Catalyzed Asymmetric Hydrogenation Reactions

Alexander Bayer,[a] Petra Murszat,[a] Ulf Thewalt,[b] and Bernhard Rieger*[a]

Keywords: Chiral pool / P ligands / Rhodium / Asymmetric catalysis / Hydrogenation

The new monodentate phosphoramidites **8a**–**g** and bidentate phospholanes **13a**–**e** are prepared in an ex-chiral-pool synthesis from D-mannitol. Chiral diols **7a**–**g**, obtained via nucleophilic ring opening of bis(epoxides) **6a**–**b**, are the key intermediates for the production of both classes of ligands. Treatment of **8a**–**g** or **13a**–**e** with $[PdCl_2(COD)]$ or $[Rh(COD)_2][SO_3CF_3]$ yield the corresponding Pd (**10a, 10f, 15a**) and Rh compounds (**9a**–**g** and **14a**–**e**), respectively. The C_2 symmetry of the complexes in the solid state is demonstrated by X-ray structure investigations performed on **10a**, **10f** and **15a**. Surprisingly high enantioselectivities in the asymmetric hydrogenation of itaconic acid (94% *ee*) and α-acetamidocinnamic acid (89% *ee*) are observed on using the Rh complex **9g** bearing two monodentate phosphoramidite ligands. Although the chelating bis(phospholanes) described herein are more effective, the adjustable synthesis of the monodentate phosphoramidites may permit the optimization of asymmetric catalytic reactions.
(© Wiley-VCH Verlag GmbH, 69451 Weinheim, Germany, 2002)

Introduction

The enantioselective hydrogenation of prochiral olefins plays an important role in the application of homogeneous catalysts. The development of suitable ligands for rhodium(I) species started in 1968 with Wilkinson-type complexes.[1,2] They used chiral monophosphane ligands, e.g. methyl(phenyl)(*n*-propyl)phosphane, which led to poor enantioselectivities in rhodium(I)-catalyzed hydrogenation reactions (3−15% *ee*). Also, other monodentate ligands failed to produce high enantioselectivities, while cyclohexyl(*o*-anisyl)methylphosphane (CAMP) was one of the rare exceptions (90% *ee* for hydrogenation of dehydroamino acids).[3] With the introduction of Kagan's DIOP, the first chiral diphosphane,[4] the research focussed on bidentate ligands. Knowles et al. showed that DIPAMP, another chelating diphosphane, is superior to PAMP, the corresponding monodentate species, with respect to rhodium-catalyzed hydrogenation reactions.[5] The use of bidentate ligands such as BINAP[6] and DuPHOS,[7] have also led to extremely high enantiomeric excess values. These chelating compounds are supposed to be superior because of the resulting rigid catalysts which favor effective chiral induction.[8] Monodentate ligands have been neglected in asymmetric hydrogenation reactions until Pringle et al. questioned the superiority of the bidentate species. They found higher enantioselectivities (92% *ee*) when using an asymmetric monophosphonite compared with the corresponding C_2-symmetric diphosphonite in the hydrogenation of methyl 2-(acetamido)acrylate.[9] Excellent enantioselectivities (> 99% *ee*) are also reported with monodentate phosphites[10] and phosphoramidites.[11] These new monodentate ligands have an enantiomerically pure binaphthol fragment in common. Based on the X-ray data of a platinum(II) complex, Pringle showed that the *cis* coordination of two sterically demanding monophosphonite ligands favors one stable conformation at the metal center, so that rotation about the M−P bond is prevented. Quadrant diagrams demonstrate the edge-on conformation of the bulky binaphthol moiety, presumably causing the asymmetric induction.[9]

Our approach to achieve high enantioselectivities in asymmetric hydrogenation reactions is not based on a single chiral auxiliary group. We present a highly variable ex-chiral-pool synthesis in order to generate monodentate phosphoramidites bearing four stereogenic centers, differing in the absolute configuration of carbon atoms and the steric demand of the substituents. This synthetic protocol also offers access to functionalized bidentate DuPHOS derivatives. Both types of ligands were tested in the rhodium(I)-catalyzed hydrogenation reaction of itaconic and α-(acetamido)-cinammic acid. The hydrogenation results can be explained with the help of quadrant diagrams based on X-ray data of corresponding palladium(II) complexes.

Ligand and Complex Synthesis

Our approach starts with the chiral building block D-mannitol[12] (**1**, Figure 1), which is converted into the

[a] Department of Inorganic Chemistry II, Materials and Catalysis, University of Ulm
Albert-Einstein-Allee 11, 89069 Ulm, Germany
Fax: (internat.) + 49-(0)731/502-3039
E-mail: bernhard.rieger@chemie.uni-ulm.de
[b] Section for X-ray and Electron Diffraction, University of Ulm
Albert-Einstein-Allee 11, 89069 Ulm, Germany

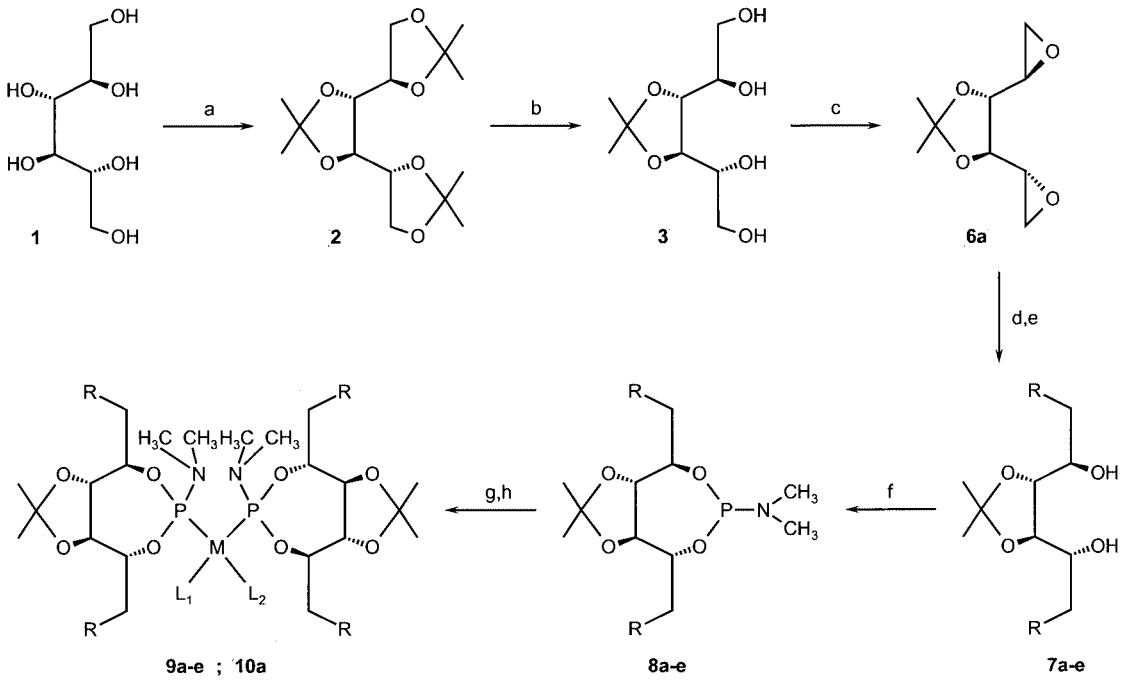

Figure 1. a) acetone, H_2SO_4; b) AcOH, H_2O, 40 °C; c) (i) trimethyl orthoacetate, PPTS, (ii) NEt_3, AcBr, (iii) K_2CO_3, MeOH; d) $LiAlH_4$, Et_2O, R = H (**7a**); e) CuBr·SMe_2, RMgBr, THF/Et_2O, −40 °C, R = CH_3 (**7b**), C_2H_5 (**7c**), iC_4H_9 (**7d**), C_6H_5 (**7e**); f) HMTAP, toluene, reflux; g) $[Rh(COD)_2][SO_3CF_3]$, CH_2Cl_2, **9a**−**e**: M = Rh, L_1-L_2 = COD; h) $[PdCl_2(COD)]$, CH_2Cl_2, **10a**: M = Pd, $L_1 = L_2$ = Cl

1,2;3,4;5,6-tri-*O*-isopropylidene (**2**) and the 3,4-*O*-isopropylidene derivative (**3**).[13,14] The syntheses of 1,2;5,6-dianhydro-3,4-*O*-isopropylidene-D-mannitol (**6a**),[15] the corresponding chiral diols **7a**−**e**,[16,17] the monodentate phosphoramidites **8a**−**e**, the Rh complexes **9a**−**e** and the Pd complex **10a** were recently reported by us.[18]

The highly variable synthetic strategy allows for the conversion of compound **3** (Figure 1) to the diastereomeric bis(epoxide) 1,2;5,6-dianhydro-3,4-*O*-isopropylidene-L-iditol (**6b**, Figure 2), with a changed configuration at carbon atoms C2 and C5 (dibenzoylation of **3**, ditosylation of **4**, subsequent transesterification with concomitant intramole-

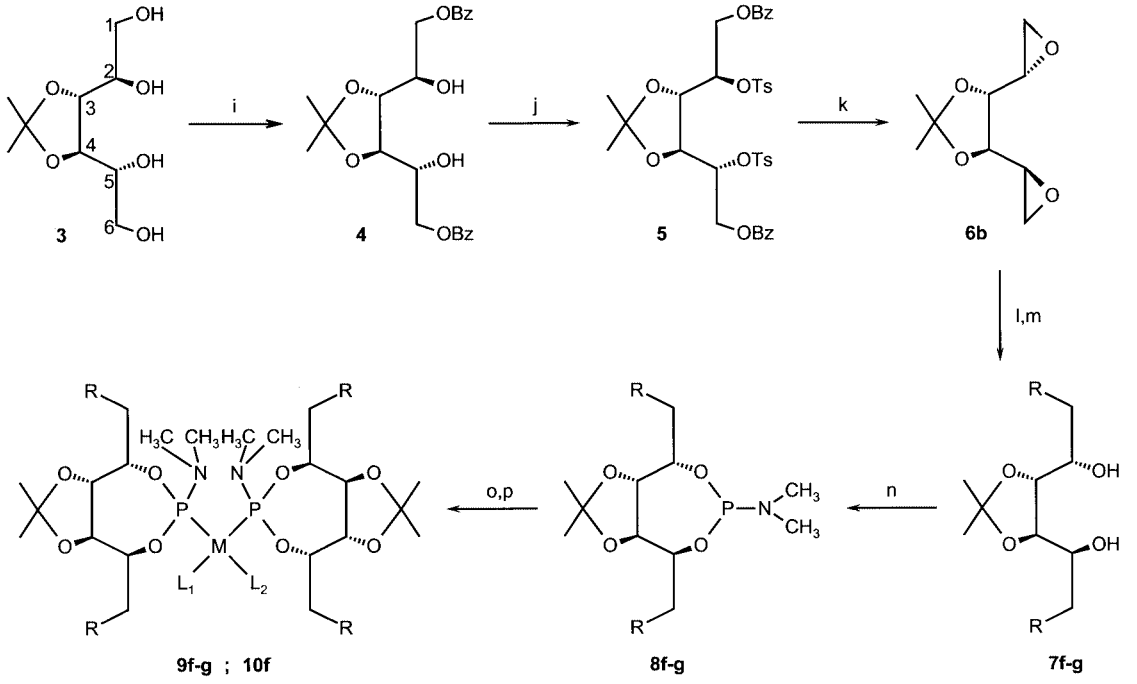

Figure 2. i) benzoyl chloride, pyridine, CH_2Cl_2, −80 °C; j) tosyl chloride, NEt_3, 4-(dimethylamino)pyridine, CH_2Cl_2; k) K_2CO_3, MeOH; l) $LiAlH_4$, Et_2O, R = H (**7f**); m) CuBr·SMe_2, PhMgBr, THF/Et_2O, −40 °C, R = C_6H_5 (**7g**); n) HMTAP, toluene, reflux; o) $[Rh(COD)_2][SO_3CF_3]$, CH_2Cl_2, **9f**−**g**: M = Rh, L_1-L_2 = COD; p) $[PdCl_2(COD)]$, CH_2Cl_2, **10f**: M = Pd, $L_1 = L_2$ = Cl

cular S_N2 reaction of **5**).[13] Nucleophilic attack of $LiAlH_4$ opens the epoxide rings of **6b** to form (2*S*,3*R*,4*R*,5*S*)-3,4-*O*-isopropylidene-2,3,4,5-hexanetetraol (**7f**) in a clean reaction.[16,19] Larger substituents [e.g. (2*S*,3*R*,4*R*,5*S*)-3,4-*O*-isopropylidene-1,6-diphenyl-2,3,4,5-hexanetetraol, **7g**, R = phenyl] can be introduced by nucleophilic ring-opening of **6b** with organocuprate reagents generated from the copper(I) bromide−dimethylsulfide complex and suitable Grignard reagents in diethyl ether.[17,20] Subsequently, the monodentate phosphoramidites **8f**−**g** were synthesized in high yields by refluxing **7f**−**g** and hexamethyltriaminophosphane (HMTAP) in toluene. The corresponding orange Rh complexes **9f**−**g** and the pale yellow Pd compound **10f** were prepared by stirring 2 equiv. of monodentate ligand **9f**−**g** with $[Rh(COD)_2][SO_3CF_3]$ or $[PdCl_2(COD)]$ in dichloromethane.

Access to functionalized DuPHOS ligands was offered by branching off from the key intermediates **7a**−**e** (Figure 3), which were readily converted into the corresponding cyclic sulfates **11a**−**e** by reaction with thionyl chloride, followed by in situ oxidation of the intermediate cyclic sulfite with catalytic amounts of RuO_4.[21,22] The 1,2-bis(phospholano)-benzenes **12a**−**e** were prepared by successive treatment of 1,2-bis(phosphanyl)benzene with 2 equiv. of *n*BuLi, followed by the addition of 2 equiv. of the corresponding cyclic sulfate **11a**−**e** and an additional 2.2 equiv. of *n*BuLi.[8] The chiral bis(phospholanes) **13a**−**e** bearing four free hydroxy groups were synthesized by cleavage of the protecting groups (refluxing **12a**−**e** with methanesulfonic acid in water/methanol).[23−25] The resulting chiral bis(phospholanes) **13a**−**e** were converted into the corresponding yellow-orange Rh complexes **14a**−**e** and the pale yellow Pd analog **15a** by stirring 1 equiv. of **13a**−**e** with $[Rh(COD)_2][SO_3CF_3]$ or $[PdCl_2(COD)]$ in tetrahydrofuran or dichloromethane, respectively.

Structure of $PdCl_2$ Complexes

We were not able to grow suitable crystals of the rhodium complexes for X-ray analysis, but we succeeded in crystallizing the isoelectronic $PdCl_2$ species **10a**, **10f** (from methanol) and **15a** (from acetone/ethyl acetate). The crystallographic data of **10a** (Figure 4) were already reported on in our latest report.[18] The X-ray structure of **10a** (C2, C11, C5, C14: *R*; C3, C12, C4, C13: *S*; "*RSSR*") indicates the *cis* coordination of the two monodentate ligands **8a**, and the expected square-planar coordination environment of Pd^{II} [see (a) in Figure 4, front-view] with a chiral, C_2-symmetric arrangement of both ligands [see (b) in Figure 4, side-view]. Furthermore, Figure 4 (b) clearly shows that the tunable substituents (Figure 1, CH_2−R) of the monodentate phosphoramidites (Figure 4; C1, C10: R = H) occupy the top-left and bottom-right quadrants [see (c) in Figure 4], thereby defining a chiral cage around the metal center. The size of the cage is influenced by the nucleophile (R) used for the epoxide ring opening.

The diastereomeric $PdCl_2$ complex **10f** (C2−C5, C11−C14: *S*; "*SSSS*") also bears two *cis*-coordinated monodentate phosphoramidites **8f**. The C_2 symmetry and the square-planar geometry around the Pd^{II} center was determined by an X-ray structure investigation (Figure 5). The corresponding crystallographic data are listed in Table 1

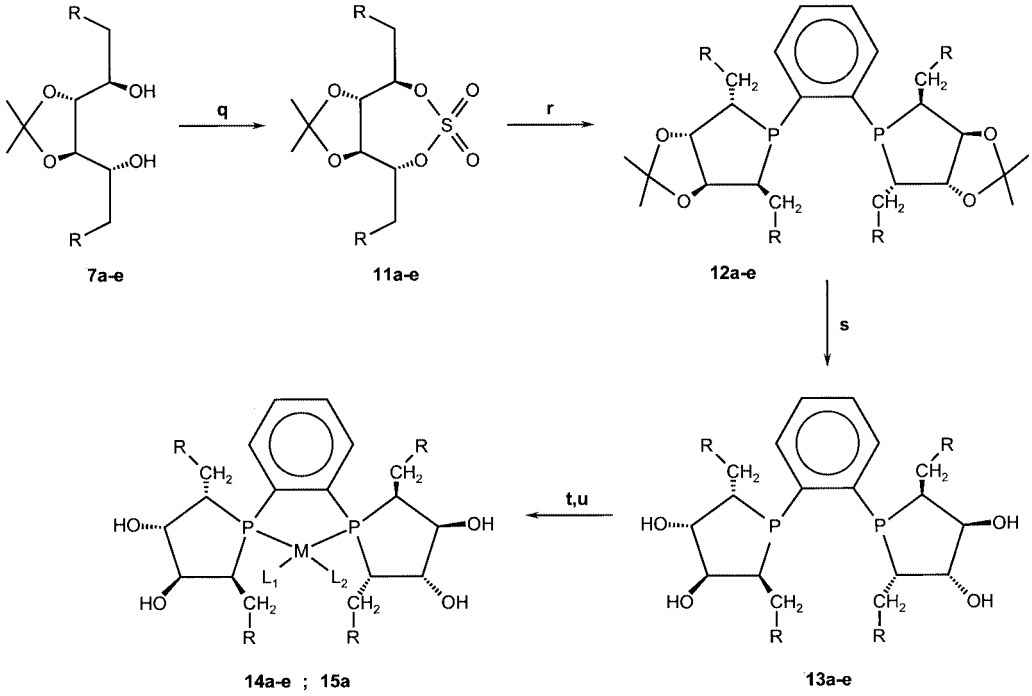

Figure 3. q) (i) $SOCl_2$, NEt_3, CH_2Cl_2; (ii) $NaIO_4/RuCl_3$, $CH_2Cl_2/MeCN/H_2O$; r) (i) 1,2-bis(phosphanyl)benzene, *n*BuLi, THF; (ii) *n*BuLi, THF; s) CH_3SO_3H, MeOH/H_2O, reflux; t) $[Rh(COD)_2][SO_3CF_3]$, THF, **14a**−**e**: M = Rh, L_1-L_2 = COD; u) $[PdCl_2(COD)]$, CH_2Cl_2, **15a**: M = Pd, $L_1 = L_2$ = Cl

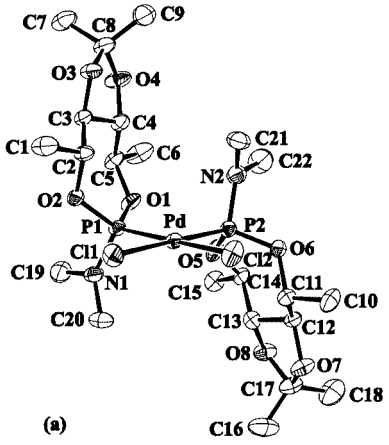

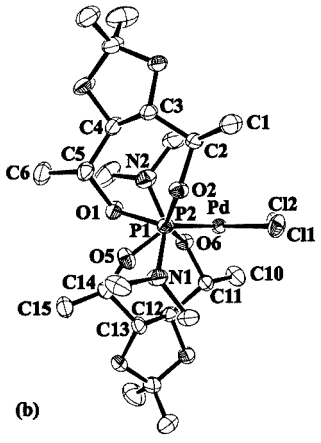

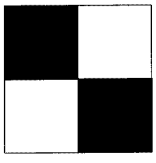

Figure 4. Molecular structure of **10a** (*RSSR*); (a) front-view: square-planar environment of Pd^{II}; (b) side-view: C_2-symmetric arrangement; hydrogen atoms have been omitted for clarity; (c) quadrant diagram

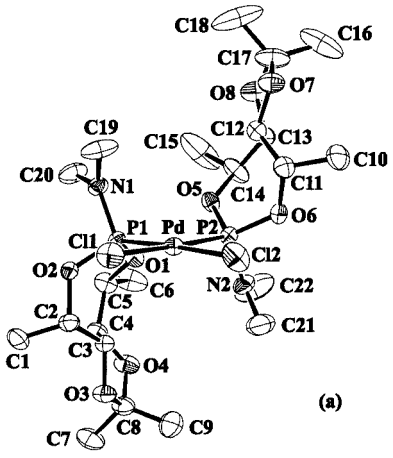

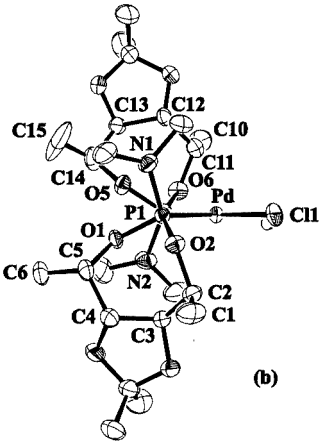

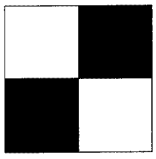

Figure 5. Molecular structure of **10f** (*SSSS*); (a) front-view: square-planar environment of Pd^{II}; (b) side-view: C_2-symmetric arrangement; hydrogen atoms have been omitted for clarity; (c) quadrant diagram

and 3. The side-view shows that the tunable substituents (Figure 2, CH_2-R) of the monodentate ligands (Figure 5; C1, C10: R = H) now occupy the top-right and bottom-left quadrants less effectively than in **10a** [see (c) in Figure 5].

In contrast to **10a** and **10f**, which bear two monodentate ligands each, the Pd^{II} complex **15a** (C2−C5, C8−C11: *S*; "*SSSS*") consists of a chelating bis(phospholane) (**13a**). Figure 6 (a) shows the five-membered phospholane rings and the planarity of the 1,2-phenylene moiety. The top view in Figure 6 (b) verifies the almost perpendicular orientation of the substituents (C1, C6, C7, C12 = CH_3) in the equatorial positions of the phospholane ring relative to the square-planar Pd^{II} environment. The effective occupation of the top-right and bottom-left quadrants is especially due to the free hydroxy groups (O2, O4) in the axial positions of the five-membered rings [Figure 6 (c); Table 2 and 3].

Results in the Asymmetric Hydrogenation Reactions

The synthesized Rh^{I} complexes bearing two monodentate phosphoramidite ligands (**9a**−**g**) or a chelating bis(phospholan)e (**14a**−**e**) were tested in the asymmetric hydrogenation reactions of α-(acetamido)cinnamic acid (**16**) and itaconic acid (**18**). Complexes **9a**−**e** ["*RSSR*", see (A) in Figure 7] produce a small excess of *N*-acetyl-(*R*)-phenylalanine in the hydrogenation of **16** (Table 4, Entries 1−5), ranging

Table 1. Selected bond lengths [Å] and angles [°] in **10f**

Bond lengths			
Pd−Cl1	2.3581(11)	C1−C2	1.501(6)
Pd−Cl2	2.3518(10)	C2−C3	1.499(5)
Pd−P1	2.2412(8)	C3−C4	1.506(5)
Pd−P2	2.2324(10)	C4−C5	1.534(5)
P1−O1	1.585(2)	C5−C6	1.510(6)
P1−O2	1.599(2)	C7−C8	1.512(6)
P1−N1	1.631(3)	C8−C9	1.498(7)
N1−C19	1.471(6)	O3−C3	1.420(4)
N1−C20	1.441(5)	O3−C8	1.441(5)
O1−C5	1.461(4)	O4−C4	1.426(5)
O2−C2	1.475(4)	O4−C8	1.430(5)
Bond angles			
Cl1−Pd−Cl2	90.20(5)	C1−C2−C3	116.5(3)
P1−Pd−Cl1	88.57(4)	C2−C3−C4	115.8(3)
P1−Pd−P2	90.77(4)	C2−C3−O3	113.4(3)
P2−Pd−Cl2	90.53(5)	C3−O3−C8	106.4(3)
P1−Pd−Cl2	177.57(3)	O3−C3−C4	102.2(3)
P2−Pd−Cl1	177.82(4)	O3−C8−C7	107.8(4)
Pd−P1−O1	113.13(10)	O3−C8−C9	110.4(4)
Pd−P1−O2	115.58(9)	O3−C8−O4	106.1(3)
Pd−P1−N1	113.88(12)	C7−C8−C9	113.8(4)
O1−P1−O2	103.14(13)	C7−C8−O4	111.1(4)
O1−P1−N1	106.15(15)	C9−C8−O4	107.4(4)
O2−P1−N1	103.80(15)	C8−O4−C4	106.4(3)
P1−N1−C19	121.3(3)	O4−C4−C5	114.3(3)
P1−N1−C20	123.4(3)	O4−C4−C3	100.1(3)
C19−N1−C20	114.6(3)	C3−C4−C5	116.8(3)
P1−O1−C5	124.4(2)	C4−C5−C6	113.8(4)
P1−O2−C2	123.2(2)	C4−C5−O1	110.9(3)
C1−C2−O2	105.8(3)	O1−C5−C6	106.1(4)
C3−C2−O2	106.8(3)		

from 3 to 36% *ee*. The highest value in this series (36% *ee*) is achieved with **9e** which bears the sterically most demanding benzyl substituent. The absolute configuration (*R*) of our hydrogenation products is in accordance with the prediction of Knowles[26] that the reaction to form (*R*)-amino acids is favored if the top-right quadrant of the catalyst's chiral cage is not occupied [Figure 4 (c)]. On the other hand, the diastereomeric Rh^{I} complexes **9f−g** ["*SSSS*", Figure 7 (B)], with the opposite quadrant geometry [cf. Pd^{II} complex **10f**, Figure 5 (c)], deliver an excess of the (*S*) form of *N*-acetylphenylalanine (**17**) (Entries 6−7). Complex **9g** remarkably yields an 89% *ee* (*S*) due to the benzyl groups, whereas the methyl-substituted analog **9f** only gives a 14% *ee* (*S*).

The methyl substituents in **9a** [Figure 7 (a), *RSSR*, C1, C10] occupy the "front-side" of the catalyst, whereas the same groups in **9f** [Figure 7 (B), *SSSS*, C1, C10] are oriented "sidewards". This leads to overall low enantioselectivities in the case of the methyl derivatives **9a**, **9f** (R = H), but with a trend to better results for **9a**. This situation changes completely for the benzyl-substituted species **9e** [Figure 7 (A)] and **9g** [Figure 7 (B)]. Computer models suggest that the sterically demanding benzyl groups (R = Ph) in **9e** are most probably oriented away from the P1−Pd−P2 plane, pointing into the "free-areas" above and below the coordination plane [Figure 7 (A)]. The changed stereochemistry of C2 and C11 (both *S*) in **9g** provides a "tight chiral cage" in the case of the demanding benzyl substituents in

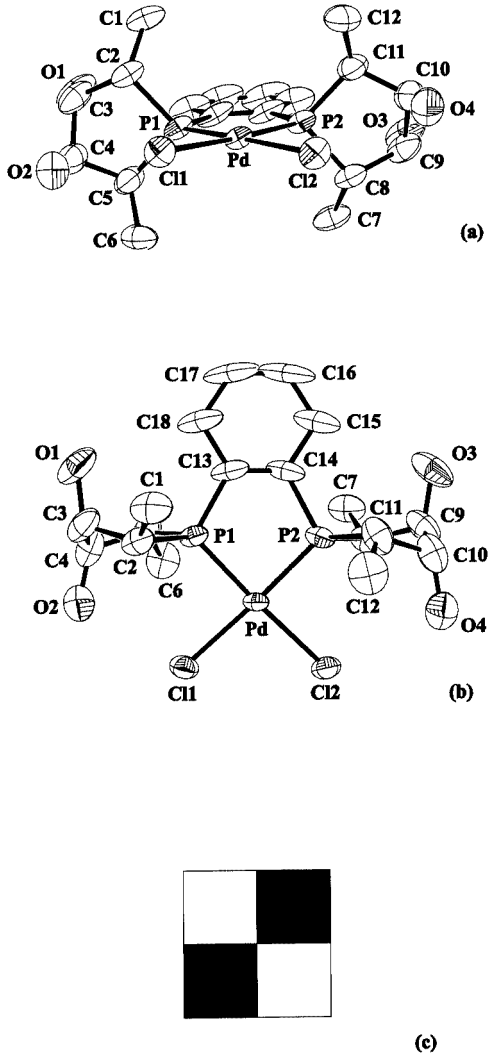

Figure 6. Molecular structure of **15a** (*SSSS*); (a) front-view: square-planar environment of Pd^{II}; (b) top-view: C_2-symmetric arrangement; hydrogen atoms have been omitted for clarity; (c) quadrant diagram

9g, and induces high enantioselectivities due to the "front orientation" of the phenyl fragments. In contrast, the small methyl substituents in **9f** lead to an "open chiral cage" of low enantioselectivity.

Itaconic acid (**18**), our second test olefin, gave the (*S*)-configured product after hydrogenation with **9a−e** ("*RSSR*"). The % *ee* values are higher with increasing steric demand of the substituents at the stereogenic centers C2 and C11 (Table 5, Entries 1−5). Therefore, **9e** gives the best result (61% *ee*) in this series; **9f** also produces a small excess (10% *ee*) of (*S*)-methylsuccinic acid (**19**); **9g** follows the opposite quadrant geometry relative to the former diastereomeric complexes, yielding **19** in an outstanding 94% *ee* (*R*) (Entries 6−7). This indicates that the steric arguments used above (Figure 7) also hold true for other substrates.

The Rh^{I} complexes **14a−e** bearing bidentate ligands once again demonstrate their outstanding ability to induce excellent enantioselectivities in asymmetric hydrogenation reactions. Compounds **14a−e**, with a quadrant diagram ident-

Table 2. Selected bond lengths [Å] and angles [°] in **15a**

Bond lengths			
Pd−Cl1	2.3786(7)	C3−C4	1.535(5)
Pd−P1	2.2301(7)	C4−O2	1.417(4)
P1−C2	1.852(3)	C4−C5	1.555(5)
P1−C5	1.856(4)	C5−C6	1.528(5)
P1−C13	1.815(3)	C13−C14	1.386(7)
C1−C2	1.525(5)	C13−C18	1.399(5)
C2−C3	1.542(4)	C17−C18	1.375(6)
C3−O1	1.421(4)	C16−C17	1.371(10)
Bond angles			
Cl1−Pd−Cl2	94.85(3)	C13−C18−C17	118.6(4)
P1−Pd−Cl1	88.66(2)	C18−C17−C16	121.2(3)
P1−Pd−P2	87.95(4)	C1−C2−C3	116.1(3)
P1−Pd−Cl2	175.73(3)	C2−C3−C4	108.5(2)
Pd−P1−C2	113.95(10)	C2−C3−O1	112.5(3)
Pd−P1−C5	121.13(11)	O1−C3−C4	107.8(3)
Pd−P1−C13	107.90(11)	C3−C4−C5	106.6(3)
P1−C2−C1	114.9(2)	C3−C4−O2	111.6(3)
P1−C2−C3	105.2(2)	O2−C4−C5	113.9(3)
P1−C5−C6	117.4(2)	C4−C5−C6	114.8(3)
P1−C5−C4	105.9(2)	C2−P1−C5	95.09(15)
P1−C13−C14	118.11(10)	C2−P1−C13	110.33(14)
P1−C13−C18	121.7(3)	C5−P1−C13	107.73(15)
C14−C13−C18	120.2(2)		

Table 3. Crystal data and refinement details for **15a** and **10f**

	15a	**10f**
Formula	$C_{18}H_{28}Cl_2O_4P_2Pd$	$C_{22}H_{44}Cl_2N_2O_8P_2Pd$
M_r	547.64	703.83
Crystal system	trigonal	orthorhombic
Space group	$P3_121$	$P2_12_12_1$
T [K]	203	293
a [Å]	10.554(1)	13.969(3)
b [Å]	10.554(1)	14.464(3)
c [Å]	17.876(2)	15.756(4)
V [Å^3]	1724.3(2)	3183.5(12)
Z	3	4
$D_{calcd.}$ [g cm^{-3}]	1.582	1.469
μ [mm^{-1}]	1.20	0.89
Crystal size [mm]	0.30 × 0.18 × 0.12	0.50 × 0.50 × 0.30
θ range [°]	2.23-25.85	2.82−25.98
Measured reflections	13451	33823
Unique reflections	2218	6165
R_{int}	0.048	0.060
Reflections with $I > 2\sigma(I)$	2049	5008
Goodness-of-fit	0.949	0.993
$R_1[F, I > 2\sigma(I)]$	0.020	0.029
$R_1(F$, all data)	0.023	0.041
$wR_2(F^2$, all data)	0.047	0.067
Min./Max. in ΔF [e Å^{-3}]	−0.33/0.33	−0.23/0.39
Absolute struct. parameter	−0.01(3)	−0.02(2)

ical to **10f**, also produce the (*S*) form of **17** in excellent enantioselectivities (up to 99% *ee* for *N*-acetylphenylalanine). This is clearly a consequence of the enhanced rigidity of the phenylene backbone (Table 4, Entries 8−12). The %

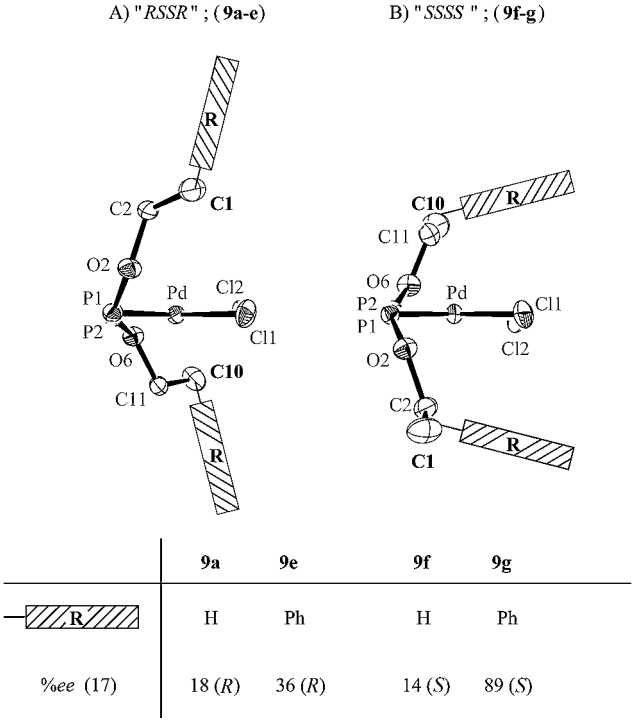

Figure 7. A) Section of Figure 4 (b); "*RSSR*" stereochemistry: aryl substituents occupy top-left and bottom-right quadrant "face-on"; B) section of Figure 5 (b); "*SSSS*" stereochemistry: "edge-on" orientation of aryl substituents in top-right and bottom-left quadrant, defining an effective chiral cage; the given % *ee* values of asymmetric hydrogenation reactions using **9a**,**e**,**f**,**g** are related to *N*-acetylphenylalanine (**17**)

Table 4. Asymmetric hydrogenation of α-(acetamido)cinnamic acid (**16**); the reactions were carried out at room temp. under 1.3 bar of H_2 for 20 h in 5 mL of MeOH with a substrate/[Rh] (10 μmol) ratio of 244; all reactions achieved 100% conversion; the absolute configurations and % *ee* values were determined by chiral HPLC using Daicel chiral column Chiralpak WH 10 μm (250 mm × 4.6) with a Waters HPLC 2690 with UV/Vis detection (λ = 254 nm)

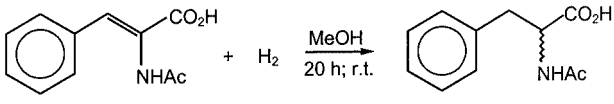

16 **17**

Entry	Catalyst	*ee* (%)
1	**9a**	18 (*R*)
2	**9b**	3 (*R*)
3	**9c**	5 (*R*)
4	**9d**	10 (*R*)
5	**9e**	36 (*R*)
6	**9f**	14 (*S*)
7	**9g**	89 (*S*)
8	**14a**	99 (*S*)
9	**14b**	98 (*S*)
10	**14c**	98 (*S*)
11	**14d**	97 (*S*)
12	**14e**	96 (*S*)

Table 5. Asymmetric hydrogenation of itaconic acid (**18**); the reactions were carried out at room temp. under 1.3 bar of H_2 for 20 h in 5 mL of MeOH with a substrate/[Rh] (10 μmol) ratio of 192; all reactions achieved 100% conversion; the absolute configurations and % *ee* values were determined by chiral HPLC using Daicel chiral column Chiralcel OD 10 μm (250 mm × 4.6) with a Waters HPLC 2690 with UV/Vis detection (λ = 220 nm)

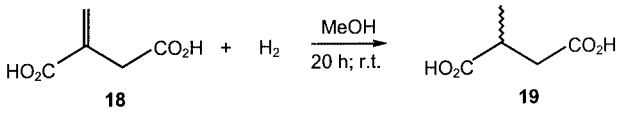

18 **19**

Entry	Catalyst	*ee* (%)
1	**9a**	18 (*S*)
2	**9b**	27 (*S*)
3	**9c**	27 (*S*)
4	**9d**	44 (*S*)
5	**9e**	61 (*S*)
6	**9f**	10 (*S*)
7	**9g**	94 (*R*)
8	**14a**	> 99 (*R*)
9	**14b**	> 99 (*R*)
10	**14c**	98 (*R*)
11	**14d**	99 (*R*)
12	**14e**	98 (*R*)

ee values obtained with the hydroxy-substituted bis(phospholanes) **13a**−**e** are as high as that for the DuPHOS case, but we did not find a maximal enantioselectivity for the *n*-propyl derivative.[8] An increase in the steric demand of our tunable ligands **13a**−**e** lowers the resulting enantiomeric excess of the amino acids produced. Figure 6 (b) shows that mainly the free hydroxy groups in the axial positions claim the top-right and bottom-left quadrant. Raising the steric demand of the equatorial substituents cannot improve the occupation of the crucial areas.

The (*R*) form of methylsuccinic acid (**19**) is produced throughout with very high enantiomeric excess values (up to > 99% *ee*) (Table 5, Entries 8−12). The best enantioselectivities are again produced with the catalysts **14a**,**b** with the smallest substituents in the 2,5-positions of the phospholane moiety.

Conclusion

Recently developed chiral monodentate P-ligands based on binaphthol as the chiral building block show remarkable selectivities in asymmetric hydrogenation reactions. Here, we presented an efficient ex-chiral-pool synthesis starting from D-mannitol, which allows for the tailoring of monodentate phosphoramidites and bidentate phospholanes. The diastereoisomers of these new monodenate ligands allow the exact positioning of substituents with a defined steric demand at the stereogenic centers. The benzyl-substituted Rh^I complex **9g** (up to 94% *ee*) proved that monodentate ligands can be designed for high enantioselectivities in asymmetric catalytic reactions of different substrates. This opens the possibility to fine-tune our ligands and the corresponding metal complexes for given prochiral substrates. A suitable design strategy can be based on relatively simple steric considerations, e.g. the "quadrant model" of Knowles et al. Our results were in accordance with the carefully drawn structure-selectivity relations based on such quadrant diagrams derived from X-ray structures of the corresponding Pd^{II} species.

Experimental Section

General Remarks: All reactions and manipulations were performed using standard Schlenk techniques. The reagents were obtained from Aldrich, Fluka, Merck and Strem and used without purification. Diethyl ether, tetrahydrofuran, toluene and pentane were distilled from $LiAlH_4$, dichloromethane was distilled from CaH_2 under nitrogen. Dry methanol (secco solv) was purchased from Merck. Melting points were determined using a Büchi Melting Point B-540 apparatus and are uncorrected. Optical rotations were obtained using a POLAR monitor from IBZ Messtechnik. Elemental analyses were carried out using an Elementar Vario EL. Mass spectrometry was performed using a Finnigan MAT, TSQ 7000 (FAB; matrix: 2-nitrophenyl octyl ether) and a Finnigan MAT, SSQ 7000 (CI: CH_4; EI: 70 eV). ^1H, ^{13}C, ^{31}P NMR spectra were recorded with a Bruker DRX 400 spectrometer. Chemical shifts are reported in ppm downfield from tetramethylsilane, with the solvent as the internal standard or 85% H_3PO_4 as the external standard. Enantiomeric excess (% *ee*) values were measured using Daicel chiral HPLC columns Chiralcel OD and Chiralpak WH 10 μ m (250 mm × 4.6) with a Waters HPLC 2690 with a Knauer variable UV/Vis detector. Hydrogen (5.0) was purchased from mti. All compounds shown in Figure 1 were reported in our latest report.[18]

Synthesis of Chiral Diols 7f−g

(2*S*,3*R*,4*R*,5*S*)-3,4-*O*-Isopropylidene-2,3,4,5-hexanetetraol (7f): A solution of **6b** (8.85 g, 47.5 mmol) in 50 mL of diethyl ether was slowly added to a stirred suspension of $LiAlH_4$ (3.61 g, 95.1 mmol) in 130 mL of diethyl ether. After refluxing for 3 h, the reaction mixture was carefully hydrolyzed at 0 °C, subsequently with water and diluted sulfuric acid until the white precipitate dissolved. Extraction with diethyl ether, washing the organic layer with $NaHCO_3$, drying with Na_2SO_4 and evaporation of the solvent yielded **7f** as a colorless oil. Yield: 5.60 g, 62.0%. $[\alpha]_D^{25}$ = +26.1 (*c* = 0.44, $CHCl_3$). ^1H NMR (400 MHz, $CDCl_3$): δ = 1.21 (d, 6 H, CH_3), 1.40 (s, 6 H, CH_3), 3.68−3.75 (m, 2 H, CH), 3.76−3.78 (m, 2 H, CH) ppm. ^{13}C NMR: δ = 20.1, 27.4, 67.1, 81.4, 109.4 ppm. MS (CI): *m*/*z* = 335 [MH^+] (+MSTFA). $C_9H_{18}O_4$ (190.24): calcd. C 56.82, H 9.54; found C 54.43, H 9.31.

(2*S*,3*R*,4*R*,5*S*)-3,4-*O*-Isopropylidene-1,6-diphenyl-2,3,4,5-hexanetetraol (7g): $CuBr{\cdot}SMe_2$ (0.62 g, 3 mmol) was added to a stirred suspension of phenylmagnesium bromide (120 mmol) in 100 mL of diethyl ether at −40 °C. After stirring at −40 °C for 2 h, a solution of **6b** (5.59 g, 30 mmol) in 30 mL of tetrahydrofuran was added. After 1 h of stirring at room temp., the mixture was poured into a saturated NH_4Cl solution. The organic layer was extracted, washed with water, dried with Na_2SO_4 and the solvents were evaporated to dryness to give **7g**, after flash chromatography (eluting with hexane/EtOAc, 7:3), as a colorless oil. Yield: 7.82 g, 76.1%. $[\alpha]_D^{21}$ = +10.2 (*c* = 0.53, $CHCl_3$). ^1H NMR (400 MHz, $CDCl_3$): δ = 1.43 (s, 6 H, CH_3), 2.70−2.83 (m, 4 H, CH_2), 3.66−3.71 (m, 2 H, CH), 3.95−3.99 (m, 2 H, CH), 7.13−7.26 (m, 10 H, $CH_{arom.}$) ppm. ^{13}C

NMR: δ = 27.1, 41.1, 70.9, 78.6, 109.3, 126.4, 128.4, 129.2, 137.9 ppm. MS (CI): *m*/*z* = 343 [MH$^+$]. $C_{21}H_{26}O_4$ (342.4): calcd. C 73.66, H 7.65; found C 72.44, H 7.62.

General Procedure for the Synthesis of 8f−g: Chiral diols **7f−g** (6.2 mmol) and NH_4Cl (10 mg) were refluxed in 150 mL of toluene. HMTAP (1.24 mL, 6.8 mmol) was added to this refluxing solution and stirred for a further 8 h. The mixture was concentrated under reduced pressure affording colorless oils.

(4*S*,5*S*,6*S*,7*S*)-5,6-*O*-Isopropylidene-2-(dimethylamino)-4,7-dimethyl-1,3,2-dioxaphosphepane-5,6-diol (8f): Yield: 1.59 g, 97.3%. $[\alpha]_D^{23}$ = −67.1 (*c* = 0.41, $CHCl_3$). ^{1}H NMR (400 MHz, $CDCl_3$): δ = 1.24 (d, 3 H, CH_3), 1.36 (s, 3 H, CH_3), 1.37 (s, 3 H, CH_3), 1.42 (d, 3 H, CH_3), 2.57 (s, 3 H, N−CH_3), 2.60 (s, 3 H, N−CH_3), 4.24−4.27 (m, 1 H, CH), 4.41−4.56 (m, 3 H, CH) ppm. ^{13}C NMR: δ = 15.0, 16.4, 27.2, 34.8, 35.0, 68.4, 69.8, 75.7, 76.3, 110.3 ppm. ^{31}P NMR: δ = 140.48 (s) ppm. MS (CI): *m*/*z* = 264 [MH$^+$]. $C_{11}H_{22}NO_4P$ (263.3): calcd. C 50.18, H 8.42, N 5.32; found C 48.38, H 8.41, N 6.21.

(4*S*,5*S*,6*S*,7*S*)-5,6-*O*-Isopropylidene-2-(dimethylamino)-4,7-dibenzyl-1,3,2-dioxaphosphepane-5,6-diol (8g): Yield: 2.38 g, 92.4%. $[\alpha]_D^{21}$ = −50.0 (*c* = 0.01, $CHCl_3$). ^{1}H NMR (400 MHz, $CDCl_3$): δ = 1.49 (s, 6 H, CH_3), 2.45 (s, 3 H, N−CH_3), 2.48 (s, 3 H, N−CH_3), 2.70−2.78 (m, 1 H, CH_2), 3.09−3.25 (m, 3 H, CH_2), 4.43−4.61 (m, 3 H, CH), 4.73−4.79 (m, 1 H, CH), 7.17−7.29 (m, 10 H, $CH_{arom.}$) ppm. ^{13}C NMR: δ = 27.0, 27.2, 34.3, 34.8, 35.0, 36.7, 73.3, 74.8, 76.4, 77.3, 110.6, 126.09, 126.13, 128.1, 128.2, 129.6, 129.8, 138.8, 139.1 ppm. ^{31}P NMR: δ = 140.24 (s) ppm. MS (CI): *m*/*z* = 417 [MH$^+$]. $C_{23}H_{30}NO_4P$ (415.5): calcd. C 66.49, H 7.28, N 3.37; found C 62.56, H 7.07, N 3.56.

General Procedure for the Synthesis of Rhodium(I) Complexes 9f−g: A solution of 2 equiv. of the corresponding monodentate phosphoramidite **8f−g** in 20 mL of dichloromethane was added to a stirred solution of $[Rh(COD)_2][SO_3CF_3]$ (300 mg, 0.64 mmol) in 30 mL of dichloromethane at 0 °C. After stirring for 2 h at room temp., the solvent was removed under reduced pressure. The resulting orange solid was washed twice with 50 mL of pentane and dried in vacuo.

{Bis[(4*S*,5*S*,6*S*,7*S*)-5,6-*O*-isopropylidene-2-(dimethylamino)-4,7-dimethyl-1,3,2-dioxaphosphepane]Rh^I(COD)} Trifluoromethanesulfonate (9f): Yield: 528 mg, 93.0%. ^{1}H NMR (400 MHz, $CDCl_3$): δ = 1.23 (d, 6 H, CH_3), 1.33 (d, 6 H, CH_3), 1.38 (s, 12 H, CH_3), 2.31−2.57 (m, 8 H, $CH_{2,COD}$), 2.97−3.01 (m, 12 H, N−CH_3), 4.29−4.35 (m, 2 H, CH), 4.41−4.46 (m, 2 H, CH), 4.52−4.64 (m, 4 H, CH), 5.10−5.17 (m, 2 H, CH_{COD}), 5.52−5.59 (m, 2 H, CH_{COD}) ppm. ^{31}P NMR: δ = 117.06 (d) ppm. MS (FAB): *m*/*z* = 737 [(M − $SO_3CF_3^-$)$^+$]. $C_{31}H_{56}F_3N_2O_{11}P_2RhS$ (886.7): calcd. C 41.99, H 6.37, N 3.16; found C 41.87, H 6.48, N 2.55.

{Bis[(4*S*,5*S*,6*S*,7*S*)-5,6-*O*-isopropylidene-2-(dimethylamino)-4,7-dibenzyl-1,3,2-dioxaphosphepane]Rh^I(COD)} Trifluoromethanesulfonate (9g): Yield: 734 mg, 96.2%. ^{1}H NMR (400 MHz, $CDCl_3$): δ = 1.37 (s, 6 H, CH_3), 1.39 (s, 6 H, CH_3), 2.17−2.54 (m, 8 H, CH_{2COD}), 2.38−2.44 (m, 12 H, N−CH_3), 2.60−2.75 (m, 4 H, CH_2), 2.95−3.06 (m, 4 H, CH_2), 4.10−4.16 (m, 2 H, CH), 4.26−4.31 (m, 2 H, CH), 4.45−4.53 (m, 2 H, CH), 4.53−4.59 (m, 2 H, CH), 4.78−4.86 (m, 2 H, CH_{COD}), 5.45−5.53 (m, 2 H, CH_{COD}), 7.05−7.32 (m, 20 H, $CH_{arom.}$) ppm. ^{31}P NMR: δ = 116.60 (d) ppm. MS (FAB): *m*/*z* = 1041 [(M − $SO_3CF_3^-$)$^+$]. $C_{55}H_{72}F_3N_2O_{11}P_2RhS$ (1191.1): calcd. C 55.46, H 6.09, N 2.35; found C 54.28, H 6.22, N 2.31.

{Bis[(4*S*,5*S*,6*S*,7*S*)-5,6-*O*-isopropylidene-2-(dimethylamino)-4,7-dimethyl-1,3,2-dioxaphosphepane]}PdCl$_2$ (10f): A solution of 2 equiv. of the monodentate ligand **8f** in 50 mL of dichloromethane was added to a stirred solution of $[PdCl_2(COD)]$ (500 mg, 1.75 mmol) in 70 mL of dichloromethane at 0 °C. After stirring at room temp. for 2 h, the solvent was removed under reduced pressure. Washing of the residue twice with 50 mL of diethyl ether and drying in vacuo resulted in a pale yellow powder. Yield: 1.13 g, 91.7%. ^{1}H NMR (400 MHz, $CDCl_3$): δ = 1.34 (d, 6 H, CH_3), 1.37 (s, 12 H, CH_3), 1.38 (d, 6 H, CH_3), 2.86−2.89 (m, 12 H, N−CH_3), 4.34−4.44 (m, 4 H, CH), 4.73−4.81 (m, 2 H, CH), 5.20−5.28 (m, 2 H, CH) ppm. ^{13}C NMR: δ = 15.4, 16.7, 26.7, 26.9, 38.1, 72.9, 74.4, 75.4, 75.9, 111.8 ppm. ^{31}P NMR: δ = 101.47 (s) ppm. MS (FAB): *m*/*z* = 669 [(M − Cl$^-$)$^+$]. $C_{22}H_{44}N_2O_8P_2PdCl_2$ (703.9): calcd. C 37.54, H 6.30, N 3.98; found C 35.66, H 6.45, N 4.18.

General Procedure for the Synthesis of the Cyclic Sulfates 11a−e: **11a**,**b** have already been reported.[24] A solution of thionyl chloride (1.91 mL, 26 mmol) in 20 mL of dichloromethane was added to a stirred solution of the corresponding chiral diol **7c−e** (24 mmol) and pyridine (4.26 mL, 53 mmol) in 100 mL of dichloromethane at 0 °C. After 3 h at room temp., the reaction mixture was washed with water and the organic layer extracted, dried with Na_2SO_4 and the solvents were evaporated to dryness. The resulting oil was redissolved in 40 mL of dichloromethane and 40 mL of acetonitrile, and $NaIO_4$ (10.25 g, 48 mmol) and $RuCl_3{\cdot}nH_2O$ (34 mg) in 60 mL of water were then added. After 1 h at room temp., the organic layer was extracted with dichloromethane, washed with brine, dried with Na_2SO_4 and the solvents were evaporated to dryness. The products were isolated by filtration through silica (eluent: dichloromethane). After concentration to dryness, the cyclic sulfates **11c−d** were obtained as colorless crystals, **11e** as a pale yellow oil.

(4*R*,5*S*,6*S*,7*R*)-5,6-*O*-Isopropylidene-4,7-di-*n*-propyl-1,3,2-dioxathiepane 2,2-Dioxide (11c): Yield: 5.48 g, 74.2%; m.p. 36−38 °C. $[\alpha]_D^{24}$ = +45.4 (*c* = 1.0, $CHCl_3$). ^{1}H NMR (400 MHz, $CDCl_3$): δ = 0.94 (t, 6 H, CH_3), 1.38 (s, 6 H, CH_3), 1.41−1.49 (m, 2 H, CH_2), 1.55−1.64 (m, 2 H, CH_2), 1.81−1.86 (m, 4 H, CH_2), 3.98−4.04 (m, 2 H, CH), 4.25−4.31 (m, 2 H, CH) ppm. ^{13}C NMR: δ = 13.5, 18.0, 26.7, 34.2, 79.6, 84.6, 110.5 ppm. MS (CI): *m*/*z* = 309 [MH$^+$]. $C_{13}H_{24}O_6S$ (308.4): calcd. C 50.63, H 7.84; found C 49.81, H 7.69.

(4*R*,5*S*,6*S*,7*R*)-4,7-Diisopentyl-5,6-*O*-isopropylidene-1,3,2-dioxathiepane 2,2-Dioxide (11d): Yield: 7.22 g, 82.6%; m.p. 36−38 °C. $[\alpha]_D^{24}$ = +45.3 (*c* = 1.0, $CHCl_3$). ^{1}H NMR (400 MHz, $CDCl_3$): δ = 0.88−0.90 (m, 12 H, CH_3), 1.23−1.34 (m, 2 H, CH_2), 1.39 (s, 6 H, CH_3), 1.42−1.50 (m, 2 H, CH_2), 1.51−1.61 (m, 2 H, CH), 1.77−1.93 (m, 4 H, CH_2), 3.99−4.04 (m, 2 H, CH), 4.22−4.28 (m, 2 H, CH) ppm. ^{13}C NMR: δ = 22.2, 22.5, 26.8, 27.7, 30.2, 33.6, 79.7, 85.3, 110.6 ppm. MS (CI): *m*/*z* = 365 [MH$^+$]. $C_{17}H_{32}O_6S$ (364.5): calcd. C 56.02, H 8.85; found C 55.41, H 8.89.

(4*R*,5*S*,6*S*,7*R*)-4,7-Dibenzyl-5,6-*O*-isopropylidene-1,3,2-dioxathiepane 2,2-Dioxide (11e): Yield: 8.07 g, 83.2%. $[\alpha]_D^{23}$ = +54.2 (*c* = 1.0, $CHCl_3$). ^{1}H NMR (400 MHz, $CDCl_3$): δ = 1.44 (s, 6 H, CH_3), 3.07−3.18 (m, 4 H, CH_2), 4.02−4.07 (m, 2 H, CH), 4.39−4.45 (m, 2 H, CH), 7.18−7.28 (m, 10 H, $CH_{arom.}$) ppm. ^{13}C NMR: δ = 26.8, 38.1, 78.7, 84.5, 110.9, 127.1, 128.5, 129.6, 135.1 ppm. MS (CI): *m*/*z* = 405 [MH$^+$]. $C_{21}H_{24}O_6S$ (404.49): calcd. C 62.39, H 5.98; found C 59.56, H 5.95.

General Procedure for the Synthesis of the Bis(phospholanes) 12a−e: **12a**,**b** have already been reported.[24] A solution of 1.6 M *n*-butyllithium (8.0 mL, 12.8 mmol) in *n*-hexane was added to a stirred solution of 1,2-bis(phosphanyl)benzene (0.91 g, 6.4 mmol) in 50 mL of

tetrahydrofuran. After 2 h at room temp., the corresponding cyclic sulfate **11c−e** (12.8 mmol) in 50 mL of tetrahydrofuran was added. After an additional 4 h at room temp., *n*-butyllithium (8.8 mL of 1.6 M solution, 14.1 mmol) in *n*-hexane was added. After 16 h at room temp., the excess *n*-butyllithium was hydrolyzed with 3 mL of methanol. The reaction solvents were evaporated to dryness. The resulting yellow oil was extracted twice with 50 mL *n*-pentane. After concentrating to dryness, the bidentate ligands were obtained as a white powder (**12d−e**) or a colorless oil (**12c**).

1,2-Bis[(2*S*,3*S*,4*S*,5*S*)-3,4-*O*-isopropylidene-2,5-diisopropylphospholanyl]benzene (12c): Yield: 2.37 g, 65.8%. $[\alpha]_D^{24}$ = +189.3 (*c* = 0.783, $CHCl_3$). ^{1}H NMR (400 MHz, $CDCl_3$): δ = 0.57 (t, 6 H, CH_3), 0.69−0.78 (m, 2 H, CH_2), 0.85 (t, 6 H, CH_3), 0.95−1.05 (m, 2 H, CH_2), 1.23−1.35 (m, 6 H, CH_2), 1.37−1.42 (m, 2 H, CH_2), 1.44 (s, 6 H, CH_3), 1.45 (s, 6 H, CH_3), 1.47−1.56 (m, 2 H, CH_2), 1.81−1.97 (m, 2 H, CH_2), 2.24−2.29 (m, 2 H, CH), 2.61−2.73 (m, 2 H, CH), 4.33−4.46 (m, 4 H, CH), 7.30−7.38 (m, 4 H, $CH_{arom.}$) ppm. ^{13}C NMR: δ = 13.90, 13.91, 21.6, 22.9, 27.2, 27.3, 29.8, 29.9, 30.6, 30.9, 81.3, 82.2, 117.0, 129.2, 131.1, 141.2 ppm. ^{31}P NMR: δ = 35.95 (s) ppm. MS (CI): *m*/*z* = 563 [MH^+]. $C_{32}H_{52}O_4P_2$ (562.7): calcd. C 68.30, H 9.31; found 64.18, H 8.56.

1,2-Bis[(2*S*,3*S*,4*S*,5*S*)-2,5-diisopentyl-3,4-*O*-isopropylidenephospholanyl]benzene (12d): Yield: 3.00 g, 69.3%; m.p. 125−130 °C. $[\alpha]_D^{23}$ = +136.5 (*c* = 0.31, $CHCl_3$). ^{1}H NMR (400 MHz, $CDCl_3$): δ = 0.48 (d, 6 H, CH_3), 0.59 (d, 6 H, CH_3), 0.72−0.81 (m, 4 H, CH), 0.85 (d, 12 H, CH_3), 0.85−0.90 (m, 2 H, CH_2), 1.04−1.13 (m, 4 H, CH_2), 1.15−1.24 (m, 2 H, CH_2), 1.26−1.42 (m, 4 H, CH_2), 1.46 (s, 6 H, CH_3), 1.47 (s, 6 H, CH_3), 1.47−1.56 (m, 2 H, CH_2), 1.87−2.00 (m, 2 H, CH_2), 2.15−2.20 (m, 2 H, CH), 2.54−2.66 (m, 2 H, CH), 4.32−4.49 (m, 4 H, CH), 7.31−7.37 (m, 4 H, $CH_{arom.}$) ppm. ^{13}C NMR: δ = 22.3, 22.4, 22.6, 22.7, 25.2, 26.1, 27.31, 27.33, 28.2, 28.4, 31.3, 31.4, 38.3, 38.9, 81.3, 82.4, 117.1, 129.2, 131.3, 141.2 ppm. ^{31}P NMR: δ = 36.71 (s) ppm. MS (CI): *m*/*z* = 676 [MH^+]. $C_{40}H_{68}O_4P_2$ (674.9): calcd. C 71.18, H 10.15; found C 67.24, H 9.69.

1,2-Bis[(2*S*,3*S*,4*S*,5*S*)-2,5-dibenzyl-3,4-*O*-isopropylidenephospholanyl]benzene (12e): Yield: 2.64 g, 54.6%; m.p. 136−140 °C. $[\alpha]_D^{23}$ = +28.1 (*c* = 0.089, $CHCl_3$). ^{1}H NMR (400 MHz, $CDCl_3$): δ = 1.47 (s, 12 H, CH_3), 2.05−2.10 (m, 2 H, CH_2), 2.49−2.55 (m, 2 H, CH_2), 2.67−2.73 (m, 2 H, CH_2), 2.79−2.88 (m, 2 H, CH_2), 3.12−3.26 (m, 4 H, CH), 4.43−4.63 (m, 4 H, CH), 6.89−7.44 (m, 24 H, $CH_{arom.}$) ppm. ^{13}C NMR: δ = 27.3, 27.4, 30.9, 32.2, 24.0, 35.1, 81.0, 81.9, 117.8, 125.6, 126.0, 127.8, 128.2, 128.6, 128.9, 129.0, 129.7, 130.8, 141.3, 141.4 ppm. ^{31}P NMR: δ = 42.39 (s) ppm. MS (CI): *m*/*z* = 755 [M^+]. $C_{48}H_{52}O_4P_2$ (754.9): calcd. C 76.37, H 6.94; found C 75.04, H 6.65.

General Procedure for the Synthesis of the Bis(phospholanes) 13a−e: 13a,**b** have already been reported.[24,25] Methanesulfonic acid (1 mL of a 70% solution) in water was added to a stirred solution of the corresponding bis(phospholane) **12c−e** (2.11 mmol) in 50 mL of methanol at room temp. After 2.5 h of stirring under reflux, the reaction solvents were evaporated to dryness. The residue was dissolved in 30 mL of ethyl acetate and 30 mL of water. K_2CO_3 was then added until neutral reaction of litmus. After stirring for several hours, the organic layer was separated and dried with Na_2SO_4. Concentration to dryness yielded bis(phospholanes) **13c−e** as white solids.

1,2-Bis[(2*S*,3*S*,4*S*,5*S*)-3,4-dihydroxy-2,5-di-*n*-propylphospholanyl]benzene (13c): Yield: 0.73 g, 71.9%; m.p. 100−103 °C. $[\alpha]_D^{26}$ = +103.7 (*c* = 0.52, MeOH). ^{1}H NMR (400 MHz, MeOD): δ = 0.69−0.72 (t, 6 H, CH_3), 0.77−0.82 (t, 6 H, CH_3), 1.12−1.36 (m, 12 H, CH_2), 1.53−1.66 (m, 2 H, CH_2), 1.68−1.83 (m, 2 H, CH_2), 2.53−2.66 (m, 2 H, CH), 2.82−2.89 (m, 2 H, CH), 4.14−4.19 (m, 4 H, CH), 7.18−7.22 (m, 2 H, $CH_{arom.}$), 7.89−7.93 (m, 2 H, $CH_{arom.}$) ppm. ^{13}C NMR: δ = 14.9, 15.0, 23.8, 24.4, 30.6, 32.9, 41.7, 45.3, 80.0, 81.0, 129.1, 135.3, 144.8 ppm. ^{31}P NMR: δ = −10.36 (s) ppm. MS (CI): *m*/*z* = 483 [MH^+]. $C_{26}H_{44}O_4P_2$ (482.5): calcd. C 64.72, H 9.19; found C 62.77, H 9.00.

1,2-Bis[(2*S*,3*S*,4*S*,5*S*)-3,4-dihydroxy-2,5-diisopentylphospholanyl]benzene (13d): Yield: 1.13 g, 90.2%; m.p. 150−155 °C. $[\alpha]_D^{24}$ = +89.2 (*c* = 0.25, MeOH). ^{1}H NMR (400 MHz, MeOD): δ = 0.68−0.81 (m, 24 H, CH_3), 0.83−0.90 (m, 4 H, CH), 1.04−1.27 (m, 6 H, CH_2), 1.31−1.40 (m, 4 H, CH_2), 1.42−1.52 (m, 2 H, CH_2), 1.53−1.65 (m, 2 H, CH_2), 1.77−1.91 (m, 2 H, CH_2), 2.50−2.63 (m, 2 H, CH), 2.77−2.87 (m, 2 H, CH), 4.16−4.20 (m, 4 H, CH), 7.18−7.22 (m, 2 H, $CH_{arom.}$), 7.88−7.92 (m, 2 H, $CH_{arom.}$) ppm. ^{31}P NMR: δ = −10.04 (s) ppm. MS (CI): *m*/*z* = 595 [M^+]. $C_{34}H_{60}O_4P_2$ (594.7): calcd. C 68.67, H 10.17; found C 66.22, H 9.89.

1,2-Bis[(2*S*,3*S*,4*S*,5*S*)-2,5-dibenzyl-3,4-dihydroxyphospholanyl]benzene (13e): Yield: 0.81 g, 56.9%; m.p. 178−183 °C. $[\alpha]_D^{24}$ = +37.9 (*c* = 0.174, MeOH). ^{1}H NMR (400 MHz, MeOD): δ = 2.05−2.27 (m, 2 H, CH_2), 2.75−2.85 (m, 2 H, CH_2), 2.89−3.04 (m, 4 H, CH_2), 3.06−3.18 (m, 2 H, CH), 3.31−3.43 (m, 2 H, CH), 3.83−3.93 (m, 2 H, CH), 3.99−4.06 (m, 2 H, CH), 6.80−7.37 (m, 24 H, $CH_{arom.}$) ppm. ^{31}P NMR: δ = −11.13 (s) ppm. MS (CI): *m*/*z* = 675 [M^+]. $C_{42}H_{44}O_4P_2$ (674.7): calcd. C 74.77, H 6.57; found C 73.34, H 6.58.

General Procedure for the Synthesis of the Rhodium(I) Complexes 14a−e: A solution of 1 equiv. of the corresponding bis(phospholane) **13a−e** in 30 mL of tetrahydrofuran was added to a solution of $[Rh(COD)_2][SO_3CF_3]$ (400 mg, 0.85 mmol) in 50 mL of tetrahydrofuran at room temp. After 3 h of stirring at room temp., the reaction solvents were evaporated to dryness. The orange residue was washed twice with 50 mL of diethyl ether and dried in vacuo.

[{1,2-Bis[(2*S*,3*S*,4*S*,5*S*)-3,4-dihydroxy-2,5-dimethylphospholanyl]benzene}Rh^I(COD)] Trifluoromethanesulfonate (14a): Yield: 582 mg, 93.3%. ^{1}H NMR (400 MHz, MeOD): δ = 0.91−0.96 (m, 6 H, CH_3), 1.34−1.40 (m, 6 H, CH_3), 2.17−2.64 (m, 8 H, CH_{2COD}), 2.79−2.89 (m, 4 H, CH), 4.06−4.14 (m, 2 H, CH), 4.16−4.24 (m, 2 H, CH), 5.54−5.61 (m, 2 H, CH_{COD}), 5.95−6.04 (m, 2 H, CH_{COD}), 7.55−7.58 (m, 2 H, $CH_{arom.}$), 8.62−8.66 (m, 2 H, $CH_{arom.}$) ppm. ^{31}P NMR: δ = 78.20 (d) ppm. MS (FAB): *m*/*z* = 581 [(M − $SO_3CF_3^-$)$^+$]. $C_{27}H_{40}F_3O_7P_2RhS$ (730.5): calcd. C 44.39, H 5.52; found C 43.36, H 5.78.

[{1,2-Bis[(2*S*,3*S*,4*S*,5*S*)-3,4-dihydroxy-2,4-diethylphospholanyl]benzene}Rh^I(COD)] Trifluoromethanesulfonate (14b): Yield: 615 mg, 91.5%. ^{1}H NMR (400 MHz, MeOD): δ = 0.85−0.88 (t, 6 H, CH_3), 0.93−0.96 (t, 6 H, CH_3), 1.43−1.54 (m, 2 H, CH_2), 1.81−1.91 (m, 2 H, CH_2), 1.91−2.04 (m, 2 H, CH_2), 2.14−2.22 (m, 2 H, CH_2), 2.29−2.65 (m, 8 H, CH_{2COD}), 2.57−2.65 (m, 2 H, CH), 2.67−2.75 (m, 2 H, CH), 4.18−4.34 (m, 4 H, CH), 5.53−5.58 (m, 2 H, CH_{COD}), 5.89−5.95 (m, 2 H, CH_{COD}), 7.54−7.57 (m, 2 H, $CH_{arom.}$), 8.65−8.69 (m, 2 H, $CH_{arom.}$). ^{31}P NMR: δ = 71.50 (d) ppm. MS (FAB): *m*/*z* = 637 [(M − $SO_3CF_3^-$)$^+$]. $C_{31}H_{48}F_3O_7P_2RhS$ (786.6): calcd. C 47.33, H 6.15; found C 46.7, H 6.13.

[{1,2-Bis[(2*S*,3*S*,4*S*,5*S*)-3,4-dihydroxy-2,5-di-*n*-propylphospholanyl]benzene}Rh^I(COD)] Trifluoromethanesulfonate (14c): Yield: 679 mg, 94.4%. ^{1}H NMR (400 MHz, MeOD): δ = 0.74−0.80 (m, 12 H, CH_3), 0.82−1.68 (m, 10 H, CH_2), 1.79−1.98 (m, 4 H, CH_2),

2.13−2.26 (m, 2 H, CH_2), 2.27−2.67 (m, 8 H, CH_{2COD}), 2.68−2.76 (m, 2 H, CH), 2.79−2.88 (m, 2 H, CH), 4.12−4.33 (m, 4 H, CH), 5.46−5.57 (m, 2 H, CH_{COD}), 5.88−5.99 (m, 2 H, CH_{COD}), 7.55−7.60 (m, 2 H, $CH_{arom.}$), 8.65−8.69 (m, 2 H, $CH_{arom.}$) ppm. ^{31}P NMR: δ = 71.87 (d) ppm. MS (FAB): *m*/*z* = 693 [(M − $SO_3CF_3^-$)$^+$]. $C_{35}H_{56}F_3O_7P_2RhS$ (842.7): calcd. C 49.89, H 6.70; found C 50.31, H 6.75.

[{1,2-Bis[(2*S*,3*S*,4*S*,5*S*)-3,4-dihydroxy-2,5-diisopentylphospholanyl]benzene}Rh^I(COD)] Trifluoromethanesulfonate (14d): Yield: 763 mg, 93.5%. ^{1}H NMR (400 MHz, MeOD): δ = 0.66−0.69 (m, 12 H, CH_3), 0.78 (d, 6 H, CH_3), 0.83 (d, 6 H, CH_3), 0.86−0.95 (m, 4 H, CH), 0.99−1.66 (m, 12 H, CH_2), 1.71−1.83 (m, 2 H, CH_2), 2.00−2.14 (m, 2 H, CH_2), 2.14−2.65 (m, 8 H, CH_{2COD}), 2.65−2.80 (m, 4 H, CH), 4.15−4.34 (m, 4 H, CH), 5.50−5.57 (m, 2 H, CH_{COD}), 5.94−6.03 (m, 2 H, CH_{COD}), 7.53−7.61 (m, 2 H, $CH_{arom.}$), 8.62−8.69 (m, 2 H, $CH_{arom.}$) ppm. ^{31}P NMR: δ = 73.36 (d) ppm. MS (FAB): *m*/*z* = 805 [(M − $SO_3CF_3^-$)$^+$]. $C_{43}H_{72}F_3O_7P_2RhS$ (954.9): calcd. C 54.09, H 7.60; found C 52.00, H 7.47.

[{1,2-Bis[(2*S*,3*S*,4*S*,5*S*)-2,5-dibenzyl-3,4-dihydroxyphospholanyl]benzene}Rh^I(COD)] Trifluoromethanesulfonate (14e): Yield: 803 mg, 90.9%. ^{1}H NMR (400 MHz, MeOD): δ = 2.19−2.63 (m, 8 H, CH_{2COD}), 2.68−2.89 (m, 4 H, CH_2), 2.91−2.99 (m, 2 H, CH_2), 3.00−3.08 (m, 2 H, CH_2), 3.09−3.24 (m, 2 H, CH), 3.41−3.53 (m, 2 H, CH), 3.91−4.16 (m, 4 H, CH), 5.41−5.49 (m, 2 H, CH_{COD}), 6.04−6.11 (m, 2 H, CH_{COD}), 6.77−8.85 (m, 24 H, $CH_{arom.}$) ppm. ^{31}P NMR: δ = 72.40 (d) ppm. MS (FAB): *m*/*z* = 885 [(M − $SO_3CF_3^-$)$^+$]. $C_{51}H_{56}F_3O_7P_2RhS$ (1034.8): calcd. C 59.19, H 5.45; found C 58.04, H 5.38.

{1,2-Bis[(2*S*,3*S*,4*S*,5*S*)-3,4-dihydroxy-2,5-dimethylphospholanyl]benzene}Pd^{II}Cl$_2$ (15a): A solution of **12a** (2.10 g, 4.66 mmol) in 50 mL of dichloromethane was added to a solution of [$PdCl_2$(COD)] (1.10 g, 3.85 mmol) in 50 mL of dichloromethane. The yellow solution was stirred for 1 h at room temp. and the solvents were evaporated to dryness. The residue was washed twice with 50 mL of *n*-pentane and dissolved in 50 mL of dichloromethane. On addition of 20 mL of water, and a small amount of hydrochloric acid, a pale yellow powder precipitated. After stirring for 1 h at room temp., the precipitate was filtered off, washed with dichloromethane and dried in vacuo. Yield: 1.87 g, 88.6%. ^{1}H NMR (400 MHz, MeOD): δ = 0.91−0.99 (m, 6 H, CH_3), 1.35−1.44 (m, 6 H, CH_3), 3.09−3.19 (m, 2 H, CH), 3.51−3.60 (m, 2 H, CH), 3.97−4.08 (m, 2 H, CH), 4.15−4.25 (m, 2 H, CH), 7.73−7.79 (m, 2 H, $CH_{arom.}$), 8.49−8.55 (m, 2 H, $CH_{arom.}$) ppm. ^{31}P NMR: δ = 104.99 (s) ppm. MS (FAB): *m*/*z* = 513 [(M − Cl^-)$^+$]. $C_{18}H_{28}Cl_2O_4P_2Pd$ (547.7): calcd. C 39.47, H 5.15; found C 39.47, H 5.09.

General Procedure for the Asymmetric Hydrogenation: Hydrogenation reactions were performed using standard Schlenk techniques. Methanol Secco Solv was purchased from Merck and stored over molecular sieves. In a Schlenk tube, the corresponding Rh^I complex, **9a**−**g**, **14a**−**e**, (10 μmol) and **16** (500 mg, 2.44 mmol) or **18** (250 mg, 1.92 mmol) were dissolved in 5 mL of methanol. After three vacuum/nitrogen cycles, followed by one vacuum/hydrogen cycle (1.3 bar), the reaction mixture was stirred at room temp. for 20 h. The reaction products were filtered through a short silica column and subjected to *ee* determination. Conversions were determined by means of ^{1}H NMR spectroscopy.

X-ray Crystallography of 15a and 10f: The crystals used in this study were mounted onto the ends of glass fibers. X-ray data were collected with a STOE IPDS unit (Imaging Plate Diffraction System). Graphite-monochromatized Mo-K_α radiation (λ = 0.71073 Å) was used. Crystal data are listed in Table 3, together with refinement details. The lattice constants correspond to the temperatures indicated there. Absorption corrections were not applied. The structures were solved by the Patterson method with the SHELXS-86 program.[27] The atomic coordinates and anisotropic thermal parameters of the non-hydrogen atoms were refined using the SHELXL-97 program;[28] full-matrix method on F^2 data. Hydrogen atoms were included in the final refinement cycles, except those of atoms C15, C16, C18, C19 and C22 of **10f**, since these were highly anisotropic. The riding model was used for the hydrogen atoms. By using the absolute structure parameter[29] as a criterion, it could be decided which of the enantiomers in both cases corresponds to the crystal investigated, and that in the case of **15a**, $P3_121$ is the correct space group and not $P3_221$. CCDC-177475 and -177476 for **15a** and **10f** contain the supplementary crystallographic data for this paper. These data can be obtained free of charge at www.ccdc.cam.ac.uk/conts/retrieving.html or from the Cambridge Crystallographic Data Centre, 12, Union Road, Cambridge CB2 1EZ, UK [Fax: (internat.) + 44-1223/336-033; E-mail: deposit@ccdc.cam.ac.uk].

Acknowledgments

We thank the Deutsche Forschungsgemeinschaft for financial support of this work (Ri613/5-1). A. B. was further supported by a scholarship of the state of Baden-Württemberg.

[1] L. Horner, H. Siegel, H. Büthe, *Angew. Chem.* **1968**, *80*, 1034−1035; *Angew. Chem. Int. Ed. Engl.* **1968**, *7*, 942−943.
[2] W. S. Knowles, M. J. Sabacky, *J. Chem. Soc., Chem. Commun.* **1968**, 1445−1446.
[3] W. S. Knowles, M. J. Sabacky, B. D. Vineyard, *J. Chem. Soc., Chem. Commun.* **1972**, 10−11.
[4] T. P. Dang, H. P. Kagan, *J. Chem. Soc., Chem. Commun.* **1971**, 481.
[5] W. S. Knowles, M. J. Sabacky, B. D. Vineyard, D. J. Weinkauff, *J. Am. Chem. Soc.* **1975**, *97*, 2567−2568.
[6] A. Miyashita, A. Yasuda, H. Takaya, K. Toriumi, T. Ito, T. Souchi, R. Noyori, *J. Am. Chem. Soc.* **1980**, *102*, 7932−7934.
[7] M. J. Burk, *J. Am. Chem. Soc.* **1991**, *113*, 8518−8519.
[8] M. J. Burk, J. E. Feaster, W. A. Nugent, R. L. Harlow, *J. Am. Chem. Soc.* **1993**, *115*, 10125−10138.
[9] C. Claver, E. Fernandez, A. Gillon, K. Heslop, D. J. Hyett, A. Martorell, A. G. Orpen, P. G. Pringle, *Chem. Commun.* **2000**, 961−962.
[10] M. T. Reetz, G. Mehler, *Angew. Chem.* **2000**, *112*, 4047−4049; *Angew. Chem. Int. Ed.* **2000**, *39*, 3889−3891.
[11] M. Berg, Van den, A. J. Minnaard, E. D. Schudde, J. Esch, van, A. H. M. Vries, de, B. L. Feringa, *J. Am. Chem. Soc.* **2000**, *122*, 11539−11540.
[12] D-Mannitol is the chiral starting material for the synthesis of the RoPHOS ligands, too: J. Holz, M. Quirmbach, U. Schmidt, D. Heller, R. Stürmer, A. Börner, *J. Org. Chem.* **1998**, *63*, 8031−8034.
[13] Y. Merrer, A. Dureault, C. Greck, D. Micas-Languin, C. Gravier, J. Depezay, *Heterocycles* **1987**, *25*, 541−548.
[14] L. F. Wiggins, *J. Chem. Soc.* **1946**, 13−14.
[15] B. B. Lohray, M. Chatterjee, Y. Jayamma, *Synth. Commun.* **1997**, *27*, 1711−1724.
[16] L. F. Wiggins, D. J. C. Wood, *J. Chem. Soc.* **1950**, 1566−1575.
[17] P. Allevi, M. Anastasia, P. Ciufredda, A. M. Sanvito, *Tetrahedron: Asymmetry* **1994**, *5*, 927−934.

[18] A. Bayer, U. Thewalt, B. Rieger, *Eur. J. Inorg. Chem.* **2002**, 199−203.
[19] Y.-Y. Yan, T. V. RajanBabu, *J. Org. Chem.* **2000**, *65*, 900−906.
[20] A. K. Ghosh, S. P. McKee, W. J. Thompson, *Tetrahedron Lett.* **1991**, *41*, 5729−5732.
[21] Y. Gao, K. B. Sharpless, *J. Am. Chem. Soc.* **1988**, *110*, 7538−7539.
[22] B. M. Kim, K. B. Sharpless, *Tetrahedron Lett.* **1989**, *30*, 655−658.
[23] W. Li, Z. Zhang, D. Xiao, X. Zhang, *Tetrahedron Lett.* **1999**, *40*, 6701−6701.
[24] **11a−b**,**12a−b**,**13a−b** were already reported in: W. Li, Z. Zhang, D. Xiao, X. Zhang, *J. Org. Chem.* **2000**, *65*, 3489−3496. We assume, that Zhang. et al. received **13a−b** as syrup-like phosphonium salts.
[25] **13a−b** were first obtained in pure state by: T. V. RajanBabu, Y.-Y. Yan, S. Shin, *J. Am. Chem. Soc.* **2001**, *123*, 10207−10213.
[26] W. S. Knowles, *Acc. Chem. Res.* **1983**, *16*, 106−112.
[27] G. M. Sheldrick, *SHELXS-86, Program for the solution of Crystal Structures*, Göttingen, **1986**.
[28] G. M. Sheldrick, *SHELXL-97, Program for the Refinement of Crystal Structures*, Göttingen, **1997**.
[29] H. D. Flack, D. Schwarzenbach, *Acta Crystallogr., Sect. A* **1988**, *44*.

Received March 11, 2002
[I02125]

Metal Complexes of the Tetradentate Ligands *rac*- and *meso*-N,P,P,N: Synthesis, Separation and Structural Characterization

Gabi Müller,[a] Martti Klinga,[b] Markku Leskelä,[b] and Bernhard Rieger*[a]

Keywords: N ligands / P ligands / Iron / Palladium / Cobalt

The N,P,P,N ligand 1,2-bis[(2-quinolinemethyl)(phenyl)phosphanyl]ethane (**2**) which contains two stereogenic phosphane units in the ligand backbone [***rac*-2** (*R*/*R*, *S*/*S*) and ***meso*-2** (*R*/*S*)] and two pendant quinaldine moieties was synthesized. The diastereomeric forms were separated after conversion of the ligands to the corresponding palladium(II) diiodide complexes (***rac*-3**, ***meso*-3**). The structure of both compounds was determined by X-ray structure analysis and revealed a bidentate coordination through phosphorus leading to the expected square-planar geometry. The free ligands were regenerated by treatment of the palladium(II) diiodides with potassium cyanide and the coordination behavior of ***rac*-2** and ***meso*-2** towards iron(II) and cobalt(II) dichloride (***rac*-5, *meso*-5**, M = Fe; ***rac*-6, *meso*-6**, M = Co) was investigated by the means of IR and UV/Vis spectroscopy. The results indicate that in the case of Fe^{II} and Co^{II} the quinaldine moieties are not coordinated to the metal center and the ligands therefore act, as in the case of Pd^{II}, as bidentate systems. UV/Vis investigations suggest a tetrahedral coordination environment for the Co^{II} complexes. The Fe^{II} and Co^{II} derivatives were tested for ethene polymerization and the bis(acetonitrile)-palladium compounds (***rac*-4**, ***meso*-4**) for ethene/CO copolymerization reactions.

(© Wiley-VCH Verlag GmbH, 69451 Weinheim, Germany, 2002)

Introduction

A variety of late-transition-metal polymerization catalysts with different ligand (mono-, bi-, tri- or tetradentate)-metal combinations are known in the literature.[1–3] Bidentate ligands are often used in nickel-catalyzed olefin homopolymerization and palladium-catalyzed olefin/CO copolymerization reactions. Highly active iron and cobalt complexes with tridentate pyridyl-diimine systems were discovered recently.[4,5] However less attention has been directed towards iron and cobalt complexes with tetradentate ligands.

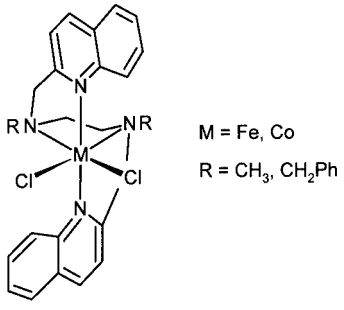

Figure 1. Octahedral C_2-symmetric complexes containing ligand **1**

Recently, our group reported the synthesis of a tetradentate quinaldine-amine ligand **1** and on the application of the corresponding palladium complexes for norbornene polymerization.[6,7] When coordinated to iron(II) or cobalt(II) dichloride, **1** exclusively forms an octahedral, C_2-symmetric complex [**(1)Fe/CoCl$_2$**, Figure 1].

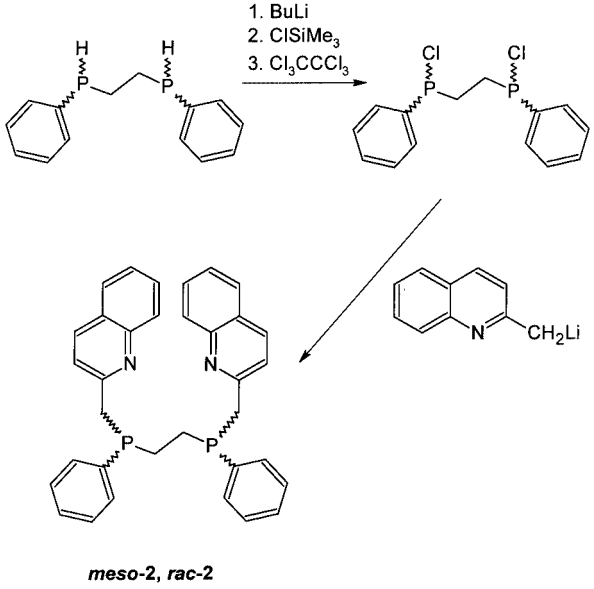

Figure 2. Synthesis of the N,P,P,N ligand **2** (***rac*-2** and ***meso*-2**)

[a] Department of Materials and Catalysis, Inorganic Chemistry II, University of Ulm,
89069 Ulm, Germany,
Fax: (internat.) +49-(0)731/502-3039
E-mail: bernhard.rieger@chemie.uni-ulm.de
[b] Laboratory of Inorganic Chemistry, Department of Chemistry, P. O. Box 55, 00014 University of Helsinki, Finland

After activation with MAO, **(1)CoCl$_2$** (R = CH_2Ph) forms an active catalyst for the polymerization of ethene.[8] The molecular weight of the product is relatively high ($M_w \approx 1.5 \times 10^6$ g/mol), however the activity (10 kg PE/[Co]h) of this system is poor due to the low stability of the activated complex.[8] We report here on the synthesis of a tetradentate, mixed nitrogen/phosphorus-containing ligand **2** which, instead of the donor-amine groups of ligand **1**, carries donor/acceptor phosphane functionalities in the ligand backbone. The overall arrangement with the pendant quinaldine moieties was left unchanged to ensure the formation of the C_2-symmetric, octahedral coordination compound. Pd^{II}, Fe^{II} and Co^{II} complexes bearing the new N,P,P,N ligands were synthesized and tested in ethene and ethene/CO copolymerization reactions.

Results and Discussion

Ligand and Complex Synthesis

The ligand **2** (***rac*-2** and ***meso*-2**) was prepared following the synthetic pathway depicted in Figure 2.[9]

1,2-Bis(phenylphosphanyl)ethane was converted into 1,2-bis(chlorophenylphosphanyl)ethane by treating the bis(Li phosphide) with $ClSiMe_3$, followed by the addition of hexachloroethane. Subsequent reaction of Li-quinaldine with 1,2-bis(chlorophenylphosphanyl)ethane afforded the tetradentate N,P,P,N ligand **2** which was isolated as a mixture of two diastereoisomers due to the two stereogenic phosphorus atoms [***rac*-2** (*R*/R and *S*/*S*) and ***meso*-2** (*S*/*R*)]. The ratio of ***rac*-2**/***meso*-2** was 1.7:1, indicating a preferred

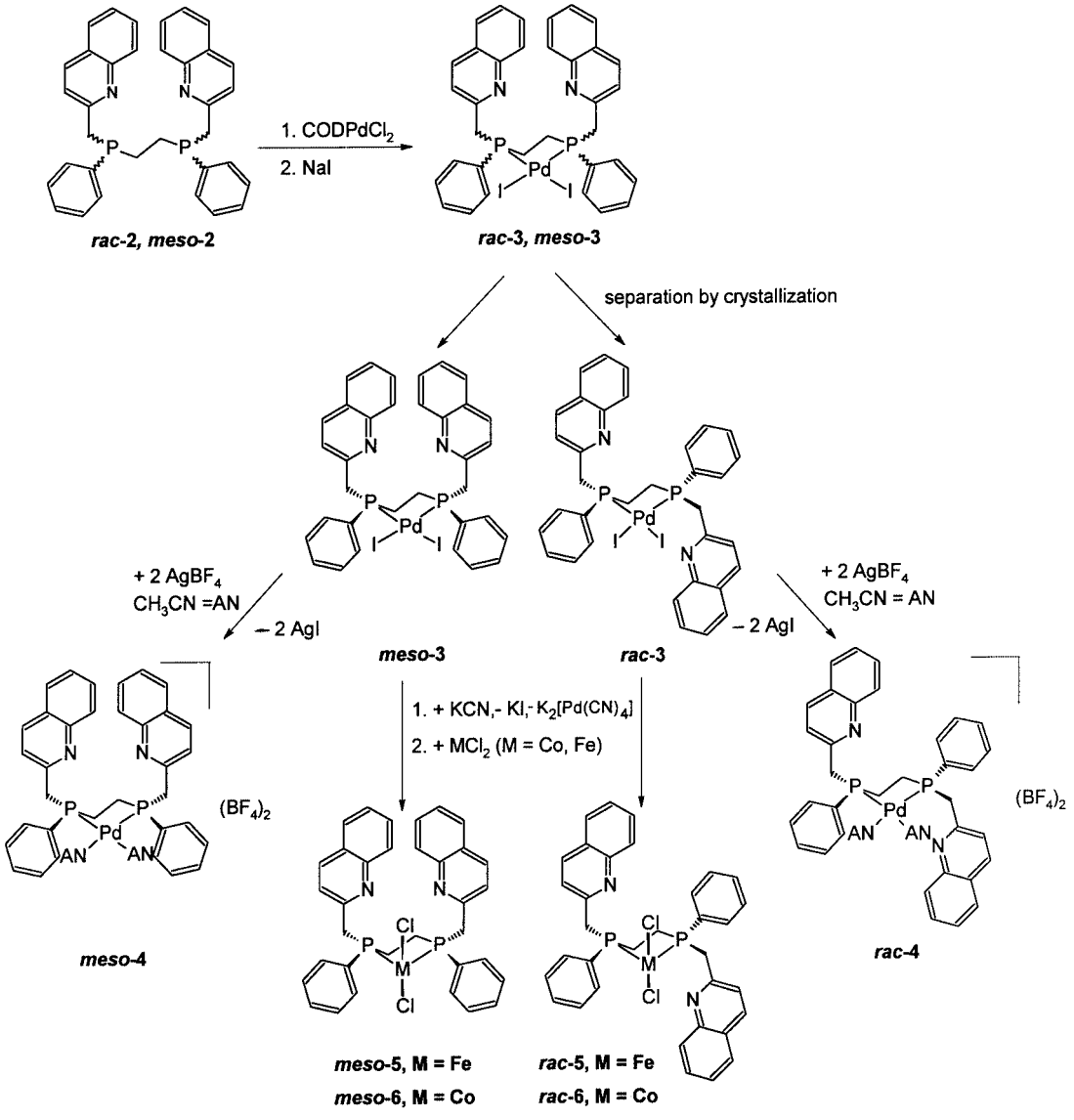

Scheme 1

formation of the *rac*-form. Attempts to separate the two ligands were unsuccessful.

The mixture of ***rac*-2** and ***meso*-2** was converted into the corresponding, air-stable palladium(II) diiodide complexes (Scheme 1, ***rac*-3**, ***meso*-3**) by treatment with [$PdCl_2$(COD)] in the presence of sodium iodide.[10] After purification of the mixture by column chromatography, ***rac*-3** could be separated by repeated crystallization from CH_2Cl_2/EtOAc. A pure sample of ***meso*-3** was isolated by crystallization from hot acetone.

To investigate the catalytic properties of our diastereomeric Pd^{II} complexes for ethene/CO copolymerizations the palladium diiodide compounds were converted into the bis(acetonitrile) complexes ***rac*-4** and ***meso*-4** by treating the diiodides with silver tetrafluoroborate in acetonitrile.

The diastereomeric ligands ***rac*-2** and ***meso*-2** were isolated in pure form after treatment of the corresponding PdI_2 species with aqueous KCN solution. The iron(II) and cobalt(II) dichloride complexes of ***rac*-2** and ***meso*-2** were synthesized by treatment of the free ligands with the appropriate metal(II) salt (***rac*-5**, ***meso*-5**, M = Fe; ***rac*-6, *meso*-6**, M = Co). Elemental analysis and FAB-MS indicated a 1:1 metal to ligand ratio.

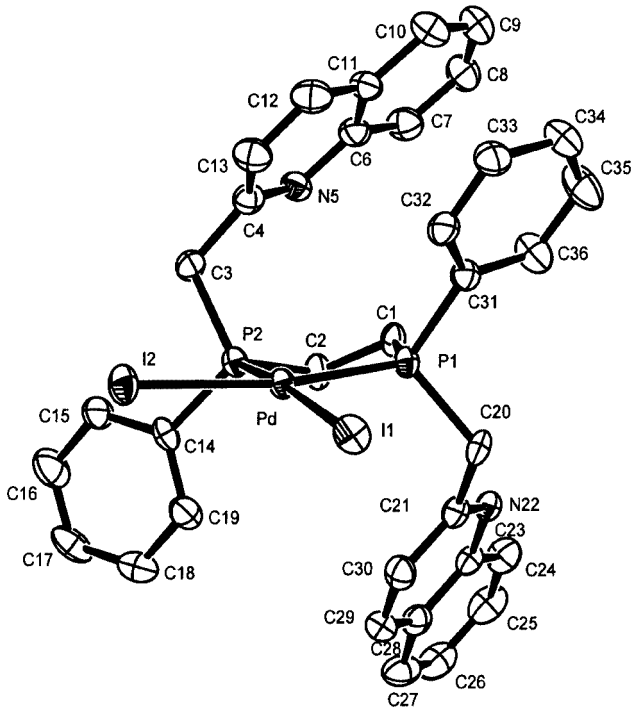

Structural Characterization

Solid State Structures

Single crystals of the palladium(II) diiodide compounds suitable for an X-ray structure determination were obtained by crystallization from CH_2Cl_2/EtOAc (***rac*-3**) or from acetone/toluene (***meso*-3**) (Figure 3).

For both complexes a water molecule was located in the unit cell which forms intermolecular hydrogen bonds to neighboring quinaldine moieties. Both compounds crystallize in the monoclinic form. The two iodides (I1 and I2) and the two phosphorus units (P1 and P2) form the expected square-planar coordination sphere around the palladium center. Small deviations might result from crystal packing (Table 1). Bond lengths and angles are within the range expected for this type of complex (Table 2).[11–13] In ***rac*-3** one of the quinaldine moieties is located above, and the second below, the Pd–P1–P2–I1–I2 coordination plane, while in ***meso*-3** both units lie on the same side of the plane. Considering this geometrical arrangement it is obvious that only the *rac*-form of the ligand is able to coordinate as a tetradentate ligand in a manner identical to the N,N,N,N ligand **1** (see Figure 1), with the quinaldine fragments occupying both axial positions.[6] Attempts to obtain single crystals of ***rac*-5,6** or ***meso*-5,6** suitable for an X-ray structure analysis were unsuccessful.

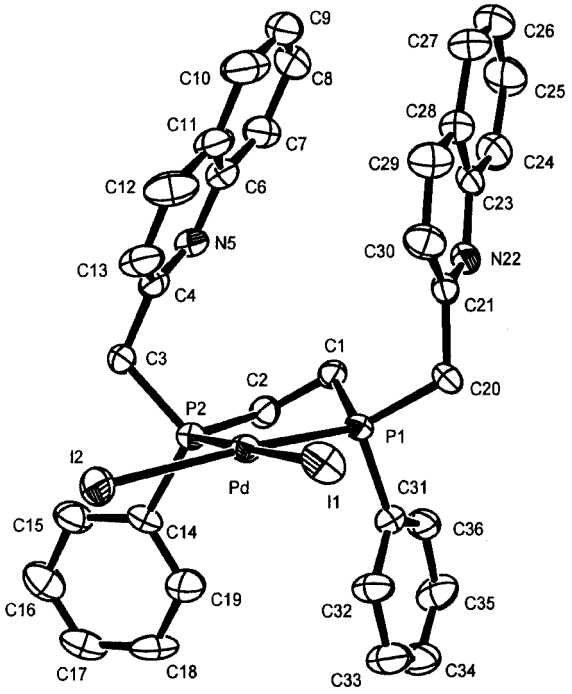

Figure 3. The structure of ***rac*-3** (upper) and ***meso*-3** (lower)

IR Analysis

For structure elucidation IR analysis was performed on the free ligands **1**, ***rac*-2** and ***meso*-2** as well as on the corresponding Fe^{II} and Co^{II} complexes. Coordination of an N-heteroaromatic unit to a metal center is indicated by a frequency shift of the heteroaromatic ring vibrations.[14–16] The IR spectra of the octahedral Fe^{II} and Co^{II} complexes of ligand **1** [**(1)$FeCl_2$** and **(1)$CoCl_2$**] were used as references, since in this case the coordination of the quinaldine moieties has been confirmed by an X-ray structure determination.[6,8]

Table 1. Crystallographic data for ***rac*-3** and ***meso*-3**

	***rac*-3**·H_2O	***meso*-3**·0.5(C_7H_8)·H_2O
Chemical formula	$C_{34}H_{32}I_2N_2OP_2Pd$	$C_{37.5}H_{36}I_2N_2OP_2Pd$
Molecular weight [g/mol]	906.76	952.82
Crystal color and form	yellow plate	yellow prism
Crystal system	monoclinic	monoclinic
Space group	*P*21/*n*	*C*2/*c*
a [Å]	12.518(5)	35.069(7)
b [Å]	11.243(5)	10.734(2)
c [Å]	23.584(5)	22.419(4)
β [°]	100.63(3)	120.44(3)
Volume [Å^3]	3262(2)	7276(2)
Z	4	8
$D_{calcd.}$ [mg/m^3]	1.846	1.740
Absorption coefficient [mm^{-1}]	2.590	2.327
F(000)	1760	3720
Crystal size [mm]	0.44 × 0.38 × 0.16	0.48 × 0.45 × 0.43
θ_{max} [°]	25.01	25.03
Number of observed reflections [$I > 2\sigma(I)$]	4923	5508
Number of collected reflections	5714	6173
Number of unique reflections	5461	6070
Number of parameters	409	418
Index range	$0 \le h \le 14$	$0 \le h \le 41$
	$0 \le k \le 13$	$0 \le k \le 12$
	$-28 \le l \le 27$	$-26 \le l \le 22$
Goodness-of-fit on F^2	1.039	1.021
Final *R* indices [$I > 2\sigma(I)$][a][b]	*R*1 = 0.0368	*R*1 = 0.0620
	*wR*2 = 0.0881	*wR*2 = 0.1579
R indices (all data)[a,b]	*R*1 = 0.0427	*R*1 = 0.0665
	*wR*2 = 0.0912	*wR*2 = 0.1626
Largest differential peak and hole [e/ Å^3]	1.310 and −0.836	2.438 and −2.046

[a] $R1 = \Sigma||F_0| - |F_c||/\Sigma|F_0|$. [b] $wR2 = \{\Sigma[w(F_0^2 - F_c^2)^2]/\Sigma[wF_o^4]\}^{1/2}$.

Table 2. Selected bond lengths and angles for ***rac*-3** and ***meso*-3**

Bond lengths [Å]	***rac*-3**·H_2O	***meso*-3**·0.5(C_7H_8)·H_2O
I1−Pd	2.6514(9)	2.6528(8)
I2−Pd	2.6468(8)	2.6499(12)
Pd−P2	2.2429(15)	2.2527(17)
Pd−P1	2.2526(14)	2.2554(17)
P1−C1	1.830(5)	1.828(6)
P1−C20	1.850(5)	1.832(6)
P2−C3	1.832(5)	1.826(6)
P2−C2	1.833(5)	1.834(6)
Bond angles [°]	***rac*-3**·H_2O	***meso*-3**·0.5(C_7H_8)·H_2O
P2−Pd−P1	87.10(5)	84.78(6)
P2−Pd−I2	87.73(4)	87.23(4)
P1−Pd−I2	170.50(4)	170.55(4)
P2−Pd−I1	171.48(4)	177.22(4)
P1−Pd−I1	90.15(4)	92.44(4)
I2−Pd−I1	96.06(3)	95.55(2)
Pd−P2−C3	115.81(19)	114.0(2)
Pd−P1−C20	117.22(18)	124.1(2)

The high frequency region (1700−1400 cm^{-1}) of the ring deformations of the aromatic and heteroaromatic units is depicted in Figure 4.[17,18] The IR diagrams **1** (ligand **1** and complexes), **2** (***rac*-2** and complexes) and **3** (***meso*-2** and complexes) show the spectra of the free ligand (top), and the iron (middle) and cobalt (bottom) complexes. The ring vibration of the free ligands at 1614 cm^{-1} and 1595 cm^{-1} (**1**), 1617 cm^{-1} and 1597 cm^{-1} (***rac*-2**), 1614 cm^{-1} and 1595 cm^{-1} (***meso*-2**) were attributed to the quinaldine moiety.[17]

The spectra of the Fe^{II} and Co^{II} complexes of ligand **1** show a high frequency band at 1647 and 1648 cm^{-1}, respectively, which is not present in the spectrum of the free ligand. Also, a distinct shift of the bands in the 1400−1570 cm^{-1} region is detectable upon coordination of the quinaldine moiety. No differences of band positions and intensities in the spectra of the Fe^{II} and Co^{II} complexes were observed.

In the case of the Fe^{II} and Co^{II} complexes of the N,P,P,N ligands ***rac*-2** and ***meso*-2** no band at higher frequencies is detectable, which would indicate a coordination of the quinaldine moiety. The slight variation in the 1400−1570 cm^{-1} region might be due to the coordination of the phosphane units to the metal center. These investigations imply that, in contrast to **1**, which coordinates as a tetradentate ligand, ***rac*-2** and ***meso*-2** form Fe^{II} and Co^{II} complexes where the heteroaromatic unit is not coordinated to the metal center and the ligands therefore act as bidentate systems.

UV/Vis Spectroscopy

To support this hypothesis, UV/Vis measurements were performed on the Co^{II} complexes ***rac*-6** and ***meso*-6** in solution (Figure 5). The spectra of both isomers show a similar structure of band positions and intensities, suggesting the

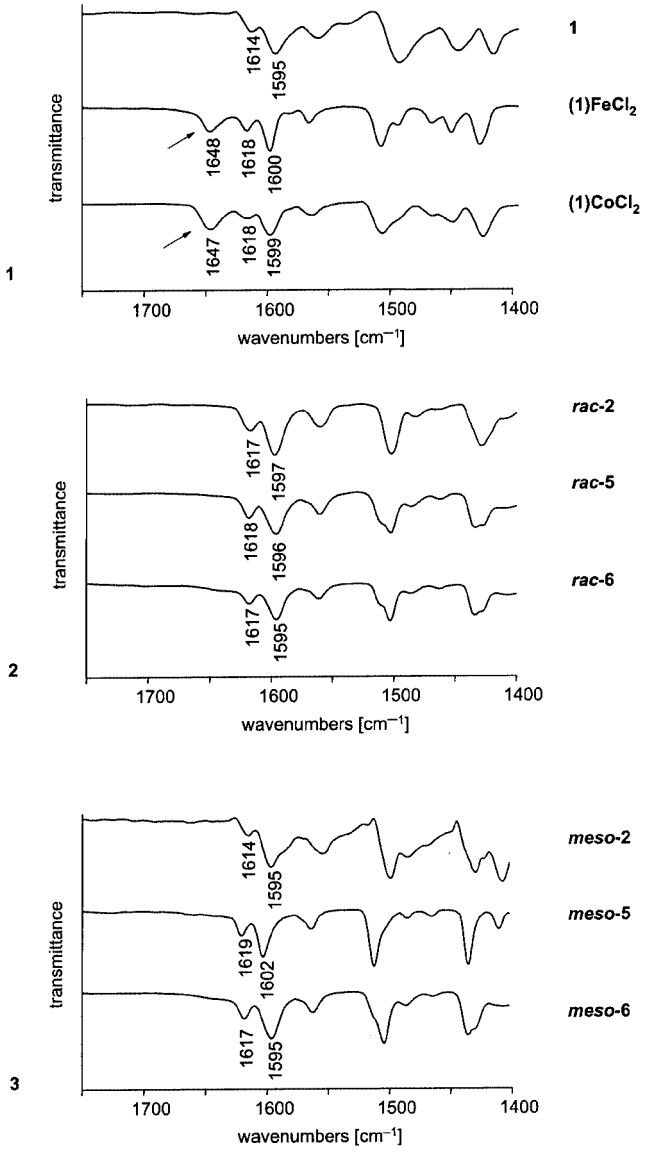

Figure 4. IR spectra of the free ligands (top), the Fe^{II} (middle) and the Co^{II} (bottom) complexes of the ligands **1** (diagram 1), ***rac*-2** (diagram 2) and ***meso*-2** (diagram 3)

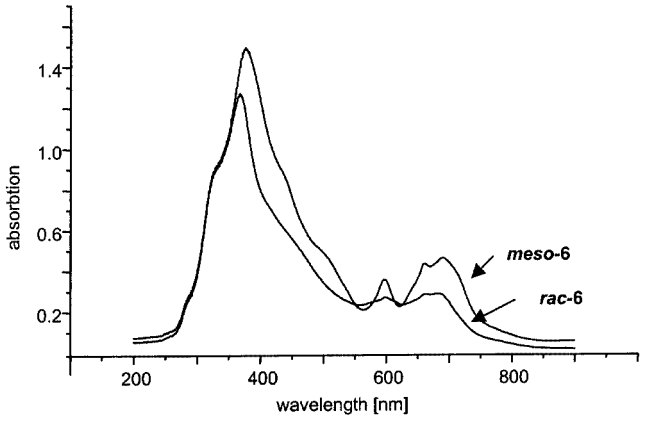

Figure 5. UV/Vis spectra of a solution of ***rac*-6** and ***meso*-6** in CH_2Cl_2

same overall coordination geometry for both complexes (Table 3).

Table 3. Positions of the band maxima and molar extinction coefficient of the UV/Vis spectra of a solution of ***rac*-6** and ***meso*-6** in CH_2Cl_2

	λ_{max} [nm] (ε_{max} [L·mol^{-1}·cm^{-1}])			
***rac*-6**	368 (852)	599 (329)	663 (375)	683 (381)
***meso*-6**	377 (985)	597 (316)	661 (390)	690 (414)

UV/Vis investigations on other tetrahedral $CoCl_2L_2$ complexes (L = P donor) have shown that the absorption in the 500−800 nm region can be attributed to the spin-allowed transition $^4A_2 \rightarrow {}^4T_1$.[19−25] The observed absorption spectra for ***rac*-6** and ***meso*-6** resemble the reported spectra for the tetrahedral complex $[CoCl_2(PPh_3)_2]$, indicating a bidentate coordination of ***rac*-2** and ***meso*-2** (through the P units) to give the corresponding tetrahedral $CoCl_2$ complexes (Figure 6).[20,24] We assume a similar coordination behavior for the Fe^{II} complexes.

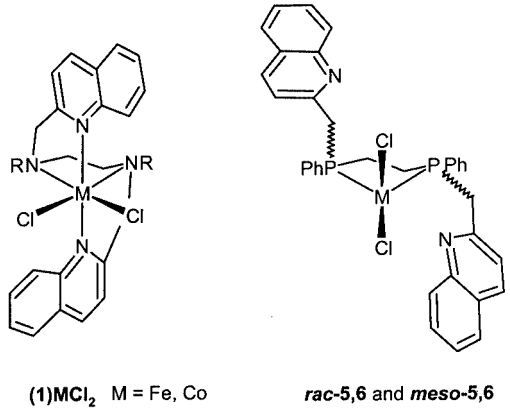

Figure 6. Coordination behavior of **1** and proposed coordination behavior of ***rac*-2** and ***meso*-2** in their Fe^{II} and $Co^{II}Cl_2$ complexes

Analysis of the bond lengths and angles found for the strained, octahedral complex **(1)$FeCl_2$** revealed an Fe−N(R)−CH_2 angle of 107°.[6] This angle, together with the N(R)−Fe bond length determines the distance of the quinaldine moiety from the axial coordination site in the complexes. The strained structure of **(1)$FeCl_2$** indicates that an angle of 107° together with an N−Fe bond length of 2.25 Å is necessary to allow coordination of the quinaldine moieties.[6] In the square-planar Pd^{II} complexes ***rac*-3** and ***meso*-3**, where the quinaldine moieties are not coordinated to the metal center, a Pd−P−CH_2 angle of 116° was observed. It is likely that bidentate coordination of the N,P,P,N ligands stabilizes the tetrahedral $CoCl_2P_2$ complexes (P−Co ≈ 2.2 Å [26]) sufficiently so that there is no need to diminish this angle considerably, forming a highly constrained ring systems.

The Fe^{II} and Co^{II} complexes were tested for the polymerization of ethene. However, in contrast to the octahedral **(1)$CoCl_2$**, the tetrahedral complexes ***rac*-5,6** and ***meso*-5,6** of the present study decomposed upon addition of MAO to

give a suspension of the complexes in toluene (black precipitate, most likely Fe^0 or Co^0). Initial experiments showed that the diastereomeric bis(acetonitrile)palladium complexes ***rac*-4** and ***meso*-4** are suitable catalyst precursors for the copolymerization of ethene and CO using methanol as cocatalyst. Further investigations on the behavior of the diastereomeric complexes towards the polymerization of 1-olefins and CO are in progress.

Conclusion

Exchanging the backbone nitrogen functionalities in the tetradentate N,N,N,N ligand **1** for phosphorus leads to the formation of two stable diastereoisomers ***rac*-2** and ***meso*-2**. At the same time a distinct variation in the coordination behavior of the new N,P,P,N ligands is induced. While the N,N,N,N ligand **1** forms octahedral Fe^{II} and Co^{II} complexes, a tetrahedral environment is suggested for the Fe^{II} and Co^{II} complexes of ***rac*-2** and ***meso*-2**. Whereas **(1)$CoCl_2$** shows some activity for ethene polymerization, the tetrahedral ***rac*-5,6** and ***meso*-5,6** complexes undergo fast decomposition upon treatment with MAO. However, the Pd^{II} analogues ***rac*-4** and ***meso*-4** show some activity in the ethene/CO copolymerization reaction; this will be investigated further.

Experimental Section

General Remarks: All manipulations except the handling of the palladium diiodide complexes were carried out in dry solvents under an inert atmosphere of argon using standard Schlenk techniques. THF, diethyl ether and toluene were distilled from $LiAlH_4$, and CH_2Cl_2 and petroleum ether were distilled from CaH_2. All solvents were stored over molecular sieves. Commercially available anhydrous acetonitrile and ethanol, BuLi (1.6 M in hexane), hexachloroethane, KCN, anhydrous $FeCl_2$ and $CoCl_2$ were used without further purification. Quinaldine and chlorotrimethylsilane were purified by distillation. (*cis*,*cis*-Cycloocta-1,5-diene)dichloropalladium,[27] 1,2-bis(phenylphosphanyl)ethane,[28] ligand **1**, as well as the corresponding iron and cobalt complexes,[6] were prepared according to literature procedures.

Polymerization experiments were performed in a 100 mL steel autoclave (Roth) with a glass inlet and mechanical stirring. Ethene (BASF, 2.7) and CO (BASF, 2.0) were used without further purification. MAO (10% in toluene) was purchased from Witko.

NMR measurements were conducted on a Bruker DRX 400 spectrometer at 400 MHz (^1H) and 162 MHz (^{31}P). Chemical shifts are reported in ppm. Tetramethylsilane and 85% phosphoric acid were used as references. IR spectra were measured on a Bruker IFS 113v spectrometer, FAB-MS spectra on a Finnigan MAT TSQ 7000 spectrometer using *meta*-nitrobenzyl alcohol (*m*-NBA), 2,3,4-trimethoxyacetophenone (TMAP) or 2-nitrophenyloctyl ether (2-NPOE) as matrices. Elemental analysis were measured on an Vario EL elementar. UV/Vis absorption spectra were conducted on a J & M spectrometer using 2 mm solutions in CH_2Cl_2.

Synthesis of *rac*-2, *meso*-2: BuLi (55.2 mL, 88 mmol) was added slowly to a solution of 1,2-bis(phenylphosphanyl)ethane (10.9 g, 44 mmol) in THF (300 mL) cooled to −78 °C. The reaction mixture was warmed to 0 °C and chlorotrimethylsilane (11.4 mL, 90 mmol) was added slowly with a syringe. The solvent was removed under reduced pressure and CH_2Cl_2 (300 mL) was added. The reaction mixture was cooled to 0 °C and hexachloroethane (20.9 g, 88 mmol) was added in small portions. The reaction mixture was stirred at room temperature for 72 hours. The solvent was removed under reduced pressure and the solid was suspended in THF (250 mL). In a separate flask BuLi (55.2 mL, 88 mmol) was added slowly to a solution of quinaldine (12 mL, 88 mmol) in 200 mL of THF cooled to −78 °C. The dark red solution of the quinaldine anion was allowed to reach room temperature and was then added to the suspension of the chlorophosphane at −78 °C until the red color of the quinaldine anion remained. A further 10 mL of quinaldine solution was added to ensure the complete transformation of the chlorophosphane. The reaction mixture was allowed to reach room temperature and was stirred overnight. Water (10 mL) was added and the solvent was removed under reduced pressure. The remaining solid was dissolved in water (300 mL) and CH_2Cl_2 (500 mL). The organic layer was separated and the water layer was extracted with two 200 mL portions of CH_2Cl_2. The organic layers were dried over sodium sulfate. Evaporation of the solvent left a red oil which contained a 1:1.7 *meso*:*rac* mixture of the ligand. The crude product was used without further purification. Yield: 80% (18.6 g).

Synthesis of *rac*-3, *meso*-3: [$PdCl_2$(COD)] (10.5 g, 36.7 mmol) was added to a solution of the ligand (36.7 mmol) in CH_2Cl_2 (300 mL). NaI (22 g, 1.47 mol) was added after 10 minutes and the reaction mixture was stirred for 12 hours. CH_2Cl_2 (500 mL) was added and the solution was stirred for a further 24 hours. The reaction mixture was filtered and the solvent was removed under reduced pressure. The product was purified by column chromatography on silica using a 10:1 (v:v) mixture of CH_2Cl_2 and ethyl acetate as eluent. The *rac* form was separated by crystallization of the diastereomeric mixture from CH_2Cl_2 and ethyl acetate. A pure sample of the *meso*-isomer was obtained by crystallization of a *meso*-enriched fraction from hot acetone. Overall yields: 37% (12.1 g) ***rac*-3**, 25% (8.1 g) ***meso*-3**.

***rac*-3:** ^1H NMR ($CDCl_3$): δ = 2.13 (m, 1 H), 2.22 (m, 1 H), 2.50 (m, 2 H), 4.14 (dd, J_1 = 15.9, J_2 = 13.1 Hz, 2 H), 4.80 (dd, J_1 = 12.9, J_2 = 10.1 Hz, 2 H), 6.80 (m, 4 H), 7.12 (dd, 2 H), 7.24 (m, 4 H), 7.53−7.61 (m, 4 H), 7.65 (d, J = 8.1 Hz, 2 H), 7.83 (d, J = 8.1 Hz, 2 H), 8.08 (d, J = 8.4 Hz, 2 H), 8.15 (d, J = 8.7 Hz, 2 H) ppm. ^{31}P NMR ($CDCl_3$): δ = 69.48 ppm. FAB-MS (matrix: 2-NPOE): *m*/*z* (%) = 889 (22) [MH^+], 761 (100) [M^+ − I]. $C_{34}H_{30}I_2N_2P_2Pd{\cdot}H_2O$ (906.8): calcd. C 45.03, H 3.56, N 3.09; found C 44.65, H 3.45, N 2.95.

***meso*-3:** ^1H NMR ($CDCl_3$): δ = 1.78−1.96 (m, 2 H), 2.02−2.19 (m, 2 H), 4.27 (dd, J_1 = 14.9, J_2 = 13.6 Hz, 2 H), 4.65 (dd, J_1 = 13.5, J_2 = 10.5 Hz, 2 H), 7.34 (m, 4 H), 7.41−7.50 (m, 4 H), 7.55 (d, J = 8.3 Hz, 2 H), 7.59−7.64 (m, 4 H), 7.74−7.82 (m, 8 H) ppm. ^{31}P NMR ($CDCl_3$): δ = 67.33 ppm. FAB-MS (matrix: 2-NPOE): *m*/*z* (%) = 889 (25) [MH^+], 761 (100) [M^+ − I]. $C_{34}H_{30}I_2N_2P_2Pd$ (888.8): calcd. C 45.95, H 3.40, N 3.15; found C 45.54, H 3.71, N 2.96.[29]

Synthesis of *rac*-4, *meso*-4: Silver tetrafluoroborate (223 mg, 1.13 mmol) was added to a suspension of the palladium diiodide (0.5 g, 0.56 mmol) in acetonitrile (50 mL). The reaction mixture was stirred overnight and the solution was filtered through celite. The solvent was removed under reduced pressure and the remaining solid was extracted twice with 20 mL portions of CH_2Cl_2. Evaporation of the solvent left a yellow, microcrystalline solid. Yield: 90−95% (0.45−0.47 g).

***rac*-4:** ^{1}H NMR (CD_3CN): δ = 2.26 (s, CH_3CN), 2.96−3.20 (m, 4 H), 4.34 (m, 2 H), 4.65 (m, 2 H), 7.25 (m, 4 H), 7.47 (m, 2 H), 7.60 (m, 4 H), 7.67−7.71 (m, 4 H), 7.86 (m, 2 H), 8.00 (d, J = 8.1 Hz, 2 H), 8.09 (d, J = 8.6 Hz, 2 H), 8.44 (d, J = 8.5 Hz, 2 H) ppm. ^{31}P NMR (CD_3CN): δ = 86.09 ppm. FAB-MS (matrix: TMAP): *m*/*z* (%) = 721 (10) [$M^+ - 2CH_3CN - BF_4$], 653 (92) [$M^+ - 2CH_3CN - BF_4 - BF_3$], 633 (100) [$M^+ - 2CH_3CN - BF_4 - BF_3 - HF$]. IR (KI): $\tilde{\nu}$ = 2320 cm^{-1}, 2292 (N≡C−CH_3, m), 1057 (ν BF_4, bs).

***meso*-4:** ^{1}H NMR (CD_3CN): δ = 2.25 (s, CH_3CN), 2.80−3.18 (m, 4 H), 4.30−4.70 (m, 4 H), 7.25 (m, 2 H), 7.45−7.71 (m, 10 H), 7.84 (m, 4 H), 7.98−8.10 (m, 4 H), 8.43−8.48 (m, 2 H) ppm. ^{31}P NMR (CD_3CN): δ = 86.40 ppm. FAB-MS (matrix: *m*-NBA): *m*/*z* (%) = 721 (2) [$M^+ - 2CH_3CN - BF_4$], 653 (52) [$M^+ - 2CH_3CN - BF_4 - BF_3$], 633 (100) [$M^+ - 2CH_3CN - BF_4 - BF_3 - HF$]. IR (KI): $\tilde{\nu}$ = 2321 cm^{-1}, 2293 (N≡C−CH_3, m), 1060 (ν BF_4, bs).

Synthesis *rac*-2: *rac*-3 (1 g, 1.125 mmol) and KCN (1.4 g, 22.5 mmol) were added to a mixture of water (20 mL) and toluene (25 mL). The two-phase system was stirred overnight. The water phase was separated and the organic phase was washed four times with 20 mL portions of water. The organic phase was dried over $MgSO_4$ and the solvent was removed under reduced pressure to leave the ligand as a colorless solid. Yield: 84% (0.50 g). ^{1}H NMR ($CDCl_3$): δ = 1.77−1.88 (m, 4 H), 3.38 (dd, J_1 = 14.8, J_2 = 13.1 Hz, 4 H), 6.99 (d, J = 8.4 Hz, 2 H), 7.19−7.29 (m, 6 H), 7.34 (m, 4 H), 7.45 (m, 2 H), 7.63 (m, 2 H), 7.70 (d, J = 8.1 Hz, 2 H), 7.87 (d, J = 8.4 Hz, 2 H), 7.94 (d, J = 8.5 Hz, 2 H) ppm. ^{31}P NMR ($CDCl_3$): δ = −14.82 ppm.

Synthesis of *meso*-2: *meso*-3 (500 mg, 0.56 mmol) and KCN (730 mg, 11.25 mmol) were added to a mixture of water (20 mL) and CH_2Cl_2 (15 mL). The two-phase system was stirred for 2 h. The water phase was separated and the organic phase was washed four times with 20 mL portions of water. The organic phase was dried over $MgSO_4$ and the solvent was removed under reduced pressure to leave the ligand as a colorless solid. Yield: 80% (0.24 g). ^{1}H NMR ($CDCl_3$): δ = 1.79−1.92 (m, 4 H), 3.39 (s, 4 H), 6.96 (d, J = 8.5 Hz, 2 H), 7.21−7.30 (m, 6 H), 7.37 (m, 4 H), 7.44 (m, 2 H), 7.63 (m, 2 H), 7.70 (d, J = 8.2 Hz, 2 H), 7.86 (d, J = 8.4 Hz, 2 H), 7.92 (d, J = 8.5 Hz, 2 H) ppm. ^{31}P NMR ($CDCl_3$): δ = −14.23 ppm.

Synthesis of *rac*-5, ***rac*-6**, ***meso*-5 and *meso*-6:** A solution of the ligand (between 0.4−0.8 mmol) in 15 mL of CH_2Cl_2 was added to a solution of the metal chloride (1 equiv.) in 5 mL of ethanol. The reaction mixture was stirred overnight and the solvent was reduced to 5 mL. The precipitate was isolated and dried under vacuum. Yields: 90−95% (0.25−0.41 mg).

***rac*-5:** FAB-MS (matrix: TMAP): *m*/*z* (%) = 619 (100) [$M^+ - Cl$]. $C_{34}H_{30}Cl_2FeN_2P_2 \cdot H_2O$ (673.3): calcd. C 60.65, H 4.79, N 4.16; found C 60.23, H 4.71, N 3.99.

***meso*-5**: FAB-MS (matrix: 2-NPOE)**:** *m*/*z* (%) = 619 (100) [$M^+ - Cl$]. $C_{34}H_{30}Cl_2FeN_2P_2$ (655.3): calcd. C 62.32, H 4.61, N 4.27; found C 62.48, H 4.85, N 4.23.

***rac*-6**: FAB-MS (matrix: 2-NPOE)**:** *m*/*z* (%) = 622 (100) [$M^+ - Cl$], 587 (61) [$M^+ - 2Cl$]. $C_{34}H_{30}Cl_2CoN_2P_2 \cdot H_2O$ (676.4): calcd. C 60.37, H 4.77, N 4.14; found C 59.92, H 4.60, N 4.08.

***meso*-6**: FAB-MS (matrix: 2-NPOE): *m*/*z* (%) = 622 (100) [$M^+ - Cl$], 587 (35) [$M^+ - 2Cl$]. $C_{34}H_{30}Cl_2CoN_2P_2 \cdot H_2O$ (676.4): calcd. C 60.37, H 4.77, N 4.14; found C 59.86, H 4.85, N 4.05.[30]

Ethene/CO Copolymerization: A 100 mL stainless steel autoclave equipped with a glass inlet and a stirring bar was purged with argon. The appropriate amount of the complex (50 μmol catalyst), solvent (50 mL of CH_2Cl_2) and methanol (Cat.:Cocat. = 1:200) were added and the autoclave was pressurized with the ethene (20 bar) and CO (60 bar). After stirring for 1 h at room temp. the gases were vented off and the polymer was isolated by filtration. Yields: 50 mg (***meso*-4**), 65 mg (***rac*-4**). IR: ECO (***meso*-4**): 2912.3 cm^{-1} (ν CH_2), 1693.6 (ν C≡O); ECO (***rac*-4**): 2912.3 cm^{-1} (ν CH_2), 1693.9 (ν C≡O)

X-ray Crystallographic Study: Crystal data of the compounds ***rac*-3** and ***meso*-3** were collected with a Rikagu AFC7S single-crystal diffractometer at 193(2) K using Mo-K_α radiation (graphite monochromator, λ = 0.71073 Å; omega scans). Intensities were corrected for Lorentz and polarization effects.[30] A psi-scan absorption correction was performed, $0.592 < T < 1.000$ (***rac*-3**), $0.920 < T < 1.000$ (***meso*-3**).[31] Solution and refinement: SHELX97 (Sheldrick, 1997).[32,33] The structure was solved by direct methods. All non-hydrogen atoms were refined anisotropically and hydrogen atoms were refined isotropically with their displacement factors 1.2-times that of the host atom. The hydrogen atoms of the lattice water were picked up from the final electron density map and were not further refined. The solid-state structures are stabilized by hydrogen bonds. The water molecule in both compounds is H-bonded to N5 and N22, the nitrogen acceptor atoms being situated in different complex molecules. In ***meso*-3** a toluene molecule is present in the unit cell which lies on a twofold rotation axis and is slightly disordered. All the final electron densities greater than one lie within one angsterom unit from palladium or iodine atoms.

CCDC-175209 (***rac*-3**) and -175208 (***meso*-3**) contain the supplementary crystallographic data for this paper. These data can be obtained free of charge at www.ccdc.cam.ac.uk/conts/retrieving.html [or from the Cambridge Crystallographic Data Centre, 12, Union Road, Cambridge CB2 1EZ, UK; Fax: (internat.) +44−1223/336−033; E-mail: deposit@ccdc.cam.ac.uk].

Acknowledgments

The Fonds der Chemischen Industrie and the DAAD are gratefully acknowledged for their financial support.

[1] G. J. P. Britovsek, V. C. Gibson, D. F. Wass, *Angew. Chem.* **1999**, *111*, 448−468; *Angew. Chem. Int. Ed.* **1999**, *38*, 428−448.
[2] S. D. Ittel, L. K. Johnson, M. Brookhart, *Chem. Rev.* **2000**, *100*, 1169−1203.
[3] *Applied Homogeneous Catalysis with Organometallic Compounds* Vol 1 (Eds.: B. Cornils, W. A. Herrmann), Wiley-VCH, Weinheim, **1996**.
[4] B. L. Small, M. Brookhart, A. M. A. Bennett, *J. Am. Chem. Soc.* **1998**, *120*, 4049−4050.
[5] G. J. P. Britovsek, V. C. Gibson, B. S. Kimberley, P. J. Maddox, S. J. McTavish, G. A. Solan, A. J. P. White, D. J. Williams, *Chem. Commun.* **1998**, 849−850.
[6] B. Rieger, A. S. Abu-Surrah, R. Fawzi, M. Steiman, *J. Organomet. Chem.* **1995**, *497*, 73−79.
[7] A. S. Abu-Surrah, U. Thewalt, B. Rieger, *J. Organomet. Chem.* **1999**, *587*, 58−66.
[8] A. M. S. Abu-Surrah, PhD Dissertation, Universität Ulm **1997**.
[9] Attempts to synthesize ligand **2** following the procedures applied for the N,N,N,N ligand **1** by treating the Li phosphide with bromoquinaldine were unsuccessful due to metal-halogen exchange reactions.
[10] The diiodide compounds were prepared instead of the dichloro complexes because of their higher solubility.
[11] U. Nagel, T. Krink, *Chem. Ber.* **1993**, *126*, 1091−1100.
[12] CRC, *Handbook of Chemistry and Physics*, 59th edition, CRC Press, inc., Boca Raton, Florida, F-215.

[13] U. Nagel, B. Rieger, *Chem. Ber.* **1988**, *121*, 1123−1131.
[14] S. Yurdakul, S. Akyuz, J. E. D. Davies, *J. Mol. Struct.* **1989**, *197*, 355−359.
[15] M. M. da Mota, J. Rodgers, S. M. Nelson, *J. Chem. Soc.* **1969**, 2036−2044.
[16] S. Yurdakul, S. Akyüz, J. E. D. Davies, *J. Mol. Struct.* **1988**, *174*, 435−441.
[17] A. R. Katritzky, R. A. Jones, *J. Chem. Soc.* **1960**, *14*, 2942−2947.
[18] R. M. Silverstein, G. C. Bassler, T. C. Morrill, *Spectrometric Identification of Organic Compounds*, John Wiley & Sons, Inc. **1991**.
[19] W. E. Hatfield, J. T. Yoke, *Inorg. Chem.* **1962**, *3*, 470−474.
[20] F. A. Cotton, D. M. L. Goodgame, M. Goodgame, A. Sacco, *J. Am. Chem. Soc.* **1961**, *83*, 4157−4161.
[21] J. Ellermann, W. H. Gruber, *Zeitschr. Anorg. Allg. Chem.* **1969**, *364*, 55−68.
[22] K. Heinze, G. Huttner, L. Zsolnai, P. Schober, *Inorg. Chem.* **1997**, *36*, 5457−5469.
[23] W. V. Dahlhoff, T. R. Dick, S. M. Nelson, *J. Chem. Soc. (A)* **1969**, 2919−2923.
[24] F. A. Cotton, O. D. Faut, D. M. L. Goodgame, R. H. Holm, *J. Am. Chem. Soc.* **1961**, *83*, 1780−1785.
[25] W. E. Hatfield, J. T. Yoke, *Inorg. Chem.* **1962**, *3*, 475−481.
[26] Common P−Co distance, source: Cambridge Crystallographic Data Centre.
[27] F. H. Allen, O. Kennard, *Chem. Design Automatation News* **1993**, *8*, 31.
[28] G. Brauer, *Handbuch der Präparativen Anorganischen Chemie*, 3. Band, Ferdinand-Enke-Verlag, Stuttgart **1981**, 1904−1905.
[29] T.-S. Chou, C.-H. Tsao, S. C. Hung, *J. Org. Chem.* **1985**, *50*, 4329−4332.
[30] In different cases, we were not able to obtain solvent-free samples of the metal complexes due to instability at higher temperature (especially the iron and cobalt complexes). We assume, therefore, that the deviation of the elemental analysis is due to solvent residues.
[31] *teXsan, Single Crystal Structure Analysis Software, Version 1.6*, Molecular Structure Corporation, 3200 Research Forest Drive, The Woodlands, TX 77381, USA **1993**.
[32] A. C. T. North, D. C. Phillips, F. S. Mathews, *Acta Crystallogr., Sect. A* **1968**, *24*, 351−359.
[33] G. M. Sheldrick SHELXTL/PC, Siemens Analytical X-ray Instruments Inc., Madison, Wisconsin, USA **1990**.
[34] G. M. Sheldrick, *SHELX97, Program for the Solution and Refinement of Crystal Structures* **1997**.

Received March 14, 2002
[I02129]

Synthesis, Structural and Chemical Characterization of Unsaturated C_4- and C_{10}-Bridged Group-4 *ansa*-Metallocenes Obtained Through a Ring-Closing Olefin Metathesis Reaction

Doris Hüerländer,[a] Nina Kleigrewe,[a] Gerald Kehr,[a] Gerhard Erker,*[a] and Roland Fröhlich[a][‡]

Keywords: Carbenes / Metallocenes / Metathesis / Olefins / Ruthenium / Zirconium

Bis[(5-hexenyl)cyclopentadienyl]zirconium dichloride (**3**) underwent ring-closure olefin metathesis with loss of ethylene when treated with 10 mol % of the $[Cl_2(PCy_3)_2Ru{=}CHPh]$ catalyst in refluxing dichloromethane, to yield the large *ansa*-zirconocene complex [dec-5-ene-1,10-diylbis(η^5-cyclopentadienyl)]$ZrCl_2$ (*trans*-**4**). Characterization by NMR and by X-ray diffraction revealed that the isolated complex contained a *trans*-C=C double bond inside the *ansa* bridge. Similarly, bis[(allyl)cyclopentadienyl]$ZrCl_2$ (**7**) gave the *ansa*-metallocene [but-2-ene-1,4-diylbis(η^5-cyclopentadienyl)]zirconium dichloride (*cis*-**8**) when treated with the same ruthenium metathesis catalysts (10 mol %) under similar conditions, except that a *cis*-C=C double bond was now found to be present (shown by NMR and X-ray diffraction). The *cis*-**8** complex was used as a homogeneous Ziegler–Natta catalyst for ethylene polymerization [after activation of the metallocene dichloride **8** with MAO (methylalumoxane) or treatment of the corresponding dimethylmetallocene complex **9** with $B(C_6F_5)_3$]. Complex **8** was also converted into a mixture of (*s-cis*- and *s-trans*-η^4-butadiene)-*ansa*-metallocene complexes (*s-cis*-**15**/*s-trans*-**15** = 4:5) by treatment with (butadiene)-magnesium. The C=C double bond of *cis*-**8** could be hydroborated with 9-BBN or with the $H{-}B(C_6F_5)_2$ reagent. $Li^+[B(C_6F_5)_4^-]$ added to *cis*-**8** to yield an interesting solid-state chain structure in which the $[Zr]Cl_2$ unit and the *o*-/*m*-F pairs of two $-C_6F_5$ groups were found to be in contact with the central lithium cation in a distorted octahedral coordination environment (as shown by X-ray diffraction).
(© Wiley-VCH Verlag GmbH, 69451 Weinheim, Germany, 2002)

Introduction

ansa-Metallocenes of the Group 4 metals have become of great importance, especially as components of homogeneous Ziegler−Natta catalyst systems.[1] Their synthesis in most cases involves nucleophilic substitution routes with Cp-anion equivalents and the respective bis(electrophile) of the bridging unit to build up the ligand framework before it is attached to the transition metal atom. This synthetic scheme has been followed in many cases, providing the ubiquitous *ansa*-metallocenes with small bridging units (e.g. SiR_2, $CH_2{-}CH_2$ etc.)[2−6] as well as the few examples of "large *ansa*-metallocenes" so far described in the literature.[7−10] A sizeable number of alternatives of linked bis(Cp) ligand syntheses has been reported in the literature,[11−19] but only very few in which selective organic transformations were carried out by coupling functional groups at the Cp ligands at the Group 4 metallocene stage.[20,21]

The C=C double bonds of alkenyl side chains at the Cp rings are functional groups compatible with many Group 4 metallocene features, and are easily introduced.[8,9,22−25] Modern variants of the olefin metathesis reaction, employing defined molecular Group 6 or Group 8 alkylidene complexes, can efficiently use alkenyl functional groups for carbon−carbon coupling.[26−28] Intramolecular variants ("ring-closure metathesis", RCM) has become an especially useful tool in organic synthesis.[29−36] We have employed such an olefin metathesis reaction for the intramolecular C−C coupling of bis[(ω-alkenyl)cyclopentadienyl]$ZrCl_2$ complexes to yield the respective C=C unsaturated *ansa*-metallocene complexes. Two representative examples are described, including their structural characterization and some chemical features of these easily available new systems.[37]

Results and Discussion

Synthesis and Characterization of the *ansa*-Metallocenes

Bis[(5-hexen-1-yl)cyclopentadienyl]zirconium dichloride (**3**) was prepared by a procedure analogous to that described by us in the literature: treatment of Cp−sodium

[a] Organisch-Chemisches Institut der Universität Münster, Corrensstrasse 40, 48149 Münster, Germany
[‡] X-ray crystal structure analyses
Supporting information for this article is available on the WWW under http://www.eurjic.org or from the author.

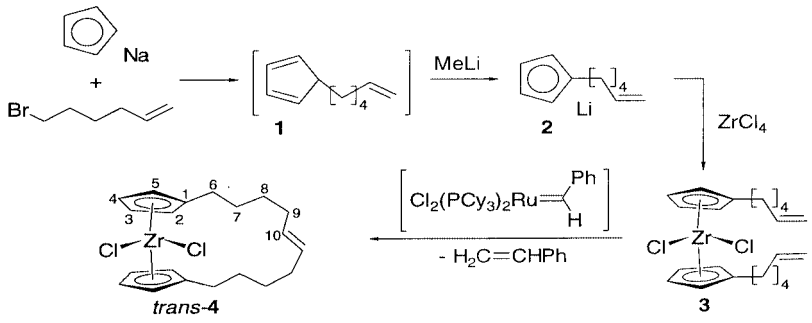

Scheme 1

with hexenyl bromide, followed by deprotonation (MeLi) and transmetallation furnished complex **3** in 38% yield (see Scheme 1).[8,22] Intramolecular olefin metathesis was carried out catalytically on **3** by treatment with 10 mol % of the "Grubbs catalyst" benzylidenedichlorobis(tricyclohexylphosphane)ruthenium.[38,39] In dilute solution, with use of a syringe pump for addition of **3** in dichloromethane to the metathesis catalyst, the reaction can largely be kept in the intramolecular regime. Crystallization from toluene gave the "large *ansa*-zirconocene dichloride complex" as a white crystalline solid in 25% yield.

Single crystals of **4** suitable for X-ray crystal structure analysis were obtained from [D_6]benzene at room temperature. The crystals were very thin needles, and the diffraction power was therefore weak, giving data of limited accuracy. The structure features an *ansa*-metallocene containing a *trans*-C=C double bond [C10−C11: 1.291(18) Å] in its centre. The large "13-membered" ring displays a crown-shaped conformation. The metallocene conformation is such that the bridging ring system is completely oriented toward a lateral sector of the bent metallocene wedge ["bis(lateral) *syn*" conformation, see Figure 1].[10,40,41] The zirconium atom in complex **4** is pseudotetrahedrally coordinated by the two η^5-Cp rings [Cp(centroid)−Zr: 2.193 and 2.216 Å, Cp(centroid)−Zr−Cp(centroid) angle 129.4°, Zr−Cl2 2.430(3) Å, Zr−Cl1 2.437(3) Å, Cl1−Zr−Cl2 angle: 98.2(1)°] in a largely unstrained fashion.

In the NMR spectra the signals of a major (> 95%) and a minor component could be seen. Whereas the minor compound has remained unidentified so far (it could be the *cis* isomer or an oligomer), the major product is likely to be identical to *trans*-**4** as identified by X-ray diffraction. This is indicated by the typical ^{13}C NMR shift of the allylic $-CH_2-CH=$ resonance (C-9) at δ = 31.9 ppm [δ(C-10) = 131.5 ppm]. The remaining CH_2 shifts of the bridging hydrocarbyl chain are found at δ = 29.3 (C-6), 26.4 (C-7) and 28.5 (C-8) ppm (for atom numbering scheme see Scheme 1). The corresponding ^1H NMR resonances occur at δ = 2.52 (6-H), 1.22 (7-H), 1.30 (8-H), 2.01 (9-H) and 5.25 (olefinic 10-H) ppm.

The synthesis of bis(allylcyclopentadienyl)zirconium dichloride (**7**) was carried out analogously to the procedure described by us previously (Scheme 2).[22] The ring-closing metathesis reaction was carried out by treatment of **7** with $Cl_2(PCy_3)_2Ru=CHPh$ under high-dilution reaction conditions. Oligomeric by-products were removed by filtration and the product **8** was purified by fractional crystallization. Eventually, the isomerically pure complex *cis*-**8** was obtained as a colourless, crystalline material in ca. 50% yield.

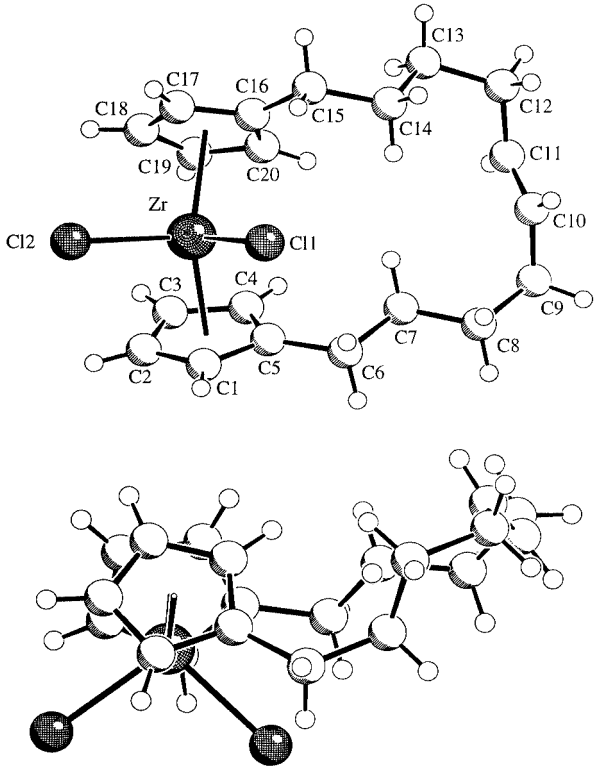

Figure 1. Two views of the organometallic olefin metathesis product **4**; selected bond lengths [Å] and angles [°]: Zr−Cl1 2.437(3), Zr−Cl2 2.430(3), C5−C6 1.526(14), C6−C7 1.489(14), C7−C8 1.516(14), C8−C9 1.500(17), C9−C10 1.472(19), C10−C11 1.291(18), C11−C12 1.455(23), C12−C13 1.538(22), C13−C14 1.505(20), C14−C15 1.528(19), C15−C16 1.510(16); Cl1−Zr−Cl2 98.2(1), C5−C6−C7 113.6(9), C6−C7−C8 113.8(9), C7−C8−C9 112.3(9), C8−C9−C10 111.7(11), C9−C10−C11 128.0(15), C10−C11−C12 126.7(16), C11−C12−C13 114.0(13), C12−C13−C14 112.0(12), C13−C14−C15 116.3(13), C14−C15−C16 118.0(11); C5−C6−C7−C8 −175.4(10), C6−C7−C8−C9 179.2(11), C7−C8−C9−C10 71.2(14), C8−C9−C10−C11 -107.6(15), C9−C10−C11−C12 176.2(14), C10−C11−C12−C13 -108.4(16), C11−C12−C13−C14 65.1(19), C12−C13−C14−C15 -175.6(13), C13−C14−C15−C16 74.4(18)

The X-ray crystal structure analysis of **8** (single crystals were obtained from [D_6]benzene at room temperature) again shows the presence of an unconstrained *ansa*-metallo-

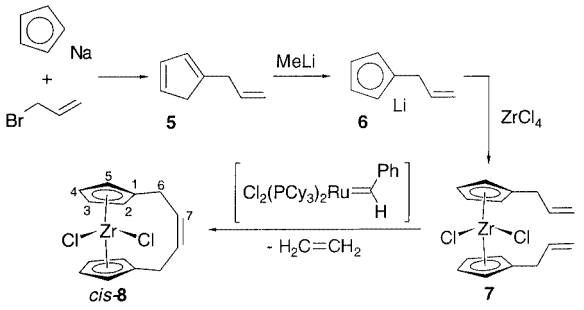

Scheme 2

cene framework. The metal−C(Cp) bond lengths are in a rather narrow range between 2.486(2) Å (Zr−C13) and 2.536(2) Å (Zr−C11). The Cp(centroid)−Zr−Cp(centroid) angle amounts to an ideal bent metallocene value of 130.0°.[42] The Cl1−Zr−Cl2 angle in **8** [95.95(2)°] is only marginally smaller than that in the parent compound Cp_2ZrCl_2.[43] Zr−Cl1 [2.437(1) Å] and Zr−Cl2 [2.455(1) Å] are very similar in lengths.

The *ansa*-metallocene complex **8** features an endocyclic *cis*-carbon−carbon double bond [C16−C26 1.319(3) Å]. This value is in the range typical for an uncoordinated C=C bond.[44] Close inspection reveals that there is no immediate coordinative interaction between the *cis*-C=C double bond inside the *ansa* bridge and its adjacent, slightly electron-deficient Group 4 metal centre. The observed Zr···C16/C26 distances of ca. 4 Å rule out any significant direct interaction. Consequently, an eclipsed metallocene conformation is attained in complex *cis*-**8**, with the C10−C15 and C20−C25 vectors oriented to the same lateral sector of the bent metallocene wedge and the $-CH_2-CH=CH-CH_2-$ unit bent back towards the back side of the metallocene framework (as illustrated by the top view projection of *cis*-**8** in Figure 2).

In solution one finds a single set of NMR signals, indicating that there is only one isomer present. This shows a ^{13}C NMR signal of the allylic C-6 $CH_2-CH=$ carbon centre (see Scheme 1) at δ = 24.8 ppm, consistent with the *cis*-**8** structure (*trans*-**4** shows the analogous $-CH_2-CH=$ signal at δ = 31.9 ppm, see above). In addition, there are the olefinic −CH= resonance at δ = 129.7 ppm and three Cp signals at δ = 119.3, 115.3 (both *C*H) and δ = 121.2 ppm (*C*). The pairwise identical C-2/C-5 and C-3/C-4 resonances indicate rapid conformational equilibration of *cis*-**8** on the NMR timescale. Probably both the Cp−Zr rotation *and* the inversion of the metallacycle that includes the *ansa* bridge atoms are fast.[45] Consequently, only two C_5H_4 resonances are observed in the ^1H NMR spectrum of *cis*-**8** at "high" temperatures. In a $CDFCl_2/CDF_2Cl$ mixture[46] at 253 K this pair of ^1H NMR Cp signals is observed at δ = 6.32 and 6.66 ppm. On lowering the temperature these signals each decoalesce to a new pair of Cp signals that at 128 K have become separated by 517 and 128 Hz, respectively (see Figure 7). From these temperature-dependent ^1H NMR spectra an averaged activation barrier has been calculated as $\Delta G^{\ddagger}_{inv}$ (128 K) = 5.1 ± 0.3 kcal mol^{-1}.[47] We assume

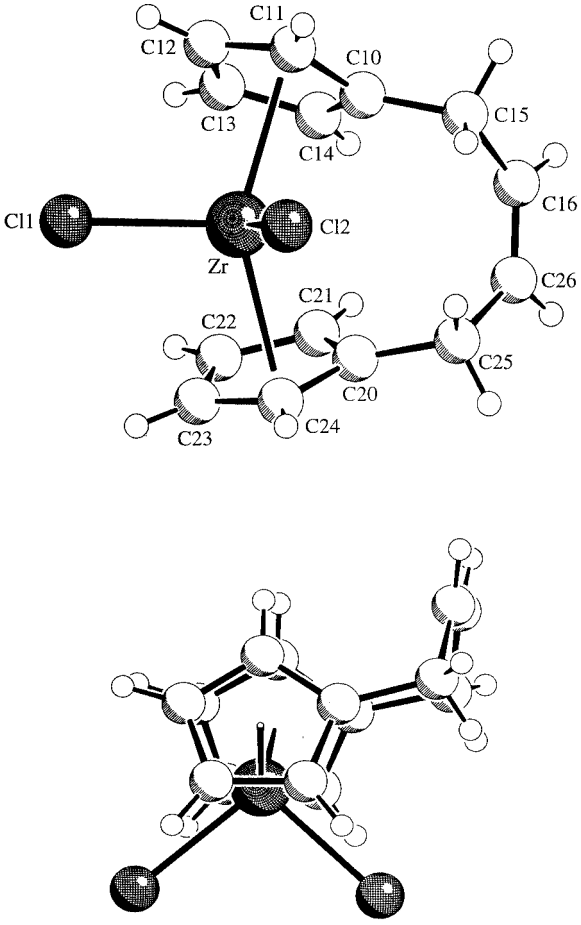

Figure 2. Top and side views of the molecular structure of complex *cis*-**8**; selected bond lengths [Å] and angles [°]: Zr−Cl1 2.437(1), Zr−Cl2 2.455(1), C10−C15 1.513(3), C15−C16 1.496(3), C16−C26 1.319(3), C26−C25 1.503(3), C25−C20 1.518(3); Cl1−Zr−Cl2 95.95(2), C10−C15−C16 114.7(2), C15−C16−C26 126.2(2), C16−C26−C25 126.1(2), C26−C25−C20 112.5(2); C10−C15−C16−C26 −83.5(3), C15−C16−C26−C25 0.9(3), C16−C26−C25−C20 86.0(3)

that this Gibbs activation energy primarily characterises the inversion barrier of the *ansa*-metallacycle, but it is in principle possible that this has coincided with "freezing" of the Cp−M rotation on the NMR timescale at this very temperature.[48−50]

Reactions of the *ansa*-Metallocenes

Treatment of the *ansa*-zirconocene dichloride **8** with methyllithium (2 equiv.) gave the corresponding dimethylmetallocene complex **9** {$^1H/^{13}C$ NMR of [Zr]$(CH_3)_2$: δ = −0.05/31.0 ppm ($^1J_{CH}$ = 117 Hz) in [D_6]benzene}. Treatment of **9** with $B(C_6F_5)_3$ in [D_8]toluene with NMR monitoring generated the ion-pair **10** {^1H NMR of [Zr]CH_3/[B]CH_3: δ = 1.34/0.94}. Compound **10** separated from the solution as a red oil after some time. An attempt to crystallise **10** from [D_6]benzene resulted in partial hydrolysis of the moisture-sensitive complex, and we isolated single crystals of the corresponding dinuclear μ-oxobis(*ansa*-metallo-

cene) compound **11** suitable for an X-ray crystal structure determination (see Scheme 3 and Figure 3).

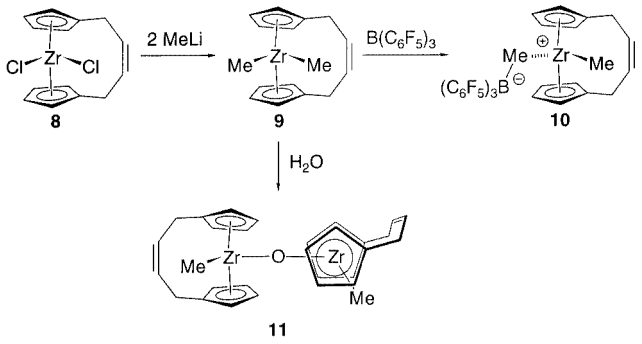

Scheme 3

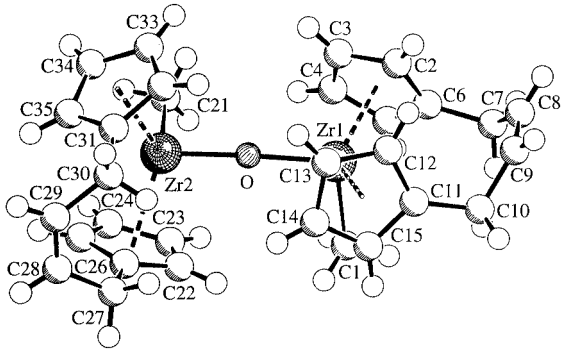

Figure 3. A projection of the molecular structure of the μ-oxobis(*ansa*-metallocene) complex **11**; selected bond lengths [A] and angles [°]: Zr1−O 1.951(2), Zr1−C1 2.294(3), Zr2−O1 1.954(2), Zr2−C21 2.291(3), C6−C7 1.509(4), C7−C8 1.499(4), C8−C9 1.312(4), C9−C10 1.503(4), C10−C11 1.502(4), C26−C27 1.514(4), C27−C28 1.483(4), C28−C29 1.317(4), C29−C30 1.489(4), C30−C31 1.503(4); Zr1−O−Zr2 170.53(9), C1−Zr1−O 97.55(9), C21−Zr2−O 97.97(9), C6−C7−C8 113.7(2), C7−C8−C9 124.4(3), C8−C9−C10 123.8(2), C9−C10−C11 112.8(2), C26−C27−C28 114.7(3), C27−C28−C29 124.0(3), C28−C29−C30 124.0(3), C29−C30−C31 113.6(2); C6−C7−C8−C9 84.3(3), C7−C8−C9−C10 −0.9(5), C8−C9−C10−C11 −88.9(3), C26−C27−C28−C29 −81.7(4), C27−C28−C29−C30 0.2(5), C28−C29−C30−C31 88.8(4)

The X-ray crystal structure analysis of **11** shows the presence of two C_4-*ansa*-metallocene subunits, bridged by a close to linear μ-oxobridge [angle Zr1−O−Zr2: 170.53(9)°]. Both the zirconium−oxygen bonds are rather short, at 1.951(2) Å (Zr1−O) and 1.954(2) Å (Zr2−O), respectively. This indicates considerable μ-oxygen ligand-to-metal π-backbonding,[51] making use of the available acceptor orbital at the (formally) 16-electron metal centre.[52] Consequently, the overall structural arrangement of the two metallocene subunits of **11** along the metal-oxygen-metal vector is close to perpendicular (dihedral angle C1−Zr1···Zr2−C21 −85.8°). The conformational arrangement of the strongly bent *ansa*-bridge is noteworthy, as it is different in the two metallocene subunits. On both sides the $-CH_2-CH=CH-CH_2-$ bridge is oriented toward a lateral sector of the bent metallocene wedge, and this is toward the oxygen side in both cases, but the *ansa* bridge at Zr1 is bent in the direction toward the front side of the bent metallocene, whereas at Zr2 this hydrocarbyl bridge is bent away from the μ-oxygen atom and prefers to point toward the narrow back side of the bent metallocene wedge.

Both the complexes **8** and **9** were used as starting materials for the generation of active homogeneous Ziegler−Natta catalysts. In the case of the dimethylzirconium complex, activation was achieved by treatment with $B(C_6F_5)_3$ in a close to equimolar ratio (the active species probably being **10**, see Scheme 3).[53] The *ansa*-metallocene dichloride **8** was activated by treatment with a large excess of methylalumoxane in toluene solution (Al/Zr > 1000).[1,54] Both systems turned out to be excellent ethylene polymerization catalysts (see Table 1). They also polymerized propene at room temperature, although not with high activities (a = 38). The obtained polypropylene was atactic.

We had previously shown that Cp-bound alkenyl groups can undergo a C−C coupling reaction with metal-coordinated butadiene ligands at the Group 4 metallocene frameworks.[22] The formation of **14** from **12** via **13** is a typical example.

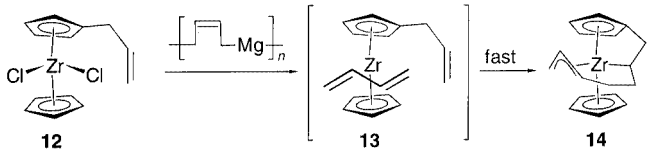

We were curious to see whether there would be any interaction between the endocyclic *cis*-C=C double bond in the *ansa*-metallocene framework and a butadiene ligand attached at, for example, the framework of complex **8**. We therefore treated complex **8** directly with 1 mol-equiv. of the (butadiene)Mg·(THF)$_n$ reagent[55] in [D_8]toluene at room temperature. Formation of the (butadiene)metallocenes took place. NMR analysis revealed the presence of the (*s-cis*- and *s-trans*-η^4-butadiene)[Zr] complex isomers (*s-cis*-**15**;

Table 1. Ethylene polymerization with homogeneous Ziegler−Natta catalysts derived from the complexes **8** and **9**

Cat. precursor[a]	Activator	Al(B)/Zr ratio	T [°C]	Reaction time [min]	PE [g]	M.p. [°C]	Act.[b]
9	$B(C_6F_5)_3$	1.1	25	4	12.8	128	2600
8	MAO	1000	25	10	43.6	128	3660
9	$B(C_6F_5)_3$	1.1	60	10	25.0	129	2150
8	MAO	1250	60	10	37.1	126	3750

[a] In toluene solution at 2 bar ethene pressure. [b] Catalyst activity in kg(polymer)/mol[Zr]·h·bar(ethene).

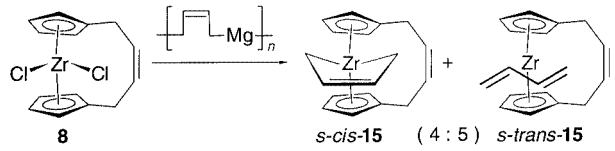

Scheme 4

s-trans-**15**, see Scheme 4) in a 4:5 ratio. The *s-cis* isomer is easily identified by its dynamic NMR behaviour, due to a rapid inversion of its five-membered σ^2,π-metallacyclopentene core on the NMR timescale at room temperature, becoming frozen at low temperature.[56] This results in the observation of a 1:1 pair of ^{1}H NMR singlets at 298 K (δ = 5.09, 4.88 ppm) that decoalesces to a set of four Cp signals of equal intensity at 213 K in the [D_8]toluene solvent (δ = 5.55, 4.91, 4.78, 4.53 ppm). In contrast, the chiral (averaged C_2-symmetric) *s-trans*-**15** isomer exhibits temperature-invariant NMR spectra showing four separate ^{1}H NMR Cp resonances (213 K: δ = 4.87, 4.85, 4.53, 4.35 ppm) throughout this temperature range. The ^{1}H/^{13}C NMR shifts of the (*s-cis*-η^4-butadiene)[Zr] complex [213 K: δ = 4.76, 3.42, −0.59 (H_{meso}, H_{syn}, H_{anti})/112.1, 49.7 (C-2/3, C-1/4) ppm] and its *s-trans*-**15** isomer [213 K: δ = 3.04, 3.14, 1.38 ppm (^{1}H)/96.7, 59.1 ppm (^{13}C)] are characteristically different.[56] The *s-cis*- and *s-trans*-**15** complexes are stable as such in the examined temperature range. We have so far found no evidence of the occurrence of a C−C coupling reaction with the disubstituted C=C double bond of the adjacent *ansa* bridge.

The C=C double bond in *cis*-**8** undergoes reactions typical of olefins, however. Catalytic hydrogenation (H_2, Pd/C) cleanly yields the saturated tetramethylene-bridged *ansa*-

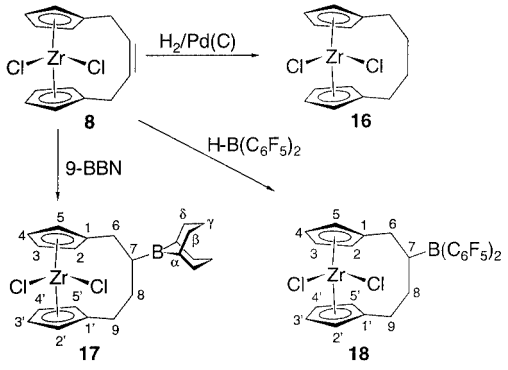

Scheme 5

zirconocene dichloride complex **16** (see Scheme 5). Hydroboration takes place equally facilely and also leaves the metallocene nucleus untouched. We have used two sterically and electronically quite different boranes for this purpose. 9-BBN[57,58] adds to the endocyclic double bond in *cis*-**8** to yield the product **17**. The borylated complex **18** was formed by treatment of *cis*-**8** with the electrophilic borane H−B(C_6F_5)$_2$.[59,60] As expected, each of these products now shows eight ^{1}H NMR signals of the pair of monosubstituted Cp ligands [**17**: δ = 6.53, 6.45 (2 H), 6.42, 6.40, 6.35, 6.33, 6.25 ppm]. It is interesting to note that complex **18** has an electrophilic −B(C_6F_5)$_2$ unit covalently bonded to its *ansa*-metallocene framework. Future studies should show if this can be utilized as an internal activator component for the generation of an active single-component metallocene Ziegler−Natta catalyst system.[61,62]

L_nM^+ cations can sometimes be generated by treatment of the respective metal halide complexes (e.g., L_nM−Cl) with alkali metal cations in combination with anions of low nucleophilicity.[63] An interesting alternative reaction, namely Li^+ addition, was observed in one case starting from **8**. When we treated the *ansa*-metallocene complex *cis*-**8** with $Li^+[B(C_6F_5)_4^-]$ in [D_8]toluene at room temperature, the crystalline adduct **19** was obtained. Its rather interesting structure was determined by X-ray diffraction (see Figures 4 and 5).

The X-ray crystal structure analysis revealed that the Li^+ cations of two independent molecules are (electrostatically) coordinated to the pair of chloride ligands[64,65] at the zirconium center in a chelate fashion. The coordination sphere around the lithium ion is complemented by two additional

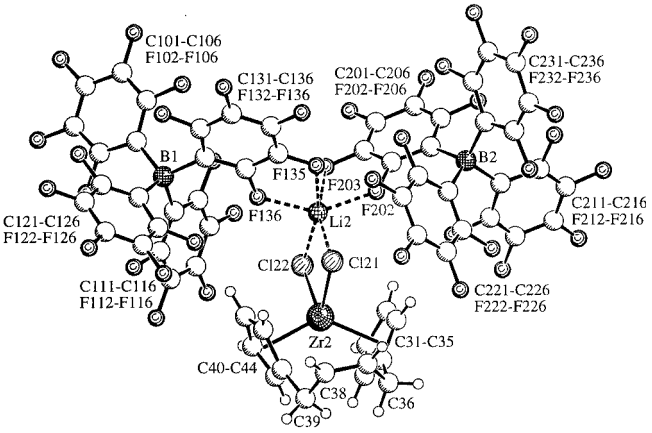

Figure 4. A view of the *cis*-**8**·$Li^+[B(C_6F_5)_4^-]$ adduct structure (**19**); selected bond lengths [A] and angles [°]: Zr1−Cl11 2.479(1), Zr1−Cl21 2.487(1), Zr2−Cl21 2.454(1), Zr2−Cl22 2.477(1), C11−C16 1.518(5), C31−C36 1.504(6), C16−C17 1.480(6), C36−C37 1.517(10), C17−C18 1.327(5), C37−C38 1.436(12), C18−C19 1.467(5), C38−C39 1.445(12), C19−C20 1.516(4), C39−C40 1.480(8); Cl11−Zr1−Cl12 87.53(2), Cl21−Zr2−Cl22 89.50(3), C11−C16−C17 112.5(3), C31−C36−C37 115.3(4), C16−C17−C18 126.0(4), C36−C37−C38 117.8(5), C17−C18−C19 125.5(4), C37−C38−C39 116.9(6), C18−C19−C20 112.4(3), C38−C39−C40 105.0(8); C11−C16−C17−C18 −85.4(5), C31−C36−C37−C38 80.7(8), C16−C17−C18−C19 0.4(6), C36−C37−C38−C39 −0.8(7), C17−C18−C19−C20 87.5(5), C37−C38−C39−C40 −102.7(6); Li1−Cl11 2.376(5), Li1−Cl12 2.385(5), Li2−Cl21 2.379(6), Li2−Cl22 2.420(6), Li1−F115 2.812(6), Li1−F116 1.985(5), Li2−F203 2.567(6), Li2−F202 2.045(5), Li1−F235 2.235(5), Li1−F236 2.087(5), Li2−F135 2.223(6), Li2−F136 2.052(5); Cl11−Li1−Cl12 92.4(2), Cl21−Li2−Cl22 92.7(2), Cl11−Li1−F115 159.1(2), Cl21−Li2−F203 160.8(2), Cl11−Li1−F116 101.9(2), Cl21−Li2−F202 96.9(2), Cl11−Li1−F235 91.6(2), Cl21−Li2−F135 86.1(2), Cl11−Li1−F236 115.8(2), Cl21−Li2−F136 105.2(2), Cl12−Li1−F115 78.9(2), Cl22−Li2−F203 83.4(2), Cl12−Li1−F116 105.0(2), Cl22−Li2−F202 110.0(2), Cl12−Li1−F235 168.5(2), Cl22−Li2−F135 165.9(3), Cl12−Li1−F236 96.1(2), Cl22−Li2−F136 93.3(2), F115−Li1−F116 63.1(2), F203−Li2−F202 67.2(2), F115−Li1−F235 100.7(2), F203−Li2−F135 102.1(2), F115−Li1−F236 84.2(2), F203−Li2−F136 93.8(2), F116−Li1−F235 84.8(2), F202−Li2−F135 84.1(2), F116−Li1−F236 135.9(3), F202−Li2−F136 147.0(3), F235−Li1−F236 72.5(2), F135−Li2−F136 73.5(2)

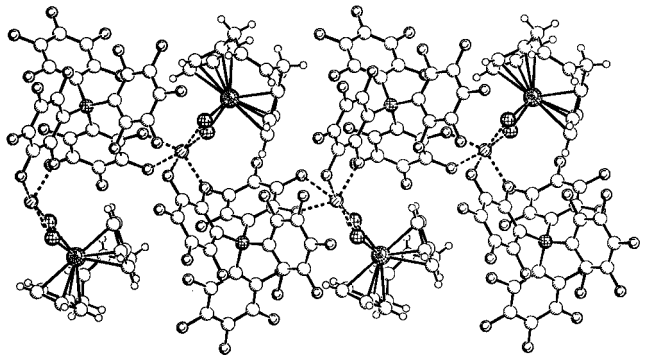

Figure 5. A projection of the chain structure of the adduct **19** in the crystal

chelate interactions, each with a pair of *ortho*- and *meta*-fluorine atoms of one C_6F_5 substituent from two different adjacent $[B(C_6F_5)_4^-]$ anions. This complements a distorted octahedral coordination sphere around the alkali metal cation (see Figure 4). The octahedral geometry is, however, markedly distorted. Of the (idealised) three 180° bonding angles around the central (alkali) metal ion, only two are close to linear [F135−Li2−Cl22: 165.9(3)° and Cl21−Li2−F203: 160.8(2)°; only the data of one of the crystallographically independent units (here around Li2) are given, those around Li1 are similar], whereas the third is markedly smaller at 147.0(3)° (F202−Li2−F136). Most of the remaining twelve bonding angles at the origin of the distorted octahedron are reasonably close to the expected 90° [F202−Li2−F135: 84.1(2)°, F202−Li2−Cl21: 96.9(2)°, F135−Li2−Cl21: 86.1(2)°, F136−Li2−Cl22: 93.3(2)°, Cl21−Li2−Cl22: 92.7(2)°, F136−Li2−F203: 93.8(2)°, Cl22−Li2−F203: 83.4(2)°], with the exception of the two narrow internal *o*-/*m*-F chelate angles [F136−Li2−F135: 73.5(2)° and F202−Li2−F203: 67.2(2)°] and some secondary deviation, caused by this chelate effect [F136−Li2−Cl21: 105.2(2)°, F202−Li2−Cl22: 110.0(2)°, F135−Li2−F203: 102.1(2)°].

The lithium chloride contact lengths in the adduct **19** amount to 2.379(6) Å (Li2−Cl21) and 2.420(6) Å (Li2−Cl22). The Li−F distances cover a wider range [Li2−F202: 2.045(5) Å, Li2−F136: 2.052(5) Å, Li2−F135: 2.223(6) Å, and Li2−F203: 2.567(6) Å]. Each $[B(C_6F_5)_4^-]$ anion in the adduct **19** contains two C_6F_5 units that exhibit chelate contacts to two different Li^+ cations, whereas the remaining C_6F_5 pair of substituents is oriented away from the alkali metal centres. This results in a chain-type suprastructure of **19**, depicted in Figure 5.

The electrostatic Li^+ coordination has changed the $[Zr]Cl_2$ geometry slightly. In comparison with the starting material **8**, the Zr−Cl bond lengths in the adduct **19** are slightly longer [Zr1−Cl11: 2.479(1) Å, Zr1−Cl12: 2.487(1) Å, Zr2−Cl21: 2.454(1) Å, Zr2−Cl22: 2.477(1) Å; see for comparison: *cis*-**8** Zr−Cl1: 2.437(1) Å, Zr−Cl2: 2.455(1) Å]. Consequently, the Cl11−Zr1−Cl12 angle in **19** is markedly smaller [87.53(2)°; Cl21−Zr2−Cl22: 89.50(3)] than in *cis*-**8** [Cl1−Zr2−Cl2: 95.95(2)°].

It is also noteworthy that the conformational arrangement of the $-CH_2-CH=CH-CH_2-$ *ansa* bridge in *cis*-**8** and in the adduct **19** are quite different. In the former, the C=C double bond in the strongly bent structural subunit is oriented toward the back side (Zr···C=C separation ca. 4 Å), whereas in the latter it is found in the inverted position (see Figure 6), which brings the C=C π-system closer to the electron-deficient d^0-configurated Group 4 metal centre (in **19** the Zr···C=C separation is only ca. 3.5 Å).

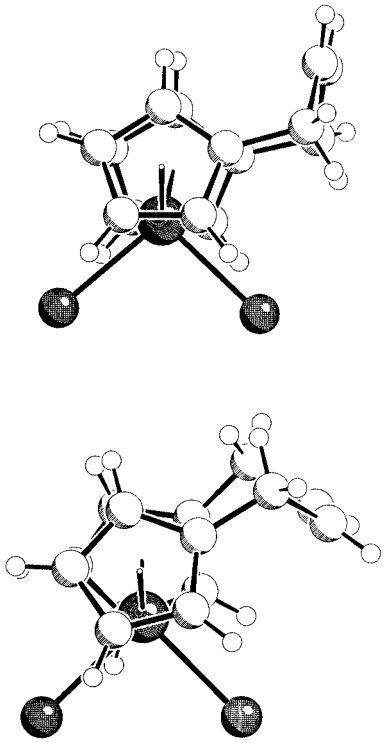

Figure 6. A comparison of the *ansa*-metallocene core conformation as found in *cis*-**8** (top) and the adduct **19** (bottom)

We conclude that olefin metathesis at the Cp−alkenyl unit of Group 4 metallocenes can easily be carried out intramolecularly, cleanly yielding the respective unsaturated *ansa*-metallocenes with loss of ethene. The C=C bond inside the *ansa*-metallocene bridge undergoes a variety of typical reactions without affecting the Group 4 metallocene backbone. Such combinations of reactions may potentially open up new synthetic pathways to functionalized bent metallocene complexes that may turn out to be useful for the development of improved catalysts for rapid and selective C−C coupling reactions and/or for use as reagents in organic synthesis. Studies aimed at finding out about such properties are being carried out in our laboratory.

Experimental Section

General: All reactions were carried out under dry argon in Schlenk-type glassware or in a glove-box. Solvents, including deuterated solvents used for NMR spectroscopy, were dried and distilled prior to use. For additional general conditions, including a list of instruments used for physical characterization of the compounds, see

ref.[41b] or ref.[66] NMR assignments were usually secured by carrying out a variety of 2D NMR experiments.[67] The starting materials **3** and **7** were prepared according to literature procedures.[8,22]

Preparation of [Dec-5-ene-1,10-diylbis(η⁵-cyclopentadienyl)]zirconium Dichloride (*trans*-4): A solution containing [$Cl_2(PCy_3)_2Ru$=CHPh] (45.3 mg, 0.06 mmol, 10 mol %) in 400 mL of dichloromethane was brought to reflux temperature in a three-necked flask, equipped with stirrer, reflux condenser and a septum. Over 6 h a solution of bis[η⁵-(5-hexen-1-yl)cyclopentadienyl]$ZrCl_2$ (**3**, 250 mg, 0.55 mmol) in 100 mL of dichloromethane was added by syringe pump. The mixture was heated under reflux for an additional 3 h, and then cooled to room temperature and filtered. Solvent was removed in vacuo, and the residue was washed with pentane (2 × 20 mL). Fractional crystallization from toluene (10 mL) gave 58.9 mg (25%) of *trans*-**4** as a white solid, m.p. 162 °C. IR (KBr): $\tilde{\nu}$ = 3103 w, 2929 m, 2856 w, 2387 w, 1497 w, 1263 m, 1102 s, 1035 s, 969 w, 841 w, 828 s, 825 vs cm^{-1}. ^1H NMR ([D_6]benzene, 599.9 MHz, 298 K): δ = 5.97 (m, 4 H, 3,4-H), 5.73 (m, 4 H, 2,5-H), 5.25 (m, 2 H, 10-H), 2.52 (m, 4 H, 6-H), 2.01 (m, 4 H, 9-H), 1.30 (m, 4 H, 8-H), 1.22 (m, 4 H, 7-H) ppm. $^{13}C\{^1H\}$ NMR ([D_6]benzene, 150.8 MHz, 298 K): δ = 139.3 (C, C-1), 131.5 (CH, C-10), 115.1 (CH, C-3,4), 111.0 (CH, C-2,5), 31.9 (CH_2, C-9), 29.3 (CH_2, C-6), 28.5 (CH_2, C-8), 26.4 (CH_2, C-7) ppm. $C_{20}H_{26}Cl_2Zr$ (428.5): calcd. C 56.05, H 6.12; found C 56.35, H 6.63.

X-ray Crystal Structure Analysis of *trans*-4: Single crystals were obtained from [D_6]benzene at ambient temperature. $C_{20}H_{26}Cl_2Zr$, M = 428.53, yellow crystal, 0.30 × 0.04 × 0.03 mm, a = 6.581(1), b = 20.480(1), c = 14.451(1) Å, β = 97.47(1)°, V = 1931.2(3) $Å^3$, $\rho_{calcd.}$ = 1.474 g cm^{-3}, μ = 8.43 cm^{-1}, empirical absorption correction by SORTAV (0.786 ≤ T ≤ 0.975), Z = 4, monoclinic, space group $P2_1/c$ (no. 14), λ = 0.71073 Å, T = 198 K, ω and φ scans, 5920 reflections collected (±h, ±k, ±l), [(sinθ)/λ] = 0.59 $Å^{-1}$, 3401 independent (R_{int} = 0.066) and 2048 observed reflections [$I \geq 2\sigma(I)$], 209 refined parameters, R = 0.094, wR^2 = 0.165, max. (min.) residual electron density 1.46 (−1.19) e $Å^{-3}$, weakly diffracting crystal due to its shape; therefore the accuracy of the resulting data is poor, hydrogen atoms calculated and refined as riding atoms.

Synthesis of [But-2-ene-1,4-diylbis(η⁵-cyclopentadienyl)]zirconium Dichloride (*cis*-8): Analogously to the procedure described above, bis[η⁵-(2-propen-1-yl)cyclopentadienyl]$ZrCl_2$ (**7**, 1.60 g, 4.30 mmol) was metathesized by treatment with [$Cl_2(PCy_3)_2Ru$=CHPh] (248 mg, 0.30 mmol, 7 mol %) in a total of 500 mL of dichloromethane under high-dilution conditions. The mixture was heated under reflux for an additional 6 h, cooled to room temperature and filtered. The volume of the resulting solution was reduced to 20 mL in vacuo. Crystallization at −30 °C overnight gave a crystalline precipitate that was washed with pentane (15 mL) and dried in vacuo to give 740 mg (50%) of *cis*-**8** as a microcrystalline solid, m.p. 182 °C. IR (KBr): $\tilde{\nu}$ = 3117 w, 2968 w, 2922 w, 2848 w, 2373 w, 1487 w, 1447 m, 1430 w, 1269 m, 1098 w, 1046 s, 960 w, 903 m, 829 s, 817 vs, 795 s cm^{-1}. ^1H NMR ([D_6]benzene, 599.9 MHz, 298 K): δ = 6.02 (m, 4 H, 2,5-H), 6.00 (m, 4 H, 3,4-H), 5.61 (m, 2 H, 7-H), 2.74 (m, 4 H, 6-H) ppm. ^1H NMR ($CDFCl_2/CDF_2Cl$, 599.9 MHz): δ (253 K) = 6.66, 6.32 (each m, each 4 H, 2,5-H, 3,4-H), 6.31 (m, 2 H, 7-H), 3.35 (m, 4 H, 6-H); δ (128 K) = 6.83/6.61, 6.74/5.87 (each br., each 2 H, 2,5-H, 3,4-H), 6.33 (br., 2 H, 7-H), 3.29, 3.25 (each br., each 2 H, 6-H) ppm. $^{13}C\{^1H\}$ NMR ([D_6]benzene, 150.8 MHz, 298 K): δ = 129.7 (CH, $^1J_{CH}$ = 145 Hz, C-7), 121.2 (C, C-1), 119.3 (CH, $^1J_{CH}$ = 176 Hz, C-2,5), 115.3 (CH, $^1J_{CH}$ = 175 Hz, C-3,4), 24.8 (CH_2, $^1J_{CH}$ = 129 Hz, C-6) ppm. $C_{14}H_{14}Cl_2Zr$ (344.4): calcd. C 48.83, H 4.10; found C 48.70, H 4.84. The dynamic behaviour of *cis*-**8** was monitored by ^1H NMR over a temperature range of 253 to 128 K (Figure 7). The AA′BB′ spin system of the Cp protons at high temperature changed to an ABCD spin system at low temperature. The activation energies were estimated as $\Delta G^{\neq}_{inv}$ [T_c: 153 K; Δν (128 K): 517 Hz] = 5.22 kcal·mol^{-1} for one group of protons and $\Delta G^{\neq}_{inv}$ [T_c: 138 K; Δν (128 K) = 128 Hz] = 5.07 kcal·mol^{-1} for the other. The average activation energy was calculated as $\Delta G^{\neq}_{inv}$ = 5.1 ± 0.3 kcal·mol^{-1}.

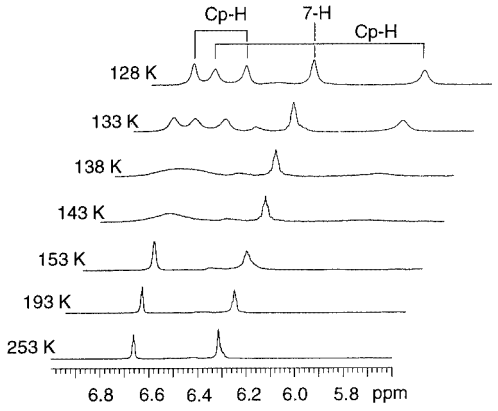

Figure 7. Dynamic ^1H NMR spectrum of *cis*-**8** (in $CDFCl_2$/CDF_2Cl)

X-ray Crystal Structure Analysis of *cis*-8: Single crystals of the *ansa*-metallocene were obtained from [D_6]benzene at room temperature. $C_{14}H_{14}Cl_2Zr$, M = 344.37, light yellow crystal, 0.40 × 0.20 × 0.10 mm, a = 7.798(1), b = 12.887(1), c = 13.044(1) Å, V = 1310.8(2) $Å^3$, $\rho_{calcd.}$ = 1.745 g cm^{-3}, μ = 12.19 cm^{-1}, empirical absorption correction by SORTAV (0.641 ≤ T ≤ 0.888), Z = 4, orthorhombic, space group $P2_12_12_1$ (no. 19), λ = 0.71073 Å, T = 198 K, ω and φ scans, 10,955 reflections collected (±h, ±k, ±l), [(sinθ)/λ] = 0.67 $Å^{-1}$, 3159 independent (R_{int} = 0.037) and 3025 observed reflections [$I \geq 2\sigma(I)$], 156 refined parameters, R = 0.020, wR^2 = 0.043, max. (min.) residual electron density 0.29 (−0.40) e $Å^{-3}$, refined as racemic twin, Flack parameter 0.17(3), hydrogen atoms calculated and refined as riding atoms.

[But-2-ene-1,4-diylbis(η⁵-cyclopentadienyl)]dimethylzirconium (9): [But-2-ene-1,4-diylbis(η⁵-cyclopentadienyl)]zirconium dichloride (**8**, 50 mg, 0.15 mmol) and methyllithium (6.4 mg, 0.3 mmol) were suspended in 2 mL of toluene, precooled to −78 °C. The suspension was allowed to warm up to room temperature and stirred overnight. The reaction mixture was filtered through Celite. After removal of the solvent in vacuo, product **9** was isolated as a brown solid (yield: 32 mg, 72%), m.p. 48 °C. IR (KBr): $\tilde{\nu}$ = 3115 w, 2961 m, 2926 w, 2869 w, 1458 w, 1412 w, 1269 vs, 1097 s, 1028 s, 965 w, 867 w, 793 vs, 729 m cm^{-1}. ^1H NMR ([D_6]benzene, 599.9 MHz, 298 K): δ = 6.01, 5.62 (each m, each 4 H, Cp-H), 5.58 (m, 2 H, 7-H), 2.66 (m, 4 H, 6-H), −0.05 (s, 6 H, CH_3) ppm. $^{13}C\{GATED\}$ NMR ([D_6]benzene, 150.8 MHz, 298 K): δ = 129.6 (dm, $^1J_{CH}$ = 158 Hz, C-7), 120.8 (s, C-1), 111.9 (d, $^1J_{CH}$ = 172 Hz, Cp), 110.2 (d, $^1J_{CH}$ = 171 Hz, Cp), 31.0 (q, $^1J_{CH}$ = 117 Hz, CH_3), 24.4 (t, $^1J_{CH}$ = 128 Hz, C-6) ppm. $C_{16}H_{20}Zr$ (303.56): calcd. C 63.31, H 6.64; found C 61.64, H 6.72. Single crystals of the partial hydrolysis product **11**, suitable for X-ray diffraction, were obtained from a concentrated [D_6]benzene solution of **9**.

X-ray Crystal Structure Analysis of 11: $C_{30}H_{34}OZr_2$, M = 593.01, colourless crystal 0.60 × 0.20 × 0.08 mm, a = 8.218(1), b =

10.985(1), c = 27.805(1) Å, β = 94.07(1)°, V = 2503.8(4) Å^3, $\rho_{calcd.}$ = 1.573 g cm^{-3}, μ = 8.53 cm^{-1}, empirical absorption correction by SORTAV (0.629 ≤ T ≤ 0.935), Z = 4, monoclinic, space group $P2_1/c$ (no. 14), λ = 0.71073 Å, T = 198 K, ω and φ scans, 17976 reflections collected (±h, ±k, ±l), [(sinθ)/λ] = 0.66 Å^{-1}, 5886 independent (R_{int} = 0.048) and 4599 observed reflections [I ≥ 2 σ(I)], 300 refined parameters, R = 0.035, wR^2 = 0.061, max. (min.) residual electron density 0.39 (−0.52) e Å^{-3}, hydrogen atoms calculated and refined as riding atoms.

Ethene Polymerization Reactions: These were carried out in a 1-L Büchi glass autoclave, charged with 300 mL of toluene. In the cases in which the *ansa*-metallocene dichloride *cis*-**8** was used as a precursor, methylalumoxane (MAO) in toluene (10.5%, 20 mL, 9.05 mmol) was added. In the case of the dimethylmetallocene/$B(C_6F_5)_3$ catalysts, triisobutylaluminium (0.5 mL) was added instead as a water scavenger. The autoclave was brought to the desired temperature and the solution was then saturated with ethene at a 2 bar pressure with stirring (800 rpm) for ca. 40 min. Either *cis*-**8** or the **9**/$B(C_6F_5)_3$ mixture (see Table 1 for details) was injected. To end the polymerization reaction, the ethene addition was terminated, excess monomer was allowed to vent, and the mixture was quenched by injection of 40 mL of a solution of dilute aqueous HCl/methanol (1:1). After 20 min of stirring, 100 mL of H_2O was added. The precipitated polyethylene was collected by filtration, and washed with 50 mL of 2 N aqueous HCl and then with water. The polymer was dried in vacuo for 24 h. The observed ethene polymerization activities of the homogeneous Ziegler−Natta catalyst derived from **8** or **9** (Table 1) are in a range similar to those obtained with related unbridged systems under similar conditions (e.g., **7**/MAO: a ≈ 2400 kg PE/mol [Zr]·h·bar at 25 °C). Propene polymerization reactions were carried out analogously (2 bar propene pressure). The **9**/$B(C_6F_5)_3$ system gave atactic polypropylene (stereochemical analysis by ^{13}C NMR spectroscopy) with a catalyst activity of a = 38 kg PP/mol [Zr]·h·bar at 25 °C. The **8**/MAO catalyst system produced atactic polypropylene at 25 °C with a = 38 (Al/Zr = 800) at 60 °C with a = 40 (Al/Zr = 1050).

Preparation of (Butadiene)metallocene Complexes *s-cis*-15 and *s-trans*-15: Samples of [but-2-ene-1,4-diylbis(η^5-cyclopentadienyl)]-zirconium dichloride (**8**, 80 mg, 0.23 mmol) and 2-butene-1,4-diylbis(tetrahydrofuran)magnesium (95.1 mg, 0.23 mmol) were mixed as solids and then dissolved in 3 mL of toluene. The reaction mixture spontaneously changed colour to deep red, and a white precipitate was formed. Because of the rapid decomposition of the product upon filtration, all volatile components were removed in vacuo to obtain the product **15**·$MgCl_2(THF)_n$ (112 mg, 85%) as a red solid (in [D_8]toluene solution at 298 K both the *s-cis*-**15** and the *s-trans*-**15** isomers were detected in a 4:5 ratio). $(C_{18}H_{20}Zr)\cdot(THF)_2MgCl_2$ (327.58 + 239.42 = 567.00): calcd. C 55.08, H 6.40; found C 53.22, H 6.43. IR (KBr): $\tilde{\nu}$ = 2962 w, 2915 m, 2849 m, 1635 w, 1449 m, 1262 m, 1042 s, 797 s, 729 m cm^{-1}. *s-cis*-**15**: ^1H NMR ([D_8]toluene, 599.9 MHz, 298 K): δ (298 K) = 5.81 (m, 2 H, 7-H), 5.09 (br., 4 H, Cp-H), 4.88 (br. m, 4 H, Cp-H), 4.73 (m, 2 H, H_{meso}), 2.91 (m, 4 H, 6-H), 1.24 (br., 4 H, H_{syn}, H_{anti}) ppm; δ (213 K) = 5.89, 5.75 (each m, each 1 H, 7-H), 5.55, 4.91, 4.53 (each br., each 2 H, Cp-H), 4.78 (m, 2 H, Cp-H), 4.76 (m, 2 H, H_{meso}), 3.42 (m, 2 H, H_{syn}), 2.97 (m, 2 H, 6-H), 2.81 (m, 2 H, 6-H), −0.59 (m, 2 H, H_{anti}) ppm. $^{13}C\{^1H\}$ NMR ([D_8]toluene, 150.8 MHz): δ (298 K) = 130.2 (CH, $^1J_{CH}$ = 157 Hz, C-7), 118.6 (C, C-1), 112.8 (CH, $^1J_{CH}$ = 157 Hz, butadiene-CH), 100.9 (CH, $^1J_{CH}$ = 173 Hz, Cp), 25.8 (CH_2, $^1J_{CH}$ = 121 Hz, C-6) ppm; δ (213 K) = 130.5, 129.4 (each CH, C-7), 121.5, 115.1 (each C, C-1), 112.1 (CH, butadiene-CH), 107.9, 101.1, 101.1(4) (each CH, Cp), 96.0 o. 97.6 (CH, Cp), 49.7 (butadiene-CH_2), 25.3, 25.0 (each CH_2, C-6) ppm. ***s-trans*-15:** ^1H NMR ([D_8]toluene, 599.9 MHz): δ (298 K) = 5.81 (m, 2 H, 7-H), 4.96, 4.93, 4.57, 4.39 (each m, each 2 H, Cp-H), 3.02 (m, 2 H, H_{syn}), 2.99 (m, 4 H, 6-H), 2.97 (m, 2 H, H_{meso}), 1.24 (m, 2 H, H_{anti}); δ (213 K) = 5.79 (m, 2 H, 7-H), 4.87, 4.85, 4.53, 4.35 (br) (each m, each 2 H, Cp-H), 3.14 (m, 2 H, H_{syn}), 3.04 (m, 2 H, H_{meso}), 2.97 (m, 4 H, 6-H), 1.38 (m, 2 H, H_{anti}) ppm. $^{13}C\{^1H\}$ NMR ([D_8]toluene, 150.8 MHz, 298 K): δ = 130.2 (CH, $^1J_{CH}$ = 157 Hz, C-7), 112.1 (C, C-1), 104.4 (CH, $^1J_{CH}$ = 170 Hz, C-Cp), 101.7 (CH, $^1J_{CH}$ = 172 Hz, C-Cp), 98.0 (CH, $^1J_{CH}$ = 174 Hz, C-Cp), 96.1 (CH, $^1J_{CH}$ = 149 Hz, butadiene-CH), 95.9 (CH, $^1J_{CH}$ = 175 Hz, C-Cp), 59.5 (CH_2, $^1J_{CH}$ = 157, $^1J_{CH}$ = 146 Hz, butadiene-CH_2), 25.5 (CH_2, $^1J_{CH}$ = 125 Hz, C-6); δ (213) = 129.8 (CH, C-7), 111.1 (C, C-1), 104.0, 101.1(4) (CH, Cp), 97.6 o. 96.0 (CH, Cp), 95.7 (CH, butadiene-CH), 95.3 (CH, Cp), 59.1 (CH_2, butadiene-CH_2), 24.9 (CH_2, C-6) ppm.

Catalytic Hydrogenation of *cis*-8. Preparation of 16: Complex *cis*-**8** (77 mg, 0.22 mmol) was dissolved in dichloromethane (20 mL). Heterogeneous Pd(C) catalyst (10% palladium, 80 mg) was added. Hydrogen was passed through the solution through a frit at 1 bar with stirring for 2 h. The catalyst was removed by filtration and the solvent was evaporated in vacuo to yield 43 mg (56%) of the *ansa*-metallocene **16**. ^1H NMR ([D_2]dichloromethane, 599.9 MHz, 298 K): δ = 6.40 (m, 4 H, 2,5-H), 6.38 (m, 4 H, 3,4-H), 2.84 (br. m, 4 H, 6-H), 1.90 (m, 4 H, 7-H) ppm. $^{13}C\{^1H\}$ NMR ([D_2]dichloromethane, 150.8 MHz, 298 K): δ = 128.1 (C, C-1), 118.5 (CH, C-3,4), 117.6 (CH, C-2,5), 27.5 (CH_2, C-6), 26.1 (CH_2, C-7) ppm.

Treatment of *cis*-8 with 9-BBN. Preparation of 17: A mixture of [but-2-ene-1,4-diylbis(η^5-cyclopentadienyl)]zirconium dichloride (**8**, 50 mg, 0.15 mmol) and 9-borabicyclo[3.3.1]nonane (17.7 mg, 0.15 mmol) was dissolved in 2 mL of dichloromethane at room temperature. The solution was stirred for 12 h and then concentrated to dryness in vacuo. The product (67.1 mg, 96%) was isolated as a white solid, m.p. 170 °C. IR (KBr): $\tilde{\nu}$ = 3094 w, 2911 m, 2837 m, 2362 w, 1492 w, 1452 m, 1355 w, 1309 w, 1195 w, 1012 m, 880 w, 817 vs cm^{-1}. ^1H NMR ([D_2]dichloromethane, 599.9 MHz, 298 K): δ = 6.53, 6.33 (each m, each 1 H, 2,5-H), 6.45, 6.25 (each m, each 1 H, 3,4-H), 6.45, 6.35 (each m, each 1 H, 2′,5′-H), 6.42, 6.40 (each m, each 1 H, 3′,4′-H), 3.03 (*A*BM, ^2J = 16.1, ^3J = 2.3 Hz, 1 H, 6-H), 2.99 (*A*BMN, ^2J = 16.2, ^3J = 3.0, ^3J = 7.1 Hz, 1 H, 9-H), 2.89 (A*B*MN, ^2J = 16.2, ^3J = 2.6, ^3J = 10.9 Hz, 1 H, 9-H′), 2.75 (A*B*M, ^2J = 16.1, ^3J = 9.0 Hz, 1 H, 6-H′), 2.09 (m, 1 H, 8-H), 1.88 (m, 1 H, 8-H′), 1.94, 1.72 (each m, each 4 H, β, δ-H), 1.93, 1.28 (each m, each 2 H, γ-H), 1.82 (m, 2 H, α-H), 1.71 (m, 1 H, 7-H) ppm. $^{13}C\{^1H\}$ NMR ([D_2]dichloromethane, 150.8 MHz, 298 K): δ = 129.4 (C, C-1), 128.1 (C, C-1′), 122.0, 115.1 (each CH, C-2,5), 120.5, 113.6 (each CH, C-2′,5′), 120.4, 117.4 (each CH, C-3,4), 118.4, 117.3 (each CH, C-3′,4′), 34.0, 33.9 (each CH_2, C-β, δ), 31.3 (br. CH, C-7), 30.7 (br. CH, C-α), 27.8 (CH_2, C-9), 27.4 (CH_2, C-6), 26.4 (CH_2, C-8), 23.5 (CH_2, C-γ) ppm. $^{11}B\{^1H\}$ NMR ([D_6]benzene, 64.2 MHz, 298 K): δ = 87 ($\nu_{1/2}$ = 329 Hz) ppm. $C_{22}H_{29}BCl_2Zr$ (466.41): calcd. C 56.65, H 6.27; found C 55.72, H 6.16.

Treatment of *cis*-8 with H-B(C_6F_5)$_2$. Preparation of 18: A mixture of [but-2-ene-1,4-diylbis(η^5-cyclopentadienyl)]zirconium dichloride (**8**, 50 mg, 0.15 mmol) and bis(pentafluorophenyl)borane (50.2 mg, 0.145 mmol) was dissolved in 2 mL of dichloromethane at room temperature. The solution was stirred for 1 h. Solvent was removed in vacuo to yield 90.3 mg (90%) of the product as a light brown solid, m.p. 238 °C. IR (KBr): $\tilde{\nu}$ = 3103 w, 2934 m, 2861 m, 1648 m, 1520 s, 1467 vs, 1386 m, 1316 m, 1288 w, 1094 m, 974 s, 813 s cm^{-1}. ^1H NMR ([D_2]dichloromethane, 599.9 MHz, 298 K): δ = 6.56, 6.43

(each m, each 1 H, 2,5-H), 6.49, 6.38 (each m, each 1 H, 3′,4′-H), 6.48, 6.47 (each m, each 1 H, 2′,5′-H), 6.40, 6.28 (each m, each 1 H, 3,4-H), 3.12 (*A*BMN, ^2J = 16.8, ^3J = 2.7, ^3J = 10.5 Hz, 1 H, 9-H), 3.05 (d, $^{2\text{ or }3}J$ = 15.9 Hz, 1 H, 6-H), 2.92 (A*B*MN, ^2J = 16.8, ^3J = 2.8, ^3J = 7.7 Hz, 1 H, 9-H′), 2.85 (m, 1 H, 6-H′), 2.56 (m, 1 H, 7-H), 2.16 (m, 1 H, 8-H), 1.96 (m, 1 H, 8-H′) ppm. $^{13}C\{^1H\}$ NMR ([D$_2$]dichloromethane, 150.8 MHz, 298 K): δ = 148.3 [dm, ^1J = 247.2 Hz, B(C_6F_5)$_2$], 139.4 [dm, ^1J = 253.0 Hz, B(C_6F_5)$_2$], 145.0 (dm, ^1J = 265.0 Hz, B(C_6F_5)$_2$], 128.4 (C, C-1), 128.3 (C, C-1′), 124.5, 117.9 (each CH, C-2,5), 121.5, 121.2 (CH, C-2′,5′), 120.4, 114.6 (each CH, C-3′,4′), 119.4, 118.6 (each CH, C-3,4), 115.0 [br., B(C_6F_5)$_2$], 30.2 (CH_2, C-9), 29.9 (CH_2, C-6), 27.5 (CH_2, C-8), (C-7 not observed) ppm. $^{11}B\{^1H\}$ NMR ([D$_6$]benzene, 64.2 MHz, 298 K): δ = 76 ($\nu_{1/2}$ = 340 Hz) ppm. ^{19}F NMR ([D$_6$]benzene, 563.6 MHz, 298 K): δ = −127.3 (br. m, 4 F, *o*-C_6F_5), −146.2 (br. m, 2 F, *p*-C_6F_5), −159,4 (br. m, 4 F, *m*-C_6F_5) ppm. $C_{26}H_{15}BCl_2F_{10}Zr$ (690.33): calcd. C 45.24, H 2.19; found C 45.02, H 2.42.

Adduct Formation between *cis*-8 and $Li^+[B(C_6F_5)_4^-]$. Generation of 19: In an NMR experiment, *cis*-**8** (23 mg, 0.07 mmol) was mixed with $Li^+[B(C_6F_5)_4^-]$ (46 mg, 0.07 mmol), and [D$_8$]toluene (1.0 mL) was then added. NMR spectra of the mixture were not distinguished from those of the single components, but the coordination product **19** crystallised from the mixture after ca. 1 d at ambient temperature to allow an X-ray crystal structure analysis.

X-ray Crystal Structure Determination of 19: $C_{14}H_{14}Cl_2Zr{\cdot}LiBC_{24}F_{20}$, M = 1030.36, colourless crystal, 0.50 × 0.40 × 0.15 mm, a = 13.8212(1), b = 14.7217(1), c = 18.2205(2) Å, α = 88.406(1), β = 77.278(1), γ = 89.484(1)°, V = 3614.92(5) Å^3, $\rho_{calcd.}$ = 1.893 g cm^{-3}, μ = 5.88 cm^{-1}, empirical absorption correction by SORTAV (0.758 ≤ T ≤ 0.917), Z = 4, triclinic, space group $P\bar{1}$ (no. 2), λ = 0.71073 Å, T = 198 K, ω and φ scans, 26503 reflections collected (±h, ±k, ±l), [(sinθ)/λ] = 0.67 Å^{-1}, 17598 independent (R_{int} = 0.025) and 14617 observed reflections [$I \geq 2\sigma(I)$], 1135 refined parameters, R = 0.043, wR^2 = 0.105, max. (min.) residual electron density 1.24 (−1.44) e Å^{-3}, hydrogen atoms calculated and refined as riding atoms.

Data sets were collected with a Nonius KappaCCD diffractometer, equipped with a Nonius FR591 rotating anode generator. Programs used: data collection COLLECT[68], data reduction DenzoSMN[69], absorption correction SORTAV[70], structure solution SHELXS-97[71], structure refinement SHELXL-97[72], graphics SCHAKAL[73]. CCDC-180478 to -180481 contain the supplementary crystallographic data for this paper. These data can be obtained free of charge at www.ccdc.cam.ac.uk/conts/retrieving.html or from the Cambridge Crystallographic Data Centre, 12, Union Road, Cambridge CB2 1EZ, UK [Fax: (internat.) + 44-1223/336-033; E-mail: deposit@ccdc.cam.ac.uk].

Supporting Information Available: 2D NMR spectroscopic data of the complexes *trans*-**4**, *cis*-**8**, **9**, *s-cis*-/*s-trans*-**15**, **16**, **17** and **18** (see also the footnote on the first page of this article).

Acknowledgments

Financial support from the Fonds der Chemischen Industrie (and the BMBF) and the Deutsche Forschungsgemeinschaft is gratefully acknowledged.

[1] Review: H.-H. Brintzinger, D. Fischer, R. Mülhaupt, B. Rieger, R. M. Waymouth, *Angew. Chem.* **1995**, *107*, 1255−1283; *Angew. Chem. Int. Ed. Engl.* **1995**, *34*, 1143−1171.
[2] J. A. Smith, J. von Seyerl, G. Huttner, H. H. Brintzinger, *J. Organomet. Chem.* **1979**, *173*, 175−185.
[3] F. R. W. P. Wild, L. Zsolnai, G. Huttner, H.-H. Brintzinger, *J. Organomet. Chem.* **1982**, *232*, 233−247.
[4] F. R. W. P. Wild, M. Wasiucionek, G. Huttner, H. H. Brintzinger, *J. Organomet. Chem.* **1985**, *288*, 63−67.
[5] F. Wochner, L. Zsolnai, G. Huttner, H. H. Brintzinger, *J. Organomet. Chem.* **1985**, *288*, 69−77.
[6] S. Collins, B. A. Kuntz, N. J. Taylor, D. G. Ward, *J. Organomet. Chem.* **1988**, *342*, 21−29.
[7] G. Erker, C. Mollenkopf, M. Grehl, R. Fröhlich, C. Krüger, R. Noe, M. Riedel, *Organometallics* **1994**, *13*, 1950−1955.
[8] T. H. Warren, G. Erker, R. Fröhlich, B. Wibbeling, *Organometallics* **2000**, *19*, 127−134.
[9] M. Horáček, P. Štěpnička, R. Gyeped, I. Císařová, I. Tišlerová, J. Zemánek, J. Kubišta, K. Mach, *Chem. Eur. J.* **2000**, *6*, 2397−2408.
[10] T. Jödicke, F. Menges, G. Kehr, G. Erker, U. Höweler, R. Fröhlich, *Eur. J. Inorg. Chem.* **2001**, 2097−2106.
[11] R. L. Halterman, A. Tretyakov, M. A. Khan, *J. Organomet. Chem.* **1998**, *568*, 41−51.
[12] R. L. Halterman, D. Combs, J. G. Kihega, M. A. Khan, *J. Organomet. Chem.* **1996**, *520*, 163−170.
[13] R. L. Halterman, D. Combs, M. A. Khan, *Organometallics* **1998**, *17*, 3900−3907.
[14] H. Schwemlein, H. H. Brintzinger, *J. Organomet. Chem.* **1983**, *254*, 69−73.
[15] J. A. Ewen, R. L. Jones, A. Razavi, J. D. Ferrara, *J. Am. Chem. Soc.* **1988**, *110*, 6255−6256.
[16] A. Razavi, J. L. Atwood, *J. Organomet. Chem.* **1996**, *520*, 115−120.
[17] M. Könemann, G. Erker, R. Fröhlich, S. Kotila, *Organometallics* **1997**, *16*, 2900−2908.
[18] G. Erker, C. Psiorz, C. Krüger, M. Nolte, *Chem. Ber.* **1994**, *127*, 1551−1553.
[19] G. Erker, C. Psiorz, R. Fröhlich, M. Grehl, C. Krüger, R. Noe, M. Nolte, *Tetrahedron* **1995**, *51*, 4347−4358.
[20] G. Erker, S. Wilker, C. Krüger, R. Goddard, *J. Am. Chem. Soc.* **1992**, *114*, 10983−10984.
[21] G. Erker, S. Wilker, C. Krüger, M. Nolte, *Organometallics* **1993**, *12*, 2140−2151.
[22] G. Erker, R. Aul, *Chem. Ber.* **1991**, *124*, 1301−1310.
[23] H. G. Alt, M. Jung, *J. Organomet. Chem.* **1999**, *580*, 1−16.
[24] H. G. Alt, M. Jung, *J. Organomet. Chem.* **1998**, *562*, 229−253.
[25] R. E. v. H. Spence, W. E. Piers, *Organometallics* **1995**, *14*, 4617−4624.
[26] T. M. Trnka, R. H. Grubbs, *Acc. Chem. Res.* **2001**, *34*, 18−29, and references cited therein.
[27] R. R. Schrock, *Tetrahedron* **1999**, *55*, 8141−8153.
[28] C. Bruneau, P. H. Dixneuf, *Acc. Chem. Res.* **1999**, *32*, 311−323.
[29] R. H. Grubbs, S. Chang, *Tetrahedron* **1998**, *54*, 4413−4450.
[30] N. Schuster, S. Blechert, *Angew. Chem.* **1997**, *109*, 2124−2144; *Angew. Chem. Int. Ed. Engl.* **1997**, *36*, 2036−2055.
[31] A. Fürstner, *Top. Catal.* **1997**, *4*, 285−299.
[32] R. H. Grubbs, S. J. Miller, G. C. Fu, *Acc. Chem. Res.* **1995**, *28*, 446−452.
[33] M. J. Marsella, H. D. Maynard, R. H. Grubbs, *Angew. Chem.* **1997**, *109*, 1147−1150; *Angew. Chem. Int. Ed. Engl.* **1997**, *36*, 1101−1103.
[34] R. R. Schrock, *Acc. Chem. Res.* **1990**, *23*, 158−165.
[35] T. Weskamp, F. J. Kohl, W. Hieringer, D. Gleich, W. A. Herrmann, *Angew. Chem.* **1999**, *111*, 2573−2576; *Angew. Chem. Int. Ed.* **1999**, *38*, 2416−2419.
[36] A. Fürstner, O. R. Thiel, C. W. Lehmann, *Organometallics* **2002**, *21*, 331−335.
[37] Olefin metathesis has been relatively seldom used as a tool in organometallic synthesis. For representative examples see: [37a] J. Ruwwe, J. M. Martín-Alvarez, C. R. Horn, E. B. Bauer, S. Szafert, T. Lis, F. Hampel, P. C. Cagle, J. A. Gladysz, *Chem. Eur. J.* **2001**, *7*, 3931−3950. [37b] H. E. Blackwell, D. J. O'Leary,

A. K. Chatterjee, R. A. Washenfelder, D. A. Bussmann, R. H. Grubbs, *J. Am. Chem. Soc.* **2000**, *122*, 58−71. [37c] P. L. Ng, J. N. Lambert, *Synlett* **1999**, 1749−1750.

[38] P. Schwab, M. B. France, J. W. Ziller, R. H. Grubbs, *Angew. Chem.* **1995**, *107*, 2179−2181; *Angew. Chem. Int. Ed. Engl.* **1995**, *34*, 2039.

[39] M. Gandelman, B. Rybtchinski, N. Ashkenazi, R. M. Gauvin, D. Milstein, *J. Am. Chem. Soc.* **2001**, *123*, 5372−5373.

[40] [40a] M. Knickmeier, G. Erker, T. Fox, *J. Am. Chem. Soc.* **1996**, *118*, 9623−9630. [40b] G. Erker, M. Aulbach, M. Knickmeier, D. Wingbermühle, C. Krüger, M. Nolte, S. Werner, *J. Am. Chem. Soc.* **1993**, *115*, 4590−4601, and references cited therein.

[41] See also: [41a] M. D. Bruce, G. W. Coates, E. Hauptmann, R. M. Waymouth, J. W. Ziller, *J. Am. Chem. Soc.* **1997**, *119*, 11174−11182. [41b] T. Dreier, G. Erker, R. Fröhlich, B. Wibbeling, *Organometallics* **2000**, *19*, 4095−4103.

[42] A. G. Orpen, L. Brammer, F. H. Allen, O. Kennard, D. G. Watson, R. Taylor, *J. Chem. Soc., Dalton Trans.* **1989**, S1−S83.

[43] C. Saldarriaga-Molina, A. Clearfield, I. Bernal, *J. Organomet. Chem.* **1974**, *80*, 79−90.

[44] F. H. Allen, O. Kennard, D. G. Watson, L. Brammer, A. G. Orpen, R. Taylor, *J. Chem. Soc., Perkin Trans. 2* **1987**, S1−S19.

[45] See for a related example: G. Erker, K. Engel, J. L. Atwood, W. E. Hunter, *Angew. Chem.* **1983**, *95*, 506−507, *Angew. Chem. Int. Ed. Engl.* **1983**, *22*, 494−495.

[46] J. S. Siegel, F. A. Anet, *J. Org. Chem.* **1988**, *53*, 2629−2630.

[47] M. L. H. Green, L.-L. Wong, A. Seela, *Organometallics* **1992**, *11*, 2660−2668, and references cited therein.

[48] R. Benn, H. Grondey, R. Nolte, G. Erker, *Organometallics* **1988**, *7*, 777−778.

[49] G. Erker, R. Nolte, G. Tainturier, A. Rheingold, *Organometallics* **1989**, *8*, 454−460.

[50] R. Benn, H. Grondey, G. Erker, R. Aul, R. Nolte, *Organometallics* **1990**, *9*, 2493−2497, and references cited therein.

[51] G. Erker, U. Dorf, C. Krüger, Y.-H. Tsay, *Organometallics* **1987**, *6*, 680−682, and references cited therein.

[52] J. W. Lauher, R. Hoffmann, *J. Am. Chem. Soc.* **1976**, *98*, 1729−1742.

[53] Review: E. Y.-X. Chen, T. J. Marks, *Chem. Rev.* **2000**, *100*, 1391−1434.

[54] H. Sinn, W. Kaminsky, *Adv. Organomet. Chem.* **1980**, *18*, 99−149.

[55] H. Yasuda, Y. Kajihara, K. Mashima, K. Nagasuna, K. Lee, A. Nakamura, *Organometallics* **1982**, *1*, 388−396, and references cited therein.

[56] G. Erker, C. Krüger, G. Müller, *Adv. Organomet. Chem.* **1985**, *24*, 1−39, and references cited therein.

[57] R. Köster, *Angew. Chem.* **1960**, *72*, 626−627.

[58] E. F. Knights, H. C. Brown, *J. Am. Chem. Soc.* **1968**, *90*, 5280−5281.

[59] D. J. Parks, R. E. v. H. Spence, W. E. Piers, *Angew. Chem.* **1995**, *107*, 895−897; *Angew. Chem. Int. Ed. Engl.* **1995**, *34*, 809−901.

[60] D. J. Parks, W. E. Piers, G. P. A. Yap, *Organometallics* **1998**, *17*, 5492−5503.

[61] B. Temme, G. Erker, J. Karl, H. Luftmann, R. Fröhlich, S. Kotila, *Angew. Chem.* **1995**, *107*, 1867−1869; *Angew. Chem. Int. Ed. Engl.* **1995**, *34*, 1755−1757.

[62] Review: G. Erker, *Acc. Chem. Res.* **2001**, *34*, 309−317.

[63] S. Döring, G. Erker, R. Fröhlich, *J. Organomet. Chem.* **2002**, *643/644*, 61−67, and references cited therein.

[64] K. A. Butakoff, D. A. Lemenovskii, P. Mountford, L. G. Kuz′mina, A. V. Churakov, *Polyhedron* **1996**, *15*, 489−499.

[65] A. Demsar, A. Pevec, L. Golic, S. Petricek, A. Petricec, H. Roesky, *Chem. Commun.* **1998**, 1029−1030.

[66] M. Dahlmann, G. Erker, K. Bergander, *J. Am. Chem. Soc.* **2000**, *122*, 7986−7998.

[67] S. Braun, H.-O. Kalinowski, S. Berger, *150 and More Basic NMR Experiments*, VCH, Weinheim, **1998**, and references cited therein.

[68] Nonius B.V., **1998**.

[69] Z. Otwinowski, W. Minor, *Methods Enzymol.* **1997**, *276*, 307−326.

[70] R. H. Blessing, *Acta Crystallogr., Sect. A* **1995**, *51*, 33−37; R. H. Blessing, *J. Appl. Crystallogr.* **1997**, *30*, 421−426).

[71] G. M. Sheldrick, *Acta Crystallogr., Sect. A* **1990**, *46*, 467−473.

[72] G. M. Sheldrick, Universität Göttingen, **1997**.

[73] E. Keller, Universität Freiburg, **1997**.

Received March 26, 2002
[I02157]

Bismuthanides and Bismuthanediides − Synthesis and Structural Characterization of $[R_2Bi]^-$ and $[(RBi)_{12}Na_{21}]^{3-}$ Salts with Bulky Silyl Substituents

Gerald Linti,*[a] Wolfgang Köstler,[a] and Hans Pritzkow[a]

Dedicated to Prof. Dr. Gottfried Huttner on the occasion of his 65th birthday

Keywords: Bismuth / Lithium / Sodium / Silicon / Cluster compounds

The reaction of bismuth trihalides with the bulky alkali metal silanides $[(THF)_3LiSi(SiMe_3)_3]$ and $[(THF)_2NaSi(CMe_3)_3]$ affords the cyclotetrabismuthanes $(RBi)_4$ **1** and **3**, the alkali metal bismuthanides $[Li(THF)_4][Bi\{Si(SiMe_3)_3\}_2]$ (**2**) and $Na(THF)_3[Bi\{Si(CMe_3)_3\}]_2$ (**4**) and the bismuthanediide $Na_3(THF)_{14}[Na_{21}\{BiSi(CMe_3)_3\}_{12}]$ (**5**). Compound **2** features a two-coordinate bismuth atom. The core of **5** is a Bi_{12} icosahedron which is face-capped by 20 sodium atoms. The cluster is filled with a sodium atom. All structures were confirmed by single crystal X-ray crystallography. In addition, the bismuthanides and bismuthanediides were investigated by quantum chemical calculations.
(© Wiley-VCH Verlag GmbH, 69451 Weinheim, Germany, 2002)

Introduction

Alkali metal amides, phosphides and arsanides are common reagents, and their structural chemistry, especially that of the heavier homologous, has been explored recently.[1] This interest focused mainly on lithiated species and, consequently, relatively little is known about heavier alkali metal derivatives.[2] The structural chemistry of doubly metalated phosphanes and arsanes M_2PR revealed a high diversity of cluster compounds.[3,4]

Metalated bismuthanes have been known for 60 years, when the synthesis of $MBi(C_6H_5)_2$ (M = Li, Na, K) by reduction of $(C_6H_5)_2BiI$ with alkali metals in liquid ammonia was described.[5] About 40 years later, the first lithium bismuthanide $[(dme)LiBi(SiMe_3)_2]$ was structurally characterized.[6] MER_2 and M_2ER (E = P, As) compounds are normally prepared by metalation of phosphanes and arsanes and the lack of stable hydrogen compounds of bismuth might have caused the low interest in metalated bismuthanes;[7] only very recently was the first stable diarylbismuthane reported.[8] We report here on the reduction of bismuth halides with alkali metal silanides resulting in cyclotetrabismuthanes[9] and bismuthanides and bismuthanediides. The reaction of $SbCl_3$ with $NaSi(CMe_3)_3$ leads to the isolation of the cyclotetrastibane $[(Me_3C)_3SiSb]_4$.[10]

[a] Anorganisch-Chemisches Institut, Universität Heidelberg, Im Neuenheimer Feld 270, Heidelberg, Germany
Fax: (internat.) + 49-(0)6221/546-617
E-mail: gerald.linti@urz.uni-heidelberg.de

Results and Discussion

Reactions

The reaction of $BiBr_3$ with three equivalents of $[(THF)_3LiSi(SiMe_3)_3]$ in toluene affords the cyclotetrabismuthane **1** in good yields [Equation (1)].[9] If $BiCl_3$ in THF is used instead, **1** forms as the main product of the reaction, too. Initially a green solution is observed during warming of the reaction mixture from −78 °C to ambient temperatures. On stirring at room temperature the color changes to brown. Workup allows isolation of **1** as pentane soluble red crystals. The green component is soluble in THF. The dark green crystals obtained proved to be **2** [Equation (1), nonstoichiometric]. If $NaSi(CMe_3)_3$ dissolved in THF is reacted with $BiBr_3$ [Equation (2), nonstoichiometric] the reaction proceeds similarly to Equation (1).

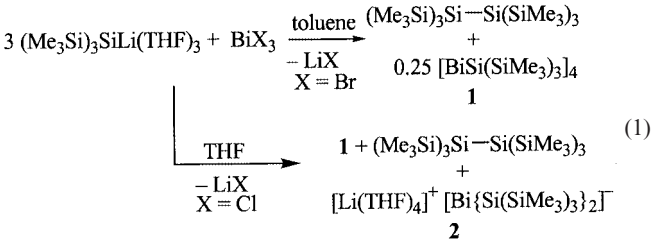

(1)

Table 1. Data for the X-ray structure determinations of **2**, **3**, **4** and **5**.

Compound	**2**	**3**·2THF	**4**	**5**
Chemical formula	$C_{34}H_{86}BiLiO_4Si_8$	$C_{48}H_{108}Bi_4Si_4{\cdot}2C_4H_8O$	$C_{36}H_{78}BiNaO_3Si_2$	$C_{200}H_{436}Bi_{12}Na_{24}O_{14}Si_{12}$
Molecular weight	999.7	1777.8	847.1	6462.1
T [K]	190	210	203	210
Crystal system	monoclinic	monoclinic	trigonal	trigonal
Space group	$P2_1/c$	$C2/c$	$P3_1$	$R\bar{3}$
a [pm]	1928.4(2)	2379.0(5)	1252.8(2)	2255.8(3)
b [pm]	1494.2(2)	1328.0(3)	1252.8(2)	2255.8(3)
c [pm]	1882.1(2)	2410.6(5)	2413.3(5)	4893(1)
β [°]	91.053(2)	112.28(3)	–	–
V [nm^3]	422(1)	7.05(1)	3.2809(1)	21.56(1)
Z	4	4	3	3
Density (calcd.) [g cm^{-3}]	1.225	1.676	1.286	1.497
Absorption coefficient [mm^{-1}]	3.457	10.059	4.124	7.445
F(000)	2080	3456	1320	9576
Crystal color	green	red	red	black
Crystal size [mm]	0.3 × 0.24 × 0.12	0.3 × 0.3 × 0.15	0.25 × 0.25 × 0.15	0.35 × 0.35 × 0.3
Scan type	CCD area detection	image plate area detection	ω-scan	image plate area detection
2θ-range [°]	4.0–49.5	3.6–48.0	3.6–50.0	3.6–48.0
Abs. corr.	multi-scan	numerical	-	numerical
Min/max. transm.	0.346/1.00	0.062/0.437	-	0.169/0.249
Refl. collected	9671	26501	2265	18194
Independent reflections	9265	5543	2258	7340
Observed refl. [$I > 2\sigma(I)$]	5765	4233	1811	3477
x (weighting scheme)	0.1035	0.0126	0.120	0.0291
y (weighting scheme)	0.1073	468.3614	5.6147	0
Parameters	454	316	227	508
$R1$ [$F > 4\sigma(F)$]	0.064	0.064	0.072	0.051
wR_2 (all data)	0.189	0.168	0.199	0.117
$R1$ (all data)	0.116	0.082	0.103	0.123
GOOF	1.023	1.239	1.166	0.766
Largest difference peak/hole [e·nm^{-3}]	2540/–2100 (near Bi)	2170/–2080	1220/–1110	1040/–1050

$$BiBr_3 + 3\ Na(THF)_2Si(CMe_3)_3 \xrightarrow[-\ LiBr]{THF} \begin{array}{l} (Me_3C)_3Si{-}Si(CMe_3)_3 \\ + \\ 0.25\ [BiSi(CMe_3)_3]_4 \\ \mathbf{3} \\ + \\ Na(THF)_3Bi[Si(CMe_3)_3]_2 \\ \mathbf{4} \\ + \\ Na_3(THF)_{14}[Na_{21}Bi_{12}\{Si(CMe_3)_3\}_{12}] \\ \mathbf{5} \end{array} \quad (2)$$

The cyclotetrabismuthane **3** is formed predominantly. In addition, the bismuthanide **3** and the bismuthanediide **4** can be isolated. Compound **4** is the first example of a bismetalated bismuthane and a highly aggregated structure is expected as alkali metal phosphanediides and arsanediides form a large variety of cage compounds.[3]

Crystal Structure Analysis

The molecule structure of **3** resembles that of **1**.[9] The tetrabismuthane **3** crystallizes in the monoclinic space group $C2/c$ (Table 1, Figure 1) together with two molecules of THF. No direct intermolecular contacts are observed. The molecule of **3** with a folded Bi_4 core resides on a crystallographic twofold axis (angle between Bi_3 planes: 150°). This folding angle is even flatter than in **1** (angle between Bi_3 planes 138°). $[(Me_3Si)_2CHBi]_4$ [11] with less bulky substituents than **1** and **3** has a more folded Bi_4 core (angle between Bi_3 planes: 113°). The Bi–Bi–Bi bond angles are near 90°, as expected. The Bi–Bi–Si angles are wider, and

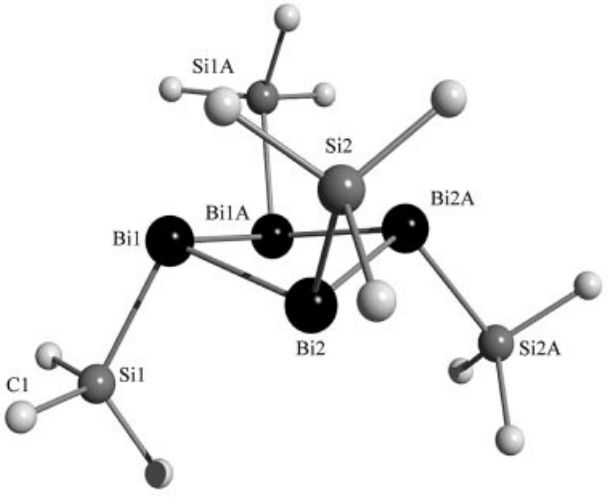

Figure 1. View of a molecule of **3**; disordered methyl groups are omitted from the plot for clarity; selected bond lengths [pm] and angles [°]: Bi(1)–Bi(2) 301.3(1), Bi(1)–Bi(1A) 303.1(2), Bi(2)–Bi(2A) 303.8(2), Bi(1)–Si(1) 275.0(6), Bi(2)–Si(2) 276.5(5); Bi(1)–Bi(2)–Bi(2A) 87.97(2), Bi(2)–Bi(1)–Bi(1A) 88.10(2), Bi(2)–Bi(1)–Si(1) 100.3(1), Bi(1A)–Bi(1)–Si(1) 101.4(1), Bi(1)–Bi(2)–Si(2) 108.9(1), Bi(2A)–Bi(2)–Si(2) 105.8(1)

range from 100° to 109° due to the steric demand of the substituents.

The Bi−Bi distances [(d_{Bi-Bi} = 301.3(1)−303.8(2) pm)] are similar to those in **1**. $[(Me_3Si)_2CHBi]_4$ has more alternating Bi−Bi bonds [d_{Bi-Bi} = 297.0(5)−304.4(2) pm]. The Bi−Si bond lengths (d_{BiSi} = 275.8 pm on average) are longer than those in **1** by approx. 5 pm. This difference is typical for the substituents under consideration and is observed in other cases, too.[12] This difference in the Bi−Si bond lengths and the increasing flattening of the Bi_4 cores in the known cyclotetrabismuthanes is due to the increased steric demand of the substituents.

Compound **2** crystallizes in the monoclinic space group $P2_1/a$. In this $LiBiR_2$ compound, the ions are separated. The lithium cation is coordinated by four THF molecules in a distorted tetrahedral manner. The BiR_2 anion (Figure 2) has a two-coordinate Bi atom. The shortest nonbonding intramolecular distances (except H) are 390 pm (for Bi−C_{methyl}), and the nearest Bi atom of a neighboring anion is 1100 pm away. The Bi−Si distances [d_{Bi-Si} = 267 pm on average] are shorter than those in **1** by 4 pm. This is due to the lower coordination number at the Bi atom. The Si−Bi−Si angle (114.4°) is larger than 90°, the usual angle observed in BiR_3 compounds. The wide range for the Si−Si−Si and Si−Si−Bi angles observed makes the distortion of the hypersilyl group obvious.

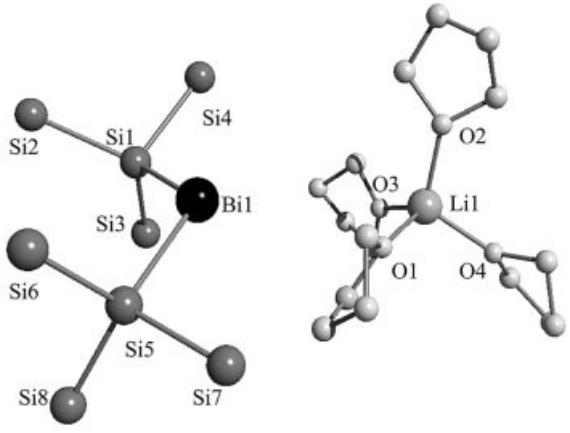

Figure 2. View of a molecule of **2**; disordered methyl groups are omitted from the plot for clarity; selected bond lengths [pm] and angles [°]: Bi(1)−Si(1) 266.8(5), Bi(1)−Si(5) 267.2(4), Si(1,5)−Si 234.2 (aver.); Si(1)−Bi(1)−Si(5) 112.2(1), Si−Si(1,5)−Si 103.1(3)−110.1(3), Bi(1)−Si(1)−Si(4) 123.1(3), Bi(1)−Si(1)−Si(3) 113.1(3), Bi(1)−Si(1)−Si(2) 99.5(2), Bi(1)−Si(5)−Si(6) 115.2(2), Bi(1)−Si(5)−Si(7) 120.6(2), Bi(1)−Si(5)−Si(8) 92.8(2)

For $[Bi(SiH_3)_2]^-$ an Si−Bi−Si angle of 93.4° is calculated by MP2 calculations.[13] This angle is nearly unaffected by the coordination of a lithium or sodium atom to the bismuth atom (see Table 2, Figure 3).[13] $[(dme)LiBi(SiMe_3)_3]$[6] is the only structurally characterized lithium bismuthanide so far. In this polymeric structure the Bi atom is tetracoordinated by two Si and two Li atoms, with an Si−Bi−Si angle of 91.8(4)°.

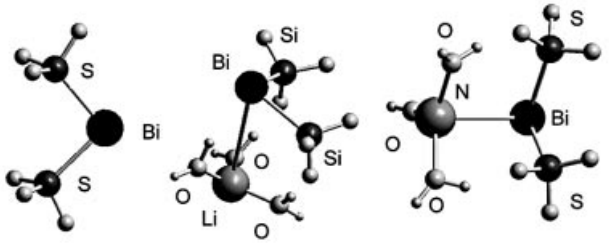

Figure 3. Calculated structures of $[(H_3Si)_2Bi]^-$ and $[(H_3Si)_2Bi-M(OH_2)_3]$ (M = Li, Na)

Compound **4** crystallizes in the trigonal space group $P3_1$ with Z = 3. Here, unlike **2**, a separated ion pair is not present. The alkali metal ion is coordinated by three THF molecules and the fourth coordination site is occupied by the Bi atom of the $BiSi_2$ unit. Thus, the Bi atom in **4** (Figure 4) is three-coordinated by two Si atoms (d_{BiSi} = 271.7 pm on average) and a sodium atom [d_{Bi-Na} = 311(1) pm]. Similar to the differences in **1** and **2**, the Bi−Si distances in **4** are

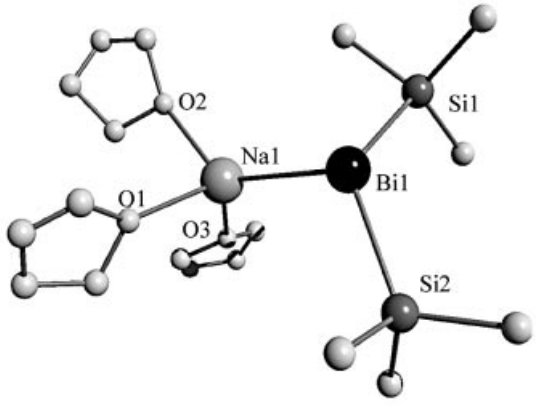

Figure 4. View of a molecule of **4**; disordered methyl groups are omitted from the plot for clarity; selected bond lengths [pm] and angles [°]: Bi(1)−Si(1) 272.6(10), Bi(1)−Si(2) 270.7(8), Bi(1)−Na(1) 311(1); Si(1)−Bi(1)−Si(2) 122.3(2), Na(1)−Bi(1)−Si(1) 113.7(4), Na(1)−Bi(1)−Si(2) 98.6(3)

Table 2. Results of MP2 calculations on bismuthanides

	d(Bi-Si) [pm]	*d*(Bi−M) [pm]	Si−Bi−Si [°]	M−Bi−Si [°]	M−Bi/Si−Bi−Si [°]
$[(H_3Si)_2Bi]^-$	267.8	–	93.4	–	
$(H_3Si)_2BiLi(OH_2)_3$	267.1	308.2	92.7	81.0, 88.4	85
$(H_3Si)_2BiNa(OH_2)_3$	267.4	367.3	92.7	74.9, 85.0	80
for comparison: crystal structure of $(Me_3Si)_2BiLi(dme)$[6] (c.n. Bi and Li = 4)	263 (1)	292(3)	91.8	96(1), 106(1)	

shorter than those in **3** by 4 pm. The Si−Bi−Si angle is even wider (122.3°) than that in **2**. Here, the higher steric demand of the $Si(CMe_3)_3$ group compared to the $Si(SiMe_3)_3$ group becomes obvious again. The line Bi(1)−Na(1) is not orthogonal to the Si_2Bi plane, as might be expected, and as proposed by the quantum chemical calculations (Table 2). The angle of the line Bi(1)−Na(1) to the Si_2Bi plane is 143.8°, which means that the Bi atom is only 82 pm above the Si_2Na plane.

Compound **5** crystallizes in the trigonal space group $R\bar{3}$ with $Z = 3$, and is the sodium salt of an RBi^{2-} ion, which means that a highly aggregated structure can be expected. In fact, **5** forms an RBi dodecamer (Figure 5a) in which 12 bismuth atoms and 20 sodium atoms form a ball-like cage. Of the remaining four sodium atoms two show up as $[Na(THF)_4]^+$ and one as $[Na(THF)_6]^+$. In the structural model applied, the fourth is in a disordered position in the center of the $Bi_{12}Na_{20}$ cage. The disordered sodium atom takes the positions of an internal icosahedron.

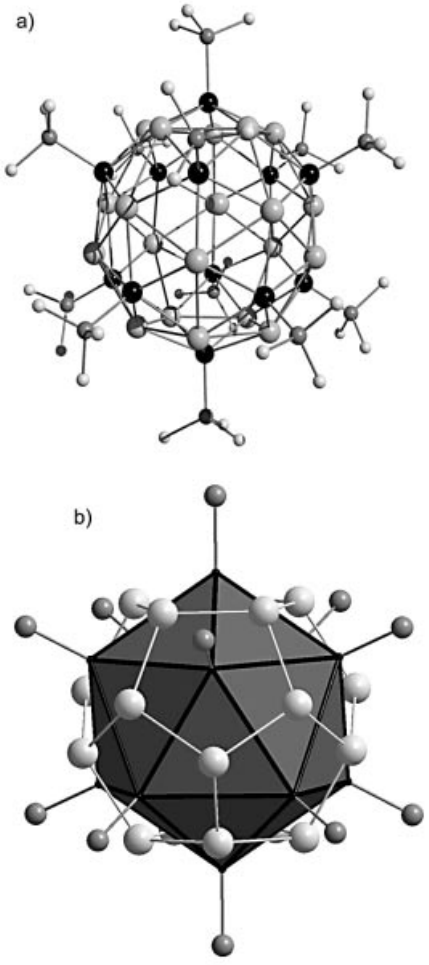

Figure 5. View of the cluster anion of **5**: a) showing only one position of the disordered central sodium atom (methyl groups are omitted for clarity); b) polyhedral representation of the Bi_{12} icosahedron with capping sodium atoms in pentagon dodecahedral arrangement; only the silicon atoms are shown for the $Si(CMe_3)_3$ substituents; selected bond lengths [pm] and angles [°] Bi(1)−Si(1) 263.0(4), Bi(2)−Si(2) 264.4(4), Bi−Na 317.2(6)−324.4(6); Si(1)−Bi(1)−Na 106.8(1)−113.5(1)

In the cage, 12 Bi atoms form an icosahedron (d_{BiBi} = 527−536 pm), whose faces are capped by 20 sodium atoms (Figure 5b). These sodium atoms themselves form a pentagonal dodecahedron ($d_{Na\text{-}Na}$ = 351−363 pm). All Bi atoms are bonded to the central silicon atom of a $Si(CMe_3)_3$ substituent (d_{BiSi} = 263.7 pm on average), which is severely disordered, as usual. The Bi−Si bond is even shorter than in **3** and **4**, which is expected in the series $R-BiX_2$, R_2Bi^- and RBi^{2-}. The $(RBi)_{12}Na_{20}$ cage is unique in the chemistry of bismuth, although $(R'P)_{12}Li_{20}$ and $(R'As)_{12}R_{20}$ (R = Li, Na) clusters with an analogous arrangement of the pnicogen and alkali metal atoms as in **5** are known.[3] These clusters are filled, too. In most cases M_nO (n = 2,6) units are present in the center of the cages. RI-DFT calculations[14] were performed on an empty $[(HBi)_{12}Na_{20}]^{4-}$ shell (Figure 6a). The resulting structure was quite similar to the observed structure of **5**. If a sodium cation is placed in the center of this $[(HBi)_{12}Na_{20}]^{4-}$ shell, the final position for this cation is out of the center of the shell and in a position similar to that of one position for the disordered encapsulated sodium atom. Adding this additional positive charge inside the cage results in a shrinking of the cage. This means the diameter of the $Bi_{12}Na_{20}$ shell decreases from 1044 pm to 1020 pm (Figure 6b). The Bi−Na interactions in **5**, as well as the Bi-(Li, Na) contacts in **2** and **4**, are mostly ionic, as is revealed by Aldrich−Heinzmann population analyses.[15] This is expressed in the shared electron numbers, which are as low as 0.22 to 0.29 for the Bi−Na interactions.

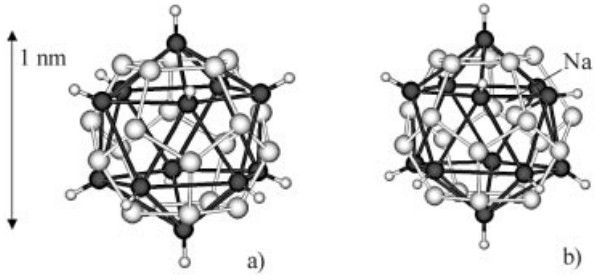

Figure 6. View of a) $[(HBi)_{12}Na_{20}]^{4-}$ and b) $[(HBi)_{12}Na_{21}]^{3-}$ as derived from RI-DFT calculations; average selected bond lengths [pm] a) Bi−Na 330.7, Bi−H 184.5, Bi···Bi 548.0, Na···Na 364.0; b) Bi−Na 328.6, Bi−H 184.0, Bi···Bi 545.0, Na···Na 361.6

Conclusion

The reaction of bismuth halides with bulky silanides has proved to be a valuable entry to the chemistry of bismuth ring compounds as well as for the synthesis of anionic bismuthanides R_2Bi^- and RBi^{2-}. In particular, the latter opens a novel field for bismuth. Whether these compounds are useful for synthetic applications will depend on their improved availability.

Experimental Section

General: All experiments were performed under purified nitrogen or in vacuo with Schlenk techniques. All yields are referenced to

BiX_3. Chemical analysis for **3** gave unreliable results, due to the partial loss of THF from the crystals, and for the ionic species **2**, **4** and **5** due to their sensitivity. NMR: Bruker ACP 250; Mass spectra: Varian MAT 711; X-ray crystallography: Suitable crystals were mounted with a perfluorinated polyether oil on the tip of a glass fiber and cooled immediately on the goniometer head. Data collections were performed with Mo-K_α radiation on a Bruker AXS (**2**), STOE IPDS (**3**, **5**) or a STOE STADI4 diffractometer (**4**). Absorption correction was performed numerically with XRED (STOE) for **3,5** and empirically using equivalent reflections for **2**. Structures were solved and refined with the Bruker AXS SHELXTL 5.1 program package. Refinement in full-matrix against F^2. All hydrogen atoms were included as a riding model with fixed isotropic U values in the final refinement. For further data see Table 1. The structures of **4** and **5** are influenced by disorder of the CMe_3 groups. In part, we attempted to describe this by a split model. The crystal structure of **4** was refined as a merohedral twin (BASF 0.49, Flack parameter −0.03). The low parameter/data ratio and the lack of an absorption correction due to decomposition of the crystal together with the severe disorder of the silyl groups allows no detailed discussion of the structure.
CCDC-174922 (**2**), -174923 (**3**) -174924 (**4**) and -174925 (**5**) contain the supplementary crystallographic data for this paper. These data can be obtained free of charge at www.ccdc.cam.ac.uk/conts/retrieving.html [or from the Cambridge Crystallographic Data Centre, 12, Union Road, Cambridge CB2 1EZ, UK; Fax: (internat.) +44-1223/336-033; E-mail: deposit@ccdc.cam.ac.uk].

Compounds 1 and 2: A solution of $[(THF)_3LiSi(SiMe_3)_3]$[16−18] (2.58 g, 5.49 mmol) in 20 mL THF was added dropwise to a stirred solution of $BiCl_3$ (0.58 g, 1.84 mmol) in 20 mL THF at −78 °C within 10 min. The dark-colored mixture was stirred for an additional 10 min at low temperature and was then quickly warmed to ambient temperature. After stirring for 1 h the dark green solution was stripped down. The residue was extracted with 50 mL of pentane in several portions. After filtration an orange-red solution was obtained, from which **1** was isolated as tiny red crystals by cooling to −20 °C. The solid, dark colored residue after the pentane extraction was treated with 15 mL of THF. After filtration a dark green solution of **2** (pure by NMR spectroscopy) was obtained. Upon cooling to −20 °C, green crystals of **2** formed; yield: 0.92 g (51%; with reference to Bi).
1:[9] ^{1}H NMR (250 MHz, C_6D_6): δ = 0.49 ppm. ^{13}C NMR: δ = 5.6 ppm. ^{29}Si NMR: δ = −124 (Si) −2.2 ($SiMe_3$).
2: ^{1}H NMR (250 MHz, C_6D_6): δ = 0.64 (s, 54 H, $SiMe_3$), 1.66 (m, 16 H, CH_2), 3.40 (m, 16 H, OCH_2) ppm. ^{13}C NMR: δ = 5.9 ($SiMe_3$), 26.0 (CH_2), 68.9 (OCH_2), ppm. ^{29}Si NMR: δ = −110 (Si) −8.6 ($SiMe_3$) (approx. 6% **1** as impurity, as indicated by ^{1}H NMR integration).

Compounds 3, **4 and 5:** $[NaSi(CMe_3)_3]$ (6.80 mmol),[10] dissolved in 10 mL THF, was added dropwise with a syringe into a stirred solution of $BiBr_3$ (1.02 g, 2.27 mmol) in 40 mL of THF at −78 °C. The dark-colored solution was stirred for an additional 30 min at −78 °C. The THF was removed in vacuo before ambient temperature was reached. The residue was extracted with 50 mL of pentane and 20 mL of THF. The pentane solution was reduced to a volume of 10 mL. Upon cooling to −20 °C red crystals of **3** were isolated [yield: 0.30 g (32%)]. From the THF solution dark-red crystals of **4** were isolated, which were accompanied by traces of **3** and several nearly dark black crystals of **5**. Attempts to purify **4** by recrystallization resulted in decomposition of **4** to **3**.
3: ^{1}H NMR (250 MHz; C_6D_6): δ = 1.15 ppm. ^{13}C NMR: δ = 30.9 ppm. MS (EI, 70 eV): *m/z* (%) = 816 (5) $[Bi_2\{Si(CMe_3)_3\}_2]^{+\cdot}$, 607 (4) $[Bi\{Si(CMe_3)_3\}_2]^+$, 550 (2) $[Bi\{Si(CMe_3)_3\}\{Si(CMe_3)_2\}]^{+\cdot}$, 408 (5) $[BiSi(CMe_3)_3]^{+\cdot}$, 57 (100) $[C(CMe_3)_3]^+$.
4: $C_{36}H_{78}BiNaO_3Si_2$ (847.2): calcd. C 51.04, H 9.28; found C 56.53, H 11.30. ^{1}H NMR (250 MHz; C_6D_6): δ = 1.41 (m, 12 H, CH_2), 1.49 (s, 54 H, CMe_3), 3.56 (m, 12 H, OCH_2) ppm. ^{13}C NMR: δ = 25.8 (CH_2), 34.6 (CMe_3), 67.9 (OCH_2).
5: $C_{200}H_{436}Bi_{12}Na_{24}O_{14}Si_{12}$ (6462.2): calcd. C 37.17, H 6.80; found C 36.96, H 7.94.

Acknowledgments

We are grateful to the Deutsche Forschungsgemeinschaft and the Fonds der Chemischen Industrie for their generous financial support.

[1] A.-M. Sapse, P. v. R. Schleyer, *Lithium Chemistry*, Wiley, New York **1995**.
[2] G. W. Rabe, G. P. A. Yap, L. M. Liable-Sands, I. A. Guzei, A. L. Rheingold, *Phosphorus, Sulfur Silicon Relat. Elem.* **1999**, *144−146*, 269−272.
[3] M. Driess, *Acc. Chem. Res.* **1999**, *32*, 1017−1025.
[4] N. Wiberg, A. Wörner, D. Fenske, H. Nöth, J. Knizek, K. Polborn, *Angew. Chem.* **2000**, *112*, 1908−1912; *Angew. Chem. Int. Ed.* **2000**, *39*, 1838−1842.
[5] H. Gilman, H. L. Yablunky, *J. Am. Chem. Soc.* **1941**, *63*, 212−216.
[6] O. Mundt, G. Becker, M. Rössler, C. Witthauer, *Z. Anorg. Allg. Chem.* **1983**, *506*, 42−58.
[7] C. Silvestru, H. J. Breuning, H. Althaus, *Chem. Rev.* **1999**, *99*, 3277−3327.
[8] N. J. Hardman, B. Twamley, P. P. Power, *Angew. Chem.* **2000**, *112*, 2884−2886; *Angew. Chem. Int. Ed.* **2000**, *39*, 2771−2773.
[9] G. Linti, W. Köstler, *Z. Anorg. Allg. Chem.* **2002**, *628*, 63−66.
[10] N. Wiberg, *Coord. Chem. Rev.* **1997**, *163*, 217−252.
[11] H.-J. Breunig, R. Rösler, E. Lork, *Angew. Chem.* **1998**, *110*, 3361−3363; *Angew. Chem. Int. Ed.* **1998**, *37*, 3175−3177.
[12] M. Kehrwald, W. Köstler, G. Linti, A. Rodig, T. Blank, N. Wiberg, *Organometallics* **2001**, *20*, 860−867.
[13] MP2 calculations: LANL2DZ-base, Gaussian 98W: M. J. Frisch, G. W. Trucks, H. B. Schlegel, G. E. Scuseria, M. A. Robb, J. R. Cheeseman, V. G. Zakrzewski, J. A. Montgomery Jr., R. E. Stratmann, J. C. Burant, S. Dapprich, J. M. Millam, A. D. Daniels, K. N. Kudin, M. C. Strain, O. Farkas, J. Tomasi, V. Barone, M. Cossi, R. Cammi, B. Mennucci, C. Pomelli, C. Adamo, S. Clifford, J. Ochterski, G. A. Petersson, P. Y. Ayala, Q. Cui, K. Morokuma, D. K. Malick, A. D. Rabuck, K. Raghavachari, J. B. Foresman, J. Cioslowski, J. V. Ortiz, A. G. Baboul, B. B. Stefanov, G. Liu, A. Liashenko, P. Piskorz, I. Komaromi, R. Gomperts, R. L. Martin, D. J. Fox, T. Keith, M. A. Al-Laham, C. Y. Peng, A. Nanayakkara, C. Gonzalez, M. Challacombe, P. M. W. Gill, B. Johnson, W. Chen, M. W. Wong, J. L. Andres, C. Gonzalez, M. Head-Gordon, E. S. Replogle, J. A. Pople, Gaussian Inc., Pitsburgh **1998**.
[14] RI-DFT calculations with BP86 functional and SV(P) base. TURBOMOLE program package: O. Treutler, R. Ahlrichs, *J. Chem. Phys.* **1995**, *102*, 346−354; A. D. Becke, *Phys. Rev. A* **1998**, *38*, 3098−3100; J. P. Perdew, *Phys. Rev. B* **1996**, *33*, 8822−8824; K. Eichkorn, O. Treutler, H. Ohm, M. Häser, R. Ahlrichs, *Chem. Phys. Lett.* **1995**, *242*, 652−660; K. Eichkorn, F. Weigend, O. Treutler, R. Ahlrichs, *Theor. Chem. Acc.* **1997**, *97*, 119−124.
[15] R. Ahlrichs, R. Heinzmann, *Theoret. Chim. Acta* **1976**, *42*, 33.
[16] G. Gutekunst, A. G. Brook, *J. Organomet. Chem.* **1982**, *225*, 1−3.
[17] H. Gilman, C. L. Smith, *J. Organomet. Chem.* **1968**, *14*, 91−94.
[18] A. Heine, R. Herbst-Irmer, G. M. Sheldrick, D. Stalke, *Inorg. Chem.* **1993**, *32*, 2694−2698.

Received December 5, 2002
[I01498]

Evaluation of 3,4-Hydroxypyridinecarboxylic Acids as Possible Bidentate Chelating Agents for Aluminium(III): Synthesis and Metal−Ligand Solution Chemistry

Valerio B. Di Marco,[a] Robert A. Yokel,[b] Maria Grazia Ferlin,[c] Andrea Tapparo,[a] and G. Giorgio Bombi*[a]

Keywords: Aluminium / Carboxylate ligands / Potentiometry / Chelation therapy

In view of a possible application to aluminium(III) chelation therapy, 3-hydroxy-4-pyridinecarboxylic acid (3H4P) and 4-hydroxy-3-pyridinecarboxylic acid (4H3P) were synthesised, and their chemical interactions with the metal ion were investigated in aqueous 0.6 m (Na)Cl at 25 °C by means of potentiometric titrations. Only mononuclear complexes of the type AlL_lH_h (l = 1, 2 and 3; h = 0, 1, ..., l) were formed. The qualitative and quantitative results obtained were confirmed by UV spectrophotometry and ^1H NMR spectroscopy. The efficiencies of the ligands to chelate aluminium(III) were evaluated at physiological pH and ionic strength (in vitro), together with the *n*-octanol/water distribution coefficients of the free ligands and of the ligand–metal complexes. The results suggest that 3H4P and 4H3P lack sufficient chelation efficacy to be proposed as chelation therapy agents for aluminium(III). However, the results do suggest a strategy for the synthesis of more promising compounds.

(© Wiley-VCH Verlag GmbH, 69451 Weinheim, Germany, 2002)

Introduction

The therapy for metal overload pathologies usually involves the administration of suitable chelating agents to selectively remove the metal from the body. Regarding aluminium(III) and iron(III), medical research continuously emphasises the need for new safe, efficient and orally effective chelators.[1−3] The existing chelating agents, desferrioxamine and deferiprone, have a number of drawbacks, including oral inefficacy and high cost for the former,[4−6] and several toxic side effects and controversial efficiency for the latter.[5−8] An attempt to address this need is the chemical modification of existing chelating agents, to improve their in vivo properties.[9−11] Another important approach is the synthesis of new hexadentate ligands.[12−16] However, although there is some evidence that hexadentate ligands may be more efficient than bidentate and tridentate ligands, they are more expensive and thought to be less absorbed orally.[5,17,18] There are very few attempts to synthesise new tridentate ligands[19] and, to the best of our knowledge, no attempts to synthesise new bidentate ones other than deferiprone analogues.

Hydroxypyridinecarboxylic acids (HPs) represent a class of compounds that have not been considered for metal chelation therapy. The limited data in biomedical literature seems to demonstrate their lack of toxicity. Some have been proposed as drugs.[20−23] Their structure suggests a good ligating capability towards aluminium(III) and iron(III). The interactions between 2-hydroxy-3-pyridinecarboxylic acid (2H3P) and 3-hydroxy-2-pyridinecarboxylic acid (3H2P) with aluminium(III) have been investigated.[24] Although complexes with reasonably high stability constants form in solution, their stability is much lower than those of the corresponding desferrioxamine and deferiprone complexes. Therefore, neither 2H3P nor 3H2P appear to be good candidates for chelation therapy.

It is known, for hydroxypyridinones, that the 3,4 derivatives form significantly more stable complexes with aluminium(III) and iron(III), than the 2,3 derivatives.[25] The same behaviour is expected for HPs, which are structurally very similar to hydroxypyridinones. Therefore, an investigation of the stability of the metal complexes of 3,4-HPs is advisable.

In this work, the formation of complexes of aluminium(III) and 3-hydroxy-4-pyridinecarboxylic acid (3H4P),

[a] Department of Inorganic, Organometallic and Analytical Chemistry, University of Padova,
Via Marzolo 1, 35131 Padova, Italy
E-mail: g.g.bombi@unipd.it
[b] College of Pharmacy, 501B Pharmacy Building, University of Kentucky Medical Center,
Rose Street, Lexington, KY 40536-0082, U.S.A.
E-mail: ryokel1@uky.edu
[c] Department of Pharmaceutical Sciences, University of Padova,
Via Marzolo 5, 35131 Padova, Italy
E-mail: mariagrazia.ferlin@unipd.it

and 4-hydroxy-3-pyridinecarboxylic acid (4H3P) (Figure 1) have been studied in aqueous solutions by means of potentiometric titrations. The speciation data obtained has been integrated and confirmed by UV/Vis spectrophotometry, NMR spectroscopy and elemental analysis. The efficiency of the ligands to chelate aluminium(III) at physiological pH and ionic strength in vitro, and the octanol/water distribution of both the free ligands and the metal−ligand complexes, have been determined according to a method developed by Yokel et al.[26] For comparison, the efficiency and the octanol/water distribution of 2H3P and 3H2P have also been analysed.

Figure 1. 3-Hydroxy-4-pyridinecarboxylic acid (3H4P, left) and 4-hydroxy-3-pyridinecarboxylic acid (4H3P, right), shown as the H_2L forms

Results And Discussion

Synthesis of the Ligands

Among the methods proposed for the synthesis of 3H4P,[27,28−31] we selected the three-step procedure starting from 4-methylpyridine described by Dejarden.[27] The advantage of this pathway lies in the bromination of the starting material, which gives the precursor 3-monobromo derivative of 3H4P as the main reaction product as a result of the deactivation caused by the bromine atom itself. In all cases the yields were lower than those reported; for the hydrolysis of the bromo acid of 3H4P, no product was obtained under the literature conditions;[27] the use of a water/methanol mixture (6:4, v:v) for 12−24 h yielded over 40% of pure 3H4P (ref.[27] 80%).

The synthesis of 4H3P was accomplished via butadienedicarbonitriles according to the method of Mittelbach,[32] that produces the desired isomeric compound. This pathway, although requiring five steps, is quite straightforward and has proven to be more convenient (17% overall yield) than others.[33−36]

Thermodynamic Study

Acidity Constants of the Ligands

The pK_a values for H_2L and HL (here and in the following, charges are omitted for simplicity), corresponding to the deprotonation of the pyridine nitrogen atom and the phenol oxygen atom, respectively, were computed for the potentiometric titration data of the free ligands (Table 1).[24,37]

Table 1. Acidic properties of 3H4P and 4H3P, at 25 °C in aqueous (Na)Cl 0.6 m

Species	3H4P pK_a	n[a]	4H3P pK_a	n[a]	Source
H_3L	0.64 ± 0.03	4	−0.06 ± 0.04	3	UV
H_2L	4.713 ± 0.001	30	5.955 ± 0.002	24	pot.
HL	10.300 ± 0.004	15	10.85 ± 0.01	12	pot.

[a] n is the number of experiments from which the data were obtained; the reported uncertainty is the standard deviation of the mean.

Accurate potentiometric measurements at pH values lower than ca. 1.5 cannot be executed, because under these conditions the pH modification induced by the acid-base equilibria is negligible. Therefore, the more acidic pH region has been explored by means of UV spectrophotometric measurements, which allowed for the detection of H_3L and the calculation of its pK_a value (Table 1). This deprotonation has been assigned to the carboxylic group.[37] It may be noted that for the carboxylic group in nicotinic acid, $pK_{a1} \approx 2$;[38] as the *ortho*-phenol group can be expected to produce a significant increase in the acidity (for example, the carboxylic pK_a of salicylic acid is ca. 1.2 units lower than that of benzoic acid[38]), the values obtained for H_3L appear to be reasonable.

Metal−Ligand Complexes − Potentiometric Results

The potentiometric titrations of solutions containing both the metal ion and the ligand allowed for the identification of a large number of complexes, 9 in the case of 3H4P and 8 in the case of 4H3P; their stoichiometries are reported in Table 2, together with the values of their stability constants. The distribution diagrams for the two systems, containing an excess ligand concentration, are reported in Figure 2. It is worth noting that the precipitation of aluminium hydroxide was not observed in any systems in the presence of an excess ligand concentration (at least three-

Table 2. Stability constants for Al−L complexes, at 25 °C in aqueous (Na)Cl 0.6 m (reactions: $m\,Al + l\,L + h\,H \rightleftarrows Al_mL_lH_h$; pK_a values refer to the equilibrium $Al_mL_lH_h \rightleftarrows Al_mL_lH_{h-1} + H$)

	3H4P			4H3P		
m, l, h	log β	pK_a	n[a]	log β	pK_a	n[a]
1, 1, 1	15.97 ± 0.05	5.13	5	18.19 ± 0.09		8
1, 1, 0	10.84 ± 0.06		4	−		
1, 2, 2	30.78 ± 0.02	5.31	20	35.15 ± 0.03	6.4	16
1, 2, 1	25.47 ± 0.04	5.97	4	28.7 ± 0.1	8.2	6
1, 2, 0	19.50 ± 0.03		10	20.5 ± 0.1		3
1, 3, 3	44.05 ± 0.03	5.36	16	50.76 ± 0.06	7.84	16
1, 3, 2	38.69 ± 0.07	6.02	10	42.92 ± 0.07	8.15	7
1, 3, 1	32.67 ± 0.06	6.58	10	34.77 ± 0.05	9.01	7
1, 3, 0	26.09 ± 0.07		6	25.76 ± 0.09		7

[a] n is the number of experiments from which the data were obtained; the reported uncertainty is the standard deviation of the mean.

fold), due to the high affinity of the ligands towards the metal ion.

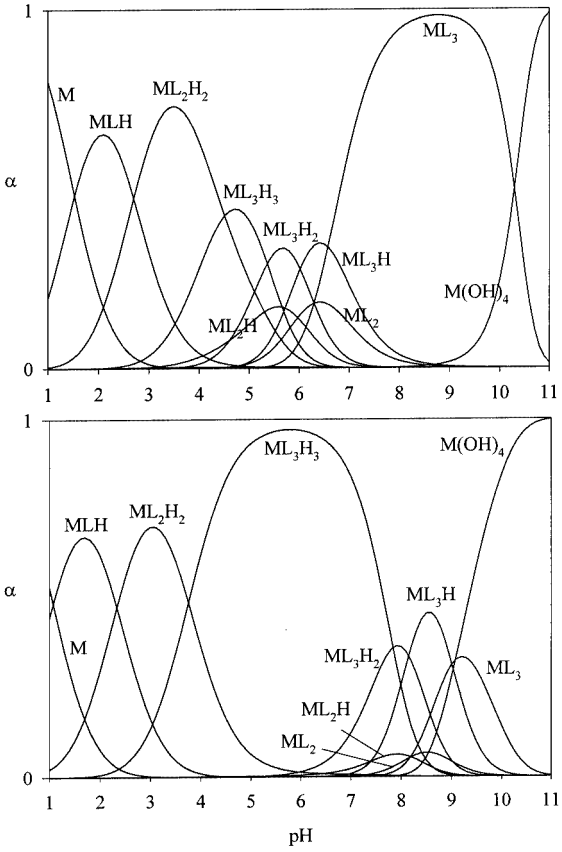

Figure 2. Distribution diagrams of the most important aluminium species in the presence of 3H4P (above) and 4H3P (below) in aqueous (Na)Cl 0.6 m, $T = 25$ °C; $[Al]_0 = 5{\cdot}10^{-4}$ m, $[ligand]_0 = 4{\cdot}10^{-3}$ m

Owing to the large number of species, the simultaneous optimisation of the metal−ligand complexation constants led to strong correlations between the various values. Therefore, the data has been elaborated in a sequential manner, considering the titrations with large metal/ligand ratios (1:1, 1:2) separately from the others. In this way, some of the complexes could be neglected in the former titrations and optimised only in the latter, and most of the correlations could be avoided. Of course the consistency of the above procedure needed to be verified a posteriori: distribution diagrams like those reported in Figure 2 have been drawn for the actual metal and ligand concentrations adopted for the former titrations in order to verify that the species rejected were actually negligible.

In some of the titrations of the system Al^{III}/3H4P, the precipitation of a white powder was observed (for $[Al]_0 >$ ca. $8{\cdot}10^{-4}$ m, $[Al]_0/[L]_0 \leq 1{:}3$ and pH > ca. 5−6). The solid was examined by elemental analysis (C = 37.9, H = 3.1, Al = 6.92, N = 7.1, Na = 4.22). The relative mol ratios between aluminium, carbon and nitrogen were calculated. The values obtained, 1:12.3:1.96, are in close agreement with the theoretical ratios 1:12:2 expected for an AlL_2 species (= $C_{12}H_8AlN_2O_6$). The 1:2 metal/ligand stoichiometry is also suggested by the observation that in all the titrations, the precipitation occurred when the concentration of the neutral species AlL_2H (as calculated from the stability constants reported in Table 2) reached a value of about $3{\cdot}10^{-4}$ m. The solid obtained is likely to be coordinated with water molecules (elemental analysis suggests two) and with NaCl (elemental analysis suggests Na/Al = 0.7). Unfortunately, the stoichiometry and the structure of this solid cannot be defined exactly because no crystals suitable for X-ray analysis could be obtained.

The distribution curves in Figure 2 show that the speciation in the two aluminium−ligand systems is very similar at acidic pH values, where only the free metal ion and the complexes AlLH and AlL_2H_2 exist in solution. At pH > 4, 3H4P forms a large number of complexes, which include AlL_3H_3 and the deprotonation products of the 1:2 and 1:3 metal/ligand species; AlL_3 and $Al(OH)_4$ are the only existing metal species at pH values larger than ca. 8. On the contrary, 4H3P forms only one main species, AlL_3H_3, in the pH range 4−6, and the deprotonation products only appear at higher pH values; among these, AlL_3 is not as predominant as in 3H4P. The different behaviour of 3H4P and 4H3P is due to the different acidity of the pyridine hydrogen atom of the two ligands (pK_{a2}, Table 1), the pK_a value of 3H4P is 1.2 log units lower. This acidity difference is further increased in the metal complexes (pK_a values, Table 2), and therefore, the deprotonation products of the Al/3H4P species are more stable than those of Al/4H3P. For the same reason, the species AlL is not present in a significant amount in the Al/4H3P system.

Two interesting properties regarding the acidity of the complexes in both aluminium/ligand systems should be noted. (i) For the Al/3H4P system, the acidity decreases systematically (i.e. pK_a increases) in the order $H_2L >$ AlLH > $AlL_2H_2 > AlL_3H_3$ (Table 2). For the Al/4H3P system, no pK_a value for AlLH is available, but the acidity order for the other species is the same. The decrease in the acidities is less marked for 4H3P than for 3H4P. (ii) The increase in the pK_a values of the complexes having the same number of ligands (namely AlL_2H_2 and AlL_2H; AlL_3H_3, AlL_3H_2 and AlL_3H) by decreasing the number of acidic protons is close to that expected on statistical grounds (for example, the K_a ratio of the 3H4P complexes AlL_2H_2/AlL_2H is 4.6, the statistical value is 4). All these results are very similar to those obtained for the complexes formed by 2H3P and 3H2P with aluminium(III)[24] and iron(III).[39] In ref.[24] an explanation is given for both the effects.

In order to confirm the potentiometric results with some independent techniques, UV spectrophotometric quantitative data and NMR spectroscopic qualitative and semiquantitative data have also been obtained.

Metal−Ligand Complexes − UV Spectrophotometric Results

UV spectra for the Al/4H3P system at several pH values are reported in Figure 3. The following value was obtained

for log β (AlLH): log $\beta_{1,1,1}$ = 18.03 ± 0.10 (fitting of 5 spectra, values at three λs). This value compares well (*t*-test) with the corresponding potentiometric value (18.19 ± 0.09). The agreement between these results suggests the absence of any bias on final results.

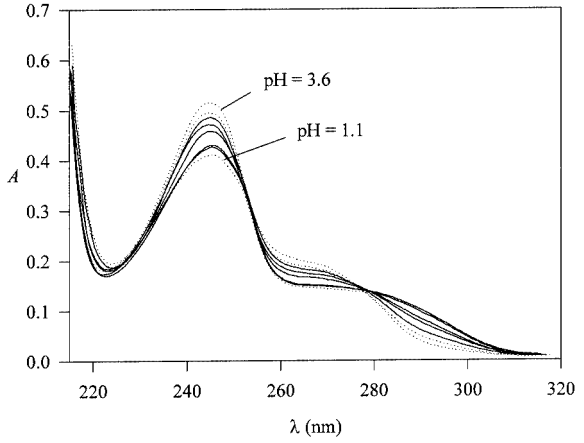

Figure 3. UV spectrophotometric study for Al/4H3P; see Table 6 for experimental details; dashed curves were excluded for the log β calculation

Metal−Ligand Complexes − NMR Spectroscopic Results

^{1}H NMR spectra were collected for both 4H3P and 3H4P systems at various pD values in D_2O solutions containing only the free ligand or the ligand with the metal ion. As an example, the spectra obtained for the 4H3P system are shown in Figure 4.

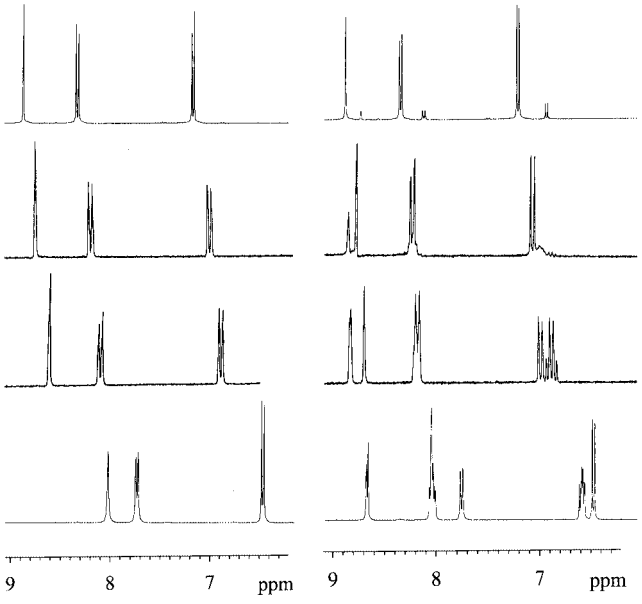

Figure 4. Left side: ^{1}H NMR spectra of 4H3P alone (0.050 m); right side: ^{1}H NMR spectra of Al^{III} (0.010 m) + 4H3P (0.050 m); from top to bottom: pD = 0.11, 1.73, 5.20, 8.58

On complexation with aluminium, three new groups of peaks in addition to those of the free ligand are observed. At pD = 0.11 the multiplicity and the shape of the "new" peaks are almost identical to those of the free ligand; according to the potentiometric data, these signals can be assigned to the AlLH complex. On increasing the pH, the peaks of the complexes become more complicated, since under these conditions different species coexist in solution (AlL_2H_x and AlL_3H_x). Furthermore, as the ligands are not symmetric and may chelate the metal ion in different spatial configurations, AlL_2H_x and AlL_3H_x can form with 4 and 2 different diastereoisomers, respectively, each with a slightly different NMR response. At pD = 5.20 and 8.58, the patterns of the signals become more simple, because, according to potentiometric data, only the AlL_3H_x species (and therefore fewer diastereoisomers) exist in solution.

The dependence of the chemical shift of the different signals on the pD can be explained by the acid-base properties of the ligand and the complexes: deprotonation of the pyridine nitrogen atom causes a shift of the ligand signals towards lower ppm values; this shift is maximal at pD = pK_a. However, for a correct interpretation it is necessary to take into account the difference in the pK_a values of the acid in D_2O and in H_2O due to isotopic effects. In order to estimate the pK_a difference, the empirical equation p$K_a(D_2O)$ = 0.41 + 1.02·p$K_a(H_2O)$ has been proposed[40] (for example, the pK_a values for 4H3P in heavy water are: pK_{a1} ≈ 0.3, pK_{a2} ≈ 6.5 and pK_{a3} ≈ 11.5). Considering the NMR spectra in the light of the above, the lowest-field signal at pD = 0.11 is due to the free ligand, whereas the signals at pD = 1.73 and 5.20 are assigned to the complexes since the free ligand deprotonates between pD = 0.11 and 1.73 ($H_3L \rightarrow H_2L$) and the complex species do not [for example, for AlL_2H_2 p$K_a(D_2O)$ ≈ 6.9]. For a similar reason, at pD = 8.58 the chemical shift difference between the same lowest-field signals of the complexes and of the free ligands become significantly larger than in the spectrum at pD = 5.20. This is because in this pD range the free ligand further deprotonates ($H_2L \rightarrow HL$), whereas the complexes deprotonate only partially [for example, for AlL_3H_3 p$K_a(D_2O)$ ≈ 8.4]. These semi-quantitative data are in good agreement with the potentiometric results.

The integration of the signals of the free ligand and of the complexes gives the relative amount of free and complexed ligand; the values obtained are reported in Table 3, together with the corresponding values calculated from the stability constants reported in Table 1 and Table 2. The agreement between the two sets of data is good, in view of the uncertainties of the NMR integration values, and of the presence of isotopic and solvent effects introduced by the change in solvent from H_2O to D_2O.

n-Octanol/Water Distribution and Chelation Efficacy Study

The results obtained for each ligand are summarised in Table 4. 2H3P and 3H2P have also been analysed for comparison.

A significant increase in efficiency can be observed for the 3,4-HPs, and especially for 4H3P, with respect to the

Table 3. Percentages of free and complexed ligand (Al/4H3P spectra)

pD	from NMR spectroscopic data		from potentiometric/UV results	
0.11	free ligand	88.8	$H_3L + H_2L$	90.4
	complexed ligand	11.2	$AlLH + 2\ AlL_2H_2$	9.6
1.73	free ligand	61.5	$H_3L + H_2L$	64.2
	complexed ligand	38.5	$AlLH + 2\ AlL_2H_2 + 3\ AlL_3H_3$	35.8
5.20	free ligand	42.7	$H_2L + HL$	40.1
	complexed ligand	57.3	$2\ AlL_2H_2 + 3\ AlL_3H_3 + 3\ AlL_3H_2$	59.9
8.58	free ligand	44.2	$H_2L + HL + L$	40.3
	complexed ligand	55.8	$3\ AlL_3H_3 + 3\ AlL_3H_2 + 3\ AlL_3H + 3\ AlL_3$	59.7

Table 4. Octanol/water distribution coefficients, and Al^{III} chelation efficiencies

Ligand	$D_{o/w}$ free ligand	$D_{o/w}$ Al complexes	Chelation efficiency (%)
3H4P	0.014 ± 0.001	0.005	20 ± 2
4H3P	0.004 ± 0.001	0.002	43 ± 6
2H3P	0.0006 ± 0.0001	–	4 ± 1
3H2P	0.006 ± 0.001	–	13 ± 2

2,3-HPs. This is in agreement with the thermodynamic data. The very low lipophilicity of all the ligands and the metal−ligand complexes at physiological pH values should be noted; in fact, from thermodynamic data it is known that at pH = 7.4 both the free ligand and the metal−ligand complexes are predominantly in the charged form (HL^- and deprotonated $AlL_3H_x^{(3-x)-}$ species, respectively). Actually, the octanol/water distribution of the Al ligand complexes could not accurately be calculated from its distribution in the presence and the absence of Al borate, because a significant (if not predominant) percentage of the ligand was not complexed with Al, as evidenced by the generally low efficiency obtained. The values obtained for 3H4P and 4H3P suggest that the metal−ligand complexes are slightly more hydrophilic than the free ligand.

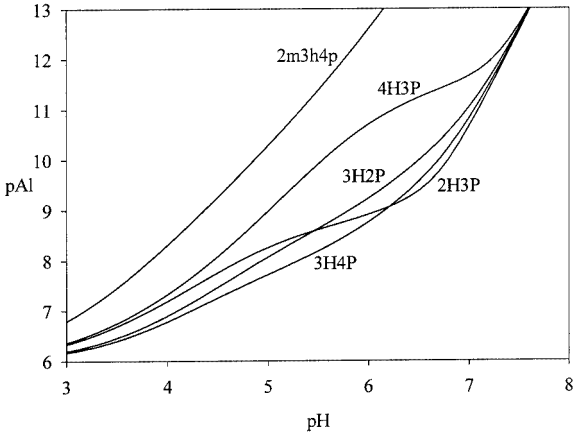

Figure 5. pAl for several ligands (see text); $[Al]_0 = 10^{-6}$ m, $[ligand]_0 = 5{\cdot}10^{-5}$ m

Conclusions

Both 3H4P and 4H3P form strong complexes in solution with aluminium(III) such that no metal hydroxide precipitates at neutral pH in the presence of a threefold (or higher) ligand excess. The speciation patterns of the two ligands with aluminium(III) are similar, and a number of 1:1, 1:2 and 1:3 metal/ligand species are formed in solution.

In order to compare the affinities of the various HPs (3H4P, 4H3P, 3H2P and 2H3P) for the metal, the direct analysis of the data reported in Table 2 (and in the corresponding Table of ref.[24]) is not useful since the competition arising from the proton (i.e. the basicity of the ligand) cannot be taken into account. The comparison could be accomplished by computing the conditional stability constants of the complexes, however, in the literature the calculation of pAl (= $-\log [Al^{3+}]$) vs. pH at a given metal and ligand concentration is much more common. Generally,[41] the pAl is computed at a metal concentration of 10^{-6} m and at a ligand concentration of $5{\cdot}10^{-5}$ m. For different systems, the higher the pAl, the stronger the complexes. In Figure 5, pAl plots for the four HPs are shown, together with that of a deferiprone-like molecule (2-methyl-3-hydroxy-4-pyridinone, 2m3h4p, data taken from ref.[42]). It is evident that 4H3P forms significantly more stable complexes with aluminium than the other HPs, especially at slightly acidic and neutral pH values. This result is as expected (see Introduction) and confirms that 3,4-HPs are more promising chelating agents than 2,3-HPs. Surprisingly, the pAl of 3H4P is quite low, similar to those of the 2,3-HPs; this latter data cannot be explained as yet. However, it is important to note from Figure 5 that the pAl of 4H3P is significantly lower than that of the deferiprone-like molecule at all pH values.

The chelation efficiencies give an indication of the ability of the ligands to solubilise aluminium(III) at physiological pH. The data obtained correlate well with the thermodynamic results, and a reasonably high efficiency, 43%, was obtained for only 4H3P.

Table 5. Potentiometric titrations (titrant: NaOH)

Titrations	Conditions			
	$[Al]_0/10^{-3}$ m	$[L]_0/10^{-3}$ m	$[Al]_0/[L]_0$	pH
1.				
3H4P + HCl	–	0.51–1.27	–	2.7–10.5
4H3P + HCl	–	0.36–2.98	–	2.1–10.5
2.				
Al + HCl	0.50–2.88	–	–	2.4–3.5
	1.01–3.39	–	–	
3.				
Al + 3H4P + HCl	0.50–3.81	1.88–4.01	1:1;1:2;1:4;1:8	1.7–10.0
Al + 4H3P + HCl	0.31–3.01	1.58–4.95		

The octanol/water distribution coefficients $D_{o/w}$ indicate that all HPs and their aluminium complexes show a marked hydrophilic behaviour. Porter[43] has suggested that an orally effective Fe (or Al) chelator should probably have a $D_{o/w}$ of 0.2 or greater to be absorbed. However, in our evaluation of a series of 3,4-hydroxypyridinones we found that some compounds with a $D_{o/w}$ much lower were among the most orally bioavailable and effective chelators of Al.[44–46]

In conclusion, the thermodynamic data and the chelation efficiencies suggest that the HPs considered in this work cannot be regarded as possible alternatives to desferrioxamine and deferiprone in the chelation therapy of aluminium(III). The synthesis of more lipophilic HPs with higher stability constants towards the metal ion is advisable. For deferiprone-like molecules, both of these characteristics have been obtained by introducing electron-donating, lipophilic groups into the pyridinic ring. The synthesis of 1- and 2-methyl HP derivatives is therefore now in progress.

Experimental Section

Synthesis of the Ligands: The ligands 3H4P and 4H3P (which are not commercially available) were prepared acording to reported multi-step methods,[27,32] with some modifications. All chemicals and solvents were obtained from Aldrich Chimica or Janssen Chimica (now Acros). The identity and purity of all intermediates and final compounds were checked by melting point (m.p.) measurements (Gallenkamp MFB 595 010 M/B capillary m.p. apparatus), ^{1}H NMR spectra (Bruker 300 MHz), TLC (Merck silica gel 60 F-254 glass plates), mass spectrometry (Mat 112 Varian Mat Bremen mass spectrometer) and elemental analyses (Perkin–Elmer Elemental Analyzer Model 240B).

3H4P: White needles. Yield 24% (4 g). M.p. 321 °C (ref.[32] 316–319 °C). ^{1}H NMR (in [D$_6$]DMSO), δ = 7.83 (d, $J_{5,6}$ = 5.2 Hz, 1 H, 5-H), 8.10 (d, $J_{6,5}$ = 5.2 Hz, 1 H, 6-H), 8.39 (s, 1 H, 2-H) ppm. $C_6H_5NO_3$ (139.11): calcd. C 51.80, H 3.62, N 10.07; found C 51.72, H 3.65, N 9.97.

4H3P: White needles. Yield 17% (4 g). ^{1}H NMR ([D$_6$]DMSO): δ = 6.73 (d, $J_{5,6}$ = 5 Hz, 1 H, 5-H), 8.07 (d, $J_{6,5}$ = 5 Hz, 1 H, 6-H), 8.61 (s, 1 H, 2-H), 12.99 (s, 1 H, OH), 15.70 (s, 1 H, COOH) ppm. EI MS (70 eV): *m/z* (%) = 139 (100) [M$^+$], 122 (80.66) [M$^+$ – OH], 94 (63.94) [M$^+$ – COOH]. $C_6H_5NO_3$ (139.11): calcd. C 51.80, H 3.62, N 10.07, found C 51.74, H 3.59, N 10.00.

Thermodynamic Study: The experimental apparatus, reagents and measurement methods were almost the same as those reported previously.[47] In the following, a summary will be given; details are reported only when different from those described previously.

Apparatus: All potentiometric measurements were performed using a Radiometer ABU93 Triburette apparatus. UV spectra were recorded using Perkin–Elmer Lambda 20 and Lambda 5 instruments, ^{1}H NMR spectra using Varian Gemini 200 MHz and Bruker 300 MHz instruments. The elemental analyses were performed using an Iris Intrepid ICP-AES for Al and Na, and a Perkin–Elmer Elemental Analyzer Model 240B for C, N and H.

Reagents: All analyte concentrations were expressed using the molality scale (mol/kg of water). For potentiometric and UV spectrophotometric measurements, working solutions of HCl (0.1 m), NaOH (0.1 m) and $AlCl_3$ (0.05 m, containing HCl 0.01 m) were prepared and standardised as described previously;[47] 3H4P and 4H3P were used as synthesised to prepare 0.004 m and 0.05 m working solutions, respectively, (the concentrations correspond to about 80% of their water solubility). The ionic strength of all the solutions was adjusted to 0.6 m (≈ 0.594 M) (Na)Cl. Solutions for ^{1}H NMR spectroscopic measurements were prepared by dissolving weighted amounts of ligand, $AlCl_3$ (Fluka, ≥ 99%) and NaCl in D_2O.

Potentiometric Measurements: Titrations were carried out at 25 ± 0.1 °C; duplicate potentiometric measurements were performed using two different glass electrodes (Radiometer pHG201 and BDH 309/1015/02) and an Ag/AgCl/0.6 m NaCl reference electrode,[48,49] with a J-shaped junction; its acidic liquid junction potential has been determined previously[39] and can be represented by the equation[49] $E_j = -S\cdot\log(1 + J\cdot[H^+])$, with J = 4.251 ± 0.003. Besides the calibration and the base standardisation experiments,[47] the titrations reported in Table 5 were performed. All stability constants were calculated using the computer program PITMAP.[50] The hydroxometal species reported by Öhman[51] have been considered and the corresponding log β values were kept constant during the processing of the data. After the addition of the metal ion and either of the two ligands to an acidic solution (pH < 3), the measured e.m.f. drifted and reached a constant value only after ca. 1 h, suggesting a low complex formation rate. The kinetics of the aluminium–ligand reaction became "normal" (equilibration after ca. 1 min) at pH values > 3. These findings are in agreement with previous results with 2,3-HPs.[24,52] Experimental details regarding the treatment of the slow kinetics during the titrations are reported.[24]

UV Spectrophotometric Measurements: The measurements reported in Table 6 were performed. The pH of the solutions was computed

Table 6. UV spectrophotometric measurements

System	Conditions				
	$[Al]_0/10^{-4}$ m	$[L]_0/10^{-4}$ m	pH	λ [nm] for calculation	Cell length [cm]
3H4P	–	6.00	0.30–2.90	215; 245; 322; 346	0.1
4H3P	–	6.61	0.23–1.80	226; 248; 283	0.1
Al + 4H3P	0.806	1.16	1.10–3.60	245; 262; 290	1

from the stoichiometric concentration of HCl,[53] because the changes in $[H^+]$ produced by the other species were always negligible under the chosen conditions. The pK_a for the equilibrium $H_3L^+ \leftrightarrows H_2L + H^+$ (for both ligands) and the log β for the equilibrium $H_2L + Al^{3+} \leftrightarrows AlLH^{2+} + H^+$ (for 4H3P only) were computed using a described method.[24,47]

^{1}H NMR Spectroscopic Measurements: Spectra were obtained in D_2O for solutions containing only the ligand (0.0041 m in the case of 3H4P and 0.050 m in the case of 4H3P) and for solutions also containing aluminium (0.010 m and 0.0012 m, respectively, with the same ligand concentration as before) at various pH values, in the presence of (Na)Cl 0.6 m. The pH was adjusted with small additions of concentrated HCl or NaOH solutions (prepared in D_2O), and was measured with a glass electrode BDH 309/1025/02 previously calibrated in aqueous solutions containing (Na)Cl 0.6 m and known concentrations of HCl. 0.41 pH units were added to the pH-meter readings to correct for isotopic and solvent effects,[54] i.e. "pD" rather than "pH" values were measured.

***n*-Octanol/Water Distribution and Chelation Efficacy Studies**

Materials: NaCl, KCl, $NaHCO_3$, H_3BO_3 and *n*-octanol were obtained from EM, Fisher, or Sigma; Al borate from Pfaltz and Bauer (Waterbury, CT) and an Al atomic absorption standard from Sigma. Polypropylene test tubes (10 mL) with polyethylene caps were purchased from VWR.

Method: The octanol/water distribution of the ligands (3H4P, 4H3P, 2H3P and 3H2P), their ability to solubilise Al as an indicator of chelation potential, and the octanol/water distribution of the aluminium–ligand complex were assessed in an octanol/aqueous system, as described previously;[26] 4 mL of *n*-octanol and 4 mL of an aqueous buffer were added to 10-mL test tubes. The tubes also contained Al borate, ligand or Al borate + ligand. Al borate (7–8 mg) was added as a source of Al, which is quite insoluble, but not kinetically inert. The ligand was introduced in the aqueous phase at $1 \cdot 10^{-3}$ M. The aqueous phase contained 125 mM NaCl, 25 mM $NaHCO_3$, 5 mM KCl and 100 mM H_3BO_3 at pH = 7.4. The tubes were shaken overnight at room temperature in order to achieve equilibrium. Al was quantitated in the aqueous and octanol phases of tubes that contained Al borate, using a Perkin–Elmer 4100 ZL atomic absorption spectrophotometer, S-70 sampler and DEC workstation. All samples were analysed at least twice at λ = 309.3 nm. The concentration of the ligand, both in the presence and absence of Al borate, was determined in the aqueous and octanol phases using a Shimadzu UV2501PC recording spectrophotometer. Samples were compared, at the isosbestic point of absorbance of the ligand (λ = 306.0, 298.3, 257.0 and 305.4 nm for 3H4P, 4H3P, 2H3P and 3H2P, respectively), to aqueous standards containing the ligand in the absence of Al borate. The amount of Al in each phase in the absence of ligand was subtracted from the amount of Al in the presence of ligand, as a measure of the Al solubilised by the chelator. Since 1:3 complexes form for all compounds (see thermodynamic results above and ref.[24]), the efficiency of the test compound to solubilise (chelate) Al was calculated as threefold the sum of the increase in Al (in mol) in the two phases in the presence of ligand, divided by the molar concentration of the ligand introduced into the aqueous phase ($1 \cdot 10^{-3}$ M). The octanol/water distribution of each ligand was determined from its concentration in the octanol/aqueous phase (in the absence of Al borate). The octanol/water distribution of the Al–ligand complex was calculated from the total ligand concentration in each phase (determined by UV spectrophotometry in the presence of Al borate) minus the calculated free ligand concentration, as described.[55] The total free ligand concentration was calculated from (1-% efficiency/100) × the total chelator concentration. The free ligand concentration in each phase was calculated from the octanol/water distribution of the ligand. The results are the mean of three or four independent experiments containing duplicate observations for each aluminium–ligand system.

Acknowledgments

We would like to thank Professor Gianfranco Chiarelotto for helpful suggestions for the synthesis, the graduate students Alessandro Gnocchi, Angela M. Peagler and Maria Rosa Trestin for their careful work, and Chelab S. r. l. (Resana, Treviso, Italy) for the ICP analysis.

[1] A. V. Hoffbrand, *J. Lab. Clin. Med.* **1998**, *131*, 290–291.
[2] M. J. Pippard, D. J. Weatherall, *Brit. J. Haematol.* **2000**, *111*, 2–5.
[3] R. C. Hider, R. Choudhury, B. L. Rai, L. S. Dehkordi, S. Singh, *Acta Haematol.* **1996**, *95*, 6–12.
[4] G. J. Kontoghiorghes, *Analyst* **1995**, *120*, 845–851.
[5] G. Faa, G. Crisponi, *Coord. Chem. Rev.* **1999**, *184*, 291–310.
[6] R. A. Yokel, P. Ackrill, E. Burgess, J. P. Day, J. L. Domingo, T. P. Flaten, J. Savory, *J. Toxicol. Environ. Health* **1996**, *48*, 667–683.
[7] M. L. Albina, M. Belles, D. J. Sanchez, J. L. Domingo, *Teratology* **2000**, *62*, 86–92.
[8] N. F. Olivieri, G. M. Brittenham, C. E. McLaren, D. M. Templeton, R. G. Cameron, R. A. McClelland, A. D. Burt, K. A. Fleming, *N. Eng. J. Med.* **1998**, *339*, 417–423.
[9] P. R. Dragsten, P. E. Hallaway, G. J. Hanson, A. E. Berger, B. Bernard, B. E. Hedlund, *J. Lab. Clin. Med.* **2000**, *135*, 57–65.
[10] B. Faller, C. Spanka, T. Sergejew, V. Tschinke, *J. Med. Chem.* **2000**, *43*, 1467–1475.
[11] Z. D. Liu, H. H. Khodr, S. L. Lu, R. C. Hider, *J. Pharm. Pharmacol.* **2000**, *52*, 263–272.
[12] B. L. Rai, H. Khodr, R. C. Hider, *Tetrahedron* **1999**, *55*, 1129–1142.
[13] C. Bazzicalupi, A. Bencini, A. Bianchi, F. Vieri, C. Giorgi, L. Messori, M. Migliorini, P. Paoletti, B. Valtancoli, *J. Chem. Soc., Dalton Trans.* **1998**, 359–367.
[14] P. Baret, C. Béguin, G. Gellon, J. L. Pierre, T. Serratrice, G. Fabrice, J. P. Laulhére, E. Saint-Aman, *Eur. J. Inorg. Chem.* **2000**, 1219–1227.
[15] M. Gaspar, R. Grazina, A. Bodor, E. Farkas, M. A. Santos, *J. Chem. Soc., Dalton Trans.* **1999**, 799–806.
[16] G. Rivkin, G. Link, E. Simhon, R. I. Cyjon, J. Y. Klein, C. Hershko, *Blood* **1997**, *90*, 4180–4187.

[17] R. A. Yokel, A. M. Fredenburg, P. W. Durbin, J. Xu, M. K. Rayens, K. N. Raymond, *J. Pharm. Sci.* **2000**, *89*, 545−555.
[18] R. C. Hider, J. B. Porter, S. Singh, "The design of therapeutically useful iron chelators", in *The development of iron chelators for clinical use* (Eds.: R. J. Bergeron, G. M. Brittenham), CRC Press, Boca Raton, Florida, USA, **1994**.
[19] D. R. Richardson, P. Ponka, *J. Lab. Clin. Med.* **1998**, *131*, 306−315.
[20] W. O. Foye, J. M. Kauffman, *Chim. Ther.* **1967**, *2*, 462−466.
[21] H. Tandeloo, F. Broekman, V. Stroer, J. Siemelink, Neth. Appl. 70 11,749, **1972**.
[22] R. Gleckman, S. Alvarez, D. W. Joubert, S. J. Matthews, *Am. J. Hosp. Pharm.* **1979**, *36*, 1071−1074.
[23] K. Spear, C. Johnson, H. W. Gschwend, PCT Int. Appl. WO 94 20,527, **1993**.
[24] V. B. Di Marco, A. Tapparo, G. G. Bombi, *Ann. Chim. (Rome)* **1999**, *89*, 535−546.
[25] R. C. Scarrow, P. E. Riley, K. Abu-Dari, D. L. White, K. N. Raymond, *Inorg. Chem.* **1985**, *24*, 954−967.
[26] R. A. Yokel, H. B. Kostenbauder, *Toxicol. Appl. Pharmacol.* **1987**, *91*, 281−294.
[27] J. V. Dejarden, C. L. Lapiere, *Bull. Soc. Chim. Fr.* **1976**, *3−4*, 530−532.
[28] J. Abbalard, C. Decoret, I. Cronenberger, H. Pacheco, *Bull. Soc. Chim. Fr.* **1972**, *6*, 2466−2481.
[29] H. Meyer, V. Graf, *Ber. Dtsch. Chem. Ges.* **1928**, *61*, 2202.
[30] S. Gabriel, J. Colman, *Ber. Dtsch. Chem. Ges.* **1902**, *35*, 1358−1367.
[31] S. Gabriel, J. Colman, *Ber. Dtsch. Chem. Ges.* **1902**, *35*, 2831−2852.
[32] M. Mittebach, G. Kastner, H. Junek, *Arch. Pharm.* **1985**, *318*, 481−486.
[33] H. W. Schmidt, H. Junek, *Monatsh. Chem.* **1977**, *108*, 895.
[34] T. Wieland, C. Fest, G. Pfleiderer, *Justus Liebigs Ann. Chem.* **1961**, *642*, 163−173.
[35] E. C. Taylor, J. S. Driscoll, *J. Am. Chem. Soc.* **1960**, *82*, 31419.
[36] W. C. J. Ross, *J. Chem. Soc. C* **1966**, 1816−1819.
[37] B. A. Korolev, L. G. Stolyarova, L. D. Smirnov, K. M. Dyumaev, *Bull. Acad. Sci. USSR Div. Chem. Sci. (Engl. Transl.)* **1979**, 1159−1164.
[38] A. E. Martell, R. M. Smith, *Critical stability constants*, vol. 1−4 and first supplement, Plenum Press, New York, **1979**.
[39] V. B. Di Marco, A. Tapparo, G. G. Bombi, *Ann. Chim. (Rome)* **2001**, *91*, 595−603.
[40] A. O. McDougall, F. A. Long, *J. Phys. Chem.* **1962**, *66*, 429−433.
[41] T. Kiss, E. Farkas, *Perspec. Bioinorg. Chem.* **1996**, *3*, 199−250.
[42] D. J. Clevette, W. O. Nelson, A. Nordin, C. Orvig, S. Sjöberg, *Inorg. Chem.* **1989**, *28*, 2079−2081.
[43] J. B. Porter, E. R. Huehns, R. C. Hider, *Clin. Haematol.* **1989**, *2*, 257−292.
[44] R. A. Yokel, A. M. Fredenburg, K. A. Meurer, T. L. Skinner, *Drug Metab. Dispos.* **1995**, *23*, 1178−1180.
[45] R. A. Yokel, K. A. Meurer, T. L. Skinner, A. M. Fredenburg, *Drug Metab. Dispos.* **1996**, *24*, 105−111.
[46] R. A. Yokel, K. A. Meurer, C. B. Hong, K. M. Dickey, T. L. Skinner, A. M. Fredenburg, *Drug Metab. Dispos.* **1997**, *25*, 182−190.
[47] V. B. Di Marco, A. Tapparo, G. G. Bombi, *Ann. Chim. (Rome)* **1999**, *89*, 397−407.
[48] G. J. Janz, "Silver − Silver Halide Electrodes", in *Reference Electrodes: Theory and Practice* (Eds.: D. J. G. Ives, G. J. Janz), Academic Press, New York, London, **1961**.
[49] G. Biedermann, L. G. Sillén, *Ark. Kemi* **1953**, *5*, 425−440.
[50] V. B. Di Marco, PhD Thesis, University of Padova, **1998**.
[51] L. O. Öhman, *Inorg. Chem.* **1988**, *27*, 2565−2570.
[52] C. Baiocchi, E. Mentasti, *Ann. Chim. (Rome)* **1981**, *71*, 631−647.
[53] A. K. W. Stephens, C. Orvig, *Inorg. Chim. Acta* **1998**, *273*, 47−53.
[54] A. K. Covington, M. Paabo, R. A. Robinson, R. G. Bates, *Anal. Chem.* **1968**, *40*, 700−706.
[55] R. A. Yokel, *J. Toxicol. Environ. Health* **1994**, *41*, 131−174.

Received February 21, 2002
[I02094]

(Tetramethylcyclobutadiene)cobalt Complexes − Syntheses of Tris(ligand) Derivatives and Structures of $[(C_4Me_4)Co(CO)_3]BF_4$ and $[(C_4Me_4)Co(NCMe)_3]PF_6$

Mikhail V. Butovskii,[a] Ulli Englert,[a] Alexei A. Fil'chikov,[b] Gerhard E. Herberich,*[a] Ulrich Koelle,[a] and Alexander R. Kudinov*[b]

Keywords: Cobalt / Cyclobutadiene complexes / Metallo-electrophiles

Photolysis of $[Cb^*Co(C_6H_6)]PF_6$ (**6**) ($Cb^* = C_4Me_4$) in acetonitrile solution produces the red solvento complex $[Cb^*Co(NCMe)_3]PF_6$ (**8**) in quantitative yield. Alternatively, heating of the acetonitrile solution to reflux temperature may effect the displacement of the benzene ligand. Photolysis of **6** in liquid ammonia gives $[Cb^*Co(NH_3)_3]PF_6$ (**9**). Compound **8** is substitution-labile and reacts with a wide variety of Lewis bases to produce substitution products $[Cb^*CoL_3]PF_6$ with L = $P(OMe)_3$ (**10**), py (**11**), CN*t*Bu (**12**), and the related compound $(NEt_4)_2[Cb^*Co(CN)_3]$ (**13**). Thermal reaction of $[Cb^*Co(CO)_3]BF_4$ (**7**) with PMe_3 takes place spontaneously at ambient temperature and produces the monosubstitution product $[Cb^*Co(CO)_2(PMe_3)]BF_4$ (**14**), while irradiation combined with a purging stream of N_2 effects an exhaustive decarbonylation and affords $[Cb^*Co(PMe_3)_3]BF_4$ (**16**). Irradiation of **7** in acetonitrile produces mixtures of the mono- and disubstitution products; if a purging stream of N_2 is applied, $[Cb^*Co(CO)(NCMe)_2]BF_4$ (**18**) is formed with a small admixture of $[Cb^*Co(NCMe)_3]BF_4$. The iodide $Cb^*CoI(CO)_2$ reacts with 2,2′-bipyridine to produce the monocarbonyl complex $[Cb^*Co(CO)(bipy)]I$ (**15**). Single-crystal structure determinations of $[Cb^*Co(CO)_3]BF_4$ (**7**) with Co–Cb(ring plane) 1.777(2) Å (av.) and of $[Cb^*Co(NCMe)_3]PF_6$ (**8**) with Co–Cb(ring plane) 1.68(1) Å (av.) are reported. Synthetic procedures for the preparation of $[Cb^*Co(CO)_3]BF_4$ (**7**), $Cb^*CoI(CO)_2$ (**2**), and $[Cb^*Co(C_6H_6)]PF_6$ (**6**) are also given. An electrochemical study of the compounds **8**, **10**–**13**, and **16** reveals chemically fully reversible oxidation reactions. Hard σ-donor ligands (CN^-, py, NCMe) stabilize the corresponding 17e species much more so than soft donor ligands [PMe_3, CN*t*Bu, and $P(OMe)_3$].

(© Wiley-VCH Verlag GmbH, 69451 Weinheim, Germany, 2002)

Introduction

Electrophilic complex fragments or metallo-electrophiles of the general type $[L_xM(solv)_y]^{n+}$ are useful synthons in organometallic chemistry. Our interest in metallo-electrophiles developed during our quest for new triple-decker complexes.[1,2] Early examples of metallo-electrophiles are the 1,5-cyclooctadiene complex $[(COD)Rh(THF)_x]^+$ [3] and the cation $[Cp^*Rh(OCMe_2)_3]^{2+}$.[4] These species are usually generated from corresponding chlorides by dehalogenation with Ag^+ or Tl^+ salts with nonbasic anions such as BF_4^-, PF_6^-, or $CF_3SO_3^-$. Weakly coordinating solvents such as nitromethane, dichloromethane, THF, acetone, or acetonitrile are used in the generation of the metallo-electrophiles to provide a maximum reactivity and a minimal stabilization. The number of coordinated solvent units is often unknown, especially in the cases of the most weakly bonded solvent molecules. On the other hand, the acetonitrile ligand provides sufficient stabilization to the electrophilic metal center to allow the isolation of less reactive, but well-defined compounds. The species $[CpFe(NCMe)_3]^+$,[5,6] $[Cp^*Fe(NCMe)_3]^+$,[7] $[CpRu(NCMe)_3]^+$,[6,8] $[Cp^*Ru(NCMe)_3]^+$,[9] and $[CpOs(NCMe)_3]^+$ [10] are pertinent examples, and the more recently discovered species $[Cb^*Co(solv)_x]^+$ ($Cb^* = C_4Me_4$, solv = inter alia MeCN)[11] is related to these by virtue of the isolobal analogy.

Complex fragments of the (cyclobutadiene)cobalt type are well known in complexes with Cp counterligands, e.g. Cb^*CoCp,[12] or $(C_4Ph_4)CoCp$,[13] whereas comparatively little is known about (cyclobutadiene)cobalt complexes with counterligands other than Cp. There are several general reviews on (cyclobutadiene)metal complexes,[14] and also specialized reviews that center on the chemistry of (cyclobutadiene)cobalt complexes.[15]

In pioneering work Pauson et al.[16] have shown that the zwitterionic cyclobutenyl species $Me_4C_4AlCl_3$ [17] readily re-

[a] Institut für Anorganische Chemie, Technische Hochschule Aachen
52056 Aachen, Germany
Fax: (internat.) + 49-(0)241/809-2288
E-mail: gerhard.herberich@ac.rwth-aachen.de
[b] A. N. Nesmeyanov Institute of Organoelement Compounds, Russian Academy of Sciences,
28 ul. Vavilova, 119991 Moscow, Russian Federation
Fax: (internat.) + 7-095/135-5085
E-mail: arkudinov@ineos.ac.ru

acts with $Co_2(CO)_8$ to form the cation $[Cb^*Co(CO)_3]^+$ ($\mathbf{1}^+$). On this basis they developed syntheses of $Cb^*Co-I(CO)_2$ (**2**), and $[Cb^*Co(C_6H_6)]^+$ ($\mathbf{3}^+$). The goal of the present work is the further development of the chemistry of the (tetramethylcyclobutadiene)cobalt complex fragment and especially of the new metallo-electrophile $[Cb^*Co(NCMe)_3]^+$ ($\mathbf{4}^+$). We also present the first structural characterizations of tris(ligand) species $[Cb^*CoL_3]^+$ with L = CO and MeCN.

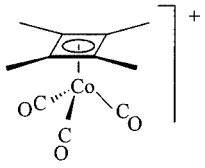

$\mathbf{1}^+$

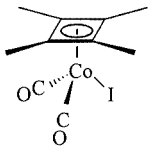

2

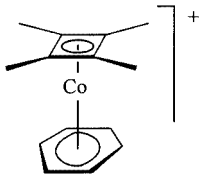

$\mathbf{3}^+$

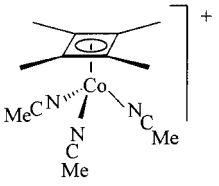

$\mathbf{4}^+$

Results and Discussion

Starting Materials

In the work of Pauson et al.[16] the salt $[Cb^*Co(CO)_3]PF_6$ (**5**) was isolated from the reaction of $Me_4C_4AlCl_3$ [17] and $Co_2(CO)_8$. In a second step, this salt was treated with Me_3NO/Bu_4NI in dichloromethane or with K_2CO_3/Bu_4NI in dichloromethane to afford the iodide **2**. In a further transformation the iodide **2** was heated with $AlCl_3$ in benzene, and the resulting cation $\mathbf{3}^+$ was isolated as hexafluorophosphate **6** [≡ (**3**)PF_6].[16]

In part of our work we used the tetrafluoroborate **7** [≡ (**1**)BF_4] which was synthesized by a straightforward adaptation of the published synthesis of the hexafluorophosphate **5**. The iodide **2** was prepared by a simplified procedure that combines the two steps of the original work into a single protocol. After hydrolysis of the primary reaction mixture, Me_3NO and NaI were added to the raw aqueous solution containing $\mathbf{1}^+$, producing the uncharged iodide **2** as a brown precipitate. This procedure gave a somewhat lower yield (37%; ref.[16] 45−52%), but requires less work.

When we repeated the synthesis of the benzene complex **6**, we found that some tricarbonyl cation $\mathbf{1}^+$ was also formed as was readily seen from the product IR spectrum or from ^{1}H NMR spectra in nitromethane or dichloromethane solution. It is recommendable to use a tenfold excess of $AlCl_3$, to add petroleum ether (octane fraction, 60% by volume), and to run the reaction at ca. 130 °C. Under these conditions the CO formed is removed more efficiently from the reaction mixture, and the formation of $\mathbf{1}^+$ is largely suppressed. The by-product may also be removed during workup of the reaction mixture, by adding a little Me_3NO and NaI to the aqueous solution. The yield of **6** varies somewhat erratically between 50 and 80% (ref.[16] 25%), presumably because traces of water seem to be favorable while larger amounts of water are detrimental.

Photolysis of $[Cb^*Co(C_6H_6)]PF_6$ (6) and Alternative Thermal Ligand Displacement

The sandwich cation $\mathbf{3}^+$ is rather light-sensitive, and solutions of **6** can be photolyzed with any light source at hand (cf. Exp. Sect.). In this context the most useful solvent is acetonitrile. During irradiation, the color changes from yellow to red, and subsequent removal of the volatiles affords the product $[Cb^*Co(NCMe)_3]PF_6$ (**8**) as red crystalline solid in quantitative yield. When acetonitrile solutions of **6** are heated, the benzene ligand is displaced almost completely. This thermal ligand displacement reaction may be forced to go to completion if the volatiles are largely pumped off and the reaction mixture is heated once more in fresh solvent (Scheme 1). The number of acetonitrile units in **8** was determined by elemental analysis and from the relative intensities of the ^{1}H NMR spectrum in [D_6]acetone; these were found to be 8.95:12 for the methyl signals of acetonitrile and Cb*, respectively. It was also finally confirmed by a single-crystal structure analysis (see below). The new compound **8** is sensitive to air, especially in solution. It undergoes slow oxidation by CH_2Cl_2 that is seen as a fast deterioration in the NMR spectra performed in the same solvent.

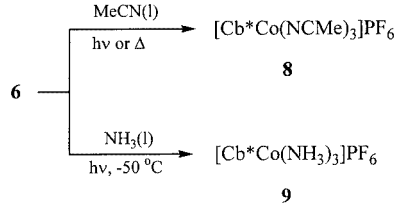

Scheme 1. Substitution reactions of $[Cb^*Co(C_6H_6)]PF_6$ (**6**)

^{1}H NMR spectra of **8** in [D_3]acetonitrile, measured at 200 MHz and at ambient temperature, show a single signal for the methyl groups of acetonitrile. An ^{1}H NMR spectrum in [D_6]acetone/[D_3]acetonitrile mixtures (with comparable quantities of free and coordinated acetonitrile), taken at 500 MHz, showed line-broadening at ambient temperature, decoalescence at −10 °C, and below two signals corresponding to a low-temperature exchange regime; at −84 °C, these two signals were sharp with chemical shifts of δ = 2.50 ppm for coordinated acetonitrile and of δ = 2.12 ppm for free acetonitrile.

The photolysis of **6** works equally well in liquid ammonia and affords the red crystalline salt $[Cb^*Co(NH_3)_3]PF_6$ (**9**). The crystals of **9** are sensitive to air and humidity and smell of ammonia; they melt at about 170 °C, apparently without

decomposition. NMR spectra could be recorded in [D_6]acetone that was charged with gaseous NH_3.

Ligand Substitution Reactions of [Cb*Co(NCMe)$_3$]PF$_6$ (8)

Complex **8** readily undergoes ligand substitution reactions with a wide variety of neutral and anionic reagents. The in situ reaction with the carbaborane anion [9-(Me_2S)-7,8-$C_2B_9H_{10}$]$^-$ to give the metallacarbaborane Cb*Co[9-(Me_2S)-7,8-$C_2B_9H_{10}$] has been described in previous work,[11] and sandwich complexes with bora- and boratabenzene counter-ligands have been made with complex **8** as the starting material.[18] Herein we describe the new compounds **10**−**13** (Scheme 2). In the cases of pyridine and of the phosphorus ligands $P(OMe)_3$ and PMe_3, the third substitution step is slow, and gentle heating may be required to complete the substitution. We treated, for instance, compound **8** with an excess of PMe_3 at only ambient temperature. After removal of the volatiles under vacuum, the solid residue showed a virtual triplet for the protons of the *P*-methyl groups, thereby indicating the presence of two PMe_3 ligands. Similarly, treatment of **8** with excess pyridine at 20 °C for 3 h and subsequent removal of all volatiles left a red solid whose ^{1}H NMR spectroscopic data showed a pyridine/acetonitrile ratio of 2:1. Substitution of the third acetonitrile ligand required prolonged heating at temperatures of 40−50 °C. On the other hand, the slim and strong carbon nucleophiles CN*t*Bu and Et_4NCN readily effected substitution of all three acetonitrile ligands.

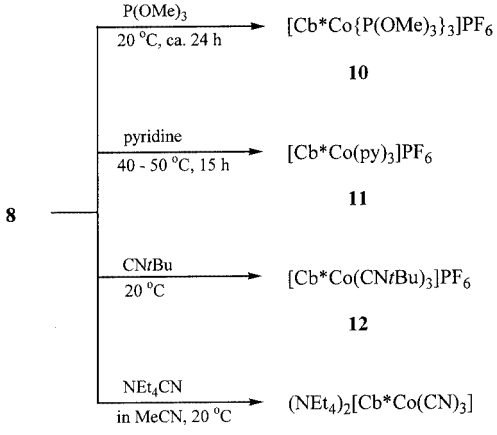

Scheme 2. Thermal ligand substitution reactions of [Cb*Co(NCMe)$_3$]PF$_6$ (**8**)

There are some obvious limitations to this method. The ligand to be introduced should either bind strongly to the metal atom or should be less volatile than acetonitrile. For instance, it is not possible to replace acetonitrile with dimethyl sulfide.

Ligand Substitution Reactions of [Cb*Co(CO)$_3$]BF$_4$ (7) and Cb*CoI(CO)$_2$ (2)

The cation **1**$^+$ is prone to thermal ligand substitution reactions. In favorable cases product formation is highly chemoselective. Thus, the tetrafluoroborate **7** reacts with trimethylphosphane in dichloromethane at ambient temperature with spontaneous evolution of CO to give the monosubstitution product [Cb*Co(CO)$_2$(PMe_3)]BF$_4$ (**14**) in good yield (Scheme 3). In contrast to this simple case, the analogous reaction with the weaker donor ligand $P(OMe)_3$ showed little selectivity. When **7** was treated with $P(OMe)_3$ in [D_6]-acetone, warming to 40−50 °C was required to effect the reaction, and in ^{1}H NMR spectra signals of the mono- and the disubstitution product were observed besides those of the starting material. Thermal substitution of **1**$^+$ with 2,2′-bipyridine (bipy), at somewhat elevated temperatures, produced the cation [Cb*Co(CO)(bipy)]$^+$; the same cation can be obtained more conveniently from the reaction of the iodide **2** to give the iodide [Cb*Co(CO)(bipy)]I (**15**) (Scheme 4).

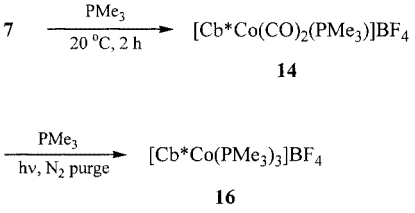

Scheme 3. Trimethylphosphane derivatives of [Cb*Co(CO)$_3$]BF$_4$ (**7**)

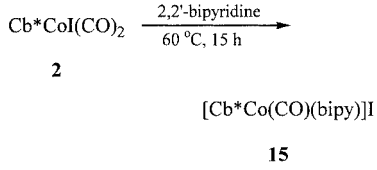

Scheme 4. An ionic 2,2′-bipyridine derivative of Cb*CoI(CO)$_2$ (**2**)

Photochemically induced ligand substitution reactions provide a synthetic alternative. Irradiation of **7** in CH_2Cl_2 in the presence of PMe_3 or $P(OMe)_3$ effects the stepwise replacement of one, two and, much more slowly, even of all three carbonyl groups. For practical purposes it is necessary to purge the reaction mixture with a slow stream of dinitrogen. We used this method to produce the salt [Cb*Co(PMe_3)$_3$]BF$_4$ (**16**) by exhaustive decarbonylation (Scheme 3). The closely related trimethyl phosphite compound **10** can be prepared analogously; however, the synthesis from **8** described above seems more convenient.

We were especially interested in the replacement of the CO ligands of cation **1**$^+$ with acetonitrile. The first substitution step has already been described by Pauson et al.[16] to give the red salt [Cb*Co(CO)$_2$(NCMe)]BF$_4$ (**17**). Irradiation of an acetonitrile solution of **7** effects a slow second substitution and affords mixtures of **17** and the disubstitution product [Cb*Co(CO)(NCMe)$_2$]BF$_4$ (**18**). If a slow stream of dinitrogen purges the reaction mixture, the rates of these reactions are greatly increased. After a few hours, complex **17** is completely consumed, but the monocarbonyl complex **18** is now contaminated by an admixture of the

tris(acetonitrile) complex $[Cb^*Co(NCMe)_3]BF_4$ (**19**) (typically 10%). The monocarbonyl complex **18** is highly reactive and rather sensitive to traces of air and humidity.

Structure Determinations

To the best of our knowledge no tris(ligand) complex of the Cb*Co fragment has yet been structurally characterized. Therefore, the structure of **7** was elucidated. Crystallization from acetone/THF gave small light-yellow crystals that turned out to be systematically twinned platelets. This situation is expected to limit the quality of the final structural model. The crystals possess the monoclinic space group $P2_1/m$ with two very similar independent formula units in the elemental cell. Both cations and anions display crystallographic mirror symmetry. One of the cations (cation 1, all labels beginning with a leading 1) is shown in Figure 1.

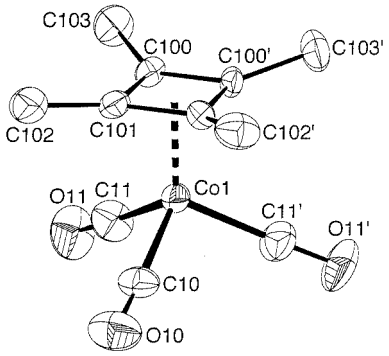

Figure 1. Structure of one of two independent cations $\mathbf{1}^+$ (PLATON plot, see ref.[19] at the 50% probability level) in the crystal of **7**; selected bond lengths [Å]: Co1−C10 1.826(13), Co1−C11/Co1−C11′ 1.852(10), Co1−C100/Co1−C100′ 2.061(8), Co1−C101/Co1−C101′ 2.048(8), Co2−C22 1.739(13), Co2−C21/Co2−C21′ 1.817(10), Co2−C200/Co2−C200′ 2.029(8), Co2−C201/Co2−C201′ 2.061(8)

The cation $\mathbf{1}^+$ possesses the expected piano-stool structure. The planes defined by the cyclobutadiene carbon atoms (plane C_4), the carbonyl carbon atoms (plane C_3), and the carbonyl oxygen atoms (plane O_3) are roughly parallel [largest deviation 3.8(6)° between the two carbon planes C_4 and C_3 of cation 1]. The metal-to-ring distance amounts to 1.769(2) for cation 1 and 1.785(2) Å for cation 2, and is remarkably long. In the family of CoCbCp complexes this distance ranges from 1.68 to 1.70 Å,[20a] and is 1.681 Å for the parent complex CoCbCp[20b] and 1.692 Å for $Co(C_4Ph_4)Cp$.[20a] With reference to the general bonding characteristics of (cyclobutadiene)metal complexes such as $Fe(CO)_3(C_4H_4)$,[21] we expect that the lower energy of the 2e valence orbital set of the $Co(CO)_3^+$ fragment, as compared to that of the uncharged CoCp fragment, results in an e MO set of more metal character and hence weaker Co−Cb bonding in the cation $\mathbf{1}^+$.

Crystals of **8**, that were suitable for a structural study, were obtained by crystallization of **8** from an acetonitrile/ether mixture. The structure determination of **8** (Figure 2) was hampered by disorder of the cyclobutadiene rings. In the final structural model this disorder is largely resolved showing two dispositions of the rings with almost equal (0.52 and 0.48) occupancies. The best ring planes C_4 (with the atoms C1, C2, C3, C4) and C_4B (with C1B, C2B, C3B, C4B; not shown in Figure 2) of the minor orientation display an interplanar angle of 6.8(16)°. The metal-to-ring distance amounts to 1.680(10) for the major disposition and to 1.670(10) Å for the minor disposition. In this case the weak π-acceptor property of the acetonitrile ligands allows for a much stronger Co−Cb interaction as compared to **7**.

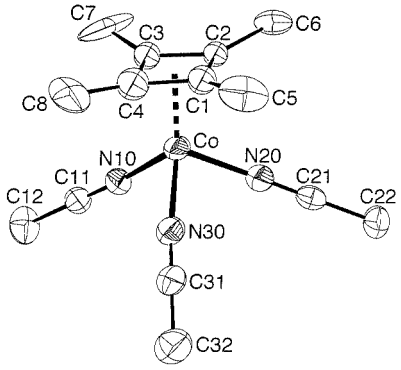

Figure 2. Structure of the major disposition of cation $\mathbf{4}^+$ (PLATON plot, see ref.[19] at the 30% probability level) in the crystal of **8**; for details of the disorder problem see text; selected bond lengths [Å]: Co−N10 1.943(6), Co−N20 1.951(7), Co−N30 1.957(7), Co−C1 1.95(4), Co−C2 2.043(12), Co−C3 1.989(13), Co−C(4) 1.856(19); the positional coordinates of C1 are most severely affected by the disorder of the Cb* ring

Electrochemical Studies

The redox behaviour of the complexes **8**, **10**−**13**, and **16** was studied by cyclic voltammetry. All these complexes show a chemically fully reversible oxidation. No reduction was found down to the solvent/electrolyte limit at about −2 V. Table 1 lists the electrochemical data obtained, with the compounds arranged in order of increasing oxidation potential. The data show that hard donor ligands tend to ease oxidation; in other words, hard donor ligands stabilize the $CbCo^{2+}$ fragment more than the soft donors PMe_3, CN*t*Bu, and $P(OMe)_3$. The 17e acetonitrile cation $\mathbf{4}^{2+}$ shows a second irreversible oxidation at about 0.8 V. The 17e monoanion $[Cb^*Co(CN)_3]^-$, derived from monoelectronic oxidation of **13**, is not further oxidized up to about 0.4 V, i.e. it exhibits a stability window of at least 1 V. The dianion of **13** is highly air-sensitive. However, the green air oxidation product seems to be different from the electrochemical oxidation product since it cannot be re-reduced electrochemically. Further investigation of the cyano compounds would seem desirable and rewarding.

The redox behaviour classifies the Cb^*Co^+ fragment as a relatively hard organometallic metallo-electrophile, similar to $CpFe^+$. This feature is illustrated by the fact that complexes $[Cb^*CoL_3]^{n+}$ could be prepared with ligands of predominant σ-donor character as well as with π-acceptor ligands. However, in both cases of Cb^*Co^+ and $CpFe^+$,

Table 1. Cyclovoltammetric data for **8**, **10**−**13**, and **16**

Electroactive species	Solvent	$E_{1/2}$/V vs. SCE	ΔE/mV	v/mV s^{-1}
$[Cb^*Co(CN)_3]^{2-}$ in **13**	acetonitrile	−0.616	146	50
$[Cb^*Co(py)_3]^+$ in **11**	acetonitrile	0.155	80	100
$[Cb^*Co(NCMe)_3]^+$ in **8**	acetonitrile	0.23	77	50
$[Cb^*Co(PMe_3)_3]^+$ in **16**	CH_2Cl_2	0.70	65	100
$[Cb^*Co(CNtBu)_3]^+$ in **12**	CH_2Cl_2	0.97	94	100
$[Cb^*Co\{P(OMe)_3\}_3]^+$ in **10**	CH_2Cl_2	1.02	74	100

ligands placed to the left of ammonia and acetonitrile in the spectrochemical series, such as water, lead to decomplexation of the carbocyclic ligand.

Conclusions

This paper documents an improved access to the (tetramethylcyclobutadiene)cobalt complexes $Cb^*CoI(CO)_2$ (**2**) and $[Cb^*Co(C_6H_6)]^+$ ($\mathbf{3}^+$) (as hexafluorophosphate **6**) which may serve as versatile starting materials in this chemistry. Photolysis of the salt **6** in solution produces synthetically useful, reactive metallo-electrophiles of the type $[Cb^*Co(solv)_x]^+$. The generation of a very reactive species of this type in dichloromethane allowed the synthesis of triple-decker sandwich complexes with a bridging cyclopentadienyl ligand.[22] One main aim of this paper was the full characterization of the cation $[Cb^*Co(NCMe)_3]^+$ ($\mathbf{4}^+$). This species is not only prepared from $\mathbf{3}^+$ by the photolytic method, but also by thermal ligand displacement in acetonitrile solution. With the improved accessibility of Cb*Co complexes achieved in this work the metallo-electrophiles $[Cb^*Co(solv)_x]^+$ should from now on belong to the standard armory of the synthetic organometallic chemist.

Experimental Section

General Remarks: Reactions were carried out under dinitrogen by means of conventional Schlenk techniques. THF and Et_2O were distilled from sodium benzophenone ketyl, acetonitrile and CH_2Cl_2 from CaH_2. A 400-W Philips sodium lamp SON-T or the pyrex-filtered output of a 150-W mercury lamp were used in photolytic reactions. Elemental analyses were performed by Analytische Laboratorien Prof. Dr. H. Malissa und G. Reuter GmbH, 51789 Lindlar, Germany. Melting points were determined with a Büchi 510 melting point apparatus and are uncorrected. NMR spectra were recorded with a Varian 200 (^{1}H, 200 MHz. $^{13}C\{^1H\}$, 50.29 MHz. $^{31}P\{^1H\}$, 80.96 MHz) or, in special cases, with a Varian Unity 500 (^{1}H, 499.6 MHz. ^{13}C, 125.6 MHz) instrument. Chemical shifts are given in ppm; they were measured at ambient temperature and are referenced to internal TMS for ^{1}H and ^{13}C, and relative to H_3PO_4 (85%) as external reference for ^{31}P. IR spectra were measured with a Nicolet Avatar 360 FT IR instrument.

$[Cb^*Co(CO)_3]BF_4$ (7): A suspension of anhydrous aluminium chloride (16.5 g, 124 mmol) in CH_2Cl_2 (40 mL) was cooled to 0 °C. A solution of 2-butyne (8.93 mL, 114 mmol) in dichloromethane (25 mL) was added dropwise while stirring for 30 min. After addition of more CH_2Cl_2 (35 mL), the mixture was allowed to warm to 20 °C and stirred for 1 h at 20 °C. Octacarbonyldicobalt (9.78 g, 28.6 mmol) was then added and stirring was continued for 80 h. The reaction mixture was hydrolyzed with cold water at 0 °C. The organic phase was removed and the water phase was filtered. $NaBF_4$ (8.0 g, 73 mmol) was added and the mixture was cooled to 0 °C overnight. The precipitate was collected and dried under vacuum. The raw product was dissolved in acetone, and the solution was passed through a 2-cm layer of alumina. Concentration of the filtrate and addition of ether gave **7** (6.67 g, 19.7 mmol, 35%) as a pale yellow powder. $C_{11}H_{12}CoF_4O_3$ (338.0): calcd. C 39.09, H 3.58; found C 39.09, H 3.60. $^{13}C\{^1H\}$ NMR (CD_3NO_2): δ = 9.9 ($C_4\mathit{Me}_4$), 106.6 (C_4Me_4), 197.8 (br, CO) ppm.

$Cb^*CoI(CO)_2$ (2): To the aqueous solution from a similar preparation [$AlCl_3$ (10.6 g, 80 mmol) in CH_2Cl_2 (40 mL), 2-butyne (5.74 mL, 73.5 mmol) in CH_2Cl_2 (25 mL), $Co_2(CO)_8$ (6.29 g, 18.4 mmol)] were added trimethylamine *N*-oxide $Me_3NO{\cdot}2H_2O$ (1.99 g, 17.9 mmol) and NaI (18 g, 0.12 mol). The mixture was stirred for 15 h. The brown precipitate that formed was collected and dried under vacuum; the filtrate did not form any more product when further Me_3NO was added. The raw product was dissolved in CH_2Cl_2, and the solution was passed through a 4-cm layer of alumina. After concentration of the filtrate and addition of a sixfold volume of octane, the solution was kept at −30 °C for 15 h to give **2** (4.79 g, 37%) as dark brown crystals. $^{13}C\{^1H\}$ NMR ([D$_6$]acetone): δ = 10.2 ($C_4\mathit{Me}_4$), 94.2 (C_4Me_4) ppm; signals of CO groups not observed. For further data see ref.[16]

$[Cb^*Co(C_6H_6)]PF_6$ (6): A round-bottomed flask was charged with benzene (20 mL), octane (30 mL), iodide **2** (3.5 g, 10 mmol), and anhydrous aluminium chloride (13.4 g, 100 mmol). The mixture was stirred and heated under reflux at ca.130 °C for 8 h. After cooling to 20 °C, the reaction mixture was carefully hydrolyzed with ca. 100 mL of cold water. The organic phase was separated and the water phase was filtered. Addition of NH_4PF_6 (1.63 g, 10 mmol) to the filtrate gave a yellow precipitate. For further purification, the solution of the dry raw product was passed through a 2-cm layer of alumina. Concentration of the filtrate and addition of a large volume of ether gave **6** (2.44 g, 63%) as a pale yellow powder. $^{13}C\{^1H\}$ NMR ([D$_6$]acetone): δ = 10.1 ($C_4\mathit{Me}_4$), 94.7 (C_4Me_4), 99.8 (C_6H_6) ppm. For further data see ref.[16]

$[Cb^*Co(NCMe)_3]PF_6$ (8). By Photochemical Synthesis: A solution of **6** (390 mg, 1.00 mmol) in acetonitrile (20 mL) was irradiated with a sodium lamp at ambient temperature for 2 h. The color of the solution changed from yellow to red. Removal of the solvent under vacuum afforded **8** (434 mg, 100%) as an air-sensitive, red crystalline solid; m.p. 175 °C (dec.). $C_{14}H_{21}CoF_6N_3P$ (435.2): calcd. C 38.63, H 4.86, N 9.65; found C 38.51, H 4.83, N 9.66. **By Thermal Ligand Displacement:** A solution of **6** (392 mg, 1.00 mmol) in acetonitrile (20 mL) was heated to reflux temperature for 2.5 h. After removal of the volatiles, fresh acetonitrile (20 mL) was added, and the solution was re-heated for 1 h. The volatiles were pumped

off to leave **8** (436 mg, 100%) as spectroscopically pure (^{1}H NMR) product. **Data:** ^{1}H NMR ([D$_6$]acetone): δ = 0.91 (s, Cb*), 2.41 (s, 3 Me) ppm. ^{13}C{^{1}H} NMR ([D$_6$]acetone): δ = 2.9 (*Me*CN), 8.9 (C$_4$*Me*$_4$), 74.8 (*C*$_4$Me$_4$), 124.6 (CN) ppm.

[Cb*Co(NH$_3$)$_3$]PF$_6$ (9): A Schlenk tube with a suspension of complex **6** (195 mg, 0.5 mmol) in liquid ammonia (20 mL) was irradiated with a sodium lamp, while the reaction mixture was stirred at −50 °C. The color of the reaction mixture changed to red and finally, when all the starting material had dissolved, it was a transparent solution (5−7 h). The ammonia was removed by allowing the system to slowly warm to ambient temperature, thus affording **9** (180 mg, 99%) as an air-sensitive, red crystalline solid; m.p. 170 °C, dec. 240 °C. $C_8H_{21}CoF_6N_3P$ (363.2): calcd. C 26.46, H 5.83, N 11.57; found C 26.41, H 5.67, N 11.37. ^{1}H NMR ([D$_6$]acetone, saturated with NH$_3$): δ = 0.84 (s, Cb*), 1.44 (s, 3 NH$_3$) ppm. ^{13}C{^{1}H} NMR ([D$_6$]acetone, saturated with NH$_3$): δ = 8.9 (C$_4$*Me*$_4$), 61.7 (*C*$_4$Me$_4$).

[Cb*Co{P(OMe)$_3$}$_3$]PF$_6$ (10): Trimethyl phosphite (3 mL, 27 mmol) was added to the tris(acetonitrile) complex **8** (434 mg, 1 mmol) in acetonitrile (10 mL). The mixture was stirred at room temperature overnight. The solution was then concentrated in a gentle vacuum to ca. 3 mL, and stirring was continued for 24 h. Addition of ether (20 mL) precipitated a crystalline powder, which was collected on a frit, washed with ether (20 mL), and dried under vacuum to give **7** (680 mg, 100%) as a yellow powder; dec. 210−230 °C. $C_{17}H_{39}CoF_6O_9P_4$ (684.3): calcd. C 29.84, H 5.74; found C 29.81, H 5.83. ^{1}H NMR ([D$_6$]acetone): δ = 1.51 (q, J_{PH} = 5.4 Hz, Cb*), 3.80 [m, 3 P(OMe)$_3$] ppm. ^{13}C{^{1}H} NMR ([D$_6$]acetone): δ = 9.4 [q, not well resolved, J_{PC} = 1.4 Hz, C$_4$*Me*$_4$), 53.8 [vq, J_{PC} = 2.7 Hz, P(OMe)$_3$], 86.6 [q, not well resolved, J_{PC} = 2 Hz, *C*$_4$Me$_4$] ppm. ^{31}P{^{1}H} NMR ([D$_6$]acetone): δ = −140.8 (sept, PF_6^-), 163.0 [s, P(OMe)$_3$] ppm.

[Cb*Co(py)$_3$]PF$_6$ (11): A solution of **8** (434 mg, 1 mmol) in pyridine (10 mL) was stirred at 40−50 °C overnight. The solution was then concentrated to 2−3 mL under vacuum at the same temperature. Addition of ether precipitated **11** in large crystal blocks, which were washed with ether (40 mL), and dried under vacuum to afford **11** (547 mg, 100%) as a dark red, crystalline solid; dec. 90 °C, very air-sensitive. Sharp NMR spectra could only be recorded when a trace of [D$_5$]pyridine was added. $C_{23}H_{27}CoF_6N_3P$ (549.4): calcd. C 50.28, H 4.95, N 7.65; found C 49.83, H 5.08, N 7.55. ^{1}H NMR ([D$_6$]acetone with a drop of [D$_5$]pyridine): δ = 0.62 (s, Cb*), 7.41 (m, 6 H$_\beta$), 7.76 (tt, 3 H$_\gamma$), 8.79 (d, 6 H$_\alpha$) ppm. ^{13}C{^{1}H} NMR ([D$_6$]acetone with a drop of [D$_5$]pyridine): δ = 8.8 (C$_4$*Me*$_4$), 70.4 (*C*$_4$Me$_4$), 125.0 (C$_\beta$), 136.0 (C$_\gamma$), 150.6 (C$_\alpha$) ppm.

[Cb*Co(CN*t*Bu)$_3$]PF$_6$ (12): Preparation similar to that of **10**; with *tert*-butyl isocyanide (1.0 mL, 9 mmol) the reaction was completed in 2 h and gave **12** (560 mg, 100%) as a yellow crystalline solid; m.p. 178 °C, dec. 192 °C. $C_{23}H_{39}CoF_6N_3P$ (561.5): calcd. C 49.20, H 7.00, N 7.48; found C 49.31, H 7.14, N 7.48. ^{1}H NMR ([D$_6$]acetone): δ = 1.56 (s, 3 *t*Bu), 1.57 (s, Cb*) ppm. ^{13}C{^{1}H} NMR ([D$_6$]acetone): δ = 9.6 (C$_4$*Me*$_4$), 30.0 (C*Me*$_3$), 58.5 (*C*Me$_3$), 87.1 (*C*$_4$Me$_4$), 155.8 (CN) ppm. IR (MeCN): $\tilde{\nu}$ = 2140, 2174 [ν(CN)] cm^{-1}.

(NEt$_4$)$_2$[Cb*Co(CN)$_3$] (13): A solution of **8** (515 mg, 1.18 mmol) in acetonitrile (20 mL) was added to a stirred solution of Et$_4$NCN (555 mg, 3.55 mmol) in acetonitrile (15 mL). The yellow color of the mixture indicates completion of the reaction immediately after mixing. The solvent was removed under vacuum to afford a brownish yellow crystalline material. The product was separated from Et$_4$NPF$_6$ by two recrystallizations from MeCN (0.5 mL)/dry acetone (10 mL), keeping the solution at −30 °C for 18 h, to give **13** (518 mg, 87%) as a spectroscopically pure, brownish-yellow, crystalline solid; m.p. 187 °C, dec. 194 °C, very air-sensitive. $C_{27}H_{52}CoN_5$ (505.7): calcd. C 64.13, H 10.37, N 13.85; found C 63.6, H 10.0, N 14.1 (average of two determinations). ^{1}H NMR (CD$_3$CN): δ = 1.23 [tt, ^3J(^{1}H-^{1}H) = 7.3, ^3J(^{14}N-^{1}H) = 1.9 Hz, 8 Me], 1.27 (s, Cb*), 3.27 [q, br, ^3J(^{1}H-^{1}H) = 7.3 Hz, 8 CH$_2$N] ppm. ^{13}C{^{1}H} NMR (CD$_3$CN): δ = 7.8 (*C*H$_3$CH$_2$N), 10.9 (C$_4$*Me*$_4$), 53.0 [t, ^1J(^{14}N-^{13}C) = 3.0 Hz, CH$_2$N], 71.0 (*C*$_4$Me$_4$), 165.1 (CN) ppm.

[Cb*Co(CO)$_2$(PMe$_3$)]BF$_4$ (14): A solution of PMe$_3$ in CH$_2$Cl$_2$ (1 M, 20 mL, 20 mmol) was added to **5** (342 mg, 1.01 mmol), and the mixture was stirred at room temperature until the spontaneous evolution of CO had completely ceased (ca. 2 h). The solution was concentrated in a gentle vacuum to ca. 2−3 mL. Addition of ether (10 mL) precipitated the raw product that was then collected on a frit, washed with ether (20 mL), and dried under vacuum. In a further purification step, the product was dissolved in CH$_2$Cl$_2$, passed through a 0.5-cm layer of alumina, and recovered by addition of ether to give **14** (270 mg, 69%) as a pale yellow, crystalline solid; dec. 245 °C. $C_{13}H_{21}BCoF_4O_2P$ (386.0): calcd. C 40.45, H 5.48; found C 40.68, H 5.42. ^{1}H NMR ([D$_6$]acetone): δ = 1.73 (d, J_{PH} = 10.1 Hz, PMe$_3$), 1.89 (d, J_{PH} = 4.0 Hz, Cb*) ppm. ^{13}C{^{1}H} NMR ([D$_6$]acetone): δ = 9.5 (s, C$_4$*Me*$_4$), 17.7 (d, J_{PC} = 31.1 Hz, PMe$_3$), 96.9 (s, *C*$_4$Me$_4$) ppm. ^{31}P{^{1}H} NMR ([D$_6$]acetone): δ = 7.6 ppm. IR (CH$_2$Cl$_2$): $\tilde{\nu}$ = 2025 and 2064 [ν(CO)] cm^{-1}.

[Cb*Co(CO)(bipy)]I (15): A solution of complex **2** (349 mg, 1.00 mmol) and 2,2′-bipyridine (156 mg, 1.00 mmol) in acetonitrile (5 mL) was stirred overnight at 50−60 °C. The product was precipitated by addition of ether (40 mL), washed with ether (40 mL), and dried under vacuum to afford **15** (471 mg, 99%) as a crystalline powder; dec. 130−140 °C. $C_{19}H_{20}CoIN_2O$ (478.2): calcd. C 47.72, H 4.22, N 5.86; found C 47.79, H 4.29, N 6.05. ^{1}H NMR ([D$_6$]acetone): δ = 1.32 (s, Cb*), 7.86 (m, 4-/4′-H), 8.28 (m, 5-/5′-H), 8.81 (m, 6-/6′-H), 9.04 (m, 3-/3′-H) ppm. ^{13}C{^{1}H} NMR ([D$_6$]acetone): δ = 9.1 (C$_4$*Me*$_4$), 89.6 (*C*$_4$Me$_4$), 124.3 (C-6,6′), 127.9 (C-4,4′), 139.6 (C-5,5′), 154.8 (C-3,3′), 155.9 (C-2,2′). Assignments within the 2,2′-bipyridine ligand were made on the basis of COSY and HETCOR spectra. IR (KBr): $\tilde{\nu}$ = 1960.3 [ν(CO)] cm^{-1}.

[Cb*Co(PMe$_3$)$_3$]BF$_4$ (16): A solution of PMe$_3$ in CH$_2$Cl$_2$ (1 M, 20 mL, 20 mmol) was added to **14** (180 mg, 0.46 mmol) in a Schlenk tube, equipped with a capillary as a gas outlet, and irradiated with a mercury lamp at ambient temperature. A very slow stream of N$_2$ was passed through the solution for 5 h. Concentration of this solution to 5 mL and addition of diethyl ether (20 mL) afforded the raw product which was collected, washed with ether (20 mL) and dried under vacuum to give **16** (210 mg, 93%) as a deep yellow powder; dec. 150−160 °C. $C_{17}H_{39}BCoF_4P_3$ (540.3): calcd. C 42.35, H 8.15; found C 42.15, H 8.05. ^{1}H NMR ([D$_6$]acetone): δ = 1.48 (q, J_{PH} = 3.1 Hz, Cb*), 1.50 (d, J_{PH} = 7.2 Hz, PMe$_3$) ppm. ^{13}C{^{1}H} NMR ([D$_6$]acetone): δ = 10.5 (s, C$_4$*Me*$_4$), 21.6 (8 lines between 21.3 and 21.9, PMe$_3$), 78.5 (s, *C*$_4$Me$_4$) ppm. ^{31}P{^{1}H} NMR ([D$_6$]acetone): δ = 7.3.

[Cb*Co(CO)(NCMe)$_2$]BF$_4$ (18): A sample of **7** (338 mg, 1.00 mmol) in a Schlenk tube, equipped with a capillary as a gas outlet, was dissolved in acetonitrile (20 mL). The solution was photolyzed while N$_2$ was passed through the solution for 8 h. Product formation was monitored by ^{1}H NMR spectroscopy in CD$_3$NO$_2$ on samples taken from the reaction mixture. The acetonitrile was removed completely under vacuum. The residue was dissolved in CH$_2$Cl$_2$, and the product was precipitated with ether and dried under vacuum; yield not determined. $C_{13}H_{18}BCoF_4N_2O$ (364.0): calcd. C 42.89, H 4.98 N 7.70; found C 43.01, H 5.13, N 6.54. ^{1}H

NMR ([D$_6$]acetone): δ = 1.33 (s, Cb*), 2.50 (s, 2 Me) ppm. ^{1}H NMR ([D$_6$]MeNO$_2$): δ = 1.33 (s, Cb*), 2.39 (s, 2 Me) ppm. ^{13}C{^{1}H} NMR ([D$_3$]nitromethane): δ = 3.6 (*Me*CN), 9.2 (C$_4$*Me*$_4$), 92.2 (*C*$_4$Me$_4$), 128.9 (CN), 202.7 (CO) ppm.

X-ray Crystal Structure Determinations:[23] Diffraction intensity data were collected with ENRAF-Nonius CAD4 diffractometers, equipped with graphite monochromators. Crystal data, data collection parameters, and convergence results are listed in Table 2. Numerical absorption corrections[24] were applied before averaging symmetry-equivalent data. The structures were solved by direct methods[25] and refined on F^2.[26] Hydrogen atoms were calculated in standard geometry and treated as riding on the corresponding C atoms. In the case of **7** all crystals tested proved to be twinned. In the diffraction pattern reflections of the type *hkl*, *l* = 0 for both domains coincide, and reflections *hkl*, *l* = 10 show partial overlap and were omitted from the refinement. Despite this modest loss of information, the final completeness of the data set amounts to 0.94. The structure suffers from strongly anisotropic displacement parameters, especially for the methyl substituents on the Cb* rings and the BF_4^- anion; rigid bond[27] restraints and, in the case of the fluorine atoms, additional distance restraints were introduced to ensure a physically reasonable model. The Cb* ligand in **8** shows disorder; C atoms belonging to this moiety were assigned isotropic displacement parameters, and distance restraints were used to ensure a stable refinement of the alternative orientations.

Table 2. Crystal data, data collection parameters, and convergence results for **7** and **8**

	7	**8**
Empirical formula	$C_{11}H_{12}BCoF_4O_3$	$C_{14}H_{21}CoF_6N_3P$
Formula mass	337.95	435.24
Crystal system	monoclinic	monoclinic
Space group	$P2_1/m$	$C2/c$
Radiation (λ [Å])	Mo-K_α (0.71073)	Mo-K_α (0.71073)
a [Å]	10.057(3)	19.276(6)
b [Å]	11.402(5)	10.841(2)
c [Å]	12.2362(16)	19.621(2)
β [°]	93.476(19)	103.48(2)
V [Å^3]	1400.6(8)	3987(2)
Z	4	8
$d_{calcd.}$ [g/cm^3]	1.60	1.45
F(000)	680	1776
μ [mm^{-1}]	1.267	0.992
Absorption correction	numerical	numerical
Max./min. transmission	0.902/0.571	0.896/0.751
θ range [°]	3.1−26.0	2.7−26.0
Temperature [K]	213	213
Scan mode	ω−2θ	ω−2θ
Crystal size [mm]	0.67 × 0.48 × 0.10	0.25 × 0.23 × 0.12
Reflections collected	9436	8098
Reflections unique	3402	3915
Reflections observed	1391	1335
Criterion for observation	$I > 2\sigma(I)$	$I > 2\sigma(I)$
Variables	204	272
R_1[a], observed	0.084	0.079
wR_2 [b], all data	0.190	0.148
GOF[c]	0.832	0.872
Max. resd. density [e/Å^3]	2.27	0.60

[a] $R_1 = \|\|F_o\| - \|F_c\|\|/\|F_o\|$. [b] $wR_2 = [w(F_o^2 - F_c^2)^2/w(F_o^2)^2]^{1/2}$, where $w = 1/[\sigma^2(F_o^2) + (aP)^2]$ and $P = [\max(F_o^2,0) + 2F_c^2]/3$. [c] GOF = $[w(F_o^2 - F_c^2)^2/(n - p)]^{1/2}$.

Electrochemical Measurements: The redox behaviour of the complexes **8**, **10**−**13**, and **16** was investigated by cyclic voltammetry with an IJ Cambria Scientific CHI630A potentiostat at the Pt electrode in the solvents indicated in Table 1 using tetrabutylammonium hexafluorophosphate as the supporting electrolyte. Potentials are vs. SCE and have been standardized towards a ferrocene/ferrocenium potential vs. SCE of 0.400 V in either solvent.

Acknowledgments

This work was generously supported by the Fonds der Chemischen Industrie.

[1] A. R. Kudinov, M. I. Rybinskaya, Yu. T. Struchkov, A. I. Yanovskii, P. V. Petrovskii, *J. Organomet. Chem.* **1987**, *336*, 187−197.
[2] [2a] G. E. Herberich, U. Englert, F. Marken, P. Hofmann, *Organometallics* **1993**, *12*, 4039−4045. [2b] G. E. Herberich, U. Englert, D. Pubanz, *J. Organomet. Chem.* **1993**, *459*, 1−9.
[3] R. R. Schrock, J. A. Osborn, *J. Am. Chem. Soc.* **1971**, *93*, 3089−3091.
[4] C. White, S. J. Thompson, P. M. Maitlis, *J. Chem. Soc., Dalton Trans.* **1977**, 1654−1661.
[5] T. P. Gill, K. R. Mann, *Inorg. Chem.* **1983**, *22*, 1986−1991.
[6] K. R. Mann, A. M. Blough, J. L. Schrenk, R. S. Koefod, D. A. Freedman, J. R. Matachek, *Pure Appl. Chem.* **1995**, *67*, 95−101.
[7] [7a] D. Catheline, D. Astruc, *Organometallics* **1984**, *3*, 1094−1100. [7b] G. E. Herberich, A. Gaffke, H. J. Eckenrath, *Organometallics* **1998**, *17*, 5931−5932.
[8] T. P. Gill, K. R. Mann, *Organometallics* **1982**, *1*, 485−488.
[9] [9a] As hexafluorophosphate: B. Steinmetz, W. A. Schenk, *Organometallics* **1999**, *18*, 943−946. [9b] J. L. Schrenk, A. M. McNair, F. B. McCormick, K. R. Mann, *Inorg. Chem.* **1986**, *25*, 3501−3504. [9c] As triflate: P. J. Fagan, M. D. Ward, J. C. Calabrese, *J. Am. Chem. Soc.* **1989**, *111*, 1698−1719.
[10] [10a] D. A. Freedman, T. B. Gill, A. M. Blough, R. S. Koefod, K. R. Mann, *Inorg. Chem.* **1997**, *36*, 95−102. [10b] D. A. Freedman, J. R. Matachek, K. R. Mann, *Inorg. Chem.* **1993**, *32*, 1078−1080.
[11] A. R. Kudinov, V. I. Meshcheryakov, P. V. Petrovskii, M. I. Rybinskaya, *Izv. Akad. Nauk, Ser. Khim.* **1999**, 177−179; *Russ. Chem. Bull.* **1999**, *48*, 176−178.
[12] [12a] U. Koelle, *Inorg. Chim. Acta* **1981**, *47*, 13−18. [12b] R. Bruce, P. M. Maitlis, *Can. J. Chem.* **1967**, *45*, 2017−2022.
[13] M. D. Rausch, R. A. Genetti, *J. Org. Chem.* **1970**, *35*, 3888−3897.
[14] [14a] P. K. Baker, H. Silgram, *Trends Organomet. Chem.* **1999**, *3*, 21−33. [14b] A. Efraty, *Chem. Rev.* **1977**, *77*, 691−744. [14c] P. M. Maitlis, *Adv. Organomet. Chem.* **1966**, *4*, 95−143.
[15] [15a] R. Gleiter, *Angew. Chem.* **1992**, *104*, 29−46; *Angew. Chem. Int. Ed. Engl.* **1992**, *31*, 27−44. [15b] R. Gleiter, D. Kratz, *Angew. Chem.* **1990**, *102*, 304−307; *Angew. Chem. Int. Ed. Engl.* **1990**, *29*, 276. [15c] R. S. Dickson, P. J. Fraser, *Adv. Organomet. Chem.* **1974**, *12*, 323−377.
[16] M. R. Cook, P. Härter, P. L. Pauson, J. Šraga, *J. Chem. Soc., Dalton Trans.* **1987**, 2757−2760.
[17] [17a] J. B. Koster, G. J. Timmermans, H. van Bekkum, *Synthesis* **1971**, 139−140. [17b] C. Krüger, P. J. Roberts, Y.-H. Tsay, J. B. Koster, *J. Organomet. Chem.* **1974**, *78*, 69−74.
[18] G. E. Herberich, T. S. Basu Baul, U. Englert, *Eur. J. Inorg. Chem.* **2002**, 43−48.
[19] A. L. Spek, *Acta Crystallogr., Sect. A* **1990**, *46*, C34.
[20] [20a] M. D. Rausch, G. F. Westover, E. Mintz, G. M. Reisner, I. Bernal, A. Clearfield, J. M. Troup, *Inorg. Chem.* **1979**, *18*, 2605−2615. [20b] P. E. Riley, R. E. Davis, *J. Organomet. Chem.* **1976**, *113*, 157−66.

[21] T. A. Albright, J. K. Burdett, M. H. Whangbo, *Orbital Interactions in Chemistry*, John Wiley & Sons, **1985**, p. 386.
[22] A. R. Kudinov, A. A. Fil'chikov, P. V. Petrovskii, M. I. Rybinskaya, *Izv. Akad. Nauk, Ser. Khim.* **1999**, 1364−1367; *Russ. Chem. Bull.* **1999**, *48*, 1352−1355.
[23] CCDC-182899 [(**1**)BF_4] and -182900 (**5**) contain the supplementary crystallographic data for this paper. These data can be obtained free of charge at www.ccdc.cam.ac.uk/conts/retrieving.html or from the Cambridge Crystallographic Data Centre, 12, Union Road, Cambridge CB2 1EZ, UK [Fax: (internat.) + 44-1223/336-033; E-mail: deposit@ccdc.cam.ac.uk].
[24] P. Coppens, L. Leiserowitz, D. Rabinovich, *Acta Crystallogr.* **1965**, *18*, 1035−1038.
[25] G. M. Sheldrick, *SHELXS-97, Program for Structure Solution*, University of Göttingen, Göttingen, Germany, **1997**.
[26] G. M. Sheldrick, *SHELXL-97, Program for Structure Refinement*, University of Göttingen, Göttingen, Germany, **1997**.
[27] F. L. Hirshfeld, *Acta Crystallogr., Sect. A* **1976**, *32*, 239−244.

Received April 11, 2002
[I02188]

Synthesis and Structural Characterization of Trinuclear, Amidate-Bridged Heterobimetallic Complexes $[\{Pt(NH_3)_2(NHCOtBu)_2\}_2M]X_n$ (M = Mn, Fe, Co, Ni, Cu; X = BF_4^-, ClO_4^-; *n* = 2 or 3)

Wanzhi Chen[a] and Kazuko Matsumoto*[a]

Keywords: N ligands / Bridging ligands / Platinum / Manganese / Iron / Cobalt / Nickel / Copper

A family of trinuclear heterometallic complexes of the formula $[\{Pt(NH_3)_2(NHCOtBu)_2\}_2M]X_n$ (M = Mn^{2+}, Fe^{3+}, Co^{2+}, Ni^{2+}, Cu^{2+}; X = BF_4^-, ClO_4^-) have been prepared by reacting $[Pt(NH_3)_2(NHCOtBu)_2]\cdot 2H_2O$ and the corresponding metal ions in water. They were characterised by elemental analysis, and their structures were determined by X-ray crystallography. The crystal structures of all the complexes consist of trinuclear $[\{Pt(NH_3)_2(NHCOtBu)_2\}_2M]^{n+}$ (M = Mn^{2+}, Fe^{3+}, Co^{2+}, Ni^{2+}, Cu^{2+}) cations with M located at the centre. The platinum atoms are linked to the central metal atom through their amidate ligands also by Pt–M interactions. The coordination sphere of the Pt atom is completed by two NH_3 and two amidate ligands in *cis* positions to each other. The central heterometal ions are coordinated by four oxygen atoms of the amidate ligands, adopting either a square-planar or a tetrahedral conformation. Crystal structure determinations of all the complexes revealed extensive systems of N–H···O hydrogen bonds between the coordinated NH_3 ligands and the counteranions.

(© Wiley-VCH Verlag GmbH, 69451 Weinheim, Germany, 2002)

Introduction

Heterometallic cluster complexes containing direct M−M interactions are expected to create a new era of transition metal chemistry, especially in the fields of multimetallic catalysis and functional materials, due to their versatile chemical and physical properties, and thus the chemistry of heterotransition metal complexes has received great attention in recent years.[1] Multimetallic complexes are also promising precursors in developing nanostructured materials, including molecular-scale electronic, optical, and chemical devices.[2] A number of these complexes have been shown to exhibit unique spectroscopic properties that are associated with the metal-metal interactions.[3]

We became interested in $[Pt(NH_3)_2(NHCOtBu)_2]\cdot 2H_2O$[4] because this compound is the core of a number of amidate-bridged dimeric and oligomeric platinum complexes containing metal-metal interactions and mixed oxidation states of the metals.[5] Partially oxidized tetranuclear platinum complexes have been applied to the activation of C−H bonds of ketones to give ketonylplatinum(III) dinuclear complexes, and the coordination of olefins in water to give hydroxyalkylplatinum complexes.[6] It was also found that amidate-bridged Pt^{III} complexes catalyze the oxidation of terminal olefins to ketones in acidic water and promote the dihydroxylation of alkenes in neutral aqueous solutions.[7] We have recently described the preparation and structural characterization of $[Pt(NH_3)_2(NHCOtBu)_2]\cdot 2H_2O$, which acts as a versatile building block for the construction of dinuclear platinum and platinum-palladium complexes.[4] In addition, many transition metal ions of the first row are known to play an important role in oxidation reactions. Therefore, it was of interest to prepare amidate-bridged heterometallic compounds with the transition metal ions of the first row, and to study their redox chemistry and catalysis. As a continuation of our work on the platinum amidate chemistry, we report here the preparation and X-ray structural characterization of heterometallic trinuclear complexes of the formula $[\{Pt(NH_3)_2(NHCOtBu)_2\}_2M]X_n$ (M = Mn^{2+} **1**, Fe^{3+} **2**, Co^{2+} **3**, Ni^{2+} **4**, Cu^{2+} **5** and **6**; X = BF_4^-, ClO_4^-).

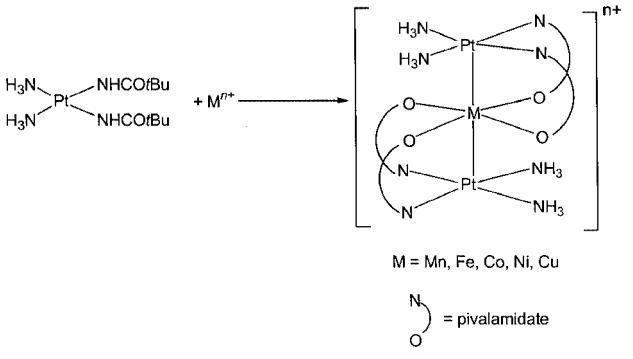

[a] Department of Chemistry, Advanced Research Institute for Science and Engineering,
Waseda University, 3-4-1 Okubo, Shinjuku-ku,
Tokyo 169-8555, Japan
Fax: (internat.) +81-3/5273-3489
E-mail: kmatsu@waseda.jp

Results and Discussion

Synthesis

The square-planar platinum complex $[Pt(NH_3)_2(NHCOtBu)_2]\cdot 2H_2O$, readily prepared by basic hydrolysis of $[Pt(NH_3)_2(NCtBu)_2](ClO_4)_2$, reacts with Mn^{2+}, Fe^{2+}, Co^{2+}, Ni^{2+} or Cu^{2+} salts in water to form trinuclear complexes with the formula $[\{Pt(NH_3)_2(NHCOtBu)_2\}_2M]X_n$, where X is either perchlorate or tetrafluoroborate. Remarkably, regardless of the Pt:M ratio (1:1 or 2:1) the trinuclear Pt_2M complexes were formed exclusively in high yield. Attempts to prepare the platinum-copper dimeric complex with the formula $[Pt(NH_3)_2(NHCOtBu)_2Cu(en)](ClO_4)_2$ by reacting $[Cu(en)_2(H_2O)](SO_4)$ with $[Pt(NH_3)_2(NHCOtBu)_2]\cdot 2H_2O$ in a 1:1 ratio were not successful, and $[\{Pt(NH_3)_2(NHCOtBu)_2\}_2Cu](ClO_4)_2$ was the only isolated complex. However, both dimeric *cis*-$[(NH_3)_2Pt(1\text{-}MeU)_2Cu(H_2O)_2]SO_4\cdot 4.5H_2O$,[8] and trimeric *cis*-$[(NH_3)_2Pt(1\text{-}MeU)_2Cu(1\text{-}MeU)_2Pt(NH_3)_2]^{2+}$ (1-MeU = 1-methyluracilato)[9] have long been known. Reaction of $FeSO_4\cdot 7H_2O$ with $[Pt(NH_3)_2(NHCOtBu)_2]\cdot 2H_2O$ did afford the red $Pt_2^{II}Fe^{III}$ complex rather than $Pt_2^{II}Fe^{II}$, and a gradual colour change in water was observed from light green to red.

Structural Characterisation

Since the NMR spectroscopic data of the paramagnetic complexes were not particularly informative, suitable single crystals were grown by slow evaporation and cooling of an H_2O/acetone solution. All of the complexes were characterised by X-ray diffraction analysis.

The crystal structures of all of the complexes consist of trinuclear $[\{Pt(NH_3)_2(NHCOtBu)_2\}_2M]^{n+}$ (M = Mn^{2+}, Fe^{3+}, Co^{2+}, Ni^{2+}, Cu^{2+}) cations with M located at the centre. Within the cations each platinum atom is linked to the central heterometal atom through two amidate ligands and a Pt−M interaction. The coordination sphere of the Pt atom is completed by two NH_3 and two amidate ligands in *cis* positions to each other. The central metal atoms are coordinated by four oxygen atoms of the amidate ligands. Two pairs of pivalamidate ligands are arranged head-to-head. The head-to-head orientation of the amidate ligands in these complexes is not straightforward from X-ray crystallographic arguments, but is reasonable on the basis of the method of preparation and the properties of the central metal ions. The Pt−N bond lengths and N−Pt−N angles are normal and similar to the values found in the starting compound $[Pt(NH_3)_2(NHCOtBu)_2]\cdot 2H_2O$. These data as well as the M−O distances and O−M−O angles are listed in Table 1 and 2. The Pt−M−Pt axes in **1b, 4−7** are roughly perpendicular to both of the coordination planes of Pt and M. In complex **1b**, **4−7**, the Pt−M−Pt axes are virtually linear with a Pt−M−Pt angle of 180°, whereas in **1a** and **3**, the Pt−M−Pt axes are bent with a Pt−M−Pt angle of 114.13(7)° and 176.39(8)° for **1a** and **3**, respectively. The structures of the complexes with the linearly ordered Pt−M−Pt cores are essentially the same.

Crystal Structures of $[\{Pt(NH_3)_2(NHCOtBu)_2\}_2Mn](ClO_4)_2\cdot 4H_2O$ (1)

Crystallographic analysis of the manganese complex revealed that the asymmetric unit comprises of one molecule of **1a** and half of a molecule of **1b**. The structure of **1b** is generated by the inversion centre (1/2, 0, 1/2) at Mn(2). The structure of the cations of **1a** and **1b** are illustrated in Figure 1a and 1b. It is interesting to note that in **1a** the central Mn atom adopts a tetrahedral geometry, which is completed by the four amidate oxygen atoms, or a bicapped tetrahedron when the two rather long Pt−Mn contacts are considered. In **1b**, however, the Mn ion adopts a square-planar geometry, or it may be viewed as octahedrally coordinated with the platinum atoms sitting above and below the coordination plane. The distance between the Pt and Mn

Table 1. Selected bond lengths (Å) for complexes **1−6**

Compound	Pt−N_{amine}	Pt−N_{amide}	M−O	C−N	C−O	Pt−M
1a	2.006(16)	2.031(12)	2.044(8)	1.327(16)	1.246(14	2.8807(18)
	2.028(11)	1.996(10)	2.084(9)	1.293(15)	1.298(14)	2.9995(18)
	2.049(13)	1.995(12)	2.088(10)	1.312(18)	1.268(14)	
	2.042(11)	1.989(10)	2.089(9)	1.315(16)	1.310(13)	
1b	2.026(13)	2.019(11)	2.074(10)	1.275(16)	1.246(16)	2.6644(5)
	2.071(12)	2.007(10)	2.110(9)	1.293(15)	1.305(15)	
2	2.066(10)	1.999(9)	1.950(8)	1.294(15)	1.314(14)	2.5566(15)
	2.079(9)	2.018(11)	1.983(8)	1.266(17)	1.283(15	2.5718(15)
	2.058(9)	1.993(10)	2.003(8)	1.333(16)	1.293(15)	
	2.046(10)	2.010(9)	2.025(8)	1.301(16)	1.318(15)	
3	2.046(6)	1.991(6)	2.023(4)	1.258(10)	1.295(8)	2.6197(4)
	2.055(6)	1.991(6)	2.054(4)	1.318(8)	1.241(7)	
4	2.064(9)	2.036(9)	2.005(7)	1.321(13)	1.263(13)	2.5870(4)
	2.051(9)	2.000(9)	2.008(7)	1.286(12)	1.279(11)	
5	2.058(5)	1.995(5)	1.949(4)	1.314(7)	1.263(7)	2.6795(3)
	2.053(5)	1.985(5)	1.964(4)	1.315(7)	1.267(6)	
6	2.047(6)	2.017(5)	1.958(4)	1.283(8)	1.271(8)	2.6957(3)
	2.059(5)	2.011(5)	1.960(4)	1.308(7)	1.273(7)	

Table 2. Selected bond angles (°) for complexes **1**−**6**

Angles	**1a**	**1b**	**2**	**3**	**4**	**5**	**6**
N−Pt−N	86.0(6)	92.7(5)	90.5(5)	91.8(2)	91.5(4)	90.2(2)	91.4(2)
	93.6(6)	93.8(5)	88.1(4)	92.6(2)	87.8(4)	88.4(2)	87.1(2)
	95.0(4)	86.7(5)	86.4(4)	87.4(2)	88.5(4	92.8(2)	88.4(2)
	85.5(5)	86.8(5)	94.9(4)	88.0(2)	92.2(4)	88.4(2)	93.0(2)
	89.4(5)		90.3(4)				
	89.6(5)		87.9(4)				
	89.2(5)		92.6(4)				
	91.9(6)		89.2(4)				
O−M−O	145.4(4)	89.0(5)	96.6(4)	89.7(2)	89.0(3)	90.84(18)	89.12(19)
	89.6(4)	91.0(5)	89.6(3)	90.3(2)	91.0(3)	89.16(18)	90.88(19)
	101.6(4)		86.8(4)				
	99.2(4)		87.3(4)				
	101.3(4)						
	106.1(4)						
Pt−M−Pt	114.12(6)	180.000(10)	176.40(8)	180.0	180.0	180.0	180.0

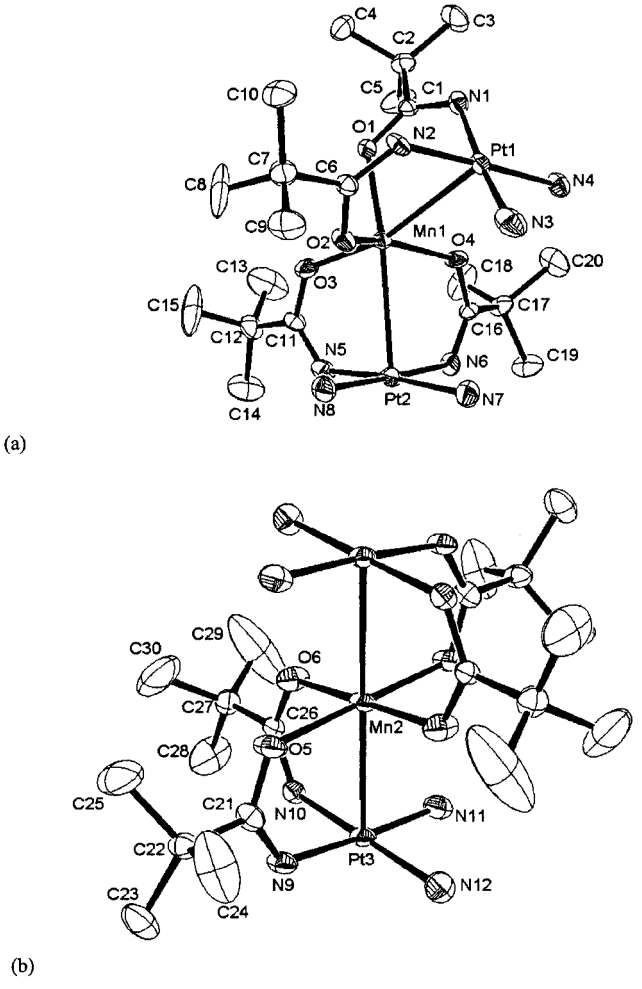

Figure 1. (a) ORTEP view of the bent $[\{Pt(NH_3)_2(NHCOtBu)_2\}_2Mn]^{2+}$ cation in complex **1a**, showing the numbering of the atoms; (b) ORTEP view of the linear $[\{Pt(NH_3)_2(NHCOtBu)_2\}_2Mn]^{2+}$ cation in complex **1b**, showing the numbering of the atoms; thermal ellipsoids are drawn at the 30% probability level

atoms within the cation of **1b** [2.6644(5)] is much shorter than those in the cation of **1a** [2.8807(18) Å and 2.9995(18) Å]. The Pt−Mn distance in **1b** is also shorter than that in $[(NH_3)_2Pt(1\text{-}MeT)_2Mn(1\text{-}MeT)_2Pt(NH_3)_2]^{2+}$ (1-Met = 1-methylthymine) [2.704(1) Å],[10] which has a similar Mn^{II} coordination environment, and it is even shorter than that in $[(dppe)(CH_3)PtMn(CO_5)]$ (2.795 Å),[2a] in which the Pt−Mn bond is thought to be typical of a covalent single bond. The shorter Pt−Mn distance in **1b** is probably a consequence of the square-planar coordination of the Mn^{II} atoms which enables a closer approach to the square-planar Pt atoms than the Mn^{II} ion in the tetrahedral arrangement in **1a**. The Mn−O distances in both **1a** and **1b** fall in the range of 2.044(8)−2.110(9) Å, and are consistent with those found for octahedral complexes with oxygen atoms coordinated to Mn^{II} ions. The Pt−Mn−Pt axis in **1b**, which is linear by space group symmetry, is approximately perpendicular to both of the coordination planes of Pt and Mn. These coordination planes are tilted towards each other by an angle of 17.34°.

Crystals containing both **1a** and **1b** have four lattice water molecules in the unit cell. All of the water molecules and perchlorate ions participate in short contacts with the coordinated NH_3. The N−H···O contacts fall in the range of 3.011(15)−3.49(3) Å, suggesting hydrogen bonding. These hydrogen bonds link the cations, counteranions and the lattice water molecules into a two-dimensional network structure. Selected hydrogen bonds are listed in Table 3.

Crystal Structure of $[\{Pt(NH_3)_2(NHCOtBu)_2\}_2Fe](ClO_4)_3$ (2)

The crystal structure of **2** is shown in Figure 2. The Pt_2Fe complex crystallises in a chiral orthorhombic space group $P2_12_12_1$. The platinum(II) and iron(III) atoms are held together through the four bridging pivalamidate ligands. The Pt−Fe−Pt is slightly bent with an angle of 176.40(8)°, but still close to a linear arrangement. The Pt−Fe distances are rather short [2.5566(15) Å and 2.5718(15) Å], and are similar to the values [2.5062(9)−2.673(4) Å] in the dppm-bridged Pt−Fe complexes.[11,12] The short Pt−Fe distances are attributed to the smaller Fe^{III} radius and the geometry requirement of the pivalamidate ligands. The coordination sphere of the Fe^{III} ion is completed by the four equatorial

Table 3. Selected hydrogen bonds (Å and °) for complexes **1**−**5**

D−H···A[a]	*d*(D−H)	*d*(H···A)	*d*(D···A)	<(DHA)
1				
N(3)−H(3D)···O(18)#2	0.89	2.29	3.13(3)	158.4
N(3)−H(3F)···O(22)#2	0.89	2.28	3.02(3)	140.6
N(4)−H(4E)···O(19)#3	0.89	2.25	3.111(18)	161.8
N(4)−H(4F)···O(4)	0.89	2.38	3.113(15)	139.9
N(7)−H(7A)···O(23)	0.89	2.28	3.14(3)	163.3
N(7)−H(7B)···O(22)#2	0.89	2.21	3.03(3)	153.0
N(7)−H(7C)···O(13)	0.89	2.26	3.04(2)	146.8
N(8)−H(8D)···O(2)	0.89	2.25	3.017(15)	144.1
N(8)−H(8E)···O(21)#4	0.89	2.22	3.10(3)	171.3
N(11)−H(11B)···O(17)#1	0.89	2.40	3.19(2)	147.7
N(11)−H(11C)···O(5)#1	0.89	2.21	3.011(15)	150.2
N(12)−H(12A)···O(6)#1	0.89	2.32	3.069(17)	142.4
N(12)−H(12B)···O(16)#1	0.89	2.27	3.04(2)	144.6
N(12)−H(12C)···O(11)	0.89	2.31	3.09(3)	146.3
2				
N(8)−H(8C)···O(2)	0.89	2.37	3.108(15)	141.0
N(8)−H(8B)···O(6)#5	0.89	2.19	3.074(16)	173.5
N(7)−H(7C)···O(7)#5	0.89	2.32	3.167(17)	157.8
N(7)−H(7B)···O(1)	0.89	2.17	2.906(12)	139.5
N(7)−H(7A)···O(9)#5	0.89	2.43	3.038(19)	126.3
N(4)−H(4B)···O(12)	0.89	2.37	3.046(15)	133.1
N(3)−H(3C)···O(3)	0.89	2.33	3.074(14)	141.0
N(3)−H(3B)···O(10)	0.89	2.40	3.031(17)	127.7
N(3)−H(3B)···O(12)	0.89	2.37	3.244(16)	166.6
3				
N(3)−H(3A)···O(1)#7	0.89	2.11	2.895(8)	146.9
N(3)−H(3B)···O(9)#8	0.89	2.30	3.157(10)	161.3
N(3)−H(3C)···O(5)#9	0.89	2.20	3.087(10)	175.3
N(4)−H(4A)···O(7)#8	0.89	2.31	3.158(15)	158.3
N(4)−H(4B)···O(9)#8	0.89	2.15	3.007(8)	160.7
N(4)−H(4C)···O(2)#7	0.89	2.16	2.937(7)	145.3
4				
N(3)−H(3D)···O(20)	0.89	2.25	3.120(15)	164.4
N(3)−H(3F)···O(1)	0.89	2.18	2.906(12)	139.0
N(4)−H(4D)···O(2)#10	0.89	2.13	2.899(12)	144.7
N(4)−H(4E)···O(15)#14	0.89	2.36	3.24(2)	169.0
N(4)−H(4F)···O(22)#15	0.89	2.29	3.16(2)	163.0
N(7)−H(7C)···O(3)#12	0.89	2.15	2.888(13)	140.3
N(8)−H(8D)···O(4)#12	0.89	2.20	2.923(12)	138.7
N(8)−H(8E)···O(11)	0.89	2.47	3.127(17)	131.4
N(11)−H(11A)···O(9)#16	0.89	2.29	3.178(15)	172.9
N(11)−H(11B)···O(14)#17	0.89	2.15	2.983(16)	154.5
N(11)−H(11C)···O(5)#11	0.89	2.09	2.865(12)	145.2
N(12)−H(12A)···O(6)	0.89	2.10	2.871(11)	145.0
N(12)−H(12C)···O(23)#12	0.89	2.43	3.32(2)	172.3
N(15)−H(15F)···O(7)#13	0.89	2.18	2.910(11)	139.0
N(16)−H(16A)···O(8)#13	0.89	2.13	2.906(10)	144.6
N(16)−H(16C)···O(20)#14	0.89	2.28	3.163(15)	169.6
5				
N(3)−H(3A)···O(1)#19	0.89	2.31	3.044(6)	139.3
N(3)−H(3B)···O(4)	0.89	2.31	3.181(10)	164.8
N(3)−H(3C)···O(5)#20	0.89	2.28	3.166(8)	172.5
N(4)−H(4A)···O(2)	0.89	2.22	2.983(6)	143.2
N(4)−H(4B)···O(6)#21	0.89	2.37	3.221(8)	161.1
N(4)−H(4C)···O(3)	0.89	2.39	3.143(9)	142.4

[a] Symmetry transformations used to generate equivalent atoms: #1: $-x+1, -y, -z+1$; #2: $x-1, y, z-1$; #3: $x-1, y, z$; #4: $x, y, z-1$; #5: $x+1, y, z$; #6: $-x+2, y+1/2, -z+3/2$; #7: $-x+2, -y+1, -z$; #8: $x+1, y, z$; #9: $-x+3/2, y+1/2, -z+1/2$; #10: $-x+1, -y+2, -z$; #11: $-x+2, -y+1, -z$; #12: $-x+1, -y+1, -z+1$; #13: $-x+2, -y+2, -z+1$; #14: $-x+1, -y+2, -z+1$; #15: $x, y+1, z-1$; #16: $x+1, y, z-1$; #17: $x, y, z-1$; #18: $x+1, y+1, z$; #19: $-x+1, -y, -z+1$; #20: $-x+2, -y, -z+1$; #21: $x-1/2, -y+1/2, -z+1$.

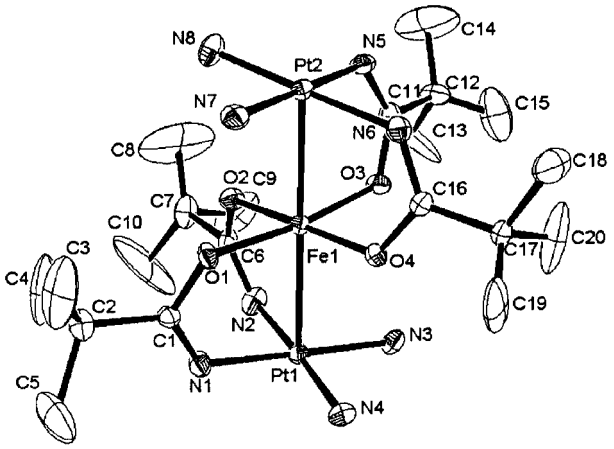

Figure 2. ORTEP view of the $[\{Pt(NH_3)_2(NHCOtBu)_2\}_2Fe]^{3+}$ cation in complex **2**, showing the numbering of the atoms; thermal ellipsoids are drawn at the 30% probability level

oxygen atoms of the amidate ligands and the two platinum atoms sitting above and below the FeO_4 coordination plane, if the two Pt−Fe interactions are taken into account. The Pt−N and Fe−O bond lengths are normal and not very different from those observed in **1**. The whole molecules are also organized in the two-dimensional structure involving hydrogen bonds both of intercationic and between cations and perchlorate anions. Some hydrogen bonds are collected in Table 3.

Crystal Structure of $[\{Pt(NH_3)_2(NHCOtBu)_2\}_2Co](ClO_4)_2$ (3)

Crystal data and selected bond lengths and angles are presented in Table 1 and 2. The structure of **3** consists of a centrosymmetric trinuclear Pt−Co−Pt core and two perchlorate counteranions (Figure 3). The Pt−Co bond length [2.6197(4) Å] within the cation is longer than those found in the Pt−Co clusters $[PtCo_2(CO)_7(cod)]$ [2.515(1) Å and 2.514(1) Å] and $[Pt_2Co_2(CO)_8(\mu_3\text{-}EtC_2Et)]$ [2.551(1) Å and 2.556(1) Å],[13] and is also longer than in the $(Ph_2P)_2NH$-

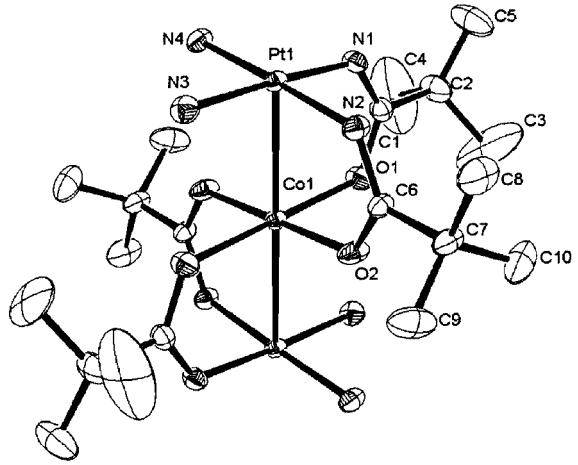

Figure 3. ORTEP view of the $[\{Pt(NH_3)_2(NHCOtBu)_2\}_2Co]^{2+}$ cation in complex **3**, showing the numbering of the atoms; thermal ellipsoids are drawn at the 30% probability level

bridged Pt−Co carbonyl complexes [2.531(2)−2.508(2) Å].[14] The cation and the counteranions are linked by hydrogen bonds between the coordinated NH_3 and the perchlorate oxygens. Intermolecular hydrogen bonds between the NH_3 and amidate oxygen atoms are also observed, and thus form two-dimensional networks.

Crystal Structure of $[\{Pt(NH_3)_2(NHCOtBu)_2\}_2Ni](ClO_4)_2$ (4)

The asymmetric unit of the Pt_2Ni complex comprises four half units of a molecule of the complex, and their structures are generated by the inversion centre (1/2, 1, 0; 1/2, 1/2, 1/2; 1, 1/2, 0; 1, 1, 1/2) at Ni(1), Ni(2), Ni(3) and Ni(4), respectively. The four molecules are essentially the same, and one of the structures of the four cations is shown in Figure 4. The Pt−Ni−Pt angles in all of the four independent molecules are 180°. The platinum and nickel centres are bridged by triatomic NCO groups of the amidate ligands. Each nickel ion is coordinated to four oxygen and two platinum atoms at the axial sites. The *cis* O−N−O angles lie within the range 89.0(3)°−91.3(3)°. The *trans* O−Ni−O angles are both 180°. The Ni−O bond lengths [2.005(7) Å and 2.008(7) Å] are almost identical. The Pt−Ni distance within the cation is 2.5870(4) Å. The hydrogen atoms of the coordinated NH_3 ligands are engaged in hydrogen bonding interactions with the oxygen atoms of the perchlorate anions, resulting in the formation of a three-dimensional network.

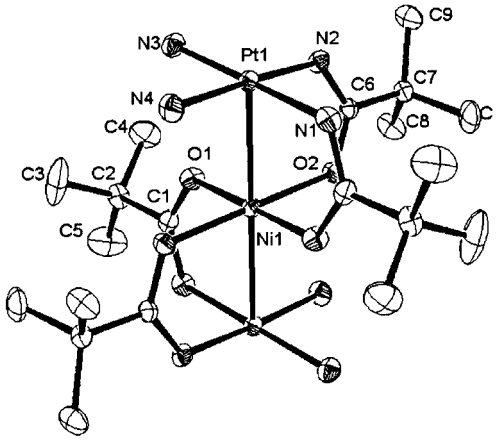

Figure 4. ORTEP view of the $[\{Pt(NH_3)_2(NHCOtBu)_2\}_2Ni]^{2+}$ cation in complex **4**, showing the numbering of the atoms; thermal ellipsoids are plotted at the 30% probability level

Crystal Structure of $[\{Pt(NH_3)_2(NHCOtBu)_2\}_2Cu](ClO_4)_2$ (5) and $[\{Pt(NH_3)_2(NHCOBu)_2\}_2Cu](BF_4)_2$ (6)

Although the two complexes crystallise in different space groups, their structures are essentially the same. A molecular view of **5** is shown in Figure 5. Within the trimers, the Cu atoms are located at the special position (1/2, 0, 1/2) for both **5** and **6**. The Pt−Cu distances are 2.6795(3) Å and 2.6955(2) Å in **5** and **6,** respectively, and are therefore shorter than that in the Pt/Cu dimer, *cis*-$[(NH_3)_2Pt(1\text{-}MeU)_2Cu(H_2O)_2]^{2+}$,[9] and the Pt_2Cu trimer, *cis*-$[(NH_3)_2Pt(1\text{-}MeU)_2Cu(1\text{-}MeU)_2Pt(NH_3)_2]^{2+}$ (1-MeU = 1-methyluracilato),[10] and much shorter than those in the platinum-copper complexes bridged by alkynyl ligands.[15]

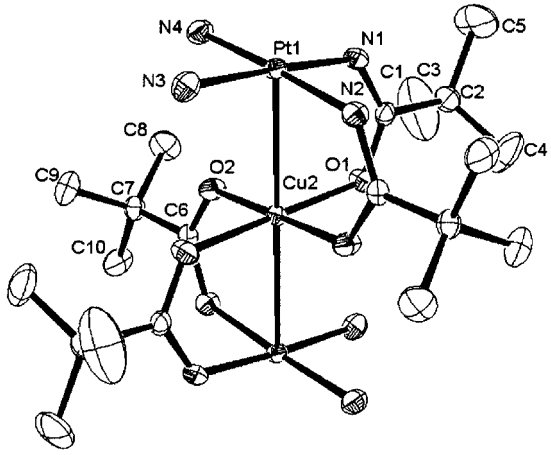

Figure 5. ORTEP view of the $[\{Pt(NH_3)_2(NHCOtBu)_2\}_2Cu]^{2+}$ cation in complex **5**, showing the numbering of the atoms; thermal ellipsoids are plotted at the 30% probability level

Similar to the complexes described above, the trinuclear cations and counteranions in **5** and **6** are connected by N−H···O and N−H···F hydrogen bonding, with N···O distances in the range from 2.983(6) Å to 3.221(8) Å, and the N−H···F distances from 2.961(9) to 3.092(13) Å. Short N−H···F and N−H···O contacts are presented in Table 3. The short contacts indicate strong hydrogen bonds between the hydrogen atoms of the NH_3 ligands and the fluorine or oxygen atoms of the anions. These interactions make two- and three-dimensional hydrogen bond networks for **5** and **6,** respectively.

All of the complexes presented here have provided unequivocal evidence for the formation of Pt−M (2:1) amidate-bridged complexes. X-ray diffraction analysis showed that the Pt atoms have an essentially planar conformation, and the central metal ions are similarly coordinated by four equatorial oxygen atoms with two platinum atoms occupying the two axial sites in **1b**, and **2**−**7**. The metal-metal distances in these complexes with linear Pt−M−Pt conformation are found to follow the order: Pt−Cu > Pt−Mn > Pt−Co > Pt−Ni > Pt−Fe. The metal-metal distances between the platinum and Mn^{II} (d^5), Fe^{III} (d^5), Co^{II} (d^7), Ni^{II} (d^8) and Cu^{II} (d^9) are rather short in complexes **2**−**7**. It was thought that these short intermetallic distances within the cations do not reflect a significant electronic interaction between the Pt and heterometals, and they are rather attributed to the geometric requirement caused by the two bridging ligands.[9] Most probably this also applies to our complexes. However, a weak metal-metal interaction should probably not be ruled out, on the basis of the Pt and the heterometal radii. The redox chemistry of these cationic trinuclear heterometallic complexes is currently being explored.

Experimental Section

General Remarks: $[Pt(NH_3)_2(NHCOtBu)_2{\cdot}2H_2O]$ was prepared according to our published procedure.[4] All other chemicals and solvents were purchased and used as received.

Table 4. Crystal data and structure refinement for the complexes **1**−**6**

	1	**2**	**3**	**4**	**5**	**6**
Empirical formula	$C_{20}H_{56}Cl_2MnN_8O_{14}Pt_2$	$C_{20}H_{52}Cl_3FeN_8O_{16}Pt_2$	$C_{20}H_{52}Cl_2CoN_8O_{12}Pt_2$	$C_{20}H_{52}Cl_2N_8NiO_{12}Pt_2$	$C_{20}H_{52}Cl_2CuN_8O_2Pt_2$	$C_{20}H_{52}B_2CuF_8N_8O_4Pt_2$
Molecular weight	1148.70	1213.08	1116.71	1116.49	1121.32	1096.04
Crystal size	0.28 × 0.38 × 0.44	0.20 × 0.22 × 0.43	0.15 × 0.22 × 0.26	0.21 × 0.30 × 0.32	0.12 × 0.18 × 0.26	0.14 × 0.17 × 0.27
Crystal system	monoclinic	orthorhombic	monoclinic	triclinic	orthorhombic	monoclinic
Space group	$P2_1/n$	$P2_12_12_1$	$P2_1/n$	$P\bar{1}$	*P*bca	$P2_1/n$
a, Å	11.4228(17)	10.8505(15)	13.451(2)	15.4742(10)	10.7665(17)	10.5401(7)
b, Å	34.480(5)	18.607(3)	11.0189(19)	15.5319(11)	18.178(3)	16.1012(11)
c, Å	16.128(3)	22.350(3)	16.056(3)	17.0866(12)	19.570(3)	12.1744(8)
α, deg	90	90	90	87.5750(10)	90	90
β, deg	91.481(3)	90	97.477(3)	83.976(2)	90	110.3520(10)
γ, deg	90	90	90	86.810(2)	90	90
V, Å^3	6350.1(17)	4512.5(11)	2359.6(7)	4074.9(5)	3830.3(11)	1937.1(2)
Z	6	4	2	4	4	2
$D_{calcd.}$ Mg/m^3	1.817	1.786	1.572	1.820	1.944	1.879
θ range	1.39−27.56	1.42−27.67	1.86−27.60	1.31−27.56	2.08−27.52	2.19−27.54
Reflections collected	38339	28144	14336	15008	16631	12043
Independent reflections (R_{int})	14358 (0.1407)	10323 (0.0728)	5355 (0.1025)	13829 (0.0355)	4386 (0.0904)	4416 (0.0313)
Goodness-of-fit	1.030	1.035	1.098	0.965	0.915	1.023
*R*1, *wR*2 [$I > 2\sigma(I)$]	0.0769, 0.1969	0.0501, 0.1485	0.0434, 0.1171	0.0463, 0.1201	0.0355, 0.0741	0.0327, 0.0937
*R*1, *wR*2 (all data)	0.1156, 0.2172	0.0600, 0.1553	0.0512, 0.1222	0.0732, 0.1318	0.0620, 0.0828	0.0454, 0.0988

Preparation of [{Pt(NH$_3$)$_2$(NHCO*t*Bu)$_2$}$_2$Mn](ClO$_4$)$_2$·4H$_2$O (1): A solution of $MnCl_2·4H_2O$ (20 mg, 0.10 mmol) in 2 mL of water was added to a solution of [Pt(NH$_3$)$_2$(NHCO*t*Bu)$_2$]·2H$_2$O (93 mg, 0.20 mmol) in 1 mL of water. A pale-yellow precipitate was formed immediately by the addition of $NaClO_4$ (50 mg) to the pale-yellow solution. Yield: 95 mg (83%). $C_{20}H_{52}Cl_2N_8MnO_{12}Pt_2·4H_2O$ (1148.70): calcd. C 20.28, H 5.10, N 9.46; found C 20.42, H 5.03, N 9.46.

Preparation of [{Pt(NH$_3$)$_2$(NHCO*t*Bu)$_2$}$_2$Fe](ClO$_4$)$_3$ (2): This compound was prepared from $FeSO_4·7H_2O$ (27.8 mg, 0.10 mmol), [Pt(NH$_3$)$_2$(NHCO*t*Bu)$_2$·2H$_2$O], and $NaClO_4$ (50 mg) as for **1**, and was isolated as red crystals. Yield: 98 mg (81%). $C_{20}H_{52}Cl_3FeN_8O_{16}Pt_2$ (1213.08): calcd. C 19.80, H 4.32, N 9.24; found C 19.90, H 4.15, N 9.26.

Preparation of [{Pt(NH$_3$)$_2$(NHCO*t*Bu)$_2$}$_2$Co](ClO$_4$)$_2$ (3): This compound was prepared from $Co(NO_3)_2·6H_2O$, [Pt(NH$_3$)$_2$(NHCO*t*Bu)$_2$·2H$_2$O] and $NaClO_4$ (50 mg) as for **1**, and was isolated as blue crystals. Yield: 102 mg (91%). $C_{20}H_{52}Cl_2CoN_8O_{12}Pt_2$ (1116.71): calcd. C 21.51, H 4.69, N 10.03; found C 21.36, H 4.55, N 9.78.

Preparation of [{Pt(NH$_3$)$_2$(NHCO*t*Bu)$_2$}$_2$Ni](ClO$_4$)$_2$ (4): This compound was prepared from $Ni(NO_3)_2·6H_2O$ (18.2 mg, 0.1 mmol), [Pt(NH$_3$)$_2$(NHCOBu)$_2$]·2H$_2$O (46 mg, 0.1 mmol), and $NaClO_4$ (50 mg) as for **1**, and was isolated as light-green crystals. Yield: 80 mg, (72%). $C_{20}H_{52}Cl_2N_8NiO_{12}Pt_2$ (1116.49) C, 21.52, H 4.69, N 10.04; found C 21.75, H 4.88, N 9.70.

Preparation of [{Pt(NH$_3$)$_2$(NHCO*t*Bu)$_2$}$_2$Cu](ClO$_4$)$_2$ (5): This compound was prepared from [Cu(en)(H$_2$O)](SO$_4$) (25 mg, 0.1 mmol), [Pt(NH$_3$)$_2$(NHCO*t*Bu)$_2$·2H$_2$O] (46 mg, 0.1 mmol), and $NaClO_4$ (50 mg) as for **1**. The compound can also be prepared directly from $Cu(ClO_4)_2·2H_2O$. Yield: 82 mg, (73%). $C_{20}H_{52}Cl_2CuN_8O_{12}Pt_2$ (1121.32): calcd. C 21.42, H 4.67, N 9.99; found C 21.46, H 4.43, N 9.82.

Preparation of [{Pt(NH$_3$)$_2$(NHCO*t*Bu)$_2$}$_2$Cu](BF$_4$)$_2$ (6): This compound was prepared from $Cu(BF_4)_2·6H_2O$ (23.7 mg, 0.10 mmol) and [Pt(NH$_3$)$_2$(NHCO*t*Bu)$_2$·2H$_2$O] (93 mg, 0.2 mmol) as for **1** and isolated as light green crystals. Yield: 84 mg (77%). $C_{20}H_{52}B_2CuF_8N_8O_4Pt_2$ (1096.04): calcd. C 21.92, H 4.78, N 10.22; found C 21.89, H 4.79, N 10.21.

X-ray Crystallographic Study: Data collection was performed on a Bruker Smart-CCD diffractometer by using monochromatized Mo-K_α radiation (λ = 0.71073 Å) at room temperature. Data reduction was performed by using the SAINT+ Version 6.02 software.[16] The data were corrected for absorption by using the program SADBAS within the SAINTPLUS package. The structures were solved by direct methods. This solution yielded metal atoms, N O, and some C atoms. Subsequent Fourier synthesis gave the remaining C-atom positions. The hydrogen atoms, except those of the amidate and water hydrogen atoms, were geometrically fixed, allowed to ride on their attached atoms, and refined with the XSHELL software.[17] The final refinement included anisotropic thermal parameters for all of the non-hydrogen atoms and converged to the *R*1 and *wR*2 values listed in Table 4.

CCDC-183354 (**1**), -183355 (**2**), -183356 (**3**), -183357 (**4**), -183358 (**5**) and CCDC-183359 (**6**) contain the supplementary crystallographic data for this paper. These data can be obtained free of charge at www.ccdc.cam.ac.uk/conts/retrieving.html [or from the Cambridge Crystallographic Data Centre, 12, Union Road, Cambridge CB2 1EZ, UK; Fax: (internat.) +44-1223/336-033; E-mail: deposit@ccdc.cam.ac.uk].

[1] [1a] M. A. Bennett, M. Contel, D. C. R. Hockless, L. L. Welling, A. C. Willis, *Inorg. Chem.* **2002**, *41*, 844−855. [1b] T. Kawashima, K. Takai, H. Aso, T. Manabe, K. Takizawa, C. Kachi-Terajima, T. Ishii, H. Miyasaka, H. Matsuzaka, M. Yamashita, H. Okamoto, H. Kitagawa, M. Shiro, K. Toriumi, *Inorg. Chem.* **2001**, *40*, 6651−6655. [1c] L. Hao, J. Xiao, J. J. Vittal, R. J. Puddephatt, *Organometallics* **1997**, *16*, 2165−2174.

[2] [2a] V. W. W. Yam, K. L. Yu, K. M. C. Wong, K. K. Cheung, *Organometallics* **2001**, *20*, 721−726. [2b] S. Komiya, S. Muroi, M. Furuya, M. Hirano, *J. Am. Chem. Soc.* **2000**, *122*, 170−171.

[3] [3a] A. F. Heyduk, D. J. Krodel, E. E. Meyer, D. G. Nocera, *Inorg. Chem.* **2002**, *41*, 634−636. [3b] E. J. Fernández, P. G.

Jones, A. Laguna, J. M. López-de-Luzuriaga, M. Monge, J. Pérez, M. E. Olmos, *Inorg. Chem.* **2002**, *41*, 1056−1063. [3c] J. R. Berenguer, J. Forniés, J. Gómez, E. Lalinde, M. T. Moreno, *Organometallics* **2001**, *20*, 4847−4851. [3d] J. Forniés, J. Gómez, E. Lalinde, M. T. Moreno, *Inorg. Chem.* **2001**, *40*, 5415−5419.

[4] K. Matsumoto, K. Sakai, *Adv. Inorg. Chem.* **1999**, *49*, 375−427 and references therein.

[5] W. Chen, K. Matsumoto, *Inorg. Chim. Acta* in press.

[6] [6a] Y. Lin, H. Misawa, J. Yamada, K. Matsumoto, *J. Am. Chem. Soc.* **2001**, *123*, 569−575. [6b] K. Matsumoto, J. Matsunami, K. Mizuno, H. Uenura, *J. Am. Chem. Soc.* **1996**, *118*, 8959−8960.

[7] [7a] Y. Lin, S. Takeda, K. Matsumoto, *Organometallics* **1999**, *18*, 4897−4899. [7b] W. Chen, J. Yamada, K. Matsumoto, *Synth. Commun.* **2002**, *32*, 17−22. [7c] K. Matsumoto, Y. Nagai, J. Matsunami, K. Mizuno, T. Abe, R. Somazawa, J. Kinoshita, H. Shimura, *J. Am. Chem. Soc.* **1998**, *120*, 2900−2907.

[8] D. Neugebauer, B. Lippert, *J. Am. Chem. Soc.* **1982**, *104*, 6596−6601.

[9] B. Lippert, U. Thewalt, H. Schlhorn, D. M. L. Goodgame, R. W. Rollins, *Inorg. Chem.* **1984**, *23*, 2807−2813.

[10] B. Lippert, U. Schubert, *Inorg. Chim. Acta* **1981**, *56*, 15−20.

[11] [11a] X. L. R. Fontaine, G. B. Jacobsen, B. L. Shaw, M. Thornton-Pett, *J. Chem. Soc., Dalton Trans.* **1988**, 741−750. [11b] X. L. R. Fontaine, G. B. Jacobsen, B. L. Shaw, M. Thornton-Pett, *J. Chem. Soc., Dalton Trans.* **1988**, 1185−1196.

[12] [12a] M. Knorr, P. B. Braunstein, A. DeCian, J. Fischer, *Organometallics* **1995**, *14*, 1302−1309. [12b] R. D. Adams, I. Arafa, G. Chen, J. C. Li, J. G. Wang, *Organometallics* **1990**, *9*, 2350−2357.

[13] R. D. Adams, G. Chen, W. G. Wu, J. G. Yin, *Inorg. Chem.* **1990**, *29*, 4208−4214.

[14] [14a] I. Bachert, I. Bartusseck, P. Braunstein, E. Guillon, J. Rose, G. Kickelbick, *J. Organomet. Chem.* **1999**, *588*, 144−151. [14b] I. Bachert, I. Bartusseck, P. Braunstein, E. Guillon, J. Rose, G. Kickelbick, *J. Organom. Chem.* **1999**, *580*, 257−264.

[15] [15a] V. W. W. Yam, K. L. Yu, K. K. Cheung, *J. Chem. Soc., Dalton Trans.* **1999**, 2913−2916. [15b] J. P. H. Charmant, J. Forniés, J. Gomez, E. Lalinde, R. I. Merino, M. T. Moreno, A. C. Orpen, *Organometallics* **1999**, *18*, 3353−3358. [15c] J. Forniés, E. Lalinde, A. Martin, M. T. Moreno, *J. Organomet. Chem.* **1995**, *490*, 179−188. [15d] P. Espinet, J. Forniés, F. Martinez, M. Tomas, E. Lalinde, M. T. Moreno, A. Ruiz, A. J. Welch, *J. Chem. Soc., Dalton Trans.* **1990**, 791−798.

[16] G. M. Sheldrick, *SHELXS-97, Program for X-ray Crystal Structure Solution*; University of Göttingen: Götingen, Germany, **1997**.

[17] G. M. Sheldrick, *SHELXL-97, Program for X-ray Crystal Structure Refinement*; University of Götingen: Götingen, Germany, **1997**.

Received February 21, 2002
[I02197]

Dioxygenation of Sterically Hindered (Ethene)Rh^{I} and -Ir^{I} Complexes to (Peroxo)Rh^{III} and (Ethene)(peroxo)Ir^{III} Complexes

Bas de Bruin,*[a] Theo P. J. Peters,[a] Jos B. M. Wilting,[a] Simone Thewissen,[a] Jan M. M. Smits,[a] and Anton W. Gal*[a]

Keywords: Alkene ligands / Iridium / O−O activation / Oxidations / Peroxo ligands

New cationic, five-coordinate bis(ethene)iridium(I) complexes [(κ^3-Me_3-tpa)Ir^{I}(ethene)$_2$]$^+$ (**12**$^+$) and [(κ^3-Me_2-dpa-Me)Ir^{I}(ethene)$_2$]$^+$ (**13**$^+$) have been prepared {Me_3-tpa = *N*,*N*,*N*-tris[(6-methyl-2-pyridyl)methyl]amine, Me_2-dpa-Me = *N*-methyl-*N*,*N*-bis[(6-methyl-2-pyridyl)methyl]amine}. Complexes **12**$^+$ and **13**$^+$ lose one ethene fragment in solution, yielding the five-coordinate mono(ethene) complex [(κ^4-Me_3-tpa)Ir^{I}(ethene)]$^+$ (**14**$^+$) and the four-coordinate mono-(ethene) complex [(κ^3-Me_2-dpa-Me)Ir^{I}(ethene)]$^+$ (**15**$^+$), respectively. [(κ^4-Me_3-tpa)Rh^{I}(ethene)]$^+$ (**11**$^+$), the rhodium analogue of **14**$^+$, was also prepared. Whereas rhodium complex **11**$^+$ is stable in acetonitrile at room temperature, the iridium analogue **14**$^+$ converts to the cyclometallated (acetonitrile)(hydrido) complex **16**$^+$ within 72 h by dissociation of the unique 6-methylpyridyl fragment and oxidative addition of the 6-methylpyridyl C^3–H bond. The four-coordinate mono(-ethene) complex **15**$^+$ is even less stable in solution; it converts to a mixture of compounds within 18 h. Reaction of the mono(ethene)Rh^{I} complex **11**$^+$ with O_2 yields the peroxo complex **17**$^+$ by ethene displacement. In contrast, the mono(-ethene)Ir^{I} complexes **14**$^+$ and **15**$^+$ bind O_2 without the loss of ethene, leading to unprecedented (ethene)(peroxo)Ir^{III} complexes **18**$^+$ and **19**$^+$. At room temperature, peroxo complex **17**$^+$ does not react with ethene and, quite remarkably, C–O bond formation does not occur in the (ethene)(peroxo) complexes **18**$^+$ and **19**$^+$.
(© Wiley-VCH Verlag GmbH, 69451 Weinheim, Germany, 2002)

Introduction

Mechanistic aspects of oxygenation reactions with environmentally benign dioxygen are poorly understood. In the late transition metal (LTM) catalyzed oxidation of olefins, peroxo and (olefin)peroxo complexes,[1] 3-metalla-1,2-dioxolanes,[1,2] and 2-metallaoxetanes[3,4] have been proposed as crucial intermediates. In an attempt to collect more mechanistic insight in LTM-mediated oxygenation of olefins we are investigating the stoichiometric oxygenation of rhodium(I)- and iridium(I)-coordinated olefins by O_2.

We have previously observed the selective oxygenation of the cationic (ethene)Rh^{I} and -Ir^{I} complexes **1**$^+$−**4**$^+$ by H_2O_2 *in solution* (various solvents), to give 2-rhoda(III)- and 2-irida(III)oxetanes (1-oxa-2-metalla(III)cyclobutanes) **5**$^+$−**8**$^+$ (Scheme 1).[5,6] Recently, we also observed monooxygenation of cationic (ethene)Ir^{I} complexes by O_2; reaction of **4**$^+$ with air or O_2 in CH_2Cl_2 led to formation of approximately 25% of **8**$^+$.[6]

Furthermore we observed slow, selective dioxygenation of *solid* **1** with air or O_2 to the 3-metalla-1,2-dioxolanes **9a**$^+$ and **9b**$^+$. The ratio between these geometrical isomers proved to be counterion-dependent.[7] Recently, we observed a similar reaction for the iridium analogue **3**$^+$ yielding **10a**$^+$ and **10b**$^+$.[8]

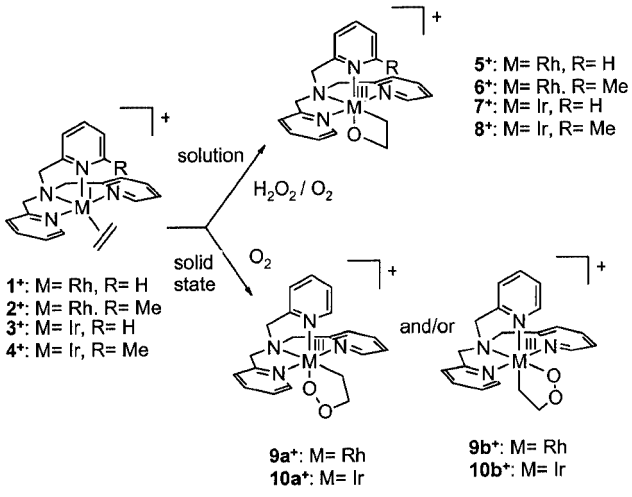

Scheme 1. Mono- and dioxygenation of (ethene)Rh^{I} and -Ir^{I} complexes by O_2

In order to improve our understanding of the mechanisms by which the above reactions proceed, we have now studied the reactivity of [(ethene)(N-ligand)M^{I}]$^+$ (M = Rh, Ir) complexes containing the more bulky N-ligands Me_3-tpa and Me_2-dpa-Me.

[a] Department of Inorganic Chemistry, University of Nijmegen, Toernooiveld 1, 6525 ED Nijmegen, The Netherlands
Fax: (internat.) + 31-24/355-34 50
E-mail: BdeBruin@sci.kun.nl
gal@sci.kun.nl

Results and Discussion

1. Synthesis of (Ethene)Rh^{I} and -Ir^{I} Complexes

We synthesized the cationic ethene complex [(Me_3TPA)-$Rh^{I}(C_2H_4)]^+$ (**11**$^+$) using the route in Scheme 2. Stirring of $[\{(C_2H_4)_2Rh^{I}(\mu\text{-Cl})\}_2]$ with Me_3-tpa in MeOH at −78 °C resulted in the formation of **11**$^+$, which was isolated as [**11**]PF_6 by precipitation with KPF_6.

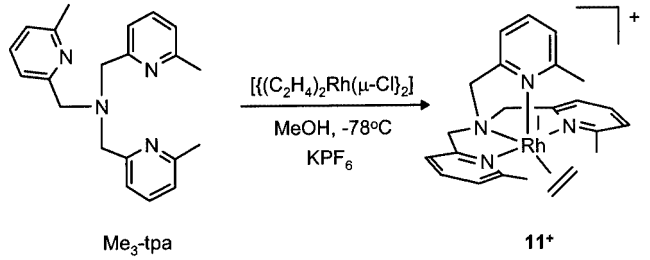

Scheme 2. Preparation of (ethene)Rh^{I} complex **11**$^+$

A similar reaction of $[(C_2H_4)_4Ir^{I}(Cl)]$[9] (generated in situ from the reaction of $[\{(coe)_2Ir^{I}(\mu\text{-Cl})\}_2]$[10] with ethene; coe = cyclooctene) in MeOH with Me_3-tpa and Me_2-dpa-Me yielded the bis(ethene)iridium complexes [(Me_3-tpa)$Ir^{I}(C_2H_4)_2]^+$ (**12**$^+$) and [(Me_2-dpa-Me)$Ir^{I}(C_2H_4)_2]^+$ (**13**$^+$), respectively (Scheme 3). The cations **12**$^+$ and **13**$^+$ were isolated as PF_6^- salts by precipitation with KPF_6.

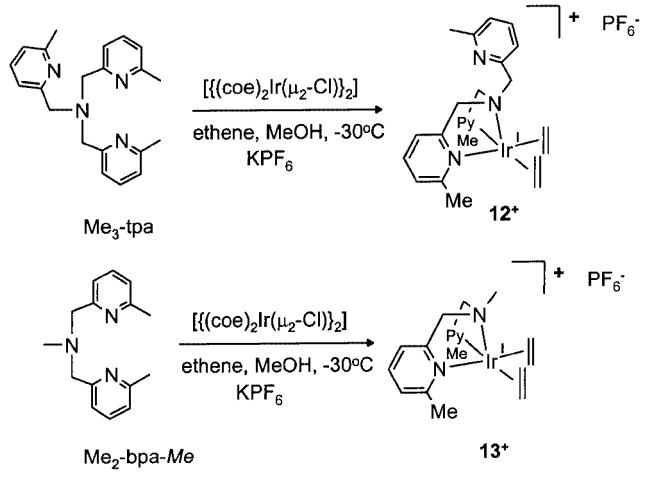

Scheme 3. Synthesis of bis(ethene)Ir^{I} complexes **12**$^+$ and **13**$^+$

The ^1H and ^{13}C NMR spectroscopic data of **12**$^+$ and **13**$^+$ reveal two equivalent N-CH_2-Py^{Me} groups. The ^1H NMR methyl signals of these two groups have shifted by approximately 0.7 ppm downfield relative to the free ligand, in both **12**$^+$ and **13**$^+$. As expected, the diastereotopic methylene protons of the two equivalent N-CH_2-Py^{Me} groups give rise to two AB-type doublets. The ^1H NMR methyl signal of the unique N-CH_2-Py^{Me} group of **12**$^+$ at δ = 2.6 ppm is close to the value of that of the free ligand (δ = 2.56 ppm). In the ^1H NMR spectra of **12**$^+$ and **13**$^+$, the ethene fragments are observed as two broad signals between δ = 2.1 and 1.6 ppm at room temperature.

The X-ray structure of **12**$^+$ was determined. Despite of the poor quality of the data set obtained, the X-ray analysis clearly shows the presence of the κ^3-*N,N,N-fac*-coordinated Me_3-tpa ligand with a noncoordinated 6-methylpyridyl group. The structure is in good agreement with the NMR spectroscopic data in solution (Figure 1).

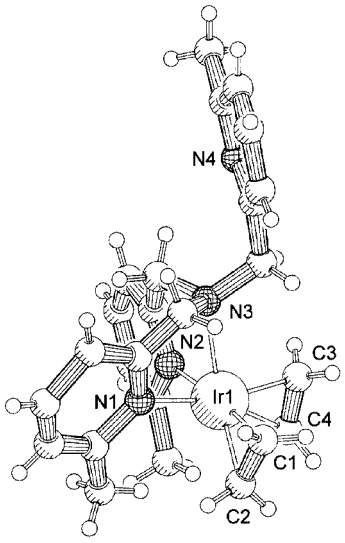

Figure 1. X-ray structure of **12**$^+$

The coordination mode of **12**$^+$ is best described as pseudo square-pyramidal (sqpy). Analogously, complex **13**$^+$ will most probably be square-pyramidal, too.

2. Ethene Dissociation from Bis(ethene)Ir^{I}

Solutions of the bis(ethene) complexes **12**$^+$ and **13**$^+$ are not stable. One of the two ethene fragments dissociates in [D_6]acetone, CD_2Cl_2, or MeCN within 4 h at room temperature (Scheme 4). For **12**$^+$, substitution of the ethene fragment by the unique 6-methylpyridyl group results in the mono(ethene) complex [(κ^4-Me_3-tpa)Ir^{I}(ethene)]$^+$ (**14**$^+$), which is the iridium analogue of **11**$^+$. Ethene dissociation from **13**$^+$ results in the four-coordinate mono(ethene) complex **15**$^+$.

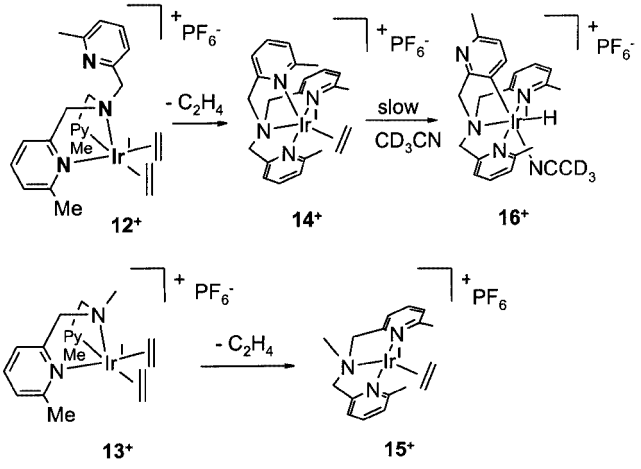

Scheme 4. Ethene dissociation from bis(ethene)Ir^{I} complexes **12**$^+$ and **13**$^+$ resulting in the mono(ethene) complexes **14**$^+$ and **15**$^+$ and the cyclometallated complex **16**$^+$

At room temperature the ^{1}H and ^{13}C NMR spectra of **14^{+}** show two equivalent and one unique N-CH_2-Py^{Me} fragment, consistent with a κ^4-coordination mode of the Me_3-tpa ligand. The ^{1}H and ^{13}C NMR spectra of **15^{+}** show signals for two equivalent N-CH_2-Py^{Me} groups. The ethene signals of both **14^{+}** and **15^{+}** are observed as two sharp triplets, indicating that the ethene fragment does not rotate on the NMR time scale.

The ^{1}H NOE patterns of **15^{+}** are characteristic of a *mer*-coordination mode of the Me_2-dpa-Me ligand; clear NOE contacts are observed between N-*CH_3* and the equatorial N-*CH_2*-Py^{Me} methylene protons (one of the two AB-type doublets). The latter also show NOE contacts with the Py-H^3 protons. The axial N-*CH_2*-Py^{Me} methylene protons (the other AB-type doublet) do not show NOE contacts with either N-*CH_3* or Py^{Me}-*H^3*.

The mono(ethene) complexes **14^{+}** and **15^{+}** are only moderately stable at room temperature, in solution. Complex **14^{+}** is in marked contrast with the less substituted tpa and (Me-tpa)Ir^{I}(ethene) complexes **3^{+}** and **4^{+}**, which are stable in solution over a period of days. Complex **15^{+}** decomposes in CD_2Cl_2 or CD_3CN to a complex mixture of products within 18 h. In CD_3CN, complex **14^{+}** selectively converts in 72 h to cyclometallated complex **16^{+}**, presumably by chelate ring opening, oxidative addition of the 6-methylpyridyl C^3−H bond to the Ir^{I} center and substitution of ethene by CD_3CN (Scheme 4). The hydride in **16^{+}** is observed as a sharp ^{1}H NMR signal at $\delta = -18.6$ ppm. The presence of a coordinated CD_3CN was confirmed by ESI-MS and elemental analysis. The observed cyclometallation also occurs in acetone or CH_2Cl_2. In these solvents, however, ^{1}H NMR spectroscopy indicates that the 6th coordination site is still occupied by ethene.

A solution of **15^{+}** in CD_2Cl_2 contains only **15^{+}**. In CD_3CN, however, **15^{+}** and **15^{+}**(CD_3CN) are present in a ratio of 3:1. Although they have separate ^{1}H NMR signals, they show exchange signals in the EXSY spectrum, indicating that **15^{+}** and **15^{+}**(CD_3CN) are in slow exchange on the ^{1}H NMR time scale. The ethene ^{1}H NMR signals of **15^{+}**(CD_3CN) are very similar to those of **14^{+}**. The ethene signals of **15^{+}**, both in CD_3CN and CD_2Cl_2, have clearly shifted downfield relative to those of **14^{+}**. Computer-generated space-filling models of **15^{+}** indicate that the methyl substituents on the pyridyl fragments must hinder a true square-planar coordination geometry (see also Figure 4 and the discussion of the structure of complex **19^{+}**). Therefore, we propose that **15^{+}** has a distorted square-planar geometry, in which the ethene fragment has moved to a position below the *mer*-(Me-dpa-Me)Ir plane, away from the N_{amine}-Me and the Py-6-Me substituents (Scheme 4). From MO calculations it is known that such a distortion towards a mono-vacant trigonal-bipyramidal coordination geometry increases the reactivity of d^8-metal centers towards oxidative addition of a C−H bond.[11] This could explain the apparent reactivity of **15^{+}** in solution at room temperature. Dissociation of the unique 6-methyl-pyridyl fragment of **14^{+}** would lead to a similar distorted square-planar geometry, thus accounting for its intramolecular C−H activation.

3. Electrochemical Oxidation of the (Ethene)Rh^{I} and -Ir^{I} Complexes

The electrochemical oxidation of the ethene complexes **11^{+}**−**15^{+}** (Schemes 2 and 3) was studied by means of cyclic voltammetry. Table 1 summarizes the electrochemical data.

Table 1. Electrochemical data for complexes **11^{+}**−**15^{+}** [measured in MeCN (0.1 M TBAH); potentials in mV vs. the Fc/Fc^{+} couple]

	M	E^{p}_{anode}	$E^{p}_{cathode}$	$E_{1/2}$	I_b/I_f	ΔE
12^{+}	Ir	188	57	124[a]	0.53	114
13^{+}	Ir	156	90	123	1.00	66
11^{+}	Rh	−272	−426	−349[a]	0.48	154
14^{+}	Ir	−330	−399	−365	1.00	69
15^{+}/15^{+}(MeCN)	Ir	−226	−	−	0.00	−

[a] Quasi-reversible.

Clearly, the mono(ethene) complexes **11^{+}**, **14^{+}**, and **15^{+}**/**15^{+}**(MeCN) are oxidized at much lower potentials (−226 to −330 mV vs. Fc/Fc^{+}) than the bis(ethene) complexes **12^{+}** and **13^{+}** (+156 to +188 V vs. Fc/Fc^{+}). This presumably stems from an increased electron density at the metal center (due to decreased π-back donation) as a result of the loss of one ethene fragment. As expected, the (N_4-ligand)-Rh^{I} complex **11^{+}** is oxidized at a higher potential than the (N_4-ligand)Ir^{I} complex **14^{+}**.

The five-coordinate bis- and mono(ethene)Ir^{I} complexes **13^{+}** and **14^{+}** (Scheme 4) undergo reversible one-electron oxidation at 100 mV/s in MeCN (0.1 M TBAH). The five-coordinate mono(ethene)Rh^{I} complex **11^{+}** and bis(ethene)Ir^{I} complex **12^{+}** both undergo quasi-reversible one-electron oxidation. In contrast, the mono(ethene) complex **15^{+}**/**15^{+}**(MeCN) is oxidized irreversibly in MeCN at 100mV/s.

During conversion of the bis(ethene) complexes **12^{+}** and **13^{+}** to the mono(ethene) complexes **14^{+}** and **15^{+}**, respectively, the redox pairs **12^{+}**/**14^{+}** and **13^{+}**/**15^{+}** are both seen as separate waves in the cyclic voltammogram. Therefore the bis(ethene) complexes are not in equilibrium with the mono(ethene) complexes on the electrochemical time scale.

4. Oxidation of the (Olefin)Rh^{I} and -Ir^{I} Complexes by O_2

The reactivity of the (ethene)rhodium complex **11^{+}** and the (ethene)iridium complexes **12^{+}**−**15^{+}** towards O_2 has been investigated. For the rhodium complex **11^{+}**, we observed clean ethene displacement by O_2. In contrast, the iridium complexes **14^{+}** and **15^{+}** react aselectively. For 25% the complexation of O_2 occurs without dissociation of ethene, giving **18^{+}** and **19^{+}** (Scheme 5).

Treatment of a CD_2Cl_2 solution of the Rh^{I} complex **11^{+}** with O_2 resulted in selective formation of the (peroxo)Rh^{III} complex **17^{+}**, according to ^{1}H NMR spectroscopy and ESI-MS. Loss of ethene was confirmed by ^{1}H NMR spectroscopy. The ^{1}H and ^{13}C NMR spectroscopic data of **11^{+}**, showing two equivalent and one unique N-CH_2-Py^{Me} frag-

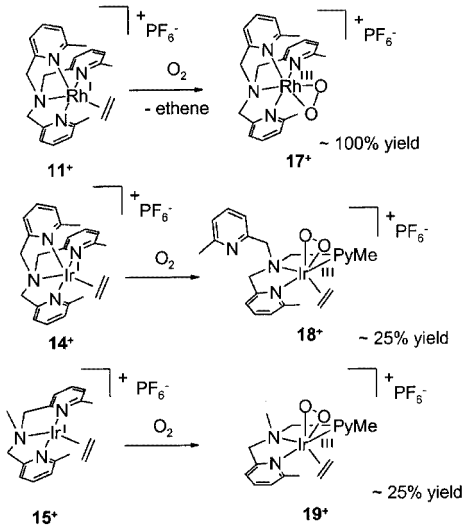

Scheme 5. Reaction of (ethene)Rh^{I} and -Ir^{I} complexes to (peroxo)Rh^{III} and (ethene)(peroxo)Ir^{III} complexes

ment, are in accordance with a κ^4-coordination mode of the Me_3TPA ligand. ^{1}H NMR and ESI-MS indicate that the reaction of [(Me_2-tpa)Rh^{I}(ethene)]$^+$ with O_2 also results in selective formation of the (peroxo)Rh^{III} complex [(Me_2-tpa)$Rh^{II}(O_2)$]$^+$. In solution, Me_x-tpa complexes with less Me substituents, viz. [(Me_x-tpa)Rh^{I}(ethene)]$^+$ (x = 0, 1) lose ethene upon contact with O_2 or air in an aselective reaction.

Upon reaction of (mono)etheneIr^{I} complex **14**$^+$ with 1.2 bar O_2 in CD_2Cl_2, the ^{1}H NMR spectrum showed intense signals from the (ethene)(peroxo) complex **18**$^+$ and very broad signals, probably from paramagnetic species (Scheme 5). Based on the intensity of the ^{1}H NMR signals of **18**$^+$ relative to the internal standard dichloroethane, the starting complex **14**$^+$ has been converted into **18**$^+$ for approximately 25%, and approximately 70% of (a) paramagnetic compound(s). The reaction of complex **15**$^+$ with 1.2 bar O_2 in CD_2Cl_2 proceeds similarly to that of **14**$^+$. Again, approximately 25% of the (ethene)(peroxo) complex **19**$^+$ and approximately 70% of unidentified paramagnetic species are formed (Scheme 5). Any attempts to improve the selectivity of these reactions, e.g. by treatment of [**14**]PF_6 or [**15**]PF_6 with only 1 equiv. O_2 or by performing the reactions at lower temperatures, were not successful. Nevertheless, we succeeded in the isolation of pure [**18**]PF_6 and [**19**]PF_6 through crystallization.

The ^{1}H and ^{13}C NMR spectra of **18**$^+$ and **19**$^+$ show signals for two equivalent N-CH_2-Py^{Me} groups. The equatorial N−CH_2−Py^{Me} group of **18**$^+$ gives rise to a ^{1}H NMR methyl signal at δ = 2.65 ppm, close to the value for the free ligand (δ = 2.56 ppm). The methyl signals of the two equivalent 6-methylpyridyl groups of **18**$^+$ and **19**$^+$ are approximately 0.4 ppm downfield from those in the free ligand. The diastereotopic methylene protons of the two equivalent N-CH_2-Py^{Me} groups give rise to two AB-type doublets.

On going from (ethene)Ir^{I} compounds **14**$^+$ and **15**$^+$ to the (ethene)(peroxo)Ir^{III} species **18**$^+$ and **19**$^+$ the rate of ethene rotation increases. In the 200 MHz ^{1}H NMR spectra of **18**$^+$ and **19**$^+$ at room temperature, the ethene fragments are observed as very broad signals at δ = 4.48 and 4.22 ppm, respectively. At 500 MHz, the broad signals have split into two sharp triplets at 233 K for both **18**$^+$ (δ = 4.84 and 4.14 ppm, $^3J_{H,H}$ = 9.70 Hz) and **19**$^+$ (δ = 4.56 and 3.77 ppm, $^3J_{H,H}$ = 9.40 Hz). For both **18**$^+$ and **19**$^+$, at 500 MHz, coalescence of these triplets into one signal occurs at T_c = 273 K. From these data, the free energy of activation ($\Delta G_c^{\neq}$) for ethene rotation in **18**$^+$ and **19**$^+$ at T_c was estimated to be ca. 12 kcal/mol. The ethene fragments of **14**$^+$ and **15**$^+$ do not rotate on the ^{1}H NMR time scale at room temperature (298 K, 200 MHz). The free energy of activation for ethene rotation ($\Delta G_c^{\neq}$) of **14**$^+$ and **15**$^+$, as estimated from line-width analysis of the ethene ^{1}H NMR signals, must be at least 17 kcal/mol.

The structures of [**18**]PF_6 (Figure 2) and [**19**]PF_6 (Figure 3) were determined by single-crystal X-ray diffraction.

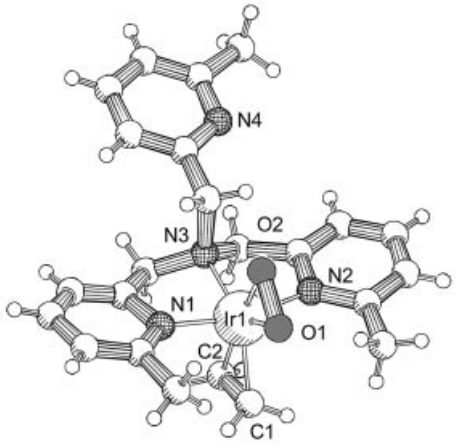

Figure 2. X-ray structure of **18**$^+$; selected bond lengths [Å] and angles [°]: Ir1−N1 2.071(12), Ir1−N2 2.085(12), Ir1−N3 2.073(11), Ir1−O1 2.014(10), Ir1−O2 2.011(9), Ir1−C1 2.119(14), Ir1−C2 2.162(14), O1−O2 1.430(13), C1−C2 1.40(2); N1−Ir1−N2 162.3(5), N1−Ir1−N3 80.7(5), N2−Ir1−N3 81.6(5), O1−Ir1−N3 136.7(4), O2−Ir1−N3 95.1(4), C1−Ir1−N3 128.4(5), C2−Ir1−N3 90.1(5), O1−Ir1−C1 94.9(5), O1−Ir1−C2 133.1(5), O2−Ir1−C1 136.5(5), O2−Ir1−C2 174.6(5)

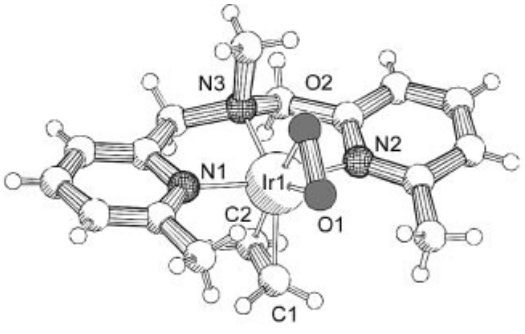

Figure 3. X-ray structure of **19**$^+$; selected bond lengths [Å] and angles [°]: Ir1−N1 2.083(6), Ir1−N2 2.076(5), Ir1−N3 2.098(5), Ir1−O1 2.046(5), Ir1−O2 2.023(5), Ir1−C1 2.122(7), Ir1−C2 2.136(7), O1−O2 1.446(8), C1−C2 1.404(11); N1−Ir1−N2 164.0(2), N1−Ir1−N3 81.5(2), N2−Ir1−N3 82.7(2), O1−Ir1−N3 136.0(2), O2−Ir1−N3 94.4(2), C1−Ir1−N3 127.1(3), C2−Ir1−N3 88.8(3), O1−Ir1−C1 96.8(3), O1−Ir1−C2 135.1(3), O2−Ir1−C1 138.4(3), O2−Ir1−C2 176.1(5)

The X-ray structure of **18**$^{+}$ reveals a κ^3-*mer*-coordinated Me_3-tpa ligand with a noncoordinated 6-methylpyridyl group, in accordance with the NMR spectroscopic data. Thus, dissociation of the unique pyridyl group probably precedes the reaction of **14**$^{+}$ with O_2. It is therefore not surprising that the reaction of **15**$^{+}$ with O_2 proceeds similarly.

The O−O distances in **18**$^{+}$ [1.430(13) Å] and **19**$^{+}$ [1.446(8) Å] indicate that the coordinated η^2-O_2 is best described as an η^2-peroxo fragment. Consequently the iridium center is formally in the +III oxidation state. The Ir−C and C−C distances for coordinated ethene in **18**$^{+}$ and **19**$^{+}$, however, fit well within the Ir−C and C−C ranges reported for (ethene)Ir^{I} complexes (ranges found in the Cambridge Structural Database: Ir^{I}−C: 2.036−2.191 Å, C−C: 1.351−1.444 Å).

Viewing the stick representation of (ethene)(peroxo) complex **19**$^{+}$ along the N1−Ir1−N2 axis reveals that folding of Me_2-dpa-Me to its *mer*-coordination mode leaves a relatively small compartment for *cis* coordination to the N3-Me fragment and a relatively large compartment for *trans* coordination to the N3-Me fragment (*cis* and *trans* with respect to the Ir1−N3 axis, Figure 4).

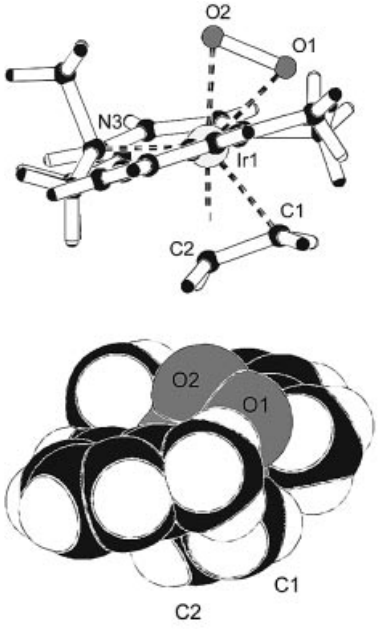

Figure 4. X-ray structure of **19**$^{+}$; top: stick representation; bottom: CPK representation

Viewing the CPK representation of **19**$^{+}$ (Figure 4, right) suggests that *mer*-Me_2-dpa-Me in the ethene complex **15**$^{+}$ allows ethene coordination neither in the small *cis* compartment (resulting in a mono-vacant trigonal-bipyramidal geometry) nor at a position *trans* to N3, in between the Py-Me groups (resulting in a square-planar geometry). It is therefore tempting to assume that **15**$^{+}$ (Scheme 4) has a mono-vacant trigonal-bipyramidal coordination geometry, with ethene coordinated *trans* to the N3-Me fragment, close to the structure of **19**$^{+}$ without the peroxo fragment. Binding of O_2 to **15**$^{+}$ would thus involve only small structural rearrangements.

5. π-Back Bonding in (Ethene)Rh^{I}, -Ir^{I} and -Ir^{III} Complexes

The ethene signals of four-coordinate **15**$^{+}$ have shifted down-field relative to those of five-coordinate **14**$^{+}$, both in ^{1}H NMR (**15**$^{+}$: δ = 3.54 and 2.34 ppm; **14**$^{+}$: δ = 1.85 and 1.37 ppm) and ^{13}C NMR (**15**$^{+}$: δ = 37.0 and 25.1 ppm; **14**$^{+}$: δ = 3.7 and 0.2 ppm). The ethene signals of the five-coordinate Rh^{I} complex **11**$^{+}$ (^{1}H NMR: δ = 2.41 and 2.11 ppm; ^{13}C NMR: δ = 29.5 and 26.3 ppm) have also shifted down-field relative to those of its Ir^{I} analogue **14**$^{+}$. Furthermore, the (N_4-ligand)Rh^{I} complex **11**$^{+}$ is oxidized at a potential 60 mV higher than that of the (N_4-ligand)Ir^{I} complex **14**$^{+}$. These data are consistent with weaker M→C=C π-back donation upon removal of a donor atom (from **14**$^{+}$ to **15**$^{+}$) and upon substitution of rhodium(I) for iridium(I) (from **14**$^{+}$ with **11**$^{+}$).

The increased rate of ethene rotation on going from (ethene)Ir^{I} compounds **14**$^{+}$ and **15**$^{+}$ to (ethene)(peroxo)Ir^{III} species **18**$^{+}$ and **19**$^{+}$ (vide infra) most likely results from decreased Ir→C=C π-back bonding for Ir^{III} relative to Ir^{I}.

Discussion and Conclusions

Complexes **18**$^{+}$ and **19**$^{+}$ are very rare examples of (olefin)(peroxo) complexes. In the only other structurally characterized (peroxo)(olefin)transition-metal complex **20**, the olefin fragment is part of the stabilizing P-ligand (Figure 5).[12] Olefin coordination in **20** must be promoted by the chelate effect, in contrast to ethene coordination in **18**$^{+}$ and **19**$^{+}$.

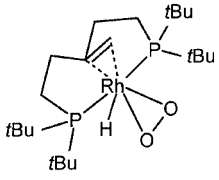

20

Figure 5. (Olefin)(peroxo)rhodium complex **20**[12]

For **18**$^{+}$, **19**$^{+}$, and **20** it is quite remarkable that the olefin fragment does not insert into the M−O bond of the η^2-peroxo fragment. The approach of the peroxo fragment by the olefin fragment might be hindered by geometrical constraints, i.e. the fixed position of the olefin in the rigid chelating diphosphane ligand in **20** and for steric reasons in **18**$^{+}$ and **19**$^{+}$. However, there seems to be no obvious geometrical constraint for the peroxo fragment to move towards the olefin. Nevertheless, intramolecular C−O bond formation is not observed.

The (peroxo)Rh^{III} complex **17**$^{+}$ and the unprecedented (ethene)(peroxo)Ir^{III} complexes **18**$^{+}$ and **19**$^{+}$ add to the list of species observed upon reaction of [(N-ligand)M^{I}(ethene)]$^{+}$ (M = Rh, Ir) with O_2 (**a** and **b** in

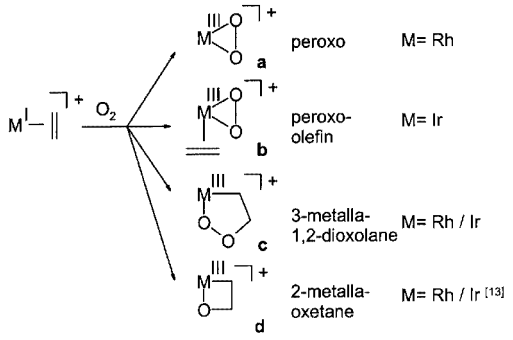

Scheme 6. Observed oxygenations of $[(\text{N-ligand})\text{M}^{\text{I}}(\text{olefin})]^+$ (M = Rh, Ir) by O_2

Scheme 6). The reactivity of (ethene)Rh^{I} and -Ir^{I} fragments towards dioxygen thus varies from ethene displacement (**a**) and formation of mixed (ethene)(O_2) complexes (**b**) to C−O bond formation (to give a 3-metalla-1,2-dioxolane; **c**) and to C−O bond formation plus O−O bond breaking (to give a 2-metallaoxetane; **d**).[13] Apparently, the outcome of the oxygenation reaction subtly depends on the metal and the N-ligand (Scheme 6).

The remarkable effects of variation of metal and N-ligand on the obtained products are best demonstrated by comparing **11**$^+$ (Scheme 5), **14**$^+$ (Scheme 5), and **4**$^+$ (Scheme 1) in their solution-phase reactivity towards O_2. Changing the metal from rhodium in **11**$^+$ to iridium in **14**$^+$ results in (η^2-ethene)(η^2-peroxo) complex **18**$^+$ instead of η^2-peroxo complex **17**$^+$. Apparently ethene binds stronger to iridium(III) than to rhodium(III).[14] Changing the ligand from Me_3-tpa in **14**$^+$ to Me-tpa in **4**$^+$ results in 2-iridaoxetane **8**$^+$, instead of the (ethene)(peroxo) complex **18**$^+$, as the observed product.

One could imagine peroxo species of type **a** (analogues of **17**; Scheme 5) to react with olefins, yielding 3-metalla-1,2-dioxolanes **c** (analogues of **9**$^+$ or **10**$^+$; Scheme 1) or 2-metallaoxetanes **d** (analogues of **1**−**4**; Scheme 1). Insertion of ethene into the Ir−O bond of (ethene)(peroxo) complexes **b** (analogues of **18**$^+$ or **19**$^+$; Scheme 5) would seem a simple and viable route to 3-metalla-1,2-dioxalanes **c**. However, at room temperature, the (peroxo)Rh^{III} species **17**$^+$ shows no further reactivity towards ethene, and the (ethene)(peroxo)Ir^{III} complexes **18**$^+$ and **19**$^+$ do not undergo insertion of ethene into the Ir−O bond. The 3-metalla-1,2-dioxolane isomers **9**$^+$ and **10**$^+$ (Scheme 1) are only formed from **1**$^+$ and **3**$^+$ in the *solid state*, whereas *in solution* very aselective reactions yield other products without any indication for the formation of **9**$^+$ or **10**$^+$. It is hard to believe that chelate ring opening, which would be required to form a (ethene)(peroxo) complex analogous to **18**$^+$, plays a role in the *solid state* reactions. Therefore, 3-metalla-1,2-dioxolanes **c** probably form by alternative routes in the *solid state*.

In **14**$^+$, relieving the steric strain by the Me substituents in the κ^4-coordination mode of the Me_3-tpa ligand through dissociation of a 6-methylpyridyl fragment apparently opens up the "κ^3-route" to the formation of **18**$^+$. As such strain is absent in the Me-tpa complex **4**$^+$, formation of 2-iridaoxetane **8**$^+$ might proceed by a "κ^4-route". However, we cannot exclude that the formation of the (ethene)-(peroxo) complex **18**$^+$, instead of an analogue of 2-iridaoxetane **8**$^+$ (Scheme 1), merely reflects a thermodynamic preference, resulting from the weaker N-donor capacity of the Me_3-tpa ligand.

Experimental Section

General Methods: All procedures were performed under N_2 using standard schlenk techniques unless otherwise indicated. Solvents (p.a.) were deoxygenated by bubbling a stream of N_2 through the solvent or by the freeze-pump-thaw method. Room temperature corresponds to ca. 20 °C. NMR spectroscopic experiments were carried out with a Bruker DPX200 (200 MHz and 50 MHz for ^{1}H and ^{13}C, respectively), a Bruker AC300 (300 MHz and 75 MHz for ^{1}H and ^{13}C, respectively), a Varian Inova 400 (400 MHz and 100 MHz for ^{1}H and ^{13}C, respectively) and a Bruker AM500 (500 MHz and 125 MHz for ^{1}H and ^{13}C, respectively). Solvent shift reference for ^{1}H NMR spectroscopy: [D_6]acetone δ_H = 2.05, CD_3CN δ_H = 1.94, CD_2Cl_2 δ_H = 5.31. For ^{13}C NMR: [D_6]acetone δ_C = 29.50, CD_3CN δ_C = 1.25, CD_2Cl_2 δ_C = 54.20. Abbreviations used are s = singlet, d = doublet, dd = doublet of doublets, t = triplet, dt= doublet of triplets, q = quadruplet, dq = doublet of quadruplets, m = multiplet and br = broad. Py^A represents the two equivalent 6-methylpyridyl groups, Py^B represents the unique 6-methylpyridyl group. Elemental analyses (C,H,N) were carried out with a Carlo Erba NCSO analyzer. Mass spectra (FAB, ESI) were recorded with a MAT 900 XL mass spectrometer or a JEOL JMS SX/SX102A four-sector mass spectrometer. Cyclic voltammetry measurements were performed using an Eco Chemie Autolab PGSTAT20. A conventional three-electrode cell, with Pt working and auxiliary electrodes and 0.1 M [(nBu)$_4$N]PF_6 (TBAH) electrolyte was used. An Ag/AgI reference electrode (grain of AgI, 0.02 M [(nBu)$_4$N]I (TBAI) and 0.1 M TBAH) was employed. Me_3-tpa,[15] [{(C_2H_4)$_2$Rh(μ-Cl)}$_2$],[16] and [{(coe)$_2$Ir(μ-Cl)}$_2$][10] were prepared according to literature procedures. All other chemicals were commercially available and were used without further purification, unless otherwise stated.

X-ray Diffraction: Single crystals were mounted in air on glass fibers. Intensity data were collected at room temperature. An Enraf−Nonius CAD4 single-crystal diffractometer was used, applying graphite-monochromatized Cu-K_α or Mo-K_α radiation. Unit cell dimensions were determined from the angular setting of 22 reflections for [**12**]PF_6, 24 reflections for [**18**]PF_6 and 25 reflections for [**19**]PF_6. Intensity data were corrected for Lorentz and polarization effects. Semiempirical absorption correction (ψ-scan) was applied for all compounds.[17] The structures were solved by the program system DIRDIF[18] using the program PATTY[19] to locate the heavy atoms. All structures were refined with standard methods (refinement against F^2 of all reflections with SHELXL-97[20]) with anisotropic parameters for the non-hydrogen atoms. Hydrogen atoms were placed at calculated positions and were subsequently refined isotropically in riding mode. For [**18**]PF_6 and [**19**]PF_6 geometrical data with regard to O1, O2, C1, and C2 are rather similar. The assignment of atomic species has been made on the basis of prior occupancy factor refinement and comparison of thermal displacement parameters. Selected bond lengths and angles are summarized in Figures 1−3. Drawings were generated with the program PLATON.[21] Other relevant crystal data are summarized in Table 2. Crystallographic data (excluding structure factors) for the

Table 2. Crystallographic data for [**12**]PF_6, [**18**]PF_6, and [**19**]PF_6

	[**12**]PF_6·CH_3OH·1/2H_2O	[**18**]PF_6·1/2H_2O	[**19**]PF_6
Empirical formula	$C_{25.5}H_{36}F_6IrN_4O_{1.5}P$	$C_{23}H_{29}F_6IrN_4O_{2.5}P$	$C_{17}H_{23}F_6IrN_3O_2P$
Formula mass	759.75	738.67	638.55
Crystal size [mm]	0.63 × 0.28 × 0.13	0.36 × 0.11 × 0.10	0.52 × 0.38 × 0.20
T [K]	293(2)	293(2)	293(2)
Crystal system	orthorhombic	monoclinic	triclinic
Space group	*Pbcn*	$P2_1/c$	$P\bar{1}$
a [Å]	31.9939(19)	9.583(2)	7.001(3)
b [Å]	12.1203(8)	24.768(5)	12.081(4)
c [Å]	14.7332(8)	12.0374(13)	12.414(3)
α [°]	90	90	90.91(2)
β [°]	90	100.420(12)	90.74(2)
γ [°]	90	90	100.699(17)
V [Å^3]	5713.2(6)	2809.8(9)	1031.5(6)
$\rho_{calcd.}$ [gcm^{-3}]	1.767	1.746	2.056
Z	8	4	2
Diffractometer	Enraf−Nonius CAD4	Enraf−Nonius CAD4	Enraf−Nonius CAD4
Scan	ω-scan	ω-scan	ω/2θ-scan
Radiation	Cu-K_α	Mo-K_α	Mo-K_α
Wavelength [Å]	1.54184	0.71073	0.71073
F(000)	3000	1444	616
θ range [°]	3.90−54.96	3.11−27.49	2.96−27.48
Index ranges	$-33 \le h \le 0$	$-12 \le h \le 12$	$0 \le h \le 9$
	$-12 \le k \le 0$	$0 \le k \le 32$	$-15 \le k \le 15$
	$-15 \le l \le 0$	$0 \le l \le 15$	$-16 \le l \le 16$
Measured reflections	3586	6705	5112
Unique reflections	3586	6408	4724
Observed refl. [$I_o > 2\sigma(I_o)$]	1688	2563	4273
Refined parameters	357	337	274
Goodness-of-fit on F^2	1.110	0.907	1.142
R [$I_o > 2\sigma(I_o)$]	0.0844	0.0784	0.0423
$wR2$ (all data)	0.2202	0.1808	0.1111
ρ_{fin} (max/min) [e·Å^{-3}]	1.017/−0.891	0.784/−0.785	2.889/−3.954

structures reported in this paper have been deposited with the Cambridge Crystallographic Data Centre as supplementary publication no. CCDC-176106 for [**12**]PF_6, -176105 for [**18**]PF_6, and -176104 for [**19**]PF_6. Copies of the data can be obtained free of charge on application to CCDC, 12 Union Road, Cambridge CB2 1EZ, UK [Fax: (internat.) + 44-1223/336-033; E-mail: deposit@ccdc.cam.ac.uk].

[12]PF_6: The structure determination was hampered by the poor quality of the data caused by the inferior quality of the crystals, which was, unfortunately, the best that could be achieved. The crystal diffracted very weakly, and no reliable data could be collected at θ > 55° (resolution 0.95 Å). Moreover a more than average crystal decay was observed, up to 17%. No attempt was made to locate the hydrogen atoms attached to the disordered CH_3OH and partially occupied H_2O moieties; they cannot be calculated and no indication whatsoever of their location was found in the difference fourier map. From the anisotropic thermal displacement parameters for the PF_6 moiety it is clear that these atoms show a large positional disorder. Although it is possible to use several partially occupied positions for these atoms, no physically reasonable model results from these parameters, at least not any better than the model presented here. Because the EMPABS procedure,[17] by itself, was not adequate enough, presumably caused by the poor quality of the data and hence the ψ-scans, an additional absorption correction was applied using the DIFABS procedure.[22] Even then it was necessary to use the SIMU option in the least-squares refinement to end up with physically acceptable anisotropic thermal displacement parameters. Geometrical calculations (PLATON-93)[21] revealed neither unusual geometric features, nor unusual short intermolecular contacts. The calculations revealed no higher symmetry and no (further) solvent accessible areas.

[18]PF_6: Unfortunately the crystal structure determination was influenced by a rather severe but regular crystal decay of up to 43%. From the anisotropic thermal displacement parameters for the PF_6 moiety it is clear that these atoms show a large positional disorder. Although it is possible to use several partially occupied positions for these atoms, no physically reasonable model results from these parameters, at least not any better than the model presented here. Moreover, the model presented here was the only one that was stable by itself without the need for additional restraints. Calculations (PLATON-93)[21] showed a small void of 162 Å^3, containing at least 6 electrons, around 0,1/2,0. This electron density is assumed to be a disordered water molecule, and the SQUEEZE (PLATON-93) procedure was applied to account for this electron density. This assumption accounts for the physical molecular properties as given in Table 2.

[19]PF_6: Geometrical calculations (PLATON-93)[21] revealed neither unusual geometric features, nor unusual short intermolecular contacts. The calculations revealed no higher symmetry and no solvent accessible areas.

Syntheses

Methylbis[(6-methyl-2-pyridyl)methyl]amine (Me_2-dpa-Me): To CH_3CN (300 mL), 2-(chloromethyl)-6-methylpyridine·HCl[23] (7.98

g, 44.8 mmol), CH_3NH_2·HCl (2.27 g, 33.6 mmol), Na_2SO_4 (25.00 g), and Na_2CO_3 (47.50 g) were added. The resulting suspension was heated to reflux for 16 h. The mixture was filtered and the filtrate was concentrated yielding a brown oil, to which Et_2O (100 mL) was added. Partial evaporation of the solvent resulted in precipitation of Me_2-dpa-Me as a white solid (> 95% pure according to GC), which was crystallized as white crystals from a saturated hexane solution at −20 °C. Yield 2.52 g (16.8 mmol, 50%). An alternative synthetic route to Me_2-dpa-Me has been reported, mentioning its melting point and C,H,N analysis.[24] ^{1}H NMR (200.13 MHz, $CDCl_3$, 289 K): δ [ppm] = 7.54 (t, $^3J_{H,H}$ = 7.7 Hz, 2 H, Py-H^4), 7.34 (d, $^3J_{H,H}$ = 7.7 Hz, 2 H, Py-H^3), 7.00 (d, $^3J_{H,H}$ = 7.7 Hz, 2 H, Py-H^5), 3.74 (s, 4 H, N-*CH*$_2$-Py^{Me}), 2.54 (s, 6 H, Py-*CH*$_3$), 2.30 (s, 3 H, N-*CH*$_3$). ^{13}C{^{1}H} NMR (75.47 MHz, $CDCl_3$, 289 K): δ [ppm] = 158.6 (Py-C^2), 157.4 (Py-C^6), 136.4 (Py-C^4), 121.2 (Py-C^5), 119.6 (Py-C^3), 63.6 (N-*C*H$_2$-Py^{Me}), 42.6 (N-*C*H$_3$), 24.3 (Py-*C*H$_3$).

[(κ^4-Me$_3$-tpa)Rh^I(C$_2$H$_4$)]PF$_6$ ([11]PF$_6$): [(C$_2$H$_4$)$_2$Rh(μ-Cl)]$_2$ (270 mg, 0.69 mmol) and Me_3-tpa (375 mg, 1.13 mmol) were stirred in MeOH (55 mL) at −78 °C for about 4 h until a clear solution was obtained. Subsequently, KPF_6 (127 mg, 0.69 mmol) was added. Partial evaporation of the solvent caused the precipitation of [**11**]PF_6 as a yellow powder, which was collected by filtration and dried under vacuum. Yield 370 mg (0.61 mmol, 63%). ^{1}H NMR 200.13 MHz, CD_2Cl_2, 298 K): δ [ppm] = 7.42 (t, $^3J_{H,H}$ = 7.8 Hz, 3 H, Py^A-H^4 and Py^B-H^4), 7.16 (d, $^3J_{H,H}$ = 7.3 Hz, 1 H, Py^B-H^3 or Py^B-H^5), 7.04 (d, $^3J_{H,H}$ = 7.6 Hz, 2 H, Py^A-H^3 or Py^B-H^5), 6.89 (d, $^3J_{H,H}$ = 7.6 Hz, 3 H, Py^B-H^3 or -H^5 or Py^A-H^3 or -H^5), 5.63 (d[AB], $^2J_{H,H}$ = 15.3 Hz, 2 H, N-*CH*$_2$-Py^A), 4.80 (d[AB], $^2J_{H,H}$ = 15.3 Hz, 2 H, N-*CH*$_2$-Py^A), 4.41 (s, 2 H, N-*CH*$_2$-Py^B), 3.71 (s, 3 H, Py^B-*CH*$_3$), 2.87 (s, 6 H, Py^A-*CH*$_3$), 2.54−2.34 (m, 2 H, *CH*$_2$=CH$_2$), 2.25−2.05 (m, 2 H, CH$_2$=*CH*$_2$). ^{13}C{^{1}H} NMR (50.32 MHz, CD_2Cl_2, 289 K): δ [ppm] = 163.8 (Py^B-C^2), 163.6 (Py^A-C^2), 161.0 (Py^B-C^6), 159.6 (Py^A-C^6), 138.0 (Py^B-C^4), 137.8 (Py^A-C^4), 125.5 (Py^A-C^3), 124.5 (Py^B-C^3), 120.5 (Py^A-C^5), 119.9 (Py^B-C^5), 70.5 (N-*C*H$_2$-Py^A), 63.7 (N-*C*H$_2$-Py^B), 31.7 (Py^B-*C*H$_3$), 29.5 (d, $^1J_{Rh,H}$ = 16.9 Hz, *CH*$_2$=CH$_2$), 28.2 (Py^A-*C*H$_3$), 26.3 (d, $^1J_{Rh,H}$ = 19.9 Hz, CH$_2$=*CH*$_2$). FAB$^+$-MS: *m*/*z* = 463 [M − PF$_6$]$^+$. $C_{23}H_{28}F_6N_4PRh$ (608.37): calcd. C 45.41, H 4.64, N 9.21; found C 45.18, H 4.71, N 9.40.

[(κ^3-Me$_3$-tpa)Ir^I(C$_2$H$_4$)$_2$]PF$_6$ ([12]PF$_6$): [Ir(coe)$_2$Cl)$_2$ (350 mg, 0.39 mmol) was dissolved in methanol (14 mL). Ethene was bubbled through the solution until a clear solution was obtained. The solution was cooled to −30 °C and Me_3-tpa (260 mg, 0.78 mmol) was added under ethene. The reaction mixture was stirred until the Me_3-tpa had dissolved. Subsequently, KPF_6 (170 mg, 0.92 mmol) was added and the solution was stirred for 1 h at −30 °C, after which the solution was cooled to −78 °C causing the precipitation of [**12**]PF_6. A second portion was obtained by adding KPF_6 (25 mg, 0.14 mmol) to the filtrate, stirring for 1 h at −50 °C, and leaving overnight at −20 °C. The yellow solid thus obtained was collected by filtration, washed three times with cold methanol (−78 °C) under nitrogen and dried under vacuum. Yield: 311 mg (0.43 mmol, 55%). ^{1}H NMR (200.13 MHz, CD_2Cl_2, 289 K): δ [ppm] = 7.80 (t, $^3J_{H,H}$ = 7.7 Hz, 1 H, Py^B-H^4), 7.71 (t, $^3J_{H,H}$ = 7.7 Hz, 2 H, Py^A-H^4), 7.38 (d, $^3J_{H,H}$ = 7.7 Hz, 2 H, Py$^{A/B}$-H$^{3/5}$), 7.34 (d, $^3J_{H,H}$ = 7.7 Hz, 2 H, Py$^{A/B}$-H$^{3/5}$), 7.24 (d, $^3J_{H,H}$ = 7.7 Hz, 2 H, Py$^{A/B}$-H$^{3/5}$), 5.26 (d[AB], $^2J_{H,H}$ = 16.0 Hz, 2 H, N-*CH*$_2$-Py^A), 4.94 (s, 2 H, N-*CH*$_2$-Py^B), 3.92 (d[AB], $^2J_{H,H}$ = 16.0 Hz, 2 H, N-*CH*$_2$-Py^A), 3.28 (s, 6 H, CH$_3$-Py^A). 2.62 (s, 3 H, CH$_3$-Py^B), 2.02 (br, 4 H, CH$_2$=CH$_2$), 1.81 (br, 4 H, CH$_2$=CH$_2$). $C_{25}H_{32}F_6IrN_4P$ (725.74): calcd. C 41.38, H 4.44, N 7.72, found C 41.19, H 4.20, N 7.80.

[(κ^3-Me$_2$-dpa-Me)Ir^I(C$_2$H$_4$)$_2$]PF$_6$ ([13]PF$_6$): [Ir(coe)$_2$Cl]$_2$ (350 mg, 0.39 mmol) was dissolved in methanol (14 mL), ethene was bubbled through the solution until a clear solution was obtained. The solution was cooled to −30 °C and Me_2-dpa-Me (190 mg, 0.79 mmol) was added under ethene. The reaction mixture was stirred until the Me_2-dpa-Me had dissolved. Subsequently, KPF_6 (170 mg, 0.92 mmol) was added and the solution was stirred for 1 h at −30 °C, after which the solution was cooled to −78 °C causing precipitation of [**13**]PF_6. A second portion was obtained by adding KPF_6 (25 mg, 0.14 mmol) to the filtrate, stirring for 1 h at −50 °C, and leaving overnight at −20 °C. The resulting yellow solid was collected by filtration, washed three times with cold methanol (−78 °C) under nitrogen and dried under vacuum. Yield: 234 mg (0.37 mmol, 47%). ^{1}H NMR (200.13 MHz, CD_3CN, 289 K): δ [ppm] = 7.73 (t, $^3J_{H,H}$ = 7.7 Hz, 2 H, Py-H^4), 7.37 (d, $^3J_{H,H}$ = 7.7 Hz, 2 H, Py-H$^{3/5}$), 7.27 (d, $^3J_{H,H}$ = 7.7 Hz, 2 H, Py-H$^{3/5}$), 4.64 (d[AB], $^2J_{H,H}$ = 15.8 Hz, 2 H, CH$_2$-Py), 4.10 (d[AB], $^2J_{H,H}$ = 15.8 Hz, 2 H, CH$_2$-Py), 3.34 (s, 3 H, CH$_3$-N), 3.18 (s, 6 H, CH$_3$-Py), 1.83 (br, 4 H, CH$_2$=CH$_2$), 1.67 (br, 4 H, CH$_2$=CH$_2$). $C_{19}H_{27}F_6IrN_3P$ (634.63): calcd. C 35.96, H 4.29, N 6.62; found C 35.66, H 4.10, N 6.39.

[(κ^4-Me$_3$-tpa)Ir^I(C$_2$H$_4$)]PF$_6$ ([14]PF$_6$): Compound [**12**]PF_6 (100 mg, 0.14 mmol) was dissolved in acetone (5 mL) and stirred for 4 h under nitrogen at room temp. The gas phase was flushed with fresh nitrogen every hour. Subsequently, 25 mL of hexane was added causing precipitation of [**14**]PF_6. The resulting orange solid was collected by filtration, washed 3 times with cold hexane and dried under vacuum. Yield 42 mg (0.07 mmol, 50%). ^{1}H NMR (200.13 MHz, CD_3CN, 289 K): δ [ppm] = 7.54 (t, $^3J_{H,H}$ = 7.7 Hz, 1 H, Py^B-H^4), 7.50 (t, $^3J_{H,H}$ = 7.7 Hz, 2 H, Py^A-H^4), 7.24 (d, $^3J_{H,H}$ = 7.7 Hz, 2 H, Py^A-H^3/Py^B-H$^{3\&5}$), 7.09 (d, $^3J_{H,H}$ = 7.7 Hz, 2 H, Py^A-H$^{5/3}$/Py^B-H$^{3\&5}$), 7.02 (d, $^3J_{H,H}$ = 7.7 Hz, 2 H, Py^A-H^5/Py^B-H$^{3\&5}$), 5.29 (d[AB], $^2J_{H,H}$ = 15.3 Hz, N-*CH*$_2$-Py^A), 4.85 (d[AB], $^2J_{H,H}$ = 15.3 Hz N-*CH*$_2$-Py^A), 4.64 (s, N-*CH*$_2$-Py^B), 3.65 (s, 3 H, Py^B-CH$_3$), 2.85 (s, 6 H, Py^A-CH$_3$), 1.85 (t, 2 H, $^3J_{H,H}$ = 8.6 Hz, *CH*$_2$=CH$_2$), 1.37 (t, 2 H, $^3J_{H,H}$ = 8.58 Hz, CH$_2$=*CH*$_2$). ^{1}H NMR (400.14 MHz, [D$_6$]acetone, 289 K): δ [ppm] = 7.72 (t, $^3J_{H,H}$ = 7.8 Hz, 1 H, Py^B-H^4), 7.60 (t, $^3J_{H,H}$ = 7.8 Hz, 2 H, Py^A-H^4), 7.35 (d, $^3J_{H,H}$ = 7.2 Hz, 1 H, Py^B-H^3), 7.26 (d, $^3J_{H,H}$ = 7.6 Hz, 2 H, Py^A-H^3), 7.15 (d, $^3J_{H,H}$ = 7.3 Hz, 1 H, Py^B-H^5), 7.81 (d, $^3J_{H,H}$ = 7.8 Hz, 2 H, Py^A-H^5), 5.49 (d[AB], $^2J_{H,H}$ = 15.2 Hz, N-*CH*$_2$-Py^A), 5.11 (d[AB], $^2J_{H,H}$ = 15.2 Hz, N-*CH*$_2$-Py^A), 4.90 (s, N-*CH*$_2$-Py^B), 3.75 (s, 3 H, Py^B-*CH*$_3$), 2.94 (s, 6 H, Py^A-*CH*$_3$), 1.89 (t, 2 H, $^3J_{H,H}$ = 8.6 Hz, *CH*$_2$=CH$_2$), 1.47 (t, 2 H, $^3J_{H,H}$ = 8.79 Hz, CH$_2$=*CH*$_2$). ^{13}C{^{1}H} NMR (100.61 MHz, [D$_6$]acetone, 289 K): δ [ppm] = 164.6 (Py^A-C^6), 163.2 (Py^A-C^2), 161.8 (Py^B-C^6), 160.2 (Py^B-C^2), 138.4 (Py^B-C^4), 136.9 (Py^A-C^4), 124.7 (Py^A-C^5), 123.5 (Py^B-C^5), 119.8 (Py^A-C^3), 118.9 (Py^B-C^3), 71.7 (N-*C*H$_2$-Py^A), 65.2 (N-*C*H$_2$-Py^B), 32.5 (Py^B-*C*H$_3$), 27.2 (Py^A-*C*H$_3$), 3.7 (*C*H$_2$=CH$_2$), 0.2 (CH$_2$=*C*H$_2$). ESI$^+$-MS: *m*/*z* = 553 [M − PF$_6$]$^+$. $C_{23}H_{28}F_6IrN_4P$ (697.69): calcd. C 39.60, H 4.04, N 8.03; found C 39.43, H 4.17, N 8.20.

[(κ^3-Me$_2$-dpa-Me)Ir^I(C$_2$H$_4$)]PF$_6$ ([15]PF$_6$): Dissolving [**13**]PF_6 in CD_2Cl_2 resulted in the formation of [**15**]PF_6 within 2 h. ^{1}H NMR (200.13 MHz, CD_2Cl_2, 289 K): δ [ppm] = 7.59 (t, $^3J_{H,H}$ = 7.7 Hz, 2 H, Py-H^4), 7.17 (d, $^3J_{H,H}$ = 7.5 Hz, 2 H, Py-H^3), 7.05 (d, $^3J_{H,H}$ = 7.9 Hz, 2 H, Py-H^5), 5.07 (d[AB], $^2J_{H,H}$ = 14.9 Hz, N-*CH*$_2$-Py), 4.75 (d[AB], $^2J_{H,H}$ = 14.9 Hz, N-*CH*$_2$-Py), 3.59 (t, $^3J_{H,H}$ = 9.7 Hz, 2 H, *CH*$_2$=CH$_2$), 3.15 (s, 3 H, N-CH$_3$), 2.66 (s, 6 H, Py-CH$_3$), 2.36 (t, $^3J_{H,H}$ = 9.7 Hz, 2 H, CH$_2$=*CH*$_2$). ^{1}H NMR (400.14 MHz, CD_3CN, 289 K): δ [ppm] = 7.63 (t, $^3J_{H,H}$ = 7.9 Hz, 2 H, Py-H^4), 7.18 (d, $^3J_{H,H}$ = 7.4 Hz, 2 H, Py-H^3), 7.11 (d, $^3J_{H,H}$ = 7.9 Hz, 2

H, Py-H^5), 5.06 (d[AB], $^2J_{H,H}$ = 15.1 Hz, N-*CH*$_2$-Py), 4.71 (d[AB], $^2J_{H,H}$ = 15.1 Hz, N-*CH*$_2$-Py), 3.54 (t, $^3J_{H,H}$ = 9.7 Hz, 2 H, *CH*$_2$=CH$_2$), 3.11 (s, 3 H, N-CH$_3$), 2.64 (s, 6 H, Py-CH$_3$), 2.34 (t, $^3J_{H,H}$ = 9.7 Hz, 2 H, CH$_2$=*CH*$_2$). ^{13}C{^{1}H} NMR (75.47 MHz, CD$_3$CN, 289 K): δ [ppm] = 166.6 (Py-C^6), 164.4 (Py-C^2), 138.7 (Py-C^4), 127.2 (Py-C^5), 121.9 (Py-C^3), 72.2 (N-*C*H$_2$-Py), 52.4 (N-*C*H$_3$), 37.0 (*C*H$_2$=CH$_2$), 27.1 (Py-*C*H$_3$), 25.1 (CH$_2$=*C*H$_2$). Due to the instability of [**15**]PF$_6$, reliable elemental analytical data were not obtained.

[(κ^3-Me$_2$-dpa-Me)Ir^{I}(C$_2$H$_4$)]PF$_6$ ([15(MeCN)]PF$_6$): Dissolving [**13**]PF$_6$ in CD$_3$CN resulted in a 3:1 mixture of [**15**]PF$_6$ and [**15**(MeCN)]PF$_6$ within 2 h. ^{1}H NMR (400.14 MHz, CD$_3$CN, 289 K): δ [ppm] = 7.63 (t, $^3J_{H,H}$ = 7.8 Hz, 2 H, Py-H^4), 7.20 (d, $^3J_{H,H}$ = 7.9 Hz, 2 H, Py-H^3), 7.16 (d, $^3J_{H,H}$ = 7.8 Hz, 2 H, Py-H^5), 4.95 (d[AB], $^2J_{H,H}$ = 14.9 Hz, N-*CH*$_2$-Py), 4.57 (d[AB], $^2J_{H,H}$ = 14.9 Hz, N-*CH*$_2$-Py), 2.91 (s, 6 H, Py-CH$_3$), 2.78 (s, 3 H, N-CH$_3$), 1.94 (t, $^3J_{H,H}$ = 8.7 Hz, 2 H, *CH*$_2$=CH$_2$), 1.28 (t, $^3J_{H,H}$ = 8.7 Hz, 2 H, CH$_2$=*CH*$_2$). ^{13}C{^{1}H} NMR (75.47 MHz, CD$_3$CN, 289 K): δ [ppm] = 166 (Py-C^6), 164 (Py-C^2), 137.0 (Py-C^4), 127.2 (Py-C^5), 120.0 (Py-C^3), 72.6 (N-*C*H$_2$-Py), 51.4 (N-*C*H$_3$), 27.6 (Py-*C*H$_3$). ^{13}C NMR signals of the ethene fragment could not be observed at 289 K. Due to the instability of [**15**(MeCN)]PF$_6$, reliable elemental analytical data were not obtained.

[(κ^4-C,*N*,*N*′,*N*′′-Me$_3$-tpa)Ir(H)(CD$_3$CN)]PF$_6$ ([16]PF$_6$): Compound [**14**]PF$_6$ (20 mg, 0.03 mmol) was dissolved in MeCN (1 mL) and was kept for 3 d under nitrogen. Sample prepared in CD$_3$CN: CPy represents the unique cyclometallated pyridyl group (at C^3). ^{1}H NMR (500 MHz, CD$_3$CN, 289 K): δ [ppm] = 7.81 (d, $^3J_{H,H}$ = 7.7 Hz, CPy-H^5), 7.63 (t, $^3J_{H,H}$ = 7.7 Hz, 2 H, Py^A-H^4), 7.25 (d, $^3J_{H,H}$ = 7.2 Hz, 2 H, Py^A-H^3), 7.23 (d, $^3J_{H,H}$ = 7.7 Hz, 2 H, Py^A-H^5), 6.48 (d, $^3J_{H,H}$ = 7.7 Hz, CPy-H^4), 5.09 (d[AB], $^2J_{H,H}$ = 15.3 Hz, 2 H, N-*CH*$_2$-Py^A), 5.04 (d[AB], $^2J_{H,H}$ = 15.3 Hz, 2 H, N-*CH*$_2$-Py^A), 4.41 (s, 2 H, N-*CH*$_2$-CPy), 2.81 (s, 6 H, Py^A-CH$_3$), 2.13 (s, 3 H, CPy-CH$_3$), −18.58 (s, Ir-H). ^{13}C{^{1}H} NMR (75.47 MHz, CD$_3$CN, 289 K): δ [ppm] = 169.6 (CPy-C^6), 167.0 (Py^A-C^6), 164.6 (CPy-C^2), 151.8 (CPy-C^5), 151.2 (Py^A-C^2), 139.0 (Py^A-C^4), 127.3 (CPy-C^3-Ir), 124.9 (Py^A-C^5), 121.9 (CPy-C^4), 121.7 (Py^A-C^3), 70.4 (N-*C*H$_2$-Py^A), 68.8 (N-*C*H$_2$-CPy), 31.6 (*C*H$_3$-Py^A), 23.2 (*C*H$_3$-CPy). ESI-MS: *m*/*z* = 569 [M − PF$_6$]$^+$. Sample prepared in CH$_3$CN: ESI-MS: *m*/*z* = 566 [M − PF$_6$]$^+$. C$_{23}$H$_{27}$F$_6$IrN$_5$P (710.68): calcd. C 38.87, H 3.83, N 9.85; found C 39.07, H 4.01, N 9.99.

[(κ^4-C,*N*,*N*′,*N*′′-Me$_3$TPA)Ir(H)(C$_2$H$_4$)](PF$_6$): [**14**]PF$_6$ (10 mg, 0.015 mmol) was dissolved in CD$_2$Cl$_2$ (1 mL) and kept for 3 d under nitrogen. ^{1}H NMR: (200 MHz, CD$_2$Cl$_2$): δ [ppm] = 8.23 (d, CPy-H^5, $^3J_{H,H}$ = 7.4 Hz), 7.58 (t, 2 H, Py^A-H^4, $^3J_{H,H}$ = 7.9 Hz), 7.22 (d, 2 H, CPy-H^3, $^3J_{H,H}$ = 7.7 Hz), 7.13 (d, 2 H, Py^A-H^5, $^3J_{H,H}$ = 7.7 Hz), 6.70 (d, CPy-H^4, $^3J_{H,H}$ = 7.7 Hz), 5.50 (d[AB], N-*CH*$_2$-Py^A, $^2J_{H,H}$ = 16.0 Hz), 5.27 (d[AB], N-*CH*$_2$-Py^A, $^2J_{H,H}$ = 16.0 Hz), 4.68 (s, 2 H, N-*CH*$_2$-CPy), 3.53 (s, 4 H, *CH*$_2$=*CH*$_2$), 2.75 (s, 6 H, Py^A-*CH*$_3$), 2.22 (s, 3 H, CPy-*CH*$_3$), -15.87 (s, Ir-*H*).

[(k^4-Me$_3$-tpa)Rh^{III}(O$_2$)]PF$_6$ ([17]PF$_6$): A solution of [**11**]PF$_6$ (50 mg, 0.082 mmol) in CH$_2$Cl$_2$ (2 mL) was vigorously stirred at room temperature in contact with O$_2$ for about 30 min. The peroxo complex **17** was formed in 100% yield. Addition of hexane to the solution caused precipitation of [**17**]PF$_6$ as a light-brown solid, which was collected by filtration and dried under vacuum. ^{1}H NMR (200.13 MHz, CD$_2$Cl$_2$, 298 K): δ [ppm] = 7.63 (t, $^3J_{H,H}$ = 7.7 Hz, 2 H, Py^A-H^4), 7.60 (t, $^3J_{H,H}$ = 7.7 Hz, 1 H, Py^B-H^4), 7.34 (d, $^3J_{H,H}$ = 7.6 Hz, 1 H, Py^B-H^3 or -H^5), 7.24 (d, $^3J_{H,H}$ = 7.6 Hz, 2 H, Py^A-H^3 or -H^5), 7.11 (d, $^3J_{H,H}$ = 7.8 Hz, 1 H, Py^B-H^3 or -H^5), 7.10 (d, $^3J_{H,H}$ = 8.1 Hz, 2 H, Py^A-H^3 or -H^5), 5.64 (d[AB], $^2J_{H,H}$ = 15.5 Hz, 2 H, N-C*H*$_2$-Py^A), 5.15 (d[AB], $^2J_{H,H}$ = 15.5 Hz, 2 H, N-C*H*$_2$-Py^A), 4.68 (s, 2 H, N-C*H*$_2$-Py^B), 3.56 (s, 3 H, Py^B-C*H*$_3$), 3.03 (s, 6 H, Py^A-C*H*$_3$). ^{13}C{^{1}H} NMR (50.31 MHz, CD$_2$Cl$_2$, 298 K): δ [ppm] = 165.4, 162.7, 162.6, 160.3 (Py^B- and Py^A-C^2, Py^B- and Py^A-C^6), 139.8 (Py^A-C^4), 139.5 (Py^B-C^4), 127.6 (Py^A-C^3), 126.3 (Py^B-C^3), 120.8 (Py^A-C^5), 119.9 (Py^B-C^5), 72.0 (N-*C*H$_2$-Py^A), 67.5 (N-*C*H$_2$-Py^B), 31.3 (Py^B-*C*H$_3$), 24.2 (Py^A-*C*H$_3$). FAB$^+$-MS: *m*/*z* = 467 [M − PF$_6$]$^+$: *m*/*z* = 1079 [2 M − PF$_6$]$^+$. ESI-MS with argon as a collision gas: *m*/*z* = 467 [M − PF$_6$]$^+$. C$_{21}$H$_{24}$F$_6$N$_4$O$_2$PRh (612.32): calcd. C 41.19, H 3.95, N 9.15; found C 40.29, H 4.72, N 8.46.

[(κ^3-Me$_3$-tpa)Ir^{III}(C$_2$H$_4$)(O$_2$)]PF$_6$ ([18]PF$_6$): Compound [**14**]PF$_6$ (40 mg, 0.06 mmol) was dissolved in dichloromethane (4 mL) and placed under 1.6 bar of O$_2$ for 30 min. The solution was filtered and dried under vacuum. Yellow/brown crystals of [**18**]PF$_6$, suitable for X-ray diffraction, were obtained by vapor-vapor diffusion of diethyl ether and a solution of [**18**]PF$_6$ in MeCN. A separate volumetric gas-uptake measurement indicated consumption of 1 mol of O$_2$ per mol of [**14**]PF$_6$. During this reaction [**14**]PF$_6$ (150 mg, 0.15 mmol) consumed ca. 3.40 mL of O$_2$ (0.14 mmol). Isolated yield 7.3 mg (0.01 mmol, 16%). ^{1}H NMR (400.14 MHz, [D$_6$]acetone, 289 K): δ [ppm] = 7.97 (t, $^3J_{H,H}$ = 7.8 Hz, 2 H, Py^A-H^4), 7.82 (t, $^3J_{H,H}$ = 7.6 Hz, 1 H, Py^B-H^4), 7.63 (d, $^3J_{H,H}$ = 7.8 Hz, 2 H, Py^A-H^3), 7.43 (d, $^3J_{H,H}$ = 7.4 Hz, 1 H, Py^B-H^5), 7.41 (d, $^3J_{H,H}$ = 7.8 Hz, 2 H, Py^A-H^5), 7.37 (d, $^3J_{H,H}$ = 7.6 Hz, 1 H, Py^B-H^3), 5.79 (d[AB], $^3J_{H,H}$ = 16.0 Hz, 2 H, Py^A-*CH*$_2$-N), 5.05 (d[AB], $^3J_{H,H}$ = 16.0 Hz, 2 H, Py^A-*CH*$_2$-N), 4.80 (s, 2 H, Py^B-*CH*$_2$-N), 4.48 (br, 4 H, *CH*$_2$=*CH*$_2$), 2.96 (s, 6 H, Py^A-CH$_3$), 2.65 (s, 3 H, Py^B-CH$_3$). ^{13}C{^{1}H} NMR (75.47 MHz, [D$_6$]acetone, 289 K): δ (ppm) = 166 (Py^A-C^2), 166 (Py^A-C^2), 165 (Py^A-C^6), 159.5 (Py^B-C^6), 151 (Py^B-C^2), 140.2 (Py^A-C^4), 137.9 (Py^B-C^4), 128 (Py^A-C^5), 124.5 (Py^B-C^3), 124 (Py^B-C^5), 122 (Py^A-C^3), 65.5 (N-*C*H$_2$-Py^A), 62.7 (N-*C*H$_2$-Py^B), 22.0 (Py^A-*C*H$_3$ & Py^B-*C*H$_3$). ^{13}C NMR signals of the ethene fragment could not be observed at 289 K. ESI-MS: 585 [M − PF$_6$]$^+$, 557 [M − PF$_6$ − C$_2$H$_4$]$^+$, 553 [M − PF$_6$ − O$_2$]$^+$, 566 [M − PF$_6$ − O$_2$ − C$_2$H$_4$ + CH$_3$CN]$^+$. C$_{23}$H$_{28}$F$_6$IrN$_4$O$_2$P (729.68): calcd. C 37.86, H 3.87, N 7.68; found C 38.05, H 4.03, N 7.85.

[(κ^3-Me$_2$-dpa-Me)Ir^{III}(C$_2$H$_4$)(O$_2$)]PF$_6$ ([19]PF$_6$): [**15**]PF$_6$ (40 mg, 0.112 mmol) was dissolved in 4 mL of dichloromethane and placed under of 1.6 bar of O$_2$ for 30 min. The solution was filtered and dried under vacuum. Light-brown crystals of [**19**]PF$_6$, suitable for X-ray diffraction, were obtained by vapor-vapor diffusion of hexane and a solution of [**19**]PF$_6$ in acetone. Isolated yield 7.7 mg (0.012 mmol, 16%). ^{1}H NMR (400.14 MHz, CD$_3$CN, 289 K): δ [ppm] = 7.78 (t, $^3J_{H,H}$ = 7.8 Hz, 2 H, Py-H^4), 7.35 (d, $^3J_{H,H}$ = 7.8 Hz, 1 H, Py-H^3), 7.22 (d, $^3J_{H,H}$ = 8.1 Hz, 2 H, Py-H^5), 4.93 (d[AB], $^2J_{H,H}$ = 15.6 Hz, 2 H, N-*CH*$_2$-Py), 4.86 (d[AB], $^2J_{H,H}$ = 15.6 Hz, 2 H, N-*CH*$_2$-Py), 4.22 (br, 4 H, C$_2$H$_4$), 3.23 (s, 3 H, N-CH$_3$), 2.82 (s, 6 H, Py-CH$_3$). ^{1}H NMR (400.14 MHz, [D$_6$]acetone, 289 K): δ [ppm] = 7.93 (t, $^3J_{H,H}$ = 7.8 Hz, 2 H, Py-H^4), 7.56 (d, $^3J_{H,H}$ = 7.8 Hz, 1 H, Py-H^3), 7.37 (d, $^3J_{H,H}$ = 7.8 Hz, 2 H, Py-H^5), 5.53 (d[AB], $^2J_{H,H}$ = 15.6 Hz, 2 H, N-*CH*$_2$-Py), 5.21 (d[AB], $^2J_{H,H}$ = 15.6 Hz, 2 H, N-*CH*$_2$-Py), 4.36 (br, 4 H, *CH*$_2$=*CH*$_2$), 3.41 (s, 3 H, N-*CH*$_3$), 2.92 (s, 6 H, Py-*CH*$_3$). ^{13}C{^{1}H} NMR (75.47 MHz, CD$_3$CN, 289 K): δ [ppm] = 166.1 (Py-C^2), 165.5 (Py-C^6), 140.7 (Py-C^4), 128.6 (Py-C^5), 122.5 (Py-C^3), 71.3 (N-*C*H$_2$-Py), 52.7 (N-*C*H$_3$), 23.0 (Py-*C*H$_3$). ^{13}C NMR signals of the ethene fragment could not be observed at 289 K. C$_{17}$H$_{23}$F$_6$IrN$_3$O$_2$P (638.57): calcd. C 31.98, H 3.63, N 6.58; found C 32.14, H 3.61, N 6.38.

[1] [1a] H. Mimoun, *Pure Appl. Chem.* **1981**, *53*, 2389. [1b] F. Di Furia, G. Modena, *Pure Appl. Chem.* **1982**, *54*, 1853. [1c] O.

Bortolini, F. Di Furia, G. Modena, R. Seraglia, *J. Mol. Catal.* **1984**, *22*, 313. [1d] K. Takao, Y. Fujiwara, T. Imanaka, S. Teranishi, *Bull. Chem. Soc. Jpn.* **1970**, *43*, 1153. [1e] K. Takao, M. Wayaku, Y. Fujiwara, T. Imanaka, S. Teranishi, *Bull. Chem. Soc. Jpn.* **1970**, *43*, 3898. [1f] C. Dudley, G. Read, *Tetrahedron Lett.* **1972**, 5273. [1g] G. Read, P. J. C. Walker, *J. Chem. Soc., Dalton Trans.* **1977**, 883. [1h] L. Carlton, G. Read, M. Urgelles, *J. Chem. Soc., Chem. Commun.* **1983**, 586. [1i] G. Read, M. Urgelles, *J. Chem. Soc., Dalton Trans.* **1985**, 1591. [1j] H. Mimoun, M. M. P. Machirant, I. S. de Roch, *J. Am. Chem. Soc.* **1978**, *100*, 5437. [1k] F. Igersheim, H. Mimoun, *Nouv. J. Chim.* **1980**, *4*, 161.

[2] G. Strukul, R. A. Michelin, *J. Am. Chem. Soc.* **1985**, *107*, 7563.

[3] G. Read, *J. Mol. Catal.* **1988**, *44*, 15.

[4] [4a] K. A. Jørgensen, *Chem. Rev.* **1989**, *89*, 431. [4b] K. A. Jørgensen, B. Schiøtt, *Chem. Rev.* **1990**, *90*, 1483.

[5] [5a] B. de Bruin, M. J. Boerakker, J. J. J. M. Donners, B. E. C. Christiaans, P. P. J. Schlebos, R. de Gelder, J. M. M. Smits, A. L. Spek, A. W. Gal, *Angew. Chem. Int. Ed. Engl.* **1997**, *36*, 2064; *Angew. Chem.* **1997**, *109*, 2153. [5b] B. de Bruin, M. J. Boerakker, R. de Gelder, J. M. M. Smits, A. W. Gal, *Angew. Chem. Int. Ed.* **1999**, *38*, 219; *Angew. Chem.* **1999**, *111*.118. [5c] B. de Bruin, M. J. Boerakker, J. A. W. Verhagen, R. de Gelder, J. M. M. Smits, A. W. Gal, *Chem. Eur. J.* **2000**, *6*, 298. [5d] B. de Bruin, J. A. Brands, J. J. J. M. Donners, M. P. J. Donners, R. de Gelder, J. M. M. Smits, A. L. Spek, A. W. Gal, *Chem. Eur. J.* **1999**, *5*, 2921.

[6] R. J. N. A. M. Kicken, Thesis ("Oxidation of Iridium Olefin Complexes by H_2O_2 and O_2"), University of Nijmegen, **2001**.

[7] M. Krom, R. G. E. Coumans, J. M. M. Smits, A. W. Gal, *Angew. Chem. Int. Ed. Eng.* **2001**, *40*, 2106−2108, *Angew. Chem.* **2001**, *113*, 2164−2166.

[8] M. Krom, T. P. J. Peters, A. W. Gal, to be published.

[9] A. L. Onderlinden, A. van der Ent, *Inorg. Chim. Acta* **1972**, *6*, 420−426.

[10] J. L. Herde, J. C. Lambert, C. V. Senoff, *Inorg. Synth.* **1974**, *15*, 18−20.

[11] R. Hoffmann, J. Saillard, *J. Am. Chem. Soc.* **1984**, *106*, 2006−2026.

[12] A. Vigalok, L. J. W. Shimon, D. Milstein, *Chem. Commun.* **1996**, 1673.

[13] This kind of reactivity (path **d**) has been observed for (ethene)Ir^{I} (see ref.[6]) and (cod)Rh^{I} complexes (see ref.[5d]).

[14] See also: R. Jiménez-Cantaño, S. Niu, M. B. Hall, *Organometallics* **1997**, 1962−1968.

[15] H. Nagao, N. Komeda, M. Mukaida, M. Suzuki, K. Tanaka, *Inorg. Chem.* **1996**, *35*, 6809−6815.

[16] R. Cramer, J. A. McCleverty, J. Bray, *Inorg. Synth.* **1990**, *28*, 86.

[17] A. C. T. North, D. C. Phillips, F. C. Mathews, *Acta Crystallogr., Sect. A* **1968**, *24*, 351.

[18] P. T. Beurskens, G. Beurskens, W. P. Bosman, R. de Gelder, S. Garcia-Granda, R. O. Gould, R. Israel, J. M. M. Smits, *DIRDIF-96, A computer program system for crystal structure determination by Patterson methods and direct methods applied to difference structure factors*, Laboratory of Crystallography, Department of Inorganic Chemistry, University of Nijmegen, The Netherlands, **1996**.

[19] P. T. Beurskens, G. Beurskens, M. Strumpel, C. E. Nordman, in: *Patterson and Pattersons* (Eds.: J. P. Glusker, B. K. Patterson, M. Rossi), Clarendon Press, Oxford, **1987**, p. 356.

[20] G. M. Sheldrick, *SHELXL-97, Program for the refinement of crystal structures*, University of Göttingen, Germany, **1997**.

[21] A. L. Spek, *PLATON-93*, *Program for display and analysis of crystal and molecular structures*, University of Utrecht, The Netherlands, **1995**.

[22] N. Walker, D. Stuart, *Acta Crystallogr., Sect. A* **1983**, *39*, 158.

[23] W. Baker, K. M. Bugg, J. F. McOmie, D. A. Watkins, *J. Chem. Soc.* **1958**, 3595.

[24] M. M. da Mota, J. Rodgers, S. M. Nelson, *J. Chem. Soc. A* **1969**, 2036−2044.

New Aspects in the Coordination Chemistry of Magnesium Hydrazides

Hermann Sachdev[a]

Keywords: Hydrazides / Coordination chemistry / Magnesium / N ligands

The coordination chemistry of alkaline earth metal hydrazides has been investigated, and the synthesis and crystal structures of monomeric magnesium bis[*N*-phenyl-*N*′,*N*′-bis-(trimethylsilyl)hydrazide] (**1**) and dimeric magnesium bis[*N*,*N*-dimethyl-*N*′-(trimethylsilyl)hydrazide] (**2**) are presented. An unusual coordination sphere of the magnesium atom was observed in the first structurally characterized monomer magnesium hydrazide **1**, a highly reactive compound with side-on coordinated hydrazide ligands forming a bent butterfly-type structure. The Mg–N distances range from 1.92 to 2.45 Å and intramolecular C–H···Mg interactions in the range 2.42 to 2.63 Å are observed. This structural motif is unprecedented in the coordination chemistry of magnesium hydrazides.
(© Wiley-VCH Verlag GmbH, 69451 Weinheim, Germany, 2002)

Low-coordinated compounds of main-group metals are highly desired to study their structural chemistry and reactivity. They are considered to be potential candidates for the synthesis of ceramic composite materials by CVD techniques. Different ligand systems have been investigated to achieve low-coordinated, volatile compounds.[1,2] Hydrazines are interesting ligands due to an additional donor atom in the α-position, and metalated hydrazines exhibit a different coordination chemistry than the corresponding amides. Due to a second nitrogen atom in the adjacent α-position, intramolecular (**A**), as well as intermolecular (**B**) coordination of the metal centers is possible by the ligands.

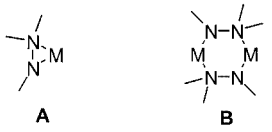

The structural chemistry of the amides of group-1, -2 and -13 metals has already been widely characterized and indicates the formation of oligomeric or polymeric ring and cage structures.[3–5] Some recent aspects of the coordination chemistry of alkali metal hydrazides have been reported,[6–8] and the syntheses of aluminium and gallium hydraziedes were studied as possible precursors for AlN[3] and GaN.[10,11] These metal hydrazides share some common features with the corresponding amides, but also show significant differences in their coordination chemistry. Monomeric magnesium complexes containing monoanionic bidentate ligands are rare and the coordination chemistry of alkaline earth metal hydrazides is quite unexplored. The alkaline earth metal hydrazides were studied in order to compare the structures with the corresponding alkali metal hydrazides.

In this report, the structures of two magnesium hydrazides are presented. The aim was to investigate the coordination chemistry of alkaline earth metal hydrazides without the influence of donor solvents on the coordination sites at the metal atoms, hence a straightforward synthesis of the corresponding compounds was carried out. The deprotonation of the hydrazines was achieved by a solution of dibutylmagnesium in hexane according to Equations (1) and (2). This gave magnesium bis[*N*-phenyl-*N*′,*N*′-bis(trimethylsilyl)hydrazide] (**1**) and magnesium bis[*N*,*N*-dimethyl-*N*′-(trimethylsilyl)hydrazide] (**2**).

$$2\,(Me_3Si)_2N-N(H)Ph + MgBu_2 \rightarrow [(Me_3Si)_2N-N-Ph]_2Mg\,(\mathbf{1}) + 2\,Bu\text{-}H \quad (1)$$

$$2\,Me_2N-N(H)SiMe_3 + MgBu_2 \rightarrow [Me_2N-N-SiMe_3]_2Mg\,(\mathbf{2}) + 2\,Bu\text{-}H \quad (2)$$

In the case of hydrazide **1**, two isomers (**C**, **D**) are likely since migration of the silyl groups is a common feature of silylated hydrazines.[12] Silyl group migration also occurs during metalation and the resulting isomers are sometimes difficult to predict, as indicated by the formation of mixed isomers in lithiated silylhydrazines.[7,8] Structural characterizations of metalated phenylhydrazines have shown that a phenyl group is able to stabilize the negative charge of a hydrazide nitrogen atom better than a silyl group leading to an η^n coordination of the metal center ($n = 2-6$) by the π-electron system, hence the formation of isomer **C** is expected.[7b–7d]

[a] Institute for Inorganic Chemistry FR 8.11, University of Saarland,
P. O. Box 1150, 66041 Saarbrücken, Germany
E-mail: h.sachdev@mx.uni-saarland.de

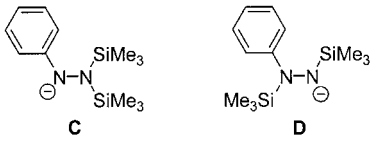

Compound **1** was obtained from the reaction of *N*-phenyl-*N*′,*N*′-bis(trimethylsilyl)hydrazine and dibutylmagnesium in hexane in a 73% yield in the form of colorless platelets according to Equation (1). It was characterized by ^{1}H, ^{13}C, and ^{29}Si NMR spectroscopy and X-ray crystallography.

The ^{29}Si NMR spectrum in hexane solution, as well as the spectrum of the isolated crystals of **1** in C_6D_6, exhibits only one resonance at $\delta = 8.70$ ppm. The ^{1}H and ^{13}C NMR data reveal a single resonance for the silyl groups, and four signals in the ^{13}C NMR for the phenyl group, which indicates the free rotation of the aryl unit. The data reveal a high symmetry for compound **1**.

The magnesium hydrazide **1** could be isolated from a hexane solution and it crystallizes in the monoclinic system (space group $P2_1/n$) containing four molecules per unit cell. The most remarkable feature of compound **1** is that it is monomeric in the solid state and no intermolecular interactions could be observed. The molecular structure of **1** is depicted in Figure 1.

In spite of the tetrahedral coordination geometry of the magnesium atom, which is common in e.g. donor-coordinated magnesium amides, an unprecedented type of coordination is adopted by the magnesium atom of compound **1** which displays an unusual arrangement of the hydrazide ligands. The magnesium atom Mg(1) exhibits four bonds with the nitrogen atoms of two side-on-coordinated hydrazide ligands giving a butterfly-shaped conformation. The individual molecule reveals a symmetry close to C_2. There are two types of Mg–N distances, short ones to the atoms N(1) and N(3) [Mg(1)–N(1) 1.918(2) Å, Mg(1)–N(3) 1.917(2) Å], both linked to the phenyl groups of the hydrazide ligands and which can be considered equal, and longer distances to the nitrogen atoms N(2) and N(4) of the NSi_2 groups [Mg(1)–N(4) 2.399(2) Å, Mg(1)–N(2) 2.448(2) Å]. The structural features of **1** resemble an sp^2-type hybridization for all nitrogen atoms in each hydrazide unit [sum of the bond angles at N(1) 360.0°, N(2) 359.9°, N(3) 359.8°, N(4) 359.4°], indicating that the basicity of the atoms N(2) and N(4) is low and an sp^3-type hybridization does not occur from the coordinative interaction of the $-NSi_2-$ nitrogen atoms with the magnesium atom. The nearest C–H···Mg interactions occur with the trimethylsilyl groups of the atoms Si(2) and Si(4), involving the carbon atoms C(6) and C(12), and are in the range of 2.417 to 2.625 Å. The shortest Mg–C distances [Mg(1)···C(6) 2.688 Å, Mg(1)···C(12) 2.696 Å] are longer than those reported for a monomeric dialkylmagnesium compound $Mg[CH(SiMe_3)_2]_2$ [Mg···C 2.535(4) Å],[13] but are of comparable magnitude as those found in a monomeric magnesium diamide $Mg[N(SiPh_2Me)_2]_2$,[14] and can be considered as quite weak. The Si–N distances involving the silyl groups Si(2) and Si(4) [1.760(2), 1.771(2) Å, respectively] are significantly longer than the distances involving the silyl groups Si(1) and Si(3) without C–H···Mg contacts [1.745(2), 1.749(2) Å], and are in general longer than the Si–N distances of tetrameric $[Ph(Li)N-N(SiMe_3)_2]_4$ and of the ether adducts of $Ph(Na)N-N(SiMe_3)_2$, which all exhibit coordinative metal–aryl interactions.[7b–7d] According to the solid-state structure of **1**, the silyl groups of the $-NSi_2$ unit are different, but the ^{29}Si NMR spectrum displays only one signal indicating a more symmetric species in solution.

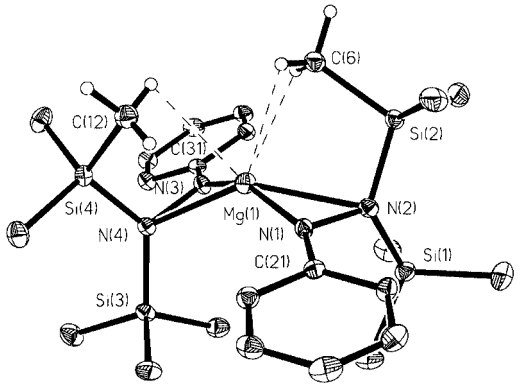

Figure 1. Molecular structure of monomeric magnesium bis[*N*-phenyl-*N*′,*N*′-bis(trimethylsilyl)hydrazide] (**1**); thermal ellipsoids are shown at a 25% probability level and only hydrogen atoms at C(6) and C(12) are shown; selected atom distances [Å] and angles [°]: N(1)–N(2) 1.497(2), N(3)–N(4) 1.493(2), Mg(1)–N(3) 1.917(2), Mg(1)–N(1) 1.918(2), Mg(1)–N(4) 2.399(2), Mg(1)–N(2) 2.448(2), Si(1)–N(2) 1.760(2), Si(2)–N(2) 1.745(2), Si(3)–N(4) 1.771(2), Si(4)–N(4) 1.749(2), N(1)–C(21) 1.372(2), N(3)–C(31) 1.372(2); N(3)–Mg(1)–N(1) 151.17(8), N(3)–Mg(1)–N(4) 38.47(6), N(1)–Mg(1)–N(4) 128.78(6), N(3)–Mg(1)–N(2) 130.34(6), N(1)–Mg(1)–N(2) 37.70(6), N(4)–Mg(1)–N(2) 144.85(6), C(21)–N(1)–N(2) 117.77(13), C(21)–N(1)–Mg(1) 151.48(12), N(2)–N(1)–Mg(1) 90.75(10), N(1)–N(2)–Si(2) 111.03(11), N(1)–N(2)–Si(1) 118.25(11), Si(2)–N(2)–Si(1) 130.61(9), N(1)–N(2)–Mg(1) 51.56(7), C(31)–N(3)–N(4) 117.72(13), C(31)–N(3)–Mg(1) 153.56(12), N(4)–N(3)–Mg(1) 88.51(9), N(3)–N(4)–Si(4) 110.82(11), N(3)–N(4)–Si(3) 118.64(11), Si(4)–N(4)–Si(3) 129.96(9), N(3)–N(4)–Mg(1) 53.02(7)

The Si–N–Si and C–N–Mg planes are almost orthogonal to each other [C(21)N(1)Mg(1)/Si(1)N(2)Si(2) 81.1°, C(31)N(3)Mg(1)/Si(3)N(4)Si(4) 98.8°], but the tilt is greater than in the corresponding lithium hydrazide (cf. 87.6°/92.3°).

The interplanar angle of the phenyl group and the N–N–Mg plane is quite small (4.2°), indicating a π interaction between the aromatic ring system and the lone pair of electrons at the nitrogen atom.

The N–Mg–N angles resulting from the side-on-coordinated hydrazide ligands are small [N(1)Mg(1)N(2) 37.70(6)°, N(3)Mg(1)N(4) 38.47(6)°], whereas the N(1)–Mg(1)–N(3) angle of 151.17(8)°, involving the deprotonated nitrogen atoms N(1) and N(3) of the hydrazide ligands, is in a similar range as reported for the monomeric magnesium bis(amide) $Mg[N(SiPh_2Me)_2]_2$ [N–Mg–N 162.8(3)°],[14] or the monomeric dialkylmagnesium com-

pound $Mg[CH(SiMe_3)_2]_2$ [C−Mg−C 140.0(2)°].[13] The angle N(2)−Mg(1)−N(4), involving both NSi_2 groups is 144.85(6)°, and the N−Mg−N angles involving different hydrazide nitrogen atoms are in the range of ca. 130° [N(1)Mg(1)N(4) 128.78(6)°, N(2)Mg(1)N(3) 130.34(6)°]. There are two types of N−N−Mg angles of comparable magnitude, those centered at the deprotonated nitrogen atoms N(1) [90.75(10)°] and N(3) [88.51(10)°], and those involving the sp^2-type $-NSi_2$ groups at N(2) [51.56(7)°] and N(4) [53.02(7)°].

A significant difference in the coordination chemistry of comparable alkali metal phenylhydrazides, where the aromatic ring system may act as an η^n ligand ($n = 2-6$) to the metal atom, is the fact that the phenyl groups do not participate in the coordinative saturation of the magnesium atom. This difference is also the reason for the larger C−N distances between the nitrogen atom of the hydrazide unit and the *i*-C of the phenyl group [1.372(2) Å] than the corresponding C−N distances of the tetrameric lithium hydrazide $[Ph-N(Li)-N(SiMe_3)_2]_4$ [1.346(5), 1.349(5) Å] or of the ether adducts of the corresponding sodium hydrazides (1.34−1.36 Å).[7c][7d]

Table 1 depicts an overview of the bond lengths involving the $Ph-N^{-}-N(SiMe_3)_2$ hydrazide ligand and different metal atoms. Although the N−N distances of the *N*-phenyl-*N*′,*N*′-bis(trimethylsilyl)hydrazides of lithium, sodium, cesium[7b−7d] and magnesium are of comparable magnitude, a significant difference is seen in the C−N and Si−N bond lengths.

Compound **2** was obtained from the reaction of *N*,*N*-dimethyl-*N*′-(trimethylsilyl)hydrazine and dibutylmagnesium in hexane in a 86% yield, in the form of colorless crystals according to Equation (2). It was characterized by ^1H, ^{13}C and ^{29}Si NMR spectroscopy and X-ray crystallography.

The ^{29}Si NMR spectrum of the hexane solution indicates two peaks at $\delta = -2.62$ and -9.43 ppm, which is identical to the spectrum of the isolated crystals in C_6D_6. The ^1H and ^{13}C NMR spectra reveal two resonances each for the silyl groups and methyl groups, and indicate two different hydrazide ligands. No change was observed up to a temperature of 60 °C in the high-temperature ^{29}Si NMR spectra. The resonances observed in the ^{29}Si NMR spectrum can be interpreted as silyl groups located at three- and four-coordinated deprotonated nitrogen atoms.

Single crystals of the magnesium hydrazide **2** could be obtained from a hexane solution and they crystallize in the monoclinic system and space group $P2_1/n$ with four formula units per unit cell.

The crystal structure of the hydrazide **2** is shown in Figure 2. It is aggregated in the form of centrosymmetric dimers in the solid state with terminal and bridging hydrazide units. The magnesium atoms are coordinated by five nitrogen atoms with Mg−N distances ranging from 1.971(2) to 2.232(2) Å.

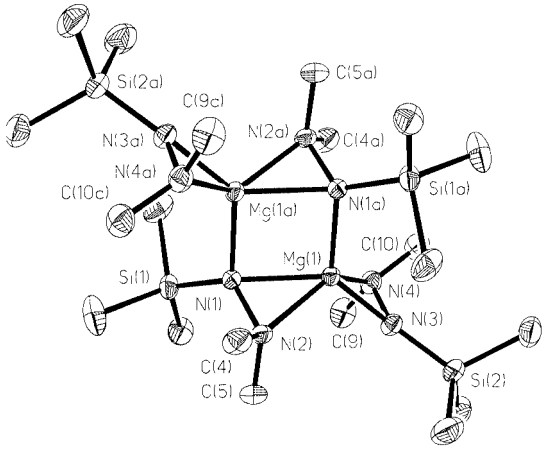

Figure 2. Molecular structure of dimeric magnesium bis[*N*,*N*-dimethyl-*N*′-(trimethylsilyl)hydrazide] (**2**); thermal ellipsoids are shown at a 25% probability level and hydrogen atoms are omitted for clarity; selected atom distances [Å] and angles [°]: Mg(1)−N(3) 1.971(2), Mg(1)−N(1a) 2.107(2), Mg(1)−N(2) 2.125(2), Mg(1)−N(1) 2.139(2), Mg(1)−N(4) 2.232(3), Mg(1)−Mg(1a) 2.9659(18), Si(1)−N(1) 1.726(2), N(1)−N(2) 1.501(3), N(1)−Mg(1a) 2.107(2), N(2)−C(4) 1.463(4), N(2)−C(5) 1.473(4), Si(2)−N(3) 1.696(2), N(3)−N(4) 1.474(3), N(4)−C(10) 1.451(5), N(4)−C(9) 1.469(5), Mg(1)−Mg(1a) 2.966(2); N(3)−Mg(1)−N(1a) 132.28(10), N(3)−Mg(1)−N(1) 136.19(10), N(2)−Mg(1)−N(4) 132.05(10), N(1a)−Mg(1)−N(1) 91.40(9), Mg(1a)−N(1)−Mg(1) 88.60(9), N(1)−Mg(1)−N(4) 121.53(10), N(3)−Mg(1)−Mg(1a) 176.87(9), N(2)−N(1)−Si(1) 124.59(16), N(2)−N(1)−Mg(1a) 111.70(15), N(2)−N(1)−Mg(1) 68.88(12), N(1)−N(2)−Mg(1) 69.91(12), N(4)−N(3)−Si(2) 126.58(18), N(4)−N(3)−Mg(1) 79.34(14), Si(2)−N(3)−Mg(1) 151.56(15), C(4)−N(2)−C(5) 109.6(3), C(10)−N(4)−C(9) 109.3(3)

If the coordination sphere of the magnesium atoms is considered with respect to the deprotonated hydrazine nitrogen atoms only, they exhibit a trigonal-planar coordination sphere [sum of the bond angles at Mg(1) involving N(1), N(1a) and N(3): 359.9°], indicating that the coordination of the NMe_2 groups to the magnesium atoms does not cause a tetrahedron-type coordination. The coordination sphere of the nitrogen atoms N(3) and N(3a) of the ter-

Table 1. Bond lengths of *N*-phenyl-*N*′,*N*′-bis(trimethylsilyl)hydrazides

Compound	$Mg[N(Ph)-N(SiMe_3)_2]_2$	$LiN(Ph)-N(SiMe_3)_2$ [7c]	$NaN(Ph)-N(SiMe_3)_2 \cdot nOR_2$ [7d]	$Cs(Ph)-N(SiMe_3)_2$ [7c]
Aggregation	monomeric	tetrameric	monomeric to polymeric	polymeric
N−N [Å]	1.497(2), 1.493(2)	1.486(5), 1.493(5)	1.47−1.51	1.501(8)
N−Si [Å]	1.760(2), 1.745(2), 1.771(2), 1.749(2)	1.733(4), 1.736(4)	1.71−1.74	1.724(6), 1.735(6)
M−N [Å]	1.917(2), 1.918(2)	1.881(9), 1.883(9)	2.30−2.33	2.991(6)
C−N [Å]	1.372(2)	1.346(5), 1.349(5)	1.34−1.36	1.351(9)

minal hydrazide units are almost trigonal-planar (sum of the bond angles: 357.5°), whereas the remaining nitrogen atoms are four-coordinate. The N−N bond length of the terminal hydrazide ligand [N(3)−N(4) 1.474(3) Å] is slightly shorter than the bond length of the hydrazide ligand bridging the magnesium atoms [N(1)−N(2) 1.501(3) Å], due to the different coordination geometries of the nitrogen atoms involved. The N−Mg−N angles of the terminal and bridging hydrazide ligands are of comparable magnitude [N(1)Mg(1)N(2) 41.21(8)°, N(3)Mg(1)N(4) 40.47(9)°], and are only slightly larger as the corresponding N−Mg−N angles of **1**. The N−N−Mg angles range from 60.2 to 79.34°, and the angles of the central Mg_2N_2 unit are close to 90° [N(1)Mg(1)N(1a) 91.40(9)°, Mg(1a)N(1)Mg(1) 88.60(9)°]. The NMR spectra of the solution are in accordance with the dimeric structure of **2**.

The dimeric structure of **2** can be explained either as an association of two molecules with both side-on- and end-on-coordinated hydrazide units each (**E**), or as an arrangement of two monomeric hydrazide units with bent, side-on-coordinated ligands (**F**). The latter explanation arises since the structural unit of the bent coordination sphere in the monomer magnesium hydrazide **1** is also detected in the structure of the dimeric molecule **2**.

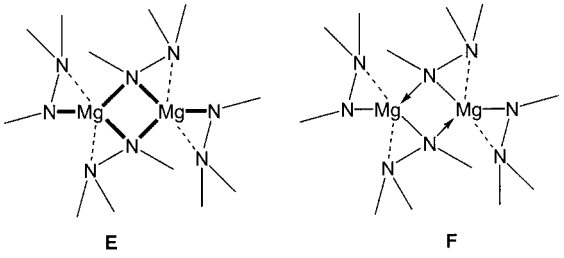

E **F**

The structural arrangement of the nitrogen atoms in dimeric **2** ($\mathbf{2}_2$) reveals some strong similarities with the corresponding dimeric magnesium amides.[15] When only the deprotonated hydrazide nitrogen atoms N(1), N(3), N(1a) and N(3a) are considered, the remaining core structure of $\mathbf{2}_2$ is almost planar, with the exocyclic nitrogen atoms inclined by 3.1° from the central Mg_2N_2 plane. This structural motif is related to the structure of the dimeric magnesium amide $Mg[N(SiMe_3)_2]_2$, and the Mg−N and Si−N distances, as well as the N−Mg−N angles of the core structure of **2** and the latter magnesium amide are similar.

In spite of an expected tetrahedral coordination geometry, the magnesium atom in compound **1** displays a side-on coordination of the hydrazine ligands, whereas magnesium bis[*N*,*N*-dimethyl-*N*′-(trimethylsilyl)hydrazide] (**2**) reveals a dimeric structure in the solid state. The unusual coordination sphere of **1** explains its high reactivity, e.g. towards ethers or toluene. In the case where these solvents are used, a reaction of **1** with the solvents occurs with the formation of phenylbis(trimethylsilyl)hydrazine, which is identified using NMR spectroscopy,[7c] and other reaction products. It has been reported that magnesium amides are able to generate arene anions, which might also be likely to react with these low-coordinated magnesium hydrazides.[16]

Since the substituents of the hydrazine unit are not extremely bulky, the bent coordination sphere at the magnesium center can result from a weak Mg···H−C interaction involving the methyl groups of the silyl substituents. Regarding heavier alkaline earth metals, a bent coordination sphere of the two-coordinate species is due to core polarization effects, as indicated by theoretical investigations.[17] The aryl ligand does not coordinate to the metal center in the magnesium hydrazide **1**, which is in contrast to the corresponding alkali metal hydrazides. Further investigations with other ligands leading to low-coordinate magnesium compounds need to be carried out in order to explain the different coordinative behavior and the bent N−Mg−N moiety.

Experimental Section

General: All reactions were performed by using modified Schlenk techniques under argon. Solvents were freshly distilled from an Na/K alloy. Dibutylmagnesium (1 M in heptane) was obtained from commercial suppliers and used as received, and starting materials were prepared according to literature methods. NMR spectra were recorded in C_6D_6 solution by using a Bruker ACP 200 spectrometer (TMS as external standards; ^{1}H: 200 MHz; ^{13}C: 55.0 MHz; ^{29}Si: 39.7 MHz). Compounds **1** and **2** react with ethers and toluene and can ignite when exposed to air. Deviations in elemental analyses are attributed to the formation of silicon carbide during combustion. The data for the crystal structure of compound **1** were collected with a Siemens P4 automated four-circle diffractometer with CCD detector and LT2 cooling device (Mo-K_α, λ= 0.71073 Å, graphite monochromator). For the X-ray structure determination of **2**, a STOE IPDS diffractometer was used (Mo-K_α, λ= 0.71073 Å, graphite monochromator). The programs XS, SHELXTL Plus and SHELX97 were used for data collection, structure solution and refinement.[18] The structures of the compounds were solved by direct methods and refined by full-matrix least-square methods. Anisotropic thermal parameters for all non-hydrogen atoms in the final cycles, isotropic refinement for hydrogen atoms positioned by geometry. CCDC-168700 and -168701 contain the supplementary crystallographic data for this paper. These data can be obtained free of charge at www.ccdc.cam.ac.uk/conts/retrieving.html or from the Cambridge Crystallographic Data Centre, 12, Union Road, Cambridge CB2 1EZ, UK [Fax: (internat.) + 44-1223/336-033; E-mail: deposit@ccdc.cam.ac.uk].

Magnesium Bis[*N*-phenyl-*N*′,*N*′-bis(trimethylsilyl)hydrazide] (1): A solution of freshly distilled *N*-phenyl-*N*′,*N*′-bis(trimethylsilyl)hydrazine (0.84 g, 3.3 mmol) in 15 mL of hexane was allowed to react at room temperature with dibutylmagnesium (1.7 mL of a 1 M solution; 1.7 mmol) in heptane. The mixture became light yellow and colorless crystals were formed at −18 °C within several days. Yield: 0.65 g (73%); m.p. 93−95 °C (dec.). ^{1}H NMR (C_6D_6): δ = 0.10 (s, Me_3Si, 18 H), 6.63−7.17 (m, Ph-N, 5 H) ppm. ^{13}C NMR: δ = 1.00 (Me_3Si), 112.58, 129.27 (o, *m*-C), 118.60 (*p*-C), 151.9 (*i*-C1) ppm. ^{29}Si NMR: δ = 8.70 ppm. $C_{24}H_{46}MgN_4Si_4$ (527.32): calcd. C 54.67, H 8.79, Mg 4.61, N 10.63; found C 52.64, H 8.29, Mg 4.36, N 10.99.

Magnesium Bis[*N*,*N*-dimethyl-*N*′-(trimethylsilyl)hydrazide] (2): Dibutylmagnesium (3.0 mL of a 1 M solution; 3.0 mmol) in heptane was added dropwise to a stirred solution of *N*,*N*-dimethyl-*N*′-(trimethylsilyl)hydrazine (0.79 g, 6.0 mmol) in 15 mL of hexane at am-

bient temperature. The evolution of butane occurred immediately. Colorless crystals separated from the solution within several days at room temperature. Yield 0.74 g (86%), m.p. 107−109 °C (dec.). ^{1}H NMR (C_6D_6): δ = 0.30 (s, Me_3Si, 9 H), 0.36 (s, Me_3Si, 9 H), 2.58 (s, Me_2N−, 6 H), 2.61 (s, Me_2N−, 6 H) ppm. ^{13}C NMR: δ = 4.77 (Me_3Si), 5.65 (Me_3Si), 52.17 (Me_2N−), 53.39 (Me_2N−) ppm. ^{29}Si NMR: δ = −2.62 [$^1J(^{13}C^{29}Si)$ = 54.0 Hz], −9.43 [$^1J(^{13}C^{29}Si)$ = 52.4 Hz] ppm. $C_{10}H_{30}MgN_4Si_2$ (286.87): calcd. C 41.87, H 10.54, Mg 8.47, N 19.53; found C 41.24, H 10.22, Mg 8.33, N 19.38.

Crystal Data and Data Collection Parameters: 1: $C_{24}H_{46}MgN_4Si_4$, M_r = 527.32, crystal size 0.22 × 0.36 × 0.48 mm, monoclinic, $P2_1/n$, a = 11.0017(2), b = 12.4958(2), c = 22.5633(4) Å, β = 96.119(1)°, V = 3084.22(9) Å^3, Z = 4, $\rho_{calcd.}$ = 1.136 Mg/m^3, μ = 0.232 mm^{-1}, F(000) = 1144, index range: $-14 \le h \le 10$, $-16 \le k \le 16$, $-27 \le l \le 28$, 2θ = 57.96°, T = 193 K, refl. collected 17422, refl. unique 5969, refl. observed (4σ) 5324, R(int.) = 0.0352, no. of variables 367, weighting scheme x/y = 0.0272/2.5741, GOOF = 1.226, final R(4σ) = 0.0476, final $wR2$ = 0.1039, largest residual peak 0.281 e/Å^3, with: $w^{-1} = \sigma^2F_o^2 + (xP)^2 + yP$; $P = (F_o^2 + 2F_c^2)/3$. **2:** $C_{10}H_{30}MgN_4Si_2$, M_r = 286.87, T = 293(2) K; monoclinic, $P2_1/n$, a = 10.320(2), b = 12.755(3), c = 14.102(3) Å, β= 98.19(3)°, V = 1837.3(7) Å^3, Z = 4, $\rho_{calcd.}$ = 1.037 Mg/m^3, μ = 0.217 mm^{-1}, F(000) = 632, crystal size: 0.35 × 0.5 × 0.5 mm, θ range for data collection: 2.16−22.51°, index ranges: $0 \le h \le 11$, $-13 \le k \le 0$, $-15 \le l \le 15$; reflections collected: 2400, independent reflections: 2400; refinement method: full-matrix least squares on F^2; data/restraints/parameters: 2400/0/274; GOOF on F^2: 1.193; final R indices [$I > 2\sigma(I)$]: $R1$ = 0.0410, $wR2$ = 0.0946; R indices (all data): $R1$ = 0.0627, $wR2$ = 0.1095; largest difference peak and hole: 0.166 and −0.179 e/Å^3.

Acknowledgments

H. S. is grateful to Prof. Dr. H. Nöth for collecting data of a low-temperature X-ray analysis of compound **1** and acknowledges financial support of the Fonds der Chemischen Industrie and the Deutsche Forschungsgemeinschaft, as well as Chemetall for the donation of alkyllithium compounds. Experimental assistance of S. Scholl is also acknowledged.

[1] M. Veith, A. Altherr, H. Wolfanger, *Chem. Vap. Deposition* **1999**, *5*, 87−90.
[2] M. Veith, *Mat. Sci. For.* **2000**, *343−346*, 531−538.
[3] C. Schade, P. v. Rague Schleyer, *Adv. Organomet. Chem.* **1987**, *27*, 169−209.
[4] M. Veith, *Chem. Rev.* **1990**, *90*, 3−16.
[5] R. E. Mulvey, *Chem. Soc. Rev.* **1991**, *20*, 167−209.
[6] C. Drost, C. Jäger, S. Freitag, U. Klingebiel, M. Noltemeyer, G. M. Sheldrick, *Chem. Ber.* **1994**, *127*, 845−947.
[7] [7a] U. Klingebiel, S. Dielkus, C. Drost, R. Herbst-Irmer, *Angew. Chem.* **1993**, *105*, 1689−1690; *Angew. Chem. Int. Ed. Engl.* **1993**, *32*, 1625. [7b] H. Nöth, H. Sachdev, M. Schmidt, H. Schwenk, *Chem. Ber.* **1995**, *128*, 105−113. [7c] B. Gemünd, H. Nöth, H. Sachdev, M. Schmidt, *Chem. Ber.* **1996**, *129*, 1335−1344. [7d] J. Knizek, I. Krossing, H. Nöth, T. Seifert, *Chem. Ber./Recueil* **1997**, *130*, 1053−1062.
[8] [8a] N. Metzler, H. Nöth, H. Sachdev, *Angew. Chem.* **1994**, *106*, 1837−1839, *Angew. Chem. Int. Ed. Engl.* **1994**, *33*, 1746−1748. [8b] K. Bode, U. Klingebiel, M. Noltemeyer, H. Witte-Abel, *Z. Anorg. Allg. Chem.* **1995**, *621*, 500−505.
[9] [9a] W. Uhl, J. Moltar, R. Koch, *Eur. J. Inorg. Chem.* **2000**, 2255−2262. [9b] H. Nöth, T. Seifert, *Eur. J. Inorg. Chem.* **1998**, 1931−1938.
[10] D. Cho, J. E. Park, B. J. Bae, K. Lee, B. Kim, J. T. Park, *J. Organomet. Chem.* **1999**, *592*, 162−167.
[11] D. W. Peters, M. P. Power, E. D. Bourret, J. Arnold, *J. Chem. Soc., Chem. Commun.* **1998**, 753−754.
[12] [12a] R. West, M. Ishikawa, R. E. Bailey, *J. Am. Chem. Soc.* **1966**, *88*, 4448−4454. [12b] R. West, *Adv. Organomet. Chem.* **1977**, *16*, 1−33.
[13] P. B. Hitchcock, J. A. K. Howard, M. F. Lappert, W. P. Leung, S. A. Mason, *J. Chem. Soc. Chem. Commun.* **1990**, 847−848.
[14] R. A. Barthlett, M. M. Olmstead, P. P. Power, *Inorg. Chem.* **1994**, *33*, 4800−4803.
[15] [15a] M. Westerhausen, W. Schwarz, *Z. Anorg. Allg. Chem.* **1992**, *609*, 39−44. [15b] M. Westerhausen, *Trends Organomet. Chem.* **1997**, *2*, 89−105.
[16] D. R. Armstrong, A. R. Kennedy, R. E. Mulvey, R. B. Rowlings, *Angew. Chem.* **1999**, *111*, 231−233; *Angew. Chem. Int. Ed.* **1999**, *38*, 131−133.
[17] [17a] M. Kaupp, P. v. R. Schleyer, *J. Am. Chem. Soc.* **1992**, *114*, 491−497. [17b] M. Kaupp, P. v. R. Schleyer, *Inorg. Chem.* **1996**, *35*, 2247−2252. [17c] M. Kaupp, P. v. R. Schleyer, H. Stoll, H. Preuss, *J. Chem. Phys.* **1991**, *94*, 1360−1366. [17d] C. Elschenbroich, A. Salzer, *Organometallchemie*, 3rd ed., B. G. Teubner, Stuttgart, **1993**, p. 58.
[18] [18a] G. M. Sheldrick, University of Göttingen, **1997**. [18b] *Shelxtl*, version 5, Siemens Analytical Instruments, Madison, **1994**.

Received January 29, 2002
[I02046]

Synthesis, Variable Temperature and Pressure ^{17}O NMR Study of Bis(alkylamide) Derivatives of $[(Gd\text{-}DTPA)(H_2O)]^{2-}$ − An Assessment of the Substitution Effect on Water Exchange Kinetics

François Botteman,[a] Gaëlle M. Nicolle,[b] Luce Vander Elst,[a] Sophie Laurent,[a] André E. Merbach,[b] and Robert N. Muller*[a]

Keywords: Water exchange / MRI contrast agents / DTPA-bis(amide) derivatives / Substituent effects / ^{17}O

In this work, primary, secondary and tertiary bis(amide) derivatives of DTPA have been synthesized and the residence time of the water molecule coordinated to their gadolinium complexes has been measured by variable temperature ^{17}O NMR spectroscopy. The influence of substituent characteristics (molecular mass, hydrophobicity, volume) has been studied. For the primary and secondary bis(amide) complexes, increasing the length of the lateral chains decreases the water residence time. It varies from 1171±38 ns for [Gd(DTPA-BA)(H_2O)] to 673±32 ns for [Gd(DTPA-BHeptA)(H_2O)]. The activation volumes of 5 bis(amide) complexes {[Gd(DTPA-BA)(H_2O)], [Gd(DTPA-BEA)(H_2O)], [Gd(DTPA-BnBA)(H_2O)], [Gd(DTPA-BAA)(H_2O)], and [Gd(DTPA-BHA)(H_2O)]} have been measured by a variable pressure ^{17}O NMR spectroscopic study. No change in the activation volume is observed when the substituent size is increased. The inner sphere is therefore not disturbed by the substitution on the amide groups. The slight decrease in water residence time can be attributed to the hydrophobicity increase of the complexes which, in turn, leads to a hydrophobic environment favorable to water molecule exchange. The water residence time of tertiary bis(amide) complexes is similar to the fastest secondary bis(amide) complex. For the tertiary bis(amide) complexes, a length increase by the substituent does not change the residence time. According to these results, we suspect that a disruption of the hydration shell of the complexes by amide substituents occurs that can influence coordinated water exchange by a factor of two, at most.
(© Wiley-VCH Verlag GmbH, 69451 Weinheim, Germany, 2002)

Introduction

Most of the contrast agents used in Magnetic Resonance Imaging (MRI) are paramagnetic complexes of gadolinium. Their efficiency, expressed by their relaxivity, r_1 (water proton relaxation rate enhancement induced by 1 millimole per liter of paramagnetic complex), depends on water exchange kinetics, electronic relaxation, and molecular tumbling, as well as on the number of water molecules in the first coordination sphere of the gadolinium cation (q). The influence of these parameters has been extensively described and the ways in which to modify some of them, for instance the rotational correlation time of the complex (τ^r) and the number q, are well known.[1] By comparison, the strategies towards changing the electronic relaxation times (τ_{Si}, $i = 1, 2$) and the residence time of the water-coordinated molecule (τ_M) are poorly understood.

[a] NMR Laboratory, Department of Organic Chemistry, University of Mons-Hainaut,
7000 Mons, Belgium
Fax: (internat.) + 32-65/373520
E-mail: robert.muller@umh.ac.be
[b] Institute of Molecular and Biological Chemistry, Swiss Federal Institute of Technology, EPFL-BCH,
1015 Lausanne, Switzerland

τ_M is not a limiting factor for the relaxivity of commercially available T_1 low molecular weight agents, like Magnevist® (Schering, Berlin, Germany), Omniscan® (Amersham Health, Amersham, United Kingdom), Dotarem® (Guerbet, Aulnay, France) or Prohance® (Bracco, Milan, Italy), at physiological temperatures and magnetic fields normally used in MRI, but this parameter may play an important role when covalent or noncovalent coupling to a macromolecule is involved.[2,3] Indeed, in order to improve the relaxivity, high molecular weight contrast agents have been developed. To reach optimal relaxivity, the residence time must, however, fulfil the condition: $T_{1M} > \tau_M > \tau_{Si}$, τ_R, where T_{1M} is the longitudinal relaxation time of nuclei in the first coordination sphere. The adjustment of τ_M is therefore of paramount importance.

Up to now, it has been reported that the water exchange rate of monoaquagadolinium chelates decreases by several orders of magnitude as compared to the aqueous ion.[4] Micksei et al. showed that the water exchange rate of $[Gd(DTPA)(H_2O)]^{2-}$ is about 200 times slower than that for aqueous gadolinium $[Gd(H_2O)_8]^{3+}$.[5] The presence of amide groups further decreases the exchange rate of Ln^{III}-DTPA derivatives.[6−9] The determination of water exchange rates for a set of lanthanide complexes of DTPA-

BMA (from Nd^{3+} to Ho^{3+}) has shown that the exchange rate increases when the ionic radius of the lanthanide decreases.[10] These two latter observations show the importance of steric hindrance in the coordination cage on the water exchange rate. Furthermore, the charge has also been invoked as a factor affecting residence times which are particularly long, as for $[Gd(DTMA)(H_2O)]^{3+}$ (τ_M= 17 μs at 278 K),[11] or short, as for $[Gd(PCTP\text{-}[13])(H_2O)]^{3-}$ (τ_M = 8 ns at 278 K).[12] Further substitution of the DTPA backbone on the ethylene bridge decreases the residence time by about 30% as compared to $[Gd(DTPA)(H_2O)]^{2-}$ at 310 K as is the case for the Gd^{III} chelates of EOB-DTPA and MS-325.[13,14]

From the literature, no simple relationship can be clearly established between the structure of Gd complexes and water exchange kinetics. To unravel some relationship, we have studied a series of equally charged but diversely amide-substituted chelates of Gd-DTPA bis(amide) derivatives (Table 1). Proton and oxygen-17 relaxometry at variable temperatures and pressures have been carried out to analyze the influence of the lengthening of the amide substituent on the water residence time.

Results and Discussion

Primary and Secondary Bis(amide) DTPA Gd^{III}-Chelates

The proton relaxivity of primary and secondary chelates measured at 20 MHz and 310 K is given in Table 2. The data for the variable temperature study is presented in Figure 1. The proton longitudinal relaxivity reflects the molecular mass increase of the complexes as expected by the Solomon−Bloembergen theory.[15,16] The relaxivity is the sum of inner- and outer-sphere contributions. The outer-sphere relaxation is not influenced by the residence time of water and increases when the temperature decreases due to the reduction of the water molecule translational diffusion. On the contrary, the inner-sphere contribution depends on the water residence time as expressed in Equations (1) and (2).

When the water residence time is short as compared to T_{1M} ($\tau_M << T_{1M}$), the inner-sphere contribution increases and the total relaxivity is enhanced when the temperature decreases, as for $[Gd(DTPA)(H_2O)]^{2-}$.[17] If the water exchange is slow, the inner-sphere contribution decreases when the temperature is reduced, as is the case for [Gd(DTPA-BMA)(H_2O)]. As a result, the total relaxivity may remain approximately constant or decrease at low temperature. The proton relaxivity of all the bis(amide) complexes studied in this work is clearly limited at low temperatures and reflects a long water residence time (Figure 1).

For the determination of the residence time from ^{17}O NMR spectroscopic measurements, the experimental ^{17}O NMR spectroscopic data were fitted assuming q = 1 (the temperature dependence of the logarithm of the ^{17}O reduced transverse relaxation rates is shown in Figure 2 for four of the studied complexes). This assumption was supported by the values of the hyperfine-coupling constant ($A/\hbar$) and relaxivities that are similar to those measured for DTPA complexes with one coordinated water molecule. Table 2 shows the parameters obtained by the fitting of the experimental points. Since the ^{17}O transverse relaxation rates have been measured at one magnetic field (7.05 T in this study), the electronic parameters obtained are relatively

Table 1. Structures of the ligands

	Bis(amide) derivative	Ligand abbreviation	
			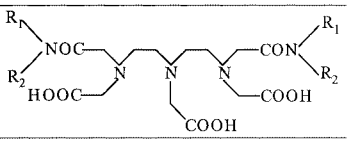
1	*Bis*(*a*mide)	DTPA-BA	$R_1 = R_2 = H$
2	*Bis*(*m*ethyl*a*mide)	DTPA-BMA	$R_1 = CH_3$, $R_2 = H$
3	*Bis*(*e*thyl*a*mide)	DTPA-BEA	$R_1 = CH_2CH_3$, $R_2 = H$
4	*Bis*(*n-p*ropyl*a*mide)	DTPA-BnPA	$R_1 = CH_2CH_2CH_3$, $R_2 = H$
5	*Bis*(*n-b*utyl*a*mide)	DTPA-BnBA	$R_1 = CH_2CH_2CH_2CH_3$, $R_2 = H$
6	*Bis*(*a*myl*a*mide)[a]	DTPA-BAA	$R_1 = CH_2CH_2CH_2CH_2CH_3$, $R_2 = H$
7	*Bis*(*h*exyl*a*mide)	DTPA-BHA	$R_1 = CH_2CH_2CH_2CH_2CH_2CH_3$, $R_2 = H$
8	*Bis*(*hept*yl*a*mide)	DTPA-BHeptA	$R_1 = CH_2CH_2CH_2CH_2CH_2CH_2CH_3$, $R_2 = H$
9	*Bis*[*bis*(*m*ethyl*a*mide)]	DTPA-BBMA	$R_1 = CH_3$, $R_2 = CH_3$
10	*Bis*[*bis*(*e*thyl*a*mide)]	DTPA-BBEA	$R_1 = CH_2CH_3$, $R_2 = CH_2CH_3$
11	*Bis*[*bis*(*n-p*ropyl*a*mide)]	DTPA-BBnPA	$R_1 = CH_2CH_2CH_3$, $R_2 = CH_2CH_2CH_3$
12	*Bis*(*t-b*utyl*a*mide)	DTPA-BtBA	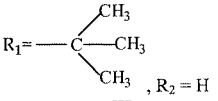
13	*Bis*(*i-p*ropyl*a*mide)	DTPA-BiPA	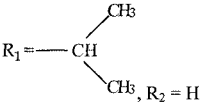
14	(*R,S*)-Bis(2-*h*ydroxy*p*ropyl*a*mide)	DTPA-(R,S)BHPA	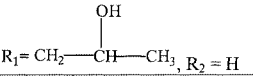

[a] The abbreviation BAA [*Bis*(*a*myl*a*mide)] for the pentyl derivative has been selected to avoid confusion with the propyl derivative (BnPA)

Table 2. Parameters obtained from the fitting of experimental ^{17}O NMR spectroscopic data at variable temperature and proton longitudinal relaxivity of the studied bis(amide) complexes

	Complexes	r_1 [s^{-1} mM^{-1}] (310 K at 20 MHz)	τ_M^{310} [ns]	$\Delta H^{\neq}$ [kJ mol^{-1}]	$\Delta S^{\neq}$ [Jmol^{-1} K^{-1}]	$A/\hbar$ [10^6 rad s^{-1}]	B [10^{20} s^{-2}]	τ_v [ps] (298 K)
	$[Gd(DTPA)(H_2O)]^{2-}$ [a]	3.8	143±25	51.5±0.3	52.1±0.6	−3.4±0.1	2.60±0.06	12.3±0.3
1	$[Gd(DTPA\text{-}BA)(H_2O)]$	3.6	1171±38	43.3±0.1	8.2±0.1	−2.8±1.5	2.45±0.07	36.5±1.2
2	$[Gd(DTPA\text{-}BMA)(H_2O)]$[b]	3.8	967±36	48.0±0.1	24.9±0.2	−3.2±0.1	2.04±0.06	21.2±0.6
3	$[Gd(DTPA\text{-}BEA)(H_2O)]$	3.7	927±31	46.8±0.1	21.2±0.1	−2.8±1.3	2.73±0.10	39.2±1.4
4	$[Gd(DTPA\text{-}BnPA)(H_2O)]$	4.0	845±35	47.2±0.1	23.4±0.2	−2.8±0.1	2.09±0.18	24.8±2.1
5	$[Gd(DTPA\text{-}BnBA)(H_2O)]$	4.4	713±31	48.5±0.1	29.2±0.2	−3.4±0.2	2.03±0.21	17.1±1.9
6	$[Gd(DTPA\text{-}BAA)(H_2O)]$	4.3	575±29	48.4±0.1	20.4±0.3	−3.6±0.1	1.96±0.17	14.8±1.3
7	$[Gd(DTPA\text{-}BHA)(H_2O)]$	4.5	681±23	45.7±0.1	20.5±0.2	−2.8±1.6	1.37±0.05	25.2±0.8
8	$[Gd(DTPA\text{-}BHeptA)(H_2O)]$	4.5	673±32	45.7±0.1	20.5±0.2	−3.0±0.3	2.27±0.14	17.9±1.1
9	$[Gd(DTPA\text{-}BBMA)(H_2O]$	3.8	624±44	48.9±0.1	31.5±0.4	−3.5±0.1	3.46±0.31	25.9±2.4
10	$[Gd(DTPA\text{-}BBEA)(H_2O)]$	3.9	654±78	48.3±0.1	29.2±0.6	−3.3±0.4	2.00±0.16	18.5±1.5
11	$[Gd(DTPA\text{-}BBPA)(H_2O)]$	4.5	672±38	42.3±0.1	9.4±0.2	−3.0±0.3	1.67±0.28	22.2±3.8
12	$[Gd(DTPA\text{-}BiPA)(H_2O)]$	4.1	654±29	52.6±0.1	42.9±0.1	−4.5±1.4	3.34±0.31	15.2±1.3
13	$[Gd(DTPA\text{-}BtBA)(H_2O)]$	4.2	659±27	44.2±0.1	15.8±0.2	−3.0±0.1	2.56±0.08	35.9±1.2
14	$[Gd(DTPA\text{-}(R,S)BHPA)(H_2O)]$	4.5	1128±95	43.2±0.1	8.1±0.3	−2.8±1.1	1.58±0.15	26.7±3.2

[a] See ref.[15] [b] The reduced ^{17}O transverse relaxation rates measured at variable temperature have been refitted with the equations used in this study.

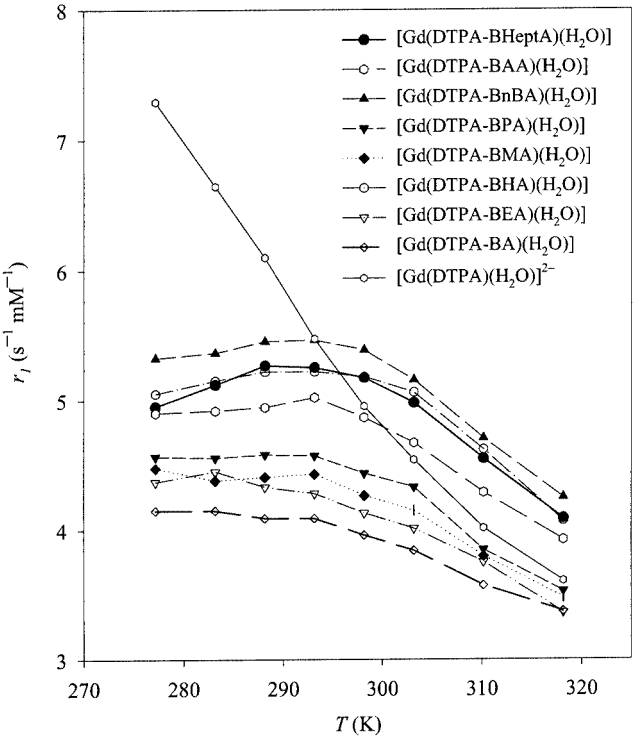

Figure 1. Temperature dependence of the proton relaxivity of linear bis(amide) complexes of $[Gd(DTPA)(H_2O)]^{2-}$ and of the parent compounds at 20 MHz

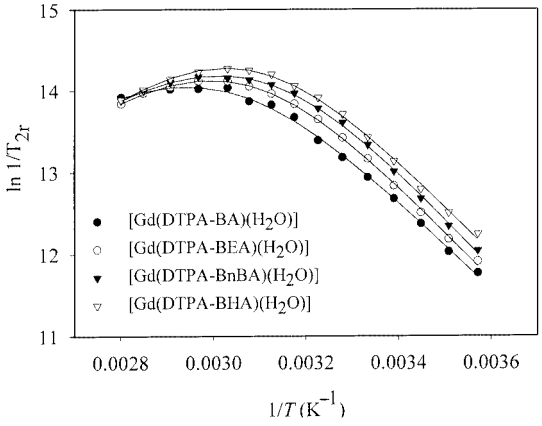

Figure 2. Temperature dependence of the reduced transverse ^{17}O relaxation rate for four linear bis(amide) complexes at 7.05 T; the straight lines represent the fitted curves

less reliable. Nevertheless, this is not a problem for the determination of the water residence time, which is nearly unaffected by the value of the electronic parameters. Table 2 indicates that the substituent size (or the substituent mass in Figure 3) has an effect on the water residence time: the larger the substituent, the faster the water exchange rate. The energy difference between the initial state and the transition state of the exchange seems thus to be reduced for a larger substituent. Steric hindrance can be invoked since it could reduce the energy necessary to reach the transition state assumed to have identical energy whatever the complex.

The ^{17}O transverse relaxation rate of the paramagnetic solutions, $1/T_2^r$, and of the acidified water reference, $1/T_2^{dia}$, were also measured at high pressure. This allows the calculation of the reduced transverse relaxation rate as described above in the variable temperature section. For the fitting of the high pressure data, T_{2M} was then fixed to the value calculated at 400 MHz with the parameters obtained at 300 MHz in the variable temperature study using Equations (7)−(10). The pressure dependence of $1/T_2^r$ at 298.15 K is presented in Figure 4 for five of the studied complexes. The decrease of $1/T_2^r$ as pressure increases, indicates a slowing down of the water exchange process, which has been checked to be reversible for all the studied Gd^{III} chelates. The fitted parameters are given in Table 3. The replacement of two carboxylic groups by two amide groups induces a nearly twofold decrease in the activation volume, as seen by

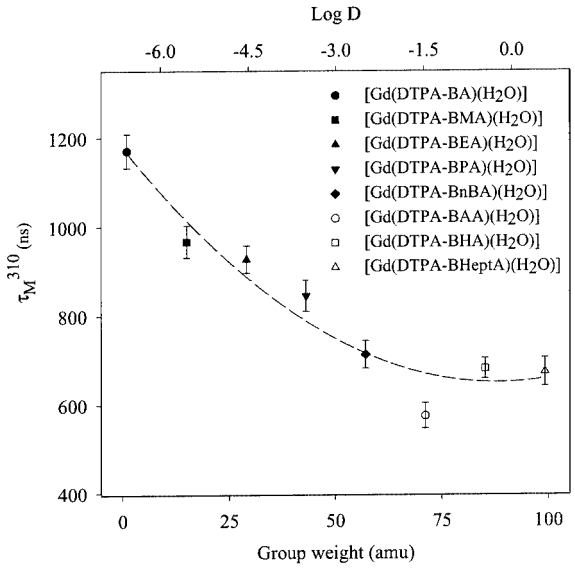

Figure 3. Dependence of the water residence time for linear bis(amide) complexes as a function of the group mass and of the hydrophobicity of the ligand (log D)

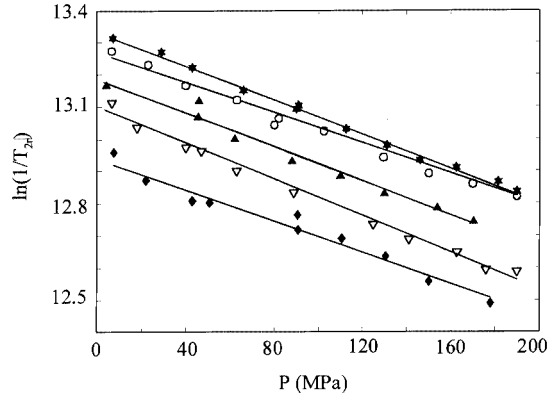

Figure 4. Pressure dependence of the reduced transverse ^{17}O relaxation rate at 298.15 K and 9.4 T for $[Gd(DTPA\text{-}BA)(H_2O)]$ (black diamonds), $[Gd(DTPA\text{-}BEA)(H_2O)]$ (white triangles), $[Gd(DTPA\text{-}BnBA)(H_2O)]$ (black triangles), $[Gd(DTPA\text{-}BAA)(H_2O)]$ (black stars) and $[Gd(DTPA\text{-}BHA)(H_2O)]$ (white circles);the straight lines represent the fitted curves

comparing $[Gd(DTPA\text{-}BA)(H_2O)]$ to $[Gd(DTPA)(H_2O)]^{2-}$. For the $[Gd(DTPA\text{-}BA)(H_2O)]$ complex, the incoming water molecule is therefore more implicated in the water exchange process than it is for the $[Gd(DTPA)(H_2O)]^{2-}$ complex. The decrease of the water exchange rate constant for $[Gd(DTPA\text{-}BA)(H_2O)]$ compared to $[Gd(DTPA)(H_2O)]^{2-}$, by one order of magnitude, therefore is not interpretable in terms of activation volume but could be attributed to the difference between their entropy of activation (see Table 2). The variation of the substituent site, on going from the methyl to the hexyl group, does not affect the value of the activation volume within the experimental errors. The activation volumes are in accordance with the one obtained for the $[Gd(DTPA\text{-}BMA)(H_2O)]$ complex in a previous study (< 7.5 cm^3 mol^{-1}) and indicates a dissociative interchange I_d mechanism.[4] The activation volume is therefore independent of the nature of the alkyl substituent. This shows in turn that the substituent does not have a major influence on the first coordination sphere nor on its steric crowding.

As stated above, the similar values obtained for the activation volumes for the series have revealed that the inner sphere is not affected by the substitution on the amide group. This result is in agreement with the available crystallographic data of various Gd-DTPA-bis(amide) complexes.[18−21] In fact, it shows that as compared to $[Gd(DTPA)(H_2O)]^{2-}$, the formation of an amide bond does not markedly modify the distances between Gd^{III} and its coordinates (Table 4). A folding of lateral chains in solution, however, is not excluded. The decrease of the residence time when the lateral chain is lengthened could be explained by such a folding due to the hydrophobic repulsion between the complex and the bulk. This phenomenon could disrupt the hydration shell of the complexes and favor the water exchange by modifying the hydrogen bonds between the exchanging water molecule and the hydration shell. For instance, the presence of a hydroxy group in $[Gd(DTPA\text{-}(R,S)BHPA)(H_2O)]$ causes an increase of about 30% of the water residence time (Table 2) as compared to $[Gd(DTPA\text{-}BnPA)(H_2O)]$. Furthermore, this folding occurs outside of the coordination cage and this could thus explain why the

Table 3. Parameters obtained from the fit of the high pressure ^{17}O NMR spectroscopic data; the high pressure study has been performed at 9.4 T and at $T = 298.15$ K if not stated otherwise; the values in parentheses are the water exchange rate constants obtained from the fit of variable temperature ^{17}O NMR spectroscopic data at 298.15 K; T_{2M} was fixed for the fit

Gd complexes	$(k_{ex})_0^T/10^6$ s^{-1} variable P	$\Delta V^{\neq}$/cm^{3}mol^{-1}	$T_{2M}/10^{-7}$ s
$[Gd(DTPA)(H_2O)]^{2-}$ [a]	1.37	+12.5±0.2	–
$[Gd(DTPA\text{-}BA)(H_2O)]$	0.44±0.01 (0.42)	+6.3±0.4	1.30
$[Gd(DTPA\text{-}BMA)(H_2O)]$[b]	0.206	+7.3±0.2	–
$[Gd(DTPA\text{-}BEA)(H_2O)]$	0.52±0.01 (0.49)	+7.3±0.2	1.36
$[Gd(DTPA\text{-}BnBA)(H_2O)]$	0.58±0.01 (0.64)	+7.0±0.4	1.54
$[Gd(DTPA\text{-}BAA)(H_2O)]$	0.68±0.01 (0.78)	+7.1±0.2	1.54
$[Gd(DTPA\text{-}BHA)(H_2O)]$	0.62±0.01 (0.71)	+6.5±0.3	1.14

[a] $T = 291.2$ K.[16] [b] $T = 285.6$ K.[4]

Table 4. Distances obtained from crystallographic data

Average distances [Å] Gd−N	Gd−O_{amide}	Gd−$O_{carboxylate}$	Gd−O_{water}	Complexes
2.64	−	2.40	2.49	$Na_2[Gd(DTPA)(H_2O)]$[a]
2.61−2.74	2.33−2.42		−	[Gd(DTPA-BMA)(H_2O)][b]
2.67	2.44	2.38	2.44	[Gd(DTPA-BBA)(H_2O)][c]
2.70	2.39	2.36	2.42	[Gd(DTPA-BEA)(H_2O)][d]

[a] From ref.[18] [b] From ref.[21] [c] BBA = *B*is(*b*enzyl*a*mide); from ref.[20] [d] From ref.[19]

activation volume is not affected by the nature of the substituent.

In order to characterize the hydrophobicity of our bis(amide) complexes carrying aliphatic linear chains, the log D coefficient of the corresponding ligands was used.[22] At a fixed pH, this log D coefficient reflects the hydrophobicity for the different ligands in solution and takes into account the contribution of ionizable groups. For the calculation of log D, the pH was set to 12 since the ligand structure is similar to the one in the complex (the carboxylate groups and nitrogen atoms are not protonated). The calculated hydrophobicity of bis(amide) ligands is reported in Figure 3. The residence time decreases with increasing hydrophobicity and remains quite similar for larger groups. This plateau could be explained due to the fact that only the first carbon atoms of the chain disturb the hydration shell that contributes to the exchange process.

The influence of the substituent volume on the water residence time was also investigated. The volumes of 4 substituents (R_1 = hydrogen, methyl, isopropyl, *tert*-butyl) were calculated using the van der Waals radii of atoms. The volumes of linear chains were not calculated because their flexibility does not allow a correct description of their volumes. The evolution of the residence times shown in Figure 5 is similar to the one observed in Figure 3. The measured values for [Gd(DTPA-BiPA)(H_2O)] and [Gd(DTPA-BtBA)(H_2O)] (Table 2) confirm a fact previously observed in this study: the only hindrance arising from the first carbon atoms of the substituent leads to a shortening of the residence time.

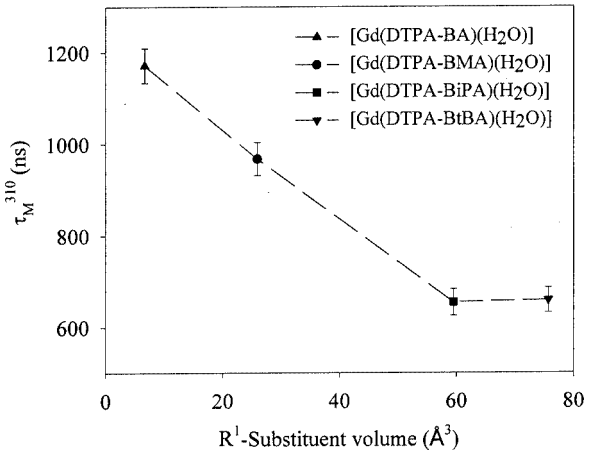

Figure 5. Volume substituent dependence of the residence time for bis(amide) complexes

An alternative explanation can be proposed. The bis(alkylamide) DTPA derivatives present four diastereoisomers in solution.[23] It has been shown for the complex $[Eu(DOTAM)(H_2O)]^{3+}$ that the diastereoisomers have different exchange rates.[24] Recently, the study of interconversion mechanisms between the diastereoisomers proved that the global value of the residence time was mainly fixed by the minor stereoisomer.[25] The exchange rates measured for the bis(alkylamide) derivatives are therefore averages weighted by the molar fractions of the stereoisomers. Like for tetrakis(amide) DOTA derivatives,[26] the alkyl chains could influence the equilibrium between the stereoisomers. According to Figure 3, the lengthening of lateral chains could favor the faster stereoisomer, but this must still be demonstrated.

Study of Tertiary Bis(amide) DTPA Complexes

For the tertiary bis(amides), the evolution of proton relaxivity at varying temperatures also demonstrates a limitation by the residence time (Figure 6). The values of the residence times are similar to those measured for the larger linear bis(amide) complexes [Gd(DTPA-BnBA)(H_2O)], [Gd(DTPA-BAA)(H_2O)], [Gd(DTPA-BHA)(H_2O)], and [Gd(DTPA-BHeptA)(H_2O)] (Table 2). The reduction of the

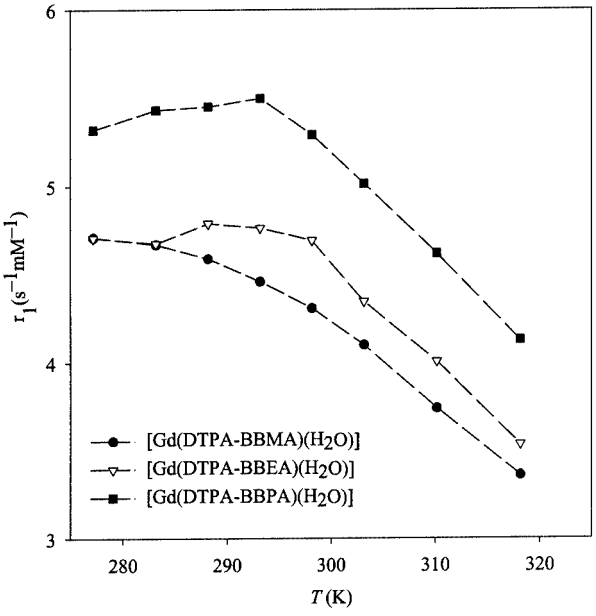

Figure 6. Temperature dependence of the proton relaxivity for tertiary bis(amide) complexes of $[Gd(DTPA)(H_2O)]^{2-}$

residence time of [Gd(DTPA-BBMA)(H_2O)] compared to [Gd(DTPA-BMA)(H_2O)], as well as the similarity of the residence time of the tertiary bis(amides), once again confirm the importance of steric hindrance at the level of the nitrogen atom from the amide group.

Conclusions

For the first time an extensive series of Gd-DTPA bis(amide) derivatives has been studied to assess the influence of the amide substituents on the water exchange rate. ^{17}O NMR spectroscopic studies carried out at variable temperatures and high pressures reveal that the substituents, which are close to the first coordination sphere, influence the residence time of bis(amide) DTPA derivatives without modifying the activation volume. However, this influence is relatively weak since the water exchange rate is doubled, at the most, for [Gd(DTPA-BA)(H_2O)] as compared to [Gd(DTPA-BHeptA)(H_2O)] and does not reach the exchange rate of $[Gd(DTPA)(H_2O)]^{2-}$. To explain the decrease of τ_M along the series, both the hydrophobicity and the hindrance of the complexes have been addressed, since these complexes are all neutral. The relative influence of these factors depends on the complexes studied. However, another hypothesis is that the lengthening of alkyl substituents favors the stereoisomers with the faster exchange rates and therefore influences the global exchange rate.

Experimental Section

Chemicals: DTPA-BMA was provided by Nycomed (Amersham Health, Amersham, United Kingdom). All chemicals and $GdCl_3 \cdot 6H_2O$ were purchased from Aldrich (Bornem, Belgium).

Ligand Synthesis: The bis(amide) derivatives of DTPA were synthesized by adding an excess of amine to DTPA-bis(anhydride).[19,27] Amine (16.8 mmol) was added to a stirred suspension of DTPA-bis(anhydride) (2 g, 5.6 mmol) in anhydrous DMF (50 mL) and heated at 325 K. After 12 h, the yellow solution was concentrated under reduced pressure. The residue was dissolved in water (50 mL) and the pH of the aqueous phase was adjusted to 7 with saturated $NaHCO_3$ solution. The aqueous phase was extracted with diethyl ether (5 × 30 mL). The organic phase was discarded and the pH of the aqueous solution was adjusted to 2−3 with 3 M HCl and the solvents evaporated once again. The residue was dissolved in a minimum of methanol and filtered. Solvent A (Table 5) was slowly added whilst stirring. The white precipitate was filtered, suspended in solvent B (Table 5) and heated until dissolution. The warm solution was filtered and cooled to 273 K. Cold solvent C (Table 5) was then slowly added whilst stirring to precipitate the ligand. The ligand was filtered, washed with diethyl ether and dried under vacuum. The yields are reported in Table 5. For the synthesis of DTPA-BHeptA, when the pH of the aqueous phase was adjusted to 7 with saturated $NaHCO_3$ solution, the aqueous phase was continuously extracted with diethyl ether for 48 h (to avoid emulsion formation). The purity and structure of the compounds were identified by ^1H, ^{13}C NMR spectroscopy with a Bruker AMX-300 (Bruker, Karlsruhe, Germany) and by LSIMS mass spectrometry (VG Analytical Autospec 6F, Manchester, UK). For this technique, samples were dissolved in water and deposited on a glycerol matrix.

NMR Spectroscopic Data

DTPA-BnPA (4): $C_{20}H_{37}N_5O_8$: 475.54 amu. ^1H NMR (D_2O, 298 K, pH ≈ 6): δ = 0.55 (t, 6 H, 2 × CH_3), 1.2 (sext, 4 H, 2 × CH_2), 2.8 (t, 4 H, 2 × CH_2), 2.9 (t, 4 H, 2 × CH_2), 3.0 (t, 4 H, 2 × CH_2), 3.1 (m, 8 H, 4 × CH_2), 3.55 (s, 2 H, 1 × CH_2) ppm. ^{13}C NMR (D_2O, 298 K, pH ≈ 6, reference pyridine): δ = 10.0, 21.1, 40.1, 49.6, 51.9, 53.6, 58.1, 58.2, 169.5, 172.2, 177.8 ppm.

DTPA-BAA (6): $C_{24}H_{45}N_5O_8$: 531.64 amu. ^1H NMR (D_2O, 298 K, pH ≈ 13): δ = 0.75 (t, 6 H, 2 × CH_3), 1.1−1.3 (m, 8 H, 4 × CH_2), 1.4 (quint, 4 H, 2 × CH_2), 2.3−2.6 (m, 8 H, 4 × CH_2), 2.9−3.2 (m, 14 H, 2 × CH_2 + 5 × CH_2) ppm. ^{13}C NMR (D_2O at 298 K, pH ≈ 13, reference MeOH): δ = 14.0, 22.4, 28.9, 32.6, 39.3, 52.1, 52.6, 58.6, 59.1, 59.4, 173.4, 179.2, 179.6 ppm.

DTPA-BHeptA (8): $C_{28}H_{53}N_5O_8$: 587.75 amu. ^1H NMR (D_2O, 298 K, pH ≈ 11): δ = 0.7 (t, 6 H, 2 × CH_3), 1−1.3 (m, 16 H, 8 × CH_2), 1.3−1.5 (quint, 4 H, 2 × CH_2), 1.8 (m, 4 H, 2 × CH_2), 2.3−2.6 (m, 6 H, 3 × CH_2), 2.9−3.3 (m, 12 H, 6 × CH_2) ppm. ^{13}C NMR (D_2O, 298 K, pH ≈ 11, reference pyridine): δ = 13.5, 22.2, 23.1, 23.2, 26.6, 28.7, 28.8, 31.5, 38.8, 52.1, 52.6, 57.9, 58.3, 58.9, 172.6, 178.5, 181.2 ppm.

DTPA-BBEA (10): $C_{22}H_{41}N_5O_8$: 503.59 amu. ^1H NMR (D_2O, 298 K, pH ≈ 6): δ = 1−1.2 (dt, 12 H, 4 × CH_3), 3.15 (t, 4 H, 2 × CH_2), 3.2−3.4 (m, 8 H, 4 × CH_2), 3.45 (s, 2 H, 1 × CH_2), 3.65 (s, 4 H, 2 × CH_2), 4.05 (s, 4 H, 2 × CH_2) ppm. ^{13}C NMR (D_2O, 298 K, pH ≈ 6, reference pyridine): δ = 14.9, 15.1, 15.9, 16.1, 43.9, 44.7, 53.4, 54.9, 58.2, 58.7, 60.6, 169.8, 176.4, 178.1 ppm.

DTPA-BBPA (11): $C_{26}H_{49}N_5O_8$: 559.70 amu. ^1H NMR (D_2O, 298 K, pH ≈ 1): δ = 0.6 (dt, 12 H, 4 × CH_3), 1.3 (m, 8 H, 4 × CH_2), 2.7−3.1 (m, 10 H, 5 × CH_2), 3.3 (m, 8 H, 4 × CH_2), 4.05 (s, 4 H, 2 × CH_2), 4.25 (s, 4 H, 2 × CH_2) ppm. ^{13}C NMR (D_2O, 298 K, pH ≈ 6, reference pyridine): δ = 6.9, 7.2, 16.6, 17.5, 44.4, 45.1, 45.5, 45.6, 50.0, 52.6, 53.4, 160.9, 165.8, 168.8 ppm.

DTPA-BiPA (13): $C_{20}H_{37}N_5O_8$: 475.54 amu. ^1H NMR (D_2O, 298 K, pH ≈ 3): δ = 0.9 (d, 12 H, 4 × CH_3), 2.95 (t, 4 H, 2 × CH_2), 3.3 (t, 4 H, 2 × CH_2), 3.4 (s, 2 H, 1 × CH_2), 3.7 (2 H, sept,

Table 5. Solvents used and yields for the syntheses of bis(amide) derivatives

Ligands	Solvent A	Solvent B	Solvent C	Yield (%)
DTPA-BnPA	acetone	2-propanol	diethyl ether	69
DTPA-BAA	acetone	ethanol	diethyl ether	51
DTPA-BHeptA	ethyl acetate	ethanol/ethyl acetate (2:2)	acetone	55
DTPA-BBEA	diethyl ether	ethanol	diethyl ether	57
DTPA-BBPA	diethyl ether	ethanol/ethyl acetate (5:5)	diethyl ether	49
DTPA-(R,S)BHPA	acetone	2-propanol	diethyl ether	47
DTPA-BiPA	diethyl ether	2-propanol/ethanol (3:1)	acetone	47

2 × CH), 3.9 (s, 4 H, 2 × CH_2), 4.0 (s, 4 H, 2 × CH_2) ppm. ^{13}C NMR (D_2O, 298 K, pH ≈ 6, reference pyridine): δ = 17.9, 38.7, 47.1, 48.6, 51.0, 53.3, 53.5, 162.7, 168.1, 169.2 ppm.

DTPA-(R,S)BHPA (14): $C_{20}H_{37}N_5O10$: 507.53 amu. ^1H NMR (D_2O, 298 K, pH ≈ 6: δ = 0.9 (d, 6 H, 2 × CH_3), 2.8 (t, 4 H, 2 × CH_2), 2.9−3.0 (m, 8 H, 4 × CH_2), 3.0−3.2 (m, 8 H, 4 × CH_2), 3.55 (s, 2 H, 1 × CH_2), 3.65 (2 H, sext, 2 × CH) ppm. ^{13}C NMR (D_2O, 298 K, pH ≈ 6, reference pyridine): δ = 18.9, 45.3, 49.7, 52.3, 53.8, 58.2, 63.2, 65.4, 169.7, 172.8, 178.0 ppm.

Preparation of the Gadolinium Complexes: The gadolinium complexes were prepared by mixing a slight excess (5%) of ligand with gadolinium chloride. The pH of the solution was adjusted to 6−7. The absence of free gadolinium ions was checked with xylenol orange indicator.[28] In order to eliminate the excess of ligand, the bis(amide) complexes were filtered through a Sep-Pak Vac 6cc cartridge, OH^- form from Waters (Brussels, Belgium) and eluted with demineralized water. The mass was confirmed by ElectroSpray spectrometry (Micromass, Manchester, UK) and the purity of the chelates was checked by HPLC (Waters, Milford, USA), C18 column, inverse phase, pH = 6.5, triethylammonium buffer 0.05 M, flow 1 mL/min, diode array and fluorescence detectors. The concentration of the Gd complex solutions was measured by proton relaxometry after decomplexation of Gd^{3+} and by Induced Coupled Plasma methods (Jobin-Yvon 38+, Jobin-Yvon ISA, Longjumeau, France).

Variable Temperature and High Pressure ^{17}O NMR Spectroscopy: Variable temperature ^{17}O NMR spectroscopic measurements were recorded with a Bruker AMX-300 spectrometer (7.05T, 40.65 MHz). The temperature was controlled by a BVT-2000 unit. ^{17}O NMR spectroscopic measurements at natural abundance were performed in 2-mL samples contained in 10-mm (o.d.) tubes. The concentration of the solutions was lower than 30 mM. ^{17}O diamagnetic transverse relaxation times of water were measured using a Carr-Purcell-Meiboom-Gill sequence (90° and 180° pulse lengths were 25 and 50 μs, respectively). All ^{17}O NMR spectra were proton-decoupled. ^{17}O transverse relaxation times of water in solutions containing Gd complexes were calculated from the spectral linewidth. High pressure ^{17}O NMR spectroscopic measurements were performed up to 200 MPa at 298.15 K and with a Bruker ARX 400 spectrometer (9.4T, 54.2 MHz) equipped with a homebuilt probe head.[29] The Gd^{III} complex solutions were enriched to 3%, using in all cases 10% ^{17}O-enriched water (Yeda R&D Co., Rehovot, Israel). Their Gd^{III} concentration was checked as previously described. The pH of the solutions, measured with a combined glass electrode, was between 4.0 and 6.1. The reference used was 2% ^{17}O-enriched bidistilled water acidified with perchloric acid. The temperature was externally controlled by a circulating flow from an external temperature bath and measured using a built-in Pt resistor. The transverse relaxation times were obtained by the CPMG spin-echo technique.[30]

Proton Relaxometry: The relaxivities were measured at 0.47T with a Bruker Minispec PC-120 thermostatted by a tetrachloroethylene flow at temperatures between 278.15 and 318.15 K. To avoid prototropic exchange, measurements were carried out at pH = 6−7.

Data Analysis: Fitting of variable temperature ^{17}O NMR spectroscopic data was performed with Minuit software (CERN library). Least-squares fits of the ^{17}O high pressure data were performed by Scientist for Windows. The log D coefficients were calculated using log D Suite developed by Advanced Chemistry Development (Toronto, Canada). The volumes of substituents were calculated with the software Molecular Modeling Pro (ChemSW Software, Fairfield, USA). All the equations that are used in the treatment of ^{17}O NMR spectroscopic data and relaxivity measurements are given here.

Relaxivity Measurement: The measured proton relaxivities contain both inner- and outer-sphere contributions [Equation (1)].

$$r_1 = r_1^{is} + r_1^{os} \tag{1}$$

The inner-sphere term is given by Equation (2), where P is the molar fraction of paramagnetic centers and q is the number of coordinated water molecules.

$$\frac{1}{T_1^{is}} = \frac{Pq}{T_{1M} + \tau_M} \tag{2}$$

Variable Temperature ^{17}O NMR Spectroscopy: The residence time of inner-sphere water molecules can be estimated by the analysis of the temperature dependence of the ^{17}O transverse relaxation rate. The observed transverse relaxation rate is the sum of a paramagnetic ($1/T_2^p$) and a diamagnetic ($1/T_2^{dia}$) contribution [Equation (3).]

$$\frac{1}{T_2} = \frac{1}{T_2^p} + \frac{1}{T_2^{dia}} \tag{3}$$

The paramagnetic term itself arises from outer-sphere ($1/T_2^{os}$) and inner-sphere ($1/T_2^{is}$) mechanisms [Equation (4)].

$$\frac{1}{T_2^p} = \frac{1}{T_2^{os}} + \frac{1}{T_2^{is}} \tag{4}$$

The inner-sphere contribution is given by the classical Equation (5), where $\Delta\omega_M$ is the chemical shift difference between bound and bulk water and T_{2M} is the transverse relaxation time of the bound water.

$$\frac{1}{T_2^{is}} = \frac{Pq}{\tau_M} \frac{T_{2M}^{-2} + \tau_M^{-1} T_{2M}^{-1} + \Delta\omega_M^2}{\left(\tau_M^{-1} + T_{2M}^{-1}\right)^2 + \Delta\omega_M^2} \tag{5}$$

It has been shown that for gadolinium complexes the outer-sphere contribution is negligible.[4] $\Delta\omega_M$ is defined by Equation (6), where g_L is the Landé factor (equal to 2 for Gd^{3+}), μ_B is the Bohr magneton, S is the electron spin (3.5 for Gd^{3+}), k_B is the Boltzmann constant, $A/\hbar$ is the hyperfine coupling constant, and T is the temperature.

$$\Delta\omega_M = \frac{g_L \mu_B S(S+1) B_o}{3 k_B T} \frac{A}{\hbar} \tag{6}$$

The transverse relaxation rate of ^{17}O coordinated to the gadolinium ion is predominantly described by the scalar interaction [Equation (7)]. The dipolar and quadrupolar contributions can be neglected since their contribution to the relaxation is 5% at the most.[4] Therefore, T_{2M} is given by Equation (7), where ω_S is the resonance frequency of the electron.

$$\frac{1}{T_{2M}} = \frac{S(S+1)}{3} \left(\frac{A}{\hbar}\right)^2 \left(\tau_{e1} + \frac{\tau_{e2}}{1 + \omega_S^2 \tau_{e2}^2}\right) \tag{7}$$

The scalar correlation times τ_{ei} are defined by Equation (8).

$$\frac{1}{\tau_{ei}} = \frac{1}{\tau_M} + \frac{1}{\tau_{Si}} \text{ with } i = 1,2 \tag{8}$$

The electronic relaxation times (τ_{Si}) are described by the contribution of the zero-field splitting interaction (no contribution of the spin rotation has been considered) and are expressed by Equation (9) and (10), where τ_v is the correlation time related to the modulation of the zero-field splitting (ZFS) and B is a parameter related to the ZFS and is independent of the temperature.

$$\frac{1}{\tau_{S1}} = B \tau_V \left[\frac{1}{1 + \omega_S^2 \tau_V^2} + \frac{4}{1 + 4\omega_S^2 \tau_V^2}\right] \tag{9}$$

$$\frac{1}{\tau_{S2}} = \frac{B\,\tau_V}{2}\left[3 + \frac{5}{1+\omega_S{}^2\,\tau_V{}^2} + \frac{2}{1+4\,\omega_S{}^2\,\tau_V{}^2}\right] \quad (10)$$

At high magnetic fields, $\omega_S\tau_{e2} >> 1$ and Equation (7) becomes Equation (11).

$$\frac{1}{T_{2M}} = \frac{S(S+1)}{3}\left(\frac{A}{\hbar}\right)^2 \tau_{e1} \quad (11)$$

A reduced relaxation rate given by Equation (12) was used in this study, where f is the ratio [paramagnetic complexes]/[water].

$$\frac{1}{T_2^r} = \frac{\left(\frac{1}{T_2^{is}}\right)}{f \times q} \quad (12)$$

The reduced transverse relaxation depends thus on the electronic relaxation time τ_{S1}, the hyperfine coupling constant $A/\hbar$, and the water residence time τ_M. The parameters $A/\hbar$ and B are independent of temperature. The temperature dependence of the water residence time and of the correlation time τ_v can be described according to the theories of Eyring and Arrhenius [Equation (13) and (14)], where $\Delta S^{\neq}$ and $\Delta H^{\neq}$ are the entropy and enthalpy of activation, respectively, for the water exchange process and E_v is the activation energy related to τ_v; τ_v^{298} is the correlation time for the modulation of the zero-field splitting interaction at 298.15 K.

$$\frac{1}{\tau_M} = \frac{k_B\,T}{h}\exp\left(\frac{\Delta S^{\neq}}{R} - \frac{\Delta H^{\neq}}{RT}\right) \quad (13)$$

$$\tau_v = \tau_v{}^{298}\exp\left(\frac{E_V}{R}\left(\frac{1}{T} - \frac{1}{298.15}\right)\right) \quad (14)$$

The temperature dependence of the ^{17}O reduced transverse relaxation rate, $1/T_2^r$, can thus be used to determine the water residence time and the related activation parameters ($\Delta S^{\neq}$ and $\Delta H^{\neq}$).

Variable Pressure ^{17}O NMR Spectroscopy: By neglecting $\Delta\omega_M$ in Equation (5) and using Equation (12), the reduced transverse relaxation rate, $1/T_2^r$, can be simplified by Equation (15), where $1/T_{2M}$ is expressed as in Equation (7).[21]

$$\frac{1}{T_2^r} = \frac{1}{T_{2M} + \tau_M} \quad (15)$$

Previous studies have shown that the logarithm of the water exchange rate varied almost linearly with pressure, as long as the compressibility coefficient of activation is negligible, as expressed by Equation (16),[31] where $\Delta V^{\ddagger}$ is the activation volume independent of pressure and $(k_{ex})_0^T$ is the water exchange rate at zero pressure and temperature T; $1/T_{2M}$ is small and therefore can be assumed to be independent of the pressure since a pressure dependence of $1/T_{2M}$ with a $\Delta V_M^{\ddagger}$ between +5 and −5 cm^3mol^{-1} does not affect the value of $\Delta V^{\ddagger}$ within the experimental errors.

$$\frac{1}{\tau_M} = k_{ex} = (k_{ex})_0^T \exp\{-\frac{\Delta V^{\ddagger}}{RT}P\} \quad (16)$$

Acknowledgments

We thank the Fonds pour la Recherche dans l'Industrie et l'Agriculture (FRIA) of Belgium. We are also grateful to the Swiss OFES as part of the EU-COST D18 Action and the Swiss National Science Foundation. The authors thank Mrs. Patricia de Francisco for her help in preparing the manuscript.

[1] P. Caravan, J. J. Ellison, T. J. McMurry, R. B. Lauffer, *Chem. Rev.* **1999**, *99*, 2293.
[2] *The Chemistry of Contrast Agents in Medical Magnetic Resonance Imaging* (Eds.: A. E. Merbach, E. Tóth), John Wiley & Sons, Ltd., **2001**, pp. 78.
[3] E. Tóth, A. E. Merbach, *Mod. Chem.* **1998**, *135*, 873.
[4] K. Micskei, L. Helm, E. Brücher, A. E. Merbach, *Inorg. Chem.* **1993**, *32*, 3844.
[5] K. Micskei, D. H. Powell, L. Helm, E. Brücher, A. E. Merbach, *Magn. Reson. Chem.* **1993**, *31*, 1011.
[6] S. Aime, M. Botta, M. Fasano, S. Paoletti, L. Anelli, F. Uggeri, M. Virtuani, *Inorg. Chem.* **1994**, *33*, 4707.
[7] E. Toth, D. Pubanz, S. Vauthey, L. Helm, A. E. Merbach, *Chem. Eur. J.* **1996**, *2*, 1607.
[8] S. W. A. Bligh, A. H. M. S. Chowdhury, D. Kennedy, C. Luchinat, G. Parigi, *Magn. Reson. Med.* **1999**, *41*, 767.
[9] C. F. G. C. Geraldes, A. M. Urbano, M. C. Alpoim, A. D. Sherry, K. T. Kuan, R. Rajagopalan, F. Maton, R. N. Muller, *Mag. Reson. Imag.* **1995**, *13*, 401.
[10] D. Pubanz, G. Gonzalez, D. H. Powell, A. E. Merbach, *Inorg. Chem.* **1995**, *34*, 4447.
[11] S. Aime, A. Barge, M. Botta, D. Parker, A. S. De Sousa, *J. Am. Chem. Soc.* **1997**, *119*, 4767.
[12] S. Aime, M. Botta, S. G. Crich, G. B. Giovenzana, R. Pagliarin, M. Piccinini, M. Sisti, E. Terreno, *J. Biol. Inorg. Chem.* **1997**, *2*, 470.
[13] L. Vander Elst, F. Maton, S. Laurent, F. Seghi, F. Chapelle, R. N. Muller, *Magn. Reson. Med.* **1997**, *38*, 604.
[14] R. N. Muller, B. Radüchel, S. Laurent, J. Platzek, C. Piérart, P. Mareski, L. Vander Elst, *Eur. J. Inorg. Chem.* **1999**, 1949.
[15] I. Solomon, *Phys. Rev.* **1955**, *55*, 559.
[16] N. Bloembergen, *J. Chem. Phys.* **1957**, *27*, 572.
[17] S. Laurent, L. Vander Elst, S. Houzé, N. Guérit, R. N. Muller, *Helv. Chim. Acta* **2000**, *83*, 394.
[18] H. Gries, H. Miklautz, *Physiol. Chem. Phys. Med.* **1984**, *16*, 105.
[19] M. S. Konings, W. C. Dow, D. B. Love, K. N. Raymond, S. C. Quay, S. M. Rocklage, *Inorg. Chem.* **1990**, *29*, 1488.
[20] S. W. A. Bligh, A. H. M. S. Chowdhury, M. McPartlin, I. J. Scowen, *Polyhedron* **1995**, *14*, 567.
[21] G. Gonzalez, H. D. Powell, V. Tissières, A. E. Merbach, *J. Phys. Chem.* **1994**, *98*, 53.
[22] C. Hansch, A. J. Leo, in *Substituent Constants for Correlation Analysis in Chemistry and Biology*, Wiley, New York, **1979**.
[23] C. F. G. C. Geraldes, A. M. Urbano, M. A. Hoefnagel, J. A. Peters, *Inorg. Chem.* **1993**, *32*, 2426.
[24] S. Aime, A. Barge, M. Botta, A. S. De Sousa, D. Parker, *Ang. Chem. Int. Ed.* **1998**, *37*, 2673.
[25] F. A. Dunand, S. Aime, A. E. Merbach, *J. Am. Chem. Soc.* **2000**, *122*, 1506.
[26] S. Aime, A. Barge, J. I. Bruce, M. Botta, J. A. K. Howard, J. M. Moloney, D. Parker, A. S. de Sousa, M. Woods, *J. Am. Chem. Soc.* **1999**, *121*, 5762.
[27] S. Laurent, L. Vander Elst, F. Copoix, R. N. Muller, *Invest. Radiol.* **2001**, *36*, 115.
[28] G. Brunisholz, M. Randin, *Helv. Chim. Acta* **1959**, *42*, 1927.
[29] A. Cusanelli, L. Nicula-Dadci, U. Frey, A. E. Merbach, *Inorg. Chem.* **1997**, *36*, 2211.
[30] S. Meiboom, D. Gill, *Rev. Sci. Instrum.* **1958**, *29*, 688.
[31] C. Cossy, L. Helm, A. E. Merbach, *Inorg. Chem.* **1989**, *28*, 2699.

Received February 20, 2002
[I02088]

A Study of the Method of Synthesis and Chromatic Properties of the Cr-SnO_2 Pigment

Beatriz Julián,[a] Héctor Beltrán,[a] Eloisa Cordoncillo,[a] Purificación Escribano,*[a] José Vicente Folgado,[b] Maria Vallet-Regí,[c] and Rafael P. del Real[c]

Keywords: Ceramics / Chromium / Chromium-tin pigment / Solid-state reactions / Tin

Chromium-doped tin dioxide has long been used as a violet pigment in the ceramic industry. However, traditional ceramic synthesis involves slow diffusion processes, high processing temperatures and serious environmental problems due to the use of carcinogenic Cr^{VI} precursors. This paper addresses the synthesis of Cr-SnO_2 by a novel, wet route that uses $Cr(acac)_3$ and $Sn(OiPr)_4$ as raw materials. The new wet method does not require handling of Cr^{VI} reagents and allows a reduction in the heat-treatment temperature from 1400 to 800 °C, which are promising economic and environmental improvements. The coloring mechanism in this pigment, currently the subject of debate, was also studied. The results indicate that the violet color is produced by the chromium ions incorporated in the cassiterite structure (SnO_2), while the quantity of chromium exceeding the network dissolution limit gives rise to Cr_2O_3 segregation, producing a greenish color. Electron spin resonance (ESR) and magnetic measurements show that chromium ions are present in the pigment in various oxidation states, reduced chromium species such as Cr^{III} and/or Cr^{IV} being responsible for the violet color.

(© Wiley-VCH Verlag GmbH, 69451 Weinheim, Germany, 2002)

Introduction

Cr-doped structures have been widely studied as ceramic pigments.[1−3] The influence of the host structure in the chromium ion crystal field produces a different coloring of the solid in which it acts as a chromophore.

Tin dioxide (cassiterite) exhibits a rutile structure consisting of infinite chains of octahedral SnO_6 linked by sharing of edges and corners to form a three-dimensional framework. This lattice has attracted attention as a host lattice for the incorporation of coloring metal ions such as transition metals, and also as a sealant for the inclusion of glaze-unstable colored pigments. When chromium ions are introduced into the SnO_2 structure in low quantities, they produce a violet color, yielding a pigment classified by DCMA (Dry Colour Manufacturer's Assn.) as 11-23-5.[4]

This pigment is usually synthesized by the conventional ceramic method, involving mixture dispersion of the metal oxides in a planetary ball mill and heat treatment of the mixture at 1200−1500 °C for a solid-state reaction. This procedure presents some drawbacks. Since the product formation rate is controlled by slow diffusion processes,[5] high reaction temperatures are required, with the energy costs entailed. These high temperatures produce losses of volatile reagents and hence departure from starting system stoichiometric conditions. To improve these interdiffusion processes, small quantities of various additives (mineralizers) need to be introduced. These mineralizers often contain toxic components. Furthermore, the Cr^{VI} precursors[6−9] used in Cr^{III} synthesis or oxidation to more oxidized species during heat treatment are highly toxic carcinogens.

To avoid the above disadvantages of the traditional ceramic method, a new method of synthesis for obtaining the reaction mixture has been tested. In this method the reagents are dissolved and begin to react at very low temperatures (70 °C). This synthesis route provides a high degree of homogeneity and low particle size, raising diffusion process efficiency, reducing heat-treatment temperature and avoiding the use of toxic mineralizers.

The Cr-SnO_2 pigment is an economically important material with a long history in the ceramic industry. However, its coloring mechanism is essentially unknown and a subject of debate.[9] The main difficulty could be related to determination of the oxidation states of the chromium ions in the network. Thus, little information on Cr-doped tin(IV) oxide materials is available.

[a] Departamento de Química Inorgánica y Orgánica, Universitat Jaume I
Campus Riu Sec, 12071 Castellón de la Plana, Spain
Fax: (internat.) + 34-964/728214
E-mail: escriban@qio.uji.es
[b] Institut de Ciència de Materials, Universitat de València
46071 Paterna (Valencia), Spain
[c] Departamento de Química Inorgánica y Bioinorgánica, Facultad de Farmacia, Universidad Complutense de Madrid, 28040 Madrid, Spain

To attempt to clarify some of these aspects, a study was undertaken, (i) to determine the optimum chromium content in the structure that yields the best color development by the traditional ceramic method, (ii) to design a new method of synthesis to reduce thermal treatment, and (iii) to determine the chromium oxidation states responsible for the violet color.

Results and Discussion

A preliminary study was carried out on five samples synthesized by the ceramic method (Method 1, see Table 5) to determine the relation between chromium starting quantity in synthesis and the resulting color after heat treatment. Phase evolution in the 1000−1400 °C range was studied by X-ray diffraction (XRD). Figure 1 shows the evolution of the crystalline phases for sample SC2.

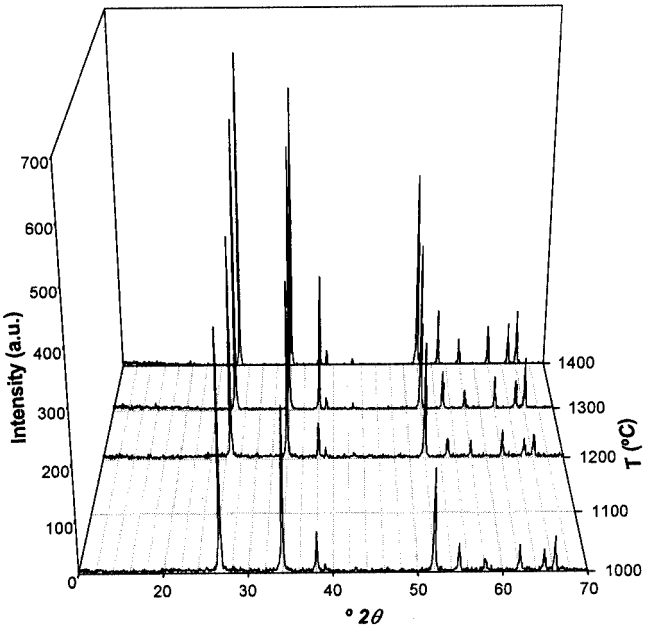

Figure 1. XRD diffractograms of sample SC2 after heat treatment at 1000, 1200, 1300 and 1400 °C for 6 h

SnO_2 (cassiterite) is the major phase in all the samples, the crystallinity of which increases with temperature. Some of the samples also exhibit peaks attributable to Cr_2O_3. The tin dioxide phase content in each sample was approximately estimated from the cassiterite (110) and Cr_2O_3 (012) peak intensities (JCPDS patterns no. 41-1445 and 38-1479, respectively) from Equation (1).

$$\%_{SnO_2} = \frac{I_{SnO_2}}{I_{SnO_2} + I_{Cr_2O_3}} \text{x}100 \quad (1)$$

Of course, for accurate analysis, a calibration curve is required for this method. XRD analysis showed a single SnO_2 phase for compositions SC1 and SC2 at all temperatures, while Cr_2O_3 was also detected for compositions SC3−SC5. In these last samples, the chromium(III) oxide phase content decreased when the temperature increased. Figure 2 plots these results. It shows that, in the samples in which the chromium content rises, high temperatures are required to produce a single phase, 1200 °C for sample SC3, 1300 °C for sample SC4, etc.

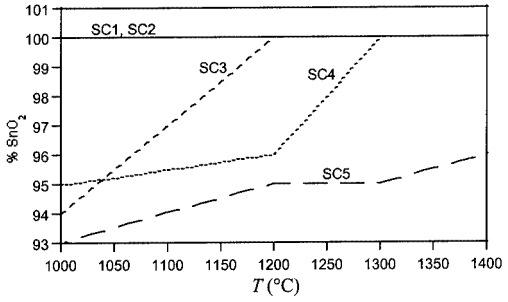

Figure 2. SnO_2 content (%) versus temperature for samples SC1, SC2, SC3, SC4 and SC5

Table 1. Colours of the samples produced by the dry method after heat treatment

Sample	1000 °C/6 h	1200 °C/6 h	1300 °C/6 h	1400 °C/6 h
SC1	pale pink	pale pink	pink-violet	violet
SC2	pale pink	pink	violet	intense violet
SC3	grey	pink-grey	pink-grey	violet-grey
SC4	grey-green	grey-pink	grey-pink	grey-pink
SC5	green	grey-green	grey-green	grey-green

Table 1 details the color of the ceramic samples heat-treated at different temperatures. For compositions with chromium contents lower than that in SC3, the violet color develops after heat treatment at 1300−1400 °C for 6 h, the SC2 composition having the most intense color. However, in samples with a chromium quantity exceeding that in SC2, a greenish shade overlies the characteristic violet color, giving rise to a greyish color for compositions SC3 and SC4, and greenish colors for SC5 at all temperatures.

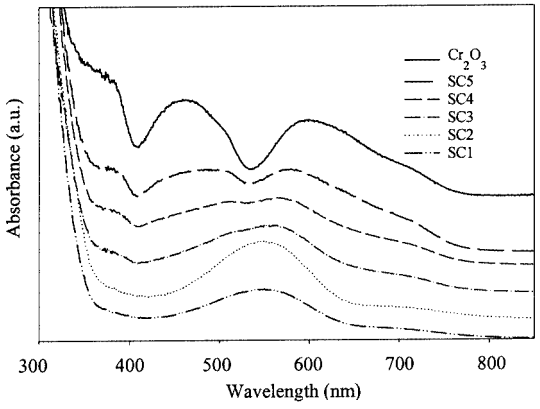

Figure 3. Diffuse reflectance spectra of ceramic samples calcined at 1400 °C for 6 h and of Cr_2O_3

Figure 3 depicts the diffuse reflectance spectra of the ceramic samples after calcination at 1400 °C for 6 h, showing the evolution of the bands with chromium content (from SC1 to SC5). The Cr_2O_3 spectrum is also included as a

reference. It is to be noted that the color of pure chromium(III) oxide is green.

In the Cr_2O_3 spectrum, two bands at 460 and 600 nm can be observed. The Cr^{III} ion, with a $3d^3$ electronic configuration, tends to an octahedral coordination. According to the Tanabe-Sugano diagram these bands can be attributed to $^4A_{2g} \rightarrow {}^4T_{2g}$ and $^4A_{2g} \rightarrow {}^4T_{1g}(F)$ spin-allowed transitions, respectively. SC1 and SC2 sample spectra exhibit a wide absorption band centerd at 18182 cm^{-1} (550 nm) and a shoulder at 14286 cm^{-1} (700 nm). In the samples with higher Cr content, however, a progressive twofold splitting of the wide absorption band can be seen. Thus, as sample SC2 developed the most intense color, the violet shade can be associated with absorption at 550 nm.

The above results indicate that, under the working conditions used, SC2 is the optimum composition. A doping ion quantity higher than that contained in $Sn_{0.985}Cr_{0.02}O_2$ cannot be fully accommodated by the host lattice, resulting in Cr_2O_3 segregation (detected by XRD), causing the greenish shade in the pigment.

It is difficult to establish where and how the chromium ion is located in the pigment, due especially to the small doping content in the violet samples (SC1 and SC2). The fact that XRD spectra of these samples detected a single tin dioxide phase at all temperatures could suggest the formation of a solid solution.

From a review of the experimental results on alloy formation, it is suggested that a difference of 15% in the radii of the metal atoms that are replacing each other is the most that can be tolerated if a substantial solid solution range is to be formed. For solid solutions in nonmetallic systems, the limiting acceptable difference in size appears to be rather larger than 15%, although difficult to quantify because it is difficult to quantify the sizes of the ions themselves.[10]

If a solid solution were formed in this system, a shift in the SnO_2 diffraction peaks should be detected, because the idealized cation radii of chromium(III) and tin(IV) ions in octahedral coordination are 75.5 and 83 pm, respectively.[11] However, comparison of XRD spectra of doped and undoped tin dioxide showed no deviations in peak positions. On the other hand, if there is free Cr_2O_3 outside the tin dioxide lattice, the amount must be below the sensitivity threshold of the instrument. XRD analysis therefore does not enable solid solution formation to be established.

The Cr-SnO_2 pigment composition was thus optimized (sample SC2) by the ceramic method. This composition was therefore prepared by the wet method (sample referenced SC6). Undoped tin dioxide was also synthesized as a reference under the same conditions (sample S2).

XRD characterization of the powders produced by Method 2 (after heating under reflux and evaporation of the solvent) showed that they were amorphous. To determine the cassiterite crystallization temperature and to design an appropriate heat treatment to remove organic matter, differential thermal (DTA) and thermogravimetric (TG) analyses were performed. Figure 4 shows the DTA/TG data for sample SC6 in the 25−1200 °C range.

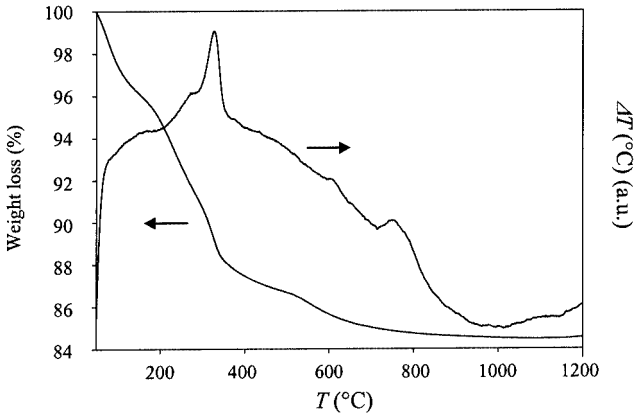

Figure 4. DTA/TG curves found for sample SC6

The DTA curve of SC6 displayed several broad exothermic peaks below 650 °C, which were accompanied by a gradual weight loss of 15% as detected by TG measurements. These bands can be assigned to solvent evaporation (below 150 °C) and decomposition/combustion of the organic groups. An exothermic peak without weight loss at 750 °C was also detected. This latter peak could be tentatively associated with cassiterite crystallization. To confirm this, the sample was heat-treated at several temperatures below and above 750 °C, followed by XRD analysis. The resulting XRD patterns indicated that SnO_2 crystallization occurred at 400 °C. The crystallization peak in the DTA curve is probably overlapped by organic matter burnout (between 150 and 650 °C) and cannot be detected. Moreover, the same peak was also observed in the undoped sample (SC2). This exothermic peak was therefore associated with SnO_2 phase transformation.

In spite of the detection of SnO_2 crystallization at 400 °C, heat-treatment design needed to ensure complete removal of organic matter. Taking this into account and also to enable comparison of the results of the two methods of synthesis, the following heat-treatment schedule was adopted. Samples SC2 and SC6 (with the same composition but synthesized by different methods) were calcined in air at a heating rate of 10 °C/min at 800, 1000, 1200, 1300, and 1400 °C for 6 h, with a hold at 500 °C for 1 h. The diffractograms of the samples indicate the presence of SnO_2 as single phase, while the diffraction peak intensity increases with temperature.

Table 2 shows the color and CIELAB (L*a*b*) parameters of samples SC2 and SC6 after heat treatment at several temperatures.

In Table 2 the same color evolution can be observed for both samples from 1000 to 1400 °C. However, at 800 °C the ceramic sample exhibited a yellow color, whereas sample SC6 exhibited a violet color with L*a*b* parameters similar to those found for the SC2 sample after calcination at 1400 °C for 6 h. The wet method thus reduced the synthesis temperature by 600 °C.

The diffuse reflectance spectra of the SC2 and SC6 samples under different heat-treatment conditions are dis-

Table 2. L* a* b* parameters for SC2 and SC6 samples heat treated at different temperatures

	800 °C/6 h		1000 °C/6 h		1200 °C/6 h		1400 °C/6 h	
Sample	SC2	SC6	SC2	SC6	SC2	SC6	SC2	SC6
Color	yellow	violet	pale pink	pale pink	pink	pink	violet	intense violet
L*	79.83	61.06	83.66	78.26	82.10	83.61	63.28	50.83
a*	2.15	15.95	3.71	6.65	4.63	3.89	15.33	15.92
b*	7.26	−12.48	2.71	2.01	1.16	4.49	−12.08	−12.74

played in Figure 5, part a) (ceramic method) and part b) (dissolution method).

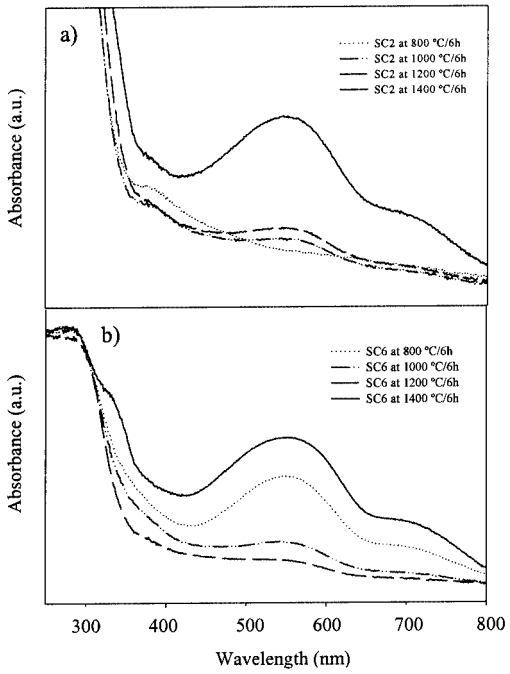

Figure 5. Diffuse reflectance spectra of samples (a) SC2 and (b) SC6 heat-treated at 800, 1000, 1200 and 1400 °C for 6 h

All the spectra show a strong absorption band in the ultraviolet zone (from 200 to around 350 nm) but different behavior is observed in the two synthesis methods. The most remarkable fact is the similarity between the spectra of the SC2 sample, calcined at 1400 °C for 6 h, and the SC6 sample calcined at 800 °C for 6 h, producing the same color in the two samples (Table 2). The spectrum of sample SC6 heat treated at 1400 °C shows a high intensity for the band centerd at 550 nm, which explains the very intense violet color exhibited by this sample.

Although exhaustive study for thorough understanding of the pigment-coloring mechanism is still pending, exploratory studies were performed to determine the origin of the differences found in the colors of samples SC2 and SC6 heat-treated under the same conditions.

The first explanation advanced was that the violet color was related to the quantity of chromium introduced into the SnO_2 framework. This would allow a ready explanation of the violet color found in the sample prepared by the wet method at 800 °C, since the degree of homogeneity and the reaction rate are much higher than in the ceramic method.

An estimation was therefore made of the Cr content inside and outside the framework for the SC2 and SC6 samples calcined at 800 and 1200 °C for 6 h. These two temperatures were chosen because at 800 °C/6 h the colors of the two samples were quite different, while at 1200 °C/6 h the color was the same. The samples were washed by the procedure described in the Exp. Sect. Acid attack and oxidation to Cr^{VI} were performed to remove the unretained chromium in the SnO_2 lattice. The Cr^{VI} content in the washing liquids was determined by atomic absorption spectrometry (AAS), and the Cr content in the washed powders was analysed by X-ray fluorescence (XRF). The values, expressed in mol Cr/g pigment, are summarized in Table 3.

Table 3. Cr^{VI} content in washing liquids and Cr content in washed powders

Sample	800 °C/6 h	1200 °C/6 h
SC2 (washing liquids)	3.034×10^{-5}	1.283×10^{-5}
SC2 (powders)	1.171×10^{-4}	1.355×10^{-4}
SC6 (washing liquids)	2.657×10^{-5}	1.794×10^{-5}
SC6 (powders)	1.118×10^{-4}	1.013×10^{-4}

The initial chromium content was 1.334×10^{-4} mol/g pigment. Table 3 shows that the Cr^{VI} content in the washing liquids is slightly higher in samples heat-treated at 800 °C for 6 h. This is a reasonable finding, if it is taken into account that the introduction of chromium into the SnO_2 structure requires slow diffusion processes, which improve with increasing temperature. However, no significant difference in Cr^{VI} content, that could be responsible for the drastic difference in color (at 800 °C), was found between the washing liquids of samples SC2 and SC6. Moreover, the color of the washed and unwashed samples does not differ significantly. On the other hand, the Cr content detected in the solid by XRF for both samples at the two temperatures is also similar (it is to be noted that measurement was at the detection limit of this technique).

Due to the similarity of the Cr content in both samples, the differences in color can be considered mainly due to variations in the oxidation state of the chromium ions, and not to the chromium content introduced into the SnO_2 structure.

In order to analyse the chromium oxidation states, electron spin resonance (ESR) analysis was performed for samples SC2 and SC6 heat-treated at 800 and 1200 °C. The ESR spectra found are depicted in Figure 6.

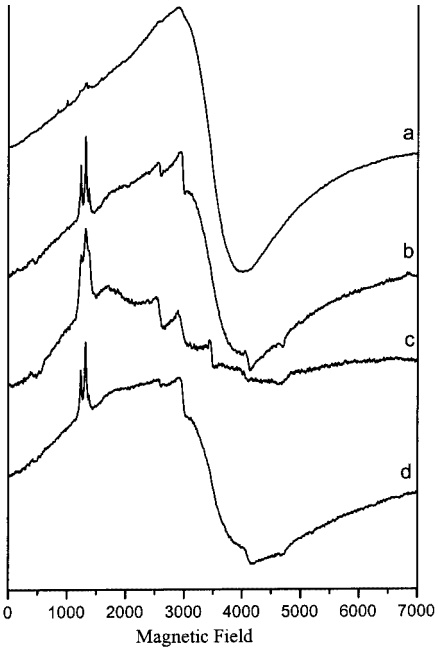

Figure 6. ESR spectra of sample SC2 heat-treated at 800 °C/6 h (a) and 1200 °C/6 h (b), and sample SC6 heat-treated at 800 °C/6 h (c) and 1200 °C/6 h (d)

The four spectra are each dominated by a very broad signal centerd at a g value of ca. 2, with other, narrower, superimposed peaks. The ratio between the narrow and the broad signals depends on the method of synthesis and the heat-treatment temperature. These facts indicate the presence of Cr^{3+} in the samples. The broad isotropic signal can be attributed to Cr_2O_3-like clusters, whereas the narrow signals correspond to isolated Cr^{3+} ions (i.e., diluted in a diamagnetic lattice[12−14]). Broad signals at $g = 2$ have also been observed in mixed-valence trimers of the type $Cr^{VI}-O-Cr^{III}-O-Cr^{VI}$ with an average oxidation state of +5.[15,16]

The spectra of sample SC2 at 800 °C/6 h are dominated by the signal at $g = 2$, indicating that the chromium ions are predominantly forming clusters. In contrast, for sample SC6 at the same temperature, the chromium ions basically appear as isolated species and the relative quantity of clusters is smaller. Moreover, in the latter sample, a very weak sharp signal at $g = 2$ may indicate the presence of a small quantity of Cr^{V} or tetrahedrally coordinated Cr^{IV} ions.[17] Almost identical spectra were found for the SC2 and SC6 samples heat-treated at 1200 °C for 6 h. In these samples, isolated Cr^{3+} ions and clusters are observed and, although the cluster fraction is still significant, it is lower than that in SC2 at 800 °C for 6 h.

With regard to the set of signals associated with isolated Cr^{3+} ions, at least seven features are observed in each spectrum. Careful study of these signals indicates that they are due to the presence of Cr^{3+} in two different polyhedral coordinations, both corresponding to orthorhombically distorted octahedra.[12−14] Cr^{III} is an $S = 3/2$ ion and exhibits a zero field splitting (characterized by D and E parameters), which is very sensitive to small variations of the local crystal field. In our case, the spectra are typical of $2D >> h\nu$ and $E \neq 0$, and two groups of five signals should be expected under the experimental conditions used. Although no accurate calculations can be performed, due to overlapping and poor resolution of the signals, a value of $D > 0.6$ cm^{-1} and an E/D ratio of ca. 0.22 and 0.28 can be estimated for the two slightly different sites. The higher E value corresponds to a major orthorhombic distortion of the site. These values are very similar to those found in Cr^{3+} diluted in TiO_2-rutile,[12−14] and suggest that Cr^{3+} is incorporated into the Sn sites in the SnO_2 lattice.

This study reflects the tendency of paramagnetic chromium ions to form clusters with strong Cr−Cr interactions. Since no remarkable differences in chromium oxidation states were found in the different samples and no clear signal associated with isolated Cr^{V} species and Cr^{IV} ions was detected, the color difference could be related to the quantity of chromium in each oxidation state. The clustering effect may modify the color slightly, but would not be expected to produce the drastic changes in color found in these samples.

To confirm the presence of Cr^{III} in the two different distorted octahedral environments, the band observed in the UV/Vis spectra at 550 nm was deconvoluted by a Gaussian function. Figure 7 shows that this band can be resolved into two bands centerd at 578 and 510 nm, which matches ESR results.

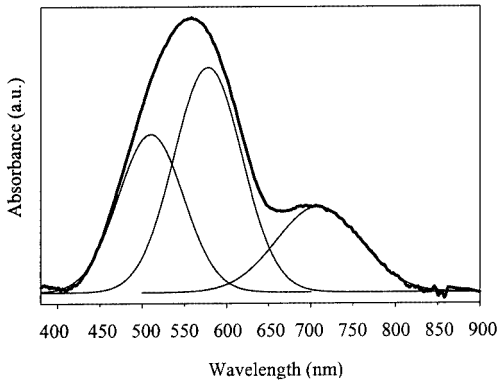

Figure 7. Deconvolution in Gaussian functions of the band centerd at 550 nm

According to the Tanabe-Sugano diagram, two other bands should be observed in the UV/Vis region. The most energetic band should appear in the UV zone and cannot be detected. The second band associated with a $^4A_{2g} \rightarrow {}^4T_{2g}$ transition should appear at around 380 nm, but is overlapped by a broad charge-transfer band in the UV zone.

The presence of Cr^{IV} ions was also studied in the absorption spectra, but no characteristic signals of this species were found (in the IR region, at 1000−1200 nm).[18] If any Cr^{IV} ions are contained in the pigment, they must be in

small quantities as they are not detected within the sensitivity limits of the instrument.

As the presence of Cr^{II} ions was precluded under the synthesis conditions used, the existence of chromium ions in more than one oxidation state (Cr^{VI}, Cr^{V}, Cr^{IV} and Cr^{III}) was determined from measurements of magnetic moment (*m*) vs. magnetic field (*H*) at a constant temperature of 77 K. For this purpose the magnetic response of a sample is assumed to be generated from the paramagnetic contributions of the chromium ions in each oxidation state. It was further assumed that the chromium ions in a sample are only contained in two oxidation states, Cr^{VI} (with no magnetic response) and Cr in another oxidation state (III, IV or V, each having its own magnetic response). Table 4 summarizes the calculated quantity of Cr^{VI} contained in the structure for each pair of oxidation states (Cr^{III} and Cr^{VI}, Cr^{IV} and Cr^{VI}, or Cr^{V} and Cr^{VI}).

Table 4. Cr^{VI} content (%) in the samples for each pair of oxidation states

	Cr^{VI} (%)			
Oxidation state	SC2 at 800 °C/6 h	SC6 at 800 °C/6 h	SC2 at 1200 °C/6 h	SC6 at 1200 °C/6 h
Cr^{III}	82	40	91	81
Cr^{IV}	66	0	84	64
Cr^{V}	8	−	57	5

The Cr^{VI} content (%) was found from the slope (*m* vs. *H*) and quantity of Cr in the samples.[19]

The data indicate that all samples contain chromium ions in different oxidation states. Sample SC6 at 800 °C shows a high magnetic response, which could be attributable to all the chromium ions being in oxidation state IV (and no Cr^{VI} would be present). However, since Cr^{III} was detected by ESR, it must also contain Cr^{VI}, so that this sample must mainly contain species in low oxidation states (Cr^{III} and Cr^{IV}) and a minor quantity of Cr^{VI}. All the other samples show low magnetization values indicating a very high Cr^{VI} content, this being especially notable for sample SC2 at 1200 °C for 6 h. Samples SC2 at 800 °C and SC6 at 1200 °C exhibit the same magnetic behavior, but different colors. This can be explained by the assumption of a different distribution of chromium ions in the various oxidation states.

The ESR results and magnetic measurements therefore indicate that differences in color are directly related to the quantity of chromium in each different oxidation state, and must be mainly generated by reduced species such as Cr^{III} and Cr^{IV}. Emission measurements are currently under further investigation in order to achieve a better understanding of the coloring mechanism.

Conclusion

A new synthesis method to prepare chromium-doped tin dioxide from a mixture of Sn^{IV} and Cr^{III} precursors has been devised, and compared with the traditional ceramic method. The composition that developed the best violet color under the working conditions used was $Sn_{0.985}Cr_{0.02}O_2$. The great advantage of this dissolution method is that the intense violet color can be produced after heat treatment at 800 °C for 6 h, whereas the traditional method requires heat treatment at 1400 °C for 6 h. An excess of chromium content in the SnO_2 structure causes the segregation of Cr_2O_3, giving rise to a greenish shade.

ESR studies reflect the tendency of paramagnetic chromium ions to form clusters with strong Cr−Cr interactions and reveal that the main chromium oxidation state in all the samples is Cr^{III}. The presence of Cr^{IV} ions was also studied by diffuse reflectance spectra but no characteristic signals of this species were found.

All the studies performed to establish the coloring mechanism indicate that the origin of the violet color is unrelated to the quantity of chromium introduced in the structure, but is directly associated with the quantity of chromium present in different oxidation states, the reduced chromium species (Cr^{III} and/or Cr^{IV}) being mainly responsible for the violet color.

This new synthesis method presents promising results for the ceramic industry from an economic and environmental standpoint.

Experimental Section

General Remarks: Two different synthesis routes for preparing the precursor mixture for the solid-state reaction were developed, the traditional ceramic method from Sn^{IV} and Cr^{III} oxides (Method 1) and a method in which the Sn^{IV} and Cr^{III} reagents are dissolved (Method 2). The nominal compositions and references of the samples synthesized are summarized in Table 5. In a first step, the optimum Cr content was established for samples produced by the ceramic method and the best composition (SC2 sample) was also synthesized by the dissolution method (SC6 sample). In Method 1, the following precursors were used: SnO_2 (Panreac, analytical grade) and Cr_2O_3 (Merck, analytical grade). These samples were prepared by mixing and homogenizing stoichiometric amounts of each precursor in a planetary ball mill, with acetone used as a dispersant. After evaporation of the dispersant at room temperature, the samples were dried under infrared lamps. In Method 2, synthesis was performed by heating the appropriate amount of $Cr(acac)_3$ (Merck, pure grade) under reflux in a 2-propanol solution of $Sn(OiPr)_4 \cdot i$PrOH adduct (ABCR, analytical grade). Sample

Table 5. Nominal composition of the samples

Sample	Composition	Method of synthesis
SC1	$Sn_{0.992}Cr_{0.01}O_2$	1
SC2	$Sn_{0.985}Cr_{0.02}O_2$	1
SC3	$Sn_{0.956}Cr_{0.06}O_2$	1
SC4	$Sn_{0.927}Cr_{0.1}O_2$	1
SC5	$Sn_{0.86}Cr_{0.2}O_2$	1
S2	SnO_2	2
SC6	$Sn_{0.985}Cr_{0.02}O_2$	2

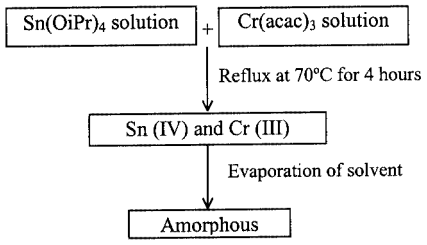

Figure 8. Synthesis diagram of S2 and SC6 samples

preparation is set out in the flow diagram in Figure 8. As an SnO_2 structure is generated during heat treatment in this method of synthesis, an undoped sample (referenced S2) was prepared by the same experimental procedure. All the samples were heat-treated in an electric furnace at different temperatures (from 800 to 1400 °C for 6 h) at a heating rate of 10 °C/min. In order to refine and homogenize the particle size after calcination, the resulting product was ground in an agate mortar with acetone, followed by sieving to 50 μm.

Instrumentation: Crystalline phase evolution of the calcined powders was monitored by X-ray powder diffraction (XRD) with a SIEMENS D5000 diffractometer with Cu-K_α radiation. Data were collected by step-scanning from $2\theta = 10$ to 70° with a step size of $2\theta = 0.050°$ and 1 s counting time per step. The automatic diffractometer was controlled by "SIEMENS DIFFRACT plus" software, which records diffraction peak positions and intensities. Differential thermal (DTA) and thermogravimetric (TG) analyses were performed in a Mettler Toledo model SDTA 851^e. All experiments were run in air from 25 to 1200 °C with a heating rate of 10 °C/min. UV/Vis spectra (diffuse reflectance) and CIELAB parameters were determined at room temperature with a spectrophotometer (CARY 500 SCAN) and a coupled analytical software for color measurements. The data were registered from 200 to 1400 nm with a PTFE blank as reflecting standard. CIELAB color parameter measurements were conducted using a D65 standard illuminant. ESR experiments were performed at 100 K with a Bruker spectrophotometer (ER200D) in the X-band at 9.5 GHz. Magnetic susceptibilities were recorded as a function of the magnetic field at 20 K with a SQUID magnetometer ($H_{max} = 5$ T). In view of the high carcinogenicity of Cr^{VI} ions, the Cr^{VI} content in the washing liquids of the samples was determined by atomic absorption. 1 g of sample was subjected to successive washings with hot 0.3 M HNO_3 until 100 mL of solution was obtained. Measurements were conducted with a Varian Spectra 640 atomic absorption spectrophotometer. Besides these analyses, the chromium content was determined on solid samples by X-ray fluorescence spectrometry with a PHILIPS instrument (Model PW 2400) fitted with an Rh tube and eight single crystals for analysis: LiF200, LiF220, GE(111), InSn, PE, TLAP, PX1 and PX3.

Acknowledgments

The financial support of the Spanish CICYT (project No. PB98-1042) is gratefully acknowledged. We thank the Spanish government for a doctoral fellowship (B. J.).

[1] S. A. Chronister, W. Chen, *Am. Ceram. Soc. Bull.* **1994**, *73*, 71−75.
[2] A. C. Airey, W. Roberts, *Ceram. Eng. Sci. Proc.* **1987**, *8*, 1168−1187.
[3] E. Cordoncillo, F. Del Rio, J. Carda, M. Llusar, P. Escribano, *J. Eur. Ceram. Soc.* **1998**, *18*, 1115−1120.
[4] *DCMA Classification and Chemical Description of the Mixed Metal Oxide Inorganic Coloured Pigments*, 2nd ed., Metal Oxides and Ceramics Colours Subcommittee, Dry Colour Manufacturer's Assn., Washington DC, **1982**.
[5] W. D. Kingery, H. K. Bowen, D. R. Uhlmann, *Introduction to Ceramics*, 2nd ed., John Wiley and Sons, New York, **1976**, p. 314.
[6] A. M. Heyns, P. M. Harden, *J. Phys. Chem. Solids* **1999**, *60*, 277−284.
[7] D. G. Park, J. M. Burlitch, R. F. Geray, R. Dieckmann, D. B. Barber, C. R. Pollock, *Chem. Mater.* **1993**, *5*, 518−524.
[8] S. Ishida, S. Kanaoka, I. Kato, M. Hayashi, *Yogyo-Kyokai-Shi* **1985**, *94*, 457−463.
[9] P. G. Harrison, N. C. Lloyd, W. Daniell, C. Bailey, W. Azelee, *Chem. Mater.* **1999**, *11*, 896−909.
[10] A. R. West, *Solid State Chemistry and its Applications*, John Wiley and Sons, New York, **1992**, p. 359.
[11] R. D. Shannon, *Acta Crystallogr., Sect. A* **1976**, *32*, 359.
[12] R. Biasi, A. Fernandes, M. Grillo, *J. Am. Ceram. Soc.* **1993**, *76*, 223−225.
[13] S. Ishida, M. Hayasi, Y. Fujimura, *J. Am. Ceram. Soc.* **1990**, *73*, 3351−3355.
[14] S. Doeuff, M. Henry, C. Sanchez, J. Livage, *J. Non-Cryst. Solids* **1987**, *89*, 84−97.
[15] P. G. Harrison, N. C. Lloyd, W. Daniell, *J. Phys. Chem. B* **1998**, *102*, 10672−10679.
[16] C. S. Sunandana, *Mater. Res. Bull.* **1985**, *20*, 531−537.
[17] P. S. Devi, H. D. Gafney, V. Petricevic, R. R. Alfano, D. He, K. E. Miyano, *Chem. Mater.* **2000**, *12*, 1378−1385.
[18] H. Eilers, U. Hommerich, S. M. Jacobsen, W. M. Yen, *Phys. Rev. B* **1994**, 15505.
[19] B. D. Cullity, *Introduction to magnetic materials*, Addison Wesley, Reading, MA, **1972**.

Received March 22, 2002
[I02150]

Synthesis and Structures of Triorganotelluronium Pseudohalides

Thomas M. Klapötke,*[a] Burkhard Krumm,[a] Peter Mayer,[a][‡] Holger Piotrowski,[a][‡] Ingo Schwab,[a] and Martin Vogt[a][‡]

Dedicated to Professor D. Naumann on the occasion of his 60th birthday

Keywords: Tellurium / Azides / NMR spectroscopy / Noncovalent interactions

The syntheses of $[(CH_3)_3Te]X$ {X = N_3 (**1**), OCN (**2**), SCN (**3**), SeCN (**4**), $[Ag(CN)_2]$ (**5**)} and $[(C_6H_5)_3Te]X$ {X = N_3 (**6**), SeCN (**7**), $[Ag(CN)_2]$ (**8**)}, their NMR spectroscopic data, vibrational spectra and single crystal structures are described. Compounds **1**–**4** are the first trimethyltelluronium pseudohalides, while the known compounds **6** and **7** have been prepared for completion of their analytical and structural properties. The occurrence of intermolecular Te···N, Te···O, Te···S and Te···Se contacts is thoroughly studied. The dicyanoargentates **5** and **8** were obtained in an attempt to prepare telluronium cyanides. Low-temperature ^{13}C NMR spectroscopy of the $[Ag(CN)_2]^-$ ion in solution has been carried out, with determination of the ^{13}C–$^{107/109}Ag$ coupling.

(© Wiley-VCH Verlag GmbH, 69451 Weinheim, Germany, 2002)

Introduction

Telluronium salts $[R_3Te]X$ have been known for more than a hundred years.[1,2] Some experimental work has been carried out since then, synthesizing telluronium cations with various substituents. In the 1970s Ziolo reported on the first telluronium pseudohalides $[(C_6H_5)_3Te]X$ (X = N_3, CN, OCN, SCN, SeCN),[3,4] with no NMR spectroscopic characterization, but single-crystal X-ray data for $[(C_6H_5)_3Te]OCN$ and $[(C_6H_5)_3Te]SCN$.[5–7]

The preparation and characterization of tris(perfluorophenyl)tellurium(IV) halides $(R_F)_3TeCl$ and $(R_F)_3TeBr$ (R_F = C_6F_5, $CF_3C_6F_4$) was achieved recently.[8] Their X-ray crystallographic analysis and properties revealed structures consistent with a rather covalent constitution.

Telluronium halides and pseudohalides bearing nonfluorinated substituents are in most cases widely ionic and show strong electrolyte behavior in solution.[9,10] Dihalotelluranes R_2TeX_2 feature intermolecular interactions in the solid state, whose distances lie between those of the sum of covalent and van der Waals radii.[11–13] Similar secondary interactions[14] have also been found in telluronium salts.[15,16]

To the best of our knowledge, no trimethyltelluronium pseudohalide has been reported, and continuing our efforts to explore the chemistry of main-group element azides, we report here on the first single-crystal structural determination of telluronium azides. $[(CH_3)_3Te]N_3$ (**1**) and $[(C_6H_5)_3Te]N_3$ (**6**) complete the series $R_nTe(N_3)_{4-n}$ (R = CH_3 or C_6H_5; n = 1, 2, 3), of which both $(CH_3)_2Te(N_3)_2$ and $CH_3Te(N_3)_3$, as well as $(C_6H_5)_2Te(N_3)_2$ and $C_6H_5Te(N_3)_3$ were recently synthesized and characterized.[17,18]

Pursuing the work of Ziolo, we intended to complete his examinations of **6** and **7** with modern spectroscopic and crystallographic methods. Moreover, the scope of telluronium pseudohalides should be extended to the smallest compounds, trimethyltelluronium salts. Thus, the preparation of a series of trimethyltelluronium chalcogenocyanates **2**–**4** was of further interest.

An attempt to prepare telluronium cyanides, omitting the use of an anion exchange resin,[4] will be reported. This work can be seen in context with a very recent report, dealing with structural investigations of several triphenyltelluronium transition metallates.[19]

Results and Discussion

Synthesis

Suitable precursors for the synthesis of telluronium compounds $[R_3Te]X$ are the corresponding telluronium halides. These can be obtained either by the reaction of Grignard reagents with tellurium tetrachloride,[2] or the aqueous ha-

[‡] X-ray structure analyses
[a] Department Chemie, Ludwig-Maximilians-Universität, Butenandtstr. 5–13 (D), 81377 München, Germany
Fax: (internat.) + 49-(0)89/2180-7492
E-mail: tmk@cup.uni-muenchen.de

logenation of tetraalkyl- or tetraaryltelluranes, generated in situ [Equation (1)].[20]

$$TeCl_4 + 4\,RLi \xrightarrow[-4\,LiCl]{Et_2O,\ -70\ ^\circ C} R_4Te \xrightarrow[-RH]{H_2O/KI} [R_3Te]I \qquad R = CH_3, C_6H_5 \qquad (1)$$

Another method for the preparation of $[(C_6H_5)_3Te]Cl$ is the Friedel−Crafts type arylation of tellurium tetrachloride with benzene and aluminum trichloride.[21] Some references stated this as a method suitable for the preparation of $[(C_6H_5)_3Te]Cl$. However, it was found by tracing this reaction at different temperatures up to 90 °C, that the latter approach is somewhat slower than reported.[21] Additionally, minor impurities of $(C_6H_5)_2TeCl_2$ are always present in the isolated product, which was proven by ^{125}Te NMR spectroscopy with a resonance at $\delta = 920$ ppm.

The synthesis of trimethyltelluronium pseudohalides **1**−**4** is achieved by reaction of the corresponding silver pseudohalides with trimethyltelluronium iodide in aqueous or ethanolic solutions [Equation (2)].

$$[(CH_3)_3Te]I + AgX \xrightarrow[-AgI]{H_2O\ or\ EtOH} [(CH_3)_3Te]X \qquad X = N_3, OCN, SCN, SeCN \qquad (2)$$
$$(1)\quad (2)\quad (3)\quad (4)$$

The trimethyltelluronium pseudohalides are colorless salt-like substances which slowly release dimethyltellane as a product of their reductive decomposition [Equation (3)].

$$[(CH_3)_3Te]X \xrightarrow{slow\ dec.,\ 25\ ^\circ C} (CH_3)_2Te + CH_3X \qquad (3)$$

Another method of preparation of telluronium pseudohalides is employed for the preparation of **6** and **7**. As previously described,[4] they can be obtained by a two-phase exchange reaction of $[(C_6H_5)_3Te]Cl$ with an excess of NaN_3 (**6**), and by simply precipitating a hot aqueous solution with excess KSeCN (**7**) [Equation (4)]. Since **6** and **7** are known compounds, they have been prepared for further spectroscopic and structural characterization and in order to compare the properties of telluronium pseudohalides with different cations.

$$[(C_6H_5)_3Te]Cl \xrightarrow[-NaCl]{NaN_3/H_2O/CHCl_3} [(C_6H_5)_3Te]N_3\ (6) \qquad [(C_6H_5)_3Te]Cl \xrightarrow[-KCl]{KSeCN/H_2O} [(C_6H_5)_3Te]SeCN\ (7) \qquad (4)$$

Of further interest in this study would be a telluronium cyanide. The only report of such a compound was also given by Ziolo, who stated that its synthesis had succeeded with the use of an anion exchange resin.[4] Applying the methods mentioned before, mostly led to the formation of an unidentified red decomposition product, after trimethyl- or triphenyltelluronium chloride had been treated with excess of KCN and evaporated subsequently. The use of silver cyanide produced the highly stable dicyanoargentate salts $[(CH_3)_3Te][Ag(CN)_2]$ (**5**) and $[(C_6H_5)_3Te][Ag(CN)_2]$ (**8**), since the complex dicyanoargentate anion formed during the reaction is more stable than the corresponding silver halides [Equation (5)]. Although their synthesis was not an initial goal, they were fully characterized including X-ray crystallography.

$$[R_3Te]I + 2\,AgCN \xrightarrow[-AgI]{H_2O} [R_3Te][Ag(CN)_2] \qquad R = CH_3, C_6H_5 \qquad (5)$$
$$(5)\quad (8)$$

Vibrational Spectra

In their IR (strong), as well as their Raman (weak) spectra, the antisymmetric stretching vibration $\nu_{as}N_3$ is visible for both telluronium azides **1** and **6**. They are found in the region of 2030−2000 cm^{-1} similar as found for the $\nu_{as}N_3$ of covalent tellurium(IV) azides.[17,18] Since **1** and **6** exhibit ionic character, the difference between their $\nu_{as}N_3$ frequencies and that of ionic azide ion in NaN_3 ($\nu_{as}N_3 = 2041$ cm^{-1}, $\nu_sN_3 = 1344$ cm^{-1})[22] is negligible. The symmetric stretching vibration, ν_sN_3, is visible in the Raman spectra at 1376 cm^{-1} for **1**, and 1328 cm^{-1} for **6** with medium intensity and in the IR spectra with weak intensity.

Compounds **2**−**4** and **7** are chemically related and may be described together. Again, comparison of their vibrational spectra, namely the $\nu_{as}XCN$ vibration, shows only minor differences from the precursors. As found for **1** and **6**, the telluronium chalcogenocyanates exhibit ionic nature as well. No coordination effects in solution have been proven (NMR section), but the coordination in the solid state shows a significant effect, accounting for a shift of 20 cm^{-1} on the S−C stretching vibration of the SCN^- moiety in the Raman spectrum of **3** (732 cm^{-1}), compared to 749 cm^{-1} in KSCN (Table 1).

Table 1. IR/Raman vibrational frequencies of trimethyltelluronium pseudohalides

[a]	**1**	**2**	**3**	**4**
ν_3	2027, 1998/1999	2170/2135	2076, 2058/2058	2065/2065
$\nu_3(KN_3/KXCN)$	1998[b]/[c]	2155[23]	2060/2058[24] [d]	2071/2076[25]
ν_1	−/1323	1288/1290	732	[e]
$\nu_1(NaN_3/KXCN)$	1342[b]	1282[23]	741/749[24] [d]	561[25]/556

[a] In cm^{-1}. [b] See ref.[26] and references therein. [c] Inactive. [d] Refers to $[Me_4N]NCS$. [e] Not observed due to overlapping with other vibrations.

Table 2. NMR spectroscopic data

[a][b]		**1**	**2**	**3**	**4**	**5**	**6**	**7**	**8**[c]
^{1}H		2.29	2.28	2.31	2.31	2.30	7.79−7.31	7.79−7.31	7.61−7.48
	$^{2}J_{H-Te}$	23.7	23.7	24.6	23.7	23.7			
^{13}C		4.4	128.8 (OCN), 4.5 (CH_3)	133.7 (SCN), 4.5 (CH_3)	120.6 (SeCN), 4.5 (CH_3)	149.0 (CN), 4.4 (CH_3)	134.3 (C2), 131.3 (C4), 130.2 (C3), 127.9 (C1)	134.7 (C2), 131.9 (C4), 130.7 (C3), 125.9 (C1), 117.3 (SeCN)	147.0 (CN), 134.7 (C2), 132.7 (C4), 131.1 (C3), 123.5 (C1)
	$^{1}J_{C-Te}$	158.3	147.6	147.6	147.6	150.6	249.3	247.5	245.6
	$^{2}J_{C-Te}$						30.8	31.6	33.1
	$^{1}J_{C-N(Se)}$		21.1		268.7			256.2	
^{14}N ($\Delta\nu_{1/2}$)		−132 (N_β, 20), −266 ($N_{\alpha\gamma}$, 60)	−304 (10)	−176 (90)	−144 (140)	−106 (400)	−133 (N_β, 50), −260 ($N_{\alpha\gamma}$, 20)	−130 (1000)	−110 (>2000)
^{77}Se					−324			−144 (br)	
^{125}Te		456	443	δ = 441	441	441	795	759	773
	$^{2}J_{Te-H}$	24.6	24.1	23.7	23.6	23.6			

[a] **1**−**5** in D_2O, **6**−**8** in $CDCl_3$. [b] J and $\Delta\nu_{1/2}$ in Hz. [c] ^{109}Ag shift δ = 593 ppm.

Comparison of the Raman spectra of $[(CH_3)_3Te][Ag(CN)_2]$ (**5**) and $[(C_6H_5)_3Te][Ag(CN)_2]$ (**8**) with the Raman spectrum of crystalline $K[Ag(CN)_2]$ (νCN = 2140 cm^{-1})[27] shows that νCN is slightly shifted to 2132 cm^{-1} (**5**) and 2135 cm^{-1} (**8**). Further deviations are not detected.

The vibrational data indicate that all compounds consist of discrete ions in the solid state.

NMR Spectra

The NMR spectroscopic data (Table 2) confirm the salt-like nature of the compounds. In case of the azides, two resonances were observed in the ^{14}N NMR spectra at δ = −132 (N_β) and −266 ($N_{\alpha\gamma}$) ppm for **1** and δ = −132 (N_β) and −272 ($N_{\alpha\gamma}$) ppm for **6**. This strongly suggests, that in solution **1** and **6** are completely dissociated into telluronium cations and azide anions, since for covalently bound azides, three distinct ^{14}N resonances are observed.[17,18] The ^{125}Te NMR spectra show resonances at δ = 443 ppm (D_2O) and δ = 456 ppm ($CDCl_3$) for **1** and δ = 795 ppm ($CDCl_3$) for **6**, which, as expected, are very similar to the shifts of the starting materials $[(CH_3)_3Te]I$ [δ = 441 ppm (D_2O)] and $[(C_6H_5)_3Te]Cl$ [δ = 759 ppm ($CDCl_3$)], respectively. The corresponding triorganoselenonium azides are discrete ions in solution as well.[28]

For compounds **2**−**5**, **7**, and **8**, only minor variations of the ^{125}Te chemical shift are found, proving the negligible effect of the counterion on the telluronium cation in solution. This is consistent with the ^{125}Te NMR spectroscopic data of $[(C_6H_5)_3Te]_2[MCl_6]$ (M = Ir, Pt) and $[(C_6H_5)_3Te][AuCl_4]$.[19]

The ^{77}Se NMR shift of $[(CH_3)_3Te]SeCN$ (**4**) in D_2O is δ = −324 ppm, which is very similar to that of KSeCN in D_2O (δ = −340 ppm) and $[(CH_3)_3Se]SeCN$ [δ(SeCN) = −328 ppm],[28] but notably different to that of $[(C_6H_5)_3Te]$-SeCN (**7**) in $CDCl_3$ (δ = −144 ppm). This is believed to be mainly a solvent effect.[10] On going from cyanate **2** to thiocyanate **3** and selenocyanate **4**, the linewidth of the ^{14}N NMR resonance increases with the chemical shift. This reflects the change in electronegativity and shielding properties of the chalcogen atom in the chalcogenocyanate moiety.

An interesting temperature-dependent behavior is observed for the ^{13}C NMR resonance of $[(C_6H_5)_3Te][Ag(CN)_2]$ (**8**). At 25 °C, a single resonance at δ = 143 ppm is detected for the cyano resonance. Variable-temperature measurements of the ^{13}C NMR spectra of **8** between −100 °C and 60 °C in $[D_8]THF$ show, that below 25 °C the CN resonance broadens, and at ca. −80 °C two resonances become visible (Figure 1a). Finally, at −100 °C, both the $^{1}J^{13}C-^{107}Ag$ (J = 183 Hz) and the $^{1}J^{13}C-^{109}Ag$ (J = 209 Hz) coupling is resolved (Figure 1b). A similar feature has been reported for $K[Ag(CN)_2]$ in DMF upon cooling below −50 °C.[29]

The coupling with silver isotopes ^{107}Ag (I = −1/2, 51.82%) and ^{109}Ag (I = −1/2, 48.18%)[30] can be observed only at low temperatures, often explained as a result of fast exchange mechanisms.[31−34] For **8**, the calculated ratio of the coupling constants 0.876 is very close to that predicted by the theoretical ratio of the gyromagnetic constants $\gamma^{107}Ag/\gamma^{109}Ag$ = 0.869.

Crystal Structures

As indicated earlier, the crystal structures of $[Ph_3Te]X$ (X = OCN, SCN)[5−7] are known, but for X = N_3 (**6**) and X = SeCN (**7**) only powder diffraction data existed.[3] Hence, for all compounds described in the synthesis section, single-crystal structure determinations have been carried out. Our focus has been set especially on the interactions between the telluronium cations and the different anions, leading to an extended coordination sphere around the tellurium centre (Table 3). The concept of secondary interactions[14] also applies for telluronium compounds[5,6,19,35,36] and was subject to a detailed study.[15,16]

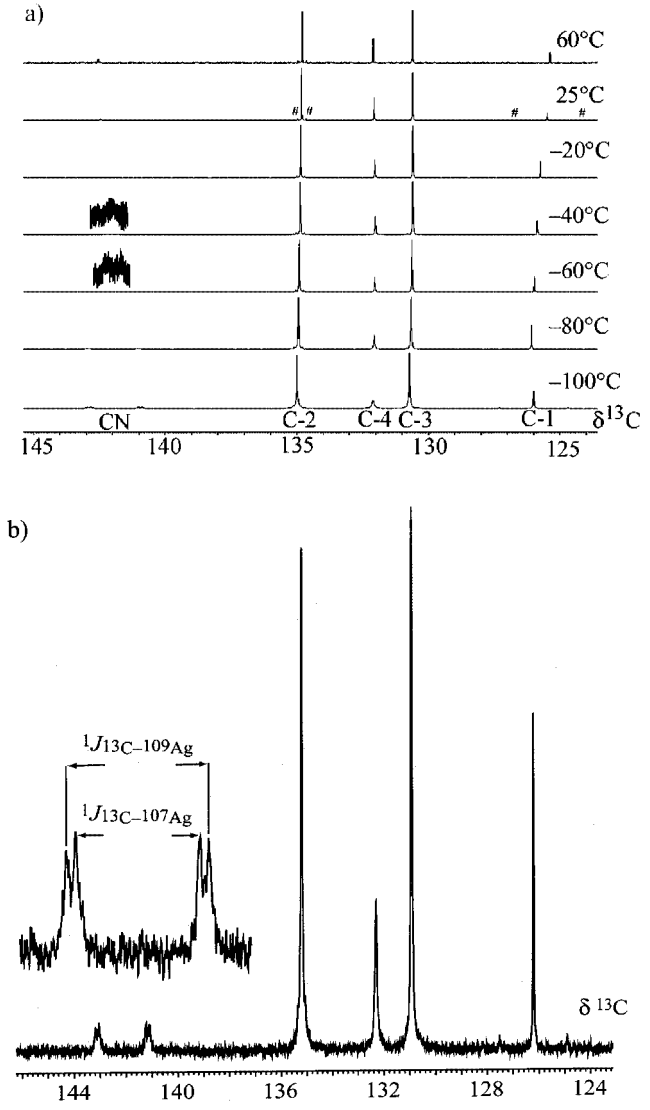

Figure 1: (a) Variable-temperature ^{13}C NMR spectra of $[Ph_3Te][Ag(CN)_2]$ (**8**) in $[D_8]$THF; asterisks denoting ^{125}Te satellites; (b) ^{13}C NMR spectrum of **8** in $[D_8]$THF at −100 °C

In covalent tellurium azides, $R_2Te(N_3)_2$ and $RTe(N_3)_3$, including the free electron pair at the tellurium centre, hepta- and octacoordination of Te is found,[17,18] containing almost linear azide groups connected to the tellurium ion with Te−C bond lengths of ca. 2.2 Å. The interatomic Te···N distances are in the range of 2.7−3.5 Å.

In contrast, the structures of $[(CH_3)_3Te]N_3$ (**1**) (Figure 2) and $[(C_6H_5)_3Te]N_3$ (**6**) (Figure 3) show almost perfectly linear azide groups connected on both sides to different layers of telluronium cations. The azide **6** crystallizes as a chloroform solvate (see Table 4). In both azides **1** and **6**, the N−N bond lengths (1.15−1.18 Å) differ only slightly from each other. This is in agreement with the crystal structure of the azide anion in $[(CH_3)_4N]N_3$, and demonstrates the minor influence of the secondary bonds on the bonding situation of the azide group.[26] The average secondary bonding Te···N distances amount to 3.0 Å, which is well below the sum of the tellurium−nitrogen van der Waals radii (ΣvdWr Te−N 3.61 Å).[37] This leads mostly to a monocapped distorted octahedral AX_3Y_3E environment and a complex three-dimensional network of cations and anions (Figure 2).

The Te−C bond lengths for the telluronium cations $[(CH_3)_3Te]^+$ (in **1**−**5**) and $[(C_6H_5)_3Te]^+$ (in **6**−**8**) span ranges between 2.11 and 2.14 Å, and are together with the resulting bond angles in good agreement with those of $[(CH_3)_3Te]I$[38] and $[(C_6H_5)_3Te]SCN$.[7] Regarding only Te−C bonds, a typical AX_3E trigonal-pyramidal arrangement around the tellurium centre is formed.

Similarly, the C−N and C−O(S)(Se) bond lengths in the chalcogenocyanate anions of **2**−**4** and **7** exhibit only marginal deviations to those found in the potassium salts. The bond lengths of the cyanate anions in **2** [C−N 1.168(4) Å, C−O 1.217(4) Å] are very similar to those of $[(C_6H_5)_3Te]OCN{\cdot}1/2CHCl_3$[5] and KOCN.[39] For $[(CH_3)_3Te]SCN$ (**3**), the distances are very similar, the C−N [1.143(8) Å] and C−S [1.662(5) Å] bonds being negligibly shortened when compared to KSCN [C−N 1.15(1) Å, C−S 1.69(1) Å].[40] The selenocyanate ions in **4** [C−N 1.146(7) Å, C−Se 1.816(5) Å] and **7** [C−N 1.142(8)/1.148(6) Å, C−Se 1.804(5)/1.817(6) Å] feature bond lengths, which also cannot be considered significantly different from those in KSeCN.[41] As discussed for AgSeCN,[42] this is in agreement with a slightly elongated C−N triple bond and a C−Se bond with minor multiple bond contribution.

Table 3. Summary of Te···X interactions [Å]

	1	**2**	**3**	**4**	**5**	**6**	**7**	**8**
Te···N	2.938(4)	2.983(3)	3.185(3)	3.252(4)	3.154(5)	2.772(4)	3.122(5)	3.162(4)
	3.006(4)	3.103(3)			3.270(5)	2.867(4)		3.346(5)
	3.032(3)				3.407(6)	2.946(4)		3.501(5)
	3.018(5)					3.000(4)		
	3.037(3)					3.027(4)		
Te···O		3.095(2)						
Te···S			3.390(1)					
			3.488(1)					
Te···Se				3.4712(5)			3.4424(6)	
				3.5534(6)			3.5413(6)	

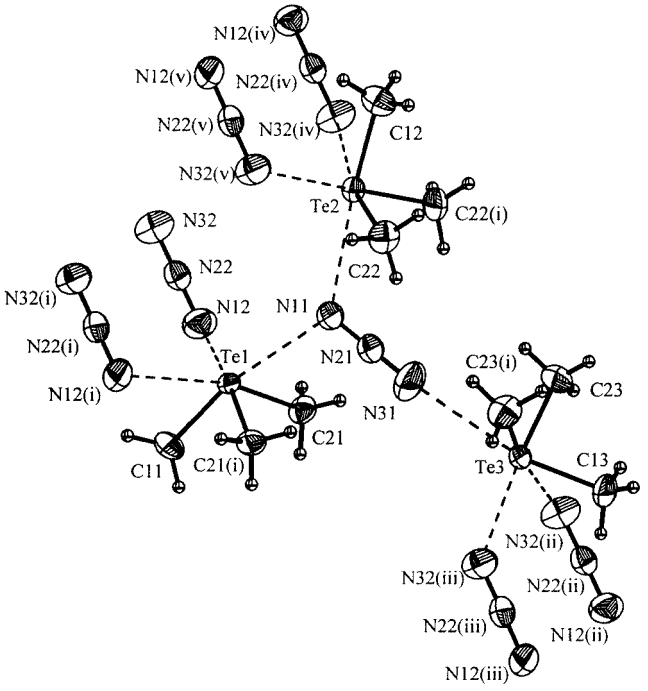

Figure 2. ORTEP plot of **1**; selected bond lengths [Å] and angles [°]: N12−N22 1.164(4), N22−N32 1.173(4), Te1−C11 2.112(4), Te1−C21 2.114(3), Te2−C12 2.143(5), Te2−C22 2.122(3), Te3−C13 2.107(5), Te3−C23 2.111(3), Te1···N11 3.006(4), Te1···N12 3.032(3), Te2···N11 2.938(4), Te3···N31 3.018(5), Te3···N32(*ii*) 3.037(3), N12−N22−N32 179.3(4), C11−Te1−C21 93.9(1); with $i = x, 1/2 - y, z$; $ii = 1 + x, y, z$; $iii = 1 + x, 1/2 - y, z$; $iv = -x, -y, -z$; $v = -x, 1/2 + y, -z$

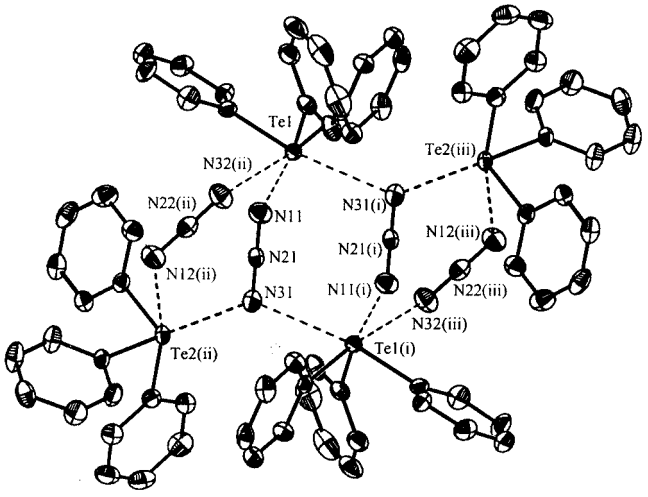

Figure 3. ORTEP plot of **6**; solvate molecules and H atoms omitted for clarity; selected bond lengths [Å] and angles [°]: Te−C 2.121(4)−2.146(4), N11−N21 1.181(5), N21−N31 1.161(5), N12(*ii*)−N22(*ii*) 1.184(5), N22(*ii*)−N32(*ii*) 1.170(5), Te1···N11 2.867(4), Te2(*ii*)···N12(*ii*) 2.772(4), Te2(*ii*)···N31 3.027(4), C−Te−C 92.6(2)−98.8(2), N11(*ii*)−N21(*ii*)−N31(*ii*) 179.6(5), N12−N22−N32 179.1(5); with $i = -x, -y, 1 - z$; $ii = -1 + x, y, z$; $iii = 1$

For compounds **2**−**4** and **7** (Figure 4−7), similar network-like structures as for the azides **1** and **6** exist. Distorted monocapped octahedral AX_3Y_3E environments indicate secondary bonding between cations and anions as well. An analogous structure was reported for β-[TeCl_3][$AlCl_4$], considering primary Te−Cl and secondary Te···Cl bonds.[15] As chalcogenocyanates are ambidentate ligands, it is of interest, whether Te···X [X = O, S, Se; ΣvdWr TeO(S)(Se) 3.58, 3.86, 3.96 Å)], or Te···N contacts or both are preferred. The crystal structures show, that Te···N as well as Te···X coordination is present. Compounds **3**, **4** and **7** exhibit two Te···S(Se) and one Te···N contact each, **3** and **4** crystallize isotypically. The cyanate ion in **2**, which has the oxygen atom as its "hard end", shows an inverted situation. This can be explained according to the HSAB concept,[43,44] considering a telluronium cation as a rather weak acid, preferring coordination to the softer ends of the particular anions. In the solid state the N···Te contacts in **2**−**4**

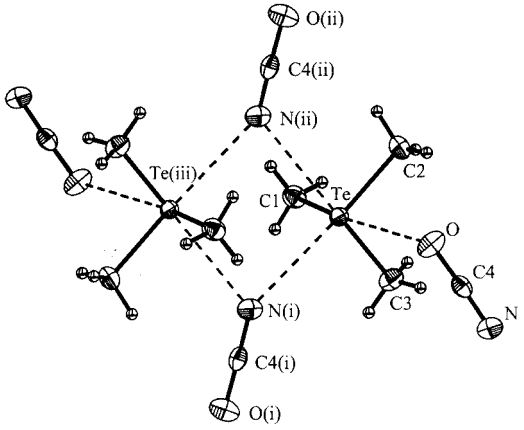

Figure 4. ORTEP plot of **2**; selected bond lengths [Å] and angles [°]: Te−C1 2.113(3), Te−C2 2.121(3), Te−C3 2.110(3), O−C4 1.217(4), N−C4 1.168(4), Te···O 3.095(2), Te···N(*i*) 2.983(3), Te···N(*ii*) 3.103(3), C1−Te−C2 94.8(1), C3−Te−C1 93.3(1), C3−Te−C 2 95.4(1), N−C4−O 178.5(3), Te···N(*i*)···Te(*iii*) 83.14(7), N(*i*)···Te···N(*ii*) 96.86(7); with $i = 11/2 - x, y - 1/2, -1/2 - z$; $ii = x - 1/2, 1/2 - y, 1/2 + z$; $iii = 1 - x, -y, -z$

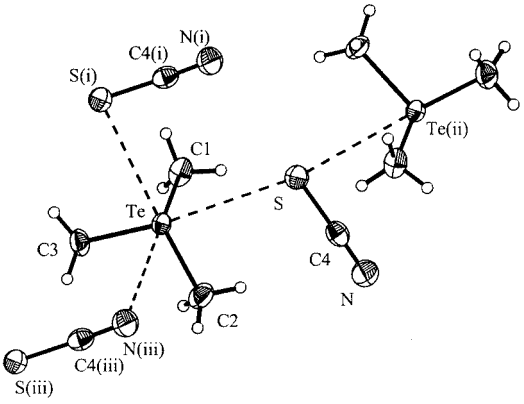

Figure 5. ORTEP plot of **3**; selected bond lengths [Å] and angles [°]: Te−C1 2.115(3), Te−C2 2.113(4), Te−C3 2.120(3), Te···S 3.488(1), Te···S(*i*) 3.390(1), Te(*ii*)···S 3.390(1), Te···N(*iii*) 3.185(3), S−C4 1.662(5), N−C4 1.143(8), C1−Te−C3 92.7(2), C2−Te−C1 93.7(2), C2−Te−C3 96.7(2), N−C4−S 178.5(4), Te···S···Te(*ii*)···167.83(3); with $i = 1 - x, 1 - y, 1/2 + z$; $ii = 1 - x, 1 - y, z - 1/2$; $iii = 1 - x + 1/2, 2 - y, 1/2 + z$

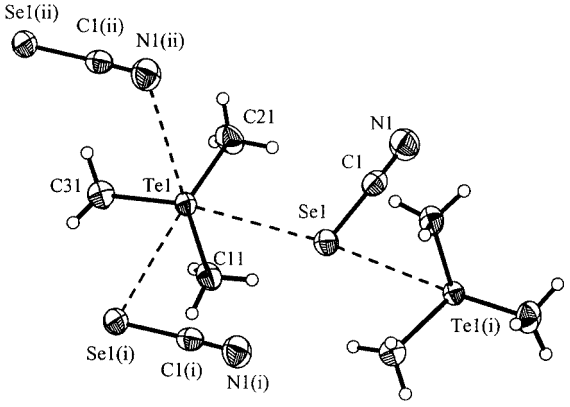

Figure 6. ORTEP plot of **4**; selected bond lengths [Å] and angles [°]: Te1−C11 2.107(3), Te1−C21 2.124(4), Te1−C31 2.121(4), C1−N1 1.146(7), Se1−C1 1.816(5), Te1···N1(*ii*) 3.252(4), Te1···Se1 3.5534(6), Te1···Se1(*i*) 3.4712(5), C11−Te1−C21 93.5(2), C11−Te1−C31 93.3(2), C31−Te1−C21 96.6(2), N1−C1−Se1 178.0(4); with *i* = 1 − *x*, 1 − *y*, −1/2 + *z*; *ii* = 1 − *x*, −*y*, −1/2 + *z*; *iii* = 1 − *x*, 1 − *y*, 1/2 + *z*

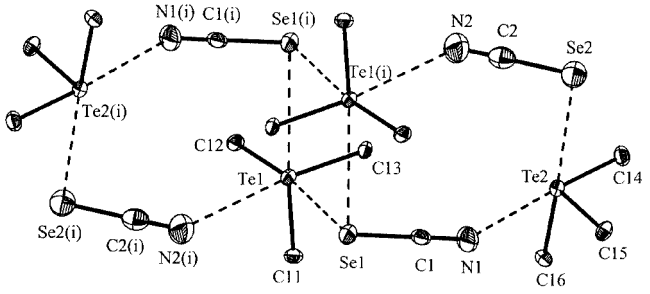

Figure 7. ORTEP plot of **7**; only *Te*-bonded atoms of phenyl groups shown; selected bond lengths [Å] and angles [°]: Te1−C11 2.126(5), Te1−C12 2.139(5), Te1−C13 2.137(4), Te2−C14 2.128(5), Te2−C15 2.120(5), Te2−C16 2.128(5), N1−C1 1.148(6), N2−C2 1.142(8), Se1−C1 1.804(5), Se2−C2 1.817(6), Te1···N2(*i*) 3.122(5), Te2···N1 2.810(5), Te1···Se1 3.4424(6), Te1···Se1(*i*) 3.5413(6), Te2···Se2 3.4321(7), C11−Te1−C12 94.8(2), C11−Te1−C13 93.4(2), C13−Te1−C12 99.9(2), C14−Te2−C15 97.5(2), C14−Te2−C16 94.8(2), C15−Te2−C16 95.3(2), N2−C2−Se2 179.2(6), N1−C1−Se1 177.6(5); with *i* = 1 − *x*, −*y*, 1 − *z*

and in **7** are always shorter than the Te···O/S/Se contacts. The latter have approximately the same distance as reported for Te···Se contacts in $[R_3Te][SeR]$.[36] The coordination sphere of azide **1**, and the other pseudohalides **2**−**4** and **7** are very similar, with all anions being threefold coordinated (e.g. in **1**: Te1···N11, Te2···N11, Te3···N31 (Figure 2)].

The crystal structures of the dicyanoargentates $[(CH_3)_3Te][Ag(CN)_2]$ (**5**) and $[(C_6H_5)_3Te][Ag(CN)_2]$ (**8**) contain short Ag···Ag contacts that account for 3.167 Å and 2.985 Å, respectively, which is at the lower distance limit of known Ag···Ag contacts (2.99−4.2 Å),[45−47] but no significant effect on the bonding parameters of both the telluronium cation and the dicyanoargentate anion are found. The rod-like dicyanoargentate anions are able to mediate interactions between ions in the crystal which are far away from each other. In the structure of the methyl derivative **5** (Figure 8), infinite chains of two crystallographically independent perfectly linear $[Ag(CN)_2]^-$ ions (C−Ag−C 180°) are oriented staggered in an angle of 75° to each other, alternately coordinated to telluronium cations. In the phenyl derivative **8**, the corresponding angle is 84° (Figure 9). The coordination sphere around tellurium consists of two shorter and one longer Te···N contacts, the latter being only 0.1 Å below the sum of the van der Waals radii of Te−N 3.61 Å. This again can be regarded as a distorted monocapped octahedral AX_3Y_3E arrangement.

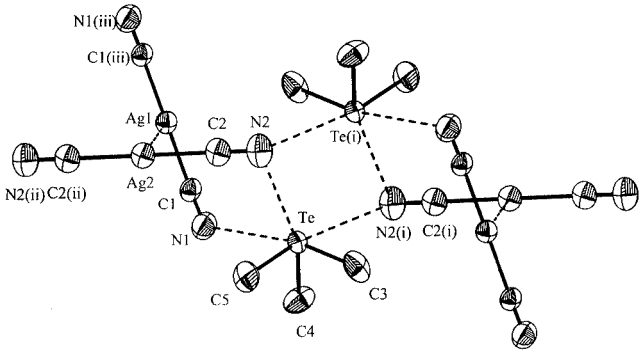

Figure 8. ORTEP plot of **5**; selected bond lengths [Å] and angles [°]: Te−C3 2.102(5), Te−C4 2.100(5), Te−C5 2.109(6), C1−N1 1.098(6), C2−N2 1.143(7), Ag1−C1 2.074(5), Ag2−C2 2.055(6), Te···N1 3.270(5), Te···N2 3.407(6), Te···N2(*i*) 3.154(5), Ag1···Ag2 3.1670(3), C4−Te−C3 95.9(2), C4−Te−C5 95.1(3), C3−Te−C5 93.6(3), C1−Ag1−C1(*iii*) 180.000(1), C2−Ag2−C2(*ii*) 180.000(1), N1−C1−Ag1 178.3(5), N2−C2−Ag2 178.6(5), C1−Ag1−Ag2−C2 −74.9(2); with *i* = −*x*, −*y*, 1 − *z*; *ii* = 1 − *x*, −*y*, 2 − *z*; *iii* = −*x*, −*y*, 2 − *z*

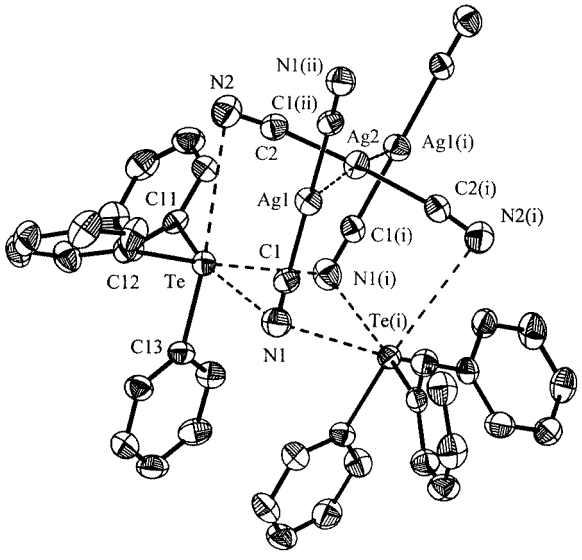

Figure 9. ORTEP plot of **8**; selected bond lengths [Å] and angles [°]: Te−C11 2.119(5), Te−C12 2.121(5), Te−C13 2.120(5), N1−C1 1.142(6), N2−C2 1.138(7), Ag1−C1 2.055(5), Ag2−C2 2.069(6), Te···N1 3.346(5), Te1···N1(*i*) 3.162(4), Te···N2 3.501(5), Ag1···Ag2 2.9847(1), C11−Te−C13 94.4(2), C11−Te−C12 99.5(2), C13−Te−C12 96.0(2), N1−C1−Ag1 174.8(5), N2−C2−Ag2 173.7(5), C1−Ag1−C1(*ii*), 180.0, C2−Ag2−C2(*i*) 175.9(3), Te−N1−Te(*i*) 92.8(1) Ag1−Ag2−Ag1(i) 170.63(2), C1−Ag1−Ag2−C2 91.6(2); with *i* = 1 − *x*, *y*, 1/2 − *z*; *ii* = 1 − *x*, 1 − *y*, 1 − *z*

Conclusion

The syntheses, spectroscopic, and structural studies of triorganotelluronium azides, pseudohalides, and dicyanoargentates have been described. Multinuclear NMR spectroscopy established that total dissociation occurs in solution. Variable-temperature ^{13}C NMR studies of the $[Ag(CN)_2]^-$ ion in solution revealed discrete couplings of ^{13}C to both silver isotopes (^{107}Ag and ^{109}Ag). In the crystal structures of all compounds, secondary interactions, Te···N(O)(S)(Se), are present between cations and anions.

Experimental Section

General Remarks: Commercially available chemicals ($TeCl_4$, 1.6 M MeLi in diethyl ether, 1.8 M PhLi in cyclohexane/diethyl ether) were used without further purification. The silver salts AgX (X = N_3, OCN, SCN, SeCN) were obtained by precipitation of aqueous solutions of silver nitrate with the corresponding Na/K pseudohalides. $[Me_3Te]I$ was prepared according to a standard procedure,[20,48] $[Ph_3Te]Cl$ by a similar reaction or according to ref.[21] IR: Perkin−Elmer Spektrum One FT-IR or Nicolet 520 FT-IR Spektrometer (as KBr pellets or between KBr plates). Raman: Perkin−Elmer Spectrum 2000 NIR FT-Raman (Nd:YAG laser, 1064 nm, 200 mW). NMR spectroscopy: JEOL Eclipse 400 and EX400 instruments; chemical shifts are reported with respect to $(CH_3)_4Si$ (^1H, 399.8 MHz; ^{13}C, 100.5 MHz), CH_3NO_2 (^{14}N, 28.9 MHz), $(CH_3)_2Se$ (^{77}Se, 76.3 MHz), aqueous $AgNO_3$ (^{109}Ag, 18.6 MHz), $(CH_3)_2Te$ (^{125}Te, 126.1 MHz). The ^{77}Se and ^{125}Te spectra were recorded at 25 °C. All chemical shifts are presented in Table 2. MS: JEOL MStation JMS 700 Spektrometer. Multi-isotope containing fragments refer to the isotope with the highest natural abundance (for example ^{130}Te). The FAB mass spectra were recorded using 3-nitrobenzyl alcohol (NBA) as matrix. Elemental analyses: in-house.

X-ray Crystallography: For compounds **1**−**4** and **8** a Nonius Kappa CCD, and for **5**−**7** a STOE IPDS area detector device was employed for data collection using Mo-K_α radiation. All structures were solved by direct methods using SIR97[49] (**1**−**4**, **7**, **8**) and SHELXS (**5**, **6**) and refined by means of the full-matrix least-squares procedures using SHELXL-97[50] (Table 4). CCDC-184294 (**1**), -184288 (**2**), -184289 (**3**), -184293 (**4**), -184290 (**5**), -184295 (**6**), -184291 (**7**) and -184292 (**8**) contain the supplementary crystallographic data for this paper. These data can be obtained free of charge at www.ccdc.cam.ac.uk/conts/retrieving.html or from the Cambridge Crystallographic Data Centre, 12, Union Road, Cambridge CB2 1EZ, UK [Fax: (internat.) + 44-1223/336-033; E-mail: deposit@ccdc.cam.ac.uk].

CAUTION! Silver azide is potentially explosive. This necessitates meticulous safety precautions during its preparation and handling. Although both azides **1** and **6** reported in this section are ionic, they do exhibit a noticeable fizzling when exposed to heat!

Trimethyltelluronium Azide, $[Me_3Te]N_3$ (1): Into a solution of 3 mmol of trimethyltelluronium iodide in 40 mL of H_2O, was added 4.2 mmol of moist AgN_3 in one portion. After stirring for 4 h at ambient temperature, the mixture was filtered and the solvent removed from the filtrate in vacuo. After recrystallization from ethanol/diethyl ether, **1** was obtained as colorless, hygroscopic powder (84%), m.p. 110 °C. IR (KBr): $\tilde{\nu}$ = 3009 s, 2027 vs/1998 s ($\nu_{as}N_3$), 1416 m, 1376 m, 1216 w, 1115 vs, 1054 s, 906 s, 618 s, 594 w, 543 m, 439 w cm^{-1}. Raman: $\tilde{\nu}$ = 3023 (5), 2924 (20), 1999 (5, $\nu_{as}N_3$), 1990 (5), 1414 (5), 1323 (35, ν_sN_3), 1225 (5), 1042 (5), 546 (100), 528 (90), 226 (10), 135 (25) cm^{-1}. FAB^+ MS: *m*/*z* (%) = 328 (10) [Me_3Te^+ + NBA], 175 (100) [Me_3Te^+]. $C_3H_9N_3Te$ (214.72): calcd. C 16.8, H 4.2, N 19.6; found C 16.5, H 4.1, N 18.3.

Trimethyltelluronium Cyanate, $[Me_3Te]OCN$ (2): Into a solution of 1 mmol of trimethyltelluronium iodide in 50 mL of H_2O, was added

Table 4. Crystal data and structure refinements

	1	**2**	**3**[a]	**4**[b]	**5**	2(**6**·$CHCl_3$)[c]	**7**	**8**
Empirical formula	$C_3H_9N_3Te$	C_4H_9NOTe	C_4H_9NSTe	C_4H_9NSeTe	$C_5H_9AgN_2Te$	$C_{37}H_{31}Cl_3N_6Te_2$	$C_{19}H_{15}NSeTe$	$C_{21}H_{16}AgCl_3N_2Te$
Formula mass	214.72	214.72	230.79	277.68	332.61	921.23	463.89	638.19
Temperature [K]	200(2)	200(2)	200(2)	200(2)	200(2)	200(3)	200(2)	200(2)
Crystal size [mm]	0.56 × 0.24 × 0.20	0.17 × 0.15 × 0.07	0.24 × 0.11 × 0.09	0.16 × 0.10 × 0.02	0.36 × 0.18 × 0.06	0.18 × 0.18 × 0.08	0.33 × 0.26 × 0.20	0.31 × 0.17 × 0.13
Crystal system	orthorhombic	monoclinic	orthorhombic	orthorhombic	monoclinic	triclinic	orthorhombic	orthorhombic
Space group	*Pnma*	$P2_1/n$	$Pna2_1$	$Pna2_1$	$P2_1/n$	$P\bar{1}$	*Pbca*	*Pbcn*
a [Å]	11.2220(1)	6.5637(2)	11.5352(3)	11.6595(2)	6.3340(6)	12.1279(9)	15.7423(9)	31.0459(5)
b [Å]	9.7746(1)	10.6046(3)	6.5142(2)	6.6326(1)	15.331(1)	12.620(1)	20.363(1)	12.4486(2)
c [Å]	19.2919(3)	9.6477(3)	10.0654(2)	10.1745(2)	9.622(1)	13.648(1)	21.668(1)	11.8989(2)
β [°]	90	93.288(1)	90	90	98.79(1)	114.408(9)	90	90
V [Å^3]	2116.14(4)	670.43(3)	756.34(3)	786.82(2)	923.4(2)	1856.0(3)	6945.8(7)	4598.7(1)
Z	12	4	4	4	4	2	16	8
$\rho_{calcd.}$ [g cm^{-3}]	2.022	2.127	2.027	2.344	2.393	1.649	1.774	1.844
μ [mm^{-1}]	4.116	4.334	4.106	8.307	5.208	1.823	3.805	2.478
F(000)	1200	400	432	504	608	900	3552	2448
θ range [°]	3.5−27.5	3.65−23.99	3.53−30.03	3.5−27.5	2.52−24.00	2.14−28.0	1.89−24.0	3.27−24.0
Index ranges	$-14 \le h \le 14$ $-12 \le k \le \le 12$ $-24 \le l \le 25$	$-7 \le h \le 7$ $-12 \le k \le 12$ $-11 \le l \le 10$	$-15 \le h \le 16$ $-9 \le k \le 9$ $-14 \le l \le 14$	$-15 \le h \le 15$ $-8 \le k \le 8$ $-13 \le l \le 13$	$-7 \le h \le 7$ $-16 \le k \le 17$ $-11 \le l \le 11$	$-14 \le h \le 14$ $-16 \le k \le 16$ $-17 \le l \le 17$	$-18 \le h \le 18$ $-23 \le k \le 23$ $-24 \le l \le 24$	$-33 \le h \le 35$ $-14 \le k \le 12$ $-13 \le l \le 10$
Reflections collected	28232	6166	7241	15675	5065	16215	42898	23151
Reflections unique	2569 (R_{int} = 0.0714)	1054 (R_{int} = 0.0422)	2203 (R_{int} = 0.0526)	1808 (R_{int} = 0.0524)	1379 (R_{int} = 0.0426)	8276 (R_{int} = 0.0470)	5451 (R_{int} = 0.0718)	3607 (R_{int} = 0.0667)
*R*1, *wR*2 (2σ data)	0.0250, 0.0580	0.0155, 0.0353	0.0251, 0.0521	0.0213, 0.0442	0.0199, 0.0406	0.0338, 0.0607	0.0277, 0.0596	0.0355, 0.0794
*R*1, *wR*2 (all data)	0.0282, 0.0595	0.0177, 0.0359	0.0333, 0.0546	0.0235, 0.0455	0.0302, 0.0420	0.0673, 0.0663	0.0454, 0.0624	0.0570, 0.0893
Max./min. transm.	0.4377/0.2811	0.7464/0.4819	0.7109/0.4377	0.8184/0.2956	0.7469/0.3413	0.9017/0.7383	0.5321/0.4589	0.7628/0.5196
Data/restr./param.	2569/0/116	1054/0/101	2203/1/65	1808/1/64	1379/0/85	8276/0/557	5451/0/397	3607/0/255
GOOF on F^2	1.153	1.120	1.056	1.071	0.965	0.831	0.938	1.061
Larg. diff. peak/hole [e/Å^3]	0.906/−1.086	0.749/−0.494	1.133/−0.805	0.765/−0.415	0.476/−0.572	0.559/−0.633	0.530/−1.130	0.832/−0.746

[a] Flack parameter: −0.01(3). [b] Racemic twin, volume fraction from refinement: 0.40(1). [c] Compound **6**: α = 95.58(1)°, γ = 97.96(1)°.

2 mmol of freshly precipitated AgOCN in one portion. After stirring for 1 d at ambient temperature, the mixture was filtered and the solvent removed from the filtrate in vacuo. After recrystallization from ethanol/diethyl ether, **2** was obtained as colorless powder (93%), m.p. 141 °C. IR (KBr): $\tilde{\nu}$ = 3011 m, 2916 w, 2170 vs/2138 s/2113 m (ν_{as}OCN), 1414 s, 1318 w, 1301 s, 1288 s, 1269 w, 1249 m, 1237 m, 1224 w, 1206 vs, 1185 w, 907 vs, 900 vs, 831 m, 822 m, 662 w, 638 s, 628 s, 623 s, 580 w, 546 s, 537 s cm^{-1}. Raman: $\tilde{\nu}$ = 3025 (15), 2930 (35), 2135 (20, ν_{as}OCN), 1428 (5), 1290 (15), 1203 (10), 551 (85), 540 (100), 234 (15) cm^{-1}. FAB$^+$ MS: *m/z* (%) = 328 (10) [Me_3Te^+ + NBA], 175 (100) [Me_3Te^+]. C_4H_9NOTe (214.72): calcd. C 22.1, H 4.2, N 6.5; found C 22.4, H 4.2, N 6.5.

Trimethyltelluronium Thiocyanate, [Me_3Te]SCN (3): Into a solution of 1 mmol of trimethyltelluronium iodide in 15 mL of H_2O, was added 2 mmol of freshly precipitated AgSCN in one portion. After stirring for 4 h at ambient temperature, the mixture was filtered and the solvent removed from the filtrate in vacuo. After recrystallization from ethanol/diethyl ether, **3** was obtained as colorless powder (89%), m.p. 86−88 °C. IR (KBr): $\tilde{\nu}$ = 3004 m, 2916 w, 2076 s/2058 vs (ν_{as}SCN), 1793 w, 1759 w, 1631 m, 1515 w, 1412 s, 1385 m, 1262 m, 1251 m, 1228 m, 1214 s, 1096 m, 1022 m, 937 m, 925 m, 894 vs, 822 m, 804 m, 730 s, 544 s, 534 s, 468 m, 463 m cm^{-1}. Raman: $\tilde{\nu}$ = 3018 (5), 2936 (5), 2058 (30, ν_{as}SCN), 1405 (5), 1251 (5), 1232 (5), 1216 (5), 932 (10), 732 (10), 545 (100), 534 (98), 215 (10), 112 (10) cm^{-1}. FAB$^+$ MS: *m/z* (%) = 328 (10) [Me_3Te^+ + NBA], 175 (100) [Me_3Te^+]. C_4H_9NSTe (230.79): calcd. C 20.8, H 3.9, N 6.1, S 13.9; found C 20.7, H 4.0, N 5.9, S 13.2.

Trimethyltelluronium Selenocyanate, [Me_3Te]SeCN (4): Into a solution of 1 mmol of trimethyltelluronium iodide in 100 mL of H_2O, was added 2 mmol of freshly precipitated AgSeCN in one portion. After stirring for 8 h at ambient temperature, the mixture was filtered and the solvent removed from the filtrate in vacuo. After recrystallization from methanol/chloroform/diethyl ether, **4** was obtained as slightly pinkish powder (58%), m.p. 106−109 °C. IR (KBr): $\tilde{\nu}$ = 3421 (br), 3011 m, 2065 vs/2018 m (ν_{as}SeCN), 1757 w, 1640 w, 1503 w, 1409 s, 1385 m, 1249 m, 1226 m, 1215 s, 890 vs, 826 w, 816 m, 540 s, 530 s, 414 m cm^{-1}. Raman: $\tilde{\nu}$ = 3014 (5), 2918 (15), 2065 (40, ν_{as}SeCN), 1217 (5), 542 (85), 531 (100), 227 (br, 10), 120 (br, 5) cm^{-1}. FAB$^+$ MS: *m/z* (%) = 328 (10) [Me_3Te^+ + NBA], 175 (100) [Me_3Te]$^+$. C_4H_9NSeTe (277.68): calcd. C 17.3, H 3.2, N 5.0; found C 17.5, H 3.3, N 4.9.

Trimethyltelluronium Dicyanoargentate, [Me_3Te][Ag(CN)$_2$] (5): Into a solution of 1 mmol of trimethyltelluronium iodide in 100 mL of H_2O, was added 2 mmol of AgCN in one portion. After stirring for 20 h at 50 °C, the mixture was filtered and the solvent removed from the filtrate in vacuo; **5** was obtained as slightly grayish crystals (85%), m.p. 118−122 °C. IR (KBr): $\tilde{\nu}$ = 3007 m, 2962 m, 2929 m, 2873 m, 2135 s/2126 s (νCN), 1728 m, 1563 m, 1416 m, 1290 m, 1251 m, 1222 m, 1125 w, 898 s, 832 m, 550 m, 537 m, 391 s cm^{-1}. Raman: $\tilde{\nu}$ = 3027 (20), 2932 (50), 2132 (70, νCN), 1412 (10), 1226 (10), 550 (90), 540 (100), 213 (30) cm^{-1}. FAB$^+$ MS: *m/z* (%) = 328 (10) [Me_3Te^+ + NBA], 175 (100) [Me_3Te]$^+$. FAB$^-$ MS: *m/z* (%) = 427 [$Ag_3(CN)_4^-$], 292 [$Ag_2(CN)_3^-$], 159 [$Ag(CN)_2^-$]. $C_5H_9AgN_2Te$ (332.6): calcd. C 18.1, H 2.7, N 8.4; found C 20.9, H 3.1, N 7.6.

Triphenyltelluronium Azide, [Ph_3Te]N_3 (6): Into a solution of 2.5 mmol of triphenyltelluronium chloride in 50 mL of chloroform, was poured in one portion a solution of 20 mmol of NaN_3 in 50 mL H_2O. After stirring for 45 min at ambient temperature, the chloroform extract was separated and dried with anhydrous $MgSO_4$. After removal of the solvent, recrystallization from chloroform or 2-propanol yielded **6** as colorless crystals (82%), m.p. 155 °C (ref.[4] 155.5−156.5 °C). IR (KBr): $\tilde{\nu}$ = 3293 w, 3051 w, 2017 vs/1993 s ($\nu_{as}N_3$), 1572 w, 1478 w, 1434 w, 1182 w, 1055 w, 996 w, 735 m, 688 w cm^{-1}. Raman: $\tilde{\nu}$ = 3145 (10), 3058 (70), 1989 (25, $\nu_{as}N_3$), 1574 (35), 1478 (10), 1328 (40), 1240 (5), 1188 (10), 1160 (10), 1056 (15), 1020 (55), 1001 (100), 655 (50), 614 (10), 464 (5), 365 (10), 284 (45), 269 (40), 258 (70), 233 (40), 134 (70) cm^{-1}. FAB$^+$ MS: *m/z* (%) = 361 (100) [Ph_3Te^+], 284 (10) [Ph_2Te^+], 207 (5) [$PhTe^+$]. $C_{18}H_{15}N_3Te\cdot 1/2CHCl_3$ (460.62): calcd. C 48.2, H 3.4, N 9.1, Cl 11.6; found C 48.7, H 3.4, N 9.0, Cl 11.3.

Triphenyltelluronium Selenocyanate, [Ph_3Te]SeCN (7): Into a solution of 0.5 mmol of triphenyltelluronium chloride in 10 mL of H_2O, was added 1 mL of a hot aqueous solution of 2 mmol of KSeCN in one portion. After stirring for 15 min at 50 °C, filtration of the residue and subsequent rinsing with diethyl ether yielded **7** as a colorless powder (98%), m.p. 164.5−165.5 °C (ref.[4] 164.5−165.5 °C). IR (KBr): $\tilde{\nu}$ = 3048 w, 2960 m, 2077 vs/2062 vs (ν_{as}SeCN), 1572 m, 1477 s, 1436 vs, 1331 w, 1313 w, 1262 s, 1180 w, 1160 w, 1096 vs, 1064 s, 1056 s, 1017 vs, 995 s, 802 vs, 746 s, 730 vs, 685 s, 467 m, 452 m, 403 m cm^{-1}. Raman: $\tilde{\nu}$ = 3142 (10), 3053 (8), 2079 (75, ν_{as}SeCN), 1574 (35), 1479 (10), 1332 (40), 1271 (5), 1188 (10), 1162 (10), 1056 (15), 1020 (55), 1000 (100), 657 (50), 613 (10), 570 (5), 550 (5), 470 (5), 452 (5), 281 (95), 270 (60), 255 (90), 228 (75), 179 (30), 117 (45) cm^{-1}. FAB$^+$ MS: *m/z* (%) = 361 (100) [Ph_3Te^+], 284 (10) [Ph_2Te^+], 207 (5) [$PhTe^+$]. $C_{19}H_{15}NSeTe$ (463.89): calcd. C 49.2, H 3.3, N 3.0; found C 49.0, H 3.2, N 3.0.

Triphenyltelluronium Dicyanoargentate, [Ph_3Te][Ag(CN)$_2$] (8): Into a solution of 1 mmol of triphenyltelluronium chloride in 40 mL of H_2O, was added 1.5 mmol of KI in one portion. The resulting precipitate was collected and washed with water and diethyl ether. To a suspension of this precipitate in 50 mL of H_2O was added 2 mmol of AgCN. After stirring for 20 h at 50 °C, the mixture was filtered and the solvent removed from the filtrate in vacuo. Recrystallization from chloroform/hexane yielded **8** as colorless crystals (42%), m.p. 130−132 °C. IR (KBr): $\tilde{\nu}$ = 3055 w, 2921 w, 2126 s/1999 s (νCN), 1573 s, 1477 w, 1436 s, 1384 m, 1250 m, 1182 w, 1149 w, 1042 m, 1016 s, 994 s, 958 s, 915 m, 817 s, 732 s, 6685 s, 649 s, 502 m cm^{-1}. Raman: $\tilde{\nu}$ = 3056 (55), 2135 (30), 1575 (40), 1020 (45), 1000 (100), 658 (55), 613 (20), 263 (50), 231 (50) cm^{-1}. FAB$^+$ MS: *m/z* (%) = 361 (100) [Ph_3Te^+], 284 (10) [Ph_2Te^+], 207 (5) [$PhTe^+$]. FAB$^-$ MS: *m/z* (%) = 427 [$Ag_3(CN)_4^-$], 292 [$Ag_2(CN)_3^-$], 159 [$Ag(CN)_2^-$].

Acknowledgments

Financial support of this work by the University of Munich and the Fonds der Chemischen Industrie is gratefully acknowledged.

[1] A. Cahours, *Justus Liebigs Ann. Chem.* **1865**, *135*, 352−357.
[2] C. Lederer, *Ber. Dtsch. Chem. Ges.* **1911**, *44*, 2287−2292.
[3] R. F. Ziolo, D. D. Titus, *J. Appl. Crystallogr.* **1976**, *9*, 506−507.
[4] R. F. Ziolo, K. Pritchett, *J. Organomet. Chem.* **1976**, *116*, 211−217.
[5] D. D. Titus, J.-S. Lee, R. F. Ziolo, *J. Organomet. Chem.* **1976**, *120*, 381−388.
[6] J.-S. Lee, D. D. Titus, R. F. Ziolo, *J. Chem. Soc., Chem. Commun.* **1976**, 501−502.
[7] J.-S. Lee, D. D. Titus, R. F. Ziolo, *Inorg. Chem.* **1977**, *16*, 2487−2492.
[8] T. M. Klapötke, B. Krumm, P. Mayer, K. Polborn, O. P. Ruscitti, *J. Fluorine Chem.* **2001**, *112*, 207−212.
[9] M. T. Chen, J. W. George, *J. Am. Chem. Soc.* **1968**, *90*, 4580−4583.
[10] F. H. Musa, W. R. McWhinnie, *J. Organomet. Chem.* **1978**, *159*, 37−45.
[11] R. F. Ziolo, J. M. Troup, *J. Am. Chem. Soc.* **1983**, *105*, 229−235.

[12] D. Naumann, L. Ehmanns, K.-F. Tebbe, W. Crump, *Z. Anorg. Allg. Chem.* **1993**, *619*, 1269−1276.
[13] T. M. Klapötke, B. Krumm, P. Mayer, K. Polborn, O. P. Ruscitti, *Inorg. Chem.* **2001**, *40*, 5169−5176.
[14] N. W. Alcock, *Adv. Inorg. Chem. Radiochem.* **1972**, *15*, 1−58.
[15] B. H. Christian, M. J. Collins, R. J. Gillespie, J. F. Sawyer, *Inorg. Chem.* **1986**, *25*, 777−788.
[16] M. J. Collins, J. A. Ripmeester, J. F. Sawyer, *J. Am. Chem. Soc.* **1988**, *110*, 8583−8590.
[17] T. M. Klapötke, B. Krumm, P. Mayer, O. P. Ruscitti, *Inorg. Chem.* **2000**, *39*, 5426−5427.
[18] T. M. Klapötke, B. Krumm, P. Mayer, H. Piotrowski, O. P. Ruscitti, A. Schiller, *Inorg. Chem.* **2002**, *41*, 1184−1193.
[19] R. Oilunkaniemi, J. Pietikäinen, R. Laitinen, M. Ahlgrén, *J. Organomet. Chem.* **2001**, *640*, 50−56.
[20] D. Hellwinkel, G. Fahrbach, *Chem. Ber.* **1968**, *101*, 574−584.
[21] W. H. H. Günther, J. Nepywoda, J. Y. C. Chu, *J. Organomet. Chem.* **1974**, *74*, 79−84.
[22] K. Nakamoto, *Infrared and Raman spectra of inorganic and coordination compounds*, 5th ed., Wiley, New York, **1997**.
[23] O. H. Ellestad, P. Klaeboe, E. E. Tucker, J. Songstad, *Acta Chem. Scand.* **1972**, *26*, 1721−1723.
[24] K. W. Hipps, U. Mazur, *J. Phys. Chem.* **1987**, *91*, 5218−5224.
[25] S. S. Ti, S. F. A. Kettle, *Spectrochim. Acta* **1976**, *32A*, 1765−1769.
[26] K. O. Christe, W. W. Wilson, R. Bau, S. W. Bunte, *J. Am. Chem. Soc.* **1992**, *114*, 3411−3414.
[27] G. L. Bottger, *Spectrochim. Acta, Part A* **1968**, *24*, 1821−1829.
[28] T. M. Klapötke, B. Krumm, P. Mayer, H. Piotrowski, K. Polborn, I. Schwab, *Z. Anorg. Allg. Chem.* **2002**, *628*, 1831−1834.
[29] R. Eujen, B. Hoge, D. J. Brauer, *Inorg. Chem.* **1997**, *36*, 1464−1475.
[30] J. Mason, *Multinuclear NMR*, 2nd ed., Plenum Press, New York, **1989**.
[31] L. H. Jones, R. Pennemann, *J. Chem. Phys.* **1954**, *22*, 965−971.
[32] A. J. Leusink, G. Van Koten, J. W. Marsman, J. G. Noltes, *J. Organomet. Chem.* **1973**, *55*, 419−425.
[33] R. D. Sanner, R. G. Austin, M. S. Wrighton, W. D. Honnick, C. U. Pittman, Jr., *Inorg. Chem.* **1979**, *18*, 928−932.
[34] P. S. Pregosin, *Transition metal nuclear magnetic resonance*, Elsevier, Amsterdam, **1991**.
[35] R. F. Ziolo, M. Extine, *Inorg. Chem.* **1980**, *19*, 2964−2967.
[36] J. Jeske, W.-W. du Mont, P. G. Jones, *Angew. Chem.* **1996**, *108*, 2822−2824; *Angew. Chem. Int. Ed. Engl.* **1996**, *35*, 2653−2655.
[37] A. Bondi, *J. Phys. Chem.* **1964**, *68*, 441−451.
[38] Z.-L. Zhou, Y.-Z. Huang, Y. Tang, Z.-H. Chen, L.-P. Shi, X.-L. Jin, Q.-C. Yang, *Organometallics* **1994**, *13*, 1575−1581.
[39] E. L. Wagner, *J. Chem. Phys.* **1965**, *43*, 2728−2735.
[40] C. Akers, S. W. Peterson, R. D. Willett, *Acta Crystallogr., Sect. B* **1968**, *24*, 1125−1126.
[41] D. D. Swank, R. D. Willett, *Inorg. Chem.* **1965**, *4*, 499−501.
[42] H. Bürger, W. Schmid, *Z. Anorg. Allg. Chem.* **1972**, *388*, 67−77.
[43] R. G. Pearson, *Hard and soft acids and bases*, Dowden Hutchinson and Ross, Stroudsburg, PA, USA, **1973**.
[44] R. G. Pearson, *Science* **1966**, *151*, 1721−1727.
[45] C. Kappenstein, A. Ouali, M. Guerin, J. Cernak, J. Chomic, *Inorg. Chim. Acta* **1988**, *147*, 189−197.
[46] J. Cernak, F. Gerard, J. Chomic, *Acta Crystallogr., Sect. C: Cryst. Struct. Commun.* **1993**, *C49*, 1294−1296.
[47] T. Soma, T. Iwamoto, *Inorg. Chem.* **1996**, *35*, 1849−1856.
[48] W. A. Herrmann, G. Brauer, F. T. Edelmann, D. K. Breitinger, H. H. Karsch, N. Auner, *Synthetic methods of organometallic and inorganic chemistry*, Georg Thieme Verlag, Stuttgart, **1996**.
[49] A. Altomare, M. C. Burla, M. Camalli, G. L. Cascarano, C. Giacovazzo, A. Guagliardi, A. G. G. Moliterni, G. Polidori, R. Spagna, *J. Appl. Crystallogr.* **1999**, *32*, 115−119.
[50] G. M. Sheldrick, *SHELXL-97*, version 97-2, Universität Göttingen, Germany, **1997**.

Received April 24, 2002
[I02214]

Synthesis, Structure and Characterisation of New Phenolato-Bridged Manganese Complexes $[L_2Mn_2]^{2+}$ − Formation by Ligand Oxidation in L_aH [L_aH = *N*-(2-hydroxybenzyl)-*N*,*N*′-bis(2-pyridylmethyl)ethane-1,2-diamine]

Christelle Hureau,[a] Elodie Anxolabéhère-Mallart,[a] Martine Nierlich,[b] Florence Gonnet,[d] Eric Rivière,[a] and Geneviève Blondin*[a]

Keywords: Manganese / N,O ligands / Electrochemistry / EPR spectroscopy

A mononuclear $[L_aMn^{III}OAc](ClO_4)\cdot 0.5H_2O$ [**2**$(ClO_4)\cdot 0.5H_2O$] complex with a new amino-containing pentadentate ligand L_aH with a $[N_4O]$ coordination sphere has been obtained. Magnetic susceptibility measurements of **2**$(ClO_4)\cdot 0.5H_2O$ indicated a high spin electronic configuration for the Mn^{III} ion. In cyclic voltammetry the reversible wave observed at $E_{1/2}$ = 0.15 V vs. SCE was attributed to the reduction of Mn^{III} into Mn^{II}. In acetonitrile solution complex **2** spontaneously evolved into phenolato-bridged $Mn^{II}Mn^{II}$ dimeric complexes with the concomitant oxidation of the ligand. X-ray diffraction structures revealed that there is indeed a 1:1 mixture of two closely related complexes: in one case both ligands L_a^- have been oxidised to the imine form leading to the $[L_iMn^{II}Mn^{II}L_i]^{2+}$ cation (**1a**), whereas in the other, only one ligand has been oxidised, leading to the $[L_aMn^{II}Mn^{II}L_i]^{2+}$ cation (**1b**). In both **1a** and **1b**, Mn^{II} ions are in a distorted octahedral environment. Crystallographic data indicated that the Mn_2O_2 core is similar for **1a** and **1b.** The complete spectroscopic and electrochemical studies performed on powder samples and on acetonitrile solutions did not allow one to distinguish between the two cations. The magnetic susceptibility measurements performed on a powder sample of **1**$(BPh_4)_2\cdot 2CH_3COCH_3$ was characteristic of a weak antiferromagnetic coupling interaction between the two high-spin Mn^{II} ions (g = 1.95 and J = –1.5 cm^{-1}). Similar behaviour was observed for the powder sample of **1**$(ClO_4)_2\cdot H_2O$ (g = 1.96 and J = –2.9 cm^{-1}). Powder samples of **1**$(BPh_4)_2\cdot 2CH_3COCH_3$ and **1**$(ClO_4)_2\cdot H_2O$ showed EPR intensity variations with temperature indicating that the signal was mainly due to the S = 2 spin state. EPR spectra run on the acetonitrile solutions indicated that the dinuclear structure of **1** is maintained. In cyclic voltammetry, complex **1**$(ClO_4)_2\cdot H_2O$ exhibited a quasi-reversible wave in oxidation at E_p = 0.71 V vs. SCE, attributed to the slow electron transfer of the $Mn^{II}Mn^{II}/Mn^{II}Mn^{III}$ redox process ($k_s^{app} = 1.10^{-4}$ $cm^2\cdot s^{-1}$).

(© Wiley-VCH Verlag GmbH, 69451 Weinheim, Germany, 2002)

Introduction

Manganese is involved in several essential processes of life.[1] One famous example is the oxidation, under light, of water into dioxygen that is catalysed by the tetranuclear (oxo)Mn cluster of the Oxygen Evolving Complex (OEC) located in the photosystem II of green plants.[2,3] Dinuclear manganese clusters are present in several metalloproteins.[4,5] Among them, one can quote the manganese catalases, arginase and manganese ribonucleotide reductase.

In the last decade, X-ray diffraction studies were performed on an increasing number of metalloproteins, allowing new insight into the active sites. Resolution may, however, not be sufficient to predict either, the nature of the ligands[6] or the spatial arrangement of the metal ions.[7,8] The determination of the nature of the active sites still relies on the analysis of spectroscopic data. For instance, different hypotheses are formulated for the Mn_4 cluster of the OEC based on X-ray absorption investigations in conjunction with electronic spin resonance techniques (EPR, ENDOR, ESEEM).[3,9−11] Another example is the magnetisation studies run on catalases.[12]

Synthesising new complexes is still a challenge for the chemists along with the investigation of spectroscopic characteristics of such molecules and the perspective of elaborating new catalysts.

[a] Laboratoire de Chimie Inorganique, UMR 8613, Institut de Chimie Moléculaire d'Orsay, Université Paris-Sud, 91405 Orsay Cedex, France
Fax: (internat.) + 33-1/69154754
E mail: gblondin@icmo.u-psud.fr
[b] CEA Saclay, DRECAM/SCM Bat 125, 91191 Gif-Sur-Yvette, France
[c] Laboratoire de Chimie Structurale Organique et Biologique, Université Pierre et Marie Curie, 75005 Paris, France
[d] Present address: Laboratoire Analyse et Environnement, UMR 8587, Bâtiment des Sciences, Université d'Evry Val d'Essonne, Boulevard François Mitterrand, 91025 Evry Cedex, France

Supporting information for this article is available on the WWW under http://www.eurjic.org or from the author.

In relation to the OEC, we are interested in the EPR signatures of mixed-valent dinuclear $Mn^{III}Mn^{IV}$ systems for which the chemical nature of the bridge appears to have a great influence on the EPR signature. At the X-band, both the $[Mn^{III}-(\mu\text{-}O)_2-Mn^{IV}]^{3+}$ [13,14] and $[Mn^{III}-(\mu\text{-}O)_2(\mu\text{-}OAc)-Mn^{IV}]^{2+}$ [15,16] core systems present 16-line spectra that differ in their relative line intensities while the only mono(μ-oxo) complex reported in the literature, $[L'_iMn^{III}-(\mu\text{-}O)-Mn^{IV}L'_i]^{3+}$ (see Scheme 1), exhibits a peculiar 18-line spectrum.[17] In order to synthesise a new $Mn^{III}-(\mu\text{-}O)-Mn^{IV}$ system, we designed a ligand very similar to the one (L'_iH) used by Horner et al. In the laboratory, we previously used these ligands in the amine form (noted L_aH and L'_aH in Scheme 1) to synthesise $Fe^{III}-(\mu\text{-}O)-Fe^{III}$ systems and found that both ligands behave the same.[18,19] We will show here that this is not the case when the trivalent metal used is manganese. Following the same synthetic route reported for the formation of $[L'_iMn^{III}-(\mu\text{-}O)-Mn^{III}L'_i]^{2+}$, a mononuclear Mn^{III} complex is isolated when ligand L_aH is used instead of L'_aH. We found that this complex evolves into a bis(μ-phenolato)bis(Mn^{II}) complex with the concomitant dehydrogenation of the amine function of the ligand. Only three out of four ligands are indeed oxidised and we will designate LH to the mixture of L_aH and L_iH present in the isolated dinuclear Mn^{II} complex.

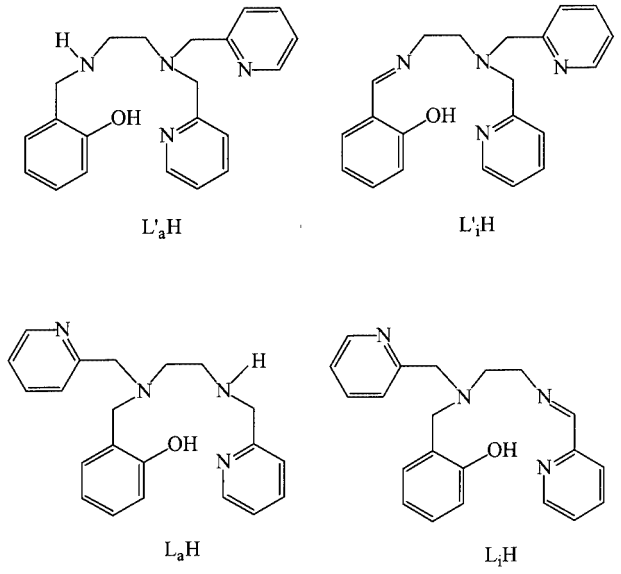

Scheme 1

Results and Discussion

Starting from $Mn(OAc)_3{\cdot}nH_2O$ and the ligand L_aH, a mononuclear Mn^{III} complex **2** was isolated as a perchlorate salt. No X-ray structure could be obtained, but the entire characterisation allows us to propose the formula $[L_aMnOAc]^+$ for **2**, which is in good agreement with all the measurements that were taken. Complex **2** evolves spontaneously in solution and leads to the formation of the dinuclear Mn^{II} complex **1** that was isolated using BPh_4^- or ClO_4^-. The two powdered samples $[\mathbf{1}](BPh_4)_2{\cdot}2CH_3COCH_3$ and $[\mathbf{1}](ClO_4)_2{\cdot}H_2O$ were characterised. Crystals were only obtained with tetraphenylborate as a counterion. Based on the whole characterisation of $[\mathbf{1}](BPh_4)_2{\cdot}2CH_3COCH_3$ and $[\mathbf{1}](ClO_4)_2{\cdot}H_2O$ discussed below, it is shown that the cation is the same in the two complexes. The dehydrogenation of the secondary amine which goes with the conversion of **2** into **1** is corroborated by the IR spectra. The vibration detected at 1665 cm^{-1} for $[\mathbf{1}](BPh_4)_2{\cdot}2CH_3COCH_3$ or 1661 cm^{-1} for $[\mathbf{1}](ClO_4)_2{\cdot}H_2O$ may be assigned to a coordinated imine function. No such vibration is detected for **2** indicating that the ligand remains as introduced.

X-ray Crystal Structure of $[L_2Mn_2](BPh_4)_2{\cdot}2CH_3COCH_3$

The structure consists of one $[LMn^{II}Mn^{II}L]^{2+}$ complex cation, two tetraphenylborate anions and two acetone molecules. The structure reveals that the complex is indeed a mixture of two closely related complexes in a 1:1 ratio. In complex **1a**, both ligands have been oxidised and exhibit an imine function conjugated to one pyridine group in place of the secondary amine function present in L_a^-. In complex **1b**, only one ligand has been oxidised while the second is the unchanged amine. A view of the cations is presented in Figure 1 and selected bond lengths and angles are listed in Table 1.

In both cations **1a** and **1b**, the two manganese ions are coordinated by the four nitrogen atoms of one ligand and by two oxygen atoms from phenolato groups, one belonging to the same ligand, and the other to the ligand coordinating the other metallic site. The metallic ions in **1a** and **1b** are in a distorted octahedral environment as shown by the angle values listed in Table 1. Such angle values are commonly observed in hexacoordinated Mn^{II} complexes.

The imine function is identified by the short C24−N6 and C3A−N2A bond lengths [1.310 (8) Å and 1.32 (2) Å] in the ligand coordinated to the Mn2 and Mn1 sites respectively. Moreover, the sum of the angles around the nitrogen atoms N6 or N2A approaches 360° (351° around N6, 343° around N2A), clearly demonstrating the sp^2 hybridisation of the nitrogen atoms.

The $Mn^{II}-N$ bond lengths in **1a** and **1b** are close to the values commonly observed for Mn^{II} complexes[20−26] except for the Mn1−N2A distance (2.375 Å) in **1a**. This distance is longer than the observed $Mn^{II}-N$ bond lengths (2.20−2.32 Å) where the nitrogen atom belongs to a phenolate conjugated imine function.[27−29]

The Mn2 moiety is common to the cations **1a** and **1b**. A comparison of the Mn1 moieties is shown in Figure 2. The folding of the ligand L_i^- around the metal centre is the same for Mn1 and Mn2 in complex **1a**, but the folding of the ligand L_a^- is not the same, leading to a different environment around the Mn1 atom in **1b**: (i) the phenolate ring planes are almost orthogonal (81°), (ii) the tertiary amine nitrogen atom to which this phenolate group is linked (N1A in **1a** and N1B in **1b**) is *cis* to the bridging phenolate O2

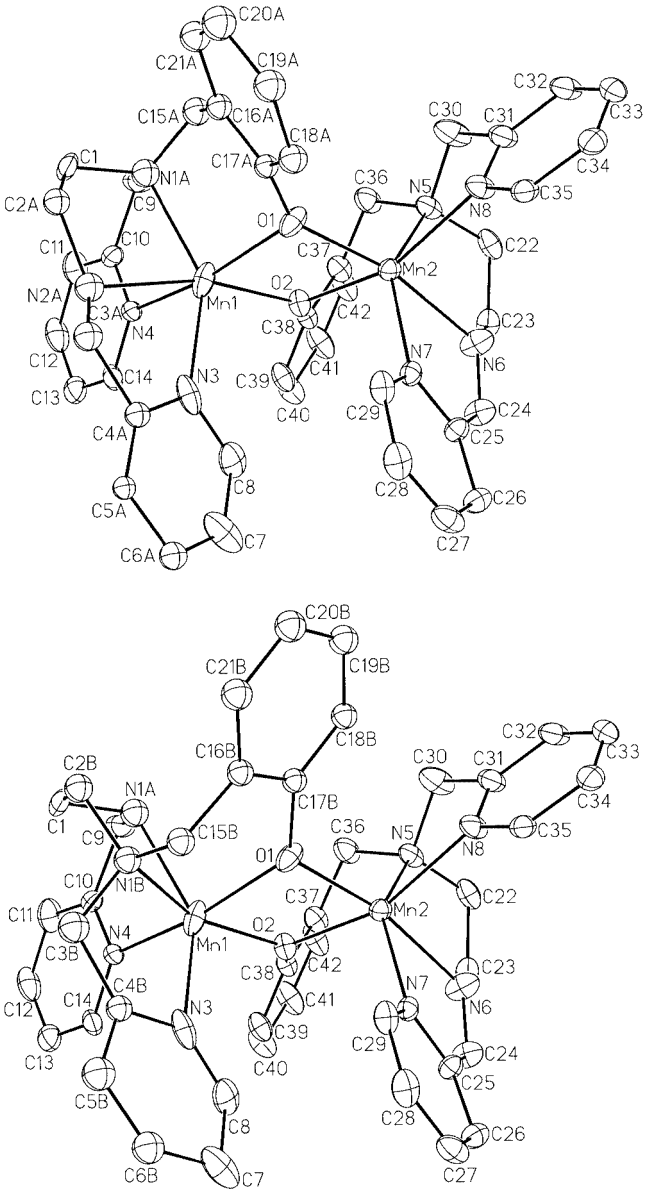

Fiugre 1. Views of the cations **1a** (top) and **1b** (bottom)

Table 1. Selected bond lengths [Å] and angles [°] for **1a** and **1b**; values are common to **1a** and **1b** unless specified

Mn1−O1	2.144(4)	Mn2−O1	2.129(4)
Mn1−O2	2.104(4)	Mn2−O2	2.103(4)
Mn1−N1A	2.278(6)	Mn2−N5	2.336(5)
Mn1−N2A (**1a**)	2.375(14)	Mn2−N6	2.279(6)
Mn1−N1B (**1b**)	2.327(10)		
Mn1−N3	2.266(7)	Mn2−N7	2.256(5)
Mn1−N4	2.284(5)	Mn2−N8	2.232(5)
O1−Mn1−N4	160.4(2)	O2−Mn2−N8	156.2(2)
N1A−Mn1−N3	144.5(2)	N5−Mn2−N7	145.7(2)
N2A−Mn1−O2 (**1a**)	164.9(3)	N6−Mn2−O1	166.9(2)
N1B−Mn1−O2 (**1b**)	156.7(3)		
Mn1−O1−Mn2	100.3(2)	Mn1−O2−Mn2	102.5(2)

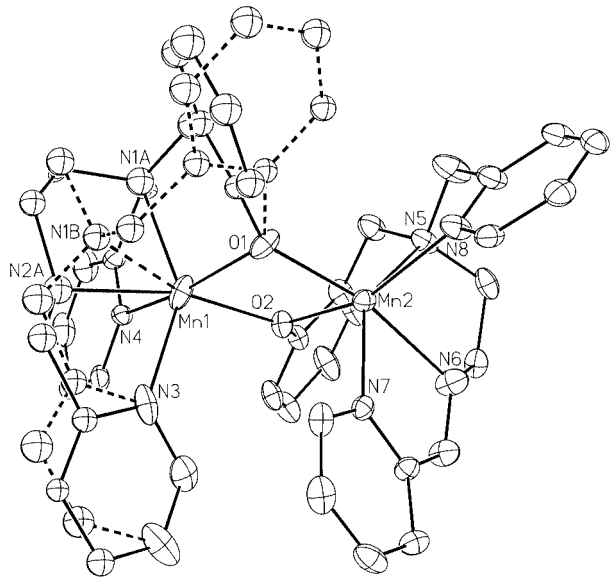

Figure 2. Comparison of the cations **1a** and **1b**, showing the differences in the Mn1 moieties; N1A of **1a** and N2B of **1b** are superimposed

atom in **1a** [N1A−Mn1−O2 113.8(2)°] while it is in the *trans* position in **1b** [N1B−Mn1−O2 156.7(3)°], (iii) the pyridine ring, slightly different in its orientation in the two Mn1 moieties, which contains the N3 atom, is linked to the imine nitrogen atom N2A atom in **1a** but to the tertiary amine N1B atom in **1b**, (iv) consequently, the two aromatic group substituents of the tertiary amine are *cis* to each other in **1b** [O1−Mn1−N3 102.7(2)°] while they are *trans* to each other in **1a** [O1−Mn1−N4 160.4(2)°] as it is around the Mn2 site [O2−Mn2−N8 156.2(2)°].

Such foldings can be compared to the ones of the same or closely related pentadentate ligands around Mn^{III} or Fe^{III} dinuclear complexes. The complexes $[L'_iMn-(\mu\text{-}O)-MnL'_i]^{n+}$ (n = 2, 3) have been characterised by X-ray crystallography.[17] The folding of the isomeric ligand L'^{-}_{i} presents the same characteristics as that of the ligand L^{-}_{i}, that is (i) the two aromatic groups anchored to the tertiary amine nitrogen atom are *trans* to each other, (ii) the tertiary amine nitrogen atom is *trans* to the group linked to the imine nitrogen atom (the phenolate ring in L'^{-}_{i}) and (iii) the imine nitrogen atom is *trans* to the exogeneous ligand. The same folding is observed for the ligand L'^{-}_{a} around the Fe^{III} ion in the complex $[L'_aFe-(\mu\text{-}O)-FeL'_a]^{2+}$,[18,19] and the secondary amine nitrogen atom in L'^{-}_{a} and the imine nitrogen atom in L'^{-}_{i} behave the same. In contrast, the ligand L^{-}_{a} adopts another folding in the complex $[L_aFe-(\mu\text{-}O)-FeL_a]^{2+}$.[18,19] The common features observed with the coordination around the Mn1 site just described in **1b** are (i) the two aromatic rings linked to the tertiary amine nitrogen atom are *cis* to each other and (ii) the tertiary amine nitrogen atom is *trans* to the extra ligand. The main difference lies in the ligation of the secondary amine nitrogen atom that is *trans* to the phenolate group. The variety of foldings observed when the ligand is in the reduced form (L^{-}_{a} and L'^{-}_{a}) compared to the unique ligating mode ob-

served when the ligand is oxidised (L_i^- and L'^-_i) is a signature of the greater flexibility when the conjugated imine function is absent.

Both Mn_2O_2 diamond core structures in **1a** and **1b** formed by the two metallic sites and the two oxygen atoms of the phenolate rings present features characteristic of such a motif. The $Mn^{II}-O$ distances (average 2.110 Å), and the $Mn^{II}-O-Mn^{II}$ bridging angles (average 101.4°) with a Mn···Mn separation of 3.280 Å, lie in the range observed for similar complexes.[20,21,25,27–34] One can note that the Mn_2O_2 diamond core structure is not planar and has a dihedral angle of 11.5°. Owing to the similarities in the Mn_2O_2 core in **1a** and **1b**, the two cations were considered identical in the following solid state studies.

Solution studies of **1** are prepared from powder samples [**1**$(ClO_4)_2$·H_2O or **1**$(BPh_4)_2$·$2CH_3COCH_3$]. One expects the same mixture of complex **1a** and **1b** observed in the crystals to exist in the powder samples and in solution.

Magnetic Susceptibility Measurements

The molar magnetic susceptibility χ_M of a powder sample of **1**$(BPh_4)_2$·$2CH_3COCH_3$ was measured as a function of temperature. The $\chi_M T$ value as a function of T is reported in Figure S1 in the Supporting Information (see also footnote on the first page of this article), together with the values obtained for **1**$(ClO_4)_2$·H_2O. For **1**$(BPh_4)_2$·$2CH_3COCH_3$, $\chi_M T$ decreases very slowly from 8.13 $cm^3 \cdot mol^{-1} \cdot K$ at 300 K to 7.91 $cm^3 \cdot mol^{-1} \cdot K$ at 100 K. Below 100 K, $\chi_M T$ decreases more rapidly to 0.9 $cm^3 \cdot mol^{-1} \cdot K$ at 2 K. This behaviour suggests a weak antiferromagnetic coupling interaction between the two high-spin Mn^{II} ions ($S_1 = S_2 = 5/2$). The best fit was obtained assuming identical parameters for the cations **1a** and **1b**: $g = 1.95$ and $J = -1.5$ cm^{-1}. These values are in agreement with those reported in the literature for complexes where two Mn^{II} ions are bridged by two phenolate ligands.[27,29,31,34]

Comparable results are obtained for **1**$(ClO_4)_2$·H_2O: $g = 1.96$ and $J = -2.9$ cm^{-1}. Small deformations of the $[Mn_2O_2]$ diamond core unit could lead to the slight differences in the g and J values determined for compound **1**, depending on the counterion.

The product of the molar magnetic susceptibility χ_M and the temperature T for a powder sample of **2**(ClO_4)·$0.5H_2O$ has a constant value of 3 $cm^3 \cdot mol^{-1} \cdot K$ from room temperature down to 30 K (see Figure S1 in the Supporting Information; see also footnote on the first page of this article). This indicates a +III oxidation state and a high-spin electronic configuration for the manganese ion ($S_{Mn^{III}} = 2$). $\chi_M T$ decreases below 30 K to reach 1.8 $cm^3 \cdot mol^{-1} \cdot K$ at 2 K. This behaviour is the signature of the zero-field splitting on the high-spin Mn^{III} ion. The best fits were obtained with a g factor close to 2 with either a positive or a negative D parameter: $g = 2.008$ and $D = +4.3$ cm^{-1} or $g = 2.006$ and $D = -4.5$ cm^{-1}. A weak intermolecular antiferromagnetic coupling between high-spin Mn^{III} ions can also contribute to the drop of $\chi_M T$ below 30 K. Mn^{III} complexes usually present an elongated octahedral geometry which corresponds to a negative D parameter.[35] The g and D values deduced here are in agreement with those determined by high-frequency EPR spectroscopy on other Mn^{III} complexes.[36–39]

EPR Spectroscopy

X-band EPR spectra of a powder sample of **1**$(BPh_4)_2$·$2CH_3COCH_3$ were recorded at several temperatures between 4.2 and 50 K using the perpendicular detection mode. The series is shown in Figure S2 in the Supporting Information (see also footnote on the first page of this article). All spectra exhibit features extending from 0 to 800 mT. Increasing temperature from 4.2 to 50 K does not affect the line positions but only their relative intensities. In addition, the signal intensity calculated as the double integral of the recorded spectrum does not follow a Curie law and reaches a maximum at 10 K.

The overall shape of the detected signals in conjunction with the deviation from the Curie law of the temperature dependence of the intensity is typical of dinuclear Mn^{II} complexes.[23,24,27,40–43] As previously reported in the literature, the complexity of the EPR spectra originating from weakly coupled dinuclear Mn^{II} complexes comes from the superposition of the signatures of the various paramagnetic spin states ($S = 1-5$) weighted by the Boltzmann distribution. Deconvolution procedures have been performed on systems presenting a relatively large antiferromagnetic exchange interaction.[44,45] In such systems, only the $S = 1$ and $S = 2$ excited spin states are sufficiently populated at low temperature to contribute to the EPR signal. In the present study, the exchange interaction is too small to allow for such an analysis.

A powder sample of the compound **1**$(ClO_4)_2$·H_2O was also tested in X-band EPR at 4.2 K and the observed spectrum is almost superimposable with the one of **1**$(BPh_4)_2$·$2CH_3COCH_3$.

The EPR was also run on frozen acetonitrile solutions of both compounds, either in the absence or in the presence of 0.1 M tetrabutylammonium perchlorate. The spectra recorded at 4.2 K present the same features as the ones detected on powder samples using the perpendicular or the parallel detection mode. This proves that the dinuclear structure of complex **1** is maintained in solution.

No X-band EPR signal was detected using the perpendicular detection mode on a powder sample of compound [**2**](ClO_4)·$0.5H_2O$. This is expected for integer spin states presenting a zero-field splitting much larger than the microwave quantum as is usually the case for monomeric Mn^{III} systems.

The EPR spectrum recorded on a freshly prepared acetonitrile solution of **2** displays a characteristic signature of **1**, together with signatures of free Mn^{II} ions (6 lines) and mixed valent $Mn^{III}Mn^{IV}$ species as impurities. These observations are the first indications that complex **2**(ClO_4)·$0.5H_2O$ is not stable in acetonitrile solution (vide infra).

Electrochemical Properties

The cyclic voltammogram of [**1**]$(ClO_4)_2 \cdot H_2O$ at 4×10^{-3} M in acetonitrile containing 0.1 M tetrabutylammonium perchlorate under argon is shown in Figure 3a. **1**$(BPh_4)_2 \cdot 2CH_3COCH_3$ was also investigated under reduction and showed similar results. The counterion BPh_4^- being easily oxidised, this sample was not investigated in the high potential ranges.

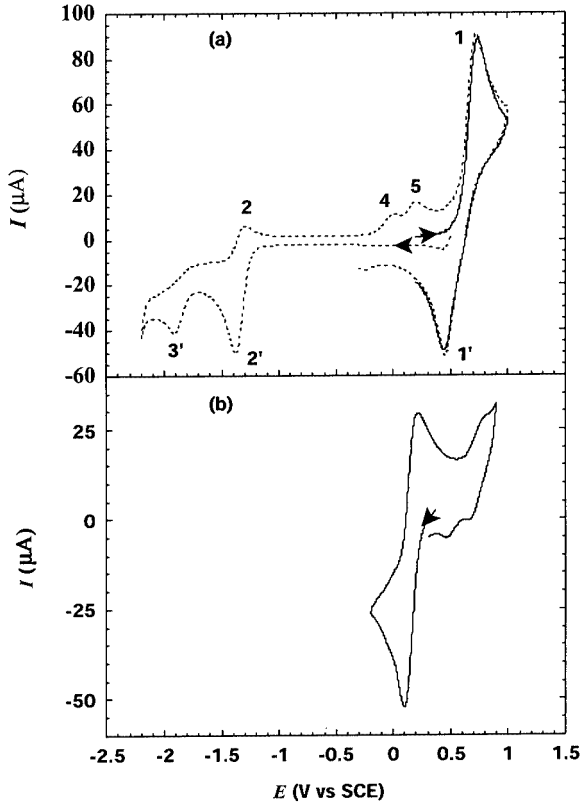

Figure 3. Cyclic voltammograms of **1**$(ClO_4)_2 \cdot H_2O$ (a) and **2**$(ClO_4)_2 \cdot 0.5H_2O$ (b) in acetonitrile containing 0.1 M of tetrabutylammonium perchlorate, $T = 20$ °C and scan rate = 100 mV·s^{-1}

The cyclic voltammetry trace of [**1**]$(ClO_4) \cdot H_2O$ shows a well-defined anodic wave (labelled wave 1 in Figure 3a) at $E_p = 0.710$ V vs. SCE, accompanied on the reverse scan by a well-defined cathodic wave (labelled 1′, $E_p = 0.450$ V vs. SCE). This oxidation process is attributed to the oxidation of the Mn^{II} ion being complexed by the imine form of the ligand in both **1a** and **1b**. This Mn^{II} oxidation potential is fairly high. $Mn^{II}Mn^{II}/Mn^{II}Mn^{III}$ oxidation potentials have been reported in the literature at about 0.35 V vs. SCE for the $[LMn_2Cl_2]$[30] or $[L'Mn_2(OAc)]^{2+}$ [46] cation where LH_2 and L′H are related to L_aH.[47] In complex **1**, the higher potential value is related to the lower number of the charged ligand around the Mn^{II} ion. A value of 0.598 V vs. SCE is reported in the literature for the $Mn^{II}Mn^{II}/Mn^{II}Mn^{III}$ oxidation potential in the case of the neutral bis(phenolato)-bridged $[Mn_2^{II}(SALPS)_2]$ dinuclear complex.[27,48] The Mn^{II} ion complexed by the amine ligand is expected to be oxidised at a higher potential. Indeed other oxidation waves are detected when scanning the potential up to 1.7 V vs. SCE. Those irreversible, ill defined cyclic voltammetry traces are attributed to oxidation of the ligand (phenolic part) and overlay with the oxidation trace of the Mn^{II} ion complexed by the amine ligand.

The cyclic voltammogram displayed in Figure 3a shows a large difference in peak potential ($\Delta E_p = 260$ mV) for wave 1/1′. This indicates that the associated electron transfer is slow. In the case of slow electron transfer, determination of n, the number of electrons involved in the redox process, is not easy. For a system undergoing irreversible charge transfer kinetics (i.e. slow electron transfer), it has been shown that $|E_p - E_{p/2}|$[49] is related to αn through Equation (1), where α is the charge transfer coefficient.[50]

$$\alpha n = \frac{0.048}{|E_p - E_{p/2}|} \quad (1)$$

In the present case, considering the symmetrical shape of the entire wave, a value of 0.5 can be taken for α. At this point one must be concerned with the influence of solution resistance since it can affect the position of the peak potential. Therefore particular care was taken to insure that the present ohmic drop was correctly compensated. From $|E_p - E_{p/2}|$ values listed in Table 2, one can establish that $n = 1$. This value was confirmed by chronocoulometry measurements. A step potential ($E = +1$ V vs. SCE, $t = 500$ ms or 250 ms) was applied to the working electrode of known surface area.[51] The chronocoulometry response gives the total charge passed Q vs. time t from the initial step. From the linear relationship[52] between Q and $\sqrt{t}$, a value of 1.2 was found for n. Thus, at the time scale of cyclic voltammetry (v range 50−500 mV·s^{-1}), or for chronocoulometry with time steps shorter than 1 s, the first oxidation step corresponds to Equation (2).

Table 2. Potential peak values and electron transfer rate constants for the $Mn^{II}Mn^{II}/Mn^{II}Mn^{III}$ oxidation in **1**$(ClO_4)_2 \cdot H_2O$

v [mV·s^{-1}]	E_{pa} [a] [V vs. SCE]	$E_{pa/2}$ [a] [V vs. SCE]	E_{pc} [a] [V vs. SCE]	ΔE_p [b] [mV]	k_s^{app} [c] [cm·s^{-1}]
50	0.705	0.595	0.460	245	7.7×10^{-4}
75	0.705	0.600	0.465	240	9.9×10^{-4}
100	0.710	0.610	0.450	260	9.4×10^{-4}
200	0.730	0.625	0.435	295	9.4×10^{-4}
300	0.730	0.625	0.445	285	1.3×10^{-3}
400	0.725	0.625	0.435	290	1.4×10^{-3}
500	0.730	0.630	0.440	290	1.5×10^{-3}
1000	0.750	0.650	0.410	340	1.4×10^{-3}

[a] E_{pa} and E_{pc} are the values of the anodic and of the cathodic peak potential, respectively, of the wave of interest. [b] ΔE_p is defined as the difference between the anodic and the cathodic peak potentials. [c] k_s^{app} is calculated according to Equation (3) given in the text with $\alpha = 0.5$, $D = 15 \times 10^{-6}$ cm$^2 \cdot$ s^{-1} and $T = 298$ K.

$$Mn^{II}Mn^{II} \rightarrow Mn^{II}Mn^{III} + e^- \quad (2)$$

It was not possible to confirm this stoichiometry by controlled potential electrolysis at $E = +1$ V vs. SCE, due to the instability of the $Mn^{II}Mn^{III}$ state on the electrolysis time

scale, even when lowering the temperature down to −30 °C. The quasi-reversibility of this oxidation step was studied by cyclic voltammetry, which showed that the peak separation, ΔE_p, for the redox couple $Mn^{II}Mn^{II}/Mn^{II}Mn^{III}$ varied between ca. 240 and 340 mV as the scan rate was increased from v = 50 to 2000 mV·s^{-1}. Table 2 gives the measured ΔE_p values for a series of voltammograms at different scan rates. Values of the apparent charge transfer rate constant (k_s^{app}) can be obtained using the procedure of Nicholson[50] for peak separations smaller than 210 mV. When ΔE_p exceeds this value, k_s^{app} [cm^{-1}] can be calculated using Equation (3), where D is the diffusion coefficient of the species of interest [cm^2·s^{-1}] and v the scan rate [m^{-1}].

$$k_s^{app} = 2.18\sqrt{\frac{D\alpha nFv}{RT}}\exp\left(\alpha^2\frac{nF}{RT}\Delta E_p\right) \quad (3)$$

Values of k_s^{app} obtained for different values of v are listed in Table 2 and a mean value of 1.2×10^{-3} cm·s^{-1} is found. This is in agreement with what is found in the literature for slow electron transfer in inorganic compounds. For example, a value of 10^{-3} cm·s^{-1} is found for the electron transfer constant of the reduction of a (porphyrin)Mn^{III} compound in dimethyl sulfoxide.[53]

This low value of the electron transfer can mainly be attributed to the fact that the oxidation process requires structural reorganisation of the original $Mn^{II}Mn^{II}$ cation. Indeed the geometry around the Mn^{III} ion should become axially distorted, due to the Jahn−Teller effect. The constraint of the structure imposed by the phenolato bridges makes this reorganisation difficult. Moreover, it was never possible to generate an $Mn^{II}Mn^{III}$ species that is stable in solution when running exhaustive electrolysis at E = +1 V vs. SCE. EPR spectra recorded on such an electrolysed solution did not show the expected $Mn^{II}Mn^{III}$ signature. Indeed, the observed signal is characteristic of monomeric Mn^{II} species, suggesting that most of the complexes remaining in solution are monomeric EPR-silent Mn^{III} entities. These observations sustain the fact that the phenolato bridges cannot support the dimeric structure in a mixed-valent state.

When scanning towards low potentials, two cathodic waves (noted as 2′ and 3′, see a in Figure 3) are observed. The first appears at E_p = −1.380 V vs. SCE and the second at −1.910 V vs. SCE. When scanning back to the oxidative potential, a first anodic wave is observed at E_p = −1.300 V vs. SCE (wave 2) and is related to the cathodic wave 2′. Scanning back towards higher potentials generates two new anodic waves (denoted 4 and 5) at E_p = 0.005 V and E_p = 0.190 V, respectively. The waves 2′ and 3′ are attributed to the [2e$^-$,1H$^+$] reductive process of the imine function of the ligand. Indeed the addition of perchloric acid to the solution results in the shift of the peak potentials towards positive values (not shown). Increasing the scan rate results in the increase of reversibility of wave 2′/2, thus showing that the reduction process associated with wave 2 generates a very reactive species. We propose this first reduced species to be an anion radical, the unpaired electron being located on the nitrogen atom of the imine part of the ligand. This very reactive anion radical is immediately protonated and further reduced at −1.910 V (wave 3′). Waves 4 and 5 are tentatively attributed to monomeric Mn^{II} species, most likely generated consecutively by the reduction process 2′ and 3′. Indeed, the monomeric **2**$(ClO_4)_2$ species exhibits an Mn^{II}/Mn^{III} redox process in the potential range of waves 4 and 5.

The cyclic voltammogram of **2**$(ClO_4)_2$·H_2O in acetonitrile containing 0.1 M tetrabutylammonium perchlorate under Ar is shown in Figure 3b. The most intense wave at $E_{1/2}$ = 0.150 V vs. SCE [$E_{1/2} = (E_{pa} + E_{pc})/2$, ΔE_p = 180 mV] is attributed to the reduction of the Mn^{III} into Mn^{II} species. This value lies between the ones measured on acetonitrile solutions of {[$py_2(NMe)_2$]$Mn^{II}Cl_2$} ($E_{1/2}$ = 0.55 V vs. SCE) and {[$py_2(NMe)_2$]$Mn^{III}F_2$}$^+$ ($E_{1/2}$ = −0.07 V vs. SCE) where $py_2(NMe)_2$ stands for *N*,*N*′-dimethyl-2,11-diaza[3,3]-(2,6)pyridinophane.[38] The fairly low value for the reduction potential of **2** agrees with the coordination of two negatively charged ligands, the phenolate and the acetate, to the Mn^{III} site. In the anodic part of the voltammogram, a second and less intense wave is observed at $E_{1/2}$ = 0.770 V and is related to the conversion of **2** into **1** (vide infra).

UV/Vis Spectroscopy

The UV/Vis spectrum of complex **2** was recorded on a freshly prepared acetonitrile solution and is reproduced in Figure 4 [curve (a)]. Three bands are found at 373 (ε = 1770 M^{-1}·cm^{-1}), 502 (940) with a shoulder at 475 (1050),

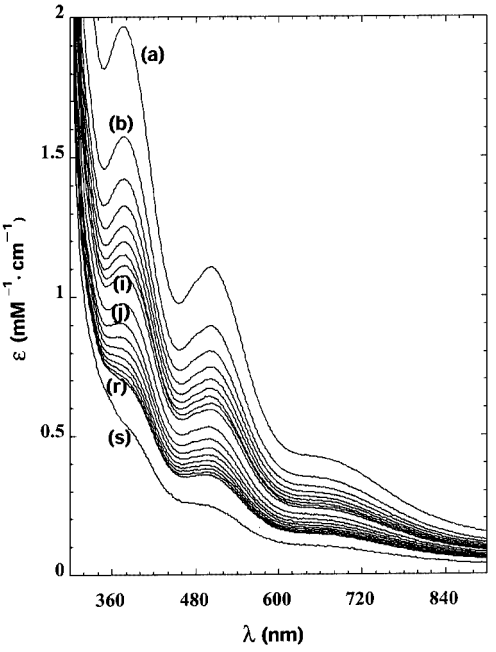

Figure 4. Time evolution of the UV/Vis spectrum of **2**$(ClO_4)_2$·0.5H_2O, 10^{-3} M in acetonitrile; spectrum (a) corresponds to the freshly prepared solution (t = 0); spectra (b) to (i) are recorded every 15 min (t = 15−120 min) and spectra (j) to (r) every hour (t = 180−660 min); spectrum (s) was recorded 46 h after spectrum (a)

and 670 nm (330). The more intense band detected in the near UV region is also observed in Mn^{III}-based complexes containing phenolato ligands and may be assigned to a phenolato-to-Mn^{III} charge transfer (LMCT) transition.[46,54,55] The last two transitions may be attributed to d-d transitions of the Mn^{III} ion according to the literature.[56,57] The low extinction coefficient measured at 670 nm enforces such an attribution. The greater absorption detected around 500 nm suggests that this band does not arise only from a d-d transition and may overlap with other LMCT bands. Resonance Raman experiments performed on dinuclear Mn^{III} complexes presenting the bis(μ-acetato)(μ-oxo) core unit suggest that the acetato-to-Mn^{III} charge transfer transition occurs in the range 450 to 500 nm rather than around 400 nm.[58] We thus propose that the absorption observed in **2** could originate from the $AcO^- \rightarrow Mn^{III}$ LMCT transition but we cannot reject a contribution from a phenolato $\rightarrow Mn^{III}$ LMCT transition.[59]

Complex **1** presents features only in the UV region [282 (ε = 2850 $cm^{-1}\cdot M^{-1}$), 262 (3960), 238 (6000) and 210 nm (15400)] associated with π-π* transitions of the ligand, in agreement with the +II oxidation state of the manganese ions.

Evolution of 2 into 1

All the attempts to obtain crystals of complex **2** ineluctably led to the formation of crystals of complex **1**. Thus, we decided to investigate the transformation of **2** into **1**, using different techniques.

A freshly prepared acetonitrile solution of **2** was allowed to evolve at room temperature and the UV/Vis spectra were recorded every 15 min. The evolution is presented in Figure 4. 36% of the initial absorption is lost in 1 h. It was not possible to interpret the series of spectra assuming the existence in solution of only two chromophores. Indeed, the band at 502 nm and the shoulder at 475 nm do not obey the same kinetic law. This implies the formation of at least one intermediate species (not identified).

The transformation was also monitored by EPR spectroscopy. As mentioned above, a signal attributed to **1** was detected on the freshly prepared acetonitrile solution of **2**, which significantly increased with time. Cyclic voltammetry and mass measurements confirmed the fast generation of **1** from **2**.

Electrospray mass spectra were recorded on freshly prepared acetonitrile solutions of complexes **1** and **2**. For complex **1**, peaks at *m*/*z* values of 901 and 903 are detected and attributed to the $\{[L_iMn^{II}Mn^{II}L_i](ClO_4)\}^+$ and $\{[L_iMn^{II}Mn^{II}L_a](ClO_4)\}^+$ entities, respectively. For complex **2**, no peak was detected at the expected *m*/*z* value of 461 for the monocationic $[L_aMn^{III}(OAc)]^+$ species. On the other hand, the above-mentioned peaks at *m*/*z* values of 901 and 903 were well observed, clearly indicating the conversion of **2** into **1** in acetonitrile solution.

Conclusion

Mn^{III} coordination chemistry has been investigated with a new pentadentate ligand L_aH with an $[N_4O]$ coordination sphere. It was expected to form a new dimeric $Mn^{III}-(\mu\text{-}O)-Mn^{IV}$ system, as has previously been obtained with an isomeric $[N_4O]$ ligand[17] (L_i'), but a mononuclear $[L_aMn^{III}]^{2+}$ complex **2** was obtained. It was found that this monomeric complex spontaneously evolves in acetonitrile solution into phenolato-bridged $Mn^{II}Mn^{II}$ dimeric complexes with the concomitant oxidation of the ligand. The formation of this bridge is made possible owing to the fairly flexible phenolate arm, when the conjugated imine function is absent in contrast to what has been observed in $[L_i'Mn-(\mu\text{-}O)-MnL_i']^{n+}$ (n = 2, 3). X-ray crystal structure analyses revealed that there is indeed a mixture of two closely related complexes: in one case both ligands L_a have been oxidised to the imine form leading to the $[L_iMn^{II}Mn^{II}L_i]^{2+}$ cation **1a**, whereas in the other only one ligand has been oxidised leading to the $[L_aMn^{II}Mn^{II}L_i]^{2+}$ cation **1b**. One can note that the oxidation of the ligand L_aH into L_iH is a $(2e^-,2H^+)$ process, while the concomitant reduction of Mn^{III} into Mn^{II} implies only one electron. We thus propose that the mononuclear complex **2** evolves in solution according to Equation (4).

$$6\ [L_aMn(OAc)]^+ \rightarrow [L_iMnMnL_i]^{2+} + [L_iMnMnL_a]^{2+} + [L_aMnMnL_a]^{2+} + 6\ OAc^- + 6\ H^+ \quad (4)$$

The three complexes would present the same bis(μ-phenolato)-bridged core unit and would be indistinguishable by EPR spectroscopy for instance. Complex $[L_aMn^{II}Mn^{II}L_a]^{2+}$ would remain in solution during the crystallisation process. Further investigation on the mechanism of this evolution was not pursued. A complete study would require controlling the pH value and the amount of acetate ions during the synthesis and crystallisation processes. In order to avoid the oxidation of the secondary amine of the L_aH ligand, methylation of the nitrogen atom has been performed. Manganese coordination chemistry of both the Mn^{II} and Mn^{III} oxidation states with this pentadentate ligand is under investigation.

Experimental Section

General Remarks: Reagents and solvents were purchased commercially and used as received. Elemental analysis: Analyses were performed by the Service Central d'Analyse du CNRS (Vernaison-France) for C, H, B, Cl, Mn, N. Infrared spectroscopy: Spectra were recorded on KBr pellets in the range of 4000 to 200 cm^{-1} with a Perkin–Elmer Spectrum 1000 spectrophotometer. The synthesis of L_aH has been described previously.[18]

Caution: *Perchlorate salts of metal complexes with organic ligands are potentially explosive. Only small quantities of these compounds should be prepared and handled behind suitable protective shields.*

Syntheses

[1](BPh$_4$)$_2$·2CH$_3$COCH$_3$: An ethanol solution (5 mL) of L_aH (348 mg, 1.0 mmol) and triethylamine (0.2 mL, 2.0 mmol) was added to an ethanol solution (5 mL) of Mn(OAc)$_3$·2H$_2$O (268 mg, 1.0 mmol) while stirring. The resulting brown solution was stirred for an extra hour and filtered at least twice in order to eliminate the remaining Mn(OAc)$_3$·2H$_2$O. To the filtrate sodium tetraphenylborate (342 mg, 1.0 mmol) was added. The brownish powder thus obtained, was then washed with ethanol, dried on a frit, and redissolved in acetone. Crystals suitable for X-ray crystallography were obtained by slow evaporation of acetone. 170 mg (ρ = 11%) of crystallised complex was collected by filtration. IR (KBr): $\tilde{\nu}$ = 3461 (w), 3254 (w), 3053 (m), 1710 (m), 1665 (s), 1597 (w), 1580 (m), 1569 (m), 1479 (w), 1453 (m), 1443 (m), 1360 (s), 1265 (w), 1220 (m), 1156 (s), 1101 (s), 1031 (s), 1015 (s), 974 (s), 882 (s), 841 (s), 751 (m), 733 (w), 706 (w), 643 (s), 624 (s), 611 (m), 581 (s), 528 (s), 470 (s), 412 (s) cm^{-1}. $C_{96}H_{95}B_2Mn_2N_8O_4$ (1556.3): calcd. C 74.09, H 6.15, B 1.36, Mn 7.06, N 7.20; found C 73.68, H 6.11, B 2.06, Mn 7.00, N 6.97.

[1](ClO$_4$)$_2$·H$_2$O: An ethanol solution (5 mL) of L_aH (348 mg, 1.0 mmol) and triethylamine (0.2 L, 2 mmol) was added to an ethanol solution (5 mL) of Mn(OAc)$_3$·2H$_2$O (268 mg, 1.0 mmol) while stirring. The resulting brown solution was stirred for several hours and filtered at least twice in order to eliminate the remaining Mn(OAc)$_3$·2H$_2$O. To the filtrate sodium perchlorate (122 mg, 1.0 mmol) was added. The pale brownish powder thus obtained, was then washed with ethanol, and dried on a frit. IR (KBr): $\tilde{\nu}$ = 3440 (s), 3278 (m), 3059 (w), 2912 (m), 1661 (w), 1595 (s), 1570 (m), 1479 (s), 1453 (m), 1442 (m), 1294 (m), 1265 (s), 1152 (m), 1094 (s), 1017 (m), 884 (w), 838 (w), 769 (m), 762 (m), 725 (w), 636 (w), 624 (w), 611 (m), 579 (w), 472 (w), 412 (w) cm^{-1}. $C_{42}H_{45}Cl_2Mn_2N_8O_{11}$ (1018.6): calcd. C 49.52, H 4.45, Cl 6.96, N 11.00; found C 49.61, H 4.63, Cl 7.33, N 10.82.

[2](ClO$_4$)·0.5H$_2$O: An ethanol solution (5 mL) of L_aH (348 mg, 1.0 mmol) was added to an ethanol solution (5 mL) of Mn(OAc)$_3$·2H$_2$O (268 mg, 1.0 mmol) while stirring. The resulting dark purple solution was stirred for 5 min and filtered at least twice in order to eliminate the remaining Mn(OAc)$_3$·2H$_2$O. To the filtrate sodium perchlorate (122 mg, 1.0 mmol) was added. The solution was stirred for an extra hour and the purple powder thus obtained, was then washed with ethanol, and dried on a frit. IR (KBr): $\tilde{\nu}$ = 3416 (s), 3148 (m), 2970 (w), 2926 (w), 1607 (w), 1568 (m), 1479 (s), 1450 (s), 1445 (s), 1428(m), 1375(s), 1327 (s), 1283 (m), 1263 (s), 1160 (w), 1088 (s), 1017 (m), 974(w), 944 (w), 930 (w), 887 (w), 852 (w), 783 (s), 765 (s) 56 (s), 724 (w), 658 (w), 640 (m), 623 (s), 584 (w), 579 (w), 415 (w) cm^{-1}. $C_{23}H_{27}ClMnN_4O_{7.5}$ (569.9): calcd C 48.48, H 4.78, Cl 6.22, N 9.83; found C 48.35, H 4.72, Cl 6.65, N 9.58.

Crystallographic Data Collection and Refinement of the Structure of [1](BPh$_4$)$_2$·2CH$_3$COCH$_3$: The crystal data of [**1**](BPh$_4$)$_2$·2CH$_3$COCH$_3$ and the parameters of data collection are summarized in Table 3. A honey-colored crystal of approximate dimensions 0.30 × 0.20 × 0.15 mm was selected. The diffraction collection was carried out with a Nonius diffractometer, equipped with a CCD detector. The lattice parameters were determined from ten images recorded with 2° Φ-scans and later refined on all data. The data were recorded at 123 K. A 180° Φ-range was scanned with 2° steps with a crystal-to-detector distance fixed at 30 mm. Data were corrected for Lorentz polarisation. The structure was solved by direct methods and refined by full-matrix least squares on F^2 with anisotropic thermal parameters for all non-H atoms. One ligand was found disordered on two positions with a 0.5 occupation factor. H atoms were introduced at calculated positions (except for atoms of the disordered ligands) and constrained to ride on their parent C atom. All calculations were performed with an O2 Silicon Graphics Station with the SHELXTL package.[60] Crystal data are summarized in Table 3. CCDC-178266 contains the supplementary crystallographic data for this paper. These data can be obtained free of charge at www.ccdc.cam.ac.uk/conts/retrieving.html or from the Cambridge Crystallographic Data Centre, 12, Union Road, Cambridge CB2 1EZ, UK [Fax: (internat.) + 44-1223/336-033; E-mail: deposit@ccdc.ac.uk].

Table 3. Crystallographic data for [**1**](BPh$_4$)$_2$·2CH$_3$COCH$_3$

Empirical formula	$C_{96}H_{95}B_2Mn_2N_8O_4$
Formula mass	1556.3
Temperature [K]	123
Wavelength [Å]	0.71073
a [Å]	24.502(5)
b [Å]	14.805(3)
c [Å]	25.626(5)
β [°]	115.86(3)
Volume [Å^3]	8365(3)
Z	4
Density [g·cm^{-3}]	1.236
μ [mm^{-1}]	0.359
θ_{max} [°]	24.69
hkl ranges	$0 \le h \le 28$ $0 \le k \le 17$ $-30 \le l \le 27$
Reflections measured	51714
Reflections independent	14126
Reflections with $I > 2\sigma(I)$	7772
Parameters	962
$R1 = \Sigma\|\|F_o\| - \|F_c\|\|/\Sigma\|F_o\|$	0.1004
$wR2 = \{\Sigma[w(F_o^2 - F_c^2)^2]^2/\Sigma w(F_o^2)^2]\}^{1/2}$ $w = 1/[\sigma^2(F_o^2) + (0.1000P)^2]$ where $P = (F_o^2 + 2F_c^2)/3$	0.2120
(Δ/σ)max	0.016
$\Delta\rho_{max}$ [e·Å^{-3}]	0.566
$\Delta\rho_{min.}$ [e·Å^{-3}]	−0.475

Magnetic Susceptibility Measurements: Magnetic susceptibility data were recorded with an MPMS5 magnetometer (Quantum Design, Inc.). The calibration was made at 298 K using a palladium reference sample furnished by Quantum Design, Inc. The data were collected over a temperature range of 2−300 K at a magnetic field of 0.5 or 1 T and were corrected for diamagnetism. In the case of **1**, the $\chi_M T$ vs. T curves were fitted using the van Vleck formula and assuming the same g factor for each spin state S. The energies appearing in the exponential arguments are derived from the Heisenberg−Dirac-van Vleck Hamiltonian $-JS_1 \cdot S_2$. The total spin S runs from $|S_1 - S_2|$ to $S_1 + S_2$ by unit steps. The fitting procedure used for complex **2** is derived from magnetisation calculations described previously.[61]

EPR Spectroscopy: EPR Spectra were recorded with a Bruker 200D spectrometer at the X-band. For low-temperature studies, an Oxford Instrument continuous-flow liquid helium cryostat and a temperature control system were used.

Cyclic Voltammetry and Chronocoulometry: Cyclic voltammetry and chronocoulometry measurements were recorded with an EGG PAR potentiostat (M273 model). The counter electrode was an Au wire, the working electrode, a glassy carbon disk, was carefully polished before each voltammogram with a 1 μm diamond paste, sonicated in an ethanol bath and then washed carefully with eth-

anol. It is worth noting that in the absence of such treatment of the working electrode surface, the successive cyclic voltammograms were not reproducible. The reference electrode was an $Ag/AgClO_4$ electrode (0.530 V vs. NHE electrode), isolated in a fritted bridge. The solvent used was distilled acetonitrile where tetrabutylammonium perchlorate was added to obtain a 0.1 M supporting electrolyte, when the experiments were carried out at room temperature, or 0.2 M, when the experiments were carried out at low temperature (below 10 °C). Low-temperature regulation was insured by a Julabo circulation cryostat.

UV/Vis Spectroscopy: UV/Vis spectra were recorded with a Cary 300 Bio spectrophotometer at 20 °C with 1-cm quartz cuvettes.

Electrospray Ionisation Ion Trap Mass Spectrometry: All experiments were performed with an ESQUIRE ion trap (Bruker-Franzen Analytic GmbH, Bremen, Germany). The used instrument has a fundamental RF frequency of 781 kHz and was used here in the *standard* mode with a mass-to-charge ratio up to 2000 Th, using a 260.3 kHz frequency as axial modulation. The ion trap operated at an uncorrected partial He buffer gas pressure of 3.4×10^{-5} Torr ($4.5\ 10^{-3}$ Pa). A differentially pumped interface transferred the ions from the electrospray source (Analytica of Brandford, Inc., Brandford, CT) to the mass spectrometer. No Ion Current Control (ICC) was used, allowing the adjustment of the ion accumulation time. Some applied parameters were unchanged for all experiments, such as the RF frequency amplitude of the hexapole (700 V), and the voltage applied on the electron multiplier (−1500 V). The dynode voltage of the electron multiplier was −5 kV, the delay before scanning 10 ms and the exit lens voltage −50 V, with the low *m/z* cutoff value at 50 Th.

Infused Solutions: The complexes were analysed in the positive-ion mode. Diluted samples (ca. 10^{-4} M) in pure acetonitrile were infused into the ESI source using a Cole−Parmer Instrument Company (74900 series) syringe pump at a flow rate of 120 μL/h. The capillary entry voltage was about −3500 V. The N_2 drying gas temperature was 150 °C with a flow rate of 200 L/h.

[1] E. J. Larson, V. L. Pecoraro, in *Manganese Redox Enzymes* (Ed.: V. L. Pecoraro), VCH Publishers, Inc., New York, **1992**, p. 1−28.
[2] R. J. Debus, *Biochim. Biophys. Acta* **1992**, *1102*, 269−352.
[3] V. K. Yachandra, K. Sauer, M. P. Klein, *Chem. Rev.* **1996**, *96*, 2927−2950.
[4] G. C. Dismukes, *Chem. Rev.* **1996**, *96*, 2909−2926.
[5] N. A. Law, M. T. Caudle, V. L. Pecoraro, *Adv. Inorg. Chem.* **1998**, *46*, 305−440.
[6] V. V. Barynin, M. M. Whittaker, S. V. Antonyuk, V. S. Lamzin, P. M. Harrison, P. J. Artymiuk, J. W. Whittaker, *Structure* **2001**, *9*, 725−738.
[7] A. Zouni, H.-T. Witt, J. Kern, P. Fromme, N. Krauß, W. Saenger, P. Orth, *Nature* **2001**, *409*, 739−743.
[8] A. W. Rutherford, P. Faller, *Trends Biochem. Sci.* **2001**, *26*, 341−344.
[9] K. Hasegawa, T.-A. Ono, Y. Inoue, M. Kusunoki, *Bull. Chem. Soc. Jpn.* **1999**, *72*, 1013−1023.
[10] J. M. Peloquin, K. A. Campbell, D. W. Randall, M. A. Evanchik, V. L. Pecoraro, W. H. Armstrong, R. D. Britt, *J. Am. Chem. Soc.* **2000**, *122*, 10926−10942.
[11] T. G. Carrell, A. M. Tyryshkin, G. C. Dismukes, *J. Biol. Inorg. Chem.* **2002**, *7*, 2−22.
[12] L. Le Pape, E. Perret, I. Michaud-Soret, J.-M. Latour, *J. Biol. Inorg. Chem.* **2002**, *7*, 445−450.
[13] P. A. Goodson, J. Glerup, D. J. Hodgson, K. Michelsen, H. Weihe, *Inorg. Chem.* **1991**, *30*, 4909−4914.
[14] Y. Frapart, A. Boussac, R. Albach, E. Anxolabéhère-Mallart, M. Delroisse, J.-B. Verlach, G. Blondin, J.-J. Girerd, J. Guilhem, M. Cesario, A. W. Rutherford, D. Lexa, *J. Am. Chem. Soc.* **1996**, *118*, 2669−2678.
[15] W. Zweygart, R. Bittl, K. Wieghardt, W. Lubitz, *Chem. Phys. Lett.* **1996**, 272−276.
[16] K.-O. Schäfer, R. Bittl, W. Zweygart, F. Lendzian, G. Haselhorst, T. Weyhermüller, K. Wieghardt, W. Lubitz, *J. Am. Chem. Soc.* **1998**, *120*, 13104−13120.
[17] O. Horner, E. Anxolabéhère-Mallart, M.-F. Charlot, L. Tchertanov, J. Guilhem, T. A. Mattioli, A. Boussac, J.-J. Girerd, *Inorg. Chem.* **1999**, *38*, 1222−1232.
[18] S. Poussereau, PhD Thesis, Université Paris-Sud,Orsay, France, **1999**.
[19] S. Poussereau, G. Blondin, E. Anxolabéhère-Mallart, T. A. Mattioli, L. Tchertanov, J.-J. Girerd, manuscript in preparation.
[20] C. Fraser, L. Johnston, A. L. Rheingold, B. S. Haggerty, G. K. Williams, J. Whelan, B. Bosnich, *Inorg. Chem.* **1992**, *31*, 1835−1844.
[21] S. C. Shoner, P. P. Power, *Inorg. Chem.* **1992**, *31*, 1001−1010.
[22] K. Yamato, I. Miyahara, A. Ichimura, K. Hirotsu, Y. Kojima, H. Sakurai, D. Shiomi, K. Sato, T. Takui, *Chem. Lett.* **1999**, 295−296.
[23] T. Howard, J. Telser, V. J. Derose, *Inorg. Chem.* **2000**, *39*, 3379−3385.
[24] I. Romero, M.-N. Collomb, A. Deronzier, A. Llobet, E. Perret, J. Pécaut, L. Le Pape, J.-M. Latour, *Eur. J. Inorg. Chem.* **2001**, 69−72.
[25] D. J. Hodgson, B. J. Schwartz, T. N. Sorrell, *Inorg. Chem.* **1989**, *28*, 2226−2228.
[26] S.-B. Yu, S. J. Lippard, I. Shweky, A. Bino, *Inorg. Chem.* **1992**, *31*, 3502−3504.
[27] D. P. Kessissoglou, W. M. Butler, V. L. Pecoraro, *Inorg. Chem.* **1987**, *26*, 495−503.
[28] S.-B. Yu, C.-P. Wang, E. P. Day, R. H. Holm, *Inorg. Chem.* **1991**, *30*, 4067−4074.
[29] E. Gallo, E. Solari, N. Re, C. Floriani, A. Chiesi-Villa, C. Rizzoli, *J. Am. Chem. Soc.* **1997**, *119*, 5144−5154.
[30] H.-R. Chang, S. K. Larsen, P. D. W. Boyd, C. G. Pierpont, D. N. Hendrickson, *J. Am. Chem. Soc.* **1988**, *110*, 4565−4576.
[31] D. Coucouvanis, K. Greiwe, A. Salifoglou, P. Challen, A. Simopoulos, A. Kostikas, *Inorg. Chem.* **1988**, *27*, 593−594.
[32] J. C. Jeffery, P. Thornton, M. D. Ward, *Inorg. Chem.* **1994**, *33*, 3612−3615.
[33] S. Theil, Y. Ratnamala, R. Chikate, F. Dahan, A. Bousseksou, S. Padhye, J.-P. Tuchagues, *Inorg. Chem.* **1997**, *36*, 6279−6286.
[34] T. C. Higgs, K. Spartalian, C. J. O'Connor, B. F. Matzanke, C. J. Carrano, *Inorg. Chem.* **1998**, *37*, 2263−2272.
[35] H. J. Gerritsen, E. S. Sabisky, *Phys. Rev.* **1963**, *132*, 1507−1512.
[36] A.-L. Barra, D. Gatteschi, R. Sessoli, G. L. Abbati, A. Cornia, A. C. Fabretti, M. G. Uytterhoeven, *Angew. Chem. Int. Ed. Engl.* **1997**, *36*, 2329−2331.
[37] J. Limburg, J. S. Vrettos, R. H. Crabtree, G. W. Brudvig, J. C. De Paula, A. Hassan, A.-L. Barra, C. Duboc-Toia, M.-N. Collomb, *Inorg. Chem.* **2001**, *40*, 1698−1703.
[38] R. Carina, B. Albela, C. Policar, S. Poussereau, J. Cano-Boquera, J. Guilhem, L. Tchertanov, S. Un, G. Blondin, M. Delroisse, J.-J. Girerd, manuscript in preparation.
[39] A. Marvilliers, PhD Thesis, Université Paris-Sud, Orsay, France, **1999**.
[40] E. J. Laskowski, D. N. Hendrickson, *Inorg. Chem.* **1978**, *17*, 457−470.
[41] H. Adams, N. A. Bailey, N. Debaeker, D. E. Fenton, W. Kanda, J.-M. Latour, H. Okawa, H. Sakiyama, *Angew. Chem. Int. Ed. Engl.* **1995**, *34*, 2535−2537.
[42] B. E. Schultz, B.-H. Ye, X.-Y. Li, S. I. Chan, *Inorg. Chem.* **1997**, *36*, 2617−2622.
[43] B. Albela, M. Corbella, J. Ribas, I. Castro, J. Sletten, H. Stoeckli-Evans, *Inorg. Chem.* **1998**, *37*, 788−798.

[44] S. V. Khangulov, P. J. Pessiki, V. V. Barynin, D. E. Ash, G. C. Dismukes, *Biochemistry* **1995**, *34*, 2015−2025.
[45] A. E. Meier, M. M. Whittaker, J. W. Whittaker, *Biochemistry* **1996**, *35*, 348−360.
[46] H. Diril, H.-R. Chang, M. J. Nigles, X. Zhang, J. A. Potenza, H. J. Schugar, S. S. Isied, D. N. Hendrickson, *J. Am. Chem. Soc.* **1989**, *111*, 5102−5114.
[47] LH_2 is the Schiff base condensation of 2 mol of 1,3-diaminopropane with 2 mol of 4-*tert*-butyl-2,6-diformylphenol; L′H is 2,6-bis[bis(2-pyridylmethyl)aminomethyl)-4-methylphenol, also called BPMPH.
[48] $SALPS^{2-}$ is the *N*,*N*′-[1,1′-dithiobis(phenylene)]bis(salicylidene)aminato ligand.
[49] E_p is the peak potential of the considered wave and $E_{p/2}$ the potential value at half the intensity of the peak current. Both potential are expressed in V.
[50] R. S. Nicholson, I. Shain, *Anal. Chem.* **1964**, *36*, 706−723.
[51] The surface *S* of the working electrode was measured by cyclic voltammetry and chronocoulometry on a known concentration of ferrocene in acetonitrile assuming a diffusion coefficient $D = 2.3 \cdot 10^{-5}$ $cm^2 \cdot s^{-1}$.
[52] A plot of *Q* vs. $t^{1/2}$ transforms the data into a linear relationship whose slope is $2nSFC(D/\pi)^{1/2}$ where *F* is the Faraday constant and *C* the concentration.
[53] K. M. Kadish, M. Sweetland, J. S. Cheng, *Inorg. Chem.* **1978**, *17*, 2795−2797.
[54] J. A. Bonadies, M. J. Maroney, V. L. Pecoraro, *Inorg. Chem.* **1989**, *28*, 2044−2051.
[55] M. G. Patch, C. J. Carrano, *Inorg. Chim. Acta* **1981**, *56*, L71.
[56] T. S. Davies, J. P. Fackler, M. J. Weeks, *Inorg. Chem.* **1968**, *7*, 1994−2002.
[57] R. Dingle, *Acta Chem. Scand.* **1966**, *20*, 33−44.
[58] J. E. Sheats, R. S. Czernuszewicz, G. C. Dismukes, A. L. Rheingold, V. Petrouleas, J. Stubbe, W. H. Armstrong, R. H. Beer, S. J. Lippard, *J. Am. Chem. Soc.* **1987**, *109*, 1435−1444.
[59] A. Neves, S. M. D. Erthal, I. Vencato, A. S. Ceccato, Y. P. Mascarambas, O. R. Nascimento, M. Hörner, A. A. Batista, *Inorg. Chem.* **1992**, *31*, 4749−4755.
[60] G. M. Sheldrick, *SHELXTL: Program for the Refinement of Crystal Structures*, University of Gottingen, Germany, **1993**.
[61] O. Horner, E. Rivière, G. Blondin, S. Un, A. W. Rutherford, J.-J. Girerd, A. Boussac, *J. Am. Chem. Soc.* **1998**, *120*, 7924−7928.

Received January 22, 2002
[I02037]

Syntheses, Crystal Structure, and Nuclease Activity of Oxalato-Bridged Dicopper(II) Complexes with Planar N-Donor Heterocyclic Bases

Anitha M. Thomas,[a] Girish Neelakanta,[b] Subramony Mahadevan,[b] Munirathinam Nethaji,[a] and Akhil R. Chakravarty*[a]

Keywords: Catalysis / Copper / Crystal structure / Magnetic properties / Nuclease activity

Oxalato-bridged dicopper(II) complexes [{CuL(H_2O)}$_2$(μ-ox)]-(ClO_4)$_2$ (**1**–**4**), where L is a bidentate chelating heterocyclic base such as 2,2′-bipyridine (bpy, **1**), 1,10-phenanthroline (phen, **2**), dipyridoquinoxaline (dpq, **3**) and dipyridophenazine (dppz, **4**), were prepared by treatment of copper(II) perchlorate hexahydrate with sodium oxalate and L in aqueous ethanol. Complex **3** has been structurally characterised. The coordination geometry of the copper centres is essentially square-pyramidal. The {CuL(H_2O)} units are bridged by an oxalate moiety to form the discrete dimeric core. Magnetic studies in the 20–300 K temperature range show the presence of an antiferromagnetically coupled dicopper(II) unit, giving $-2J$ values in the 346–384 cm^{-1} range. The redox-active complexes retain the dimeric core in solution, and two quasireversible Cu^{II}/Cu^{I} couples are observed in the potential range from 0.2 to –0.4 V vs. SCE in a DMF/tris–HCl/0.1 M KCl buffer system (1:1, v/v, pH = 7.2) with a glassy carbon working electrode. The binding and cleavage of DNA by the complexes have been studied. The intercalating ability of the planar bases, determined from the decrease of the fluorescence intensity of ethidium bromide bound calf thymus DNA on addition of the complex, gave the order: **3** > **4** > **2** >> **1**. The nuclease activity of the complexes with supercoiled pUC19 DNA in DMF/tris–HCl/NaCl buffer (pH = 7.2) in the presence of ascorbic acid follows the order: **3** > **2** >> **4** ≈ **1**. The dpq complex exhibits the most efficient DNA binding and cleavage activity. The dppz complex shows good binding ability but poor nuclease activity.
(© Wiley-VCH Verlag GmbH, 69451 Weinheim, Germany, 2002)

Introduction

Coordination complexes that oxidatively cleave DNA under physiological conditions are of current interest in the development of artificial nucleases.[1−3] In view of the important role played by copper ions in enzymatic catalysis, efforts to develop the chemistry of redox-active copper complexes as chemical nucleases are underway.[1−6] It has been suggested that metallointercalators such as the bis(1,10-phen) complex of copper(I), on activation by hydrogen peroxide in the presence of a reducing agent, cleave DNA through the formation of a hydrogen-abstracting active oxygen species.[6] It has also been postulated that the active oxo species react with the H1′ or H4′ deoxyribose protons of the nucleotide in the vicinity of the binding site at the minor groove to initiate a series of reactions resulting in the cleavage of DNA.[5a,7] The cleavage efficiency is generally dependent on the DNA binding ability and the metal-based redox potential of the complex.

[a] Department of Inorganic and Physical Chemistry
Bangalore 560012, India
Fax: (internat.) + 91-80/3600683
E-mail: arc@ipc.iisc.ernet.in
[b] Department of Molecular Reproduction, Development and Genetics, Indian Institute of Science,
Bangalore 560012, India
Supporting information for this article is available on the WWW under http://www.eurjic.org or from the author.

Although the true binding mode of the bis(phen) complex to DNA is currently unknown, it has been indicated by several research groups that the nuclease activity of the complex is related to the partial intercalation or binding of one phen ligand to the minor DNA groove, with the other phen ligand making favourable contacts within the groove.[8−11] Rill and co-workers have observed that the phen complex displays efficient nuclease activity at a phenanthroline/copper ratio of greater than 2:1, regardless of the reducing agent used in the cleavage reaction.[8] This current work stems from our interest in covalently linking two mono(phen) and related copper units through an oxalate moiety to form a dinuclear complex with an N-donor base/copper ratio of 1:1 and studying the DNA binding and nuclease activity of the complexes. The objective of the use of the oxalate as a linker is to provide a planar skeleton in the {LCu−ox−CuL} moiety. In addition, the bio-relevant oxalate ligand is an oxidized product of ascorbic acid (vitamin C), used extensively in copper-mediated enzymatic reactions.[12] An essentially planar $N_4O_4Cu_2$ unit with planar N-donor bases should be expected to show good binding ability to the DNA minor groove. Previous studies on oxalato-bridged dicopper(II) complexes have shown that an estimate of the planarity of the core can readily be obtained from the singlet-triplet energy gap, which varies over a wide range depending upon the nature of the terminal

Table 1. Spectral and magnetic data for the complexes $[\{CuL(H_2O)\}_2(\mu\text{-ox})](ClO_4)_2$ (**1**−**4**)

Complex	IR[a]/cm^{-1} oxalate	ClO_4^-	d-d band[b] λ_{max}/nm	ε/dm^3 mol^{-1} cm^{-1}	Magnetic data[c] $-2J$/cm^{-1}	g (ρ)	μ_{eff}/μ_B
1	1653	1091	650	140	358	2.18 (0.01)	1.3
2	1651	1098	665	120	370	2.19 (0.029)	1.5
3	1655	1085	667	114	384	2.19 (0.015)	1.4
4	1662	1077	710	[d]	346	2.19 (0.049)	1.4

[a] KBr phase. [b] Aqueous DMF (1:1, v/v). [c] μ_{eff} per copper at 298 K; ρ: paramagnetic impurity. [d] Not measured due to solubility problem.

ligands.[13−17] Here we report the synthesis, structure and nuclease activity of the dicopper(II) complexes $[\{CuL(H_2O)\}_2(\mu\text{-ox})](ClO_4)_2$ (**1**−**4**) with planar heterocyclic bases as terminal ligands [L: 2,2′-bipyridine (bpy), **1**; 1,10-phenanthroline (phen), **2**; dipyrido[3,2-*d*:2′,3′-*f*]quinoxaline (dpq), **3**; and dipyrido[3,2-*a*:2′,3′-*c*]phenazine (dppz), **4**]. The significant result of this study is the observation of varied DNA binding and nuclease activity of the structurally similar complexes **1**−**4**. A preliminary report on the crystal structure of complex **1** has already appeared.[18]

Results and Discussion

Synthesis and Characterization

Complexes **1**−**4**, prepared by treatment of $Cu(ClO_4)_2\cdot 6H_2O$ with the bidentate N-donor heterocyclic base (L) and sodium oxalate in aqueous ethanol, belong to the general class of oxalato-bridged dicopper(II) complexes of formulation $[LCu(\mu\text{-}C_2O_4)CuL]X_n$, where X is a counteranion or solvent molecule.[13] The physicochemical data for **1**−**4** are given in Table 1. The complexes are moderately soluble in methanol and MeCN, soluble in DMF or DMSO. While the bpy and phen complexes are moderately water-soluble, the dpq and dppz complexes show poor solubility in water. They display characteristic infrared bands in the 1651−1662 and 1077−1098 cm^{-1} ranges for the oxalate and perchlorate, respectively. The complexes show a d-d band in the 650−710 nm range in aqueous DMF solution.

Crystal Structure and Magnetic Properties

Complex **3**, crystallised as $[Cu_2(ox)(dpq)_2(H_2O)_2](ClO_4)_2\cdot 2H_2O$, has been structurally characterised by single-crystal X-ray diffraction. A perspective view of the complex is shown in Figure 1. The crystallographic data and the data collection parameters are summarized in Table 5 and the selected bond lengths and angles are given in Table 2. The structure consists of a centrosymmetric complex in which $Cu(dpq)(H_2O)$ units are bridged by oxalate to give a copper−copper distance of 5.138 Å. Each copper centre is essentially in a 4 + 1 coordination environment, with the N(1), N(2), O(1), and O(2) atoms forming a basal plane and the Ow(1) atom of the bound water occupying the axial position. The perchlorate anion, involved in the hydrogen-bonding interactions with the water molecules, also shows a very weak axial contact to the copper centre through oxygen atom O(11) [Cu(1)···O(11), 2.696 Å]. The planar dpq ligand exhibits a bidentate chelate mode of bonding and non-involvement of the quinoxaline moiety in any metal−ligand interaction. The deviation of the copper atom from the basal plane is 0.062 Å, which is the shortest among known copper−oxalate species.[14] The angle formed between the basal plane containing the copper atom and the oxalate plane is 2.55°. This angle gives a measure of the coplanarity, an important factor for derivation of the orbital topologies.

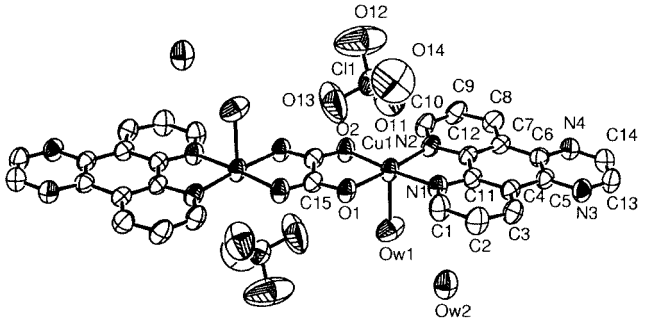

Figure 1. An ORTEP view of $[\{(dpq)Cu(H_2O)\}_2(\mu\text{-ox})](ClO_4)_2\cdot 2H_2O$ (**3**·2H$_2$O) showing the atom labelling scheme and thermal ellipsoids at a 50% probability level

Table 2. Selected bond lengths [Å] and bond angles [°] for the complex $[\{Cu(dpq)(H_2O)\}_2(\mu\text{-ox})](ClO_4)_2\cdot 2H_2O$ (**3**.2H$_2$O)

Cu(1)···Cu(1)′	5.138(1)	O(1)−Cu(1)−O(2)	84.87(12)
Cu(1)−O(1)	1.979(3)	O(1)−Cu(1)−Ow(1)	88.54(16)
Cu(1)−O(2)	1.970(3)	O(2)−Cu(1)−Ow(1)	93.77(14)
Cu(1)−Ow(1)	2.256(4)	O(2)−Cu(1)−N(1)	175.83(15)
Cu(1)−N(1)	1.992(4)	O(1)−Cu(1)−N(1)	98.00(13)
Cu(1)−N(2)	1.977(4)	O(2)−Cu(1)−N(2)	94.04(13)
O(1)−C(15)	1.253(5)	O(1)−Cu(1)−N(2)	175.66(15)
O(2)−C(15)′	1.232(5)	N(2)−Cu(1)−Ow(1)	95.73(16)
C(15)−C(15)′	1.555(8)	N(2)−Cu(1)−N(1)	82.88(14)
N(3)−C(5)	1.347(5)	N(1)−Cu(1)−Ow(1)	89.35(15)
N(3)−C(13)	1.324(7)	O(1)−C(15)−C(15)′	115.7(5)
N(4)−C(14)	1.320(6)	O(2)′−C(15)−O(1)	126.7(4)
N(4)−C(6)	1.353(6)	O(2)′−C(15)−C(15)′	117.3(5)
C(13)−C(14)	1.386(8)	C(14)−N(4)−C(6)	116.2(4)
C(5)−C(6)	1.401(6)	C(13)−N(3)−C(5)	115.7(4)

The complexes **1**−**4** are antiferromagnetically (AF) coupled dimeric species. Magnetic susceptibility measurements from 20 to 300 K with polycrystalline samples of the complexes gave a singlet-triplet separation ($-2J$) in the 346−384 cm^{-1} range from theoretical fitting of the $\chi_M T$ vs. T plots (Figure 2; Table 1). It has been theoretically predicted that, for a coplanar orbital topology with the $d_{x^2-y^2}$-type orbital coplanar with the oxalate molecule [i.e., both singly occupied molecular orbitals (SOMOs) being in the

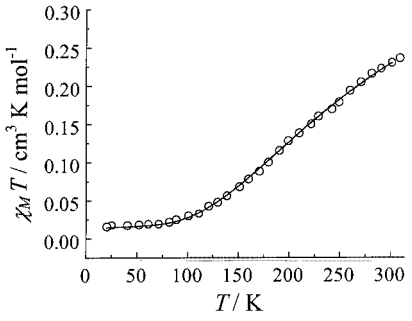

Figure 2. Plot of $\chi_M T$ vs. T for a polycrystalline sample of [{(phen)Cu(H$_2$O)}$_2$(μ-ox)](ClO$_4$)$_2$ (**2**); the solid line shows a theoretical fit to the experimental data

plane of the oxalate bridge], the $-2J$ (S-T gap) value should fall in the 300−400 cm^{-1} range, with the singlet being the ground state.[13] The observed $-2J$ values for the complexes **1**−**4** suggest a coplanar orbital topology in which the copper(II) $d_{x^2-y^2}$ orbitals, being in the plane of the oxalate molecule, result in the strong overlap of both SOMOs and the oxalate-based molecular orbitals.

Electrochemical and Catalytic Properties

In a DMF−50 mM tris−HCl/0.1 M KCl (1:1, v/v) buffer (pH = 7.2) and with a glassy carbon working electrode, complexes **1**−**3** show two cyclic voltammetric responses attributable to the $Cu_2^{II}/Cu^{II}Cu^{I}$ and $Cu^{II}Cu^{I}/Cu_2^{I}$ couples in the 0.2 to −0.4 V (vs. SCE) potential range (Figure 3; Table 3). The observation of these redox couples, with similar current heights, suggests a dimeric nature of the complexes in solution. The ratio of unity of the cathodic to anodic peak currents (i_{pc}/i_{pa}) at different scan rates and the ΔE_p values in the 100−250 mV range at 50 mV·s^{-1} indicate the quasireversible nature of the electron-transfer processes. Because of poor solubility, the redox chemistry of the dppz complex was studied by differential pulse voltammetry (DPV). The electrochemical data suggest the stability order for the copper(I) species as: **4** (dppz) > **3** (dpq) > **2** (phen) > **1** (bpy). The observed differences in the $E_{1/2}$ values could be due to the effect of the quinoxaline and phenazine moieties in dpq and dppz ligands, stabilizing the copper(I) state. When the potential is scanned up to −1.7 V, the complexes show an irreversible reduction peak in the range of −1.0 to −1.5 V and two anodic counterparts, with the one near −0.1 V showing high anodic current indicating absorption of the reduced species on the electrode surface.

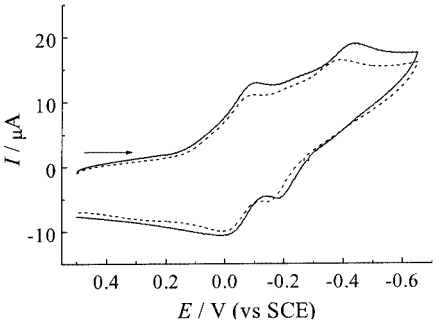

Figure 3. Cyclic voltammograms showing the $Cu_2^{II}/Cu^{II}Cu^{I}$ and $Cu^{II}Cu^{I}/Cu_2^{I}$ couples for [{LCu(H$_2$O)}$_2$(μ-ox)](ClO$_4$)$_2$ in DMF−50 mM tris−HCl/0.1 M KCl buffer (1:1, v/v, pH = 7.2) at 50 mV s^{-1} [L = bpy, −; phen, ---]

Table 3. Electrochemical data for the complexes [{CuL(H$_2$O)}$_2$(μ-ox)](ClO$_4$)$_2$ (**1**−**4**) in DMF−50 mM tris−HCl/0.1 M KCl buffer (1:1, v/v, pH = 7.2) at 50 mV s^{-1}

Complex[a]	$E_{1/2}$/V (ΔE_p/mV) $Cu_2^{II}/Cu^{II}Cu^{I}$	$Cu^{II}Cu^{I}/Cu_2^{I}$	E_{pc}/V (E_{pa}/V)[b]
1	−0.05 (100)	−0.31 (250)	−1.45 (0.25, −0.17)
2	−0.04 (100)	−0.27 (240)	−1.30 (0.30, −0.10)
3	0.02 (200)	−0.22 (250)	−1.15 (0.36, −0.11)
4	0.07	−0.20	

[a] CV data for **1**−**3**; DPV data for **4**. [b] Irreversible process.

The complexes undergo facile reduction with ascorbic acid (H$_2$A) in a DMF/50 mM tris−HCl buffer medium (1:1, v/v, pH = 7.2) to form an unstable brown copper(I) species, which converts into the oxidized species on exposure to dioxygen (Scheme 1). The catalytic cycle is effective with mol ratios of H$_2$A and the complex of ca. 100 for **1** and **2** and ca. 60 for **3** and **4**. The product from such a reaction in the presence of excess ascorbic acid has been analysed as polymeric copper(II) oxalate by the powder X-ray diffraction method.[19] The oxalic acid is formed by hydrolytic ring-rupture and oxidation of dehydroascorbate through the formation of L-threonic and 2,3-diketo-L-gulonic acids.[12] Additionally, the reduced species of **3** and **4** are susceptible to dimer formation through the extended aromatic rings of the quinoxaline and phenazine moieties.[8] Attempts to isolate the cuprous complex of **1** under anaerobic condition over a period of 7 d were unsuccessful. The brown single crystals formed in low yield were analysed from the unit cell dimensions as the bis(bpy) complex of copper(I).[20] The reduced species isolated by rapid precipitation of the solid from the reaction mixture was tentatively analysed as [Cu(bpy)(H$_2$O)(ClO$_4$)]. The solid mass did not show any IR band for the oxalate ion. We believe that the dicopper cores in **1**−**4** undergo cleavage due to a concomitant two-electron and two-proton transfer process by ascorbic acid [H$_2$A → A + 2 H$^+$ + 2 e$^-$]. The reduced monomeric species regenerates the dimeric core on exposure to dioxygen in the presence of oxalic acid in solution.

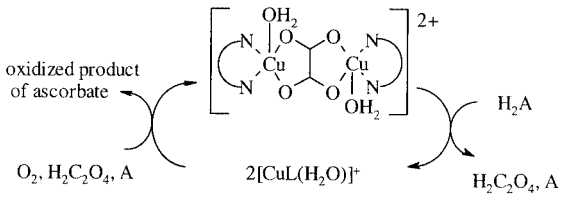

Scheme 1. Catalytic oxidation reaction of ascorbic acid (H$_2$A) by dioxygen, mediated by [{LCu(H$_2$O)}$_2$(μ-ox)](ClO$_4$)$_2$ (L = bpy, **1**; phen, **2**; dpq, **3**; dppz, **4**) in a DMF/tris−HCl buffer (1:1, v/v, pH = 7.2)

DNA Binding and Cleavage Studies

The binding of the complexes **1**−**4** and $[Cu(phen)_2(H_2O)](ClO_4)_2$ to calf thymus DNA was studied by fluorescence spectroscopy. Measurements were made with ethidium bromide bound (EB-bound) DNA, and showed enhanced emission intensity relative to the free EB. Competitive binding of the copper complex to CT DNA results in the displacement of the bound EB. This causes a reduction in the emission intensity, due to fluorescence quenching of the free EB by the solvent molecules.[21−23] Figure 4 shows the decrease in the emission intensity of EB on addition of the complexes, including the bis(phen)copper(II) complex. Complexes **3** and **4**, showing higher slopes than the bis(phen) complex, indicate significant binding abilities of the dpq and dppz complexes (Figure 4). The bpy complex, with a near zero slope, does not show any binding affinity to CT DNA. The binding ability of the complexes to the CT DNA follows the order: **3** ≥ **4** > **2** ≥ $Cu(phen)_2^{2+}$ >> **1**. The

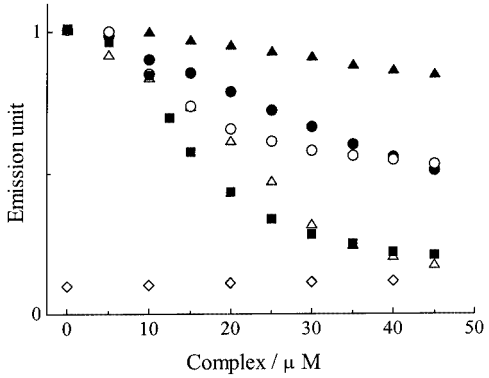

Figure 4. Effect of addition of $[\{LCu(H_2O)\}_2(\mu\text{-ox})](ClO_4)_2$ (L = bpy, black triangle; phen, whithe circles; dpq, black squares; dppz, whithe triangles) and the bis(phen)copper(II) species (black circles) on the emission intensity of the CT DNA bound ethidium bromide (12.5μM) at different complex concentrations in 5 mM tris−HCl + 50 mM NaCl buffer (pH = 7.2) containing 3% DMF at 25 °C; the concentration of CT DNA was 125 μM; the emission intensity of EB (in the absence of DNA) at various concentrations of the $[\{(dpq)Cu(H_2O)\}_2(\mu\text{-ox})](ClO_4)_2$ complex is also shown (whithe diamonds)

binding constant (K_b) for the bis(phen)copper(I) complex is known to be 5×10^4 M^{-1} (base pairs).[9] The K_b value for the copper(II) species is 2.7 times lower, as evidenced by differential pulse voltammetric (DPV) studies.[23] Although it was not possible for us to estimate the K_b values for **1**−**4**, due to the absence of any intense band in the visible spectra of the complexes, the emission data suggest a significantly higher binding constant for **3** and **4** than for the bis(phen)-copper(II) species.

The nuclease activity of **1**−**4**, together with that of the bis(phen)copper complex, was studied with pUC19 DNA in a medium of DMF/tris−HCl buffer (1:1, v/v, pH = 7.2) in the presence of ascorbic acid. The cleavage efficiency of the complexes was determined by gel electrophoresis, from their ability to convert supercoiled (SC) to nicked circular

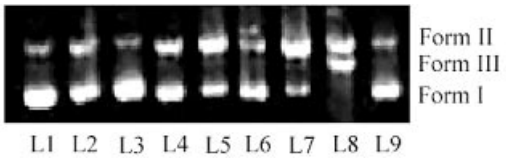

Figure 5. Cleavage of supercoiled pUC19 DNA (0.5 μg) by $[\{LCu(H_2O)\}_2(\mu\text{-ox})](ClO_4)_2$ (**1**−**4**) in DMF in the presence of ascorbic acid (H_2A, 100 μM) in a 50 mM tris−HCl + 50 mM NaCl buffer at 37 °C; cleavage by the mono- and bis(phen) complexes of copper are also shown for comparison; Lane 1, DNA control; Lane 2, DNA + H_2A; Lane 3, DNA + complex **3**; Lane 4, DNA + H_2A + mono(phen)copper(II) complex; Lane 5, DNA + H_2A + bis(phen)copper(II) complex; Lane 6, DNA + H_2A + **1**; Lane 7, DNA + H_2A + **2**; Lane 8, DNA + H_2A + **3**; Lane 9, DNA + H_2A + **4**; complex concentration was 30 μM; forms I−III are supercoiled, nicked circular and linear, respectively

(NC) DNA (Table 4; Figure 5).[24] The dpq complex has the greatest ability to cleave DNA. The mechanistic aspects of the cleavage reactions are of importance. Oxalato-bridged dicopper(II) complexes containing terminal 2,2′-bipyridyl or 2,2′:6′,2"-terpyridyl ligands (L) are known to exist in equilibria with two mononuclear complexes of formulations CuL^{2+} and CuL(ox) at pH values ranging between 2.0 and 6.0.[25,26] At pH values higher than 7.5, the mononuclear

Table 4. A comparison of the DNA cleavage efficiency of **1**−**4** along with the mono- and bis(phen) complexes of copper(II) in the presence of ascorbic acid

Sl. no.[a]	Reaction condition[b]	Form (%) I	II	III
1	DNA control	90	10	
2	DNA + H_2A	83	17	
3	DNA + $[Cu_2(dpq)_2(H_2O)_2(ox)](ClO_4)_2$ (**3**)	90	10	
4	DNA + H_2A + $[Cu(phen)(H_2O)_2](ClO_4)_2$	70	30	
5	DNA + H_2A + $[Cu(phen)_2(H_2O)](ClO_4)_2$	40	60	
6	DNA + H_2A + $[Cu_2(bpy)_2(H_2O)_2(ox)](ClO_4)_2$ (**1**)	80	20	
7	DNA + H_2A + $[Cu_2(phen)_2(H_2O)_2(ox)](ClO_4)_2$ (**2**)	28	72	
8	DNA + H_2A + $[Cu_2(dpq)_2(H_2O)_2(ox)](ClO_4)_2$ (**3**)	0	55	45
9	DNA + H_2A + $[Cu_2(dppz)_2(H_2O)_2(ox)](ClO_4)_2$ (**4**)	78	22	

[a] The serial numbers correspond to the lanes shown in Figure 5. [b] Concentration: H_2A 100 μM; copper complexes 30 μM. Reaction medium: DMF−50 mM tris−HCl/50 mM NaCl buffer (1:1, v/v, pH = 7.2). Forms I−III are supercoiled (SC) pUC19, nicked circular and linear DNA, respectively.

[Cu(L)(ox)] species predominates. Such mononuclear copper(II) complexes, with one terminal ligand, show poor cleavage activity when L is an intercalating ligand such as 1,10-phen. Although we cannot exclude the possibility of such an equilibrium involving the present complexes, the cleavage efficiency data indicate that the dimeric structure in **1**−**4** is generally retained in pH = 7.2 DMF/tris−HCl buffer.

There are several important findings in this study pertaining to the binding and cleavage of DNA. Complexes **1**−**4** are dicationic and have a Cu/heterocyclic base ratio of 1:1. The bpy complex has been found to be nuclease-inactive and a poor binder to DNA. This suggests that DNA binding in the form of intercalation could be an important factor for the cleavage activity. The luminescence experiments monitoring the emission of the DNA-bound ethidium bromide strongly support an intercalative binding mode for the copper(II) complexes. Complexes **2**−**4** are powerful binders to DNA. The high affinities of the dpq and dppz ligands for intercalative binding could be related to the presence of extended aromatic rings, making noncovalent interactions between the π-system of the ligand and the DNA base pairs more favourable. The ability of the dppz ligand to approach deep into the DNA helix would be expected to be greater than that of the dpq ligand. However, the emission data indicate equal CT DNA helix binding affinities for both complexes. The complexes differ drastically in their abilities to cleave DNA in the presence of a reducing agent such as ascorbic acid. The anomalous nuclease activity of **4** could be related either to the difference in groove selectivity[27−32] or to an enhancement of the stability of the cuprous complex in the presence of hydrophobic interactions.

Conclusions

Four dicopper(II) complexes with $[Cu(\mu\text{-ox})Cu]^{2+}$ cores and planar N-donor heterocyclic bases as terminal ligands show interesting DNA-binding and -cleavage properties. The phen, dpq and dppz complexes were found to be powerful binders to CT DNA. While the phen and dpq complexes show good cleavage properties, the dppz complex is nuclease-inactive. The results are explained in terms of intercalative binding of the complexes to DNA. The cleavage activity of the dpq complex is significantly greater than that of the phen complexes. The results are of significance, as the dpq complex may find use as a new DNA-binding and -cleaving agent in nucleic acids chemistry.

Experimental Section

General Methods: All reagents and chemicals were purchased from commercial sources and used without further purification. Solvents were purified by standard procedures. The calf thymus (CT) DNA and supercoiled (SC) pUC19 DNA were purchased from Bangalore Genie (India). Agarose (molecular biology grade) and ethidium bromide were from Sigma (USA). Tris−HCl buffer solution was prepared with deionised, sonicated, triply distilled water. Dipyridoquinoxaline and dipyridophenazine ligands were prepared by literature methods.[24,33] The elemental analyses were done with a Perkin−Elmer 2400 CHN analyser. The infrared, electronic and fluorescence spectra were recorded with Bruker Equinox 55, Hitachi U-3000 and Perkin−Elmer LS 50B spectrophotometers, respectively. Variable-temperature magnetic susceptibility data in the 20−300 K range were obtained for polycrystalline samples with a George Associates Inc. Lewis-coil-force magnetometer system equipped with a closed-cycle cryostat (Air products) and a Cahn balance. $Hg[Co(NCS)_4]$ was used as a calibrant. Experimental susceptibility data were corrected for diamagnetic contributions[34] and temperature-independent paramagnetism ($N\alpha = 60\times10^{-6}$ $cm^3\cdot mol^{-1}$ per copper). The molar magnetic susceptibilities were fitted by the modified Bleaney−Bowers expression[35,36] based on the isotropic form of the Heisenberg−Dirac−van Vleck (HDvV) model with a spin Hamiltonian $H = -2JS_1S_2$ ($S_1 = S_2 = 1/2$ for d^9-d^9 configuration): $\chi_{Cu} = [Ng^2\beta^2/kT][3 + \exp(-2J/kT)]^{-1}(1 - \rho) + (Ng_{\parallel}^2\beta^2/4kT)\rho + N\alpha$, where ρ is the fraction of monomeric impurity and $-2J$ is the singlet-triplet energy separation, with the singlet being the ground state. The magnetic moments at various temperatures were calculated in μ_B units [$\mu_B \approx 9.274\cdot10^{-24}$ $J\cdot T^{-1}$]. Electrochemical measurements were made at 25 °C with an EG&G PAR Model 253 Versastat Potentiostat/Galvanostat with electrochemical analysis software 270 for voltammetric work with a three-electrode set-up comprising a glassy carbon working electrode, a platinum wire auxiliary electrode and a saturated calomel reference (SCE) electrode. The electrochemical data were uncorrected for junction potentials.

Preparation of $[\{CuL(H_2O)\}_2(\mu\text{-ox})](ClO_4)_2$ (1−4): The complexes were prepared by a general procedure in which the heterocyclic base (L, 1.0 mmol; 156 mg bpy; 198 mg phen; 232 mg dpq; 282 mg dppz) was treated with $Cu(ClO_4)_2\cdot6H_2O$ (1.0 mmol; 371 mg) in aqueous ethanol (70 cm^3), followed by addition of an aqueous solution (5 mL) of sodium oxalate (0.5 mmol; 67 mg). The reaction mixture was stirred for 10 min. Complexes were isolated as pale blue solids after washing with ethanol and water followed by drying in vacuo over P_4O_{10} (yield: 70%). ***Caution!*** Perchlorate salts are potentially explosive and should be handled in small quantities with care. Single crystals of **3**, suitable for X-ray studies, were obtained by slow concentration of an aqueous methanolic solution of the complex $C_{22}H_{16}Cl_2Cu_2N_4O_{12}$ (**1**) (726.38): calcd. C, 36.36, H 2.20, N 7.71; found C 36.51, H 2.48, N 7.62. $C_{26}H_{20}Cl_2Cu_2N_4O_{14}$ (**2**) (810.45): calcd. C, 38.52, H 2.47, N 6.91; found C 38.92, H 2.23, N 6.93. $C_{30}H_{20}Cl_2Cu_2N_8O_{14}$ (**3**) (914.55): calcd. C, 39.36, H 2.19, N 12.25; found C 38.97, H 2.34, N 11.96. $C_{38}H_{24}Cl_2Cu_2N_8O_{14}$ (**4**) (1014.64): calcd. C, 44.97, H 2.37, N 11.05%; found C 44.71, H 2.63, N 10.86.

X-ray Crystal Structure Analysis: All geometric and intensity data were collected with an automated Enraf−Nonius CAD4 diffractometer equipped with Mo-K_α radiation (λ = 0.71073 Å) with a crystal mounted on a fibre by epoxy cement (Table 5). Intensity data, collected by an ω-2θ scan technique, were corrected for Lorentz polarisation effects and for absorption.[37] The structure was solved by the combination of Patterson and Fourier techniques and refined by full-matrix least squares. During refinement, positional disorder of the oxygen atoms of the perchlorate anion were observed. The four oxygen peaks concerned were refined with restraints. The ClO_4 moiety refined well, but showed a highest peak of 1.01 e·Å^{-3} near the O(11) atom ($x = 0.7932$; $y = 0.2161$; $z = 0.3594$). All the non-hydrogen atoms were refined anisotropically. Hydrogen atoms were located from the difference Fourier map and

Table 5. Crystallographic data for compound $[Cu_2(dpq)_2(H_2O)_2(ox)](ClO_4)_2 \cdot 2H_2O$

Empirical formula	$C_{30}H_{24}N_8O_{16}Cl_2Cu_2$
Formula mass	950.55
Crystal system	monoclinic
Space group	$P2_1/n$ (no. 1014)
a [Å]	8.738(2)
b [Å]	13.691(4)
c [Å]	15.181(4)
β [°]	98.23(2)
V [Å^3]	1797.3(8)
Z	2
D_c [g cm^{-3}]	1.756
μ [mm^{-1}]	1.419
Crystal colour and habit	bluish green needle
Crystal size [mm]	0.32 × 0.18 × 0.08
$2\theta_{max}$ [°]	50
Index range	$0 \le h \le 10$, $0 \le k \le 16$, $-18 \le l \le 17$
Reflns. collected	3158
Independent reflns [$I > 2\sigma(I)$]	2536
R_{int}	0.0118
Parameters refined	310
$F(000)$	960
R(obsd.data)	0.0481
wR(obsd.data)[a]	0.1329
R(all data)	0.0611
wR(all data)	0.1411
Goodness of fit	1.078
Largest diff. peak and hole [e Å^{-3}]	1.011 and −0.562

[a] $w = 1/[\sigma^2(F_o^2) + (0.0690\ P)^2 + (3.0700\ P)]$ where $P = [\mathrm{Max}(F_o^2,0) + 2\ F_c^2]/3$.

were refined isotropically, except for those attached to the water oxygen atoms, which were treated as rigid groups. All calculations were performed with PC versions of the SHELX system of programs.[38] The perspective view of the complex was obtained by use of ORTEP.[39] CCDC-159021 contains the supplementary crystallographic data for this paper. These data can be obtained free of charge at www.ccdc.cam.ac.uk/conts/retrieving.html or from the Cambridge Crystallographic Data Centre, 12, Union Road, Cambridge CB2 1EZ, UK [Fax: (internat.) + 44-1223/336-033; E-mail: deposit@ccdc.cam.ac.uk].

DNA-Binding and -Cleavage Experiments: The concentration of the CT DNA was determined by recording the absorption intensity at 260 nm, with a known molar extinction coefficient value of 6600 dm^3 mol^{-1} cm^{-1}.[40] The experiments were performed with 0.1 mM complex solution in the absence and in the presence of CT DNA, varying from 0 to 250 μM. In order to compare the relative binding of the complexes to DNA with that of the bis(phen) complex of copper(II), ethidium bromide bound CT DNA solution in tris−HCl/NaCl buffer (pH = 7.2) was treated with an increasing amount of the complex solution. The fluorescence intensities of the ethidium bromide in the bound form at 601 nm (510 nm excitation) were plotted against the complex concentration. The cleavage of DNA was monitored by agarose gel electrophoresis. Supercoiled pUC19 DNA (6 μL, ca. 500 ng) in tris−HCl buffer (50 mM) with 50 mM NaCl (pH = 7.2) was treated with the metal complex (30 μM) and ascorbic acid (100 μM), followed by dilution with the tris−HCl buffer to a total volume of 20 μL. The samples were incubated for 1 h at 37 °C, loading buffer [25% bromophenol blue, 0.25% xylene cyanol, 30% glycerol (3 μL)] was added and then loaded on 0.8% agarose gel containing 1.0 μg/mL ethidium bromide. Electrophoresis was carried out at 40 V for 3 h in TBE buffer. Bands were viewed under UV light and photographed. The cleavage efficiency was measured by determining the ability of the complex to convert the supercoiled DNA (SC) to nicked circular form (NC). After electrophoresis, the proportion of DNA in each fraction was estimated quantitatively from the intensities of the bands by use of the BIORAD Gel Documentation System. The fraction of the original supercoiled DNA, converted into the NC (nicked circular) at the end of the reaction, was calculated after correction for the low level of NC present in the original sample and the low affinity of ethidium bromide binding to SC compared to NC and linear forms of DNA.[24]

Acknowledgments

We thank the Department of Science and Technology, Government of India, and the Council of Scientific and Industrial Research, New Delhi, for financial support. Thanks are due to the Alexander von Humboldt Foundation, Germany, for the donation of an electroanalytical system. We also thank Mr. P. A. N. Reddy for his help in DNA-binding and -cleavage studies and the Bioinformatic Center of the Indian Institute of Science, Bangalore, for a database search.

[1] [1a] D. S. Sigman, *Biochemistry* **1990**, *29*, 9097−9105. [1b] D. S. Sigman, T. W. Bruice, A. Mazumder, C. L. Sutton, *Acc. Chem. Res.* **1993**, *26*, 98−104. [1c] D. S. Sigman, A. Mazumder, D. M. Perrin, *Chem. Rev.* **1993**, *93*, 2295−2316. [1d] D. S. Sigman, *Acc. Chem. Res.* **1986**, *19*, 180−186.

[2] [2a] G. Pratviel, J. Bernadou, B. Meunier, *Angew. Chem. Int. Ed. Engl.* **1995**, *34*, 746−769. [2b] B. Meunier, *Chem. Rev.* **1992**, *92*, 1411−1456. [2c] G. Pratviel, J. Bernadou, B. Meunier, *Adv. Inorg. Chem.* **1998**, *45*, 251−312.

[3] [3a] W. K Pogozelski, T. D. Tullius, *Chem. Rev.* **1998**, *98*, 1201−1220. [3b] C. J. Burrows, J. G. Muller, *Chem. Rev.* **1998**, *98*, 1109−1152.

[4] [4a] O. Bandoin, M.-P. Teulade-Fichou, J.-P. Vigneron, J.-M. Lehn, *Chem. Commun.* **1998**, 2349−2350. [4b] T. Itoh, H. Hisada, T. Sumiya, M. Hosono, Y. Usui, Y. Fujii, *Chem. Commun.* **1997**, 677−678. [4c] S. Kawanishi, K. Yamamoto, *Biochemistry* **1991**, *30*, 3069−3075. [4d] B. C. Gilbert, S. Silvester, P. H. Walton, A. C. Whitwood, *J. Chem. Soc., Perkin Trans.* **1999**, 1891−1895. [4e] E. Lamour, S. Routier, J.-L. Bernier, J.-P. Catteau, C. Bailly, H. Vezin, *J. Am. Chem. Soc.* **1999**, *121*, 1862−1869. [4f] D. K. Chand, H.-J. Schneider, A. Bencini, A. Bianchi, C. Giorgi, S. Ciattini, B. Valtancoli, *Chem. Eur. J.* **2000**, *6*, 4001−4008. [4g] M. Pitie, J. D. V. Horn, D. Brion, C. J. Burrows, B. Meunier, *Bioconjugate Chem.* **2000**, *11*, 892−900.

[5] [5a] T. B. Thederahn, M. D. Kuwabara, T. A. Larsen, D. S. Sigman, *J. Am. Chem. Soc.* **1989**, *111*, 4941−4946. [5b] D. R. Graham, D. S. Sigman, *Inorg. Chem.* **1984**, *23*, 4188−4191.

[6] [6a] O. Zelenko, J. Gallagher, D. S. Sigman, *Angew. Chem. Int. Ed. Engl.* **1997**, *36*, 2776−2778. [6b] M. M. Meijler, O. Zelenko, D. S. Sigman, *J. Am. Chem. Soc.* **1997**, *119*, 1135−1136.

[7] T. E. Goyne, D. S. Sigman, *J. Am. Chem. Soc.* **1987**, *109*, 2846−2848.

[8] J. M. Veal, K. Merchant, R. L. Rill, *Nucleic Acids Res.* **1991**, *19*, 3383−3388.

[9] [9a] J. M. Veal, R. L. Rill, *Biochemistry* **1991**, *30*, 1132−1140. [9b] J. M. Veal, R. L. Rill, *Biochemistry* **1988**, *27*, 1822−1827.

[10] L. D. Williams, J. Thivierge, I. H. Goldberg, *Nucleic Acids Res.* **1988**, *16*, 11607−11615.

[11] J. C. Stockert, *J. Theor. Biol.* **1989**, *137*, 107−111.

[12] S. Lewin, in: *Vitamin C: Its Molecular Biology and Medical Potential*, Academic Press, London, **1976**.

[13] J. Cano, P. Alemany, S. Alvarez, M. Verdaguer, E. Ruiz, *Chem. Eur. J.* **1998**, *4*, 476−484.

[14] S. Alvarez, M. Julve, M. Verdaguer, *Inorg. Chem.* **1990**, *29*, 4500−4507.

[15] A. Gleizes, M. Julve, M. Verdaguer, J. A. Real, J. Faus, X. Solans, *J. Chem. Soc., Dalton Trans.* **1992**, 3209−3216.

[16] M. Julve, M. Verdaguer, A. Gleizes, M. Philoche-Levisalles, O. Kahn, *Inorg. Chem.* **1984**, *23*, 3808−3818.

[17] [17a] O. Castillo, I. Muga, A. Luque, J. M. Gutiérrez-Zorilla, J. Sertucha, P. Vitoria, P. Roman, *Polyhedron* **1999**, *18*, 1235−1245. [17b] Y. Akhriff, J. S. Carrio, A. Sancho, J. G. Lozano, E. Escriva, J. V. Folgado, L. Soto, *Inorg. Chem.* **1999**, *38*, 1174−1185. [17c] M. L. Calatayud, I. Castro, S. Sletten, F. Lloret, M. Julve, *Inorg. Chim. Acta* **2000**, *300−302*, 846−854. [17d] L. Zhang, W.-M. Bu, S.-P. Yan, Z.-H. Jiang, D. Z. Liao, G.-L. Wang, *Polyhedron* **2000**, *19*, 1105−1110. [17e] A. Bencini, A. C. Fabretti, C. Zanchini, P. Zannini, *Inorg. Chem.* **1987**, *26*, 1445−1449.

[18] A. M. Thomas, G. C. Mandal, S. K. Tiwari, R. K. Rath, A. R. Chakravarty, *J. Chem. Soc., Dalton Trans.* **2000**, 1395−1396.

[19] [19a] M. R. Sundberg, R. Kivekas, J. K. Koskimies, *J. Chem. Soc., Chem. Commun.* **1991**, 526−527. [19b] E. L. Prien, C. Frondel, *J. Urology* **1947**, *57*, 949.

[20] M. Munakata, S. Kitagawa, A. Asahara, H. Masuda, *Bull. Chem. Soc. Jpn.* **1987**, *60*, 1927−1929.

[21] [21a] M. J. Waring, *J. Mol. Biol.* **1965**, *13*, 269−282. [21b] J.-B. LePecq, C. Paoletti, *J. Mol. Biol.* **1967**, *27*, 87−106.

[22] L. Changzheng, W. Jigui, W. Liufang, R. Min, J. Naiyong, G. Jie, *J. Inorg. Biochem.* **1999**, *73*, 195−202.

[23] S. Mahadevan, M. Palaniandavar, *Inorg. Chem.* **1998**, *37*, 3927−3934.

[24] J. Bernadou, G. Pratviel, F. Bennis, M. Girardet, B. Meunier, *Biochemistry* **1989**, *28*, 7268−7275.

[25] I. Castro, J. Faus, M. Julve, M. C. Munoz, W. Diaz, X. Solans, *Inorg. Chim. Acta* **1991**, *179*, 59−66.

[26] I. Castro, J. Faus, M. Julve, A. Gleizes, *J. Chem. Soc., Dalton Trans.* **1991**, 1937−1944.

[27] J. G. Collins, A. D. Sleeman, J. R. Aldrich-Wright, I. Greguric, T. W. Hambley, *Inorg. Chem.* **1998**, *37*, 3133−3141.

[28] J. V. Fry, J. G. Collins, *Inorg. Chem.* **1997**, *36*, 2919−2921.

[29] I. Greguric, J. R. Aldrich-Wright, J. G. Collins, *J. Am. Chem. Soc.* **1997**, *119*, 3621−3622.

[30] K. E. Erkkila, D. T. Odom, J. K. Barton, *Chem. Rev.* **1999**, *99*, 2777−2796.

[31] R. E. Holmlin, E. D. A. Stemp, J. K. Barton, *Inorg. Chem.* **1998**, *37*, 29−34.

[32] C. M. Dupureur, J. K. Barton, *Inorg. Chem.* **1997**, *36*, 33−43.

[33] [33a] J. E. Dickeson, L. A. Summers, *Aust. J. Chem.* **1970**, *23*, 1023−1027. [33b] E. Amouyal, A. Homsi, J.-C. Chambron, J.-P. Sauvage, *J. Chem. Soc., Dalton Trans.* **1990**, 1841−1845.

[34] P. W. Selwood, *Magnetochemistry*, 2nd ed., John Wiley & Sons, New York, **1956**.

[35] B. Bleaney, K. D. Bowers, *Proc. R. Soc. London, A* **1952**, *214*, 451−465.

[36] O. Kahn, *Molecular Magnetism*, VCH Publishers, New York, **1993**.

[37] N. Walker, D. Stuart, *Acta Crystallogr., Sect. A* **1983**, *39*, 158−166.

[38] G. M. Sheldrick, *SHELX-97, Programs for crystal structure solution and refinement*, University of Göttingen, Germany, **1997**.

[39] C. K. Johnson, *ORTEP*, Report ORNL − 5138, Oak Ridge National Laboratory, Oak Ridge, TN, **1976**.

[40] M. E. Reichmann, S. A. Rice, C. A. Thomas, P. Doty, *J. Am. Chem. Soc.* **1954**, *76*, 3047−3053.

Received October 26, 2001
[I01422]

A New Oligomeric Complex of Cyclic Hydrogenphosphonates with Calcium Perchlorate

Elsa Sutra,[a] Lydia Lamandé,[a] Heinz Gornitzka,[b] and Jacques Bellan*[a]

Keywords: Phosphorus heterocycles / Calcium / P ligands / Self-assembly / Noncovalent interactions

A hybrid organic/inorganic material is obtained with calcium as the structural building block. The structure of this new oligomeric complex was confirmed by a single crystal X-ray diffraction, which shows the bridging position of the calcium ions between four dioxazaphosphocane moieties.

(© Wiley-VCH Verlag GmbH, 69451 Weinheim, Germany, 2002)

Methylenebisphosphonates, also known as geminal bisphosphonates, are analogues of pyrophosphates and are also characterized by a P−C−P bond. These compounds with various side chains linked to the central carbon atom, like Etidronate® or Clodronate®, have been extensively studied and widely used in treating various diseases of bone and calcium metabolism.[1−3]

Whereas monophosphonates have been reported to be inactive with respect to calcium related disorders,[4] the presence of a potential donor group adjacent to the phosphonate moiety (as in α-acylphosphonates or α-hydroxyiminophosphonates) restores this activity.[5] Despite the large number of bis-phosphonates investigated for their biological activity or even used clinically, structural studies of their calcium complexes are very limited. However, a common feature of the few structural studies reported is that the Ca ion forms bidentate chelates with two oxygen atoms.[6−7]

In this field, we have synthesized, in the past few years, new eight-membered cyclic hydrogenophosphonates named dioxazaphosphocanes. These cyclic and nonionizable phosphodiesters, with two donor groups (carbonyl and phosphoryl) in the same molecule, display interesting complexing properties towards alkaline earth metal cations.[8]

The complexing properties of the dioxazaphosphocane moiety have been demonstrated in the solid state by an X-ray structure determination. It revealed an original polymeric arrangement which is in accordance with the previously claimed stoichiometry and the data obtained by classical physical methods (NMR and IR spectroscopy).

[a] Synthèse et Physicochimie de Molécules d'Intérêt Biologique, UMR 5068 CNRS, Université Paul Sabatier Toulouse III, 118 rte de Narbonne, 31062 Toulouse cedex 04 France
Fax: (internat.) +33-5/6155-6011
E-mail: bellan@chimie.ups-tlse.fr
[b] Hétérochimie Fondamentale et Appliquée, UMR 5069 CNRS, Université Paul Sabatier Toulouse III, 118 rte de Narbonne, 31062 Toulouse cedex 04 France

The synthesis of dioxazaphosphocanes, based on the reactivity of a constrained bicyclophosphane, was developed in our laboratory.[9] Scheme 1 shows the synthesis of compound **2**, studied in this paper, which is obtained by an oxidative addition reaction of acetic acid to the bicyclophosphane **1**.[10]

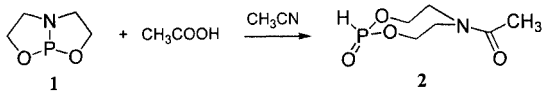

1 **2**

Scheme 1

By a single crystal X ray diffraction analysis, we have recently demonstrated that the dioxazaphosphocane **2** adopts a crown conformation in the solid state.[11] This conformation is retained in solution according to the ^{1}H and ^{13}C NMR spectra, thus meaning that the phosphoryl and carbonyl groups are in favourable positions for complexation.

We have already observed the formation of a well-defined complex from the reaction of dioxazaphosphocane **2** with calcium perchlorate. Comparison of the IR spectra of the free ligand and of the complex shows shifts to lower frequencies for the carbonyl ($\Delta\nu_{C=O}$ = 22 cm^{-1}) and phosphoryl ($\Delta\nu_{P=O}$ = 14 cm^{-1}) stretching vibrations; hence they are both involved in the complexation. Moreover, interaction of the phosphoryl group with calcium was confirmed by ^{31}P NMR spectroscopy ($\Delta\delta^{31}{}_{P}$ = 0.9 ppm; $\Delta^{1}{}_{JPH}$ = 32 Hz). The chemical formula of complex **3** [$CaL_2{\cdot}(ClO_4)_2$ (with L = compound **2**)] is consistent with a 1:2 stoichiometry (one calcium atom for two heterocycles) as determined by elemental analysis, and from these results we previously proposed a sandwich-type structure, with the calcium atom being located between two dioxazaphosphocane moieties.

A single crystal X-ray diffraction analysis of this complex (Figure 1) confirmed that the complexation actually involves the phosphoryl and carbonyl groups.

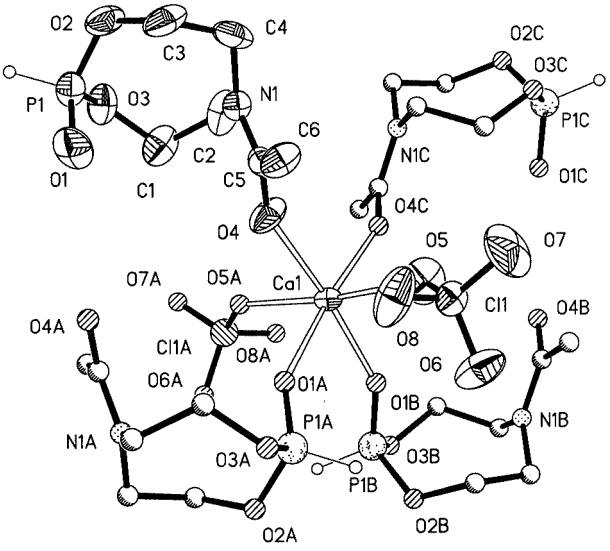

Figure 1. Structure of **3** in the solid state; the asymmetric unit is drawn as a thermal ellipsoid diagram at the 50% probability level; the figure shows the coordination environment of the Ca cation; except for the hydrogen atom bonded to the phosphorus, all others hydrogen atoms have been omitted for clarity; selected bond lengths [Å] and angles [°]: Ca−O1A 2.280(6), Ca−O4 2.281(5), Ca−O5 2.36(4), O1A−Ca−O1B 85.0(4), O1A−Ca−O4 92.5(2), O1A−Ca−O4C 174.3(2), O1A−Ca−O5 91.5(5), O1A−Ca−O5C 92.9(5)

However, calcium is not located between two dioxazaphosphocane moieties, but is bridged between four heterocycles leading to the formation of a one-dimensional polymeric material in which the metal plays the role of a template element. However, and in contrast to the solid state, the sandwich-type structure is not unlikely in solution. It is important to notice that in complex **3** the dioxazaphosphocane moieties retain the crown conformation previously determined for the free ligand.

Ca^{2+} generally accepts a coordination number of eight or nine,[12] and its coordination shell is either full, or completed with one molecule of solvent (e.g. H_2O, CH_3CN, THF). A coordination number of six, while less common, leads to well-defined octahedral complexes.[13] This latter arrangement is found in antibiotics like Benastatine A[14] or Griseocheline.[15] In complex **3** the calcium atom is coordinated to six oxygen atoms, four from four different dioxazaphosphocane moieties and two from perchlorate anions. The charge neutrality of the complex is maintained by perchlorate anions located on both parts of the mean plane formed by the other complexing oxygen atoms from two carbonyl groups and two phosphoryl groups for each calcium ion. The Ca−O distances are in the range 2.37−2.26 Å and there are no other Ca−O contacts less than 3.2 Å to indicate any additional coordination of Ca.

The most prominent common structural feature is the arrangement of the $[CaL_2]\cdot(ClO_4)_2$ units (L = dioxazaphosphocane **2**) in polymeric chains, where the metal centers are connected by bridging dioxazaphosphocane groups (Figure 2).

An examination of Ca/dioxazaphosphocane complex formation under physiological conditions is in progress, because in many biomineralizing systems organized organic assemblies serve as inductive templates for mediating the nucleation and growth of inorganic crystals.

Experimental Section

3: $[Ca(ClO_4)_2\cdot 6H_2O]$ (0.37 g, 1.08 mmol) in MeCN (30 mL) was added to a solution of dioxazaphosphocane **2** (0.42 g, 2.17 mmol) in MeCN (50 mL). The mixture was stirred at room temperature for 10 min. Slow evaporation of the solvent produced colorless crystals of **3** (0.48 g, 70%). ^{31}P NMR (80.96 MHz, CH_3CN, 298 K): $\delta = 8.8$ ($^1J_{PH} = 760$ Hz) ppm. $C_{12}H_{24}CaCl_2N_2O_{16}P_2$ (624.98): calcd. C 23.04, H 3.84, N 4.48; found C 23.13, H 3.65, N 4.49.

Crystal Data for 3: $C_{12}H_{24}CaCl_2N_2O_{16}P_2$, $M = 625.25$, monoclinic, $C2/c$, $a = 15.067(5)$ Å, $b = 12.271(4)$ Å, $c = 13.564(4)$ Å, $\beta = 94.792(6)°$, $V = 2499.2(13)$ Å^3, $Z = 4$, $\rho_c = 1.662$ Mg m^{-3}, $F(000) = 1288$, $\lambda = 0.71073$ Å, $T = 193(2)$ K, μ(Mo-K_α) = 0.669 mm^{-1}, crystal size 0.2 × 0.2 × 0.05 mm, $2.14° < \Theta < 23.25°$, 4459 reflections (1761 independent with $R_{int} = 0.0638$) were collected at low temperatures with an oil-coated shock-cooled crystal on a Bruker-AXS CCD 1000 diffractometer. The structure was solved by direct methods (SHELXS-97)[16] and 209 parameters were refined using the least-squares method on F^2.[17] All non-hydrogen atoms were refined anisotropically. The hydrogen atoms of the molecules were idealized geometrically and refined using a riding model. The hydrogen atom bonded to the phosphorus atom was located by a difference Fourier procedure. A disorder of the ClO_4 anion was refined anisotropically with the help of 202 ADP and distance restraints. Largest electron density residue: 0.599 e·Å^{-3}, R_1 [for $I > 2\sigma(I)$] = 0.0711 and $wR_2 = 0.1795$ (all data) with $R_1 = \Sigma||F_o| - |F_c||/\Sigma|F_o|$ and $wR_2 = [\Sigma w(F_o^2 - F_c^2)^2/\Sigma w(F_o^2)^2]^{0.5}$.

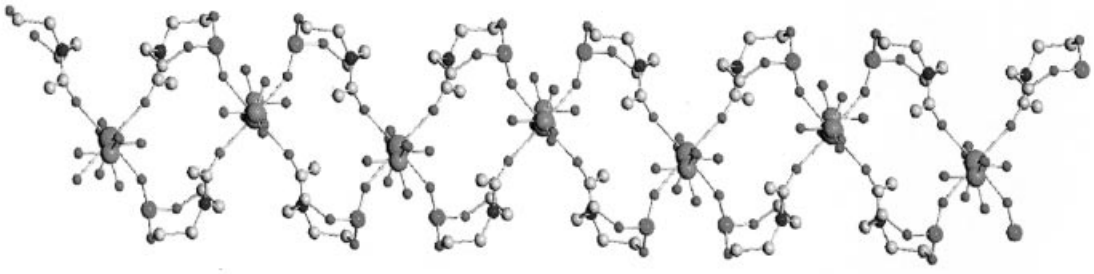

Figure 2. Ball-and-stick view showing the polymeric nature of **3**

CCDC-178965 contains the supplementary crystallographic data for this paper. These data can be obtained free of charge at www.ccdc.cam.ac.uk/conts/retrieving.html [or from the Cambridge Crystallographic Data Centre, 12, Union Road, Cambridge CB2 1EZ, UK; Fax: (internat.) +44-1223/336-033; E-mail: deposit@ccdc.cam.ac.uk].

[1] G. R. Mundy, *Bone* **1987**, *8*, S9−S16.
[2] F. J. Schoen, H. Harasaki, K. M. Kim, H. C. Anderson, R. J. Levy, *J. Biomed. Mater. Res.* **1988**, *22*, 11−36.
[3] H. Fleisch, *Bisphosphonates in Bone Disease. From the Laboratory to the Patient, 2nd ed.*; The Parthenon Publishing Group; New York, **1995**.
[4] H. Fleisch, *Bone* **1987**, *8*, S23−S28.
[5] M. Mathew, B. O. Fowler, E. Breuer, G. Golomb, I. S. Alferiev, N. Eidelman, *Inorg. Chem.* **1998**, *37*, 6485−6494.
[6] P. G. Jones, O. Kennard, *Acta Crystallogr., Sect. B* **1978**, *34*, 2309−2311.
[7] D. Gibson, R. Karaman, *J. Chem. Soc., Dalton Trans.* **1989**, 1911−1914.
[8] [8a] L. Lamandé, J.-M. Grévy, D. Houalla, L. Cazaux, J. Bellan, *Tetrahedron Lett.* **1995**, *45*, 8201−8204. [8b] A. Pujo-Bouteillé, L. Lamandé, L. Lopez, L. Cazaux, J. Bellan, *Tetrahedron* **1998**, *54*, 3817−3826.
[9] B. Duthu, D. Houalla, R. Wolf, *Can. J. Chem.* **1988**, *66*, 2965−2974.
[10] 2,8-Dioxa-5-aza-1-σ^3,λ^3-phosphabicyclo[3.3.0] octane (or bicyclophosphane **1**) has been synthesized according to a method developed in our laboratory by reaction of tris(dimethylamino)-phosphane, $[(CH_3)_2N]_3P$, with 3-azapentane-1,5-diol, $HN(CH_2CH_2OH)_2$.
[11] D. Houalla, J. Bellan, J.-M. Grévy, L. Lamandé, J. Jaud, *Phosphorus, Sulfur & Silicon* **2000**, *159*, 1−22.
[12] J. P. Roux, G. J. Kruger, *Acta Crystallogr., Sect. B* **1976**, *32*, 1171−1175.
[13] T. Pigot, M.-C. Duriez, C. Picard, L. Cazaux, P. Tisnès, *Tetrahedron* **1992**, *48*, 4359−4368.
[14] T. Aoyama, H. Naganawa, Y. Muraoka, H. Nakamura, T. Aoyagi, T. Takeuchi, Y. Litaka, *J. Antibiot.* **1992**, *45*, 1391−1396.
[15] D. Scharfenberg-Pfeiffer, M. Czugler, *Pharmazie* **1991**, *46*, 781−783.
[16] G. M. Sheldrick, *Acta Crystallogr., Sect. A* **1990**, *46*, 467−473.
[17] SHELXL-97, *Program for Crystal Structure Refinement*, G. M. Sheldrick, University of Göttingen **1997**.

Received February 14, 2002
[I02079]

The Structure and Fluorescence Properties of Two Novel Mixed-Ligand Supramolecular Frameworks with Different Structural Motifs

Zhi-Yong Fu,[a,b] Xin-Tao Wu,*[a] Jing-Cao Dai,[a] Sheng-Min Hu,[a] Wen-Xin Du,[a] Han-Hui Zhang,[c] and Rui-Qing Sun[c]

Keywords: Crystal engineering / Cobalt / Fluorescence / Supramolecular chemistry

Two novel coordination polymers formed by cobalt nitrate and 1,2-bis(4-pyridyl)ethane with the homologous ligands 2-aminoterephthalic acid and terephthalic acid, respectively, have been prepared. One displays a fivefold diamond-type feature while the other exhibits a twofold interpenetrating structural motif. The thermal and photoluminescence properties associated with their structures have been characterized and studied.
(© Wiley-VCH Verlag GmbH, 69451 Weinheim, Germany, 2002)

Introduction

The construction of functional metal-organic frameworks is of great interest due to their intriguing network topologies and their potential applications as microporous,[1] magnetic,[2] nonlinear optical[3] and fluorescent materials.[4] Molecular self-assembly has been proven as an effective way of constructing various fascinating supramolecular frameworks. The basic building blocks recognize each other in a reaction system and aggregate to form the bulk structure.[5] Lots of supramolecular frameworks have already been produced in the past decade based upon the principle of crystal engineering.[6] However, the mechanism of molecular self-assembly is unclear and the result of self-assembly is unpredictable, therefore an understanding of the factors that govern the assembly process is necessary for technological development. Recently, considerable attention has been focused on the influence of the factors involved in molecular self-assembly processes, such as the solvent system,[7] template,[8] counterion,[9] and the conformational freedom of the ligands.[10] We are particularly interested in self-assembly and the functionalities associated with different coordination conformations. Here, we report two novel mixed organic ligand supramolecular compounds [Co{1,2-bis(4-pyridyl}ethane)(2-aminoterephthalate)] (**1**) and [Co{1,2-bis(4-pyridyl)ethane}(terephthalate)] (**2**). The O,O′-donor ligands adopt different coordination modes forming different kinds of building blocks, which finally aggregate to generate different supramolecular architectures, due to the influence of the substituent groups. These different structures show similar fluorescence spectra: they both display strong fluorescence emission at 400 nm.

[a] State Key Laboratory of Structural Chemistry, Fujian Institute of Research on the Structure of Matter, Chinese Academy of Sciences,
Fuzhou, Fujian350002, China
Fax: (internat.) +86-591/371-4946
E-mail: wxt@ms.fjirsm.ac.cn
[b] Graduate School of the Chinese Academy of Sciences
Fuzhou, Fujian350002, China
[c] Department of Chemistry, Fuzhou University
Fuzhou, Fujian 350002, China

Results and Discussion

2-Aminoterephthalic acid and terephthalic acid were chosen as starting materials as one has a substituted amino group while the other has none. These two organic acids react with 1,2-bis(4-pyridyl)ethane and cobalt nitrate in a 1:1:1 ratio under the same conditions. The O-donors accept different coordination modes (Scheme 1), which finally results in different coordination frameworks.

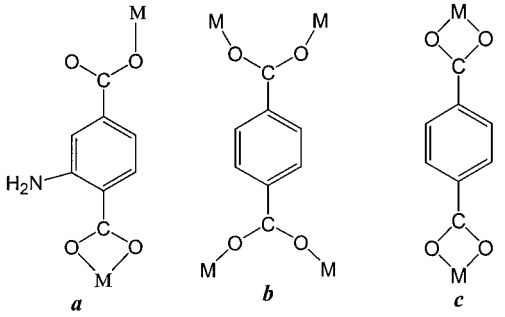

Scheme 1. The coordination modes of the carboxylate group: *a*) unidentate and chelating bis-bidentate; *b*) bidentate; *c*) chelating bidentate

Crystal Structures

An ORTEP view of a Co center of compound **1** is shown in Figure 1. The Co atom has a distorted tetrahedral coordination geometry, being coordinated by two N atoms of two 1,2-bis(4-pyridyl)ethane molecules [Co1−N2b = 2.101(11) Å, Co1−N3 = 2.063(11) Å], two O atoms from one chelating bis-bidentate carboxylate group [Co1−O1a = 2.050(10) Å, Co(1)−O2a = 2.224(10) Å], and one O atom of one unidentate carboxylate group [Co1−O3 = 2.024(9) Å], which provide the four connecting nodes resulting in an unsymmetrical adamantane-type unit (Figure 2). No guest molecules were found in the cage of the adamantane unit and distortions of the unit can arise from the application of different ligands. Four 2-aminoterephthalate ligands and two 1,2-bis(4-pyridyl)ethane ligands bridge six Co atoms to form a hexagonal circuit. The distance between the Co centers is determined by the length of 2-aminoterephthalate (10.729 Å) or 1,2-bis(4-pyridyl)ethane (13.349 Å). Figure 3 shows that five independent equivalent networks are interpenetrated within the structure (fivefold diamondoid mode). The nodes of four other nets are arranged between the top-most and bottom-most extremities of an adamantane unit of the first net. Although many diamond-related nets displaying various interpenetration modes ranging from two- to ninefold have been reported,[13] the fivefold interpenetration of **1** is novel in the presence of the mixed organic ligands with different lengths. To the best of our knowledge, with coordination polymers only two other examples of a fivefold diamond-type net have been previously observed. They are $[Cu(L_2)](BF_4)$ (L = 1,4-dicyanobenzene) and $[Cu(bpe)_2](BF_4)$ generated by the reaction of $CuBF_4$ with 1,4-dicyanobenzene and bpe, respectively.[14]

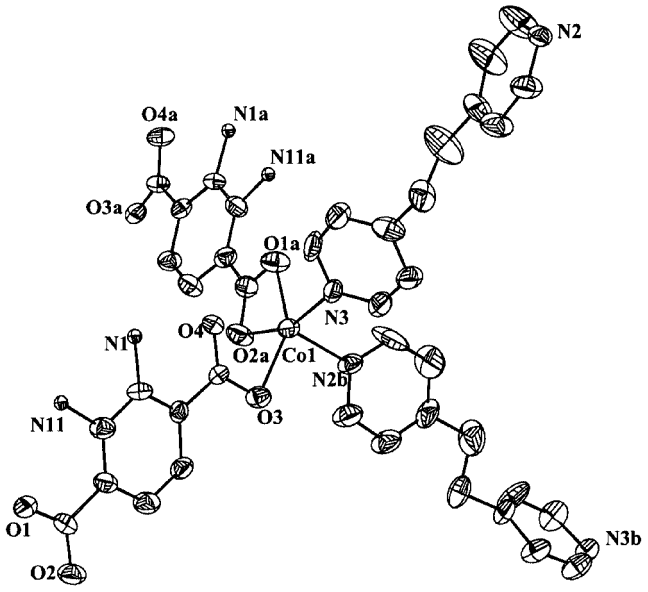

Figure 1. ORTEP drawing of **1** around the Co center (ellipsoids at 30% probability); the hydrogen atoms are omitted for clarity; the N1 and N11 atoms of compound **1** were located from the E-map directly, and the displacement parameters of them were of 0.5 to 0.5 statistically; symmetry codes: $a = -x, 1 + y, z - 1/4$; $b = x, 2 - y, z + 1/4$

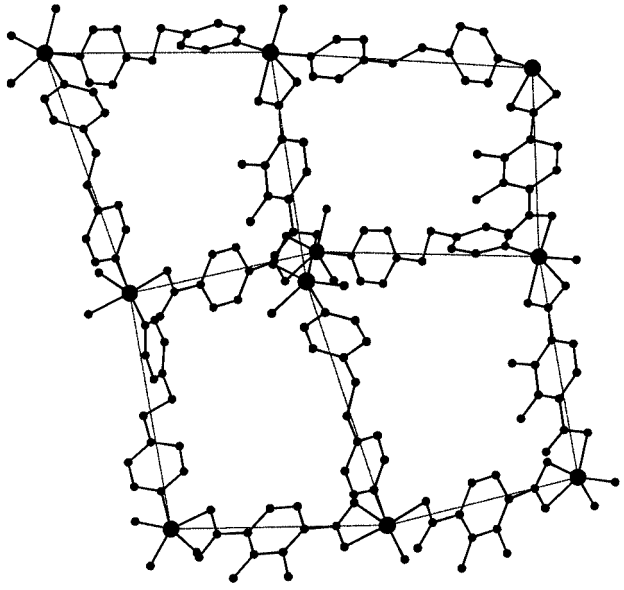

Figure 2. View of the adamantane units of **2**; the large black balls represent the Co atoms

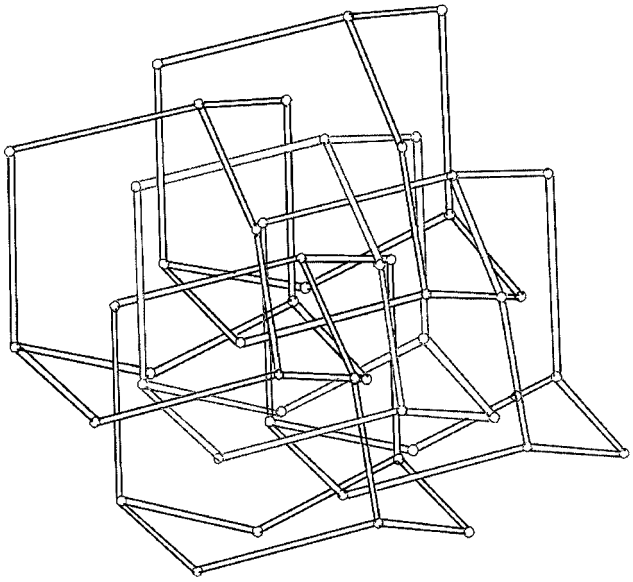

Figure 3. The interpenetration model for complex **1**

For the preparation of compound **2**, the terephthalate ligand was used instead of 2-aminoterephthalate ligand. The Co center has a distorted octahedral coordination geometry, with two oxygen donors of one chelating bis-bidentate carboxylate group [Co1−O1 = 2.200(3) Å, Co1−O2 = 2.192(3) Å] and two oxygen donors of two bridging bidentate carboxylate groups in the horizontal direction (Co1−O3 = 2.017 Å, Co1−O4a = 2.028 Å). The coordination sphere is completed by two nitrogen donors of 1,2-bis(4-pyridyl)ethane [Co1−N1 = 2.163(3) Å, Co1−N2b =

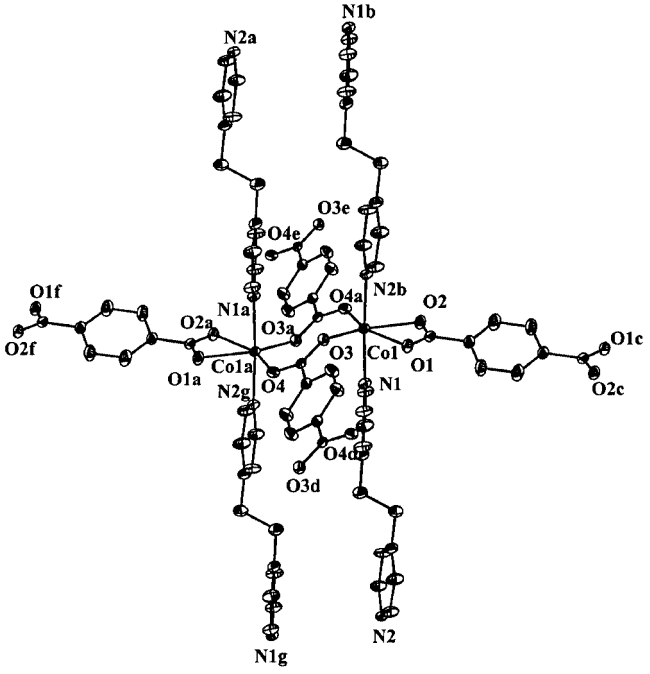

Figure 4. View of the dimetal unit of **2**; hydrogen atoms have been omitted, and the ellipsoids at 30% probability represent C, N O, and Co; symmetry codes: $a = -x, -y, -z$; $b = x, y + 1, z - 1$; $c = 1 - x, -1 - y, -1 - z$; $d = 1 - x, -y, -z$; $e = -1 + x, y, z$; $f = -1 + x, 1 + y, 1 + z$; $g = -x, -1 - y, 1 - z$

2.152(3) Å] in the axial direction (Figure 4). The coordination mode in compound **2** generates a novel cuboidal building block (Figure 5). Each corner of the cuboidal block is occupied by a binuclear subunit and the Co···Co separation in the binuclear subunit is 4.27 Å. Eight terephthalate ligands form the length and width of the cuboidal block while eight 1,2-bis(4-pyridyl)ethane ligands make up the height of it. No guest molecule is included in the cuboidal box. The aggregation of the building blocks results in a 3-D framework, and the 3-D networks interlock with each other displaying a twofold-interpenetrating mode. As shown in Figure 6, in the axial direction every two rods (rod a and b) in the cuboidal block are associated with one particular quadrate ring (ring 1) of the other framework through which they pass, while in the horizontal direction one rod (rod c) is associated with two particular quadrate rings (ring 2 and 3) of the other framework through which it penetrates.

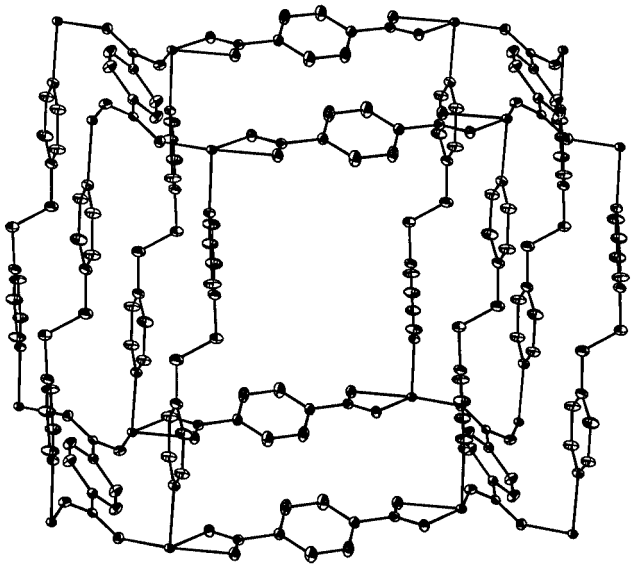

Figure 5. Structure of the cuboidal block of **2**, showing eight Co2 units linked by eight terephthalate anions and eight 1,2-bis(4-pyridyl)ethane units

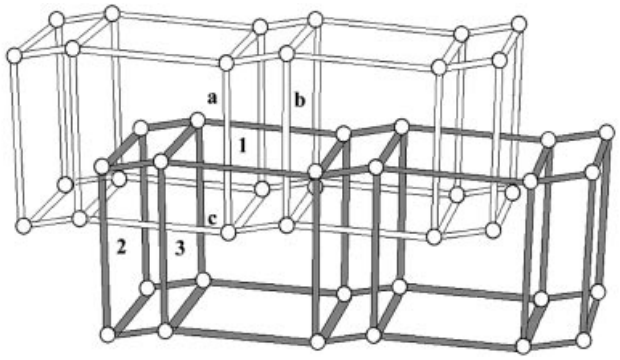

Figure 6. The interpenetration model for complex **2**

Under the same reaction conditions, compounds **1** and **2** exhibit different structural motifs. The coordination mode of the carboxylate group is an essential factor in affecting the bulk structures of **1** and **2**. One of the characteristics of these reactions is that the substituent groups in the homologous O,O′-donor ligands are slightly different, which affects the pH values in the reaction systems (obsd. 6.22 in **1** and 5.13 in **2**). These different basicities, which most probably make the carboxylate groups in **1** and **2** accept different coordination modes, lead to different supramolecular architectures.

IR Spectroscopy

The IR spectrum of compound **1** shows the characteristic bands of the dicarboxylate groups of the 2-aminoterephthalate ligands at 1618−1549 cm^{-1} for the asymmetric vibration and at 1421−1396 cm^{-1} for the symmetric vibration. While the IR spectrum of compound **2** shows the characteristic bands of the dicarboxylate groups of the terephthalate ligands at 1610−1552 cm^{-1} for the asymmetric vibration and at 1410−1394 cm^{-1} for the symmetric vibration. The splitting of $\nu_{asym}(CO_2)$ in compound **1** and compound **2** confirms that the carboxylate groups have two different coordination modes,[15] in agreement with their crystal structures. The absence of the expected characteristic bands at 1730−1690 cm^{-1} for the protonated carboxylate groups indicates the complete deprotonation of 2-aminoterephthalic acid and terephthalic acid in the reaction with Co ions.[16]

Thermal and Fluorescent Properties

Compounds **1** and **2** were heated to 600 °C under N_2. Their thermal decomposition behavior (Figure 7) is very similar. No obvious decomposition was observed in until ca 430 °C. The TGA data show that **1** has an obvious weight loss starting at about 435 °C (437 °C for **2**).

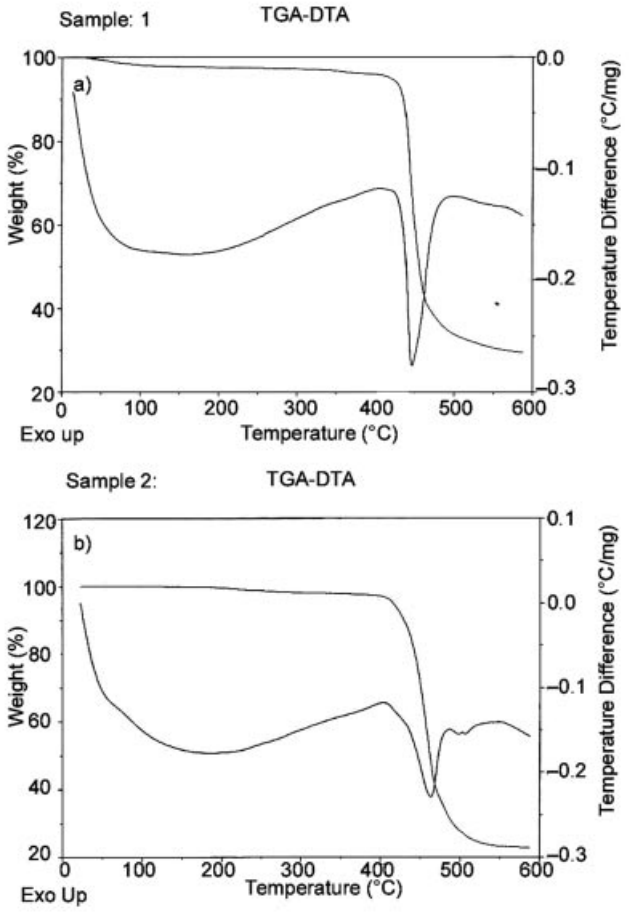

Figure 7. The TGA-DTA diagram for the coordination polymers: *a*) compound **1**; *b*) compound **2**

The emission spectra of compounds **1** and **2** in the solid state at room temperature are shown in Figure 8. It can be seen that **1** exhibits an intense photoluminescence emission at 400 nm (Figure 8a, λ_{ex} = 300 nm) while **2** also exhibits an intense photoluminescence emission at 400 nm (Figure 8b, λ_{ex} = 310 nm). These emissions may be assigned as ligand-to-metal charge transfer (LMCT).[17] Due to their high thermal stability, **1** and **2** may be good candidates for emitting diode devices.

It is very interesting to note that **1** and **2** exhibit similar thermal behaviors and photoluminescence spectra despite having different structural motifs. What is the reason for these phenomena? Due to the fact that thermal behaviors and photoluminescence behavior are closely associated with the metal ions and the ligands coordinated around them, we decided to look again at the coordination environments of the metal ions in **1** and **2**. In **1** the Co atom has a distorted tetrahedral coordination geometry while in **2** the Co

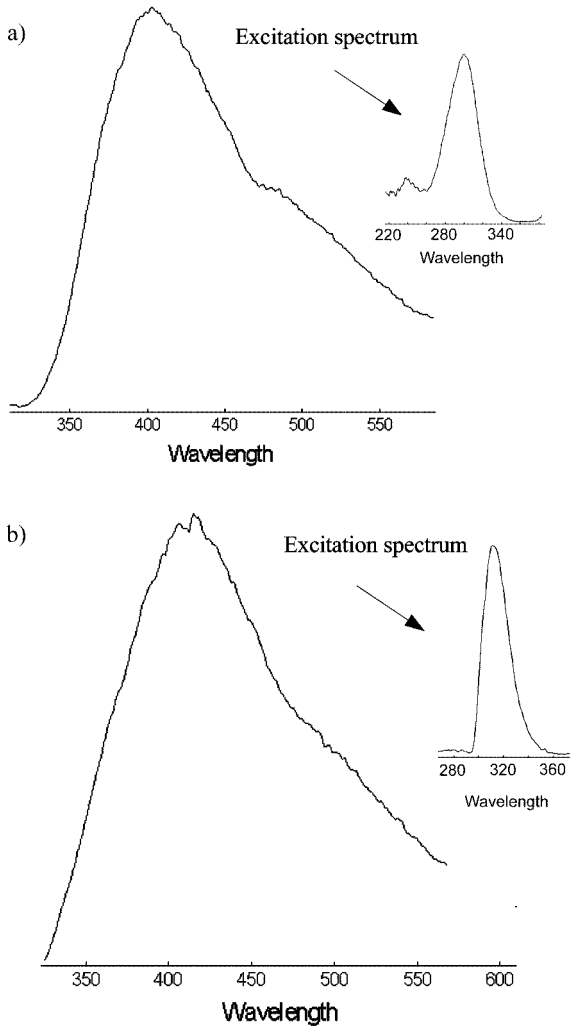

Figure 8. Solid-state emission spectra of the coordination polymers at room temperature: *a*) compound **1**; *b*) compound **2**

atom has a distorted octahedral coordination geometry. However, despite this distinct disparity, the ligands coordinated around the metal ions in **1** and **2** are similar (Figure 1 and Figure 4). The Co center in **1** has one chelating bis-bidentate carboxylate group, one unidentate carboxylate group, and two 1,2-bis(4-pyridyl)ethane ligands while in **2** there are one chelating bis-bidentate carboxylate group, two bridging bidentate carboxylate groups, and two 1,2-bis(4-pyridyl)ethane ligands. These similar environments may be the reason, for the similar thermal and photoluminescence behaviors (Figure 7 and 8).

Conclusion

Two novel coordination polymers formed by cobalt nitrate and 1,2-bis(4-pyridyl)ethane with the homologous ligands 2-aminoterephthalic acid and terephthalic acid have been prepared and characterized. Compound **1** displays a fivefold diamond-type net while compound **2** exhibits a twofold-interpenetrating structural motif. The two com-

pounds have similar thermal behaviors and photoluminescence spectra. In this paper, we have shown that the amino group in 2-aminoterephthalic acid plays an important role in affecting the coordination mode of the carboxylate group, causing **1** to have a structural motif that is clearly different from that of **2**. Their thermal and photoluminescence properties are closely associated with the coordination environments around the metal centers.

Experimental Section

General Remarks: All reactions were carried out in hydrothermal conditions. All chemicals are commercially available and used as received without further purification. The C, H and N microanalyses were carried out with a Vario EL III elemental analyzer. Infrared spectra (KBr pellets) were recorded in the range from 4000−400 cm^{-1} on a Nicolet Magna 750 FT-IR spectrometer. Thermogravimetric analyses (**TGA**) were performed under nitrogen with a heating rate of 10 °C·min^{-1} using a TA5200/MDSC2910 system. Fluorescent spectra were measured with an Edinburgh FL-FS90 TCSPC system at the Spectroscopy Lab of Fuzhou University.

Synthesis of [Co{1,2-bis(4-pyridyl)ethane}(2-aminoterephthalate)] (1): An aqueous mixture (10 cm^3) containing $Co(NO_3)_2·6H_2O$ (0.292 g, 1 mmol), 1,2-bis(4-pyridyl)ethane (0.184 g, 1 mmol), 2-aminoterephthalic acid (0.181 g, 1 mmol) and NaOMe (0.108 g, 2 mmol) was placed in a Parr Teflon-lined stainless steel bomb (25 cm^3). The bomb was heated at 5 °C·min^{-1} to 160 °C; after 24 h at 160 °C it was cooled to 90 °C at the rate of 0.1 °C·min^{-1}, then maintained at that temperature for 12 h. Finally, it was cooled at 0.1 °C·min^{-1} to 20 °C. The bomb was opened to give red block crystals in 62% yield. $C_{20}H_{17}CoN_3O_4$ (422.3): calcd. C 56.86, H 4.06, N 9.95; found C 56.96, H 4.01, N 9.97. IR (KBr): $\tilde{\nu}$ = 3442m, 3338m, 3055w, 2945w, 1618s, 1564s, 1549s, 1498m, 1446m, 1421s, 1396s, 1375m, 1333w, 1261s, 1072w, 1028s, 847s, 816m, 768s, 702w, 536w, 517w cm^1.

Table 1. Crystal data and refinement details for the structures of **1** and **2**

Complex	**1**	**2**
Empirical formula	$C_{20}H_{17}CoN_3O_4$	$C_{20}H_{16}CoN_2O_4$
Space group	$P4_1$	$P\bar{1}$
a, Å	9.1737(4)	10.0719(3)
b, Å	9.1737(4)	10.23420(10)
c, Å	24.6489(16)	10.8551(3)
α	90°	80.34°
β	90°	66.6430(10)°
γ	90°	75.474(2)°
V, Å^3	2074.37(19)	991.45(4)
Z	4	2
μ(Mo-K_α), mm^{-1}	0.856	0.891
d_{calcd}, g/cm^3	1.352	1.364
Measured reflections	5098	5139
Independent reflections	2051	3450
Observed reflections [$I > 2\sigma(I)$]	1247	2612
R	0.0790	0.0502
wR	0.1465	0.1145
Max/mean shift in final cycle	0.000/0.000	0.000/0.000

Synthesis of [Co{1,2-bis(4-pyridyl)ethane}(terephthalate)] (2): An aqueous mixture (10 cm^3) containing $Co(NO_3)_2·6H_2O$ (0.292 g, 1 mmol), 1,2-bis(4-pyridyl)ethane (0.184 g, 1 mmol), terephthalic acid (0.166 g, 1 mmol) and NaOMe (0.108 g, 2 mmol) was placed in a Parr Teflon-lined stainless steel bomb (25 cm^3). The bomb was heated at 5 °C·min^{-1} to 160 °C; after 24 h at 160 °C it was cooled to 90 °C at the rate of 0.1 °C·min^{-1}, then maintained at that temperature for 12 h. Finally, it was cooled at 0.1 °C·min^{-1} to 20 °C. The bomb was opened to give red block crystals in 75% yield. $C_{20}H_{16}CoN_2O_4$ (407.3): calcd. C 58.98, H 3.96, N 6.88; found C 58.87, H 3.92, N 6.89. IR (KBr): $\tilde{\nu}$ = 3057w, 2933w, 1610s, 1568s, 1552s, 1510m, 1500m, 1427m, 1410s, 1394s, 1306w, 1221w, 1018m, 841s, 818m, 748s, 550s, 523m cm^1.

X-ray Crystallographic Study: Crystallographic data for compound **1** and compound **2** are listed in Table 1. For compound **1**, a red block crystal with dimensions of 0.40 × 0.14 × 0.14 mm was used. For compound **2**, a red block crystal with dimensions of 0.30 × 0.22 × 0.12 mm was used. Data for **1** and **2** were collected at room temperature on a Siemens SMART-CCD area-detector diffractometer with Mo-K_α radiation (λ = 0.71073 Å) and a graphite monochromator using the ω-scan mode. Data reductions and absorption corrections were performed with SMART and SADABS software, respectively. For all structural analyses, all calculations were performed on an indy workstation from Silicon Graphics with the program SHELXTL.[11] The structures were solved by direct methods. The refinement of structures was performed by full-matrix least-squares techniques on F^2 using SHELXL-97.[12] All non-hydrogen atoms were treated anisotropically. The nitrogen atoms of 2-aminoterephthalate exhibit disorder. They were located from

Table 2. Selected bond lengths (Å) and bond angles (deg) for **1** and **2**

[Co{1,2-bis(4-pyridyl)ethane}(2-aminoterephthalate)] (**1**)[a]

Co(1)−O(3)	2.024(9)	N(2)−Co(1c)	2.101(11)
Co(1)−O(1a)	2.050(10)	O(2)−Co(1d)	2.224(10)
Co(1)−N(3)	2.063(11)	O(1)−Co(1d)	2.050(10)
Co(1)−N(2b)	2.101(11)	Co(1)−O(4)	2.347(9)
Co(1)−O(2a)	2.224(10)		
O(3)−Co(1)−O(1a)	147.2(4)	N(3)−Co(1)−O(2a)	157.9(4)
O(3)−Co(1)−N(3)	106.5(4)	N(2b)−Co(1)−O(2a)	88.6(4)
O(1a)−Co(1)−N(3)	97.7(4)	O(3)−Co(1)−O(4)	60.0(4)
O(3)−Co(1)−N(2b)	96.9(4)	O(1a)−Co(1)−O(4)	99.2(4)
O(1a)−Co(1)−N(2b)	101.2(4)	N(3)−Co(1)−O(4)	89.6(4)
N(3)−Co(1)−N(2b)	98.5(5)	N(2b)−Co(1)−O(4)	156.9(4)
O(3)−Co(1)−O(2a)	93.4(4)	O(2a)−Co(1)−O(4)	92.1(4)
O(1a)−Co(1)−O(2a)	60.3(4)		

[Co{1,2-bis(4-pyridyl)ethane}(terephthalate)] (**2**)[b]

Co(1)−O(3)	2.017(3)	Co(1)−O(2)	2.192(3)
Co(1)−O(4a)	2.028(3)	Co(1)−O(1)	2.200(3)
Co(1)−N(2b)	2.152(3)	O(4)−Co(1a)	2.028(3)
Co(1)−N(1)	2.163(3)	N(2b)−Co(1)−O(2)	90.90(11)
O(3)−Co(1)−O(4a)	110.08(11)	N(1)−Co(1)−O(2)	85.36(11)
O(3)−Co(1)−N(2b)	88.43(12)	O(3)−Co(1)−O(1)	155.72(11)
O(4a)−Co(1)−N(2b)	89.31(11)	O(4a)−Co(1)−O(1)	93.97(11)
O(3)−Co(1)−N(1)	92.04(12)	N(2b)−Co(1)−O(1)	88.58(12)
O(4a)−Co(1)−N(1)	94.00(11)	N(1)−Co(1)−O(1)	89.47(12)
N(2b)−Co(1)−N(1)	176.26(12)	O(2)−Co(1)−O(1)	60.01(10)
O(3)−Co(1)−O(2)	95.95(10)	O(4a)−Co(1)−O(2)	153.96(11)

[a] Symmetry codes: (a) $-x$, $y + 1$, $z - 1/4$, (b) x, $2 - y$, $z + 1/4$; (c) $-x + 2$, y, $z - 1/4$; (d) $x - 1$, $-y$, $z + 1/4$. [b] Symmetry codes: (a) $-x$, $-y$, $-z$; (b) x, $y + 1$, $z - 1$

the E-map directly, and the displacement parameters were of 0.5 to 0.5 statistically. The positions of the hydrogen atoms were generated geometrically. Selected bond lengths and bond angles for the cluster cores of **1** and **2** are listed in Table 2.

CCDC-181331 (**1**) and -181332 (**2**) contain the supplementary crystallographic data for this paper. These data can be obtained free of charge at www.ccdc.cam.ac.uk/conts/retrieving.html [or from the Cambridge Crystallographic Data Center, 12, Union Road, Cambridge CB2 1EZ, UK; fax: (internat.) +44−1223/336−033; E-mail: deposit@ccdc.cam.ac.uk].

Acknowledgments

This work is supported by grants from the State Key Laboratory of Structural Chemistry, Fujian Institute of Research on the Structure of Matter, Chinese Academy of Sciences (CAS), the Ministry of Science and Technology of China (001CB1089), the National Science Foundation (29733090, 29890210, 29873053) of China and the Science Foundation of the Chinese Academy of Sciences

[1] [1a] M. J. Zaworotko, *Angew. Chem. Int. Ed.* **2000**, *39*, 3052−3054. [1b] V. A. Russell, C. C. Evans, W. J. Li, M. D. Ward, *Science* **1997**, *276*, 575−579. [1c] M. Fujita, D. Oguro, M. Miyazawa, H. Oka, K. Yamaguchi, K. Ogura, *Nature* **1995**, *378*, 469−471.

[2] D. Armentano, G. D. Munno, J. Faus, F. Lloret, M. Julve, *Inorg. Chem.* **2001**, *40*, 655−660.

[3] W. B. Lin, O. R. Evans, R. G. Xiong, Z. Y. Wang, *J. Am. Chem. Soc.* **1998**, *120*, 13272−13273.

[4] [4a] M. L. Tong, X. M. Chen, B. H. Ye, L. N. Ji, *Angew. Chem. Int. Ed.* **1999**, *38*, 2237−2240. [4b] Z. Y. Fu, X. T. Wu, J. C. Dai, L. M. Wu, C. C. Cui, S. M. Hu, *Chem. Commun.* **2001**, 1856−1857.

[5] [5a] S. Leininger, B. Olenyuk, P. J. Stang, *Chem. Rev.* **2000**, *100*, 853−908. [5b] B. Moulton, M. J. Zaworoko, *Chem. Rev.* **2001**, *101*, 1629−1658.

[6] S. R. Batten, R. Robson, *Angew. Chem. Int. Ed.* **1998**, *37*, 1460−1494.

[7] R. Robson, B. F. Abrahams, S. R. Batten, R. W. Gable, B. F. Hoskins, J. Liu. *Supramolecular Architecture* (ACS Symp, Ser., **1992**, 499, Chap. 19).

[8] M. L. Tong, B. H. Ye, J. W. Cai, X. M. Chen, S. W. Ng, *Inorg. Chem.* **1998**, *37*, 2645−2649.

[9] M. A. Withersby, A. J. Blake, N. R. Champness, P. Hubberstey, W. S. Li, M. Schröder, *Angew. Chem. Int. Ed. Engl.* **1997**, *36*, 2327−2329.

[10] T. L. Hennigar, D. C. MacQuarrie, P. Losier, R. D. Rogers, M. J. Zaworoko, *Angew. Chem. Int. Ed. Engl.* **1997**, *36*, 972−973.

[11] G. M. Sheldrick, SHELXTL, Version 5; Siemens Analytical X-ray Instruments Inc., Madison, WI, **1990**.

[12] G. M. Sheldrick, *SHELXL-97, Program for X-ray Crystal Structure Refinement*; University of Göttingen: Göttingen, Germany, **1997**.

[13] S. R. Batten, R. Robson, *Angew. Chem. Int. Ed.* **1998**, *37*, 1460−1494.

[14] [14a] R. Robson, B. F. Abrahams, S. R. Batten, R. W. Gable, B. F. Hoskins, J. Liu, in *Supramolecular Architecture: Synthetic Control in Thin Films and Solids* (Ed.: T. Bein), American Chemical Society, Washington DC, 1992, pp. 256−273. [14b] A. J. Blake, N. R. Champness, S. S. M. Chung, W. S. Li, M. Schröder, *Chem. Commun.* **1997**, 1005−1006.

[15] K. Nakamoto, *Infrared and Raman Spectra of Inorganic and Coordination Compounds*, John Wiley & Sons: New York, 1986.

[16] L. J Bellamy, *The Infrared Spectra of Complex Molecules*, Wiley: New York, 1958.

[17] [17a] A. Meijerink, G. Blasse, M. Glasbeek, *J. Phys.: Condense. Matter* **1990**, *2*, 6303−6313. [17b] R. Bertoncello, M. Bettinelli, M. Casarin, A. Gulino, E. Tondello, A. Vittadini, *Inorg. Chem.* **1992**, *31*, 1558−1565. [17c] J. Tao, M. L. Tong, J. X. Shi, X. M. Chen, S. W. Ng. *Chem. Commun.* **2000**, 2043−2044.

Received March 19, 2002
[I02143]

New Dimetallic Palladium and Platinum Complexes Containing the Tetrakis-(1-pyrazolyl)borate Ligand − Crystal Structures of $[\{(C_6F_5)_2Pd\}_2(\mu\text{-}pz)_2B(\mu\text{-}pz)_2]^-$, $[\{(C_6F_5)(t\text{BuNC})Pd\}_2(\mu\text{-}pz)_2B(\mu\text{-}pz)_2]^+$ and $[(C_6F_5)_2Pd(\mu\text{-}pz)_2B(\mu\text{-}pz)_2Pd(\eta^3\text{-}C_4H_7)]$

José Ruiz,*[a] Félix Florenciano,[a] Venancio Rodríguez,[a] Concepción de Haro,[a] Gregorio López,[a] and José Pérez[b]

Keywords: Palladium / Platinum / N ligands / Bridging ligands / Structure elucidation

New dimetallic palladium and platinum complexes containing the tetrakis(pyrazol-1-yl)borate ligand of the type $[\{(C_6F_5)_2M\}_2(\mu\text{-}pz)_2B(\mu\text{-}pz)_2]^-$ (M = Pd, Pt), $[\{(C_6F_5)(L)Pd\}_2(\mu\text{-}pz)_2B(\mu\text{-}pz)_2]^+$ (L = CN*t*Bu, NCPh, PR_3, AsR_3) and $[\{(C_6F_5)(Cl)Pd\}_2(\mu\text{-}pz)_2B(\mu\text{-}pz)_2]^-$ have been prepared using the benzonitrile complexes *cis*-$[(C_6F_5)_2M(NCPh)_2]$ (M = Pd, Pt) or the halide bridged complexes $[\{(C_6F_5)LPd(\mu\text{-}X)\}_2]$ (L = CN*t*Bu, NCPh, PR_3, AsR_3, tht; X = Cl or Br), and $[B(pz)_4]^-$ as starting materials. The monometallic $[(C_6F_5)(t\text{BuNC})Pd(\mu\text{-}pz)_2B(pz)_2]$ and the asymmetric dinuclear $[(C_6F_5)_2Pd(\mu\text{-}pz)_2B(\mu\text{-}pz)_2Pd(\eta^3\text{-}C_4H_7)]$ complexes have also been prepared. The crystal structures of $[\{(C_6F_5)_2Pd\}_2(\mu\text{-}pz)_2B(\mu\text{-}pz)_2]^-$, $[\{(C_6F_5)(t\text{BuNC})Pd\}_2(\mu\text{-}pz)_2B(\mu\text{-}pz)_2]^+$ and $[(C_6F_5)_2Pd(\mu\text{-}pz)_2B(\mu\text{-}pz)_2Pd(\eta^3\text{-}C_4H_7)]$ have been established by X-ray diffraction.

(© Wiley-VCH Verlag GmbH, 69451 Weinheim, Germany, 2002)

Introduction

Poly(pyrazolyl)borates have become an important class of ligands with unique properties, as indicated by the variety of species they form with most metals and metalloids,[1,2] including those of palladium and platinum.[3] This family of ligands has found great favor in studies of structure and reactivity[1−6] relevant to catalysis[7,8] and inorganic biochemistry.[5,9] From a structural coordination chemistry point of view, these polydentate nitrogen-donor ligands offer unique opportunities to look into the detailed dynamic behavior in solution, particularly by use of NMR spectroscopy.[10] Although an important number of monomeric palladium(II) poly(pyrazol-1-yl)borate complexes that have already been structurally characterized by X-ray crystallography exists ($[Pd(COMe)\{(Me_2pz)_2BH\text{-}N,N'\}(PCy_3)]$,[11] $[Pd(CH_2SiMe_3)\{(Me_2pz)_2BH\text{-}N,N'\}(PMe_3)]$,[12] $[Pd(\eta^3\text{-}C_3H_5)\{(pz)_3BH\text{-}N,N'\}]$, $[PdPh\{(pz)_3BH\text{-}N,N'\}]$, $[PdR\{(pz)_4B\text{-}N,N'\}(PPh_3)]$ (R = Me, Ph),[13] $[Pd\{2\text{-}(NMe_2CH_2)C_{10}H_6\text{-}C,N\}\{(pz)_3BH\text{-}N,N'\}]$,[14] $[Pd\{2\text{-}CH_2\text{-}C_6H_4P(o\text{-tolyl})_2\text{-}C,P\}\{(pz)_3BH\text{-}N,N'\}]$, $[Pd(C_6H_4C_5H_4N\text{-}C^2,N)\{(pz)_3BH\text{-}N,N'\}]$[15]), surprisingly, to the best of our knowledge (3D Search using the Cambridge Structural Database, October 2001 release) there are no dimeric palladium complexes yet fully characterized by X-ray diffraction.

Here, we describe the synthesis and characterization of some new dimetallic palladium and platinum complexes with the tetrakis(pyrazol-1-yl)borate ligand. The crystal structures of $[\{(C_6F_5)_2Pd\}_2(\mu\text{-}pz)_2B(\mu\text{-}pz)_2]^-$, $[\{(C_6F_5)(t\text{BuNC})Pd\}_2(\mu\text{-}pz)_2B(\mu\text{-}pz)_2]^+$ and $[(C_6F_5)_2Pd(\mu\text{-}pz)_2B(\mu\text{-}pz)_2Pd(\eta^3\text{-}C_4H_7)]$ have been established by X-ray diffraction. The benzonitrile complexes *cis*-$[(C_6F_5)_2M(NCPh)_2]$ (M = Pd, Pt) and the halide-bridged complexes $[\{(C_6F_5)LPd(\mu\text{-}X)\}_2]$ (L = CN*t*Bu, NCPh, PR_3, AsR_3, tht; X = Cl or Br) have been shown to be good precursors for the synthesis of the binuclear compounds reported herein.

Results and Discussion

Homodimetallic Complexes 1 and 2

The ready reaction of *cis*-$[(C_6F_5)_2M(NCPh)_2]$ (M = Pd, Pt) in CH_2Cl_2 with $K[B(pz)_4]$ (pz = pyrazolyl) in a 2:1 molar ratio gives the dimetallic complexes **1** and **2** (Scheme 1). The replacement of PhCN by $[B(pz)_4]^-$ takes place without isomerization, and the reaction products are the *cis* isomers. The complexes are air-stable, both in the solid state and in solution, and they are white. The new complexes have been characterized by partial elemental analyses and spectroscopic (IR and ^1H and ^{19}F NMR)

[a] Departamento de Química Inorgánica, Universidad de Murcia, 30071 Murcia, Spain
Fax: (internat.) + 34-968/364148
E-mail: jruiz@um.es
[b] Departamento de Ingeniería Minera, Geológica y Cartográfica, Area de Química Inorgánica, Universidad Politécnica de Cartagena, 30203 Cartagena, Spain

methods. In an acetone solution, these complexes behave as 1:1 electrolytes.[16]

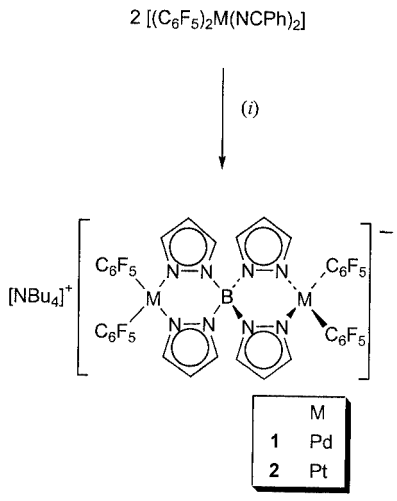

Scheme 1. (*i*) $K[B(pz)_4]/Bu_4NCl$

The IR spectra of complexes **1** and **2** show the characteristic absorptions of the C_6F_5 group [17] at 1630, 1490, 1450, 1050, 950 cm^{-1}, and a split band at ca. 800 cm^{-1}, derived from the so-called X-sensitive mode in C_6F_5 halogen molecules, which is characteristic of the *cis*-$M(C_6F_5)_2$ fragment[18,19] and behaves like a ν(M−C) band.[20]

The ^1H NMR spectra of **1** and **2** at room temperature show a unique set of three resonances for the pyrazolyl ring protons, which suggests the occurrence of a very fast intramolecular interconversion between the conformational isomers **A** and **B** that arises from the boat like $M(N-N)_2B$ ring inversions of these compounds (Scheme 2) for which a spiro structure is expected. The same spectra are observed when the temperature is lowered to −90 °C in CD_2Cl_2. The 3-H and 5-H resonances of complex **1** appear as doublets, owing to coupling with 4-H. The resonance assigned to 4-H appears as a pseudo-triplet. Assignment of the signals to the 3-H and 5-H protons of complex **1** was possible by comparison with the spectrum of complex **2**, for which the 3-H resonance is flanked by satellites (1:4:1) arising from a small hydrogen-platinum coupling. Furthermore, the assignment is also in accordance with the usual criterion for pyrazoles where $^3J_{45} > {}^3J_{34}$.[21]

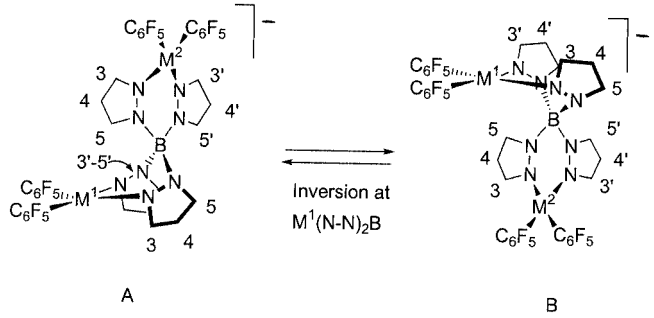

Scheme 2

We have performed ^1H-^{13}C COSY on **1** in order to examine the Onishi criterion[22] for the pyrazolyl C-3 and C-5 NMR assignments in transition-metal poly(1-pyrazolyl)borate complexes, and we have also found that the resonance assigned to the pyrazolyl C-3 CH carbon atoms is at a lower field than that of C-5.

The ^{19}F NMR spectra of **1** and **2** show the presence of four equivalent freely rotating C_6F_5 rings giving three resonances with relative intensities of 2:1:2, due to the *ortho*-, *para*- and *meta*-F atoms, respectively. As expected, the *ortho*-F signal of complex **2** is flanked by satellites due to coupling to ^{195}Pt.

The structure of **1** is shown in Figure 1 and selected bond lengths and angles in Table 1. Insofar as we know, this is the first dipalladium tetrakis(pyrazol-1-yl)borate species to be structurally characterized. The X-ray structure determination of **1** shows the existence of the spiro structure. Both six-membered chelate $Pd(1)N_4B$ and $Pd(2)N_4B$ rings adopt a boat conformation. Each of the palladium atoms essentially has a square-planar geometry. The four distances Pd−N [2.089(2), 2.098(2), 2.068(2) and 2.100(3) Å] are very similar and are in the range found for other Pd−N distances in polypyrazolylborate complexes [e.g., 2.113(3) and 2.079(2) Å in $[PdPh\{(pz)_4B\text{-}N,N'\}(PPh_3)]$].[13] The bridging tetrakis(pyrazolyl)borate ligand forms chelate angles of 91.04(9) and 89.43(9)° at Pd(1) and Pd(2), respectively. The Pd−C_6F_5 distances [2.003(3), 2.006(6), 2.002(3), 2.005(3) Å] are in the range found in the literature.[23,24]

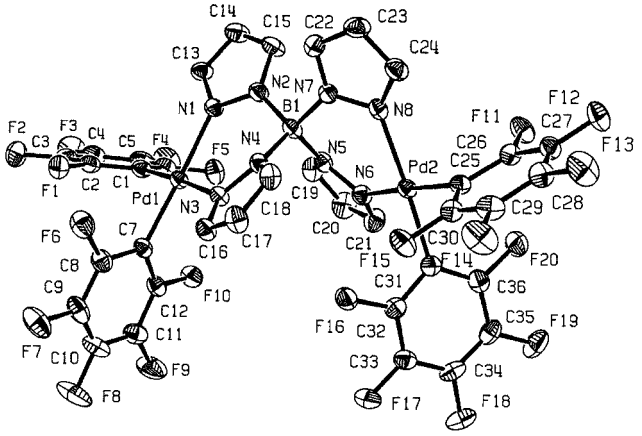

Figure 1. Structure of the anion of **1** showing the atom numbering scheme; hydrogen atoms have been omitted for clarity

Homodimetallic Complexes 3−9

The reaction of $[\{(C_6F_5)LPd(\mu\text{-}X)\}_2]$ (X = Cl, L = *t*BuNC, PhCN, PPh_3, $AsPh_3$; X = Br, L = PEt_3, PMe_2Ph) with $AgClO_4$ (1:2 molar ratio) in acetone, followed by the addition of $K[B(pz)_4]$ (1:1 molar ratio) gives the corresponding dimetallic complexes **3**−**8** (Scheme 3). The reaction of $[\{(C_6F_5)LPd(\mu\text{-}Cl)\}_2]$ [L = tetrahydrothiophene (tht)] with $K[B(pz)_4]$ and Bu_4NCl (1:1:1 molar ratio) leads to the formation of complex **9** (Scheme 3). In an acetone solution, complexes **3**−**9** behave as 1:1 electrolytes.[16]

Table 1. Selected bond lengths [Å] and angles [°] for complex **1**

Bond lengths		Bond angles	
Pd(1)−C(7)	2.003(3)	C(7)−Pd(1)−C(1)	85.13(12)
Pd(1)−C(1)	2.006(3)	C(7)−Pd(1)−N(3)	91.90(10)
Pd(1)−N(3)	2.089(2)	C(1)−Pd(1)−N(3)	177.00(11)
Pd(1)−N(1)	2.098(2)	C(7)−Pd(1)−N(1)	176.98(11)
Pd(2)−C(25)	2.002(3)	C(1)−Pd(1)−N(1)	91.93(11)
Pd(2)−C(31)	2.005(3)	N(3)−Pd(1)−N(1)	91.04(9)
Pd(2)−N(6)	2.068(2)	C(25)−Pd(2)−C(31)	86.73(12)
Pd(2)−N(8)	2.100(3)	C(25)−Pd(2)−N(6)	175.03(11)
		C(31)−Pd(2)−N(6)	90.49(11)
		C(25)−Pd(2)−N(8)	93.59(11)
		C(31)−Pd(2)−N(8)	176.64(11)
		N(6)−Pd(2)−N(8)	89.43(9)

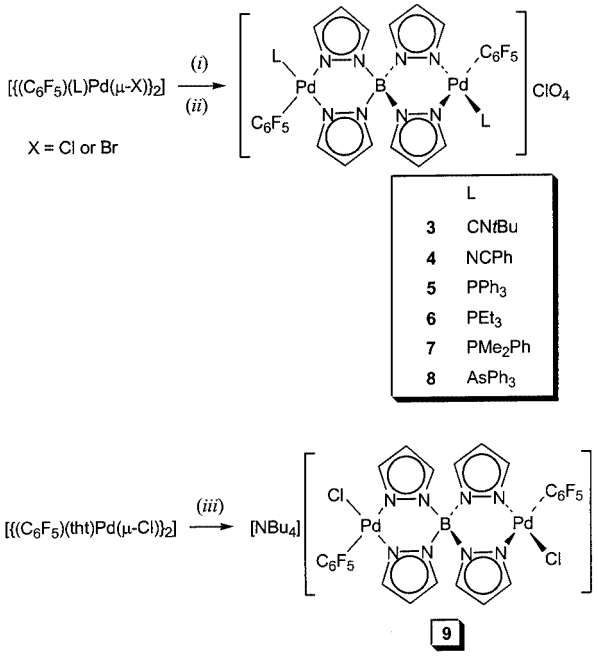

Scheme 3. (*i*) 2 $AgClO_4$; (*ii*) $K[B(pz)_4]$; (*iii*) $K[B(pz)_4]/Bu_4NCl$

The IR spectra of complexes **3**−**9** show an absorption at 790 cm^{-1} that is observed as a single band for the so-called X-sensitive mode,[20] as expected from the presence of only one C_6F_5 group in the coordination sphere of the palladium atom. Two absorptions at 1100 and 620 cm^{-1}, which are typical of the uncoordinated ClO_4^- (T_d) anion are observed for complexes **3**−**8**.[25] IR spectra of **3** and **4** also show an absorption assigned to ν(CN) at ca. 2230 cm^{-1} (*t*BuNC group[26−28] for **3**) or at 2280 cm^{-1} (PhCN ligand[28,29] for **4**). Complex **9** exhibits a Pd−Cl stretching vibration at 326 cm^{-1}.[30] The NMR spectroscopic data show that they exist in solution in a unique arrangement. Thus, the ^{19}F NMR spectra of **3**−**9** exhibit only one resonance for the *para*-fluorine atoms corresponding to only one type of pentafluorophenyl ring, and the ^{31}P NMR spectra of complexes **5**−**7** only show a resonance for the phosphane ligands. The ^1H NMR spectrum of complex **3** shows a singlet resonance for the *t*BuNC groups at δ = 1.56 ppm. On the other hand, the ^1H NMR spectra of complexes **3**−**9** exhibit two distinct sets of pyrazolyl signals of equal intensities, one assigned to the pyrazolyl group *trans* to C_6F_5 and the other to the pyrazolyl group *trans* to L (with three resonances 1:1:1 each). This suggests the occurrence of a very fast intramolecular interconversion between the conformational isomers that arises from the boat like $M(N-N)_2B$ ring inversions of these compounds for which a spiro structure is expected. The resonances assigned to the pyrazolyl groups in the ^1H NMR spectrum of complex **3** are assigned by considering the NOE between the 3′-H and the *t*BuNC singlet, the usual criterion for pyrazoles where $^3J_{45} > {}^3J_{34}$,[21] and from two-dimensional ^1H-^1H COSY experiments. Furthermore, we have also performed ^1H-^{13}C COSY on **3** (Figure 2), and we have also found that the resonance assigned to the pyrazolyl C-3 CH carbon atoms is at a lower field than that of C-5.[22]

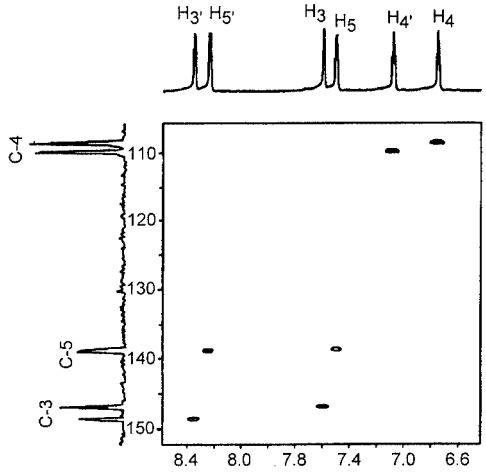

Figure 2. ^1H-^{13}C COSY of **3** in $[D_6]$acetone at 25 °C

The *ortho*- and *meta*-fluorine resonances of complexes **3**−**9** are duplicated, suggesting hindered rotation around the Pd−C_6F_5 bond.

The structure of **3** is shown in Figure 3 and selected bond lengths and angles in Table 2. The Pd(1)−N(2) bond length (*trans* to the C_6F_5 group) is longer (ca. 0.06 Å) than the Pd(1)−N(6) bond (*trans* to the *t*BuNC ligand), reflecting the stronger *trans* influence of the aryl group relative to the carbon donor group of the *t*BuNC ligand. The Pd−CN*t*Bu distances are very similar to those observed in the related complexes $[\{(C_6F_5)LPd(\mu\text{-}X)\}_2]$ (L = *t*BuNC; X = HNPh,[27] N=CPh_2 [26] and PhNNNPh[28]).

Monometallic Complexes 10−12

The reaction of $[\{(C_6F_5)(L)Pd(\mu\text{-}X)\}_2]$ (X = Cl, L = CN*t*Bu) with $AgClO_4$ (1:2 molar ratio) in acetone, followed by the addition of $K[B(pz)_4]$ (1:2 molar ratio) gives the monometallic complex **10** (Scheme 4). The IR spectrum shows an absorption assigned to ν(CN) of the *t*BuNC group[26−28] at ca. 2230 cm^{-1}. The ^{19}F NMR spectrum at room temperature shows a unique set of sharp resonances, indicating the presence of only one type of C_6F_5 group.

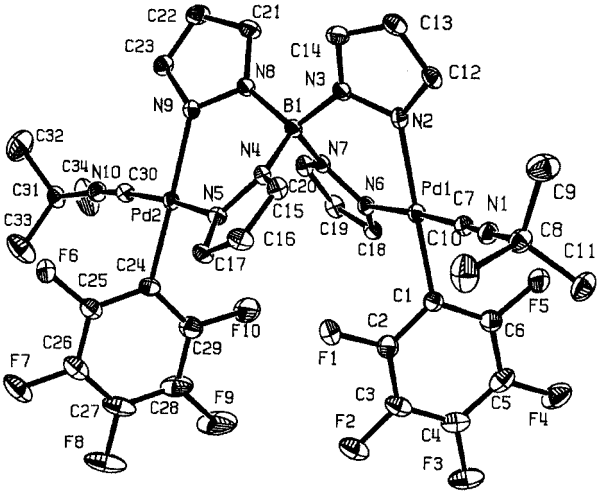

Figure 3. Structure of the cation of **3** showing the atom numbering scheme; hydrogen atoms have been omitted for clarity

Table 2. Selected bond lengths [Å] and angles [°] for complex **3**

Bond lengths		Bond angles	
Pd(1)−C(7)	1.946(4)	C(7)−Pd(1)−C(1)	87.59(16)
Pd(1)−C(1)	2.000(4)	C(7)−Pd(1)−N(6)	175.25(15)
Pd(1)−N(6)	2.026(3)	C(1)−Pd(1)−N(6)	90.71(14)
Pd(1)−N(2)	2.088(3)	C(7)−Pd(1)−N(2)	92.26(15)
Pd(2)−C(30)	1.931(4)	C(1)−Pd(1)−N(2)	179.44(15)
Pd(2)−C(24)	2.007(4)	N(6)−Pd(1)−N(2)	89.48(13)
Pd(2)−N(5)	2.026(3)	C(30)−Pd(2)−C(24)	84.46(17)
Pd(2)−N(9)	2.077(3)	C(30)−Pd(2)−N(5)	175.11(15)
		C(24)−Pd(2)−N(5)	91.42(15)
		C(30)−Pd(2)−N(9)	94.22(15)
		C(24)−Pd(2)−N(9)	178.54(15)
		N(5)−Pd(2)−N(9)	89.87(12)

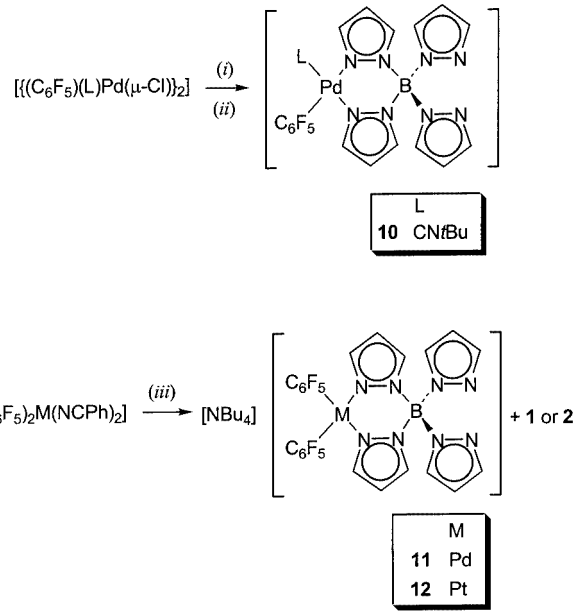

Scheme 4. (*i*) 2 $AgClO_4$; (*ii*) 2 K[B(pz)$_4$]; (*iii*) 2 K[B(pz)$_4$]/2 *n*Bu$_4$Cl

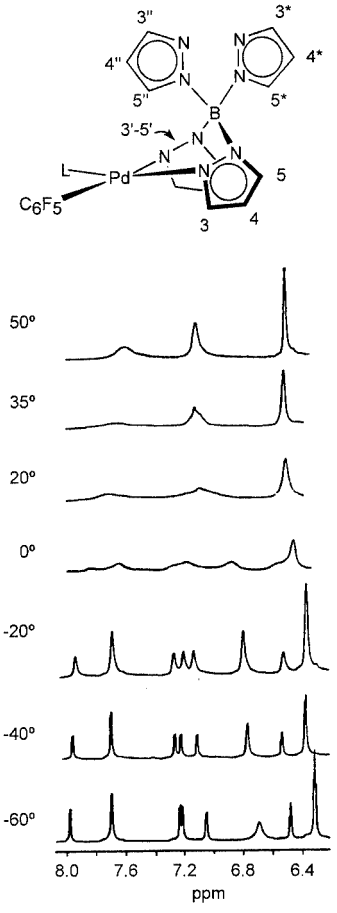

Figure 4. Temperature-dependent ^{1}H NMR (300 MHz) of pyrazolyl protons in **10** in [D$_6$]acetone

However, in the ^{1}H NMR spectrum broad bands are observed due to exchanges between the four pyrazolyl groups. Fluxional motions of (η^2-BPz$_4$)palladium(II) complexes have been considered to involve the additional coordination of one uncoordinated pyrazolyl group near the palladium atom [via a tridentate tetrakis(pyrazolyl)borate−palladium structure], dissociation of one pyrazolyl group coordinated previously, and inversion of the boat-like six-membered Pd−(N−N)$_2$−B ring.[22] Variable-temperature ^{1}H NMR spectra of **10** have been recorded (Figure 4). At −60 °C the ^{1}H NMR spectrum exhibits eight different resonances in the pyrazolyl region with relative intensities of 1:2:1:1:1:2:1:3 (the two coordinated and the two uncoordinated pyrazolyl groups should all be nonequivalent, although casual overlaps of some signals are observed). The ^{1}H signals (nearly apparent triplets) at δ = 6.7−6.3 are readily assigned to 4-H protons of the BPz$_4$ ligand. A singlet resonance is observed for the *t*BuNC group at δ = 1.6 ppm.

The reaction of *cis*-[(C$_6$F$_5$)$_2$M(NCPh)$_2$] (M = Pd or Pt) in CH_2Cl_2 with K[B(pz)$_4$] (pz = pyrazolyl) in a 1:1 molar ratio was attempted, in order to obtain the corresponding mononuclear complexes. However, mixtures containing both the dimetallic and the monometallic complexes **1** and **11** (for palladium), or **2** and **12** (for platinum), respectively,

were obtained (Scheme 4). All attempts to separate them were unsuccessful.

Asymmetric Dinuclear Complex 13

The reaction of *cis*-$[(C_6F_5)_2Pd(NCPh)_2]$ with the monomeric palladium tetrakis(pyrazol-1-yl)borate complex $[(\eta^3\text{-}CH_2CCH_3CH_2)Pd(\mu\text{-}pz)_2B(pz)_2]$[31] in a 1:1 molar ratio yields the asymmetric dinuclear complex **13** (Scheme 5).

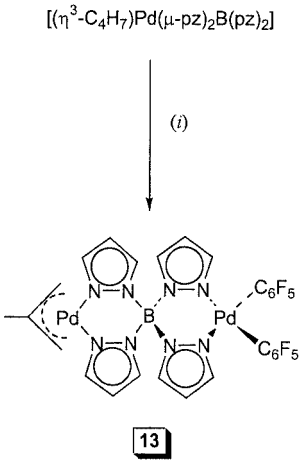

Scheme 5

The new complex has been characterized on the basis of partial elemental analysis and spectroscopic data. A split absorption located at ca. 800 cm^{-1} in the IR spectrum is observed, which indicates that the *cis* arrangement[18,19] of the $Pd(C_6F_5)_2$ fragment is kept in the reaction. The ^1H NMR spectrum at room temperature shows the presence of three types of pz groups in a 2:1:1 ratio (Figure 5). No changes are observed in the temperature range −70 to + 50 °C. The ^{19}F NMR spectrum exhibits two resonances for the *para*-fluorine atoms, which is indicative of the existence of two different C_6F_5 rings. ^1H NMR resonances are assigned on the basis of a strong NOE between H_{syn} and 3*-H,[10] and selective decoupling experiments, and assuming that the 5′-H proton will be in a magnetic environment that is most similar to that of the 5*-H proton (Figure 5).[31,32] These findings are reconcilable with a structure where one ring is undergoing rapid inversion even at low temperatures, and the other is puckered in a boat conformation (Figure 5). Presumably, the puckered system is the $B(\mu\text{-}pz)_2Pd(\eta^3\text{-}CH_2CRCH_2)$ ring. The same pattern has been found previously in the *B*,*B*-bis(1-pyrazolyl)pyrazabole complexes $[(Et_2B(\mu\text{-}pz)_2B(\mu\text{-}pz)_2Pd(\eta^3\text{-}CH_2CRCH_2)]^+$ (R = Me or Ph).[31]

The structure of **13** has been established by X-ray diffraction and is shown in Figure 6 and selected bond lengths and angles in Table 3. Each of the palladium atoms essentially has a square-planar geometry. The Pd−N distances are very similar for Pd(1) and Pd(2), these values are similar to the distances found in polypyrazolylborate complexes of Pd^{II}.[13] The bridging tetrakis(pyrazolyl)borate ligand forms chelate angles of 88.9(2) and 88.7(2) Å at Pd(1) and Pd(2),

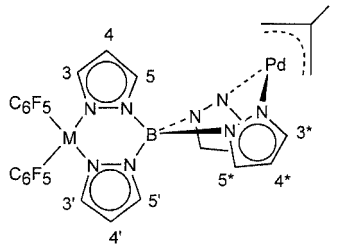

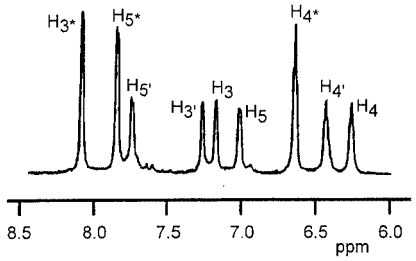

Figure 5. ^1H NMR (300 MHz) of pyrazolyl protons in **13** in $[D_6]$acetone

respectively. The $Pd(2)N_4B$ ring adopts a shallow boat conformation, the palladium and boron atoms are on the same side of the plane defined by the nitrogen atoms; in $Pd(1)N_4B$ the boat is distorted giving a twist-like conformation.

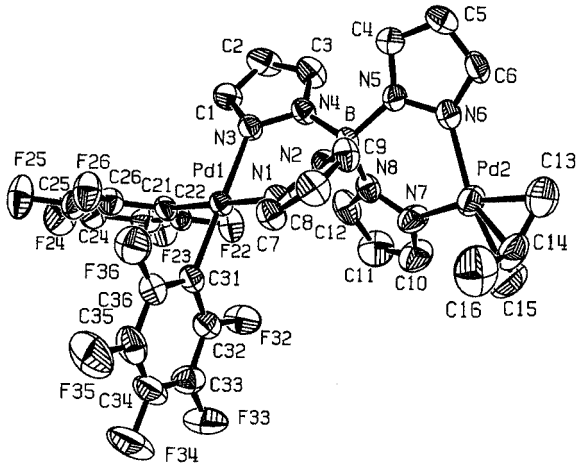

Figure 6. Structure of complex **13** showing the atom numbering scheme; hydrogen atoms have been omitted for clarity

The geometry of the allyl group is similar to that usually found in (η^3-allyl)palladium(II) complexes.[24,32] Thus, the allyl plane is not normal to the "$Pd(1)N_2$" plane, giving a dihedral angle of 114.5(5)°. The methyl group on the central carbon atom is 0.29(3) Å out of the allyl plane, on the same side as the Pd atom. The central carbon atom lies 0.55(1) Å to one side of the plane. The three carbon atoms bonded to the palladium atom are approximately equidistant from Pd [2.084(8), 2.121(7) and 2.127 (7) Å], and the carbon−carbon bond lengths of the η^3-allyl group are al-

Table 3. Selected bond lengths [Å] and angles [°] for complex **13**

Bond lengths		Bond angles	
Pd(1)−C(31)	2.013(6)	C(31)−Pd(1)−C(21)	85.2(2)
Pd(1)−C(21)	2.012(6)	C(31)−Pd(1)−N(1)	93.2(2)
Pd(1)−N(1)	2.081(5)	C(21)−Pd(1)−N(1)	176.6(2)
Pd(1)−N(3)	2.108(5)	C(31)−Pd(1)−N(3)	177.5(2)
Pd(2)−N(7)	2.056(6)	C(21)−Pd(1)−N(3)	92.8(2)
Pd(2)−C(15)	2.084(8)	N(1)−Pd(1)−N(3)	88.9(2)
Pd(2)−N(6)	2.099(5)	N(7) −Pd(2)−C(15)	101.1(3)
Pd(2)−C(13)	2.121(8)	N(7)−Pd(2)−N(6)	88.7(2)
Pd(2)−C(14)	2.127(8)	C(15)−Pd(2)−N(6)	169.1(3)
		N(7)−Pd(2)−C(31)	168.7(3)
		C(15)−Pd(2)−C(13)	67.8(4)
		N(6)−Pd(2)− C(13)	102.1(3)
		N(7)−Pd(2)−C(14)	132.9(3)
		C(15)−Pd(2)−C(14)	38.7(3)
		N(6)−Pd(2)−C(14)	134.4(3)
		C(13)−Pd(2)−C(14)	38.5(3)

most equal [1.397(12), 1.401(12) Å]. The Pd−C(1) bond lengths [2.013(6) and 2.012(6) Å] are similar to the values observed in other (pentafluorophenyl)palladium complexes.[23,24]

Experimental Section

General Methods: Calcd. C, H, N analyses were performed with a Carlo Erba model EA 1108 microanalyzer. Decomposition temperatures were determined with a Mettler TG-50 thermobalance at a heating rate of 5 °C min^{-1}. Conductance measurements were performed in an acetone solution ($c \approx 5 \times 10^{-4}$ mol L^{-1}) with a Crison 525 conductimeter. The NMR spectra were recorded with a Bruker AC 200E (^1H) or Varian Unity 300 (^1H, ^{19}F) spectrometer, using $SiMe_4$ or $CFCl_3$ as standards, respectively. NOE difference spectra were recorded with the following acquisition parameters: spectral width 4000 Hz, acquisition time 2.5 s, pulse width 5 μs (45°), relaxation delay 10 s, irradiation power 35−251 L, number of scans 100. Infrared spectra were recorded with a Perkin−Elmer 16F PC FT-IR spectrophotometer using Nujol mulls between polyethylene sheets. The compounds $[(C_6F_5)_2M(NCPh)_2]$ (M = Pd,[29] Pt[34]) and $[\{(C_6F_5)(L)Pd(\mu\text{-}Cl)\}_2]$ (L = PPh_3, tht, CN*t*Bu),[35,36] $K[B(pz)_4]$[37] were prepared as described elsewhere.

Safety Note: Perchlorate salts of metal complexes with organic ligands are potentially explosive. Only small amounts of material should be prepared, and these should be handled with great caution.

$[Bu_4N][\{(C_6F_5)_2M\}_2(\mu\text{-}pz)_2B(\mu\text{-}pz)_2]$ [M = Pd (1) or Pt (2)]: $K[B(pz)_4]$ (19.6 mg, 0.06 mmol), followed by $[Bu_4N]Cl$ (16.7 mg, 0.06 mmol) was added to a solution of $[(C_6F_5)_2M(NCPh)_2]$ (M = Pd or Pt) (0.12 mmol) in dimethylformamide (DMF) (5 mL) . The resulting solution was stirred for 30 min at room temperature. Addition of water caused the precipitation of a white solid, which was collected by filtration and air-dried. It was recrystallized from dichloromethane/hexane.

1: Yield 73%. $C_{52}H_{48}BF_{20}N_9Pd_2$ (1402): calcd. C 44.5, H 3.4, N 9.0; found C 44.1, H 3.3, N 8.9. M.p. 300 °C (dec.). Λ_M = 84 S cm^2 mol^{-1}. IR (nujol): $\tilde{\nu}$ = 794, 784 cm^{-1} (Pd−C_6F_5). ^1H NMR ([D$_6$]acetone, TMS): δ = 7.75 (d, J_{45} = 2.5 Hz, 4 H, 5-H,), 7.23 (d, J_{34} = 1.4 Hz, 4 H, 3-H), 6.42 (pseudo-t, 4 H, 4-H) ppm. $^{13}C\{^1H\}$ NMR ([D$_6$]acetone, TMS): δ = 145.7 (C-3), 138.2 (C-5), 107.6 (C-4) ppm. ^{19}F NMR ([D$_6$]acetone, $CFCl_3$): δ = −114.7 (m, 8 F_o), −163.7 (t, 4 F_p, J_{mp} = 19.7 Hz), −165.4 (m, 8 F_m) ppm.

2: Yield 77%. $C_{52}H_{48}BF_{20}N_9Pt_2$ (1580): calcd. C 39.5, H 3.1, N 8.0; found C 39.1, H 3.2, N 7.7. M.p. 288 °C (dec.). Λ_M = 86 S cm^2 mol^{-1}. IR (nujol): $\tilde{\nu}$ = 806, 798 cm^{-1} (Pt−C_6F_5). ^1H NMR ([D$_6$]acetone, TMS): δ = 7.73 (d, J_{45} = 2.5 Hz, 4 H, 5-H), 7.33 (d, J_{34} = 1.7 Hz, J_{HPt} = 10 Hz, 4 H, 3-H), 6.29 (pseudo-t, 4 H, 4-H) ppm. ^{19}F NMR ([D$_6$]acetone, $CFCl_3$): δ = −118.4 (d, J_{om} = 25.9 Hz, J_{PtF_o} 456 Hz, 8 F_o), −163.7 (t, J_{mp} = 19.7 Hz, 4 F_p), −165.3 (m, 8 F_m) ppm.

$[\{(C_6F_5)(L)Pd\}_2(\mu\text{-}pz)_2B(\mu\text{-}pz)_2]ClO_4$ [L = CN*t*Bu (3), NCPh (4), PPh_3 (5), PEt_3 (6), PMe_2Ph (7), $AsPh_3$(8): $AgClO_4$ (53.0 mg, 0.26 mmol) was added to a solution of $[\{(C_6F_5)(L)Pd(\mu\text{-}X)\}_2]$ (X = Cl, L = CN*t*Bu, PhCN, PPh_3, $AsPh_3$; X = Br, L = PEt_3, PMe_2Ph) (0.13 mmol) in acetone (15 mL). The solution was stirred at room temperature for 30 min, while it was protected from light. The white AgCl was then filtered off. $K[B(pz)_4]$ (40.0 mg, 0.13 mmol) was then added to the resulting solution. The solution was stirred for 30 min at room temperature and concentrated under vacuum. The addition of ether/hexane caused the precipitation of a white solid, which was collected by filtration and air-dried. The complexes were recrystallized from dichloromethane/hexane.

3: Yield 80%. $C_{34}H_{30}BClF_{10}N_{10}O_4Pd_2$ (1092): calcd. C 37.4, H 2.8, N 12.8; found C 37.1, H 2.6, N 12.8. M.p. 157 °C (dec.). Λ_M = 117 S cm^2 mol^{-1}. IR (nujol): $\tilde{\nu}$ = 2234 cm^{-1} [ν(CN)], 798 cm^{-1} (Pd−C_6F_5 str). ^1H NMR ([D$_6$]acetone, TMS): δ = 8.34 (d, $J_{3'4'}$ = 1.6 Hz, 2 H, 3′-H), 8.23 (d, $J_{4'5'}$ = 2.6 Hz, 2 H, 5′-H), 7.39 (d, J_{34} = 1.6 Hz, 2 H, 3-H), 7.30 (d, J_{45} = 2.6 Hz, 2 H, 5-H), 6.87 (pseudo-t, 2 H, 4′-H), 6.55 (pseudo-t, 2 H, 4-H), 1.56 (s, 18 H, *t*BuNC) ppm. $^{13}C\{^1H\}$ NMR ([D$_6$]acetone, TMS): δ = 148.5 (C-3′), 146.7 (C-3), 138.8 (C-5′), 138.6 (C-5), 109.7 (C-4′), 108.5 (C-4), 30.1 (Me_3C) ppm. ^{19}F NMR ([D$_6$]acetone, $CFCl_3$): δ = −119.1 (m, 4 F_o), −159.6 (t, 2 F_p, J_{mp} = 19.7 Hz), −163.6 (m, 4 F_m) ppm.

4: Yield 81%. $C_{38}H_{22}N_{10}BClF_{10}O_4Pd_2$ (1132): calcd. C 40.3, H 2.0, N 12.4; found C 39.9, H 1.8, N 12.4. M.p. 122 °C (dec.). Λ_M = 125 S cm^2 mol^{-1}. IR (nujol): $\tilde{\nu}$ = 2280 cm^{-1} [ν(CN)], 798 cm^{-1} (Pd−C_6F_5 str). ^1H NMR ($CDCl_3$, TMS): δ = 8.07 (unresolved d, 4 H, 3′-H + 5′-H), 7.72 (m, 4 H_m + 2 H_p), 7.57 (m, 4 H_o), 7.10 (m, 4 H, 3-H + 5-H), 6.87 (pseudo-t, 2 H, 4′′-H), 6.43 (pseudo-t, 2 H, 4-H) ppm. ^{19}F NMR ($CDCl_3$, $CFCl_3$): δ = −121.1 (m, 2 F_o, J_{om} = 25.9 Hz), −122.5 (m, 2 F_o, J_{om} = 29.0 Hz), −157.4 (t, 2 F_p, J_{mp} = 19.7 Hz), −162.0 (m, 4 F_m) ppm.

5. Yield 84%. $C_{60}H_{42}BClF_{10}O_4N_8P_2Pd_2$ (1450): calcd. C 49.7, H 2.9, N 7.7; found C 49.4, H 2.8, N 7.6. M.p. 278 °C (dec.). Λ_M = 106 S cm^2 mol^{-1}. IR (nujol): $\tilde{\nu}$ = 796 (Pd−C_6F_5 str). ^1H NMR ([D$_6$]acetone, TMS): δ = 7.83 (unresolved d, 2 H, 3′-H), 7.5 (m, 34 H, PPh_3 + 2 5′-H + 2 × 3-H), 7.09 (unresolved d, 2 H, 5-H), 6.67 (unresolved pseudo-t, 2 H, 4′-H), 6.48 (unresolved pseudo-t, 2 H, 4-H) ppm. ^{19}F NMR ([D$_6$]acetone, $CFCl_3$): δ = −117.9 (m, 4 F_o), −160.1 (t, 2 F_p, J_{mp} = 19.7 Hz), −161.2 (m, 2 F_m), −161.9 (m, 2 F_m) ppm. ^{31}P NMR ([D$_6$]acetone, H_3PO_4): δ = 30.9 (s) ppm.

6: Yield 75%. $C_{36}H_{42}N_8BClF_{10}O_4P_2Pd_2$ (1162): calcd. C 37.2, H 3.6, N 9.6; found C 36.9, H 3.8, N 9.8. M.p. 271 °C (dec.). Λ_M = 110 S cm^2 mol^{-1}. IR (nujol): $\tilde{\nu}$ = 800 cm^{-1} (Pd−C_6F_5 str). ^1H NMR ([D$_6$]acetone, TMS): δ = 8.22 (unresolved d, 2 H, 3′-H), 8.03 (unresolved m, 2 H, 3-H), 7.32 (unresolved d, 2 H, 5′-H), 7.19 (unresolved d, 2 H, 5-H), 6.76 (unresolved pseudo-t, 2 H, 4′-H), 6.57 (unresolved m, 2 H, 4-H), 1.8 (m, 12 H, CH_2P), 1.1 (m, 18 H,

CH_3CH$_2$P) ppm. ^{19}F NMR ([D$_6$]acetone, CFCl$_3$): δ = −117.4 (m, 4 F$_o$), −159.3 (t, J_{mp} = 19.7 Hz, 2 F$_p$), −161.7 (m, 2 F$_m$), −162.3 (m, 2 F$_m$) ppm. ^{31}P NMR ([D$_6$]acetone, H$_3$PO$_4$): δ = 29.7 (s) ppm.

7: Yield 84%. $C_{40}H_{34}BClF_{10}N_8O_4P_2Pd_2$ (1202): calcd. C 40.0, H 2.9, N 9.3; found C 39.6, H 3.1, N 9.1. M.p. 244 °C (dec.). Λ_M = 115 S cm^2 mol^{-1}. IR (nujol): $\tilde{\nu}$ = 792 cm^{-1} (Pd−C$_6$F$_5$ str). ^{1}H NMR ([D$_6$]acetone, TMS): δ = 7.95 (unresolved m, 2 H, 3-H), 7.83−7.73 (m, 4 H, Ph), 7.65 (unresolved d, 2 H, 5′-H), 7.60−7.54 (m, 8 H, Ph + 2 × 3′-H), 7.36 (unresolved d, 2 H, 5-H), 6.71 (unresolved pseudo-t, 2 H, × 4′-H), 6.61 (unresolved m, 2 H, 4-H), 1.64 (d, J_{HP} = 19.5 Hz, 6 H, Me), 1.57 (d, J_{HP} = 19.6 Hz, 6 H, Me) ppm. ^{19}F NMR ([D$_6$]acetone, CFCl$_3$): δ = −117.9 (m, 2 F$_o$), −118.3 (m, 2 F$_o$), −159.6 (t, 1 F$_p$, J_{mp} = 20.0 Hz), −161.9 (m, 2 F$_m$), −162.5 (m, 2 F$_m$) ppm. ^{31}P NMR ([D$_6$]acetone, H$_3$PO$_4$): δ = 6.49 (s) ppm.

8: Yield 77%. $C_{60}H_{42}As_2BClF_{10}N_8O_4Pd_2$ (1538): calcd. C 46.7, H 2.7, N 7.3; found C 49.8, H 3.6, N 6.4. M.p. 213 °C (dec.). Λ_M = 120 S cm^2 mol^{-1}. IR (nujol): $\tilde{\nu}$ = 796 cm^{-1} (Pd−C$_6$F$_5$ str). ^{1}H NMR ([D$_6$]acetone, TMS): δ = 7.94 (d, $J_{4'5'}$ = 2.4 Hz, 2 H, 5′-H), 7.62 (unresolved d, 2 H, 3′-H), 7.5−7.3 (m, 32 H, AsPh$_3$ and 5-H), 7.27 (unresolved d, 2 H, 3-H), 6.69 (pseudo-t, 2 H, 4′-H), 6.55 (pseudo-t, 2 H, 4-H) ppm. ^{19}F NMR ([D$_6$]acetone, CFCl$_3$): δ = −117.0 (m, 4 F$_o$), −159.2 (t, J_{mp} = 19.7 Hz, 2 F$_p$), −160.7 (m, 2 F$_m$), −161.2 (m, 2 F$_m$).

[Bu$_4$N][{(C$_6$F$_5$)(Cl)Pd}$_2$(μ-pz)$_2$B(μ-pz)$_2$] (9): K[B(pz)$_4$] (32.0 mg, 0.10 mmol), followed by [Bu$_4$N]Cl (29.6 mg, 0.10 mmol) was added to a solution of [{(C$_6$F$_5$)LPd(μ-Cl)}$_2$] [L = tetrahydrothiophene (tht)] (80.0 mg, 0.10 mmol) in acetone (15 mL).The resulting solution was stirred for 30 min at room temperature and concentrated under vacuum. The addition of ethanol/water caused the precipitation of a yellow solid, which was collected by filtration and air-dried. Yield 84%. $C_{40}H_{48}BCl_2F_{10}N_9Pd_2$ (1139): calcd. C 42.2, H 4.3, N 11.1; found C 41.8, H 4.0, N 11.2. M.p. 246 °C (dec.). Λ_M = 90 S cm^2 mol^{-1}. IR (nujol): $\tilde{\nu}$ = 796 cm^{-1} (Pd−C$_6$F$_5$ str), 326 cm^{-1} [ν(Pd−Cl)]. ^{1}H NMR ([D$_6$]acetone, TMS): δ = 8.43 (d, $J_{3'4'}$ = 1.6 Hz, 2 H, 3′-H), 7.95 (d, $J_{4'5'}$ = 2.6 Hz, 2 H, 5′-H), 7.35 (d, J_{34} = 1.6 Hz, 2 H, 3-H), 7.15 (d, 2 H, 5-H, J_{45} = 2.6 Hz), 6.60 (pseudo-t, 2 H, 4′-H), 6.37 (pseudo-t, 2 H, 4-H) ppm. ^{19}F NMR ([D$_6$]acetone, CFCl$_3$): δ = −118.7 (m, 4 F$_o$), −163.9 (t, 2 F$_p$, J_{mp} 19.7 Hz), −166.1 (m, 4 F$_m$) ppm.

[(C$_6$F$_5$)(CN*t*Bu)Pd(μ-pz)$_2$B(pz)$_2$] (10): AgClO$_4$ (46.0 mg, 0.20 mmol) was added to a solution of [{(C$_6$F$_5$)(*t*BuNC)Pd(μ-Cl)}$_2$] (80.0 mg, 0.10 mmol) in acetone (15 mL). The solution was stirred at room temperature for 30 min, while it was protected from light. The white AgCl was then filtered off. K[B(pz)$_4$] (64.8 mg, 0.20 mmol) was then added to the resulting solution. The solution was stirred for 30 min at room temperature and concentrated under vacuum. The addition of ether/hexane caused the precipitation of a white solid, which was collected by filtration and air-dried. The complex was recrystallized from dichloromethane/hexane. Yield 90%. $C_{23}H_{21}BF_5N_9Pd$ (636): calcd. C 43.5, H 3.3, N 19.8; found C 43.8, H 3.5, N 19.8. M.p. 182 °C (dec.). IR (nujol): $\tilde{\nu}$ = 2230 cm^{-1} [ν(CN)], 796 (Pd−C$_6$F$_5$ str). ^{1}H NMR ([D$_6$]acetone, TMS, 20 °C): δ = 7.7 (br, 3 H), 7.0 (br, 5 H), 6.3 (br, 4 H). ^{1}H NMR ([D$_6$]acetone, TMS, −60 °C): δ = 7.98 (d, J = 1.8 Hz, 1 H), 7.69 (unresolved d, 2 H), 7.23 (d, J = 2.4 Hz, 1 H), 7.21 (d, J = 2.1 Hz, 1 H), 7.05 (d, J = 2.4 Hz, 1 H), 6.69 (br, 2 H), 6.48 (pseudo-t, 1 H), 6.31 (pseudo-t, 3 H), 1.6 (s, 18 H, *t*BuNC) ppm. ^{19}F NMR ([D$_6$]acetone, CFCl$_3$, 20 °C): δ = −117.2 (m, 2 F$_o$), −159.7 (t, 1 F$_p$, J_{mp} 20.3 Hz), −163.5 (m, 4 F$_m$) ppm.

[(C$_6$F$_5$)$_2$Pd(μ-pz)$_2$B(μ-pz)$_2$Pd(η^3-C$_4$H$_7$)] (13): [(C$_6$F$_5$)$_2$Pd(NCPh)$_2$] (88.0 mg, 0.14 mmol) was added to a solution of [(η^3-CH$_2$CCH$_3$CH$_2$)Pd(μ-pz)$_2$B(pz)$_2$] (60.0 mg, 0.14 mmol) in acetone (10 mL). The resulting solution was stirred for 30 min at room temperature and concentrated under vacuum. The addition of ethanol/water caused the precipitation of a white solid, which was collected by filtration and air-dried. Yield 88%. $C_{28}H_{19}F_{10}N_8Pd_2$ (870): calcd. C 38.2, H 2.2, N 12.7; found C 38.2, H 2.3, N 12.5. M.p. 185 °C (dec.). IR (nujol): $\tilde{\nu}$ = 782, 808 (Pd−C$_6$F$_5$ str) cm^{-1}. ^{1}H NMR ([D$_6$]acetone, TMS): δ = 8.06 (unresolved d, 2 H, 3*-H), 7.82 (d, J_{4*5*} = 2.4 Hz, 2 H, 5*-H), 7.72 (d, $J_{4'5'}$ = 2.2 Hz, 1 H, 5′-H), 7.26 (unresolved d, 1 H, 3-H), 7.22 (unresolved d, 1 H, 3-

Table 4. Crystal structure determination details

	1	**3**	**13**
Empirical formula	$C_{52}H_{48}BF_{20}N_9Pd_2$	$C_{46}H_{32}BCl_3F_{10}N_8O_4Pd_2$	$C_{29}H_{21}BCl_2F_{10}N_8Pd_2$
Formula mass	1402.60	1176.67	966.05
Crystal system	monoclinic	monoclinic	triclinic
Unit cell dimensions			
a [Å]	9.2970(10)	14.2510(10)	11.8552(12)
b [Å]	17.1590(10)	17.9360(10)	12.8142(10)
c [Å]	35.642(3)	17.5860(10)	13.1023(10)
α [°]	90	90	89.809(5)
β [°]	93.510(10)	95.350(10)	64.431(6)
γ [°]	90	90	73.584(6)
Unit cell volume [Å^3]	5675.2(8)	4475.5(5)	1706.0(3)
Temperature [K]	173(2)	173(2)	298(2)
Space group	$P2_1/n$	$P2_1/c$	$P\bar{1}$
Z	4	4	2
μ [mm^{-1}]	0.744	1.075	1.301
Reflections collected	11161	9865	6870
Independent reflections	9959	7851	5933
R(int)	0.0278	0.0247	0.0313
*R*1 [$I > 2\sigma(I)$][a]	0.0309	0.0368	0.0508
wR_2 (all data)[b]	0.0779	0.0992	0.1206

[a] $R1 = \Sigma||F_o| - |F_c||/\Sigma|F_o|$, $wR2 = [\Sigma[w(F_o^2-F_c^2)^2]/\Sigma\, w(F_o2)^2]^{0.5}$. [b] $w = 1/[\sigma^2(F_o^2) + (aP)^2 + bP]$, where $P = (2F_c^2 + F_o^2)/3$ and *a* and *b* are constants set by the program.

H), 7.02 (d, J_{45} = 2.4 Hz, 1 H, 5-H), 6.65 (unresolved pseudo-t, 2 H, 4*-H), 6.45 (unresolved pseudo-t, 1 H, 4′-H), 6.28 (unresolved pseudo-t, 1 H, 4-H), 4.04 (s, 2 H, H_{syn}), 3.23 (s, 2 H, H_{anti}), 2.12 (s, 3 H, CH_3) ppm. ^{19}F NMR ([D$_6$]acetone, $CFCl_3$): δ = −114.0 (m, 4 F_o), −162.8 (m, 2 F_p), −164.7 (m, 4 F_m) ppm.

Determination of the X-ray Crystal Structures of 1, 3 and 13: Crystals of **1**, **3**·CH_2Cl_2 and **13**·CH_2Cl_2 suitable for X-ray diffraction studies were grown from dichloromethane/toluene/hexane solution, mounted on glass fibers, and transferred to the diffractometer (Siemens P4) as summarized in Table 4. Cell constants were refined from 82 (**1**), 57 (**3**) and 44 (**13**) reflections in the 2θ range of 9.5−25°. The structures were solved by direct methods (**1**, **13**) and by the Patterson method (**3**) using the SHELXS-97 program,[38] and refined anisotropically on F^2 (program SHELXL-97[38]). Hydrogen atoms were included using a riding model. CCDC-182373 (**1**), -182374 (**3**) and -182372 (**13**) contain the supplementary crystallographic data for this paper. These data can be obtained free of charge at www.ccdc.cam.ac.uk/conts/retrieving.html or from the Cambridge Crystallographic Data Centre, 12 Union Road, Cambridge CB2 1EZ, UK 9Fax: (internat.) + 44-1223/336-033; E-mail: deposit@ccdc.cam.ac.uk].

Acknowledgments

This work was supported by the Dirección General de Investigación del Ministerio de Ciencia y Tecnología (Project No. BQU2001-0979-C02-01), Spain, and the Fundación Séneca de la Comunidad Autónoma de la Región de Murcia (Project No. PI-72-00773-FS-01 and a grant to V. R.). F. F. thanks the University of Murcia for a research grant. We thank Dr. M. D. Santana, Dr. G. García and Mr. A. Lozano for helpful discussions.

[1] S. Trofimenko, *Chem. Rev.* **1993**, *93*, 943.
[2] S. Trofimenko, *Scorpionates: The Coordination Chemistry of Polypyrazolylborate Ligands*, Imperial College Press, London, **1999**.
[3] P. K. Byers, A. J. Canty, R. T. Honeyman, *Adv. Organomet. Chem.* **1992**, 34.
[4] G. Parkin, *Adv. Inorg. Chem.* **1995**, *42*, 291.
[5] N. Kitajima, W. B. Tolman, *Prog. Inorg. Chem.* **1995**, *43*, 419.
[6] Y. Alvarado, O. Boutry, E. Gutierrez, A. Monge, M. C. Nicasio, M. C. Poveda, P. J. Pérez, C. Ruiz, C. Bianchini, E. Carmona, *Chem. Eur. J.* **1997**, 860.
[7] H. V. R. Dias, H.-L. Lu, H.-J. Kim, S. A. Polach, T. K. H. Goh, R. G. Browning, C. J. Lovely, *Organometallics* **2002**, *21*, 1466.
[8] M. M Díaz-Requejo, P. J. Pérez, *J. Organomet. Chem.* **2001**, *617−618*, 110.
[9] W. B. Tolman, *Adv. Chem. Ser.* **1995**, *246*, 195.
[10] K. Ohkita, H. Kurosawa, T. Hasegawa, T. Shirafuji, I. Ikeda, *Inorg. Chim. Acta* **1992**, *198−200*, 275.
[11] M. M Díaz-Requejo, M. C. Nicasio, T. R. Belderrain, P. J. Pérez, M. C. Puerta, P. Valerga, *Eur. J. Inorg. Chem.* **2000**, 1359.
[12] E. Gutierrez, M. C. Nicasio, M. Paneque, C. Ruiz, V. Salazar, *J. Organomet. Chem.* **1997**, *549*, 165.
[13] A. J. Canty, H. Jin, A. S. Roberts, P. R. Traill, B. W. Skelton, A. H. White, *J. Organomet. Chem.* **1995**, *489*, 153.
[14] J.-M. Valk, F. Maassarani, P. van der Sluis, A. L. Spek, J. Boersma, G. van Koten, *Organometallics* **1994**, *13*, 2320.
[15] A. J. Canty, J. L. Hoare, B. W. Skelton, A. H. White, G. van Koten, *J. Organomet. Chem.* **1998**, *552*, 23.
[16] W. J. Geary, *Coord. Chem. Rev.* **1971**, *7*, 81.
[17] D. A. Long, D. Steel, *Spectrochim. Acta* **1963**, *19*, 1955.
[18] G. López, J. Ruiz, C. Vicente, J. M. Martí, G. García, P. A. Chaloner, P. B. Hitchcock, R. M. Harrison, *Organometallics* **1992**, *11*, 4090.
[19] E. Alonso, J. Forniés, C. Fortuño, M. Tomás, *J. Chem. Soc., Dalton Trans.* **1995**, 3777.
[20] E. Maslowski, *Vibrational Spectra of Organometallic Compounds*, Wiley, New York, **1977**, p. 437.
[21] L. A. Oro, M. Esteban, R. M. Claramunt, J. Elguero, C. Fóces-Fóces, F. H. Cano, *J. Organomet. Chem.* **1984**, *276*, 79.
[22] M. Onishi, K. Hiraki, *Inorg. Chim. Acta* **1994**, *224*, 131.
[23] J. Forniés, F. Martínez, R. Navarro, E. P. Urriolabeitia, *J. Organomet. Chem.* **1995**, *495*, 185.
[24] J. Ruiz, F. Florenciano, M. A. Sánchez, G. López, M. C. Ramírez de Arellano, J. Pérez, *Eur. J. Inorg. Chem.* **2000**, 943.
[25] J. Hathaway, A. E. Underhill, *J. Chem. Soc.* **1961**, 3091.
[26] J. Ruiz, V. Rodríguez, N. Cutillas, F. Florenciano, J. Pérez, G. López, *Inorg. Chem. Commun.* **2001**, *4*, 23.
[27] J. Ruiz, M. T. Martínez, C. Vicente, G. García, G. López, P. A. Chaloner, P. B. Hitchcock, *Organometallics* **1993**, *30*, 1594.
[28] J. Ruiz, J. F. J. López, V. Rodríguez, J. Pérez, M. C. Ramírez de Arellano, G. López, *J. Chem. Soc., Dalton Trans.* **2001**, 2683.
[29] C. de Haro, G. García, G. Sánchez, G. López, *J. Chem. Res. Synop.* **1986**, *119; J. Chem. Res., Miniprint* **1986**, 1128.
[30] G. Minghetti, M. A. Cinellu, L. Bandini, G. Banditelli, F. Demartin, M. Manassero, *J. Organomet. Chem.* **1986**, *315*, 289.
[31] J. Bielawski, T. G. Hodgkins, W. J. Layton, K. Niedenzu, J. Serwatowski, *Inorg. Chem.* **1986**, *25*, 87.
[32] M. K. Das, K. Niedenzu, S. Roy, *Inorg. Chim. Acta* **1988**, *150*, 47.
[33] J. Cermak, S. D. Perera, B. L. Shaw, M. Thorton-Pett, *Inorg. Chim. Acta* **1996**, *244*, 115.
[34] G. López, J. Ruiz, G. García, C. Vicente, J. M. Martí, J. A. Hermoso, A. Vegas, M. Martínez-Ripoll, *J. Chem. Soc., Dalton Trans.* **1992**, 53.
[35] R. Usón, J. Forniés, R. Navarro, M. P. García, *Inorg. Chim. Acta* **1979**, *33*, 69.
[36] R. Usón, J. Forniés, P. Espinet, E. Lalinde, *J. Organomet. Chem.* **1983**, *254*, 371.
[37] S. Trofimenko, *Inorg. Synth.* **1970**, *12*, 99.
[38] G. M. Sheldrick, *SHELX-97, Programs for Crystal Structure Analysis*, release 97-2, University of Göttingen, Germany, **1998**.

Received April 1, 2002
[I02167]

EurJIC
European Journal of Inorganic Chemistry

November 2002
Issue 11
Pages 2745–3048

Papers available ahead of print in Early View at www.interscience.wiley.com

Earliest available Table of Contents:
Automatically, free of charge by e-mail through
www.interscience.wiley.com/alerts

COVER PICTURE

The cover picture shows the familiar depiction of an sp^3-hybrid orbital. Each lobe highlights an example of one of the emerging classes of heavy alkaline earth organometallic compounds, specifically those in which the central metal (calcium, strontium and barium) displays direct metal–carbon bonds. Clockwise around the orbital, these classes are: di- and triphenylmethanides, dibenzyl species, acetylides, and "ate" complexes. Atoms in green depict the alkaline earth metal centers, carbon atoms are black, silicon atoms pink, oxygen atoms red and nitrogen atoms blue. Details are discussed in the Microreview by J. S. Alexander and K. Ruhlandt-Senge on pp. 2761 ff. The cover image was generated by Dr. Jesse Taylor (Syracuse University).

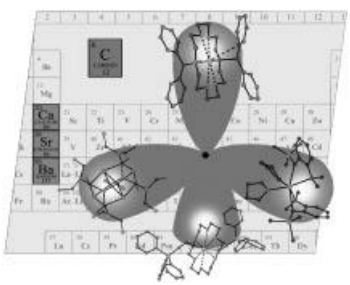

MICROREVIEW

Contents

2761 **J. S. Alexander, K. Ruhlandt-Senge***

Not Just Heavy "Grignards": Recent Advances in the Organometallic Chemistry of the Alkaline Earth Metals Calcium, Strontium and Barium

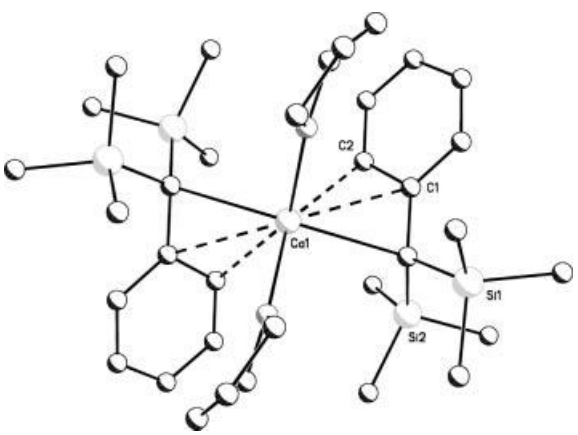

Keywords: Calcium / Strontium / Barium / σ-bound organometallics / Synthesis / Structural characterization

 © 2002 WILEY-VCH Verlag GmbH & Co. KGaA, 69451 Weinheim 1434–1948/02/1111–2749 $ 20.00+.50/0

SHORT COMMUNICATIONS

2775 **N. Takagi, S. Nagase***

Theoretical Study of an Isolable Compound with a Short Silicon-Silicon Triple Bond, $(t\mathrm{Bu_3Si})_2\mathrm{MeSiSi{\equiv}SiSiMe}(\mathrm{Si}t\mathrm{Bu_3})_2$

Keywords: Silicon / Multiple bonds / Substituent effects / Density functional calculations

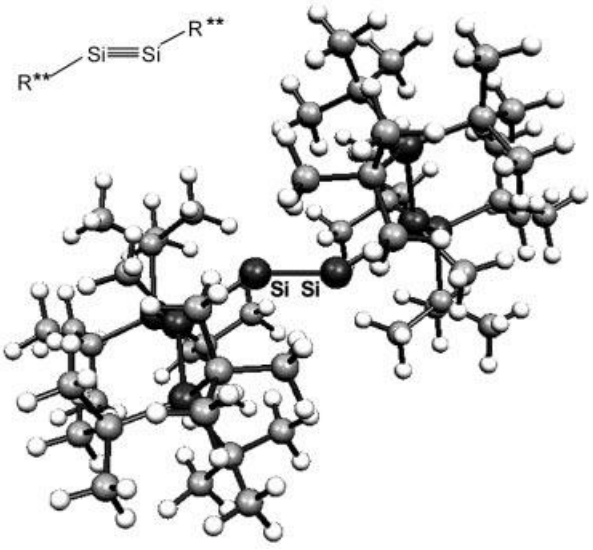

2779 **R. C. Smith,* T. Ren, J. D. Protasiewicz***

A Robust, Reactive, and Remarkably Simple to Prepare Sterically Encumbered *meta*-Terphenyl Ligand

Keywords: Terphenyl / Diphosphene / Insertion / Phosphaalkene

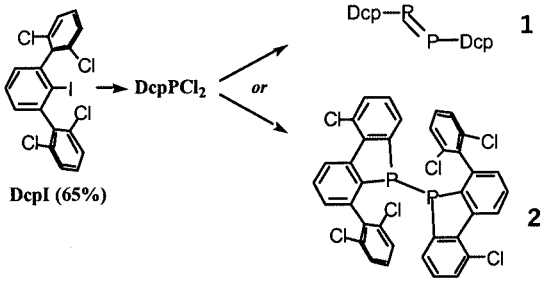

2784 **P. L. Shutov, S. S. Karlov,* K. Harms, A. V. Churakov, J. A. K. Howard, J. Loberth,* G. S. Zaitseva**

Synthesis and Characterization of Group 14 1-Haloazametallatranes

Keywords: Azametallatranes / Silicon / Germanium / Tripodal ligands / Tin

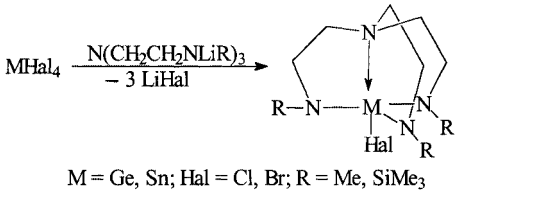

FULL PAPERS

2789 **C. Höltke, G. Erker,* G. Kehr, R. Fröhlich, O. Kataeva**

The Reaction of (Butadiene)zirconocene with Imines

Keywords: Template synthesis / Zirconium / Metallocenes / Polymerizations

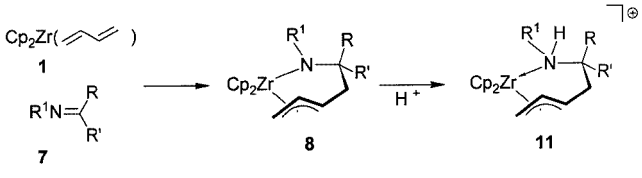

2800 **S. Rau, L. Böttcher, S. Schebesta, M. Stollenz, H. Görls, D. Walther***

Simultaneous Cation/Anion Coordination by Bifunctional 1,2-Diimine/1,2-Diamine Type Ligands: Synthesis, Structures, and Properties of Tight Ion Pair Complexes of Ruthenium and Iron

Keywords: Iron / Hydrogen bonds / N ligands / Ruthenium

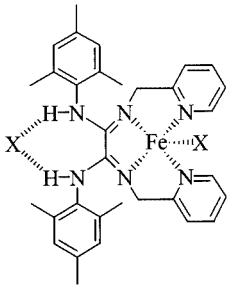

2810 **F. Amor, J. Sánchez-Nieves, P. Royo,* H. Jacobsen, O. Blacque, H. Berke, M. Lanfranchi, M. A. Pellinghelli, A. Tiripicchio**

Competitive Insertion of Isocyanide into Tantalum–Amido and Tantalum–Methyl Bonds

Keywords: Tantalum / Competitive insertion / Isocyanide insertion / Density functional calculations

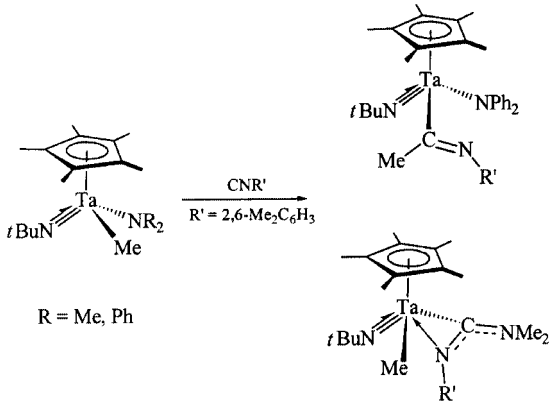

2818 **K. D. Benkstein, C. L. Stern, K. E. Splan, R. C. Johnson, K. A. Walters, F. W. M. Venhelmont, J. T. Hupp***

Collapsed Molecular Rectangles Based on Rhenium(I) Coordination of Ethynylpyridyl Porphyrins – Synthesis, Structure, and Bending-Induced Charge-Transfer Behavior

Keywords: Porphyrins / Rhenium / Supramolecular chemistry / Molecular rectangles / Electroabsorption spectroscopy

2823 **F. A. Almeida Paz, Y. Z. Khimyak, A. D. Bond, J. Rocha, J. Klinowski***

Synthesis and Characterization of a Novel Modular Cadmium-Organic Framework with Biphenyl-4,4′-dicarboxylate

Keywords: Coordination polymers / Cadmium / Supramolecular chemistry / O ligands

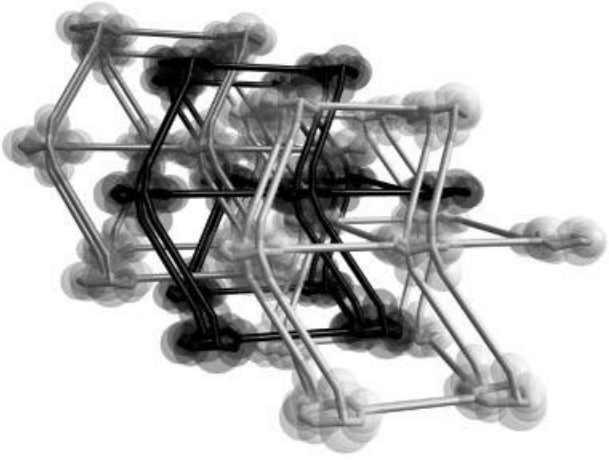

2829 **J. Bley-Escrich, J.-P. Gisselbrecht, E. Vogel, M. Gross***

Electrochemical and Spectroelectrochemical Investigations of "Figure-Eight" Octapyrrolic Macrocycles, Free Bases, and Their Mononuclear, Homo- and Heterodinuclear Complexes with Divalent Transition Metals

Keywords: Macrocyclic ligands / Octaphyrins / Transition metal complexes / Electrochemistry

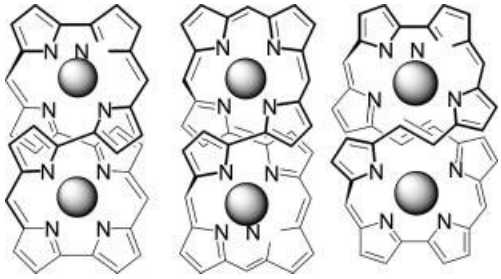

2838 **T. Azaïs, L. Bonhomme-Coury, H. Vaissermann, J. Maquet, C. Bonhomme***

The First Aluminophosphonate Cluster Analogue of the 4=1 SBU of Zeolites: Structure and Multinuclear Solid-State NMR Study, Including ^{1}H NMR

Keywords: Aluminium / Cluster compounds / NMR spectroscopy / Phosphorus / Solid state

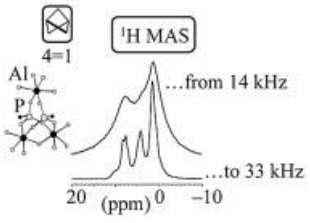

2844 **T. Devic, B. Domercq, P. Auban-Senzier, P. Molinié, M. Fourmigué***

Cyano-Halogen Interactions in [EDT-TTF-I]$_2$-[Ni(mnt)$_2$] and [EDT-TTF-I$_2$]$_2$[Ni(mnt)$_2$] and Geometrical Evolutions within Mixed-Valence or Fully Oxidized TTF Dyads

Keywords: Radical ions / S ligands / Magnetic properties / Crystal engineering / Non-covalent interactions

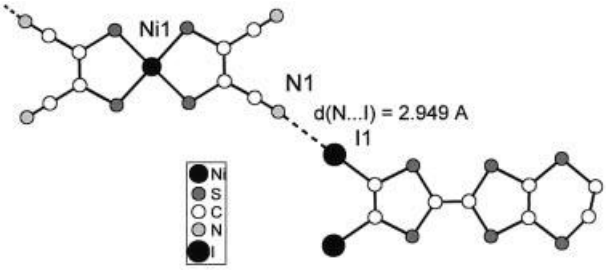

2850 **S. Chardon-Noblat,* P. Da Costa, A. Deronzier,* T. Mahabiersing, F. Hartl***

Novel Complexes *trans*(Cl)-[Os(bpy)(CO)-(CH$_3$CN)Cl$_2$]^n (n = 0, +1; bpy = 2,2′-Bipyridine): Photo- and Electrochemical Syntheses and Comparative Study of Their Bonding and Redox Properties

Keywords: Osmium / N ligands / Charge-transfer photochemistry / Electrochemical oxidation / Decarbonylation

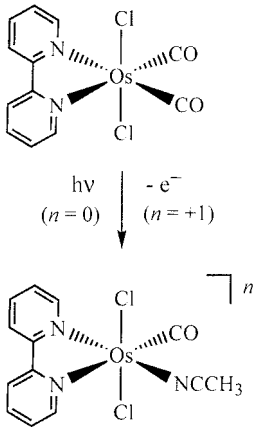

2857 **H. Ma, M. Allmendinger, U. Thewalt, A. Lenz, M. Klinga, B. Rieger***

Dioxygen Activation Using Schiff Base Macrocyclic Dinuclear Copper(I) Complexes: Structurally Characterized Dioxygen Reaction Products

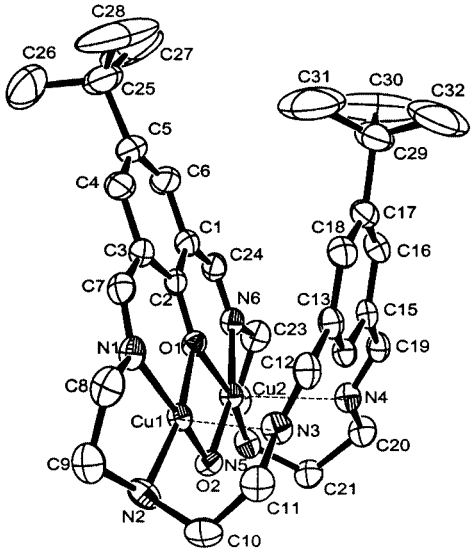

Keywords: Macrocyclic ligands / Dinuclear copper complexes / Oxygenation reactions / O−O activation / X-ray crystal structures

2868 **T. Spaniel, H. Schmidt, C. Wagner, K. Merzweiler, D. Steinborn***

(Phenylalkyl)palladium Complexes Containing β-Hydrogen Atoms: Synthesis and Characterization of $[PdR_2(dppe)]$, $[PdR(SPh)(dppe)]$ (R = CH_2CH_2Ph, $CH_2CH_2CH_2Ph$, $CH_2CHMePh$), and $[Pd(CH_2CH_2CH_2Ph)X(dppe)]$ (X = I, Br, Cl)

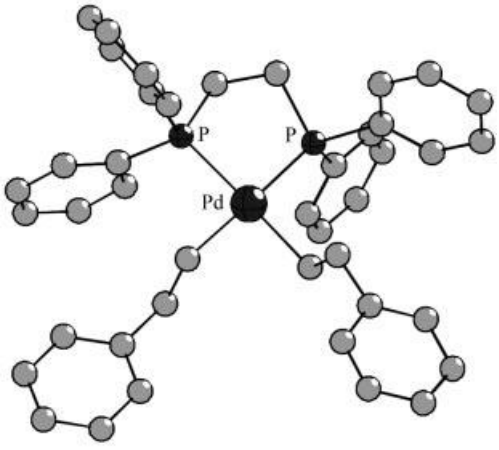

Keywords: Phenylalkyl complexes / Palladium / β-Hydrogen-containing alkyl ligands / P ligands

2878 **J. Baldamus, C. Berghof, M. L. Cole, E. Hey-Hawkins, P. C. Junk,* L. M. Louis**

Studies of Aryl Substituent and Solvent Donor Imposed Structural Diversity in *N,N′*-Diarylformamidinate Complexes of Lithium

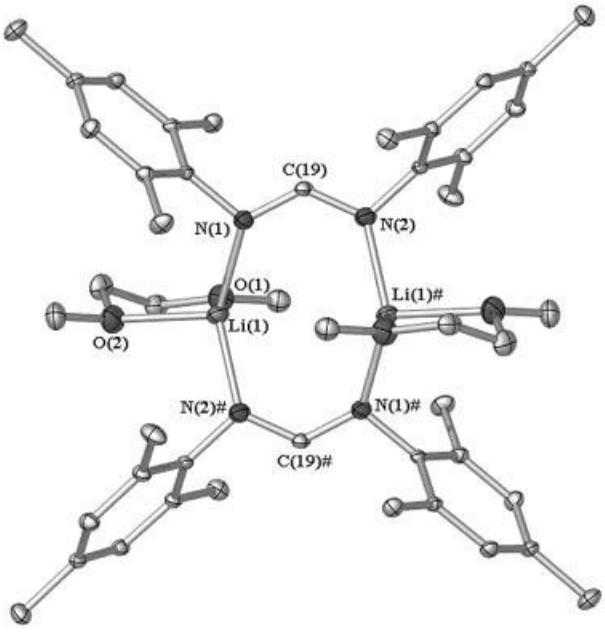

Keywords: Lithium / Formamidinates / Coordination modes / N ligands

2885 **R. Dreos,* G. Nardin, L. Randaccio, P. Siega, G. Tauzher**

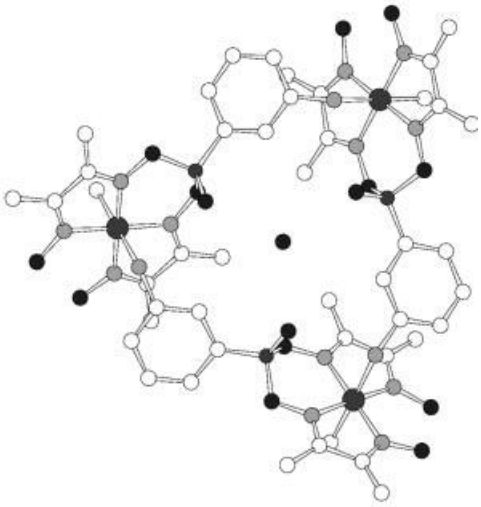

Self-Assembly of Cobaloximes and Rhodoximes with 3-Aminophenylboronic Acid: A Molecular Triangle and a Polymer

Keywords: Cobalt / Rhodium / Boronic acid / Self assembly

2891 **O. Fazio, M. Gnida, W. Meyer-Klaucke, W. Frank, W. Kläui***

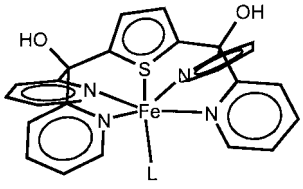

An Iron(II) Complex with an N_4S Ligand − A Novel Model Compound to Mimic Cytochrome P450 Activity

Keywords: Metalloenzymes / Tetrapodal pentadentate ligand / Iron / Homogeneous catalysis / O−O activation / N,S ligands / Epoxidation / EXAFS spectroscopy

2897 **M. Hoogenraad, H. Kooijman, A. L. Spek, E. Bouwman, J. G. Haasnoot, J. Reedijk***

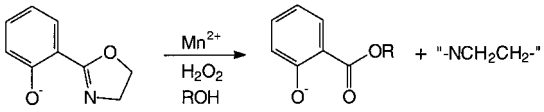

Manganese Oxidation Catalysts with 2-(2′-Hydroxyphenyl)oxazoline Ligands: Catalyst Intermediates and Degradation Products − Crystal Structure of Bis[{2-(2′-oxazolinyl)phenolato}-bis(1-methylimidazole)manganese(III)] Perchlorate

Keywords: Catalysis / Manganese / Mass spectrometry / Oxazolines / Oxidation

2904 **R. Wang, M. Hong,* J. Luo, R. Cao, Q. Shi, J. Weng**

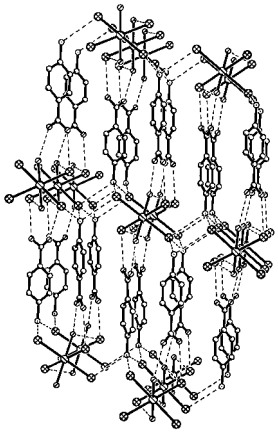

Syntheses and Crystal Structures of Five Cadmium(II) Complexes Derived from 4-Aminobenzoic Acid

Keywords: Cadmium / Hydrogen bonds / N,O ligands / Supramolecular chemistry

2913 **J. M. Schveigkardt, A. C. Rizzi, O. E. Piro, E. E. Castellano, R. C. de Santana, R. Calvo, C. D. Brondino***

Structural and Single Crystal EPR Studies of the Complex Copper L-Glutamine: A Weakly Exchange-Coupled System with *syn-anti* Carboxylate Bridges

Keywords: EPR spectroscopy / Carboxylate ligands / Through bond interactions / Copper / Magnetic Properties / Layered compounds

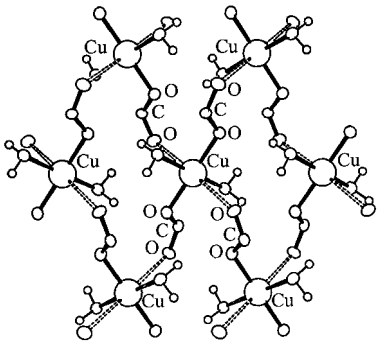

2920 **M. Calligaris,* L. Randaccio**

Stereochemical Analysis of Cobalt(III) Complexes with Tridentate Imino- and Amino-Oxime Ligands

Keywords: Stereochemistry / Molecular mechanics / Tridentate ligands / Cobalt / Vitamin B_{12}

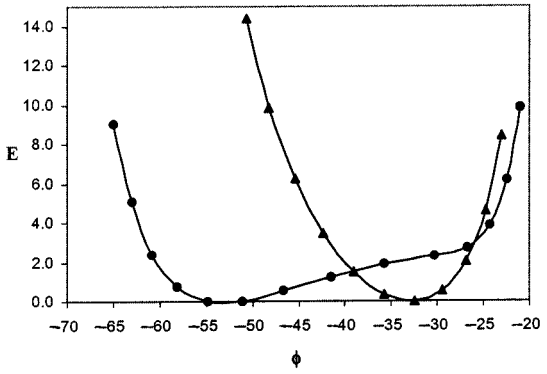

2928 **A. C. Filippou,* S. Schneider, B. Ziemer**

Syntheses and Molecular Structures of Chromium(IV) Halides and Pseudohalides Bearing a Triamidoamine Ligand

Keywords: Chromium / Tripodal ligands / N ligands / Halides / Pseudohalides / Oxidations

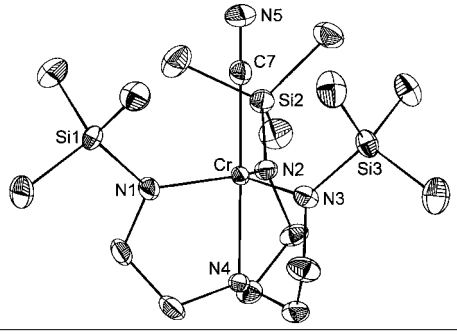

2936 **L. Engelke, C. Näther, W. Bensch***

Two New Layered Thioantimonate(III) Compounds: Solvothermal Syntheses, Crystal Structures, and Properties of (*trans*-1,4-$C_6N_2H_{15}$)-Sb_3S_5 and (*trans*-1,2-$C_6N_2H_{15}$)$Sb_3S_5{\cdot}H_2O$

Keywords: Crystal structure / Hydrogen bonds / Solvothermal synthesis / Thioantimonate

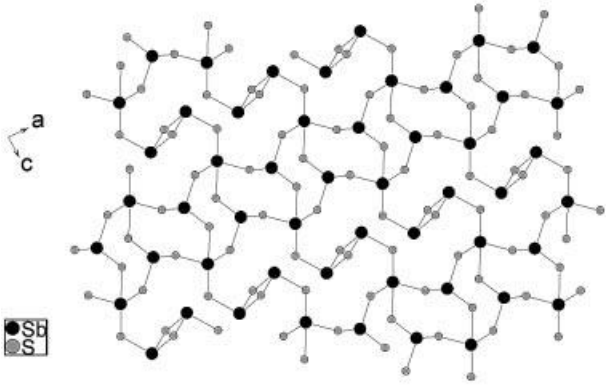

2942 **T. Köhler, J. Faderl, H. Pritzkow, W. Siebert***

Synthesis and Properties of Bis(2-heteroaryl)-borane Derivatives

Keywords: Boranes / Porphyrinogens / Lithiation / Grignard reaction / Bromination

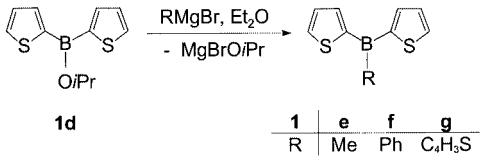

2947 **V. G. Shtyrlin,* A. V. Zahkharov,* A. M. Kuznetsov, O. V. Kukushnika, P. P. Chernov**

Thermodynamics of Redox Processes and Kinetics and Mechanism of Electron Self-Exchange Reactions in the Bis(*N*,*N*-diethyldithiocarbamato)-copper(II)/Iodine/Dichloromethane System

Keywords: Copper / Electron-transfer kinetics / Reaction mechanisms / Redox reactions thermodynamics / S ligands

$Cu^{II}L_2 + n/2I_2 \rightleftharpoons [Cu^{III}L_2]I_3$ ($n = 3, 5$)

$Cu^{II}L_2 + [{}^*Cu^{III}L_2]I_n \overset{k_e}{\rightleftharpoons} [Cu^{III}L_2]I_n + {}^*Cu^{II}L_2$ ($n = 3, 5$)

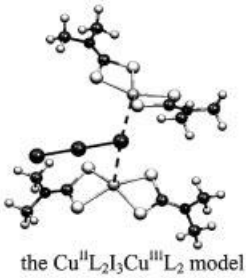

the $Cu^{II}L_2I_3Cu^{III}L_2$ model

2956 **S. Gazeau, J. Pécaut, R. Haddad, J. A. Shelnutt,* J.-C. Marchon***

Twisting the Porphyrin Ring to Enhance Epoxidation Enantioselectivity

Keywords: Porphyrinoids / Manganese / Enantioselectivity / Asymmetric catalysis / Epoxidation

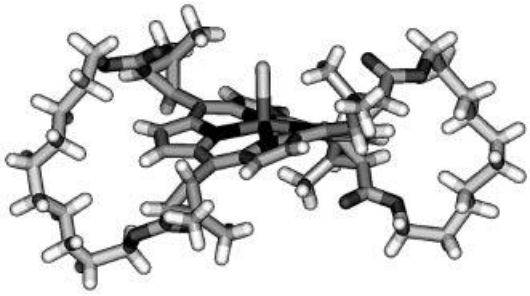

2961 **M. Driess,* J. Aust, K. Merz**

P−H Activation By Zirconium Amido Complexes: From New Phosphanidozirconium Complexes to the First Zr_2P_6 Cluster with the $[RP-P-PR]^{3-}$ Ligand [R = $Me_2(iPrMe_2C)Si$]

Keywords: Phosphanides / Bond activation / Cluster compounds / Zirconium / Phosphanes

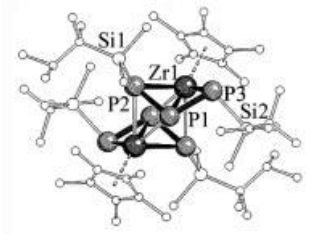

2965 **R. Lomoth, P. Huang, J. Zheng, L. Sun,* L. Hammarström,* B. Åkermark, S. Styring***

Synthesis and Characterization of a Dinuclear Manganese(III,III) Complex with Three Phenolate Ligands

Keywords: Manganese / Ligand design / Redox chemistry

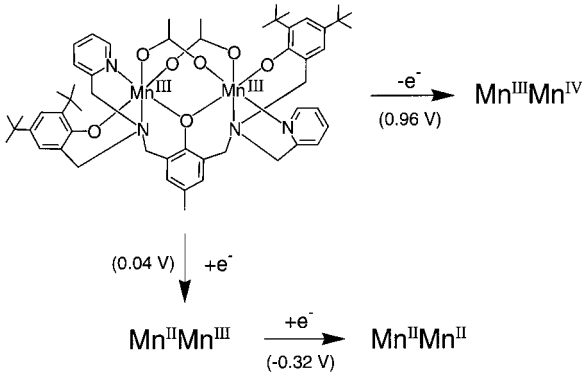

2975 **S. Blaurock, E. Hey-Hawkins***

Syntheses, Crystal Structures and Reactivity of Organometallic Tantalum(IV) Phosphinidene Complexes: *trans*-[{Cp*TaCl(μ-PR)}$_2$] (Cp* = C_5Me_5, R = Cy, *t*Bu, Ph), *cis*- and *trans*-[{Cp* TaCl(μ-PMes)}$_2$] (Mes = 2,4,6-$Me_3C_6H_2$) and *cis*-[{Cp′TaCl(μ-PMes)}$_2$] (Cp′ = C_5H_4Me)

Keywords: Tantalum / P ligands / Oxo ligands / Isocyanide ligands

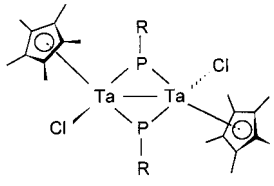

2985 **I. Shevchenko,* V. Andrushko, E. Lork, G.-V. Röschenthaler***

Bis[bis(dialkylamino)phosphanyl]methanes and Bis(trifluoromethyl)acrylonitrile − Reactions and Derivatives

Keywords: Ylides / Phosphanes / Nitriles / Hexafluoroacetone

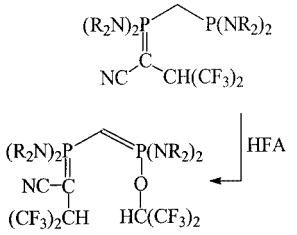

2991 **S. Delagrange, C. Gateau, D. Chapon, C. Lebrun, P. Delangle,* P. Vottéro**

Lipophilic Ligands Derived from 1,3,5-Triamino-1,3,5-trideoxy-*cis*-inositol (Taci) for Trivalent Lanthanide Complexation in Aqueous and Organic Solutions

Keywords: Lanthanides / Complexes / N,O ligands / Substituent effects / Stability constants

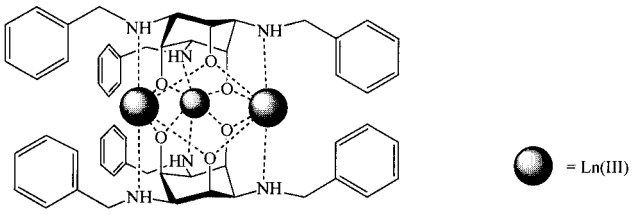

2999 **G. Esquius, J. Pons, R. Yáñez, J. Ros,* R. Mathieu,* B. Donnadieu, N. Lugan**

Synthesis of a New Potentially Hemilabile Ligand: 1-[2-(Diphenylphosphanyl)ethyl]-3,5-dimethylpyrazole, and Comparison of its Bonding Properties with the Related 1-[2-(Ethylamino)-ethyl]-3,5-dimethylpyrazole Ligand toward Rh^{I}

Keywords: Rhodium / P ligands / N ligands / Hemilabile ligands / Hydroformylations

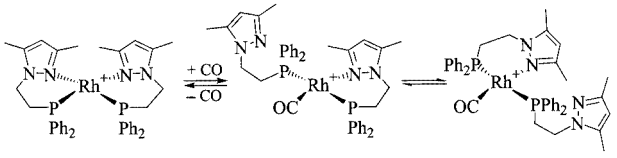

3007 **H. V. Huynh, T. Lügger, F. E. Hahn***

Synthesis and X-ray Molecular Structure of $[W^{VI}(C_6H_4S_2\text{-}1,2)_3]$ Completing the Structural Characterization of the Series $[W(C_6H_4S_2\text{-}1,2)_3]^{n-}$ (n = 0, 1, 2): Trigonal-Prismatic versus Octahedral Coordination in Tris(benzene-1,2-dithiolato) Complexes

Keywords: Tungsten / S ligands / Structure elucidation / Coordination modes

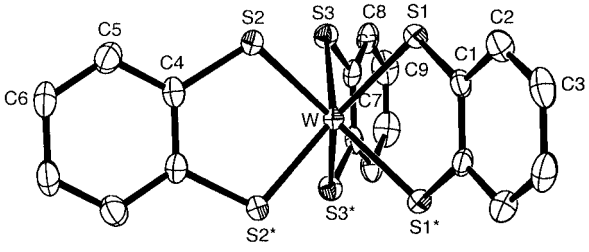

3010 **H. E. Toma,* A. D. P. Alexiou, S. Dovidauskas**

Extended Electronic Interactions in a Triangular μ-Oxotriruthenium Acetate Cluster Containing Nitric Oxide

Keywords: Ruthenium / Nitrogen oxides / Carboxylate ligands / Cluster compounds / Pi interactions

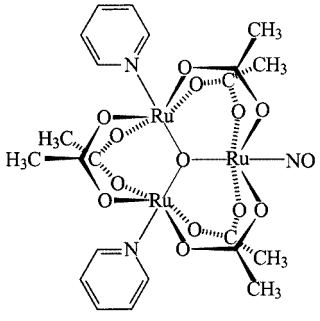

3018 **A. R. Kudinov,* D. A. Loginov, Z. A. Starikova, P. V. Petrovskii, M. Corsini, P. Zanello**

Iron- and Ruthenium-Containing Triple-Decker Complexes with a Central Pentaphospholyl Ligand − X-ray Structures of $[(\eta\text{-}C_5H_5)Fe(\mu\text{-}\eta\text{:}\eta\text{-}P_5)Ru(\eta\text{-}C_5Me_5)]PF_6$ and $[(\eta\text{-}C_5Me_5)Ru(\mu\text{-}\eta\text{:}\eta\text{-}P_5)Ru(\eta\text{-}C_5Me_5)]PF_6$

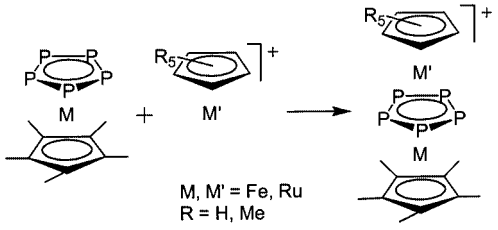

Keywords: Electrochemistry / Iron / Phosphorus / Ruthenium / Sandwich compounds / Triple-decker complexes

3028 **A. Marson, A. B. van Oort, W. P. Mul***

In Situ Preparation of Palladium Diphosphane Catalysts

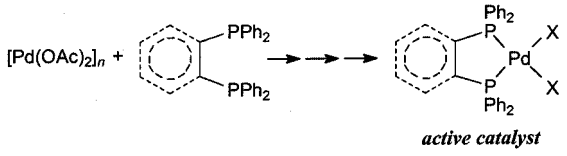

Keywords: Palladium / Phosphanes / Homogeneous catalysis / Copolymerization

3032 **R. Ferreira, C. Freire,* B. de Castro,* A. P. Carvalho, J. Pires, M. B. de Carvalho**

Encapsulation of Copper(II) Complexes with Pentadentate N_3O_2 Schiff Base Ligands in a Pillared Layered Clay

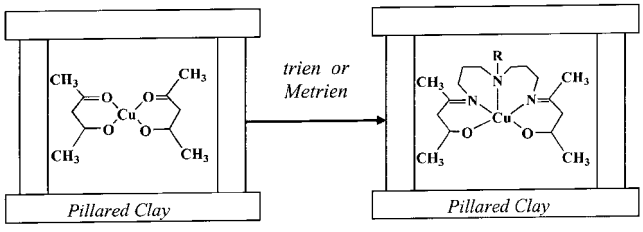

Keywords: Clays / Microporous materials / Copper / Schiff bases

3039 **S. Fox, J. P. Dunne, M. Tacke,* D. Schmitz, R. Dronskowski**

Synthesis and Structural Characterisation of a Novel Chiral *ansa*-Cobaltocenium Hexafluorophosphate

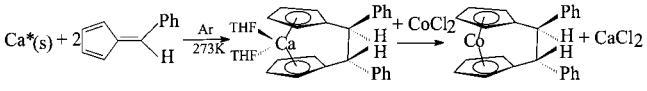

Keywords: Metallocenes / Structural analysis / Density functional calculations / Cobalt

CORRECTION

3047 **H. Brunner,* J. Klankermayer, M. Zabel**

Synthesis, Stereochemistry and Molecular Structures of Chiral-at-Metal (Cycloheptatrienyl)-molybdenum Complexes Containing the Diphosphane Prophos

Not Just Heavy "Grignards": Recent Advances in the Organometallic Chemistry of the Alkaline Earth Metals Calcium, Strontium and Barium

Jacob S. Alexander[a] and Karin Ruhlandt-Senge*[a]

Keywords: Calcium / Strontium / Barium / σ-bound organometallics / Synthesis / Structural characterization

Since their initial development in the early 1900's, Grignard reagents have proven to be immensely useful and are among the most common organometallic reagents. The nature of the reagents in solution is complex and depends on substituents, solvent, concentration and temperature. Despite continuing questions about their solid state and solution composition and conformation, organomagnesium reagents find new applications continually. In contrast, little information about the heavier alkaline earth organometallic compounds RMX and R_2M (R = alkyl, aryl; M = Ca, Sr, Ba, X = halide) exists. High reactivity due to the predominantly ionic character of the metal-ligand bond and increased lability complicates synthetic access.

Recent interest in the organometallic chemistry of the alkaline earth metals calcium, strontium and barium has been sparked by the realization that heavy alkaline earth metal organometallics play unique roles in synthetic applications, such as polymerization initiators and as reagents to modify polymers. As a result, the organometallic chemistry of calcium, strontium and barium has received significant attention over the last few years. This article summarizes recent results in this emerging area of chemistry.
(© Wiley-VCH Verlag GmbH, 69451 Weinheim, Germany, 2002)

1. Introduction
2. Scope of this Microreview
3. Synthetic Methodology
3.1 Transamination
3.2 Direct Metallation
3.3 Alkene/arene Elimination
3.4 Transmetallation
4. Historical Examples
5. Dibenzyl Derivatives of the Heavy Alkaline Earth Metals
6. "Ate" Complexes of Calcium, Strontium and Barium
7. Acetylides of the Heavy Group 2 Metals
8. Di- and Triphenylmethanes, Contact and Ion Pairs
9. Conclusions

[a] Department of Chemistry, 1-014 Center for Science and Technology, Syracuse University
Syracuse, NY 13244-4100, USA
Fax: (internat.) + 1-315/443-4070
E-mail: kruhland@syr.edu

Jacob S. Alexander was born in Nashville, Tennessee in 1975. He obtained his B.S. in Chemistry from Tennessee Technological University in 1997. He received his M.S. in inorganic chemistry in 2000 and is currently pursuing his Ph.D. at Syracuse University where he studies organometallic main group chemistry and crystallography with Karin Ruhlandt-Senge. His research interests include a wide range of issues concerning alkali and alkaline earth metal organometallics, including structural chemistry and applications in organic synthesis.

Karin Ruhlandt-Senge studied chemistry at the Gutenberg University in Mainz (Germany) and the Philipps University in Marburg, Germany. She received her doctorate in 1991 working with Ulrich Müller (Marburg) on transition metal chemistry and crystallography, and with Philip P. Power and Håkon Hope at the University of California, Davis (U.S.A.) where she was concerned with main group III chemistry and crystallography. After her return to Davis for postdoctoral work in P.P. Power's group (1992−1993), she started her independent career in fall 1993 at Syracuse University (U.S.A.). Her current research interests focus on various aspects of alkali and alkaline earth metal chemistry.

MICROREVIEWS: This feature introduces the readers to the authors' research through a concise overview of the selected topic. Reference to important work from others in the field is included.

1. Introduction

The organometallic chemistry of the heavy alkaline earth metals dates back to the early 1900's, with the intent to synthesize highly reactive "Grignard analogs" for synthetic applications.[1] The assumption that the organometallic chemistry of these metals roughly resembles that of the lighter congener, magnesium, prompted attempts to synthesize candidate molecules bearing small organic ligands. However, the formation of either unstable and/or sparsely soluble compounds with little opportunity to be utilized for synthesis discouraged further efforts. These compounds continued to be viewed as obscure, and rather recently a popular organometallic textbook remarked: "Since the heavier alkaline earth organometallics do not offer any advantages over Grignard reagents, their chemistry has not been studied extensively [..]."[2] In consideration of the recent prominence organometallic calcium, strontium, and barium derivatives have received, this view is now changing. Still, most applications rely on the preparation of reagents in situ, and little information exists with regard to the reactive species.

Organometallic derivatives of the heavy alkaline earth metals have been most intensely studied for cyclopentadienyl systems, dating back to 1956 with the preparation of $(C_5H_5)_2Ca$.[3] Since then, many related derivatives have been prepared due to the unique capability of this system to stabilize the alkaline earth metal centers both sterically and electronically.[4−6] Similar work has been extended to fluorenyl, indenyl and related π-ligand systems.[7−10]

This progress did not however extend towards σ-bonded ligand systems and, aside from the early studies mentioned above and some activity in the latter part of the last century,[9,11−21] little attention has been devoted to them. High reactivity and low solubility complicated the isolation and detailed characterization of these systems, resulting in reports of the in situ preparation of the candidate molecules, whose identity was predominantly verified by the products from chemical reactions.

Examples of well-characterized σ-bonded organometallic calcium, strontium, and barium derivatives are heavily based on heteroleptic compounds, incorporating cyclopentadienyl (Cp) ligation in addition to a σ-bonded organometallic ligand system, taking advantage of the stabilizing effect provided by the Cp ligand.[4−6,22] Well-characterized organometallic compounds relying purely on σ-bonded ligands remain scarce, the original examples being the now familiar $[Ca\{CH(SiMe_3)_2\}_2(1,4\text{-dioxane})_2]$,[23] available by co-condensation of metal and ligand at 77 K, and $Ca[C(SiMe_3)_3]_2$, prepared by treatment of CaI_2 with two equivalents of $KC(SiMe_3)_3$.[24] Treatment of the latter with diethyl ether results in immediate ether scission and formation of the parent hydrocarbon and $Ca(OEt)_2$, illustrating the problems associated with the organometallic chemistry of these elements: severe limitation of synthetic variables due to high reactivity, low solubility caused by the high ionic character of the metal-ligand bond, high lability, and a prominent tendency towards the formation of oligomeric or polymeric species associated with a dramatic reduction of solubility.

The ability to reproducibly and cleanly prepare organometallic derivatives in good yield and purity and analyze their structure and function is critical for the progress of this emerging area of chemistry. Several recent studies have provided much needed information to improve the performance and utility of existing applications while establishing a new branch of organometallic chemistry with room for considerable growth.

2. Scope of This Microreview

This review examines recent examples of structurally characterized σ-bound and charge-separated organometallic complexes of calcium, strontium and barium with a focus on synthetic access strategies and structural features. Compounds of magnesium and beryllium will not be addressed. Numerous π-bound calcium, strontium and barium derivatives are now known, such as the families of cyclopentadienyl-, fluorenyl- and indenyl-stabilized organometallics; with a few exceptions these lie outside of the chemistry reviewed here. Similarly, allyl or vinyl systems will not be discussed; instead we refer to the several excellent review articles on these subjects.[4−6,25]

3. Synthetic Strategies

Multiple synthetic strategies towards the target compounds have been explored; among the most successful are transamination, direct metallation, alkane/arene elimination and transmetallation.

3.1 Transamination

The ready availability of the alkaline earth metal amides $M[N(SiMe_3)_2]_2$,[26] their solubility in many different solvent systems, and the easy removal of $HN(SiMe_3)_2$ make this an attractive route for the synthesis of alkaline earth metal organometallics [Equation (1)].[27]

$$M[N(SiMe_3)_2]_2 + 2\,HR \longrightarrow MR_2 + 2\,HN(SiMe_3)_2 \quad (1)$$

R = alkyl, aryl M = Ca, Sr, Ba

A limiting factor in this reaction is the pK_a range of hydrocarbon sources: only those with a higher acidity than $HN(SiMe_3)_2$ can be utilized. Highly acidic substrates, however, induce a competing side reaction involving protonation of the liberated secondary amine and formation of the silane [Equation (2)].

$$HN(SiMe_3)_2 + HR \longrightarrow Me_3SiR + 2\,H_2NSiMe_3 \quad (2)$$

R = alkyl, aryl

This side reaction may be suppressed by careful and dilute addition of the acid.[28] An additional complication stems from the basic amide starting material promoting ether cleavage. This may be avoided using low temperature conditions.

3.2 Direct Metallation

The ease of the reaction and ready availability of precursors adds to the attractive nature of this route [Equation (3)].

$$2\,HR + M_{act} \longrightarrow MR_2 + H_2 \quad (3)$$

R = alkyl, aryl, Act.= activated, M = Ca, Sr, Ba

Necessary requirements for this reaction include the presence of highly active and pure alkaline earth metal. Activation methods include the distillation or sublimation of the metals,[29] the reduction of metal iodides with alkali metals,[30] or by dissolving the metals in anhydrous, deoxygenated liquid ammonia.[31] The reactivity of the metals plays a major role: barium will react smoothly, while the less reactive strontium and calcium generally require reflux conditions in liquid ammonia.

Problems associated with the ammonia route focus on difficulties in evolving a viable solvent system. Often, cosolvent systems are necessary along with the ammonia, but the sparse solubility of many organometallic complexes upon removal of NH_3 precludes crystallographic and spectroscopic characterization, and, more importantly, use of the target compound as a soluble precursor. If the system allows, this obstacle may be overcome by using donor systems in addition to the ammonia.

3.3 Arene Elimination

Until recently, this method was not applicable for the synthesis of heavy alkaline earth organometallics due to the unavailability of suitable precursor materials. The widely known and easily available cyclopentadienyl (Cp) complexes as basic substrates are not suitable due to the inherent stability of the Cp^- anion. In addition, the tendency of liberated C_5H_6 to dimerize causes significant difficulties in separation and purification. Fortunately, during the last few years several dibenzyl derivatives of calcium,[32,33] strontium[34] and barium[35] have become available, making arene elimination an attractive route. This method takes advantage of the strong thermodynamic drive towards the formation of toluene (and/or substituted phenylmethanes), resulting in the facile metallation of a variety of acidic hydrocarbons [Equation (4)].[52]

$$M(C_7H_7)_2(THF)_2 + 2HR \longrightarrow MR_2 + 2C_7H_8 \quad (4)$$

R = alkyl, aryl M = Ca, Sr, Ba

This method is particularly attractive as it forms simple hydrocarbons as the reaction products that can be easily removed from the reaction mixture. Again, similar pK_a limitations as discussed above apply (see section 3.1), as well as the lack of flexibility in solvent selection for some of the heavier analogs. Particularly for the heavier metal congeners, the high ionic character of the complexes precludes solvation in all but the most polar solvents, such as THF. This limitation makes the separation of the two solid reaction products difficult due to the lack of differentiation in solubility. In addition, great care must be applied to choose the appropriate reaction conditions as alkaline earth metal arene systems are extremely basic and will readily promote ether scission.

3.4 Transmetallation/Metal Exchange

Several possible variations of these schemes may be considered: the use of organomercury reagents in conjunction with activated alkaline earth metals [Equation (5)], or the reaction of organolithium compounds with alkaline earth metal alkoxides, aryloxides [Equation (6)], or amides [Equation (7)]. The chemistry as successfully employed in Equation (6) and (7) has been applied in the synthesis of dibenzylcalcium, -strontium and -barium derivatives [Equation (8)],[32−35] whereas organomercury chemistry [Equation (5)] has been employed to prepare the related organolanthanides.[36]

$$HgR_2 + M_{act} \longrightarrow MR_2 + Hg \quad (5)$$

$$2LiR + M(OR)_2 \longrightarrow MR_2 + 2LiOR \quad (6)$$

$$M[N(SiMe_3)_2]_2 + 2\,LiR \longrightarrow MR_2 + 2\,LiN(SiMe_3)_2 \quad (7)$$

$$M[N(SiMe_3)_2]_2 + 2\,LiCH_2Ph \longrightarrow M(CH_2Ph)_2 + 2LiN(SiMe_3)_2 \quad (8)$$

R = alkyl, aryl M = Ca, Sr, Ba

Although these reactions often proceed smoothly and with few side products, the toxicity of mercury and its compounds make this route less attractive, and have therefore not been applied extensively towards the alkaline earth metal systems. In the case of the reactions shown in Equation (6) and (7), the separation of the two solid reaction products remains the key challenge. Necessary for successful separation are sufficient differences in the solubility of the products, sometimes achievable by careful choice of ligands or by addition of donors.[37]

4. Historical Examples

Successful structurally authenticated investigations into the area of σ-bonded organometallic compounds of the heavy alkaline earth metals opened in 1991 with the now-familiar isolation and structural characterization of $[Ca\{CH(SiMe_3)_2\}_2(C_4H_8O_2)_2]$ (**1**).[23] This four-coordinate complex arose from a co-condensation of calcium vapor and bis(trimethylsilyl)bromomethane in THF at 77 K, presumably to give $RCaBr(THF)_n$, with subsequent formation of the target compound via a Schlenk-type equilibrium. This calcium compound was a starting point for observing

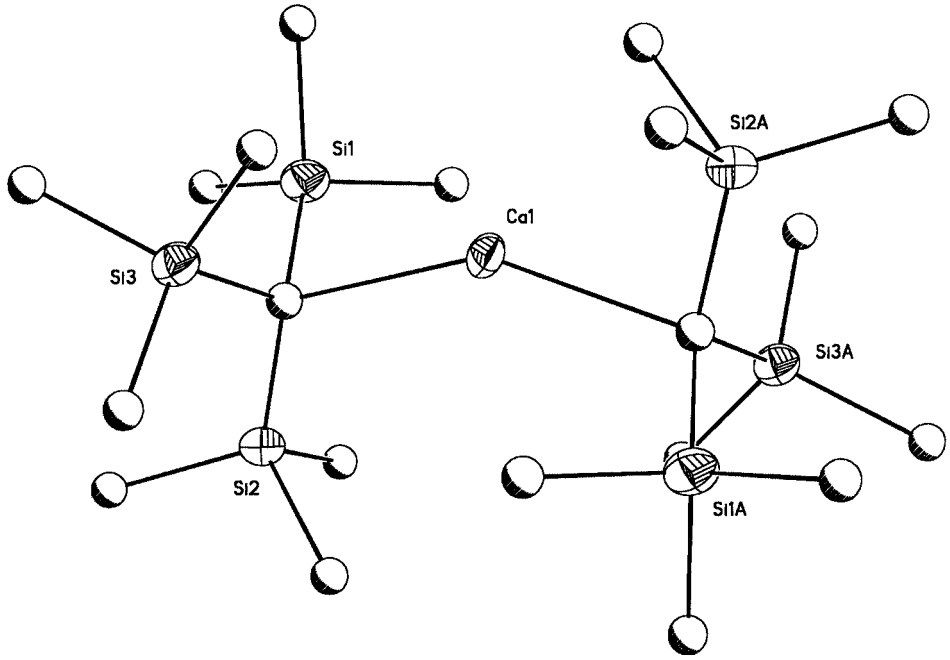

Figure 1. Molecular structure of **2**; heavy atoms displayed anisotropically with ellipsoids at 30% probability; hydrogen atoms have been omitted for clarity

σ-type alkaline earth metal-carbon interactions in Group 2 organometallics.

The first, and to date only, example of an unsolvated, two-coordinate complex of a heavy Grignard analog came with the report of the remarkable calcium bis(tristrimethylsilyl)methanide (**2**; Figure 1).[24] Reaction of the potassium methanide with calcium iodide in benzene over extended periods of time, followed by recrystallization from benzene/heptane, led to the isolation of extremely thin plates suitable for X-ray diffraction. While considerable disorder exists in the structure, the structural information is reliable and agrees well with other σ-bonded alkaline earth organometallics. Interestingly, there is little evidence for strong agostic interactions, although the compound still adopts the bent geometry predicted for compounds of this type.[38]

5. Dibenzyl Derivatives of the Heavy Alkaline Earth Compounds

Early studies on alkaline earth metal benzyl derivatives focussed on the use of organomercury reagents; the reaction products were solely characterized by NMR studies and no definitive structural information exists. Very recently, a facile synthesis of homoleptic dibenzylbarium became available by treatment of barium bis[bis(trimethylsilyl)]amide or barium *tert*-butoxide with two equivalents of the TMEDA (*N*,*N*,*N*′,*N*′-tetramethylethylenediamine) adduct of benzyllithium in diethyl ether.[35] This promising result, coupled with the known activity of dibenzylbarium as a polymerization initiator, led to intense efforts to provide a wider array of derivatives of this type, as summarized in Table 1. Major impediments in this chemistry lie in the relative insolubility of dibenzylbarium in hydrocarbons, in addition to difficulties separating pure compounds for the lighter metals, calcium and strontium, from a mixture of reaction products of varying solubility. These problems were addressed by altering the substitution pattern of the benzyl moiety in an attempt to tune the solubility of the resulting compounds.

As a result, the first benzylcalcium complex (**3**; Figure 2) was reported from the reaction of the potassium salt of an α,α-bis(trimethylsilyl)-substituted toluene derivative with calcium iodide.[32] This compound crystallizes as the bis-THF adduct with a four-coordinate metal center with some additional weak π-contacts to the attendant phenyl rings. Interestingly, beyond these contacts (2.89−2.95 Å) no agostic interactions to the trimethylsilyl moieties are seen, probably as a result of the THF-metal interaction.

A related approach improved the solubility properties with intramolecular stabilization by means of a tethered dimethylamino moiety to give the diastereomeric benzylcalcium complex as its bis-THF adduct (**4**; Figure 3).[33] This benzene soluble derivative exhibits a six-coordinate distorted octahedral metal center with slightly shorter $Ca-C_\alpha$ distances than the α,α-disubstituted benzylide **3** as well as mixed hybridization of the α-carbons, with angles summing to 342(1)° and 346(1)°. Unlike **3**, this bidentate compound shows no additional aryl interactions. In solution, a temperature- and concentration-dependant exchange between diastereomers is observed; the addition of THF assists this exchange.

The first example of a heteroleptic benzylcalcium derivative displays fluorenyl stabilization with a distorted η^5 coordination (**5**).[39] One additional THF completes the coordination sphere of the metal. The metal-C_α distance of 2.50 Å is noticeably shorter than the purely σ-bound species **3**

Table 1. Details of dibenzylcalcium, -strontium and -barium derivatives

Compound	Aggr.	CN	M−C [Å]	D	M−D [Å]	ref.
$[Ca\{C_7H_5(SiMe_3)_2\}_2(THF)_2]$ (**3**)	1	4	2.65	THF	2.38	32
$[Ca\{C_8H_{10}N(SiMe_3)\}(THF)_2]_2$ (**4**)	1	6	2.64, 2.62	THF	2.44, 2.37	33
				NMe_2	2.56, 2.63	
$[Ca\{C_8H_{10}N(SiMe_3)(C_{13}H_8SiMe_3)\}(THF)]$ (**5**)	1	3+5[a]	2.50, 2.69−2.78	THF	2.30, 2.46	39
				NMe_2		
$[Na(OEt_2)][Ca(2\text{-}MeO\text{-}C_6H_4CHPPh'_2)_3]$ (**7**)[b]	1	6	2.53−2.57	OMe	2.42−2.44	40
$[Ca(2\text{-}O\text{-}C_6H_4CHPPh'_2)(THF)]_4$ (**8**)[b]	4	6	2.59	Ph−O$^-$	2.34−2.43,	40
				PPh'_2	2.99	
$[Sr\{C_8H_{10}N(SiMe_3)\}(THF)_2]_2$ (**6**)	1	6	2.77, 2.79	THF	2.53, 2.56	34
				NMe_2	2.76, 2.78	
$[Ba\{Ph_2P(CH_2C_6H_4\text{-}4\text{-}Me)_2\}_2]$ (**9**)	1	6+4[c]	2.98−4.07	PPh_2	3.71, 3.94	41

[a] Fluorenyl stabilized. [b] Ph′ = *p*-tolyl. [c] Two η^3- and two η^2-metal-carbon interactions.

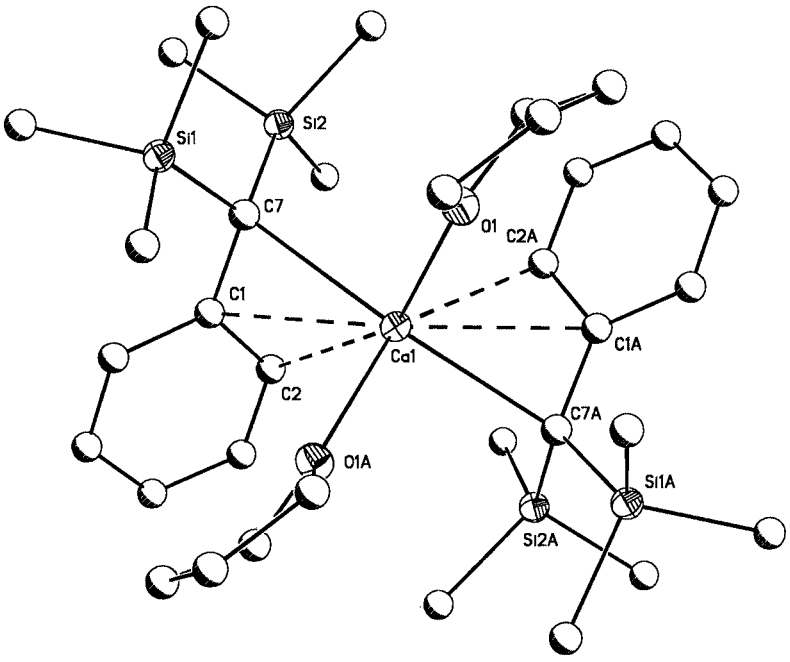

Figure 2. Molecular structure of **3**; heavy atoms displayed anisotropically with ellipsoids at 30% probability; hydrogen atoms have been omitted for clarity

and **4**, and is rationalized as a result of the π-stabilization afforded by the fluorenyl system.

Currently, the only example of a simple homoleptic dibenzylstrontium complex is the well-defined bis[(2-dimethylamino-α-trimethylsilyl)benzyl]strontium (**6**).[34] Like the calcium congener, this internally stabilized compound crystallizes as the bis-THF adduct. Unlike the calcium compound, however, there are several close contacts to the aryl rings, which may indicate an η^3-interaction. The geometry around the metal is strongly distorted, and takes up a nearly trigonal prismatic arrangement, with a bridging $C_\alpha-Sr-C_\alpha'$ angle of 143.5°, versus 157.5° for the calcium congener. This compound also crystallizes as a set of diastereomers, and shows slow exchange from the heterochiral to the homochiral orientation similar to that of the calcium compound. As in that example, the extra intramolecular stabilization afforded by the NMe_2 ligation and the added bulk of the $SiMe_3$ moiety result in a low coordination number at the metal center and good solubility, although apparently at the expense of the efficacy of the compound as a polymerization initiator. There appears to be a clear connection between the steric bulk and the reactivity of these compounds for polymerization; for detailed discussions on this topic we refer the reader to the original literature.[32−35]

The concept of internal stabilization and modification of the benzyl group was also utilized in the synthesis of two closely related organometallic complexes of calcium.[40] The first uses the stabilization of PPh_2' (Ph′ = *p*-tolyl) on the α-carbon along with internal coordination from a methoxy substituent on the benzyl ring to afford an example of a benzylcalcium complex (**7**; Figure 4). The parent hydrocarbon was lithiated in Et_2O, then transmetallated with sodium *tert*-butoxide followed by salt elimination with CaI_2. This compound assumes a coordination number of six, with the geometry around the metal lying between octahedral and trigonal prismatic. There are several agostic interactions be-

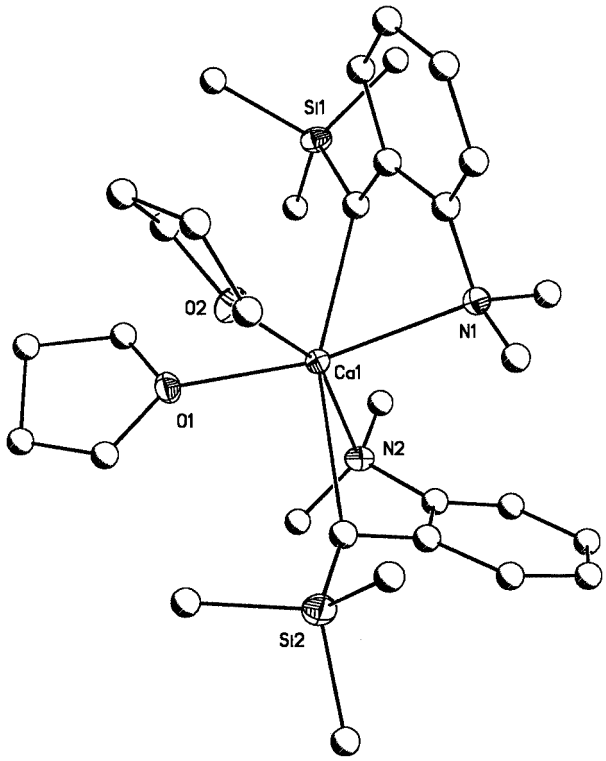

Figure 3. Molecular structure of **4**; heavy atoms displayed anisotropically with ellipsoids at 30% probability; hydrogen atoms have been omitted for clarity

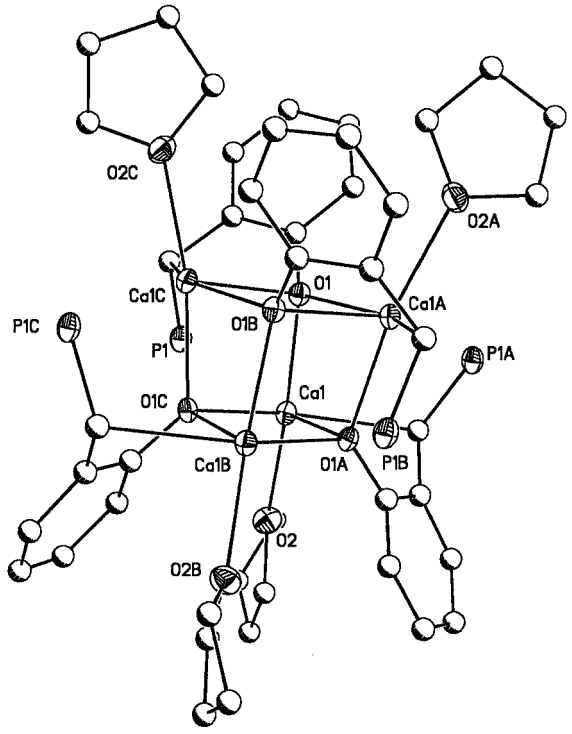

Figure 5. Molecular structure of **8**; heavy atoms displayed anisotropically with ellipsoids at 30% probability; hydrogen atoms and *p*-tolyl groups have been omitted for clarity

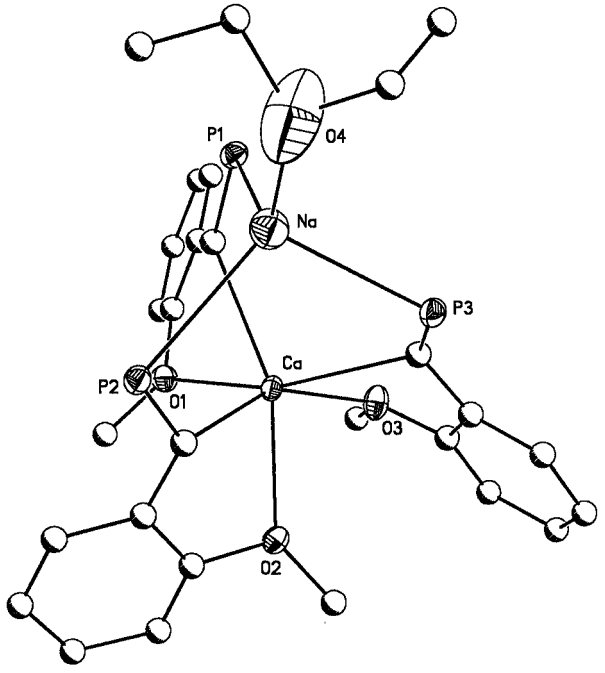

Figure 4. Molecular structure of **7**; heavy atoms displayed anisotropically with ellipsoids at 30% probability; hydrogen atoms and *p*-tolyl groups have been omitted for clarity

tween H_α and the metal center of 2.41 Å, possibly as a consequence of the calcium being situated out of the plane of the π-bound benzyl moieties. The phosphanyl groups do not coordinate to the calcium, but rather to the sodium counterion.

If the salt elimination reaction is instead carried out in THF, an ether cleavage occurs on the methoxy substituent leading to the formation of a tetrameric benzyl alkoxide derivative (**8**; Figure 5) in very low yield. The mechanism is explained by nucleophilic attack of the iodide ion at the carbon of the calcium-coordinated methoxy group. The resulting compound displays a distorted cuboidal structure with the oxygen atoms at alternate corners. This reaction illustrates one of the most prevalent problems in the organometallic chemistry of the heavy group 2 metals: ether cleavage is a common occurrence, limiting solvent and donor choices.

Another example of the use of phosphorus-bearing substituents is observed in barium phosphonium dibenzylide (**9**; Figure 6).[41] This example of a heavy organoalkaline earth metal compound is accessible through the reduction of the phosphonium ylide bromide with potassium amide followed by addition of 0.5 equivalents of barium amide. The ylidic ligand easily fills the coordination sphere of barium with numerous η^2- and η^3-interactions; the added bulk of the substituents affords a complex which is readily soluble in toluene, benzene and THF. The benzyl planes occupy four different orientations with respect to the metal, and the contact distances vary. For all four ylidic carbons, the angles add up to perfectly planar sp^2-bonding geometries.

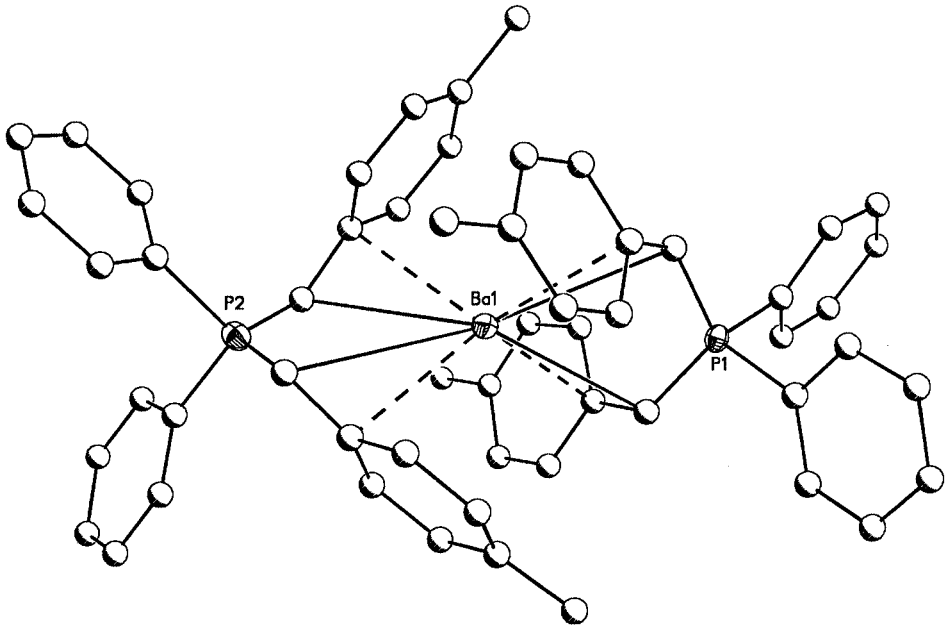

Figure 6. Molecular structure of **9**; heavy atoms displayed anisotropically with ellipsoids at 30% probability; hydrogen atoms have been omitted for clarity

The solubility of the dibenzyl derivatives can be adjusted by a careful choice of substituents, allowing for increased utility of these organometallics in an array of synthetic applications. The internal stabilization appears to play a key role in isolation and characterization.

6. "Ate" Complexes of Calcium, Strontium and Barium

The structural chemistry of "ate" complexes of the alkaline earth metals has been mostly limited to compounds of magnesium and beryllium.[42] There are many examples of anionic transition and main group organometallic compounds with beryllium and magnesium counterions, usually with a coordinating donor, but rarely in these cases do the metals display metal-carbon contacts. Several recent examples of such complexes involving heavy alkaline earth cations displaying metal-carbon bonds have been reported, as summarized in Table 2.

The addition of tris(trimethylsilylmethyl)alane and unsolvated calcium bis[bis(trimethylsilyl)amide] in a 2:1 molar ratio in toluene affords the dimeric calcium bis(trimethylsilyl)amide-tetrakis(trimethylsilylmethyl) aluminate (**10**; Figure 7).[43] The central Ca_2N_2 core of the complex is planar. The complex exhibits calcium-carbon distances of 2.68 and 2.64 Å. The close calcium-aluminum contact (3.25 Å) and the small Ca−C−Al angles (85.5° and 86.3°) might indicate the presence of three-center, two-electron bonding. There are several agostic interactions from the methylene hydrogens, also explaining the short Ca−Al contacts.

Several "ate" complexes have been obtained by the reaction of bis[(trimethylsilyl)methyl]zinc with freshly distilled alkaline earth metals with extrusion of elemental zinc. Utilizing this route, the reaction of freshly distilled strontium metal with bis[(trimethylsilyl)methyl]zinc in THF at room temperature over 24 hours yielded the strontium zincate (**11**; Figure 8).[44] This complex assumes a coordination number of six at the strontium center in a slightly distorted octahedral geometry as a result of the small chelation angle

Table 2. Details of -ate complexes of calcium, strontium and barium

Compound	Aggr.	CN	M−C [Å]	D	M−D [Å]	ref.
$Ca_2[Al(CH_2(SiMe_3)_4]_2[N(SiMe_3)_2]_2$ (**10**)	2	4	2.68, 2.63			43
$Sr(THF)_2[Zn(SiMe_3)(CH_2SiMe_3)_2]_2$ (**11**)	1	6	2.08, 2.02 2.10	THF	2.53	44
$Ba(THF)_4[Zn(SiMe_3)(CH_2SiMe_3)_2]_2$ (**12**)	1	8	3.09, 3.23 3.18, 3.17	THF	2.78−2.87	44
$Ba(Tol)_2[Zn(SiMe_3)(CH_2SiMe_3)_2]_2$ (**13**)	1	6	3.03, 3.05	Tol	3.37−3.41	44
$[Ba(THF)_3OZn_2(CH_2SiMe_3)_2(SiMe_2)]_2$ (**14**)	2	7	3.18, 3.24	O THF	2.51, 2.57 2.79−2.86	44
$Ba_4[Zn_6(CH_2SiMe_3)_4(CHSiMe_3)_3]_2$ (**15**)	2	5, 6	2.83−3.20			45

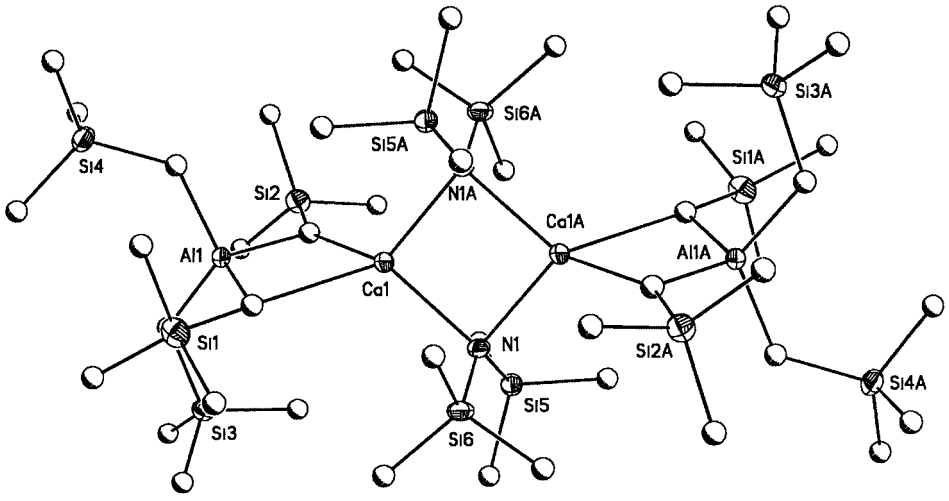

Figure 7. Molecular structure of **10**; heavy atoms displayed anisotropically with ellipsoids at 30% probability; hydrogen atoms have been omitted for clarity

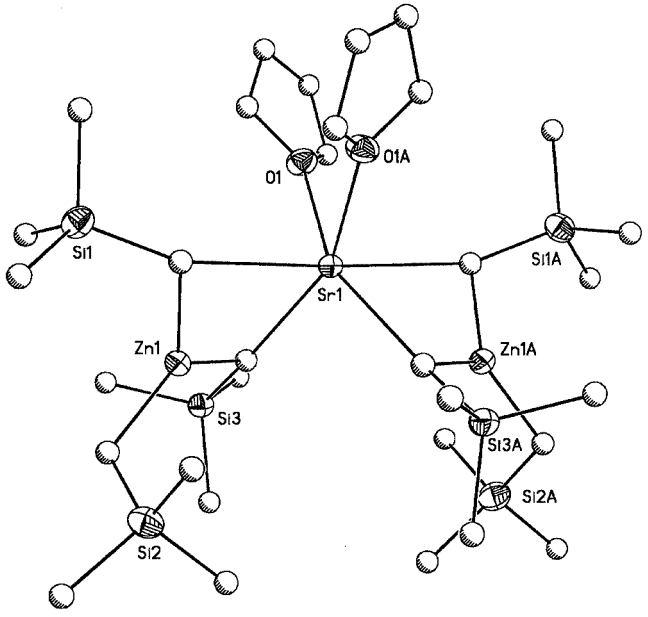

Figure 8. Molecular structure of **11**; heavy atoms displayed anisotropically with ellipsoids at 30% probability; hydrogen atoms have been omitted for clarity

afforded by the anion. The somewhat longer strontium-carbon contacts, as compared to other organostrontium compounds, are probably the result of the higher coordination number of the strontium as well as the result of a proposed Sr−C−Zn three-center, two-electron bonding mode through the core of the complex.

An analogous reaction between freshly distilled barium metal and a dialkylzinc derivative in THF affords the barium congener (**12**).[44] The larger radius of barium allows for an expanded coordination sphere filled by two additional THF donor molecules. Overall, the barium center possesses a coordination number of eight in a rather irregular geometry. As a result, the barium-carbon contacts are considerably longer than those of the strontium congener.

Repeating the reaction in toluene affords the bis-toluene adduct (**13**) of the zincate, with the toluene molecules π-bound to the barium metal center.[44] If each toluene is counted as filling one coordination site, then the coordination number of the barium is six, allowing a slightly distorted octahedral metal environment. This low coordination state, coupled with the steric shielding provided by the closely coordinated toluene donors also allows for shorter metal-carbon contacts than in the THF adduct (3.05 vs. 3.23 Å).

An attempt to obtain donor-free derivatives by using *n*-heptane as the solvent did not lead to a crystalline product. However, dropwise addition of THF to the reaction mixture led to a barium zincate/oxide (**14**; Figure 9).[44] This barium complex features a dimeric barium oxide with numerous contacts to THF donors and silyl substituents. An apparent rearrangement and elimination leads to the concurrent formation of a zinc silanide in situ, indicating the possibility of water or oxygen contamination causing the unexpected side reactions. The low coordinate zinc centers exhibit very short contacts to the oxygen atoms, while the barium-carbon distances are extremely long due to the lack of anionic charge located in these carbon centers.

A complex reaction of barium bis[tris(trimethylsilylmethyl)zincate] with excess barium, with extrusion of zinc metal, leads to the formation of a proposed alkylbarium moiety in situ. This highly reactive substrate reacts immediately with subsequently added metal and excess zincate to form the unique barium cubane (**15**; Figure 10) with extrusion of tetramethylsilane.[45] This distorted, face-sharing double cube possesses agostic interactions between the methylene groups and the nearby barium centers, in addition to metal-carbon σ-bonds within the range observed for other σ-bonded compounds.

In addition, this complex shows carbon ligands in the unusual coordination state of six, resulting in rather long contacts to the nearly trigonal planar environments of the zinc centers.

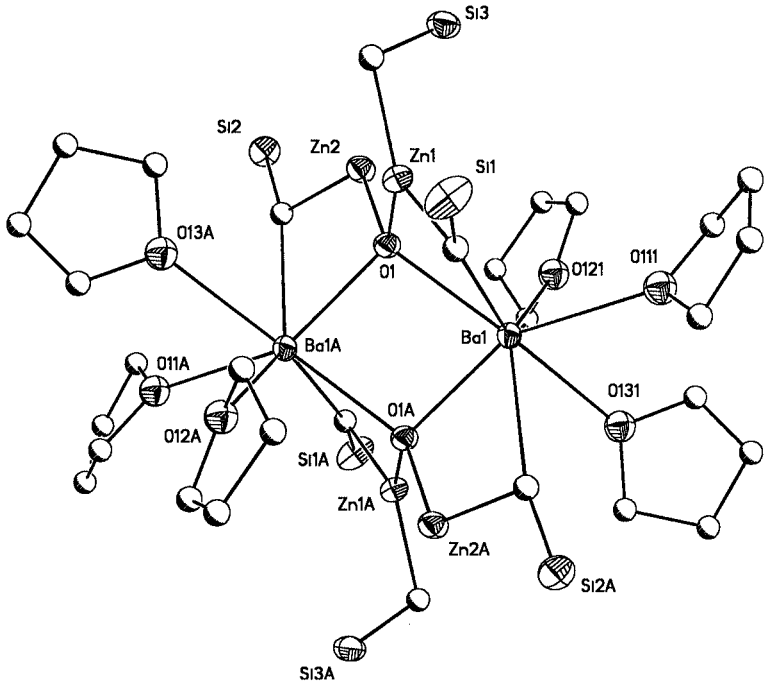

Figure 9. Molecular structure of **14**; heavy atoms displayed anisotropically with ellipsoids at 30% probability; hydrogen atoms and methyl groups have been omitted for clarity

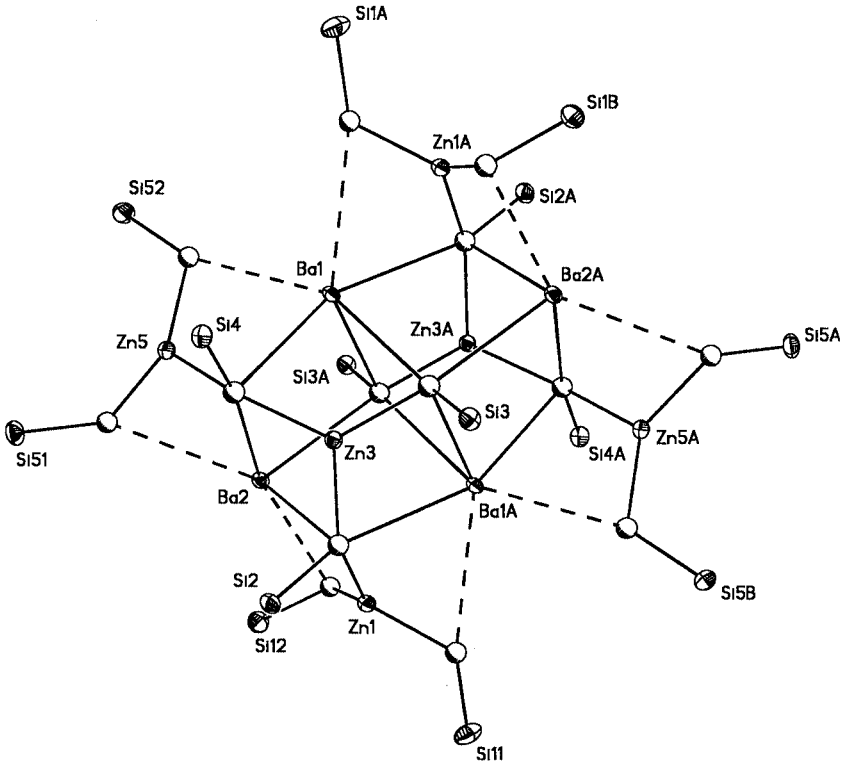

Figure 10. Molecular structure of **15**; heavy atoms displayed anisotropically with ellipsoids at 30% probability; hydrogen atoms and methyl groups have been omitted for clarity

Table 3. Details of σ-bonded complexes of the heavy alkaline earth metals

Compound	CN	M−C [Å]	C−M−C [°]	M−C_{ipso}−C [°]	ref.
$[Ca\{CH(SiMe_3)_2\}_2(C_4H_8O_2)_2]$ (**1**)	4	2.48	133.7		23
$[Ca\{C(SiMe_3)_3\}_2]$ (**2**)	2	2.46	149.7		24
$[Ca(CCSiMe_3)_2$(18-crown-6)] (**16**)	6	2.52, 2.56	168.7	162.4, 164.0	46
$[Sr(CCSiMe_3)_2$(18-crown-6)] (**17**)	6	2.69, 2.72	166.0	158.9, 159.7	46
$[Sr(CCPhtBu)_2$(18-crown-6)] (**19**)	6	2.69, 2.71[a]	180, 180[a]	166.4,167.0	48
$[Ba(CCSiMe_3)_2$(18-crown-6)] (**18**)	6	2.85	162.7	126.6, 141.3	46
$[Ba(CCPhtBu)_2$(18-crown-6)] (**20**)	6	2.86	180	115.8−145.7[b]	48

[a] Two independent molecules. [b] Acetylide ligands disordered over three positions.

7. Acetylides of the Heavy Group 2 Metals

The first examples of homoleptic heavy alkaline earth metal acetylides were reported recently;[46] these examples are summarized in Table 3.

The heavy Group 2 acetylides were prepared by transamination: reacting triphenylsilylethyne with a metal amide in THF at −78 °C with the addition of 18-crown-6. The geometry of these acetylides (**16**−**18**; the structure of **18** is shown in Figure 11) can be envisioned as distorted, pseudo-octahedral with the crown ether occupying the equatorial plane and the ligands filling the axial positions. The presence of the crown ether is critical for the formation of the acetylides. The complexes react with trace amounts of water to form siloxides and acetylene.[47]

The structural composition of the calcium, strontium and barium derivatives reveals a number of interesting trends, beginning with a smooth increase of metal-C_α distances with increasing size of the metal. Of particular note is an unexpected bend angle through the presumably sp-hybridized *ipso*-carbon, with a value of 168° for the calcium congener decreasing to 127° for the barium complex. This unexpected geometry led to several suggestions to explain the surprising results, including a lack of directionality in the ethyne sp orbital and subsequent freedom of motion. Other possibilities include the potential for partial rehybridization of the acetylide moiety, a possible side-on π-interaction of the ligand with the heavier metals, or crystal packing effects.

To further probe these trends, the effects of the ligands on the structural features were examined with the synthesis of less sterically demanding acetylides. Utilization of the same transamination pathway with *para-tert*-butylphenylethyne led to the formation of the strontium and barium acetylides (**19**; Figure 12) and **20**.[48] It was expected that the smaller phenyl substituents would experience a reduced steric repulsion with the crown ether ring and allow for more flexibility and perhaps an even closer approach of the ligand to the crown ether than in the bulkier triphenylsilyl analogs.

Intriguingly, very similar geometrical features were observed for both groups of acetylides, suggesting that simple steric models do not satisfactorily explain the unexpected geometry. DFT calculations to shed further light on this topic are currently underway.[49]

8. Di- and Triphenylmethanides

Organometallic di- and triphenylmethanide complexes of the alkali metals are well-known.[50] In contrast, such compounds of the heavier alkaline earth metals are rare; only the compounds shown in Table 4 have been structurally characterized.[51] Of particular interest in these systems is the structural geometry about the methyl carbon, as the

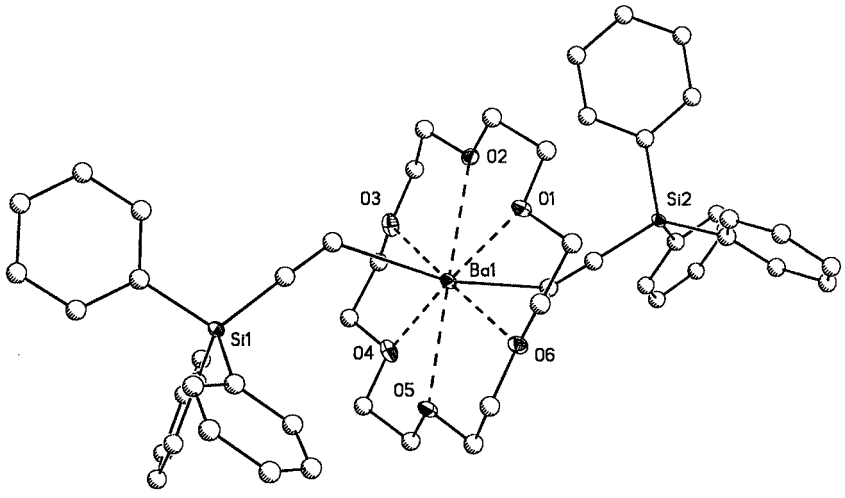

Figure 11. Molecular structure of **18**; heavy atoms displayed anisotropically with ellipsoids at 30% probability; hydrogen atoms have been omitted for clarity

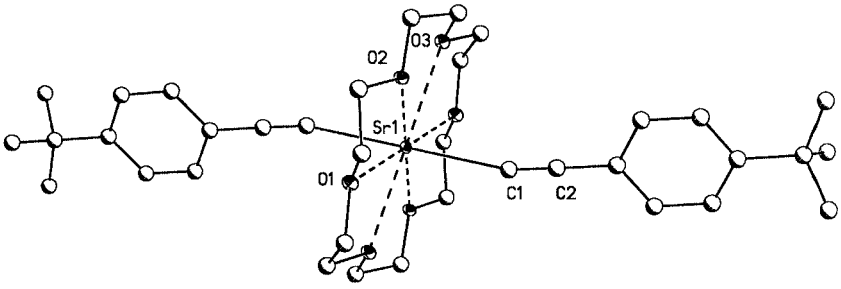

Figure 12. Molecular structure of **19**; heavy atoms displayed anisotropically with ellipsoids at 30% probability; hydrogen atoms have been omitted for clarity

Table 4. Di- and triphenylmethanes, contact and ion pairs

Compound	CN	M−R [Å]	D	M−D [Å]	ref.
$[Sr(CPh_3)_2(HMPA)_2(18\text{-crown-6})]$ (**24**)[a]	6		HMPA	2.41	53
			18-c-6	2.68−2.72	
$[Sr\{N(SiMe_3)_2\}]_2(C_{12}H_{23}O_2)$ (**23**)	7	2.57[b]	O[c]	2.47, 2.42	53
			18-c-6[d]	2.72−2.88	
$[Ba(CPh_3)_2(HMPA)_2(18\text{-crown-6})]$ (**22**)	6		HMPA	2.59	52
			18-c-6	2.78−2.79	
$[Ba\{N(SiMe_3)_2\}(C_{12}H_{23}O_2)]_2$ (**21**)	7	2.71[b]	O[c]	2.57, 2.61	52
			18-c-6[d]	2.61−2.95	
$[Ba(HCPh_2)_2(18\text{-crown-6})]$ (**25**)	7	3.07, 3.10 3.39[e]	18-c-6	2.75−2.80	54
$[Ba\{\eta^5\text{-}PhCH(C_5H_4N)\}(THF)(diglyme)]$ (**26**)	4 + 5[f]	2.76−3.30	THF	2.82	56
			Diglyme	2.77−2.86	

[a] HMPA = Hexamethylphosphoramide. [b] Metal-amide distance. [c] Bridging alkoxy anion. [d] Cleaved crown ether distances. [e] Close phenyl contact. [f] Two η^5-metal-carbon interactions.

level of resonance through the phenyl rings can be derived from studies of this type.

Early attempts to synthesize group 2 triphenylmethanides focussed on the transamination route employed successfully to prepare the acetylides (**16**−**20**). Reaction of triphenylmethane and barium bis[bis(trimethylsilyl)]amide in the presence of 18-crown-6 in THF at low temperature did not afford the desired product; instead, cleavage of the crown ether and subsequent elimination of free amine led to the formation of the heteroleptic vinyl ether amide (**21**; Figure 13).[52]

This heteroleptic barium amide exists as a dimer, with two slightly asymmetrically bridging alkoxide moieties connecting the two metal centers. The opposite face is filled by an amide ligand, and the vinyl ether wraps around the equator of the barium atom giving four additional metal-oxygen interactions for a total coordination number of seven. This reproducible product continued to form even with the switch to an arene elimination route utilizing dibenzylbarium. It was not until the addition of HMPA (HMPA = hexamethylphosphoramide) in conjunction with the arene elimination route that charge separation was induced and the desired product observed.

The barium triphenylmethanide crystallizes as a separated ion pair, with the metal center occupying a center of symmetry (**22**; Figure 14). The crown ether fills the equatorial plane, while two HMPA molecules occupy the axial sites. The metal lies almost directly at the center of the crown ether ring, at an average M−O distance of 2.78 Å. The triphenylmethanide anions exhibit a "propeller" geometry, with the center of the anion fully planarized, suggesting considerable resonance through the phenyl rings. The rings are too sterically demanding to be coplanar and so twist out of the plane by an average of 31.1°. One of the phenyl substituents exhibits a slightly longer bond length to the methyl center; this ring possesses the greatest twist angle, reducing the possible orbital overlap and subsequent resonance stabilization. It is noteworthy that the crown ether is cleaved rather than the THF solvent.

Similarly, the strontium congeners (**23**) and (**24**) of these complexes can be prepared.[53] Reaction of triphenylmethane with strontium bis[bis(trimethylsilyl)]amide with 18-crown-6 in THF at low temperatures leads to the heteroleptic vinyl ether amide (**23**). This compound adopts the same basic geometry as the barium congener, with a similar bridged dimeric structure. As expected, the bonds in the strontium complex overall are slightly shorter than those in the barium compound. The metal centers are still seven coordinate with the cleaved ether wrapping around to complete the coordination sphere.

The strontium triphenylmethanide can be synthesized analogously to the barium congener.[53] Preparation via arene elimination with dibenzylstrontium in the presence of triphenylmethane and HMPA in THF at low temperature

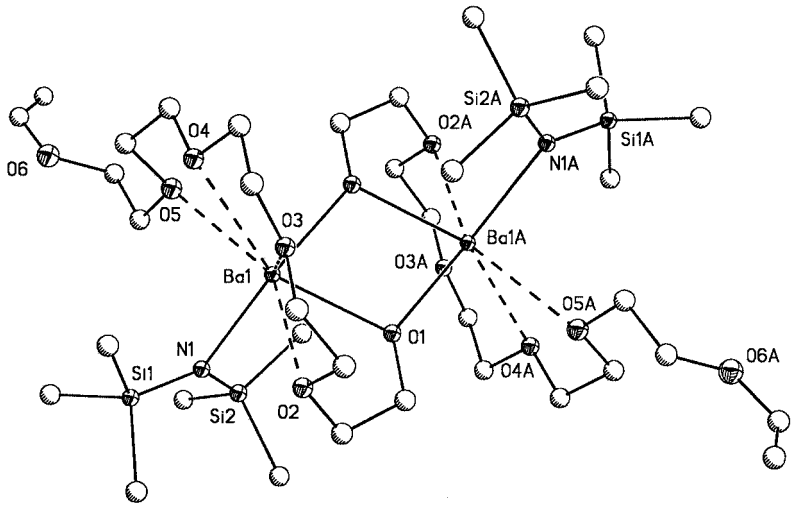

Figure 13. Molecular structure of **21**; heavy atoms displayed anisotropically with ellipsoids at 30% probability; hydrogen atoms have been omitted for clarity

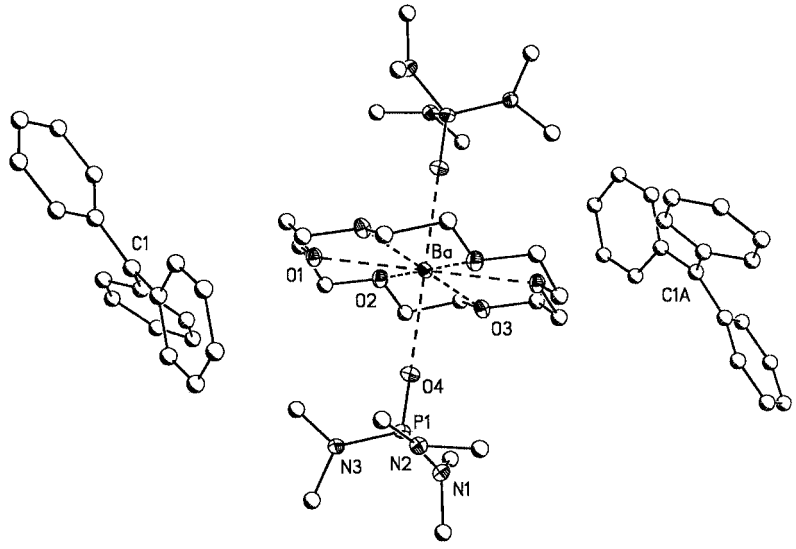

Figure 14. Molecular structure of **22**; heavy atoms displayed anisotropically with ellipsoids at 30% probability; hydrogen atoms have been omitted for clarity

leads to the charge-separated strontium triphenylmethanide (**24**). This complex adopts a structure analogous to the barium congener, with the anions exhibiting a "propeller" geometry. The methyl center is planar, and the phenyl rings twist out of the plane by an average of 30.6°. The ring showing the greatest twist angle leads to the longest C-C distance. If dibenzylbarium is treated with diphenylmethane in the presence of 18-crown-6, the contact barium diphenylmethanide (**25**; Figure 15) stabilized by 18-crown-6 is observed.[54]

Compound **25** crystallizes out of warm THF as a nine-coordinate distorted pseudo-octahedron with the methanide anions capping the axial positions over the crown ether encapsulated metal. The α-carbons in the ligand are slightly pyramidal. The phenyl rings are not coplanar, and are twisted slightly away from the methyl center by an average of 5.5°. Curiously, this compound is stable enough in THF to allow for recrystallization without any of the ether cleavage reactions observed for the triphenylmethanide system. It is possible that the lower steric demand of the diphenylmethanide anion plays a key role. Similar chemistry using dibenzylbarium, diphenylmethane and six equivalents of HMPA led to a charge-separated diphenylmethanide compound with six HMPA donors stabilizing the barium cation. Insufficient crystal quality has thus far prevented a satisfactory structure elucidation.[55]

An earlier example of a heavy alkaline earth dibenzyl system comes with the metallation of 2-pyridylphenylmethane in liquid NH_3/THF with barium and the addition of diglyme (**26**; Figure 16).[56] This "open metallocene" has the potential to add stabilization through coordination of the pyridyl moiety. The metal center is saturated with two η^3-contacts, two pyridyl contacts, one diglyme and one THF molecule. Although the ligands show conjugation through

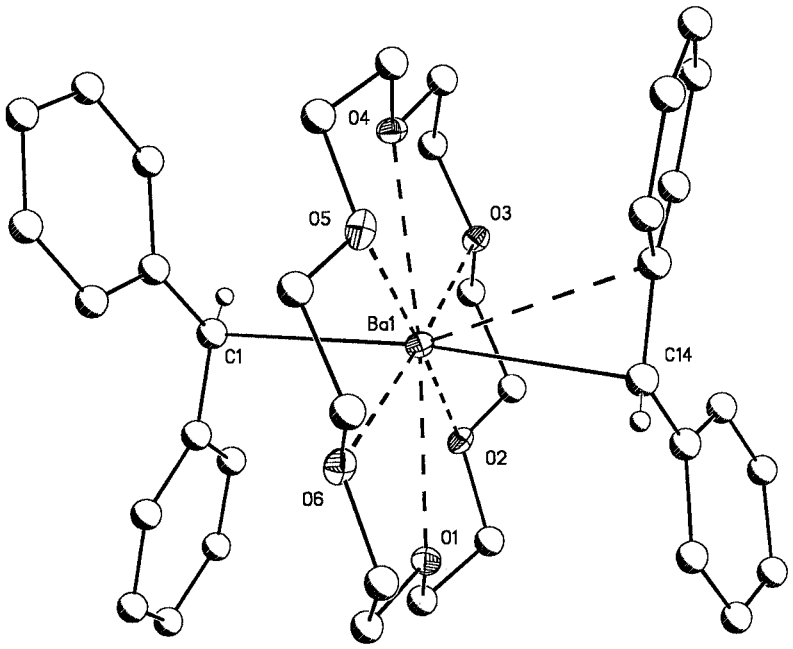

Figure 15. Molecular structure of **25**; heavy atoms displayed anisotropically with ellipsoids at 30% probability; hydrogen atoms except those on the *ipso* carbons have been omitted for clarity

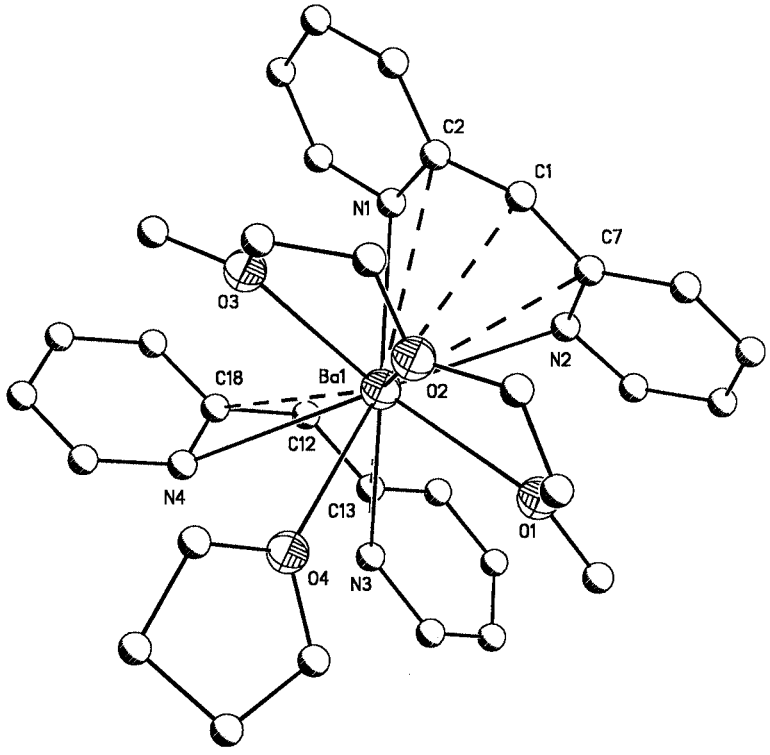

Figure 16. Molecular structure of **26**; heavy atoms displayed anisotropically with ellipsoids at 30% probability; hydrogen atoms have been omitted for clarity

the *ipso*-carbons (C_{ipso}−C distances of 1.41−1.43 Å) the rings are tilted away from the metal center (dihedral angles of 16.0°, 21.8°). Interestingly, the steric bulk of the ligands appears to be of little consequence, as they are pushed quite near each other by the approach of the donor.

9. Conclusions

With the advent of new synthetic methods and an array of possible applications the once sparsely investigated organometallic chemistry of calcium, strontium and barium

is coming to the forefront of main group chemistry. A wide variety of compounds once thought inaccessible are now being prepared simply and efficiently, and the interesting structural features of these complexes and the questions they raise demand further examination. With the synthesis and structural characterization of new targets, information on the relationship between structure and reactivity is slowly becoming clear. This will have a profound effect on the possible applications of the target molecules. Future investigations will extend to new ligand systems and alternative synthetic pathways to probe the fascinating geometry, unusual chemical properties and various applications exhibited by this exciting new collection of compounds.

Note added in proof (July 24, 2002): After submission of this article we became aware of two publications which are of importance to this review.[57,58]

Acknowledgments

We are deeply indebted to Professor Dr. Matthias Westerhausen and Priv. Doz. Dr. Sjoerd Harder for sharing information prior to publication. We are also grateful to Dr. Jesse Taylor for his assistance in designing illustrations.

[1] G. E. Coates, M. L. H. Green, K. Wade, *The Main Group Elements*, Meuthen & Co., London, **1969**;Vol. 1.
[2] C. Elschenbroich, A. Salzer, *Organometallics* 2nd ed., VCH: New York, **1992**.
[3] K. Ziegler, H. Froitzheim-Kehlhorn, K. Hafner, *Chem. Ber.* **1956**, *89*, 434−443.
[4] T. P. Hanusa, *Polyhedron* **1990**, *9*, 1345−1362.
[5] [5a] T. P. Hanusa, *Chem. Rev.* **1993**, *93*, 1023−1036. [5b] T. P. Hanusa, *Organometallics* **2002**, *21*, 2559−2571.
[6] D. J. Burkey, T. P. Hanusa, *Comments Inorg. Chem.* **1995**, *17*, 41−77.
[7] J. Overby, T. P. Hanusa, *Organometallics* **1996**, *15*, 2205−2212.
[8] G. Masges, F. Hampel, P. v. R. Schleyer, *Organometallics* **1992**, *11*, 1769−1770.
[9] K. Allan, B. G. Gowenlock, W. E. Lindsell, *J. Organomet. Chem.* **1974**, *65*, 1−7.
[10] S. Drake, D. Otway, *Polyhedron* **1992**, *11*, 745−758.
[11] K. A. Allen, B. G. Gowenlock, W. E. Lindsell, *J. Organomet. Chem.* **1973**, *55*, 229−235.
[12] B. Gowenlock, W. E. Lindsell, B. Singh, *J. Chem. Soc., Dalton Trans.* **1978**, 657−664.
[13] R. Masthoff, G. Kreig, *Z. Chem.* **1966**, *6*, 433−434.
[14] R. Masthoff, H. Schyler, G. Kreig, *J. Organomet. Chem.* **1968**, *13*, 37−43.
[15] V. Masthoff, C. Vieroth, *J. Prakt. Chem.* **1968**, 182−189.
[16] D. Bryce-Smith, A. Skinner, *J. Chem. Soc. A.* **1963**, 577−585.
[17] M. Coles, F. Hart, *J. Organomet. Chem.* **1971**, *32*, 279−284.
[18] N. Kawabata, A. Matsumura, S. Yamashita, *Tetrahedron* **1973**, *28*, 1069−1071.
[19] N. Kawabata, A. Matsumura, S. Yamashita, *J. Org. Chem.* **1973**, *38*, 4268−4270.
[20] K. Takahishi, Y. Kondo, R. Asami, *J. Chem. Soc., Perkin Trans. 2* **1978**, 577−580.
[21] D. J. Payne, R. T. Sanderson, *J. Am. Chem. Soc.* **1958**, *80*, 5324.
[22] See for example: K. C. Jayaratne, L. S. Fitts, T. P. Hanusa, V. G. Young, Jr, *Organometallics* **2001**, *20*, 3638−3640.
[23] F. G. Cloke, P. Hitchcock, M. Lappert, G. Lawless, B. Royo, *J. Chem. Soc., Chem. Commun.* **1991**, 724−726.
[24] C. Eaborn, S. Hawkes, P. Hitchcock, J. D. Smith, *Chem. Commun.* **1997**, 1961−1962.
[25] [25a] M. Westerhausen, *Angew. Chem. Int. Ed.* **2001**, *40*, 2975−2977. [25b] T. P. Hanusa, *Coord. Chem. Rev.* **2000**, *210*, 329−367, and references therein.
[26] [26a] W. A. Herrmann, N. Auner, U. Klingebeil, *Synthetic Methods of Organometallic and Inorganic Chemistry, Vol. 2* **1996**, Thieme, NY, 62−63. [26b] M. Westerhausen, *Inorg. Chem.* **1991**, *30*, 96−101.
[27] S. Chadwick, U. Englich, B. C. Noll, K. Ruhlandt-Senge, *Inorg. Chem.* **1998**, *37*, 4718−4725.
[28] See for example: S. Chadwick, U. Englich, K. Ruhlandt-Senge, *Angew. Chem. Int. Ed.* **1998**, *37*, 3007−3009.
[29] See for example: M. Westerhausen, M. Digeser, C. Gueckel, H. Nöth, J. Knizek, W. Ponikwar, *Organometallics* **1999**, *18*, 2491−2496.
[30] M. J. McCormick, K. B. Moon, S. P. Jones, T. P. Hanusa, *J. Chem. Soc., Chem. Commun.* **1990**, 778−779.
[31] See for example: J. D. Woolius, *Inorganic Experiments*, 1994, VCH, New York, 260.
[32] F. Fiel, S. Harder, *Organometallics* **2000**, *19*, 5010−5015.
[33] S. Harder, F. Fiel, A. Weeber, *Organometallics* **2001**, *20*, 1044−1046.
[34] F. Fiel, S. Harder, *Organometallics* **2001**, *20*, 4616−4622.
[35] A. Weeber, S. Harder, H. Britzinger, *Organometallics* **2000**, *19*, 1325−1332.
[36] See for example: [36a] G. B. Deacon, D. Stellfeldt, G. Meyer, *Z. Anorg. Allg. Chem.* **2000**, *626*, 623−624. [36b] C. Forsyth, G. B. Deacon, *Organometallics* **2000**, *19*, 1205−1207.
[37] D. M. Jenkins, W. Teng, U. Englich, D. Stone, K. Ruhlandt-Senge, *Organometallics* **2001**, *20*, 4600−4606.
[38] M. Kaupp, *Angew. Chem. Int. Ed.* **2001**, *40*, 3534−3565.
[39] S. Harder, F. Feil, K. Knoll, *Angew. Chem. Int. Ed.* **2001**, *40*, 4261−4264.
[40] V. Knapp, G. Müller, *Angew. Chem. Int. Ed.* **2001**, *40*, 183−186.
[41] S. Harder, M. Lutz, *Organometallics* **1997**, *16*, 225−230.
[42] S. Chadwick, PhD dissertation, Syracuse University, 1997.
[43] M. Westerhausen, H. Birg, H. Nöth, J. Knizek, T. Siefert, *Eur. J. Inorg. Chem.* **1999**, 2209−2214.
[44] M. Westerhausen, C. Gückel, T. Habereder, M. Vogt, M. Warchhold, H. Nöth, *Organometallics* **2001**, *20*, 893−899.
[45] M. Westerhausen, C. Gückel, P. Mayer, *Angew. Chem. Int. Ed.* **2001**, *40*, 2666−2668.
[46] D. C. Green, U. Englich, K. Ruhlandt-Senge, *Angew. Chem. Int. Ed.* **1999**, *38*, 354−357.
[47] D. C. Green, M. S. Thesis, Syracuse University, **1999**.
[48] J. S. Alexander, K. Ruhlandt-Senge, manuscript in preparation.
[49] J. S. Alexander, K. Ruhlandt-Senge, B. Hudson, manuscript in preparation.
[50] See for example: [50a] J. J. Brooks, G. D. Stucky, *J. Am. Chem. Soc.* **1972**, *94*, 7333−7338. [50b] R. A. Bartlett, H. V. R. Dias, P. P. Power, *J. Organomet. Chem.* **1988**, *341*, 1−9. [50c] H. Koster, E. Weiss, *J. Organomet. Chem.* **1979**, *168*, 273−279. [50d] D. Hoffman, W. Bauer, P. R. von Schleyer, U. Pieper, D. Stalke, *Organometallics* **1993**, *12*, 1193−1200. [50e] H. Viebrock, T. Panther, U. Behrens, U. Weiss, *J. Organomet. Chem.* **1995**, *491*, 19−25.
[51] L. M. Engelhardt, S. Harvey, C. L. Raston, A. H. White, *J. Organomet. Chem.* **1988**, *341*, 39−51.
[52] J. S. Alexander, K. Ruhlandt-Senge, *Angew. Chem. Int. Ed.* **2001**, *40*, 2658−2660.
[53] J. S. Alexander, K. Ruhlandt-Senge, unpublished results.
[54] J. S. Alexander, K. Ruhlandt-Senge, manuscript in preparation.
[55] J. S. Alexander, K. Ruhlandt-Senge, unpublished results.
[56] M. G. Gardiner, C. L. Raston, H. Viebrock, *Chem. Commun.* **1996**, 1795−1796.
[57] S. Harder, F. Fiel, *Organometallics* **2002**, *21*, 2268−2274.
[58] M. Westerhausen, C. Gueckel, H. Piotrowski, *Z. Anorg. Allg. Chem.* **2002**, *628*, 735−740.

Received March 21, 2002
[I02148]

Theoretical Study of an Isolable Compound with a Short Silicon-Silicon Triple Bond, $(t\mathrm{Bu_3Si})_2\mathrm{MeSiSi{\equiv}SiSiMe}(\mathrm{Si}t\mathrm{Bu_3})_2$

Nozomi Takagi[a] and Shigeru Nagase*[a]

Keywords: Silicon / Multiple bonds / Substituent effects / Density functional calculations

The effects of a very bulky silyl group [R**, -SiMe(Si-tBu$_3$)$_2$] — developed recently by Wiberg and co-workers — on silicon-silicon triple bonding have been investigated by density functional theory in search of a stable disilyne. These calculations predict that R**Si≡SiR** is stable enough to be isolated and has a short Si-Si bond length of 2.072 Å that is short enough to be a triple bond.

(© Wiley-VCH Verlag GmbH, 69451 Weinheim, Germany, 2002)

Introduction

Since the first isolation of a stable disilene ($R_2Si{=}SiR_2$) in 1981,[1] a variety of synthetic methods have been developed for the synthesis of silicon-silicon doubly bonded compounds, as summarized in recent reviews.[2−4] However, stable silicon-silicon triply bonded compounds [disilynes (RSi≡SiR)] are still unknown, despite several attempts to isolate them,[5] except for their transient existence as intermediates.[6,7] It is the focus of much current interest whether disilynes are synthetically accessible and isolable as stable compounds.[3,4,8,9] The major difficulty in synthesizing and isolating disilynes is due to their high reactivities, especially toward isomerization and dimerization.[10−14] To suppress these reactivities, substituent effects have been extensively investigated.[10−14] Bulky aryl groups such as Tbt [C_6H_3-2,4,6-{$CH(SiMe_3)_2$}$_3$] and Ar* [C_6H_3-2,6-(C_6H_2-2,4,6-iPr$_3$)$_2$][15] have been suggested as sterically promising substituents.[12,13]

According to theoretical investigations,[10,11] substitution by electropositive silyl groups is electronically much more effective in realizing a less trans-bent disilyne structure with a short silicon-silicon multiple bond. Thus, silyl groups such as SitBu$_3$ and SiDep$_3$ (Dep = 2,6-diethylphenyl) have been tested as bulky candidates.[10,11] However, it has been found that they are not sufficiently bulky to make disilynes isolable under normal conditions.[12,16] Therefore, the availability of much bulkier silyl groups has been anticipated. In this context, it is worthy to note that Wiberg and co-workers have very recently developed the extremely bulky silyl group R** [SiMe(SitBu$_3$)$_2$] and succeeded in synthesizing and isolating a stable 1,2-dichlorodisilene, R**ClSi=SiClR**, with the R** groups in trans positions, as reported in this journal.[17] It has been suggested that dechlorination of R**ClSi=SiClR** could lead to an isolable disilyne, R**Si≡SiR**. To confirm this interesting suggestion, we have performed theoretical calculations on R**Si≡SiR**.

Results and Discussion

Hybrid density functional calculations at the B3LYP level[18] were performed with the 3-21G* basis set,[19] as in a series of previous studies,[10−14] using the Gaussian 98 program.[20] Since the structure of R**ClSi=SiClR** has been determined by X-ray crystal analysis,[17] its geometry optimization was first carried out to calibrate the B3LYP/3-21G* calculations. As found for the X-ray crystal structure, it was calculated that R**ClSi=SiClR** has a planar structure around the Si-Si double bond with C_i symmetry. The calculated bond lengths and angles were R**-Si = 2.397 Å, Cl−Si = 2.116 Å, R**-Si-Si = 135.9°, and Cl−Si−Si = 108.0°. These values agree very well with the X-ray crystal data of R**-Si = 2.401 Å, Cl−Si = 2.091 Å, R**-Si-Si = 132.0°, and Cl−Si−Si = 106.8°. The Si-Si double bond length was calculated to be 2.171 Å, this being only 0.008 Å longer than the X-ray crystal structure value of 2.163 Å.

The optimized structure of R**Si≡SiR** is shown in Figure 1; it has C_2 symmetry. Owing to the two bulky R** groups, the skeleton of R**Si≡SiR** is only twisted around the central Si-Si bond by 1.0°, as shown by the dihedral R**-Si-Si-R** angle (ω) of 179.0°. However, the two bulky R** groups help to protect the central Si-Si bond from the attack of reactive reagents (see Figure 1). Silicon has a low tendency to form an ideal hybrid orbital because of the size difference between valence s and p orbitals.[10,11,21] For this reason, it is normal that disilynes prefer a highly trans-bent structure with some lone pair character at each Si atom, in contrast to the well-known linear

[a] Department of Theoretical Studies, Institute for Molecular Science,
Okazaki 444-8585, Japan
E-mail: nagase@ims.ac.jp

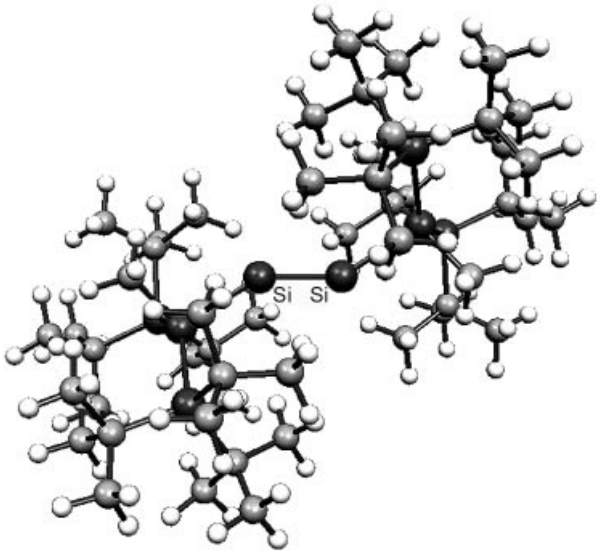

Figure 1. Optimized structure of R**Si≡SiR**; Si-Si = 2.072 Å and R**-Si-Si = 148.0°

structure of the carbon analogues. For R**Si≡SiR**, the R**-Si-Si bond angle (θ) was calculated to be 148.0°. It is noticeable that the trans-bending is 23.1° smaller than that for HSi≡SiH (θ = 124.9°). In addition, the energy difference between trans-bent and linear structures is only 5.5 kcal/mol for R**Si≡SiR**, while it is 20.3 kcal/mol for HSi≡SiH.

More interesting is the central Si-Si bond length of 2.072 Å calculated for R**Si≡SiR**, which is shorter than that of 2.093 Å for HSi≡SiH and considerably shorter than those of 2.121 and 2.136 Å calculated at the same level of theory for TbtSi≡SiTbt (θ = 130.9° and ω = 180.0°)[12] and Ar*Si≡SiAr* (θ = 129.0° and ω = 171.2°),[13b] owing to the much less trans-bent structure. The advantage of the R** group in the Si-Si bond shortening and skeletal linearization for R**Si≡SiR** is due to the fact that the SiR** components have a very small doublet-quadruplet energy difference of 28.5 kcal/mol because of the electropositive character of R**, as compared with the values of 42.6, 50.1, and 55.1 kcal/mol for SiH, SiTbt, and SiAr*, respectively; for the importance of the small doublet-quadruplet energy gap, see refs.[10,11]

The Si-Si bond length of 2.072 Å for R**Si≡SiR** is 0.1 Å shorter than the Si-Si double bond length of R**ClSi=SiClR** and 0.13−0.18 Å shorter than those of 2.202−2.251 Å determined for tetrasilyldisilenes $R_2Si=SiR_2$ (R = $SiMe_2t$Bu, $SiMei$Pr$_2$, and SiiPr$_3$).[22] These results clearly suggest that R**Si≡SiR** possesses an additional bond between the Si atoms, as compared with disilenes; it is interesting that the Si-Si distance is very close to an "idealized" Si-Si triple bond length of 2.025 Å in the linear structure of R**Si≡SiR**.[23] In an attempt to reduce the crowding of the substituents, the Me group in R** [$SiMe(Sit$Bu$_3)_2$] was replaced by an H atom. After this replacement the Si-Si distance increased to 2.081 Å, and the trans-bending and twisting were enhanced by 4.6 and 6.1°, respectively, thus showing that even the small Me group in R** plays an important role.[24]

The bulk of the R** group helps to destabilize the 1,2-R**-shifted isomer SiSiR**R**, because the two R** groups crowd more around one end of the Si-Si bond, as is apparent from Figure 2. Thus, R**Si≡SiR** was calculated to be 33.4 kcal/mol more stable than SiSiR**R**. This energy difference is large enough to prevent the 1,2-R** shift in R**Si≡SiR**. The corresponding energy differences are 18.5 and 37.9 kcal/mol for TbtSi≡SiTbt[12] and Ar*Si≡SiAr*,[13b] while they are only 9.8 and 12.0 kcal/mol for tBu$_3$SiSi≡SiSitBu$_3$ [10] and Dep$_3$SiSi≡SiSiDep$_3$,[10] respectively.

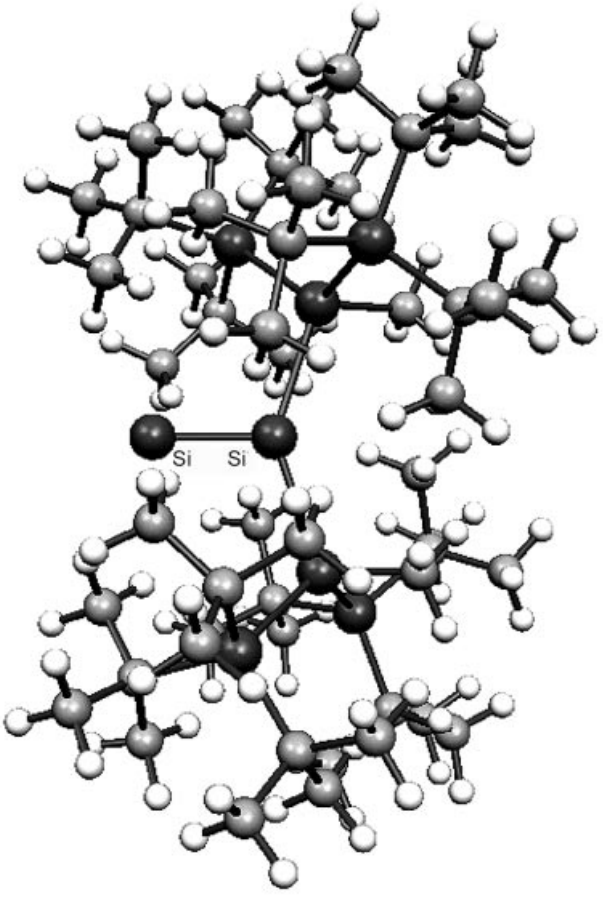

Figure 2. Optimized structure of the SiSiR**R** isomer; Si-Si = 2.187 Å and R**-Si-R** = 143.9°

Because of the bulk of the R** group, it may be argued that R**Si≡SiR** dissociates readily in solution. However, the energy required to cleave the central Si-Si bond (leading to two SiR** fragments in the doublet ground-state) was calculated to be 55.1 kcal/mol, this value being larger than those of 51.8 and 37.9 kcal/mol calculated for TbtSi≡SiTbt[12] and Ar*Si≡SiAr*,[13b] respectively. The dissociation energy of R**Si≡SiR** is 20.3 kcal/mol larger than the value of 34.8 kcal/mol calculated for R**ClSi=SiClR** (leading to two SiClR** fragments in the singlet ground-state), confirming that the two central Si atoms are strongly bonded in R**Si≡SiR**. According to orbital analysis, the

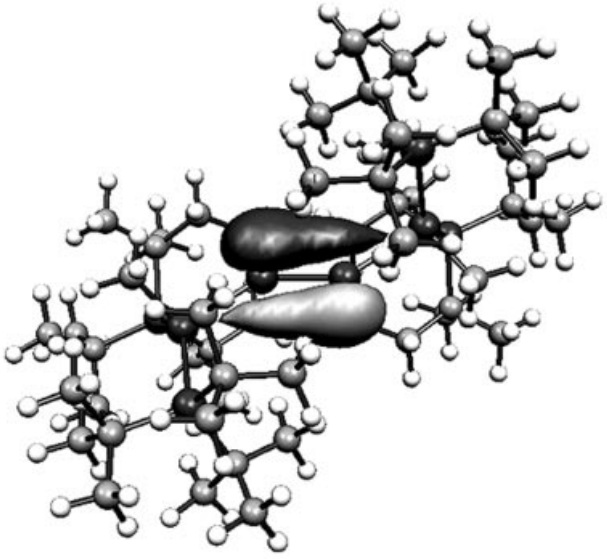

Figure 3. The Si-Si π-bonding orbital in the R*-Si-Si-R* plane of R**Si≡SiR** plotted with a value of 0.05 au

Figure 4. Optimized tetrasilabutadiene structure of the R**Si≡SiR** dimer; Si−Si = 2.227−2.534 Å and Si−Si−Si = 88.7−91.0°

Si≡Si bonding consists of a slightly distorted σ-bond, an out-of-plane π-bond, and a slipped in-plane π-bond due to the σ* mixing.[23] There has been much debate on the bonding contribution of a slipped π-bond.[3,5,8] As Figure 3 shows, however, the slipped in-plane π-orbital of R**Si≡SiR** has considerable bonding character between the Si atoms and helps to form a strong triple bond, though it is localized on each Si atom and becomes nonbonding as the trans-bending increases.

The most important obstacle to the isolation of disilynes is their facile dimerization to form tetrasilatetrahedrane or more stable tetrasilacyclobutadiene structures. To investigate to what extent R**Si≡SiR** is stable towards dimerization, calculations were carried out for a dimer of large size (a total of 1660 basis functions at the B3LYP/3-21G* level). Up to now, it has been predicted that the dimerization of tBu$_3$SiSi≡SiSitBu$_3$ [12] and Dep$_3$SiSi≡SiSiDep$_3$ [16] to form tetrasilatetrahedrane structures is exothermic by 80 and 32 kcal/mol, respectively. In this context, it is interesting to note that a stable tetrasilatetrahedrane has been synthesized using a reaction that involves most probably tBu$_3$SiSi≡SiSitBu$_3$ as a transient intermediate.[25] In contrast, the dimerization of R**Si≡SiR** to a tetrasilacyclobutadiene structure (Figure 4) was calculated to be endothermic by 49.9 kcal/mol owing to the steric congestion of four bulkier R** groups. This large endothermicity confirms that R**Si≡SiR** is highly unlikely to dimerize.

In conclusion, R**Si≡SiR** is very stable towards both isomerization and dimerization. In addition, it has the least trans-bent structure and the shortest triple bond among isolable silicon analogues of alkynes that have ever been investigated.[10−14] It is expected that R**Si≡SiR** will soon be successfully isolated[26] and open up a new area in silicon chemistry.

Acknowledgments

This work was supported in part by a Grand-in-Aid from the Ministry of Education, Culture, Sports, Science, and Technology of Japan.

[1] R. West, M. J. Fink, J. Michl, *Science* **1981**, *214*, 1343−1344.
[2] R. Okazaki, R. West, *Adv. Organomet. Chem.* **1996**, *39*, 231−273.
[3] P. P. Power, *Chem. Rev.* **1999**, *99*, 3463−3503; P. P. Power, *J. Chem. Soc., Dalton Trans.* **1998**, 2939−2951.
[4] M. Weidenbruch, *Eur. J. Inorg. Chem.* **1999**, 373−381; M. Weidenbruch, *J. Organomet. Chem.* **2002**, *646*, 39−52.
[5] For a recent discussion on a Ga-Ga bond length as short as triple bonds, see: G. H. Robinson, *Acc. Chem. Res.* **1999**, *32*, 773−782; N. Takagi, M. W. Schmidt, S. Nagase, *Organometallics* **2001**, *20*, 1646−1651.
[6] A. Sekiguchi, S. S. Zigler, R. West, *J. Am. Chem. Soc.* **1986**, *108*, 4241−4242.
[7] R. Pietschnig, R. West, D. R. Powell, *Organometallics* **2000**, *19*, 2724−2729.
[8] K. W. Klinkhammer, *Angew. Chem.* **1997**, *109*, 2414−2416; *Angew. Chem. Int. Ed. Engl.* **1997**, *36*, 2320−2322.
[9] P. Jutzi, *Angew. Chem.* **2000**, *112*, 3953−3957; *Angew. Chem. Int. Ed.* **2000**, *39*, 3797−3800.
[10] K. Kobayashi, S. Nagase, *Organometallics* **1997**, *16*, 2489−2491.
[11] S. Nagase, K. Kobayashi, N. Takagi, *J. Organomet. Chem.* **2000**, *611*, 264−271.
[12] K. Kobayashi, N. Takagi, S. Nagase, *Organometallics* **2001**, *20*, 234−236.
[13] [13a] N. Takagi, S. Nagase, *Chem. Lett.* **2001**, 966−967. [13b] It has recently been found that the structure with the central aryl rings of the terphenyl groups (Ar*) nearly coplanar to the Si≡Si part is 6.2 kcal/mol more stable than the somewhat more twisted structure (Si-Si = 2.126 Å, θ = 130.5 °, and ω = 163.9°) with the central aryl rings perpendicular to Si≡Si.[13a] This trend has also been found for Ar*Ge≡GeAr* and Ar*Sn≡SnAr* (to be published).
[14] N. Takagi, S. Nagase, *Organometallics* **2001**, *20*, 5498−5500.

[15] For recent reviews on the stabilization and synthesis of doubly bonded compounds using the Tbt and Ar* groups, see: B. Twamley, S. T. Haubrich, P. P. Power, *Adv. Organomet. Chem.* **1999**, *44*, 1−65; J. A. C. Clyburne, N. McMullen, *Coord. Chem. Rev.* **2000**, *210*, 73−99; R. Okazaki, N. Tokitoh, *Acc. Chem. Res.* **2000**, *33*, 625−630; T. Sasamori, Y. Arai, N. Takeda, R. Okazaki, Y. Fuyukawa, M. Kimura, S. Nagase, N. Tokitoh, *Bull. Chem. Soc. Jpn.* **2002**, *75*, 1−15. For the synthesis and isolation of silabenzene, see: K. Wakita, N. Tokitoh, R. Okazaki, S. Nagase, *Angew. Chem.* **2000**, *112*, 648−650; *Angew. Chem. Int. Ed.* **2000**, *39*, 634−636; K. Wakita, N. Tokitoh, R. Okazaki, N. Takagi, S. Nagase, *J. Am. Chem. Soc.* **2000**, *122*, 5648−5649.

[16] K. Kobayashi, S. Nagase, to be published.

[17] N. Wiberg, W. Niedermayer, G. Fischer, H. Nöth, M. Suter, *Eur. J. Inorg. Chem.* **2002**, 1066−1070.

[18] A. D. Becke, *Phys. Rev.* **1988**, *A38*, 3098−3100; A. D. Becke, *J. Chem. Phys.* **1993**, *98*, 5648−5652; C. Lee, W. Yang, R. G. Parr, *Phys. Rev.* **1988**, *B37*, 785−789.

[19] W. J. Pietro, M. M. Francl, W. J. Hehre, D. J. DeFrees, J. A. Pople, J. S. Binkley, *J. Am. Chem. Soc.* **1982**, *104*, 5039−5048.

[20] M. J. Frisch, G. W. Trucks, H. B. Schlegel, G. E. Scuseria, M. A. Robb, J. R. Cheeseman, V. G. Zakrzewski, J. A. Montgomery Jr., R. E. Stratmann, J. C. Burant, S. Dapprich, J. M. Millam, A. D. Daniels, K. N. Kudin, M. C. Strain, O. Farkas, J. Tomasi, V. Barone, M. Cossi, R. Cammi, B. Mennucci, C. Pomelli, C. Adamo, S. Clifford, J. Ochterski, G. A. Petersson, P. Y. Ayala, Q. Cui, K. Morokuma, D. K. Malick, A. D. Rabuck, K. Raghavachari, J. B. Foresman, J. Cioslowski, J. V. Ortiz, B. B. Stefanov, G. Liu, A. Liashenko, P. Piskorz, I. Komaromi, R. Gomperts, R. L. Martin, D. J. Fox, T. Keith, M. A. Al-Laham, C. Y. Peng, A. Nanayakkara, C. Gonzalez, M. Challacombe, P. M. W. Gill, B. Johnson, W. Chen, M W. Wong, J. L. Andres, M. Head-Gordon, E. S. Replogle, J. A. Pople, Gaussian 98, Gaussian, Inc., Pittsburgh, PA, **1998**.

[21] W. Kutzelnigg, *Angew. Chem.* **1984**, *96*, 262−286; *Angew. Chem. Int. Ed. Engl.* **1984**, *23*, 272−295.

[22] M. Kira, T. Maruyama, C. Kabuto, K. Ebata, H. Sakurai, *Angew. Chem.* **1994**, *106*, 1575−1577; *Angew. Chem. Int. Ed. Engl.* **1994**, *33*, 1489−1491.

[23] Upon the trans-bending, the low-lying vacant σ*-orbital is mixed into the in-plane π-orbital (a second-order Jahn−Teller effect); this orbital mixing contributes to stabilization but makes the π-bond slipped and weakened.

[24] For the possible intermediate formation of RSi≡SiR [R = SiH(Si*t*Bu$_3$)$_2$], see: N. Wiberg, W. Niedermayer, H. Nöth, M. Warchhold, *Z. Anorg. Allg. Chem.* **2001**, *627*, 1717−1722.

[25] N. Wiberg, C. M. M. Finger, K. Polborn, *Angew. Chem.* **1993**, *105*, 1140−1142; *Angew. Chem. Int. Ed. Engl.* **1993**, *32*, 1054−1056; N. Wiberg, *Coord. Chem. Rev.* **1997**, *163*, 217−252.

[26] It has been reported that the reduction of R**ClSi=SiClR** with LiC$_{10}$H$_8$ in THF leads to a reaction mixture containing a Cl-free product that shows a low field ^{29}Si NMR signal at δ = 91.5 ppm.[17] In an attempt to estimate ^{29}Si NMR chemical shifts of triply bonded Si atoms, GIAO-B3LYP calculations were carried out using B3LYP/3-21G* optimized structures; a larger 6-311G(3d) basis set was employed only for Si because of the size of molecules. At this level, the ^{29}Si NMR chemical shifts of H$_3$SiSi≡SiSiH$_3$ and MeSi≡SiMe were calculated at δ = 95.0 and 26.9 ppm, respectively. It may be informative that the ^{29}Si NMR chemical shift at δ = 111.2 ppm calculated for R**Si≡SiR** is much closer to the observed signal than that at δ = 180.4 ppm calculated for R**ClSi=SiClR**.

Received May 22, 2002
[I02264]

A Robust, Reactive, and Remarkably Simple to Prepare Sterically Encumbered *meta*-Terphenyl Ligand

Rhett C. Smith,*[a] Tong Ren,[b] and John D. Protasiewicz*[a]

Keywords: Terphenyl / Diphosphene / Insertion / Phosphaalkene

A cost-efficient, high yield and simple one-pot route to the sterically encumbered iodoterphenyl DcpI [Dcp = 2,6-(2,6-$Cl_2C_6H_3)_2C_6H_3$] is developed in which the necessary addition of external Grignard reagent is avoided. This material is employed as a convenient precursor to low-coordinate phosphorus compounds, such as DcpP=PDcp (**1**), DcpP=C(H)Ph (**4**), and DcpP=PMe_3. The resultant aryl is found to provide robust steric protection for **1** and **4** once in place, but reactive intermediates leading to insertion chemistry must be avoided in the course of their synthesis. A new bis(dibenzophosphole) **2** resulting from insertion of a phosphorus atom into vicinal C–Cl bonds was isolated and characterized. The single crystal X-ray structures of **1**, **2**, and **4** are presented.

(© Wiley-VCH Verlag GmbH, 69451 Weinheim, Germany, 2002)

Sterically encumbered *meta*-terphenyl ligands represent an exciting class of protective groups. Recent reviews have detailed their widespread success for stabilizing new compounds having novel element−element multiple bonds, generating interesting molecular geometries and coordination environments, and synthesis of models for biological systems.[1] Yet despite their great success in stabilizing reactive functional groups, these types of ligands can be susceptible to intramolecular attack by high-energy intermediates. For example, it was recently noted that both reduction of 2,6-$Trip_2C_6H_3PCl_2$ with magnesium, and photolysis of $Trip_2C_6H_3P{=}PMe_3$, lead to the same phosphafluorene [Equation (1)].[2−4]

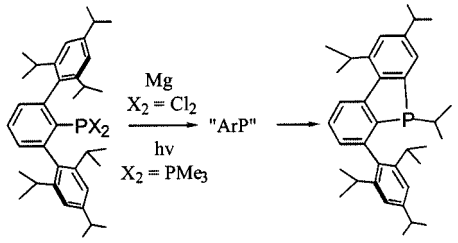

(1)

Presumably, the phosphinidene ("ArP"), generated from either process, inserts into an Ar−*i*Pr carbon−carbon bond to account for the final product. While phosphinidenes, the phosphorus analogues of carbenes, have been invoked in many reactions to justify a variety of products, direct evidence for such species is still quite limited.[5−7]

Our interest in examining the scope of this type of process and finding more convenient and economical variations of *meta*-terphenyl ligands led us to investigate systems based upon the 2,6-bis(2,6-dichlorophenyl)phenyl (Dcp) group. This terphenyl was first isolated in 22% yield by Kress from the black sludge that resulted from the thermal decomposition (exothermic) of 2,6-dichlorophenyllithium at temperatures above −45 °C (Scheme 1).[8] Hart subsequently found that the corresponding Grignard reagent was much more stable and could be used to prepare 2,6-bis(2,6-dichlorophenyl)benzene (DcpH) in moderate yields (44%).[9] This discovery led to the development of a convenient route to a range of terphenyls (2,6-$Ar_2C_6H_3E$, Scheme 1) using *meta*-dichlorobenzene and various Grignard reagents. The maximum steric screening provided by terphenyl ligands for reactive atoms and functional groups is largely defined by the *ortho* substituents on the outer aromatic rings. Hence, another particularly attractive facet of the Dcp terphenyl is its steric similarity to the widely used terphenyl 2,6-$Mes_2C_6H_3$ (Dmp). Because of the similar van der Waals radii for chlorine and methyl groups, one should be able to obtain the same steric coverage as the Dmp system at reduced cost and effort. We now report that the modification of the original Kress reaction and subsequent quenching with iodine leads to a high yield and convenient synthesis of DcpI, as well as its unusual stability and reactivity in low-coordinate phosphorus compounds.

The reaction first reported to yield DcpH was thus modified by not allowing the initial dichlorobenzene/butyllithium mixture to warm above −50 °C, and by the subsequent addition of I_2. A 65% yield of DcpI is achieved

[a] Department of Chemistry, Case Western Reserve University
Cleveland, OH 44106-7078, USA
Fax: (internat.) + 1-216/368-3006
E-mail: jdp5@po.cwru.edu
[b] Department of Chemistry, University of Miami
Coral Gables, FL 33124, USA
Fax: (internat.) + 1-305/284-1880
E-mail: tren@miami.edu

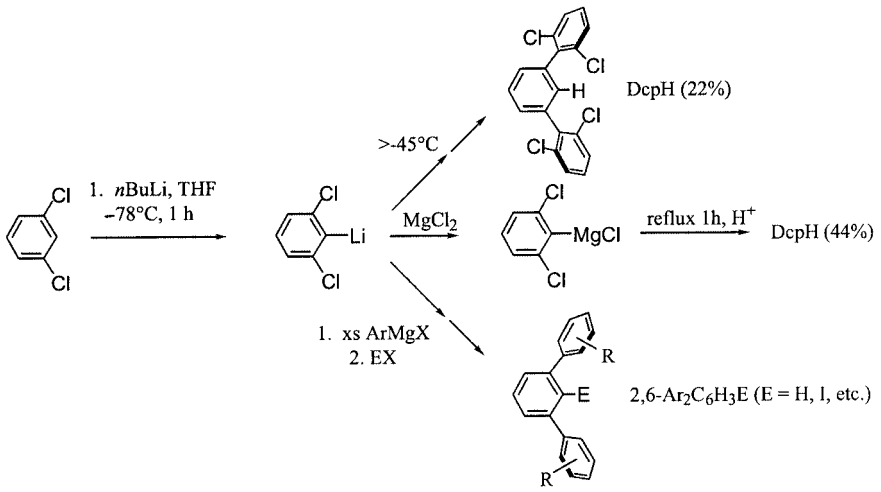

Scheme 1

after single recrystallization by an exceptionally convenient and simple procedure that provides better yields than many conventional iodoterphenyl syntheses (Scheme 1). With this pure material in hand, the synthesis of $DcpPCl_2$ was effected by standard methods (metallation of DcpI by *n*BuLi at −78 °C in THF, followed by addition of three equivalents of PCl_3 and warming to room temperature).

Synthesis of the diphosphene DcpP=PDcp (**1**) was then undertaken to assess the steric screening capabilities of the Dcp ligand. Attempts to prepare this material by reduction of $DcpPCl_2$ by proven and established methods[10] (by either ultrasound/magnesium or 2 equiv. Na[Napth]) surprisingly failed to provide any evidence of the desired diphosphene. Instead, two other major products (**2** and **3**) were observed in about equal amounts (Scheme 2, top). This result was puzzling, since the diphosphene bearing the nearly isosteric terphenyl Dmp ligand is quite robust and stable.[11] The identity (and perhaps the origins) of **2** became clearer when the synthesis of the phosphanylidene-σ^4-phosphorane $DcpP{=}PMe_3$ was undertaken (Scheme 2). Reduction of $DcpPCl_2$ by either Zn/PMe_3 or excess PMe_3 cleanly leads to $DcpP{=}PMe_3$ [^{31}P NMR (THF): δ = 6.7, −121.1 ppm, J_{PP} = 573 Hz] having NMR spectroscopic properties similar to its $DmpP{=}PMe_3$ analogue.[12] This material,

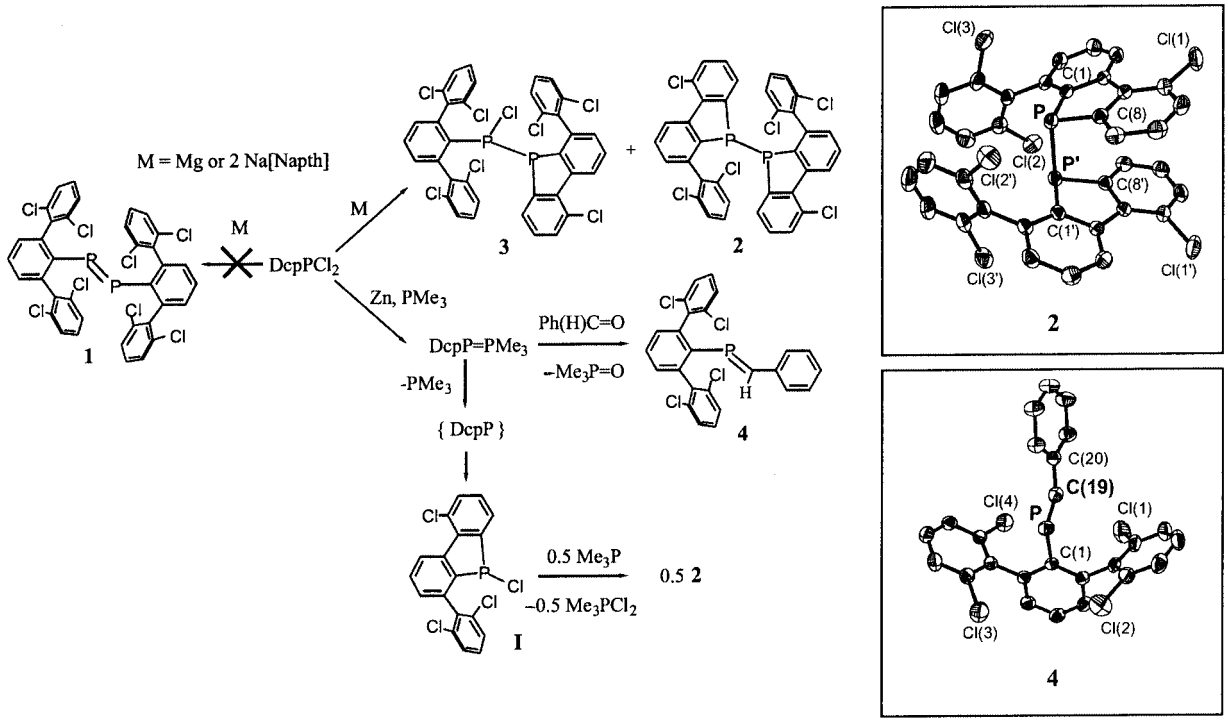

Scheme 2. Selected bond lengths [Å] and angles [°] for **2**: P−C(8) 1.810(2), P−C(1) 1.813(2), P−P′ 2.248(1), C(8)−P−C(1) 89.3(1), C(8)−P−P′ 101.69(8), C(1)−P−P′ 97.36(9); selected bond lengths [Å] and angles [°] for **4**: P−C(19) 1.634(3), P−C(1) 1.841(3), C(19)−P−C(1) 102.9(1), C(20)−C(19)−P 125.4(2)

however, quickly (10−15 min) and cleanly transforms to **2** [^{31}P NMR (THF): δ = −27.6 ppm].

Interestingly, as the results of an X-ray diffraction study show (Scheme 2), two phosphorus atoms have inserted into the carbon−chlorine bonds of two terphenyl ligands and coupled to one another to provide bis(dibenzophosphole) **2**.[13] Despite the crowded nature about the P−P bond, a relatively normal P−P single bond length of 2.248(1) Å is found. The structure of **2** is remarkably similar to the disilane postulated to arise by insertion of a silylene into the carbon−carbon bonds of a Dmp terphenyl.[14]

The nature of **2** makes it tempting to speculate that the unstable phosphanylidene-σ^4-phosphorane loses PMe_3 in an initial step to generate a highly reactive phosphinidene (Scheme 2, bottom). This behavior would stand in contrast to the related phosphanylidene-σ^4-phosphoranes ArP=PMe_3 (Ar = Dmp, Mes*, 2,6-$Trip_2C_6H_3$) that are thermally stable at room temperature, but extrude PMe_3 upon photolysis.[3] The presumed product of phosphinidene insertion into the carbon−chlorine bond, chlorophosphafluorene **I**, has, however, proven to be much more difficult to detect than the analogous product derived from phosphinidene insertion into a carbon−carbon bond [Equation (1)]. It appears that the P−Cl bond in **I** must be more susceptible to further reduction than $DcpPCl_2$. For example, reactions of $DcpPCl_2$ and either 1 equiv. of Na[Napth] or 1/2 equiv. of Mg yield mixtures of **2** and unchanged $DcpPCl_2$. Likewise, the proposed intermediate **I** must also be very susceptible to trialkylphosphane-promoted dehalogenation and P−P coupling processes.[15]

The unstable DcpP=PMe_3 was trapped by excess benzaldehyde to give the new phosphaalkene DcpP=C(H)Ph [**4**, ^{31}P NMR ($CDCl_3$): δ = 233.0] (> 95% by ^{31}P NMR, 62% isolated yield) by our version of a phospha-Wittig reaction (Scheme 2).[12,16] Scheme 2 also shows the results of a single-crystal X-ray diffraction study of **4**.[13] The main feature of interest, the P=C bond length of 1.634(3) Å, is at the shorter end of the spectrum of reported values for such compounds.[17−21] The phosphaalkene unit itself resides within the protective cleft of the large Dcp ligand.

The other major product produced by reduction of $DcpPCl_2$ by magnesium has been assigned as **3**, based on its ^{31}P NMR spectrum [δ = 96.3 ppm (d, J_{PP} = 305 Hz), −5.0 (d, J_{PP} = 305 Hz)]. The identity of this product was more firmly established by its independent synthesis. Bis(dibenzophosphole) **2** was reductively cleaved by excess Na metal to a dibenzophospholide anion[22,23] [^{31}P NMR (THF): δ = 21.9 ppm], which was treated with $DcpPCl_2$ to give **3** as the main product. Interestingly, this material does *not* appear to be an intermediate to **2** during the thermal decomposition of DcpP=PMe_3, as it does not react with Zn or PMe_3.

Though the Dcp ligand might be very susceptible to attack by phosphinidene (or other) intermediates, it is a very effective protective unit once in place. In fact, the diphosphene **1** is very stable and robust. Compound **1** was readily prepared by the stepwise process described in Scheme 3, which avoids potential generation of phosphinidenes. While

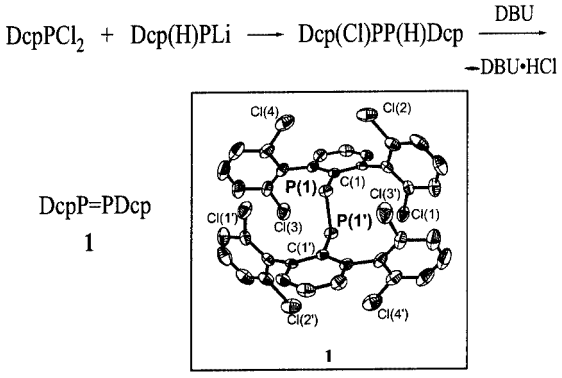

Scheme 3. Selected bond lengths [Å] and angles [°] for **1**; (only one of two independent molecules shown); P(1)−C(1) 1.847(4), P(1)−P(1′) 2.039(2), C(1)−P(1)−P(1′) 98.46(15)

1 exhibits a typical ^{31}P NMR chemical shift value of δ = 500.3 ppm, the compound has two notable features that distinguish it from the Dmp analogue. First, the presumed π-π* electronic transition of **1** is blue-shifted by approximately 19 nm compared to DmpP=Dmp (solid **1** is yellow, while DmpP=PDmp is orange). Secondly, the structure of **1** (Scheme 3) reveals a different orientation of the terphenyl groups.[13] Specifically, the two central rings of each terphenyl are nearly parallel to one another (and related by an inversion center). Similar orientations of the terphenyl groups of DmpPE=EDmp (E = As, Sb) are adopted in the solid state.[2]

For the phosphorus species, it appears that the smaller central atom size and bond lengths disfavor this orientation due to steric clashes between Dmp groups across the P=P unit. Compound **1** lacks the *para* substituents present on the Dmp system, and thus interactions of the Dcp groups across the P=P unit are not as severe. Average P−P distances of 2.030 Å (two independent molecules in unit cell) and C−P−P bond angles spanning 98.5(2) to 98.9(1)° are otherwise unexceptional for **1**.

The facile self-destruction reactions of the Dcp ligand (as in **2** and **3**) bear some likeness to similar reactions of low-coordinate phosphorus compounds bearing the Mes* (Mes* = 2,4,6-$tBu_3C_6H_2$) group. In these materials the phosphorus atoms insert into the vicinal C−H bonds of the *tert*-butyl groups. For example, reduction of Mes*PCl_2 with activated magnesium gives rise to a phosphaindane.[4] In addition, photolysis of the diphosphene Mes*P=PMes* readily leads to such products, and therefore it was anticipated that under photolysis **1** would yield products such as **2** or **3**.[24] The remarkable stability of **1** is amply demonstrated by its complete inertness to continued photolysis (by either irradiation in a 254-nm photochemical reactor or by 355-nm laser light). In this regard, **1** behaves like the terphenyl-protected diphosphenes DmpP=PDmp[3] and ArP=PAr[25] (Ar = 2,6-Mes_2-4-MeC_6H_2).

We have thus shown that a relatively inexpensive and sterically encumbered *meta*-terphenyl ligand can rapidly be constructed for applications in low-coordinate phosphorus chemistry. Highly reactive phosphorus centers can insert into the carbon−chlorine bonds of the Dcp ligand and pro-

vide access to novel phosphafluorene-derived materials. If these high-energy intermediates can be avoided, then the resulting materials bearing the Dcp unit are very robust. This finding should also serve as another reminder for others searching for new compounds having multiply bonded elements, that the size of the ligand is not everything. In other applications, where an economically more desirable sterically demanding protecting group is required, the Dcp unit should also be useful.

Experimental Section

General: Air sensitive materials were handled in a dry box or using modified Schlenk line techniques under dry nitrogen. Solvents were obtained by distillation from Na-benzophenone ketyl under nitrogen. ^{1}H NMR and ^{31}P NMR spectra were acquired on a Varian Gemini 300 MHz spectrometer and are referenced to TMS and 85% H_3PO_4, respectively.

DcpI: 54.8 mL of *n*BuLi (2.5 M in hexanes, 138 mmol) was added dropwise to a solution of 1,3-dichlorobenzene (20.0 g, 136 mmol) in THF (250 mL) at −78 °C. The resulting white suspension was stirred for 1.5 h at −78 °C (dry ice/acetone bath), and then warmed to −50 °C (bath temperature) over a 30 min period. Elemental iodine (14.0 g, 55.2 mmol) was added under positive pressure of N_2 and the mixture was allowed to warm to room temperature over a 2 h period. Excess iodine was quenched with aqueous Na_2SO_3, and the organic products were extracted with diethyl ether. The combined organic layers were washed with water and then dried with Na_2SO_4. Removal of all volatiles under reduced pressure yielded a sticky light brown solid. Recrystallization from hot EtOH gave 14.9 g (65% yield) of pure white DcpI; m.p. 176−178 °C. ^{1}H NMR ($CDCl_3$): δ = 7.56 (t, J = 7.0 Hz, 2 H), 7.43 (d, J = 7.0 Hz, 4 H), 7.29 (t, J = 8.0 Hz, 1 H) 7.22 (d, J = 8.0 Hz, 2 H) ppm. ^{13}C NMR (300 MHz, $CDCl_3$): δ = 143.5, 141.9, 135.0, 129.6, 129.1, 128.6, 127.8, 104.8 ppm. HR-MS (FAB): calcd. for $C_{18}H_9Cl_4I$: 491.8503; found 491.8509 [M + H$^+$].

DcpPCl$_2$: Prepared in 52% yield using literature methods.[11] ^{1}H NMR (C_6D_6): δ = 7.09 (t, J = 8.0 Hz, 1 H), 6.97 (d, J = 8.0 Hz, 4 H), 6.81 (dd, $^3J_{H,H}$ = 8, $^4J_{PH}$ = 3 Hz, 2 H), 6.55 (d, J = 8.0 Hz, 2 H) ppm. ^{31}P NMR (C_6D_6): δ = 155.4 (s) ppm.

DcpPH$_2$: Prepared in 47% yield using literature methods.[11] ^{1}H NMR (C_6D_6): δ = 7.13 (t, J = 8.0 Hz, 1 H), 7.02 (d, J = 8.0 Hz, 4 H), 6.96 (d, $J_{H,H}$ = 8, $^4J_{PH}$ = 2 Hz, 2 H), 6.57 (t, J = 8.0 Hz, 2 H), 3.23 (d, J_{PH} = 208 Hz) ppm. ^{31}P NMR (C_6D_6): δ = −148.1 (t, J_{PH} = 208 Hz) ppm.

2: To a stirred mixture of DcpPCl$_2$ (0.30 g, 0.60 mmol) and Zn dust (0.05 g, 0.76 mmol) in 10 mL of THF was added a solution of PMe_3 (0.19 g, 2.5 mmol) in 5 mL of THF. The solution immediately turned bright yellow, and a ^{31}P NMR spectrum of an aliquot, run after 5 min of reaction, indicated complete conversion into DcpP=PMe$_3$. After 20 min, the solvent was removed in vacuo, and the solids were extracted with hexanes. Removal of hexanes in vacuo yielded 0.16 g of **3** as a white solid (70% yield). Crystals suitable for X-ray structure determination were grown from hexanes/$CDCl_3$. ^{1}H NMR (C_6D_6): δ = 8.83 (d, J = 8.0 Hz, 2 H), 7.33 (t, J = 8.0 Hz, 2 H), 7.14 (d, J = 8.0 Hz, 4 H), 6.94 (d, J = 8.0 Hz, 2 H), 6.84 (d, J = 8.0 Hz, 2 H), 6.63 (t, J = 8.0 Hz, 2 H), 6.34 (t, J = 8.0 Hz, 2 H), 6.00 (d, J = 8.0 Hz, 2 H) ppm. ^{31}P NMR (THF): δ = −27.6 ppm. HR-MS (FAB):calcd. for $C_{36}H_{19}Cl_6P_2$ 722.9093; found 722.9128 [M + H$^+$].

DcpP=C(H)Ph (4): To a stirred mixture of DcpPCl$_2$ (0.10 g, 0.21 mmol), zinc dust (0.02 g, 0.3 mmol), and benzaldehyde (0.090 g, 0.85 mmol) in 5 mL of THF in a 20-mL vial was added a solution of PMe_3 (0.10 g, 1.32 mmol) in 3 mL of THF. After 1 h of stirring, the solvent was removed in vacuo. The solid was extracted with hexanes, and the hexanes were evaporated to yield 0.060 g of **4** as a white powder (62%). Crystals suitable for X-ray structure determination were grown by slow concentration of a $CDCl_3$ solution. ^{1}H NMR ($CDCl_3$): δ = 9.08 (d, J = 24.0 Hz, 1 H), 7.49 (t, J = 7.0 Hz, 1 H), 7.27 (d, J = 7.0 Hz, 4 H), 7.20−7.08 (m, 10 H) ppm. ^{31}P NMR ($CDCl_3$): δ = 233.0 ppm. HR-MS (FAB): calcd. for $C_{25}H_{16}Cl_4P$ 486.9743; found 486.9718 [M + H$^+$].

DcpP=PDcp (1): To a rapidly stirred solution of DcpPCl$_2$ (0.87 g, 1.9 mmol) in ether (50 mL), a suspension of DcpPH[Li·OEt$_2$] (0.90 g, 2.0 mmol) in 50 mL of diethyl ether was added dropwise over 30 min. After 1 h, a solution of DBU (0.26 g, 1.7 mmol) in 5 mL of diethyl ether was added and the mixture stirred for 2 h. The bright yellow mixture was then filtered and the solvent removed in vacuo to afford a crude yellow solid. The solid was taken up in THF/hexanes (4:1) and cooled to −35 °C to yield **1** as a yellow powder (0.31 g, 23%). ^{1}H NMR (C_6D_6): δ = 7.02 (t, J = 8.0 Hz, 1 H), 6.97 (d, J = 8.0 Hz, 4 H), 6.88 (d, J = 8.0 Hz, 2 H), 6.61 (t, J = 8.0 Hz, 2 H) ppm. ^{31}P NMR (C_6D_6): δ = 500.3. UV/Vis (THF): ε (448 nm) = 626 cm^{-1} M^{-1}; ε (352 nm) = 8551 cm^{-1} M^{-1}. $C_{36}H_{18}P_2Cl_8$: calcd. C 54.31, H 2.28; found C 53.91, H 2.53.

Acknowledgments

This work was supported the National Science Foundation (CAREER CHE-9733412 to J. D. P.) and by the University of Miami CCD diffractometer fund.

[1] [1a] B. Twamley, S. T. Haubrich, P. Power, *Adv. Organomet. Chem.* **1999**, 1−65. [1b] J. A. C. Clyburne, N. McMullen, *Coord. Chem. Rev.* **2000**, *210*, 73−99. [1c] G. H. Robinson, *Acc. Chem. Res.* **1999**, *32*, 773−782. [1d] W. B. Tolman, L. Que, Jr., *J. Chem. Soc., Dalton Trans.* **2002**, 653−660. [1e] H. Hart, *Pure Appl. Chem.* **1993**, *65*, 27−34.
[2] B. Twamley, C. D. Sofield, M. M. Olmstead, P. P. Power, *J. Am. Chem. Soc.* **1999**, *121*, 3357−3367.
[3] S. Shah, M. C. Simpson, R. C. Smith, J. D. Protasiewicz, *J. Am. Chem. Soc.* **2001**, *123*, 6925−6926.
[4] R. C. Smith, S. Shah, J. D. Protasiewicz, *J. Organomet. Chem.* **2002**, *646*, 255−261.
[5] F. Mathey, in *Multiple Bonds and Low Coordination in Phosphorus Chemistry* (Eds.: M. Regitz, O. J. Scherer), Thieme Verlag, Stuttgart, **1990**, pp. 33−47.
[6] X. Li, S. I. Weissman, T.-S. Lin, P. P. Gaspar, A. H. Cowley, A. I. Smirnov, *J. Am. Chem. Soc.* **1994**, *116*, 7899−7900.
[7] X. Li, D. Lei, M. Y. Chiang, P. P. Gaspar, *J. Am. Chem. Soc.* **1992**, *114*, 8526−8531.
[8] T. H. Kress, M. R. Leanna, *Synthesis* **1988**, 803−805.
[9] A. Saednya, H. Hart, *Synthesis* **1996**, 1455−1458.
[10] L. Weber, *Chem. Rev.* **1992**, *92*, 1839−1906.
[11] E. Urnezius, J. D. Protasiewicz, *Main Group Chem.* **1996**, *1*, 369−372.
[12] S. Shah, J. D. Protasiewicz, *Chem. Commun.* **1998**, 1585−1586.
[13] Crystal data of **1**: $C_{36}H_{18}Cl_8P_2$, M_r = 796.04, monoclinic, space group $P21/c$, a = 19.442(3), b = 12.083(2), c = 14.737(2) Å, β = 90.335(3)°, V = 3461.8(8) Å^3, Z = 4, $\rho_{calcd.}$ =1.527 g cm^{-3}, $2\theta_{max}$ = 50°, Mo-K_α radiation, λ = 0.71073 Å, μ = 0.771 mm^{-1}. Crystal data for **2**·*n*-C_6H_{14}: $C_{42}H_{18}Cl_6P_2$, M_r = 797.20, monoclinic, space group $C2/c$, a = 21.271(3), b =

12.587(2), c = 14.940(2) Å, β = 103.499(2)°, V = 3889.4(9) Å^3, Z = 4, $\rho_{calcd.}$ = 1.361 g cm^{-3}, $2\theta_{max}$ = 50°, Mo-K_α radiation, λ = 0.71073 Å, μ = 0.554 mm^{-1}. Crystal data for **4**: $C_{25}H_{15}Cl_4P$, M_r = 488.14, monoclinic, space group $C2/c$, a = 30.200(7), b = 8.335(2), c = 18.698(4) Å, β = 91.947(4)°, V = 4704(2) Å^3, Z = 8, $\rho_{calcd.}$ = 1.379 g cm^{-3}, $2\theta_{max}$ = 50°, Mo-K_α radiation, λ = 0.71073 Å, μ = 0.581 mm^{-1}. All data sets were collected with a Bruker SMART CCD diffractometer at 300(2) K. Lorentz polarization and empirical (SADABS) absorption corrections were applied. The structures were solved by direct methods and refined using SHELXTL. Non-hydrogen atoms were refined with anisotropic displacement parameters, and hydrogen atoms were placed in idealized positions and included as riding with U_{iso}(H) =1.3 U_{eq}(non-H). Of 17736 collected reflections for **1**, 6090 were unique (R_{int} = 0.0663). Final figures of merit for **1**: R = 0.0568 [$I > 2\sigma(I)$], Rw = 0.1142 (F^2, all data). Of 9341 collected reflections collected for **2**, 3360 were unique (R_{int} = 0.0326). Final figures of merit for **2**: R = 0.0425 [$I > 2\sigma(I)$], Rw = 0.1196 (F^2, all data). Of 11278 collected reflections for **4**, 4086 were unique (R_{int} = 0.0563). Final figures of merit for **4**: R = 0.0540 [$I > 2\sigma(I)$], Rw = 0.1161 (F^2, all data). The highest peaks in the final difference map were 0.609, 0.318 and 0.318 e Å^{-3} for **1**, **2** and **4**, respectively. CCDC-184750 (**1**), -184749 (**2**), and -184748 (**4**) contain the supplementary crystallographic data for this paper. These data can be obtained free of charge at www.ccdc.cam.ac.uk/conts/retrieving.html or from the Cambridge Crystallographic Data Centre, 12, Union Road, Cambridge CB2 1EZ, UK [Fax: (internat.) + 44-1223/336-033; E-mail: deposit@ccdc.cam.ac.uk].

[14] R. Pietschnig, R. West, D. R. Powell, *Organometallics* **2000**, *19*, 2724−2729.
[15] [15a] S. E. Frazier, R. P. Nielsen, H. H. Sisler, *Inorg. Chem.* **1964**, *3*, 292−294. [15b] S. F. Spangenberg, H. H. Sisler, *Inorg. Chem.* **1969**, *8*, 1006−1010. [15c] J. C. Summers, H. H. Sisler, *Inorg. Chem.* **1970**, *9*, 862−869.
[16] S. Shah, J. D. Protasiewicz, *Coord. Chem. Rev.* **2000**, *210/211*, 181−201.
[17] R. Appel, F. Knoll, I. Ruppert, *Angew. Chem. Int. Ed. Engl.* **1981**, *20*, 731.
[18] R. Appel, F. Knoll, *Adv. Inorg. Chem.* **1989**, *33*, 259−361.
[19] L. N. Markovskii, V. D. Romanenko, *Tetrahedron* **1989**, *45*, 6019−6090.
[20] F. Mathey, *Acc. Chem. Res.* **1992**, *25*, 90−96.
[21] L. Weber, *Eur. J. Inorg. Chem.* **2000**, 2425−2441.
[22] A. D. Britt, E. T. Kaiser, *J. Org. Chem.* **1966**, 112−114.
[23] F. Nief, L. Ricard, *J. Organomet. Chem.* **1994**, *464*, 149−154.
[24] M. Yoshifuji, T. Sato, N. Inamoto, *Chem. Lett.* **1988**, 1735−1738.
[25] [25a] K. Tsuji, Y. Fujii, S. Sasaki, M. Yoshifuji, *Chem. Lett.* **1997**, 855−856. [25b] K. Tsuji, S. Sasaki, M. Yoshifuji, *Heteroatom Chem.* **1998**, *9*, 607−613

Received June 18, 2002
[I02322]

Synthesis and Characterization of Group 14 1-Haloazametallatranes

Pavel L. Shutov,[a] Sergey S. Karlov,*[b] Klaus Harms,[a] Andrei V. Churakov,[c] Judith A. K. Howard,[c] Jörg Lorberth,*[a] and Galina S. Zaitseva[b]

Keywords: Azametallatranes / Silicon / Germanium / Tripodal ligands / Tin

The reaction between $MHal_4$ (M = Ge, Sn; Hal = Cl, Br) and $N(CH_2CH_2NRLi)_3$ (R = Me, $SiMe_3$) yields 1-haloazametallatranes **1**–**8**, $N(CH_2CH_2NR)_3M$–Hal (**1**, M = Ge, Hal = Cl, R = Me; **2**, M = Ge, Hal = Br, R = Me; **3**, M = Ge, Hal = Cl, R = $SiMe_3$; **4**, M = Ge, Hal = Br, R = $SiMe_3$; **5**, M = Sn, Hal = Cl, R = Me; **6**, M = Sn, Hal = Br, R = Me; **7**, M = Sn, Hal = Cl, R = $SiMe_3$; **8**, M = Sn, Hal = Br, R = $SiMe_3$). The composition and structures of the new compounds were established by elemental analyses, ^1H and ^{13}C NMR spectroscopy and mass spectrometry. Single crystal structures of **1** and **3** were determined by X-ray diffraction studies: both compounds show transannular Ge–N_{ax} interactions.
(© Wiley-VCH Verlag GmbH, 69451 Weinheim, Germany, 2002)

Introduction

The chemistry of pentacoordinate complexes of the group 14 elements has attracted much attention, mostly from a theoretical point of view, with the nature of the intramolecular interaction the main subject of interest.[1–4] In addition, these species are ideal models for the investigation of nucleophilic substitution pathways in group 14 element chemistry.[5] During the last decade we have focussed our research interests on metallatranes containing symmetrical tripodal ligands of type **A** (Scheme 1).[4,6–10]

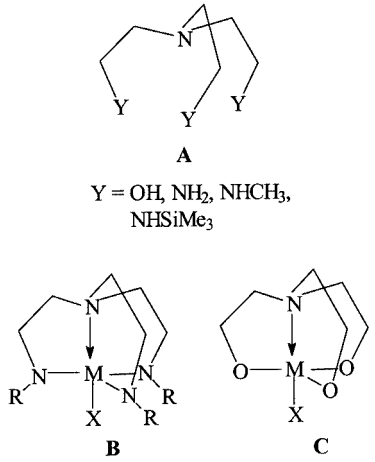

Scheme 1

[a] Fachbereich Chemie, Philipps-Universität Marburg, Hans-Meerwein-Strasse, 35032 Marburg-Lahn, Germany
E-mail: lorberth@chemie.uni-marburg.de
[b] Chemistry Department, Moscow State University, Leninskie Gory 1, str. 3, 119899 Moscow, Russia
E-mail: sergej@org.chem.msu.su
[c] Department of Chemistry, University of Durham, South Road, DH1 3LE Durham, UK

Metal derivatives of tripodal amines — azametallatranes (type **B**) — have greater chemical and structural flexibility than the "usual" metallatranes (type **C**) due to the influence of various substituents R (for example, R = H, Me, $SiAlk_3$, C_6F_5 etc.) on the structure and the chemical properties of these derivatives. Although azasilatranes have been known for some twenty years,[2] azagermatranes and azastannatranes are compounds which have been very little studied.[11–19]

Compounds containing an $SiAlk_3$ group apart from the equatorial nitrogen atoms (N_{eq}) of the azatrane skeleton are the subject of special interest among the group 14 element azametallatranes (**B**). Due to the extremely long Si–N_{ax} distance in the only structurally characterized example $[N(CH_2CH_2NSiMe_3)_3Si{-}CH_3]$[20] Verkade et al. coined the term "*quasi-azasilatranes*" for these rare silicon species.[2] The corresponding azastannatranes (**B**, R = $SiMe_3$) are as yet unknown and for germanium only $N(CH_2CH_2NSiMe_3)_3Ge$–allyl has been reported amongst the $N(CH_2CH_2NSiMe_3)_3Ge$–X derivatives prior to this work.[12]

In this paper we report on the synthesis of 1-haloazametallatranes (M = Ge, Sn) by metathetical exchange reactions between $MHal_4$ (M = Ge, Sn; Hal = Cl, Br) and the trilithium salts of the parent amines $N(CH_2CH_2NHMe)_3$ (Me_3-tren) and $N(CH_2CH_2NHSiMe_3)_3$ (TMS_3-tren). Details of the X-ray crystal and molecular structures of $N(CH_2CH_2NMe)_3GeCl$ (**1**) and $N(CH_2CH_2NSiMe_3)_3GeCl$ (**3**) are also described.

Results and Discussion

Our aim was to obtain 1-haloazametallatranes as precursors for further synthetic applications and to find a new

improved method of preparation for azametallatranes of group 14 elements. 1-Haloazatranes of group 14 elements are those bearing reactive apical groups which have the possibility for further derivatization at the metal centre. Verkade et al. reported only a relatively complicated multistep procedure involving $N(CH_2CH_2NMe)_3Si-H$ and $N(CH_2CH_2NMe)_3Sn-NMe_2$ as intermediate products leading finally to 1-chloro-*N*,*N*′,*N*′′-trimethylazasilatranes and 1-chloro(bromo)-*N*,*N*′,*N*′′-trimethylazastannatranes.[16,21] We prepared azagermatranes **1** and **2** by transamination reactions of $HalGe(NMe_2)_3$ with Me_3-tren.[13]

Another method for building the main group element azatrane framework was previously only used for transition metals.[22] Tetrahalides (Hal = Cl, Br) of germanium and tin react readily with the trilithium salts of Me_3-tren and TMS_3-tren (in toluene at room temperature) to give 1-haloazametallatranes **1**−**8** in high yield (Scheme 2). The derivatives with Me_3-tren were purified by recrystallization from toluene/*n*-pentane while those of TMS_3-tren were purified by recrystallization from *n*-pentane. Lithium salts of Me_3-tren and TMS_3-tren are conveniently generated in situ by treatment of Me_3-tren or TMS_3-tren with the equivalent amount of *n*BuLi.

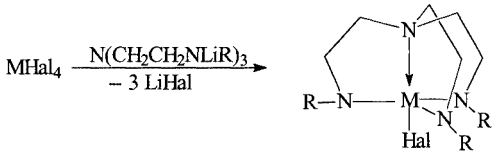

M = Ge; **1**, R = Me, Hal = Cl; **2**, R = Me, Hal = Br
3, R = $SiMe_3$, Hal = Cl; **4**, R = $SiMe_3$, Hal = Br
M = Sn; **5**, R = Me, Hal = Cl; **6**, R = Me, Hal = Br
7, R = $SiMe_3$, Hal = Cl; **8**, R = $SiMe_3$, Hal = Br

Scheme 2

The structures of **1**−**8** were confirmed by ^1H and ^{13}C NMR spectroscopy. In the ^1H NMR spectra of **1**−**8** the signals of the methylene protons of the azatrane skeleton appear as a set of two pseudo-triplets, forming an AA′BB′ spin system. This pattern is a general feature of the "atrane" framework for a variety of metallatranes.[1,2,4]

The reaction of silicon derivatives ($SiCl_4$, $SiBr_4$) with lithium salts of Me_3-tren and TMS_3-tren resulted in unidentifiable polymeric products.

To the best of our knowledge, compounds **1** and **3** (Figure 1 and 2, respectively) are the first structurally characterized azagermatranes. Molecules of **1** lie on a crystallographic threefold axis, while molecules of **3** possess approximate C_3 symmetry. The coordination polyhedron of the germanium atom in both compounds is a distorted trigonal bipyramid with the N(4) [for compound **3**; N(1) for compound **1**] and Cl atoms in the axial positions and the three nitrogen atoms in equatorial sites. The germanium atoms are displaced by 0.25 Å (for **3**) and by 0.22 Å (for **1**) from a plane defined by the three equatorial nitrogen atoms towards the chlorine substituent. The $N_{ax}-Ge-Cl$ angles are exactly 180° for **1** and 179.53(7)° for **3**. The Ge−Cl distances observed in **3** [2.2727(8) Å] and in **1** [2.2968(9) Å] are significantly longer than in the closely related 1-chlorogermatrane $N(CH_2CH_2O)_3Ge-Cl$ (**9**) [2.209(1) Å].[23] The $Ge-N_{ax}$ bonds [2.278(2) Å for **3** and 2.167(4) Å for **1**] are also longer than in **9** [2.096(3) Å]. Thus, a formal substitution of the oxygen atom in molecule **9** by a NCH_3 group (molecule **1**) results in a simultaneous increase of the Ge−Cl and $Ge-N_{ax}$ distances by 0.088 Å and 0.051 Å, respectively. With the same formal substitution in silatranes this leads to the opposite change in the Si−X and $Si-N_{ax}$ bond lengths, as found previously for the compounds $N(CH_2CH_2O)_3Si-OEt$ [$d(Si-O_{ax})$ = 1.699(2) Å, $d(Si-N_{ax})$ = 2.135(2) Å] and $N(CH_2CH_2NMe)_3Si-OEt$

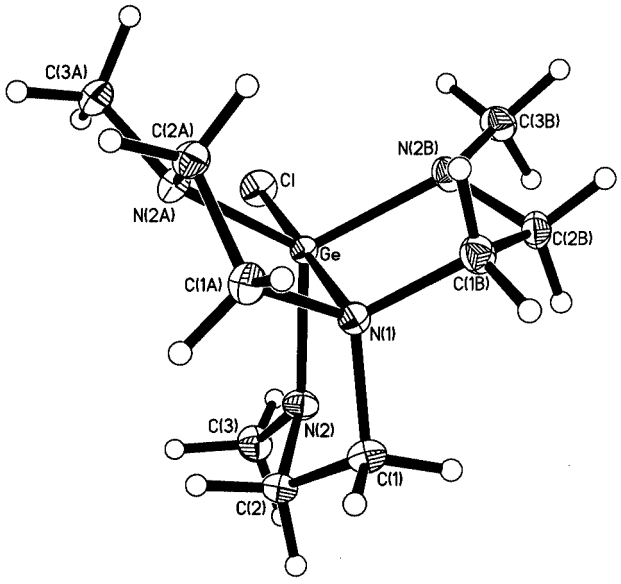

Figure 1. Molecular structure of compound **1**

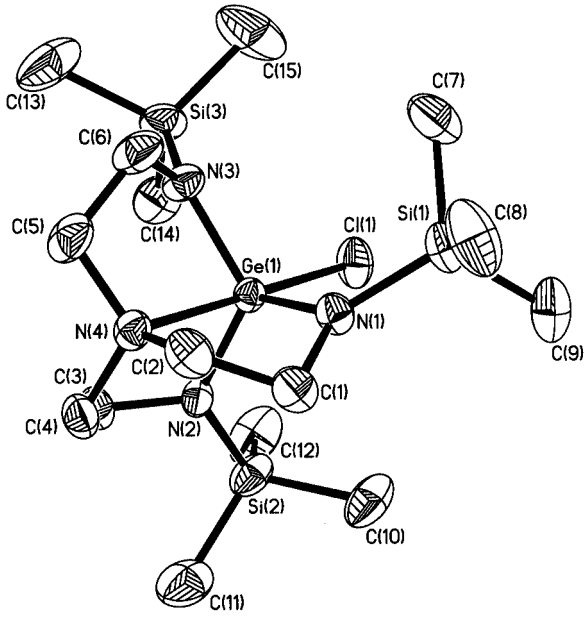

Figure 2. Molecular structure of compound **3**; hydrogen atoms have been omitted for clarity

[d(Si−O_{ax}) = 1.658 Å, d(Si−N_{ax}) = 2.152 Å (averaged for two independent molecules)].[24,25] The Ge−N_{ax} distance in **3** [2.278(2) Å] lies within the typical range for germatranes [2.081(5)−2.32(1) Å][26,27] and clearly verifies the existence of a Ge−N transannular bond in **3**. In contrast, the Si analogue of **3**, $N(CH_2CH_2NSiMe_3)_3Si-CH_3$, possesses an extremely long Si−N_{ax} bond [2.775(7) Å].[20] The Ge−N_{ax} bond length in **1** [2.167(4) Å] is noticeably shorter than that in **3** [2.278(2) Å]; the Ge−N_{eq} distances are 1.837(2) Å, 1.838(2) Å and 1.838(2) Å for **3** and 1.858(1) Å for **1**.

The environment at the N_{ax} atoms is approximately tetrahedral with C−N_{ax}−C and C−N_{ax}−Ge angles ranging between 104.1(2)° and 114.4(3)° for **3** and 106.3(2)° and 112.5(2)° for **1**. The axial nitrogen atoms are displaced by 0.37 Å (for **3**) and by 0.42 Å (for **1**) from a plane defined by the three carbon atoms towards germanium.

All five-membered rings of the atrane skeleton in **1** and **3** adopt an ''envelope''-like conformation; for both **1** and **3** all carbon atoms in the positions β to the N_{ax} atom occupy ''flap'' sites, while the C-α atoms form the base of an envelope plane, the latter being unusual for germatranes without C-β substituents.[9]

Conclusion

In summary, metathetical exchange reactions between $MHal_4$ (M = Ge, Sn; Hal = Cl, Br) and the lithiated parent amines afford compounds **1**−**8** in good yields. The presence of a transannular Ge←N interaction in **1** and **3** was confirmed by X-ray diffraction analyses. Further studies on the application of this reaction for the synthesis of main group element azametallatranes and an investigation of their chemical behaviour are in progress.

Experimental Section

General Remarks: All manipulations were performed under dry, oxygen-free argon atmosphere using standard Schlenk techniques. Solvents were dried by standard methods and distilled prior to use. $MHal_4$ (M = Si, Ge, Sn; Hal = Cl, Br) (Aldrich) were used as supplied. Starting materials Me_3-tren[28] and TMS_3-tren[12] were prepared according to the literature. C_6D_6 was obtained from Deutero GmbH and dried over sodium. ^{1}H and ^{13}C NMR spectra were recorded on a Bruker AC200 spectrometer. ^{1}H and ^{13}C chemical shifts are reported in ppm relative to Me_4Si as external standard. Elemental analyses were carried out by the Microanalytical Laboratory of the Chemistry Department of the Moscow State University and by that of the Fachbereich Chemie of the Philipps-University of Marburg (Heraeus-Rapid-Analyser). Mass spectra (EI-MS) were recorded on a VARIAN CH-7a device using electron impact ionization at 70 eV; mass spectra (FD-MS) were recorded on a HP-5989B device; all assignments were made with reference to the most abundant isotopes.

1-Chloro-*N*,*N*′,*N*′′-trimethylazagermatrane (1): A 1.6 M *n*BuLi solution (4.88 mL, 7.8 mmol) in hexane at room temperature was added dropwise to a stirred solution of Me_3-tren (0.48 g, 2.6 mmol) in 40 mL of toluene. The reaction mixture was stirred for 5 h and a solution of $GeCl_4$ (0.55 g, 2.6 mmol) in 10 mL of toluene was added dropwise at room temperature. After stirring for a further 24 h a white precipitate of LiCl was filtered off. Most of the volatiles were then evaporated in vacuo and 10 mL of *n*-pentane was added. A white crystalline solid was separated by filtration, washed with cold *n*-pentane (3 × 5 mL) and dried in vacuo. Yield: 0.50 g (65%). ^{1}H NMR and ^{13}C NMR spectroscopic data were consistent with those already reported.[13]

1-Bromo-*N*,*N*′,*N*′′-trimethylazagermatrane (2): Following the same experimental procedure as above for **1** using Me_3-tren (0.50 g, 2.7 mmol), a 1.6 M *n*BuLi solution in hexane (5.06 mL, 8.1 mmol) and $GeBr_4$ (1.04 g, 2.7 mmol), colourless crystals (0.63 g, 69%) were obtained. ^{1}H NMR, ^{13}C NMR and EI MS data were consistent with those already reported.[13]

1-Chloro-*N*,*N*′,*N*′′-tris(trimethylsilyl)azagermatrane (3): A 1.6 M *n*BuLi solution in hexane (4.67 mL, 7.5 mmol) at room temperature was added dropwise to a stirred solution of TMS_3-tren (0.90 g, 2.5 mmol) in 40 mL of toluene. The reaction mixture was stirred for 5 h and a solution of $GeCl_4$ (0.53 g, 2.5 mmol) in 10 mL of toluene was added dropwise at room temperature. The mixture was stirred for another 24 h. Removal of all volatiles in vacuo followed by extraction of the residue with 20 mL of *n*-pentane gave a yellowish extract. The solution was reduced in volume by 50% and stored at −30 °C to obtain colourless crystals **3** (0.81 g, 70%). ^{1}H NMR (C_6D_6, 200.13 MHz): δ = 0.40 (s, 27 H, $SiCH_3$), 1.81 (t, ^1J = 6 Hz, 6 H, CH_2N), 2.59 (t, ^1J = 6 Hz, 6 H, CH_2NSi) ppm. ^{13}C NMR (C_6D_6, 50.32 MHz): δ = 2.41 ($SiCH_3$), 41.03 (CH_2N), 58.79 (CH_2NSi) ppm. EI MS: *m*/*z* (%) = 468 (13) [M^+], 453 (21) [M^+ − CH_3], 433 (7) [M^+ − Cl], 367 (100) [M^+ − Me_3SiNCH_2], 353 (17) [M^+ − $Me_3SiNCH_2CH_2$]. $C_{15}H_{39}ClGeN_4Si_3$ (467.8): calcd. C 38.51, H 8.40, N 11.98; found C 38.21, H 8.63, N 11.73.

1-Bromo-*N*,*N*′,*N*′′-tris(trimethylsilyl)azagermatrane (4): Using the same experimental procedure as above for **3** employing TMS_3-tren (1.85 g, 5.1 mmol), 9.56 mL of a 1.6 M *n*BuLi solution (15.3 mmol) in hexane and $GeBr_4$ (2.00 g, 5.1 mmol), colourless crystals **4** (1.72 g, 66%) were obtained from an *n*-pentane solution at −30 °C. ^{1}H NMR (C_6D_6, 200.13 MHz): δ = 0.43 (s, 27 H, $SiCH_3$), 1.82 (t, ^1J = 6 Hz, 6 H, CH_2N), 2.59 (t, ^1J = 6 Hz, 6 H, CH_2NSi) ppm. ^{13}C NMR (C_6D_6, 50.32 MHz): δ = 2.63 ($SiCH_3$), 41.34 (CH_2N), 59.14 (CH_2NSi). FD-MS: *m*/*z* (%) = 512 (21) [M^+], 433 (100) [M^+ − Br]. $C_{15}H_{39}BrGeN_4Si_3$ (512.3): calcd. C 35.17, H 7.67, N 10.94; found C 35.43, H 7.49, N 11.15.

1-Chloro-*N*,*N*′,*N*′′-trimethylazastannatrane (5): The procedure was analogous to that for **1**: reaction of Me_3-tren (1.06 g, 5.6 mmol) with 10.56 mL of a 1.6 M *n*BuLi solution (16.9 mmol) in hexane and then with $SnCl_4$ (1.46 g, 5.60 mmol) gave **5** as a white crystalline solid. Yield: 1.31 g (69%). ^{1}H NMR and ^{13}C NMR spectroscopic data were consistent with those already reported.[16]

1-Bromo-*N*,*N*′,*N*′′-trimethylazastannatrane (6): The procedure was analogous to that for **1**: reaction of Me_3-tren (1.77 g, 9.4 mmol) with 17.63 mL of a 1.6 M *n*BuLi solution (28.2 mmol) in hexane and then with $SnBr_4$ (4.12 g, 9.4 mmol) gave **6** as a white crystalline solid. Yield: 2.58 g (71%). ^{1}H NMR and ^{13}C NMR spectroscopic data were consistent with those already reported.[16]

1-Chloro-*N*,*N*′,*N*′′-tris(trimethylsilyl)azastannatrane (7): The procedure was analogous to that for **3**: reaction of TMS_3-tren (0.93 g, 2.6 mmol) with 4.81 mL of a 1.6 M *n*BuLi solution (7.7 mmol) in hexane and then with $SnCl_4$ (0.68 g, 2.6 mmol) gave **7** as a white crystalline solid. Yield: 0.84 g (63%). ^{1}H NMR (C_6D_6, 200.13 MHz): δ = 0.38 (s, 27 H, $SiCH_3$), 1.81 (t, ^1J = 6 Hz, 6 H, CH_2N), 2.71 (t, ^1J = 6 Hz, 6 H, CH_2NSi) ppm. ^{13}C NMR (C_6D_6,

Table 1. Crystal data, data collection, structure solution and refinement parameters for **1** and **3**

Compound	**1**	**3**
Empirical formula	$C_9H_{21}Cl_1Ge_1N_4$	$C_{15}H_{39}Cl_1Ge_1N_4Si_3$
Molecular weight	293.34	467.81
Colour, habit	Colorless block	Colorless prism
Crystal size [mm]	0.60 × 0.30 × 0.30	0.36 × 0.24 × 0.18
Crystal system	Trigonal	Monoclinic
Space group	*R*3c	$P2_1/c$
a [Å]	11.2754(2)	16.341(1)
b [Å]		10.081(1)
c [Å]	16.5461(4)	15.144(1)
β [°]		93.76(1)
Volume [Å^3]	1821.75(6)	2489.4(3)
Z	6	4
Density (calcd.)[g·cm^{-3}]	1.604	1.248
Absorption coefficient [mm^{-1}]	2.718	1.488
F(000)	912	992
Diffractometer	Bruker SMART CCD	Enraf Nonius CAD4
Temperature [K]	100.0(2)	203(2)
Radiation [λ/Å]	graphite-monochromated Mo-K_α (0.71073)	
θ range [°]	3.23 to 27.49	2.38 to 24.99
Index ranges	$-14 \le h \le 14$	$-19 \le h \le 0$
	$-14 \le k \le 14$	$-11 \le k \le 0$
	$-21 \le l \le 21$	$-17 \le l \le 18$
Reflections collected	6253	4401
Independent reflections	934 [R_{int} = 0.0316]	3994 [R_{int} = 0.0500]
Data reduction	Bruker SAINT[29]	XCAD4[30]
Absorption correction type	Empirical	Empirical
Min. and Max. transmission	0.2028 and 0.3508	0.6163 and 0.7755
Solution method	Direct methods (SHELXS-97)[31]	
Refinement method	Full-matrix least-squares on F^2 (SHELXL-97)[32]	
Hydrogen treatment	Isotropic refinement	Riding model
Data/restraints/parameters	934/1/75	3994/0/227
Reflections with $I > 2\sigma(I)$	906	3301
Goodness-of-fit on F^2	1.033	1.018
Final *R* indices [$I > 2\sigma(I)$]	*R*1 = 0.0135, *wR*2 = 0.0358	*R*1 = 0.0338, *wR*2 = 0.0797
R indices (all data)	*R*1 = 0.0142, *wR*2 = 0.0364	*R*1 = 0.0468, *wR*2 = 0.0858
Absolute structure parameter	−0.005(8)	−
Extinction coefficient	0.0007(2)	0.0004(2)
Largest diff. peak and hole [e Å^{-3}]	0.382 and −0.183	0.303 and −0.465

50.32 MHz): δ = 2.57 ($SiCH_3$), 41.17 (CH_2N), 59.27 (CH_2NSi) ppm. $C_{15}H_{39}ClN_4Si_3Sn$ (513.9): calcd. C 35.06, H 7.65, N 10.90; found C 35.27, H 7.94, N 10.79.

1-Bromo-*N*,*N*′,*N*′′-tris(trimethylsilyl)azastannatrane (8): The procedure was analogous to that for **3**: reaction of TMS_3-tren (2.65 g, 7.3 mmol) with 13.70 mL of a 1.6 M *n*BuLi solution (21.9 mmol) in hexane and then with $SnBr_4$ (3.21 g, 7.3 mmol) gave **8** as a white crystalline solid. Yield: 2.81 g (69%). ^{1}H NMR (C_6D_6, 300.13 MHz): δ = 0.40 (s, 27 H, $SiCH_3$), 1.83 (t, ^1J = 6 Hz, 6 H, CH_2N), 2.71 (t, ^1J = 6 Hz, 6 H, CH_2NSi) ppm. ^{13}C NMR (C_6D_6, 50.32 MHz): δ = 2.83 ($SiCH_3$), 41.39 (CH_2N), 59.76 (CH_2NSi) ppm. EI MS: *m*/*z* (%) = 479 (1.03) [M^+ − Br], 443 (4.30) [M^+ − $Me_3SiNCH_2CH_2$], 364 (7.15) [M^+ − Br − $Me_3SiNCH_2CH_2$]. $C_{15}H_{39}BrN_4Si_3Sn$ (558.4): calcd. C 32.27, H 7.04, N 10.03; found C 31.85, H 7.26, N 9.82.

Attempted Syntheses of $N(CH_2CHNR)_3Si-Hal$: Reactions of trilithium salts of Me_3-tren and TMS_3-tren with $SiCl_4$ and $SiBr_4$ were carried out as for **1** and **3**, respectively, resulting (according to ^{1}H NMR spectra) in a complex mixture of products which were difficult to separate and to identify.

X-ray Crystallographic Study: Crystal data, data collection, structure solution and refinement parameters for compounds **1** and **3** are presented in Table 1.

CCDC-178804 (**1**) and -184337 (**3**) contain the supplementary crystallographic data for this paper. These data can be obtained free of charge at www.ccdc.cam.ac.uk/conts/retrieving.html [or from the Cambridge Crystallographic Data Centre, 12, Union Road, Cambridge CB2 1EZ, UK; Fax: (internat.) +44-1223/336-033; E-mail: deposit@ccdc.cam.ac.uk].

Acknowledgments

This work was supported by the Russian Foundation for Basic Research under Grant No 01-03-32474 for A. V. C and INTAS under Grant No YSF 2001/2-135 for S. S. K. as well as by the Philipps-University Marburg, Chemistry Department, with a grant for P. L. S.

[1] M. G. Voronkov, V. M. D'yakov, S. V. Kirpichenko, *J. Organomet. Chem.* **1982**, *233*, 1−147.
[2] J. G. Verkade, *Coord. Chem. Rev.* **1994**, *137*, 233−295.

[3] V. Pestunovich, S. Kirpichenko, M. Voronkov, in *The Chemistry of Organic Silicon Compounds* (Ed.: Z. Rappoport, Y. Apeloig), John Wiley & Sons, **1998**, volume 2, part 1, chapter 24.
[4] S. S. Karlov, G. S. Zaitseva, *Chem. Heterocycl. Comp.* **2001**, *37*, 1325−1357.
[5] C. Chuit, R. J. P. Corriu, C. Reye, J. C. Young, *Chem. Rev.* **1993**, *93*, 1371−1448.
[6] M. Nasim, L. I. Livantsova, G. S. Zaitseva, J. Lorberth, *J. Organomet. Chem.* **1991**, *403*, 85−91.
[7] G. S. Zaitseva, L. I. Livantsova, M. Nasim, S. S. Karlov, A. V. Churakov, J. A. K. Howard, E. V. Avtomonov, J. Lorberth, *Chem. Ber./Recueil* **1997**, *130*, 739−746.
[8] G. S. Zaitseva, S. S. Karlov, A. V. Churakov, J. A. K. Howard, E. V. Avtomonov, J. Lorberth, *Z. Anorg. Allg. Chem.* **1997**, *623*, 1144−1150.
[9] G. S. Zaitseva, S. S. Karlov, B. A. Siggelkow, E. V. Avtomonov, A. V. Churakov, J. A. K. Howard, J. Lorberth, *Z. Naturforsch., Teil B* **1998**, *53*, 1247−1254.
[10] G. S. Zaitseva, S. S. Karlov, G. V. Pen'kovoy, A. V. Churakov, J. A. K. Howard, B. A. Siggelkow, E. V. Avtomonov, J. Lorberth, *Z. Anorg. Allg. Chem.* **1999**, *625*, 655−660.
[11] Y. Wan, J. G. Verkade, *Inorg. Chem.* **1993**, *32*, 79−81.
[12] G. S. Zaitseva, B. A. Siggelkow, S. S. Karlov, G. V. Pen'kovoy, J. Lorberth, *Z. Naturforsch., Teil B* **1998**, *53*, 1255−1258.
[13] P. L. Shutov, S. S. Karlov, J. Lorberth, G. S. Zaitseva, *Z. Naturforsch., Teil B* **2001**, *56*, 137−140.
[14] A. Tzschach, K. Jurkschat, C. Mugge, *Z. Anorg. Allg. Chem.* **1982**, *492*, 135−138.
[15] W. Plass, J. G. Verkade, *Inorg. Chem.* **1993**, *32*, 5145−5152.
[16] W. Plass, J. G. Verkade, *Inorg. Chem.* **1993**, *32*, 5153−5159.
[17] W. Plass, J. Pinkas, J. G. Verkade, *Inorg. Chem.* **1997**, *36*, 1973−1978.
[18] W. Plass, J. G. Verkade, *J. Am. Chem. Soc.* **1992**, *114*, 2275−2276.
[19] W. Plass, J. G. Verkade, *Inorg. Chem.* **1993**, *32*, 3762−3765.
[20] D. Gudat, L. M. Daniels, J. G. Verkade, *J. Am. Chem. Soc.* **1989**, *111*, 8520−8522.
[21] Y. Wan, J. G. Verkade, *J. Am. Chem. Soc.* **1995**, *117*, 141−156.
[22] R. R. Schrock, *Acc. Chem. Res.* **1997**, *30*, 9−16.
[23] R. Eujen, E. Petrauskas, A. Roth, D. J. Brauer, *J. Organomet. Chem.* **2000**, *613*, 86−92.
[24] R. J. Garant, L. M. Daniels, S. K. Das, M. N. Janakiraman, R. A. Jacobson, J. G. Verkade, *J. Am. Chem. Soc.* **1991**, *113*, 5728−5735.
[25] D. Gudat, J. G. Verkade, *Organometallics* **1989**, *8*, 2772−2779.
[26] S. P. Narula, S. Soni, R. Shankar, R. K. Chadha, *J. Chem. Soc., Dalton Trans.* **1992**, 3055−3056.
[27] S. N. Gurkova, S. N. Tandura, A. V. Kisin, A. I. Gusev, N. V. Alekseev, T. K. Gar, N. Yu. Khromova, I. R. Segel'man, *Zh. Strukt. Khim.* **1982**, *23*, 101−106.
[28] H. Schmidt, C. Lensink, S. K. Xi, J. G. Verkade, *Z. Anorg. Allg. Chem.* **1989**, *578*, 75−80.
[29] *SAINT Version 5.0.,* Bruker AXS Inc., Madison, Wisconsin, USA, **1997**.
[30] K. Harms, *XCAD4, Program for the Lp-Correction of Nonius CAD4 Data*, Marburg, Germany, **1997**.
[31] G. M. Sheldrick, *Acta Crystallogr., Sect. A* **1990**, *46*, 467−473.
[32] G. M. Sheldrick, *SHELXL-97, Program for the Refinement of Crystal Structures*, University of Göttingen, Germany, **1997**.

Received April 27, 2002
[I02241]

The Reaction of (Butadiene)zirconocene with Imines

Carsten Höltke,[a] Gerhard Erker,*[a] Gerald Kehr,[a] Roland Fröhlich,[a][‡] and Olga Kataeva[a][‡]

Keywords: Template synthesis / Zirconium / Metallocenes / Polymerizations

(Butadiene)zirconocene (*s-trans-*/*s-cis-***1** equilibrium mixture) reacts with the imine MeN=CHPh (**7a**) to form the 1:1 carbon-coupling product [κ*N*-MeN–CHPh–CH_2–η^3-(CHCHCH_2)]ZrCp_2 (**8a**). The X-ray crystal structure analysis of **8a** revealed a metallacyclic structure featuring a distorted π-allyl moiety and a planar-tricoordinate nitrogen atom. Only one of the two possible diastereoisomers is found in the crystal (*cis*-**8a**) as well as in solution. Treatment of **1** with the more bulky aldimine $PhCH_2N$=CHPh (**7b**) selectively gave the corresponding 1:1 addition product *trans*-**8b**. Ketimines $PhCH_2N=C(CH_2)_4$ (**7c**), HN=CPh_2 (**7d**), or Δ^1-2-methylpyrroline (**7e**) also reacted selectively with (butadiene)zirconocene to yield the analogous metallacyclic C–C coupling products **8c**–**e**. Treatment of **8e** with $B(C_6F_5)_3$ proceeded cleanly by abstraction of a hydride anion from the carbon atom α to the nitrogen atom to form the intramolecularly coordinated imine product **10a** {with the [$HB(C_6F_5)_3^-$] anion}. Similarly, Ph_3C^+ abstracts a hydride ion from **8e** to yield **10b** {isolated with the [$B(C_6H_5)_4^-$] anion}. Proton addition from HNR_3^+ reagents takes place selectively at the Zr–amido nitrogen atom of the complexes **8a** or **8d** to yield the substituted (π-allyl)zirconocene cation complexes **11** or **12**, respectively, The cationic complexes **10**, **11**, and **12** polymerize ethene at room temperature/2 bar of ethene with moderate catalytic activities.

(© Wiley-VCH Verlag GmbH, 69451 Weinheim, Germany, 2002)

Introduction

(Butadiene)zirconocene (**1**) has been used repeatedly as a reagent in organometallic and organic synthesis[1] as well as in catalysis.[2] Compound **1** is remarkable since it exists as a mixture of the two stereoisomers, (*s-cis-*) and (*s-trans-*η^4-C_4H_6)ZrCp_2.[3] It is readily prepared by treatment of the metallocene dihalide with "butadiene−magnesium".[4,5] Several alternative syntheses of **1** have been described in the literature.[3,6]

The (η^4-butadiene)zirconocene system reacts with a variety of unsaturated organic or organometallic reagents with carbon−carbon coupling. In many cases 1:1 or 1:2 addition products were obtained selectively. Their further transformation including hydrolytic workup has opened attractive synthetic pathways to novel Fischer carbene complexes,[1,7] stable conjugated primary enamines,[8] β,γ-unsaturated ε-hydroxycarboxylic acids,[9] and other organic building blocks.[10] Typical examples of organometallic products formed in these addition reactions are shown in Scheme 1.

It is noteworthy that the addition of organic carbonyl compounds leads to seven-membered metallacycles **4** that exhibit a strong metal−oxygen interaction caused by a marked oxygen-to-Zr π-backbonding component,[11] whereas the formally related zirconoxycarbene complexes **3** typically show a metallacyclic π-allyl structure.[7] Five-mem-

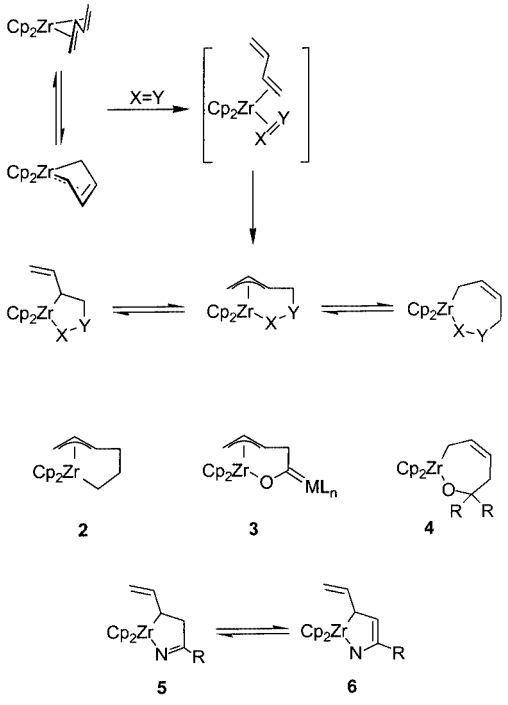

Scheme 1

[a] Organisch-Chemisches Institut der Universität Münster, Corrensstr. 40, 48149 Münster, Germany
[‡] X-ray crystal structure analyses.
Supporting information for this article is available on the WWW under http://www.eurjic.org or from the author.

bered tautomeric mixtures (**5** ⇄ **6**) were observed in the case of the 1:1 addition products between **1** and nitriles.[8] The metallacyclic structural type actually favored in such systems thus seems to depend strongly on the specific electronic features of the subunits involved, especially on the π-backbonding ability of the heteroatom that is σ-attached to the zirconocene unit.[2,5] We have now treated (butadiene)-zirconocene with a variety of organic imines and found that the formation of metallacyclic 1:1 addition products is favored. The systems were structurally characterized and their remarkable reaction with some electrophiles was studied.

Results and Discussion

Addition of Aldimines

We have employed the benzaldimines **7a** and **7b** for the addition reaction with (butadiene)zirconocene (**1**). The reactions were carried out in toluene solution at ambient temperature. Both addition reactions required ca. 2 d of reaction time under these conditions to go to completion. The 1:1 addition products **8a** and **8b** were formed selectively (see Scheme 2). We did not observe the formation of any 1:2 addition products, even in the presence of excess imine.[12] The products were isolated as yellow to orange-colored solids in 60% (**8a**) and 45% (**8b**) yield.

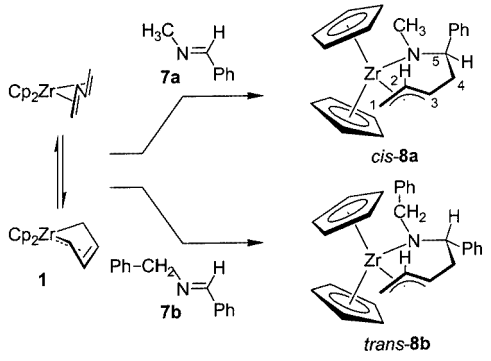

Scheme 2

Single crystals of **8a** were obtained from dichloromethane (Figure 1). The structure shows that a new C−C connection has been formed between the heterocarbonyl carbon atom of the imine reagent **7a** and a terminal sp^2-carbon center of the butadiene ligand in **1** [C4−C5: 1.525(4) Å]. The metallocene complex **8a** contains a metallacyclic substructure located in the bent metallocene σ-plane, that contains a distorted η^3-allyl moiety. It exhibits short Zr−C1 [2.472(3) Å] and Zr−C2 [2.487(3) Å] bonds and a markedly longer Zr−C3 contact [2.618(3) Å]. The carbon−carbon bond lengths inside the π-allyl unit are distorted towards a σ,π-type structure [C1−C2: 1.417(4) Å; C2−C3: 1.356(4) Å].[13] The Zr−N bond in **8a** is rather short at 2.157(2) Å. The nitrogen center in complex **8a** is trigonally planar coordinated (sum of bonding angles at N: 354.7°).

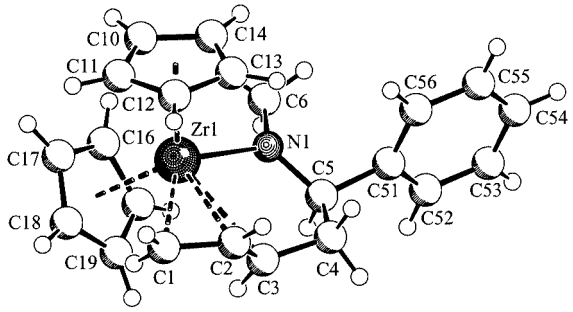

Figure 1. Molecular structure of **8a**; selected bond lengths [Å] and angles [°]: Zr1−N1 2.157(2), Zr1−C1 2.472(3), Zr1−C2 2.487(3), Zr1−C3 2.618(3), C1−C2 1.417(4), C2−C3 1.356(4), C3−C4 1.481(4), C4−C5 1.525(4), C5−N1 1.459(3), N1−C6 1.453(3); N1−Zr1−C1 123.9(1), N1−Zr1−C2 91.7(1), N1−Zr1−C3 67.4(1), C1−Zr1−C2 33.2(1), C1−Zr1−C3 57.3(1), C2−Zr1−C3 30.7(1), Zr1−N1−C5 128.0(2), Zr−N1−C6 116.6(2), Zr1−C1−C2 74.0(2), C1−C2−Zr1 72.8(2), C3−C2−Zr1 80.0(2), C2−C3−Zr1 69.3(2), C4−C3−Zr1 109.1(2), C1−C2−C3 123.7(3), C2−C3−C4 124.3(3), C3−C4−C5 107.6(2), C4−C5−N1 108.0(2), C5−N1−C6 110.1(2); C1−C2−C3−C4 160.9(3)

The formation of a new bond to the former imine sp^2-carbon atom has created a chiral center (C5) in **8a**. In addition, the substituted (π-allyl)$ZrCp_2$ subunit contains an element of planar chirality. Thus, two diastereoisomers could have been formed. However, only one is observed in the crystal. It is characterized by a *cis* orientation of the phenyl group at C5 and the π-allyl "*meso*"-hydrogen atom at C2 (*cis*-**8a**).

Single crystals of **8b** suitable for an X-ray crystal structure analysis were obtained from a toluene solution. In the asymmetric unit there are two crystallographically almost identical enantiomeric molecules. It exhibits an analogous metallacyclic framework to that of **8a**, containing a σ,π-distorted π-allyl unit [Zr−C1: 2.479(5) Å; Zr−C2: 2.511(4) Å; Zr−C3: 2.597(3) Å; C1−C2: 1.409(7) Å; C2−C3: 1.370(6) Å; values taken from molecule A]. The Zr−N σ-bond length in **8b** is found to be 2.185(3) Å and the nitrogen center is coordinated in a trigonally planar manner (sum of bonding angles: 358.0°). The major difference from **8a** is that the phenyl substituent of **8b** at C5 is *trans*-oriented relative to the 2-H at the π-allyl unit (see Figure 2). This may derive from a steric basis: in **8b**, the bulky C_6H_5 group of the *N*-benzyl substituent is found clearly oriented away from the C5 phenyl group.

In solution, only a single diastereoisomer of **8a** was observed, which is probably the *cis*-**8a** isomer. It exhibits a diastereotopic pair of ^{1}H NMR Cp singlets at δ = 5.87 and 5.82 ppm (in CD_2Cl_2 at 298 K). The (*E*)-configured monosubstituted π-allyl unit of **8a** is characterized by ^{13}C NMR signals at δ = 42.9 (C1), 124.7 (C2), and 110.5 (C3) as well as ^{1}H NMR resonances at δ = 2.19/1.89 (1-H, 1-H′), 5.80 (2-H), and 5.02 (3-H) with a characteristic set of coupling constants [^2J(1-H, 1-H′) = 3.0 Hz, ^3J(1-H_{syn}, 2-H) = 8.0 Hz, ^3J(1-H_{anti}, 2-H) = 14.5 Hz, and ^3J(2-H, 3-H) = 15.0 Hz]. The proton 5-H (δ = 4.60 ppm) shows a

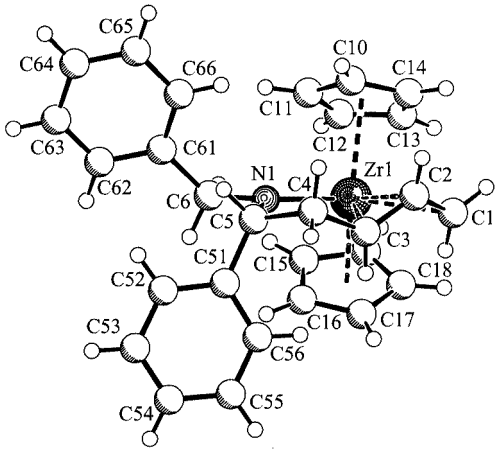

Figure 2. A view of the molecular structure of *trans*-**8b**; selected bond lengths [A] and angles [°] (molecule A): Zr1−N1 2.185(3), Zr1−C1 2.479(5), Zr1−C2 2.511(4), Zr1−C3 2.597(4), C1−C2 1.409(7), C2−C3 1.370(6), C3−C4 1.487(6), C4−C5 1.535(5), C5−N1 1.473(5), N1−C6 1.462(5); N1−Zr1−C1 123.7(2), N1−Zr1−C2 92.4(2), N1−Zr1−C3 67.2(2), C1−Zr1−C2 32.8(2), C1−Zr1−C3 57.0(2), C2−Zr1−C3 31.1(1), Zr1−N1−C5 129.9(2), Zr−N1−C6 118.2(2), Zr1−C1−C2 74.9(3), C1−C2−Zr1 72.3(3), C3−C2−Zr1 77.9(2), C2−C3−Zr1 71.0(3), C4−C3−Zr1 110.5(3), C1−C2−C3 121.3(5), C2−C3−C4 125.9(4), C3−C4−C5 110.1(3), C4−C5−N1 107.3(3), C5−N1−C6 109.9(3); C1−C2−C3−C4 −162.5(4)

large (anti-periplanar) coupling of ^3J(4-H′, 5-H) = 11.5 Hz and a small (gauche) coupling of ^3J(4-H, 5-H) = 7.2 Hz. Together with the coupling constants at 4-H/4-H′ of ^2J(4-H′, 4-H) = 12.0 Hz, ^3J(4-H′, 3-H) = 11.5 Hz, and ^3J(4-H, 3-H) = 3.5 Hz, this places the C5 phenyl substituent of complex **8a**, in solution, in a *cis* orientation relative to the 2-H *meso*-proton, just as it is found in the solid state structure. The NMR spectroscopic features of complex **8b** are similar (see Tables 1 and 2), but in detail specifically different. In **8b**, the 5-H proton shows only small coupling to 4-H/4-H′ (ca. 7 Hz) which indicates the presence of the *trans*-**8b** isomer in solution, analogously as it is found in the solid state (see Scheme 2).

Table 1. Selected ^{1}H NMR spectroscopic features of the complexes **8**, **10** and **11**

	1-H	1-H′	2-H	3-H	4-H	4-H′	5-H	N−CH$_3$	N−H
8a[a]	2.19	1.89	5.80	5.04	2.41	1.72	4.60	2.24	
8b[b]	2.30	1.88	6.06	5.67	2.33		4.91		
8c[c]	2.22	1.88	5.83	4.87	2.44	1.68			
8d[a]	2.16	1.97	5.43	5.08	3.22	1.45			1.71
8e[a]	2.12	1.83	5.68	5.22	2.27	1.35			
10a[d]	2.05	1.70	5.44	4.34	2.11	1.35			
10b[a]	2.47	2.14	5.93	4.89	2.56	1.78			
11a[e]	2.47	2.26	5.90	4.92	2.64	2.20	4.11	2.15	2.89
11b[a]	2.59	2.35	5.92	4.95	2.85	2.18	4.09	2.27	2.55

[a] Chemical shifts in CD_2Cl_2 at 298 K. [b] 253 K. [c] 273 K. [d] In [D_5]bromobenzene at room temperature. [e] Room temperature [D_6] benzene/[D_8] THF (4:1).

Reaction of (Butadiene)zirconocene with Ketimines

The reaction of **1** with imine **7c** of *N*-benzylcyclopentanone in toluene at room temperature required 2 d to go to completion. Again, only a 1:1 addition product was detected (**8c**), which was isolated in ca. 80% yield. Single crystals of **8c** were obtained from toluene. There are two crystallographically independent but chemically equivalent molecules of **8c** in the asymmetric unit; the values given below correspond to molecule A. The X-ray crystal structure analysis showed the presence of the typical metallacyclic framework (see Figure 3), featuring a nitrogen center that is close to being sp^2-hybridized [sum of bonding angles: 355.3°; angle Zr−N−C5: 128.5(2)°] and bonded to the zirconium atom [Zr−N: 2.178(3) Å], and a distorted η^3-allyl moiety [Zr−C1: 2.473(4) Å; Zr−C2: 2.491(4) Å; Zr−C3: 2.635(4) Å; C1−C2: 1.406(6) Å; C2−C3: 1.373(5) Å] inside a rigid metallacycle. The benzyl substituent at the nitrogen atom in **8c** attains a similar conformational orientation as was observed for **8b** (see above). The spiro-annelated carbocyclic five-membered ring at C5 occupies a pseudoaxial and a pseudoequatorial substituent position with its C−C bonds at the slightly crown-shaped central heterometallacycle.

In solution, complex **8c** shows the typical ^{1}H/^{13}C NMR spectroscopic features of the metallacyclic π-allyl complex systems (see Tables 1 and 2), so we can assume that the structures of **8c** in solution are similar to that of the solid state.

Imine **7d** of benzophenone also adds cleanly to (butadiene)zirconocene. The reaction takes only ca. 7 h to go to completion. The metallacyclic 1:1 addition product **8d** was

Table 2. Selected ^{13}C NMR chemical shifts of the framework atoms of the complexes **8** and **11**

	C-1	C-2	C-3	C-4	C-5
8a[a]	42.9	124.7	110.5	46.6	96.4
8b[b]	44.0	126.9	112.7	40.9	88.4
8c[c]	44.9	125.3	109.4	44.0	97.2
8d[a]	41.2	124.8	114.2	47.6	97.3
8e[a]	41.7	125.2	117.4	49.1	98.9
11a[d]	47.6	128.9	103.6	41.6	82.5
11b[a]	47.8	128.6	102.4	41.7	83.1

[a] Chemical shifts in CD_2Cl_2 at 298 K. [b] 253 K. [c] 273 K. [d] Room temperature [D_6] benzene/[D_8] THF (4:1).

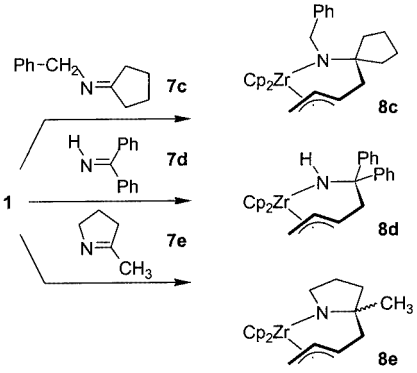

Scheme 3

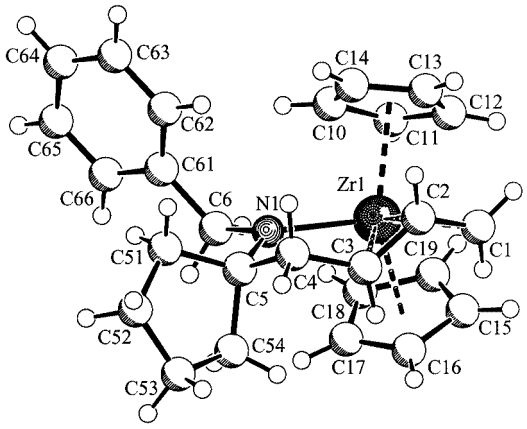

Figure 3. Molecular structure of complex **8c**; selected bond lengths [Å] and angles [°]: Zr1−N1 2.178(3), Zr1−C1 2.473(4), Zr1−C2 2.491(4), Zr1−C3 2.635(4), C1−C2 1.406(6), C2−C3 1.373(5), C3−C4 1.476(5), C4−C5 1.534(5), C5−N1 1.487(5), N1−C6 1.476(5); N1−Zr1−C1 123.3(1), N1−Zr1−C2 91.4(1), N1−Zr1−C3 67.2(1), C1−Zr1−C2 32.9(1), C1−Zr1−C3 57.1(1), C2−Zr1−C3 30.9(1), Zr1−N1−C5 128.5(2), Zr−N1−C6 115.0(2), Zr1−C1−C2 74.3(2), C1−C2−Zr1 72.8(2), C3−C2−Zr1 80.3(2), C2−C3−Zr1 68.8(2), C4−C3−Zr1 108.8(2), C1−C2−C3 123.2(4), C2−C3−C4 125.7(4), C3−C4−C5 110.0(3), C4−C5−N1 105.2(3), C5−N1−C6 111.8(3); C1−C2−C3−C4 −160.5(4)

isolated in 74% yield as a pale yellow solid. The ^{1}H NMR spectrum of **8d** (in CD_2Cl_2) shows a large separation of the signals of the diastereotopic Cp ligands (δ = 5.85 and 5.26 ppm). The typical π-allyl resonances of **8d** are listed in Tables 1 and 2. The broad NH ^{1}H NMR resonance of **8d** is found at δ = 1.71 ppm (in CD_2Cl_2). Figure 4 shows a typical ^{1}H NMR spectrum of complex **8d**.

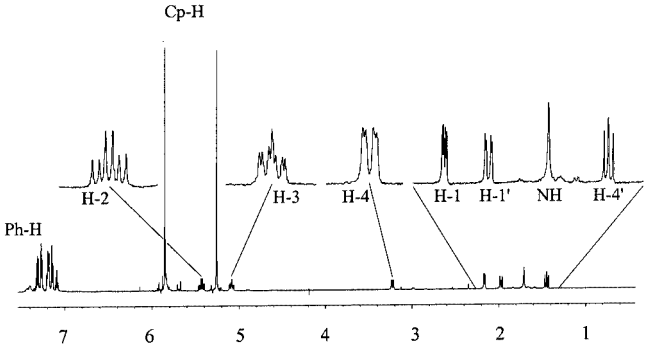

Figure 4. ^{1}H NMR spectrum of **8d** (CD_2Cl_2, 600 MHz, 298 K, δ in ppm)

Addition of the cyclic imine Δ^1-2-methylpyrroline (**7e**) to **1** at room temperature gave **8e** (single diastereomer, 60% isolated, for characterization see Tables 1 and 2, and the Exp. Sect.). The complexes **8c**−**e** were also characterized by ^{15}N NMR spectroscopy.[14] They showed ^{15}N NMR resonances at δ = −279 (**8c**), δ = −254 (**8d**), and δ = −249 ppm (**8e**) (external reference: nitromethane, δ = 0 ppm). These values are in a range that is typical for trigonal-planar nitrogen derivatives[15] including zirconocene-bound amido ligands.[16]

Reaction of 2-Methyl-2-oxazoline with (Butadiene)zirconocene

The reaction of **1** with the oxazoline reagent **7f** takes place slowly at room temperature in toluene solution (see Scheme 4). Workup after 20 h of reaction time gave the product **9** in ca. 80% yield, which was different from the expected simple addition product **8f**. Single crystals were obtained from toluene solution that allowed **9** to be structurally characterized by X-ray diffraction. The result of the X-ray crystal structure analysis (see Figure 5) revealed that the oxazoline heterocycle had been opened in the course of the reaction, and that a thermodynamically favorable zirconium−oxygen bond had been formed. Related ring-opened products have previously been obtained by Rosenthal et al. in the reaction of a [η^2-bis(trimethylsilyl)acetylene]zirconocene complex with thiazoles or benzoxazole.[17]

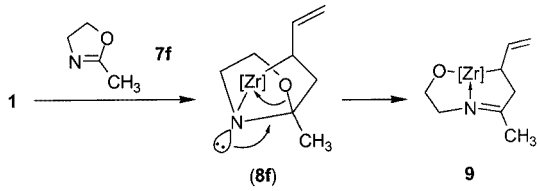

Scheme 4

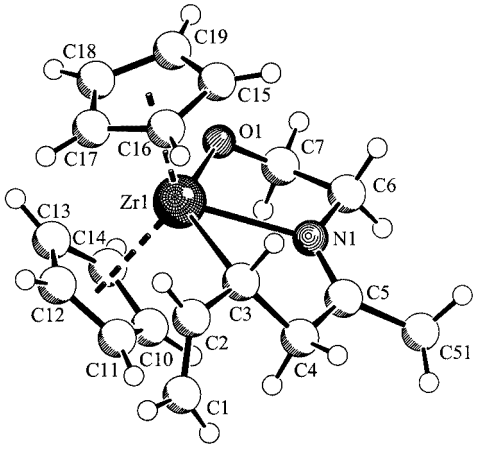

Figure 5. Molecular structure of complex **9**; selected bond lengths [Å] and angles [°]: Zr1−O1 2.094(2), Zr1−N1 2.378(2), Zr1−C3 2.448(2), C1−C2 1.336(4), C2−C3 1.470(3), C3−C4 1.517(3), C4−C5 1.491(4), C5−N1 1.279(3), N1−C6 1.467(3), C6−C7 1.492(4), C7−O1 1.365(3); O1−Zr1−N1 69.8(1), O1−Zr1−C3 135.2(1), N1−Zr1−C3 66.2(1), C7−O1−Zr1 123.4(2), Zr1−N1−C5 122.9(2), Zr−N1−C6 114.6(2), C2−C3−Zr1 118.8(2), C4−C3−Zr1 110.5(2), C1−C2−C3 128.3(3), C2−C3−C4 114.0(2), C3−C4−C5 110.6(2), C4−C5−N1 115.9(2), C5−N1−C6 121.8(2), N1−C6−C7 106.2(2), C6−C7−O1 111.2(2); C1−C2−C3−C4 −13.3(4)

In the reaction a metallabicyclic framework has been formed. The structural core is made up of an eight-membered ring comprising the zirconium atom, the −O−CH_2−CH_2−N=C(CH_3)− core of the oxazoline reagent, and two butadiene carbon atoms. The metallabicyclic structure is formed from building up a close transannular

zirconium−nitrogen contact. In **9** the Zr−O bond length is 2.094(2) Å, which is rather long and indicates the absence of a significant O→Zr π-interaction.[18] Consequently, the Zr−O−C7 bond angle is in the "normal" range at 123.4(2)°.

The N−C5 bond length is 1.279(3) Å, which clearly indicates the presence of an imine-type N=C double bond.[19] Consequently, the remaining lone pair on the N atom is used to coordinate to the zirconium atom [Zr−N: 2.378(2) Å]. The coordination geometry at the nitrogen atom in **9** is trigonal-planar (sum of bonding angles: 359.3°) as is the adjacent sp^2-hybridized carbon atom C5 (360°). The lateral Zr−C σ-bond length is 2.448(2) Å. The σ-ligand angle at the five-coordinate zirconium atom in **9** is rather large [O−Zr−C3: 135.2(1)°]. It is divided almost equally by the central N−Zr dative bond [O−Zr−N: 69.8(1)°; N−Zr−C3: 66.2(1)°]. The remaining vinyl group at C3 does not interact with the zirconium atom. It is pointing away from the metal center and is rotated out of the σ-plane [dihedral angle C4−C3−C2−C1: −13.3(4)°]. Consequently, a typical $C(sp^3)-C(sp^2)$ σ-bond length is observed for C2−C3 [1.470(3) Å]. The C1−C2 length [1.336(4) Å] denotes the presence of a C=C double bond.[19]

The ^{13}C NMR spectrum of complex **9** shows a typical imine carbon resonance of the N=C unit at δ = 187.2 ppm and a corresponding ^{15}N NMR signal at δ = −105.6.[14] The C4 ^{13}C NMR resonance of **9** is observed at δ = 48.8 ppm with a $^1J_{CH}$ coupling constant of 121 Hz, similar to the C3 resonance (δ = 52.6 ppm, $^1J_{CH}$ = 125 Hz). The C1 (δ = 97.5 ppm, $^1J_{CH}$ = 157 Hz and 151 Hz) and C2 (δ = 147.9 ppm, $^1J_{CH}$ = 144 Hz) signals indicate the presence of a σ-allyl group [^1H NMR signals at δ = 6.23 (2-H), 4.36, and 4.19 (1-H/1-H′) ppm]. Complex **9** exhibits a pair of equal-intensity ^1H NMR signals for the diastereotopic Cp ligands at δ = 5.95 and 5.70 ppm.

It is conceivable that the reaction of **1** with the oxazoline **7f** initially takes the usual course, and the addition product **8f**, that already contains the essential newly formed carbon−carbon bond, is actually formed. The applied reaction conditions probably favor thermodynamically controlled product formation. A subsequent β-oxygen elimination pathway that transforms **8f** to the more stable product **9** is viable (see Scheme 4).

Reactions of the Complexes 8 with Electrophiles

The reaction of alkylzirconocene complexes with activator Lewis acids, such as $B(C_6F_5)_3$[19,20] or the salt $[Ph_3C^+][B(C_6H_5)_4^-]$,[21] mostly proceeds with abstraction of an alkyl anion equivalent from the metal center with formation of a metallocene-derived cation.[22] Such cations often serve as very active homogeneous Ziegler−Natta catalysts for α-olefin polymerization.[23] In this context we were interested to learn about the favored reaction pathways that might be followed upon treatment of the heteroatom-functionalized metallacycles **8** with such electrophilic reagents.

We first reacted the bicyclic (butadiene)zirconocene/imine addition product **8e** with tris(pentafluorophenyl)borane (Scheme 5). The starting materials were dissolved in dichloromethane at 0 °C, and their reaction was then allowed to go to completion over 1 h at room temperature. The resulting product **10a** was isolated as an amorphous solid in greater than 80% yield. The NMR spectroscopic analysis showed that the $B(C_6F_5)_3$ electrophile had not attacked the Zr−allyl group (see Table 1). Instead, the borane had selectively abstracted a hydride from the C8 methylene group adjacent to the nitrogen atom, with formation of a κ*N*-coordinated imine.[24] The ^{11}B NMR spectrum of the salt shows a characteristic doublet (δ = −24.9 ppm, $^1J_{BH}$ = 85 Hz) of the $[HB(C_6F_5)_3^-]$ anion. In addition, the typical $^1H/^{13}C$ NMR spectroscopic features of the metal−imine moiety are observed at δ = 7.42 (8-H) and 183.5 ppm (C8), which were shifted drastically from the respective resonances of the starting material [**8e**: δ = 3.22, 2.90 (8-H); δ = 56.0 ppm (C8)].

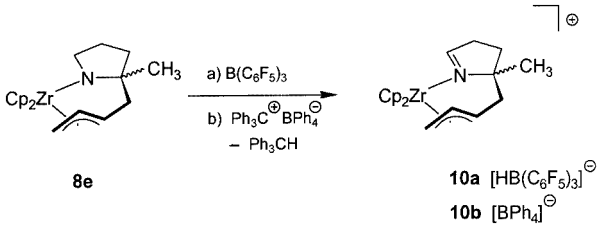

Scheme 5

An even more pronounced $\Delta\delta^{15}N$ value was observed upon transforming the neutral starting material **8e** ($\delta^{15}N$ = −249 ppm) to the salt **10a** ($\delta^{15}N$ = −89 ppm). Figure 6 shows the characteristic appearance of the ^1H NMR spectrum of complex **10a** in [D_5]bromobenzene (the *H*BAr_3^- ^1H NMR resonance was not observed).

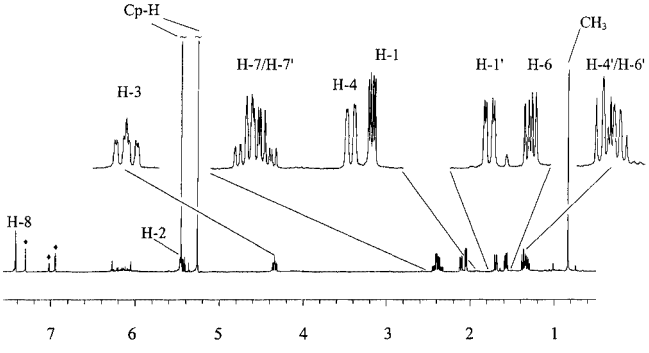

Figure 6. ^1H NMR spectrum of **10a** in [D_5]bromobenzene (600 MHz, 298 K, δ in ppm, black diamonds = solvent peaks)

Treatment of **8e** with trityl tetraphenylborate proceeded similarly. Hydride abstraction[25] from C8 takes place cleanly with formation of triphenylmethane and the organometallic salt **10b**.

We then treated the complexes **8a** and **8d** with both the ammonium Brønsted acids $[Bu_3NH^+][B(C_6H_5)_4^-]$ and $[PhNMe_2H^+][B(C_6F_5)_4^-]$.[26,27] Again, the Zr(π-allyl) moiety proved to be inert to electrophilic attack. Instead, in both cases it is the amido nitrogen atom that picks up the proton. We isolated the respective salts **11** and **12** [with

BPh_4^- (**a**) or $B(C_6F_5)_4^-$ (**b**) anions, respectively, see Scheme 6]. Both systems show the typical ^1H and ^{13}C NMR spectroscopic features of the remaining substituted (η^3-allyl)zirconocene moiety (see Tables 1 and 2). Protonation at the nitrogen atom has resulted in characteristic ^1H NMR spectroscopic features of **11b**, such as the $N-CH_3$ doublet at $\delta = 2.27$ ppm and the characteristic triplet of doublets of 5-H at $\delta = 4.09$ ppm (see Figure 7).

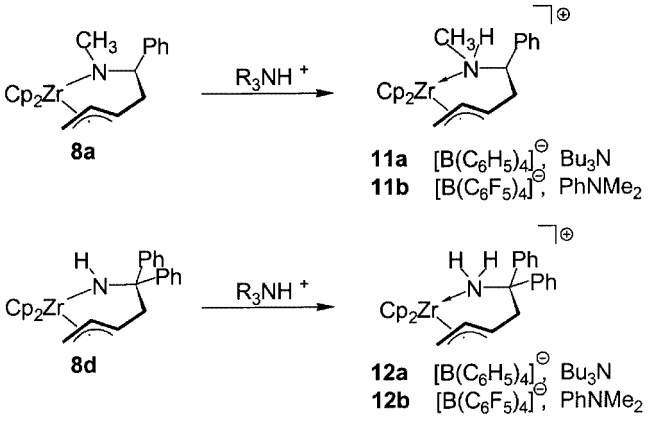

Scheme 6

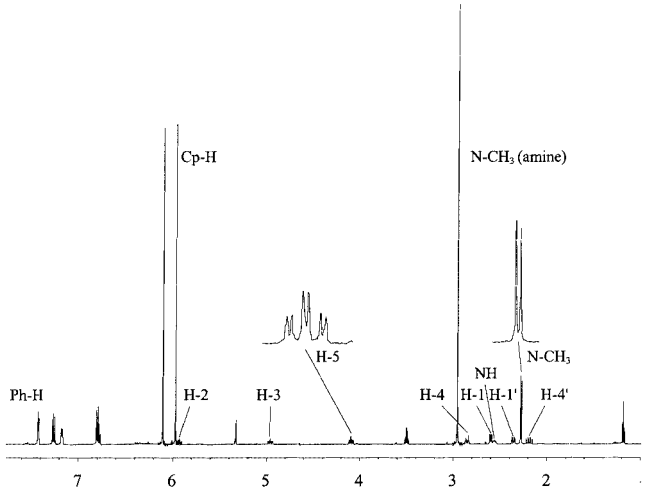

Figure 7. ^1H NMR spectrum of the salt **11b** [with $B(C_6F_5)_4^-$ anion]; the sample contains ca. 1 mol-equiv. of *N*,*N*-dimethylaniline (δ in ppm)

All the isolated samples of the complexes **11** and **12** contained ca. 1 mol-equiv. of the respective tertiary amine base, which could not readily be removed during the workup procedure. This has led us to assume an equilibrium of intra- and intermolecular amine coordination to the strongly electrophilic group-4 transition metal in these systems. For simplicity, the structures with intramolecular amine coordination to the zirconocene cation moiety are drawn in Scheme 6, although this has not been strictly proven.

We have employed the complexes **10a**, **11b**, and **12b** {all with $[HB(C_6F_5)_3^-]$ or $[B(C_6F_5)_4^-]$ anions} in polymerization experiments. Ethene polymerization was carried out with these systems in toluene solution (200 mL) at room temperature (2 bar of ethylene). The solution contained 0.5 mL of triisobutylaluminum as a "scrubbing agent" to prevent hydrolysis of the very sensitive homogeneous Ziegler–Natta catalyst systems at the very low concentrations that were used. The organometallic single component catalyst systems were injected as bromobenzene/toluene solutions to the pre-equilibrated reaction mixtures. All three systems turned out to be catalysts with moderate activity in the ethene polymerization experiments. Linear polyethylenes were obtained in all three cases (see Table 3).

Table 3. Ethene polymerization with the metallocene cation complexes **10**, **11**, and **12**

[a]	Catalyst [mg]	PE [g]	Activity[b]	M.p. [°C]
10a	15.0	2.24	65	129
11b	15.0	2.74	110	129
12b	15.0	4.30	177	131

[a] In 200 mL of toluene/0.5 mL of Bu_3Al, 1 h, room temperature, 2 bar of ethene. [b] Catalyst activities in kg(polymer)/[mol(cat.)·h·bar(ethene)].

We conclude that the (butadiene)zirconocene reagent is just reactive enough to add to the organic imines. It seems that in these cases the limit of the reactivity of these organometallic reagents is approached, since a subsequent carbon–carbon coupling at the other former diene terminus could not be achieved in these reactions. The nitrogen lone pair of the resulting metal amides does not seem to be substantially involved in bonding to the zirconocene unit.[26] This becomes apparent from the structural data of the complexes characterized here, which all feature relatively long Zr–N bonds. It also shows up in the reactions of these (π-allyl)zirconacycles: protonation occurs at the rather basic Zr–N bond, but not at the allyl carbanion equivalent, and hydride abstraction α to the nitrogen atom is also a favorable reaction of the systems **8**. Overall, this provides interesting selectivity features. We will explore whether the resulting cationic systems **10**, **11**, **12** can be used in selective stoichiometric carbon–carbon coupling reactions with functionalized unsaturated organic reagents. The observed moderate ethene polymerization activity of these systems allows us to believe that this can be achieved.

Experimental Section

General: Reactions with organometallic compounds were carried out under argon using Schlenk-type glassware or a glove-box. Solvents were dried and distilled under argon before use. NMR spectroscopic experiments were carried out with a Varian Unity plus 600 or a Bruker AC 200 NMR spectrometer. The NMR assignments were usually secured by carrying out a series of 2D NMR spectroscopy experiments.[29] For details see the Supporting Information. The following instruments were used for additional physical characterization: IR spectroscopy: Nicolet 5DXC FT-IR spectrometer; melting points: DSC 2010 (TA instruments); elemental analyses:

Foss Heraeus CHN-O-Rapid. (Butadiene)zirconocene (**1**)[3] and tris(pentafluorophenyl)borane[20] were prepared according to literature procedures. Commercially available imines [imine of benzophenone, Δ^1-2-methylpyrroline, benzylidene(methyl)amine, benzyl(benzylidene)amine] were distilled under argon prior to use. The other imines used in this study were prepared by condensation reactions of the respective carbonyl compound with the amine using 4 Å molecular sieves. The molecular sieves were activated by heating them to approx. 600 °C in vacuo, prior to use. The aldehyde or ketone (50.0 mmol) and the amine (50.0 mmol) were dissolved in dry toluene (150 mL) and stirred overnight with the activated molecular sieves at ambient temperature under argon. The molecular sieves were filtered off and the solvent removed in vacuo. The remaining crude imine was then purified by distillation and kept at 7 °C under argon.

Reaction of (Butadiene)zirconocene with Benzylidene(methyl)amine. Formation of 8a: Benzylidene(methyl)amine (**7a**, 0.24 g, 2.00 mmol) was added to a solution of (butadiene)zirconocene (**1**) (0.55 g, 2.00 mmol) in toluene (150 mL). After stirring at room temperature for 40 h the mixture was filtered and the solvent evaporated in vacuo. The crude residue was then treated with pentane (40 mL) to precipitate the insertion product (**8a**) as a yellow amorphous solid. The product was collected by filtration, washed with pentane (20 mL) and dried in vacuo. Yield: 0.60 g (75%). M.p. 194 °C. IR (KBr): $\tilde{\nu}$ = 3088 w, 2897 w, 2840 m, 2754 s, 1450 m, 1004 s, 999 s, 979 s, 877 m, 804 vs, 763 s, 703 s cm^{-1}. ^{1}H NMR (599.9 MHz, CD_2Cl_2, 298 K): δ = 7.25 (pt, 2 H, ph-H$_{meta}$), 7.14 (pt, 1 H, ph-H$_{para}$), 7.12 (pd, 2 H, ph-H$_{ortho}$), 5.87 (s, 5 H, cp-H), 5.8 (m, 1 H, 2-H), 5.82 (s, 5 H, cp-H), 5.04 (m, 1 H, 3-H), 4.60 (dd, $^3J_{H,H}$ = 11.5, $^3J_{H,H}$ = 4.5 Hz, 1 H, 5-H), 2.41 (m, 1 H, 4-H), 2.24 (s, 3 H, 6-H), 2.19 (dd, $^3J_{H,H}$ = 8.0, $^2J_{H,H}$ = 2.5 Hz, 1 H, 1-H), 1.89 (dd, $^3J_{H,H}$ = 14.5, $^2J_{H,H}$ = 2.5 Hz, 1 H, 1′-H), 1.72 (m, 1 H, 4′-H) ppm. ^{13}C{^{1}H} NMR (150.8 MHz, CD_2Cl_2, 298 K): δ = 148.1 (ph-C$_{ipso}$), 128.3 (ph-C$_{meta}$), 127.2 (ph-C$_{ortho}$), 126.4 (ph-C$_{para}$), 124.7 (C-2), 110.5 (C-3), 108.4 (cp-C), 106.6 (cp-C), 96.4 (C-5), 46.6 (C-4), 45.6 (C-6), 42.9 (C-1) ppm.

X-ray Crystal Structure Analysis of 8a: Crystals were obtained by slow concentration of a dichloromethane solution. Formula $C_{22}H_{25}NZr$, M = 394.65, green-yellow crystal 0.35 × 0.10 × 0.05 mm, a = 20.995(1), c = 8.039(1) Å, V = 3543.5(5) Å^3, ρ$_{calcd.}$ = 1.480 g·cm^{-3}, μ = 6.23 cm^{-1}, empirical absorption correction (0.812 ≤ T ≤ 0.970), Z = 8, tetragonal, space group $I\bar{4}$ (no. 82), λ = 0.71073 Å, T = 198 K, ω and φ scans, 6355 reflections collected (±h, ±k, ±l), [(sinθ)/λ] = 0.65 Å^{-1}, 3654 independent (R_{int} = 0.032) and 3400 observed reflections [$I \geq 2\sigma(I)$], 218 refined parameters, R = 0.028, wR^2 = 0.054, Flack parameter −0.02(4), max. residual electron density 0.27 (−0.25) e·Å^{-3}, hydrogen atoms calculated and refined as riding atoms.

Reaction of (Butadiene)zirconocene with Benzyl(benzylidene)amine. Formation of 8b: Benzyl(benzylidene)amine (**7b**, 1.97 g, 10.0 mmol) was added to a solution of (butadiene)zirconocene (**1**) (2.26 g, 10.0 mmol) in toluene (200 mL). After stirring for 60 h, the mixture was filtered and the solvent evaporated in vacuo. The crude residue was then treated with pentane (150 mL) to precipitate the insertion product as a yellow powder. The product was collected by filtration, washed twice with pentane (50 mL) and dried in vacuo. Yield: 2.12 g (45%). M.p. 114 °C. IR (KBr): $\tilde{\nu}$ = 3078 w, 3024 w, 2892 m, 2831 m, 2796 m, 2767 m, 1598 m, 1570 s, 1489 s, 1450 s, 1344 s, 1261 s, 1190 m, 1024 vs, 875 m, 811 vs, 740 vs, 702 s cm^{-1}. ^{1}H NMR (599.9 MHz, CD_2Cl_2, 253 K): δ = 7.34 (pt, 2 H, ph-H$_{meta/B}$), 7.24 (pt, 2 H, ph-H$_{meta/A}$), 7.1 (m, 4 H, ph-H$_{para/A}$, ph-H$_{para/B}$, ph-H$_{ortho/B}$), 7.01 (pd, 2 H, ph-H$_{ortho/A}$), 6.06 (m, 1 H, 2-H), 5.83 (s, 5 H, cp-H), 5.80 (s, 5 H, cp-H), 5.67 (m, 1 H, 3-H), 4.91 (m, 1 H, 5-H), 4.24 (d, $^2J_{H,H}$ = 17.2 Hz, 1 H, 6-H), 3.48 (d, $^2J_{H,H}$ = 17.2 Hz, 1 H, 6′-H), 2.39−2.28 (m, 3 H, 4-H/4′-H/1-H), 1.88 (m, 1 H, 1′-H) ppm. ^{13}C{^{1}H} NMR (150.8 MHz, CD_2Cl_2, 253 K): δ = 146.9 (ph-C$_{ipso/A}$), 142.4 (ph-C$_{ipso/B}$), 128.1 (ph-C$_{meta/B}$), 127.9 (ph-C$_{meta/A}$), 127.6 (ph-C$_{ortho/A}$), 127.5 (ph-C$_{ortho/B}$), 126.9 (C-2), 126.2 (ph-C$_{para/A}$), 125.7 (ph-C$_{para/B}$), 112.7 (C-3), 108.4 (cp-C), 106.7 (cp-C), 88.4 (C-5), 60.0 (C-6), 44.0 (C-1), 40.9 (C-4) ppm. $C_{28}H_{29}NZr$ (470.7): calcd. C 71.44, H 6.21, N 2.98; found C 71.21, H 6.32, N 2.66.

X-ray Crystal Structure Analysis of 8b: Crystals were obtained from a saturated toluene solution. Formula $C_{28}H_{29}NZr$, M = 470.74, yellow crystal 0.15 × 0.15 × 0.05 mm, a = 11.516(1), b = 17.227(1), c = 22.510(1) Å, V = 4465.7(5) Å^3, ρ$_{calcd.}$ = 1.400 g·cm^{-3}, μ = 5.07 cm^{-1}, empirical absorption correction (0.928 ≤ T ≤ 0.975), Z = 8, orthorhombic, space group $P2_12_12_1$ (no. 19), λ = 0.71073 Å, T = 198 K, ω and φ scans, 37107 reflections collected (±h, ±k, ±l), [(sinθ)/λ] = 0.66 Å^{-1}, 10611 independent (R_{int} = 0.077) and 7135 observed reflections [$I \geq 2\sigma(I)$], 541 refined parameters, R = 0.050, wR^2 = 0.080, Flack parameter 0.01(4), max. residual electron density 0.33 (−0.51) e·Å^{-3}, hydrogen atoms calculated and refined as riding atoms, two almost identical independent molecules in the asymmetric unit, being enantiomers of each other.

Reaction of (Butadiene)zirconocene with Benzyl(cyclopentylidene)-amine. Formation of 8c: Benzyl(cyclopentylidene)amine (**7c**, 0.87 g, 5.0 mmol) was added to a solution of (butadiene)zirconocene (**1**) (1.38 g, 5.0 mmol) in toluene (120 mL). After stirring for 16 h, the mixture was filtered and the solvent was evaporated in vacuo. The crude residue was then treated with pentane (100 mL) to precipitate the insertion product **8c** as a yellow powder. The product was collected by filtration, washed with pentane (50 mL) and dried in vacuo. Yield: 1.82 g (81%). M.p. 130 °C. IR (KBr): $\tilde{\nu}$ = 3072 w, 2951 m, 2863 m, 2792 w, 1575 w, 1446 m, 1087 m, 1017 s, 803 vs, 736 s cm^{-1}. ^{1}H NMR (599.9 MHz, CD_2Cl_2, 273 K): δ = 7.34 (pd, 2 H, ph-H$_{ortho}$), 7.29 (pt, 2 H, ph-H$_{meta}$), 7.15 (t, $^3J_{H,H}$ = 7.5 Hz, 1 H, ph-H$_{para}$), 5.83 (ddd, $^3J_{H,H}$ = 14.5, $^3J_{H,H}$ = 14.5, $^3J_{H,H}$ = 7.2 Hz, 1 H, 2-H), 5.81 (s, 5 H, cp-H), 5.66 (s, 5 H, cp-H), 4.87 (ddd, $^3J_{H,H}$ = 14.5, $^3J_{H,H}$ = 11.5, $^3J_{H,H}$ = 3.5 Hz, 1 H, 3-H), 4.41 (d, $^2J_{H,H}$ = 18.5 Hz, 1 H, 8-H), 3.91 (d, $^2J_{H,H}$ = 18.5 Hz, 1 H, 8′-H), 2.44 (dd, $^3J_{H,H}$ = 3.5, $^2J_{H,H}$ = 11.5 Hz, 1 H, 4-H), 2.22 (dd, $^3J_{H,H}$ = 7.2, $^2J_{H,H}$ = 2.5 Hz, 1 H, 1-H), 1.88 (dd, $^3J_{H,H}$ = 14.5, $^2J_{H,H}$ = 2.5 Hz, 1 H, 1′-H), 1.81−1.73 (m, 1 H, 6-H$_a$), 1.68 (m, 1 H, 4′-H), 1.65−1.50 (m, 3 H, 6-H$_b$/7-H$_{a+b}$), 1.45−1.27 (m, 2 H, 7′-H$_{a+b}$), 1.09−0.93 (m, 2 H, 6′-H$_{a+b}$) ppm. ^{13}C{^{1}H} NMR (150.8 MHz, CD_2Cl_2, 273 K): δ = 148.6 (ph-C$_{ipso}$), 127.5 (ph-C$_{meta}$), 127.2 (ph-C$_{ortho}$), 125.3 (C-2), 124.8 (ph-C$_{para}$), 109.4 (C-3), 108.1 (cp-C), 106.2 (cp-C), 97.2 (C-5), 55.8 (C-8), 44.9 (C-1), 44.0 (C-4), 40.7 (C-6′), 29.6 (C-6), 23.5 (C-7′), 21.1 (C-7) ppm. (^{1}H-^{15}N)-GHMBC (599.9 MHz/60.0 MHz, CD_2Cl_2, 273 K): δ^{1}H/δ^{15}N = 4.41, 3.91/−279.5 ppm. $C_{26}H_{31}NZr$ (448.7): calcd. C 69.59, H 6.96, N 3.12; found C 67.94, H 6.62, N 2.50.

X-ray Crystal Structure Analysis of 8c: Single crystals were obtained from a saturated toluene solution. Formula $C_{26}H_{31}NZr$, M = 448.74, light yellow crystal 0.15 × 0.10 × 0.03 mm, a = 8.206(1), b = 25.367(1), c = 20.260(1) Å, β = 90.84(1)°, V = 4216.9(6) Å^3, ρ$_{calcd.}$ = 1.414 g·cm^{-3}, μ = 5.33 cm^{-1}, empirical absorption correction (0.924 ≤ T ≤ 0.984), Z = 8, monoclinic, space group $P2_1/c$ (no. 14), λ = 0.71073 Å, T = 198 K, ω and φ scans, 42299 reflections collected (±h, ±k, ±l), [(sinθ)/λ] = 0.66 Å^{-1}, 9977 independent (R_{int} = 0.124) and 5583 observed reflections [$I \geq 2\sigma(I)$], 505 refined parameters, R = 0.060, wR^2 = 0.086, max.

residual electron density 0.57 (−0.77) e·Å^{-3}, hydrogen atoms calculated and refined as riding atoms, two almost identical independent molecules in the asymmetric unit.

Reaction of (Butadiene)zirconocene with the Imine of Benzophenone. Formation of 8d: Imine **7d** (0.91 g, 5.0 mmol) of benzophenone was added to a solution of (butadiene)zirconocene (**1**) (1.38 g, 5.0 mmol) in toluene (150 mL). After stirring for 7 h, the solvent was evaporated in vacuo and the crude residue was treated with pentane (100 mL) to precipitate the insertion product **8d** as a light-yellow powder. The product was collected by filtration, washed with pentane (50 mL) and dried in vacuo. Yield: 1.69 g (74%). M.p. 129 °C. IR (KBr): $\tilde{\nu}$ = 3052 s, 2936 m, 2912 s, 2849 m, 1643 s, 1604 s, 1576 s, 1493, 1450 s, 1228 m, 1173 s, 1064 s, 1020 s, 800 vs, 712 s, 611 s cm^{-1}. ^{1}H NMR (599.9 MHz, CD_2Cl_2, 298 K): δ = 7.47−7.06 (m, 10 H, ph-H), 5.85 (s, 5 H, cp-H), 5.43 (ddd, $^3J_{H,H}$ = 14.8, $^3J_{H,H}$ = 14.8, $^3J_{H,H}$ = 8.1 Hz, 1 H, 2-H), 5.26 (s, 5 H, cp-H), 5.08 (ddd, $^3J_{H,H}$ = 14.8, $^3J_{H,H}$ = 11.2, $^3J_{H,H}$ = 3.8 Hz, 1 H, 3-H), 3.22 (dd, $^3J_{H,H}$ = 3.8, $^2J_{H,H}$ = 12.7 Hz, 1 H, 4-H), 2.16 (dd, $^3J_{H,H}$ = 8.1, $^2J_{H,H}$ = 3.2 Hz, 1 H, 1-H), 1.97 (dd, $^3J_{H,H}$ = 14.8, $^2J_{H,H}$ = 3.2 Hz, 1 H, 1′-H), 1.71 (br, 1 H, NH), 1.45 (dd, $^3J_{H,H}$ = 11.2, $^2J_{H,H}$ = 12.7 Hz, 1 H, 4′-H) ppm. ^{13}C{^{1}H} NMR (150.8 MHz, CD_2Cl_2, 298 K): δ = 155.4, 151.6, 128.2, 127.8, 127.5, 126.1, 125.7, 125.6 (ph-C), 124.8 (C-2), 114.2 (C-3), 108.6, 106.3 (cp-C), 97.3 (C-5), 47.6 (C-4), 41.2 (C-1). (^{1}H-^{15}N)-GHMBC (599.9 MHz/60.0 MHz, CD_2Cl_2, 273 K): δ^{1}H/δ^{15}N = 1.71/−254.3 (d, $^1J_{HN}$ = 62 Hz) ppm. $C_{27}H_{27}NZr$ (456.74): calcd. C 71.00, H 5.96, N 3.07; found C 71.14, H 5.93, N 2.93.

Reaction of (Butadiene)zirconocene with Δ^1-2-Methylpyrroline. Formation of 8e: Δ^1-2-Methylpyrroline (**7e**, 0.84 g, 10.0 mmol) was added to a solution of (butadiene)zirconocene (**1**) (2.76 g, 10.0 mmol) in toluene (200 mL). After stirring for 16 h, the mixture was filtered and the solvent evaporated in vacuo. The residue was washed with three portions of pentane (3 × 50 mL). The filtrate was concentrated in vacuo until precipitation of the product occurred, and then stored at −18 °C overnight. The resulting product was collected by filtration and washed with cold pentane (20 mL). Subsequent concentration of the mother liquor and crystallization gave a combined yield of 2.15 g (60%) of the insertion product **8e**. M.p. 70 °C. IR (KBr): $\tilde{\nu}$ = 3088 w, 2951 m, 2863 m, 1628 w, 1441 w, 1015 s, 797 vs, 740 vs cm^{-1}. ^{1}H NMR (599.9 MHz, CD_2Cl_2, 298 K): δ = 5.79 (s, 5 H, cp-H), 5.71 (s, 5 H, cp-H), 5.68 (ddd, $^3J_{H,H}$ = 14.5, $^3J_{H,H}$ = 14.5, $^3J_{H,H}$ = 7.7 Hz, 1 H, 2-H), 5.22 (ddd, $^3J_{H,H}$ = 14.5, $^3J_{H,H}$ = 11.5, $^3J_{H,H}$ = 3.5 Hz, 1 H, 3-H), 3.22 (m, 1 H, 8-H), 2.90 (m, 1 H, 8′-H), 2.27 (dd, $^3J_{H,H}$ = 3.5, $^2J_{H,H}$ = 11.5 Hz, 1 H, 4-H), 2.12 (dd, $^3J_{H,H}$ = 7.7, $^2J_{H,H}$ = 3.2 Hz, 1 H, 1-H), 1.83 (dd, $^3J_{H,H}$ = 14.5, $^2J_{H,H}$ = 3.2 Hz, 1 H, 1′-H), 1.68−1.61 (m, 2 H, 7-H/7′-H), 1.53 (m, 1 H, 6-H), 1.35 (m, 1 H, 4′-H), 1.26 (m, 1 H, 6′-H), 1.06 (s, 3 H, 9-H) ppm. ^{13}C{^{1}H} NMR (150.8 MHz, CD_2Cl_2, 298 K): δ = 125.2 (C-2), 117.4 (C-3), 109.2 (cp-C), 107.7 (cp-C), 98.9 (C-5), 56.0 (C-8), 49.1 (C-4), 42.9 (C-6), 41.7 (C-1), 28.0 (C-7), 24.1 (C-9, s, $^1J_{CH}$ = 124 Hz) ppm. (^{1}H-^{15}N)-GHMBC (599.9 MHz/60.0 MHz, CD_2Cl_2, 273 K): δ^{1}H/δ^{15}N = 3.22, 2.90/−249.3 ppm. $C_{19}H_{25}NZr$ (358.64): calcd. C 63.63, H 7.03, N 3.91; found C 62.42, H 6.80, N 3.56.

Reaction of (Butadiene)zirconocene with 2-Methyl-2-oxazoline. Formation of 9: 2-Methyl-2-oxazoline (**7f**, 171 mg, 2.00 mmol) was added to a solution of butadiene(zirconocene) (**1**) (551 mg, 2.00 mmol) in toluene (50 mL). After stirring for 17 h, the mixture was filtered and the solvent evaporated in vacuo. The crude residue was then treated with pentane (20 mL) to precipitate the insertion product as a light brown powder. The product was collected by filtration, washed twice with pentane (10 mL) and dried in vacuo. Yield: 613 mg (85%). IR (KBr): $\tilde{\nu}$ = 3060 m, 2826 m, 2673 w, 1654 s, 1589 s, 1448 w, 1368 w, 1106 s, 1015 s, 821 s, 795 vs, 765 m cm^{-1}. ^{1}H NMR (599.9 MHz, CD_2Cl_2, 298 K): δ = 6.23 (ddd, $^3J_{H,H}$ = 10.5, $^3J_{H,H}$ = 16.9, $^3J_{H,H}$ = 5.4 Hz, 1 H, 2-H), 5.95 (s, 5 H, cp-H), 5.70 (s, 5 H, cp-H), 4.36 (ddd, $^3J_{H,H}$ = 10.5, $^2J_{H,H}$ = 2.2, $^4J_{H,H}$ = 2.1 Hz, 1 H, 1-H), 4.19 (ddd, $^3J_{H,H}$ = 16.9, $^2J_{H,H}$ = 2.2, $^4J_{H,H}$ = 2.1 Hz, 1 H, 1′-H), 3.90 (ddd, $^3J_{H,H}$ = 5.7, $^3J_{H,H}$ = 5.8, $^2J_{H,H}$ = 9.8 Hz, 1 H, 7-H), 3.71 (ddd, $^3J_{H,H}$ = 5.4, $^3J_{H,H}$ = 6.6, $^2J_{H,H}$ = 9.8 Hz, 1 H, 7′-H), 3.28 (m, 1 H, 6-H), 3.11 (m, 1 H, 6′-H), 2.95 (m, 1 H, 4-H), 2.80 (m, 1 H, 4′-H), 2.53 (m, 1 H, 3-H), 2.03 (s, 3 H, 8-H) ppm. ^{13}C{^{1}H} NMR (150.8 MHz, CD_2Cl_2, 298 K): δ = 187.2 (C-5, s), 147.9 (C-2, d, $^1J_{CH}$ = 144 Hz), 111.0 (cp-C, d, $^1J_{CH}$ = 171 Hz), 110.6 (cp-C, d, $^1J_{CH}$ = 171 Hz), 97.5 (C-1, dd, $^1J_{CH}$ = 151, $^1J_{CH}$ = 157 Hz), 69.0 (C-7, t, $^1J_{CH}$ = 139 Hz), 56.4 (C-6, t, $^1J_{CH}$ = 137 Hz), 52.6 (C-3, d, $^1J_{CH}$ = 125 Hz), 48.8 (C-4, t, $^1J_{CH}$ = 121 Hz), 20.2 (C-8, q, $^1J_{CH}$ = 128 Hz) ppm. (^{1}H-^{15}N)-GHMBC (599.9 MHz/60.0 MHz, CD_2Cl_2, 273 K): δ^{1}H/δ^{15}N = 3.28, 3.11/−105.6 ppm. $C_{18}H_{23}NOZr$ (360.61): calcd. C 59.95, H 6.43, N 3.88; found C 58.74, H 6.53, N 3.48.

X-ray Crystal Structure Analysis of 9: Single crystals were obtained from a saturated toluene solution. Formula $C_{18}H_{23}NOZr$, M = 360.59, light yellow crystal 0.15 × 0.15 × 0.10 mm, a = 10.486(1), b = 13.273(1), c = 11.591(1) Å, β = 94.73(1)°, V = 1607.7(2) Å^3, $\rho_{calcd.}$ = 1.490 g·cm^{-3}, μ = 6.83 cm^{-1}, empirical absorption correction (0.905 ≤ T ≤ 0.935), Z = 4, monoclinic, space group $P2_1/c$ (no. 14), λ = 0.71073 Å, T = 198 K, ω and φ scans, 13970 reflections collected (±h, ±k, ±l), [(sinθ)/λ] = 0.66 Å^{-1}, 3845 independent (R_{int} = 0.048) and 3039 observed reflections [$I \geq 2\sigma(I)$], 191 refined parameters, R = 0.033, wR^2 = 0.072, max. residual electron density 0.63 (−0.61) e·Å^{-3}, hydrogen atoms calculated and refined as riding atoms.

Data sets were collected with a Nonius Kappa CCD diffractometer, equipped with a rotating anode generator Nonius FR591. Programs used: data collection COLLECT (Nonius B.V., **1998**), data reduction Denzo-SMN (Z. Otwinowski, W. Minor, *Methods Enzymol.* **1997**, *276*, 307−326), absorption correction SORTAV (R. H. Blessing, *Acta Crystallogr.* **1995**, *A51*, 33−37; R. H. Blessing, *J. Appl. Crystallogr.* **1997**, *30*, 421−426), structure solution SHELXS-97 (G. M. Sheldrick, *Acta Crystallogr.* **1990**, *A46*, 467−473), structure refinement SHELXL-97 (G. M. Sheldrick, Universität Göttingen, **1997**), graphics SCHAKAL (E. Keller, Universität Freiburg, **1997**). CCDC-183380 to -183383 contain the supplementary crystallographic data for this paper. These data can be obtained free of charge at www.ccdc.cam.ac.uk/conts/retrieving.html or from the Cambridge Crystallographic Data Centre, 12, Union Road, Cambridge CB2 1EZ, UK [Fax: (internat.) + 44-1223/336-033; E-mail: deposit@ccdc.cam.ac.uk].

Reaction of 8e with Tris(pentafluorophenyl)borane. Formation of 10a: Compound **8e** (0.36 g, 1.0 mmol) was treated with tris(pentafluorophenyl)borane (0.51 g, 1.0 mmol) in dichloromethane (20 mL) at 0 °C for 1 h. Evaporation of the solvent yielded a semi-solid material, which was suspended in pentane (30 mL) and stirred for 2 d at ambient temperature to precipitate the reaction product. Filtration gave 0.77 g (88%) of complex **10a**. M.p. 244 °C (decomp.). IR (KBr): $\tilde{\nu}$ = 3124 w, 2973 m, 2368 m, 1643 m, 1511 s, 1461 vs, 1272 m, 1103 s, 968 s, 821 s cm^{-1}. ^{1}H NMR (599.9 MHz, C_6D_5Br, 298 K): δ = 7.42 (s, 1 H, 8-H), 5.45 (s, 5 H, cp-H), 5.44 (ddd, $^3J_{H,H}$ = 15.2, $^3J_{H,H}$ = 14.5, $^3J_{H,H}$ = 7.8 Hz, 1 H, 2-H), 5.26 (s, 5 H, cp-H), 4.34 (ddd, $^3J_{H,H}$ = 15.2, $^3J_{H,H}$ = 11.9, $^3J_{H,H}$ = 2.9 Hz, 1 H, 3-H), 2.46-2.32 (m, 2 H, 7-H, 7′-H), 2.11 (dd, $^3J_{H,H}$ = 2.9, $^2J_{H,H}$ = 13.0 Hz, 1 H, 4-H), 2.05 (dd, $^3J_{H,H}$ = 7.8, $^2J_{H,H}$ = 3.7 Hz, 1 H, 1-H), 1.70 (dd, $^3J_{H,H}$ = 14.5, $^2J_{H,H}$ = 3.7 Hz, 1 H, 1′-

H), 1.58 (m, 1 H, 6-H), 1.37−1.30 (m, 2 H, 4′-H, 6′-H), 0.84 (s, 3 H, 9-H) ppm. The $H-B(C_6F_5)_3^-$ resonance was not observed. $^{13}C\{^1H\}$ NMR (150.8 MHz, C_6D_5Br, 298 K): δ = 183.5 (C-8, d, $^1J_{CH}$ = 181 Hz), 127.6 (C-2), 107.9 (cp-C), 107.3 (cp-C), 102.0 (C-3), 98.8 (C-5), 45.2 (C-1), 43.1 (C-4), 38.1 (C-7), 36.9 (C-6), 23.4 (C-9) ppm. ^{11}B NMR (64.2 MHz, C_6D_5Br, 298 K): δ = −24.9 (d, $^1J_{BH}$ = 85 Hz) ppm. (^1H-^{15}N)-GHMBC (599.9 MHz/60.0 MHz, CD_2Cl_2, 273 K): $\delta^1H/\delta^{15}N$ = 7.42/−88.8 ppm. HRMS (EI): calcd. for $C_{19}H_{24}NZr^+$ 356.0956, found 356.0965.

Reaction of Complex 8e with Trityl Tetraphenylborate. Formation of 10b: A sample of **8e** (0.36 g, 1.00 mmol) was treated with trityl tetraphenylborate (0.57 g, 1.00 mmol) in dichloromethane (20 mL) at −78 °C. The mixture was then warmed to ambient temperature and stirred overnight. Evaporation of the solvent yielded a white, solid material, which was suspended in pentane (30 mL) and stirred for 17 h at ambient temperature to precipitate the product and to dissolve triphenylmethane. Filtration and washing with pentane yielded 0.58 g (85%) of complex **10b**. M.p. 215 °C (decomp.). ^1H NMR (599.9 MHz, CD_2Cl_2, 298 K): δ = 7.45−7.40 (m, 8 H, ph-H_{borate}), 7.23 (m, 1 H, 8-H), 7.08 (pt, 8 H, ph-H_{borate}), 6.93 (pt, 4 H, ph-H_{borate}), 5.93 (m, 1 H, 2-H), 5.88 (s, 5 H, cp-H), 5.62 (s, 5 H, cp-H), 4.89 (ddd, $^3J_{H,H}$ = 2.8, $^3J_{H,H}$ = 11.5, $^3J_{H,H}$ = 14.9 Hz, 1 H, 3-H), 2.59−2.53 (m, 3 H, 4-H, 7-H, 7′-H), 2.47 (dd, $^3J_{H,H}$ = 7.7, $^2J_{H,H}$ = 3.6 Hz, 1 H, 1-H), 2.14 (dd, $^3J_{H,H}$ = 14.1, $^2J_{H,H}$ = 3.6 Hz, 1 H, 1′-H), 1.99 (m, 1 H, 6-H), 1.78 (dd, $^3J_{H,H}$ = 11.5, $^2J_{H,H}$ = 13.0 Hz, 1 H, 4′-H), 1.65 (m, 1 H, 6′-H), 1.25 (s, 3 H, 9-H) ppm. $^{13}C\{^1H\}$ NMR (150.8 MHz, CD_2Cl_2, 298 K): δ = 184.6 (C-8), 164.5 (q, ph-$C_{ipso/borate}$, $^1J_{BC}$ = 49.5 Hz), 136.2 (ph-$C_{ortho/borate}$), 128.2 (C-2), 126.3 (q, ph-$C_{meta/borate}$, $^3J_{BC}$ = 2.8 Hz), 122.4 (ph-$C_{para/borate}$), 108.6 (cp-C), 108.0 (cp-C), 102.6 (C-3), 99.6 (C-5), 46.1 (C-1), 44.0 (C-4), 38.9 (C-7), 37.7 (C-6), 24.4 (C-9) ppm. HRMS (EI): calcd. for $C_{19}H_{24}NZr^+$ 356.0956, found 356.0987.

Reaction of 8a with Tri(*n*-butyl)ammonium Tetraphenylborate. Formation of 11a: A sample of **8a** (0.39 g, 1.00 mmol) was treated with tri(*n*-butyl)ammonium tetraphenylborate (0.51 g, 1.00 mmol) in diethyl ether (20 mL) at −78 °C. The mixture was then warmed to ambient temperature and stirred overnight. Evaporation of the solvent yielded a white solid, which was suspended in pentane (30 mL) and stirred for 17 h at ambient temperature. Filtration gave 0.79 g (88%) of complex **11a**. M.p. 204 °C. ^1H NMR (599.9 MHz, C_6D_6/[D_8]THF ≈ 4:1, 298 K): δ = 7.39−7.33 (m, 3 H, ph-H), 7.31−7.27 (m, 8 H, ph-H_{borate}), 7.27−7.24 (m, 2 H, ph-H), 6.86 (pt, 8 H, ph-H_{borate}), 6.72 (pt, 4 H, ph-H_{borate}), 6.04 (s, 5 H, cp-H), 5.93 (s, 5 H, cp-H), 5.90 (dt, $^3J_{H,H}$ = 14.5, $^3J_{H,H}$ = 8.2 Hz, 1 H, 2-H), 4.92 (ddd, $^3J_{H,H}$ = 14.5, $^3J_{H,H}$ = 11.2, $^3J_{H,H}$ = 3.5 Hz, 1 H, 3-H), 4.11 (m, 1 H, 5-H), 2.89 (m, 1 H, NH), 2.64 (m, 1 H, 4-H), 2.47 (dd, $^3J_{H,H}$ = 8.2, $^2J_{H,H}$ = 3.2 Hz, 1 H, 1-H), 2.43 (br, 6 H, α-H_{amine}) 2.27−2.24 (m, 1 H, 1′-H), 2.20 (m, 1 H, 4′-H), 2.15 (d, $^3J_{H,H}$ = 6.2 Hz, 3 H, 6-H), 1.40 (m, $^3J_{H,H}$ = 7.4 Hz, 6 H, β-H_{amine}), 1.31 (m, $^3J_{H,H}$ = 7.4 Hz, 6 H, γ-H_{amine}), 0.90 (t, $^3J_{H,H}$ = 7.4 Hz, 9 H, δ-H_{amine}) ppm. $^{13}C\{^1H\}$ NMR (150.8 MHz, [D_6]benzene/[D_8]THF ≈ 4:1, 298 K): δ = 165.2 (q, $C_{ipso/borate}$, $^1J_{BC}$ = 50.2 Hz), 139.0 (ph-C), 137.2 ($C_{ortho/borate}$), 129.8, 128.2, 127.9 (ph-C), 128.9 (C-2), 125.8 (q, $C_{meta/borate}$, $^3J_{BC}$ = 2.5 Hz), 121.9 ($C_{para/borate}$), 110.3 (cp-C), 109.8 (cp-C), 103.6 (C-3), 82.5 (C-5), 54.6 (α-C_{amine}), 47.6 (C-1), 41.6 (C-4), 39.6 (C-6), 29.6 (β-C_{amine}, only visible in the 50 MHz spectrum), 21.2 (γ-C_{amine}), 14.3 (δ-C_{amine}) ppm. HRMS (EI): calcd. for $C_{22}H_{26}NZr^+$ 394.1112, found 394.1147.

Reaction of Complex 8a with *N,N*-Dimethylammonium Tetrakis(pentafluorophenyl)borate. Formation of 11b: A mixture of **8a** (395 mg, 1.00 mmol) and *N,N*-dimethylanilinium tetrakis(pentafluorophenyl)borate (800 mg, 1.00 mmol) was dissolved in diethyl ether (50 mL) at −78 °C. The mixture was then warmed to ambient temperature and stirred overnight. Evaporation of the solvent yielded a white solid, which was suspended in pentane (30 mL) and stirred for 17 h at ambient temperature to precipitate the product. Filtration gave 0.88 g (74%) of complex **11b**. M.p. 267 °C (decomp.). ^1H NMR (599.9 MHz, CD_2Cl_2, 298 K): δ = 7.42 (m, 3 H, ph-H), 7.26 (m, 2 H, ph-H_{amine}), 7.17 (m, 2 H, ph-H), 6.78 (m, 3 H, ph-H_{amine}), 6.10 (s, 5 H, cp-H), 5.96 (s, 5 H, cp-H), 5.92 (m, 1 H, 2-H), 4.95 (ddd, $^3J_{H,H}$ = 15.3, $^3J_{H,H}$ = 11.3, $^3J_{H,H}$ = 3.6 Hz, 1 H, 3-H), 4.09 (dt, $^3J_{H,H}$ = 3.6, $^3J_{H,H}$ = 12.1 Hz, 1 H, 5-H), 2.95 [s, 6 H, $N(CH_3)_{amine}$], 2.85 (dt, $^3J_{H,H}$ = 3.6, $^2J_{H,H}$ = 14.5 Hz, 1 H, 4-H), 2.59 (dd, $^3J_{H,H}$ = 8.1, $^2J_{H,H}$ = 3.6 Hz, 1 H, 1-H), 2.55 (m, 1 H, NH), 2.35 (dd, $^3J_{H,H}$ = 14.3, $^2J_{H,H}$ = 3.6 Hz, 1 H, 1′-H), 2.27 (d, $^3J_{H,H}$ = 6.2 Hz, 3 H, N-CH_3), 2.18 (ddd, $^3J_{H,H}$ = 15.3, $^3J_{H,H}$ = 12.1, $^2J_{H,H}$ = 14.5 Hz, 1 H, 4′-H) ppm. $^{13}C\{^1H\}$ NMR (150.8 MHz, CD_2Cl_2, 298 K): δ = 150.5 ($C_{ipso/amine}$), 148.6 (dm, $C_{ortho/borate}$, $^1J_{C,F}$ = 241 Hz), 138.6 (dm, $C_{para/borate}$, $^1J_{C,F}$ = 247 Hz), 137.3 (ph-C_{ipso}), 136.7 (dm, $C_{meta/borate}$, $^1J_{C,F}$ = 245 Hz), 130.1 (ph-C), 130.0 (ph-C), 129.5 ($C_{meta/amine}$), 128.6 (C-2), 126.4 (ph-C), 124.7 ($C_{ipso/borate}$), 118.0 ($C_{para/amine}$), 113.4 ($C_{ortho/amine}$), 109.5 (cp-C), 108.9 (cp-C), 102.4 (C-3), 83.1 (C-5), 47.8 (C-1), 41.7 (C-4), 41.2 [$N(CH_3)_{amine}$], 39.6 (N-CH_3) ppm. HRMS (EI): calcd. for $C_{22}H_{26}NZr^+$ 394.1112, found 394.1099.

Reaction of Complex 8d with Tri(*n*-butyl)ammonium Tetraphenylborate. Formation of 12a: A sample of complex **8d** (457 mg, 1.00 mmol) and tri(*n*-butyl)ammonium tetraphenylborate (0.51 g, 1.00 mmol) was suspended in diethyl ether (20 mL) at −78 °C. The mixture was then warmed to ambient temperature and stirred overnight. Evaporation of the solvent yielded a white solid, which was stirred in pentane (30 mL) for 17 h at ambient temperature. Filtration gave 0.71 g (74%) of complex **12a**. M.p. 247 °C (decomp.). Due to rapid decomposition of compound **12a** in solution only ^1H and $^1H/^1H$-correlation NMR spectra were recorded. ^1H NMR (599.9 MHz, C_6D_6/[D_8]THF = 2:1, 298 K): δ = 7.72 (m, 8 H, Ph-H_{borate}), 7.25 (m, 1 H, Ph-H), 7.23 (m, 1 H, Ph-H), 7.19 (pt, 8 H, Ph-H_{borate}), 7.17 (m, 4 H, Ph-H), 7.09 (pt, 2 H, Ph-H), 7.03 (pt, 4 H, Ph-H_{borate}), 6.90 (pd, 2 H, Ph-H), 5.46 (ddd, $^3J_{H,H}$ = 14.2, $^3J_{H,H}$ = 15.1, $^3J_{H,H}$ = 8.0 Hz, 1 H, H-2), 5.39 (s, 5 H, Cp-H), 5.09 (s, 5 H, Cp-H), 4.63 (m, 1 H, H-3), 3.69 (d, $^2J_{H,H}$ = 12.3 Hz, 1 H, NH), 3.27 (d, $^2J_{H,H}$ = 14.5 Hz, 1 H, H-4), 3.01 (d, $^2J_{H,H}$ = 12.3 Hz, 1 H, NH′), 2.17 (dd, $^3J_{H,H}$ = 8.0, $^2J_{H,H}$ = 3.3 Hz, 1 H, H-1), 2.10 (br, 6 H, α-H_{amine}) 1.93 (dd, $^3J_{H,H}$ = 14.2, $^2J_{H,H}$ = 3.3 Hz, 1 H, H-1′), 1.86 (dd, $^3J_{H,H}$ = 11.9, $^2J_{H,H}$ = 14.5, 1 H, H-4′), 1.02 (br, 6 H, γ-H_{amine}), 0.98 (br, 6 H, β-H_{amine}), 0.90 (br, 9 H, δ-H_{amine}) ppm.

Reaction of Complex 8d with *N,N*-Dimethylanilinium Tetrakis(pentafluorophenyl)borate. Formation of 12b: A mixture of compound **8d** (457 mg, 1.00 mmol) and *N,N*-dimethylanilinium tetrakis(pentafluorophenyl)borate (800 mg, 1.00 mmol) was suspended in diethyl ether (50 mL) at −78 °C. The mixture was then warmed to ambient temperature and stirred overnight. Evaporation of the solvent yielded a white solid, which was suspended in pentane (30 mL) and stirred for 17 h at ambient temperature. Filtration gave 1.02 g (81%) of complex **12d**. M.p. 288 °C (decomp.). ^1H NMR (599.9 MHz, CD_2Cl_2, 298 K): δ = 7.60 (m, 2 H, Ph-H_{meta}), 7.52 (m, 1 H, Ph-H_{para}), 7.43 (m, 2 H, Ph-H_{ortho}), 7.38 (m, 2 H, Ph-H_{meta}), 7.32 (m, 1 H, Ph-H_{para}), 7.26 (m, 2 H, Ph-H_{amine}), 7.03 (m, 2 H, Ph-H_{ortho}), 6.81 (m, 3 H, Ph-H_{amine}), 5.98 (m, 1 H, H-2), 5.96, 5.54 (s, each 5 H, Cp-H), 5.13 (ddd, $^3J_{H,H}$ = 14.9, $^3J_{H,H}$ = 11.9, $^3J_{H,H}$ = 2.8 Hz, 1 H, H-3), 3.76 (dd, $^3J_{H,H}$ = 14.9, $^2J_{H,H}$ = 15.6 Hz, 1 H, H-4), 3.57, 3.30 (d, $^2J_{H,H}$ = 12.5 Hz, each 1 H, NH, and NH′), 2.95 [s, 6 H, $N(CH_3)_{amine}$], 2.60 (dd, $^3J_{H,H}$ = 8.2, $^2J_{H,H}$ =

3.7 Hz, 1 H, H-1), 2.38 (dd, $^3J_{H,H}$ = 14.2, $^2J_{H,H}$ = 3.7 Hz, 1 H, H-1′), 2.31 (dd, $^3J_{H,H}$ = 11.9, $^2J_{H,H}$ = 15.6 Hz, 1 H, H-4′) ppm. $^{13}C\{^1H\}$ NMR (150.8 MHz, CD_2Cl_2, 298 K): δ = 149.9 (C, Ph-$C_{ipso/amine}$), 148.6 (CF, dm, Ph-$C_{ortho/borate}$, $^1J_{C,F}$ = 242 Hz), 146.4, 140.1 (C, Ph-C_{ipso}), 138.7 (CF, dm, Ph-$C_{para/borate}$, $^1J_{C,F}$ = 242 Hz), 136.7 (CF, dm, Ph-$C_{meta/borate}$, $^1J_{C,F}$ = 248 Hz), 130.5 (CH, Ph-C), 130.3 (CH, C-2), 129.9, 129.7 (CH, Ph-C), 129.6 (CH, Ph-$C_{meta/amine}$), 128.7, 126.8, 124.2 (CH, Ph-C), 124.0 (C, br, Ph-$C_{ipso/borate}$), 118.7 (CH, Ph-$C_{para/amine}$), 113.8 (CH, Ph-$C_{ortho/amine}$), 108.7, 108.4 (CH, Cp-C), 102.1 (CH, C-3), 85.9 (C, C-5), 46.6 (CH_2, C-1), 44.6 (CH_2, C-4), 41.6 [CH_3, $N(CH_3)_{amine}$] ppm. HRMS (EI): calcd. for $C_{27}H_{28}NZr^+$ 456.1269, found 456.1231.

Polymerization Experiments: The polymerization experiments were carried out in a thermostatted 1-L Büchi glass autoclave. The reaction mixtures contained toluene (200 mL) and triisobutylaluminum (0.5 mL) as the scavenger. The stirred (700 rpm) solution was saturated with ethylene at 2 bar for 45 min before the polymerization reactions were started by injection of the group-4 metal catalyst precursors, dissolved in 3−7 mL of a toluene/bromobenzene mixture. The polymerization reactions were stopped after 1 h by the addition of ca. 20 mL of a 1:1 mixture of 1 N aqueous HCl in methanol after the pressure had been released and the excess ethylene vented. The mixture was stirred for an additional 30 min. The polymer formed was collected by filtration, washed with aqueous HCl and water and dried in vacuo at an elevated temperature. Further information is provided in Table 3.

Acknowledgments

Financial support from the Fonds der Chemischen Industrie and the Deutsche Forschungsgemeinschaft is gratefully acknowledged.

[1] Reviews: [1a] H. Yasuda, K. Tatsumi, A. Nakamura, *Acc. Chem. Res.* **1985**, *18*, 120−126. [1b] G. Erker, C. Krüger, G. Müller, *Adv. Organomet. Chem.* **1985**, *24*, 1−39. [1c] H. Yasuda, A. Nakamura, *Angew. Chem.* **1987**, *99*, 745−764; *Angew. Chem. Int. Ed. Engl.* **1987**, *26*, 723−742. [1d] G. Erker, *Angew. Chem.* **1989**, *101*, 411−426; *Angew. Chem. Int. Ed. Engl.* **1989**, *28*, 397−412.

[2] [2a] B. Temme, G. Erker, J. Karl, H. Luftmann, R. Fröhlich, S. Kotila, *Angew. Chem.* **1995**, *107*, 1867−1869; *Angew. Chem. Int. Ed. Engl.* **1995**, *34*, 1755−1757. [2b] D. D. Devore, F. J. Timmers, D. L. Hasha, R. K. Rosen, T. J. Marks, P. A. Deck, C. L. Stern, *Organometallics* **1995**, *14*, 3132−3134. [2c] B. Temme, J. Karl, G. Erker, *Chem. Eur. J.* **1996**, *2*, 919−924. [2d] J. Karl, G. Erker, R. Fröhlich, *J. Organomet. Chem.* **1997**, *535*, 59−62. [2e] G. J. Pindado, M. Thornton-Pett, M. Bowkamp, A. Meetsma, B. Hessen, M. Bochmann, *Angew. Chem.* **1997**, *109*, 2457−2460; *Angew. Chem. Int. Ed. Engl.* **1997**, *36*, 2358−2361. [2f] M. Dahlmann, G. Erker, M. Nissinen, R. Fröhlich, *J. Am. Chem. Soc.* **1999**, *121*, 2820−2828. [2g] M. Dahlmann, G. Erker, R. Fröhlich, O. Meyer, *Organometallics* **2000**, *19*, 2956−2967. [2h] M. Dahlmann, G. Erker, K. Bergander, *J. Am. Chem. Soc.* **2000**, *122*, 7986−7998. [2i] Review: G. Erker, *Acc. Chem. Res.* **2001**, *34*, 309−317.

[3] [3a] G. Erker, J. Wicher, K. Engel, F. Rosenfeldt, W. Dietrich, C. Krüger, *J. Am. Chem. Soc.* **1980**, *102*, 6344−6346. [3b] G. Erker, J. Wicher, K. Engel, C. Krüger, *Chem. Ber.* **1982**, *115*, 3300−3309. [3c] G. Erker, K. Engel, C. Krüger, A.-P. Chiang, *Chem. Ber.* **1982**, *115*, 3311−3323. [3d] Y. Kai, N. Kanehisa, K. Miki, N. Kasai, K. Mashima, K. Nagasuna, H. Yasuda, A. Nakamura, *J. Chem. Soc., Chem. Commun.* **1982**, 191−192. [3e] U. Dorf, K. Engel, G. Erker, *Organometallics* **1983**, *2*, 462−463. [3f] G. Erker, K. Engel, C. Krüger, G. Müller, *Organometallics* **1984**, *3*, 128−133. [3g] C. Krüger, G. Müller, G. Erker, U. Dorf, K. Engel, *Organometallics* **1985**, *4*, 215−225. [3h] T. Okamoto, N. Kanehisa, A. Nakamura, H. Yasuda, Y. Kai, N. Kasai, *J. Am. Chem. Soc.* **1988**, *110*, 5008−5017. [3i] M. Dahlmann, G. Erker, R. Fröhlich, O. Meyer, *Organometallics* **1999**, *18*, 4459−4461. [3j] M. Dahlmann, J. Schottek, R. Fröhlich, D. Kunz, M. Nissinen, G. Erker, G. Fink, R. Kleinschmidt, *J. Chem. Soc., Dalton Trans.* **2000**, 1881−1886.

[4] [4a] H. E. Ramsden, U. S. Patent 3388179, **1968**. [4b] Y. Nakano, K. Natsukawa, H. Yasuda, H. Tani, *Tetrahedron Lett.* **1972**, 2833−2836. [4c] K. Fujita, Y. Ohnuma, H. Yasuda, H. Tani, *J. Organomet. Chem.* **1976**, *113*, 201−213. [4d] H. Yasuda, Y. Nakano, K. Natsukawa, H. Tani, *Macromolecules* **1978**, *11*, 586−592. [4e] Y. Kai, N. Kanehisa, K. Miki, N. Kasai, K. Mashima, H. Yasuda, A. Nakamura, *Chem. Lett.* **1982**, 1277−1280. [4f] See also: S. Datta, S. S. Wreford, R. P. Beatty, T. J. McNeese, *J. Am. Chem. Soc.* **1979**, *101*, 1053−1054. [4g] See also: S. S. Wreford, J. F. Whitney, *Inorg. Chem.* **1981**, *20*, 3918−3924.

[5] H. Yasuda, Y. Kajihara, K. Mashima, K. Nagasuna, K. Lee, A. Nakamura, *Organometallics* **1982**, *1*, 388−396.

[6] [6a] P. Czisch, G. Erker, H.-G. Korth, R. Sustmann, *Organometallics* **1984**, *3*, 945−947. [6b] R. Beckhaus, K.-H. Thiele, *J. Organomet. Chem.* **1986**, *317*, 23−31. [6c] U. Böhme, K.-H. Thiele, A. Rufinska, *Z. Anorg. All. Chem.* **1994**, *620*, 1455−1462.

[7] [7a] G. Erker, U. Dorf, R. Benn, R.-D. Reinhardt, J. L. Petersen, *J. Am. Chem. Soc.* **1984**, *106*, 7649−7650. [7b] G. Erker, R. Lecht, R. Schlund, K. Angermund, C. Krüger, *Angew. Chem.* **1987**, *99*, 708−710; *Angew. Chem. Int. Ed. Engl.* **1987**, *26*, 666−668. [7c] G. Erker, R. Lecht, J. L. Petersen, H. Bönnemann, *Organometallics* **1987**, *6*, 1962−1967. [7d] G. Erker, R. Lecht, Y.-H. Tsay, C. Krüger, *Chem. Ber.* **1987**, *120*, 1763−1765. [7e] G. Erker, F. Sosna, R. Zwettler, C. Krüger, *Organometallics* **1989**, *8*, 450−454. [7f] G. Erker, F. Sosna, R. Noe, *Chem. Ber.* **1990**, *123*, 821−827. [7g] G. Erker, F. Sosna, *Organometallics* **1990**, *9*, 1949−1953. [7h] G. Erker, R. Pfaff, C. Krüger, S. Werner, *Organometallics* **1991**, *10*, 3559−3568.

[8] [8a] G. Erker, R. Pfaff, C. Krüger, M. Nolte, R. Goddard, *Chem. Ber.* **1992**, *125*, 1669−1673. [8b] G. Erker, R. Pfaff, *Organometallics* **1993**, *12*, 1921−1926. [8c] G. Erker, D. Kowalski, R. Noe, C. Krüger, M. Nolte, *Tetrahedron Lett.* **1994**, *35*, 6665−6668. [8d] D. Kowalski, G. Erker, S. Kotila, *Liebigs Annalen* **1996**, 887−890.

[9] [9a] M. Berlekamp, G. Erker, B. Schönecker, R. Krieg, A. L. Rheingold, *Chem. Ber.* **1993**, *126*, 2119−2126. [9b] G. Erker, M. Berlekamp, L. López, M. Grehl, B. Schönecker, R. Krieg, *Synthesis* **1994**, 212−222. [9c] H. C. Strauch, G. Erker, R. Fröhlich, *Chem. Ber.* **1996**, *129*, 1029−1034. [9d] M. Berlekamp, G. Erker, R. Fröhlich, *Z. Naturforsch., Teil B* **1996**, *51*, 1649−1654. [9e] H. C. Strauch, T. Rinderknecht, G. Erker, R. Fröhlich, E. Wegelius, F. Zippel, S. Höppener, H. Fuchs, L. Chi, *Eur. J. Org. Chem.* **2000**, 187−192.

[10] [10a] G. Erker, K. Engel, U. Dorf, J. L. Atwood, W. E. Hunter, *Angew. Chem.* **1982**, *94*, 915−916; *Angew. Chem. Int. Ed. Engl.* **1982**, *21*, 914. [10b] L. Lopez, M. Berlekamp, D. Kowalski, G. Erker, *Angew. Chem.* **1994**, *106*, 1168−1170; *Angew. Chem. Int. Ed. Engl.* **1994**, *33*, 1114−1116.

[11] [11a] G. Erker, K. Engel, J. L. Atwood, W. E. Hunter, *Angew. Chem.* **1983**, *95*, 506−507; *Angew. Chem. Int. Ed. Engl.* **1983**, *22*, 494−495. [11b] G. Erker, U. Dorf, *Angew. Chem.* **1983**, *95*, 800; *Angew. Chem. Int. Ed. Engl.* **1983**, *22*, 777−778. [11c] H. Yasuda, K. Nagasuna, M. Akita, K. Lee, A. Nakamura, *Organometallics* **1984**, *3*, 1470−1478. [11d] H. Yasuda, A. Nakamura, *Angew. Chem.* **1987**, *99*, 745−764; *Angew. Chem. Int. Ed. Engl.* **1987**, *26*, 723−742. [11e] H. Yasuda, T. Okamoto, K. Mashima, A. Nakamura, *J. Organomet. Chem.* **1989**, *363*, 61−76. [11f] H. Yasuda, T. Okamoto, Y. Matsuoka, A. Nakamura, Y. Kai, N. Kanehisa, N. Kasai, *Organometallics* **1989**, *8*, 1139−1152. [11g] See also: H. C. Strauch, G. Erker, R. Fröhlich, *Organometallics* **1998**, *17*, 5746−5757.

[12] Rosenthal et al. have observed coupling of two benzaldimines at Cp_2Ti or Cp_2Zr in the reaction of the respective [η^2-bis(tri-

methylsilyl)acetylene]metallocene complexes with PhN=CHPh.[12a,12b] We have some indication that in the reaction of the bulky ansa-metallocene complex $Me_2Si(C_5Me_4)CpZr$(butadiene) with MeN=CHPh such imine coupling (with extrusion of butadiene) is competing with the imine/butadiene addition reaction. [12a] C. Lefeber, P. Arndt, A. Tillack, W. Baumann, R. Kempe, V. V. Burlakov, U. Rosenthal, *Organometallics* **1995**, *14*, 3090−3093. [12b] C. Lefeber, W. Baumann, A. Tillack, R. Kempe, H. Görls, U. Rosenthal, *Organometallics* **1996**, *15*, 3486−3490.

[13] [13a] G. Erker, K. Berg, K. Angermund, C. Krüger, *Organometallics* **1987**, *6*, 2620−2621. [13b] See for a comparison: E. G. Hoffmann, R. Kallweit, G. Schroth, K. Seevogel, W. Stempfle, G. Wilke, *J. Organomet. Chem.* **1975**, *97*, 183−202.

[14] See for a comparison: H. G. Alt, K. Föttinger, W. Milius, *J. Organomet. Chem.* **1999**, *572*, 21−30.

[15] [15a] S. Berger, S. Braun, H. Kalinowski, *NMR-Spektroskopie von Nichtmetallen*, vol. 2, Georg Thieme Verlag, Stuttgart **1992**. [15b] G. J. Martin, M. L. Martin, J. Gouesnard, *^{15}N NMR-Spectroscopy*, Springer Verlag, Berlin **1981**. [15c] The ^{15}N NMR chemical shifts of formamide ($\delta = -267.6$ ppm) or benzamide ($\delta = -275.2$ ppm) are in a similar range: M. Hesse, H. Meier, B. Zech, *Spektroskopische Methoden in der organischen Chemie*, Georg Thieme Verlag, Stuttgart, **1995**. [15d] For ^{15}N NMR shifts of imines see: P. W. Westerman, R. E. Botto, J. C. Roberts, *J. Org. Chem.* **1978**, *43*, 2590−2596. [15e] ^{15}N NMR of iminium ions: C. Rabiller, G. Ricolleau, M. L. Martin, G. J. Martin, *Nouv. J. Chim.* **1980**, *4*, 35−42.

[16] J. Pflug, A. Bertuleit, G. Kehr, R. Fröhlich, G. Erker, *Organometallics* **1999**, *18*, 3818−3826.

[17] P. Arndt, C. Lefeber, R. Kempe, U. Rosenthal, *Chem. Ber.* **1996**, *129*, 207−211.

[18] G. Erker, U. Dorf, C. Krüger, Y.-H. Tsay, *Organometallics* **1987**, *6*, 680−682, and references cited therein.

[19] F. H. Allen, O. Kennard, D. G. Watson, L. Brammer, A. G. Orpen, R. Taylor, *J. Chem. Soc., Perkin Trans. 2* **1987**, S1−S19.

[20] [20a] A. G. Massey, A. J. Park, F. G. A. Stone, *Proc. Chem. Soc., London* **1963**, 212. [20b] A. G. Massey, A. J. Park, *J. Organomet. Chem.* **1964**, *2*, 245−250. [20c] A. G. Massey, A. J. Park, in: *Organometallics Syntheses* (Eds.: R. B. King, J. J. Eisch), Elsevier, New York, **1986**, vol. 3, p. 461−462. [20d] X. Yang, C. L. Stern, T. J. Marks, *J. Am. Chem. Soc.* **1994**, *116*, 10015−10031. [20e] Review: E. Y.-X. Chen, T. J. Marks, *Chem. Rev.* **2000**, *100*, 1391−1434.

[21] J. C. W. Chien, W.-M. Tsai, M. D. Rausch, *J. Am. Chem. Soc.* **1991**, *113*, 8570−8571.

[22] R. F. Jordan, *Adv. Organomet. Chem.* **1991**, *32*, 325−397.

[23] [23a] T. J. Marks, *Acc. Chem. Res.* **1992**, *25*, 57−65. [23b] M. Aulbach, F. Küber, *Chem. Unserer Zeit* **1994**, *28*, 197−208. [23c] H.-H. Brintzinger, D. Fischer, R. Mülhaupt, B. Rieger, R. Waymouth, *Angew. Chem.* **1995**, *107*, 1255−1283; *Angew. Chem. Int. Ed. Engl.* **1995**, *34*, 1143−1170. [23d] M. Bochmann, *J. Chem. Soc., Dalton Trans.* **1996**, 255−270.

[24] See for a comparison: [24a] G. Erker, B. Temme, *J. Organomet. Chem.* **1995**, *488*, 177−182. [24b] N. Coles, M. C. J. Harris, R. J. Whitby, J. Blagg, *Organometallics* **1994**, *13*, 190−199. [24c] N. Coles, R. J. Whitby, J. Blagg, *Synlett* **1992**, 143−145. [24d] S. L. Buchwald, B. T. Watson, M. W. Wannamaker, C. Dewan, *J. Am. Chem. Soc.* **1989**, *111*, 4486−4494. [24e] J. M. Meyer, C. J. Curis, J. E. Bercaw, *J. Am. Chem. Soc.* **1983**, *105*, 2651−2660.

[25] P. D. Bartlett, F. E. Condon, A. Schneider, *J. Am. Chem. Soc.* **1944**, *66*, 1531−1539.

[26] M. Bochmann, A. J. Jaggar, J. C. Nicholls, *Angew. Chem.* **1990**, *102*, 830−832; *Angew. Chem. Int. Ed. Engl.* **1990**, *29*, 780−782.

[27] See also: [27a] G. Kehr, R. Roesmann, R. Fröhlich, C. Holst, G. Erker, *Eur. J. Inorg. Chem.* **2001**, 535−538. [27b] D. Vagedes, G. Erker, R. Fröhlich, *J. Organomet. Chem.* **2002**, *641*, 148−155.

[28] The occupied p-orbital at the nitrogen atom is oriented perpendicular to the available acceptor orbital at the zirconium atom: [28a] J. W. Lauher, R. Hoffmann, *J. Am. Chem. Soc.* **1976**, *98*, 1729−1742. [28b] J. C. Green, *Chem. Soc. Rev.* **1998**, *27*, 263−271.

[29] S. Braun, H.-O. Kalinowski, S. Berger, in: *150 and More Basic NMR Experiments*, VCH, Weinheim, **1998**, and references cited therein.

Received May 10, 2002
[I02242]

Simultaneous Cation/Anion Coordination by Bifunctional 1,2-Diimine/1,2-Diamine Type Ligands: Synthesis, Structures, and Properties of Tight Ion Pair Complexes of Ruthenium and Iron

Sven Rau,[a] Lars Böttcher,[a] Sebastian Schebesta,[a] Michael Stollenz,[a] Helmar Görls,[a] and Dirk Walther*[a]

Keywords: Iron / Hydrogen bonds / N ligands / Ruthenium

The reaction between $[(\eta^6\text{-}p\text{-cymene})RuCl_2]_2$ and tetra-*p*-tolyloxalic amidine (*oxam1*) results in a coupled cation/anion coordination forming the ion-paired complex $[(\eta^6\text{-}p\text{-cymene})RuCl(oxam1)Cl]$ (**1a**). According to an X-ray single crystal diffraction analysis the Ru moiety is coordinated at the 1,2-diimine part yielding a five-membered chelate ring. Furthermore, the 1,2-diamine group on the opposite side binds to a chloride anion via two N–H groups. Exchange of the chloride anion by trifluoractetate yields $[(\eta^6\text{-}p\text{-cymene})RuCl(oxam1)CF_3CO_2]$ (**1c**) in which the C=O group is bonded to the diamine part. Similarly, bis(mesityl)bis(pyridylmethyl)oxalic amidine (*oxam2*) reacts with FeX_2 to yield the ion-paired complexes **3a** (X: Cl), and **3b** (X: Br). X-ray diffraction studies of both compounds reveal that the oxalic amidine ligand acts as a four-dentate chelating ligand. One halide is fixed in the same way as in **1a**. The complex **1a** reacts with $Pd(acac)_2$ (acac: acetylacetonate) to give the tetranuclear heterobimetallic complex $[(\eta^6\text{-}p\text{-cymene})RuCl(oxam1)PdCl]_2$ (**2**). The related complexes $[(tbbpy)_2Ru(bbimH_2)(OOC\text{–}CF_3)](PF_6)$ (**4**), $[(tbbpy)_2Ru(bbimH_2)\{OOC(CF_2)_7CF_3\}][OOC(CF_2)_7CF_3]$ (**5**), $[\{(tbbpy)_2Ru(bbimH_2)\}_2(OOC\text{–}C_6F_4\text{–}COO)](PF_6)_2$ (**6**), and $[\{(tbbpy)_2Ru(bbimH_2)\}_2(OOC\text{–}C_6F_4\text{–}COO)]$ (**7**), ($bbimH_2$: bibenzimidazole; tbbpy: 4,4′-di-*tert*-butyl-2,2′-bipyridine) also form ion-paired compounds. According to the X-ray diffraction analyses of **4**–**6** both oxygen atoms of the carboxylate ions are coordinated to the two N–H functions via strong N–H···O bonds. Although **5** contains a dication, the compound is soluble in solvents of low polarity, even in supercritical carbon dioxide.

(© Wiley-VCH Verlag GmbH, 69451 Weinheim, Germany, 2002)

Introduction

Oxalic amidines containing the structural element **A** are not only variable building blocks for bi- and oligonuclear complexes[1–8] but can also be considered as bifunctional ligands which should be capable of coupled cation/anion coordination forming tight contact ion-paired complexes according to Scheme 1.

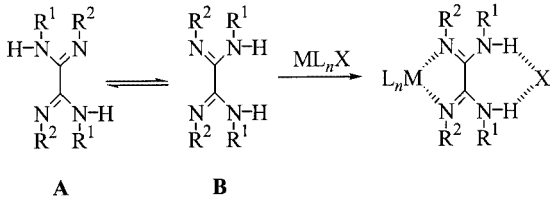

Scheme 1. Formation of ion-paired complexes by coupled cation/anion coordination

Structure **B**, the tautomer of **A** can be stabilized by formation of a 1,2-diimine metal compound provided a suitable metal complex fragment is used. Additionally, anion bonding via hydrogen bonds on the opposite 1,2-diamine side of the oxalic amidine system may stabilize the mononuclear complex preventing undesired coordination polymerization.

The general principle behind this process is strongly reminiscent of anion recognition events in supramolecular chemistry between cationic diamine-based hosts and anionic guests.[9] The stability of the resulting aggregates is commonly influenced by steric and electronic tuning of the host molecule with regard to the guest. The application of these construction principles in metallorganic and coordination chemistry is still relatively underdeveloped even so multinuclear supramolecular aggregates are promising candidates for multistep catalytic processes or biomimetic analogues, such as light harvesting complexes.

Simultaneous cation/anion coordination could therefore result in the generation of "supramolecularly" protected metalloligands, useful as starting products for the construction of heterobi- or oligometallic complexes, but also for the formation of ion-paired metal complexes with untypical high solubilities in solvents of low polarity. In addition, in-

[a] Institut für Anorganische und Analytische Chemie, Universität Jena
August-Bebel-Straße 2, 07743 Jena, Germany
Fax (internat) + 49-(0)3641/948102
E-mail: cdw@rz.uni-jena.de

teraction of dicarboxylates as dianions with appropriately designed 1,2-diamine containing complexes should result in the formation of hydrogen-bonded stable dimers. Furthermore, this type of reaction may be used to force ligands bearing additional donor groups in R^1 into untypical coordination modes. Additionally, the generation of 1,2-diimine metal species containing cationic electrophilic parts may be of special interest because of their well-known catalytic potential.[10,11]

We describe here the first examples for simultaneous cation/anion bonding using oxalic amidines as ligands and investigate the structures and properties of the new compounds. Furthermore, we report on ion-paired complexes consisting of the photoactive fragment $(tbbpy)_2Ru(bbimH_2)^{2+}$ and carboxylates that are hydrogen bonded to the related bibenzimidazole ligand. Although in these complexes a dication is part of the tight ion-paired compound, these compounds show surprisingly high solubilities in nonpolar solvents if long chained perfluoro-substituted carboxylates are coordinated to the N−H groups.

Results and Discussion

Reaction between $[(\eta^6\text{-}p\text{-cymene})RuCl_2]_2$ and tetra-*p*-tolyloxalic amidine (*oxam1*) in refluxing toluene resulted in the formation of $[(\eta^6\text{-}p\text{-cymene})RuCl(oxam1)Cl]$, **1a**, which was isolated as an orange-red crystalline compound at room temperature. Elemental analysis and a mass spectrum confirmed its composition. In the ESI-mass spectrum the complex ion $[\mathbf{1a} - Cl]^+$ (m/z =716) was detected. The ^1H NMR spectrum of **1a**, recorded in $[D_8]$THF at room temperature supports the assumption of a C_s symmetrical complex. It showed one doublet belonging to the methyl protons of the isopropyl group at δ = 1.14 and 1.17 ppm and a singlet for the methyl group of coordinated cymene at δ = 2.27 ppm. Two singlets for the methyl groups of the coordinated *oxam1* were detected at δ = 2.09 and 2.18 ppm. The relative intensities of these resonances are, as expected, (1:1):(1:2):2. The multiplet corresponding to the CH proton of the isopropyl group was detected at δ = 2.50 ppm. The aromatic protons of the *p*-cymene ligand (δ = 4.59 ppm), and the protons of the aromatic substituents (δ = 6.66 and 7.60 ppm) were detected with the expected intensities. Furthermore, the ^1H NMR spectrum shows one sharp singlet for both NH groups at δ = 12.83 ppm, which is in agreement with a strong chloride binding to the N−H functions according to Figure 1. The ^{13}C NMR spectrum for **1a** in $[D_8]$THF also showed the expected simple pattern corresponding to a symmetrical complex.

The molecular structure of compound **1a** has been confirmed by X-ray crystallography (Figure 1). The compound consists of a cationic portion in which the metal center is surrounded by the *p*-cymene, the diimine part of the oxalic amidine ligand and one chloride to form a typical "piano stool" complex in which the arene acts as the "bench" and the other ligands form "the legs" of the stool. The ruthenium coordination environment is best described as a distorted trigonal pyramidal geometry considering the aromatic ring as a unique coordination site, represented by the middle of the benzene unit, occupying one position of the polygon. The second chloride is bonded to the two N−H groups of the 1,2 diamine part of the oxalic amidine via two hydrogen bonds. Bond lengths and angles are listed in the figure caption and lie within typical ranges (see Figure 1 caption). The C1−N1 and C2−N2 bond lengths of 1.301(4), and 1.298(4) Å clearly indicate that the ligand coordinates with the 1,2-diimine part. Typically, due to the partial delocalization of the double bonds of the coordinated 1,2 diimine, the C1−C2 bond length 1.497(4) Å is shorter than that of a C−C single bond. The N3−Cl2 and N4−Cl2 distances of 3.077(2) and 3.088(2) Å, respectively, are in the accepted range for these distances. Furthermore, the angles for the N3−H···Cl group, and the N4−H···Cl group (167 and 170°, respectively) show very little deviation from linearity. These findings clearly indicate a strong bonding between the N−H functions of the 1,2-diamine system and the chloride counterion. In the related compound tris(*N*,*N*′-diphenyloxalic amidine−*N*,*N*′)cobalt(II) dichloride, the peripheral primary amine functions form tight hydrogen bonds to one chloride anion resulting in a polymeric three-dimensional network.[12]

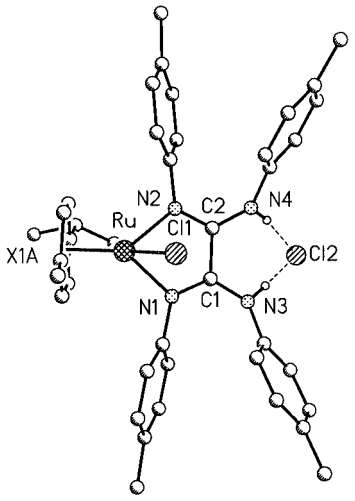

Figure 1. Molecular structure of complex **1a**, selected distances [Å] and bond angles [deg]: Ru−Cl1 2.398(1), Ru−X1A 1.692(4), Ru−N1 2.088(3), Ru−N2 2.079(3), C1−N1 1.301(4), C1−N3 1.436(4), C1−C2 1.497(4), C2−N2 1.298(4), C2−N4 1.350(5), Cl2−N3 3.077(2), Cl2−N4 3.088(2); X1A−Ru−Cl1 128.60(7), X1A−Ru−N1 83.9(2), X1A−Ru−N2 83.5(2), Cl1−Ru−N1 83.93(9), Cl1−Ru−N2 83.54(8), N1−Ru−N2 75.9(1), N1−C1−N3 127.2(3), N2−C2−N4 127.4(3), C1−C2−N2 114.1(3), C1−C2−N4 118.2(3), C2−C1−N1 114.1(3), C2−C1−N3 118.6(3)

The complex **1a** has been proven to be a suitable "protected" ligand for the construction of oligonuclear complexes containing different metals. For example, reaction with $Pd(acac)_2$ resulted in the formation of the tetranuclear complex **2** containing palladium atoms in the inner part and two ruthenium centers on the peripheries (Scheme 2). Elemental analysis and a mass spectrum confirmed its composition. In the ESI-mass spectrum the complex cation [M

$- Cl]^+$ $m/z = 1679$ was detected and the obtained isotope pattern agrees well with the calculated molecular formula $C_{80}H_{84}Cl_3N_8Pd_2Ru_2$. Furthermore, the ^1H NMR and the ^{13}C NMR spectra of **2** ([D$_8$]THF at room temperature) show the expected signals for a symmetrical complex and are similar to those of **1a**, except for the absence of the signals of the N−H protons. Red single crystals of compound **2** obtained from toluene were subjected to an X-ray diffraction analysis. Figure 2 displays the molecular structure of **2**.

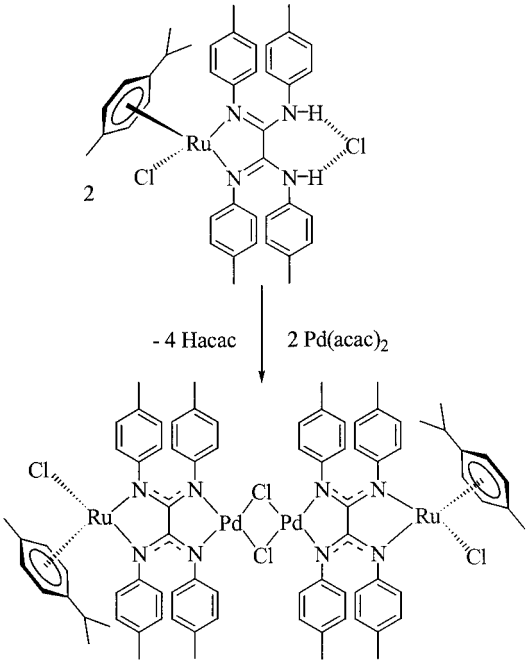

Scheme 2. Formation of the tetranuclear heterobimetallic complex **2**

The Ru(*oxam1*)PdCl$_2$Pd(*oxam1*)Ru core of **2** is essentially planar and the peripheral ligands cymene and chloride are *trans* with respect towards each other. The coordination geometry around the ruthenium centers is the same as in **1a**.

Exchange of the hydrogen bonded chloride in **1a** by BF_4^- or trifluoroacetate anions in THF resulted in the formation of the complexes [(η^6-*p*-cymene)RuCl(*oxam1*)BF$_4$] (**1b**), and [(η^6-*p*-cymene)RuCl(*oxam1*)OOCCF$_3$] (**1c**). The ^1H NMR spectra of both compounds in [D$_8$]THF showed nearly identical signals for all of the CH groups; however the signals for the NH protons were very different. In **1b** this signal appeared at $\delta = 9.05$ ppm as a sharp singlet. The magnitude of this upfield shift ($\delta = 3.8$ ppm) is indicative of a weaker hydrogen bond interaction compared with **1a**. In contrast, the trifluoroacetate complex **1c** showed very broad NH signals between $\delta = 11$ and $\delta = 12$ ppm, characteristic of a fast proton exchange or rotational effect. At lower temperature the signal became sharper at around $\delta = 11.6$ ppm. This low-field shift is indicative of a stronger hydrogen bond than that in **1b**.

The solid-state structure of **1b** and **1c** could be determined by X-ray analyses. Both ruthenium cymene moieties

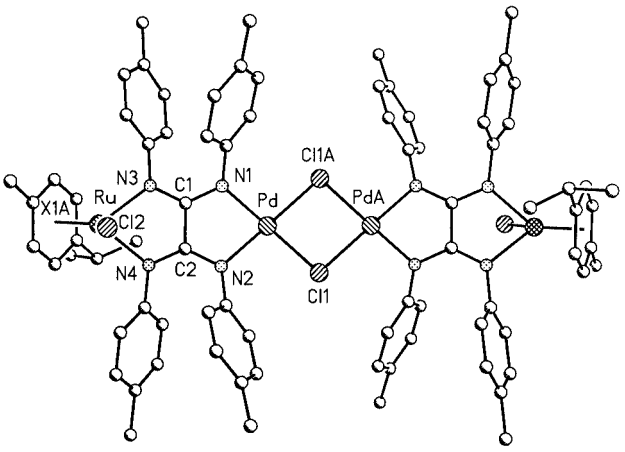

Figure 2. Molecular structure of complex **2**, selected distances [Å] and bond angles [deg]: Ru−Cl2 2.431(1), Ru−X1A 1.681(4), Ru−N4 2.104(3), Ru−N3 2.082(3), Pd−Cl1 2.333(1), Pd−Cl1A 2.341(1), Pd−N1 1.989(4), Pd−N2 2.011(3), C1−N1 1.342(5), C1−N3 1.312(5), C1−C2 1.495(5), C2−N2 1.332(5), C2−N4 1.318(5); X1A−Ru−Cl2 127.8(1), X1A−Ru−N3 86.5(2), X1A−Ru−N4 83.8(2), Cl2−Ru−N3 86.8(1), Cl2−Ru−N4 83.8(1), N3−Ru−N4 76.7(1), Cl1−Pd−Cl1A 82.99(4), Cl1−Pd−N1 179.4(1), Cl1−Pd−N2 97.7(1), N1−Pd−N2 81.7(1), N1−Pd−Cl1A 97.6(1), N2−Pd−Cl1A 179.3(1), N1−C1−N3 129.8(4), N2−C2−N4 130.9(4), C1−C2−N2 114.9(3), C1−C2−N4 114.2(3), C2−C1−N1 114.7(3), C2−C1−N3 115.5(3)

(**1b** not depicted) are identical to **1a** within experimental errors. One fluoro substituent of the BF_4^- anion does form a hydrogen bond to both NH function [N3−F4 2.825(4) and N4−F4 3.034(4) Å]. The surprisingly short N3−F4 distance might be due to packing effects. Similar N−H···F hydrogen bond patterns have been observed in related copper azophenine complexes.[13]

The trifluoroacetate anion in **1c** does form a hydrogen bond with both NH functions of the coordinated oxalic amidine (Figure 3). However, in contrast to the usual bonding mode of carboxylate anions in previously reported related metal complexes containing a diimine/diamine[14–16] in **1c** only the oxygen of the C=O group [C41−O2 = 1.176(7) Å] is involved in the hydrogen bond network. The relatively short N−H···O distances of 2.771(3), and 2.761(3) Å, respectively suggest a very strong interaction.

The formation of the complexes **3a** and **3b** between bis(mesityl)bis(pyridylmethyl)oxalic amidine (*oxam2*) and FeX_2 (X: Cl, Br) clearly demonstrates that coupled cation/anion coordination can also be used for realizing untypical coordination modes (Scheme 3). Whereas in transition metal complexes containing additional coordinating anionic chelate ligands (such as acetylacetonate), *oxam2* typically acts as a three-dentate bridging ligand in dinuclear complexes[18−20] whereas it forms mononuclear tetradentate complexes with iron halides.

The solid-state structure of **3a** determined by X-ray diffraction analysis shows the oxalic amidine ligand to be coordinated as tetradentate ligand in its prototropic form (Figure 4). The 1,2-diimine now residing on the picolyl based nitrogens is coordinated together with the pyridine donor sites to the five-coordinated Fe^{II} with the chloride ligand in the apical position resulting in a square-planar

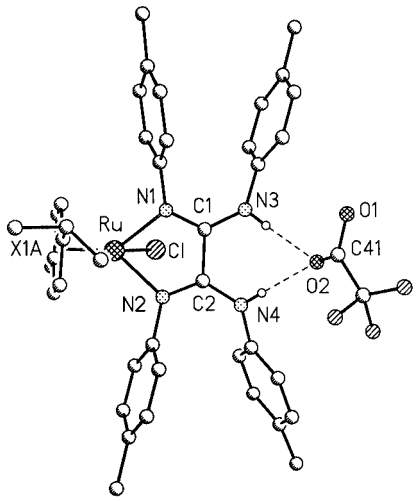

Figure 3. Molecular structure of complex **1c**, selected distances [Å] and bond angles [deg]: Ru−Cl 2.406(1), Ru−X1A 1.687(4), Ru−N1 2.079(3), Ru−N2 2.084(3), C1−N1 1.304(5), C1−N3 1.344(5), C1−C2 1.513(6), C2−N2 1.308(5), C2−N4 1.347(5), O2−N3 2.761(3), O2−N4 2.771(3); X1A−Ru−Cl 128.3(1), X1A−Ru−N1 85.4(2), X1A−Ru−N2 84.4(2), Cl−Ru−N1 85.2(1), Cl−Ru−N2 84.4(1), N1−Ru−N2 75.8(1), N1−C1−N3 129.0(4), N2−C2−N4 127.5(4), C1−C2−N2 113.5(4), C1−C2−N4 118.9(4), C2−C1−N1 113.6(3), C2−C1−N3 117.4(4)

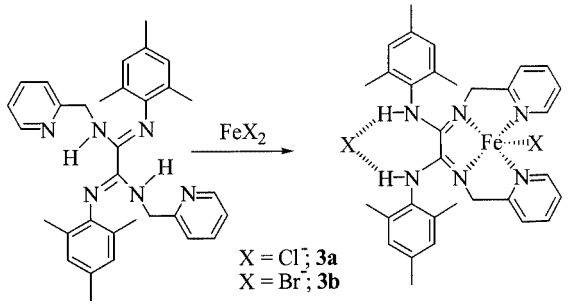

Scheme 3. Structure of the free ligand bis(mesityl)bis(pyridylmethyl)-oxalic amidine, and coordination mode in the iron complexes **3a** and **3b**

pyramidal coordination environment. Similarly to complex **1a**, one halide is coordinated to the two N−H groups on the opposite side of the oxalic amidine frame yielding a zwitterionic complex [Cl2−N5 = 3.051(1) Å, Cl2−N6 = 3.152(1) Å]. Other relevant bond lengths and angles fall in the range of typical values. The internal bond length and angles of the central oxalic amidine are similar to those in **1a**. In contrast to **1a**, the plane arranged by the four nitrogen donor atoms of the central oxalic amidine frame of **3a** is slightly distorted. More significant are the differences between the bond angles Cl1−Fe−N2 [104.27(7)°] and Cl1−Fe−N4 [107.66(7)°] respectively to Cl1−Fe−N1 [109.27(7)°] and Cl1−Fe−N3 [114.36(7)°]. These differences result in a distorted square pyramidal coordination arrangement in **3a**. In this arrangement the iron center is "out of plane" coordinated similar to well-known hem iron systems. According to X-ray structural analysis, **3b** has the same ion-paired structure as **3a**.

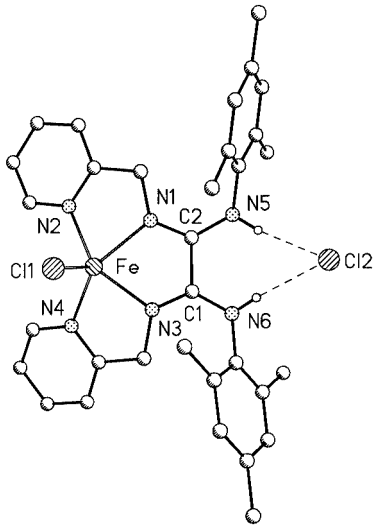

Figure 4. Molecular structure of complex **3a**, selected distances [Å] and bond angles [deg]: Fe−Cl1 2.663(9), Fe−N1 2.091(2), Fe−N2 2.148(2), Fe−N3 2.089(2), Fe−N4 2.181(2), C1−N3 1.296(3), C1−N6 1.336(3), C1−C2 1.535(4), C2−N1 1.284(3), C2−N5 1.350(3), Cl2−N5 3.051(1), Cl2−N6 3.152(1); Cl1−Fe−Nl 109.27(7), Cl1−Fe−N2 104.27(7), Cl1−Fe−N3 114.36(7), Cl1−Fe−N4 107.66(7), Nl−Fe−N2 76.98(9), N1−Fe−N3 75.64(9), N1−Fe−N4 140.04(9), N2−Fe−N3 138.13(9), N2−Fe−N4 108.03(9), N3−Fe−N4 75.70(9), N6−C1−N3 128.8(3), N1−C2−N5 128.5(3), C1−C2−N1 113.6(2), C1−C2−N5 117.9(2), C2−C1−N3 112.7(2), C2−C1−N6 118.5(2)

The cores of bibenzimidazole (*bbimH*$_2$) and biimidazole (*bimH*$_2$) are structurally related to the oxalic amidine ligand family. However, electronic differences exist which manifest themselves in different pK_a values of the coordinated ligands.[3,17] Since ruthenium polypyridyl complexes of these ligands are photoactive it was our aim to use the coupled cation/anion coordination for the formation of tight ion-paired, photoactive complexes. The appropriate choice of anions should lead to stable assemblies of potentially higher nuclearity and in addition a tuning of their solubility in nonpolar solvents could be envisaged.

It is known that some biimidazole (*bimH*$_2$) can form complexes in which one anion is linked to the imidazole based NH groups via hydrogen bonds;[21−28] however, in most cases polymeric networks resulted.[21,22−24] In contrast, well-defined mononuclear ion-paired bibenzimidazole complexes are rare. Ag^I and Cu^I complexes containing associated chloride or acetate anions have been characterized by de Souza Lemos.[25,26] Iron(II) complexes with *bbimH*$_2$ exhibit complex hydrogen bonding patterns where cationic complexes are linked via hydrogen bonds to their respective anions.[15] Recently, Beauchamp et al. have shown that some *bimH*$_2$ Re^{III} complexes form hydrogen bonds with halides or benzoate anions resulting in ion pairs that are stable in organic solvents.[16,27,28]

In an initial work we have shown that N−H groups of *bbimH*$_2$ Ru complexes bind water molecules resulting in hydrogen bonded networks. The variation of the noncoordinating anion determined the supramolecular aggregation in these compounds.[29]

Based on these observations we choose to employ carboxylate anions in an attempt to obtain stable aggregates. The trifluoroacetate complex $[(tbbpy)_2Ru(bbimH_2)(OOC-CF_3)](PF_6)$ (**4**), could easily be prepared by deprotonation of $[(tbbpy)_2Ru(bbimH_2)](PF_6)_2$ followed by reaction of the deprotonated complex with the trifluoroacetic acid. $[(tbbpy)_2Ru(bbimH_2)\{OOC(CF_2)_7CF_3\}][OOC(CF_2)_7CF_3]$ (**5**) was prepared by deprotonation of $[(tbbpy)_2Ru(bbimH_2)](Cl)_2$ followed by reaction of the fully deprotonated complex with the corresponding acid. The ^1H NMR spectra of both **4** and **5** show a new signal at δ = 16.4 ppm in deuterated acetone in addition to the other signals for the complex cation (see Exp. Sect.). Its broadness and extreme low-field shift suggests that it corresponds to the N−H protons. Since a signal for these protons in other ruthenium polypyridyl complexes with $bbimH_2$ as ligand has never been observed,[29] we assume that strong ion paring may explain this effect. The ESI-mass spectroscopical investigation confirmed the nature of the complex cation.

The solid-state structure of **4** elucidated by an X-ray diffraction study showed the expected complex cation where the bibenzimidazole ligand coordinates via the 1,2-diimine part to the Ru^{II} atom that exhibits distorted-octahedral geometry. The peripheral NH functions form hydrogen bonds to the carboxylate anion resulting in an ion-paired structure (Figure 5). The distances between hydrogen atoms of the N−H functions and the oxygens of the carboxylate [N3−O1 = 2.703(3), N4−O1 = 2.659(3) Å] are in the range of strong hydrogen bonds.[29] In contrast to the hydrogen bond association in **1c**, *both* NH function interact with both carboxylate oxygens in **4**. The complementary topology of the secondary amines of coordinated bibenzimidazole and the carboxylate anions allows a more efficient interaction between both parts leading to two strong N−H···O bonds (see also Figure 3).

In order to understand why the two strongly related complexes, **1c** and **4**, form different hydrogen bonding networks with trifluoroacetate the central cores of **1b** and **4** were superimposed on each other (Figure 6). It is clearly evident from Figure 6 that the steric demand of the aryl substituents at the nitrogens in **1c** determines the C1−N3−H angle in such a way that a favorable hydrogen bond interaction is only possible with one hydrogen bond acceptor. In contrast, the bibenzimidazole ligand in **4** is bent around the ruthenium center[29] that results in the orientation of the two NH functions towards two hydrogen bond acceptors.

Although the diffraction data for complex **5**, containing perfluorooctylcarboxylate instead of trifluoroacetate, were insufficient for satisfactory refinement of all parameters, the data show without doubt that the perfluorooctylcarboxylate is anchored via the two imidazole NH to the complex cation, as is similar in **4** (O1−N4 = ca. 2.660 Å, O2−N3 = ca. 2.706 Å). The structural motif of **5** is displayed in Figure 7.

Complex **5** contains a twofold positively charged cation as part of the ion-paired unit but also a discrete anion. Surprisingly, **5** is even soluble in supercritical CO_2, which is known to be an extremely poor solvent for ionic compounds. This suggests that the tight ion-paired compound **5** is also stable in such nonpolar solvents. This could be explained by the interaction of the hydrophilic moieties, cationic 1,2-diamine and carboxylate with each other in such a way that only the lipophilic *tert*-butyl- and perfluorooctyl moieties interact with the solvent. In contrast, the ionic complex $[(tbbpy)_3Ru][OOC(CF_2)_7CF_3]_2$, which can be obtained by simple anion-exchange, is completely insoluble in $scCO_2$. Due to the lack of N−H functions in this complex no hydrogen bonds can be formed, additionally confirming that the supramolecular association via hydrogen bonds is essential for this unexpected effect.

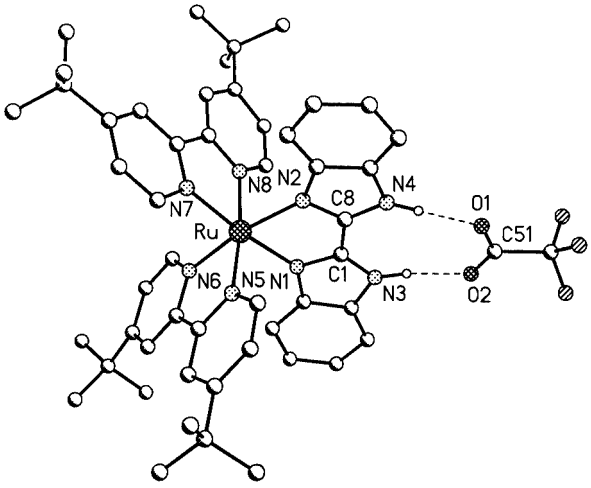

Figure 5. Molecular structure of complex **4**, selected distances [Å] and bond angles [deg]: Ru−N1 2.086(3), Ru−N2 2.109(3), Ru−N5 2.038(2), Ru−N6 2.037(3), Ru−N7 2.042(3), Ru−N8 2.074(3), C1−N11.332(5), C1−N3 1.336(6), C1−C8 1.433(6), C8−N2 1.328(6), C8−N4 1.359(6), N4−O1 2.659(3), N3−O2 2.703(3), O1−C51 1.257(6), O2−C51 1.223(6), N1−Ru−N2 77.5(1); N1−Ru−N5 88.3(1), N1−Ru−N6 93.6(1), N1−Ru−N7 173.4(1), N1−Ru−N8 97.2(1), N1−C1−N3 114.0(4), C1−C8−N2 117.3(4), C1−C8−N4 129.1(4), C8−C1−N1 115.9(4), C8−C1−N3 130.0(4), O1−C51−O2 131.2(5)

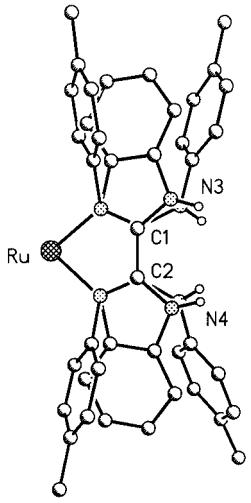

Figure 6. Least square fit of parts of complex **1c** and **4**, torsion angles N3−C1−C2−N4: for **1c** −1.2° and for **4** −2.4°; distance N3−N4: for **1c** 2.784(4) Å and for **4** 3.184(4) Å

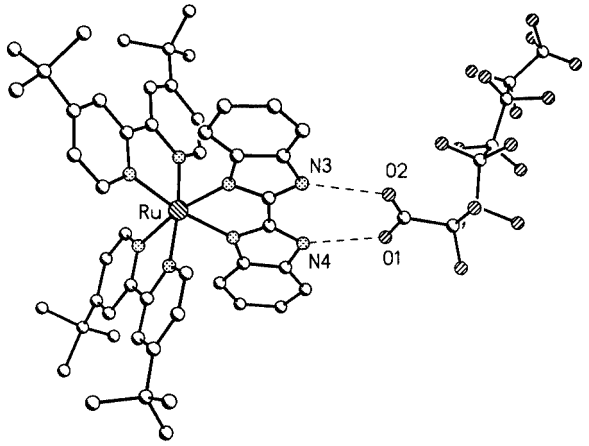

Figure 7. Structural motif of complex **5**

Deprotonation of $[(tbbpy)_2Ru(bbimH_2)](PF_6)_2$ and subsequent reaction with tetetrafluoroterephthalic acid in a molar ratio 2:1 in acetone/water resulted in the formation of complex **6**. Upon recrystallization of **6** from acetonitrile/water the deep red complex **7** was obtained. Both complexes could be isolated as single crystals.

Figure 8 shows the molecular structure for compound **6** and lists relevant bond lengths and angles in the figure captions.

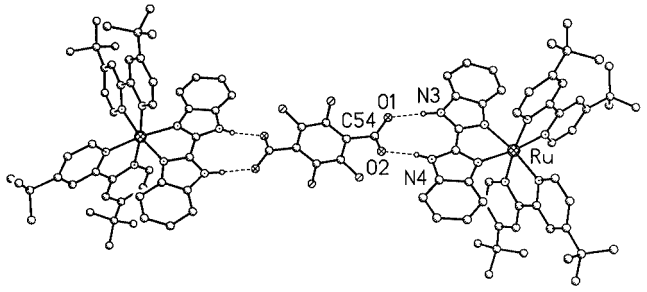

Figure 8. Molecular structure of complex **6**, selected distances [Å] and bond angles [deg]: O1−N3 2.673(5), O2−N4 2.652(5), O1−C54 1.240(5), O2−C54 1.232(5); O1−C54−O2 128.5(4)

In the solid state two ruthenium bibenzimidazole units are connected via a deprotonated tetrafluoroterephthalic acid dianion. Two PF_6 anions remain isolated. Both imidazole based NH functions interact with both oxygen atoms of one carboxylate function, resulting in N···O distances of 2.673(5) and 2.652(5) Å, respectively. The interaction between the ruthenium complex units and the carboxylate moiety is very similar to that observed in **4**. Both ruthenium complexes are twisted out of the plane defined by the two coplanar carboxylate moieties by 152.8°. The Ru···Ru distance defined by this supramolecular arrangement is 1.957 nm. Although the combination of two inherently chiral ruthenium complexes may lead to a mixture of diastereomers[3] the crystals of **6** only contained the MESO isomer.

According to the X-ray analysis of single crystals, **7** contains two monodeprotonated ruthenium units, also connected by the terephthalate bridge (Figure 9 and Scheme 4). However, only the protonated imidazole nitrogen forms a hydrogen bond to one oxygen of the carboxylate group [N3−O2 = 2.693(5) Å] whereas the deprotonated imidazole nitrogen acts as a hydrogen bond acceptor for an additional water molecule [N4−O3 = 2.871(5) Å].

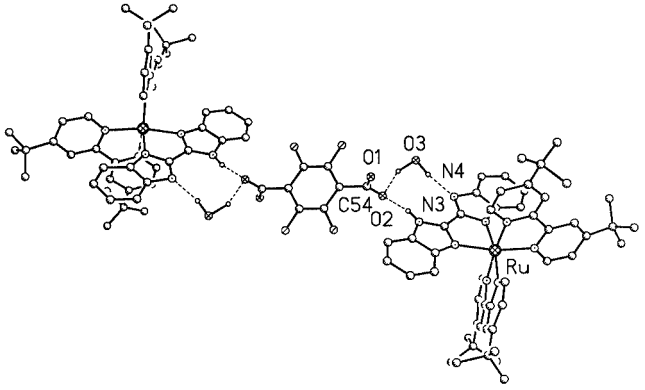

Figure 9. Molecular structures of complex **7**, selected distances [Å] and bond angles [deg]: O3−N4 2.871(5), O2−N3 2.693(4), O2−O3 2.926 (5), O1−C54 1.230(5), O2−C54 1.248(5); O1−C54−O2 127.9(4)

The ruthenium complexes are consequently twisted out of the plane defined by the two carboxylate moieties by 65.0°. This is a difference of 87.8° compared with the value obtained for **6**. As expected, the Ru···Ru distance in **7** (2.025 nm) is longer than in **6** (1.957 nm). The isolated compound **7** contains, as in **6**, only the MESO isomer.

The dimeric arrangement is therefore stable even if the essential ruthenium based NH functions are monodeprotonated.

Conclusion

Tight ion-paired complexes with different anions can be synthesized using diimine/diamine type bridging ligands, which are able to split M−X bonds under formation of a coupled cation/anion coordination. The resulting ion-paired complexes can be considered as ''protected metalloligands'' useful for the construction of oligonuclear organometallic complexes, as demonstrated by the reaction of **1a** with $Pd(acac)_2$ resulting in the formation of the tetranuclear mixed metal complex **2**. The hydrogen bonded anion in **1** can be varied in a wide range. The novel hydrogen bonding pattern displayed in **1a−c** between the cationic oxalic amidine fragment and one specific spatially well defined point opens the possibility of designing supramolecular compounds using new, ''single point'' bridging components such as the redox active 1,4-benzoquinone and similar systems.

The connection of chromophores such as ruthenium polypyridyl complexes employing supramolecular construction principles is strongly reminiscent of the building principles of the naturally occurring Light Harvesting Complexes (LHA). Additionally, the simple building blocks em-

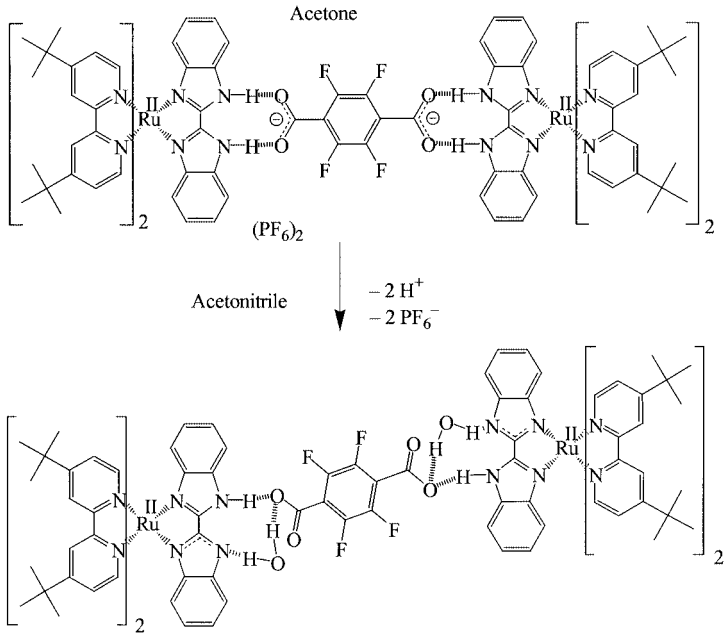

Scheme 4. Structural formula of complexes **6** and **7**

ployed here, as in **6**, would allow a wide variation of the structures obtained, for example simply by switching the coordination mode by altering the pH values. Furthermore, the enhanced solubility of **5** offers the interesting possibility of investigating reactions of the photoactive complex **5** and related complexes in supercritical CO_2. Further studies along these lines are now in progress.

Experimental Section

General: *p*-Tolyl oxalic amidine ligand (*oxam1*);[30] the ligand *N*,*N*′-bis(2-pyridylmethyl)-1,2-bis(2,4,6-trimethylphenylimino)ethane-1,2-diamine (*oxam2*),[20,31] and [(tbbpy)$_2$Ru]Cl$_2$ and [(tbbpy)$_2$Ru-(bbimH$_2$)](X)$_2$ (X = Cl, PF$_6$)[3,29] were prepared according to described methods. The complexes (η^6-*p*-cymene)RuCl$_2$, PdCl$_2$(CH$_3$CN)$_2$, and trifluoroacetic acid (Aldrich) and perfluorooctylcarboxylic acid (ABCR) were used without additional purification. All manipulations were carried out under Argon using standard Schlenk techniques and the solvents used were dried and distilled.

^{1}H NMR and ^{13}C NMR spectra were recorded at ambient temperature unless otherwise stated on a Bruker AC 200 MHz spectrometer. All spectra were referenced to TMS or deuterated solvent as an internal standard. FAB-mass spectra were obtained on a Finnigan MAT SSQ 710 system (2,4-dimethoxybenzyl alcohol as matrix), ESI-mass spectra were recorded on a Finnigan MAT, MAT 95 XL. IR measurements were carried out on a Perkin−Elmer System 2000 FT-IR.

Complex 1a: A solution of *oxam1* (1.30 g, 2.92 mmol) in toluene (30 mL) was added to a suspension of [(η^6-*p*-cymene)RuCl$_2$]$_2$ (0.89 g, 1.46 mmol) in toluene (30 mL) and the mixture was refluxed for 2 hours. After cooling to room temperature, the orange-red microcrystalline solid was filtered, washed with diethyl ether (20 mL) and dried in vacuo. Single crystals of **1** were obtained by recrystallization from hot toluene. Yield: 1.75 g (79%). $C_{40}H_{44}Cl_2N_4Ru$ (752.8): calcd.: C 63.82, H 5.89, N 7.44, Cl 9.42; found C 63.52, H 6.23, N 7.05, Cl 9.24. ^{1}H NMR ([D$_8$]THF): δ = 1.14, 1.17 [d, $^3J_{H\text{-}H}$ = 6.9 Hz, 6 H, −CH(CH_3)$_2$ cymene], 2.09, 2.18 (2 s, 6 H each, −CH$_3$ tolyl), 2.27 (s, 3 H, −CH$_3$ cymene), 2.50 [five lines, $^3J_{H\text{-}H}$ = 7.0 Hz, 1 H, −C*H*(CH$_3$)$_2$ cymene], 4.55, 4.58, 4.60, 4.64 (2 d, $^3J_{H\text{-}H}$ = 6.2 Hz, 2 H each, H^{2,3,5,6} cymene), 6.62, 6.66, 6.74, 6.78 [2 d$_{AA'BB'}$, $^3J_{H\text{-}H}$ = 8.3 Hz, 6 H each, −CH tolyl), 7.02, 7.60 (2 s$_{broad}$, 2 H each, −CH tolyl), 12.83 (s, 2 H, −NH) ppm. ^{13}C NMR ([D$_8$]THF): δ = 15.5 (−CH$_3$ cymene), 20.9 (−CH$_3$ tolyl), 22.6 (−CH(**C**H$_3$)$_2$ cymene), 31.0 [−*C*H(CH$_3$)$_2$ cymene], 84.8, 86.5 (C^{2,3,5,6} cymene), 102.0, 104.3 (C^{1,4} cymene), 123.9, 126.2, 128.6, 129.3 (CH tolyl), 124.7, 126.3 (**C**−CH$_3$ tolyl), 138.3 (NH−C tolyl), 148.8 (=N−C tolyl), 155.6 (C$_{bridge}$) ppm. MS (ESI in THF): *m*/*z* (%) = 716 (100) [M − Cl]$^+$, 680 (20) [M − 2 Cl]$^+$.

The red-orange complex **1b** was prepared by reaction of **1a** in THF with equimolar amounts of NaBF$_4$. yield: 80% $C_{40}H_{44}BClF_4N_4Ru$ (804.2) calcd.: C 59.74, H 5.52, N 6.97; found C 58.63, H 5.43, N 6.53. ^{1}H NMR ([D$_8$]THF): δ = 1.13, 1.17 [d, $^3J_{H,H}$ = 6.9 Hz, 6 H, −CH(CH_3)$_2$ cymene], 2.10 (s, 12 H, −CH$_3$ tolyl), 2.19 (s, 3 H, −CH$_3$ cymene), 2.63 [m, $^3J_{H,H}$ = 6.8 Hz, 1 H, −C*H*(CH$_3$)$_2$ cymene], 4.63 (s, 4 H, H^{2,3,5,6} cymene), 6.69, 6.84, 6.96, 7.17, 7.50 (four broad signals, one s, 16 H overall, −CH tolyl), 9.05 (s$_{broad}$, 2 H, −NH) ppm. ^{13}C NMR ([D$_8$]THF): δ = 15.9 (−CH$_3$ cymene), 20.7 (−CH$_3$ tolyl), 22.5 [−CH(*C*H$_3$)$_2$ cymene], 31.7 [−*C*H(CH$_3$)$_2$ cymene], 84.7, 87.3 (C^{2,3,5,6} cymene), 102.0, 104.3 (C^{1,4} cymene), 123.7, 128.8 (CH tolyl), 134.2 (*C*−CH$_3$ tolyl), 136.5 (NH−C tolyl), 149.7 (=N−C tolyl), 156.7 (C$_{bridge}$).

Analogously, **1c** was synthesized by reaction of **1a** in THF with an equimolar quantity of Ag(OOCCF$_3$). yield: nearly quantitative $C_{42}H_{44}ClF_3N_4O_2Ru$ (830.4) calcd.: C 60.75 H 5.33 N 6.75 Cl 4.27 found C 60.01 H 5.13 N 6.44. ^{1}H NMR ([D$_8$]THF): δ = 1.14, 1.18 [d, $^3J_{H,H}$ = 6.9 Hz, 6 H, −CH(CH_3)$_2$ cymene], 2.10 (s, 12 H, −CH$_3$ tolyl), 2.18 (s, 3 H, −CH$_3$ cymene), 2.51 [m, 1 H, −C*H*(CH$_3$)$_2$ cymene], 4.57, 4.60, 4.62, 4.65 (s, 1 H each, $^3J_{H,H}$ = 4.3 Hz, H^{2,3,5,6} cymene), 6.67, 6.87, 7.56 (m, 16 H, −CH tolyl), 11−12 (s$_{very\ broad}$, 2 H, −NH).

Single crystals of these complexes, suitable for an X-ray diffraction analysis, were obtained from THF or toluene.

Complex 2: Complex **1** (0.38 g, 0.5 mmol) and $Pd(acac)_2$ (0.154 g, 0.5 mmol) were suspended in toluene (20 mL) and refluxed for 4 h or until a clear, dark red solution resulted. The solution was concentrated to 5 mL and pentane (20 mL) was added. The red microcrystalline solid was filtered, washed with pentane (20 mL) and dried in vacuo. Single crystals of **2** were obtained by recrystallization from diethyl ether or toluene. Yield: 0.28 g (65%). $C_{80}H_{84}Cl_4N_8Pd_2Ru_2$ (1714.35) calcd.: C 56.04, H 4.94, N 6.53, Cl 8.27; found C 55.63, H 5.49, N 5.90, Cl 8.25. ^{1}H NMR (400 MHz, [D$_8$]THF): δ = 1.11, 1.13 [d, $^3J_{H\text{-}H}$ = 6.9 Hz, 6 H, −CH(CH_3)$_2$ cymene], 2.00 (s, 24 H, −CH_3 tolyl), 2.09 (s, 6 H, −CH_3 cymene), 2.43 [m, $^3J_{H\text{-}H}$ = 7.0 Hz, 2 H, −CH(CH$_3$)$_2$ cymene], 4.07, 4.09, 4.21, 4.23 (2 d, $^3J_{H\text{-}H}$ = 5.9 Hz, 4 H each, H^{2,3,5,6} cymene), 6.45, 6.47, 6.49, 6.51 (2 $d_{AA'BB'}$, $^3J_{H\text{-}H}$ = 8.0 Hz, 8 H each, −CH tolyl), 6.65, 6.68, 7.22, 7.24 (2 $d_{AA'BB'}$, $^3J_{H\text{-}H}$ = 8.0 Hz, 8 H each, −CH tolyl) ppm. ^{13}C NMR (100.6 MHz, [D$_8$]THF): δ = 19.0 (−CH_3 cymene), 20.8, 21.0 (2 s, −CH_3 tolyl), 22.7 [−CH(CH_3)$_2$ cymene], 31.5 [−CH(CH$_3$)$_2$ cymene], 82.7, 85.5 (C^{2,3,5,6} cymene), 100.2, 101.6 (C^{1,4} cymene), 125.9, 127.5, 127.7, 128.6 (CH tolyl), 132.9, 133.3 (C−CH_3 tolyl), 144.7, 151.1 (−N−C tolyl), 167.8 (C_{bridge}) ppm. MS (ESI in toluene + methanol): *m*/*z* (%) = 1679 (46) [M − Cl]$^+$ (isotope pattern found), 854 (100) [M − $C_{40}H_{42}N_4Cl_2RuPd]^+$, 680 [M − $C_{40}H_{42}N_4Cl_4Pd_2Ru]^+$.

Complex 3a: This compound was prepared as a crystalline bright orange solid analogously to **3b** from $FeCl_2$ (66 mg, 0.52 mmol) using *N*,*N*′-bis(2-pyridylmethyl)-1,2-bis(2,4,6-trimethylphenylimino)-ethane-1,2-diamine (*oxam2*) (262 mg, 0.52 mmol). Single crystals suitable for X-ray determination were obtained from THF. Yield: 286 mg (87%). $C_{36}H_{44}Cl_2FeN_6O$ (703.6) calcd.: C 61.46, H 6.30, N 11.95; found C 61.91, H 6.55, N 12.15. MS (FAB in NBA): *m*/*z* (%) = 630 (1) [M]$^+$, 595 (58) [M − Cl]$^+$, 560 (33) [M − 2 Cl]$^+$, 559 (83) [M − 2 Cl]$^+$.

Complex 3b: $FeBr_2$·2THF (181 mg, 0.50 mmol) and *N*,*N*′-bis(2-pyridylmethyl)-1,2-bis(2,4,6-trimethylphenylimino)ethane-1,2-diamine (*oxam2*) (261 mg, 0.52 mmol) were dissolved in THF (40 mL) and stirred overnight, at room temperature. After concentrating the solution to 10 mL, the precipitate was filtered off, washed with THF (3 × 10 mL) and dried by oil pump vacuum (9 h) at room temperature. A light orange solid was obtained. Yield: 317 mg (88%). Single crystals suitable for X-ray-determination were obtained from THF. $C_{32}H_{36}Br_2FeN_6$ (720.33): calcd. C 53.36; H 5.04; N 11.67; found C 52.44; H 5.22; N 11.07. IR (Nujol): $\tilde{\nu}$ = 3127 (m, NH), 1605, 1622, 1554 cm^{-1}. MS (FAB in NBA): *m*/*z* (%) = 639 (17) [M − Br]$^+$, 560 (14)[M − 2 Br]$^+$, 559 (83)[M − 2 Br−H]$^+$.

Complex 4: [(tbbpy)$_2$Ru(bbimH$_2$)](PF$_6$)$_2$ (500 mg, 0.43 mmol) was dissolved in predistilled THF. Freshly prepared NaOMe (0.43 mmol) in MeOH was then added, resulting in a bathochromic shift of the absorption. The solution was stirred for 20 min. CF_3COOH (49 mg, 0.43 mmol,) was added to this solution, which resulted in a hypsochromic shift of absorption, the solution was stirred for 20 min, the solvent removed and the precipitate recrystallized from acetone/water resulting in single crystals. ^{1}H NMR spectra were recorded in deuterated acetone. Yield: 410 mg (84.4%). $C_{55}H_{64}F_9N_8O_3PRu$ (1188.21): calcd. C 55.59, H 5.43, N 9.43; found C 55.87, H 5.13, N 8.84. ^{1}H NMR ([D$_6$]acetone): δ = 16.4 (s, 1 H, NH), 8.85 (s, 2 H, 3a-H), 8.75 (s, 2 H, 3b-H), 8.04 (m, 2 H, 6a-H), 8.04 (m, 2 H, 6b-H), 7.76 (d, 2 H, 6-H), 7.61 (d, 2 H, 5a-H), 7.45 (d, 2 H 5b-H), 7.37 (t, 2 H, 5-H) 7.01 (t, 2 H, 4-H), 5.72 (d, 2 H, 3-H), 1.47 (s, 18 H, C_4H_9), 1.35 (s, 18 H, C_4H_9) ppm. MS (ESI in methanol): *m*/*z* (%) = 871 (100) [M − H − PF$_6$ − $CF_3COO]^+$ (isotope pattern found) IR (Nujol): $\tilde{\nu}$ = 3060 (m, NH), 1776 (s, C=O), 1614 (s, C=N) cm^{-1}.

Complex 5: [(tbbpy)$_2$Ru(bbimH$_2$)](Cl)$_2$ (405 mg, 0.43 mmol) was dissolved in predistilled THF. Freshly prepared NaOMe (0.87 mmol) in MeOH was then added, resulting in a bathochromic shift of the absorption. The solution was stirred for 30 min. $C_7F_{15}COOH$ (358 mg, 0.87 mmol) was added to this solution, which resulted in a hypsochromic shift of the absorption, the solution was stirred for 20 min, the solvent removed and the precipitate recrystallized from acetone/water. ^{1}H NMR spectra were recorded in deuterated acetone. Yield 705 mg, 92%, ^{1}H NMR ([D$_6$]acetone): δ = 16.4 (s, 1 H, NH), 8.85 (s, 2 H, 3a-H), 8.75 (s, 2 H, 3b-H), 8.04 (m, 2 H, 6a-H), 8.04 (m, 2 H, 6b-H), 7.76 (d, 2 H, 6-H), 7.61 (d, 2 H, 5a-H), 7.45 (d, 2 H, 5b-H), 7.37 (t, 2 H, 5-H) 7.01 (t, 2 H, 4-H), 5.72 (d, 2 H, 3-H), 1.47 (s, 18 H, C_4H_9), 1.35 (s, 18 H, C_4H_9) ppm. MS (ESI in methanol): *m*/*z* (%) = 871 (100) [M − H − 2 $C_7F_{15}COO]^+$ (isotope pattern found) IR (Nujol): $\tilde{\nu}$ = 3060 (m, NH), 1730 (s, C=O), 1612 (s, C=N) cm^{-1}.

Complex 6: [(tbbpy)$_2$Ru(bbimH$_2$)](PF$_6$)$_2$ (500 mg, 0.43 mmol) was dissolved in THF. Freshly prepared NaOMe (0.43 mmol) in MeOH was then added, resulting in a bathochromic shift of the color. After stirring for 20 min $COOHC_6F_4COOH$ (0.43 mmol, 103 mg) was added to this solution resulting in a hypsochromic shift of the color. The solution was then stirred for 20 min, the solvent removed and the precipitate recrystallized from acetone/water. Yield 404 mg, 75%, ^{1}H NMR ([D$_6$]acetone): δ = 8.85 (s, 2 H, 3a-H), 8.75 (s, 2 H, 3b-H), 8.04 (m, 2 H, 6a-H), 8.04 (m, 2 H, 6b-H), 7.76 (d, 2 H, 6-H), 7.61 (d, 2 H, 5a-H), 7.45 (d, 2 H, 5b-H), 7.37 (t, 2 H, 5-H) 7.01 (t, 2 H, 4-H), 5.72 (d, 2 H, 3-H), 1.47 (s, 18 H, C_4H_9), 1.35 (s, 18 H, C_4H_9) ppm. MS (ESI in methanol): *m*/*z* (%) = 871 (100) [M − (tbbpy)$_2$Ru(bbimH$_2$) − H − 2 PF$_6$ − $COOC_6F_4COO]^+$ (isotope pattern found) IR (Nujol): $\tilde{\nu}$ = 3410 (w, OH), 3177 (m, NH), 1704 (m, C=O), 1613 (s, C=N) cm^{-1}.

Complex 7: Compound **6** (200 mg) was dissolved in acetonitrile/water (80:20). The color of the solution changed from bright orange to red. The solvent was allowed to evaporate slowly and the small crystals that appeared were collected by filtration. X-ray suitable crystals were obtained by recrystallization from acetonitrile/water. Yield 110 mg 55%, ^{1}H NMR ([D$_6$]acetonitrile): δ = 8.51 (s, 2 H, 3a-H), 8.42 (s, 2 H, 3b-H), 7.87 (d, 2 H, 6a-H), 7.76 (m, 4 H, 6b/6-H), 7.48 (d, 2 H, 5a-H), 7.43 (t, 2 H, 5-H) 7.35 (d, 2 H, 5b-H), 7.06 (t, 2 H, 4-H), 5.68 (d, 2 H, 3-H), 1.47 (s, 18 H, C_4H_9), 1.35 (s, 18 H, C_4H_9) ppm. MS (ESI in methanol): *m*/*z* (%) = 871 (100) [M − (tbbpy)$_2$Ru(bbimH$_2$) − H − $COOC_6F_4COO]^+$ (isotope pattern found) IR (Nujol): $\tilde{\nu}$ = 3460 (m, OH), 3177 (m, NH), 1674 (m, C=O), 1607 (s, C=N) cm^{-1}.

(tbbpy)$_3$Ru(C$_7$F$_{15}$COO)$_2$: Triethylamine (45 mg, 0.44 mmol) was added to a solution of perfluorooctanoic acid (177 mg, 0.44 mmol) in CH_2Cl_2 while stirring. After 15 minutes this solution was poured into a suspension of [(tbbpy)$_3$Ru](PF$_6$)$_2$ (250 mg, 0.21 mmol in CH_2Cl_2/H_2O, 50:50). This mixture was stirred rapidly for 48 hours. The bright orange-red organic layer was separated and the solvent was removed. The remaining solid was recrystallized from acetone/water (10:1). The absence of the PF_6^- anion was established via ^{31}P NMR spectroscopy. Yield 363 mg, quantitative $C_{70}H_{72}F_{30}O_4N_6Ru$ (1732.4) calcd.: C 48.53, H 4.19, N 4.85 found C 46.33, H 3.93, N 4.42. ^{1}H NMR (298 K, 400 MHz, CD_2Cl_2): δ = 1.410 (s, 9 H, CH_3), 7.436 (dd, 1 H, CH-arom.), 7.605 (d, 1 H, CH-arom.), 8.529 (s, 1 H, CH-arom.) ppm. IR (Nujol): $\tilde{\nu}$ = 1695 (s, C=O), 1237, 1202 cm^{-1} (s, CF). MS (ESI in methanol): *m*/*z* (%) = 1319 (100) [M − $C_7F_{15}COO$ + 1]$^+$, 905 (16) [M − 2 $C_7F_{15}COO]^+$.

Crystal Structure Determination: The intensity data for the compounds were collected on a Nonius−Kappa CCD diffractometer, using graphite-monochromated Mo-K_α radiation. Data were corrected for Lorentz and polarization effects, but for absorption were only corrected for **3b**.[32,33] The structures were solved by direct methods (SHELXS[34]) and refined by full-matrix least-squares techniques against F_o^2 (SHELXL-97[35]). The diffraction data obtained for compound **5** were insufficient for satisfactory refinement of the structure parameters. However, the data were sufficient to show the structural motif of the molecule (Figure 7), the hydrogen-bridging system, and the crystallographic data. The data for compound **5** were not deposited in the Cambridge Crystallographic Data Centre.

For all compounds the hydrogen atoms of the diamine groups and the hydrogen atoms of the water molecule of **7** were located by difference Fourier synthesis and refined isotropically. All other hydrogen atoms were included at calculated positions with fixed thermal parameters. All non-hydrogen atoms (without the acetone and the disordered $[PF_6]^-$) were refined anisotropically.[36] XP (SIEMENS Analytical X-ray Instruments, Inc.) was used for structure representations.

Crystal Data for 1a:[36] $C_{40}H_{44}Cl_2N_4Ru$, Mr = 752.76 g·mol^{-1}, orange prism, size 0.10 × 0.10 × 0.09 mm, monoclinic, space group $P2_1/n$, a = 12.0053(3), b = 18.2083(4), c = 17.2697(3) Å, β = 95.763(2)°, V = 3756.01(14) Å^3, T= −90 °C, Z = 4, $\rho_{calcd.}$ = 1.331 g·cm^{-3}, μ(Mo-K_α) = 5.92 cm^{-1}, F(000) = 1560, 15215 reflections in h (−15/15), k (−23/21), l (−22/22), measured in the range 2.27° ≤ Θ ≤ 27.50°, completeness Θ_{max} = 98.8%, 8535 independent reflections, R_{int} = 0.036, 7120 reflections with $F_o > 4\sigma(F_o)$, 427 parameters, 0 restraints, $R1_{obs.}$ = 0.0547, $wR^2_{obs.}$ = 0.142, $R1_{all}$ = 0.067, wR^2_{all} = 0.152, GOOF = 1.085, largest difference peak and hole: 1.219/−1.074 e·Å^{-3}.

Crystal Data for 1b:[36] $[C_{40}H_{44}ClN_4Ru(BF_4)]$, Mr = 804.12 g·mol^{-1}, red-orange prism, size 0.10 × 0.10 × 0.03 mm, orthorhombic, space group $P2_12_12_1$, a = 11.0377(2), b = 18.0910(3), c = 19.2852(4) Å, V = 3850.93(12) Å^3, T= −90 °C, Z = 4, $\rho_{calcd.}$ = 1.387 g·cm^{-3}, μ(Mo-K_α) = 5.29 cm^{-1}, F(000) = 1656, 8625 reflections in h (−14/14), k (−23/23), l (−24/25), measured in the range 2.41° ≤ Θ ≤ 27.47°, completeness Θ_{max} = 98.7%, 8625 independent reflections, R_{int} = 0.042, 8018 reflections with $F_o > 4\sigma(F_o)$, 466 parameters, 0 restraints, $R1_{obs}$ = 0.032, wR^2_{obs} = 0.079, $R1_{all}$ = 0.037, wR^2_{all} = 0.084, GOOF = 1.036, Flack-parameter −0.04(2), largest difference peak and hole: 0.484/−0.501 e·Å^{-3}.

Crystal Data for 1c:[36] $[C_{40}H_{44}ClN_4O_2Ru(CF_3COO)]$, Mr = 830.33 gmol^{-1}, red-orange prism, size 0.10 × 0.10 × 0.05 mm, triclinic, space group $P\bar{1}$, a = 10.9028(8), b = 13.4278(8), c = 13.5573(9) Å, α = 92.835(5), β = 93.959(4), γ = 93.280(4)°, V = 1974.0(2) Å^3, T= −90 °C, Z = 2, $\rho_{calcd.}$ = 1.397 g·cm^{-3}, μ(Mo-K_α) = 5.19 cm^{-1}, F(000) = 856, 13866 reflections in h (−14/11), k (−15/17), l (−16/17), measured in the range 1.88° ≤ Θ ≤ 27.46°, completeness Θ_{max} = 98.7%, 8921 independent reflections, R_{int} = 0.042, 6350 reflections with $F_o > 4\sigma(F_o)$, 486 parameters, 0 restraints, $R1_{obs}$ = 0.059, wR^2_{obs} = 0.128, $R1_{all}$ = 0.097, wR^2_{all} = 0.148, GOOF = 1.037, largest difference peak and hole: 0.634/−0.701 e·Å^{-3}.

Crystal Data for 2:[36] $C_{80}H_{84}Cl_4N_8Pd_2Ru_2$·$4C_7H_8$, Mr = 2082.83 g·mol^{-1}, black-red prism, size 0.10 × 0.09 × 0.06 mm, monoclinic, space group $P2_1/c$, a = 13.6852(4), b = 18.2930(7), c = 19.9623(7) Å, β = 101.706(2)°, V = 4893.5(3) Å^3, T= −90 °C, Z = 2, $\rho_{calcd.}$ = 1.414 g·cm^{-3}, μ(Mo-K_α) = 8.25 cm^{-1}, F(000) = 2136, 14535 reflections in h (−15/17), k (−20/23), l (−25/25), measured in the range 3.74° ≤ Θ ≤ 27.46°, completeness Θ_{max} = 88.8%, 9942 independent reflections, R_{int} = 0.028, 8442 reflections with $F_o > 4\sigma(F_o)$, 559 parameters, 0 restraints, $R1_{obs}$ = 0.048, wR^2_{obs} = 0.120, $R1_{all}$ = 0.062, wR^2_{all} = 0.134, GOOF = 1.099, largest difference peak and hole: 1.328/−0.865 e·Å^{-3}.

Crystal Data for 3a:[36] $C_{32}H_{36}Cl_2FeN_6$·C_4H_8O, Mr = 703.52 g·mol^{-1}, orange prism, size 0.10 × 0.09 × 0.08 mm, monoclinic, space group $P2_1/c$, a = 9.7875(2), b = 13.6051(3), c = 27.9561(5) Å, β = 98.710(1)°, V = 3679.70(13) Å^3, T = −90 °C, Z = 4, $\rho_{calcd.}$ = 1.270 g·cm^{-3}, μ(Mo-K_α) = 5.91 cm^{-1}, F(000) = 1480, 27538 reflections in h (−12/12), k (−17/17), l (−36/35), measured in the range 2.10° ≤ Θ ≤ 27.46°, completeness Θ_{max} = 99.3%, 8375 independent reflections, R_{int} = 0.066, 6324 reflections with $F_o > 4\sigma(F_o)$, 411 parameters, 10 restraints, $R1_{obs}$ = 0.060, wR^2_{obs} = 0.165, $R1_{all}$ = 0.081, wR^2_{all} = 0.184, GOOF = 1.020, largest difference peak and hole: 0.931/−0.577 e·Å^{-3}.

Crystal Data for 3b:[36] $C_{32}H_{36}Br_2FeN_6$·$2.5C_4H_8O$, Mr = 900.60 g·mol^{-1}, red-brown prism, size 0.08 × 0.08 × 0.06 mm, triclinic, space group $P\bar{1}$, a = 15.9361(7), b = 18.4001(8), c = 18.5403(6) Å, α = 97.792(3), β = 113.089(3), γ = 108.091(2)°, V = 4543.2(3) Å^3, T= −90 °C, Z = 4, $\rho_{calcd.}$ = 1.317 g·cm^{-3}, μ(Mo-K_α) = 21.31 cm^{-1}, semi-empirical, transmin: 0.5701, transmax: 0.6280, F(000) = 1864, 34660 reflections in h (−20/20), k (−22/23), l (−24/22), measured in the range 2.59° ≤ Θ ≤ 27.42°, completeness Θ_{max} = 91.2%, 18862 independent reflections, R_{int} = 0.067, 10654 reflections with $F_o > 4\sigma(F_o)$, 929 parameters, 0 restraints, $R1_{obs.}$ = 0.095, $wR^2_{obs.}$ = 0.232, $R1_{all}$ = 0.169, wR^2_{all} = 0.286, GOOF = 1.034, largest difference peak and hole: 2.981/−1.214 e·Å^{-3}.

Crystal Data for 4:[36] $[C_{50}H_{58}N_8Ru(C_2F_3O_2)][PF_6]$·$C_3H_6O$, Mr = 1188.18 g·mol^{-1}, orange prism, size 0.12 × 0.10 × 0.10 mm, monoclinic, space group $P2_1/n$, a = 16.499(3), b = 18.947(4), c = 18.518(4) Å, β = 99.09(3)°, V = 5716(2) Å^3, T = −90 °C, Z = 4, $\rho_{calcd.}$ = 1.381 g·cm^{-3}, μ(Mo-K_α) = 3.81 cm^{-1}, F(000) = 2456, 46833 reflections in h (−20/21), k (−23/24), l (−21/24), measured in the range 2.10° ≤ Θ ≤ 27.51°, completeness Θ_{max} = 98%, 12884 independent reflections, R_{int} = 0.089, 7991 reflections with $F_o > 4\sigma(F_o)$, 673 parameters, 36 restraints, $R1_{obs.}$ = 0.072, $wR^2_{obs.}$ = 0.205, $R1_{all}$ = 0.114, wR^2_{all} = 0.224, GOOF = 1.336, largest difference peak and hole: 1.452/−1.101 e·Å^{-3}.

Crystal Data for 5: $[C_{50}H_{58}N_8Ru(C_7F_{15}COO)](C_7F_{15}COO)$, Mr = 1578.17 g·mol^{-1}, red-brown prism, size 0.20 × 0.18 × 0.12 mm, triclinic, space group $P\bar{1}$, a = 15.880(3), b = 21.334(4), c = 29.081(6) Å, α = 75.96(3), β = 88.66(3), γ = 86.98(3)°, V = 9544(3) Å^3, T = −90 °C, Z = 4, $\rho_{calcd.}$ = 1.098 g·cm^{-3}, μ(Mo-K_α) = 2.58 cm^{-1}, F(000) = 3184, 43889 reflections in h (−20/20), k (−27/22), l (−35/36), measured in the range 1.07° ≤ Θ ≤ 27.47°, completeness Θ_{max} = 78%, 34097 independent reflections.

Crystal Data for 6:[36] $[(C_{50}H_{58}N_8Ru)_2\{C_4F_4(COO)_2\}](PF_6)_2$·$3(CH_3)_2CO$, Mr = 2462.50 g·mol^{-1}, red-brown prism, size 0.10 × 0.09 × 0.08 mm, triclinic, space group $P\bar{1}$, a = 13.6330(4), b = 14.2867(5), c = 16.7479(5) Å, α = 98.356(2), β = 94.201(2), γ = 100.148(2)°, V = 3160.47(17) Å^3, T = −90 °C, Z = 2, $\rho_{calcd.}$ = 1.294 g·cm^{-3}, μ(Mo-K_α) = 3.46 cm^{-1}, F(000) = 1276, 20848 reflections in h (−17/17), k (−14/18), l (−21/21), measured in the range 3.07° ≤ Θ ≤ 27.47°, completeness Θ_{max} = 96.3%, 13947 independent reflections, R_{int} = 0.028, 11364 reflections with $F_o > 4\sigma(F_o)$, 731 parameters, 1 restraints, $R1_{obs.}$ = 0.060, wR^2_{obs} = 0.159, $R1_{all}$ = 0.078, wR^2_{all} = 0.1775, GOOF = 1.055, largest difference peak and hole: 1.351/−0.589 e·Å^{-3}.

Crystal Data for 7:[36] $[(C_{50}H_{59}N_8Ru)_2\{C_4F_4(COO)_2\}][C_4F_4(COO)_2]$·$H_2O$·$3CH_3CN$, Mr = 2155.50 g·mol^{-1}, red-brown prism,

size 0.12 × 0.10 × 0.09 mm, triclinic, space group $P\bar{1}$, a = 10.3448(2), b = 15.5248(4), c = 19.5865(5) Å, α = 88.110(1), β = 78.075(1), γ = 70.915(1) °, V = 2906.52(12) Å^3, T = −90 °C, Z = 1, $\rho_{calcd.}$ = 1.231 g·cm^{-3}, μ(Mo-K_α) = 3.26 cm^{-1}, $F(000)$ = 1126, 20157 reflections in h (−12/13), k (−19/17), l (−22/25), measured in the range 7.07° ≤ Θ ≤ 27.45°, completeness Θ_{max} = 95.3%, 12680 independent reflections, R_{int} = 0.033, 10139 reflections with $F_o > 4\sigma(F_o)$, 668 parameters, 0 restraints, $R1_{obs.}$ = 0.060, $wR2_{obs}$ = 0.150, $R1_{all}$ = 0.083, $wR2_{all}$ = 0.169, GOOF = 1.053, largest difference peak and hole: 1.171/−0.567 e·Å^{-3}.

Acknowledgments

Financial support for this work from the Deutsche Forschungsgemeinschaft (SFB 436), and the Fonds der Chemischen Industrie is gratefully acknowledged.

[1] D. Walther, T. Döhler, N. Theyssen, H. Görls, *Eur. J. Inorg. Chem.* **2001**, 2049−2060.
[2] T. Döhler, H. Görls, D. Walther, *Chem. Commun.* **2000**, 945−946.
[3] M. Ruben, S. Rau, A. Skirl, K. Krause, H. Görls, D. Walther, J. G. Vos, *Inorg. Chim. Acta* **2000**, *303*, 206−214.
[4] M. Döring, P. Fehling, H. Görls, W. Imhof, R. Beckert, D. Lindauer, *J. Prakt. Chem.* **1999**, *341*, 748−756.
[5] P. Feeling, M. Döring, F. Knoch, R. Beckert, H. Görls, *Chem. Ber.* **1995**, *128*, 405−412.
[6] M. Döring, H. Görls, R. Beckert, *Z. Anorg. Allg. Chem.* **1994**, *620*, 551− 560.
[7] R. Beckert, S. Vorwerk, D. Lindauer, M. Döring, *Z. Naturforsch., Teil B* **1993**, *48*, 1386−1390.
[8] M. Pasquali, C. Floriani, A. Chiesi-Villa, C. Guastini, *J. Am. Chem. Soc.* **1979**, *101*, 4740 4742.
[9] J. M. Lehn, Supramolecular Chemistry: Concepts and Perspectives, VCH, **1995**.
[10] For recent reviews see: G. J. P. Britovsek, V. C. Gibson, *Angew. Chem.* **1999**, *111*, 448−468; *Angew. Chem. Int. Ed.* **1999**, *38*, 428−447.
[11] S. D. Ittel, L. K. Johnson, *Chem. Rev.* **2000**, *100*, 1169−1203.
[12] M.-C- Liaw, M.-C. Cheng, S.-M. Peng, *Bull. Inst. Chem. Academica, Sini*ca. **1991**, *38*, 55−63.
[13] J. Rall, A. F. Stange, K. Hübler, W. Kaim, *Angew. Chem.* **1998**, *110*, 2827−2829, *Angew. Chem. Int. Ed.* **1998**, *37*, 2682−2682.
[14] B.-H. Ye, F. Xue, G.-Q. Xue, L.-N. Ji, T. C. W. Mak, *Polyhedron* **1999**, 1785−1790.
[15] D. Boinnard, P. Cassoux, V. Petrouleas, J.-M. Savariault, J.-P. Tuchagues, *Inorg. Chem.* **1990**, *29*, 4114−4121.
[16] S. Fortin, A. L. Beauchamp, *Inorg. Chem.* **2001**, *40*, 105−112.
[17] S. Rau, T. Büttner, C. Temme, M. Ruben, H. Görls, D. Walther, M. Duati, F. Fanni, J. G. Vos, *Inorg. Chem.* **2000**, *39*, 1621−1624.
[18] D. Walther, M. Stollenz, H. Görls, Organometallics **2001**, *20*, 4221−4229.
[19] D. Walther, M. Stollenz, L. Böttcher, H. Görls, *Z. Anorg. Allg. Chem.* **2001**, *627*, 1560−1570.
[20] J. Wuckelt, M. Döring, H. Görls, P. Langer, *Eur. J. Inorg. Chem.* **2001**, 805−811.
[21] J. Cancela, M. J. Gonzales Gasmedia, M. Quiros, *Inorg. Chim. Acta* **2001**, *313*, 156−159.
[22] M. A. Martinez Lorente, F. Dahan, Y. Sanakis, V. Petrouleas, A. Bousseksou, J.-P. Tuchagues, *Inorg. Chem.* **1995**, *34*, 5346−5357.
[23] J. G. Dance, A. S. Abushamleh, H. A. Goodwin, *Inorg. Chim. Acta* **1980**, *43*, 217−221.
[24] A. D. Mighell, C. W. Reimann, F. A. Mauer, *Acta Crystallogr., Sect. B* 1969, *25*, 60−66.
[25] S. de Souza Lemos, K. E. Bessler, E. Schulz Lang, *Z. Anorg. Allg. Chem.* **1998**, *624*, 30−34.
[26] S. de Souza Lemos, K. E. Bessler, E. Schulz Lang, *Z. Anorg. Allg. Chem.* **1998**, *624*, 701−707.
[27] S. Fortin, A. L. Beauchamp, *Inorg. Chem.* **2000**, *39*, 4886−4893.
[28] S. Belanger, L. Beauchamp, *Acta Cryst* 1995, *C55*, 517−521.
[29] S. Rau, M. Ruben, T. Büttner, C. Temme, S. Dautz, H. Görls, M. Rudolph, D. Walther, A. Brodkorb, M. Duati, C. O′Connor, J. G. Vos, *J. Chem. Soc., Dalton Trans.* **2000**, 3649−3657.
[30] R. Bauer, *Ber. Dtsch. Chem. Ges.* **1907**, *40*, 2650−2662.
[31] D. Lindauer, R. Beckert, M. Döring, P. Fehling, H. Görls, *J. Prakt. Chem.* **1995**, *337*, 143−152.
[32] *COLLECT*, Data Collection Software; Nonius B. V., Netherlands, **1998**.
[33] Z. Otwinowski, W. Minor, "Processing of X-ray Diffraction Data Collected in Oscillation Mode", in: *Methods in Enzymology*, Vol. 276, Macromolecular Crystallography, Part A, (Eds.: C. W. Carter, R. M. Sweet), pp. 307−326, *Academic Press, San Diego*, **1997**.
[34] G. M. Sheldrick, *Acta Crystallogr., Sect. A* **1990**, *46*, 467−473.
[35] G. M. Sheldrick, *SHELXL-97*, University of Göttingen, Germany, **1993**.
[36] Further details of the crystal structure investigations are available on requests from the director of the Cambridge Crystallographic Data Centre, 12 Union Road, GB-Cambridge CB2 1 EZ, on quoting the depository number CCSD-182291 to CCSD-182299, the names of the authors, and the journal citation.

Received March 28, 2002
[I02164]

Competitive Insertion of Isocyanide into Tantalum−Amido and Tantalum−Methyl Bonds

Francisco Amor,[a] Javier Sánchez-Nieves,[a] Pascual Royo,*[a] Heiko Jacobsen,[b] Olivier Blacque,[b] Heinz Berke,[b] Maurizio Lanfranchi,[c] Maria Angela Pellinghelli,[c] and Antonio Tiripicchio[c]

Keywords: Tantalum / Competitive insertion / Isocyanide insertion / Density functional calculations

The (amido)methyl complexes [Ta(η^5-C_5Me_5)(N*t*Bu)Me(NR_2)] [R = Ph (**3**), $SiMe_3$ (**4**)] were prepared by reaction of [Ta(η^5-C_5Me_5)(N*t*Bu)ClMe] (**1**) with the appropriate lithium amides. Attempts to isolate the analogous NHMe derivative afforded a mixture of complexes [Ta(η^5-C_5Me_5)(N*t*Bu)Me(NHMe)] (**5**) and [Ta(η^5-C_5Me_5)(NMe)Me(NH*t*Bu)] (**6**), resulting from hydrogen exchange between the amido and imido ligands. Insertion of CN(2,6-$Me_2C_6H_3$) into the Ta–Me bond of complexes **3** and **4** gave the η^1-iminoacyl derivatives [Ta(η^5-C_5Me_5)(N*t*Bu)(NR_2){η^1-C(Me)=N(2,6-$Me_2C_6H_3$)}] [R = Ph (**7**), $SiMe_3$ (**8**)], while insertion into the Ta–NRMe (R = H, Me) bond of the complexes [Ta(η^5-C_5Me_5)(N*t*Bu)Me(NRMe)] [R = H (**5**), Me (**2**)] gave the η^2-iminocarbamoyl compounds [Ta(η^5-C_5Me_5)(N*t*Bu)Me{η^2-C(NRMe)=N(2,6-$Me_2C_6H_3$)}] [R = H (**10**), Me (**9**)]. All of the new compounds were characterized by ^{1}H and ^{13}C NMR spectroscopy. The X-ray crystal structure of **9** is reported. DFT calculations were carried out to justify the preference of the insertion either into the Ta–C or the Ta–N bond.

(© Wiley-VCH Verlag GmbH, 69451 Weinheim, Germany, 2002)

Introduction

It is well known that isocyanides can be inserted into early transition metal−alkyl[1−5] and metal−amido[1,6−10] bonds to give η^2-iminoacyl and η^2-iminocarbamoyl compounds, respectively. These are versatile and potentially useful reagents in many synthetic applications.[1]

We reported[11] the insertion of isocyanide into the tantalum−methyl bond of various (η^5-pentamethylcyclopentadienyl)(imido) complexes of the type [Ta(η^5-C_5Me_5)(NR)MeX] to verify that this insertion takes place into the tantalum−methyl bond[12] not only for X = Cl, OR (R = Me, *t*Bu), noncompetitive ligands, but also for X = NH*t*Bu, which could behave as a competitive ligand to give η^2-iminocarbamoyl derivatives. We concluded that the steric demands of the X substituent influence these reactions more significantly than its π-donor capacity, the reaction being easier for X = Cl, Me, OMe (immediate at room temperature) than for X = O*t*Bu (7 h at room temperature) and X = NH*t*Bu (3 d at 75 °C). We also observed that the double insertion of isocyanide into the tantalum−iminoacyl bond is preferred over the insertion into the Ta−NH*t*Bu bond, allowing for the isolation of [Ta(η^5-C_5Me_5)(N*t*Bu)(NH*t*Bu){η^2-C(CMe=NR)=NR}] (R = 2,6-$Me_2C_6H_3$) complexes. Consequently, formation of η^2-iminocarbamoyl derivatives by insertion into tantalum−amido bonds would only be possible if no alkyl substituent were present, as observed for [Ta(η^5-C_5Me_5)(N*t*Bu)Cl{NH*t*Bu)][12] and related (amido)niobium compounds.[13]

However, an unexpected behaviour was observed when [Ta(η^5-C_5Me_5)(N*t*Bu)Me(NMe_2)], which contains a less bulky dimethylamido ligand, was used. This reaction was immediate at room temperature affording the η^2-iminocarbamoyl derivative with preferential insertion into the tantalum−amido rather than the tantalum−methyl bond. For this reason we decided to thoroughly investigate these insertion reactions using different amido ligands. Meanwhile, a similar preferential insertion into a metal−dimethylamido bond was reported for related [Nb(η^5-$C_5H_4SiMe_3$){N(2,6-$Me_2C_6H_3$)}Me(NMe_2)] and [Ta(η^5-C_5Me_5){N(2,6-$Me_2C_6H_3$)}Me(NMe_2)] complexes.[14]

Here we report the synthesis of new (amido)methyltantalum complexes [Ta(η^5-C_5Me_5)(N*t*Bu)Me(NR_2)] [R_2 = HMe, Ph_2, $(SiMe_3)_2$] and the competitive insertion of

[a] Departamento de Química Inorgánica, Universidad de Alcalá, Campus Universitario,
28871 Alcalá de Henares, Spain
Fax: (internat.) + 34-91/885-4683
E-mail: pascual.royo@uah.es
[b] Anorganisch-chemische Institut, Universität Zürich-Irchel, Winterthurerstrasse 190, 8057 Zürich, Switzerland
[c] Dipartimento di Chimica Generale ed Inorganica, Chimica Analitica, Chimica Fisica, Università di Parma, Parco Area delle Scienze 17A, 43100 Parma, Italy

Supporting information for this article is available on the WWW under http://www.eurjic.org or from the author.

$CN(2,6\text{-}Me_2C_6H_3)$ into their Ta−Me and Ta−NR_2 bonds. The X-ray molecular structure of the η^2-iminocarbamoyl complex $[Ta(\eta^5\text{-}C_5(CH_3)_5](NtBu)Me\{\eta^2\text{-}C(NMe_2)=N(2,6\text{-}Me_2C_6H_3)\}]$ is also reported, as well as DFT calculations carried out to justify the notion of preferential insertion into Ta−dimethylamido bonds.

Results and Discussion

As previously reported[15] the dimethylamido complex $[Ta(\eta^5\text{-}C_5Me_5)(NtBu)Me(NMe_2)]$ (**2**) was isolated in high yield as a dark yellow oil by addition of $LiNMe_2$ to an ethereal solution of the (chloro)(methyl) derivative $[Ta(\eta^5\text{-}C_5Me_5)(NtBu)ClMe]$ (**1**). As shown in Equation (1), the same procedure afforded complex $[Ta(\eta^5\text{-}C_5Me_5)(NtBu)Me(NPh_2)]$ (**3**) as a yellow oil in 90% yield. It is an air-sensitive compound that can be stored for long periods under an inert gas. The complex $[Ta(\eta^5\text{-}C_5Me_5)(NtBu)Me\{N(SiMe_3)_2\}]$ (**4**), which was not isolated as a solid, was prepared in quantitative yield by the same reaction in a sealed NMR tube, and is stable in C_6D_6 solution for long periods.

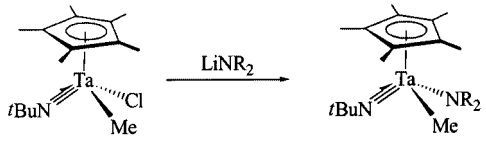

(1)

1 R = Ph, **3**; $SiMe_3$, **4**

It was found[15] that **2** shows dynamic NMR spectroscopic behaviour, indicating free rotation of the amido ligand and making the two methyl groups equivalent, to give a unique broad signal in both ^1H and ^{13}C NMR spectra at room temperature. Dynamic NMR spectroscopy experiments showed a coalescence temperature of ca. 302 K and a Gibbs activation energy $\Delta G^{\neq}$ of 58.15 kJ/mol for this process, in agreement with reported values for analogous complexes.[16] However, the ^1H NMR spectra of complexes **3** and **4** show the presence of two nonequivalent phenyl- and silylamido substituents, respectively, every aryl ring proton of **3** appearing as a sharp signal (δ = 6.7−7.2 ppm) while two sharp signals for the $SiMe_3$ groups of **4** were observed at δ = 0.18 and 0.50 ppm. Resonances for the methyl, *tert*-butyl and pentamethylcyclopentadienyl groups in complexes **3** and **4** appear in the usual region (see Exp. Sect.).

In an attempt to complete the series of (amido)(imido) complexes analogous to **2**, we tried the reaction of **1** with LiNHMe in THF. This reaction was not so simple and gave a mixture of $[Ta(\eta^5\text{-}C_5Me_5)(NtBu)Me(NHMe)]$ (**5**) and $[Ta(\eta^5\text{-}C_5Me_5)(NMe)Me(NHtBu)]$ (**6**) in ca. 1:1 ratio [Equation (2)], as a pale yellow oil from which they could not be separated. No interconversion between **5** and **6** was observed when the mixture was heated up to 80 °C in the NMR tube, indicating that the temperature does not substantially modify the equilibrium.

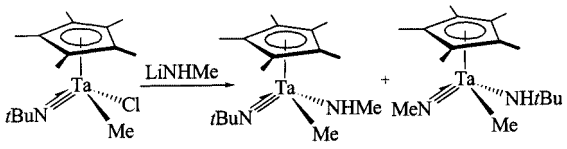

(2)

1 **5** **6**

Complexes **5** and **6** were easily distinguished by their ^1H NMR spectrum, which shows the methyl resonance of the amido ligand as a doublet (δ = 3.63 ppm, $^3J_{H,H}$ = 7 Hz) whereas that of the imido ligand appears as a singlet (δ = 3.77 ppm). Two sets of signals for the methyl, *tert*-butyl and pentamethylcyclopentadienyl groups were observed for the mixture of complexes **5** and **6**. The amido proton of the corresponding NHMe and NH*t*Bu appears as a broad signal at δ = 4.62 and 4.88 ppm, respectively. The values of $\Delta\delta$ ($\Delta\delta = \delta_{quat} - \delta_{Me}$) observed in the ^{13}C NMR spectra of **5** (30.2 ppm) and **6** (21.6 ppm) are consistent with the presence of the *tert*-butylimido and *tert*-butylamido ligands, respectively.[17]

Therefore, formation of **5**, followed by proton transfer from the methylamido to the more basic *tert*-butylimido ligand,[16,18−25] affords complex **6**, and the kinetic barrier for interconversion between **5** and **6** must be high.

Treatment of complexes **3** and **4** with $CN(2,6\text{-}Me_2C_6H_3)$ resulted in insertion into the Ta−Me bond, to give the η^1-iminoacyl compounds $[Ta(\eta^5\text{-}C_5Me_5)(NtBu)(NPh_2)\{\eta^1\text{-}C(Me)=N(2,6\text{-}Me_2C_6H_3)\}]$ (**7**) and $[Ta(\eta^5\text{-}C_5Me_5)(NtBu)[N(SiMe_3)_2]\{\eta^1\text{-}C(Me)=N(2,6\text{-}Me_2C_6H_3)\}]$ (**8**), after heating at 80 °C for 8 h and 20 h, respectively [Equation (3)]. This is the same behaviour previously observed for $[Ta(\eta^5\text{-}C_5Me_5)(NtBu)Me(NHtBu)]$.[12]

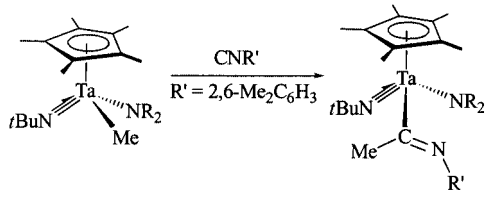

(3)

R_2 = Ph_2, **3**; $(SiMe_3)_2$, **4** R_2 = Ph_2, **7**; $(SiMe_3)_2$, **8**

Formation of the iminoacyl compounds **7** and **8** was confirmed by the low-field shift ($\delta > 1$ ppm) of the ^1H NMR signal of the migrated methyl group and the ^{13}C resonance of the iminoacyl sp^2-carbon atom observed at δ = 249.3 (**7**) and 251.9 ppm (**8**), as expected for complexes of this type.

In contrast, an almost immediate and complete reaction of the dimethylamido complex **2** with 1 equiv. of $CN(2,6\text{-}Me_2C_6H_3)$ took place at room temperature in hexane to afford the η^2-iminocarbamoyl compound $[Ta(\eta^5\text{-}C_5Me_5)(NtBu)Me\{\eta^2\text{-}C(NMe_2)=N(2,6\text{-}Me_2C_6H_3)\}]$ (**9**) [Equation (4)], which was recrystallized from pentane and isolated as colourless air-stable crystals soluble in all the usual organic solvents. Its crystal structure was determined by X-ray diffraction methods.

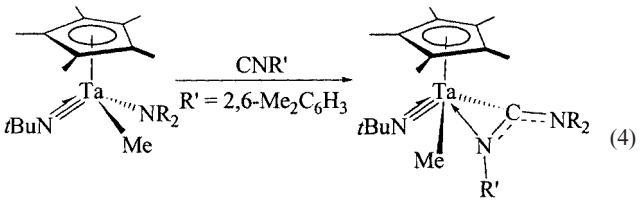

(4)

$R_2 = Me_2$, **2**; HMe, **5** $R_2 = Me_2$, **9**; HMe, **10**

Addition of 2 equiv. of CN(2,6-$Me_2C_6H_3$) to a C_6D_6 solution of a ca. 1:1 mixture of **5** and **6** proceeded with darkening of the solution and isocyanide insertion into the Ta−NHMe bond of complex **5** to give [Ta(η^5-C_5Me_5)(N*t*Bu)Me{η^2-C(NHMe)=N(2,6-$Me_2C_6H_3$)}] (**10**) after 24 h at room temperature [Equation (4)]. Under these conditions complex **6** remained unaltered. No insertion into the Ta−Me bond was observed even after heating to 80 °C, which caused complex **6** to decompose, while **10** remained unchanged.

Formation of the η^2-iminocarbamoyl compounds **9** and **10** was confirmed by the high-field shift ($\delta \approx 1$ ppm) of the methylamido signal, the very slight displacement of the Ta-Me resonance and the presence in the ^{13}C NMR spectra of a low-field signal ($\delta > 200$ ppm) due to the iminocarbamoyl sp^2-carbon atom.[26] Three ν(C=N) IR stretching vibrations were observed[6] for the η^2-iminocarbamoyl complex **9**.

The transformation of the (benzyl)(η^2-iminocarbamoyl) species into the corresponding (amido)(η^2-iminoacyl) derivative, typical in related (amido)niobium compounds,[13] was not observed for complex **9**, which decomposed on heating to over 100 °C. It can therefore be concluded that insertion occurred directly into the Ta−NMe_2 rather than the Ta−Me bond.

An X-ray diffraction study of complex **9** confirms that the isocyanide was inserted into the tantalum−amido bond. A view of the molecular structure of complex **9**, together with the atomic labeling system, is shown in Figure 1. Selected bond lengths and angles are given in Table 1.

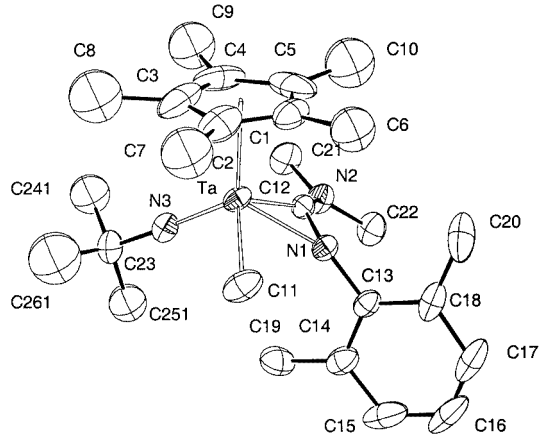

Figure 1. ORTEP view of the molecular structure of **9**; thermal ellipsoids are drawn at 30% probability level; hydrogen atoms are omitted for the sake of clarity

Table 1. Selected bond lengths [Å] and angles [°] with e.s.d.s in parentheses for compound **9** [CE(1) is the centroid of the C(1)···C(5) cyclopentadienyl ring and M(1) the midpoint of the N(1)−C(12) double bond]

Ta−N(3)	1.785(4)	Ta−C(4)	2.406(6)
Ta−C(11)	2.230(5)	Ta−C(5)	2.503(6)
Ta−N(1)	2.164(4)	N(1)−C(12)	1.303(5)
Ta−C(12)	2.146(5)	N(1)−C(13)	1.418(6)
Ta−CE(1)	2.182(6)	C(12)−N(2)	1.339(6)
Ta−M(1)	2.054(5)	N(2)−C(21)	1.444(6)
Ta−C(1)	2.567(5)	N(2)−C(22)	1.464(7)
Ta−C(2)	2.485(6)	N(3)−C(23)	1.441(7)
Ta−C(3)	2.441(6)		
CE(1)−Ta−C(11)	106.8(3)	N(1)−Ta−C(12)	35.2(1)
CE(1)−Ta−N(3)	122.6(2)	Ta−N(1)−C(12)	71.7(3)
CE(1)−Ta−M(1)	120.7(2)	Ta−N(1)−C(13)	150.0(3)
CE(1)−Ta−N(1)	122.6(2)	C(12)−N(1)−C(13)	133.6(4)
CE(1)−Ta−C(12)	115.7(2)	Ta−C(12)−N(1)	73.1(3)
C(11)−Ta−N(3)	97.0(2)	Ta−C(12)−N(2)	155.5(3)
C(11)−Ta−M(1)	98.4(2)	N(1)−C(12)−N(2)	130.3(4)
C(11)−Ta−N(1)	81.4(2)	C(12)−N(2)−C(21)	119.1(5)
C(11)−Ta−C(12)	115.5(2)	C(12)−N(2)−C(22)	124.6(4)
N(3)−Ta−M(1)	105.7(2)	C(21)−N(2)−C(22)	116.3(5)
N(3)−Ta−N(1)	111.9(2)	Ta−N(3)−C(23)	176.8(4)
N(3)−Ta−C(12)	98.2(2)		

The tantalum atom shows a four-legged piano stool arrangement involving the pentamethylcyclopentadienyl ring [Ta−CE(1) = 2.182(6) Å], [CE(1) being the centroid of the ring], the methyl carbon atom [Ta−C(11) = 2.230(5) Å], the nitrogen atom of the *tert*-butylimido ligand [Ta−N(3) = 1.785(4) Å], and the carbon and nitrogen atoms of the η^2-iminocarbamoyl ligand [Ta−C(12) = 2.146(5) and Ta−N(1) = 2.164(4) Å]. The dihedral angle between the cyclopentadienyl ring and the N(3)C(11)N(1)C(12) mean plane is 5.2(2)°. This arrangement can also be viewed as a three-legged piano-stool if the midpoint [M(1)] of the N(1)−C(12) bond is taken into consideration [Ta−M(1) = 2.054(5) Å]. The coordination geometry around the Ta atom can be described also as pseudotetrahedral if the centroid CE(1) and the midpoint M(1) are considered as coordination sites. The complex is chiral, and both enantiomers are present in the crystals. The insertion of CN(2,6-$Me_2C_6H_3$) into the coordinated dimethylamido group is stereoselective; in fact the η^2-iminocarbamoyl shows the N atom in a *cis* position with respect to the coordinated methyl group. Only one of the two possible stereoisomers is so formed. This stereoselectivity is probably mainly due to steric factors.

The *inside* coordination of the N(1) iminocarbamoyl nitrogen atom located between C(12) and C(11) is similar to that found for similar (chloro)(iminoacyl)(imido)(pentamethylcyclopentadienyl)- or (iminoacyl)(imido)(methyl)(pentamethylcyclopentadienyl)tantalum complexes[11,12,14,27] in which the N(1) iminoacyl nitrogen atom is located between the iminoacyl carbon atom and the chlorine atom or the methyl carbon atom. The values of the Ta−N(3) bond length, consistent with triple bond character, and of the nearly linear Ta−N(3)−C(23) bond angle of 176.8(4)° are as expected for an imido ligand and compare well with

those found in other (imido)(pentamethylcyclopentadienyl)-tantalum complexes.[11,12,14,27−30] The Ta−C(11) bond length presents the normal value for a $Ta-CH_3$ bond. The Cp* (C_5Me_5) ring is bound to the Ta atom in a nearly symmetric η^5-fashion; a slight trend towards η^3-coordination is observed, as indicated by three short [Ta−C(2) = 2.485(6), Ta−C(3) = 2.441(6), Ta−C(4) = 2.406(6) Å] and two long $Ta-C_{Cp^*}$ ring carbon distances [Ta−C(1) = 2.567(5) and Ta−C(5) = 2.503(6) Å], involving the C(1)−C(5) bond nearly *trans* to the imido group[30] {τ[N(3)−Ta−CE(1)−C(1)] = 159.7(4), τ[N(3)−Ta−CE(1)−C(5)] = −128.6(6), τ[N(3)−Ta−CE(1)−C(3)] = 17.3(7)°}. The midpoint of the N(1)−C(12) bond nearly eclipses the C(5) atom of Cp* {τ[M(1)−Ta−CE(1)−C(5)] = 10.3(7)°}. The Ta−N(1) and Ta−C(12) bond lengths are similar to those found in (η^2-*C*,*N*-iminoacyl)Ta complexes.[11,12,14,27] The N(1)−C(12) [1.303(5) Å], and the C(12)−N(2) [1.339(6) Å] bond lengths reveal π delocalizaton in the η^2-*C*,*N*-iminocarbamoyl moiety. The N(1)C(12)N(2)C(21)C(22) fragment is quite planar {max. dev. 0.050(7) Å for C(21), τ[N(1)−C(12)−N(2)−C(21)] = 173.4(5), τ[N(1)−C(12)−N(2)−C(22)] = −6.8(8)°} and forms dihedral angles of 4.5(2) and 81.7(2)° with the TaN(1)C(12) and the aryl groups, respectively.

The close similarity between the symmetry properties of the frontier orbitals of (cyclopentadienyl)(imido)metal [Ta(η^5-C_5Me_5)(N*t*Bu)] and the metallocene [Ti(η^5-C_5Me_5)$_2$] fragments[30] suggests that the $1a_1$ metal orbital is used for π-bonding by the NMe_2 ligand. The dynamic behaviour observed for **2** at room temperature indicates that this $1a_1$ orbital is energetically accessible for ligand binding, allowing the isocyanide to be located at any of the two positions appropriate for insertion into either the Ta−Me or $Ta-NMe_2$ bonds. Insertion into the Ta−NRMe (R = H, Me) bonds is the most favorable, being followed by rotation around the Ta−C bond to give the η^2-iminocarbamoyl compound, and similar behaviour should be expected for the NH*t*Bu derivatives **6** and [Ta(η^5-C_5Me_5)(N*t*Bu)-Me(NH*t*Bu)].[12] However steric effects from the presence of the bulky *tert*-butyl substituent are more important than the electronic effects and probably prevent this reaction, leaving the energetically less favorable insertion into the Ta−Me bond as the only possible pathway, which requires heating at 75 °C for 3 d in the case of [Ta(η^5-C_5Me_5)-(N*t*Bu)Me(NH*t*Bu)].[12] Complexes **3** and **4** favor preferential insertion into the Ta−Me bond when heated at 80 °C for 8 and 20 h, respectively, probably due to electronic effects of the amido substituents.

To help answer the question why compound **3** shows a preference for insertion into the tantalum−methyl bond, rather than insertion into the tantalum−amido bond, as observed for compound **2**, we performed density functional calculations on possible insertion products of the reaction of **2** and **3** with CN(2,6-$Me_2C_6H_3$). The relative energies and coordination geometries are collected in Scheme 1.

According to our calculations, the most stable insertion product for compound **2** is the η^2-iminocarbamoyl complex **9** based on the approach of the isocyanide between the alkyl and the amido ligands. However, the corresponding iminoacyl derivative is only 3 kJ/mol higher in energy. Furthermore, the optimized geometry shows that the iminoacyl ligand is bound in an η^1-fashion, with the two N groups in a *cis* position with respect to the Ta−C bond. A rotation around the latter bond leads to a complex with an η^2-iminoacyl ligand. This compound, however, is 40 kJ/mol higher in energy than the one bearing an η^1-iminoacyl ligand. The possibility of an attack of the isocyanide from the other "side" of the amido ligand (between the amido and imido ligands) has also been investigated but the η^2-iminocarbamoyl insertion product is about 36 kJ/mol higher in energy.

Turning to the insertion products for compound **3**, the calculations show that the iminoacyl complex **7** is the energetically favored insertion product. Again, the iminoacyl group acts as an η^1-ligand, and the corresponding η^2 complex is 44 kJ/mol higher in energy. Also, the η^2-iminocarbamoyl complexes are energetically disfavored by 49 and 68 kJ/mol.

An analysis of the charge distributions in complexes **2** and **3** holds an answer for the observed preferences in coordination geometry. Charges (in a.u.) at the atoms forming the Ta−C and Ta−N bonds of **2** and **3** are displayed in Scheme 2.

For both compounds, the imido N atom as well as the methyl C atom carry a negative charge, whereas the metal center is positively charged. However, whereas for compound **2** the electron-rich dimethylamido ligand carries a sizeable amount of negative charge at the N atom, the N atom of the diphenlyamido group of compound **3** carries almost no charge at all. Also, in this compound, the central metal atom as well as the imido N atom are more positively charged by 0.2 and 0.1 a.u., when compared with **2**. This suggests that the diphenylamido ligand possesses some electron-withdrawing properties, since charge can be effectively delocalized over the two aromatic phenyl groups. This assumption is supported when the total charge on the NMe_2 and NPh_2 in compounds **2** and **3** is analyzed. Summing up the individual contributions of all atoms of the NMe_2 group, we find a charge value of +0.10 a.u., indicating that the dimethylamido group is acting as an electron-donating group. On the other hand, the total charge of the NPh_2 group amounts to −0.61 a.u. This indicates that electron delocalization over the phenyl groups indeed induces some electron-withdrawing properties. The same behaviour should be expected for compound **4** by electron delocalization onto the silicon d orbitals. Thus, the isocyanide ligand will insert into that Ta−R (R = C, N) bond, in which R carries a sizeable amount of negative charge. In this case, the attack of R at the LUMO of the CN(2,6-$Me_2C_6H_3$) molecule, which is the first step in the formation of the new R−CN(2,6-$Me_2C_6H_3$) bond, is facilitated. We also note that when steric bulk is provided by alkyl groups, the sterically most hindered M−C bond can also be expected to contain the C atom with the largest amount of negative charge.

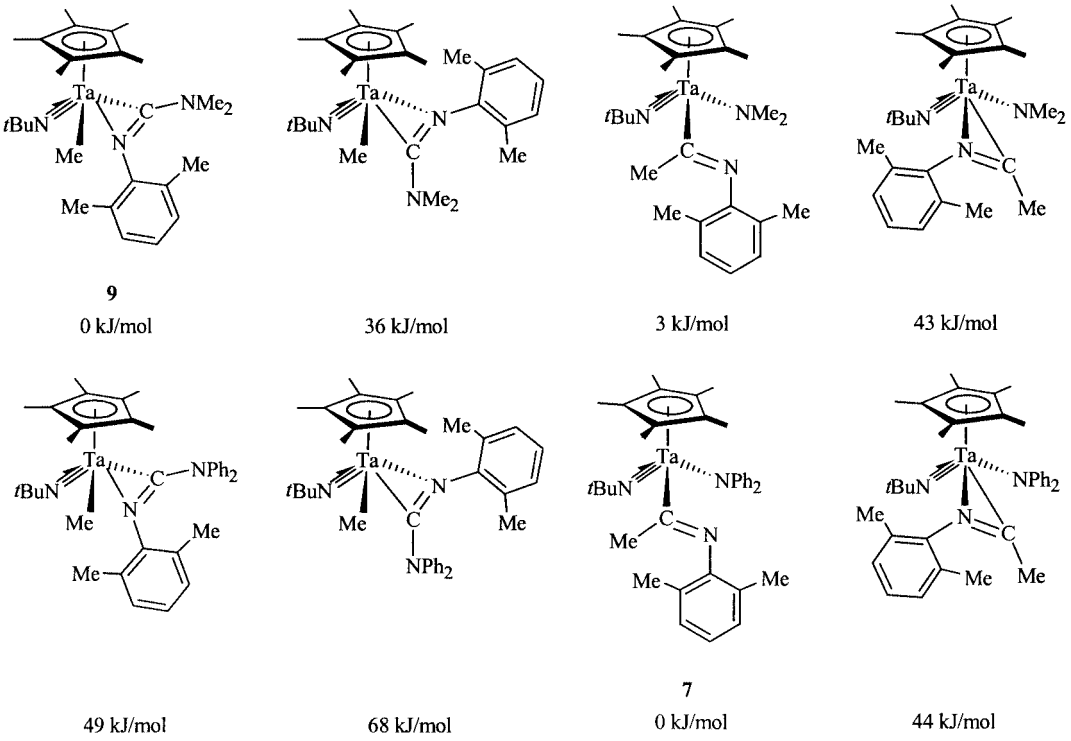

Scheme 1

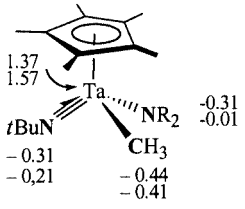

R = Me, **2**
R = Ph, **3**

Scheme 2

Comparing the small energy difference between **9** and the corresponding η^1-iminoacyl complex, it becomes clear that thermodynamic considerations do not explain the preference for insertion into the Ta−NMe_2 bond. In order to gain further insight into the nature of the frontier orbitals, we carried out an orbital analysis of the (amido)(imido) compound **2**. As expected, the lone pair of the amido ligand interacts in a π-fashion with the empty $1a_1$ metal orbital. The π-bonding interaction takes place in the highest occupied molecular orbital of the complex (Figure 2), while the corresponding π-antibonding interaction is mainly localized in the LUMO.

The resulting metal−nitrogen π-bonding interaction leads to a more stable orientation with one of the amido substituents pointing towards the Cp* ring. For the real insertion process of the $CN(2,6\text{-}Me_2C_6H_3)$ molecule into the Ta−amido bond, we may then take the attack of the lone pair of the amido group in the HOMO (π-bonding orbital) on the π* LUMO of the isocyanide molecule as the major orbital transformation of this process (Scheme 3). The preference of Ta−N over Ta−C insertion is therefore governed by frontier orbital arguments, and is preferred on kinetic, rather than thermodynamic, grounds.

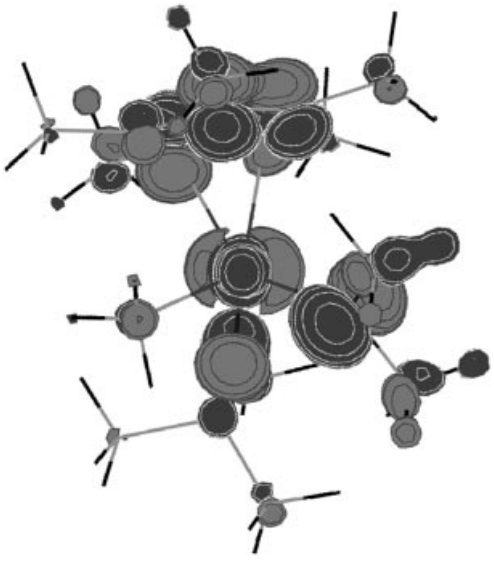

Figure 2. Calculated HOMO of the amido imido complex **2** showing the π-bonding interaction between the metal orbital and the amido lone pair

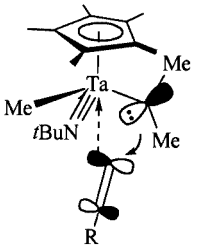

Scheme 3

Conclusions

Various (amido)methyltantalum complexes [Ta(η^5-C_5Me_5)(N*t*Bu)Me(NR_2)] [R_2 = HMe, Ph_2, $(SiMe_3)_2$] were prepared by reaction of the (chloro)(methyl) derivative with appropriate lithium amides Li(NR_2). Easy hydrogen exchange between methylamido (NHMe) and the more basic *tert*-butylimido (N*t*Bu) groups was observed.

According to density functional calculations, coordination of isocyanide CN(2,6-$Me_2C_6H_3$) followed by nucleophilic attack initiates the insertion, either into Ta−amido or Ta−methyl bonds, that is governed by kinetic factors. Insertion into Ta−methyl bonds is preferred for amido NR_2 [R_2 = Ph_2, $(SiMe_3)_2$] complexes to give the η^1-iminoacyl [Ta(η^5-C_5Me_5)(N*t*Bu)(NR_2){η^1-C(Me)=N(2,6-$Me_2C_6H_3$)}] derivatives, whereas stereoselective insertion into the Ta−amido bonds is preferred for NRMe (R = H, Me) yielding *inside-N*-coordinated η^2-iminocarbamoyl [Ta(η^5-C_5Me_5)(N*t*Bu)Me{η^2-C(NRMe)=N(2,6-$Me_2C_6H_3$)}] complexes.

Experimental Section

General: All operations were performed under argon using standard Schlenk-line or glovebox techniques. Hexane and pentane were distilled from a sodium/potassium alloy and diethyl ether from sodium benzophenone ketyl. H_2NMe (Aldrich), $HNPh_2$ (Aldrich), $HN(SiMe_3)_2$ (Aldrich), CN(2,6-$Me_2C_6H_3$) (Fluka) were used as received. LiBu (Aldrich) was titrated prior to use.[31] Complexes [Ta(η^5-C_5Me_5)(N*t*Bu)ClMe] (**1**)[12] and [Ta(η^5-C_5Me_5)(N*t*Bu)Me(NMe_2)] (**2**)[15] were prepared by known procedures. IR: Perkin−Elmer 583 spectrophotometer (4000−200 cm^{-1}). ^{1}H and ^{13}C NMR: Varian Unity 300 MHz spectrometer (^{1}H, 299.95 MHz; ^{13}C, 75.43 MHz). Chemical shifts (in ppm) were referenced internally using the residual solvent resonances and were reported relative to tetramethylsilane. Elemental analyses: Perkin−Elmer 2400 CHNO.

Preparation of [Ta(η^5-C_5Me_5)(N*t*Bu)Me(NPh_2)] (3): Cooled THF (30 mL) was added to a solid mixture of **1** (1.36 g, 3.11 mmol) and $LiNPh_2$ (0.59 g, 3.42 mmol) at 0 °C. The mixture was allowed to warm slowly to room temperature. All volatiles were removed and pentane (2 × 15 mL) was added to give a brown-yellow solution. The solution was filtered and the solvent was completely removed to give **3** as a yellow oil. Yield 1.60 g (90%). IR (Nujol, CsI): $\tilde{\nu}$ = 1273 (s) cm^{-1}. ^{1}H NMR ($CDCl_3$, 298 K): δ = 0.39 (s, 3 H, Ta*Me*), 0.79 (s, 9 H, NC*Me*$_3$), 1.89 (s, 15 H, C_5Me_5), 6.7−7.2 (s, 10 H, N*Ph*$_2$) ppm. ^{13}C{^{1}H} NMR ($CDCl_3$, 298 K): δ = 11.2 (C_5Me_5), 28.0 (Ta*Me*), 32.0 (NC*Me*$_3$), 64.5 (N*C*Me$_3$), 115.4 (C_5Me_5), 122.8, 125.3, 128.1, 129.3 (N*Ph*$_2$) ppm. $C_{27}H_{37}N_2Ta$ (570.55): calcd. C 56.84, H 6.49, N 4.91; found C 56.59, H 6.25, N 4.52.

NMR Tube Scale Preparation of [Ta(η^5-C_5Me_5)(N*t*Bu)Me{N($SiMe_3$)$_2$}] (4): C_6D_6 was added to a solid mixture of **1** (0.034 g, 0.077 mmol) and $LiN(SiMe_3)_2$ (0.013 g, 0.077 mmol) in a sealed NMR tube and the mixture was monitored by ^{1}H NMR spectroscopy. After 24 h at 90 °C, the signals of complex **1** disappeared leaving a solution that contained **4** in quantitative yield. ^{1}H NMR (C_6D_6, 298 K): δ = 0.18 [s, 9 H, N(Si*Me*$_3$)$_2$], 0.47 (s, 3 H, Ta*Me*), 0.5 [s, 9 H, N(Si*Me*$_3$)$_2$], 1.32 (s, 9 H, NC*Me*$_3$), 1.91 (s, 15 H, C_5Me_5) ppm. ^{13}C{^{1}H} NMR (C_6D_6, 298 K): δ = 6.6, 7.7 [N(Si*Me*$_3$)$_2$], 12.2 (C_5Me_5), 20.3 (Ta*Me*), 33.5 (NC*Me*$_3$), 65.5 (N*C*Me$_3$), 116.4 (C_5Me_5) ppm.

Preparation of [Ta(η^5-C_5Me_5)(N*t*Bu)Me(NHMe)] (5) and [Ta(η^5-C_5Me_5)(NMe)Me(NH*t*Bu)] (6): According to a similar procedure to that used for **3**, compound **1** (1.06 g, 2.42 mmol) was treated with LiNHMe (0.11 g, 2.91 mmol) in hexane (30 mL) at −78 °C, to give a ca. 1:1 mixture of **5** and **6** as a pale yellow oil. Yield 0.76 g (72%). **5:** ^{1}H NMR (C_6D_6, 298 K): δ = 0.33 (s, 3 H, Ta*Me*), 1.37 (s, 9 H, NC*Me*$_3$), 1.84 (s, 15 H, C_5Me_5), 3.63 (d, $^3J_{H,H}$ = 7 Hz, 3 H, NH*Me*), 4.62 (br, 1 H, N*H*Me) ppm. ^{13}C{^{1}H} NMR (C_6D_6, 298 K): δ = 11.1 (C_5Me_5), 20.4 (Ta*Me*), 33.9 (NC*Me*$_3$), 45.5 (NH*Me*), 64.1 (N*C*Me$_3$), 114.0 (C_5Me_5) ppm. **6:** ^{1}H NMR (C_6D_6, 298 K): δ = 0.29 (s, 3 H, Ta*Me*), 1.35 (s, 9 H, NHC*Me*$_3$), 1.82 (s, 15 H, C_5Me_5), 3.77 (s, 3 H, N*Me*), 4.88 (br, 1 H, N*H*CMe$_3$) ppm. ^{13}C{^{1}H} NMR (C_6D_6, 298 K): δ = 10.6 (C_5Me_5), 20.4 (Ta*Me*), 34.7 (NHC*Me*$_3$), 45.9 (N*Me*), 56.3 (NH*C*Me$_3$), 113.3 (C_5Me_5) ppm.

Preparation of [Ta(η^5-C_5Me_5)(N*t*Bu)(NPh_2){η^1-C(Me)=N(2,6-$Me_2C_6H_3$)}] (7): A solution of **3** (1.79 g, 3.14 mmol) in toluene (20 mL) was treated with CN(2,6-$Me_2C_6H_3$) (0.42 g, 3.20 mmol) and the mixture was heated (80 °C) and stirred for 8 h. The solution was filtered and the solvent completely removed. The residue was washed with hexane (2 × 15 mL) to give **7** as a brown oil. Yield 1.65 g (75%). IR (Nujol CsI): $\tilde{\nu}$ = 1594 (s), 1260 (s) cm^{-1}. ^{1}H NMR ($CDCl_3$, 298 K): δ = 1.0 (s, 9 H, NC*Me*$_3$), 1.91 [s, 3 H, C(*Me*)=N], 1.98 (s, 3 H, 2,6-*Me*$_2$C$_6$H$_3$), 2.12 (s, 15 H, C_5Me_5), 2.46 (s, 3 H, 2,6-*Me*$_2$C$_6$H$_3$), 6.5−7.3 (m, 13 H, 2,6-Me$_2$C$_6$*H*$_3$, N*Ph*$_2$) ppm. ^{13}C{^{1}H} NMR ($CDCl_3$, 298 K): δ = 12.3 (C_5Me_5), 18.9, 19.3 (2,6-*Me*$_2$C$_6$H$_3$), 22.5 [C(*Me*)=N], 33.2 [NC*Me*$_3$], 65.8 [N*C*Me$_3$], 115.7 (C_5Me_5), 117.7, 120.9, 124.9, 125.0, 127.5, 127.9, 128.1, 129.3, 130.9, 142.0 (2,6-Me$_2$*C*$_6$H$_3$, N*Ph*$_2$), 249.3 [*C*(Me)=N] ppm. $C_{36}H_{46}N_3Ta$ (701.73): calcd. C 61.63, H 6.61, N 5.99; found C 61.33, H 6.39, N 5.66.

NMR Tube Scale Preparation of [Ta(η^5-C_5Me_5)(N*t*Bu){N($SiMe_3$)$_2$}{η^1-C(Me)=N(2,6-$Me_2C_6H_3$)}] (8): CN(2,6-$Me_2C_6H_3$) (0.015 g, 0.114 mmol) was added to an NMR tube containing a C_6D_6 solution of **4** (0.114 mmol) and the mixture was monitored by ^{1}H NMR spectroscopy. After ca. 20 h at 80 °C, the signals of complex **4** disappeared leaving a solution that contained **8** in quantitative yield. ^{1}H NMR (C_6D_6, 298 K): δ = 0.17, 0.63 [s, 9 H, N(Si*Me*$_3$)$_2$], 1.19 (s, 9 H, NC*Me*$_3$), 2.01 (s, 15 H, C_5Me_5), 2.04 [s, 3 H, C(*Me*)=N], 2.22, 2.38 (s, 3 H, 2,6-*Me*$_2$C$_6$H$_3$), 6.92 (m, 3 H, 2,6-Me$_2$C$_6$*H*$_3$) ppm. ^{13}C{^{1}H} NMR (C_6D_6, 298 K): δ = 8.3, 8.9 [N(Si*Me*$_3$)$_2$], 12.8 (C_5Me_5), 18.6, 19.9 (2,6-*Me*$_2$C$_6$H$_3$), 24.0 [C(*Me*)=N], 34.4 (NC*Me*$_3$), 66.3 (N*C*Me$_3$), 116.0 (C_5Me_5), 125.8, 128.5, 128.9, 132.2, 134.9, 144.0 (2,6-Me$_2$*C*$_6$H$_3$), 251.9 [*C*(Me)=N] ppm.

Preparation of [Ta(η^5-C$_5$Me$_5$)(N*t*Bu)Me{η^2-C(NMe$_2$)=N(2,6-Me$_2$C$_6$H$_3$)}] (9): A solution of **2** (1.0 g, 2.24 mmol) in hexane (20 mL) was added to CN(2,6-Me$_2$C$_6$H$_3$) (0.30 g, 2.26 mmol) and the mixture was stirred for 1 h at room temperature. The solution was filtered and the solvent was removed to give **9** as a white solid. Recrystallization from pentane gave **9** as colourless crystals. Yield 1.14 g (88%). IR (KBr pellets): $\tilde{\nu}$ = 1606 (s), 1586 (s), 1267 (s) cm^{-1}. ^{1}H NMR (CDCl$_3$, 298 K): δ = −0.29 (s, 3 H, Ta*Me*), 1.03 (s, 9 H, NC*Me*$_3$), 1.96, 2.0 (s, 3 H, 2,6-*Me*$_2$C$_6$H$_3$), 2.04 (s, 15 H, C$_5$*Me*$_5$), 2.59, 3.39 [s, 3 H, C(N*Me*$_2$)=N], 6.87 (m, 3 H, 2,6-Me$_2$C$_6$*H*$_3$) ppm. ^{13}C{^{1}H} NMR (CDCl$_3$, 298 K): δ = 11.8 (C$_5$*Me*$_5$), 14.2 (Ta*Me*), 19.7 (2,6-*Me*$_2$C$_6$H$_3$), 33.7 (NC*Me*$_3$), 36.8, 45.3 [C(N*Me*$_2$)=N], 64.1 (N*C*Me$_3$), 112.4 (*C*$_5$Me$_5$), 123.7, 127.0, 127.4, 132.0, 132.5, 143.8 (2,6-Me$_2$*C*$_6$H$_3$), 206.6 [*C*(NMe$_2$)=N] ppm. C$_{26}$H$_{42}$N$_3$Ta (577.59): calcd. C 54.07, H 7.33, N 7.28; found C 54.26, H 7.46, N 7.48.

NMR Tube Scale Preparation of Ta(η^5-C$_5$Me$_5$)(N*t*Bu)Me{η^2-C(NHMe)=N(2,6-Me$_2$C$_6$H$_3$)} (10): C$_6$D$_6$ was added to a mixture of **5** and **6** (0.054 g, 0.125 mmol) and CN(2,6-Me$_2$C$_6$H$_3$) (0.016 g, 0.125 mmol) in a sealed NMR tube and the mixture was monitored by ^{1}H NMR spectroscopy. After ca. 24 h at room temperature, the signals of complex **5** disappeared leaving a solution that contained **10**, **6** and excess isocyanide. **10:** ^{1}H NMR (C$_6$D$_6$, 298 K): δ = 0.44 (s, 3 H, Ta*Me*), 1.29 (s, 9 H, NC*Me*$_3$), 2.04 (s, 15 H, C$_5$*Me*$_5$), 2.14, 2.21 (s, 3 H, 2,6-*Me*$_2$C$_6$H$_3$), 2.66 [d, $^3J_{H,H}$ = 7 Hz, 3 H, C(NH*Me*)=N], 4.68 [br, 1 H, C(N*H*Me)=N], 6.95 (m, 3 H, 2,6-Me$_2$C$_6$*H*$_3$) ppm. ^{13}C{^{1}H} NMR (C$_6$D$_6$, 298 K): δ = 12.0 (C$_5$*Me*$_5$), 16.6 (Ta*Me*), 19.3, 19.5 (2,6-*Me*$_2$C$_6$H$_3$], 34.1 (NC*Me*$_3$), 64.3 (N*C*Me$_3$), 67.8 [C(NH*Me*)=N], 112.8 (*C*$_5$Me$_5$), 125.0, 128.8, 132.5, 132.9, 141.8, 143.6 (2,6-Me$_2$*C*$_6$H$_3$), 208.4 [*C*(NHMe)=N] ppm.

Crystal Structure Determination of 9: Crystals of compound **9** were obtained by crystallization from pentane. A suitably sized crystal in a Lindemann tube was mounted on a Philips PW 1100 diffractometer with graphite-monochromated Mo-K_α radiation (λ = 0.71073 Å). Crystallographic and experimental details are summarized in Table 2. A semi-empirical method of absorption correction was applied (maximum and minimum values for the transmission coefficient were 1.000 and 0.582).[32] A decay of 15% was observed during the data collection. The structure was solved by direct methods (SIR92)[33] and refined by least squares against F_o^2 (SHELXL-97).[34] All non-hydrogen atoms were refined anisotropically except for the methyl carbon atoms of the Cp* ring and of the *t*Bu group. These last methyl groups were found to be disordered in two positions and refined with s.o.f. of 0.5. All hydrogen atoms were introduced from geometrical calculations and refined using a riding model. All calculations were carried out with the DIGITAL AlphaStation 255 of the "Centro di Studio per la Strutturistica Diffrattometrica del C.N.R.", Parma. The programs PARST[35] and ORTEP[36] were also used. CCDC-187149 contains the supplementary crystallographic data for this paper. These data can be obtained free of charge at www.ccdc.cam.ac.uk/conts/retrieving.html or from the Cambridge Crystallographic Data Centre, 12, Union Road, Cambridge CB2 1EZ, UK [Fax: (internat.) + 44-1223/336-033; E-mail: deposit@ccdc.cam.ac.uk].

Computational Details: Gradient-corrected density functional calculations were carried out with corrections for exchange and correlation according to Becke[37] and Perdew,[38] respectively (BP86). Geometries were optimized using the program system TURBOMOLE[39] within the framework of the RI-*J* approximation.[40] The geometry was pre-optimized using a triple-ζ valence basis plus polarization TZVP[41] for Ta, and a split-valence basis set with one set of polarization functions for the non-H atoms SV(P)[42] for the remaining elements. In the final steps of the geometry optimization, all elements were treated with the TZVP basis. Atomic charges were obtained from a population analysis based on occupation numbers, and include multicenter corrections.[43] Optimized geometries and final energies are presented in the Supporting Information (see also footnote on the first page of this article).

Table 2. Summary of crystallographic data for compound **9**

Empirical formula	C$_{26}$H$_{42}$N$_3$Ta
Formula mass	577.58
Crystal system	triclinic
Space group	$P\bar{1}$
Radiation (λ [Å])	Mo-K_α (0.71073)
a [Å]	8.592(5)
b [Å]	9.874(4)
c [Å]	16.940(9)
α [°]	101.55(2)
β [°]	93.04(2)
γ [°]	102.50(2)
V [Å^3]	1367.7(12)
Z	2
$D_{calcd.}$ [Mg m^{-3}]	1.403
μ(Mo-K_α) [mm^{-1}]	4.034
F(000)	584
Crystal size [mm]	0.49 × 0.30 × 0.15
Diffractometer	Philips PW 1100
θ range [°]	3.20−30.01
Scan type	θ/2θ
Index ranges	$-12 \le h \le 12$, $-13 \le k \le 13$, $0 \le l \le 23$
No. of reflections measured	7954
No. of unique total data	7954
No. of unique observed data	6016 [$I > 2\sigma(I)$]
Data/restraints/parameters	7954/0/253
Goodness-of-fit on F^2	0.955
*R*1 [$I > 2\sigma(I)$]	0.0385
*wR*2 [$I > 2\sigma(I)$]	0.0947
*R*1 (all data)	0.0572
*wR*2 (all data)	0.1023

Acknowledgments

The authors acknowledge MCyT (project MAT2001-1309) for financial support and EC (project COST-D12/0016/98). J. S.-N. acknowledges the Ministerio de Educación y Ciencia for a fellowship.

[1] L. D. Durfee, I. P. Rothwell, *Chem. Rev.* **1988**, *88*, 1059−1079.
[2] [2a] P. J. Fagan, J. M. Manriquez, S. H. Vollmer, S. C. Day, V. W. Day, T. J. Marks, *J. Am. Chem. Soc.* **1981**, *103*, 2206−2220. [2b] J. Jeffery, M. F. Lappert, N. T. Luong-Thi, M. Webb, J. L. Atwood, W. E. Hunter, *J. Chem. Soc., Dalton Trans.* **1981**, 1593−1605. [2c] J. L. Petersen, L. Kloppenburg, *Organometallics* **1997**, *16*, 3548−3556.
[3] [3a] P. Legzdins, S. J. Rettig, K. J. Ross, *Organometallics* **1994**, *13*, 569−577. [3b] R. L. Huff, S.-Y. S. Wang, K. A. Abboud, J. M. Boncella, *Organometallics* **1997**, *16*, 1779−1785.
[4] A. Dormond, A. Aaliti, C. Moise, *J. Chem. Soc., Chem. Commun.* **1985**, 1231−1233.
[5] E. A. Boring, M. Sabat, M. G. Finn, R. N. Grimes, *Organometallics* **1997**, *16*, 3993−4000.
[6] M. H. Chisholm, C. E. Hammond, D. Ho, J. C. Huffman, *J. Am. Chem. Soc.* **1986**, *108*, 7860−7861.
[7] Z. Wu, J. B. Diminnie, Z. Xue, *Organometallics* **1999**, *18*, 1002−1010 and references therein.
[8] C. K. Broder, A. E. Goeta, J. A. K. Howard, A. K. Hughes,

A. L. Johnson, J. M. Malget, K. Wade, *J. Chem. Soc., Dalton Trans.* **2000**, 3526−3533.
[9] P. Zanella, N. Brianese, U. Casellato, F. Ossola, M. Porchia, G. Rossetto, R. Graziani, *J. Chem. Soc., Dalton Trans.* **1987**, 2039−2043.
[10] M. Galakhov, P. Gómez-Sal, A. Martín, M. Mena, C. Yélamos, *Eur. J. Inorg. Chem.* **1998**, 1319−1325.
[11] M. Gómez, P. Gómez-Sal, G. Jiménez, A. Martín, P. Royo, J. Sánchez-Nieves, *Organometallics* **1996**, *15*, 3579−3587.
[12] J. Sánchez-Nieves, P. Royo, M. A. Pellinghelli, A. Tiripicchio, *Organometallics* **2000**, *19*, 3161−3169.
[13] M. I. Alcalde, P. Gómez-Sal, P. Royo, *Organometallics* **2001**, *20*, 4623−4631.
[14] A. Castro, M. Galakhov, M. Gómez, P. Gómez-Sal, A. Martín, F. Sánchez, *J. Organomet. Chem.* **2000**, *595*, 36−53.
[15] J. Sánchez-Nieves, P. Royo, *J. Organomet. Chem.* **2001**, *621*, 299−303.
[16] A. Castro, M. V. Galakhov, M. Gómez, F. Sánchez, *J. Organomet. Chem.* **1999**, *580*, 161−168.
[17] [17a] W. A. Nugent, J. M. Mayer, *Metal-Ligand Multiple Bonds*, John Wiley & Sons, New York, **1988**, p. 133. [17b] W. A. Nugent, B. L. Haymore, *Coord. Chem. Rev.* **1980**, *31*, 123−175.
[18] D. S. Glueck, J. Wu, F. J. Hollander, R. G. Bergman, *J. Am. Chem. Soc.* **1991**, *113*, 2041−2054.
[19] R. J. Michelman, R. G. Bergman, R. A. Andersen, *Organometallics* **1993**, *12*, 2741−2751.
[20] M. P. Coles, C. I. Dalby, V. C. Gibson, W. Clegg, M. R. J. Elsegood, *Polyhedron* **1995**, *14*, 2455−2459.
[21] [21a] M. Jolly, J. P. Mitchell, V. C. Gibson, *J. Chem. Soc., Dalton Trans.* **1992**, 1329−1330. [21b] A. Bell, W. Clegg, P. W. Dyer, M. R. J. Elsegood, V. C. Gibson, E. L. Marshall, *J. Chem. Soc., Chem. Commun.* **1994**, 2247−2248.
[22] M. C. W. Chan, J. M. Cole, V. C. Gibson, J. A. K. Howard, *Chem. Commun.* **1997**, 2345−2346.
[23] P. Royo, J. Sánchez-Nieves, *J. Organomet. Chem.* **2000**, *597*, 61−68.
[24] [24a] P. E. Collier, S. C. Dunn, P. Mountford, O. V. Shishkin, D. Swallow, *J. Chem. Soc., Dalton Trans.* **1995**, 3743−3745. [24b] A. J. Blake, P. E. Collier, S. C. Dunn, W.-S. Li, P. Mountford, O. V. Shishkin, *J. Chem. Soc., Dalton Trans.* **1997**, 1549−1508. [24c] J. M. McInnes, D. Swallow, A. J. Blake, P. Mountford, *Inorg. Chem.* **1998**, *37*, 5970−5977.
[25] M. J. Humphries, M. L. H. Green, M. A. Leech, V. C. Gibson, M. Jolly, D. N. Williams, M. R. J. Elsegood, W. Clegg, *J. Chem. Soc., Dalton Trans.* **2000**, 4044−4051.
[26] [26a] R. D. Adams, D. F. Chodosh, *Inorg. Chem.* **1978**, *17*, 41−48. [26b] G. Erker, *Acc. Chem. Res.* **1984**, *17*, 103−109. [26c] L. R. Chamberlain, L. D. Durfee, P. E. Fanwick, L. Kobriger, S. L. Latesky, A. K. McMullen, I. P. Rothwell, K. Folting, J. C. Huffman, W. E. Streib, R. Wang, *J. Am. Chem. Soc.* **1987**, *109*, 390−402.
[27] M. V. Galakhov, M. Gómez, G. Jiménez, P. Royo, M. A. Pellinghelli, A. Tiripicchio, *Organometallics* **1995**, *14*, 2843−2854.
[28] M. V. Galakhov, M. Gómez, G. Jiménez, M. A. Pellinghelli, P. Royo, A. Tiripicchio, *Organometallics* **1994**, *13*, 1564−1566.
[29] P. Royo, J. Sánchez-Nieves, M. A. Pellinghelli, A. Tiripicchio, *J. Organomet. Chem.* **1998**, *563*, 15−21.
[30] D. N. Williams, J. P. Mitchell, A. D. Poole, U. Siemeling, W. Clegg, D. C. R. Hockless, P. A. O'Neil, V. C. Gibson, *J. Chem. Soc., Dalton Trans.* **1992**, 739−751.
[31] J. Suffert, *J. Org. Chem.* **1989**, *54*, 509−510.
[32] A. C. T. North, D. C. Phillips, F. S. Mathews, *Acta Crystallogr., Sect. A* **1968**, *24*, 351−359.
[33] A. Altomare, G. Cascarano, C. Giacovazzo, A. Gagliardi, M. C. Burla, G. Polidori, M. Camalli, *J. Appl. Crystallogr.* **1994**, *27*, 435−435.
[34] G. M. Sheldrick, *SHELXL-97, Program for the Refinement of Crystal Structures*, Universität Göttingen, Göttingen, Germany, **1997**.
[35] M. Nardelli, *Comput. Chem.* **1983**, *7*, 95−98.
[36] L. Zsolnai, H. Pritzkow, *ZORTEP, ORTEP original program modified for P.C.*, Universität Heidelberg, Heidelberg, Germany, **1994**.
[37] A. D. Becke, *Phys. Rev.* **1988**, *A38*, 3098−3100.
[38] J. P. Perdew, *Phys. Rev.* **1986**, *B33*, 8822−8824.
[39] [39a] R. Ahlrichs, M. Bär, M. Häser, H. Horn, C. Kölmel, *Chem. Phys. Lett.* **1989**, *162*, 165−169. [39b] O. Treutler, R. Ahlrichs, *J. Chem. Phys.* **1995**, *102*, 346−354. [39c] M. von Arnim, R. Ahlrichs, *J. Comp. Chem.* **1998**, *19*, 1746−1757.
[40] [40a] K. Eichkorn, O. Treutler, H. Öhm, M. Häser, R. Ahlrichs, *Chem. Phys. Lett.* **1995**, *242*, 652−670. [40b] K. Eichkorn, F. Weigand, O. Treutler, R. Ahlrichs, *Theor. Chem. Acc.* **1997**, *97*, 119−124.
[41] A. Schäfer, C. Huber, R. Ahlrichs, *J. Chem. Phys.* **1994**, *100*, 5829−5835.
[42] A. Schäfer, H. Horn, R. Ahlrichs, *J. Chem. Phys.* **1992**, *97*, 2571−2577.
[43] C. Ehrhardt, R. Ahlrichs, *Theor. Chim. Acta* **1985**, *68*, 231−245.

Received April 12, 2002
[I02189]

Collapsed Molecular Rectangles Based on Rhenium(I) Coordination of Ethynylpyridyl Porphyrins − Synthesis, Structure, and Bending-Induced Charge-Transfer Behavior

Kurt D. Benkstein,[a] Charlotte L. Stern,[a] Kathryn E. Splan,[a] Robert C. Johnson,[a] Keith A. Walters,[a] Frederick W. M. Vanhelmont,[a] and Joseph T. Hupp*[a]

Keywords: Porphyrins / Rhenium / Supramolecular chemistry / Molecular rectangles / Electroabsorption spectroscopy

Efforts to synthesize extremely large rectangle-shaped porphyrin systems have yielded an unusual and unexpected collapsed structure that brings the porphyrin walls into van der Waals contact. The bent geometry of the nominally rigid ethynylpyridyl porphyrin ligand edges, mandated by the collapse of the rectangle, imparts significant charge-transfer character to the rectangles' Soret and Q-region electronic transitions, as shown experimentally by Stark spectroscopy and transient DC photoconductivity measurements, and replicated by electronic structure calculations. In contrast to lower symmetry porphyrin-like pairs found in naturally occurring photosystems, however, the light-induced charge transfer is an intra-porphyrin rather than inter-porphyrin process.

(© Wiley-VCH Verlag GmbH, 69451 Weinheim, Germany, 2002)

Introduction

Cyclic molecular host compounds — squares, triangles, pentagons, hexagons, cylinders, prisms and other structures — featuring transition-metal-ion corners and multifunctional aromatic ligands as edges hold substantial promise for applications entailing selective chemical sensing, reaction catalysis, or nanoscale molecular transport.[1] As a logical next step beyond the now ubiquitous molecular-square motif, we recently reported the synthesis of tetrametallic molecular rectangles featuring frameworks of modest size: ca. 6 × 11 Å.[2,3] The resulting cavities are too narrow to host even a planar aromatic guest molecule. Nevertheless, by packing in a fashion that creates intermolecular cavities, neutral versions of the rectangles have proven effective in the solid state as hosts for selected volatile organic chemical guests (arenes)[2b] and as shape-selective thin-film coatings for condensed-phase molecular transport.[4] Here we describe the synthesis of new and much larger rectangles **2** and **3** featuring lengthy dihexyl derivatives of [5,15-bis(4-ethynylpyridyl)porphyrinato]zinc(II) (**1**) as walls. Intermolecular voids, potentially suitable for guest uptake, were again expected in the solid state. Additionally, however, our hope was that the extended walls would prove sufficiently flexible, especially in solution, to permit the rectangles to encapsulate polyaromatic guests in an intramolecular fashion. We further envisioned that the available pair of zinc sites could be used to bind a difunctional ligand axially, thereby propping open the porphyrin walls and resulting in a well-defined, but smaller, cavity. We instead found that the cavities are collapsed such that the porphyrinic walls approach within van der Waals distances and that the collapsed cavities strongly resist functionalization via Zn^{II} ligation. In addition we found that the cavity collapse alters the rectangle's electronic structure and imparts significant porphyrin-localized charge-transfer character to both B- and Q-band transitions, as evidenced by electronic Stark effect (electroabsorption) measurements, transient DC photoconductivity measurements, and electronic structure calculations.

Results and Discussion

Reaction of **1** with either $[Re_2(CO)_6Cl_2(\mu\text{-bipyrimidine})]$ or $[Re_2(CO)_8\{\mu\text{-bis(benzimidazolate)}\}]$ leads readily to the desired rectangles **2** and **3**.[5] The single-crystal X-ray structure for **3** is shown in Figure 1. Especially striking is the pronounced inward bowing of two of the four ethynylpyridine linkages (15.6° angle between the plane of the pyridine and the plane of the porphyrin + second pyridine). Thus, while the rhenium atoms define a framework 24.6 Å long and 5.7 Å wide, the porphyrins approach within 3.4 Å, slightly less than the estimated van der Waals contact distance (3.6 Å). A "top" view of the structure shows that the porphyrins are significantly laterally slipped — the zinc centers, for example, being laterally displaced from each other by 1.0 Å to give a slip angle of 19°. This offset is consistent with strong porphyrin/porphyrin π-stacking in-

[a] Department of Chemistry and Center for Nanofabrication and Molecular Self-Assembly, Northwestern University
2145 Sheridan Road, Evanston, IL, 60208, USA
Fax: (internat.) +1-847/491-7713
E-mail: jthupp@chem.nwu.edu

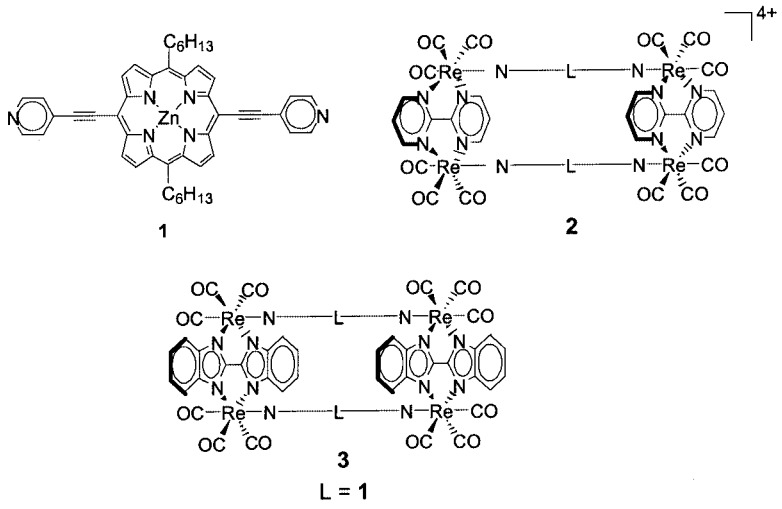

teractions and is similar to the displacements reported for other cofacial metalloporphyrin assemblies.[6] Another factor may be an intrinsic predisposition at the rhenium center for angles of less than 90° between the chelating short-edge ligand and the Re−N(imine) bond; crystal structures of closely related *Z*-shaped molecules such as *trans*-[(pyridine)$_2$Re$_2$(CO)$_8${μ-bis(benzimidazolate)}] feature angles of 82 to 84°.[7]

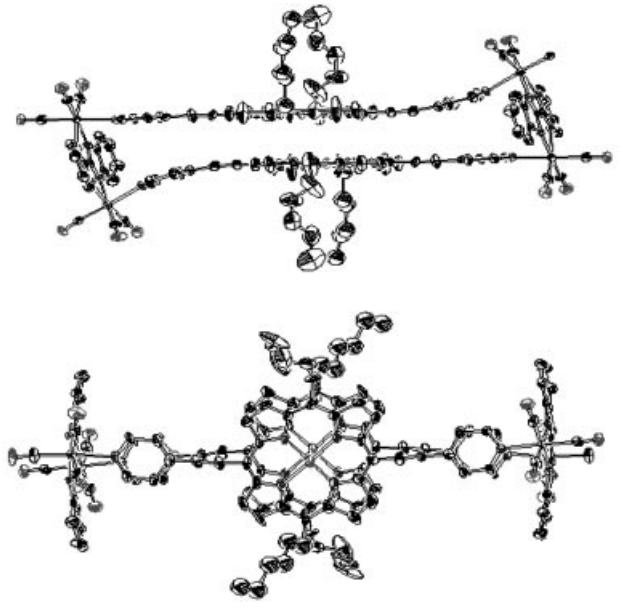

Figure 1. ORTEP representations of **3** showing the side view (top) and top view (bottom) of the co-facial porphyrin systems; hydrogen atoms have been omitted for clarity; the thermal ellipsoids represent 50% occupancy

While the collapsed cavity is too narrow for guest incorporation, as evidenced by the crystal structure, we reasoned that the flexible nature of the porphyrin walls may allow for cooperative interior binding of a single bridging ligand by the pair of Zn^{II} centers. To this end, DABCO (1,4-diazobicyclo[2.2.2]octane), a strong Lewis base, might be expected to bind inside the cavity despite being larger than the framework defined by the rhenium corners. However, DABCO is observed to bind to **3** in a 2:1 stoichiometry with no detectable preferential binding of the first equivalent ($K_b = 5 \times 10^4$ M^{-1} in $CHCl_3$) — an observation that clearly implies exterior binding. Furthermore, quinuclidine, a monofunctional, exterior-binding ligand also binds to **3** in a 2:1 stoichiometry, with $K_b = 2 \times 10^5$ M^{-1}, four times larger than the binding constant of DABCO. With other bis(porphyrinato)zinc(II) systems, the di-functionality of DABCO can favor inside binding (double ligation of a single ligand) over outside binding by as much as 300-fold, despite estimated π-stacking enthalpies of as great as −48 kJ mol^{-1}.[8] The absence of significantly favored inside binding suggests, but does not prove, even greater interactions here.

The visible-region electronic absorption spectra for **2** and **3** are dominated by porphyrin-based B- and Q-bands (Figure 2). In particular, the Q-bands for **2** and **3** are red-shifted by 20 and 10 nm, respectively, versus the Q-band for **1**, consistent with expected electron-withdrawing effects due to metal-cation coordination. Electroabsorption measurements at 77 K for **3** in a 2-methyl-THF glass (Figure 3) show that excitation in either region entails charge transfer.

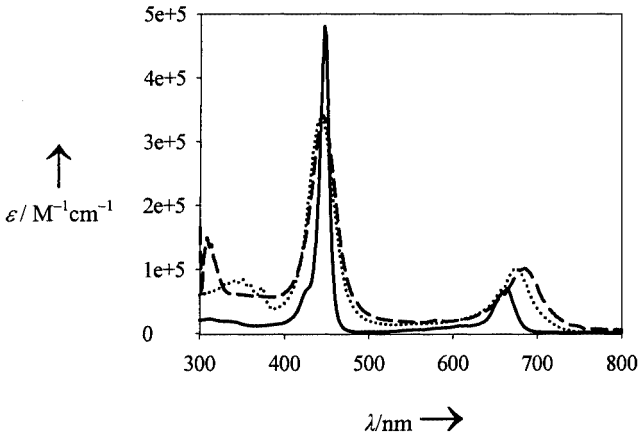

Figure 2. Electronic absorption spectra of **1** (−), **2** (---), and **3** (···) in $CHCl_3$

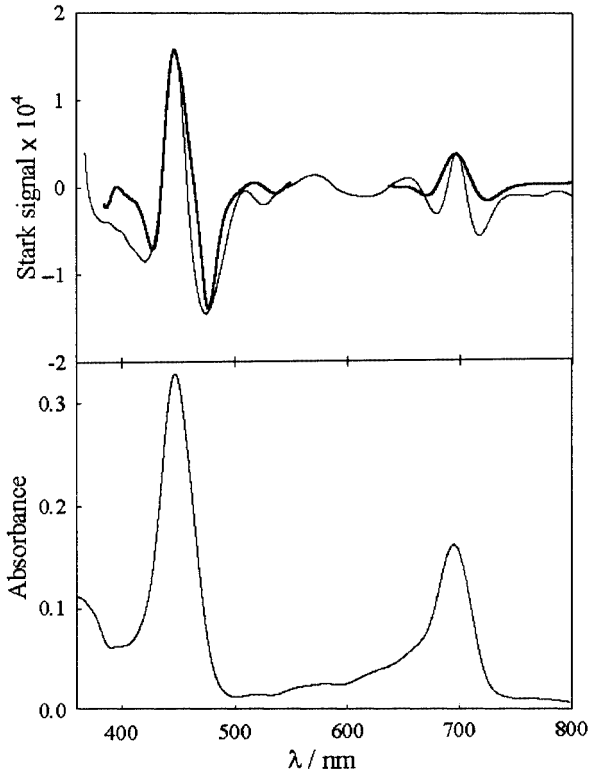

Figure 3. Electroabsorption (Stark) spectrum (top) at 77 K for **3** in a 2-methyl-THF glass at a field strength (r.m.s.) of 4.5×10^7 V/m; both B- and Q-regions of the Stark spectrum display substantial components of the second derivative (bold line) of the absorption spectrum, indicating charge-transfer character in these regions; dipole moment changes were obtained by fitting the spectra to appropriately weighted sums of zeroth-, first-, and second derivative spectra

A standard Liptay analysis of the electroabsorption spectrum,[9] neglecting local field corrections, yields ground-state to excited-state vector-dipole-moment changes, $|\Delta\mu|$, of 5 debeye for the B transition and 2 debeye for the Q transition. No charge transfer is seen in Stark measurements of **1**. That the charge-transfer observation is not peculiar to the glass environment is evidenced by liquid-phase transient DC photoconductivity measurements[10] (not shown) that demonstrate that the scalar dipole moment of the emissive excited state of **3** exceeds that of the ground state.

It is tempting, by analogy to the known low-energy charge-transfer behavior of various versions of the bacteriachlorophyl dimer (the "special pair") in photosynthetic reaction systems, to ascribe this unusual electric-field-effect behavior to photo-induced porphyrin-to-porphyrin charge-transfer. Nevertheless, the result would be most surprising given the inversion symmetry of **3**.[11] A comparison of Stark measurements made at electric-field/electromagnetic-field angles of 55° and 90° shows that in both the B- and Q-regions the change in dipole moment (charge-transfer vector) is essentially collinear with the transition dipole moment (absorption vector). This unequivocally rules out porphyrin-to-porphyrin charge-transfer, for which a vector offset of close to 90° would be expected. The behavior instead is ascribed to the remarkable structural distortions occurring in one of the two ethynylpyridines attached to each porphyrin. Bending partially attenuates electron withdrawal by the rhenium-cation-appended linkage, thereby reducing the symmetry of the porphyrin in an electronic sense and creating a porphyrin-localized dipole moment. AM1 calculations (HyperChem. 5.02), using a bent and doubly-pyridyl-protonated ligand **1** as a surrogate for one-half of **3** (in the absence of parameters for Re), corroborate the explanation. The anti-parallel arrangement of the porphyrins, of course, leads to a net molecular dipole moment of zero in the ground electronic state. Local excitation of only one of the two available porphyrins eliminates the inversion symmetry, leaving **3** with a calculated net charge-transfer polarization of 2 debeye in the lowest singlet excited state.

Finally, ambient temperature photo-excitation of **1**, **2**, and **3** in THF leads to singlet emission. Corrected emission maxima are red-shifted for the rectangles in comparison to free porphyrin: $\lambda_{em}(\mathbf{1}) = 677$ nm, $\lambda_{em}(\mathbf{2}) = 694$ nm, $\lambda_{em}(\mathbf{3}) = 714$ nm. Emission lifetimes are: $\tau(\mathbf{1}) = \tau(\mathbf{2}) =$ 1.3 ns, with emission too weak for reliable assessment of $\tau(\mathbf{3})$. Cyclic voltammetry in THF yielded the following reversible reduction potentials, measured vs. Ag/AgCl, for **1**: −0.96 and −1.39 V; for **2**: −0.70, −0.95, −1.06, −1.18 V; and for **3**: −0.89, −1.08, and −1.20 V. All are assigned as porphyrin reductions, except the first and fourth reductions for **2**; these are multi-electron reductions and are assigned as overlapping one-electron reductions of the widely separated pair of bipyrimidine ligands.[12] The relatively good reductive accessibility of the coordinated bipyrimidine edges suggests redox quenching and may account for the attenuation of the fluorescence of **2**. The splitting of nominally equivalent one-electron porphyrin reduction waves, on the other hand, suggests significant Por^-/Por^- electrostatic repulsion and/or Por^-/Por^0 electronic interactions. Combining the voltammetry and emission data, the estimated excited-state reduction potentials for **1** and **3** are both approximately +0.87 V; with less certainty, because of the intervening bipyrimidine reduction, the excited-state reduction potential for **2** is approximately +0.82 V.

To summarize, coordination chemistry based molecular-rectangle construction using lengthy bis(4-ethynylpyridyl)-porphyrins as two of the edges yields an unusual collapsed structure that places the porphyrin faces in very close proximity and substantially distorts two of the four nominally rigid ethynylpyridyl linkages. These distortions, in turn, polarize the porphyrins sufficiently that electronic transitions in both the B- and Q-band regions develop significant charge-transfer character. While we have emphasized here the special structural and photophysical features of the new rectangles, there are also interesting prospects for chemical catalysis, particularly if reactive metals are used in place of zinc and if added oxidizing or reducing equivalents lead to porphyrin-porphyrin electrostatic repulsion, thereby opening up the collapsed cavity for substrate binding.

Experimental Section

General: $[Re_2(CO)_6Cl_2(\mu\text{-bipyrimidine})]$,[2a] $[Re_2(CO)_8\{\mu\text{-bis(benzimidazolate)}\}]$,[2b] and **1**[13] were synthesized according to literature methods. THF was dried with Na/benzophenone. All other chemicals and solvents were reagent grade and used as received. ^{1}H NMR spectra were recorded with a 400 MHz Varian Mercury spectrometer. FAB mass spectra were obtained in the Mass Spectrometry Laboratory, School of Chemical Sciences, University of Illinois. Electroabsorption experiments were performed at 77 K in neat 2-methyltetrahydrofuran glass with a Cary-14 spectrophotometer. Full experimental procedures and the data reduction method have been described in detail elsewhere.[14]

1: ^{1}H NMR ([D$_5$]pyridine/$CDCl_3$): δ = 1.04 (t, J = 7 Hz, 6 H), 1.45 (m, 4 H), 1.59 (m, 4 H), 2.65 (m, 4 H), 5.13 (t, 4 H), 8.03 (d, J = 6 Hz, 4 H), 8.98 (d, J = 6 Hz, 4 H), 9.79 (d, J = 5 Hz, 4 H) 10.05 (d, J = 5 Hz, 4 H) ppm. LR ES-MS: calcd. for $[M + H^+]$: m/z = 743; found 743. HR FAB-MS: calcd. for $[M + H^+]$: m/z = 743.2841; found 743.2840 l. UV/Vis (THF): λ_{max} = 446, 664 nm.

2: Porphyrin rectangle **2** was formed by first refluxing 15.5 mg (0.0201 mmol) of $[Re_2(CO)_6Cl_2(\mu\text{-bipyrimidine})]$ with slightly more than two equivalents of AgOTf (10.9 mg, 0.424 mmol) in 20 mL of acetone under N_2 for 4 hours. The solution was passed through celite and concentrated to leave a red film. This film, $[OTf(CO)_3Re]_2(\mu\text{-bipyrimidine})$, was refluxed for two days with 14.8 mg (0.0199 mmol) of **1** in 20 mL of deoxygenated THF. The desired product precipitated as a dark red power (11.3 mg, 0.0032 mmol) in 33% yield. ^{1}H NMR ([D$_6$]DMSO): δ = 0.088 (t, J = 7 Hz, 12 H), 1.31 (m, 16 H), 1.57 (m, 8 H), 1.94 (m, 8 H), 4.28 (m, 8 H), 7.98 (d, J = 6 Hz, 8 H), 8.52 (d, J = 6 Hz, 8 H), 8.66 (m, 12 H), 9.06 (d, J = 4 Hz, 8 H), 10.16 (d, J = 6 Hz, 8 H) ppm. LR ES-MS: calcd. for [M − 2OTf]: m/z = 1592.0; found 1591.6. UV/Vis (THF): λ_{max} = 446, 686 nm.

3: Equimolar amounts of $[Re_2(CO)_8\{\mu\text{-bis(benzimidazolate)}\}]$ (22.2 mg, 0.0268 mmol) and **1** (25.5 mg, 0.0255 mmol) were refluxed in 30 mL of THF for two days. Upon addition of hexanes the desired product precipitated as a dark green powder (35.4 mg, 0.0117 mmol) in 91% yield. ^{1}H NMR ($CDCl_3$): δ = 0.879 (t, J = 7 Hz, 12 H), 1.32 (m, 16 H), 1.55 (m, 8 H), 1.92 (m, 8 H), 4.34 (t, J = 8 Hz, 8 H), 7.50 (d, J = 6 Hz, 8H0, 7.60 (q, J = 3 Hz, 8 H), 8.04 (q, J = 3 Hz, 8 H), 8.24 (d, J = 6 Hz, 8 H), 8.66 (d, J = 5 Hz, 8 H), 8.92 (d, J = 5 Hz, 8 H) ppm. FTIR ($CHCl_3$): ν_{CO} = 1901, 1922, 2022, 2028 cm^{-1}; ν_{cc} =2188 cm^{-1}. LR FAB-MS: calcd. m/z = 3034.0; found 3033.4. UV/Vis (THF): λ_{max} = 444, 686 nm. X-ray quality crystals of **3** were grown by slow evaporation from a THF/toluene solution (1:1, v:v) at ambient temperature.

Crystal Data for 3·4C$_7$H$_8$: $C_{150}H_{74}N_{20}O_{12}Zn_2Re_4$; crystal dimensions 0.5 × 0.20 × 0.48 mm; triclinic; space group $P\bar{1}$ No. 2; a = 10.877 (2), b = 17.501 (2), c = 19.230 (3) Å, α = 88.657 (2)°, β = 82.615 (2)°, γ = 88.943 (2)°, V = 3628.6 (8) Å^3; Z = 1; $\rho_{calcd.}$ = 1.487 g cm^{-3}; $2\theta_{max}$ = 56.8°; Mo-K_α radiation, λ = 0.7101 Å; T = 153 K; 33040 reflections, of which 16692 were unique; 9224 of these were included in the refinement; data corrected for Lorentz polarization effects; solution by direct methods (G. M. Sheldrick, SHELX 1997) and refinement on $|F^2|$ by full-matrix least-squares procedures (TeXsan for Windows version 1.03, Molecular Structure Corporation, Texas, USA); 781 parameters; isotropic refinement of disordered solvent molecules and C61−C66, the remaining non-hydrogen atoms were refined anisotropically; methyl groups for toluene and half the disordered hexyl group were not found in the difference Fourier map. H atoms were included, except in disordered solvent molecules and the constrained carbons, but not refined; R = 0.063, R_w = 0.141.

CCDC-176672 contains the supplementary crystallographic data for this paper. These data can be obtained free of charge at www.ccdc.cam.ac.uk/conts/retrieving.html [or from the Cambridge Crystallographic Data Center, 12, Union Road, Cambridge CB2 1EZ, UK; Fax: (internat.) +44-1223/336-033; E-mail: deposit@ccdc.cam.ac.uk].

Acknowledgments

We gratefully acknowledge the U. S. Department of Energy, Office of Science (Grant DE-FG02-87ER13808), the Dow Foundation (graduate fellowship for KES), and the Swiss National Science Foundation (postdoctoral fellowship for FWMV) for financial support.

[1] For reviews, see: [1a] M. Fujita, *Chem. Soc. Rev.* **1998**, *27*, 417−425. [1b] S. Leininger, B. Olenyuk, P. J. Stang, *Chem. Rev.* **2000**, *100*, 853−908. [1c] B. J. Holliday, C. A. Mirkin, *Angew. Chem. Int. Ed.* **2001**, *40*, 2022−2043. [1d] P. H. Dinolfo, J. T. Hupp, *Chem. Mater.* **2001**, *13*, 3113−3125.

[2] [2a] K. D. Benkstein, J. T. Hupp, C. L. Stern, *J. Am. Chem. Soc.* **1998**, *120*, 12982−12983. [2b] K. D. Benkstein, J. T. Hupp, C. L. Stern, *Angew. Chem. Int. Ed.* **2000**, *39*, 2891−2893. [2c] K. D. Benkstein, J. T. Hupp, C. L. Stern, *Inorg. Chem.* **1998**, *37*, 5404−5405.

[3] For additional work see also: [3a] S. M. Woessner, J. B. Helms, Y. Shen, B. P. Sullivan, *Inorg. Chem.* **1998**, *37*, 5406−5407. [3b] T. Rajendan, B. Manimaran, F. Lee, G. Lee, S. Peng, C. Wang, K. Lu, *Inorg. Chem.* **2000**, *39*, 2016−2017. [3c] C. J. Kuehl, S. D. Huang, P. J. Stang, *J. Am. Chem. Soc.* **2001**, *123*, 9634−9641.

[4] M. E. Williams, J. T. Hupp, in *The Encyclopedia of Electrochemistry* (Eds.: A. J. Bard, M. Stratmann), Wiley-VCH Publishers, **2002**; Vol. 10, to be published.

[5] Based on the successful synthesis of molecular squares from alkyl-functionalized dipyridyl porphyrins lacking ethynyl groups (P. J. Stang, J. Fan, *Chem. Commun.* **1997**, *15*, 1453−1454; R. V. Slone, J. T. Hupp, *Inorg. Chem.* **1997**, *36*, 5422−5423) rectangle construction was initially attempted using the same porphyrins as long edges. Unfortunately, discrete rectangles could not be isolated. In retrospect, the problem almost certainly is steric, stemming from the ca. 90° orientation of the rhenium-coordinating pyridyl functionalities with respect to the porphyrin itself and the subsequent crowding likely accompanying rectangle formation. The elimination of pyridine-proximal alkyl groups and the addition of ethynyl spacers at the 5- and 15-positions permits co-planarization of the porphyrin and appended pyridines and allows for formation of the desired rectangles.

[6] See, for example: [6a] J. P. Fillers, K. G. Ravichandran, L. Abdalmuhdi, A. Tulinsky, C. K. Chang, *J. Am. Chem. Soc.* **1986**, *108*, 417−424. [6b] J. P. Collman, P. S. Wagenknecht, J. E. Hutchison, *Angew. Chem. Int. Ed. Engl.* **1994**, *33*, 1537−1554. [6c] P. D. Harvey, N. Proulx, G. Martin, M. Drouin, D. J. Nurco, K. M. Smith, F. Bolze, C. P. Gros, R. Guilard, *Inorg. Chem.* **2001**, *40*, 4134−4142. [6d] C. J. Chang, E. A. Baker, B. J. Pistorio, Y. Deng, Z.-H. Loh, S. E. Miller, S. D. Carpenter, D. G. Nocera, *Inorg. Chem.* **2002**, *41*, 3102−3109.

[7] P. H. Dinolfo, C. L. Stern, J. T. Hupp, manuscript in preparation.

[8] C. A. Hunter, M. Nafees Meah, J. K. M. Sanders, *J. Am. Chem. Soc.* **1990**, *112*, 5773−5780.

[9] W. Liptay, in *Excited States* (Ed.: E. C. Lim), Academic Press: New York, **1974**; Vol. 1, pp 129−229.

[10] [10a] S. N. Smirnov, C. L. Braun, *Rev. Sci. Instrum.* **1998**, *69*, 2875−2887. [10b] F. W. M. Vanhelmont, J. T. Hupp, *Inorg. Chem.* **2000**, *39*, 1817−1819.
[11] J. L. Moore, H. Zhou, S. G. Boxer, *Biochemistry* **1999**, *38*, 11949−11960.
[12] H. Hartmann, S. Berger, R. Winter, J. Fiedler, W. Kaim, *Inorg. Chem.* **2000**, *39*, 4977−4980.
[13] [13a] L. D. Ciana, A. Haim, *J. Heterocyclic Chem.* **1984**, *21*, 607−608. [13b] S. G. DiMagno, V. S.-Y. Lin, M. J. Therien, *J. Org. Chem.* **1993**, *58*, 5983−5993. [13c] S. M. LeCours, S. G. DiMagno, M. J. Therien, *J. Am. Chem. Soc.* **1996**, *118*, 11854−11864.
[14] L. Karki, H. P. Lu, J. T. Hupp, *J. Phys. Chem.* **1996**, *100*, 15637−15639.

Received May 7, 2002
[I02237]

Synthesis and Characterization of a Novel Modular Cadmium-Organic Framework with Biphenyl-4,4′-dicarboxylate

Filipe A. Almeida Paz,[a] Yaroslav Z. Khimyak,[a] Andrew D. Bond,[a] João Rocha,[b] and Jacek Klinowski*[a]

Keywords: Coordination polymers / Cadmium / Supramolecular chemistry / O ligands

We report the synthesis and structural characterization of a thermally stable and highly crystalline novel metal-organic framework with cadmium(II) ions. The crystal structure is formed by a threefold interpenetration of identical three-dimensional modular frameworks, assembled by the repetition of a binuclear secondary building unit. This unit contains 1,2-bis(4-pyridyl)ethane and introduces biphenyl-4,4′-dicarboxylate as an effective rigid large spacer between metal centres. Water molecules are hydrogen bonded to carboxylate groups and act as bridges between each independent framework. To the best of our knowledge, CUmof-1 is the first structure in which the paddlewheel motif is associated with a distribution of cavities in a concertina manner.

(© Wiley-VCH Verlag GmbH, 69451 Weinheim, Germany, 2002)

Introduction

Crystal engineering of polymeric coordination networks has advanced significantly since Hoskins and Robson reported the first such compounds.[1] The design and synthesis of highly ordered, porous, multi-dimensional metal-organic frameworks (MOFs) combining organic and inorganic properties is possible through the assembly of metal centres with di- or multitopic organic ligands. Consequently, features typical of purely inorganic frameworks, such as robustness, high thermal stability and a large variety of coordination geometries, can be achieved through very strong metal-to-ligand bonds (several hundreds of $kJ \cdot mol^{-1}$).[2] By closely controlling the molecular properties of the ligands, such as shape, functionality, flexibility and symmetry, frameworks with interesting and desirable properties can be created. A number of MOFs with attractive new topologies and containing several different metal centres (Cd, Co, Cu, Ni, Pt, Sn, Zn) have been reported. Many of these exhibit interesting properties, such as shape selectivity, clathration, molecular recognition, chirality, photoluminescence and unusual magnetic behaviour, and have potential applications in nonlinear optics, catalysis, and semiconductor physics.[2–23]

N,*N*′-donor spacer ligands with rod-like characteristics, such as 4,4′-bipyridine (BPY), have been extensively used.[24–30] 1,2-Bis(4-pyridyl)ethane (BPE),[6,31–33] can adopt the *gauche* and *anti* conformations which may induce supramolecular isomerism in coordination polymers.[34] Multifunctional organic molecules with one or more *exo* carboxylic acid groups have also been widely used as ligands, due to their rigidity and ability to coordinate to several metal centres in various modes.[9,22,35–37] The most common coordination forms are the unidentate, the chelating bidentate (both symmetrical and asymmetrical), several bridging systems and the free carboxylate anion.[38] Deprotonation of biphenyl-4,4′-dicarboxylic acid (H_2BPhDC) gives rise to a linear symmetrical ligand (BPhDC), which coordinates to metal ions in aqueous solutions. This ligand can serve as a bridge between metal centres because of its rigidity along the C_2 symmetry axis.

The use of large ligands such as BPhDC (ca. 10 Å between carboxylate groups) or BPE (ca. 9 Å between N-donor atoms) in MOFs increases the average distance between metal centres, leading to frameworks with large channels, cavities or windows. However, the presence of large cavities commonly leads to unusual materials, where the voids of one network are filled by one or more independent networks, which do not necessarily need to be identical or to have the same dimensionality.[27,39] Several structures reflecting these properties and containing BPE have been reported.[6,33,40–43] The design and synthesis of porous modular materials assembled by discrete aggregates (referred to as secondary building units, SBUs) has become an area of increasing interest.[12,36,44,45] This approach facilitates the design of crystal structures by selectively controlling the experimental conditions. For instance, optimal porosity of interpenetrated networks is achieved by controlling

[a] Department of Chemistry, University of Cambridge, Lensfield Road, Cambridge CB2 1EW, U.K.
Fax: (internat.) +44-1223/336-362
E-mail: jk18@cam.ac.uk
[b] Department of Chemistry, University of Aveiro, 3810-193 Aveiro, Portugal

Supporting information for this article is available on the WWW under http://www.eurjic.org or from the author.

not only the length of the spacer but also the diameter of the repeat unit.[44]

In contrast to the extensive research focused on the use of mononuclear centres, coordination polymers containing bimetallic units (both homo- and heteronuclear) are little explored. These structural units have predictable coordination environments according to the type of ligands used, and can also exhibit attractive properties due to close metal-metal interactions. Cotton and co-workers made a contribution to this field,[46] and an unusual twofold interpenetrated $4^6 6^4$ network containing copper and the $Cr_2O_7^{2-}$ ion has been reported.[47]

Here we report the synthesis and crystal structure of a novel MOF (CUmof-1) containing cadmium(II). The combination of H_2BPhDC with BPE and a cadmium(II) salt under hydrothermal conditions, and in the presence of a stoichiometric amount of triethylamine (TEA), gives a product containing a bimetallic SBU which self-assembles into a porous modular framework, interpenetrating in a threefold manner. The highly crystalline product was obtained in high yield (86.3%) using a carefully controlled temperature program for the synthesis. This was designed in order to overcome the limitations of hydrothermal synthesis, such as the formation of poorly crystalline products caused by the irreversible nature of the process,[24] and the fast kinetics of nucleation and crystal growth.[45]

Results and Discussion

Crystallography

Single-crystal X-ray diffraction revealed a remarkable extended 3D structure with the molecular formula $[Cd(BPhDC)(BPE)(H_2O)]_n$ (CUmof-1) (Figure 1 and Table 1), which reflects the molar ratios in the synthesis mixture. The structure contains only one crystallographically unique metal centre coordinated to two BPE and three BPhDC ligands, in a geometry which is best described as a distorted octahedron (Figure 1 and Table 2). BPhDC acts as a bridging ligand with two different coordination modes. It also exhibits rod-like properties despite the internal rotations about the C_2 axis. In one of the coordination modes, each carboxylate group is coordinated to only one metal centre, forming an asymmetric chelate and imposing a Cd···Cd separation of 15.554(2) Å. Hydrogen bonds to the free water molecule maintain the C−O equivalence, although the respective Cd−O distances are slightly different (Table 2). The O−C−O angle [122.4(9)°] is also close to the expected value.[38] The aromatic rings in the chelating BPhDC are coplanar, forming an average dihedral angle of 16.1(9)° with the two crystallographically equivalent carboxylate groups. The second mode has each carboxylate forming a *syn-syn* bidentate bridge between the two cadmium centres with the Cd···Cd distance being 4.375(1) Å. This leads to the formation of a binuclear SBU with a paddlewheel-like structure, with the two bridging BPhDC ligands occupying the equatorial positions (Figure 1). The minimum separation between cadmium centres

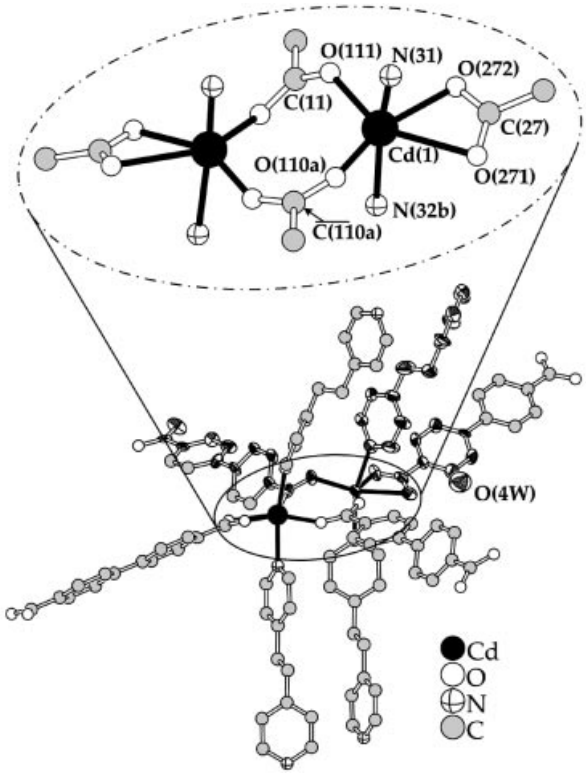

Figure 1. Binuclear building block in CUmof-1, showing the hexacoordinate environment of the cadmium centre; the top magnification shows in detail the two different coordination modes associated with the BPhDC ligand and responsible for the formation of the binuçlear SBU; the distance between the metal centres is 4.375(1) Å; bond lengths and angles are given in Table 2; the atoms from the asymmetric unit are drawn as ellipsoids at 50% of probability; hydrogen atoms have been omitted for clarity

Table 1. Crystal data and structure refinement details

	CUmof-1
Formula	$C_{26}H_{22}CdN_2O_5$
Molecular weight	554.86
Crystal system	Monoclinic
Space group	*C*2/*c*
a (Å)	18.3846(14)
b (Å)	14.9260(2)
c (Å)	16.9890(2)
β (°)	93.897(7)
Volume (Å^3)	4651.1(4)
Z	8
D_c (g cm^{-3})	1.585
μ (Mo-K_α) (mm^{-1})	0.979
Crystal size (mm)	0.07×0.01×0.01
Crystal type	Colourless needles
θ range	3.52 to 22.47
Reflections collected	12300
Independent reflections	3018 (R_{int} = 0.238)
R1 [$I > 2\sigma(I)$]	0.0693
wR2 (all data)	0.0966

across this type of BPhDC rod is 14.926(1) Å. The oxygen atoms in the two carboxylate groups are approximately equidistant from the metal centres to which they are bound, with an average Cd−O distance of 2.22 Å (Table 2). The

Table 2. Bond lengths and angles

Bond lengths [Å][a]		Bond angles [°]	
Cd(1)−N(31)	2.349(7)	O(272)−Cd(1)−O(111)	91.8(2)
Cd(1)−N(32b)	2.310(7)	O(111)−Cd(1)−O(110)	114.4(2)
Cd(1)−O(110a)	2.227(7)	O(110a)−Cd(1)−O(271)	100.5(3)
Cd(1)−O(111)	2.215(6)	O(271)−Cd(1)−O(272)	53.0(2)
Cd(1)−O(271)	2.597(6)	N(31)−Cd(1)−N(32b)	157.6(3)
Cd(1)−O(272)	2.282(6)	N(31)−Cd(1)−O(271)	82.4(2)
C(11)−O(111)	1.258(8)	N(31)−Cd(1)−O(272)	83.4(2)
C(110)−O(110)	1.245(8)	N(31)−Cd(1)−O(110a)	80.2(2)
C(27)−O(271)	1.249(13)	N(31)−Cd(1)−O(111)	97.9(2)
C(27)−O(272)	1.258(12)	N(32b)−Cd(1)−O(271)	86.2(2)
O(4 W)···O(271)	2.974(13)	N(32)−Cd(1)−O(272)	104.9(2)
O(4 W)···O(271c)	3.190(11)	N(32b)−Cd(1)−O(110a)	83.0(3)
		N(32b)−Cd(1)−O(111)	102.5(2)
		O(271)−Cd(1)−O(111)	144.7(2)
		O(272)−Cd(1)−O(110a)	150.7(2)

[a] Symmetry codes: (a) x, 1 + y, z; (b) 1/2 + x, 1/2 − y, 1/2 + z; (c) 1/2 − x, 1/2 − y, 1 − z

dihedral angle between the two aromatic rings is 44.4(3)°. Although one carboxylic group is essentially coplanar with the benzene residue to which it is bound, the other is tilted by 25.6(3)° to the respective aromatic ring. The BPE ligands are *trans*-coordinated to the metal centres acting as axial linkers in a distorted *anti* conformation. The dihedral angle between the 4-pyridyl groups is 50.4(3)°.

The 3D assembly of the binuclear SBU gives a coordinatively bonded open framework (Figure 2). This structure has decorated square-grid perforated layers formed by dicarboxylate and cadmium ions, with each pair of opposite sides of the cavity containing one of the two previously discussed types of BPhDC (Figure 2, bottom perspective). The layers can be described as a 4.8^2 net,[48] a topology common to structures with the paddlewheel motif.[44] However, to the best of our knowledge, CUmof-1 is the first structure where this motif is associated with a distribution of the cavities in a concertina manner. The BPE axial linkers act as pillars between the 4.8^2 sheets, producing several types of channels. The most prominent channels run along the *b* direction of the unit cell and have a cross-section of ca. 8.0 × 12.1 Å^2 (Figure 2). A second type of perforated sheet can be described as a distorted rectangular 4^4 net, again presented in a concertina manner (Figure 2, top perspective). A BPE molecule acting as a pillar has also been found in other structures.[6,33]

The open framework can be seen as the [ABAB...] alternation, in the *ac* plane, of two different highly distorted cuboidal [$Cd_{16}(BPhDC)_8(BPE)_6$] units (Figure 3), which are mirror images of one another. Tao et al. have reported three frameworks resembling the CUmof-1 structure, with one of the structures containing cadmium ions.[49] However, in those cases the cuboidal units are significantly more regular, possibly due to the use of the 4,4′-bipyridine ligand, which is a more rigid pillar between the acid sheets.

Interpenetration occurs in CUmof-1 as in several other structures, and involves two identical frameworks filling the voids in another framework (Figure 4). This threefold inter-

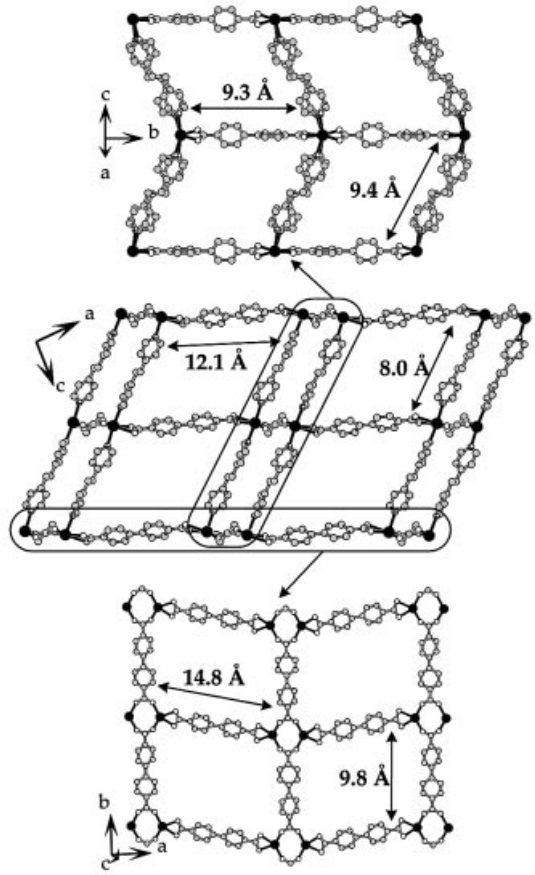

Figure 2. Overhead view along the crystallographic *b* axis of the framework constructed by assembly of the SBU; the structure has two types of perforated and interconnected concertina layers running along this axis, creating a porous 3D network; cavities inside each layer are shaded grey, and their dimensions are based on van der Waals radii; hydrogen atoms have been omitted for clarity

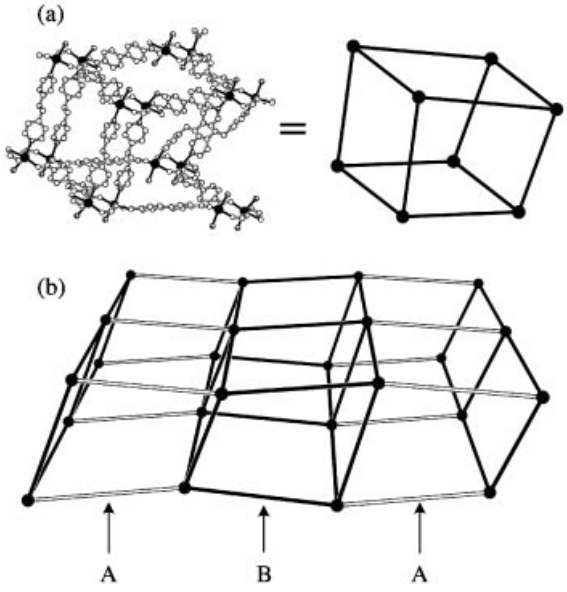

Figure 3. (a) The highly distorted cuboidal [$Cd_{16}(BPhDC)_8(BPE)_6$] unit and its simplified representation (a node is taken in the centre of each SBU); (b) The framework is constructed by [ABAB...] alternation in the *ac* plane of the two cuboidal units

penetration gives a nonporous material, as confirmed by nitrogen adsorption measurements (the adsorption isotherm of evacuated CUmof-1 reveals a BET surface area of about 2 m^2/g). The existence of an additional interpenetrating framework in CUmof-1 rather than the twofold interpenetration in the Cd-based compound reported by Tao et al.,[49] is probably the result not only of the greater length of the ligands, but also of the higher flexibility of BPE, which allows it to bend inside the cavities (Figure 4c). Such flexibility occurs in other MOF structures containing the BPE ligand: in NbO-like[42] and adamantoid networks,[43] layers[4,41] and chains.[32,41] We believe that this property of the BPE ligand is also responsible for the high distortion of the cuboidal units.

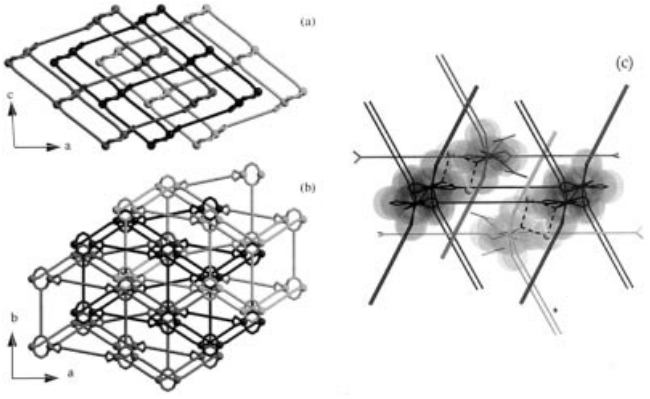

Figure 4. Crystal structure of CUmof-1, showing the presence of three interpenetrated networks, viewed along the (a) *b* and (b) *c* crystallographic axes; in view of the complexity of the structure, the aromatic rings have been omitted for clarity; for BPE the nitrogen atoms were connected directly one to each other [N(31) to N(32)], for BPhDC the connection is between the carboxylate carbon atoms [C(27) to C(27*x*), where *x* represents a different symmetry operation; C(11) to C(110)]; (c) projection showing two frameworks filling the voids of the third one; the van der Waals volume of the SBUs is also represented, along with the bridging water molecules and hydrogen bonds (dashed black lines)

Another remarkable feature of CUmof-1 is the structural function of the solvent molecules. Each individual framework is bridged to the other two by hydrogen bonding between the free water molecules and the O(271) bifurcated acceptor atoms (Figure 4c and Figure 5). These two strong O−H···O hydrogen bonds create an $R_4^2(8)$ motif with two different O···O distances (Table 2).

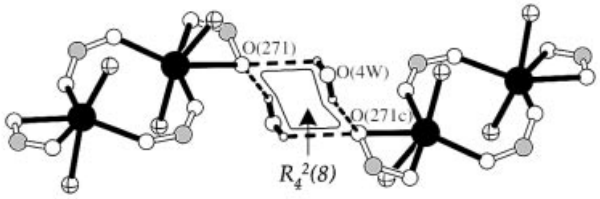

Figure 5. The chemical environment of the free solvent molecules, showing their function as bridges between different interpenetrated networks; bond lengths are given in Table 2

Other Techniques

The phase purity and crystallinity of the bulk were confirmed by a direct comparison between the experimental high-resolution PXRD pattern and a simulation based on the single-crystal X-ray diffraction results (see Supporting Information). This was also confirmed by elemental analysis. ^{113}Cd MAS NMR spectroscopy confirms the existence of only one cadmium site in CUmof-1, with a chemical shift of $\delta = 21.3$ ppm.

TGA shows a very slow and gradual release of approximately 0.71 water molecules per formula unit in the 28−140 °C temperature range. The slow kinetics of dehydration, along with the fact that not all the molecules were released, implies that the water is either strongly bonded or trapped inside the compact structure of CUmof-1. The two most significant weight losses occur between 330 and 440 °C, and are attributable to the complete oxidation of the sample to cadmium(II) oxide. This conclusion is supported by the 23.7% of residue which agrees with the expected value, considering the formation of a stoichiometric amount of CdO (23.1%). DSC analysis is in good agreement with the TGA, showing three endothermic processes corresponding to thermal decomposition of the MOF.

FT-IR and FT-Raman confirm the presence of the water molecule hydrogen bonded to the structure, and also the two organic ligands used in the synthesis. The typical antisymmetric (1577 cm^{-1}) and symmetric (1526 and 1400 cm^{-1}) stretching bands of carboxylate ions are also evident in the FT-IR spectrum. The respective $\Delta[\nu_{assym}(CO_2) - \nu_{sym}(CO_2)]$ values clearly indicate the presence of chelate (51 cm^{-1}) and bridging coordination modes (177 cm^{-1}) in CUmof-1 (Table 2), as is shown by the crystal structure.[38,50]

Conclusions

A novel modular coordination polymer with cadmium(II) ions was synthesised using a new organic bridging ligand, BPhDC, and a well-known flexible bidentate bridging molecule with two 4-pyridyl donor groups, BPE. A highly crystalline product was obtained using close control of the temperature in hydrothermal synthesis. The structure contains a single framework, assembled by the repetition of a binuclear SBU, which leads to the formation of BPhDC layers pillared by the BPE ligand. A cuboidal unit can also be isolated from the framework. Its distorted nature is attributed to the high flexibility of the BPE ligand. A threefold interpenetration leads to the formation of a nonporous compound, CUmof-1.

Experimental Section

Elemental analysis for C, N and H was performed on an Exeter Analytical CE-440 Elemental Analyser. The sample was combusted under oxygen at 975 °C for 1 minute, with He as the purge gas. TGA was carried out using Shimadzu TGA-50 and DSC on Shim-

adzu DSC-50 analyzers. Measurements were performed with a heating rate of 5 °C/min under a nitrogen atmosphere with a flow rate of 20 cm^3/min. The FT-IR spectrum was acquired using KBr pellets (Aldrich 99% +, FT-IR grade) on a Mattson 7000 FT-IR spectrometer. The FT-Raman spectrum was measured on a Bruker RFS 100 spectrometer with a Nd: YAG coherent laser (λ = 1064 nm). ^{113}Cd MAS NMR spectra were recorded at 88.71 MHz using a Chemagnetics CMX-400 spectrometer equipped with a 9.4 T magnet and zirconia rotors 7.5 mm in diameter spun in nitrogen at 5.0 kHz, using 6 μs pulse length and 180 s repetition time. Chemical shifts are quoted in ppm with respect to a 0.1 M aqueous solution of $Cd(NO_3)_2$.

Reagents: All chemicals are available from commercial sources and were used as received. The synthesis was carried out in a Teflon-lined autoclave under autogeneous pressure and static conditions (8 cm^3 total volume, filling rate 70%). The autoclave was obtained from Parr Instruments. The temperature profile used for the synthesis is described in Scheme 1.

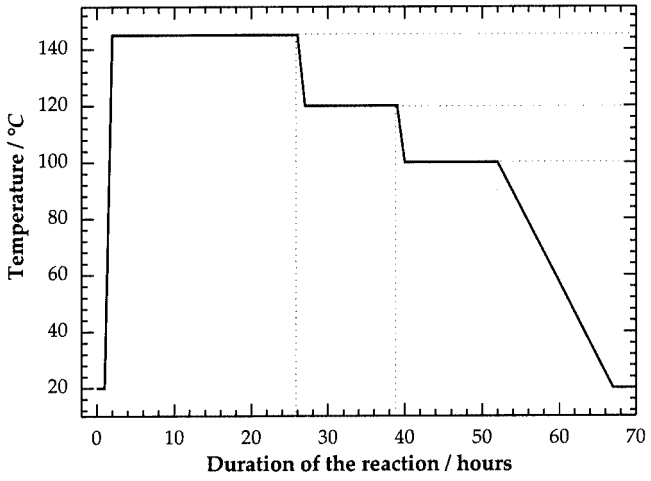

Scheme 1

Characterization: A suitable single crystal of CUmof-1 was mounted on a glass fibre, directly from the autoclave solution, using perfluoropolyether oil.[51] Data were collected on a Nonius Kappa CCD diffractometer with Mo-K_α graphite-monochromated radiation (λ = 0.7107 Å). The crystals were very thin needles and diffracted weakly: data were collected only to θ = 22.5° (equivalent to 0.93 Å resolution) and weak data at high angle contributes to a relatively large R_{int} value of 0.238). The structure was solved by direct methods and refined by full-matrix least-squares on F^2 with anisotropic displacement parameters for all non-hydrogen atoms,[52,53] with multi-scan absorption corrections also being applied.[54] All hydrogen atoms bound to carbon were placed geometrically, and refined using a riding model with an isotropic displacement parameter fixed at 1.2-times U_{eq} for the atom to which they are connected. Bond length restraints were not applied, except for H(1O) and H(2O), associated with the water molecule, for which the O−H distances were restrained to be 0.85(1) Å and the H−O−H angle was also restrained to be 1.39(2) Å. These restraints ensure a chemically reasonable geometry for the water molecule. Cavity dimensions were calculated by overlapping rigid spheres with van der Waals radii for each element: Cd^{2+} 2.20 Å; O 1.52 Å; N 1.55 Å; C 1.7 Å. Hydrogen atoms were omitted in all cases for simplicity. Information concerning crystallographic data collection and structure refinement for CUmof-1 is summarised in Table 1, while selected bond lengths and angles are presented in Table 2. CCDC-178338 contains the supplementary crystallographic data for this paper. These data can be obtained free of charge at www.ccdc.cam.ac.uk/conts/retrieving.html [or from the Cambridge Crystallographic Data Centre, 12, Union Road, Cambridge CB2 1EZ, UK; Fax: (internat.) +44-1223/336-033; E-mail: deposit@ccdc.cam.ac.uk].

The PXRD pattern was measured at ambient temperature on a STOE STADI-P high-resolution diffractometer with Ge(111)-monochromated Cu-K_α radiation (λ = 1.5406 Å) and a position-sensitive detector covering 6° 2θ angle (40 kV, 40 mA). Data were collected using the step counting method (step 1.0°, time 150 s) in the 2° ≤ 2θ ≤ 60° range. Theoretical PXRD calculations were performed using the STOE Win XPOW software package.[55]

Synthesis of CUmof-1: 1,2-Bis(4-pyridyl)ethane (BPE, 0.188 g, Aldrich), biphenyl-4,4′-dicarboxylic acid (H_2BPhDC, 0.244 g, Fluka) and triethylamine (TEA, 0.211 g, Avocado) were added to a solution of $Cd(NO_3)_2{\cdot}4H_2O$ (0.318 g, Aldrich) in distilled water (6.15 g) and the mixture was stirred thoroughly for 1 hour at ambient temperature. The suspension, with a composition of 1.00 H_2BPhDC:1.02 Cd^{2+}:1.01 BPE:2.07 TEA:339 H_2O, was autoclaved at 145 °C. A white crystalline product was obtained. Crystals suitable for single-crystal X-ray diffraction were separated manually and preserved in a portion of the autoclave aqueous solution. The powder was washed with 50 cm^3 distilled water and three times with 50 cm^3 absolute ethanol, and air-dried at 70 °C to give crystalline CUmof-1. This MOF proved to be air- and light-stable, as well as insoluble in distilled water and common organic solvents (ethanol, acetone, dichloromethane and toluene). The elemental composition found was: C 55.91%, H 3.85%, N 4.92%. The calculated composition was: C 56.30%, H 4.00%, N 5.05%. TGA (weight loss for an initial sample of 11.82 mg): 28−140 °C 2.3%; 330−380 °C 31.8% (DTG peak at 368 °C); 380−440 °C 41.6% (DTG peak at 435 °C). DSC data: three endothermic processes with peaks at 63, 371 and 433 °C. Selected FT-IR data (cm^{-1}): ν(O−H) 3664w and 3426 m,vb; ν(C−H) 3070w; overtones and combinations in substituted benzene rings, 1940w and 1815w; *p*-disubstituted benzene and pyridine rings ν(C=C) 1608vs, 1577vs, 1526vs, 1400vs,vb; ν(C−O) 1230m and 1175m; 1103w; 1071m; δ(=C−H) 1016m and 1006m; 963w; γ(O−H) 877w; *p*-substituted pyridine ring γ(C−H) 851s, 829s, 816s and 800m; *m*-substituted benzene ring ω(C−H) 773s; γ(C=O) 703m, 685m and 672m; pyridines δ(=C−H) 629w; *p*-disubstituted benzene ring δ and γ(=C−H) 547m, 528m; ρ[(C=O)−O] 493m; substituted benzenes γ(C−H) 420s. Selected FT-Raman data (cm^{-1}): ν(C−H) 3067 m; ν(C=C, pyridines and aromatic compounds) 1608vs; δ(O−H) 1415m; ν(C−O) 1295m and 1280m; 1141m; δ(=C−H) 1016w; γ(C−H) 861m and 846m; depolarized δ(C=C) 667w; 628w; 412w; 335w.

Acknowledgments

We are grateful to the Fundação Para a Ciência e Tecnologia (FCT), Portugal, for financial support for F. A. A. P. through the SFRH/BD/3024/2000 scholarship, and to the Cambridge Oppenheimer Fund for a Research Fellowship for Y. Z. K.

[1] B. F. Hoskins, R. Robson, *J. Am. Chem. Soc.* **1990**, *112*, 1546−1554.
[2] D. Braga, A. Angeloni, L. Maini, A. W. Gotz, F. Grepioni, *New J. Chem.* **1999**, *23*, 17−24.
[3] E. G. Bakalbassis, M. Korabik, A. Michailides, J. Mrozinski,

C. Raptopoulou, S. Skoulika, A. Terzis, D. Tsaousis, *J. Chem. Soc., Dalton Trans.* **2001**, 850−857.
[4] G. De Munno, F. Cipriani, D. Armentano, M. Julve, J. A. Real, *New J. Chem.* **2001**, *25*, 1031−1036.
[5] B. L. Fei, W. Y. Sun, T. Okamura, W. X. Tang, N. Ueyama, *New J. Chem.* **2001**, *25*, 210−212.
[6] Z. Y. Fu, X. T. Wu, J. C. Dai, L. M. Wu, C. P. Cui, S. M. Hu, *Chem. Commun.* **2001**, 1856−1857.
[7] M. Muthuraman, R. Masse, J. F. Nicoud, G. R. Desiraju, *Chem. Mat.* **2001**, *13*, 1473−1479.
[8] F. M. Tabellion, S. R. Seidel, A. M. Arif, P. J. Stang, *Angew. Chem. Int. Ed.* **2001**, *40*, 1529−1533.
[9] G. Yang, H. G. Zhu, B. H. Liang, X. M. Chen, *J. Chem. Soc., Dalton Trans.* **2001**, 580−585.
[10] T. Ezuhara, K. Endo, K. Matsuda, Y. Aoyama, *New J. Chem.* **2000**, *24*, 609−613.
[11] C. J. Kepert, T. J. Prior, M. J. Rosseinsky, *J. Am. Chem. Soc.* **2000**, *122*, 5158−5168.
[12] J. S. Seo, D. Whang, H. Lee, S. I. Jun, J. Oh, Y. J. Jeon, K. Kim, *Nature* **2000**, *404*, 982−986.
[13] C. B. Aakeroy, A. M. Beatty, D. S. Leinen, *Angew. Chem. Int. Ed.* **1999**, *38*, 1815−1819.
[14] B. L. Chen, K. F. Mok, S. C. Ng, M. G. B. Drew, *New J. Chem.* **1999**, *23*, 877−883.
[15] S. S. Y. Chui, S. M. F. Lo, J. P. H. Charmant, A. G. Orpen, I. D. Williams, *Science* **1999**, *283*, 1148−1150.
[16] C. R. Kagan, D. B. Mitzi, C. D. Dimitrakopoulos, *Science* **1999**, *286*, 945−947.
[17] C. J. Kepert, M. J. Rosseinsky, *Chem. Commun.* **1999**, 375−376.
[18] H. Li, M. Eddaoudi, M. O′Keeffe, O. M. Yaghi, *Nature* **1999**, *402*, 276−279.
[19] T. M. Reineke, M. Eddaoudi, M. Fehr, D. Kelley, O. M. Yaghi, *J. Am. Chem. Soc.* **1999**, *121*, 1651−1657.
[20] R. G. Xiong, J. L. Zuo, X. Z. You, H. K. Fun, S. S. S. Raj, *New J. Chem.* **1999**, *23*, 1051−1052.
[21] L. Carlucci, G. Ciani, P. Macchi, D. M. Proserpio, *Chem. Commun.* **1998**, 1837−1838.
[22] O. M. Yaghi, G. M. Li, H. L. Li, *Nature* **1995**, *378*, 703−706.
[23] M. Fujita, Y. J. Kwon, S. Washizu, K. Ogura, *J. Am. Chem. Soc.* **1994**, *116*, 1151−1152.
[24] M. J. Zaworotko, *Chem. Commun.* **2001**, 1−9.
[25] Y. B. Dong, M. D. Smith, R. C. Layland, H. C. zur Loye, *Chem. Mater.* **2000**, *12*, 1156−1161.
[26] P. J. Hagrman, D. Hagrman, J. Zubieta, *Angew. Chem. Int. Ed.* **1999**, *38*, 2639−2684.
[27] S. R. Batten, R. Robson, *Angew. Chem. Int. Ed.* **1998**, *37*, 1461−1494.
[28] S. Kitagawa, M. Kondo, *Bull. Chem. Soc. Jpn.* **1998**, *71*, 1739−1753.
[29] M. Fujita, M. Aoyagi, K. Ogura, *Bull. Chem. Soc. Jpn.* **1998**, *71*, 1799−1804.
[30] C. Janiak, *Angew. Chem. Int. Ed. Engl.* **1997**, *36*, 1431−1434.
[31] S. A. Bourne, J. J. Lu, B. Moulton, M. J. Zaworotko, *Chem. Commun.* **2001**, 861−862.
[32] M. Fujita, Y. J. Kwon, M. Miyazawa, K. Ogura, *J. Chem. Soc., Chem. Commun.* **1994**, 1977−1978.
[33] Q. M. Wang, G. C. Guo, T. C. W. Mak, *Chem. Commun.* **1999**, 1849−1850.
[34] T. L. Hennigar, D. C. MacQuarrie, P. Losier, R. D. Rogers, M. J. Zaworotko, *Angew. Chem. Int. Ed. Engl.* **1997**, *36*, 972−973.
[35] O. M. Yaghi, H. L. Li, T. L. Groy, *J. Am. Chem. Soc.* **1996**, *118*, 9096−9101.
[36] O. M. Yaghi, H. L. Li, C. Davis, D. Richardson, T. L. Groy, *Acc. Chem. Res.* **1998**, *31*, 474−484.
[37] B. L. Chen, M. Eddaoudi, T. M. Reineke, J. W. Kampf, M. O′Keeffe, O. M. Yaghi, *J. Am. Chem. Soc.* **2000**, *122*, 11559−11560.
[38] C. Oldham, in *Comprehensive Coordination Chemistry*, Vol. 2, First ed. (Ed.: G. Wilkinson), Pergamon Press, **1987**, pp. 435.
[39] J. Y. Lu, A. M. Babb, *Chem. Commun.* **2001**, 821−822.
[40] L. Carlucci, G. Ciani, D. M. Proserpio, S. Rizzato, *Chem. Commun.* **2000**, 1319−1320.
[41] D. Hagrman, R. P. Hammond, R. Haushalter, J. Zubieta, *Chem. Mater.* **1998**, *10*, 2091−2100.
[42] K. N. Power, T. L. Hennigar, M. J. Zaworotko, *Chem. Commun.* **1998**, 595−596.
[43] A. J. Blake, N. R. Champness, S. S. M. Chung, W. S. Li, M. Schroder, *Chem. Commun.* **1997**, 1005−1006.
[44] M. Eddaoudi, D. B. Moler, H. L. Li, B. L. Chen, T. M. Reineke, M. O′Keeffe, O. M. Yaghi, *Acc. Chem. Res.* **2001**, *34*, 319−330.
[45] J. C. MacDonald, P. C. Dorrestein, M. M. Pilley, M. M. Foote, J. L. Lundburg, R. W. Henning, A. J. Schultz, J. L. Manson, *J. Am. Chem. Soc.* **2000**, *122*, 11692−11702.
[46] F. A. Cotton, C. Lin, C. A. Murillo, *Acc. Chem. Res.* **2001**, *34*, 759−771.
[47] L. Pan, N. Ching, X. Y. Huang, J. Li, *Chem. Commun.* **2001**, 1064−1065.
[48] A. F. Wells, *Structural Inorganic Chemistry*, Fourth ed., Oxford University Press, Oxford, **1975**.
[49] J. Tao, M. L. Tong, X. M. Chen, *J. Chem. Soc., Dalton Trans.* **2000**, 3669−3674.
[50] G. B. Deacon, R. J. Phillips, *Coord. Chem. Rev.* **1980**, *33*, 227−250.
[51] T. Kottke, D. Stalke, *J. Appl. Crystallogr.* **1993**, *26*, 615−619.
[52] G. M. Sheldrick, SHELXL 97, *Program for Crystal Structure Refinement*, University of Göttingen **1997**.
[53] G. M. Sheldrick, SHELXS 97, *Program for Crystal Structure Solution*, University of Göttingen **1997**.
[54] R. H. Blessing, *Acta Crystallogr., Sect. A* **1995**, *51*, 33.
[55] STOE, Cie GmbH, *Win XPOW THEO* Version 1.15 **1999**.

Received May 23, 2002
[I02268]

Electrochemical and Spectroelectrochemical Investigations of "Figure-Eight" Octapyrrolic Macrocycles, Free Bases, and Their Mononuclear, Homo- and Heterodinuclear Complexes with Divalent Transition Metals

Jordi Bley-Escrich,[a] Jean-Paul Gisselbrecht,[a] Emanuel Vogel,[b] and Maurice Gross*[a]

Keywords: Macrocyclic ligands / Octaphyrins / Transition metal complexes / Electrochemistry

This work reports on electrochemical investigations of "figure-eight"-shaped cyclooctapyrrolic macrocycles (octaphyrins) **1**–**3** and of some of their mono- and dinuclear transition metal complexes. The octaphyrins **1**–**3** differ mainly in the size of the main conjugation pathway, which involves either $4n$ π-electrons for **1** and **3**, or $(4n + 2)$ π-electrons for **2**. All species studied undergo six redox steps, namely two reductions and four oxidations. The two reductions and the first three oxidations are reversible one-electron transfers. The fourth oxidation is either reversible, or irreversible due to a subsequent chemical reaction. Depending on the complex studied, the third and fourth oxidations occur either at similar potentials, so that a global two-electron step is observed, or at distinct potentials, leading to two well-separated signals. Spectroelectrochemical investigations demonstrate that all redox processes are ligand centred. The reported results clearly indicate that the redox potential changes in these new octapyrrolic macrocycles depend much more on structural contributions, due to their figure-eight topography, than on characteristics such as ionic radius or electronegativity of the coordinated metal. The HOMO-LUMO gap in the series of octaphyrins studied is rather small (about 1 eV), and is not only related to the macrocyclic ring size, but also depends on whether the main conjugation pathway involves $4n$ or $(4n + 2)$ π-electrons.

(© Wiley-VCH Verlag GmbH, 69451 Weinheim, Germany, 2002)

Introduction

Expanded porphyrinoids with five or more conjugated pyrrolic rings have attracted interest since the discovery of the pentapyrrolic sapphyrin by Woodward, Dolphin, and Johnson.[1−3] Subsequent to this early work, various cyclopolypyrroles, namely penta- and hexapyrrolic ring systems[4−8] have been prepared and identified. More recently, a new cyclodecapyrrole called turcasarin,[9] and a family of cyclooctapyrroles, named octaphyrins,[10−12] belonging to figure-eight-shaped cyclopolypyrroles have been obtained. Giant cycles containing up to 16 pyrrole units have also been synthesised and identified very recently.[13−15]

Despite this very large set of polypyrrolic macrocycles now available, the complexing abilities of these new expanded macrocycles have only been investigated for a few compounds,[16] and electrochemical studies remain scarce.[17]

The cyclooctapyrroles (COP) presently known,[10−12] i.e., **1** {[32]COP(1.0.1.0.1.0.1.0)},[18] **2** {[34]COP(1.1.1.0.1.1.1.0)},[18] and **3** {[36]COP(2.1.0.1.2.1.0.1)}[18] (all three series studied in this publication), are employed as hexadecaethyl derivatives (Figure 1) for reasons of solubility. A characteristic feature of these cyclooctapyrroles is that they are folded in such a way so as to adopt figure-eight conformations with approximate D_2 symmetry, both in solution and in the solid state as confirmed by NMR spectroscopic studies and X-ray crystallographic analysis.[19−20] NMR spectroscopic studies of these cyclooctaphyrin free bases confirmed their nonaromatic character, whether they possess $(4n + 2)$ [**2** (34)] or $4n$ [**1** (32) and **3** (36)] π-electrons in their main conjugation pathway. The figure-eight-shaped structure of cyclooctaphyrins provides two equivalent porphyrin-sized cavities for metal complexation, enabling the generation of mononuclear, homodinuclear and heterodinuclear complexes. However, depending on the ring size, all three types of complexes could be prepared with **1** and **2**. On the other hand, only homodinuclear complexes could be obtained and identified with ligand **3**.[21]

Until now, electrochemical investigations of macrocyclic polypyrroles containing more than four pyrrole units remain rather scarce,[17] and studies on octapyrrolic macrocycles are restricted to preliminary studies on the free bases and some complexes of **1** and **3** in CH_2Cl_2.[22] In the present paper the electrochemical behaviour of a new series of cyclooctaphyrins, namely **2**, has been investigated in dry benzonitrile. Its behaviour will be compared with previously

[a] Laboratoire d'Electrochimie et de Chimie Physique du Corps Solide, UMR 7512 − CNRS Université Louis Pasteur, 4, rue Blaise Pascal, 67000 Strasbourg, France
Fax: (internat.) + 33-3/90241431
E-mail: gross@chimie.u-strasbg.fr
[b] Institut für Organische Chemie, Universität zu Köln, Greinstrasse 4, 50939 Köln, Germany

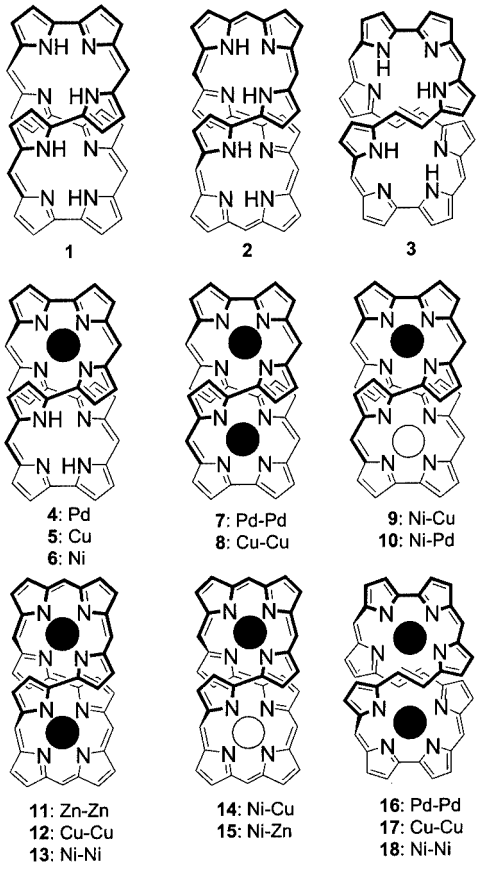

Figure 1. Free bases and complexes, studied in the three hexadecaethylcyclooctaphyrin series; the ethyl groups are omitted for clarity

published data[22] involving **1** and **3**. However, to obtain a better insight into the redox behaviour of the three series of COP and to allow consistent comparison, the previously studied COP (**1**, **3**−**10**, **16**−**18**) have been reinvestigated here in dry benzonitrile by hydrodynamic voltammetry, by cyclic voltammetry, and by UV/Vis spectroelectrochemistry.

Results and Discussion

Results

In order to obtain useful information on the redox properties of the cyclooctaphyrins **1**, **2**, and **3** and their complexes (Figure 1), studies were carried out by cyclic voltammetry (CV) and hydrodynamic voltammetry on a platinum RDE in dry PhCN + 0.1 M Bu_4NPF_6 solutions at 25 °C on the three series of cyclooctaphyrins.

Hydrodynamic voltammetry of **1** and its complexes **4**−**10** show similar redox behaviour. Indeed, all species exhibit, as illustrated for the Pd−Pd complex **7** (Figure 2), two reduction waves of equal amplitude, as well as three oxidation waves. The first two oxidation waves have the same limiting current as the reduction waves, whereas the current for the third oxidation is twice that of the previous steps. For the complexes **4**−**10**, this later wave is broader, depending on the complex studied. Wave analysis, using Tomeš criteria,[23] give slopes $|E_{3/4} - E_{1/4}|$ close to 56.4 mV for the two reductions and the first two oxidations, whereas the third oxidations have slopes ranging from 60 to 170 mV, depending on the coordinated metal ion(s). For the two reductions and the first two oxidations, the observed slopes are consistent with reversible one-electron exchanges, whereas the slope for the third oxidation, involving two electrons will be studied by CV to obtain more information on its electron transfer mechanism. The potentials obtained by hydrodynamic voltammetry are in agreement with those observed by CV, and they are reported in Table 1.

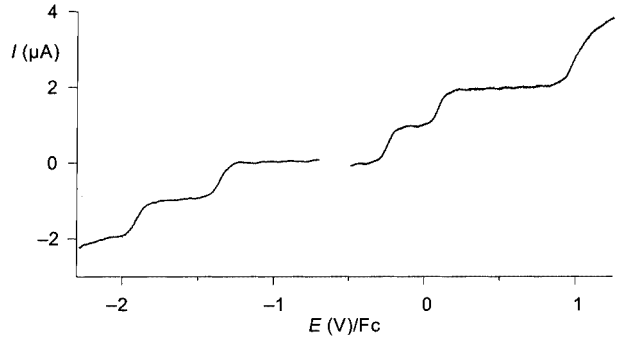

Figure 2. Hydrodynamic voltammetry of **7** in PhCN + 0.1 M Bu_4NPF_6, on Pt working electrode; scan rate: 0.01 V/s (potentials vs. Fc)

The CVs for **1** and its complexes are given in Figure 3 and their redox potentials are reported in Table 1. For the free base, as well as for the complexes studied, two one-electron reversible reductions are observed. For the oxidations, the first two electron transfers are also one-electron reversible oxidations, as confirmed by the monitoring of their peak current (I_p) and peak potentials (E_p) with scan rate. The corresponding peak potentials are constant with scan rates of up to 5 V/s, the peak current ratio I_{pa}/I_{pc} is close to unity at any v, the peak potential difference $\Delta E = E_{pc} - E_{pa}$ is approximately 60 mV up to 5 V/s, and a linear correlation intercepting the origin is observed by plotting I_p vs. $v^{1/2}$.

Further oxidation steps deserve specific comments. The free base **1** and the mononuclear complexes **4**−**6** exhibit a third oxidation step, which is irreversible at scan rates lower than 1 V/s. At scan rates higher than 1 V/s, this third step becomes reversible for complexes **4**−**6**, and reversible only at scan rates higher than 5 V/s for **1**. Analysis of the peak characteristics show that the plot I_{pa} vs. $v^{1/2}$ is a straight line intercepting the origin for scan rates lower than 0.2 V/s. Its slope is twice that of the first and second oxidation, consistent with a two-electron transfer, as indicated from the results obtained in hydrodynamic voltammetry. At scan rates higher than 0.2 V/s, the peak current evolution was slightly curved to the x axis. In addition, the peak current ratio I_{pa}/I_{pc} increases with scan rate to unity. The peak shape ($E_p - E_{p/2}$) is specific to the species studied (45 mV for **1**, 100 mV for **4** and 60 mV for **5** at v = 0.1 V/s) and increases with scan rate. Although no clear conclusion

Table 1. Redox potentials obtained by cyclic voltammetry, in PhCN + 0.1 M Bu_4NPF_6, on Pt working electrode; scan rate: 0.1 V/s; $E = (E_{pc} + E_{pa})/2$ (potentials vs. Fc)

COP(1.0.1.0.1.01.0)	$Ered_2$ [V]	$Ered_1$ [V]	Eox_1 [V]	Eox_2 [V]	Eox_3 [V]	Eox_4 [V]	$Eox_1 - Ered_1$ [V]
H_4COP (**1**)	−2.02	−1.64	−0.18	0.08	1.01[a]	1.06[a]	1.46
PdH_2COP (**4**)	−1.91	−1.42	−0.20	0.16	0.99[b]	1.07[b]	1.22
CuH_2COP (**5**)	−2.06	−1.30	−0.26	0.10	1.05[b]	1.09[b]	1.04
NiH_2COP (**6**)	−1.96	−1.44	−0.27	0.10	0.95	1.08	1.17
Pd_2COP (**7**)	−1.93	−1.38	−0.27	0.07	0.87	0.91	1.11
Cu_2COP (**8**)	−2.07	−1.29	−0.39	0.00	0.97	1.01	0.90
NiCuCOP (**9**)	−2.00	−1.26	−0.33	0.04	0.91	0.95	0.93
NiPdCOP (**10**)	−1.90	−1.34	−0.26	−0.02	0.95	0.99	1.08
COP(1.1.1.0.1.1.1.0)	$Ered_2$ [V]	$Ered_1$ [V]	Eox_1 [V]	Eox_2 [V]	Eox_3 [V]	Eox_4 [V]	$Eox_1 - Ered_1$ [V]
H_4COP (**2**)	−1.88	−1.40	−0.30	0.13	0.83	1.21	1.10
Zn_2COP (**11**)	−1.89	−1.38	−0.35	0.09	0.78	1.01	1.03
Cu_2COP (**12**)	−1.92	−1.37	−0.36	0.13	0.80	1.03	1.01
Ni_2COP (**13**)	−1.87	−1.35	−0.37	0.11	0.72	0.76	0.98
NiCuCOP (**14**)	−1.89	−1.36	−0.36	0.12	0.76	0.80	1.00
NiZnCOP (**15**)	−1.88	−1.37	−0.35	0.11	0.72	0.76	1.02
COP(2.1.0.1.2.1.0.1)	$Ered_2$ [V]	$Ered_1$ [V]	Eox_1 [V]	Eox_2 [V]	Eox_3 [V]	Eox_4 [V]	$Eox_1 - Ered_1$ [V]
H_4COP (**3**)	−1.68	−1.37	−0.15	0.08	0.89[c]	0.93[c]	1.22
Pd_2COP (**16**)	−1.58	−1.18	−0.25	0.09	0.78	0.82	0.93
Cu_2COP (**17**)	−1.69	−1.18	−0.38	−0.08	0.69	0.73	0.80
Ni_2COP (**18**)	−1.64	−1.22	−0.32	0.08	0.55	0.59	0.90

[a] Reversible above scan rate 5 V/s. [b] Reversible above scan rate 1 V/s. [c] Reversible above scan rate 0.5 V/s.

could be drawn from these data from known criteria,[24] these results are fully consistent with a third oxidation obeying an $E_{rev}E_{rev}C_{irr}$ mechanism. Such a mechanism is indeed observed for complex **6** (belonging to the same series of species studied), with distinct potentials for both steps. Actually, the NiH_2 complex **6** undergoes distinct third and fourth one-electron oxidations. Reversing the scan after the third oxidation confirms the reversibility of the third oxidation, whereas the fourth oxidation remains irreversible at scan rates lower than 1 V/s. Digital simulation using DIGISIM software[25] confirms the proposed mechanism, as illustrated for **1** in Figure 4, and allows us to access to the corresponding potentials. The final species generated could not be identified. However, the species generated is electroactive and could be identified by its reduction around +0.7 V/Fc on the reverse scan.

The complexes **7**−**10** exhibit a two-electron, reversible third oxidation at all scan rates. The redox potentials are presented in Table 1. For this third step, wave analysis gives slopes close to 60 mV in hydrodynamic voltammetry, and the peak potential difference $\Delta E_p = E_{pa} - E_{pc}$ is close to 60 mV up to 1 V/s. These characteristics are in agreement with two overlapping reversible one-electron transfers, whose redox potentials are separated by 35.6 mV, as predicted by Savéant[26] for hydrodynamic voltammetry and Shain[27] for CV. The latter transfers occur at two independent redox centres whose potentials are given in Table 1.

For **2** and its homo- and heterodinuclear complexes **11**−**15**, the redox behaviour is similar to the results reported above. All these species undergo two one-electron reversible reductions. Oxidation of the free base **2** gives four well-separated one-electron reversible steps, whereas for complexes **11** and **12** the fourth oxidation is irreversible as shown by CV (Figure 5). Oxidation of **13**, **14** and **15** occurs in three steps, the first two are one-electron reversible oxidations, and the third step is a reversible two-electron step. Analysis of the peak characteristics indicate that the third oxidation involves two reversible overlapping one-electron steps whose potentials are reported in Table 1.

Ligand **3** and its homodinuclear complexes **16**−**18** all have similar redox behaviour, namely two one-electron reduction steps, as well as three oxidations as shown in Figure 6. The first two oxidations are reversible one-electron transfers, whereas the third oxidation has the characteristics of two overlapping one-electron reversible transfers. Indeed, wave analysis of the third oxidation step gives a slope close to 60 mV by hydrodynamic voltammetry, whereas the peak potential difference in CV, $E_{pc} - E_{pa}$, is approximately 60 mV at scan rates up to 1 V/s. As two electrons are involved in the third step, these characteristics are in agreement with two one-electron transfers separated by 35.6 mV,[26,27] which occur at two independent redox centres. In order to identify the electron-transfer sites, spectroelectrochemical studies have also been carried out.

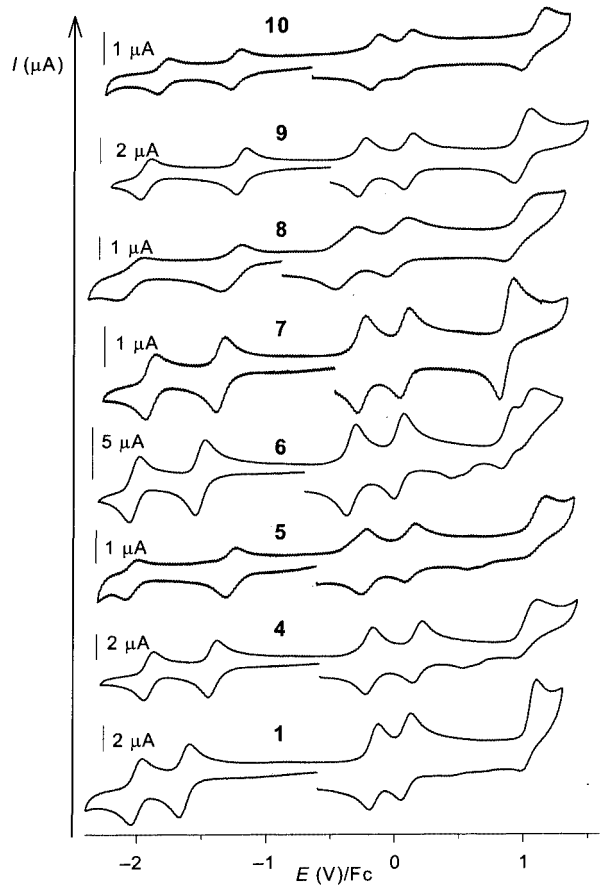

Figure 3. Cyclic voltammetry of **1** and **4**−**10** in PhCN + 0.1 M Bu_4NPF_6, on Pt working electrode; potential vs. Fc; scan rate: 1 V/s for **1** and 0.2 V/s for **4**−**10**

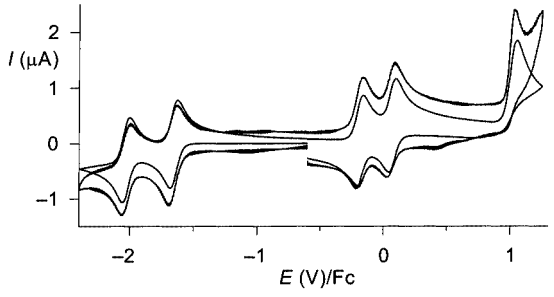

Figure 4. Cyclic voltammetry of **1** (solid line) in PhCN + 0.1 M Bu_4NPF_6, on Pt working electrode (scan rate: 0.1 V/s) and simulation using the software DIGISIM[25] (dashed line) for an oxidation mechanism involving four subsequent one electron oxidations at distinct potentials (E_1−E_4), the fourth step is followed by an irreversible chemical reaction (C_{irr}); the global reaction scheme may be the represented as $E_1E_2E_3E_4C_{irr}$; parameters used for oxidation: $E_1 = -0.18$ V ($k_s = 10^4$ cm/s); $E_2 = +0.08$ V ($k_s = 10^4$ cm/s); $E_3 = +1.01$ V ($k_s = 0.01$ cm/s); $E_4 = +1.06$ V ($k_s = 0.01$ cm/s) and for the chemical reaction: $Ox_4 \rightarrow X$, the equilibrium constant was $K_{eq} = (k_f/k_b) = 1000$; parameters used for reduction: $E_1' = -1.65$ V ($k_s = 10^4$ cm/s); $E_2' = -2.02$ V ($k_s = 10^4$ cm/s) (potentials vs. Fc)

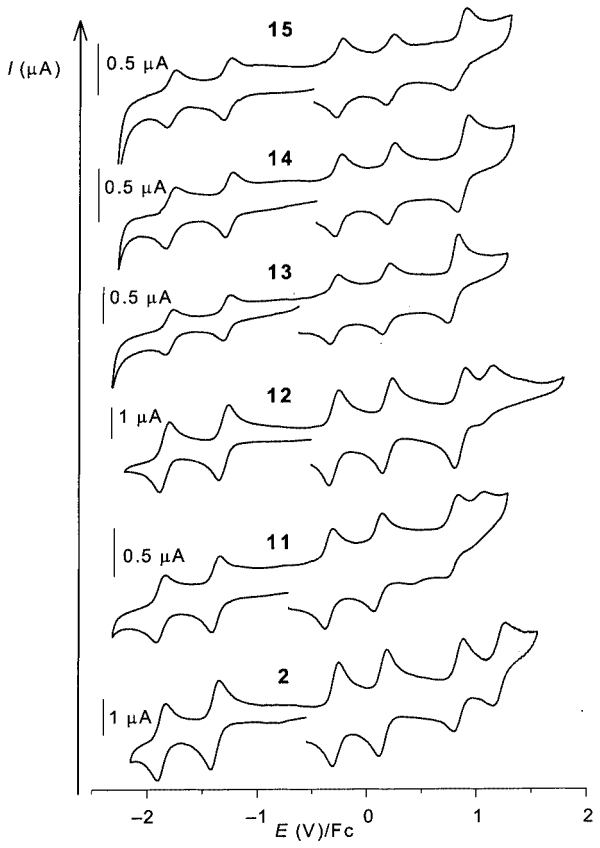

Figure 5. Cyclic voltammetry of **2** and **11**−**15** in PhCN + 0.1 M Bu_4NPF_6, on Pt working electrode; scan rate: 0.05 V/s (potentials vs. Fc)

Spectroelectrochemistry

Spectroelectrochemistry was carried out on each compound. The spectra showing the two reduction steps and the four oxidations exhibit, in general, well-defined isosbestic points. During the two reductions and the first two oxidations, the species generated exhibit specific absorbance bands. The initial spectrum could be recovered quantitatively by stepwise electrochemical restoration of the initial cyclooctaphyrin. This indicates that the two electroreduced and the two electrooxidised species are chemically stable on the time scale of the spectroelectrochemical experiments, i.e. about 30 min, a good indication of the high stability of the electrogenerated species under the experimental conditions.

In general, the third and fourth oxidations do not revert to the initial spectrum after spectroelectrochemical measurements, due to the chemical reaction coupled to the fourth oxidation step, hence leading to global irreversibility. When the third and fourth oxidations occur at quite distinct potentials (i.e. for the Zn_2 and Cu_2 complexes **11** and **12**), allowing for the trioxidised and the tetraoxidised species to be obtained separately, the trioxidised species quantitatively reverts to the initial spectrum by stepwise electrochemical restoration of the initial species.

The spectral changes during electrolysis are similar for **1** and its complexes **4**−**10**, as well as for **3** and its complexes **16**−**18**. Therefore, the behaviour of one representative compound, Pd_2 complex **16**, will be described for these two series (**a**, **b** in Figure 7). The neutral species presents a main absorbance band at 660 nm, and no bands are detected

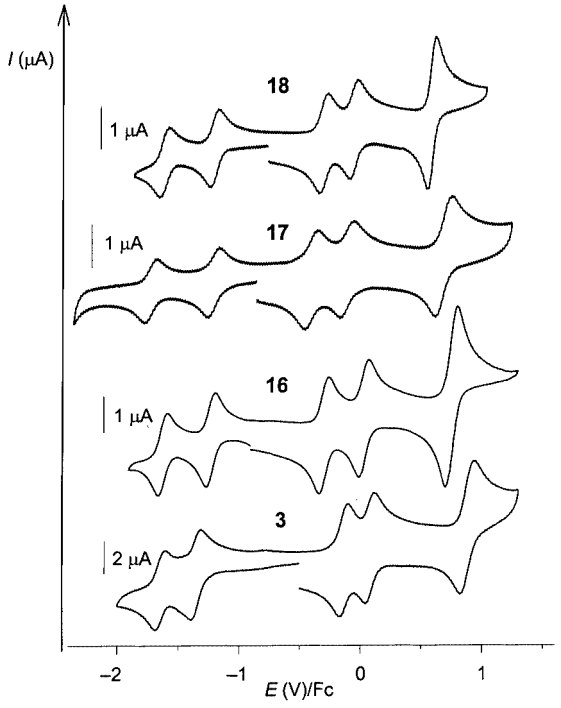

Figure 6. Cyclic voltammetry of **3** and **16**−**18** in PhCN + 0.1 M Bu_4NPF_6, on Pt working electrode; scan rate: 1 V/s for **3** and 0.2 V/s for **16**−**18** (potentials vs. Fc)

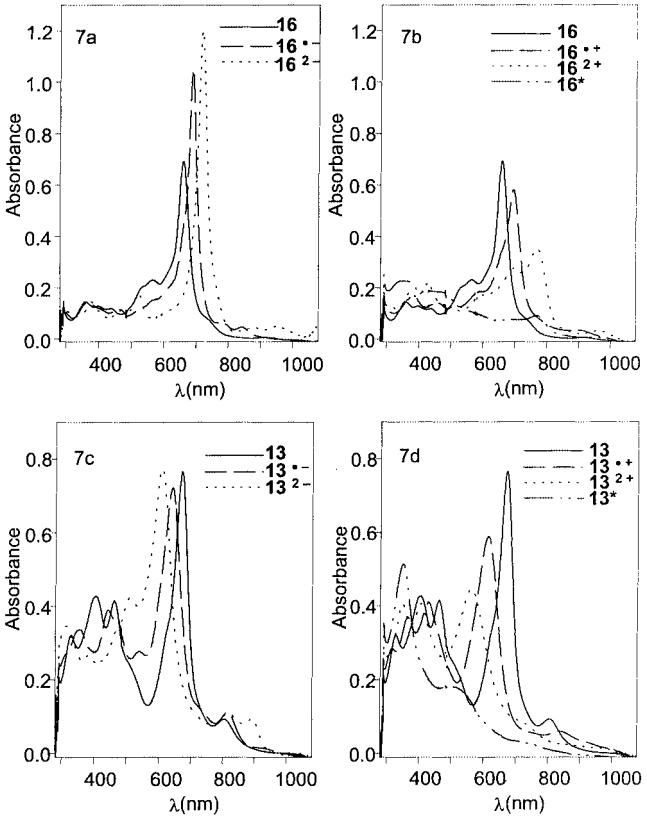

Figure 7. Spectroelectrochemistry of COP **16** and **13**, in PhCN + 0.1 M Bu_4NPF_6; reductions (see **a**) and oxidations (see **b**) of **16**; reductions (see **c**) and oxidations (see **d**) of **13**; *: spectrum corresponding to the species resulting from the irreversible chemical reaction following the fourth oxidation

from 800 to 1100 nm. During electrolysis on the plateau potential corresponding to the first reduction, the main band shifts to the red (691 nm) and its intensity increases by 75%, while some small bands appear between 800 and 900 nm. The main band shifts to a lower energy (720 nm) and its intensity increases again by 20%, after further electrolysis at the potential of the second reduction. Small bands appear between 900 and 1000 nm and an absorbance band is detected at 1078 nm. Spectra of the neutral, mono- and di-reduced species are presented in Figure 7 (see **a**). For the oxidation, the behaviour is quite similar for the first and second steps: the main absorbance band undergoes a red shift during the first oxidation electrolysis (696 nm), while its intensity decreases relative to the intensity of the neutral compound. The electrolysis at the second oxidation potential leads to a spectrum in which the main absorbance band also undergoes a red shift (771 nm) and is less intense.

During the third oxidation step, the intensity of all bands beyond 550 nm decreases considerably, or the bands completely disappear. This step is not reversible on the time scale of spectroelectrochemistry. Spectra characterising the species generated during oxidative electrolysis are presented in Figure 7 (see **b**).

The spectroelectrochemical behaviour of **2** and its complexes **11**−**15** is similar to the results presented above. However, a blue shift of the main absorbance band is observed during reduction, as well as during oxidation, as illustrated in the case of complex **13** (see **c**, **d** in Figure 7). The most intense main absorbance band is observed in the neutral compound spectrum, and not for the di-reduced species as observed previously with **1**, **3**, and their respective complexes.

These redox and spectral characteristics unambiguously indicate that the metal complexes of the cyclooctaphyrins studied undergo redox processes very similar to those of the free bases. Comparison of these reduction and oxidation potentials of the free bases with those of their metal complexes, as well as the spectral modifications associated with electron transfer in each redox step, lead to the reasonable conclusion that the electron transfer processes occur on the cyclooctapyrrolic ligand in the free bases and also in the complexes studied.

Discussion

The present electrochemical investigations clearly demonstrate that all the free bases and complexes studied above undergo six one-electron transfers on the conjugated cyclooctapyrrolic ring, namely two well-separated reversible one-electron reduction and four oxidation steps. The first three oxidations are reversible one-electron steps, whereas the fourth oxidation is either reversible, in most cases, or is irreversible in the species **1**, **4**, **5**, **6**, **11**, and **12**. For almost all the species studied, the last two oxidations occur at fairly close potentials ($Eox_4 - Eox_3 = 35.6$ mV), giving, macroscopically, a unique two-electron transfer, except in **2**, **6**,

11, **12** where the third and fourth oxidation potentials are separated by more than 80 mV. The third oxidation step observed, involving two-electron transfers separated by 35.6 mV and corresponding to oxidations at almost independent redox centres, is not well understood for COP. It could either result from non-interacting redox centres in the ligand, or from geometric changes occurring after the third electron exchange, which raises the energy level of the HOMO, making the removal of the fourth electron easier.[28] Theoretical approaches should be undertaken in order to obtain a better insight into these new families of compounds. Nevertheless, it should be stressed that unlike other polypyrrolic macrocycles, such as porphyrins, the COP ligands studied here are not planar[19,20] and do not possess an aromatic π-electron system, although they are fully conjugated. Therefore, it is possible that the removal of two electrons from the same HOMO orbital, occurring at two distant sites in the ligand, avoiding any coulombic repulsion, occurs in a unique step. However, until further information is made available, conformational changes triggered by the third oxidation thus allowing for the removal of the fourth electron at the same potential may not be ruled out, since geometric and steric factors contribute to the electrochemical behaviour, as pointed out hereafter.

Comparison of the redox potentials lead to interesting observations. Disregarding the species involving **3**, for which the number of complexes studied is too small (free base **3** and complexes **16**−**18**) to allow significant comparisons, it may be observed from Table 1 that **2** and its complexes **11**−**15**, possessing ($4n$ + 2) π-electrons in the main conjugation pathway, present very close mean reduction potentials values ($E\text{red}_1$ = −1.36±0.04 V, $E\text{red}_2$ = −1.89±0.03 V/Fc). In contrast, **1** and its complexes **4**−**10**, possessing $4n$ π-electrons, present a greater spread in their mean reduction potentials values ($E\text{red}_1$ = −1.35±0.09 V, $E\text{red}_2$ = −1.98±0.08 V/Fc). However, the difference between these two values remain similar for **2** and its complexes ($E\text{red}_1 - E\text{red}_2$ = +0.52±0.03 V) and for **1** and its complexes ($E\text{red}_1 - E\text{red}_2$ = +0.53±0.03 V), except for the complexes of **1** that contain copper (0.75 V). The similarity in these values is a good indication that all the reductions occur on the ligand, and they are also consistent with the possible explanation that the potential difference corresponds to the energy repulsion between two electrons filling the same orbital.[29]

The same conclusions are observed for the oxidation processes. For **2** and its complexes, the first two oxidation potentials are quite similar ($E\text{ox}_1$ = −0.37±0.02 V, $E\text{ox}_2$ = +0.10±0.03 V), whereas **1** and its complexes present more dispersed mean potential values ($E\text{ox}_1$ = −0.29±0.09 V, $E\text{ox}_2$ = +0.06±0.10 V). The potential difference between the first and second oxidations in each series are also quite similar. Indeed $E\text{ox}_1 - E\text{ox}_2$ = +0.46±0.03 V for **2** and its complexes, and $E\text{ox}_1 - E\text{ox}_2$ = +0.36±0.03 V for **1** and its complexes, except for **10** (0.24 V). As observed recently by Guyard et al.,[30] who studied the oxidation behaviour of several pyrrole oligomers, namely pyrrole to tetrapyrrole, the longer the chain, the easier the oxidations. The tetrapyrrole was easily oxidised (stepwise) at −0.16 and +0.12V/Fc like COP. The low potentials associated with the first two oxidations of COP agree with those results, assuming that COP behave like polypyrroles, independent of their cyclic or conjugation characteristics. It has to be mentioned that in the present set of cyclooctaphyrins studied, no correlation between the observed redox potentials and the electronegativity of the complexed metals could be established, in contrast with results observed with porphyrins or porphyrin isomers.[31−33] This suggests that geometric and steric factors contribute in good part to the electrochemical behaviour of COP.

In a given set of molecules, advantage may be taken from the existing correlation between the energy of the HOMO orbital and at least the first oxidation potential, and also between the LUMO and the first reduction potential. In such a case the difference $E\text{ox}_1 - E\text{red}_1$ may be taken as a good approximation of the energy gap between the HOMO and the LUMO orbitals.[32,34] The energy gaps for cyclooctaphyrins are relatively low (Table 1), compared with aromatic polypyrrolic macrocycles like porphyrins (2.25±0.15 V)[32] or porphycenes (1.85±0.15 V),[33,35−37] but they are similar to that of expanded porphycenes containing 26 π-electrons (1.01 V).[38] This low energy gap observed in cyclooctaphyrins is therefore related to the extension of the π-conjugation pathway. However, as observed in free bases **1**−**3**, the gap does not decrease on increasing the size of the conjugated macrocycle. Indeed, the highest value belongs to the smallest cyclooctaphyrin **1** (ΔE = 1.46 V), followed by the largest macrocycle **3** (ΔE = 1.22 V), and finally the smallest gap corresponds to the middle-sized cyclooctaphyrin **2** (ΔE = 1.10 V). These values are in agreement with the observed lowest energy bands observed in CH_2Cl_2, as shown in Figure 8. Indeed, **2** gives well-defined bands, the less energetic band being located at 1280 nm (0.97 eV). In contrast, both free-bases **1** and **3** only exhibit small amplitude absorbance bands at 865 (1.43 eV) and 932 nm (1.33 eV), respectively. However, this is parallel to the energy sequence of the most intense bands in the UV/Vis spectra of these macrocycles (λ = 534 nm for **1**, λ = 596 nm for **3**, and λ = 660 nm for **2**), illustrated in Figure 8.

For the species studied (Figure 9), **2**, **11**−**15** [($4n$ + 2) π-electrons] exhibit an almost constant gap within the series of the five complexes studied (ΔE =1.00±0.10 V). In complexes of **1** and **3** ($4n$ π-electrons), this difference decreases drastically from the free base to mononuclear complexes, and further to dinuclear complexes (Figure 9). For example, in mononuclear complexes **4**−**6** these values change drastically in the series, the highest belonging to **4** and the lowest to **5**. These variations could not successfully be correlated to any metal characteristics (electronegativity, ionization potential, ionic radius, ...), and therefore we are inclined to conclude that this evolution is basically related to geometric and steric parameters characterising the cations in the cavity of cyclooctaphyrins.

The results obtained from spectroelectrochemical studies on cyclooctaphyrins confirm that all redox steps occur on the ligand, and that no metal-centred transfer is observed

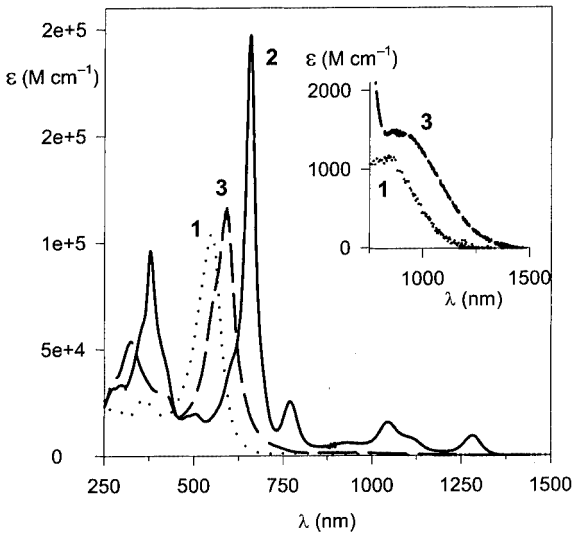

Figure 8. UV/Vis absorbance spectra of the three free bases **1**, **2**, and **3**, in CH_2Cl_2

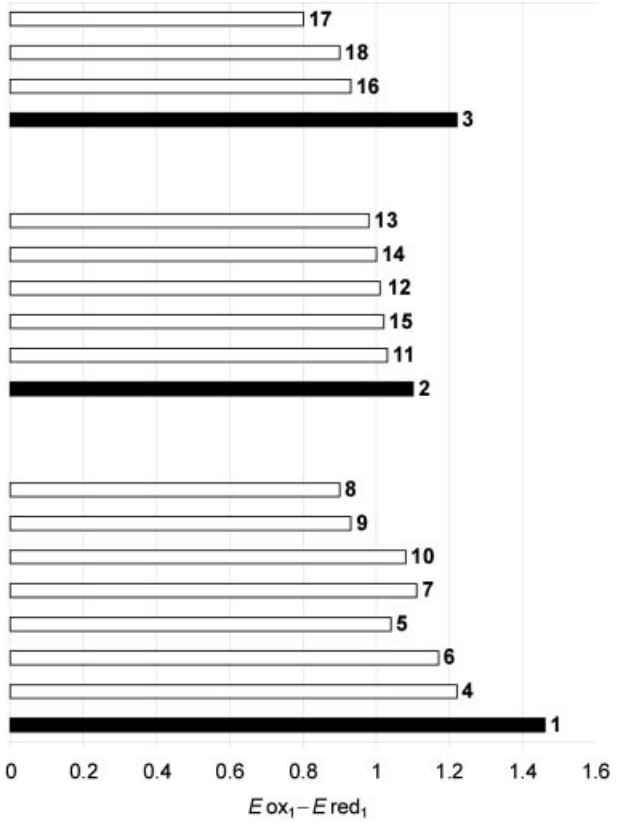

Figure 9. Potential difference $E\text{ox}_1 - E\text{red}_1$ [V], estimation of the HOMO−LUMO gap, for the three cyclooctaphyrin series

in the series studied. Some unexpected trends within the three series of compounds studied are observed. Indeed, although none of the species studied involves an aromatic ligand (even though they have 34 or 38 π-electrons [(4*n* + 2) π-electrons]),[11,39] the observed spectra obtained from spectroelectrochemistry are markedly different, depending on whether the ligands possess 4*n* or (4*n* + 2) π-electrons.

Such unexpected spectral changes are documented from comparison among the three COP families, more specifically when comparing the families with 4*n* π-electrons with the family with (4*n* + 2) π-electrons. Indeed, the spectra of the families with 4*n* π-electrons show a red shift during the two reductions and the first two oxidations, both corresponding to changes from 4*n* to (4*n* + 2) π-electrons. More explicitly, the species with (4*n* + 2) π-electrons exhibit a narrow and intense band whose wavelength depends on the family studied: this absorbance band is located close to 660 nm for the neutral species **2** and its complexes, and close to 725 nm for the di-reduced species **1**, **3**, and their complexes. The intensity and the geometry of this band is reminiscent of the characteristics of a Soret band, although the species are not aromatic.[11,39] On the contrary, the spectra of the family initially possessing (4*n* + 2) π-electrons shifts to the blue during the reductions and the oxidations, i.e. when changing from (4*n* + 2) to 4*n* π-electrons. Based on such related 4*n* or (4*n* + 2) π-electron numbers, the two evolutions are consistent. Another interesting observation was carried out for cyclooctaphyrins containing (4*n* + 2) π-electrons, including di-reduced **1** and **3**, as well as the neutral ligands **2**, and their respective metal complexes: all exhibit a particular similarity in their UV/Vis absorbance spectra. On the contrary, the absorbance band wavelength of the species having 4*n* π-electrons in their main conjugation pathway depends to a large extent on the chemical nature of the complexed metal(s).

The presence of this intense and sharp band in the species possessing (4*n* + 2) π-electrons is surprising for these macrocycles, in particular because of their twisted ("figure-eight") conformation. Still more surprising is the observation that the absorbance bands of the neutral ligand **2** and its complexes and those of the di-reduced species **3** and its complexes are perfectly located on the linear correlation (established previously by Franck et al. for aromatic planar expanded porphyrins)[40] between the wavelength of the Soret-like band and the number of conjugated π-electrons belonging to expanded macrocycles, named Babuška Porphyrins.

In the absence of any study or review available on macrocyclic polypyrroles analysing their spectral evolution with the size of the conjugated macrocycles, we plotted the wavelength of the most intense band of known polypyrrolic macrocycles, versus the number of π-electrons in the main conjugation pathway. The data collected, shown in Figure 10, involve species containing (4*n* + 2) π-electrons as well as 4*n* π electrons, their conformation being either planar or twisted "figure-eight". Two linear correlations are obtained (Figure 10) for species with (4*n* + 2) and with 4*n* π-electrons, respectively. These two correlations differ in their slopes. A greater slope is obtained for the correlation involving macrocycles with (4*n* + 2) π-electrons. Both correlations intercept at a common point, which has no physical meaning. Such correlations were never reported previously on polypyrrolic macrocycles. However, the same kind of

correlation has been established by Märkl et al.[41] for tetraoxaporphyrins, possessing (4*n* + 2) π-electrons, and also for tetraepoxyannulenes with 4*n* π-electrons. The two correlations were linear and differed mainly in their slopes. It has to be mentioned here that the two linear correlations with macrocycles involving (4*n* + 2) π-electrons containing either N or O heteroatoms overlap, whereas for macrocycles containing 4*n* π-electrons the two correlations possess similar slopes, but with different ordinates (the wavelength of the macrocycles with O heteroatoms is blue-shifted relative to the polypyrrolic macrocycles).[41]

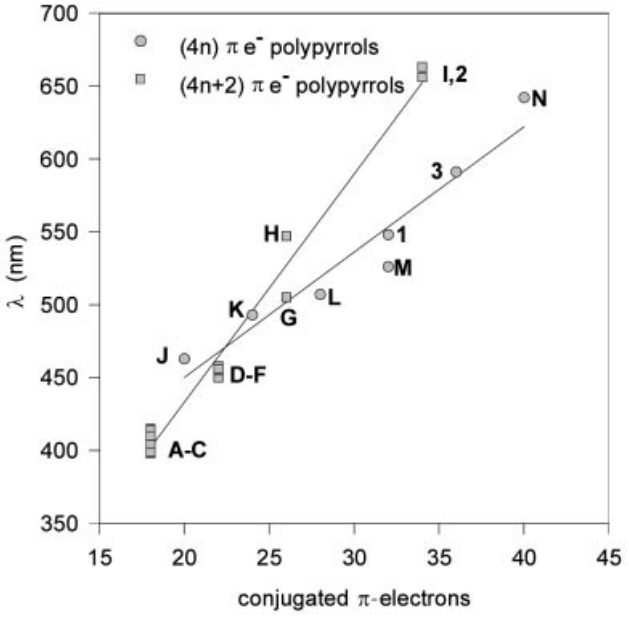

Figure 10. Correlation established for the main absorbance bands in UV/Vis spectra of polypyrrolic macrocycles versus the number of π-electrons involved in the main conjugation pathway; **A**: porphyrin;[40,42] **B**: corrphycene;[43,44] **C**: hemiporphycene;[45,46] **D**: sapphyrin;[3,42,47,48] **E**: pentaphyrin;[4] **F**: smaragdyrine;[49] **G**: rubyrine;[7] **H**: (3.3.3.3)porphyrin;[40] **I**: (5.5.5.5)porphyrin;[40] **J**: orangarin;[50] **K**: amethyrin;[50] **L**: heptaphyrin;[12] **M**: octaphyrin(1.0.0.0.1.0.0.0);[12] **N**: turcasarin;[9] **1**;[10] **2**;[11] **3**[11]

The observed correlations (Figure 10) with two different slopes rationalise the results of the spectroelectrochemical experiments. As reported above, the spectra from cyclooctaphyrins possessing 4*n* π-electrons undergo a red shift after two one-electron reductions, generating (4*n* + 2) π-electron species. Spectral evolutions for cyclooctaphyrins with (4*n* + 2) π-electrons undergo a blue shift under the same conditions, which is in agreement with the observed evolutions given in Figure 10, above the intercept.

The data reported above and correlations clearly indicate that the polypyrrolic macrocycles containing (4*n* + 2) π-electrons exhibit greater homogeneous characteristics. For instance, the redox potentials of **2** and its complexes **11**−**15** are identical, and the observed HOMO−LUMO gap is very similar for the series. Also their UV/Vis spectra give strong Soret-like bands at similar wavelengths. The homogeneity of such data for macrocycles containing (4*n* + 2) π-electrons most likely results from a stabilised structure, due to the presence of (4*n* + 2) π-electrons in cyclooctaphyrins. From the spectroelectrochemical studies, the dianion of **1**, **3**, and of their complexes also exhibit well-resolved sharp bands located at 725 nm.

Conclusion

The studied cyclooctaphyrins undergo six redox steps, two one-electron reversible reductions and four one-electron oxidations, the first three oxidations are one-electron reversible transfers. For some derivatives, the fourth oxidation is irreversible. The potential difference between the third and fourth oxidation is rather small in most of the species studied (close to 40 mV), resulting in a unique reversible two-electron exchange on the time scale of the experiments. The latter step, involving two overlapping electron transfers, involves two independent redox centres. Spectroelectrochemical studies confirm that all electron transfers are ligand-centred and that the species generated are stable on the time scale of the spectroelectrochemical measurements, namely for at least 30 min, except for the species generated by the fourth oxidation. This tetracation generated undergoes further chemical reaction(s) and renders the fourth oxidation irreversible on the spectroelectrochemical time scale.

The present study also demonstrates that cyclooctaphyrins with (4*n* + 2) π-electrons possess more homogeneous electrochemical and spectral characteristics, whereas cyclooctaphyrins with 4*n* π-electrons exhibit a greater spread in the redox potentials and UV/Vis absorbance bands. The spectra of the species with (4*n* + 2) π-electrons exhibit an intense and sharp absorbance band, clearly resulting from an intense conjugation in the ligand.

Further studies are under way, especially on cyclooctaphyrins containing electroactive metals that are, up to now, rather scarce. Also, more insight into these new classes of compounds will be provided by theoretical approaches.

Experimental Section

General: All of the presently studied cyclooctapyrroles were, for reasons of solubility, employed as hexadecaethyl derivatives. The synthesis of compound **1**, namely 2,3,6,7,11,12,15,16,20,21,24,25,29,30,33,34-hexadecaethylcyclooctapyrrol-(1.0.1.0.1.0.1.0), and for species **2**, namely 2,3,7,8,12,13,16,17,21,22,26,27,31,32,35,36-hexadecaethylcyclooctapyrrol-(1.1.1.0.1.1.1.0), and **3**, namely 2,3,6,7,11,12,17,18,22,23,26,27,31,32,37,38-hexadecaethylcyclooctapyrrol-(2.1.0.1.0.2.1.0.1), have been published previously.[10,11] The figure-eight conformation confers two coordination sites on these molecules, and it has been shown that **1** and **2** are able to coordinate diverse transition metal ions to afford complexes of all three types, namely mononuclear, homo- and hetero-dinuclear complexes according to classical procedures.[19,20] Ligand **3** gave only some homodinuclear complexes according to published procedures.[20,21] The electrochemical measurements were carried out in a glove box (less than 3 ppm of H_2O and less than 2 ppm of O_2) at room temperature (25±2 °C) in PhCN containing 0.1 M Bu_4NPF_6 in a classical three-electrode cell. The electrochemical cell was con-

nected to a computerised multipurpose electrochemical device (PAR 273) interfaced with a PC computer. The working electrode was a platinum (Pt) disc electrode (diameter: 2 mm) used either motionless for cyclic voltammetry (v = 20 mV/s to 5 V/s) or as a rotating disc electrode. The auxiliary electrode was a platinum wire, and the pseudo-reference electrode was also a platinum wire. All potentials are referred to the ferrocenenium/ferrocene (Fc^+/Fc) couple used as an internal standard. Benzonitrile (PhCN, Aldrich, 99%) was dried, before use, for 2 d with $CaCl_2$ (anhydrous, Fluka, 97%), and distilled from P_2O_5 (Prolabo) under reduced pressure and argon. The main fraction was collected under argon and transferred into the glove box. The supporting electrolyte, Bu_4NPF_6 (Fluka − electrochemical grade) was dried in an oven (65 °C) under vacuum for 2 d. Bu_4NPF_6 was solubilised in PhCN inside the glove box and the solution was then percolated over activated aluminia. The available potentials on a platinum working electrode ranged from −2.5 to +1.8 V/Fc. Spectroelectrochemical measurements were carried out in PhCN in a home-made quartz cell, having an optical pathway of 1 mm. The working electrode was a platinum grid (1000 mesh) placed in the optical pathway. The reference and the auxiliary electrodes were platinum wires in individual compartments, separated from the solution by cotton. The cell was filled in the glove box, and hermetically closed, it was then placed in a diode array spectrophotometer (Hewlett−Packard 8453) and spectra were recorded during electrolysis. UV/Vis spectra were recorded in CH_2Cl_2 (Merck, spectroscopy grade, used as received) with a Varian Cary 05E UV/Vis/NIR spectrophotometer, at room temperature.

Acknowledgments

We are much indebted to the Ministère de la Recherche for a research fellowship to J. B. E. and to CNRS for financial and human resources.

[1] R. B. Woodward, in: *Aromaticity: an International Symposium*, Sheffield, UK, **1966**; special publication no. 21, The Chemical Society, London, **1966**.
[2] V. J. Bauer, D. L. J. Clive, D. Dophin, J. B. Paine, F. L. Harris, M. M. King, J. Loder, S. W. C. Wang, R. B. Woodward, *J. Am. Chem. Soc.* **1983**, *105*, 6429.
[3] M. J. Broadhurst, R. J. Grigg, A. W. Johnson, *J. Chem. Soc., Perkin Trans. 1* **1972**, 2111−2116.
[4] H. Rexhausen, A. Gossauer, *J. Chem. Soc., Chem. Commun.* **1983**, 275.
[5] A. Gossauer, *Bull. Soc. Chim. Belg.* **1983**, *92*, 793.
[6] R. Charrière, T. A. Jenny, H. Rexhausen, A. Gossauer, *Heterocycles.* **1993**, *36*, 1561.
[7] J. L. Sessler, T. Morishima, V. Lynch, *Angew. Chem. Int. Ed. Engl.* **1991**, *30*, 977−980.
[8] J. L. Sessler, S. J. Weghorn, T. Morishima, M. Rosingana, V. Lynch, V. Lee, *J. Am. Chem. Soc.* **1992**, *114*, 8306.
[9] J. L. Sessler, S. J. Weghorn, V. Lynch, M. R. Johnson, *Angew. Chem. Int. Ed. Engl.* **1994**, *33*, 1509−1512.
[10] M. Bröring, J. Jendrny, L. Zander, H. Schmickler, J. Lex, Y. D. Wu, M. Nendel, J. Chen, D. A. Plattner, K. N. Houk, E. Vogel, *Angew. Chem. Int. Ed. Engl.* **1995**, *34*, 2515−2517.
[11] E. Vogel, M. Bröring, J. Fink, D. Rosen, H. Schmickler, J. Lex, K. W. K. Chan, Y. D. Wu, D. A. Plattner, M. Nendel, K. N. Houk, *Angew. Chem. Int. Ed. Engl.* **1995**, *34*, 2511−2514.
[12] J. L. Sessler, D. Seidel, V. Lynch, *J. Am. Chem. Soc.* **1999**, *121*, 11257−11258.
[13] J. Setsune, Y. Katakami, N. Iizuna, *J. Am. Chem. Soc.* **1999**, *121*, 8957−8958.
[14] J. A. Wytko, M. Michels, L. Zander, J. Lex, H. Schmickler, E. Vogel, *J. Org. Chem.* **2000**, *65*, 8709−8714.
[15] T. D. Lash, *Angew. Chem. Int. Ed.* **2000**, *39*, 1763−1767.
[16] A. Jasat, D. Dolphin, *Chem. Rev.* **1997**, *97*, 2267−2340
[17] M. Shionoya, H. Furuta, V. Lynch, A. Harriman, J. L. Sessler, *J. Am. Chem. Soc.* **1992**, *114*, 5714.
[18] M. Gosmann, B. Franck, *Angew. Chem. Int. Ed. Engl.* **1986**, *25*, 1100−1101.
[19] L. Zander, PhD dissertation, Universität zu Köln, **1998**.
[20] M. Michels, PhD dissertation, Universität zu Köln, **1999**.
[21] A. Werner, M. Michels, L. Zander, J. Lex, E. Vogel, *Angew. Chem. Int. Ed.* **1999**, *38*, 3650−3653.
[22] J. P. Gisselbrecht, J. Bley-Escrich, M. Gross, L. Zander, M. Michels, E. Vogel, *J. Electroanal. Chem.* **1999**, *469*, 170−175.
[23] J. Tomeš, *Collect. Czech. Chem. Commun.* **1937**, *9*, 150.
[24] R. S. Nicholson, I. Shain, *Anal. Chem.* **1964**, *36*, 706−723.
[25] M. Rudolph, D. P. Reddy, S. W. Feldberg, *Anal. Chem.* **1994**, *66*, 589A−600A.
[26] F. Ammar, J. M. Savéant, *J. Electroanal. Chem.* **1973**, *47*, 215−221.
[27] R. L. Myers, I. Shain, *Anal. Chem.* **1969**, *41*, 980.
[28] D. H. Evans, M. W. Lehmann, *Acta Chem. Scand.* **1999**, *53*, 765−774.
[29] K. M. Kadish, *Prog. Inorg. Chem.* **1986**, *34*, 443.
[30] L. Guyard, P. Audebert, P. Hapiot, *J. Chem. Phys.* **1998**, *95*, 1192−1195.
[31] J. P. Gisselbrecht, M. Gross, E. Vogel, J. L. Sessler, *Inorg. Chem.* **2000**, *39*, 2850−2854.
[32] J. H. Fuhrhop, K. M. Kadish, D. G. Davis, *J. Am. Chem. Soc.* **1973**, *95*, 5140−5147.
[33] C. Bernard, J. P. Gisselbrecht, M. Gross, E. Vogel, M. Lausmann, *Inorg. Chem.* **1994**, *33*, 2393−2401.
[34] K. M. Barkigia, M. W. Renner, L. R. Furenlid, C. J. Medforth, K. M. Smith, J. Fajer, *J. Am. Chem. Soc.* **1993**, *115*, 3627−3635.
[35] J. P. Gisselbrecht, M. Gross, M. Köcher, M. Lausmann, E. Vogel, *J. Am. Chem. Soc.* **1990**, *112*, 8618−8620.
[36] C. Bernard. PhD dissertation, Université Louis Pasteur, Strasbourg, **1994**.
[37] M. W. Renner, A. Forman, W. Wu, C. K. Chang, J. Fajer, *J. Am. Chem. Soc.* **1989**, *111*, 8618−8621.
[38] C. Bernard, J. P. Gisselbrecht, M. Gross, N. Jux, E. Vogel, *J. Electroanal. Chem.* **1995**, *381*, 159−166.
[39] E. Hückel, *Z. Phys.* **1931**, *72*, 310.
[40] B. Franck, A. Nonn, *Angew. Chem. Int. Ed. Engl.* **1995**, *34*, 1795−1811.
[41] G. Märkl, T. Knott, P. Kreitmeier, T. Burgemeister, F. Kastner, *Helv. Chim. Acta* **1998**, *81*, 1480−1505.
[42] R. A. Berger, E. LeGoff, *Tetrahedron Lett.* **1978**, *44*, 4225−4228.
[43] J. L. Sessler, E. A. Bruker, S. J. Weghorn, M. Kisters, M. Schäfer, J. Lex, E. Vogel, *Angew. Chem. Int. Ed. Engl.* **1994**, *33*, 2308−2312.
[44] D. M. Guldi, P. Neta, A. Heger, E. Vogel, J. L. Sessler, *J. Phys. Chem.* **1998**, *102*, 960−967.
[45] H. J. Callot, A. Roher, T. Tschamber, B. Metz, *New J. Chem.* **1995**, *19*, 155−159.
[46] E. Vogel, M. Bröring, S. J. Weghorn, P. Scholz, R. Deponte, J. Lex, H. Schmickler, K. Schaffner, S. E. Braslavsky, M. Müller, S. Pörting, C. J. Fowler, J. L. Sessler, *Angew. Chem. Int. Ed. Engl.* **1997**, *36*, 1651−1654.
[47] J. L. Sessler, M. Cyr, A. K. Burrell, *Tetrahedron.* **1992**, *48*, 9661−9672.
[48] J. L. Sessler, M. J. Cyr, A. K. Burrell, *Synlett* **1991**, 127−134.
[49] J. L. Sessler, S. J. Weghorn. *Expanded, Contracted & Isomeric Porphyrins*, Elsevier Science Ltd., Redwood Books, Wiltshire, **1997**.
[50] J. L. Sessler, S. J. Weghorn, Y. Hiseada, V. Lynch, *Chem. Eur. J.* **1995**, *1*, 56−67.

Received March 12, 2002
[I02128]

The First Aluminophosphonate Cluster Analogue of the 4=1 SBU of Zeolites: Structure and Multinuclear Solid-State NMR Study, Including ^{1}H NMR

Thierry Azaïs,[a] Laure Bonhomme-Coury,[b] Jacqueline Vaissermann,[c] Jocelyne Maquet,[a] and Christian Bonhomme*[a]

Keywords: Aluminium / Cluster compounds / NMR spectroscopy / Phosphorus / Solid state

The first Al–O–P analogue of the so-called 4=1 Secondary Building Unit (SBU) of zeolites is presented and characterized by single-crystal X ray diffraction (compound **1**). The 4=1 building unit structure is very rarely encountered in zeolites and microporous materials. Compound **1** was carefully studied by ^{31}P and ^{27}Al solid-state MAS NMR, resulting in the precise spectroscopic description of the phosphorus and aluminium sites. Unusual ^{27}Al quadrupolar parameters were measured. Moreover, we also present a high-resolution solid-state ^{1}H NMR study of **1** at 600 MHz and 33 kHz MAS; a remarkable improvement in resolution is observed, allowing definite assignments. The new opportunities offered by very high speed ^{1}H NMR at high field were further demonstrated with the study of a cubane-shaped Al–O–P cluster (compound **2**) and of phenylphosphonic acid.

(© Wiley-VCH Verlag GmbH, 69451 Weinheim, Germany, 2002)

Introduction

Description of zeolites and porous aluminophosphate derivatives in terms of Secondary Building Units (SBUs) is now well established.[1] The geometrical features of each structural type are adequately described by connecting these small portions of solids. The synthesis of clusters mimicking SBUs[2] remains a great chemical challenge for the following reasons: (i) the SBUs may be considered as intermediates in the synthesis of microporous materials, and so it follows that reactions between these well-defined entities could give rise to new framework structures, and (ii) these clusters are suitable for fine spectroscopic studies, including solid-state NMR. Interactions such as the chemical shift anisotropy (CSA) or the quadrupolar interaction (for nuclei with $I > 1/2$) can be related to structural features around nuclei. These parameters are therefore of prime importance for NMR studies of more complex derivatives, such as microporous compounds.

Among the 18 SBUs described in the literature,[1] six types have synthetic analogues. If we restrict the list to Al−O−P-containing entities, only five types of clusters mimicking the following SBUs have been reported: the S4R (or 4) ring,[3] the S6R (or 6) ring,[4] the cubane-shaped D4R (or 4−4),[3c,3h,5] the prismatic D6R (6−6),[3h,5c] and the 6≡1 SBU.[6] Here we present the first cluster involving Al−O−P bonds to mimic the so-called 4=1 SBU: [(μ$_2$-hydroxo)bis{μ$_3$-phenylphosphonato(2−)-*o*,*o*′,*o*"}-decaethanoltrialuminium](4+) chloride·water(1:1): $[Al_3(\mu_2\text{-}OH)(\mu_3\text{-}C_6H_5PO_3)_2(C_2H_5OH)_{10}]Cl_4\cdot H_2O$ (compound **1**). The 4=1 SBU is encountered only very rarely; only three zeolites can be considered as derivatives of 4=1 units: natrolite ($Na_2Al_2Si_3O_{10}\cdot 2H_2O$), thomsonite ($NaCa_2Al_5Si_5O_{20}\cdot 6H_2O$), and edingtonite ($Ba_{2.02}Al_{4.03}Si_{5.07}O_{20}\cdot 7.8H_2O$).[1,7−9] These compounds exclusively involve Al−O−Si bonds. No aluminophosphate (-onate, -inate) derivative containing the 4=1 SBU has ever been described. We conjecture that it might be possible to synthesize such a derivative, as compound **1** definitely shows that the 4=1 Al−O−P architecture is realistic. Only two clusters involving Ga−O−P bonds and resembling the 4=1 SBU have previously been reported in the literature.[10] Finally, we stress the fact that compound **1** is an analogue of the 4=1 SBU but differs in terms of Al coordination: Al atoms are sixfold coordinated in compound **1**, whereas the Al atoms in zeolites are fourfold coordinated.

Cluster analogues of SBUs have generally been characterized by IR and solution NMR (^{1}H, ^{13}C, ^{27}Al, ^{31}P) techniques, after dissolution. Surprisingly, these compounds have never been studied by solid-state NMR, whereas this technique has been extensively applied to the structural characterization of microporous aluminophosphates (such as $AlPO_4$-*n*). Very recently, we have fully characterized

[a] Université P. et M. Curie
4, Place Jussieu, 75252 Paris Cedex 05, France
Fax: (internat.) + 33-1/44274769
E-mail: bonhomme@ccr.jussieu.fr
[b] Laboratoire Céramiques et Matériaux Minéraux, E.S.P.C.I.
10, rue Vauquelin, 75231 Paris Cedex 05, France
[c] Laboratoire de Chimie Inorganique et Matériaux Moléculaires, Université P. et M. Curie,
4, Place Jussieu, 75252 Paris Cedex 05, France

S4R[11] and D4R[12] Al−O−P analogues by high-resolution ^{27}Al and ^{31}P MAS NMR spectroscopy. In this paper we present the structure of compound **1**, which was obtained as single crystals, and a multinuclear solid-state study, ^{31}P and ^{27}Al NMR for the inorganic core, and ^{13}C and ^{1}H NMR for the organic part. We have extracted precise data related to CSA (^{31}P) and quadrupolar interaction (^{27}Al) for compound **1** and analyze them in terms of the crystallographic structure. We also introduce (for the first time in the field of the study of inorganic clusters) ^{1}H MAS experiments at high field (600 MHz, 14 T) and at very high rotation frequency (up to 33 kHz). Spectacular improvements have been observed in terms of resolution, and these allow clear interpretation of spectra. These new opportunities in solid-state ^{1}H NMR are further illustrated by results obtained for the cubane-shaped Al−O−P cluster $[Al_4(HPO_4)_4(C_2H_5OH)_{12}]Cl_4{\cdot}4C_2H_5OH$ (compound **2**)[12] and phenylphosphonic acid [$C_6H_5PO(OH)_2$, precursor of **1**]. One original insight of this paper concerns the solid-state ^{1}H MAS experiments.

Results and Discussion

The structure of compound **1** is presented in Figure 1, a). It presents a very unusual geometry. Two Al atoms (Al2, Al3) and two P atoms (P1, P2), linked through oxo bonds, form a ring. On one side, this ring is capped with a third Al atom (O2Al1O3) between P atoms, and there is a hydroxo bridge (O5) on the other side between Al atoms [Figure 1, b)]. All Al atoms are sixfold coordinated, involving three (Al2, Al3) or four (Al1) ethanol ligands. Selected bond lengths are reported in Table 1. Average bond lengths involving oxo bridges are 1.84 Å around Al2 and Al3 atoms and 1.80 Å around Al1. Distances between O of ethanol ligands and Al atoms are much longer: 1.94 Å (Al2, Al3) and 1.93 Å (Al1). The mean bond length for the μ-OH bridge is about 1.85 Å. Distortions of polyhedra are discussed quantitatively below. P atoms are fourfold coordinated; in addition to three O atoms, each P atom is bonded to one phenyl ring (C11→C16 and C21→C26). The average P−O bond length is 1.52 Å, whereas the mean P−C bond length is about 1.79 Å. Cl^- counter-ions (Cl1→Cl4) are present in the structure. H···Cl hydrogen bonds are strongly suggested by O···Cl distances shorter than 3.35 Å.[13] All Cl atoms are involved in several hydrogen bonds, two for Cl1 (with O11 and O12) and for Cl4 (with O15 and O17), three for Cl2 (with O8, O14, and O16), and four for Cl3 (with O5, O9, O10, and O13). The inorganic core of **1** strongly mimics the geometry of the 4=1 SBU [Figure 1, c)]. In the case of compound **1**, however, a μ-OH bridge is observed between Al2 and Al3, although there is no such bridge in the 4=1 SBU. We note that the Ga−O cluster,[10] which also looks like the 4=1 SBU, has a marked difference with the SBU; a phosphonate group links two Al atoms, as does the μ-OH bridge in compound **1**.

Compound **1** was fully characterized by solid-state ^{31}P, ^{27}Al, and ^{13}C MAS NMR spectroscopy (Figure 2). The ^{31}P CP (cross polarization from ^{1}H) MAS spectrum of **1** exhibits two sharp lines located at δ = 1.7 and 2.8 ppm, in agreement with the crystallographic data. At 3 kHz, numerous spinning sidebands are observed, allowing the principal values of the chemical shift tensors δ_{ii} to be determined. All data are reported in Table 2. In terms of NMR parameters (δ_{iso}, η_{CSA}, and $\Delta\delta$), the two sites are clearly distinguished, whereas crystallographic data show that the chemical environments of the P atoms are very similar. The next challenge is therefore to correlate NMR spectroscopic data with slight distortions of polyhedra around P atoms by ab initio CSA calculations. In other words, the next step of our research is to assign P1 and P2 definitely to the two observed ^{31}P lines.

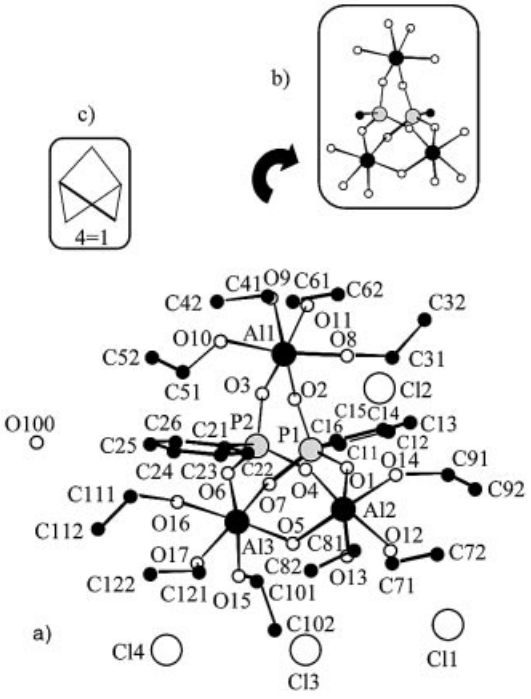

Figure 1. a) Representation of compound **1**: H atoms are omitted for clarity; b) the inorganic core of compound **1**, mimicking the 4=1 SBU of zeolites [c)]

Table 1. Selected bond lengths [Å] for $[Al_3(\mu_2\text{-}OH)(\mu_3\text{-}C_6H_5PO_3)_2(C_2H_5OH)_{10}]Cl_4{\cdot}H_2O$ (**1**)

	Distances [Å]		Distances [Å]
Al1−O2	1.805(4)	Al1−O9	1.932(4)
Al1−O3	1.804(3)	Al1−O10	1.935(4)
Al1−O8	1.925(4)	Al1−O11	1.932(4)
Al2−O1	1.842(4)	Al2−O12	1.937(4)
Al2−O4	1.833(4)	Al2−O13	1.953(4)
Al2−O5	1.845(4)	Al2−O14	1.944(4)
Al3−O6	1.835(4)	Al3−O15	1.969(4)
Al3−O7	1.840(3)	Al3−O16	1.928(4)
Al3−O5	1.852(4)	Al3−O17	1.932(4)
P1−O1	1.528(4)	P1−O7	1.512(3)
P1−O2	1.519(4)	P1−C11	1.787(5)
P2−O3	1.515(3)	P2−O6	1.519(3)
P2−O4	1.516(4)	P2−C21	1.784(5)

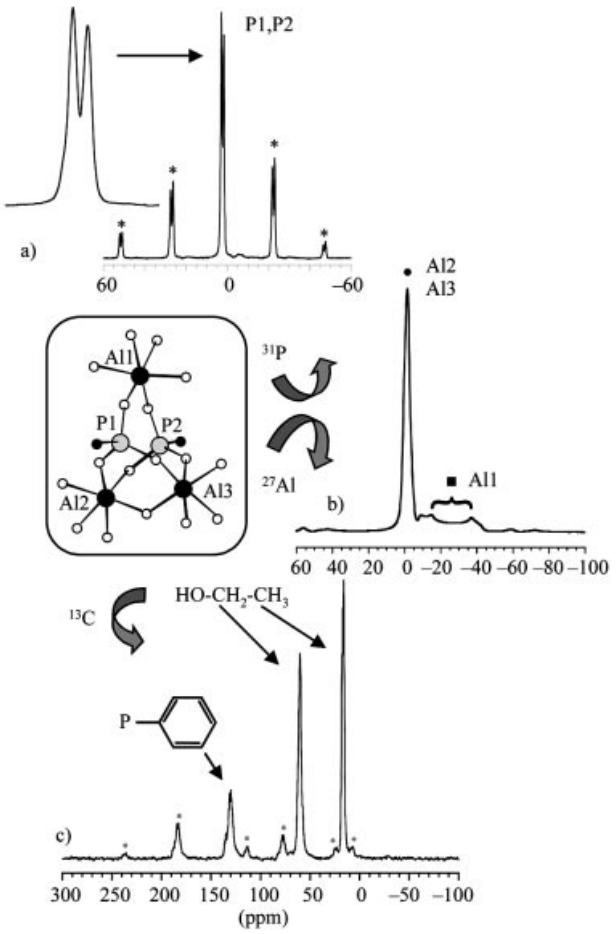

Figure 2. a) ^{31}P CP MAS NMR spectrum of compound **1**; b) ^{27}Al MAS NMR spectrum; c) ^{13}C CP MAS spectrum (see Exp. Sect.)

Table 2. ^{31}P and ^{27}Al NMR spectroscopic data for compound **1**; for CSA: $\delta_{iso} = 1/3(\delta_{11} + \delta_{22} + \delta_{33})$ with $|\delta_{33} - \delta_{iso}| \geq |\delta_{11} - \delta_{iso}| \geq |\delta_{22} - \delta_{iso}|$; $\eta_{CSA} = (\delta_{22} - \delta_{11})/(\delta_{33} - \delta_{iso})$; $\Delta\delta = \delta_{33} - (\delta_{11} + \delta_{22})/2$; $\delta_{iso}(^{31}P)$: ± 0.1; $\eta_{CSA}(^{31}P)$: ±0.05; for the quadrupolar interaction: $C_Q = (e^2qQ)/h$ (±0.05 MHz); $\eta_Q = (V_{22} - V_{11})/V_{33}$ (±0.02)

^{31}P			^{27}Al		
δ_{iso} [ppm]	η_{CSA}	$\Delta\delta$ [ppm]	δ_{iso} [ppm]	C_Q [MHz]	η_Q
1.7	0.60	70.1	−2.2 (Al1)	4.92 (Al1)	0.2 (Al1)
2.8	0.75	73.1	1.5 (Al2,3)	<< 1[a]	–

[a] The quadrupolar interaction for (Al2, Al3) is very small(see text).

The ^{27}Al MAS spectrum of **1** [Figure 2, b)] exhibits two major lines. The first one is centered at $\delta \approx 1.5$ ppm and is narrow. The second is strongly broadened and exhibits the characteristic features of a second-order quadrupolar broadened line (i.e. "horns" at $\delta \approx -15$ and -35 ppm). Quantitative experiments[14] show that the two lines are in the ratio 2:1. Therefore, the line centered at $\delta \approx 1.5$ ppm is assigned to Al2 and Al3, the other to Al1. At low rotation frequency (4.5 kHz), the sub-spectrum corresponding to Al1 is a complex superposition of the central transition, spinning sidebands of the central transition (full square), and spinning sidebands of satellite transitions (open square) [Figure 3, a)]. However, the full spectrum can be satisfactorily simulated by the SIMPSON program, available on the web (see the Exp. Sect.).[15] The quadrupolar parameters are very precisely determined (see Table 2), as all the discontinuities of the spectrum are sensitive to (C_Q, η_Q). For instance, the calculated shift of one particular discontinuity (boxed **1**) versus η_Q is plotted in Figure 3, b). The experimental shift unambiguously gives $\eta_Q = 0.2 \pm 0.02$. The final set of quadrupolar parameters for Al1, including second-order corrections for the chemical shift,[16] is: Al1 ($\delta_{iso} = -2.2$ ppm; $C_Q = 4.92$ MHz; $\eta_Q = 0.2$). Chemical shifts for Al2 and Al3 are located at $\delta_{iso} = 1.5$ ppm. The C_Q values for (Al2, Al3) are very small, as shown in Figure 3 (a). Indeed, only two spinning sidebands corresponding to (Al2, Al3) are observed at a rotation frequency of 4.5 kHz (open circle). At this stage, the C_Q parameters can be analyzed in terms of the correlation established by Ghose et al:[17] C_Q of octahedrally coordinated aluminium atoms increases with the longitudinal strain $|\alpha|$ with

$$|\alpha| = \sum_{i=1}^{6} |\ln(l_i / l_0)|$$

where l_i are the individual Al−O bond lengths and l_0 is the ideal bond length for a perfect octahedron with the same volume as the distorted polyhedron.

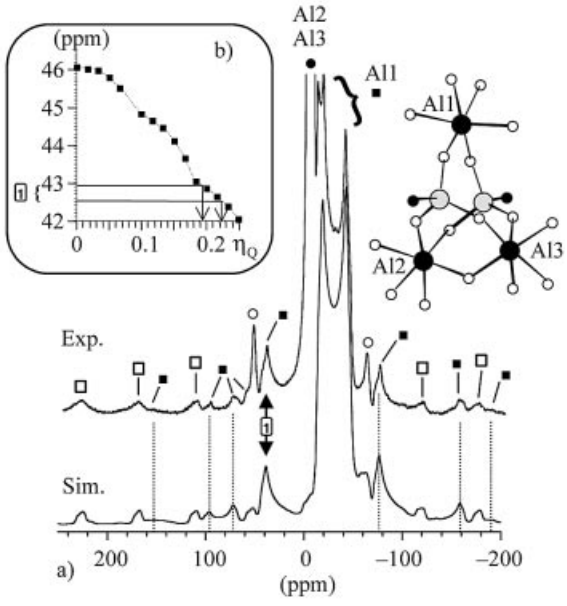

Figure 3. a) ^{27}Al MAS {^{1}H dec} spectrum of compound **1** at moderate spinning frequency (4.5 kHz); full circle: central transition of (Al2,Al3); open circle: spinning sidebands related to the satellite transitions; full square: central transition of Al1 and corresponding sidebands; open square: spinning sidebands related to the satellite transitions; simulation obtained by use of the SIMPSON program with: $\delta_{iso} = -2.2$ ppm, $C_Q = 4.92$ MHz, and $\eta_Q = 0.2$; b) calculated shift of the discontinuity (boxed **1**) versus η_Q; the experimental shift (with uncertainty) is shown by boxed **1** {; arrows indicate the derived values of η_Q

From the crystallographic data of compound **1**, the following calculated longitudinal strains are obtained: $|\alpha|$ = 0.155 and 0.165 for Al1 and Al2, respectively; $|\alpha|$ = 0.182 for Al3. These values are high and should be connected to $C_Q > 8$ MHz, as stated by Ghose et al. for aluminium oxide derivatives.[12,17] Obviously, the extracted experimental data are not in agreement with the previously reported results: (i) the C_Q values for Al1, Al2, and Al3 are much lower than 8 MHz, and (ii) C_Q(Al1,Al2) << C_Q(Al3) although $|\alpha|$ is almost identical for Al1, Al2, and Al3. This study proves unambiguously that a simple approach of the electric field gradient, taking into account only the first oxygen neighbors of Al atoms, is not suitable for the fine description of clusters such as **1**.

The ^{13}C CP MAS spectrum of **1** [Figure 2, c)] shows three main groups of resonances centered at δ = 17.3, 60.2, and 132.5 ppm and corresponding to $^{13}CH_3$, $^{13}CH_2$, and aromatic groups, respectively. The resolution is not high enough to count C atoms in the asymmetric unit (ten $^{13}CH_3$, ten $^{13}CH_2$, and twelve aromatic C). Experiments at higher field (up to 17.5 T) should allow a much improved resolution of spectra, and therefore direct counting of C atoms.

The ^{1}H MAS NMR spectra of phenylphosphonic acid [$C_6H_5PO(OH)_2$] and of compound **1** are presented in Figure 4. At $\nu_0(^1H)$ = 300 MHz and high rotation frequency (up to 14 kHz), the spectra are broad and almost featureless [Figure 4, a) and c)]. This is mainly due to the homogeneous character of the strong ^{1}H-^{1}H homonuclear dipolar interaction.[18] In the case of inhomogeneous interactions, such as CSA or first-order quadrupolar interaction, MAS is efficient even at low spinning frequency: sharp isotropic lines and sharp spinning sidebands are obtained [see, for instance, the ^{31}P CP MAS spectrum of compound **1** in Figure 2, a)]. It follows that high resolution is obtained. In contrast, slow MAS is inefficient to remove the broadening due to strong homonuclear coupling, unless the MAS frequency equals or exceeds the magnitude of the interaction. The problem was partially circumvented by the use of the so-called Combined Rotation And Multi Pulse Spectroscopy (CRAMPS), combining MAS and multi-pulse irradiation during the acquisition of the ^{1}H signal.[19] CRAMPS is a very demanding technique and is rarely implemented in laboratories. In this paper we present a second approach, involving a high field [14 T, $\nu_0(^1H)$ = 600 MHz] − to increase resolution − and a very high rotation frequency (33 kHz) − to average the homonuclear interaction efficiently. The observed increase of resolution is indeed dramatic [Figure 4, b) and d)]. In the case of the phenylphosphonic acid, two main lines located at δ = 8 ppm and 12 ppm [experimental intensity ratio: 5.6:2; calculated ratio for $C_6H_5PO(OH)_2$: 5:2] are observed and can safely be assigned to phenyl and P−OH groups, respectively. In the case of compound **1**, three main groups of resonances located at δ = 1.5, 4.5, and ca. 8 ppm are observed. The first two lines are attributable to CH_3 and CH_2 groups of ethanol molecules, respectively. The line at δ ≈ 8 ppm is complex, and involves several resonances. These are related to phenyl groups, OH (ethanol and μ-OH), and H_2O. Deconvolution of groups of resonances at δ = 1.5, 4.5, and ca. 8 ppm by Gaussian lines gives the following experimental integration: 30 (CH_3):16 (CH_2):16 (OH, H_2O, phenyl); the integrals of signals include the contributions of the first spinning sidebands, which represent ca. 10% of the total signal. The calculated integral for compound **1** gives: 30 (CH_3):20 (CH_2):23 (OH, H_2O, phenyl). The experimental results therefore indicate good general trends. The noted discrepancies between calculated and experimental data may be attributed to the strong overlapping of lines in the δ = 7−12 ppm region.

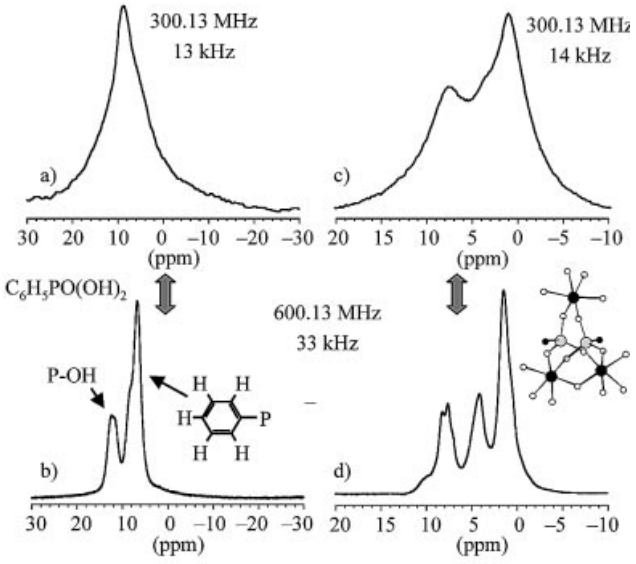

Figure 4. ^{1}H MAS NMR spectra (single pulse experiment) of phenylphosphonic acid: at $\nu_0(^1H)$ = 300.13 MHz and ν_{rot} = 13 kHz [a)]; at $\nu_0(^1H)$ = 600.13 MHz and ν_{rot} = 33 kHz [b)]; compound **1**: at $\nu_0(^1H)$ = 300.13 MHz and ν_{rot} = 14 kHz [c)]; at $\nu_0(^1H)$ = 600.13 MHz and ν_{rot} = 33 kHz [d)]

In order to highlight the new possibilities offered by ^{1}H very fast MAS NMR, we present experimental data (Figure 5) related to the cubane-shaped Al−O−P cluster $[Al_4(HPO_4)_4(C_2H_5OH)_{12}]Cl_4{\cdot}4C_2H_5OH$ (compound **2**).[12] For compound **2**, four types of protons may be distinguished, namely CH_3 and CH_2 groups from ethanol ligands and solvates, OH groups from ethanol, and OH groups from P−OH entities. Once again, at $\nu_0(^1H)$ = 600 MHz and 33 kHz, a spectacular gain in resolution is demonstrated. Assignments can be safely proposed (Figure 5). Experimental integration of lines at δ = 1.2 (CH_3), 3.9 (CH_2), 7.4 (OH), and 8.7 ppm (P-OH) gives 48:32.3:13.7:2. The calculated values for compound **2** are 48:32:16:4. An excellent agreement is noted between experimental and calculated data.

The examples presented above clearly show that solid-state ^{1}H NMR is now available as an analytical tool for the study of Al−O−P clusters, or more generally, for inorganic cores linked to organic groups. Very high MAS frequencies (up to 33 kHz) result (in these particular cases), in sufficient

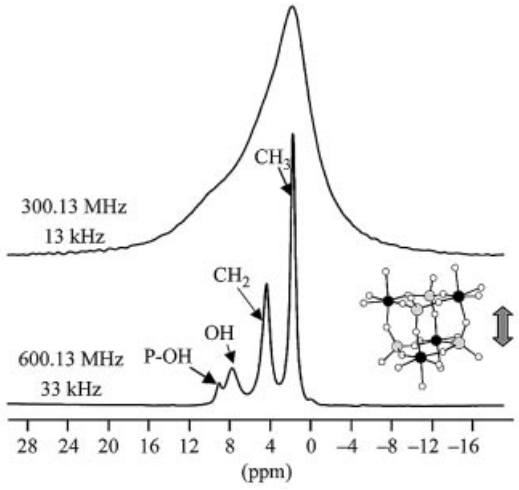

Figure 5. ^{1}H MAS NMR spectra (single pulse experiment) of compound **2** at [$\nu_0(^1H)$ = 300.13 MHz, ν_{rot} = 13 kHz] and [$\nu_0(^1H)$ = 600.13 MHz and ν_{rot} = 33 kHz]; each Al atom is coordinated to three ethanol ligands; four ethanol solvate molecules (per each cube) are present; each P atom is bonded to an OH group; see ref.[12]

averaging of the strong ^{1}H-^{1}H homonuclear interaction. Caution must be taken to ensure that no degradation due to high rotation frequency (heating[20] and gigantic pressure inside the rotor) occurs in samples. Spectra were first recorded at low rotation speeds, and the frequency of rotation was then increased. After high rotation speed experiments, checking of the integrity of the products was performed by recording spectra at low speed, and comparing them to the initial spectra.

Solid-state NMR therefore offers a two-level approach for the study of Al−O−P clusters. Firstly, the inorganic core can be studied by standard ^{31}P and ^{27}Al MAS NMR. The latest developments in ab initio calculation of chemical shifts and quadrupolar interaction[21] show that it is now possible to calculate these parameters safely for structures involving a reasonable number of atoms per cell. SBUs could act as good candidates for precise comparison between calculated and experimental data. Secondly, the organic part of the cluster, which acts as a link between inorganic cores, may now be investigated by high-resolution ^{1}H MAS NMR.

Finally, we believe that compound **1** could serve as a valuable precursor for the direct synthesis of complex aluminophosphonate frameworks. Our experience is that such a compound is slightly soluble in ethanol (see Exp. Sect.) and that the structure is preserved in solution (as checked by solution-state ^{31}P NMR). The compound may appear much more soluble in other solvents such as DMF, CH_3CN, etc., but the structure is usually not preserved in solution (several resonances with various intensities are observed in the corresponding ^{31}P spectra; see also refs.[11,12]). However, we note that treatment of **1** under solvothermal conditions (with ethanol) resulted in highly crystalline compounds with interesting solid-state NMR features. These compounds are under investigation in the laboratory.

Experimental Section

Synthesis of $[Al_3(\mu_2\text{-}OH)(\mu_3\text{-}C_6H_5PO_3)_2(C_2H_5OH)_{10}]Cl_4\cdot H_2O$ (1): Anhydrous $AlCl_3$ (4.33 g, 32.5 mmol) was slowly added to cooled ethanol (25 mL, 0 °C, exothermic reaction). $C_6H_5PO(OH)_2$ (5.14 g, 32.5 mmol) was then added to the solution. After 48 h at 5 °C, colorless crystals were obtained. Yield: 65%. Elemental analysis (Vernaison, France): $C_{32}H_{73}Al_3Cl_4P_2O_{18}$ (1030.6): calcd. C 37.29, H 7.14, Al 7.85, Cl 13.76, P 6.01; found C 35.87, H 6.63, Al 7.60, Cl 14.48, P 6.35. Chemical analyses were hardly reliable due to the extreme instability of compound **1** to air and moisture (several attempts were made).

Simultaneous Differential Thermal and Thermogravimetric Analyses: TA Instrument SDT 2960; air flow, 5 °C·min^{-1}, 25 °C up to 1250 °C; 25 to 1250 °C, TGA, 71.3 wt% loss (calcd. 71.4%); 25 to 160 °C: 50.3 wt% loss, endothermic event: ethanol loss; 500 to 650 °C: 11.3 wt% loss, complex exothermic event: phenyl decomposition/combustion; 1035 °C: weak exothermic event: poor crystallization into cristobalite and tridymite ($AlPO_4$) (powder XRD); 1180 to 1240 °C, 3.0 wt% loss, exothermic event: residual carbon combustion. End of DTA-TGA: gray powder containing traces of carbon, poorly crystallized (cristobalite and tridymite); no crystalline alumina detected.

Crystal Data for 1: $[Al_3(\mu_2\text{-}OH)(\mu_3\text{-}C_6H_5PO_3)_2(C_2H_5OH)_{10}]Cl_4\cdot H_2O$, (0.1 × 0.1 × 0.1 mm, rapidly brought out of the mother liquor, put in a capillary with oil), Enraf−Nonius MACH-3, monoclinic, $P2_1/a$, a = 20.083(5), b = 12.011(4), c = 24.36(1) Å, β = 114.00(3)°, V = 5368(3) Å^3, $\rho_{calcd.}$ = 1.28 ·cm^{-3}, Mo-K_α (λ = 0.71069 Å), ω/2θ, θ = 1−26°, T = 200 K, measured reflections: 11383, independent reflections: 10524, reflections included in the refinement: 6484 with $(F_o)^2 > 3\sigma(F_o)^2$, data corrected for Lorentz and polarization effects, no absorption correction, 534 parameters, $R = \Sigma||F_o| - |F_c||/\Sigma|F_o| = 0.0812$; $wR = [\Sigma w(|F_o| - |F_c|)^2/\Sigma w|F_o|^2]^{1/2} = 0.0985$, $w = w'\,[1 - (||F_o| - |F_c||/6\sigma(F_o)^2]^2$ with $w' = 1/\Sigma_r A_r T_r(X)$ with 3 coefficients 12.1, 5.48, and 8.53 for the Chebyshev series for which X is $F_C/F_{C(max)}$, Δρ(min.) = −0.81, Δρ(max.) = 1.85 e·Å^{-3}. Scattering factors corrections for anomalous absorption were taken from ref.[22] Structures were solved by direct methods (SHELXS)[23] and refined by full-matrix, least-squares with anisotropic thermal parameters for all non-hydrogen atoms. Hydrogen atoms were introduced in calculated positions as fixed contributors in the last refinement. CCDC-182720 (**1**) contains the supplementary crystallographic data for this paper. These data can be obtained free of charge at www.ccdc.cam.ac.uk/conts/retrieving.html or from the Cambridge Crystallographic Data Center, 12, Union Road, Cambridge CB2 1EZ, UK [Fax: (internat.) + 44-1223/336-033; E-mail: deposit@ccdc.cam.ac.uk].

Solid-State NMR: All ZrO_2 rotors were filled under argon in a dried glove-box, as compounds **1** and **2** were very sensitive to air moisture. ^{31}P CP MAS: Ξ^{31}P: 121.44 MHz; δ = 0 ppm: H_3PO_4 (85%); diameter of rotor (φ): 4 mm; MAS: ν_{rot} = 3−5 kHz. ^{1}H 90° pulse duration: 4 μs; for each ν_{rot}, the Hartmann−Hahn (H-H) condition was matched with compound **2**; contact time: 3 ms; relaxation delay (RD): 15 s, number of scans (NS): 40. ^{31}P (in ethanol-OD): Ξ^{31}P: 161.92 MHz, δ = 2.3 ppm (relative to H_3PO_4). ^{13}C CP MAS: Ξ^{13}C: 75.43 MHz; spectra referenced to TMS via solid adamantane; φ: 4 mm; MAS: 4 kHz. ^{1}H 90° pulse duration: 5 μs; H-H condition was matched with adamantane; contact time: 3 ms; RD = 15 s; NS = 2000. ^{27}Al MAS: Ξ^{27}Al: 78.17 MHz; δ = 0 ppm: $Al(NO_3)_3$, HNO_3 (1 M); φ: 4 mm; flip angles ≤ π/12; MAS-{^{1}H} high power decoupling: 4.5−15 kHz; RD = 1 s; NS = 7200.

^{1}H MAS: Ξ^1H: 600.13 MHz; spectra referenced to TMS via solid adamantane; φ: 2.5 mm; very high speed Bruker probe; MAS: 33 kHz; RD = 15 s; NS = 8.

Simulation of Spectra: See the SIMPSON package, available on the web.[15] Simulations of second-order ^{27}Al spectra (Figure 3) include the following parameters: ^{27}Al frequency, MAS frequency, quadrupolar Hamiltonian up to second-order, central transition and all satellite transitions, isotropic chemical shift δ_{iso} (no CSA), quadrupolar parameters (C_Q, η_Q), powder averaging type.

Acknowledgments

Professor G. Bodenhausen is warmly thanked for access time on the 600 MHz spectrometer of the Ecole Normale Supérieure (Paris).

[1] C. Baerlocher, W. M. Meier, D. H. Olson in *Atlas of Zeolite Framework Types*, 5th ed., Elsevier, Amsterdam, **2001**.
[2] M. G. Walawalkar, H. W. Roesky, R. Murugavel, *Acc. Chem. Res.* **1999**, *32*, 117.
[3] [3a] S. A. Sangokoya, W. T. Pennington, G. H. Robinson, D. C. Hrncir, *J. Organomet. Chem.* **1990**, *385*, 23. [3b] J. M. Corker, D. J. Browning, M. Webster, *Acta Crystallogr., Sect. C* **1996**, *52*, 583. [3c] M. R. Mason, R. M. Matthews, M. S. Mashuta, J. F. Richardson, *Inorg. Chem.* **1996**, *35*, 5756. [3d] J. Pinkas, D. Chakraborty, Y. Yang, R. Murugavel, M. Noltemeyer, H. W. Roesky, *Organometallics* **1999**, *18*, 523. [3e] C. G. Lugmair, T. D. Tilley, A. L. Rheingold, *Chem. Mater.* **1999**, *11*, 1615. [3f] D. Chakraborty, S. Horchler, H. W. Roesky, M. Noltemeyer, H-G. Schmidt, *Inorg. Chem.* **2000**, *39*, 3995. [3g] K. L. Fujdala, T. Don Tilley, *J. Am. Chem. Soc.* **2001**, *123*, 10133. [3h] M. R. Mason, A. M. Perkins, V. V. Ponomarova, A. Vij, *Organometallics* **2001**, *20*, 4833. [3i] for a review: M. R. Mason, *J. Cluster Sci.* **1998**, *9*, 1.
[4] Y. Yang, J. Pinkas, M. Noltemeyer, H. W. Roesky, *Inorg. Chem.* **1998**, *37*, 6404.
[5] [5a] J. E. Cassidy, J. A. J. Jarvis, R. N. Rothon, *J. Chem. Soc., Dalton Trans.* **1975**, 1497. [5b] Y. Yang, H.-G. Schmidt, M. Noltemeyer, J. Pinkas, H. W. Roesky, *J. Chem. Soc., Dalton Trans.* **1996**, 3609. [5c] Y. Yang, M. G. Walawalkar, J. Pinkas, H. W. Roesky, *Angew. Chem.* **1998**, *37*, 96. [5d] J. Pinkas, H. Wessel, Y. Yang, M. L. Montero, M. Noltemeyer, M. Froba, H. W. Roesky, *Inorg. Chem.* **1998**, *37*, 2450.
[6] Y. Yang, J. Pinkas, M. Schafer, H. W. Roesky, *Angew. Chem.* **1998**, *37*, 2650.
[7] W. M. Meier, *Z. Kristallog.* **1960**, *113*, 430.
[8] E. Galli, *Acta Crystallogr., Sect. B* **1976**, *32*, 1623.
[9] A. Alberti, G. Vezzalini, V. Tazzoli, *Zeolites* **1981**, *1*, 91.
[10] [10a] M. R. Mason, A. M. Perkins, R. M. Matthews, J. D. Fisher, M. S. Mashuta, A. Vij, *Inorg. Chem.* **1998**, *37*, 3734. [10b] C. C. Landry, W. M. Cleaver, I. A. Guzci, A. L. Rheingold, *Organometallics* **1998**, *17*, 5209.
[11] T. Azaïs, L. Bonhomme-Coury, J. Vaissermann, P. Bertani, J. Hirschinger, J. Maquet, C. Bonhomme, *Inorg. Chem.* **2002**, *41*, 981.
[12] T. Azaïs, C. Bonhomme, L. Bonhomme-Coury, J. Vaissermann, Y. Millot, P. P. Man, P. Bertani, J. Hirschinger, J. Livage, *J. Chem. Soc., Dalton Trans.* **2002**, 609.
[13] T. Steiner, *Angew. Chem. Int. Ed.* **2002**, *41*, 48.
[14] D. Massiot, C. Bessada, J-P. Coutures, F. Taulelle, *J. Magn. Reson.* **1990**, *90*, 251.
[15] [15a] SIMPSON, http://NMR.imsb.au.dk [15b] M. Bak, J. T. Rasmussen, N. C. Nielsen, *J. Magn. Reson.* **2000**, *147*, 296.
[16] P. P. Man in *Encyclopedia of Nuclear Magnetic Resonance*, Wiley, Chichester, **1996**, p. 3838.
[17] S. Ghose, T. Tsang, *Am. Mineral.* **1973**, *58*, 748.
[18] K. Schmidt-Rohr, H. W. Spiess in *Multidimensional Solid-State NMR and Polymers*, Academic Press, London, **1996**, p. 115.
[19] B. C. Gerstein, R. G. Pembleton, P. C. Wilson, L. M. Ryan, *J. Chem. Phys.* **1977**, *66*, 361.
[20] J. Brus, *Solid State Nucl. Magn. Reson.* **2000**, *16*, 151.
[21] C. J. Pickard, F. Mauri, *Phys. Rev. B* **2001**, *63*, 245101-1-13.
[22] D. T. Cromer in *International Tables for X-ray Crystallography*, Kynoch Press, Birmingham, **1974**, vol. IV.
[23] G. M. Sheldrick, *SHELXS-86, Program for the Solution of Crystal Structures*, University of Göttingen, Göttingen,Germany, **1986**.

Received June 6, 2002
[I02299]

Cyano-Halogen Interactions in $[EDT\text{-}TTF\text{-}I]_2[Ni(mnt)_2]$ and $[EDT\text{-}TTF\text{-}I_2]_2[Ni(mnt)_2]$ and Geometrical Evolutions within Mixed-Valence or Fully Oxidized TTF Dyads

Thomas Devic,[a] Benoît Domercq,[b] Pascale Auban-Senzier,[c] Philippe Molinié,[b] and Marc Fourmigué*[a]

Keywords: Radical ions / S ligands / Magnetic properties / Crystal engineering / Non-covalent interactions

The structure of the iodo-substituted tetrathiafulvalene derivative EDT-TTF-I is described, with neutral molecules associated into inversion-centred dyads; no short intermolecular I···I contacts are observed. Electrocrystallisation of EDT-TTF-I (**1**) or EDT-TTF-I_2 (**2**) in the presence of $[nBu_4N][Ni(mnt)_2]$ afforded 2:1 salts, formulated as $[\mathbf{1}]_2[Ni(mnt)_2]$ and $[\mathbf{2}]_2[Ni(mnt)_2]$. In both salts the organic donor molecules **1** or **2** are associated into inversion-centred dyads, connected to the $[Ni(mnt)_2]$ species through a short, directional CN···I interaction. The dyads alternate with the nickel dithiolene complex into mixed ...DDADDADDA... stacks. Comparisons in both salts of intramolecular bond lengths, intra-dyad overlap modes, and magnetic susceptibilities, indicate a full charge-transfer in $[\mathbf{1}]_2[Ni(mnt)_2]$, formulated as $[\mathbf{1}]_2^{2+}[Ni(mnt)_2]^{2-}$, while a mixed-valence state is observed in $[\mathbf{2}]_2^{+\cdot}[Ni(mnt)_2]^{-\cdot}$.
(© Wiley-VCH Verlag GmbH, 69451 Weinheim, Germany, 2002)

Introduction

Intermolecular CN···I interactions[1,2] have been known for a long time in the solid state chemistry of organic molecules[3] and were recently investigated theoretically.[4] Mainly associated with the most polarisable halogens (Br, I), they are characterised by a N···Hal distance far shorter than the sum of the van der Waals radii [N···I = 3.0−3.15 Å; Σ_{vdW}(N···I) = 3.53 Å] together with a strong tendency to linearity.[5,6] Recent ab initio intermolecular perturbation theory calculations showed that the attractive nature of the N···I interaction is mainly due to electrostatic effects while its directionality can be explained by the anisotropic electron distribution around the halogen atom.[4] This directional interaction has been used deliberately in the synthesis of several organic salts derived from iodinated tetrathiafulvalenes such as TTF-I,[7] EDT-TTF-I,[8,9] EDO-TTF-I_2,[10] or DIETS[11] and cyano-containing anions such as $Ag(CN)_2^-$, $Pd(CN)_4^{2-}$ or $[Pd(mnt)_2]^{2-}$. It is also elegantly used in a TTF molecule containing both a pyrazino and two iodo moieties,[12] or by the inclusion in the anionic layer of neutral iodinated molecules.[13] Among those various cyanide-containing counterions, only one example has been described which involves an open-shell anion, namely the $[Ni(mnt)_2]^{-\cdot}$ nickel dithiolene complex, in a 2:1 salt with EDO-TTF-I_2.[14] In this salt, the metallic conductivity is due to the one-dimensional chains of EDO-TTF-I_2, while the localised spins of the $[Ni(mnt)_2]^-$ anions behave as a one dimensional ferromagnet, and interact with conduction electrons. In a search for similar systems where localised and itinerant spins coexist and eventually interact,[15] we investigated the salts derived from the mono- and diiodo-substituted tetrathiafulvalene derivatives EDT-TTF-I (**1**) and EDT-TTF-I_2 (**2**) with the open-shell anion $[Ni(mnt)_2]^{-\cdot}$ and describe here their structural and electronic properties, paying special attention to the CN···I and the magnetic organic/inorganic interactions.

[a] Laboratoire Chimie Inorganique, Matériaux et Interfaces, FRE 2447 CNRS-Université d'Angers, UFR Sciences,
Bât. K, 2 bd. Lavoisier, 49045 Angers, France
Fax: (internat.) + 33-241/735-405
E-mail: marc.fourmigue@univ-angers.fr
[b] Institut Jean Rouxel, CNRS-Université de Nantes,
2, rue de la Houssinière, BP32229, 44322 Nantes, France
[c] Laboratoire de Physique des Solides, UMR 8502 CNRS-Université Paris-Sud,
Bât. 510, 91405 Orsay cedex, France

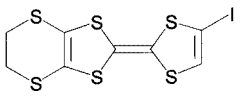
I-EDT-TTF (1)

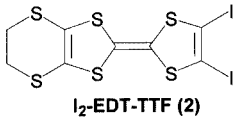
I_2-EDT-TTF (2)

Results and Discussion

Solid-State Structures

Compounds **1** and **2** were prepared as described previously[16] and recrystallised from toluene. Molecule **1**, in the neutral state, crystallises in the triclinic system, space group $P\bar{1}$ with two crystallographically independent molecules in the unit cell (Figure 1). One of these exhibits strong distortions from planarity with folding angles along the S···S hinge of the two dithiole rings of 14.3(1) and 14.0(1)° for the dithiole rings bearing the dithioethylene and iodo substituents, respectively. The other crystallographically independent molecule is almost planar,[17] except for the dithioethylene bridge, which is also disordered over two positions with a 55:45 distribution. The intramolecular bond lengths and angles differ only slightly from those observed in the unsubstituted EDT-TTF.[18] The molecules are associated into inversion-centred dyads with plane-to-plane distances of 3.43(2) and 3.51(2) Å in the two independent dyads, respectively, while the shortest intermolecular I···I contacts are observed at 4.47 Å, thus excluding the presence of I···I interactions in the solid state.[16,19,20] (NB The structure of the neutral diiodo derivative **2** could not be fully determined due to the poor quality of the crystals.[21]) Electrocrystallisation of **1** and **2** in the presence of [nBu$_4$N][Ni(mnt)$_2$] afforded in both cases a 2:1 salt, formulated as [**1**]$_2$[Ni(mnt)$_2$] and [**2**]$_2$[Ni(mnt)$_2$]. They crystallise in the triclinic system, space group $P\bar{1}$, and exhibit almost identical gross structural features (Figure 2 and 3), with the organic donor molecules **1** or **2** associated into inversion-centred dyads connected to the [Ni(mnt)$_2$] moiety through a short, directional CN···I interaction with the following characteristics: N···I = 2.926(4) Å, C≡N···I = 177.9(2)° in [**1**]$_2$[Ni(mnt)$_2$]; N···I = 2.949(9) Å, C≡N···I = 171.6(9)° in [**2**]$_2$[Ni(mnt)$_2$]. It should be stressed that the CN···I distances observed here are much shorter than the distances observed in the neutral *p*-iodobenzonitrile, for example (3.0−3.15 Å). This striking shortening suggests an enhanced interaction due to the electrostatic nature of the CN···I interaction. Indeed, in those systems where the iodine atom is covalently linked to the *cationic* tetrathiafulvalene and the nitrile group is part of an *anionic* dithiolene complex, this polarised interaction is expected to be enhanced, as observed here and in the salts of the iodinated TTF's mentioned above. Such an activation of iodinated molecules has also been performed by the incorporation of neighbouring electron-withdrawing fluorinated groups, leading to enhanced N···I interactions.[22,23] To further demonstrate the electrostatic character of this interaction, the *reverse polarisation*, which involves a cyanide-bound tetrathiafulvalene cation and halogenated anions, has recently been addressed:[24] the interaction was completely suppressed in these cases.

In both salts, as shown in Figure 4, the oxidised donor molecules are associated into inversion-centred dyads which alternate with the nickel dithiolene complex into mixed ...DDADDADDA... stacks. This alternating structure is in sharp contrast with the EDO-TTF-I$_2$ salt described by Enoki et al.,[14] where segregated stacks were observed.

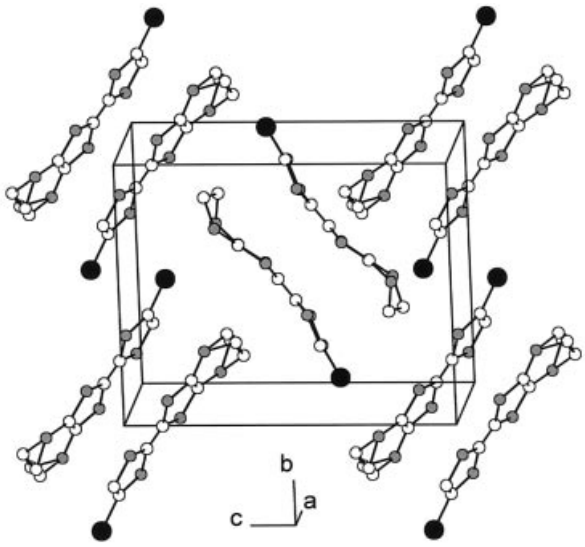

Figure 1. A view of the unit cell of neutral EDT-TTF-I (**1**); sulfur atoms are in dark grey, iodine atoms in black; note the folding of the dithiole rings of the molecule located at the centre of the unit cell

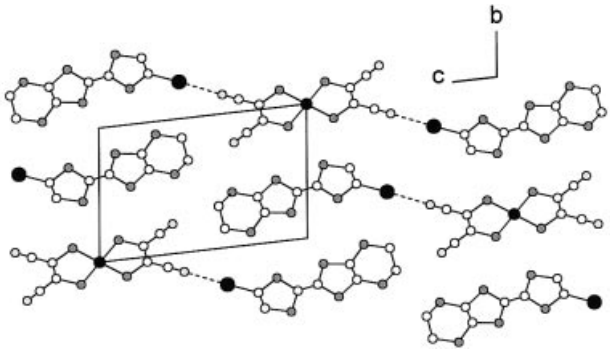

Figure 2. Projection view (along *a*) of a molecular plane in [**1**]$_2$[Ni(mnt)$_2$] showing the CN···I interaction (dotted line)

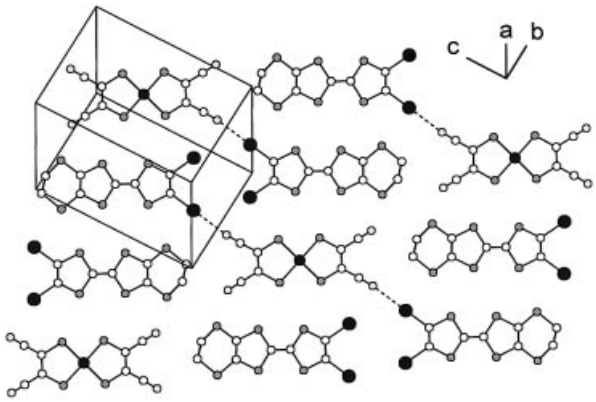

Figure 3. View of a molecular plane in [**2**]$_2$[Ni(mnt)$_2$] showing the CN···I interaction (dotted line)

The magnetic susceptibilities of both salts, as determined from SQUID measurements, are very different (Figure 5).

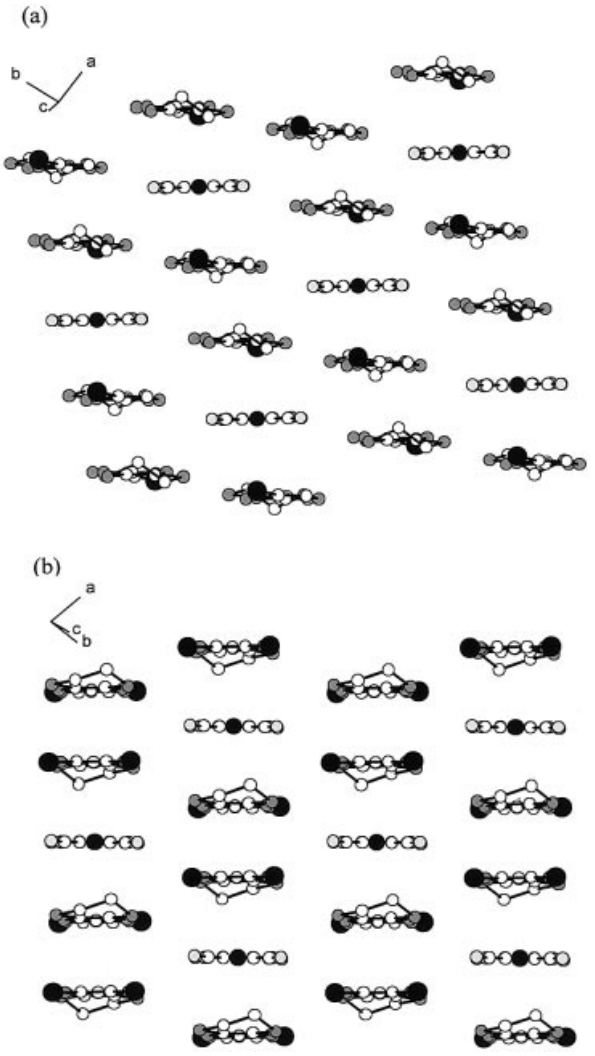

Figure 4. Views along the long molecular axis of the mixed ...DDADDADDA... chains arranged into slabs in $[\mathbf{1}]_2[Ni(mnt)_2]$ (a) and $[\mathbf{2}]_2[Ni(mnt)_2]$ (b)

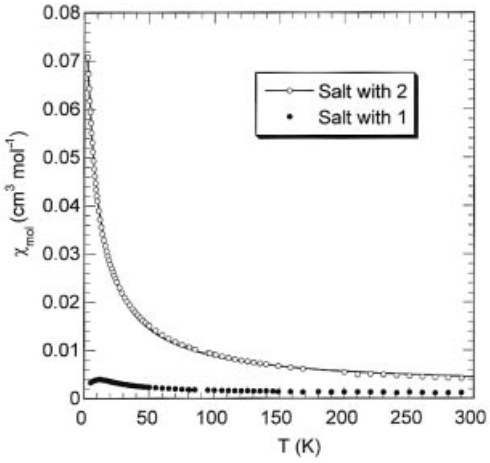

Figure 5. Temperature dependence of the magnetic susceptibility in $[\mathbf{1}]_2[Ni(mnt)_2]$ and $[\mathbf{2}]_2[Ni(mnt)_2]$; the solid line for $[\mathbf{2}]_2[Ni(mnt)_2]$ is the fit to the Curie−Weiss model, $\chi_{mol} = \chi_0 + C/(T - \theta)$, with $\chi_0 = 0.002$ cm^3·mol^{-1}, C = 0.71 cm^3·K·mol^{-1} and $\theta = -8$ K

Indeed, $[\mathbf{2}]_2[Ni(mnt)_2]$ follows a Curie−Weiss-type law, $\chi = C/(T\text{-}\theta)$, with $C = 0.71$ and $\theta = -8$ K — the signature of two localised, weakly interacting spin carriers — while $[\mathbf{1}]_2[Ni(mnt)_2]$ exhibits a weak paramagnetism (see below). Single crystal conductivity measurements performed on $[\mathbf{2}]_2[Ni(mnt)_2]$ show a semi-conducting behaviour with a low room-temperature conductivity ($\sigma_{RT} = 6 \times 10^{-3}$ S cm^{-1}) and an activation energy of 1700 K (0.14 eV).[25] These contrasting behaviours raise several questions concerning the actual oxidation state of both the donor molecules and the nickel dithiolene complex in the two salts. A precise examination of the two structures and their differences is expected to reveal the actual nature of these salts. Are we in presence of mixed-valence organic dyads, $[\mathbf{1}]_2^{+\cdot}$ or $[\mathbf{2}]_2^{+\cdot}$, together with a paramagnetic $[Ni(mnt)_2]^{-\cdot}$ radical anion, or in the presence of fully oxidised donor molecules, $[\mathbf{1}]_2^{2+}$ or $[\mathbf{2}]_2^{2+}$ with the reduced diamagnetic $[Ni(mnt)_2]^{2-}$ complex?

A comparison of the redox potentials favours the mixed-valence solution. Indeed, as shown in Scheme 1, both donor molecules oxidise at potentials far above the $Ni(mnt)_2^{2-/1-}$ couple, and **1** oxidises at a slightly lower potential than **2**, illustrating the electron-withdrawing effect of the iodine atom. The evolution of the bond lengths within the donor molecules and the dithiolene complexes is also a very efficient tool for evaluating the degree of charge transfer. As observed in Table 1, the lengthening of the central C=C bond and shortening of the C−S bonds within the TTF cores upon oxidation is observed to a larger extent in $[\mathbf{1}]_2[Ni(mnt)_2]$ than in $[\mathbf{2}]_2[Ni(mnt)_2]$. Similarly, the bond lengths' evolution within the $Ni(mnt)_2$ complex in both salts (Table 2) more clearly reveals that the monoanionic[26] $Ni(mnt)_2^{-\cdot}$ is present in $[\mathbf{2}]_2[Ni(mnt)_2]$, while most probably the dianionic $Ni(mnt)_2^{2-}$ moiety[27] is found in $[\mathbf{1}]_2[Ni(mnt)_2]$. This assignment is further confirmed by the ν_{CN} stretching frequency (Table 2). We are therefore faced here with two totally different electronic distributions: mixed-valence organic $[\mathbf{2}]_2^{+\cdot}$ dyads alternating with an anionic $[Ni(mnt)_2]^{-\cdot}$ moiety in $[\mathbf{2}]_2[Ni(mnt)_2]$, and dicationic $[\mathbf{1}]_2^{2+}$ dyads alternating with a dianionic $[Ni(mnt)_2]^{2-}$ moiety in $[\mathbf{1}]_2[Ni(mnt)_2]$.

Besides the intramolecular bond length variations, this electronic distribution is also reflected in the overlap geometry within the organic dyads. Indeed, as shown in Figure 6, the overlap interaction between two donor molecules within a dyad in $[\mathbf{1}]_2[Ni(mnt)_2]$ is of the eclipsed type, with a short plane-to-plane distance at 3.396(1) Å, characteristic of a fully oxidized $[\mathbf{1}]_2^{2+}$ dyad. The eclipsed configuration indeed favours the best overlap between SOMOs and, as a consequence, the pairing of the two spin carriers in their bonding combination. The corresponding calculated $\beta_{HOMO\cdots HOMO}$ overlap interaction amounts to 1.03 eV, a large value which also confirms the dicationic character of the dyad. On the other hand, a so-called bond-over-ring overlap is observed in the dyads in $[\mathbf{2}]_2[Ni(mnt)_2]$ together with a larger plane-to-plane distance [3.418(1) Å] and a much reduced $\beta_{HOMO\cdots HOMO}$ overlap interaction

Table 2. Characteristic averaged bond lengths (Å) and ν_{CN} IR band (cm^{-1}) in Ni(mnt)$_2^x$ ($x = -2, -1$) in different salts

	x	Ni−S bonds	C−S bonds	C=C bonds	ν_{CN}	Ref.
[Et$_4$N]$_2$[Ni(mnt)$_2$]	−2	2.174(2)	1.742(5)	1.35(1)	2191	27
[**1**]$_2$[Ni(mnt)$_2$]	−2	2.171(1)	1.731(4)	1.362(6)	2191	this work
[**2**]$_2$[Ni(mnt)$_2$]	−1	2.142(2)	1.723(9)	1.369(11)	2204	this work
[Et$_4$N][Ni(mnt)$_2$]	−1	2.147(3)	1.720(10)	1.369(12)	2207	26

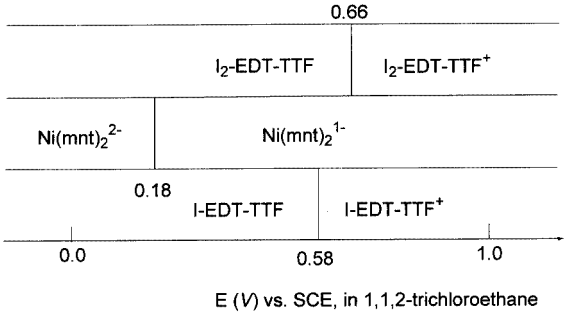

Scheme 1

Table 1. Characteristic bond lengths in the donor molecules, in various oxidation states

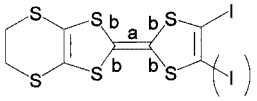

	ρ	C=C bond (a)	C−S bonds (b)	ref.
EDT-TTF-I (**1**)	0	1.332(8)	1.763(7)	this work
[**1**]$_2$[Ag(CN)$_2$]	0.5	1.369(4)	1.736(4)	9
[**1**]$_2$[Ni(mnt)$_2$]	0.5	1.382(6)	1.723(4)	this work
[**2**]$_2$[I$_3$]	0.5	1.365(10)	1.741(8)	16
[**2**]$_2$[Ni(mnt)$_2$]	1	1.389(11)	1.731(9)	this work
[**2**][I$_3$]	1	1.40(2)	1.718(9)	unpubl. results

(0.435 eV) — another confirmation of its mixed-valence character. Note also that the calculated β values for the interactions between the mixed-valence dyads are much smaller albeit not negligible (≈ 40 meV).

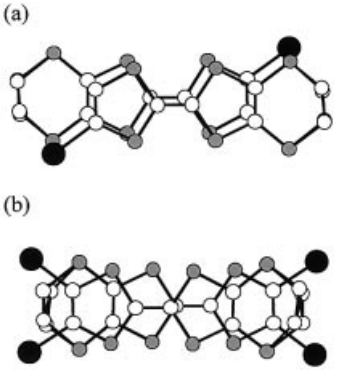

Figure 6. The overlap within each donor dyad in [**1**]$_2$[Ni(mnt)$_2$] (a) and [**2**]$_2$[Ni(mnt)$_2$] (b)

All these results confirm the above-mentioned formulations, i.e. a full charge-transfer in [**1**]$_2^{2+}$[Ni(mnt)$_2$]$^{2-}$ and a mixed-valence state in [**2**]$_2^{+\cdot}$[Ni(mnt)$_2$]$^{-\cdot}$. A fully oxidised dyad has already been observed in [TTF-I]$_2$[Pd(mnt)$_2$], a similar system described by Bryce et al. with a closely related structure and CN··I interaction.[7] In this salt, TTF-I is more easily oxidised than **1** while [Pd(mnt)$_2$]$^{2-}$ oxidises at higher potentials than Ni(mnt)$_2^{2-}$. It is therefore understandable that this salt was formulated as [TTF-I]$_2^{2+}$[Pd(mnt)$_2$]$^{2-}$. The same formulation in [**1**]$_2^{2+}$[Ni(mnt)$_2$]$^{2-}$ appears more surprising given the potential difference between the two redox centres (−0.40 V, Scheme 1). Furthermore, from the [TTF-I]$_2^{2+}$[Pd(mnt)$_2$]$^{2-}$ and [**1**]$_2^{2+}$[Ni(mnt)$_2$]$^{2-}$ formulations, one would expect a fully diamagnetic behaviour, in contrast to the temperature dependence of the magnetic susceptibility in both salts. [TTF-I]$_2^{2+}$[Pd(mnt)$_2$]$^{2-}$ was indeed reported to behave as a one-dimensional Heisenberg chain with an isotropic nearest-neighbour exchange interaction of $J \approx -50$ K. The temperature dependence of the magnetic susceptibility in [**1**]$_2$[Ni(mnt)$_2$] (Figure 5) shows a similar shape even though the fits we performed with the Bonner−Fisher model[28] are consistent with a J value of −18 K but with a contribution of only 0.25 mol of $S = 1/2$, a behaviour which we cannot explain at present, although one possibility would be the contribution of a sizeable TIP arising from the inorganic moiety. However, a control susceptibility measurement performed on [Et$_4$N]$_2$[Ni(mnt)$_2$] confirmed the diamagnetic character of the dianionic [Ni(mnt)$_2$]$^{2-}$ component with a χ_{mol} value of -340×10^{-6} cm^3·mol^{-1}, attributable to the diamagnetic contribution of the different atoms, as evaluated from the Pascal constants (-290×10^{-6} cm^3·mol^{-1}). This observation of a paramagnetic contribution in Bryce's [TTF-I]$_2$[Pd(mnt)$_2$] complex as well as in [**1**]$_2$[Ni(mnt)$_2$] could also originate from a minority polymorph. However, an X-ray powder diagram of the polycrystalline sample used for the magnetic susceptibility measurements confirmed the identity of [**1**]$_2$[Ni(mnt)$_2$] as determined from the single-crystal diffraction experiment.

The observation of a mixed-valence salt in [**2**]$_2$[Ni(mnt)$_2$] is confirmed by the SQUID magnetic susceptibility, which shows that both paramagnetic entities, the [**2**]$_2^{+\cdot}$ dyad and the [Ni(mnt)$_2$]$^{-\cdot}$ complex, contribute to the susceptibility, hence the Curie−Weiss law for two almost-independent spin carriers. The weak, negative θ value (−8 K) found in the temperature dependence of the magnetic susceptibility of [**2**]$_2$[Ni(mnt)$_2$] cannot find its origin in a ZFS of the nickel complex since the [Ni(mnt)$_2$]$^{-\cdot}$ moieties have a spin of 1/2; it must therefore stem from weak intermolecular in-

teractions between the $[\mathbf{2}]_2^{+\cdot}$ moieties since the $[Ni(mnt)_2]^{-\cdot}$ moieties are fully isolated from each other in the structure. Indeed, as mentioned above, the calculated $\beta_{HOMO\cdots HOMO}$ overlap interaction between donor molecules pertaining to neighbouring dyads amounts to approximately 40 meV and can explain the Curie−Weiss behaviour observed here. Preliminary EPR measurements at room temperature performed on a polycrystalline sample of $[\mathbf{2}]_2[Ni(mnt)_2]$ show a single asymmetric line centred at $g = 2.032$ with a ΔH value of 240 G (Figure 7). Taking into account the presence of two types of spin carriers in the salt, the line can be tentatively decomposed as the sum of two lines of equal intensity, centred at the g values of 2.012 and 2.062. These values compare favourably with those reported in the literature for similar TTF dyads ($g = 2.005-2.008$)[29] and for $[Ni(mnt)_2]^{-\cdot}$ ($g = 2.0633$).[30]

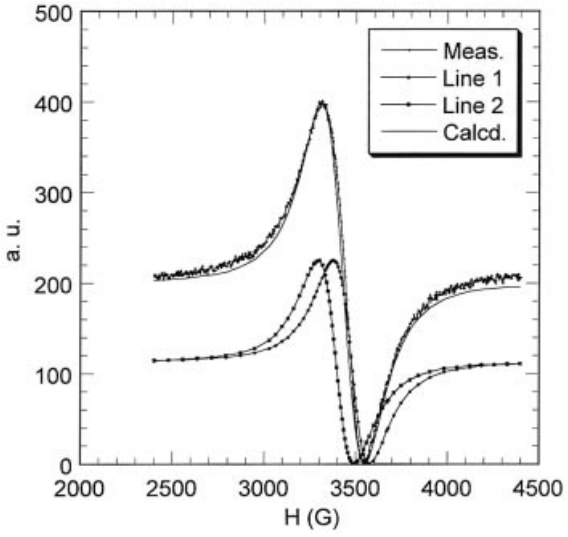

Figure 7. EPR signal obtained for $[\mathbf{2}]_2[Ni(mnt)_2]$; the solid line is the sum of the line 1 and line 2 components

Experimental Section

Synthesis: The donor molecules **1** and **2** were prepared as previously described. Electrocrystallization experiments were performed in two-compartment cells in 1,1,2-trichloroethane (10 mL) with $[n Bu_4N][Ni(mnt)_2]$ (20 mg) as electrolyte and **1** or **2** (4 mg). Crystals were obtained on the anode after galvanostatic electrolysis (0.25 μA, 16 days for **1** and 0.5 μA, 12 days for **2**).

Crystallography: Details of the data collection and structure refinement are given in Table 3. For neutral **1** and $[\mathbf{1}]_2[Ni(mnt)_2]$ data were collected on a Stoe-IPDS or an Enraf−Nonius Mach3 diffractometer at 293 K with graphite-monochromatized Mo-K_α radiation ($\lambda = 0.71073$ Å). The Stoe software was used for data collection and reduction, and numerical absorption correction using crystal faces. For $[\mathbf{2}]_2[Ni(mnt)_2]$ data were collected on an Enraf−Nonius Mach 3 diffractometer, reduction of the data was performed with XCAD4 (Harms, 1986) and absorption correction from a ψ-scan (SHELXPREP). The structures were solved by direct methods (SHELXS-86) and refined using SHELXL. All atoms were refined anisotropically except hydrogen atoms and some carbon atoms of the disordered ethylene bridge (C15B in neutral **1**, C7, C7′, C8, C8′ in $[\mathbf{1}]_2[Ni(mnt)_2]$ and $[\mathbf{2}]_2[Ni(mnt)_2]$). Hydrogen atoms were introduced at calculated positions (riding model) and not refined. Crystallographic data (excluding structure factors) for the structures reported in this paper have been deposited with the Cambridge Crystallographic Data Centre as supplementary publication no. CCDC-178087, -178088 and -178089 for **1**, $[\mathbf{1}]_2[Ni(mnt)_2]$ and $[\mathbf{2}]_2[Ni(mnt)_2]$ respectively. Copies of the data can be obtained free of charge on application to CCDC, 12 Union road, Cambridge CB2 1EZ, UK [Fax: (internat.) +44-1223/336-033; E-mail: deposit@ccdc.cam.ac.uk].

Table 3. Crystallographic data

Formula	EDT-TTF-I (**1**) $C_8H_5IS_6$	$[\mathbf{1}]_2[Ni(mnt)_2]$ $C_{12}H_5IN_2Ni_{0.5}S_8$	$[\mathbf{2}]_2[Ni(mnt)]$ $C_{24}H_8I_4N_4NiS_{16}$
Formula mass	420.38	589.92	1431.61
Crystal system	triclinic	triclinic	triclinic
Space group	$P\bar{1}$	$P\bar{1}$	$P\bar{1}$
a/ Å	6.4507(7)	7.7632(16)	8.3183(10)
b/ Å	12.6268(15)	8.8071(18)	9.6862(10)
c/ Å	16.197(2)	13.951(3)	12.8455(10)
α/degrees	89.662(15)	94.52(3)	85.657(10)
β/degrees	84.568(15)	104.80(3)	80.218(10)
γ/degrees	79.988(15)	95.25(3)	80.595(10)
V/ Å^3	1293.2(3)	913.2(3)	1005.01(18)
Z	4	2	1
d_{calc}/g cm^{-3}	2.159	2.145	2.365
μ/mm^{-1}	3.408	3.165	4.414
Data collected	12511	8957	4049
Abspt. corr.	numerical	numerical	psi-scan
T_{min}, T_{max}	0.594, 0.725	0.657, 0.952	0.327, 0.451
Ind. data	4600	3311	3867
R_{int}	0.0883	0.0425	0.0129
Obs. data $[I > 2\sigma(I)]$	3175	2460	2867
Param. refined	285	213	222
$R(F)$	0.0496	0.0284	0.0390
$wR(F^2)$	0.1238	0.0608	0.1732
Residual d/e·Å^{-3}	1.6, −1.0	1.0, −0.35	0.87, −0.78.

Magnetic Measurements: Magnetic susceptibility measurements were performed on a Quantum Design MPMS5 SQUID magnetometer operating in the range 5−300 K with polycrystalline samples. Data were corrected for Pascal diamagnetism and sample holder contribution. Room temperature EPR measurements were obtained from a Bruker ER200D spectrometer operating in X-band (9.782 GHz) with a modulation of 1.25 G.

[1] O. Hassel, *Mol. Phys.* **1958**, *1*, 241−246.
[2] O. Hassel, C. Romming, *Q. Rev. Chem. Soc.* **1962**, *16*, 1−18.
[3] D. Britton, *Persp. Struct. Chem.* **1967**, *1*, 109−171.
[4] J. P. M. Lommerse, A. J. Stone, R. Taylor, F. H. Allen, *J. Am. Chem. Soc.* **1996**, *18*, 3108−3116.
[5] G. R. Desiraju, R. L. Harlow, *J. Am. Chem. Soc.* **1989**, *111*, 6757−6764.
[6] A. S. Batsanov, M. R. Bryce, A. Chesney, J. A. K. Howard, D. E. John, A. J. Moore, C. L. Wood, H. Gershtenman, J. Y. Becker, V. Y. Khodorkovsky, A. Ellern, J. Bernstein, I. F. Perepichka, V. Rotello, M. Grey, A. O. Cuello, *J. Mater. Chem.* **2001**, *11*, 2181−2191.
[7] A. S. Batsanov, A. J. Moore, N. Roberston, A. Green, M. R. Bryce, J. A. K. Howard, A. E. Underhill, *J. Mater. Chem.* **1997**, *7*, 387−389.

[8] T. Imakubo, H. Sawa, R. Kato, *J. Chem. Soc., Chem. Commun.* **1995**, 1097−1098.
[9] T. Imakubo, H. Sawa, R. Kato, *Synth. Metals* **1997**, *86*, 1847−1848.
[10] Y. Kuwatani, E. Ogura, H. Nishikawa, I. Ikemoto, M. Iyoda, *Chem. Lett.* **1997**, 817−818.
[11] T. Imakubo, H. Sawa, R. Kato, *J. Chem. Soc., Chem. Commun.* **1995**, 1667−1668.
[12] T. Imakubo, T. Maruyama, H. Sawa, K. Kobayashi, *Chem. Commun.* **1998**, 2021−2022.
[13] H. M. Yamamoto, J.-I. Yamaura, R. Kato, *J. Am. Chem. Soc.* **1998**, *120*, 5905−5913.
[14] J. Nishijo, E. Ogura, J. Yamaura, A. Miyazaki, T. Enoki, T. Takano, Y. Kuwatani, M. Iyoda, *Solid State Commun.* **2000**, *116*, 661−664.
[15] E. Coronado, J. R. Galan-Mascaros, C. J. Gomez-Garcia, V. Laukhin, *Nature* **2000**, *408*, 447−449 and references therein.
[16] B. Domercq, T. Devic, M. Fourmigué, P. Auban-Senzier, E. Canadell, *J. Mater. Chem.* **2001**, *11*, 1570−1575.
[17] The corresponding folding angles of the dithiole rings amount to 4.8(1) and 1.7(2)°.
[18] B. Garreau, D. De Montauzon, P. Cassoux, J.-P. Legros, J.-M. Fabre, K. Saoud, S. Chakroune, *New. J. Chem.* **1995**, *19*, 161−171.
[19] G. R. Desiraju, R. Parthasarathy, *J. Am. Chem. Soc.* **1989**, *111*, 8725−8726.
[20] S. L. Price, A. J. Stone, J. Lucas, R. S. Rowland, A. E. Thornley, *J. Am. Chem. Soc.* **1994**, *116*, 4910−4918.
[21] Compound **2** crystallises in the orthorhombic system with a = 12.6757(13), b = 13.8122(9), c = 16.4095(13) Å, V = 2873.0(7) Å^3.
[22] E. Corradi, S. V. Meille, M. T. Messina, P. Metrangolo, G. Resnati, *Angew. Chem. Int. Ed.* **2000**, *39*, 1782−1786.
[23] R. B. Walsh, C. W. Padgett, P. Metrangolo, G. Resnati, T. W. Hanks, W. T. Pennington, *Cryst. Growth Des.* **2001**, *1*, 165−175.
[24] T. Devic, J. N. Bertran, B. Domercq, E. Canadell, N. Avarvari, P. Auban-Senzier, M. Fourmigué, *New J. Chem.* **2001**, *25*, 1418−1424.
[25] No reliable conductivity data could be obtained from [**1**]$_2$[Ni(mnt)$_2$] as the crystals were too small.
[26] A. Kobayashi, Y. Susuki, *Bull. Chem. Soc. Jpn.* **1977**, *50*, 2650−2656.
[27] C. Mahadevan, M. Seshasayee, A. Radha, P. T. Manoharan, *Acta Crystallogr., Sect. C* **1984**, *40*, 2032−2034.
[28] O. Kahn, in *Molecular Magnetism*, VCH, Weinheim, 1993, ch. 11.
[29] A. Dolbecq, M. Fourmigué, P. Batail, C. Coulon, *Chem. Mater.* **1994**, *6*, 1413−1418 and references therein.
[30] A. Davison, N. Edelstein, R. H. Holm, A. H. Maki, *Inorg. Chem.* **1963**, *2*, 1227−1232.

Received January 28, 2002
[I02045]

Novel Complexes *trans*(Cl)-[Os(bpy)(CO)(CH_3CN)Cl_2]^n (n = 0, +1; bpy = 2,2′-Bipyridine): Photo- and Electrochemical Syntheses and Comparative Study of Their Bonding and Redox Properties

Sylvie Chardon-Noblat,*[a] Philippe Da Costa,[a] Alain Deronzier,*[a] Taasje Mahabiersing,[b] and František Hartl*[b]

Keywords: Osmium / N ligands / Charge-transfer photochemistry / Electrochemical oxidation / Decarbonylation

Photoirradiation of the complex *trans*(Cl)-[Os(bpy)($CO)_2Cl_2$] in acetonitrile with $\lambda \geq 320$ nm light gives rise to substitution of a CO ligand, with the formation of *trans*(Cl)-[Os(bpy)-(CO)(CH_3CN)Cl_2]. The bonding properties and redox reactions of the novel photoproduct were thoroughly investigated by several methods such as nanosecond time-resolved UV/Vis absorption and resonance Raman spectroscopy, cyclic voltammetry, and IR and UV/Vis spectroelectrochemistry. Its one-electron electrochemical oxidation in acetonitrile produces the stable cation *trans*(Cl)-[Os(bpy)(CO)(CH_3CN)Cl_2]$^+$. This complex is also formed as the major product during one-electron oxidation of the dicarbonyl precursor *trans*(Cl)-[Os(bpy)($CO)_2Cl_2$] in acetonitrile at room temperature. By contrast, the initial dicarbonyl oxidation product *trans*(Cl)-[Os(bpy)($CO)_2Cl_2$]$^+$ remains stable in dry noncoordinating dichloromethane and in butyronitrile at low temperatures. The CO-loss reactivity of *trans*(Cl)-[Os(bpy)($CO)_2Cl_2$], induced by the partial oxidation of the formally osmium(II) centre, is dramatically lower compared to the corresponding ruthenium(II) complex due to the stronger Os–CO bonds. Replacement of one CO or Cl ligand in *trans*(Cl)-[Os(bpy)-($CO)_2Cl_2$] by a stronger σ-donor CH_3CN or isopropoxycarbonyl [–C(O)O*i*Pr] ligands strengthens the Os–CO bond(s) and results in photostable derivatives.
(© Wiley-VCH Verlag GmbH, 69451 Weinheim, Germany, 2002)

Introduction

In the past two decades considerable attention has been paid to the synthesis,[1−3] electrochemistry,[4−6] photochemistry[7−10] and (photo-, electro-)catalytic properties[11−17] of the complex *trans*(Cl)-[Ru(bpy)($CO)_2Cl_2$] (bpy = 2,2′-bipyridine) and its derivatives. The active species in the electrocatalytic reduction of CO_2 with this complex is the insoluble polymer [Ru(bpy)($CO)_2$]$_n$ resulting from a two-electron reduction pathway. Its physicochemical properties and reactivity can be finely tuned by attachment of different substituents at the bpy rings.[5] We have been particularly interested whether a major difference in this regard can be achieved by replacement of the ruthenium centre by the heavier osmium. In general, osmium complexes are less reactive and therefore better suited for mechanistic studies. The properties of the corresponding precursor osmium complex *trans*(Cl)-[Os(bpy)($CO)_2Cl_2$] (**1**) have been relatively unexplored. Apart from its synthesis and brief spectroscopic characterisation,[18] only a preliminary electrochemical study has recently been reported.[19] In addition, an analogous complex **1a** with 4,4′-dimethyl-2,2′-bipyridine (dmb) was prepared as a precursor of the luminescent complex *trans*($SnPh_3$)-[Os(dmb)($CO)_2$($SnPh_3$)$_2$].[20−22] As a part of our continued studies of bonding properties and reactivity of complex **1** and its derivatives, we describe in the present work its charge-transfer photochemical reactivity [Equation (1)] and electrochemical oxidation [Equation (2)], both promoting CO substitution reaction by the donor solvent acetonitrile. The studied osmium complexes will also be compared with the corresponding ruthenium compounds.

[a] Laboratoire d'Electrochimie Organique et de Photochimie Rédox, UMR CNRS 5630, Université Joseph Fourier, Grenoble 1,
B. P. 53, 38041 Grenoble Cedex 9, France
Fax: (internat.) + 33-4/76514267
E-mail: alain.deronzier@ujf-grenoble.fr
[b] Institute of Molecular Chemistry, Universiteit van Amsterdam, Nieuwe Achtergracht 166, 1018 WV Amsterdam, The Netherlands
Fax: (internat.) + 31-20/525-6456
E-mail: hartl@science.uva.nl

$$[Os(bpy)(CO)_2Cl_2] \xrightarrow[CH_3CN]{h\nu} [Os(bpy)(CO)(CH_3CN)Cl_2] + CO \quad (1)$$

$$[Os(bpy)(CO)_2Cl_2] \xrightarrow[CH_3CN]{-e^-} [Os(bpy)(CO)(CH_3CN)Cl_2]^+ + CO \quad (2)$$

Results and Discussion

Photochemical Formation and Characterization of [Os(bpy)(CO)(CH_3CN)Cl_2] (2)

Irradiation of *trans*(Cl)-[Os(bpy)(CO)$_2$Cl$_2$] (**1**) in CH_3CN with a 250-W Xe lamp into its predominantly Os-to-bpy charge transfer band at 364 nm produces within a few hours exclusively the photostable monocarbonyl complex *trans*(Cl)-[Os(bpy)(CO)(CH_3CN)Cl_2] (**2**) (Figure 1). The composition of the photoproduct has been verified by mass spectrometry and elemental analysis. Its *trans*(Cl) geometry can be deduced from the corresponding ^{1}H NMR spectrum, in particular from the coinciding signals of the 2,2′-bipyridine hydrogen atoms 6-H and 6′-H at δ = 9.05 ppm (see Scheme 1 and Exp. Sect.).[23] The identity of complex **2** has further been confirmed by IR spectroscopy. During the irradiation, the two ν(CO) bands of the parent complex **1** (2038 and 1968 cm^{-1}; CH_3CN) are replaced by a single band at 1933 cm^{-1}. Such a large wavenumber drop is quite normal for CO substitution in a dicarbonyl complex, resulting in considerably increased π-back-bonding to the remaining CO ligand. For comparison, a similar situation applies for *cis*(Cl)-[Ru(bpy)(CO)$_2$Cl$_2$] [ν(CO) at 2067 and 2001 cm^{-1}; CH_3CN] and *cis*(Cl)-[Ru(bpy)(CO)(CH_3CN)Cl_2] [ν(CO) at 1969 cm^{-1}; CH_3CN].[9] The typically smaller ν(CO) wavenumbers for the osmium(II) compounds compared to their ruthenium(II) derivatives [$\Delta\nu$(CO) $\approx$ 30 cm^{-1} for corresponding bands] reflect the stronger bond between CO and the 5d metal atom.

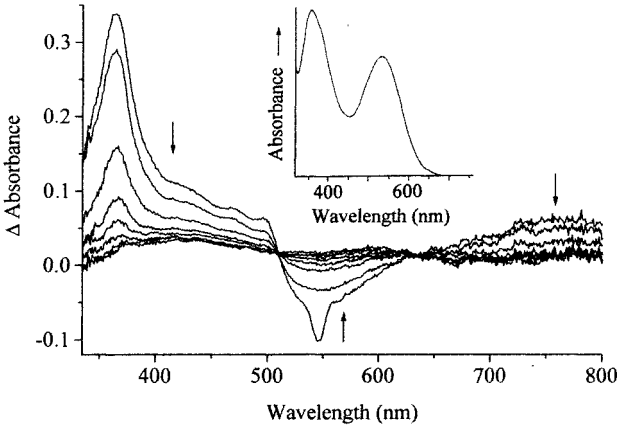

Figure 1. Nanosecond TA spectra of complex **2** in acetonitrile (λ_{exc} = 545 nm, time increment 5 ns, 50 accumulations); the MLCT/XLCT (X = Cl; L = 2,2-bipyridine) excited-state lifetime τ = 12.6 ns at 293 K; inset: UV/Vis spectrum of complex **2** in acetonitrile

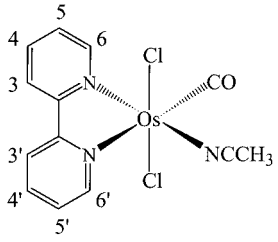

Scheme 1. Schematic molecular structure of complex **2** with numbering of 2,2′-bipyridine proton nuclei for assignment of ^{1}H NMR signals

In the course of the photoreaction the initially yellow solution of **1** (λ_{max} = 364 nm in acetonitrile) turns progressively purple due to the appearance of a new visible absorption band of complex **2** at λ_{max} = 535 nm; in addition, a new band also grows at 362 nm (Figure 1, in set). This spectral change is consistent with a significantly higher energy of the largely d_π(Os)-centred highest occupied molecular orbital (HOMO) of complex **2** compared to that of precursor **1**. The higher energy of the HOMO is evidenced by the much less positive $E_{1/2}(Os^{II}/Os^{III})$ oxidation potential for **2** (see below), reflecting sensitively the substitution of the π-acceptor carbonyl ligand by the stronger σ-donor acetonitrile ligand. On the other hand, the lowest unoccupied π^* (bpy) orbital (LUMO) rises by much less energy upon the photosubstitution than the HOMO, as can be concluded from the close $E_{1/2}$(bpy/bpy$^{\cdot-}$) reduction potentials for **1** and **2** (see below).

In order to assign the lowest-energy electronic transition of complex **2**, nanosecond time-resolved absorption (TA) spectra (Figure 1) and resonance Raman spectra (Figure 2) were recorded upon irradiation into the visible absorption band at 535 nm. The difference UV/Vis absorption spectra in Figure 1 show a bleaching between 500 and 630 nm due to the disappearance of complex **2** (inset to Figure 1) that completely regenerates in 35 ns after the laser pulse. The transient absorption between 630 and 800 nm can be ascribed to the lowest π^*-π^* transitions of the aromatic [bpy]$^{\cdot-}$ ligand;[24] another set of π^*-π^* transitions is observed as a band with two characteristic absorption maxima at 467 and 497 nm. The strong transient band at 363 nm probably belongs to the π-π^* transition of [bpy]$^{\cdot-}$. The shoulder at 418 nm may reflect the presence of the formally Os^{III} centre in the excited transient, as a similar absorption band appears in the UV/Vis spectrum of the electrochemically one-electron-oxidised Os^{III} species **2**$^+$ (see below and Figure 3). The TA data thus indicate that the lowest optically accessible excited state has an osmium(II)-to-bpy charge-transfer (MLCT) character. On the other hand, resonance Raman spectra of nonluminescent **2**, dispersed in KNO_3 and irradiated with 514.5 nm (Figure 2) and 543 nm light, show only a weak rR effect of ν_s(CO) at 1917 cm^{-1}. [For comparison, the ν(CO) band of complex **2**, dispersed in KBr, occurs at 1927 cm^{-1}, i.e. lower by 6 cm^{-1} than found in acetonitrile, see above]. This implies that the Os-to-CO π-back-bonding is not strongly affected by this electronic transition. Characteristic resonance-enhanced Raman bands of the bpy ligand are found at 1606, 1557 [both ν(C=C)], 1493, 1325 [both ν(C=N)], 1278 [ν(C−C) inter-ring], 1177 [δ(CCH) in-plane], 1031 (ring breathing) and 669 [δ(CCC) inter-ring] cm^{-1}. Importantly, an apparent Raman band due to ν_s(Os−Cl) is observed at 302 cm^{-1}, consistent with a relatively strong rR effect on the Os−Cl bonds. However, the overall rR effect is rather weak and,

hence, the normal coordinates of complex **2** are less affected by the electron transfer to π*(bpy) than would be expected for an MLCT transition. Instead, the rR spectra of complex **2** agree with a mixed MLCT/XLCT (X = Cl) character of the lowest optically accessible excited state. Its lifetime τ = 12.6 ns at 293 K has been determined from the TA data (see above).

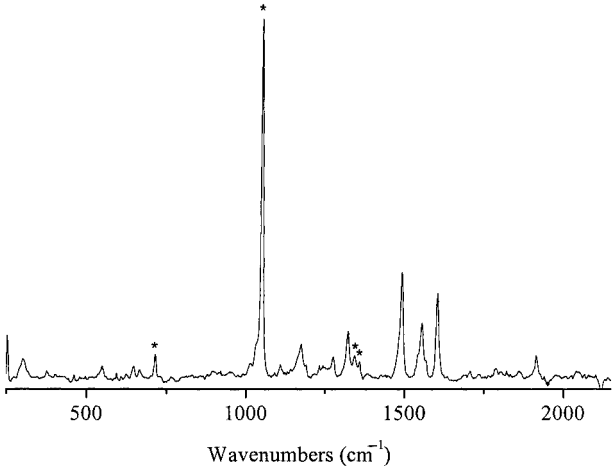

Figure 2. Resonance Raman spectrum of complex **2** dispersed in a KNO_3 pellet; λ_{exc} = 514.5 nm; bands due to KNO_3 indicated by an asterisk

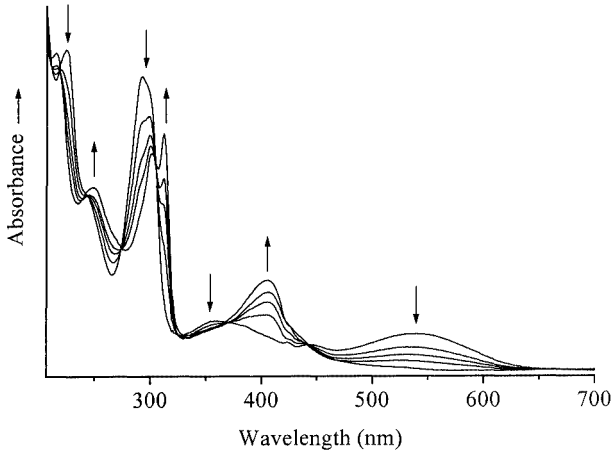

Figure 3. UV/Vis spectral changes recorded during the one-electron oxidation of complex **2** (10^{-3} M) in acetonitrile; electrolysis within an OTTLE cell[38] at 293 K

Unfortunately, the CO-loss photoreactivity and luminescence of complex **1** prevented the recording of both TA and resonance Raman spectra for this complex and comparison with complex **2**.

A similar difference in the CO-loss reactivity was also observed between the corresponding cations $\mathbf{1}^+$ and $\mathbf{2}^+$ produced by electrochemical oxidation (see below). This observation is consistent with removal of electron density from the highest occupied molecular orbital, similarly to the situation in the mixed lowest-energy charge-transfer excited state of the Os^{II} complexes **2**. The cyclic voltammogram (CV) of the photoproduct **2** dissolved in $CH_3CN/10^{-1}$ M TBAP indeed shows a completely reversible Os^{II}/Os^{III} redox couple at $E_{1/2}$ = 0.45 V vs. Ag/Ag^+ that is positioned less positively by 0.80 V than the one-electron oxidation of parent complex **1**.[19] This observation agrees with the strong σ-donor ability of the CH_3CN ligand compared to the expulsed π-acceptor carbonyl ligand, thereby stabilizing the formal osmium(III) oxidation state in $\mathbf{2}^+$. Exhaustive oxidation of complex **2** at 0.55 V upon bulk electrolysis or within a thin-layer spectroelectrochemical cell produced the corresponding inherently stable cation $\mathbf{2}^+$ quantitatively. The UV/Vis spectrum of the oxidised product exhibits a low-energy absorption band at 406 nm (ε_{max} = 5500 M^{-1} cm^{-1}) tailing down to 550 nm. The UV/Vis spectral changes accompanying the formation of $\mathbf{2}^+$ within an OTTLE cell are shown in Figure 3. In the infrared region the single ν(CO) band of $\mathbf{2}^+$ (2047 cm^{-1}) is shifted to larger wavenumbers by 114 cm^{-1} compared to parent complex **2** (1933 cm^{-1}). The large ν(CO) difference testifies to the predominantly Os-localised oxidation, resulting in strongly diminished Os-to-CO π-back-bonding.[25]

Unlike the completely irreversible reduction of the dicarbonyl precursor **1** in CH_3CN electrolyte at room temperature and moderate cyclic voltammetric scan rates,[19] complex **2** is reduced under the same experimental conditions in a nearly chemically reversible one-electron step at $E_{1/2}$ = −1.80 V (I_{pa}/I_{pc} = 0.93 at v = 100 mV s^{-1}). As mentioned above, the π*(bpy) LUMO energy for complex **2** is slightly higher than complex **1**, which is reversibly reduced at a less negative potential: $E_{1/2}$ −1.64 V (THF, 293 K)[19] and −1.62 V (PrCN, 273 K). Exhaustive electrolysis of **2** in acetonitrile at −1.90 V leads to the formation of a dark film, weakly adherent to the working electrode surface, together with a green solution containing 1 mol-equiv. of free chloride ions, as revealed by voltammetry on a rotating disk electrode.[29] In situ IR spectroelectrochemical study of this cathodic process in acetonitrile/10^{-1} M TBAP at room temperature showed disappearance of the ν(CO) band of **2** at 1933 cm^{-1} and formation of a new reduced complex **2R**, absorbing at 1890 cm^{-1}. The parallel thin-layer cyclic voltammetric scan shows that **2R** is not the one-electron-reduced radical anion $\mathbf{2}^{\cdot-}$ [stable in PrCN at 253 K, ν(CO) at 1895 cm^{-1}], as its reverse oxidation occur 0.45 V less negatively than the initial reduction of precursor **2**. Further reduction of **2R** is chemically reversible ($E_{1/2}$ = −1.96 V), causing a shift of the ν(CO) band to 1857 cm^{-1}. This behaviour of complex **2** upon reduction closely resembles that of complex **1**,[19] pointing to the formation of an Os−Os-bonded species. Detailed experimental studies of the reduction paths of complexes **1** and **2** are in progress and will be published in a separate paper.

Electrochemical Formation of [Os(bpy)(CO)(CH_3CN)Cl_2] (2)

Electrochemical oxidation of complex **1** to the formally osmium(III) species $\mathbf{1}^+$ ($E_{1/2}$ = 1.23 V vs. Ag/Ag^+ in acetonitrile[19]) is completely reversible on the time scale of cyclic voltammetry at room temperature, independently of the solvent used {acetonitrile [see Figure 4 (a)], butyronitrile, dichloromethane}. The less positive oxidation potential

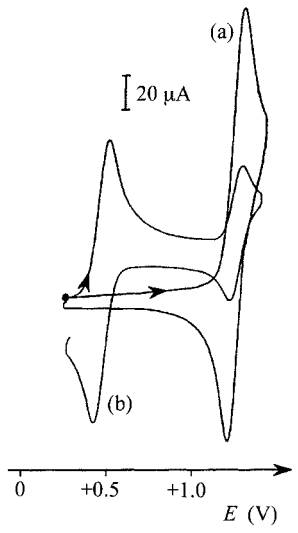

Figure 4. Cyclic voltammograms recorded (a) before and (b) after exhaustive one-electron oxidation of complex **1** (2.71×10^{-3} M) at 1.35 V and subsequent back reduction of the oxidised species $\mathbf{1}^+$ and $\mathbf{2}^+$ at 0.25 V at a Pt sheet electrode; conditions: acetonitrile containing 10^{-1} M TBAP and 1 μL of H_2O per 10 mL of CH_3CN, Pt disk electrode (5 mm diameter), scan rate 100 mV s^{-1}, T = 293 K

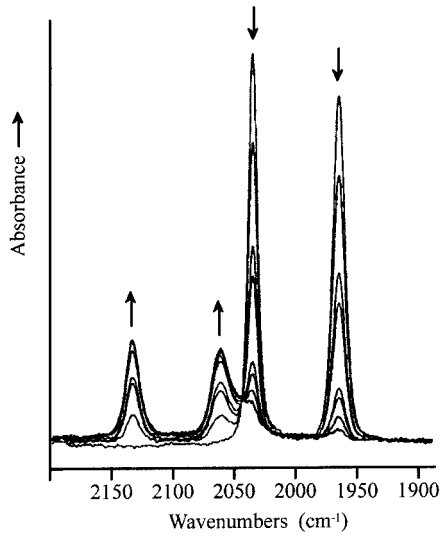

Figure 5. Spectral changes in the IR ν(CO) region recorded during the reversible oxidation of complex **1** (ca. 5×10^{-3} M) to $\mathbf{1}^+$ in butyronitrile; electrolysis within an OTTLE cell[39] at 273 K

of complex **1** compared to *trans*(Cl)-[Ru(bpy)($CO)_2Cl_2$] ($E_{1/2}$ = 1.45 V vs. Ag/Ag^+)[4,5] is generally encountered also for other types of Ru^{II} and Os^{II} complexes, such as classical $[M(bpy)_3]^{2+}$ (M = Ru, Os) and their numerous derivatives.[30] Bulk electrolysis of **1** at +1.35 V, carried out in acetonitrile containing a small amount of water (0.01%),[4] produced a mixture of $\mathbf{1}^+$ and $\mathbf{2}^+$ in 30% and 70% yield, respectively. Their quantitative back reduction at 0.25 V gave the corresponding neutral complexes **1** and **2** that were analysed by cyclic voltammetry [Figure 4 (b)]. Notably, both cations $\mathbf{1}^+$ and $\mathbf{2}^+$ are unstable during the bulk electrolysis in dry acetonitrile.

On the other hand, cation $\mathbf{1}^+$ could be completely stabilised in dry noncoordinating dichloromethane (at 293 K) or in dry butyronitrile electrolyte (at 273 K). The corresponding IR spectroelectrochemical studies showed the complete conversion of **1** [ν(CO) at 2037, 1967 cm^{-1} in dichloromethane (293 K); 2036, 1966 cm^{-1} in butyronitrile (273 K)], into $\mathbf{1}^+$ [ν(CO) at 2129 and 2056 cm^{-1} in dichloromethane (293 K); 2144 and 2063 cm^{-1} in butyronitrile (273 K)]. Notably, the ν(CO) bands of the cationic product $\mathbf{1}^+$ possess much lower intensity than those of the parent complex (see Figure 5). The large CO-stretching wavenumbers for $\mathbf{1}^+$ again imply one-electron oxidation predominantly localised on the osmium centre.[25] The UV/Vis spectrum of $\mathbf{1}^+$ in dichloromethane is very similar to that of the electrochemically oxidised photoproduct $\mathbf{2}^+$ in acetonitrile (see Figure 3), the maximum of the new lowest-lying absorption band of $\mathbf{1}^+$ being merely shifted to 385 nm. Apparently, the corresponding electronic transition in the formally osmium(III) complexes $\mathbf{1}^+$ and $\mathbf{2}^+$ with *trans*(Cl) geometry is not much affected by the substitution of the CO ligand by acetonitrile. Its assignment, however, has not been attempted, as support from theoretical MO studies is needed for a precise description of the molecular orbitals involved.

In contrast, when the butyronitrile electrolyte is replaced with acetonitrile, the oxidation of complex **1** within the IR OTTLE cell at 273 K produces besides $\mathbf{1}^+$ [ν(CO) at 2135, 2063 cm^{-1}] also CO-substituted $\mathbf{2}^+$ [ν(CO) at 2048 cm^{-1}] as the minor secondary product ($\mathbf{1}^+/\mathbf{2}^+ \approx 3:1$). At room temperature $\mathbf{2}^+$ becomes the major product ($\mathbf{1}^+/\mathbf{2}^+ \approx 1:4$). When the one-electron oxidation of complex **1** is nearly completed, two additional secondary products begin to form both at 293 and 273 K. At the same time the concentrations of $\mathbf{1}^+$ and $\mathbf{2}^+$ decrease. These cations are apparently in equilibrium. One of the ultimate products can be assigned as $[Os^{II}(bpy)(CO)_2(CH_3CN)Cl]^+$ [ν(CO) at 2066 and 2003 cm^{-1}], based on the comparison with $[Ru^{II}(bpy)(CO)_2(CH_3CN)Cl]^+$ [ν(CO) at 2091 and 2035 cm^{-1}][31] and taking into account the likely ν(CO) wavenumber difference of ca. 30 cm^{-1} (see above). The other tertiary product [ν(CO) at 2058 and 1991 cm^{-1}] has remained unassigned. Possibly, two different structural isomers of $[Os^{II}(bpy)(CO)_2(CH_3CN)Cl]^+$ are formed in similar amounts. As a plausible explanation of the observed anodic behavior, CO liberated during the formation of $\mathbf{2}^+$ cannot escape from the thin electrolyte layer within the spectroelectrochemical cell and remains dissolved in the vicinity of the working electrode. At the end of the electrolysis the CO concentration increased sufficiently to trigger the reaction with cations $\mathbf{1}^+$ or $\mathbf{2}^+$ and the replacement of one chloride ligand with the formation of $[Os^{III}(bpy)(CO)_2(CH_3CN)Cl]^{2+}$. Importantly, the thin-layer cyclic voltammetric scan recorded during the oxidation of complex **1,** has proven that $[Os^{II}(bpy)(CO)_2(CH_3CN)Cl]^+$ is not further oxidised to the corresponding dication before the anodic limit of the potential "window" of the acetonitrile electrolyte is reached. The generation of the oxidised transient $[Os^{III}(bpy)(CO)_2(CH_3CN)Cl]^{2+}$ from complex $\mathbf{2}^+$, even though inefficient,

must therefore be coupled to its instantaneous one-electron reduction at the applied electrode potential of the **1/1**$^+$ redox couple, resulting in the stable complex $[Os^{II}(bpy)(CO)_2(CH_3CN)Cl]^+$. In this way $[Os^{II}(bpy)(CO)_2(CH_3CN)Cl]^+$ is formed at the expense of **1**$^+$ and **2**$^+$ until the process becomes inhibited owing to decreased CO concentration.

Comparison of the CO-Loss Reactivity of Complexes $[M(bpy)(CO)_n(CH_3CN)_{2-n}Cl_2]$ (M = Ru, Os; n = 1, 2)

It is important to recall that electrochemical oxidation of the complex *trans*(Cl)-$[Ru(bpy)(CO)_2Cl_2]$ in acetonitrile, containing a small amount of water, induces decoordination of one CO and one Cl ligand, producing the Ru^{III} complex $[Ru(bpy)(CO)(CH_3CN)_2Cl]^{2+}$. The completely decarbonylated Ru^{III} compound $[Ru(bpy)(CH_3CN)_2Cl_2]^{2+}$ is also formed in low yield (5%) in this medium.[4] In contrast to this, for the corresponding Os^{II} complex **1** it proved possible to substitute merely a single CO ligand, by electrochemical one-electron oxidation producing the cationic species **2**$^+$. Moreover, the CO substitution is incomplete even in aqueous CH_3CN electrolyte at ambient temperature and a mixture of cations **1**$^+$ and **2**$^+$ is produced. Substitution of a chloride ligand in the course of the oxidation of complex **1**, producing ultimately the Os^{II} complex $[Os(bpy)(CO)_2(CH_3CN)Cl]^+$, could only be achieved under special conditions of locally increased CO concentration in the acetonitrile electrolyte. These results point to much stronger Os−CO bonds in complex **1**$^+$, but also in **2**$^+$, compared to the corresponding ruthenium derivatives. This conclusion is supported by the lower ν(CO) frequencies for the Os^{II} complexes (see above). The σ,π-donation from the chloride ligands is assumed to play an important role in the stabilization of the formal metal(III) oxidation state, strengthening the metal-to-CO π-backbonding and, hence, the metal(III)−CO bonds. A comparison of ν(CO) frequencies for the corresponding Os^{III} and Ru^{III} complexes would be useful in this regard. Unfortunately, the oxidised Ru^{III} complexes *trans*(Cl)-$[Ru(bpy)(CO)_2Cl_2]^+$ and $[Ru(bpy)(CO)(CH_3CN)Cl_2]^+$ have not been characterised so far by IR spectroscopy.

Similar arguments can be used to explain the relatively slow dissociative photosubstitution reaction of complex **1** in acetonitrile, producing the monocarbonyl complex *trans*(Cl)-$[Os(bpy)(CO)(CH_3CN)Cl_2]$ (**2**). Resonance Raman spectra of the latter photostable complex have shown that its lowest-energy optically populated excited state has a mixed MLCT/XLCT character. This unreactive excited state apparently does not interact with any reactive state from which a CO-loss reaction would occur [e.g. ligand-field (LF) or metal-to-CO charge-transfer (MLCT) states[10,32]. In contrast to this, the related 4d-ruthenium complex *cis*(Cl)-$[Ru(bpy)(CO)(CH_3CN)Cl_2]$ is readily photoreactive and converts into $[Ru(bpy)(CH_3CN)_2Cl_2]$.[7] Time-resolved spectroscopic studies and theoretical MO calculations are needed to describe the reactive (dissociative) state in the latter case.

Time-dependent DFT calculations on the complex *trans*(Cl)-$[Ru(Me\text{-}DAB)(CO)_2Cl_2]$ (Me-DAB = *N*,*N*′-dimethyl-1,4-diaza-1,3-butadiene) have revealed a mixed XLCT/MLCT character of its lowest-energy allowed electronic transition, while CASSCF/CASPT2 ab initio calculations favour its predominant MLCT assignment.[33] The CO-loss reactions of the analogous ruthenium complex *trans*(Cl)-$[Ru(bpy)(CO)_2Cl_2]$ and the studied complex **1** probably occur upon optical preparation of a similar Franck-Condon excited state. Upon light absorption and electron transfer to the π*(bpy) orbital the metal centre becomes partly oxidised, resulting in diminished π-backbonding toward the CO ligands bound in the equatorial metal−bpy plane. The stabilization of the metal−CO bonds by increased donation of electron density to the $M(CO)_2$ unit from the axial donor ligands plays a crucial role in tuning the photoreactivity. Thus, incorporation of a stronger σ-donor isopropoxycarbonyl [−C(O)O*i*Pr] ligand instead of chloride results in a photostable complex $[Os(bpy)(CO)_2\{C(O)OiPr\}Cl]$.[34] Under identical experimental conditions, the isomeric ruthenium(II) photoproduct *cis*(Cl)-$[Ru(bpy)(CO)(CH_3CN)Cl_2]$ is formed from *trans*(Cl)-$[Ru(bpy)(CO)_2Cl_2]$ markedly more rapidly (within a few minutes),[7,9] again consistent with weaker Ru−CO bonds in the reactive excited state and in analogy with the electrochemical oxidation. It is also possible that for the less photoreactive 5d-Os complex **1** a branching of the Franck-Condon excited state evolution occurs, resulting in a competition between CO-loss reactivity from the dissociative state and parallel population of an unreactive excited state.[10,32] Again, time- and temperature-dependent studies and theoretical support are needed. The CO-loss-induced photoisomerisation is characteristic for this class of dicarbonylruthenium and -osmium complexes with the lowest-energy optically accessible XLCT/MLCT excited states. Another example is the complex *trans*,*cis*-$[Ru(CO)_2(dmb)(Me)I]$ (dmb = 4,4′-tetramethyl-bpy) isomerising via the monocarbonyl transient [Ru(CO)(dmb)(Sv)(Me)I] (Sv = donor solvent) to *cis*,*cis*-$[Ru(CO)_2(dmb)(Me)I]$.[36] In this regard it is remarkable that both complex **1** and its ultimate photoproduct **2** are *trans*(Cl) isomers; although, the proposed stucture of complex **2** (see above) has not been yet confirmed by a single-crystal X-ray diffraction study.

Experimental Section

General Remarks: The supporting electrolyte Bu_4NClO_4 (TBAP; Fluka) and HPLC-grade acetonitrile (Rathburn) were used as received. Analytical-grade acetontrile and butyronitrile (purchased from Acros) were distilled from CaH_2. All syntheses and measurements were performed under dry nitrogen or argon, in a dry-box and/or using standard Schlenk techniques. For photolysis experiments, the samples were placed in a pyrex glass vessel and irradiated under argon with unfiltered light of Oriel Instruments 500-W Hg or Osram XBO 250-W Xe discharge lamps. Cyclic voltammetric measurements and bulk electrolyses were performed using a PAR Model 173 potentiostat. All cyclic voltammograms were recorded with a conventional single-compartment three-electrode cell in a

dry box (Jaram). All electrode potentials reported in this work are given relative to Ag/Ag^+ (10^{-2} M in CH_3CN containing 10^{-1} M TBAP). Conversion into the ferrocene/ferrocenium reference system can be easily done by adding −0.087 V.[37] The working electrodes for cyclic voltammetry were platinum or glassy carbon (GC) discs (active surface areas of 0.19 and 0.07 cm^2, respectively), polished carefully with a 2 μm diamond paste (Mecaprex Presi). Exhaustive electrolyses were carried out in the same cell on a platinum sheet (2 cm^2). The auxiliary electrode was a Pt wire in acetonitrile/10^{-1} M TBAP. The electrolysed solutions of complex **1** were handled in the dark to avoid photoreactions. IR and UV/Vis spectroelectrochemical experiments at variable temperatures were carried out with home-made OTTLE cells[38,39] equipped with a Pt minigrid working electrode (32 wires/cm) and CaF_2 windows. The spectroelectrochemical samples typically contained 3×10^{-3} M osmium complex and 3×10^{-1} M supporting electrolyte. The working electrode potential of the OTTLE cells was controlled with PA4 (EKOM, Czech Republic) or PAR Model 173 potentiostats. Electronic absorption spectra were recorded with Hewlett−Packard 8452 A or 8453 diode array spectrophotometers, IR spectra with Perkin−Elmer Spectrum GX FTIR or Bio-Rad FTS 7 spectrometers, and ^1H NMR spectra with a Bruker AC 250 MHz spectrometer. Mass spectra (FAB^+) were obtained with a ZAB-HF-VB analytical apparatus in a *m*-nitrobenzyl alcohol matrix. Nanosecond time-resolved absorption (TA) spectra of complex **2** were obtained by irradiating the sample with 5-ns pulses (fwhm) of a 545 nm line of a continuously tunable (360−700 nm) Coherent Infinity XPO laser. The employed experimental setup has been described previously.[40] Resonance Raman (rR) spectroscopic measurements were performed with a Dilor XY spectrometer, equipped with a Wright Instruments CCD detector. A Spectra Physics 2040E argon ion laser in combination with Coherent CR490 and CR590 dye lasers (with Coumarine 6 and Rhodamine 6G dyes) served as excitation sources under a 180° backscattering geometry. Data acquisition was controlled by Dilor Labspec 2.08 software. Wavenumbers of the resonance-enhanced Raman bands were calibrated with respect to the Raman bands of NO_3^- at 1051 and 716 cm^{-1}. Baseline deviations were corrected by using Grams software. Elemental analyses (C, H, N) were carried out in the Microanalytisches Laboratorium of Dornis & Kolbe, Mülheim a. d. Ruhr, Germany. Determination of Cl was performed argentometrically after pyrolysis according to the method of Schöniger.[41,42]

Synthesis of *trans*(Cl)-[Os(bpy)(CO)(CH_3CN)Cl_2] (2): The precursor complex *trans*(Cl)-[Os(bpy)(CO)$_2Cl_2$] (**1**) was prepared as previously described.[19] A solution of complex **1** (20 mg, 4.2×10^{-5} mol) in acetonitrile (20 mL) was illuminated with unfiltered light of a 250-W Xe lamp with continuous stirring and incidental purging with argon gas. The progress of the photoreaction was monitored by UV/Vis and IR spectroscopy. Under these conditions the complete photochemical conversion of **1** into **2** was achieved in 18 h (Figure 1). The resulting solution of **2** was concentrated to dryness, leaving behind a purple powder. Yield: ca. 18 mg (90%). ^1H NMR (250 MHz, CD_3CN, 298 K): δ = 1.96 (s, 3 H, CH_3CN), 7.40 (td, ^3J = 5.6, ^4J = 1.6 Hz, 1 H, 5′-H), 7.75 (2 td, 2 H, 4′,5-H), 8.17 (td, ^3J = 5.6, ^4J = 1.6 Hz, 1 H, 4-H), 8.33 (d, ^3J = 8.7 Hz, 1 H, 3′-H), 8.41 (d, ^3J = 8.7 Hz, 1 H, 3-H), 9.05 (d, ^3J = 5.6 Hz, 2 H, 6,6′-H) ppm. IR (CH_3CN): $\tilde{\nu}$ = 1933 [vs, ν(CO)] cm^{-1}; CsI pellet: $\tilde{\nu}$ = 1929 [vs, ν(CO)], 317 (w, ν(Os-Cl)] cm^{-1}. UV/Vis (CH_3CN): λ_{max} = 362, 534 nm. FAB-MS: *m*/*z* = 487.4 $[M + H]^+$, 446.3 $[M + H - CH_3CN]^+$, 418.3 $[M + H - CH_3CN - CO]^+$. $C_{13}H_{11}Cl_2N_3OOs$ (486.36): calcd. C 32.10, H 2.28, Cl 14.58, N 8.64; found C 31.90, H 2.19, Cl 14.81, N 8.39.

Acknowledgments

We gratefully acknowledge the Ministère des Affaires Etrangères and the Netherlands Organization for Scientific Research (NWO; project VGP 71-126) for the financial support of this work undertaken as a part of the bilateral Dutch-French Van Gogh Programme. Many thanks are owed to Mr. Frank W. Vergeer and Mr. Theo L. Snoeck (both University of Amsterdam) for recording the nanosecond TA and resonance Raman spectra, respectively.

[1] D. S. C. Black, G. B. Deacon, N. C. Thomas, *Aust. J. Chem.* **1982**, *35*, 2445−2453.
[2] D. S. C. Black, G. B. Deacon, N. C. Thomas, *Polyhedron* **1983**, *2*, 409−412.
[3] P. A. Anderson, G. B. Deacon, K. H. Haarmann, F. R. Keene, T. J. Meyer, D. A. Reitsma, B. W. Skelton, G. F. Strouse, N. C. Thomas, J. A. Treadway, A. H. White, *Inorg. Chem.* **1995**, *35*, 6145−6157.
[4] M.-N. Collomb-Dunand-Sauthier, A. Deronzier, R. Ziessel, *J. Electroanal. Chem.* **1993**, *350*, 43−55.
[5] C. Caix-Cecillon, S. Chardon-Noblat, A. Deronzier, M. Haukka, T. A. Pakkanen, R. Ziessel, D. Zsoldos, *J. Electroanal. Chem.* **1999**, *466*, 187−196.
[6] S. Chardon-Noblat, P. Da Costa, A. Deronzier, M. Haukka, T. A. Pakkanen, R. Ziessel, *J. Electroanal. Chem.* **2000**, *490*, 62−69.
[7] M.-N. Collomb-Dunand-Sauthier, A. Deronzier, R. Ziessel, *J. Organomet. Chem.* **1993**, *444*, 191−198.
[8] M.-N. Collomb-Dunand-Sauthier, A. Deronzier, R. Ziessel, *J. Phys. Chem.* **1993**, *97*, 5973−5979.
[9] E. Eskelinen, M. Haukka, T. Venäläinen, T. A. Pakkanen, M. Wasberg, S. Chardon-Noblat, A. Deronzier, *Organometallics* **2000**, *19*, 163−169.
[10] S. Luukkanen, M. Haukka, E. Eskelinen, T. A. Pakkanen, V. Lehtovuori, J. Kallioinen, P. Myllyperkiö, J. Korppi-Tommola, *Phys. Chem. Chem. Phys.* **2001**, *3*, 1992−1998.
[11] M.-N. Collomb−Dunand-Sauthier, A. Deronzier, R. Ziessel, *Inorg. Chem.* **1994**, *33*, 2961−2967.
[12] S. Chardon-Noblat, A. Deronzier, R. Ziessel, D. Zsoldos, *J. Electroanal. Chem.* **1998**, *444*, 253−260.
[13] M. Haukka, J. Kiviaho, M. Ahlgrén, T. A. Pakkanen, *Organometallics* **1995**, *14*, 825−833.
[14] S. Luukkanen, P. Homanen, M. Haukka, T. A. Pakkanen, A. Deronzier, S. Chardon-Noblat, D. Zsoldos, R. Ziessel, *Appl. Catal., A* **1999**, *185*, 157−164.
[15] M. Haukka, L. Alvila, T.A. Pakkanen, *J. Mol. Catal.* **1995**, *102*, 79−92.
[16] M. Haukka, T. Venäläinen, M. Kallinen, T.A. Pakkanen, *J. Mol. Catal.* **1998**, *136*, 127−134.
[17] J.-M. Lehn, R. Ziessel, *J. Organomet. Chem.* **1990**, *382*, 157−173.
[18] E. Z. Jandrasics, F. R. Keene, *J. Chem. Soc., Dalton Trans.* **1997**, 153−159.
[19] S. Chardon-Noblat, A. Deronzier, F. Hartl, J. van Slageren, T. Mahabiersing, *Eur. J. Inorg. Chem.* **2001**, 613−617.
[20] J. van Slageren, D. J. Stufkens, *Inorg. Chem.* **2001**, *40*, 277−285.
[21] J. van Slageren, F. Hartl, D. J. Stufkens, D. M. Martino, H. van Willigen, *Coord. Chem. Rev.* **2000**, *208*, 309−320.
[22] J. A. Weinstein, J. van Slageren, D. J. Stufkens, S. Záliš, M. W. George, *Dalton Trans.* **2001**, 2587−2592.
[23] For related isomeric ruthenium(II) complexes, e.g. *trans*(Cl)- and *cis*(Cl)-[Ru(bpy)(CO)$_2Cl_2$], the 6-H and 6-H′ signals are well separated by 0.7−0.9 ppm if one of the Cl ligands occupies an equatorial position, the signal of 6-H at the pyridine ring *trans* to the Cl ligand being shifted to values at δ > 9.6 ppm.[9]
[24] J. Víchová, F. Hartl, A. Vlček, Jr., *J. Am. Chem. Soc.* **1992**, *114*, 10903−10910.
[25] In order to underline the large shift in the ν(CO) wavenumbers observed for the predominantly metal-centred oxidation of complexes **1** and **2**, a comparison with a ligand-centred

redox series is given. Suitable examples of complexes containing Ru(CO) and $Ru(CO)_2$ moieties are $[Ru^{II}(CO)(PPh_3)(DBDiox)_2]^n$ and *cis*(CO)-$[Ru^{II}(CO)_2(DBDiox)_2]^n$, respectively; DBDiox = 3,5-di-*tert*-butyl-1,2-dioxobenzene, existing in three redox forms, as neutral *o*-quinone (Q), *o*-semiquinone (SQ) radical anion and catecholate (Cat) dianion.[26,27] The assignment of the formal oxidation states of the ruthenium(II) centre and the DBDiox ligands throughout the redox series has been supported by resonance Raman spectroscopic data.[28] Infrared CO-stretching wavenumbers for the members of the redox series $[Ru^{II}(CO)_2(DBDiox)_2]^n$ (dichloromethane, 228 K): $\tilde{\nu}$ = 2112, 2060 cm^{-1} (n = +2; DBQ/DBQ); 2091, 2037 cm^{-1} (n = +1; DBQ/DBSQ); 2056, 1998 cm^{-1} (n = 0; DBSQ/DBSQ; analogous to complex **1**); 2016, 1942 cm^{-1} (n = −1; DBSQ/DBCat); 1985, 1893 cm^{-1} (n = −2; DBCat/DBCat). Infrared CO-stretching wavenumbers for the members of the redox series $[Ru^{II}(CO)(PPh_3)(DBDiox)_2]^n$ (acetonitrile, 243 K): $\tilde{\nu}$ = 2012 cm^{-1} (n = +2; DBQ/DBQ); 1987 cm^{-1} (n = +1; DBQ/DBSQ); 1961 cm^{-1} (n = 0; DBSQ/DBSQ; analogous to complex **2**); 1909 cm^{-1} (n = −1; DBSQ/DBCat); 1861 cm^{-1} (n = −2; DBCat/DBCat).[28]

[26] C. G. Pierpont, C. W. Lange, *Prog. Inorg. Chem.* **1994**, *41*, 331−442.

[27] S. Bhattacharya, C. G. Pierpont, *Inorg. Chem.* **1994**, *33*, 6038−6042.

[28] F. Hartl, unpublished results.

[29] G. Cauquis, A. Deronzier, B. Sillion, D. Damin, J. Garapon, *J. Electroanal. Chem.* **1981**, *117*, 139−146.

[30] F. M. Calvert, R. H. Schmehl, B. P. Sullivan, J. S. Facci, T. J. Meyer, R. W. Murray, *Inorg. Chem.* **1983**, *22*, 2151−2162.

[31] S. Chardon-Noblat, G. H. Cripps, A. Deronzier, J. S. Field, S. Gouws, R. J. Haines, F. Southway, *Organometallics* **2001**, *20*, 1668−1675.

[32] A. Vlček, Jr., *Coord. Chem. Rev.* **2000**, *200−202*, 933−977.

[33] M. Turki, C. Daniel, S. Záliš, A. Vlček Jr., J. van Slageren, D. J. Stufkens, *J. Am. Chem. Soc.* **2001**, *123*, 11431−11440.

[34] The complex [Os(bpy)$(CO)_2${C(O)O*i*Pr}Cl] is usually formed as a minor side product (yield 15−20%) during the synthesis of complex **1** conducted in 2-propanol.[19] Its purification was not attempted. A similar side reaction has also been reported for the corresponding ruthenium complexes.[35] [Os(bpy)$(CO)_2${C(O)O*i*Pr}Cl] was characterised in a mixture with complex **1**. IR (in CH_3CN): ν(CO) at $\tilde{\nu}$ = 2012, 1933 cm^{-1}. MS (FAB^+): m/z = 527 $[M + H]^+$, 491 $[M + H - Cl]^+$, 467 $[M + H - C(O)OiPr]^+$. The smaller ν(CO) wavenumbers of [Os(bpy)$(CO)_2${C(O)O*i*Pr}Cl] compared to complex **1** testify to stronger donation of electron density from the isopropoxycarbonyl ligand compared to Cl, resulting in stronger Os−CO bonds. Indeed, in contrast to complex **1**, [Os(bpy)$(CO)_2${C(O)O*i*Pr}Cl] is photostable in acetonitrile at ambient temperature and CO substitution does not occur.

[35] S. Chardon-Noblat, A. Deronzier, R. Ziessel, D. Zsoldos, *Inorg. Chem.* **1997**, *36*, 5384−5389.

[36] C. J. Kleverlaan, D. J. Stufkens, *J. Photochem. Photobiol. A: Chem.* **1998**, *116*, 109−118.

[37] V. V. Pavlishchuk, A. W. Addison, *Inorg. Chim. Acta* **2000**, *298*, 97−102.

[38] M. Krejčík, M. Daněk, F. Hartl, *J. Electroanal. Chem.* **1991**, *317*, 179−187.

[39] F. Hartl, H. Luyten, H. A. Nieuwenhuis, G. C. Schoemaker, *Appl. Spectrosc.* **1994**, *48*, 1522−1528.

[40] C. J. Kleverlaan, D. J. Stufkens, I. P. Clark, M. W. George, J. J. Turner, D. M. Martino, H. van Willigen, A. Vlček, Jr., *J. Am. Chem. Soc.* **1998**, *120*, 10871−10879.

[41] W. Schöniger, *Mikrochim. Acta* **1955**, 123−129.

[42] W. Schöniger, *Mikrochim. Acta* **1956**, 869−876.

Received February 20, 2002
[I02086]

Dioxygen Activation Using Schiff Base Macrocyclic Dinuclear Copper(I) Complexes: Structurally Characterized Dioxygen Reaction Products

Haiyan Ma,[a] Markus Allmendinger,[a] Ulf Thewalt,[b][‡] Axel Lentz,[c] Martti Klinga,[d][‡‡] and Bernhard Rieger*[a]

Keywords: Macrocyclic ligands / Dinuclear copper complexes / Oxygenation reactions / O−O activation / X-ray crystal structures

Schiff-base condensation of diethylenetriamine with a series of dialdehydes [isophthalaldehyde (**2a**), 5-*tert*-butylisophthalaldehyde (**2b**), 2-methylisophthalaldehyde (**2c**), and *p*-phthalaldehyde (**2d**)] affords four hexaaza macrocyclic ligands [$L^{H,H}$ (**3a**), $L^{tBu,H}$ (**3b**), $L^{H,Me}$ (**3c**), $L^{p\text{-}H,H}$ (**3d**)] bearing different substituents on the aromatic units that connect the two metal ion binding sites. The dinuclear copper(I) complexes $[L^{H,H}Cu_2(MeCN)_2](ClO_4)_2$ (**4a**), $[L^{tBu,H}Cu_2(MeCN)_2](ClO_4)_2$ (**4b**), $[L^{H,Me}Cu_2(MeCN)_2](ClO_4)_2$ (**4c**), and $[L^{p-H,H}Cu_2(MeCN)_2](CF_3SO_3)_2$ (**4d**) are obtained in good yields by reaction with Cu^I salts. X-ray diffraction studies performed on **4a** and **4d** reveal a distorted tetrahedral coordination geometry around each Cu^I ion, which is constructed by three nitrogen donors of the macrocyclic ligand and one acetonitrile solvent molecule. Treatment of these complexes with molecular dioxygen shows that their reactivity can be fine-tuned by the nature of the aromatic unit of the dialdehyde building blocks. Thus two different dinuclear Cu^{II} complexes resulting from the reaction of **4a** and **4b** with dioxygen were isolated and characterized by single crystal X-ray diffraction, XPS and magnetic measurements. The introduction of a methyl group in the 2-position of the aromatic spacers in **4c** hinders such oxygen transfer reactions but may allow the characterization of stable dioxygen binding species.
(© Wiley-VCH Verlag GmbH, 69451 Weinheim, Germany, 2002)

Introduction

The study of copper-dioxygen interactions and reactivity is of great interest in chemical systems that involve redox activity or oxidative transformations. In biological systems copper proteins are known to provide a variety of functions including dioxygen transport by hemocyanin (Hc), oxygenation and dehydrogenation of substrates combined with the transformation of O_2 to either H_2O_2 or water.[1−3] With the hope of mimicking the mild and selective biological oxygenation reactions,[4−10] a great variety of mononuclear[11−15] and dinuclear[16−21] copper(I) complexes ligated by polydentate N-ligands (containing amine or imine groups) have been synthesized and investigated. In most cases, two interacting copper centers were found to be included in dioxygen binding and activation process just as hemocyanins and tyrosinases do in the natural systems.[4,10,22]

Tolman and co-workers[22−25] suggested an equilibrium between $Cu_2(\mu\text{-}\eta^2\text{:}\eta^2\text{-peroxo})$ and $Cu_2(\mu\text{-oxo})_2$ cores using mono- or binucleating 1,4,7-3R-1,4,7-triazacyclonoanes ligands (R = alkyl or aryl), which was strongly influenced by ligand geometry, solvent donor ability and temperature. It was further found that either of the cores might be responsible for oxygenation of substrates. Karlin and coworkers thoroughly investigated the reaction of dioxygen with a series of dinuclear Cu^I complexes ligated by alkyl- or aryl-bridged bis[2-(pyrid-2-yl)ethyl]amine.[26−30] The alkyl bridge afforded in some cases the reversible binding of dioxygen to the copper centers, identified by UV/Vis or resonance Raman spectroscopy.[26−28] The replacement of the alkyl bridge by an aryl group, however, usually resulted in hydroxylation at the 2-position of the arene spacer, leading to $[Cu_2^{II}(R-XYL-O^-)(OH^-)]^{2+}$ (XYL: *m*-xylylene) species.[20,29,30] Surveying back the development of copper(I) complexes used in the oxygenation reaction, much of the research work has been focused on the use of "open" (non-macrocyclic) ligands. Only a few macrocyclic copper com-

[‡] X-ray diffraction (**4a**, **5a** and **5b**).
[‡‡] X-ray diffraction (**4d**).

[a] University of Ulm, Department of Materials and Catalysis, Albert-Einstein-Allee 11, 89069 Ulm, Germany
E-mail: bernhard.rieger@chemie.uni-ulm.de
[b] University of Ulm, Sektion für Röntgen- und Elektronenbeugung, Albert-Einstein-Allee 11, 89069 Ulm, Germany
[c] University of Ulm, Inorganic Chemistry I, Albert-Einstein-Allee 11, 89069 Ulm, Germany
[d] University of Helsinki, Department of Chemistry, 00014 Helsinki, Finland

plexes have been reported for oxygenation reactions during the past several decades.[31−35]

According to the active sites of type III copper proteins (hemocyanins, tyrosinases), two copper ions coordinated by two or three nitrogen ligands per Cu unit and a suitable copper-copper distance for dioxygen binding are necessary aspects for the formation of stable copper-dioxygen adducts.[1−3] In our opinion, Schiff-base macrocyclic ligands fulfil these requirements. At the same time, a freely adjustable Cu···Cu distance can be realized by designing ligands of various sizes. Martell, Schindler et al. reported the first example of oxygenation reaction of a copper(I) complex ligated by a Schiff-base macrocyclic ligand. A possible oxygenation mechanism[32] and kinetic details[34] were provided in their work. However, they did not provide structural characterization of Cu^{I} or Cu^{II} complexes, leaving many structural and mechanistic questions unanswered. It is found that a minor modification of the ligand environment around the copper center will lead to a dramatic variation in oxygenation activity of the copper(I) complexes.[26,27] For a better understanding of the relation between a complex's structure and its reactivity towards dioxygen, we report here a series of Schiff-base macrocycles of different size and substitution, which provide structural insight into a tyrosinase model system.

Results and Discussion

Syntheses of Ligands

The macrocyclic compounds used in our investigations (Scheme 1) were prepared by a Schiff-base condensation reaction of diethylenetriamine (**1**) with four different aromatic aldehydes (**2a**−**d**) under dilute conditions.[36]

The dropwise addition of aldehydes in acetonitrile to a solution of amine in the same solvent affords the formation of macrocycles, which precipitate as white crystalline solids. This one step procedure gives all [2+2][37] cycles in good to quantitative yields. The products were characterized by a combination of different MS techniques (CI, FAB, MALDI-Tof: size distribution), by elemental analysis, and by IR and NMR spectroscopy. The ^{1}H NMR spectra of the macrocycles **3a**−**c** suggest the existence of isomers in solution. This can be explained by a facile nucleophilic attack of an NH group to one of the neighboring imine fragments, leading to the reversible formation of 18-membered diimine imidazolidine macrocycles.[33] According to ^{1}H and ^{13}C NMR spectroscopy at 25 °C, **3b** exists predominantly in the form of the bisimidazolidine isomer, while for **3a** and **3c** no preference can be found.

Syntheses and Characterization of Copper(I) Complexes

Cu^{I} complexes of the macrocycles **3a**−**d** were obtained by an addition of in situ generated Cu^{I} perchlorate[38] or Cu^{I} triflate to the ligand solution in dichloromethane (Scheme 2).

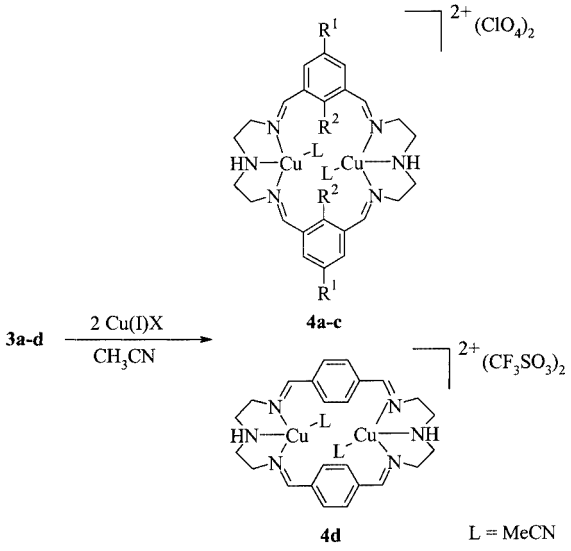

Scheme 2. Formation of dinuclear Cu^{I} complexes

The yellow to red crystalline compounds obtained were isolated and in selected cases characterized by single-crystal X-ray analysis. Suitable crystals of **4a** and **4d** were obtained by diffusion of diethyl ether into an acetonitrile solution

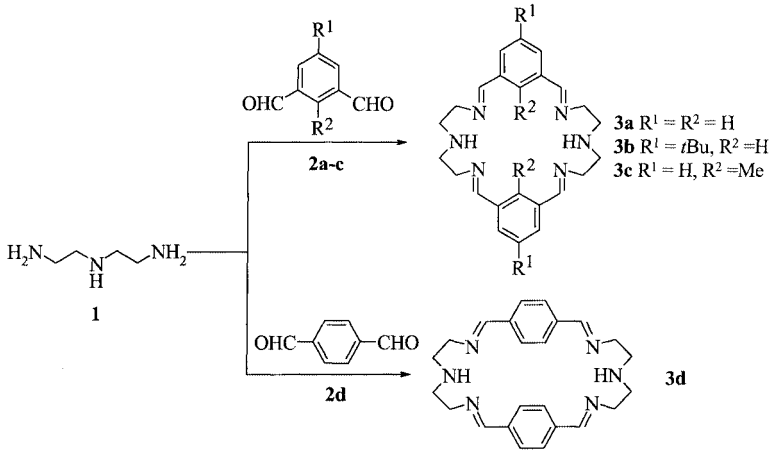

Scheme 1. Reaction of diethylenetriamine (**1**) with dialdehydes **2a**−**d** to form macrocyclic ligands **3a**−**d**

Table 1. Crystallographic data overview for **4a** and **4d**

	4a	**4d**
Empirical formula	$C_{28}H_{36}Cl_2Cu_2N_8O_8$	$C_{30}H_{36}Cu_2F_6N_8O_6S_2$
Formula mass [g/mol]	810.65	909.87
Crystal size [mm]	0.61 × 0.38 × 0.27	0.52 × 0.48 × 0.42
Crystal color	yellow	red
Crystal system	monoclinic	monoclinic
Space group	*I*2/*a*	$P2_1/n$
a [Å]	19.085(2)	13.178(2)
b [Å]	11.416(1)	11.505(2)
c [Å]	31.613(4)	25.048(3)
β [°]	95.09(2)	97.340(10)
V [Å^3]	6860.5(14)	3766.5(10)
Z	8	4
$D_{calcd.}$ [g/cm^3]	1.570	1.605
μ [mm^{-1}]	1.46	1.32
Temperature [K]	220(2)	193(2)
θ range [°]	2.08−25.93	2.56−25.26
Refl. collected	23000	7104
R_{int}	0.076	0.020
Refl. unique	6337	6792
Refl. observed [$I > 2\sigma(I)$]	4762	5309
*R*1, *wR*2 [$I > 2\sigma(I)$]	0.038/0.084	0.0409/0.0954
*R*1, *wR*2 (all data)	0.054/0.088	0.0603/0.1016
Goodness-of-fit on F^2	0.99	1.031
Largest diff. peak and hole [e Å^{-3}]	0.50 and −0.37	0.63 and −0.41

of the complex. The crystallographic analysis of **4a** and **4d** (Table 1) confirms in both cases the coordination of two copper atoms to the hexadentate macrocycle. Additionally, a coordinated acetonitrile molecule completes the distorted tetrahedral coordination geometry of the copper centers (Figures 1 and 2). In the case of **4a** the *meta*-substituted aromatic spacer units afford a C_2-symmetric arrangement of both copper(I)-containing subunits relative to each other leading to a short Cu···Cu distance of 4.28 Å, which is indeed similar to that found in tyrosinase (ca. 3.6 Å) and in the solid state of oxygenated and deoxygenated haemocyanin (3.6 and 4.6 Å).[1−3] Thereby the two copper centers are pointing towards each other, enforced by a pocket-like orientation of the macrocyclic ligand array (Figure 1).

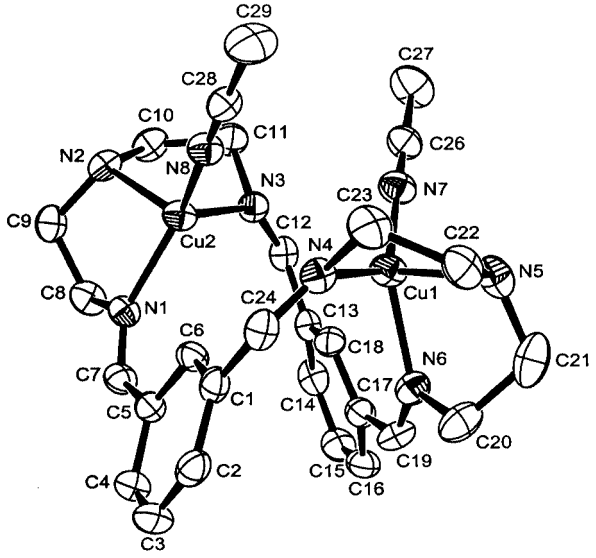

Figure 1. An ORTEP view of $[L^{H,H}Cu_2(MeCN)_2](ClO_4)_2$ (**4a**); hydrogen atoms and anions are omitted for clarity

Compound **4d** contains two tridentate metal binding sites that are separated by *para*-substituted aromatic spacer units. This leads to a "linear" arrangement of the two copper sub-structures with a larger Cu···Cu distance (relative to **4a**) of 6.86 Å. The two triflate anions show no direct interaction with the metal centers. In contrast to a recently published crystal structure of a similar complex with perchlorate anions,[35] the metal centers in **4d** are oriented to the same side of the plane defined by the macrocycle (Figure 2).

Reaction of Copper(I) Complexes with O_2

The dinuclear copper(I) complexes **4a**−**d** were exposed to oxygenation reactions.[39] Dioxygen was bubbled directly via a gas releasing apparatus into the solution of **4a** in a mixture of acetonitrile, dichloromethane and methanol at room temperature. A clear green solution developed gradually. After workup, green prismatic crystals of **5a** could be isolated by recrystallization from acetonitrile. Single crystal analysis indicates **5a** to be a dinuclear bis(μ-methoxy)-copper complex still bearing the initial macrocyclic ligand (Scheme 3). This is a clear difference to the bis(μ-hydroxo)dicopper(II) complex or the aromatic hydroxylation Cu^{II} complex proposed by Menif et al.[32,34] Complex **5a** displays sharp signals for the aromatic units of the ligand in the ^{1}H NMR spectrum. A broad peak appears at δ = 5−6 ppm which could be assigned to the bridging methoxy groups. Thus the existence of two strongly-coupled copper(II) centers is suggested for **5a**. This hypothesis is further supported

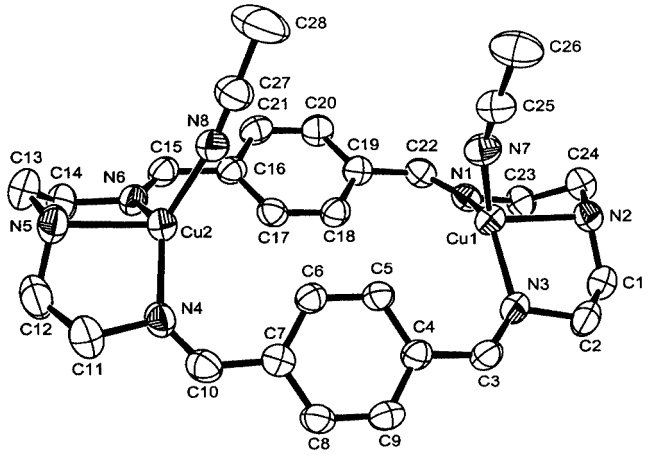

Figure 2. An ORTEP view of $[L^{p\text{-}H,H}Cu_2(MeCN)_2](CF_3SO_3)_2$ (**4d**); hydrogen atoms and anions are omitted for clarity

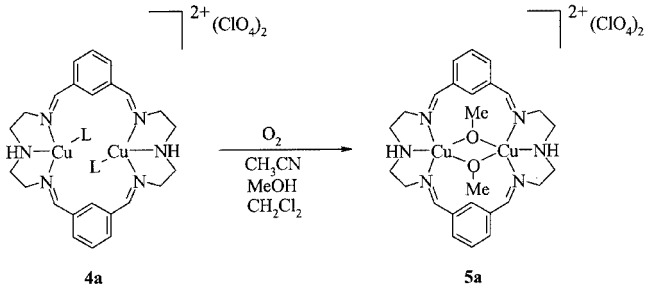

Scheme 3

by temperature-dependent magnetic susceptibility measurements and by X-ray photoelectron spectroscopy.

Compound **5a** is not the first example of a methoxy-bridged Cu^{II} complex. The isolation of similar Cu^{II} species from the reaction of Cu^{I} precursors bearing noncyclic ligands with dioxygen has been reported by other groups [7,16,40,41]. However, the formation process is still not understood. We assume here that the formation of **5a** occurs most likely via the reaction of the oxygenated species [either the dioxygen-binding species **I** or the bis(μ-hydroxo)dicopper complex **II**, Scheme 4] with solvent molecules.[42] Unfortunately, we were not able to demonstrate the formation of hydrogen peroxide or water. Direct synthesis of the bis(μ-hydroxo)dicopper(II) species from Cu^{II} salts also failed due to the decomposition of the Schiff-base ligands in the presence of water or a base.

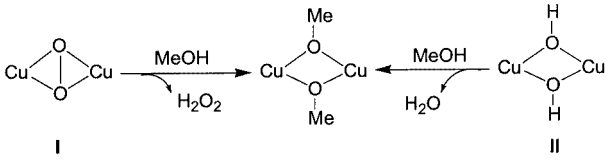

Scheme 4

To gain a better understanding, the reaction of **4a** with dioxygen was further investigated by UV/Vis spectroscopy in *N*,*N*-dimethylformamide. A single absorption at 400 nm is displayed initially for **4a**. By bubbling dioxygen into this

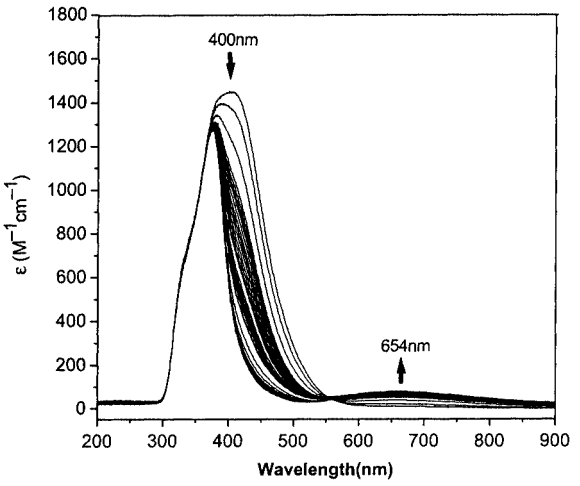

(A)

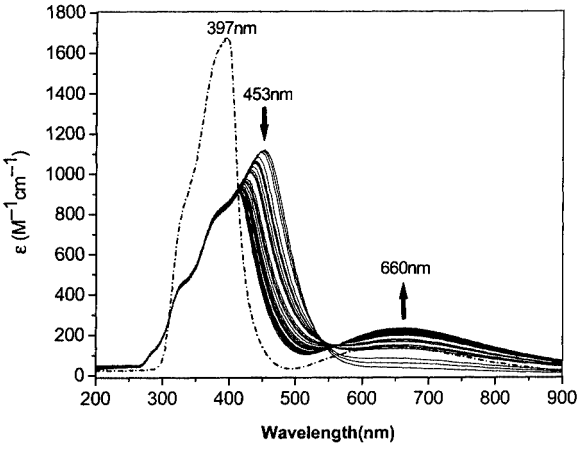

(B)

Figure 3. Reaction of (A) $[L^{H,H}Cu_2(MeCN)_2](ClO_4)_2$ (**4a**), (B) $[L^{tBu,H}Cu_2(MeCN)_2](ClO_4)_2$ (**4b**) with dioxygen in dry *N*,*N*-dimethylformamide; the initial trace shows the electronic spectrum of **4a** or **4b**; the subsequent traces were obtained upon adding dioxygen continually at room temperature for 2 h; the dashed line in (B) is the spectrum of $[(L^{tBu,H}O)Cu_2(\mu\text{-}OH)](ClO_4)_2$ (**5b**) in DMF

solution continually, this absorption shifts gradually to shorter wavelength with decreasing intensity. At the same time, a new absorption around 650−700 nm appears with lower intensity [Figure 3 (A)]. The final trace (after oxygenation is complete) shows a strong absorption at 375 nm and a weak one at 654 nm, which are only slightly different from the data reported by Menif (362 nm and 620 nm).[32] However, it suggests the formation of phenoxo- hydroxo-bridged dinuclear copper(II) complexes in DMF.[1,17,27,32] The absorption at 375 nm can be assigned to the ligand to metal charge transfer transition (from phenoxide to the Cu^{II} center). The high wavelength absorption at 654 nm is due to the d-d transition band, which is characteristic for Cu^{II} complexes.[1,7] The existence of the proposed bis(μ-hydroxo)dicopper complex[32−34] could not be identified definitely, however, the deviation of the low energy absorption (654 nm instead of 620 nm) might indicate its formation.

The reaction of **4b** with dioxygen in dichloromethane proved to be even faster than **4a**. Complex **5b**, which was

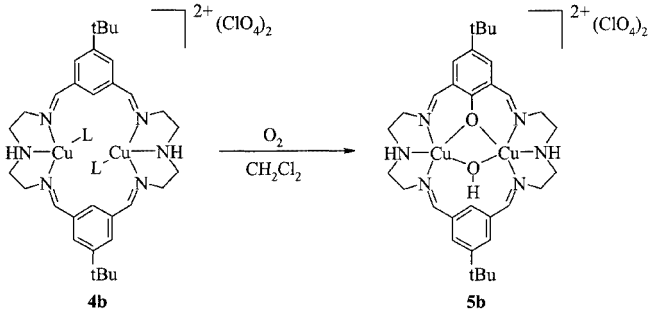

Scheme 5

isolated from this reaction in high yield, is the product of an intramolecular oxygen transfer and bears the dioxygen molecule after reductive O−O bond cleavage (Scheme 5, Figure 6). Such aromatic hydroxylation products obtained from noncyclic Cu^{I} precursors and dioxygen are already well known.[29,30] However, to the best of our knowledge, **5b** is the first characterized structure obtained from the reaction of a Schiff-base macrocyclic Cu^{I} complex and O_2.

An electrophilic attack of the μ-η^2:η^2-peroxo moiety to the aryl part of the ligand is proposed for the formation of such hydroxylation products.[29,30] This suggestion is supported by our observation that *tert*-butyl substitution at the 5-position of the aromatic spacer unit increases the rate of the C−H activation process in the 2-position and leads to higher yields of the insertion product **5b**. It is further found that a lower reaction temperature or addition of toluene inhibits the hydroxylation reaction. However, the presence of benzyl alcohol[43] increases the ratio of **5b** to the rest of oxidation products up to 88%. This is consistent with the result of Casella et al.[44] whereby the increase of the proton donor ability of the reaction medium favors the formation of the hydroxylation products (Table 2).

The UV spectrum of **4b** in the presence of dioxygen displays a similar reactivity to complex **4a**. The initial absorption at 453 nm of **4b** is gradually replaced by new absorptions at 397 nm and 660 nm, indicating the formation of the phenoxo- hydroxo-bridged dicopper complex **5b** [Figure 3, (B), solid lines)]. Nevertheless, the proposed dioxygen adduct intermediates which are responsible for the formation of **5b**, are again undetectable due to fast subsequent oxygen transfer.[1−10,14] By comparing the UV spectrum of pure **5b** [isolated crystals, Figure 3 (B), dashed line] with the final trace of **4b** after oxygenation, a good agreement is obtained except for the low energy region. Compound **5b** displays a d-d transition band at 640 nm (in contrast to the absorption at 660 nm of the reaction mixture), indicating most probably the formation of some other Cu^{II} species during the oxygenation reaction. One suitable suggestion might be the formation of bis(μ-hydroxo)dicopper(II) complexes. This is supported by the findings of Karlin and co-workers on dinuclear Cu^{I}−dioxygen reaction products ligated by substituted pyridine ligands.[19,20,29,30]

The reaction of **4c**, bearing methyl substituents on the aromatic rings of the macrocyclic frame, with dioxygen shows a completely different reactivity than **4a** and **4b** (Figure 4 vs. Figure 3). The initial absorption at 433 nm shifts gradually to *longer* wavelength with *increasing* intensity and a weaker absorption appears at ca. 550 nm. Furthermore the intensity of this new absorption ($\varepsilon \approx 800$ $M^{-1}cm^{-1}$) is significantly higher than the comparable d-d bands in Figure 3 ($\varepsilon < 200$ $M^{-1}cm^{-1}$). This suggests the formation of new species [instead of phenoxo- hydroxo-bridged dicopper complex or bis(μ-hydroxo)dicopper complex] by reaction with dioxygen.[1,11]

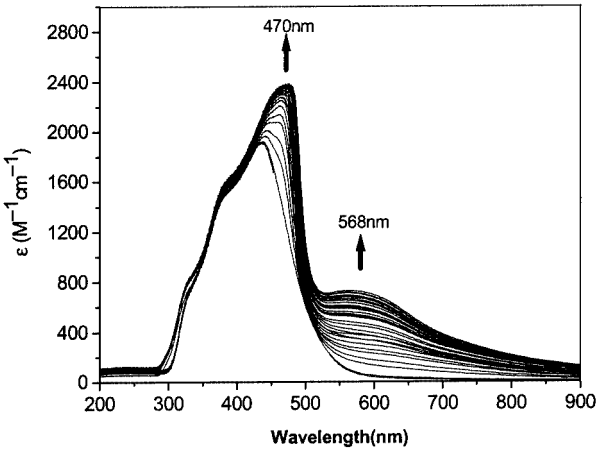

Figure 4. Reaction of $[L^{H,Me}Cu_2(MeCN)_2](ClO_4)_2$ (**4c**) with dioxygen in dry *N*,*N*-dimethylformamide; the initial trace shows the electronic spectrum of **4c**; the subsequent traces were obtained upon continuous addition of dioxygen at room temperature for 2 h

The features depicted in Figure 4 are more similar to what was reported for μ-peroxo-bridged complexes. These species show absorptions near 550 nm with moderate molar

Table 2. Aspects influencing the reaction of **4b** with O_2

	Conc. [mM]	Solvent	BzOH (BzOH/Cu)	Temp. [°C]	Time [h]	**5b**[a] (%)
1	0.58	CH_2Cl_2/toluene (20:1)	-	-80/25	5/15	13
2	3.09	CH_2Cl_2/toluene (20:1)	-	25	20	44
3	3.60	CH_2Cl_2	-	25	20	50
4	1.45	CH_2Cl_2	1:1	-80/25	5/15	70
5	1.45	CH_2Cl_2	1:1	25	20	88
6	10	CH_2Cl_2	1:1	25	24	80[b]
7	10	CH_2Cl_2	2:1	25	24	79[b]

[a] Determined after hydrolysis of the reaction mixture by the ratio of hydroxylated dialdehydes to their nonhydroxylated counterparts.[32] [b] Dioxygen was bubbled for 1 min.

absorbance of about 1000 $M^{-1}cm^{-1}$,[42] which is similar to the observed absorption at 568 nm. The absorption at ca. 470 nm (ca. 2000 $M^{-1}cm^{-1}$) after oxygenation of **4c** is again assigned to a ligand to metal charge transfer transition. The relatively low intensity[42] of this band can result either from a generally low absorption of our macrocyclic ligands or − most probably − from a low concentration of the peroxo species, which seems to be stable for hours even at room temperature.

The reaction of **4c** with dioxygen was also performed on a synthetic scale in dichloromethane at room temperature. The color of the solution changed gradually to yellow-greenish and a solid of the same color precipitated. No pure green color developed as in the cases of **4a** and **4b**. After workup, a yellow-greenish powder was isolated, which shows the existence of a $[L^{H,Me}Cu_2(O_2)]^{2+}$ fragment by means of MS spectrometry. Unfortunately, all attempts to purify the products by crystallization failed, due to the poor solubility in suitable solvents. The analysis of products obtained after hydrolysis by addition of 4 N HCl and subsequent extraction with dichloromethane gave the original dialdehyde, 4-hydroxy-2-methylisophthalaldehyde, and a tetraaldehyde coupling product (Scheme 6).[45] Thus, the introduction of 2-methyl substituents in **4c** has not blocked the binding of dioxygen but has effectively inhibited the intramolecular hydroxylation reactions. The formation of 4-hydroxy-2-methylisophthalaldehyde might be explained by assuming that an intermolecular hydroxylation process occurs. If an electrophilic attack is suggested for this process,[29,40,46] the hydroxylation should happen in the 5-position of the aromatic unit. Thus 4-hydroxy-2-methylisophthalaldehyde and even the coupling product are most likely formed via a free radical process before or during acidic decomposition.[47]

Compared to the oxygenation activity of **4a**−**c**, the *para*-subsituted Cu^I complex **4d** is completely inert to dioxygen. No oxygenation or even decomposition was observed in solution or in the solid state after exposure to dioxygen.[35] This surprising effect becomes clear by comparing the Cu···Cu distances in the *meta*-bridged complex **4a** and the "linear", *para*-bridged complex **4d**. The *para*-substituted aromatic units restrict the free location of the two Cu^I centers relative to each other and leads to a separation of the Cu centers (Cu···Cu: 6.86 Å). This implies that no dioxygen can be activated. The *meta*-aromatic bridges force the two copper(I) centers into a chiral, "pocket-like" arrangement (cf. Figure 1) with a short Cu···Cu distance (4.28 Å) allowing both copper centers to bind and activate the dioxygen molecule simultaneously.[4−10]

Characterization of Copper(II) Complexes

Solid State Structures

Single crystals of dinuclear copper(II) complexes **5a** (Figure 5) and **5b** (Figure 6) were obtained and characterized

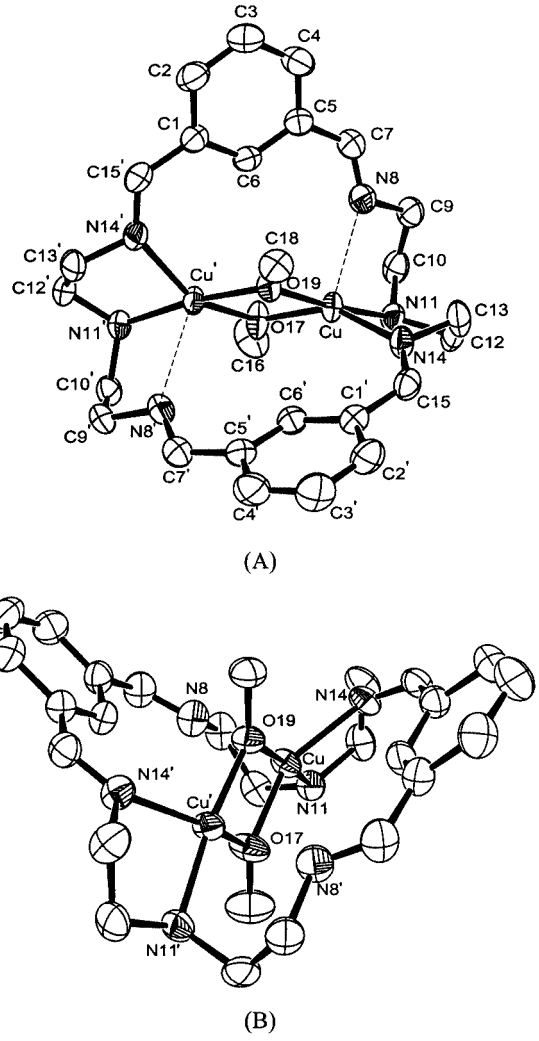

Figure 5. Two ORTEP views of $[L^{H,H}Cu_2(\mu\text{-}OMe)_2](ClO_4)_2$ (**5a**); hydrogen atoms and anions are omitted for clarity

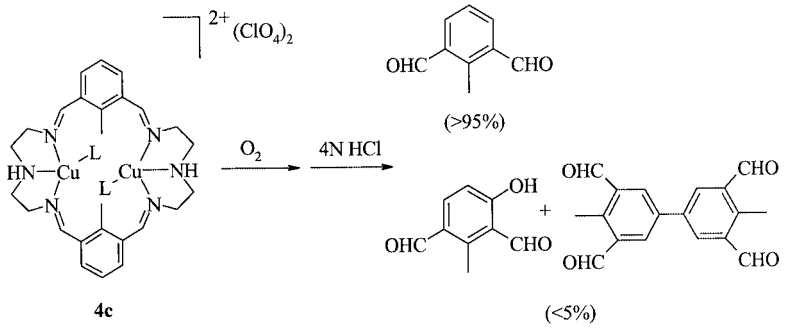

Scheme 6

by X-ray diffraction (Table 3). The dicationic portion of **5a** shows a chiral, C_2-symmetric coordination around the dinuclear Cu^{II} core in the solid state. Compared to the quasi-tetrahedral coordination adopted by **4a**, the coordination geometry around each Cu^{II} ion in **5a** is most likely distorted square planar with a Cu···Cu separation of about 3.03 Å. This distance is typical for dinuclear copper complexes containing two single-atom bridging ligands.[23,27] The $Cu-N_{imine}$, $Cu-N_{amine}$ distances in **5a** do not differ from each other and are in the expected region for nitrogen-coordinated copper complexes of that type (Table 4).[10,11,22,27]

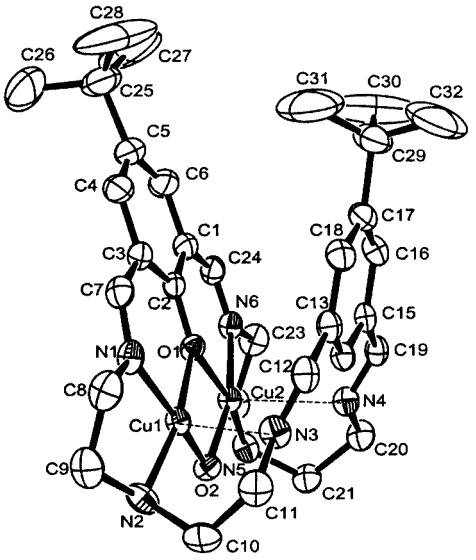

Figure 6. ORTEP view of $[(L^{tBu,H}O)Cu_2(\mu\text{-}OH)](ClO_4)_2$ (**5b**); hydrogen atoms and anions are omitted for clarity

However, the imine nitrogen atoms N8 (N8′) are also relatively close to the respective copper centers (N8−Cu, N8′−Cu′: 2.62 Å), thus a distorted square pyramidal environment can be assumed for both Cu centers[29,30] [Figure 5 (A)]. The $[Cu_2(\mu\text{-}OMe)_2]^{2+}$ core unit forms an ideal plane (torsion angle O19−Cu−O17−Cu = 0°), which is located perpendicular to the "macrocyclic pocket" structure [Figure 5 (B)] and N8, N8′ are disposed *anti* relative to it.

The nonsymmetric complex **5b** is the product of an intramolecular oxygenation reaction bearing bridging phenoxide and hydroxy units (Figure 6). Each Cu^{II} ion adopts a slightly distorted square pyramidal coordination environment. The nitrogen atom N1 (N6), N2 (N5) and the two oxygen atoms O1, O2 form the basal equatorial plane (the sum of the angles is 358°). In contrast to **5a**, the two axial imine donors (N3, N4) are deposited *cis* with respect to the Cu_2O_2 plane, which leads to the observed unusual "U"-form of the macrocyclic ligand system. However, this coordination is less pronounced than in literature reports of five-coordinated species (2.409−2.437 Å relative to 2.0 −2.3 Å, Table 4).[20,22,46] The effect is probably due to repulsive steric interactions of the bulky *tert*-butyl substituents of **5b**.

Magnetic Measurements

The magnetic susceptibilities of complexes **5a** and **5b** from 2 to 400 K (or 300 K) were determined by variable temperature magnetic susceptibility measurements. The curve of complex **5a** shows a pronounced antiferromagnetic behavior over the whole temperature range, due to the coupling of the two copper(II) ions in the same molecule, where the superexchange is mediated by the bridging me-

Table 3. Crystallographic data overview for **5a** and **5b**

	5a	**5b**
Empirical formula	$C_{26}H_{36}Cl_2Cu_2N_6O_{10}$	$C_{32}H_{46}Cl_2Cu_2N_6O_{10}$
Formula mass [g/mol]	790.61	872.73
Crystal size [mm]	0.40 × 0.30 × 0.10	0.35. × 0.31× 0.04
Crystal color	green	green
Crystal system	monoclinc	monoclinc
Space group	*A2/a*	$P2_1/a$
a [Å]	15.261(2)	11.816(2)
b [Å]	10.105(2)	13.583(2)
c [Å]	22.544(3)	24.471(5)
β [°]	112.000(16)	99.02(2)
V [Å^3]	3223.6(10)	3879.0(12)
Z	4	4
$D_{calcd.}$ [g/cm^3]	1.621	1.494
μ [mm^{-1}]	1.55	1.30
Temperature [K]	293(2)	223(2)
θ range [°]	2.24−25.94	2.26−25.92
Refl. collected	12348	29855
R_{int}	0.048	0.085
Refl. unique	3005	7464
Refl. observed[$I > 2\sigma(I)$]	2285	5167
*R*1, *wR*2 [$I > 2\sigma(I)$]	0.046/0.122	0.0468/0.1120
*R*1, *wR*2 (all data)	0.061/0.128	0.073/0.121
Goodness-of-fit on F^2	0.99	0.95
Largest diff. peak and hole [e Å^{-3}]	0.62 and −0.64	075 and −0.39

Table 4. Selected lengths [Å] and angles [°] of some dinuclear Cu^{I}, Cu^{II} complexes

	Lengths [Å]					Angles [°]		Ref.
	Cu···Cu	O···O	Cu−O	Cu−N_{eq}	Cu−N_{ax}	Cu−O−Cu	O−Cu−O	
4a	4.28	–	–	2.003(2), 2.092(2), 2.034(2), 2.043(2)	2.200(2), 2.192(2)	–	–	this work
4d	6.86	–	–	2.0212(8), 2.0221(9), 2.0106(8), 2.0791(9)	2.1743(9), 2.1374(10)	–	–	this work
5a	3.0278(9)	2.410	1.948(2), 1.9215(19)	2.027(3), 2.029(3)	2.624	101.99, 103.95	77.01(11)	this work
5b	3.0206(7)	2.470	1.905(3), 1.988(3), 1.978(3), 1.925(3)	1.931(3), 2.043(3), 2.028(3), 1.948(3)	2.437(3), 2.409(3)	99.23(10), 104.11(14)	78.17(11), 77.94(11)	this work
6[a]	7.04	–	–	2.022(5), 2.045(4)	2.185(4)	–	–	[35]
7[b]	3.560(3)	1.412(12)	1.903(11)	2.000(8), 1.993(14)	2.258(8)	136.7(5)	43.3(4)	[13]
8[c]	2.794(2)	2.287(2)	1.808(5), 1.803(5)	1.986(6), 1.987(6)	2.298(6)	101.4(2)	78.6(2)	[23]
9[d]	2.9769(9)	2.454(2)	1.940(4), 1.921(5), 1.924(5), 1.949(4)	2.087(5), 2.054(4), 2.085(5), 2.029(5)	2.289(5), 2.266(5)	100.8(2), 100.5(2)	78.6(2)	[23]
10[e]	2.990(2)	–	1.968(4), 1.909(4), 1.967(4), 1.911(4)	1.933(6), 1.996(5), 1.939(5), 1.991(5)	–	–	78.3(2), 78.3(2)	[46]

[a] **6**: $[L^{p\text{-}H,H}Cu_2(MeCN)_2](ClO_4)_2$. [b] **7**: $[(HB(3,5\text{-}iPr_2pz)_3]Cu]_2(\mu\text{-}\eta^2\text{:}\eta^2\text{-}O_2)$. [c] **8**: $[(Bz_3TACD)Cu]_2(\mu\text{-}O)_2(SbF_6)_2$. [d] **9**: $[(Bz_3TACN)(HBz_2TACN)Cu]_2(\mu\text{-}OH)_2(CF_3SO_3)_2$; [e] **10**: $[(m\text{-}XYLO)Cu_2(\mu\text{-}OH)](BF_4)_2$.

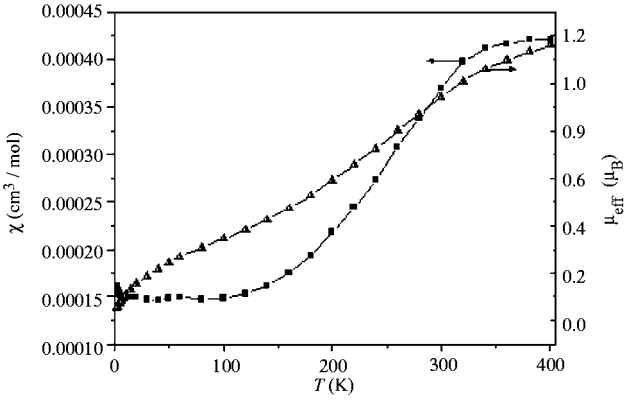

Figure 7. Temperature dependence of the corrected molar susceptibility of $[L^{H,H}Cu_2(\mu\text{-}OMe)_2](ClO_4)_2$ (**5a**)

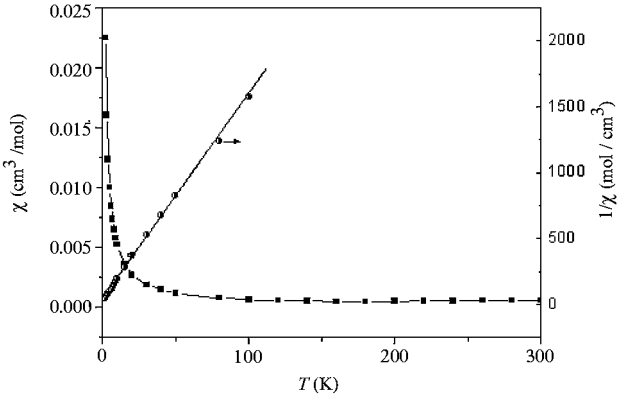

Figure 8. Temperature dependence of the corrected molar susceptibility of $[(L^{tBu,H}O)Cu_2(\mu\text{-}OH)](ClO_4)_2$ (**5b**)

thoxy groups (Figure 7). The effective magnetic moment per copper (μ_{eff}/Cu) is about 1.2 μ_B in solid state. A value of $-2J = 587\ cm^{-1}$ is obtained at room temperature, indicating a strong coupling between the two copper ions even at room temperature. This is however in accordance with the result of the ^1H NMR spectra.

The magnetic behavior of the phenoxo- hydroxo-bridged dicopper complex **5b** is significantly different from **5a**, despite the relatively similar Cu···Cu distance. The data obtained for **5b** suggest that the copper ions are essentially independent centers or, at best, very weakly coupled (Figure 8). In the low temperature range, the molar susceptibility of **5b** is in a good agreement with the Curie−Weiss law[48,49] as indicated by the linear relation of $1/\chi$ over T below 100 K.

Conclusion

Our results show that macrocycles containing suitable sites for transition metal coordination can be designed to hold two metal centers at a well-defined distance and orientation relative to each other. In agreement with natural oxidation catalysts, such as monooxygenase tyrosinase, this seems to be a major requirement to fine-tune the reactivity of artificial cyclic di- or multinuclear structures. In our case, *meta*-substituted dialdehyde building blocks resulted in macrocyclic complexes with Cu···Cu distances that allowed the activation and transfer of molecular dioxygen. It has been shown that subsequent oxygen transfer reactions can follow multiple pathways from which one intra- and one intermolecular reaction product could be isolated and characterized. Interestingly, the unwanted intramolecular reaction could be blocked effectively by introduction of methyl substituents in the 2-position of the bridging aromatic spacer, favoring other oxygen-transfer routes. This gives good hope that macrocyclic complexes can be designed to bind oxygen and allow selective transfer to substrates of technical importance.

Experimental Section

General Remarks: All operations concerning air- or moisture sensitive substances were performed under argon with standard Schlenk

techniques. Reagents and solvents were purchased from commercial sources and were used as received unless stated otherwise. Acetonitrile and methanol were purchased as dry solvents (water <0.005%) and were subsequently kept together with activated 3 Å or 4 Å molecular sieves. Dichloromethane and diethyl ether were refluxed with CaH_2 and $LiAlH_4$, respectively, and stored over activated molecular 4 Å sieves. All dry solvents were degassed prior to use. 2-Methylisophthalaldehyde[50], 5-*tert*-butylisophthalaldehyde[51] as well as **3a**[33] and **3d**[35] were prepared according to literature methods[32]. ^{1}H NMR and ^{13}C NMR spectra were recorded with a Bruker AMX400. Infrared measurements were obtained on KBr pellets using a Bruker IFS 113V and IFS 66V instrument. UV/Vis scan spectra were recorded with a J&M detector connected to a TIDAS spectrometer at room temperature. MS measurements were carried out using a Finnigan SSQ 7000 spectrometer with the methods of CI, FAB and MALDI. Magnetic measurement was carried out with a SQUID Magnetometer with constant field of 10000 Gauss. Elemental analyses were determined in the Microanalytical Laboratory of the University of Ulm.

Caution! *Perchlorate salts of metal complexes with organic ligands are potentially explosive. Only small amounts of material should be prepared and handled with great care.*

General Synthesis of Macrocyclic Imine Ligands: In a typical reaction the aldehyde (1 mmol) in 20 mL of acetonitrile was added dropwise to a stirred solution of the amine (1 mmol) in about 30 mL of acetonitrile. The addition was done over 1−2 h at room temperature. After stirring the reaction mixture for 24 h the crystalline precipitates were filtered and washed with acetonitrile in small portions. If necessary the products can be recrystallized from chloroform/acetonitrile. The compounds were characterized by ^{1}H NMR, ^{13}C NMR, IR spectroscopy, and by MS and elemental analysis.

$L^{tBu,H}$ (3b): Yield 78%. FT IR (KBr): ν(C=N) = 1650 (s) cm^{-1}. $C_{32}H_{46}N_6$ (514.76): calcd. C 74.67, H 9.01, N 16.33; found C 74.51, H 8.98, N 16.25. ^{1}H NMR ($CDCl_3$): δ = 8.1 (d, 2 H), 7.83 (m, 2 H), 7.44 (m, 2 H), 7.35 (m, 2 H), 3.13−4.0 (m, 14 H), 2.25−2.39 (m, 4 H), 1.85 (s, 2 H), 1.21 (m, 18 H) ppm. ^{13}C NMR ($CDCl_3$): δ = 160.8, 150.3, 140.1, 135.9, 128.2, 126.0, 120.6, 83.4, 58.4, 51.4, 51.1, 43.9, 33.6, 30.3 ppm. CI-MS, FAB-MS, MH$^+$: 515 (2+2 macrocycle), MALDI-Tof (dithranol): *m*/*z* = 514.38.

$L^{H,Me}$ (3c): Yield 79%. FT IR (KBr): ν(C=N) = 1629 (s) cm^{-1}. $C_{26}H_{34}N_6$ (430.34): calcd. C 72.50, H 7.90, N 19.52, found C 72.09, H 7.74, N 19.48. CI-MS, FAB-MS, MH$^+$: 431 (2+2 macrocycle), minor amount 646 (3+3 macrocycle), MALDI-Tof (dithranol): *m*/*z* = 514.38. The ^{1}H and ^{13}C NMR spectra in $CDCl_3$ are complex, suggesting the presence of isomers of the macrocycle.

General Preparation Method for Cu^I Complexes: Cu^I precursors were synthesized from Cu^{II} salts according to literature procedures in a mixture of oxygen-free methanol/acetonitrile (1:1). This solution was filtered directly into a degassed solution of the ligand in dichloromethane. After stirring for several hours at room temperature, the complexes can be either isolated by evaporating the solvent to dryness or by precipitating the product with degassed diethyl ether after concentration of the solution. The yellow to orange products were characterized by a combination of ^{1}H NMR and IR spectroscopy and elemental analysis.

$[L^{H,H}Cu_2(MeCN)_2](ClO_4)_2$ (4a): Yield 95%. FT IR (KBr): ν(C=N) = 1640 (s) cm^{-1}; ν(ClO_4^-) = 1111 (s), 1091 (s), 624 (s) cm^{-1}. $C_{28}H_{36}N_8Cu_2Cl_2O_8$ (810.26): calcd. C 41.46, H 4.44, N 13.82, found C 41.38, H 4.46 N 13.79. ^{1}H NMR (CD_3CN): δ = 9.3−8.3 (m, 6 H), 7.65 (s, 4 H), 7.1 (s, 2 H), 3.5 (s, 8 H), 3.25 (s, 2 H), 2.85 (m, 8 H) ppm. ^{13}C NMR (CD_3CN): δ = 164.2, 152.2, 135.9, 132.0, 129.6, 60.3, 48.5 ppm.

$[L^{tBu,H}Cu_2(MeCN)_2](ClO_4)_2$ (4b): Yield 93%. FT IR (KBr): ν(C=N) = 1621(s) cm^{-1}; ν(ClO_4^-) = 1111 (s), 1091 (s), 624 (s) cm^{-1}. $C_{36}H_{52}Cu_2Cl_2N_8O_8$ (922.08): calcd. C 46.85, H 5.64, N 12.15, found C 46.49, H 5.68, N 12.27. ^{1}H NMR (CD_3CN): δ = 9.24 (s, 2 H), 8.25 (s, 4 H), 7.62 (s, 4 H), 3.45 (m, 8 H), 3.2 (s, 2 H), 2.9 (m, 8 H), 1.3 (m, 18 H) ppm.

$[L^{H,Me}Cu_2(MeCN)_2](ClO_4)_2$ (4c): Yield 90%. FT IR (KBr, cm^{-1}): ν(C=N) = 1619 (s), ν(ClO_4^-) = 1111 (s), 1091 (s), 624 (s). $C_{30}H_{40}Cu_2Cl_2N_8O_8$ (838.4): calcd. C 42.94, H 4.77, N 13.36, found C 41.66, H 4.85, N 13.51. ^{1}H NMR spectra could not be obtained, due to the very low solubility of the complex.

$[L^{p\text{-}H,H}Cu_2(MeCN)_2](CF_3SO_3)_2$ (4d): Yield 95%. FT IR (KBr, cm^{-1}): ν(C=N) = 1626 (s). $C_{30}H_{36}Cu_2F_6N_8O_6S_2$ (909.14): calcd. C 39.59, H 3.96, N 12.32, found C 39.84, H 4.18, N 12.12. ^{1}H NMR (CD_3CN): δ = 8.5 (s, 4 H), 8.0 (s, 8 H), 3.6 (m, 8 H), 3.3 (s, 2 H), 2.9 (m, 8 H) ppm.

Isolation of $[L^{H,H}Cu_2(\mu\text{-}OMe)_2](ClO_4)_2$ (5a): Blue crystals of $Cu(ClO_4)_2{\cdot}6H_2O$ (0.370 g, 1 mmol) were added to a suspension of excess Cu powder in acetonitrile (25 mL) and methanol (25 mL). The reaction mixture was stirred for 3 h. After filtration, the obtained clear colourless solution was added dropwise to a solution of macrocyclic ligand **3a** (0.402 g, 1 mmol) in dichloromethane (30 mL). An orange solution was obtained at once and was stirred overnight. Dioxygen was then bubbled gently via a gas releasing apparatus into the above solution at room temperature for 2 days. The solution became green within the first 10 minutes. After removal of the solvents, 50 mL of acetonitrile was injected to dissolve the dark green powder. Trace amounts of impurities were removed by filtration. The clear solution was concentrated to about 15 mL (warming the solution during this process slightly), and kept at room temperature for one day. Green prismatic crystals were separated from the solution (50 mg), and characterized as **5a**. MS (*m*/*z*, FAB): 627 (52) [M + H − ClO_4^- − Cu^{2+}], 565 (22) [M + H − ClO_4^- − 2 MeO^-] 527 (30) [M − 2 ClO_4^- − Cu^{2+}], 500 (19) [M − $HClO_4$ − 2 Cu^{2+} − 2 MeO^-], 465 (100) [M − 2 ClO_4^- − Cu^{2+} − 2 MeO^-]. IR (KBr): $\tilde{\nu}$ = 3436 br, 3270 m, 3077 w, 2930 m, 2819 m, 1642 s, 1604 sh, 1580 sh, 1456 m, 1434 sh, 1336 m, 1294 w, 1258 w, 1232 m, 1011 s, 1081 s, 1054 s, 967 m, 891 m, 794 m, 685 m, 622 s, 538 m, 450 m cm^{-1}. $C_{26}H_{36}Cl_2Cu_2N_6O_{10}$: calcd. C 39.50, H 4.58, N 10.63; found C 39.69, H 4.44, N 10.89. ^{1}H NMR (CD_3CN): δ = 10.6 (br, 4 H), 8.2 (s, 2 H, Ar-*H*), 7.85 (m, 2 H, Ar-*H*), 7.4 (d, 4 H, Ar-*H*), 4.8−6.2 (br, 6 H, C*H*$_3$O), 3.2 (d, 8 H), 2.1 (s, 2 H, N-*H*), 1.8 (m, 8 H) ppm.

Isolation of $[(L^{tBu,H}O)Cu_2(\mu\text{-}OH)](ClO_4)_2$ (5b): Dioxygen was bubbled gently through a violently stirred solution of **4b** (500 mg, 0.54 mmol) in dichloromethane (150 mL) at room temperature. The solution turned green immediately and some green precipitate appeared. After 24 h, the reaction mixture was concentrated to dryness to afford a green powder. Acetonitrile (15 mL) was added to dissolve it and a trace amount of impurities was removed by filtration. The filtrate was then concentrated to about 3−4 mL (warming the solution during this process slightly), and kept at room temperature. Green planar crystals were obtained in a yield of 45% (190 mg), which were characterized as complex **5b**. MS (FAB): *m*/*z* = 655 (100) [M − 2 ClO_4^- − OH], 672 (31) [M − 2 ClO_4^-]. IR (KBr): $\tilde{\nu}$ = 3566 s, 3267 s, 2960 s, 2871 m, 1647 s, 1597 w, 1559 m, 1455 m, 1395 w, 1366 w, 1399 m, 1287 w, 1238 m, 1098 s, 1010 m, 968 m, 889 w, 766 w, 706 w, 621 s, 575 w, 481 w, 445 m cm^{-1}.

$C_{32}H_{46}Cl_2Cu_2N_6O_{10}$: calcd. C 44.04, H 5.31, N 9.63; found C 44.62, H 5.30, N 9.71.

Magnetic Susceptibility Measurements: Solid-state magnetic susceptibility measurements of copper complexes **5a** and **5b** were obtained at a constant field of 10KOe on a SHE SQUID magnetometer operating between 2 and 400 K. Determinations were made on crystalline samples loaded into gelatine capsules. Diamagnetic corrections for the capsules were made by direct measurements, while corrections for the ligands were calculated by use of Pascal's constants.[49] A fixed TIP correction of 60×10^{-6} cm^3/mol was adopted.[48]

X-ray Photoelectron Spectroscopy: Measurements for **5a** were carried out under the conditions of 5.85 eV, 250.0 W at 45.0° over 83.33 min for the Cu2p energy region. The same curve was also obtained by combining the energy bands reported for $CuCl_2$ and CuO.

X-ray Crystallographic Study: The crystal data of copper(I) complexes **4a** and **4d** and copper(II) complexes **5a** and **5b** were collected on a Rigaku AFC7S four-circle diffractometer or a STOE IPDS unit (Imaging Plate Diffraction System) using graphite monochromatized Mo-K_α radiation, $\lambda = 0.71073$ Å, ω-scans. Intensities were corrected for Lorentz and polarization effect.[52] A psi-scans absorption correction was applied for **4d**.[53] The structures of **4a** and **5b** were solved by the Patterson method (SHELXS-86 program), while the structures of **4d** and **5a** were solved primarily by direct methods. A refinement of full-matrix least-squares on F^2 was performed for all reflections with the SHELXL-97 program. All non-hydrogen atoms were refined anisotropically. Hydrogen atoms were included in the final refinement cycle in a riding mode except for those of the methoxy bridges in **5a** and the *tert*-butyl groups of **5b**. In the case of **4d**, one triflate anion is disordered with site occupation factors of 0.25 and 0.75. DFIX was needed to refine both ordered and disordered triflate anions, which stabilize the structure by H bonds through oxygen atom with the macrocycle or its symmetry equivalent.[54,55] The perchlorate anions in **5a** are also disordered. Four oxygen atoms were represented by eight half-populated oxygen atoms. Crystal data of **4a**, **4d**, **5a** and **5b**, details about data collection, analysis and refinement were listed in Tables 1 and 3. CCDC-182382, -182229, -182383 and -182384 for **4a**, **4d**, **5a,** and **5b** contain the supplementary crystallographic data for this paper. These data can be obtained free of charge at www.ccdc.cam.ac.uk/conts/retrieving.html or from the Cambridge Crystallographic Data Centre, 12, Union Road, Cambridge CB2 1EZ, UK [Fax: (internat.) + 44-1223/336-033; E-mail: deposit@ccdc.cam.ac.uk].

[1] E. I. Solomon, U. M. Sundaram, T. E. Machonkin, *Chem. Rev.* **1996**, *96*, 2563−2605.
[2] J. P. Klinman, *Chem. Rev.* **1996**, *96*, 2541−2561.
[3] S. Ferguson-Miller, G. T. Babcock, *Chem. Rev.* **1996**, *96*, 2889−2907.
[4] R. Than, A. A. Feldmann, B. Krebs, *Coord. Chem. Rev.* **1999**, *182*, 211−241.
[5] K. D. Karlin, Y. Gultneh, *Prog. Inorg. Chem.* **1987**, *35*, 219−327.
[6] T. N. Sorrell, *Tetrahedron* **1989**, *45*, 3−68.
[7] N. Kitajima, Y. Moro-oka, *Chem. Rev.* **1994**, *94*, 737−757.
[8] K. D. Karlin, S. Kaderli, A. D. Zuberbühler, *Acc. Chem. Res.* **1997**, *30*, 139−147.
[9] P. L. Holland, W. B. Tolman, *Coord. Chem. Rev.* **1999**, *190−192*, 855−869.
[10] S. Schindler, *Eur. J. Inorg. Chem.* **2000**, 2311−2326.
[11] M. Schatz, M. Becker, F. Thaler, F. Hampel, S. Schindler, R. R. Jacobson, Z. Tyeklár, N. N. Murthy, P. Ghosh, Q. Chen, J. Zubieta, K. D. Karlin, *Inorg. Chem.* **2001**, *40*, 2312−2322.
[12] R. R. Jacobson, Z. Tyeklar, A. Farooq, K. D. Karlin, S. Liu, J. Zubieta, *J. Am. Chem. Soc.* **1988**, *110*, 3690−3692.
[13] N. Kitajima, K. Fujisawa, Y. Moro-oka, *J. Am. Chem. Soc.* **1989**, *111*, 8975−8976.
[14] S. Mahapatra, J. A. Halfen, E. C. Wilkinson, G. Pan, C. J. Cramer, L. Que Jr., W. B. Tolman, *J. Am. Chem. Soc.* **1995**, *117*, 8865−8866.
[15] V. Mahadevan, Z. Hou, A. P. Cole, D. E. Boot, T. K. Lal, E. I. Solomon, T. D. P. Stack, *J. Am. Chem. Soc.* **1997**, *119*, 11996−11997.
[16] T. N. Sorrell, M. R. Malachowski, D. L. Jameson, *Inorg. Chem.* **1982**, *21*, 3250−3252.
[17] S. Ryan, H. Adams, D. E. Fenton, M. Becker, S. Schindler, *Inorg. Chem.* **1998**, *37*, 2134−2140.
[18] M. Kodera, K. Katayama, Y. Tachi, K. Kano, S. Hirota, S. Fujinami, M. Suzuki, *J. Am. Chem. Soc.* **1999**, *121*, 11006−11007.
[19] C. X. Zhang, H.-C. Liang, E. Kim, Q.-F. Gan, Z. Tyeklár, K.-C. Lam, A. R. Rheingold, S. Kaderli, A. D. Zuberbühler, K. D. Karlin, *Chem. Commun.* **2001**, 631−632.
[20] N. N. Murthy, M. M. Tahir, K. D. Karlin, *Inorg. Chem.* **2001**, *40*, 628−635.
[21] E. Pidcock, H. V. Obias, M. Abe, H.-C. Liang, K. D. Karlin, E. I. Solomon, *J. Am. Chem. Soc.* **1999**, *121*, 1299−1308.
[22] W. B. Tolman, *Acc. Chem. Res.* **1997**, 227−237.
[23] S. Mahapatra, J. A. Halfen, E. C. Wilinson, G. Pan, X. Wang, V. C. Young Jr., C. J. Cramer, L. Que Jr., W. B. Tolman, *J. Am. Chem. Soc.* **1996**, *118*, 11555−11574.
[24] J. Cahoy, P. L. Holland, W. B. Tolman, *Inorg. Chem.* **1999**, *38*, 2161−2168.
[25] B. M. T. Lam, J. A. Halfen, V. G. Young, Jr., J. R. Hahadorn, P. L. Holland, A. Lledós, L. C. Sánchez, J. I. Novoa, S. Alvarez, W. B. Tolman, *Inorg. Chem.* **2000**, *39*, 4059−4072.
[26] K. D. Karlin, M. S. Haka, R. W. Cruse, Y. Gultneh, *J. Am. Chem. Soc.* **1985**, *107*, 5828−5829.
[27] K. D. Karlin, R. W. Cruse, Y. Gultneh, A. Farooq, J. C. Hayes, J. Zubieta, *J. Am. Chem. Soc.* **1987**, *109*, 2668−2679.
[28] K. D. Karlin, Z. Tyeklár, *Adv. Inorg. Biochem.* **1994**, *9*, 123−172.
[29] K. D. Karlin, M. S. Nasir, B. I. Cohen, R. W. Cruse, S. Kaderli, A. D. Zuberbühler, *J. Am. Chem. Soc.* **1994**, *116*, 1324−1336.
[30] K. D. Karlin, J. C. Hayes, Y. Gultneh, R. W. Cruse, J. W. McKown, J. P. Hutchinson, J. Zubieta, *J. Am. Chem. Soc.* **1984**, *106*, 2121−2128.
[31] S. M. Nelson, *Copper Coordination Chemistry: Biochemical and Inorganic Perspectives* (Eds: K. D. Karlin, J. Zubieta), Adenine Press, New York, **1994**.
[32] R. Menif, A. E. Martell, *J. Chem. Soc., Chem. Commun.* **1989**, 1521−1523.
[33] R. Menif, A. E. Martell, P. J. Squattrito, A. Clearfield, *Inorg. Chem.* **1990**, *29*, 4723−4729.
[34] M. Becker, S. Schindler, R. van Eldik, *Inorg. Chem.* **1994**, *33*, 5370−5371.
[35] P. Comba, T. W. Hambley, P. Hilfenhaus, D. T. Richens, *J. Chem. Soc., Dalton Trans.* **1996**, 533−539.
[36] J. Jazwinski, J.-M. Lehn, R. Méric, J.-P. Vigneron, M. Cesario, J. Guilhem, C. Pascard, *Tetrahedron Lett.* **1987**, *28*, 3489−3492.
[37] Two amine molecules and two aldehyde molecules afford the [2 + 2] products. In some cases, [3 + 3], [4 + 4] or even bigger size products could be formed also under the same conditions.
[38] J. van Rijn, J. Reedijk, M. Dartmann, B. Krebs, *J. Chem. Soc., Dalton Trans.* **1987**, 2576.
[39] Complex **4a** was originally synthesized and investigated by Menif et al.;[32,33] Schindler's group added further details on the kinetics of oxygen activation.[34]
[40] P. L. Holland, K. R. Rodgers, W. B. Tolman, *Angew. Chem. Int. Ed.* **1999**, *38*, 1139−1142.

[41] K. D. Karlin, J. Shi, J. C. Hayes, J. W. Mckowm, J. P. Hutchinson, J. Zubieta, *Inorg. Chim. Acta* **1984**, *91*, L3−L7.
[42] N. Kitajima, T. Koda, Y. Iwata, Y. Moro-oka, *J. Am. Chem. Soc.* **1990**, *112*, 8833−8839.
[43] Benzyl alcohol was added to check our complexes for intermolecular oxygenation; however, no benzyl alcohol oxidation products could be detected.
[44] L. Casella, M. Gullotti, G. Pallanza, L. Rigoni, *J. Am. Chem. Soc.* **1988**, *110*, 4221−4227.
[45] 4-Hydroxy-2-methylisophthalaldehyde was characterized by ^{1}H NMR($CDCl_3$): δ = 2.95 (s, 3 H, C*H*$_3$), 10.21 (s, 1 H, C*H*O), 10.48 (s, 1 H, C*H*O), 12.65 (s, 1 H, O*H*) (see: J. N. Chatterjea, K. R. R. P. Singh, I. S. Iha, Y. Prasad, S. C. Shaw, *Ind. J. Chem.* **1986**, 796−798); GC-MS: *m*/*z* = 164. Tetraaldehyde coupling product: ^{1}H NMR ($CDCl_3$): δ = 3.05 (s, 6 H, C*H*$_3$), 8.33 (s, 4 H, Ar-*H*), 10.51−10.53 (s, 4 H, C*H*O); GC-MS: *m*/*z* = 294.
[46] O. J. Gelling, F. v Bolhuis, A. Meetsma, B. L. Feringa, *J. Chem. Soc., Chem. Commun.* **1988**, 552−554.
[47] Complex **4c** was also tested for oxidation reactions of external substances, such as phenol or *o*-diphenol, under aerobic conditions. Unfortunately, no diphenol (from phenol) or *o*-quinone could be detected by GC-MS.
[48] R. L. Carlin, A. J. van Duyneveldt, *Magnetic Properties of Transition Metal Compounds*, Springer-Verlag, New York, Heidelberg, Berlin, **1977**.
[49] A. Weiss, H. Witte, *Magnetochemie*, Verlag Chemie, Berlin, **1973**.
[50] R. H. Mitchell, V. Boekelheide, *J. Am. Chem. Soc.* **1974**, *96*, 1547−1557.
[51] Y. L. Bennani, K. S. Marron, D. E. Mais, K. Flatten, A. M. Nadzan, M. F. Boehm, *J. Org. Chem.* **1998**, *63*, 543−550.
[52] *Single Crystal Structure Analysis Software*, version 1.6, Molecular Structure Corporation, The Woodlands, TX 77381, USA, **1993**.
[53] A. C. T. North, D. C. Phillips, F. S. Mathews, *Acta Crystallogr., Sect. A* **1968**, *24*, 351−359.
[54] G. M. Sheldrick, *SHELX-97, Program for the Solution and Refinement of Crystal Structures*, University of Göttingen, Germany, **1997**.
[55] *ORTEP3 for Windows:* L. J. Farrugia, *J. Appl. Crystallogr.* **1997**, *30*, 565.

Received April 5, 2002
[I02175]

(Phenylalkyl)palladium Complexes Containing β-Hydrogen Atoms: Synthesis and Characterization of [PdR_2(dppe)], [PdR(SPh)(dppe)] (R = CH_2CH_2Ph, $CH_2CH_2CH_2Ph$, $CH_2CHMePh$), and [Pd($CH_2CH_2CH_2Ph$)X(dppe)] (X = I, Br, Cl)

Thomas Spaniel,[a] Harry Schmidt,[a] Christoph Wagner,[a] Kurt Merzweiler,[a] and Dirk Steinborn*[a]

Keywords: Phenylalkyl complexes / Palladium / β-Hydrogen-containing alkyl ligands / P ligands

Reactions of HgR_2 (R = CH_2CH_2Ph, **1a**; $CH_2CH_2CH_2Ph$, **1b**; $CH_2CHMePh$, **1c**) (prepared from $HgCl_2$ and the requisite Grignard compounds) with lithium in toluene afforded (phenylalkyl)lithium compounds LiR (**2a**–**c**) in yields of between 64 and 81%. At –30 °C, they react with [$PdCl_2$(dppe)] [dppe = 1,2-bis(diphenylphosphanyl)ethane] yielding bis(phenylalkyl)palladium(II) complexes [PdR_2(dppe)] (**3a**–**c**) which were isolated (T_{dec} = 159 °C, **3a**; 80 °C, **3b**; 145 °C, **3c**) and fully characterized by ^1H, ^{13}C, and ^{31}P NMR spectroscopy. Single-crystal X-ray diffraction of [Pd(CH_2CH_2Ph)$_2$(dppe)] (**3a**) showed that the palladium atom is square-planar coordinated by two 2-phenylethyl ligands and the dppe ligand. The two CH_2CH_2Ph ligands exhibite nearly a fully staggered conformation. Overall, a good approximation for the complex is that it has C_2 symmetry with the C_2 axis defined by the Pd atom and the midpoint of the central C–C bond of the dppe ligand. Bis(phenylalkyl)palladium complexes **3a** and **3b** reacted with PhSH in a 1:1 ratio yielding [PdR(SPh)(dppe)] (R = CH_2CH_2Ph, **5a**; $CH_2CH_2CH_2Ph$, **5b**), whereas in the case of complex **3c**, besides [Pd($CH_2CHMePh$)(SPh)(dppe)] (**5c**), a considerable amount of [Pd(SPh)$_2$(dppe)] (**6a**) was formed. Reactions of **3b** with the less acidic alkanethiols *i*PrSH and *t*BuSH resulted in the formation of [Pd($CH_2CH_2CH_2Ph$)(SR′)(dppe)] (R′ = *i*Pr, **5d**; *t*Bu, **5e**) along with smaller amounts of [Pd(SR′)$_2$(dppe)] (**6**) and [Pd(dppe)$_2$] (**7**). Furthermore, complex **3b** was found to react in THF with disulfides R′SSR′ (R′ = Ph, Bz, Me), yielding [Pd($CH_2CH_2CH_2Ph$)(SR′)(dppe)] (R′ = Ph, **5b**; Bz, **5f**, Me, **5g**) with small amounts (3–13%) of [Pd(SR′)$_2$(dppe)] (**6**) as side products. The corresponding reaction with MeSeSeMe afforded [Pd($CH_2CH_2CH_2Ph$)(SeMe)(dppe)] (**8a**) and 3% of [Pd(SeMe)$_2$(dppe)] (**9a**) and [Pd(dppe)$_2$] (**7**). Reactions of complex **5b** with MeI and H_2C=$CHCH_2Br$ in tetrahydrofuran and with neat H_2C=$CHCH_2Cl$ readily proceeded at –30 °C to give halo(3-phenylpropyl)palladium complexes [Pd($CH_2CH_2CH_2Ph$)X(dppe)] (X = I, **10a**; Br, **10b**; Cl, **10c**). They were isolated as pale yellow powdery/microcrystalline substances and fully characterized by ^{13}C and ^{31}P NMR spectroscopy. Solutions of complexes **10** in THF decompose rapidly above –30 °C.

(© Wiley-VCH Verlag GmbH, 69451 Weinheim, Germany, 2002)

1. Introduction

The Heck reaction has been proven to be a powerful method for the arylation and vinylation of olefins (Scheme 1).[1] Despite the continuous debate on its mechanism,[2] oxidative addition of RX (R = aryl, vinyl, heteroaryl, ...; X = halide, tosylate, triflate, ...) to the Pd catalyst complex yielding an $L_xPd(R)X$ complex (**I**, Scheme 1) followed by olefin insertion (**II**, Scheme 1) are crucial reaction steps in the classic Heck cycle. The reactions of ethene with phenyl and benzyl halides yielding styrene and allylbenzene, respectively, can be considered as the most simple prototypic model reactions for Heck reactions. Complexes of type **I** in Scheme 1 (R = Ph, Bz) are well known.[3] Contrary to type **I**, those of type **II**, (2-phenylethyl)- and (3-phenylpropyl)palladium complexes, have not yet been described. Due to β-hydrogen atoms in the phenylalkyl ligands the thermal stability of these complexes can be expected to be low. Facile β-hydride elimination reactions, in Heck-type catalysts, are discussed as a reason for the alkylation of olefins being restricted to special cases. Alkyl halides R′CH−CH_2X react to form intermediates **I** [$L_xPd(CH_2-CHR')X$], which undergo β-hydride elimination more easily than insertion of the olefin, giving intermediate **II** and opening the reaction channel to the desired products.

Several mononuclear palladium complexes with β-hydrogen-containing acyclic alkyl ligands have been isolated as solids and characterized. These include: (i) dialkyl− and alkyl/aryl−Pd^{II} complexes [PdR_2L_2] [R = Et, *n*Pr, *n*Bu; L_2 = (PR′$_3$)$_2$, dppe, bpy, ...; R_2 = Et/Ar, *n*Bu/Ar, Ar = Aryl],[4] (ii) monoalkyl−Pd^{II} complexes with an anionic

[a] Institut für Anorganische Chemie der Martin-Luther-Universität Halle-Wittenberg,
Kurt-Mothes-Straße 2, 06120 Halle (Saale), Germany
Fax: (internat.) + 49-345/552-7028
E-mail: steinborn@chemie.uni-halle.de

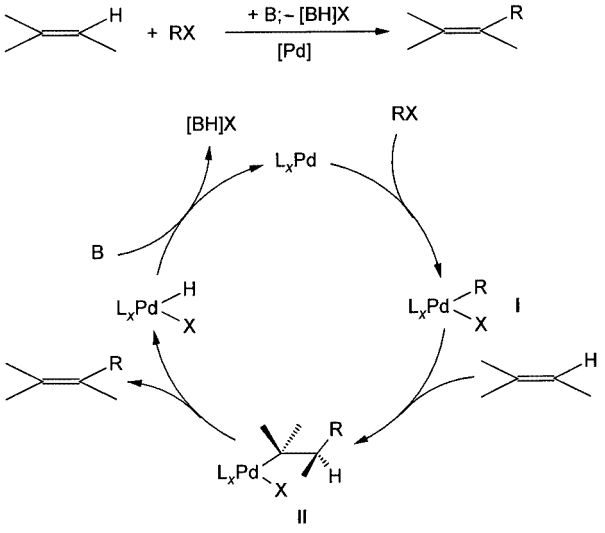

Scheme 1

ligand *trans*-[PdEt(X)(PR′$_3$)$_2$] (X = Cl, Br, I, SPh, OPh, O$_2$CR′),[5] [Pd(CH$_2$CH$_2$CH=CH$_2$)Cl(dppe)],[6] and [PdR(S$_2$CNR′$_2$)(PR′$_3$)] (R = *n*Pr, *i*Pr, *n*Bu, *s*Bu, ...),[7] and (iii) cationic Pd^{II} complexes [PdR{N(CH$_2$CH$_2$PPh$_2$)$_3$}]X (R = Et, *n*Pr, *n*Bu; X = I, BPh$_4$)[8] and [PdEt(η^2-C$_2$H$_4$)(phen)][B{C$_6$H$_3$(CF$_3$)$_2$}$_4$];[9] furthermore, (iv) alkyl-(Et, *n*Pr)–Pd^{IV} complexes with tripodal N-donor and bipyridine co-ligands have been synthesized.[10] Only a few of these complexes could be structurally characterized, namely *trans*-[PdEt(X)(PMe$_3$)$_2$] (X = Br,[5b] SPh[5c]), [PdR{S$_2$CN-(CH$_2$)$_4$}(PEt$_3$)] (R = *n*Pr, *i*Pr),[7b] and [PdEtMe$_2$-{(pz)$_3$BH}].[10d]

Palladium complexes with acyclic β-hydrogen-containing alkyl ligands cover a wide range of stability: PdEtI without supporting ligands already decompose at −100 °C[11] whereas toluene solutions of complexes with dithiocarbamato[7] and tris(pyrazolyl)borate[10d] co-ligands were found to be stable to 60 °C and to at least 80 °C, respectively. On the other hand, many of the above-mentioned complexes are unstable in solution even at room temperature. Preferred decomposition pathways are β-hydrogen elimination and/or reductive elimination in the case of dialkyl complexes. For stereoelectronic reasons organopalladium complexes with β-hydrogen-containing cycloalkyl ligands are thermally more stable.[4b,4c,4f,6,12]

(Phenylalkyl)palladium complexes containing the structural unit Pd–[CH$_2$]$_n$Ph with $n > 1$ [benzyl complexes (n = 1), for which β-hydrogen elimination is lacking, will not be considered here] have not yet been synthesized. Pd(CH$_2$CH$_2$Ph)Cl was proposed as an intermediate in reactions of PdCl$_2$/HgPhCl with ethene and [PdCl$_4$]$^{2-}$ with Hg(CH$_2$CH$_2$Ph)Cl followed by cleavage of the Pd–C bond with CuCl$_2$/LiCl.[13] Furthermore, complexes with CH$_2$–CH$_2$Ph and CHPh–CH$_2$Ph ligands were detected by NMR spectroscopy as intermediates in reactions of phenylpalladium complexes with ethene and styrene, respectively.[14]

Here we report on the synthesis and characterization of (2-phenylethyl)- as well as (2- and 3-phenylpropyl)palladium complexes with bis(diphenylphosphanyl)ethane (dppe) as a stabilizing co-ligand. Reactions of [PdCl$_2$(dppe)] with LiR (R = CH$_2$CH$_2$Ph, CH$_2$CH$_2$CH$_2$Ph, CH$_2$CHMePh) afforded the diorgano complexes [PdR$_2$(dppe)]. Partial protolysis with phenylthiol resulted in formation of mono(phenylalkyl) complexes [PdR(SPh)-(dppe)], whose reactions with organo halides, disulfides and diselenides are described. Furthermore, the molecular structure of the first palladium complex with two β-hydrogen-containing alkyl ligands, [Pd(CH$_2$CH$_2$Ph)$_2$(dppe)], is presented.

2. Results and Discussion

2.1. Synthesis and Characterization of (Phenylalkyl)lithium and -mercury Compounds

The synthesis of (2-phenylethyl)lithium was described in the literature by either a direct synthesis (PhCH$_2$CH$_2$Br + Li),[15] or a lithium/iodide exchange reaction (PhCH$_2$CH$_2$I + *t*BuLi)[16] in diethyl ether. We and others[16b] failed to obtain LiCH$_2$CH$_2$Ph by direct synthesis. By a lithium/iodide exchange reaction we succeeded to obtain LiCH$_2$CH$_2$Ph, although severe impurities due to ether cleavage prevented its use as starting material for the synthesis of organopalladium complexes. Thus, we prepared (phenylalkyl)lithium compounds by transmetalation according to Scheme 2.

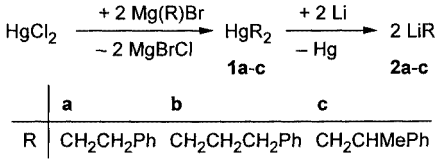

Scheme 2

The bis(phenylalkyl)mercury compounds **1a–c** were obtained (Scheme 2) by reaction of the Grignard compounds with mercury chloride in THF/diethyl ether as colorless liquids in moderate to good yields (66–84%). They were characterized by ^{1}H and ^{13}C NMR spectroscopy; all chemical shifts and couplings ($^nJ_{Hg,H}$ and $^nJ_{Hg,C}$, see Exp. Sect.) are in full agreement with expectations. Due to its two equivalent substituted stereogenic centers, the ^{13}C NMR spectrum of Hg(CH$_2$*C*HMePh)$_2$ (**1c**) shows two sets of signals of equal intensity corresponding to *rac* and *meso* forms. Comparison of the $^1J_{Hg,C}$ coupling constants (706 Hz, **1a**; 692 Hz, **1b**; 720 Hz, **1c**) with those of the corresponding non-phenyl-substituted compounds HgEt$_2$ (647 Hz)[17] and Hg(*n*Pr)$_2$ (660 Hz),[17] shows that phenyl substitution in the 2- (**1a**/**1c**) and 3-position (**1b**) gives rise to an increase of the $^1J_{Hg,C}$ coupling constants by 59/60 Hz and 32 Hz, respectively. In terms of Bent's model[18] this indicates a higher electronegativity of phenylalkyl ligands compared with their pure alkyl analogues.

Reactions of bis(phenylalkyl)mercury compounds **1a−c** with lithium in toluene resulted in the formation of (phenylalkyl)lithium compounds **2a−c** in moderate to good yields (64−81%) (Scheme 2). The compounds are stable in toluene at room temperature for days. Despite the use of highly toxic organomercury compounds these transmetalation reactions are superior to all other methods[15,16] because they essentially proceed without side reactions and can be performed in a solvent (toluene) in which the organolithium reagents **2a−c** are stable.

Instead of toluene as a solvent, *n*-pentane can be used for the synthesis of (3-phenylpropyl)lithium (**2b**). This is due to the excellent solubility of **2b** in aliphatic hydrocarbons at room temperature. Without obvious reason the homologous compounds **2a** and **2c** are insoluble in aliphatic hydrocarbons and the transmetalation in these solvents failed. The ^{13}C NMR spectrum of **2b** in perdeuterated *n*-hexane gave evidence for its identity. The signal of the carbon atom attached to the lithium atom is broadened ($b_{1/2} \approx 75$ Hz) due to dynamic processes and/or the quadrupole moment of Li (^{7}Li: $I = 3/2$, 92.6% rel. abund.). Its chemical shift ($\delta = 10.1$ ppm) is in the expected range as compared with other alkyllithium compounds [$\delta(^{13}C_\alpha)$, median: 12.5 ppm; lower/upper quartile: 10.2/17.0 ppm; 17 observations[19]]. The lithium-induced shift in **2b** [$\delta(^{13}C_\alpha)$ in LiR − $\delta(^{13}C_\alpha)$ in HR] amounts to $\delta = 10.1-14.6$ ppm[20] $= -4.5$ ppm, and is somewhat larger than expected for the correlation given in ref.[19] The $^1J_{C,H}$ coupling constant (ca. 94 Hz) is in the range expected for alkyllithium compounds ($^1J_{C,H}$ in $LiCH_3$: 98 Hz[21]).

2.2. Synthesis and Characterization of Bis(phenylalkyl)palladium Complexes

The (phenylalkyl)lithium compounds **2a−c** reacted with [$PdCl_2$(dppe)] in toluene at −30 °C to give bis(phenylalkyl){bis(diphenylphosphanyl)ethane}palladium complexes **3a−c** (Scheme 3). Addition of *n*-pentane resulted in the precipitation of complexes **3a−c**. Note that the choice of solvent determins the success of the synthesis: Despite its low vapor pressure at −30 °C, resulting in a long-lasting procedure to remove it in vacuo at that temperature, toluene is the most preferable one. The (phenylalkyl)lithium compounds **2** are freely soluble in toluene even at −78 °C and they are indefinitely stable in toluene, which is not the case for ethereal solvents.

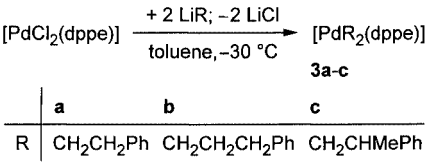

Scheme 3

Complexes **3a−c** were isolated in yields between 68 and 84% as colorless (**3a/b**) and yellowish (**3c**) microcrystalline substances that are moderately air-sensitive. Heating by a rate of about 4 K/min resulted in decomposition at about 159 °C (**3a**), 80 °C (**3b**) and 145 °C (**3c**). Solutions of these complexes in toluene are stable at −30 °C for several days although decomposition occurs at room temperature within several hours.

The identities of complexes **3** were unambiguously confirmed by ^1H, ^{13}C and ^{31}P NMR spectroscopy and also by X-ray crystallography for **3a**. Selected NMR spectroscopic data are shown in Table 1 along with the data of the dimethyl complex [$PdMe_2$(dppe)] (**4**) for comparison. As for the mercury compound **1c**, ^1H, ^{13}C, and ^{31}P NMR spectra of the 2-phenylpropyl complex [$Pd(CH_2CHMePh)_2$(dppe)] (**3c**) show two sets of signals in a 1:1 ratio due to the existence of *rac* and *meso* forms. Furthermore, in the ^{13}C NMR spectrum of **3c** a further signal splitting for the phenyl carbon atoms of the dppe ligand (e.g. four different C_o signals with coupling to the phosphorus atom, see Exp. Sect.) was observed indicating a pairwise inequivalence of the phenyl groups of the dppe ligand. This was expected as the two asymmetric carbon atoms reduce the symmetry (C_{2v} in terms of the NMR time scale) of simple [PdR_2(dppe)] complexes to C_2 in the *rac* form and C_s in the *meso* form.

Coupling with the magnetically inequivalent P atoms resulted in higher order multiplets of AA′X or − taking into account the isotopic shift of ^{13}C − ABX spin systems (A, B = ^{31}P; X = ^{13}C) for the ^{13}C resonances. For the dimethyl compound [$PdMe_2$(dppe)] (**4**) a complete set of $^nJ(^{31}P,^{13}C)$ coupling constants was obtained by spectral analysis using the program package PERCH[22] (cf. Table 1 and Exp. Sect.). For the methyl carbon atoms (signal pattern 'dd', pseudo-doublet of doublet with roof effect) and the methylene carbon atoms (signal pattern 't', pseudo-triplet) the results obtained by computer analysis are very similar to the results obtained when the signals are handled as first-order multiplets: CH_3: $^2J(P,C_{trans}) = 107.3$ Hz vs. 107.5 Hz, $^2J(P,C_{cis}) = 10.1$ Hz vs. 9.7 Hz; CH_2: $^{1+4}J_{P,C}/^{2+3}J_{P,C} = 19.7/21.9$ Hz (with opposite sign, assignment tentative) vs. 21.5 Hz. Thus, it seems to be justified to obtain approximate coupling constants by a "first-order treatment" as was done for complexes **3** (cf. Table 1).

The α-carbon signals in (phenylalkyl)palladium complexes **3a−c** are strongly lowfield-shifted compared with that in [$PdMe_2$(dppe)] (**4**) ($\delta = 24.9-33.6$ ppm vs. 1.9 ppm). In the couplings of α-carbon atoms to phosphorus atoms ($^2J_{P,C}$) only smaller differences between **3a−c** (*trans* coupling 100−101 Hz; *cis* coupling 9 Hz) and the dimethyl complex **4** (*trans* coupling 107.3 Hz; *cis* coupling 10.1 Hz) were found. The phosphorus chemical shifts are in the order 2-phenyl-substituted alkyl (**3a/c**: $\delta = 38.6-40.3$ ppm) < 3-phenyl-substituted alkyl (**3b**: $\delta = 43.6$ ppm) < Me (**4**: $\delta = 45.6$ ppm).

Single crystals of the 2-phenylethyl complex **3a**, which were suitable for X-ray diffraction analysis were grown from THF/pentane. The molecular structure of complex **3a** is shown in Figure 1, and selected bond lengths and angles are compiled in Table 2. Complex **3a** crystallizes as separate molecules without unusual intermolecular interactions; the shortest ones between non-hydrogen atoms are C···C distances of more than 3.5 Å. The palladium atom, to a good

Table 1. Selected NMR spectroscopic data (δ in ppm, *J* in Hz) for complexes $[PdR_2(dppe)]$ (**3**); data of $[PdMe_2(dppe)]$ (**4**) are given for comparison

R	Me (**4**)[a]	CH_2CH_2Ph (**3a**)	$CH_2CH_2CH_2Ph$ (**3b**)	$CH_2CHMePh$ (**3c**)
C1, δ(^{13}C)	1.9	28.6	24.9	33.5/33.6
$^2J_{P,C}$ *trans*	107.3	101	101	100/101
$^2J_{P,C}$ *cis*	10.1	9	9	9/9
C2, δ(^{13}C)		39.7	35.9	42.4/42.5
C3, δ(^{13}C)			44.0	25.9/26.6
$^4J_{P,C}$ *trans*			11	
PdCH_2, δ(^{1}H)	0.41 (m)	1.62 (m)	1.44 (m)	1.22−2.49 (m)[b]
δ(^{31}P)	45.6	40.3	43.6	38.6/39.7

[a] Coupling constants of complex **4** were calculated by spectral analysis. Couplings given for complexes **3** are only approximate values because they were derived from line distances, see text. [b] Superimposed by other signals.

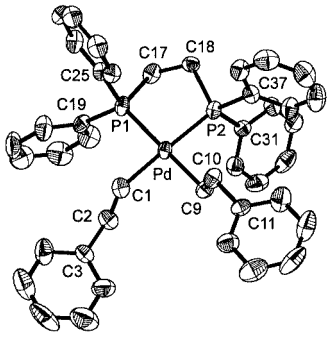

Figure 1. Molecular structure in the solid state with atomic labelling scheme for $[Pd(CH_2CH_2Ph)_2(dppe)]$ (**3a**); hydrogen atoms are omitted for clarity; thermal ellipsoids are drawn with 50% probability

Table 2. Selected bond lengths [Å], bond angles [°] and dihedral angles [°] of complex **3a**

Pd−C1	2.096(5)	C1−C2	1.526(6)
Pd−C9	2.107(6)	C2−C3	1.515(7)
Pd−P1	2.288(3)	C9−C10	1.524(8)
Pd−P2	2.291(1)	C10−C11	1.511(8)
C1−Pd−C9	85.8(2)	C9−Pd−P1	178.7(1)
P1−Pd−P2	85.53(8)	Pd−C1−C2	112.6(4)
C1−Pd−P1	93.1(2)	Pd−C9−C10	111.2(3)
C9−Pd−P2	95.5(2)	C1−C2−C3	112.6(5)
C1−Pd−P2	177.8(2)	C9−C10−C11	114.8(4)
Pd−C1−C2−C3	178.0(4)	Pd−C9−C10−C11	165.0(3)

approximation, is square-planar coordinated by two carbon atoms and two phosphorus atoms [greatest deviation of the least-squares plane: Pd 0.018(1) Å]. The five-membered PdP_2C_2 ring is twisted about C17−C18. The phenyl rings of the dppe ligand are arranged in a typical "face-to-edge"[23] position (face: Ph37/Ph19; edge: Ph31, Ph25; phenyl groups are designated by Ph*x*, where *x* is the number of the *ipso*-carbon atom). The bite of the dppe ligand [P1−Pd−P2 85.53(8)°] is as expected (median: 85.0°; lower/higher quartile: 84.3/85.6°; number of values: 52[24]). The opposite C1−Pd−C9 angle [85.8(2)°] is also markedly smaller than 90°.

As shown by the torsion angles Pd−C1−C2−C3 [178.0(4)°] and Pd−C9−C10−C11 [165.0(4)°] the two 2-phenylethyl ligands exhibit a nearly fully staggered conformation. The Pd−C1−C2/Pd−C9−C10 [112.6(4)/111.2(3)°] and C1−C2−C3/C9−C10−C11 [112.6(5)/114.8(4)°] angles are nearly tetrahedral. The phenyl groups of the 2-phenylethyl ligands are nearly parallel to the complex plane [Ph3/PdP_2C_2 10.8(2)°; Ph11/PdP_2C_2 14.2(3)°] and nearly perpendicular to the face-positioned phenyl groups of the dppe ligand [Ph3/Ph19 80.7(3)°; Ph11/Ph37 89.8(3)°]. Thus, the complex, to a good approximation, is C_2-symmetric with the C_2 axis defined by the Pd atom and the midpoint of the central C17−C18 bond of the dppe ligand.

2.3. Synthesis and Characterization of (Phenylalkyl)(thiolato)palladium Complexes

Yamamoto[5b,25] showed that *trans*-$[PdEt_2(PMe_3)_2]$ and $[PdMe_2(dppe)]$ react selectively with equimolar amounts of PhSH with protolytic cleavage of one of the two Pd−C bonds yielding *trans*-$[PdEt(SPh)(PMe_3)_2]$ and [PdMe(SPh)(dppe)], respectively. The analogous reaction of bis(phenylalkyl)palladium complexes **3a−c** proceeded according to Scheme 4. In the case of the 2-phenylethyl (**3a**) and 3-phenylpropyl (**3b**) complexes the protolytic cleavage of the first Pd−C bond proceeded faster than that of the second one. Thus, at −30 °C using a 1:1 ratio of **3a/3b** and PhSH the desired (phenylalkyl)(thiolato) complexes **5a** and **5b** were obtained. On the other hand, under the same reaction conditions the 2-phenylpropyl complex **3c** reacted with PhSH (1:1) to yield both the mixed complex **5c** (15%) and $[Pd(SPh)_2(dppe)]$ (**6a**) to a remarkable extent (16%) as shown by ^{31}P NMR spectroscopy. Successive additions of further quantities of PhSH (calculated 1:1 in relation to the amount of unchanged starting complex **3c** detected in the

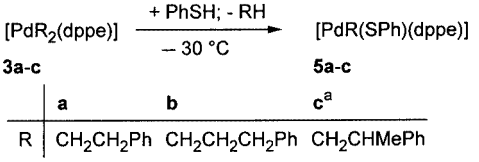

Scheme 4. [a] $[Pd(SPh)_2(dppe)]$ (**6a**) was also formed

^{31}P NMR spectrum) until **3c** had been completely consumed resulted in a mixture of **5c** and **6a** of about 3:1.

The less acidic alkanethiols *i*PrSH and *t*BuSH reacted slower with the 3-phenylpropyl complex **3b** than with PhSH (Scheme 5): At −30 °C the reaction was incomplete even after six days of reaction time. Increasing the temperature to −15 °C for one day and to 0 °C for eight days, resulted in the formation of [Pd($CH_2CH_2CH_2Ph$)(SR′)(dppe)] in 77% (R′ = *i*Pr, **5d**) and 82% yield (R′ = *t*Bu, **5e**). Side products were the bis(thiolato) complexes **6b** (R′ = *i*Pr; 13%) and **6c** (R′ = *t*Bu; 8%), and [Pd(dppe)$_2$] (**7**; 2% for R′ = *i*Pr; 7% for R′ = *t*Bu) as the reduction product. Comparing *i*PrSH and *t*BuSH, the protolytic cleavage of the second Pd−C bond yielding **6c** is less favoured, although the reduction yielding **7** is more favoured with *t*BuSH, which might be explained because of its lower acidity *and* its greater bulkiness.

[PdR$_2$(dppe)] + R′SH → [PdR(SR′)(dppe)] + [Pd(SR′)$_2$(dppe)] + [Pd(dppe)$_2$]

t, *T* [a]	**3b**	**5d/5e**	**6b/6c**	**7**
6 d, -30 °C	38/41[b]	56/55	5/1	1/3
1 d, -15 °C	29/35	62/60	8/2	1/3
8 d, 0 °C	8/3	77/82	13/8	2/7

Scheme 5. R = $CH_2CH_2CH_2Ph$; [a] temperature regime, see text; [b] composition of reaction mixture in % for R′ = *i*Pr/*t*Bu

The (phenylalkyl)(thiolato) complexes **5a** and **5b** were isolated as colorless (**5a**) and pale pink (**5b**) slightly air-sensitive, microcrystalline substances. The solids decomposed at 145 °C (**5a**) and 90 °C (**5b**). Solutions in tetrahydrofuran were stable at −30 °C; at room temperature they decomposed slowly. The identities of (phenylalkyl)(thiolato) complexes **5a** and **5b** were confirmed by ^{1}H, ^{13}C and ^{31}P NMR spectroscopy. The bis(thiolato) complexes **6** were characterized by ^{31}P NMR spectroscopy and by comparison with authentic samples prepared by reaction of [PdCl$_2$(dppe)] with LiSR′. Substitution of a phenylalkyl ligand by PhS (**3a/b** → **5a/b**) gives rise to a slight (δ = 1.5/4.1 ppm) lowfield shift of the C1 signal of the remaining phenylalkyl ligand. In complexes **5a/b** the signals of the P atoms *trans* to the carbon atoms are shifted to higher field [**5a/b**: δ($^{31}P_{trans\ to\ C}$) = 34.5/34.0 ppm] relative to those in the analogous bis(phenylalkyl) complexes [**3a/b**: δ(^{31}P) = 40.3/43.6 ppm] and those *trans* to sulfur atoms are lowfield-shifted [**5a/b**: δ($^{31}P_{trans\ to\ S}$) = 53.2/53.1 ppm]. Very similar to the latter one is the phosphorus shift in the bis(thiolato) complex [Pd(SPh)$_2$(dppe)] (**6a**) (δ = 55.4 ppm).

Apart from protolytic cleavage of the Pd−C bonds with alkanethiols (vide supra), reactions of bis(phenylalkyl)palladium complexes **3** with diorgano disulfides are another access to (phenylalkyl)(thiolato)palladium complexes **5**. Thus, reactions of R′SSR′ (R′ = Ph, Bz, Me) with the (3-phenylpropyl)palladium complex **3b** were performed (Scheme 6). PhSSPh exhibited the highest reactivity. It reacted already at −30 °C (to a small extent even at −50 °C) whereas for reactions of BzSSBz and MeSSMe, the temperature had to be increased to 0 °C and 15 °C, respectively. Side products were the bis(thiolato) complexes [Pd(SR′)$_2$(dppe)] (**6**) in all cases.

[PdR$_2$(dppe)] (**3b**) + R′SSR′ → [PdR(SR′)(dppe)] (**5b, 5f, 5g**) + [Pd(SR′)$_2$(dppe)] (**6a, 6d, 6e**)

R′	*t*, *T*	**3b**	**5**	**6**
Ph	5 d, -30 °C	7[a]	90 (**5b**)	3 (**6a**)
Bz	19 d, 0 °C	75	17 (**5f**)	8 (**6d**)
Me	6 d, 15 °C	64	22 (**5g**)	13 (**6e**)[b]

Scheme 6. R = $CH_2CH_2CH_2Ph$; [a] composition of reaction mixture in %; [b] small amounts of [Pd(dppe)$_2$] (**7**) were formed

In analogous reactions diorgano diselenides exhibited a higher reactivity than diorgano disulfides. Thus, at −30 °C, in tetrahydrofuran, reactions of MeSeSeMe with [Pd($CH_2CH_2CH_2Ph$)$_2$(dppe)] (**3b**) afforded the formation of [Pd($CH_2CH_2CH_2Ph$)(SeMe)(dppe)] (**8a**) (73%) and [Pd(SeMe)$_2$(dppe)] (**9a**) (3%), within one day. Formation of 3% [Pd(dppe)$_2$] (**7**) after a further day of reaction indicated a relatively low stability of **8a**. [PdMe$_2$(dppe)] (**4**) reacted with PhSeSePh at −30 °C completely, yielding 91% [PdMe(SePh)(dppe)] (**8b**) and 9% [Pd(SePh)$_2$(dppe)] (**9b**), within one day. No indication for the formation of organopalladium(IV) complexes as intermediates was found in any of the reactions. Analogous reactions between [PdMe$_2$L$_2$] (L$_2$ = bpy, phen) and PhEEPh (E = S, Se) afforded complexes [PdMe$_2$(EPh)$_2$L$_2$] that are unstable for E = S and moderately stable for E = Se.[26] This is further support for the far greater versatility of nitrogen-donor ligands in stabilizing palladium(IV) than that of phosphane ligands.[27]

2.4. Synthesis and Characterization of Halo(3-phenylpropyl)palladium Complexes

The (3-phenylpropyl)(phenylthiolato) complex **5b** reacted with organo halides RX with substitution of the phenylthiolato ligand by the halide yielding halo(3-phenylpropyl)palladium complexes **10a−c** (Scheme 7). Due to the low thermal stability of the products, reactions were performed at −30 °C in tetrahydrofuran as solvent or in neat RX. The reactivity of RX followed the expected order of X (I > Br > Cl) and R (allyl > alkyl). To obtain a complete degree

[Pd($CH_2CH_2CH_2Ph$)(SPh)(dppe)] (**5b**) + RX; − RSPh (thf; −30 °C) → [Pd($CH_2CH_2CH_2Ph$)X(dppe)] (**10a-c**)

	a	**b**	**c**
X	I	Br	Cl
R	Me	$H_2C{=}CHCH_2$	$H_2C{=}CHCH_2$

Scheme 7

of conversion, a threefold excess of methyl iodide was necessary; ethyl bromide did not react at all. Allyl bromide reacted quantitatively when a 50-fold excess was used. In neat allyl chloride complex **10c** was obtained with a 94% degree of conversion whereas allyl fluoride did not react at all. *trans*-[PdEt(SPh)(PMe_3)$_2$] proved to be more reactive than complex **5b** and reacted with MeI, $PhCH_2Br$ and $H_2C{=}CHCH_2Cl$ in a 1:1 ratio yielding *trans*-[PdEt(X)(PMe_3)$_2$] (X = I, Br, Cl) in > 80% yields.[5b]

The iodo (**10a**), bromo (**10b**) and chloro (**10c**) complexes were isolated as yellow (**10a**) and pale yellow (**10b**, **c**) powdery/microcrystalline substances that are moderately air-sensitive. Heating by about 4 K/min results in a decomposition at about 80 °C (**10b**) and 140 °C (**10c**). Solids can be handled at room temperature without noticeable decomposition for a short period of time. Solutions in tetrahydrofuran decompose rapidly above −30 °C, turning intensively violet.

The identities of complexes **10** were confirmed by ^{13}C and ^{31}P NMR spectroscopy. Selected values are shown in Table 3. Substitution of the 3-phenylpropyl ligand by bromide and chloride (**3b** → **10b/c**) gives rise to a lowfield shift of C1 by 4.1 and 6.1 ppm, respectively, whereas substitution by iodide (**3b** → **10a**) leaves the C1 chemical shift practically unchanged. Analogous to mono(phenylalkyl)(thiolato) complexes **5**, P atoms *trans* to the carbon atom resonate at higher fields than those *trans* to the halide ligand (δ = 27.7−30.2 vs. 56.1−59.5 ppm).

Table 3. Selected NMR spectroscopic data (δ in ppm, *J* in Hz) for complexes [Pd($CH_2CH_2CH_2Ph$)X(dppe)] (**10**)

X	I (**10a**)	Br (**10b**)	Cl (**10c**)
C1, δ(^{13}C)	24.3	29.0	31.0
$^2J_{P,C}$ *trans*	100.6	100.4	101.2
C2, δ(^{13}C)	35.8	34.6	34.0
$^3J_{P,C}$ *trans*			4.5
C3, δ(^{13}C)	42.9	42.4	42.2
$^4J_{P,C}$ *trans*	13.9	15.3	15.3
$^4J_{P,C}$ *cis*			3.2
P *trans* to C, δ(^{31}P)	30.2	28.9	27.7
P *trans* to X, δ(^{31}P)	56.1	59.5	59.4
$^{2+3}J_{P,P}$	29.3	29.5	29.5

In the present investigation (2- and 3-phenylalkyl)palladium complexes have been prepared and fully characterized for the first time. All of them contain β-hydrogen atoms and proved to be − at least in solution − of low thermal stability. This is especially pronounced in the *cis*-halo(3-phenylpropyl)palladium complexes [Pd($CH_2CH_2CH_2Ph$)X(dppe)] (**10a**−**c**; X = I, Br, Cl) that are − most likely − intermediates in the catalytic Heck cycle.[1b]

Experimental Section

1. General Comments: All reactions were performed under argon using standard Schlenk techniques. Solvents were dried prior to use: Et_2O, THF, and toluene with Na/benzophenone, *n*-hexane, *n*-pentane and [D_8]THF with $LiAlH_4$. ^1H, ^{13}C, and ^{31}P NMR spectra were recorded with Gemini 200, VXR 400 and Unity 500 NMR spectrometers (Varian). For ^1H and ^{13}C NMR spectra the protio impurities of the deuterated solvent or the solvent signals were used as internal references. For ^{31}P NMR spectra H_3PO_4 (85%) was used as the external reference. In higher order multiplets *N* gives the distance between the two most intense lines. In pseudo-triplets ('t') and pseudo-doublets of doublets ('dd') *N* was derived like couplings in first-order triplets and doublets of doublets, respectively. A CP9000 chromatograph (Chrompack) was used for chromatographic analyses. GC/MS investigations were carried out with an HP 5890 Series II/HP 5972 (Hewlett−Packard). [$PdCl_2$(dppe)] and [Pd(dppe)$_2$] were prepared according to literature methods.[28,29] Reactions of LiSR (R = Ph, *i*Pr, *t*Bu, Bz, Me) [obtained from RSSR and (*n*BuLi)] with [$PdCl_2$(dppe)] afforded complexes [Pd(SR)$_2$(dppe)] (**6a**−**e**) in yields between 40 and 85%. ^{31}P NMR (81 MHz, [D_8]THF): δ = 55.4 (in $CDCl_3$; R = Ph, **6a**), 56.7 (R = *i*Pr, **6b**), 54.3 (R = *t*Bu, **6c**), 58.2 (R = Bz, **6d**), 57.6 (R = Me, **6e**) ppm. Other chemicals were commercially available.

2. HgR_2 (R = CH_2CH_2Ph, 1a; $CH_2CH_2CH_2Ph$, 1b; $CH_2CHMePh$, 1c): Solutions of Grignard compounds RMgBr in diethyl ether (0.7−0.9 M) were prepared following a standard procedure[30] from Mg and RBr. Yields (93−97%) were determined by acidimetric titration. Only solutions of Grignard compounds free from unchanged RBr (checked by GC/MS) were used. These solutions of RMgBr (40.5 mmol) were added dropwise to a solution of $HgCl_2$ (5.0 g, 18.4 mmol) in THF (20 mL) at −78 °C. The reaction mixture was slowly warmed to room temperature and stirred for 2 days. At −78 °C, water (20 mL) was added dropwise. The organic phase was separated, washed with water and dried with Na_2SO_4. The solvent was removed in vacuo. Finally, the temperature was raised to 50 °C (0.1 Torr) to remove all volatile substances. ***Warning!*** All manipulations with the highly toxic organomercurials were done in a separate fume hood using appropriate safety requirements, above all, a special combination of gloves.[31] All glassware used in these syntheses was treated with a solution of bromine in methanol to convert highly toxic organomercurials into less toxic $HgBr_2$.

Compound 1a (R = CH_2CH_2Ph): Colorless oil. Yield: 5.3 g (70%). ^1H NMR (200 MHz, $CDCl_3$): δ = 1.29 ('t' + dt, *N* = 7.7, $^2J_{Hg,H}$ = 96.7 Hz, 4 H, $HgCH_2$), 3.05 ('t' + dt, *N* = 7.7, $^3J_{Hg,H}$ = 112.3 Hz, 4 H, $HgCH_2CH_2$), 7.12−7.33 (m, 10 H, Ph) ppm. ^{13}C NMR (100 MHz, $CDCl_3$): δ = 34.8 (s, $HgCH_2CH_2$), 45.0 (s + d, $^1J_{Hg,C}$ = 706.5 Hz, $HgCH_2$), 125.4 (s, *m*-*C*),[32] 127.9 (s, *p*-*C*), 128.4 (s, *o*-*C*), 147.3 (s, *i*-*C*).

Compound 1b (R = $CH_2CH_2CH_2Ph$): Colorless oil. Yield: 5.3 g (66%). ^1H NMR (400 MHz, $CDCl_3$): δ = 0.77 ('t' + dt, *N* = 7.2, $^2J_{Hg,H}$ = 100.0 Hz, 4 H, $HgCH_2$), 2.13 ('quint' + dt, *N* = 7.2, $^3J_{Hg,H}$ = 112.3 Hz, 4 H, $HgCH_2CH_2$), 2.58 ('t', *N* = 7.2 Hz, 4 H, $HgCH_2CH_2CH_2$), 7.13−7.19 (m, 6 H, Ph), 7.27−7.30 (m, 4 H, Ph) ppm. ^{13}C NMR (100 MHz, $CDCl_3$): δ = 30.5 (s + d, $^2J_{Hg,C}$ = 33.2 Hz, $HgCH_2CH_2$), 40.2 (s + d, $^3J_{Hg,C}$ = 83.8 Hz, $HgCH_2CH_2CH_2$), 41.7 (s + d, $^1J_{Hg,C}$ = 692.0 Hz, $HgCH_2$), 125.7 (s, *p*-*C*), 128.3/128.6 (s/s, *o*-, *m*-*C*), 142.9 (s, *i*-*C*) ppm.

Compound 1c (R = $CH_2CHMePh$, 1:1 Mixture of Two Diastereomers): Colorless oil. Yield: 6.8 g (84%). ^1H NMR (400 MHz, $CDCl_3$): δ = 1.22 (d, $^3J_{H,H}$ = 7.0 Hz, 2 × 6 H, CH_3), 1.28 (centered, m, 2 × 4 H, $HgCH_2$), 3.41−3.52 (m, 2 × 2 H, $HgCH_2CH$), 7.11−7.18, 7.22−7.28 (m, 2 × 10 H, Ph) ppm. ^{13}C NMR (100 MHz, $CDCl_3$): δ = 26.50/26.51 (s/s, CH_3), 39.46/39.49 (s/s, $HgCH_2CH$), 54.46/54.49 (s + d/s + d, $^1J_{Hg,C}$ = 720.2/720.2, $HgCH_2$), 2 × 125.6 (s, *p*-*C*), 2 × 126.3/128.3/128.4 (s/s/s, *o*-, *m*-*C*), 151.66/151.68 (s/s, *i*-*C*) ppm.

3. Synthesis of LiR (R = CH_2CH_2Ph, 2a; $CH_2CH_2CH_2Ph$, 2b; $CH_2CHMePh$, 2c): A solution of HgR_2 (**1**) (ca. 7 mmol) in toluene (ca. 15 mL) was stirred for 2 days with freshly cut lithium chips (ca. 75 mmol) at room temperature. The lithium amalgam formed was allowed to settle and the supernatant was filtered [yield (acidimetric): 64%, **2a**; 81%, **2b**; 80%, **2c**]. For isolation of compound **2b**, the reaction was performed in *n*-pentane. Removal of solvent in vacuo resulted in an orange oil that was dissolved in $[D_{14}]$*n*-hexane for NMR spectroscopic investigations.

Compound 2b (R = $CH_2CH_2CH_2Ph$): ^{13}C NMR (100 MHz, $[D_{14}]$*n*-hexane): δ = 10.1 (br., t, $^1J_{C,H} \approx 94$ Hz, Li*C*H_2), 31.0 (t, $^1J_{C,H}$ = 121.8 Hz, LiCH$_2$*C*H_2), 44.2 (t, $^1J_{C,H}$ = 126.6 Hz, LiCH$_2$CH$_2$*C*H_2), 125.7 (dt, $^1J_{C,H}$ = 159.9, $^2J_{C,H}$ = 7.4 Hz, *p*-*C*), 128.3 (dd, $^1J_{C,H}$ = 158.9, $^2J_{C,H}$ = 7.6 Hz, *o*-*C*), 128.7 (dt, $^1J_{C,H}$ = 156.3, $^2J_{C,H}$ = 5.9 Hz, *m*-*C*), 142.6 (s, *i*-*C*). Couplings refer to H-coupled spectrum.

4. [PdR$_2$(dppe)] (R = CH_2CH_2Ph, 3a; $CH_2CHMePh$, 3c): At −78 °C, 1.9 equiv. of LiCH_2CH_2Ph (**2a**) or Li$CH_2CHMePh$ (**2c**) in toluene (20−25 mL) was added to [PdCl$_2$(dppe)] (ca. 3 mmol). The reaction mixture was slowly warmed to −30 °C and stirred overnight. The filtered solution was concentrated to about 5 mL in vacuo at −30 °C. Cooling to −78 °C and addition of *n*-pentane (ca. 25 mL) resulted in precipitation of **3a** or **3c**, respectively, that were filtered off, washed with *n*-pentane (2 × 5 mL) and dried in vacuo at −30 °C.

Complex 3a (R = CH_2CH_2Ph): Colorless microcrystalline powder. Yield: 68%. ^1H NMR (400 MHz, $[D_8]$THF): δ = 1.62 (m, 4 H, PdCH_2), 2.25 (m, *N* = 17.8 Hz, 4 H, PCH_2), 2.65 (m, 4 H, PdCH$_2$CH_2), 6.87 (m, 6 H, Ph), 7.01 (m, 4 H, Ph), 7.43 (m, 12 H, Ph), 7.65 (m, 8 H, Ph) ppm. ^{13}C NMR (125 MHz, −30 °C, $[D_8]$THF): 27.9 ('t', *N* = 21.2 Hz, P*C*H$_2$), 28.6 ('dd', *N* = 101.4/9.3 Hz, Pd*C*H$_2$), 39.7 (s, PdCH$_2$*C*H$_2$), 124.7 (s, *p*-C_{Ph}), 128.4/128.6 (s/s, *o*-C_{Ph}/*m*-C_{Ph}), 129.5 (m, *N* = 8.7 Hz, *m*-C_{dppe}), 130.9 (s, *p*-C_{dppe}), 134.3 (m, *N* = 12.6 Hz, *o*-C_{dppe}), 134.4 (m, superposed, *N* = 29.4 Hz, *i*-C_{dppe}), 150.3 (m, *N* = 10.7 Hz, *i*-C_{Ph}) ppm. ^{31}P NMR (202 MHz, −30 °C, $[D_8]$THF): δ = 40.3 (s) ppm.

Complex 3c (R = $CH_2CHMePh$; 1:1 Mixture of Two Diastereomers): Yellow microcrystalline powder. Yield: 69%. ^1H NMR (200 MHz, $CDCl_3$): δ = 0.92/0.99 (m/m, *N*/*N* = 6.8/6.8 Hz, 6/6 H, CHCH_3), 1.22−2.49 (m, 2 × 8 H, PCH_2 + PdCH_2), 3.05 (m, 2 × 2 H, C*H*Me), 6.9−7.2, 7.3−7.7 (m, 2 × 30 H, Ph) ppm. ^{13}C NMR (125 MHz, $CDCl_3$): δ = 25.9/26.6 (s/s, CH*C*H$_3$), 26.9/26.9 ('t', *N* = 20.9 Hz, P*C*H$_2$), 33.5/33.6 ('dd'/'dd', *N* = 99.7/9.0 Hz/100.8/8.9 Hz, Pd*C*H$_2$), 42.4/42.5 (s/s, PdCH$_2$*C*H), 124.1/124.2 (s/s, *p*-*C*), 126.5/126.6/127.6/127.7 (s/s/s/s, *o*-*C*, *m*-*C*), 128.4/128.5/128.6/128.7 (m/m/m/m, *N* = 9.0/9.0/9.0/9.0 Hz, *m*-C_{dppe}), 129.5/2 × 129.9/130.4 (s/s/s, *p*-C_{dppe}), 132.5/133.3/133.5/134.3 (m/m/m/m, *N* = 10.9/11.9/13.9/13.9 Hz, *o*-C_{dppe}), 132.7/133.9 (m, *N* = 29.0/30.0 Hz, *i*-C_{dppe}, 2 × *i*-C_{dppe} not found due to superposition), 154.0/154.2 (m/m, *N* = 8.0/9.0 Hz, *i*-*C*) ppm. ^{31}P NMR (81 MHz, $CDCl_3$): δ = 38.6/39.7 (s/s) ppm.

5. [Pd(CH$_2$CH$_2$CH$_2$Ph)$_2$(dppe)] (3b): At −78 °C, a solution of Li$CH_2CH_2CH_2Ph$ (**2b**) (34.2 mmol) in toluene (50 mL) was added to [PdCl$_2$(dppe)] (3.30 g, 5.73 mmol). The reaction mixture was slowly warmed to −30 °C and stirred overnight. The colorless precipitate was filtered off and washed at room temperature with *n*-pentane as long as the filtrate remained colorless (ca. 20 mL). The precipitate was dissolved in toluene (100 mL) at room temperature and immediately filtered. At −30 °C, the solution was concentrated in vacuo to about 10 mL. Cooling to −78 °C and addition of *n*-pentane (ca. 50 mL) resulted in the formation of **3b** as a colorless microcrystalline precipitate that was filtered off, washed with *n*-pentane (2 × 5 mL) and dried in vacuo at −30 °C. Yield: 3.56 g (84%). ^1H NMR (400 MHz, $[D_8]$THF): δ = 1.44 (m, 4 H, PdCH_2), 1.67 (m, 4 H, PdCH$_2$CH_2), 2.20 (m, *N* = 17.8 Hz, 4 H, PCH_2), 2.31 ('t', *N* = 7.8 Hz, 4 H, PdCH$_2$CH$_2$CH_2), 6.87−7.60 (m, 30 H, Ph) ppm. ^{13}C NMR (125 MHz, $[D_8]$THF, −30 °C): δ = 24.9 ('dd', *N* = 100.7/9.1 Hz, Pd*C*H$_2$), 28.2 ('t', *N* = 20.9 Hz, P*C*H$_2$), 35.9 (s, PdCH$_2$*C*H$_2$), 44.0 (m, *N* = 10.9 Hz, PdCH$_2$CH$_2$*C*H$_2$), 125.3 (s, *p*-C_{Ph}), 128.3/129.1 (s/s, *o*-C_{Ph}, *m*-C_{Ph}), 129.3 (m, *N* = 9.9 Hz, *m*-C_{dppe}), 130.6 (s, *p*-C_{dppe}), 134.1 (m, *N* = 12.9 Hz, *o*-C_{dppe}), 134.9 (m, *N* = 26.9 Hz, *i*-C_{dppe}), 145.1 (s, *i*-C_{Ph}) ppm. ^{31}P NMR (81 MHz, $[D_8]$THF): δ = 43.6 (s) ppm.

6. [PdMe$_2$(dppe)] (4): In a modified synthesis to that described in ref.[33], a solution of MeLi (6.25 mmol) in diethyl ether (24 mL) was added to [PdCl$_2$(dppe)] (2.00 g, 3.47 mmol) at −78 °C. The reaction mixture was slowly warmed to −30 °C, stirred overnight and filtered. At −30 °C the solvent was distilled off in vacuo and toluene (20 mL) was added to the residue. The precipitated LiCl was filtered off and the solution was concentrated to about 5 mL in vacuo at −30 °C. At −78 °C the addition of *n*-pentane (ca. 30 mL) resulted in the formation of **4** as a colourless precipitate that was filtered off, washed with *n*-pentane (2 × 10 mL) and dried in vacuo at −30 °C. Yield: 0.95 g (51%). ^1H NMR (400 MHz, $CDCl_3$): δ = 0.41 (m, *N* = 0.8 Hz, *N*′ = 14.1 Hz, 6 H, PdCH_3; *N*′: distance of the two outer lines lower in intensity), 2.22 (m, *N* = 18.2 Hz, 4 H, PCH_2), 7.32−7.42 (m, 12 H, Ph), 7.57−7.83 (m, 8 H, Ph) ppm. ^{13}C NMR (100 MHz, $[D_8]$THF), for analysis PERCH[22] program package was used: δ = 1.95 (m, *trans*-$^2J_{P,C}$ = 107.3 Hz, *cis*-$^2J_{P,C}$ = 10.1 Hz, Pd*C*H$_3$), 28.5 (m, $^{1+4}J_{P,C}$/$^{2+3}J_{P,C}$ = 19.7/21.9 Hz, P*C*H$_2$; with opposite signs, assignment tentative), 129.5 (m, $^3J_{P,C}$ = 8.6, $^5J_{P,C}$ = 0.5 Hz, *m*-*C*), 130.9 (s, *p*-*C*), 134.2 (m, $^2J_{P,C}$ = 13.6, $^4J_{P,C}$ = −1.1 Hz, *o*-*C*), 135.0 (m, $^1J_{P,C}$ = 28.8 Hz, $^{3+4}J_{P,C}$ = 1.9 Hz, *i*-*C*) ppm. ^{31}P NMR (81 MHz, $[D_8]$THF): δ = 45.6 (s) ppm.

7. [Pd(CH$_2$CH$_2$Ph)(SPh)(dppe)] (5a): At −78 °C, PhSH (77 mg, 0.70 mmol) in THF (15 mL) was added to a solution of [Pd(CH$_2$CH$_2$Ph)$_2$(dppe)] (**3a**) (500 mg, 0.70 mmol) in THF (15 mL). After warming to −30 °C, the reaction mixture was stirred overnight. At −30 °C, the precipitate formed was filtered off, washed with pentane (2 × 10 mL) and dried in vacuo. Yield: 251 mg (50%). ^1H NMR (200 MHz, $CDCl_3$): δ = 1.53 (m, 2 H, PdCH_2), 2.00−2.48 (m, 4 H, PCH_2), 2.22 (m, 2 H, PdCH$_2$CH_2), 6.0−6.2, 6.8−7.0, 7.2−7.8 (m, 30 H, Ph) ppm. ^{13}C NMR (100 MHz, $CDCl_3$): δ = 26.1 (dd, $^{1+4}J_{P,C}$ = 24.7 Hz, $^{2+3}J_{P,C}$ = 14.7 Hz, P*C*H$_2$), 29.4 (dd, $^{1+4}J_{P,C}$ = 28.2 Hz, $^{2+3}J_{P,C}$ = 22.0 Hz, P*C*H$_2$), 30.1 (d, $^2J_{Ptrans,C}$ = 91.6 Hz, Pd*C*H$_2$), 37.0 (d, $^3J_{Ptrans,C}$ = 4.2 Hz, PdCH$_2$*C*H$_2$), 122.9 (s, *p*-C_{SPh}), 124.2 (s, *p*-C_{Ph}), 127.3/127.4/128.0 (s/s/s, *o*-C_{Ph}, *m*-C_{Ph}, *m*-C_{SPh}), 128.8 (d, $^3J_{P,C}$ = 9.6 Hz, *m*-C_{dppe}), 129.0 (d, $^3J_{P,C}$ = 10.4 Hz, *m*-C_{dppe}), 130.3 (d, $^1J_{P,C}$ = 43.1 Hz, *i*-C_{dppe}), 130.4 (d, $^4J_{P,C}$ = 2.5 Hz, *p*-C_{dppe}), 131.0 (d, $^4J_{P,C}$ = 2.5 Hz, *p*-C_{dppe}), 132.1 (d, $^1J_{P,C}$ = 28.6 Hz, *i*-C_{dppe}), 133.3 (d, $^2J_{P,C}$ = 12.5 Hz, *o*-C_{dppe}), 133.7 (d, $^2J_{P,C}$ = 12.0 Hz, *o*-C_{dppe}), 135.7 (d, $^4J_{Ptrans,C}$ = 1.6 Hz, *o*-C_{SPh}), 144.5 (m, *i*-C_{Ph}), 147.0 (dd, $^3J_{Ptrans,C}$ = 13.1, $^3J_{Pcis,C}$ = 3.1 Hz, *i*-C_{SPh}) ppm. ^{31}P NMR (81 MHz, $CDCl_3$): δ = 34.5 (d, $^{2+3}J_{P,P}$ = 26.9 Hz, P_{trans} to CH_2CH_2Ph), 53.2 (d, $^{2+3}J_{P,P}$ = 26.9 Hz, P_{trans} to SPh) ppm.

8. [Pd(CH$_2$CH$_2$CH$_2$Ph)(SPh)(dppe)] (5b): At −78 °C, PhSH (244 mg, 2.21 mmol) in THF (90 mL) was slowly added to a solution of [Pd(CH$_2$CH$_2$CH$_2$Ph)$_2$(dppe)] (**3b**) (1.644 g, 2.21 mmol) in THF (90 mL). After warming to −30 °C, the reaction mixture was stirred overnight. At −30 °C the solution was concentrated in vacuo to 5 mL and at −78 °C pentane (25 mL) was added. At −30

°C the pale pink precipitate that formed was filtered off, washed with pentane (2 × 10 mL) and dried in vacuo. Yield: 1.54 g (95%). ^{1}H NMR (200 MHz, $CDCl_3$): δ = 1.12 (m, 2 H, PdCH_2), 1.37 (m, 2 H, PdCH$_2$CH_2), 1.71 (m, 2 H, PdCH$_2$CH$_2$CH_2), 1.94−2.43 (m, 4 H, PCH_2), 6.6−6.7, 6.9−7.2, 7.4−7.8 (m, 30 H, Ph) ppm. ^{13}C NMR (125 MHz, $CDCl_3$): δ = 25.9 (dd, $^{1+4}J_{P,C}$ = 25.0 Hz, $^{2+3}J_{P,C}$ = 15.0 Hz, P*C*H$_2$), 28.9 (dd, $^{1+4}J_{P,C}$ = 27.9 Hz, $^{2+3}J_{P,C}$ = 22.0 Hz, P*C*H$_2$), 29.0 (d, $^{2}J_{Ptrans,C}$ = 90.8 Hz, Pd*C*H$_2$), 33.3 (d, $^{3}J_{Ptrans,C}$ = 4.0 Hz, PdCH$_2$*C*H$_2$), 41.3 (dd, $^{4}J_{Ptrans,C}$ = 14.9, $^{4}J_{Pcis,C}$ = 3.0 Hz, PdCH$_2$CH$_2$*C*H$_2$), 122.6 (s, *p*-C_{SPh}), 124.5 (s, *p*-C_{Ph}), 126.8 (s, *m*-C_{SPh}), 127.5/128.2 (s/s, *o*-C_{Ph}, *m*-C_{Ph}), 128.5 (d, $^{3}J_{P,C}$ = 9.0 Hz, *m*-C_{dppe}), 128.7 (d, $^{3}J_{P,C}$ = 11.0 Hz, *m*-C_{dppe}), 130.1 (s, *p*-C_{dppe}), 130.3 (d, $^{1}J_{P,C}$ = 42.9 Hz, *i*-C_{dppe}), 130.7 (s, *p*-C_{dppe}), 132.0 (d, $^{1}J_{P,C}$ = 27.9 Hz, *i*-C_{dppe}), 133.1 (d, $^{2}J_{P,C}$ = 12.0 Hz, *o*-C_{dppe}), 133.3 (d, $^{2}J_{P,C}$ = 12.1 Hz, *o*-C_{dppe}), 135.4 (s, *o*-C_{SPh}), 143.2 (s, *i*-C_{Ph}), 144.6 (d, $^{3}J_{Ptrans,C}$ = 9.9 Hz, *i*-C_{SPh}) ppm. ^{31}P NMR (81 MHz, $CDCl_3$): δ = 34.0 (d, $^{2+3}J_{P,P}$ = 26.8 Hz, P_{trans} to CH$_2$CH$_2$CH$_2$Ph), 53.1 (d, $^{2+3}J_{P,P}$ = 25.6 Hz, P_{trans} to SPh) ppm.

9. [Pd(CH$_2$CHMePh)(SPh)(dppe)] (5c)/[Pd(SPh)$_2$(dppe)] (6a): At −78 °C, PhSH (115 mg, 1.04 mmol) was added to a solution of [Pd(CH$_2$CHMePh)$_2$(dppe)] (**3c**) (770 mg, 1.04 mmol) in THF (50 mL). After stirring overnight at −30 °C, the degree of conversion was determined by ^{31}P NMR spectroscopy. Then, PhSH was added in a quantity that corresponded to the unchanged amount of **3c** and stirring (−30 °C) was continued. This procedure was repeated until all of **3c** had been consumed (final ratio **3c**/PhSH = 1:6). At −30 °C, THF was removed in vacuo. The residue was taken up in toluene (10 mL). Addition of pentane (50 mL) at −78 °C resulted in the precipitation of a mixture of **5c/6a** (74/26%) that was filtered, washed with pentane and dried in vacuo at −30 °C.

Complex 5c: ^{31}P NMR (81 MHz, [D$_8$]THF): δ = 35.6 (d, $^{2+3}J_{P,P}$ = 25.7 Hz, P_{trans} to CH$_2$CHMePh), 51.3 (d, $^{2+3}J_{P,P}$ = 25.7 Hz, P_{trans} to SPh) ppm.

Complex 6a: ^{31}P NMR (81 MHz, $CDCl_3$): δ = 55.4 ppm.

10. [Pd(CH$_2$CH$_2$CH$_2$Ph)X(dppe)] (X = I, 10a; Br, 10b; Cl, 10c): At −78 °C, MeI (290 mg, 2.04 mmol), H$_2$C=CHCH$_2$Br (4.12 g, 34.1 mmol), or H$_2$C=CHCH$_2$Cl (10 mL, without THF) was added to [Pd(CH$_2$CH$_2$CH$_2$Ph)(SPh)(dppe)] **5b** (500 mg, 0.68 mmol) in THF (10 mL). After stirring overnight at −30 °C, solvent and unchanged RX compound were removed in vacuo. The residue was taken up in toluene (10 mL) and cooled to −78 °C. Addition of pentane (ca. 30 mL) resulted in precipitation of complexes **10** that were filtered off, washed with pentane (2 × 5 mL) and dried in vacuo. All manipulations were performed at a maximum temperature of −30 °C.

Complex 10a (X = I): Yellow solid. Yield: 500 mg (98%). ^{13}C NMR (125 MHz, −30 °C, [D$_8$]THF): δ = 24.3 (d, $^{2}J_{Ptrans,C}$ = 100.6 Hz, Pd*C*H$_2$), 30.2 (dd, $^{1+4}J_{P,C}$ = 30.0 Hz, $^{2+3}J_{P,C}$ = 22.6 Hz, P*C*H$_2$; other P*C*H$_2$ not found, probably beneath solvent signal), 35.8 (s, PdCH$_2$*C*H$_2$), 42.9 (d, $^{4}J_{Ptrans,C}$ = 13.9 Hz, PdCH$_2$CH$_2$*C*H$_2$), 125.6 (s, *p*-C_{Ph}), 128.5/128.9 (s/s, *o*-C_{Ph}, *m*-C_{Ph}), 129.2 (d, $^{3}J_{P,C}$ = 9.2 Hz, *m*-C_{dppe}), 129.9 (d, $^{3}J_{P,C}$ = 10.3 Hz, *m*-C_{dppe}), 130.2 (d, $^{1}J_{P,C}$ = 47.4 Hz, *i*-C_{dppe}), 131.1 (s, *p*-C_{dppe}), 132.1 (s, *p*-C_{dppe}), 133.6 (d, $^{1}J_{P,C}$ = 28.9 Hz, *i*-C_{dppe}), 134.5 (d, $^{2}J_{P,C}$ = 11.8 Hz, *o*-C_{dppe}), 134.7 (d, $^{2}J_{P,C}$ = 11.7 Hz, *o*-C_{dppe}), 143.8 (s, *i*-C_{Ph}) ppm. ^{31}P NMR (202 MHz, −30 °C, [D$_8$]THF): δ = 30.2 (d, $^{2+3}J_{P,P}$ = 29.3 Hz, P_{trans} to CH$_2$CH$_2$CH$_2$Ph), 56.1 (d, $^{2+3}J_{P,P}$ = 29.3 Hz, P_{trans} to I) ppm.

Complex 10b (X = Br): Pale yellow solid. Yield: 456 mg (95%). ^{13}C NMR (125 MHz, −30 °C, [D$_8$]THF): δ = 24.0 (dd, $^{1+4}J_{P,C}$ = 25.6 Hz, $^{2+3}J_{P,C}$ = 11.9 Hz, P*C*H$_2$), 29.0 (d, $^{2}J_{Ptrans,C}$ = 100.4 Hz, Pd*C*H$_2$), 30.4 (dd, $^{1+4}J_{P,C}$ = 31.3 Hz, $^{2+3}J_{P,C}$ = 24.1 Hz, P*C*H$_2$), 34.6 (s, PdCH$_2$*C*H$_2$), 42.4 (d, $^{4}J_{Ptrans,C}$ = 15.3 Hz, PdCH$_2$CH$_2$*C*H$_2$), 125.5 (s, *p*-C_{Ph}), 128.5/129.0 (s/s, *o*-C_{Ph}, *m*-C_{Ph}), 129.3 (d, $^{3}J_{P,C}$ = 9.7 Hz, *m*-C_{dppe}), 129.8 (d, $^{3}J_{P,C}$ = 9.7 Hz, *m*-C_{dppe}), 130.6 (d, $^{1}J_{P,C}$ = 49.0 Hz, *i*-C_{dppe}), 131.0 (s, *p*-C_{dppe}), 132.0 (s, *p*-C_{dppe}), 134.0 (d, $^{1}J_{P,C}$ = 27.3 Hz, *i*-C_{dppe}), 134.5 (d, $^{2}J_{P,C}$ = 9.7 Hz, *o*-C_{dppe}), 144.1 (s, *i*-C_{Ph}) ppm. ^{31}P NMR (202 MHz, −30 °C, [D$_8$]THF): δ = 28.9 (d, $^{2+3}J_{P,P}$ = 29.5 Hz, P_{trans} to CH$_2$CH$_2$CH$_2$Ph), 59.5 (d, $^{2+3}J_{P,P}$ = 29.5 Hz, P_{trans} to Br) ppm.

Complex 10c (X = Cl): Pale yellow solid. Yield: 420 mg (94%). ^{13}C NMR (125 MHz, −30 °C, [D$_8$]THF): δ = 23.2 (dd, $^{1+4}J_{P,C}$ = 26.3 Hz, $^{2+3}J_{P,C}$ = 11.0 Hz, P*C*H$_2$), 30.3 (dd, $^{1+4}J_{P,C}$ = 32.7 Hz, $^{2+3}J_{P,C}$ = 23.9 Hz, P*C*H$_2$), 31.0 (d, $^{2}J_{Ptrans,C}$ = 101.2 Hz, Pd*C*H$_2$), 34.0 (d, $^{3}J_{P,C}$ = 4.5 Hz, PdCH$_2$*C*H$_2$), 42.2 (dd, $^{4}J_{Ptrans,C}$ = 15.3, $^{4}J_{Pcis,C}$ = 3.2 Hz, PdCH$_2$CH$_2$*C*H$_2$), 125.5 (s, *p*-C_{Ph}), 128.5/129.0 (s/s, *o*-C_{Ph}, *m*-C_{Ph}), 129.4 (d, $^{3}J_{P,C}$ = 8.8 Hz, *m*-C_{dppe}), 129.7 (d, $^{3}J_{P,C}$ = 10.1 Hz, *m*-C_{dppe}), 130.7 (d, $^{1}J_{P,C}$ = 49.0 Hz, *i*-C_{dppe}), 131.0 (s, *p*-C_{dppe}), 131.9 (s, *p*-C_{dppe}), 134.1 (one line of d, other one superposed, *i*-C_{dppe}), 134.3 (d, $^{2}J_{P,C}$ = 11.3 Hz, *o*-C_{dppe}), 134.5 (d, $^{2}J_{P,C}$ = 11.3 Hz, *o*-C_{dppe}), 144.2 (s, *i*-C_{Ph}) ppm. ^{31}P NMR (202 MHz, −30 °C, [D$_8$]THF): δ = 27.7 (d, $^{2+3}J_{P,P}$ = 29.5 Hz, P_{trans} to CH$_2$CH$_2$CH$_2$Ph), 59.4 (d, $^{2+3}J_{P,P}$ = 29.5 Hz, P_{trans} to Cl) ppm.

11. Experiments Monitored by ^{31}P NMR Spectroscopy: The corresponding amounts of sulfur or selenium compounds were added with a syringe to solutions of the palladium complex in THF/[D$_8$]THF (ca. 4:1). The reaction mixtures were transferred to NMR tubes that were then sealed. The reactions were monitored by ^{31}P{^{1}H} NMR spectroscopy.

[Pd(CH$_2$CH$_2$CH$_2$Ph)(SPh)(dppe)] (5b) from 3b and PhSSPh: ^{31}P NMR (81 MHz): δ = 34.0 (d, $^{2+3}J_{P,P}$ = 25.6 Hz, P_{trans} to CH$_2$CH$_2$CH$_2$Ph), 53.1 (d, $^{2+3}J_{P,P}$ = 25.6 Hz, P_{trans} to SPh) ppm.

[Pd(CH$_2$CH$_2$CH$_2$Ph){S(*i*Pr)}(dppe)] (5d) from 3b and *i*PrSH: ^{31}P NMR (81 MHz): δ = 40.7 (d, $^{2+3}J_{P,P}$ = 22.0 Hz, P_{trans} to CH$_2$CH$_2$CH$_2$Ph), 55.9 [d, $^{2+3}J_{P,P}$ = 22.0 Hz, P_{trans} to S(*i*Pr)] ppm.

[Pd(CH$_2$CH$_2$CH$_2$Ph){S(tBu)}(dppe)] (5e) from 3b and tBuSH: ^{31}P NMR (81 MHz): δ = 35.3 (d, $^{2+3}J_{P,P}$ = 23.2 Hz, P_{trans} to CH$_2$CH$_2$CH$_2$Ph), 56.9 [d, $^{2+3}J_{P,P}$ = 22.0 Hz, P_{trans} to S(*t*Bu)] ppm.

[Pd(CH$_2$CH$_2$CH$_2$Ph)(SBz)(dppe)] (5f) from 3b and BzSSBz: ^{31}P NMR (81 MHz): δ = 41.9 (d, $^{2+3}J_{P,P}$ = 23.2 Hz, P_{trans} to CH$_2$CH$_2$CH$_2$Ph), 56.6 (d, $^{2+3}J_{P,P}$ = 23.2 Hz, P_{trans} to SBz) ppm.

[Pd(CH$_2$CH$_2$CH$_2$Ph)(SMe)(dppe)] (5g) from 3b and MeSSMe: ^{31}P NMR (81 MHz): δ = 41.3 (d, $^{2+3}J_{P,P}$ = 23.2 Hz, P_{trans} to CH$_2$CH$_2$CH$_2$Ph), 55.6 (d, $^{2+3}J_{P,P}$ = 23.2 Hz, P_{trans} to SMe) ppm.

[Pd(CH$_2$CH$_2$CH$_2$Ph)(SeMe)(dppe)] (9a) from 3b and MeSeSeMe: ^{31}P NMR (81 MHz): δ = 46.1 (d, $^{2+3}J_{P,P}$ = 23.2 Hz, P_{trans} to CH$_2$CH$_2$CH$_2$Ph), 52.4 (d, $^{2+3}J_{P,P}$ = 23.2 Hz, P_{trans} to SeMe) ppm.

[PdMe(SePh)(dppe)] (9b) from 4 and PhSeSePh: ^{31}P NMR (81 MHz): δ = 45.0 (d, $^{2+3}J_{P,P}$ = 23.2 Hz, P_{trans} to Me), 56.8 (d, $^{2+3}J_{P,P}$ = 23.2 Hz, P_{trans} to SePh) ppm.

12. X-ray Structure of [Pd(CH$_2$CH$_2$Ph)$_2$(dppe)] (3a): Single crystals of complex **3a** suitable for X-ray diffraction analysis were grown at −30 °C by slow diffusion of *n*-pentane into a solution of **3a** in THF. Intensity data for complex **3a** were collected at 200(2) K with a Stoe STADI4 diffractometer with Mo-K_α radiation (0.71073 Å, graphite monochromator). A summary of crystallographic data, data collection parameters, and refinement parameters is given in

Table 4. The structure was solved by direct methods with SHELXS-86[34] and refined using full-matrix least-squares routines against F^2 with SHELXL-93.[34] Non-hydrogen atoms were refined with anisotropic displacement parameters. All hydrogen atoms were found in the difference Fourier map and were refined isotropically. CCDC-184402 contains the supplementary crystallographic data for this paper. These data can be obtained free of charge at www.ccdc.cam.ac.uk/conts/retrieving.html or from the Cambridge Crystallographic Data Centre, 12, Union Road, Cambridge CB2 1EZ, UK [Fax: (internat.) + 44-1223/336-033; E-mail: deposit@ccdc.cam.ac.uk].

Table 4. Crystal data and details of the structure determination for complex **3a**

Empirical formula	$C_{42}H_{42}P_2Pd$
Formula mass	715.10
Crystal system	orthorhombic
Space group	*Pbca*
a [Å]	12.97(2)
b [Å]	22.000(5)
c [Å]	25.545(6)
Z	8
V [Å^3]	7290(12)
$D_{calcd.}$[g cm^{-3}]	1.303
F(000)	2960
μ(Mo-K_α) [cm^{-1}]	6.24
2θ range [°]	1.59−26.04
Recip. latt. segment (*h*, *k*, *l*)	0 → 8, 0 → 27, 0 → 31
Measured reflections	7659
Independent reflections [$R_{int.}$]	4775 [0.0387]
Observed reflections	3590
Parameters	575
*R*1, *wR*2 [$I > 2\sigma(I)$]	0.0387, 0.0794
*R*1, *wR*2 (all data)	0.0647, 0.0930
Goodness-of-fit on F^2	1.108
Min. and max. resd. electron density [e·Å^{-3}]	−0.558 and 0.333

Acknowledgments

This work is supported by the Deutsche Forschungsgemeinschaft and by the Fonds der Chemischen Industrie. Gifts of chemicals by the companies Degussa (Hanau) and Merck (Darmstadt) are gratefully acknowledged.

[1] [1a] R. F. Heck, in *Comprehensive Organic Synthesis* (Eds: B. M. Trost, I. Fleming), Pergamon Press, Oxford, **1991**, vol. 4, p. 833−863. [1b] W. Cabri, I. Candiani, *Acc. Chem. Res.* **1995**, *28*, 2−7.

[2] [2a] G. T. Crisp, *Chem. Soc. Rev.* **1998**, *27*, 427−436. [2b] B. L. Shaw, *New J. Chem.* **1998**, 77−79.

[3] A. J. Canty, in *Comprehensive Organometallic Chemistry II* (Eds.: E. W. Abel, F. G. A. Stone, G. Wilkinson), Pergamon/Elsevier, Oxford, **1995**, vol. 9, p. 225−290.

[4] [4a] R. Van Der Linde, R. O. De Jongh, *J. Chem. Soc. D* **1971**, 563. [4b] P. Diversi, G. Ingrosso, A. Lucherini, *J. Chem. Soc., Chem. Commun.* **1978**, 735−736. [4c] P. Diversi, G. Ingrosso, A. Lucherini, S. Murtas, *J. Chem. Soc., Dalton Trans.* **1980**, 1633−1637. [4d] F. Ozawa, T. Ito, A. Yamamoto, *J. Am. Chem. Soc.* **1980**, *102*, 6457−6463. [4e] F. Ozawa, T. Ito, Y. Nakamura, A. Yamamoto, *Bull. Chem. Soc. Jpn.* **1981**, *54*, 1868−1880. [4f] F. Ozawa, A. Yamamoto, T. Ikariya, R. H. Grubbs, *Organometallics* **1982**, *1*, 1481−1485. [4g] J. Lau, R. Sustmann, *Tetrahedron Lett.* **1985**, *26*, 4907−4910. [4h] R. Sustmann, J. Lau, *Chem. Ber.* **1986**, *119*, 2531−2541. [4i] R. Sustmann, J. Lau, M. Zipp, *Recl. Trav. Chim. Pays-Bas* **1986**, *105*, 356−359. [4j] F. Ozawa, A. Yamamoto, *Nippon Kagaku Kaishi* **1987**, 773−784. [4k] F. Ozawa, K. Kurihara, M. Fujimori, T. Hidaka, T. Toyoshima, A. Yamamoto, *Organometallics* **1989**, *8*, 180−188. [4l] F. Ozawa, T. Son, S. Ebina, K. Osakada, A. Yamamoto, *Organometallics* **1992**, *11*, 171−176. [4m] D. Drago, P. S. Pregosin, *J. Chem. Soc., Dalton Trans.* **2000**, 3191−3196.

[5] [5a] F. Ozawa, T. Sugimoto, Y. Yuasa, M. Santra, T. Yamamoto, A. Yamamoto, *Organometallics* **1984**, *3*, 683−692. [5b] K. Osakada, Y. Ozawa, A. Yamamoto, *J. Chem. Soc., Dalton Trans.* **1991**, 759−764. [5c] K. Osakada, Y. Ozawa, A. Yamamoto, *Bull. Chem. Soc. Jpn.* **1991**, *64*, 2002−2004. [5d] F. Kawataka, Y. Kayaki, I. Shimizu, A. Yamamoto, *Organometallics* **1994**, *13*, 3517−3524.

[6] P. Barabotti, P. Diversi, G. Ingrosso, A. Lucherini, F. Nuti, *J. Chem. Soc., Dalton Trans.* **1984**, 2517−2523.

[7] [7a] D. L. Reger, D. G. Garza, J. C. Baxter, *Organometallics* **1990**, *9*, 873−874. [7b] D. L. Reger, D. G. Garza, L. Lebioda, *Organometallics* **1991**, *10*, 902−906. [7c] D. L. Reger, D. G. Garza, L. Lebioda, *Organometallics* **1992**, *11*, 4285−4292.

[8] [8a] C. A. Ghilardi, S. Midollini, S. Moneti, A. Orlandini, *J. Chem. Soc., Chem. Commun.* **1986**, 1771−1772. [8b] F. Cecconi, C. A. Ghilardi, S. Midollini, S. Moneti, A. Orlandini, G. Scapacci, *J. Chem. Soc., Dalton Trans.* **1989**, 211−216.

[9] F. C. Rix, M. Brookhart, *J. Am. Chem. Soc.* **1995**, *117*, 1137−1138.

[10] [10a] P. K. Byers, A. J. Canty, *J. Chem. Soc., Chem. Commun.* **1988**, 639−641. [10b] D. G. Brown, P. K. Byers, A. J. Canty, *Organometallics* **1990**, *9*, 1231−1235. [10c] A. J. Canty, P. R. Traill, R. Colton, I. M. Thomas, *Inorg. Chim. Acta* **1993**, *210*, 91−97. [10d] A. J. Canty, H. Jin, A. S. Roberts, B. W. Skelton, P. R. Traill, A. H. White, *Organometallics* **1995**, *14*, 199−206. [10e] A. J. Canty, J. L. Hoare, N. W. Davies, P. R. Traill, *Organometallics* **1998**, *17*, 2046−2051.

[11] [11a] K. J. Klabunde, J. Y. F. Low, *J. Am. Chem. Soc.* **1974**, *96*, 7674−7680. [11b] K. J. Klabunde, *Angew. Chem.* **1975**, *87*, 309−314.

[12] P. Diversi, G. Ingrosso, A. Lucherini, T. Lumini, F. Marchetti, V. Adovasio, M. Nardelli, *J. Chem. Soc., Dalton Trans.* **1988**, 133−140.

[13] J.-E. Bäckvall, R. E. Nordberg, *J. Am. Chem. Soc.* **1980**, *102*, 393−395.

[14] [14a] M. E. Cucciolito, A. De Renzi, F. Giordano, F. Ruffo, *Organometallics* **1995**, *14*, 5410−5414. [14b] V. De Felice, M. E. Cucciolito, A. De Renzi, F. Ruffo, D. Tesauro, *J. Organomet. Chem.* **1995**, *493*, 1−11. [14c] M. Ludwig, S. Strömberg, M. Svensson, B. Akermark, *Organometallics* **1999**, *18*, 970−975.

[15] A. Maercker, M. Passlack, *Chem. Ber.* **1982**, *115*, 540−577.

[16] [16a] W. F. Bailey, E. R. Punzalan, *J. Org. Chem.* **1990**, *55*, 5404−5406. [16b] E. Negishi, D. R. Swanson, C. J. Rousset, *J. Org. Chem.* **1990**, *55*, 5406−5409.

[17] J. Browning, P. L. Goggin, R. J. Goodfellow, N. W. Hurst, L. G. Mallinson, M. Murray, *J. Chem. Soc., Dalton Trans.* **1978**, 872−876.

[18] H. A. Bent, *Chem. Rev.* **1961**, *61*, 275−311.

[19] R. D. Thomas, M. T. Clarke, T. C. Young, *J. Organomet. Chem.* **1987**, *328*, 239−248.

[20] C. J. Pouchert, J. Behnke, *The Aldrich Library of ^{13}C and ^{1}H FT NMR Spectra*, Aldrich, Milwaukee, Wisconsin, **1993**.

[21] H.-O. Kalinowski, S. Berger, S. Braun, *^{13}C NMR-Spektroskopie*, Thieme, Stuttgart **1984**, p. 447.

[22] *PERCH, an integrated software for analysis of NMR spectra on a personal computer*, version 1/2000, University of Kuopio, Finland, **2000**.

[23] R. E. Gawley, J. Aubé, *Principles of Asymmetric Synthesis, Tet-*

rahedron Organic Chemistry Series (Eds.: J. E. Baldwin, P. D. Magnus), Pergamon/Elsevier, Oxford, **1996**, vol. 14.

[24] Cambridge Structural Database (CSD). Cambridge Crystallographic Data Centre, University Chemical Laboratory, Cambridge, England.

[25] Y.-J. Kim, K. Osakada, K. Sugita, T. Yamamoto, A. Yamamoto, *Organometallics* **1988**, *7*, 2182−2188.

[26] A. J. Canty, H. Jin, B. W. Skelton, A. H. White, *Inorg. Chem.* **1998**, *37*, 3975−3981.

[27] A. J. Canty, *Acc. Chem. Res.* **1992**, *25*, 83−90.

[28] D. W. Meek, P. E. Nicpon, V. I. Meek, *J. Am. Chem. Soc.* **1970**, *92*, 5351−5359.

[29] W. Goertz, PhD Thesis; RWTH Aachen, Aachen, **1998**.

[30] K. Schwetlick (Ed.), *Organikum*, 20th ed., Barth Verlag, Heidelberg, **1996**.

[31] H. Strasdeit, *Nachr. Chem. Tech. Lab.* **1998**, *46*, 846−848.

[32] Here and in the following, assignment of phenyl carbon atoms is based on calculations with ACD software; Advanced Chemistry Development Inc., Richmond, **1997**.

[33] G. Calvin, G. E. Coates, *J. Chem. Soc.* **1960**, 2008−2016.

[34] G. M. Sheldrick, *SHELXS-86, SHELXL-93, Programs for Crystal Structure Determination*; University of Göttingen, Göttingen, **1986**, **1993**.

Received April 24, 2002
[I02212]

Studies of Aryl Substituent and Solvent Donor Imposed Structural Diversity in *N*,*N*′-Diarylformamidinate Complexes of Lithium[‡]

Jens Baldamus,[a][+] Christiane Berghof,[a][+] Marcus L. Cole,[a] Evamarie Hey-Hawkins,[b] Peter C. Junk,*[a] and Lance M. Louis[c]

Keywords: Lithium / Formamidinates / Coordination modes / N ligands

Treatment of *N*,*N*′-bis(2,4,6-trimethylphenyl)formamidine, (2,4,6-$Me_3C_6H_2$)NC(H)NH(2,4,6-$Me_3C_6H_2$) (HFMes) with *n*-butyllithium in DME leads to deprotonation of the amidine affording the dimeric compound [{Li(FMes)(dme)}$_2$] (**1**). Similar treatment of the less sterically encumbered formamidine *N*,*N*′-bis(*o*-tolyl)formamidine, (2-MeC_6H_4)NC(H)NH(2-MeC_6H_4) (HFTolO) in DME (1,2-dimethoxyethane) or HFMes in hexane/TMEDA (*N*,*N*,*N*′,*N*′-tetramethylethylenediamine) yields the compounds [Li(dme)$_3$][Li(FTolO)$_2$] (**2**) and [Li(FMes)(tmeda)] (**3**), respectively. Both the anion of **2** and **3** are the first monomeric group 1 formamidinates to exhibit η^2-chelation in the solid state, and **3** is the first Lewis base stabilised mononuclear group 1 formamidinate complex. Complexes **1**–**3** have been characterised by spectroscopy (^{1}H and ^{13}C NMR, FTIR) and X-ray crystallography, and are discussed herein vis-à-vis formamidinate binding modes exhibited by *N*,*N*′-diarylformamidinates of smaller steric size, e.g. *N*,*N*′-bis(*p*-tolyl)formamidine, (4-MeC_6H_4)NC(H)NH-(4-MeC_6H_4) (HFTolP).

Introduction

The fundamental role of group 1 amido complexes, particularly those of lithium, as synthetic reagents in inorganic chemistry and strong Bronsted bases or nucleophiles in organic synthesis[1−5] has led to considerable advances in the field of metal amide chemistry.[6] Within this arena, knowledge of reagent structure both in solution and in the solid state is crucial, permitting the synthetic chemist to tailor syntheses or transformations. In both, association is to be expected due to the high polarity of the Li−N bond.[7−13] However, aggregation can be frustrated if ligands of adequate steric bulk are employed.[14]

In contrast to the actively investigated area of transition metal formamidinate chemistry (formamidinate = [RNC(H)NR]$^-$, R = aryl, alkyl, silyl),[15,16] literature detailing the full characterisation of s-block systems has been conspicuously absent.[17] As a result there is a scarcity of structural data pertaining to this class of amidinate complex, which are generally perceived as metathesis reagents, their isolation and characterisation largely being ignored. It has been suggested that this shortage of structural data, there being just one structurally authenticated lithium formamidinate complex ([{Li(FTolP)(Et_2O)}$_2$]), results from the facility by which group 1 formamidinates lose solvent.[18] However, to compliment the vast array of coordination modes observed for formamidinates in d-block systems we have engaged in a program of s-block metal formamidinate structural characterisation using solvent donors that either chelate or have recognised strong donor characteristics. Thus far, this has identified several group 1 diarylformamidinate bonding motifs, e.g. μ_2:η^2:η^1 (in [{Li_2(FTolP)$_2$(tmeda)}$_\infty$])[17] and η^6:η^1 (in [K(FMes)(HFMes)]),[19] that are either rare or unprecedented in transition metal chemistry. To date several known bonding motifs like discrete η^2-chelation, have not been observed in group 1 systems. Furthermore, there is potential for new binding modes, e.g. η^3-diazaallyl, as seen for η^3-*N*-aryl diarylketeneiminates,[20] where the carbon atom of the NCN backbone would interact with a metal centre that sits perpendicular to the NCN plane either as part of symmetrical NCN donation or as a discrete C=N π-donor. In order to assess the likelihood of these, and advance our study, we have now chosen to focus our attention on formamidine ligands of greater steric bulk, in this case *N*,*N*′-bis(2,4,6-trimethylphenyl)formamidine, (2,4,6-$Me_3C_6H_2$)NC(H)NH(2,4,6-$Me_3C_6H_2$) (HFMes). Herein we present a preliminary lithium study employing HFMes and relate the findings to new and archival structural data.

[‡] On leave from the Institut für Anorganische Chemie, Universität Leipzig, Johannisallee 29, 04103 Leipzig, Germany.
[a] School of Chemistry, Monash University, P. O. Box 23, Clayton, Victoria 3800, Australia
Fax: (internat.) + 61-3/9905-4597
E-mail: peter.junk@sci.monash.edu.au
[b] Institut für Anorganische Chemie, Universität Leipzig, Johannisallee 29, 04103 Leipzig, Germany
[c] Department of Chemistry, James Cook University, Townsville, Queensland 4811, Australia

 © 2002 WILEY-VCH Verlag GmbH & Co. KGaA, 69451 Weinheim 1434−1948/02/1111−2878 $ 20.00+.50/0 *Eur. J. Inorg. Chem.* **2002**, 2878−2884

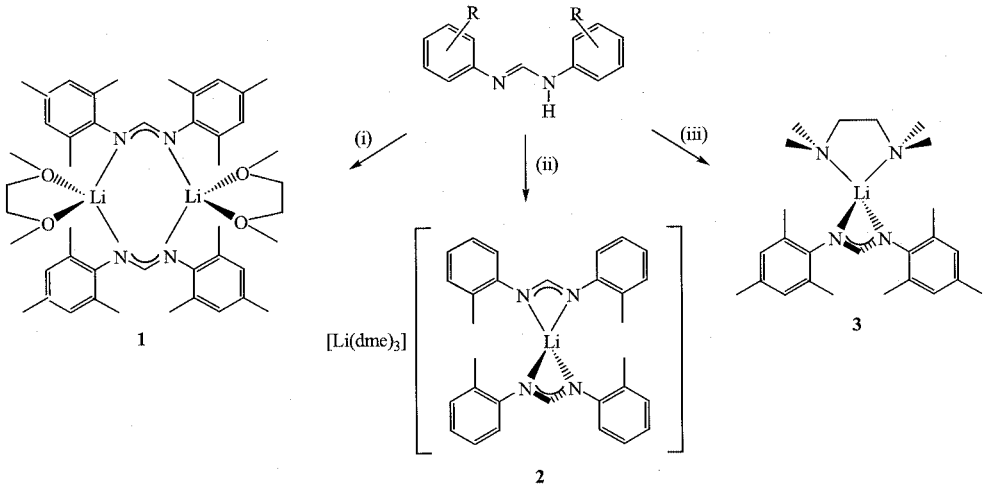

Scheme 1. Reagents and conditions: (i) R = 2,4,6-Me_3, 1.0 equiv. *n*BuLi, DME; (ii) R = 2-Me, 1.0 equiv. *n*BuLi, DME; (iii) R = 2,4,6-Me_3, 1.0 equiv. *n*BuLi, hexane/TMEDA

Results and Discussion

Treatment of HFMes with *n*-butyllithium in the coordinating solvent DME (1,2-dimethoxyethane) results in clean deprotonation of the amino group (see Scheme 1), after moderate heating, yielding a colourless crystalline product that characterises as [Li(FMes)$(dme)_{3/2}$] (**1**) by ^{1}H NMR (C_6D_6). Spectroscopic evidence confirms deprotonation via the absence of a resonance attributable to the amino proton of HFMes and the lack of an N−H stretch at ca. 3200−3300 cm^{-1} [^{1}H NMR (C_6D_6): δ = 5.71 ppm (NH); FTIR: $\tilde{\nu}$ = 3228 cm^{-1} (HFMes N−H stretch)].[21] The appearance of a broad NC(*H*)N resonance at δ = 7.60 ppm is also indicative of deprotonation, that of the ligand appearing at δ < 7.07 ppm.[21] Similarly, the NCN backbone carbon resonance at δ = 157.6 ppm (C_6D_6) is suggestive of deprotonation, the analogous resonance of HFMes appearing at δ = 145.0 ppm. Attempts to obtain ^{7}Li NMR spectroscopic data for **1** were thwarted by low solubility in nondonating solvents (employed to preclude further solvation). Overall, NMR resonances for **1** compare favourably to those of the FTolP ligands in the ionic complex [Li$(dme)_3$][$Li_2(\mu_2{:}\eta^1{:}\eta^1$-FTolP$)_3$] (**4**) although the NC(*H*)N resonance is shifted to lower frequency, that of **4** appearing at δ = 8.88 ppm.[17] This intimates a differing structural preference for **1** viz. **4**, as does the abated decomposition temperature of 112 °C, which would intuitively be in excess of that for **4** were they to assume a congruent solid-state motif (**4**: dec. At 130 °C).[17]

To assess this, X-ray quality crystals of **1**, which proved extremely air-sensitive and prone to solvent loss, were isolated and a structure determination undertaken. A POV-RAY depiction of **1** can be seen in Figure 1 (30% thermal ellipsoids), whilst selected bond lengths and angles are listed in the caption. Crystallographic data for compounds

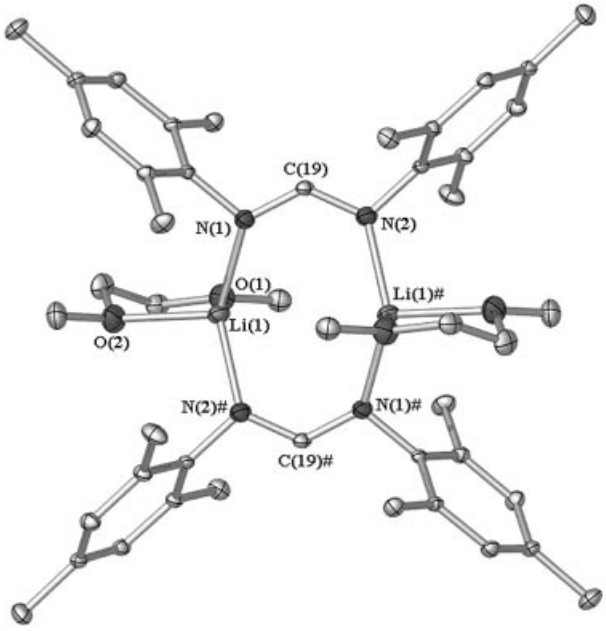

Figure 1. Molecular structure of [{Li($\mu_2{:}\eta^1{:}\eta^1$-FMes)$(dme)\}_2$] (**1**), all hydrogen atoms omitted for clarity; selected bond lengths [Å] and angles [°]: N(1)−Li(1) 2.035(6), N(2)−Li(1)# 2.033(6), N(1)−C(19) 1.312(4), N(2)−C(19) 1.314(4), Li(1)−O(1) 2.043(6), Li(1)−O(2) 2.093(6), N(1)−Li(1)−N(2)# 133.5(3), O(1)−Li(1)−O(2) 78.9(2), N(1)−Li(1)−O(1) 101.4(3), N(1)−Li(1)−O(2) 111.0(3), Li(1)−N(1)−C(19) 129.7(3), N(1)−C(19)−N(2) 127.7(2), C(1) ring−NCN 66.5(3), C(10) ring−NCN 66.6(3), C(1) ring−C(10) ring 87.2(1)

1−**3** are listed in Table 1. Compound **1** crystallises in the monoclinic space group $P2_1/n$ with half a dinuclear [{Li($\mu_2{:}\eta^1{:}\eta^1$-FMes)$(dme)\}_2$] and half a DME of solvation in the asymmetric unit. Unlike **4**, compound **1** is not ionic, displaying both solvent and formamidinate coordination to

Table 1. Summary of crystal data for compounds **1**−**3**

	[{Li(FMes)(dme)}$_2$]·DME (**1**)	[Li(dme)$_3$][Li(FTolO)$_2$] (**2**)	[Li(FMes)(tmeda)] (**3**)
Empirical formula	$C_{25}H_{38}LiN_2O_3$	$C_{42}H_{60}Li_2N_4O_6$	$C_{25}H_{39}LiN_4$
Molecular mass	421.53	730.82	402.54
Temperature [K]	123(2)	296(2)	123(2)
Space group	$P2_1/n$	$C2/c$	$P\bar{1}$
a [Å]	12.1580(14)	14.28(7)	8.2180(16)
b [Å]	15.6552(18)	18.57(9)	12.235(2)
c [Å]	14.4561(16)	17.62(8)	13.348(3)
α [°]	90	90	103.84(3)
β [°]	111.533(2)	103.27(18)	91.92(3)
γ [°]	90	90	103.45(3)
Volume [Å^3]	2559.5(5)	4546(37)	1261.7(4)
Z	2	4	2
D_c [g cm^{-3}]	1.035	1.068	1.060
μ [mm^{-1}]	0.066	0.070	0.062
Reflections collected	16124	9664	23286
Reflections unique	5801	3248	6195
Parameters	289	255	281
R_{int}	0.1207	0.1984	0.0671
R_1	0.0782	0.0698	0.0581
wR_2	0.1665	0.1475	0.1530

each lithium centre. This results from the increased steric bulk of FMes with respect to FTolP, which not only inhibits discrete ion formation, as in **4**, but also precludes μ_2:η^2:η^1-formamidinate coordination as seen for both [{$Li_2(\mu_2$:η^2:η^1-FTolP)$_2$(μ_2-tmeda)}$_\infty$] (**5**)[17] and [{Li(μ_2:η^2:η^1-FTolP)(Et_2O)}$_2$],[18] the Li(1)#−N(1) distance of 3.3723(60) Å testifies to this. Interestingly, the donation of two singular DME ligands in **1** is representative of the overall steric coordination number[22] of [$Li_2(\mu_2$:η^1:η^1-FTolP)$_2$(THF)$_2$(μ_2-thf)],[17] which exhibits analogous formamidinate binding modes with one chelating and one bridging THF interaction completing each lithium coordination sphere. The lithium atoms of **1** sit in a distorted tetrahedral environment [N(1)−Li(1)−N(2)# 133.5(3)°, N(2)#−Li(2)−O(2) 115.6(3)°, O(1)−Li(1)−O(2) 78.9(2)°, whilst the Li−N bond lengths of 2.035(6) Å and 2.033(6) Å are abated relative to those deposited in the Cambridge structural database (mean 2.082 Å),[23] extended with respect to those of **4** (mean 1.992 Å)[17] and similar to those displayed by the similarly dimeric lithium amide complex [{Li[NHC_6H_4(*o*-$AsMe_2$)](THF)$_2$}$_2$] [24] (mean 2.064 Å). As per **4**, the considerable strain involved in formamidinate bridging to two separate metal atoms has repercussions regarding ligand geometry. This includes the opening of the NCN backbone angle to 127.7(3)° (**4**: mean 123.0°) and the C(19)−N(1)−Li(1) angle to 129.7(3)° (**4**: mean 122.2°), these are in stark contrast to the comparatively acute angles of the bis(η^2-chelate) complex [Mg(FTolP)$_2$(THF)$_2$] (mean 117.0 and 90.14°, respectively).[25] Consequently, C(19) sits 0.023 Å out of the N_4 plane, whilst the Li centres sit 0.670 Å out of the N_4 plane [N(2)#−Li(1)−N(1) plane at 56.55(33)° to the N_4 plane). Given the orthogonal orientation of the FMes ligands to the lithium−lithium vector, these projections are insignificant regarding possible Li(1)/Li(1)#···C(19) interactions. Intriguingly, the structural motifs of **1** and **4** are reminiscent of the "lantern-type" structures popularised by the transition metal studies of Cotton and Murillo et al.,[15,16,26] e.g. [Mo_2(PhNC(Ph)NPh)$_4$],[27] the lower ratio of ligand/metal resulting from the restricted space in which the formamidinate ligands can orientate themselves around the diminutive dilithium core. Conversely, unlike the close-contact-enforced metal−metal bonding observed for d-block systems, which lead to magnetic and electronic phenomena,[15,16] the metal−metal distance of complex **1** [3.508(11) Å] precludes similar interaction (**4**: mean 2.580 Å). Furthermore, the steric congestion of **1** is exemplified by the near orthogonal torsion angle of the mesityl rings to one another [87.19(12)°] and the large dihedral angles of both rings to the NCN plane [C(1) ring 66.5(3)°, C(10) ring 66.6(3)°]. These impose a differing structural motif and lower formamidinate aggregation for **1**, with respect to **4**, which necessitates augmentative DME donation to achieve an equivalent degree of coordinative saturation. Meanwhile, the formamidinate backbone N−C bond lengths of 1.312(4) and 1.314(4) Å are indicative of symmetrical amidinate ligation (**4**: mean 1.326 Å; HFTolP dimer mean C−N bonds: imino 1.294 Å and amino 1.347 Å).[17] Lastly, the symmetrical dilithium di-β-dinitrogen ligand eight-membered metallacycle exhibited by **1** is not an uncommon feature of lithium structural chemistry (22 examples),[23] however, the lithium−lithium distance described (listed above) does testify to significant steric congestion about the core, there being just two polymetallacyclic examples wherein the distance of **1** is exceeded; [(Li{*t*BuNC(*t*Bu)N*t*Bu})$_4$] (max. Li···Li 3.809 Å)[28] and [Li_2\{1,2-*trans*-[NC(*para*-Tol)N(*para*-Tol)]$_2C_6H_{10}$\}] (max. Li···Li 4.391 Å).[29]

If complex **1** represents double *o*-methylaryl substitution (i.e. 2,6-dimethyl) and **4** represents no *o*-methylaryl substitution, the considerable variation in the solid-state motifs of **1** and **4** invites speculation as to the likely solid-state

nature of a singularly *o*-methylated *N*,*N*′-diarylformamidinate lithium complex. As such, an identical preparation to that of **1** was undertaken employing *N*,*N*′-bis(*o*-tolyl)formamidine (HFTolO), see Scheme 1. As per the synthesis of **1**, treatment of HFTolO in DME with *n*-butyllithium renders a colourless crystalline compound devoid of amino-attributable resonances or stretches (^{1}H NMR and FTIR), with a composition that indicates two formamidinate ligands to three DME molecules; [Li(FTolO)(dme)$_{3/2}$] (**2**) (^{1}H NMR). The NC(H)N-attributable resonances of **2** at δ = 8.72 ppm and 160.4 ppm (^{1}H and ^{13}C NMR, respectively) are representative of **4** rather than **1** (^{1}H NMR: **4**: δ = 8.88 ppm; **1**: δ = 7.60 ppm) as is the decomposition temperature of 122 °C (**1**: 112 °C; **4**: 130 °C).[17] Correspondingly, block-like crystals of **2** were grown from DME and an X-ray structure determination undertaken (Figure 2; POV-RAY illustration, 30% thermal ellipsoids, relevant bond lengths and angles listed in the caption).

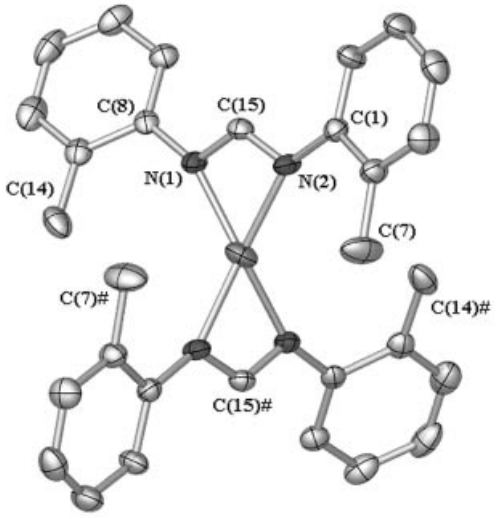

Figure 2. Molecular structure of the anion of **2** [Li(η^1:η′-FTolO)$_2$], all hydrogen atoms omitted for clarity; selected bond lengths [Å] and angles [°]: N(1)−Li(1) 2.063(11), N(2)−Li(1) 2.073(10), N(1)−C(15) 1.323(8), N(2)−C(15) 1.315(8), N(1)−Li(1)−N(1)# 135.5(8), N(1)−Li(1)−N(2)# 130.7(3), N(1)−Li(1)−N(2) 67.3(3), N(1)−C(15)−N(2) 120.6(7), NCN−NCN# 82.5(4), C(1) ring−NCN 13.3(7), C(8) ring−NCN 33.1(6), C(1) ring−C(8) ring 28.0(4)

Akin to complex **4**, compound **2** crystallises in the space group *C*2/*c* as discrete anions and cations, of which there is half an anion/cation pair in the asymmetric unit. The cationic lithium unit, which is solvated by three DME molecules to form a distorted octahedron (mean O−Li−O bite 76.34°), is not uncommon,[23] structurally unexceptional and will not be discussed further. However, the anion (see Figure 2) is a mononuclear [Li(FTolO)$_2$] unit that presents two η^2-FTolO ligands forming a distorted tetrahedral geometry about a lithium centre without solvent interaction [N(1)−Li(1)−N(2) bite 67.3(3)°, N(1)−Li(1)−N(1)# 135.5(8)°]. The Li−N bond lengths vary in the range 2.063(11)−2.073(10) Å and are therefore closer to the mean average Li−N bond length deposited in the Cambridge structural database (2.082 Å)[23] than the appropriate bonds of **1** and **4**. This perhaps results from lessened steric strain and the absence of bridging interactions. Likewise, the NCN backbone angle of 120.6(7)° bares a closer resemblance to the analogous angles of [Mg(FTolP)$_2$(THF)$_2$] (mean: 117.0 Å),[25] than those of **1** [127.7(3)°] due to the chelate motif described. The depreciated tolyl−tolyl steric buttressing described by **2** vis-à-vis **1** can be seen in the dihedral angle of either tolyl ring to the NCN backbone plane [C(1) ring 13.3(7)°, C(8) ring 33.1(6)°] and the relative torsion angle of 28.0(4)°. Thus, in complex **2** we can state that whilst the imposition of two *o*-methyl groups upon the formamidinate frame, as in FMes, results in nonionic **1**, the addition of a singular *o*-methyl group renders an ionic complex, similar to **4**, with lower anion aggregation. This modification creates a complex devoid of formamidinate bridging interactions, which cannot merely result from *o*-methyl addition relative to **4** because complex **1** exhibits similar μ$_2$:η^1:η^1 interactions. To rationalise this, it appears that the relative cation and anion sizes of **2** and **4** are comparable, thereby presenting lattice energies of adequate magnitude for salt formation. Meanwhile, an ionic composition for complex **1** is thermodynamically unfavourable due to the sheer steric bulk of the included amidinate ligands. These create a cation/anion size disparity. This has precedent in group 1 cyclopentadienide crown ether chemistry[30,31] where the ionic complex [K{15-crown-5}$_2$][Cp] forms whilst use of 18-crown-6 yields solely the monomer [K(18-crown-6)Cp].[32] Irrespective, it remains that the ionic nature of **2** introduces a new type of lithium-based formamidinate anion.

To increase the steric encumbrance observed for complex **1**, and thereby potentially frustrate bridging interactions and generate new bonding motifs, a bulkier solvent donor; *N*,*N*,*N*′,*N*′-tetramethylethylenediamine (TMEDA) was utilised in a preparative procedure similar to that for **1** using hexane as solvent. Treatment of HFMes with *n*-butyllithium in hexane resulted in instant deposition of an insoluble colourless material, presumably polymeric in nature, which dissolved upon addition of excess TMEDA (see Scheme 1). Subsequent recrystallisation of the reaction mother liquor yielded colourless prisms that characterised as [Li(FMes)(tmeda)] (**3**) by ^{1}H NMR, and were devoid of the resonances and stretches (NMR and FTIR, respectively) attributable to the HFMes ligand. Unlike compounds **1** and **2**, compound **3** appears to be stable to solvent loss but is extremely air-sensitive decomposing to a dark brown material upon brief exposure to air. Solid samples of **3** are thermally robust decomposing above 145 °C (cf. **1**: 112 °C; **2**: 122 °C; **4**: 130 °C).[17] The spectroscopic data for **3** bare a resemblance to those of both **4** and the related TMEDA compound [{Li$_2$(μ$_2$:η^2:η^1-FTolP)$_2$(μ$_2$-tmeda)}$_\infty$] (**5**) in that compound **3** possesses a ^{1}H NMR resonance at δ = 8.02 ppm (**4**: δ = 8.88 ppm; **5**: δ = 8.25 ppm, respect-

ively);[17] however, the solvent/formamidinate ligand ratios of 1:1 mitigate against a solid-state motif analogous to **5** unless half an equivalent of TMEDA is contained as lattice solvent. In order to evaluate the above, an X-ray structure determination of **3** was undertaken (Figure 3; POV-RAY illustration, 30% thermal ellipsoids, selected bond lengths and angles listed in the caption).

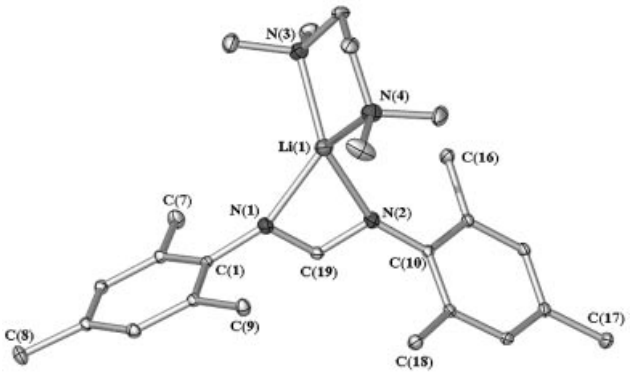

Figure 3. Molecular structure of [Li(η^1:η^1-FMes)(tmeda)] (**3**), all hydrogen atoms omitted for clarity; selected bond lengths [Å] and angles [°]: Li(1)−N(1) 2.036(3), Li(1)−N(2) 2.011(3), Li(1)−N(3) 2.087(3), Li(1)−N(4) 2.057(3), N(1)−C(19) 1.314(2), N(2)−C(19) 1.328(2), $NLiN_{FMes}$−$NLiN_{TMEDA}$ 72.95(6), N(1)−Li(1)−N(2) 68.84(10), N(3)−Li(1)−N(4) 86.94(12), N(1)−Li(1)−N(3) 125.52(15), N(2)−Li(1)−N(4) 112.57(14), N(1)−C(19)−N(2) 120.04(15), C(1) ring−NCN 86.9(2), C(10) ring−NCN 50.6(1), C(1) ring−C(10) ring 58.07(5)

Compound **3** represents the first structurally authenticated lithium formamidinate complex that displays neither μ_2:η^2:η^1/μ_2:η^1:η^1-bridging interactions or an ionic composition. It appears that the added steric buttressing of TMEDA relative to DME imposes enough hindrance to cause **3** to exist as discrete [Li(FMes)(tmeda)] units without intermolecular contacts. Inspite of this, the tetrahedral geometry about the metal centre of **3** is deficient in symmetry [N(1)−Li(1)−N(4) 131.94(15)°, N(2)−Li(1)−N(3) 137.92(15)°, N(3)−Li(1)−N(4) 86.94(12)°]. For example, the N−Li−N planes of the two dinitrogen ligands exist at a dihedral angle of 72.95(6)° to one another, this exacerbates the interaction of the C(11)-bound mesityl ring with the tmeda C(23)-bound NMe_2 group. This group counterintuitively leans toward the N(2) side of the formamidinate ligand [N(2)−Li(1)−N(4) 112.57(14)°, N(1)−Li(1)−N(3) 125.52(15)°]. In the absence of an apparent energetic benefit to this, such an anomaly must surely result as a crystal-packing phenomenon. Correspondingly, the disparate dihedral angles of the mesityl rings to the NCN plane [C(1) ring 86.92(15)°, C(11) ring 50.61(14)°] cannot be explained by intramolecular interactions alone. Indeed, one would expect the two mesityl groups to lie orthogonal to the NCN plane, and therefore flat to one another, thereby minimising interaction with the TMEDA ligand. Instead, the mesityl rings exist at a relative torsional angle of 58.07(5)°, which seemingly decries the rationale proposed for the structure exhibited. Reassuringly, the NCN FMes backbone of **3** displays nearly equivalent C−N bond lengths of 1.314(2) and 1.328(2) Å (symptomatic of symmetrical η^2-chelation) without interaction of C(19) to the metal centre [C(19) projects 0.024 Å above/below the NCN plane). Lastly, the bond lengths N(1)−Li(1) and N(2)−Li(1) [2.036(3) and 2.011(3) Å, respectively) are similar to other symmetrically bonded FMes compounds (**1**, mean: 2.034 Å), whilst the FMes backbone angle of **3** is acute with respect to the μ_2:η^1:η^1-bound FMes ligands of **1** [120.04(15)°; **1**: 127.7(3)°], and comparable those of the μ_2:η^2:η^1-formamidinate complexes **5** [120.8(3)°][17] and [{Li(μ_2:η^2:η^1-FTolP)(Et_2O)}$_2$] [120.0(4)°],[18] and hence closer to the sp^2-hybridised ideal of 120°.

Conclusion

The solid-state structures of **1**−**3** exhibit structural diversity borne out of the rational exchange and substitution of both solvent and aryl substituents. In tandem with archival structural data, we can assert that *N*,*N*′-diarylformamidinates are versatile ligands for lithium, exhibiting an ever increasing number of binding modes and structural motifs. In particular, we have identified the first complexes to display solely η^2-formamidinate chelation (**2** and **3**), and the first mononuclear Lewis base stabilised group 1 formamidinate to be structurally authenticated (**3**). These studies expand our understanding of the structural ramifications of increased diaryl steric bulk in group 1 systems, which in the extreme negate the interaction of solvent donors, as in the anion of **2**, or frustrate salt formation, as in **1**. In summary, with respect to known FTolP complexes,[17,18] it appears that the presence of *o*-methyl group(s) upon the aryl substituents frustrate, and to a certain extent limit, dimer formation such that μ_2:η^2:η^1-formamidinate bridging is not viable (lithium−lithium proximity hindered). This enforces either supplementary solvent coordination or, as seen for **2**, low aggregate lithium−formamidinate anion composition. We are presently extending these studies to ligands of greater steric bulk, e.g. *N*,*N*′-bis(2,6-diisopropylphenyl)formamidine (HFIso), and heavy group 2 and f-block metals. The outcome of these will form the basis of forthcoming publications.

Experimental Section

General: The formamidinate ligand precursors *N*,*N*′-bis(2,4,6-trimethylphenyl)- and *N*,*N*′-bis(*o*-tolyl)formamidine, HFMes and HFTolO, respectively, were synthesised according to published procedures.[18,33] *n*-Butyllithium (1.6 M solution in hexanes) was purchased from Aldrich. 1,2-Dimethoxyethane (DME/dme) and hexane were dried with sodium, freshly distilled from sodium/benzophenone, and freeze-thaw-degassed prior to use. *N*,*N*,*N*′,*N*′-Tetramethylethylenediamine (TMEDA/tmeda) was dried with sodium, freshly distilled from sodium, and freeze-thaw-degassed prior to use. All manipulations were performed using conventional Schlenk or glovebox techniques under high-purity argon or dinitrogen in flame-dried glassware. Infrared spectra were recorded as Nujol mulls using sodium chloride plates with a Nicolet Nexus FTIR

spectrophotometer. ^{1}H NMR spectra were recorded at 300.13 MHz and ^{13}C NMR spectra were recorded at 75.46 MHz using Bruker BZH 300/52 and DPX 300 spectrometers with Varian or Bruker consoles and chemical shifts were referenced to the residual ^{1}H or ^{13}C resonances of the deuteriobenzene solvent employed. Melting points were determined in sealed glass capillaries under argon or dinitrogen and are uncorrected. The high aerobic and moisture sensitivity of compounds **1**−**3**, combined with the facile loss of solvent from both **1** and **2** (as seen for [{Li(μ_2:η^2:η^1-FTolP)(Et_2O)}$_2$], see ref.[18]), frustrated the acquisition of meaningful mass spectrometric and C,H,N microanalytical data. Microanalyses for **1** and **2** were consistently high in carbon and nitrogen, and low in hydrogen, whilst those of **3** were repeatedly low in nitrogen.

[{Li(μ_2:η^1:η^1-FMes)(dme)}$_2$].DME (1): *n*-Butyllithium (0.80 mL, 1.28 mmol) was added dropwise to a stirred ambient-temperature solution of HFMes (0.36 g, 1.28 mmol) in DME (30 mL). Heating of the resultant clear colourless solution to 50 °C for 1 h yielded an opaque-white slurry that was filtered and the filtrate placed at −20 °C. This yielded the title compound as small colourless needles (0.36 g, 67%), m.p. 112 °C (dec.). ^{1}H NMR (C_6D_6, 300 K): δ = 2.24 (s, 12 H, *p*-CH_3), 2.32 (s, 24 H, *o*-CH_3), 3.04 (s, 18 H, OCH_3), 3.11 (s, 12 H, OCH_2), 6.85 (s, 8 H, *m*-H), 7.60 [br. s, 2 H, NC(H)N] ppm. ^{13}C NMR (C_6D_6, 300 K): δ = 18.4 (s, *p*-CH_3), 19.6 (s, *o*-CH_3), 57.4 (s, OCH_3), 70.6 (s, OCH_2), 127.7 (s, *m*-C), 128.0, 128.1, 130.7 (s, Ar-C), 157.6 [s, NC(H)N] ppm. IR (Nujol): $\tilde{\nu}$ = 850 m, 872 m, 1022 m, 1090 m, 1124 m, 1146 m, 1209 s, 1246 w, 1294 w, 1564 s, 1614 m, 1639 m cm^{-1}.

[Li(dme)$_3$][Li(η^2-FTolO)$_2$] (2): *n*-Butyllithium (0.80 mL, 1.28 mmol) was added dropwise to a stirred solution of HFTolO (0.29 g, 1.29 mmol) in DME (30 mL) producing an opaque-yellow solution. Cessation of stirring after 2 h, followed by filtration gave a solution that yielded colourless crystals of the title compound (upon storage at −30 °C) as large solvent-dependent blocks (0.33 g, 71%), m.p. 122 °C (dec.). ^{1}H NMR (C_6D_6, 300 K): δ = 2.13 (s, 12 H, *o*-CH_3), 2.86 (s, 18 H, OCH_3), 2.88 (s, 12 H, OCH_2), 6.94 (m, 4 H, Ar-H), 7.03 (m, 4 H, Ar-H), 7.15 (m, 8 H, Ar-H), 8.72 [br. s, 2 H, NC(H)N] ppm. ^{13}C NMR (C_6D_6, 300 K): δ = 19.2 (s, *o*-CH_3), 58.9 (s, OCH_3), 71.1 (s, OCH_2), 118.2, 120.1, 127.1, 129.9, 130.6, 150.7 (s, Ar-C), 160.4 [s, NC(H)N] ppm. IR (Nujol): $\tilde{\nu}$ = 811 m, 831 m, 867 m, 921 w, 995 w, 1028 w, 1083 s, 1122 m, 1178 w, 1205 m, 1222 m, 1245 w, 1549 s, 1568 m, 1664 w cm^{-1}.

[Li(η^2-FMes)(tmeda)] (3): *n*-Butyllithium (1.10 mL, 1.76 mmol) was added dropwise to a stirred solution of HFMes (0.48 g, 1.71 mmol) in hexane (60 mL), instantly yielding a white precipitate. Addition of TMEDA (300 μL, 1.99 mmol) resulted in dissolution of the precipitate, rendering a clear yellow solution that was concentrated in vacuo (ca. 40 mL) and filtered. Placement of the filtrate at −5 °C for one week yielded the title product as a microcrystalline powder and a small quantity of colourless prisms (single product by ^{1}H NMR, 0.49 g, 71%), m.p. 145 °C (dec.). ^{1}H NMR (C_6D_6, 300 K): δ = 1.80 (s, 4 H, NCH_2), 1.92 (s, 12 H, NCH_3), 2.29 (s, 6 H, *p*-CH_3), 2.38 (s, 12 H, *o*-CH_3), 6.97 (s, 4 H, *m*-H), 8.02 [br. s, 1 H, NC(H)N] ppm. ^{13}C NMR (C_6D_6, 300 K): δ = 20.0 (s, *o*-CH_3), 21.0 (s, *p*-CH_3), 45.3 (s, NCH_3), 56.5 (s, NCH_2), 129.0 (s, *m*-C), 129.4, 131.0, 140.4 (s, Ar-C), 166.1 [br. s, NC(H)N] ppm. IR (Nujol): $\tilde{\nu}$ = 792 m, 851 m, 944 m, 998 m, 1018 m, 1061 w, 1158 m, 1212 m, 1285 s, 1302 m, 1536 s, 1609 w, 1644 w cm^{-1}.

X-ray Crystallography: Crystalline samples of compounds **1** and **3** were mounted upon glass fibres in silicone grease at −150 °C (123 K). A crystalline sample of **2** was mounted in a 0.5 mm capillary and sealed under argon at ambient temperature. Crystal data for compounds **1** and **3** were obtained using an Enraf−Nonius Kappa CCD. Data for **2** were obtained with a Bruker SMART CCD diffractometer. Data were corrected for absorption using the SADABS program.[34] Structural solution and refinement was carried out using SHELXL-97[35] and SHELXS-97[36] utilising the graphical interface X-Seed.[37] Crystal data and refinement parameters for all complexes are compiled in Table 1. Crystallographic data (excluding structure factors) for the structures reported in this paper have been deposited with the Cambridge Crystallographic Data Centre as supplementary publication no. CCDC-186011 (**1**), -186013 (**2**) and -186012 (**3**). Copies of the data can be obtained free of charge on application to the CCDC, 12 Union Road, Cambridge CB2 1EZ, UK [Fax: (internat.) + 44-1223/336-033; E-mail: deposit@ccdc.cam.ac.uk].

Acknowledgments

The authors gratefully acknowledge the continued financial support of the Australian Research Council (RIEFP grant for Bruker SMART CCD X-ray diffractometer). J. B. and C. B. thank the Deutsche Studienstiftung and Friedrich Ebert Stiftung, respectively, for financial support. M. L. C. would like to acknowledge the Royal Society, UK, for the provision of a postdoctoral fellowship.

[1] M. Majewski, D. M. Gleave, *J. Organomet. Chem.* **1994**, *470*, 1.
[2] B. J. Wakefield, *Organolithium Methods*, Academic Press, New York, **1988**.
[3] A. M. Sapsa, P. v. R. Schleyer (Eds.), *Lithium Chemistry: A Theoretical and Experimental Overview*, Wiley-Interscience, New York, **1995**.
[4] M. Gray, M. Tinkl, V. Snieckus, in *Comprehensive Organometallic Chemistry*, 2nd ed. (Eds.: E. W. Abel, F. G. A. Stone, G. Wilkinson), Pergamon, Oxford, **1995**, vol. 11, p. 1.
[5] C. H. Heathcock, in *Comprehensive Carbanion Chemistry* (Eds.: E. Buncel, T. Durst), Elsevier, New York, **1980**, vol. B, chapter 4.
[6] M. F. Lappert, P. P. Power, A. R. Sanger, R. C. Srivastava, *Metal and Metalloid Amides*, Ellis Horwood Ltd., Chichester, **1980**.
[7] W. N. Setzer, P. v. R. Schleyer, *Adv. Organomet. Chem.* **1985**, *24*, 353.
[8] K. Gregory, P. v. R. Schleyer, R. Snaith, *Adv. Inorg. Chem*,. **1991**, *37*, 47.
[9] R. E. Mulvey, *Chem. Soc. Rev.* **1991**, *20*, 176.
[10] D. S. Wright, M. A. Beswick, in *Comprehensive Organometallic Chemistry*, 2nd ed. (Eds.: E. W. Abel, F. G. A. Stone, and G. Wilkinson), Pergamon, Oxford, **1995**, vol. 1, chapter 1, p.1.
[11] D. Seebach, *Angew. Chem. Int. Ed. Engl.* **1988**, *27*, 1624.
[12] D. R. Armstrong, D. Barr, W. Clegg, R. E. Mulvey, D. Reed, R. Snaith, K. Wade, *J. Chem. Soc., Chem. Commun.* **1986**, 869.
[13] T. Fjeldberg, P. B. Hitchcock, M. F. Lappert, A. J. Thorne, *J. Chem. Soc., Chem. Commun.* **1984**, 822.
[14] J. A. R. Schmidt, J. Arnold, *Chem. Commun.* **1999**, 2149.
[15] J. Barker, M. Kilner, *Coord, Chem. Rev.* **1994**, *133*, 219.
[16] F. T. Edelmann, *Coord, Chem. Rev.* **1994**, *137*, 403.
[17] M. L. Cole, P. C. Junk, L. M. Louis, *J. Chem. Soc., Dalton Trans.,* in press.
[18] F. A. Cotton, S. C. Haefner, J. H. Matonic, X. Wang, C. A. Murillo, *Polyhedron* **1997**, *16*, 541.
[19] J. Baldamus, C. Berghof, M. L. Cole, D. J. Evans, E. Hey-Hawkins, P. C. Junk, *J. Chem. Soc., Dalton Trans.* **2002**, 2802.
[20] T. Sielisch, U. Behrens, *J. Organomet. Chem.* **1987**, *327*, 85.
[21] M. L. Cole, D. J. Evans, P. C. Junk, E. Robertson, M. K. Smith, unpublished results.

[22] From the steric coordination number defined for lanthanoid and actinoid complexes, defined in: J. Marçalo, A. Pires de Matos, *Polyhedron* **1989**, *8*, 2431. Included as, like f-block elements, the coordination of group 1 metals appears to be largely nondirectional (isotropic) contrary to d-block elements where metallic geometry is rigid due to electronic constraints.
[23] Obtained from a survey of the Cambridge Crystallographical Structural Database (CCSD).
[24] M. L. Cole, C. Jones, P. C. Junk, *New J. Chem.* **2002**, 89.
[25] M. L. Cole, D. J. Evans, P. C. Junk, L. M. Louis, *New J. Chem.* **2002**, 1015.
[26] F. A. Cotton, L. M. Daniels, C. A. Murillo, *Inorg. Chem.* **1993**, *32*, 2881.
[27] F. A. Cotton, T. Inglis, M. Kilner, T. R. Webb, *Inorg. Chem.* **1975**, *14*, 2023.
[28] T. Chivers, M. Parvez, G. Schatte, *J. Organomet. Chem.* **1998**, *550*, 213.
[29] G. D. Whitener, J. R. Hagadorn, J. Arnold, *J. Chem. Soc., Dalton Trans.* **1999**, 1249.
[30] M. L. Cole, C. Jones, P. C. Junk, *J. Chem. Soc., Dalton Trans.* **2002**, 896.
[31] H. Chen, P. Jutzi, M. M. Olmstead, P. P. Power, *Organometallics* **1991**, *10*, 1282.
[32] S. Neander, F. E. Tio, R. Buschmann, U. Behrens, F. Olbrich, *J. Organomet. Chem.* **1999**, *582*, 58.
[33] R. M. Roberts, *J. Org. Chem.* **1949**, *14*, 277.
[34] R. H. Blessing, *Acta Crystallogr., Sect. A* **1995**, *51*, 33.
[35] G. M. Sheldrick, *SHELXL-97*, University of Göttingen, Germany, **1997**.
[36] G. M. Sheldrick, *SHELXS-97*, University of Göttingen, Germany, **1997**.
[37] L. J. Barbour, *X-Seed, Crystallographic Interface*, University of Missouri−Columbia, MO, USA, **1999**.

Received May 21, 2002
[I02266]

Self-Assembly of Cobaloximes and Rhodoximes with 3-Aminophenylboronic Acid: A Molecular Triangle and a Polymer

Renata Dreos,*[a] Giorgio Nardin,[a] Lucio Randaccio,*[a] Patrizia Siega,[a] and Giovanni Tauzher[a]

Keywords: Cobalt / Rhodium / Boronic acid / Self assembly

The reactions of methylaquacobaloxime and ethylaquacobaloxime with 3-aminophenylboronic acid in water produce supramolecular triangles **3a** and **3b** respectively, through the reaction of boron with the oxime oxygens of the alkylcobaloxime and the coordination of pyridine to cobalt. The reaction is reversible and strongly pH dependent. The complexes **3a** and **3b** precipitate immediately from the solution at pH 7, but dissolve quickly at both acidic (below 4) and basic (above 9) pH values. The aggregates are re-formed by readjusting the pH to neutrality and the precipitation-dissolution cycle may be repeated several times without an apparent decrease in yield. The complexes were fully characterised by ^{1}H and ^{13}C NMR spectroscopy. The X-ray structure shows that the neutral chiral supramolecule **3a** is a triangle of cobalt atoms with an approximate C_3 symmetry. The side of the triangle is about 9.5 Å. The ring closure is ensured by the torsion angles around the B–C and C–NH_2 bonds, which vary in the range 25–30° and 97–109°, respectively. The reaction of methylaquarhodoxime with 3-aminophenylboronic acid in water at pH 7 results in the displacement of H_2O by 3-aminophenylboronic acid only. The polymeric form **4** precipitates from CD_3OD in the NMR tube with time. The X-ray structure shows that **4** is a polymeric species with a zig-zag chain arrangement, with Rh···Rh distances of 9.2 Å. The chain arrangement is characterized by torsion angles around the B–C and C-NH_2 bonds of 61° and 92°, respectively.
(© Wiley-VCH Verlag GmbH, 69451 Weinheim, Germany, 2002)

Introduction

Use of the metal-ligand interaction to form inorganic supramolecules from mononuclear building blocks is a rapidly developing field in supramolecular chemistry.[1] Transition metal-directed self-assembly has been used to construct a large variety of molecular polygons and polyhedra, but molecular triangles with metal ions in vertex positions are still relatively rare, mainly due to the impossibility of generating the required 60° angle in a metal fragment of common coordination number. The majority of molecular triangles with metal ions at the corners are based on the square-planar geometry of Pt^{II} and Pd^{II} complexes [2] and display right-angled vertices. The closure of the triangle is made possible by ligands with appropriate coordinate vectors or by rather flexible ligands. The latter approach often results in low yields, owing to the formation of equilibrium mixtures, in which larger species, typically squares, are also present.[1] We report here the selective formation, in high yield, of neutral supramolecular triangles by reaction of octahedral organoaquacobaloximes with 3-aminophenylboronic acid. Furthermore, we show that changing the metal atom from Co to Rh causes a dramatic change in the structure and an inorganic polymer is formed.

[a] Dipartimento di Scienze Chimiche, Università degli Studi di Trieste,
Via L. Giorgieri 1, 34127 Trieste, Italy
Fax: (internat.) +39-040/676-3903
E-mail: dreos@univ.trieste.it
randaccio@univ.trieste.it
Supporting information for this article is available on the WWW under http://www.eurjic.org or from the author.

Results and Discussion

Synthesis

Alkylaquabis(dimethylglyoximates) of Co^{III} (alkylaquacobaloximes, Scheme 1) have already been shown to be suit-

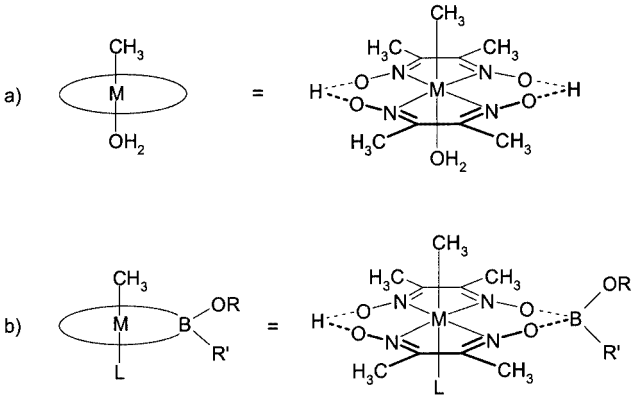

Scheme 1. Structural (right) and schematic (left) representation of a) alkylaquabis(dimethylglyoximate) (M = Co, Rh); b) monoborylated alkylbis(dimethylglyoximate)

able for self-assembly with functionalized arylboronic acids, such as 3- and 4-PyB(OH)$_2$.[3] In fact, similar to *cis*-diols,[4] the oxime bridges are very reactive towards boronic acids and the axial water ligand can easily be replaced by the pyridinyl group. The reaction of methylaquacobaloxime with 3-pyB(OH)$_2$ gives cyclic dimer **1**, with coplanar pyridinyl moieties, whereas the reaction with 4-pyB(OH)$_2$ gives cyclic dimer **2**, with parallel pyridinyl rings (Scheme 2). The reactions are strongly pH dependent, because the formation of the dinuclear species **1** and **2** requires the neutral (or zwitterionic) form of the boronic acid.[3b]

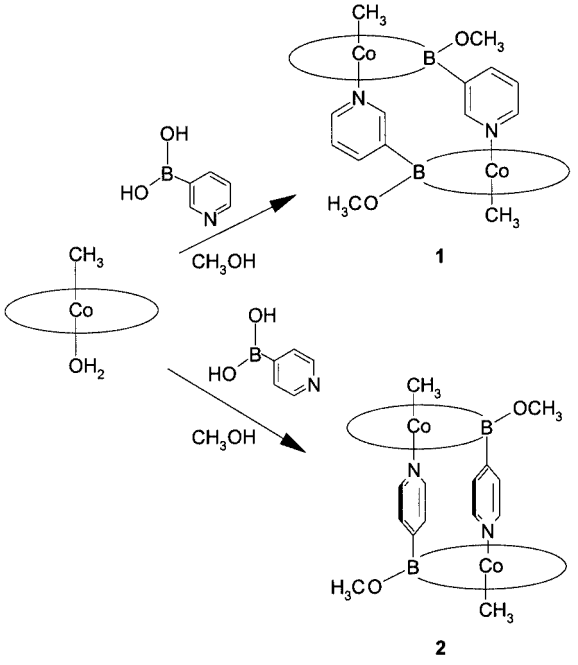

Scheme 2

The macroscopic pK_a values for the first and the second deprotonation of the 3-aminophenylboronic acid, determined by spectrophotometric titration, are 9.14 and 4.56, respectively. These values suggest, by analogy with the reactions with pyridinylboronic acids, that self-assembly should occur within this pH range. Indeed, when the pH of an aqueous solution of organoaquacobaloxime containing 3-aminophenylboronic acid in slightly less than an equimolar amount is adjusted to about 7, complexes **3a** and **3b** precipitate immediately from the solution (Scheme 3). Further acidification of the solution to below pH 4 results in the dissolution of the precipitate. The aggregate is re-formed by restoring the pH of the solution back to neutrality and is redissolved at alkaline pH values (above pH 9). The precipitation/dissolution cycle may be repeated at least twenty times without an apparent decrease in yield. The same trimer **3a** can be synthesized in methanol, without esterification of the B(OH) groups, provided the reagent concentration is sufficiently high to induce an immediate precipitation. If the precipitation occurs after a longer time, or if the precipitate is left in contact with the solution, the ^{1}H NMR spectrum shows a mixture of several products.

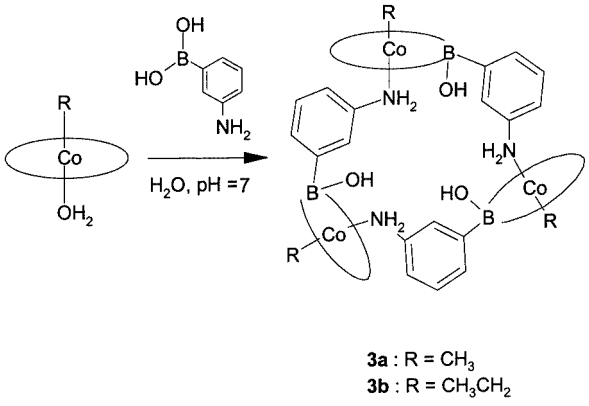

Scheme 3

The reaction of [CH$_3$Rh(DH)$_2$H$_2$O] with 3-aminophenylboronic acid in water at pH 7 (Scheme 4) results in the displacement of H$_2$O by 3-aminopheylboronic acid only, as suggested by an incomplete X-ray structural analysis and by the ^{1}H NMR spectrum in CD$_3$OD. The polymeric form **4** precipitates from CD$_3$OD in the NMR tube with time (Scheme 3). A ^{1}H NMR study in D$_2$O of a solution containing [CH$_3$Rh(DH)$_2$H$_2$O] and 3-aminophenylboronic acid in equimolar amounts does not give any evidence of a condensation reaction between the oxime bridge and the boronic acid in the pH range 9.5−0.6.

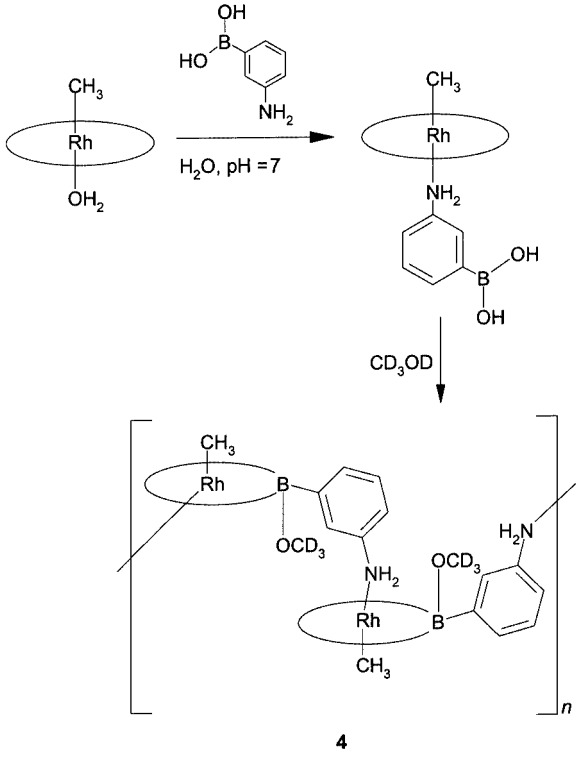

Scheme 4

X-ray Structure Determination of 3a

The structure of one enantiomer of the racemic crystal of **3a** is depicted in Figure 1. The molecule has an approx-

imate C_3 symmetry, with the threefold axis perpendicular to the plane of the cobalt atoms. Each B−OH group makes an intramolecular H-bond with the amino group coordinated to Co (Figure 1), with relatively short NH···O distances in the range 2.95(1)−3.04(1) Å. The conformational freedom of B and the torsion around the Co−NH_2 bond are thereby "frozen", so that the structure is essentially defined by the values of the torsion angles around the B−C and C−NH_2 bonds, which have very similar values in the three independent units. The torsion angles HO−B−C−C_α and Co−NH_2−C−C_α (where C_α = C40, C46, and C52, Figure 1) vary in the ranges 25−30° and 97−109°, respectively. The mean plane of the three carbon atoms of the methyl groups, each from one bis(dimethylglyoximate) moiety, is nearly parallel to that of the Co triangle [at an interplanar distance of 1.35(1) Å]. The Co plane is 1.76 Å from the approximately parallel mean plane of the O atoms of the boron OH groups. Therefore, one side of **3a** is hydrophilic (OH groups), while the other side is hydrophobic. A water molecule (O2W) is H-bonded to the three boron OH groups at distances in the range 2.82(1)−2.85(1) Å (Figure 1) and lies approximately at the mid-point of the three hydroxyl O atoms. It is interesting to note that the trimer/OW2 aggregates are held together by a network of H-bonds between the $(OH)_3$···OW2 grouping of one aggregate and that of the neighbouring aggregate, related by a crystallographic twofold axis along z (at x = 1/2, y = 1/4). Figure 2 shows the H-bond network, with O···O distances in the range 2.82−3.02 Å. Two distributions of the H atoms with half occupancy, related by the twofold axis, are represented. Each O atom has a distorted tetrahedral arrangement with four O···O H-bonds around OW2 and with two O···O, one NH···OH, and one O−B bond around each O atom of the boron (OH) groups.

Characterization of 3a and 3b by NMR Spectroscopy

The ^{1}H NMR spectrum of **3a** in $CDCl_3$ is in agreement with the trimeric structure of Figure 1. Four signals are observed for the equatorial methyl groups of each cobaloxime moiety, due to the loss of equivalence caused by the self-assembly process. One signal is shifted considerably upfield (δ = 1.39 ppm) in comparison with the usual range found for alkylcobaloximes.[5] This signal has been assigned to the protons on C18, C21 and C31, which lie above the plane of the phenyl rings and in the cone of their magnetic shielding. The protons of the NH_2 groups are diastereotopic and give rise to two doublets, one of which is in the aromatic part of the spectrum and the other in the range δ = 3.0−3.5 ppm. The protons on B(OH) and the oximic protons give rise to two singlets at δ = 4.48 and 18.0 ppm, respectively. In the spectrum of complex **3b**, the methylene protons of the ethyl groups are diastereotopic and give rise to the AB part of an ABM_3 pattern. All the other signals are almost superimposable onto those of **3a**. The strong similarity of the spectra suggests a trimeric structure also for **3b**.

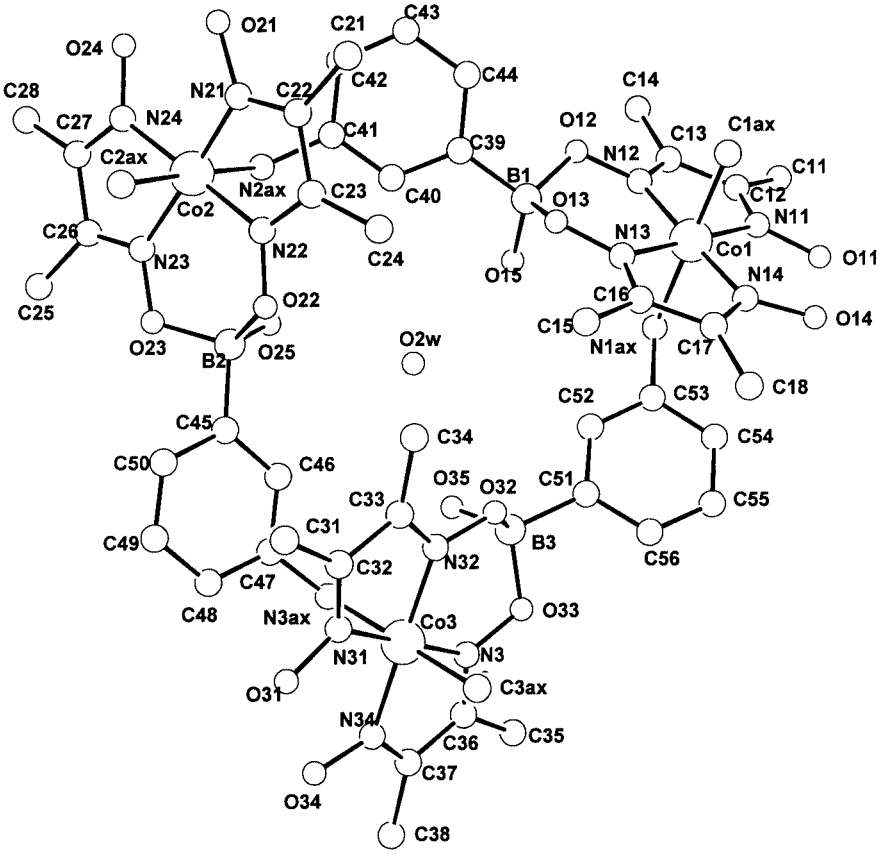

Figure 1. Molecular structure of one enantiomer of **3a**, with the labelling scheme for the atoms

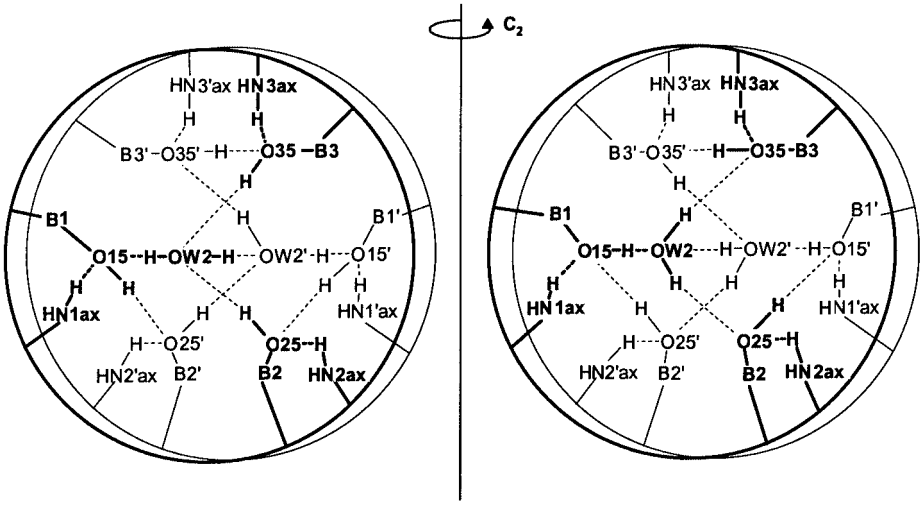

Figure 2. Two H-bond distributions, with half occupancy H atoms, in the network involving OW2 and boron OH groups; the superimposition of the two schemes has C_2 symmetry

The spectra show little variation with concentration (except for the NH_2 protons) in the range 2×10^{-2} to 1×10^{-3} M or with temperature in the range −60 to +50 °C. Therefore, the trimers are very stable in $CDCl_3$ solution and do not coexist in equilibrium with other species, even if a model inspection suggests that a tetranuclear square species is sterically allowed.

X-ray Structure Determination of 4

The structure of **4** is shown in Figure 3. In spite of the increase of about 0.1 Å in the coordination distances of rhodoximes with respect to those of the analogous cobaloximes, the local geometry of each unit is very similar to that of the unit in **3a**. An intramolecular H-bond between the coordinated amino group and the axially directed OCD_3 group, arising from the esterification of B(OH) in CD_3OD [NH···OCD_3 distance of 2.88(1) Å], is still present. Conformational changes, essentially due to a significant variation in the B−C and C−NH_2 torsion angles with respect to **3a**, lead to the chain arrangement shown in Figure 3, with a Rh···Rh distance of 9.159(4) Å. The O5−B1−C9−C10 and Rh−N5−C11−C12 torsion angles are 61(1) and 92(1)°, respectively. The polymer **4** is too insoluble in non-coordinating solvents to be studied by ^{1}H NMR spectroscopy.

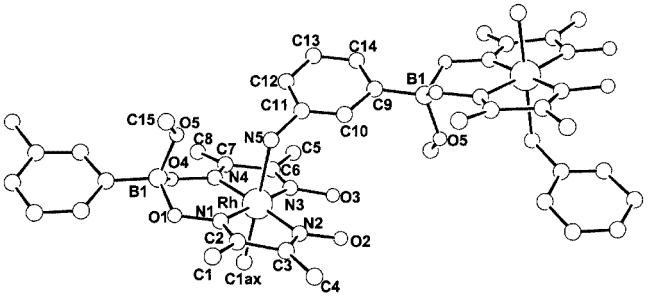

Figure 3. The chain arrangement of the polymeric species **4** with the labelling scheme for the atoms

Conclusion

The neutral trimers **3a** and **3b** are one of the few examples of triangular supramolecular structures based on an octahedral metal centre,[6] and show some novel elements. The fast assembly/disassembly process is reversible and "triggered" by a pH variation.[7] Furthermore, the 3-aminophenylboronic acid does not connect the cobaloxime units through two direct metal-ligand interactions, as occurs in most of the reported triangles.[1,2] The connection is created, on one side, by the reaction of the $B(OH)_2$ group with the oxime bridge at the periphery of the equatorial ligand and, on the other side, by the coordination of the amino group to cobalt. The chirality of **3** is a consequence of this way of binding. A further consequence of the use of the asymmetric linker is the complete diastereoselectivity in the formation of **3** and **4**. The ^{1}H NMR spectra of **3** do not show epimerization even at elevated temperatures ($CDCl_3$, 50 °C).

Methylaquacobaloxime and methylaquarhodoxime give very different products under similar conditions. As both the geometry and the coordination properties of the complexes are very similar, we believe that the relevant point is the esterification of the OH groups in **4**, due to their prolonged contact with deuterated methanol. This hypothesis is supported by evidence that complex **3a** can be recovered from methanol, without esterification of the B(OH) groups, but decomposes if left in contact with the solvent for a longer time. Probably, esterification reduces the stabilization arising from the H-bonds between the water molecule (OW2) and the three boron OH groups in the cyclic form **3** (Figure 2). The steric hindrance of OCH_3 could contribute to prevent the cyclization in **4**.

Experimental Section

General Remarks: NMR spectra were recorded on a Jeol EX-400 spectrometer (^{1}H at 400 MHz and ^{13}C at 100.4 MHz) with TMS

as internal standard. $[CH_3Co(DH)_2H_2O]$, $[CH_3CH_2Co(DH)_2H_2O]$[8] and $[CH_3Rh(DH)_2H_2O]$[9] were prepared according to literature procedures. All other reagents were reagent grade and used without further purification.

Synthesis of 3a and 3b: The appropriate alkylaquacobaloxime (0.40 mmmol) was dissolved in an aqueous alkaline solution (10 mL) with a pH of about 11 and 3-aminophenylboronic acid (0.37 mmol) was added. After filtration, the pH of the solution was lowered to about 7.0 with concentrated $HClO_4$. A highly insoluble yellow precipitate formed immediately, which was filtered and washed with water. X-ray quality crystals of **3a** were obtained by slow diffusion of a solution of the complex into CH_2Cl_2 in *n*-heptane.

3a: Yield: 70 mg (40%). $C_{45}H_{75}B_3Co_3N_{15}O_{18}$ (1323, with $3H_2O$): calcd: C 40.8, H 5.71, N 15.8; found C 40.4, H 5.51, N 15.2. ^{1}H NMR (400 MHz, $CDCl_3$, TMS): δ = 0.64 (s, 9 H, axial CH_3), 1.39 (s, 9 H, eq. CH_3), 1.90 (s, 9 H, eq. CH_3), 2.13 (s, 9 H, eq. CH_3), 2.27 (s, 9 H, eq. CH_3), 3.26 (d, $^2J_{H\text{-}H}$ = 8.3 Hz, 3 H, NH_2), 4.48 (s, 3 H, BOH), 6.67 (d, $^3J_{H\text{-}H}$ = 7.8 Hz, 3 H, ar. H), 6.88 (d, $^2J_{H\text{-}H}$ = 8.3 Hz, 3 H, NH_2) 7.04 (m, 3 H, ar. H), 7.09 (s, 3 H, ar. H), 7.35 (d, $^3J_{H\text{-}H}$ = 7.1 Hz, 3 H, ar. H), 18.01 (s, 3 H, OHO) ppm. ^{13}C NMR (100.4 MHz, $CDCl_3$, TMS): δ = 11.46, 12.18, 13.10, 14.60 (equatorial CH_3), 118.74, 124.36, 126.49, 129.44, 137.38 (aromatic carbons), 148.77, 149.62, 154.27, 156.69 (C=N).

3b: Yield: 90 mg (50%). $C_{48}H_{81}B_3Co_3N_{15}O_{18}$ (1365, with $3H_2O$): calcd: C 42.2, H 5.98, N 15.4; found C 41.0, H 5.60, N 15.0. ^{1}H NMR (400 MHz, $CDCl_3$, TMS): δ = 0.24 (t, $^3J_{H\text{-}H}$ = 7.6 Hz, 9 H, CH_3 of ethyl), 1.37 (s, 9 H, eq. CH_3), 1.57 (m, $^2J_{H\text{-}H}$ = 7.6 Hz, 6 H, CH_2 of ethyl), 1.87 (s, 9 H, eq. CH_3), 2.09 (s, 9 H, eq. CH_3), 2.26 (s, 9 H, eq. CH_3), 3.38 (d, $^2J_{H\text{-}H}$ = 8.3 Hz, 3 H, NH_2), 4.47 (s, 3 H, BOH), 6.66 (d, $^3J_{H\text{-}H}$ = 7.6 Hz, 3 H, ar. H), 6.73 (d, $^2J_{H\text{-}H}$ = 8.3 Hz, 3 H, NH_2), 7.03 (m, 3 H, ar. H), 7.09 (s, 3 H, ar. H), 7.32 (d, $^3J_{H\text{-}H}$ = 7.1 Hz, 3 H, ar. H), 17.87 (s, 3 H, OHO) ppm. ^{13}C NMR (100.4 MHz, $CDCl_3$, TMS): δ =15.83 (axial CH_3), 25.63 (axial CH_2) 11.47, 12.24, 13.20, 14.77 (equatorial CH_3), 118.75, 124.46, 126.56, 129.31, 137.60 (aromatic carbons), 148.80, 149.73, 154.42, 156.86 (C=N).

Synthesis of 4: Methylaquarhodoxime (0.10 mmmol) was dissolved in an aqueous alkaline solution (3 mL) with a pH of about 11 and 3-aminophenylboronic acid (0.12 mmol) was added. The pH of the solution was lowered to about 7.0 with concentrated $HClO_4$ and the solution left to stand. After some days yellow needle crystals were collected. Both an incomplete X-ray structure (due to the very low resolution) and the ^{1}H NMR spectrum in CD_3OD strongly suggested that the yellow product was a rhodoxime with coordinated aminophenylboronic acid. After some days, X-ray quality crystals of **4** were collected from the CD_3OD solution in the NMR tube. Yield: 10 mg (20%) $[C_{16}H_{25}N_5BO_5Rh + 1H_2O]_n$: calcd. C 38.5, H 5.45, N 14.0; found C 37.8, H 5.10, N 13.9. The polymer **4** is too insoluble in non-coordinating solvents to be studied by ^{1}H or ^{13}C NMR spectroscopy.

Equilibrium Studies: The deprotonation constants of the 3-aminophenylboronic acid were determined by spectrophotometric titration as previously described.[3b]

Structure Determination of 3a and 4: Single crystals, suitable for X-ray data collection, were obtained as reported above. X-ray diffraction data for **3a** and **4** were collected at room temperature with a Nonius DIP 1030 H System, using graphite-monochromated Mo-K_α radiation. For all compounds a total of 36 frames were collected, using the Xpress program,[10] over a half of reciprocal space, with a rotation of 5° about the axis. A Mac Science Image Plate (diameter = 300 mm) was used and the crystal-to-plate distance was fixed at 90 mm. The determination of unit-cell parameters, integration of reflection intensities and data scaling were performed using MOSFLM and SCALA from the CCP4 program suite.[11] Reflections, which were measured on previous and later frames, were used to scale the frames onto each other, a procedure that partially eliminated absorption effects, taking into account also any crystal decay. The structures were solved by direct methods,[12] followed by Fourier syntheses, and refined by full-matrix least-squares (on F^2) cycles.[13] Compounds **3a** and **4** co-crystallized with water molecules and 0.5 molecules of CH_2Cl_2 in the case of **3a**, and 1.5 molecules of CD_3OD in the case of **4**. All solvent molecules were refined isotropically. The H atoms were not refined but were included at calculated positions in the final refinements. The solvent H atoms and the disordered hydrogen of the B−OH were not included. A suite of programs[14] was also used for the geometrical and final calculations. Crystal and refinement data are given in Table 1. CCDC-175792 (**3a**) and CCDC-175793 (**4**) contain the supplementary crystallographic data for this paper. These data can be obtained free of charge at www.ccdc.cam.ac.uk/conts/retrieving.html [or from the Cambridge Crystallographic Data Centre, 12, Union Road, Cambridge CB2 1EZ, UK; Fax: (internat.) +44-1223/336-033; E-mail: deposit@ccdc.cam.ac.uk].

Table 1. Crystallographic data for **3a** and **4**

	3a	4
Formula	$C_{45.5}H_{66}ClCo_3N_{15}O_{19.5}$	$C_{17.5}H_{29.5}BN_5O_9Rh$
Mol. wt.	1379.8	567.7
System	Orthorhombic	Orthorhombic
Space group	Ibca	$P2_12_12_1$
a, Å	28.829(3)	11.468(2)
b, Å	29.662(4)	14.503(3)
c, Å	33.896(4)	16.216(4)
V, Å^3	28985(5)	2691(1)
Z	16	4
ρ_{calc}, g·cm^{-3}	1.27	1.40
T, K	293	293
μ (Mo-K_α), mm^{-1}	0.785	0.683
*R*1 [$I > 2\sigma(I)$][a]	0.084	0.071
w*R*2 (all data)[b]	0.262	0.192

[a] $R1 = \||F_o| - |F_c|\|/|F_o|$. [b] $wR2 = [w(|F_o|^2 - |F_c|^2)^2/w|F_o^2|^2]^{1/2}$.

Acknowledgments

This work was supported by Italian MIUR MM 03185591 and CNR Agenzia 2000 (Roma).

[1] [1a] S. Leininger, B. Olenyuk, P. J. Stang, *Chem. Rev.* **2000**, *100*, 853−908 and references therein. [1b] G. F. Swiegers, T. J. Malefetse, *Chem. Rev.* **2000**, *100*, 3483−3537 and references therein. [1c] B. J. Holliday, C. A. Mirkin, *Angew. Chem. Int. Ed.* **2001**, *40*, 2022−2043.

[2] For some recent references, see for example: [2a] M. Fujita, O. Sasaki, T. Mitsuhashi, T. Fujita, J. Yazaki, K. Yamaguchi, K. Ogura, *Chem. Commun.* **1996**, 1535−1536. [2b] S. B. Lee, S. G. Hwang, D. S. Chung, H. Yun, J.-I. Hong, *Tetrahedron Lett.* **1998**, *39*, 873−876. [2c] R. -D. Schnebeck, L. Randaccio, E. Zangrando, B. Lippert, *Angew. Chem. Int. Ed.* **1998**, *37*, 119−121. [2d] S.-W. Lai, M. C.-W. Chan, S.-M. Peng, C.-M. Che, *Angew. Chem. Int. Ed.* **1999**, *38*, 669−671. [2e] R. F. Carina, A. F. Williams, G. Bernardinelli, *Inorg. Chem.* **2001**, *40*,

1826−1832. [2f] M. Schweiger, R. S. Seidel, A. M. Arif, P. J. Stang, *Angew. Chem. Int. Ed.* **2001**, *40*, 3467−3469.

[3] [3a] R. Dreos, G. Nardin, L. Randaccio, G. Tauzher, S. Vuano, *Inorg. Chem.* **1997**, *36*, 2463−2464. [3b] R. Dreos, G. Nardin, L. Randaccio, P. Siega, G. Tauzher, V. Vrdoljak, *Inorg. Chem.* **2001**, *40*, 5536−5540.

[4] For comprehensive reviews: [4a] T. D. James, K. R. A. S. Sandanayake, S. Shinkai, *Angew. Chem. Int. Ed. Engl.* **1996**, *35*, 1910−1922. [4b] T. D. James, P. Linnane, S. Shinkai, *Chem. Commun.* **1996**, 281−287.

[5] N. Bresciani Pahor, M. Forcolin, L. G. Marzilli, L. Randaccio, M. F. Summers, P. J. Toscano, *Coord. Chem. Rev.* **1985**, *63*, 1−125 and references therein.

[6] S. Sun, A. J. Lees, *Inorg. Chem.* **1999**, *38*, 4181−4182.

[7] For further examples of pH-dependent self-assembly of triangles: [7a] T. Habereder, M. Warchhold, H. Nöth, K. Severin, *Angew. Chem. Int. Ed.* **1999**, *38*, 3225−3228. [7b] H. Chen, M. M. Olmstead, P. D. Smith, M. F. Maestre, R. H. Fish, *Angew. Chem. Int. Ed. Engl.* **1995**, *34*, 1514−1516.

[8] G. N. Schrauzer, in *Inorganic Syntheses, Vol. 11*, (Ed.: R. Parry), Wiley, New York, **1968**, p.61.

[9] [9a] J. H. Espenson, R. C. Mc Hatton, *Inorg. Chem.* **1981**, *20*, 3090−3092. [9b] R. Dreos Garlatti, G. Tauzher, G. Costa, *Inorg. Chim. Acta* **1986**, *121*, 27−32.

[10] B. Schierbeek, *Nonius*; Delft: The Netherlands, **1998**.

[11] Collaborative Computational Project, Number 4, *Acta Crystallogr., Sect. A* **1990**, *46*, 467−473.

[12] SIR92 − *A program for crystal structure solution:* A. Altomare, G. Cascarano, C. Giacovazzo, A. Guagliardi, *J. Appl. Crystallogr.* **1993**, *26*, 343−350.

[13] G. M. Sheldrick, SHELXL-97 − *Programs for Structure Refinement.* Universität Göttingen, Göttingen, Germany, **1998**.

[14] L. J. Farrugia, *Appl. Crystallogr.* **1999**, *32*, 837−838.

Received December 28, 2001
[I01531]

An Iron(II) Complex with an N_4S Ligand − A Novel Model Compound to Mimic Cytochrome P450 Activity

Oliver Fazio,[a] Manuel Gnida,[b,c] Wolfram Meyer-Klaucke,[b] Walter Frank,[a] and Wolfgang Kläui*[a]

Dedicated to Prof. Dr. K. Wieghardt on the occasion of his 60th birthday

Keywords: Metalloenzymes / Tetrapodal pentadentate ligand / Iron / Homogeneous catalysis / O−O activation / N,S ligands / Epoxidation / EXAFS spectroscopy

The ligand 2,5-Bis[hydroxybis(2-pyridyl)methyl]thiophene (bhpmt) was designed to mimic the coordination sphere of cytochrome P450. With the ligand's four coplanar nitrogen atoms and an axial sulfur donor group it is the first nonporphyrin model compound to form a similar arrangement. The structure of the corresponding iron(II) perchlorate complex was determined by EXAFS and XPS measurements. The bond lengths of the first coordination sphere are remarkably similar to known porphyrin-based P450 model compounds. It is shown that the iron complex of bhmpt is able to perform epoxidation reactions with open-chain olefins and aqueous hydrogen peroxide (30%) as the oxidizing agent.
(© Wiley-VCH Verlag GmbH, 69451 Weinheim, Germany, 2002)

Introduction

Iron complexes are widely known in nature and play an essential part as biological redox catalysts in almost all life forms. Especially the heme proteins are of importance. Aside from hemoglobin, a great number of structurally related compounds, such as the cytochromes in the oxidative chain, are known.[1] Designing ligands that can mimic the structural aspects and, consequently, the catalytic properties of an enzyme has been the subject of extensive research in the field of biomimetic chemistry. It is one such model that we would like to report here. As a natural counterpart for our model system we have chosen the ubiquitous enzyme cytochrome P450, one of a class of heme-containing enzymes that catalyze the hydroxylation of C−H bonds, epoxidation of carbon−carbon double bonds, and the oxidation of heteroatoms.[2] Unlike many of the other heme-containing enzymes, P450 features a thiolate function at the apical position of the octahedral iron complex rather than another nitrogen donor group. It appears that thiolate ion ligation of the metal center is the main reason for the different reactivity of P450 compounds compared to other heme-based enzymes.[3] To understand the extraordinary properties of this enzyme many model compounds have been developed to date. While these mostly porphyrin-based complexes can sufficiently mimic the exact steric properties of the natural counterpart, their catalytic activities are limited.[4] So far only the Woggon group has developed a system that is able to perform oxygen insertion with dioxygen into nonactivated C−H bonds. Since the insertion occurs at a side chain of the model compound, the functional properties of P450 cannot be sufficiently mimicked.[4e] Simple, non-porphyrin iron-containing model compounds with an N_4S-donor set are unknown to the best of our knowledge. In contrast to the few known pentadentate ligands that usually carry N_5-donor sets,[5,6] we wanted to introduce a sulfur atom to occupy one axial position in an octahedral metal complex. However, the introduction of a thiolate moiety into a metal complex proves to be difficult, since it readily forms disulfides in the presence of O_2. In nature this problem is circumvented by creating hydrophobic cavities to protect the sulfur atom from oxidation.[4b] Trading stability for higher donor strength, we chose thiophene instead of thiolate as the axial donor group. Here we report the synthesis of the novel ligand 2,5-bis[hydroxybis(2-pyridyl)methyl]thiophene (bhmpt), the iron perchlorate complex of bhmpt, its catalytic properties in the epoxidation of simple olefins, and the structural characterization of its active site.

[a] Institut für Anorganische Chemie und Strukturchemie der Heinrich-Heine-Universität Düsseldorf,
Universitätsstraße 1, 40225 Düsseldorf, Germany
Fax: (internat.) + 49-211/81-12287
E-mail: klaeui@uni-duesseldorf.de
[b] European Molecular Biology Laboratory (EMBL), Outstation at DESY,
Notkestraße 85, 22603 Hamburg, Germany
[c] Institut für Physik, Medizinische Universität zu Lübeck,
Ratzeburger Allee 160, 23538 Lübeck, Germany

Results and Discussion

According to a procedure recently published by Feringa,[6a] who created a similar N_5-ligating system, bhpmt can be synthesized by treating 2,5-thiophenedicarbonyl dichloride with 2-lithiopyridine. However, treatment of 2,5-dilithiothiophene with bis(2-pyridyl) ketone gives much higher yields (Figure 1).

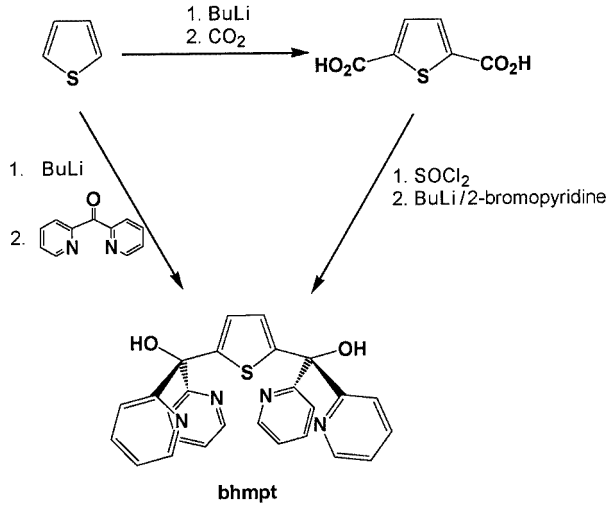

Figure 1. Synthesis of 2,5-bis[hydroxybis(2-pyridyl)methyl]thiophene (bhpmt)

The ligand is well soluble in halogenated solvents, toluene, THF as well as methanol and displays a high stability towards oxidation and hydrolysis.

Reaction of bhpmt with anhydrous iron(II) perchlorate in THF gives the corresponding metal complex. The compound is a yellow solid, paramagnetic and solely soluble in acetonitrile and dimethyl sulfoxide (DMSO). Due to disorder problems we have not been able to solve the crystal structure of the complex. The same problems were observed with the complexes of other divalent metal ions such as Co^{2+}, Ni^{2+} and Zn^{2+}. Only the corresponding copper perchlorate complex of bhpmt gave crystals suitable for X-ray analysis. It would not be reasonable to expect iron to exhibit the same coordination geometry as the copper complex. However, as is shown below, the X-ray data of the copper complex have helped to interpret the XPS and EXAFS data of the iron complex in the solid state and in solution.

The crystal structure of the copper complex shows that the thiophene moiety does not participate in the coordination of the metal center. Instead a dimer of two units of $[Cu(bhmpt)]^{2+}$ is formed, which allows the copper atoms to adopt the preferred square arrangement of four donor atoms. Both copper atoms are coordinated in a nearly planar fashion by three nitrogen atoms and one oxygen atom (Figure 2).

Vapour-pressure osmometric measurements, as well as conductivity measurements, suggest that the dimer is cleaved in solution to give monomers of as-yet-unknown structure.

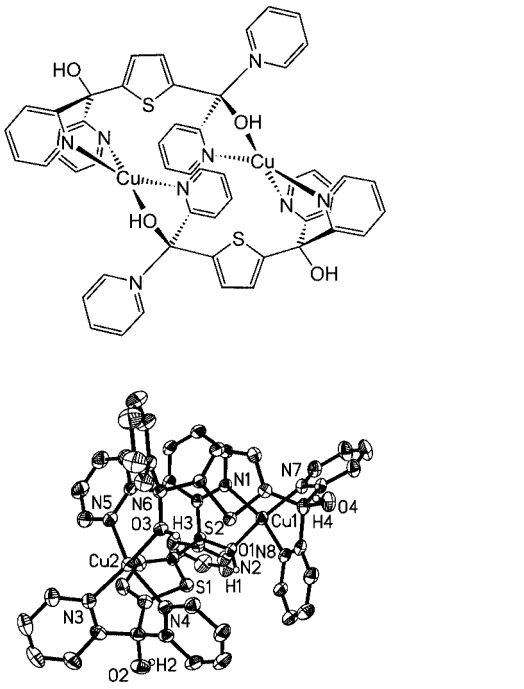

Figure 2. Molecular structure of the cation $[\{Cu(bhpmt)\}_2]^{4+}$; selected bond lengths [Å]: Cu1−O1 1.877(3), Cu1−N1 2.001(3), Cu1−N7 1.980(3), Cu1−N8 2.022(2), Cu1−O33′ 2.716(6) (perchlorate O), Cu2−O3 1.869(2), Cu2−N3 1.974(3), Cu2−N4 2.022(3), Cu2−N5 1.998(3), Cu2−O12 2.691(4) (perchlorate O); ′: $-x$, $2-y$, $-z$; selected H atoms, perchlorate anions and solvent molecules have been omitted for clarity; two of the perchlorate ions are weakly bonded to the two copper metal ions; by way of moderate hydrogen bonding two THF molecules are bonded to the OH moieties O2 and O4; additional disordered water and THF is situated among the ionic groups; displacement ellipsoids are drawn at the 25% probability level

Since the crystal structure of the corresponding iron complex of bhpmt could not be solved, spectroscopic measurements were used. X-ray photoelectron spectroscopy (XPS) measurements of $[Fe(bhpmt)](ClO_4)_2$ show four equivalent nitrogen atoms with binding energies in the range of coordinated pyridine, whereas for the corresponding copper complex the signal is broadened, indicating different electronic environments for the pyridine groups. According to the crystal structure of $[Cu_2(bhpmt)_2](ClO_4)_4$ the thiophene moiety does not participate in the coordination of the metal center. The XPS signal of thiophene is found at 164.3 eV. For the iron complex this signal is shifted to 164.0 eV. This decrease of binding energy at the sulfur atom is probably due to coordination of the sulfur atom to the iron atom.

The binding of bhmpt to the iron atom was investigated by means of Fe-*K*-edge X-ray absorption spectroscopy (XAS). The iron coordination environment was determined for solid $[Fe(bhpmt)](ClO_4)_2$·thf as well as for the metal complex dissolved in acetonitrile. Comparison of the normalized absorption edges for both samples shows that the step-like edge jump for the dissolved compound appears at lower energies than for the solid complex (Figure 3, separation of about 2−3 eV over the entire edge). Its energetic position is connected to the charge on the absorbing ion,[7]

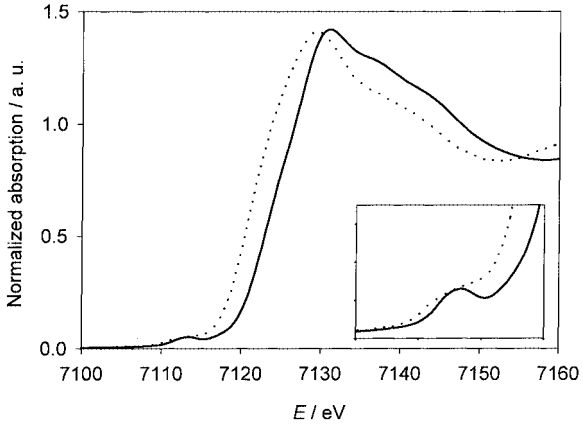

Figure 3. Normalized Fe-*K*-absorption edges of the solid compound (−) and the compound in solution (···); the inset displays the enlarged pre-edge region; abbreviations: a.u. = arbitrary units; *E* = X-ray energy

allowing the assignments of Fe^{II} for the solution and Fe^{III} for the solid-state complex. The Fe^{III} state is presumably a result of aerobic handling of the solid during sample preparation (see Exp. Sect.).

Both edge spectra exhibit a pre-edge peak at about 7113 eV (inset in Figure 3). It is due to a formally dipole-forbidden 1s → 3d electronic transition and its intensity is related to the coordination number and geometry of the iron site.[8] For both complexes the pre-edge peak areas (solid: 10.1 units; dissolved: 9.7 units; 1 unit = 10^{-2} eV) are in between the typical ranges for five- and six-coordinate complexes, indicating a significant distortion from octahedral symmetry.[8,9]

Further information on the iron coordination environment is derived from the extended X-ray absorption fine structure (EXAFS) of the absorption edge. Fourier transformation of the EXAFS signal allows the radial distribution of neighbouring atoms around the central absorbing metal ion to be explored (Figure 4, Table 1).

The structural composition of the first coordination shell of the iron atom is summarized in Table 1. In the solid as well as in the solution sample, the iron atom is coordinated by four nitrogen atoms (solid: 2.13 Å; solution: 2.11 Å) and one sulfur donor (solid: 2.29 Å; solution: 2.27 Å). Thus, the ligand binds in the desired pentadentate fashion with thiophene occupying the apical position (Figure 5). The sixth coordination site is most likely occupied by THF (Fe−O: 1.90 Å) and acetonitrile (Fe−N: 2.21 Å) in the solid state and in solution, respectively. No indication was found that dimerization occurs, as is the case for the corresponding Cu^{II} complex.

Comparison of the obtained data with EXAFS data of a heme-based P450-model compound by Higuchi's group shows very similar bond lengths (Fe−S 2.20 Å, Fe−N 2.00 Å).[4d] This indicates that the structural aspects of P450 can be adequately mimicked even by a simple model compound such as bhmpt in the solid state as well as in solution.

Epoxidation reactions were performed in order to investigate the catalytic activity, and consequently the ability of

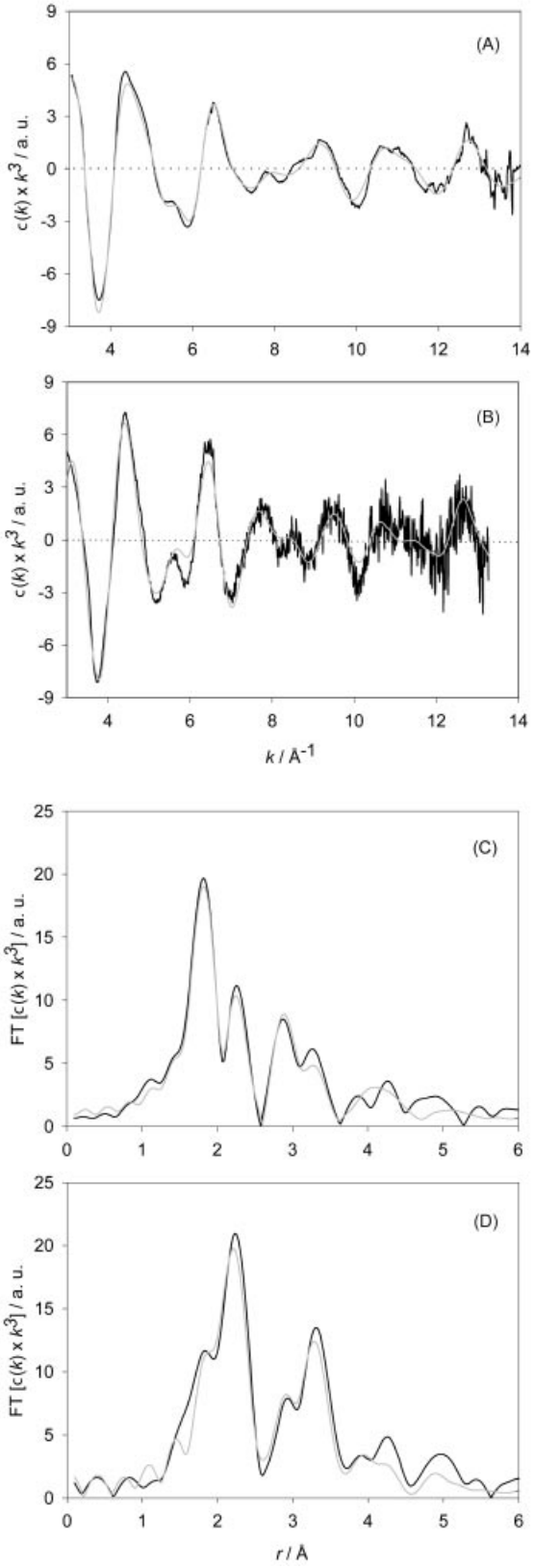

Figure 4. EXAFS (A, B) and corresponding Fourier transforms (C, D) of the solid (A, C) and dissolved (B, D) compound; experimental (black curves) and calculated (gray curves) spectra are compared; abbreviations: a.u. = arbitrary units; χ = EXAFS amplitude; *k* = photoelectron wave number; FT = Fourier transform amplitude; *r* = distance

Table 1. Structural parameters for the first iron coordination sphere, derived from EXAFS analysis

Atom[a]	Solid		Solution	
	r/Å	$2\sigma^2$/Å^2	r/Å	$2\sigma^2$/Å^2
1 O	1.903(2)	0.004(1)	–	–
4 N	2.127(7)	0.036(1)[b]	2.109(8)	0.029(2)[b]
1 N	–	–	2.212(6)	0.003(2)
1 S	2.291(11)	0.036(1)[b]	2.269(19)	0.029(2)[b]
E_F/eV	−15.2(2)		−12.1(4)	
R/%	19.8		35.5	

[a] r: distance; $2\sigma^2$: Debye−Waller parameter; E_F: Fermi energy (related to edge position, see manual of EXCURV98);[10] R: R factor (goodness of refinement).[10] [b] Constrained to have the same value during refinement; values in brackets are the numerical uncertainties (twice the standard deviation) of the last digit.

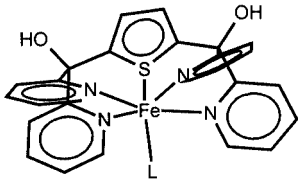

Figure 5. Molecular structure of the P-450 mimic investigated in this study; in the solid L is THF whereas CH_3CN binds to the iron ion in the dissolved complex

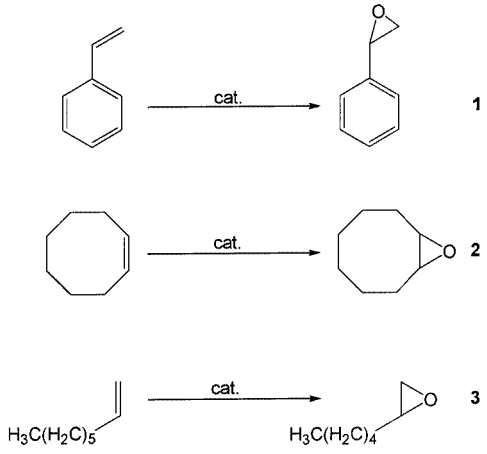

Figure 6. Performed epoxidation reactions

[Fe(bhpmt)]$^{2+}$ to mimic its biological counterpart (Figure 6).

For all reactions the catalyst was charged with a 50-fold excess of the substrate and the same amount of aqueous hydrogen peroxide (30%). The course of the catalytic reaction was monitored by gas chromatography (GC) and the resulting products were identified by gas chromatography/mass spectrometry (GC/MS). Surprisingly, the catalysis with a relatively unreactive olefin such as 1-octene displays similar efficiencies to that of more reactive substrates like styrene and cyclooctene (Figure 7).

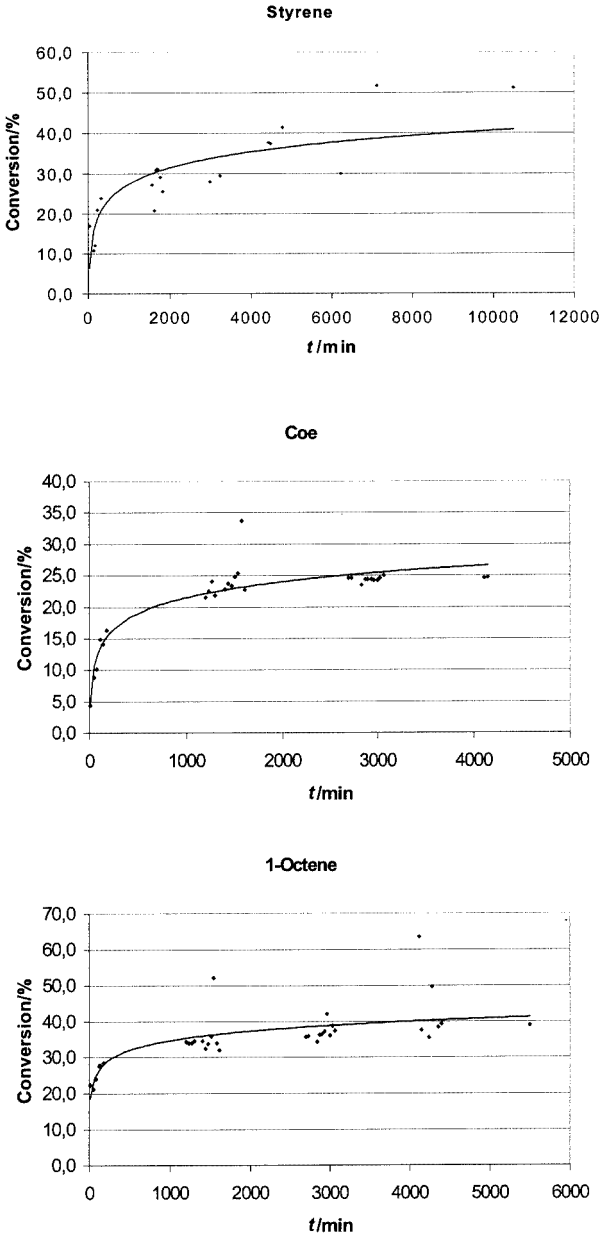

Figure 7. Conversion vs. time plots of the epoxidation reactions with styrene, cyclooctene (coe) and 1-octene

When norbornene is used as a substrate, significantly less epoxide is formed. This leads to the conclusion that the steric demands of the substrate and thus accessibility to the metal center determine the conversion rate, while the electronic properties of the substrate only have a minor effect on the catalysis. Since none of the other model compounds of P450 have been reported to show similar behavior we cannot decide whether this is typical for these types of iron complexes.

The only other iron complex to catalyze the epoxidation of open-chain olefins has been reported by Valentine. In this case, however, the ligand system is based on cyclam, thus having only four nitrogen donor groups. With a turnover of 20 for [Fe(bhpmt)]$(ClO_4)_2$, the epoxidation of 1-

octene shows significantly higher turnover numbers based on the iron complex than the one obtained with [Fe(cyclam)]$(CF_3SO_3)_2$ which reaches only 7 turnovers (Table 2).[11]

Table 2. Substrates used and resulting conversions to the corresponding epoxides

Substrate	Conversion	Turnover[a]
Styrene	51%	25
1-Octene	40%	20
Cyclooctene	25%	13
Norbornene	10%	5

[a] mmol of epoxide per mmol of catalyst.

The catalytic reactions proceed slowly with moderate conversions of the substrates. After approximately one day, the termination stage of each reaction is reached and the efficiency cannot be increased by further addition of either substrate or hydrogen peroxide. This suggests that the catalyst, which displays an unusually high durability in an aqueous medium for an iron(II) complex, does decompose after a while, forcing the catalytic activity to subside. At present, we do not know the nature or structure of the decomposition products. We believe that the ligand is oxidized after a while, releasing iron perchlorate. This is known to catalyze the decomposition of hydrogen peroxide, which could be another reason for the comparatively low efficiency of the catalyst. When using $Fe(ClO_4)_2$ as the catalyst in a control experiment, no epoxidation product could be detected.

Conclusions

With the iron complex of bhpmt we were able to mimic the structural aspects as well as the catalytic activity of cytochrome P450. We believe the latter is possible due to sulfur ligation of the central atom. Unusually for iron(III) complexes, which mostly form insoluble hydroxides in the presence of water, the metal complex of bhpmt displays a high tolerance for small amounts of water and is able to perform the catalysis with aqueous hydrogen peroxide. We discovered that higher conversion rates are obtained with sterically less demanding (albeit less strained) substrates. Therefore, styrene and 1-octene display conversion rates in the same range, whereas substrates with considerably higher ring strain, such as cyclooctene, are much harder to epoxidize. Norbornene, with the highest steric demand shows hardly any conversion into the corresponding epoxide. This is unlike the reactivity of other epoxidation catalysts such as porphyrin−iron complexes[12] and manganese[13] and chromium[14] complexes of salen-type ligands, where electronic factors play a more important role than the steric factor.

Experimental Section

CAUTION! Although no problems were encountered in this work, transition metal perchlorate complexes with organic ligands are potentially explosive and should be handled with due precaution. All reagents were commercial samples and were used as received.

Materials and Instrumentation: When not stated otherwise, experiments were performed under nitrogen using standard Schlenk techniques and freshly dried solvents. Filtration was done with 1-μm membrane filters (regenerated cellulose, Schleicher & Schuell). Infrared spectra were recorded by using a Bruker IFS 66 FT spectrometer. GC analysis was done with an HP-5890 series II chromatograph with an FID detector and an MSD 5970 integrator. As a standard for gas chromatography 0.8 mL of mesitylene was added to each catalysis experiment. Elemental analyses were performed using a Perkin−Elmer CHN-2400/II elemental analyzer.

2,5-Bis[hydroxybis(2-pyridyl)methyl]thiophene (bhpmt): *n*-Butyllithium (8.0 mL, 3 mmol) was dissolved in *n*-hexane (40 mL) and treated with an equimolar amount of tetramethylethylenediamine (tmeda; 1.5 g). After slow addition of freshly distilled thiophene (0.43 g, 5.1 mmol) in *n*-hexane (50 mL), the reaction mixture was heated to reflux for 1 h. The mixture was then transferred to a flask, containing bis(2-pyridyl) ketone (2.4 g, bis 13 mmol) in diethyl ether, and stirred overnight. After hydrolyzing with iced water and neutralization with hydrochloric acid, the precipitate was filtered off and washed with diethyl ether until a white solid remained. Recrystallization from THF/*n*-hexane yielded 1.1 g (47%). ^{1}H NMR (500 MHz, $CDCl_3$, 298 K): δ = 6.95 (s, 2 H, C_4H_2S), 7.19 (dt, $^3J_{H,H}$ = 6, $^4J_{H,H}$ = 1 Hz, 4 H, C_5H_4N), 7.94 (dt, $^3J_{H,H}$ = 8, $^4J_{H,H}$ = 2 Hz, 4 H, C_5H_4N), 7.98 (d, $^3J_{H,H}$ = 8 Hz, 4 H, C_5H_4N), 8.49 (d, $^3J_{H,H}$ = 5 Hz, 4 H, C_5H_4N) ppm. $^{13}C\{^1H\}$ NMR (500 MHz, $CDCl_3$, 298 K): δ = 78.7 (s, COH), 122.6 (s, C_5H_4N), 122.8 (s, C_5H_4N), 125.9 (s, C_4H_2S), 137.1 (s, C_5H_4N), 147.7 (s, C_5H_4N), 150.6 (s, C_5H_4N), 162.7 (s, C_4H_2S) ppm. IR (KBr): $\tilde{\nu}$ = 3375 br, 1585 vs, 1569 s, 1463 vs, 1432 vs, 1363 br, 1328 m, 1190 s, 1154 m, 1142 m, 1104 s, 1068 m, 967 w, 864 m, 774 s, 749 s, 700 s, 674 s, 662 s, 627 m, 513 w cm^{-1}. UV/Vis (THF): λ_{max} (ε) = 259 nm (22000), 210 nm (28000). MS (FAB+NBA): *m*/*z* (%) = 453 (61) [M^+ + H], 435 (92) [M^+ − OH], 268 ([M − $py_2COH]^+$). $C_{26}H_{20}N_4O_2S$ (452.5): calcd. C 69.0, H 4.4, N 12.4; found C 68.6, H 3.9, N 11.9.

[Fe(bhpmt)]$(ClO_4)_2$·thf: bhpmt (0.36 g, 0.65 mmol) was treated with anhydrous iron(II) perchlorate (0.17 mg, 0.65 mmol) in THF and stirred overnight. The resulting solid was filtered and recrystallized from acetonitrile/THF. Yield 0.31 g (60%). IR (KBr): $\tilde{\nu}$ = 3431 br, 3098 w, 1602 s, 1521 w, 1468 m, 1437 m, 1297 w, 1096 vs, 772 s, 624 s cm^{-1}. Conductivity Λ = 234 S·cm^2·mol^{-1} (acetonitrile). $C_{30}H_{28}Cl_2FeN_4O_{11}S$ (779.4): calcd. C 46.2, H 3.6, N 7.2; found C 46.8, H 3.5, N 7.5.

[Cu_2(bhpmt)$_2$]$(ClO_4)_4$: The compound was prepared according to the procedure described for the iron complex; bhpmt (0.13 g, 0.29 mmol), copper(II) perchlorate dihydrate (0.11 g, 0.29 mmol), recrystallization from acetonitrile/THF. Yield 0.12 g (80%). IR (KBr): $\tilde{\nu}$ = 3429 br, 1602 s, 1514 w, 1469 m, 1441 m, 1294 w, 1121 vs, 1101 m, 1090 w, 772 s, 627 s cm^{-1}. $C_{64}H_{67}Cl_4Cu_2N_8O_{24.5}S_2$ (1673.2):calcd. C 45.9, H 4.0, N 6.7; found C 42.7, H 3.4, N 7.0.

Crystal Structure Analysis of [Cu_2(bhmpt)$_2$]$(ClO_4)_4$·3C_4H_8O·1.5H_2O: M_r = 1673.26; crystal dimensions: 0.32 × 0.45 × 0.61 mm, *a* = 13.787(3) Å, *b* = 15.753(2) Å, *c* = 19.182(4) Å, α = 89.69(2)°, β = 81.12(2)°, γ = 65.85(2)°, *V* = 3748.2(12) $Å^3$, *Z* =

2, $\rho_{calcd.}$ = 1.483 Mg/m^3, triclinic, space group $P\bar{1}$. Stoe IPDS, Mo-K_α radiation (λ = 0.71073 Å), graphite monochromator, T = 20 °C, Θ_{max} = 30.31°, $-19 < h < 16$, $-20 < k < 18$, $-27 < l < 27$, 76976 reflections were detected, 20254 independent (R_{int} = 0.0595), 7640 were classified as "observed" with $I > 2\sigma(I)$, μ = 0.847 mm^{-1}, Direct method (SHELXS-97) and difference Fourier syntheses (SHELXL-97), minimizing of $\Sigma w(F_o^2 - F_c^2)^2$ with $w = 1/[\sigma^2(F_o^2) + 0.03P^2]$ and $P = (F_o^2 + 2F_c^2)/3$, 1048 refined parameters, R_1 = 0.0592, wR_2 = 0.1131, $(\Delta/\sigma)_{max}$ = 0.001, $\Delta\rho_{max}/\Delta\rho_{min}$ = 0.615/−0.358 e Å^{-3}. CCDC-190219 contains the supplementary crystallographic data for this paper. These data can be obtained free of charge at www.ccdc.cam.ac.uk/conts/retrieving.html or from the Cambridge Crystallographic Data Centre, 12, Union Road, Cambridge CB2 1EZ, UK [Fax: (internat.) + 44-1223/336-033; E-mail: deposit@ccdc.cam.ac.uk].

General Preparation for the Synthesis of Epoxides: [Fe(bhpmt)](ClO$_4$)$_2$ (8.4 mg, 1.0 μmol) and the substrate (50 μmol) were dissolved in acetonitrile (15 mL) and treated with 30% hydrogen peroxide (50 μL, 50 μmol). This mixture was stirred for 3 d at room temperature. The substrates used and resulting conversions are displayed in Table 2.

XAS Samples: Solution sample: A 3.2 mM solution of Fe(bhpmt)(ClO$_4$)$_2$ in acetonitrile (75 μL), with 5 vol.% glycerine, was poured into a sample cell of HESAR glass, covered with Kapton windows. Solid sample: In order to avoid "thickness effects" in the X-ray absorption spectrum, [Fe(bhpmt)](ClO$_4$)$_2$ (28 mg) in THF was mixed with boron nitride (59 mg, under aerobic conditions) in order to obtain an absorbance less than unity.[15] The mixture was pasted homogeneously into a sample cell of HESAR glass and was sealed with Kapton windows.

XAS Data Collection: Data were collected at the EMBL bending magnet EXAFS beam line D2 at DESY (Hamburg, Germany) using an Si(111) double crystal monochromator and a double focusing mirror. As detectors ionization chambers (absorption mode for solid sample) and a 13-element solid-state Canberra fluorescence detector (fluorescence mode for solution sample) were used. Absolute energy calibration of the spectra was achieved recording Bragg reflections of a static Si(220) crystal in back-reflection geometry.[16] During data collection, the samples were kept in an He closed-cycle cryostat (modified Oxford instruments) at temperatures below 55 K.

XAS Data Analysis: Data reduction such as background removal and extraction of the EXAFS signal was performed using the EXPROG program package (H. F. Nolting, C. Hermes, EMBL Hamburg) and assuming an Fe-K-edge position of E_0 = 7112 eV. EXAFS data were analyzed with EXCURV98,[10] considering multiple scattering from the units of pyridine, tetrahydrofuran, thiophene, and acetonitrile. Pre-edge peak areas were determined by fitting one (solid) or two (solution) Gaussians to the X-ray absorption spectra (solid: 7100−7121 eV; solution: 7100−7118). In addition, a Lorentzian was used as background function (rising edge).

Acknowledgments

We thank Dr. P. Albers and Dr. M. Pfeifer at dmc^2 for their kind support and XPS measurements. The authors are grateful to Dr. G. Barone (Department of Inorganic Chemistry, University of Palermo, Italy) for providing us with optimized structures of the multiple scattering units used in the EXAFS analysis. We gratefully acknowledge the Fonds der Chemischen Industrie for supporting our research.

[1] A. Lombardi, F. Nastri, V. Pavone, *Chem. Rev.* **2001**, *101*, 3165−3189.
[2] P. R. Ortiz de Montellano, *Cytochrome P450. Structure, Mechanism and Biochemistry*, 2nd ed., Plenum Press, New York, **1995**.
[3] T. L. Poulos, *Advances in Inorganic Biochemistry*, Elsevier, Amsterdam, **1988**, vol. 7.
[4] [4a] J. P. Collman, S. E. Groh, *J. Am. Chem. Soc.* **1982**, *104*, 1391−1403. [4b] B. Stäubli, H. Fretz, U. Piantini, W.-D. Woggon, *Helv. Chim. Acta* **1987**, *70*, 1173−1193. [4c] H. Aissaoui, S. Ghirlanda, C. Gmür, W.-D. Woggon, *J. Mol. Cat., A: Chem.* **1996**, *113*, 393−402. [4d] T. Higuchi, M. Hirobe, *J. Mol. Cat., A: Chem.* **1996**, *113*, 403−422. [4e] H. Patzelt, W.-D. Woggon, *Helv. Chim. Acta* **1992**, *75*, 523−530.
[5] C. Dietz, F. W. Heinemann, J. Kuhnigk, C. Krüger, M. Gerdan, A. X. Trautwein, A. Grohmann, *Eur. J. Inorg. Chem.* **1998**, 1041−1049.
[6] [6a] M. E. de Vries, R. M. LaCrois, G. Roelfes, H. Kooijman, A. L. Spek, R. Hage, B. L. Feringa, *Chem. Commun.* **1997**, 1549−1550. [6b] G. Roelfes, M. Lubben, K. Chen, R. Y. N. Ho, A. Meetsma, S. Genseberger, R. M. Hermant, R. Hauge, S. K. Mandal, V. G. Young, Jr., Y. Zang, H. Kooijman, A. L. Spek, L. Que, Jr., B. L. Feringa, *Inorg. Chem.* **1999**, *38*, 1929−1936.
[7] R. G. Shulman, Y. Yafet, P. Eisenberger, W. E. Blumberg, *Proc. Natl. Acad. Sci. USA* **1976**, *73*, 1384−1388.
[8] A. L. Roe, D. J. Schneider, R. J. Mayer, J. W. Pyrz, J. Widom, L. Que, *J. Am. Chem. Soc.* **1984**, *106*, 1676−1681.
[9] T. E. Westre, P. Kennepohl, J. G. DeWitt, B. Hedman, K. O. Hodgson, E. I. Solomon, *J. Am. Chem. Soc.* **1997**, *119*, 6279−6314.
[10] N. Binsted, R. W. Strange, S. S. Hasnain, *Biochemistry* **1992**, *31*, 12117−12125.
[11] W. Nam, R. Ho, J. S. Valentine, *J. Am. Chem. Soc.* **1991**, *113*, 7052−7054.
[12] J. T. Groves, T. E. Nemo, *J. Am. Chem. Soc.* **1983**, *105*, 5786−5791.
[13] X.-D. Du, X.-D. Yu, *J. Mol. Cat., A: Chem.* **1997**, *126*, 109−113.
[14] E. G. Samsel, K. Srinivasan, J. K. Kochi, *J. Am. Chem. Soc.* **1985**, *107*, 7606−7617.
[15] E. A. Stern, K. Kim, *Phys. Rev., B* **1981**, *23*, 3781−3787.
[16] R. F. Pettifer, C. Hermes, *J. Appl. Crystallogr.* **1985**, *18*, 404−412.

Received March 8, 2002
[I02121]

Manganese Oxidation Catalysts with 2-(2′-Hydroxyphenyl)oxazoline Ligands: Catalyst Intermediates and Degradation Products − Crystal Structure of Bis[{2-(2′-oxazolinyl)phenolato}bis(1-methylimidazole)manganese(III)] Perchlorate

Marcel Hoogenraad,[a] Huub Kooijman,[b] Anthony L. Spek,[b] Elisabeth Bouwman,[a] Jaap G. Haasnoot,[a] and Jan Reedijk*[a]

Keywords: Catalysis / Manganese / Mass spectrometry / Oxazolines / Oxidation

Manganese complexes with phox ligands [Hphox = 2-(2′-hydroxyphenyl)oxazoline] act as oxidation catalysts with dihydrogen peroxide. Their catalytic efficiency is strongly affected by the presence of a base, such as 1-methylimidazole (1-Meim). The crystal structure of an Mn–phox complex with two axial 1-Meim ligands, $[Mn(phox)_2(1\text{-}Meim)_2](ClO_4)$, is reported. The $[Mn(phox)_2]^+$ and $[Mn(phox)_2(1\text{-}Meim)]^+$ species have been detected in catalytic reaction mixtures by electrospray mass spectrometry. In the catalytic oxidation of styrene, turnover numbers of 428 and 456 have been obtained for styrene oxide in the presence of $[Mn(phox)_3]$ and of $[Mn(5'\text{-}NO_2phox)_3]$, respectively. During these reactions, catalyst degradation occurs, and is the main obstacle to obtaining higher turnover numbers. GC-MS analysis of the degradation products of $[Mn(5'\text{-}Clphox)_3]$ after catalytic reactions indicates that the oxazoline group is decomposed. The same decomposition products are also observed with electrospray mass spectrometry at higher ionisation potentials.
(© Wiley-VCH Verlag GmbH, 69451 Weinheim, Germany, 2002)

Introduction

Oxidations are versatile reactions for the synthesis of various fine chemicals and pharmaceuticals.[1] Traditionally, these reactions are performed with stoichiometric amounts of inorganic oxidants such as chromium or manganese oxides. However, the use of such reagents is environmentally unacceptable and there is an increasing demand for clean synthetic methods.[2,3] A very attractive method for oxidation reactions is the use of manganese catalysts with clean and cheap oxidants such as molecular oxygen or dihydrogen peroxide. Various manganese complexes with, for example, substituted tacn (1,4,7-triazacyclononane), porphyrin, salen [H_2salen = bis(salicylidene)ethylenediamine] or phox [Hphox = 2-(2′-hydroxyphenyl)oxazoline] ligands, have successfully been used in oxidation reactions and bleaching processes with dihydrogen peroxide.[4,5] In most reactions with these complexes, however, catalyst degradation results in loss of catalytic activity. Catalyst degradation is often a problem in oxidation catalysis,[6] and provision of increased stability in the manganese catalysts is therefore of great interest. A significant increase in stability has been accomplished by modification of the ligands. For instance, the introduction of halogen or nitro groups onto porphyrin catalysts results in a higher resistance towards oxidative degradation.[7] Similarly, the stability, and thus the catalytic efficiency, of Mn−salen complexes (or Jacobsen−Katsuki catalysts) has been reported to be improved by introduction of electron-withdrawing nitro substituents,[8] although in catalysed asymmetric epoxidation reactions this change results in significantly lower enantiomeric excesses (*ee*s) in the epoxides.[9] Alternatively, the addition of *N*-oxides[10] or, for reactions with dihydrogen peroxide,[11] of bases improves the catalytic efficiency without significantly reducing the *ee*s of the products. A base effect[12] and a substituent effect[13] have also been found for oxidations catalysed by the Mn−phox complexes. The didentate Hphox ligands, like the salen ligands, have a mixed N,O-donor set and are readily accessible. They are also known to be more stable to hydrolysis than the salen ligands.[14] However, the Mn−phox complexes also show a loss of catalytic activity over time during oxidation reactions.

The reactions causing the degradation of the complexes with the salen and similar phox ligands are not yet clearly understood. Dual-mode EPR spectroscopy has been used to gain insight into the mechanism of catalyst degradation of Mn−salen epoxidation catalysts.[15] This paper reports studies of the Mn−phox complexes during oxidation reac-

[a] Leiden Institute of Chemistry, Gorlaeus Laboratories, Leiden University,
P. O. Box 9502, 2300 RA Leiden, The Netherlands
Fax: (internat.) + 31-71/527-4671
E-mail: reedijk@chem.leidenuniv.nl
[b] Bijvoet Centre for Biomolecular Research, Crystal and Structural Chemistry, Utrecht University,
Padualaan 8, 3584 CH Utrecht, The Netherlands

tions, showing the effect of the reaction conditions on the catalytic efficiency, and the identification of various catalyst intermediates and degradation products.

Results and Discussion

Molecular Structure of $[Mn(phox)_2(1\text{-}Meim)_2](ClO_4)$

X-ray analysis of $[Mn(phox)_2(1\text{-}Meim)_2](ClO_4)$ (1-Meim = 1-methylimidazole) shows two similar independent molecules present in the unit cell, with $Z = 2$.

The structure of these molecules consists of a C_i-symmetric manganese(III) ion with two phox ligands *trans*-coordinated in the equatorial plane and two monodentate axial 1-Meim ligands (Figure 1), together with a noncoordinating perchlorate anion. Selected bond lengths and angles are given in Table 1.

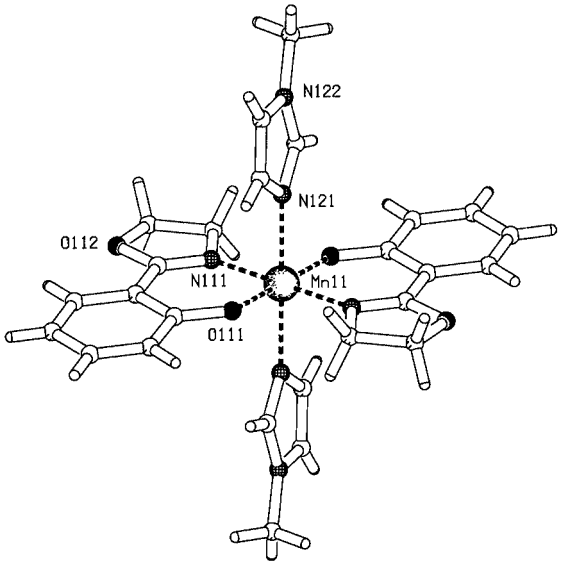

Figure 1. PLATON projection of the structure of one of the $[Mn(phox)_2(1\text{-}MeIm)_2]^+$ ions

Table 1. Selected bond lengths [Å] and angles [°] of one of the molecules of $[Mn(phox)_2(1\text{-}MeIm)_2](ClO_4)_2$; symmetry operation: $'$: $-x, -y, 1 - z$

Mn11−O111	1.867(2)	Mn11−N121	2.235(3)
Mn11−N111	2.045(3)		
O111−Mn11−N111	90.59(11)	O111−Mn11−N121′	89.88(10)
O111−Mn11−N111′	89.41(11)	N111−Mn11−N121	89.40(10)
O111−Mn11−N121	90.12(10)	N111−Mn11−N121′	90.60(10)

The differences in the ligand-to-metal bond lengths between the independent units are within 0.03 Å, while the differences in the bond angles are within 0.06°. The axial bonds of 2.235(3) (Mn1−N121) and 2.261(3) Å (Mn2−N221) are longer than the coordination bonds between the manganese ion and the phox ligands, as is to be expected for a Jahn−Teller-distorted d^4 ion. The Mn1−O111 and Mn−O211 bond lengths are similar to the bond lengths found in the $[Mn(phox)_2(MeOH)_2]^+$ units of the other Mn−phox complexes,[16] while the bonds of the manganese ion to the oxazoline nitrogen atoms are slightly longer.

Manganese(III) complexes with similar N_4O_2 coordination have been characterised for various Mn−salen complexes with pyridine molecules as axial ligands.[17] The main differences are the longer axial coordination bonds (between 2.30[18] and 2.48 Å[19]) for these complexes, as compared to $[Mn(phox)_2(1\text{-}Meim)_2](ClO_4)$. A manganese(III) complex with two axially coordinated imidazole groups from 1,4-di(1-imidazolyl)butane has been synthesised; in this case the two imidazole groups of one ligand coordinate to different manganese atoms, resulting in a network structure.[20] The bond lengths of the Mn−N bonds in this complex (2.28 and 2.29 Å) are only slightly longer than those in $[Mn(phox)_2(1\text{-}Meim)_2](ClO_4)$.

Catalysis

The solvent employed has a large effect on $[Mn(phox)_3]$-catalysed oxidation reactions;[13] the most interesting solvents were found to be methanol and acetone. The catalytic efficiency in the reactions in acetone (similarly to that in the reactions in methanol[12]) is increased by the addition of a base such as 1-Meim. In acetone, however, much higher turnover numbers have been obtained. It has been proposed that an acetone adduct of dihydrogen peroxide would be formed under these conditions, and that this would slowly release dihydrogen peroxide during the reaction,[21] although the adduct itself might also act as the actual oxidant. Gas evolution due to dihydrogen peroxide decomposition is visible during the reactions in acetone, and hydrogen peroxide decomposition is the limiting factor for these reactions. In methanol, ligand degradation limits the cumulative turnover numbers; after 15 min, hydrogen peroxide is still present and activity can be restored by addition of fresh quantities of the ligand. The amounts of dihydrogen peroxide used were varied to study the result on the turnover numbers, as well as the efficiency, relative to the oxidant (Table 2).

The results in Table 2 clearly show that the use of only 2.1 mmol of dihydrogen peroxide (10% of the standard amount) already results in a turnover number of 22 in methanol, an efficiency of 14.7% relative to dihydrogen peroxide. With larger amounts of dihydrogen peroxide, the turnover numbers level off, with a concomitant decrease in the efficiency based on the oxidant. This efficiency and the turnover number can be slightly increased by slow addition of the oxidant (five times 4.2 mmol in 15 min), resulting in a turnover number of 40 towards styrene oxide (efficiency of 2.7% based on H_2O_2) and of 4 towards benzaldehyde.

In acetone, contrary to the situation in methanol, an increase in the amount of oxidant from 5.3 mmol to 21 mmol results in a significant increase in the turnover numbers. The highest efficiency (15.8%) towards the oxidant is obtained on addition of 15.8 mmol of dihydrogen peroxide. At higher amounts of the oxidant, added at once, the turnover

Table 2. Effect of the amount of 1-Meim and dihydrogen peroxide on the turnover numbers and efficiency towards H_2O_2 in the [Mn(phox)$_3$]-catalysed oxidation of styrene

1-Meim Amount [mmol]	H_2O_2 Amount [mmol]	Turnover numbers towards styrene oxide[a] Methanol	Acetone	Yield of styrene oxide based on H_2O_2 (%) Methanol	Acetone
0.0	21.0	4	9	0.3	0.6
2.0	2.1	22	3	14.7	2.0
2.0	5.3	33	16	8.7	4.2
2.0	10.5	33	104	4.4	13.9
2.0	15.8	34	178	3.0	15.8
2.0	21.0	34	220	2.3	14.7
2.0	21.0[b]	40	n.d.	2.7	n.d.
2.0	4 × 21.0[c]	34	428	0.6	7.1

[a] Reactions in methanol were carried out with stirring by dissolving [Mn(phox)$_3$] (14 μmol) in methanol (20 mL) at room temperature; subsequently, the substrate (14 mmol), 1-MeIm (2.0 mmol) and the indicated amount of dihydrogen peroxide were added (t = 0); turnover numbers are the total turnover numbers at t = 15 min; reactions in acetone were carried out by stirring acetone (10 mL) and the indicated amount of dihydrogen peroxide at 0 °C for 30 min; subsequently, the substrate (14 mmol), 1-MeIm (2.0 mmol) and [Mn(phox)$_3$] (14 μmol) were added (t = 0); turnover numbers are the total turnover numbers at t = 15 min. [b] Slow addition of the oxidant (five times 4.2 mmol in 15 min); n.d. = not determined. [c] 21.0 mmol was added before the reaction; additional amounts of 21.0 mmol of the oxidant, dissolved in 5 mL of acetone, were added, at t = 15, 30 and 45 min.

numbers appear to reach a maximum. It may be that a maximum activity is found at a certain dihydrogen peroxide concentration, or it may indicate that by this time most of the extra dihydrogen peroxide added is decomposed into water and dioxygen. In contrast to the reactions in methanol,[12] the catalytic activity could not be restored by addition of fresh Hphox ligand. Subsequent addition of extra dihydrogen peroxide instead of the ligand, however, results in an increase in the total turnover number. After three consecutive additions of quantities of 21 mmol of dihydrogen peroxide in 5 mL of acetone at t = 15, 30, and 45 min (by which time the solution had turned colourless), a turnover number of up to 428 was obtained. The addition of even more dihydrogen peroxide did not result in any further increase in the turnover number, but gas evolution still continued. To regain catalytic epoxidation activity at this point, addition of fresh Hphox ligand appeared to be necessary, indicating that the catalyst had been degraded by this time.

Higher turnover numbers have been obtained with the more stable [Mn(5′-NO_2phox)$_3$] catalyst, similarly to the case of the reactions in methanol.[13] For [Mn(5′-NO_2phox)$_3$], the obtained turnover number of 456 towards styrene oxide obtained for the reaction in acetone (4×21 mmol H_2O_2) corresponds to a yield of 46% relative to styrene. The addition of extra dihydrogen peroxide increases the turnover numbers, but lowers the efficiency relative to the oxidant to 7.1% (reaction with [Mn(phox)$_3$]) and 7.6% (reaction with [Mn(5′-NO_2phox)$_3$]).

Catalyst Degradation

The major obstacle to the obtainment of higher turnover numbers in the Mn−phox-catalysed oxidation reactions is catalyst degradation. It has been reported that the decrease in catalytic activity during the reactions in methanol coincides with a change in the original green colour of the solution to pale yellow or colourless and the appearance of a manganese(II) EPR signal, while the addition of fresh free ligand results in regeneration both of the green solution and of the catalytic activity, indicating that the ligand decomposes during the catalytic reactions.[12] Similarly, the appearance of the manganese(II) EPR signal and decolouration of the solution also occur for the reactions in acetone, although loss of the catalytic activity due to catalyst degradation and the related decolouration of the solution both proceed less quickly (45 min) than in methanol (15 min, see above).

ES-MS studies were performed during the oxidation of styrene with [Mn(phox)$_3$] and [Mn(5′-NO_2phox)$_3$] in methanol and in acetone. In the absence of the oxidant, the main fragments detected for the [Mn(phox)$_3$] and [Mn(5′-NO_2phox)$_3$] complexes (both in the methanol and in the acetone solutions) are the $[MnL_2]^+$ and the $[MnL_2(1\text{-Meim})]^+$ ions. These two fragments may originate from species of the type $[MnL_3]$ or $[MnL_2L'_xL''_y]^+$ (with L′ and L″ being, for instance, 1-methylimidazole or solvent molecules) after dissociation of one or two coordinating groups. After addition of dihydrogen peroxide, the $[MnL_2]^+$ and $[MnL_2(1\text{-Meim})]^+$ fragments are still the most important species observed in

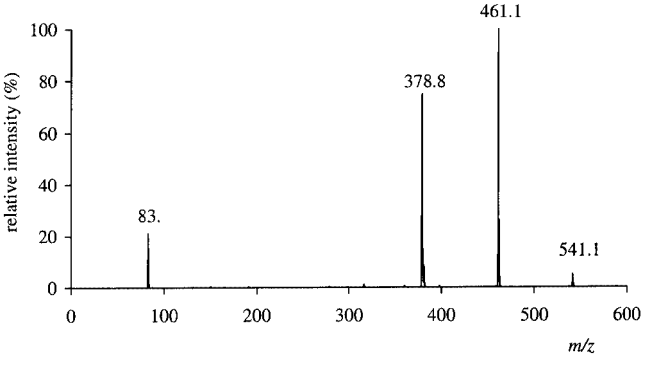

Figure 2. Electrospray mass spectrum at the start (t = 1 min) of the oxidation of styrene with [Mn(phox)$_3$] and dihydrogen peroxide in methanol: m/z = 83.0 [1-MeIm + H^+], 378.8 $[Mn(phox)_2]^+$, 461.1 $[Mn(phox)_2(1\text{-MeIm})]^+$, 541.1 $[Mn(phox)_3]^+$

both solvents during the first minutes of the reaction (Figure 2).

A few minutes after the start of the reaction, the ES-MS spectra of all reaction mixtures show decreases in the intensities of the $[MnL_2]^+$ and $[MnL_2(1\text{-Meim})]^+$ peaks. In these spectra, the parent peak originates from the [1-Meim + H^+] fragment, while various other peaks of low intensity are also present; these could not be clearly assigned. In mass spectra of reaction mixtures taken towards the end of all reactions, only various small peaks are observed. Apart from the peaks already assigned, no other peaks that could be clearly assigned to a manganese-containing species or a ligand degradation product have been observed.

In order to try to identify the ligand degradation products, catalysis experiments were performed. During these, an excess of fresh ligand (2×30 equiv. with respect to Mn) was added. GC-MS analysis of the oxidation products of H-5′-Clphox in an ethanol/methanol solution showed nearly quantitative conversion of the ligand. The main product appeared to be 5-chlorosalicylic acid; the secondary products methyl 5-chlorosalicylate and ethyl 5-chlorosalicylate, which are due to the acidic alcoholic conditions used for GC-MS, are also observed. The formation of these products indicates degradation of the catalyst at the oxazoline moiety. No traces of derivatives of the $-NCH_2CH_2-$ part of the oxazoline group were found.

Further indications that the oxazoline group is the part of the ligand most susceptible towards degradation are obtained by analysis of the ES-MS spectra of the pure $[Mn(5'\text{-Clphox})_3]$, $[Mn(phox)_3]$ and $[Mn(phox)_2(MeOH)_2]$-$[Mn(phox)_2(ClO_4)_2](H_2O)_2$ complexes. With a +70 V nozzle ionisation potential, the main fragments observed are the $[MnL_2]^+$ and the $[HL + H]^+$ fragments. Additional information can be obtained by use of other ionisation potentials. For $[Mn(5'\text{-Clphox})_3]$, $[Mn(phox)_3]$ and $[Mn(phox)_2(MeOH)_2][Mn(phox)_2(ClO_4)_2](H_2O)_2$, the application of a +170 V nozzle ionisation potential results in mass spectra showing fragments that might be related to catalyst degradation products. In the mass spectra of $[Mn(phox)_3]$ and $[Mn(phox)_2(MeOH)_2][Mn(phox)_2(ClO_4)_2](H_2O)_2$ (Figure 3), the $[Mn(phox)_2]^+$ fragments can be observed at m/z = 379.0. The mass difference of m/z = 42.2 between this signal and the signal at m/z = 336.8 corresponds to the loss of an $-NCH_2CH_2-$ fragment. A small signal at m/z = 121.0, corresponding to the $(Ar-C=O)^+$ fragment (see Figure 4) of a decomposed ligand, can also be observed.

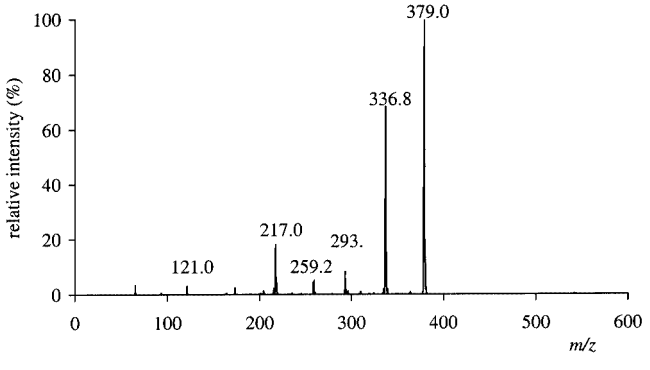

Figure 3. Ligand degradation observed in the electrospray mass spectrum of $[Mn(phox)_2(MeOH)_2][Mn(phox)_2(ClO_4)_2](H_2O)_2$ at a 170 V nozzle ionisation potential: m/z = 121.0 $[Ar\text{-}C=O]^+$, 217.0 $[Mn(phox)]^+$, 259, 293 unidentified, 336.8 $[Mn(phox)(Ar-C=O)]^+$, 379.0 $[Mn(phox)_2]^+$

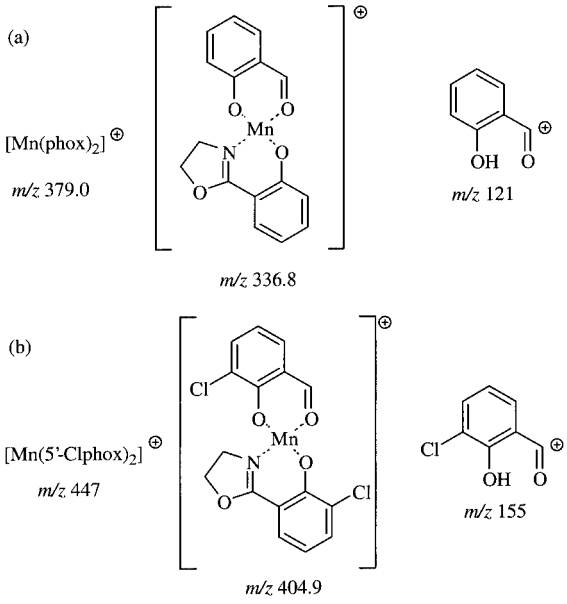

Figure 4. Schematic overview of degradation products (with m/z) observed in the ES-MS spectra of: (a) $[Mn(phox)_3]$, (b) $[Mn(5'\text{-Clphox})_3]$

A similar complex degradation pattern is found in the mass spectrum of $[Mn(5'\text{-Clphox})_3]$. The degradation of the $[MnL_2]^+$ fragment (m/z = 447.0) results in the $[Mn(5'\text{-Clphox})(Ar-C=O)]^+$ ion, which is clearly observed at m/z = 404.9. The isotope pattern of the latter fragment confirms the presence of two chlorine atoms. The $(Ar-C=O)^+$ fragment in this mass spectrum is observed at m/z = 155 (Figure 4). The reaction of the $(Ar-C=O)^+$ fragment, found in the ES-MS measurements, with water or an alcohol results in salicylic acid or one of its esters, which are the ligand decomposition products identified after the oxidation reaction with $[Mn(5'\text{-Clphox})_3]$ and excess of the H-5′-Clphox ligand (see above). Fragments containing the $-NCH_2CH_2-$ part of the oxazoline group were not identified.

The $\{[MnL_2]^+ - 42\}$ fragment is present with higher relative intensities in the mass spectra of $[Mn(phox)_2(MeOH)_2][Mn(phox)_2(ClO_4)_2](H_2O)_2$ and $[Mn(phox)_3]$ than in the spectra of $[Mn(5'\text{-Clphox})_3]$. In the mass spectrum of $[Mn(5'\text{-}NO_2phox)_3]$, no such signal is observed at all. In the reactions in methanol, $[Mn(5'\text{-}NO_2phox)_3]$ remains active for a longer time than the other catalysts.[12] This indicates that the complexes containing Hphox ligands with electron-withdrawing substituents are more resistant towards oxidative degradation, which is similar to the trend found for manganese complexes with porphyrin[7] and Mn−salen[8] ligands.

Conclusion

The most important reactions occurring during oxidation catalysis with the Mn−phox complexes are substrate oxidation, dihydrogen peroxide decomposition and catalyst degradation. The choice of the catalyst and the reaction conditions have considerable influence on all these reactions and therefore also on the catalyst efficiency. For instance, the addition of a base such as 1-Meim to the reaction mixtures is required to improve the catalytic efficiency. 1-Meim can coordinate to the manganese complex, as shown by the crystal structure of $[Mn(phox)_2(1\text{-}Meim)_2](ClO_4)$. The presence of $[Mn(phox)_2(1\text{-}Meim)]^+$ species during the catalytic reactions has been observed with ES-MS. Furthermore, coordination of 1-Meim significantly influences the electrochemical properties of the complexes containing the $Mn(phox)_2$ unit, as indicated by the changes in the cyclic voltammograms.[16] Therefore, the higher catalytic efficiency observed in the presence of 1-Meim is likely to be caused by coordination of 1-Meim to manganese atoms, thus resulting in a more active or stable catalyst.

In the reactions in acetone, oxygen evolution caused by dihydrogen peroxide decomposition is visible. Upon addition of extra dihydrogen peroxide, higher turnover numbers can be obtained in styrene oxidation, but the efficiency relative to dihydrogen peroxide is decreased. Despite the addition of extra dihydrogen peroxide, the reactions finally cease completely because of catalyst degradation, and the maximum turnover numbers obtained are 428 with $[Mn(phox)_3]$ and 456 with $[Mn(5'\text{-}NO_2phox)_3]$ as catalysts.

Changes in the solvent used or the addition of a base notwithstanding, the catalytic reactions cease in the end due to ligand degradation, which is the main obstacle to obtaining high turnover numbers. The decolouration of the reaction solution, and the appearance of an Mn^{II} EPR signal coincide with decreasing catalytic activity.[12] In methanol, the activity could easily be regenerated by addition of fresh Hphox ligand, which simultaneously restored the green colour of the solution. ES-MS measurements and analysis of the oxidation products of H-5′-Clphox indicate that the oxazoline group is the part of the Mn−phox catalysts most susceptible towards oxidative degradation. The introduction of a nitro substituent resulted in a more stable catalyst, as shown by the catalytic experiments and the ES-MS studies. The higher catalytic efficiency and the prolonged catalytic activity of $[Mn(5'\text{-}NO_2phox)_3]$ in styrene oxidation in methanol[13] directly reflects higher stability of the catalyst, as shown by electrochemistry (the irreversible oxidation of $[Mn(5'\text{-}NO_2phox)_3]^+$ occurs at the highest potentials)[13] and ES-MS, which is in accordance with the disappearance of the green colour being slower than in the reactions with the other catalysts. These results indicate that the introduction of strongly electron-withdrawing substituents decreases the susceptibility of the oxazoline group towards degradation. The first step of ligand degradation is presumably an oxidation reaction. In the literature, decomposition of oxazoline groups has been reported in reactions with the oxidants *m*-chloroperbenzoic acid (*m*-CPBA)[22] and sodium hypochlorite.[23] The oxidation products may be the oxaziridine and the oxazoline *N*-oxide,[22] with the ring still intact, as well as ring-opening products such as various esters,[22,23] which have also been found after oxidation of the excess H-5′-Clphox, indicating that similar oxazoline degradation reactions occur.

As shown in this study, Mn−phox- and Mn−salen-catalysed oxidation reactions with hydrogen peroxide have similar characteristics. Examples are the decolouration of the reaction solutions, the beneficial effect of the addition of bases on the catalytic efficiency and the increased stability upon introduction of electron-withdrawing substituents. Two oxidative conversions of Mn−salen complexes have been reported. Treatment of an Mn−salen complex in pyridine with dioxygen resulted in the oxidation of one imine group to an amide,[24] while complex degradation by visible light photolysis resulted in 2-(2′-hydroxyphenyl)benzimidazole, salicylaldehyde and a manganese(II) ion.[25] The products formed in the latter reaction, salicylaldehyde and manganese(II), are similar to the observed Mn−phox degradation products after the oxidation reactions. These results emphasise that for the Mn−phox complexes, the oxazoline group is the most oxidation-sensitive, while it is indicated that the imine group is the most sensitive position of the Mn−salen catalysts. Replacement of these groups should therefore be required to enhance the catalyst stability and indeed, for a similar catalyst system, the replacement of an imine by a tertiary amine group has resulted in a significantly more stable catalyst.[26] Given the potential of the Mn−salen complexes as asymmetric (ep)oxidation catalysts, further studies of stabilisation of these complexes are of paramount importance.

Experimental Section

General Remarks: All manganese complexes were synthesised by published procedures.[12,13,16] Solvents were used as technical grade, p.a. grade or, for acetonitrile, as HPLC grade (Rathburn) and, unless noted otherwise, were used as received. All p.a. grade solvents were purchased from Baker, except for acetone (Acros). Dihydrogen peroxide (35% in water) and styrene were supplied by Merck, all other chemicals used were obtained from Acros.

Equipment: A Varian Star 3400CX gas chromatograph with a J&W Scientific/Fisons DB-1701 (14% cyanopropylphenyl-methylpolysiloxane) column was used for analysis of the oxidation experiments. UV/Vis/NIR measurements were performed with a Perkin−Elmer Lambda 900 UV/Vis/NIR spectrometer. EPR measurements were performed at 77 K with a Jeol Esprit RE-2X spectrometer with a Jeol Esprit 330 ESRE data system. EPR *g* values were determined relative to DPPH as an external "*g*-mark" (g = 2.0037). GC-MS analysis of the ligand degradation products was recorded with a Finnigan MAT ITD 700 (EI mode) coupled with a Hewlett−Packard 438a GC. Electrospray mass spectra at higher ionisation potentials and before and during the oxidation reactions were performed at the Pharmacy department of the University of Groningen and were recorded with a NERMAG R 3010 triple quadrupole mass spectrometer equipped with an in-house atmospheric pressure ionisation source and ion spray interface.[27,28] The

PE-Sciex API 3 data system with an in-house and digital interface was used for data acquisition and data processing.

Catalysis: The catalytic reactions were carried out in methanol and in acetone, usually with a catalyst/substrate/oxidant ratio of 1:1000:1500. All flasks and stirrer bars used were thoroughly cleaned with acid to remove traces of metal, after which they were washed with an aqueous sodium carbonate solution. The turnover numbers given are the total turnover numbers per manganese ion after the indicated period of time. All reactions were performed at least in duplicate. ***Caution!*** The combination of acetone and dihydrogen peroxide is potentially explosive, especially under acidic conditions.[29] However, it can be handled safely by performing reactions on a small scale at 0 °C under slightly alkaline conditions, as used in the experiments described below.

In Methanol: The catalyst (14 μmol) was dissolved with stirring in 20 mL of methanol at room temperature. Styrene (14 mmol), chlorobenzene (5.0 mmol) and 1-methylimidazole (1-Meim, 2.0 mmol) were added to the resulting green solution, followed (at $t = 0$ min) by dihydrogen peroxide (35% in water, 21 mmol). Except for the reaction mixture with [Mn(5′-NO_2phox)], which slowly started to turn pale yellow after $t = 10$ min, the colours of the reaction mixtures changed to slightly yellow to colourless within the first few minutes of the reactions. At $t = 15$ min, a sample was taken and analysed by gas chromatography, with chlorobenzene as the internal standard.

In Acetone: Dihydrogen peroxide (35% in water, 21 mmol) and acetone (10 mL) were stirred for 30 min at 0 °C. Next, styrene (14 mmol), chlorobenzene (5.0 mmol) and 1-Meim (2.0 mmol) were added, followed by the powdered catalyst (14 μmol, $t = 0$). The green solution became slightly red-brown within the first few minutes of the reactions. After 10 min, the solution slowly turned pale green-yellow. At $t = 15$ min, a sample was taken and analysed by gas chromatography, with chlorobenzene as the internal standard.

Addition of Extra Dihydrogen Peroxide to the Oxidation of Styrene with [Mn(phox)$_3$] and [Mn(5′-NO_2phox)$_3$]: Dihydrogen peroxide (35% in water, 21 mmol) and acetone (10 mL) were stirred for 30 min at 0 °C. Styrene (14 mmol) and 1-Meim (2.0 mmol) were then added, followed by [Mn(phox)$_3$] (14 μmol, $t = 0$ min). At $t = 15$ min, a sample was taken from the pale green-yellow solution and analysed by gas chromatography, with chlorobenzene as the internal standard. Subsequently, 5 mL of a solution of dihydrogen peroxide (42 mmol) in acetone (20 mL), which had been stirring for 30 min at 0 °C, was added. At $t = 30$ and 45 min, a sample was taken for analysis, after which an additional 5 mL of the dihydrogen peroxide solution was added. At this time, the solution had turned almost colourless to pale yellow. A final sample was taken at $t = 60$ min.

Oxidation of the H-5′-Clphox Ligand: [Mn(5′-Clphox)$_3$] (14 μmol) was dissolved at room temperature, with stirring, in a mixture of methanol (10 mL) and ethanol (10 mL). Styrene (1.4 mmol) was added to this green solution, followed by dihydrogen peroxide (35% in water, 21 mmol). After 15 min, during which the solution turned from green to colourless, a sample was taken and analysed by gas chromatography, with chlorobenzene as the internal standard. Next, H-5′-Clphox (0.42 mmol) was added, resulting in the regeneration of the green color of the reaction solution. Samples were taken each 15 min and were analysed by gas chromatography, with chlorobenzene as the internal standard. The H-5′-Clphox peak could be clearly detected. The reaction was monitored over time by gas chromatography until the solution had become almost colourless and most of the ligand had disappeared. Further H-5′-Clphox (0.42 mmol) and dihydrogen peroxide (21 mmol) were added. After disappearance of most of the ligand, a sample was taken and analysed by GC-MS.

Electrospray Mass Spectrometry: Electrospray mass spectra of [Mn(phox)$_3$], [Mn(5′-phox)$_3$], [Mn(5′-NO_2phox)$_3$] and [Mn(phox)$_2$-(MeOH)$_2$][Mn(phox)$_2$(ClO_4)$_2$](H_2O)$_2$ were recorded in methanol and acetone, both in the absence and in the presence of water and/or 1-Meim. Mass spectra were also recorded on samples taken during the oxidation of styrene with [Mn(phox)$_3$] or [Mn(5′-NO_2-phox)$_3$] and dihydrogen peroxide. For these reactions, the standard conditions in methanol and acetone were used, with exception of the use of 10.5 mmol of dihydrogen peroxide instead of 21 mmol.

X-ray Data Collection and Structure Determination of [Mn(phox)$_2$(1-Meim)$_2$](ClO_4): The data were collected with an Enraf−Nonius Kappa CCD area detector on a rotating anode, with graphite-monochromated Mo-K_α radiation ($\lambda = 0.71073$ Å). The crystallographic data of the complex are presented in Table 3. The unit cell parameters were checked for the presence of lattice symmetry.[30] The structures were solved by automated direct methods (SHELXS-86).[31] Refinement on F^2 was carried out by full-matrix, least squares (SHELXL-97-2).[32] Neutral atom scattering factors and anomalous dispersion corrections were taken from the International Tables for Crystallography.[33] Geometrical calculations and illustrations were performed with PLATON.[34] All calculations were performed with a DEC Alpha 255. Hydrogen atoms were included in the refinement on calculated positions riding on their carrier atoms. All non-hydrogen atoms were refined with anisotropic thermal parameters; hydrogen atoms were refined with a fixed isotropic thermal parameter related to the value of the equivalent isotropic displacement parameter of their carrier atoms. CCDC-181805 contains the supplementary crystallographic data for this paper. These data can be obtained free of charge at www.ccdc.cam.ac.uk/conts/retrieving.html or from the Cambridge Crystallographic Data Centre, 12, Union Road, Cambridge CB2 1EZ, UK [Fax: (internat.) + 44-1223/336-033; E-mail: deposit@ccdc.cam.ac.uk].

Table 3. Crystallographic data for [Mn(phox)$_2$(1-MeIm)$_2$](ClO_4)

Empirical formula	$C_{26}H_{28}ClMnN_6O_8$
Formula mass	642.93
Crystal dimensions [mm]	0.06 × 0.20 × 0.30
Crystal system	triclinic
Space group	$P\bar{1}$ (no. 2)
a [Å]	8.5401(10)
b [Å]	9.6127(15)
c [Å]	19.153(3)
α [°]	83.522(7)
β [°]	89.034(8)
γ [°]	65.008(7)
Cell volume [Å^3]	1415.2(4)
Z	2
F(000)	664
$D_{calcd.}$ [g·cm^{-3}]	1.5088(4)
μ(Mo-K_α) [mm^{-1}]	0.62
T [K]	150
No. of measured reflections	17005
No. of independent reflections	5013
R_{int}	0.060
R	0.053 {for 4302 [$F_o > 4\sigma(F_o)$]}
wR_2	0.138
S	1.08
No residual density outside [e·Å^{-3}]	−0.52, 0.89 (near Mn)

Acknowledgments

This work was carried out as part of the Innovation Oriented Research Programme on Catalysis (IOP Katalyse, no. IKA94056) sponsored by the Netherlands Ministry of Economic Affairs. This work was supported in part (A. L. S.) by the Council for Chemical Sciences of the Netherlands Organisation for Scientific Research (CW-NWO). We would like to acknowledge Mrs. C. M. Jeronimus-Stratingh and Dr. A. P. Bruins (Pharmacy Department, University of Groningen) for performing the ES-MS measurements and Dr. J. G. de Vries (DSM, The Netherlands) and Dr. R. Hage (Unilever, The Netherlands) for useful discussions.

[1] R. A. Sheldon, *ChemTech* **1991**, 566−576.
[2] W. F. Hoelderich, F. Kollmer, *Pure Appl. Chem.* **2000**, *72*, 1273−1287.
[3] W. R. Sanderson, *Pure Appl. Chem.* **2000**, *72*, 1289.
[4] G. B. Shul'pin, G. Suss-Fink, L. S. Shul'pina, *J. Mol. Catal., A* **2001**, *170*, 17−34.
[5] T. Katsuki, *Adv. Synth. Catal.* **2002**, *344*, 131−147.
[6] T. J. Collins, *Acc. Chem. Res.* **1994**, *27*, 279−285.
[7] A. M. d'A. Rocha Gonsalves, M. M. Pereira, *J. Mol. Catal., A* **1996**, *113*, 209−221.
[8] K. Srinivasan, P. Michaud, J. K. Kochi, *J. Am. Chem. Soc.* **1986**, *108*, 2309−2320.
[9] M. Palucki, N. S. Finney, P. J. Pospisil, M. L. Güler, T. Ishida, E. N. Jacobsen, *J. Am. Chem. Soc.* **1998**, *120*, 948−954.
[10] K. Miura, T. Katsuki, *Synlett* **1999**, *37*, 783−785.
[11] P. Pietikäinen, *Tetrahedron Lett.* **1994**, *35*, 941−944.
[12] M. Hoogenraad, K. Ramkisoensing, H. Kooijman, A. L. Spek, E. Bouwman, J. G. Haasnoot, J. Reedijk, *Inorg. Chim. Acta* **1998**, *279*, 217−220.
[13] M. Hoogenraad, K. Ramkisoensing, S. Gorter, W. L. Driessen, E. Bouwman, J. G. Haasnoot, J. Reedijk, T. Mahabiersing, F. Hartl, *Eur. J. Inorg. Chem.* **2002**, 377−387.
[14] H. R. Hoveyda, V. Karunanatne, S. J. Rettig, C. Orvig, *Inorg. Chem.* **1992**, *31*, 5408−5416.
[15] K. A. Campbell, M. R. Lashley, J. K. Wyatt, M. H. Nantz, R. D. Britt, *J. Am. Chem. Soc.* **2001**, *123*, 5710−5719.
[16] M. Hoogenraad, K. Ramkisoensing, W. L. Driessen, H. Kooijman, A. L. Spek, E. Bouwman, J. G. Haasnoot, J. Reedijk, *Inorg. Chim. Acta* **2001**, *320*, 117−126.
[17] Y. Sunatsuki, M. Mimura, H. Shimada, F. Kai, N. Matsumoto, *Bull. Chem. Soc. Jpn.* **1998**, *71*, 167−173.
[18] R. G. Pritchard, C. A. McAuliffe, R. V. Parish, A. A. J. Nabhan, F. M. Ashmawy, A. Garcia-Deibe, A. Sousa, M. R. Bermejo, *Acta Crystallogr., Sect. C* **1991**, *47*, 2453−2454.
[19] K. Bertoncello, G. D. Fallon, K. S. Murray, *Inorg. Chim. Acta* **1990**, *174*, 57−60.
[20] N. Matsumoto, N. Takemoto, A. Ohyosi, H. Okawa, *Bull. Chem. Soc. Jpn.* **1988**, *61*, 2984−2986.
[21] D. E. De Vos, T. Bein, *J. Organomet. Chem.* **1996**, *520*, 195−200.
[22] M. Kobayakawa, Y. Langlois, *Tetrahedron Lett.* **1992**, *33*, 2353−2356.
[23] J. I. Levin, S. M. Weinreb, *Tetrahedron Lett.* **1982**, *23*, 2347−2350.
[24] E. Gallo, E. Solari, N. Re, C. Floriani, A. Chiesi-Villa, C. Rizzoli, *Angew. Chem. Int. Ed. Engl.* **1996**, *35*, 1981−1983.
[25] T. Fukuda, F. Sakamoto, M. Sato, Y. Nakano, X. S. Tan, Y. Fujii, *Chem. Commun.* **1998**, 1391−1392.
[26] R. M. La Crois, PhD thesis, University of Groningen, The Netherlands, **2000**.
[27] A. P. Bruins, C. Beaugrand, in *Proceedings of the 36th ASMS conference on mass spectrometry and allied topics*, **1988**, pp. 1241.
[28] A. P. Bruins, T. R. Covey, J. D. Henion, *Anal. Chem.* **1987**, *59*, 2642−2646.
[29] C. J. M. Stirling, *Chem. Br.* **1969**, *5*, 36.
[30] A. L. Spek, *J. Appl. Crystallogr.* **1988**, *21*, 578−579.
[31] G. M. Sheldrick, *SHELXS-86 Program for Crystal Structure Determination*, University of Göttingen, Germany, **1986**.
[32] G. M. Sheldrick, *SHELXL-97-2 Program for Crystal Structure Determination*, University of Göttingen, Germany, **1997**.
[33] *International Tables for Crystallography*, vol. C (Ed.: A. J. C. Wilson), Kluwer Academic Publishers, Dordrecht, **1992**.
[34] A. L. Spek, *PLATON, A multipurpose crystallographic tool*, Utrecht University, The Netherlands, **2002**; internet: http://www.cryst.chem.uu.nl/platon/

Received March 22, 2002
[I02156]

Syntheses and Crystal Structures of Five Cadmium(II) Complexes Derived from 4-Aminobenzoic Acid

Ruihu Wang,[a] Maochun Hong,*[a] Junhua Luo,[a] Rong Cao,*[a] Qian Shi,[a] and Jiabao Weng[a]

Keywords: Cadmium / Hydrogen bonds / N,O ligands / Supramolecular chemistry

Five cadmium(II) complexes, $[CdClL\cdot H_2O]_n$ (**1**), $[CdBrL\cdot H_2O]_n$ (**2**), $CdI_2(HL)_2$ (**3**), $\{[Cd(dca)_2(HL)_2]\cdot 2H_2O\}_n$ (dca^- = dicyanamide) (**4**), and $(H_2L)_2[CdCl_4(H_2O)_2]$ (**5**), have been synthesized by the reaction between 4-aminobenzoic acid (HL) and Cd^{2+}. In **1** and **2**, L^- serves as a tridentate ligand and bridges six-coordinate Cd^{II} centers to form $[Cd^{II}–L]_n$ chains; halide anions link adjacent chains into two-dimensional layers. Complex **3** is a typical metallic carboxylic acid synthon. In **3**, HL acts as a monodentate ligand coordinating to Cd^{II} through the nitrogen atom, and the head-to-tail hydrogen bonds of carboxylic groups result in a zigzag chain. The weak Cd···I interactions between adjacent chains extend the zigzag chain-like structure into a two-dimensional structure. Complex **4** consists of $[Cd(dca)_2(HL)_2]_n$ chains and free water molecules. The twelve-membered rings formed by water molecules and carboxylic groups through hydrogen bonds link the adjacent chains to yield a two-dimensional layer. Complex **5** consists of discrete $[CdCl_4(H_2O)_2]^{2-}$ anions and H_2L^+ organic cations, which are linked by intermolecular hydrogen-bonding interactions to form a three-dimensional structure.

(© Wiley-VCH Verlag GmbH, 69451 Weinheim, Germany, 2002)

Introduction

The design and synthesis of novel complexes with unusual and tailorable structures are fundamental steps for the discovery and fabrication of various functional supramolecular devices or technologically useful materials.[1] Recently, a great deal of attention has been paid to the design and construction of organic-inorganic hybrid frameworks from synthons or building blocks, owing to their fascinating structural diversity and promising potential application in chemistry, biology, and material science.[2,3] Coordination covalent bonds, hydrogen bonds, and combinations of the two have been powerful tools for linking synthons or building blocks into extended structural topologies;[2–5] likewise, organic counterions are frequently used as templating agents – based on their shape and hydrogen-bonding capability – to form frameworks such as perovskites.[6] Through careful selection of organic ligands with hydrogen-bonding functionalities, structural frameworks can be confidently established and predicted, and their physical properties, such as magnetic, optical, and electronic properties, can be controlled and tailored.[2,4–6] By the aforementioned synthetic methods, it is possible to prepare and modify complexes with different structural frameworks through control of synthetic conditions such as counterions, pH value, reaction temperature, solvent, template, and the ratio of metal/ligand.

In previous studies, we have synthesized a series of novel organic-inorganic hybrid complexes based on covalent bonds through the use of simple organic ligands such as pyridine-2-thiol and pyrimidine2-thiol.[7] Recently, we have extended our work by the selection of multifunctional organic ligands that may form both coordination covalent bonds and hydrogen bonds as synthons or building blocks. 4-Aminobenzoic acid (HL) has been extensively studied in coordination chemistry, thanks to the richness of its coordination modes (Scheme 1, **a–i**): 1) HL can act as a carboxylic acid synthon and also as a good monodentate ligand through the amine group.[8] 2) deprotonated 4-aminobenzoic acid (L^-) can act as a monodentate ligand through a carboxylate oxygen atom,[9] chelating and/or bridging ligands through its amide and/or carboxylate groups,[10,11] and 3) HL may be protonated to form organic cation templating agents. Previous reports showed that the association of d^{10}-configured cadmium(II) with HL resulted in two kinds of complexes, in which HL acts as a carboxylic acid synthon[8] and as a bridging ligand.[11] Our aim is to study self-assembly processes of Cd^{II}–HL complexes, especially the influence of co-ligand and reaction medium on the coordination behaviour of HL and thereby the structural topology of the complexes obtained. Here we report the syntheses and crystal structures of five cadmium complexes: $[CdClL\cdot H_2O]_n$ (**1**), $[CdBrL\cdot H_2O]_n$ (**2**), $CdI_2(HL)_2$ (**3**),

[a] State Key Laboratory of Structural Chemistry, Fujian Institute of the Research on the Structure of Matter, Chinese Academy of Sciences,
Fuzhou, Fujian 350002, China
Fax: (internat.) + 86-591/371-4946
E-mail: hmc@ms.fjirsm.ac.cn

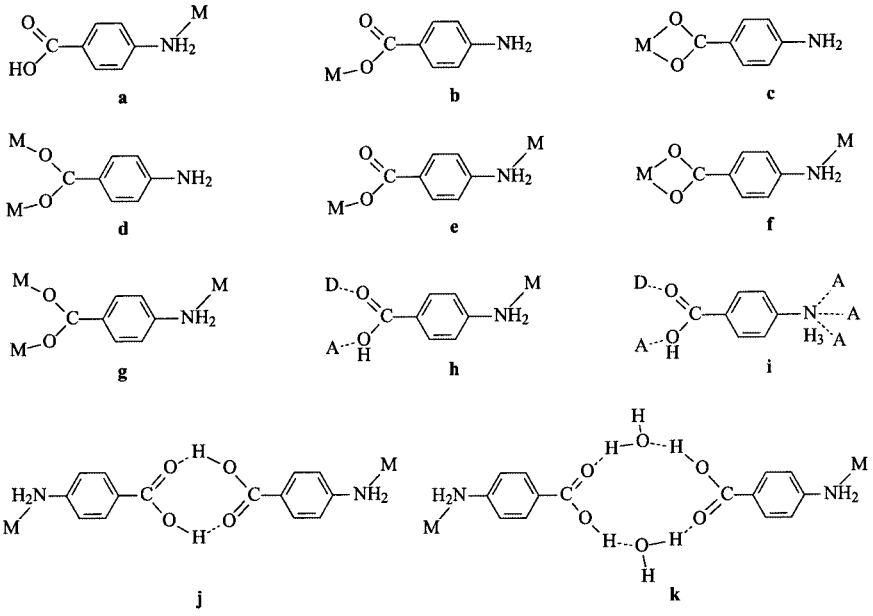

Scheme 1. Possible coordination modes of HL, L^- and H_2L^+; M = metal ion, A = hydrogen bond acceptor, D = hydrogen bond donor

$\{[Cd(dca)_2(HL)_2]\cdot 2H_2O\}_n$ (**4**), and $(H_2L)_2[CdCl_4(H_2O)_2]$ (**5**).

Results and Discussion

Syntheses and IR Spectra

Treatment of L^- with $CdCl_2\cdot 2.5H_2O$ and $CdBr_2\cdot 4H_2O$ in MeOH/H_2O (2:1) resulted in the formation of the corresponding mixed-anion cadmium(II) complexes **1** and **2**, respectively. However, treatment of L^- with CdI_2 under the same conditions failed to produce the expected complex containing mixed-anion ligands. Instead, a straightforward reaction between HL and CdI_2 in MeOH/H_2O (2:1) yielded a two-dimensional complex **3**, formed by head-to-head carboxylic acid hydrogen bonding (Scheme 1, **j**) and weak Cd···I interactions. The successful isolation of **3** prompted us to replace I^- with bridging ligands, such as SCN^-, dca^-, and N_3^-, in order to obtain layer complexes containing head-to-head carboxylic acid hydrogen bonds. Use of $Cd(NO_3)_2\cdot 6H_2O$, NH_4SCN, and HL in MeOH/H_2O (2:1) generated the expected complex $[Cd(SCN)_2(HL)_2]_n$,[8b] but employment of $Cd(NO_3)_2\cdot 6H_2O$, Na(dca), and HL in MeOH/H_2O (2:1) produced complex **4**, comprising twelve-membered rings made up of water molecules and carboxylic groups through hydrogen bonds (Scheme 1, **k**). Isolation of $[Cd(N_3)_2(HL)_2]_n$ from the reaction between $Cd(NO_3)_2\cdot 6H_2O$, NaN_3, and HL in EtOH/H_2O (2:1) was not successful; instead, HL was deprotonated by NaN_3 and a known compound $[(CdL_2\cdot H_2O)\cdot 2H_2O]_n$ [11] was obtained. As mentioned above, HL may be protonated to form an organic ammonium ion H_2L^+, which can act as an organic cation templating agent for perovskite complexes. When the reaction between $CdCl_2\cdot 2.5H_2O$ and HL was carried out in aqueous HCl solution, HL did accept a proton to form H_2L^+ and produced a perovskite-type complex **5**.

The IR spectra of complexes **1** and **2** confirm the presence of the carboxylate group, by the strong peaks at 1608 and 1398 cm^{-1} for **1** and at 1610, 1597, 1414 and 1402 cm^{-1} for **2**. The separations (Δ) between the antisymmetric stretching ν_{asym}(COO) and the symmetric stretching ν_{sym}(COO) are 210 cm^{-1} for **1**, and 197 and 195 cm^{-1} for **2**. The characteristic carboxylic acid group bands are observed at 1684, 1441, and 1423 cm^{-1} for **3** and at 1678, 1626, 1443 (m), and 1423 (m) cm^{-1} for **4**. Moreover, the IR spectrum in complex **4** displays a very strong absorption band at 2175 cm^{-1}, indicating the presence of C≡N in dca^-. The carboxylic group in complex **5** is characterized by the presence of strong peaks at 1701 and 1678 cm^{-1} for antisymmetric stretching and at 1487 and 1433 cm^{-1} for symmetric stretching. Several strong bands in the 3550 to 2750 cm^{-1} range may be assigned to N−H and O−H stretching frequency in H_2L^+.

Structures

[CdClL·H₂O]ₙ (1)

Complex **1** consists of two-dimensional layers formed by interconnection of neighboring $[Cd^{II}-L]_n$ chains through bridging Cl^- in a *trans* mode. As shown in Figure 1 (a), each Cd^{II} is coordinated by two chelating carboxylate oxygen atoms from one L^- ligand, a nitrogen atom from the other L^- ligand, two bridging Cl^- ions, and one coordinated water molecule in a distorted octahedral geometry. The two bridging Cl^- ions stand at the apical positions [Cd−Cl = 2.580(1) and 2.646(1) Å, Cl−Cd−Cl(A) = 171.13(2)°], while the two carboxylate oxygen atoms [O(1) and O(2)], the nitrogen atom [N(0B)], and the water oxygen atom (O_w) form the equatorial plane. Cd^{II} is approximately coplanar with the mean plane of O1, O2, O_w, and N(0B), with a deviation of 0.0625 Å. L^- adopts a chelating/

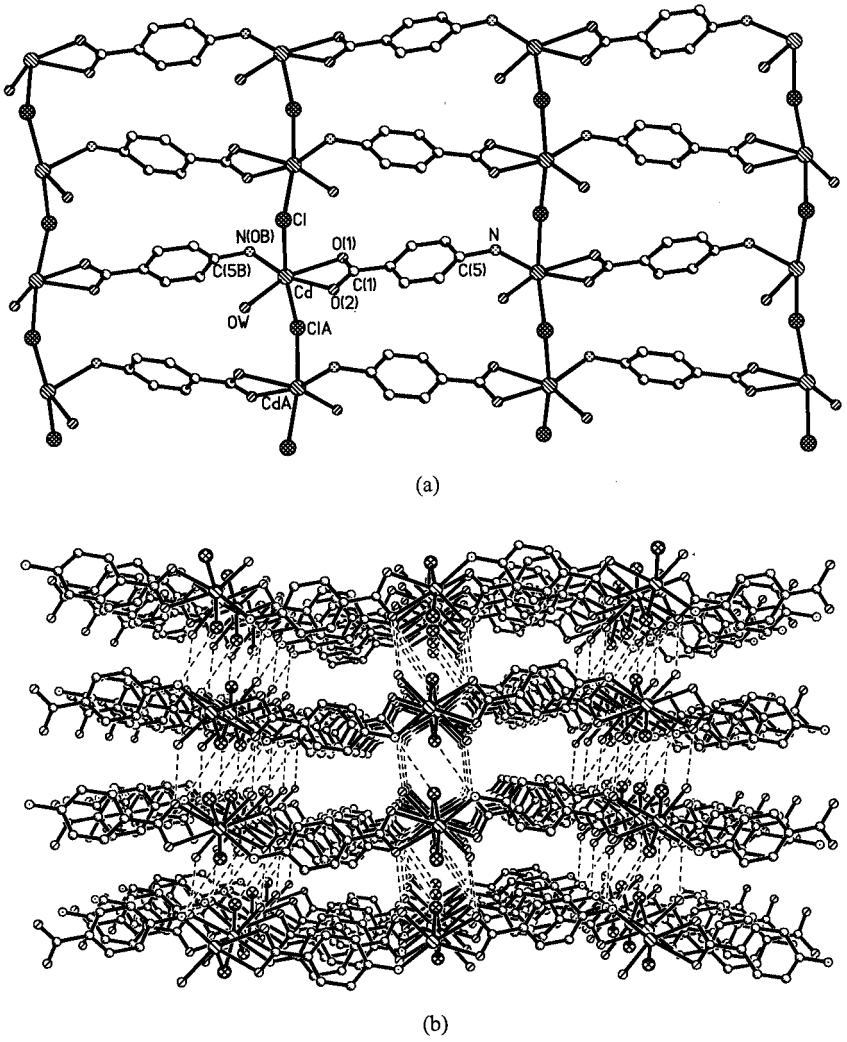

Figure 1. (a) View of the two-dimensional layer in **1** along the *b* axis with atomic numbering; (b) view of a packing diagram showing the three-dimensional structure of **1** along the *a* axis

bridging coordination mode to link two Cd^{II} centers (Scheme 1, **f**), similar to those in reported Cd^{II} complexes.[11] Cl^- acts as a μ_2-bridge and lies at the apical site occasionally reported in Cd^{II} complexes with mixed carboxylate and Cl^- ligands.[12] The Cd^{II} components can thus be viewed as linkers connecting L^- and Cl^- to form a two-dimensional layer consisting of rectangular grids with dimensions of 4.397 × 9.881 Å based on Cd···Cd distances. It should be noted that the water ligand forms hydrogen bonds with carboxylate oxygen atoms of L^- [O_w−H···O(1)^i 2.776(4) Å and O_w−H···O(2)^{ii} 2.773(5) Å; symmetry modes: i: $x + 1/2, -y + 1/2, -z + 1$; ii: $-x + 1, -y + 1, -z + 1$], and the amide of L^- also forms a hydrogen bond with Cl^- [N−H···Cl^{iii} 3.186(4) Å; symmetry mode: iii: $-x + 1/2, -y + 1, z - 1/2$]. Such hydrogen bonding interactions consolidate the structural architecture and further extend the two-dimensional layers into a three-dimensional structure (Figure 1, b).

[CdBrL·H$_2$O]$_n$ (2)

Complex **2** consists of two-dimensional layers formed by the interconnection of neighboring $[Cd^{II}-L]_n$ chains through bridging Br^- in a *cis* mode. As shown in Figure 2 (a), each Cd^{II} is coordinated by two chelating carboxylate oxygen atoms of one L^-, a nitrogen atom of the other L^-, two bridging Br^- moieties, and one coordinated water molecule in a highly distorted octahedral geometry; the equatorial plane is formed by the two carboxylate oxygen atoms [O(1) and O(2)], a nitrogen atom [N(0A)], and one bromide ion (Br) [with the shorter Cd−Br distance of 2.787(1) Å], while the water oxygen atom (O_w) and the other bromide ion [with the longer Cd−Br(B) distance of 2.829(1) Å] occupy the axial positions. The deviation of Cd^{II} from the equatorial plane defined by O(1), O(2), N(0A), and Br is 0.197 Å. Two adjacent Cd^{II} atoms are bridged by two Br^- moieties to form a Cd_2Br_2 four-membered ring[13] with a Cd···Cd separation of 3.795 Å. Such four-membered rings

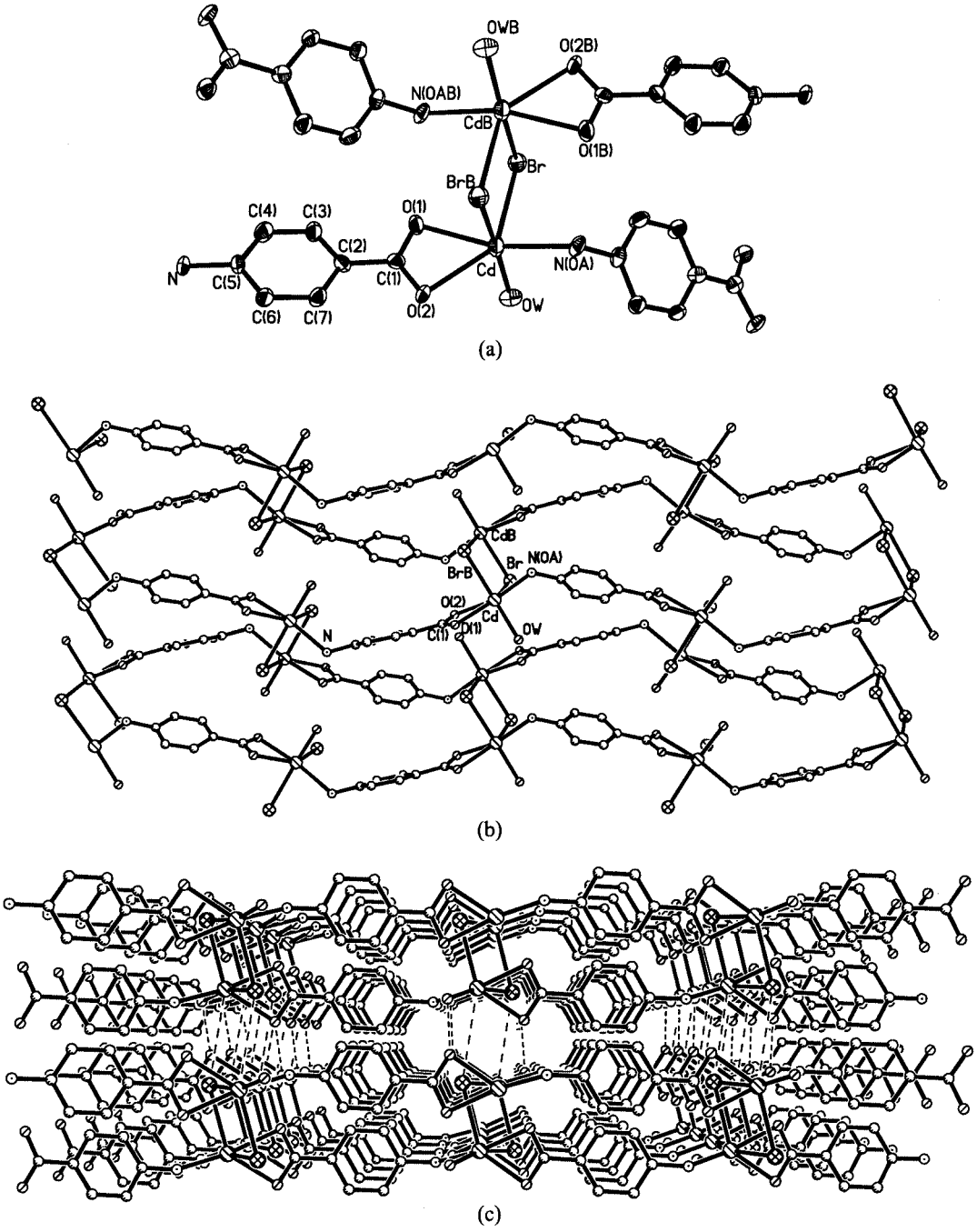

Figure 2. (a) The coordination geometry of Cd^{II} in **2**, thermal ellipsoids are shown with 50% probability; (b) view of the two-dimensional layer in **2** along the *a* axis; (c) view of the stacking layers in **2** along the *b* axis

act as nodes, and L^- links the nodes to yield a two-dimensional layer. The coordination mode of L^- is the same as in **1** (Scheme 1, **f**), but the layer is very different from that of **1** owing to the *cis* orientations of Br^- in **2**. The Cd···Cd distance separated by L^- (9.907 Å) is close to that in **1** (9.881 Å). It is noteworthy that the weak inter-layer Br···Cd interaction (3.798 Å) and hydrogen bonding interactions may play important roles in consolidating the crystal architecture. As shown in Figure 2 (c), hydrogen bonds of the water ligand and two oxygen atoms of different L^- ligands [$O_w-H\cdots O1^{i}$ 2.716(7) and $O_w-H\cdots O2^{ii}$ 2.818(7) Å; symmetry modes: i: $1-x$, $1-y$, $-z$; ii: $-x$, $1-y$, $-z$], and of Br^- and amide [$Br\cdots H-N^{iii}$ 3.376(6) Å; symmetry mode: iii: $-x$, $y-0.5$, $-0.5-z$] along with the weak Br···Cd interaction extend the two-dimensional layers into a three-dimensional structure.

$CdI_2(HL)_2$ (3)

The structure of complex **3** is made up of $HL-CdI_2-HL$ metallic synthons. As shown in Figure 3 (a), each Cd^{II} is coordinated by two I^- and two nitrogen atoms of HL in a distorted tetrahedral geometry [Cd–N = 2.347(5) Å,

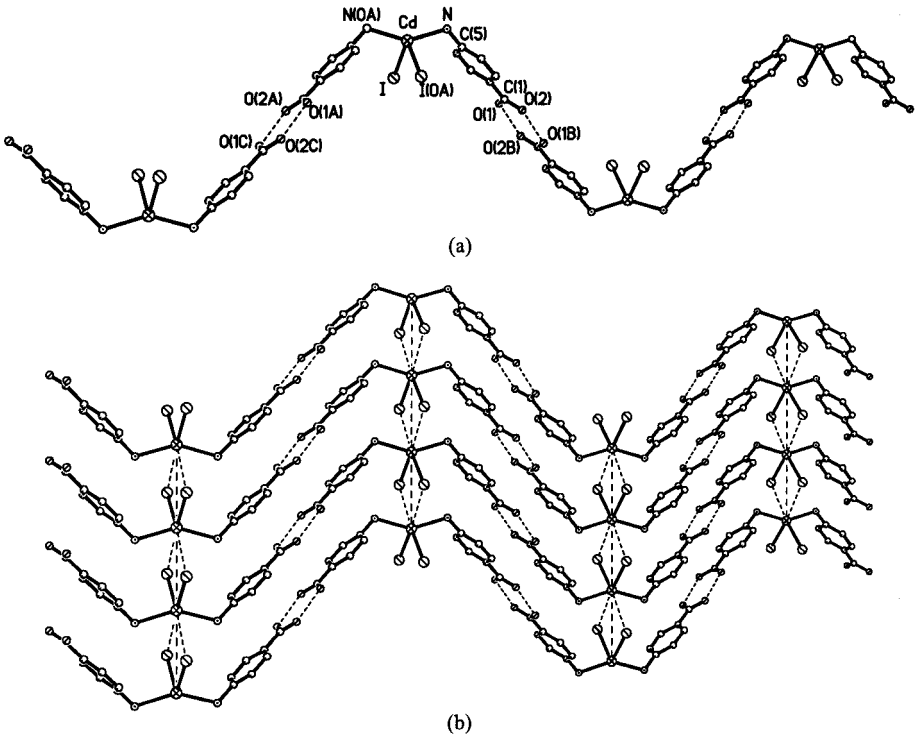

Figure 3. (a) One-dimensional hydrogen bonding zigzag chain in **3**; (b) two-dimensional layer is formed through weak Cd−I and hydrogen bonding interactions in **3**

Cd−I = 2.8276(8) Å, N−Cd−N(0A) = 148.8(3)°]. Each HL acts as a monodentate ligand, coordinating to Cd^{II} through its amine nitrogen atom, and forms hydrogen bonds through the carboxylic group (Scheme 1, **h**). The two HL components coordinated to the same Cd^{II} atom are approximately perpendicular, with a dihedral angle of 83.8°, similar to those in synthons of four-coordinate metal centers and pyridine derivatives.[5] In **3**, HL−CdI_2−HL units propagate by head-to-head hydrogen bonds between the carboxylic acid groups of HL (Scheme 1, **j**) into a zigzag chain [O(1)···H−O(2)^{i} 2.631(7) Å; symmetry code: i: $-x + 1/2, -y + 5/2, -z + 1$]. Such zigzag chains are further extended into a two-dimensional network through weak inter-chain Cd···I interactions [I···Cd^{ii} 3.3365(9) Å, Cd−I···Cd^{ii} 93.727(13)°; symmetry code: ii: $x, y + 1, z$] (Figure 3, b). The inter-chain adjacent Cd···Cd separation is 4.511 Å.

{[Cd(dca)$_2$(HL)$_2$]·2H$_2$O}$_n$ (4)

The crystal structure of complex **4** consists of one-dimensional cadmium chains and free water molecules (Figure 4, a). Each Cd^{II} is coordinated by six nitrogen atoms in a distorted octahedral geometry, in which four nitrogen atoms of different dca^- moieties form the equatorial plane [average $Cd-N_{dca}$ = 2.326(3) Å] and the nitrogen atoms of two HL units [$Cd-N_{HL}$ = 2.377(3) Å] occupy the apical positions. Each adjacent Cd^{II} pair is bridged by two inversely related dca^- units to form a neutral one-dimensional cadmium−dca chain consisting of twelve-membered $(N-C-N-C-N-Cd)_2$ rings with a Cd···Cd separation of 7.737 Å, which is slightly larger than those in the complexes comprising this type of bridge.[14] The HL ligands are situated at the two sides of the chain to saturate the six-coordinate Cd^{II} centers, adopting a monodentate coordination mode through the nitrogen atoms and forming hydrogen bonds through the carboxylic groups (Scheme 1, **h**). Unlike in **3**, adjacent one-dimensional chains in **4** are interconnected by hydrogen bonds between free water molecules and carboxylic groups to produce a two-dimensional structure [O_w···O(2) 2.608(3), O_w−H···O(1)^{i} 2.783(4) Å; symmetry code: i: $-x + 1, -y + 2, -z + 1$] (Figure 4, b). The O(2)−C(11) bond of 1.327(4) Å in HL is longer than those in **3**, $[Cd(SCN)_2(HL)_2]_n$,[8b] and the free HL ligand.[15] Formula **k** in Scheme 1 shows the twelve-membered ring formed by hydrogen bonds of water molecules and carboxylic acid groups. To the best of our knowledge, this is a unique structural motif in supramolecular chemistry. As shown in Figure 4 (c), the two-dimensional layers are further extended into a three-dimensional framework through weak inter-layer hydrogen bonds between free water molecules and oxygen atoms from HL [O_w···O(2)^{ii} 2.924(4) Å; symmetry code: ii: $-x + 1, y + 1/2, -z + 1/2$].

(H$_2$L)$_2$[CdCl$_4$(H$_2$O)$_2$] (5)

Complex **5** consists of discrete octahedral $[CdCl_4(H_2O)_2]^{2-}$ anions linked by H_2L^+ organic cations through extensive intermolecular hydrogen bonding interactions. As shown in Figure 5 (a), cadmium(II) is coordinated by four Cl^- ions [Cd−Cl = 2.5687(7) or 2.5699(7) Å] and two water oxygen atoms [$Cd-O_w$ = 2.364(2) Å] in a compressed octahedral geometry, in which the Cl^- units lie in the equatorial plane and the oxygen atoms are situated at

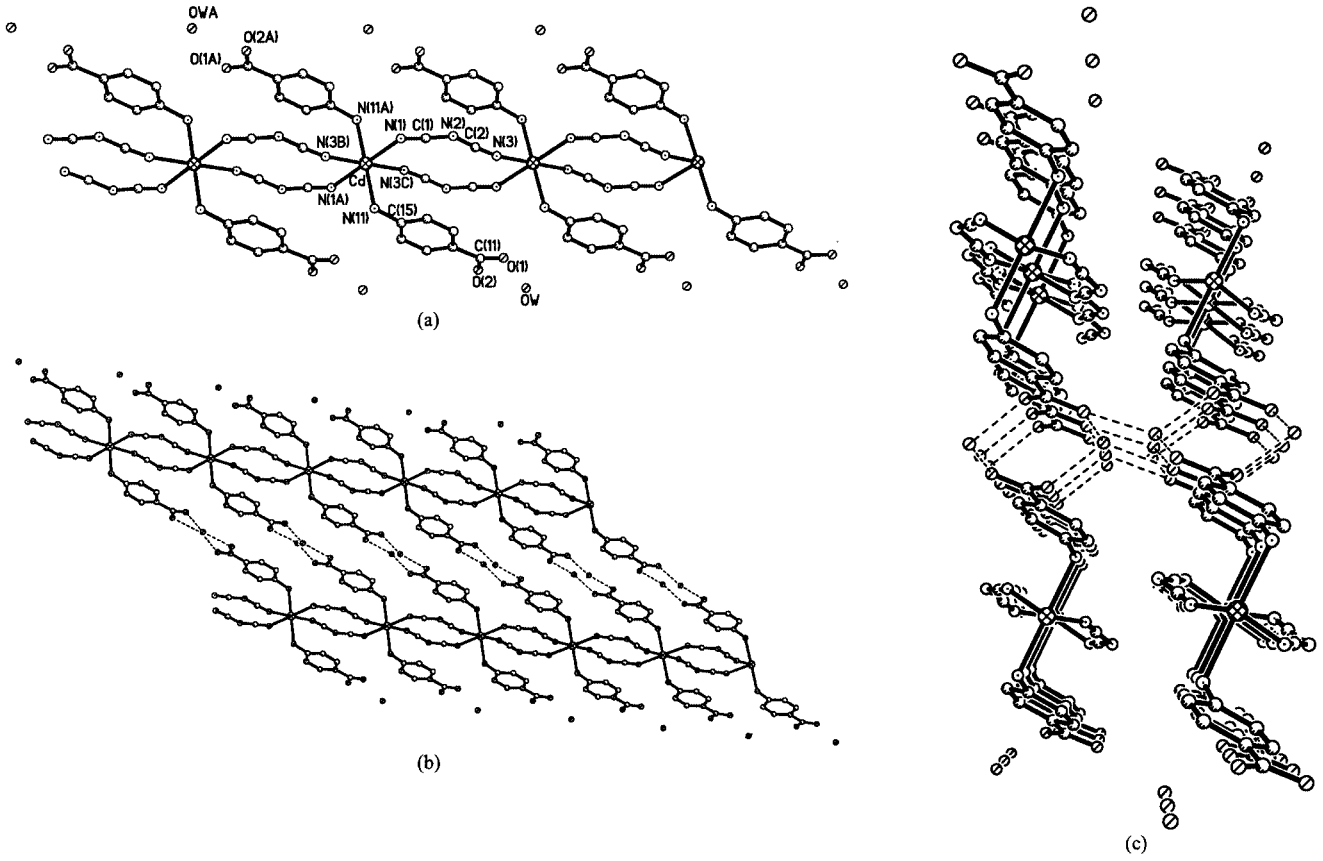

Figure 4. (a) View of one-dimensional chain and lattice water molecules in **5** with atomic numbering; (b) view of the hydrogen bonding between adjacent chains to form a two-dimensional layer along the *c* axis; (c) view of three-dimensional structure in **4** along the *a* axis

the axial positions. The coordination environment around Cd^{II} is similar to that in $[CdCl_2(H_2O)_2{\cdot}2Cyt]_n$ (Cyt = cytosine).[16] Cd^{II} is coplanar with the four Cl^- units and lies in the center of the equatorial plane. The bond lengths and angles are very similar to those in $[CdCl_2(H_2O)_2{\cdot}2Cyt]_n$.[16] As shown in Figure 5 (b), H_2L^+ cations act as linkers to link discrete $[CdCl_4(H_2O)]^{2-}$ units into a three-dimensional supramolecular structure through hydrogen bonding. There is no interaction between adjacent $[CdCl_4(H_2O)]^{2-}$ units, and the shortest Cd−Cd separation is 5.833 Å. Formula **i** in Scheme 1 shows the hydrogen bonds formed by H_2L^+: $-NH_3^+$ is surrounded by three Cl^- units [N−H···Cl(2) 3.228(3), N−H···Cl(2)^{i} 3.193(3), N−H···Cl(2)^{ii} 3.233(3) Å; symmetry codes: i: x, $y + 1$, z; ii: $-x + 1$, $y + 1/2$, $-z + 1/2$], −OH forms a hydrogen bond with a Cl^- ion [O(1)−H···Cl^{iii} 3.031(3) Å; symmetry code: iii: $-x + 2$, $y + 1/2$, $-z + 1/2$], and −C=O forms a hydrogen bond with a coordinated water molecule (O_w) [O_w−H···O(2)^{iv} 2.753(4) Å; symmetry code: iv: $x - 1$, $-y + 3/2$, $z - 1/2$]. To the best of our knowledge, this is the first complex comprising discrete $[CdCl_4(H_2O)]^{2-}$ anions and the first complex to use protonated 4-aminobenzoic acid (H_2L^+) as an organic cation templating agent.

Conclusion

Through the use of the multifunctional 4-aminobenzoic acid (HL) ligand and different synthetic strategies, we have successfully synthesized five Cd^{II} complexes that display hydrogen-bonding interactions. Complexes **1** and **2** may be regarded as extensions of the one-dimensional chain structure of $[(CdL_2{\cdot}H_2O){\cdot}2H_2O]_n$ [11] into two-dimensional networks through bridging Cl^- or Br^- instead of L^- and are further extended into three-dimensional structures by interlayer hydrogen bonding interactions. Moreover, Cl^- and Br^-, occupying different coordination sizes around Cd^{II}, result in two completely differentstructural topologies. Complex **3** is a typical metallic carboxylic acid synthon. The twelve-membered ring formed by H_2O and the carboxylic acid group of HL through hydrogen bonding in **4** is a unique structural motif in supramolecular chemistry. In complex **5**, N−H···Cl, O−H···Cl, O_w−H···Cl, and O_w−H···O hydrogen bonds link compressed octahedral $[CdCl_4(H_2O)]^{2-}$ anions and H_2L^+ cations into a three-dimensional structure. To the best of our knowledge, this is the first complex comprising discrete $[CdCl_4(H_2O)]^{2-}$ anions and the first complex to use protonated 4-aminobenzoic acid (H^2L^+) as an organic cation templating agent. In summary, this work demonstrates that the combination of coordination covalent bonds and hydrogen bonds is an important tool for the construction of supramolecular architectures, and that the presence of counterions or co-ligands in the synthetic reaction plays an important role in the formation of different structures.

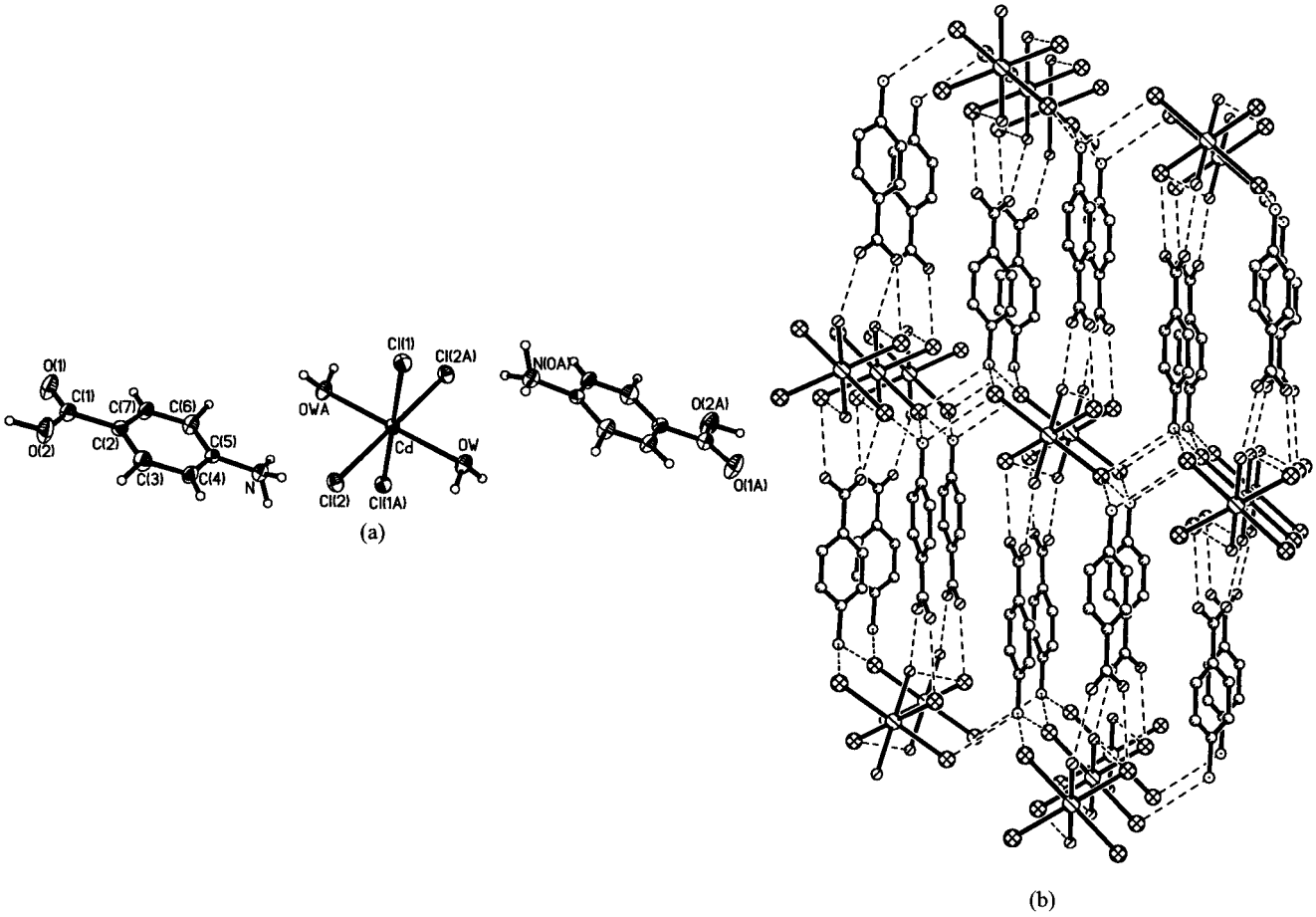

Figure 5. (a) View of discrete $[CdCl_4(H_2O)_2]^{2-}$ and H_2L^+ organic cations in **5**; thermal ellipsoids are shown with 30% probability; (b) packing diagram in **5** along the *a* axis

Table 1. Crystallographic data for the five crystal structures

Compound	**1**	**2**	**3**	**4**	**5**
Empirical formula	$C_7H_8CdCl_3NO_3$	$C_7H_8BrCdNO_3$	$C_7H_7Cd_{0.5}INO_2$	$C_9H_9Cd_{0.50}N_4O_3$	$C_7H_{10}Cd_{0.5}Cl_2NO_3$
Formula mass	301.99	346.45	320.24	277.40	283.26
Crystal size [mm]	0.64 × 0.50 × 0.12	0.58 × 0.36 × 0.09	0.62 × 0.20 × 0.14	0.48 × 0.35 × 0.19	0.68 × 0.60 × 0.44
Crystal system	orthorhombic	monoclinic	monoclinic	monoclinic	monoclinic
Space group	*Pbca*	$P2_1/c$	$C2/c$	$P2_1/c$	$P2_1/c$
a [Å]	8.7606(3)	6.4357(2)	15.8720(2)	11.5381(10)	12.0794(11)
b [Å]	10.6930(3)	7.2533(3)	4.5115(1)	7.7374(6)	5.8333(5)
c [Å]	19.7616(7)	19.7258(6)	25.0187(7)	12.4261(11)	14.8963(13)
β [°]		90.890(2)	97.474(2)	90.979(2)	100.376(1)
V [Å^3]	1851.21(10)	920.69(6)	1776.28(7)	1109.18(16)	1032.47(16)
Z	8	4	8	4	4
D_c [g·cm^{-3}]	2.167	2.499	2.395	1.661	1.822
μ [mm^{-1}]	2.619	6.683	4.724	1.037	1.608
F(000)	1168	656	1192	556	564
T [K]	293(2)	293(2)	293(2)	293(2)	293(2)
λ(Mo-K_α) [Å]	0.71073	0.71073	0.71073	0.71073	0.71073
Reflns. collected	5826	2833	2852	3332	2995
Unique reflns.	1646	1596	1555	1918	1825
Obsd. reflns.[$F > 4.0\sigma(F)$]	1418	1333	1259	1591	1744
Parameters	119	119	106	151	165
S on F^2	1.176	1.020	1.024	1.098	1.194
R_1	0.0348	0.0539	0.0453	0.0309	0.0245
wR	0.1056	0.1413	0.1206	0.0914	0.0713
$\Delta\rho_{min.}$ and $_{max.}$ [e Å^{-3}]	0.863 and −0.639	1.276 and −1.453	1.143 and −1.043	0.565 and −0.629	0.388 and −0.718

Experimental Section

General: All reagents are commercially available and were used as purchased without further purification. The IR spectra were recorded with a Magna 750 FT-IR spectrophotometer from KBr disks. Elemental analyses were recorded with an Elementar Vario ELIII elemental analyzer.

$[CdClL\cdot H_2O]_n$ (1): A solution of $CdCl_2\cdot 2.5H_2O$ (0.11 g, 0.5 mmol) in H_2O (5 mL) was added slowly to a solution of HL (0.07 g, 0.5 mmol) in MeOH (10 mL). Aqueous NaOH (1 mol·L^{-1}) was then added dropwise to the reaction mixture until a small amount of precipitate had formed. The precipitate was filtered off and the clear filtrate was allowed to stand at room temperature. After one week, light yellow crystals were obtained. Yield: 68%. $C_7H_8CdClNO_3$ (302.0): calcd. C 27.84, H 2.65, N 4.64; found C 28.27, H 2.76, N 4.52. IR (KBr): $\tilde{\nu}$ = 3329 (s), 3280 (s), 3217 (s), 3134 (m), 1928 (vw), 1693 (vw), 1637 (vw), 1608 (vs), 1597 (m), 1520 (s), 1518 (s), 1433 (m), 1398 (vs), 1327 (w), 1302 (w), 1240 (w), 1176 (w), 1142 (w), 1076 (s), 1034 (m), 964 (w), 856 (m), 843 (vw), 787 (m), 777 (m), 702 (vw), 636 (m), 617 (vw), 517 (vw), 503 (vw) cm^{-1}.

$[CdBrL\cdot H_2O]_n$ (2): The procedure was similar to the synthesis of complex **1**, except that $CdBr_2\cdot 4H_2O$ (0.17 g, 0.5 mmol) was used instead of $CdCl_2\cdot 2.5H_2O$. Yield: 53%. $C_7H_8BrCdNO_3$ (346.5): calcd. C 24.27, H 2.31, N 4.04; found C 24.32, H 2.43, N 4.12. IR (KBr): $\tilde{\nu}$ = 3286 (br, vs), 1923 (vw), 1911 (vw), 1668 (w), 1610 (vs), 1597 (vs), 1502 (vs), 1414 (vs), 1402 (vs), 1302 (m), 1246 (s), 1184 (m), 1146 (w), 1101 (m), 1055 (vs), 951 (w), 868 (s), 852 (s), 785 (s), 702 (m), 636 (s), 596 (m), 530 (m) cm^{-1}.

$CdI_2(HL)_2$ (3): A solution of CdI_2 (0.09 g, 0.25 mmol) in H_2O (5 mL) was added slowly to a solution of HL (0.07 g, 0.5 mmol) in MeOH (10 mL). The reaction mixture was stirred for 30 min and the resulting colourless solution was filtered. Light yellow crystals of complex **3** were obtained by allowing the filtrate to stand in air for one week. Yield: 56%. $C_7H_7Cd_{0.5}INO_2$ (320.2): calcd. C 26.25, H 2.19, N 4.37; found C 26.37, H 2.24, N 4.43. IR (KBr): $\tilde{\nu}$ = 3460 (s), 3363 (s), 3329 (s), 3215 (m), 2978 (m), 2669 (m), 2551 (m), 1684 (s), 1605 (s), 1574 (m), 1512 (vw), 1441 (m), 1423 (m), 1387 (w), 1319 (s), 1290 (s), 1261 (m), 1174 (s), 1128 (w), 1097 (vw), 1012 (w), 1018 (w), 964 (w), 899 (vw), 843 (w), 773 (m), 694 (vw), 617 (w), 550 (vw), 499 (vw) cm^{-1}.

$\{[Cd(dca)_2(HL)_2]\cdot 2H_2O\}_n$ (4): A solution of $Cd(NO_3)_2\cdot 6H_2O$ (0.15 g, 0.5 mmol) and Na(dca) (0.09 g, 1 mmol) in H_2O (5 mL) was added slowly to a solution of HL (0.07 g, 0.5 mmol) in MeOH (10 mL). The reaction mixture was stirred for 30 min and gave a colourless solution. After filtration, the filtrate was allowed to stand in air for two weeks to give light yellow crystals of complex **4**. Yield: 50%. $C_9H_9Cd_{0.5}N_4O_3$ (277.4): calcd. C 38.97, H 3.24, N 20.19; found C 39.02, H 3.27, N 20.23. IR (KBr): $\tilde{\nu}$ = 3575 (vw), 3460 (m), 3383 (w), 3365 (m), 3307 (w), 3165 (vw), 2663 (vw), 2291 (m), 2268 (m), 2235 (w), 2175 (vw), 1678 (s), 1626 (s), 1605 (s), 1576 (vw), 1518 (vw), 1443 (w), 1423 (w), 1365 (vw), 1327 (s), 1315 (s), 1292 (s), 1263 (w), 1176 (m), 1128 (vw), 1012 (vw), 964 (vw), 943 (vw), 918 (vw), 845 (vw), 771 (vw), 698 (vw), 619 (vw), 553 (vw), 509 (vw) cm^{-1}.

$(H_2L)_2[CdCl_4(H_2O)_2]$ (5): An aqueous solution (10 mL) of $CdCl_2\cdot 2.5H_2O$ (0.11 g, 0.5 mmol) was added slowly to a solution of HL (0.07 g, 0.5 mmol) in HCl (6 mol·L^{-1}, 20 mL). After stirring for 30 min, the colourless reaction mixture was filtered. Light yellow crystalline complex **5** was obtained by keeping the filtrate in

Table 2. Selected bond lengths [Å] and angles [°] for the five complexes; symmetry codes: **1** (A): $x + 1/2, -y + 1/2, -z + 1$; (B): $x, -y + 1/2, z + 1/2$; **2** (A): $x, -y + 1/2, z + 1/2$; (B): $-x, -y, -z$; **3** (A): $-x + 1, y, -z + 1/2$; **4** (A): $-x, -y, -z + 1$; (B): $-x, -y + 1, -z + 1$; (C): $x, y - 1, z$; **5** (A): $-x + 1, -y + 1, -z$

Complex **1**			
Cd−O(1)	2.395(3)	Cd−N(0B)	2.304(3)
Cd−O(2)	2.351(3)	O(1)−C(1)	1.257(5)
Cd−O_w	2.266(3)	O(2)−C(1)	1.280(5)
Cd−Cl	2.646(1)	N−C(5)	1.435(5)
Cd−ClA	2.580(1)		
O(2)−Cd−O(1)	55.35(10)	O_w−Cd−N(0B)	98.24(13)
O(1)−Cd−Cl	82.53(8)	N(0B)−Cd−O(2)	163.65(12)
O(2)−Cd−Cl	82.26(8)	N(0B)−Cd−O(1)	109.76(11)
O(1)−Cd−ClA	88.62(8)	N(0B)−Cd−ClA	94.34(10)
O(2)−Cd−ClA	92.11(8)	N(0B)−Cd−Cl	89.38(10)
O_w−Cd−O(1)	151.94(12)	ClA−Cd−Cl	171.13(2)
O_w−Cd−O(2)	96.64(12)	CdA−ClA−Cd	114.60(4)
O_w−Cd−Cl	96.35(9)	C(5B)−N(0B)−Cd	119.8(3)
O_w−Cd−ClA	91.09(9)	O(1)−C(1)−O(2)	120.7(4)
Complex **2**			
Cd−O(1)	2.392(6)	Cd−Br(B)	2.830(1)
Cd−O(2)	2.413(5)	N−C(5)	1.430(9)
Cd−O_w	2.236(6)	O(1)−C(1)	1.286(9)
Cd−Br	2.7875(9)	O(2)−C(1)	1.266(10)
Cd−N(0A)	2.353(6)		
O(1)−Cd−O(2)	54.57(17)	O_w−Cd−N(0A)	94.8(2)
O(1)−Cd−Br	82.41(12)	N(0A)−Cd−O(1)	164.1(2)
O(2)−Cd−Br	136.98(12)	N(0A)−Cd−O(2)	133.3(2)
O(1)−Cd−Br(B)	87.15(13)	N(0A)−Cd−Br	88.42(15)
O(2)−Cd−Br(B)	84.24(13)	N(0A)−Cd−Br(B)	80.72(15)
O_w−Cd−O(1)	99.4(2)	Br−Cd−Br(B)	95.01(3)
O_w−Cd−O(2)	89.4(2)	Cd−Br−Cd(B)	84.99(3)
O_w−Cd−Br	98.23(13)	O(2)−C(1)−O(1)	119.3(7)
O_w−Cd−Br(B)	165.90(14)		
Complex **3**			
Cd−N	2.347(5)	O(1)−C(1)	1.249(7)
Cd−I	2.8276(8)	O(2)−C(1)	1.289(8)
N−C(5)	1.429(8)		
N−Cd−I	103.35(14)	N−Cd−I(0A)	97.57(15)
N(0A)−Cd−N	148.8(3)	I(0A)−Cd−I	95.12(3)
N(0A)−Cd−I	97.57(15)	C(5)−N−Cd	119.7(4)
N(0A)−Cd−I(0A)	103.35(14)	O(1)−C(1)−O(2)	123.3(6)
Complex **4**			
Cd−N(1)	2.338(3)	N(11)−C(15)	1.413(4)
Cd−N(11)	2.377(3)	O(1)−C(11)	1.216(4)
Cd−N(3B)	2.314(3)	O(2)−C(11)	1.327(4)
Cd−N(3C)	2.314(3)		
N(1)−Cd−N(11)	90.43(11)	N(3B)−Cd−N(11A)	87.13(11)
N(1)−Cd−N(1A)	180.0	N(3C)−Cd−N(11A)	92.87(11)
N(1)−Cd−N(11A)	89.57(11)	N(3C)−Cd−N(3B)	180.0
N(1A)−Cd−N(11)	89.57(11)	N(3C)−Cd−N(1)	96.36(11)
N(1A)−Cd−N(11A)	90.43(11)	N(3C)−Cd−N(1A)	83.64(11)
N(11A)−Cd−N(11)	180.0	N(3C)−Cd−N(11)	87.13(11)
N(3B)−Cd−N(1)	83.64(11)	C(15)−N(11)−Cd	115.1(2)
N(3B)−Cd−N(1A)	96.36(11)	O(1)−C(11)−O(2)	121.4(3)
N(3B)−Cd−N(11)	92.87(11)		
Complex **5**			
Cd−O_w	2.364(2)	Cd−Cl(2)	2.5687(7)
Cd−Cl(1)	2.5699(7)	N−C(5)	1.464(4)
O(2)−C(1)	1.188(4)	O(1)−C(1)	1.310(4)
O_w−Cd−O_wA	180.00(9)	Cl(2A)−Cd−Cl(1)	86.90(2)
O_w−Cd−Cl(2A)	86.52(7)	Cl(2)−Cd−Cl(1)	93.10(2)
O_wA−Cd−Cl(2A)	93.48(7)	O_w−Cd−Cl(1A)	92.83(6)
O_w−Cd−Cl(2)	93.48(7)	O_wA−Cd−Cl(1A)	87.17(6)
O_wA−Cd−Cl(2)	86.52(7)	Cl(2A)−Cd−Cl(1A)	93.10(2)
Cl(2A)−Cd−Cl(2)	180.00(3)	Cl(2)−Cd−Cl(1A)	86.90(2)
O_w−Cd−Cl(1)	87.17(6)	Cl(1)−Cd−Cl(1A)	180.00(3)
O_wA−Cd−Cl(1)	92.83(6)	O(2)−C(1)−O(1)	124.6(3)

air for one month. Yield: 65% (based on HL). $C_{14}H_{18}CdCl_6N_2O_4$ (603.4): calcd. C 27.87, H 2.98, N 4.64; found C 27.91, H 2.93, N 4.69. IR (KBr): $\tilde{\nu}$ = 3496 (m), 3275 (m), 3066 (br, s), 2920 (br, s), 2677 (m), 2617 (m), 2546 (m), 1950 (vw), 1701 (vs), 1678 (vs), 1612 (vs), 1589 (s), 1558 (m), 1522 (m), 1510 (s), 1487 (m), 1433 (m), 1419 (m), 1387 (w), 1319 (m), 1284 (s), 1211 (m), 1182 (m), 1119 (m), 1107 (m), 1063 (vw), 1020 (w), 957 (vw), 906 (vw), 856 (w), 833 (vw), 762 (s), 739 (w), 692 (w), 638 (w), 596 (w), 542 (w), 525 (w), 480 (m) cm^{-1}.

X-ray Crystallography: Intensity data for the five complexes were measured with a Siemens Smart CCD diffractometer with graphite-monochromated Mo-K_α radiation (λ = 0.71073 Å) at 298 K. Empirical absorption corrections were applied by use of the SADABS program. The structures were solved by direct methods and all calculations were performed with the aid of the SHELXL PC program. The positions of H atoms in complexes **1**−**4** were generated geometrically (C−H bond fixed at 0.96 Å) and the positions of H atoms in complex **5** were generated from difference Fourier maps, assigned isotropic thermal parameters, and allowed to ride on their parent carbon atoms before the final cycle of refinement. The structures were refined by full-matrix, least-squares minimization of $\Sigma(F_o - F_c)^2$ with anisotropic thermal parameters for all atoms except the H atoms. The crystallographic data for complexes **1**−**5** are listed in Table 1, selected bond lengths and angles in Table 2. CCDC-180374 to -180376 contain the supplementary crystallographic data for this paper. These data can be obtained free of charge at www.ccdc.cam.ac.uk/conts/retrieving.html or from the Cambridge Crystallographic Data Centre, 12, Union Road, Cambridge CB2 1EZ, UK [Fax: (internat.) + 44-1223/336-033; E-mail: deposit@ccdc.cam.ac.uk].

Acknowledgments

The authors are grateful to the National Nature Science Foundation of China and the Key Project of the Chinese Academy of Science for financial support.

[1] [1a] P. J. Hagrman, D. Hagrman, J. Zubieta, *Angew. Chem. Int. Ed.* **1999**, *38*, 2638−2684. [1b] J. Makarevic, M. Jokic, B. Peric, V. Tomisic, B. Kojic-Prodic, M. Zinic, *Chem. Eur. J.* **2001**, *7*, 3328−3341. [1c] L. R. MacGillivray, J. L. Reid, J. A. Ripmeester, *Chem. Commun.* **2001**, 1034−1035.

[2] [2a] B. Moulton, M. J. Zaworotko, *Chem. Rev.* **2001**, *101*, 1629−1658. [2b] L. Pan, N. Ching, X. Huang, J. Li, *Chem. Eur. J.* **2001**, *7*, 4431−4437. [2c] E. Breuning, U. Ziener, J.-M. Lehn, E. Wegelius, K. Rissanen, *Eur. J. Inorg. Chem.* **2001**, 1515−1521. [2d] A. R. Kennedy, M. P. Hughes, M. L. Monaghan, E. Staunton, S. J. Teat, W. E. Smith, *J. Chem. Soc., Dalton Trans.* **2001**, 2199−2205. [2e] J. Rojo, F. J. Romero-Salguero, J.-M. Lehn, G. Baum, D. Fenske, *Eur. J. Inorg. Chem.* **1999**, 1421−1428. [2f] G. R. Desiraju, *Angew. Chem. Int. Ed. Engl.* **1995**, *34*, 2311−2327.

[3] [3a] S. A. Bourne, J. Lu, A. Mondal, B. Moulton, M. J. Zaworotko, *Angew. Chem. Int. Ed.* **2001**, *40*, 2111−2113. [3b] D. J. Chesnut, D. Hagrman, P. J. Zapf, R. P. Hammond, R. L. La Duca, R. C. Haushalter, J. Zubieta, *Coord. Chem. Rev.* **1999**, *190*−*192*, 737−769. [3c] S. Leininger, B. Olenyuk, P. J. Stang, *Chem. Rev.* **2000**, *100*, 853−908. [3d] D. L. Caulder, K. N. Raymond, *Acc. Chem. Res.* **1999**, *32*, 975−982. [3e] B. J. Holliday, C. A. Mirkin, *Angew. Chem. Int. Ed.* **2001**, *40*, 2022−2043. [3f] C. Janiak, S. Deblon, H.-P. Wu, M. J. Kolm, P. Klüfers, H. Piotrowski, P. Mayer, *Eur. J. Inorg. Chem.* **1999**, 1507−1521.

[4] [4a] S. Tanase, M. Andruh, A. Müller, M. Schmidtmann, C. Mathonière, G. Rombaut, *Chem. Commun.* **2001**, 1084 −1085. [4b] Y. Diskin-Posner, G. K. Patra, I. Goldberg, *Eur. J. Inorg. Chem.* **2001**, 2515−2523. [4c] A. D. Burrows, R. W. Harrington, M. F. Mahon, C. E. Price, *J. Chem. Soc., Dalton Trans.* **2001**, 3845−3854.

[5] C. J. Kuehl, F. M. Tabellion, A. M. Arif, P. J. Stang, *Organometallics* **2001**, *20*, 1956−1959.

[6] [6a] K. D. Karlin, *Progress in Inorg. Chem.* **2001**, *48*, 1−122. [6b] D. B. Mitzi, S. Wang, C. A. Feild, C. A. Chess, A. M. Guloy, *Science* **1995**, *267*, 1473−1476. [6c] S. Haddad, R. D. Willett, *Inorg. Chem.* **2001**, *40*, 809−811. [6d] M. Wei, R. D. Willett, K. W. Hipps, *Inorg. Chem.* **1996**, *35*, 5300−5303 and references therein.

[7] [7a] W. Su, M. Hong, J. Weng, R. Cao, S. Lu, *Angew. Chem. Int. Ed.* **2000**, *39*, 2911−2914. [7b] Y. Zhao, M. Hong, Y. Liang, R. Cao, W. Li, J. Weng, S. Lu, *Chem. Commun.* **2001**, 1020−1021. [7c] M. Hong, W. Su, R. Cao, W. Zhang, W.-T. Wong, J. Lu, *Inorg. Chem.* **1999**, *38*, 600−602. [7d] W. Su, R. Cao, M. Hong, W. Zhang, W.-T. Wong, J. Lu, *Inorg. Chem. Commun.* **1999**, *2*, 241−243. [7e] W. Su, M. Hong, J. Weng, Y. Liang, Y. Zhao, R. Cao, Z. Zhou, A. S. C. Chan, *Inorg. Chim. Acta*, in press.

[8] [8a] Y. L. Fur, R. Masse, *Acta Crystallogr., Sect. C* **1996**, *52*, 2183−2185. [8b] H.-J. Chen, X.-M. Chen, *Inorg. Chim. Acta* **2002**, *329*, 13−21.

[9] [9a] M. R. Sundberg, J. K. Koskimies, J. Matikainen, H. Tylli, *Inorg. Chim. Acta* **1998**, *268*, 21−30. [9b] V. Chandrasekhar, R. O. Day, J. M. Holmes, R. R. Holmes, *Inorg. Chem.* **1988**, *27*, 958−964. [9c] I. R. Amiraslanov, K. S. Mamedov, E. M. Movsumov, F. N. Musaev, G. N. Nadzhafov, *Zh. Strukt. Khim.* **1979**, *20*, 1075−1077.

[10] [10a] S.-L. Zheng, M.-L. Tong, X.-L. Yu, X.-M. Chen, *J. Chem. Soc., Dalton Trans.* **2001**, 586−592. [10b] L. P. Battaglia, A. C. Bonamartini, S. Lanelli, M. A. Zoroddu, G. Sanna, *J. Chem. Soc., Faraday Trans.* **1991**, *87*, 3863−3867. [10c] Z. Rzaezynska, V. K. Belskii, *Pol. J. Chem.* **1994**, *68*, 309−312.

[11] [11a] P. J. Smith, R. O. Day, V. Chandrasekhar, J. M. Holmes, R. R. Holmes, *Inorg. Chem.* **1986**, *25*, 2495−2499. [11b] R. W. Turner, N. G. Charles, E. L. Amma, *Cryst. Struct. Comm.* **1982**, *11*, 241−245. [11c] R. Hauptmann, M. Kondo, S. Kitagawa, *Z. Kristallogr. - New Cryst. Struct.* **2000**, *215*, 169−172.

[12] S. L. Li, T. C. W. Mak, *Inorg. Chim. Acta* **1997**, *258*, 11−24.

[13] [13a] D.-D. Wu, T. C. W. Mak, *Polyhedron* **1996**, *15*, 655−664. [13b] C. Zhang, D. Xu, Y. Xu, Y. Huang, *Acta Crystallogr., Sect. C* **1996**, *52*, 591−593. [13c] G. Reinhard, B. Hirle, U. Schubert, M. Knorr, P. Braunstein, A. Decian, J. Fischer, *Inorg. Chem.* **1993**, *32*, 1656−1661. [13d] M. Nieuwenhuyzen, C. J. Wilkins, *J. Chem. Soc., Dalton Trans.* **1993**, 2673−2681.

[14] [14a] I. Dasna, S. Golhen, L. Ouahab, O. Pena, J. Guillevic, M. Fettouhi, *J. Chem. Soc., Dalton Trans.* **2000**, 129−132. [14b] G. A. Albada, M. E. Quiroz-Castro, I. Mutikainen, U. Turpeinen, J. Reedijk, *Inorg. Chim. Acta* **2000**, *298*, 221−225. [14c] S. R. Batten, P. Jensen, C. J. Kepert, M. Kurmoo, B. Moubaraki, K. S. Murray, D. J. Price, *J. Chem. Soc., Dalton Trans.* **1999**, 2987−2997. [14d] J. L. Manson, A. M. Arif, C. D. Incarvito, L. M. Liable-Sands, A. L. Rheingold, J. S. Miller, *J. Solid State Chem.* **1999**, *145*, 369−378.

[15] T. F. Lai, R. E. Marsh, *Acta Crystallogr.* **1967**, *22*, 885−893.

[16] G. D. Munno, S. Mauro, T. Pizzino, D. Viterbo, *J. Chem. Soc., Dalton Trans.* **1993**, 1113−1119.

Received April 3, 2002
[I02178]

Structural and Single Crystal EPR Studies of the Complex Copper L-Glutamine: A Weakly Exchange-Coupled System with *syn-anti* Carboxylate Bridges

José M. Schveigkardt,[a] Alberto C. Rizzi,[a] Oscar E. Piro,[b] Eduardo E. Castellano,[c] Ricardo Costa de Santana,[d] Rafael Calvo,[a,e] and Carlos D. Brondino*[a]

Keywords: EPR spectroscopy / Carboxylate ligands / Through bond interactions / Copper / Magnetic Properties / Layered compounds

We report the molecular structure and a single crystal EPR study at 9.8 and 33.9 GHz of a new copper(II) compound with the amino acid L-Glutamine, $Cu[NH_2CO_2CH(CH_2)_2CONH_2]_2$. The Cu^{II} ion is in an elongated octahedral environment equatorially *trans*-coordinated by two glutamine molecules acting as bidentate ligands through the nitrogen atom and one oxygen atom of each amino acid group, and axially by two carboxylate oxygen atoms of two neighboring glutamine molecules. Copper ions are arranged in layers connected by *syn-anti* carboxylate bridges that provide equatorial and apical ligands to the copper ions. Neighboring layers are connected by long chemical paths, which include two amino acid side chains connected by H bonds. Single crystal EPR spectra show a single exchange-collapsed resonance at both microwave frequencies for any magnetic field orientation. The evaluation of the molecular ***g***-tensor from the angular variation of the EPR line position yielded $g_\perp = 2.051$ and $g_\parallel = 2.248$, which indicates a $d_{x^2-y^2}$ ground orbital for the Cu ions. The angular variation of the EPR line width displays a contribution that is typical of a 2-D magnetic system, and another contribution depending on the microwave frequency, which is attributed to the incomplete collapse of the resonances corresponding to magnetically nonequivalent copper ions. A quantitative analysis of the line width data allowed us to estimate a mean exchange coupling constant $|J/k| = 0.42(2)$ K, which is assigned to the *syn-anti* carboxylate chemical path that connects neighboring copper ions within a layer. The results are discussed and compared with those observed in similar systems.

(© Wiley-VCH Verlag GmbH, 69451 Weinheim, Germany, 2002)

Introduction

Copper complexes with amino acids are appropriate compounds for the study of magnetic properties of weakly exchange-coupled systems. They are also of biological interest as amino acids provide ligands to the metal ions in metalloproteins.[1] Additional biological interest arises because chemical paths for superexchange interactions, such as carboxylate bridges, saturated and nonsaturated sigma bonds, hydrogen bonds, stacking of aromatic rings, or mixed paths integrated by fragments of the previous ones, have been identified as possible pathways for electron transfer in several biological systems.[2] These paths are responsible for the transmission of weak exchange interactions ($0.0005\ K \leq |J/k| \leq 2\ K$) that have been related to the matrix element for electron transfer between redox centers in metalloproteins.[3] Small exchange interactions are difficult to evaluate by standard magnetic susceptibility measurements, but they can be accurately and selectively measured employing EPR spectroscopy.[4−6]

Most solid copper compounds with α-amino acids have the Cu^{II} ions coordinated to the nitrogen and one of the carboxylate oxygen atoms of the amino acid group of two amino acid molecules, while the remaining carboxylate oxygen atoms are bonded to copper ions of neighboring molecules. This gives rise to copper ion networks having 1-, 2-, or 3-D structures, connected by carboxylate bridges of the *syn-anti* type that provide equatorial and apical ligands to the copper ions.[7−12] A different situation occurs in the copper complexes with aspartic acid,[13,14] glutamic acid,[15,16] and asparagine.[17] In these compounds, the copper ions are coordinated to one amino acid molecule as

[a] Departamento de Física, Facultad de Bioquímica y Ciencias Biológicas, Universidad Nacional del Litoral
C.C. 242, 3000 Santa Fe, Argentina
Fax: (internat.) + 54−342/4575221
E-mail: brondino@dfbioq.unl.edu.ar
[b] Departamento de Física, Facultad de Ciencias Exactas, Universidad Nacional de La Plata and Instituto IFLP (CONICET)
C.C. 67, 1900 La Plata, Argentina
[c] Instituto de Física de São Carlos, Universidade de São Paulo
C.P. 369, 13560 São Carlos (SP), Brazil
[d] Instituto de Física, Universidade Federal de Goiás, Campus Samambaia,
C.P. 131, 74001−970, Goiânia-GO, Brazil
[e] INTEC (CONICET−UNL)
Güemes 3450, 3000 Santa Fe, Argentina

in the compounds described above, and, in addition, are coordinated to the side chain carboxylate group of the other amino acid molecule in the case of aspartic and glutamic acids, and by the side chain amide in the case of asparagine. This coordination gives rise to polymeric chains, where the sigma skeleton of the amino acid molecule connects two neighboring copper ions.

We report herein the crystal and molecular structure and a single-crystal EPR study of the copper complex with the amino acid L-glutamine. According to the information given above, this compound was expected to exhibit a polymeric structure. However, our results indicate that this complex has a molecular structure and a magnetic behaviour different from that observed in polymeric compounds.

Results and Discussion

Molecular Structure

X-ray structural characterizations of the title compound reveal that it crystallizes in the monoclinic space group *C*2. The copper ion has an elongated octahedral coordination, trans coordinated by two glutamine molecules with a nearly square planar equatorial N_2O_2 ligand group. Figure 1 is an ORTEP[18] drawing of the complex showing the coordination around the Cu^{II} ion, hereafter called $Cu(gln)_2$. Selected bond lengths and angles are given in Table 1. The axial ligands are the carboxylate oxygen atoms O22 and O12, each belonging to one of two symmetry related neighboring glutamine molecules.

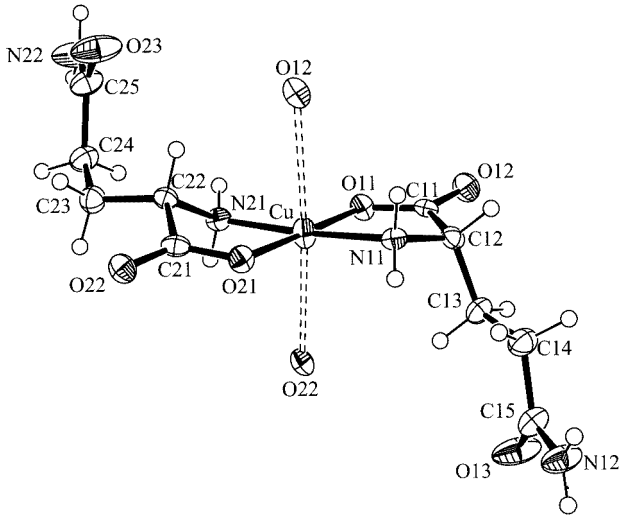

Figure 1. Drawing of the $Cu(gln)_2$ molecule showing the coordination around Cu^{II}, the labeling scheme of the non-H atoms and their displacement ellipsoids at 50% probability level; full lines indicate copper-ligand bonds

The four symmetry related copper ions in the unit cell of $Cu(gln)_2$ lie in two layers parallel to the *cb* plane 14.1 Å apart . One of them, shown in Figure 2, contains the copper atoms in the general positions (*x,y,z*) and ($-x + 1/2$, $y + 1/2$, $-z$) (positions I and IV, respectively, of the crystallographic space group *C*2). The other one contains the copper atoms in positions ($-x$, y, $-z$) and ($x + 1/2$, $y + 1/2$, z) (positions II and III, respectively).[19]

Table 1. Selected bond lengths (Å) and angles (deg) around copper(II) for $Cu(gln)_2$; symmetry code: (i) $3/2-x$, $y-1/2$, $2-z$; (ii) $3/2-x$, $y + 1/2$, $1-z$.

Bond lengths		Bond angles	
Cu−O(11)	1.941(2)	O(21)−Cu−O(11)	179.10(7)
Cu−O(21)	1.951(2)	O(11)−Cu−N(11)	84.39(7)
Cu−N(11)	1.985(2)	O(11)−Cu−N(21)	95.62(8)
Cu−N(21)	1.984(2)	O(21)−Cu−N(21)	84.11(7)
Cu−O(12^{i})	2.848(3)	N(11)−Cu−N(21)	175.44(9)
Cu−O(22^{ii})	2.778(3)	O(12^{i})−Cu- O(22^{ii})	176.11(13)

Two different types of chemical paths connect copper ions within each layer. Cu^{I} and Cu^{IV} are connected by two similar carboxylate bridges of the *syn-anti* type ($-Cu-O_{ap}-C-O_{eq}-Cu-$), which gives rise to a 2-D network of copper ions (see Figure 2). The same situation occurs for Cu^{II} and Cu^{III} in the other layer (not shown). A similar equatorial-apical copper interaction in the layered compounds has been observed in the copper complexes with the amino acids phenylalanine,[7] methionine,[8] leucine,[9] alanine,[10,11] and α-aminobutyric acid.[12] The second path is provided by double hydrogen bonds N−H···O that connect the copper ions with identical spatial orientation (Figure 2). This connection, which involves equatorial ligands to the copper ions, gives rise to infinite polymeric chains along the *b* crystal axis. Copper ions having the same spatial orientation, but in neighboring layers, are connected by chemical paths that involve the skeleton of two amino acid molecules and double N−H···O hydrogen bonds (see Figure 3).

Crystal and Molecular *g*-Factor

The room temperature EPR spectra of $Cu(gln)_2$ display a single Lorentzian-shaped resonance line for any magnetic field orientation at the microwave frequencies of 9.8 and 33.9 GHz. Figure 4 shows the angular variation of the squared *g*-factor [$g^2(\theta,\varphi)$] observed at 9.8 GHz. A similar result is obtained at 33.9 GHz (data not shown). Since Cu^{I} and Cu^{III} sites [as well as Cu^{II} and Cu^{IV}] are related by a [1/2, 1/2, 0] translation, they have identical spatial orientation and consequently give rise to identical EPR spectra for any magnetic field orientation. Within each layer Cu^{I} and Cu^{IV} sites [as well Cu^{II} and Cu^{III}] are related by a C_{2b} rotation, and consequently the angular variation of their EPR spectra will also be related by the same symmetry operation. Therefore, two-symmetry related EPR spectra associated with copper ion pairs I−III and II−IV are expected for any magnetic field orientation except in the *ca* plane and along the *b* crystal axis, in which the four copper ions are magnetically equivalent. These resonance lines should be split by hyperfine interactions with the copper nuclear spin ($I = 3/2$) and the nitrogen ligands ($I = 1$). The fact that a single Lorentzian-shaped resonance line is observed for the

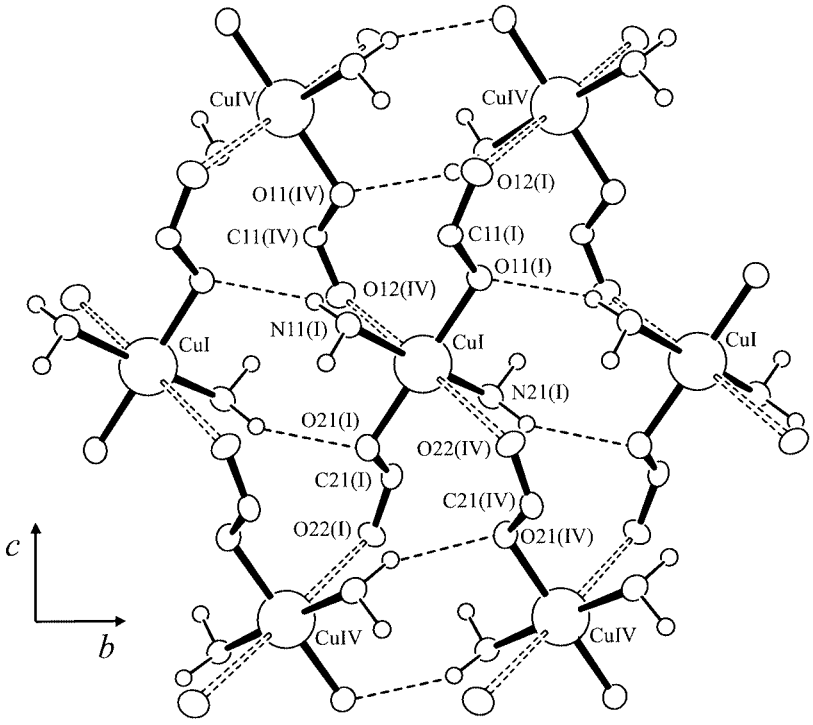

Figure 2. Orthogonal projection of $Cu(gln)_2$ along $a^* = b \times c$ crystal axis showing a copper atom and its six nearest copper neighbors within a layer; only the layer containing copper ions at symmetry positions I and IV is shown

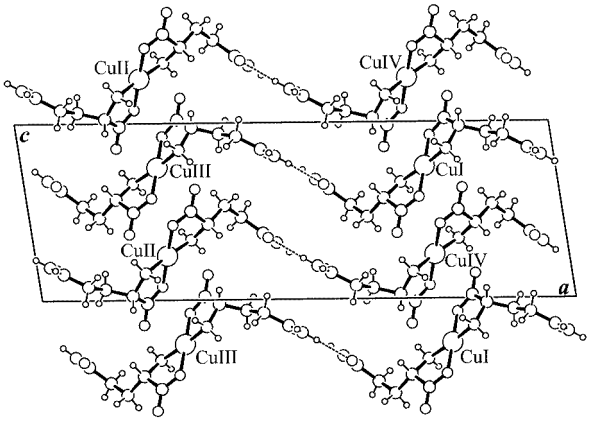

Figure 3. Orthogonal projection of $Cu(gln)_2$ along the b crystal axis showing the copper atom layers and the chemical paths connecting them

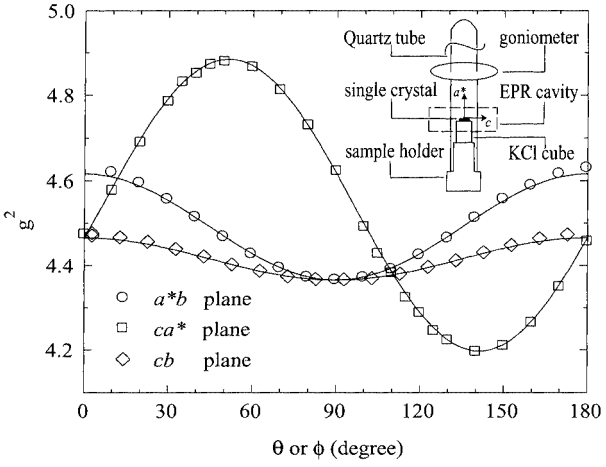

Figure 4. Angular variation of the squared g-factor measured at 298 K and 9.8 GHz in three orthogonal crystalline planes of $Cu(gln)_2$; the solid lines were obtained by fitting a symmetric $\boldsymbol{g}^2$ second-order tensor to the data; the parameters of the fit are included in Table 2; the inset schematizes the orientation of the sample for the EPR experiment

measured crystal planes, even at 33.9 GHz, indicates that the exchange interaction between the Cu^{II} ions is large enough to collapse both the expected hyperfine splitting and the resonance lines due to magnetically nonequivalent Cu^{II} ions.

For a magnetic system showing a single exchange-collapsed resonance line, the position of the observed resonance lines is described by the Zeeman Hamiltonian in Equation (1) where μ_B is the Bohr magneton, **S** is the effective spin operator ($S = 1/2$), $\boldsymbol{g}$ is the crystal $\boldsymbol{g}$-tensor defined as the average of the molecular $\boldsymbol{g}_i$-tensors (i = I,···IV), and **B** is the applied magnetic field.

$$H = \mu_B \mathbf{S} \cdot \boldsymbol{g} \bullet \mathbf{B} \quad (1)$$

The components of the crystal $\boldsymbol{g}$-tensor defined in Equation (1) were obtained by least-squares fitting the function $g^2(\theta,\phi) = \mathbf{h}\cdot\boldsymbol{g}^2\cdot\mathbf{h}$ to the experimental data, where $\mathbf{h} = \mathbf{B}/|\mathbf{B}| = (\sin\theta\cos\phi, \sin\theta\sin\phi, \cos\theta)$ is the direction of the applied magnetic field **B**. The components of $\boldsymbol{g}^2$ at both microwave frequencies, its eigenvalues and eigenvectors, are

given in Table 2. They were employed to calculate the solid lines shown in Figure 4.

Table 2. Values of the components of the g^2 tensor obtained by least-squares analyses of the data at both microwave frequencies. $(g^2)_1$, $(g^2)_2$ and $(g^2)_3$ and α_1, α_2 and α_3 are the eigenvalues and eigenvectors of the g^2 tensor in the $xyz = a^*bc$ coordinates system ($a^* = b\times c$); the values of $g_\perp$ and $g_\parallel$, the polar and azimuthal angles θ_m and ϕ_m of the normal to the square of ligands to copper ion in site I, and the angle 2α between the normals to copper ions in sites I and IV (identical to those of sites II and III) were calculated like in ref.[20]

9.8 GHz	33.9 GHz
$(g^2)_{xx} = 4.616(1)$	$(g^2)_{xx} = 4.6036(5)$
$(g^2)_{yy} = 4.366(1)$	$(g^2)_{yy} = 4.3918(5)$
$(g^2)_{zz} = 4.466(1)$	$(g^2)_{zz} = 4.4865(5)$
$(g^2)_{zx} = 0.33(5)$	$(g^2)_{zx} = 0.3255(5)$
$(g^2)_{xy} = (g^2)_{zy} = 0$	$(g^2)_{xy} = (g^2)_{zy} = 0$
$(g^2)_1 = 4.197(1)$	$(g^2)_1 = 4.2143(5)$
$(g^2)_2 = 4.884(1)$	$(g^2)_2 = 4.8758(5)$
$(g^2)_3 = 4.366(1)$	$(g^2)_3 = 4.3918(5)$
$\alpha_1 = [0.625(1), 0, 0.7808(1)]$	$\alpha_1 = [0.6415(3), 0, 0.7672(3)]$
$\alpha_2 = [0.7808(1), 0, -0.625(1)]$	$\alpha_2 = [0.7672(3), 0, -0.6415(3)]$
$\alpha_3 = [0, 1, 0]$	$\alpha_3 = [0, 1, 0]$
$g_\perp = 2.049$	$g_\perp = 2.053$
$g_\parallel = 2.248$	$g_\parallel = 2.248$
$2\alpha = 127.3°$	$2\alpha = 125.2°$
$\theta_m = 124.1$	$\theta_m = 124.7$
$\phi_m = 32.3$	$\phi_m = 34.0$

The components and principal directions of the copper molecular g_i-tensor shown in Table 2 were evaluated following the procedure described elsewhere assuming axial symmetry.[20] θ_m and φ_m are, respectively, the polar and azimuthal angles of the symmetry axis of the Cu^I site [identical to Cu^{III} site] referred as to the a^*bc crystal system, and 2α is the angle between the normals to the Cu^I and Cu^{IV} sites [identical to $Cu^{II}-Cu^{III}$]. The values for θ_m, φ_m and 2α are in a good agreement with the crystallographic ones ($\theta_c = 120.4°$, $\varphi_c = 29.0°$, and $2\alpha_c = 130.4°$), supporting the assumption of axial symmetry for this copper complex. The result obtained for the molecular g-tensor (Table 2) indicates a $d_{x^2-y^2}$ ground state orbital situated in the equatorial ligand plane of the Cu^{II} ion.[21]

EPR Line Width and Superexchange Paths

Figure 5 shows the angular variation of the peak-to-peak line width $[\Delta B_{pp}(\theta,\phi)]$ at 9.8 and 33.3 GHz. To analyze the variation of the line width with the magnetic field orientation, the data shown in Figure 5 were least-squares fitted with the function presented in Equation (2), where θ_n is the angle between the applied external magnetic field and the normal to the layers ($\cos\theta_n = \sin\theta\cos\phi$). The a_i coefficients, given in Table 3, were used to obtain the solid lines shown in Figure 5.

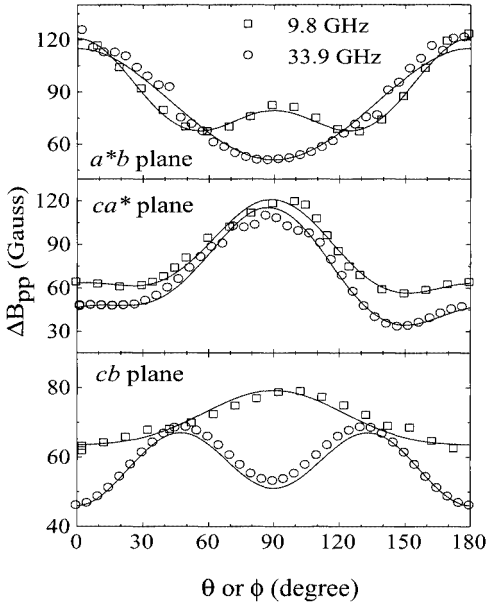

Figure 5. Angular variation of the peak-to-peak line width measured at 9.8 GHz and 33.9 GHz and 298 K in three orthogonal crystalline planes of $Cu(gln)_2$; the solid lines were obtained by fitting the data with Equation (2); the parameters of the fit are included in Table 3

Table 3. Values of the coefficients a_i (in Gauss) obtained at each microwave frequency by least-squares analyses of the line width data to Equation (2)

	9.8 GHz	33.9 GHz
a_1	75(1)	63(1)
a_2	66(1)	38(1)
a_3	52(1)	34(1)
a_4	7(1)	17(2)
a_5	11.7(1)	13.2(5)
a_6	n.d.[a]	1801(81)

[a] n.d. not detectable

$$\Delta B_{pp}(\theta,\phi) = a_1 \sin^2\theta\cos^2\phi + a_2 \sin^2\theta\sin^2\phi + a_3\cos^2\theta + a_4 \sin\theta\cos\theta\cos\phi + a_5(1-3\cos^2\theta_n)^2 + a_6[g_I(\theta,\phi) - g_{IV}(\theta,\phi)]^2 \quad (2)$$

Several mechanisms, such as dipolar interactions and incomplete collapse of the hyperfine splitting and/or the resonances corresponding to nonequivalent copper ions, contribute to the EPR line width in copper amino acid complexes.[22–25] The terms a_{1-4} in Equation (2) consider the contributions to the EPR line width of interactions having a second order angular variation, like the crystal g-tensor, such as the incomplete collapse of the hyperfine structure, as well as other smaller interactions (e.g. anisotropic and antisymetric exchange).[4] They are not important in our study, and therefore will not be analyzed further.

The term a_5 describes the dipolar contribution for a 2-D magnetic system.[26] The typical angular variation originat-

ing from this interaction can be visualized at the X-band in Figure 5. At the Q-band, the contribution of the dipolar interaction in both *a*b* and *cb* planes is masked by the contribution described by the term a_6, which is negligible at the X-band but not at the Q-band (see below).

The term a_6 in Equation (2) takes into account the contribution to the line width arising from the presence of two magnetically nonequivalent copper sites in the crystal lattice of $Cu(gln)_2$. As discussed elsewhere,[27,28] this interaction depends on both the microwave frequency and the number of neighboring nonequivalent Cu^{II} ions connected by the bridge. Its contribution can be identified at the Q-band in the *cb* and, though less noticeable, *a*b* crystal planes (see Figure 5 and Table 3). On the contrary, in the *ca** crystal plane, where the four copper ions are magnetically equivalent, the line width does not show significant differences at both frequencies, except for a small constant shift. This shift is attributed to nonsecular terms of the Zeeman interaction that only make a contribution at the X-band.[29]

For a system having two magnetically nonequivalent copper ions per unit cell, the coefficient a_6 in Equation (2) is given by Equation (3),[28,30] where $g = 1/3\ \mathrm{tr}(\boldsymbol{g})$ is the isotropic *g*-factor, ω_o is the Larmor frequency, and ω_e is the exchange frequency.

$$a_6 = (2/3\pi)^{1/2}\, \omega_o^2\, \hbar/4\, g^3\, \omega_e\, \mu_B \qquad (3)$$

Using Equation (3) and the a_6 value obtained from the fitting (Table 3 and Figure 5) we calculated $\omega_e = 1.089 \times 10^{11}\ s^{-1}$, which is related to the exchange parameters through Equation (4)[28] where J_i's are the exchange parameters associated with the chemical paths connecting magnetically nonequivalent copper ion pairs and z_i is the number of the nearest neighboring copper ions connected by the ith chemical path.

$$\hbar\,\omega_e = (\Sigma_i z_i J_i^2)^{1/2} \qquad (4)$$

As shown in Figures 2 and 3, each copper ion is connected to only four nonequivalent neighboring copper ions through two similar *syn-anti* carboxylate bridges. Further, since line-width data indicate a 2-D magnetic behaviour, it is reasonable to assume $J_1 \approx J_2$, where J_1 and J_2 are the exchange parameters associated with each carboxylate bridge. Then, from Equation (4) we obtain a mean exchange parameter $|J|/k = 0.42(2)$ K for the intralayer bridge connecting magnetically nonequivalent copper ions (Figure 2).[31] This value is supported by the lowest limit $|J|/k \geq 0.13$ K estimated from the collapse condition $J \geq \Delta g\, \mu_B\, B$ at Q-band. The model employed to analyze the EPR data does not allow for the measurement of exchange couplings between magnetically equivalent copper ions associated with intra- or interlayer bridges (Figures 2 and 3). However, the observed 2-D spin dynamic indicates that the interlayer exchange couplings are negligible (Figure 3). Thermodynamic measurements at very low temperatures (< 1 K) performed on the copper compounds with the amino acids L-alanine[32,33] and α-aminobutyric acid[34] indicate that *syn-anti* carboxylate bridges involving equatorial and apical ligands to the copper ions transmit antiferromagnetic interactions. Therefore, a similar magnetic behaviour is expected for all copper amino acid compounds that show this characteristic.

Levstein and Calvo observed that the magnitude of *J* decreases linearly with an increase in the $Cu-O_{ap}$ bond length for three Cu^{II} amino acid complexes.[35] According to their results, the *J* value for $Cu(gln)_2$ should be smaller than 0.1 K. A similar discrepancy was obtained for the copper complexes with L-alanine[32] and L-α-aminobutyric acid.[12] Thus, the length of the $Cu-O_{ap}$ bond is not the only factor that determines the magnitude of the magnetic interactions, but other structural factors should also be considered. Table 4 shows the *J* values, the $Cu-O_{ap}$ distances and the dihedral angles between the plane of the carboxylate bridge and the planes (eq and eq′) of the equatorial ligands of the two magnetically nonequivalent Cu^{II} ions connected by the bridge for six layered Cu^{II} L-amino acid complexes. As seen in Table 4, the compounds studied in ref.[35] have similar dihedral angles, deviating by about two degrees from the mean value. Meanwhile, the compounds that do not follow the proposed dependence of the magnitude of *J* with the $Cu-O_{ap}$ length have smaller dihedral angles when the longer $Cu-O_{ap}$ bond is taken into account. For the shorter $Cu-O_{ap}$ bond, there is a dual behaviour: on the one hand no significant changes are observed for the higher angles (< eq−OCO in Table 4); on the other hand, a slight increase of the angle value is observed for the lower angles (< eq′−OCO in Table 4). Consequently, the results in Table 4 suggest that the values of the angles between the magnetic orbitals of the Cu^{II} ion and the OCO plane, play a key role regarding the *J* value. They indicate that the higher the planarity of the Cu−OCO−Cu bridge, the larger the magnitude of the exchange interaction. This is in line with previous observations for some copper dimers, which yielded the same conclusion.[36]

Table 4. *J*-values, copper-apical ligand bond lengths, and angles between the carboxylate group bridging equatorial ligand planes of two nearest magnetically nonequivalent Cu^{II} ions (eq and eq′) in six layered Cu^{II}-L-amino acid complexes

Compound	$\lvert J/k\rvert$ [K]	d Cu−O_{ap} [Å]	<eq−OCO [°]	<eq′−OCO [°]	Ref
$Cu(met)_2$	0.10(1)	2.675	75.2	17.7	[8,35]
		2.751	67.8	10.8	
$Cu(leu)_2$	0.23(1)	2.628	79.2	18.1	[9,35]
		2.749	72.2	12.0	
$Cu(phe)_2$	0.38(2)	2.578	77.4	16.4	[7,35]
		2.690	71.0	10.9	
$Cu(ala)_2$	0.33(1)	2.698	75.9	21.8	[10,11,32]
		2.904	58.5	6.6	
$Cu(but)_2$	0.36(3)	2.676	73.1	16.3	[12]
		2.783	64.9	9.1	
$Cu(gln)_2$	0.42(2)	2.778	72.4	19.7	This work
		2.848	59.9	7.7	

Conclusion

This work demonstrates that $Cu(gln)_2$ belongs to the family of copper amino acid complexes in which the amino acid R group is not involved in the Cu^{II} coordination resulting in a layered structure of copper ions connected by equatorial-apical *syn-anti* carboxylate bridges. Cu^{II} complexes of amino acids are among the few examples of equatorial-apical *syn-anti* carboxylate-bridged compounds magnetically characterized so far.[37] In this work we show that the magnitude of the exchange interaction depends on both the $Cu-O_{ap}$ distance and the angles between the equatorial ligand plane and the bridging ligand plane. The larger the co-planarity between the Cu^{II} equatorial ligand plane and the OCO plane, the larger the J value.

Experimental Section

Sample Preparation: All commercially available chemicals were reagent grade and used without further purification. Single crystals of $Cu(gln)_2$, $Cu[NH_2CO_2CH(CH_2)_2CONH_2]_2$, were obtained by dissolving L-glutamine (730.5 mg, 5 mmol) and basic copper carbonate (276.4 mg, 2.5 mmol) in ion-exchanged water (40 mL). This solution was stirred for a few minutes until a light-blue colour developed, and the solid was filtered out, using a 0.22 μm Millipore filter. The pH of the resulting solution was adjusted to 9 and left to evaporate at room temperature. Thin blue plates were obtained after one week. The crystals are elongated along the b direction and show well defined bc lateral faces.

X-ray Structural Determination. Data Collection, Solution, and Refinement of the Structure. X-ray data were collected at 120 and 293 K on an Enraf−Nonius KappaCCD diffractometer with Mo-K_α (λ = 0.71073 Å) graphite monochromated radiation. Diffraction data were reduced and corrected using the DENZO and SCALEPACK Programs.[38] Structures were solved by direct methods with the help of the SHELXS-97 program[39] and refined on reflection intensities (F^2) using the SHELXL-97 program.[40]

Table 5. Summary of the crystal data, intensity collection, and structure refinement parameters for $Cu(gln)_2$.

Formula	$C_{10}H_{18}CuN_4O_6$
Crystal size (mm)	0.08 × 0.06 × 0.02
Molecular mass	353.82
Space group	$C2$
Crystal system	monoclinic
a (Å)	28.0610(5)
b (Å)	5.0756(1)
c (Å)	9.3719(2)
β (deg)	99.5139(8)
Z	4
$d_{calcd.}$ (g/cm^3)	1.785
Absorption coefficient (mm^{-1})	1.695
θ range for data collection (deg)	2.20 to 25.77
Reflections collected/unique	12752/2288 [R(int) = 0.092]
Data/restraints/parameters	2288/5/206
Goodness-of-fit on F^2	1.069
Final R indices [$I > 2\sigma(I)$][a]	$R1$ = 0.0214, $wR2$ = 0.0559

[a] R indices defined as: $R1 = \Sigma||Fo| - |Fc||/\Sigma|Fo|$, $wR_2 = [\Sigma w(Fo^2 - Fc^2)^2/\Sigma w(Fo^2)^2]^{1/2}$.

Crystal data, structure determination methods and refinement results at 120 K are summarized in Table 5. All H atoms were located among the first 18 peaks of a difference Fourier map. As expected, the terminal amine H atoms were found close to the OCN plane. These hydrogen atoms were therefore positioned stereochemically on the corresponding planes and refined with the riding model. The hydrogen atoms of the amine group coordinated to the copper(II) ion were refined isotropically with N−H bond lengths restrained to a target value of 0.89(1) Å. The remaining glutamine H atoms were also positioned on a stereochemical basis and refined with the riding model. The room temperature solid is isomorphous to that of the low temperature one.

CCDC-179785 contains the supplementary crystallographic data for this paper. These data can be obtained free of charge at www.ccdc.cam.ac.uk/conts/retrieving.html [or from the Cambridge Crystallographic Data Centre, 12, Union Road, Cambridge CB2 1EZ, UK; Fax: (internat.) +44-1223/336-033; E-mail: deposit@ccdc.cam.ac.uk].

EPR Measurements: EPR spectra at 9.8 GHz (X-band) and 33.9 GHz (Q-band) were acquired on Bruker ER-200 and Bruker ESP300 spectrometers, respectively, using a Bruker rectangular cavity ER4102ST (X-band) and a cylindrical cavity ER5101Q (Q-band). The field modulation was 100 kHz in both cases. All the experiments were carried out at room temperature.

The samples were oriented by gluing the single crystal bc face to a cleaved KCl cubic holder, which defines a set of x,y,z orthogonal axes with the x axis along the $a^* = b\times c$ direction, and the y and z directions along the b and c crystal axes, respectively. For the X-band measurements, the sample holder was positioned on the horizontal plane at the top of a pedestal, which was introduced into a 4 mm OD Quartz tube (see inset on Figure 4). For the Q-band measurements, the samples were mounted only on the pedestal. Both devices were introduced into the cavity, and the EPR spectra were taken with the magnetic field along several directions of the crystal planes a^*b, ca^* and cb of the sample. Positions and peak-to-peak line widths (ΔB_{pp}) of the resonance lines were obtained by least-squares fitting of the spectra to a Lorentzian derivative line.

Acknowledgments

This work was supported by the Universidad Nacional del Litoral (CAI+D 291) (Argentina), the Consejo Nacional de Investigaciones Científicas y Técnicas (CONICET) (Argentina), Fundación Antorchas (Argentina), the Conselho Nacional de Pesquisas (CNPq) (Brazil), and the Fundação de Amparo a Pesquisa do Estado de São Paulo (FAPESP) (Brazil). We thank Dr. Fernando Pelegrini (UFG, Brazil) in whose lab we performed the Q-band EPR measurements.

[1] S. J. Lippard, J. M. Berg, *Principles of Bioinorganic Chemistry*, University Science Books, Mill Valley, California, **1994**.
[2] M. J. Romão, J. Knäblein, R. Huber, J. J. G. Moura, *Prog. Biophys. Molec. Biol.* **1997**, *68*, 121−144.
[3] R. Calvo, E. C. Abresch, R. Bittl, G. Feher, W. Hofbauer, R. A. Isaacson, W. Lubitz, M. Y. Okamura, M. L. Paddock, *J. Am. Chem. Soc.* **2000**, *122*, 7327−7341.
[4] A. Bencini, D. Gatteschi, *Electron Paramagnetic Resonance of Exchange Coupled Systems*, Springer, Berlin, **1989**.
[5] S. K. Hoffmann, W. Hilczer, J. Goslar, *Appl. Magn. Reson.* **1994**, *7*, 289−321 and references therein.
[6] M. C. G. Passeggi, R. Calvo, *J. Magn. Reson. A* **1995**, *114*, 1−11.

[7] D. van der Helm, M. B. Lawson, E. L. Enwall, *Acta Crystallog. B* **1971**, *27*, 2411−2418.
[8] C. C. Ou, D. A. Powers, J. A. Thich, T. R. Felthouse, D. N. Hendrickson, J. A. Potenza, H. J. Schugar, *Inorg. Chem.* **1978**, *17*, 34−40.
[9] T. G. Fawcett, M. Ushay, J. P. Rose, R. A. Lalancette, J. A. Potenza, H. J. Schugar, *Inorg. Chem.* **1979**, *18*, 327−332.
[10] A. Dijkstra, *Acta Crystallog.* **1966**, *20*, 588−590.
[11] M. A. Hitchman, L. Kwan, L. M. Engelhardt, A. H. White, *J. Chem. Soc., Dalton Trans.* **1987**, 457−465.
[12] P. R. Levstein, R. Calvo, E. E. Castellano, O. E. Piro, B. E. Rivero, *Inorg. Chem.* **1990**, *29*, 3918−3922.
[13] R. Calvo, C. A. Steren, O. E. Piro, T. Rojo, F. J. Zuñiga, E. E. Castellano, *Inorg. Chem.* **1993**, *32*, 6016−6022.
[14] R. F. Baggio, R. Calvo, C. D. Brondino, M. T. Garland, A. M. Atria, E. Spodine, *Acta Crystallog. C.* **1995**, *51*, 382−385.
[15] C. M. Gramaccioli, R.E. Marsh, *Acta Crystallog.* **1966**, *21*, 594−605.
[16] L. Antolini, G. Marcotrigiano, L. Menabue, G. C. Pellacani, M. Saladini, M. Sola, *Inorg. Chem.* **1985**, *24*, 3621−3626.
[17] F. S. Stephens, R. S. Vagg, P. A. Williams, *Acta Crystallog. B* **1974**, *27*, 841−845.
[18] C. K. Johnson, ORTEP. Report ORNL-3794, Oak Ridge, TN, **1965**.
[19] *International Tables for X-ray Crystallography*, Vol. IV, Kynoch Press, Birmingham, **1974**.
[20] R. Calvo, M. A. Mesa, *Phys. Rev. B* **1983**, *28*, 1244−1248.
[21] H. J. Zeiger, G. W. Pratt, *Magnetic Interactions in Solids*, Oxford University Press, London, **1973**.
[22] A. M. Gennaro, P. R. Levstein, C. A. Steren, R. Calvo, *Chem. Phys.* **1987**, *111*, 431−438.
[23] H. Yokoi, S. Ohsawa, *Bull. Chem. Soc. Japan* **1973**, *46*, 2766−2768.
[24] P. R. Newman, J. M. Imes, J. A. Cowen, *Phys. Rev. B* **1976**, *13*, 4093−4097.
[25] R. Calvo, H. Isern, M. A. Mesa, *Chem. Phys.* **1985**, *100*, 89−99.
[26] P. M. Richards, M. B. Salamon, *Phys. Rev. B* **1974**, *9*, 32−45.
[27] C. D. Brondino, N. M. C. Casado, M. C. G. Passeggi, R. Calvo, *Inorg. Chem.* **1993**, *32*, 2078−2084.
[28] P. R. Levstein, C. A. Steren, A. M. Gennaro, R. Calvo, *Chem. Phys.* **1988**, *120*, 449−459.
[29] A. M. Gennaro, R. Calvo, *J. Phys. Condens. Matter* **1989**, *1*, 7061−7068.
[30] In Equations (3) and (4) a Heisenberg exchange Hamiltonian $H_{ex} = -J\mathbf{S}_i.\mathbf{S}_j$ was assumed.
[31] EPR spectroscopy cannot determine the sign of the exchange interaction.
[32] R. Calvo, M. C. G. Passeggi, M. A. Novak, O. G. Symko, S. B. Oseroff, O. R. Nascimento, M. C. Terrile, *Phys. Rev. B* **1991**, *43*, 1074−1083.
[33] R. E. Rapp, H. Godfrin, R. Calvo, *J. Phys. Condens. Matter* **1995**, *7*, 9595−9606.
[34] M. L. Siqueira, R. E. Rapp, R. Calvo, *Phys. Rev. B* **1993**, *48*, 3257−3263.
[35] P. R. Levstein, R. Calvo, *Inorg. Chem.* **1990**, *29*, 1581−1582.
[36] O. Kahn, *Molecular Magnetism*, VCH Publishers, Inc., New York, **1993**, chapter 8.
[37] E. Colacio, M. Ghazi, R. Kivekäs, J. M. Moreno, *Inorg. Chem.* **2000**, *39*, 2882−2890 and references therein.
[38] Z. Otwinowski, W. Minor in *Methods in Enzymology* (Eds.: C.W. Carter Jr., R. M. Sweet), Academic Press, New York, **1997**, *276*, 307−326.
[39] G. M. Sheldrick, *SHELXS-97, Program for Structure Solution*, University of Göttingen, Göttingen, Germany, **1997**.
[40] G. M. Sheldrick, *SHELXL-97, Program for Structure Refinement*, University of Göttingen, Göttingen, Germany, **1997**.

Received April 14, 2002
[I02195]

Stereochemical Analysis of Cobalt(III) Complexes with Tridentate Imino- and Amino-Oxime Ligands

Mario Calligaris*[a] and L. Randaccio[a]

Keywords: Stereochemistry / Molecular mechanics / Tridentate ligands / Cobalt / Vitamin B_{12}

The stereochemistry of a new class of models of the vitamin B_{12} system, containing tridentate pyridyl-imino-oxime [$C_6H_5N(CH_2)_nNC(CH_3)C(CH_3)NO^-$; n = 1, L^1; n = 2, L^2] and pyridyl-amino-oxime [$C_6H_5N(CH_2)_nNHCH(CH_3)$-$C(CH_3)NO^-$; n = 1, L^3; n = 2, L^4] ligands, has been investigated through molecular mechanics calculations based on a specific force field. It is shown that, among all the possible diastereomers of the imino complexes $[Co(L^{1,2})_2]^+$, the minimum strain energy is exhibited in a *mer* configuration. For the amino complexes $[Co(L^{3,4})(HL^{3,4})]^{2+}$, the minimum is exhibited in a *fac* configuration, with the amino nitrogen atoms all having the same chirality, opposite to that of the adjacent carbon atoms. Furthermore, comparison of the effect of five- (L^1, L^3) or six-membered (L^2, L^4) chelate rings on the complexes indicates that the strain energy decreases upon passing from L^1 to L^2 complexes, while it increases upon passing from L^3 to L^4 complexes. The effect of rotation around the axial pyridyl Co–N bond on the coordination geometry has also been studied through a conformational analysis of the methyl (R = Me) and adamantyl (R = Adam) organocobalt derivatives $[RCo(L^4)(HL^4)]^+$. The most important result is that the rotation is rather hindered in the case of the bulky Adam group, while in the Me case the pyridyl group can rotate across a wide angular range. In both cases, the rotation causes a significant change in the Co–N bond length, while the Co–C distance is almost unaffected. It is also shown that the aromatic base is oriented with respect to the equatorial ligand in a fashion quite different from other B_{12} models.
(© Wiley-VCH Verlag GmbH, 69451 Weinheim, Germany, 2002)

Introduction

In recent years,[1−3] tridentate imino- and amino-oxime ligands, obtained by condensation of biacetyl monoxime with 2-(aminomethyl)pyridine and 2-(2-aminoethyl)pyridine (see Scheme 1), have been used to prepare stable alkylcobalt complexes, which differ in a number of respects from the widely studied tetradentate ligand derivatives.[4] Thus, it has recently been shown[3] that organocobalt(III) complexes of formula $[RCo(L^4)(HL^4)]^+$ (Figure 1, a), containing the tridentate 3-[2-(2-pyridyl)ethylamino]butane-2-one-oximato ligand (L^4) and its protonated form (HL^4), constitute a new type of model of alkylcobalamins (vitamin B_{12} system).[5] Their geometry is reminiscent of the lariat-type complexes (Figure 1, b),[6] which combine the corrin-like features of iminocobaloximes with an appended axial base, but differs by having a more crowded equatorial moiety. Structural evidence[3] indicates that their properties are closer to those of alkylcobalamins (particularly for the C−Co−N axial fragment) than that of any of the other previously reported models,[7] such as the well documented alkylcobaloximes, $RCo(DH)_2L$ (DH = monoanion of dimethylglyoxime). This has been attributed to the more crowded nature of the equatorial moiety (planar in cobaloximes), which would cause stronger steric interactions with the axial ligands.[2,3] Therefore, these compounds offer the opportunity to study the influence of the electronic and steric factors on the axial Co−C and Co−N bonds, thereby extending the previous molecular mechanics (MM) investigation on alkylcobaloximes.[8]

Structural investigations of lariat-type complexes[6] and alkylcobaloximes[7,8] have shown that the Co−N axial bond length is significantly affected by the relative orientation of the N and equatorial ligands. This feature becomes relevant in light of the evidence of substitution in some B_{12} enzymes of the Co-bound benzimidazole residue with a histidine group of the protein chain.[9] Therefore, the study of the nature of the Co−N bond in simple models,[6a,10] and particularly of the influence of the orientation of the nitrogen base with respect to the equatorial ligand, is of special interest.[8,11]

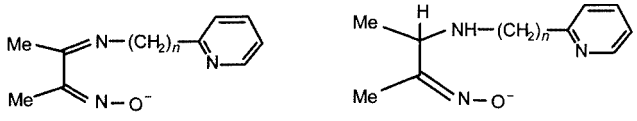

n = 1, L1 n = 2, L2 n = 1, L3 n = 2, L4

Scheme 1

[a] Centro di Eccellenza di Biocristallografia, Dipartimento di Scienze Chimiche, Università degli Studi di Trieste
Via L. Giorgieri 1, 34127 Trieste, Italy
Fax: (internat.) +39−040/558-3903
E-mail: calligaris@univ.trieste.it
Supporting information for this article is available on the WWW under http://www.eurjic.org or from the author.

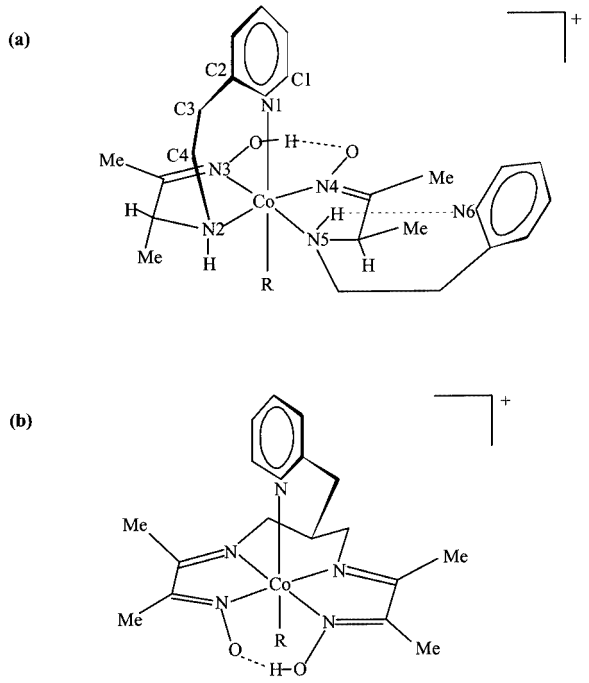

Figure 1. (a) Sketch of the structure of $[RCo(L^4)(HL^4)]^{2+}$ with a numbering scheme for the relevant atoms. (b) Sketch of the structure of a lariat type complex

$[RCo(L^4)(HL^4)]^+$ species may be obtained from $[Co(L^4)(HL^4)]^{2+}$ by reduction and successive oxidative alkylation.[3] In turn, the latter complex may be obtained by hydrogenation of the imino-oxime derivative $[Co(L^2)_2]^+$ (Figure 2).[2] Interestingly, starting from the 2-(aminomethyl)pyridine complex $[Co(L^1)_2]^+$ and under the same conditions, the metal reduction and alkylation reactions do not occur and only the hydrogenation product $[Co(L^3)(HL^3)]^{2+}$ is obtained.[2] This difference has been attributed to a more strained coordination in the L^1 complex with respect to that in the L^2 derivative.[2]

In order to provide some insight into the different strain energies of the $[Co(L^1)_2]^+ - [Co(L^2)_2]^+$ and $[Co(L^3)(HL^3)]^{2+} - [Co(L^4)(HL^4)]^{2+}$ complexes, a stereochemical investigation has been carried out through MM calculations, by implementation of the previously derived cobaloxime force field.[8] Furthermore, the present investigation includes an analysis of all the possible diastereomers of these complexes, denoted as $[Co(A\hat{}B\hat{}C)_2]$, where A^B^C represents the tridentate ligand with its three different nitrogen donors, A, B, and C (Figure 3). In the cases of the L^3 and L^4 complexes, ligand chirality, arising from the presence of stereogenic nitrogen and carbon centres in the equatorial ligand (N2, N5, and their adjacent C atoms, see Figure 2, b), has also been taken into account. This appears to be of some interest for an investigation of the possible species present in solution, considering that the $[Co(L^1)_2]^+$ [12] and $[Co(L^2)_2]^+$ complexes have been found in the solid state in a *mer* configuration, while the $[Co(L^3)(HL^3)]^{2+}$ and $[Co(L^4)(HL^4)]^{2+}$ complexes have been isolated in the *fac* configuration with *trans* pyridyl groups and *cis* amino and oxime nitrogen atoms.[2]

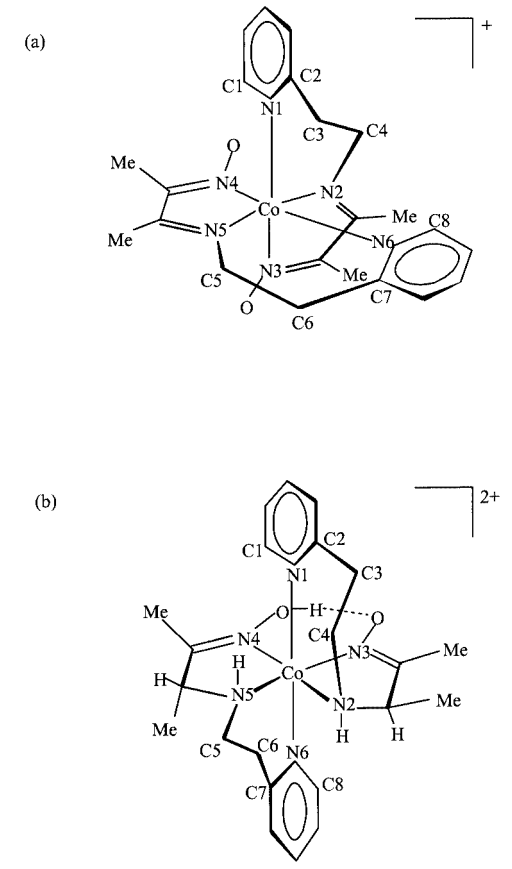

Figure 2. Sketch of the structure of $[Co(L^2)_2]^+$ (a) and $[Co(L^4)(HL^4)_2]^{2+}$ (b), with a numbering scheme for the relevant atoms. Hydrogen atoms are shown for H bonds and the chiral C and N atoms

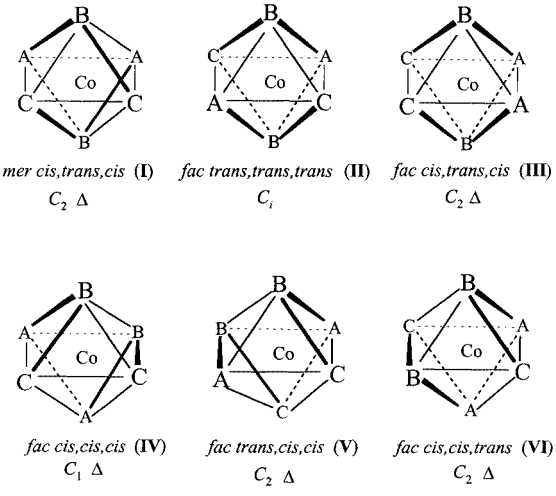

Figure 3. Schematic depiction of the six possible diastereomers for octahedral cobalt complexes containing two tridentate ligands A^B^C. Point symmetry and complex chirality are also shown. Larger letters define the octahedron upper triangular face. Thick lines represent the ligand bites

After validation of the force field, the effect of rotation around the axial Co−N bond on the metal coordination geometry has been investigated for the $[MeCo(L^4)(HL^4)]^+$

complex. The study has also been extended to the much bulkier adamantyl (Adam) derivative, even if not thus far isolated, in order to address the effects of the alkyl bulkiness. The results of the conformational analysis are also useful for a comparison between sterically different equatorial ligands, such as $(L^4)(HL^4)$ and $(DH)_2$.[4,5]

Results

Methods

Energy calculations have been performed with a Pentium III PC, using the HyperChem 6.01 molecular modelling system.[13] The Polak−Ribiere version of the conjugate gradient method was used in all energy minimisation calculations with a convergence criterion of 0.001 kcal·mol^{-1}·Å^{-1}.

The AMBER force field,[14] already implemented for the stereochemical investigation of cobaloximes,[8] has been used after further addition of the new atom types, NP_R, NI_R, NH_R, NE_R, and NO_R (R = X, Y, Z) for the pyridyl (py), imino (im), amino (am), protonated and nonprotonated oximato (ox) nitrogen atoms, respectively. The relative stretching and bending force field constants (Table 1) have been derived by the methods and optimisation procedure previously described,[8,15] which are based on the crystal structure atom parameters of the Co−L^{1-4} complexes.[3] The minimised function is GOF = $[\Sigma_i w_i \Delta_i^2/(n_{obsd.} - n_p)]^{1/2}$, where $n_{obsd.}$ is the number of observables (388 in the present case) with weights $w_i = 1/\sigma_i^2$, n_p is the number of variable parameters (11), the summation being extended to all the differences, Δ_i, between each observed and calculated value. In order to simulate crystal packing effects that can affect the torsion angles and yield to strained geometries, the pyridyl endocycle N−Co−N−C and N−C−C−C torsion angles were restrained to the observed values by force constants of 20 kcal·mol^{-1}. In order to estimate the electrostatic contribution to the total strain energy, E, the dielectric constant D = 7.8 has been used, as for cobaloximes.[8]

Table 1. Optimised force field stretching [k^d (kcal·mol^{-1}·Å^{-2}), d^o (Å)] and bending [k^θ (kcal·mol^{-1}·rad^{-2}), θ^o (°)] constants

[a]	k^d	d^o
CO3−NE_R	104.03	1.9712
CO3−NP_R	123.30	1.9255
CO3−NI_R	108.37	1.9600
CO3−NH_R	101.69	1.9776
CO3−NO_R	108.27	1.9602
NO_R−O1	647.61	1.2713
	k^θ	θ^o
CO3−NH_R−CT	61.89	110.40
CO3−NI_R−CDH	53.22	120.10
CO3−NI_R−CT	48.36	125.50
CO3−NO_R−CDH	51.15	122.50
CO3−NO_R−O1	65.57	121.10

[a] R = X, Y, Z.

Atomic charges for each molecule have been calculated by the semi-empirical ZINDO/1 method, using restricted Hartree Fock functions,[13] and then averaged over chemically equivalent atoms. At convergence GOF was 4.786, with a difference between the lowest and highest GOF values of less than 0.0001.

In order to explore, as thoroughly as possible, the conformational space of the complexes of type $[Co(L)_2]^+$ and $[Co(L)(HL)]^{2+}$ (L = L^3, L^4), all possible stereoisomers have been built using HyperChem, considering all combinations of nitrogen and carbon chiralities. The strain energies of all these diastereomers have been calculated by molecular energy minimisation, without any torsion restraint and with $D = r_{ij}$, in order to simulate solvent effects.[14]

Because of the uncertainty in the location of the oxime bridge hydrogen atoms, it has been assumed, as in the case of cobaloximes,[8] that the hydrogen atom (atom type HDH) lies on the median of the O···O segment (atom types ODH). The energy of the H-bonding interaction is given by electrostatic interactions and by the stretching of the ODH−HDH bond (d^o = 1.269, k^d = 198.9 kcal·mol^{-1}·Å^{-2}). Where it has been assumed that this H bond is not present (L^o ligands), one ODH−HDH bond has been substituted by an ODH−HO bond (d^o = 0.96 Å, k^d = 553.0 kcal·mol^{-1}·Å^{-2}) and the other oxygen atom treated as type O1. In this case, when properly oriented, the O1 atom can give rise to a hydrogen bond interaction with HO only through electrostatic interactions.

For the conformational analysis of the alkyl derivatives $[RCo(L^4)(HL^4)]^+$, with R = Me and Adam, the strain energy has been minimised (D = 7.8) by rotating about the Co−N(py) bond (torsion angle φ_1 = N2−Co−N1−C2, see Figure 1) in steps of 5°, with a restraint constant of 1000 kcal·mol^{-1}. For these complexes, the force field constants derived for the axial ligands of the relative alkyl/pyridine cobaloxime have been adopted.[8] The Δ isomer with S and R configurations for the nitrogen and carbon atoms, respectively, has been used in the calculations, maintaining the intramolecular N5···N6 hydrogen bond (Figure 1, a) present in the solid state.

In all calculations, the same improper torsion parameters have been assigned to trigonal carbon atoms (atom type CA) and trigonal nitrogen atoms, taking the parameters of CA given in AMBER.[14] As in previous calculations,[8] torsion barriers around the coordination bonds have not been considered.

A local program[16] has been used for all the geometrical calculations, including the ring puckering parameter Q,[17] and the conformation discriminator Δ_c.[18]

Validation of the Force Field

As shown in Table 2, the agreement between observed and calculated bond lengths and angles for the Co−L^{1-4} complexes is quite satisfactory, on the basis of the values of the average differences $<\Delta>$ and the root-mean-square deviations, rms = $[(\Sigma_i \Delta_i^2)/n]^{1/2}$.

Moreover, the consistency of the force field is well illustrated (Table 3) by its ability to reproduce the observed vari-

Table 2. Average differences, <Δ>, between observed and calculated bond lengths [Å] and angles [°], together with rms values (Å) and number of observations, *n*; X, Y, and Z represent generic non-metal atoms

Distances	<Δ>	rms	n
Co−X	−0.006	0.019	24
X−Y	−0.015	0.022	116
Angles			
X−Co−Y	−0.2	1.6	60
Co−X−Y	−0.4	1.5	48
X−Y−Z	0.3	1.4	140

Table 3. Selected average observed and calculated bond lengths [Å] and angles [°] for $[Co(L)_2]^+$ (L = L^1, L^2), and $[Co(L)(HL)]^{2+}$ (L = L^3, L^4)

	L^1 obsd.	L^2 obsd.	L^1 calcd.	L^2 calcd.
Co−N(py)	1.953	2.038	1.926	2.018
N(py)−Co−N(im)	83.8	93.8	85.2	94.1
	99.5	94.6	96.6	93.1
N(py)−Co−N(ox)	166.1	174.9	168.2	174.6
Co−N(py)−C_α[a]	125.7	119.0	127.3	121.3
Co−N(py)−C_β[a]	113.9	123.8	112.9	121.7
Co−N(im)−C [b]	118.1	123.2	118.6	125.3
	116.2	114.0	116.0	114.1
	L^3 obsd.	L^4 obsd.	L^3 calcd.	L^4 calcd.
Co−N(py)	1.916	2.026	1.921	2.042
N(py)−Co−N(am)	83.5	88.3	84.7	89.1
	92.1	89.7	93.3	88.5
N(py)−Co−N(ox)	89.9	84.8	87.4	86.3
	94.7	93.0	94.6	92.2
Co−N(py)−C_α[a]	126.0	116.8	126.8	119.1
Co−N(py)−C_β[a]	114.3	126.5	113.8	124.8
Co−N(am)−C [c]	106.9	114.9	107.7	115.0
	111.1	111.5	109.5	110.5

[a] C_α and C_β represent, respectively, the pyridyl carbon atoms like C1, C2 and C8, C7 in Figure 2. [b] The first line refers to the pyridyl bridge, the second one to the oxime ring. [c] The first line refers to the pyridyl bridge, the second one to the equatorial ring.

ations[2] of both bond lengths and angles on passing from $[Co(L^1)_2]^+$ to $[Co(L^2)_2]^+$, as well as from $[Co(L^3)(HL^3)]^{2+}$ to $[Co(L^3)(HL^3)]^{2+}$, that is on passing from complexes with ligands L^1, L^3 [$-(CH_2)-$ bridges] to complexes with ligands L^2, L^4 [$-(CH_2)_2-$ bridges]. The conformational parameters of the calculated structures are also in good agreement with those observed (Table 4).

In the case of the methyl derivative, $[MeCo(L^4)(HL^4)]^+$, the agreement between observed and calculated coordination bond lengths (Table 5) is not as good (rms = 0.033 Å) as that found in the Co−L^{1-4} complexes (rms = 0.019 Å). This indicates that the force field is not completely transferable to the organometallic derivatives. However, for the limited scope of this work, it is sufficient that the trend in the Co−N bond lengths, Co−N(ox) < Co−N(am) < Co−N(py), as well as the deviations from 90° of the coordination bond angles involving the coordinated pyridyl ligand (Table 5), are well reproduced. Furthermore, it is to be stressed that the perchlorate anion and the methyl group in the crystal structure are affected by thermal motion, reducing the accuracy of the crystal structure determination.[3] Correction of the experimental distances for this effect (riding model) reduces the rms deviation of the Co−X distances to 0.022 (Table 5).

Table 4. Conformational parameters of the two pyridyl chelate rings for $[Co(L)_2]^+$ (L = L^1, L^2) and $[Co(L)(HL)]^{2+}$ (L = L^3, L^4). The two rings are defined by the bites N1−N2 and N5−N6, respectively

	L^1 obsd.	L^1 calcd.	L^2 obsd.	L^2 calcd.
Conformation	planar	planar	half-chair[a]	half-chair[a]
	planar	planar	half-chair [b]	half-chair[b]
Helicity			δ	δ
			δ	δ
Discriminator (Δ_c)	5.4	1.6	10.9	12.5
	5.7	1.6	11.4	12.5
Puckering (Q)	0.073	0.025	0.62	0.63
	0.081	0.025	0.63	0.63
	L^3 obsd.	L^3 calcd.	L^4 obsd.	L^4 calcd.
Conformation	envelope[c]	envelope[c]	sofa[c]	sofa[c]
	envelope[d]	envelope[d]	half-chair[e]	half-chair[e]
Helicity	λ	λ	λ	λ
	λ	λ	λ	λ
Discriminator (Δ_c)	2.2	3.7	4.0	1.4
	2.9	3.7	1.8	6.9
Puckering (Q)	0.35	0.32	0.52	0.51
	0.39	0.32	0.53	0.53

[a] Flag: Co,N1−C3,C4. [b] Flag: Co,N6−C6,C7. [c] Flag: C3. [d] Flag: N5. [e] Flag: N5,C5−N6,C7.

Table 5. Selected bond lengths [Å] and angles [°] for $[MeCo(L^4)(HL^4)]^+$. Torsion (φ, °), and bending angles (α, °) and Co out-of-plane displacement (*d*, Å) are also reported

Distances	calcd.	obsd.[a]
Co−C	2.013	1.960(7), 1.982[b]
Co−N(ox)	1.924	1.888(6), 1.900[b]
Co−N(am)	2.016	1.996(5), 2.003[b]
	2.034	2.017(5), 2.018[b]
Co−N(py)	2.117	2.134(5), 2.137[b]
Angles		
N(py)−Co−N(am)	93.0 89.0	92.2(2) 88.7(2)
N(py)−Co−N(ox)	92.0 89.3	92.1(2) 89.2(2)
N(py)−Co−C	177.3	177.3(3)
Co−N(py)−C1	119.0	117.0(4)
Co−N(py)−C2	124.4	126.4(5)
φ	−37.0	−38.3
α	6.5	9.1
d	0.029	0.018

[a] Molecule A; esd in parentheses. [b] The second value refers to the bond length corrected for thermal motion using the riding model.

Table 6. Scaled minimum strain energies (kJ·mol^{-1}) for the possible diastereomers of the [Co(A^B^C)$_2$] type complexes: [Co(L)$_2$]$^+$, (L = L^1, L^2), and [Co(L)(HL)]$^{2+}$, (L = L^3, L^4, L^{3o} and L^{4o}). L^{3o} and L^{4o} represent the L^3 and L^4 ligands without the oxime intramolecular hydrogen bond (O···H···O). For the L^3−L^4 type ligands, the chirality of the stereogenic centres (in the order: N2, N5, and their adjacent C atoms, see Figure 2, b) are also reported, for the minimum energy structures

Isomer	Configuration[a]	L^1	L^2	L^3	L^4	L^{3o}	L^{4o}
I	Δ *mer cis,trans,cis*	0	0	3292 *RSSR*	119.3 *SSRR*	3182 *RSSR*	57.8 *SSRR*
II	*fac trans,trans,trans*	117.3	63.3	1249 *RRRR*	249.4 *RSSR*	251.7 *RRRR*	95.4 *SSRR*
III	Δ *fac cis,trans,cis*	129.8	49.3	146.7 *RSSR*	90.2 *SSRR*	14.6 *SSRR*	14.1 *SSRR*
IV	Δ *fac cis,cis,cis*	144.1	61.2	72.7 *SSRR*	125.3 *RSSR*	253.5 *RSRR*	26.7 *RSRR*
V	Δ *fac trans,cis,cis*	146.4	100.7	0 *SSRR*	0 *SSRR*	0 *SSRR*	0 *SSRR*
VI	Δ *fac cis,cis,trans*	134.9	57.4	910 *SSRR*	1008 *SSRR*	31.7 *SSRR*	27.2 *SSRR*

[a] The *cis*/*trans* descriptors refer, in the order, to the pairs of the nitrogen atoms of the tridentate ligands, N(py), N(am)/N(im), and N(ox), labelled, respectively, A, B, and C in Figure 3.

Diastereomers of Complexes Co−L$^{1-4}$

The relative minimum energies for the six possible diastereomers of the [Co(L)$_2$]$^+$ (L = L^1, L^2) and [Co(L)(HL)]$^{2+}$ (L = L^3, L^4) complexes are reported in Table 6. Structures **I**−**VI** refer to those depicted in Figure 3, that is, the bis-tridentate ligand octahedral complexes [Co(A^B^C)$_2$], where A = N(pyridyl), B = N(imine), and C = N(nonprotonated oxime) for L^1 and L^2, and A = N(pyridyl), B = N(amine), and C = N(protonated oxime) for L^3 and L^4.

It is evident that the L^1 and L^2 complexes are stable only in the *mer cis,trans,cis* configuration (**I**), the *cis*/*trans* descriptors referring, respectively, to the pairs of A, B, and C nitrogen atoms of the tridentate ligands in [Co(A$_2$B$_2$C$_2$)]. On the other hand, the L^3 and L^4 complexes have a minimum strain energy in the *fac trans,cis,cis* configuration (**V**). In order to address the possibility of the opening of the O···H···O oxime hydrogen bond, especially in the highly strained configurations with *trans* NE atoms, Table 6 also lists the relative strain energies for the [Co(HL^{3o})$_2$]$^{2+}$ and [Co(HL^{4o})$_2$]$^{2+}$ complexes, where HL^{3o} and HL^{4o} represent the HL^3 and HL^4 ligands without the symmetric oxime intramolecular hydrogen bond.

It should be noted that the high values of the strain energies of some diastereomers (Table 6) are merely indicative of highly distorted improbable structures, having been calculated by the harmonic force field functionals of AMBER.[14]

Δ/Λ descriptors can be applied to designate the chirality of the complexes, on the basis of the 'skew lines' convention.[19] In this work, because of the different nature of the three donor atoms and the different number of skew lines, the descriptor is defined by the orientation of the two lines AB, or, when they are parallel as in **VI**, by the skew lines AB and BC. This convention is applied to the descriptors given in Figure 3.

Conformational Analysis of [RCo(L^4)(HL^4)]$^+$

Figure 4 shows the variation of the total strain energy E for the methyl and adamantyl derivatives as a function of the rotation angle φ = C1−N1−Co−N*, where N* represents the midpoint between the oxime nitrogen atoms (N3, N4 in Figure 1, a). Moreover, according to the usual convention, the sign of φ, as well as of all torsion angles, is positive for anticlockwise rotations and negative for clockwise rotations. According to the definition of the two torsion angles, (φ_1 − φ) is approximately 50°, that is, half the N3−Co−N4 bond angle (Figure 1, a).

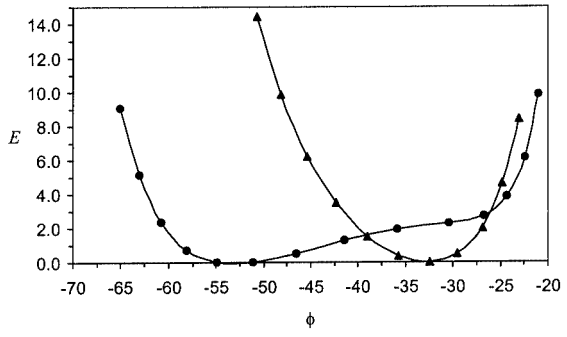

Figure 4. Plot of the scaled strain energy (E, kJ·mol^{-1}) as a function of the rotation angle φ around the axial Co−N bond for [RCo(L^4)(HL^4)]$^+$ with R = Me (circles) and Adam (triangles)

The E/φ plot of the methyl derivative is characterised by a broad asymmetric minimum (E < 2.5 kJ·mol^{-1}), in the range −60° < φ < −25°, with E = 0 at φ = −53°. For the adamantyl derivative, the energy plot is nearly symmetric, with a narrower minimum (−42° < φ < −26°, for E < 2.5 kJ mol^{-1}) centred at φ = −32°.

Figure 5 shows the variation of the axial Co−C and Co−N bond lengths as a function of the rotation angle φ. Figure 6 (see a) reports the α/φ plot, where α is the dihedral angle between the two moieties of the equatorial ligand (Figure 1, a), while Figure 6 (see b) shows the trend of the cobalt out-of plane displacement (d) from the least-squares plane defined by the four equatorial nitrogen atoms. The plots refer to the φ range corresponding to low energy regions of the methyl and adamantyl derivatives.

Tables S1 and S2 in the Supplementary Information (see also footnote on the first page of this article), report for R = Me and R = Adam, respectively, the scaled total strain

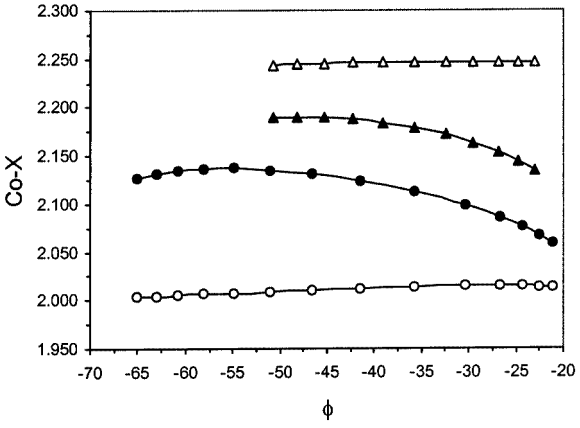

Figure 5. Plot of the axial Co−X distances [Å] as a function of the rotation angle φ [°] for $[RCo(L^4)(HL^4)]^+$. Circles refer to R = Me, with open circles for X = C, and full circles for X = N. Triangles refer to R = Adam, open for X = C, full for X = N

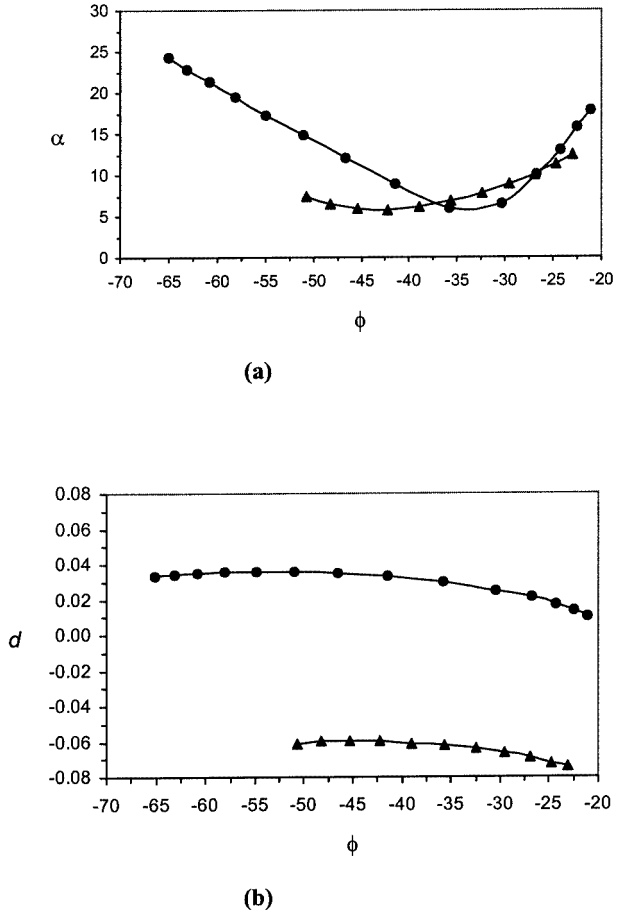

Figure 6. Plot of the dihedral angle α [°] (a), and of the cobalt out-of-plane displacement *d* [Å] (b), as a function of the rotation angle φ (°) for $[RCo(L^4)(HL^4)]^+$. Circles refer to R = Me, triangles to R = Adam

energy (*E*) calculated as a function of the torsion angle φ_1 (C2−N1−Co−N2), together with the rotation angle φ, the ethylene bridge torsion angle φ_2 (C2−C3−C4−N2), the cobalt out-of-plane displacement (*d*), the dihedral angle α, and the axial Co−C and Co−N bond lengths.

Discussion

Stereochemical Features of the Bis(tridentate ligand)cobalt Complexes

Octahedral metal complexes with bis-tridentate ligands of the type $[M(A\hat{}B\hat{}C)_2]$, where A, B, and C represent three different coordinating atoms, can in principle[19b,20] give rise to the six diastereomers illustrated in Figure 3 for M = Co, where A = N(py), B = N(im, or am), and C = N(ox). Of these, only the facial isomer **II**, with its C_i point symmetry, is achiral (ignoring the possible inherent ligand chirality), while all the others are chiral and exist as Δ/Λ enantiomeric pairs (Table 6).[19b,20]

The different stability of the six isomers depends on the nature of the donor atoms and on the length of the chelate bridge. Thus, in the case of $[Co(L^1)_2]^+$ it is evident from molecular models that all the *fac* isomers (**II**−**VI**) can be built only with great difficulty because of the trigonal nature of the imino nitrogen atoms (B) and the short A−(CH_2)−B bridge. In fact, MM calculations show (Table 6) that the *mer cis,trans,cis* arrangement (**I**) has the lowest strain energy, with the closest *fac* arrangement *trans,trans,trans* (**II**) at a significantly higher energy (117.3 kJ·mol^{-1} higher), thereby corresponding to an unrealistic structure. Owing to the longer bridge A−$(CH_2)_2$−B, the $[Co(L^2)_2]^+$ complex is more flexible and the energy difference between the minimum energy isomer (**I**) and the closest *fac* isomer *cis,trans,cis* (**III**) is reduced to 49.3 kJ·mol^{-1}, although this difference is still rather high. These results are in perfect agreement with the observation that, both in the solid state and in solution, only isomer **I** has been detected.[2]

Isomer stability is more complicated in the case of the L^3 and L^4 derivatives, $[Co(L^3)(HL^3)]^{2+}$ and $[Co(L^4)(HL^4)]^{2+}$, because of the presence of tetrahedral amino nitrogen atoms at B. Moreover, in this case, chiral centres are present at the positions of the amine nitrogen atoms (N2, N5) and of their adjacent carbon atoms in the equatorial five-membered rings (Figure 2, b), which gives rise to further possible diastereomers. On the other hand, molecular model inspection suggests that the nitrogen atom chirality is a crucial factor for the ring closure, so that a limited number of reasonable diastereomers is to be expected. Further restriction arises from formation of intramolecular hydrogen bonds involving the oxime nitrogen atoms (atom type NE, atom C in Figure 3). If these are to be maintained, all structures with *trans* NE atoms would be highly strained with respect to those with *cis* NE atoms.

The results of the present MM calculations show that both $[Co(L^3)(HL^3)]^{2+}$ and $[Co(L^4)(HL^4)]^{2+}$ complexes exhibit minimum strain energy in the configuration *fac trans,cis,cis* (isomer **V**), with *S* and *R* configurations for the nitrogen and carbon atoms, respectively (see Table 6). All other diastereomers have markedly higher energies. As expected, isomers **II** and **VI**, with *trans* oxime nitrogen atoms have exceedingly high energies, indicating that they cannot exist. When the constraint on the oxime hydrogen bond is re-

moved, the energy values decrease on passing from $L^{3,4}$ to $L^{3o,4o}$ ligands, but again isomers of type **V** have the lowest energy.

Data in Table 6 show that in the minimum energy structures of the $[Co(L^3)(HL^3)]^{2+}$ and $[Co(L^4)(HL^4)]^{2+}$-complexes the chirality of the nitrogen and carbon atoms depends on the isomer type. Nevertheless, any change from the *SSRR* chirality to the other configurations does not significantly lower the energy of the nonminimum energy isomers.

Further elements of chirality could derive from the helicity of the chelate rings. However, the oxime five-membered rings are essentially planar and the helicity of the metallacycles formed by the pyridyl ligands, as defined by the IUPAC rules,[19] is rather small (pseudo-torsion angles, defined by the N···N and C···C skew lines, of 10°−12°). Therefore, it seems likely that in solution the helicity can be easily reversed, so this factor can be neglected.

Another important conformational feature is defined by the torsion angle (φ_2) around the C−C bonds of the six-membered rings in the L^2 and L^4 complexes. MM calculations show that for $[Co(L^2)_2]^+$ inverting the sign of both the torsion angles increases the strain energy by only 1.0 kJ·mol^{-1}, while a significant increase (28.7 kJ·mol^{-1}) occurs by changing the sign of one only. On the contrary, for $[Co(L^4)(HL^4)]^{2+}$ all changes in the torsion angles cause a significant increase in the strain energy.

As experimentally observed and confirmed by the present MM calculations (Table 3), passage from N(py)−(CH_2)−N(am,im) to N(py)−$(CH_2)_2$−N(am,im) bridges (that is, on meeting the ring closure condition by passing from five- to six-membered chelate rings) causes a lengthening of about 0.10 Å of the Co−N(py) bond lengths together with significant angular changes in the pyridyl metallacycles. The largest effect, observed in both the L^1, L^2 and L^3, L^4 pairs, is the narrowing of the pyridyl exo-cycle bond angles (av. calcd. Co−N(py)−C_α, from 127.0(3)° to 120(1)°], which is paralleled by a widening of the endo-cycle angles (av. calcd. Co−N(py)−C_β, from 113.4(5)° to 123(2)°]. These observations are in very good agreement with the experimental X-ray data (see Table 3, where C_α and C_β represent, respectively, the pyridyl carbon atoms like C1, C2 and C8, C7 in Figure 2)

However, the total strain energy of $[Co(L^1)_2]^+$ is 19.1 kJ·mol^{-1} higher than that of $[Co(L^2)_2]^+$, while in $[Co(L^3)(HL^3)]^{2+}$ it is 67.9 kJ·mol^{-1} lower than in $[Co(L^4)(HL^4)]^{2+}$, paralleling the ring strain energies (sum of only stretching and bending contributions). These results suggest that the pyridyl ring closure introduces a severe strain in the $[Co(L^1)_2]^+$ (five-membered rings) and $[Co(L^4)(HL^4)]^{2+}$ (six-membered rings) complexes with respect to their L^2 and L^3 analogues.

Stereochemical Features of the Organometallic Complexes $[RCo(L^4)(HL^4)]^+$

The results of the conformational analysis of the organocobalt methyl derivative $[MeCo(L^4)(HL^4)]^+$ (see Figure 4 and Table S1 show that the pyridyl group can rotate around the axial Co−N bond across a rather wide range ($-60° < \varphi \leq -25°$) while maintaining the total strain energy within a limit of 2.5 kJ·mol^{-1}. This is in agreement with the observation that in the solid state two crystallographically independent molecules are present, with φ values of −38° and −48°, and that similar values were also found for the ethyl and trifluoroethyl derivatives, with φ = −36° and −44°, respectively.[3] This corresponds to the pyridyl ring being more or less parallel to the N2−Co−N4 axis ($-15° < \varphi_1 < 24°$).

In the case of the adamantyl group, the minimum strain energy is also observed at a similar torsion angle ($\varphi \approx -32°$), but the MM calculations show that, in the case of this much bulkier alkyl group, the pyridyl rotation is rather restricted ($\Delta\varphi \approx \pm 8°$ with $\Delta E < 2.5$ kJ·mol^{-1}) (Figure 4, Table S2).

Thus, the present results confirm the observation that in complexes with tridentate amino-oxime ligands the orientation of the planar nitrogen base is quite different from that commonly found in cobaloximes and lariat-type complexes ($\varphi \approx 0°$),[6] and in iminocobaloximes ($\varphi \approx 90°$).[3]

Interestingly, the variation of φ is accompanied by significant changes in the geometry of the pyridyl metallacycle, such as the variation of the torsion angle φ_2. Of particular interest is the significant increase of the Co−N(py) bond length with decrease (more negative values) of the rotation angle φ (Figure 5). This confirms the appreciable effect of steric factors in determining the *trans* influence of an alkyl group.[3]

On the contrary, the Co−C bond length of both the Me and Adam derivatives show negligible variations (Figure 5), in agreement with FT-Raman studies which do no detect any change in the Co−C force constants even in base-on and base-off cobalamins.[10a]

In order to maintain the total strain energy around its minimum, the variation of φ also causes distortions in the equatorial ligand, as shown by the variation of the dihedral angle α between its two moieties. This is the combination of bending and twisting deformations of the two equatorial five-membered rings. Inspection of molecular diagrams shows that when α is less than 7° ($-36° < \varphi < -30°$ for R = Me; $-46° < \varphi < -35°$ for R = Adam) the two rings are essentially twisted without significant bending, while for higher values the latter component becomes more appreciable. The calculations indicate that this effect is stronger in the methyl derivative (see Figure 6, a), in which the equatorial ligand is bent away from the axial alkyl group when φ increases from −30°. This trend is in good agreement with that experimentally observed.[3] The opposite bending occurs when φ is less than −36°. The variation of α with φ (in the low strain energy region) is much lower in the adamantyl derivative (Figure 6, a) because the bending towards the alkyl group is hindered by the alkyl bulkiness.

Finally, it is interesting to observe that while in the Me derivative the cobalt atom is displaced towards the pyridyl nitrogen atom, in the Adam derivative the displacement is nearly doubled and reversed, the Co atom moving towards the carbon atom (Figure 6, b).

Acknowledgments

This work has been supported by MIUR (PRIN: MM03185591, Rome) and Agenzia 2000 (CNR, Rome).

[1] R. Dreos, G. Tauzher, D. H. Trendafilova, G. Nardin, L. Randaccio, *Inorg. Chem.* **1996**, *35*, 2715−2716.
[2] L. Catalano, R. Dreos, G. Nardin, L. Randaccio, G. Tauzher, S. Vuano, *J. Chem. Soc., Dalton Trans.* **1996**, 4269−4274.
[3] R. Dreos, A. Felluga, G. Nardin, L. Randaccio, P. Siega, G. Tauzher, *Eur. J. Inorg. Chem.* **2001**, 267−276.
[4] L. Randaccio, N. Bresciani Pahor, E. Zangrando, L. G. Marzilli, *Chem. Soc. Rev.* **1989**, *18*, 225−250.
[5] *Chemistry and Biochemistry of Vitamin B_{12}* (Ed.: R. Banerjee), Wiley, New York, **1999**.
[6] [6a] A. Gerli, M. Sabat, L. G. Marzilli, *J. Am. Chem. Soc.* **1992**, *114*, 6711−6718. [6b] L. G. Marzilli, A. Gerli, A. M. Calafat, *Inorg. Chem.* **1992**, *31*, 4617−4627.
[7] L. Randaccio, *Comments, Inorg. Chem.* **1999**, *21*, 327−376.
[8] S. Geremia, M. Calligaris, L. Randaccio, *Eur. J. Inorg. Chem.* **1999**, 981−992.
[9] [9a] R. Reitzer, C. Kratky, *Biochemistry* **1999**, *38*, 891−902. [9b] F. Mancia, N. H. Keep, A. Nakagawa, P. F. Leadlay, S. McSweeney, B. Rasmussen, P. Böske, O. Diat, P. R. Evans, *Structure* **1996**, *4*, 339−350. [9c] C. L. Drennan, S. Huang, J. T. Drummond, R. G. Mattews, M. L. Ludwig, *Science* **1994**, *226*, 1669−1670.
[10] [10a] S. J. Moore, A. Kutikov, R. J. Lachicotte, L. G. Marzilli, *Inorg. Chem.* **1999**, *38*, 768−776. [10b] J. M. Sirovatka, R. G. Finke, *J. Am. Chem. Soc.* **1997**, *119*, 3057−3067.
[11] [11a] R. Cini, S. J. Moore, L. G. Marzilli, *Inorg. Chem.* **1998**, *37*, 6890−6897. [11b] S. Hirota, S. M. Polson, J. M. Puskett, Jr., S. J. Moore, M. B. Mitchell, L. G. Marzilli, *Inorg. Chem.* **1996**, *35*, 5646−5663.
[12] E. Uhlig, D. Schneider, H. Hildebrand, *Z. Anor. Allg. Chem.* **1966**, *346*, 173−180.
[13] *HyperChem*, Hypercube Inc., Waterloo, Ontario, **2000**.
[14] W. D. Cornell, P. Cieplak, I. R. Bayly, I. R. Gould, K. M. J. Merz, Jr., D. M. Ferguson, D. C. Spellmeyer, T. Fox, J. W. Caldwell, P. A. Kollman, *J. Am. Chem. Soc.* **1995**, *117*, 5179−5197.
[15] S. Geremia, M. Calligaris, *J. Chem. Soc., Dalton Trans.* **1997**, 1541−1547.
[16] M. Calligaris, GEOM, **2001**, University of Trieste, Trieste, Italy.
[17] D. Cremer, J. A. Pople, *J. Am. Chem. Soc.* **1975**, *97*, 1354−1358.
[18] S. Geremia, L. Vicentini, M. Calligaris, *Inorg. Chem.* **1998**, *37*, 4094−4103.
[19] [19a] *Nomenclature of Inorganic Chemistry* **1990** (Ed.: G. L. Leigh); Blackwell: Oxford. [19b] A. von Zelewsky, *Stereochemistry of Coordination Compounds* **1995**, Wiley, Chichester.
[20] D. Heineke, S. J. Franklin, K. N. Raymond, *Inorg. Chem.* **1994**, *33*, 2413−2421.

Received April 18, 2002
[I02203]

Syntheses and Molecular Structures of Chromium(IV) Halides and Pseudohalides Bearing a Triamidoamine Ligand

Alexander C. Filippou,*[a] Sven Schneider,[a] and Burkhard Ziemer[a]

Keywords: Chromium / Tripodal ligands / N ligands / Halides / Pseudohalides / Oxidations

A general method for the synthesis of chromium(IV) halides and pseudohalides of the general formula [Cr(N_3N)X] (**2**: X = F; **3**: X = Cl; **4**: X = Br; **5**: X = I; **6**: X = CN) is presented. It involves the one-electron oxidation of the Cr^{III} triamidoamine complex [Cr(N_3N)] {($(N_3N)^{3-}$ = [($Me_3SiNCH_2CH_2)_3N]^{3-}$} (**1**) with silver(I) salts. The oxidation of **1** with one equivalent of $AgBF_4$ or [Ag(CN*t*Bu)$_2$](BF_4) (**7**) affords the chromium(IV) fluoride [Cr(N_3N)F] (**2**), and treatment of **1** with AgX (X = Cl, Br, I, CN) gives the complexes **3**–**6**. Alternatively, the complexes **4** and **5** can be obtained by halogenation of **1** with 0.5 equivalents of X_2 (X = Br, I). The magnetic moments of **2**–**6** range from 2.7–3.0 μ_B at 297 K, indicating the presence of high spin d^2 chromium complexes, and their ^1H NMR spectra suggest an averaged C_{3v} symmetry in solution. X-ray crystallography shows that complexes **4** and **6** have a distorted trigonal-bipyramidal coordination geometry, with the halide(pseudohalide) ligand and the bridgehead amine nitrogen atom occupying the apical positions. The triamidoamine ligand is disposed, approximately with a three-fold symmetry about the chromium centre. The chromium centre is displaced out of the equatorial plane defined by the three amido nitrogen atoms towards the halide(pseudohalide) ligand, by 0.212 (**4**) and 0.191 Å (**6**). The molecular structures of **4** and **6** are compared with that of **3** and other chromium(IV) triamidoamine complexes and show a strong effect of the ligand X on the conformation of the N_3N ligand and the $Cr–N_{amine}$ bond length.

(© Wiley-VCH Verlag GmbH, 69451 Weinheim, Germany, 2002)

Introduction

The coordination and organometallic chemistry of chromium(IV) is much less developed than that of chromium in the oxidation states +II, +III, and +VI.[1] This can be traced back to the greater oxidising power of most chromium(IV) compounds and their inclination to valence disproportionation or reductive elimination.[2] Most of the isolable chromium(IV) complexes are stabilised by electronegative and strong σ- or π-donor ligands as exemplified by [CrF_4],[3] the ionic fluorides $M^I[CrF_5]$, $M^I_2[CrF_6]$, and $M^{II}[CrF_6]$ (M^I = Li, K, Rb, Cs, Ag; M^{II} = Mg, Ca, Sr, Ba, Zn, Cd, Hg),[4] and the homoleptic chromium(IV) alkyls [CrR_4] {R = CH_2SiMe_3, CH_2tBu, CH_2CMe_2Ph, CH_2CPh_3, 1-adamantylmethyl, *i*Pr, Cy (cyclohexyl), 2-adamantyl, *t*Bu, 1-camphyl, 1-norbornyl},[5] dialkylamides [Cr(NRR′)$_4$] (R, R′ = Et, Pr; R = Me, R′ = Bu; RR′ = C_5H_{10})[6] and alkoxides [Cr($OR)_4$] {R = C(H)(Me)*t*Bu, $CHtBu_2$, *t*Bu, CMe_2Et, $CMeEt_2$, CEt_3, 1-adamantyl, $SiEt_3$}.[7]

Some chromium(IV) imido-,[8] oxo-,[9] peroxo-,[10] sulphido-,[11] pentamethylcyclopentadienyl-,[8c,9f,11a,12] and carbaborane complexes[13] are also known. Representative examples are the compounds [Cr^{IV}Cl(NEt)(dmpe)$_2$]OTf {dmpe = 1,2-bis(dimethylphosphanyl)ethane, OTf = CF_3SO_3},[8a] [Cr^{IV}(NAr)$_2L_2$] (Ar = C_6H_3-2,6-*i*Pr_2; L = PMe_3, PMe_2Ph),[8e] [Cr^{IV}(O)(porphyrinato)],[9a–9e] [$Tp^{tBu,Me}Cr^{IV}$(O)OPh] {$Tp^{tBu,Me}$ = hydridotris(3-*tert*-butyl-5-methylpyrazol-1-yl)borate},[9h] [$Cr^{IV}(O_2)_2(NH_3)_3$],[10a] [{Cr^{IV}-(NRR′)$_2$}$_2$(μ-S)$_2$] (R, R′ = Cy; R = 1-adamantyl, R′ = C_6H_3-3,5-Me_2)[11b] and [(Cp*$Cr^{IV}Me_2)_2$(μ-O)] (Cp* = C_5Me_5).[9f] In comparison, chromium(IV) halides (halide = Cl, Br, I) and pseudohalides are rare and include the hydroxo derivatives [{Cr($OH)_2(X)_2$(pyridine)}$_2$] (X = Cl, Br, I),[14] the cyanochromate(IV) K_2[Cr($CN)_4$(O)(pyridine)]·H_2O,[15] and the Cr^{IV} iodide [Cr($I)_2$($NRAr_F)_2$] {R = $C(CD_3)_2CH_3$, Ar_F = C_6H_3-2,5-F,Me}.[16]

Chromium(IV) halides are promising starting materials for the preparation of chromium(IV) alkyls. These compounds have attracted considerable interest since the recent reports of S. L. Scott et al. on the polymerization of α-olefins by silica-supported Cr^{IV} species,[17] and the theoretical studies of T. Ziegler et al. which predict that the chromium(IV) model compounds [$Cr(NR_2)_2R']^+$ (R = H, Me, SiH_3; R′ = Me Et) should be active ethylene polymerization catalysts.[18] Therefore, a general approach to stable chromium(IV) halides bearing amido ligands would be very valuable.

We have recently described the synthesis and molecular structure of the triamidoamine complex [Cr(N_3N)Cl] {($(N_3N)^{3-}$ = [($SiMe_3NCH_2CH_2)_3N]^{3-}$} (**3**), which is a remarkably stable chromium(IV) chloride (m.p. 155–158

[a] Institut für Chemie, Humboldt-Universität zu Berlin, Brook-Taylor Straße 2, 12489 Berlin, Germany
Fax: (internat.) +49–(0)30/2093 6939
E-mail: filippou@chemie.hu-berlin.de

°C),[19] considering the thermal instability of $CrCl_4$.[1a] In continuation of our studies in this field, here, we present a general method for the synthesis of chromium(IV) halides and pseudohalides of the general formula $[Cr(N_3N)X]$ (X = F, Br, I, CN) and describe their spectroscopic properties, as well as the molecular structures of the bromo and cyano derivatives.

Results and Discussion

Syntheses and Characterisation

The starting material for the reactions described below was the Cr^{III} triamidoamine complex $[Cr(N_3N)]$ (**1**), which was obtained from $CrCl_3(THF)_3$ and $Li_3(N_3N)$, as described recently.[19] Treatment of **1** with one equivalent of $AgBF_4$ in THF at −78 °C resulted in the rapid precipitation of elemental silver and a colour change from green to dark brown, indicating the fast oxidation of **1**. After evaporation of the solvent and extraction of the residue with pentane, the chromium(IV) fluoride $[Cr(N_3N)F]$ (**2**) was isolated as a dark brown/black crystalline solid in a 43% yield (Scheme 1).[20]

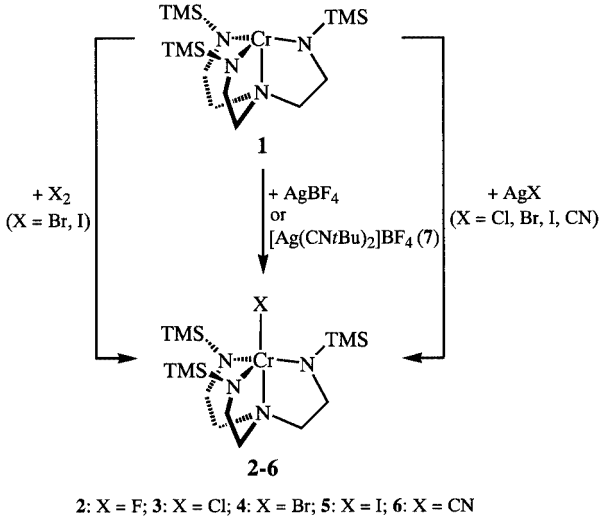

Scheme 1. Syntheses of $[Cr(N_3N)X]$ (X = F, Cl, Br, I, CN) (**2**−**6**) (TMS = $SiMe_3$)

The formation of **2** suggests that a cationic species $[Cr(N_3N)]^+$, which was expected as the primary product of the one-electron oxidation of **1** with Ag^+, is electrophilic enough (as other inorganic electrophiles[21]) to abstract a fluoride ion from BF_4^-. In an attempt to trap such a species with *t*BuNC, the oxidation of **1** with the silver(I) isocyanide complex $[Ag(CNtBu)_2](BF_4)$ (**7**) was investigated. Complex **7** was synthesised for this purpose by the reaction of $AgBF_4$ with two equivalents of *t*BuNC in CH_2Cl_2 and was isolated as a white solid in a 89% yield. It was characterised by elemental analysis and spectroscopic methods (vide infra). Treatment of **1** with **7** in THF at −78 °C also led to the rapid precipitation of elemental silver and a reddish-black solution indicating the fast oxidation of **1**, as in the case of $AgBF_4$. IR spectroscopic monitoring of the reaction revealed the fast replacement of the ν(C≡N) absorption of $[Ag(CNtBu)_2](BF_4)$ at 2212 cm^{-1} by that of uncoordinated *t*BuNC at 2134 cm^{-1}, and gave no evidence for the formation of any stable Cr^{IV} isocyanide complexes even at low temperatures. Workup of the reaction mixture afforded $[Cr(N_3N)F]$ (**2**) as the only pentane-soluble product in a 52% yield (Scheme 1, Table 1).

Table 1. Preparation of **2**−**6** by oxidation of $[Cr(N_3N)]$ (**1**)

Oxidant	Product	Yield (%)
$AgBF_4$	$[Cr(N_3N)F]$ (**2**)	43
$[Ag(CNtBu)_2](BF_4)$		52
AgCl	$[Cr(N_3N)Cl]$ (**3**)[a]	54
$CrCl_3(THF)_3$		50
$PhICl_2$		28
AgBr	$[Cr(N_3N)Br]$ (**4**)	64
Br_2		16
AgI	$[Cr(N_3N)I]$ (**5**)	71
I_2		29
AgCN	$[Cr(N_3N)CN]$ (**6**)	57

[a] Ref.[19]

Oxidation of **1** with Ag^I salts has proven to be a versatile route for obtaining chromium(IV) triamidoamine complexes as shown by the syntheses of $[Cr(N_3N)X]$ (**4**: X = Br; **5**: X = I; **6**: X = CN) via the reactions of **1** with AgX (X = Br, I, CN) in THF (Scheme 1). Complexes **4**−**6** were isolated after crystallisation from diethyl ether or pentane as black crystalline solids in good yields (Table 1). The chloro complex **3** was previously obtained using the same method (Scheme 1, Table 1).[19] Alternatively, the halides **4** and **5** can be prepared by halogenation of **1** with 0.5 equivalents of X_2 (X = Br, I) in THF, albeit in lower yields (Table 1). The chromium(IV) complexes **2**−**6** are moderately air-sensitive solids, and their melting points are 159 (**2**), 155−158 (**3**), 175 (**4**), 177 (**5**), and 166 °C (**6**). They are very soluble in pentane, diethyl ether, toluene, and THF, giving dark brown (**2**), dark red (**3**, **6**), reddish-black (**4**), and yellowish-black (**5**) solutions. The thermal stability of the halides **3**, **4**, and **5** is remarkable, given the very low thermodynamic stability of CrX_4 (X = Cl, Br).[1a] This can be attributed to the strong π-donating ability of the N_3N ligand.

Complexes **2**−**6** have very similar IR spectra in nujol, indicating the structural similarity of these compounds. It is worth noting that the IR spectrum of **6** in nujol lacks an absorption for the ν(C≡N) vibration of the cyano ligand, as was previously observed for the analogous molybdenum and tungsten complexes $[M(N_3N)(CN)]$.[22] The Ag^I isocyanide complex **7** is stable in CH_2Cl_2 and THF solutions at ambient temperature, as shown by the IR spectra, which display only one intense absorption band for the ν(C≡N) vibrations of the isocyanide ligands at 2225 and 2212 cm^{-1}, respectively. This absorption is assigned to the Σ_u^+ mode

and indicates a local $D_{\infty h}$ symmetry of the Ag(C≡N−C)$_2$ core in **7**.[23] In comparison, the IR spectrum of **7** in KBr shows two ν(C≡N) absorption bands at very different wavenumbers (2245 and 2185 cm^{-1}) from that in solution, which indicates that **7** reacts with the KBr matrix under pressure.[24] The opposite behaviour is shown by [Ag(CN*t*Bu)$_4$](BF$_4$) (**8**), which is stable in pressed KBr discs but unstable in CH_2Cl_2 solution, in which it exists in a dissociation equilibrium with [Ag(CN*t*Bu)$_3$](BF$_4$) (**9**) and *t*BuNC.[25] Thus, in KBr complex **8** gives rise to only one ν(C≡N) absorption band at 2184 cm^{-1}, which is assigned to the T_2 stretching mode and suggests a local T_d symmetry of the Ag(C≡N−C)$_4$ core of the cation.[23] However, in CH_2Cl_2 two ν(C≡N) absorption bands are observed at 2200 and 2140 cm^{-1}, in addition to the band at 2183 cm^{-1} assigned to **8**, which by comparison with authentic samples are assigned to **9** and *t*BuNC, respectively.[25]

The effective magnetic moments of **2**−**6** were determined in C_6D_6 solution at 297 K by the method of Evans (Table 2).[26,27] These range from 2.8−3.0 μ_B, and are similar to the spin-only value for a d^2 high-spin configuration (2.83 μ_B). The ^{1}H NMR spectra of **2**−**6** in C_6D_6 at 297 K display three very broad, strongly shifted signals due to the presence of the two unpaired electrons. On the basis of integration of these signals, two are assigned to the backbone methylene groups and one to the trimethylsilyl groups of the N_3N ligand. This suggests an averaged C_{3v} symmetry of these complexes in solution on the ^{1}H NMR spectroscopic time scale (Table 2).

Table 2. ^{1}H NMR spectroscopic data and magnetic moments of **2**−**6**

Compound[a]	δ(Si*Me*$_3$)[b]	δ(C*H*$_2$)[b]	δ(C*H*$_2$)[b]	μ_{eff} [μ_B]
[Cr(N_3N)F] (**2**)	3.28 (190)	−33.1 (1400)	−208 (5100)	3.0
[Cr(N_3N)Cl] (**3**)[c]	4.47 (220)	−40.8 (1300)	−211 (6000)	2.6
[Cr(N_3N)Br] (**4**)	5.17 (250)	−47.4 (1000)	−185 (2700)	2.8
[Cr(N_3N)I] (**5**)	5.88 (150)	−54.1 (950)	−145 (2100)	3.0
[Cr(N_3N)CN] (**6**)	3.49 (220)	−39.0 (1400)	−188 (6900)	2.9

[a] ^{1}H NMR spectra and magnetic moments in C_6D_6 at 297 K. [b] Chemical shifts in ppm relative to the residual proton resonance of the deuterated solvent [δ(C_6D_5H) = 7.15 ppm], $\Delta\nu_{1/2}$ [Hz] in parentheses. [c] Ref.[19]

Molecular Structures

The solid-state structures of **4** and **6** were determined by single-crystal X-ray diffraction.[28] Complex **6** is the first chromium(IV) cyano complex to be structurally characterised. DIAMOND plots of the molecular structures of **4** and **6** are shown in Figures 1 and 2, respectively, and selected bond lengths and angles are listed in Table 3. For comparative purposes, the corresponding bonding parameters of complex **3**[19] are also summarised in Table 3.

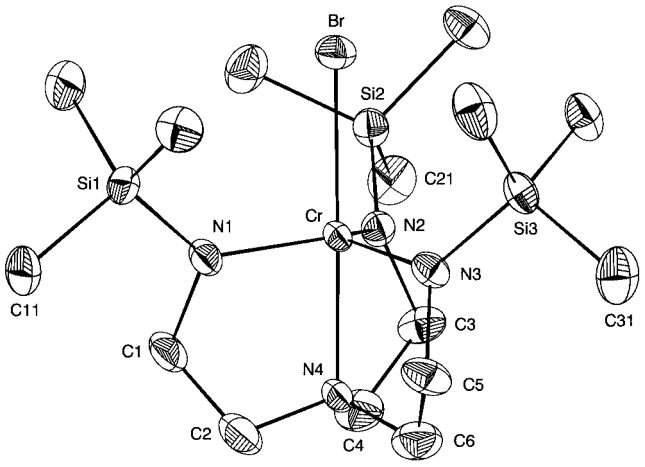

Figure 1. DIAMOND plot of the molecular structure of [Cr(N_3N)Br] (**4**) with thermal ellipsoids drawn at the 50% probability level; hydrogen atoms are omitted for clarity

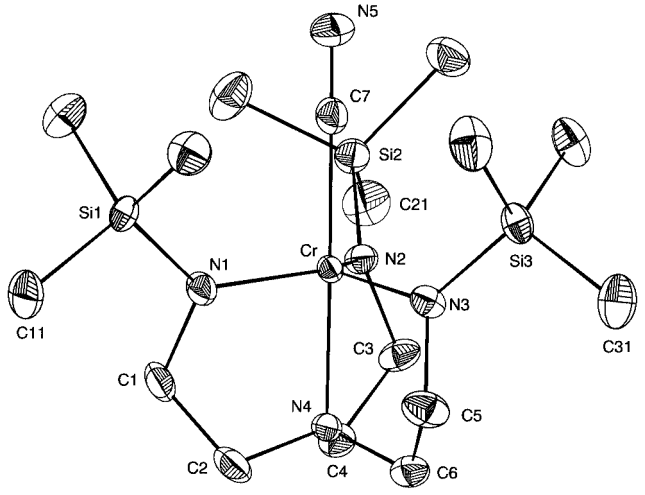

Figure 2. DIAMOND plot of the molecular structure of [Cr(N_3N)CN] (**6**) with thermal ellipsoids drawn at the 50% probability level; hydrogen atoms are omitted for clarity

As for the case of **3**, both complexes are distorted trigonal-bipyramidal, with the bridgehead amine nitrogen atom N4 of the tetradentate N_3N ligand and the bromo (**4**) or cyano ligand (**6**) residing at the apexes of the trigonal bipyramid. Distortion arises as a result of the displacement of the chromium atom out of the equatorial plane defined by the three amido nitrogen atoms N1−N3, toward the halide (pseudohalide) ligand. The distance of the chromium atom from the equatorial plane is 0.212 (**4**) and 0.191 Å (**6**), larger than that in the chloro complex **3** (0.189 Å). This results in a slightly smaller mean $N_{amido}-Cr-N_{amine}$ bond angle of 83.5(2) (**4**) and 84.13(6)° (**6**), compared with that of **3** [84.2(2)°] (Table 3). In **4** and **6**, as in **3**, the amido groups approach an "upright" conformation, as shown by the torsion angles N4−Cr−N1−Si1, N4−Cr−N2−Si2 and N4−Cr−N3−Si3 (Table 3). The amido nitrogen atoms are sp^2 hybridised, as shown by the mean sum of the bond

Table 3. Selected bond lengths, bond angles and dihedral angles of complexes **4** and **6** (corresponding bonding parameters of **3** are also listed for comparative purposes).

	4	**6**	**3**[19]
Bond Lengths [Å]			
Cr−X	2.440(1)	2.062(2)	2.269(2)
Cr−N1	1.875(3)	1.869(2)	1.886(3)
Cr−N2	1.868(3)	1.870(2)	1.869(4)
Cr−N3	1.877(3)	1.876(2)	1.877(4)
Cr−N4	2.135(3)	2.140(2)	2.043(3)
Bond Angles [deg]			
N4−Cr−X	179.0(1)	179.06(7)	179.4(1)
N1−Cr−N4	83.8(2)	83.90(6)	84.2(2)
N2−Cr−N4	83.6(2)	84.53(6)	84.2(2)
N3−Cr−N4	83.1(2)	83.96(6)	84.3(2)
N1−Cr−N2	119.3(2)	119.15(7)	120.6(2)
N2−Cr−N3	118.2(2)	118.65(7)	117.9(2)
N1−Cr−N3	118.8(2)	119.10(7)	118.6(2)
Dihedral Angles [deg]			
N4−Cr−N1−Si1	158.8(3)	161.2(2)	164.0(3)
N4−Cr−N2−Si2	158.2(3)	160.3(2)	162.2(3)
N4−Cr−N3−Si3	156.4(2)	159.7(2)	163.8(3)

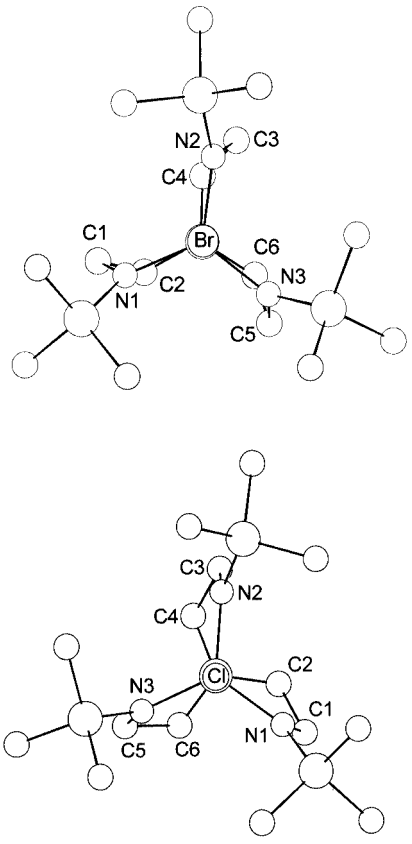

Figure 3. View of **4** (top) and of **3** (bottom) down the X−Cr−N4 axis showing the different conformation of the N_3N ligand in the two complexes

angles at the atoms N1−N3, which is 360.0° in both compounds (**3**: 359.1°). In addition, the $Cr-N_{amido}$ bond lengths have an average value of 1.873(3) Å in the bromo complex **4** and 1.872(2) Å in the cyano complex **6**, which is similar to that of **3** [1.877(4) Å], but are considerably shorter than the $Cr-N_{amine}$ bond lengths in these compounds, e.g. **4** [$Cr-N_{amine}$ = 2.135(3) Å] (Table 3). All these structural features indicate extensive π-electron donation of the N_3N ligand to the chromium centre.

In complexes **4**, **6**, and **3** the tetradentate N_3N ligand is disposed with an approximate C_3 symmetry about the chromium centre. The nearly linear $N_{amine}-Cr-X$ atom sequence corresponds to the principal axis. The $SiMe_3$ groups form a pocket in which the ligand X is located, as shown by the torsion angles Cr−N1−Si1−C11, Cr−N2−Si2−C21, and Cr−N3−Si3−C31 of −155.8(3), −164.6(3), and −160.2(2)° (**4**), and −156.5(2), −166.5(2), and −161.6(2)° (**6**), respectively. However, complexes **4** and **6** differ from **3** by the envelope conformation of the three five-membered chelate rings (Cr−N1−C1−C2−N4, Cr−N2−C3−C4−N4, and Cr−N3−C5−C6−N4) (Figure 3). In complexes **4** and **6** the N_{amido}-bonded methylene carbon atoms C1, C3, and C5 form the "flap" of the envelope, whereas in complex **3** the N_{amine}-bonded methylene carbon atoms C2, C4, and C6 are "tipped up" (Figure 3).

It is suggested that this conformational change results from the increased steric repulsion as the auxiliary ligand becomes more sterically demanding. This causes the $SiMe_3$ groups to twist out of the apical pocket, as shown by the mean torsion angle $N_{amine}-Cr-N_{amido}-Si$ (**4**: 157.8°; **6**: 160.4°; **3**: 163.3°). Additional evidence for the influence of steric strain on the conformation of the N_3N ligand is also found in other chromium(IV) and related molybdenum(IV) triamidoamine complexes. For example, a similar conformation as in [Cr(N_3N)Cl] (**3**) is adopted by the N_3N ligand in [Cr(N_3N)H][29] containing the 'small' hydrido ligand, or in [Mo(N_3N)Cl],[30a] whereas the complexes [Cr(N_3N)Me],[29] [Mo(N_3N)CD_3],[30b] and [Mo(N_3N)OTf][30b] bearing "large" auxiliary ligands have the same N_3N ligand conformation as in **4** and **6**.

The Cr−Br distance of 2.440(1) Å in **4** is similar to that found in [$Cr^{IV}Br(\eta^5$-Cp*)(μ-NCy)]$_2$·toluene [Cr−Br = 2.470(2) Å],[8c] and the Cr−CN bond length of 2.063(2) Å in **6** is similar to those of six-coordinate Cr^{III} and Cr^{V} cyano complexes.[31] The $Cr-N_{amine}$ bond length depends on the *trans*-influence[32] of the ligand X, as seen by the longer $Cr-N_{amine}$ bond of [Cr(N_3N)Me] [$Cr-N_{amine}$ = 2.250(2) Å][29] relative to that of **4** [$Cr-N_{amine}$ = 2.135(3) Å] or **6** [$Cr-N_{amine}$ = 2.140(2) Å], and the longer $Cr-N_{amine}$ bond of [Cr(N_3N)H] [$Cr-N_{amine}$ = 2.140(2) Å][29] relative to that of **3** [$Cr-N_{amine}$ = 2.043(3) Å] (Table 3). The steric repulsion between the ligand X and the $SiMe_3$ groups, which is transmitted via the chelate backbone (see different conformations of **4** and **3** in Figure 3), also seems to affect the $Cr-N_{amine}$ bond length, as indicated, for example, by the larger $Cr-N_{amine}$ distance of **4** relative to that of **3** (Table 3).

Conclusion

The one-electron oxidation of the chromium(III) triamidoamine complex [Cr(N_3N)] {($(N_3N)^{3-}$ = [(Me_3Si-$NCH_2CH_2)_3N]^{3-}$} (**1**) with silver(I) salts is a very valuable method for the synthesis of rare, thermally stable chromium(IV) halides and pseudohalides of the general formula [Cr(N_3N)X] (X = F, Cl, Br, I, CN). Their molecular structures, magnetic moments, and ^{1}H NMR spectra show the presence of distorted trigonal-bipyramidal, high-spin d^2 chromium complexes with threefold symmetry, in which the bridgehead amine nitrogen atom of the tetradendate N_3N ligand and the halide (pseudohalide) ligand occupy the apical positions. The strong π-donating ability of the N_3N ligand is expected to reduce the oxidising power of these compounds making them promising starting materials for the development of the organometallic chemistry of chromium(IV).

Experimental Section

General Remarks: All syntheses and sample manipulations were carried out under an atmosphere of argon using Schlenk and glovebox techniques.[33] The solvents were dried using standard methods (pentane with CaH_2 or sodium wire/benzophenone/tetraglyme, diethyl ether and THF with sodium wire/benzophenone and CH_2Cl_2 with Sicapent (Merck) and Na/Pb alloy), and freshly distilled and deoxygenated prior to use. Complex **1** was prepared as described recently.[19] AgBr and AgI were dried under exclusion of light in vacuo for 4 h at 70 °C. Br_2 was dried with concentrated sulphuric acid and distilled. $SiMe_4$ was dried with sodium, trap-to-trap distilled in vacuo and stored over 4 Å molecular sieves. All other commercially available chemicals were used as purchased. Elemental analyses were obtained from the Central Analytical Group of the Chemistry Department of the Humboldt-Universität zu Berlin. The IR spectra of the compounds were recorded on a Bruker IFS-55 spectrometer either in solution using a cell of NaCl plates, as dispersions in pressed KBr discs or as nujol mulls between KBr plates (**6** - between NaCl plates). The following abbreviations are used for the intensities and the shape of the absorption bands: vs = very strong, s = strong, m = medium, w = weak, vw = very weak, br = broad, sh = shoulder. The ^{1}H, ^{13}C{^{1}H}, and ^{19}F NMR spectra were recorded on a Bruker AM-300 spectrometer in dry deoxygenated C_6D_6 and CD_2Cl_2. The ^{1}H and ^{13}C{^{1}H} NMR spectra were calibrated against the internal residual proton resonance and the natural abundance ^{13}C resonance of the solvent, respectively (C_6D_6, δ_H = 7.15 and δ_C = 128.0 ppm; CD_2Cl_2, δ_H = 5.32 and δ_C = 53.8 ppm). The ^{19}F NMR spectra were calibrated against external $CFCl_3$. Magnetic moments were determined in C_6D_6 at 297 K by the Evans method as modified by Sur[26,27] using the shift of the proton resonance of internal $SiMe_4$. The diamagnetic correction was performed using Pacault's method.[34] Melting points were determined using a Büchi 530 melting point apparatus and are corrected. The samples were sealed under vacuum in capillary tubes and heated slowly until the compounds melted.

Preparation of [Cr(N_3N)F] (2) by Oxidation of 1 with $AgBF_4$: A precooled solution (−78 °C) of [Cr(N_3N)] (**1**) (0.356 g, 0.86 mmol) in 25 mL of THF was rapidly added, via a double ended needle, to a stirred solution of $AgBF_4$ (0.168 g, 0.86 mmol) in 20 mL of THF that was kept in the dark at −78 °C. The green solution of **1** quickly turned dark brown and elemental silver precipitated out of the solution. The reaction mixture was allowed to warm to ambient temperature and stirred in the dark for 15 h. The solvent was evaporated to dryness and the residue extracted twice with 25 mL of pentane. The red-brown extracts were filtered through a filter cannula and the filtrate was evaporated to dryness leaving 180 mg of a dark brown microcrystalline residue. The residue was recrystallised from pentane at −78 °C affording **2** as a black crystalline solid. Yield 0.16 g (43%). $C_{15}H_{39}CrFN_4Si_3$ (430.75): calcd. C 41.83, H 9.13, N 13.01; found C 42.39, H 9.15, N 12.63. The product was shown by ^{1}H NMR spectroscopy to be identical to that obtained from oxidation of **1** with **7** (vide infra).

Preparation of [Cr(N_3N)F] (2) by Oxidation of 1 with 7: Under exclusion of light, a solution of [Ag(CN*t*Bu)$_2$](BF_4) (**7**) (0.36 g, 1.00 mmol) in 50 mL of THF was slowly added, via a double ended needle, to a stirred solution of [Cr(N_3N)] (**1**) (0.42 g, 1.02 mmol) in 50 mL of THF, at −78 °C. The green solution of **1** rapidly turned reddish-black and elemental silver started to precipitate. The suspension was stirred at −78 °C for 0.5 h and then allowed to warm to ambient temperature in the dark. IR spectra of the reaction solution were recorded in the region of 2300−1500 cm^{-1} to monitor the progress of the reaction. These revealed the fast replacement of the ν(C≡N) absorption of [Ag(CN*t*Bu)$_2$](BF_4) at 2212 cm^{-1} by that of uncoordinated *t*BuNC at 2134 cm^{-1}. In addition, a weak ν(C≡N) absorption band of an intermediate was observed at 2203 cm^{-1}, which disappeared after stirring the reaction mixture for ca. 3.5 h at ambient temperature. All volatiles were removed after 4 h in vacuo. The residue was extracted twice with 40 mL of pentane and the extract filtered through a filter cannula. The filtrate was evaporated to dryness and the residue was washed with a minimum amount of pentane at −78 °C affording **2** as a dark brown microcrystalline solid (0.17 g). A second crop of **2** was obtained from the wash solution on crystallisation at −78 °C (0.06 g). Overall yield 0.23 g (52% relative to **1**), m.p. 159 °C. IR (nujol mull): $\tilde{\nu}$ [cm^{-1}] = 2726 vw, 2655 vw, 1458 m, 1450 m, 1421 w, 1408 vw, 1400 vw, 1344 w, 1331 w, 1310 vw, 1286 w, 1259 sh, 1245 sh, 1238 s, 1210 vw, 1180 vw, 1151 vw, 1131 w, 1090 m, 1077 m, 1062 m, 1025 w, 958 s, 944 s, 922 s, 887 m, 840 vs br, 793 s br, 756 m, 748 sh, 724 sh, 685 sh, 679 m, 632 w, 593 s, 577 m, 535 w, 493 m. ^{1}H NMR (300.1 MHz, C_6D_6, 297 K): δ [ppm] = 3.28 [s, $\Delta\nu_{1/2}$ = 190 Hz, 27 H, 3 × Si(CH_3)$_3$], −33.1 (s, $\Delta\nu_{1/2}$ = 1400 Hz, 6 H, 3 × CH_2), −208 (s, $\Delta\nu_{1/2}$ = 5100 Hz, 6 H, 3 × CH_2). μ_{eff} = 3.0 μ_B. $C_{15}H_{39}CrFN_4Si_3$ (430.75): calcd. C 41.83, H 9.13, N 13.01; found C 41.47, H 8.85, N 13.13.

Preparation of [Cr(N_3N)Br] (4) by Oxidation of 1 with AgBr: [Cr(N_3N)] (**1**) (0.42 g, 1.02 mmol) was dissolved in 40 mL of THF, the solution was cooled to −60 °C and transferred via a double ended needle to a Schlenk tube, which was charged with AgBr (0.192 g, 1.02 mmol) and cooled to −60 °C. The suspension was allowed to warm to ambient temperature and stirred in the dark for 16 h. During this time the colour of the solution turned from green to reddish-black and a black precipitate of elemental silver was formed. The volatiles were removed in vacuo and the residue was extracted with 30 mL of diethyl ether. The extract was filtered through a filter cannula and the filtrate was concentrated to approximately 5 mL. Crystallisation was completed by storing the solution at −35 °C, affording **4** as a brown-black microcrystalline solid. Yield 0.32 g (64%), m.p. 175 °C. IR (nujol mull): $\tilde{\nu}$ [cm^{-1}] = 2724 vw, 2642 vw, 1448 m, 1400 vw, 1366 w, 1335 w, 1325 w, 1302 vw br, 1262 m, 1245 s, 1212 vw, 1181 vw, 1150 vw, 1132 w, 1119 sh, 1066 m, 1052 s, 1030 w, 942 s, 919 s, 905 m, 841 vs br, 796 m, 777 s, 753 s, 742 m, 689 w, 671 m, 632 w, 602 m, 575 m, 563 w, 545

vw, 482 w. ^{1}H NMR (300.1 MHz, C_6D_6, 297 K): δ [ppm] = 5.17 [s, $\Delta\nu_{1/2}$ = 250 Hz, 27 H, 3 × Si(CH_3)$_3$], −47.4 (s, $\Delta\nu_{1/2}$ = 1000 Hz, 6 H, 3 × CH_2), −185 (s, $\Delta\nu_{1/2}$ = 2700 Hz, 6 H, 3 × CH_2). μ_{eff} = 2.8 μ_B. $C_{15}H_{39}BrCrN_4Si_3$ (491.66): calcd. C 36.64, H 8.00, Br 16.25, N 11.40; found C 36.66, H 7.65, Br 16.32, N 11.28.

Preparation of [Cr(N$_3$N)Br] (4) by Oxidation of 1 with Br$_2$: A solution of [Cr(N$_3$N)] (**1**) (0.26 g, 0.63 mmol) in 50 mL of pentane was treated at −78 °C with a solution of Br_2 (0.016 mL, 0.31 mmol) in 1 mL of pentane. The colour of the reaction solution instantly turned black. After stirring for 2.5 h at ambient temperature, the solution was concentrated in vacuo to half of its volume and filtered from a black solid through a glass frit. The brownish-red filtrate was evaporated to dryness to yield 0.16 g of an oily residue. Crystallisation of the crude product from diethyl ether at −78 °C afforded **4** as black cubes. A second crop of **4** could be obtained after evaporation of the mother liquor to dryness and crystallisation of the residue from pentane at −78 °C. Overall yield 0.05 g (16%). The product was shown by ^{1}H NMR spectroscopy to be identical to that obtained from oxidation of **1** with AgBr.

Preparation of [Cr(N$_3$N)I] (5) by Oxidation of 1 with AgI: A mixture of [Cr(N$_3$N)] (**1**) (0.41 g, 1.00 mmol) and AgI (0.24 g, 1.02 mmol) was treated in the dark with 40 mL of THF at −78 °C. On warming to room temperature, the green solution of **1** turned yellowish-black and elemental silver precipitated out of the solution. After stirring for 16 h at room temperature in the dark, the solvent was removed in vacuo and insoluble material was removed by extraction of the residue with 40 mL of diethyl ether and filtration. The filtrate was concentrated to approximately 5 mL, then 10 mL of pentane was added and the volume of the solution was reduced in vacuo again to approximately 5 mL. Crystallisation of the product was completed by storing the solution overnight at −78 °C, thus providing **5** as black crystals, which were found by ^{1}H NMR spectroscopy to be more than 95% pure. Yield: 0.46 g (86%). Analytically pure **5** was obtained after recrystallisation of the crude product from diethyl ether and washing of the obtained crystals with pentane at −78 °C. Yield 0.38 g (71%), m.p. 177 °C. IR (nujol mull): $\tilde{\nu}$ [cm^{-1}] = 2635 w, 2080 w br, 2014 w, 1992 vw, 1925 w br, 1871 w br, 1447 m, 1401 w, 1366 vw, 1358 w, 1331 w, 1321 w, 1304 w, 1261 s, 1246 vs, 1211 w, 1136 m, 1115 w, 1069 m, 1050 sh, 1044 vs, 1024 m, 938 vs, 912 vs, 840 vs br, 781 vs br, 753 s, 740 s, 689 m, 674 m, 630 w, 574 s. ^{1}H NMR (300.1 MHz, C_6D_6, 297 K): δ [ppm] = 5.88 [s, $\Delta\nu_{1/2}$ = 140 Hz, 27 H, 3 × Si(CH_3)$_3$], −54.1 (s, $\Delta\nu_{1/2}$ = 950 Hz, 6 H, 3 × CH_2), −145 (s, $\Delta\nu_{1/2}$ = 2100 Hz, 6 H, 3 × CH_2). μ_{eff} = 3.0 μ_B. $C_{15}H_{39}CrIN_4Si_3$ (538.66): calcd. C 33.45, H 7.30, I 23.56, N 10.40; found C 33.16, H 7.36, I 23.32, N 10.25.

Preparation of [Cr(N$_3$N)I] (5) by Oxidation of 1 with I$_2$: A solution of I_2 (0.127 g, 0.50 mmol) in 30 mL of THF was added dropwise to a solution of **1** (0.42 g, 1.02 mmol) in 50 mL of THF at −78 °C. The colour of the solution instantly changed to yellowish-black. The resulting reaction mixture was stirred at room temperature for 15 h. The volatiles were removed in vacuo and the residue was extracted with 40 mL of pentane and then with 10 mL of diethyl ether. The extracts were filtered and evaporated to dryness in vacuo providing 0.48 g of a brown-black sticky solid. This was crystallised from 10 mL of diethyl ether at −78 °C affording black crystals of **5**. Yield: 0.16 g (29% relative to **1**). $C_{15}H_{39}CrIN_4Si_3$ (538.66): calcd. C 33.45, H 7.30, I 23.56, N 10.40; found C 32.21, H 7.17, I 23.88, N 10.37. The product was shown by ^{1}H NMR spectroscopy to be identical to that obtained from the oxidation of **1** with AgI.

Preparation of [Cr(N$_3$N)CN] (6): A solution of **1** (0.59 g, 1.43 mmol) in 30 mL of THF was added to a suspension of AgCN (0.22 g, 1.64 mmol) in 30 mL of THF at −50 °C. The reaction mixture was allowed to warm to ambient temperature under the exclusion of light. The colour of the solution slowly changed to red, and a black precipitate of elemental silver was formed. The suspension was stirred overnight at room temperature in the dark. The volatiles were removed in vacuo and the residue was extracted with 70 mL of diethyl ether. The blood-red extract was filtered, the filtrate was concentrated to approximately 15 mL and stored overnight at −78 °C to complete crystallisation of the product. After decanting the supernatant solution, the black crystals were washed with a minimum amount of diethyl ether at −78 °C and dried in vacuo. Yield: 0.36 g (57%), m.p. 166 °C. IR (nujol mull): $\tilde{\nu}$ [cm^{-1}] = 2642 vw, 1929 vw, 1871 vw, 1402 m, 1367 m, 1335 w, 1323 m, 1309 w, 1265 m, 1259 m, 1246 s, 1211 w, 1180 vw, 1169 vw, 1150 vw, 1132 m, 1118 sh, 1069 sh, 1051 s, 1029 m, 1015 sh, 941 vs, 919 vs, 841 vs br, 778 vs br, 750 s, 743 s, 732 sh, 687 m, 676 m, 633 m, 629 w, 601 m, 575 s, 562 m, 490 m, 466 m, 444 w, 417 m. ^{1}H NMR (300.1 MHz, C_6D_6, 297 K): δ [ppm] = 3.49 (s, $\Delta\nu_{1/2}$ = 220 Hz, 27 H, 3 × Si(CH_3)$_3$], −39.0 (s, $\Delta\nu_{1/2}$ = 1400 Hz, 6 H, 3 × CH_2), −188 (s, $\Delta\nu_{1/2}$ = 6900 Hz, 6 H, 3 × CH_2). μ_{eff} = 2.9 μ_B. $C_{16}H_{39}CrN_5Si_3$ (437.77): calcd. C 43.90, H 8.98, N 16.00; found C 44.14, H 9.06, N 15.75.

Preparation of [Ag(CN*t*Bu)$_2$](BF$_4$) (7): A suspension of $AgBF_4$ (0.625 g, 3.21 mmol) in 15 mL of CH_2Cl_2 was treated in the dark with *t*BuNC (0.72 mL, 6.37 mmol) and the reaction mixture was stirred at room temperature. After 5 min, an IR spectrum of the solution was recorded in the region of 2300−1500 cm^{-1} to follow the progress of the reaction. This showed two strong ν(C≡N) absorptions at 2225 and 2200 cm^{-1}, indicating the formation of the cations $[Ag(CNtBu)_2]^+$ and $[Ag(CNtBu)_3]^+$. After stirring for 30 min at ambient temperature, the IR spectrum of the reaction solution revealed that the ν(C≡N) absorption of $[Ag(CNtBu)_3]^+$ at 2200 cm^{-1} had disappeared. The solution was then filtered and the filtrate was concentrated in vacuo to a few millilitres and pentane was added to precipitate complex **7**. The supernatant solution was discarded and the precipitate washed once with pentane and dried in vacuo to afford **7** as a white solid. Yield 1.03 g (89%). IR (CH_2Cl_2): $\tilde{\nu}$ [cm^{-1}] = 2225 vs [ν(*t*BuN≡C)]. IR (THF): $\tilde{\nu}$ [cm^{-1}] = 2212 vs [ν(*t*BuN≡C)]. IR spectra in KBr showed extensive decomposition of **7** due to reaction with the matrix. ^{1}H NMR (300.1 MHz, CD_2Cl_2, 248 K): δ [ppm] = 1.52 (s, 18 H, 2 × CMe_3). ^{13}C{^{1}H} NMR (75.5 MHz, CD_2Cl_2, 222 K): δ [ppm] = 29.3 (s, 2 × CMe_3), 58.6 (s, 2 × CMe_3), 132.7 (s, 2 × CNCMe_3). ^{19}F NMR (282.4 MHz, CD_2Cl_2, 248 K): δ [ppm] = −152.65 (s, $^{11}BF_4$), −152.60 (s, $^{10}BF_4$). $C_{10}H_{18}AgBF_4N_2$ (360.94): calcd. C 33.28, H 5.03, N 7.76; found C 33.24, H 4.99, N 7.59.

X-ray Crystallographic Study: Suitable single crystals of **4** and **6** were grown by slow cooling of a saturated pentane (**4**) or diethyl ether (**6**) solution from ambient temperature to −35 °C. A summary of the crystal data, data collection and refinement is given in Table 4.

Data collection was performed on a STOE IPDS diffractometer (area detector) equipped with a low- temperature device (Cryostream, Oxford Cryosystems) using graphite monochromated Mo-K_α radiation (λ = 0.71073 Å). Unit cell parameters of **4** and **6** were determined from least-squares analyses using 5000 reflections (5.6° < 2θ < 50.0°). Intensities were measured by φ-oscillation scans and corrected for background, polarisation and Lorentz effects. DIFABS was applied for absorption correction of the data set of **4**.[35] The structures were solved by direct methods and refined anisotropically by the least-squares procedure implemented in the SHELX program system.[36] Hydrogen atoms were included iso-

Table 4. Crystallographic data for the complexes **4** and **6**

	4	**6**
Empirical formula	$C_{15}H_{39}BrCrN_4Si_3$	$C_{16}H_{39}CrN_5Si_3$
Molecular weight	491.68	437.79
Crystal colour	Black	Black
Crystal size [mm]	0.32 × 0.32 × 0.20	0.42 × 0.40 × 0.28
Crystal system	Monoclinic	Monoclinic
space group	*Cc*	*Cc*
a [Å]	17.210(2)	17.168(4)
b [Å]	9.574(2)	9.589(2)
c [Å]	15.835(2)	16.028(4)
β [deg]	110.46(2)	110.85(3)
V [Å^3]	2444.5(6)	2465.9(9)
Z	4	4
$D_{calcd.}$ [g·cm^{-3}]	1.336	1.179
T [K]	180(2)	180(2)
μ [mm^{-1}]	2.256	0.619
$T_{min.}/T_{max.}$	0.532/0.661	0.781/0.845
2θ min./max. [deg]	5.22/50.50	5.20/50.48
h/*k*/*l* ranges	−20,20/−11,11/−18,18	−20,20/−11,11/−19,19
Number of reflections collected	7867	7959
Number of unique reflections, *n*	4411	4403
R_{int} [$I > 2\sigma(I)$]	0.0622	0.0178
Parameters, *p*	217	226
Refinement method	full-matrix on F^2	full-matrix on F^2
R_1,[a] wR_2[b] [$I > 2\sigma(I)$]	0.0341, 0.0791	0.0226, 0.0568
R_1, wR_2 (all data)	0.0387, 0.0807	0.0236, 0.0572
GoF[c]	0.993	1.038
Largest peak/hole [e·Å^{-3}]	0.856/−0.565	0.255/−0.185

[a] $R_1 = \Sigma||F_o| - |F_c||/\Sigma|F_o|$. [b] $wR_2 = \{\Sigma[w(F_o^2 - F_c^2)^2]/\Sigma[w(F_o^2)^2]\}^{1/2}$. [c] GoF $= S = \{\Sigma[w(F_o^2 - F_c^2)^2]/(n - p)\}^{1/2}$.

tropically using the riding model on the bound carbon atoms. Geometrical calculations were performed with PLATON[37] and illustrations with DIAMOND.[38]

CCDC-183384 and CCDC-183385 contain the supplementary crystallographic data for this paper. These data can be obtained free of charge at www.ccdc.cam.ac.uk/conts/retrieving.html [or from the Cambridge Crystallographic Data Centre, 12 Union Road, Cambridge CB2 1EZ, UK; Fax: (internat.) + 44-1223/336-033; E-mail: deposit@ccdc.cam.ac.uk].

Acknowledgments

We thank the Fonds der Chemischen Industrie and the Humboldt-Universität zu Berlin for financial support, P. Neubauer for the crystal structure analyses of **4** and **6**, and Dr. U. Hartmann, U. Kursawe, and U. Kätel for the elemental analyses.

[1] [1a] L. F. Larkworthy, K. B. Nolan, P. O'Brien, in: *Comprehensive Coordination Chemistry*, 1st edition (Eds.: G. Wilkinson, R. D. Gillard, J. A. McCleverty), Pergamon Press, Oxford, **1987**, vol. 3, pp. 699−969. [1b] S. W. Kirtley, in: *Comprehensive Organometallic Chemistry*, 1st edition (Eds.: G. Wilkinson, F. G. A. Stone, E. W. Abel), Pergamon Press, Oxford, **1982**, vol. 3, pp. 783−951. [1c] M. J. Winter, S. Woodward, in: *Comprehensive Organometallic Chemistry II*, 1st edition, (Eds.: E. W. Abel, F. G. A. Stone, G. Wilkinson), Pergamon, Oxford, **1995**, vol. 5, pp. 281−329.

[2] [2a] M. Rahman, J. Rocek, *J. Am. Chem. Soc.* **1971**, *93*, 5455−5462, and: M. Rahman, J. Rocek, *J. Am. Chem. Soc.* **1971**, *93*, 5462−5464. [2b] K. B. Wiberg, S. K. Mukherjee, *J. Am. Chem. Soc.* **1971**, *93*, 2543−2544. [2c] S. L. Scott, A. Bakac, J. H. Espenson, *J. Am. Chem. Soc.* **1992**, *114*, 4205−4213.

[3] [3a] H. von Wartenberg, *Z. Anorg. Allg. Chem.* **1941**, *247*, 135−146. [3b] E. G. Hope, P. J. Jones, W. Levason, J. S. Ogden, M. Tajik, J. W. Turff, *J. Chem. Soc., Dalton Trans.* **1985**, 1443−1449.

[4] [4a] E. Huss, W. Klemm, *Z. Anorg. Allg. Chem.* **1950**, *262*, 25−32. [4b] H. Bode, E. Voss, *Z. Anorg. Allg. Chem.* **1956**, *286*, 136−141. [4c] H. C. Clark, Y. N. Sadana, *Can. J. Chem.* **1964**, *42*, 50−56. [4d] D. H. Brown, K. R. Dixon, R. D. W. Kemmit, D. W. A. Sharp, *J. Chem. Soc.* **1965**, 1559−1560. [4e] G. Siebert, R. Hoppe, *Z. Anorg. Allg. Chem.* **1972**, *391*, 126−136.

[5] [5a] W. Mowat, A. Shortland, G. Yagupsky, N. J. Hill, M. Yagupsky, G. Wilkinson, *J. Chem. Soc., Dalton Trans.* **1972**, 533−542. [5b] W. Kruse, *J. Organomet. Chem.* **1972**, *42*, C39−C42. [5c] W. Mowat, A. Shortland, N. J. Hill, G. Wilkinson, *J. Chem. Soc., Dalton Trans.* **1973**, 770−778. [5d] B. K. Bower, H. G. Tennent, *J. Am. Chem. Soc.* **1972**, *94*, 2512−2514. [5e] J. Müller, W. Holzinger, *Angew. Chem.* **1975**, *87*, 781−782, *Angew. Chem. Int. Ed. Engl.* **1975**, *14*, 760−761. [5f] R. R. Schrock, G. W. Parshall, *Chem. Rev.* **1976**, *76*, 243−268. [5g] C. J. Cardin, D. J. Cardin, A. Roy, *J. Chem. Soc., Chem. Commun.* **1978**, 899−900. [5h] M. Bochmann, G. Wilkinson, G. B. Young, *J. Chem. Soc., Dalton Trans.* **1980**, 1879−1887. [5i] P. Stavropoulos, P. D. Savage, R. P. Tooze, G. Wilkinson, B. Hussain, M. Motevalli, M. B. Hursthouse, *J. Chem. Soc., Dalton Trans.* **1987**, 557−562. [5j] A. Haaland, K. Rypdal, H. V. Volden, R. A. Andersen, *Acta Chem. Scand.* **1991**, *45*, 955−957.

[6] [6a] J. S. Basi, D. C. Bradley, M. H. Chisholm, *J. Chem. Soc. A* **1971**, 1433−1436. [6b] D. C. Bradley, M. H. Chisholm, *Acc. Chem. Res.* **1976**, *9*, 273−280.

[7] [7a] N. Hagihara, H. Yamazaki, *J. Am. Chem. Soc.* **1959**, *81*, 3160−3161. [7b] H.-L. Krauss, G. Münster, *Z. Anorg. Allg. Chem.* **1967**, *352*, 24−26. [7c] E. C. Alyea, J. S. Basi, D. C. Bradley, M. H. Chisholm, *J. Chem. Soc. (A)* **1971**, 772−776. [7d] G. Dyrkacz, J. Rocek, *J. Am. Chem. Soc.* **1973**, *95*, 4756−4757. [7e] M. Bochmann, G. Wilkinson, G. B. Young, *J. Chem. Soc., Dalton Trans.* **1980**, 901−910. [7f] M. Bochmann, G. Wilkinson,

M. B. Hursthouse, K. M. A. Malik, *J. Chem. Soc., Dalton Trans.* **1980**, 1863−1871. [7g] E. G. Thaler, K. Rypdal, A. Haaland, K. G. Caulton, *Inorg. Chem.* **1989**, *28*, 2431−2434.

[8] [8a] A. R. Barron, J. E. Salt, G. Wilkinson, M. Motevalli, M. B. Hursthouse, *J. Chem. Soc., Dalton Trans.* **1987**, 2947−2954. [8b] A. A. Danopoulos, G. Wilkinson, T. K. N. Sweet, M. B. Hursthouse, *J. Chem. Soc., Dalton Trans.* **1995**, 2111−2123. [8c] A. A. Danopoulos, G. Wilkinson, T. K. N. Sweet, M. B. Hursthouse, *J. Chem. Soc., Dalton Trans.* **1996**, 271−281. [8d] A. A. Danopoulos, G. Wilkinson, T. K. N. Sweet, M. B. Hursthouse, *Polyhedron* **1996**, *15*, 873−879. [8e] K. C. Chew, W. Clegg, M. P. Coles, M. R. J. Elsegood, V. C. Gibson, A. J. P. White, D. J. Williams, *J. Chem. Soc., Dalton Trans.* **1999**, 2633−2639.

[9] [9a] J. W. Buchler, K. L. Lay, L. Castle, V. Ullrich, *Inorg. Chem.* **1982**, *21*, 842−844. [9b] J. T. Groves, W. J. Kruper, Jr., R. C. Haushalter, W. M. Butler, *Inorg. Chem.* **1982**, *21*, 1363−1368. [9c] L.-C. Yuan, T. C. Bruice, *J. Am. Chem. Soc.* **1985**, *107*, 512−513. [9d] D. J. Liston, B. O. West, *Inorg. Chem.* **1985**, *24*, 1568−1576. [9e] S. E. Creager, R. W. Murray, *Inorg. Chem.* **1985**, *24*, 3824−3828. [9f] S.-K. Noh, R. A. Heintz, B. S. Haggerty, A. L. Rheingold, K. H. Theopold, *J. Am. Chem. Soc.* **1992**, *114*, 1892−1893. [9g] K. B. P. Ruppa, K. Feghali, I. Kovacs, K. Aparna, S. Gambarotta, G. P. A. Yap, C. Bensimon, *J. Chem. Soc., Dalton Trans.* **1998**, 1595−1605. [9h] A. Hess, M. R. Hörz, L. M. Liable-Sands, D. C. Lindner, A. L Rheingold, K. H. Theopold, *Angew. Chem.* **1999**, *111*, 126−128; *Angew. Chem. Int. Ed.* **1999**, *38*, 166−168. [9i] J. Hesschenbrouck, E. Solari, C. Floriani, N. Re, C. Rizzoli, A. Chiesi-Villa, *J. Chem. Soc., Dalton Trans.* **2000**, 191−198.

[10] [10a] G. B. Kauffman, G. Acero, *Inorg. Synth.* **1966**, *8*, 132−135 and references cited therein. [10b] R. Stromberg, *Ark. Kemi* **1964**, *22*, 49−64. [10c] R. Stromberg, *Ark. Kemi* **1965**, *23*, 401−430 and *24*, 47−71.

[11] [11a] H. Brunner, J. Wachter, E. Guggolz, M. L. Ziegler, *J. Am. Chem. Soc.* **1982**, *104*, 1765−1766. [11b] D. Reardon, I. Kovacs, K. B. P. Ruppa, K. Feghali, S. Gambarotta, J. Petersen, *Chem. Eur. J.* **1997**, *3*, 1482−1488.

[12] W. A. Herrmann, W. R. Thiel, E. Herdtweck, *J. Organomet. Chem.* **1988**, *353*, 323−336.

[13] [13a] A. R. Oki, H. Zhang, J. A. Maguire, N. S. Hosmane, H. Ro, W. E. Hatfield, *Organometallics* **1991**, *10*, 2996−2998. [13b] A. R. Oki, H. Zhang, J. A. Maguire, N. S. Hosmane, H. Ro, W. E. Hatfield, M. Moscherosch, W. Kaim, *Organometallics* **1992**, *11*, 4202−4213.

[14] S. Sarkar, R. C. Maurya, S. C. Chaurasia, S. K. Srivastava, *Indian J. Chem.* **1977**, *15A*, 744−745.

[15] S. Sarkar, B. Sharma, R. C. Maurya, S. C. Chaurasia, S. K. Srivastava, *Indian J. Chem.* **1977**, *15A*, 747−748.

[16] D. J. Mindiola, C. C. Cummins, *Angew. Chem.* **1998**, *110*, 983−986; *Angew. Chem. Int. Ed.* **1998**, *37*, 945−947.

[17] [17a] J. Amor Nait Ajjou, S. L. Scott, *Organometallics* **1997**, *16*, 86−92. [17b] J. Amor Nait Ajjou, S. L. Scott, V. Paquet, *J. Am. Chem. Soc.* **1998**, *120*, 415−416. [17c] J. Amor Nait Ajjou, G. L. Rice, S. L. Scott, *J. Am. Chem. Soc.* **1998**, *120*, 13436−13443. [17d] J. Amor Nait Ajjou, S. L. Scott, *J. Am. Chem. Soc.* **2000**, *122*, 8968−8976. [17e] R. Schmid, T. Ziegler, *Can. J. Chem.* **2000**, *78*, 265−269.

[18] R. Schmid, T. Ziegler, *Organometallics* **2000**, *19*, 2756−2765.

[19] S. Schneider, A. C. Filippou, *Inorg. Chem.* **2001**, *40*, 4674−4677.

[20] A violet-red, THF-soluble product of presently unknown composition is also formed in the oxidation of **1** with $AgBF_4$. This product is insoluble in pentane and can thereby be separated easily from **2**.

[21] S. H. Strauss, *Chem. Rev.* **1993**, *93*, 927−942.

[22] G. E. Greco, M. O′Donoghue, S. W. Seidel, W. M. Davis, R. R. Schrock, *Organometallics* **2000**, *19*, 1132−1149.

[23] I.-P. Lorenz, *Gruppentheorie und Molekülsymmetrie*, Attempto Verlag, Tübingen, Germany, **1992**.

[24] The lower-energy ν(C≡N) absorption band of **7** in KBr appears at nearly the same position as that of analytically pure $[Ag(CN\textit{t}Bu)_4](BF_4)$ (**8**) in KBr (2184 cm^{-1}). This let us suggest that **8** might be one of the products of the reaction of **7** with KBr under pressure. It is interesting to note, that $[Ag(CN\textit{t}Bu)_3](PF_6)$ has been previously reported to give two ν(C≡N) absorption bands in KBr at positions (2241 and 2184 cm^{-1}) very close to those of **7**: Y. Yamamoto, K. Aoki, H. Yamazaki, *Inorg. Chim. Acta* **1982**, *68*, 75−78.

[25] Complexes **8** and **9** were prepared in CH_2Cl_2 by the reaction of $AgBF_4$ with four and three equivalents of *t*BuNC, respectively. These were isolated as analytically pure, white solids in very high yields and were fully characterised: D. Wössner, Dissertation, **1997**, Humboldt-Universität zu Berlin, Cuviller Verlag, Göttingen, Germany, **1997**.

[26] D. F. Evans, *J. Chem. Soc.* **1959**, 2003−2005.

[27] S. K. Sur, *J. Magn. Res.* **1989**, *82*, 169−173.

[28] The determination of the solid-state structure of the iodo derivative **5** was also attempted by single-crystal X-ray diffraction. So far the crystal structure of **5** could not be refined satisfactory due to a disorder in the crystal. It revealed, however, the same configuration of complex **5** with that of **4** and **6**.

[29] A. C. Filippou, S. Schneider, manuscript in preparation.

[30] [30a] Z. Duan, J. G. Verkade, *Inorg. Chem.* **1995**, *34*, 1576−1578. [30b] R. R. Schrock, S. W. Seidel, N. C. Mösch-Zanetti, K.-Y. Shih, M. B. O′Donoghue, W. M. Davis, W. M. Reiff, *J. Am. Chem. Soc.* **1997**, *119*, 11876−11893.

[31] [31a] J. H. Enemark, M. S. Quinby, L. L. Reed, M. J. Steuck, K. K. Walthers, *Inorg. Chem.* **1970**, *9*, 2397−2403. [31b] D. G. Fu, J. Chen, X. S. Tan, L. J. Jiang, S. W. Zhang, P. J. Zheng, W. X. Tang, *Inorg. Chem.* **1997**, *36*, 220−225. [31c] J. Bendix, K. Meyer, T. Weyhermüller, E. Bill, N. Metzler-Nolte, K. Wieghardt, *Inorg. Chem.* **1998**, *37*, 1767−1775. [31d] M. Ohba, N. Usuki, N. Fukita, H. Okawa, *Inorg. Chem.* **1998**, *37*, 3349−3354.

[32] [32a] T. G. Appleton, H. C. Clark, L. E. Manzer, *Coord, Chem. Rev.* **1973**, *10*, 335−422. [32b] K. B. Yatsimirskii, *Pure Appl. Chem.* **1974**, *38*, 341−361. [32c] E. M. Shustorovich, M. A. Porai-Koshits, Yu. A. Buslaev, *Coord, Chem. Rev.* **1975**, *17*, 1−98. [32d] J. K. Burdett, T. A. Albright, *Inorg. Chem.* **1979**, *18*, 2112−2120.

[33] D. F. Shriver, M. A. Drezdzon, *The Manipulation of Air Sensitive Compounds*, 2nd edition, Wiley, New York, **1986**.

[34] [34a] A. Pacault, J. Hoarau, A. Marchand, *Adv. Chem. Phys.* **1961**, *3*, 171−238. [34b] W. Klemm, *Z. Anorg. Allg. Chem.* **1940**, *244*, 377−396 and **1941**, *246*, 347−362.

[35] N. Walker, D. Stuart, *Acta Crystallogr., Sect. A* **1983**, *39*, 158−166.

[36] G. M. Sheldrick, *SHELX-97*, Universität Göttingen, Göttingen, Germany, **1997**.

[37] A. L. Spek, *PLATON-98*, University of Utrecht, Utrecht, The Netherlands, **1998**.

[38] K. Brandenburg, *DIAMOND 2.1c*, Crystal Impact GbR, Bonn, Germany, **1999**.

Received April 15, 2002
[I02217]

Two New Layered Thioantimonate(III) Compounds: Solvothermal Syntheses, Crystal Structures, and Properties of (*trans*-1,4-$C_6N_2H_{15}$)Sb_3S_5 and (*trans*-1,2-$C_6N_2H_{15}$)$Sb_3S_5 \cdot H_2O$

Lars Engelke,[a] Christian Näther,[a] and Wolfgang Bensch*[a]

Keywords: Crystal structure / Hydrogen bonds / Solvothermal synthesis / Thioantimonate

Two new thioantimonate(III) compounds (*trans*-1,4-chxnH)Sb_3S_5 (**I**) and (*trans*-1,2-chxnH)$Sb_3S_5 \cdot H_2O$ (**II**) (chxn = diaminocyclohexane = $C_6N_2H_{14}$) were prepared under solvothermal conditions. Structure-directing arrangements of the organic molecules are formed under the conditions of synthesis; these consist of hydrogen-bonded chains (**I**) and of double chains of the amine molecules indirectly joined by water molecules through hydrogen bonding (**II**). In both compounds the structure-directing counter-ions are arranged in a layer-like fashion and because of the similar arrangements the topologies of the thioantimonate(III) layers $^2_\infty[Sb_3S_5]^-$ are nearly identical. The anionic layers are formed by interconnection of SbS_3 trigonal pyramids and SbS_4 moieties. The layers containing Sb_2S_2, Sb_4S_4, and $Sb_{10}S_{10}$ heterorings as secondary building units are stacked parallel to the *b* axis. The anionic layers and the structure-directing aggregates are stacked in a sandwich-like fashion. The water molecule in **II** can be removed at low temperatures, and this process is partially reversible. Interestingly, the removal of water is accompanied by a pronounced colour change from bright yellow to red.

(© Wiley-VCH Verlag GmbH, 69451 Weinheim, Germany, 2002)

Introduction

Structure-directing molecules such as alkylamines or their ammonium salts are widely used for the solvothermal synthesis of new main group thiometallates. A large number of thioantimonates(III) have been synthesized over recent years. The high flexibility of the coordination behaviour of the Sb^{III} atom, with coordination numbers between 3 and 6[1–4] due to the lone pair effect,[5,6] has allowed the preparation of a large variety of thioantimonate(III) compounds.

With alkali or alkaline metal cations, a size dependence of the anion dimensionality is observed. With decreasing ionic radius the formation of one-dimensional chains,[7] layered anions,[8] or three-dimensional networks[9] is preferred. In cases of transition metal amine complexes[10–12] or pure alkylammonium cations[13–15] no simple relationship between the size and the dimensionality of the thioantimonate(III) anion could be observed; thus, other factors must play a dominant role during the anionic framework formation. Systematic investigations are required in order to obtain a deeper knowledge of the factors influencing the formation and crystallization of thioantimonates(III). One approach to study the influence of the structure-directing molecules is the application of amines of similar size and charge but with their amino groups at different positions. Such an amine pair is *trans*-1,2-diaminocyclohexane and *trans*-1,4-diaminocyclohexane. In this contribution we report the syntheses, crystal structures, thermal stabilities, and optical properties of the two new thioantimonate(III) (chxnH)$[Sb_3S_5]$ species, with chxnH being the protonated amines *trans*-1,2-diaminocyclohexane and *trans*-1,4-diaminocyclohexane.

[a] Institut für Anorganische Chemie, Universität Kiel, Olshausenstr. 40, 24098 Kiel, Germany

Results and Discussion

Both (*trans*-1,4-chxnH)Sb_3S_5 (**I**) and (*trans*-1,2-chxnH)$Sb_3S_5 \cdot H_2O$ (**II**) crystallize in the triclinic space group $P\bar{1}$ with two formula units in the unit cell (Table 1). The Sb(1) and Sb(2) atoms in both **I** and **II** are coordinated by three sulfur atoms, forming the well-known SbS_3 pyramids. The Sb–S distances range from 2.396(1) to 2.5993(8) Å in **I** (Table 2) and from 2.393(1) to 2.599(1) Å in **II** (Table 3). In both compounds the Sb(3) atoms are coordinated by four S atoms to form an SbS_4 unit with two shorter Sb–S distances [2.4299(8) and 2.452(1) Å in **I** and 2.435(1) and 2.450(1) Å in **II**] and two significantly longer Sb–S separations [2.684(1) and 2.777(1) Å in **I** and 2.615(1) and 2.908(1) Å in **II**]. Such SbS_4 building units are common, and the two longer Sb–S distances are always in *trans* relationships to each other.[16–19] The coordination spheres of the antimony atoms are completed by S atoms at greater distances, giving coordination numbers of five [Sb–S: 2.978(1) to 3.546(1) and 2.973(1) to 3.519(1) Å, respectively]

to form distorted SbS_5 trigonal bipyramids (Table 4 and Figure 1).

The $Sb(1)S_3$ and $Sb(2)S_3$ pyramids each share a common corner with the $Sb(3)S_4$ moiety, yielding the $Sb_3S_5^-$ anion. Further interconnection to produce the two-dimensional

Table 1. Details of the data collections and some refinement results for the two compounds (*trans*-1,4-chxnH)Sb_3S_5 (**I**) and (*trans*-1,2-chxnH)Sb_3S_5 (**II**)

	(1,4-chxn)Sb_3S_5	(1,2-chxn)$Sb_3S_5{\cdot}H_2O$
a [Å]	6.713(1)	6.660(1)
b [Å]	10.059(2)	10.889(2)
c [Å]	12.368(3)	12.430(3)
α [°]	83.34(3)	105.43(3)
β [°]	84.15(3)	94.58(3)
γ [°]	73.13(3)	106.42(3)
V [Å^3]	791.7(3)	821.7(3)
Temperature [K]	293(2)	293(2)
Z	2	2
μ [mm^{-1}]	5.719	5.518
Formula mass [g/mol]	640.75	658.77
Space group	$P\bar{1}$	$P\bar{1}$
Density (calcd.) [g/cm^3]	2.688	2.663
Diffractometer	PHILIPS 4-circle	NONIUS CAD4
2Θ range [°]	3−60	4−60
Data collected	4991	5143
Unique data	4625	4763
Data [$F_o > 4\sigma(F_o)$]	4179	3874
Δρ [e/Å^3]	0.55/−0.67	1.06/−2.07
Refined parameters	206	183
y, z[a]	0.0244/0.28	0.0422/0.54
$R1[F_o > 4\sigma(F_o)]$	0.0177	0.0277
$wR2$ for all data	0.0455	0.0700
Goodness of fit	1.054	1.017

[a] $w = 1/[\sigma^2(F_o^2) + (yP)^2 + zP]$; $P = [\mathrm{Max}(F_o^2,0) + 2F_c^2]/3$.

Table 2. Distances [Å] and angles [°] in (*trans*-1,4-chxnH)Sb_3S_5 (**I**); estimated standard deviations are given in parentheses

Sb(1)−S(1)	2.419(1)	Sb(1)−S(1a)	2.5993(8)
Sb(1)−S(5)	2.460(1)	Sb(2)−S(2)	2.462(1)
Sb(2)−S(3)	2.396(1)	Sb(2)−S(4)	2.5812(8)
Sb(3)−S(2)	2.4299(8)	Sb(3)−S(3)	2.777(1)
Sb(3)−S(4)	2.452(1)	Sb(3)−S(5)	2.684(1)
Long contacts			
Sb(1)−S(2)	3.357(1)	Sb(1)−S(5a)	2.978(1)
Sb(2)−S(3a)	3.020(1)	Sb(2)−S(4a)	3.397(1)
Sb(3)−S(1)	3.546(1)		
S(1)−Sb(1)−S(1a)	88.79(2)	S(1)−Sb(1)−S(2)	80.17(1)
S(1)−Sb(1)−S(5)	95.12(2)	S(1a)−Sb(1)−S(5a)	82.44(1)
S(1a)−Sb(1)−S(2)	81.50(1)	S(1a)−Sb(1)−S(5)	100.47(2)
S(2)−Sb(1)−S(5a)	97.15(1)	S(5)−Sb(1)−S(5a)	87.80(1)
S(1a)−Sb(1)−S(5a)	171.13(2)	S(2)−Sb(1)−S(5)	174.90(1)
S(2)−Sb(2)−S(3a)	81.26(1)	S(2)−Sb(2)−S(3)	95.59(1)
S(2)−Sb(2)−S(4)	85.97(1)	S(3)−Sb(2)−S(4)	88.70(1)
S(3)−Sb(2)−S(3a)	87.42(1)	S(3)−Sb(2)−S(4a)	77.42(1)
S(3a)−Sb(2)−S(4)	95.59(1)	S(4)−Sb(2)−S(4a)	96.45(1)
S(2)−Sb(2)−S(4a)	172.50(1)	S(3a)−Sb(2)−S(4)	166.23(2)
S(1)−Sb(3)−S(2)	78.52(1)	S(1)−Sb(3)−S(3)	110.18(1)
S(1)−Sb(3)−S(5)	72.54(1)	S(2)−Sb(3)−S(3)	87.06(1)
S(2)−Sb(3)−S(4)	99.44(1)	S(2)−Sb(3)−S(5)	83.65(1)
S(3)−Sb(3)−S(4)	90.04(1)	S(4)−Sb(3)−S(5)	86.89(1)
S(1)−Sb(3)−S(4)	159.42(1)	S(3a)−Sb(3)−S(5)	169.59(1)

Table 3. Distances [Å] and angles [°] in (*trans*-1,2-chxnH)$Sb_3S_5{\cdot}H_2O$ **II**; estimated standard deviations are given in parentheses

Sb(1)−S(1)	2.415(1)	Sb(1)−S(1a)	2.524(1)
Sb(1)−S(5)	2.494(1)	Sb(2)−S(2)	2.485(1)
Sb(2)−S(3)	2.393(1)	Sb(2)−S(4)	2.599(1)
Sb(3)−S(2)	2.435(1)	Sb(3)−S(3)	2.908(1)
Sb(3)−S(4)	2.450(1)	Sb(3)−S(5)	2.615(1)
Long contacts			
Sb(1)−S(2)	3.385(1)	Sb(1)−S(5a)	3.139(2)
Sb(2)−S(3a)	2.973(1)	Sb(2)−S(4a)	3.519(1)
Sb(3)−S(1)	3.419(2)		
S(1)−Sb(1)−S(1a)	89.61(4)	S(1)−Sb(1)−S(2)	83.66(3)
S(1)−Sb(1)−S(5)	98.39(4)	S(1)−Sb(1)−S(5a)	79.97(4)
S(1a)−Sb(1)−S(2)	80.95(3)	S(1a)−Sb(1)−S(5)	97.20(4)
S(2)−Sb(1)−S(5a)	91.48(3)	S(5)−Sb(1)−S(5a)	90.68(3)
S(1a)−Sb(1)−S(5a)	167.78(4)	S(2)−Sb(1)−S(5)	177.25(3)
S(4)−Sb(2)−S(4a)	98.24(3)	S(2)−Sb(2)−S(4)	86.44(4)
S(3)−Sb(2)−S(4)	90.55(4)	S(3)−Sb(2)−S(4a)	77.64(3)
S(3a)−Sb(2)−S(4a)	91.49(3)	S(2)−Sb(2)−S(3)	97.74(4)
S(2)−Sb(2)−S(3a)	83.39(4)	S(3)−Sb(2)−S(3a)	85.69(4)
S(2)−Sb(2)−S(4a)	173.39(4)	S(3a)−Sb(2)−S(4)	168.58(4)
S(1)−Sb(3)−S(2)	81.43(3)	S(1)−Sb(3)−S(3)	103.69(3)
S(1)−Sb(3)−S(5)	74.69(3)	S(2)−Sb(3)−S(4)	98.33(4)
S(2)−Sb(3)−S(3)	85.67(4)	S(2)−Sb(3)−S(5)	86.27(4)
S(3)−Sb(3)−S(4)	90.18(4)	S(4)−Sb(3)−S(5)	91.36(4)
S(1)−Sb(3)−S(4)	166.04(3)	S(3a)−Sb(3)−S(5)	171.94(4)

Table 4. Differences [Å] for Sb−S bonds expressed as Δ(Sb−S in **II** − Sb−S in **I**)

Sb(1)−S(1)	−0.004	Sb(1)−S(1a)	−0.075
Sb(1)−S(5)	+0.034	Sb(2)−S(2)	+0.023
Sb(2)−S(3)	−0.003	Sb(2)−S(4)	+0.018
Sb(3)−S(2)	+0.005	Sb(3)−S(3)	+0.131
Sb(3)−S(4)	−0.002	Sb(3)−S(5)	−0.069
Long contacts			
Sb(1)−S(2)	+0.028	Sb(1)−S(5a)	+0.161
Sb(2)−S(3a)	−0.047	Sb(2)−S(4a)	+0.122
Sb(3)−S(1)	−0.127		

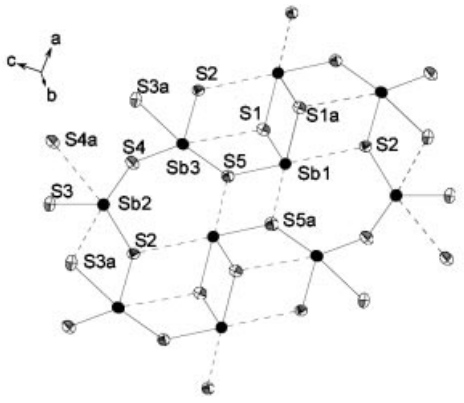

Figure 1. The environment of the Sb atoms, atom labelling and the long Sb−S contacts shown as dotted lines; the probability ellipsoids are drawn at the 50% level

layered anion is achieved by corner- and edge-sharing in the different primary building units. Two symmetry-related $Sb(1)S_3$ pyramids share a common edge to form a *trans*-Sb_2S_4 unit, and two $Sb(3)S_4$ and two $Sb(2)S_3$ have common corners, yielding a puckered, eight-membered Sb_4S_4 ring (8MR). The 8MR units are condensed into rods running along the *a* axis. Adjacent rods are connected by the *trans*-Sb_2S_4 building units, giving the two-dimensional $[Sb_3S_5]^-$ anion extending within the *a*−*c* plane shown in Figure 2. The connection of the rods by the Sb_2S_4 units gives rise to the formation of ellipsoidal 20-membered $Sb_{10}S_{10}$ heterorings (20MR) with approximate dimensions of 9.2×3 Å (measured from coordinate to coordinate). The layers are stacked perpendicular to the *b* axis (interlayer spacing about 6.9 Å) with a parallel alignment of the 8MR and 20MR units. The thickness of the individual layers is about 3.5 Å.

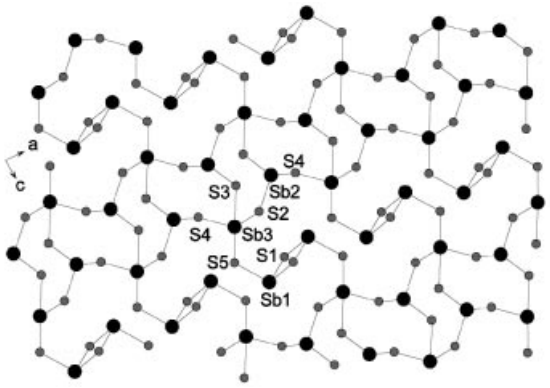

Figure 2. The $[Sb_3S_5^-]_\infty$ layer viewed parallel to [010], with numbering scheme and the four-, eight-, and 20-membered rings

In compound **I**, protonation of one of the two NH_2 groups yields the charge-balancing *trans*-1-amino-4-ammoniocyclohexane cation. Strong hydrogen bonds [N···H distance: 1.86(2) Å; N−H···N angle: 172.26(4)°] between adjacent cations (see Figure 3) force the arrangement of nearly linear chains running parallel to the *a* axis. The chains are oriented parallel to one another to form pseudo-layers within the *a*−*c* plane. As shown in Figure 4, the anionic Sb_3S_5 layers and cationic pseudo-layers are stacked in a sandwich-like manner perpendicular to the *b* axis.

Figure 3. Hydrogen bonds in the *trans*-1-amino-4-ammoniocyclohexane chains; the displacement ellipsoids are drawn at the 50% probability level

In compound **II**, one of the amino groups is again protonated to form the *trans*-1-amino-2-ammoniocyclohexane cation for charge-balancing. Hydrogen bonds between the

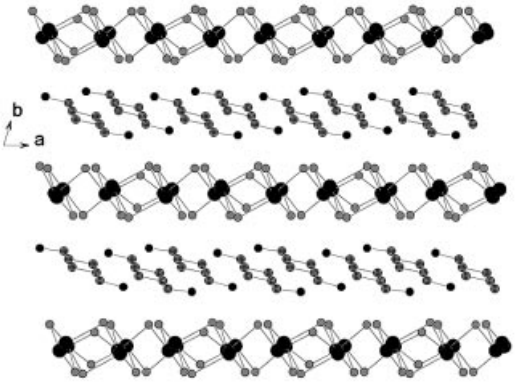

Figure 4. The sandwich-like arrangement of alternating anionic and cationic layers viewed along [001] in compound **I**

NH_2 and NH_3^+ groups in the 1- and 2-positions cannot give rise to the formation of linear chains as observed for the *trans*-1-amino-4-ammoniocyclohexane cation. In this compound, pairs of cations are formed, connected through hydrogen bonds involving two water molecules (Figure 5). The O···H distance of 1.85(5) Å and the N···H distance of 1.87(7) Å, with corresponding angles of 165.5° and 175.6°, are indicative of strong hydrogen bonds. An additional, weaker O···H hydrogen bond between the NH_3^+ groups and the water molecules interconnects the pairs to produce double chains. The O···H distance of 2.03(4) Å, the corresponding angle of 177.4°, and the N···O distance of 2.87(4) Å are common values for weaker hydrogen bonds.[20] The double chains running along the *a* axis are arranged in a layer-like fashion within the *a*−*c* plane. As in compound **I**, a sandwich-like structure consisting of alternating anionic and cationic layers stacked perpendicular to the *b* axis is observed. The differences between the arrangements of the cations in the two compounds are presumably due to the type of H bonding. In compound **I**, the amine molecules are joined by direct hydrogen bonds, whereas the connection in compound **II** involves a bridging water molecule. This acts as a donor and acceptor to two adjacent cations and is an acceptor for a third amine molecule.

At first glance, the two anionic network structures seem to be identical. However, a more detailed analysis reveals several differences, demonstrating the high flexibility of Sb^{III} coordination spheres for optimization of the packing (see Table 4). If only the short Sb−S bonds are taken into account, the average Sb−S distances of 2.526 Å (**I**) and 2.532 Å (**II**) are identical (Table 4). A small difference is observed when the long bonds are also considered [<Sb−S> = 2.771 Å for **I** and 2.783 Å for **II**]. The flexible behaviour can be demonstrated by comparing the environments of Sb(3) in the two compounds. In **I** the Sb(3)−S(3) and Sb(3)−S(5) separations are 2.777(1) Å and 2.684(1) Å, whereas in **II** these values amount to 2.908(1) Å and 2.615(1) Å. Because the bond order of the S(5) atom has to remain constant, the Sb(1)−S(5) bond in **I** [2.460(1) Å] is shorter than in **II** [2.494(1) Å].

Some remarkable differences are also observed for the S−Sb−S angles. In **I**, these values range from about 72.5

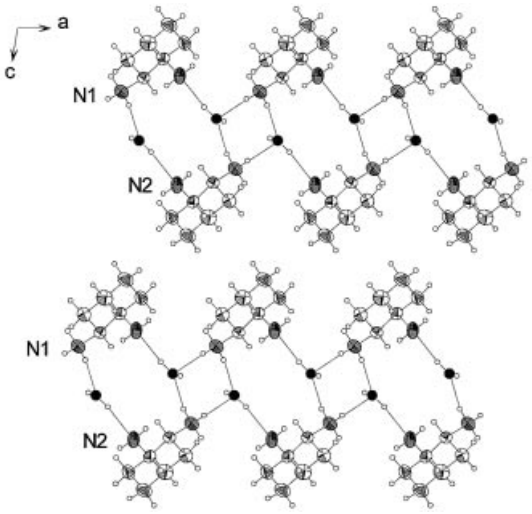

Figure 5. View of the *trans*-1-amino-2-ammoniocyclohexane cations and the water molecules forming double chains in the $a-c$ plane (displacement ellipsoids are drawn at the 50% probability level; hydrogen bonds are shown as dotted lines)

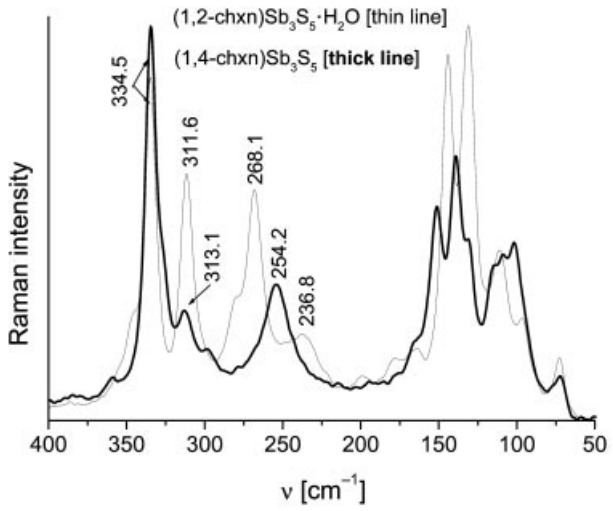

Figure 6. Raman spectra of (*trans*-1,4-chxnH)Sb_3S_5 and (*trans*-1,2-chxnH)$Sb_3S_5{\cdot}H_2O$; the numbers are the frequencies of some of the most intense resonances

to 110.2° whereas in **II** the analogous values extend from 74.7 to 103.7° (note: *trans*-S−Sb−S angles are not considered). Individual angles show differences of up to about 6.5° [S(1)−Sb(3)−S(3)], again demonstrating the flexibility of the thioantimonate(III) network for achievement of optimum packing.

As previously demonstrated, the bonding properties of a lone-pair atom are best detected from changes of the bond angles, whereas interatomic bond lengths are only slightly affected,[21] and the local environment of the Sb^{III} atoms exhibits no significant alterations of the Sb−S distances. Raman spectroscopy is a powerful tool for the detection of differing bonding properties; the Raman spectra are shown in Figure 6. Both compounds show intense bands located at 334.5 cm^{-1} (**I** and **II**) and at 313.1 cm^{-1} (**I**) or 311.6 cm^{-1} (**II**), due to SbS_3 and SbS_4 units.[22] Because of the similar average Sb−S bond lengths in **I** and **II**, the main resonances show only minute differences. However, small shoulders on the high-frequency side of the first band are caused by the different Sb environments in the two compounds. The assignments of the Sb−S modes are in accordance with the results reported by Pfitzner for Cu_3SbS_3 and $(CuI)_2Cu_3SbS_3$.[23] In the former compound, two maxima were observed at 321 and 290 cm^{-1}, reflecting the weaker bonding interaction due to the 3 + 5 environment. In the latter, the [SbS_3^{3-}] anion has no next-nearest S atoms, yielding Raman bands at 362 and 339 cm^{-1}. For $Mn_2Sb_2S_4$, with one Sb^{III} atom in a sixfold environment of S atoms and the other Sb^{III} atom in a sevenfold one, Raman bands occur at even lower frequencies, being located between about 280 and 310 cm^{-1}.[24]

A brief comparison of the crystal structures of **I** and **II** with structures of composition RSb_3Q_5 (R = cation, Q = S, Se) should serve to highlight the uniqueness of the thioantimonate(III) layers in the title compounds. In $RbSb_3S_5{\cdot}H_2O$[16] and $RbSb_3Se_5$,[25] layered anions are found. In these two compounds, however, remarkably different modes of interconnection of the primary building units to form SbS/SbSe heterorings are found. In the selenide, six- and eight-membered rings are formed, while in the sulfide the interconnection yields four- and 16-membered rings. Compounds $[M^{II}(en)_3]Sb_3S_5$ with M = Ni, Co[26] contain isolated $[Sb_3S_5]^-$ anions. With large organic cations such as Tpa [tetrapropylammonium, $(C_3H_7)_4N^+$] or PPh_4 (tetraphenylphosphonium), the SbS_x units are joined to form one-dimensional chains, as found in $(Tpa)Sb_3S_5$ [11] and $(PPh_4)Sb_3S_5$.[27] With the smaller Tma [tetramethylammonium, $(CH_3)_4N^+$] cation, three-dimensional interconnection of the primary units of the Sb_3S_5 anion was proposed.[28] The ternary compound $TlSb_3S_5$ [29] shows a three-dimensional anionic framework. We note that the two title compounds are the first examples of thioantimonate(III) moieties with $[Sb_3S_5]^-$ networks containing 4MR, 8MR, and 20MR components as secondary building units.

With respect to the syntheses of the compounds, several observations are remarkable. Compound **I** forms under a wide range of conditions, with factors such as temperature, amine concentration, and amine/antimony ratio having virtually no influence on product formation. Several unsuccessful attempts were made to introduce transition metal cations into the anionic thioantimonate(III) framework. In all experiments compound **I** was obtained. Hence, we conclude that, under the reaction conditions used, *trans*-1,4-diaminocyclohexane forms a very stable arrangement that forces the growth of $^2_\infty[Sb_3S_5]^-$ layers with the topology found in the title compound. In contrast, the synthesis of **II** requires very precise conditions, suggesting a lower stability of the hydrogen-bonded 1,2-substituted amine. Parameters such as temperature, amine concentration, and amine/antimony ratio were varied in a large number of experiments. Small deviations from the synthesis conditions reported in the Exp. Sect., though, always yield thioanti-

monates of different composition. In addition, application of Mn, Ni, or Co results in the formation of compounds composed of isolated $[M(chxn)_3]^{2+}$ and SbS_4^{3-} ions (M = Co, Ni) or of $[M(chxn)_2(SbS_4)_2]^{4-}$ ions (M = Mn). Obviously, the formation of the structure-directing arrangement of the cations requires precise conditions, and deviations from exact stoichiometric quantities suppress the "template" formation.

Thermal Investigations

The DTA-TG curves are shown in Figure 7. Compound **I** starts to decompose at T_{onset} = 250 °C. A weight loss of 18.9% occurs in one step, and is accompanied by an endothermic signal with a peak temperature T_p of 257 °C. The mass loss is in good agreement with that calculated for the emission of the amine molecules ($-\Delta m_{theo}$ = 17.98%). In the X-ray powder pattern of the decomposition product, the reflections of crystalline Sb_2S_3 as well as of elemental antimony are found. Obviously, the Sb/S ratio in the starting material (0.6) results in a partial reduction of Sb^{III} to elemental Sb and the formation of Sb_2S_3. A C,H,N analysis of the residue yields a very low contamination level of about 0.5%.

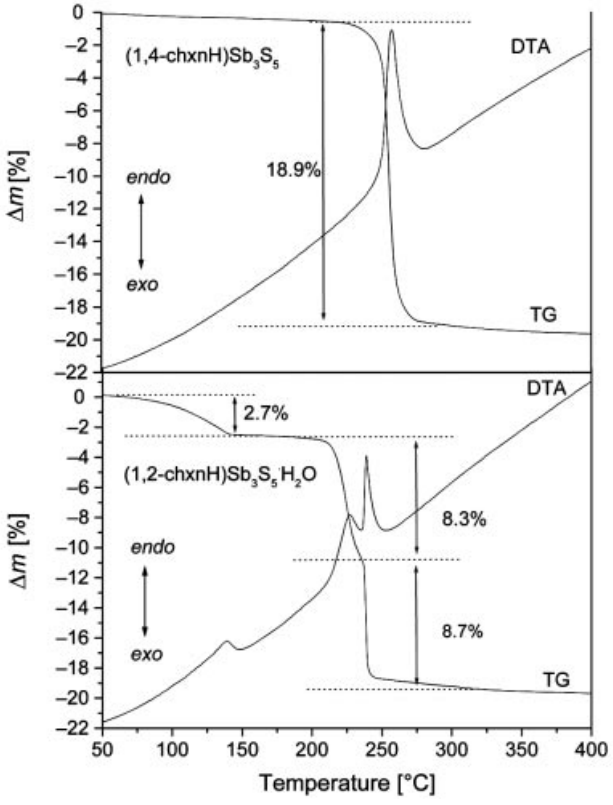

Figure 7. DTA/TG curves for compound **I** (top) and for compound **II** (bottom; mass changes are given in %)

For compound **II** the decomposition reaction is more complex. In the first step, a weight loss of 2.7% is observed at T_{onset} = 80 °C, accompanied by an endothermic signal at T_p = 139 °C. This weight change is in agreement with the emission of the water molecule ($-\Delta m_{theo}$ = 2.7%). On further heating, two strongly endothermic signals occur at T_{onset} = 220 and 230 °C, with DTA signals at T_p = 227 and 239 °C. The total weight loss is about 17.0%, suggesting successive decomposition of the amine. The experimental mass change is close to the value expected for the removal of the amine ($-\Delta m_{theo}$ = 17.4%). The X-ray powder pattern of the final product is identical with that obtained for the decomposition product of **I**.

In a further experiment, thermal decomposition was interrupted after the emission of the water molecule. The formerly yellow compound exhibited a significant darkening to red. The X-ray powder pattern shows a significant shift of the (0*k*0) reflections to larger 2θ values (see Figure 8), representing a reduction of the interlayer distance from 9.95 to 9.52 Å. The removal of H_2O is partly reversible, and the X-ray powder pattern after a few days in humid air is similar to that of the pristine material. The positions of the (010) and (020) reflections shifted to 2θ values very close to those determined for the original material. The alteration of the reflection profiles indicate that the process is not fully reversible. This is further supported by the orange colour of the sample, in comparison to the yellow colour of the pristine material.

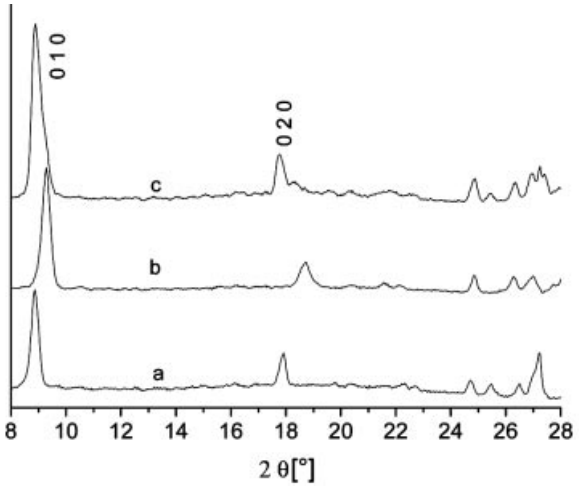

Figure 8. X-ray powder patterns of compound **II**: as prepared (a), after removal of water (b), and after treatment of the water-free sample in humid air (c); for two reflections the indices are given

Conclusion

The crystal structures of the two new thioantimonate(III) compounds are excellent examples demonstrating the structure-directing effect of the amines used under solvothermal conditions. The topologies of the $^2_\infty[Sb_3S_5]^-$ layers in **I** and **II** are very similar, but with some distinct differences demonstrating the high flexibility of Sb^{III} coordination spheres. The structure-directing cations are formed in situ, and the stability seems to be determined mainly by the location of the two amino functions. Compound **I** is formed under a wide range of reaction conditions, strong intermolecular hy-

drogen bonds resulting in the stable arrangement of the cations. In contrast, compound **II** is only formed in a very narrow window of reaction conditions, and water molecules are necessary for the formation of the structure-directing arrangement. The anionic layers and the structure directors are stacked in a sandwich-like manner. The removal of water from **II** is partially reversible and is accompanied by a significant change of the colour from bright yellow to red. We are currently investigating whether the uptake of other polar molecules into the water-free material is possible. In addition, the 1,3-diamino- and 1,3,5-triaminocyclohexane should be used in further solvothermal syntheses to provide information on the influence of the structure-directing molecules on product formation.

Experimental Section

Syntheses of (*trans*-1,4-chxnH)Sb_3S_5 (I) and (*trans*-1,2-chxnH)$Sb_3S_5 \cdot H_2O$ (II) (chxn = Diaminocyclohexane, $C_6H_{14}N_2$): The two compounds were prepared under solvothermal conditions in a Teflon-lined steel autoclave with an inner volume of 30 mL. For **I**, a mixture of elemental antimony (122 mg, 1 mmol) and sulfur (80 mg, 2.5 mmol) was heated with *trans*-1,4-diaminocyclohexane (0.65 g, 5.7 mmol) and water (2.5 mL) to 140 °C for 5 d. For **II**, the same amounts of Sb and S were applied, but a mixture of water (1.5 mL) and *trans*-1,2-diaminocyclohexane (1.5 mL, 12.5 mmol) was used (120 °C for 5 d). The products were filtered and washed with water and acetone. Single crystals suitable for X-ray investigations were obtained under static conditions. Pale yellow, air-stable platelets were obtained in yields of about 75% based on antimony. Both compounds could also be prepared whilst stirring. For **I**, a mixture of Sb (122 mg, 1 mmol), S (64 mg, 2 mmol), amine (0.8 g, 7 mmol), and water (2 mL) was heated in a Teflon-lined autoclave of 7 mL internal volume, while for **II**, the amine (1.5 mL, 12.5 mmol) was diluted with water (0.5 mL). When the slurry was stirred, the reactions were complete after 3 h, with yields of 90% based on antimony. The yellow microcrystalline powders were shown to be phase-pure by X-ray powder diffraction. **I:** (640.75): calcd. C 11.24, H 2.36, N 4.37; found C 11.06, H 2.29, N 4.30. **II:** (658.77): calcd. C 10.94, H 2.58, N 4.25; found C 10.70, H 2.51, N 4.18.

X-ray Crystallography: The intensity data were collected with PHILIPS PW1100 four-circle (**I**) and NONIUS CAD4 (**II**) diffractometers, with graphite-monochromated Mo-K_α radiation (λ = 0.71073 Å). The structures were solved by use of SHELXS-97[28] and structure refinements were done against F^2 with SHELXL-97.[29] All non-hydrogen atoms were refined with anisotropic displacement parameters. All H atoms in **I** and those bound to N and O in **II** were located in the difference Fourier maps and were refined with varying coordinates and varying isotropic displacement parameters. In compound **II**, the H atoms bound to carbon atoms were positioned with idealized geometries and refined with fixed isotropic displacement parameters by use of a riding model. The details of data acquisition and some refinement results are listed in Table 1, and atom distances and angles are listed in Tables 2−3. CCDC-178624 (**I**) and -178625 (**II**) contain the supplementary crystallographic data for this paper. These data can be obtained free of charge at www.ccdc.cam.ac.uk/conts/retrieving.html or from the Cambridge Crystallographic Data Centre, 12, Union Road, Cambridge CB2 1EZ, UK [Fax: (internat.) + 44-1223/336-033; E-mail: deposit@ccdc.cam.ac.uk].

X-ray Powder Diffraction: The X-ray powder patterns were recorded in transmission geometry with a STOE Stadi-P diffractometer with Cu-$K_{\alpha 1}$ radiation (λ = 1.540598 Å).

Thermal Analysis: The thermal investigations were performed with a Netzsch STA 429 DTA-TG device. The samples were heated in Al_2O_3 crucibles, with a heating rate of 3 °C min^{-1}, up to 600 °C and purged in an argon stream (approximately 100 mL min^{-1}). The data were corrected for buoyancy effects.

Raman Spectroscopy: The Raman spectra were measured from 50 to 3500 cm^{-1} with a Bruker IFS 66 Fourier transform Raman spectrometer (wavelength: 1064 nm).

Acknowledgments

This work was supported by the state of Schleswig-Holstein and the Fonds der Chemischen Industrie.

[1] W. S. Sheldrick, M. Wachold, *Angew. Chem. Int. Ed. Engl.* **1997**, *36*, 206−226.
[2] C. L. Cahill, B. Gugliotta, J. B. Parise, *Chem. Commun.* **1998**, 1715−1716.
[3] C. L. Bowes, G. A. Ozin, *Adv. Mater.* **1996**, *8*, 13−28.
[4] W. S. Sheldrick, M. Wachhold, *Coord. Chem. Rev.* **1998**, *176*, 211−322.
[5] C. L. Bowes, A. Lough, A. Malek, G. A. Ozin, S. Petrov, D. Young, *Chem. Ber.* **1996**, *129*, 283−287.
[6] W. S. Sheldrick, H. Braunbeck, *Z. Naturforsch.* **1990,** *45B*, 1643−1646.
[7] G. Cordier, H. Schäfer, C. Schwidetzky, *Z. Naturforsch.* **1984,** *39b*, 131−134.
[8] W. S. Sheldrick, H.-J. Häusler, *Z. Anorg. Allg. Chem.* **1988**, *557*, 105−111.
[9] H. A. Graf, H. Schäfer, *Z. Naturforsch.* **1972,** *27b*, 735−739.
[10] R. Stähler, C. Näther, W. Bensch, *Chem. Commun.* **2001**, 477−478.
[11] H.-O. Stephan, M. G. Kanatzidis, *Inorg. Chem.* **1997**, *36*, 6050−6057.
[12] W. Bensch, M. Schur, *Z. Naturforsch.* **1997,** *52b*, 405−409.
[13] J. B. Parise, Y. Ko, *Chem. Mater.* **1992**, *4*, 1446−1450.
[14] X. Wang, *Chem. Ber.* **1995**, *32*, 303−312.
[15] A. V. Powell, S. Boissière, A. Chippindale, *Chem. Mater.* **2000**, *12*, 182−187.
[16] B. Eisenmann, H. Schäfer, *Z. Naturforsch.*, **1979**, *34B*, 383−385.
[17] X. Wang, F. Liebau, *J. Solid State Chem.* **1994**, *111*, 385−389.
[18] G. Schimek, J. Kolis, *Inorg. Chem.* **1997**, *36*, 1689−1693.
[19] R. Stähler, C. Näther, W. Bensch, *Eur. J. Inorg. Chem.* **2001**, 3073−3078.
[20] R. Taylor, O. Kennard, *Acta Crystallogr., Sect. B* **1983**, *39*, 133−138.
[21] X. Wang, F. Liebau, *Acta Crystallogr., Sect. B* **1996**, *52*, 7−15.
[22] X. Wang, F. Liebau, *Z. Kristallogr.* **1996**, *211*, 437−439.
[23] A. Pfitzner, *Chem. Eur. J.* **1997**, *3*, 2032−2038.
[24] A. Pfitzner, D. Kurowski, *Z. Kristallogr.* **2000**, *215*, 373−376.
[25] H. Rijnberk, C. Näther, W. Bensch, *Monatsh. Chem.* **2000**, *131*, 721−726.
[26] J. B. Parise, *Science* **1991**, *291*, 293−294.
[27] M. Gostojic, W. Nowacki, P. Engel, *Z. Kristallogr.* **1982**, *159*, 217−224.
[28] G. M. Sheldrick, *SHELXS-97, Program for Crystal Structure Determination*, University of Göttingen, Germany, **1997**.
[29] G. M. Sheldrick, *SHELXL-97, Program for the Refinement of Crystal Structures*, University of Göttingen, Germany, **1997**.

Received May 3, 2002
[I02219]

Synthesis and Properties of Bis(2-heteroaryl)borane Derivatives

Thomas Köhler,[a] Jürgen Faderl,[a] Hans Pritzkow,[a] and Walter Siebert*[a]

Dedicated to Professor Gottfried Huttner on the occasion of his 65th birthday

Keywords: Boranes / Porphyrinogens / Lithiation / Grignard reaction / Bromination

The reaction of (isopropyloxy)bis(2-thienyl)borane (**1d**) with Grignard reagents leads to methylbis(2-thienyl)borane (**1e**) and to phenylbis(2-thienyl)borane (**1f**). Treatment of monolithiated heterocycles with dichloroboranes yields the bis(2-heteroaryl)boranes **1b**, **1c**, and **3a**, which are dibrominated with NBS to give the 5,5′-dibromo products **1b**′, **2a**′, and **3a**′. NMR spectroscopic and MS data confirm the composition of the compounds. The [2+2] cyclization of the dibromo derivatives yields, in the case of **2a**′, the macrocycle **4b**, as confirmed by HR-MS data.
(© Wiley-VCH Verlag GmbH, 69451 Weinheim, Germany, 2002)

Introduction

We are interested in the electronic structure and ligand properties of tetraboraporphyrinogens **B**, which formally derive from isophlorins (*N*,*N*′-dihydroporphyrins) **A**[1] (X = NR) by exchange of the *meso*-carbon atoms for boron atoms. In **B** the empty p_z orbitals of the boron atoms may allow macrocyclic conjugation when **B** (16 π-electrons) is reduced to the dianion **C**. As a first example of a tetraboraporphyrinogen we recently synthesized the tetrathia macrocycle **B** (X = S; R = N*i*Pr$_2$) in good yield via the bis(2-thienyl)borane **1a**.[2] Attempts to incorporate the corresponding *N*-methylpyrrole derivative **2a** into **B** (X = NMe) were not successful.[3a,3b] The formation of silyl- and stannyl-bridged macrocycles has been reported.[4a,4b]

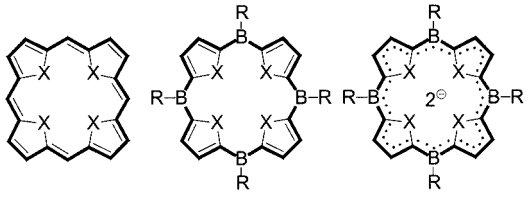

A X = NR, O, S **B** X = NR, O, S **C** X = NR, O, S

Bis(2-heteroaryl)boranes were first prepared via tin/boron exchange and characterized by NMR spectroscopic studies.[5a,5b] Recently, we reported the formation of (diisopropylamino)bis(1-methyl-2-pyrrolyl)borane (**2a**) and its *N*-benzyl analogue.[6] Besides **1a**[2] some bis(2-thienyl)boranes are already known.[7,8] For the synthesis of furan- and *N*-methylpyrrole-containing macrocycles we investigated the 5,5′-dibromination of the corresponding bis(heteroaryl)boranes with *N*-bromosuccinimide. In the following we report on the new derivatives **1b**, **1c**, and **3a** of bis(2-heteroaryl)boranes, as well as on a new synthesis for methylbis(2-thienyl)borane (**1e**) and phenylbis(2-thienyl)borane (**1f**), and a high-yield bromination method for bis(2-heteroaryl)boranes and their reactivity in [2+2] cyclizations.

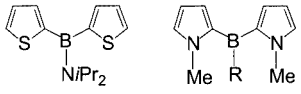

1a **2a** R = N*i*Pr$_2$ **2b** R = C_4H_3NMe

Results and Discussion

1. Syntheses, Spectra of Aminobis(2-heteroaryl)boranes (1b, 1c, 3a), and Structure of 3b

(Dialkylamino)bis(2-thienyl)boranes are obtained when 2-lithiothiophene is treated at low temperatures with dichloro(diethylamino)borane and dichloro(2,2,6,6-tetramethylpiperidino)borane in a 2:1 ratio to give colorless and moisture-sensitive (diethylamino)bis(2-thienyl)borane (**1b**) and (2,2,6,6-tetramethylpiperidino)bis(2-thienyl)borane (**1c**) in yields of 72 and 85%, respectively. Their compositions follow from spectroscopic data. The ^{1}H NMR spectrum of **1b** exhibits a triplet for the CH_3 and a quadruplet for the CH_2 protons. At low field the thienyl protons appear as doublets of doublets. Sharp ^{13}C NMR signals for the heteroaromatic carbon atoms and a broad signal for the boron-bound car-

[a] Anorganisch-Chemisches Institut der Universität,
Im Neuenheimer Feld 270, 69120 Heidelberg, Germany
Fax: (internat.) + 49-(0)6221/54-5609
E-mail: ci5@ix.urz.uni-heidelberg.de

bon atom are observed. Its ^{11}B NMR shift at $\delta = 35$ ppm is similar to that of other aminobis(2-thienyl)boranes.[7,8] Compound **1c** shows similar NMR shifts to that of **1b** in the heteroaromatic region. The 2,2,6,6-tetramethylpiperidino substituent (tmp) of **1c** yields a multiplet for the ring methylene protons and a singlet for the ring-bound methyl protons. The composition of both compounds was confirmed by HR-EI mass spectra.

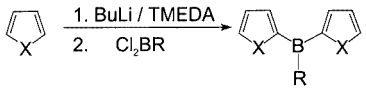

	1b	1c	3a	3b
X	S	S	O	O
R	NEt_2	tmp	$NiPr_2$	C_4H_3O

Addition of a suspension of monolithiated furan to a solution of Cl_2BNiPr_2 yields (diisopropylamino)bis(2-furanyl)borane (**3a**, 45%) as a colorless liquid that is sensitive to air and moisture. When the reaction is carried out by addition of the dichloroborane to monolithiated furan, only a small amount of **3a** is obtained, the main product being tris(2-furanyl)borane (**3b**). The ^1H NMR spectrum of **3a** shows the signals of the isopropyl groups and three doublets of doublets for the ring protons. Because of the coupling constants and the shift, the signal at $\delta = 6.19$ ppm is assigned to 4-H.[5a] Similarly, the ^{13}C NMR signal at $\delta = 110.4$ ppm is assigned to C-4 which is confirmed by a ^1H-^{13}C COSY NMR spectrum. The ^{11}B NMR shift at $\delta = 30$ ppm is in the expected region. The composition of **3a** is confirmed by a high-resolution mass spectrum.

Crystals of **3b** (Figure 1) suitable for X-ray analysis were grown from a hexane solution. Crystal data and structure refinement are shown in Table 1. The B1−C1 bond lengths in **3b** are similar to those in **1g**[9] but significantly shorter than the B−C bonds in triphenylborane[10] (1.585 Å). The O1−C1 bond (1.398 Å) in **3b** is slightly longer than O1−C4 (1.353 Å). This corresponds to **1g**, where the S1−C1 bond is longer than S1−C4. The boron atom in **3b** is tricoordinated and the C−B−C angles are 120°. As in **1g** the bond angle O1−C1−C4 (107.4°) is more acute than O1−C2−C3 (111.0°).

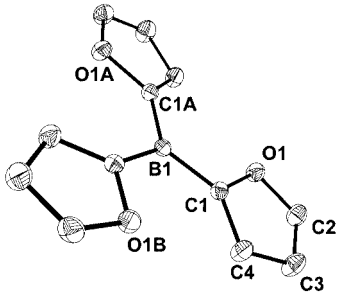

Figure 1. Molecular structure of **3b** in the crystal; selected bond lengths [Å] and angles [°]: O1−C2 1.353(1), O1−C1 1.389(1), B1−C1 1.537 (1), C1−C4 1.368(2), C2−C3 1.338(2), C3−C4 1.415 (2); C1−O1−C2 107.39(9), C4−C1−O1 107.43(9), C4−C1−B1 133.35(9), O1−C1−B1 119.20(8), C3−C2−O1 111.03(10), C2−C3−C4 106.28(11), C1-B1-C1A 120.00(1)

2. Syntheses of Alkylbis(2-thienyl)boranes (1e, 1f)

Methylbis[2-(5-methyl)thienyl]borane[8] (**1e**) was obtained from a redox reaction between 2-iodo-5-methylthiophene and $MeBI_2$ with elimination of elemental iodine. Because of the low yield an alternative approach to **1e** was developed. (Isopropyloxy)bis(2-thienyl)borane[7] (**1d**) was treated with methylmagnesium bromide in diethyl ether to give **1e** in almost quantitative yield. Its NMR spectroscopic and mass spectrometric data are in accordance with those reported previously.[5b,11] The reaction of phenylmagnesium bromide with **1d** analogously yielded phenylbis(2-thienyl)borane (**1f**) (53%). The composition of the colorless air-sensitive solid follows from ^{11}B and ^1H NMR spectroscopic data, the ^{13}C NMR spectrum exhibits six sharp signals for aryl and thienyl carbon atoms and two broad signals for the boron-bound carbon atoms.[12] Attempts to obtain the corresponding furan and pyrrole derivatives were not successful, because the reactions led to tris(1-methyl-2-pyrrolyl)borane (**2b**) and tris(2-furanyl)borane (**3b**), respectively.

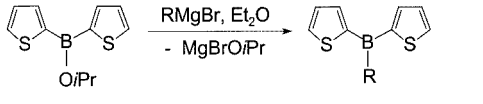

1	e	f	g
R	Me	Ph	C_4H_3S

3. 5,5′-Dibromination of 1b, 2a, and 3a with *N*-Bromosuccinimide

For the syntheses of new macrocycles we need reactive *N*-methylpyrrole and furan derivatives as building blocks. Because of the very low tendency of the bis(2-pyrrolyl)borane **2a** and bis(2-furanyl)borane **3a** to yield dilithiated products[3a,3b] the bromination of the heterocycles at C-5 and C-5′ was investigated by using *N*-bromosuccinimide in THF. The bis(2-heteroaryl)boranes **1b**, **2a**, and **3a** react at −78 °C with *N*-bromosuccinimide in THF to give the dibromo derivatives **1b′**, **2a′**, and **3a′** in 89, 75, and 70% yield, respectively. Compound **3a′** is a yellow oil, which decomposes rapidly at room temperature. The ^{11}B NMR spectra exhibit signals for **1b′** at $\delta = 34$ ppm, for **2a′** at $\delta = 35$ ppm, and for **3a′** at $\delta = 29$ ppm. The shifts for the heteroaromatic protons of each compound show a coupling pattern of two doublets (AB spectrum). The three dibromo compounds **1b′**, **2a′**, and **3a′** were identified by EI-mass and HR EI-mass spectrometry.

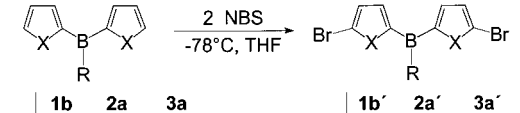

	1b	2a	3a
X	S	NMe	O
R	NEt_2	$NiPr_2$	$NiPr_2$

	1b′	2a′	3a′
X	S	NMe	O
R	NEt_2	$NiPr_2$	$NiPr_2$

4. Formation of 4b

As the [2+2] cyclization of **1b** led only to products with a quaternary boron atom, **1b′** was treated with lithium at

low temperatures and quenched with Cl_2BNiPr_2. However, cyclization did not take place, and only decomposition was noticed. Compound **2a′** reacted in a [2+2] cyclization to yield the first *N*-methylpyrrole-containing tetraboraporphyrinogen **4b**. The ^{11}B NMR shift of δ = 33 ppm and the HR-EI mass spectrometric analysis confirm the existence of macrocycle **4b**, however, purification of the dark brown oil was not successful. The oily residue obtained by performing the same reaction with the furan derivative **3a′** did not contain the macrocycle **4c**.

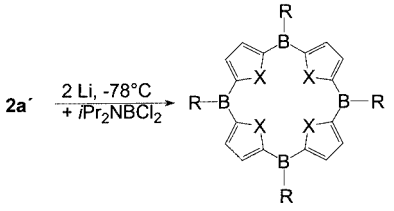

4b X = NMe, R = N*i*Pr$_2$

Conclusion

Quenching of 2 equiv. of 2-lithioheteroarenes with dichloro(2,2,6,6-tetramethylpiperidino)borane and dichloro(diisopropylamino)borane yields the corresponding aminobis(2-heteroaryl)boranes **1b**, **1c**, and **3a**. Interestingly, the bromination of the aminobis(2-heteroaryl)boranes **1b**, **2a**, and **3a** with 2 equiv. of *N*-bromosuccinimide leads to new dibromo derivatives **1b′**, **2a′**, and **3a′**. Methyl- and phenylmagnesium bromide were treated with (isopropoxy)bis(2-thienyl)borane (**1d**) to give the organyl-substituted bis(2-thienyl)boranes **1e** and **1f**. In summary, new organyl- and amino-substituted building blocks containing heteroarenes of the new tetraboraporphyrinogens are obtained in good yields. The [2+2] cyclization of the dibromo derivatives **1b′**, **2a′**, **3a′** give in the case of **2a′** the first *N*-methylpyrrole-containing tetraboraporphyrinogen **4b**.

Experimental Section

General: Reactions were carried out under dry nitrogen using standard Schlenk techniques. Solvents and chemicals were dried, distilled and saturated with nitrogen. Glassware was dried with a heat-gun under high vacuum. ^1H, ^{11}B, ^{13}C NMR: Bruker DRX 200 spectrometer, shift references are $(CH_3)_4Si$ and $F_3B{\cdot}OEt_2$. Mass spectra were obtained with a ZAB-2F VH Micromass CTD spectrometer, HR mass spectra with a JEOL MS Station JMS 700 spectrometer both using the EI ionization technique. (Isopropyloxy)-bis(2-thienyl)borane (**1d**),[7] dichloro(diisopropylamino)borane,[13] dichloro(diethylamino)borane,[14] and dichloro(2,2,6,6-tetramethylpiperidino)borane[15] were prepared according to literature procedures.

(Diethylamino)bis(2-thienyl)borane (1b): *n*-Butyllithium (2.5 M in hexane; 6 mL, 15 mmol) was added to a solution of thiophene (1.3 g, 15 mmol) in diethyl ether (30 mL) at −25 °C. After warming to room temperature, the reaction mixture was stirred for 1 h and then cooled to −50 °C. Dichloro(diethylamino)borane (1.2 g, 7.6 mmol) in diethyl ether (15 mL) was added dropwise to this solution. The mixture was allowed to warm to room temperature and was stirred overnight. Volatile compounds were removed under vacuum, the residue dissolved in pentane and filtered. The solvent was evaporated under vacuum and the colorless oil crystallized at −15 °C. Yield: 1.4 g (5.5 mmol, 72%) of colorless **1b**, m.p. 103 °C. ^1H NMR ($CDCl_3$, 200 MHz): δ = 1.21 (t, CH_3CH_2, $^3J_{H,H}$ = 7.0 Hz, 6 H), 3.38 (q, CH_3CH_2, $^3J_{H,H}$ = 7.0 Hz), 4 H, 7.10 (m, 4 H, CH_{th}), 7.50 ppm (m, 2 H, CH_{th}). ^{11}B NMR ($CDCl_3$, 64 MHz): δ = 35 ppm. ^{13}C NMR ($CDCl_3$, 50 MHz): δ = 16.1 (CH_3CH_2), 44.3 (CH_3CH_2), 127.7, 129.8, 135.2 (CH_{th}), 142 ppm (br, CB). MS: *m*/*z* (%) = 249 (28) [M^+], 234 (78) [$M^+ - CH_3$]. HR-MS: *m*/*z* (%) = 249.0845 [M^+]; calcd. for $^{12}C_{12}{}^1H_{16}{}^{11}B^{14}N^{32}S_2$ 249.0817 (Δmmu = 2.8).

(2,2,6,6-Tetramethylpiperidino)bis(2-thienyl)borane (1c): *n*-Butyllithium (2.5 M in hexane; 6 mL, 15.0 mmol) was added to a solution of thiophene (1.3 g, 15 mmol) in diethyl ether (30 mL) at −25 °C. The reaction mixture was stirred for 1 h at room temperature. At −20 °C a solution of dichloro(2,2,6,6-tetramethylpiperidino)borane (1.7 g, 7.6 mmol) in diethyl ether (15 mL) was added dropwise. The mixture was allowed to warm to room temperature and stirred overnight. Volatile compounds were removed under vacuum, and the residue was dissolved in pentane and filtered. The solvent was evaporated under vacuum leaving a white solid. Yield: 2.1 g (6.5 mmol, 85%) of colorless **1c**, m.p. 116−118 °C. ^1H NMR ($CDCl_3$, 200 MHz): δ = 1.28 (s, 12 H, $CH_{3,tmp}$), 1.68 (m, 6 H, $CH_{2,tmp}$), 6.98 (m, 2 H, CH_{th}), 7.08 (m, 2 H, CH_{th}), 7.41 ppm (m, 2 H, CH_{th}). ^{11}B NMR ($CDCl_3$, 64 MHz): δ = 42 ppm. ^{13}C NMR ($CDCl_3$, 50 MHz): δ = 16.1 ($CH_{2,tmp}$), 35.0 ($CH_{3,tmp}$), 37.7 ($CH_{2,tmp}$), 56.3 (C_{tmp}), 127.0, 130.7, 133.5 (CH_{th}), 151 ppm (br, CB). MS: *m*/*z* (%) = 317 (4) [M^+], 302 (100) [$M^+ - CH_3$]. HR-MS: *m*/*z* (%) = 317.1413 [M^+]; calcd. for $^{12}C_{17}{}^1H_{24}{}^{11}B^{14}N^{32}S_2$ 317.1444 (Δmmu = 3.1).

Methylbis(2-thienyl)borane (1e): Methylmagnesium bromide (3.0 M in diethyl ether; 1.7 mL, 5.1 mmol) was added dropwise to a solution of **1d** (1.1 g, 4.7 mmol) in diethyl ether (50 mL) at −25 °C. The mixture was allowed to warm for 30 min and stirred at room temp. for 3 h until a colorless solid was formed. Volatile compounds were removed under vacuum, the residue was dissolved in diethyl ether and filtered. The solvent was evaporated under vacuum and the wax-like residue dried. Yield: 0.9 g (4.5 mmol, 95%) of colorless **1e**. ^1H NMR (C_6D_6, 200.1 MHz): δ = 1.37 (s, 3 H, BCH_3), 6.96 (dd, $^3J_{H,H}$ = 3.6, $^3J_{H,H}$ = 4.7 Hz, 2 H, C4-H_{th}), 7.37 (dd, $^3J_{H,H}$ = 4.7, $^4J_{H,H}$ = 0.9 Hz, 2 H, CH_{th}), 7.87 ppm (dd, $^3J_{H,H}$ = 3.6, $^4J_{H,H}$ = 0.9 Hz, 2 H, CH_{th}). ^{11}B NMR (C_6D_6, 64 MHz): δ = 57. ^{13}C NMR (C_6D_6, 50 MHz): δ = 12.3 (CB), 129.1 [CH_{th} (C-4)], 136.1, 140.0 ppm (CH_{th}), $C_{th}B$ signal not observed. EI-MS: *m*/*z* (%) = 192 (62) [M^+], 177 (100) [$M^+ - CH_3$].

Phenylbis(2-thienyl)borane (1f): Phenylmagnesium bromide (3.0 M in diethyl ether; 1.7 mL, 5.1 mmol) was added dropwise to a solution of **1d** (1.2 g, 5.1 mmol) in diethyl ether (50 mL) at −20 °C. The mixture was allowed to warm for 20 min and stirred at room temperature for 26 h. Volatile compounds were removed under vacuum, the residue was dissolved in hexane/CH_2Cl_2 (1:4) and filtered. The solvent was evaporated under vacuum and the solid recrystallized from hexane at −80 °C. Yield: 0.7 g (2.7 mmol, 53%) of colorless **1f**, m.p. 85 °C. ^1H NMR (C_6D_6, 200 MHz): δ = 7.04 (m, 2 H, CH_{th}), 7.28 (m, 2 H, CH_{th}), 7.59−8.01 ppm (m, 7 H, CH_{ar}). ^{11}B NMR (C_6D_6, 64 MHz): δ = 49 ppm. ^{13}C NMR (C_6D_6, 50 MHz): δ = 128.1, 129.6, 130.5, 136.7, 136.8, 141.8 (CH_{ar}), 146, 149 ppm (2 × br, CB). EI-MS: *m*/*z* (%) = 254 (100) [M^+].

(Diisopropylamino)bis(2-furanyl)borane (3a): *n*-Butyllithium (2.5 M in hexane; 10.0 mL, 25. mmol) was added at room temperature to a solution of TMEDA (2.7 g, 24. mmol) in hexane (50 mL). The solution was stirred for 30 min and furan (1.4 g, 21 mmol) was added at room temperature. After stirring the mixture for 90 min, it was added to a solution of Cl_2BNiPr_2 (2.2 g, 12. mmol) in hexane (100 mL), within 80 min, at −25 °C. The mixture was allowed to warm to room temperature and stirred for 20 h. Volatile compounds were removed under vacuum, the residue was dissolved in hexane and filtered. The solvent was evaporated under vacuum and the crude product was distilled to give colorless **3a** (1.4 g, 5.5 mmol, 45%), b.p. 65 °C/5·10^{-3} mbar. ^{1}H NMR (C_6D_6, 200 MHz): δ = 1.21 [d, $^3J_{H,H}$ = 6.9 Hz, 12 H, CH(CH_3)$_2$], 3.95 [sept, $^3J_{H,H}$ = 6.9 Hz, 2 H, CH(CH$_3$)$_2$], 6.19 (dd, $^3J_{H,H}$ = 1.7, $^3J_{H,H}$ = 3.3 Hz, 2 H, C4-H$_{fu}$), 6.63 (dd, $^3J_{H,H}$ = 3.3, $^4J_{H,H}$ = 0.7 Hz, 2 H, CH$_{fu}$), 7.39 ppm (dd, $^3J_{H,H}$ = 1.7, $^4J_{H,H}$ = 0.7 Hz, 2 H, CH$_{fu}$). ^{11}B NMR (C_6D_6, 64 MHz): δ = 30 ppm. ^{13}C NMR (C_6D_6, 50 MHz): δ = 23.5 [CH(*C*H$_3$)$_2$], 49.4 [*C*H(CH$_3$)$_2$], 110.4 [CH$_{fu}$ (C-4)], 123.4, 145.2 ppm (CH$_{fu}$), CB signal not observed. EI-MS: *m*/*z* (%) = 245 (16) [M$^+$], 230 (100), [M$^+$ − CH$_3$]. HR EI-MS: *m*/*z* (%) = 245.1608 [M$^+$]; calcd. for $^{12}C_{12}{}^1H_{16}{}^{11}B^{14}N^{32}S_2$ 245.1587 (Δmmu = 2.1).

Bis(5-bromo-2-thienyl)(diethylamino)borane (1b′): A solution of **1b** (1.3 g, 5.0 mmol) in THF (65 mL) was cooled to −78 °C and *N*-bromosuccinimide (1.5 g, 10 mmol) was added in portions. The mixture turned yellow to orange and was allowed to warm to room temperature. The solvent was removed under vacuum and pentane was added to the residue. After filtering the succinimide off, the solvent of the yellow solution was evaporated. The yellow viscous oil was crystallized from pentane at −30 °C to give colorless **1b′** (1.5 g, 3.8 mmol, 75%), m.p. 132 °C. ^{1}H NMR (CDCl$_3$, 200 MHz): δ = 1.15 (t, CH_3CH$_2$, $^3J_{H,H}$ = 7.0 Hz, 6 H), 3.28 (q, CH$_3$CH_2, $^3J_{H,H}$ = 7.0 Hz, 4 H), 6.79 (m, 4 H, CH_{th}), 6.90 ppm (m, 2 H, CH_{th}). ^{11}B NMR (CDCl$_3$, 64 MHz): δ = 34 ppm. ^{13}C NMR (CDCl$_3$, 50 MHz): δ = 16.3 (*C*H$_3$CH$_2$), 44.9 (CH$_3$*C*H$_2$), 114.1, 130.0, 135.4 (C$_{th}$), 144 ppm (br, CB). MS: *m*/*z* (%) = 407 (12) [M$^+$], 392 (15) [M$^+$ − CH$_3$].

Bis(5-bromo-1-methyl-2-pyrrolyl)(diisopropylamino)borane (2a′): This compound was prepared analogously to **1b′** from **2a** (1.4 g , 5.0 mmol) and *N*-bromosuccinimide (1.5 g, 10 mmol) of. Yield: 1.9 g (4.5 mmol, 89%) of colorless **2a′**, m.p. 145 °C. ^{1}H NMR (CDCl$_3$, 200 MHz): δ = 1.15 [d, $^3J_{H,H}$ = 6.9 Hz, 12 H, CH(CH_3)$_2$], 3.02 (s, 6 H, NCH$_3$), 3.94 [sept,$^3J_{H,H}$ = 6.9 Hz, CH(CH$_3$)$_2$, 2 H], 6.08 (d, $^3J_{H,H}$ = 3.7 Hz, 2 H, CH$_{py}$), 6.22 ppm (d, $^3J_{H,H}$ = 3.7 Hz, 2 H, CH$_{py}$). ^{11}B NMR (CDCl$_3$, 64 MHz): δ = 35 ppm. ^{13}C NMR (CDCl$_3$, 50 MHz): δ = 25.0 [CH(*C*H$_3$)$_2$], 34.5 (N−CH$_3$), 49.3 [*C*H(CH$_3$)$_2$], 105.2, 110.2, 116.4 (CH$_{py}$), 139 ppm (br, CB). MS: *m*/*z* (%) = 429 (60) [M$^+$], 350 (15) [M$^+$ − Br]. HR-MS: *m*/*z* (%) = 427.0409 [M$^+$]; calcd. for $^{12}C_{16}{}^1H_{24}{}^{11}B^{79}Br_2{}^{14}N_3$ 427.0430 (Δmmu = 2.1).

Bis(5-bromo-2-furanyl)(diisopropylamino)borane (3a′): This compound was prepared analogously to **1b′** from **3a** (1.2 g, 5.0 mmol) and *N*-bromosuccinimide (1.5 g, 10 mmol). The mixture turned dark brown and was allowed to warm to room temp. for 16 h. The solvent was removed under vacuum and pentane was added. After filtering the succinimide off, the solvent of the yellow solution was evaporated. The yellow, viscous oil turned orange and needed no further purification. Yield: 1.4 g (3.5 mmol, 70%) of orange **3a′**. ^{1}H NMR (CDCl$_3$, 200 MHz): δ = 1.16 [d, $^3J_{H,H}$ = 6.9 Hz, 12 H, CH(CH_3)$_2$], 3.82 [sept,$^3J_{H,H}$ = 6.9 Hz, 2 H, CH(CH$_3$)$_2$], 6.21 (d, $^3J_{H,H}$ = 3.7 Hz, 2 H, CH$_{fu}$), 6.41 ppm (d, $^3J_{H,H}$ = 3.7 Hz, 2 H, CH$_{fu}$). ^{11}B NMR (CDCl$_3$, 64 MHz): δ = 29 ppm. ^{13}C NMR (CDCl$_3$, 50 MHz): δ = 23.8 [CH(*C*H$_3$)$_2$], 48.3 [*C*H(CH$_3$)$_2$], 112.0, 125.7, 145.5 ppm (CH$_{fu}$), CB signal not observed . MS: *m*/*z* (%) = 403 (6) [M$^+$], 324 (60) [M$^+$ − Br]. HR-MS: *m*/*z* (%) = 400.9823 [M$^+$]; calcd. for $^{12}C_{14}{}^1H_{18}{}^{11}B^{79}Br_2{}^{14}N^{16}O_2$ 400.9797 (*Δmmu* = 2.6).

Macrocycle 4b: A solution of bis(5-bromo-1-methyl-2-pyrrolyl)(diisopropylamino)borane [**2a′**, 481 mg (1.1 mmol)] was added to a suspension of lithium powder (13 mg, 2.2 mmol) in THF (30 mL) at −78 °C. The color of the suspension changed to bright orange. After 2 h of stirring, the mixture was allowed to warm to −20 °C. Excess lithium was filtered off and the solution cooled to −40 °C. A solution of dichloro(diisopropylamino)borane (0.21 g, 1.2 mmol) in pentane (20 mL) was added over 2 h and warmed overnight to room temperature. Insoluble salts were filtered and the volatile compounds evaporated leaving a brown oily residue that could not be purified by column chromatography or crystallization. ^{11}B NMR (CDCl$_3$, 64 MHz): δ = 33 ppm. MS: *m*/*z* (%) = 760 (13) [M$^+$], 717 (3) [M$^+$ − *i*Pr]. HR-MS: *m*/*z* (%) = 760.6600 [M$^+$]; calcd. for $^{12}C_{44}{}^1H_{76}{}^{11}B_4{}^{14}N_8$ 760.6565 (Δmmu = 3.5).

X-ray Structure Determination of 3b: Crystal data and details of the structure determination are listed in Table 1. Intensity data for **3b** were collected at −83 °C with a Bruker AXS SMART 1000 diffractometer (Mo-K_α radiation, λ = 0.71073 Å, graphite monochromator, ω-scan). An empirical absorption correction was applied. The structure was solved by direct methods (SHELXS-86)[16] and refined by least-squares methods based on F^2 with all measured reflections (SHELXL-97).[16] All non-hydrogen atoms are refined anisotropically. Hydrogen atoms were located in difference Fourier maps and refined isotropically. CCDC-177342 (**3b**) contains the supplementary crystallographic data for this paper. These data can be obtained free of charge at www.ccdc.cam.ac.uk/conts/retrieving.html or from the Cambridge Crystallographic Data Centre, 12, Union Road, Cambridge CB2 1EZ, UK [Fax: (internat.) + 44-1223/336-033; E-mail: deposit@ccdc.cam.ac.uk].

Table 1. Crystal data and structure refinement for **3b**

Empirical formula	$C_{12}H_9BO_3$
Formula mass	212.00
Crystal system	cubic
Space group	$P2_13$
Unit cell dimensions	a = 10.2961(4) Å
Volume	1091.49(7) Å^3
Z	4
Density (calculated)	1.29 g/cm^3
Absorption coefficient	0.091 mm^{-1}
F(000)	440
Crystal size	0.36 × 0.30 × 0.20 mm
θ_{max}	32.40°
Reflections collected	7894
Independent reflections	1272 [R(int) = 0.0332]
Final R indices [$I > \sigma(I)$]	$R1$ = 0.0387, $wR2$ = 0.1004
R indices (all data)	$R1$ = 0.0463, $wR2$ = 0.1084
Largest diff. peak/hole	0.288/-0.124 e·Å^{-3}

Acknowledgments

Support of this work by the Deutsche Forschungsgemeinschaft (SFB 247), the Fonds der Chemischen Industrie and the BASF AG is gratefully acknowledged. J. F. thanks the Graduiertenkolleg "Selektivität in der Organischen und Metallorganischen Synthese und Katalyse" for support.

[1] R. B. Woodward, *Angew. Chem.* **1960**, *72*, 651−662.
[2] F. H. Carré, R. J.-P. Corriu, T. Deforth, W. E. Douglas, W. Siebert, W. Weinmann, *Angew. Chem.* **1998**, *110*, 654−656; *Angew. Chem. Int. Ed.* **1998**, *37*, 652−654.
[3] [3a] J. Faderl, Inaugural Dissertation, Universität Heidelberg, **1998**. [3b] T. Köhler, Diploma Thesis, Universität Heidelberg, **1999**.
[4] [4a] B. König, M. Rödel, P. Bubenitschek, P. G. Jones, *Angew. Chem.* **1995**, *107*, 752−754; *Angew. Chem. Int. Ed. Engl.* **1995**, *34*, 661−663. [4b] B. König, M. Rödel, P. Bubenitschek, P. G. Jones, I. Thondorf, *J. Org. Chem.* **1995**, *60*, 7406−7410.
[5] [5a] B. Wrackmeyer, H. Nöth, *Chem. Ber.* **1976**, *109*, 1075−1088. [5b] J. D. Odom, T. F. Moore, R. Goetze, H. Nöth, B. Wrackmeyer, *J. Organomet. Chem.* **1979**, *173*, 15−32.
[6] J. Faderl, B. Deobald, R. Guilard, H. Pritzkow, W. Siebert, *Eur. J. Inorg. Chem.* **1999**, 399−404.
[7] K. R. Lawson, W. R. Mound, W. G. Whittingham, International Patent WO97/11951, 1-33, **1997**.
[8] W. Siebert, *Chem. Ber.* **1970**, *103*, 2308−2316.
[9] B. Wrackmeyer, W. Milius, E. Molla, *Z. Naturforsch., Teil B* **1996**, *51*, 1811−1814.
[10] F. Zettler, H.D. Hausen, H. Hess, *J. Organomet. Chem.* **1974**, *72*, 157−159.
[11] H. Nöth, B. Wrackmeyer, *Chem. Ber.* **1976**, *109*, 1075−1088.
[12] Signals for boron-bound carbon atoms in standard proton-decoupled ^{13}C NMR spectra measured at room temperature are normally broadened or cannot even be observed. This is caused by relaxation effects of the boron nuclei. For details see: H. Nöth, B. Wrackmeyer, *NMR Spectroscopy of Boron Compounds*, Springer Verlag, Heidelberg, **1978**, pp. 6−104.
[13] W. Gerrard, H. R. Hudson, E. F. Mooney, *J. Chem. Soc.* **1960**, 5168−5172.
[14] H. Noeth, H. Vahrenkamp, *J. Organomet. Chem.* **1968**, *11*, 399−405.
[15] W. Einholz, G. Frey, W. Haubold, *Z. Naturforsch., Teil B* **1989**, *44*, 47−54.
[16] G. M. Sheldrick, *SHELXS-86*, Univ. Göttingen, **1986**; G. M. Sheldrick, *SHELXL-97*, Univ. Göttingen, **1997**.

Received May 6, 2002
[I02229]

Thermodynamics of Redox Processes and Kinetics and Mechanism of Electron Self-Exchange Reactions in the Bis(*N*,*N*-diethyldithiocarbamato)copper(II)/Iodine/Dichloromethane System

Valery G. Shtyrlin,*[a] Alexey V. Zakharov,*[a] Andrey M. Kuznetsov,[b] Ol'ga V. Kukushkina,[a] and Pavel P. Chernov[a]

Keywords: Copper / Electron-transfer kinetics / Reaction mechanisms / Redox reactions thermodynamics / S ligands

The thermodynamics of complex formation between Et_4NI and I_2 in CH_2Cl_2 and the redox processes in the bis(*N*,*N*-diethyldithiocarbamato)copper(II) $[Cu^{II}L_2]/I_2/CH_2Cl_2$ system have been studied spectrophotometrically. The reversibility of the reactions of formation of copper(III) complexes was established and their thermodynamic parameters determined: $Cu^{II}L_2 + {}^3/_2I_2 \rightleftarrows [Cu^{III}L_2]I_3$ {log$K$ = 5.80 (298 K), ΔH = –35.0 kJ·mol^{-1}, and ΔS = –6.7 J·K^{-1}·mol^{-1}} and $[Cu^{III}L_2]I_3 + I_2 \rightleftarrows [Cu^{III}L_2]I_5$ {log$K$ = 2.02 (298 K), ΔH = –11.1 kJ·mol^{-1}, and ΔS = 1.3 J·K^{-1}·mol^{-1}}. The rate constants and activation parameters for the electron self-exchange reactions between $Cu^{II}L_2$ and $[Cu^{III}L_2]I_n$ (n = 3, 5) in the CD_2Cl_2 solutions were determined by NMR line-broadening of the ligand L protons: $k_e = 3.0 \cdot 10^8$ M^{-1}·s^{-1} (298 K), $\Delta H^{\neq} = 6.1$ kJ·mol^{-1}, and $\Delta S^{\neq} = -62.3$ J·K^{-1} mol^{-1}. To account for the kinetic parameters, an unusual mechanism for the self-exchange reaction was suggested. This mechanism involves the prior formation of the $Cu^{II}L_2I_nCu^{III}L_2$ intermediate, in which considerable delocalization of electron density through the orbitals of copper and bridging iodine atoms is achieved, followed by electron transfer. The formation of the intermediate was supported by ESR data and quantitative analysis of the activation parameters with the use of quantum chemical computations by the DFT method at the B3LYP/3-21G* level.
(© Wiley-VCH Verlag GmbH, 69451 Weinheim, Germany, 2002)

Introduction

The study of redox reactions of Cu^I, Cu^{II}, and Cu^{III} complexes with sulfur-containing ligands is of interest for fundamental understanding of electron-transfer mechanisms. In this regard, the interconversions of copper(II) and copper(III) dithiocarbamates deserve particular attention. The electrochemical oxidation of the copper(II) dithiocarbamates to copper(III) is a reversible process at a platinum electrode.[1] With a "soft" oxidative agent such as iodine, one would also expect a reversible copper(II)/copper(III) transformation in solution. This would in principle allow one to evaluate both the thermodynamic parameters of the redox processes and the kinetic characteristics of the copper(II)/copper(III) electron self-exchange reactions. A first attempt to turn these possibilities into reality has been undertaken in this work.

We have investigated the thermodynamics of the redox processes and kinetics of the electron self-exchange reactions in the bis(*N*,*N*-diethyldithiocarbamato)copper(II) $[Cu^{II}L_2]/I_2/CH_2Cl_2$ (CD_2Cl_2) system by means of spectrophotometric, NMR, and ESR methods. Moreover, for the characterization of polyiodide anions forming in these solutions, the thermodynamics of complex formation in the $Et_4NI/I_2/CH_2Cl_2$ system have been studied spectrophotometrically.

Previously,[1–5] treatment of copper(II) *N*,*N*-dialkyldithiocarbamates ($Cu^{II}L'_2$) with iodine had resulted in the isolation of copper(III) complexes of compositions $[Cu^{III}L'_2]I_3$[1–5] and $[Cu^{III}L'_2]I_5$[4] as crystals. Two of these, $[Cu^{III}(S_2CNnBu_2)_2]I_3$ and $[Cu^{III}(S_2CNEt_2)_2]I_3$, have been characterized by X-ray data.[3,5] No thermodynamic or kinetic parameters of reactions of this type have been reported in the literature.

To the best of our knowledge, the only directly studied copper(II)/copper(III) electron self-exchange reaction was the electron transfer between the copper complexes with the deprotonated tripeptide tris-α-aminoisobutyrate $[Aib_3H_{(-2)}{}^{3-}]$ in aqueous medium.[6] Those authors[6] had suggested an outer-sphere electron exchange mechanism, but not ruled out bridging by an axially bound water molecule. In this investigation we have attempted to elucidate the mechanism of the electron self-exchange reaction between the copper(II) and copper(III) dithiocarbamates.

[a] Department of Inorganic Chemistry, Kazan State University, Kremlevskaya st., 18, Kazan, 420008, Russian Federation
E-mail: Valery.Shtyrlin@ksu.ru, Alexey.Zakharov@ksu.ru
[b] Department of Inorganic Chemistry, Kazan State Technological University, Marx st., 68, Kazan, 420015, Russian Federation
Supporting information for this article is available on the WWW under http://www.eurjic.org or from the author.

Results and Discussion

Thermodynamics of Complex Formation and Redox Processes

For interpretation of the experimental data in the $Cu^{II}L_2/I_2/CH_2Cl_2$ system, previous investigations of complex formation between Et_4NI and I_2 in CH_2Cl_2 are of considerable significance. The I_2 concentration-dependence of the molar absorption coefficient (ε) of Et_4NI in CH_2Cl_2 solutions (Figure 1) is adequately computer-simulated by two equilibria with consecutive addition of two I_2 molecules to Et_4NI, but the first equilibrium constant (K_1) cannot be exactly estimated at these concentration conditions. The K_1 values were therefore deduced from the dependence of the molar absorption coefficient of the I_2 solution ($c_{I_2} = 2\cdot10^{-5}$ M) upon the Et_4NI concentration ($2\cdot10^{-6}$ to $8\cdot10^{-5}$ M) at λ 365 nm (Table S1, Supporting Information), and these values were then fixed at computations of the addition constant of I_2 to Et_4NI_3 (K_2) from the above-mentioned $\varepsilon - c_{I_2}$ dependence at λ 400 nm (Table S2). The enthalpy (ΔH) and entropy (ΔS) of each equilibrium were calculated from the log $K_{1,2}$ magnitudes at different temperatures. The derived $\log K_{1,2}$, $\Delta H_{1,2}$, and $\Delta S_{1,2}$ parameters are given in Table 1. With the aid of the computed mol fractions of the Et_4NI_3 and Et_4NI_5 compounds their electronic absorption spectra were reconstructed (Figure 2).

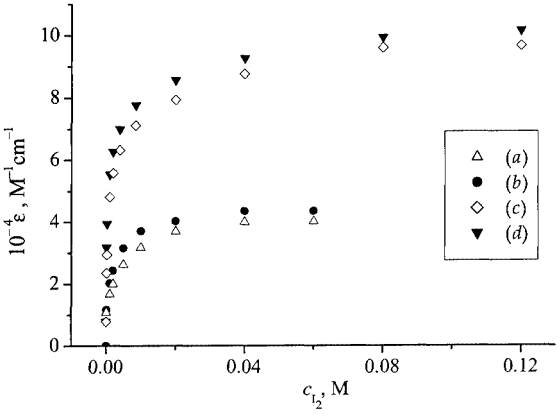

Figure 1. Dependence of the molar absorption coefficient (ε) upon the I_2 concentration in the systems $Et_4NI/I_2/CH_2Cl_2$ (*a*, *b*) and $Cu^{II}L_2/I_2/CH_2Cl_2$ (*c*, *d*) at 298 K (*a*, *c*) and 278 K (*b*, *d*), $c_{CuL_2} = 1\cdot10^{-4}$ M (*a*, *b*), $c_{Et_4NI} = 6.25\cdot10^{-5}$ M (*c*, *d*); λ = 400 nm

Table 1. Thermodynamic parameters of equilibria in the systems $Et_4NI/I_2/CH_2Cl_2$ and $Cu^{II}L_2/I_2/CH_2Cl_2$

Equilibrium	log*K* (298 K)	Δ*H* [kJ·mol^{-1}]	Δ*S* [J·K^{-1}·mol^{-1}]
$Et_4NI + I_2 \rightleftarrows Et_4NI_3$	7.20±0.10	−60.0±4.4	−63.6±15.1
$Et_4NI_3 + I_2 \rightleftarrows Et_4NI_5$	2.33±0.03	−16.8±1.0	−11.6±3.4
$Cu^{II}L_2 + 3/2I_2 \rightleftarrows [Cu^{III}L_2]I_3$	5.80±0.04	−35.0±1.3	−6.7±4.6
$[Cu^{III}L_2]I_3 + I_2 \rightleftarrows [Cu^{III}L_2]I_5$	2.02±0.06	−11.1±1.0	1.3±3.5

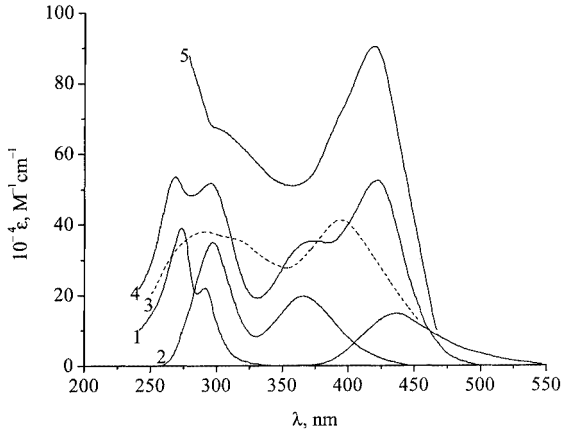

Figure 2. Electronic absorption spectra of $Cu^{II}L_2$ (1), Et_4NI_3 (2), Et_4NI_5 (3), $[Cu^{III}L_2]I_3$ (4), and $[Cu^{III}L_2]I_5$ (5) in CH_2Cl_2 at 298 K

Two absorption bands of the I_3^- spectrum in CH_2Cl_2 have the parameters λ_{max} 363 nm (ε_{max} $2.5\cdot10^4$ M^{-1}·cm^{-1}) and λ_{max} 293 nm (ε_{max} $4.3\cdot10^4$ M^{-1}·cm^{-1}), which are essentially coincident with those reported for triiodide anion in CH_2Cl_2,[7] acetonitrile, and 1,2-dichlorethane[8] and somewhat different from those found for I_3^- in water.[9,10] These two bands correspond[7,11–13] to the allowed singlet-singlet transitions $\pi_g \rightarrow \sigma_u^*$ and $\sigma_g \rightarrow \sigma_u^*$, respectively, for the linear I_3^- anion with nominal $D_{\infty h}$ symmetry (in theoretical studies this symmetry is predicted for the gas phase[11–17] but it can be slightly broken by solvation[18,19]).

The I_5^- spectrum in CH_2Cl_2 exhibits bands at λ_{max} 392 nm (ε_{max} $5.0\cdot10^4$ M^{-1}·cm^{-1}) and λ_{max} 288 nm (ε_{max} $4.6\cdot10^4$ M^{-1}·cm^{-1}) with a "shoulder" at λ_{sh} 312 nm (ε_{sh} $4.4\cdot10^4$ M^{-1}·cm^{-1}); these differ from those in acetonitrile (λ_{max} 390 nm, ε_{max} $2.5\cdot10^4$ M^{-1}·cm^{-1}; λ_{max} 310 nm, ε_{max} $2.1\cdot10^4$ M^{-1}·cm^{-1})[20] and in *tert*-butyl alcohol (λ_{max} 395 nm, ε_{max} $3.1\cdot10^4$ M^{-1}·cm^{-1}; λ_{max} 315 nm, ε_{max} $2.5\cdot10^4$·M^{-1} cm^{-1}).[20] In solid compounds, the I_5^- anion exhibits either a bent structure (symmetry C_{2v})[12,21–23] or a linear structure (symmetry $D_{\infty h}$).[24–28] According to calculations,[15,29] however, interconversions between these I_5^- conformations under vacuum require little or no energy expenditure. In our opinion the band at 392 nm (25510 cm^{-1}) in the I_5^- spectrum can be assigned to the allowed $4\sigma_u \rightarrow 5\sigma_g^*$ transition for the $D_{\infty h}$ symmetry or the $6b_1 \rightarrow 8a_1^*$ transition for the C_{2v} symmetry (see notations in ref.[15]) and the band at 288 nm (34720 cm^{-1}) and the "shoulder" at λ_{sh} 312 nm (32050 cm^{-1}) are attributable to the allowed transitions $3\pi_u \rightarrow 5\sigma_g^*$ ($D_{\infty h}$ symmetry) and $3b_2 \rightarrow 8a_1^*$ (C_{2v} symmetry), respectively. This assignment is in good accordance with the theoretically calculated difference between the $4\sigma_u$ and $3\pi_u$ orbital energies (9130 cm^{-1})[15] or between the $6b_1$ and $3b_2$ orbital energies (7290 cm^{-1}).[15]

The $\log K_1$ value obtained (Table 1) is very similar to the reported values of $\log K_1$ in nitromethane (6.7[30] and 7.4[31] at 293 K), nitrobenzene (8.0),[32] sulfolane (7.4),[33] ethylene carbonate (6.6 at 313 K),[34] propylene carbonate (7.9),[35] acetonitrile (6.6,[30] 7.0,[31] 7.4,[36] 6.85,[37] 6.75,[38] and

6.80[39]), dimethylacetamide (7.4),[39] DMF (7.0),[39] and DMSO (6.9),[39] while differing fundamentally from the $\log K_1$ values in methanol (4.94[38] and 4.30[39]), ethanol (4.13[38] and 4.70[38]), and water (2.85,[9] 2.86,[10] and 2.84[38]). The $\log K_2$ value found (Table 1) is fairly close to the $\log K_2$ values in nitrobenzene (2.7),[32] ethylene carbonate (1.8 at 313 K),[34] propylene carbonate (1.9),[35] acetonitrile (2.0−2.3),[20] and *tert*-butyl alcohol (2.03)[20] (the data for water are contradictory: $\log K_2 = 0.95$[40] or 2.3[41]). As is evident from Table 1, the difference between $\log K_1$ and $\log K_2$ is mainly the result of the enthalpy constituent. This also governs the decrease in $\log K_1$ on going from CH_2Cl_2 to H_2O ($\Delta H_1 = -21.3$[9] or -19.9[10,40] kJ·mol^{-1}). The more positive ΔS_2 value relative to ΔS_1 (Table 1) accounts for the rigid I_3^- structure and the flexible I_5^- structure with interconversions between the bent and linear I_5^- conformers,[15,29] as mentioned above.

Let us consider the $Cu^{II}L_2/I_2/CH_2Cl_2$ system. The excellently reproducible dependence of the molar absorption coefficient of the $Cu^{II}L_2$ solutions on the I_2 concentration can be computer-simulated equally well by two alternative equilibrium models involving formation of the following pairs of complexes: 1) $[Cu^{III}L_2]I$ and $[Cu^{III}L_2]I_3$, or 2) $[Cu^{III}L_2]I_3$ and $[Cu^{III}L_2]I_5$ (Table S3). The electronic absorption spectra were reconstructed for each pair of complexes on the basis of their respective calculated equilibrium constants, and these pointed unambiguously to the suitability of the second model only. Indeed, the reconstructed spectra of $[Cu^{III}L_2]I_3$ and $[Cu^{III}L_2]I_5$ (Figure 2) are superpositions of the I_3^- and I_5^- spectra discussed above and the spectrum of the $[Cu^{III}L_2]^+$ cation produced by the electrochemical oxidation of $Cu^{II}L_2$.[1] Note that the asymmetric band at λ_{max} 435 nm for $Cu^{II}L_2$ (Figure 2) is attributable to the composition of two ligand-to-metal charge-transfer transitions,[42,43] $\pi S \rightarrow 3d_{x^2-y^2}$ (two bands with λ_{max} 270 and 290 nm in the $Cu^{II}L_2$ spectra (Figure 2) correspond to pure ligand $\pi \rightarrow \pi^*$ transitions).[43] By analogy, the band at λ_{max} 418 nm for $[Cu^{III}L_2]^+$ (Figure 2) can be assigned to the $\pi S \rightarrow 3d_{x^2-y^2}$ transitions. Thus, according to the spectrophotometric data, the following equilibria operate in the $Cu^{II}L_2/I_2/CH_2Cl_2$ system:

$$Cu^{II}L_2 + 3/2I_2 \overset{K_3}{\rightleftharpoons} [Cu^{III}L_2]I_3 \quad (1)$$

$$[Cu^{III}L_2]I_3 + I_2 \overset{K_4}{\rightleftharpoons} [Cu^{III}L_2]I_5 \quad (2)$$

The validity of reactions according to Equations (1) and (2) was supported by the isolation of $[Cu^{III}L_2]I_3$ and $[Cu^{III}L_2]I_5$ crystals under suitable concentration conditions (see Exp. Sect.). The reversibility of process (2) is apparent from its similarity to the Et_4NI_5 formation reaction described above. The reversibility of process (1) was established by ESR in the following manner. Dissolution of the diamagnetic $[Cu^{III}L_2]I_3$ crystals in CH_2Cl_2 ($c_{Cu} = 1\cdot10^{-3}$ M) gives rise to the ESR spectrum with the spin-Hamiltonian parameters $g_o = 2.048\pm0.001$ and $A_o = (75.8\pm0.5)\cdot10^{-4}$ cm^{-1} (298 K), which correspond to the $Cu^{II}L_2$ complex. The integral intensity of the ESR signals of the $[Cu^{III}L_2]I_3$ solution in question is 25(±3)% of that for the $Cu^{II}L_2$ solution at the same concentration ($1\cdot10^{-3}$ M). This value is nearly equal to the $Cu^{II}L_2$ fraction (22.1%) calculated for the $[Cu^{III}L_2]I_3$ dissociation from the obtained K_3 and K_4 constants. This leftward shift of equilibrium (1) is suppressed by introduction of iodine into the $Cu^{II}L_2$ solution: at $c_{I_2} = 0.1$ M the ESR spectrum disappeared entirely.

The equilibrium constants of Equations (1) and (2) and the thermodynamic parameters computed from the temperature-dependence of $\log K_3$ and $\log K_4$ are listed in Table 1. The $\log K_3$ constant can be presented as a sum of three contributions [Equation (3)]

$$\log K_3 = -\frac{\Delta G_3^0}{2.3RT} = \frac{nF}{2.3RT}\cdot\Delta E^0 + \log K_{M^+I^-} + \log K_{MI_3} \quad (3)$$

where ΔG_3^0 is the standard free energy of the reaction (1), ΔE^0 is the standard electromotive force[44] of the reaction $Cu^{II}L_2 + {}^1/_2I_2 \rightleftarrows [Cu^{III}L_2]^+ + I^-$, $K_{M^+I^-}$ is the constant of the association process $[Cu^{III}L_2]^+ + I^- \rightleftarrows [Cu^{III}L_2]I$, and K_{MI_3} is the constant of the equilibrium $[Cu^{III}L_2]I + I_2 \rightleftarrows [Cu^{III}L_2]I_3$. With the requirement that replacement of $M^+ = [Cu^{III}L_2]^+$ by $M^+ = Et_4N^+$ has little or no effect on the constants above, it is possible to take $\log K_{MI_3} = K_1 = 7.20$ and $\log K_{M^+I^-} = 4.9$.[44] With these values and $\log K_3 = 5.80$ (Table 1), according to Equation (3), a value of $\Delta E^0 = -0.375$ V (298 K) would be estimated. The ΔE^0 value in CH_2Cl_2 has not been determined by electrochemical methods, but the ΔE^0 value obtained above is reasonably close to the difference between the normal electrode potential for the reaction ${}^1/_2I_2 + e^- \rightarrow I^-$ (0.36 V in acetone)[30] and the half-wave potential for the oxidation process $Cu^{II}L_2 \rightleftarrows [Cu^{III}L_2]^+ + e^-$ (0.70 V in acetone).[1] Thus, the spontaneous course of reaction (2) in dichloromethane is provided by the energy-favorable processes of triiodide anion formation and ionic association.

The thermodynamic description achieved for the $Cu^{II}L_2/I_2/CH_2Cl_2$ system allows one to regulate the Cu^{II} and Cu^{III} contents by varying the I_2 concentration and to study the kinetics of electron self-exchange reactions between the complexes $Cu^{II}L_2$ and $[Cu^{III}L_2]I_n$ ($n = 3, 5$) at different temperatures on this basis.

Kinetics of Electron Self-exchange

^{1}H NMR spectra of the $Cu^{II}L_2$ solutions in CD_2Cl_2 display only the signal of the methyl protons of the coordinated L ligand, with the chemical shift (δ) varying from 0.36 to 0.67 ppm and the line-width ($\Delta\nu_{1/2}$) decreasing from 86 to 46 Hz as the temperature increases from 248 to 298 K; the ^{1}H NMR signal of the L methylene protons is so broad that it defies observation. As iodine is added to the $Cu^{II}L_2$ solution ($c_{I_2} \leq 1\cdot10^{-3}$ M), the NMR signal of the CH_3-protons is progressively narrowed and shifted to low field (the signal of the CH_2-protons remains unobservable). Such a situation corresponds to a "fast exchange"[45] of the L methyl protons between two different environments **A** (dia-

magnetic $[Cu^{III}L_2]I_n$) and **B** (paramagnetic $Cu^{II}L_2$) through electron self-exchange. On a further increase in the I_2 concentration (above $1\cdot10^{-2}$ M), multiplet structures of the ^1H NMR signals appear for both methyl and methylene protons, and their chemical shifts cease to be changed and range up to 1.41−1.43 and 3.81−3.85 ppm, respectively. In the I_2 concentration interval from 0.03 to 0.12 M, with decreasing I_2 content (and correspondingly increasing $Cu^{II}L_2$ fraction), the line-widths of the methyl triplet are essentially unaffected, while the lines of the methylene quadruplet are significantly broadened. The line-widths of the CH_3-protons decrease and those of the CH_2-protons increase with increasing temperature from 268 to 298 K (Figure 3). All these facts clearly attest to the "fast exchange" limiting case being reached for the methyl protons and the "slow exchange" limiting case for the methylene protons (see ref.[45]).

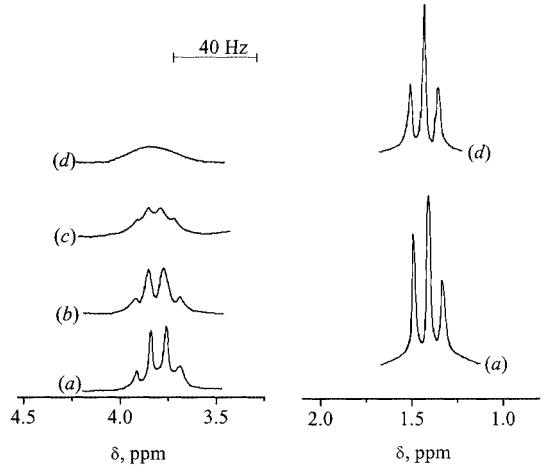

Figure 3. ^1H NMR spectra of the $Cu^{II}L_2$ solutions in CD_2Cl_2 with I_2 (0.04 M) at 268 K (*a*), 278 K (*b*), 288 K (*c*), and 298 K (*d*); $c_{CuL_2} = 1.5\cdot10^{-3}$ M

Under conditions suitable for the quantitative kinetic experiments ($c_{I_2} = 0.03-0.12$ M and $T = 268-298$ K) the mol fractions (P) calculated from the K_3 and K_4 constants change from $3.7\cdot10^{-7}$ to $5.0\cdot10^{-5}$ for $Cu^{II}L_2$, from 0.048 to 0.238 for $[Cu^{III}L_2]I_3$, and from 0.952 to 0.762 for $[Cu^{III}L_2]I_5$. Consequently, the condition [**A**] >> [**B**] is obeyed, and with this the exchange between **A** ($[Cu^{III}L_2]I_n$) and **B** ($Cu^{II}L_2$) is described by the Swift−Connick equation,[46] which at $\Delta\omega_{AB} \approx 0$ is reduced to relation (4)

$$\pi\Delta\Delta\nu_{1/2} = \frac{1}{T_2} = \frac{1}{T_{2A}} + \frac{P_B}{T_{2B} + \tau_B} \qquad (4)$$

where P_B is the mol fraction of $Cu^{II}L_2$, T_{2A} and T_{2B} denote the transverse relaxation times of the protons in the dia- and paramagnetic positions, respectively, and τ_B is the lifetime of the protons in the latter position. Equation (4) holds for the bimolecular electron self-exchange reaction according to Equation (5)

$$Cu^{II}L_2 + [{}^{*}Cu^{III}L_2]I_n \underset{k_e}{\rightleftharpoons} [Cu^{III}L_2]I_n + {}^{*}Cu^{II}L_2 \quad (n = 3, 5) \qquad (5)$$

under the condition that the chemical shifts of the **A** form, the T_{2A} relaxation times, and the electron self-exchange rate constants (k_e) are independent on the size of the I_n^- counter-ion (n = 3, 5) with $\tau_B^{-1} = k_e[Cu^{III}L_2I_n]$ in this case. From the above values of P_B and $\Delta\nu_{1/2} = (\pi\cdot T_{2B}{}^{CH_3})^{-1}$ for the CH_3-protons in $Cu^{II}L_2$ it follows that at c_{I_2} = 0.03−0.12 M the contribution of the last term in Equation (4) to the methyl proton line-widths is negligibly small (< 0.01 Hz). Because of this, for the "slow exchange" of the L methylene protons ($T_{2B}{}^{CH_2} << \tau_B$), the difference of the NMR line-widths of the CH_2- and CH_3-protons ($\Delta\Delta\nu_{1/2}$) can be represented by Equation (6) {with $P_B[Cu^{III}L_2I_n] = [Cu^{II}L_2]$}

$$\pi\Delta\Delta\nu_{1/2} = \pi\left(\Delta\nu_{1/2}^{CH_2} - \Delta\nu_{1/2}^{CH_3}\right) = \left(\frac{1}{T_{2A}^{CH_2}} - \frac{1}{T_{2A}^{CH_3}}\right) + k_e\left[Cu^{II}L_2\right] \qquad (6)$$

The application of the $\pi\Delta\Delta\nu_{1/2}$ parameter has the advantage that this enables one to eliminate almost fully the $\Delta\nu_{1/2}{}^{CH_2}$ contributions from the variation of the solution viscosity, the magnetic field inhomogeneity, the signal acquisition regime, and so on as $T_{2A}{}^{CH_2} << T_{2A}{}^{CH_3}$. As Figure 4 suggests, plots of the $\pi\Delta\Delta\nu_{1/2}$ parameter as a function of $[Cu^{II}L_2]$ are linear, with small intercepts. Therefore, all discussed conditions for the use of Equation (6) are fulfilled. True, it should be pointed out that the k_e constant accounts mainly for the $Cu^{II}L_2/[Cu^{III}L_2]I_5$ exchange because of a predominance of the last form at the kinetic experiment conditions (Table S4). (The experimental relationship $T_{2B}{}^{CH_2} << T_{2B}{}^{CH_3}$, as used above, can reasonably be explained in terms of a dipole−dipole mechanism of the proton relaxation[45] by virtue of a greater distance from the paramagnetic center for the methyl protons of L than for the methylene protons). From the k_e constants derived by Equation (6) at different temperatures (Table S4), the activation enthalpy ($\Delta H^{\neq}$) and entropy ($\Delta S^{\neq}$) of the electron self-exchange reaction were determined by application of the Eyring equation. The obtained values of k_e, $\Delta H^{\neq}$, and

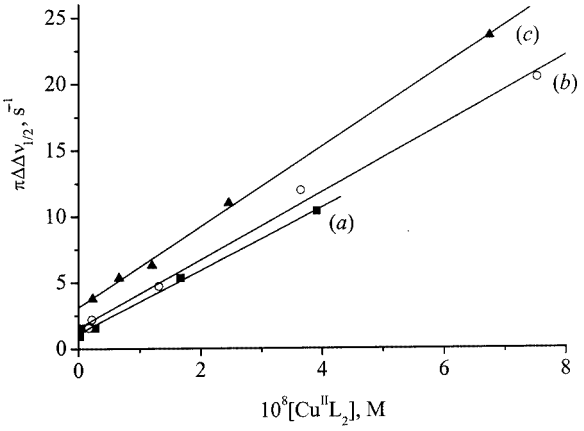

Figure 4. Dependence of the $\pi\Delta\Delta\nu_{1/2}$ parameter on $[Cu^{II}L_2]$ in the $Cu^{II}L_2/I_2/CD_2Cl_2$ system at 278 K (*a*), 288 K (*b*), and 298 K (*c*)

Table 2. Rate constants and activation parameters of the electron self-exchange reaction in the CD_2Cl_2 solution

$$Cu^{II}L_2 + [{}^{*}Cu^{III}L_2]I_n \underset{}{\overset{k_e}{\rightleftharpoons}} [Cu^{III}L_2]I_n + {}^{*}Cu^{II}L_2 \quad (n = 3,5)$$

T, K	k_e [$M^{-1}\,s^{-1}$]	
268	$(2.04\pm0.21)\cdot10^8$	
278	$(2.38\pm0.09)\cdot10^8$	$\Delta H^{\neq} = 6.1\pm0.9$ kJ·mol^{-1}
288	$(2.57\pm0.09)\cdot10^8$	$\Delta S^{\neq} = -62.3\pm3.0$ J·K^{-1}·mol^{-1}
298	$(3.04\pm0.07)\cdot10^8$	

$\Delta S^{\neq}$ are listed in Table 2 and are essentially different from those found for the related electron self-exchange reaction between the copper(II) and copper(III) complexes (with tris-α-aminoisobutyrate as a ligand) in aqueous medium ($k_e = (5.5\pm0.1)\cdot10^4$ M^{-1}·s^{-1} (298 K), $\Delta H^{\neq} = 29\pm2$ kJ·mol^{-1}, and $\Delta S^{\neq} = -54\pm8$ J·K^{-1}· mol^{-1}).[6]

Mechanism of the Electron Self-exchange Reactions

The remarkably high values of the rate constants and some unusual $\Delta H^{\neq}$ magnitude for the exchange of the σ* ($3_{dx^2-y^2}$) electron between the $Cu^{II}L_2$ and $[Cu^{III}L_2]I_n$ complexes are difficult to account for by an ordinary outer-sphere mechanism. We therefore suggest a special outer-sphere mechanism of this process, involving prior formation of a fairly stable associate of reagents (intermediate) − $Cu^{II}L_2I_nCu^{III}L_2$ − in which the essential delocalization of the electron density through the orbitals of the copper and the bridging iodine atoms is achieved, followed by an efficient electron transfer.

Direct evidence of the formation of the $Cu^{II}L_2I_3Cu^{III}L_2$ intermediate was deduced by us from comparison of the ESR spectra of the $5\cdot10^{-3}$ M $Cu^{II}L_2$ solutions in CH_2Cl_2 (or CH_2Cl_2/toluene 1:1) without and with I_2 ($3.8\cdot10^{-3}$ M). At this I_2 concentration − according to the thermodynamic data (Table 1) − as much $[Cu^{III}L_2]I_3$ complex arises as $Cu^{II}L_2$ remains (ca. $2.5\cdot10^{-3}$ M). In liquid solutions at 293 K, the obtained isotropic spin-Hamiltonian parameters for $Cu^{II}L_2$ without and with I_2 are the same within the limits of experimental error [$g_o = 2.048\pm0.001$ and $A_o = (75.8\pm0.5)\cdot10^{-4}$ cm^{-1}] and close to the literature data for $Cu^{II}L_2$ solutions in other noncoordinating solvents.[47,48] In frozen solutions at 77 K, alternatively, the anisotropic ESR spectra of $Cu^{II}L_2$ without and with I_2 differ from one another markedly [Figure 5 (*a*) and (*b*)]. Computer simulation of the ESR spectra in view of the known relations[49] by the program produced previously[50] enabled the following parameters of the axial-symmetry spin-Hamiltonian to be determined: $g_\parallel = 2.087$, $g_\perp = 2.025$, $A_\parallel^{63} = 163.4\cdot10^{-4}$ cm^{-1}, $A_\parallel^{65} = 174.8\cdot10^{-4}$ cm^{-1}, $A_\perp = 43.1\cdot10^{-4}$ cm^{-1} for the (*a*) spectrum, as well as $g_\parallel = 2.090$, $g_\perp = 2.027$, $A_\parallel^{63} = 160.5\cdot10^{-4}$ cm^{-1}, $A_\parallel^{65} = 171.8\cdot10^{-4}$ cm^{-1}, $A_\perp = 41.0\cdot10^{-4}$ cm^{-1} for the (*b*) spectrum (the *g* and *A* parameters were calculated with an accuracy of ±0.001 and $\pm0.5\cdot10^{-4}$ cm^{-1}, respectively; in parallel orientation the hyperfine lines due to the two isotopes ^{63}Cu and ^{65}Cu are clearly resolved). The anisotropic parameters of the (*a*) spectrum agree closely with those reported for $Cu^{II}L_2$ in noncoordinating solvents.[47,48] Increases in the $g_\parallel$ and $g_\perp$ values and decreases in the $A_\parallel$ and $A_\perp$ values in going from spectrum (*a*) to spectrum (*b*) (Figure 5) are typical both for the axial adduct formation and for the self-association of copper(II) complexes.[47,48] Consequently, the spectrum (*b*) parameters are consistent with the formation of the $Cu^{II}L_2I_3Cu^{III}L_2$ intermediate with the axial bridging iodine atom or the self-associated complex,[47] which involves fairly strong axial Cu−S interactions, as with the Cu_2L_4 dimeric unit of the $Cu^{II}L_2$ monocrystal.[51] However the comparatively small changes in the *g* and *A* parameters with the $[Cu^{III}L_2]I_3$ present correlate better with the first of the intermediate structures.

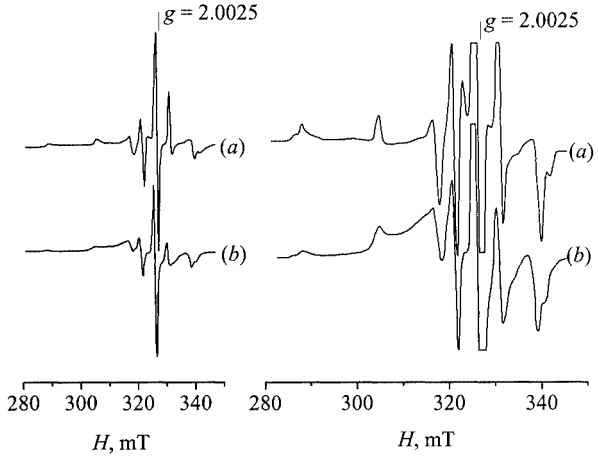

Figure 5. ESR spectra of the $5\cdot10^{-3}$ M $Cu^{II}L_2$ solutions in CH_2Cl_2/toluene 1:1 (*a*) and CH_2Cl_2 (*b*) without (*a*) and with I_2 (*b*) at 77 K, $c_{I_2} = 3.8\cdot10^{-3}$ M

The formation of the $Cu^{II}L_2I_3Cu^{III}L_2$ intermediate with the bridge coordination of the I_3^- terminal iodine atom was confirmed by density functional theory (DFT) quantum-chemical computations (B3LYP version) with the Gaussian 98 and Jaguar program packages.[52,53] To save computation time, four ethyl groups of the ligands in the copper(II) or copper(III) complexes were in all cases replaced by methyl groups on the assumption that this should not essentially influence the geometry characteristics and electron density distribution in the immediate environment of the metal atom. The calculations were performed in three steps. Initially, optimization of the $Cu^{II}L_2$ and $[Cu^{III}L_2]^+$ geometry in vacuum was carried out by application of the Gaussian 98 program with the use of the standard 3-21G* basis set on the assumption that both complexes have D_{2h} symmetry. Some computation results are given in Table 3. Note that the deduced surroundings of copper in the $Cu^{II}L_2$ and $[Cu^{III}L_2]^+$ species are close to square-planar and the calculated Cu−S bond lengths in $Cu^{II}L_2$ (2.328 Å) and $[Cu^{III}L_2]^+$ (2.194 Å) are in good agreement with those obtained by X-ray structure analysis for crystals of $Cu^{II}L_2$ (2.31 Å[51]) and $[Cu^{III}L_2]I_3$ (2.21 Å[5]). In addition, for the I_3^- anion in vacuum the calculated I−I distances are 2.998 Å and the effective atomic charges are −0.060 and −0.470

Table 3. Total energies (E_0), averaged Cu−S bond lengths (R), effective atomic charges (Q), and atomic spin densities (ASD) computed at the B3LYP/3-21G* level for the $Cu^{II}L_2$, $[Cu^{III}L_2]^+$, $Cu^{II}L_2$*, and $[Cu^{III}L_2$*$]^+$ species in vacuum, as well as for $Cu^{II}L_2$, $Cu^{III}L_2I_3$, and $Cu^{II}L_2I_3Cu^{III}L_2$ intermediate in dichloromethane ($Cu^{II}L_2$* is the $Cu^{II}L_2$ species with the fixed geometry optimized for the Cu^{III} complex and $[Cu^{III}L_2$*$]^+$ is the $[Cu^{III}L_2]^+$ species with the geometry optimized for the Cu^{II} complex)

Species	E_0 [Hartree]	R(Cu−S) [Å]	Q(Cu) [a.u.]	Q(S) [a.u.]	ASD(Cu) [a.u.]
In vacuum					
$Cu^{II}L_2$	−3561.503209	2.328	0.511	−0.125	0.711
$[Cu^{III}L_2]^+$	−3561.287141	2.194	0.357	0.093	0
$Cu^{II}L_2$*	−3561.488716	2.194	0.360	−0.092	0.631
$[Cu^{III}L_2$*$]^+$	−3561.273059	2.328	0.523	0.061	0
In dichloromethane					
$Cu^{II}L_2$	−3561.540925	2.338	0.544	−0.181	0.743
$Cu^{III}L_2I_3$	−24233.310823	2.216	0.307	0.033	0
$Cu^{II}L_2I_3Cu^{III}L_2$	−27794.863923	2.320[a]	0.497[a]	−0.180[a]	0.719[a]
		2.214[b]	0.303[b]	0.034[b]	0[b]

[a] For the $Cu^{II}L_2$ fragment. [b] For the $Cu^{III}L_2$ fragment.

a.u. for the central and the terminal iodine atoms, respectively. These results are consistent with the data from previous I_3^- computations.[17−19]

In the second step, the total energy of the $Cu^{II}L_2$ complex at the fixed geometry optimized for the Cu^{III} complex {$Cu^{II}L_2$*} and that of the $[Cu^{III}L_2]^+$ species at the geometry optimized for the Cu^{II} complex {$[Cu^{III}L_2$*$]^+$} were computed with the Gaussian 98 program for vacuum (Table 3). The difference between the $Cu^{II}L_2$* and $Cu^{II}L_2$ species energies gives the inner-sphere reorganization energy[54−56] of the $Cu^{II}L_2$ complex at electron transfer, and amounts to 38.1 kJ/mol (see Table 3). Similarly, the $[Cu^{III}L_2]^+$ inner-sphere reorganization energy is defined as the difference between the $[Cu^{III}L_2$*$]^+$ and $[Cu^{III}L_2]^+$ energies (37.0 kJ/mol, Table 3). By this means the total inner-sphere reorganization energy (λ_{in}) for the electron self-exchange reaction is λ_{in} = 38.1 + 37.0 = 75.1 kJ/mol. Because the values of the $Cu^{II}L_2$ and $[Cu^{III}L_2]^+$ inner-sphere reorganization energies are very close, the λ_{in} magnitude can also be calculated by assuming a parabolic approximation (Marcus equation)[54,55] and starting from the experimental data.

The Marcus equation gives λ_{in} in Equation (7)[54−56]

$$\lambda_{in} = \sum_j \frac{f_j^R f_j^P}{f_j^R + f_j^P} \cdot (\Delta q_j)^2 \qquad (7)$$

where f_j^R is the jth normal mode force constant in the reactants, f_j^P is that in the products, and Δq_j is the difference in equilibrium value of the jth normal coordinate in the oxidized and reduced states. We restrict our consideration only to the full-symmetric vibrations $\nu(a_1)$. For these vibrations, by using the Cu−S stretching frequencies in the dithiocarbamate complexes $Cu^{II}L'_2$ (376−404 cm^{-1}), $[Cu^{III}L'_2]I_3$ (400−402 cm^{-1}), and $[Cu^{III}L'_2]I_5$ (390−404 cm^{-1}),[4] we set $f_j^R \approx f_j^P \approx f$ = 300 N·m^{-1}. On the basis of the X-ray data for $Cu^{II}L_2$ [51] and $[Cu^{III}L_2]I_3$,[5] the Δq_j value is 0.10 Å. At the f and Δq_j values given, from Equation (7) we have: λ_{in} = 72.4 kJ/mol. Hence, the λ_{in} values obtained above by the DFT calculations and Equation (7) are in close agreement. In the third step of the quantum-chemical computations, the full geometry optimization of the $Cu^{II}L_2$ and $[Cu^{III}L_2]I_3$ species and the intermediate $Cu^{II}L_2I_3Cu^{III}L_2$ in dichloromethane solutions was performed by application of the Jaguar program[53] at the B3LYP/3-21G* level, with the Poisson−Boltzman SCRF model. Certain of the computed parameters are given in Table 3. We emphasize that no imaginary frequencies were found either for the initial complexes or for the optimized $Cu^{II}L_2I_3Cu^{III}L_2$ intermediate; this eliminates the possibility of the consideration of the intermediate as a transition state. From the frequency computations, the thermal correction to enthalpies required for going from 0 to 298 K were deduced. The optimized structure of the $Cu^{II}L_2I_3Cu^{III}L_2$ intermediate is rather intriguing (Figure 6). In particular, two metallo-chelates are not coplanar, with the $Cu^{II}-I_1-Cu^{III}$ angle with the bridging I_3^- iodine atom (I_1) and the dihedral angle $C(S_2)-Cu^{III}-I_1-I_2$ being 153.5° and 87.0°, respectively. The $Cu^{III}-I_1$, $Cu^{II}-I_1$, and $Cu^{II}-Cu^{III}$ distances were found to be 2.978, 4.008, and 6.805 Å, respectively. The $Cu^{III}-I_1$ distance is very close to the length of the axial $Cu^{II}-I$ bond in the crystal of (2,6-diacetylpyridine dihydrazone)diiodocopper(II)·1/2I_2 (2.974 Å),[57] but markedly different from the $Cu^{III}-I$ distance in the $[Cu^{III}L_2]I_3$ monocrystal (3.48 Å),[5] in which each copper(III) atom is axially bound with two terminal iodine atoms of two I_3^- groups. In the bridged I_3^- anion, the I_1-I_2 and I_2-I_3 bond lengths are 3.184 and 3.094 Å, respectively, and differ slightly from those in the optimized $[Cu^{III}L_2]I_3$ complex (3.166 and 3.098 Å), but far exceed the equal I−I distances in the I_3^- anion of the $[Cu^{III}L_2]I_3$ crystal (2.92 Å).[5]

The calculated values of the effective charges on the bridging (I_1), central (I_2), and terminal (I_3) iodine atoms of I_3^- are −0.231, −0.061, and −0.385, respectively, in the intermediate, as compared to −0.292 (I_1), −0.071 (I_2), and −0.391 (I_3) in the initial $[Cu^{III}L_2]I_3$ complex. Hence, part of the bridged I_3^- charge (−0.324) is delocalized on the $Cu^{III}L_2$ fragment (−0.265) and the $Cu^{II}L_2$ fragment (−0.059) of the $Cu^{II}L_2I_3Cu^{III}L_2$ intermediate. According to the data in Table 3, the formation energy of the intermediate in CH_2Cl_2 is $E_0 = E_0(Cu^{II}L_2I_3Cu^{III}L_2) - E_0(Cu^{II}L_2)$

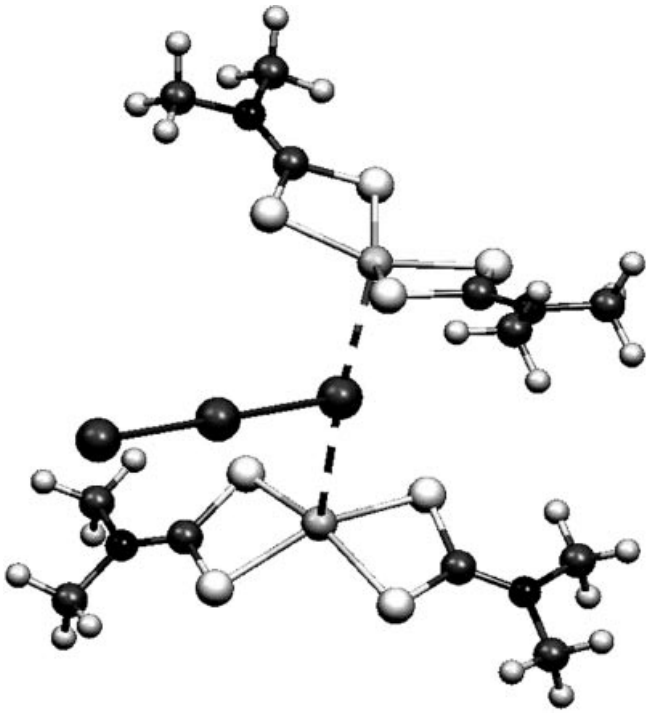

Figure 6. The structure of the $Cu^{II}L_2I_3Cu^{III}L_2$ model intermediate for the copper(II)/copper(III) electron self-exchange reaction optimized by the DFT method (the copper(III) chelate is positioned below)

$- E_0(Cu^{III}L_2I_3) = -0.012175$ a.u. $= -32.0$ kJ/mol. If the thermal correction to enthalpies ($\delta H = 1.8$ kJ/mol) is taken into account, the $Cu^{II}L_2I_3Cu^{III}L_2$ intermediate formation enthalpy can be estimated as -30.2 kJ/mol. From similar computations it follows that the alternative intermediate with the 1,3-bridging mode of triiodide at the designed C_i symmetry has a formation enthalpy of only -21.1 kJ/mol and can be regarded as less probable than the above fully optimized intermediate. It should be added that the intermediate of composition $Cu^{II}L_2I_5Cu^{III}L_2$ differs from $Cu^{II}L_2I_3Cu^{III}L_2$ (Figure 6) only by the addition of I_2 to one of the terminal atoms of the I_3^- anion.

It is appropriate to compare the value of the $Cu^{II}L_2I_3Cu^{III}L_2$ intermediate formation enthalpy discussed above with the estimation of this parameter for the dichloromethane solution following from an analysis of the activation enthalpy (Table 2) under the conditions of adiabatic electron transfer. To do this we examine the relation for the electron self-exchange rate constant k_e[55,56,58]

$$k_e = K_A \nu_n \kappa_{el} \Gamma_\lambda \exp(-\Delta G^*/RT) \quad (8)$$

with

$$\Delta G^* = \Delta G^*_{out} + \Delta G^*_{in} \quad (9)$$

where K_A is the stability constant for the formation of an encounter complex with an appropriately oriented configuration (intermediate), ν_n is an effective nuclear vibration frequency that takes the activated reactants on to products, κ_{el} is an electronic transmission coefficient ($\kappa_{el} \leq 1$), Γ_λ is a nuclear tunneling factor ($\Gamma_\lambda \geq 1$), and ΔG^* is the free energy of activation related to the reorganization energy (λ) for electron transfer ($\lambda = 4\Delta G^*$), including contributions from both the outer-sphere reorganization energy ($\lambda_{out} = 4\Delta G^*_{out}$) and the inner-sphere reorganization energy ($\lambda_{in} = 4\Delta G^*_{in}$). Let us evaluate the ΔG^*_{out} contribution for the reaction under investigation.

From the X-ray data,[5,51] the $[Cu^{III}L_2]I_n$ and $Cu^{II}L_2$ reactants can be thought of as two identical extended ellipsoids with semi-axes $a = 7.5$ Å, $b = 2.5$ Å, and $c = 1.5$ Å (the I_3^- and I_5^- anions are not taken into account because they retain their charges during the course of the electron-transfer reaction and their polarizability may be regarded as approximating the CD_2Cl_2 polarizability). In the framework of the dielectric continuum model, Equations (10) and (11) were obtained for interaction of two conducting non-polarizable ellipsoids contacting along the short semi-axis c.[59]

$$\Delta G^*_{out} = \frac{(\Delta e)^2}{4}\left(\frac{1}{D_{op}} - \frac{1}{D_s}\right)\left(\frac{F(\nu,q)}{\sqrt{a^2-c^2}} - \frac{1}{R}\cdot g\right) \quad (10)$$

$$g = 1 + \frac{2c^2 - a^2 - b^2}{3R^2} + \frac{abc}{R^3} + \frac{4\left[8c^4 + 3\left(a^4+b^4\right) - 8c^2\left(a^2+b^2\right) + 2a^2c^2\right]}{15R^4} \quad (11)$$

In these equations, Δe denotes the charge transferred from one reactant to the other, D_s and D_{op} are the static and optical (square of refractive index) dielectric constants of the solvent, respectively, R is the center-to-center separation distance in the reacting pair during the electron transfer, and $F(\nu,q)$ is the elliptic integral of the first kind[60] with $\nu = \arcsin[(a^2 - c^2)/a^2]^{1/2}$ and $q = [(a^2 - b^2)/(a^2 - c^2)]^{1/2}$. At the ellipsoid parameters specified above, the $F(\nu,q)$ value is 2.03[60] and the $[(a^2 - c^2)]^{1/2}/F(\nu,q)$ ratio is 3.62 Å. For the intermediate in CD_2Cl_2 at $R = 6.8$ Å (Figure 6), $D_s = 8.93$, and $D_{op} = 2.020$[61] (298 K), it follows from Equations (10) and (11) that $\Delta G^*_{out} = 2.2$ kJ/mol. We emphasize that the low value of ΔG^*_{out} for the reaction under consideration is caused both by the moderate magnitude of the $(D_{op}^{-1} - D_s^{-1})$ parameter for dichloromethane and by the close contact of two ellipsoids with quite large volumes.

Thus, according to Equation (9) with the above value λ_{in} (75.1 kJ/mol), we can assume that $\Delta G^* = \Delta G^*_{out} + \Delta G^*_{in} = 2.2 + 18.8 = 21.0$ kJ/mol. Knowledge of ΔG^* enables the enthalpy of the intermediate formation (ΔH_A) to be calculated for the corresponding stability constant K_A. At $\Delta S^* \approx 0$,[55] from relations (8) and $K_A = \exp[(-\Delta H_A + T\Delta S_A)/RT]$, in conjunction with the Eyring equation, we obtain: $\Delta H^{\neq} = \Delta H_A + \Delta G^*$. Hence, with regard to the experimentally determined $\Delta H^{\neq}$ value (Table 2), it follows that $\Delta H_A = \Delta H^{\neq} - \Delta G^* = 6.1 - 21.0 = -14.9$ kJ/mol. The difference between the values of the $Cu^{II}L_2I_3Cu^{III}L_2$ intermediate formation enthalpy calculated by the semiempiric approach (-14.9 kJ/mol) and by the DFT method (-30.2 kJ/mol) can be assigned both to the approximations of the dielectric continuum model[59] and to incomplete accounting for solvation effects in the DFT computations. In any case the reasonable ΔH_A values obtained provide considerable support for the stability of the proposed and found intermediate (Figure 6).

Hence, in terms of the proposed mechanism, the remarkably high values of the electron-transfer rate constants for the system involved derive both from the particular structure of the intermediate and the favorable dielectric properties of dichloromethane. To obtain greater insight into the given mechanism we are performing further investigations of the solvent effects on the kinetics of electron self-exchange reactions between the copper(II) and copper(III) dithiocarbamates.

Experimental Section

Materials. The CH_2Cl_2 and CD_2Cl_2 solvents were purified prior to use by standard method,[62] dried, and stored over 4 Å molecular sieves. Crystal iodine, $CuSO_4 \cdot 5H_2O$, $NaS_2CNEt_2 \cdot 3H_2O$ (analytical grade, Reakhim), and Et_4NI, after recrystallization, were used for preparation of solutions. The $Cu^{II}L_2$ and $[Cu^{III}L_2]I_3$ complexes were synthesized by literature methods.[4,5] For the $Cu^{II}L_2$, $C_{10}H_{20}CuN_2S_4$ (360.08), calcd. C 33.36, H 5.60, N 7.78, S 35.62; found C 32.98, H 5.62, N 7.79, S 35.32; for the $[Cu^{III}L_2]I_3$, $C_{10}H_{20}CuI_3N_2S_4$ (740.80), calcd. C 16.21, H 2.72, N 3.78, S 17.31; found C 16.27 H 2.50, N 3.62, S 17.70. The $[Cu^{III}L_2]I_5$ compound was isolated for the first time.

Synthesis of Bis(*N*,*N*-diethyldithiocarbamato)copper(III) Pentaiodide, $[Cu^{III}L_2]I_5$: A benzene solution (4 mL) of I_2 (20.3 mg, $1.6 \cdot 10^{-4}$ mol) was added to a dichloromethane solution (8 mL) of $Cu^{II}L_2$ (5.8 mg, $1.6 \cdot 10^{-5}$ mol). The resulting solution was allowed to stand in the refrigerator for a week. The grown crystals were collected, washed with hexane, and dried. The product constitutes lustrous brown-black crystals, m.p. 140−141 °C. For the $[Cu^{III}L_2]I_5$, $C_{10}H_{20}CuI_5N_2S_4$ (994.60), calcd. C 12.08; H 2.03; N 2.82; S 12.90; found C 12.02; H 1.92; N 2.73; S 12.94. Unfortunately it was impossible to perform Cu and I elemental analyses for technical reasons.

Investigation Methods: The UV/Vis absorption spectra were obtained on a LOMO Model SF 46 spectrophotometer with a thermostat in the 278−308 K temperature range, in 1.0 and 0.1 cm quartz cells. The optical densities were measured with an accuracy of ±1%. The ^1H NMR spectra were recorded on a Bruker WH 90 spectrometer (ν = 90 MHz) by 400−1000 acquisitions in CD_2Cl_2 solutions at temperatures from 248 to 298 K. Variable-temperature measurements were monitored by a Bruker temperature control unit. Signals from residual solvent protons were used as internal references. Transverse relaxation times (T_2) for protons of the methyl and methylene groups of the coordinated L ligands were evaluated from the NMR line-widths ($\Delta\nu_{1/2}$, Hz) by the relation[45] $T_2^{-1} = \pi\Delta\nu_{1/2}$ with an accuracy of ±5%. ESR spectra were recorded on a Model RE-1306 ESR spectrometer (ν = 9.2 GHz), at 100 KHz magnetic-field modulation.

Constants and thermodynamic parameters of equilibria in the above two systems were determined from the dependence of the molar absorption coefficient (ε) upon the Et_4NI or I_2 concentrations at 5−7 values of temperature and λ = 365 or 400 nm. All calculations of the equilibrium constants were made with the aid of the CPESSP computer program.[63] This program is based on the minimization of a F function,[64] $F = \Sigma_j(X_{exptl,j} - X_{calc,j})^2 \cdot (\sigma X_{exptl,j})^{-2}$, where $X_{exptl,j}$ and $X_{calc,j}$ are the experimental and calculated properties, respectively, j is the experiment number (N experiments), and σ is the relative error of the measurement. The reliability of the results obtained with this procedure was evaluated by the Fisher criterion by using the computed F_{min} value and the experimental error as described.[64]

Rate constants and activation parameters of the electron self-exchange reactions in the $Cu^{II}L_2/I_2/CD_2Cl_2$ system were calculated from the dependence of the NMR line-widths upon the I_2 and $Cu^{II}L_2$ concentrations at several temperatures with regard to the equilibrium constants obtained. Precipitation of a quantity of the copper(III) compounds at low temperatures was controlled by the integral intensity of the NMR signals. A poor solubility of these compounds at $T < 268$ K has given no way of estimating the NMR line widths at lower temperatures.

Electronically Published Supporting Information: Tables of data for the computations of the equilibrium constants with the Et_4NI_3, Et_4NI_5, $[Cu^{III}L_2]I_3$, and $[Cu^{III}L_2]I_5$ formation and the rate constants of the electron self-exchange reactions at different temperatures (4 pages, Tables S1−S4). Ordering information is given on any current masthead page (see footnote on the first page of this article).

Acknowledgments

We thank Dr. A. L. Kon'kin, A. V. Matveev, and O. I. Silkin for participation in the performance of the experiment and R. R. Garipov for help in the preparation of this paper. This work was supported by the Russian Foundation for Basic Research (Grant No 96-03-32708).

[1] A. R. Hendrickson, R. L. Martin, N. M. Rode, *Inorg. Chem.* **1976**, *15*, 2115−2119.
[2] H. C. Brinkhoff, *Recl. Trav. Chim. Pays-Bas* **1971**, *90*, 377−380.
[3] J. G. Wijnhoven, Th. E. M. Van den Hark, P. T. Beurskens, *J. Cryst. Mol. Struct.* **1972**, *2*, 189−196.
[4] S. V. Larionov, L. A. Patrina, A. N. Shan'shin, I. M. Oglezneva, E. M. Uskov, *Koord. Khim.* **1984**, *10*, 92−99.
[5] G. M. Larin, G. A. Zvereva, P. A. Koz'min, T. B. Larina, M. D. Surazhskaya, *Izv. Akad. Nauk SSSR, Neorg. Mater.* **1984**, *20*, 530−533.
[6] C. A. Koval, D. W. Margerum, *Inorg. Chem.* **1981**, *20*, 2311−2318.
[7] W. Gabes, D. J. Stufkens, *Spectrochim. Acta A* **1974**, *30*, 1835−1841.
[8] A. I. Popov, R. F. Swensen, *J. Am. Chem. Soc.* **1955**, *77*, 3724−3726.
[9] A. D. Awtrey, R. E. Connick, *J. Am. Chem. Soc.* **1951**, *73*, 1842−1843.
[10] G. Daniele, *Gazz. Chim. Ital.* **1960**, *90*, 1068−1081.
[11] W. Gabes, M. A. M. Nijuman-Meester, *Inorg. Chem.* **1973**, *12*, 589−592.
[12] E. H. Wiebenga, D. Kracht, *Inorg. Chem.* **1969**, *8*, 738−746.
[13] G. A. Bowmaker, P. D. Boyd, R. J. Sorrenson, *J. Chem. Soc., Faraday Trans. II* **1984**, *80*, 1125−1143.
[14] R. W. Hollingworth, S. Hacobian, *Aust. J. Chem.* **1974**, *27*, 1381−1389.
[15] S. N. Datta, C. S. Ewig, J. R. Van Wazer, *J. Mol. Struct.* **1978**, *48*, 407−416.
[16] L. J. Saethre, O. Gropen, J. Sletten, *Acta Chem. Scand., Ser. A* **1988**, *42*, 16−26.
[17] J. J. Novoa, F. Mota, S. Alvarez, *J. Phys. Chem.* **1988**, *92*, 6561−6566.
[18] H. Sato, F. Hirata, A. B. Myers, *J. Phys. Chem. A* **1998**, *102*, 2065−2071.
[19] Y. Ogawa, O. Takahashi, O. Kikuchi, *J. Mol. Struct. (Theochem)* **1998**, *424*, 285−292.
[20] P. Fornier de Violet, R. Bonneau, J. Joussot-Dubien, *J. Chim. Phys. et Phys.-Chim. Biol.* **1975**, *72*, 855−858.

[21] C. L. Raston, A. H. White, D. Petridis, D. Taylor, *J. Chem. Soc., Dalton Trans.* **1980**, 1928−1931.
[22] K. F. Tebbe, T. Gilles, *Z. Anorg. Allg. Chem.* **1996**, *622*, 1587−1593.
[23] K. F. Tebbe, L. Loukili, *Z. Anorg. Allg. Chem.* **1998**, *624*, 1175−1186.
[24] F. H. Herbstein, M. Kapon, *Acta Crystallogr., Sect. A* **1972**, *28*, S74.
[25] R. C. Teitelbaum, S. L. Ruby, T. J. Marks, *J. Am. Chem. Soc.* **1978**, *100*, 3215−3217.
[26] H. R. Luss, D. L. Smith, *Acta Crystallogr., Sect. B* **1980**, *36*, 1580−1588.
[27] T. Dong, H. Lin, M. Hwang, T. Lee, L. Tseng, S. Peng, G. Lee, *J. Organomet. Chem.* **1991**, *414*, 227−244.
[28] T. Akutagawa, Y. Abe, Y. Nezu, T. Nakamura, M. Kataoka, A. Yamanaka, K. Inoue, T. Inabe, C. A. Christensen, J. Becher, *Inorg. Chem.* **1998**, *37*, 2330−2331.
[29] M. Kertész, F. Vonderviszt, *J. Am. Chem. Soc.* **1982**, *104*, 5889−5893.
[30] I. V. Nelson, R. T. Iwamoto, *J. Electroanalyt. Chem.* **1964**, *7*, 218−221.
[31] J.-C. Marchon, *C. R. Acad. Sc. Paris, Ser. C* **1968**, *267*, 1123−1126.
[32] S. Tribalat, M. Grall, *C. R. Acad. Sc. Paris, Ser. C* **1966**, *263*, 399−402.
[33] R. L. Benoit, M. Guay, J. Desbarres, *Can. J. Chem.* **1968**, *48*, 1261−1266.
[34] J.-Y. Cabon, M. L′Her, M. Le Demezet, *C. R. Acad. Sc. Paris, Ser. C* **1975**, *280*, 357−360.
[35] J. Courtot-Coupez, M. L′Her, *C. R. Acad. Sc. Paris, Ser. C* **1968**, *266*, 1286−1289.
[36] J. Desbarres, *Bull. Soc. Chim. France* **1961**, 502−506.
[37] C. Barraqué, J. Vedel, B. Trémillon, *Anal. Chim. Acta* **1969**, *46*, 263−269.
[38] A. A. Ramadan, P. K. Agasyan, S. I. Petrov, *Zh. Obsh. Khim.* **1974**, *44*, 2293−2304.
[39] R. Alexander, E. C. F. Ko, Y. C. Mac, A. J. Parker, *J. Am. Chem. Soc.* **1967**, *89*, 3703−3712.
[40] R. W. Ramette, R. W. Sandford, Jr., *J. Am. Chem. Soc.* **1965**, *87*, 5001−5005.
[41] E. Makrlík, *Collect. Czechosl. Chem. Commun.* **1990**, *55*, 2602−2605.
[42] A. B. P Lever, *Inorganic Electronic Spectroscopy*, 2nd edn., Elsevier, Amsterdam, **1984**.
[43] M. V. Rajasekharan, C. N. Sethulakshmi, P. T. Manoharan, H. Gudel, *Inorg. Chem.* **1976**, *15*, 2657−2662.
[44] N. A. Izmailov, *Electrochemistry of Solutions*, 3rd edn., Khimia, Moscow, **1976**.
[45] J. A. Pople, W. G. Schneider, H. J. Bernstein, *High-Resolution Nuclear Magnetic Resonance*, McGraw-Hill Book Company, New York, **1959**.
[46] T. J. Swift, R. E. Connick, *J. Chem. Phys.* **1962**, *37*, 307−320.
[47] N. D. Yordanov, D. Shopov, *J. Chem. Soc., Dalton Trans.* **1976**, 883−886.
[48] I. N. Marov, N. A. Kostromina, *EPR and NMR in Chemistry of Coordination Compounds*, Nauka, Moscow, **1979**.
[49] G. M. Zhidomirov, Ya. S. Lebedev, S. N. Dobryakov, N. Ya. Shteinshneider, A. K. Chirkov, V. A. Gubanov, *Interpretation of Complex EPR Spectra*, Nauka, Moscow, **1975**.
[50] A. L. Kon'kin, V. G. Shtyrlin, N. G. Zabirov, A. V. Aganov, L. E. Zapechelnyuk, S. V. Kashevarov, A. V. Zakharov, *Zh. Neorg. Khim.* **1996**, *41*, 1156−1167.
[51] M. Bonamico, G. Dessy, A. Mugnoli, A. Vaciago, L. Zambonelli, *Acta Crystallogr.* **1965**, *19*, 886−897.
[52] *Gaussian 98*, M. J. Frisch, G. W. Trucks, H. B. Schlegel, G. E. Scuseria, M. A. Robb, J. R. Cheeseman, V. G. Zakrzewski, J. A. Montgomery, Jr., R. E. Stratmann, J. C. Burant, S. Dapprich, J. M. Millam, A. D. Daniels, K. N. Kudin, M. C. Strain, O. Farkas, J. Tomasi, V. Barone, M. Cossi, R. Cammi, B. Mennucci, C. Pomelli, C. Adamo, S. Clifford, J. Ochterski, G. A. Petersson, P. Y. Ayala, Q. Cui, K. Morokuma, D. K. Malick, A. D. Rabuck, K. Raghavachari, B. Foresman, J. Cioslowski, J. V. Ortiz, B. B. Stefanov, G. Liu, A. Liashenko, P. Piskorz, I. Komaromi, R. Gomperts, R. L. Martin, D. J. Fox, T. Keith, M. A. Al-Laham, C. Y. Peng, A. Nanayakkara, C. Gonzalez, M. Challacombe, P. M. W. Gill, B. Johnson, W. Chen, M. W. Wong, J. L. Andres, C. Gonzalez, M. Head-Gordon, E. S. Replogle, J. A. Pople, Gaussian, Inc., Pittsburgh PA, **1998**.
[53] *Jaguar 4.1*, Schrodinger, Inc., Portland, Oregon, **2000**.
[54] R. A. Marcus, *Disc. Faraday Soc.* **1960**, *29*, 21−31.
[55] R. A. Marcus, N. Sutin, *Biochim. Biophys. Acta* **1985**, *811*, 265−322.
[56] M. D. Newton, N. Sutin, *Ann. Rev. Phys. Chem.* **1984**, *35*, 437−480.
[57] M. Belicchi Ferrari, G. Gasparri Fava, and C. Pelizzi, *Acta Crystallogr.,* **1981**, *B 37*, 924−926.
[58] P. Chen, T. J. Meyer, *Chem. Rev.* **1998**, *98*, 1439−1477.
[59] Yu. I. Kharkats, *Electrokhim.* **1976**, *12*, 1284−1291.
[60] E. Janke, F. Emde, F. Lösch, *Tafeln höherer Funktionen*, Sechste Auflage, B. G. Teubner Verlagsgesellschaft, Stuttgart, **1960**.
[61] E. D. German, A. M. Kuznetsov, *Itogi Nauki i Techniki, VINITI, Ser. Kinetika, Kataliz.* **1990**, *20*, 3−150.
[62] A. J. Gordon, R. A. Ford, *The Chemist's Companion*, Wiley, New York, **1972**.
[63] Yu. I. Sal'nikov, A. N. Glebov, F. V. Devyatov, *Polynuclear Complexes in Solutions*, KSU, Kazan, **1989**.
[64] E. S. Shcherbakova, I. P. Gol'dshtein, E. I. Gurjanov, K. A. Kocheshkov, *Izv. Akad. Nauk SSSR, Ser. Khim.* **1975**, 1262−1271.

Received May 14, 2002
[I02257]

Twisting the Porphyrin Ring to Enhance Epoxidation Enantioselectivity

Stéphanie Gazeau,[a] Jacques Pécaut,[a] Raid Haddad,[b] John A. Shelnutt,*[b] and Jean-Claude Marchon*[a]

Keywords: Porphyrinoids / Manganese / Enantioselectivity / Asymmetric catalysis / Epoxidation

A series of bridled chiroporphyrins has been prepared in which the distortion of the porphyrin ring is controlled solely by the length of the bridles. The influence of ring distortion on the enantioselectivity of catalytic epoxidation by their manganese complexes has been investigated. Twisting the porphyrin ring is found to enhance the enantioselectivity of dihydronaphthalene epoxidation.

(© Wiley-VCH Verlag GmbH, 69451 Weinheim, Germany, 2002)

Introduction

Despite numerous recent advances in the area of asymmetric catalysis by chiral metal complexes,[1] the specific features (steric, conformational, electronic, etc.) of the chiral ligand that influence the enantiomeric excess (*ee*) are far from being completely understood. Among stereochemical factors, steric exclusion is widely considered a major determinant of asymmetric induction in a host of metal-catalyzed reactions. The influence of conformation is less clear; the impact of the distortion of a nominally planar ligand has been suspected only recently.[2,3] In this report, we examine the influence of porphyrin ring distortion on the enantioselectivity of catalytic epoxidation by manganese chiroporphyrins.

Steric crowding by bulky *meso* substituents is known to result in a ruffling distortion of the porphyrin[4] which influences the spectral and chemical properties of the molecule.[5] The asymmetric epoxidation of dihydronaphthalene by iodosylbenzene induced by ruffled manganese(III) chiroporphyrin complexes was investigated recently in our laboratories: the *ee* of the epoxide product has been found to increase as the porphyrin becomes more ruffled.[6] Since the origin of the ruffled distortion is the congestion induced by the bulky *meso* substituents near the porphyrin ring in an αβαβ conformation, we have not been able to determine whether the asymmetric induction is due to a conformational or a steric effect, or both. In an attempt to resolve these two influences, we have designed a series of chiroporphyrins H_2Bn (Scheme 1) in which the ester functions on adjacent *meso* substituents are linked by a strap of adjustable length (n = 8 to 16 methylene groups). We expected that the ruffling induced by the αβαβ conformation could be restricted by these bridles, and that the resulting distortion could be tuned by the strap length while the substituent volume and electronic effects would remain unchanged. Here we report our investigations of the ruffling of the bridled chiroporphyrin free bases and nickel(II) complexes by ^{1}H NMR and resonance Raman spectroscopy. We show that the ruffling in solution can indeed be controlled by the bridle length, and that it has a positive influence on the epoxidation enantioselectivity.

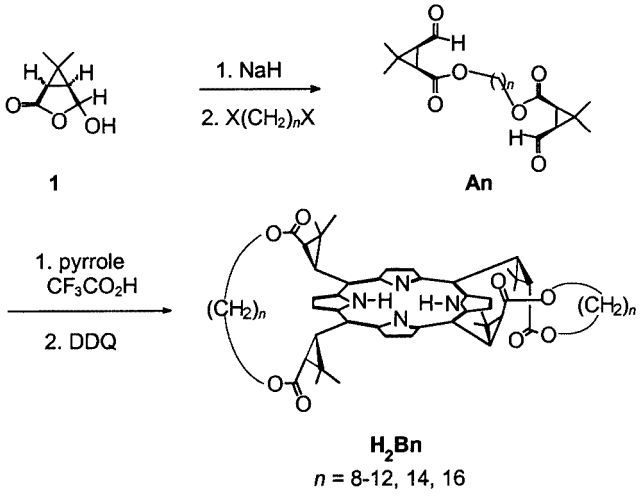

Scheme 1. Synthesis of the bridled chiroporphyrins

[a] Laboratoire de Chimie Inorganique et Biologique (UMR 5046 CEA-CNRS-UJF), Département de Recherche Fondamentale sur la Matière Condensée, CEA-Grenoble,
38054 Grenoble, France
Fax: (internat.) +33-438/785-497
E-mail: jcmarchon@cea.fr
[b] Biomolecular Materials and Interfaces Department, Sandia National Laboratories, Albuquerque, NM 87185, and Department of Chemical and Nuclear Engineering, University of New Mexico
Albuquerque, NM 87131, USA
Fax: (internat.) +1-505/272-7077
E-mail: jasheln@unm.edu

Results and Discussion

The bridled chiroporphyrins H_2B9−16 were obtained in 3−12% yield following the procedure outlined in Scheme 1, which we designed earlier for the synthesis of H_2B8 from biocartol **1**.[7] In contrast to H_2B8, which is obtained as the αααα isomer,[7] the αβαβ conformation of the free bases with longer bridles (H_2B9−16) is apparent from their D_2-symmetric ^{1}H NMR spectra, with a pair of singlets for the β-pyrrolic protons and a single signal for each group of *meso* protons. The resonances of the methylene protons of H_2B9−16 appear near δ = 1.6−1.8 ppm, indicating that the two straps are directed away from the ring current and connect adjacent substituents on opposite faces of the porphyrin. Metal insertion gave the nickel complexes NiB8−16 as pure αβαβ conformers, and the manganese complexes MnClB8−16 as a mixtures of αβαβ and αααα conformers, which were separated by TLC on silica gel and identified by X-ray crystallography. The more abundant isomer was assigned the αβαβ conformation, and the more polar, less abundant one was assigned the αααα conformation. Single crystals were obtained by slow diffusion of *n*-hexane into a chloroform solution of MnClB10. The determination of the X-ray structure showed that the asymmetric unit contains one αβαβ-MnClB10 complex and two very similar, but crystallographically distinct, αααα-MnClB10 complexes, and it confirmed the assignments made on the basis of the relative polarities observed in TLC. Views of the X-ray structures of the two conformers are illustrated in Figure 1. Notable features of these structures are the ruffled porphyrin conformation of the αβαβ conformer and the two straps connecting adjacent *meso* substituents on opposite faces, and the slightly domed porphyrin conformation of the αααα conformer and the two straps connecting adjacent *meso* substituents on the same face. Also noteworthy is the variable conformation of the four ester moieties, which have their carbonyl group inwardly directed in the αβαβ isomer and outwardly directed in the αααα isomer.

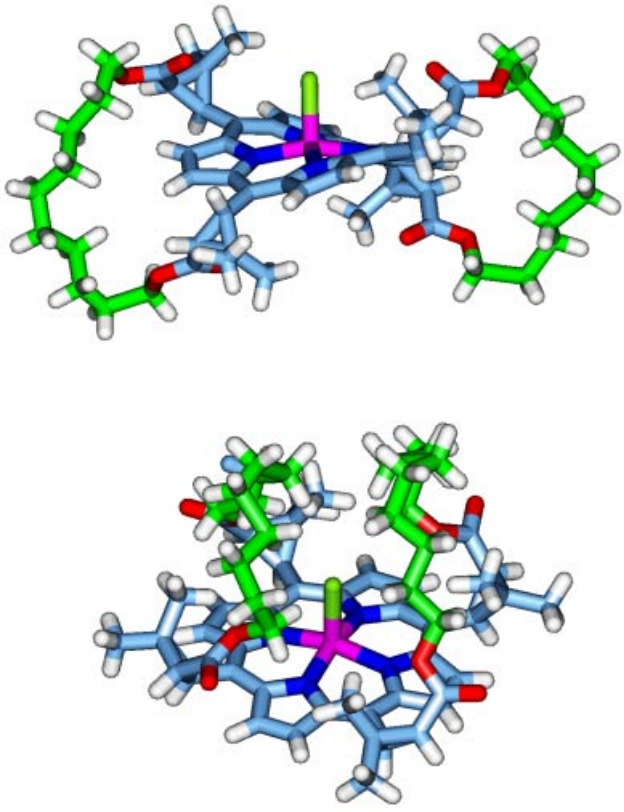

Figure 1. X-ray structures of the bridled manganese(III) complex MnClB10; (top) stick representation of the αβαβ-MnClB10 molecule showing the ruffled porphyrin conformation and the two straps connecting adjacent *meso* substituents on opposite faces; selected bond lengths (Å): Mn(1)−N(1) 1.983(8); Mn(1)−N(2) 1.987(8); Mn(1)−N(3) 1.968(8); Mn(1)−N(4) 1.993(8); Mn(1)−Cl(1) 2.371(3); (bottom) stick representation of one of the two αααα-MnClB10 molecules showing the slightly domed porphyrin conformation and the two straps connecting adjacent *meso* substituents on the same face; selected bond lengths (Å): Mn(2)−N(11) 2.024(9); Mn(2)−N(12) 2.053(8); Mn(2)−N(13) 2.033(8); Mn(2)−N(14) 2.057(8); Mn(2)−Cl(2) 2.365(3). Mn(3)−N(21) 2.019(8); Mn(3)−N(22) 2.014(8); Mn(3)−N(23) 2.018(8); Mn(3)−N(24) 2.037(9); Mn(3)−Cl(3) 2.360(3)

High-frequency Raman lines in the region 1340−1640 cm^{-1} have been shown to be especially sensitive to the ruffling mode of deformation of nickel(II) porphyrins.[5] In the resonance Raman spectra of the bridled nickel(II) complexes NiB8−16 (Figure 2), all of the high-frequency marker lines show a similar frequency dependence on bridle length. The correlation between frequency and the number of methylene groups in a bridle is depicted in Figure 3 for ν_2. At first ($8 \leq n \leq 12$), lengthening the bridle induces a decrease of the line frequency, indicating increased ruffling of the ring as we expected. Apparently the constraints imposed by the bridles, which prevent adjacent *meso* substituents on opposite faces from moving away from each other, are gradually relaxed as the number of methylene groups increases, thus allowing the porphyrin to reach a more distorted conformation until a maximum is attained for n = 12. Further lengthening of the bridles beyond n = 12 unex-

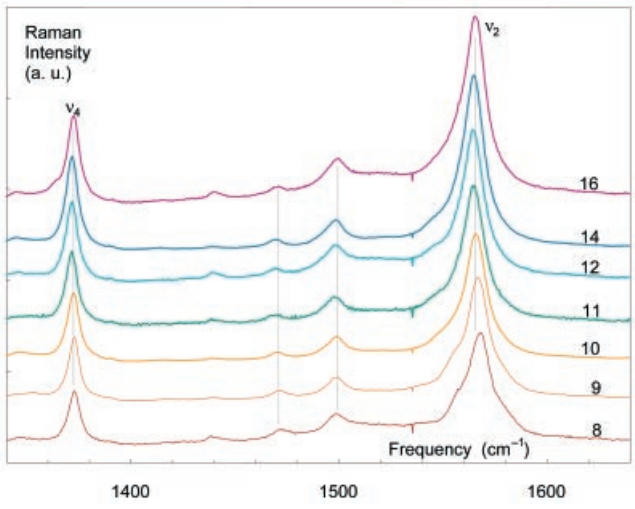

Figure 2. High-frequency region of the resonance Raman spectra for the bridled nickel(II) complexes NiB8−16 obtained at 407.6 nm laser excitation in carbon disulfide; the number on each spectrum refers to the number of methylene groups in a bridle of the complex

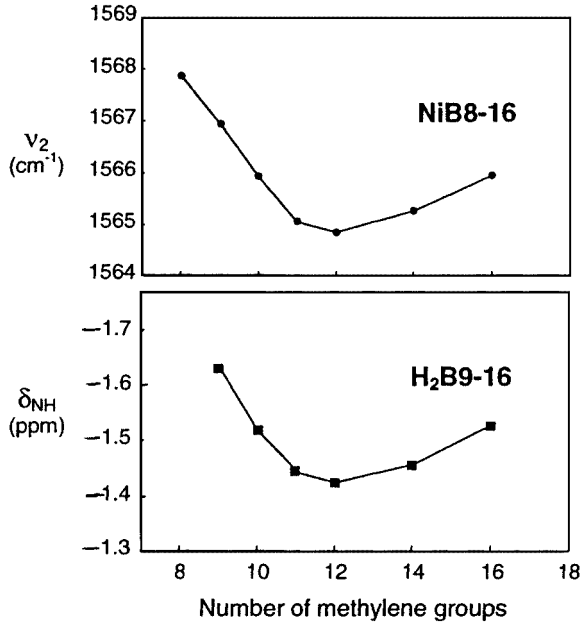

Figure 3. Dependence of the frequency of the structure-sensitive line ν_2 for the nickel(II) complexes αβαβ-NiB8−16 (upper trace), and of the chemical shift of central protons δ_{NH} for the free base chiroporphyrins αβαβ-H_2B9−16 (lower trace) on the number of methylene groups in a bridle

pectedly induces a small decrease in the ruffling, as evidenced by the small increase in the marker line frequencies.

An entirely similar biphasic behavior has been detected for the free bases H_2B9−16 by ^{1}H NMR spectroscopy (Figure 3), using the chemical shift δ_{NH} of the central protons as a probe of the ring current; the latter is directly related to the nonplanar distortion of the porphyrin. The similar trends found for the free bases and their nickel(II) complexes is a strong indication that in these intrinsically ruffled compounds the amount of distortion of the porphyrin ring arises mainly from the restraints imposed by the bridles, and that it is not strongly influenced by the size of the metal center. Molecular dynamics simulations also give average structures for NiB8−16 that indicate a dependence of the magnitude of ruffling similar to that shown in Figure 3.[10]

We surmise that long straps ($n \geq 12$) have sufficient flexibility to allow other conformational states of the ester group to be populated, for example by rotation of their oxo and alkoxy substituents. Conformations in which the carbonyl group is either inwardly or outwardly directed, as seen in Figure 1, have been observed earlier in the X-ray structure of the nickel chiroporphyrin derived from the bornyl ester of **1**.[6] In a chiroporphyrin with long bridles, a change from an outwardly to an inwardly directed carbonyl group would result in an effective shortening of the strap, and therefore to a less-distorted porphyrin ring.[10] In agreement with this proposed mechanism, the conformational flexibility of the 16-methylene chains of H_2B16 is apparent from the presence of a single signal at $\delta = 3.62$ ppm for the two diastereotopic protons of the methyleneoxy groups, which are in fast exchange on the NMR time scale. In contrast, the shorter-chain congeners are more conformationally rigid, as indicated by the anisochronicity of the two diastereotopic protons of the methyleneoxy groups, which give two broad signals. It is also possible that additional flexibility in the straps introduces new ways in which the straps can influence the out-of-plane macrocycle distortion

Table 1. Yields, enantiomeric excesses, and enantiomeric compositions obtained in the asymmetric epoxidation of 1,2-dihydronaphthalene by iodosylbenzene induced by catalysts MnClB8−16[a]

Number of methylene groups in bridle	Yield[b] (%)		*ee*[c] (%)		Enantiomeric composition (%)	
8	64	average 62	46	average 44(2)	73	average 72(1)
	61		45		73	
	62		42		71	
9	61	average 63	54	average 51(3)	77	average 76(1)
	65		47		74	
	64		52		76	
10	57	average 58	65	average 63(4)	83	average 82(1)
	61		66		83	
	56		59		80	
11	51	average 54	59	average 61(2)	79	average 80(1)
	55		62		81	
	56		62		81	
12	63	average 60	62	average 61(2)	81	average 80(1)
	58		59		79	
	60		63		81	
14	51	average 48	51	average 53(3)	76	average 77(1)
	46		54		77	
	47		53		77	
16	48	average 47	69	average 64(5)	85	average 82(2)
	45		62		81	
	49		60		80	

[a] Reaction conditions: catalyst/substrate/PhIO 1:1000:100 μmol at room temperature in 2 mL CH_2Cl_2. [b] Yield relative to PhIO. [c] Measured by GC on a Cyclodex-B chiral column.

through nonbonding interactions or additional degrees of freedom at the meso substituents.

Each catalyst of the series αβαβ-MnClB8−16 was carefully purified by TLC on silica gel. The yields and *ee*'s obtained in the catalytic epoxidation of 1,2-dihydronaphthalene by iodosylbenzene are collected in Table 1. Figure 4 shows a plot of the enantiomer composition (ec) of the major 1*S*,2*R* epoxide versus the ν_2 frequency of NiB8−16. The observed correlation suggests that similar distortions of the ring are obtained irrespective of the core metal (Ni or Mn). It also indicates that the enantioselectivity induced by the manganese catalysts increases as the ruffling of the porphyrin increases, i.e. that twisting the porphyrin ring is beneficial to the asymmetric induction.

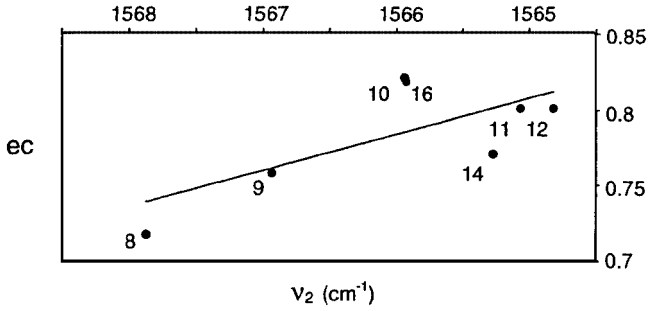

Figure 4. Plot of the enantiomer composition (ec) of the major 1*S*,2*R* epoxide obtained in the asymmetric epoxidation of 1,2-dihydronaphthalene by iodosylbenzene induced by catalysts αβαβ-MnClB8−16 as a function of the frequency of the structure-sensitive line ν_2 of NiB8−16; the number of methylene groups *n* in each bridle is indicated for each data point

The subtle effect by which a conformation change can influence the enantioselectivity of a catalyst is intriguing. We speculate that this influence may be mediated by several factors, either steric or electronic in origin. For example, a folding, or twisting, of the porphyrin ring would put more bulk near the metal center, or induce more asymmetry of charge distribution in the reactive species, respectively. Coming back to the chiroporphyrin catalysts of the first generation,[6] which were the starting point of this investigation, we can now conclude that the extent of their asymmetric induction is the result of several effects. The favorable steric influences of the ester or amide substituents in their various possible conformations are corroborated by the resulting propitious effect of porphyrin ruffling. This finding reveals a novel facet of the origins of stereoinduction in asymmetric catalysis, and it may have implications in catalyst design.

Conclusion

In summary, bridled chiroporphyrins provide the unprecedented possibility of controlling the distortion of the porphyrin ring without substantially modifying the steric and electronic influences of the macrocycle substituents. The dependence of the ruffling on the bridle length shows two opposite trends. Like the structure-sensitive Raman frequencies of the nickel complexes, the ^{1}H NMR chemical shift of the central protons of the free bases is a very sensitive probe of the ruffled distortion of the porphyrin ring in solution. Our finding that this distortion has a positive influence on stereoinduction may open new possibilities for the design or improvement of asymmetric catalysts.

Experimental Section

General Spectroscopic Information: All compounds were characterized by electrospray mass spectrometry (Finnigan MAT LCQ), UV/Vis (Perkin−Elmer Lambda 9), and NMR spectroscopy. The purity of all products was ascertained by TLC, UV/Visible and NMR spectroscopy; elemental analytical data were not obtained due to the generally low yields. ^{1}H NMR spectra of $CDCl_3$ solutions of the compounds (ca. 3 mg in 0.5 mL) were recorded at room temperature on a Bruker AC200 or a Varian Avance 400 NMR spectrometer. Parameters for acquiring proton spectra were the following: 200 MHz, 16 scans, spectral window 4 kHz, 16 K data points; 400 MHz, 8 scans, spectral window 8 kHz, 58.5 K data points. Chemical shifts were measured relative to $CHCl_3$ and they are referenced to tetramethylsilane. Resonance Raman spectra were obtained as reported in a an earlier publication.[8]

Catalytic epoxidations were carried out according to standard procedures.[6,9] Measurements of enantiomeric compositions were carried out at least in triplicate by chiral chromatography on a Cyclodex-B column with a Fisons GC 9000 system.

Synthesis of a Bridle An: A typical procedure is described below for A10. NaH (1.13 g, 28 mmol) was added in small portions to a dry THF (30 mL) solution of biocartol **1** (4 g, 28 mmol) under argon at 10 °C. The mixture was then stirred for 30 min at room temperature and 2.76 mL of 1,10-diiododecane (7 mmol) in dry DMF (120 mL) was added. After stirring for 24 h under argon at room temperature, diethyl ether was added and the organic layer was washed and dried over Na_2SO_4. The solvent was then removed under reduced pressure. The residue was purified by silica gel chromatography with dichloromethane/methanol (97:3) as eluent to afford A10 as a colorless oil (2.96 g, >99% relative to diiododecane). ^{1}H NMR (200 MHz, $CDCl_3$): δ = 9.73 (d, *J* = 6.3 Hz, 2 H, CHO), 4.09 (dt, *J* = 6.8, *J* = 1 Hz, 4 H, OCH_2), 2.10 (d, *J* = 8.8 Hz, 2 H, CH−C(O)O), 1.82 (dd, *J* = 6.3, *J* = 8.8 Hz, 2 H, C*H*−CHO), 1.62 (m, 4 H, O−CH_2−CH_2), 1.54 (s, 6 H, CH_3), 1.28 (b, 12 H, CH_2), 1.25 (s, 6 H, CH_3).

Synthesis of a Bridled Chiroporphyrin H_2Bn: A typical procedure is described below for H_2B10. A degassed dichloromethane (1.9 L) solution containing A10 (3.54 g, 8.4 mmol), 1.4 mL (20 mmol) of pyrrole and 1.55 mL (20 mmol) of TFA was stirred at room temperature under argon for 6 days. The reaction mixture was diluted to 5.7 L by adding 3.8 L of dichloromethane and then oxidized with DDQ (3.8 g, 16.6 mmol). After stirring for 4 h, the solvent was removed under reduced pressure. The residue was chromatographed on an alumina column eluting with dichloromethane/methanol (98:2), then on silica gel plates eluting with the same solvent mixture. The porphyrin H_2B10 was obtained as a purple solid (530 mg, 12%). MS (ES): *m*/*z* = 1035.7 [MH^+]. UV/Vis (CH_2Cl_2): λ_{max} = 429 nm (Soret), 530, 565, 607, 662. ^{1}H NMR (400 MHz, $CDCl_3$): δ = 9.12 and 9.08 (2s, 8 H, Hβ), 4.80 (d, *J* = 8.8 Hz, 4 H, H^2), 4.0 (m, 4 H, OCH_2), 3.55 (m, 4 H, OCH_2), 2.74 (d, *J* = 8.8 Hz, 4 H,

H^1), 1.93 (s, 12 H, CH_3), 1.82 and 1.69 (2b, 32 H, CH_2), 0.79 (s, 12 H, CH_3), −1.52 (b, 2 H, NH) ppm. ^{13}C NMR (200 MHz, $CDCl_3$): δ = 169.8 (C=O), 153.0 (Cα), 149.3 (Cα), 131.3 (Cβ), 127.3 (Cβ), 111.0 (*meso* C^{IV}), 64.3 (OCH_2), 38.4 (CH^2), 32.9 (CH^1), 29.7 (Me), 29.2 (CH_2), 28.9 (CH_2), 28.6 (CH_2), 27.7 (C^{IV}), 27.3 (CH_2), 17.9 (Me) ppm.

MnClBn: A typical procedure is described below for MnClB10. A saturated $MnCl_2{\cdot}4H_2O$ solution (20 mL) in ethanol was added to a solution H_2B10 (20 mg, 19.3 μmol) in 10 mL of chloroform. The mixture was stirred under reflux for 72 h. The solvent was removed under reduced pressure and the residue was purified twice by TLC on silica eluting with dichloromethane/methanol (92:8). The resulting product (20.5 mg, 95%) gave a single spot in TLC on silica. MS (ES): m/z = 1087.5 [M^+ − Cl]. UV/Vis (CH_2Cl_2): λ_{max} = 383, 402, 486, 596, 638 nm.

X-ray Crystallographic Study: Dark green single crystals were obtained by slow diffusion of *n*-hexane into a chloroform solution of the complex. Data collection was carried out on a Bruker AXS Smart CCD area-detector diffractometer. The structure was solved by direct methods using the SHELX-TL software package. Crystal data for MnClB10: $3C_{64}H_{80}N_4O_8MnCl{\cdot}CHCl_3$, M = 3490.50, trigonal, space group $P3_2$, a = 27.3710(8), b = 27.3710(8), c = 23.2007(9) (Å), γ = 120°, V = 15052.6(9) Å^3, T = 193(2) K, Z = 3, μ(Mo-K_α) = 0.329 mm^{-1}, 63323 reflections, 42452 independent reflections (R_{int} = 0.0820) which were used in all calculations. The final R was 0.0965, the final $wR(F^2)$ was 0.2263 [$I > 2\sigma(I)$].

CCDC-156317 contains the supplementary crystallographic data for this paper. These data can be obtained free of charge at www.ccdc.cam.ac.uk/conts/retrieving.html [or from the Cambridge Crystallographic Data Centre, 12 Union Road, Cambridge CB2 1EZ, UK; Fax: (internat.) +44-1223/336-033; E-mail: deposit@ccdc.cam.ac.uk].

Acknowledgments

We thank Pierre-Alain Bayle, Nathalie Gon, and Colette Lebrun for their help, and the CNRS and the MENRT for support. Sandia is a multiprogram laboratory operated by Sandia Corp., a Lockheed-Martin company, for the US Department of Energy under contract DE-AC04-94AL85000.

[1] *Comprehensive Asymmetric Catalysis* (Eds.: E. N. Jacobsen, A. Pfaltz and H. Yamamoto), Springer-Verlag, New York, **1999**; *Catalytic Asymmetric Synthesis Special Issue* (Eds.: S. E. Denmark and E. N. Jacobsen), *Acc. Chem. Res.* **2000**, *33*, 323−440.
[2] P. J. Pospisil, D. H. Carsten, E. N. Jacobsen, *Chem. Eur. J.* **1996**, *2*, 974−980.
[3] K. B. Lipkowitz, S. Schefzick, D. Avnir, *J. Am. Chem. Soc.* **2001**, *123*, 6710−6711.
[4] W. R. Scheidt, Y. J. Lee, *Struct. Bonding (Berlin)* **1987**, *64*, 1−70.
[5] J. A. Shelnutt, X.-Z. Song, J.-G. Ma, S.-L. Jia, W. Jentzen, C. J. Medforth, *Chem. Soc. Rev.* **1998**, *27*, 31−41.
[6] C. Pérollier, J. Pécaut, R. Ramasseul, J.-C. Marchon, *Inorg. Chem.* **1999**, *38*, 3758−3759.
[7] S. Gazeau, J. Pécaut, J.-C. Marchon, *Chem. Commun.* **2001**, 1644−1645.
[8] W. Jentzen, M. C. Simpson, J. D. Hobbs, X. Song, T. Ema, N. Y. Nelson, C. J. Medforth, K. M. Smith, M. Veyrat, M. Mazzanti, R. Ramasseul, J. C. Marchon, T. Takeuchi, W. A. Goddard III, J. A. Shelnutt, *J. Am. Chem. Soc.* **1995**, *117*, 11085−11097.
[9] S. Gazeau, *Thèse de Doctorat*, Université Joseph Fourier, Grenoble, **2001**.
[10] Note added in proof (August 28, 2002): dynamics simulations clearly indicate that exchange processes occur between inward/equatorial and outward/axial conformations of the carbonyl groups. The length of the strap influences these interconversions: R. Haddad, S. Gazeau, J. Pécaut, J.-C. Marchon, C. J. Medforth, J. A. Shelnutt, *J. Am. Chem. Soc.*, submitted.

Received May 16, 2002
[I02260]

P−H Activation By Zirconium Amido Complexes: From New Phosphanidozirconium Complexes to the First Zr_2P_6 Cluster with the $[RP-P-PR]^{3-}$ Ligand [R = Me_2(*i*PrMe_2C)Si]

Matthias Driess,*[a] Joachim Aust,[a] and Klaus Merz[a]

Dedicated to Prof. Karl Wieghardt on the occasion of his 60th birthday

Keywords: Phosphanides / Bond activation / Cluster compounds / Zirconium / Phosphanes

A new, efficient and salt-free method to synthesize phosphanidozirconium complexes is reported. Treatment of $[Cp_2Zr(PHR)_2]$ **3** [R = Me_2(*i*PrMe_2C)Si] with $[Zr(NEt_2)_4]$ furnishes the first unsymmetrically substituted 1,3-dizircona-2,4-diphosphetane $[Cp_2Zr(PR)_2Zr(NEt_2)_2]$ (**1**; Cp = η^5-C_5H_5) in quantitative yield, which undergoes intermolecular ligand exchange reactions at 140 °C to form the mixed substituted derivative $[Cp_2Zr(PR)_2ZrCp(NEt_2)]$ (**2**) in 28% yield. An X-ray diffraction analysis of **2** revealed that the four-membered Zr_2P_2 ring is only slightly puckered. The Brønsted acid-base reaction of $[Cp^*Zr(NMe_2)_3]$ (**4**; Cp^* = C_5Me_5) with the P–H acidic silylphosphane RPH_2 affords the corresponding tris-(phosphanido) complex $[Cp^*Zr(PHR)_3]$ (**5**) in the form of a red-brown oil in quantitative yield. Heating of the latter at 140 °C leads to the first dinuclear zirconium phosphanide cluster $[(Cp^*Zr)_2(R_2P_3)_2]$ (**6**), which has been isolated in the form of dark green crystals in 12% yield and structurally characterized by X-ray diffraction analysis.
(© Wiley-VCH Verlag GmbH, 69451 Weinheim, Germany, 2002)

Introduction

During the last few years substantial progress has been achieved in the development of nucleophilic, and at the same time soft, phosphorus-transfer reagents, in which Zr−P compounds play an excellent role as versatile building blocks for the synthesis of organophosphorus compounds. Since the initial work on phosphanidozirconium compounds by Issleib and Häckert[1] it has become well established that $Cp_2Zr(+4)$ and $Cp_2Zr(+3)$complexes (Cp = η^5-C_5H_5) with bridging and/or terminal phosphanido ligands can serve as soluble, mild and selective PR_2^-, PR^{2-} and P^{3-} equivalents.[2] The latter types of complexes are superior to the respective ionogenic alkali and alkaline earth metal phosphanides since, during their synthesis, they can initiate simultaneous Zr-assisted P−P and/or P−C cross-coupling reactions between several primary organophosphorus moieties, affording new polyphosphorus ligands. This synthetic potential is impressively demonstrated by the $[Cp_2Zr]$-induced cyclooligomerisation of phosphaalkynes[3] and the formation of Zr−P complexes with unsubstituted phosphorus atoms, starting from P_4 and $[Cp_2Zr]$ complex fragments.[4] The formation of Zr−P bonds in phosphanidozirconocene compounds is usually achieved by salt metathesis reactions between lithium phosphanides and $[Cp_2ZrX_2]$ (X = halogen) or through oxidative addition of (oligo)phosphanenes, P−C multiple bonds and P_4 to $[Cp_2Zr]$ fragments as reactive intermediates.[5] The latter methods also frequently involve redox processes at the zirconium and phosphorus atoms, which make product predictions more difficult. Here we report a new method for the synthesis of Zr−P complexes through σ-metathesis reactions, starting from strong Brønsted-basic amidozirconium complexes ($[Zr]-NR_2$) and P−H-acidic silylphosphanenes. Hitherto, only the reverse process, that is, the simple protolytic fission of the Zr−P bond with NH-containing amines, has been described.[6] Furthermore, we report the preparation of the first zirconium tris(silylphosphanido)-complex **5**, which can be converted into the $(ZrP_3)_2$ cluster **6**.

[a] Lehrstuhl für Anorganische Chemie I: Molekül- und Koordinationschemie
Ruhr Universität Bochum, Fakultät für Chemie
Universitätsstrasse 150, 44801 Bochum, Germany
Fax: (internat.) + 49-234/321-4378
E-mail: matthias.driess@ruhr-uni-bochum.de

Results and Discussion

The Zr_2P_2 complex **1** is furnished in almost quantitative yield by heating the diphosphanido complex **3** with $[Zr(NEt_2)_4]$ in boiling benzene, while compound **3** is accessible upon reaction of $[Cp_2ZrCl_2]$ with RP(H)Li in 71% yield [molar ratio 1:2, toluene, 0 °C; R = Me_2(*i*PrMe_2C)Si; $\delta(^{31}P)$ = −51.0 (d, $^1J_{P,H}$ = 214 Hz)]. In contrast to the $[Cp_2Zr(PHR)_2]$ derivatives (R = *t*Bu, Aryl) hitherto known,[7] **3** is not only easily accessible and thermally resist-

ant up to 120 °C but also suitable for selective P−H bond activation.

Compound **1** was isolated in the form of a red-brown oil. Its structure can be deduced from the simple features of the ^{1}H and ^{31}P NMR spectra, while its composition is proven by the EI mass spectrum. The ^{31}P NMR spectrum of **1** shows a singlet for both μ_2-bridging P atoms at relatively low field (δ = 287.6 ppm), as expected for Zr_2P_2 complexes.[9]

Surprisingly, **1** undergoes metathesis reactions in boiling xylene at 140 °C to give the unsymmetrical **2**, which contains one $Cp(Et_2N)$- and one Cp_2-substituted Zr atom, in 28% yield (Scheme 1). The mechanism of this unprecedented Cp/NEt_2 exchange reaction at the zirconium atoms is still unknown. However, the formation of **2** probably occurs intermolecularly, as indicated by the strong concentration dependence of the reaction. The complex is formed in only 1.5% yield if **3** is reacted with $[Zr(NEt_2)_4]$ in boiling xylene. The ^{31}P NMR spectrum of **2** at 28 °C shows one singlet at δ = 273.8 ppm which is consistent with an fast inversion of configuration at phosphorus on the time scale of the experiment. This inversion process could not be frozen out at low temperature due to the moderate solubility of **2** in CH_2Cl_2, $CHCl_3$, Et_2O and aromatic solvents. Its ^{1}H NMR spectrum shows, as expected, three anisotropic sets of Cp groups and one type of ethyl protons. Additionally, the constitution of **2** has been corroborated by an single-crystal X-ray diffraction analysis. The four-membered Zr_2P_2 skeleton is slightly puckered (Zr1-Zr2-P1/Zr1-Zr2-P2 = 3.2°). The Zr1−P1 [2.552(3) Å] and Zr1−P2 [2.527(3)] bond lengths are similar to the values for Zr2−P1 [2.550(3) Å] and Zr2−P2 [2.615(3) Å] (Figure 1).

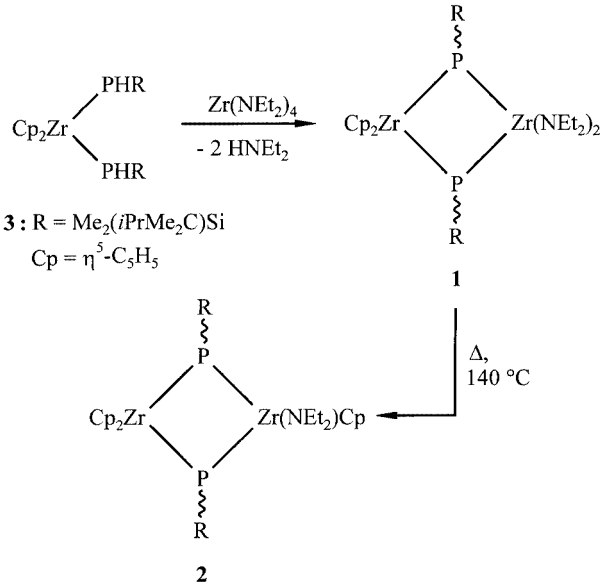

Scheme 1

The Zr−P distances are practically identical to the values observed in other Zr(+4)-phosphanide complexes but ca. 4% shorter than the single bonds in isostructural Zr_2P_2

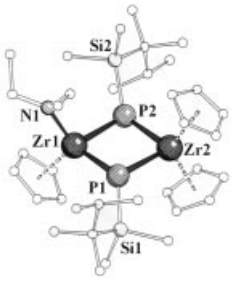

Figure 1. Molecular structure of **2**; hydrogen atoms are omitted for clarity; selected distances [Å] and angles [°]: Zr1−N1 1.958(11), Zr1−P1 2.552(3), Zr1−P2 2.527(3), Zr2−P1 2.550(3), Zr2−P2 2.615(3), P1−Si1 2.225(4), P2−Si2 2.210(4); P2−Zr1−P1 89.8(1), P1−Zr2−P2 87.90(9)

complexes with Zr(+3) centers.[1,9] The Zr−N and Si−P distances are unexceptional. The P atoms are pyramidal coordinated (ΣP1 = 344.5°, ΣP2 = 340.0°) and possess practically identical endocyclic angles at the Zr centers.

In another P−H/Zr−N σ-metathesis reaction, starting from the tris(amido) complex **4** and H_2PR in the molar ratio of 1:3 in boiling toluene, the first zirconium tris(phosphanido) complex $[Cp^*Zr(PHR)_3]$ (**5**; $Cp^* = \eta^5$-C_5Me_5) has been prepared (Scheme 2).

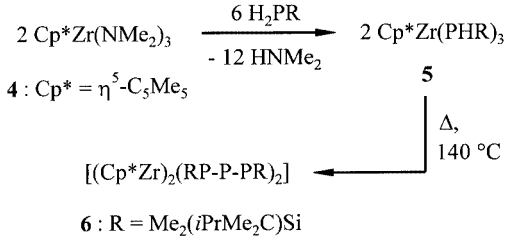

Scheme 2

This compound can be isolated in the form of a red-brown oil in quantitative yield and has been characterized by its ^{1}H and ^{31}P NMR spectra and mass spectrum. Its temperature-independent ^{31}P NMR spectrum shows a shielded ^{31}P nucleus at δ = −173.5 [$^1J_{P,H}$ = 182.4 Hz] with significantly different δ and $^1J_{P,H}$ values compared with $[Cp_2Zr(PHR)_2]$ complexes of type **3** [R = silyl; δ = −51 to −78 ppm, $^1J_{P,H}$ = 204 to 215 Hz].[7,9c] Prolonged heating of a solution of **5** in xylene at 140 °C (four days) furnishes a reaction mixture from which the novel cluster **6** can be isolated by fractional crystallization in 12% yield. The dark green crystals are only sparingly soluble in common organic solvents. Its temperature-invariable ^{31}P NMR spectrum shows an AA′BB′CC′ spin system of higher order which is in accordance with an identical chelating coordination mode of both [RP−P−PR] ligands toward the Zr centers. Since the appearance of the spectrum remains unchanged in polar solvents (THF, DMF) even at low temperature, there is no indication for a dissociation process in solution. However, the structure of **6** could only be established by an X-ray diffraction analysis. This revealed a Zr_2P_6 cluster core with a center of symmetry as a characteristic structural mo-

tif, which can be simply described as a dimer of two butterfly-like ZrP_3 frameworks (Figure 2).

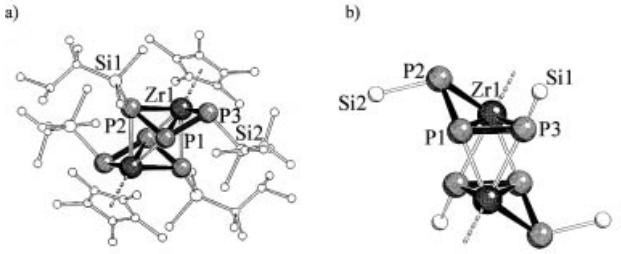

Figure 2. a) Molecular structure of **6**; hydrogen atoms are omitted for clarity; selected distances [Å] and angles [°]: Zr1−P1 2.731(3), Zr1−P2 2.665(3), Zr1−P3 2.593(3), Zr1−P1A 2.617(3), Zr1−P2A 2.796(3), P1−P3 2.175(4), P1−P2 2.184(4), P3−Si2 2.267(4), P2−Si1 2.284(4); P3−Zr1−P2 83.05(9), P3−Zr1−P1 48.14(8), P2−Zr1−P1 47.73(9), P1−P3−Zr1 69.2(1), P3−P1−Zr1 64.57(9), P2−P1−P3 106.2(1); b) view along the distorted octahedral connection between the two hypothetical ZrP_3 halves in **6**; organo groups are omitted for clarity

The hypothetical ZrP_3 halves have a distorted octahedral geometry and are connected to each other through the two Zr1−P1−P3 and Zr1A−P1A−P3A triangular faces (see Figure 2b), which leads to significantly different Zr−P distances between the ZrP_3 moieties [Zr1−P2A 2.796(3) Å, Zr1−P1A 2.617(3) Å]. However, the Zr−P distances within the butterfly-like ZrP_3 framework are also quite different: the Zr1−P1 distance of the bridgehead bond [2.731(3) Å] is, as expected, longer than the Zr1−P2 [2.665(3) and Zr1−P3 bonds [2.593(3) Å], due to ring strain. Apparently, a stabilization of the hypothetical ZrP_3 halves is achieved by the formation of Zr,P,P multiple-center bonds and the closing of vacant coordination sites at the Zr atom. While the P1 atom is substituent-free, the P2 and P3 atoms bear terminal silyl groups, which are *exo*,*endo* configured with respect to the hypothetical ZrP_3 butterfly-like framework. The almost equal P-P distances in the ZrP_3 halves [2.175(4) and 2.184(4) Å] lie between the values observed in the related complexes **A** (2.10 Å)[10] and **B** (2.24 Å) shown in

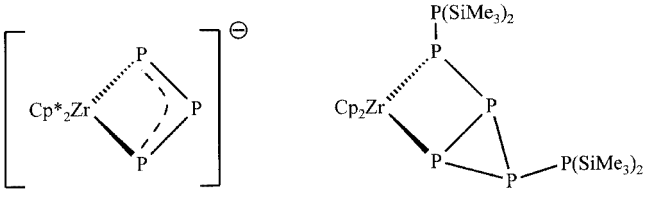

A : Cp* = η^5-C_5Me_5 **B** : Cp = η^5-C_5H_5

Scheme 3

Scheme 3,[11] and they imply, in contrast to the electronic situation in **A**, no contribution of stabilizing P-P π-interactions in the R_2P_3 ligand. The geometric features suggest that **6** is the first zirconium oligophosphanide cluster containing an $[RP-P-PR]^{3-}$ anion. The synthesis of the parent anion $[HP-P-PH]^{3-}$ by reduction of P_4 with alkali metals in liquid ammonia has recently been reported.[12]

Experimental Section

General Remarks: All manipulations were carried out under anaerobic conditions in dry argon using standard Schlenk techniques. Solvents were refluxed over an appropriate drying agent, and distilled and degassed prior to use. NMR spectra were recorded on a Bruker Avance250 spectrometer at ambient temperature operating at 250.1 MHz (^{1}H) and 101.3 MHz (^{31}P). Chemical shifts are reported relative to TMS at 0.00 (^{1}H) and to 85% H_3PO_4 in D_2O at 0.00 (^{31}P). Mass spectra were measured on a Varian MAT CH7 spectrometer. Elemental analyses were performed by the microanalytical service of the department. The starting materials H_2PR [R = Me_2(*i*PrMe$_2$C)Si],[13] [$Zr(NEt_2)_4$] and [Cp*$Zr(NMe_2)_3$] (**4**)[14] were prepared according to literature procedures.

Preparation of 1: [$Zr(NEt_2)_4$] (0.79 g, 2.1 mmol) was added to a solution of **3** (1.21 g, 2.1 mmol) in benzene and refluxed for 8 h. Subsequently, the volatile components of the mixture were evaporated off at 80 °C (10^{-3} Torr), affording the oily red-brown product in pure form according to NMR spectroscopy and EI mass spectrometry. Yield: (1.67 g, 2.07 mmol), 99%. ^{1}H NMR (C_6D_6): δ = 0.53 (d, $^3J_{P,H}$ = 3.7 Hz, 12 H, $SiMe_2$), 1.12 (d, $^3J_{H,H}$ = 6.6 Hz, 12 H, $CHMe_2$), 1.16 (s, 12 H, $SiCMe_2$), 1.98 (t,$^3J_{H,H}$ = 7.4 Hz, 12 H, NCH_2Me), 2.15 (sept., $^3J_{H,H}$ = 6.6 Hz, 2 H, $CHMe_2$), 3.23 (q, $^3J_{H,H}$ = 7.4 Hz, 8 H, NCH_2Me), 5.89 (t, $^3J_{P,H}$ = 1.9 Hz, 10 H, Cp) ppm. ^{31}P NMR (C_6D_6): δ = 287.6 (s) ppm. MS (EI, 70 eV): *m*/*z* (%) = 805 (3) [M^+], 720 (4) [M − (*i*PrMe$_2$C)]$^+$, 65 (100) [Cp^+].

Preparation of 2: A solution of **1** (1.10 g, 1.36 mmol) in xylene was heated at 140 °C for 2 days, affording a deep-brown reaction mixture. After removal of the solvent and other volatile components at 80 °C and 10^{-3} Torr, the resulting residue was taken up in ca. 5 mL hexane. The desired product crystallized after several days at −15 °C in the form of green-brown crystals. Yield: (0.31 g, 0.38 mmol), 28%. ^{1}H NMR (C_6D_6): δ = 0.52 (d, $^3J_{P,H}$ = 3.7 Hz, 12 H, $SiMe_2$), 1.14 (d, $^3J_{H,H}$ = 6.6 Hz, 12 H, $CHMe_2$), 1.15 (s, 12 H, $SiCMe_2$), 2.04 (t,$^3J_{H,H}$ = 7.4 Hz, 6 H, NCH_2Me), 2.15 (sept., $^3J_{H,H}$ = 6.6 Hz, 2 H, $CHMe_2$), 3.31 (q, $^3J_{H,H}$ = 7.4 Hz, 4 H, NCH_2Me), 5.89 (t, $^3J_{P,H}$ = 2.0 Hz, 5 H, Cp), 5.92 (t, $^3J_{P,H}$ = 1.8 Hz, 5 H), 5.97 (t, $^3J_{P,H}$ = 1.1 Hz, 5 H, Cp) ppm. ^{31}P NMR (C_6D_6): δ = 273.8 (s) ppm. MS (EI, 70 eV): *m*/*z* (%) = 720 (4) [M − (*i*PrMe$_2$C)]$^+$, 648(8) [M − (*i*PrMe$_2$C) − NEt_2]$^+$, 65 (80) [Cp^+], 29 (100) [Et^+]. correct C, H-combustion analysis: $C_{35}H_{63}NP_2Si_2Zr_2$ (798.4): calcd. C 52.65, H 7.95; found C 51.98, H 7.90.

Preparation of 3: A solution of LiP(H)R [R = Me_2(*i*PrMe$_2$C)Si] (6.8 mmol) in 20 mL toluene, freshly prepared from H_2PR (1.20 g, 6.8 mmol) and 4.26 mL of a 1.6 M solution of BuLi in hexane (Aldrich) in 50 mL toluene at 0 °C, was added to a solution of [Cp_2ZrCl_2] (1.0 g, 3.4 mmol) in 50 mL toluene at −70 °C. The reaction mixture was allowed to warm to room temperature within 8 h and then stirred for one day. After filtration, the solvent was removed under reduced pressure affording a solid residue. The latter was redissolved in ca. 20 mL hexane from which the desired product crystallized after a few days in the form of pale red crystals. Yield: (1.38 g, 2.41 mmol), 71%. ^{1}H NMR (C_6D_6): δ = 0.54 (s, 12 H, $SiMe_2$), 1.12 (d, $^3J_{H,H}$ = 6.6 Hz, 12 H, $CHMe_2$), 1.14 (s, 12 H, $SiCMe_2$), 2.12 (sept., $^3J_{H,H}$ = 6.6 Hz, 2 H, $CHMe_2$), 2.61 (d $^1J_{P,H}$ = 214 Hz, 2 H, PH,), 5.93 (s, 10 H, Cp) ppm. ^{31}P NMR (C_6D_6): δ = −51.0 (d, $^1J_{P,H}$ = 214 Hz) ppm. MS (EI, 70 eV): *m*/*z* (%) = 394 (9) [M − PH(*i*PrMe$_2$C)$SiMe_2$]$^+$, 143 (98) [*i*PrMe$_2$C)$SiMe_2$]$^+$. Correct C, H combustion analysis: $C_{26}H_{50}P_2Si_2Zr$ (572.0): calcd. C 54.59, H 8.81; found C 54.12, H 8.80.

Preparation of 5: A solution of **4** (1.72 g, 5.24 mmol) in 50 mL toluene was treated with H_2PR [R = Me_2(*i*PrMe$_2$C)Si] (2.76 g,

15.72 mmol) and refluxed at 110 °C for 3 h, resulting in an clear dark solution. After removal of all volatile components at ca. 60 °C and 10^{-3} Torr, the oily red-brown product was isolated in practically quantitative yield. Yield: (3.94 g, 5.23 mmol), 99.8%. ^{1}H NMR (C_6D_6): δ = 0.56 (s, 18 H, $SiMe_2$), 1.14 (d, $^3J_{H,H}$ = 6.6 Hz, 18 H, $CHMe_2$), 1.15 (s, 18 H, $SiCMe_2$), 1.87 (m, $^1J_{P,H}$ = 182.4 Hz, 3 H, PH), 2.13 (sept., $^3J_{H,H}$ = 6.6 Hz, 3 H, $CHMe_2$), 2.22 (s, 15 H, C_5Me_5) ppm. ^{31}P NMR (C_6D_6): δ = −173.5 (d, $^1J_{P,H}$ = 182 Hz) ppm. MS (EI, 70 eV): *m*/*z* (%) = 752 (3) [M^+], 577 (5)[M − PH(*i*PrMe$_2$C)SiMe$_2$]$^+$, 143 (98) [*i*PrMe$_2$C)SiMe$_2$]$^+$, 73 (100) [$SiMe_3^+$].

Preparation of 6: A red-brown solution of **5** (1.36 g, 1.8 mmol) in 10 mL xylene was heated at 140 °C for three days, affording a dark green solution. After removal of all volatile components under vacuum (10^{-3} Torr) at a maximum of 100 °C (oil bath), the solid residue was redissolved in ca. 10 mL hexane, from which dark green crystals precipitated after six days. Yield: (0.26 g, 0.21 mmol), 12%. ^{1}H NMR (C_6D_6): δ = 0.52 (s, 12 H, $SiMe_2$), 0.54 (s, 12 H, $SiMe_2$), 1.11 (d, $^3J_{H,H}$ = 6.6 Hz, 12 H, $CHMe_2$), 1.13 (d, $^3J_{H,H}$ = 6.6 Hz, 12 H, $CHMe_2$), 1.16 (br. s, 24 H, $SiCMe_2$), 2.15 (br. m, 4 H, $CHMe_2$), 2.05 (s, 30 H, C_5Me_5) ppm. ^{31}P NMR (C_6D_6, assignment according to $[RP_A-P_B-P_CR]_2$ and simulations [16]): $\delta(P_A)$ = −123.0 (m, $^1J_{P_A,P_B}$ = 374, $^2J_{P_A,P_C}$ = 68 Hz), $J_{P_A,P_{A'}}$ = 23.0, $J_{P_A,P_{B'}}$ = 3.0, $J_{P_A,P_{C'}}$ = 2.5 Hz; other long-range couplings = 0), δ_{P_B} = −62.6 (m, $^1J_{P_B,P_A}$ = 374, $^1J_{P_B,P_C}$ = 269, $J_{(P_B,P_{B'}}$ = 8.6, $J_{P_B,P_{A'}}$ = 3.0 Hz; other long-range couplings = 0), δ_{P_C} = −85.4 (m, $^1J_{P_C,P_B}$ = 269, $^2J_{P_C,P_A}$ = 68, $J_{P_C,P_{C'}}$ = 4.9, $J_{P_C,P_{A'}}$ = 2.5 Hz; other long-range couplings = 0). Correct C, H combustion analysis: $C_{52}H_{106}P_6Si_4Zr_2$ (1212.0): calcd. C 51.53, H 8.81; found C 51.12, H 8.76.

X-ray Crystallographic Study

1: Triclinic, space group $P\bar{1}$, a = 10.1276(18), b = 21.453(5), c = 17.066(3) Å, α = 83.016(9)°, β = 73.063(9)°, γ = 83.157(9)°, V = 2007.2(4) Å^3, 5230 independent reflections [$I > 2\sigma(I)$], 349 parameters, $R1$ = 0.0823 (observed reflections), $wR2$ = 0.1951 (all data).

6: Monoclinic, space group $P2_1/c$, a = 11.719(8), b = 12.861(9), c = 20.817(14) Å, β = 90.643(15)° Volume = 3137(4) Å^3, 4024 independent reflections [$I > 2\sigma(I)$], 281 parameters, $R1$ = 0.0843 (observed reflections), $wR2$ = 0.2390 (all data).

The intensities were measured with a Bruker-axs-SMART diffractometer. (Mo-K_α radiation, λ = 0.71707 Å, ω-scan, The structures were solved by direct methods (SHELXS 97). Refinements were carried out with the SHELXL-97 package.[16] All non-hydrogen atoms were refined with anisotropic temperature factors. The hydrogen atoms were placed in calculated positions and refined isotropically in riding mode. All refinements were made by full-matrix least-squares on F^2.

CCDC-158194 (**1**) and -158195 (**6**) contain the supplementary crystallographic data for this paper. These data can be obtained free of charge at www.ccdc.cam.ac.uk/conts/retrieving.html [or from the Cambridge Crystallographic Data Centre, 12, Union Road, Cambridge CB2 1EZ, UK; fax: (internat.) +44-1223/336-033; E-mail: deposit@ccdc.cam.ac.uk].

Acknowledgments

We are grateful to the Deutsche Forschungsgemeinschaft, the Fonds der Chemischen Industrie and the Ministry of Science and Education of Nordrhein-Westfalen for financial support.

[1] K. Issleib, H. Häckert, *Z. Naturforsch., Teil B* **1966**, *21*, 519−521.
[2] Review: E. Hey-Hawkins, *Chem. Rev.* **1994**, *94*, 1661−1717; T. L. Breen, D. W. Stephan, *J. Am. Chem. Soc.* **1995**, *117*, 11914−11921.
[3] [3a] P. Binger, in *Multiple Bonds and Low Coordination in Phosphorus Chemistry* (Eds.: M. Regitz, O. J. Scherer), Thieme, New York, **1990**, p. 90. [3b] P. Binger, B. Biedenbach, A. T. Herrmann, F. Langhauser, P. Betz, R. Goddard, C. Krüger, *Chem. Ber.* **1990**, *123*, 1617−1623. [3c] T. Wettling, B. Geissler, R. Schneider, S. Barth, P. Binger, M. Regitz, *Angew. Chem.* **1992**, *104*, 761−762; *Angew. Chem. Int. Ed. Engl.* **1992**, *31*, 758−759.
[4] [4a] O. J. Scherer, M. Swarowsky, H. Swarowsky, G. Wolmershäuser, *Angew. Chem.* **1988**, *100*, 738−739; *Angew. Chem. Int. Ed. Engl.* **1988**, *27*, 694−695. [4b] O. J. Scherer, *Angew. Chem.* **1990**, *102*, 1137−1155; *Angew. Chem. Int. Ed. Engl.* **1990**, *29*, 1104−1122. [4c] O. J. Scherer, *Acc. Chem. Res.* **1999**, *32*, 751−762. [4d] K. H. Whitmire, *Adv. Organomet. Chem.* **1998**, *42*, 1−145.
[5] Review: D. W. Stephan, *Angew. Chem.* **2000**, *112*, 322−338; *Angew. Chem. Int. Ed.* **2000**, *39*, 314−328.
[6] [6a] F. Lindenberg, E. Hey-Hawkins, G. Baum, *Z. Naturforsch., Teil B* **1995**, *50*, 1359−1361. [6b] S. R. Wade, M. G. H. Wallbridge, G. R. Willey, *J. Chem. Soc., Dalton Trans.* **1983**, 2555−2559.
[7] [7a] F. Lindenberg, E. Hey-Hawkins, *J. Organomet. Chem.* **1992**, *435*, 291−297. [7b] E. Hey-Hawkins, S. Kurz, *J. Organomet. Chem.* **1994**, *479*, 125−133. [7c] Z. Hou, T. L. Breen, D. W. Stephan, *Organometallics* **1993**, *12*, 3158−3167. [7d] B. L. Benac, R. A. Jones, *Polyhedron* **1989**, *8*, 1774−1777.
[8] [8a] T. L. Breen, D. W. Stephan, *Organometallics* **1996**, *15*, 4509−4514. [8b] J. Ho, D. W. Stephan, *Organometallics* **1991**, *10*, 3001−3003. [8c] J. Ho, Z. Hou, R. J. Drake, D. W. Stephan, *Organometallics* **1993**, *12*, 3145−3157.
[9] [9a] M. Y. Chiang, S. Gambarotta, F. van Bolhuis, *Organometallics* **1988**, *7*, 1864−1865. [9b] E. Hey, S. G. Bott, J. L. Atwood, *Chem. Ber.* **1988**, *121*, 561−563. [9c] J. Aust, PhD Thesis, Ruhr-Universität Bochum, **2000**.
[10] [10a] M. C. Fermin, J. Ho, D. W. Stephan, *Organometallics* **1995**, *14*, 4247−4256. [10b] M. C. Fermin, J. Ho, D. W. Stephan, *J. Am. Chem. Soc.* **1994**, *116*, 6033−6034.
[11] E. Hey, M. F. Lappert, J. L. Atwood, S. Bott, *J. Chem. Soc., Chem. Commun.* **1987**, 597−598.
[12] N. Korber, J. Aschenbrenner, *J. Chem. Soc., Dalton Trans.* **2001**, 1165−1166.
[13] O. Scherer, R. Mergner, *J. Organomet. Chem.* **1972**, *40*, C64−C66.
[14] D. C. Bradley, I. M. Thomas, *J. Chem. Soc.* **1960**, 3857−3861.
[15] Perch, Version 1/96, University of Kuopio (Finland).
[16] G. M. Sheldrick, SHELXTL-97, University of Göttingen, **1997**.

Received June 18, 2002
[I02321]

Synthesis and Characterization of a Dinuclear Manganese(III,III) Complex with Three Phenolate Ligands

Reiner Lomoth,[a] Ping Huang,[b] Jiutian Zheng,[c] Licheng Sun,*[c] Leif Hammarström,*[a] Björn Åkermark,[c] and Stenbjörn Styring*[b]

Keywords: Manganese / Ligand design / Redox chemistry

A dinuclear manganese complex ($[Mn_2L(\mu\text{-}OAc)_2]PF_6$) has been synthesized, where L is the trianion of 2,6-bis{[(2-hydroxy-3,5-di-*tert*-butylbenzyl)(2-pyridylmethyl)amino]-methyl}-4-methylphenol, a ligand with three phenolate groups. The two pseudo-octahedrally coordinated Mn ions are bridged via the two bidentate acetate ligands and the 4-methylphenolate group of the ligand. We have characterized the complex with electrochemistry, spectroelectrochemistry and EPR spectroscopy. Electrochemically the $Mn_2^{III,III}$ complex undergoes two metal-centered quasi-reversible one-electron reduction steps ($E_{1/2}$ = 0.04 and −0.32 V vs. SCE). Reduction to the $Mn_2^{II,III}$ state results in transformation into a modified complex with slightly different redox properties. One-electron oxidation ($E_{1/2}$ = 0.96 V vs. SCE) affords the $Mn_2^{III,IV}$ state while further one-electron oxidation ($E_{1/2}$ = 1.13 V vs. SCE) presumably involves ligand oxidation. High valent Mn complexes involving Mn^{IV} or Mn^{V} centers are of particular interest as intermediates in catalytic water oxidation. The redox potentials of $[Mn_2L(\mu\text{-}OAc)_2]^+$ show the expected stabilization of higher manganese oxidation states compared with the related complex, $[Mn_2(bpmp)(\mu\text{-}OAc)_2]^+$.

(© Wiley-VCH Verlag GmbH, 69451 Weinheim, Germany, 2002)

Introduction

A major reason for the interest in higher valent multinuclear manganese complexes is the catalytic activity of the $(Mn)_4$ cluster in photosynthetic water oxidation.[1] This is a key reaction in nature that provides the electrons needed for the reduction of CO_2 resulting in energy rich reduced carbon products. Therefore, synthetic Mn complexes have potential importance for the construction of artificial photosynthetic systems to convert solar energy into fuels.[2] The oxygen evolving center (OEC) in photosynthesis, as well as artificial systems aiming for fuel production by light-induced water splitting, has to involve a catalyst that can store four oxidation equivalents generated by subsequent light-induced one-electron oxidations. Finally the catalyst has to retrieve all four electrons from water since oxidation of water can be accomplished at a reasonable potential (0.82 V vs. NHE at pH 7) only in a four-electron process. In photosynthesis catalytic water oxidation is carried out in Photosystem II by the OEC, an oxo-bridged tetranuclear manganese complex that cycles between five redox states.[1]

In our attempts to mimic the electron transfer reactions on the electron donor side of Photosystem II we have, earlier, studied the light-induced oxidation of manganese complexes sensitized by $[Ru(bpy)_3]^{2+}$ (bpy = 2,2′-bipyridine) and we recently observed the light-induced three-step oxidation of the $Mn_2^{II,II}$ dimer $[Mn_2(bpmp)(\mu\text{-}OAc)_2]^+$ [3] to a $Mn_2^{III,IV}$ dimer in an aqueous/acetonitrile medium.[4]

Although the exact mechanism of photosynthetic water oxidation is not solved, it is clear that some of the steps in the cyclic redox reactions (the so called S-cycle) involve Mn-centered oxidations.[5] It is also clear that the Mn ions in the higher oxidation states of the S-cycle are at the Mn^{III} state or higher. A $Mn^{V}{=}O$ moiety has been proposed to play a key-role in O−O bond formation in both photosynthesis[6] as well as in a model complex.[7] With regard to the importance of high-valent manganese species for catalytic water oxidation, we have commenced with the synthesis of manganese complexes with an increased number of negatively charged ligand functions to stabilize higher oxidation states of manganese. In this paper we on report the synthesis and characterization of complex **4**, which is the $Mn_2^{III,III}$ dimer $[Mn_2L(\mu\text{-}OAc)_2]^+$, where L is the trianion of 2,6-bis{[(2-hydroxy-3,5-di-*tert*-butylbenzyl)(2-pyridylmethyl)amino]methyl}-4-methylphenol. The complex con-

[a] Department of Physical Chemistry, Uppsala University, P. O. Box 532, 751 21 Uppsala, Sweden
Fax: (internat.) + 46-18/508542
E-mail: Leifh@fki.uu.se
[b] Department of Biochemistry, Center for Chemistry and Chemical Engineering, Lund University, P. O. Box 124, 221 00 Lund, Sweden
Fax: (internat.) + 46-46/2224534
E-mail: stenbjorn.styring@biokem.lu.se
[c] Department of Organic Chemistry, Arrhenius Laboratories, Stockholm University, 106 91 Stockholm, Sweden
Fax: (internat.) + 46-8154908
E-mail: licheng.sun@organ.su.se
Supporting information for this article is available on the WWW under http://www.eurjic.org or from the author.

tains a bridging phenolate and two additional phenolate groups that replace two of the pyridyl groups in the $[Mn_2(bpmp)(\mu\text{-}OAc)_2]^+$ complex resulting in considerably lowered redox potentials for the manganese redox couples. Thus, the high valent Mn states that are of interest for water oxidation may also be accessible with photochemical oxidation, using photo-oxidants such as $[Ru(bpy)_3]^{2+}$.

Results and Discussion

Synthesis

A ligand similar to the one used here has been employed for the preparation of $Fe_2^{II,III}$ and $Fe_2^{III,III}$ complexes[8] but no Mn dimer with this type of $(N_2O_2)_2$-μ-O compartmental ligand has been prepared. We have introduced *tert*-butyl substituents on the phenol groups of the ligand to increase their electron donating effect and to improve the solubility of the complex. Apart from that the *tert*-butyl groups seem to ease the isolation of the Mn complex since we were not able to isolate the analogue Mn complexes with unsubstituted or methyl-substituted phenol groups.

The synthesis of the ligand precursors is shown in Scheme 1. The Schiff base intermediate was made by a condensation reaction of 3,5-di-*tert*-butyl-2-hydroxybenzaldehyde and picolylamine. The reduction of the Schiff base by sodium hydroborate gave the secondary amine **1**. 2,6-dichloromethyl-4-methylphenol **2** was synthesized by reaction of 2,6-dihydroxy-4-methylphenol, which was prepared by the procedure shown in Scheme 1 (see b).

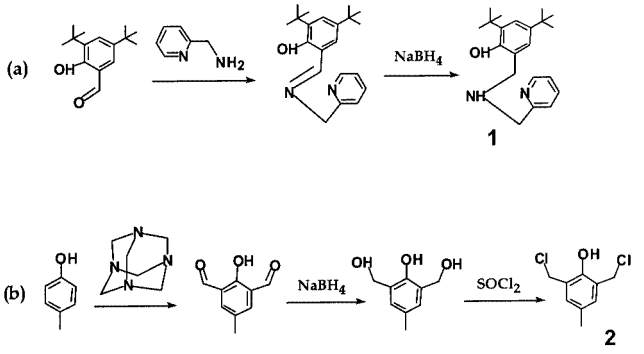

Scheme 1

Two different routes have been used to synthesize the ligand **3** in reasonable yields (Scheme 2). In route A, the secondary amine **1** was reacted directly with *p*-cresol and paraformaldehyde in a modified Mannich reaction in an ethanol/water mixture. Alternatively, **3** was obtained from the reaction of the secondary amine **1** and 2,6-dichloromethyl-4-methylphenol **2** according to route B.

Reaction of manganese(III) acetate in ethanol with **3** gave the manganese(III,III) dimer complex $[Mn_2L(\mu\text{-}OAc)_2]^+$, **4**, where L is the trianion of **3**. Elemental analysis, ESI-MS (see Exp. Sect.), electrochemistry, spectroelectrochemistry, and EPR spectroscopy (see below) were used to characterize the complex. In ESI-MS spectra the base peak was attributed to the mono-charged $Mn_2^{III,III}$ dimer complex.

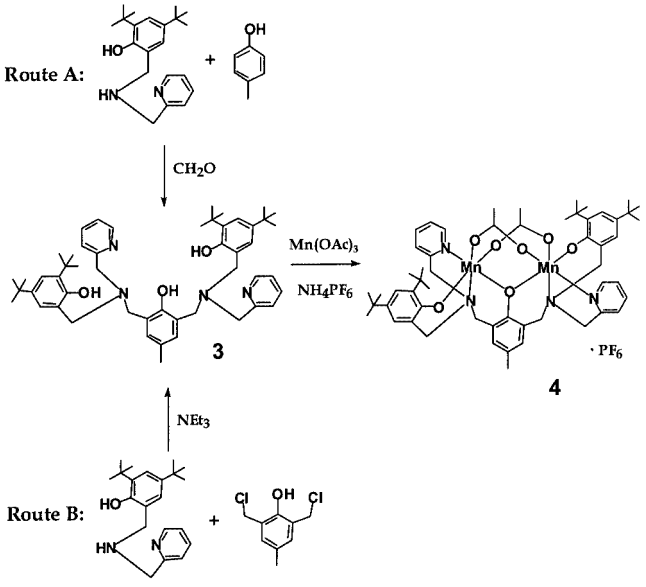

Scheme 2

In addition to the base peak a minor peak at a higher *m*/*z* region was observed that can be assigned to a trace of a $Mn_4^{III,III,III,III}$ tetramer $[\{Mn_2L(\mu\text{-}OAc)_2\}_2(PF_6)]^+$ with one counterion. The tetramer has exactly twice the mass of the dimer, suggesting either a weak association between two structurally intact dimers, or a true tetramer with acetates crossbridging between the dimer units. The tetramer could be formed during the ionization process in ESI-MS, but the fact that these tetramers may have been formed during the synthesis cannot be excluded.

Complex **4** can be expected to exist in two diastereomeric forms with the pyridine nitrogens *syn* or *anti* to the Mn−O(phenolate)−Mn plane. Within the limits of spectral resolution no indication for a mixture of different diastereomers in the preparation of **4** was obtained by any of the spectroscopic methods applied.

Several attempts to crystallize **4** failed.

Spectroscopic and Electrochemical Characterization of 4

We will begin by describing the spectroscopic and electrochemical characterization of **4**. In the following sections we will then describe the characterization of the different products obtained by reduction or oxidation of **4**.

Magnetic Susceptibility Measurements

The molar magnetic susceptibility χ in a powder sample of **4**(PF_6) was measured as a function of temperature between 2 and 300 K. The product χT amounts to 5.34 $cm^3mol^{-1}K$ at 300 K and decreases to 0.21 $cm^3mol^{-1}K$ at 2 K (not shown). The temperature behavior reveals antiferromagnetic coupling between the Mn^{III} sites and the high value of χT at 300 K indicates a weak coupling interaction. The best fit of the data was obtained with a *g*-factor of 1.99

and a fraction of dimer of $F = 0.961$ and resulted in an exchange coupling constant of $J = -8.5$ cm^{-1}. Weak antiferromagnetic coupling with similar values of $-J = 5-8$ cm^{-1} has been reported for other $Mn_2^{II,III}$ and $Mn_2^{II,II}$ complexes with a (μ-phenoxo)bis(μ-acetato) core.[9] No reference data is available for $Mn_2^{III,III}$ complexes with the same bridging structure but the difference between the $Mn_2^{II,III}$ and $Mn_2^{II,II}$ states of $[Mn_2(bpmp)(\mu\text{-}RCOO)_2]^{+/2+}$ [10] is small and similar behavior might be expected for the $Mn_2^{III,III}$ complex **4**, supporting its (μ-phenoxo)bis(μ-acetato) formulation.

EPR Spectroscopy

The perpendicular mode EPR spectrum of **4** is shown in Figure 1 (see c). This spectrum is essentially silent as expected for a $Mn_2^{III,III}$ dimer with an integral spin. Moreover, no signals were detected with parallel mode EPR (not shown). The absence of a parallel mode signal has been interpreted as an indication for antiferromagnetic coupling between two Mn^{III} ions, resulting in an $S = 0$ singlet ground spin state.[11] Magnetic susceptibility measurements of **4** clearly reveal weak antiferromagnetic coupling between the two Mn^{III} ions (see above). Weak multiline signals centered at $g \approx 2$ in the perpendicular mode spectrum (see c in Figure 1) can be assigned to traces of a $Mn_2^{II,III}$ species (ca. 4100−4600 G) and a $Mn_2^{III,IV}$ species (ca. 2900−4000 G) that amount to $< 5\%$ and $< 1\%$ of the total Mn, respectively (for details of the quantification see Exp. Sect.). Thus, the dominating part ($> 94\%$) of the material is an EPR silent $Mn_2^{III,III}$ dimer, as expected. The $Mn_2^{II,III}$ signal probably arises from the reduced state of **4**.

UV/Vis Spectroscopy

Figure 2 shows the electronic spectrum of **4** and its oxidation and reduction products in acetonitrile. On the basis of similarities with the spectra of other Mn complexes and the spectral changes observed upon oxidation and reduction (see below), the following assignments of the electronic transitions are suggested: The UV absorption with the pronounced peak at $\lambda = 260$ nm is observed with the complex as well as with the protonated ligand (not shown). This can be assigned to LC transitions of the aromatic groups, which are only slightly affected in energy and intensity by the oxidation state of the Mn ions. The band at 400 nm ($\varepsilon = 4600$ M^{-1}cm^{-1}) is presumably a CT transition from the bridging phenolate to Mn^{III} that has been observed between 320 and 400 nm with other phenoxo bridged $Mn_2^{II,III}$ and $Mn_2^{III,III}$ complexes.[9] The intensity of this bridging phenolate-Mn^{III} LMCT band has been reported to amount to as much as $\varepsilon = 2100$ M^{-1}cm^{-1} per phenoxo bond.[12] This value is in good agreement with the spectrum of **4** ($\varepsilon = 2300$ M^{-1}cm^{-1} per bridging phenoxo bond). The additional visible absorption might originate from LMCT transitions from other ligands, i.e. the nonbridging phenolate ligands or the pyridyl ligands, and also from a splitting of the metal d-orbitals due to the reduced symmetry of the complex. LF transitions of six-coordinated Mn^{III} complexes can occur in the visible

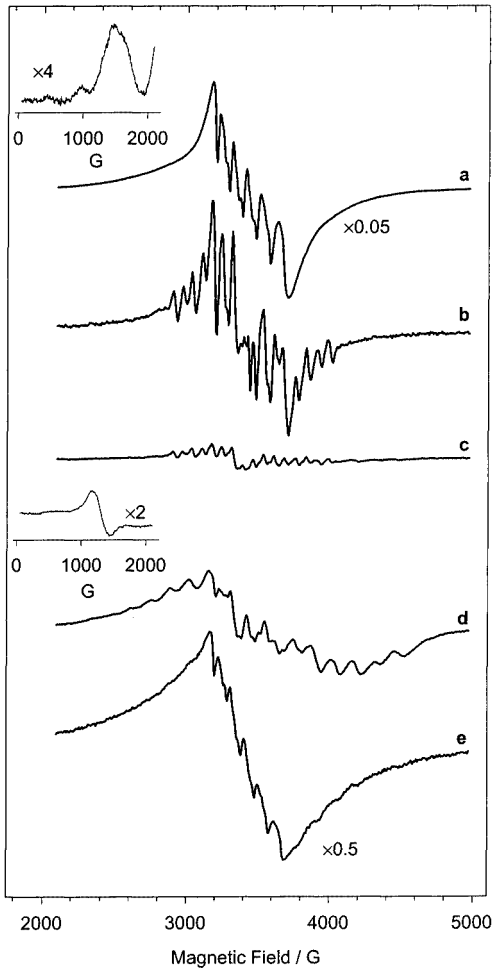

Figure 1. EPR spectra of **4** (1 mm, spectrum c) and its oxidation and reduction products in CH_3CN [0.1 M $N(n\text{-}C_4H_9)_4PF_6$] observed after electrolysis at −0.05 V (d), −0.50 V (e), 0.92 V (b) and 1.25 V (a). EPR parameters. *T*, 4 K; microwave frequency, 9.62 GHz; modulation amplitude, 10 G; microwave power, 3 mW (a, c, d), 0.3 mW (b, e). The spectra are normalized in amplitude (to the same microwave power, number of spectrometer scans, gain etc.) such that their size is approximately similar to facilitate comparison

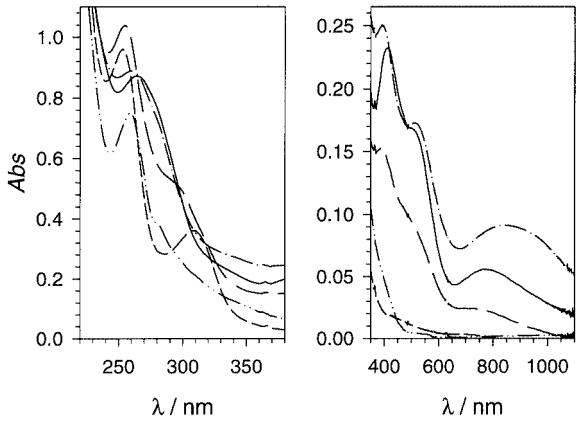

Figure 2. Electronic absorption spectrum of **4** ($5 \cdot 10^{-4}$ M, −) and spectra recorded after electrolysis at −0.05 V (− −), −0.60 V (---), 1.08 V (− · −), and 1.30 V (− · · −) in acetonitrile [0.1 M $N(n\text{-}C_4H_9)_4PF_6$]. $l = 1$ mm

region[13] but are of low intensities (typically $\varepsilon < 500$ $M^{-1}cm^{-1}$ [9a,14]).

IR Spectroscopy

IR spectra of ligand **3** and complex **4** (**4** as PF_6^- salt, see Supplementary Material) were recorded between 4000 and 400 cm^{-1}. Based on characteristic frequencies and comparison with the spectrum of **3,** the following assignments are suggested for the bands observed with **4** in agreement with the composition of the complex: 3082 cm^{-1}(w, ν C−H, aryl); 2954, 2907, 2868 cm^{-1} (s, ν C−H, alkyl); 1579cm^{-1} (s, ν_a C=O, carboxylate); 1605, 1571, 1478 cm^{-1}(m, ν C=C, aryl); 1430 cm^{-1}(m, ν_s C=O, carboxylate); 1384, 1361 cm^{-1} (w, δ C−H, alkyl); 844 cm^{-1}(s, ν_a P−F, PF_6^-); 761, 810 cm^{-1}(m, γ C−H, aryl); 558 cm^{-1} (m, δ P−F, PF_6^-). No assignment could be made for a number of weaker bands at 1247, 1171, 663, 617, 591 cm^{-1} of which the bands at 663 and 591 cm^{-1} were clearly absent in the spectrum of **3** and probably involve metal to ligand modes as ν Mn−O−Mn that were observed between 550 and 750 cm^{-1} with μ-oxo-bis(μ-carboxylato) $Mn^{III,III}$ complexes.[15]

The IR spectrum of **3** shows additional bands at about 3000 cm^{-1} (s, very broad, ν O−H with intramolecular H-bond), 1300 cm^{-1} (m, δ O−H) and 1111 cm^{-1} (m, ν C−O) that are diagnostic for the phenol functions of the ligand. These bands are not observed in the spectrum of **4** providing evidence that all phenol functions are deprotonated and ligated to the metal ions in **4** and that no or very little of the free ligand **3** is present in this preparation of **4**.

The value of Δν between the asymmetric and symmetric C=O stretch modes of the acetate ligands of **4** [$\Delta\nu = (\nu_a$ C=O) − (ν_s C=O) = 149 cm^{-1}], indicates that both acetate ligands are symmetrically bridging the two manganese(III) ions: For monodentate acetate ligands Δν is known to substantially exceed the free ionic value of $\Delta\nu = 164$ cm^{-1}, and for chelating acetate ligands Δν is usually smaller than the value observed with **4**.[16] Asymmetrically bridging carboxylates have been reported to show a greater Δν, similar to monodentate ligands.[17]

Electrochemistry

Cyclic and differential pulse voltammograms of **4** are shown in Figures 3 and 4 and the electrochemical data are summarized in Table 1. All potentials are reported vs. SCE (see Exp. Sect.). The cyclic voltammograms (see a in Figure 3) show two major quasi-reversible reduction waves labeled (1) and (2) and two almost merged oxidation waves labeled (3) and (4) that cannot be fully resolved even in differential pulse voltammetry (see b in Figure 3). A small reverse peak for the first oxidation is already observed with the low sweep rates (10 $mV{\cdot}s^{-1}$, not shown) but the minor reverse peak for the second oxidation only appears at higher sweep rates (≥ 500 $mV{\cdot}s^{-1}$). The one-electron nature of the reductions was confirmed coulometrically. Separate coulometric measurements on the individual oxidations are impeded by the small potential separation but the two oxidations correspond to two electrons in total.

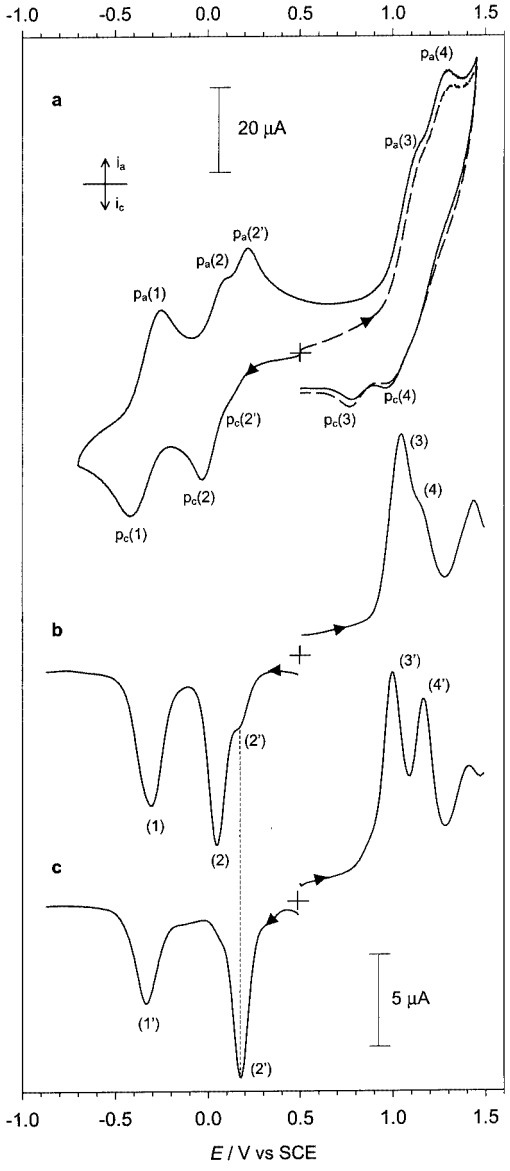

Figure 3. Cyclic voltammograms ($v = 500$ $mV{\cdot}s^{-1}$) (a) and differential pulse voltammogram (b) of **4** (1 mM) in acetonitrile (0.1 M $N(n\text{-}C_4H_9)_4PF_6$). Differential pulse voltammogram of a solution of **4** after exhaustive electrolysis at −0.10 V (c). Arrows indicate scanning direction

The minor quasi-reversible reduction wave (2′) in the cyclic voltammograms, that appears as a shoulder of the first reduction peak (2) in the differential pulse voltammogram (see b in Figure 3), is assigned to a different complex **4′** that is initially present, to a small extent, but is subsequently formed upon one-electron reduction of **4**. Evidence for this assignment comes from voltammograms observed immediately after exhaustive reduction of **4** at −0.10 V showing that the peak for the first reduction has shifted completely from $E(2)$ to $E(2')$ (compare b and c in Figure 3). A corresponding shift is observed for the re-oxidation peak when starting from the reduced complex. The conversion is quantitative (> 95%) as judged from the disappearance of the initial reduction peak (2) of **4**.

Table 1. Electrochemical data in acetonitrile

Complex	$E_{1/2}$ /V[a] (ΔE_p/mV)[b]			
	1	**2**	**3**	**4**
	$Mn_2^{II,III}/Mn_2^{II,II}$	$Mn_2^{III,III}/Mn_2^{II,III}$	$Mn_2^{III,IV}/Mn_2^{III,III}$	[c]
4[d]	−0.32 (140)	0.04 (130)	0.96 (360)	1.13 (340)
4′[d]	−0.34 (275)	0.17 (90)	0.95 (300)	1.13 (300)
$[Mn_2(bpmp)(\mu\text{-}OAc)_2]^{+}$ [e]	0.50 (70[f])	1.06 (120[f])	−[g]	−

[a] From cyclic voltammetry in CH_3CN, ±0.03 V. [b] v = 500 mV·s^{-1}. [c] The final oxidation product is a monomeric Mn^{II} or possibly Mn^{IV} complex. [d] As PF_6^- salt with 0.1 M $N(n\text{-}C_4H_9)_4PF_6$ as supporting electrolyte. [e] As ClO_4^- salt with 0.1 M $N(n\text{-}C_4H_9)_4ClO_4$ as supporting electrolyte. [f] v = 100 mV·s^{-1}. [g] No oxidation to the $Mn_2^{III,IV}$ state in CH_3CN.

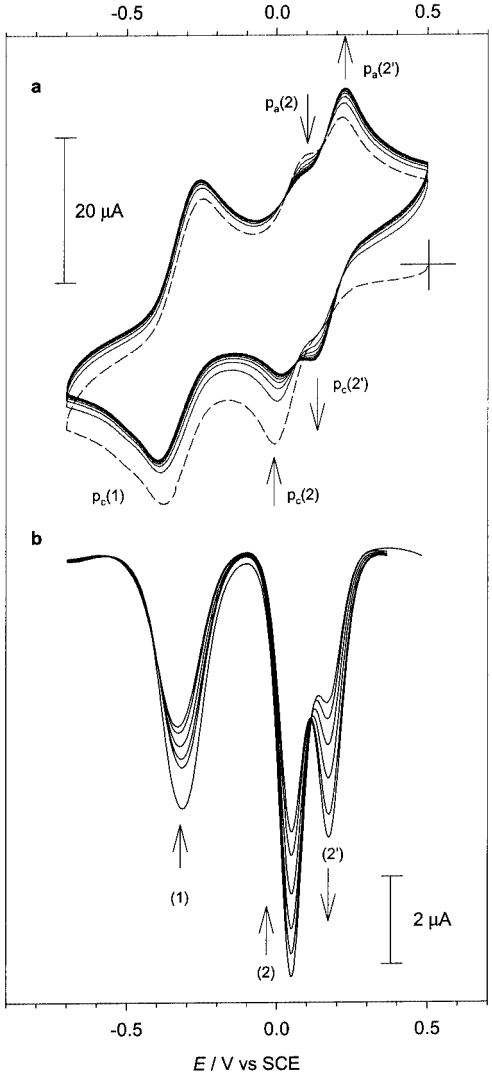

Figure 4. Voltammograms of **4** (1 mm) in acetonitrile [0.1 M $N(n\text{-}C_4H_9)_4PF_6$]. a) Cyclic voltammograms (v = 500 mV·s^{-1}). Scan 1 (- - -) and scans 2 to 10 (−). Arrows indicate the effect of increasing number of scans. b) Differential pulse voltammograms after increasing duration (0, 2, 5, 10, 20, 50 s) of pre-electrolysis at −0.10 V. Arrows indicate the effect of increasing pre-electrolysis time

A set of subsequent cyclic voltammograms of **4** (see a in Figure 4) shows how the reduction wave of **4′** grows with the expense of the reduction wave of **4**, as indicated by the arrows.

The same transformation was followed by differential pulse voltammograms (see b in Figure 4) recorded with increasing time of pre-electrolysis at −0.10 V, providing further evidence that the transformation to **4′** occurs in the one-electron reduced state of **4**.

The effect of this transformation on the potential for the first reduction is $\Delta E_{1/2}$ = 130 mV, while the effect on the second reduction (at −0.3 V) and the two oxidations (around 1 V) is comparatively small ($|\Delta E_{1/2}| \leq 0.05$ V) (see c in Figures 3, 4, Table 1).

The two reductions of both **4** and **4′** exhibit quasi-reversible CV waves (see a in Figure 4) but they are not reversible on the longer time-scale of the bulk electrolysis experiments (see below). For the oxidations of **4′** only small cathodic counter-peaks at $E_{pc}(3')$ = 0.80 V and $E_{pc}(4')$ = 0.98 V are observed on the reverse scan of the cyclic voltammograms (500 mV·s^{-1}, not shown) recorded after exhaustive electrolysis of **4** at −0.10 V. **4′** is unstable in its initial reduced state since well-defined voltammograms of **4′** were obtained only a few minutes after reduction of **4**. This will presumably impede isolation of **4′**. However, spectroscopic characterization of the reduced states of **4′** could be made immediately after reduction of **4**. (see below).

According to its EPR spectrum (see below) **4′** in its one-electron reduced state is a magnetically coupled $Mn_2^{II,III}$ dimer, the exact structure of which we cannot elucidate from our data. The loss of an acetate bridge from **4** as a charge compensating reaction due to reduction of the complex could explain the potential shift of the first reduction. However, with the loss of a negatively charged ligand a larger shift of *all* metal centered reduction and oxidation processes towards higher potentials would be expected. Therefore we suggest that the transformation of **4** into **4′** might instead represent a geometric re-arrangement of the reduced complex rather than loss or exchange of ligands.

Spectroscopic Characterization of the Reduced and Oxidized Products of 4

The products of the two reduction and the two-oxidation processes have been characterized by UV/Vis-spectroelectrochemistry and by EPR spectroscopy on samples prepared by electrolysis of **4** at appropriate potentials. Exhaustive electrolysis in the spectroelectrochemical experiments as well as for preparation of EPR samples occurs on

the time-scale of minutes, i.e. the species observed by these techniques upon *reduction* will be the reduction products of **4′**. The results of these experiments are discussed in the following paragraphs.

First Reduction

The first one-electron reduction of **4** can be assigned to a metal centered process [Equation (1)] resulting in a $Mn_2^{II,III}$ complex as evidenced by EPR spectroscopy.

$$[Mn_2^{III,III}L(\mu\text{-}OAc)_2]^+ + e^- \rightarrow [Mn_2^{II,III}L(\mu\text{-}OAc)_2] \qquad E_{1/2} = 0.04\ V \qquad (1)$$

The EPR spectrum of, **4** after exhaustive reduction at −0.05 V, displays a partially resolved multiline signal centered at $g \approx 2$ and a weak featureless signal at $g \approx 5.3$ (see d in Figure 1). The $g \approx 2$ multiline signal has a total line width of ca. 2300 G. The hyperfine lines are clearly visible but they are somewhat broadened. The relative amplitude of the $g \approx 2$ signal decreases while the $g \approx 5.3$ signal increases with increased temperature (not shown). This indicates that the $g \approx 2$ signal originates from a ground spin state while the $g \approx 5.3$ signal originates from an excited spin state. Similar overall behavior has been reported earlier for the EPR signals from $[Mn_2^{II,III}(bpmp)(\mu\text{-}OAc)_2]^{2+}$ [18], that is weakly antiferromagnetically coupled with a ground spin state $S = {}^1/_2$. In $[Mn_2^{II,III}(bpmp)(\mu\text{-}OAc)_2]^{2+}$ a featureless signal at $g \approx 5.4$ became detectable only above 7.5 K, while the multiline signal centered at $g \approx 2$ dominated at 4 K. In our case, however, the appearance of the relatively large $g \approx 5.3$ signal together with the $g \approx 2$ multiline signal already at 4 K, indicates that the excited spin state is lower in energy than in $[Mn_2^{II,III}(bpmp)(\mu\text{-}OAc)_2]^{2+}$. There are no parallel mode EPR signals of this sample (not shown), which is expected for an $S = {}^1/_2$ system. From EPR spectroscopy we therefore conclude that one electron reduction of **4** gives a weakly antiferromagnetically coupled $Mn_2^{II,III}$ species.

This assignment is in agreement with the spectrophotometrical changes observed during electrolysis at −0.05 V (Figure 2, − −): Upon the first reduction of **4** about half of the visible absorption disappears. Absorption at $\lambda >$ 400 nm has been assigned to the Mn^{III} subunit in the mixed valence $Mn_2^{II,III}$ state[9a] of the similar phenoxo bridged dinuclear manganese complex $[Mn_2(bpmp)(\mu\text{-}OAc)_2]^{2+}$. Therefore, the electronic spectrum corroborates the assignment of the first cathodic process to the formation of a $Mn^{II,III}$ complex. Several isosbestic points are observed in the course of the first reduction (not shown). This suggests that the structural changes of the reduced complex, that lead to the formation of **4′**, as indicated by voltammetry (see above), do not affect the absorption spectrum. Thus, they have a negligible effect on the phenolate to Mn^{III} CT transitions in the visible region and the ligand centered transitions in the UV part of the electronic spectrum.

Re-oxidation of the one-electron reduction product by bulk electrolysis was carried out at 0.60 V after exhaustive reduction at −0.05 V. According to coulometry only 55% of the material could be re-oxidized pointing to a limited stability of the one-electron reduction product. This is supported by the EPR spectrum of the re-oxidized sample (not shown) that can be assigned to uncoupled Mn^{II}, presumably from decomposition of the reduced complex, while the re-oxidized $Mn_2^{III,III}$ species can be expected to be EPR-silent. Note that the time-scale of bulk electrolysis is several minutes, which is much longer than that for the voltammetry experiments (Figures 3 and 4, and above).

Second Reduction

Further one-electron reduction of the $Mn_2^{II,III}$ complex at −0.50 V probably gives rise to both a dimeric $Mn_2^{II,II}$ and a monomeric Mn^{II} complex [Equation (2)].

$$[Mn_2^{II,III}L(\mu\text{-}OAc)_2] + e^- \rightarrow [Mn_2^{II,II}L(\mu\text{-}OAc)_2]^- + \text{monomeric } Mn^{II} \text{ species} \qquad E_{1/2} = -0.32\ V \qquad (2)$$

The EPR spectrum shows a broadened 6-line spectrum in the $g \approx 2$ region (see e in Figure 1) that can be assigned to a monomeric Mn^{II} species. Quantification of the EPR signal reveals that about 48% of the complex was found in the monomeric Mn^{II} form after the second reduction. Since all of the $Mn_2^{II,III}$ signals disappeared it is reasonable to assume that the residual 52% of the complex was kept in the $Mn_2^{II,II}$ state after the second reduction.

This is supported by the observation of an EPR spectrum with parallel mode EPR (Figure 5). This featureless spectrum covers the spectral range from 0−3000 G and indicates the presence of a species with integral spin. Monomeric Mn^{II} species with $S = {}^1/_2$ are not expected to give rise to spectra of this kind. To the best of our knowledge there are no literature reports of parallel mode EPR studies for $Mn^{II,II}$ compounds but spectra of this kind cannot be excluded for antiferromagnetically coupled dimers.

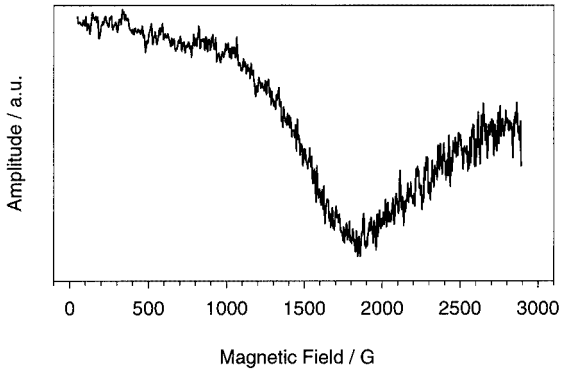

Figure 5. EPR spectrum recorded in parallel mode after bulk electrolysis of **4** at −0.50 V. The spectrum is recorded on the same sample as in Figure 1e. $T = 4$ K; microwave power 16 mW; modulation amplitude 10 G; microwave frequency 9.47 GHz

Reductive degradation of the ligand is unlikely at this potential and presumably a $Mn_2^{II,II}$ complex is formed initially that undergoes some subsequent dissociation reaction giving the monomeric Mn^{II} species observed by EPR.

The assignment of the second reduction to the reduction of Mn^{III} centers to Mn^{II} is in agreement with the spectrophotometric changes: Most of the residual visible absorption of the $Mn_2^{II,III}$ complex disappears upon the second one-electron reduction (Figure 2, ---) as expected from the usually low intensity of MLCT transitions of Mn^{II}. Similar spectral changes have been reported for the reduction of $[Mn_2^{II,III}(bpmp)(\mu\text{-}OAc)_2]^{2+}$ to the $Mn_2^{II,II}$ state.[9a]

First Oxidation

4 can be oxidized in two irreversible one-electron steps that occur very close in potential (Figure 3), making the study of the individual oxidation products of the respective oxidation process more complicated. Still the first oxidation can be assigned to a metal centered process resulting in a $Mn_2^{III,IV}$ dimer [Equation (3)] detected by EPR spectroscopy.

$$[Mn_2^{III,III}L(\mu\text{-}OAc)_2]^{+} \rightarrow [Mn_2^{III,IV}L(\mu\text{-}OAc)_2]^{2+} + e^{-} \qquad E_{1/2} = 0.96\ V \qquad (3)$$

The EPR spectrum in Figure 1 (see b) was observed after partial oxidation of **4** at 0.92 V, i.e. at a potential 40 mV *below* $E_{1/2}$ for the first oxidation. At this potential only a minor fraction of the complex can be expected to be oxidized but further oxidation due to the nearby second anodic process is avoided. The resulting EPR spectrum displays a well-resolved multiline signal (see b in Figure 1). This multiline signal consists of 18−19 lines centered at $g \approx 2$, with an overall line width of 1115 G, and an average hyperfine splitting of ca. 73 G. The spectrum is thus much narrower than that for the one-electron reduced $Mn_2^{II,III}$ product of **4** (see above). A narrow multiline EPR signal of this character (see b in Figure 1) is typical for a $Mn_2^{III,IV}$ dimer that is strongly antiferromagnetically coupled with a resulting spin of $S = {}^1/_2$.[19] Integration of the signal and comparison with a $Mn_2^{III,IV}$ standard (see Exp. Sect.) shows that this multiline spectrum corresponds to about 0.2 mM of $Mn_2^{III,IV}$ after oxidation of a 1 mM solution of **4**. This is similar to the 0.3 charge equivalents determined coulometrically for oxidation of the EPR sample demonstrating that oxidation at 0.92 V is predominantly a metal centered reaction resulting in $Mn_2^{III,IV}$. The multiline signal from the $Mn_2^{III,IV}$ disappeared almost completely (not shown) after re-reduction at 0.50 V. However, for this reduction only 0.04 charge equivalents were consumed, pointing to limited stability of the $Mn_2^{III,IV}$ state. This might also explain that the concentration of $Mn_2^{III,IV}$ after bulk electrolysis is somewhat lower than expected from coulometry.

At higher potentials, such as 1.05 V, electrolysis results in a mixture of oxidation products as the EPR spectra (not shown) are a superposition of a multiline signal from $Mn_2^{III,IV}$ as described above and a 6-line signal that is probably due to monomeric Mn^{II} (see below). Upon re-reduction of this sample at 0.50 V, the multi-line spectrum disappeared while the 6-line spectrum remained, supporting the assignment of the spectra to a $Mn_2^{III,IV}$ complex and Mn^{II}, respectively. Since no 6-line signal was observed upon oxidation at lower potentials, such as 0.92 V (see above), the species giving rise to this signal is presumably a product of the second anodic process.

The spectrophotometrical changes observed upon oxidation of **4** at 1.05 V corroborate the conclusions drawn from the EPR results. The increased absorption in the region 500−1100 nm upon oxidation at 1.08 V (Figure 2, − · −) can be assigned to the $Mn_2^{III,IV}$ complex detected by EPR spectroscopy. Absorption bands observed between 500 and 935 nm have been assigned to phenolate to Mn^{IV} LMCT transitions in Mn^{IV} monomeric complexes[20] as well as $Mn_2^{III,IV}$ and $Mn_2^{IV,IV}$ dimers[21] and bands at $\lambda > 700$ nm have been assigned to intervalence transitions in mixed-valence μ-oxo $Mn_2^{III,IV}$ complexes.[22] Isosbestic points were observed at the outset ($t < 300$ s) of the spectroelectrochemical experiment (not shown). Throughout the course of electrolysis, however, the isosbestic points were not maintained either due to instability of the $Mn_2^{III,IV}$ species or parallel formation of oxidation products from the second oxidation process. This is consistent with the EPR spectroscopic results that show a 6-line spectrum besides the spectrum of the Mn_2III,IV complex after oxidation at this potential (1.05 V).

Second Oxidation

Oxidation at 1.25 V [Equation (4)] gives rise to EPR spectra dominated by a 6-line signal centered at $g \approx 2$ with a hyperfine coupling of ca. 95 G (see a in Figure 1).

$$[Mn_2^{III,IV}L(\mu\text{-}OAc)_2]^{2+} \rightarrow \text{oxidation products} + e^{-} \qquad E_{1/2} = 1.13\ V \qquad (4)$$

The EPR spectrum of the product is identical to the 6-line signal for the sample oxidized at 1.05 V (not shown, see above). A detailed inspection of the lower field region reveals the presence of a very weak signal at g ≈ 4 (inset in Figure 1). The 6-line spectral feature (see a in Figure 1) is very similar to a typical spectrum from monomeric Mn^{II} and we assign this spectrum to Mn^{II}. This assignment is also based on the spectroelectrochemical studies where the complete disappearance of visible and near infrared absorption upon the second oxidation (Figure 2, − · · −) suggests that the second oxidation process generates monomeric Mn^{II} rather than Mn^{IV}, since Mn^{IV} phenolate complexes are known to show intense LMCT transitions in the visible region.[20] Thus, it seems that **4** is degraded during the second oxidation step probably involving ligand oxidation at the relatively high potential that is employed. In the course of the second oxidation isosbestic points are absent (not shown). This is in agreement with a more complicated reaction scheme that possibly involves phenolate ligand oxidation[23] finally resulting in the release of monomeric Mn^{II}.

The very weak EPR signal at $g \approx 4$ might however originate from a trace of Mn^{IV} remaining after the oxidation although the fraction is too small to give a measurable absorption in UV/Vis spectroelectrochemistry (Figure 2). Monomeric Mn^{IV} has been reported to give rise to a 6-line signal around $g \approx 2$, quite similar in shape to the signal

from Mn^{II}, in addition to the weak $g \approx 4$ signal.[20e] It is thus difficult to distinguish Mn^{IV} from Mn^{II} in the $g \approx 2$ region while the $g \approx 4$ region probably is more indicative.

The possible generation of a Mn^{IV} containing state at a high potential in **4** is interesting, although one has to use techniques more rapid than bulk electrolysis to trap and detect it and possibly utilize its oxidative power.

Conclusions

The negative charge of the three phenolate groups in **4** results in a considerable stabilization of higher oxidation states of the Mn ions compared to the case of $[Mn_2(bpmp)(\mu\text{-}OAc)_2]^+$ [9a] that has only one bridging phenoxo group of the bpmp ligand. The stabilization is reflected in the electrochemical potentials summarized in Table 1. The potentials for the $Mn_2^{II,III}/Mn_2^{II,II}$, and $Mn_2^{III,III}/Mn_2^{II,III}$ couples of **4** are lowered by 0.8 and 1.0 V compared with $[Mn_2(bpmp)(\mu\text{-}OAc)_2]^+$, and a third metal centered process attributable to the $Mn_2^{III,IV}/Mn_2^{III,III}$ couple is observed with **4** before oxidative degradation of the complex occurs. With regard to our interest in systems as functional mimics of the water oxidizing complex in Photosystem II, it is worth pointing out that due to the stabilization of high valent Mn states all four of the reported oxidation steps of **4** could be driven with photogenerated $Ru(bpy)_3^{3+}$ ($E_{1/2}$ = 1.32 V). However, accumulation and subsequent use of oxidative equivalents would require a rapid redox cycling in order to outcompete degradation of the less stable states of **4**.

Experimental Section

Materials: Triethylamine and ammonium hexafluorophosphate were purchased from Aldrich and used as received. Silica gel 60 (230−400 mesh) from Merck, Darmstadt, Germany and Aluminum oxide from Aldrich. All solvents were dried by standard methods. 2-aminomethylpyridine was purchased from Lancaster. 3,5-di-*tert*-butyl-2-hydroxybenzaldehyde was purchased from Aldrich and used without further purification.

General Methods: NMR spectra were measured either on Bruker-400 MHz spectrometer for 1D or on a Bruker-500 MHz spectrometer for 2D. The positions of the signals are reported on δ scale in ppm units. The splitting of the signal is described as singlets (s), doublets (d), triplets (t), quadruplets (q), doublets of doublets (dd), or multiplets (m).

The electrospray ionization mass spectrometry (ESI-MS) experiments were performed on a ZacSpec mass spectrometer (VG Analytical, Fisons Instrument). Electrospray conditions were: Needle potential, 3 kV; acceleration voltage, 4 kV; bath and nebulizing gas, nitrogen. The liquid flow was 75 μL per min from a syringe pump (Phoenix 20, Carlo−Erba, Fisons instrument). Solvent, CH_3CN. Accurate mass measurements were obtained by the use of polyethylene glycol (PEG) as an internal standard.

Thin-layer chromatography (TLC) was performed using silica gel (Kieselgel F_{254}) adsorbent.

Column chromatography was performed using silica gel (Kieselgel 60, 0.040−0.063 mm).

Synthesis of *N*-(3,5-Di-*tert*-butyl-2-hydroxy)-*N*-(2-pyridylmethyl)-amine (1): 3,5-di-*tert*-butyl-2-hydroxybenzaldehyde (1.48 g, 6.32 mmol) and picolylamine (0.68 g, 6.32 mmol) were dissolved in MeOH (30 mL) and stirred for 4 hours at 50° C. After cooling to room temperature, $NaBH_4$ (0.34 g, 9 mmol) was added to the solution in small amounts and the solution was stirred for another 4 hours at room temperature. After evaporating the solvent to dryness, the residue was dissolved in CH_2Cl_2 and washed with an aqueous solution of NH_4Cl and dried with Na_2SO_4. 1.20 g (61%) of product was obtained after purification by flash chromatography on silica gel eluting with CH_2Cl_2. ^1H NMR ($CDCl_3$, 400 MHz): δ = 8.58 (d, H-Py); 7.66 (t, H-Py); 7.23 (m, 2 H-Py); 6.84 (d, 2 H-Ph); 3.98 (s, N-CH_2-Py); 3.94 (s, N-CH_2-Ph); 1.43 (s, *tert*-Butyl); 1.28 (s, *tert*-Butyl) ppm.

Synthesis of 2,6-Bis(chloromethyl)-4-methylphenol (2):[24] A solution of 2,6-bis(hydroxymethyl)-4-methylphenol (2.5 g,,15 mmol) in dichloromethane (12.5 mL) was added to a solution of thionyl chloride (7.0 g,60 mmol) in dichloromethane (25 mL). After stirring for 24 hours the mixture was poured over ice (25 mL) and adjusted to pH = 6 with aqueous NaOH. The aqueous solution was extracted with three 25 mL portions of dichloromethane, washed with brine and dried with anhydrous Na_2SO_4. The solution was evaporated to dryness at reduced pressure yielding a pale-yellow solid. By recrystallization from hexane 1.85 g (yield: 60%) of the product was obtained and stored in a freezer. mp: 80° C. ^1H NMR ($CDCl_3$, 400 MHz, ppm): 7.09 (s, 2 H, Ar-H), 4.66 (s, 4 H, Ar-CH_2-Cl), 2.28 (s, 3 H, Ar-CH_3).

Synthesis of 2,6-Bis{[(3,5-di-*tert*-butylbenzyl-2-hydroxy)(2-pyridylmethyl)amino]methyl}-4-methylphenol (3)[25] A solution of (3,5-di-*tert*-butylbenzyl-2-hydroxy)(2-pyridylmethyl)amine (2.1 g, 6.4 mmol) and triethylamine (1.3 g, 13 mmol) in THF (20 mL) was added dropwise to 10 mL of a stirred solution of 2,6-bis(chloromethyl)-4-methylphenol (0.6 g, 3.2 mmol) in THF at 0° C under nitrogen atmosphere. The reaction mixture was stirred for 12 hours at room temperature. Then the solution was filtered to remove the TEA salts, the filtrate was evaporated to dryness and the residue was dissolved in CH_2Cl_2 (80 mL) and washed with brine. The organic phase was dried with anhydrous Na_2SO_4. The product was purified by flash chromatography on silica gel, eluting with CH_2Cl_2. 1.32 g of product was obtained, yield: 52%. ^1H NMR ($CDCl_3$, 400 MHz, ppm): 8.60 (d, H-Py); 7.65 (t, H-Py); 7.31 (d, H-Py); 7.22 (t, H-Ph); 7.16 (d, H-Ph); 6.93 (s, H-Ph); 6.83 (d, H-Ph); 3.83 (s, N−CH_2-Py); 3.78 (s, N−CH_2-Ph); 3.76 (s, N−CH_2-Ph); 2.22 (s, CH_3-Ph); 1.32 (s, *tert*-butyl-Ph); 1.25 (s, *tert*-butyl-Ph).

The Complex of $Mn(OAc)_3(H_2O)_2$ with 2,6-Bis{[(3,5-di-*tert*-butylbenzyl-2-hydroxy)(2-pyridylmethyl)amino]methyl}-4-methylphenol (4):[9a] $Mn(OAc)_3(H_2O)_2$ (95.0 mg, 0.35 mmol) was added to 2,6-bis{[(3,5-di-*tert*-butylbenzyl-2-hydroxy)(2-pyridylmethyl)amino]-methyl}-4-methylphenol (**3**) (135.0 mg, 0.17 mmol) in 85% ethanol (3 mL). The mixture was heated at 50 °C for 30 min and cooled to room temperature. NH_4PF_6 (81 mg, 0.49 mmol) in 85% ethanol (1 mL) was added to the red-brown solution whilst stirring, and the solution was stored in a freezer overnight. The solid was filtered off and washed with 85% ethanol (1.5 mL) at 0° C, H_2O (2 mL) and 99% ethanol (1.5 mL). After drying under vacuum, 151 mg of solid product was obtained. Yield: 86%. ESI-MS: (*m*/*z*): 1009.4 [M − PF_6]$^+$ (calcd. for $C_{55}H_{71}N_4O_7Mn_2$: 1010.06), 2163.8 [2 M − PF_6]$^+$ (calcd. for $C_{110}H_{142}N_8O_{14}F_6PMn_4$: 2165.08); $C_{55}H_{71}F_6Mn_2N_4O_7P$ (1155.02): calcd. C 57.19, H 6.20, N 4.85, Mn 9.51; found C 57.16, H 6.26, N 4.82, Mn 9.44.

Electrochemistry: Cyclic voltammetry, differential pulse voltammetry, and controlled potential electrolysis were performed with an Autolab potentiostat and a GPES electrochemical interface in a 3-electrode cell with the counter electrode separated from the bulk by a fritted disk. The working electrode was a glassy carbon disc (diameter 3 mm) for voltammetry or a platinum grid cylinder (15 mm × 15 mm diameter) for bulk electrolysis, respectively. The reference electrode was a nonaqueous Ag/Ag^+ electrode (10 mM $AgNO_3$ in acetonitrile) of double-junction design. The reference electrode has a potential of −0.08 V vs. the ferrocene/ferrocenium couple in acetonitrile as an external standard. All potentials reported here are vs. the saturated calomel electrode (SCE) and have been converted by adding 0.30 V to the potentials measured vs. the Ag/Ag^+ electrode according to $E_{1/2} = 0.38$ V vs. SCE for the ferrocene/ferrocenium couple.[26]

Electrolyte solutions were prepared from dry acetonitrile (Merck, spectroscopy grade, dried with MS 3 Å) with 0.1 M tetrabutylammonium hexafluorophosphate (Fluka, electrochemical grade, dried at 373 K) as supporting electrolyte. The glassware used was oven dried, assembled and flushed with argon while hot. Before all measurements, the solutions were deoxygenated by bubbling solvent saturated argon through the stirred solutions for 10 minutes. Whilst measuring the samples were kept under an argon atmosphere.

The electrochemical preparation of EPR samples was performed by bulk electrolysis of 1 mm (3 mL) solutions at controlled potentials. The electrolysis was followed by amperometry and coulometry. After electrolysis, samples of 250 μL were taken with an argon filled syringe via a septum from the electrolysis vessel and transferred to argon flushed EPR tubes. The samples were immediately frozen and kept in liquid nitrogen.

UV/Vis Spectroelectrochemistry: Spectroelectrochemical measurements were made in an OTTLE-type quartz cell with an optical path length of 1 mm. A platinum grid of size 10 × 30 mm^2 and 400 meshes per cm^2 was used as working electrode. The counter and reference electrodes were of the same type as described for electrochemistry. Solvent saturated argon was bubbled through samples for 15 min, and they were then transferred to the argon flushed cell with an argon stream. The spectra were recorded on an UV/Vis diode array spectrophotometer (Hewlett Packard 8435).

IR Spectroscopy: IR spectra were recorded on a FT-IR spectrometer (Bruker IFS 66v/S) with the sample as a KBr pellet.

EPR Spectroscopy: All EPR spectra were recorded on a Bruker E580-ELEXSYS spectrometer equipped with an Oxford 900 liquid helium cryostat and an ITC 503 temperature controller. An ER4116DM dual mode X-band resonator of rectangular type (TE_{102} for perpendicular and TE_{012} for parallel mode) was used for all measurements. Data analysis was carried out with either the X-Epr or X-Winpro software packages.

Quantification of **4** in different oxidation states was carried out by double integration of the perpendicular EPR mode signal studied within the selected spectral region. The signal intensity was then converted into spin concentration by comparison with the signal intensity in a standard sample in the same oxidation state with known concentration. All EPR spectra used for the evaluation of the different concentrations were recorded using nonsaturating microwave power.

The amount of $Mn_2^{II,III}$ found in the preparation of **4** was obtained by comparison with the signal in the $g = 2$ region recorded after exhaustive one electron reduction of **4** to the $Mn_2^{II,III}$ state. The reduction was monitored coulometrically providing the exact concentration of $Mn_2^{II,III}$ after electrolysis.

$[Mn_2^{III,IV}(\mu\text{-}O)_2(bpy)_4]^{3+}$ was utilized as the standard for quantification of the $Mn_2^{III,IV}$ complex formed after one-electron oxidation of **4**. The precise concentration of the $[Mn_2^{III,IV}(\mu\text{-}O)_2(bpy)_4]^{3+}$ standard was determined spectrophotometrically at 684 nm.[27]

Mn^{II} acetate (purity > 99.9%) in 10% water/90% acetonitrile was used as standard for quantification of monomeric Mn^{II} species formed, e.g. after two-electron reduction. Mn^{II} acetate was used as purchased.

Magnetic Susceptibility Measurements: Magnetic susceptibility measurements were performed on an MPMS5 magnetometer (Quantum Design Inc.) over a temperature range of 2−300 K and at a magnetic field of 1.0 T. A palladium reference (Quantum Design Inc.) was used for callibration at 298 K. Data were corrected for diamagnetism and the χT vs. T plot was fitted according to the procedure described in ref.[28]

Acknowledgments

Eric Rivière (Université Paris-Sud, Orsay) is gratefully acknowledged for performing and analyzing the magnetic susceptibility measurements. This work was supported by the Knut and Alice Wallenberg Foundation, the Swedish National Energy Administration, the Swedish Research Council, and DESS.

[1] [1a] Thematic issue: *Biochim. Biophys. Acta* **2001**, *1503*, 1− 259. [1b] R. D. Britt, in: *Oxygenic Photosynthesis: The Light Reactions* (Ed.: D. R. Ort, C. F. Yocum), Kluwer Academic Publishers, Dordrecht, **1996**, pp 137−164. [1c] W. Ruttinger, G. C. Dismukes, *Chem. Rev.* **1997**, *97*, 1−24.

[2] [2a] L. Sun, L. Hammarström, B. Åkermark, S. Styring, *Chem. Soc. Rev.* **2001**, *30*, 36−49. [2b] M. Yagi, M. Kaneko, *Chem. Rev.* **2001**, *101*, 21−35. [2c] See ref.[1c]

[3] bpmp = 2,6-bis[bis(2-pyridylmethyl)amino]methyl-4-methylphenol.

[4] [4a] L. Sun, M. K. Raymond, A. Magnuson, D. LeGourriérec, M. Tamm, M. Abrahamsson, P. Huang-Kenéz, J. Mårtensson, G. Stenhagen, L. Hammarström, S. Styring, B. Åkermark, *J. Inorg. Biochem.* **2000**, *78*, 15−22. [4b] P. Huang-Kenéz, A. Magnuson, R. Lomoth, M. Abrahamsson, M. Tamm, L. Sun, B. van Rotterdam, J. Park, L. Hammarström, B. Åkermark, S. Styring, *J. Inorg. Biochem.* **2002**, *91*, 159−172.

[5] [5a] J. H. Robblee, R. M. Cinco, V. K. Yachandra, *Biochim. Biophys. Acta* **2001**, *1503*, 7−23 and references therein. [5b] D. Kuzek, R. J. Pace, *Biochim. Biophys. Acta* **2001**, *1503*, 123−137. [5c] G. Renger, *Biochim. Biophys. Acta* **2001**, *1503*, 210−228. [5d] V. K. Yachandra, K. Sauer, M. P. Klein, *Chem. Rev.* **1996**, *96*, 2927−2950.

[6] P. E. M. Siegbahn, R. H. Crabtree, *J. Am. Chem. Soc.* **1999**, *121*, 117−127.

[7] [7a] J. Limburg, J. S. Vrettos, L. M. Liable-Sands, A. L. Rheingold, R. H. Crabtree, G. W. Brudvig, *Science* **1999**, *283*, 1542−1527. [7b] J. Limburg, J. S. Vrettos, H. Chen, J. C. de Paula, R. H. Crabtree, G. W. Brudvig, *J. Am. Chem. Soc.* **2001**, *123*, 423−430. [7c] J. S. Vrettos, J. Limburg, G. W. Brudwig, *Biochim. Biophys. Acta* **2001**, *1503*, 229−245.

[8] A. Neves, M. A. de Brito, I. Vencato, V. Drago, K. Griesar, W. Haase, *Inorg. Chem.* **1996**, *35*, 2360−2368.

[9] [9a] H. Diril, H.-R. Chang, M. J. Nilges, X. Zhang, J. A. Potenza, H. J. Schugar, S. S. Isied, D. N. Hendrickson, *J. Am. Chem. Soc.* **1989**, *111*, 5102−5114. [9b] M. Suzuki, M. Miku-

riya, S. Murata, A. Uehara, H. Oshio, S. Kida, K. Saito, *Bul. Chem. Soc. Jpn.* **1987**, *60*, 4305−4312.
[10] See ref.[14b]
[11] [11a] K. A. Campbell, PhD thesis, University of California, Davis, **1999**. [11b] T. Yamauchi, H. Mino, T. Matsukawa, A. Kawamori, T. Ono, *Biochemistry* **1997**, *36*, 7520−7526.
[12] J. B. Vincent, K. Folting, J. C. Huffman, G. Christou, *Inorg. Chem.* **1986**, *25*, 996−999.
[13] E. König, S. Kremer, *Ligand Field Energy Diagrams*, Plenum Press, New York, **1977**, 175−200.
[14] K. Yamaguchi, D. T. Sawyer, *Inorg. Chem.* **1985**, *24*, 971−976.
[15] J. E. Sheats, R. S. Czernuszewicz, G. C. Dismukes, A. L. Rheingold, V. Petrouleas, J. Stubbe, W. H. Armstrong, R. H. Beer, S. J. Lippard, *J. Am. Chem. Soc.* **1987**, *109*, 1435−1444.
[16] G. B. Deacon, R. J. Phillips, *Coord. Chem. Rev.* **1980**, *23*, 227−250.
[17] M. Suzuki, M. Mikuriya, S. Murata, A. Uehara, H. Oshio, S. Kida, K. Saito, *Bull. Chem. Soc. Jpn.* **1987**, *60*, 4305−4312.
[18] [18a] H. Diril, H.-R. Chang, X. Zhang, S. K. Larsen, J. A. Potenza, C. G. Pierpont, H. J. Schugar, S. S. Isied, D. N. Hendrickson, *J. Am. Chem. Soc.* **1987**, *109*, 6207−6208. [18b] H-R. Chang, S. K. Larsen, P. W. Boyd, C. G. Pierpont, D. N. Hendrickson, *J. Am. Chem. Soc.* **1988**, *110*, 4565−4576.
[19] [19a] M. Zheng, S. V. Khangulov, G. C. Dismukes, V. V. Barynin, *Inorg. Chem.* **1994**, *33*, 382−387. [19b] P. J. Pessiki, S. V. Khangulov, D. M. Ho, G. C. Dismukes, *J. Am. Chem. Soc.* **1994**, *116*, 891−897.
[20] [20a] H. Okawa, M. Nakamura, S. Kida, *Bull. Chem. Soc. Jpn.* **1982**, *55*, 466−470. [20b] D. P. Kessisoglou, X. Li, W. M. Butler, V. L. Pecoraro, *Inorg. Chem.* **1987**, *26*, 2487−2492. [20c] U. Auerbach, T. Weyhermüller, K. Wieghardt, B. Nuber, E. Bill, C. Butzlaff, A. X. Trautwein, *Inorg. Chem.* **1993**, *32*, 508−519. [20d] A. Neves, S. M. D. Erthal, I. Vencato, A. S. Ceccato, Y. P. Mascarenhas, O. R. Nascimento, M. Hörner, A. A. Batista, *Inorg. Chem.* **1992**, *31*, 4749−4755. [20e] S. K. Chandra, A. Chakravorty, *Inorg. Chem.* **1992**, *31*, 760−765. [20f] S. K. Chandra, P. Basu, D. Ray, S. Pal, A. Chakravorty, *Inorg. Chem.* **1990**, *29*, 2423−2428.
[21] [21a] O. Horner, E. Anxolabéhère-Mallart, M.-F. Charlot, L. Tchertanov, J. Guilhem, T. A. Mattioli, A. Boussac, J.-J. Girerd, *Inorg. Chem.* **1999**, *38*, 1222−1232. [21b] M. J. Baldwin, T. L. Stemmler, P. J. Riggs-Gelasco, M. L. Kirk, J. E. Penner-Hahn, V. L. Pecoraro, *J. Am. Chem. Soc.* **1994**, *116*, 11349−11356.
[22] P. A. Goodson, J. Glerup, D. J. Hodgson, K. Michelsen, E. Pedersen, *Inorg. Chem.* **1990**, *29*, 503−508.
[23] Mn(Ph−O$^{\cdot}$) states of monomeric complexes have been reported (ref.[23]) and generation of a $Mn_2^{III,IV}$(Ph−O$^{\cdot}$) species has also been observed in a dimer with nonbridging phenolates (ref.[21a]). In our case no Ph−O$^{\cdot}$ species was sufficiently stable to be observed on the time-scale of electrolysis. [23a] J. Müller, A. Kikuchi, E. Bill, T. Weyhermüller, P. Hildebrandt, L. Ould-Moussa, K. Wieghardt, *Inorg. Chim. Acta* **2000**, *297*, 265−277. [23b] H. Schmitt, R. Lomoth, A. Magnuson-Styring, J. Park, J. Fryxelius, M. Kritikos, J. M Årtensson, L. Hammarström, L. Sun, B. Åkermark, *Chem. Eur. J.* **2002**, *8*, 3757−3768.
[24] [24a] A. S. Borovik, V. Papaefthymiou, L. F. Taylor, O. P. Anderson, L. Que Jr., *J. Am. Chem. Soc.* **1989**, *111*, 6183−6195. [24b] H. P. Berends, D. W. Stephan, *Inorg. Chem.* **1987**, *26*, 749−754.
[25] K. J. Oberhausen, J. F. Richardson, R. M. Buchanan, J. K. McCusker, D. N. Hendrickson, J. M. Latour, *Inorg. Chem.* **1991**, *30*, 1357−1365.
[26] V. V. Pavlishchuk, A. W. Addison, *Inorg. Chim. Acta* **2000**, *298*, 97−102.
[27] R. Manchanda, G. W. Brudvig, R. H. Crabtree, *New J. Chem.* **1994**, *18*, 561−568.
[28] S. Poussereau, G. Blondin, G. Chottard, J. Guilhelm, L. Tchertanov, E. Rivière, J.-J. Girerd, *Eur. J. Inorg. Chem.* **2001**, 1057−1062.

Received February 6, 2002
[I02060]

Syntheses, Crystal Structures and Reactivity of Organometallic Tantalum(IV) Phosphinidene Complexes: *trans*-[{Cp*TaCl(μ-PR)}$_2$] (Cp* = C_5Me_5, R = Cy, *t*Bu, Ph), *cis*- and *trans*-[{Cp*TaCl(μ-PMes)}$_2$] (Mes = 2,4,6-$Me_3C_6H_2$) and *cis*-[{Cp′TaCl(μ-PMes)}$_2$] (Cp′ = C_5H_4Me)

Steffen Blaurock[a] and Evamarie Hey-Hawkins*[a]

Keywords: Tantalum / P ligands / Oxo ligands / Isocyanide ligands

The reaction of [Cp*TaCl$_4$] (Cp* = C_5Me_5) with LiPHR (1:1 or 1:2) gives the phosphinidene-bridged tantalum(IV) complexes *trans*-[{Cp*TaCl(μ-PR)}$_2$] [R = Cy (**1**), *t*Bu (**2**), Ph (**3**), 2,4,6-$Me_3C_6H_2$ (Mes) (**4b**)]. When the reaction with LiPHMes is carried out in a 1:1 ratio, *cis*-[{Cp*TaCl(μ-PMes)}$_2$] (**4a**) is also formed besides **4b**. For comparison, *cis*-[{Cp′TaCl(μ-PMes)}$_2$] (**5**) was prepared from [Cp′TaCl$_4$] (Cp′ = C_5MeH_4) and LiPHMes (1:1). **1**–**5** are diamagnetic and were characterised spectroscopically (IR, MS; ^{1}H, ^{31}P, ^{13}C NMR). Crystal structure determinations on **1**–**5** showed the presence of dimeric phosphinidene-bridged Ta^{IV} complexes. The phosphinidene-bridged complexes **1**, **3** and **4b** do not react with acetone, benzophenone, acetonitrile, CS_2 (**1**, **3**), acetaldehyde (**4b**), or ethylaluminum dichloride (**3**). **3** reacts with moist acetone in the presence of traces of air to give the trinuclear cluster [{Cp*TaCl(μ$_2$–O)}$_3$(μ$_3$-O)(μ$_2$-O_2PHPh)] (**6**) in very low yield. With an excess of CyNC, **3** gives [Cp*TaCl(CNCy)$_4$]Cl (**7**), which was characterised by ^{1}H and ^{13}C NMR spectroscopy and by crystal structure determination. As a minor product, [(Cp*TaCl$_2$)$_2$(μ$_2$-O)(η^2,μ$_2$-P_2Cy_2)] (**8**) was also obtained in the reaction of [Cp*TaCl$_4$] with LiPHCy. **6** and **8** were only characterised by crystal structure determination.
(© Wiley-VCH Verlag GmbH, 69451 Weinheim, Germany, 2002)

Introduction

Organometallic dialkyl- and diarylphosphanido complexes of early transition metals have been studied intensively, while complexes derived from functionalised phosphanes which exhibit a reactive phosphorus-ligand bond have largely been neglected.[1] To date, only a few phosphanido derivatives of organometallic[2,3] and inorganic[4,5] tantalum compounds, one phosphinidene-bridged dimeric Ta^{IV} complex[3] and two stable terminal phosphinidene complexes[5,6] have been described in the literature.

Recently, we reported the syntheses and structures of the primary phosphane complexes [Cp′TaCl$_4$(PH$_2$Tipp)] (Cp′ = C_5H_4Me, Tipp = 2,4,6-*i*Pr$_3$C$_6$H$_2$)[3] and [Cp*MCl$_4$(PH$_2$R)] [Cp* = C_5Me_5; M = Nb, Ta; R = *t*Bu, Ad, Cy, Ph, 2,4,6-$Me_3C_6H_2$ (Mes)],[7] which we expected to be suitable precursors for the preparation of phosphanido and phosphinidene complexes. However, when [Cp*TaCl$_4$(PH$_2$R)] (R = *t*Bu, Cy, Ad, Ph, Mes) were treated with DBU an internal redox reaction occurred with formation of [(DBU)H][Cp*TaCl$_4$] (DBU = 1,8-diazabicyclo[5.4.0]undec-7-ene) and the corresponding diphosphane ($P_2H_2R_2$) or decomposition products thereof.[8] For the aryl-substituted phosphane complexes, there was also an indication from the ^{31}P NMR spectra of the formation of tantalum phosphinidene complexes, which could, however, not be isolated.

We now report the targeted synthesis of these and other dimeric Ta^{IV} phosphinidene complexes, which are accessible from [Cp^{R}TaCl$_4$] (Cp^R = Cp*, Cp′) and LiPHR′, and some reaction products thereof. The related tantalum(IV) phenylimido complex *trans*-[{Cp*TaCl(μ-NPh)}$_2$] is also known.[9]

Results and Discussion

Synthesis and Properties of *trans*-[{Cp*TaCl(μ-PR)}$_2$] [R = Cy (1), *t*Bu (2), Ph (3)], *cis*- and *trans*-[{Cp*TaCl(μ-PMes)}$_2$] (4a,b) and *cis*-[{Cp′TaCl(μ-PMes)}$_2$] (5)

When [Cp*TaCl$_4$][7,10] was treated with two equivalents of LiPHR[11–14] in toluene (to keep the concentration of LiPHR low in solution) at low temperature (to reduce side reactions), the deep red phosphinidene-bridged tantalum(IV) complexes *trans*-[{Cp*TaCl(μ-PR)}$_2$] [R = Cy (**1**), *t*Bu (**2**), Ph (**3**), Mes (**4b**)] were obtained after workup in 73 to 86% yield (based on [Cp*TaCl$_4$]; Scheme 1).

In the ^{31}P NMR spectra of the reaction mixtures, one singlet is observed for the *t*Bu, Ph and Mes derivatives, while for the Cy derivative, two singlets are observed in the low-field region, one of which has only a low intensity [δ = 437.6 (major) and 433.7 (minor) ppm]. The major signal

[a] Institut für Anorganische Chemie der Universität Leipzig
Johannisallee 29, 04103 Leipzig (Germany)
Fax: (internat.) + 49–(0)341/9739319
E-mail: hey@rz.uni-leipzig.de

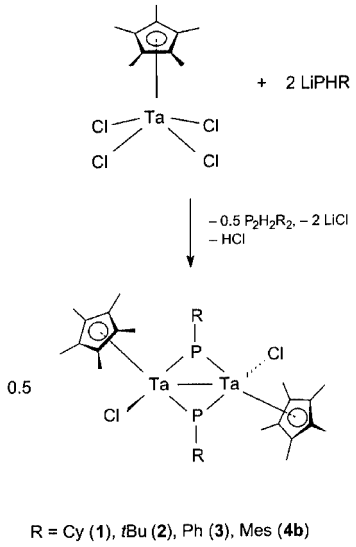

Scheme 1

was shown to belong to the *trans* isomer, while the minor signal presumably belongs to the *cis* isomer.

When the reaction of [Cp*$TaCl_4$] with LiPHMes was carried out in a 1:1 ratio, *cis*-[{Cp*TaCl(μ-PMes)}$_2$] (**4a**) was also formed along with **4b**. An additional signal was observed in the ^{31}P NMR spectrum at δ = 485.8 ppm [ratio ca. 1 (**4a**): 6 (**4b**): 3], which indicates the formation of a terminal phosphinidene complex, [Cp*$TaCl_2$(PMes)] (cf. the stable terminal phosphinidene complex [Cp*$TaCl_2${P(Tipp)}], which shows a singlet at δ = 488.0 ppm).[15] The mesitylphosphinidene complex could, however, not be obtained in its pure form. Complexes **4a** and **4b** could be separated by fractional crystallisation from *n*-hexane.

For comparison, *cis*-[{Cp′TaCl(μ-PMes)}$_2$] (**5**) was prepared from [Cp′$TaCl_4$][16] and LiPHMes (1:1). In the ^{31}P NMR spectrum of the reaction mixture, only one signal was observed, which indicates the exclusive formation of the *cis* isomer.

In these reactions, the lithium reagent acts as a reducing agent, base and substitution reagent. The products of these reactions, that is, the oxidation product $P_2H_2R_2$, the free phosphane RPH_2, and the corresponding Ta^{IV} phosphinidene complex were detected by ^{31}P NMR spectroscopy.

The formation of **1**–**4b** was also observed when only one equivalent of LiPHR was used, but the yield was lower.

Related tantalum phosphinidene complexes include *trans*-[(Cp′TaCl{μ-P(Tipp)})$_2$] (**I**),[3] which was obtained by treating [Cp′$TaCl_4${PH_2(Tipp)}] with DBU (1:2 or 1:3), and the stable terminal phosphinidene complexes [N{$CH_2CH_2N(SiMe_3)$}$_3$Ta=PR] [δ(^{31}P) = 175.1 (R = Cy) and 227.3 (R = *t*Bu) ppm][6] and [(tBu$_3$SiO)$_3$Ta=PPh][5] [δ(^{31}P) = 334.6 ppm]. These ^{31}P chemical shifts indicate the presence of a linear MPR unit (bent MPR unit: δ = 660 to 800 ppm).[17] For **1**–**5** and **I**, ^{31}P chemical shifts of δ = 390.3 ppm (for **4b**) to 482.0 ppm (for **2**) are observed [for **I**, δ(^{31}P) = 391.5 ppm], and Δδ (phosphane vs. phosphinidene complex) ranges from δ = 526 to 562 ppm (Table 1).

Apparently, the influence of the substituted cyclopentadienyl ligand on the ^{31}P NMR chemical shift is negligible, as shown by the similar values for **4b** (Cp* complex) and **I** (Cp′ complex), while alkyl-substituted phosphinidene complexes **1** and **2** exhibit low-field shifts compared to aryl-substituted phosphinidene complexes **3**–**5**. The same trend is observed for the corresponding primary phosphanes (Table 1).

In the ^{13}C NMR spectra of **1**–**4**, the signals of the carbon atoms of the Cp* ring are shifted to high field by Δδ = 16.5–18 relative to the starting material [Cp*$TaCl_4$] (δ = 132.9 ppm).

Molecular ion peaks were observed in the mass spectra of **1**–**4**.[18] For **1**, **3**, and **4a**, signals for monomeric [Cp*TaCl(PR)]$^+$ and fragmentation products thereof were also observed.

In the UV/Vis spectra in pentane, **1**–**4** exhibit four absorptions in the ranges 682 – 753 (ν_1), 473 – 528 (ν_2), 337 – 396 (ν_3), and 313 – 319 nm (ν_4), with molar absorption coefficients of 10^2 – 10^3 (for ν_1, d-d transition), $2{\cdot}10^3$ – 10^4 (for ν_2 and ν_3; CT transitions), and 10^4 – $3{\cdot}10^4$ cm^2/mol (for ν_4, π -π * transition of Cp*).

Molecular Structures of *trans*-[{Cp*TaCl(μ-PR)}$_2$] [R = Cy (1), *t*Bu (2), Ph (3), Mes (4b)], *cis*-[{Cp*TaCl(μ-PMes)}$_2$] (4a) and *cis*-[{Cp′TaCl(μ-PMes)}$_2$] (5)

Single crystals of **1**–**5** were obtained from concentrated solutions in diethyl ether (**1**, **3**), pentane (**2**) or hexane (**4a**,**b**, **5**) at 5 °C. The *trans* complexes **1**–**3** crystallise in the monoclinic space group $P2_1/n$, **4b** in the monoclinic space group $P2_1/c$ and have two formula units per unit cell; the *cis* complexes **4a** and **5** crystallise in the triclinic space group $P\bar{1}$ with two formula units in the unit cell (Table 2). The unit

Table 1. Comparison of the ^{31}P NMR spectroscopic data of compounds **1**–**5** and [(Cp′TaCl{μ-P(Tipp)})$_2$] (**I**)[3] (NMR in C_6D_6) with the ^{31}P{^{1}H} NMR spectroscopic data of the corresponding primary phosphanes

	1 (*trans*) R = Cy	**2** (*trans*) R = tBu	**3** (*trans*) R = Ph	**4a** (*cis*) R = Mes	**4b** (*trans*) R = Mes	**5** (*cis*) R = Mes	**I** (*trans*)
δ(^{31}P, ppm)	437.6	482.0	403.9	399.0	390.3	396.0	391.5
	PH_2Cy[39]	PH_2Bu[36b]	PH_2Ph[36b]	PH_2Mes[36b,40,41]	PH_2Mes[36b,40,41]	PH_2Mes[36b,40,41]	PH_2(Tipp)[36b]
δ(^{31}P, ppm)	–111.3	–80.5	–122.1	–153.8	–153.8	–153.8	–158.2
Δ δ	549.0	562.4	526.0	552.8	544.1	549.8	549.7

Table 2. Crystal data and structure refinement for **1**–**8**

Compound	**1**·2Et$_2$O	**2**	**3**	**4a** (*cis*)	**4b**
Empirical formula	$C_{36}H_{62}OCl_2P_2Ta_2$	$C_{28}H_{48}Cl_2P_2Ta_2$	$C_{32}H_{40}Cl_2P_2Ta_2$	$C_{38}H_{52}P_2Cl_2Ta_2$· hexane	$C_{38}H_{52}P_2Cl_2Ta_2$
Molecular mass	1005.76	879.40	919.38	1003.54	1003.54
Temperature [K]	220(2)	220(2)	220(2)	220(2)	220(2)
Crystal system	monoclinic	monoclinic	monoclinic	triclinic	monoclinic
Space group	$P2_1/n$ (no. 14)	$P2_1/n$ (no. 14)	$P2_1/n$ (no. 14)	$P\bar{1}$ (no. 2)	$P2_1/c$ (no. 14)
Unit cell dimensions					
a [Å]	12.168(2)	12.386(3)	8.813(2)	8.7270(3)	11.1373(5)
b [Å]	9.219(2)	9.288(2)	13.214(3)	12.6329(4)	9.7817(4)
c [Å]	18.841(4)	14.166(3)	14.724(3)	21.2748(8)	17.5396(8)
α [°]	90	90	90	104.018(1)	90
β [°]	106.95(3)	96.25(3)	105.53(3)	91.234(1)	90.052(1)
γ [°]	90	90	90	99.577(1)	90
V [Å^3]	2021.7(7)	1619.9(6)	1652.1(6)	2239.2(2)	1910.8(2)
Z	2	2	2	2	2
$\rho_{calcd.}$ [g cm^{-3}]	1.556	1.803	1.848	1.552	1.744
μ(Mo-K_α) [mm^{-1}]	5.644	7.029	6.897	5.099	5.971
F(000)	972	852	884	1030	980
$\Theta_{min.}$, Θ_{max} [°]	1.78–24.74	2.08–27.93	2.11–27.86	1.73–28.54	1.83–27.85
Index ranges					
	−13 h 13	−15 h 14	−11 h 11	−11 h 11	−14 h 10
	−10 k 10	−12 k 11	−17 k 9	−8 k 16	−12 k 12
	−21 l 18	−18 l 17	−19 l 19	−27 l 28	−20 l 21
Reflections collected	8166	14304	9194	13684	
Independent reflections	3295	3601	3568	9902	4145
R(int)	0.0182	0.0405	0.0336	0.0186	0.0430
Parameters	240	178	237	432	281
Goodness-of-fit on F^2	0.974	1.060	1.029	0.946	1.029
Final R indices [$I > 2\sigma(I)$]					
R_1	0.0275	0.0228	0.0269	0.0290	0.0364
wR_2	0.0747	0.0554	0.0631	0.0911	0.0860
R indices (all data)					
R_1	0.0301	0.0267	0.0360	0.0406	0.0572
wR_2	0.0798	0.0575	0.0679	0.0946	0.1034
Largest diff. peak and hole [e Å^{-3}]	0.95 and −0.87	1.07 and −1.47	1.02 and −1.24	2.07 and −1.44	2.28 and −2.34

Compound	**5**	**6**	**7**	**8**
Empirical formula	$C_{36}H_{36}P_2Cl_2Ta_2$	$C_{36}H_{51}O_6PCl_3Ta_3$·acetone	$C_{38}H_{59}N_4Cl_2Ta$	$C_{32}H_{52}OP_2Cl_4Ta_2$
Molecular mass	891.33	1318.01	823.74	1018.38
Temperature [K]	220(2)	220(2)	220(2)	220(2)
Crystal system	triclinic	monoclinic	monoclinic	monoclinic
Space group	$P\bar{1}$ (no. 2)	$P2_1/n$ (no. 14)	$P2_1/n$ (no. 14)	Cc (no. 9)
Unit cell dimensions				
a [Å]	9.0480(3)	11.5431(3)	15.056(2)	20.6118(1)
b [Å]	13.4376(4)	24.6455(5)	15.261(2)	16.1667(1)
c [Å]	13.9232(4)	16.1917(3)	16.911(2)	11.3250(2)
α [°]	77.837(1)	90	90	90
β [°]	75.24	105.062(1)	91.16(2)	96.195(1)
γ [°]	77.024(1)	90	90	90
V [Å^3]	1573.83(8)	4448.1(2)	3884.8(8)	3760.7(7)
Z	2	4	4	2
$\rho_{calcd.}$ [g cm^{-3}]	1.881	1.967	1.408	1.799
μ(Mo-K_α) [mm^{-1}]	7.236	7.622	2.997	6.208
F(000)	852	2524	1688	1984
$\Theta_{min.}$, Θ_{max} [°]	1.53–27.89	1.54–27.85	1.79–28.04	1.60–27.45
Index ranges				
	−11 h 11	−14 h 14	−19 h 19	−10 h 26
	−12 k 17	−32 k 30	−19 k 20	−19 k 20
	−18 l 17	−21 l 20	−22 l 22	−14 l 12
Reflections collected	8814	35789	35585	9147
Independent reflections	6373	9691	8761	4526
R(int)	0.0698	0.0472	0.0320	0.0415
Parameters	325	482	642	370
Goodness-of-fit on F^2	0.891	1.168	1.105	1.114
Final R indices [$I > 2\sigma(I)$]				
R_1	0.0473	0.0290	0.0297	0.0272
wR_2	0.1257	0.0730	0.0682	0.0696
R indices (all data)				
R_1	0.0761	0.0374	0.0372	0.0278
wR_2	0.1629	0.0848	0.0717	0.0761
Largest diff. peak and hole [e Å^{-3}]	2.02 and −1.94	0.76 and −1.86	0.57 and −0.92	1.33 and −2.13

cell of **1** contains four noninteracting diethyl ether molecules, and that of **4a** two hexane molecules.

The pronounced tendency of Ta^{IV} to form binuclear complexes is also evident in the molecular structures of **1**−**5**. The *trans* complexes **1**−**4b** are centrosymmetric dimers in which two Ta atoms are bound by two bridging phosphinidene [PCy (**1**) (Figure 1), P*t*Bu (**2**) (Figure 2), PPh (**3**) (Figure 3), PMes (Figure 4)] groups. Each Ta atom also bears a terminal chloro ligand, and a Cp* ligand completes the coordination sphere of the Ta atom (Table 3). The four-membered metallacycles Ta−P−Ta′−P′ are planar and almost square (the centres of the planar Ta_2P_2 rings in **1**−**4b** coincide with crystallographic inversion centres); this indicates substantial pπ -dπ backbonding (P→ Ta) of the phosphorus lone pair. Complex **I** exhibits comparable structural parameters.[3]

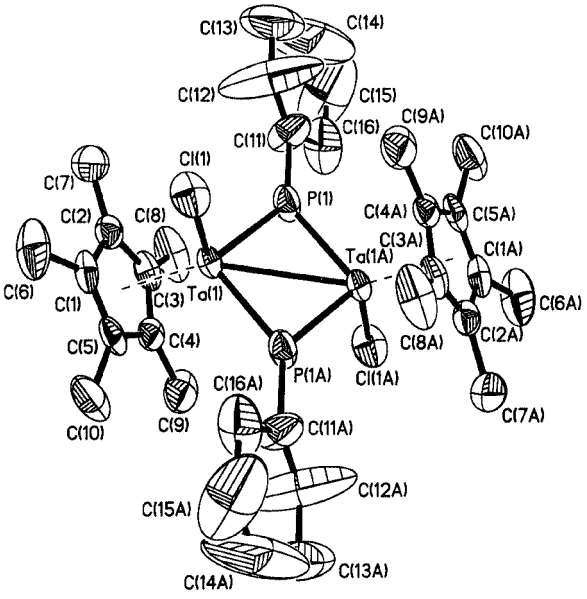

Figure 1. Molecular structure of *trans*-[{Cp*TaCl(μ-PCy)}$_2$] (**1**) showing the atom numbering scheme employed (ORTEP plot, 50% probability, SHELXTL PLUS; XP[37]). Hydrogen atoms are omitted for clarity.

In the *cis* complexes **4a** (Figure 5) and **5** (Figure 6), a butterfly-type central Ta_2P_2 ring is observed [dihedral angle for **4a**: Ta(1)−P(1)−Ta(2)/Ta(1)−P(2)−Ta(2) 27.61(6)°, **5**: Ta(1)−P(1)−Ta(2)/Ta(1)−P(2)−Ta(2) 10.4(2)°]. Due to geometric requirements, the aryl rings in **4a** are almost perpendicular to the Ta_2P planes [dihedral angles 89.9(4)° and 88.9(4)°]. This structure is also retained in solution, as indicated by two signals for the nonequivalent *meta*-H atoms (^{1}H NMR) and the *ortho*-methyl groups in the ^{1}H and ^{13}C NMR spectra. In **5**, both mesityl rings are also almost perpendicular to the Ta_2P planes [dihedral angles 86.6(4)° for P(2)-mesityl and 73.8(4)° for P(1)-mesityl]. However, in this case free rotation around the P−C_{ipso}(Mes) bond is possible in solution, as indicated by the presence of only one broad signal for the equivalent *meta*-H atoms and the *ortho*-methyl groups (^{1}H NMR).

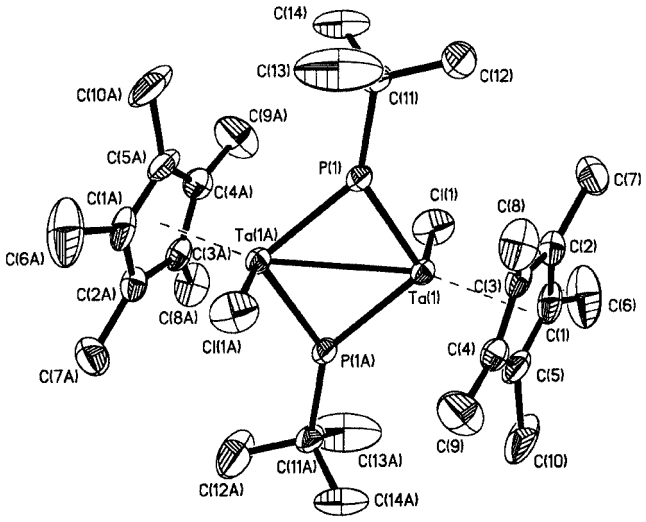

Figure 2. Molecular structure of *trans*-[{Cp*TaCl(μ-P*t*Bu)}$_2$] (**2**) showing the atom numbering scheme employed (ORTEP plot, 50% probability, SHELXTL PLUS; XP[37]). Hydrogen atoms are omitted for clarity.

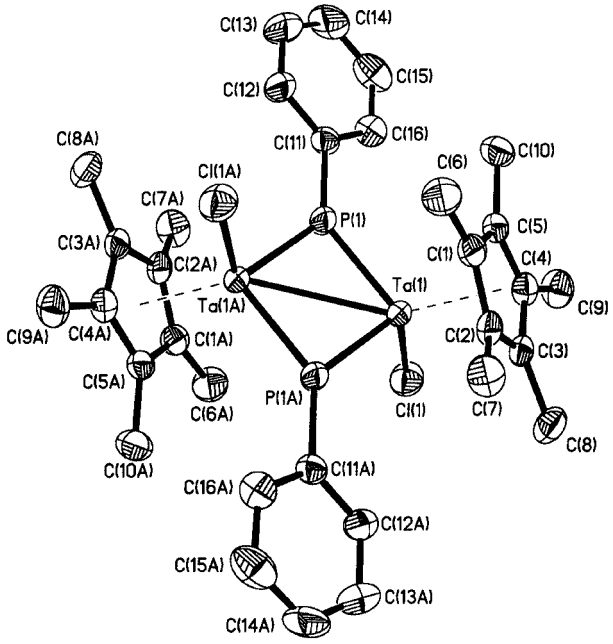

Figure 3. Molecular structure of *trans*-[{Cp*TaCl(μ-PPh)}$_2$] (**3**) showing the atom numbering scheme employed (ORTEP plot, 50% probability, SHELXTL PLUS; XP[37]). Hydrogen atoms are omitted for clarity.

Complexes **1**−**5** are diamagnetic, thus the presence of a Ta−Ta single bond can be assumed. For other dimeric complexes it was observed that the Ta−Ta bond length[19] is strongly dependent on the number and type of ligands (e.g., hydrido-bridged complexes generally have shorter Ta−Ta bonds than comparable halogen-bridged complexes[20]). A comparable value of 3.165 Å was observed for [{$TaCl_3(SMe_2)$(μ-SPh)}$_2$],[21] in which a Ta−Ta single bond is present according to theoretical calculations.[22]

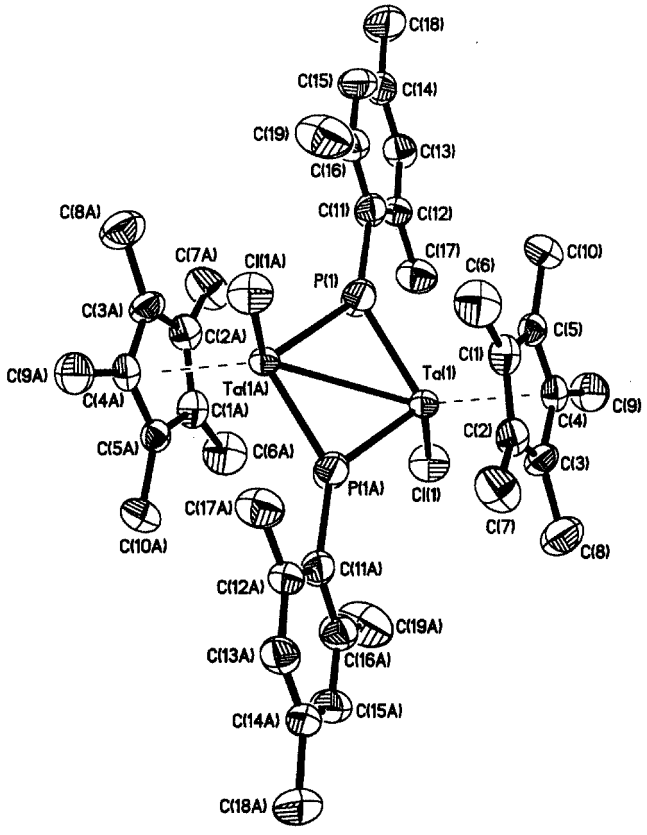

Figure 4. Molecular structure of *trans*-[{Cp*TaCl(μ-PMes)}$_2$] (**4b**) showing the atom numbering scheme employed (ORTEP plot, 50% probability, SHELXTL PLUS; XP[37]). Hydrogen atoms are omitted for clarity.

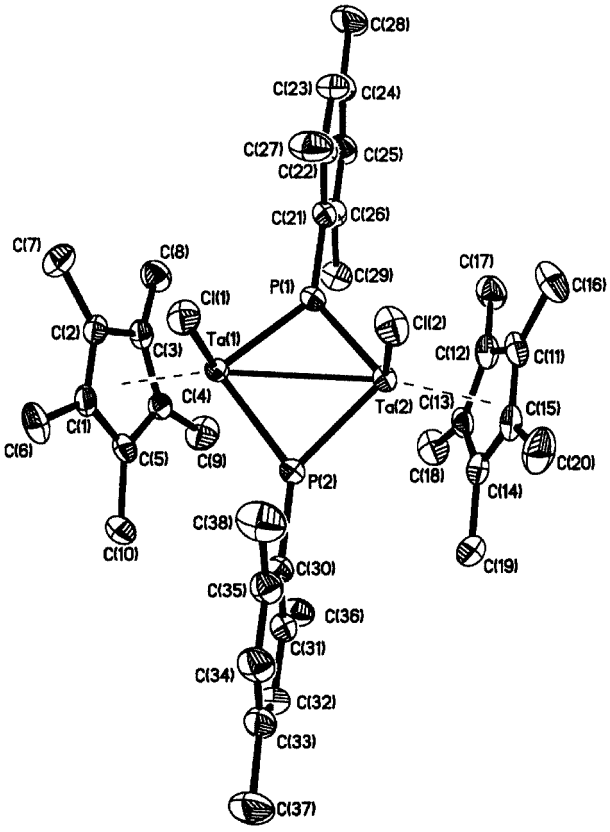

Figure 5. Molecular structure of *cis*-[{Cp*TaCl(μ-PMes)}$_2$] (**4a**) showing the atom numbering scheme employed (ORTEP plot, 50% probability, SHELXTL PLUS; XP[37]). Hydrogen atoms are omitted for clarity.

Table 3. Selected bond lengths [Å] and angles [°] of compounds **1**–**5** and [(Cp′TaCl{μ-P(Tipp)})$_2$] (**I**)[3]

Compound	Ta–P	Ta–Ta	Ta–Cl	Ta–P–Ta	P–Ta–P
1	2.334(2), 2.336(2)	3.132(1)	2.358(2)	84.26(6)	95.74(6)
2	2.354(1), 2.357(1)	3.1759(8)	2.360(1)	84.78(4)	95.22(4)
3	2.345(1), 2.344(1)	3.1957(6)	2.357(1)	85.92(4)	94.08(4)
4a	3 × 2.344(2), 2.349(1)	3.0881(3)	2.347(2), 2.352(2)	82.31(5), 82.39(5)	93.87(5), 94.00(5)
4b	2.328(2), 2.331(2)	3.0773(5)	2.364(2)	82.68(7)	97.32(7)
5	2.348(3), 2.358(3) 2.336(3), 2.357(3)	3.1253(7)	2.351(3), 2.365(3)	83.0(1), 83.7(1)	95.9(1), 96.3(1)
I	2.317(6), 2.338(2)	3.100(3)	2.350(2)	83.51(8)	96.49(8)

The Ta–P bond lengths in **1**–**5** are similar to those of **I**[3] (Table 3) and the terminal phosphinidene complex [(*t*Bu$_3$SiO)$_3$Ta=PPh][5] [2.317(4) Å] with a bent TaPC arrangement [Ta–P–C 110.2(4)°], while [N{CH$_2$CH$_2$N(SiMe$_3$)}$_3$Ta=PCy][6] has a linear TaPC arrangement and a shorter Ta–P bond of 2.145(7) Å. However, all these distances are shorter than the sum of the covalent radii of Ta and P (2.44 Å).[23] Longer bonds are observed for bridging phosphanido ligands (e.g., [{Cp′Ta(PPh$_2$)(μ-PPh$_2$)}$_2$], Ta–P$_{br}$ 2.486(2), 2.458(2) Å].[3]

The trigonal-planar geometry of the P atoms of the bridging phosphinidene group in the *trans* complexes **1**–**4b** (sum of bond angles ca. 360°) indicates that the PR group acts as a three-electron donor. In the *cis* complexes **4a** and **5**, the P atoms also have a trigonal-planar environment [sum of bond angles **4a**: P(1): 358.0(2)°, P(2): 357.8(2)°, **5**: P(1): 356.8(4)°, P(2): 358.8(4)°].

The Ta–Cl bonds in **1**–**5** (Table 3) are shorter than those in the Ta chloro phosphane complexes (e.g., [{TaCl$_2$(μ-Cl)(μ-PMe$_2$CH$_2$PMe$_2$)}$_2$], Ta–Cl (terminal) 2.435(7), 2.457(6) Å;[24] *trans*-[CpTaCl$_2$(CO)(PMe$_2$Ph)$_2$], Ta–Cl 2.518(4), 2.539(4) Å;[25] [Cp*TaCl$_3$(PMe$_3$)], Ta–Cl 2.395(3) to 2.416(3) Å;[26] *cis*-[Cp*TaCl$_2$(CO)$_2$(PMe$_3$)], Ta–Cl 2.504(2), 2.512(2) Å[26]).

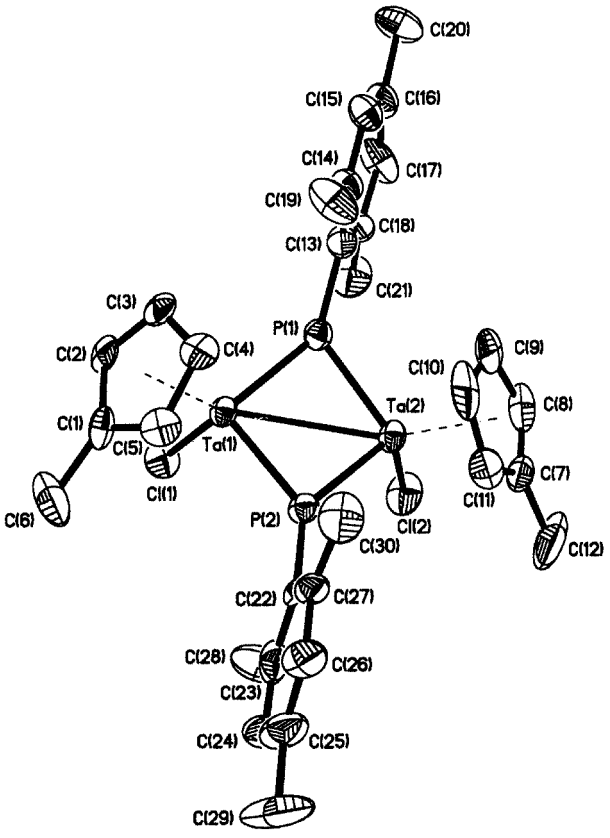

Figure 6. Molecular structure of *cis*-[{Cp′TaCl(μ-PMes)}$_2$] (**5**) showing the atom numbering scheme employed (ORTEP plot, 50% probability, SHELXTL PLUS; XP[37]). Hydrogen atoms are omitted for clarity.

Reactivity of 1, 3 and 4

While terminal electrophilic phosphinidene complexes are highly reactive,[27] **1**−**5** are air-stable as solids for at least several hours. **1**, **3** and **4b** also exhibit a remarkable stability towards acetone, benzophenone, acetonitrile, CS_2 (**1** and **3**), acetaldehyde (**4b**), or $EtAlCl_2$ (**3**), even at elevated temperatures.

Complex **3** reacts with moist acetone (50-fold excess) in the presence of traces of air to give the trinuclear cluster [{Cp*TaCl(μ$_2$-O)}$_3$(μ$_3$-O)(μ-O$_2$PHPh)}] (**6**) in very low yield (Scheme 2). **6** was only characterised by crystal structure determination.

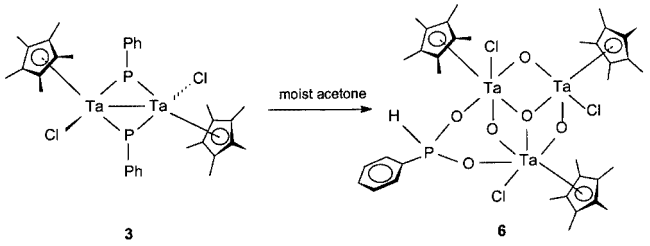

3 6

Scheme 2

Complex **6** crystallises as yellow prismatic crystals in the monoclinic space group $P2_1/n$ with four molecules of acetone in the unit cell. The central structural fragment is a Ta_3O_4 cluster, in which the Ta^V and O atoms alternatingly occupy the corners of a heterocubane with one missing corner (Figure 7). Related clusters have been reported for Zr, Nb, Ta and Mo.[28] Each Ta atom is coordinated by a Cp* and one terminal chloro ligand. Two Ta atoms have a coordination number of six [Ta(1) and Ta(2)]; Ta(3) is five-coordinate. The Ta−Ta distances range from 3.1185(3) to 3.3378(3) Å. There are two types of O atoms: one triply-bridging [O(6)] and three doubly-bridging oxo ligands [O(3), O(4), and O(5); Ta−O 1.910(3) to 2.003(3) Å]. The latter Ta−O bond lengths are in the range for single bonds,[28a,28b] while the Ta−O(6) bond lengths differ by

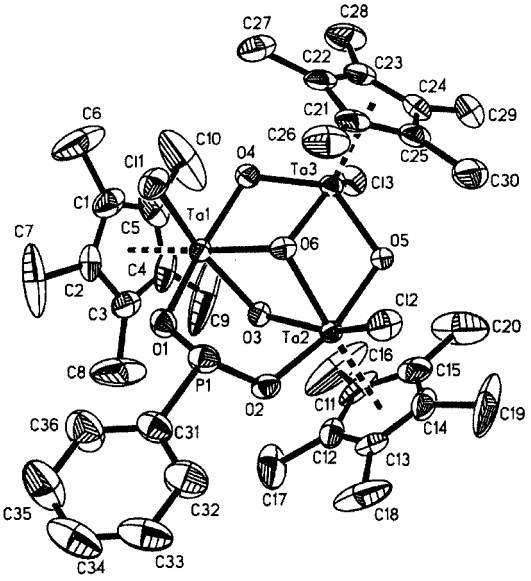

Figure 7. Molecular structure of [{Cp*TaCl(μ$_2$-O)}$_3$(μ$_3$-O)(μ$_2$-O$_2$PHPh)}] (**6**) showing the atom numbering scheme employed (ORTEP plot, 50% probability, SHELXTL PLUS; XP[37]). Hydrogen atoms are omitted for clarity. Bond lengths [Å] and angles [°]: Ta(1)−O(4) 1.960(3), Ta(1)−O(3) 1.991(3), Ta(1)−O(1) 2.127(3), Ta(1)−O(6) 2.148(3), Ta(2)−O(5) 1.964(3), Ta(2)−O(3) 2.003(3), Ta(2)−O(2) 2.117(3), Ta(2)−O(6) 2.136(3), Ta(3)−O(5) 1.910(3), Ta(3)−O(4) 1.915(3), Ta(3)−O(6) 2.058(3), Ta(1)−Cl(1) 2.506(1), Ta(2)−Cl(2) 2.491(1), Ta(3)−Cl(3) 2.429(1), Ta(1)−Ta(3) 3.1185(3), Ta(1)−Ta(2) 3.3378(3), Ta(2)−Ta(3) 3.1206(3), P(1)−O(1) 1.510(4), P(1)−O(2) 1.514(4), P(1)−C(31) 1.778(6); O(4)−Ta(1)−O(3) 98.6(1), O(4)−Ta(1)−O(1) 155.9(1), O(3)−Ta(1)−O(1) 86.6(1), O(4)−Ta(1)−O(6) 74.0(1), O(3)−Ta(1)−O(6) 71.2(1), O(1)−Ta(1)−O(6) 85.7(1), O(4)−Ta(1)−Cl(1) 86.9(1), O(3)−Ta(1)−Cl(1) 148.8(1), O(1)−Ta(1)−Cl(1) 77.1(1), O(6)−Ta(1)−Cl(1) 81.05(9), O(5)−Ta(2)−O(3) 97.7(1), O(5)−Ta(2)−O(2) 156.1(1), O(3)−Ta(2)−O(2) 86.2(1), O(5)−Ta(2)−O(6) 74.0(1), O(3)−Ta(2)−O(6) 71.2(1), O(2)−Ta(2)−O(6) 85.1(1), O(5)−Ta(2)−Cl(2) 87.6(1), O(3)−Ta(2)−Cl(2) 148.7(1), O(2)−Ta(2)−Cl(2) 77.5(1), O(6)−Ta(2)−Cl(2) 80.91(9), O(5)−Ta(3)−O(6) 76.9(1), O(4)−Ta(3)−O(6) 77.0(1), O(5)−Ta(3)−Cl(3) 86.0(1), O(4)−Ta(3)−Cl(3) 85.4(1), O(6)−Ta(3)−Cl(3) 136.68(9), O(1)−P(1)−O(2) 112.5(2), O(1)−P(1)−C(31) 109.4(3), O(2)−P(1)−C(31) 109.2(2), P(1)−O(1)−Ta(1) 123.7(2), P(1)−O(2)−Ta(2) 124.8(2), Ta(1)−O(3)−Ta(2) 113.4(2), Ta(3)−O(4)−Ta(1) 107.2(2), Ta(3)−O(5)−Ta(2) 107.3(2), Ta(3)−O(6)−Ta(2) 96.1(1), Ta(3)−O(6)−Ta(1) 95.7(1), Ta(2)−O(6)−Ta(1) 102.4(1), C(36)−C(31)−P(1) 122.1(5), C(32)−C(31)−P(1) 120.0(5).

ca. 0.1 Å [Ta(3)−O(6) 2.058(3), Ta(1)−O(6) 2.148(3), Ta(2)−O(6) 2.136(3) Å]. For Ta(1) and Ta(2), the *trans* effect of the Cp* ligand apparently affects the Ta−O bond lengths. Similar structural data were found for [(Cp*TaCl)$_3$(μ_2-Cl)(μ_2−O)$_2$(μ_3-O)(μ-O$_2$Si*t*Bu$_2$)].[28b]

In addition, a P(H)(Ph)O$_2^-$ ligand, the anion of phenyl phosphinic acid, bridges Ta(1) and Ta(2). However, the PH proton could not be localised. Due to the small amount of **6** available, no ^{31}P NMR spectrum could be obtained to verify the presence of the PH proton. However, since tantalum(v) is present in this cluster, the presence of an anionic P(H)(Ph)O$_2^-$ ligand must be assumed. The P−O bond lengths indicate multiple bond character (ca. 1.51 Å).[28f]

While no reaction of **3** with one or two equivalents of CyNC was observed, a 10-fold excess of CyNC gave the tantalum(III) complex [Cp*TaCl(CNCy)$_4$]Cl (**7**) (Scheme 3), which was characterised by ^{1}H, ^{13}C NMR spectroscopy and

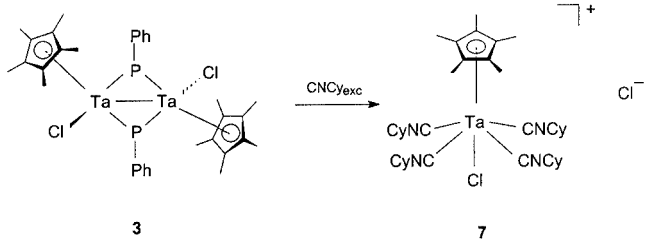

Scheme 3

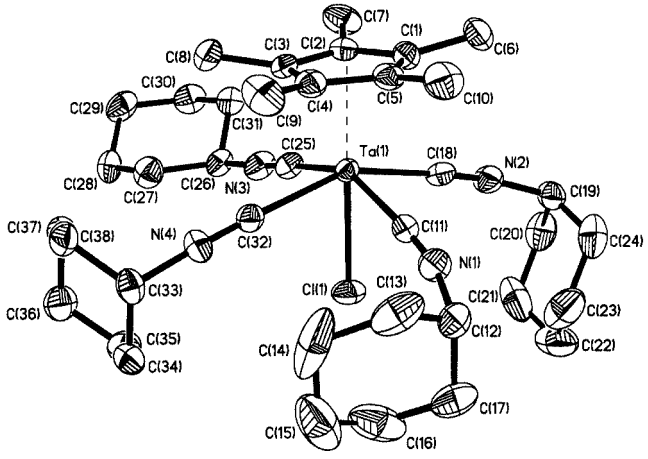

Figure 8. Molecular structure of [Cp*TaCl(CNCy)$_4$]Cl (**7**) showing the atom numbering scheme employed (ORTEP plot, 50% probability, SHELXTL PLUS; XP[37]). Only the cation is shown. Hydrogen atoms are omitted for clarity; selected bond lengths [Å] and angles [°]: Ta(1)−C(11) 2.179(4), Ta(1)−C(32) 2.185(4), Ta(1)−C(18) 2.187(4), Ta(1)−C(25) 2.187(4), Ta(1)−Cl(1) 2.5146(9), N(1)−C(11) 1.151(5), N(1)−C(12) 1.460(5), N(2)−C(18) 1.147(5), N(2)−C(19) 1.452(5), N(3)−C(25) 1.154(5), N(3)−C(26) 1.452(5), N(4)−C(32) 1.152(5), N(4)−C(33) 1.459(5); C(11)−Ta(1)−C(32) 84.69(13), C(11)−Ta(1)−C(18) 87.54(14), C(32)−Ta(1)−C(18) 153.37(13), C(11)−Ta(1)−C(25) 153.23(13), C(32)−Ta(1)−C(25) 86.15(13), C(18)−Ta(1)−C(25) 89.51(14), C(11)−Ta(1)−Cl(1) 76.99(10), C(32)−Ta(1)−Cl(1) 76.98(10), C(18)−Ta(1)−Cl(1) 76.46(10), C(25)−Ta(1)−Cl(1) 76.45(10), C(11)−N(1)−C(12) 165.6(4), C(18)−N(2)−C(19) 166.5(4), C(25)−N(3)−C(26) 174.6(4), C(32)−N(4)−C(33) 175.5(4), N(1)−C(11)−Ta(1) 176.1(3), N(2)−C(18)−Ta(1) 176.0(3), N(3)−C(25)−Ta(1) 177.2(3), N(4)−C(32)−Ta(1) 177.7(3).

by crystal structure determination. A molecular ion peak was observed for the cation in **7** by FAB-MS (3-nitrobenzaldehyde as matrix) at m/z = 786. In the ^{31}P NMR spectrum of the reaction mixture, signals for the oxidation products (PPh)$_n$ (n = 4−6)[29] were observed. In addition, two doublets (δ = −57.8 ppm and −121.4 ppm, $^1J_{PP}$ = 311 Hz) were observed, which we could not assign.

Complex **7** crystallises as orange rhombic crystals from THF in the monoclinic space group $P2_1/n$. In the cation (Figure 8), the NC group occupies the axial position in three of the four cyclohexyl groups of the isocyanide ligands. The reason for this unexpected arrangement is the formation of hydrogen bonds between the hydrogen atom of the α-C atom C(26) of the isocyanide ligand in which the NC group is in the equatorial position and the hydrogen atom on the β-C atom of an isocyanide ligand of a second molecule to a chloride anion (Figure 9). However, in solution the four isocyanide ligands are equivalent (^{13}C NMR).

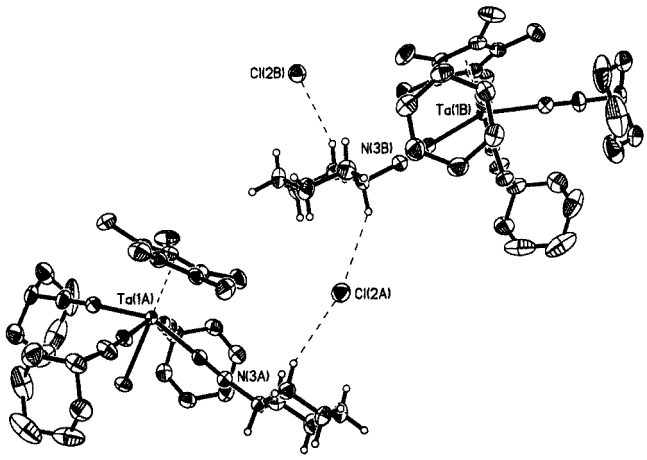

Figure 9. Hydrogen bonding in [Cp*TaCl(CNCy)$_4$]Cl (**7**) (ORTEP plot, 50% probability, SHELXTL PLUS; XP[37]).

For the TaCN group, two mesomeric structures can be formulated (as for carbonyl groups):

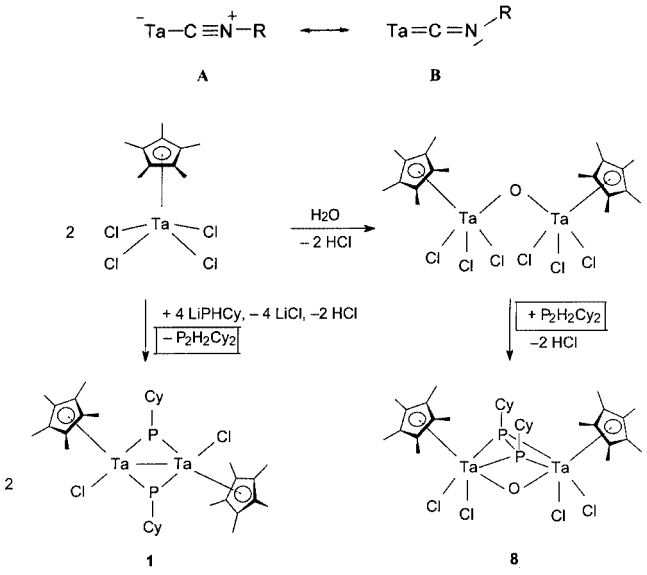

Scheme 4

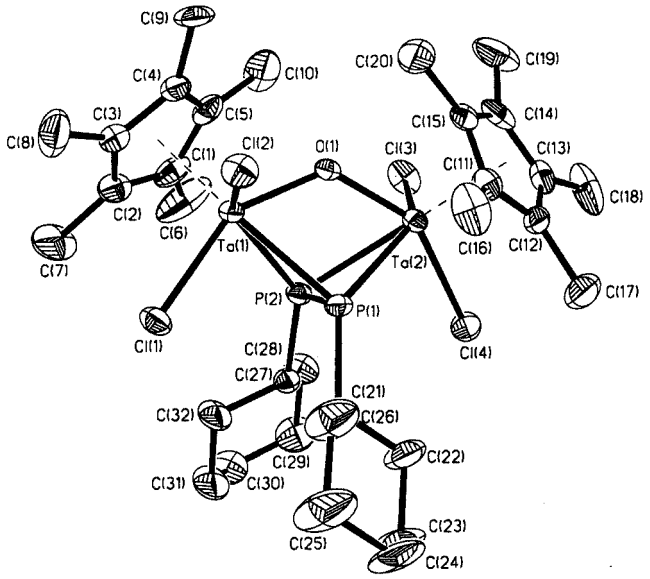

Figure 10. Molecular structure of $[(Cp^*TaCl_2)_2(\mu_2\text{-}O)(\eta^2,\mu_2\text{-}P_2Cy_2)]$ (**8**) showing the atom numbering scheme employed (ORTEP plot, 50% probability, SHELXTL PLUS; XP[37]). Hydrogen atoms are omitted for clarity. Bond lengths [Å] and angles [°]: Ta(2)−O(1) 1.974(6), Ta(2)−Cl(3) 2.413(2), Ta(2)−Cl(4) 2.425(2), Ta(2)−P(1) 2.580(2), Ta(2)−P(2) 2.600(2), Ta(1)−O(1) 1.978(6), Ta(1)−Cl(2) 2.407(2), Ta(1)−Cl(1) 2.413(2), Ta(1)−P(2) 2.578(2), Ta(1)−P(1) 2.602(2), P(1)−C(21) 1.884(9), P(1)−P(2) 2.188(3), P(2)−C(27) 1.864(9); O(1)−Ta(2)−Cl(3) 94.31(18), O(1)−Ta(2)−Cl(4) 148.73(17), Cl(3)−Ta(2)−Cl(4) 88.86(9), O(1)−Ta(2)−P(1) 69.02(17), Cl(3)−Ta(2)−P(1) 137.96(8), Cl(4)−Ta(2)−P(1) 88.01(8), O(1)−Ta(2)−P(2) 67.73(17), Cl(3)−Ta(2)−P(2) 88.14(8), Cl(4)−Ta(2)−P(2) 81.33(8), P(1)−Ta(2)−P(2) 49.97(8), O(1)−Ta(1)−Cl(2) 94.81(17), O(1)−Ta(1)−Cl(1) 148.85(16), Cl(2)−Ta(1)−Cl(1) 90.28(8), O(1)−Ta(1)−P(2) 68.17(17), Cl(2)−Ta(1)−P(2) 137.60(8), Cl(1)−Ta(1)−P(2) 87.57(7), O(1)−Ta(1)−P(1) 68.49(16), Cl(2)−Ta(1)−P(1) 87.88(8), Cl(1)−Ta(1)−P(1) 81.04(8), P(2)−Ta(1)−P(1) 49.97(8), C(21)−P(1)−P(2) 111.3(4), C(21)−P(1)−Ta(2) 138.1(3), P(2)−P(1)−Ta(2) 65.49(9), C(21)−P(1)−Ta(1) 131.2(3), P(2)−P(1)−Ta(1) 64.45(9), Ta(2)−P(1)−Ta(1) 87.02(7), C(27)−P(2)−P(1) 111.2(3), C(27)−P(2)−Ta(1) 138.2(3), P(1)−P(2)−Ta(1) 65.57(9), C(27)−P(2)−Ta(2) 131.0(3), P(1)−P(2)−Ta(2) 64.55(9), Ta(1)−P(2)−Ta(2) 87.10(7), Ta(2)−O(1)−Ta(1) 129.1(3).

As the Ta−C bond lengths of the isocyanide ligands [2.179(4) to 2.187(4) Å] are in the range of Ta−C single bonds and the C−N−C(Cy) groups are almost linear [165.6(4)° to 175.5(4)°], mesomeric structure **A** can be assumed. The Ta atom is located 0.502(2) Å above the plane of the four isocyanide carbon atoms.

As a minor product, $[(Cp^*TaCl_2)_2(\mu_2\text{-}O)(\eta^2,\mu_2\text{-}P_2Cy_2)]$ (**8**) was also obtained in the reaction of $[Cp^*TaCl_4]$ with one equivalent of LiPHCy. **8** was only characterised by crystal structure determination; in the ^{31}P NMR spectrum of the reaction mixture a singlet of low intensity at $\delta = 538.6$ ppm was observed, which could be attributed to **8** or a precursor complex thereof. As two doublets are observed in the high-field region of the ^{31}P NMR spectrum of $[Cp_2TaH(\eta^2\text{-}P_2R_2)]$ (R = Ph:[2a,30] $\delta = -145.1$ ppm and -162.8 ppm, R = Cy:[30] $\delta = -123.1$ ppm and -143.3 ppm) the latter seems more likely.

A possible route for the formation of **8** is hydrolysis of $[Cp^*TaCl_4]$ to give $[(Cp^*TaCl_3)_2(\mu\text{-}O)]$, which can then react with $P_2H_2R_2$ (formed in the redox reaction which gives **1**) to yield the observed product (Scheme 4).

Complex **8** crystallises in the monoclinic space group *Cc*. In **8**, two Cp^*TaCl_2 fragments are bridged by one oxo ligand and a diphosphanediyl group $P_2Cy_2^{2-}$; this indicates the presence of Ta^V (Figure 10). In general, free diphosphenes P_2R_2 are only stable when sterically demanding R groups are present;[31] however, unstable derivatives can be stabilised by coordination to a transition metal.[32] The Ta−P bond lengths [Ta(2)−P(1) 2.580(2), Ta(2)−P(2) 2.600(2), Ta(1)−P(2) 2.578(2), Ta(1)−P(1) 2.602(2) Å] are in the range observed for other tantalum diphosphene complexes [2.602(5) to 2.632(5) Å].[32]

In **8**, the P(1)−P(2) bond length of 2.188(3) Å indicates a single bond. In the tantalum diphosphene complexes $[Cp_2TaH(\eta^2\text{-}P_2R_2)]$ (R = Cy, H) the P−P bond lengths are shorter [2.131(3) and 2.136(6) Å].[30]

Experimental Section

All experiments were carried out under purified dry argon. Solvents were dried and freshly distilled under argon. The NMR spectra were recorded with an AVANCE DRX 400 spectrometer (Bruker), ^1H NMR: internal standard solvent (benzene or $CDCl_3$), external standard $SiMe_4$. ^{13}C NMR: external standard $SiMe_4$, internal standard solvent. ^{31}P NMR: external standard 85% H_3PO_4. The IR spectra were recorded with a FT-IR spectrometer Perkin−Elmer System 2000 in the range 350−4000 cm^{-1}. UV/Vis spectra were recorded in pentane with a LAMBDA 900 (Perkin−Elmer) in an inert-gas cuvette. The melting points were determined in sealed capillaries under argon and are uncorrected. LiPHCy,[11] LiPH*t*Bu,[12] LiPHPh,[13] LiPHMes,[14] [Cp′$TaCl_4$][16] and $[Cp^*TaCl_4]$[10] were prepared by literature procedures.

General Procedure for the Preparation of *trans*-[{Cp*TaCl(μ-PR)}$_2$] [R = Cy (1), *t*Bu (2), Ph (3), Mes (4b)]: A suspension of $[Cp^*TaCl_4]$ in toluene (30 mL) was cooled to −70 °C, and two equivalents of LiPHR were added to the stirred reaction mixture over 2 h. The resulting suspension was slowly warmed to room temperature and stirred overnight. The solvent was removed and the solid dissolved in diethyl ether (**1**, **3**), pentane (**2**), or hexane (**4b**). The mixture was filtered. Deep red crystals were obtained by cooling the filtrate to 5 °C.

The Ta^{IV} phosphinidene complex (Table 1) and the oxidation products $P_2H_2R_2$ (or their decomposition products: cyclic oligophosphanes and the free phosphane RPH_2) were detected by ^{31}P NMR spectroscopy. The following signals were observed for the oxidation products:

*t*Bu: $\delta = -57.5$ ppm [s, $(PtBu)_4$],[29] −71.7 (d) and −108.0 (t) $(PtBu)_3$ ppm.[33]

Cy: $\delta = -68.3$ (s, $PCy)_4$, −84.3 and −87.5 (m, *rac*- and *meso*-$P_2H_2Cy_2$),[29] −111.0 (t, PH_2Cy) ppm.

Ph: δ = ca. 3 [m, $(PPh)_5$], −21.3 [s, $(PPh)_6$], −47.6 [s, $(PPh)_4$][29,34] −67.4, −70.9 (m, *meso*- and *rac*-$P_2H_2Ph_2$; the signal for the unstable diphosphane disappears after two days),[35,36] −122.1 (t, PH_2Ph) ppm.

Mes: $\delta = -43.2$ [s, $(PMes)_4$], −109.3 (d), −143.9 (t) $(PMes)_3$, −110.4, −117.5 (m, *meso*- and *rac*-$P_2H_2Mes_2$), −153.8 (t, PH_2Mes) ppm.

1: (0.45 g, 0.98 mmol) [Cp*$TaCl_4$], (0.48 g, 1.96 mmol) LiPHCy, rhombohedral deep red crystals of **1**·2 Et_2O, yield: 0.40 g (81% rel. [Cp*$TaCl_4$]), m.p. 319 °C (dec.). ^{1}H NMR (400 MHz, C_6D_6, 25 °C): δ = 1.12 [t, $^3J_{H,H}$ = 7.0 Hz, 6 H, CH_3 in ether], 1.38 (m, 4 H, 4-H in Cy), 1.46 (m, 8 H, 3-H/5-H in Cy), 1.76 (m, 8 H, 2-H/6-H in Cy), 2.00 (m, 2 H, 1-H in Cy), 2.20 (s, 30 H, CH_3 in Cp*), 3.27 [q, $^3J_{H,H}$ = 7.0 Hz, 4 H, CH_2 in ether] ppm. ^{13}C{^{1}H} NMR (100.61 MHz, C_6D_6, 25 °C): δ = 14.0 (*C*H_3 in C_5Me_5), 16.2 (*C*H_3 in ether), 27.5 (C-4 in Cy), 30.0 [d, $^3J_{P,C}$ = 19 Hz; C-3/C-5 in Cy], 35.9 [d, $^2J_{P,C}$ = 79 Hz; C-2/C-6 in Cy], 52.1 (br; C-1 in Cy), 66.6 (*C*H_2 in ether), 114.9 (*C*$_5$Me$_5$) ppm. Solvent-free **1**, $C_{32}H_{52}Cl_2P_2Ta_2$ (931.51): C 41.3, H 5.6, Cl 7.6; found C 40.4, H 5.3, Cl 7.2.

2: (0.40 g, 0.87 mmol) [Cp*$TaCl_4$], (0.17 g, 1.77 mmol) LiPH*t*Bu, yield: 0.33 g (86% rel. [Cp*$TaCl_4$]), m.p. 341 °C (dec.), prismatic deep red crystals. ^{1}H NMR (400 MHz, C_6D_6, 25 °C): δ = 1.48 [d, $^3J_{P,H}$ = 14 Hz, 18 H, *t*Bu], 2.18 (s, 30 H, CH_3 in Cp*) ppm. ^{13}C{^{1}H} NMR (100.61 MHz, C_6D_6, 25 °C): δ = 14.8 (*C*H_3 in C_5Me_5), 35.1 [C(*C*H_3)$_3$], 35.6 [*C*(CH$_3$)$_3$], 116.4 (*C*$_5$Me$_5$) ppm. $C_{28}H_{48}Cl_2P_2Ta_2$ (879.40): calcd. C 38.3, H 5.5, Cl 8.1; found C 38.8, H 5.6, Cl 8.1.

3: (0.50 g, 1.09 mmol) [Cp*$TaCl_4$], (0.25 g, 2.20 mmol) LiPHPh, yield: 0.42 g (85% rel. [Cp*$TaCl_4$]), m.p. 341 °C (dec.), rhombohedral deep red crystals. ^{1}H NMR (400 MHz, C_6D_6, 25 °C): δ = 2.03 (s, 30 H, CH_3 in Cp*), 6.97 (br, 2 H, *p*-H in Ph), 7.36 [pseudo t, $^3J_{H,H}$ = 14, $^3J_{P,H}$ = 14 Hz, 4 H, *o*-H in Ph], 8.17 [t, $^3J_{H,H}$ = 14 Hz, 4 H, *m*-H in Ph] ppm. ^{13}C{^{1}H} NMR (100.61 MHz, C_6D_6, 25 °C): δ = 13.6 (*C*H_3 in C_5Me_5), 115.3 (*C*$_5$Me$_5$), 129.7 (*p*-C in Ph), 125.2 (*m*-C in Ph), 136.0 (*o*-C in Ph), 148.6 (*ipso*-C in Ph) ppm. $C_{32}H_{40}Cl_2P_2Ta_2$ (919.38): calcd. Cl 7.7; found Cl 8.1.

4b: (0.40 g, 0.87 mmol) [Cp*$TaCl_4$], (0.28 g, 1.8 mmol) LiPHMes, yield: 0.32 g (73% rel. [Cp*$TaCl_4$]), m.p. 321 °C (dec.), rhombohedral deep red crystals. ^{1}H NMR (400 MHz, C_6D_6, 25 °C): δ = 2.01 (s, 30 H, CH_3 in Cp*), 2.22 (s, 6 H, *p*-Me in Mes), 2.72 (s, 12 H, *o*-Me in Mes), 7.01 (s, 4 H, *m*-H in Mes) ppm. ^{13}C{^{1}H} NMR (100.61 MHz, C_6D_6, 25 °C): δ = 13.3 (*C*H_3 in C_5Me_5), 22.0 (*p*-Me in Mes), 25.9 (*o*-Me in Mes), 115.2 (*C*$_5$Me$_5$), 130.5 (*m*-C in Mes), 132.9 (*p*-C in Mes), 139.4 (*o*-C in Mes), 144.8 (*ipso*-C in Mes) ppm. $C_{38}H_{52}Cl_2P_2Ta_2$ (1003.54): calcd. C 45.5, H 5.2; Cl 7.1; found C 45.9, H 5.4, Cl 7.0.

Synthesis of *cis*-[{Cp*TaCl(μ-PMes)}$_2$] (4a): A suspension of one equivalent of [Cp*$TaCl_4$] (0.5 g, 1.09 mmol) in toluene (30 mL) was cooled to −70 °C, and one equivalent of LiPHMes (0.17 g, 1.09 mmol) was added to the stirred reaction mixture over 3 h. The resulting suspension was stirred at −70 °C for 2 h, and then slowly warmed to room temperature and stirred overnight. The solvent was removed under vacuum, and the solid recrystallised twice from *n*-hexane. Yield: 80 mg (29% rel. LiPHMes); m.p. 289 °C (dec.). ^{1}H NMR (400 MHz, C_6D_6, 25 °C): δ = 2.05 (s, 30 H, CH_3 in Cp*), 2.26 (s, 6 H, *p*-Me in Mes), 2.39 (s, 6 H, *o*-Me in Mes), 2.56 (s, 6 H, *o*-Me in Mes), 6.91 (s, 2 H, *m*-H in Mes), 6.97 (s, 2 H, *m*-H in Mes) ppm. ^{13}C{^{1}H} NMR (100.61 MHz, C_6D_6, 25 °C): δ = 12.9 (*C*H_3 in C_5Me_5), 21.8 (*p*-Me in Mes), 23.1 (*o*-Me in Mes), 24.3 (*o*-Me in Mes), 115.5 (*C*$_5$Me$_5$), 128.0 (*m*-C in Mes), 130.9 (*m*-C in Mes),139.7 (*p*-C in Mes), 142.1 (*o*-C in Mes), 145.7 (*o*-C in Mes), 149.3 (*ipso*-C in Mes) ppm. $C_{38}H_{52}Cl_2P_2Ta_2$ (1003.54): calcd. C 45.5, H 5.2; Cl 7.1; found C 45.8, H 6.0, Cl 6.8.

Synthesis of *cis*-[{Cp′TaCl(μ-PMes)}$_2$] (5): A suspension of [Cp′$TaCl_4$] (0.4 g, 0.99 mmol) in toluene (20 mL) was cooled to −70 °C, and one equivalent of LiPHMes (0.15 g, 0.98 mmol) was added to the stirred reaction mixture over 3 h. The resulting suspension was stirred at −70 °C for 2 h, and then slowly warmed to room temperature and stirred overnight. The solvent was removed in vacuo, and the solid recrystallised twice from *n*-hexane. Yield: 0.19 g (43.5% rel. LiPHMes), rhombohedral orange-red crystals; m.p. 276 °C (dec.). ^{1}H NMR (400 MHz, C_6D_6, 25 °C): δ = 2.00 (s, 6 H, C_5MeH_4), 2.34 (s, 6 H, *p*-Me in Mes), 2.49 (br, 12 H, *o*-Me in Mes), 5.72 (t, $J_{H,H}$ = 2.6 Hz, 4 H, C_5MeH_4), 6.27 (t, $J_{H,H}$ = 2.6 Hz, 4 H, C_5MeH_4), 6.64 (br, 4 H, *m*-H in Mes) ppm. $C_{30}H_{36}Cl_2P_2Ta_2$ (891.33): C 40.4, H 4.1, Cl 8.0; found C 40.6, H 4.2, Cl 7.7.

Synthesis of [Cp*TaCl(CNCy)$_4$]Cl (7): Cyclohexyl isocyanide (0.17 g, 1.6 mmol) was added to a solution of **3** (0.15 g, 0.16 mmol) in toluene (20 mL). Over 3 days, the red solution turned orange. The solvent was removed under vacuum, and the solid recrystallised from THF to give **7** as rhombic orange crystals (0.10 g, 38% rel. to **3**); m.p. 345 °C (dec.). ^{1}H NMR (400 MHz, $CDCl_3$, 25 °C): δ = ca. 1.3 (m, 24 H, 3-H, 4-H, 5-H in Cy), ca. 1.7 (m, 16 H, 2-H, 6-H in Cy), 2.29 (s, 15 H, CH_3 in Cp*), 4.45 (br, 4 H, 1-H in Cy) ppm. ^{13}C{^{1}H} NMR (100.61 MHz, $CDCl_3$, 25 °C): δ = 13.7 (*C*H_3 in C_5Me_5), 23.5 (C-4 in Cy), 26.1 (C-3 and C-5 in Cy), 33.5 (C-2 and C-6 in Cy), 55.4 (C-1 in Cy), 70.3 (*C*NCy) 102.2 (*C*$_5$Me$_5$) ppm. $C_{38}H_{59}Cl_2N_4Ta$ (823.74): C 55.4, H 7.2, Cl 8.6; found C 55.0, H 7.8, Cl 8.4.

Data Collection and Structural Refinement of 1−8: Details of the data collection and crystal structure refinement are summarised in Table 2. Data (Mo-*Kα* , λ = 0.71073 Å) were collected with a Siemens CCD (SMART). All observed reflections were used for determination of the unit cell parameters. The structures were solved by direct methods (SHELXTL PLUS[37]) and subsequent difference Fourier syntheses and refined by full-matrix least-squares on F^2 (SHELXTL PLUS[37]). Restrictions for **1−8**: Ta, Cl, C, O, N and P atoms anisotropic, H atoms located or in calculated positions and refined isotropically. Absorption correction with SADABS[38]. CCDC-181631 (**1**), −181629 (**2**), −181627 (**3**),- 181633 (**4a**), −181635 (**4b**), −181632 (**5**), −181630 (**6**), −181628 (**7**) and CCDC-181634 (**8**) contain the supplementary crystallographic data for this paper. These data can be obtained free of charge at www.ccdc.cam.ac.uk/conts/retrieving.html [or from the Cambridge Crystallographic Data Centre, 12, Union Road, Cambridge CB2 1EZ, UK; Fax: (internat.) +44-1223/336-033; E-mail: deposit@ccdc.cam.ac.uk].

Acknowledgments

We gratefully acknowledge support of this work by the Landesgraduiertenförderung Sachsen (scholarship for S. B.). We thank the company H. C. Starck GmbH & Co. KG for a generous donation of $TaCl_5$.

[1] Eds. E. W. Abel, F. G. A. Stone, G. Wilkinson, *Comprehensive Organometallic Chemistry II*, Volumes 4 and 5, Pergamon Press, **1995**.

[2] [2a] J. C. Leblanc, C. Moïse, *J. Organomet. Chem.* **1989**, *364*, C3−C4. [2b] R. T. Baker, J. C. Calabrese, R. L. Harlow, I. D. Williams, *Organometallics* **1993**, *12*, 830−841. [2c] G. I. Nikonov, L. G. Kuzmina, P. Mountford, D. A. Lemenovskii, *Organometallics* **1995**, *14*, 3588−3591. [2d] G. Bonnet, O. Lavastre, J. C. Leblanc, C. Moïse, *New. J. Chem.* **1988**, *12*, 551−552. [2e] C. Poulard, G. Boni, P. Richard, C. Moïse, *J. Chem. Soc., Dalton Trans.* **1999**, 2725−2730. [2f] O. Lavastre, G. Bonnet, G. Boni, M. M. Kubicki, C. Moïse, *J. Organomet. Chem.* **1997**, *547*, 141−147. [2g] P. Sauvageot, O. Blacque, M. M. Kubicki, S. Juge, C. Moïse, *Organometallics* **1996**, *15*, 2399−2403. [2h] S. Challet, O. Lavastre, C. Moïse, J.-C. Leblanc, *New J. Chem.* **1994**, *18*, 1155−1161.

[3] G. A. A. Hadi, K. Fromm, S. Blaurock, S. Jelonek, E. Hey-Hawkins, *Polyhedron* **1997**, *16*, 721−731.
[4] P. J. Domaille, B. M. Foxmann, T. J. McNeese, S. S. Wreford, *J. Am. Chem. Soc.* **1980**, *102*, 4114−4120.
[5] J. B. Bonanno, P. T. Wolczanski, E. B. Lobkovsky, *J. Am. Chem. Soc.* **1994**, *116*, 11159−11160.
[6] C. C. Cummins, R. R. Schrock, W. M. Davis, *Angew. Chem.* **1993**, *105*, 758−761; *Angew. Chem. Int. Ed. Engl.* **1993**, *32*, 756−759.
[7] S. Blaurock, E. Hey-Hawkins, *Z. Anorg. Allg. Chem.*, in press.
[8] S. Blaurock, E. Hey-Hawkins, *Z. Anorg. Allg. Chem.* **2002**, *628*, 37−40.
[9] M. Culmsee, T. Kruck, G. Meyer, M. S. Wickleder, *Z. Anorg. Allg. Chem.* **2001**, *627*, 1111−1112.
[10] R. D. Sanner, S. T. Carter, W. J. Bruton, Jr., *J. Organomet. Chem.* **1982**, *240*, 157−162.
[11] E. Hey-Hawkins, S. Kurz, *Phosphorus, Sulfur, and Silicon* **1994**, *90*, 281−284.
[12] E. Hey-Hawkins, S. Kurz, J. Sieler, G. Baum, *J. Organomet. Chem.* **1995**, *486*, 229−235.
[13] C. Frenzel, E. Hey-Hawkins, *Phosphorus, Sulfur* **1998**, *143*, 1−17.
[14] E. Hey, F. Weller, *J. Chem. Soc., Chem. Commun.* **1988**, 782−783.
[15] U. Segerer, R. Felsberg, S. Blaurock, G. A. Hadi and E. Hey-Hawkins, Phosphorus, Sulfur **1999**, *144−146*, 477−480; S. Blaurock, *Dissertation*, Universität Leipzig, **2000**; S. Blaurock, G. A. Hadi, E. Hey-Hawkins, *Angew. Chem.* (in preparation).
[16] M. J. Bunker, A. de Cian, M. L. H. Green, J. J. E. Moreau, N. Siganporia, *J. Chem. Soc., Dalton Trans.* **1980**, 2155−2161.
[17] P. B. Hitchcock, M. F. Lappert, W. P. Leung, *Chem. Commun.* **1987**, 1282−1283.
[18] EI for **1−3**, FAB for **4a, 4b**. The mass spectra were recorded with a Varian MAT 711 (EI, 70 eV, source temperature 180 °C. FAB in nitrobenzaldehyde as matrix).
[19] [19a] J. A. M. Canich, F. A. Cotton, *Inorg. Chem.* **1987**, *26*, 3473−3478. [19b] F. A. Cotton, M. P. Diebold, W. J. Roth, *Polyhedron* **1985**, *4*, 1103−1108. [19c] A. J. Scioly, M. L. Luetkens, R. B. Wilson, J. C. Huffmann, A. P. Sattelberger, *Polyhedron* **1987**, *6*, 741−757. [19d] A. P. Sattelberger, R. B. Wilson Jr., J. C. Huffmann, *Inorg. Chem.* **1982**, *21*, 4179−4184. [19e] F. A. Cotton, M. P. Diebold, S. A. Duraj, W. J. Roth, *Polyhedron* **1985**, *4*, 1479−1484.
[20] L. Messerle, *Chem. Rev.* **1988**, *88*, 1229−1254.
[21] G. C. Campbell, J. A. M. Canich, F. A. Cotton, S. A. Duraj, J. F. Haw, *Inorg. Chem.* **1986**, *25*, 287−290.
[22] M. B. Hall, R. F. Fenske, *Inorg. Chem.* **1972**, *11*, 768−775.
[23] L. Pauling, *Die Natur der chemischen Bindung*, Verlag Chemie, Weinheim, **1962**.
[24] A. R. Chakravarty, F. A. Cotton, M. P. Diebold, D. B. Lewis, W. J. Roth, *J. Am. Chem. Soc.* **1986**, *108*, 971−976.
[25] R. J. Burt, G. J. Leigh, D. L. Hughes, *J. Chem. Soc., Dalton Trans.* **1981**, 793−799.
[26] V. C. Gibson, T. P. Kee, W. Clegg, *J. Chem. Soc., Dalton Trans.* **1990**, 3199−3210.
[27] [27a] D. W. Stephan, *Angew. Chem.* **2000**, *112*, 322−328; *Angew. Chem.* **2000**, *39*, 314−329. [27b] F. Mathey, *Multiple Bonds and Low Coordination in Phosphorus Chemistry*, M. Regitz, O. J. Scherer (eds), Thieme, Stuttgart, **1990**, p.38. [27c] F. Mathey, *Angew. Chem.* **1987**, *99*, 285−296; *Angew. Chem. Int. Ed. Engl.* **1987**, *26*, 275−286. [27d] K. D. Dillon, F. Mathey, J. F. Nixon, *Phosphorus: The Carbon Copy*, Wiley, Chichester, **1998**, p.19. [27e] M. J. M. Vlaar, A. W. Ehlers, F. J. J. de Kanter, M. Schakel, A. L. Spek, K. Lammertsma, *Angew. Chem.* **2000**, *112*, 3071−3074; *Angew. Chem. Int. Ed.* **2000**, *39*, 2943−2945. [27f] M. J. M. Vlaar, P. Valkier, A. W. Ehlers, F. J. J. de Kanter, M. Schakel, A. L. Spek, M. Lutz, K. Lammertsma, *Chem. Eur. J.* **2001**, *7*, 3551−3557. [27g] M. J. M. Vlaar, A. W. Ehlers, F. J. J. de Kanter, M. Schakel, A. L. Spek, M. lutz, N. Sigal, Y. Apeloig, K. Lammertsma, *Angew. Chem.* **2000**, *112*, 4296−4299; *Angew. Chem. Int. Ed.* **2000**, *39*, 4127−4130. [27h] M. J. M. Vlaar, F. J. J. de Kanter, M. Schakel, A. L. Spek, M. Lutz, K. Lammertsma, *J. Organomet. Chem.* **2001**, *617−618*, 311− 317. [27i] M. J. M. Vlaar, S. G. A. van Assema, F. J. J. de Kanter, M. Schakel, A. L. Spek, M. Lutz, K. Lammertsma, *Chem. Eur. J.* **2002**, *8*, 58−65. [27j] M. J. M. Vlaar, A. W. Ehlers, M. Schakel, S. B. Clendenning, J. F. Nixon, M. Lutz, A. L. Spek, K. Lammertsma, *Chem. Eur. J.* **2001**, *7*, 3545−3549. [27k] J. B. M. Wit, G. Th. van Eijkel, F. J. J. de Kanter, M. Schakel, A. W. Ehlers, M. Lutz, A. L. Spek, K. Lammertsma, *Tetrahedron* **2000**, *56*, 137−141. [27l] J. B. M. Wit, G. Th. van Eijkel, F. J. J. de Kanter, M. Schakel, A. W. Ehlers, M. Lutz, A. L. Spek, K. Lammertsma, *Angew. Chem.* **1999**, *111*, 2716−2719; *Angew. Chem. Int. Ed.* **1999**, *38*, 2596−2599. (and references therein)
[28] [28a] P. Jernakoff, C. de Meric de Bellefon, G. L. Geoffroy, A. L. Rheingold, S. J. Geib, *Organometallics* **1987**, *6*, 1362−1364. [28b] H.-J. Gosink, H. W. Roesky, H.-G. Schmidt, M. Noltemeyer, E. Irmer, R. Herbst-Irmer, *Organometallics* **1994**, *13*, 3420−3426. [28c] E. Benory, A. Bino, D. Gibson, F. A. Cotton, Z. Dori, *Inorg. Chim. Acta* **1985**, *99*, 137−142. [28d] D. T. Richens, L. Helm, P.-A. Pittet, A. E. Merbach, F. Nicolõ, G. Chapuis, *Inorg. Chem.* **1989**, *28*, 1394−1402. [28e] F. Boutonnet, M. Zablocka, A. Igau, J. Jaud, J.-P. Majoral, J. Schamberger, G. Erker, S. Werner, C. Krüger, *J. Chem. Soc., Chem. Commun.* **1995**, 823−824. [28f] J. de la Mata, R. Fandos, M. Gómez, P. Gómez-Sal, S. Martinez-Carrera, P. Royo, Organometallics **1990**, *9*, 2846−2850. [28g] N. Wiberg, *Lehrbuch der Anorganischen Chemie*, Walter de Gruyter & Co., Berlin, **1985**.
[29]]M. Baudler, K. Glinka, *Chem. Rev.* **1993**, *93*, 1623−1667.
[30] N. Etkin, M. T. Benson, S. Courtenay, M. J. McGlinchey, A. D. Bain, D. W. Stephan, *Organometallics* **1997**, *16*, 3504−3510.
[31] M. Yoshifuji, I. Shima, N. Inamoto, K. Hirotsu, T. Higuchi, *J. Am. Chem. Soc.* **1981**, *103*, 4587−4589.
[32] [32a] J. C. Green, M. L. H. Green, G. E. Morris, *J. Chem. Soc., Chem. Commun.* **1974**, 212−213. [32b] P. S. Elmers, M. L. Scudder, B. O. West, *J. Organomet. Chem.* **1976**, *122*, 281−288. [32c] B. Deppisch, H. Schäfer, *Acta Crystallogr., Sect. B* **1982**, *38*, 748−751. [32d] M. M. Olmstead, P. P. Power, *J. Am. Chem. Soc.* **1984**, *106*, 1495−1496. [32e] J. Chatt, P. B. Hitchcock, A. Pidcock, C. P. Warrens, K. R. Dixon, *J. Chem. Soc., Chem. Commun.* **1982**, 932−933. [32f] A. H. Cowley, J. E. Kilduff, J. G. Lasch, N. C. Norman, M. Pakulski, F. Ando, T. C. Wright, *Organomet.* **1984**, *3*, 1044−1050. [32g] S. Kurz, E. Hey-Hawkins, *J. Organomet. Chem.* **1993**, *462*, 203−207.
[33] M. Baudler, J. Hahn, H. Dietsch, G. Fürstenberg, *Z. Naturforsch., Teil B* **1976**, *31*, 1305−1310.
[34] [34a] M. Baudler, B. Carlsohn, W. Böhm, G. Z. Reuschenbach, *Z. Naturforsch., Teil B* **1976**, *31*, 558−564. [34b] M. Baudler, G. Reuschenbach, *Z. Anorg. Allg. Chem.* **1980**, *464*, 9−16.
[35] M. Baudler, B. Carlson, D. Koch, P. K. Medda, *Chem. Ber.* **1978**, *111*, 1210−1216.
[36] [36a] G. Becker, M. Rössler, E. Schneider, *Z. Anorg. Allg. Chem.* **1978**, *439*, 121−133. [36b] C. Frenzel, *Dissertation*, Universität Leipzig, **1999**.
[37] SHELXTL PLUS, Siemens Analyt. X-ray Inst. Inc., **1990**, XS: *Program for Crystal Structure Solution*, XL: *Program for Crystal Structure Determination*, XP: *Interactiv Molecular Graphics.*
[38] R. H. Blessing, *Acta Crystallogr., Sect. A* **1995**, *51*, 33−38.
[39] S. Kurz, *Dissertation*, Universität Leipzig, **1994**.
[40] D. Feitler, G. M. Whitesides, *Inorg. Chem.* **1976**, *15*, 466−469.
[41] A. Cowley, N. C. Norman, M. Pakulski, *Inorg. Syn.* **1990**, *27*, 235−240.

Received March 15, 2002
[I02138]

Bis[bis(dialkylamino)phosphanyl]methanes and Bis(trifluoromethyl)acrylonitrile — Reactions and Derivatives

Igor Shevchenko,*[a] Vasyl Andrushko,[a] Enno Lork,[b] and Gerd-Volker Röschenthaler*[b]

Keywords: Ylides / Phosphanes / Nitriles / Hexafluoroacetone

The reaction of bis[bis(dialkylamino)phosphanyl]methanes **1a,b** with bis(trifluoromethyl)acrylonitrile **8** led to the ylides **10a,b** which showed an interesting ability for self-fluorination involving trifluoromethyl groups to give the P–F derivatives **13a,b**. An X-ray analysis and NMR spectroscopic data showed that molecules of **10a,b** have different conformations in solution and in the crystal. Compounds **10a,b** reacted further with **8** to give either the symmetrical diylide **16a** or the P–F derivative **13b**. The addition of hexafluoroacetone to **10a,b** resulted in the formation of unsymmetrical diylides **19a,b**.

(© Wiley-VCH Verlag GmbH, 69451 Weinheim, Germany, 2002)

Introduction

Previously we have described the unusual reaction of hexafluoroacetone (HFA) with bis[bis(dialkylamino)phosphanyl]methanes **1a,b**, which does not lead to the expected phosphoranes **2a,b**,[1–4] in which one of the phosphorus atoms is included into 1,3,2-dioxaphospholane heterocycles, but yields quantitatively the carbodiphosphoranes **3a,b** (Scheme 1).[5,6]

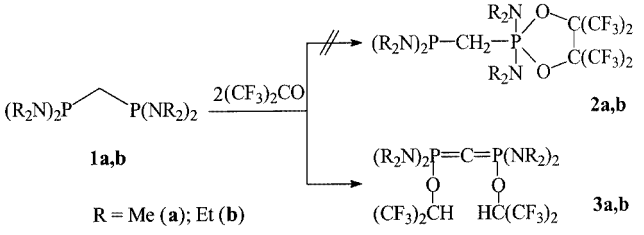

Scheme 1

Taking into account the unusual nature of this reaction we were interested in studying its scope by substituting the carbonyl function of hexafluoroacetone with a C=C double bond. In this paper we describe the reaction of the bis[bis(dialkylamino)phosphanyl]methanes **1a,b** with alkenes in which the C=C double bond is activated by two trifluoromethyl groups.

[a] Institute of Bioorganic Chemistry,
Murmanskaya Street 1, 02094 Kiev, Ukraine
Fax: (internat.) +38-044/573-2552
E-mail: ishev@bpci.kiev.ua
[b] Institute of Inorganic and Physical Chemistry, Universität Bremen, NW2, C2350,
Leobener Str, 28334 Bremen, Germany
Fax: (internat.) + 49-(0)421/218-4267
E-mail: gvr@chemie.uni-bremen.de

The interaction of tertiary phosphanes with compounds containing activated carbon-carbon double bonds to give phosphorus ylides is well known. The first step of this interaction is the formation of the intermediate zwitterionic compounds **A** (Scheme 2), containing a carbanion in the β-position to the phosphorus atom. Sometimes such intermediates can be isolated as stable compounds.[7–10] Then, a migration of the more acidic α-proton to the β-carbon is observed to give the appropriate ylides **B**. In some cases a similar migration is found for fluorine.[11,12] The forms **A** and **B** are in equilibrium with each other, and this equilibrium is usually shifted completely to the thermodynamically more stable form **B**. When this interconversion is separated by a high barrier, the two forms can be isolated as separate stable isomers.[13]

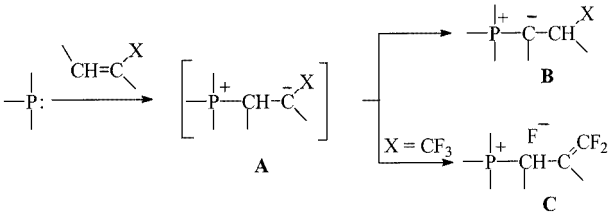

Scheme 2

We reasoned that if the C=C double bond of the starting alkene is activated by a CF_3 group (X = CF_3) the intermediate zwitterionic compound **A** can be alternatively stabilized by the elimination of a fluoride anion to give structure **C**. Such reactions have not been studied yet in the chemistry of phosphorus ylides, although the elimination of F^- from the α-position of a carbanion is well-known in fluorine chemistry.[14–17]

The second objective of the present investigation was to use methylenediphosphanes containing the fragment

P−C−P. Such compounds have not yet been investigated in their reactions with alkenes, to the best of our knowledge. The only known close example is the reaction of methylenebis(diphenylphosphane) (**4**) with the methyl ester of acetylenedicarboxylic acid,[18] which gave a mixture of *E*/*Z* isomers of the stable cyclic ylide **5** (Scheme 3)

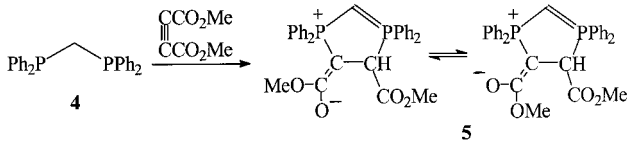

Scheme 3

Results and Discussion

The activation of ethylene by two trifluoromethyl groups, as in compound **6**, turned out to be insufficient for the electrophilic attack of the trivalent phosphorus atom. The reaction of **1b** even with a threefold excess of 1,1-bis(trifluoromethyl)ethylene (**6**) proceeded very slowly (Scheme 4). After heating the reaction mixture in hexane in a sealed tube at 60 °C for 18 h, only traces of product **7** were detected by ^{31}P NMR spectroscopy as two characteristic doublets at δ = 34 and 78 ppm ($^2J_{P,P}$ = 76.4 Hz). The reaction rate increased in more polar solvents (CH_2Cl_2, $CHCl_3$), although it still required heating for a long period, which led to substantial decomposition of **7** and prevented its isolation in pure form.

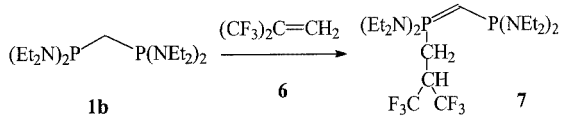

Scheme 4

The presence of a nitrile group at the double bond, as in bis(trifluoromethyl)acrylonitrile (**8**), renders this compound much more reactive towards methylenediphosphanes **1a,b**. The reaction of **8** with **1a,b** proceeds rapidly in hexane solution at −15 °C to give ylides **10a,b** almost quantitatively (Scheme 5)

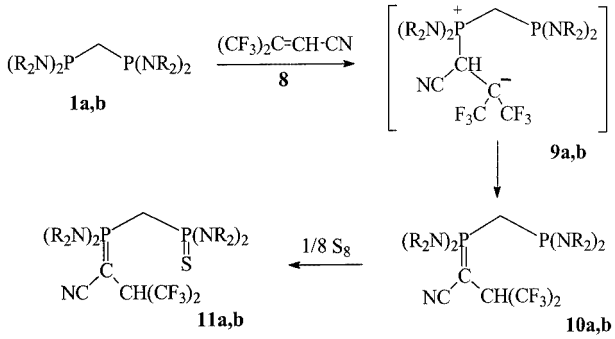

Scheme 5

The first step of this reaction is the formation of the intermediate betaines **9a,b**. However, at −15 °C the stability of these compounds is determined not by a fluoride ion elimination, but by a standard proton migration to give the ylides **10a,b**. Compounds **10a,b** can be isolated in good yields as colorless crystalline products. The structure of compounds **10a,b** and, in particular, the position of the ylidic bond, have been confirmed by NMR spectroscopy. For example the P−C−P carbon atom of **10a** appears as a doublet of doublets at δ = 26 ppm, whereas the negatively charged ylidic carbon atom P-*C*−CN appears with a characteristic high field chemical shift at δ = 10.8 ppm with a large $J_{P,C}$ coupling constant of 180 Hz. It is interesting to note that unlike the doublet of doublets of the $P-CH_2-P$ carbon atom in the ^{13}C NMR spectrum, the two equivalent protons of this unit appear in the ^1H NMR spectrum as only one doublet, probably because one of the two $^2J_{P,H}$ coupling constants is close to zero.

The second interesting peculiarity of compounds **10a,b** is the "through-space" spin-spin interaction between the $(CF_3)_2CH$ unit and the tricoordinate phosphorus atom. In the $^{31}P\{^1H\}$ NMR spectra the P^{III} phosphorus appears as a doublet of septuplets with $J_{P,F}$ = 3.0 Hz (**10a**) or 2.9 Hz (**10b**). All the fluorine atoms are equivalent and appear as a doublet of doublets in the ^{19}F NMR spectra, one of the doublets having the same $J_{P,F}$ coupling constant. In addition, the *C*H$(CF_3)_2$ carbon atom has a $J_{P,C}$ coupling constant of 6 Hz in the ^{13}C NMR spectrum. It should be noted that this spin-spin through-space interaction does not lead to a rigid cyclic conformation of compounds **10a,b**: the $(CF_3)_2CH$ group have a possibility for rotation, otherwise the equivalence of all fluorine nuclei should be accounted for by the appropriate symmetry of the molecule.

The structure of compound **10a** in the crystal was solved by X-ray analysis (Figure 1).

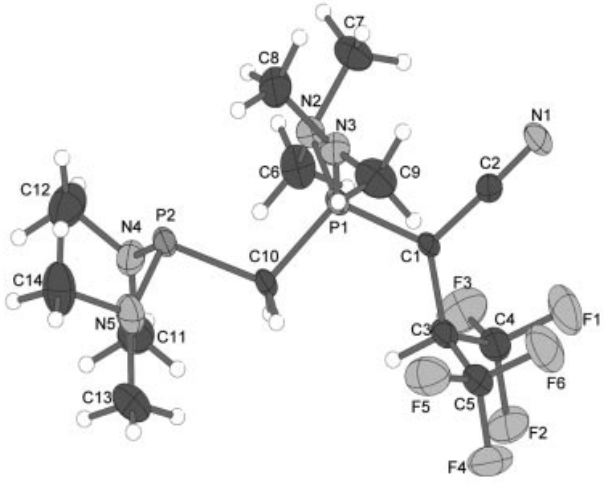

Figure 1. Perspective view and labeling scheme for the molecule **10a**; selected bond lengths [pm] and angles [°]: P(1)−C(1) 172.6(3), P(1)−C(10) 180.2(3), P(1)−N(2) 166.6(3), P(1)−N(3) 164.8(3), C(10)−P(2) 187.6(3), C(1)−C(2) 139.8(5), C(2)−N(1) 116.4(5), C(1)−C(3) 149.6(5); C(1)−P(1)−C(10) 109.07(16), P(1)−C(10)−P(2) 112.05(18), C(2)−C(1)−C(3) 121.3(3), C(2)−C(1)−P(1) 113.8(3), C(3)−C(1)−P(1) 124.9(2), N(1)−C(2)−C(1) 177.8(4); C(1)−P(1)−C(10)−P(2) −179.9(2), C(10)−P(1)−C(1)−C(2) −172.6(3), C(10)−P(1)−C(1)−C(3) 7.5(4)

In crystalline form the molecule of **10a** is rather symmetrical as the C(1), P(1), C(10), P(2) atoms are situated exactly in the same plane. The appropriate dihedral angle has a value of −179.9(2)°. The neighboring C(2) and C(3) atoms are only slightly deviated from this plane. For example, the C(10)−P(1)−C(1)−C(3) dihedral angle is 7.5(4)°. The two adjacent nitrogen atoms N(2) and N(3) have a slightly different configuration. The N(3) atom is almost flat, whereas the N(2) atom has a more pronounced tetrahedral geometry [the sums of angles are 357.3(8)° and 343.6(9), respectively]. In solution, however, both the dimethylamino groups are equivalent and display a common signal at δ = 2.49 ppm in the ^{1}H NMR spectrum.

The ylidic carbon C(1) has an ideal flat conformation which is accounted for by the delocalization of the negative charge on the nitrile group; this is why the P(1)−C(1) bond (172.6 pm) is somewhat longer than the normal ylidic bond (168 pm),[19] whereas the C(1)−C(2) distance is considerably shorter (139.8 pm) than the average single C−C bond. These data are consistent with the structure of other nitrile-substituted phosphorus ylides.[20−22]

As is seen from the structure of **10a**, because of the large distance between P(1) and the fluorine atoms their spin-spin through-space interaction is hardly possible in the crystalline form. In solution, however, the molecule should have different conformations in which the bis(dimethylamino)-phosphane unit and the trifluoromethyl groups are close to each other due to rotation around the P(1)−C(10) and C(1)−C(3) bonds. This conclusion is also supported by the fact that the spin-spin through-space interaction in compounds **10a,b** disappears upon sulfuration of the phosphane center. All the fluorine atoms of the thio derivatives **11a,b** are equivalent and appear as one clear doublet in the ^{19}F NMR spectra at δ = −67 ppm ($^3J_{H,F}$ = 8 Hz).

Compounds **10a,b** are rather stable in the crystalline form and in solution at −15 °C. At room temperature, however, they slowly decompose (over several days) into the monofluorides **13a,b** (Scheme 6). At 60 °C this process takes several hours. The stability of **10a,b** is probably determined by the presence of CF_3 groups in the α-position to the carbanion of the equilibrium forms **9a,b**. The elimination of the fluoride ion from the non-phosphorus analogs of **9a,b** can lead, in some cases, to stable products containing a perfluoroisopropenyl unit.[17] However, the elimination of F^- from **10a,b** probably goes via the unstable intermediates **12a,b**, which quickly decompose forming HF and a complex mixture of unidentified products. Thus, one half of the ylide molecules **10a,b** is formally used in their decomposition as a source of HF, which then reacts with the second half to give the monofluoro derivatives **13a,b**. Further transformation of **13a,b** into difluoro derivatives was not observed. The proposed mechanism was confirmed by the addition of HF (as $Et_3N{\cdot}3HF$) to compounds **10a,b**, giving the monofluorides **13a,b**. This result is consistent with the decomposition of carbodiphosphoranes **3a,b** and the formation of P−F bonds.[6]

The structure of compounds **13a,b** was confirmed by NMR spectroscopy and by their reaction with silylated amines, which led to the starting materials **10a,b**. One of the two phosphorus atoms in **13a,b** is asymmetric, which is why these compounds exist as a mixture of enantiomers. The diethylamino derivative **13b** was isolated as a crystalline product. Although the nucleophilicity of the phosphorus atom P^{III} in this compound is substantially reduced, it can be sulfurated with elemental sulfur to give **14b**. This process leads to the disappearance of the free rotation around one of the P−C bonds, hence **14b** was isolated as a mixture of diastereomers. Unlike starting compound **13b** the two trifluoromethyl groups in **14b** are inequivalent and appear as two quadruplets in the ^{19}F NMR spectrum. An interesting peculiarity of the sulfurated derivative is that the P−F fluorine is coupled with only one proton of the P−CH_2−P unit, the second coupling constant being equal or very close to zero. The presence of only one proton between two phosphorus is excluded as the chemical shift of the appropriate carbon atom in the ^{13}C NMR spectrum does not differ from that of compound **13b**.

The trivalent phosphorus of compounds **10a,b** is able to react further with **8**. However, the pathway of this reaction depends on the steric situation in compounds **10a,b**. The diethylamino derivative **10b** reacts slowly with **8** at room temperature and does not give the expected diylide but yields the monofluoro derivative **13b** as the main product (Scheme 7). According to the spectroscopic data the yield of monofluoride **13b** is about 70%, which is why its formation cannot be accounted for by the decomposition of the start-

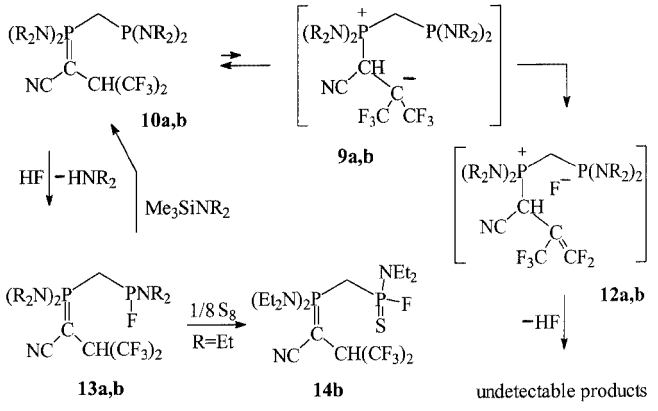

Scheme 6

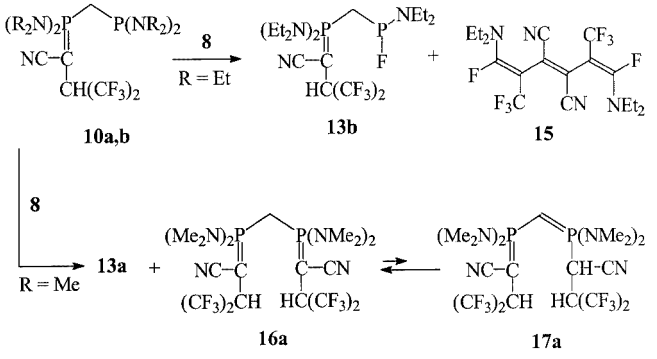

Scheme 7

ing material. Bis(trifluoromethyl)acrylonitrile (**8**) acts as a fluorinating agent in this unusual reaction, transforming into the novel fluorinated triene **15**.[23] It is interesting to note that one of the trifluoromethyl groups of the acrylonitrile **8** looses two fluorine atoms and adds one of the diethylamino groups which was initially connected to one trivalent phosphorus atom of **10b**. Triene **15** was isolated as a slightly yellow crystalline product. The detailed structure of this compound was determined by X-ray analysis.[23]

The reaction of the less bulky dimethylamino derivative **10a** with **8** is much easier and gives a mixture of monofluoro derivative **13a** and the expected diylide **16a** in the ratio 35:65. The same result was obtained when two equivalents of **8** were added to the starting bis[bis(dialkylamino)phosphanyl]methane (**1a**). The formation of compound **13a** is not a result of decomposition of **16a**, as this ratio does not change after completion of the reaction. The mechanism of fluorination of **10a** by **8** does not, therefore, include the formation of **16a** as an intermediate product.

Diylide **16a** was isolated as a stable crystalline product, the structure of which was confirmed by NMR spectroscopy. Despite the fact that the $P-CH_2-P$ hydrogen atoms are situated between the two positively charged phosphorus atoms and are therefore rather acidic, the possible unsymmetrical structure **17a** was not detected. Thus, the equilibrium between **16a** and **17a** is completely shifted to the symmetrical form. The NMR spectroscopic data showed that the two phosphorus atoms and all their substituents are equivalent. The methylene group $P-CH_2-P$ appears as a triplet and the two ylidic carbon atoms as a characteristic doublet at $\delta = 12.0$ ppm ($^1J_{P,C} = 197$ Hz) in the ^1H and ^{13}C NMR spectra. Analogously to other symmetrical compounds containing central P−P or P−C−P fragments in which two phosphorus atoms are divided by a plane of symmetry, the diylide **16a** shows characteristic signals of an AA′XX′ spin system. The two tertiary carbon atoms of the $(CF_3)_2CH$ units are equivalent and appear as a clear septet of triplets in the ^{13}C NMR spectrum, each carbon having the same coupling constants with the two phosphorus atoms and vice versa. The two protons of the $(CF_3)_2CH$ groups show the same effect. However, because of the equality of the $^3J_{P,H}$ and $^3J_{H,F}$ coupling constants the spectrum appears as a multiplet of nine lines. Earlier we observed the analogous coupling for the same protons of carbodiphosphoranes **3a,b**.[5]

The presence of ylidic and trivalent phosphorus bridged by a methylene group makes compounds **10a,b** interesting synthons for further investigations. We were interested in the reaction of **10a,b** with hexafluoroacetone as it could answer the question as to whether the formation of carbodiphosphoranes described at the beginning of this paper is an exception or is more common.

We found that HFA reacts easily with ylides **10a,b** giving compounds **19a,b**, which were isolated as stable crystalline products, quantitatively (Scheme 8). The reaction proceeds via the intermediate zwitterionic structure **18a,b**, followed by proton migration from the $P-CH_2-P$ unit to the $(CF_3)_2C^-$ carbanion. As ylidic bonds are extremely polarized, the compounds **19a,b** can be considered as structures with alternating charges $P^+-C^--P^+-C^-$. Compounds **19a,b** should be in equilibrium with the carbodiphosphorane structures **20a,b**, although according to NMR spectroscopic data this equilibrium is shifted towards **19a,b**. For example, the $P-HC^--P$ proton appears in the ^1H NMR spectra as a doublet of doublets at high field ($\delta =$ 0.63 ppm). The two negatively charged ylidic carbon atoms are clearly seen in the ^{13}C NMR spectra at $\delta = 7.6$ and 15.6 ppm. The latter value, corresponding to the $C-CN$ carbon atom, is shifted slightly to low field compared with starting ylides **10a,b** which can be accounted for by the presence of the isomeric forms **20a,b**.

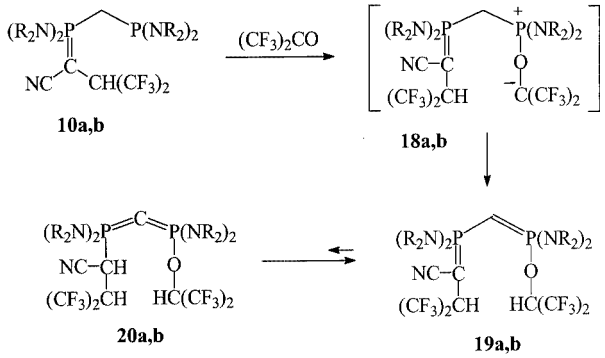

Scheme 8

Experimental Section

General Remarks: All operations were performed under nitrogen in a dry box. The solvents were dried by standard procedures. The NMR spectra were recorded with a JEOL FX-90Q and Varian 300 MHz spectrometers. The ^1H and ^{13}C chemical shifts are referenced to external tetramethylsilane (TMS). The ^{31}P chemical shifts are referenced to 85% aqueous orthophosphoric acid as an external standard. As usual, downfield shifts are given positive signs. The digital resolutions were 0.25, 0.5 Hz and 1.25 Hz for ^1H, ^{13}C and ^{31}P NMR spectra respectively.

Compound 10a: Bis(trifluoromethyl)acrylonitrile (**8**; 400 mg, 2.12 mmol) in 2 mL of diethyl ether was cooled to −15 °C and added to a solution of methylenebis(dimethylaminophosphane) (**1a**; 500 mg, 1.98 mmol) in 10 mL of hexane at the same temperature. The reaction mixture was maintained at −15 °C for 48 h. The colorless crystals of **10a** formed over this time were separated and recrystallized from chloroform/diethyl ether (1:2) at −15 °C, (681 mg, 78%), m.p. 72−74 °C. ^1H NMR ($CDCl_3$): $\delta = 2.13$ [d, $^2J_{P(1),H} = 13.5$, $^2J_{P(2),H} = 0$ Hz, 2 H, $P-CH_2-P$], 2.45 [d, $^3J_{P,H} =$ 10.0 Hz, 12 H, $N(CH_3)_2$], 2.49 [d, $^3J_{P,H} = 10.0$ Hz, 12 H, $N(CH_3)_2$], 3.34 [m, 1 H, $CH(CF_3)_2$] ppm. ^{13}C NMR ($CDCl_3$): $\delta = 10.78$ (dm, $J_{P,C} = 180.0$ Hz, 1 C, PCCN), 26.22 (dd, $^1J_{P,C} = 25.4$, $^1J_{P,C} =$ 85.8 Hz, PCP), 36.60 (d, $^2J_{P,C} = 2.9$ Hz, 2 C, NMe_2), 36.76 (d, $^2J_{P,C} = 3.9$ Hz, 2 C, NMe_2), 40.40 (d, $^2J_{P,C} = 15.6$ Hz, 4 C, NMe_2), 45.62 [sept. dd, $^2J_{P,C} = 16.6$, $J_{P,C} = 5.9$, $^2J_{F,C} = 29.3$ Hz, 1 C, $CH(CF_3)_2$], 124.20 (q, $^1J_{F,C} = 282.9$ Hz, 2 C, CF_3), 125.02 (d, $^2J_{P,C} = 10.8$ Hz, CN) ppm. ^{19}F NMR ($CDCl_3$): $\delta = -67.5$ (dd, $^3J_{H,F} = 8.3$, $J_{P,F} = 3.0$ Hz, 6 F) ppm. ^{31}P NMR ($CDCl_3$): $\delta =$ 66.94 (d, $^2J_{P,P} = 85.3$ Hz), 79.19 (sept. d, $^2J_{P,P} = 85.3$, $J_{F,P} =$

3.0 Hz) ppm. $C_{14}H_{27}F_6N_5P_2$ (441.34): calcd. C 38.10, H 6.17; found C 37.18, H 5.82.

Compound 10b: Bis(trifluoromethyl)acrylonitrile (**8**; 233 mg, 1.23 mmol) in hexane (3 mL) was cooled to −15 °C and added to a solution of methylenebis(diethylaminophosphane) (**1b**; 418 mg, 1.15 mmol) in hexane (5 mL) at the same temperature. The reaction mixture was maintained at −15 °C for 24 h. The colorless or light-yellow crystals of **10b** formed over this time were separated and washed with hexane (2 × 2 mL). Yield 496 mg (78%), 68−72% after crystallization from diethyl ether/hexane at −15 °C, m.p. 62−64 °C. ^{1}H NMR ($CDCl_3$): δ = 1.01 (t, $^3J_{H,H}$ = 7.07 Hz, 12 H, CH_2CH_3), 1.14 (t, $^3J_{H,H}$ = 7.07 Hz, 12 H, NCH_2CH_3), 2.27 [d, $^2J_{P(1),H}$ = 16.1, $^2J_{P(2),H}$ = 0 Hz, 2 H, P−CH_2−P], 3.09 (m, 16 H, N NCH_2CH_3), 3.44 [m, 1 H, $CH(CF_3)_2$] ppm. ^{13}C NMR ($CDCl_3$): δ = 13.13 (d, $^3J_{P,C}$ = 1.9 Hz, 4C, NCH_2CH_3), 13.17 (dm, $J_{P,C}$ = 214.6 Hz, 1C, $PCCN$), 13.5 (d, $^3J_{P,C}$ = 3.9 Hz, 4C, NCH_2CH_3), 28.09 (dd, $^1J_{P,C}$ = 21.5, $^1J_{P,C}$ = 80.0 Hz, PCP), 39.19 (d, $^2J_{P,C}$ = 3.9 Hz, 2C, NCH_2CH_3), 39.34 (d, $^2J_{P,C}$ = 2.9 Hz, 2C, NCH_2CH_3), 42.20 (d, $^2J_{P,C}$ = 16.6 Hz, 4C, NCH_2CH_3), 46.40 [sept. dd, $^2J_{P,C}$ = 17.8, $J_{P,C}$ = 9.0, $^2J_{F,C}$ = 29.3 Hz, 1C, $CH(CF_3)_2$], 124.12 (q, $^1J_{F,C}$ = 282.0 Hz, 2C, CF_3), 125.66 (d, $^2J_{P,C}$ = 9.9 Hz, CN) ppm. ^{19}F NMR ($CDCl_3$): δ = −66.93 (dd, $^3J_{H,F}$ = 7.8, $J_{P,F}$ = 2.9 Hz, 6F) ppm. ^{31}P NMR ($CDCl_3$): δ = 73.78 (d, $^2J_{P,P}$ = 102.4 Hz), 67.18 (sept. d, $^2J_{P,P}$ = 102.4, $J_{F,P}$ = 2.9 Hz) ppm. $C_{22}H_{43}F_6N_5P_2$ (553.56): calcd. C 47.74, H 7.83; found C 47.69, H 7.75.

Compounds 11a, 11b: Sulfur (16 mg) was added to a solution of **10a** or **10b** (0.4 mmol) in 2 mL of CH_2Cl_2 at 20 °C. After 2 h the solution was filtered, the solvent was evaporated and the residue was recrystallized from CH_2Cl_2/hexane (1:2) at −15 °C.

11a: Yield 142 mg (75%), m.p. 125−128 °C. ^{1}H NMR ($CDCl_3$): δ = 2.48 [d, $^3J_{P,H}$ = 12.6 Hz, 6 H, $N(CH_3)_2$], 2.63 [d, $^3J_{PH}$ = 10.3 Hz, 6 H, $N(CH_3)_2$], 2.83 (t, $^2J_{P(1),H}$ = $^2J_{P(2),H}$ = 15.8 Hz, 2 H, P−CH_2−P), 3.54 [m, 1 H, $CH(CF_3)_2$] ppm. ^{13}C NMR ($CDCl_3$): δ = 12.81 (dm, $J_{P,C}$ = 186.3 Hz, 1C, $PCCN$), 27.73 (dd, $^1J_{P,C}$ = 88.8, $^1J_{P,C}$ = 90.7 Hz, PCP), 36.56 (d, $^2J_{P,C}$ = 2.9 Hz, 4C, NMe_2), 37.23 (d, $^2J_{P,C}$ = 3.9 Hz, 4C, NMe_2), 46.27 [sept.d , $^2J_{P,C}$ = 14.6, $^2J_{F,C}$ = 29.3 Hz, 1C, $CH(CF_3)_2$], 124.20 [q, $^1J_{F,C}$ = 284.8 Hz, 2(CF_3)], 124.70 (d, $^2J_{P,C}$ = 13.7 Hz, CN) ppm. ^{19}F NMR ($CDCl_3$): δ = −66.95 (d, $^3J_{H,F}$ = 7.8 Hz, 6F) ppm. ^{31}P NMR ($CDCl_3$): δ = 61.46 ($^2J_{P,P}$ = 1.2 Hz), 72.12 ($^2J_{P,P}$ = 1.2 Hz) ppm. $C_{14}H_{27}F_6N_5P_2S$ (473.40): calcd. C 35.52, H 5.75; found C 35.14, H 5.35.

11b: Yield 176 mg (75%), m.p. 106−109 °C. ^{1}H NMR ($CDCl_3$): δ = 1.11 (t, $^3J_{H,H}$ = 7.03 Hz, 12 H, NCH_2CH_3), 1.16 (t, $^3J_{H,H}$ = 7.03 Hz, 12 H, NCH_2CH_3), 2.7−3.2 (m, 2 H, P−CH_2−P, 16 H, NCH_2CH_3), 3.09 (m, 16 H, NCH_2CH_3), 3.45 [m, 1 H, $CH(CF_3)_2$] ppm. ^{13}C NMR ($CDCl_3$): δ = 13.43 (d, $^3J_{P,C}$ = 3.9 Hz, 4C, NCH_2CH_3), 13.67 (d, $^3J_{P,C}$ = 2.9 Hz, 4C, NCH_2CH_3), 13.87 (dm, $J_{P,C}$ = 195.05 Hz, 1C, $PCCN$), 27.74 (dd, $^1J_{P,C}$ = 28.8, $^1J_{P,C}$ = 90.7 Hz, PCP), 39.51 (d, $^2J_{P,C}$ = 2.9 Hz, 4C, NCH_2CH_3), 40.07 (d, $^2J_{P,C}$ = 4.9 Hz, 4C, NCH_2CH_3), 46.27 [sept. d, $^2J_{P,C}$ = 14.6 Hz, $^2J_{F,C}$ = 29.3 Hz, 1C, $CH(CF_3)_2$], 124.23 [q, $^1J_{F,C}$ = 284.8 Hz, 2(CF_3)], 124.70 (d, $^2J_{P,C}$ = 13.7 Hz, CN) ppm. ^{19}F NMR ($CDCl_3$): δ = −66.70 (d, $^3J_{H,F}$ = 8.0 Hz, 6F) ppm. ^{31}P NMR ($CDCl_3$): δ = 63.71 (d, $^2J_{P,P}$ = 7.3 Hz), 69.77 (d, $^2J_{P,P}$ = 7.3 Hz) ppm. $C_{22}H_{43}F_6N_5P_2S$ (585.62): calcd. C 45.12, H 7.40, N 11.96; found C 44.89, H 6.96, N 11.23.

Compound 13b: Compound **8** (170 mg, 0.90 mmol) was added to a solution of **10b** (400 mg, 0.72 mmol) in toluene (2 mL) and the reaction mixture was left at room temperature for 7 days. If the ^{31}P NMR spectrum showed the residual starting material **10b** the reaction mixture was heated at 70 °C for about 15 min. (NB The reaction can be carried out at elevated temperature, although the yield is then lower.) The solvent was removed in vacuo and the remaining thick dark-brown oil was thoroughly washed with cold hexane (2 × 1 mL) at −15 °C. The product was then extracted with boiling hexane (5 × 3 mL) and the obtained solution was left overnight at −15 °C. Light yellow crystalline product, yield 184 mg (51%), after re-crystallization from hexane 137 mg (38%). M.p. 90−91 °C. ^{1}H NMR ($CDCl_3$): δ = 1.14 (t, $^3J_{H,H}$ = 7.03 Hz, 6 H, NCH_2CH_3), 1.16 (t, $^3J_{H,H}$ = 7.03 Hz, 12 H, NCH_2CH_3), 2.3−2.7 (m, 2 H, P−CH_2−P), 2.9−3.4 [m, 12 H, NCH_2CH_3, 1 H, $CH(CF_3)_2$] ppm. ^{13}C NMR ($CDCl_3$): δ = 12.68 (dm, $J_{P,C}$ = 238.9 Hz, 1C, $PCCN$), 13.48 (m, 4C, NCH_2CH_3), 15.13 (m, 2C, NCH_2CH_3), 34.26 (ddd, $^1J_{P,C}$ = 19.5, $^1J_{P,C}$ = 87.8, $^2J_{F,C}$ = 48.8 Hz, PCP), 39.36 (m, 4C, NCH_2CH_3), 42.89 (d, $^3J_{F,C}$ = 18.5 Hz, 2C, NCH_2CH_3), 47.44 [m, 1C, $CH(CF_3)_2$], 124.16 [q, $^1J_{F,C}$ = 281.8 Hz, 2(CF_3)], 124.90 (d, $^2J_{P,C}$ = 12.6 Hz, CN) ppm. ^{19}F NMR ($CDCl_3$): δ = −67.04 (dd, $^3J_{H,F}$ = 7.8, $^3J_{P,F}$ = 3.6 Hz, 6F), −106 (d, $^1J_{P,F}$ = 958 Hz, 1F) ppm. ^{31}P NMR ($CDCl_3$): δ = 62.23 (dd, $^2J_{P,P}$ = 68.2, $^3J_{P,F}$ = 17.1 Hz,), 155.05 (dd, $^2J_{P,P}$ = 68.2, $^1J_{F,P}$ = 958 Hz) ppm. $C_{18}H_{33}F_7N_4P_2$ (500.42): calcd. C 43.20, H 6.64, N 11.20; found C 44.39, H 6.98, N 12.20.

Compound 14b: Sulfur (10 mg) was added to a solution of **13b** (100 mg, 0.2 mmol) in $CHCl_3$ (1 mL) and the mixture was heated at 60 °C for 3.5 h. The solvent was removed in vacuo and the residue was extracted with diethyl ether (1.5 mL) at −10 °C in order to separate the product from the remaining sulfur. Evaporation of diethyl ether in vacuo yielded 77 mg (72%) of **14b**. M.p. 51−53 °C. ^{1}H NMR ($CDCl_3$): δ = 1.17 (t, $^3J_{H,H}$ = 7.03 Hz, 6 H, NCH_2CH_3), 1.20 (t, $^3J_{H,H}$ = 7.03 Hz, 12 H, NCH_2CH_3), 2.8−3.5 [m, 2 H, P−CH_2−P, 12 H, NCH_2CH_3, 1 H, $CH(CF_3)_2$] ppm. ^{13}C NMR ($CDCl_3$): δ = 13.05 (dm, $J_{P,C}$ = 195.03 Hz, 1C, $PCCN$), 13.39 (m, 4C, NCH_2CH_3), 14.17 (m, 2C, NCH_2CH_3), 33.87 (ddd, $^1J_{P,C}$ = 34.1, $^1J_{P,C}$ = 95.6, $^2J_{F,C}$ = 85.8 Hz, PCP), 39.77 (d, 2C, $^2J_{P,C}$ = 4.9 Hz, NCH_2CH_3), 39.99 (d, 2C, $^2J_{P,C}$ = 4.9 Hz, NCH_2CH_3), 40.53 (dd, $^2J_{P,C}$ = 3.9, $^3J_{F,C}$ = 1.9 Hz, 2C, NCH_2CH_3), 47.10 [m, 1C, $CH(CF_3)_2$], 124.33 [q, $^1J_{C,F}$ = 283.8 Hz, 2(CF_3)], 124.52 (d, $^2J_{P,C}$ = 13.7 Hz, CN) ppm. ^{19}F NMR ($CDCl_3$): δ = −66.52 (q, $^4J_{FF}$ = 8.5 Hz, 3F), −67.04 (q, $^4J_{FF}$ = 8.5 Hz, 3F), −41.80 (dd, $^1J_{P,F}$ = 1063, $^2J_{H,F}$ = 9.8 Hz) ppm. ^{31}P NMR ($CDCl_3$): δ = 59.75 (d, $^2J_{P,P}$ = 4.9 Hz), 84.90 (dd, $^2J_{P,P}$ = 4.9, $^1J_{F,P}$ = 1060.7 Hz) ppm. $C_{18}H_{33}F_7N_4P_2S$ (532.48): calcd. C 40.60, H 6.24, S 6.02; found C 39.86, H 6.21, S 6.24.

Compound 16a: Compound **8** (200 mg, 1.06 mmol) was added to a solution of **10a** (360 mg, 0.82 mmol) in dichloromethane (4 mL) and the reaction mixture was maintained at 20 °C for 16 h. The solvent was then removed in vacuo and compound **13a** was extracted from the residue with diethyl ether (2 × 2.5 mL). The remaining product was dried in vacuo, dissolved in the minimum amount of dichloromethane, diluted with diethyl ether until the solution became turbid and the solution was left at −15 °C. After 2 days colorless crystals of **16a** were separated and dried in vacuo (280 mg, 54%), m.p. 185−186 °C. ^{1}H NMR ($CDCl_3$): δ = 2.66 [m, 2 H, $CH(CF_3)_2$], 2.77 (d, $^3J_{PH}$ = 10.0 Hz, 24 H, NCH_3), 3.18 (t, $^2J_{PH}$ = 16.1 Hz, 2 H, P−CH_2−P) ppm. ^{13}C NMR (CD_3COCD_3): δ = 12.00 (dm, $J_{P,C}$ = 196.8 Hz, 2C, $PCCN$), 26.4 (t, $J_{P,C}$ = 93.0 Hz, PCP), 36.75 (s, 8C, NCH_3), 47.03 [sept. t, $^2J_{P,C}$ = 29.3, $J_{P,C}$ = 6.8 Hz, $CH(CF_3)_2$], 123.0 (t, $^2J_{P,C}$ = 7.1 Hz, 2 C, CN), 124.8 [q, $^1J_{F,C}$ = 279.8 Hz, 2(CF_3)] ppm. ^{19}F NMR ($CDCl_3$): δ = −67.1 (d, $^3J_{H,F}$ = 7.8 Hz, 6F) ppm. ^{31}P NMR ($CDCl_3$): δ = 59.9 (s, 2P) ppm. $C_{19}H_{28}F_{12}N_6P_2$ (630.39): calcd. C 36.20, H 4.48; found C 35.81, H 4.12.

Compounds 19a, 19b: A solution of **10a** or **10b** (0.2 mmol) in toluene (1.5 mL) was placed in a 10 mL flask. The flask was then evacuated slightly and gaseous hexafluoroacetone (4.8 mL, 0.21 mmol) was introduced with a syringe. The mixture was left for 24 h at room temperature, then the solvent was removed in vacuo. The remaining oil was dissolved in minimum amount of diethyl ether (about 2 mL), diluted with hexane and left for two days at −15 °C. Colorless crystals were separated and dried in vacuo.

19a: Yield 80 mg (66%), m.p. 88−90 °C. ^{1}H NMR ($CDCl_3$): δ = 0.64 (dd, $^2J_{P,H}$ = 5.6, $^2J_{P,H}$ = 8.1 Hz, 1 H, P−C*H*−P), 2.56 [d, $^3J_{P,H}$ = 10.0 Hz, 12 H, N(CH_3)$_2$], 2.63 [d, $^3J_{P,H}$ = 10.0 Hz, 12 H, N(CH_3)$_2$], 2.95 [sept. d, $^3J_{H,F}$ = 8.5, $^3J_{PH}$ = 8.5 Hz, 1 H, C*H*(CF$_3$)$_2$], 5.08 [sept. d, $^3J_{H,F}$ = 5.8, $^3J_{P,H}$ = 11.9 Hz, 1 H, C*H*(CF$_3$)$_2$] ppm. ^{13}C NMR ($CDCl_3$): δ = 7.67 (dd, $^1J_{P,C}$ = 168.7, $^1J_{P,C}$ = 205.8 Hz, P*C*P), 15.86 (dm, $J_{P,C}$ = 136.5 Hz, 1C, P*C*CN), 36.97 (d, $^2J_{P,C}$ = 3.9 Hz, 4C, NMe$_2$), 37.17 (d, $^2J_{P,C}$ = 4.9 Hz, 4C, NMe$_2$), 48.20 [sept. d, $^2J_{P,C}$ = 12.7, $^2J_{F,C}$ = 29.3 Hz, 1C, *C*H(CF$_3$)$_2$], 70.11 [sept. d, $^2J_{P,C}$ = 2.9, $^2J_{F,C}$ = 34.1 Hz, 1C, *C*H(CF$_3$)$_2$], 120.20 (q, $^1J_{F,C}$ = 285.7 Hz, 2C, CF$_3$), 124.68 (q, $^1J_{F,C}$ = 279.9 Hz, 2C, CF$_3$), 127.63 (d, $^2J_{P,C}$ = 14.7 Hz, CN) ppm. ^{19}F NMR ($CDCl_3$): δ = −67.29 (d, $^3J_{H,F}$ = 8.5 Hz, 6F), −73.15 (d, $^2J_{H,F}$ = 5.8 Hz, 6F) ppm. ^{31}P NMR ($CDCl_3$): δ = 60.65 ($^2J_{P,P}$ = 39.0 Hz), 63.81 ($^2J_{P,P}$ = 39.0 Hz) ppm. $C_{17}H_{27}F_{12}N_5OP_2$ (607.36): calcd. C 33.61, H 4.48, N 11.53; found C 33.24, H 4.31, N 11.80.

19b: Yield 139 mg (97%), m.p. 79−82 °C. ^{1}H NMR ($CDCl_3$): δ = 0.67 (dd, $^2J_{P,H}$ = 9.7, $^2J_{P,H}$ = 12.3 Hz, 1 H, P−C*H*−P), 1.10 (t, $^3J_{H,H}$ = 7.1 Hz, 24 H, CH_2CH_3), 2.8−3.5 [m, 16 H, CH_2CH_3, 1 H, C*H*(CF$_3$)$_2$], 5.36 [sept, $^3J_{H,F}$ = 5.9 Hz, 1 H, C*H*(CF$_3$)$_2$] ppm. ^{13}C NMR ($CDCl_3$): δ = 12.2 (dd, $^1J_{P,C}$ = 173, $^1J_{P,C}$ = 199 Hz, P*C*P), 13.1 (d, $^3J_{P,C}$ = 2.9 Hz, 4 C, NCH$_2$*C*H$_3$), 13.8 (d, $^3J_{P,C}$ = 1.9 Hz, 4 C, NCH$_2$*C*H$_3$), 38.8 (d, $^2J_{P,C}$ = 4.9 Hz, 4 C, N*C*H$_2$CH$_3$), 40.4 (d, $^2J_{P,C}$ = 4.9 Hz, 4 C, N*C*H$_2$CH$_3$), 48.7 [sept. d, $^2J_{P,C}$ = 12.7, $^2J_{F,C}$ = 28.3 Hz, 1 C, *C*H(CF$_3$)$_2$], 70.4 [sept. d, $^2J_{P,C}$ = 2, $^2J_{F,C}$ = 37 Hz, 1C, *C*H(CF$_3$)$_2$], 121.0 (q, $^1J_{F,C}$ = 279 Hz, 2C, CF$_3$), 124.7 (q, $^1J_{F,C}$ = 285 Hz, 2C, CF$_3$), 128.1 (d, $^2J_{P,C}$ = 14.7 Hz, CN) ppm. ^{19}F NMR ($CDCl_3$): δ = −66.5 (d, $^3J_{H,F}$ = 8.3 Hz, 6 F), −72.6 (d, $^3J_{H,F}$ = 5.8 Hz, 6 F) ppm. ^{31}P NMR ($CDCl_3$): δ = 61.9 (d, $^2J_{P,P}$ = 41 Hz), 64.2 (d, $^2J_{P,P}$ = 41 Hz) ppm. $C_{25}H_{43}F_{12}N_5OP_2$ (719.58): C 41.73, H 6.02, N 9.73; found C 40.89, H 6.56, N 10.23.

X-ray Crystallographic Study: The single-crystal X-ray structure determination was performed at 173(2) K on a Siemens P4 diffractometer using graphite monochromated Mo-K_α radiation (λ = 71.073 pm) and a low temperature LT2 device. The structure was solved by direct methods and refined by full-matrix least-squares on F^2 using the SHELX-97 program suite.[24] Crystal data for **10b** ($C_{14}H_{27}F_6N_5P_2$): M_w = 441.35, monoclinic, space group $P2_1/c$, a = 1195.0(2), b = 1348.9(2), c = 1397.7(4) pm, β = 110.400(10)°, V = 2.1117(8) nm^3, Z = 4, D_c = 1.388 Mg/m^3, μ = 0.266 mm^{-1}; 6078 reflections collected, 256 parameters refined using 4850 unique reflections (R_{int} = 0.0463) to final indices $R1$ [$I > 2\sigma(I)$] = 0.0651 and wR_2 (all data) = 0.1652 [$w = 1/[\sigma^2(F_o^2) + (0.0698P)^2 + P]$ where $P = (2F_c^2 + F_o^2)/3$. All non-hydrogen atoms were refined anisotropically and the position of the hydrogen atoms was calculated as a riding model. The final residual Fourier positive and negative peaks were equal to 0.401 and −0.480 e Å^{-3}.

CCDC-164430 contains the supplementary crystallographic data (for **10a**). These data can be obtained free of charge at www.ccdc.cam.ac.uk/conts/retrieving.html [or from the Cambridge Crystallographic Data Centre, 12, Union Road, Cambridge CB2 1EZ, UK; Fax: (internat.) +44-1223/336-033; E-mail: deposit@ccdc.cam.ac.uk].

Acknowledgments

We thank the Deutsche Forschungsgemeinschaft for financial support.

[1] M. Witt, K. S. Dathathreyan, H. W. Roesky, *Adv. Inorg. Chem. Radiochem.* **1986**, *30*, 223−312.
[2] R. Burgada, R. Setton, "Preparation, Properties and Reactions of Phosphoranes", in *The Chemistry of Organophosphorus Compounds* (Ed.: F. R. Hartley, in *The Chemistry of Functional Groups* (Series ed.: S. Patai), Wiley, Chichester, New York, Brisbane, Toronto, Singapore, 1994, vol. 3; pp. 185−272.
[3] F. U. Seifert, G.-V. Röschenthaler, *J. Fluorine. Chem.* **1995**, *70*, 171−174.
[4] I. Neda, C. Melnicky, A. Vollbrecht, A. Fischer, P. G. Jones, R. Schmutzler, *Z. Anorg. Allg. Chem.* **1996**, *622*, 1047−1059.
[5] I. V. Shevchenko, *Chem. Commun.* **1998**, 1203−1204.
[6] I. V. Shevchenko, R. Mikolenko, S. Loss, H. Grützmacher, *Eur. J. Inorg. Chem.* **1999**, 1665−1671.
[7] I. Yavari, M. R. Islami, H. R. Bijanzadeh, *Tetrahedron* **1999**, *55*, 5547−5554.
[8] I. Yavari, M. T. Maghsoodlou, *Tetrahedron Lett.* **1998**, 4579−4580.
[9] I. Yavari, N. N. Arasi, H. R. Bijanzadeh, *J. Fluor. Chem.* **2000**, *103*, 155−157.
[10] Y. G. Gololobov, V. A. Pinchuk, H. Thönnessen, P. G. Jones, R. Schmutzler, *Phosphorus, Sulfur and Silicon* **1996**, *115*, 19−37.
[11] R. F. Stockel, F. Megson, H. T. Beachem, *J. Org. Chem.* **1968**, *33*, 4395−4397.
[12] M. A. Howells, R. D. Howells, N. C. Baenziger, D. J. Burton, *J. Am. Chem. Soc.* **1973**, *95*, 5366−5370.
[13] I. T. Hennawy, *Collect. Czech. Chem. Commun.* **1994**, *59*, 2109−2115.
[14] P. J. Goldman, *Biol. Chem.* **1973**, *93*, 5366−5370.
[15] D. Peters, R. Miethchen, "Loss of Fluorine To Form C=C Bonds", in Houben-Weyl, *Organo-Fluorine Compounds* (Eds.: B. Baasner, H. Hagemann, J. C. Tatlov), Georg Thieme Verlag, Stuttgart, New York, 2000, vol. E10b, Part 2; pp. 345−381.
[16] W. H. Gumprecht, "Hydrolysis of Trifluoromethyl Groups", in *Chemistry of Organic Fluorine Compounds II; A Critical Review* (Ed.: M. Hudlický and A. E. Pavlath), ACS Monograph 187; American Chemical Society: Washington DC, **1995**, pp. 433−436.
[17] V. Martin, H. Molines, C. Wakselman, *J. Org. Chem.* **1992**, *57*, 5530−5532.
[18] M. A. Show, J. C. Tebby, R. S. Ward, D. H. Williams, *J. Chem. Soc. (C)* **1970**, 504−507.
[19] O. I. Kolodiazhnyi, in *Phosphorus Ylides*, Wiley-VCH; Weinheim, New York, Chichester, Brisbane, Singapore, Toronto, **1999**.
[20] I. Kawamoto, T. Hata, Y. Kishida, C. Tamura, *Tetrahedron Lett.* **1971**, 2417.
[21] H. J. Hecht, G. Ruban, *Cryst. Struct. Commun.* **1981**, 495.
[22] H. Grützmacher, H. Pritzkow, *Chem. Ber.* **1989**, 1411−1416.
[23] I. Shevchenko, V. Andrushko, E. Lork, G.-V. Röschenthaler, *Eur. J. Inorg. Chem.*, submitted.
[24] SHELX-97, G. M. Sheldrick, University of Göttingen, 1997.

Received March 21, 2002
[I02155]

Lipophilic Ligands Derived from 1,3,5-Triamino-1,3,5-trideoxy-*cis*-inositol (Taci) for Trivalent Lanthanide Complexation in Aqueous and Organic Solutions

Samuel Delagrange,[a] Christelle Gateau,[a] David Chapon,[a] Colette Lebrun,[a] Pascale Delangle,*[a] and Philippe Vottéro[a]

Keywords: Lanthanides / Complexes / N,O ligands / Substituent effects / Stability constants

New lipophilic ligands derived from 1,3,5-triamino-1,3,5-trideoxy-*cis*-inositol (taci), namely 1,3,5-trideoxy-1,3,5-tris-(ethylamino)-*cis*-inositol (L^1), 1,3,5-tris(butylamino)-1,3,5-trideoxy-*cis*-inositol (L^2), 1,3,5-trideoxy-1,3,5-tris(hexylamino)-*cis*-inositol (L^3) have been synthesized by reductive amination of taci. Their complexing properties towards trivalent lanthanide cations, together with those of 1,3,5-tris(benzylamino)-1,3,5-trideoxy-*cis*-inositol (L^4), have been investigated in solution using mass spectrometry, NMR spectroscopy and potentiometry. It has been shown that each ligand forms trinuclear complexes with the composition $[Ln_3(LH_{-3})_2]^{3+}$. The stability constants (log β_{32-6}) of these complexes have been calculated for Nd^{3+}, Eu^{3+}, and in some cases for Lu^{3+}. The affinity for the lanthanide cations follows the sequence $Lu^{3+} > Eu^{3+} > Nd^{3+}$, for all the ligands. This sequence follows the well-known electrostatic trend. The stability of the complex depends on the conjugate effects of the steric hindrance of the substituents and the basicity of the ligands: $L^1 \approx L^2 <$ taci, in water, and $L^3 < L^2 << L^4$, in water/methanol. Among the ligands studied in this work, L^4 appears to be the most effective complexing agent for the lanthanide cations in water/methanol under slightly acidic conditions.
(© Wiley-VCH Verlag GmbH, 69451 Weinheim, Germany, 2002)

Introduction

The design of selective chelating agents represents one of the basic challenges in the field of coordination chemistry.[1,2] Important medicinal and technological areas such as the treatment of metal intoxication,[3] ligands for magnetic resonance, radiochemical imaging[4,5] or luminescent probes,[6] and selective extractants in industrial processes[7,8] may greatly benefit from such studies.

Separation of trivalent lanthanide and actinide cations, both present in nuclear fuel, is required for nuclear waste management.[9,10] Due to the chemical similarity of these two cation families, their selective extraction by tailored ligands still remains a challenge. For several years, we have been engaged in the studies of polyfunctional ligands based on cyclohexanic platforms for group *f* element selective complexation.[11,12] Among the ligands studied in our laboratory, 1,3,5-triamino-1,3,5-trideoxy-*cis*-inositol (taci) was found to be a model compound of great interest for this purpose. It is a rigid receptor with preorganized N- and O-donor atoms (Scheme 1), which offer different chelating modes for metal binding. Its coordination properties have been widely investigated and described in the literature.[13,14] In particular, it has been shown that taci forms trinuclear species of the type $[M_3(taciH_{-3})_2]^{3+}$, with trivalent lanthanide cations with an original "sandwich-type" structure (Scheme 2).[15,16] In these complexes, each of the three metal cations binds to an amino group and to two alkoxo groups of each of the two deprotonated ligands. The coordination sphere is completed by peripheral ligands such as H_2O or counterions. For the purposes of our research, taci is especially attractive because, although the 4f complexes are isostructural across the lanthanide series, it shows an uncommon selectivity for the elements at the end of the series.[17]

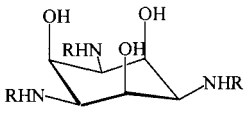

taci : R=H
L^1 : R = -CH_2-CH_3
L^2 : R = -$(CH_2)_3$-CH_3
L^3 : R = -$(CH_2)_5$-CH_3
L^4 : R = -CH_2-C_6H_5

Scheme 1

Despite the rich coordination chemistry of taci,[14] only a few derivatives have been described in the literature. Several *O*-[18] or *N*-substituted derivatives have been elaborated by Hegetschweiler et al. to modulate metal binding properties.

[a] Laboratoire de Reconnaissance Ionique, Service de Chimie Inorganique et Biologique UMR 5046, CEA/DSM/ Département de Recherche Fondamentale sur la Matière Condensée, CEA-Grenoble,
38054 Grenoble cedex 9, France
Fax: (internat.) +33−(0)4 38 78 50 90
E-mail: delangle@cea.fr

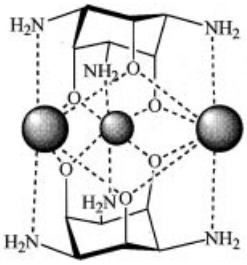

Scheme 2

Two types of substituents, with or without additional donor groups, have been introduced at the nitrogen atoms. 1,3,5-trideoxy-1,3,5-tris[(2-hydroxybenzyl)amino]-*cis*-inositol (H_3thci),[19] 1,3,5-trideoxy-1,3-bis[(2-hydroxybenzyl)amino]-*cis*-inositol (H_3bhci) and its bifunctionalized analog, 1,3,5-trideoxy-5-glutaramido-1,3-bis[(2-hydroxybenzyl)amino]-*cis*-inositol (H_3bhci-glu-H)[20] have been prepared as new types of potential hexa- and pentadentate chelators, by hydrogenation of a mixture of taci and salicylaldehyde using Pt as a catalyst. Furthermore, several methylated derivatives have been synthesized to favor one of the binding modes, for steric reasons. For this purpose, 1,3,5-trideoxy-1,3,5-tris-(dimethylamino)-*cis*-inositol (tdci)[21] was obtained by catalytic hydrogenation of taci in the presence of formaldehyde with Pt as the catalyst, and 1,3,5-trideoxy-1,3,5-tris(trimethylamino)-*cis*-inositol (ttci)[21] was obtained by complete methylation of the amino groups using an excess of methyliodide. Even if the direct treatment of taci with methylating agents resulted in *N*- rather than *O*-alkylation, the introduction of only one methyl group at each primary amine proved to be difficult. Hence, starting from taci, 1,3,5-trideoxy-1,3,5-tris(methylamino)-*cis*-inositol (tmaci) was obtained by an indirect route using the corresponding Co^{III} complex $[Co(taci)_2]^{3+}$ as an intermediate.[22] Recently, 1,3,5-tris(benzylamino)-1,3,5-trideoxy-*cis*-inositol (tbci or L^4), obtained by reductive alkylation of taci using $NaBH_4$ as the reducing agent, and 1,3,5-tris(benzylmethylamino)-1,3,5-trideoxy-*cis*-inositol (tbmci) have been reported for the preparation, in nonaqueous medium, of a new type of Ba^{2+} complex having a chiral structure.[23]

In order to develop new lipophilic ligands based on the taci framework, we decided to prepare a series of *N*-alkylated derivatives. To retain the specific coordination properties of taci towards lanthanide(III) ions, the alcohol functions, which are deprotonated during complexation in this particular case, had to remain untouched. Various lipophilic substituents were thus attached to the three nitrogen atoms of taci (Scheme 1). Here, we present the syntheses of a series of new *N*-alkylated derivatives of taci, namely 1,3,5-trideoxy-1,3,5-tris(ethylamino)-*cis*-inositol (L^1), 1,3,5-tris-(butylamino)-1,3,5-trideoxy-*cis*-inositol (L^2), and 1,3,5-trideoxy-1,3,5-tris(hexylamino)-*cis*-inositol (L^3), and the characterization of their lanthanide complexes and those of tbci (L^4) in aqueous and methanolic solutions. The affinity towards Ln^{III} ions will be discussed as a function of ligand substituents, cation size and pH.

Results and Discussion

Ligand Syntheses

The syntheses of the three ligands L^1-L^3 are summarized in Scheme 3. As previously discussed with regard to the ligand tmaci,[22] the introduction of alkyl groups is not a routine task, mainly due to the multifunctionality of taci and the possibility of forming many amines having numerous degrees of substitution. Many procedures for the specific conversion of primary to secondary amines have been reported in the literature, but there is no universal efficient method available. However, the reductive alkylation of primary amines is one of the most useful routes to secondary amines. According to the Hegetschweiler reports,[19–21] catalytic hydrogenation using Pt as the catalyst[24] is probably the best way to prepare *N*-alkylated derivatives starting from taci. This method was then chosen for the reduction of the Schiff bases formed in situ by the treatment of taci with the appropriate carbonyl compound. Indeed, catalytic hydrogenation of the taci sulfate salt in the presence of a large excess of acetaldehyde with Pt as the catalyst, and subsequent elution by ion-exchange chromatography led to L^1 in a 62% yield. Unfortunately, the introduction of butyl substituents at the three nitrogen atoms by the same method was not successful and resulted in the formation of a crude mixture of various compounds, presumably due to the steric hindrance of the imine formed in situ. This reaction was readily driven towards the formation of the desired L^2 in a 65% yield by using sodium borohydride as the reducing agent. L^3 was obtained under the same conditions using 3.3 equivalents of the appropriate carbonyl compound in a 56% yield. As expected, the replacement of the H–N hydrogen atoms by alkyl substituents generates rather lipophilic chelates. The coordination properties of this new ligand set towards trivalent lanthanide cations can be evaluated in different media, depending on the chain length: in water for L^1 and L^2 and in water/methanol for L^2, L^3, and L^4.

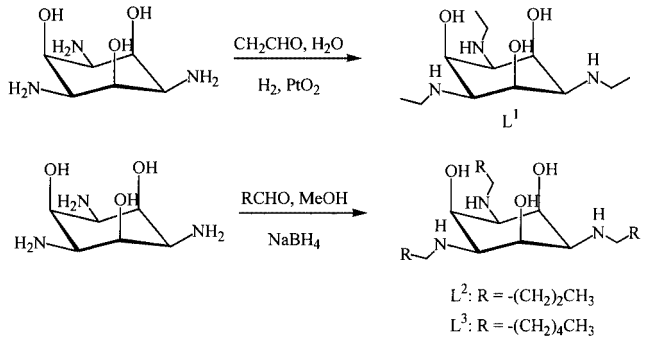

Scheme 3

Characterization of Ln^{III} Complexes in Solution by ES-MS

Electrospray ionization mass spectrometry (ES-MS) has been shown to be a suitable technique to qualitatively characterize preformed ions in solution,[25] and has moreover been used for identification of supramolecular coordination

complexes.[26−28] Aqueous and methanolic samples containing the ligand and europium(III) of different molar ratios were analyzed. Due to their characteristic isotopic patterns, the signals for the europium-containing species can easily be recognized, and indicate the number of Eu^{III} cations present in the detected complexes. Figure 1 shows a typical spectrum obtained from a water/methanol solution (1:1, v/v) of L^4 and $Eu(NO_3)_3$ at a molar ratio (M/L) of 1.5 in the absence of added base.

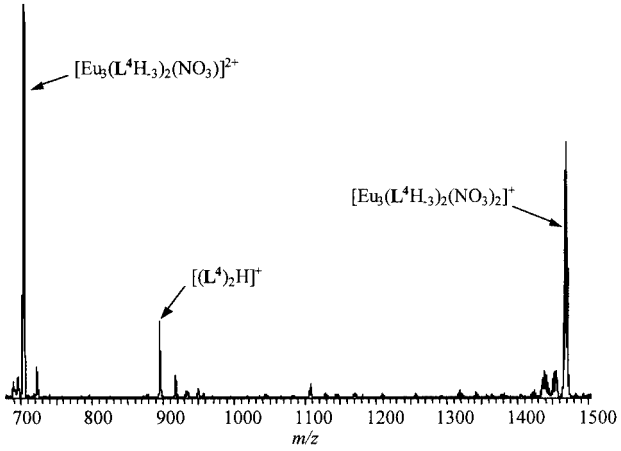

Figure 1. ES-MS spectrum of a water/methanol solution (1:1, v/v) of L^4 and $Eu(NO_3)_3$. c_L/c_M = 1:1.5; $c_L = 1{\cdot}10^{-3}$ M

The only Eu-containing species detected under our experimental conditions are $[Eu_3(LH_{-3})_2(NO_3)_2]^+$ and $[Eu_3(LH_{-3})_2(NO_3)]^{2+}$. The experimental and calculated isotopic patterns are identical. As an example, the peak envelope of $[Eu_3(L^4H_{-3})_2(NO_3)_2]^+$ is depicted in Figure 2.

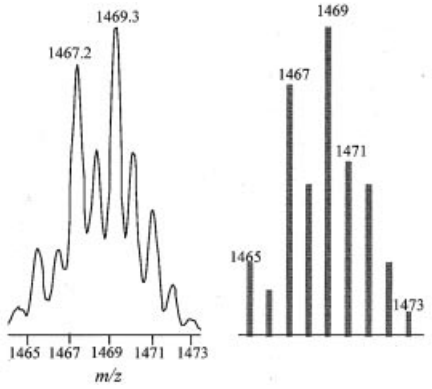

Figure 2. Experimental and calculated isotopic patterns of $[Eu_3(L^4H_{-3})_2(NO_3)_2]^+$. c_L/c_M = 1:1.5; $c_L = 1{\cdot}10^{-3}$ M

In the presence of triethylamine, the hydroxo complexes $[Eu_3(LH_{-3})_2(NO_3)(OH)]^+$ and $[Eu_3(LH_{-3})_2(OH)_2]^+$ are also detected. Fragmentation of the complex resulted in the complete destruction of this species. It is worth noting that whatever the Eu/L ratio, ranging from 1:2 to 2:1, the trinuclear complex is the only species observed. Finally, we have also checked that similar complexes were formed with a series of lanthanide cations including Pr^{3+}, Nd^{3+}, Sm^{3+}, Ho^{3+}, and Lu^{3+}. In all cases, only the ions of the type $[Ln_3(LH_{-3})_2]^{3+}$ have been evidenced in the ES-MS spectra, as was previously observed for the Ln^{III} ion complexation by taci.[17]

Protonation Equilibria

In order to analyze the stability of the metal complexes formed in solution, we first studied the protonation properties of each ligand using potentiometric methods. The protonation constants of ligands L^1, L^2, L^3, and L^4 obtained in water or in water/methanol (1:3, v/v) solutions are listed in Tables 1 and 2, respectively. For comparison, protonation constants of related compounds (taci and tdci) are also reported.

Table 1. Protonation constants ($\log K^H_i$) for taci, L^1, L^2, and tdci determined in water (25 °C; 0.10 M KCl, pK_w = 13.78) using the program HYPERQUAD

Equilibrium quotient	taci	L^1	L^2	tdci
[HL]/[L][H]	8.87(2); 8.90[a]	9.362(6)	9.40(1)	9.68[a]
$[H_2L]/[HL][H]$	7.38(3); 7.40[a]	7.777(6)	7.74(1)	7.62[a]
$[H_3L]/[H_2L][H]$	5.96(3); 5.95[a]	6.257(6)	6.20(1)	5.89[a]
$[H_3L]/[L][H]^3$	22.21	23.40	23.34	23.19

[a] From ref.[15]

Table 2. Protonation constants ($\log K^H_i$) for L^2, L^3, and L^4 determined in water/methanol (1:3, v/v) (25 °C; 0.10 M KCl, pK_w = 13.89) using the program HYPERQUAD

Equilibrium quotient	L^2	L^3	L^4
[HL]/[L][H]	8.44(3)	8.56(2)	7.65(3)
$[H_2L]/[HL][H]$	7.14(3)	7.25(3)	6.16(3)
$[H_3L]/[H_2L][H]$	5.80(6)	5.74(3)	4.48(6)
$[H_3L]/[L][H]^3$	21.38	21.55	18.29

In each case, three constants corresponding to the protonation of the amino groups have been calculated. The values obtained for L^1 and L^2 in water are roughly similar, and as expected the overall basicity of these two ligands (bearing secondary amines) is higher than that of taci (primary amine) and lower than that of tdci (tertiary amine). Due to their poor solubility in water, the protonation properties of ligands L^3 and L^4 have been investigated in water/methanol (1:3, v/v). For comparison, L^2 has also been studied under the same conditions. The protonation constants determined for L^3 are close to those determined for L^2, i.e. the chain length does not significantly affect the basicity of the amino groups. On the other hand, the overall basicity of L^4 is three orders of magnitude lower than that of the alkyl derivatives. Note that benzylamine, with a pK^H value of 9.62, is also known to be a weaker base than butylamine and hexylamine whose pK^H values are 10.78 and 10.64, respectively.[29]

The separation of the pK^H values is in the range 1.3−1.7 and is higher than the statistical separation (log3 = 0.48). This means that the protonation of an amino group is influ-

enced by other amino groups that are already protonated. This is expected since the basic sites are only separated by 3 carbon atoms.[30] Besides, the ΔpK^H values of ca. 1.5 observed between two consecutive protonation constants are similar to those calculated for 1,3,5-triaminocyclohexane (pK^H: 10.16, 8.66, 7.17),[31] and are thus consistent with the expected ligand conformation in solution, i.e. the conformation in which the hydroxy groups are in the axial positions and the amino groups are in the equatorial positions due to the steric hindrance of the bulky substituents.

Stability of the Complexes in Aqueous and H_2O/MeOH Media

The affinity of these ligands for lanthanide(III) cations was also studied by potentiometry in water or in water/methanol (1:3, v/v). The titration curves obtained for the $Ln-L^1$ and $Ln-L^4$ systems are representative of this study and are presented in Figure 3.

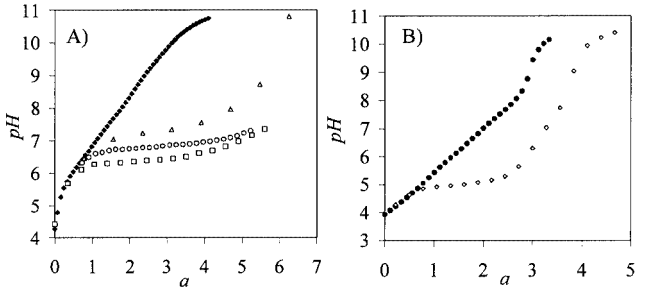

Figure 3. Potentiometric titration curves (experimental points, 25 °C, I = 0.10 M KCl) for: **A)** L^1 (♦) and different systems in water: $Nd^{3+}-L^1$ (Δ), $Eu^{3+}-L^1$ (○), $Lu^{3+}-L^1$ (□); c_L/c_M = 1:1.5; c_L = $1\cdot10^{-3}$ M; **B)** L^4 (●) and $Eu^{3+}-L^4$ (◇) system in water/methanol (1:3, v/v); c_L/c_M = 1:0.5; c_L = $0.5\cdot10^{-3}$ M. a is the number of base added per mol of ligand

The following conclusions can be drawn from the titration curves. The curves obtained for the $Ln^{III}-$ligand L^1, L^2, L^3, and L^4 systems share many features with the titration curves described for $Ln^{III}-$taci systems.[17] Each curve shows distinct regions corresponding to (i) the removal of the first proton from $[H_3L]^{3+}$, (ii) the formation of the complex characterized by the low slope of the pH curve in this range, (iii) the titration of the possible excess ligand (occurring for instance in the case of the $Ln-L^4$ system as shown in Figure 3, B), (iv) a further deprotonation of the complex at high pH values. These experiments unambiguously established the formation of the species $[M_3(LH_{-3})_2]^{3+}$ according to Equation (1):

$$H_3L^{3+} + 1.5\,M^{3+} + 6\,OH^- \rightleftarrows 0.5\,[M_3(LH_{-3})_2]^{3+} + 6\,H_2O \quad (1)$$

In all cases presented here, the HYPERQUAD 2000 program gave convergence for models containing the $[M_3(LH_{-3})_2]^{3+}$ species, and in certain cases, $[M_3(LH_{-3})_2(OH)]^{2+}$ has been suggested if sufficient experimental points in the basic region were available. All other species considered, including mono- and dinuclear complexes, were systematically rejected by the program. The values of the stability constants, β_{32-6} according to Equation (2), calculated from the experimental points using the program HYPERQUAD are compiled in Tables 3 and 4. Figure 4 gives an insight into the species distribution as a function of pH for the $Eu^{3+}-L^1$ and $Eu^{3+}-L^4$ systems.

Table 3. Formation constants ($\log\beta_{32-6} = [Ln_3(LH_{-3})_2]/[Ln]^3[L]^2[H]^{-6}$) of taci, L^1, L^2, and tdci in water (25 °C; 0.10 M KCl, pK_w = 13.78)

Ion	taci	L^1	L^2	tdci
Nd^{3+}	−24.1[a]	−26.4(2)	−27.0(2)[b]	
Eu^{3+}	−17.9[a]; −18.5[c]	−21.4(1)[b]	−21.2(2)[b]	−16.8[c]
Lu^{3+}	−12.5[a]; −11.3[c]	−16.9(2)[b]	−17.6(2)[b]	

[a] From ref.[17] [b] Constants obtained using batch ("out-of-cell") method. [c] From ref.[15]

Table 4. Formation constants ($\log\beta_{32-6} = [Ln_3(LH_{-3})_2]/[Ln]^3[L]^2[H]^{-6}$) of L^2, L^3, and L^4 determined in water/methanol (1:3, v/v) (25 °C; 0.10 M KCl, pK_w = 13.89) using the program HYPERQUAD

Ion	L^2	L^3	L^4
Nd^{3+}	−	−15.9(2)	−13.9(2)
Eu^{3+}	−10.3(2)	−11.8(1)	− 8.3(1)

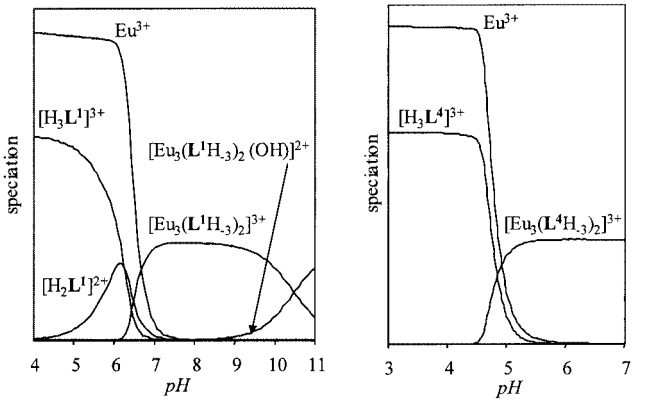

Figure 4. Species distribution as a function of pH for the $Eu^{3+}-L^1$ and $Eu^{3+}-L^4$ systems. c_L/c_M = 1:1.5; c_L = $1\cdot10^{-3}$ M. The formation constants listed in Tables 1 to 4 were used for the calculations

$$3\,Ln^{3+} + 2\,L \rightleftarrows [Ln_3L_2H_{-6}]^{3+} + 6\,H^+ \quad (2)$$

Ligands L^1 and L^2 form stable complexes with Nd^{3+}, Eu^{3+}, and Lu^{3+} in water, with stability constants lower than those previously calculated for taci and the related cations. In water/methanol solution, Nd^{3+} and Eu^{3+} complexes formed with L^4 show a higher stability than those formed with L^2 and L^3. The plots in Figure 5, giving the calculated fraction of free Eu^{3+} versus pH for the different ligands, provide another way of comparing their complexing power. The binding ability follows the sequence $L^1 \approx L^2 <$ taci, in water, and $L^3 < L^2 << L^4$, in water/

methanol. Hence, ligand L^4 is the most effective in complexing europium in water/methanol (1:3, v/v) in the pH range 4.5−5.5, due to its relatively low basicity and high stability constant.

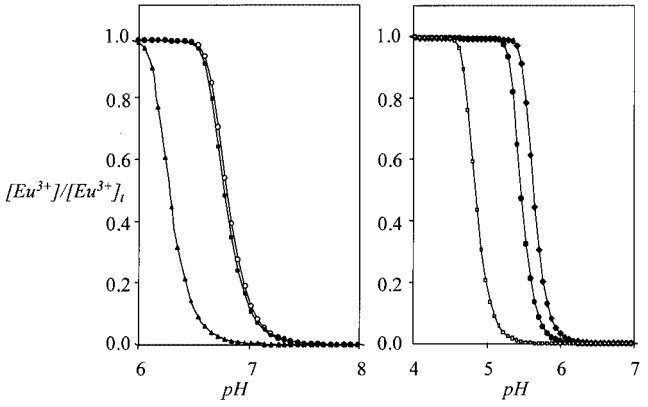

Figure 5. Fraction of calculated free europium concentration as a function of pH for taci (▲), L^1 (■), and L^2 (○) in water (left plot) and for L^2 (●), L^3 (◆), and L^4 (□) in water/methanol (1:3, v/v) (right plot). c_L/c_M = 1:1.5; $c_L = 1{\cdot}10^{-3}$ M

The differences in the Ln^{III} complex stabilities observed between taci and its *N*-functionalized derivatives may be explained by considering the effects of the basicity of the amino groups and the steric hindrance provided by the nitrogen substituent. As the Ln^{III} are very hard cations, the affinity of a family of ligands for these ions is usually correlated to their overall basicity; for a given lanthanide cation, as ΣpK^H increases, the complex stability constant also increases.[32] In this study, ligands based on the taci framework show an exceptional behavior since the more basic the amino groups are, the less effective lanthanide(III) complexation is. For taci and its derivatives, it is difficult to correlate the complexation constants with the overall ligand basicity, as has been done for several aminocarboxylic acids,[33] because the dissociation constants of the alcohol functions are not known. Under the experimental conditions used, these groups are not deprotonated in the absence of the metal, and the influence of nitrogen substitution on the alcohol dissociation constants is thus unknown. Moreover, it can obviously be assumed that the presence of the bulky groups renders the formation of the hindered sandwich-type complexes less favorable, and as a consequence the corresponding stability constant values decrease. Hence, the ligands L^1 and L^2 form less stable complexes than the unsubstituted taci in water. The same conclusion can be reached to explain the lower stability of the complexes formed with L^3 than those formed with L^2 in water/methanol solution.

The trend in the stability constants across the lanthanide series follows the well-known electrostatic trend,[34] i.e. $\log\beta_{32-6}$ increases from Nd^{III} to Lu^{III} and/or Eu^{III}, as seen in Figure 6. Lanthanide(III) complexation in water can be decomposed in two steps: the first step corresponds to dehydration, and the second step, to the reaction between the desolvated species. The compensation effect assumes that the free energy of the first step is negligible,[35] and thus the free energy of the global process reflects the second step, i.e. the interaction between the ligand and the metal ion, leading to an increase in the stability constants from La^{III} to Lu^{III}.

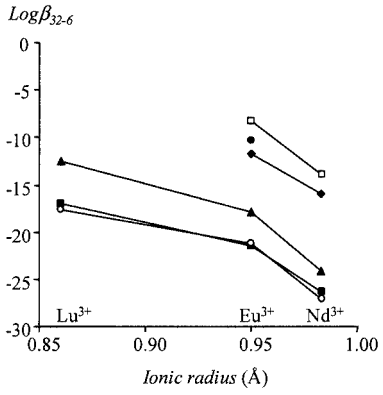

Figure 6. Variation of the $\log\beta_{32-6}$ values as a function of ionic radius for taci (▲), L^1 (■), and L^2 (○) in water and for L^2 (●), L^3 (◆), and L^4 (□) in water/methanol (1:3, v/v)

The great increase in the affinity from La^{III} to Lu^{III}, already observed with the ligand taci,[17] is also seen for the derivatives L^1-L^4. The difference in $\log\beta_{32-6}$ from Eu^{III} to Nd^{III} is 6.2 for taci, and ranges from 4.1 to 5.8 for L^1 to L^4. The simulation of the fraction of free Ln^{3+} in solution in the presence of L^4 as a function of pH clearly shows that the europium cations are totally complexed at pH 5.1, while at the same pH, the neodymium cations remain free in solution. Note that it does not mean that ligand L^4 would be able to selectively complex Eu^{3+} in the pH range 4.6 to 5.1. It would then be necessary to consider the formation of heterotrinuclear complexes, namely $[Eu_2Nd(LH_{-3})_2]^{3+}$ and $[EuNd_2(LH_{-3})_2]^{3+}$. We have already demonstrated the existence of such compounds with taci.[36]

NMR Analysis

In order to gain an insight into the solution structure of these complexes, a ^1H NMR study was undertaken. Solutions containing the water-soluble ligand L^1 and $Eu(OTf)_3$ at a molar ratio (M/L) of 1.5 were analyzed at pD values ranging from 4.70 to 8.21 at 278 K. Addition of small amounts of base (NaOD) clearly show the disappearance of the signals assigned to the ligand, and the appearance of numerous resonances within the 0 to −23 ppm region. As in the complex, each nitrogen atom becomes an asymmetric center, a mixture of diastereoisomers exists in solution and a further analysis of this region is not obvious. At pD 8.21, the spectrum of the sample only shows the resonances assigned to the complex, indicating that the ligand has totally been converted to the Eu^{III} complex. NMR spectra were also recorded at variable temperatures as seen in Figure 7, which represents the spectra of $[Eu_3(L^1)_2H_{-6}]^{3+}$ at 348 K and 278 K. A better resolution of the series of multiplets is obtained at 278 K, but it does not provide suitable informa-

tion to confirm the solution structure of the complex. At 348 K, the signals scattered within 0 and −26 ppm merge into two broad signals centered at δ = −14.2 ppm and −6.3 ppm. Considering the fact that the spectrum of the europium complex with taci only exhibits two signals at δ = −21.72 ppm and −14.49 ppm, assigned to the protons H^N and H^O,[17] the two broad signals may represent the average of all the "H^N" and "H^O" protons. This last result is consistent with the pseudo D_{3h} symmetry of the complex when interconversion around the nitrogen atom is fast. Similar observations were made for europium complexes formed with L^2, L^3, and L^4 in methanol.

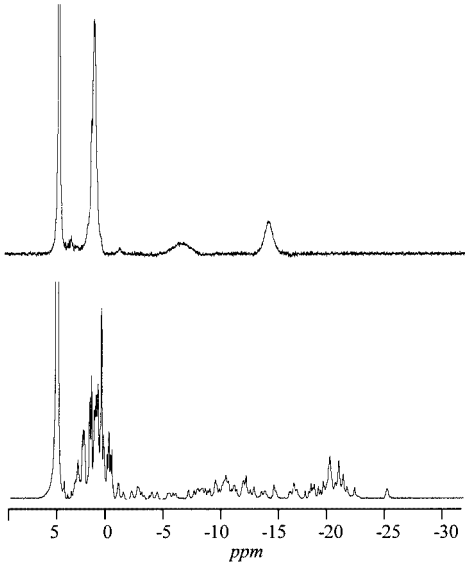

Figure 7. 400 MHz ^{1}H NMR spectra of the $Eu^{3+}-L^1$ system in D_2O (pD = 8.21) at 348 K (top) and 278 K (bottom). c_L/c_M = 1:1.5; $c_L = 1\cdot10^{-2}$ M

Conclusion

The new ligands L^1, L^2, and L^3, synthesized via alkylation of taci with various carbonated chains, as well as the trisbenzyl derivative L^4 show similar complexation properties towards lanthanide(III) cations as the ligand taci. The only species evidenced by electrospray ionization spectrometry and potentiometry is the trinuclear complex $[Ln_3L_2H_{-6}]^{3+}$. In the complex, the coordination of the nitrogen atoms to the lanthanide cations leads to several chiral centers, and thus a more detailed NMR analysis is prevented by the observation of numerous diastereoisomers in solution.

The stability constants of the lanthanide complexes of the four ligands show the well-known electrostatic trend, i.e. an increase from lanthanum to lutetium. Moreover, although ligands L^1-L^4 are more basic than taci, they give less stable complexes with Ln^{III}, indicating that the steric hindrance is the determining factor in the formation of the sandwich complex $[Ln_3L_2H_{-6}]^{3+}$. The ligands may be classified according to their Ln^{III} affinity: $L^1 \approx L^2 <$ taci, in water, and $L^3 < L^2 << L^4$, in water/methanol, and thus among this set of ligands, L^4 appears to be the most effective in binding 4f cations. The striking increase in affinity across the series, previously seen with the ligand taci, is maintained for the lipophilic derivatives L^1-L^4.

Experimental Section

General Information: All solvents and reagents were obtained from commercial suppliers and used without further purification. The precursor taci, used as the sulfate salt, and the ligand tbci (L^4) were prepared according to literature procedures.[21,23] Catalytic hydrogenation was performed within a TOP 80 reactor with controlled hydrogen pressure, temperature and rotation speed. Melting points were measured with an Electrothermal IA93000 and are uncorrected. ^{1}H and ^{13}C NMR spectra were recorded on a Varian Mercury 400 spectrometer. Chemical shifts are reported in ppm with solvent as the internal reference. When necessary, pD was adjusted with a sodium deuteroxide solution ($pD = pH_{read} + 0.41$).[37] Mass spectra were acquired on a LCQ-ion trap (Finnigan-Thermoquest, San Jose, USA) equipped with an electrospray source. Electrospray full scan spectra in the range m/z = 100−1500 were obtained by infusion through a fused silica tubing at 2−10 μL/min. The solutions were analyzed in the positive mode. The LCQ calibration (m/z = 50−2000) was achieved according to the standard calibration procedure from the manufacturer (mixture of caffeine, MRFA and Ultramark 1621). The temperature of the heated capillary for the LCQ was set to 85 °C, the ion-spray voltage was in the range 1−6 kV and the injection time was 5−200 ms. Samples for ES-MS were prepared by dissolving the ligand (10^{-3} M) and the lanthanide salt in water or in water/methanol solution, the pH was then adjusted to the desired value if necessary by adding triethylamine. Elemental analyses were performed by the Service Central d'Analyses (Vernaison-69)

Ligands Synthesis

1,3,5-Trideoxy-1,3,5-tris(ethylamino)-*cis*-inositol (L^1): A solution of the sulfate salt of taci (1.00 g, 3.08 mmol) in H_2O (160 mL) was hydrogenated under hydrogen pressure (12 bars) in the presence of PtO_2 (0.070 g, 0.31 mmol) and acetaldehyde (4.0 mL; 70.9 mmol) at room temperature for 7 days. Two additional portions of acetaldehyde (2 × 4.0 mL; 2 × 70.9 mmol) were added after 2 and 3 days. After filtration through a pad of Celite and concentration in vacuo, the crude product was purified by crystallization from H_2O/EtOH, yielding the sulfate salt of compound L^1 (0.924 g, 65%) as a white solid. ^{1}H NMR (400 MHz, D_2O, 298 K): δ (ppm) = 1.36 (t, J = 7.2 Hz, 9 H, CH_3), 3.25 (q, J = 7.3 Hz, 6 H, NCH_2),. 3.57 (t, J = 3.0 Hz, 3 H, HC_{cycle}-NH,), 4.61 (t, J = 2.9 Hz, 3 H, HC_{cycle}-OH) ppm. $C_{12}H_{30}N_3O_3\cdot SO_4\cdot HSO_4$ (457.51): calcd. C 31.5, H 6.8, N 9.1; found C 31.5, H 7.1, N.8.7.

The sulfate salt of ligand L^1 (0.924 g, 2.02 mmol) was dissolved in H_2O (50 mL) and subjected to ion-exchange chromatography (Amberlite IR 45, OH^- form). H_2O was removed under reduced pressure to afford the free base ligand L^1 (0.573 g, 96%) as a white solid. M.p. 160−161 °C (decomposition). ^{1}H NMR (400 MHz, D_2O, 298 K): δ (ppm) = 1.16 (t, J = 7.2 Hz, 9 H, CH_3), 2.83 (q, J = 7.3 Hz, 6 H, NCH_2), 2.85 (s broad, 3 H, HC_{cycle}-NH), 4.27 (t, J = 2.9 Hz, 3 H, HC_{cycle}-OH) ppm. ^{13}C NMR (100 MHz, D_2O, 298 K): δ (ppm) = 15.1 (CH_3). 41.7 (NCH_2), 59.2 (HC_{cycle}-NH), 70.0 (HC_{cycle}-OH). ES-MS: 262.2 $[M + H]^+$.

1,3,5-Tris(butylamino)-1,3,5-trideoxy-*cis*-inositol (L^2): The sulfate salt of taci (1.00 g, 3.08 mmol) in MeOH (75 mL) was refluxed with

KOH (0.675 g, 12.02 mmol) for 30 min. Butanal (1.8 mL, 20.3 mmol) was added dropwise and the solution was stirred for 3 h. The solution was then cooled to 0 °C and sodium borohydride (1.516 g, 40.08 mmol) was added in small portions. After stirring overnight at room temperature, the reaction was quenched by adding concentrated HCl. The solution was concentrated to dryness and the residue was taken up in H_2O (300 mL). The mixture was extracted with CH_2Cl_2 (150 mL) to remove excess butanal. The aqueous layer was made alkaline (pH ca. 10) by adding KOH pellets and extracted with Et_2O (8 × 200 mL). The solvent was removed in vacuo and the residue was purified by crystallization from CH_3CN, yielding compound L^2 (0.693 g, 65%) as a white solid with m.p. 117 °C. ^{1}H NMR (400 MHz, D_2O, 298 K): δ = 0.89 (t, J = 7.3 Hz, 9 H, CH_3,), 1.33 (sext, J = 7.3 Hz, 6 H, CH_2-CH_3), 1.48 (quint, J = 7.6 Hz, 6 H, -CH_2-), 2.61 (s broad, 3 H, HC$_{cycle}$-NH), 2.66 (t, J = 7.4 Hz, 6 H, NCH_2), 4.21 (s broad, 3 H, HC$_{cycle}$-OH) ppm. ^{13}C NMR (100 MHz, D_2O, 298 K): δ = 15.6 (CH_3). 22.3 (CH_2-CH_3), 33.2 (NCH_2-CH_2), 46.9 (NCH_2), 59.8 (HC_{cycle}-NH), 71.4 (HC_{cycle}-OH). ES/MS: 346.5 $[M + H]^+$, 368.3 $[M + Na]^+$. $C_{18}H_{39}N_3O_3$ (345.53): calcd. C 62.6, H 11.4, N 12.2; found C 62.3, H 11.4, N 12.2.

1,3,5-Trideoxy-1,3,5-tris(hexylamino)-*cis*-inositol (L^3): Following the same procedure as above, treatment of the sulfate salt of taci (0.300 g, 0.925 mmol) with KOH (0.202 g, 3.608 mmol), hexanal (0.37 mL, 3.053 mmol) and sodium borohydride (0.455 g, 12.02 mmol) and crystallization from ethyl acetate yielded compound L^3 (0.222 g, 56%) as a white solid with m.p. 104 °C. ^{1}H NMR (400 MHz, $CDCl_3$, 298 K): δ = 0.89 (t, J = 6.7 Hz, 9 H, CH_3), 1.32 (m, 18 H, (CH_2)$_3$$CH_3$), 1.58 (m, 6 H, C$H_2$), 2.54 (s broad, 3 H, HC$_{cycle}$-NH), 2.76 (t, J = 7.2 Hz, 6 H, NCH_2,), 4.17 (s broad, 3 H, HC$_{cycle}$-OH) ppm. ^{13}C NMR (100 MHz, $CDCl_3$, 298 K): δ = 14.2 (CH_3), 22.8 (CH_2), 27.2 (CH_2), 30.2 (CH_2), 31.9 (CH_2), 47.3 (NCH_2), 59.5 (HC_{cycle}-NH), 69.7 (HC_{cycle}-OH). ES/MS: 430.5 $[M + H]^+$. $C_{24}H_{51}N_3O_3$ (429.69): calcd. C 67.1, H 12.0, N 9.8; found C 67.3, H 12.0, N 9.9.

Potentiometric Measurements

Reagents and Solutions: Solutions of titrants, support electrolyte (KCl), metal ions and ligands were prepared in water (obtained by Millipore/Milli-Q system) or in water/methanol (1:3, v/v); methanol was of analytical grade. Carbonate-free solutions of KOH were prepared from standardized solutions and were discarded when the amount of carbonate was about 1% of the total amount of base. HCl solutions were prepared from standardized solutions. Metal ions solutions were prepared with a concentration of about $1\cdot10^{-2}$ M, from the chloride salts of the metals and standardized by titration with H_2Na_2edta. Ligand solutions were prepared at a concentration of ca. 10^{-3} M.

Equipment and Working Conditions: All potentiometric titrations were carried out at 25.0±0.1 °C. Potential values were measured with a Metrohm combined glass electrode. Atmospheric CO_2 was excluded from the cell during the titration by passing Ar across the top of the experimental solution in the reaction cell. The titrant solutions were dispensed from a Metrohm 751 piston burette. For the titrations carried out in water/methanol (1:3, v/v), the glass electrode was previously treated by soaking it in the solution for one week to prevent erratic responses.

Measurements: The $[H^+]$ of the solutions was determined by measurement of the electromotive force of the cell, $E = E'° + Q \log [H^+] + Ej$; $E'°$, and Q was obtained from previous calibrations.[38] The liquid-junction potential, Ej, was negligible under the experimental conditions used. The value of $K_w = [H^+][OH^-]$ was $10^{-13.78}$ in water. In water/methanol (1:3, v/v), K_w was determined from the alkaline region of the titration curve and was found to be equal to $10^{-13.85}$ under our experimental conditions. The potentiometric equilibrium measurements were made on 30 mL solutions containing 25−50 μmol of the ligand and at an ionic strength of 0.10 M.

For the study of Ln^{III} complexes in water, a batch ("out-of-cell") method was used: solutions of metal ion and ligand with a final concentration of about 10^{-3} M were prepared in separate vials of 2 mL, in which small volumes of standard KOH solution (0.10 M) were added. The [M]/[L] ratios used were 1.5:1 for the Ln^{III}/**L^1** systems, 0.5:1 and 1.5:1 for the Ln^{III}/**L^2** systems. The ionic strength of the solutions was kept at 0.10 M with KCl. Measurements were carried out after stabilization of the pH, which occurred within 12 h.

For the study of the Ln^{III} complexes in water/methanol (1:3, v/v) solution, [M]/[L] ratios were 0.5:1 and under such conditions, stabilization occurred within 4500 s, allowing automatic titrations to be performed. To check if complete equilibration had been achieved during titration, a back titration with HCl (0.10 M) was performed. In all the cases presented here, no hysteresis was observed.

Calculation of Equilibrium Constants: Protonation constants $K^H_i = [H_iL]/[H_{i-1}L][H]$ were calculated by fitting the potentiometric data obtained for the ligand using the program HYPERQUAD.[39,40] Stability constants of the various species formed in solution were obtained from the experimental data using the same program. The initial results were obtained in the form of overall stability constants.

$$\beta_{M_mH_hL_l} = \frac{[M_mH_hL_l]}{[M]^m[H]^h[L]^l}$$

The errors quoted correspond to the standard deviations estimated by Hyperquad 2000, multiplied by a factor of 3.

Acknowledgments

We thank the Direction du Cycle du Combustible at the Commissariat à l'Energie Atomique for financial support.

[1] R. D. Hancock, A. E. Martell, *Chem. Rev.* **1989**, *89*, 1875−1914.
[2] D. H. Busch, *Chem. Rev.* **1993**, *93*, 847−860.
[3] O. Andersen, *Chem. Rev.* **1999**, *99*, 2683−2710.
[4] S. Aime, M. Botta; M. Fasano, E. Terreno, *Chem. Soc. Rev.* **1998**, *27*, 19−29.
[5] P. Caravan, J. J. Ellison, T. J. McMurry, R. B. Lauffer, *Chem. Rev.* **1999**, *99*, 2293−2352.
[6] J.-C. G. Bünzli, G. R. Choppin, *Lanthanide Probes in Life, Chemical and Earth Sciences*; Elsevier: Amsterdam, **1989**.
[7] S. Nishihama; T. Hirai, I. Komasawa, *Ind. Eng. Chem. Res.* **2000**, *39*, 3907−3911.
[8] S. Nishihama, T. Hirai, I. Komasawa, *Ind. Eng. Chem. Res.* **1999**, *38*, 1032−1039.
[9] K. L. Nash, in: *Handbook on the Physics and Chemistry of the Rare Earths*; (Ed.: K. A. Gschneidner Jr., L. Eyring, G. R. Choppin, H. H. Lander); Elsevier, Amsterdam, **1994**; Vol. 18, pp. 197−238.
[10] K. L. Nash; M. P. Jensen, in: *Handbook on the Physics and Chemistry of the Rare Earths*; (Ed.: K. A. Gschneidner Jr, L. Eyring), Elsevier, Amsterdam, **2000**; Vol. 28, pp. 311−371.
[11] C. Husson, P. Delangle, J. Pécaut, P. J. A. Vottéro, *Inorg. Chem.* **1999**, *38*, 2012−2019.
[12] P. Delangle, C. Husson, C. Lebrun, J. Pécaut, P. J. A. Vottéro, *Inorg. Chem.* **2001**, *40*, 2953−2962.

[13] K. Hegetschweiler, *Bol. Soc. Chil. Quim.* **1997**, *42*, 257−279.
[14] K. Hegetschweiler, *Chem. Soc. Rev.* **1999**, *28*, 239−249.
[15] R. Hedinger, M. Ghisletta, K. Hegetschweiler, E. Toth, A. E. Merbach, R. Sessoli, D. Gatteschi, V. Gramlich, *Inorg. Chem.* **1998**, *37*, 6698−6705.
[16] E. Toth, L. Helm, A. E. Merbach, R. Hedinger, K. Hegetschweiler, A. Janossy, *Inorg. Chem.* **1998**, *37*, 4104−4113.
[17] D. Chapon, C. Husson, P. Delangle, C. Lebrun, P. J. A. Vottéro, *J. All. Comp.* **2001**, *323−324*, 128−132.
[18] M. Weber, D. Kuppert, K. Hegetschweiler, V. Gramlich, *Inorg. Chem.* **1999**, *38*, 859−868.
[19] K. Hegetschweiler, A. Egli, R. Alberto, H. W. Schmalle, *Inorg. Chem.* **1992**, *31*, 4027−4028.
[20] A. Kramer, R. Alberto, A. Egli, I. Novak-Hofer, K. Hegetschweiler, U. Abram, P. V. Bernhardt, P. A. Schubiger, *Bioconjugate Chem.* **1998**, *9*, 691−702.
[21] K. Hegetschweiler, I. Erni, W. Schneider, H. Schmalle, *Helv. Chim. Acta* **1990**, *73*, 97−105.
[22] K. Hegetschweiler, M. Weber, V. Hunch, R. J. Geue, A. D. Rae, A. C. Willis, A. M. Sargeson, *Inorg. Chem.* **1998**, *37*, 6136−6146.
[23] J. Sander, K. Hegetschweiler, B. Morgenstern, A. Keller, W. Amrein, T. Weyhermüller, I. Müller, *Angew. Chem. Int. Ed.* **2001**, *40*, 4180−4182.
[24] W. S. Emerson, in: *Organic Reactions*, (Ed.: R Adams, W. E. Bachmann, A. M. Blatt, L. F. Fieser, J. R. Johnson, H. R. Snyder), Wiley, New-York, **1948**; Vol. 4, pp. 174−255.
[25] R. D. Smith, J. A. Loo, C. G. Edmonds, C. J. Barinaga, H. R. Udseth, *Anal. Chem.* **1990**, *62*, 882−899.
[26] G. Hopfgartner, F. Vilbois, C. Piguet, *Rapid Commun. Mass Spectrom.* **1999**, *13*, 302−306.
[27] G. Hopfgartner, C. Piguet, J. D. Henion, *J. Am. Soc. Mass Spectrom.* **1994**, *5*, 748−756.
[28] E. Leize, A. Van Dorsselaer, R. Krämer, J.-M. Lehn, *J. Chem. Soc., Chem. Commun.* **1993**, 990−993.
[29] D. D. Perrin, *Dissociation constants of organic bases in aqueous solution*; Butterworths: London, **1965**.
[30] R. Rometsch, A. Marxer, K. Miescher, *Helv. Chim. Acta* **1951**, *34*, 1611−1618.
[31] R. M. Smith, A. E. Martell, R. J. Motekaitis, *NIST Critically Selected Stability Constants of Metal Complexes Database, NIST Standard Reference Database 46*, **2001**.
[32] G. R. Choppin, in: *Lanthanide Probes in Life, Chemical and Earth Sciences*; (Ed.: J.-C. G. Bünzli, G. R. Choppin), Elsevier: Amsterdam, **1989**, pp. 1−42.
[33] T. F. Gritmon, M. P. Goedken, G. R. Choppin, *J. Inorg. Nucl. Chem.* **1977**, *39*, 2021−2023.
[34] C. Piguet, J.-C. G. Bünzli, *Chem. Soc. Rev.* **1999**, *28*, 347−358.
[35] G. R. Choppin, *J. Less-Common Met.* **1985**, *112*, 193−205.
[36] D. Chapon, P. Delangle, C. Lebrun, *J. Chem. Soc., Dalton Trans.* **2002**, 68−74.
[37] P. K. Glasoe, F. A. Long, *J. Phys. Chem.* **1960**, *64*, 188−190.
[38] A. E. Martell, R. J. Motekaitis, *Determination and use of stability constants*; VCH, New York, **1992**.
[39] P. Gans, A. Sabatini, A. Vacca, *Talanta* **1996**, *43*, 1739−1753.
[40] P. Gans, B. O'Sullivan, *Talanta* **2000**, *51*, 33−37.

Received March 26, 2002
[I02161]

Synthesis of a New Potentially Hemilabile Ligand: 1-[2-(Diphenylphosphanyl)ethyl]-3,5-dimethylpyrazole, and Comparison of Its Bonding Properties with the Related 1-[2-(Ethylamino)ethyl]-3,5-dimethylpyrazole Ligand toward Rh^{I}

Glòria Esquius,[a] Josefina Pons,[a] Ramón Yáñez,[a] Josep Ros,*[a] René Mathieu,*[b] Bruno Donnadieu,[b] and Noël Lugan[b]

Keywords: Rhodium / P ligands / N ligands / Hemilabile ligands / Hydroformylations

The new ligand 1-[2-(diphenylphosphanyl)ethyl]-3,5-dimethylpyrazole (**2**) has been prepared by the reaction of 1-(chloroethyl)-3,5-dimethylpyrazole and PPh_2Li. The bidentate N,N ligand 1-[2-(ethylamino)ethyl]-3,5-dimethylpyrazole (**1**) and **2** react with $[Rh(COD)(THF)_2][BF_4]$ to give $[Rh(COD)(\mathbf{1})][BF_4]$ (**3**) and $[Rh(COD)(\mathbf{2})][BF_4]$ (**4**), respectively. Substitution of 1,5-cyclooctadiene with carbon monoxide in the latter complexes generates $[Rh(CO)_2(\mathbf{1})][BF_4]$ (**5**) and $[Rh(CO)_2(\mathbf{2})][BF_4]$ (**6**), respectively. Treatment of $[Rh(COD)(THF)_2][BF_4]$ with two equivalent amounts of **2** results in the complex $[Rh(\mathbf{2})_2][BF_4]$ (**7**), which converts to $[Rh(CO)(\mathbf{2})_2][BF_4]$ (**8**) on reaction with carbon monoxide. Ligand **2** in complex **8** exhibits a hemilabile character. The single-crystal X-ray structures of **3**, **4**, and **7** are reported.
(© Wiley-VCH Verlag GmbH, 69451 Weinheim, Germany, 2002)

Introduction

In recent years the use of hemilabile ligands in coordination and organometallic chemistry has increased because of their potential applications in catalysis. Many bidentate ligands containing two donor centres of different strengths, such as mixed phosphorus-heteroatom ligands, have been reviewed in recent reports and articles.[1,2,3] Their interest in catalysis arises from the easy decoordination of the weak donor centre without the displacement of the ligand, which should confer a better stability to the reaction intermediates. Mixed ligands containing phosphorus along with oxygen, nitrogen or sulphur donor atoms have specifically been designed for use in catalytic reactions such as hydrogenation,[4,5,6] oligomerisation,[7] and hydroformylation of olefins.[8]

Pyrazole-derived molecules are good candidates for the preparation of interesting N,N′ or N,P mixed ligands, owing to their ease of synthesis and the possibility of electronic and steric modulation of their properties. Pyrazole-amines have been extensively studied as ligands for hard transition metal cations.[9] These studies have led to remarkable structures for the resulting complexes, some of which can be regarded as bioinorganic models.[10,11] Some reviews about pyrazole chelating ligands in biological model systems have recently appeared.[12,13]

In pursuing investigations on pyrazole-based polydentate ligands, we have directed our efforts toward the study of their reactivity with soft transition metal ions, in order to compare their behaviour with that of the well-known tris(pyrazolyl)borate anion.[14] Very recently, we have described the coordinating properties of bis[(3,5-dimethylpyrazolyl)methyl]ethylamine toward Rh^{I}. This ligand, which contains two different N donor centres, leads to a $\kappa^2 \rightleftarrows \kappa^3$ equilibrium in solution, revealing its hemilabile character through the reversible decoordination of the amino group. The κ^3 coordination mode has been found in the solid state structure determinations.[15]

In the present paper, we extend this work to a new family of N,P ligands of the phosphanylalkylpyrazole type. Prior to our investigations, only the diphenylphosphanylmethylpyrazole has been described in this class of ligands.[16] We report the synthesis of 1-[2-(diphenylphosphanyl)ethyl]-3,5-dimethylpyrazole and the study of its bonding properties toward Rh^{I}. For comparative purposes, the reactivity of the related N,N′ bidentate ligand 1-[2-(ethylamino)ethyl]-3,5-dimethylpyrazole toward Rh^{I} has also been investigated.

Results and Discussion

The ligand 1-[2-(ethylamino)ethyl]-3,5-dimethylpyrazole (**1**) was synthesised according to a procedure previously described by Driessen.[17]

[a] Departament de Química, Universitat Autònoma de Barcelona, 08193 Bellaterra-Cerdanyola, Barcelona, Spain
Fax: (internat.) +34−(0)93/5813101
E-mail: josep.ros@uab.es
[b] Laboratoire de Chimie de Coordination du CNRS, 205 Route de Narbonne, 31077 Toulouse Cedex 4, France
Fax: (internat.) +33−561553003
E-mail: mathieu@lcc-toulouse.fr

The new ligand 1-[2-(diphenylphosphanyl)ethyl]-3,5-dimethylpyrazole (**2**) was prepared by reaction of 1-(chloroethyl)-3,5-dimethylpyrazole[18] with PPh_2Li, which is generated in situ by deprotonation of PPh_2H by *n*BuLi in tetrahydrofuran, at 0 °C (Scheme 1). The new ligand, isolated in an 83% yield as a colourless oil, was characterised by C, H, and N elemental analyses, IR, ^1H-, ^{13}C, and ^{31}P NMR spectroscopy, and by electron impact mass spectrometry. In the ^{31}P NMR spectrum, the diphenylphosphanyl moiety gives a singlet at $\delta = -20.9$ ppm.

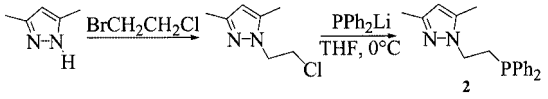

Scheme 1

1-[2-(ethylamino)ethyl]-3,5-dimethylpyrazole (**1**) or 1-[2-(diphenylphosphanyl)ethyl]-3,5-dimethylpyrazole (**2**) react with one equivalent of $[Rh(COD)(THF)_2][BF_4]$, which is generated in situ from the reaction of $[Rh(COD)Cl]_2$ and $AgBF_4$ in tetrahydrofuran, to give the complexes $[Rh(COD)(\mathbf{1})][BF_4]$ (**3**) (89% yield) and $[Rh(COD)(\mathbf{2})][BF_4]$ (**4**) (94% yield), respectively (Scheme 2). Elemental analyses of both complexes are consistent with their formulation.

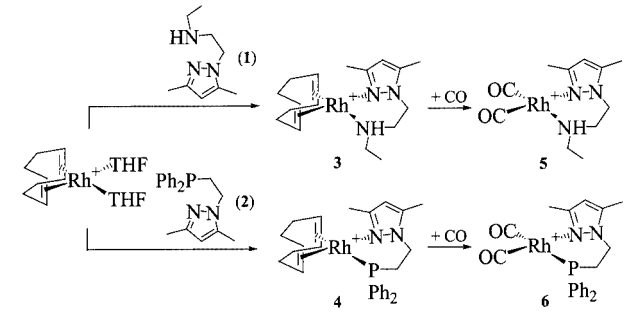

Scheme 2

We were able to prepare X-ray quality crystals of complexes **3** and **4**, and we performed a crystal structure determination for both complexes. The molecular structures of the complexes consist of discrete $[Rh(COD)(\mathbf{1})]^+$ and $[Rh(COD)(\mathbf{2})]^+$ cations, respectively, and BF_4^- anions. Perspective views of the cation complexes are given in Figures 1, and 2, respectively. Selected bond lengths and angles are provided in Table 1, and the details of the data collection and crystal data are summarised in Table 2. A slightly distorted square-planar geometry is observed around Rh in both structures. Thus, in **3**, the Rh atom deviates by 0.025 Å from the mean coordination plane formed by two N donor atoms of the ligand and the centroid of the olefinic C=C bonds of the COD ligand. In **4**, the Rh atom deviates by 0.139 Å from the mean plane formed by the donor N and P atoms of the ligand and the centroid of the olefinic C=C bonds of the COD ligand. The Rh−N distances of 2.116(3) and 2.148(3) Å for **3**, and of 2.141(2) Å for **4** fall between the experimental values reported for related complexes.[15,19,21] The Rh−P bond length of 2.274(1) Å for **4** is also similar to those found in the literature.[19,22] Due to

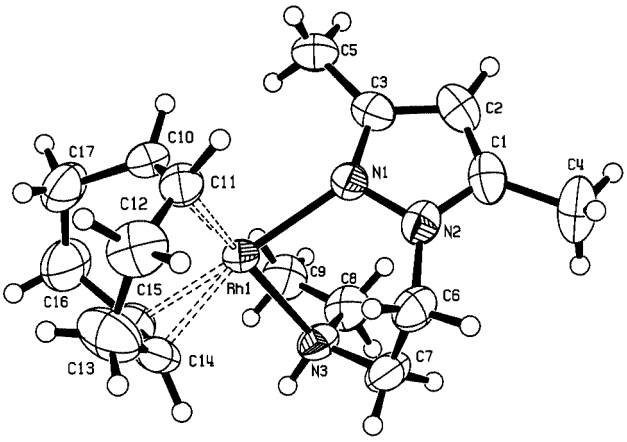

Figure 1. A perspective view of the cation $[Rh(COD)(\mathbf{1})]^+$ showing the numbering scheme

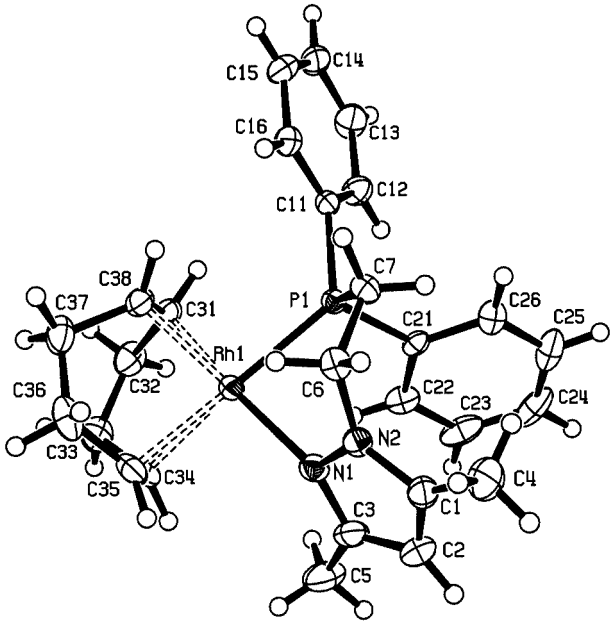

Figure 2. A perspective view of the cation $[Rh(COD)(\mathbf{2})]^+$ showing the numbering scheme

the different *trans* effect of the donor atoms in **4**, the Rh−C bonds *trans* to phosphorus [2.236(2) and 2.216(2) Å] are longer than the Rh−C bonds *trans* to nitrogen [2.132(2) and 2.129(2) Å].[19] The N1−Rh1−N3 angle [82.90(14)°] for **3** and the N1−Rh1−P1 angle [82.68(5)°] for **4** are smaller than 90°, but are consistent with the reported angles for similar complexes.[15,19] It is worth noting that in both structures the six-membered rings formed by the bidentate ligands coordinated to rhodium adopts a boat-type conformation, the Rh1 and C6 (both structures) atoms are at the apex of the boat.

The ^1H NMR spectrum for **3** recorded at 293 K (250 MHz) shows three signals with the relative intensity 2:1:1 at $\delta = 4.37$, 4.29, and 4.21 ppm for the non-equivalent olefinic protons of the 1,5-COD ligand *trans* to the pyrazole ring and *trans* to the amino group. This is fully consistent with the solid state structure, which shows that the nitrogen

Table 1. Selected bond lengths [Å] and angles [°] for compounds [Rh(COD)(**1**)][BF_4] (**3**), [Rh(COD)(**2**)][BF_4] (**4**), and [Rh(**2**)$_2$][BF_4] (**7**)

	3		**4**		**7**
C10−C11	1.385(7)	C34−C35	1.372(4)	N1−Rh1	2.119(2)
C10−Rh1	2.158(4)	C34−Rh1	2.236(2)	N3−Rh1	2.113(2)
C11−Rh1	2.133(4)	C35−Rh1	2.216(2)	P1−Rh1	2.207(1)
C14−C15	1.365(7)	C31−C38	1.392(3)	P2−Rh1	2.223(1)
C14−Rh1	2.135(4)	C31−Rh1	2.132(2)	C3−N1−N2	105.2(2)
C15−Rh1	2.125(5)	C38−Rh1	2.129(2)	C3−N1−Rh1	130.54(18)
N1−Rh1	2.116(3)	N1−Rh1	2.141(2)	N2−N1−Rh1	123.31(17)
N3−Rh1	2.148(3)	P1−Rh1	2.2743(6)	C8−N3−N4	106.1(2)
C8−N3−C7		C21−P1−C11	103.88(10)	C8−N3−Rh1	132.0(2)
C8−N3−Rh1	112.5(3)	C21−P1−C7	105.48(10)	N4−N3−Rh1	121.83(17)
C7−N3−Rh1	111.2(3)	C11−P1−C7	106.01(10)	N3−Rh1−N1	88.37(9)
N1−Rh1−C15	165.68(17)	C21−P1−Rh1	110.32(7)	N3−Rh1−P1	176.60(6)
N1−Rh1−C11	93.48(16)	C11−P1−Rh1	122.77(7)	N1−Rh1−P1	89.13(7)
C15−Rh1−C11	96.06(18)	C7−P1−Rh1	107.13(7)	N3−Rh1−P2	83.43(6)
N1−Rh1−C14	155.60(18)	C38−Rh1−C31	38.13(9)	N1−Rh1−P2	171.77(6)
C15−Rh1−C14	37.37(19)	C38−Rh1−N1	152.51(8)	P1−Rh1−P2	99.03(3)
C11−Rh1−C14	82.32(18)	C31−Rh1−N1	168.78(8)	C21−P1−C31	103.58(12)
N1−Rh1−N3	82.90(14)	C38−Rh1−C35	81.90(9)	C21−P1−C12	102.49(13)
C15−Rh1−N3	92.02(17)	C31−Rh1−C35	97.09(9)	C31−P1−C12	100.43(12)
C11−Rh1−N3	158.13(17)	N1−Rh1−C35	90.01(8)	C21−P1−Rh1	118.66(9)
C14−Rh1−N3	92.08(16)	C38−Rh1−C34	88.02(9)	C31−P1−Rh1	119.34(9)
N1−Rh1−C10	100.18(16)	C31−Rh1−C34	80.46(9)	C12−P1−Rh1	109.66(9)
C15−Rh1−C10	81.23(18)	N1−Rh1−C34	100.71(8)	C51−P2−C41	102.25(13)
C11−Rh1−C10	37.66(18)	C35−Rh1−C34	35.89(9)	C51−P2−C14	102.07(13)
C14−Rh1−C10	91.14(17)	C38−Rh1−P1	97.17(6)	C41−P2−C14	103.47(13)
N3−Rh1−C10	164.19(17)	C31−Rh1−P1	92.81(6)	C51−P2−Rh1	126.40(9)
		N1−Rh1−P1	82.68(5)	C41−P2−Rh1	111.87(10)
		C35−Rh1−P1	162.20(7)	C14−P2−Rh1	108.31(10)
		C34−Rh1−P1	161.72(7)		

atom of the amino group coordinated to rhodium constitutes a stereogenic centre. Lowering the temperature to 243 K induces the splitting of the signals at δ = 4.37 ppm. On the other hand, increasing the temperature to 323 K results in the broadening of all the signals, and the coalescence of the signals for the olefinic protons of 1,5-COD to a single signal centred at δ = 4.35 ppm is observed at 310 K. This clearly demonstrates that complex **3** undergoes a dynamic process in solution. The coalescence temperature corresponds to a $\Delta G^{\ddagger}$ value of 15(±1) kcal·mol^{-1}.[20] The averaging of the resonances for the olefinic protons of 1,5-COD can reasonably be interpreted in terms of decoordination of one end of the ligand **1**, rotation, and recoordination, thus revealing the hemilabile character of ligand **1** in complex **3**. However, the experimental data do not allow for the unambiguous determination of the end of the ligand which eventually decoordinates. Indeed, except a general broadening of the signals, there are no significant changes in the chemical shifts for the protons of the methyl and ethyl groups of the ligand. Scheme 3 shows the proposed mechanism for this process.

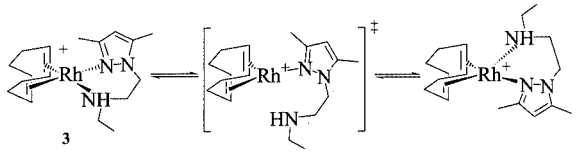

Scheme 3

In the case of complex **4**, the ^{1}H NMR spectrum at room temperature shows three signals characteristic of the CH (δ = 5.59 ppm) and the methyl substituents (δ = 2.34, 2.22 ppm) of the pyrazolyl group. The other resonances are broad signals centred at δ = 5.29 (4 H), 3.71 ppm (2 H) and a large signal between δ = 3.2 and 1.8 ppm (10 H). The signals at δ = 5.29 and 3.71 ppm are in the area characteristic of the olefinic protons of 1,5-COD *trans* to a phosphorus atom and *trans* to a nitrogen atom.[19] Thus, we can deduce that the signal at δ = 5.29 ppm is due to the two olefinic protons of 1,5-COD and the two protons of the methylene group bonded to the nitrogen of the pyrazolyl ring. The large signal is due to both the protons of the methylene group bonded to phosphorus and the alkyl protons of 1,5-COD. These observations suggest that complex **4** undergoes a fluxional process, and variable-temperature experiments were performed at 500 MHz. By lowering the temperature to 230 K, each resonance splits into two more signals at δ = 5.43 and 5.25 ppm for the olefinic protons *trans* to the phosphorus atom, and δ = 3.85 and 3.46 ppm for the olefinic protons *trans* to the nitrogen atom, leading to four signals for the non equivalent olefinic protons of 1,5-COD. The coalescence temperature of the δ = 5.43 and 5.25 ppm resonances occurs at 280 K, while the resonances at δ = 3.85 and 3.46 ppm coalescent 290 K. This corre-

sponds to a $\Delta G^{\ddagger}$ value of 13(±1) kcal·mol^{-1} [20]. No significant differences other than the narrowing of the two signals at δ = 5.33 and 3.68 ppm are observed when the temperature was raised to 333 K. The ^{31}P NMR spectra, recorded in the same temperature range, show a doublet at δ = 28.4 ppm ($^{1}J_{Rh,P}$ = 146.3 Hz), with no other changes, other than a slight displacement with temperature. From these observations it is clear that the fluxional process implies an exchange between the two protons of 1,5-COD which are *trans* to the phosphorus atom, and between the two protons which are *trans* to the nitrogen only. No exchange between the two groups of protons could be evidenced. All this has been corroborated by ^{1}H NMR spin transfer experiments on the olefinic proton resonances. The dynamic behaviour of complex **4** can thus be rationalised in terms of boat-boat configuration inversion of the six-membered ring Rh1−P1−C7−C6−N2−N1 (see Figure 2) in solution. No evidence for a hemilabile behaviour of ligand **2** in complex **4** − that would have led to an averaging of *all* the olefinic proton resonances − could be obtained in the temperature range allowed by the thermal stability of the complex.

In complexes **3** and **4**, the ligand 1,5-COD was displaced by carbon monoxide when the gas was bubbled though the solutions of the complexes in dichloromethane at room temperature, giving [Rh(CO)$_2$(**1**)][BF$_4$] (**5**) and [Rh(CO)$_2$(**2**)][BF$_4$] (**6**), respectively (Scheme 2). Complex **6** reverted back to some extent to complex **4** on evaporation of the solvent. Thus, several cycles of bubbling with carbon monoxide and vacuum drying were necessary to eliminate free 1,5-COD in order to get complex **6** in a reasonable yield.

The IR spectrum of **5** shows two strong absorption bands at 2098 and 2033 cm^{-1} due to νCO vibrations. The ^{1}H NMR spectrum proves the absence of the ligand 1,5-COD, and the appearance of two doublets at δ = 182.5 ppm ($J_{Rh,C}$ = 69.8 Hz) and δ = 181.5 ppm ($J_{Rh,C}$ = 67.3 Hz) in the ^{13}C NMR spectrum confirms the presence of two CO ligands coordinated to the rhodium atom.

The IR spectrum of **6** shows two strong absorption bands at 2103 and 2042 cm^{-1} in the νCO region. Its ^{1}H NMR spectrum confirms the decoordination of the 1,5-COD ligand. The ^{13}C NMR spectrum displays resonances assigned to the two CO ligands as doublet of doublets at δ = 184.8 ppm ($J_{Rh,C}$ = 67 Hz, $J_{P,C}$ = 16 Hz) for the CO *trans* to the nitrogen atom, and at δ = 179.9 ppm ($J_{Rh,C}$ = 60 Hz, $J_{P,C}$ = 104 Hz) for the CO *trans* to the phosphorus atom. The ^{31}P NMR spectrum of **6** displays a doublet at δ = 30.2 ppm with $J_{Rh,P}$ = 120.9 Hz.

The reaction of [Rh(COD)(THF)$_2$][BF$_4$], generated in situ from the reaction of [Rh(COD)Cl]$_2$ and AgBF$_4$ in tetrahydrofuran, and two equivalent amounts of the ligand **1** led to **3** only. This is not surprising since it is known that NN ligands cannot displace 1,5-COD in [Rh(COD)(NN)]BF$_4$ complexes.[23] The same reaction starting with **2** resulted in the formation of a yellow-orange complex **7** in a 92% yield. Elemental analyses and spectroscopic data supported the formation of the [Rh(**2**)$_2$][BF$_4$] complex. The ^{1}H and ^{13}C NMR spectra display the expected signals of the ligand, whereas the ^{31}P NMR spectrum shows a doublet at δ = 44.9 ppm with $^{1}J_{Rh,P}$ = 171 Hz. This complex was also characterised by X-ray crystallography. The molecular structure of **7** consists of discrete [Rh(**2**)$_2$]$^{+}$ cations and BF$_4^{-}$ anions. The cation complex is shown in Figure 3, selected bond lengths and angles are provided in Table 1, and the details of the data collection and crystal data are summarised in Table 2. The structure shows a planar geometry around the rhodium atom, the phosphorus atoms of the two **2** ligands are in a *cis* position. The metal slightly deviates from the mean coordination plane formed by the two N and the two P donor atoms by 0.031 Å. The Rh−N [2.119(2) and 2.113(2) Å] and the Rh−P bond lengths [2.207(1) and 2.223(1) Å] are consistent with those found in the literature.[19,21,22] Phenyl rings are oriented face to face at a distance of 3.287 Å, suggesting a π-π stacking interaction[24]. The P1−Rh1−P2 angle [99.03(3)°] is larger than 90°, and as a consequence the N3−Rh1−P2 angle [83.43(6)°] is more acute than the others [N3−Rh1−N1 = 88.37(9)°; N1−Rh1−P1 = 89.13(7)°].

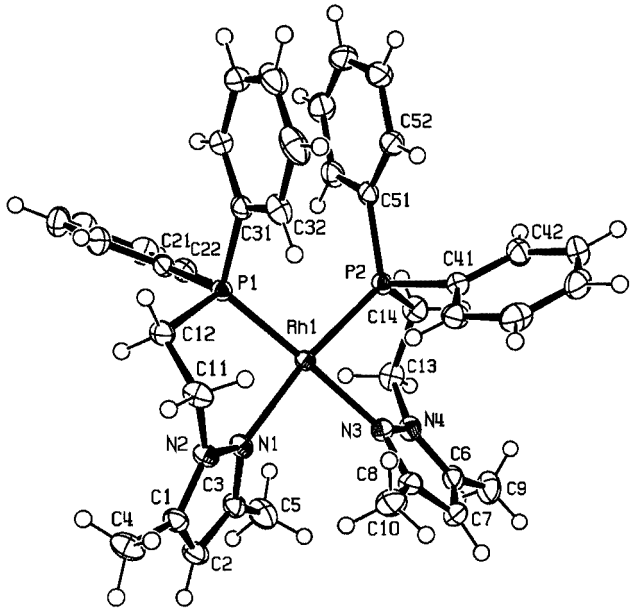

Figure 3. A perspective view of the cation [Rh(**2**)$_2$]$^{+}$ showing the numbering scheme

To prove the hemilabile behaviour of the ligand **2** in **7**, carbon monoxide was bubbled into a solution of the complex in dichloromethane. This led to the formation of a new compound that was characterised by IR and NMR spectroscopy as [Rh(CO)(**2**)$_2$][BF$_4$] (**8**). Evaporation of the solvent under vacuum or the bubbling of nitrogen into the solution of **8** slowly regenerated **7**. In solution, **8** shows a νCO absorption band at 2014 cm^{-1}. At room temperature the ^{1}H, ^{13}C, and ^{31}P NMR spectra indicate that the two **2** ligands are equivalent, thus suggesting a fluxional process in solution. Variable temperature ^{31}P{^{1}H} and ^{1}H NMR experiments were performed. The most informative results were obtained from the ^{31}P{^{1}H} experiments in CD_2Cl_2 solution. Indeed, the room temperature spectrum shows a doublet at

δ = 25.8 ppm ($J_{Rh,P}$ = 122 Hz). Lowering the temperature first induces a progressive broadening of the signal to give a broad resonance centred at δ = 23.9 ppm at 193 K. At 173 K, the lowest temperature we could attain, a slightly broad ABX spin system appears. The parameters of the system (δ_A = 28.1 ppm, δ_B = 19.5 ppm; $J_{A,B}$ = 291 Hz, $J_{A,X}$ = 120 Hz, $J_{B,X}$ = 125 Hz) are consistent with a square planar structure in which the two phosphorus atoms are in a *trans* position, and only one of the two **2** ligands is κ^2-coordinated, the second one is κ^1-coordinated by the phosphorus atom to rhodium. At the same temperature the ^{1}H NMR spectrum shows broad resonances only. The coalescence temperature, in the $^{31}P\{^1H\}$ NMR spectra lead to a $\Delta G^{\ddagger}$ value of 8($\pm$1) kcal·mol^{-1}.[20] The fluxionality observed for **8** most likely results from an exchange between the κ^2 and κ^1 modes of bonding for the two **2** ligands, by the opening of one of the rhodium-pyrazolyl bonds. The same type of dynamic process was previously observed for the [Ir(PN)$_2$(CO)][PF$_6$] complex [PN = 1-(2-pyridyl)-2-(diphenylphosphanyl)ethane],[23] and this is frequently observed in complexes containing two hemilabile bidentate ligands.[2,3] Scheme 4 summarises our observations.

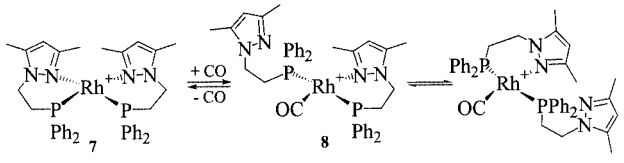

Scheme 4

The catalytic activity of complexes **4** and **7** has been evaluated for the hydroformylation of styrene. Under our experimental conditions (dichloromethane as the solvent, 20 bar of a 1:1 mixture of CO and H_2, 50 °C) a low conversion was observed (1% for **4** and 10% for **7**), and only the branched aldehyde was detected.

Conclusions

In this work we have described the synthesis of the new potentially hemilabile N,P bidentate ligand, 1-[2-(diphenylphosphanyl)ethyl]-3,5-dimethylpyrazole (**2**). The reaction of **2** and the related N,N′ bidentate ligand 1-[2-(ethylamino)ethyl]-3,5-dimethylpyrazole (**1**) with the rhodium(I) complex [Rh(COD)(THF)$_2$]BF$_4$ has led to the complexes [Rh(COD)(**1**)]BF$_4$ (**3**) and [Rh(COD)(**2**)]BF$_4$ (**4**), which have been fully characterised. Both these compounds exhibit a fluxional process in solution that can be interpreted in terms of a hemilabile behaviour of the ligand **1** in complex **3**, and a boat-boat ring inversion of the six-membered ring formed on coordination of the ligand **2** in complex **4**. The 1,5-COD ligand in complexes **3** and **4** can easily be displaced by carbon monoxide, leading to the complexes [Rh(CO)$_2$(**1**)]BF$_4$ (**5**) and [Rh(CO)$_2$(**2**)]BF$_4$ (**6**), respectively. The reaction of two equivalents of **2** with [Rh(COD)(THF)$_2$]BF$_4$ leads to [Rh(**2**)$_2$][BF$_4$] (**7**), in which the phosphorus atoms are in a *cis* position. The latter complex reversibly absorbs one molecule of CO to afford complex [Rh(**2**)$_2$(CO)][BF$_4$] (**8**). NMR studies of complex **8** show a dynamic exchange between the κ^2 and κ^1 modes of bonding for the two **2** ligands, by the opening of one of the rhodium-pyrazolyl bonds. In spite of this hemilabile property of ligand **2**, complex **7** shows a low activity for the catalytic hydroformylation of styrene.

Experimental Section

General Procedures: All chemicals were used as received from commercial suppliers, unless otherwise indicated. Reactions were carried out under a dinitrogen atmosphere using vacuum line and Schlenk techniques. Solvents were dried and distilled according to standard procedures and stored under nitrogen. NMR spectra were acquired on a Bruker AC200, AC250, Avance DPX250, or Avance DRX500 spectrometer in $CDCl_3$ solutions, unless otherwise indicated. All the chemical shifts are given in ppm and are referenced with respect to residual protons in the solvent for ^{1}H spectra, to solvent signals for ^{13}C spectra and to external H_3PO_4 for ^{31}P spectra. IR spectra were recorded on a Perkin−Elmer 2000 spectrophotometer with KBr pellets or in dichloromethane solutions with CaF_2 cells. Elemental analyses were performed at the Laboratoire de Chimie de Coordination on a Perkin−Elmer 2400 CHN analyser or at the Universitat Autònoma de Barcelona on a Carlo Erba CHNS EA-1108 apparatus. Electronic impact mass spectra were measured by the staff of the Mass Spectrometry Service at the Université Paul Sabatier (Toulouse). [Rh(COD)Cl$_2$] was prepared according to a literature procedure.[25]

Synthesis of 1-(Chloroethyl)-3,5-dimethylpyrazole:[18] 3,5-Dimethylpyrazole (1.00 g, 10.4 mmol), 40% aq. NaOH (12 mL), tetrabutylammonium bromide (TBAB, 0.483 g, 1.5 mmol), toluene (20 mL), and 1-bromo-2-chloroethane (10 mL, 17.23 g, 120 mmol) were mixed and heated to reflux for 48 h. The mixture was allowed to cool to room temperature, the phases were separated and the aqueous phase was extracted with 3 × 20 mL of dichloromethane. The extracts were combined with the organic phase and the solvents were then removed under vacuum. Addition of diethyl ether (15 mL), filtration and evaporation of the solvent yielded 1-(chloroethyl)-3,5-dimethylpyrazole as a colourless oil. Yield: 88%. M.p. 20−22 °C. $C_7H_{11}ClN_2$ (158.6) (%): calcd. C 53.00, H 6.99, N 17.66; found C 52.69, H 6.63, N 17.83. IR (neat between KBr cells): $\tilde{\nu}$ [cm^{-1}] = 3046 (νC−H$_{ar}$), 2967−2871 (νC−H$_{al}$), 1555 (νC=C$_{ar}$, νC=N$_{ar}$), 1463 (δCH$_{3as}$), 1426 (δC=C$_{ar}$, δC=N$_{ar}$), 1388−1188 (νC−N), 860 (νC−Cl). ^{1}H NMR (250 MHz, $CDCl_3$, 20 °C): δ [ppm] = 5.74 (s, 1 H, CH pyrazole), 4.19 (t, $^3J_{H,H}$ = 6.3 Hz, 2 H, CH_2CH$_2$Cl), 3.79 (t, $^3J_{H,H}$ = 6.3 Hz, 2 H, CH$_2$CH_2Cl), 2.21 (s, 3 H, CCH$_3$), 2.15 (s, 3 H, CCH$_3$). $^{13}C\{^1H\}$ NMR (63 MHz, $CDCl_3$, 20 °C): δ [ppm] = 148.2 (*C*CH$_3$), 139.7 (*C*CH$_3$), 105.1 (CH pyrazole), 49.6 (*C*H$_2$CH$_2$Cl), 43.0 (CH$_2$*C*H$_2$Cl), 13.4 (C*C*H$_3$), 11.0 (C*C*H$_3$). Mass spectroscopic data (EI, *m*/*z*): 158[M$^{+\cdot}$], 122 [M$^+$ − Cl], 109 [M$^+$ − CH$_2$Cl], 96 [M$^{+\cdot}$− C$_2$H$_3$Cl].

Synthesis of 1-[2-(Diphenylphosphanyl)ethyl]-3,5-dimethylpyrazole (2): A solution of *n*BuLi (100 μL, 1.6 mmol, 1.6 M in hexane) was added dropwise to a stirred solution of PPh$_2$H (300 μL, 1.724 mmol) in tetrahydrofuran (10 mL) at 0 °C. After 30 min, the solution of PPh$_2$Li was added dropwise to a stirred solution of 1-(chloroethyl)-3,5-dimethylpyrazole (0.325 g, 2.0 mmol) in tetrahydrofuran (20 mL) at 0 °C. The mixture was maintained at 0 °C for 1 h. The temperature was then raised to room temperature and

after 15 h of stirring the solvent was evaporated under vacuum. 40 mL of dichloromethane were added to the residue and the salts were extracted with 2 × 10 mL of distilled water. Evaporation of the solvent from the organic phase gives 1-[2-(diphenylphosphanyl)-ethyl]-3,5-dimethylpyrazole (**2**) as a colourless oil. Yield: 83%. M.p. 20−22 °C. $C_{19}H_{21}N_2P$ (308.4) (%): calcd. C 74.01, H 6.86, N 9.08; found C 73.72, H 6.68, N 9.28. IR (neat between KBr cells): ṽ [cm^{-1}]: 3074−3046 (νC−H_{ar}), 2923 (νC−H_{al}), 1553 (νC=C_{ar}, νC=N_{ar}), 1482 (δCH_{3as}), 1435 (δC=C_{ar}, δC=N_{ar}), 1387−1184 (νC−N), 764−704 (νP−C, δC−H_{oop}). ^{1}H NMR (200 MHz, $CDCl_3$, 20 °C): δ [ppm] = 7.48−7.29 (m, 10 H, PPh_2), 5.71 (s, 1 H, CH pyrazole), 4.10−3.99 (m, 2 H, CH_2CH$_2$PPh$_2$), 2.61−2.53 (m, 2 H, CH$_2$CH_2PPh$_2$), 2.19 (s, 3 H, CCH_3), 2.06 (s, 3 H, CCH_3). ^{13}C{^{1}H} NMR (63 MHz, $CDCl_3$, 20 °C): δ [ppm] = 147.3 (*C*CH_3), 138.2 (*C*CH_3), 132.7−128.3 (PPh_2), 104.8 (CH pyrazole), 45.4 (d, $^2J_{P,C}$ = 25.0 Hz, *C*H$_2$CH$_2$PPh$_2$), 29.4 (d, $^1J_{P,C}$ = 14.4 Hz, CH$_2$*C*H$_2$PPh$_2$), 13.4 (C*C*H$_3$), 10.8 (C*C*H$_3$). ^{31}P{^{1}H} NMR (81 MHz, $CDCl_3$, 20 °C): δ [ppm] = −20.9 (PPh_2). Mass spectroscopic data (EI, *m/z*): 308 [M$^{+\cdot}$], 231 [M$^+$ − Ph], 123 [M$^+$ − PPh_2], 109 [M$^+$ − CH_2PPh_2], 96 [M$^{+\cdot}$ − $C_2H_3PPh_2$].

Synthesis of [Rh(COD)(1)][BF$_4$] (3): $AgBF_4$ (0.062 g, 0.320 mmol) was added to a solution of [Rh(COD)Cl_2] (0.079 g, 0.160 mmol) in tetrahydrofuran (20 mL). A white solid precipitated (AgCl). After 30 min of stirring the solid was filtered off and 1-[2-(ethylamino)-ethyl]-3,5-dimethylpyrazole ligand (**1**) (0.054 g, 0.320 mmol) was added to the filtrate, leading to the precipitation of complex **3** as a yellow solid. The complex was crystallised in a dichloromethane/ether mixture. Yield: 89%. M.p. 135−137 °C (dec.). $C_{17}H_{29}BF_4N_3Rh$ (465.1) (%): calcd. C 43.90, H 6.28, N 9.03; found C 43.82, H 6.16, N 8.90. IR (KBr): ṽ [cm^{-1}]: 3275 (νN−H), 2960−2835 (νC−H_{al} ligand+COD), 1553 (νC=C_{ar}, νC=N_{ar}), 1469 (δCH_{3as} ligand/δCH_2 COD), 1432 (δC=C_{ar} ligand+COD, δC=N_{ar}), 1386−1188 (νC−N), 1069−964 (νB−F), 801 (δ =CH_{oop} COD), 771 (δC−H_{oop} ligand+COD). ^{1}H NMR (500 MHz, $CDCl_3$, 20 °C): δ [ppm] = 5.87 (s, 1 H, CH pyrazole), 5.51, 4.56 (AB, 2 H, CH_2CH$_2$NHEt), 4.49, 4.40, 4.30, 4.21 (m, 4 H, =CH COD), 4.15 (b, 1 H, NH), 3.54, 2.41 (AB, 2 H, CH$_2$CH_2NHEt), 2.64 (m, 2 H, CH_2 COD), 2.41 (m, 1 H, CH_2CH$_3$), 2.31 (s, 3 H, CCH_3), 2.28 (s, 3 H, CCH_3), 2.19−2.11, 1.67 (m, 6 H, CH_2 COD), 1.71−1.65 (m, 4 H, CHH_{endo} COD), 1.44 (t, $^3J_{H,H}$ = 7.0 Hz, 3 H, CH$_2$CH_3), 1.30 (m, 1 H, CH_2CH$_3$). ^{13}C{^{1}H} NMR (63 MHz, $CDCl_3$, 20 °C): δ [ppm] = 149.4 (*C*CH_3), 142.4 (*C*CH_3), 108.0 (CH pyrazole), 83.6−81.4 (m, =CH COD), 49.8, 49.3 (*C*H$_2$*C*H$_2$NHCH$_2$CH$_3$), 32.2 (*C*H$_2$CH$_3$), 29.0,28.6 (CH_2 COD), 15.6 (CH$_2$*C*H$_3$), 14.0 (C*C*H$_3$), 11.3 (C*C*H$_3$).

Synthesis of [Rh(COD)(2)][BF$_4$] (4): $AgBF_4$ (0.062 g, 0.320 mmol) was added to a solution of [Rh(COD)Cl_2] (0.079 g, 0.160 mmol) in tetrahydrofuran (20mL). A white solid precipitated (AgCl). The solid was then filtered of and 1-[2-(diphenylphosphanyl)ethyl]-3,5-dimethylpyrazole (**2**) (0.099 g, 0.320 mmol) was added to the filtrate solution. After 1 h of stirring, the solvent was evaporated under vacuum and the residue was crystallised in a dichloromethane/ether mixture to give yellow crystals of complex **4**. Yield: 94%. M.p. 208−210 °C (dec.). $C_{27}H_{33}BF_4N_2PRh$ (606.3) (%): calcd. C 53.48, H 5.50, N 4.62; found C 53.06, H 5.17, N 4.41. IR (KBr): ṽ [cm^{-1}]: 3074 (νC−H_{ar}), 2994−2828 (νC−H_{al} ligand+COD), 1555 (νC=C_{ar}, νC=N_{ar}), 1483−1467 (δCH_{3as} ligand/δCH_2 COD), 1436−1428 (δC=C_{ar} ligand+COD, δC=N_{ar}), 1389−1162 (νC−N), 1102−948 (νB−F), 862 (δ =CH_{oop} COD), 777−700 (νP−C, δC−H_{oop} ligand+COD). ^{1}H NMR (250 MHz, $CDCl_3$, 20 °C): δ [ppm] = 7.37 (b, 10 H, PPh_2), 5.59 (s, 1 H, CH pyrazole), 5.29 (b, 2 H, = CH COD *trans* P), 5.33, 5.15 (AB, 2 H, CH_2CH$_2$PPh$_2$), 3.71 (b, 2 H, =CH COD *trans* N), 2.67 (b, 2 H, CH$_2$CH_2PPh$_2$), 2.48 (b, 4 H, CHH_{exo} COD), 2.34 (s, 3 H, CCH_3), 2.22 (s, 3 H, CCH_3), 2.16 (b, 4 H, CHH_{endo} COD). ^{13}C{^{1}H} NMR (50 MHz, $CDCl_3$, 20 °C): δ [ppm] = 149.4 (*C*CH_3), 143.1 (*C*CH_3), 132.7−128.6 (PPh_2), 108.0 (CH pyrazole), 104.8−103.4 (m, =CH COD *trans* P), 78.6−77.5 (m, =CH COD *trans* N), 48.5 (d, $^2J_{P,C}$ = 5.8 Hz, *C*H$_2$CH$_2$PPh$_2$), 27.9−27.4 (*C*H_2 COD), 27.6 (d, $^1J_{P,C}$ = 27.7 Hz, CH$_2$*C*H$_2$PPh$_2$), 15.2 (C*C*H$_3$), 11.3 (C*C*H$_3$). ^{31}P{^{1}H} NMR (81 MHz, $CDCl_3$, 20 °C): δ [ppm] = 28.4 (d, $^1J_{Rh,P}$ = 146.3 Hz, PPh_2).

Synthesis of [Rh(CO)$_2$(1)][BF$_4$] (5): Carbon monoxide was bubbled for 1 h into a solution of [Rh(COD)(**1**)][BF_4] (0.098 g, 0.211 mmol) in dichloromethane (20 mL). **5** was obtained in a 98% yield after evaporation of the solvent, and 1,5-COD was liberated under vacuum. $C_{11}H_{17}BF_4N_3O_2Rh$ (413.0) (%): calcd. C 31.99, H 4.15, N 10.17; found C 32.34, H 4.12, N 9.87. IR (CH_2Cl_2 solution, CaF_2 cells): ṽ [cm^{-1}]: 2099 and 2033 (νCO). ^{1}H NMR (250 MHz, $CDCl_3$, 20 °C): δ [ppm] = 6.08 (s, 1 H,CH pyrazole), 5.60, 4.45 (AB, 2 H, CH_2CH$_2$NHEt), 4.48 (b, 1 H, NH), 3.61, 2.65 (AB, 2 H, CH$_2$CH_2NHEt), 2.88 (m, 2 H, CH_2CH$_3$), 2.43 (s, 3 H, CCH_3), 2.38 (s, 3 H, CCH_3), 1.34 (t, $^3J_{H,H}$ = 7.2 Hz, 3 H, CH$_2$CH_3). ^{13}C{^{1}H} NMR (63 MHz, $CDCl_3$, 20 °C): δ [ppm] = 182.5 (d, $J_{Rh,C}$ = 69.8 Hz, CO), 181.1 (d, $J_{Rh,C}$ = 67.3 Hz, CO), 151.3 (*C*CH_3), 144.1 (*C*CH_3), 107.6 (CH pyrazole), 50.4, 49.6, 47.8 (*C*H$_2$*C*H$_2$NHCH$_2$CH$_3$, *C*H$_2$CH$_3$), 14.5 (C*C*H$_3$), 14.6 (CH$_2$*C*H$_3$), 11.1 (C*C*H$_3$).

Synthesis of [Rh(CO)$_2$(2)][BF$_4$] (6): Carbon monoxide was bubbled for 1 h into a solution of [Rh(COD)(**2**)][BF_4] (0.170 g, 0.280 mmol) in dichloromethane (20 mL), and **6** was obtained. The complex partially reverted back to the reactants when the solvent was evaporated under vacuum, therefore, six cycles of bubbling carbon monoxide and evaporation under vacuum were carried out in order to isolate **6** in a pure form. $C_{21}H_{21}BF_4N_2O_2PRh$ (554.1) (%): calcd. C 45.52, H 3.82, N 5.06; found C 45.02, H 3.49, N 5.21. IR (CH_2Cl_2 solution, CaF_2 cells): ṽ [cm^{-1}]: 2103 and 2042 (νCO). ^{1}H NMR (200 MHz, CD_3COCD_3, 20 °C): δ [ppm] = 7.82−7.56 (m, 10 H, PPh_2), 6.01 (s, 1 H, CH pyrazole), 5.08−4.91 (m, 2 H, CH_2CH$_2$PPh$_2$), 3.30−3.19 (m, 2 H, CH$_2$CH_2PPh$_2$), 2.38 (s, 3 H, CCH_3), 2.32 (s, 3 H, CCH_3). ^{13}C{^{1}H} NMR (63 MHz, CD_2Cl_2, 20 °C): δ [ppm] = 184.8 (dd, $J_{Rh,C}$ = 67 Hz, $J_{P,C}$ = 15.8 Hz CO), 179.9 (dd, $J_{Rh,C}$ = 60 Hz, $J_{P,C}$ = 103.5 Hz CO), 151.3 (*C*CH_3), 145.0 (*C*CH_3), 133.7−128.6 (PPh_2), 108.3 (CH pyrazole), 47.2 (*C*H$_2$CH$_2$PPh$_2$), 27.2 (d, $^1J_{P,C}$ = 30.3 Hz, CH$_2$*C*H$_2$PPh$_2$), 15.3 (C*C*H$_3$), 11.5 (C*C*H$_3$). ^{31}P{^{1}H} NMR (81 MHz, CD_3COCD_3, 20 °C): δ [ppm] = 30.2 (d, $^1J_{Rh,P}$ = 120.9 Hz, PPh_2).

Synthesis of [Rh(2)$_2$][BF$_4$] (7): $AgBF_4$ (0.062 g, 0.32 mmol) was added to a solution of [Rh(COD)Cl_2] (0.079 g, 0.160 mmol) in tetrahydrofuran (20 mL). After filtration of AgCl, 1-[2-(diphenylphosphanyl)ethyl]-3,5-dimethylpyrazole (**2**) (0.221 g, 0.717 mmol) was added to the filtrate solution. The solvent was then removed under vacuum and the yellow-orange residue of complex **7** was washed with pentane and crystallised in a dichloromethane/ether mixture. Yield: 92%. M.p. 147−150 °C (dec.). $C_{39}H_{44}BCl_2F_4N_4P_2Rh$ (891.4) (%): calcd. C 52.55, H 4.98, N 6.29; found C 52.57, H 4.93, N 6.19. IR (KBr): ṽ [cm^{-1}]: 3054 (νC−H_{ar}), 2960−2919 (νC-H_{al}), 1551 (νC=C_{ar}, νC=N_{ar}), 1480−1466 (δCH_{3as}), 1435−1429 (δC=C_{ar}, δC=N_{ar}), 1392−1177 (νC−N), 1098−999 (νB−F), 744−696 (νP−C, δC−H_{oop}). ^{1}H NMR (250 MHz, $CDCl_3$, 20 °C): δ [ppm] = 7.65 (b, 20 H, PPh_2), 5.57 (s, 2 H, CH pyrazole), 4.75 (m, 4 H, CH_2CH$_2$PPh$_2$), 2.70 (m, 4 H, CH$_2$CH_2PPh$_2$), 2.29 (s, 6 H, CCH_3), 1.79 (s, 6 H, CCH_3). ^{13}C{^{1}H} NMR (63 MHz, $CDCl_3$, 20 °C): δ [ppm] = 150.6 (*C*CH_3), 140.6 (*C*CH_3), 135.2−127.8 (PPh_2), 106.7 (CH pyrazole), 47.2 (*C*H$_2$CH$_2$PPh$_2$), 33.5 (d, $^1J_{P,C}$ = 28.0 Hz,

Table 2. Crystal data for compounds [Rh(COD)(**1**)][BF_4] (**3**), [Rh(COD)(**2**)][BF_4] (**4**), and [Rh(**2**)$_2$][BF_4] (**7**)

	3	**4**	**7**
Empirical formula	$C_{17}H_{29}BF_4N_3Rh$	$C_{27}H_{33}BF_4N_2PRh$	$C_{39}H_{44}BCl_2F_4N_4P_2Rh$
Molecular weight [g]	465.15	606.24	891.34
Temperature [K]	293(2)	160(2)	160(2)
Wavelength [Å]	0.71073	0.71073	0.71069
Crystal system	triclinic	monoclinic	monoclinic
Space group	*P*1 bar	$P2_1/n$	$P2_1/n$
a [Å]	7.2584(1)	14.168(1)	10.997(5)
b [Å]	10.872(2)	14.742(1)	18.247(5)
c [Å]	13.297(2)	12.550(11)	20.073(5)
α [deg]	95.55(2)	90	90
β [deg]	104.51(2)	90.55(1)	102.518(5)
γ [deg]	98.66(2)	90	90
Volume [Å^3]	994.3(2)	2621.1(4)	3932(2)
Z	2	4	4
$D_{calcd.}$ [g·cm^{-3}]	1.554	1.536	1.506
μ [mm^{-1}]	0.900	0.760	0.705
F(000)	476	1240	1824
θ range [deg]	3.95−25.97	2.13−26.03	2.20−26.05
Index ranges	$-8 \le h \le 8$	$-17 \le h \le 17$	$-13 \le h \le 13$
	$-13 \le k \le 13$	$-18 \le k \le 18$	$-22 \le k \le 22$
	$-16 \le l \le 16$	$-15 \le l \le 15$	$-24 \le l \le 24$
Reflections collected	9568	20361	30207
Independent reflections	3530 [R_{int} = 0.0528]	5134 [R_{int} = 0.0337]	7643 [R_{int} = 0.0380]
Completeness to θ_{max} (%)	90.5	99.1	98.1
Refinement method	full-matrix least-squares on F^2		
Data/Restraints/Parameters	3530/0/233	5134/0/327	7643/0/482
goodness of fit on F^2	1.084	1.028	1.021
Final *R* indices [$I > 2\sigma(I)$]	*R*1 = 0.0436	*R*1 = 0.0266	*R*1 = 0.0395
	*wR*2 = 0.1220	*wR*2 = 0.0623	*wR*2 = 0.1016
R indices (all data)	*R*1 = 0.0456	*R*1 = 0.0369	*R*1 = 0.0421
	*wR*2 = 0.1281	*wR*2 = 0.0655	*wR*2 = 0.1041
resid. elec. density e[·Å^{-3}]	0.970 and −0.725	0.556 and −0.320	1.536 and −1.151

$CH_2CH_2PPh_2$), 13.4 (CCH_3), 11.3 (CCH_3). $^{31}P\{^1H\}$ NMR (101 MHz, $CDCl_3$, 20 °C): δ [ppm] = 44.9 (d, $^1J_{Rh,P}$ = 171.1 Hz, PPh_2).

Synthesis of [Rh(CO)(2)$_2$][BF_4] (8): [Rh(**2**)$_2$][BF_4] (0.070 g, 0.087 mmol) in dichloromethane (20 mL) was bubbled with carbon monoxide for 1 h and [Rh(CO)(**2**)$_2$][BF_4] was obtained. The complex was characterised in solution after bubbling nitrogen to eliminate dissolved carbon monoxide, as it reverted back to **7** when the solvent was evaporated under vacuum. IR (CH_2Cl_2 solution, CaF_2 cells): ν̃ [cm^{-1}]: 2088 and 2014 (νCO). ^1H NMR (250 MHz, $CDCl_3$, 20 °C): δ [ppm] = 7.96−6.70 (m, 20 H, PPh_2), 5.50 (s, 2 H, CH pyrazole), 4.53 (m, 4 H, $CH_2CH_2PPh_2$), 2.94 (broad, 4 H, $CH_2CH_2PPh_2$), 2.09 (s, 6 H, CCH_3), 1.85 (s, 6 H, CCH_3). $^{13}C\{^1H\}$ NMR (63 MHz, $CDCl_3$, 20 °C): δ [ppm] = 190.1 (broad d, CO, $J_{Rh,C}$ = 72 Hz), 148.8 (CCH_3), 141.5 (CCH_3), 135.4−127.9 (PPh_2), 106.5 (CH pyrazole), 45.9 ($CH_2CH_2PPh_2$), 29.7 (t, $J_{P,C}$ = 12.5 Hz, $CH_2CH_2PPh_2$), 14.0 (CCH_3), 10.97 (CCH_3). $^{31}P\{^1H\}$ NMR (101 MHz, $CDCl_3$, 20 °C): δ [ppm] = 25.8 (d, $^1J_{Rh,P}$ = 122.5 Hz, PPh_2).

X-ray Crystallographic Study: Crystals of **3**, **4**, and **7** suitable for X-ray diffraction were obtained through recrystallisation from dichloromethane/diethylether mixtures. Data were collected at 293 K for **3** and 160 K for **4** and **7** on a STOE IPDS diffractometer. Full crystallographic data for the three complexes are gathered in Table 2. All calculations were performed on a PC-compatible computer using the WinGX system.[26] The structures were solved by using the SIR92 program,[27] which revealed in each instance the position of most of the non-hydrogen atoms. All remaining non-hydrogen atoms were located by the usual combination of full-matrix least-squares refinement and difference electron density syntheses by using the SHELXS-97 program.[28] Atomic scattering factors were taken from the usual tabulations.[29] Anomalous dispersion terms for Rh, and P (for complexes **4** and **7**) were included in F_c.[30] All non-hydrogen atoms were allowed to vibrate anisotropically. All the hydrogen atoms were set in idealised positions [R_3CH, C−H = 0.96 Å; R_2CH_2 = 0.97 Å; $C(sp^2)$−H = 0.93 Å; U_{iso} 1.2 time greater than the U_{eq} of the carbon atom to which the hydrogen atom is attached] and held fixed during refinements.

CCDC-184360 for **3**, 184358 for **4**, and CCDC-184359 for **7** contain the supplementary crystallographic data for this paper. These data can be obtained free of charge at www.ccdc.cam.ac.uk/conts/retrieving.html [or from the Cambridge Crystallographic Data Centre, 12, Union Road, Cambridge CB2 1EZ, UK; Fax: (internat.) +44−1223/336-033; E-mail: deposit@ccdc.cam.ac.uk].

Acknowledgments

Support by the CNRS and the Ministerio de Educación y Cultura of Spain (Project BQU200-0238 and grant to G.E.) are gratefully acknowledged.

[1] P. Braunstein, F Naud, *Angew. Chem.* **2001**, *113*, 702−722; *Angew. Chem. Int. Ed.* **2001**, *40*, 680−699.
[2] A. Bader, E. Lindner, *Coord. Chem. Rev.* **1991**, *108*, 27−110.
[3] C. S Slone, D. A. Weinberger, C. A. Mirkin, *Prog. Inorg. Chem.* **1999**, *48*, 233.

[4] A. Borner, *Eur. J. Inorg. Chem.* **2001**, 327−337.
[5] C. Standfest-Hauser, C. Slugovc, K. Mereiter, R. Schmid, K. Kirchner, L. Xiao, W. Weissensteiner, *J. Chem. Soc., Dalton Trans.* **2001**, 2989−2995.
[6] H. Yang, M. Alvarez-Gressier, N. Lugan, R. Mathieu, *Organometallics* **1997**, *16*, 1401−1409.
[7] W Keim, H. Maas, S. Mecking, *Z. Naturforsch., B: Chem. Sci.* **1995**, *50*, 430.
[8] R. Weber, W. Keim, M. Mothrath, U. Englert, R. Gauter, *Chem. Commun.* **2000**, 1419−1420.
[9] R. Mukherjee, *Coord. Chem. Rev.* **2000**, *203*, 151−218.
[10] W. L Driessen, *Recl. Trav. Chim. Pays-Bas* **1982**, *101*, 441.
[11] H. L. Blonk, W. L. Driessen, J. Reedijk, *J. Chem. Soc., Dalton Trans.* **1985**, 1699−1705.
[12] E. Bouwman, W. L. Driessen, J. Reedijk, *Coord. Chem. Rev.* **1990**, *104*, 143−172.
[13] F. Mani, *Coord. Chem. Rev.* **1992**, *120*, 325−359.
[14] S. Trofimenko, *Scorpionates: The coordination chemistry of poly(pyrazolyl)borate ligands*; Imperial College Press: London, **1999**.
[15] R. Mathieu, G. Esquius, N. Lugan, J. Pons, J. Ros, *Eur. J. Inorg. Chem.* **2001**, 2683−2688.
[16] D.B. Grotjahn, D. Combs, S. Van, G. Aguirre, F. Ortega, *Inorg. Chem.* **2000**, *39*, 2080−2086.
[17] W. L. Driessen, R. M. de Vos, A. Etz, J. Reedijk, *Inorg. Chim. Acta* **1995**, *235*, 127−133.
[18] P. Cabildo, R. M. Claramunt, P. Cornago, J. L. Lavandera, D. Sanz, N. Jagerovic, M. L. Jimeno, J. Elguero, I. Gilles, J. L. Aubagnac, *J. Chem. Soc., Perkin Trans.* **1996**, *2*, 701−712.
[19] H. Yang, N. Lugan, R. Mathieu, *Organometallics* **1997**, *16*, 2089−2095.
[20] H. Friebolin, *Basic One- and Two-Dimensional NMR Spectroscopy*; VCH Verlagsgesellschaft mbH: Germany, **1993**.
[21] G. Esquius, J. Pons, R. Yáñez, J. Ros, X. Solans, M. Font-Bardía, *J. Organomet. Chem.* **2000**, *605*, 226−233.
[22] P. Suomalainen, S. Jääskeläinen, M. Haukka, R. H. Laitinen, J. Pursiainen, T. A. Pakkanen, *Eur. J. Inorg. Chem.* **2000**, 2607−2613.
[23] M. P. Anderson, A. L. Casalnuovo, B. J. Johnson, B. M. Mattson, A. N. Mueting, L. H. Pignolet, *Inorg. Chem.* **1988**, *27*, 1649−1658.
[24] G. W. Coates, A. R. Dunn, L. M. Henling, D. A. Dougherty, R. H Grubbs, *Angew. Chem.* **1997**, *109*, 290−293; *Angew. Chem. Int. Ed. Engl.* **1997**, *36*, 248.
[25] G. Giordano, R. H. Crabtree, *Inorg. Synth.* **1979**, *19*, 218.
[26] L. J. Farrugia, *J. Appl. Crystallogr.* **1999**, *32*, 837.
[27] A. Altomare, G. Cascarano, C. Giacovazzo, A. Guagliardi, *J. Appl. Crystallogr.* **1993**, *26*, 343.
[28] G. M. Sheldrick, *SHELXS-97, SHELXL-97, CIFTAB − Programs for Crystal Structure Analysis (Release 97-2)*, Institut für Anorganische Chemie der Universität, Tammanstrasse 4, 3400 Göttingen, Germany, **1998**.
[29] [29a] D. T. Cromer, J. T. Waber, *International Tables for X-ray Crystallography*; Kynoch Press: Birmingham, England, vol. 4, **1974**, Table 22B. [29b] R. F. Stewart, E. R. Davidson, W. T. Simpson, *J. Chem. Phys.* **1965**, *42*, 3175. [29c] T. Hahn (Ed.), *International Tables for Crystallography, Volume A*, Kluwer Academic Publishers, Dordrecht, The Netherlands, **1995**.
[30] D. T. Cromer, J. T. Waber, *International Tables for X-ray Crystallography*, Kynoch Press: Birmingham, England, vol. 4, **1975**, Table 2.3.1.

Received April 21, 2002
[I02215]

Synthesis and X-ray Molecular Structure of $[W^{VI}(C_6H_4S_2\text{-}1,2)_3]$ Completing the Structural Characterization of the Series $[W(C_6H_4S_2\text{-}1,2)_3]^{n-}$ (n = 0, 1, 2): Trigonal-Prismatic versus Octahedral Coordination in Tris(benzene-1,2-dithiolato) Complexes

HanVinh Huynh,[a] Thomas Lügger,[a] and F. Ekkehardt Hahn*[a]

Dedicated to Prof. Karl Wieghardt on the occasion of his 60th birthday

Keywords: Tungsten / S ligands / Structure elucidation / Coordination modes

The tris(benzene-1,2-dithiolato) complex $[W^{VI}(C_6H_4S_2\text{-}1,2)_3]$ **1** was synthesized from $[W(CH_3)_6]$ and $C_6H_4(SH)_2$-1,2 in diethyl ether. Crystals of $[W^{VI}(C_6H_4S_2\text{-}1,2)_3]$ were obtained from a saturated dichloromethane solution at room temperature. The X-ray crystal structure analysis revealed that the tungsten atom in **1** is coordinated in an almost perfect trigonal-prismatic fashion with W–S distances between 2.3724(14) Å and 2.3840(14) Å.

Introduction

The first molecular trigonal-prismatic tris(dithiolene) metal complex was reported in 1965.[1] Ever since, the reasons for the formation of complexes with a trigonal-prismatic coordination geometry over octahedral complexes have been discussed extensively.[2] In addition, the "non-innocent" nature of benzenedithiolato ligands and their derivatives has more recently become a field of considerable interest.[3] Nevertheless, the trigonal-prismatic coordination geometry is not limited to tris(dithiolene) complexes, but can also be observed for some hexaarylthiolato[4] and hexaorgano complexes with six monodentate ligands. The latter complexes have received a great deal of attention since the molecular structure of the complex $[Li(tmed)]_2[Zr(CH_3)_6]$ containing a distorted trigonal-prismatic coordinated zirconium atom was reported.[5] Recently, $[M(CH_3)_6]^{z-}$ complexes of Ta (z = 1), Nb (z = 1), Re (z = 0) and W (z = 0) have been characterized by X-ray diffraction revealing a regular to slightly distorted trigonal-prismatic coordination geometry.[6] Theoretical studies indicate that d^0 ions in particular tend to form complexes with a trigonal-prismatic geometry.[2c,2d,7] However, the pseudo-octahedral d^0 complex dianion $[Zr^{IV}(C_6H_4S_2\text{-}1,2)_3]^{2-}$ is one of the few exceptions to this postulate.[8] The coordination geometry in $[Mo^{VI}(C_6H_4S_2\text{-}1,2)_3]$ is, as expected, trigonal-prismatic (average twist angle 0°)[9] while the geometry of $[Mo^{V}(C_6H_4S_2\text{-}1,2)_3]^-$ was found to be closer to octahedral (average twist angle 33.5°)[10] than to trigonal-prismatic. Based on this observation a geometry with an even larger twist angle and therefore even closer to octahedral geometry would be expected for the structurally as-yet-uncharacterized d^2 complex $[Mo^{IV}(C_6H_4S_2\text{-}1,2)_3]^{2-}$. However, in the homologous series of tungsten complexes the derivative $[W^{V}(C_6H_4S_2\text{-}1,2)_3]^-$ exhibits a geometry analogous to the Mo^V complex in-between octahedral and trigonal-prismatic (average twist angle 33°),[11] while the complex $[W^{IV}(C_6H_4S_2\text{-}1,2)_3]^{2-}$ is clearly trigonal-prismatic (average twist angle 3.5°).[12] It appears that the stepwise reduction of the d^0 M^{VI} center does not always enhance the tendency for the formation of octahedral complexes. However, the molecular structure of $[W^{VI}(C_6H_4S_2\text{-}1,2)_3]$ has not been described. To compare the molecular structures of the complete series of complexes $[W(C_6H_4S_2\text{-}1,2)_3]^{n-}$ (n = 0, 1, 2) we prepared the missing derivative $[W^{VI}(C_6H_4S_2\text{-}1,2)_3]$ and determined its molecular structure by X-ray diffraction.

Results and Discussion

In connection with our research on helicates with benzene-1,2-dithiolato ligands[13] we investigated methods for the preparation of $[W^{VI}(C_6H_4S_2\text{-}1,2)_3]$. Published syntheses of tris(benzene-1,2-dithiolato) transition metal complexes[2d] involve the reaction of metal halides with an excess of benzene-1,2-dithiol in CCl_4 with liberation of gaseous HCl. The moderate yields as well as the solvent tox-

[a] Institut für Anorganische und Analytische Chemie,
Westfälische Wilhelms-Universität Münster,
Wilhelm-Klemm-Strasse 8, 48149 Münster, Germany
Fax: (internat.) +49-(0)251/833-3108
E-mail: fehahn@uni-muenster.de

 © 2002 WILEY-VCH Verlag GmbH & Co. KGaA, 69451 Weinheim 1434–1948/02/1111–3007 $ 20.00+.50/0

icity and the highly reactive by-product in these syntheses proved disadvantageous in our opinion. A rather exotic way to prepare hexakis(arylthiolato) zirconate complexes with six monodentate thiolato ligands using $[Zr(CH_3)_6]^{2-}$ as a precursor was reported by Giolando et al.[4] Using this approach, we have improved the synthesis for $[W^{VI}(C_6H_4S_2\text{-}1,2)_3]$ (**1**) by reacting $[W(CH_3)_6]$ with three equivalents of benzene-1,2-dithiol in diethyl ether with formation of unreactive methane gas (Scheme 1). The product can be isolated in pure form and in yields of about 70%. The perorgano precursor was prepared in situ from WCl_6 and CH_3Li in diethyl ether similar to a literature method.[14] Bright purple, air-stable crystals of **1** can be obtained from a saturated turquoise dichloromethane solution at ambient temperature.

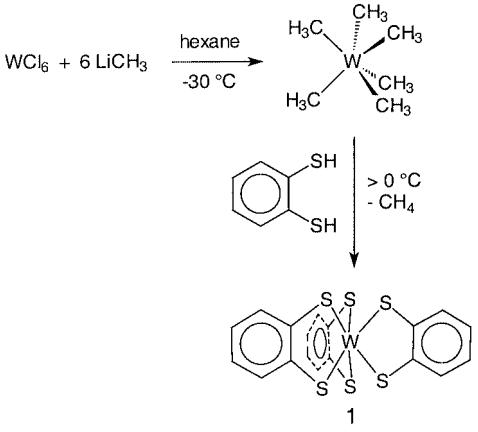

Scheme 1. Preparation of $[W^{VI}(C_6H_4S_2\text{-}1,2)_3]$ from $[W(CH_3)_6]$

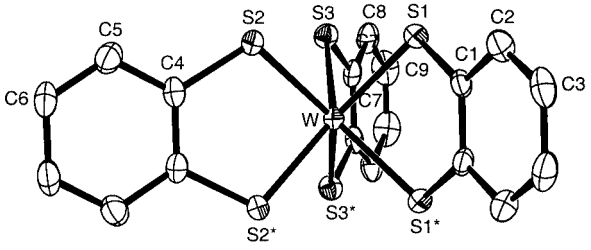

Figure 1. Molecular structure of $[W^{VI}(C_6H_4S_2\text{-}1,2)_3]$ (**1**) with the crystallographic numbering scheme; hydrogen atoms have been omitted; starred atoms are related to their corresponding atoms by a crystallographic mirror plane; selected bond lengths [Å] and angles [°]: W−S1 2.3840(14), W−S2 2.3836(13), W−S3 2.3724(14), S1−C1 1.743(5), S2−C4 1.747(5), S3−C7 1.742(6); S1−W−S1* 81.97(7), S1−W−S2 80.89(5), S1−W−S2* 134.42(5), S1−W−S3 81.96(5), S1−W−S3* 136.33(5), S2−W−S2* 81.73(6), S2−W−S3 82.02(5), S2−W−S3* 136.24(5), S3−W−S3* 82.30(7), C1−S1−W 103.21(17), C4−S2−W 107.92(18), C7−S3−W 106.17(19)

Figure 1 shows the molecular structure of the neutral complex **1** along with the crystallographic numbering scheme. The molecular geometry of complex **1** is remarkably similar to its lower homologue $[Mo^{VI}(C_6H_4S_2\text{-}1,2)_3]$.[9] The tungsten(VI) ion is coordinated by six sulfur atoms of three benzene-1,2-dithiolato ligands in an almost perfect trigonal-prismatic fashion with a crystallographically imposed twist angle of 0°. A value of 60° would be typical for an octahedron.[8,15] In addition, the WS_6 core deviates less from D_{3h} symmetry than the WC_6 core found in the organometallic precursor.[6] The mean W−S bond length of 2.380 Å, interligand S···S distance of 3.111 Å and intraligand S···S distance of 3.123 Å are slightly longer than those reported for the isostructural Mo^{VI} complex [mean values: *d*(Mo-S) 2.367 Å, *d*(S···S, interligand) 3.091 Å, *d*(S···S, intraligand) 3.110 Å]. This observation can be explained by taking into account the slightly greater ionic radius of W^{VI} compared to that of Mo^{VI}. As expected, the average C−S bond length of 1.727 Å in **1** falls in the range observed for the isostructural molybdenum(VI) complex. As observed for the Mo^{VI} complex the $S_2C_6H_4$ planes in **1** deviate from the WS_2 planes (13.5°, 22.6°, 32.7°) thereby enforcing a deviation from ideal D_{3h} symmetry for the complex (Figure 2).

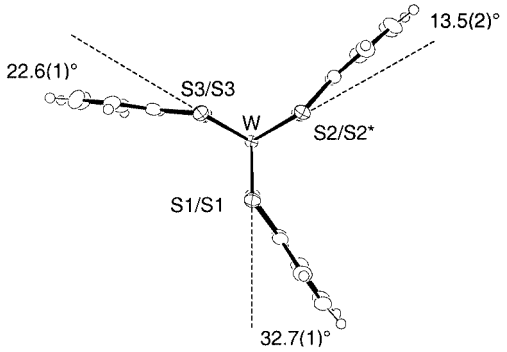

Figure 2. View of $[W^{VI}(C_6H_4S_2\text{-}1,2)_3]$ projected down the approximate molecular threefold axis, showing the bend of the ligands

A comparison of the molecular structures of the members of the series $[W(C_6H_4S_2\text{-}1,2)_3]^{n-}$ (n = 0, 1, 2) shows no clear correlation of electronic configuration or overall charge of the complexes and the molecular geometry. The one-electron reduction of trigonal-prismatic $[W^{VI}(C_6H_4S_2\text{-}1,2)_3]$ results in pseudooctahedral $[W^{V}(S_2C_6H_4)_3]$,[11] with an average twist angle of 33°. The pseudooctahedral coordination was also observed for the analogous Mo^{V} complex.[10] Here it was explained by the occupation of the π-antibonding $4a_1'$ molecular orbital causing destabilization of both S···S interactions and M−S bonds and leading to an octahedral distortion.[10] Following this argument for the tungsten complexes, dianionic $[W^{IV}(C_6H_4S_2\text{-}1,2)_3]^{2-}$ should adopt a symmetry even closer to octahedral than the W^{V} complex due to the fully occupied $4a_1'$ orbital. Surprisingly, this assumption was disproved by the close trigonal-prismatic structure found for $[W^{IV}(C_6H_4S_2\text{-}1,2)_3]^{2-}$,[12] with an average twist angle of only 3.5°. Table 1 summarizes structural parameters for the series $[W(C_6H_4S_2\text{-}1,2)_3]^{n-}$ (n = 0, 1, 2).

From the variation of the twist angles Φ in the series $[M(C_6H_4S_2\text{-}1,2)_3]^{n-}$ (M = Mo, W; n = 0, 1, 2) it appears that the d-electron configuration is not the only governing principle for the formation of a certain coordination geometry. The M^{VI} complexes exhibit a trigonal-prismatic WS_6 core and the one-electron reduction leads to a distorted octahedral geometry. Further reduction leads, at least in the case of W^{IV}, again to an almost trigonal-prismatic geometry. The recently reported structural characterization of two other tris(dithiolene) series[16] $[M\{S_2C_2(CH_3)_2\}_3]^{n-}$

Table 1. Selected mean bond lengths and twist angles for the series $[W(C_6H_4S_2\text{-}1,2)_3]^{n-}$ (n = 0, 1, 2)

	$[W^{VI}(C_6H_4S_2\text{-}1,2)_3]$[a]	$[W^{V}(C_6H_4S_2\text{-}1,2)_3]^-$ [b]	$[W^{IV}(C_6H_4S_2\text{-}1,2)_3]^{2-}$ [c]
W−S	2.380	2.386 (2.387)	2.391
S−S_{inter}	3.111	3.227 (3.235)	3.139
S−S_{intra}	3.123	3.101 (3.123)	3.101
C−S	1.744	1.713 (1.779)	1.750
Twist angle Φ	0°	33°	3.5°

[a] This study. [b] Ref.;[11a] values in parentheses from ref.[11b] [c] Ref.[12]

(M = Mo, n = 0, −1, −2; M = W, n = −1, −2) revealed distorted trigonal-prismatic structures for all members. These results indicate, once again, that the stabilization of the trigonal-prismatic structure is not only governed by electronic factors but must be considered a complicated process involving various factors.

Experimental Section

General Remarks: Unless stated otherwise, all manipulations were carried out in an atmosphere of dry argon by means of standard Schlenk techniques. Diethyl ether and hexane were freshly distilled from Na-benzophenone prior to use.

$[W^{VI}(C_6H_4S_2\text{-}1,2)_3]$ (1): WCl_6 (198 mg, 0.5 mmol) was suspended in dry diethyl ether (30 mL) and cooled to −78 °C. With vigorous stirring MeLi (2 mL of a 1.6 M solution in diethyl ether, 3.2 mmol) was added dropwise and the mixture was allowed to warm to −35 °C. After stirring for 3 h the red-brown reaction mixture was filtered through celite into a cold solution (−30 °C) of benzene-1,2-dithiol (214 mg, 1.5 mmol) in diethyl ether (10 mL). The reaction mixture was allowed to warm to ambient temperature while methane gas evolved. The product was filtered, washed with diethyl ether (5 mL) and *n*-hexane (20 mL) and dried in vacuo. Yield 236 mg (77%). $C_{18}H_{12}S_6W$ (604.50): calcd. C 35.76, H 2.00, S 31.82; found C 35.60, H 2.13, S 31.66. Additional spectroscopic parameters were identical to those reported in 1966.[2d] Crystals of **1** were obtained from a saturated dichloromethane solution.

X-ray Crystallographic Study: A suitable crystal (0.2 × 0.2 × 0.2 mm^3) was mounted on a Bruker AXS APEX diffractometer equipped with a Mo rotating anode (λ = 0.71073 Å), a cooling device and graphite monochromator. 14512 Raw structure factors ($-19 \le h \le 19$, $-13 \le k \le 14$, $-12 \le l \le 12$, $2\Theta = 4-45°$) were collected at −120 °C using omega- and phi-scans. An empirical absorption correction was applied with SADABS[17] ($T_{min}/T_{max.}$ = 0.3379) before merging. Complex **1** crystallized in the orthorhombic space group *Pnma*, a = 16.034(5), b = 11.793(4), c = 10.276(3) Å, V = 1942.9(10) $Å^3$. Structure solution with SHELXS[18] and subsequent refinement of 139 parameters against 1516 observed [$I > 2\sigma(I)$, 1794 unique collected intensities] structure factors using SHELXL[19] with anisotropic thermal parameters for all non-hydrogen atoms revealed that the unit cell contains Z = 4 molecules $C_{18}H_{12}S_6W$ (604.49 g/mol, $d_{calcd.}$ = 2.067 g/cm^3). The tungsten atom resides at a special position on a mirror plane. Hydrogen positions were determined by difference Fourier techniques and refined with isotropic thermal parameters. Final obtained residues R_{all} = 3.81, $R_{obsd.}$ = 2.94, $R_{w,obsd.}$ = 6.98%, GOF = 1.036. ORTEP[20] was used for all drawings. CCDC-185593 contains the supplementary crystallographic data for this paper. These data can be obtained free of charge at www.ccdc.cam.ac.uk/conts/retrieving.html [or from the Cambridge Crystallographic Data Centre, 12, Union Road, Cambridge CB2 1EZ, UK; fax: (internat.) +44-1223/336-033; E-mail: deposit@ccdc.cam.ac.uk].

Acknowledgments

This work was financially supported by the Deutsche Forschungsgemeinschaft and the Fonds der Chemischen Industrie

[1] [1a] R. Eisenberg, J. A. Ibers, *J. Am. Chem. Soc.* **1965**, *87*, 3376−3377. [1b] R. Eisenberg, J. A. Ibers, *Inorg. Chem.* **1966**, *5*, 411−416.
[2] [2a] D. L. Kepert, *Inorganic Stereochemistry; Inorganic Chemistry Concepts 6*, Springer Verlag, Berlin, **1982**, Chapter 8. [2b] J. E. Huheey, E. A. Keiter, R. L. Keiter, *Inorganic Chemistry: Principles of Structure and Reactivity*, 4th ed., Harper, New York, **1993**, Chapter 12. [2c] G. N. Schrauzer, V. P. Mayweg, *J. Am. Chem. Soc.* **1966**, *88*, 3235−3242. [2d] E. I. Stiefel, R. Eisenberg, R. C. Rosenberg, H. B. Gray, *J. Am. Chem. Soc.* **1966**, *88*, 2956−2966.
[3] [3a] P. Chaudhuri, C. N. Verani, E. Bill, E. Bothe, T. Weyhermüller, K. Wieghardt, *J. Am. Chem. Soc.* **2001**, *123*, 2213−2223. [3b] D. Herebian, E. Bothe, E. Bill, T. Weyhermüller, K. Wieghardt, *J. Am. Chem. Soc.* **2001**, *123*, 10012−10023.
[4] J. C. Friese, A. Krol, C. Puke, K. Kirschbaum, D. Giolando, *Inorg. Chem.* **2000**, *39*, 1496−1500.
[5] P. M. Morse, G. S. Girolami, *J. Am. Chem. Soc.* **1989**, *111*, 4114−4116.
[6] S. Kleinhenz, V. Pfennig, K. Seppelt, *Chem. Eur. J.* **1998**, *4*, 1687−1691.
[7] M. Kaupp, *Chem. Eur. J.* **1998**, *4*, 1678−1686.
[8] M. Cowie, M. J. Bennett, *Inorg. Chem.* **1976**, *15*, 1595−1603.
[9] M. Cowie, M. J. Bennett, *Inorg. Chem.* **1976**, *15*, 1584−1589.
[10] A. Cervilla, E. Llopis, D. Marco, F. Perez, *Inorg. Chem.* **2001**, *40*, 6525−6528.
[11] [11a] T. E. Burrow, R. H. Morris, A. Hills, D. L. Hughes, R. L. Richards, *Acta Crystallogr., Sect. C* **1993**, *49*, 1591−1594. [11b] F. Knoch, D. Sellmann, W. Kern, *Z. Kristallogr.* **1992**, *202*, 326−328.
[12] C. Lorber, J. P. Donahue, C. A. Goddard, E. Nordlander, R. H. Holm, *J. Am. Chem. Soc.* **1998**, *120*, 8102−8112.
[13] H. V. Huynh, C. Schulze-Isfort, W. W. Seidel, T. Lügger, R. Fröhlich, O. Kataeva, F. E. Hahn, *Chem. Eur. J.* **2002**, *8*, 1327−1335.
[14] A. J. Shortland, G. Wilkinson, *J. Chem. Soc., Dalton Trans.* **1973**, 872−876.
[15] J. L. Martin, J. Takats, *Can. J. Chem.* **1989**, *67*, 1914−1923.
[16] D. V. Formitchev, B. S. Lim, R. H. Holm, *Inorg. Chem.* **2001**, *40*, 645−654.
[17] SMART, Bruker AXS, **2000**.
[18] G. M. Sheldrick, SHELXS-97, *Acta Crystallogr., Sect. A* **1990**, *46*, 467−473.
[19] G. M. Sheldrick, SHELXL-97, Universität Göttingen, **1997**.
[20] L. J. Farrugia, ORTEP-3, University of Glasgow, **1999**.

Received May 24, 2002
[I02274]

Extended Electronic Interactions in a Triangular μ-Oxotriruthenium Acetate Cluster Containing Nitric Oxide

Henrique E. Toma,*[a] Anamaria D. P. Alexiou,[a] and Sergio Dovidauskas[a]

Keywords: Ruthenium / Nitrogen oxides / Carboxylate ligands / Cluster compounds / Pi interactions

The binding of NO to the trinuclear cluster $[Ru_3O(CH_3CO_2)_6(py)_2]^+$ (py = pyridine) leads to a stable, diamagnetic $[Ru_3O(CH_3CO_2)_6(py)_2(NO)]^+$ complex, displaying extended electronic interactions which arise from the coupling of the unpaired π^* electron of NO and the unpaired electron in the π-orbitals of the Ru_3O unit. This complex has been isolated and its spectroscopic characterization (EPR, ^1H and ^{13}C NMR, IR, UV/Vis) and electrochemical/spectroelectrochemical properties are reported in this paper. The NO^0 character in the complex is supported by spectroscopic and electrochemical results, as well as by semi-empirical theoretical calculations carried out for the complex. A remarkable point in this system is the dramatic changes in the Ru–NO electronic interactions accompanying the several successive redox states of the triangular Ru_3O center.

(© Wiley-VCH Verlag GmbH, 69451 Weinheim, Germany, 2002)

Introduction

Triangular μ-oxoruthenium acetate clusters of general formula $[Ru_3O(CH_3CO_2)_6L_3]^n$ (L = H_2O, N-heterocycles, etc.) are particularly interesting because of their rich mixed-valence chemistry, displaying catalytic properties and versatility as building blocks in supramolecular chemistry.[1] This type of complex exhibits a series of successive oxidation states and the corresponding redox potentials are dependent of the pK_a [2] and E_L parameters[3] of the terminal ligands. In general, clusters containing all ruthenium ions in the formal oxidation state +3 and above are preferentially stabilized by σ-donor ligands (L). Mixed-valence clusters with the formal oxidation state $Ru^{III}Ru^{III}Ru^{II}$, and below, are stabilized by π-acceptor molecules such as CO[4–6] or isocyanide ligands.[7,8]

Nitric oxide is a typical non-innocent ligand. It can bind to a metal center (M) yielding a metal-nitrosyl complex, where the ligand can be classified as NO^+, $NO^{\cdot}$ or NO^-.[9–12] In recent years a great number of reports dealing with NO activity in biological systems have been published,[13–20] and ruthenium nitrosyl complexes have been exploited as potential scavengers or delivery drugs for NO into biological targets.[21–27]

Because of the several available oxidation states, the interaction between NO and the triangular μ-oxoruthenium acetate clusters can be viewed as a puzzling question, especially concerning the electronic delocalization and the nature of the redox orbitals involved. Such important aspects have been focused on in this work, starting from the synthesis and characterization of the novel clusters species $[Ru_3O(CH_3CO_2)_6(py)_2(NO)]PF_6$ (Figure 1), and carrying out a detailed investigation of its spectroscopic and electrochemical properties, and a theoretical simulation of its electronic structure based on semi-empirical methods. To the best of our knowledge, except for a brief comment by Spencer and Wilkinson on the interaction of nitric oxide with $[Ru_3O(CH_3CO_2)_6L_3]^+$ [L = CH_3OH and $P(C_6H_5)_3$] complexes,[4] the chemistry of this type of nitrosyl-triruthenium acetate cluster has never been reported before.

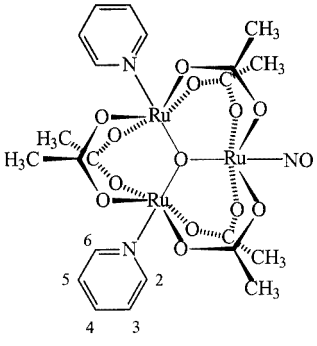

Figure 1. Structural representation of $[Ru_3O(CH_3CO_2)_6(py)_2(NO)]PF_6$; the labels of pyridine hydrogen atoms are required for the analysis of the NMR spectra

Results and Discussion

The general route for the synthesis of Ru–NO complexes based on the procedures involving $NaNO_2$ and acids[28] was initially attempted in this work, but resulted in low yields

[a] Instituto de Química, Universidade de São Paulo,
C. Postal 26077, CEP05513–970, Brazil
Fax: (internat.) +55-11/3815-5579
E-mail: henetoma@iq.usp.br

Supporting information for this article is available on the WWW under http://www.eurjic.org or from the author.

and an impure product. Surprisingly, the direct reaction of $[Ru_3O(CH_3CO_2)_6(py)_2(CH_3OH)]^+$ and NO was successful, yielding a rather stable complex, isolated as $[Ru_3O(CH_3CO_2)_6(py)_2(NO)]PF_6 \cdot CH_2Cl_2$. Its thermal stability was assayed by thermogravimetry, showing solvent loss in the range 100−253 °C and decomposition of the cluster above this temperature, indicating that the Ru−NO bonding is quite strong.

The first question concerning the nature of the $[Ru_3O(CH_3CO_2)_6(py)_2(NO)]^+$ complex refers to its valence description, for example, as $Ru^{III}Ru^{III}Ru^{III}NO^0$ or $Ru^{III}Ru^{III}Ru^{II}NO^+$, in a formal representation. For discussion purposes, the starting $[Ru_3O(CH_3CO_2)_6(py)_2(CH_3OH)]^+$ was taken as a reference compound exhibiting a formal $Ru^{III}Ru^{III}Ru^{III}$ oxidation state. In the other extreme, the $[Ru_3O(CH_3CO_2)_6(py)_2(CO)]$ complex provides a suitable model illustrating the effects of the strong π-acceptor CO ligand in preferentially stabilizing the formal $Ru^{III}Ru^{III}Ru^{II}(CO)$ oxidation state. NO^+ is a stronger π-acceptor ligand than CO, therefore if the $[Ru_3O(CH_3CO_2)_6(py)_2(NO)]^+$ complex involves NO^+, its acceptor properties would exceed those of the CO analog in terms of π-backbonding effects. In contrast, in the NO^0 form the available π*-electron can preferentially stabilize the $Ru^{III}Ru^{III}Ru^{III}$ cluster by coupling with the ruthenium d_π-electrons. In fact, such an electronic balance is supposed to be very delicate, and the NO^+ or NO^0 character will actually depend upon the relative energies of the metal cluster and NO frontier orbitals.

The complex $[Ru_3O(CH_3CO_2)_6(py)_2(NO)]PF_6 \cdot CH_2Cl_2$ exhibits a small room temperature molar paramagnetic susceptibility (6.7×10^{-4} cgs unit) very similar to that determined under the same conditions for the complex $[Ru_3O(CH_3CO_2)_6(py)_2(CO)] \cdot C_6H_6$ (6.8×10^{-4} cgs unit). Presumably, the small paramagnetism in both complexes reflects the temperature-independent paramagnetic susceptibility arising from the mixing with the excited states, which has previously been estimated to fall within the range $2.3-27 \times 10^{-4}$ cgs unit.[29,30] No EPR signal was seen at either room or liquid nitrogen temperatures for the complex $[Ru_3O(CH_3CO_2)_6(py)_2(NO)]PF_6$, thus suggesting a strong coupling between the available π*-electron in NO^0 and the ruthenium d_π-electrons in the $Ru^{III}Ru^{III}Ru^{III}$ cluster.

Infrared Spectra

The FTIR spectrum of the cluster $[Ru_3O(CH_3CO_2)_6(py)_2(NO)]PF_6$ (Figure 2) was assigned by comparison with the data for $[Ru_3O(CH_3CO_2)_6(py)_2(CH_3OH)]PF_6$ and similar compounds described in the literature[5,31−33] (FTIR data and assignments are available as Supporting Information). The characteristic peak for the nitrosyl group is found at 1865 cm^{-1} (Figure 2), corresponding to the ν(NO) vibration. This peak is very strong and symmetric, and is not observed in the spectrum of the complex $[Ru_3O(CH_3CO_2)_6(py)_2(CH_3OH)]PF_6$. Another important observation supporting the strong binding of NO is that practically all vibrational modes of the coordinated ligands are changed in the NO complex as a consequence of the electronic perturbation. For instance, the $\nu_{as}(COO^-)$ vibrational peak observed at 1550 cm^{-1} for the methanol complex, is shifted to 1585 cm^{-1} in the NO compound.

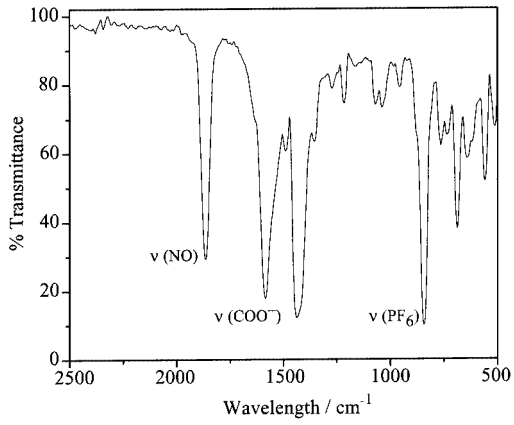

Figure 2. FT-IR spectrum of the $[Ru_3O(CH_3CO_2)_6(py)_2(NO)]PF_6$ cluster

It should be noted that the ν(NO) peak of free NO is located at 1876 cm^{-1}, but in the metal complexes it is very sensitive to the binding properties and oxidation states of the metal ion. For instance, ν(NO) frequencies for *cis*-$[Ru^{II}(bipy)_2(NO)L]$ complexes (L = N^{3-}, Cl^-, NO_2^-, NH_3, py, CH_3CN) have been observed in the range 1923−1970 cm^{-1}.[34] For $[Ru^{II}(NH_3)_5(NO)]^{3+}$ [35] and *trans*-$[Ru^{II}(NH_3)_4(NO)L]$[36] complexes [L = imidazole, L-histidine, py, isonicotinamide, pyrazine, $P(OEt)_3$], ν(NO) values span the range 1909−1941 cm^{-1}, whereas for L = SO_3^{2-}, ν(NO) = 1871 cm^{-1}. In the case of *trans*-$[Ru^{II}(py)_4(NO)L]$[37] complexes, for L = Cl^-, and Br^-, ν(NO) = 1910 and 1901 cm^{-1}, respectively, but for L = OH^-, ν(NO) = 1860 cm^{-1}. In all such examples, the ruthenium center has been considered as mainly Ru^{II}, thus imputing a predominantly NO^+ character to the nitrosyl ligand. In the case of the reduced complexes $[Ru(bipy)_2(NO)(CH_3CN)]^{2+}$ and $[Ru(bipy)_2(NO)Cl]^+$ ν(NO) is shifted to 1665 and 1640 cm^{-1}, and the spectroscopic and electrochemical data support the hypothesis of NO^+ reduction, yielding NO^0 species.[34]

In the case of *trans*-[Ru(dimethylglyoximato)(NO)Cl],[38] ν(NO) = 1878 cm^{-1} and is very close to the frequency of the free nitric oxide molecule, although a significant NO^+ character has been suggested from its observed reactivity in the presence of nucleophiles.[39] Perhaps because of its partial NO^0 character, only a small shift of ν(NO) to 1855 cm^{-1} is observed in this system upon reduction.

In the complex $[Ru_3O(CH_3CO_2)_6(py)_2(NO)]^+$, the observed ν(NO) frequency (1865 cm^{-1}) falls in the range characteristic of linear nitrosyl complexes M−NO,[12] and is closer to the vibrational frequency of free NO (1876 cm^{-1}) than of NO^+ (2273 cm^{-1}) or NO^- (1358−1374 cm^{-1}). However, it should be noted that in the NO^+ complexes the ν(NO) frequencies can also decrease significantly as a consequence of π-backbonding interactions, and typical values have been observed in the range of 1900−1970 cm^{-1} as shown by the preceding examples. In special cases (as in

the nitrosyl cluster system herein reported) where ν(NO) is close to that of the free NO molecule, the differentiation between a typical NO^0 complex and the case involving a rather strong π-backbonding to NO^+ is not obvious and cannot be carried out exclusively on the basis of the infrared vibrational data.

^{1}H and ^{13}C NMR Spectra

The ^{1}H and ^{13}C NMR spectra of the cluster were assigned by comparison with related clusters[1,5−7,40−52], using peak integration and COSY (^{1}H,^{1}H) and HMQC (^{1}H, ^{13}C) bidimensional techniques (see also Supporting Information). In the ^{1}H and ^{13}C NMR spectra one can observe two signals for the CH_3 groups, in accordance with the C_{2v} cluster symmetry. Selected NMR spectroscopic data are collected in Table 1 in order to illustrate how the signals of the ligands coordinated to the Ru_3O core depend upon the oxidation states of the ruthenium ions. Reduced clusters in the $Ru^{III}Ru^{III}Ru^{II}$ formal oxidation state, including CO species, are diamagnetic and show coordinated ligand signals close to the free ones and slightly downfield shifted. On the other hand, the oxidized clusters ($Ru^{III}Ru^{III}Ru^{III}$) are paramagnetic and their signals are not only sensitive to the inductive effects from the metal center, but also to the paramagnetic anisotropy of the Ru_3O unit.[47] Interestingly, the CH_3 and H_2 proton signals of acetate and pyridine are found at chemical shifts between the signals of the diamagnetic $[Ru_3O(CH_3CO_2)_6(py)_2CO]^0$, $[Ru_3O(CH_3CO_2)_6(py)_3]^0$ and the paramagnetic $[Ru_3O(CH_3CO_2)_6(py)_3]^+$ clusters. This rules out a description in terms of a formal $Ru^{III}Ru^{III}Ru^{II}NO^+$ oxidation state, since its corresponding NMR spectra would be similar to the CO analog.

The NMR spectroscopic data suggest a significant NO^0 character in the cluster system. The formal representation $Ru^{III}Ru^{III}Ru^{III}NO^0$ should be interpreted rather carefully, since there is a strong coupling between the NO^0 π*-electron and the ruthenium d_π-electrons, which results in a large diamagnetism according to magnetic susceptibility measurements. In fact, the increase in the π-electron density is reflected in the *J* values observed for the pyridine ligand signals [$^3J_{H,H}$ = 6.5 Hz, C(2)−H; $^4J_{H,H}$ = 1.5 Hz, C(2)−H; $^3J_{H,H}$ = 7.6 Hz, C(3)−H]. In the oxidized clusters these constants are too small to be observed because the scalar coupling decreases as the oxidation state of the coupled nucleus increases.[53] The CH_2Cl_2 molecule was detected in the ^{1}H and ^{13}C NMR spectra at δ = 5.32 and 55 ppm, respectively, corroborating the elemental analysis and thermogravimetry results.

Electronic Structure

The electronic spectrum of $[Ru_3O(CH_3CO_2)_6(py)_2(NO)]PF_6$ exhibits a series of superimposed bands in the 300−800 nm range, which can be deconvoluted as shown in Figure 3. The absorption profile is rather unusual, displaying apparently little similarity with those reported in the literature for related complexes.[2,6,7]

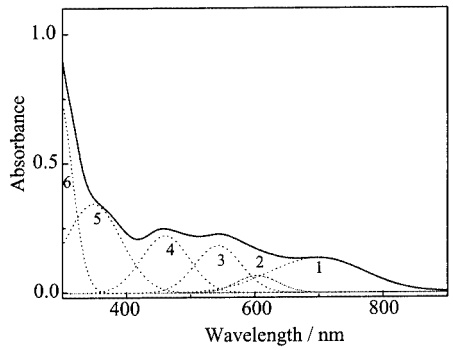

Figure 3. Electronic spectrum of a 10^{-3} M $[Ru_3O(CH_3CO_2)_6(py)_2(NO)]PF_6$ solution in acetonitrile

The electronic structure of $[Ru_3O(CH_3CO_2)_6L_3]$ clusters has been discussed in terms of a qualitative molecular orbital scheme proposed by Cotton and Norman, centered on the Ru_3O π-system in D_{3h} symmetry.[54] In this scheme, the central oxygen atom is considered to be sp^2 hybridized, leaving a single p_z orbital of π symmetry to interact with the ruthenium d_π orbitals ($d_{zy'}$, $d_{x'z}$, and $d_{x'^2-y'^2}$). The Ru $d_{zy'}$ orbitals are perpendicular to the horizontal symmetry plane of the molecule, and can combine with the O p_z orbital,

Table 1. ^{1}H and ^{13} C NMR chemical shifts (δ) for the $[Ru_3O(CH_3CO_2)_6L_3]^n$ (Ru_3L_3) clusters in CD_3CN

	$Ru_3^{III,III,III}py_3$ [47]	$Ru_3^{III,III,III}py_2NO$	$Ru_3^{III,III,II}py_2CO$[40]	$Ru_3^{III,III,II}py_3$ [a] [5]
			^{1}H (ppm)	
H_3C	4.82 (12 H)	3.96 (12 H)	2.10 (6 H)	2.14 (17.8 H)
		3.28 (6 H)	2.16[b]	
$H_{2,6}$ (L)	0.25 (6 H)	4.49 (4 H)	9.14 (4 H)	9.02 (6.0 H)
$H_{3,5}$ (L)	5.82 (6 H)	8.18 (4 H)	8.13 (4 H)	7.69 (6.1 H)
H_4 (L)	6.57 (3 H)	5.82 (2 H)	8.31 (2 H)	7.99 (3.2 H)
			^{13}C (ppm)	
H_3C	−6.4	9.1	30.8	
		16.4		
COO^-	199.3	221.2	212.5	
$C_{2,6}$ (L)	126.6	162.1	154.4	
$C_{3,5}$ (L)	114.5	113.7	126.5	
C_4 (L)	138.1	152.4	142.6	

[a] In CD_2Cl_2. [b] Overlapped with water signal.

giving rise to two a_2'' molecular orbitals, while the $d_{zy'} - d_{zy'}$ combination leads to an e'' molecular orbital. The Ru $d_{x'z}$ orbitals are localized in the Ru_3O plane and their direct combination gives rise to e'(1) and a_2' molecular orbitals. The remaining Ru $d_{x'^2-y'^2}$ orbitals can interact weakly since a considerable distance separates them. However, these orbitals can interact with the p orbitals localized on the oxygen atoms of the bridging acetates, providing a further mechanism for Ru−Ru interactions. This would remove the degeneracy of the three $d_{x'^2-y'^2}$ orbitals, giving rise to e'(2) and a_1' levels.

Under C_{2v} symmetry, the a_2'', a_2', and a_1' levels transform according to b_1, b_2, and a_1, while the e'' and e' levels split into b_1, a_2, and a_1, b_2, respectively. In principle, the qualitative molecular orbital diagram proposed by Cotton and Norman could be employed for extrapolating to C_{2v} symmetry based on a simple correlation procedure. In our case, however, this is not feasible, since the π-interactions with the NO ligand make the qualitative ordering of the molecular orbitals rather complicated.

In order to shed some light on the electronic structure of the nitrosyl cluster, a preliminary molecular orbital calculation was carried out for the model complex $[Ru_3O(CH_3CO_2)_6(NH_3)_2(NO)]^+$ using the ZINDO/S semi-empirical method after a suitable geometry optimization based on the MM^+ force field, as described in the Exp. Sect. The pyridine ligands were replaced by NH_3 in order to simplify the calculations and, specially, to facilitate the interpretation of the electronic properties of the Ru_3O-NO chromophore. It should be noticed that pyridine and NH_3 are very close in the spectrochemical series of ligands, and their influence in the $Ru^{III}Ru^{III}Ru^{III}$ cluster is expected to be rather similar.

The atomic charge distribution for the model complex can be seen in Figure 4. In this complex, the NO ligand bears a very small negative charge (δ = −0.068) while the attached ruthenium ion has a positive charge (δ = 0.593) that is significantly higher than the other two ruthenium ions (δ = 0.353). Therefore, the charge distribution within the Ru_3O-NO moiety indicates a predominant NO^0 character, and also the occurrence of substantial π-backbonding effects involving the Ru−NO bond.

According to the ZINDO/S molecular orbital calculations (Table 2) the NO ligand has a strong influence on several energy levels, particularly those involving the Ru $d_{zy'}$ (MO 99, 96, 90) and Ru $d_{x'z}$ (MO 100, 98, 91) orbitals. For instance, in the case of MO 100 (LUMO 2) the NO character is 83%, while for MO 99 (LUMO 1) there is a nearly equivalent mixture with the Ru d_π orbitals. Among the HOMO levels, MO 96 and 91 exhibit a high contribution of NO (16%), although the highest contribution is observed for MO 90 (42%).

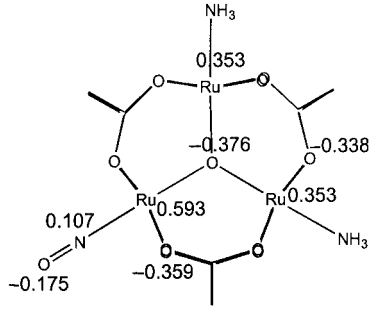

Figure 4. Atomic charge distribution for the model cluster $[Ru_3O(CH_3CO_2)_6(NH_3)_2(NO)]^+$

Table 2. Molecular orbital composition for the cluster $[Ru_3O(CH_3CO_2)_6(NH_3)_2NO]^+$

MO	% Ru	% NO	% CH_3CO_2	% O
		HOMO		
90	42	42	14	
91	63	15	13	6
92	77		22	
93	78		18	2
94	75		18	5
95	82		13	2
96	56	16	10	16
97	65		34	
		LUMO		
98	66	6	27	
99	49	34	6	9
100	14	83	2	

The ZINDO/S method successfully reproduces the observed electronic transitions in the nitrosyl cluster, as shown in Figure 3. Such transitions are also indicated in the molecular orbital scheme (Figure 5) corresponding to symmetry- and spin-allowed transitions. Transition 1, at 691 nm (ε = 1740 $M^{-1}cm^{-1}$), corresponds to the HOMO 0 → LUMO 0 excitation, involving essentially the occupied trinuclear ruthenium-acetate level of a_1 symmetry (MO 97) and the next empty b_2 level (MO 98) displaying some NO character (6%). Transition 2, at 602 nm, is relatively weak, and involves the excitation from MO 97 to MO 99 (b_1), displaying strong NO character. Transition 3, at 538 nm (ε = 2840 $M^{-1}cm^{-1}$), is more intense and involves the excitation from MO 96 (b_1) to MO 99 (b_1); both exhibiting significant NO character. Transition 4, at 451 nm (ε = 3130 $M^{-1}cm^{-1}$), corresponds to excitation from the $Ru_3O(CH_3CO_2)_6$ level [MO 93 (b_2) to MO 98], while transition 5 at 338 nm (ε = 4700 $M^{-1}cm^{-1}$) corresponds, similarly, to the excitation from MO 92 (a_1) to MO 99. The strongest band should correspond to the transition from MO 91 (b_2) to MO 100 (b_2). Unfortunately, in the pyridine complex this band is masked by the strong cluster-to-pyridine charge-transfer bands and also by the internal transitions in the aromatic ligand.

Electrochemical Behavior

The cyclic voltammogram of $[Ru_3O(CH_3CO_2)_6(py)_2(NO)]^+$ is shown in Figure 6 along with those for the reference complexes $[Ru_3O(CH_3CO_2)_6(py)_2(CH_3OH)]^+$ and $[Ru_3O(CH_3CO_2)_6(py)_2(CO)]^0$. The nitrosyl cluster exhibits four successive redox waves at −1.15, −0.44, 1.00 and 1.77 V (vs. Ag/Ag^+), which, in principle, can be ascribed to the

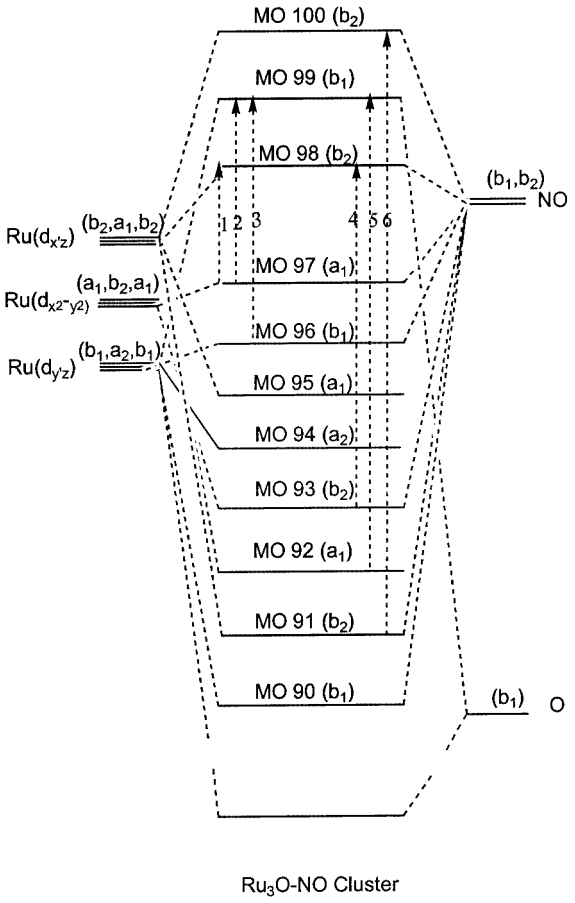

Figure 5. Molecular orbital scheme for the cluster $[Ru_3O(CH_3CO_2)_6(py)_2(NO)]^+$

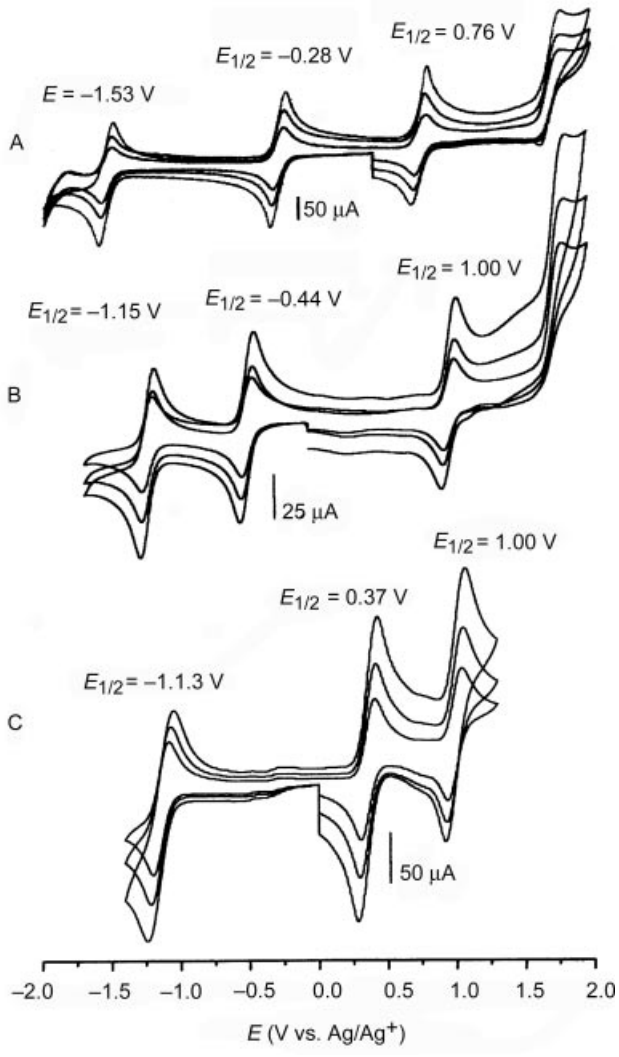

Figure 6. Cyclic voltammogram of the cluster (10^{-3} M), in acetonitrile solution containing 0.1 M $TEAClO_4$: (a) $[Ru_3O(CH_3CO_2)_6(py)_2(CH_3OH)]PF_6$; (b) $[Ru_3O(CH_3CO_2)_6(py)_2(NO)]PF_6$; (c) $[Ru_3O(CH_3CO_2)_6(py)_2(CO)]$

redox couples $Ru^{III}Ru^{II}Ru^{II}/Ru^{III}Ru^{III}Ru^{II}/Ru^{III}Ru^{III}Ru^{III}/Ru^{IV}Ru^{III}Ru^{III}/Ru^{IV}Ru^{IV}Ru^{III}$ by comparison with the reference compounds.

In our previous work we have shown that the redox potentials of $[Ru_3O(CH_3CO_2)_6L_3]$ clusters are correlated with the donor-acceptor properties of L, forming a well-behaved sequence, when the voltammograms are superimposed according to this trend. This type of behavior, however, is not apparent in Figure 6. On the other hand, the assignment of the wave at −0.44V to the NO^+/NO^0 couple cannot be totally discarded, since this process is usually observed in the range −0.6 to +0.3V vs. Ag/Ag^+ [55,56] for typical NO^+ complexes. This kind of ambiguity probably arises from the fact that the interactions of the NO ligand with the Ru d_π orbitals make the canonical structures $Ru^{III}-NO^0 \rightleftarrows Ru^{II}-NO^+$ practically equivalent, since the strong back-bonding interactions involving $Ru^{II}-NO^+$ would also lead to an electronic configuration rather close to $Ru^{III}-NO^0$. As a consequence, the NO ligand can stabilize both the $Ru^{III}Ru^{III}Ru^{III}$ (by acting as NO^0) and the $Ru^{III}Ru^{III}Ru^{II}$ (by acting as NO^+) formal oxidation states, increasing the separation between the corresponding redox waves at −0.44 and 1.00 V (ΔE = 1.44 V) in comparison with the CH_3OH (ΔE = 1.04 V) and CO (ΔE = 0.63 V) reference compounds. This exceptional ability to stabilize both oxidation states is actually responsible for the non-innocent character of the NO ligand in many transition metal complexes.

Visible-UV and IR Spectroelectrochemistry

In contrast to the electrochemical measurements, the spectroelectrochemical results were severely limited by decomposition reactions taking place over the time scale of the experiments (about ten minutes). The only completely reversible spectroelectrochemical behavior was observed at E^0 = −0.44V, corresponding to the $(Ru^{III}Ru^{III}Ru^{III}-NO^0 \rightleftarrows Ru^{III}Ru^{III}Ru^{II}-NO^+)/Ru^{III}Ru^{III}Ru^{II-}NO^0$ redox process. As shown in Figure 7a, the reduction of the $Ru^{III}Ru^{III}Ru^{III}-NO^0$ complex gives rise to a broad band in the visible-near infrared region (λ_{max} = 710 nm) consistent with intermetallic transitions within the $Ru^{III}Ru^{III}Ru^{II}-NO^0$ chromophore,[7,42,57] and to a strong band at 400 nm, characteristic of ruthenium-to-pyridine

charge-transfer transitions involving the $Ru^{III}Ru^{III}Ru^{III}$-pyridine moiety.

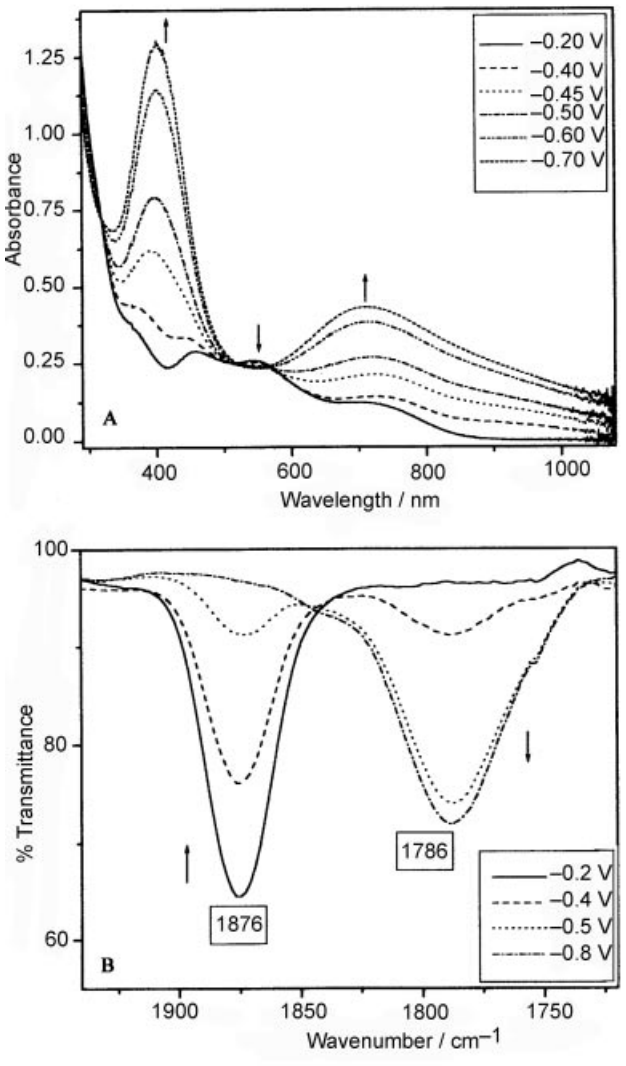

Figure 7. UV/Vis (a) and IR (b) spectroelectrochemistry of $[Ru_3O(CH_3CO_2)_6(py)_2(NO)]PF_6$ (10^{-3} M), in acetonitrile solution containing 0.10 M $TEAClO_4$

The corresponding FTIR spectroelectrochemistry (Figure 7b) exhibits a systematic conversion of the ν(NO) band at 1876 cm^{-1} into a new band at 1786 cm^{-1} indicating some NO^- character, arising from the ($Ru^{II}-NO^0$) back-bonding interactions within the $Ru^{III}Ru^{III}Ru^{II}-NO^0$ chromophore. Above 1.2V and below −1.2V the irreversible decomposition of the nitrosyl-cluster is observed, with the disappearance of the characteristic ν(NO) bands in the FTIR spectrum.

Conclusion

The interaction of NO with the complex $[Ru_3O(CH_3CO_2)_6(py)_2(CH_3OH)]^+$ leads to a stable nitrosyl-cluster system which can be formally described in terms of the delocalized electronic configuration, $Ru^{III}Ru^{III}Ru^{III}-NO^0 \rightleftarrows Ru^{III}Ru^{III}Ru^{II}-NO^+$. The strong involvement of the NO π*-orbitals is supported by theoretical calculations, as well as by the electronic, spectroscopic and magnetic properties of the complex. The remarkable contribution of NO to the LUMO levels accounts for the unusual absorption profiles observed in the electronic spectra of the cluster, as well as a significant photochemical sensitivity: the cluster releases nitric oxide upon irradiation with visible light. This interesting property is currently being investigated in our laboratory, as well as the related biological effects, including the valuation of $[Ru_3O(CH_3CO_2)_6(py)_2(NO)]PF_6$ toxicity.

Experimental Section

General: Tetraethylammonium perchlorate ($TEAClO_4$)[58] and the starting complex $[Ru_3(CH_3CO_2)_6(py)_2(CH_3OH)]PF_6$ were prepared as previously described in the literature.[5] Acetonitrile (HPLC grade, Aldrich) was kept in the presence of 3 Å dry molecular sieves. Other reagents and solvents of analytical grade were used without further purification. Thermogravimetric measurements were performed using a Shimadzu model TGA-50 instrument under the following experimental conditions: 2−4 mg of sample, platinum crucible, N_2 flow of 50 mL·min^{-1}, heating rate of 10 °C·min^{-1}. Infrared spectra were recorded in the region 4000−350 cm^{-1} on a Shimadzu FTIR model 8300 spectrophotometer. The magnetic susceptibilities of powdered samples were measured at room temperature using a Cahn model 7500 electrobalance. The studies in solution were carried out using a 10^{-3} M cluster solution in acetonitrile. X-band EPR spectrum, at 77 K, were conducted with a Bruker EMX spectrometer, operating at 9.53 GHz, 20 MW power and 4−12 G modulation amplitude. ^1H and ^{13}C NMR spectra and two-dimensional COSY (^1H, ^1H) and HMQC (^1H, ^{13}C) spectra were recorded on a Varian INOVA 1 300 MHz and Bruker DRX 500 spectrometers, using a 10^{-2} M cluster solution in CD_3CN. The electronic spectra were recorded on a Hewlett−Packard model 8453 diode-array spectrophotometer, using a 295 nm UV cut-off filter. Cyclic voltammetry and spectroelectrochemistry were carried out with an EG&G model 283 galvanostat/potentiostat. A conventional three-electrode electrochemical cell was used, with a platinum disk as working electrode, a Luggin capillary arrangement with an $Ag/AgNO_3$ (0.01 M) reference electrode in 0.10 M $TEAClO_4$ in acetonitrile, and a platinum wire as auxiliary electrode. UV/Vis spectrochemistry was conducted using a rectangular quartz cell of 0.025 cm internal optical path length, containing an optically transparent gold minigrid electrode, a platinum wire and a small $Ag/AgNO_3$ electrode as working, auxiliary and reference electrodes, respectively. IR spectroelectrochemical measurements were carried out using an acetonitrile solution containing 0.10 M $LiClO_4$ and a homemade IRTRAN thin layer cell, as previously described.[38]

Molecular mechanics geometry optimizations for the model complex $[Ru_3O(CH_3CO_2)_6(NH_3)_2(NO)]^+$ were carried out using the MM^+ module of Hyperchem 6.1 from Hypercube, starting with bond-dipole calculations and stopping at a refinement level of 10^{-3} kcal·$Å^{-1}$·mol^{-1}. In all the attempts, even when using a restricted geometry, the optimization procedure led to a pyramidal Ru_3O structure, rather than to the planar geometry characteristic of this type of system. In order to preserve the planar geometry, the cent-

ral oxygen atom was initially replaced by fluorine, thus allowing a preliminary structural refinement. In the next step, fluorine was replaced by oxygen, and the geometry refinement was carried out again, but stopping just at the point preceding the pyramidal distortion (about 30 cycles). Using this procedure, the central Ru−Ru and Ru−O distances can be adjusted, keeping the oxygen atom inside the triangular ring, without perturbing the remaining, optimized parts of the system. For this frozen undistorted geometry, single-point semi-empirical molecular orbital calculations were carried out, using the spectroscopic implementation of the ZINDO/1 method within the Hyperchem 6.1 package. The semi-empirical method provided the approximate atomic charges, which were used for a new cycle of geometry optimization (MM^+), now replacing the starting bond dipoles. This alternating semi-empirical/molecular mechanics procedure was repeated at least three times, practically ensuring convergence. In this way, the final geometry was planar, exhibiting Ru−Ru(NO) and Ru−Ru distances of 3.257 and 3.266 Å, and three similar Ru−O distances of 1.883 Å; all of them quite similar to the typical crystallographic distances reported in the literature for similar ruthenium acetate clusters.[6,59−61] The theoretical Ru−NO and NO bond lengths were 1.914 and 1.086 Å, respectively. After geometry optimization, the electronic spectra were generated by single CI excitations in an active space involving at least 12 frontier molecular orbitals (seven highest occupied and five lowest unoccupied MOs).

$[Ru_3O(CH_3CO_2)_6(py)_2(NO)]PF_6$: A solution of $[Ru_3(CH_3CO_2)_6(py)_2(CH_3OH)]PF_6$ (0.21 g; 0.21 mmol) in dichloromethane (20 mL) were saturated with Ar for 20 min, then with NO for 15 min (after which the blue solution became violet), and finally with Ar for 20 min. The product was precipitated by adding petroleum ether. The solid was collected on a filter, washed with petroleum ether and dried under vacuum. Yield: 42%. $C_{23}H_{30}Cl_2F_6N_3O_{14}PRu_3$ (1091.6): calcd. C 25.3, H 2.77, N 3.85; found C 25.2, H 2.75, N 3.80. The purity of the final product was confirmed by means of NMR spectroscopy.

Acknowledgments

We are grateful to FAPESP and CNPq for financial support, and to Prof. Ana Maria da Costa Ferreira for conducting the EPR measurements.

[1] H. E. Toma, K. Araki, A. D. P. Alexiou, S. Nikolaou, S. Dovidauskas, *Coord. Chem. Rev.* **2001**, *219−221*, 225−272.
[2] H. E. Toma, C. J. Cunha, C. Cipriano, *Inorg. Chim. Acta* **1988**, *154*, 63−66.
[3] A. D. P. Alexiou, H. E. Toma, *J. Chem. Res. (S)* **1993**, 464−465.
[4] A. Spencer, G. Wilkinson, *J. Chem. Soc., Dalton Trans.* **1974**, 786−792.
[5] J. A. Baumann, D. J. Salmon, S. T. Wilson, T. J. Meyer, W. E. Hatfield, *Inorg. Chem.* **1978**, *17*, 3342−3350.
[6] M. Abe, Y. Sasaki, Y. Yamada, K. Tsukahara, S. Yano, T. Yamaguchi, M. Tominaga, I. Taniguchi, T. Ito, *Inorg. Chem.* **1996**, *35*, 6724−6734.
[7] K. Ota, H. Sasaki, T. Matsui, T. Hamaguchi, T. Yamaguchi, T. Ito, H. Kido, C. P. Kubiak, *Inorg. Chem.* **1999**, *38*, 4070−4078.
[8] I. S. Zavarine, C. P. Kubiak, T. Yamaguchi, K. Ota, T. Matsui, T. Ito, *Inorg. Chem.* **2000**, *39*, 2696−2698.
[9] J. H. Enemark, R. D. Feltham, *Coord. Chem. Rev.* **1974**, *13*, 339−406.
[10] R. Eisenberg, C. D. Meyer, *Acc. Chem. Res.* **1975**, *8*, 26−34.
[11] F. Bottomley, *Coord. Chem. Rev.* **1978**, *26*, 7−32.
[12] B. L. Westcott, J. H. Enemark *Transition Metal Nitrosyls*; John Wiley & Sons, Inc., **1999**; Vol. II: Applications and Case Studies.
[13] E. Culotta, J. D. E. Koshland, *Science* **1992**, *258*, 1862−1865.
[14] L. J. Ignarro, *Pharm. Res.* **1989**, *6*, 651−659.
[15] S. Moncada, R. M. J. Palmer, E. A. Higgs, *Pharmacol. Rev.* **1991**, *43*, 109−142.
[16] M. J. Clarke, J. B. Gaul, *Struct. Bonding (Berlin, Ger.)* **1993**, *81*, 147−181.
[17] A. R. Butler, D. L. H. Williams, *Chem. Soc. Rev.* **1993**, 233−241.
[18] M. Fontecave, J.-L. Pierre, *Bull. Soc. Chim. Fr.* **1994**, *131*, 620−631.
[19] R. J. P. Williams, *Chem. Soc. Rev.* **1996**, 77−83.
[20] D. A. Wink, J. B. Mitchell, *Free Radic. Biol. Med.* **1998**, *25*, 434−456.
[21] S. P. Fricker, *Platinum Met. Rev.* **1995**, *39*, 150−159.
[22] N. Bettache, T. Carter, J. E. T. Corrie, D. Ogden, D. R. Trentham, *Method. Enzymol.* **1996**, *268*, 266−281.
[23] S. P. Fricker, E. Slade, N. A. Powell, O. J. Vaugham, G. R. Henderson, B. A. Murrer, I. L. Megson, S. K. Bisland, F. W. Flitney, *Br. J. Pharmacol.* **1997**, *122*, 1441−1449.
[24] T. D. Carter, N. Bettache, D. Ogden, *Br. J. Pharmacol.* **1997**, *122*, 971−973.
[25] Y. Chen, R. E. Shepherd, *J. Inorg. Biochem.* **1997**, *68*, 183−193.
[26] N. A. Davies, M. T. Wilson, E. Slade, S. P. Fricker, B. A. Murrer, N. A. Powell, G. R. Henderson, *Chem. Commun.* **1997**, 47−50.
[27] P. C. Ford, J. Bourassa, K. Miranda, B. Lee, I. Lorkovic, S. Boggs, S. Kudo, L. Laverman, *Coord. Chem. Rev.* **1998**, *171*, 185−202.
[28] J. B. Godwin, T. J. Meyer, *Inorg. Chem.* **1971**, *10*, 471−474.
[29] H. Kobayashi, N. Uryû, A. Tokiwa, T. Yamaguchi, Y. Sasaki, T. Ito, *Bull. Chem. Soc. Jpn.* **1992**, *65*, 198−202.
[30] H. Kobayashi, N. Uryû, I. Mogi, R. Miyamoto, Y. Ohba, M. Iwaizumi, Y. Sasaki, A. Ohto, T. Ito, *Bull. Chem. Soc. Jpn.* **1995**, *68*, 2551−2558.
[31] M. K. Johnson, D. B. Powell, R. D. Cannon, *Spectrochim. Acta* **1981**, *37A*, 995−1006.
[32] M. K. Johnson, R. D. Cannon, D. B. Powell, *Spectrochim. Acta* **1982**, *38A*, 307−315.
[33] A. Ohto, A. Tokiwa-Yamamoto, M. Abe, T. Ito, Y. Sasaki, K. Umakoshi, R. D. Cannon, *Chem. Lett.* **1995**, 97−98.
[34] R. W. Callahan, T. J. Meyer, *Inorg. Chem.* **1977**, *16*, 574−581.
[35] M. B. Fairey, R. J. Irving, *Spectrochim. Acta* **1966**, *22*, 359−365.
[36] M. G. Gomes, C. U. Davanzo, S. C. Silva, L. G. F. Lopes, P. S. Santos, D. W. Franco, *J. Chem. Soc., Dalton Trans.* **1998**, 601−607.
[37] F. Bottomley, M. Mukaida, *J. Chem. Soc., Dalton Trans.* **1982**, 1933−1937.
[38] I. A. Bagatin, H. E. Toma, *Spectrosc. Lett.* **1996**, *29*, 1409−1416.
[39] I. A. Bagatin, H. E. Toma, *Transition Met. Chem.* **1996**, *21*, 71−76.
[40] M. Abe, Y. Sasaki, A. Nagasawa, T. Ito, *Bull. Chem. Soc. Jpn.* **1992**, *65*, 1411−1414.
[41] T. Y. Dong, H. S. Lee, T. Y. Lee, C. F. Hsieh, *J. Chin. Chem. Soc.* **1992**, *39*, 393−399.
[42] M. Abe, Y. Sasaki, Y. Yamada, K. Tsukahara, S. Yano, T. Ito, *Inorg. Chem.* **1995**, *34*, 4490−4498.
[43] M. Abe, A. Sato, T. Inomata, T. Kondo, K. Uosaki, Y. Sasaki, *J. Chem. Soc., Dalton Trans.* **2000**, 2693−2702.
[44] A. Sato, M. Abe, T. Inomata, T. Kondo, S. Ye, K. Uosaki, Y. Sasaki, *Phys. Chem. Chem. Phys.* **2001**, *3*, 3420−3426.
[45] H. E. Toma, A. D. P. Alexiou, *J. Braz. Chem. Soc.* **1995**, *6*, 267−270.
[46] H. E. Toma, A. D. P. Alexiou, *J. Chem. Res. (S)* **1995**, 134−135.
[47] A. D. P. Alexiou, H. E. Toma, *J. Chem. Res. (S)* **1997**, 338−339.

[48] H. E. Toma, A. D. P. Alexiou, S. Nikolaou, S. Dovidauskas, *Magn. Reson. Chem.* **1999**, *37*, 322−324.
[49] S. Dovidauskas, H. E. Toma, K. Araki, H. Sacco, Y. Iamamoto, *Inorg. Chim. Acta* **2000**, *305*, 206−213.
[50] S. Dovidauskas, K. Araki, H. E. Toma, *J. Porphyrins Phthalocyanines* **2000**, *4*, 727−735.
[51] K. Araki, S. Dovidauskas, H. Winnischofer, A. D. P. Alexiou, H. E. Toma, *J. Electroanal. Chem.* **2001**, *498*, 152−160.
[52] S. Nikolaou, M. Uemi, H. E. Toma, *Spectrosc. Lett.* **2001**, *34*, 267−277.
[53] J. A. Iggo, *NMR Spectroscopy in Inorganic Chemistry*; Oxford University Press Inc.: New York, **1999**.
[54] F. A. Cotton, J. G. NormanJr, *Inorg. Chim. Acta* **1972**, *6*, 411−419.
[55] E. S. Dodsworth, A. A. Vleck, A. B. P. Lever, *Inorg. Chem.* **1994**, *33*, 1045−1049.
[56] L. G. F. Lopes, M. G. Gomes, S. S. S. Borges, D. W. Franco, *Aust. J. Chem.* **1998**, *51*, 865−866.
[57] H. E. Toma, C. J. Cunha, *Can. J. Chem.* **1989**, *67*, 1632−1635.
[58] D. T. Sawyer, J. L. Roberts, *Experimental Electrochemistry for Chemists*; John Wiley & Sons, **1974**.
[59] O. Almog, A. Bino, D. Garfinkel-Shweky, *Inorg. Chim. Acta* **1993**, *213*, 99−102.
[60] G. Powell, D. T. Richens, A. Bino, *Inorg. Chim. Acta* **1995**, *232*, 167−170.
[61] T. Yamaguchi, N. Imai, T. Ito, C. P. Kubiak, *Bull. Chem. Soc. Jpn.* **2000**, *73*, 1205−1212.

Received March 11, 2002
[I02127]

Iron- and Ruthenium-Containing Triple-Decker Complexes with a Central Pentaphospholyl Ligand − X-ray Structures of $[(\eta\text{-}C_5H_5)Fe(\mu\text{-}\eta{:}\eta\text{-}P_5)Ru(\eta\text{-}C_5Me_5)]PF_6$ and $[(\eta\text{-}C_5Me_5)Ru(\mu\text{-}\eta{:}\eta\text{-}P_5)Ru(\eta\text{-}C_5Me_5)]PF_6$

Alexander R. Kudinov,*[a] Dmitry A. Loginov,[a] Zoya A. Starikova,[a] Pavel V. Petrovskii,[a] Maddalena Corsini,[b] and Piero Zanello[b]

Keywords: Electrochemistry / Iron / Phosphorus / Ruthenium / Sandwich compounds / Triple-decker complexes

Triple-decker cationic complexes with a central pentaphospholyl (pentaphosphacyclopentadienyl) ligand $[Cp^*M(\mu\text{-}\eta{:}\eta\text{-}P_5)M'(\eta\text{-}C_5R_5)]^+$ (**3b**: M = M′ = Fe, R = Me; **4a**: M = Ru, M′ = Fe, R = H; **4b**: M = Fe, M′ = Ru, R = H; **4c**: M = Fe, M′ = Ru, R = Me; **5a**: M = M′ = Ru, R = H; **5b**: M = M′ = Ru, R = Me) were synthesized by exploitation of the stacking reactions of pentaphosphametallocenes $Cp^*M(\eta\text{-}P_5)$ (**1**: M = Fe; **2**: M = Ru) with half-sandwich fragments $[(\eta\text{-}C_5R_5)M']^+$. They were isolated as salts with BF_4^- or PF_6^- anions, and the structures of **4a**PF_6 and **5b**PF_6 were determined by X-ray diffraction. Triple-decker complexes with a central pentaphospholyl ligand are less reactive in nucleophilic degradation reactions than analogous complexes with C_4Me_4P and Cp^* ligands in the bridging position. Only **4a** and the previously known analogue **3a** (M = M′ = Fe, R = H), containing the CpFe fragment, are nucleophilically destroyed by MeCN and NaI. The electrochemical properties of **2**, **3a**, **3b**, **4a–c**, **5a** and **5b** and the related cobalt-containing complexes $[(\eta\text{-}C_4Me_4)Co(\mu\text{-}\eta{:}\eta\text{-}P_5)MCp^*]^+$ (**6**: M = Fe; **7**: M = Ru) were investigated.

(© Wiley-VCH Verlag GmbH, 69451 Weinheim, Germany, 2002)

Introduction

Several examples of triple-decker complexes with a central pentaphospholyl (pentaphosphacyclopentadienyl) ligand (*cyclo*-P_5) are known.[1] The first complexes of this type, $(\eta\text{-}C_5R_5)Cr(\mu\text{-}\eta{:}\eta\text{-}P_5)Cr(\eta\text{-}C_5R_5)$ (R = H, Me), were synthesized by Scherer[2] and other authors[3] by treatment of $[(\eta\text{-}C_5R_5)Cr(CO)_x]_2$ (x = 2, 3) with P_4. Scheer has prepared the similar complex $(\eta\text{-}C_5H_4t\text{Bu})Cr(\mu\text{-}\eta{:}\eta\text{-}P_5)Cr(\eta\text{-}C_5H_4t\text{Bu})$ by treatment of $K[(\eta\text{-}C_5H_4t\text{Bu})Cr(CO)_3]$ with $Cr(CO)_5PCl_3$.[4]

A straightforward approach to the synthesis of triple-decker complexes is based on the use of stacking reactions of coordinatively unsaturated metal complex fragments with sandwich compounds.[5] In particular, this approach has proved to be very useful for the preparation of triple-decker complexes with a central *cyclo*-P_5 ligand. By using stacking reactions of pentaphosphaferrocene $Cp^*Fe(\eta\text{-}P_5)$ (**1**) with the fragments $[CpFe]^+$ and $(CO)_3M$ (M = Cr, Mo) Scherer has prepared the triple-decker complexes $[CpFe(\mu\text{-}\eta{:}\eta\text{-}P_5)FeCp^*]^+$ (**3a**) and $(CO)_3M(\mu\text{-}\eta{:}\eta\text{-}P_5)FeCp^*$.[6] We have described the synthesis of complex $[(\eta\text{-}C_7H_7)Mo(\mu\text{-}\eta{:}\eta\text{-}P_5)FeCp^*]^+$ by treatment of **1** with the fragment $[(\eta\text{-}C_7H_7)Mo]^+$.[7]

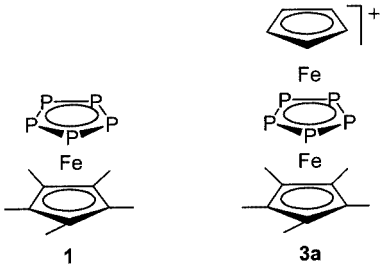

We report here the results obtained in an extension of this approach to the preparation of new iron- and ruthenium-containing triple-decker complexes with a central pentaphospholyl ligand $[Cp^*M(\mu\text{-}\eta{:}\eta\text{-}P_5)M'(\eta\text{-}C_5R_5)]^+$ (M, M′ = Fe, Ru; R = H, Me),[8] together with their electrochemical and structural properties.

Results and Discussion

Synthesis of Triple-Decker Complexes

In 1987 we described the synthesis of the first 30 VE (valence electron) triple-decker complexes with a central cyclopentadienyl ligand $[Cp^*M(\mu\text{-}\eta{:}\eta\text{-}Cp^*)M'(\eta\text{-}C_5R_5)]^+$ (M = Fe, Ru, Os; M′ = Fe, Ru).[9] These compounds were synthe-

[a] A. N. Nesmeyanov Institute of Organoelement Compounds, 28 ul. Vavilova, 119991 Moscow, GSP-1, Russian Federation
Fax: (internat.) + 7-095/1355085
E-mail: arkudinov@ineos.ac.ru
[b] Dipartimento di Chimica, University of Siena, Via Aldo Moro, 53100 Siena, Italy

sized by exploitation of the stacking reactions of decamethylmetallocenes MCp^*_2 with the coordinatively unsaturated 12 VE half-sandwich fragments $[(\eta\text{-}C_5R_5)M']^+$. In particular, the iron-containing triple-decker complexes $[CpFe(\mu\text{-}\eta\text{:}\eta\text{-}Cp^*)MCp^*]^+$ were prepared by use of the $[CpFe]^+$ fragment, generated in situ by visible light irradiation of the benzene complex $[CpFe(\eta\text{-}C_6H_6)]^+$. The same method was used later by Scherer for the preparation of complex **3a**.[6a]

Analogously, the iron-ruthenium triple-decker complex **4a** was prepared by us through the use of the stacking reaction of the fragment $[CpFe]^+$ with pentaphospharuthenocene $Cp^*Ru(\eta\text{-}P_5)$ (**2**) (Scheme 1).[10]

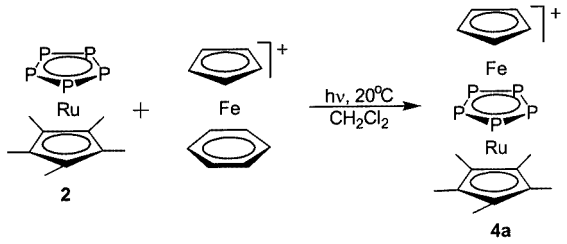

Scheme 1. Formation of complex **4a**

Since the methylated fragment $[Cp^*Fe]^+$ cannot be generated from the corresponding benzene complex $[Cp^*Fe(\eta\text{-}C_6H_6)]^+$, due to its rather high stability,[11] we used the labile acetonitrile complex $[Cp^*Fe(MeCN)_3]^+$ as the source of this fragment. The complex $[Cp^*Fe(MeCN)_3]^+$ was successfully used earlier by Herberich for the synthesis of the μ-boratabenzene triple-decker complex $[Cp^*Fe(\mu\text{-}\eta\text{:}\eta\text{-}C_5H_5BMe)FeCp^*]^+$.[12] Treatment of $[Cp^*Fe(MeCN)_3]^+$ with **1** at 20 °C affords the permethylated diiron triple-decker complex **3b** (Scheme 2). However, treatment of $[Cp^*Fe(MeCN)_3]^+$ with **2** under the same conditions failed to give the iron-ruthenium triple-decker complex $[Cp^*Fe(\mu\text{-}\eta\text{:}\eta\text{-}P_5)RuCp^*]^+$. Nevertheless, we were able to synthesize it through the stacking reaction of the fragment $[Cp^*Ru]^+$ with **1** (see below).

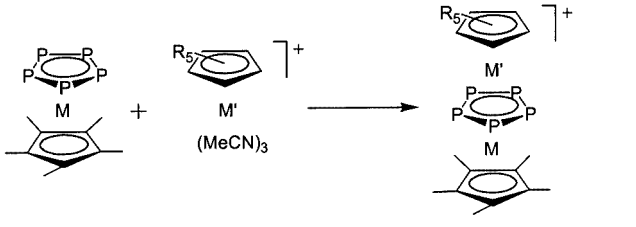

3b: M = M' = Fe, R = Me
4b: M = Fe, M' = Ru, R = H
4c: M = Fe, M' = Ru, R = Me
5a: M = M' = Ru, R = H
5b: M = M' = Ru, R = Me

Scheme 2. Formation of complexes **3b**, **4b**, **4c**, **5a** and **5b**

The ruthenium-containing triple-decker complexes $[(\eta\text{-}C_5R_5)Ru(\mu\text{-}\eta\text{:}\eta\text{-}Cp^*)MCp^*]^+$ (M = Ru, Os) had been prepared by us earlier, by use of stacking reactions of decamethylmetallocenes MCp^*_2 with the fragments $[(\eta\text{-}C_5R_5)Ru]^+$ generated by heating the acetonitrile complexes $[(\eta\text{-}C_5R_5)Ru(MeCN)_3]^+$ in $MeNO_2$.[9] We used the same method for the preparation of μ-pentaphospholyl triple-decker complexes containing the unsubstituted Cp ring at the ruthenium atom. It was shown that stacking reactions of the $[CpRu]^+$ fragment, generated from $[CpRu(MeCN)_3]^+$, with compounds **1** and **2** yield the iron-ruthenium and diruthenium triple-decker complexes **4b** and **5a**, respectively (Scheme 2). Heating was essential for successful preparation of these complexes. Under mild conditions (20 °C, CH_2Cl_2) a mixture of products was formed. In the ^{31}P NMR spectra of these mixtures, the signals of the triple-decker complex **4b** or **5a** ($\delta = -37.2$ and -54.9 ppm, respectively) were accompanied by complicated multiplets in the range between $\delta = 250$ and 20 ppm. Such multiplets are characteristic of an AA′MM′X spin system. Probably, the formation of **4b** and **5a** is complicated by side-formation of phosphane-type complexes, due to coordination of ruthenium atoms of the species $[CpRu(MeCN)_x]^+$ ($x \leq 2$) with lone pairs of phosphorus atoms of pentaphosphametallocenes.[13] It was shown by ^{31}P NMR spectroscopy that phosphane-type complexes are unstable and very slowly turn into triple-decker complexes at room temperature. This process becomes faster with increasing temperature, and complexes **4b** and **5a** were isolated in high yields when the reactions were carried out in $MeNO_2$ at 100 °C. It is noteworthy that the formation of the triple-decker complex **4a** mentioned above is also complicated by side-formation of phosphane-type complexes. In order to obtain pure complex **4a**, the crude product was heated under reflux in $MeNO_2$.

μ-Pentaphospholyl triple-decker complexes **4c** and **5b**, containing the Cp* ring at the ruthenium atom, were prepared through stacking reactions of the $[Cp^*Ru]^+$ fragment with **1** and **2** (Scheme 2). It was shown in this case that the methylated fragment $[Cp^*Ru]^+$ can also be generated from the corresponding acetonitrile complex $[Cp^*Ru(MeCN)_3]^+$ in $MeNO_2$ at 100 °C. However, it is more convenient to use labile solvent complexes $[Cp^*Ru(S)_3]^+$ (S = Me_2CO, THF) as the source of the $[Cp^*Ru]^+$ fragment. These solvates were generated in solution by treatment of $[Cp^*RuCl_2]_2$ with Zn dust and $TlBF_4$ in Me_2CO or THF at room temperature.[14] Alternatively, they could also be generated by treatment of $[Cp^*Ru(OMe)]_2$ with CF_3SO_3H.[15] The further stacking reaction of $[Cp^*Ru(S)_3]^+$ with **1** is selective at room temperature, and the iron-ruthenium triple-decker complex **4c** was isolated in 84% yield. However, similar treatment of **2** primarily yields phosphane-type complexes, which turn into the diruthenium triple-decker complex **5b** (82%) in refluxing THF or Me_2CO. Some differences in the conditions of the stacking reactions for **1** and **2** may be connected with the greater stability of phosphane-type complexes formed by **2**.

Complex **4c** was also obtained (80%) by direct treatment of **1** with $[Cp^*RuCl_2]_2$ in refluxing alcohol (Scheme 3). This method had previously been developed by us for the preparation of the arene complexes $[Cp^*Ru(arene)]^+$.[16] Unfortunately, it proved to be useless for the preparation of

5b, probably due to the rather high stability of phosphane-type complexes (formed by reaction between **2** and $[Cp^*RuCl_2]_2$), which do not turn into **5b** even after prolonged heating under reflux in alcohol.

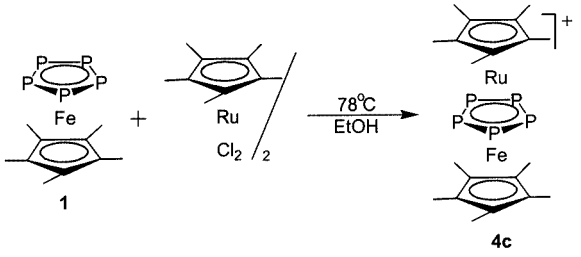

Scheme 3. Formation of complex **4c** by treatment of complex **1** with $[Cp^*RuCl_2]_2$

NMR Spectroscopy

The ^1H, ^{13}C and ^{31}P NMR spectroscopic data for triple-decker complexes **3b**, **4a**−**c**, **5a** and **5b** are given in Table 1. In the ^{31}P NMR spectra, the signals of the phosphorus atoms of the pentaphospholyl ligand are observed as singlets in the $\delta = -58.0$ to -23.0 ppm range. These signals are strongly shifted upfield from the corresponding signals for sandwich compounds **1** and **2** ($\delta = 153.0$ and 83.8 ppm, respectively); this makes ^{31}P NMR spectroscopy very informative for the establishment of the triple-decker structure. Substitution of the ruthenium atoms for iron and introduction of methyl groups also cause upfield shifts of the signal.

In the ^1H NMR spectra, the signals of Cp ring protons and of Cp* methyl groups are observed in the ranges $\delta = 4.0-4.6$ and $1.2-1.5$ ppm, respectively. In the ^{13}C NMR spectra, the signals of the C_5R_5 ring carbon atoms and of the Cp* methyl groups are observed in the ranges $\delta = 74.9-97.1$ and $7.8-9.2$ ppm, respectively. These spectroscopic data are also in accordance with the triple-decker structure.

X-ray Diffraction Study

The structures of complexes **4a**PF_6 and **5b**PF_6 were investigated by single-crystal X-ray diffraction. They contain separated **4a** or **5b** cations and PF_6^- anions. The cations have triple-decker structures formed by three cyclic frames, between which two metal atoms are located (Figures 1 and 2). Selected bond lengths and angles are given in Tables 2 and 3. In both cases the planes of the cyclic ligands are coplanar [for **4a** the dihedral angles Cp/P_5 and Cp^*/P_5 are equal to 1.3 and 3.5°; for **5b** the dihedral angles $Cp^*(1)/P_5$ and $Cp^*(2)/P_5$ are equal to 0.2 and 1.7°, respectively]. The carbon atoms of the Cp* methyl groups in **4a** and **5b** deviate somewhat from the ring planes in direction from the ruthenium atoms, these deviations amounting to 0.06−0.11 Å. The cross-orientation of all five-membered rings is perfectly eclipsed in **4a** and close to eclipsed in **5b**, the corresponding torsion angles for the latter being: P(1−5)CtCt′C(1−5) 12.4−12.8° (average 12.6°) and P(1−5)CtCt′′C(11−15) 5.1−5.2° (average 5.2°).[17] The metal atoms are located over the centres of all the rings; the metal-to-ring distances (Δ) are as follows: Fe···Cp 1.687(3), Ru···Cp* 1.837(1), Fe···P_5 1.527(1), and Ru···P_5 1.669(1) Å for **4a**; Ru(1)···Cp*(1) 1.831(1), Ru(2)···Cp*(2) 1.830(1), Ru(1)···P_5 1.675(1), and Ru(2)···P_5 1.678(1) Å for **5b**. The Fe···Ru [3.196(1) Å] and Ru(1)···Ru(2) [3.352(1) Å] distances are longer than the corresponding sums of the covalent radii for Fe−Ru (average 2.83 Å) and Ru−Ru (average 2.98 Å),[18] suggesting the absence of direct metal−metal bonds in both cases. It is noteworthy that Δ(Ru···P_5) for **4a** and **5b** are longer than the corresponding value in the sandwich compound (η-C_5Me_4Et)Ru(η-P_5) (1.652 Å).[19] The P−P bonds in **4a** (2.155−2.159 Å, average 2.157 Å) and **5b** (2.152−2.161 Å, average 2.156 Å) are longer than the corresponding bonds in (η-C_5Me_4Et)Ru(η-P_5)

Table 1. ^1H, ^{13}C and ^{31}P NMR spectroscopic data for compounds **3b**, **4a**−**c**, **5a** and **5b**

Compound[a]	^1H	$^{13}C\{^1H\}$	$^{31}P\{^1H\}$
3bBF_4 [b]	1.22 (Me)	8.14 (Me), 88.47 (C_5Me_5)	−23.0
4aPF_6 [b]	1.33 (15 H, Me), 4.00 (5 H, C_5H_5)	7.81 (Me), 74.92 (C_5H_5), 97.00 (C_5Me_5)	−35.0 (P_5), −142.7 [sept., PF_6, J(PF) = 708]
4bBF_4 [b]	1.32 (15 H, Me), 4.35 (5 H, C_5H_5)	8.20 (Me), 81.37 (C_5H_5), 88.26 (C_5Me_5)	−37.2
4cBF_4 [c]	1.27 (15 H, FeC_5Me_5 or RuC_5Me_5), 1.30 (15 H, RuC_5Me_5 or FeC_5Me_5)	8.77 ($FeC_5\mathit{Me}_5$), 9.14 ($RuC_5\mathit{Me}_5$), 87.98 (FeC_5Me_5), 96.91 (RuC_5Me_5)	−39.2
5aPF_6 [b]	1.48 (15 H, Me), 4.58 (5 H, C_5H_5)	8.17 (Me), 81.24 (C_5H_5), 97.11 (C_5Me_5)	−54.9 (P_5), −142.7 [sept.,PF_6, J(PF) = 708]
5bPF_6 [b]	1.51(Me)	8.48 (Me), 96.99 (C_5Me_5)	−58.0 (P_5), −142.7 [sept., PF_6, J(PF) = 708]

[a] Chemical shifts in ppm, coupling constants in Hz. The signals are singlets, unless otherwise stated. [b] In $(CD_3)_2CO$. [c] In CD_2Cl_2.

(2.082−2.118 Å, average 2.101 Å). The elongation of the Ru−P and P−P bonds is apparently connected with loosening of bonds upon bifacial coordination of the P_5 ring with two metal atoms as compared with its monofacial coordination with only one metal atom. The values of Δ(Ru···Cp*) for **4a** and **5b**, however, are shorter than the corresponding value in the sandwich compound (η-C_5Me_4Et)Ru(η-P_5) (1.850 Å). Probably, loosening of the Ru−P_5 bond in the triple-decker complexes causes increased occupancy of the Ru−Cp* bond. The values of Δ(Fe···P_5) and Δ(Fe···Cp) in **4a** are close to the corresponding values in the related triple-decker cation [CpFe(μ-η:η-P_5)Fe(η-C_5Me_4Et)]$^+$ [Δ(Fe···P_5) 1.534 Å and Δ(Fe···Cp) 1.679 Å].[6a] However, the P−P bonds in **4a** (average 2.157 Å) are somewhat longer than the corresponding bonds in [CpFe(μ-η:η-P_5)Fe(η-C_5Me_4Et)]$^+$ (average 2.125 Å), which suggests a greater π bond-loosening effect by the Cp*Ru fragment than by (C_5Me_4Et)Fe.

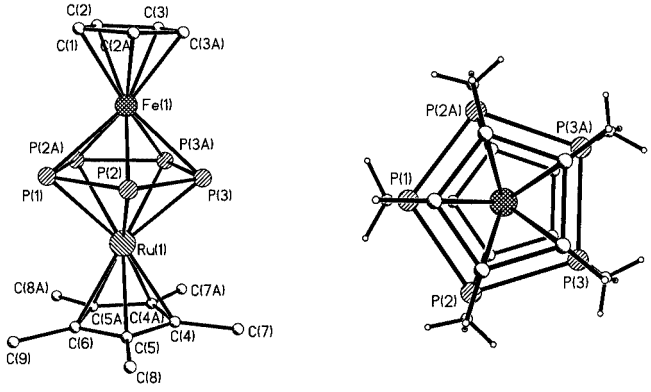

Figure 1. Structure of cation **4a**

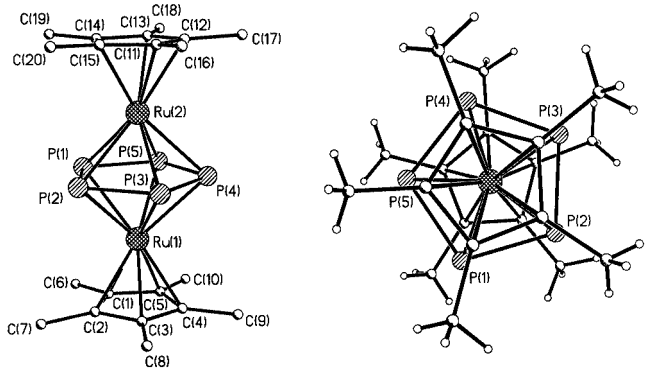

Figure 2. Structure of cation **5b**

Nucleophilic Degradation

The μ-pentaphospholyl triple-decker complexes described here have 30 VEs, which explains their stability in accordance with Hoffmann's rule for triple-decker complexes.[20] They are indefinitely stable under inert gas. However, they are stable in air only for short periods of time and lose solubility after prolonged storage. This is apparently connected with the interaction between lone electron pairs of the phosphorus atoms and oxygen.

Table 2. Selected bond lengths [Å] and angles [°] for cation **4a**

Ru(1)−P(1)	2.4960(9)	Ru(1)−C(5)	2.205(2)
Ru(1)−P(2)	2.4819(6)	Ru(1)−C(6)	2.219(3)
Ru(1)−P(3)	2.4705(6)	Fe(1)−C(1)	2.072(3)
Fe(1)−P(1)	2.3935(9)	Fe(1)−C(2)	2.074(2)
Fe(1)−P(2)	2.3931(7)	Fe(1)−C(3)	2.078(2)
Fe(1)−P(3)	2.3776(7)	P(1)−P(2)	2.1545(8)
Ru(1)−C(4)	2.200(2)	P(2)−P(3)	2.1590(9)
P(1)−P(2)−P(3)	107.96(4)	Fe(1)−P(2)−Ru(1)	81.90(2)
Fe(1)−P(1)−Ru(1)	81.60(3)	Fe(1)−P(3)−Ru(1)	82.45(2)

Table 3. Selected bond lengths [Å] and angles [°] for cation **5b**

Ru(1)−P(1)	2.4869(6)	Ru(1)−C(4)	2.209(2)
Ru(1)−P(2)	2.4835(7)	Ru(1)−C(5)	2.199(2)
Ru(1)−P(3)	2.4819(6)	Ru(2)−C(11)	2.211(2)
Ru(1)−P(4)	2.4828(7)	Ru(2)−C(12)	2.199(2)
Ru(1)−P(5)	2.4856(7)	Ru(2)−C(13)	2.193(2)
Ru(2)−P(1)	2.4778(7)	Ru(2)−C(14)	2.199(2)
Ru(2)−P(2)	2.4880(7)	Ru(2)−C(15)	2.201(2)
Ru(2)−P(3)	2.4887(6)	P(1)−P(2)	2.1613(11)
Ru(2)−P(4)	2.4813(6)	P(2)−P(3)	2.1519(11)
Ru(2)−P(5)	2.4930(7)	P(3)−P(4)	2.1562(10)
Ru(1)−C(1)	2.198(2)	P(4)−P(5)	2.1565(11)
Ru(1)−C(2)	2.204(2)	P(5)−P(1)	2.1563(11)
Ru(1)−C(3)	2.198(2)		
P(1)−P(2)−P(3)	107.87(4)	Ru(1)−P(1)−Ru(2)	84.95(2)
P(2)−P(3)−P(4)	107.99(4)	Ru(1)−P(2)−Ru(2)	84.81(2)
P(3)−P(4)−P(5)	108.29(4)	Ru(1)−P(3)−Ru(2)	84.83(2)
P(4)−P(5)−P(1)	107.64(4)	Ru(1)−P(4)−Ru(2)	84.97(2)
P(5)−P(1)−P(2)	108.21(4)	Ru(1)−P(5)−Ru(2)	84.66(2)

The properties of triple-decker complexes are insufficiently studied. The most studied reaction is nucleophilic degradation. Examples of such reactions have been described for the complexes with bifacially bonded cyclopentadienyl,[9,15d,21] borole,[22] thiadiborolene,[23] boratabenzene,[12,24] and phospholyl[25] ligands.

We studied the reactions of triple-decker complexes **3a**, **3b**, **4a**−**c**, **5a** and **5b** with MeCN and NaI. Only the CpFe-containing complexes **3a** and **4a** proved to be reactive. The reactions proceed with elimination of the [CpFe]$^+$ fragment and formation of the corresponding pentaphosphametallocenes **1** and **2** (Scheme 4). The selectivity of elimination of this fragment in the case of **3a** is apparently connected with hindrance of nucleophilic attack at the metal atom coordinated with the Cp* ring as a consequence of electronic and steric effects.

It is noteworthy that the iron-ruthenium complex **4a** is more reactive than the diiron analogue **3a** towards MeCN. From the ^{31}P NMR spectroscopic data, the degree of conversion in the case of **4a** was ca. 70% after 10 h at 80 °C, while in the case of **3a** at the same temperature it was only ca. 10% after 38 h. Addition of NaI accelerates degradation of **3a**, the degree of conversion being ca. 80% after 10 h. Unlike **3a** and **4a**, the diruthenium complex **5a**, with the same number of methyl groups, proved to be inert to nucleophilic degradation even by NaI in MeCN. This is obvi-

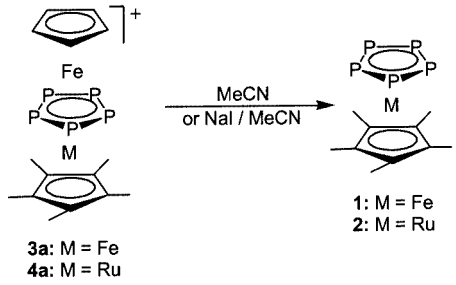

Scheme 4. Nucleophilic degradation of complexes **3a** and **4a**

ously connected with stronger bonding of *cyclo*-P_5 with the ruthenium atom than with iron. The obtained results suggest that the reactivity of μ-pentaphospholyl triple-decker complexes in nucleophilic degradation reactions decreases in the order FeRu > Fe_2 > Ru_2. It should be emphasized that the heterometallic compounds are more reactive than homometallic analogues.

The permethylated complexes **3b** and **4c** proved to be much less reactive than the pentamethylated analogues **3a** and **4a**; in fact, they are not destroyed by NaI in MeCN at 80 °C. Unfortunately, attempts to use other nucleophilic reagents (Me_2SO, $EtNH_2$, KOH, KCN, *t*BuOK and CpTl) resulted only in the formation of unidentified product mixtures.

The reactivity of the diiron triple-decker complex **3a** was compared with that of the related complexes [CpFe(μ-η:η-Cp*)FeCp*]$^+$ and [CpFe(μ-η:η-C_4Me_4P)FeCp*]$^+$, with Cp* and C_4Me_4P ligands in their bridging positions. Unlike diiron complex **3a**, which is destroyed by MeCN or NaI at 80 °C, complexes [CpFe(μ-η:η-Cp*)FeCp*]$^+$ and [CpFe(μ-η:η-C_4Me_4P)FeCp*]$^+$ are destroyed even by Me_2CO at room temperature,[9,25b] the complex with a central Cp* ring being destroyed most rapidly. Thus, the reactivity of the triple-decker complexes of the type [CpFe(ring)-FeCp*]$^+$ in nucleophilic degradation reactions greatly depends upon the central ligand and decreases in the order Cp* > C_4Me_4P > P_5.

Electrochemistry

In agreement with a previous report,[26] the iron building block **1** undergoes either a one-electron reduction or a one-electron oxidation, both showing features of chemical irreversibility. In the case of ruthenium analogue **2** we found clear evidence only of the presence of an irreversible oxidation. A possible reduction is probably localized very close to the solvent discharge. The relevant electrode potentials are compiled in Table 4, together with those for the complexes studied here.

Let us start the examination of the redox behaviour of the current triple-decker complexes with the diiron complexes **3a** and **3b**. Figure 3 shows the cyclic voltammetric response given by the permethylated complex **3b** in dichloromethane solution. It exhibits one oxidation and two separate reduction processes. Both the anodic and the first cathodic steps possess features of chemical reversibility on the cyclic voltammetric timescale [$i_{p(reverse)}/i_{p(forward)} \approx 1$], whereas the second reduction appears partially chemically reversible [$i_{p(reverse)}/i_{p(forward)} = 0.7$ at 0.2 Vs^{-1}]. A further irreversible oxidation, not shown in Figure 3, almost completely overlaps the solvent discharge.

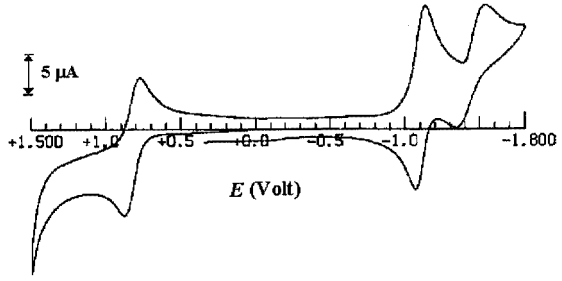

Figure 3. Cyclic voltammogram recorded at a platinum electrode on a CH_2Cl_2 solution containing **3b** (1.2×10^{-3} mol dm^{-3}); supporting electrolyte [Bu_4N][PF_6] (0.2 mol dm^{-3}); scan rate 0.2 Vs^{-1}

Consistent with the behaviour of the related complexes [(triphos)MP_3M(triphos)]$^{n+}$ (M = Ni, Co),[27] Cp* MP_6MCp^* (M = V, Mo, W),[28] Cp*Fe(As_2Se_2)FeCp*,[29]

Table 4. Formal electrode potentials (V, vs. SCE) and peak-to-peak separations (mV) for the redox changes exhibited by complexes **1**, **2**, **3a**, **3b**, **4a**−**c**, **5a**, **5b**, **6**, and **7** in dichloromethane solution; supporting electrolyte [Bu_4N]PF_6 (0.2 mol dm^{-3})

Complex	$E_{p(3+/2+)}$ [a][b]	$E^{\circ\prime}_{(2+/+)}$	i_{pc}/i_{pa} [a]	ΔE_p [a]	$E^{\circ\prime}_{(+/0)}$	i_{pa}/i_{pc} [a]	ΔE_p [a]	$E^{\circ\prime}_{(0/-)}$	i_{pa}/i_{pc} [a]	ΔE_p [a]
1		+0.92[a,b]	–	–	−1.63[a,b]	–	–			
2		+1.18[a,b]	–	–	−1.95[c]	–	–			
3a	> 1.6	+0.99	0.92	100	−0.90	1.0	120	−1.30	0.56	220
3b	+1.54	+0.84	0.87	94	−1.10	1.0	78	−1.41	0.70	150
4a	+1.5	+1.5	–	–	−0.90	0.80	160	−1.39[b]	–	–
4b	+1.30	+0.87[d]	0.6[d]	260[d]	−1.24	[e]	[e]	−1.35	[e]	[e]
4c	+1.35	+0.91	0.80	96	−1.15	1.0	76	−1.40	0.40	144
5a	+1.2[b] [f]	+1.2[b,f]	–	–	−1.10[g]	0.25	180[g]	−1.10[g]	0.25	180[g]
5b	+1.5[b,c]	+1.2[b,c]	–	–	−1.27	0.45	68	−1.27	0.45	68
6	–	+1.02	0.85	96	−1.05	1.0	88	−1.32	0.54	120
7	+1.57[f]	+1.11	0.5[e]	102	−1.22	0.90	86	−1.22	0.90	86
FcH					+0.39	1.0	88			

[a] Measured at 0.2 Vs^{-1}. [b] Peak-potential value. [c] Ill-defined. [d] Measured at 2.0 Vs^{-1}. [e] Difficult to evaluate. [f] Multielectron process. [g] Measured at 5.1 Vs^{-1}.

and in particular $Cp^*CrP_5CrCp^*$,[2] controlled potential coulometry performed in correspondence to the first cathodic step ($E_w = -1.2$ V) consumed one electron per molecule, thus supporting the involvement of one-electron transfers in all the redox processes. This means that the oxidation processes should correspond to the $Fe^{II}Fe^{II}/Fe^{II}Fe^{III}/Fe^{III}Fe^{III}$ sequence, whereas the reduction steps should correspond to the $Fe^{II}Fe^{II}/Fe^{II}Fe^{I}/Fe^{I}Fe^{I}$ sequence. In this context, it should be noted that the Fe^{I} oxidation state is not completely unusual in organometallic chemistry,[30] and the present unexpected processes could be due to cooperative electronic effects inside the triple-decker assembly.

It is interesting to note that, if allowance is made to evaluate the separation between the sequential redox changes $Fe^{II}Fe^{II}/Fe^{II}Fe^{III}/Fe^{III}Fe^{III}$ as roughly about 0.7 V, a K_{com} value of about 7×10^{11} is obtained.[31] This may well indicate that the mixed-valent $Fe^{II}Fe^{III}$ dication electrogenerated in the first oxidation process belongs to the delocalized (in the electrochemical timescale) Robin-Day class III. Analogously, the separation of 0.31 V evaluated for the $Fe^{II}Fe^{II}/Fe^{II}Fe^{I}/Fe^{I}Fe^{I}$ sequence should afford a K_{com} value of 2×10^5, which suggests that the neutral, mixed-valent $Fe^{II}Fe^{I}$ species electrogenerated in the first reduction process should be at the border of the slightly and the completely delocalized classes II and III. In this connection, a $K_{com} = 4 \times 10^{17}$ has been calculated for $Cp^*CrP_5CrCp^*$, which, also supported by EPR spectroscopic measurements, was classified as a delocalized $Cr^{II}Cr^{I}$ system.[2] It should be noted finally that, in spite of the chemical reversibility of the $Fe^{II}Fe^{II}/Fe^{II}Fe^{III}$ and $Fe^{II}Fe^{II}/Fe^{II}Fe^{I}$ redox changes on the cyclic voltammetric timescale, cyclic voltammetric tests performed after the exhaustive $Fe^{II}Fe^{II}/Fe^{II}Fe^{I}$ reduction show that the mixed-valent neutral species undergoes slow decomposition over the long timescales of macroelectrolysis.

The cyclic voltammetric profile of the pentamethylated analogue **3a** is quite similar to that of **3b**, exept for a general shift of all the redox processes towards more positive, or less negative, potential values. Indeed, as far as the anodic region is concerned, no further anodic step (which should correspond to the $Fe^{II}Fe^{III}/Fe^{III}Fe^{III}$ redox change) could be detected within the potential window of the solvent (about +1.7 V), probably because of this general anodic shift. As expected, the decrease in the number of methyl groups makes the $Fe^{II}Fe^{II}/Fe^{II}Fe^{III}$ oxidation somewhat more difficult (by 0.15 V), while favouring the $Fe^{II}Fe^{II}/Fe^{II}Fe^{I}$ reduction step (by 0.2 V) with respect to **3b**. Controlled potential coulometry at the first reduction process consumes one electron per molecule. The resulting solution no longer displays the original peak system, thus indicating that, as happens for **3b**, the neutral species is not indefinitely stable.

Let us now continue to the mixed-metal iron-ruthenium complexes **4a**–**c**. The cyclic voltammetric pattern of permethylated **4c** is very similar to that of the diiron analogue **3b**. An irreversible oxidation is also present at very positive potential values in this case, which in addition is complicated by electrode adsorption phenomena.

As illustrated in Figure 4, complex **4a**, which contains the Cp* ring at the ruthenium atom, undergoes either two discrete reductions, the first of which possesses features of partial chemical reversibility (the current ratio i_{pa}/i_{pc} is equal to 0.8 at 0.2 Vs^{-1}) whereas the second is substantially irreversible, or an irreversible oxidation, probably involving two electrons. From the redox potential of the related complex **3a**, it might be speculated that the first reduction process is centred on the iron fragment.

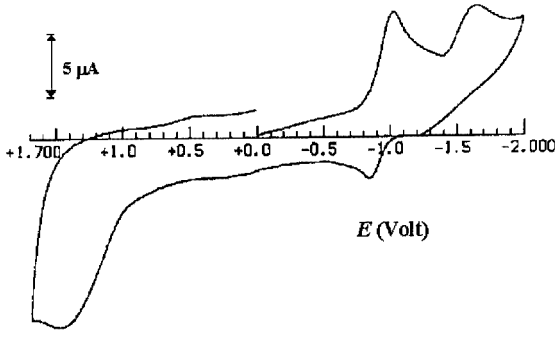

Figure 4. Cyclic voltammogram recorded at a platinum electrode of a CH_2Cl_2 solution containing **4a** (1.1×10^{-3} mol dm^{-3}) and $[Bu_4N][PF_6]$ (0.2 mol dm^{-3}); scan rate 0.2 Vs^{-1}

As illustrated in Figure 5, complex **4b**, which contains the Cp* ring at the iron atom, undergoes two separate oxidations and two apparently closely spaced reductions. In spite of the apparent irreversibility of both oxidation processes, cyclic voltammetry limited to the first oxidation step shows that a directly associated return peak can be detected at a high scan rate (see bottom inset). As far as the appearance of two slightly separated reduction processes is concerned, it must be taken into account that, as illustrated in the top inset, the second process is almost absent at low scan rates, indicating that the first step primarily involves a single two-electron reduction complicated by following chemical reactions.

Let us now examine the diruthenium complexes **5a** and **5b**. As illustrated in Figure 6, permethylated **5b** exhibits a single, partially chemically reversible, reduction process (the current ratio i_{pa}/i_{pc} is equal to 0.4 at 0.2 Vs^{-1} and 0.6 at 2.0 Vs^{-1}). Ill-defined oxidation processes are also present. Comparison with the one-electron oxidation of an equimolar amount of *N*,*N*-dimethyl-1-[1′,2-bis(diphenylphosphanyl)ferrocenyl]ethylamine ($M = 625.5$; $E_p = +0.53$ V) indicates that the cathodic process involves a two-electron addition. On the naive assumption that this process might correspond to the $Ru^{II}Ru^{II}/Ru^{I}Ru^{I}$ transition, its proceeding through a single step should suggest the absence of communication between the two ruthenium centres.

The partially methylated complex **5a** also undergoes a single two-electron reduction, as well as an ill-defined and unsplit multielectron oxidation. Analysis of the cathodic process with scan rate indicates that only at scan rates higher than 1.0 Vs^{-1} does a directly associated reoxidation peak clearly appear in the backscan. This means that the decomposition rate of the electrogenerated monoanion is

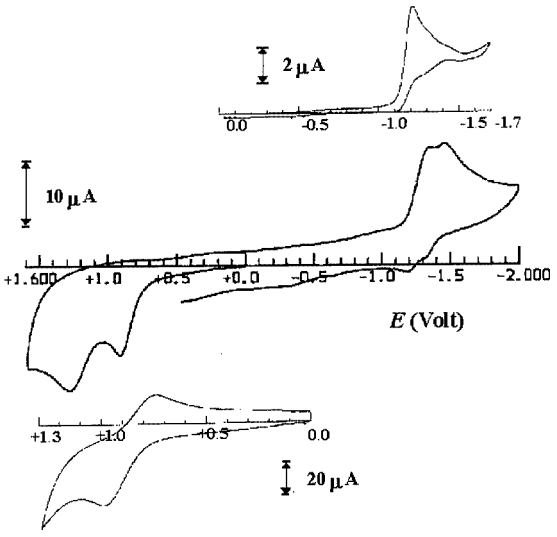

Figure 5. Cyclic voltammograms recorded at a platinum electrode of a CH_2Cl_2 solution containing **4b** (1.3×10^{-3} mol dm^{-3}) and $[Bu_4N][PF_6]$ (0.2 mol dm^{-3}); scan rate 0.2 Vs^{-1}; top inset: scan rate 0.05 Vs^{-1}; bottom inset: 2.0 Vs^{-1}

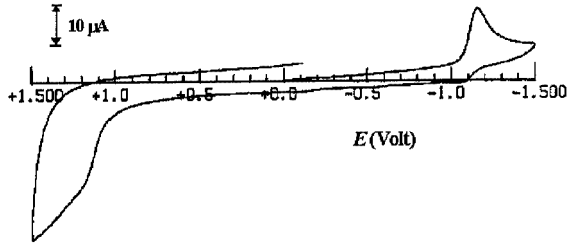

Figure 6. Cyclic voltammogram recorded at a platinum electrode of a CH_2Cl_2 solution containing **5b** (1.3×10^{-3} mol dm^{-3}) and $[Bu_4N][PF_6]$ (0.2 mol dm^{-3}); scan rate 0.2 Vs^{-1}

notably faster than that of **5b**. For **5b**, for instance, a current ratio i_{pa}/i_{pc} of 0.4 is reached at a scan rate of 0.2 Vs^{-1}, whereas for **5a** the same current ratio value is reached at 10.2 Vs^{-1}. Finally, and consistently with the partial demethylation, the reduction process occurs earlier (by 0.17 V) than that of **5b**.

Lastly, let us discuss the related cobalt-containing complexes $[(\eta\text{-}C_4Me_4)Co(\mu\text{-}\eta\text{:}\eta\text{-}P_5)MCp^*]^+$ (**6**: M = Fe; **7**: M = Ru).[32] Figure 7 immediately shows the different role played by a sandwiched iron against a ruthenium centre.

Similarly to the permethylated diiron complex **3b**, the iron-cobalt complex **6** undergoes either an oxidation or two reductions, all showing features of chemical reversibility [Figure 7, (a)]. Controlled potential coulometric experiments performed in correspondence to the first reduction process consume one electron per molecule. The exhaustively reduced solution maintains the red colour of the original species, but displays a cyclic voltammetric profile quite complementary to that shown in Figure 7. At variance with **3b**, this result testifies to the chemical reversibility of the one-electron reduction also on the long timescales of macroelectrolysis. On this basis we assign a one-electron na-

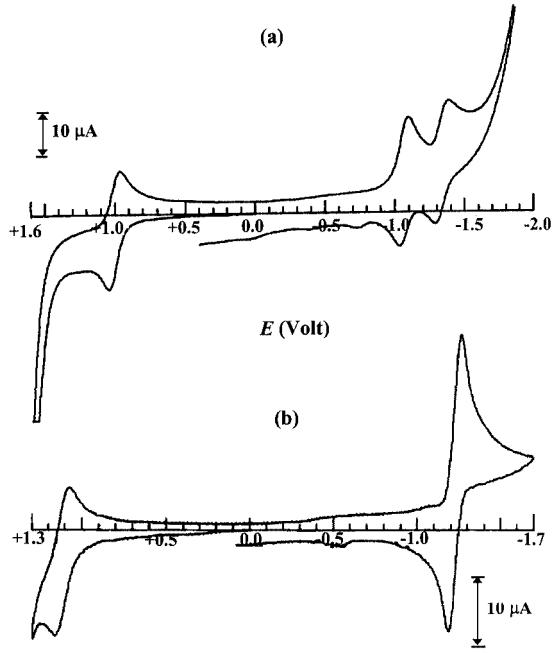

Figure 7. Cyclic voltammograms recorded at a platinum electrode of a CH_2Cl_2 solution containing $[Bu_4N][PF_6]$ (0.2 mol dm^{-3}) and: (a) **6** (1.6×10^{-3} mol dm^{-3}); (b) **7** (1.5×10^{-3} mol dm^{-3}); scan rate 0.2 Vs^{-1}

ture to all the redox processes. As far as the assignment of such redox steps is concerned, it is at the moment difficult to assign the oxidation process to the $Fe^{II}Co^{I}/Fe^{III}Co^{I}$ or to $Fe^{II}Co^{I}/Fe^{II}Co^{II}$ electron transfers, or the Co^{I} or Fe^{II} nature of the reduction processes.

The cyclic voltammetric profile exhibited by the cobalt-ruthenium complex **7** [Figure 7, (b)] is reminiscent of that of the iron-ruthenium complex **4b** and the diruthenium complex **5b**. It is evident that both the oxidation and the reduction have features of chemical reversibility. As can be seen, the height of the reduction step is about twice that of the oxidation step. Comparison of the peak heights with that of an equimolar amount of *N*,*N*-dimethyl-1-[1′,2-bis(diphenylphosphanyl)ferrocenyl]ethylamine reliably allows the cited redox changes to be assigned as two-electron and one-electron processes, respectively. It must be noted that the two-electron reduction in cyclic voltammetry at low scan rates displays a current ratio slightly lower than 1 (i_{pa}/i_{pc} is equal to 0.8 at 0.02 Vs^{-1}), thus suggesting that the electrogenerable monoanion undergoes slow decomposition. As in the case of **6**, it is difficult at the moment to assign the oxidation process as Ru^{II}- or Co^{I}-centred, whereas in this case, probably because of the reduction of the Cp*Ru system being generally more difficult than that of the Cp*Fe system (see **3b** and **5b**), the reduction process seems to involve the simultaneous reduction of both the Ru^{II} and Co^{I} centres.

In conclusion, it has been demonstrated that the presence of a ruthenium atom inside these triple-decker complexes tends to make the corresponding redox changes unstable.

Only if the ruthenium atom is bonded to the Cp* ring do the redox congeners partially increase their stability.

Conclusion

The stacking reactions of pentaphosphametallocenes **1** and **2** with half-sandwich fragments $[(\eta\text{-}C_5R_5)M']^+$ (M′ = Fe, Ru) were used to prepare triple-decker complexes **3b**, **4a**−**c**, **5a** and **5b**, in which the pentaphospholyl ligand is bifacially bonded with two metal atoms. These reactions are often complicated by side-formation of phosphane-type complexes, due to coordination of metal atoms with lone pairs of phosphorus atoms. Such complexes usually turn into triple-decker complexes on heating; the greater stability of phosphane-type complexes formed by **2** results in considerable differences in the conditions for the stacking reactions for **1** and **2**. The main structural feature of μ-pentaphospholyl triple-decker complexes is the elongation of bonds in the triple-decker fragment $M(\mu\text{-}\eta\text{:}\eta\text{-}P_5)M'$ as compared with the corresponding bonds in mononuclear sandwich compounds. Study of nucleophilic degradation reactions has shown that heterometallic (FeRu) triple-decker complexes are more reactive than their homometallic (Fe_2, Ru_2) analogues. Electrochemical data allow assignment of the diiron dication $\mathbf{3b}^{2+}$ as a class III (delocalized) mixed-valent species.

Experimental Section

General: All reactions were carried out under argon in anhydrous solvents. The isolation of products was conducted in air. Starting materials $[Cp^*Fe(CO)_2]_2$,[11] **2**,[33] $[CpFe(\eta\text{-}C_6H_6)]PF_6$,[34] $[Cp^*Fe(MeCN)_3]BF_4$,[11] $[CpRu(MeCN)_3]X$ (X = BF_4, PF_6),[35] $[Cp^*Ru(MeCN)_3]PF_6$ [36] and $[Cp^*RuCl_2]_2$ [37] were prepared as described in the literature. Complex **1** was prepared by Scherer's method,[38] with the use of the simplified isolation procedure given below. ^1H, $^{13}C\{^1H\}$ and $^{31}P\{^1H\}$ NMR spectra were recorded with a Bruker AMX 400 spectrometer operating at 400.13, 100.61 and 161.98 MHz, respectively. Materials and the apparatus for electrochemistry have been described elsewhere.[39] *N*,*N*-Dimethyl-1-[1′,2-bis(diphenylphosphanyl)ferrocenyl]ethylamine was an Aldrich product. Potential values are referenced to the saturated calomel electrode (SCE).

$(\eta\text{-}P_5)FeCp^*$ (1): A mixture of $[Cp^*Fe(CO)_2]_2$ (4.5 g, 9.1 mmol) and P_4 (5 g, 40.3 mmol) in decalin (300 mL) was stirred under reflux for 3 h. The reaction solvents were evaporated to a small volume (ca. 30 mL) under atmospheric pressure and the remaining solvent was then removed at 100 °C under water-pump vacuum. Admixed P_4 was sublimed at 100 °C at ca. 0.1 Torr. The solid residue was recrystallized from petroleum ether to give dark green crystals. Yield 3.4 g (59%). $^{31}P\{^1H\}$ NMR ($CDCl_3$): δ = 152.7 ppm.

$[CpFe(\mu\text{-}\eta\text{:}\eta\text{-}P_5)RuCp^*]PF_6$ ($\mathbf{4aPF_6}$): Dichloromethane (10 mL) was added to a mixture of **2** (60 mg, 0.15 mmol) and $[CpFe(\eta\text{-}C_6H_6)]PF_6$ (52 mg, 0.15 mmol) in a Schlenk tube (d = 15 mm). The reaction mixture was irradiated for 10 h with a 400-W high-pressure discharge lamp (sodium lamp or mercury luminescent lamp). Both the Schlenk tube and the lamp were contained in a suitable vessel covered inside with aluminium foil; cooling was accomplished with running water. The solvent was removed in vacuo. The residue was dissolved in $MeNO_2$ (ca. 4 mL) and the solution was heated under reflux for ca. 2 h in order to destroy phosphane-type by-products. After removal of the solvent, unchanged **2** (15 mg) was extracted with ether. The residue was reprecipitated twice from CH_2Cl_2 with ether to give a red-brown solid. Yield 70 mg (71%). $C_{15}H_{20}F_6FeP_6Ru$ (657.06): calcd. C 27.42, H 3.07; found C 27.76, H 3.08.

$[Cp^*Fe(\mu\text{-}\eta\text{:}\eta\text{-}P_5)FeCp^*]BF_4$ ($\mathbf{3bBF_4}$): A mixture of **1** (115 mg, 0.33 mmol) and $[Cp^*Fe(MeCN)_3]BF_4$ (129 mg, 0.32 mmol) in CH_2Cl_2 or Me_2CO (10 mL) was stirred for 2.5 h at room temperature. The solvent was removed in vacuo and the residue was reprecipitated twice from CH_2Cl_2 with ether to give a green solid. Yield 120 mg (60%). $C_{21}H_{32}BCl_2F_4Fe_2P_5$ (**3b**BF_4·CH_2Cl_2; 708.75): calcd. C 35.59, H 4.55; found C 36.22, H 4.70.

$[Cp^*M(\mu\text{-}\eta\text{:}\eta\text{-}P_5)RuCp]X$ ($\mathbf{4bBF_4}$: M = Fe; $\mathbf{5aPF_6}$: M = Ru): A mixture of **1** (or **2**) (0.2 mmol) and $[CpRu(MeCN)_3]X$ (0.21 mmol) in $MeNO_2$ (5 mL) was heated under reflux for 5 h. The solvent was removed in vacuo and the residue was reprecipitated twice from CH_2Cl_2 with ether to give a red-brown solid. Compound **4b**BF_4: Yield 75 mg (63%). $C_{15}H_{20}BF_4FeP_5Ru$ (598.91): calcd. C 30.08, H 3.37; found C 29.46, H 3.36. Compound **5a**PF_6: Yield 58 mg (41%). $C_{15}H_{20}F_6P_6Ru_2$ (702.28): calcd. C 25.65, H 2.87; found C 26.45, H 2.89.

$[Cp^*Fe(\mu\text{-}\eta\text{:}\eta\text{-}P_5)RuCp^*]BF_4$ ($\mathbf{4cBF_4}$). A: A mixture of **1** (80 mg, 0.23 mmol), $[Cp^*RuCl_2]_2$ (57 mg, 0.09 mmol), $TlBF_4$ (125 mg, 0.43 mmol) and Zn dust (100 mg, excess) in Me_2CO (5 mL) was stirred for 2 h at room temperature. The solvent was removed in vacuo and the residue was reprecipitated twice from CH_2Cl_2 with ether to give a red-brown solid. Yield 104 mg (84%). $C_{20}H_{30}BF_4FeP_5Ru$ (669.04): calcd. C 35.90, H 4.52; found C 35.23, H 4.39. **B:** A solution of **1** (87 mg, 0.25 mmol) and $[Cp^*RuCl_2]_2$ (77 mg, 0.125 mmol) in ethanol (5 mL) was heated under reflux for 1 h. The solvent was removed in vacuo and the residue was dissolved in water (5−10 mL). The solution was filtered, and the filtrate was treated with 0.2 mL (excess) of aqueous HBF_4 (48%). The precipitate formed was filtered off, washed with water, dried in vacuo and reprecipitated from CH_2Cl_2 with ether to give a red-brown solid. Yield 134 mg (80%).

$[Cp^*Ru(\mu\text{-}\eta\text{:}\eta\text{-}P_5)RuCp^*]X$ ($\mathbf{5bBF_4}$, $\mathbf{5bPF_6}$). A: A mixture of $[Cp^*RuCl_2]_2$ (32 mg, 0.05 mmol), $TlBF_4$ (70 mg, 0.24 mmol) and Zn dust (100 mg, excess) in THF (5 mL) was stirred for 0.5 h at 0 °C. The solution of the thus formed solvate $[Cp^*Ru(THF)_3]BF_4$ was treated with **2** (41 mg, 0.11 mmol) and the mixture was heated under reflux for 8 h. The solvent was removed in vacuo and the residue was reprecipitated twice from CH_2Cl_2 with ether to give complex **5b**BF_4 as a red-brown solid. Yield 61 mg (82%). $C_{20}H_{30}BF_4P_5Ru_2$ (714.26): calcd. C 33.63, H 4.23; found C 33.45, H 4.18. **B:** A mixture of **2** (30 mg, 0.08 mmol) and $[Cp^*Ru(MeCN)_3]PF_6$ (42 mg, 0.08 mmol) in $MeNO_2$ (5 mL) was heated under reflux for 7 h. The solvent was removed in vacuo and the residue was reprecipitated twice from CH_2Cl_2 with ether to give complex **5b**PF_6 as a red-brown solid. Yield 34 mg (57%). $C_{20}H_{30}F_6P_6Ru_2$ (772.41): calcd. C 31.10, H 3.92; found C 31.28, H 3.72.

Nucleophilic Degradation of 4a by MeCN: A solution of **4a** (26 mg, 0.04 mmol) in MeCN (4 mL) was heated under reflux for 10 h. The solvent was removed in vacuo and the solid residue was extracted with ether. After removal of ether in vacuo, complex **2** was obtained as an orange solid. Yield 8 mg (ca. 50%). The residue, after extrac-

Table 5. Crystal data and structure refinement parameters for **4a**PF_6 and **5b**PF_6

Compound	**4a**PF_6	**5b**PF_6
Empirical formula	$C_{15}H_{20}F_6FeP_6Ru$	$C_{20}H_{30}F_6P_6Ru_2$
Formula mass	657.05	772.40
Crystal colour, habit	Yellow plate	Dark red needle
Crystal size [mm]	0.40 × 0.20 × 0.05	0.45 × 0.30 × 0.25
Crystal system	orthorhombic	orthorhombic
Space group	*Ibam*	*Fddd*
a [Å]	15.2363(7)	21.192(1)
b [Å]	20.0508(9)	29.148(1)
c [Å]	14.9157(7)	35.561(2)
V [Å^3]	4556.7(4)	21966(2)
Z	8	32
D(calcd.) [g cm^{-3}]	1.916	1.869
Diffractometer	Bruker SMART 1000 CCD	Bruker SMART 1000 CCD
Temperature [K]	110	110
Radiation	Mo-K_α (λ = 0.71073)	Mo-K_α (λ = 0.71073)
Scan mode	φ and ω	φ and ω
θ range [°]	1.68−31.47	1.32−30.03
Abs.coeff. μ(Mo-K_α) [cm^{-3}]	17.70	15.00
Absorption correction	SADABS	SADABS
$T_{max.}$ and $T_{min.}$	0.928 and 0.471	1.000 and 0.692
Collected reflections	24940	58712
Independent reflections	3702 (R_{int} = 0.0604)	8041 (R_{int} = 0.0322)
Reflections used in refinement	3676	7998
Observed reflections [$I > 2\sigma(I)$]	2944	6875
Parameters	203	428
R_1 (on F for obs. refls.)[a]	0.0376	0.0292
wR_2 (on F^2 for all refls.)[b]	0.1069	0.0839
F(000)	2592	12224
GOF	0.779	1.055
Largest diff. peak and hole [e Å^{-3}]	3.333 and −1.017	1.518 and −0.914

[a] $R1 = \Sigma||F_o| - |F_c||/\Sigma(F_o)$ for observed reflections. [b] $wR_2 = \{\Sigma[w(F_o^2 - F_c^2)^2/\Sigma[w(F_o^2)^2]\}^{0.5}$ for all reflections.

tion with ether, was extracted with CH_2Cl_2. Addition of ether to the solution regenerated starting material **4a** (8 mg, 30%).

Nucleophilic Degradation of 3a by NaI in MeCN: A solution of **3a** (31 mg, 0.05 mmol) and NaI·$2H_2O$ (100 mg, 0.54 mmol) in MeCN (4 mL) was heated under reflux for 10 h. The solvent was removed in vacuo and the solid residue was extracted with ether. After removal of ether in vacuo, complex **1** was obtained as a green solid. Yield 12 mg (ca. 70%).

X-ray Crystal Structure Determinations: Crystals of **4a**PF_6 and **5b**PF_6 were obtained by slow diffusion of petroleum ether into CH_2Cl_2 solutions of the complexes. Data collection was carried out with a Bruker SMART 1000 diffractometer with a CCD detector by a combination of four sets of ω scans (each scan 0.3° in 20 s), each set at different φ (2θ = −28°). Low crystal temperatures were maintained with a Cryostream (Oxford Cryosystems) open-flow N_2 gas cryostat. Unit cell parameters were determined with SMART software[40] and refined with SAINT[41] on all observed reflections. Data reduction was performed with SAINT, absorption corrections were applied with the SADABS program.[42] The detailed crystal data and structure refinement parameters are listed in Table 5. The structures were solved by direct methods and refined by full-matrix, least-squares against F^2 of all data, with SHELXTL software.[43] All non-hydrogen and hydrogen atomic positions were located in difference Fourier maps and refined in anisotropic and isotropic approximations, respectively. CCDC-177284 (**4a**PF_6) and -177285 (**5b**PF_6) contain the supplementary crystallographic data for this paper. These data can be obtained free of charge at www.ccdc.cam.ac.uk/conts/retrieving.html or from the Cambridge Crystallographic Data Centre, 12, Union Road, Cambridge CB2 1EZ, UK [Fax: (internat.) + 44-1223/336-033; E-mail: deposit@ccdc.cam.ac.uk].

Acknowledgments

This work was supported by the Russian Foundation for Basic Research (Grant Nos. 99-03-33106; 00-03-32807) and the Federal Target Program "Integration" (Grant No. AO 115). P. Z. gratefully acknowledges the financial support of the University of Siena (PAR 2001).

[1] [1a] O. J. Scherer, *Angew. Chem. Int. Ed. Engl.* **1990**, *29*, 1104. [1b] M. Scheer, E. Herrmann, *Z. Chem.* **1990**, *30*, 41.
[2] O. J. Scherer, J. Schwalb, G. Wolmershäuser, W. Kaim, R. Gross, *Angew. Chem. Int. Ed. Engl.* **1986**, *25*, 363.
[3] [3a] L. Y. Goh, R. C. S. Wong, C. K. Chu, T. W. Hambley, *J. Chem. Soc., Dalton Trans.* **1990**, 977. [3b] A. K. Hughes, V. J. Murphy, D. O'Hare, *J. Chem. Soc., Chem. Commun.* **1994**, 163.
[4] M. Scheer, K. Schuster, A. Krug, H. Hartung, *Chem. Ber./Recueil* **1997**, *130*, 1299.
[5] Our recent results on this topic are summarised in the review: A. R. Kudinov, M. I. Rybinskaya, *Izv. Akad. Nauk, Ser. Khim.* **1999**, 1636 [*Russ. Chem. Bull.* **1999**, *48*, 1615 (Engl. Transl.)].
[6] [6a] O. J. Scherer, T. Brück, G. Wolmershäuser, *Chem. Ber.* **1989**, *122*, 2049. [6b] B. Rink, O. J. Scherer, G. Heckmann, G. Wolmershäuser, *Chem. Ber.* **1992**, *125*, 1011.
[7] A. R. Kudinov, P. V. Petrovskii, M. I. Rybinskaya, *Izv. Akad. Nauk, Ser. Khim.* **1999**, 1374 [*Russ. Chem. Bull.* **1999**, *48*, 1362 (Engl. Transl.)].
[8] Preliminary account of this work: A. R. Kudinov, D. A. Logi-

nov, P. V. Petrovskii, M. I. Rybinskaya, *Izv. Akad. Nauk, Ser. Khim.* **1998**, 1625 [*Russ. Chem. Bull.* **1998**, *47*, 1583 (Engl. Transl.)].
[9] A. R. Kudinov, M. I. Rybinskaya, Yu. T. Struchkov, A. I. Yanovskii, P. V. Petrovskii, *J. Organomet. Chem.* **1987**, *336*, 187.
[10] All the cationic triple-decker complexes described here were isolated as salts with the PF_6^- or BF_4^- anions (the anions are omitted in the schemes).
[11] [11a] D. Catheline, D. Astruc, *J. Organomet. Chem.* **1983**, *248*, C9. [11b] D. Catheline, D. Astruc, *Organometallics* **1984**, *3*, 1094.
[12] G. E. Herberich, U. Englert, B. Ganter, C. Lamertz, *Organometallics* **1996**, *15*, 5236.
[13] The ability of **1** to form phosphane-type complexes was illustrated by formation of the complexes $(\eta\text{-}C_5Me_5)Fe(\eta\text{-}P_5)[Cr(CO)_5]_2$ and $(\eta\text{-}C_5Me_5)Fe(\eta\text{-}P_5)[Mn(CO)_2Cp]_n$ (n = 1−4).[6a]
[14] A similar reaction of $[Cp^*RuCl_2]_2$ with Zn dust and KPF_6 in Me_2CO or THF in the presence of arenes was used earlier for the preparation of $[Cp^*Ru(arene)]^+$ complexes: B. Chaudret, F. A. Jalon, *J. Chem. Soc., Chem. Commun.* **1988**, 711.
[15] [15a] B. Chaudret, X. He, Y. Huang, *J. Chem. Soc., Chem. Commun.* **1989**, 1844. [15b] X. D. He, B. Chaudret, F. Dahan, Y.-S. Huang, *Organometallics* **1991**, *10*, 970. [15c] U. Koelle, M. H. Wang, G. Raabe, *Organometallics* **1991**, *10*, 2573. [15d] G. E. Herberich, U. Englert, F. Marken, P. Hofmann, *Organometallics* **1993**, *12*, 4039.
[16] [16a] V. S. Kaganovich, A. R. Kudinov, M. I. Rybinskaya, *Izv. Akad Nauk SSSR, Ser. Khim.* **1986**, 492 [*Bull. Acad. Sci. USSR, Div. Chem. Sci.* **1986**, *35*, 456 (Engl. Transl.)]. [16b] V. S. Kaganovich, A. R. Kudinov, M. I. Rybinskaya, *Metalloorg. Khim.* **1990**, *3*, 70 [*Organomet. Chem. USSR* **1990**, *3*, 35 (Engl. Transl.)].
[17] Ct, Ct′, and Ct′′ represent the centroids of the P_5, Cp*(1), and Cp*(2) rings, respectively.
[18] B. P. Biryukov, Yu. T. Struchkov, *Usp. Khim* **1970**, *39*, 1672. [Russ. Chem. *Rev.* **1970**, *39*, 789 (Engl. Transl.)].
[19] O. J. Scherer, T. Brück, G. Wolmershäuser, *Chem. Ber.* **1988**, *121*, 935.
[20] J. W. Lauher, M. Elian, R. H. Summerville, R. Hoffmann, *J. Am. Chem. Soc.* **1976**, *98*, 3219.
[21] [21a] A. Salzer, H. Werner, *Synth. Inorg. Met.-Org. Chem.* **1972**, *2*, 249. [21b] A. R. Kudinov, A. A. Fil'chikov, P. V. Petrovskii, M. I. Rybinskaya, *Izv. Akad. Nauk, Ser. Khim.* **1999**, 1364 [*Russ. Chem. Bull.* **1999**, *48*, 1352 (Engl. Transl.)].
[22] [22a] G. E. Herberich, B. Hessner, R. Saive, *J. Organomet. Chem.* **1987**, *319*, 9. [22b] G. E. Herberich, B. J. Dunne, B. Hessner, *Angew. Chem. Int. Ed. Engl.* **1989**, *28*, 737. [22c] G. E. Herberich, U. Büschges, B. J. Dunne, B. Hessner, N. Klaff, D. P. J. Köffer, K. M. Peters, *J. Organomet. Chem.* **1989**, *372*, 53.
[23] W. Siebert, W. Rothermel, C. Böhle, C. Krüger, D. J. Brauer, *Angew. Chem. Int. Ed. Engl.* **1979**, *18*, 949.
[24] [24a] G. E. Herberich, U. Englert, D. Pubanz, *J. Organomet. Chem.* **1993**, *459*, 1. [24b] A. R. Kudinov, D. A. Loginov, Z. A. Starikova, P. V. Petrovskii, *J. Organomet. Chem.* **2002**, *649*, 136.
[25] [25a] G. E. Herberich, B. Ganter, *Organometallics* **1997**, *16*, 522. [25b] A. R. Kudinov, D. A. Loginov, S. N. Ashikhmin, A. A. Fil'chikov, L. S. Shul'pina, P. V. Petrovskii, *Izv. Akad. Nauk, Ser. Khim.* **2000**, 1647 [*Russ. Chem. Bull.* **2000**, *49*, 1637 (Engl. Transl.)]. [25c] G. E. Herberich, B. Ganter, *Inorg. Chem. Commun.* **2001**, *4*, 100.
[26] R. F. Winter, W. E. Geiger, *Organometallics* **1999**, *18*, 1827.
[27] M. Di Vaira, L. Sacconi, *Angew. Chem. Int. Ed. Engl.* **1982**, *21*, 330.
[28] O. J. Scherer, J. Schwalb, H. Swarowsky, G. Wolmershäuser, W. Kaim, R. Gross, *Chem. Ber.* **1988**, *121*, 443.
[29] O. Blacque, H. Brunner, M. M. Kubicki, F. Leis, D. Lucas, Y. Mugnier, B. Nuber, J. Wachter, *Chem. Eur. J.* **2001**, *7*, 1342.
[30] C. Bianchini, F. Laschi, D. Masi, F. M. Ottaviani, A. Pastor, M. Peruzzini, P. Zanello, F. Zanobini, *J. Am. Chem. Soc.* **1993**, *115*, 2723.
[31] [31a] D. E. Richardson, H. Taube, *Inorg. Chem.* **1981**, *20*, 1278. [31b] R. R. Gagné, C. L. Spiro, T. J. Smith, C. A. Hamann, W. R. Thies, A. K. Shiemke, *J. Am. Chem. Soc.* **1981**, *103*, 4073. [31c] D. Astruc, in *Electron Transfer and Radical Processes in Transition-Metal Chemistry*, Wiley-VCH, New York, **1995**. [31d]B. S. Brunschwig, N. Sutin, *Coord. Chem. Rev.* **1999**, *187*, 233.
[32] A. R. Kudinov, D. A. Loginov, I. V. Pruss, Z. A. Starikova, P. V. Petrovskii, *Eur. J. Inorg. Chem.*, in preparation
[33] B. Rink, O. J. Scherer, G. Wolmershäuser, *Chem. Ber.* **1995**, *128*, 71.
[34] A. N. Nesmeyanov, N. A. Vol'kenau, I. N. Bolesova, L. S. Polkovnikova, *Koord. Khim.* **1975**, *1*, 1252 [*Sov. J. Coord. Chem.* **1975**, *1* (Engl. Transl.)].
[35] T. P. Gill, K. R. Mann, *Organometallics* **1982**, *1*, 485.
[36] J. L. Schrenk, A. M. McNair, F. B. McCormick, K. R. Mann, *Inorg. Chem.* **1986**, *25*, 3501.
[37] T. D. Tilley, R. H. Grubbs, J. E. Bercaw, *Organometallics* **1984**, *3*, 274.
[38] M. Detzel, G. Friedrich, O. J. Scherer, G. Wolmershäuser, *Angew. Chem. Int. Ed. Engl.* **1995**, *34*, 1321.
[39] F. Fabrizi de Biani, F. Laschi, P. Zanello, G. Ferguson, J. Trotter, G. M. O'Riordan, T. R. Spalding, *J. Chem. Soc., Dalton Trans.* **2001**, 1520.
[40] *SMART, Bruker Molecular Analysis Research Tool*, v. 5.059, Bruker AXS, Madison, Wisconsin, USA.
[41] *SAINTPlus Data Reduction and Correction Program*, v. 6.01, Bruker AXS, Madison, Wisconsin, USA.
[42] *SADABS, Bruker/Siemens Area Detector Absorption Correction Program*, v.2.01, Bruker AXS, Madison, Wisconsin, USA.
[43] G. M. Sheldrick, *SHELXTL, Structure Determination Software Suite*, v. 5.10, Bruker AXS, Madison, Wisconsin, USA.

Received March 20, 2002
[I02146]

In Situ Preparation of Palladium Diphosphane Catalysts

Angelica Marson,[a] A. Bart van Oort,[a] and Wilhelmus P. Mul*[a]

Keywords: Palladium / Phosphanes / Homogeneous catalysis / Copolymerization

The efficiency of a superficially simple preparation procedure for palladium-diphosphane catalysts has been examined. Preparation of $Pd(dppe)X_2$ in situ by mixing equimolar amounts of $Pd(OAc)_2$ and 1,2-bis(diphenylphosphanyl)-ethane (dppe) in methanol in the first step unexpectedly affords the bischelate $[Pd(dppe)_2](OAc)_2$ as the (main) kinetic product. Subsequently, the slow reaction of $[Pd(dppe)_2](OAc)_2$ and unreacted $Pd(OAc)_2$ forms the thermodynamically favored monochelate $[Pd(dppe)(OAc)_2]$ (following first-order kinetics). Conversion of the bischelate into the monochelate stops after addition of strong acid (HX) in the second step, thus affording a mixture of active — $Pd(dppe)X_2$ — virtually inactive — $[Pd(dppe)_2]X_2$ — and unstable — PdX_2 — species. This procedure was also evaluated for some other diphosphane ligands and methods are given to overcome the encountered problem.

The potential of homogeneous catalysis in the selective preparation of chemicals has been widely recognized, and the number of applications, both on a laboratory scale and on an industrial scale, is growing steadily.[1] In situ preparation of homogeneous catalysts from readily available precursors is a useful method, in particular when testing larger numbers of catalysts as in parallel screening. A convenient and frequently explored method to prepare cationic palladium diphosphane catalysts in situ involves two steps.[2] First, a suitable palladium source, such as $Pd(OAc)_2$, and the ligand of choice are mixed in a selected solvent [Equation (1)]. Next, a strong acid is added to exchange the anions [Equation (2)].

$$Pd(OAc)_2 + P\text{-}P \rightarrow [Pd(P\text{-}P)(OAc)_2] \quad (1)$$

$$[Pd(P\text{-}P)(OAc)_2] + 2\,HX \rightarrow [Pd(P\text{-}P)X_2] + 2\,HOAc \quad (2)$$

Although this method is often used, little attention has been given to the efficiency of catalyst preparation when using this procedure.

In the mid-eighties it was discovered that palladium(II)-based catalysts modified with the combination of a chelating diphosphane ligand and weakly or non-coordinating anions are highly active for the synthesis of perfectly alternating CO/ethene-based copolymer (PK-E). The most efficient system was based on 1,3-bis(diphenylphosphanyl)propane, which produces snow white PK-E with high rates (of 6 kg PK-E/g Pd·h and higher).[2,3] The activity of the catalyst based on its C_2-bridged counterpart, 1,2-bis(diphenylphosphanyl)ethane (dppe), was considerably lower.[2a] Moreover, the grey color of the PK-E product obtained during CO/ethene copolymerization employing the Pd(dppe)-based catalyst prepared in situ in methanol [Equations (1) and (2)] indicated significant catalyst decomposition to solid palladium(0) ("plating"). This prompted us to examine the in situ catalyst preparation procedure in methanol.

To this end, an equimolar mixture of $Pd(OAc)_2$ and dppe (32 μmol) was prepared in [D_4]methanol (0.8 mL). It was found that instead of the expected monochelate $[Pd(dppe)(OAc)_2]$ (**1**), the bischelate derivative $[Pd(dppe)_2](OAc)_2$ (**2**), characterized by a single ^{31}P NMR resonance at $\delta = 58.7$ ppm, was formed initially. Upon standing, slow conversion of **2** into **1** ($\delta = 63.4$ ppm) was observed (Scheme 1), which was virtually completed only after about 24 h, and accompanied by plating.

Mimicking the full in situ catalyst preparation procedure, six equivalents of a strong acid (CF_3CO_2H) were added well before the conversion of **2** into **1** was completed. Besides the expected exchange of the anions of the various palladium species [**1**, **2**, and unreacted $Pd(OAc)_2$], conversion of the catalytically inactive bischelate $[Pd(dppe)_2](CF_3CO_2)_2$ (**4**, $\delta = 58.6$ ppm) into the active monochelate species $[Pd(dppe)(CF_3CO_2)_2]$ (**3**, $\delta = 69.2$ ppm) also stopped (Scheme 1). This indicates that conversion of **2** into **1** is acetate-assisted. Moreover, a significant amount of palladium black was formed within a few hours due to decomposition of the co-formed palladium trifluoroacetate, a labile species in alcoholic media.

The conversion of **2** into **1** in [D_4]methanol at 20 °C was monitored by ^{31}P NMR spectroscopy and found to nicely follow first-order kinetics ($k = 0.145\ h^{-1}$; see Figure 1). At a higher degree of conversion (>80%), however, this conversion proceeded somewhat slower, which might be due to partial decomposition (plating) of $Pd(OAc)_2$ and **1**. Extrapolation of the kinetic curve to $t = 0$ h showed that, ini-

[a] Shell Research and Technology Center Amsterdam,
Shell International Chemicals B.V.,
P. O. Box 38000, 1030 BN Amsterdam, The Netherlands
Fax: (internat.) +31-20/630-3034
E-mail: pim.mul@shell.com

 © 2002 WILEY-VCH Verlag GmbH & Co. KGaA, 69451 Weinheim 1434−1948/02/1111−3028 $ 20.00+.50/0 *Eur. J. Inorg. Chem.* **2002**, 3028−3031

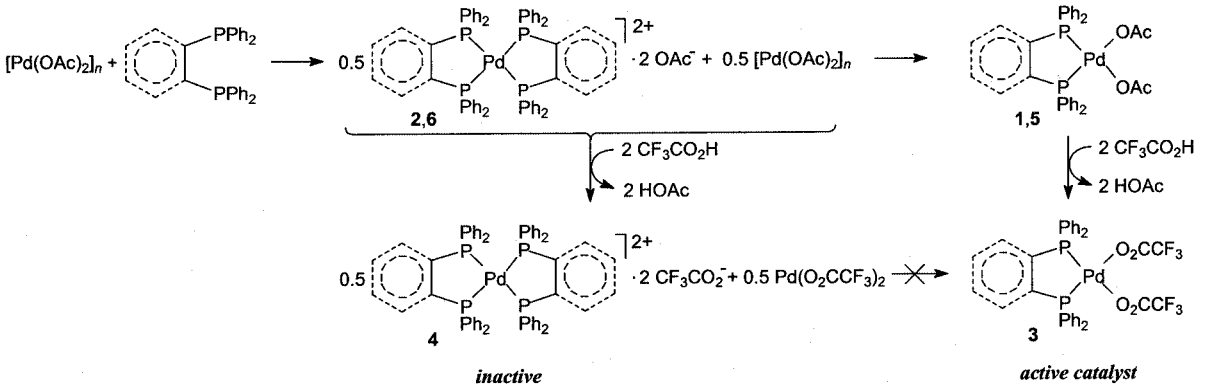

Scheme 1. Reactions observed during preparation of some palladium diphosphane catalysts in situ; P-P = dppe (**1**–**4**) or dppbz (**5**,**6**)

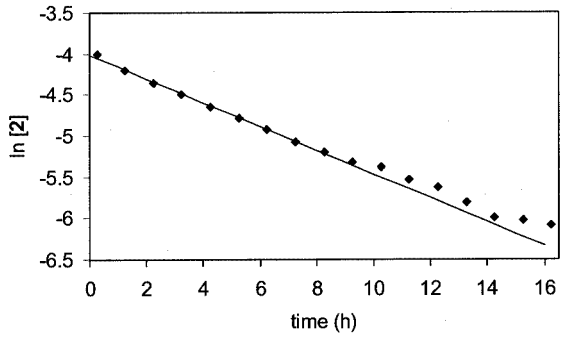

Figure 1. Conversion of **2** + $Pd(OAc)_2$ into **1** in [D_4]methanol at 20 °C

tially, **2** had formed almost quantitatively (approx. 90%). In a separate experiment equimolar amounts of isolated, pure **2** and $Pd(OAc)_2$ were dissolved in [D_4]methanol and the conversion into **1** was found to exhibit identical kinetics.

These observations clearly indicate that **2** is the kinetic product of the reaction of $Pd(OAc)_2$ and dppe, but **1** is thermodynamically favored. Further, it indicates that **1** and **2**, in contrast to Bianchini's recent conclusion,[4] are not involved in an autoionization equilibrium (2 [Pd(dppe)$(OAc)_2$] (**1**) ⇌ [Pd(dppe)$_2$]$(OAc)_2$ (**2**) + $Pd(OAc)_2$ in methanol, otherwise conversion of **2** into **1** would not have proceeded to completeness.[5] This was confirmed in a separate experiment using isolated, pure **1**: upon dissolution in [D_4]methanol, no conversion of **1** into **2** was observed (over 24 h).

It was considered that the initial formation of [Pd(dppe)$_2$]$(OAc)_2$ might be due to a relatively slow dissolution of $Pd(OAc)_2$ in methanol in comparison with dppe, causing an initial deficiency of accessible (dissolved) $Pd(OAc)_2$. To check this hypothesis, an experiment was done in which $Pd(OAc)_2$ was first dissolved in a mixture of methanol/dichloromethane (9:1) before dppe was added. Immediate formation of **2** and some **1** was observed by ^{31}P NMR spectroscopy, followed by slow conversion of **2** into **1**. Extrapolation of the kinetic curve for the conversion of **2** into **1** back to t = 0 h indicated initial formation of **2** and **1** in a ratio of about 80:20. The hypothesis of slow dissolution of $Pd(OAc)_2$ being the prime cause for the initial formation of **2** instead of **1** could therefore be discarded.

The origin of the anomalous course of the reaction is possibly related to the nature of $Pd(OAc)_2$ dissolved in methanol. It is well-known that in solution $Pd(OAc)_2$ may occur in various forms. For example, in benzene and toluene $Pd(OAc)_2$ exists as a linear trimer at 39 °C, and as a monomer at 80 °C, while an acetate-bridged cyclic trimer with D_{3h} symmetry is obtained when $Pd(OAc)_2$ is crystallized from benzene.[6] The ^1H NMR spectrum of $Pd(OAc)_2$ in methanol shows a large number of signals around δ = 2 ppm for the acetate anion, the relative intensities of the signals being dependent on the concentration and on the water content of the methanol, amongst other factors. This is indicative of the presence of $Pd(OAc)_2$ in a variety of aggregates, $[Pd(OAc)_2]_n$, with n = 1, 2, 3, etc., while even the occurrence of ionic species like $[Pd_n(OAc)_{2n-1}]^+(OAc)^-$ cannot be excluded. Apparently, the kinetically preferred pathways along which these clusters break up give rise to the preferential formation of **2**.

Subsequent conversion of **2** into **1** occurs with first-order kinetics and is acetate-assisted, suggesting the involvement of a single species in the rate-determining step. Taking the involvement of acetate into account, a possible option for this species is the adduct of **2** and acetate, five-coordinated, mono-cationic $[Pd(dppe)_2(OAc)]^+$. However, the difference in the ^{31}P chemical shift between **2** (δ = 58.7 ppm) and [Pd(dppe)$_2$]$(CF_3CO_2)_2$ (**4**, δ = 58.6 ppm) is negligible and does not point to association of an acetate anion in the former. Hence, step-wise dissociation of one of the dppe ligands starting from $[Pd(dppe)_2]^{2+}$ (**2**) seems a more likely pathway. The first, rate-determining step could well be the generation of $[Pd(\sigma,\sigma\text{-dppe})(\sigma\text{-dppe})(S)]^{2+}$, which is rapidly transferred into the more stable $[Pd(\sigma,\sigma\text{-dppe})(\sigma\text{-dppe})(OAc)]^+$, from which the dppe ligand can fully dissociate, possibly via a dppe-bridged dimer of type $[(OAc)Pd(\sigma,\sigma\text{-dppe})(\mu\text{-dppe})Pd(OAc)_2]^+$.

Next, the influence of the preparation procedure on the performance of [Pd(dppe)$(CF_3CO_2)_2$] (**3**) as a catalyst for CO/ethene copolymerization was investigated. The catalyst was either prepared in situ in methanol, by mixing dppe and $Pd(OAc)_2$, followed by addition of six equivalents of trifluoroacetic acid after about 10 min (run A) or by anion exchange starting from isolated, pure **1** (run B). The CO/ethene copolymerizations were performed under standard

catalyst screening conditions (90 °C, 5 MPa) for 2.5 h, in a solvent mixture consisting of methanol and water (98:2). In run A a grey copolymer product was obtained at a productivity of 390 g/g Pd·h, while in run B an almost white product was obtained at much higher productivity (910 g/g Pd·h). This clearly shows that preparation of catalyst **3** in methanol in situ from $Pd(OAc)_2$, ligand and acid is inferior to preparation from pure **1**, which is fully in line with the NMR studies. Interestingly, the ester to ketone end-group ratio in the copolymer products (ca. 45:55) deviated from the theoretical value of 1.[7,8] Formation of an excess of ketone end-groups is probably caused by increased partial initiation via a Pd-H species instead of via Pd-OCH_3. This can occur if initiation via the reactions given in Equations (7) to (10) efficiently competes with those given in Equation (5) and (6).

$$[Pd(P\text{-}P)]^{2+} + MeOH \rightleftharpoons [Pd(P\text{-}P)(OMe)]^{+} + H^{+} \quad (5)$$

$$[Pd(P\text{-}P)(OMe)]^{+} + CO + CH_2{=}CH_2 \rightarrow\rightarrow [Pd(P\text{-}P)\{CH_2CH_2C(O)OMe\}]^{+} \quad (6)$$

$$[Pd(P\text{-}P)(OMe)]^{+} \rightarrow [Pd(P\text{-}P)H]^{+} + CH_2O \quad (7)$$

$$[Pd(P\text{-}P)]^{2+} + H_2O \rightleftharpoons [Pd(P\text{-}P)(OH)]^{+} + H^{+} \quad (8)$$

$$[Pd(P\text{-}P)(OH)]^{+} + CO \rightleftharpoons [Pd(P\text{-}P)\{C(O)OH\}]^{+} \rightarrow [Pd(P\text{-}P)H]^{+} + CO_2 \quad (9)$$

$$[Pd(P\text{-}P)H]^{+} + CO + 2\,CH_2{=}CH_2 \rightarrow\rightarrow [Pd(P\text{-}P)\{CH_2CH_2C(O)CH_2H_3\}]^{+} \quad (10)$$

We also examined the efficiency of in situ catalyst preparation in methanol for some other palladium diphosphane systems. It was found that mixing of equimolar amounts of $Pd(OAc)_2$ and dppbz in methanol at room temp. also initially affords a mixture of monochelate $[Pd(dppbz)(OAc)_2]$ (**5**; δ = 60.3 ppm) and bischelate $[Pd(dppbz)_2](OAc)_2$ (**6**; δ = 56.0 ppm) in a ratio of about 20:80. Subsequent conversion of **6** and unreacted $Pd(OAc)_2$ into **5** proceeded about four times slower ($k = 0.037\ h^{-1}$) than for the dppe counterpart and was inevitably accompanied by plating, as unprotected $Pd(OAc)_2$ is not stable in methanol. As a result, no complete conversion of **6** into **5** took place. As for **1**, the occurrence of autoionization of **5** in methanol was discarded in a separate experiment. No conversion was observed of **5** into **6** and $Pd(OAc)_2$ (h-scale).

Preparation of $[Pd(dppp)(CF_3CO_2)_2]$ in methanol via Equation (1) and (2) was found to proceed smoothly, and no species other than the desired one was observed by ^{31}P NMR spectroscopy. This does not necessarily imply that the bischelate $[Pd(dppp)_2](OAc)_2$ is not an intermediate in the first step. $[Pd(dppp)]_2(OAc)_2$ prepared in situ was found to convert instantaneously into the monochelate $[Pd(dppp)(OAc)_2]$ upon addition of an equimolar amount of $Pd(OAc)_2$, indicating its *kinetic stability* to be much lower than that of its C_2-bridged diphosphane counterparts **2** and **6**.

An anomalous feature was observed whilst monitoring in situ preparation of $[Pd(bdompp)(CF_3CO_2)_2]$ {bdompp = 1,3-bis[di-(*o*-methoxyphenyl)phosphanyl]propane}, the catalyst employed in the manufacture of polyketone on a commercial scale.[9] Mixing $Pd(OAc)_2$ and bdompp in methanol does not afford the monochelate $[Pd(bdompp)(OAc)_2]$ nor the bischelate $[Pd(bdompp)_2](OAc)_2$ as the kinetic product, but a complex mixture of palladium-diphosphane species. It is assumed that these species are oligomeric in nature, but all attempts to characterize these species unambiguously (by NMR spectroscopy and electrospray-MS) failed. Upon standing, the complex mixture slowly converted into monomeric $[Pd(bdompp)(OAc)_2]$. Almost complete conversion (>95%) took more than 16 h at ambient temperature and was accompanied by some plating.

In conclusion, it has been shown that in situ preparation of palladium diphosphane catalysts is not a trivial affair. Instead of the desired mononuclear monochelate catalyst, $Pd(P\text{-}P)X_2$, undesired formation of inactive bischelate (dppe, dppbz) or oligomeric species (bdompp) may occur. This problem may be overcome by rational selection of the solvent in which the catalyst is prepared, or by synthesis and isolation of the $[(P\text{-}P)Pd(OAc)_2]$ intermediate prior to anion exchange in methanol.

Experimental Section

General: The ^1H, $^{13}C\{^1H\}$ and $^{31}P\{^1H\}$ NMR spectra were recorded on Varian GEMINI-300 and Varian INOVA-400 spectrometers operating at 300.1 and 400.0 for ^1H, at 75.5 MHz and 100.6 MHz for ^{13}C, and at 121.5 MHz and 161.9 MHz for ^{31}P. Deuterated solvents were used as internal reference, and the ^{31}P data are given in δ units relative to triphenylphosphane (δ = −6 ppm). All chemicals were reagent grade and were used without further purification for synthetic and spectroscopic purposes. The diphosphanes 1,2-bis(diphenylphosphanyl)ethane (dppe), 1,3-bis(diphenylphosphanyl)propane (dppp) and 1,2-bis(diphenylphosphanyl)-benzene (dppbz) were purchased from Strem Chemicals. The diphosphane 1,3-bis[di-(*o*-methoxyphenyl)phosphanyl]propane (bdompp) was synthesized according to literature procedures.[10] The CO/ethene copolymerization reactions were carried out in a 250 mL, magnetically stirred AISI-316 steel batch autoclave.

Synthesis of $[Pd(dppe)(OAc)_2]$ (1): $Pd(OAc)_2$ (0.50 g; 2.23 mmol) was dissolved in 30 mL of dichloromethane and dppe (0.89 g, 2.23 mmol) was added to the filtered red solution, which turned yellow. After 10 min half of the solvent was removed under vacuum and a pale yellow solid precipitated upon addition of diethyl ether. This solid was isolated by filtration and washed twice with diethyl ether. Yield: 1.18 g (85%). $C_{30}H_{30}O_4P_2Pd$ (622.9): calcd. C 57.84, H 4.85; found C 57.89, H 4.91. ^1H NMR (CD_3OD): δ = 1.56 [s, 6 H, $CH_3C(O)O$], 2.58 (m, 4 H, CH_2P), 7.60 (m, 12 H), 7.89 (dd, 8 H) ppm. $^{31}P\{^1H\}$ NMR (CD_3OD, 20 °C): δ = 63.4 ppm.

Synthesis of $[Pd(dppe)_2](OAc)_2$ (2): dppe (0.32 g; 0.80 mmol) was added to a solution of the isolated complex **1** (0.50 g; 0.80 mmol) in 30 mL of methanol. After 10 min the solution was concentrated to half of the original volume and diethyl ether was added resulting in the precipitation of a yellow solid, which was isolated by filtration and washed twice with diethyl ether. Yield: 0.74 g (90%). $C_{56}H_{54}O_4P_4Pd$ (1021.3): calcd. C 65.85, H 5.33; found C 65.79, H 5.28. ^1H NMR (CD_3OD): δ = 1.78 [s, 6 H, $CH_3C(O)O$], 2.79 (m, 8 H, CH_2P), 7.26 (m, 16 H), 7.44 (t, 16 H), 7.61 (t, 8 H) ppm. $^{31}P\{^1H\}$ NMR (CD_3OD, 20 °C): δ = 58.7 ppm.

Copolymerization of Carbon Monoxide and Ethene: *Catalyst preparation*. The catalyst was either prepared in situ (run A) by mixing $Pd(OAc)_2$ (2.5 mg, 11 μmol) and dppe (5.6 mg, 12 μmol) in methanol (2 mL), followed by the addition of trifluoroacetic acid (7.8 mg, 68 μmol) after 15 min, or (run B) by mixing isolated $Pd(dppe)(OAc)_2$ (**1**, 7 mg, 11 μmol) and trifluoroacetic acid (7.8 mg, 68 μmol) in methanol (2 mL).

Copolymerization. The reactor was charged with catalyst solution and with 98 mL of a methanol/water mixture (98:2 v/v). After purging the reactor with nitrogen, it was charged with ethene (2.5 MPa) and carbon monoxide (2.5 MPa), and heated to 90 °C. After 2.5 h the reaction was stopped by cooling the reactor rapidly to room temperature and venting the remaining gases. The reaction product was collected by filtration and dried at 55 °C for one day under nitrogen. The isolated grey (run A) or slightly grey copolymer (run B) was weighed and characterized by ^{13}C NMR spectroscopy in C_6D_6/1,1,1,3,3,3-hexafluoro-isopropanol, using $Cr(acac)_3$ as a relaxation reagent, providing M_n, and the methyl ester (**E**) to ethyl ketone (**K**) end-group ratio.[2]

Yield (run A) = 1.08 g, rate = 390 g/g Pd·h, M_n = 6600 Da, **E/K** ratio = 42:58, bulk density = 210 g/L; Yield (run B) = 2.27 g, rate = 910 g/g Pd·h, M_n = 4100 Da, **E/K** ratio = 45:55, bulk density = 108 g/L.

Acknowledgments

We thank Prof. Dr. E. Drent for his stimulating interest and Shell International Chemicals B. V. for giving permission to publish this paper.

[1] *Applied Homogeneous Catalysis with Organometallic Compounds: a comprehensive handbook in two volumes* (Eds.: B. Cornils and W. A. Herrmann), VCH: Weinheim, **1996**.
[2] [2a] E. Drent, J. A. M. van Broekhoven, M. J. Doyle, *J. Organomet. Chem.* **1991**, *417*, 235−251. [2b] E. Drent, P. H. M. Budzelaar, *J. Organomet. Chem.* **2000**, *593−594*, 211−225.
[3] A. Vavasori, L. Toniolo, *J. Mol. Cat. A.* **1996**, *110*, 13−23.
[4] C. Bianchini, H. M. Lee, A. Meli, W. Oberhauser, M. Peruzzini, F. Vizza, *Organometallics* **2002**, *21*, 16−33. This paper appeared during preparation of our manuscript.
[5] Autoionization is a wel-established phenomenon for nickel(II)-diphosphane complexes but has thus far not been established (convincingly) for palladium counterparts. See, for example: [5a] P. S. Jarrett, P. J. Sadler, *Inorg. Chem.* **1991**, *30*, 2098−2104. [5b] I. M. Angulo, E. Bouwman, M. Lutz, W. P. Mul, A. L. Spek, *Inorg. Chem.* **2001**, *40*, 2073−2082.
[6] [6a] T. A. Stephenson, S. M. Morehouse, A. R. Powell, J. P. Heffer, G. Wilkinson, *J. Chem. Soc.* **1965**, 3632−3640. [6b] A. C. Skapsky, M. L. Smart, *J. Chem. Soc., Chem. Commun.* **1970**, 658−659.
[7] E. Drent, P. H. M. Budzelaar, *Chem. Rev.* **1996**, *96*, 663−681.
[8] W. P. Mul, E. Drent, P. J. Jansens, A. H. Kramer, M. H. W. Sonnemans, *J. Am. Chem. Soc.* **2001**, *123*, 5350−5351.
[9] *Encyclopedia of Polymer Science and Technology 3rd·, Wiley-Interscience*, E. Drent, W. P. Mul and A. A. Smaardijk, Polyketones, **2002**.
[10] [10a] L. Brandsma, H. D. Verkruijsse, *Synth. Commun.* **1990**, *20*, 2273−2277. [10b] P. H. M. Budzelaar, J. A. van Doorn, N. Meijboom, *Recl. Trav. Chim. Pays-Bas* **1991**, *110*, 420−432.

Received February 12, 2002
[I02074]

Encapsulation of Copper(II) Complexes with Pentadentate N_3O_2 Schiff Base Ligands in a Pillared Layered Clay

Rita Ferreira,[a] Cristina Freire,*[a] Baltazar de Castro,*[a] Ana P. Carvalho,[b] João Pires,[b] and Manuela B. de Carvalho[b]

Keywords: Clays / Microporous materials / Copper / Schiff bases

Two copper(II) complexes with five-coordinate Schiff-base ligands derived from acetylacetone and with a N_3O_2 coordination sphere, namely bis(acetylacetonate)-3-amino-bis(propyldiimine) and bis(acetylacetonate)-3-methylamino-bis(propyldiimine), were entrapped in the interlayers of a pillared layered clay (PILC). A two-step process in the liquid phase was used: (i) adsorption of copper(II) acetylacetonate in the porous structure of the PILC, and (ii) in situ Schiff condensation of the copper(II) precursor complex with the corresponding triamine. The new materials were characterised by chemical analysis, surface techniques (SEM and XPS), X-ray powder diffraction, nitrogen adsorption isotherms and spectroscopic methods (FTIR, UV/Vis). These data indicate conclusively that the Cu^{II} complexes are encapsulated in the PILC, and that the entrapped complexes exhibit structural and electronic properties that are different from those of the free complexes. These differences can arise from distortions caused either by steric effects imposed by the structure of pillared clay, or by strong interactions with the matrix.

Introduction

Transition metal complexes have been proven to be efficient catalysts in several industrial chemical reactions.[1−3] A particularly strong area of research in catalysis is the immobilization of metal complexes used in homogeneous catalysis onto solid supports such as zeolites,[4,5] polymers,[6,7] carbons,[8−10] and other porous-structured materials.[11−13] This heterogenization often combines the homogeneous catalytic properties of metal complexes with some characteristics of the heterogeneous catalysts, such as shape selectivity, ease of separation from reaction media, and reusability without appreciable loss of catalytic activity.

Pillared layered clays (PILCs) are a recently developed family of porous materials obtained by exchanging the interlayered cations of swelling clays with bulky inorganic polyoxo and polyhydroxy cations.[14,15] Upon calcination they are converted into metal oxide clusters creating an interlayer space of molecular dimensions and a well-defined pore system.[14−17] Introduction of pillars between layers is an attractive route for the preparation of porous materials in which pore size and thermal stability can be tailored by the appropriate choice of the polyoxo and polyhydroxy cations.[17]

The most widely used polycation is $[Al_{13}O_4(OH)_{24}(H_2O)_{12}]^{7+}$, usually denoted as Al_{13}, mainly because its polymerisation is better understood than that of other cations. Consequently, the alumina-pillared clays (Al-pillared clays) are by far the best documented pillared clays.[15] Although metallic polyoxo or polyhydroxo cations of Al^{3+} and also of other ions, namely Zr^{4+}, Ti^{4+}, Cr^{3+}, Fe^{3+}, or Ga^{3+}, are the most widely used intercalating species, several coordination and organometallic compounds have recently been considered for this purpose.[19−21]

The catalytic properties of PILCs are mainly related to their acid character,[15,18] as seen by their uses in hydrogenation, hydrotreating and isomerisation reactions. The incorporation of transition metal elements to the composition of Al PILCs not only increases their Brönsted acidity, but also allows them to be used in catalytic redox reactions.[15,18]

In recent years, pillared clays have also been used as supports for transition metal compounds, typically their salts, which are deposited on pillared clays by ionic exchange, incipient wetness, or dry impregnation of calcined samples. Copper, vanadium, and platinum have been the preferred active phases, and, to a lesser extent, molybdenum, cobalt, and other elements.[15] Nevertheless, the use of pillared clays to act as hosts for coordination and organometallic compounds is poorly documented,[22] in contrast with what is found for other aluminosilicates, such as zeolites[4,5] and swelled clays.[23]

We have been interested in the heterogenisation of transition metal complexes in zeolites[24,25] and activated carbons[8−10] and have shown that the methodologies used

[a] CEQUP − Departamento de Química, Faculdade de Ciências, Universidade do Porto, 4169-007 Porto, Portugal
[b] Departamento de Química e Bioquímica and CCMM, Faculdade de Ciências de Lisboa, Ed. C8, Campo Grande, 1749-016 Lisboa, Portugal

 © 2002 WILEY-VCH Verlag GmbH & Co. KGaA, 69451 Weinheim 1434−1948/02/1111−3032 $ 20.00+.50/0 *Eur. J. Inorg. Chem.* **2002**, 3032−3038

for immobilisation/anchorage of the metal complexes are largely determined by the supports. The analogy between PILCs and zeolites NaX and NaY prompted us to explore the properties of the former as supports for the encapsulation of transition metal complexes. Here we use a pillared clay, denoted as BENAVILA (named after the region in Portugal from where the clay was obtained), which has been extensively characterised previously.[26] We have chosen to encapsulate two copper Schiff-base complexes, since their in situ preparation has been worked out for their immobilisation in FAU zeolites.[24,25]

The two copper(II) complexes with pentadentate N_3O_2 Schiff-base ligands derived from acetylacetone − bis(acetylacetonate)-3-amino-bis(propyldiimine) and bis(acetylacetonate)-3-methylamino-bis(propyldiimine) (Scheme 1) − were encapsulated in the pores of BENAVILA using a procedure similar to that used in the encapsulation of the same complexes in NaX and NaY zeolites.[24,25] This methodology involves in situ Schiff condensation between a Cu^{II} precursor complex, [Cu(acac)$_2$], and the corresponding triamine.

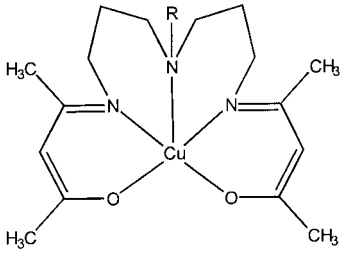

Scheme 1. [Cu(acac$_2$trien)], R = H; [Cu(acac$_2$Metrien)], R = CH_3

The BENAVILA with entrapped complexes was characterised by chemical analysis, surface techniques (SEM and XPS), X-ray powder diffraction, nitrogen adsorption isotherms and spectroscopic methods (FTIR and UV/Vis). Our data indicate that copper complexes in the PILC exhibit structural and electronic properties that are different from those of the free complexes, caused either by steric effects imposed by the structure of the pillared clay, or by strong interactions with the matrix.

Results and Discussion

Morphology and Cu Content of the Modified BENAVILA

The modified PILC with [Cu(acac)$_2$], denoted as [Cu(acac)$_2$]@BEN, was not purified by Soxhlet extraction, as the precursor square-planar complex [Cu(acac)$_2$], due to its dimensions, can diffuse out of the supporting material. Soxhlet extraction was performed only for the modified BENAVILA with the complexes [Cu(acac$_2$trien)] and [Cu(acac$_2$Metrien)]; these materials {denoted as [Cu(acac$_2$trien)]@BEN and [Cu(acac$_2$Metrien)@BEN} did not change colour after extensive extraction, and after the last extraction no bands due to copper species could be detected in the extracting solvent. These results indicate that the resulting metal complexes are too large to diffuse out of the PILC layers, and that encapsulation of metal complexes after in situ Schiff condensation has taken place.

Analysis of the SEM micrographs of the parent and modified BENAVILA indicates that there is no change in the BENAVILA morphology and structure upon complex encapsulation. In the SEM micrograph of all samples, exemplified in Figure 1 for [Cu(acac$_2$Metrien)]@BEN, two types of particles with different morphology and dimen-

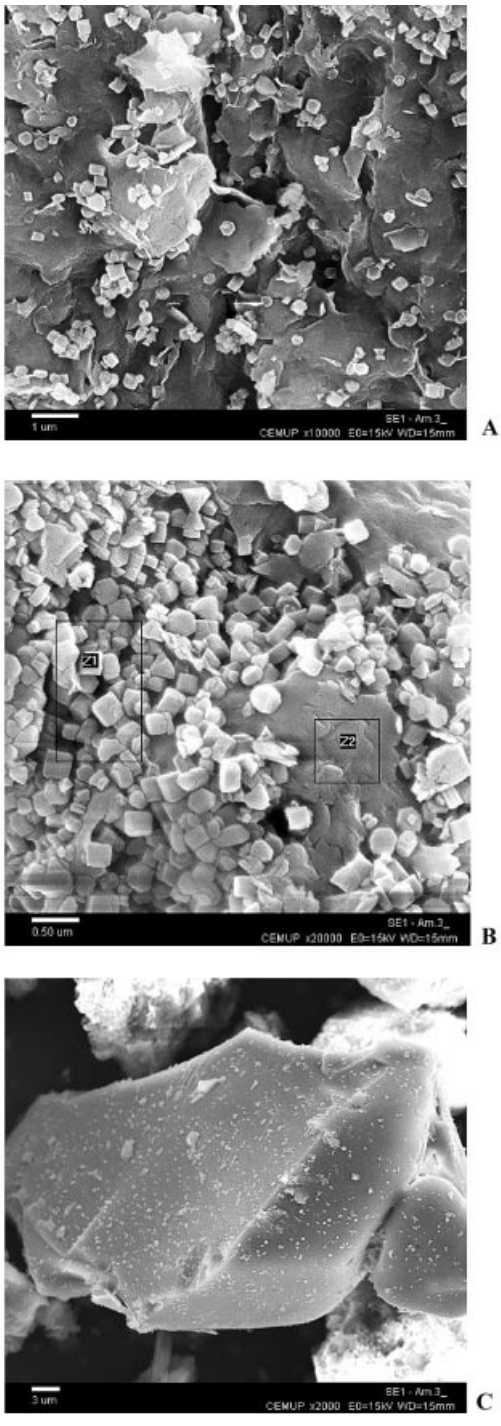

Figure 1. SEM photographs of [Cu(acac$_2$Metrien)]@BEN with different resolutions: × 10000 (A); × 20000 (B) and × 2000 (C)

sions can be observed: (i) small crystalline particles with dimensions of roughly 0.2 μm, and (ii) particles with lamellar morphology and larger dimensions (Figure 1A). By semi-quantitative EDS analysis of the different particles (Figure 1B) it is possible to assign the latter particles to the pillared clay (Figure 1C). As the small crystalline particles have high aluminium and oxygen content relative to the general composition of BENAVILA particles, we propose them to be probably aluminium oxides originating in the pillaring process. Furthermore, no crystals due to adsorbed metal complexes could be detected in any of the modified pillared clays, suggesting that the metal complexes are evenly distributed throughout the PILC.

A comparison of the X-ray diffractograms of the parent BENAVILA with those of modified PILCs (Figure 2) indicates that the structure of the PILC is retained upon metal complex immobilisation, as revealed by the proximity of the basal spacing, which is 1.8 nm for the nonencapsulated material and 1.73 nm for the encapsulated samples. As can be seen from this figure no appreciable changes are seen in the characteristic diffraction peak after encapsulation.

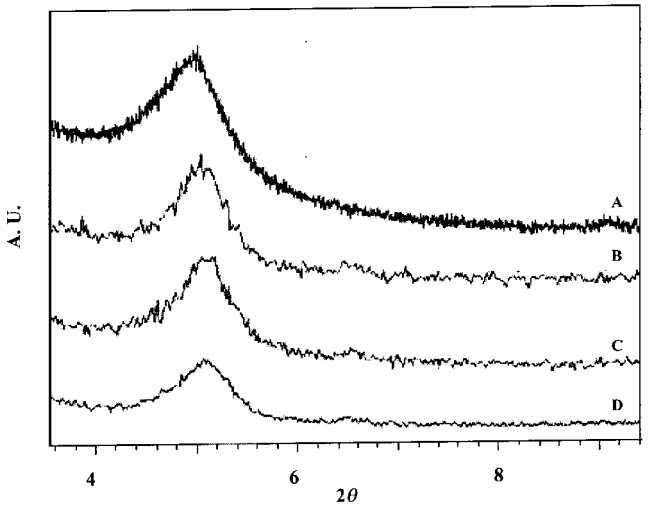

Figure 2. X-ray diffractograms for the BEN PILC: before encapsulation (A) and after encapsulation with [Cu(acac)$_2$] (B); [Cu(acac)$_2$trien] (C) and [Cu(acac)$_2$Metrien] (D)

The Si/Al, Cu/Si and Cu/Al molar ratios obtained by bulk chemical analysis and by XPS are presented in Table 1. A comparison of the Si/Al ratios obtained by chemical analysis and XPS reveals that the surface of the clay is, in general, enriched in silicon upon immobilisation of the complexes, as has been observed in several zeolites with occluded metal complexes.[27,28]

A comparison between the copper content determined by chemical analysis (Table 1) in [Cu(acac)$_2$]@BEN with that in the samples resulting from the Schiff condensation suggests that practically all adsorbed [Cu(acac)$_2$] complexes have reacted with the triamines and have became trapped inside the PILC. The Cu/Si and Cu/Al ratios obtained by chemical analysis and XPS do not differ markedly, although the values of XPS for [Cu(acac$_2$trien)]@BEN and [Cu(acac$_2$Metrien)]@BEN are slightly lower than those obtained by CA. This result suggests that upon reaction with triamines the copper complexes are located preferentially in inner pores.

Table 1. Si/Al, Cu/Si and Cu/Al ratios determined by chemical analysis (CA) and XPS in BENAVILA

Samples	Si/Al		Cu/Si		Cu/Al	
	CA	XPS	CA	XPS	CA	XPS
BENAVILA	1.16	1.17	–	–	–	–
[Cu(acac)$_2$]@BEN	1.17	1.22	0.017	0.017	0.020	0.014
[Cu(acac$_2$trien)]@BEN	1.18	1.19	0.017	0.014	0.020	0.012
[Cu(acac$_2$Metrien)]@BEN	1.22	1.21	0.020	0.016	0.024	0.013

A comparison between Cu content in BENAVILA with that in NaX[25] and in NaY[24] zeolites indicates that the loading of metal complexes occurs to a larger extent in the PILC. Despite its lower micropore volume, the PILC has a more open structure than the faujasite zeolites. Two factors can account for this behaviour: on the one hand the heights of the galleries, which have been estimated as 8.4 Å, are larger than the supercage entrances of Y and X zeolites (7.3 Å). On the other hand, the nature of the network of PILCs microporosity, in which the spacing between the pillars is not absolutely regular, can lead to the existence of regions of lower pillar density that can favour the accommodation of large molecules. Moreover, few studies have been made on the cross-linking between the pillars and the clay sheets, which leaves as an open question the possibility of the pillars also being distorted to some degree.[29]

The N_2 adsorption isotherms for parent and modified BENAVILA (Figure 3) are typical of solids which are mainly microporous, although the existence of hysteresis loops suggests some degree of mesoporosity, which is a consequence of the secondary structure of the clay particles. It is interesting to note that the loops are similar in all samples, which means that the encapsulation process does not modify the original mesoporosity of the PILC.

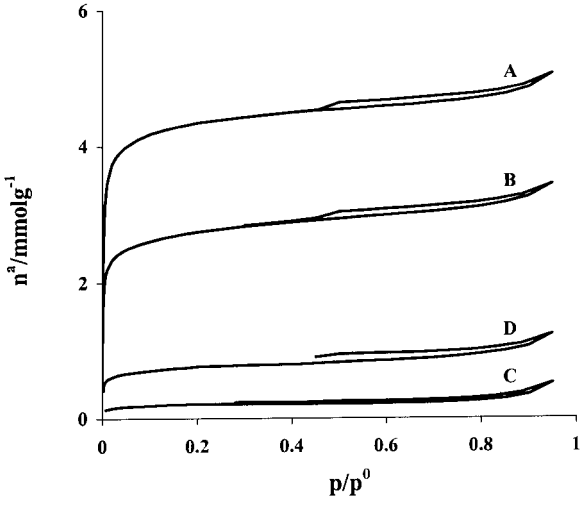

Figure 3. Nitrogen adsorption-desorption isotherms at 77 K of the samples BENAVILA (A), [Cu(acac)$_2$]@BEN (B), [Cu(acac$_2$trien)]@BEN (C), and [Cu(acac$_2$Metrien)]@BEN (D)

As expected, a decrease in adsorption capacity of the PILC was observed after immobilisation of [Cu(acac)$_2$] (to around 53% of the initial value), and a much more drastic decrease (up to 3−12% of the initial value) after Schiff-base condensation. The micropore volumes (obtained by the t-method) and the BET surface are presented in Table 2. The large reduction in micropore volume observed in the Cu-encapsulated BENAVILA is interpreted as arising from the presence of the copper compounds in the interlayers. As the copper content in all samples is roughly the same (Table 1), the observed lowering of micropore volume on going from [Cu(acac)$_2$] to [Cu(acac$_2$Metrien)] and [Cu(acac$_2$trien)] must be attributed to the larger volume of the latter complexes, thus providing indirect confirmation that Schiff condensation took place within the PILC.

Table 2. Textural properties for parent and copper-modified BENAVILA

Samples	A_{BET} (m^2/g)	V_{micro}[a] (cm^3/g)
BENAVILA	350	0.115
[Cu(acac)$_2$]@BEN	221	0.066
[Cu(acac)$_2$trien]@BEN	17	0.003
[Cu(acac)$_2$Metrien]@BEN	61	0.014

[a] Estimated using the t-method.

FTIR Spectra

Vibrational spectroscopy can provide information on both the encapsulated metal complexes and on the crystallinity of the host material. The FTIR spectra of the parent and modified BENAVILA are shown in Figure 4. The spectra of all samples are dominated by the very intense bands of BENAVILA in the range 3700−3300 cm^{-1}, due to surface hydroxyl groups, and in the range 1300−450 cm^{-1} which are assigned to lattice vibrations (Figure 4, I).[30] The bands due to the complexes are much weaker, as they are diluted in the PILC, and can only be observed in the region 1620−1200 cm^{-1}, where the BENAVILA matrix does not absorb (Figure 4, II).

No shift or broadening of the PILC structure-sensitive vibrations was observed upon inclusion of the complexes, which provides evidence, at the molecular level, that the matrix remains unchanged upon encapsulation of the copper complexes.

The IR bands of adsorbed [Cu(acac)$_2$] in the range 1620−1200 cm^{-1}, which are assigned to the coupled C=O and C=C stretching vibrations and to bending vibrations of methyl groups, occur at frequencies which are shifted by between 5 and 9 cm^{-1} from those shown by the free complex (Figure 4, II-B, E).[31] Furthermore, some changes in relative band intensities can also be observed in these bands. These observations confirm the presence of [Cu(acac)$_2$] in the PILC, and suggest that the structure of the adsorbed complex is distorted when compared with that of the square-planar free complex. This is a consequence of

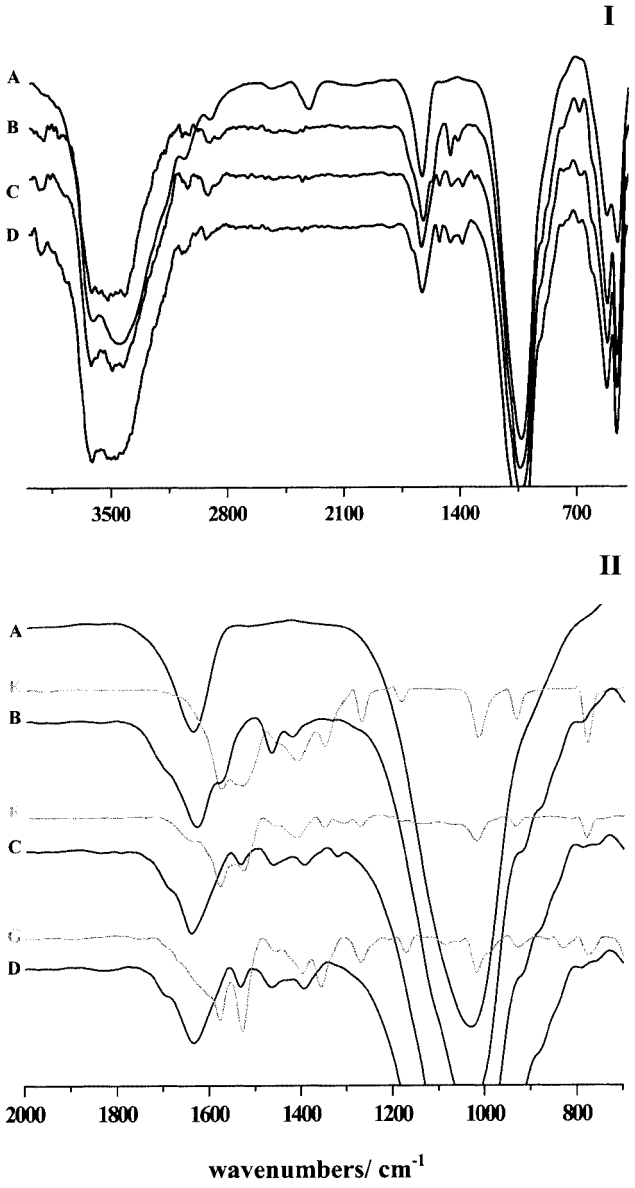

Figure 4. FTIR spectra: (I) in the range 4000−400 cm^{-1}: BENAVILA (A), [Cu(acac)$_2$]@BEN (B), [Cu(acac$_2$trien)]@BEN (C), and [Cu(acac$_2$Metrien)]@BEN (D); (II) in the region 2000−700 cm^{-1}: BENAVILA (A), [Cu(acac)$_2$]@BEN (B), [Cu(acac$_2$trien)]@BEN (C), [Cu(acac$_2$Metrien)]@BEN (D), and the free complexes [Cu(acac)$_2$] (E), [Cu(acac$_2$trien)] (F), and [Cu(acac$_2$Metrien)] (G)

host-guest interactions with the PILC, eventually to the extent of the formation of a chemical bond to the framework, as the PILC can act as a ligand to copper through its matrix oxygen atoms.

The IR spectra of [Cu(acac$_2$trien)]@BEN and [Cu(acac$_2$Metrien)]@BEN (Figure 4, II-C, D) clearly show the absence of the characteristic coupled ν(C=O) + ν(C=C) vibration of [Cu(acac)$_2$], as expected after Schiff condensation with the triamines within the PILC. The trapped complexes exhibit IR bands at 1527−1533, 1466−1464 and 1394 cm^{-1} which are similarly shifted by between 5 and 10 cm^{-1} relative to those of the free complexes (Figure 4, II-F, G). These variations in band frequency can also be at-

tributed to distortion of the complexes induced by the PILC porous structure, or to coordination of the complexes to the oxygen matrix through the sixth (free) coordination position.

UV/Vis Spectroscopy

The parent pillared layered clay exhibits, in the range 1300−200 nm, several medium-intensity broad bands at λ_{max} =265, 482 and 630 nm. These bands occur in the same range as some of the expected d-d bands for the copper complexes, which prevents a direct observation of their electronic spectra due not only to their low concentration but also to their small extinction coefficients (Figure 5).

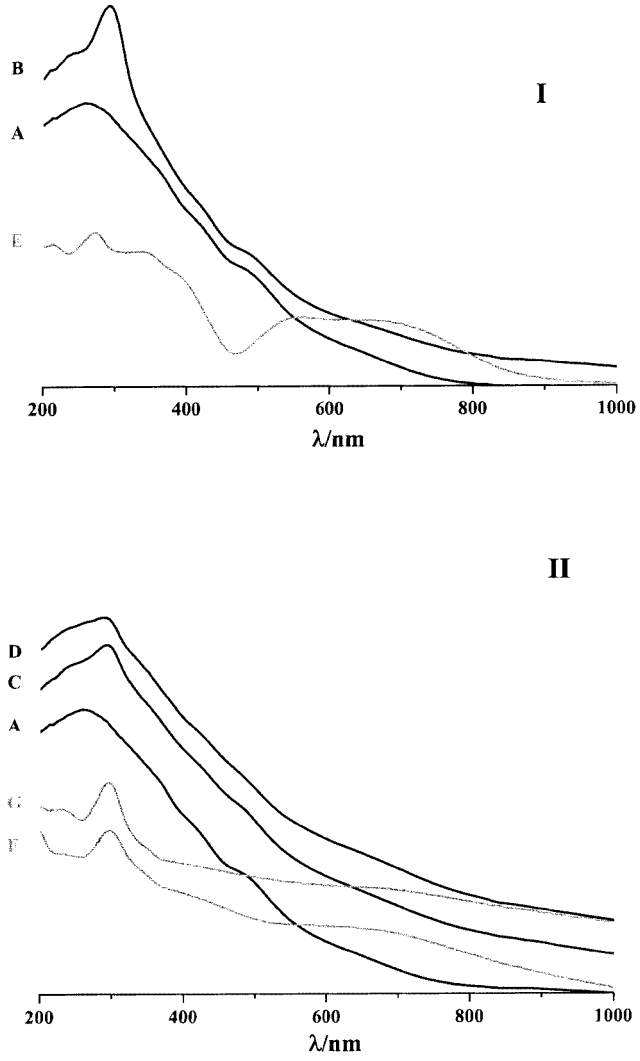

Figure 5. UV/Vis spectra: (I) BENAVILA (A), [Cu(acac)$_2$]@BEN (B), and [Cu(acac)$_2$] (E); (II) BENAVILA (A), [Cu(acac$_2$trien)]@BEN (C), [Cu(acac$_2$Metrien)]@BEN (D), [Cu(acac$_2$trien)] (F), and [Cu(acac$_2$Metrien)] (G)

The visible electronic spectrum of [Cu(acac)$_2$]@BEN is similar to that of parent BENAVILA as the d-d bands at 450−600 nm, typical of the square-planar free complex,[33] are completely masked by the PILC electronic bands, (Figure 5, I). However, a charge-transfer band due to the complex can be detected at λ_{max} = 294 nm and can be taken as a proof of the presence of the complex inside the PILC. Similarly, the visible-region spectra of [Cu(acac$_2$trien)]@BEN and [Cu(acac$_2$Metrien)]@BEN are dominated by the same features as parent BENAVILA (Figure 5, II): no d-d bands typical of pentacoordinate complexes could be observed at $\lambda \approx$ 450 and 650 nm.[33] However, as the latter band usually tails into the near-IR region, and BENAVILA does not absorb in this region, the increase in absorbance observed in the range 800−1000 nm for [Cu(acac$_2$trien)]@BEN and [Cu(acac$_2$Metrien)]@BEN, can be taken as an indication of the presence of the complexes inside the BENAVILA. Similarly to the spectrum of [Cu(acac)$_2$]@BEN, it is possible to observe one charge-transfer band at $\lambda_{max} \approx$ 290 nm in the spectra of [Cu(acac$_2$trien)]@BEN and [Cu(acac$_2$Metrien)]@BEN due to the trapped complexes, again providing a proof of the presence of the complexes inside the PILC. Due to the lack of resolution of the electronic spectra of the resulting materials, no information on the structure of the entrapped complexes could be derived from this technique.

Conclusions

By combining surface analysis and spectroscopic data it was possible to conclude that [Cu(acac$_2$trien)] and [Cu(acac$_2$Metrien)] can be encapsulated in the interlayers of BENAVILA by in situ Schiff condensation between pre-adsorbed [Cu(acac)$_2$] and the corresponding triamine, without damage of the main matrix or loss of its crystallinity. It was shown that the complex loading in the PILC is larger (approximately 0.12 mmol·g^{-1}) than for the faujasite zeolites NaX and NaY.

FTIR data suggest that copper(II) complexes entrapped in BENAVILA exhibit structural properties that are different from those of the complexes encapsulated in FAU zeolites (NaX and NaY), which have been shown to be mainly physically entrapped in the FAU supercages and with no significant interaction with the zeolite matrix. In the case of PILCs the occluded complexes exhibit distortion induced either by the porous structure or by strong interactions with the oxygen atoms of the host matrix.

The strategy used for the encapsulation of copper complexes can be extended to other metals with known catalytic properties. These novel materials may thus be used as heterogeneous catalysts, indicating that is possible to extend the potential applications of pillared clays in the field of catalysis.

Experimental Section

Reagents and Solvents: All solvents were obtained from Merck (grade *pro analysi*); copper(II) acetylacetonate was obtained from Aldrich and used as received, bis(3-aminopropyl)amine (trien) and bis(3-aminopropyl)methylamine (Metrien) were obtained from Aldrich and were distilled prior to use. The complexes [Cu-

($acac_2$trien)] and [Cu($acac_2$Metrien)] were prepared by published procedures.[32]

The BENAVILA PILC was prepared following the procedure described by Pires et al.[26] The parent material was collected from a soil in Benavila, Portugal, and purified according to published methods, with the difference that the clay was not purified by sedimentation, but only by sieving. The pillaring was achieved as described elsewhere.[26] Briefly, an oligomer solution was prepared from $AlCl_3$ and NaOH (both 0.2 M), with an OH/Al ratio of two. After mixing and aging for 2 hours the pH was increased to 6. This oligomer solution was added dropwise to the clay dispersion (2.5 g of clay in 500 mL of water) at 80 °C, whilst stirring, refluxed for 3 h and kept overnight at 25 °C. After centrifugation the solid was washed in a dialysis tube until a conductivity of less than 1 $mS \cdot m^{-1}$. After being freeze dried and calcined at 350 °C the PILC BENAVILA, with alumina pillars, was obtained. Physical properties: specific surface area of 350 m^2/g and a microporous volume of 0.115 cm^3/g. From the d_{001} reflections, which indicated a basal spacing of 1.8 nm, and subtracting the height of the sheets from the basal spacing, the heights of the galleries of this PILC were estimated to be 0.84 nm.[26]

Sample Preparation

Preparation of [Cu(acac)$_2$]@BEN: [Cu(acac)$_2$] (0.2 mmol) was dissolved in 40 cm^3 of dichloromethane and added to 1.2 g of the PILC BENAVILA (the amount of copper corresponds to about 10^{20} Cu^{2+} ions per gram of PILC). After 7 hours refluxing, the blue colour of the [Cu(acac)$_2$] solution had disappeared indicating that the complex was adsorbed by the clay, although no significant alteration of the original brown-orange colour of BENAVILA was observed. The solid material, denoted as [Cu(acac)$_2$]@BEN, was collected by filtration and dried under vacuum at 90 °C for 1 hour.

Preparation of [Cu($acac_2$trien)]@BEN and [Cu($acac_2$Metrien)]@BEN: [Cu(acac)$_2$]@BEN (0.4 g) in 40 cm^3 of dichloromethane, was refluxed for 3 h with a twofold excess of bis(3-aminopropyl)amine (trien) or bis(3-aminopropyl)methylamine (Metrien). The pillared clays changed their colour to a brownish green, providing a first indication that the Schiff condensation had taken place and the complexes [Cu($acac_2$trien)] and [Cu($acac_2$Metrien)] formed. After filtration, the solid materials, denoted as [Cu($acac_2$trien)]@BEN and [Cu($acac_2$Metrien)]@BEN, were dried under vacuum at 90 °C for 1 hour. To remove any excess triamine, unchanged [Cu(acac)$_2$] and residual Cu^{II} complexes physically adsorbed on the external surface, the solids were Soxhlet extracted with dichloromethane (4 hours) and then with acetone (4 hours). The solids were dried at 90 °C, under vacuum, for 8 hours.

Characterisation Procedures: The elemental chemical analyses (Si, Al, and Cu) were performed by Kingston Analytical Services, UK, using inductively coupled plasma atomic emission spectroscopy. X-ray photoelectron spectroscopy and scanning electron microscopy were obtained at the Centro de Materiais da Universidade do Porto (CEMUP), Porto, Portugal, on a VG Scientific ESCALAB 200A spectrometer using a non-monochromatized Mg-K_α radiation (1253.6 eV), and on a JSM-6301F Scanning Microscope with EDS (NORAN Voyager), respectively

Nitrogen adsorption measurements were performed at 77 K, using an automated apparatus (ASAP 2010). Prior to the adsorption measurements, the samples were outgassed (under vacuum) at 125 °C for 2.5 hours.

FTIR spectra were obtained at room temperature using a Shimadzu Mattson spectrometer in the 4000−400 cm^{-1} range. The transmission spectra of the samples were recorded using KBr (Merck spectroscopic grade) pellets with 32 scans and 4 cm^{-1} resolution. Diffuse reflectance electronic spectra were registered on a Shimadzu UV/3101PC spectrophotometer in the range 1500−200 nm.

X-ray diffractograms were obtained with oriented mounts, on a Philips PX 1820 instrument. To prepare the oriented films, the solids were dispersed in distilled water by ultrasound and then deposited on glass slides.

Acknowledgments

Dr. Carlos Sá performed the SEM and XPS measurements at Centro de Materiais da Universidade do Porto (CEMUP), Porto, Portugal. This work was supported by the Fundação para a Ciência e a Tecnologia (FCT, Lisboa) through Project no. POCTI/42931/QUI/2001. R. F. thanks FCT for a fellowship.

[1] L. Canali, D. C. Sherrington, *Chem. Soc. Rev.* **1999**, *28*, 85−93.
[2] L. Haughton, J. M. J. Williams, *J. Chem. Soc., Perkin Trans. 1* **2000**, 3335−3349.
[3] H. Tye, *J. Chem. Soc., Perkin Trans. 1* **2000**, 275−298.
[4] G.-J. Kim, J.-H. Shin, *Tetrahedron Lett.* **1999**, *40*, 6827−6830.
[5] M. J. Sabater, A. Corma, A. Doménech, V. Fornés, H. García, *Chem. Commun.* **1997**, 1285−1286.
[6] F. Minutolo, D. Pini, A. Petri, P. Salvadori, *Tetrahedron: Asymmetry* **1996**, *7*, 2293−2302.
[7] S. M. Islam, A. Bose, B. K. Palit, C. R. Saha, *J. Catal.* **1998**, *173*, 268−281.
[8] J. A. Alves, C. Freire, B. de Castro, J. L. Figueiredo, *Colloids Surf. A: Physicochem. Eng. Aspects* **2001**, *189*, 75−84.
[9] A. R. Silva, M. M. Freitas, C. Freire, B. de Castro, J. L. Figueiredo, *Micropor. Mesopor. Mat.* **2001**, *46*, 211−221.
[10] A. R. Silva, A. Valente, C. Freire, B. de Castro, J. L. Figueiredo, *Micropor. Mesopor. Mat.,* in press.
[11] E. Armengol, A. Corma, V. Fornés, H. García, J. Primo, *Appl. Catal. A: General* **1999**, *181*, 305−312.
[12] D. Pini, A. Mandoli, S. Orlandi, P. Salvadori, *Tetrahedron: Asymmetry* **1999**, *10*, 3883−3886.
[13] J. M. Fraile, J. I. García, J. Massam, J. A. Mayoral, *J. Mol. Catal. A: Chem.* **1998**, *136*, 47−57.
[14] T. J. Pinnavaia, *Science* **1983**, *220*, 365−371.
[15] A. Gil, L. M. Gandía, M. A. Vicente, *Catal. Rev. -Sci. Eng.* **2000**, *42*, 145−212.
[16] L. Stievano, S. Calogero, L. Storaro, M. Lenarda, F. E. Wagner, *J. Chem. Soc., Faraday Trans.* **1998**, *94*, 2627−2632.
[17] J. Pires, M. Machado, M. B. de Carvalho, *J. Mater. Chem.* **1998**, *8*, 1465−1469.
[18] G. Perez, A. De Stefanis, A. A. G. Tomlinson, *J. Mater. Chem.* **1997**, *7*, 351−356.
[19] M. Holtz, T.-R. Park, J. Amaraseka, S. A. Solin, T. J. Pinnavaia, *J. Chem. Phys.* **1994**, *100*, 3346−3350.
[20] G.-H. Liu, A.-N. Ko, Y.-C. Chang, *Micropor. Mat.* **1995**, *5*, 61−67.
[21] S. M. Thomas, J. A. Bertrand, M. L. Occelli, F. Huggins, S. A. C. Gould, *Inorg. Chem.* **1999**, *38*, 2098−2105.
[22] V. Ramaswamy, M. S. Krishnan, A. V. Ramaswamy, *J. Mol. Cat.* **2002**, *181*, 81−89.
[23] F. Bedioui, *Coord. Chem. Rev.* **1995**, *144*, 39.
[24] I. Neves, C. Freire, A. N. Zakhárov, B. de Castro, J. L. Figueiredo, *Colloids Surf. A. Physicochem. Eng. Aspects* **1996**, *115*, 249−256.
[25] R. Ferreira, M. Silva, C. Freire, B. de Castro, J. L. Figueiredo, *Micropor. Mesopor. Mat.* **2000**, *38*, 391−401.
[26] J. Pires, M. B. de Carvalho, A. P. Carvalho, *Zeolites* **1997**, *19*, 107−113.

[27] P.-P. H. J. M. Knops-Gerrits, F. C. De Schryver, M. van der Auweraer, H. Van Mingroot, X.-Y. Li, P. A. Jacobs, *Chem. Eur. J.* **1996**, *2*, 592−597.
[28] P.-P. Knops-Gerrits, D. E. De Vos, F. Thibault-Starzyk, P. A. Jacobs, *Nature* **1994**, *369*, 543−546.
[29] T. J. Pinnavaia, S. D. Landau, M.-S. Tzou, I. D. Johnson, *J. Am. Chem. Soc.* **1985**, *107*, 7222−7224.
[30] G. Coudurier, F. Lefebvre, in *Catalyst Characterisation. Physical Techniques for Solid Materials* (Eds.: B. Imelik, J. C. Vendrine), Plenum Press, New York, **1994**, p. 11−44.
[31] D. A. Thornton, *Coord. Chem. Rev.* **1990**, *104*, 173−249.
[32] Y.-Y. Chen, D. E. Chu, B. D. McKinney, L. J. Willis, S. C. Cummings, *Inorg. Chem.* **1981**, *20*, 1885−1892.
[33] F. A. Cotton, J. J. Wise, *Inorg. Chem.* **1967**, *6*, 917−924.
Received April 27, 2002
[I02221]

Synthesis and Structural Characterisation of a Novel Chiral *ansa*-Cobaltocenium Hexafluorophosphate

Shona Fox,[a] John P. Dunne,[a] Matthias Tacke,*[a] Dieter Schmitz,[b] and Richard Dronskowski[b]

Keywords: Metallocenes / Structural analysis / Density functional calculations / Cobalt

trans-[(1,2-Diphenyl-1,2-dicyclopentadienyl)ethanediyl]-cobalt(III) hexafluorophosphate (**1**) was synthesised and its structure derived by X-ray crystallography and spectroscopic methods in conjunction with theoretical calculations. To gain an insight into the effect of these bridging atoms and the exocyclic substituents on the sandwich structure, a study was undertaken in which comparisons were drawn between this *ansa*-cobaltocenium ion and other previously reported structurally characterised metallocenes and *ansa*-metallocenes. DFT calculations were also performed to provide further data for this analysis, including reaction energies for the formation of, and breaking of, the bridging C–C bond to ascertain the extent to which this moiety imposes strain on the system.

(© Wiley-VCH Verlag GmbH, 69451 Weinheim, Germany, 2002)

Introduction

The reductive dimerisation of either symmetrically or unsymmetrically substituted fulvenes leads to achiral or, in the latter case, chiral *ansa*-metallocenes. These direct syntheses can be carried out under cocondensation conditions using metal atoms like Sn, Pb[1] or Fe[2] or with electropositive metal powders like Ca,[3] Yb or Sm,[4] which reductively couple the fulvene in solution.

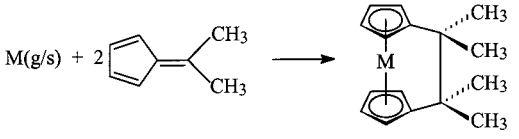

(M = Sn, Pb, Fe, Ca, Yb, Sm)

The activated metallic lanthanides Yb and Sm also form *ansa*-lanthanocenes in which the exocyclic moiety of the fulvene ligand is held in position due to its incorporation into an aromatic ring system.[5]

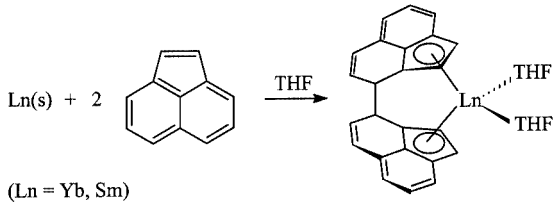

(Ln = Yb, Sm)

[a] Chemistry Department, University College Dublin, Belfield, Dublin 4, Ireland
Fax: (internat.) + 353-1-7162127
E-mail: matthias.tacke@ucd.ie
[b] Aachen University of Technology (RWTH), Institute of Inorganic Chemistry
Professor-Pirlet-Strasse 1, 52074 Aachen, Germany

The metallocenes of the transition metals have been the subject of extensive research, especially in the area of catalysis.[6,7] Many of these compounds contain an *ansa*-bridge, which restricts the geometry of the rings and therefore changes the electronic properties of the metallocene.[8,9] The rings can be the same, as in bis-cyclopentadienyl,[10,11] bis-indenyl,[12] bis-fluorenyl[13] or bis-tetrahydroindenyl[14] systems, but they can also consist of different ligands as in the case of the fluorenyl-cyclopentadienyl metallocene.[15]

We wish to report the synthesis and structural characterisation of the *trans*-[1,2-$(Ph)_2C_2H_2(\eta^5\text{-}C_5H_4)_2$]$Co^+$ cation, which was isolated as its PF_6^- salt **1**. The synthesis first involves the production of an intermediate, [1,2-$(Ph)_2C_2H_2\{\eta^5\text{-}C_5H_4\}_2$]$Ca(THF)_2$ (**2**),[16] by reacting the ligand 6-phenylfulvene with Rieke calcium. From this point, it is possible to obtain a variety of *ansa*-metallocenes,[17] simply by carrying out a transmetallation using the appropriate anhydrous metal chloride, in this case $CoCl_2$.

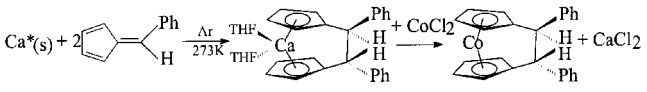

The air-sensitive, paramagnetic [1,2-$(Ph)_2C_2H_2(\eta^5\text{-}C_5H_4)_2$]Co (**3**) is then oxidised to give the cation **1**. As this compound is isoelectronic with ferrocene and its analogues, a study can be undertaken, both theoretically and experimentally, to understand the effects of the two-atom bridge on the structure of the metallocene when compared with its unbridged counterpart.

Results and Discussion

The synthesis of **1** was obtained by performing a transmetallation reaction between **2** and anhydrous $CoCl_2$ analogously to a method reported by Shapiro.[16] 6-Phenylfulvene[18] is the ligand of choice for this synthesis, undergoing reductive coupling to give solely the bridged metallocene. As reported earlier[19] this fulvene produces a radical anion that is readily formed and selective enough to give exclusive formation of the bridging moiety, thus eliminating the possibility of any unbridged metallocenes forming as an inseparable impurity.

The molecular structure of **1** (Figure 1) was determined by X-ray diffraction. Selected bond lengths can be found in Table 1, with diagrams depicting these values in Figure 2 and 3. Selected bond angles are presented in Table 2 and collection and refinement data in Table 3. From this, it can be seen that the cobalt is coordinated to the cyclopentadienyl rings in an η^5-fashion and the phenyl groups on the ethano bridge are in a *trans* position with respect to one another. Compound **1** is present only as the *S*,*S* stereoisomer, but there is no reason to believe that the *R*,*R* form is not also present as crystals and it is only the chance selection of the crystals that lead to the *S*,*S* form. The cation exhibits C_2 symmetry only, with a bridge length of 1.540 Å. In order to accommodate this bond, ring tilting from the parallel arrangement occurs, resulting in different Co^+-C bond lengths and hence a bent sandwich structure, with a ring centroid-Co^+-ring centroid angle of 163.1°. The unit cell is shown in Figure 4 where it can be seen that each PF_6^- anion is surrounded by four *ansa*-metallocene cations. The interaction between these oppositely charged ions occurs between both the cyclopentadienyl and phenyl hydrogens, and two of the fluorides.

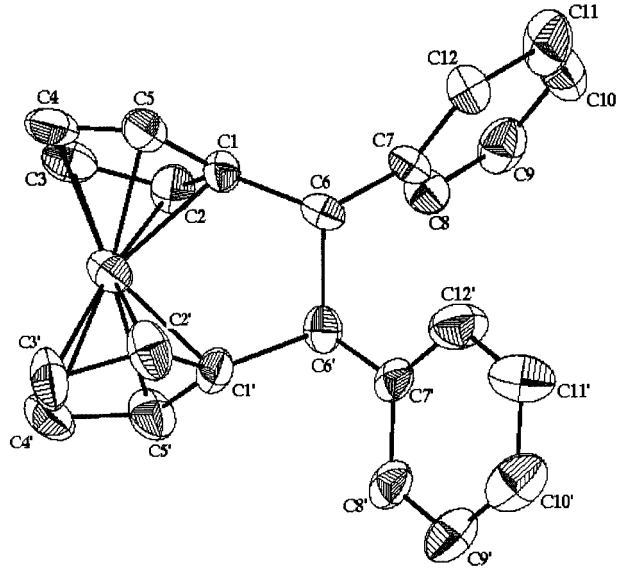

Figure 1. Molecular structure of *trans*-**1**, the PF_6^- counter anion is not shown

Table 1. Selected bond lengths in **1**

C1−C2	1.418	C1′−C2′	1.423
C2−C3	1.392	C2′−C3′	1.414
C3−C4	1.412	C3′−C4′	1.340
C4−C5	1.394	C4′−C5′	1.422
C5−C1	1.465	C5′−C1′	1.408
C1−C6	1.503	C1′−C6′	1.542
C6−R1	1.514	C6′−R1′	1.556
C6−C6′	1.540		
M−C1	1.978	M−C1′	1.963
M−C2	2.010	M−C2′	1.971
M−C3	2.054	M−C3′	2.059
M−C4	2.032	M−C4′	2.060
M−C5	1.997	M−C5′	2.004

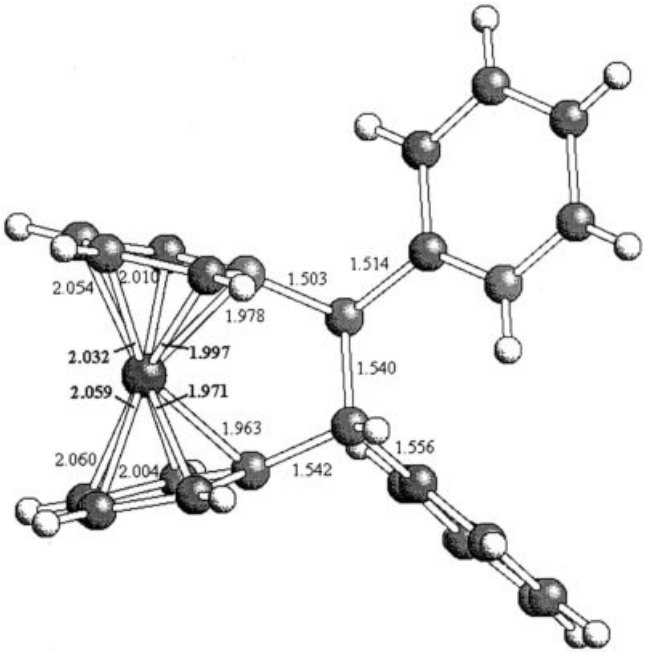

Figure 2. Side view of **1** showing the Co^+-C distances and bridging moiety bond

Structural Analysis

X-ray Crystallography

The inclusion of a two-carbon interannular bridge between the two cyclopentadienyl rings of a metallocene results in structural modification such as bending and lowering the symmetry of the metallocene. This can be demonstrated by comparing an unbridged and a bridged metallocene, namely ferrocene[20] and 1,1′-tetramethylethyleneferrocene (**4**).[21] In ferrocene, the metal is sandwiched equidistantly between the two parallel cyclopentadienyl rings, with the Fe−C distance being 2.045 Å. At room temperature, the rings adopt a staggered conformation, around 3.320 Å apart from each other with a C−C bond length of 1.403 Å. However, the presence of a two-carbon bridge in **4** introduces not only C_2 symmetry, but also a considerable amount of strain into the system, resulting in a C−C bond

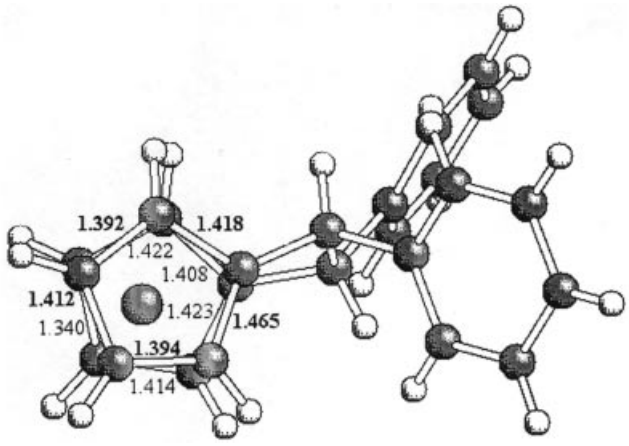

Figure 3. Top view of **1** showing the cyclopentadienyl C−C bond lengths (the C−C bond lengths of the upper ring are in bold)

Table 2. Structural comparisons of selected angles and distances of *ansa*-metallocenes **1**, **4**, **6**, and **7**

	1	4	6	7
α	22.9°	23.2°	4.2°	0.7°
β	12.4°	10.0°; 12.0°	10.8°	10.3°; 10.6°
δ	163.1°	156.8°	176.5°	179.4°
τ	9.0°	9.0°−10.0°	6.0°	2.9°
ε	37.2°; 37.4°	26.0°; 28.0°	7.9°; 8.4°	5.2°; 5.5°
D (C6−C6′)	1.540 Å	1.584 Å	2.354 Å	2.762 Å

Table 3. Summary of crystal data and intensity collection parameters

Compound	1
Molecular formula	$C_{24}H_{20}CoPF_6$
Mol. wt., g mol^{-1}	512.32
Crystal system	orthorhombic
Space group	$P2_1$
a, Å	12.363(3)
b, Å	12.615(2)
c, Å	13.321(4)
Radiation, Å	Mo-K_α (0.71073)
V, Å^3	2077.5(9)
Z	4
ρ, g·cm^{-3}	1.638
μ, mm^{-1}	0.966
F(000)	1040
Index Range	$0 \le h \le 17$, $-2 \le k \le 18$, $-6 \le l \le 18$
2θ, °	63.92
Temp, K	293(2)
Reflections Collected	3890
Reflections Unique	3572
*R*σ	0.179
*R*1 [$I > 4\sigma(I)$]	0.076
*wR*2	0.117
GOOF	0.952
Flack Parameter	−0.01(4)
Min., max. res.	−0.383, +0.418

of 1.584 Å. In order to accommodate this bond, the rings are forced to tilt by an angle (α) of 23.2° relative to one another (Table 2 and Figure 5). This, in turn, results in an

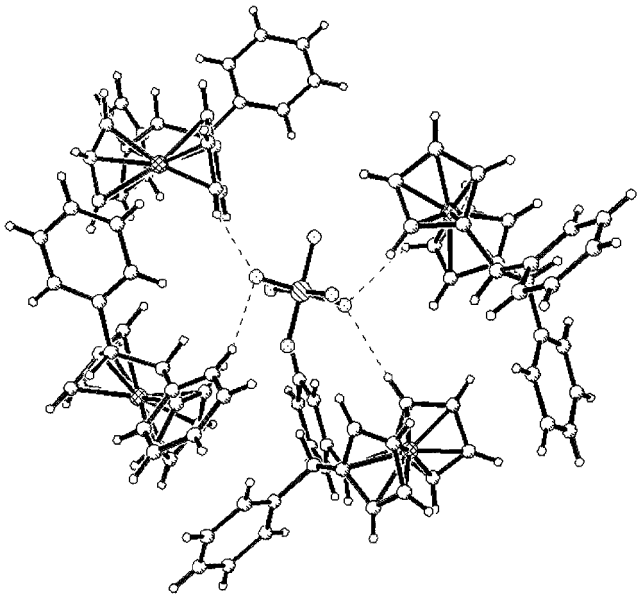

Figure 4. Crystal packing in the unit cell

angle between the metal and the ring centroids (δ) of 156.8°. The deviation from the fully eclipsed position (τ) of one ring with respect to the other is between 9.0° and 10.0°, so they are still very close to being eclipsed. As in ferrocene, the average Fe-ring C distance is 2.039 Å, but looking at each individual bond length reveals that this value actually varies from 1.965 Å to 2.099 Å. This is also the case with the inter-ring distance: the two carbons bonded to the bridge are pulled closer together (at 2.070 Å) than the carbons on the opposite side of the rings (3.600 Å and 3.650 Å). The C−C bond lengths of the rings themselves show a slight increase in going from 1.401 Å to 1.464 Å but this is still similar to ferrocene. Further evidence of strain is visible in the angles (β) occurring between the rings and the exocyclic bonds, 10.0° and 12.0°, which would not be present in an unstrained system. The two CMe_2 units of the bridge are displaced from the eclipsed arrangement by torsion angles (ε) of 26.0° and 28.0°.

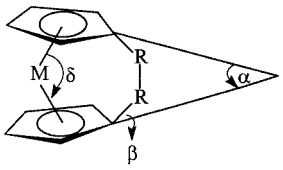

Figure 5. Selected angles from Table 2

A comparison of the structures of 1,1′-bis(benzhydryl)cobaltocenium (**5**)[22] and **1** further demonstrates the effect of the bridge. Again, the metal is sandwiched equidistantly between two parallel cyclopentadienyl rings in the unbridged metallocene, with Co-ring carbon lengths ranging from 2.016 Å to 2.068 Å. On insertion of the ethano bridge, this range increases to between 1.963 Å and 2.060 Å in order to accommodate this bond. The C−C bond lengths in the

rings vary little, however, in going from the former (1.392 Å to 1.482 Å) to the latter (1.392 Å to 1.465 Å). As **1** is isoelectronic with **4**, comparisons can be made. The C−C bond length of the bridging moiety is 1.540 Å, indicating that the substituents present around this bond do not impose a strain on it, and therefore it maintains a normal C−C single bond length. This isn't the case for **4**, where a lengthening of the bridge occurred. In addition, a less-strained situation is seen for the rest of the structure due to the differing bridge substituents between this compound (**1**) and **4**. The tilt angle (α) is found to be 22.9° which is quite similar to the above-mentioned ferrocene derivative, while the ring centroid-metal-ring centroid angle (δ) increases to 163.1°, leading to a more parallel arrangement of the cyclopentadienyl groups. As before, the twist angle (τ) is 9.0° but a slight decrease occurs in the range of the metal to ring carbon distances (1.963 Å to 2.060 Å) as a result of the less-bent structure. No further change appears to have occurred in the ring C−C bond lengths (1.392 Å to 1.465 Å). Likewise the β angles of 12.3° and 12.6° remain relatively constant. The greatest structural change to occur is in the torsion angles, ε, which are 37.2° and 37.4°, but this is mainly due to the different bridging units $(CPhH)_2$.

The types of atoms present in the bridge also influence the degree to which structural changes occur. Five important angles from the structures of cyclic ferrocenyldisilane,[23] $[Fe(\eta\text{-}C_5H_4)_2(SiMe_2)_2]$ (**6**) and 1,2-distanna(2)ferrocenophane,[24] $[Fe(\eta\text{-}C_5H_4)_2(SnMe_2)_2]$ (**7**) were examined and in almost in all cases these vary greatly from those for 1,1′-tetramethylethyleneferrocene. The length increases in going from the disilanyl bridge (2.353 Å) to the distannyl bridge (2.762 Å), due to the increase in size of these atoms. The effect of this bridge lengthening can be seen from the ring-M-ring angle (δ). The angle for **6** is 176.4° and for **7** is 179.4°, with the cyclopentadienyl rings being almost parallel in both cases. The tilt angle (α) also decreases, going from 4.2° to 0.7°. The rings are also much closer to being fully eclipsed when the bridge length is increased. Evidence of this is found from the twist angle (τ), which is 6.0° for **6** and 2.9° for **7**. The bridging units themselves, adopt a more eclipsed arrangement, ε is 7.9° and 8.4° for the silane units and decreases to 5.2° and 5.5° for the stannyl units. However, there is one set of values that remains the same and this is the angle β between the exocyclic bond and the ring plane: in **6** it is 10.8° and in **7** it is 10.3° and 10.6°.

Finally, the bonds between the bridge and the cyclopentadienyl rings also increase with replacement of the bridging moieties by larger atoms. They are found to be 1.548 Å and 1.543 Å, 1.852 Å and 1.866 Å and 2.149 Å and 2.134 Å for the C_2 (**1**), Si_2 (**6**) and Sn_2 (**7**) bridges respectively.

Theoretical Calculations

In order to get a deeper understanding of the nature of metallocene formation, a series of density functional theory (DFT) calculations were performed in which iron atoms were reacted with selected fulvenes. These calculations provide structural data and enthalpies of formation and allow a discussion of the effect of varying the substituted fulvenes, namely 6,6-dimethylfulvene, 6-phenylfulvene and 6,6-diphenylfulvene. These calculations were extended to include the reaction of the *ansa*-metallocenes **9** and **11** and the bis-fulvene complex **13** with hydrogen gas to form unbridged ferrocenes. Similar calculations were also carried out on **1**, the accuracy of which can be seen by comparing the calculated bond lengths (Table 4 and Figure 6) with the experimental values (Table 1), the difference between the two sets of results being only around 0.02 Å. Although the range of the cyclopentadienyl ring carbon bond lengths C1−C5 is shorter (1.423 Å to 1.439 Å) than the experimental values (1.392 Å to 1.465 Å) they mimic the results: bond elongation to the *ipso* carbon with shorter C−C bonds for the rest of the ring. The calculated M-ring carbon bonds also clearly show how the metallocene is bent due to the bridging moiety (1.584 Å), which is slightly longer than the actual length of 1.540 Å. As was found in the experimental values, the shortest Co^+-ring carbon bond is to the *ipso* carbon

Table 4. Calculated bond lengths (Å) for selected *ansa*-metallocenes

	8	9	10	11	**12**	**12**[a]	**13**[a]	**1**[b]
C1−C2	1.433	1.440	1.431	1.436	1.432	1.442	1.472	1.438
C2−C3	1.428	1.429	1.427	1.429	1.428	1.439	1.431	1.430
C3−C4	1.425	1.426	1.427	1.427	1.426	1.439	1.434	1.423
C4−C5	1.428	1.427	1.427	1.427	1.428	1.439	1.431	1.428
C5−C1	1.433	1.442	1.431	1.439	1.432	1.442	1.475	1.439
C1−C6	1.524	1.545	1.504	1.534	1.527	1.519	1.395	1.534
C6−R1	1.538	1.545	1.527	1.530	1.532	1.535	1.479	1.521
C6−C6′	N/A	1.631	N/A	1.570	N/A	N/A	N/A	1.584
C1′−C2′		1.440		1.436				1.438
C2′−C3′		1.429		1.429				1.430
C3′−C4′		1.426		1.427				1.423
C4′−C5′		1.427		1.427				1.428
C5′−C1′		1.442		1.439				1.439
C1′−C6′		1.545		1.534				1.534
C6′−R1′		1.545		1.530				1.521
M−C1	2.075	1.975	2.059	1.974	2.073	2.059	2.224	1.980
M−C2	2.051	2.025	2.052	2.026	2.051	2.038	2.036	2.017
M−C3	2.048	2.081	2.052	2.082	2.048	2.040	2.033	2.074
M−C4	2.048	2.087	2.052	2.089	2.048	2.040	2.039	2.080
M−C5	2.051	2.030	2.052	2.031	2.051	2.038	2.028	2.027
M−C1′		1.976		1.974				1.980
M−C2′		2.025		2.026				2.017
M−C3′		2.081		2.082				2.074
M−C4′		2.087		2.089				2.080
M−C5′		2.030		2.031				2.027

[a] Calculation performed at the B3LYP level using 3-21G as the basis set. [b] Calculation performed at the B3LYP level using 6-311G** as the basis set.

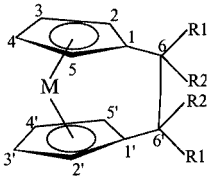

Figure 6. Numbering scheme for observed and calculated metallocene structures

(1.980 Å) and the longest to the two carbons furthest away from this (2.074 Å and 2.080 Å).

The bridged and unbridged ferrocenes that were measured were derived from 6,6-dimethylfulvene, 6-phenylfulvene and 6,6-diphenylfulvene (unbridged only). For the unbridged tetramethylferrocene (**8**), the C−C bonds in the cyclopentadienyl rings range from 1.425 Å to 1.433 Å, and are very similar to those of the bridged tetramethylferrocene **9** (1.426 Å to 1.442 Å). The difference between these two compounds is found in their Fe-ring carbon bonds (2.048 Å to 2.075 Å, compared to 1.975 Å to 2.087 Å for the bridged structure). This is a result of the C6−C6′ bridge of 1.631 Å distorting the sandwich structure of **9**. Again, these values show a slight elongation compared to the measured experimental bond lengths for 1,1′-tetramethylethyleneferrocene (**4**), whose bridge length is 1.584 Å.

In the case of the unbridged **10** and bridged diphenylferrocene **11**, the ring carbon bond lengths are very similar (1.427 Å to 1.431 Å and 1.427 Å to 1.439 Å respectively). As before, the longest bonds are to the *ipso* carbon, although the presence of a bridge (1.570 Å) causes the M-ring carbon distances to change from 2.052 Å to 2.059 Å — a parallel arrangement — to 1.974 Å to 2.089 Å — a bent structure.

The third group of calculations involved 6,6-diphenylfulvene as the ligand. Only the unbridged tetraphenylferrocene **12** was studied, as bridge formation in this case is not possible due to the large steric overload that would result.[25] As for the previous two ferrocenes, the bond lengths lie within a very similar range: the cyclopentadienyl carbon-carbon bonds are between 1.426 Å and 1.432 Å and the metal-carbon distances are between 2.048 Å and 2.073 Å.

The role of the substituents is evident from these results. In order to synthesise an *ansa*-metallocene, the groups present on the exocyclic carbon must not be so sterically demanding that they prevent dimerisation occurring, as in the case of 6,6-diphenylfulvene. Despite its suitability for radical anion stabilisation,[19] the steric hindrance between the four phenyl rings results in the sole production of the unbridged metallocene. Changing the phenyl groups for methyl groups reduces these clashes and bridge formation occurs. However, the structure still possesses substantial strain and so to compensate the C_2 bridge is elongated to 1.631 Å. Replacing the methyl groups for a phenyl and a hydrogen decreases the strain even further and this is reflected in the bridge length of 1.570 Å. This effect can also be seen in the formation energies of the respective molecules (Table 5). In both the bridged and unbridged cases, going from the tetramethylferrocene to the diphenylferrocene results in a lowering of the energy of these compounds. The energy of the unbridged tetraphenylferrocene is lower still, despite having large substituents, as these are responsible for producing the most stable radical anion. The enthaplies of bridge formation for **9** and **11** were also calculated (Scheme 1 and 2) and found to be −101.3 kcal/mol and −129.2 kcal/mol respectively. From this, it can be seen that the formation of **11** is energetically more favourable. Further ΔH values were calculated for the breaking of the bridging moiety, to give the unbridged metallocene, namely −30.2 kcal/mol (**8**) and −28.2 kcal/mol (**10**). These values show that not only does the bridge impose a strain on the metallocene, but the substituents do as well. The presence of four methyl groups on the bridge imposes greater stress on the structure than two phenyls and two hydrogens, occupying the *trans* position. Hence breaking this bond releases more energy (−30.2 kcal/mol) and thus removes the strain in the system. The ΔH value for the formation of **12** was also measured and found to be −124.3 kcal/mol (Scheme 3). This too shows that the synthesis of **12** is viable but is the lowest of the three values, for **8** the value is −131.5 kcal/mol and for **10** it is −157.4 kcal/mol.

Table 5. Calculated energies (Hartrees) and reaction enthalpies (kcal/mol) for bridged and unbridged ferrocenes

	E	ZPE	E'	ΔH
8	−1886.619006	0.339256	−1886.27975	−131.5
9	−1885.382299	0.318964	−1885.063335	−101.3
10	−2191.469967	0.318964	−2191.081835	−157.4
11	−2190.236630	0.368083	−2189.868547	−129.2
12	−2653.570935	0.550408	−2653.020527	−124.3
12[a]	−2640.004865	0.553349	−2639.451516	−169.4
13[a]	−2638.748619	0.529476	−2639.451516	−124.2

[a] Calculated with the 3-21G basis set.

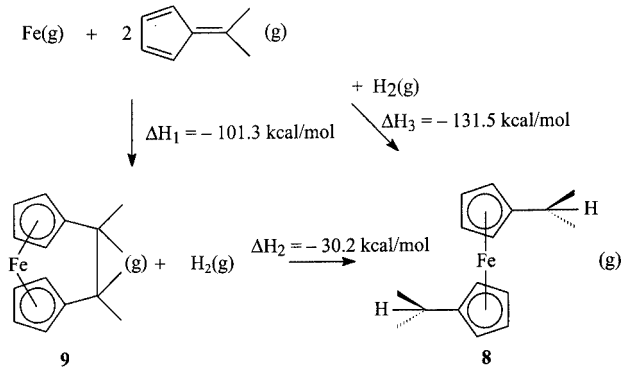

Scheme 1. Calculated reaction enthalpies for the formation of **8** and **9**, using 6,6-dimethylfulvene as the starting ligand

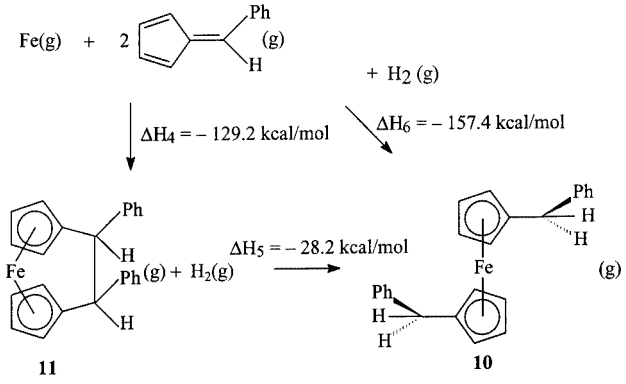

Scheme 2. Calculated reaction enthalpies for the formation of **10** and **11**, using 6-phenylfulvene as the starting ligand

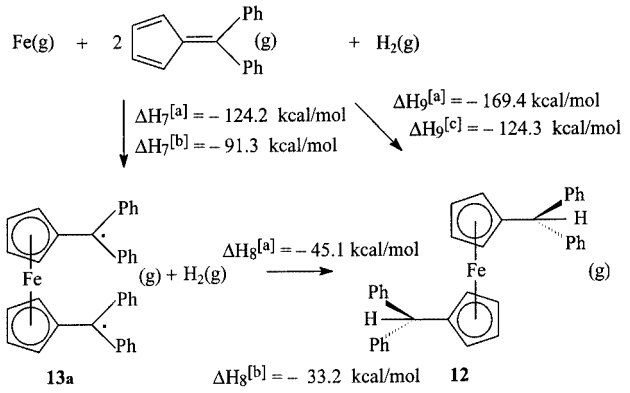

Scheme 3. Calculated reaction enthalpies for the formation of **12** and **13a**, using 6,6′-tetraphenylferrocene as the starting ligand [a] Calculations performed using the 3-21G basis set. [b] Correction factor applied to the results from the 3−21G basis set to give corresponding values from the 6-31G** basis set. [c] Calculations performed using the 6-31G** basis set

It was previously proposed[26] that a further intermediate is involved in the synthesis of these metallocenes, namely a bis-fulvene complex. This intermediate was thought to form initially from the reaction of metal atoms with fulvenes to give a complex whose metal centre has an oxidation state of zero. The next step is an electron transfer — one electron goes to each ring — resulting in an M^{2+} ion centred between two radical anions, which can then dimerise to give the *ansa*-metallocene or undergo hydrogen abstraction yielding the unbridged compound (Scheme 4). Proof of this postulate was obtained from the X-ray structure of a bis(6,6-diphenylfulvenyl)iron intermediate **13**.[26] A theoretical examination of this complex can give a further insight into its role in the reaction mechanism. The structure was calculated to obtain a minimum in the singlet state, **13a**, but this had to be performed using 3-21g* as the basis set to save calculation time. This revealed C−C ring lengths of 1.431 Å to 1.475 Å and M−C distances of 2.028 Å to 2.224 Å. These are similar to the experimentally found values of 1.406 Å to 1.452 Å for the cyclopentadienyl C−C bonds and 2.035 Å to 2.209 Å for the M−C lengths. Using these values, it can be determined whether or not **13** is really a bis-fulvene complex or a ferrocene derivative. To be the former of the two, the cyclopentadienyl rings should consist of alternating single and double bonds, with the two phenyl substituents located at the exocyclic double bond. These bond lengths should mirror the values determined both theoretically[19] and experimentally[26] for the 6,6-diphenylfulvene. Alternatively, to be the ferrocene derivative, the cyclopentadienyl rings should be more aromatic in character due to their reduction by the iron centre. The structure of the 6,6-diphenylfulvene radical anion has previously been calculated, using the 6-31G** basis set.[19] It can clearly be seen that the C−C bonds in the cyclopentadienyl ring are no longer comprised of distinct single and double bonds and lie in the range of 1.387 Å to 1.446 Å. The exocyclic bond has elongated to 1.434 Å, showing increased single bond character. A study of the crystal structure of **13** reveals that the equivalent bond in this complex is 1.408 Å and there is no clear distinction between what were formally single and double bonds in the ring. Therefore, structurally, **13** is a complex in which an Fe^{II} centre is coordinated to two fulvene radical anions with the two formally unpaired electrons in the C6 and C6′ positions. The crystal geometry also shows that the phenyl substituents are eclipsed with respect to one another, despite the steric crowding. As stated earlier, theoretical calculations found the optimised structure in the singlet state. This indicates that there is coupling occurring between the two electrons, hence allowing such an arrangement to occur, satisfying the 18 VE rule. The ΔH values for the formation of complex **13a** and the ultimate formation of **12** were also calculated at this lower level (Scheme 3). Formation of the singlet was exothermally favourable at −124.2 kcal/mol and the overall enthalpy of formation of the unbridged ferrocene was −169.4 kcal/mol. There is a considerable difference between this latter value and the original one calculated using the higher basis set (−124.3 kcal/mol). The ratio difference between these two is 1.36 and this can be used as a correction factor to get a more accurate value for the formation of the singlet. This was calculated to be −91.3 kcal/mol, and since this is too low to result in the formation of a C−C bond (−100 kcal/mol is necessary), only the unbridged metallocene is seen.

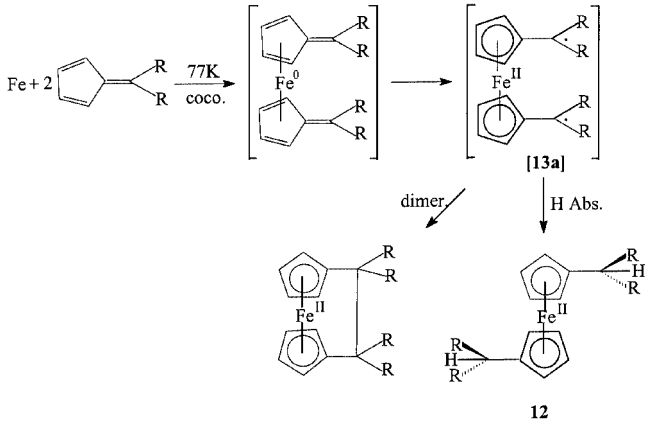

Scheme 4. Reaction mechanism for the synthesis of metallocenes, showing the role of the bis-fulvene complex **13a**

Conclusion

The formation of **1** was achieved and it was isolated as a PF_6^- salt. Theoretical calculations were also carried out in order to obtain a geometry optimised structure, and from this it was seen that these results mirror the experimental values very closely. The main difference was found in the length of the bridging moiety, which the calculations had over-estimated by about 0.04 Å. This too was also the case for the other *ansa*-metallocene calculations. Despite this, the effect of the bridge on the structure and the effect of the substituents on the bridge can be seen. From both experimental and theoretical data, it is apparent that the presence of four methyl groups on the bridge of **9** imposes strain

on the bond, elongating it. This then has a knock-on effect on the structure, causing the rings to tilt more away from the parallel and a smaller δ angle. Replacing the groups with ones that produce less steric hindrance as in **1**, results in a bridge with a normal C−C bond length. This less-strained structure is also reflected in the more parallel arrangement of the rings and the larger ring centroid-M-ring centroid angle, with respect to **9**. Finally, the structure of **13** has been proposed to be that of a ferrocene derivative, with the iron centre donating two electrons to the cyclopentadienyl rings, where they occupy the C6 and C6′ positions. Here they experience a degree of coupling which results in an eclipsed arrangement of the phenyl substituents.

Experimental Section

Synthetic Work. General: The preparation of **2** was carried out according to a literature procedure.[16] THF was dried over and distilled from Na/benzophenone prior to use. Air- and moisture-sensitive compounds were stored and handled in an argon glove box and manipulations of these substances were carried out with standard Schlenk techniques using argon to avoid calcium nitride formation.

NMR spectra were recorded on a VARIAN 300 MHz spectrometer. Chemical shifts are reported in ppm and are referenced to TMS, except for the ^{31}P NMR spectra, which are referenced to external triphenylphosphate.

The mass spectra were measured on a Finnigan MAT Incos 50 B mass spectrometer in EI mode.

Computational Study: DFT calculations were performed using the GAUSSIAN 98[27] programme implemented on an Origin 200 eight-processor cluster (SGI 180 MHz CPU/2 GB RAM). These were carried out at the B3LYP level, using either the 6-31G** or the 3-21G basis sets. The calculated electronic energies (*E*) of the complexes studied are presented in Table 5 in Hartrees. A correction value, namely the zero-point energy (ZPE), must be added to these values to give the overall energies (*E*′) of the molecules. Finally, the reaction enthalpies in Table 5 have been calculated from the energy differences between the reactants and the products. For the formation of the *ansa*-metallocenes, this was found to be the difference between the bridged ferrocene and the combined energy of the iron atom with the desired fulvene. Two pathways were studied for the unbridged metallocene: direct reaction between the iron, selected fulvene and hydrogen gas and the breaking of the bridging moiety of the *ansa*-ferrocene with subsequent reaction with the hydrogen.

Synthesis of *ansa*-Cobaltocenium Hexafluorophosphate (1): A freshly made solution of **2** was prepared according to literature methods[16] and an equimolar amount of $CoCl_2$ (0.422 g, 3.25×10^{-3} mol) was added to it under argon. This was refluxed for eight hours, producing a dark green solution of **3**. After filtration, the solution was cooled to −30 °C to produce **3** as a lime green powder, which was then dried under vacuum. Principle IR absorptions (nujol): $\tilde{\nu}$ = 2950 cm^{-1} (m), 2865 (m), 1580 (w), 1304 (w), 1260 (s), 1092 (s), 1021 (s), 867 (w), 798 (s), 722 (m). MS (EI): *m*/*z* = 367.1 (54) [M$^+$], 308.1 (8.2) [M$^+$ − Co$^+$], 306.1 (51.3) [M$^+$ − Co$^+$ − 2H$^+$], 212.9 (8.2) [M$^+$ − $C_{12}H_{10}$], 154.1 (57) [$C_{12}H_{10}$], 153.1 (100) [$C_{12}H_{10}$ − H$^+$], 58.9 (2.3) [Co$^+$]. UV/Vis (CH_3CN): λ_{max} = 364 nm. The powder was redissolved in 6 M HCl (65 mL), while exposing the solution to air. This was stirred until the olive green colour changed to yellow-green. The mixture was then filtered and the filtrate was washed with diethyl ether. The aqueous layer was separated and a saturated aqueous solution of NH_4PF_6 was added dropwise. An orange precipitate was seen to slowly drop out of the solution and upon filtration gave 0.72 g of an orange/yellow powder (yield: 43%). ^{1}H NMR (CD_3CN, 25 °C): δ = 5.20 (s, 2 H, PHC*H*Cp), 5.33, 5.71, 6.43, 6.71 (m, 8 H, C_5H_4), 7.23−7.41 (m, 10 H, C_6H_5) ppm. ^{13}C NMR (CD_3CN, 25 °C): δ = 57.1 (Ph*C*HCp), 84.1, 84.9, 89.1, 90.0, 130.9 (C_5H_4), 128.1, 128.7, 129.5, 140.3 (C_6H_5) ppm. Principle IR absorptions (KBr): $\tilde{\nu}$ = 3117 cm^{-1} (m), 3063 (m), 3015 (m), 1548 (w), 1496 (s), 1398 (s), 1032 (s), 927 (m), 836 (s), 820 (m), 777 (m), 726 (s), 704 (m). $C_{24}H_{20}CoF_6P$ (512.3): calcd. C 56.26, H 3.93, Co 11.50, F 22.25, P 6.04; found C 55.95, H 4.03, Co 11.21, F 19.91, P 5.21. MS (EI): *m*/*z* = 367.1 (54) [M$^+$ − PF_6], 213.02 (8.8) [M$^+$ − $C_{12}H_{10}$], 154.1 (48) [$C_{12}H_{10}$], 153.1 (100) [$C_{12}H_{10}$ − H$^+$], 58.9 (20) [Co$^+$]. UV/Vis (CH_3CN): λ_{max} = 422.0 nm. Crystals were grown by the slow evaporation of acetonitrile at room temperature.

X-ray Crystallography: The crystals grown were found to be suitable for X-ray diffraction. The orange cross-shaped crystals that were obtained belong to the $P2_1$ space group and the crystallographic parameters are presented in Table 3. Data were collected on an Enraf−Nonius CAD4 four-circle diffractometer with monochromatized Mo-K_α radiation. An absorption correction turned out to be unnecessary. The crystal structure was solved by direct methods[28] and refined using a least-squares method.[29] All non-hydrogen atoms were refined with anisotropic displacement parameters. The H atoms were placed at idealised positions and refined with coupled, isotropic displacement parameters. The absolute structure could be determined because of a definite Flack parameter.

CCDC-190062 contains the supplementary crystallographic data for this paper. These data can be obtained free of charge at www.ccdc.cam.ac.uk/conts/retrieving.html [or from the Cambridge Crystallographic Data Centre, 12, Union Road, Cambridge CB2 1EZ, UK; Fax: (internat.) +44-1223/336-033; E-mail: deposit@ccdc.cam.ac.uk].

Acknowledgments

The authors would like to thank Dr. Yuri Kuznetsov for useful discussions. This work was supported by the Centre for High-Performance Computing Applications at University College Dublin, Ireland. Thanks are also due to Enterprise Ireland for financial support.

[1] M. Tacke, *Organometallics* **1994**, *13*, 4124−4125.
[2] T. Tan, J. J. Fletcher, M. J. McGlinchey, *J. Chem. Soc., Chem. Commun.* **1975**, 771−772.
[3] M. Rieckhoff, U. Pieper, D. Stalke, F. T. Edelmann, *Angew. Chem. Int. Ed. Engl.* **1993**, *32*, 1079−1081.
[4] A. Recknagel, F. T. Edelmann, *Angew. Chem. Int. Ed. Engl.* **1991**, *30*, 693−694.
[5] I. L. Fedushkin, S. Dechert, H. Schumann, *Angew. Chem. Int. Ed.* **2001**, *40*, 561−563.
[6] H. G. Alt, A. Koppl, *Chem. Rev.* **2000**, *100*, 1205−1221.
[7] H. G. Alt, *J. Chem. Soc., Dalton Trans.* **1999**, 1703−1709.
[8] H. Schwemlein, L. Zsolnai, G. Huttner, H. H. Brintzinger, *J. Organomet. Chem.* **1983**, *256*, 285−289.
[9] D. M. J. Foo, P. Sinnema, B. Twamley, P. J. Shapiro, *Organometallics* **2002**, *21*, 1005−1007.

[10] J. J. Eisch, X. Shi, F. A. Owuor, *Organometallics* **1998**, *17*, 5219−5221.
[11] G. J. Matare, D. M. Foo, K. M. Kane, R. Zehnder, M. Wagener, P. J. Shapiro, T. Concolinc, A. L. Rheingold, *Organometallics* **2000**, *19*, 1534−1539.
[12] F. R. W. P. Wild, L. Zsolnai, G. Huttner, H. H. Brintzinger, *J. Organomet. Chem.* **1982**, *232*, 233−247.
[13] H. G. Alt, E. Samuel, *Chem. Soc. Rev.* **1998**, *27*, 323−329.
[14] W. Kaminsky, K. Kulper, H. H. Brintzinger, F. R. W. P. Wild, *Angew. Chem. Int. Ed. Engl.* **1985**, *24*, 507−508.
[15] J. A. Ewen, R. L. Jones, A. Razavi, J. D. Ferrara, *J. Am. Chem. Soc.* **1988**, *110*, 6255−6256.
[16] K. M. Kane, P. J. Shapiro, A. Vij, R. Cubbon, A. L. Rheingold, *Organometallics* **1997**, *16*, 4567−4571.
[17] S. Fox, J. P. Dunne, M. Tacke, J. F. Gallagher, manuscript in preparation.
[18] K. J. Stone, R. D. Little, *J. Org. Chem.* **1984**, *49*, 1849−1853.
[19] M. Tacke, S. Fox, L. Cuffe, J. P. Dunne, F. Hartl, T. Mahabiersing, *J. Mol. Struct.* **2001**, *559*, 331−339.
[20] J. D. Dunitz, L. E. Orgel, A. Rich, *Acta Crystallogr.* **1956**, *9*, 373−375.
[21] M. B. Laing, K. N. Trueblood, *Acta Crystallogr.* **1965**, *19*, 373−381.
[22] O. Koch, F. Edelmann, U. Behrens, *Chem. Ber.* **1982**, *115*, 1305−1312.
[23] W. Finckh, B. Tang, D. A. Foucher, D. B. Zamble, R. Ziembinski, A. Lough, I. Manners, *Organometallics* **1993**, *12*, 823−829.
[24] M. Herberhold, U. Steffl, W. Milius, B. Wrackmeyer, *Angew. Chem. Int. Ed. Engl.* **1996**, *35*, 1803−1804.
[25] M. Tacke, J. P. Dunne, S. Fox, G. Linti, R. Teuber, *J. Mol. Structure* **2001**, *570*, 197−202.
[26] R. Teuber, G. Linti, M. Tacke, *J. Organomet. Chem.* **1997**, 545−546, 105−110.
[27] Gaussian 98, Revision A.7, M. J. Frisch, G. W. Trucks, H. B. Schlegel, G. E. Scuseria, M. A. Robb, J. R. Cheeseman, V. G. Zakrzewski, J. A. Montgomery, Jr., R. E. Stratmann, J. C. Burant, S. Dapprich, J. M. Millam, A. D. Daniels, K. N. Kudin, M. C. Strain, O. Farkas, J. Tomasi, V. Barone, M. Cossi, R. Cammi, B. Mennucci, C. Pomelli, C. Adamo, S. Clifford, J. Ochterski, G. A. Petersson, P. Y. Ayala, Q. Cui, K. Morokuma, D. K. Malick, A. D. Rabuck, K. Raghavachari, J. B. Foresman, J. Cioslowski, J. V. Ortiz, A. G. Baboul, B. B. Stefanov, G. Liu, A. Liashenko, P. Piskorz, I. Komaromi, R. Gomperts, R. L. Martin, D. J. Fox, T. Keith, M. A. Al-Laham, C. Y. Peng, A. Nanayakkara, C. Gonzalez, M. Challacombe, P. M. W. Gill, B. Johnson, W. Chen, M. W. Wong, J. L. Andres, C. Gonzalez, M. Head-Gordon, E. S. Replogle, J. A. Pople, Gaussian Inc.: Pittsburgh PA, 1998.
[28] G. M. Sheldrick, SHELXS-86, *Program for Crystal Structure Solution*, Universitat Gottingen, **1986**.
[29] G. M. Sheldrick, SHELXL-93, *Program for Crystal Structure Refinement*, Universitat Göttingen, **1993**.

Received June 6, 2002
[I02297]

Synthesis, Stereochemistry and Molecular Structures of Chiral-at-Metal (Cycloheptatrienyl)molybdenum Complexes Containing the Diphosphane Prophos

Henri Brunner,* Jürgen Klankermayer, Manfred Zabel

Eur. J. Inorg. Chem. **2002**, 2494−2501

*In Scheme 4 on page 2496 the stereochemistry of compound **2b** was inadvertently misdrawn. The correct version of this scheme is printed below.*

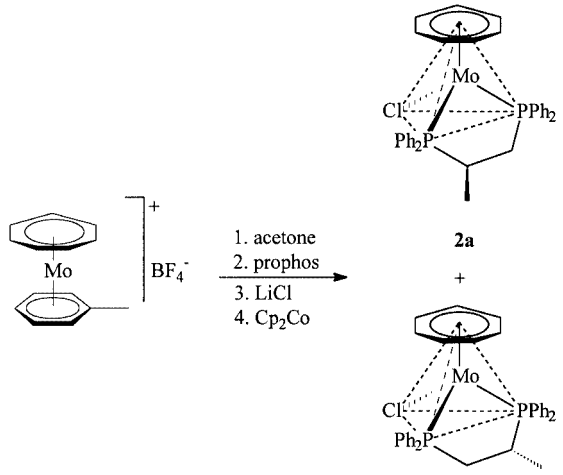

H. Brunner
[I02063 C]

 © 2002 WILEY-VCH Verlag GmbH & Co. KGaA, 69451 Weinheim 1434−1948/02/1111−3047 $ 20.00+.50/0

EurJIC
European Journal of Inorganic Chemistry

December 2002
Issue 12
Pages 3049–3374

Papers available ahead of print in Early View at www.interscience.wiley.com

Earliest available Table of Contents:
Automatically, free of charge by e-mail through
www.interscience.wiley.com/alerts

COVER PICTURE

The cover picture shows two conformations of the chiral chelate cation $[\{\kappa\text{-P(Mes)}_2\text{CH}_2\text{CH(OH)CH}_2\text{-}\kappa\text{-P(Ph}_2\}\text{Rh}(\eta^4\text{-COD})]^+$ which is active as an enantioselective hydrogenation catalyst. The δ- and λ-twist conformations of the six-membered diphosphane chelate cycle are shown together with a projection of the hypersurface relevant to the transition between these enantiomeric forms. The hypersurface is generated by force field calculations. The specific force field is derived by refinement of the relevant force field parameters by genetic algorithms on the basis of eleven compounds of this type. The predictions made by this model are in almost quantitative agreement with the experimental data: The λ-form is calculated to be 3.1 kJ•mol^{-1} more stable than the δ-form (experimental: 3.4 kJ•mol^{-1}). The δ ⇔ λ transition is predicted to be accompanied by a coupled rotation of the mesityl groups (color code in the cover picture) in full agreement with the experimental results. The upper threshold of the activation barrier of the transition is calculated to be 69.1 kJ•mol^{-1}; the experimental value is 64.4•kJ mol^{-1}. This novel approach to molecular modeling is described in the article by G. Huttner et al. on p. 3111 ff. The quantitative NMR analysis of the structure and dynamics of compounds containing six-membered diphosphane chelate cycles is presented in the accompanying article by G. Huttner et al. on p. 3129 ff.

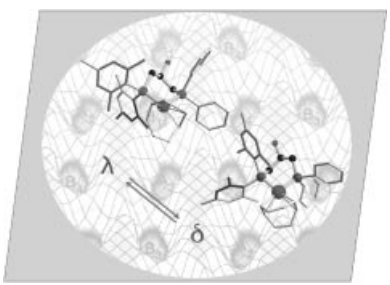

MICROREVIEW

Contents

3067 **N. J. Coville,* D. C. Levendis**

Organometallic Chemistry: Structural Isomerization Reactions in Confined Environments

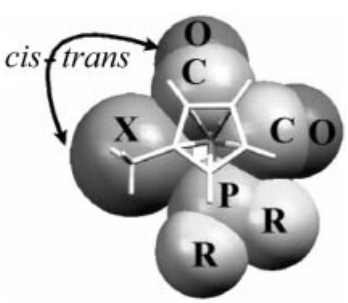

Keywords: Isomerization / Solid-state reactions / Surfaces / Organometallic chemistry / Rhenium

 © 2002 WILEY-VCH Verlag GmbH & Co. KGaA, 69451 Weinheim 1434–1948/02/1212–3053 $ 20.00+.50/0

SHORT COMMUNICATIONS

3079 **B. Zimmer, V. Bulach, M. W. Hosseini,* A. De Cian, N. Kyritsakas**

1- and 2-D Coordination Networks Based on Porphyrin and Copper: an Example of Supramolecular Isomerism

Keywords: Porphyrin / Pyridine / Isonicotinoyl / Coordination network / Copper / Atropoisomerism

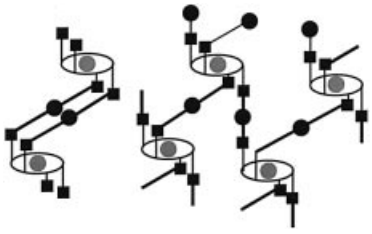

3083 **M. J. J. Mulder, J. G. Haasnoot, D. J. Stufkens, L. H. Tjeng, H.-J. Lin, C.-T. Chen, J. Reedijk***

A New Synthetic Strategy for Magnetic Metal Bis(dithiolene) Based Conductors

Keywords: Redox chemistry / Conducting materials / X-ray absorption spectroscopy / EPR spectroscopy / Raman spectroscopy

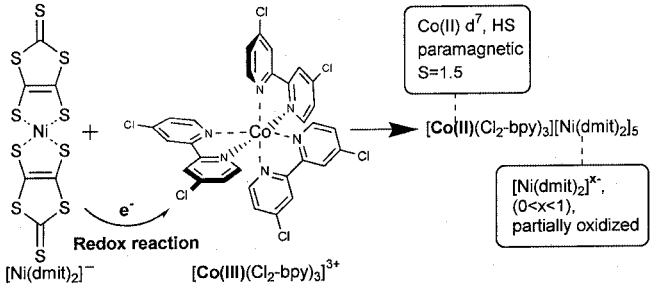

3087 **C. Belle,* I. Gautier-Luneau, L. Karmazin, J.-L. Pierre, S. Albedyhl, B. Krebs, M. Bonin**

Regio-Directed Synthesis of a $Zn^{II}Fe^{III}$ Complex from an Unsymmetrical Ligand and Its Relevance to Purple Acid Phosphatases

Keywords: Heterometallic complexes / Zinc / Iron / Unsymmetrical ligands / Phosphatases

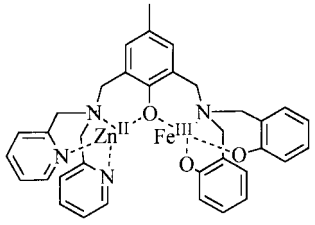

(Isolated with two diphenylphosphato bridges)

3091 **J. J. Eisch,* J. N. Gitua**

Astonishing Alkylation and Unusual Reduction Reactions of Anionic Titanium(II) Isopropoxide Complexes: Evidence for SET Processes in Transition-Metal Oxidative Additions

Keywords: Titanium / Subvalent compounds / Oxidative addition / Alkylation / Electron transfer

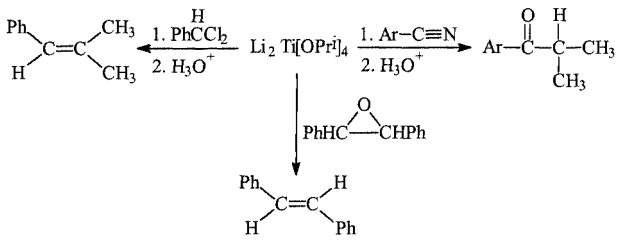

FULL PAPERS

3097 **R.-H. Wang, M.-C. Hong,* J.-H. Luo, R. Cao,* J.-B. Weng**

The First Two Novel Metallomacrocycles Constructed from Cubane-Like Cu_4I_4 Cluster Units and Ditopic Diamines

Keywords: Amine ligands / Copper / Metallacycles / X-ray diffraction

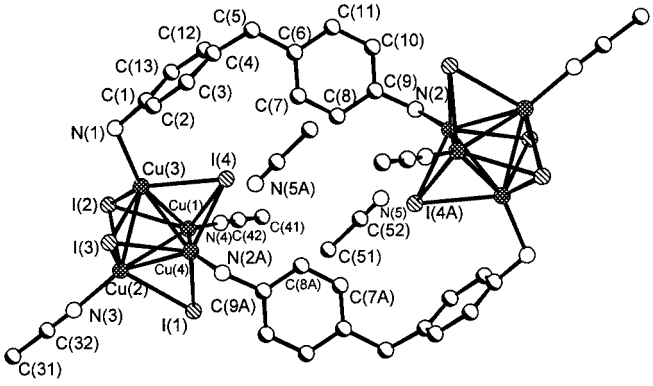

3101 **G. Muller, J. P. Riehl, K. J. Schenk, G. Hopfgartner, C. Piguet, J.-C. G. Bünzli***

Lanthanide Triple Helical Complexes with a Chiral Bis(benzimidazole)pyridine Derivative

Keywords: Lanthanides / Tridentate ligands / Chirality / Luminescence / Stability constants

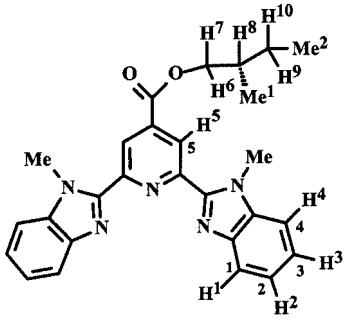

3111 **V. Schulz, A. Frick, G. Huttner***

How to Model the Conformational Behaviour of Saturated Diphosphane Chelate Cycles: The Conformational Rearrangement Processes of $[\{\kappa\text{-}PAr_2CH_2CH(OH)CH_2\text{-}\kappa\text{-}PAr'_2\}Rh\text{-}(\eta^4\text{-}COD)]^+$

Keywords: Rhodium / Phosphane ligands / Chelates / Molecular modelling / Conformation analysis

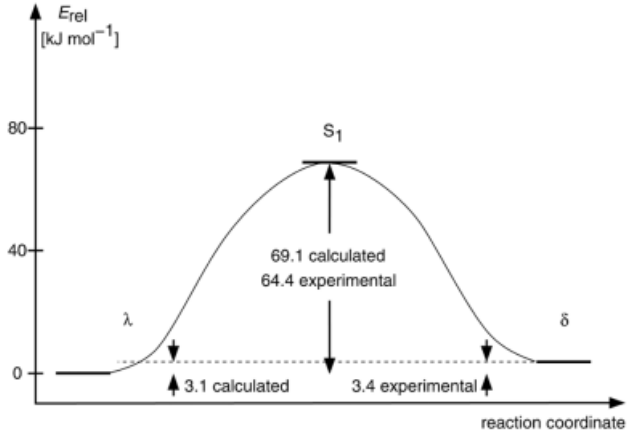

3129 **A. Frick, V. Schulz, G. Huttner***

Interconversion of δ and λ Forms of Six-Membered Chelate Cycles − A Quantitative NMR Spectroscopic Study of (Diphosphane)rhodium Compounds

Keywords: Conformational analysis / Diphosphanes / Rhodium / Kinetics / Thermodynamics

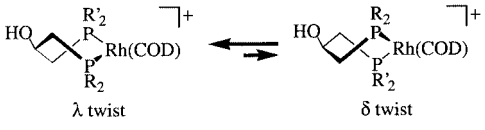

3148 **H. Suezawa,* T. Yoshida, Y. Umezawa, S. Tsuboyama, M. Nishio***

CH/π Interactions Implicated in the Crystal Structure of Transition Metal Compounds − A Database Study

Keywords: Hydrogen bonds / Noncovalent interactions / π interactions / Supramolecular chemistry

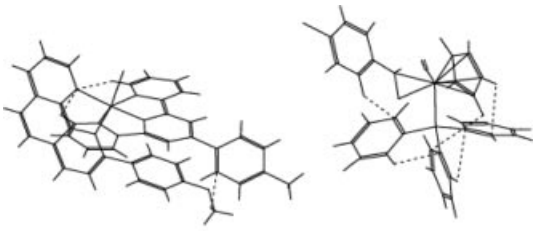

CH/ π interactions disclosed in crystal strructure of transition metal compounds

3156 **D. Harmsen, G. Erker,* R. Fröhlich, G. Kehr**

Reaction of $[(Cp_2TiCH_3)(THF)^+][BPh_4^-]$ with Tripeptide Derivatives: Formation of Cationic (Peptide)titanocene Complexes

Keywords: Bioinorganic chemistry / Peptides / Metallocenes / Titanium / Cations

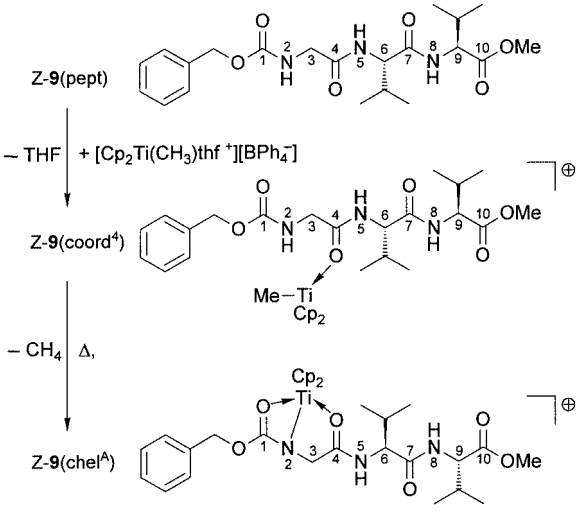

3172 **K. Müller-Buschbaum,* G. B. Deacon, C. M. Forsyth**

$[Yb(THF)_3(C_5H_4PPh_2)_2W(CO)_4]\cdot 0.5THF$ and $^1_\infty[Yb(THF)(C_5H_4PPh_2)_2(\mu\text{-}OC)W(CO)_3]$: Two New Heterobimetallic Complexes Containing Yb^{II} and W^0

Keywords: Heterometallic complexes / Ytterbium / Tungsten / Carbonyl ligands

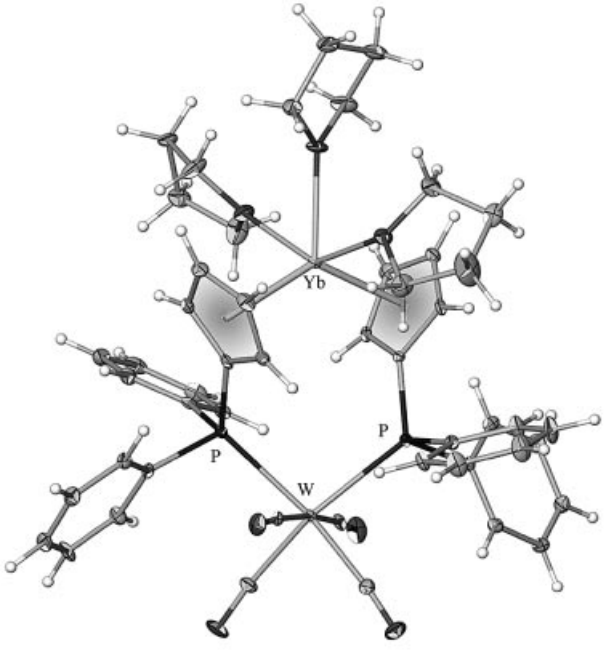

3178 **A. M. Guerrero, F. A. Jalón,* B. R. Manzano, R. M. Claramunt, M. D. Santa María, C. Escolástico, J. Elguero, A. M. Rodríguez, M. A. Maestro, J. Mahía**

Variety in the Coordination Modes of the Ligand Hexakis(pyrazol-1-yl)benzene (Hpzb) to Pd^{II}, Pt^{II} and Cu^{I} Centres

Keywords: N ligands / Conformational analysis / Palladium / Platinum / Copper / Coordination chemistry

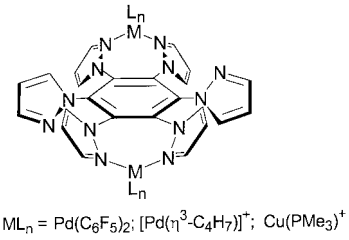

ML_n = $Pd(C_6F_5)_2$; $[Pd(\eta^3\text{-}C_4H_7)]^+$; $Cu(PMe_3)^+$

3190 **M. Hernando,* K. Boulahya, M. Parras, J. M. González-Calbet**

Synthesis, Microstructural Characterisation and Magnetic Study of Two New One-Dimensional Members of the $(A_3ZnMnO_6)_\alpha$ $(A_3Mn_3O_9)_\beta$ Homologous Series (A = Ba, Sr)

Keywords: Electron diffraction / Electron microscopy / One-dimensional oxides / Magnetic properties / Twinned microstructure

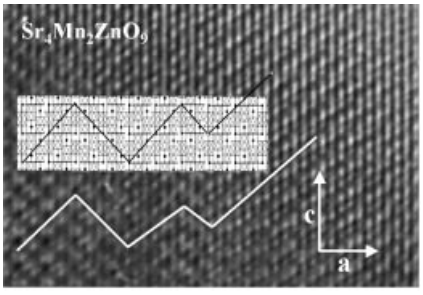

3197 **R. Horikoshi, T. Mochida,* R. Torigoe, Y. Yamamoto**

Preparation and Electrochemical Properties of Polynuclear Organometallic Complexes Derived from Ferrocene-Containing Bidentate Ligands

Keywords: Bridging ligands / Cyclic voltammetry / Ruthenium / Rhodium / Iridium / Metallocenes

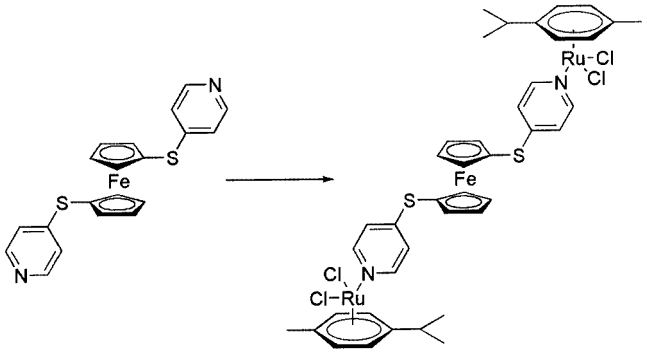

3204 **J. A. Cabeza,* I. del Río, M. Moreno, S. García-Granda, M. Pérez-Priede, V. Riera**

Reactivity of a Triruthenium Ynenyl Cluster Complex with Diynes: Cluster-Mediated Combination of up to Three Substituted Butadiyne Molecules into a Carbon-Rich Hydrocarbyl Ligand

Keywords: Ruthenium / Clusters / Alkynes / C-C bond formation / N ligands

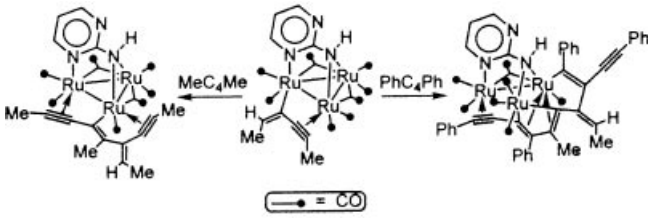

3210 **Y.-J. Shi, Y. Xu, X.-T. Chen,* Z. Xue, X.-Z. You***

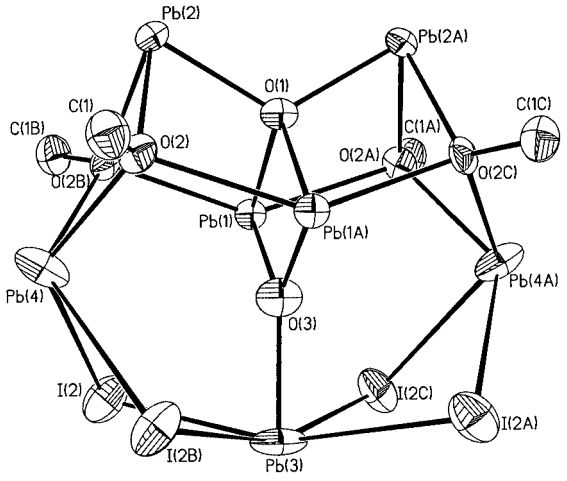

Formation and Structure of the Novel Heptanuclear Lead(II) Oxo Cluster $[Pb_7(\mu_3\text{-}O)(\mu_4\text{-}O)(\mu_3\text{-}OMe)_4(\mu_2\text{-}I)_4]I_2$ with an Unprecedented Cage Structure

Keywords: Lead / Cluster compounds / Alkoxides / Oxo ligands / Crystal structure

3214 **F. P. Pruchnik,* M. Bańbuła, Z. Ciunik, H. Chojnacki, M. Latocha, B. Skop, T. Wilczok, A. Opolski, J. Wietrzyk, A. Nasulewicz**

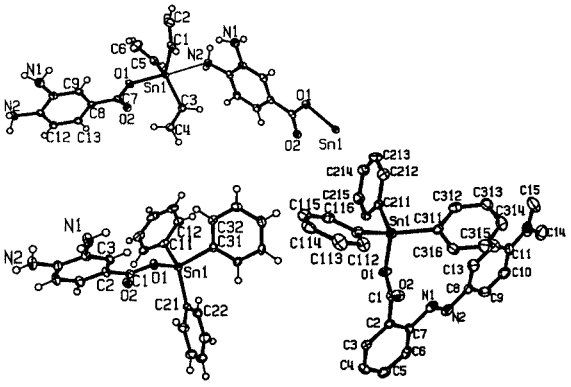

Structure, Properties and Cytostatic Activity of Triorganotin (Aminoaryl)carboxylates

Keywords: Tin / Cytostatic agents / Antitumor activity / O ligands

3222 **M. Pfeiffer, A. Murso, L. Mahalakshmi, D. Moigno, W. Kiefer, D. Stalke***

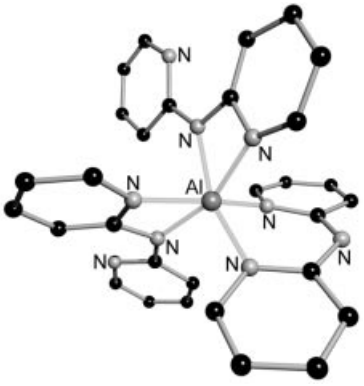

Experimental and Computational Study on a Variety of Structural Motifs and Coordination Modes in Aluminium Complexes of Di(2-pyridyl)-amides and -phosphanides

Keywords: Aluminium / Computational chemistry / Conformation analysis / N ligands / P ligands

3235 W. Malisch,* M. Hofmann, G. Kaupp, H. Käb, J. Reising

Si−H-Functionalized Ferriodisiloxanes: Synthesis from the Ferriodimethylsilanols $C_5R_5(OC)_2Fe-SiMe_2OH$ (R = H, Me) and Photoinduced Transformation into μ_2-Disiloxanediyl-Bridged Dinuclear Iron Complexes

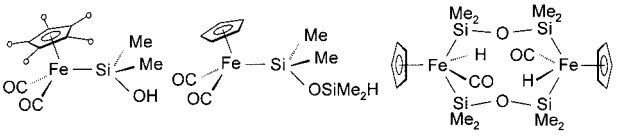

Keywords: Iron / Metallacycles / Oxidative addition / Silicon / Siloxanes

3242 W. Malisch,* M. Hofmann, M. Nieger, W. W. Schöller, A. Sundermann

Synthesis, Structural Characterization and Reactivity of the (Ferriomethyl)silanols $C_5R_5(OC)_2Fe-CH_2-SiMe(R')OH$ (R = H, Me; R′ = Me, Ph)

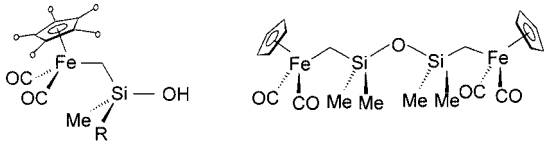

Keywords: Silicon / Iron / Oxygenation / (Metalloalkyl)silanols / Density functional calculations

3253 D. Magiera, W. Baumann, I. S. Podkorytov, J. Omelanczuk, H. Duddeck*

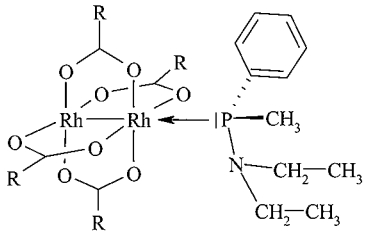

Stable $Rh_2(MTPA)_4$ Phosphane Adducts − The First Example of *P*-Chirality Recognition by ^{103}Rh NMR Spectroscopy

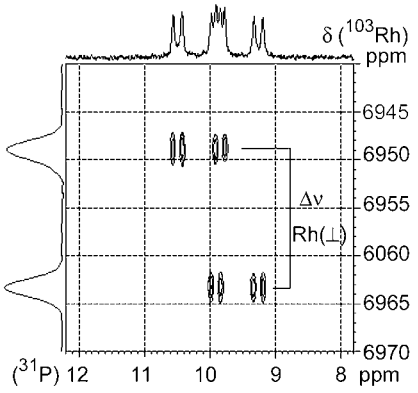

Keywords: Phosphanes / Rhodium / NMR spectroscopy / Chirality / Chiral discrimination

3258 L. Escriche,* J. A. Muñoz, R. Kivekäs, R. Sillapää, J. Casabó

Synthesis, Characterisation and Reactivity towards Pd^{II} and Pt^{II} of *ortho*-, *meta*- and *para*-Xylyl-Based Phosphorus-Containing Macrocycles

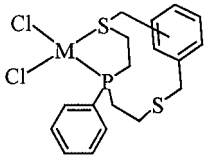

Keywords: Macrocycles / Palladium, Platinum / S ligands / Phosphanes

3264 M. Shi,* J.-K. Jiang, G.-L. Zhao

A Novel Chiral Silver(I) Complex from the Reaction of Thiazolidinethione with AgOAc

Keywords: Silver / Cluster compounds / S ligands / Structure elucidation

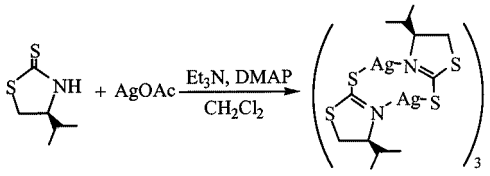

3268 C. von Hänisch,* P. Scheer, B. Rolli

Cyclic and Polycyclic Gallium-Antimony Compounds: Synthesis and Crystal Structures of $[GaCl(PnPr_2Ph)(SbSiiPr_3)]_2$ and $[(GaCl)_4(SbSiiPr_3)_4(PnPr_2Ph)_2]$

Keywords: Gallium / Antimony / Polycycles / Heterocycles / Semiconductors

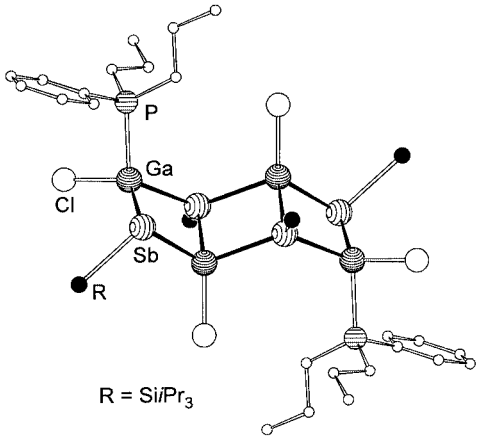

3272 L. Weber,* U. Lassahn, H.-G. Stammler, B. Neumann, K. Karaghiosoff

Synthesis and Structure of the Decanuclear Gold(I) Cluster Cation $[Au_8(AuCl)_2\{\mu_3\text{-}P(tBu)\}_2\{\mu\text{-}P(tBu)=C(NMe_2)_2\}_6]^{4+}$ with Bridging Phosphaalkene and Phosphanediide Ligands

Keywords: Cluster compounds / Gold / Phosphaalkenes / Phosphinidenes

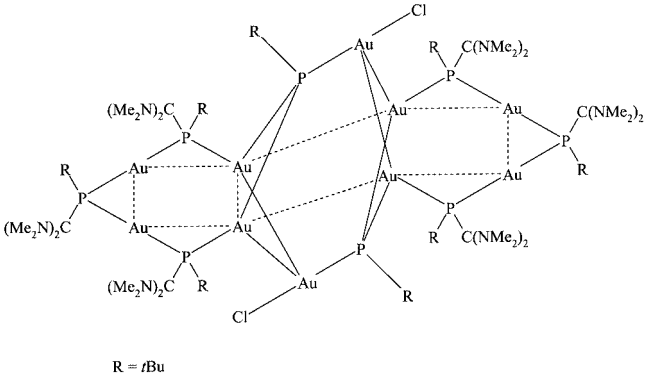

3278 O. Horner,* C. Jeandey, J.-L. Oddou, P. Bonville, C. J. McKenzie, J.-M. Latour

Hydrogenperoxo-$[(bztpen)Fe(OOH)]^{2+}$ and Its Deprotonation Product Peroxo-$[(bztpen)Fe(O_2)]^+$, Studied by EPR and Mössbauer Spectroscopy − Implications for the Electronic Structures of Peroxo Model Complexes

Keywords: EPR spectroscopy / Iron / Mössbauer spectroscopy / Peroxo ligands

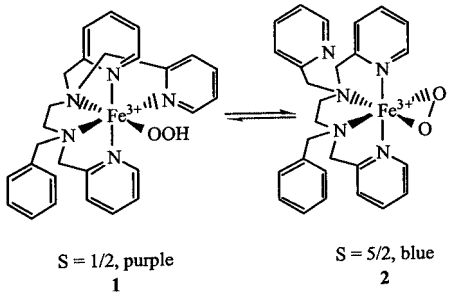

3284 **T. Darbre,* C. Dubs, E. Rusanov, H. Stoeckli-Evans**

Syntheses of Zinc Complexes with Multidentate Nitrogen Ligands: New Catalysts for Aldol Reactions

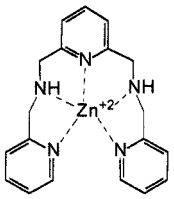

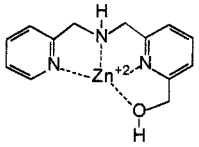

Keywords: Aldol reaction / Catalysis / N ligands / N,O ligands / Zinc

3292 **S. Dalai, P. S. Mukherjee, G. Rogez, T. Mallah,* M. G. B. Drew, N. R. Chaudhuri***

Synthesis, Crystal Structures, and Magnetic Properties of Two New 1D Copper(II) Coordination Polymers Containing Fumarate(−2) and Chelating N,N′-Donor as Ligands

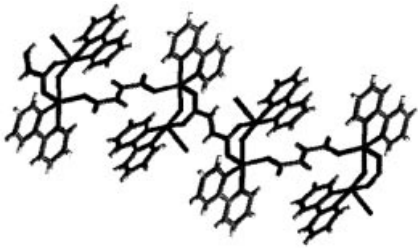

Keywords: Coordination polymers / Copper / Magnetic properties / N ligands

3298 **M. Czugler, L. Kótai,* B. Sreedhar,* A. Rockenbauer, I. Gács, S. Holly**

The Effect of HCl on the Copper(II) Chloride/Pyridine/Water System: Synthesis, Properties and Crystal Structure of $[(pyH)_2CuCl_4]$ and $[(pyH)_2Cu_3Cl_8(H_2O)_2]_n$

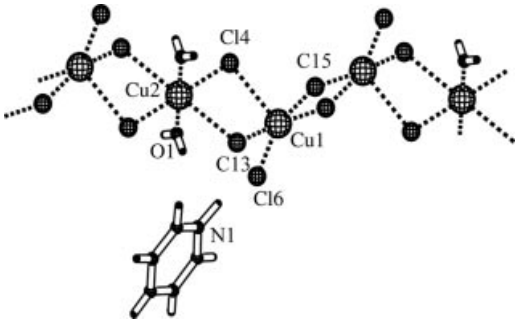

Keywords: Copper / IR spectroscopy / EPR spectroscopy / Hydrogen bonds

3305 **H.-F. Klein,* R. Beck, U. Flörke, H.-J. Haupt**

Steric Control of Cyclometallation Reactions in Schiff-Base Complexes of Cobalt(I) Containing an Anchoring Diphenylphosphanyl Group

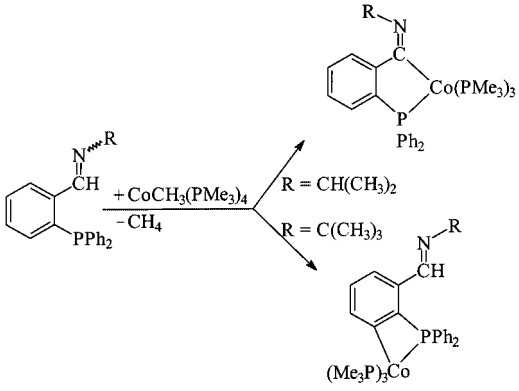

Keywords: Cyclometallation / Cobalt / P ligands / Schiff bases / Regioselectivity

3313 **S. Shova,* Gh. Novitchi, M. Gdaniec, A. Caneschi, D. Gatteschi, L. Korobchenko, V. K. Voronkova, Yu. A. Simonov, C. Turta**

Helical 1D Coordination Polymers − Structure and Magnetic Properties of *catena*-Poly[chloro-(μ-({2-[(hydroxyimino)methyl]phenoxy}acetato-*N*,*O*,*O*,O′)copper(II)]

Keywords: Copper / EPR spectroscopy / Magnetic properties / N ligands / O Ligands

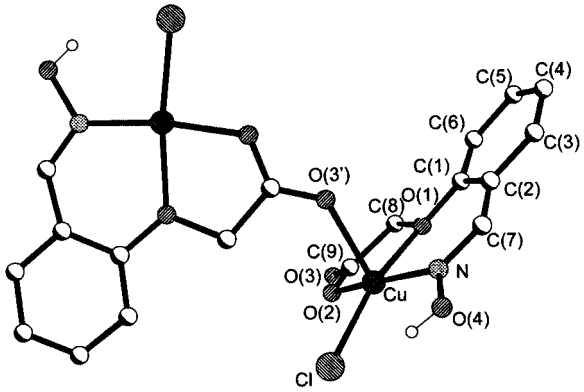

3319 **J. García-Antón, J. Pons,* X. Solans, M. Font-Bardia, J. Ros***

Synthesis of New Pd^{II} Complexes Containing Thioether−Pyrazole Hemilabile Ligands − Structural Analysis by ^{1}H and ^{13}C NMR Spectroscopy and Crystal Structures of $[PdCl_2(bddo)]$ and $[Pd(bddo)](BF_4)_2$ [bddo = 1,8-Bis(3,5-dimethyl-1-pyrazolyl)-3,6-dithiaoctane]

Keywords: Hemilabile ligands / N ligands / Palladium / S ligands

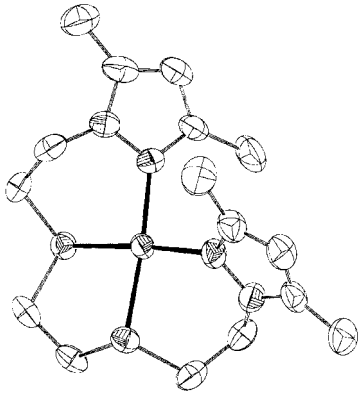

3328 **N. Millot, C. C. Santini,* B. Fenet, J. M. Basset**

Formation and Characterization of Zwitterionic Stereoisomers from the Reaction of $B(C_6F_5)_3$ and NEt_2Ph: (*E*)- and (*Z*)-$[EtPhN^+{=}CHCH_2{-}B^-(C_6F_5)_3]$

Keywords: Boranes / Aniline / Zwitterions / NMR spectroscopy

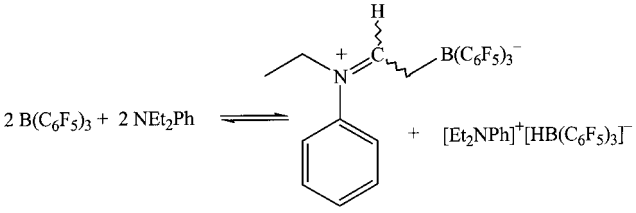

3336 **A. Zucca,* S. Stoccoro, M. A. Cinellu, G. Minghetti, M. Manassero, M. Sansoni**

Metallation of Unactivated Methyl Groups − Platinum(II) Derivatives with 6-Alkyl-2,2′-bipyridines

Keywords: Platinum / N ligands / Cyclometallation

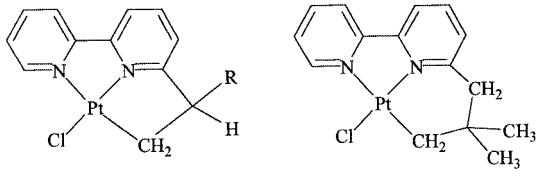

3347 **K. S. Gavrilenko, A. Vértes, G. Vanko, L. F. Kiss, A. W. Addison,* T. Weyhermüller, V. V. Pavlishchuk***

Synthesis, Magnetochemistry, and Spectroscopy of Heterometallic Trinuclear Basic Trifluoroacetates $[Fe_2M(\mu_3\text{-}O)(CF_3COO)_6(H_2O)_3]\cdot H_2O$ (M = Mn, Co, Ni)

Keywords: Heterometallic complexes / Carboxylate ligands / Magnetic properties / Iron / Manganese / Cobalt / Nickel / Trinuclear complexes

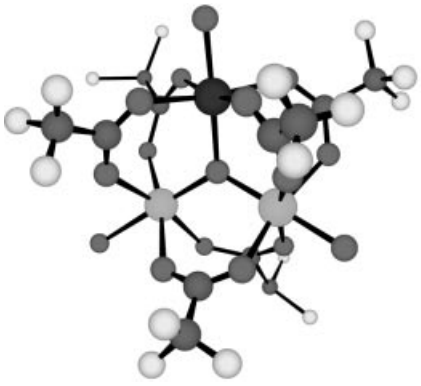

3356 **X.-J. Zheng, L.-P. Jin,* S.-Z. Lu**

Hydrothermal Syntheses, Structures, and Properties of First Examples of Lanthanide(III) 2,3-Pyrazinedicarboxylates with Three-Dimensional Framework

Keywords: Hydrothermal synthesis / Lanthanides / Coordination polymer / N ligands / O ligands

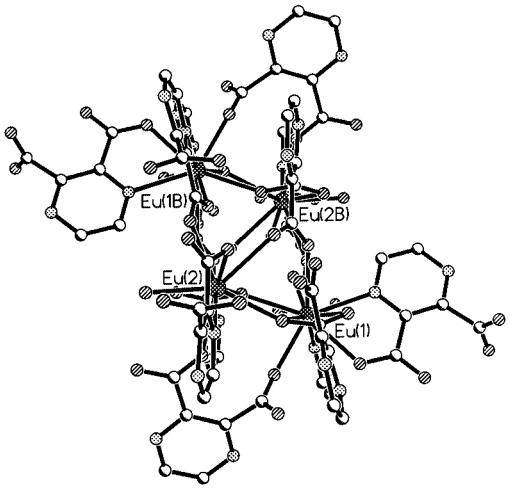

3365 **Index 2002**

Editorial staff and publishers express their thanks to all authors, referees, and readers for their continued trust, support, and interest over the past year and wish them a prosperous 2003.

Organometallic Chemistry: Structural Isomerization Reactions in Confined Environments

Neil J. Coville*[a] and Demetrius C. Levendis[a]

Keywords: Isomerization / Solid-state reactions / Surfaces / Organometallic chemistry / Rhenium

Reactions in the solution phase have dominated the development of chemistry. In recent years, however, the area of solid-state organic chemistry has undergone a renaissance, although the related area of organometallic chemistry is still in its infancy. Indeed, only a limited number of systematic studies on the reactions of organometallic compounds in a confined environment (on a surface, in a zeolite pore, in the bulk phase) have been reported. Herein we summarize some recent results on a specific reaction type in a confined environment, namely the isomerization reaction.
(© Wiley-VCH Verlag GmbH, 69451 Weinheim, Germany, 2002)

Introduction

The synthesis and characterization of ferrocene is regarded as the event that brought to life the area of organometallic chemistry.[1−3] This event, which took place in 1951, has led to the synthesis of many tens of thousands of organometallic complexes.[4,5] By the late 1980's many of the principles governing the synthesis and reactivity patterns in the discipline of organometallic chemistry had been established and the exotic complexes that had constantly been prepared were found to fit classical bonding patterns and theories.[6]

Much of this early chemistry was studied in solution, brought about by the ready availability of techniques such as IR and NMR spectroscopy. Studies in confined environments such as the solid state were more limited. While X-ray diffractometers were available, use of this technique was time consuming and studies were predominantly undertaken to determine the atom connectivity in complexes. The emphasis was certainly not on the study of reactions *in* the solid state. Developments in the last two decades in diffractometer design (such as the charge coupled device) have resulted in the determination of crystal structures now be-

[a] Molecular Sciences Institute, School of Chemistry, University of the Witwatersrand,
Johannesburg, 2050, South Africa
Fax: (internat.) +27-11/717-6749
E-mail: ncoville@aurum.chem.wits.ac.za

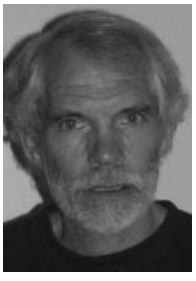

Neil Coville obtained his BSc (Hons) and MSc degrees at the University of the Witwatersrand (''Wits'') before proceeding to McGill University, Montreal where he obtained his PhD (1973) under the supervision of Ian Butler. After postdoctoral work at Harvard University with (the late) John Osborn he returned to Wits in 1976 where he has remained. He is currently the Director of the Molecular Sciences Institute and holds the Chair of Inorganic Chemistry in the School of Chemistry. His current research interests include Fischer−Tropsch chemistry, synthetic routes to carbon (and other) nanotubes, hard material synthesis and organometallic chemistry in the solid state.

Demi Levendis obtained his BSc (Hons) and MSc degrees at the University of the Witwatersrand. After obtaining his Honours degree he worked at the CSIR in Pretoria for three years, and returned to Wits to complete his PhD (1985). Thereafter he spent two years as a postdoctoral researcher with Philip Coppens at SUNY, Buffalo, New York and the Synchrotron (NLS) at Brookhaven National Laboratories. He went back to Wits to take up a full-time lecturing position. After a one year sabbatical with Ivan Bernal at the University of Houston, Texas, USA, he was promoted to Associate Professor, and in due course became team leader of the Jan Boeyens Structural Chemistry Laboratory and of the Structural and Computational Chemistry programme in the Molecular Sciences Institute of the School of Chemistry.

MICROREVIEWS: This feature introduces the readers to the author's research through a concise overview of the selected topic. Reference to important work from others in the field is included.

ing viewed as a routine analytical procedure in organometallic chemistry. Coupled to this has been the development of commercially available thermal equipment (examples include differential thermal analysis, differential scanning calorimetry, thermal gravimetric analysis, temperature programmed reduction) and surface equipment (atomic force microscopy, scanning tunneling microscopy). These and other related techniques have permitted studies of the composition/reactivity of *molecular* solids that was not available 20 years ago.

Classical inorganic complexes have been studied in the solid state for many years. Further, as pointed out by Braga and co-workers,[7] solid-state organic chemistry also has a long and rich history. The same, however, cannot be said for the area of organometallic chemistry.[8,9] The time thus seems appropriate for the development of the field of organometallic chemistry in confined environments,[10] with particular emphasis on reactions in the solid state.

There are a number of possibilities that need to be considered when describing a "confined" environment and these are listed below.

Supported Molecules

Much work has been carried out on supporting reagents on both inorganic and organic supports, for example on polymers,[11] dendrimers[12] and surfaces.[13] The study of the *chemical* interaction of molecules/ions with a surface has led to the development of SOMC (Surface Organometallic Chemistry), and the information that has been obtained has important implications for the generation of heterogeneous catalysts from organometallic precursors.[14−16] The methodology has also been exploited for the synthesis of organometallic complexes that can subsequently be extracted from surfaces.[17]

Matrix Isolated Complexes

This area of chemistry[18] constitutes another example of solid-state chemistry. In these studies, reactant molecules are generally isolated from each other by a matrix at low temperatures. Reactions are brought about typically by photolytic means and the surrounding matrix acts to modify the reactions of the deposited molecules. The information obtained has been used in the identification of reaction intermediates and pathways.

Molecules Encapsulated in Zeolites and Mesoporous Solids

The variable cavities, all of the same dimension, found in various zeolites and larger pore materials (e.g. MCM-41) provides a means of studying isolated, confined molecules.[19] The cavities range from 3−4 Å to 40−60 Å in width and thus reactions of small to very large molecules are possible.

Crystalline/Amorphous Materials

A molecule in the solid state is considered confined in a cavity generated by the other molecules surrounding it. The molecule is held rigidly in place. This type of solid contains two "types" of molecules: those in the bulk and those at the surface or situated at defects. When solids are heated they can undergo intra-atom/ligand rearrangements as well as inter-molecule rearrangements (e.g. phase changes). Interactions in the solid state *between molecules*, such as H-bonding and dipole-dipole interactions, can have similar energies to those found in covalent/ionic bonds. Braga and others have shown how interactions in organometallic molecular solids lead to the generation of 3-D networks,[7] and thus links directly to the area of supramolecular chemistry.[20]

Much of the focus of this Microreview will be on reactions in the solid state as opposed to reactions on a solid support. It will focus on isomerization reactions entailing physical (not chemical) interactions with the surrounding molecules. Others have highlighted the advantages/disadvantages in performing studies on organic materials in confined environments (e.g. the solid state). These include: solvent free synthesis, the use of enantioselective cavities, and modified reactivity patterns.[21,22] The same factors will apply to the study of organometallic chemistry in confined environments. Furthermore, the study of reversible gas adsorption by organometallic complexes in the solid state could expand the area of sensor studies,[23] while the polymerization of functional groups associated with ligands attached to metals could lead to the generation of new types of polymers.[24]

Isomerization Reactions of $[(CpMe)Re(CO)_2Br_2]$ — The Breakthrough

As with many entries into new areas of chemistry, serendipity played a crucial role for us. For many years we had been fascinated by the steric control displayed by cyclopentadienyl ligands in reactions.[25] This led us to consider methods of quantifying the size of substituted cyclopentadienyl ligands and to correlate steric measures (cone angle, solid angle) with physical parameters associated with the molecules under investigation. As part of our study we prepared a series of $[(CpR)Re(CO)_2Br_2]$ complexes and wished to determine the impact of the R group on the *cis*/*trans* isomer ratio of the complexes.[26] In attempting to purify *trans*-$[(CpMe)Re(CO)_2Br_2]$ by vacuum sublimation we noticed that the material that sublimed onto the cold probe was the *cis* isomer. We soon found that the isomerization reaction did not take place in the gas phase but occurred when the solid sample was simply heated in a flask at a temperature lower than the melting point of either of the isomers. Also surprising was the observation that in solution the isomerization reaction went in the *opposite direction* to that observed in the solid state i.e. the *cis* isomer converted into the *trans* isomer. It was clear that we had discovered a phase-dependent isomerization reaction (Figure 1). This suggested that the environment surrounding the molecule that was to rearrange (or more precisely, the cavity in which the molecule was situated) played a key role in the reaction.

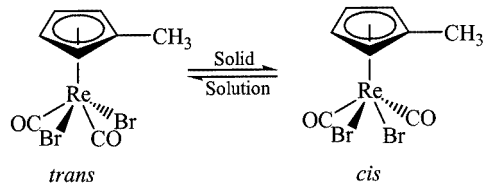

Figure 1. *cis* and *trans* isomers of $[(CpMe)Re(CO)_2Br_2]$

A procedure was developed to monitor the above solid-state reaction. This entailed placing small amounts of reactant in a degassed capillary or NMR tube and immersing the tube in an oil bath pre-set at the required temperature. At the end of a pre-determined time the material was removed from the oil bath and was ready for analysis (powder XRD, NMR or IR spectroscopy). The reaction was also monitored by optical microscopy using a specially designed temperature-controlled cell that allowed study under nitrogen.

Before proceeding with our follow up studies, it is worth digressing to indicate studies that had been undertaken by others prior to our finding, as well as some related current studies of pertinence to this Microreview.

Isomerization Reactions in the Solid State

Inorganic Molecules

Reactions of covalent molecules in the solid state have been studied for over 100 years and continue to be studied. Excellent reviews are available that have summarized the early work and thus these early studies will not be discussed in any detail here.[27,28]

Three types of isomerization reactions have been studied: racemization, *cis*/*trans* isomerization and linkage isomerization.

The *cis*/*trans* isomerization of simple four-coordinate compounds such as $[Pd(NH_3)_2X_2]$ (X = Cl, Br, I) continues to provide information on the isomerization reaction mechanism. In this specific case the reaction proceeds from the *cis* to the *trans* isomer in a process that entails the "breaking of Pd−X and Pd−N bonds".[29] Numerous six-coordinate Cr and Co compounds have also been studied.[30] It appears that the presence of water assists the *cis*/*trans* isomerization reaction of Co complexes, with dehydration playing a key role. Extensive studies, including single crystal studies, on the NO_2-ONO interconversion in complexes of the type $[Co(NH_3)_5NO_2]^{2+}$ have generated data on the role of pressure, light and cavity size on the reaction.[31] These studies provide a reference point for the study of organometallic complexes viz. typical reaction energies and reaction pathways.

Organic Molecules

Scientific investigations of solid-state organic chemistry dates back to (at least) the early 1800's but Schmidt and co-workers have been credited with the field's revival after their extensive investigations that led to the formulation of the topochemical principle.[32] One of the classic reactions that they described was the photodimerization of *ortho*-ethoxy-*trans*-cinnamic acid, a reaction that depends on which crystal polymorph is irradiated. It is cited in many reviews and textbooks, but a recent detailed analysis of three forms of *ortho*-ethoxycinnamic acid[33] has shown that factors other than the topochemical principles enunciated by Schmidt may apply. These other important factors that influence the course of solid-state reactions include the presence of solvates, planar defects, phase-transitions,[33] disorder and even crystal morphology.[34]

To date, several hundred high-yield solid-state syntheses involving numerous organic reaction types have been reported.[21] Two incentives driving the rapid development are the advantages of "solvent-free syntheses"[14] and the possibility of achieving novel or stereoselective products as a consequence of reactions in a constrained crystalline environment.

One of the predominant reaction types occurring in organic crystals is photo-dimerization/photo-polymerization, but since the 1980's many accompanying (and unique) isomerization reaction types have been reported.[35−37] These include thermal or photochemical interconversion between geometrical isomers, conformers and *E*/*Z* configurations. The interconversion between conformational isomers can occur with relatively low energy barriers in the solid, an occurrence that is sometimes referred to as conformational polymorphism.[38] However, the more space and energy demanding *E*/*Z* isomerization reactions do not generally obey the topochemical principle, and often proceed unidirectionally, either from the *Z* to *E* or from the *E* to *Z* configuration.[39] Mechanisms of solid-state isomerizations have been the subject of intense deliberation in recent years,[39−41] particularly since the application of new techniques such as scanning near field optical microscopy (SNOM) and atomic force microscopy (AFM), which have suggested, for example "phase-rebuilding" mechanisms.[39]

Organometallic Molecules

Three types of reactions can be envisaged for organometallic complexes: (i) isomerization of a ligand, (ii) isomerization at the metal, and (iii) isomerization in the crystal (phase change).

Isomerization of a Ligand

One of the earliest investigations of an isomerization/racemization reaction of an organometallic complex was the report by Ohashi and Sasada on the X-ray induced racemization reaction shown in Figure 2a [base = (*S*)-α-methylbenzylamine].[42] Of significance was the observation that the reaction occurred without crystal decay and this permitted a study of the mechanism of the reaction in a single crystal. Many publications, in which both the organic group and the base have been varied, have emanated from studies by Ohashi and co-workers since this report (Figure 2b). In these later papers they have shown:

a) racemization can be induced by exposure to a xenon lamp.[43,44]

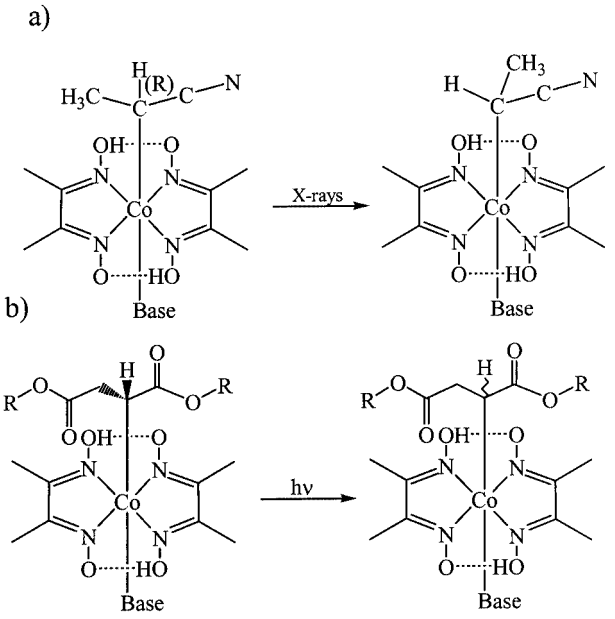

Figure 2. Cobaloxime racemization reactions: (a) X-ray induced [Base = (*S*)-α-methylbenzylamine, pyridine, PMe_2Ph etc.]; (b) light induced (bases as above, R = CH_3, C_2H_5, $CH{=}CH_2$)

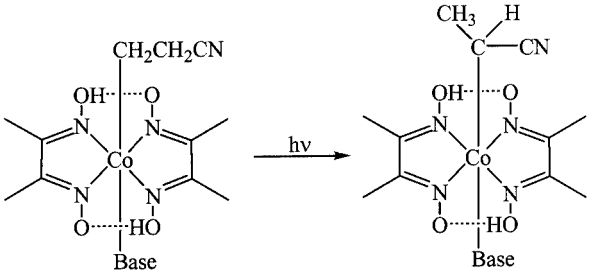

Figure 3. Cobaloxime isomerization reaction (e.g. B = 3-Mepyridine) (ref.[46])

b) isomerization reactions, for example of β-cyanoethyl to α-cyanoethyl ligands, with production of a scalemic chiral complex from a pro-chiral complex (Figure 3).[45,46]
c) asymmetric synthesis in a "cavity" i.e. generation of a preferred isomer from a racemic mixture.[47]
d) the detailed mechanism of the reaction by neutron diffraction studies entailing deuterium labelling experiments.[48–50]

By varying the R group and the base (situated below the cobaloxime ring) the ability of the R group to racemise or isomerise has been correlated with the concept of a reaction cavity.[51,52] In particular, the studies have shown that the reaction does not correlate with the density of the crystal (i.e. the packing of the whole molecule) but rather with the packing of the reactive group. The reaction cavity was defined as "*the space limited by a concave surface of spheres of the surrounding atoms around the reactive group in the crystal*".[51,52] Cavity volumes have been calculated and it has been observed that, in general, the larger the cavity volume the greater the reaction rate. For example, in a number of the complexes studied there are two crystallographically different molecules in the unit cell (i.e. two molecules per asymmetric unit). Comparison of volume data for the two independent molecules, A and B (Table 1), contained in the same crystal, reveals that inversion of the ligand only occurs when the cavity size exceeds a certain dimension and that selective reaction occurs, typically for the "B" molecules.[52] This relationship between reaction cavity size and reaction rate also holds for structures that contain only one molecule in the asymmetric unit (Table 1).

However, the *shape* of the cavity can also play a role. This is shown, for example, by studies on (cobaloxime)-Co[(*R*)-1,2-bis(ethoxycarbonyl)ethyl] (*S*)-1-phenylethylamine L complexes (Table 1).[43] Thus, the complex with L = pyridine racemizes on exposure to light, while the complex with L = PPh_2Me, with an equivalent cavity volume, does not. A detailed comparison of the shapes of the cavities revealed that movement of the ligand atoms in the cavity for L = PPh_2Me is not possible if an intact single crystal is to be maintained.

Isomerization at the Metal

Isomerization of six-coordinate complexes *in the ligand sphere* are also known. The first "organometallic-type" complexes to show *cis*/*trans* isomerization in the solid state

Table 1. Cavity volumes for cobaloxime complexes[a]

R	Base	*V* (Å^3) A	B	Molecule racemised	Ref
(*R*)-1-cyanoethyl[b]	4-cyanopyridine	7.97	10.37	B only	[51]
PPh_2Me	17.08	18.01	A and B	[51]	
3-methylpyridine	10.24	14.29	B > A	[51]	
piperidine	7.0	14.2	B	[47]	
(*R*)-1,2-bis(ethoxycarbonyl)ethyl[c]	(*S*)-1-phenylethylamine	68.8	–	none	[43]
pyridine	76.5	–	yes	[43]	
propylamine	58.9	–	none	[43]	
PPh_2Me	75.8	–	none[d]	[43]	
(*R*)-1,2-bis(methoxycarbonyl)ethyl	PPh_2Me	47.4	55.0	B only	[44]

[a] Structures are given in Figure 2. [b] Two independent molecules were found per asymmetric unit (A and B). Each has a different cavity size and the reaction only occurs in the larger cavity (ref.[51]). [c] Structures given in Figure 2b. [d] Reaction expected, but shape of the cavity did not allow for reaction.

were reported by Nelson and co-workers.[53,54] In this study a series of Ru complexes underwent *trans* to *cis* rearrangements, as shown in Figure 4, and the solution data suggested the movement of the bulky phosphane group in the isomerization reaction (ttt to ccc and ccc to cct, Figure 4a). In the solid state the reaction could occur via the interchange of only two small groups. We have recently measured the activation energy of the isomerization reaction (ttt to cct) in the solid state for a range of these complexes and find that the values fall in the range 70 ± 20 kJ·mol^{-1}, values that are consistent with a simple ligand-rotation process.[55]

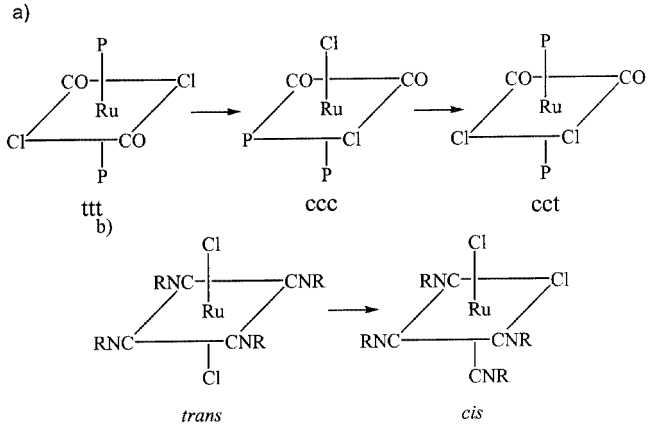

Figure 4. Solid-state isomerization reactions: (a) $[Ru(CO)_2P_2Cl_2]$ (P = phosphane) and (b) $[RuCl_2(RNC)_4]$

In a related study some Ru isocyanide complexes (Figure 4b) were also shown to undergo *trans* to *cis* isomerization in the solid state.[56]

Another type of isomerization reaction that occurs in the solid state is the η^1-acetylene to vinylidene rearrangement

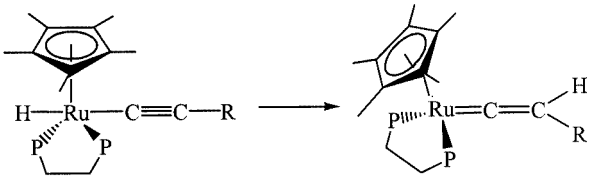

Figure 5. An η^1-alkynyl to vinylidene conversion of $[(C_5Me_5)RuH(diphos)(\eta^1\text{-}CCR)]$ in the solid state

reaction (Figure 5).[57] This reaction involves the migration of an H-atom from the metal to the ligand. Numerous examples of this reaction type have been reported.[9]

Isomerization in the Crystal

It appears that this is a little explored area in the field of solid-state organometallic chemistry. The relationship between phase transitions and chemical reactions has been the subject of continued debate.[38] One well-known example is that of ferrocene, which can exist in three distinct configurations, [staggered (D_{5d}), eclipsed (D_{5h}) and D_5] in the crystalline form, and can transform between these configurations as the crystals undergo phase transitions between different stable polymorphs.[38] In more recent work, Braga et al. reported on the fascinating solid-solid phase transition and solid-state reaction of bis(formyl)ferrocene.[58]

Isomerization of $CpML_4$ Complexes in the Solid State

The discovery of the solid-state isomerization reaction of $[(CpMe)Re(CO)_2Br_2]$ posed many interesting questions — how general is the reaction?, what are the factors that determine the direction of the reaction?, what is the mechanism of the reaction? These and other questions have provided the basis for our ongoing investigation into this area of organometallic chemistry.

Generality of the Reaction

The first issue addressed was to establish the breadth of the reaction.

Variation of the Substituents on the Cyclopentadienyl Ring

A series of $[(CpR)Re(CO)_2Br_2]$ (R = $SiMe_3$, *t*Bu, Et, C_6H_{11}) complexes was prepared but none of these complexes underwent *trans*/*cis* isomerization in the solid state.[26] Indeed, melting occurred prior to isomerization and *isomerization was found to occur in the melt.* Interestingly reaction also occurred from the *trans* to the *cis* isomer in the melt. Later studies have shown that for R = *i*Pr, a solid-state reaction does take place (Table 2).[59] Attempts to extend the reaction to disubstituted ring complexes such as $[\{Cp(SiMe_3)_2\}Re(CO)_2Br_2]$ were also made, but again the new complexes did not isomerise in the solid state.[60]

Variation of the L Groups

Substitution of CO in $[(CpR)Re(CO)_2Br_2]$ (R = Me, *t*Bu, $SiMe_3$) by L (L= phosphanes, phosphites and isocyanides) using NMe_3O-induced CO displacement techniques[61] readily gave the $[(CpR)Re(CO)LBr_2]$ complexes in good yield. Typically more than 80% of the product was synthesized as the *trans* isomer (Table 2).[62] These complexes all isomerize completely in the solid state — in every instance from the *trans* to the *cis* isomer. This is the same direction as found for the solution state isomerization reaction.

Variation of the Metal

Extension of the reaction to complexes of the type $[(CpR)M(CO)_2LX]$ (Figure 6; M = Mo, W; R = Me, Et etc.; L = phosphites, phosphanes, isocyanides; X = Br, I) has also been achieved.[63,64] Reaction of $[(CpR)M(CO)_3X]$ with L (in the presence of NMe_3O) gave a mixture of *cis*/*trans* isomers that could be separated by column chromatography. Reactions performed on either the pure *cis* or *trans* isomers gave the same *cis*/*trans* isomer equilibrium ratio (typically 65:35) in the solid state. The reaction goes from either direction to yield equilibrium mixtures of the two isomers, but the reaction is accompanied by decomposition (see below).

Interestingly, there have been two other reports of solid-state reactions of similar group 6 metal complexes in the literature. In a short comment Barnett and co-workers reported that $[CpMo(CO)_2\{P(nBu)_3\}I]$ isomerizes from the

Table 2. Thermal solid-state isomerization reactions of $[(CpR)Re(CO)LX_2]$[a]

Complex	M.p. (°C)	Reaction temp. (°C)	Yield (%)
trans-$[(\eta^5\text{-}C_5H_4Me)Re(CO)_2Br_2]$	116−118	105−107	98
cis-$[(\eta^5\text{-}C_5H_4Me)Re(CO)_2Br_2]$	158−160		
trans-$[(\eta^5\text{-}C_5H_4$*i*Pr$)Re(CO)_2Br_2]$	112−114	97−99	95
cis-$[(\eta^5\text{-}C_5H_4$*i*Pr$)Re(CO)_2Br_2]$	127−129		
trans-$[(\eta^5\text{-}C_5H_4Me)Re(CO)_2BrI]$	125−127	108−110	85
cis-$[(\eta^5\text{-}C_5H_4Me)Re(CO)_2BrI]$	135−137		
trans-$[(\eta^5\text{-}C_5H_4Me)Re(CO)\{P(OMe)_3\}Br_2]$	114−116	100−105	96
cis-$[(\eta^5\text{-}C_5H_4Me)Re(CO)\{P(OMe)_3\}Br_2]$	116−118		
trans-$[(\eta^5\text{-}C_5H_4Me)Re(CO)\{P(OPh)_3\}Br_2]$	164−166	145−150	80
cis-$[(\eta^5\text{-}C_5H_4Me)Re(CO)\{P(OPh)_3\}Br_2]$	183−185		
trans-$[(\eta^5\text{-}C_5H_4Me)Re(CO)(PPh_3]Br_2]$	186−188	145−150	72
cis-$[(\eta^5\text{-}C_5H_4Me)Re(CO)(PPh_3]Br_2]$	200−202		
trans-$[(\eta^5\text{-}C_5H_4Me)Re(CO)(NCC_6H_3Me_2)Br_2]$	154−156	140−145	86
cis-$[(\eta^5\text{-}C_5H_4Me)Re(CO)(NCC_6H_3Me_2)Br_2]$	192−194		
trans-$[(\eta^5\text{-}C_5H_4Me)Re(CO)(NCC_6H_3Me_2)BrI]$	155−157	135−140	85
cis-$[(\eta^5\text{-}C_5H_4Me)Re(CO)(NCC_6H_3Me_2)BrI]$	193−195		
trans-$[(\eta^5\text{-}C_5H_4$*t*Bu$)Re(CO)(NCC_6H_3Me_2)Br_2]$	142−144	130−135	94
cis-$[(\eta^5\text{-}C_5H_4$*t*Bu$)Re(CO)(NCC_6H_3Me_2)Br_2]$	194−196		
trans-$[(\eta^5\text{-}C_5H_4$*t*Bu$)Re(CO)\{P(OMe)_3\}Br_2]$	123−125	103−110	82
cis-$[(\eta^5\text{-}C_5H_4$*t*Bu$)Re(CO)]\{P(OMe)_3\}Br_2]$	154−156		
trans-$[(\eta^5\text{-}C_5H_4$*t*Bu$)Re(CO)\{P(O$*i*Pr$)_3\}Br_2]$	126−128	105−110	70
cis-$[(\eta^5\text{-}C_5H_4$*t*Bu$)Re(CO)\{P(O$*i*Pr$)_3\}Br_2]$	170−172		
trans-$[(\eta^5\text{-}C_5H_4$*t*Bu$)Re(CO)(PPh_3)Br_2]$	172−174	140−145	85
cis-$[(\eta^5\text{-}C_5H_4$*t*Bu$)Re(CO)(PPh_3)Br_2]$	190−192		
trans-$[(\eta^5\text{-}C_5H_4$*t*Bu$)Re(CO)\{P(OPh)_3\}Br_2]$	124−126	108−110	85
cis-$[(\eta^5\text{-}C_5H_4$*t*Bu$)Re(CO)\{P(OPh)_3\}Br_2]$	158−160		
trans-$[(\eta^5\text{-}C_5H_4SiMe_3)Re(CO)(NCC_6H_3Me_2)Br_2]$	144−146	130−135	76
cis-$[(\eta^5\text{-}C_5H_4SiMe_3)Re(CO)(NCC_6H_3Me_2)Br_2]$	179−181		
trans-$[(\eta^5\text{-}C_5H_4SiMe_3)Re(CO)\{P(O$*i*Pr$)_3\}Br_2]$	106−108	90−95	70
cis-$[(\eta^5\text{-}C_5H_4SiMe_3)Re(CO)\{P(O$*i*Pr$)_3\}Br_2]$	159−161		
trans-$[(\eta^5\text{-}C_5H_4SiMe_3)Re(CO)(PPh_3)Br_2]$	155−157	130−135	75
cis-$[(\eta^5\text{-}C_5H_4SiMe_3)Re(CO)(PPh_3)Br_2]$	187−189		
trans-$[(\eta^5\text{-}C_5H_4SiMe_3)Re(CO)\{P(OPh)_3\}Br_2]$	124−126	108−110	85
cis-$[(\eta^5\text{-}C_5H_4SiMe_3)Re(CO)\{P(OPh)_3\}Br_2]$	154−156		

[a] Reaction goes from the *trans* to the *cis* isomer.

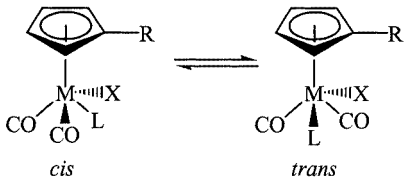

Figure 6. *cis* and *trans* isomers of $[(CpR)M(CO)_2LX]$ (M = Mo, W; L = phosphane, phosphite, isocyanide; X = halide)

cis to the *trans* isomer on standing at room temperature.[65] Also, while our work was in progress, Filippou and coworkers reported on the isomerization reaction (*cis* to *trans*) of $[(C_5R_5)W(CO)_2(PMe_3)GeCl_3]$ (R = H, Me) and $[(C_5Me_5)\text{-}Mo(CO)_2(PMe_3)GeCl_3]$ in the solid state.[66]

Variation of the Halide

$[(CpMe)Re(CO)_2I_2]$ was synthesized (see below) and, remarkably, this complex isomerized from the *cis* to the *trans*

isomer (>90%) — the reverse of the reaction for [(CpMe)Re(CO)$_2$Br$_2$].[67] The isomerization reaction, which takes place in the melt, and possibly the solid state, is more rapid for the iodo complex than for the bromo complex.[26][68] The mixed-halide complex [(CpMe)Re(CO)$_2$IBr] has also been synthesized and isomerizes from the *trans* (dihalide) to the *cis* (dihalide) isomer. More interestingly, reaction of [(CpMe)Re(CO)$_2$IBr] with 2,6-Me$_2$C$_6$H$_3$NC (RNC) yields [(CpMe)Re(CO)(RNC)IBr], a complex with *five different* substituents. This complex also undergoes a *trans* to *cis* isomerization reaction in the solid state (Table 2) and should provide interesting information on subtle features associated with the reaction mechanism (see below).[59]

From the above it can be seen that the reaction type is quite general and no doubt many other "pseudo" five-coordinate complexes will be discovered that will show solid-state isomerization behavior. However, no obvious pattern can be established that indicates which complexes will indeed isomerize and even the direction undertaken in the isomerization reaction. The data do however indicate that: (a) the isomerization can occur in the solid state if the temperatures of the melting point and the isomerization reaction are well separated, but that this in itself is not a sufficient criterion for isomerization to occur, and (b) reaction occurs from the complex with the lower melting point to that with the higher melting point.

Factors that Drive the Reaction

General Considerations

If a unidirectional isomerization reaction occurs in the solid state it suggests that the *kinetic* product is obtained during the precipitation reaction and that the *thermodynamic* product is formed on heating the solid. Either inter- or intramolecular interactions or, combinations of both factors, can drive the reaction to the thermodynamically favored product in the solid state. A more important question that has to be addressed is: does the isomerization reaction drive the change in the overall structure or do changes in the bulk structure drive the isomerization reaction?

Further, the reaction can be viewed as occurring by independent individual reactions in cavities (topotactic reaction[69]) *or* by a concerted process in which a rearrangement within a molecule (or between molecules) drives molecules in close proximity to rearrange.[70] In this latter instance the surface and defects will play an important role in the reaction.

Intramolecular Factors

Here both steric and electronic factors could play a role in determining the favored isomer. Indeed, reactions in solution are normally rationalized using these factors (e.g. *cis* and *trans* effects, cone angles, solid angles etc.). Data need to be evaluated from crystallographic analyses and it can be expected that even small *inter*molecular effects could be difficult to eliminate in the analysis.

Intermolecular Effects

The close proximity of atoms in the solid state can lead to attractive forces that could lead to the preference of one structure (e.g. isomer) over another; these forces could override intramolecular factors. These effects can, in principle, be detected by unit cell volume changes, measurement of bond lengths/angles and phase changes.

Attempts to Determine Factors that Influence the Isomerization Reaction

X-ray structural analyses

Structure determinations were undertaken for both isomers of a series of Re complexes in an attempt to evaluate the factors responsible for the reaction direction.[71−73] Three pairs of *cis*/*trans* isomers were chosen for study. The structures covered the range in which isomerization occurred with {[(CpMe)Re(CO)$_2$Br$_2$]} and without {[(CpMe)-Re(CO){P(OPh)$_3$}Br$_2$]} single crystal disintegration, and a *cis*/*trans* pair in which no isomerization was detected {[(Cp*t*Bu)Re(CO)$_2$Br$_2$]}.

Table 3. Structural parameters for *cis* and *trans* isomers of [(CpR)Re(CO)LBr$_2$] complexes [R = *t*Bu, Me; L = CO, P(OPh)$_3$] (taken from refs.[71−73])

Complex	Space group		V (Å^3)[a]		Dir[b]
	cis	trans	cis	trans	
[(CpMe)Re(CO)$_2$Br$_2$]	$P2_1/c$	$P\bar{1}$	1078	535	t→c
[(Cp*t*Bu)Re(CO)$_2$Br$_2$]	$P2_1/a$	Pbca	1375	2829	nr
[(CpMe)Re(CO){P(OPh)$_3$}Br$_2$]	$P2_1/c$	$P2_1/c$	2468	2481	t→c

[a] Note that in some instances there are half the number of molecules per unit cell. [b] Dir = direction of the isomerization reaction in the solid state.

Key data are shown in Table 3. Analysis of this data reveals that:

a) No correlation between volume changes and the isomerization reaction/direction is apparent.

b) No unusual inter-atomic bond lengths are noted (see refs.[71−73]).

c) A change in space group does not rule out an isomerization reaction.

d) The single crystal to single crystal reaction of [(CpMe)Re(CO){P(OPh)$_3$}Br$_2$] occurs in the same space group but this is not a necessary requirement for a single crystal reaction to occur.

Powder diffraction studies carried out on [(CpMe)Re-(CO)$_2$Br$_2$] revealed that the *cis* isomer generated by heating the *trans* isomer is identical to the *cis* isomer prepared independently in the solution reaction. Thus, no polymorphs were produced in the reaction.[72]

Molecular Mechanics Calculations

Attempts were made to determine the preferred isomer of [(CpMe)Re(CO)$_2$Br$_2$] by use of molecular mechanics and

semi-empirical methods, both for the isolated molecules and for the crystalline form. The data did not distinguish between the two isomers.[74] The failure of this analysis related to our inability to correctly allow for the evaluation of intermolecular interactions in our calculations. More sophisticated analyses may assist here.

Differential Scanning Calorimetry (DSC) Data

An extensive DSC study of selected Re samples revealed that the position and shape of exotherms, corresponding to the isomerization reaction, were influenced by both heating rates and crystal dimensions.[75] Indeed, at high heating rates (e.g. 20 °C/min) simultaneous melting and isomerization reactions could be detected.

Initially it appeared that the DSC technique could be used to screen isomers for their ability to transform in the solid state. However, some recent results obtained from studies on [(CpMe)Mo(CO)$_2$LI] [L = PPh$_3$, P(O*i*Pr)$_3$] have indicated cases in which isomerization occurs in the solid state but without the presence of an accompanying exotherm being detected by DSC. When the above reactions are monitored by NMR spectroscopy at temperatures below 100 °C, isomerization is noted yet no DSC exotherm is detected in the DSC profile.[63][64] The exotherms noted at temperatures above 100 °C correspond to decomposition reactions. A combination of DSC, powder XRD, solution NMR studies of reactants and optical microscopy studies of the Mo complexes reveals that isomerization commences prior to decomposition of the *cis* isomer to give as yet unidentifiable Mo complexes and OPPh$_3$.[64]

The inability to detect a DSC exotherm corresponding to a chemical reaction has been commented on by Dunitz[76] and reveals the danger of using only one technique to evaluate changes in a reaction.

Optical Microscopy Studies

An optical microscopy study of the Re complexes indicated that both crystal fragmentation and the presence of single crystal to single crystal reactions could be detected by this procedure. Two examples are described. In the first instance the isomerization of *trans*-[(CpMe)Re(CO)$_2$Br$_2$] was monitored as a function of time, and pictures taken at t = 0.5 h, 1 h, 3 h, 3 h (expanded) are shown in Figure 7. Disintegration of the crystal can be seen on the crystal edges after 1 h and indeed darkening (formation of the *cis* isomer) within the crystal can also be detected. The isomerization occurs with formation of a *new crystalline material*, as seen in Figure 7d, which is an expanded portion of the top left hand corner of Figure 7c.

Figure 8 shows the isomerization reaction of *trans*-[(CpMe)Re(CO)(2,6-Me$_2$C$_6$H$_4$NC)Br$_2$] with time (t = 0 h, 2 h, 6 h, 17 h). Darkening (corresponding to formation of the *cis* isomer) can be seen to occur at the surface as well as at cracks on the surface. The surface becomes rough with time but essentially the crystal remains single. No obvious pattern relating to the isomerization can be detected at this magnification. However, studies by Kaupp, using scanning tunneling microscopy (STM) on reactions in organic crystals, have suggested that "phase rebuilding" should be expected in many solid-state reactions, and indeed could be occurring here.[77]

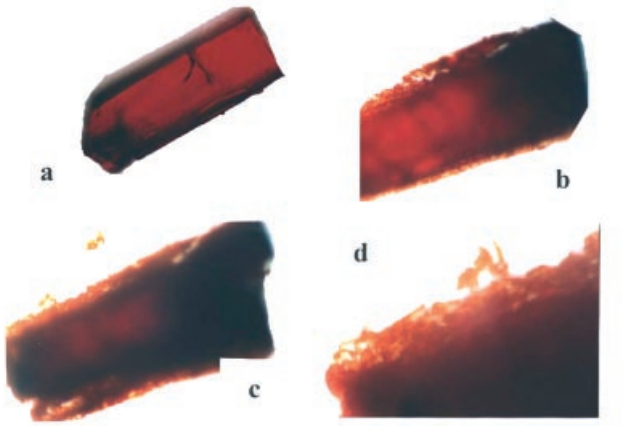

Figure 7. The isomerization of *trans* [(CpMe)Re(CO)$_2$Br$_2$] as a function of time (a = 0.5 h, b = 1 h, c = 3 h, c = 3 h − at higher magnification)

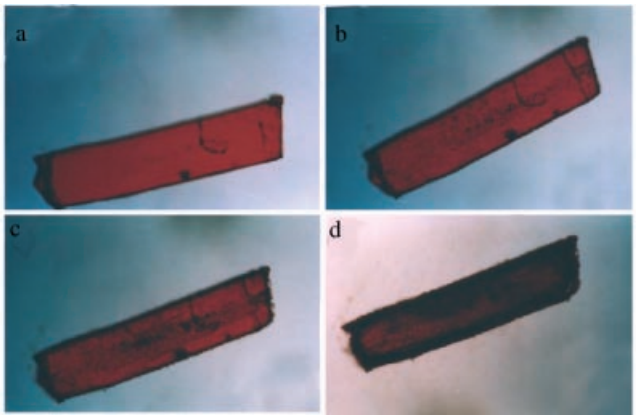

Figure 8. The isomerization of *trans*-[(CpMe)Re(CO)(2,6-Me$_2$C$_6$H$_4$NC)Br$_2$] as a function of time (a = 0 h, b = 2 h, c = 6 h, d = 17 h)

In the case of [(CpMe)Re(CO){P(OPh)$_3$}Br$_2$] (data not shown) the crystal retained its crystallinity throughout the isomerization reaction as determined by optical microscopy. Interestingly, when the crystal appeared to be completely converted, as detected by a homogeneous dark surface coloring under the optical microscope, only 22% of the *cis* isomer was detected by X-ray crystallography.

All the data is thus consistent with reactions commencing at the surface (or at defects). For all three Re compounds the pictures clearly reveal the heterogeneous nature of the reaction.

Reaction Mechanism

Two extreme mechanisms can be envisaged: (a) all ligands are attached to the metal atom, or (b) some ligands dissociate/re-associate (either as ions, atoms or molecules) in the reaction.

The reaction mechanism for the solution state *cis-trans* isomerization reaction of $[CpMo(CO)_2LX]$ complexes was studied in the 1970's by Faller,[78,79] Poilblanc[80] and coworkers. Faller proposed a mechanism based on a variation of a Berry pseudorotation model. The lowest energy pathway in the reaction involves a trigonal bipyramidal intermediate with the Cp ring and the L group in axial positions (Figure 9). In this mechanism all groups move extensively, a situation made possible in a solvent.

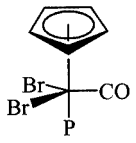

Figure 9. A proposed intermediate/transition state for the *cis*/*trans* isomerization reaction of $[CpMo(CO)_2LX]$ (ref.[79])

In an early attempt to evaluate the mechanism of the isomerization reaction in the solid state we carried out a structure correlation analysis of a wide range of ML_5 complexes using the Cambridge Structural Database.[81] Our data indicated that a modified Berry−Turnstile mechanism could fit the data (see Figure 10). For example, the isomerization of $[(CpMe)Re(CO)\{P(OPh)_3\}Br_2]$ could be rationalized with a mechanism that requires the two bulky groups [Cp, $P(OPh)_3$] to act as pivots while the movement of the three small groups undergoes rotation around a threefold axis through the metal. Some motion of the bulky groups (e.g. flexing) to accommodate the isomerization reaction is possible but the key feature entails rotation of the three non-bulky groups in the reaction.

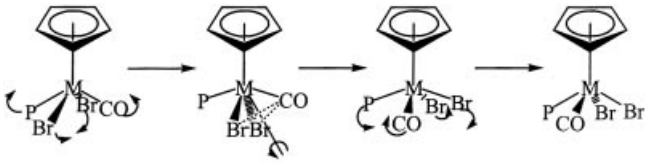

Figure 10. Proposed isomerization reaction for $[(CpMe)Re(CO)\{P(OPh)_3\}Br_2]$ based on the movement of three ligands. (ref.[81])

A recent study has led to a more detailed understanding of the reaction mechanism.[73] The single crystal to single crystal reaction of $[(CpMe)Re(CO)\{P(OPh)_3\}Br_2]$ was monitored by X-ray crystallography as a function of time. A consideration of the electron density changes indicated that only *one* of the Br ligands exchanges with the CO ligand. This suggests that the mechanism for the isomerization reaction entails rotation of the CO and one of the Br groups by 180° around an axis through the metal (Figure 11). This unexpected result relates to the size of the "cavity" in which a $[(CpMe)Re(CO)\{P(OPh)_3\}Br_2]$ molecule is confined. The second Br group is close to the ring Me group and appears to be sterically constrained in the lattice. A plot of the unit cell down the *b* axis suggests that there is a cavity of sufficient size to allow for the two-atom rotation. Notwithstanding this, the optical microscopy study also suggests that the reaction may be initiated from the "cavity surface" by a phase rebuilding process (see above).

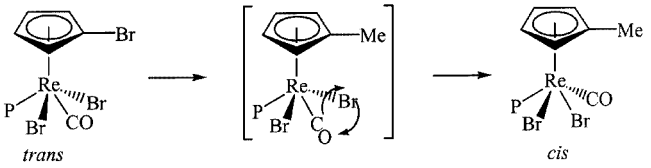

Figure 11. Proposed isomerization reaction for $[(CpMe)Re(CO)\{P(OPh)_3\}Br_2]$ based on the movement of two ligands

The electron density maps recorded as a function of isomer conversion suggested that the rotation occurs such that the CO (not the Br) ligand approaches the ring. In the rotation process, the other ligands could flex to allow for formation of a larger cavity. Indeed, the issue of a fixed versus flexible cavity *in general* is topical and currently under investigation.[82]

The *trans* to *cis* isomerization reaction of $[(CpMe)Re(CO)\{P(OPh)_3\}Br_2]$ has been monitored as a function of temperature (115−150 °C) (Figure 12).[83] The kinetic study suggests that the reaction is first order, but that two first order terms are required to give a good fit to the data. The smaller term derived from the rate expression has tentatively been assigned to an annealing process that follows the isomerization reaction.[73] An activation energy of 100 ± 9 $kJ \cdot mol^{-1}$ has been measured for the reaction.[83]

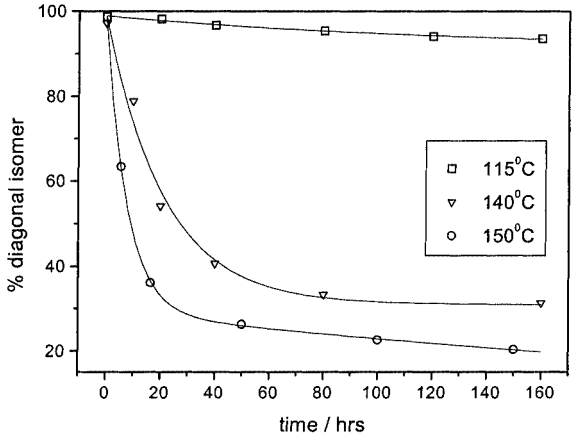

Figure 12. The *trans* to *cis* isomerization reaction of $[(CpMe)Re(CO)\{P(OPh)_3\}Br_2]$ as a function of temperature (115−150 °C)

These data do not as yet differentiate between the possibility of a process in which the two exchanging atoms (Br, CO) are bonded at all times to Re and one in which the Re−Br bond is cleaved and then reforms. (It is unlikely that CO dissociates during the reaction as the high temperatures required to induce isomerization, typically 110 °C to 145 °C, would result in loss of CO from the crystal).

Experiments to evaluate the possibility of halide-metal bond cleavage occurring during the isomerization reaction were performed. Reaction of *trans*-$[(CpMe)Re(CO_2)Br_2]$ with NaI (excess) gave *trans*-$[(CpMe)Re(CO_2)I_2]$ in quantit-

ative yield.[26] Although this suggests a mechanism entailing halide exchange the finding may not have bearing on the isomerization reaction. Studies on [(CpMe)Re(CO)$_2$BrI] are currently underway to evaluate this issue further.

Isomerization of CpML$_4$ Complexes in Matrices

Hill and co-workers have investigated photochemically induced isomerization reactions in frozen matrices for a range of CpML$_4$ complexes.[84−88] The results of the investigations can be summarized as follows:

i) For complexes of the type [CpRe(CO)$_2$Br$_2$] and [CpM(CO)$_2$LX] (Mo, W), photolysis induces *CO loss* and the intermediates formed at low temperature (e.g. 12 K) either retained (Mo, W) or lost (Re) the geometry of the starting isomer. At higher temperatures (100 K) the Mo and W *cis*/*trans* isomers inter-converted (Figure 13).[84]

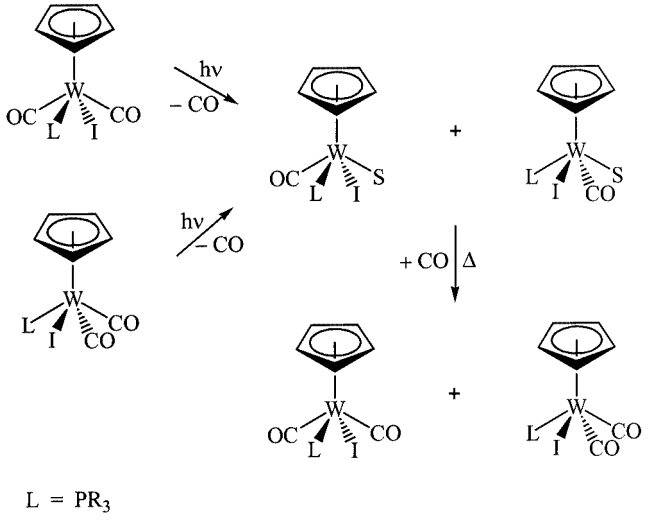

Figure 13. Photolysed low temperature *cis*/*trans* isomerization reaction of [CpW(CO)$_2$LI] (ref.[84])

ii) The isomerization ratio was similar to data observed in solution.

These data again indicate the powerful role played by the reaction cavity in the reaction. In this instance, the cavity acts to limit movement of CO away from the metal, but even under the conditions studied, preferential isomerization is seen to occur.

Isomerization of CpML$_4$ Complexes on Surfaces

Surfaces provide a range of active functional groups with which a molecule can interact. Indeed, chemical reactions between a molecule and a surface (chemisorption) provide a means to synthesize both catalysts and new reagents. To the best of our knowledge this interaction has not been exploited in isomerization reactions. However, the exploitation of the interaction of a molecule with a surface via weak dipole or van der Waals interactions to induce isomerization reactions has been reported (see below).

Hill and co-workers [88] have studied the photolytic isomerization of [(C$_5$Me$_5$)Re(CO)$_2$Br$_2$] on Si (111) surfaces at low temperature. The reaction occurred from the *cis* to the *trans* isomer, the same direction as found in solution. Photolysis of the intermediate produced at low temperature generated a second unsaturated isomer that gave the *cis* isomer on warming. (Figure 14).

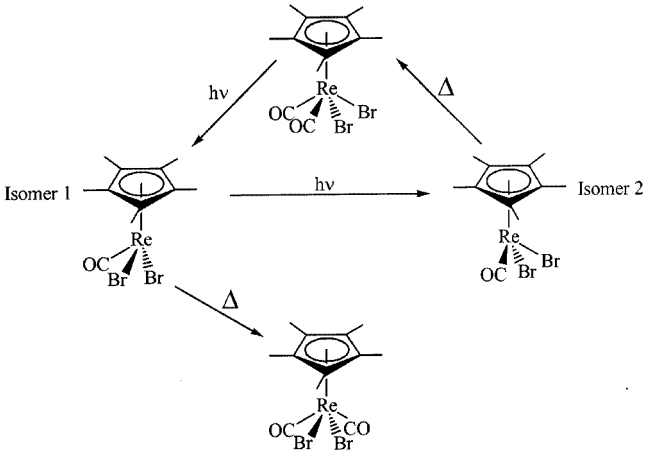

Figure 14. *cis*/*trans* isomerization reactions of [(C$_5$Me$_5$)Re(CO)$_2$Br$_2$] (film) on the surface of Si (111); irradiation of the *cis* isomer (at 77 K) gives isomer 1 which then generates both the *trans* isomer (on warming) and isomer 2; isomer 2 on warming reverts back to the *cis* isomer (ref.[88])

Addition of *cis* or *trans* isomers of [(CpR)Re(CO)$_2$X$_2$] (R = H, Me; X = Br, I)[68] and [{Cp(SiMe$_3$)$_2$}Re(CO)$_2$Br$_2$][60] to silica supports, followed by room temperature photolysis with a 200 W light source, has resulted in isomerization of the isomers to equilibrium isomer mixtures. After reaction the material can be extracted from the support to yield the isomer mixture in good yield (typically >85%). Reactions to evaluate the reaction mechanism were performed:

a) Selective removal of the surface OH groups with Me$_2$SiCl$_2$ gave a reaction that correlated with the amount of OH groups retained on the surface.

b) Irradiation of the reactants in the absence of support gave no isomerization reaction.

c) Irradiation of [(CpMe)Re(CO)$_2$Br$_2$]/NaI (excess) on SiO$_2$ gave *cis* and *trans*-[(CpMe)Re(CO)$_2$I$_2$].

d) Irradiation of a 50:50 mixture of *cis*/*trans* [(CpMe)Re(CO)$_2$Br$_2$]/[(CpMe)Re(CO)$_2$I$_2$] on SiO$_2$ gave a mixture of products that included both isomers of [(CpMe)Re(CO)$_2$BrI].

These data are consistent with interaction between the Br ligand and the surface OH groups. However, they do not distinguish between a radical or an ionic mechanism. A possible ionic mechanism involving Br interaction with a silica OH group is shown in Figure 15.[68] The kinetics of the reaction have been monitored and the data can be interpreted in terms of first order kinetics.[89] The isomerization rate on the surface follows the order [CpRe(CO)$_2$I$_2$] > [CpRe(CO)$_2$Br$_2$] > [(CpMe)Re(CO)$_2$Br$_2$], with the activation energy for all of the reactions lying in the range 60−75 kJ·mol^{-1}.

Table 4. Summary of isomerization reaction data in a confined environment[a]

Complex	Crystal/ powder	Melt	Solution	On support
$[(CpMe)Re(CO)_2Br_2]$	$t \rightarrow c$	$(t \rightarrow c)$[b]	$c \rightarrow t$	$t \rightarrow c$
$[(CpEt)Re(CO)_2Br_2]$	na	$t \rightarrow c$[c]	$c \rightarrow t$	$t \rightarrow c$
$[(CpMe)Re(CO)_2I_2]$	$c \rightarrow t$[d]	$c \rightarrow$ t	$c \rightarrow t$	$c \rightarrow t$
$[(CpMe)Re(CO)\{P(OPh)_3\}Br_2]$	$t \rightarrow c$	na	$t \rightarrow c$	$t \rightarrow c$
$[CpW(CO)_2\{P(OiPr)_3\}I]$	$t \rightleftarrows c$[e]	na	$t \rightleftarrows c$[f]	

[a] t = *trans*, c = *cis*; na = not applicable. [b] Reaction occurs in the solid. However, when the reaction is monitored by DSC at high heating rates, it appears that a reaction can be induced in the melt. [c] An equilibrium is established (ca. 65:35 *cis*/*trans*). [d] It is possible that a reaction in the solid state precedes the reaction in the melt. [e] Reaction proceeds from either isomer to yield a 30:70 *cis*/*trans* ratio of isomers. [f] In benzene (reflux) the equilibrium ratio is 70:30 *cis*/*trans*.

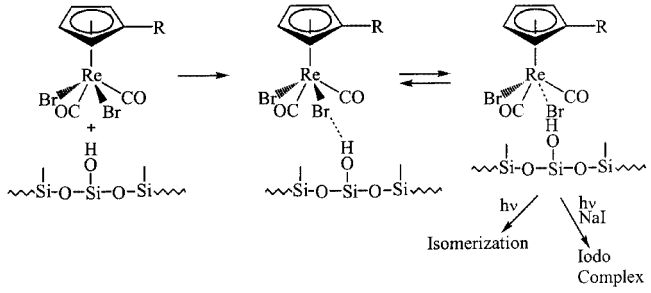

Figure 15. Possible ionic mechanism for the *trans* to *cis* isomerization of $[(CpMe)Re(CO)_2Br_2]$ on the surface of silica (ref.[67])

Isomerization of $CpML_4$ Complexes on Zeolite/Mesoporous Surfaces

The reaction described above has also been performed on high surface area MCM-41 zeolite whose pores (42 Å) are large enough to accommodate the Re molecules.[89] The data were obtained for $[(CpR)Re(CO)_2Br_2]$ (R = H, Me; both isomers) In all instances reaction occurred to yield equilibrium mixtures favoring the *cis* isomer. Only pure silica zeolites could be used, as reactions on *acidic* alumina generate $[(CpR)Re(CO)_3]$ from the $[(CpR)Re(CO)_2Br_2]$.[89]

A small-pore zeolite would only function as support by use of the external zeolite surface as the pores are too small to accommodate the reagent molecules.

Conclusions and Future Prospects

This Microreview has concentrated on a limited area of solid-state organometallic chemistry. A summary of some of the results obtained indicates the influence of the reaction environment and the reactant on the direction of a reaction (Table 4). The study has also indicated that the reaction mechanism may be different from that found in solution. Indeed, a host of mechanisms have been proposed/detected for the simple *cis*/*trans* isomerization reaction in different environments.

Clearly much work is still required to put in place the rules that permit the prediction of the reaction direction.

Other reaction types such as ligand replacement, ligand addition and ligand conversion have also been little explored in the solid state, and it is expected that such studies will yield mechanisms different from that observed in solution.

Extension of solid-state synthetic studies in organometallic chemistry to reagent mixing in the solid state to generate solventless chemical procedures has not been systematically explored to date and so the area is open for development.[90] Furthermore, the possibility of performing reactions between solids/liquids, solids/gases and carrying out reactions in the melt are still in their infancy.[9]

The remarkable success currently being achieved in the area of solid-state organic chemistry attests to the importance of the general area of solid-state chemistry. It is hoped that the same may be found true for the area of organometallic chemistry.

Acknowledgments

We would like to acknowledge the many postgraduate students in our group who have contributed to the development of this area of chemistry and in particular to Lin Cheng whose initial observations were so critical to what has since been discovered. We are also thankful to our funding sources for continued support (THRIP, SASTECH, NRF and the University of the Witwatersrand).

[1] T. J Kealy, P. L. Pauson, *Nature* **1951**, *168*, 1040.
[2] S. A. Miller, J. A. Tebboth, J. F. Tremaine, *J. Chem. Soc.* **1952**, 623.
[3] 50th Anniversary of the Discovery of Ferrocene (Ed.: R. D. Adams), *J. Organomet. Chem.* **2001**, *637−639*.
[4] *Comprehensive Organometallic Chemistry* (Eds.: G. Wilkinson, F. G. A. Stone, E. W. Abel), Pergamon, New York, 1982.
[5] *Comprehensive Organometallic Chemistry II* (Eds.: E. W. Abel, F. G. A. Stone, G. Wilkinson), Pergamon, New York, 1995.
[6] G. W. Parshall, *Organometallics* **1987**, *6*, 687.
[7] D. Braga, F. Greponi, G. R. Desiraju, *Chem. Rev.* **1998**, *98*, 1375.
[8] M. L. H. Green, J. Qin, D. O'Hare, *J. Organomet. Chem.* **1988**, *358*, 375.
[9] L. Cheng, N. J. Coville, *J. Organomet. Chem.* **1998**, *571*, 149.
[10] A. M. Rouhi, *Chem. Eng. News* **2000**, *Aug 21*, 40.
[11] *Polymer-Supported Reactions in Organic Synthesis* (Eds.: P. Hodge, D. C. Sherrington), Wiley, New York, **1980**.
[12] F. Vogtle, C. A. Schalley, *Dendrimers IV*, Springer-Verlag, Berlin, **2001**.
[13] B. C. Gates, *Chem. Rev.* **1995**, *95*, 511.
[14] R. Psaro, S. Recchia, *Catalysis Today* **1998**, *41*, 139.
[15] JM Basset, F. Lefebvre, C. Santini, *Coord. Chem. Rev.* **1998**, *178/180*, 1703.

[16] F. Lefebvre, J. M. Basset, *J. Mol. Catal.* **1999**, *146*, 3.
[17] D. Roberto, G. D'Alfonso, R. Ugo, M. Vailati, *Organometallics* **2001**, *20*, 4307.
[18] S. E. J. Goff, T. F. Nolan, M. W. George, M. Poliakoff, *Organometallics* **1998**, *17*, 2730.
[19] B. C. Gates, *Chem. Rev.* **1995**, *95*, 511.
[20] B. Moulton, M. J. Zaworotko, *Chem. Rev.* **2001**, *101*, 1629.
[21] V. Ramamurthy, K. Venkatesan, *Chem. Rev.* **1987**, *87*, 433.
[22] F. Tanaka, F. Toda, *Chem. Rev.* **2000**, *100*, 1025.
[23] M. Albrecht, M. Lutz, A. L. Spek, G. van Koten, *Nature* **2000**, *406*, 970.
[24] B. M. Foxman, P. L. Goldberg, H. Mazurek, *Inorg. Chem.* **1981**, *20*, 4368.
[25] D. White, N. J. Coville, *Adv. Organometal Chem.* **1994**, *36*, 95.
[26] L. Cheng, N. J. Coville, *Organometallics* **1996**, *15*, 867.
[27] P. O'Brien, *Polyhedron* **1983**, *2*, 233.
[28] H. E. Le May, Jr., in *Comprehensive Coordination Chemistry* (Eds.: G. Wilkinson, R. D. Gillard, J. A. McLeverty), Ch 7.5, vol 1, Pergamon, New York, **1987**.
[29] S. D. Kirik, L. A Solovyov, A. I. Blokhin, I. S. Yakimov, *Acta Crystallogr., Sect. B* **2000**, *56*, 419.
[30] R. Tsuchiya, A. Uehara, Y. Muramatsu, *Bull. Chem. Soc. Jpn.* **1982**, *55*, 3770.
[31] E. V Boldyreva, in *Reactivity of Molecular Solids* (Eds.: E. V. Boldyreva, V. Boldyrev), Wiley, New York, **1999**, 1.
[32] G. M. J. Schmidt, *Pure Appl. Chem.* **1971**, *27*, 647.
[33] M. A. Fernandes, D. C. Levendis, C. B. de Koning, *Cryst. Eng.* **2000**, *4*, 215.
[34] H. E. Zimmerman, I. V. Alabugin, W. S. Chen, Z. N. Zhu, *J. Am. Chem. Soc.* **1999**, *121*, 11930.
[35] E. Cheung, K. C. W. Chong, S. Jayaraman, V. Ramamurthy, J. R. Scheffer, J. Trotter, *Org. Lett.* **2000**, *2*, 2801.
[36] V. Chernyshev, V. A. Tafeenko, S. Yu. Ryabova, E. J. Sonneveld, H. Schenk, *Acta Crystallogr., Sect. C* **2001**, *57*, 982.
[37] M. Greenberg, V. Shteiman, M. Kaftory, *Acta Crystallogr., Sect. B* **2001**, *57*, 428.
[38] J. D. Dunitz, *Acta Crystallogr., Sect. B* **1995**, *51*, 619.
[39] G. Kaupp, *J. Photoenergy* **2001**, *3*, 55.
[40] R. H. Liu, *Acc. Chem. Res.* **2001**, *34*, 555.
[41] F. Blockhuys, R. Hoefnagels, C. Peten, C. Van Alsenoy, H. J. Geise, *J. Mol. Struct.* **1999**, *87*, 485.
[42] Y. Ohashi, Y. Sasada, *Nature* **1977**, *267*, 142.
[43] H. Sato, Y. Ohashi, *Bull. Chem. Soc. Jpn.* **1999**, *72*, 367.
[44] Y. Ohashi, Y. Sakai, A. Sekine, Y. Arai, Y. Ohgo, N. Kamiya, H. Iwasaki, *Bull. Chem. Soc. Jpn.* **1995**, *68*, 2517.
[45] Y. Ohgo, S. Takeuchi, *J. Chem. Soc., Chem. Commun.* **1985**, 21.
[46] A. Sekine, H. Tatsuki, Y. Ohashi, *J. Organomet. Chem.* **1997**, *536*, 389.
[47] T Nemoto, Y. Ohashi, *Bull. Chem. Soc. Jpn.* **1999**, *72*, 1971.
[48] T. Ohhara, H. Uekusa, Y. Ohashi, I. Tanaka, S. Kumazawa, N. Niimura, *Chem. Lett.* **1998**, 365.
[49] T. Ohhara, J. Harada, Y. Ohashi, I. Tanaka, S. Kumazawa, N. Niimura, *Acta Crystallogr., Sect. B* **2000**, *56*, 245.
[50] T. Ohhara, H. Uekusa, Y. Ohashi, I. Tanaka, S. Kumazawa, N. Niimura, *Acta Crystallogr., Sect. B* **2001**, *57*, 551.
[51] Y. Ohashi, *Acc. Chem. Res.* **1988**, *21*, 268.
[52] Y. Ohashi, A. Uchida, Y. Sasada, *Acta Crystallogr., Sect. B* **1983**, *39*, 54.
[53] D. W. Krassowski, K. Reimer, H. E. le May, J. H. Nelson, *Inorg. Chem.* **1988**, *27*, 4307.
[54] D. W. Krassowski, J. H. Nelson, K. R. Brower, D. Hauenstein, R. A. Jacobson, *Inorg. Chem.* **1988**, *27*, 4301.
[55] F. Nareetsile and N. J. Coville, unpublished results.
[56] K. Katsuki, Y. Ooyama, M. Okamoto, Y. Yamamoto, *Inorg. Chim. Acta* **1994**, *217*, 181.
[57] I. de los Rios, M. J. Tenorio, M. C. Puerta, P. Valerga, *J. Chem. Soc., Chem. Commun.* **1995**, 1757.
[58] D. Braga, F. Paganelli, E. Tagliavini, S. Casolari, G. Cojazzi, F. Grepioni, *Organometallics* **1999**, *18*, 4191.
[59] L. Cheng, Ph. D. Thesis, University of the Witwatersrand, Johannesburg, **1998**.
[60] L. Cheng, L. Carlton, N. J. Coville, *S. Afr. J. Chem.* **1998**, *51*, 127.
[61] T. Y Luh, *Coord. Chem. Rev.* **1984**, *59*, 225.
[62] L. Cheng, N. J. Coville, *J. Organomet. Chem.* **1998**, *556*, 111.
[63] O. G. Adeyemi, M. A. Fernandes, L. Cheng, U. B. Eke, D. C. Levendis, N. J. Coville, *C. R. Acad Sci.* submitted.
[64] O. G. Adeyemi, U. B. Eke, B. Mamba, N. J. Coville, to be published.
[65] D. L. Beach, M. Dattilo, K. W. Barnett, *J. Organomet. Chem.* **1977**, *140*, 47.
[66] A. C. Filippou, J. G. Winter, M. Fiest, G. Kociok-Kohn, I. Hinz, *Polyhedron* **1998**, *17*, 1103.
[67] K. Fagnou, M. Lautens, *Angew. Chem. Int. Ed.* **2002**, *41*, 26.
[68] L. Cheng, N. J. Coville, *Organometallics* **1997**, *16*, 591.
[69] M. D. Cohen, *Angew. Chem. Int. Ed. Engl.* **1975**, *14*, 386.
[70] T. Luty, C. J. Eckhardt, in *Reactivity of Molecular Solids* (Eds.: E. V. Boldyreva, V. Boldyrev), Wiley, New York, **1999**, 51.
[71] J. M. Smith, L. Cheng, N. J. Coville, J. Schulte, P. S. Dimpe, M. S. Adsetts, L. M. Cook, J. C. A. Boeyens, D. C. Levendis, *Organometallics* **2000**, *19*, 2597.
[72] J. C. A. Boeyens, L. Cheng, N. J. Coville, D. C. Levendis, *J. Chem. Crystallogr.* **1998**, *28*, 185.
[73] R. S. Bogadi, D. C. Levendis, N. J. Coville, *J. Am. Chem. Soc.* **2002**, *124*, 1104.
[74] J. Bacsa, Ph. D. Thesis, University of the Witwatersrand, Johannesburg, **1999**.
[75] L. Cheng, N. J. Coville, *Thermochim. Acta* **1998**, *319*, 27.
[76] J. D. Dunitz, *Acta Crystallogr., Sect. B* **1995**, *51*, 619.
[77] G Kaupp, in *Comprehensive Supramolecular Chemistry* (Eds.: J. L. Atwood, J. E. D. Davies, D. D. MacNicol, F. Votgle), Ch. 9, vol. 8, Pergamon, New York, **1996**.
[78] J. W. Faller, A. S. Anderson, A. Jakubowski, *J. Organomet. Chem.* **1971**, *27*, C24.
[79] J. W. Faller, A. S. Anderson, *J. Am. Chem. Soc.* **1970**, *92*, 5852.
[80] P. Kalck, R. Prince, R. Poilblanc, J. Roussel, *J. Organomet. Chem.* **1970**, *24*, 445.
[81] J. M. Smith, N. J. Coville, *Organometallics* **1996**, *15*, 3388.
[82] T. Luty, C. J. Eckhardt, *J. Am. Chem. Soc.* **1995**, *117*, 2441.
[83] R. S Bogadi, D. C Levendis, N. J. Coville, to be submitted
[84] W. Xia, R. H. Hill, *Polyhedron* **1992**, *11*, 1319.
[85] R. H. Hill, J. D. Debad, *Polyhedron* **1991**, *10*, 1705.
[86] J. D. Debad, R. H. Hill, *Can. J. Chem.* **1990**, *68*, 2216.
[87] R. H. Hill, B. J. Palmer, *Organometallics* **1989**, *8*, 1651.
[88] B. J. Palmer, A. Becalska, R. Hader, R. H. Hill, *Polyhedron* **1991**, *10*, 877.
[89] T. Magadzu and N. J. Coville, in preparation.
[90] U. B. Eke, N. J. Coville, *Inorg. Chem. Commun.* **2000**, *3*, 286.

Received April 17, 2002
[I02201]

1- and 2-D Coordination Networks Based on Porphyrin and Copper: an Example of Supramolecular Isomerism

Bertrand Zimmer,[a] Véronique Bulach,[a] Mir Wais Hosseini,*[a] André De Cian,[a] and Nathalie Kyritsakas[b]

Keywords: Porphyrin / Pyridine / Isonicotinoyl / Coordination network / Copper / Atropoisomerism

A high-yield synthesis of atropoisomers of the *meso*-tetrakis(*o*-isonicotinoylamidophenyl)porphyrin was achieved. Depending on the crystallising solvent system, the $\alpha_2\beta_2$ atropoisomer leads to the formation of either 1-D or 2-D coordination networks in the presence of $Cu(OAc)_2$.

Introduction

The design of coordination networks, i.e. infinite structures formed upon interconnection of organic tectons by metal centres, is a topic of current interest.[1] The formation of such a molecular assembly results from the interplay between the organic and the metallic tectons. With respect to the design of the organic tecton, one may use the porphyrin core which presents several interesting features. Being a tetradentate macrocycle, it binds a variety of metal cations and the resulting complex offers tuneable redox as well as photochemical properties. Furthermore, the porphyrin backbone may be functionalised either at the β-pyrrolic or *meso* positions. Thus, using this preorganised unit, one may design a variety of tectons upon anchoring additional coordination sites such as pyridine, nitrile, carboxylate etc. The porphyrin core has been widely used in materials chemistry[2] and the formation of coordination networks based on a porphyrin bearing pyridyl units directly connected at the *meso* positions has been demonstrated.[3] On the other hand, discrete polynuclear species have been also obtained when using pyridine-bearing porphyrin derivatives.[4]

Results and Discussion

Continuing our effort towards the formation and design of new types of coordination networks,[5] we thought that the porphyrin-based tecton **1** (Scheme 1) bearing four isonicotinoyl units may be of interest for the formation of coordination networks when associated with connecting transition metal complexes possessing two linearly disposed coordination sites. The tecton **1** is based on the *meso*-tetraphenylporphyrin bearing four pyridyl units. The connection between the latter and the phenyl ring is ensured at the *ortho* position through an amide junction using the *para* position of the pyridyl unit. It is worth noting that, owing to the bulkiness of the isonicotinoyl unit, four separable atropoisomers ($\mathbf{1}\alpha_4$, $\mathbf{1}\alpha_3\beta$, $\mathbf{1}\alpha_2\beta_2$, and $\mathbf{1}\alpha\beta\alpha\beta$) may be formed.[6] In terms of design principles, as previously demonstrated for catechol-bearing porphyrins,[7] this aspect is interesting since using the same units one may generate four different tectons. Although the synthesis of **1**, based on the condensation of a statistical mixture of all four atropoisomers of the amino derivative **2** with isonicotinoyl chloride, was previously reported,[8] as mentioned by the authors, the separation procedure leading to the pure atropoisomers is extremely tedious and may only be achieved by preparative thin layer chromatography affording thus small quantities of the desired species. For those reasons we developed our own strategy based on the condensation, in the presence of Et_3N and in dry THF, of purified atropoisomers of the amino derivative **2** with isonicotinoyl chloride. Thus, $\mathbf{1}\alpha_2\beta_2$,

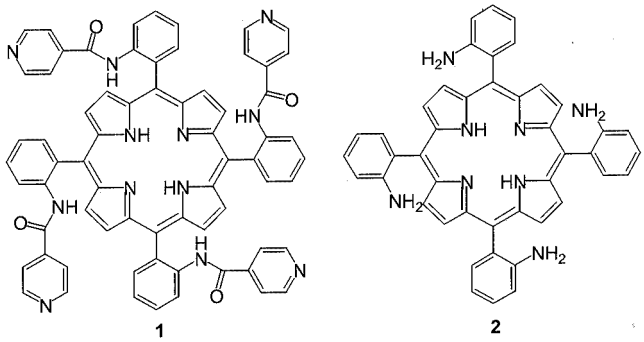

Scheme 1

[a] Laboratoire de Chimie de Coordination Organique, Université Louis Pasteur,
4, rue Blaise Pascal, 67000 Strasbourg, France
Fax: (internat.) + 33-3/90241325
E-mail: hosseini@chimie.u-strasbg.fr
[b] Service Commun des Rayons X, Institut Le Bel, Université Louis Pasteur,
4, rue Blaise Pascal, 67000 Strasbourg, France

 © 2002 WILEY-VCH Verlag GmbH & Co. KGaA, 69451 Weinheim 1434−1948/02/1212−3079 $ 20.00+.50/0

1αβαβ, and **1**α_4 could be obtained in 68, 43 and 78% yields, respectively.

Here we report on the formation of supramolecular isomeric 1-D and 2-D coordination networks formed between **1**$\alpha_2\beta_2$ and copper acetate.

Since the tecton **1**$\alpha_2\beta_2$ possesses four isonicotinoyl moieties (two adjacent pyridine units located on each face of the porphyrin), in order to generate a stair-type network the choice of a metallic tecton adopting a linear coordination geometry was obvious. Therefore, we used $Cu(OAc)_2$ which is present as a binuclear neutral complex formed upon bridging of the two Cu^{II} centres by four acetate anions.[9] This complex has been previously exploited in the formation of coordination networks using urotropine.[10]

Upon slow diffusion of compound **1**$\alpha_2\beta_2$ (5 mg) in $CHCl_3$ (0.6 mL) into a solution of $Cu(OAc)_2$ (19 mg, 25-fold excess) in 2-propanol (1.8 mL) violet crystals were obtained at room temp. over a period of one month and studied by X-ray diffraction (Figure 1). The crystal (triclinic system, $P\bar{1}$ as the space group) is composed of **1**$\alpha_2\beta_2$, Cu atoms, acetate anion, $CHCl_3$, H_2O and 2-propanol solvent molecules. Both $CHCl_3$ molecules present in the unit cell are disordered with all Cl atoms distributed over two positions. Among the 10 water molecules present, two of them are also disordered over two positions. For the organic tecton **1**$\alpha_2\beta_2$, the planar porphyrin macrocycle binds a Cu^{2+} cation adopting a square-planar coordination geometry (d_{Cu-N} = 1.99 Å). The Cu^{2+} ion, generated upon decomplexation of the copper acetate, occupies the centre of symmetry. The phenyl rings at the *meso* positions are, as expected, tilted with respect to the plane of the porphyrin with C−C−C−C dihedral angles of −67.3 and 76.6°. All four amide junctions (d_{C-N} = 1.31 and 1.36 Å; $d_{C=O}$ = 1.21 and 1.25 Å, N−C−O angle of 123 and 124°) are in *trans* configuration with the C=O fragments outwardly oriented. The pyridine units are not coplanar with the amide junctions but tilted (N−C−C−C dihedral angle of −18.2 and 44.2°). The consecutive substituted porphyrins are interconnected through the binding by all four isonicotinoyl moieties to the copper centres (average N−Cu distance of 2.17 Å) of four neutral $Cu_2(OAc)_4$ dimers leading thus to a stair-type 1-D coordination network. The structural characteristics of the bridging $Cu(OAc)_2$ dimer (O−Cu distance varying between 1.94 and 2.00 Å and Cu−Cu distance of 2.62 Å) are similar to those previously observed.[9] The 1-D networks are packed in a parallel fashion (Figure 1) with solvent molecules occupying the free space with no specific interactions between the networks and solvents. The same 1-D network was also obtained when *i*PrOH was replaced by MeOH. However, in that case the MeOH molecules were also strongly disordered.

In order to study the role played by the solvent system, the crystallisation of the same molecular components was carried out using different solvent mixtures. Upon slow diffusion of the compound **1**$\alpha_2\beta_2$ (5 mg) in 1,1′,2,2′-tetrachloroethane (TCE) (0.6 mL), or 1,2-dichlorobenzene or a TCE/$CHCl_3$ (1:1) mixture, into a solution of $Cu(OAc)_2$ (19 mg, 25 fold excess) in EtOH (1.8 mL) reddish crystals were obtained at room temp. over a period of 1 month. The single crystals were subject to X-ray diffraction which revealed, unexpectedly, the formation of a 2-D coordination network in all three solvent systems used (Figure 2).

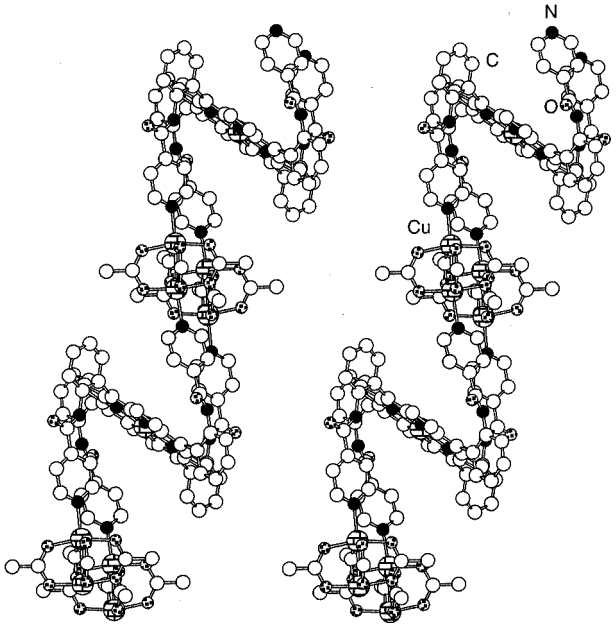

Figure 1. A portion of the crystal structures of the 1-D coordination network formed by the self-assembly of **1**$_{\alpha2\beta2}$ and copper in *i*PrOH/$CHCl_3$ showing the stair-type arrangement and the packing of two consecutive networks; solvent molecules and H atoms are not represented for clarity; for bond lengths and angles see text

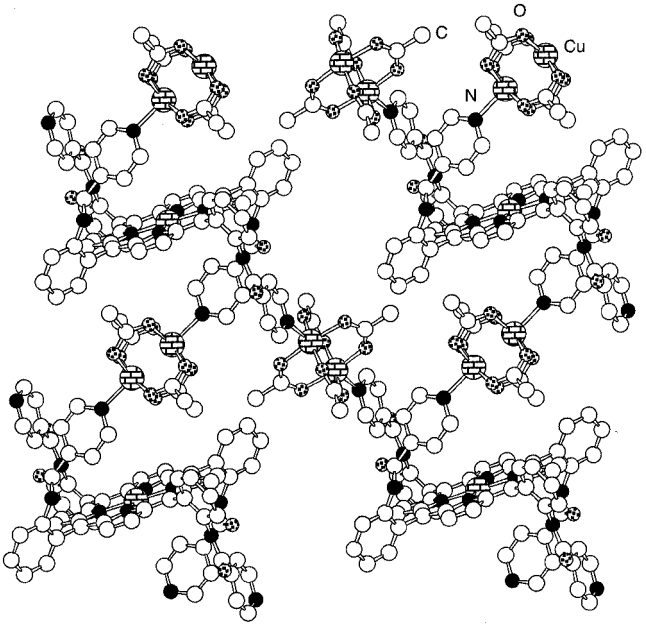

Figure 2. A portion of the crystal structures of the 2-D coordination network formed by the self-assembly of **1**$_{\alpha2\beta2}$ and copper ions in EtOH/TCE showing the connection of Cu−metallaporphyrin by $Cu_2(OAc)_4$ dimers; solvent molecules and H atoms are not represented for clarity; for bond lengths and angles see text:

The crystal (triclinic system, $P\bar{1}$ as the space group) is composed of $\mathbf{1}\alpha_2\beta_2$, Cu atoms, AcO^- anions, and TCE solvent molecules. In that case, the TCE molecules present in the lattice are not disordered and no specific interactions between them and the network structure can be spotted. Dealing with the organic tecton $\mathbf{1}\alpha_2\beta_2$, again the porphyrin macrocycle remains planar and binds a Cu^{2+} cation, formed upon decomplexation of the acetate complex, which occupies the centre of symmetry and again adopts a square-planar coordination geometry (d_{Cu-N} = 1.99 Å). The phenyl rings at the *meso* positions are differently tilted (C−C−C−C dihedral angles of −114.4 and 77.5°) with respect to the above-mentioned case . All four amide junctions (average $d_{C-N} \approx 1.35$ Å; average $d_{C=O} \approx 1.21$ Å, average N−C−O angle of ca. 124.4°) are again in *trans* configuration. The pyridine units are again not coplanar with the amide junctions but tilted (N−C−C−C dihedral angle of −17.0 and 33.3°). In marked contrast with the above-mentioned case for which the pyridine units located on the same face of the porphyrin ring are oriented almost parallel to each other, in the present case, whereas one of the two pyridine rings is almost perpendicular to the porphyrin plane, the other one is strongly tilted. As the consequence of this peculiar disposition of the coordination sites on each face of the tecton, the consecutive units are again interconnected through coordination bonds between the nitrogen atom of the isonicotinoyl moieties and the copper centres (average N−Cu distance of ca. 2.15 Å) of four neutral $Cu_2(OAc)_4$ dimers leading to a 2-D coordination network (Figure 2). Again, the structural characteristics of the bridging $Cu(OAc)_2$ dimer are similar to those obtained in the case of the 1-D network mentioned above. The packing of the 2-D networks generates channels which are filled with TCE solvent molecules with no specific interactions between the networks and the solvents molecules. As mentioned above, the same 2-D network was also obtained when TCE was replaced by 1,2-dichlorobenzene or by a mixture of TCE/$CHCl_3$ (1:1) while using EtOH.

The two networks obtained are clearly not polymorphs since they differ in their composition. However, they constitute an example of supramolecular[11] or structural[12] isomerism since both networks are based on the same molecular units and the passage from the 1-D to the 2-D network takes place through a rotational process (Figure 3).

In summary, upon self-assembly of the $\alpha_2\beta_2$, atropoisomer of the porphyrin **1** bearing four isonicotinoyl moieties and $Cu(OAc)_2$, depending on the solvent systems used, 1-D and 2-D coordination networks containing two different types of Cu^{2+} centres were formed and structurally characterised by X-ray diffraction on single crystals. The two networks obtained may be regarded as supramolecular or structural isomers. The formation of coordination networks using the other atropoisomers of **1** as well as other transition metal cations is under current investigation.

Experimental Section

Synthesis of $\mathbf{1}_{a2b2}$: 0.10 g (0.15 mmol) of $\mathbf{2}_{a2b2}$ [13] and 0.40 g (2.23 mmol, 15 equiv.) of the hydrochloride salt of isonicotinoyl chloride were placed in a round-bottom flask. 620 μL of NEt_3 (4.44 mmol, 30 equiv.) and 50 mL of freshly distilled and degassed THF were added under argon. The mixture was cooled to 0 °C and sonicated to obtain a clear solution. The course of the reaction was monitored by TLC (SiO_2, CH_2Cl_2). After ca. 3.5 h, the starting porphyrin was completely consumed. Volatiles were removed and the residue was dissolved in CH_2Cl_2 (100 mL), washed with 10% aqueous NaOH (1 × 100 mL), H_2O until neutralisation (5 × 500 mL) and finally dried with Na_2SO_4. Interestingly, due to the low solubility of $\mathbf{1}_{a2b2}$, the purification could be achieved simply by washing the solid with Et_2O (500 mL) and hexane (100 mL). The pure compound $\mathbf{1}_{a2b2}$ was obtained as a purple solid in 68% yield (0.11 g). ^{1}H NMR ($CDCl_3$, 300 MHz, 25 °C): δ = −2.65 (s, 2 H, NH pyrrole), 6.47 (dd, 8 H, J = 1.5 Hz and J = 4.4 Hz, $H_{pyridine}$), 7.61 (m, 8 H, $H_{phenyl+NHCO}$), 7.64 (broad s, 4 H, NHCO), 7.85 (dd, 8 H, J = 1.5 Hz and J = 4.4 Hz, $H_{pyridine}$), 7.90 (m, 8 H, H_{phenyl}), 8.79 (d, 4 H, J = 7.8 Hz, H_{phenyl}), 8.92 (s, 4 H, $H_{β\text{-}pyrrolic}$), 8.95 (s, 4 H, $H_{β\text{-}pyrrolic}$) ppm. ^{13}C NMR ($CDCl_3$, 75 MHz, 25 °C): δ = 114.9, 119.7, 121.9, 124.2, 130.3, 131.2, 135.2, 137.4, 140.9, 149.8, 163.3 (NH**C**O) ppm. UV/Vis ($CHCl_3$): λ_{max} (ε) = 423 (1.8 × 10^5), 517 (1.2 × 10^4), 550 (4.3 × 10^3), 590 (4.4 × 10^3), 650 (2.3 × 10^3) nm. $C_{68}H_{46}N_{12}O_4{\cdot}CH_2Cl_2$ (1180.14): calcd. C 70.21, H 4.11, N 14.24; found C 70.12, H 4.25, N 14.06.

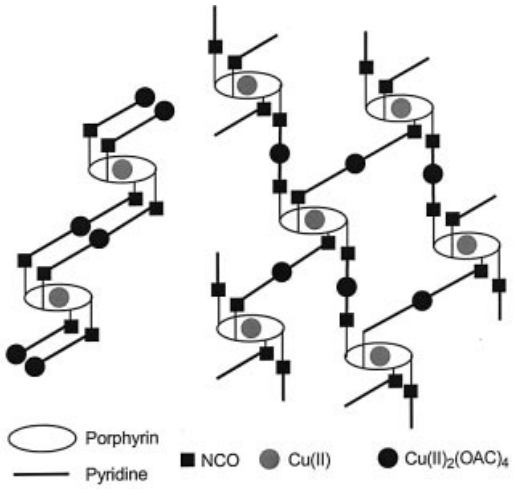

Figure 3. Schematic representation of the two supramolecular isomers based on the 1-D (left) and 2-D (right) coordination networks obtained with the same molecular components but in two different solvent systems

Crystal Structure Characterisation: X-ray diffraction data collection was carried out with a Kappa CCD diffractometer equipped with an Oxford Cryosystem liquid N_2 device, using graphite-monochromated Mo-K_α radiation. For all structures, diffraction data were corrected for absorption and analysed using the OpenMolen package.[14] All non-H atoms were refined anisotropically. Crystallographic data for the 1-D network based on $\mathbf{1}_{\alpha2\beta2}$ and $Cu_2(OAc_4)$ (violet crystals, 173 K): $C_{84}H_{68}Cu_5N_{12}O_{20}{\cdot}2CHCl_3{\cdot}10H_2O{\cdot}4C_3H_7O$, M = 2538.51, triclinic, a = 214.7082(4), b = 15.9643(4) c = 17.8289(6) Å, α = 106.851(5), β = 97.638(5), γ = 117.560(5)°, V = 3371.4(2) Å^3, space group $P\bar{1}$, Z = 1, $D_{calcd.}$ = 1.25 g cm^{-3}, μ = 0.964 mm^{-1}, 6534 data with $I > 3\sigma(I)$, R = 0.109, Rw = 0.142. Crystallographic data for the for 2-D network based on $\mathbf{1}_{\alpha2\beta2}$ and $Cu_2(OAc_4)$ (red crystals, 173 K): $C_{84}H_{68}Cu_5N_{12}O_{20}{\cdot}8C_2H_2Cl_4$, M = 3226.05, triclinic, a = 12.2094(4), b = 16.1597(5), c = 17.6546(6) Å, α = 76.557(5), β = 73.767(5), γ = 83.554(5)°, V = 3248.6(2) Å^3, space group $P\bar{1}$,

$Z = 1$, $D_{calcd.} = 1.65\ g\ cm^{-3}$, $\mu = 1.529\ mm^{-1}$, 6049 data with $I > 3\sigma(I)$, $R = 0.072$, $Rw = 0.102$. CCDC-185378 and -185379 contain the supplementary crystallographic data for this paper. These data can be obtained free of charge at www.ccdc.cam.ac.uk/conts/retrieving.html or from the Cambridge Crystallographic data Center, 12 Union Road, Cambridge CB2 1EZ, UK [Fax: (internat.) + 44-1223/336-033; E-mail: deposit@ccdc.cam.ac.uk].

Acknowledgments

We thank the Université Louis Pasteur and the Ministry of Research and Technology for financial support and a scholarship to B. Z.

[1] S. R. Batten, R. Robson, *Angew. Chem. Int. Ed.* **1998**, *37*, 1460−1494; A. J. Blake, N. R. Champness, P. Hubberstey, W.-S. Li, M. A. Withersby, M. Schöder, *Coord. Chem. Rev.* **1999**, *183*, 117−138; M. W. Hosseini, in *NATO ASI Series* (Eds.: D. Braga, F. Grepiono, G. Orpen), Series c, Kluwer, Dordrecht, Netherlands, **1999**, vol. 538, p. 181−208; M. Eddaoudi, D. B. Moler, H. Li, B. Chen, T. M. Reineke, M. O'Keeffe, O. M. Yaghi, *Acc. Chem. Res.* **2001**, *34*, 319−330; B. Moulton, M. J. Zaworotko, *Chem. Rev.* **2001**, *101*, 1629−1659.

[2] J. H. Chou, H. S. Nalwa, M. E. Kosal, N. A. Rakow, K. S. Suslick, in *The Porphyrin Handbook*, Academic Press, Orlando, FL, **2000**, vol. 6, chapter 41, p. 43−131.

[3] B. F. Abrahams, B. F. Hoskins, R. Robson, *J. Am. Chem. Soc.* **1991**, *113*, 3606−3607; E. B. Fleischer, A. M. Shachter, *Inorg. Chem.* **1991**, *30*, 3763−3769; B. F. Abrahams, B. F. Hoskins, D. M. Michail, R. Robson, *Nature* **1994**, *369*, 727−729; H. Krupitsky, Z. Stein, I. Goldberg, C. E. Strouse, *J. Inclusion Phenom. Mol. Recognit. Chem.* **1994**, *18*, 177−192; L. Pan, B. C. Noll, W. Wang, *Chem. Commun.* **1999**, 157−158; U. Michelsen, C. A. Hunter, *Angew. Chem. Int. Ed.* **2000**, *39*, 764−767; I. Goldberg, *Chem. Eur. J.* **2000**, *6*, 3863−3870.

[4] C. M. Drain, J.-M. Lehn, *J. Chem. Soc., Chem. Commun.* **1994**, 2313−2314; P. J. Stang, J. Fan, B. Olenyuk, *Chem. Commun.* **1997**, 1453−1454; R. V. Slone, J. T. Hupp, *Inorg. Chem.* **1997**, *36*, 5422−5423; A. Ikeda, M. Ayabe, S. Shinkai, S. Sakamoto, K. Yamaguchi, *Org. Lett.* **2000**, *2*, 3707−3710.

[5] For recent publications see: B. Schmaltz, A. Jouaiti, M. W. Hosseini, A. De Cian, *Chem. Commun.* **2001**, 1242−1243; A. Jouaiti, V. Jullien, M. W. Hosseini J.-M. Planeix, A. De Cian, *Chem. Commun.* **2001**, 1114−1115; C. Klein, E. Graf, M. W. Hosseini, A. De Cian, J. Fischer, *New J. Chem.* **2001**, *25*, 207−209; S. Ferlay, S. Koenig, M. W. Hosseini, J. Pansanel, A. De Cian, N. Kyritsakas, *Chem. Commun.* **2002**, 218−219 and references theiren.

[6] L. K. Gottwald, E. F. Ullman, *Tetrahedron Lett.* **1969**, 3071−3073.

[7] C. Drexler, M.W. Hosseini, J.-M. Planeix, G. Stupka, A. De Cian, J. Fischer, *Chem. Commun.* **1998**, 689−690, B. Zimmer, V. Bulach, C. Drexler, S. Erhardt, M. W. Hosseini, A. De Cian, *New. J. Chem.* **2002**, *26*, 43−57.

[8] A. Valliot, A. Adeyemo, R. F. X. Williams, L. Ricks, J. North, P. Hambright, *J. Inorg. Nucl. Chem.* **1981**, *43*, 2653−2658.

[9] V. M. Rao, D. N. Sathyanarayana, H. Manohar, *J. Chem. Soc., Dalton Trans.* **1983**, 2167−2173.

[10] B. Moulton, J. Lu, M. J. Zaworotko, *J. Am. Chem. Soc.* **2001**, *123*, 9224−9225.

[11] T. L. Hennigar, D. C. MacQuarrie, P. Losier, R. D. Rogers, M. J. Zaworotko, *Angew. Chem. Int. Ed. Engl.* **1997**, *36*, 972−973.

[12] J. A. Swift, A. M. Pivovar, A. M. Reynolds, M. D. Ward, *J. Am. Chem. Soc.* **1998**, *120*, 5887−5894.

[13] J. P. Collman, R. R. Gagne, C. A. Reed, T. R. Halbert, G. Lang, W. T. Robinson, *J. Am. Chem. Soc.* **1975**, *97*, 1427−1439.

[14] *OpenMolen, Interactive Structure Solution*, Nonius B. V., Delft, The Netherlands, **1997**.

Received June 24, 2002
[I02342]

A New Synthetic Strategy for Magnetic Metal Bis(dithiolene) Based Conductors

Martijn J. J. Mulder,[a] Jaap G. Haasnoot,[a] Derk J. Stufkens,[b] Liu Hao Tjeng,[c] Hong-Ji Lin,[d] Chien-Te Chen,[d] and Jan Reedijk*[a]

Keywords: Redox chemistry / Conducting materials / X-ray absorption spectroscopy / EPR spectroscopy / Raman spectroscopy

The combination of the $[Co^{III}(Cl_2\text{-bpy})_3]^{3+}$ complex with the $[Ni(dmit)_2]^-$ anion is a one-step reaction, which results in the partially oxidised $Ni(dmit)_2$-based material $[Co^{II}(Cl_2\text{-bpy})_3][Ni(dmit)_2]_5$ with a paramagnetic Co^{II} cation, as proven by Raman, EPR and XAS, exemplifying a, for $M(dithiolene)_2$ compounds new, synthetic strategy that may give access to a large variety of new $[Co^{II}(N,N\text{-imine})_3][M(dithiolene)_2]_n$ ($n > 2$, M = Ni, Pd) type magnetic conductors.

Introduction

One of the important relatively recent challenges in the design of molecular conductors is the combination of magnetic and conducting properties.[1] In the area of $M(dmit)_2$-based (M = Ni, Pd; dmit = 2-thioxo-1,3-dithiole-4,5-dithiolate) compounds, attempts to obtain these multiple-property materials have been made by combination of the $M(dmit)_2$ anion with either an organic radical cation[2−4] or with a paramagnetic transition-metal cation. Apart from $Cu_{0.39}[Ni(dmit)_2]$ reported by Sakai et al.,[5] no previously published $M(dmit)_2$-based material contains both (1) a paramagnetic transition-metal cation and (2) an $[M(dmit)_2]^{x-}$ anion with a non-integer formal charge ($0 < x < 1$), which is the best electronic situation for optimal conductivity.[6] Most reported $M(dmit)_2$-based materials containing a transition-metal cation are $[M'(Cp^*)_2][M(dmit)_2]$ (M′ = Fe, Mn, Ni) type compounds[7−10] with monovalent anions. These compounds exhibit various magnetic properties. Nevertheless, they can be considered precursors that need further oxidation, required to obtain a species with a non-integer formal charge. However, the major problem of these precursor materials is their poor solubility in most organic solvents, making subsequent chemical or electrolytic oxidation of the anion, virtually impossible.

[a] Leiden Institute of Chemistry, Gorlaeus Laboratories, Leiden University,
P. O. Box 9502, 2300 RA Leiden, Netherlands
Fax: (internat.) + 31-71/527-4451
E-mail: reedijk@chem.leidenuniv.nl
[b] Institute of Molecular Chemistry, University of Amsterdam, Nieuwe Achtergracht 166, 1018 WV Amsterdam, Netherlands
[c] Material Science Centre, University of Groningen, Nijenborgh 4, 9747 AG Groningen, Netherlands
[d] Synchrotron Radiation Research Centre, Hsinchu 30077, Taiwan

Here we present an elegant and powerful solution to this problem: combination of the $[M(dmit)_2]^{1-}$ anion with an oxidant that becomes a paramagnet upon its reduction and that subsequently precipitates together with the oxidised $[M(dmit)_2]^{x-}$ ($0 < x < 1$) anion, resulting in a fractionally oxidised, $M(dmit)_2$-based material containing a paramagnetic cation.

There are only a few examples in the literature where this concept of using a counter ion as an oxidant for the potentially conducting species has been exploited. $[BEDT\text{-}TTF]_{3.6}[MnCl_4]$ is an insulating compound. Replacement of some $[Mn^{II}Cl_4]^{2-}$ anions ($S = 5/2$) by $[Fe^{III}Cl_4]^-$ anions ($S = 5/2$) results in the Fe-doped salt $[BEDT\text{-}TTF]_{3.6}[(MnCl_4)_{1-x}(FeCl_4)_x]$ ($x = 0.05$) with strongly reduced resistivity and a magnetic behaviour composed of the Curie−Weiss contribution of the anions and Pauli contribution of mobile electrons in the donor lattice.[11] The semiconducting ($\sigma_{rt} = 0.025\ S\ cm^{-1}$) antiferromagnet $TMTSF(FeCl_4)$ is the product of the oxidation of the neutral TMTSF molecule to the $TMTSF^{\cdot+}$ radical cation by two $Fe^{III}Cl_3$ units that are converted into the paramagnetic counteranion $[Fe^{III}Cl_4]^-$ and "waste product" $Fe^{II}Cl_2$.[12] The compounds $(TTF)_6(Et_4N)(HPMo_{12}O_{40})$ and $(TTF)_6(Et_4N)(HPW_{12}O_{40})$ ($\sigma_{rt} = 10^{-3}-10^{-4}\ S\ cm^{-1}$) also are the result of a redox reaction between the $[PM_{12}O_{40}]^{3-}$ (M = W, Mo) anions that act as oxidants for the neutral TTF donor.[13] The redox reaction generates a paramagnetic $[PM_{12}O_{40}]^{4-}$ anion and a radical cation $TTF^{\cdot+}$. Already in 1980 some semiconducting $[CuL](TCNQ)_2$ and $[CuL_2](TCNQ)_2$ compounds ($\sigma_{rt} = 10^{-7}-1.9\ S\ cm^{-1}$) have been reported with L = en, bpy, phen. Some of these $Cu^{II}L$ and $Cu^{II}L_2$ complexes act as oxidants for the TCNQ anions, resulting in compounds with a charge distribution be-

 © 2002 WILEY-VCH Verlag GmbH & Co. KGaA, 69451 Weinheim 1434−1948/02/1212−3083 $ 20.00+.50/0

tween $Cu^{II}Ln(TCNQ^{-})_2$ and $Cu^{I}Ln(TCNQ^{-})(TCNQ^{0})$, which eliminates the paramagnetism of some of the Cu^{II} species, since the Cu^{I} d^{10} species are diamagnetic. However, these compounds do display coexistence of magnetic and conducting properties.[14−17] In the case of the $[Cu^{I}\{bis(2\text{-pyridyl})amine\}_2][TCNQ]_2$ this redox reaction is total, resulting in fractionally oxidized anions and a diamagnetic cation.[18,19]

In this communication we present, for the first time with the $[Ni(dmit)_2]^{-}$ anion, such a redox reaction, where the oxidant, a cobalt(III) cation, becomes the paramagnetic species and the $[Ni(dmit)_2]^{-}$ complex anion, the fractionally oxidised, potentially conducting species. Octahedral cobalt(III) complexes with 6 nitrogen donor atoms are d^6 systems with in general a low-spin $t_{2g}^{6}e_g^{0}$ ($S = 0$) ground state. The Co^{II} equivalent, however, is a d^7 system with a high-spin $t_{2g}^{5}e_g^{2}$ ($S = 1.5$) ground state.[20] Therefore, reduction of the Co^{III} starting compound is absolutely indispensable in order to obtain a paramagnetic cation. The electron for this reduction can be provided by the $[Ni(dmit)_2]^{-}$ anion, which then can be oxidised to its neutral form. This species then can recombine with other anions[21] to form an array of $Ni(dmit)_2$ units with formal fractional charge $x-$ ($0 < x < 1$), an optimal situation for conductivity. The desired redox reactions are described in Scheme 1.

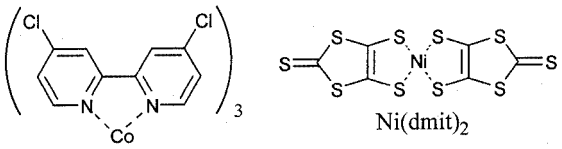

$[Co(III)(Cl_2\text{-bpy})_3]^{3+} + e^{-} \dashrightarrow [Co(II)(Cl_2\text{-bpy})_3]^{2+}$ $E_{1/2} = 0.60$ V

$1/(1\text{-}x)\ [Ni(dmit)_2]^{1-} \dashrightarrow 1/(1\text{-}x)\ [Ni(dmit)_2]^{x-} + e^{-}$ $E_{ox} = 0.24$ V

Scheme 1. Structure and redox reactions of $[Co^{III}(Cl_2\text{-bpy})_3]^{3+}$ ($E_{1/2}$ determined here) and $[Ni(dmit)_2]^{-}$ (E_{ox} redetermined here; see also ref.[22])

Below are the results of the combination of the $[Ni(dmit)_2]^{-}$ with a cationic complex that possesses these extraordinary capabilities: the $[Co^{III}(Cl_2\text{-bpy})_3]^{3+}$ complex (Cl_2-bpy = 4,4′-dichloro-2,2′-bipyridine). The $[Co^{III}(bpy)_3]^{3+}$ also has been used for comparison.

Results and Discussion

The electrochemical potentials of the starting compounds $[Co^{III}(Cl_2\text{-bpy})_3](PF_6)_3(H_2O)$, $[Co^{III}(bpy)_3](PF_6)_3(H_2O)$ and $[Bu_4N][Ni(dmit)_2]$ have been (re)determined[22,23] with cyclic voltammetry (WE, CE: Pt; RE: Ag/AgCl; CH_3CN/Bu_4NPF_6). Figure 1 shows their cyclic voltammograms. The half-wave potentials $E_{1/2,Co(III/II)}$ of $[Co(bpy)_3]^{3+}$, $E_{1/2} = 0.33$ V vs. Ag/AgCl, and $[Co(Cl_2\text{-bpy})_3]^{3+}$, $E_{1/2} = 0.60$ V vs. Ag/AgCl, are both higher than the oxidation-wave potential E_{ox} of the $[Ni(dmit)_2]^{1-/x-}$ oxidation, $E_{ox} = 0.24$ V vs. Ag/AgCl. The difference between the half-wave potential of the oxidant and the reductant, $\Delta E = E_{1/2}([Co(L)_3]^{3+/2+}) - E_{ox}([Ni(dmit)_2]^{x-/1-})$ should be at least $\Delta E > 0.1$ V,[24]

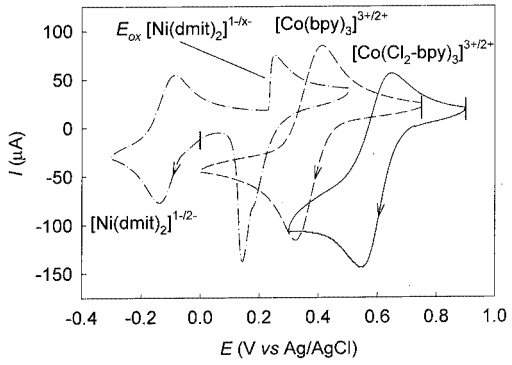

Figure 1. Cyclic voltammograms (WE, CE: Pt; RE: Ag/AgCl; CH_3CN/Bu_4NPF_6) of $[Bu_4N][Ni(dmit)_2]$ (−·), $[Co^{III}(bpy)_3](PF_6)_3{\cdot}H_2O$ (−−) and $[Co^{III}(Cl_2\text{-bpy})_3](PF_6)_3{\cdot}H_2O$ (−)

in order to have a charge transfer from anion to cation. The potential differences for $[Co(bpy)_3]^{3+}$ are $\Delta E = 0.09$, too small for this complex to be an oxidant for the $[Ni(dmit)_2]^{1-}$ anion, and for $[Co(Cl_2\text{-bpy})_3]^{3+}$ $\Delta E = 0.36$ V. Therefore, the redox reactions shown in Scheme 1 were expected to occur only for the latter cation complex. The electron-withdrawing effect of the chlorine substituents on the bpy ligand in $[Co^{III}(Cl_2\text{-bpy})_3]^{3+}$ apparently makes the difference between a normal counter cation and an effective oxidant for the $Ni(dmit)_2$ species.

Solutions of $[Co^{III}(Cl_2\text{-bpy})_3](PF_6)_3(H_2O)$ or $[Co^{III}(bpy)_3](PF_6)_3(H_2O)$ and $[Bu_4N][Ni(dmit)_2]$ in acetone have been mixed and the resulting black precipitates (product A or B, respectively) have been filtered off and washed with acetone.

In order to determine whether $[Ni(dmit)_2]^{-}$ is oxidised in the products A and B, Raman spectroscopy has been performed. Raman is a useful tool to determine the effective charge on an $Ni(dmit)_2$ anion, because of the almost linear correlation between the frequency of the ν(C=C) vibration of the dmit ligand and the charge on the anion complex.[25] The cobalt oxidation state was determined using EPR and X-ray absorption spectroscopy (XAS) at the Co $L_{2,3}$ edges. XAS is a spectroscopic technique that is very sensitive to differences in charge and spin state of a metal cation.[26]

The Raman spectra of A, [$\tilde{\nu}$(C=C) = 1331 cm^{-1}], B [$\tilde{\nu}$(C=C) = 1391 cm^{-1}] and reference $[Bu_4N][Ni(dmit)_2]$ [$\tilde{\nu}$(C=C) = 1394 cm^{-1}] (Figure 2) indicate the presence of an oxidised $Ni(dmit)_2$ species in A and a normal monovalent anion in B. This suggests that oxidation of the anion occurred only during the formation of A. The effective charge on the oxidised species in A should be 0.03− based on the previously reported correlation.[25] The asymmetry of the 1331 cm^{-1} band may indicate some variation in charge on the oxidised $Ni(dmit)_2$ species. Also some signals with low intensity are present around 1390 cm^{-1} and higher, indicating an inhomogeneous charge distribution over the $Ni(dmit)_2$ complexes in product A.

Since the Co^{III} starting compounds are diamagnetic, the equivalent Co^{II} complexes have been used as references for the EPR spectra of A and B (X-band, dpph as a standard, $T = 77$ K), that are shown together with the spectrum of

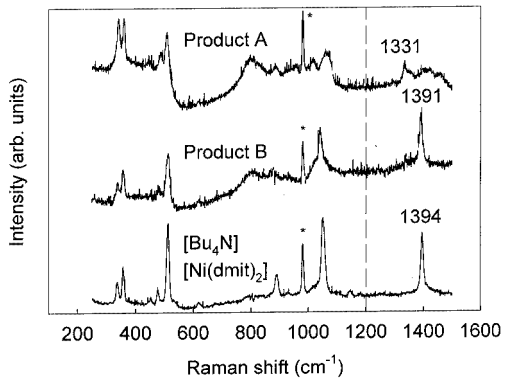

Figure 2. Raman spectra of powdered samples in rotated K_2SO_4 (*) pellets of products A ($\lambda_{exc.}$ = 514.5 nm), B and $[Bu_4N][Ni(dmit)_2]$ ($\lambda_{exc.}$ = 488 nm); right of the dotted line (> 1200 cm^{-1}) are the ν(C=C) signals of the compounds

$[Bu_4N][Ni(dmit)_2]$. The spectrum of A (Figure 3) clearly shows a signal at g = 2.06 of the radical anion $[Ni(dmit)_2]^-$ and a very broad signal with its maximum at g = 5.5, as pointed out by an arrow, indicating that a Co^{II} species must be present in A. In the spectrum of B (Figure 4) however, this signal is absent and only the anion signal is visible, which is almost identical to the signal of $[Bu_4N][Ni(dmit)_2]$. When considering the intensity of the Co^{II} EPR signal of A, no quantitative conclusions concerning the Co^{II} concentration in A can be drawn, because the intensity of the, normally very broad, Co^{II} EPR signals is, among others, strongly influenced by the relaxation times, that can differ between Co^{II} compounds.[27]

The conclusions concerning the cation charge in A and B based on the EPR spectra are confirmed by the XAS results. The spectrum (Figure 5) of A resembles very much a high-spin Co^{II} spectrum, whereas the spectrum of B agrees with a pure low-spin Co^{III} spectrum.[26]

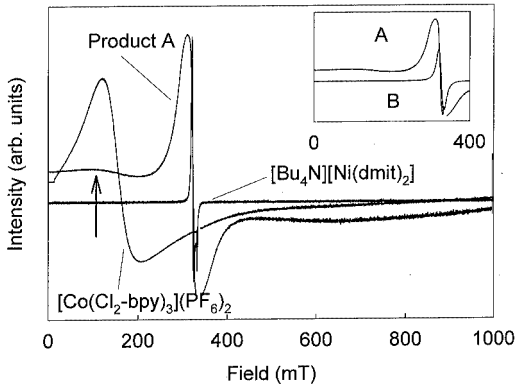

Figure 3. Powder sample EPR spectra at T = 77 K of $[Bu_4N][Ni(dmit)_2]$, $[Co(Cl_2\text{-}bpy)_3](PF_6)_2$ and product A; the inset shows comparison of spectra of products A and B

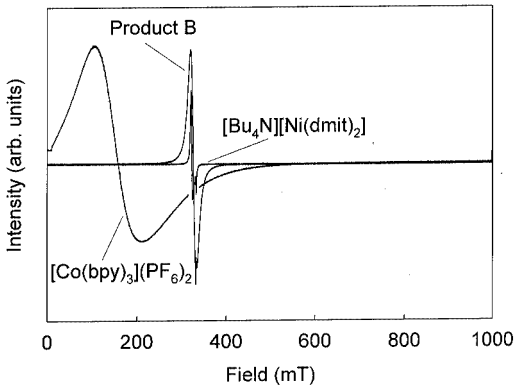

Figure 4. Powder sample EPR spectra at T = 77 K of $[Bu_4N][Ni(dmit)_2]$, $[Co(bpy)_3](PF_6)_2$ and product B

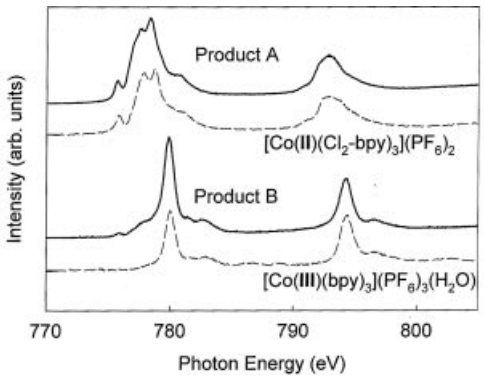

Figure 5. XAS spectra of A and B (——) and of $[Co^{II}(Cl_2\text{-}bpy)_3](PF_6)_2$ and $[Co^{III}(bpy)_3](PF_6)_3(H_2O)$ (----) as reference compounds

Product B has a cation/anion ratio of 1:3, as indicated by elemental analysis. For product A this is somewhat more difficult to determine. The elemental analysis suggests a ratio of 1:5.4, whereas the AAS indicates a ratio 1:4.5. This discrepancy between the two results is significant, but may still be within the margin of error for compounds with non-integer stoichiometries, like many $M(dmit)_2$-based compounds. It is evident that the cation/anion ratio of A, which is assumed to be 1:5 here, is significantly lower than that of B, also, like the Raman results, implying the presence of $Ni(dmit)_2$ species with formal charge x ($0 < x < 1$) in A.

The room-temperature powder conductivities of A and B are both around $\sigma_{rt} = 2 \cdot 10^{-3}$ S/cm. This similarity is remarkable considering the differences in stoichiometry and $Ni(dmit)_2$ oxidation state of the two compounds; A was expected to have a higher conductivity than B. However, the two-point powder conductivity technique is quite inaccurate for determining the true intrinsic conductivity of a compound. Contact resistance and inter-grain electron hopping in the compressed powder pellet inhibit an accurate measurement. Only single-crystal conductivity measurements can give this true intrinsic conductivity of these compounds. Studies of the magnetic properties of these materials are in progress.

Further efforts to obtain single crystals and studies on combining other $Co^{III}(N,N\text{-imine})_3$ complexes with $M(dmit)_2$ (M = Ni, Pd) are ongoing.

First findings show, that also for $Pd(dmit)_2$ anions the above described strategy is a successful one, resulting in compounds with a paramagnetic Co^{II} cation and $Pd(dmit)_2$ an-

ions with a non-integer formal charge. More detailed studies are in progress.

Conclusion

In conclusion can be stated, that combination of the appropriate ($\Delta E > 0.1$ V) $Co^{III}(N,N\text{-imine})_3$ complex with an $M(dmit)_2$ anion (M = Ni, Pd) allows the preparation of a partially oxidised, $M(dmit)_2$-based material, with a paramagnetic cation. Variation of the bis(imine) ligand enables fine tuning of the redox potential of the cobalt cation complex. In this way the oxidative power of the Co^{III} complex can be controlled.

In general can be concluded, that these $Co^{III}(N,N\text{-imine})_3$ complexes can be combined with a great variety of different $M(dithiolene)_2$ anions with a suitable $E_{ox,1-/x-}$ oxidation wave potential. A large number of such anions is already known.[6] This strategy may give access to a whole new series of compounds, all consisting of a paramagnetic cobalt(II) cation and a partially oxidised bis(dithiolato)metallate.

Experimental Section

General Remarks: Resonance Raman spectra were recorded with a Dilor XY spectrometer using a Spectra Physics 2040E Ar+ laser as excitation source. Co $L_{2,3}$ XAS data were recorded in the Fluorescence Yield mode at the SRRC Dragon beamline. The electrochemical analyses have been performed using an Autolab PGSTAT10 potentiostat, Pt working and counter electrodes and an Ag/AgCl reference electrode.

$[Bu_4N][Ni(dmit)_2]$: This starting compound has been prepared according to the well-developed procedure first described by Steimecke[28] and modified by Lindqvist.[29]

$[Co^{III}(X_2\text{-bpy})_3](PF_6)_3\cdot H_2O$ (X=H, Cl): The ligand 2,2′-bipyridine (bpy) is commercially available and has been used as received. The 4,4′-dichloro-2,2′-bipyridine ligand (Cl_2-bpy) has been synthesized according to a slightly adapted procedure described in the literature.[30] The two Co^{III} complexes have been prepared according to the literature.[31,32]

$[Co(Cl_2\text{-bpy})_3][Ni(dmit)_2]_5$ (A) and $[Co(bpy)_3][Ni(dmit)_2]_3$ (B): The cation exchange reactions to obtain products A and B involve mixing of a 2 mM solution of $[Bu_4N][Ni(dmit)_2]$ in acetone with a 2 mM $[Co^{III}(X_2\text{-bpy})_3](PF_6)_3\cdot H_2O$ solution in acetone, in a 3:1 molar ratio. The resulting black precipitates have been washed in acetone in an ultrasonic bath to wash out any enclosed starting compound, filtered off and dried under vacuum. A: Yield 50% with respect to $[Bu_4N][Ni(dmit)_2]$. IR (KBr): $\tilde{\nu}$ = 1654, 1560 (m, Cl_2-bpy), 1296 (m), 1246, 1058 (s, dmit), 922, 856, 827, 777, 747 (w, dmit), 667 (m, dmit), 497 (m, dmit) cm^{-1}. Elemental analysis found (calculated 1:5.4 cation/anion): C 22.56 (23.63), H 0.55 (0.57), N 2.53 (2.65), S 51.63 (54.59); calculated values with optimal C/N and S/N ratios. AAS found (calculated 1:4.5 cation/anion) Co 2.32 (2.17), Ni 10.25 (9.49); Co/Ni ratio 1:4.5. B: Yield 63% with respect to $[Bu_4N][Ni(dmit)_2]$. IR (KBr): $\tilde{\nu}$ = 1603, 1560 (w, bpy), 1446 (m, bpy), 1345, 1059 (s, dmit), 1025 (m, dmit), 920 (s, dmit), 757 (m, bpy), 511 (m, dmit) cm^{-1}. Elemental analysis found (calculated): C 30.29 (30.64), H 1.23 (1.29), N 4.51 (4.47), S 50.61 (51.12).

Acknowledgments

This work has been produced by collaboration within the Holland Research School for Molecular Chemistry. Theo Snoeck (Institute of Molecular Chemistry, University of Amsterdam) and Jos van Brussel (Leiden Institute of Chemistry, Gorlaeus Laboratories, Leiden University) are kindly acknowledged for performing the Raman measurements and microanalyses, respectively.

[1] P. Cassoux, *Science* **1996**, *272*, 1277−1278.
[2] H. Imai, T. Naito, K. Awaga, T. Inabe, *Synth. Met.* **2001**, *120*, 951−952.
[3] S. Aonuma, H. Casellas, C. Faulmann, B. G. de Bonneval, I. Malfant, P. Cassoux, P. G. Lacroix, Y. Hosokoshi, K. Inoue, *J. Mater. Chem.* **2001**, *11*, 337−345.
[4] C. Handrosch, R. Dinnebier, G. Bondarenko, E. Bothe, F. Heinemann, H. Kisch, *Eur. J. Inorg. Chem.* **1999**, 1259−1269.
[5] K. Sakai, T. Akutagawa, T. Hasegawa, T. Nakamura, *Synth. Met.* **2001**, *120*, 805−806.
[6] G. C. Papavassiliou, A. Terzis, P. Delhaes, *Tetrachalcogenafulvalenes, metal 1,2-dichalcogenolenes and their conducting salts* (Ed.: H. S. Nalwa), John Wiley & Sons Ltd., New York, **1997**, p. 151−227.
[7] W. E. Broderick, J. A. Thompson, M. R. Godfrey, M. Sabat, B. M. Hoffman, *J. Am. Chem. Soc.* **1989**, *111*, 7656−7657.
[8] F. Qi, Y. Xiao-Zeng, *Acta Crystallogr., Sect. C* **1993**, *49*, 1347−1350.
[9] C. Faulmann, A. E. Pullen, E. Riviere, Y. Journaux, L. Retailleau, P. Cassoux, *Synth. Met.* **1999**, *103*, 2296−2297.
[10] S. Rabaça, V. Gama, D. Belo, I. C. Santos, M. T. Duarte, *Synth. Met.* **1999**, *103*, 2302−2303.
[11] R. Kumai, A. Asamitsu, Y. Tokura, *J. Am. Chem. Soc.* **1998**, *120*, 8263−8264.
[12] R. Kumai, A. Asamitsu, Y. Tokura, *Chem. Lett.* **1996**, 753−754.
[13] L. Ouahab, *Chem. Mater.* **1997**, *9*, 1909−1926.
[14] M. Inoue, M. B. Inoue, *Inorg. Chim. Acta* **1980**, *45*, L129−L130.
[15] M. B. Inoue, M. Inoue, *Chem. Phys. Lett.* **1981**, *80*, 585−588.
[16] M. Inoue, M. B. Inoue, T. Seto, D. Nakamura, *Mol. Cryst. Liq. Cryst.* **1982**, *86*, 139−146.
[17] M. B. Inoue, M. Inoue, *Mol. Cryst. Liq. Cryst.* **1983**, *95*, 183−189.
[18] M. Inoue, M. B. Inoue, *J. Chem. Soc., Chem. Commun.* **1984**, 790−791.
[19] M. Inoue, M. B. Inoue, *Inorg. Chem.* **1986**, *25*, 37−41.
[20] A. Abragam, M. H. L. Pryce, *Proc. R. Soc. London Ser. A* **1951**, *206*, 173.
[21] J. B. Tommasino, B. Pomarede, D. Medus, D. Demontauzon, P. Cassoux, P. L. Fabre, *Mol. Cryst. Liq. Cryst. Sci. Technol., Sect. A* **1993**, *237*, 445−456.
[22] L. Valade, Thèse de 3ème cycle, no. 2823, Université Paul Sabatier, Toulouse, France, **1983**.
[23] S. A. Richert, P. K. S. Tsang, D. T. Sawyer, *Inorg. Chem.* **1989**, *28*, 2471−2475.
[24] R. C. Wheland, *J. Am. Chem. Soc.* **1976**, *98*, 3926−3930.
[25] K. I. Pokhodnya, C. Faulmann, I. Malfant, R. Andreu Solano, P. Cassoux, A. Mlayah, D. Smirnov, J. Leotin, *Synth. Met.* **1999**, *103*, 2016−2019.
[26] M. Abbate, J. C. Fuggle, A. Fujimore, L. H. Tjeng, C. T. Chen, R. Potze, G. A. Sawatzky, H. Eisaki, S. Uchida, *Phys. Rev. B* **1993**, *47*, 124−130.
[27] F. E. Mabbs, D. Collison, *Electron Paramagnetic Resonance of d Transition Metal Compounds*, Elsevier Science Publishers, Amsterdam, **1992**.
[28] G. Steimecke, H.-J. Sieler, R. Kirmse, E. Hoyer, *Phosphorus Sulfur* **1979**, *7*, 49−55.
[29] O. Lindqvist, L. Andersen, J. Sieler, G. Steimecke, E. Hoyer, *Acta Chem. Scand., Ser. A* **1982**, *36*, 855−856.
[30] P. Wehman, Thesis, University of Amsterdam, Amsterdam, **1995**.
[31] F. H. Burstall, R. S. Nyholm, *J. Chem. Soc.* **1952**, 3570−3579.
[32] R. M. L. Warren, A. G. Lappin, B. D. Mehta, H. M. Neumann, *Inorg. Chem.* **1990**, *29*, 4185−4189.

Received June 29, 2002
[I02340]

Regio-Directed Synthesis of a $Zn^{II}Fe^{III}$ Complex from an Unsymmetrical Ligand and Its Relevance to Purple Acid Phosphatases

Catherine Belle,*[a] Isabelle Gautier-Luneau,[a] Lydia Karmazin,[a] Jean-Louis Pierre,[a] Sabine Albedyhl,[b] Bernt Krebs,[b] and Michel Bonin[c]

Keywords: Heterometallic complexes / Zinc / Iron / Unsymmetrical ligands / Phosphatases

A new heterodinuclear $Zn^{II}Fe^{III}$ μ-phenoxy complex has been prepared and isolated from the unsymmetrical ligand 2-{[bis(2-hydroxybenzyl)]amino}methyl-6-{[2-pyridinylmethyl)amino]methyl}-4-methylphenol (H_3L^1), which provides two distinct N- and O-rich donor sets. The regioselective complexation is confirmed in solution by ^1H NMR studies (comparison of the spectra obtained from H_3L^1 and HL^2 – a ligand with only the N-donor set available – and a zinc salt). The crystal structure of the bis(μ-diphenylphosphato)$Zn^{II}Fe^{III}$ complex $[ZnFeL^1\{O_2P(OPh)_2\}_2]$ (**1**) is reported. The NO_5 coordination sphere around the Fe^{III} reproduces, for the first time, the oxygen-rich coordination sphere around iron(III) in red kidney bean purple acid phosphatase (KBPAP).

(© Wiley-VCH Verlag GmbH, 69451 Weinheim, Germany, 2002)

Introduction

Purple acid phosphatases (PAPs) are non redox-active dinuclear metalloenzymes representing a group of widely distributed phosphomonoesterases. Purple acid phosphatases require acidic conditions for optimum activity and are characterized by an intense purple color ($\lambda_{max} \approx 550$ nm) due to a charge-transfer transition from a tyrosine group to the iron(III).[1] Mammalian PAPs contain an $Fe^{II}Fe^{III}$ center at the active site while the most studied plant enzyme, isolated from red kidney bean (KBPAP), contains a $Zn^{II}Fe^{III}$ center. The X-ray structure of KBPAP (resolution 2.65 Å) shows that the two metal ions are 3.26 Å apart and bridged by Asp_{164}; each metal center has octahedral coordination.[2] The iron is further coordinated by Tyr_{167}, His_{325} and Asp_{135} residues, and zinc by His_{323}, His_{286} and Asn_{201} residues (Figure 1A). Three exogenous ligands are also included in the X-ray model to complete the coordination sphere: one terminal hydroxy ligand to iron, one terminal water ligand to zinc, and one hydroxy bridge between the metal ions. An important role is assigned to such unsymmetrical coordination, providing selective substrate binding and stereochemical control during the catalytic cycle.[2] The crystal structure of KBPAP with a coordinated μ-phosphate (the product of the hydrolysis reaction) (resolution 2.7 Å; Figure 1B) or with a μ-tungstate inhibitor (resolution 3.0 Å) have also been reported.[2b] Phosphate or tungstate oxoanions bind in a bidentate bridging mode to the two metals ions. The intermetallic distances have been refined to 3.33 Å and 3.20 Å, respectively.

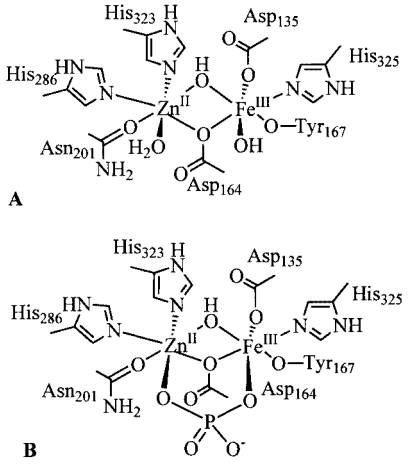

Figure 1. The active site of kidney bean purple acid phosphatase (KBPAP) (A) and of its phosphate adduct (B) from X-ray crystallography[2b]

Although the metal ions in KBPAP are in two chemically distinct environments, the heterodinuclear $Zn^{II}Fe^{III}$ complexes described as models for the active site of KBPAP[3–8] have been prepared from symmetrical ligands. Only limited examples of unsymmetrical $Zn^{II}Fe^{III}$ complexes have been

[a] LEDSS, Chimie Biomimétique, UMR CNRS 5616, Université J. Fourier,
B. P. 53, 38041 Grenoble Cedex, France
Fax: (internat.) +33-47/651-4836
E-mail: Catherine.Belle@ujf-grenoble.fr
[b] Anorganisch-Chemishes Institut, Westfälische Wilhelms-Universität
Wilhelm-Klemm-Straße 8, 48149 Münster Germany
[c] Institute of Crystallography, University of Lausanne, BSP, 1015 Lausanne, Switzerland

reported. They involve constitutionally unsymmetrical ligands with an alkoxy bridge but with identical chemical environments (two N_3O coordination spheres) around the metal ions.[9,10] The only example characterized by an X-ray structure has iron and zinc atoms bridged by an arsenate group[10] and with two different coordination environments (N_3O_3 and N_3O_2 for Fe and Zn, respectively). Currently, there is great interest in the development of new $Zn^{II}Fe^{III}$ complexes which may be used as models for enzyme-substrate/inhibitor intermediates.

We have used the known binucleating ligand H_3L^1 (Scheme 1),[11] which involves two different coordination sites connected by a phenol spacer: a hard site {a [bis(2-hydroxybenzyl)amino]methyl moiety} suited for iron(III) complexation and a softer site {a [bis(2-pyridinylmethyl)-amino]methyl moiety}, suited for zinc(II) complexation. We report here a regiodirected preparation of a heterodinuclear $Zn^{II}Fe^{III}$ complex and the X-ray structure of a diphenylphosphate adduct.

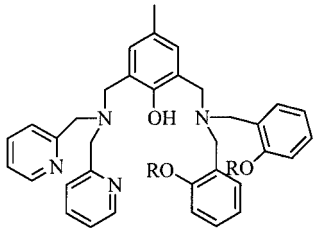

R = H (H_3L^1) or R = CH_3 (HL^2)

Scheme 1

Results and Discussion

Mononuclear zinc(II) complexes were prepared in solution in an NMR tube with either H_3L^1 or HL^2. HL^2 is the bis-methoxy derivative of H_3L^1 (Scheme 1)[12] where the terminal phenolate donor set has been suppressed and only one coordination site remains for metal ion complexation. The zinc complex of this ligand shows spectroscopic features for the complexation of Zn^{2+} by a bis(2-pyridinylmethyl)amino moiety. The complexation processes were monitored by ^1H NMR spectroscopy. The ligand resonances shifted progressively upon addition of a solution of $Zn(ClO_4)_2 \cdot 6H_2O$ in CD_3CN (Figure 2). Interestingly, the spectrum recorded for solutions containing a mixture of the ligand and the complex show that the two species are in slow exchange on the NMR time scale. Although different species are observed during the addition of the zinc salt only one species is present after addition of one molar equivalent of the zinc salt. The spectrum remains unchanged after the addition of a further equivalent of the zinc salt. The mononuclear zinc complexes prepared independently from H_3L^1 and HL^2 or obtained upon addition of the zinc salt to the ligand in the NMR tube are the same, as seen by their NMR spectra. Comparison of the spectra obtained with one molar equivalent of zinc salt and H_3L^1 instead of HL^2 reveals the similarity of the environment

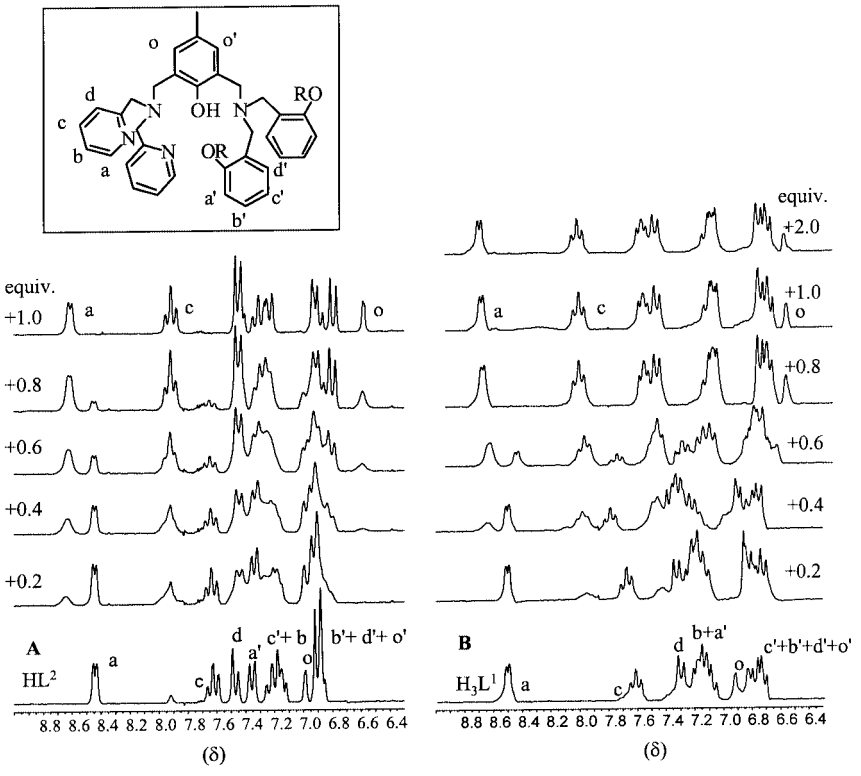

Figure 2. ^1H NMR spectra (200 MHz, CD_3CN) monitoring the formation of the mononuclear zinc complexes in the aromatic region, from HL^2(A) and H_3L^1(B) upon progressive addition of the zinc perchlorate salt; inset: ligand numbering scheme

around the zinc(II) center in the two mononuclear complexes (Figure 2). In particular, the well-resolved *ortho*- and *para*-pyridinyl resonances (protons *a* and c respectively in Figure 2) show the same behavior. In a similar manner, the resonance for the proton in the *ortho* position on the central phenyl ring and close to the pyridyl arms (signal *o* on Figure 2) appears near $\delta = 7.0$ ppm for both free ligands and is shifted to $\delta = 6.7$ ppm after complexation. Accordingly, it appears that the zinc ion is regioselectively complexed by the bis-pyridyl site of the dinucleating ligand H_3L^1.

The neutral heterobinuclear $[ZnFeL^1\{O_2P(OPh)_2\}_2]$ (**1**) complex was obtained from H_3L^1 by stepwise addition (in methanol) of zinc(II) perchlorate (1 equiv.) followed by addition of triethylamine (3 equiv.), and iron(III) perchlorate (1 equiv.). After addition of diphenylphosphate (2 equiv.) complex **1** precipitated as a violet powder. Recrystallisation by vapor diffusion of methanol into an acetonitrile solution of **1** gave crystals suitable for an X-ray diffraction study. The electronic absorption spectrum of **1** in CH_3CN displays a main feature at 501 nm ($\varepsilon \approx 3077$ M^{-1} cm^{-1}). Comparison of this spectrum with those of iron(III) complexes of μ-phenolato ligands leads to the assignment of the latter band to charge-transfer transitions from the terminal and the bridging phenolates to the iron(III).[4] The native Zn^{II}-Fe^{III} red kidney bean phosphatase displays a visible spectrum with a λ_{max} of 560 nm ($\varepsilon \approx 3360$ M^{-1} cm^{-1}).[13]

The crystal structure of **1** reveals that the two metallic atoms are triply bridged by the phenoxo group (O1) of the ligand and two μ-diphenylphosphato groups leading to the intermetallic distance of 3.7402(7) Å. An ORTEP view is shown on Figure 3, and selected bond lengths and angles are given in Table 1. The octahedral coordination geometry of the metal centers is completed by the tertiary amine (N2) and two pyridine nitrogens (N3 and N4) for Zn^{II} and by the tertiary amine (N1) and two phenolate oxygens (O2 and O3) for Fe^{III}. The distances in the $[NO_5]$ coordination sphere of the iron(III) are in the range of 1.918(2) to 2.222(3) Å and are more asymmetric than those of Zn^{II} for which the distances in the $[N_3O_3]$ coordination sphere are ranged between 2.037(3) and 2.182(3) Å. The Fe−O(phenolate) bond lengths [1.918(2) and 1.919(2) Å] are slightly longer than in the $[Fe_2L^1(\mu\text{-OMe})(OMe)]^+$ complex[14] [1.872(5) and 1.850(5) Å] where the iron has a pentacoordinate coordination sphere. The Zn···Fe distance of 3.7402(7) Å is slightly longer than in other complexes where the metals are linked by three bridges, one phenoxy and two μ-diphenylphosphate groups. In $[ZnFe(BPMP)\{O_2P(OPh)_2\}_2]^{2+}$ and $[ZnFe(BPMOP)\{O_2P(OPh)_2\}_2]^{2+}$ the intermetallic distances are 3.695(1) Å[3] and 3.7030(7) Å,[5] respectively.

Although the Zn−O1 [2.124(2) Å] and Fe−O1 [2.035(3) Å] bond lengths in complex **1** are similar to those observed in the previously cited complexes, the Zn−O1−Fe bond angle is larger [128.1(1)°] {$[ZnFe(BPMP)\{O_2P(OPh)_2\}_2]^{2+}$: Zn−O1 = 2.176(2) Å, Fe−O1 = 2.031(2) Å, Zn−O1−Fe = 122.8(1)°; $[ZnFe(BPMOP)\{O_2P(OPh)_2\}_2]^{2+}$: Zn−O1 = 2.168(2) Å, Fe−O1 = 2.047(2) Å, Zn−O1−Fe = 122.9(1)°}. Moreover, the Zn−O1−Fe angle is similar to that observed in $[ZnFe(BPBP)(MoO_4)_2]$[8] [127.4(2)°] where, due to the longer Mo−O distance [average 1.788 Å, compared to the P−O distance (average 1.478

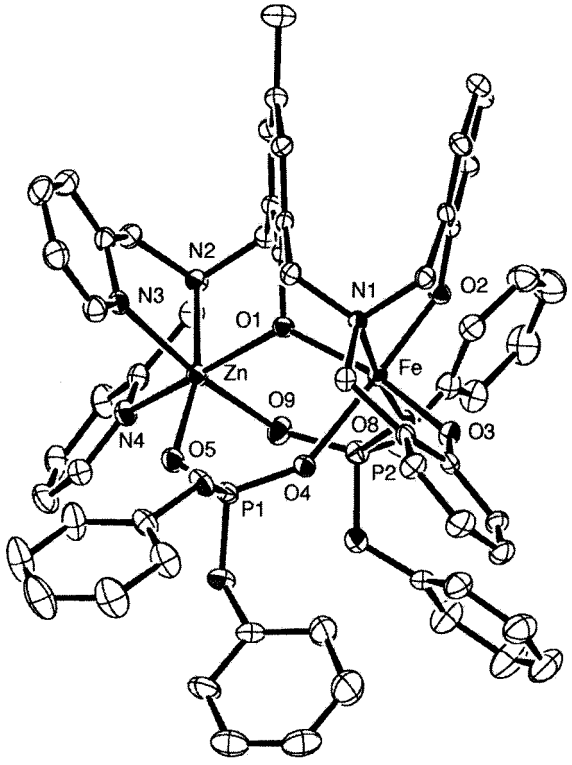

Figure 3. ORTEP plot of $[ZnFeL^1(O_2P(OPh)_2]_2]$ (**1**), with atom labels and numbering scheme; hydrogens are omitted for clarity; ellipsoids are drawn at the 30% probability level

Table 1. Selected bond lengths (Å) and angles (°) for **1**

Zn−Fe	3.7402(7)		
Zn−O1	2.124(2)	Fe−O1	2.035(3)
Zn−O5	2.037(3)	Fe−O8	2.005(2)
Zn−O9	2.130(3)	Fe−O4	2.112(2)
Zn−N2	2.182(3)	Fe−N1	2.222(3)
Zn−N3	2.180(3)	Fe−O2	1.919(2)
Zn−N4	2.151(3)	Fe−O3	1.918(2)
P1−O4	1.481(3)	P2−O8	1.484(2)
P1−O5	1.478(3)	P2−O9	1.468(3)
Zn−O1−Fe	128.1(1)		
O1−Zn−N2	91.7(1)	O1−Fe−N1	87.5(1)
O1−Zn−N4	165.5(1)	O1−Fe−O3	165.6(1)
O1−Zn−N3	89.0(1)	O1−Fe−O2	93.8(1)
O1−Zn−O9	88.2(1)	O1−Fe−O8	95.1(1)
O1−Zn−O5	96.6(1)	O1−Fe−O4	82.4(1)
O5−Zn−N2	167.3(1)	O2−Fe−N1	88.5(1)
O5−Zn−N3	91.5(1)	O2−Fe−O4	174.6(1)
O5−Zn−N4	96.0(1)	O2−Fe−O8	87.3(1)
O5−Zn−O9	97.5(1)	O3−Fe−O2	98.8(1)
O9−Zn−N4	82.9(1)	O3−Fe−N1	86.0(1)
O9−Zn−N3	170.8(1)	O3−Fe−O4	85.4(1)
O9−Zn−N2	92.3(1)	O3−Fe−O8	92.3(1)
N3−Zn−N2	79.0(1)	O4−Fe−N1	95.1(1)
N4−Zn−N3	98.0(1)	O8−Fe−N1	175.2(1)
N4−Zn−N2	77.2(1)	O8−Fe−O4	89.3(1)
Zn−O5−P1	124.0(1)	Fe−O4−P1	147.1(2)
Zn−O9−P2	139.5(2)	Fe−O8−P2	131.7(2)
O4−P1−O5	119.0(1)	O8−P2−O9	119.7(2)

Å)], the Fe−O1 [2.156(5) Å] and Zn−O1 [2.104(5) Å] bonds are longer, leading to an intermetallic distance of 3.819(4) Å. All these structures indicate a remarkable structural flexibility of the intermetallic distance, which may be important for the catalytic activity. In native KBPAP with one coordinated phosphate, the Fe···Zn distance has been refined to 3.33 Å.[2b] The bridging mode of the phosphate is nearly symmetrical (with Fe−O−P and Zn−O−P angles of 120° and 127° respectively), whereas in complex **1** the angles are larger and ranged between 124.0(1)° and 147.1(1)°. Larger angles are also observed in $[ZnFe(BPMP)\{O_2P(OPh)_2\}_2]^{2+}$ and in $[ZnFe(BPMOP)\{O_2P(OPh)_2\}_2]^{2+}$ complexes.

Conclusion

The use of an unsymmetrical ligand possessing both a hard and a softer coordination site may be considered as an interesting strategy to prepare heterobinuclear complexes in a directed, non-statistical way. This paper describes a predictable and controlled synthesis of a $Zn^{II}Fe^{III}$ complex. The zinc was complexed first and solution studies revealed that zinc(II) is bound exclusively by the N-rich donor set.; the O-rich donor remains available for the subsequent complexation of iron(III). This regiocontrolled synthesis has allowed us to describe and characterize the first example of a phosphate-bridged species with a $Zn^{II}Fe^{III}$ core in an unsymmetrical, octahedral environment. The NO_5 coordination sphere around the iron(III) models the oxygen-rich coordination sphere for this ion in KBPAP.

Experimental Section

H_3L^1 and HL^2 were synthesized as reported previously.[11−12]

$[ZnFeL^1\{O_2P(OPh)_2\}_2]$ (1): A solution of $Zn(ClO_4)_2\cdot 6H_2O$ (0.0664 g, 0.178 mmol) in methanol (3 mL) was added dropwise to a solution of H_3L^1 (0.100 g, 0.178 mmol) dissolved in methanol (4 mL). The solution was stirred for 1 h and NEt_3 (0.712 mmol) was added. After 15 min a solution of $Fe(ClO_4)_2\cdot 9H_2O$ (0.0632 g, 0.178 mmol) in methanol (3 mL) was added, and the solution, which turned dark-red, was stirred for 1 h. Diphenylphosphate (0.0893 g, 0.356 mmol) dissolved in methanol (4 mL) was then added, and the solution turned dark and a purple powder precipitated. This precipitate was collected by filtration (79.2 mg, 38%). Crystals of X-ray quality were obtained by vapor diffusion of methanol into an acetonitrile solution of **1**. $C_{59}H_{53}FeN_4O_{11}P_2Zn\cdot CH_3OH$: calcd. C 59.59, H 4.75, Fe 4.62, N 4.63, P 5.12, Zn 5.41; found C 59.49, H 4.47, Fe 4.62, P 5.13, N 4.69, Zn 5.00. UV/Vis (CH_3CN): λ_{max} = 501 nm (ε = 3077 $M^{-1}\,cm^{-1}$). FAB-MS (NBA): m/z = 1176 $[M + H]^+$.

The mononuclear zinc(II) complexes were isolated as pale yellow powders after addition of diethyl ether to a methanol solution of $Zn(ClO_4)_2\cdot 6H_2O$ (1 equiv.) and H_3L^1 (or HL^2) (1 equiv.). FAB-MS (NBA): from H_3L^1, m/z = 623 $[H_3L^1 + Zn - 2H]^+$; from HL^2, m/z = 651 $[HL^2 + Zn - 2H]^+$.

X-ray Crystallographic Study A single crystal of $[ZnFeL^1\{O_2P(OPh)_2\}_2]$ was mounted at 170 K on a Stoe IPDS diffractometer equipped with graphite-monochromated Mo-K_α radiation (λ = 0.71073 Å). $[ZnFe(C_{35}H_{33}N_4O_3)\{O_2P(OC_6H_5)_2\}_2]$ M = 1177.26, dark purple platelet (0.045 × 0.08 × 0.23 mm), monoclinic, space group $P2_1/c$, a = 19.338(4), b = 16.850(3), c = 16.851(3) Å, β = 99.12(3)°, U = 5421(2) Å^3, Z = 4, D_c = 1.44 g cm^{-3}, μ = 0.835 mm^{-1}. 43028 Reflections (10794 independent reflections) were collected and corrected for Lorentz and polarization effects but not for absorption. The structures were solved by direct methods and refined using the teXsan software package.[13] All non-hydrogen atoms were refined with anisotropic thermal parameters. Hydrogen atoms were generated in idealized positions, riding on the carrier atoms, with isotropic thermal parameters. Final cycle refinement, including 703 parameters, converged to $R(F)$ = 0.035 and $Rw(F)$ = 0.028 [for 6130 $F > 2\sigma(F)$] [s = 1.11, (Δ/σ_{max} = 0.07, $\Delta\rho_{max}$ = 0.36 e·Å^{-3}, $\Delta\rho_{min}$ = −0.26 e·Å^{-3}]. CCDC-179245 contains the supplementary crystallographic data for this paper. These data can be obtained free of charge at www.ccdc.cam.ac.uk/conts/retrieving.html [or from the Cambridge Crystallographic Data Centre, 12, Union Road, Cambridge CB2 1EZ, UK; Fax: (internat.) +44-1223/336-033; E-mail: deposit@ccdc.cam.ac.uk].

[1] M. B. Twitchett, A. G. Sykes, *Eur. J. Inorg. Chem.* **1999**, 2105−2115.
[2] [2a] N. Sträter, T. Klabunde, P. Tucker, H. Witzel, B. Krebs, *Science* **1995**, *268*, 1489−1492. [2b] T. Klabunde, N. Sträter, R. Fröhlich, H. Witzel, B. Krebs, *J. Mol. Biol.* **1996**, *259*, 737−748.
[3] K. Schepers, B. Bremer, B. Krebs, G. Henkel, E. Althaus, B. Mosel, W. Müller-Warmuth, *Angew. Chem. Int. Ed. Engl.* **1990**, *29*, 531−533.
[4] A. S. Borovik, V. Papaefthymiou, L. F. Taylor, L. P. Anderson, L. Que Jr., *J. Am. Chem. Soc.* **1989**, *111*, 6183−6195.
[5] S. Albedyhl, M. T. Averbuch-Pouchot, C. Belle, B. Krebs, J. L. Pierre, E. Saint-Aman, S. Torelli, *Eur. J. Inorg. Chem.* **2001**, 1457−1464.
[6] S. K. Dutta, R. Werner, U. Flörke, S. Mohanta, K. K. Nanda, W. Haase, K. Nag, *Inorg. Chem.* **1996**, *35*, 2292−2300.
[7] J. Kamitani, R. Kawahara, M. Yashiro, M. Komiyama, *Chem. Lett.* **1998**, 1047−1048.
[8] M. Ghiladi, C. J. McKenzie, A. Meier, A. K. Powell, J. Ulstrup, S. Wocadlo, *J. Chem. Soc., Dalton Trans.* **1997**, 4011−4018.
[9] M. Suzuki, S. Fujinami, T. Hibino, H. Hori, Y. Maeda, A. Uehara, M. Suzuki, *Inorg. Chim. Acta* **1998**, *283*, 124−135.
[10] S. Albedhyl, D. Schnieders, A. Jancsó, T. Gajda, B. Krebs, *Eur. J. Inorg. Chem.* **2002**, 1400−1409.
[11] C. Belle, G. Gellon, C. Scheer, J. L. Pierre, *Tetrahedron. Lett.* **1994**, *35*, 7019−7022.
[12] C. Belle, J. L. Pierre, E. Saint-Aman, *New J. Chem.* **1998**, *22*, 1399−1402.
[13] J. L. Beck, L. A. McConachie, A. C. Summors, W. N. Arnold, J. de Jersey, B. Zerner, M. P. Hendrich, P. G. Debrunner, *Biochem. Biophys. Acta* **1986**, *869*, 61−68.
[14] C. Belle, I. Gautier-Luneau, J. L. Pierre, C. Scheer, E. Saint-Aman, *Inorg. Chem.* **1996**, *35*, 3706−3708.
[15] Molecular Structure Corporation (1995). teXsan, Single Crystal structure Analysis Software. Version 1.7.MSC, 3200 Research Forest Drive, The Woodlands, TX 77381, USA.

Received July 8, 2002
[I02369]

Astonishing Alkylation and Unusual Reduction Reactions of Anionic Titanium(II) Isopropoxide Complexes: Evidence for SET Processes in Transition-Metal Oxidative Additions[‡]

John J. Eisch*[a] and John N. Gitua[a]

Keywords: Titanium / Subvalent compounds / Oxidative addition / Alkylation / Electron transfer

A mixture of titanium(II) isopropoxide and lithium isopropoxide (1:2), generated in THF by the treatment of titanium(IV) isopropoxide with two equivalents of *n*-butyllithium, has been shown to be an unexpected alkylating agent as well as an unusual reducing agent for a wide variety of organic substrates. Since titanium(II) isopropoxide, which is free of any lithium isopropoxide, neither causes alkylation of any of the same substrates nor is such a powerful reductant, it is proposed that the lithium isopropoxide activates titanium(II) isopropoxide for such unusual reactions by the formation of the lithium salt coordination complex $Li_2Ti[OiPr]_4$. Illustrative of the unprecedented alkylations are the transformations, after hydrolysis, of various substituted benzonitriles to isopropyl-substituted phenyl ketones, of (dichloromethyl)benzene to, principally, 2-methyl-1-phenyl-1-propene and of (trichloromethyl)benzene to isopropyl phenyl ketone. By comparing the reducing actions of $Li_2Ti[OiPr]_4$ and $Ti[OiPr]_2$ individually, it has been shown that, generally, the lithium salt is the more powerful reductant for epoxides, benzylic halides and conjugated olefins. From the reactions of $Li_2Ti[OiPr]_4$ with the benzonitriles, styrene, the isomeric stilbene oxides and *cis*-stilbene, cogent evidence is marshaled for the operation of SET processes, sensitive to steric hindrance, in such alkylations and reductions.
(© Wiley-VCH Verlag GmbH, 69451 Weinheim, Germany, 2002)

Introduction

The oxidative addition of subvalent transition metals or metal salts, $M_t^nL_x$ (**1**), where *n* is the oxidation number, to π-bonded organic substrates (**2**) with the formation of a metallacyclic intermediate (**3**) has been termed epimetallation [Equation (1)].[2]

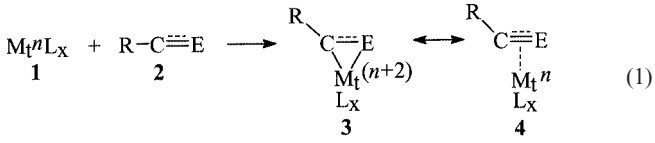

(1)

Since metallacycle **3** is one extreme of resonance structures ranging to the other extreme of a π-complex structure **4**, the term epimetallation implies that the adduct of **1** and **2** displays chemical reactions in better accord with **3**, possessing two sigma C−M_t bonds, than with **4**. The chemical behavior of **5** — the adduct of benzophenone and $Li^+CrH_2^-$ — towards D_2O[3] and towards CO_2 [2] illustrates clearly why **5** should be viewed as an oxachromacyclopropane rather than as the π-complex **6**. Were the π-complex **6** involved in the reaction with CO_2, then simple ligand displacement and reduction of CO_2 to **7** should have ensued (Scheme 1). Instead, the observed products of deuterium oxide cleavage (**8**) and of carbonation (**9**) are unambiguous proof for the presence of a C−Cr bond in **5**.

In exploring the applicability of epimetallation for organic synthesis, we have recently generated titanium(II) isopropoxide (**10**) according to Equation (2) and have employed **10** for the epimetallation of terminal alkenes, alkynes and selected carbonyl derivatives.[4]

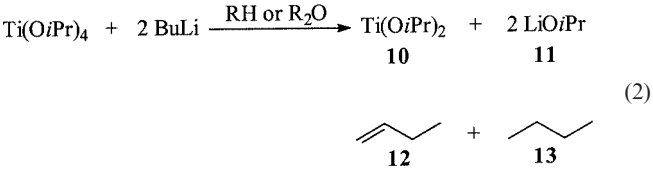

(2)

Particularly noteworthy are the by-products formed in the production of **10**, namely lithium isopropoxide (**11**), which remains in solution regardless of whether the reaction is conducted in hexane or THF, and the one equivalent of 1-butene (**12**) which is epimetallated in situ by **10** with the formation of **14** (Scheme 2). The presence of **14** was demonstrated by its chemical trapping with benzonitrile

[‡] Organic Chemistry of Subvalent Transition Metal Complexes, 24. Part 23: Ref. [1]

[a] Department of Chemistry, The State University of New York at Binghamton
P. O. Box 6016, Binghamton, New York 13902−6016 U.S.A.
Fax: (internat.) +1-607/777-4865
E-mail: jjeisch@binghamton.edu

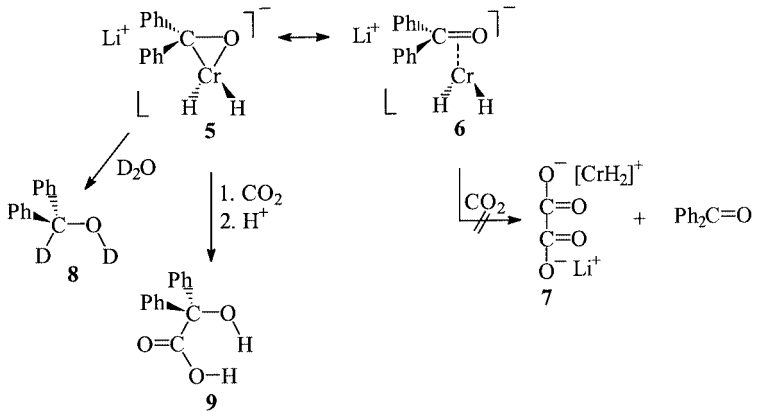

Scheme 1

(**15**) to provide **16**, whose subsequent hydrolysis yielded *n*-butyl phenyl ketone (**17**).[4] Only if the solvent is removed by warming and reduced pressure can **14** be decomposed.

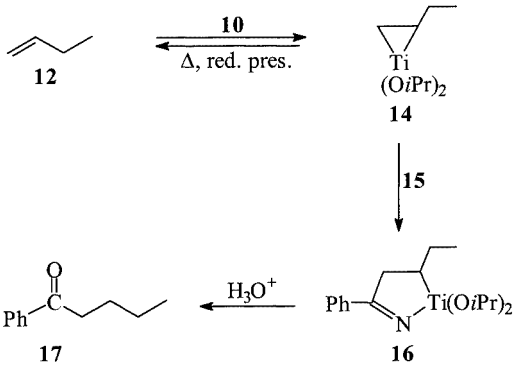

Scheme 2

Results and Discussion

In order to learn whether titanium(II) isopropoxide itself, free of any of the adduct **14**, could epimetallate benzonitrile (**15**), a solution of **10** generated in THF was freed of solvent under reduced pressure at 70°. To the black residue of **10** and **11** an equivalent of benzonitrile in toluene was then added and the solution heated at reflux. To our astonishment, upon hydrolytic workup such a reaction mixture gave 92% of isopropyl phenyl ketone (**18**) but only a small amount of **17** and a trace of 2,2-dimethyl-1,3-diphenyl-1,3-propanedione (**19**)[5] [Scheme 3, Table 1]. The formation of **18** raised the possibility that heating solutions of **10** might have produced an isopropylmetallic agent **20**, which would then have added to **15** to yield **21**, a prehydrolysis intermediate to the observed final product. That the lithium isopropoxide by-product **11** plays an essential role in this unexpected reaction was demonstrated in the following way. Recently we have reported that titanium(II) isopropoxide, free of lithium isopropoxide, can be prepared by treating titanium dichloride diisopropoxide (**22**) in hexane with two equivalents of *n*-butyllithium[6] [Equation (3)]. In this case, the lithium chloride formed is a much weaker base and more ionic salt and precipitates completely from the mixture. When this $Ti(OiPr)_2$, free of lithium isopropoxide, was heated with benzonitrile in toluene and then hydrolyzed, analogous to the reaction in Scheme 3, no trace of **18** was found whatsoever.[7] Thus, a combination of **10** and **11** is a prerequisite for the formation of isopropyl phenyl ketone (**18**) from benzonitrile (**15**).

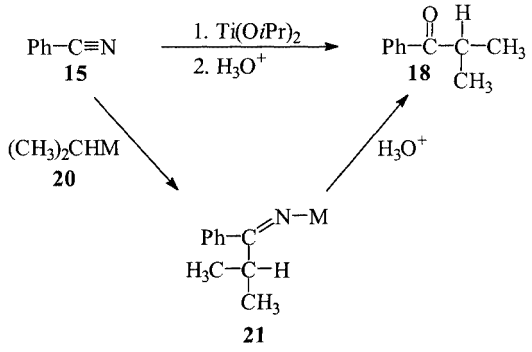

Scheme 3

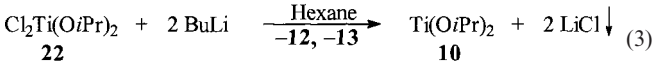

(3)

In establishing the role of **11** in activating **10** for this unusual reaction, it should be noted that titanium(II) salts form anionic complexes with alkali metal salts.[8] Therefore, **10** and **11** can be expected to be in equilibrium with complexes such as **23** [Equation (4)].

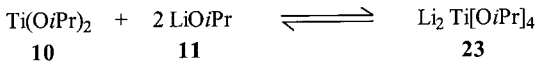

(4)

That four isopropoxyl groups can be sterically accommodated around the titanium(II) center in **23** is corroborated by the existence of stable titanium(IV) isopropoxide. One possibility for the formation of the requisite isopropyl-

Table 1. Reactions of the titanium(II) isopropoxide-lithium isopropoxide complex (23) in THF with organic substrates

Entry	Substrate[a]	Products	Yield (%)[b]
1	Benzonitrile (**15**)	Isopropyl phenyl ketone (**18**)	92
		Butyl phenyl ketone (**17**)	7
		2,2-Dimethyl-1,3-diphenyl-1,3-propanedione (**19**)	1
2	2-Methoxybenzonitrile (**26**)	Isopropyl 2-methoxybenzonitrile ketone	90
		1,3-Bis(*p*-anisyl)-2,2-dimethyl-1,3-propanedione	10
3	4-Methoxybenzonitrile (**27**)	Isopropyl 4-methoxyphenyl ketone	99
		1,3-Bis(*p*-anisyl)-2,2-dimethyl-1,3-propanedione	1
4	2,4,6-Trimethylbenzonitrile (**28**)	No Reaction	–
5	(Dichloromethyl)benzene (**29**)	2-Methyl-1-phenyl-1-propene (**30**)	40
		trans-Stilbene	1 6
		Benzyl chloride	32
		Isopropyl phenyl ketone	8
		1,2-Dichloro-1,2-diphenyl ethane	4
6	(trichloromethyl)benzene (**30a**)[c]	Isopropyl phenyl ketone (**18**)	64
		1,1,2,2-Tetrachloro-1,2-diphenylethane	30
		trans-1,2-Dichlorostilbene	6
7	Benzyl chloride (**31**)[d]	Dibenzyl (**40**)	97
		Toluene	3
8	9-Bromofluorene (**32**)[d]	Fluorene	55
		9,9′Bifluorenyl	45
9	4-Bromoanisole (**38**)	Anisole	40
10	*cis*-Stilbene oxide (**33**)[d]	*trans*-Stilbene (**36**)	91
		cis-Stilbene (**35**)	9
11	*trans*-Stilbene oxide (**34**)[d]	*trans*-Stilbene (**36**)	100
12	Diphenylacetylene (**37**)	*cis*-Stilbene (**35**)	30
		Dibenzyl (**40**)	5
13	*cis*-Stilbene (**35**)	*trans*-Stilbene (**36**)	35
		Dibenzyl (**40**)	25
14	*trans*-Stilbene (**36**)	Dibenzyl (**40**)	25
15	Styrene (**38**)	Polystyrene	100

[a] All reactions involved 10.0 mmol of $Ti(OiPr)_2$ containing the LiO*i*Pr by-product and 5.0 mmol of the organic substrate in 40 mL of THF at 25 °C for 24 h unless otherwise specified. [b] Percent yields of products were obtained from the integrated ^1H NMR spectra; recovered starting substrate = 100% −% of products. [c] The reaction was conducted at reflux for 4−8 h. [d] The reaction was conducted at 25 °C for 12 h.

ating agent **20** would be an intraanionic oxidative addition that might occur upon heating **23** that would produce isopropyllithium (**24**) and the lithium salt of the titanium(IV) complex **25** [Equation (5)]. However, the fatal flaw in this proposal is that isopropyllithium is an extremely active lithium reagent that attacks ethers and is thereby destroyed, with lithium alkoxide elimination, even at 25 °C.[9] Under the reaction conditions used to prepare a mixture **10** and **11** for reaction with benzonitrile (**15**), according to Scheme 3, no isopropyllithium would have been expected to survive.

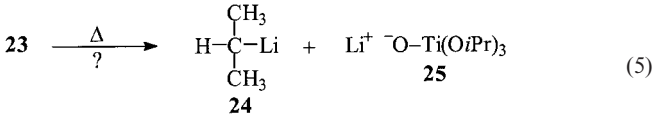

(5)

The remaining possibility, therefore, is that the ionic complex **23** itself is the actual isopropylating agent for benzonitrile (**15**). In order to evaluate this hypothesis, a series of polar substrates, ranging from substituted benzonitriles through benzylic and aryl halides to epoxides and finally to aryl-conjugated acetylenes and olefins, were individually treated with lithium complex **23**, prepared according to Equation (2). The resulting products are tabulated in Table 1.

Because of the equilibrium possible between **10** and **23** [depicted in Equation (4)], it became important to ascertain which reactions reported in Table 1 are unambiguously attributable to reagent **23** and which could equally be caused by reagent **10**. To this end, titanium(II) isopropoxide, which was essentially free of lithium isopropoxide (**11**) and hence of any **23**, was generated according to Equation (3). Reagent **10** was then individually allowed to react with many of the same polar substrates, which had previously been treated with reagent **23**, and the results are listed in Table 2.

Through a comparison of the reaction products from individual substrates towards reagent **23** (Table 1) and towards reagent **10** (Table 2), the following conclusions can be reached. First of all, only reagent **23**, not reagent **10**, can introduce an isopropyl group into any of the organic substrates, as it does with benzonitriles **15**, **26** and **27** (entries 1,2,3), (dichloromethyl)benzene (**29**, entry 5) and (trichloromethyl)benzene (**30a**, entry 6 in Table 1) [cf. Scheme 3 and Equation (6) and (7)]. Secondly, with respect to the isopropylation of benzonitriles by **23**, it is most noteworthy that some substituted benzonitriles, such as the 2-methoxy (**26**, entry 2, Table 1) and 4-methoxy (**27**, entry 3) derivat-

Table 2. Reactions of the titanium(II) isopropoxide (10, free of LiOiPr) in THF with organic substrates

Entry	Substrate[a]	Products	Yield (%)[b]
1	Benzonitrile (**15**)	Benzyl phenyl ketone	1
		Benzaldehyde	1
2	(Dichloromethyl)benzene (**29**)	*trans*-Stilbene	84
		meso-1,2-Dichloro-1,2-diphenylethane	11
		Dibenzyl	5
3	(trichloromethyl)benzene (**30a**)	1,1,2,2-Tetrachloro-1,2-diphenylethane	92
4	Benzyl chloride (**31**)	Dibenzyl	90
		Toluene	10
5	9-Bromofluorene (**32**)	Fluorene	35
		9,9′-Bifluorenyl	65
6	4-Bromoanisole (**38**)	Anisole	95
7	*trans*-Stilbene oxide (**34**)	*trans*-Stilbene (**36**)	68
		Dibenzyl (**40**)	7
8	Diphenylacetylene (**37**)	*cis*-Stilbene (**35**)	31
		Dibenzyl (**40**)	4
9	*cis*-Stilbene (**35**)	*trans*-Stilbene (**36**)	50
		Dibenzyl (**40**)	15
10	Styrene (**38**)	Polystyrene (**42**)	95
		Ethylbenzene	5

[a] Identical reaction conditions involving titanium(II) isopropoxide, prepared according to Equation (3), as those specified in footnote [a] of Table 1. [b] The percent yields of products were obtained from the integrated ^{1}H NMR spectra; recovered starting substrate = 100% − % of products.

ives underwent the isopropylation reaction readily,[5] but the 2,6-dimethyl derivative (**28**, entry 4) did not react at all. The failure of **28** to react with **23** can readily be ascribed to steric hindrance to the close approach of **23** to the C≡N group in **28** because of the flanking CH_3 groups.

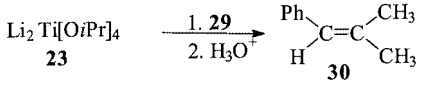

(6)

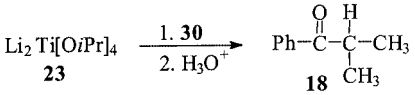

(7)

Thirdly, in those cases where no isopropylation of the organic substrate takes place, reagents **23** and **10** can effect monomolecular and bimolecular reductions, deoxygenations or dehalogenations to various degrees. Although not without exception, the results given in Table 1 and 2 indicate that reagent **23** is a more active reductant than reagent **10**. Thus in the reduction of benzyl chloride (**31**) or of 9-bromofluorene (**32**) the monomolecular and bimolecular reduction depicted in Equation (8) is complete in 12 h with **23** but requires 24 h with **10** (entries 7 and 8, Table 1, versus entries 4 and 5, Table 2). In another instance, the deoxygenation of *cis*- or *trans*-stilbene oxide (**33** or **34**) proceeds more cleanly and rapidly to the stilbenes **35** or **36** with **23** than with **10** (entries 10 and 11, Table 1, versus entry 7, Table 2; Equation (9) and (10)]. But with other substrates, such as diphenylacetylene (**37**) and the stilbenes **35** and **36**, the extent of reduction with either **23** or **10** is not markedly different. The behavior of 4-bromoanisole is anomalous in this regard, being much more readily reduced by **10** than by **23** (entry 6 in Table 2 versus entry 9 in Table 1).

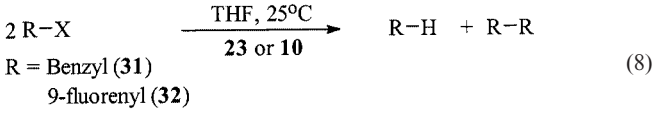

(8)

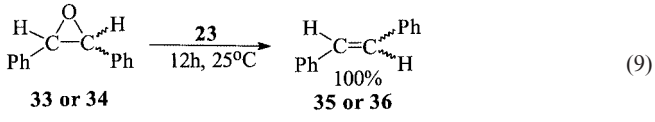

(9)

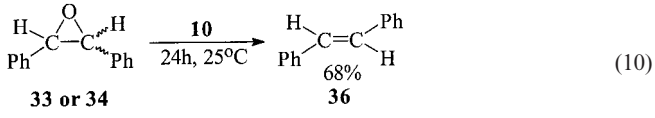

(10)

The final valuable conclusion deducible from these reductions by reagents **10** or **23** concerns their underlying mechanism of reaction. First, that *cis*-stilbene (**35**) undergoes extensive isomerization to *trans*-stilbene (**36**) in the course of epimetallation to **39** is consistent with the formation of the biradical intermediate **41** by single-electron transfer (SET). This intermediate can then either ring-close to **39** or reeliminate **23** to form the *trans*-isomer **36** (Scheme 4).[10]

Furthermore, that the *cis*- and *trans*-stilbene oxides (**33** and **34**) undergo non-stereoselective deoxygenation[11] to give chiefly *trans*-stilbene (**36**) again strongly supports an isomerizable radical ion intermediate (**42**), which can lead principally to the more stable *trans*-olefin **36** [Equation (11)]. Finally, that styrene undergoes polymerization much more rapidly than epimetallation with **23**, compared with **10**, further corroborates the superior SET donor character of **23** in forming the styrene radical-anion intermediate, crucial in such polymerization. Compelling precedents for SET mechanisms for both olefin isomerization and

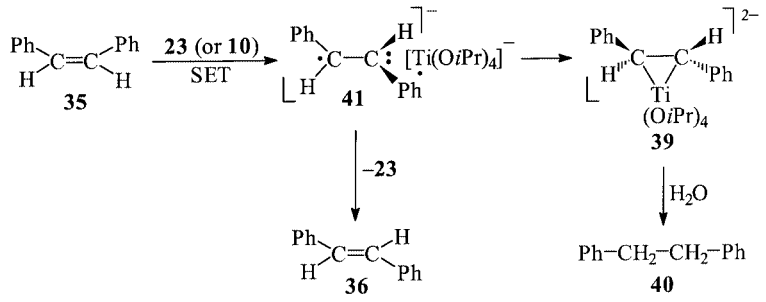

Scheme 4

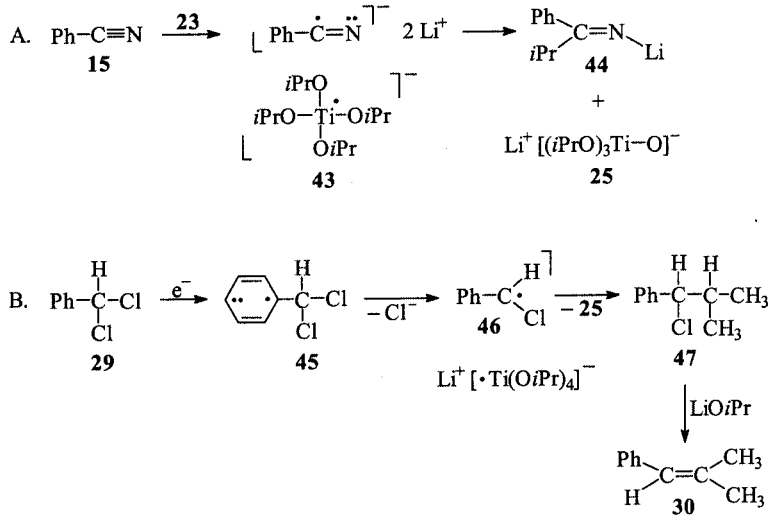

Scheme 5

conjugated olefin polymerization are available in the work of Swarc and co-workers on the "living polymerizations" of diolefins by alkali metals.[12]

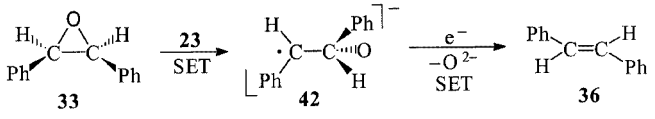

(11)

Conclusions

In light of the foregoing unexpected isopropylations of carbon centers and the nature and stereochemistry of many of the observed reductions, we conclude that the actual reagent in most of these reactions is dilithium tetraisopropoxytitanate(II) (**23**) and not titanium(II) isopropoxide (**10**) alone, and that such processes involve SET pathways. The mode of action of **23** as an isopropylating agent towards benzonitrile (**15**) is proposed in Scheme 5, Part A. The caged radical-anions formed by SET (**43**) can then undergo an isopropyl-radical transfer to the sterically accessible nitrile carbon to form the final adduct **44**. In Part B, (dichloromethyl)benzene (**29**) undergoes SET with **23** to form radical-anion **45**, which loses a Cl anion to form radical **46**. Radical **46** accepts an isopropyl radical from the caged Ti^{III} radical to form **47**. Simple dehydrohalogenation by LiO*i*Pr leads to the final product **30**.

In summary, a most unusual intramolecular oxidative addition of an ionic titanium(II) alkoxide (**23**), leading to a complex of titanium(IV), probably **25**, has been observed to occur with a variety of reducible organic substrates. The organic substrate undergoes either simple reduction or isopropylating reduction via pathways most likely involving SET processes.

Experimental Section

Instrumentation, Analysis and Starting Reagents: All reactions were carried out under a positive pressure of anhydrous, oxygen-free argon. All solvents employed with organometallic compounds were dried and distilled from a sodium metal-benzophenone ketyl mixture prior to use.[13] The IR spectra were recorded with a Perkin−Elmer instrument (model 457) and samples were measured either as mineral oil mulls or as KBr films. The NMR spectra (^1H and ^{13}C) were recorded with a Bruker spectrometer (model EM-360) and tetramethylsilane (Me_4Si) was used as the internal standard. The chemical shifts reported are expressed on the δ scale in parts per million (ppm) from the Me_4Si reference signal. The GC/MS measurements and analyses were performed with a Hewlett−Packard GC 5890/Hewlett−Packard 5970 mass-selective-

detector instrument. The gas chromatographic analyses were carried out with a Hewlett−Packard instrument (model 5880) provided with a 2-m OV-101 packed column or with a Hewlett−Packard instrument (model 4890) having a 30 m SE-30 capillary column. Melting points were determined on a Thomas-Hoover Unimelt capillary melting point apparatus and are uncorrected.

Preparation of Titanium(II) Isopropoxide (10, Free of LiO*i*Pr): *n*BuLi (1.28 g, 12.5 mL, 1.6 M solution in hexane, 20 mmol) was added slowly at −78 °C to a stirred solution of titanium(IV) chloride (1.89 g, 10 mmol) in THF (40 mL) under an argon atmosphere and the mixture stirred for 30 minutes at this temperature. Then the slow addition of isopropyl alcohol (1.20 g, 1.53 mL, 20 mmol) was performed at the same low temperature. The resulting reaction mixture was allowed to warm to 25 °C over 10 h to yield a dark brown suspension, which was then cooled to −78 °C and a further two equivalents of *n*BuLi (20 mmol) were slowly added at the same temperature. The resulting dark brown suspension was then allowed to warm to 25 °C over a 10 h period to yield a black solution of titanium(II) isopropoxide (1.66 g, 100%) from which white LiCl precipitated on standing.

Preparation of Titanium(II) Isopropoxide (23, Containing LiO*i*Pr): *n*BuLi (1.28 g, 12.5 mL, 1.6 M solution in hexane, 20 mmol) was added slowly at −78 °C to a stirred solution of titanium(IV) isopropoxide (2.84 g, 10 mmol) in THF (40 mL) under an argon atmosphere and the mixture stirred for 2 h at this temperature. The resulting light-brown reaction mixture was then allowed to warm to 25 °C over 10 h to yield a dark brown-black solution of titanium(II) isopropoxide (1.66 g, 100%).

Acknowledgments

This research has been conducted with the financial support of the U.S. National Science Foundation, a Senior Scientist Award to J.J.E. from the Alexander von Humboldt Stiftung of Bonn, Germany, and a grant from the Solvay Corporation of Brussels, Belgium. Furthermore, we are indebted to former group members, Drs. Xian Shi and Sven Thiele, for valuable orienting experiments.

[1] J. J. Eisch, F. A. Owuor, P. O. Otieno, *Organometallics* **2001**, *20*, 4132−4134.
[2] J. J. Eisch, *J. Organomet. Chem.* **2000**, *617−618*, 148−157.
[3] J. J. Eisch, J. R. Alila, *Organometallics* **2000**, *19*, 1211−1213.
[4] J. J. Eisch, J. N. Gitua, P. O. Otieno, X. Shi, *J. Organomet. Chem.* **2001**, *624*, 229−238.
[5] 1,3-Diketone **19** undoubtedly arose from the lithium isopropoxide-promoted addition of isopropyl phenyl ketone (**18**) to benzonitrile (**15**). The small amounts of diketone formed from **26** and **27** (entries 2 and 3, Table 1) were probably generated in a similar manner.
[6] J. J. Eisch, F. A. Owuor, P. O. Otieno, *Organometallics* **2001**, *20*, 4132−4134.
[7] In reactions of benzonitrile with other titanium(II) derivatives, such as $TiCl_2$, considerable amounts (30%) of benzyl phenyl ketone were isolated: J. J. Eisch, X. Shi, unpublished studies.
[8] [8a] Titanium(II) chloride, for example, forms anionic complexes of the types $[TiCl_4]^{2-}$ and $[TiCl_5]^{3-}$: G. W. A. Fowler, T. E. Lester, R. A. Walton, *J. Am. Chem. Soc. A* **1968**, 1081−1085. [8b] More recently characterized anionic titanium(II) complexes include Na_2TiCl_4 (D. J. Hinz, T. Dedecke, W. Urland, G. Meyer, *Z. Anorg. Allg. Chem.* **1994**, *620*, 801−804) and $Na_2Ti_3Cl_8$ (D. J. Hinz, G. Meyer, T. Dedecke, W. Urland, *Angew. Chem. Int. Ed. Engl.* **1995**, *34*, 71−73).
[9] P. D. Bartlett, S. Friedman, M. Stiles, *J. Am. Chem. Soc.* **1953**, *75*, 1771−1772: Isopropyllithium reacts with diethyl ether exothermally at room temperature to form lithium ethoxide and ethylene:

$$i\text{PrLi} + \text{Et}_2\text{O} \longrightarrow \text{PrH} + \text{LiOEt} + \text{H}_2\text{C=CH}_2$$

The excess *i*PrLi then adds to the ethylene to form isoamyllithium, which can be trapped with CO_2 to give, after hydrolysis, the observed diisoamyl ketone:

$$i\text{PrLi} + \text{H}_2\text{C=CH}_2 \longrightarrow i\text{Pr–CH}_2\text{–CH}_2\text{Li}$$

$$2\ i\text{Pr–CH}_2\text{–CH}_2\text{Li} \xrightarrow[2.\ \text{H}_2\text{O}]{1.\ \text{CO}_2} (i\text{Pr–CH}_2\text{–CH}_2)_2\text{C=O}$$

[10] Solutions of **23** and **10** in THF are paramagnetic as shown by ESR spectroscopic measurement at room temperature. In fact, solutions of **23** give a strong triplet signal, consistent with the presence of two unpaired electrons. However, from the magnitude of the spin coupling, the two electrons are not on the same titanium atom, and probably not even on adjacent titanium centers. (Studies in progress with Professor D. C. Doetschman).
[11] One-step deoxygenations of epoxides with polar reagents such as lithium diphenylphosphide lead stereospecifically to the olefin with inverted configuration. Deoxygenations with SET reagents, such as nickel(0) complexes, occur stereoselectively to favor the more stable olefin: J. J. Eisch, K. R. Im, *J. Organomet. Chem.* **1977**, *139*, C45−C50.
[12] [12a] M. Swarc, *Ions and Ion Pairs in Organic Reactions*, Wiley, New York, Vols. 1 and 2, **1972**. [12b] M. Swarc, in *Polynuclear Aromatic Compounds* (Ed.: L. B. Ebert), American Chemical Society, Washington, D. C., **1988**, pp. 13−37.
[13] A detailed description for conducting organometallic reactions in a safe and reproducible manner is given in: J. J. Eisch, *Organometallic Syntheses*, Vol. 2, Academic Press, New York, **1981**, pp.1−84.

Received August 9, 2002
[I02451]

The First Two Novel Metallomacrocycles Constructed from Cubane-Like Cu_4I_4 Cluster Units and Ditopic Diamines

Rui-Hu Wang,[a] Mao-Chun Hong,*[a] Jun-Hua Luo,[a] Rong Cao,*[a] and Jia-Bao Weng[a]

Keywords: Amine ligands / Copper / Metallacycles / X-ray diffraction

Two novel metallomacrocycles made up of difunctional 4,4′-diaminodiphenylmethane (DADPM) or 4,4′-diaminodiphenyl ether (DADPE) and cubane-like Cu_4I_4 cluster units have been prepared by the reaction of CuI and DADPM or DADPE in $MeCN/H_2O$. The X-ray crystal structural analyses show that the topology of the cubane-like Cu_4I_4 cluster units is maintained in the assembly process.

Introduction

Much effort has been devoted to the design and construction of metal-containing supramolecular and coordination polymers from building blocks possessing useful properties such as nonlinear optical properties, bulk magnetism, light emission and porosity.[1−8] Metallomacrocycles based on specific building blocks have recently received a great deal of attention in chemistry and material science owing to their potential applications in various materials.[9−24] A number of discrete macrocycles have been constructed by ditopic or oligotopic ligands, in particular di- or polypyridyl ligands and suitable metal ions.[15−23] For instance, discrete square or rectangular metallomacrocycles with nanometer-sized cavities have been obtained by the assembly of pyridine-based ligands, such as 4,4-bipyridine or its derivatives, and metal ions with square-planar coordination geometry, such as Pd^{II} or Pt^{II}.[15−21] However, discrete macrocycles consisting of metal clusters and organic ligands are less well-known.[23,24]

It is known that the reaction of copper(I) iodide with aniline derivatives, such as *p*-toluidine, *p*-chloroaniline, *p*-anisidine, *o*-ethylaniline, 2,6-dimethylaniline or 6-ethyl-*o*-toluidine, produces complexes containing a single cubane-like Cu_4I_4 cluster in which the aniline derivatives act as the terminal ligands coordinating to copper(I) centers.[25−28] Thus, it is reasonable to expect the formation of macrocyclic complexes constructed from Cu_4I_4 cluster units by replacing the aniline derivatives with difunctional diamine ligands containing suitable spacers. Considering the flexibility and electronic structures of diamine ligands, such as 4,4′-diaminodiphenylmethane (DADPM) and 4,4′-diaminodiphenyl ether (DADPE), we recently began work on the reaction of diamine ligands and Cu^I, with the hope of isolating some interesting complexes constructed by cubane-like Cu^I cluster units. Herein, we report two novel macrocyclic complexes $[(Cu_4I_4)(MeCN)_2(DADPM)]_2{\cdot}2MeCN$ (**1**) and $[(Cu_4I_4)(MeCN)_2(DADPE)]_2{\cdot}2MeCN$ (**2**) assembled from DADPM, DADPE and CuI, respectively. To the best of our knowledge they are the first two discrete macrocyclic complexes constructed from cubane-like Cu_4I_4 clusters.

Results and Discussion

Complex **1** was synthesized in a high yield from the reaction of DADPM and CuI with a metal-to-ligand ratio of 1:1 in $MeCN/H_2O$ at 60 °C. Single crystal X-ray diffraction analysis revealed that **1** is a discrete metallomacrocycle possessing a crystallographic center of symmetry, in which two cubane-like Cu_4I_4 cluster units are linked by two DADPM ligands (Figure 1).

Each DADPM ligand acts as a μ_2-bridge linking two cubane-like Cu_4I_4 units through its two nitrogen atoms. The dihedral angle of the two phenyl rings and the C(4)−C(5)−C(6) bond angle in the DADPM ligand are 89.2° and 112.7(10)°, respectively, resulting in a twisted-rhombus macrocycle. Two opposite phenyl rings in the macrocycle are parallel to each other at a distance of 10.53 Å, while the distance between the C(7)−C(8)−I(4A) and C(7A)−C(8A)−I(4) planes is 4.04 Å. Thus the dimension of the distorted macrocycle is 10.53 × 4.04 Å which compares well with the value of 8.36 × 4.10 Å for the macrocycle formed from DADPM and Cu^{II} ions.[22] Two uncoordinated MeCN molecules lie in two sides of the macrocycle as space fillers. Each Cu_4I_4 unit displays a cubane-like arrangement with Cu^I and iodide atoms occupying alternate corners of the cube; no crystallographic symmetry element is present for this unit. All Cu^I centers are in a distorted NI_3 tetrahedral geometry in which the coordination geometry of

[a] The State Key Laboratory of Structural Chemistry, Fujian Institute of Research on the Structure of Matter,
Chinese Academy of Sciences, Fuzhou, Fujian, 350002, China
Fax: (internat.) +86-591/371-4946
E-mail: hmc@ms.fjirsm.ac.cn

Supporting information for this article is available on the WWW under http://www.eurjic.org or from the author.

 © 2002 WILEY-VCH Verlag GmbH & Co. KGaA, 69451 Weinheim 1434−1948/02/1212−3097 $ 20.00+.50/0

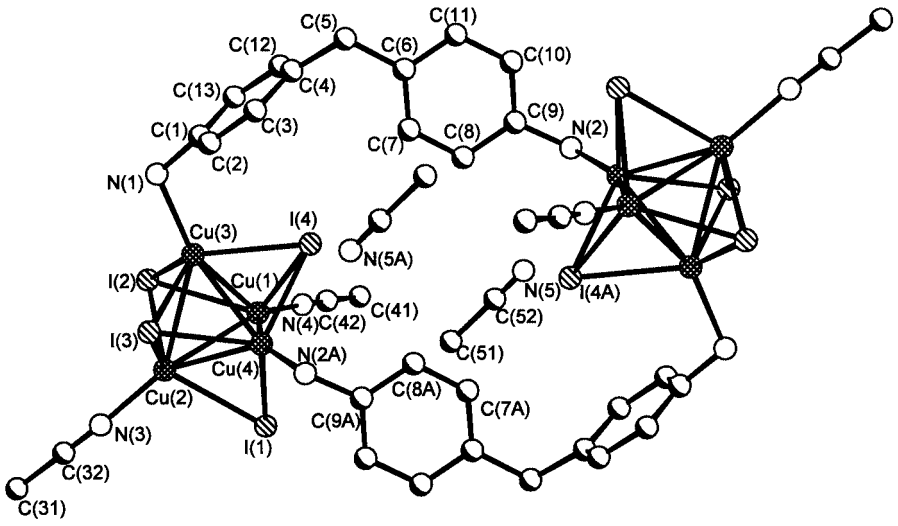

Figure 1. A view of the macrocyclic structure of **1**

two of the Cu^I ions is completed by the nitrogen atoms of two MeCN ligands and that of the other two Cu^I ions is completed by the nitrogen atoms of different DADPM ligands. All the bond lengths and bond angles of the Cu_4I_4 units in **1** are normal.[25−28] The Cu−Cu bond lengths, ranging from 2.670(3) to 2.777(3) Å (average value 2.724 Å), are within the range suggested by Mehrotra and Hoffman.[29]

Complex **2** was obtained in an analogous procedure except that DADPE was used instead of DADPM. The X-ray crystallographic analysis reveals that its structure is very similar to that of complex **1**, consisting of a centrosymmetrical metallomacrocycle formed from two cubane-like Cu_4I_4 cluster units and two bridging DADPE ligands. As shown in Figure 2, each DADPE ligand acts as a μ_2-bridge linking two Cu_4I_4 cluster units, the dihedral angle of two phenyl rings and the C(4)−O(1)−C(5) bond angle in DADPE are 90.4° and 117.1(7)°, respectively, resulting in a twisted-rhombus metallomacrocycle with dimensions of 9.99 × 3.88 Å. This is slightly smaller than in **1**, but larger than in other complexes obtained from the reaction of transitional metal ions and 1,2-bis(4-pyridyl)ethane.[19−21]

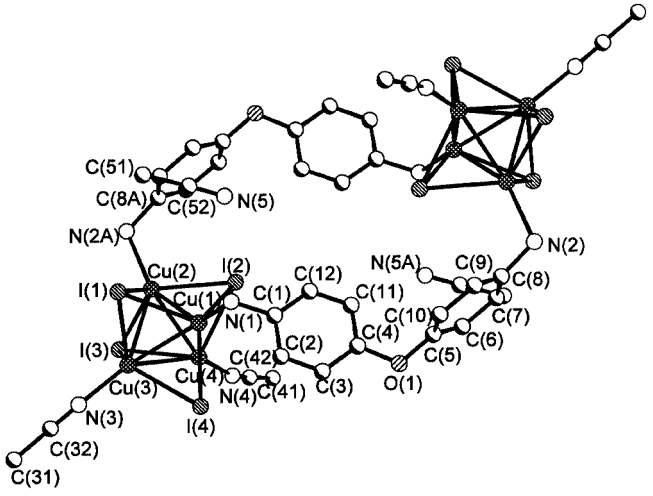

Figure 2. A view of the macrocyclic structure of **2**

There are no apparent differences in the bond lengths and bond angles in the Cu_4I_4 cluster units in complexes **1** and **2** and in the reported $[Cu_4I_4L_2(MeCN)_2]$ (L = aniline derivatives) complexes.[25−28] This result suggests that the topology of the cubane-like Cu_4I_4 cluster units is maintained during the assembly process and is not influenced by the linker ligands used.

In the solid state, the emission spectra for **1** and **2** were recorded after irradiating with light at a wavelength of 310 nm. Compounds **1** and **2** show a similar emission band in the 320−630 nm range despite the fact that free DADPM and DADPE have different emission spectra at the same excitation wavelength. Compared with single cubane-like $[Cu_4I_4L_2(MeCN)_2]$ (L = aniline derivatives) complexes[25,26] and luminescent Cu^I complexes,[30−33] the high energy emission at 350−460 nm might be ascribed to an intraligand interaction, and the weak emission which appears as a shoulder at around 500 nm might be ascribed to a metal-centered transition.

Conclusion

We have successfully assembled cubane-like Cu_4I_4 cluster units and difunctional diamines containing a spacer to form two discrete metallomacrocycles in which the topology of the Cu_4I_4 clusters is maintained. Previous reports have predicted that the tetranuclear chalcogenide Cu_4 or Ag_4 d^{10} clusters are good building blocks for the formation of materials with desirable physical and chemical properties.[33] Our report may open a new way to assembly Cu_4 clusters into desirable materials.

Experimental Section

General: All chemicals were purchased from Acros and used as received. The IR spectra were recorded as KBr discs on a Magna 750 FT-IR spectrophotometer. Elemental analyses were determined on an Elementar Vario ELIII elemental analyzer by the elemental analysis laboratory of this institute. NMR spectra were recorded on a Varian Unity 500 spectrophotometer. The fluorescent data were collected on an Edinburgh FL-FS920 TCSPC system by the Spectroscopy Laboratory of Fuzhou University.

Synthesis of $[(Cu_4I_4)(MeCN)_2(DADPM)]_2\cdot 2MeCN$ (1): A solution of DADPM (0.10 g, 0.5 mmol) in H_2O (10 mL) was added slowly to a solution of CuI (0.10 g, 0.5 mmol) in MeCN (20 mL). The reaction mixture was stirred at 60 °C for 30 min and gave a colorless solution, which was then filtered. The gray crystals of complex **1** were obtained by allowing the resulting solution to stand in the air for three days. Yield: 0.107 g, (0.049 mmol, 79% based on CuI). Addition of CuI and DADPM in a 2:1 ratio under otherwise identical experimental conditions gave the same complex. $C_{38}H_{46}Cu_8I_8N_{10}$ (2166.37): calcd. C 21.07, H 2.14, N 6.47; found C 21.23, H 2.17, N 6.54. IR (KBr): $\tilde{\nu}$ = 3396m, 3321s, 3265s, 3228m, 3140w, 3030w, 2922w, 2904w, 1612m, 1587m, 1510vs, 1433w, 1242m, 1178w, 1095w, 1018s, 985s, 941m, 850w, 825w, 812m, 777w, 766w, 704w, 577m, 515m cm^{-1}. ^1H NMR ([D_6]DMSO): δ = 2.08 (m, 9 H, MeCN), 3.68 (s, 2 H, -CH_2-), 4.33 (s, 4 H, NH_2), 6.83 and 6.37 (m, 8 H, -C_6H_4-) ppm.

Synthesis of $[(Cu_4I_4)(MeCN)_2(DADPE)]_2\cdot 2MeCN$ (2): The experimental procedure was similar to the synthesis of complex **1** except that DADPE (0.10 g, 0.5 mmol) was used instead of DADPM. Yield: 0.086 g (0.040 mmol, 63% based on CuI). Changing the metal-to-ligand ratio has no influence on the product of the reaction. $C_{36}H_{42}Cu_8I_8N_{10}O_2$ (2170.32): calcd. C 19.92, H 1.95, N 6.46; found C 20.07, H 2.03, N 6.57. IR (KBr): $\tilde{\nu}$ = 3315s, 3253s, 3128w, 3061w, 3018w, 1572m, 1498vs, 1441w, 1284m, 1265s, 1221s, 1165w, 1090w, 1014m, 978s, 926w, 877w, 843w, 825m, 785m, 552w, 517w, 503w cm^{-1}. ^1H NMR ([D_6]DMSO): δ = 2.09 (m, 9 H, MeCN), 4.29 (s, 4 H, NH_2), 6.66 and 6.43 (m, 8 H, -C_6H_4-) ppm.

Table 1. Crystallographic data for compounds **1** and **2**

	1	2
Empirical formula	$C_{38}H_{46}Cu_8I_8N_{10}$	$C_{36}H_{42}Cu_8I_8N_{10}O_2$
Mol. wt.	2166.37	2170.32
Crystal system	Monoclinic	Monoclinic
Space group	$P2_1/n$	$P2_1/c$
a, Å	10.473(3)	13.3142(2)
b, Å	21.458(8)	10.3433(3)
c, Å	13.660(7)	21.4439(6)
β, deg	94.10(3)	100.194(1)
V, Å^3	3062(2)	2906.48(13)
Z	2	2
D_c, g cm^{-3}	2.350	2.480
μ, cm^{-1}	6.789	7.155
Diffractometer	CAD4 four-circle	Siemens Smart CCD
T [K]	293(2)	293(2)
λ(Mo-K_α) [Å]	0.71073	0.71073
Reflections collected	6343	8489
Unique reflections	6008	5100
R_{int}	0.1158	0.0343
Parameters	289	289
S on F^2	1.045	1.009
$R1$ [$I > 2\sigma(I)$][a]	0.0621	0.0475,
$wR2$ (all data)[b]	0.1810	0.1318

[a] $R = \||F0| - |Fc|\|/|F0|$. [b] $wR = [w(F0^2 - Fc^2)^2/w(F0^2)^2]^{1/2}$.

Table 2. Selected bond lengths [Å] and angles [°] for compound **1**[a]

Cu(1)−N(4)	1.993(15)	Cu(2)−N(3)	1.975(12)
Cu(3)−N(1)	2.078(10)	Cu(4)−N(2A)	2.108(11)
Cu(1)−I(1)	2.709(3)	Cu(1)−I(2)	2.723(2)
Cu(1)−I(4)	2.693(2)	Cu(2)−I(1)	2.666(2)
Cu(2)−I(2)	2.742(2)	Cu(2)−I(3)	2.683(2)
Cu(3)−I(2)	2.675(2)	Cu(3)−I(3)	2.738(2)
Cu(3)−I(4)	2.675(2)	Cu(4)−I(1)	2.643(2)
Cu(4)−I(3)	2.731(2)	Cu(4)−I(4)	2.640(2)
Cu(1)−Cu(2)	2.729(3)	Cu(1)−Cu(3)	2.670(3)
Cu(1)−Cu(4)	2.733(3)	Cu(2)−Cu(3)	2.777(3)
Cu(2)−Cu(4)	2.727(3)	Cu(3)−Cu(4)	2.709(3)
N(4)−Cu(1)−I(1)	107.5(5)	N(4)−Cu(1)−I(2)	105.3(5)
N(4)−Cu(1)−I(4)	107.5(4)	N(3)−Cu(2)−I(1)	107.5(4)
N(3)−Cu(2)−I(2)	102.1(4)	N(3)−Cu(2)−I(3)	110.0(4)
N(1)−Cu(3)−I(2)	107.0(3)	N(1)−Cu(3)−I(4)	107.9(3)
N(1)−Cu(3)−I(3)	102.6(3)	N(2A)−Cu(4)−I(1)	109.8(3)
N(2A)−Cu(4)−I(3)	99.0(3)	N(2A)−Cu(4)−I(4)	108.8(3)
I(1)−Cu(1)−I(2)	113.66(8)	I(4)−Cu(1)−I(1)	108.86(8)
I(4)−Cu(1)−I(2)	113.60(8)	I(1)−Cu(2)−I(3)	112.65(8)
I(1)−Cu(2)−I(2)	114.45(8)	I(3)−Cu(2)−I(2)	109.56(7)
I(2)−Cu(3)−I(3)	109.92(7)	I(2)−Cu(3)−I(4)	115.78(8)
I(4)−Cu(3)−I(3)	112.60(7)	I(1)−Cu(4)−I(3)	111.85(7)
I(4)−Cu(4)−I(1)	112.57(7)	I(4)−Cu(4)−I(3)	113.97(7)
Cu(1)−I(2)−Cu(2)	59.91(7)	Cu(2)−I(1)−Cu(1)	61.02(7)
Cu(2)−I(3)−Cu(3)	61.63(6)	Cu(2)−I(3)−Cu(4)	60.49(6)
Cu(3)−I(2)−Cu(1)	59.28(6)	Cu(3)−I(2)−Cu(2)	61.67(6)
Cu(3)−I(4)−Cu(1)	59.65(6)	Cu(4)−I(1)−Cu(1)	61.40(6)
Cu(4)−I(1)−Cu(2)	61.83(6)	Cu(4)−I(4)−Cu(1)	61.64(6)
Cu(4)−I(3)−Cu(3)	59.37(6)	Cu(4)−I(4)−Cu(3)	61.26(6)
Cu(1)−Cu(2)−Cu(3)	58.00(7)	Cu(1)−Cu(3)−Cu(2)	60.09(8)
Cu(1)−Cu(3)−Cu(4)	61.07(7)	Cu(2)−Cu(1)−Cu(4)	59.91(7)
Cu(2)−Cu(4)−Cu(1)	59.98(7)	Cu(3)−Cu(1)−Cu(2)	61.90(7)
Cu(3)−Cu(1)−Cu(4)	60.16(7)	Cu(3)−Cu(4)−Cu(1)	58.77(7)
Cu(3)−Cu(4)−Cu(2)	61.46(7)	Cu(4)−Cu(2)−Cu(1)	60.12(7)
Cu(4)−Cu(2)−Cu(3)	58.94(7)	Cu(4)−Cu(3)−Cu(2)	59.60(7)
C(4)−C(5)−C(6)	112.7(10)		

[a] Symmetry transformations used to generate equivalent atoms: A: $-x$, $-y$, $-z$.

X-ray crystallography: The crystal data and a structure determination summary for **1** and **2** are listed in Table 1. Selected bond lengths and bond angles for **1** and **2** are listed in Table 2 and 3, respectively. Intensity data for **1** and **2** were measured on a CAD4 four-circle and Siemens Smart CCD diffractometer with graphite-monochromated Mo-K_α radiation (λ = 0.71073 Å) at 298 K, respectively. Empirical absorption corrections were applied by using the SADABS program. The structures were solved by direct methods and all calculations were performed using the SHELXL PC program. The positions of the H atoms were generated geometrically (C−H bond fixed at 0.96 Å), assigned isotropic thermal parameters, and allowed to ride on their parent carbon atoms before the final cycle of refinement. The structure was refined by full-matrix least-squares minimization of $\Sigma(F_o - F_c)^2$ with anisotropic thermal parameters for all atoms except the H atoms. CCDC-175784 (**1**) and CCDC-175785 (**2**) contain the supplementary crystallographic data for this paper. These data can be obtained free of charge at www.ccdc.cam.ac.uk/conts/retrieving.html [or from the Cambridge Crystallographic Data Centre, 12, Union Road, Cambridge CB2 1EZ, UK; Fax: (internat.) +44-1223/336-033; E-mail: deposit@ccdc.cam.ac.uk].

Table 3. Selected bond lengths [Å] and angles [°] for compound **2**[a]

Cu(1)−N(1)	2.073(8)	Cu(2)−N(2A)	2.119(8)
Cu(3)−N(3)	1.985(11)	Cu(4)−N(4)	2.005(11)
I(1)−Cu(1)	2.7357(16)	I(1)−Cu(2)	2.7299(16)
I(1)−Cu(3)	2.6892(16)	I(2)−Cu(1)	2.6192(16)
I(2)−Cu(2)	2.6777(16)	I(2)−Cu(4)	2.7087(17)
I(3)−Cu(2)	2.6597(15)	I(3)−Cu(3)	2.7289(17)
I(3)−Cu(4)	2.7602(17)	I(4)−Cu(1)	2.6367(15)
I(4)−Cu(3)	2.6844(16)	I(4)−Cu(4)	2.6743(17)
Cu(1)−Cu(2)	2.7764(19)	Cu(1)−Cu(3)	2.731(2)
Cu(1)−Cu(4)	2.772(2)	Cu(2)−Cu(3)	2.747(2)
Cu(2)−Cu(4)	2.6951(18)	Cu(3)−Cu(4)	2.765(2)
N(1)−Cu(1)−I(1)	100.6(2)	N(1)−Cu(1)−I(2)	104.6(3)
N(1)−Cu(1)−I(4)	114.0(2)	N(2A)−Cu(2)−I(1)	101.0(3)
N(2A)−Cu(2)−I(3)	107.7(2)	N(2A)−Cu(2)−I(2)	108.6(2)
N(3)−Cu(3)−I(1)	110.4(3)	N(3)−Cu(3)−I(3)	101.0(3)
N(3)−Cu(3)−I(4)	108.1(3)	N(4)−Cu(4)−I(2)	101.7(3)
N(4)−Cu(4)−I(3)	103.5(3)	N(4)−Cu(4)−I(4)	117.5(3)
I(2)−Cu(1)−I(1)	111.16(5)	I(2)−Cu(1)−I(4)	112.18(6)
I(4)−Cu(1)−I(1)	113.43(6)	I(2)−Cu(2)−I(1)	109.56(5)
I(3)−Cu(2)−I(1)	111.07(5)	I(3)−Cu(2)−I(2)	117.57(5)
I(1)−Cu(3)−I(3)	110.20(5)	I(4)−Cu(3)−I(1)	113.40(6)
I(4)−Cu(3)−I(3)	113.03(6)	I(2)−Cu(4)−I(3)	113.16(5)
I(4)−Cu(4)−I(2)	108.25(6)	I(4)−Cu(4)−I(3)	112.35(6)
Cu(1)−I(2)−Cu(2)	63.21(4)	Cu(1)−I(2)−Cu(4)	62.68(5)
Cu(1)−I(4)−Cu(3)	61.75(5)	Cu(1)−I(4)−Cu(4)	62.93(5)
Cu(2)−I(1)−Cu(1)	61.06(4)	Cu(2)−I(3)−Cu(3)	61.27(5)
Cu(2)−I(2)−Cu(4)	60.04(4)	Cu(2)−I(3)−Cu(4)	59.60(4)
Cu(3)−I(1)−Cu(1)	60.44(5)	Cu(3)−I(1)−Cu(2)	60.90(4)
Cu(3)−I(3)−Cu(4)	60.48(5)	Cu(4)−I(4)−Cu(3)	62.12(5)
Cu(1)−Cu(3)−Cu(2)	60.91(5)	Cu(1)−Cu(3)−Cu(4)	60.59(5)
Cu(2)−Cu(4)−Cu(1)	61.02(5)	Cu(2)−Cu(3)−Cu(4)	58.55(5)
Cu(2)−Cu(4)−Cu(3)	60.39(5)	Cu(3)−Cu(1)−Cu(2)	59.83(5)
Cu(3)−Cu(1)−Cu(4)	60.31(5)	Cu(3)−Cu(2)−Cu(1)	59.26(5)
Cu(3)−Cu(4)−Cu(1)	59.10(5)	Cu(4)−Cu(1)−Cu(2)	58.12(5)
Cu(4)−Cu(2)−Cu(1)	60.86(5)	Cu(4)−Cu(2)−Cu(3)	61.06(5)
C(5)−O(1)−C(4)	117.1(7)		

[a] Symmetry transformations used to generate equivalent atoms: A: $-x, -y, +1, -z$.

Acknowledgments

This work was supported by the National Nature Science Foundation of China, Nature Science Foundation of Fujian Province and the Key Project of Chinese Academy of Science.

[1] P. J. Hagrman, D. Hagrman, J. Zubieta, *Angew. Chem. Int. Ed.* **1999**, *38*, 2638−2684.
[2] S. A. Bourne, J. J. Lu, A. Mondal, B. Moulton, M. J. Zaworotko, *Angew. Chem. Int. Ed.* **2001**, *40*, 2111−2113.
[3] E. Breuning, U. Ziener, J.-M. Lehn, E. Wegelius, K. Rissanen, *Eur. J. Inorg. Chem.* **2001**, 1515−1521.
[4] M. Eddaoudi, D. B. Moler, H. Li, B. Chen, T. M. Reineke, M. O'Keeffe, O. M. Yaghi, *Acc. Chem. Res.* **2001**, *34*, 319−330.
[5] C. B. Aakeröy, A. M. Beatty, D. S. Leinen, K. R. Lorimer, *Chem. Commun.* **2000**, 935−936.
[6] S. O. H. Gutschke, D. J. Price, A. K. Powell, P. T. Wood, *Eur. J. Inorg. Chem.* **2001**, 2739−2741.
[7] A. J. Blake, N. R. Brooks, N. R. Champness, M. Crew, A. Deveson, D. Fenske, D. H. Gregory, L. R. Hanton, P. Hubberstey, M. Schröder, *Chem. Commun.* **2001**, 1432−1433.
[8] S. W. Lai, M. C. W. Chan, S. M. Peng, C.-M. Che, *Angew. Chem. Int. Ed.* **1999**, *38*, 669−671.
[9] S. W. Lai, K. K. Cheung, M. C. W. Chan, C.-M. Che, *Angew. Chem. Int. Ed.* **1998**, *37*, 182−184.
[10] P. R. Ashton, A. L. Burns, C. G. Claessens, G. K. H. Shimizu, K. Small, J. F. Stoddart, A. J. P. White, D. J. Williams, *J. Chem. Soc., Dalton Trans.* **1997**, 1493−1494.
[11] M. C. T. Fyfe, J. F. Stoddart, *Acc. Chem. Res.* **1997**, *30*, 393−401.
[12] B. Manimaran, T. Rajendran, Y.-L. Lu, G.-H. Lee, S.-M. Peng, K.-L. Lu, *J. Chem. Soc., Dalton Trans.* **2001**, 515−517.
[13] K. R. J. Thomas, J. T. Lin, Y. Y. Lin, C. Tsai, S.-S. Sun, *Organometallics* **2001**, *20*, 2262−2269.
[14] C. M. Thomas, A. Neels, H. Stockli-Evans, G. Süss-Fink, *Eur. J. Inorg. Chem.* **2001**, 3005−3008.
[15] R. V. Slone, K. D. Benkstein, S. Bélanger, J. T. Hupp, I. A. Guzei, A. L. Rheingold, *Coord. Chem. Rev.* **1998**, *171*, 221−243.
[16] S. Leininger, B. Olenyuk, P. J. Stang, *Chem. Rev.* **2000**, *100*, 853−908 and references cited therein.
[17] Y. L. Cho, H. Uh, S.-Y. Chang, H.-Y. Chang, M.-G. Choi, I. Shin, K. S. Jeong, *J. Am. Chem. Soc.* **2001**, *123*, 1258−1259.
[18] G. F. Swiegers, T. J. Malefetse, *Chem. Eur. J.* **2001**, *7*, 3636−3643.
[19] M. Fujita, S. Nagao, M. Lida, K. Ogata, K. Ogura, *J. Am. Chem. Soc.* **1993**, *113*, 1574−1576.
[20] R. V. Slone, D. I. Yoon, R. M. Calhoun, J. T. Hupp, *J. Am. Chem. Soc.* **1995**, *117*, 11813−11814.
[21] A. Hori, K. Kumazawa, T. Kusukawa, D. K. Chand, M. Fujita, S. Sakamoto, K. Yamaguchi, *Chem. Eur. J.* **2001**, *7*, 4142−4149.
[22] Y. Zhang, M. Nishiura, J. Li, D. Wei, T. Imamoto, *Inorg. Chem.* **1999**, *38*, 825−827.
[23] Y. Li, Z. Y. Lin, W.-T. Wong, *Eur. J. Inorg. Chem.* **2001**, 3163−3173.
[24] F. A. Cotton, C. Lin, C. A. Murillo, *Acc. Chem. Res.* **2001**, *34*, 759−77.
[25] N. P. Rath, E. M. Holt, K. Tanimura, *Inorg. Chem.* **1985**, *24*, 3934−3938.
[26] G. Hu, G. J. Mains, E. M. Holt, *Inorg. Chem. Acta* **1995**, *240*, 559−565.
[27] W. P. Schaefer, *Inorg. Chem.* **1986**, *25*, 2665.
[28] N. P. Rath, J. Jasinski, E. M. Holt, *Acta Crystallogr., Sect. A* **1984**, *40*, C316.
[29] P. K. Mehrotra, R. Hoffmann, *Inorg. Chem.* **1978**, *17*, 2187−2189.
[30] K. R. Kyle, C. K. Ryu, J. A. DiBenedetto, P. C. Ford, *J. Am. Chem. Soc.* **1991**, *113*, 2954−2965.
[31] P. C. Ford, A. Vogler, *Acc. Chem. Res.* **1993**, *26*, 220−226.
[32] C.-M. Che, Z. Mao, V. M. Miskowski, M. C. Tse, C. K. Chan, K. K. Cheung, D. L. Phillips, K. H. Leung, *Angew. Chem. Int. Ed.* **2000**, *39*, 4084−4088.
[33] V. W. W. Yam, K. K. W. Lo, W. K. M. Fung, C. R. Wang, *Coord. Chem. Rev.* **1998**, *171*, 17−41.

Received May 13, 2002
[I02248]

Lanthanide Triple Helical Complexes with a Chiral Bis(benzimidazole)pyridine Derivative

Gilles Muller,[a,b] James P. Riehl,[b] Kurt J. Schenk,[c] Gérard Hopfgartner,[d] Claude Piguet,[e] and Jean-Claude G. Bünzli*[a]

Keywords: Lanthanides / Tridentate ligands / Chirality / Luminescence / Stability constants

The ligand neopentyl 2,6-bis[(1-methylbenzimidazol-2-yl)]-pyridine-4-carboxylate ($\mathbf{L^{12}}$) has been synthesised to test the effect of the chiral neopentyl ester group in the 4-position of the pyridine ring on (i) the helical wrapping, (ii) the diastereomeric induction and (iii) the thermodynamic and photophysical properties of the $[Ln(\mathbf{L^{12}})_3]^{3+}$ complexes. The crystal structure of ligand $\mathbf{L^{12}}$ shows the expected *trans-trans* conformation of the tridentate binding unit. The ligand forms stable 1:3 complexes in anhydrous acetonitrile ($\log\beta_3$ in the range 17.3–19.0, $\log K_3$ in the range 2.9–4.6). The triple helical structure in solution is responsible for the four times larger specific rotary dispersion measured in the complexes. Circularly polarised luminescence of the Eu triple helical complex displays a weak effect, suggesting a small diastereomeric excess in solution. Ligand $\mathbf{L^{12}}$ appears to favour a $^3\pi\pi^*$-to-Ln energy transfer process for Eu, but temperature-dependent nonradiative processes lead to a very small quantum yield. High-resolution luminescence spectra indicate that the Eu complex has a distorted D_3 local symmetry at the metal ion site.
(© Wiley-VCH Verlag GmbH, 69451 Weinheim, Germany, 2002)

Introduction

During the last two decades, lanthanide ions Ln^{III} have proved to be powerful luminescent and magnetic probes in biology and medicine.[1−4] In the latter field, applications range from diagnosis (e.g. fluoroimmunoasssays,[5−7] luminescent specific imaging agents for tissues,[8,9] contrast agents for magnetic resonance imaging[10]) to therapeutic tools.[11] In addition, these ions are also good catalysts for the selective hydrolysis of DNA and RNA.[12,13]

These applications require the introduction of the Ln^{III} ions into functional molecular edifices able to preserve or better enhance the metal ion physicochemical properties.[14] One strategy proposed to meet this goal is the formation of induced cavities obtained by the self-assembly of carefully tailored multidentate ligands and podands.[15] A judicious design of the ligands results in weak noncovalent interstrand interactions stabilizing the molecular edifices. We have shown that tridentate aromatic ligands $\mathbf{L^1}$−$\mathbf{L^9}$, $\mathbf{L^{11}}$ derived from bis(benzimidazole)pyridine (Scheme 1) lead to triple helical assemblies displaying sizeable ππ-stacking interactions, whose structural, photophysical and thermodynamic properties can be tuned by varying the substituents R^1, R^2 and R^3.[16−18] Substitution in the R^2 position of the benzimidazole rings essentially controls the stability and the final structure of the complexes, while substitution in the R^1 and R^3 positions affects the electronic and photophysical properties.

So far, limited attention has been devoted to the inherent chirality of triple helical complexes, which often appear as racemic mixtures both in the solid state and in solution. However, Riehl et al. have shown that the $[Ln(dpa)_3]^{3-}$ racemate equilibrium (H_2dpa = dipicolinic acid) can be perturbed by adding chiral sugars.[19] Moreover, a small excess of one enantiomer can be induced in the excited state with the use of circular polarised excitation light.[20] Chiral lanthanide complexes are of potential great interest because of their use as probes for the sensing of chirality in biological substrates.[21,22] Since the high lability of the Ln^{III} ions favours easy racemisation of triple helical complexes, we are exploring the possibility of producing edifices in which the

[a] Institute of Molecular and Biological Chemistry, Swiss Federal Institute of Technology
BCH 1402,
1015 Lausanne, Switzerland
E-mail: jean-claude.bunzli@epfl.ch
[b] Department of Chemistry, University of Minnesota Duluth, Minnesota 55812−2496, USA
[c] Institute of Crystallography, BSP, University of Lausanne, 1015 Lausanne, Switzerland
[d] School of Pharmacy, University of Geneva, Switzerland,
30 quai E. Ansermet, 1211 Geneva 4, Switzerland
[e] Department of Inorganic, Analytical and Applied Chemistry, University of Geneva,
30 quai E. Ansermet, 1211 Geneva 4, Switzerland
Supporting information for this article is available on the WWW under http://www.ejic.com or from the author.

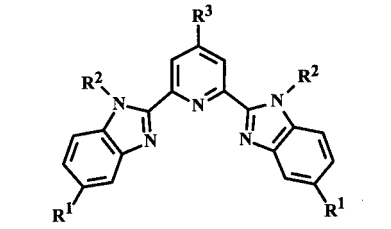

R^1	R^2	R^3	L^i
H	H	H	L^0
H	Me	H	L^1
H	Et	H	L^2
H	Pr	H	L^3
H	$Bz(OMe)_2$	H	L^4
Me	Et	H	L^5
H	$Bz(OMe)_2$	Ph	L^6
H	$Bz(OMe)_2$	$PhNO_2$	L^7
H	$Bz(OMe)_2$	$PhNEt_2$	L^8
H	Me	$PhNEt_2$	L^9
H	Oct	H	L^{10}
H		H	L^{11}
H	Me	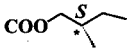	L^{12}

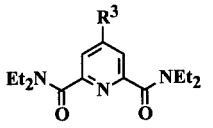

$R^3 = CH_2C^*H(CO_2Me)(NHCO_2CMe_3)$: L*

Scheme 1

chirality is brought about by the ligands, a method which can only be used if the diastereoisomers have a large enough energy difference.

Working along these lines, we have introduced a chiral substituent onto the benzimidazole side arms of bis(benzimidazole)pyridine to yield $\mathbf{L^{11}}$. Unfortunately, the bulky neopentyl group precludes the formation of stable triple helical complexes.[18] On the other hand, introducing a bulky chiral substituent in the 4-position (R^3) of a pyridine 2,6-dicarboxamide (**L***, Scheme 1) results in (i) helical wrapping of the three ligand strands around the Ln^{III} ion, (ii) thermodynamically stable 1:3 complexes ($\log K_3$ in acetonitrile is in the range 5.1−5.3), and (iii) a small excess of one diastereoisomer.[23] To further our understanding of the influence of helical wrapping on diastereomeric induction, we introduce here a chiral neopentyl ester group in the pyridine R^3 position of $\mathbf{L^1}$ ($\mathbf{L^{12}}$, Scheme 1), and investigate its influence on the thermodynamic, chiro-optical and luminescent properties of the resulting tris complexes with Ln^{III} ions.

Results and Discussion

Synthesis and Characterisation of the Ligand and its Complexes

Ligand $\mathbf{L^{12}}$ was synthesised in a 48% yield from 2,6-bis[(1-methylbenzimidazol-2-yl)]pyridine-4-carboxylic acid (**6**) by esterification with (−),(*S*)-2-methyl-1-butanol (Scheme 2), while **6** was initially obtained by a four-step

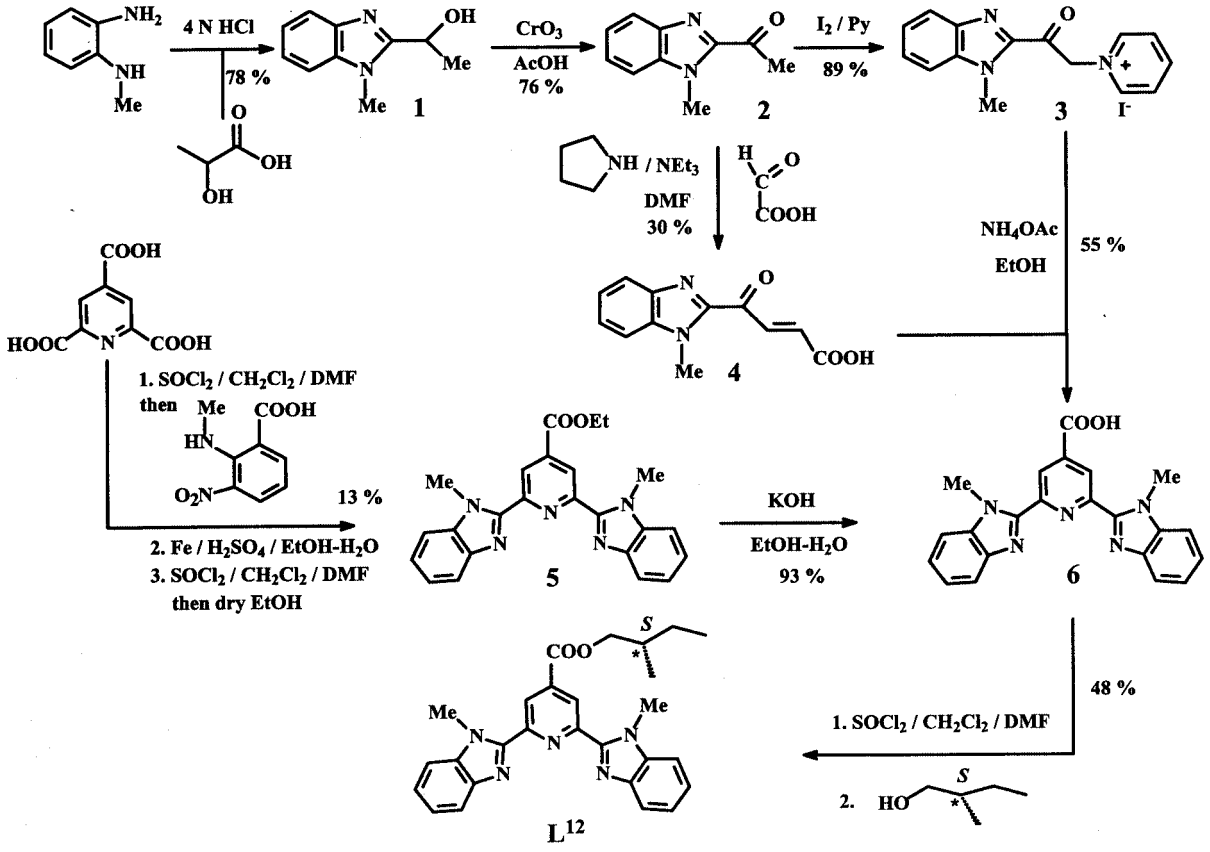

Scheme 2

procedure involving a modified double Phillips coupling reaction to form the benzimidazole unit.[24] Using an excess of *N*-ethyl-2-nitroaniline and 2,4,6-pyridinetricarboxylic acid favoured the formation of by-products such as the triamide, and significantly decreased the yield of the Phillips reaction. Consequently, we turned to a different strategy based on a procedure similar to that reported for the synthesis of $\mathbf{L^7}$ and $\mathbf{L^8}$,[25] and made use of the Kröhnke reaction[26] for the construction of the 4-substituted central pyridine ring. The required pyridinium salt **3** was prepared by an Ortoleva−King reaction[27] from 2-acetyl-1-methylbenzimidazole (**2**), while 4-(1-methylbenzimidazol-2-yl)-4-oxo-2-butanoic acid (**4**) was obtained by a Knoevenagel condensation.[26,28] Finally, **4** was synthesised by treating **2** with a mixture of glyoxylic acid monohydrate, triethylamine and pyrrolidine, which gave a better yield (30%) and resulted in an easier isolation process than the originally proposed method based on UV-irradiation.[29]

The specific rotary dispersion of $\mathbf{L^{12}}$ in degassed anhydrous acetonitrile, $[\alpha]_D^{25} = 8.1 \pm 0.4$ deg dm^2 mol^{-1}, confirms the chirality arising from the asymmetric carbon atom. At room temperature, the ^{1}H and ^{13}C NMR spectra in $CDCl_3$ (5×10^{-3} M) display 13 and 17 signals, respectively, indicating a local pseudo twofold symmetry for the bis(benzimidazole)pyridine part of the molecule (Figure 1, Figure S1). These spectra coupled with {^{1}H-^{1}H} COSY, DEPT-135, {^{1}H-^{13}C} HSQC experiments and NOE effects observed between H^4 and N−Me (NOE effects do not exist between H^5 and N−Me), clearly suggest that $\mathbf{L^{12}}$ has a *trans-trans* conformation, similar to that observed in $\mathbf{L^{11}}$. This conformation also prevails in the solid state, as demonstrated by the X-ray crystal structure (Table 1, Figure 2). The unit cell contains two independent molecules A and B, the bond lengths and angles of which differ only slightly (Table S1). All aromatic groups are planar, but the benzimidazole units are not coplanar with the pyridine group, the interplanar angles being either very similar (16.6° and 10.9°) or largely different (36.3° and 14.2°) in molecules A and B, respectively (Table S2). These angles result in an optimal packing coefficient. Finally, no noteworthy hydrogen-bonding or π-stacking interactions exist in the structure, which seems to be an example of a pure van der Waals packing.

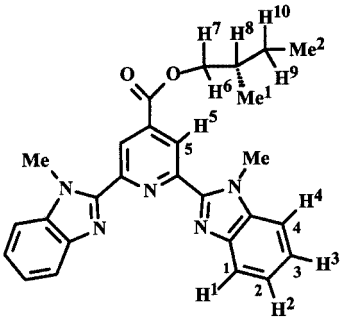

Figure 1. Numbering scheme for ligand $\mathbf{L^{12}}$.

Table 1. Crystal data for $\mathbf{L^{12}}$.

Formula	$C_{27}H_{27}N_5O_2$
M	453.54
Crystal system	orthorhombic
Space group	$P2_12_12_1$
a/ Å	7.302(5)
b/ Å	16.582(5)
c/ Å	39.001(5)
V/ Å^3	4722(4)
Z	8
T/ K	170(1)
μ(Mo-$K_α$)/ mm^{-1}	0.083
Reflections measured	15587
Independent reflections	6273 (R_{int} = 0.1013)
Observed reflections [$F_0 \geq 4\sigma(F_0)$]	4529
Final *R*1, *wR*2 [$I > 2\sigma(I)$]	0.0743, 0.1306

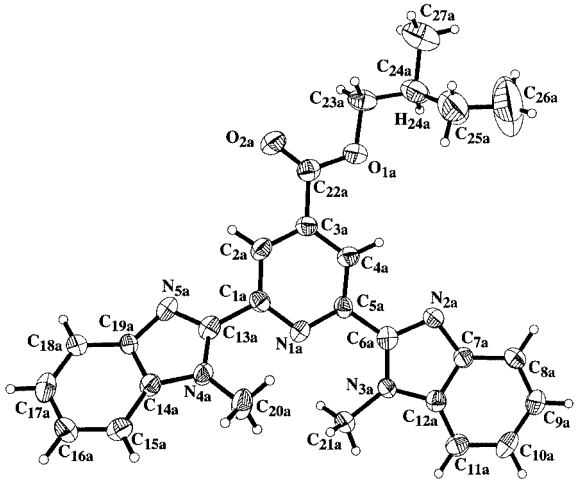

Figure 2. Molecular structure and atom numbering scheme for the two types of $\mathbf{L^{12}}$ molecules found in the unit cell.

The 1:3 complexes were obtained in 70−80% yields, by adding a solution of $\mathbf{L^{12}}$ in CH_2Cl_2 to solutions of lanthanide perchlorates in a mixture of MeCN and CH_2Cl_2. Evidence for complexation is the blue shift of the ν_{CO} and the two $\nu_{C=C}$ pyridine and benzimidazole vibrations by 4−6 cm^{-1} and 2−6 cm^{-1}, respectively. All perchlorate ions are ionic; hence the complexes are most probably nine-coordinate (see below). Single crystals for X-ray structure determination could not be obtained.

Interactions between $\mathbf{L^{12}}$ and the $\mathbf{Ln^{III}}$ Ions

The various species in solution were first identified by ESI-MS. Solutions of $\mathbf{L^{12}}$ (10^{-4} M in anhydrous acetonitrile) were titrated with $Ln(ClO_4)_3 \cdot xH_2O$ ($x = 0.2-0.6$) at 298 K, for ratios $R = [\mathbf{L^{12}}]_t/[Ln^{III}]_t = 0-3$. The spectra clearly show the successive formation of 1:*n* ($n = 1-4$) species, some of which had solvation molecules and/or were in the

Table 2. Relative intensities of the ESIMS peaks for solutions with $[\mathbf{L^{12}}]_t/[Ln^{III}]_t = 3$ (MeCN, 298 K)

Species	La	Eu	Lu
$[Ln(\mathbf{L^{12}})_3]^{3+}$	100	100	0.0
$[Ln(\mathbf{L^{12}})_4]^{3+}$	16.7	17.8	0.0
$[Ln(\mathbf{L^{12}})_2(ClO_4)]^{2+}$	7.5	9.2	0.0
$[Ln(\mathbf{L^{12}})_3(ClO_4)]^{2+}$	12.5	0.0	0.0
$[Ln(\mathbf{L^{12}})_3(MeCN)_4]^{3+}$	0.0	0.0	100
$[Ln(\mathbf{L^{12}})_2(MeCN)]^{3+}$	0.0	0.0	75

Table 4. Stability constants of $[Ln(\mathbf{L^{12}})_n]^{3+}$ complexes ($n = 1-3$) as determined by NMR spectroscopy and UV/Vis spectrometry ($\mu = 0.1$ M Et_4NClO_4, 298 K, $\pm 2\sigma$)

	Log K_1		log K_2		log K_3	
Ln	UV/Vis	NMR	UV/Vis	NMR	UV/Vis[a]	NMR
La	7.8 ± 0.4	8.0 ± 0.2	6.0 ± 0.5	6.0 ± 0.3	3.8 ± 0.6	3.8 ± 0.3
Eu	8.0 ± 0.3	[b]	6.4 ± 0.4	[b]	4.6 ± 0.5	[b]
Lu	8.0 ± 0.3	7.9 ± 0.2	6.4 ± 0.4	6.5 ± 0.3	2.9 ± 0.4	3.1 ± 0.3

[a] Values of log K_1 and log K_2 were fixed. [b] Not determined.

form of perchlorate adducts (Table 2, Table S3). For La and Eu, the 1:3 complex ($R = 3$) is most abundant, while for Lu, this species coexists in solution with the 1:2 complex. In parallel, the proportion of the $[Ln(\mathbf{L^{12}})_4]^{3+}$ species is relatively important for the larger ions (La, Eu), but this species is not seen for Lu. Such complexes have been observed for ligands derived from pyridine 2,6-dicarboxamide and were assigned to an outer-sphere association of a fourth ligand with a 1:3 complex.[23,30] The ES-MS data clearly point to the presence of stable 1:3 complexes with La and Eu, while the formation of this species with Lu appears to be less favoured.

To confirm the speciation, the titration of $\mathbf{L^{12}}$ (10^{-3} M in CD_3CN) with La^{III} and Lu^{III} ions has been monitored by 400 MHz ^1H NMR spectroscopy. Chemical shifts are reported in Table 3, while Figure S2 (see Supporting Information) presents the aromatic part of the spectra obtained with Lu. Signals for the 1:1, 1:2, and 1:3 complexes could clearly be identified for both ions. When R reaches 3, the tris species is the major complex in solution for La (> 68%) and Lu (50%); the other species in solution is the 1:2 complex. This observation confirms that the bulky neopentyl ester group increases the steric constraint in the triple helical complexes with the smaller lanthanide ions. The stability constants extracted from ^1H NMR spectroscopic data and analysed with MINEQL$^+$ [31] are reported in Table 4. The apparent ease with which the 1:3 complex forms contrasts with the situation observed with $\mathbf{L^{11}}$, and indicates that the substitution in the R^3 position of the central pyridine is less detrimental to the formation of the helical complexes compared with substitution on the benzimidazole rings.[18]

To quantify the $Ln^{III}-\mathbf{L^{12}}$ interaction further, we have performed spectrophotometric titrations of $\mathbf{L^{12}}$ with $Ln(Otf)_3$ (Ln = La, Eu, Lu; Otf = trifluoromethanesulfonate) at 298 K in MeCN, in the presence of 0.1 M Et_4NClO_4, under anhydrous conditions ($[H_2O] < 30$ ppm). Factor analysis[32] indicates the presence of three or four absorbing species and the data can be fitted to Equations (1)−(3), where solvation and anion coordination has been omitted.

$$Ln^{3+} + \mathbf{L^{12}} \rightleftarrows [Ln(\mathbf{L^{12}})]^{3+} \quad \log\beta_1 \tag{1}$$

$$Ln^{3+} + 2\,\mathbf{L^{12}} \rightleftarrows [Ln(\mathbf{L^{12}})_2]^{3+} \quad \log\beta_2 \tag{2}$$

$$Ln^{3+} + 3\,\mathbf{L^{12}} \rightleftarrows [Ln(\mathbf{L^{12}})_3]^{3+} \quad \log\beta_3 \tag{3}$$

A model including $[Ln(\mathbf{L^{12}})_4]^{3+}$ does not improve the fit, in agreement with the postulated outer-sphere nature of this species detected in the gas phase. Electronic spectra of the three complexes are correlated, which renders the fitting process difficult and generates relatively large uncertainties in the $\log\beta_i$ values (Table 4). The stability constants are in a good agreement with those extracted from NMR spectroscopic data. The interactions between $\mathbf{L^{12}}$ and the Ln^{III} ions are stronger than those with $\mathbf{L^{11}}$, as indicated by $\Delta\log K_3(\mathbf{L^{12}}-\mathbf{L^{11}}) = 2.6$ and 3.7 for La and Eu, respectively.[18] According to previous studies with ligands derived from bis(benzimidazole)pyridine,[17] the methyl substituents bound to the benzimidazole side arms in $\mathbf{L^{12}}$ favour the formation of a tight cavity around the lanthanide ions. This is not the case for the neopentyl groups in $\mathbf{L^{11}}$. This observation also confirms the large influence of the alkyl N-substituents on the formation of the 1:3 complexes. However, the size-discriminating effect along the lanthanide series, and the stability of the $[Ln(\mathbf{L^{i}})_3]^{3+}$ complexes, are largely influenced by the substituents on the benzimidazole and

Table 3. ^1H NMR shifts observed (ppm) for $\mathbf{L^{12}}$ in $CDCl_3$ and for its 1:1, 1:2, and 1:3 complexes with Ln^{III} ions in CD_3CN (10^{-3} M, 298 K).

Species	H^1	H^2	H^3	H^4	H^5	$H^{6,7}$	H^8	$H^{9,10}$	Me	Me^1	Me^2
L^{12}	7.90	7.32−7.43		7.48	8.92	4.23, 4.32	1.95	1.29, 1.56	4.24	1.04	0.97
La 1:1	8.31	7.56−7.65		7.81	8.78	4.36, 4.41	1.96	1.39, 1.62	4.32	1.10	1.02
La 1:2	7.59	7.28	6.91	7.20	8.87	4.40, 4.46	2.03	1.44, 1.66	4.34	1.14	1.05
La 1:3	7.74	7.35	6.83	7.16	8.03	4.31, 4.35	1.92	1.37, 1.56	3.82	1.07	1.02
Lu 1:1	8.12	7.67	7.63	7.87	8.91	4.39, 4.44	2.04	1.46, 1.52	4.41	1.12	1.03
Lu 1:2	7.56	7.34	7.09	6.98	9.00	4.45, 4.52	2.06	1.45, 1.68	4.24	1.17	1.07
Lu 1:3	7.82	7.43	7.49	7.68	8.81	4.25, 4.30	1.94	1.35, 1.58	4.28	1.06	0.99

central pyridine groups; the latter acting on the electron density of the pyridyl N atom. The introduction of an electron-attracting neopentyl ester group in **L12** decreases the electronic density on the pyridyl N atom, which reduces the electrostatic interaction, as indicated by $\Delta\log K_3(\mathbf{L^1}-\mathbf{L^2}) = 1.0-1.1$, but the size-discriminating effect is retained.[17]

The specific rotary dispersion of solutions of the $[Ln(\mathbf{L^{12}})_3]^{3+}$ complexes (10^{-3} M in anhydrous acetonitrile) is 33.5 ± 0.5 (La) and 31.0 ± 0.3 deg dm^2 mol^{-1} (Eu). This is about four times larger than those measured for the free ligand. We assign the greater rotary dispersion with respect to that generated by three free ligands to a structural contribution such as the formation of triple helical complexes in solution, as observed for **L***.[23] As a comparison, relatively little or no (4−5 deg dm^2 mol^{-1}) structural contribution was observed for the 1:1 and 1:2 complexes with **L11**.[18] The circularly polarised luminescence (CPL) spectrum of a 5×10^{-3} M solution of $[Eu(\mathbf{L^{12}})_3]^{3+}$ is plotted in Figure 3 in the spectral range of the $^5D_0 \rightarrow {}^7F_1$ transition,

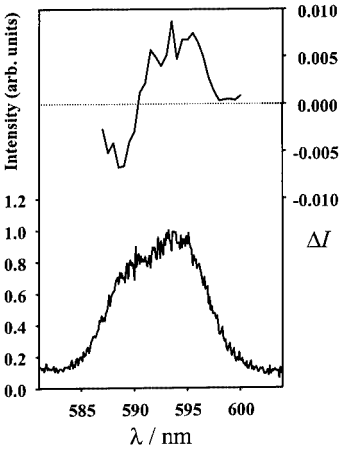

Figure 3. CPL spectrum of the $^5D_0 \rightarrow {}^7F_1$ transition of $[Eu(\mathbf{L^{12}})_3]^{3+}$ (5×10^{-3} M in anhydrous MeCN at 295 K), on ligand excitation at 386 nm.

which is particularly well-suited for CPL measurements since it satisfies the magnetic-dipole selection rule, $\Delta J = 0, \pm 1$. The spectrum depends on the polarisation of the excitation light, indicating the presence of two species in solution.[33] At the concentrations used, 93% of the Eu^{III} ion is in the form of the 1:3 complex, and 7% in the form of the 1:2 species, which is expected to generate a smaller chiral effect. The second species could also be a complex in which partial decomplexation of a ligand strand is induced by the interaction with one water molecule (see below). In conclusion, the CPL data are consistent with the presence of a small excess of one diastereoisomer in solution, on the short time scale of optical measurements, as previously observed for the corresponding complex with **L***.[23]

Photophysical Properties

The electronic spectrum of **L12** in MeCN displays two intense bands centred around 33950 and 29590 cm^{-1}, with a shoulder at higher energy (Table 5, Figure 4). Irradiation in the UV region at room temperature yields one broad unresolved fluorescence band, centred around 22885 cm^{-1} and originating from the $^1\pi\pi^*$ level (Figure 5). At 77 K, the fluorescence band is more structured and emission from the

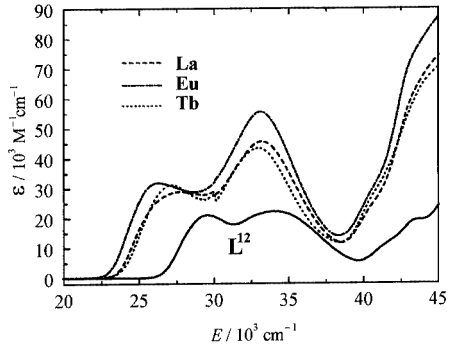

Figure 4. UV/Vis spectra of **L12** and its $[Ln(\mathbf{L^{12}})_3]^{3+}$ complexes (10^{-3} M in anhydrous MeCN at 293 K).

Table 5. Ligand-centred absorptions in acetonitrile and in the solid state (293 K), ligand-centred singlet- and triplet-state energies as determined from the emission spectra of the solids (77 K) and of the solutions (10^{-3} M in acetonitrile at 293 K) for the ligand **L12** and its triple helical complexes $[Ln(\mathbf{L^{12}})_3]^{3+}$.

Compnd	$E(x\rightarrow\pi^*)$/cm^{-1}[a] Solution[b]	solid state	$E(^1\pi\pi^*)$/cm^{-1} solution	solid state[c]	$E(^3\pi\pi^*)$/cm^{-1} solid state[c]
L^{12}	43480 (4.28) sh[d]	43480 sh			
	33950 (4.35)	33670		*23570*	*20920*
	29590 (4.32)	27100	22885	22960	17670
$[La(\mathbf{L^{12}})_3]^{3+}$	42980 (4.76) sh	45660 sh			
	33220 (4.66) 27630 (4.46)	34485		*22100*	*19750*
		24940	21210	22350	17990
$[Eu(\mathbf{L^{12}})_3]^{3+}$	43670 (4.89) sh	41490 sh			
	33115 (4.74) 26255 (4.50)	35715			
		24215	21100	[e]	[e]
$[Tb(\mathbf{L^{12}})_3]^{3+}$	43945 (4.81) sh	39215 sh			
	32980 (4.64) 27175 (4.49)	33670			
		24450	21645	22475	21050

[a] x = n or π. [b] At the concentration used, 67−85% of the metal ion is in the form of the 1:3 complex and 15−33% in the form of the 1:2 complex; Logε values are given in parentheses. [c] The 0-phonon transition is given in italics for frozen solutions in acetonitrile. [d] sh = shoulder. [e] not observed because of the **L12**-to-Ln energy transfer process.

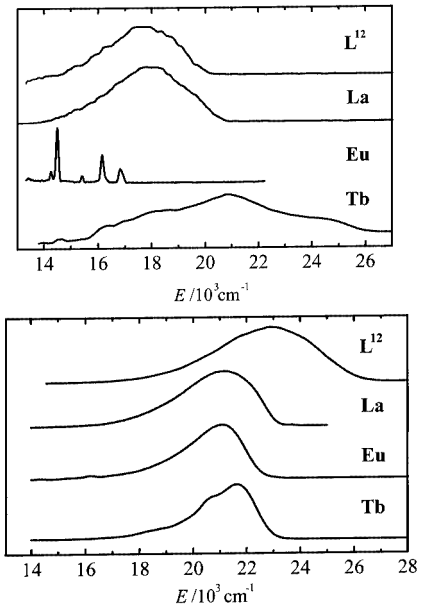

Figure 5. Top: Time-resolved emission spectra of $\mathbf{L^{12}}$ and $[Ln(\mathbf{L^{12}})_3]^{3+}$ in the solid state at 77 K and recorded with time delays of 0.01 (Eu), 0.1 (Tb) and 10 ms ($\mathbf{L^{12}}$, La). Bottom: Emission spectra of $[Ln(\mathbf{L^{12}})_3]^{3+}$ and $\mathbf{L^{12}}$ (10^{-3} M in MeCN at 293 K).

$^3\pi\pi^*$ state appears with a maximum around 17670 cm^{-1}. The decay of the latter is a single exponential with a lifetime of 210 ± 3 ms, in the range of values previously reported for similar ligands (160−323 ms).[16,34]

The higher energy component observed in the electronic (or reflectance) spectrum of $\mathbf{L^{12}}$ at 33950 cm^{-1} (33670 cm^{-1}) is only slightly modified on complexation with Ln^{III} ions, while the other band centred at 29590 cm^{-1} (27100 cm^{-1}) undergoes an important red shift (Table 5, Figure 4). This observation reflects the electronic transformations associated with the *trans-trans→cis-cis* conformational change and the complexation of the lanthanide metal ions to the tridentate binding unit.[16,25,34] On complexation of $\mathbf{L^{12}}$ to La^{III}, the 0-phonon transitions of the singlet and triplet states are red-shifted by 1470 and 1170 cm^{-1}, respectively (frozen MeCN solution, 77 K, see Figure 5), and the $^3\pi\pi^*$ lifetime decreases to 144 ± 1 ms. Emission from the $^1\pi\pi^*$ state of the ligand is still visible for the Eu and Tb complexes, suggesting an incomplete intersystem crossing. Emission from the $^3\pi\pi^*$ state disappears for the Eu solution, with a concomitant observation of the metal-centred emission bands. This is not the case for the Tb solution for which little or no ligand-to-Tb energy transfer takes place because the energy of the ligand donor level (19750 cm^{-1} in the La complex at 77 K) is located below the metal $^5D_4$ acceptor level (20350 cm^{-1}). Weak emission from the Tb^{III} ion can only be seen on direct excitation of the metal states (Figure S3, Supporting Information), and the short and temperature-dependent Tb($^5D_4$) lifetime (decreasing from 0.38 to 0.12 ms between 13 and 55 K) indicates that energy back transfer occurs in this complex.

In order to gain information on the chemical environment around the Eu^{III} ion, we have measured the high-resolution emission spectra of a solid state sample of $[Eu(\mathbf{L^{12}})_3](ClO_4)_3{\cdot}2H_2O$ (**8**) at low temperature since this complex is only faintly luminescent at room temperature. The lifetime of the $^5D_0$ level, 0.85 ± 0.01 ms, is constant between 13 and 77 K. This is shorter than the lifetimes reported for $[Eu(\mathbf{L^1})_3]^{3+}$ (1.85 ms in the range 4−77 K)[35] and $[Eu(\mathbf{L^{11}})_3]^{3+}$ (2.03 ms at 10 K),[36] but similar to that found for $[Eu(ClO_4)_2(H_2O)(\mathbf{L^{11}})_2]^+$ (0.65 ms at 10 K).[36] Therefore, we cannot rule out the interaction of one water molecule in the first coordination sphere. The decrease in the Eu($^5D_0$) lifetime from 0.85 ms to 0.27 ms between 77 and 295 K indicates temperature-dependent quenching mechanisms, e.g. a ligand-to-metal charge transfer as demonstrated for $[Eu(\mathbf{L^1})_3]^{3+}$,[37,38] and as reported for other Eu^{III} complexes[39] or other intermolecular interactions. In acetonitrile solution (10^{-3} M) at 295 K, the lifetime is longer, reaching 0.96 ± 0.01 ms; since in addition to the hydration of **8** the solvent contains about 2 mM H_2O, inner-sphere water interaction could occur. Using Horrocks equation, $q = 1.05\,(k_{H2O}-k_{D2O})$[40] and taking k_{D2O} equal to 0.51 ms^{-1} (average of the values for the anhydrous tris species with $\mathbf{L^1}$ and $\mathbf{L^{11}}$),[35,36] we find $q = 0.56$. This points to an equilibrium in solution between an anhydrous species and a monohydrate, as has been observed for triple helical complexes with terpyridine derivatives.[41] Alternatively, it has been demonstrated that fast diffusing outer-sphere H_2O molecules can contribute 0.25 ms^{-1} to the quenching of the Eu^{III} ion in complexes with cyclen derivatives.[42] Applying a similar correction for **8** results in a reduction of q by approximately a factor of 2. Therefore, given the uncertainties linked to this type of correlation, it is difficult to determine from the lifetime data whether or not a water molecule interacts in the inner coordination sphere. On the other hand, it is clear that the introduction of an electron-attracting group in the R^3 position weakens the Ln−N(py) bond, consistent with the relatively high energy of the $^5D_0 \leftarrow {}^7F_0$ transition (17258 cm^{-1} at 295 K). Using the correlation proposed by Frey and Horrocks[43] and the nephelauxetic parameter $\delta_{N(het)} = -15.3$ cm^{-1} that we reported previously,[44] we get $\delta_{N(py)} = -8.1$ cm^{-1}, a value much lower than those proposed (−12 to −17 cm^{-1}).[43,45]

The emission spectra recorded at 13 K on excitation through the ligand band, or direct laser excitation of the $^5D_0 \leftarrow {}^7F_0$ transition, display fairly broad bands which are compatible with a distorted D_3 symmetry environment for the metal ion (Figure S4). The relative intensities of the $^5D_0 \rightarrow {}^7F_J$ transitions are 0.07, 1.00, 1.28, <0.01 and 4.11 for $J = 0$, 1, 2, 3, and 4, respectively. The $^5D_0 \rightarrow {}^7F_1$ transition displays two main components, one of them appearing as a doublet with a splitting of 17 cm^{-1}, while the $^5D_0 \rightarrow {}^7F_2$ transition shows two doublets with a splitting of 13 and 14 cm^{-1}, respectively. Finally, the $^5D_0 \rightarrow {}^7F_4$ transition displays four main components, three of them having a very weak intensity, again compatible with a distorted D_3 local symmetry.

To get a better insight into the various energy conversion processes occurring in the $[Ln(\mathbf{L^{12}})_3]^{3+}$ complexes, we have determined the quantum yields of both the ligand- and

metal-centred luminescence of 10^{-3} M solutions at 295 K, and the ratio between the integrated triplet and singlet state emissions, $I^{(T)}/I^{(S)}$ for the free ligand and its La^{III} complex at 77 K. The quantum yield of $[La(\mathbf{L^{12}})_3]^{3+}$ (Q^F = 5.5%) decreases by a factor of 9 with respect to that of the free ligand (Q^F = 51%), and the ligand-centred phosphorescence increases, as indicated by $I^{(T)}/I^{(S)}$ which increases from 8×10^{-5} to 9.8×10^{-3} on complexation of $\mathbf{L^{12}}$ with La^{III}, that is by a factor of 122. The better intersystem crossing (isc) efficiency in the La^{III} complex may be explained by (i) the reduced energy gap between the $^1\pi\pi^*$ and $^3\pi\pi^*$ states: 2350 cm^{-1}, determined from the energy of the 0-phonon transitions, in contrast to 2650 cm^{-1} in the free ligand (Figure 6) and (ii) the spin-orbit mixing of the singlet and triplet states induced by the complexation with La^{III}.[46] The quantum yield of the metal-centred luminescence of $[Eu(\mathbf{L^{12}})_3]^{3+}$ obtained on ligand excitation remains very small, $Q_L^{Eu} = 5 \times 10^{-3}$ %, not only because the efficiency of the isc process stays small, but most probably because of photoinduced electron transfer processes, as already pointed out for the triple helical complex with $\mathbf{L^1}$.[37,38]

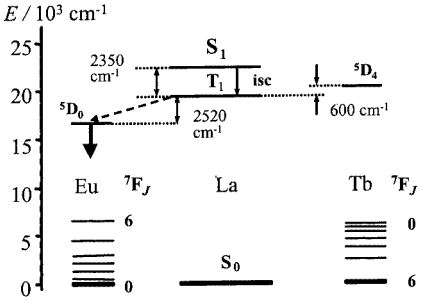

Figure 6. Schematic energy diagram for $[Ln(\mathbf{L^{12}})_3]^{3+}$ complexes. Data for S_1 and T_1 are those of the La^{III} complex in the solid state at 77 K (0-phonon transitions).

Conclusion

The introduction of a chiral neopentyl ester group in the 4-position of the central pyridine ring of ligand $\mathbf{L^1}$ to yield $\mathbf{L^{12}}$ leads to the formation of thermodynamically stable 1:3 complexes with lanthanide ions in acetonitrile, as shown by the logK_3 values in the range 2.9−4.6. Chiro-optical data clearly suggest the helical wrapping of the ligand strands around the Ln^{III} ions. As a comparison, the bulky neopentyl groups grafted onto the benzimidazole side arms in $\mathbf{L^{11}}$ precluded helical wrapping, a fact confirmed by the specific rotary dispersion measurements.[18] Although only a small excess of one diastereoisomer is induced in solution by the chiral ligand $\mathbf{L^{12}}$, as was observed for complexes with $\mathbf{L^*}$,[23] this work reveals that structural chirality may be induced in triple helical complexes by a suitable design of the ligand. The substitution also significantly modifies the photophysical properties of the tris complexes, compared with those with $\mathbf{L^{11}}$.[36] In particular, the ligand-to-metal energy transfer is amplified for Eu, but cancelled for Tb.

Therefore, this study demonstrates that, in addition to the electronic and photophysical properties which may be modulated by varying the substituent in the R^3 position, a diastereomeric excess can be induced in solution if this substituent is chiral. The combination of these properties opens new perspectives for the design of lanthanide triple helical complexes acting as probes for chiral recognition.

Experimental Section

Solvents and Starting Materials: Acetonitrile, dichloromethane, chloroform, tetrahydrofuran, pyridine and triethylamine were purified in the usual way.[47] Silica gel (Merck 60, 0.04−0.06 mm) was used for preparative column chromatography. Other products were purchased from Fluka AG (Buchs, Switzerland) or Merck and used without further purification. 2,4,6-pyridinetricarboxylic acid was prepared according to a literature procedure.[48] Lanthanide perchlorates were obtained as described previously.[49]

Caution: Dry perchlorates and their complexes with aromatic amines may easily explode and should be handled in small quantities and with extreme caution.[50]

Spectroscopic and Analytical Measurements: Electronic spectra in the UV/Vis range were recorded at 293 K with a Perkin−Elmer Lambda 900 spectrometer and 1.0 and 0.1 cm quartz cells. Reflectance spectra were recorded on finely ground powders dispersed in MgO (5%), with MgO as the reference, on the same spectrometer equipped with a Labsphere PELA-1000 integration sphere. Specific rotary dispersion values were measured from 10^{-3} M solutions in degassed anhydrous acetonitrile at 298 K with the help of a JASCO DIP-370 polarimeter (sodium D line). IR spectra were obtained from KBr pellets with a Mattson α-Centauri FT-IR spectrometer. Pneumatically assisted electrospray (ESIMS) mass spectra were recorded from MeCN solutions on API III or API 3000 tandem mass spectrometers (PE Sciex) by infusion at 10 μL min^{-1}. The spectra were recorded under low up-front declustering or collision-induced dissociation (CID) conditions, typically ΔV = 0−30 V between the orifice and the first quadrupole of the spectrometer. ^1H, ^{13}C NMR spectra and 2-D experiments were recorded at 25 °C on Bruker AM-360 or Bruker AVANCE 400-DRX spectrometers. Chemical shifts are reported in parts per million with respect to TMS. Ligand excitation and emission spectra were recorded on a Perkin−Elmer LS-50B spectrometer equipped for low temperature (77 K) measurements. The experimental procedures for high resolution, laser-excited luminescence studies have been published previously.[51] Emission spectra are corrected for the instrumental function. Quantum yields of the ligand-centred emission were measured relative to quinine sulfate in 0.05 M H_2SO_4 (A_{347} = 0.05, absolute quantum yield: 0.546).[52] Quantum yields of the metal-centred emission were determined as described previously[53] at excitation wavelengths at which (i) the Lambert−Beer law is obeyed and (ii) the absorption of the reference $[Ln(terpy)_3]^{3+}$ closely matches that of the sample. CPL measurements were made on an instrument described previously, operating in a differential photon-counting mode.[33] Elemental analyses were performed by Dr H. Eder (Microchemical Laboratory, University of Geneva).

Spectrophotometric Titrations: The electronic spectra in the UV/Vis range were recorded at 298 K from 10^{-4} M solutions in acetonitrile containing Et_4NClO_4 (0.1 M) as the inert electrolyte with a Perkin−Elmer Lambda 7 spectrometer connected to an external computer and in quartz cells of 0.100 cm path length. Solutions were prepared in a thermostatted vessel (Metrohm 6.1418.220) and the titrant solution was added with an automated burette from Me-

trohm (6.1569.150 or .210) fitted with an anti-diffusion device. In a typical experiment, 5−10 cm^3 of **L^{12}** were titrated with a solution of Ln^{III} triflate (10^{-4} M) in acetonitrile. After each addition of 0.20 cm^3 and a delay of 2 min, the spectrum was measured and transferred to the computer. In some instances, reverse titrations, i.e. with **L^{12}** as the titrating species, were also performed to confirm the values of the stability constants. All the experiments were conducted in a dry box and the water content of the solutions, measured at the end of the titration by the Karl Fischer method, was always <30 ppm. Factor analysis and stability constant determinations were carried out with the program SPECFIT, version 2.10.[54]

Crystal Structure of L^{12}: The pale yellowish, lathlike crystals were directly transferred from the mother liquor into a drop of Hostinert 216 oil kept at 210 K. A specimen was selected and placed in a glass capillary. The data collection, at 170 K, took place on a Stoe IPDS system equipped with Mo-K_α radiation (Table 1). The image plate − crystal distance was set to 80 mm, and a φ interval of 1° was chosen. Two hundred images were then exposed for 20 min each. Inspection of the reciprocal space revealed that about three quarters of the diffraction spots could be accounted for by the cell given in Table 1. The integration was based on an effective mosaic spread of 0.012 and a profile between 11 and 21 pixels. A peak overlap of 2 pixels was tolerated in order to retain the maximum number of reflections. Nevertheless, over 2700 reflections were eliminated because of severe peak overlap. The intensities were corrected for Lorentz and polarisation effects. No absorption correction could be applied since the crystal was all but invisible in the frozen oil, but the absorption coefficient appeared to be small. The decay during the measurement was negligible. The structure was solved in the space group $P2_12_12_1$ with the help of SIR 97.[55] The oxygen and nitrogen atoms were refined anisotropically and the carbon and hydrogen atoms isotropically; the latter were allowed to ride on their associated carbon atoms. The refinement seems to favour the *S* configuration for the chirality centre C24 for both molecules, as expected from the synthesis and the observed rotary dispersion, but the value of Flack's parameter (2 ± 2) is not conclusive.[56] CCDC-186842 contains the supplementary crystallographic data for this paper, which can be obtained free of charge at www.ccdc.cam.ac.uk/conts/retrieving.html [or from the Cambridge Crystallographic Data Centre, 12 Union Road, Cambridge CB2 1EZ, UK; fax: (internat) +44−1223/336−033; E-mail: deposit@ccdc.cam.ac.uk].

Preparation of the Ligand. (±)-2-(1-Hydroxyethyl)-1-methylbenzimidazole (1): A mixture of *N*-Methyl-1,2-phenylenediamine (0.93 cm^3, 8.18 mmol) and (±)-2-hydroxypropionic acid (0.91 cm^3, 12.21 mmol) was refluxed for 45 min in 4 N hydrochloric acid (10 cm^3). After cooling, the mixture was neutralised to pH = 7.1 with NH_4OH (25%). The resulting brown crude solid was filtered, washed with water and recrystallised from hot water to give 1.13 g of **1** (6.41 mmol, 78%). M.p. 106−108 °C. ^{1}H NMR (360 MHz, CD_3OD): δ = 1.73 (d, ^3J = 7.0 Hz, 3 H), 3.94 (s, 3 H), 4.93 (s, 1 H), 5.20 (q, ^3J = 7.0 Hz, 1 H), 7.25−7.34 (m, 2 H), 7.50 (m, 1 H), 7.66 (m, 1 H) ppm. ^{13}C NMR (360 MHz, CD_3OD): δ = 21.65, 30.67, 64.15, 110.79, 119.59, 123.33, 124.06, 137.37, 142.35, 157.45 ppm. IR (KBr): $\tilde{\nu}$ = 1105 ($\nu_{C\text{-}OH}$) cm^{-1}. ESI-MS (MeOH): *m*/*z* = 177.2 [L + H]$^+$.

2-Acetyl-1-methylbenzimidazole (2): A solution of chromium trioxide (494 mg, 4.94 mmol) in water (3 cm^3) was added dropwise to a solution of **1** (1.13 g, 6.41 mmol) in glacial acetic acid (5 cm^3) at 90 °C. The reaction mixture was heated at 100 °C for 10 min and poured into water (60 cm^3). The resulting precipitate was extracted with dichloromethane (3 × 30 cm^3), and the combined extracts dried (Na_2SO_4) and the solvents evaporated. The resulting crude solid was recrystallised from methanol to give 849 mg of **2** (4.87 mmol, 76%) as white crystals. M.p. 72−74 °C. ^{1}H NMR (360 MHz, $CDCl_3$): δ = 2.83 (s, 3 H), 4.11 (s, 3 H), 7.33−7.37 (m, 1 H), 7.41 (m, 2 H), 7.87 (m, 1 H) ppm. ^{13}C NMR (360 MHz, $CDCl_3$): δ = 28.18, 32.38, 110.64, 122.02, 123.82, 126.06, 137.07, 141.71, 146.28, 193.46 ppm. IR (KBr): $\tilde{\nu}$ = 1684 (ν_{CO}) cm^{-1}. ESI-MS (MeOH): *m*/*z* = 175.1 [L + H]$^+$.

1-{[(Methylbenzimidazol-2-yl)carbonyl]methyl}-1-pyridinium Iodide (3): **2** (211 mg, 1.21 mmol) and I_2 (307 mg, 1.21 mmol) were dissolved in dry distilled pyridine (4 cm^3) under an inert atmosphere. After 20 min at room temp., the mixture was heated at 100 °C for 15 h, then cooled to room temperature. The resulting brown precipitate was filtered, washed once with pyridine/diethyl ether (1:1, 5 cm^3) and twice with diethyl ether (10 cm^3). The dried crude product was recrystallised from ethanol with charcoal to give 410 mg of **3** (1.08 mmol, 89%) as dark yellow needles. M.p. 205−207 °C. ^{1}H NMR (360 MHz, [D$_6$]DMSO): δ = 4.11 (s, 3 H), 6.54 (s, 2 H), 7.46 (m, 1 H), 7.56 (m, 1 H), 7.84 (m, 1 H), 7.94 (m, 1 H), 8.30 (m, 2 H), 8.76 (m, 1 H), 9.03 (m, 2 H) ppm. ^{13}C NMR (360 MHz, [D$_6$]DMSO): δ = 31.96, 66.56, 111.86, 121.22, 124.22, 126.47, 127.74, 136.65, 141.07, 143.47, 145.56, 146.46, 184.43 ppm. IR (KBr): $\tilde{\nu}$ = 1705 (ν_{CO}) cm^{-1}. FAB-MS (MeOH): *m*/*z* = 252.1 [L − I]$^+$.

4-(1-Methylbenzimidazol-2-yl)-4-oxobut-2-enoic Acid (4): Glyoxylic acid monohydrate (1 g, 10.86 mmol), triethylamine (1.52 cm^3, 10.86 mmol) and pyrrolidine (0.33 cm^3, 3.8 mmol) were sequentially added to a solution of **2** (631 mg, 3.62 mmol) in DMF (10 cm^3). The mixture was stirred at room temp. for 48 h and 1% hydrochloric acid was then added until pH = 1. The solution was extracted with diethyl ether (3 × 20 cm^3) and the combined organic layers were dried (Na_2SO_4) and the solvents evaporated. The resulting crude solid was redissolved with 10% $NaHCO_3$ (5 cm^3) to pH = 8 and washed with dichloromethane (2 × 10 cm^3). The aqueous phase was acidified to pH = 1 by addition of 10% hydrochloric acid and extracted with diethyl ether (3 × 10 cm^3). The combined organic layers were washed with water (2 × 30 cm^3), dried (Na_2SO_4) and the solvents evaporated. The resulting crude solid was recrystallised by slow diffusion of hexane into an ethyl acetate solution to give 251 mg of **4** (1.09 mmol, 30%) as brownish-red needles. M.p. 194−196 °C. ^{1}H NMR (360 MHz, [D$_6$]DMSO): δ = 4.15 (s, 3 H), 6.83 (d, ^3J = 15.9 Hz, 1 H), 7.39 (m, 1 H), 7.50 (m, 1 H), 7.75 (m, 1 H), 7.88 (m, 1 H), 8.28 (d, ^3J = 15.9 Hz, 1 H) ppm. ^{13}C NMR (360 MHz, [D$_6$]DMSO): δ = 32.18, 111.64, 121.45, 123.85, 126.32, 132.46, 136.65, 137.03, 141.22, 146.17, 166.24, 181.66 ppm. IR (KBr): $\tilde{\nu}$ = 1707, 1670 (ν_{CO}) cm^{-1}. ESI-MS (MeOH): *m*/*z* = 231.2 [L + H]$^+$.

Ethyl 2,6-Bis[(1-methylbenzimidazol-2-yl)]pyridine-4-carboxylate (5): A mixture of 2,4,6-pyridinetricarboxylic acid (1 g, 4.7 mmol), freshly distilled thionyl chloride (15 cm^3, 207 mmol) and DMF (0.12 cm^3) was refluxed for 90 min in dry dichloromethane (40 cm^3), evaporated and dried under vacuum for 60 min. The resulting solid was dissolved in dry dichloromethane (45 cm^3), and a mixture of 2-nitro-*N*-ethylaniline (1.08 g, 7.1 mmol) and triethylamine (6.6 cm^3, 47 mmol) in dry dichloromethane (30 cm^3) was added dropwise under inert atmosphere. The solution was stirred for 2 h at room temperature, refluxed for 6 h and the solvents evaporated. The brown residue was partitioned between dichloromethane (3 × 100 cm^3) and half-saturated aqueous NH_4Cl solution (100 cm^3). The combined organic phases were dried (Na_2SO_4) and the solvents evaporated. The crude product was dissolved in a mixture of ethanol/water (250:55 cm^3), and freshly activated iron powder (8 g,

143 mmol) and 25% hydrochloric acid (45.7 cm^3, 352 mmol) were added. The solution was refluxed for 8 h under inert atmosphere. The excess of iron was filtered off, and the ethanol was distilled off under vacuum. Water was then added to bring the total volume to 100 cm^3. The resulting solution was poured into dichloromethane (150 cm^3). $Na_2H_2edta{\cdot}2H_2O$ (84 g, 236 mmol) in 150 cm^3 water was then added, and the resulting mixture was neutralised to pH = 7 with 5 M aqueous potassium hydroxide; 30% H_2O_2 (1 cm^3) was added and the pH adjusted to 8.3. After vigorous stirring for 30 min, the organic layer was separated and the aqueous phase extracted with dichloromethane (3 × 150 cm^3). The combined organic phases were dried (Na_2SO_4) and the solvents evaporated. The resulting crude solid was dissolved in dry dichloromethane (40 cm^3), then freshly distilled thionyl chloride (15 cm^3, 207 mmol) and DMF (0.12 cm^3) were added. The mixture was refluxed for 90 min, evaporated and dried under vacuum for 60 min. The crude product was cooled to 0 °C, then dry ethanol (20 cm^3) was added dropwise. The resulting solution was allowed to stand at room temperature, stirred for 60 min, evaporated and dried under vacuum for 60 min. The residue was partitioned between dichloromethane (3 × 40 cm^3) and half-saturated aqueous NH_4Cl solution (40 cm^3). The combined organic phases were dried (Na_2SO_4) and the solvents evaporated. The resulting brownish-red crude solid was purified by column chromatography (silica gel, CH_2Cl_2/MeOH, 100:0 → 99:1) to give 251 mg of **5** (0.61 mmol, 13%). ^{1}H NMR (400 MHz, $CDCl_3$): δ = 1.46 (t, ^3J = 7.0 Hz, 3 H), 4.25 (s, 6 H), 4.49 (q, ^3J = 7.0 Hz, 2 H), 7.39 (m, 4 H), 7.48 (m, 2 H), 7.91 (m, 2 H), 8.95 (s, 2 H) ppm. ^{13}C NMR (400 MHz, $CDCl_3$): δ = 14.97, 33.24, 62.89, 110.69, 121.05, 123.78, 124.66, 125.26, 137.91, 141.03, 143.36, 150.32, 151.33, 164.85 ppm. IR (KBr): $\tilde{\nu}$ = 1712 (ν_{CO}), 1597, 1562 ($\nu_{C=C}$) cm^{-1}. ESI-MS (MeCN): *m*/*z* = 412.2 $[L + H]^+$.

2,6-Bis[(1-methylbenzimidazol-2-yl)]pyridine-4-carboxylic Acid (6). Procedure A: 3 (410 mg, 1.08 mmol), **4** (226 mg, 0.98 mmol) and ammonium acetate (3 g, 38.92 mmol) were dissolved in ethanol (25 cm^3). The mixture was refluxed for 24 h under an inert atmosphere, and then slowly cooled to room temperature. The resulting white crystals were separated by filtration and recrystallised from hot methanol to give 230 mg of **6** (0.60 mmol, 55%). **Procedure B:** A solution of **5** (251 mg, 0.61 mmol) in a mixture of ethanol/water, 1:4 (5:20 cm^3) containing potassium hydroxide (17 g, 303 mmol) was refluxed for 24 h. Ethanol was distilled off and the aqueous phase acidified to pH = 3 with 25% hydrochloric acid. The resulting precipitate was filtered off and washed with water to give 218 mg of **6** (0.57 mmol, 93%) as a white powder. M.p. >260 °C. ^{1}H NMR (360 MHz, $[D_6]$DMSO): δ = 4.37 (s, 6 H), 7.38−7.47 (m, 4 H), 7.78 (m, 2 H), 7.87 (m, 2 H), 8.81 (s, 2 H) ppm. ^{13}C NMR (360 MHz, $[D_6]$DMSO): δ = 36.51, 114.78, 123.45, 126.27, 127.10, 128.81, 141.06, 146.18, 146.70, 153.00, 154.41, 166.54 ppm. IR (KBr): $\tilde{\nu}$ = 1716 (ν_{CO}), 1617, 1560 ($\nu_{C=C}$) cm^{-1}. ESI-MS (MeCN): *m*/*z* = 384.2 $[L + H]^+$, 767.4 $[2L + H]^+$.

Neopentyl 2,6-Bis[(1-methylbenzimidazol-2-yl)]pyridine-4-carboxylate (L^{12}): A mixture of **6** (430 mg, 1.12 mmol), freshly distilled thionyl chloride (3.62 cm^3, 50 mmol) and DMF (0.03 cm^3) was refluxed for 90 min in dry dichloromethane (10 cm^3), evaporated and dried under vacuum for 60 min. A solution of (−)-(*S*)-2-methyl-1-butanol (1.2 cm^3, 11.2 mmol) dried on molecular sieves was added to the resulting crude solid. After stirring for 30 min at room temp., the resulting violet solution was evaporated and the residue was redissolved in $CHCl_3$ (10 cm^3). The organic phase was washed with water (3 × 20 cm^3), then with half-saturated aqueous NH_4Cl (20 cm^3), dried (Na_2SO_4) and the mixture evaporated to dryness. The resulting crude solid was purified by column chromatography (silica gel, CH_2Cl_2/MeOH, 100:0 → 99:1) and recrystallised by slow diffusion of hexane into a dichloromethane solution to give 245 mg of $\mathbf{L^{12}}$ (0.54 mmol, 48%) as white crystals. M.p. 186−188 °C. ^{1}H NMR (360 MHz, $CDCl_3$): δ = 0.97 (t, ^3J = 7.3 Hz, 3 H), 1.04 (d, ^3J = 6.8 Hz, 3 H), 1.29 (m, ^3J = 7.3 Hz, 1 H, ^2J = 13.6 Hz), 1.56 (m, ^3J = 7.3 Hz, 1 H, ^2J = 13.6 Hz), 1.95 (1 H, pseudo-oct., ^3J = 6.3−7.3 Hz), 4.23 (dd, 1 H, ^3J = 6.3 Hz), 4.24 (s, 6 H), 4.32 (dd, 1 H, ^3J = 6.3 Hz), 7.35−7.43 (m, 4 H), 7.48 (m, 2 H), 7.90 (m, 2 H), 8.92 (s, 2 H) ppm. ^{13}C NMR (360 MHz, $CDCl_3$): δ = 11.35, 16.59, 26.20, 32.68, 34.34, 70.96, 110.15, 120.60, 123.20, 124.10, 124.68, 137.35, 140.51, 142.79, 149.78, 150.79, 164.44 ppm. IR (KBr): $\tilde{\nu}$ = 1730 (ν_{CO}), 1587, 1564 ($\nu_{C=C}$) cm^{-1}. ESI-MS (MeCN): *m*/*z* = 454.2 $[L + H]^+$. $C_{27}H_{27}N_5O_2{\cdot}0.11CH_2Cl_2$: calcd. C 70.3, H 5.9, N 15.1; found C 70.3, H 6.0, N 15.1.

Preparation of the Complexes: The 1:3 complexes $[Ln(\mathbf{L^{12}})_3](ClO_4)_3{\cdot}xH_2O$ (La, *x* = 2, (7); Eu, *x* = 2, (8); Tb, *x* = 3, (9)] were prepared by mixing $\mathbf{L^{12}}$ with stoichiometric amounts of $Ln(ClO_4)_3{\cdot}nH_2O$ (Ln = La, Eu, Tb and *n* = 0.2−0.6) in dichloromethane/acetonitrile. The complexes may be crystallised in 70−80% yields by slow diffusion of *tert*-butyl methyl ether into an acetonitrile solution. [$C_{81}H_{81}N_{15}O_{18}Cl_3La{\cdot}2H_2O$: found C 53.2, H 4.6, N 11.6, calcd. C 53.1, H 4.7, N 11.5; $C_{81}H_{81}N_{15}O_{18}Cl_3Eu{\cdot}2H_2O$: found C 52.5, H 4.7, N 11.4, calcd. C 52.7, H 4.6, N 11.4; $C_{81}H_{81}N_{15}O_{18}Cl_3Tb{\cdot}3H_2O$: found C 51.9, H 4.5, N 11.1; calcd. C 52.0, H 4.7, N 11.2]. IR (KBr): $\tilde{\nu}$ = 1736 (La), 1735 (Eu), 1734 (Tb), (ν_{CO}); 1593, 1568 (La), 1591, 1570 (Eu), 1589, 1570 (Tb), ($\nu_{C=C}$) and 1092, 625 (ionic ClO_4^-) cm^{-1}.

Acknowledgments

This work is supported through grants from the Swiss National Science Foundation. We thank Prof. Pierre Vogel for the use of his polarimeter, Dr. Anne-Sophie Chauvin for her help in the ligand synthesis and the Fondation Herbette (Lausanne) for the gift of spectroscopic equipment.

[1] J.-C. G. Bünzli in *Lanthanide Probes in Life, Chemical and Earth Sciences. Theory and Practice*, (Eds.: J.-C. G. Bünzli, G. R. Choppin), Elsevier Science Publ. B. V., Amsterdam, **1989**, Ch. 7, 219−293.
[2] C. H. Evans, *Biochemistry of the Lanthanides*, Plenum Press, New York, **1990**.
[3] D. Parker, *Coord. Chem. Rev.* **2000**, *205*, 109−130.
[4] J.-C. G. Bünzli, C. Piguet in *Encyclopedia of Materials: Science and Technology* (Eds.: K. H. J. Buschow, R. W. Cahn, M. C. Flemings, B. Ilschner, E. J. Kramer, S. Mahajan), Elsevier Science Ltd, Oxford, **2001**, 10, Ch. 1.10.4, 4465−4476.
[5] G. Mathis in *Rare Earths*, (Eds.: R. Saez Puche, P. Caro), Editorial Complutense, Madrid, **1998**, 285−297.
[6] I. Hemmilä, T. Ståhlberg, P. Mottram, *Bioanalytical Applications of Labelling Technologies*, Wallac Oy, Turku, **1995**.
[7] V. W. W. Yam, K. K. W. Lo, *Coord. Chem. Rev.* **1999**, *184*, 157−240.
[8] D. J. Bornhop, D. S. Hubbard, M. P. Houlne, C. Adair, G. E. Kiefer, B. C. Pence, D. L. Morgan, *Anal. Chem.* **1999**, *71*, 2607−2615.
[9] G. E. Kiefer, L. Jackson, D. J. Bornhop, **1999**, US patent 5,928,627.
[10] A. E. Merbach, E. Toth, *The chemistry of contrast agents in medical magnetic resonance imaging*, Wiley, London, **2001**.
[11] Z. J. Guo, P. J. Sadler, *Angew. Chem. Intl. Ed. Engl.* **1999**, *38*, 1513−1531.
[12] M. Komiyama, N. Takeda, H. Shigekawa, *Chem. Commun.* **1999**, 1443−1451.

[13] G. Pratviel, J. Bernardou, B. Meunier, *Adv. Inorg. Chem.* **1998**, *45*, 251−312.
[14] J.-C. G. Bünzli in *Rare Earths*, (Eds.: R. Saez Puche, P. Caro), Editorial Complutense, Madrid, **1998**, 223−259.
[15] C. Piguet, J.-C. G. Bünzli, *Chem. Soc. Rev.* **1999**, *28*, 347−358.
[16] C. Piguet, J.-C. G. Bünzli, G. Bernardinelli, C. G. Bochet, P. Froidevaux, *J. Chem. Soc., Dalton Trans.* **1995**, 83−97.
[17] S. Petoud, J.-C. G. Bünzli, F. Renaud, C. Piguet, K. J. Schenk, G. Hopfgartner, *Inorg. Chem.* **1997**, *36*, 5750−5760.
[18] G. Muller, J.-C. G. Bünzli, K. J. Schenk, C. Piguet, G. Hopfgartner, *Inorg. Chem.* **2001**, *40*, 2642−2651.
[19] E. Huskowska, J. P. Riehl, *Inorg. Chem.* **1995**, *34*, 5615−5621.
[20] S. C. J. Meskers, H. P. J. M. Dekkers, *J. Phys. Chem. A* **2001**, *105*, 4589−4599.
[21] H. Tsukube, S. Shinoda, *Chem. Rev.* **2002**, *102*, 2389−2404.
[22] L. J. Govenlock, C. E. Mathieu, C. L. Maupin, D. Parker, J. P. Riehl, G. Siligardi, J. A. G. Williams, *Chem. Commun.* **1999**, 1699−1700.
[23] G. Muller, B. Schmidt, J. Jiricek, G. Hopfgartner, J. P. Riehl, J.-C. G. Bünzli, C. Piguet, *J. Chem. Soc., Dalton Trans.* **2001**, 2655−2662.
[24] C. Piguet, B. Bocquet, G. Hopfgartner, *Helv. Chim. Acta* **1994**, *77*, 931−942.
[25] C. G. Bochet, C. Piguet, A. F. Williams, *Helv Chim. Acta* **1993**, *76*, 372−384.
[26] F. Kröhnke, *Synthesis* **1976**, 1−24.
[27] F. Kröhnke, *Angew. Chem. Intl. Ed. Engl.* **1963**, *2*, 225−228.
[28] M. I. Ali, A. M. Abd-Elfattah, H. A. Hammouda, *Z. Naturforsch., Teil B* **1976**, *31*, 254−256.
[29] M. J. Melo, F. Pina, A. L. Macanita, E. C. Melo, C. Herrmann, R. Förster, H. Koch, H. Wamhoff, *Z. Naturforsch., Teil B* **1992**, *47*, 1431−1437.
[30] F. Renaud, C. Piguet, G. Bernardinelli, J.-C. G. Bünzli, G. Hopfgartner, *Chem. Eur. J.* **1997**, *3*, 1660−1667.
[31] W. Schecher, MINEQL$^+$ version 2.1, MD Environmental Research Software, Edgewater, NY, **1991**.
[32] E. R. Malinowski, D. G. Howery, *Factor Analysis in Chemistry*, John Wiley, New York, Chichester, Brisbane, Toronto, **1980**.
[33] J. P. Riehl, F. S. Richardson, *Chem. Rev.* **1986**, *86*, 1−18.
[34] C. Piguet, A. F. Williams, G. Bernardinelli, E. Moret, J.-C. G. Bünzli, *Helv. Chim. Acta* **1992**, *75*, 1697−1717.
[35] C. Piguet, A. F. Williams, G. Bernardinelli, J.-C. G. Bünzli, *Inorg. Chem.* **1993**, *32*, 4139−4149.
[36] G. Muller, PhD. Dissertation, University of Lausanne, **2000**.
[37] S. Petoud, J.-C. G. Bünzli, T. Glanzman, C. Piguet, Q. Xiang, R. P. Thummel, *J. Lumin.* **1999**, *82*, 69−79.
[38] F. R. Gonçalves e Silva, R. L. Longo, O. L. Malta, C. Piguet, J.-C. G. Bünzli, *Phys. Chem. Chem. Phys* **2000**, *2*, 5400−5403.
[39] J. Bartis, M. Dankova, J. J. Lessmann, Q. H. Luo, W. deW. Horrocks, Jr., L. C. Francesconi, *Inorg. Chem.* **1999**, *38*, 1042−1053.
[40] W. deW. Horrocks, Jr., D. R. Sudnick, *Acc. Chem. Res.* **1981**, *14*, 384−384.
[41] C. Mallet, R. P. Thummel, C. Hery, *Inorg. Chim. Acta* **1993**, *210*, 223−231.
[42] A. Beeby, I. M. Clarkson, R. S. Dickins, S. Faulkner, D. Parker, L. Royle, A. S. de Sousa, J. A. G. Williams, M. Woods, *J. Chem. Soc., Perkin Trans. 2* **1999**, 493−503.
[43] S. T. Frey, W. deW. Horrocks, Jr., *Inorg. Chim. Acta* **1995**, *229*, 383−390.
[44] S. Petoud, J.-C. G. Bünzli, K. J. Schenk, C. Piguet, *Inorg. Chem.* **1997**, *36*, 1345−1353.
[45] M. Latva, J. Kankare, *J. Coord. Chem.* **1998**, *43*, 121−142.
[46] S. Tobita, M. Arakawa, I. Tanaka, *J. Phys. Chem.* **1985**, *89*, 5649−5654.
[47] D. D. Perrin, W. L. F. Armarego, *Purification of Laboratory Chemicals*, Pergamon Press, Oxford, **1988**.
[48] L. Syper, K. Kloc, J. Mlochowski, *Tetrahedron* **1980**, *36*, 123−129.
[49] J.-C. G. Bünzli, J.-R. Yersin, C. Mabillard, *Inorg. Chem.* **1982**, *21*, 1471−1476.
[50] W. C. Wolsey, *J. Chem. Educ.* **1973**, *50*, A335−A337.
[51] N. Martin, J.-C. G. Bünzli, V. McKee, C. Piguet, G. Hopfgartner, *Inorg. Chem.* **1998**, *37*, 577−589.
[52] S. R. Meech, D. C. Phillips, *J. Photochem.* **1983**, *23*, 193−217.
[53] H.-R. Mürner, E. Chassat, R. P. Thummel, J.-C. G. Bünzli, *J. Chem. Soc., Dalton Trans.* **2000**, 2809−2816.
[54] H. Gampp, M. Maeder, C. J. Meyer, A. D. Zuberbühler, *Talanta* **1985**, *23*, 1133−1139.
[55] A. Altomare, M. C. Burla, M. Camalli, G. L. Cascarano, C. Giacovazzo, A. Guagliardi, G. G. Moliterni, G. Polidori, R. Spagna, *J. Appl. Cryst.* **1999**, *32*, 115−119.
[56] H. D. Flack, *Acta Crystallogr., Sect. A* **1983**, *39*, 876−881. H. D. Flack, G. Bernardinelli, *J. Appl. Crystallogr.,* **2000**, *33*, 1143−1148.

Received June 3, 2002
[I02292]

How to Model the Conformational Behaviour of Saturated Diphosphane Chelate Cycles: The Conformational Rearrangement Processes of [{κ-$PAr_2CH_2CH(OH)CH_2$-κ-PAr'_2}Rh-(η^4-COD)]$^+$

Volker Schulz,[a] Axel Frick,[a] and Gottfried Huttner*[a]

In memoriam Dr. Laszlo Zsolnai[†]

Keywords: Rhodium / Phosphane ligands / Chelates / Molecular modelling / Conformation analysis

Eleven solid state structures of eight compounds **1**–**8** of the type [{κ-$PAr_2CH_2CH(OH)CH_2$-κ-PAr'_2}Rh-(η^4-COD)]$^+PF_6^-$ are used as a basis for deriving a force field model for this class of compound by Genetic Algorithms. By a complete search in the conformational space of [{κ-$PMes_2CH_2$-$CH(OH)CH_2$-κ-PPh_2}Rh-(η^4-COD)]$^+PF_6^-$ (**1**) it is shown that the model is not only capable of reproducing the structures but as well capable to predict the stability of individual conformers and the conformational reaction pathways in full agreement with experimental observations. The model predicts that the λ twist conformation is the most stable conformation of **1**. The δ twist conformation is calculated 3.1 kJ·mol^{-1} above this minimum. The experimental value is 3.4 kJ·mol^{-1}. The model predicts that there are two mechanistic pathways for the λ ⇄ δ isomerization process. Both of them are characterised by a strictly coupled rotation of the mesityl groups of the $PMes_2$ entity of **1**. These two pathways differ only in the sense of this rotation. The activation enthalpy for the λ ⇄ δ isomerization process as a whole is calculated as $\Delta H^{\#}$ = 69.1 kJ·mol^{-1}. The experimental value is $\Delta H^{\#}$ = 64.4 kJ·mol^{-1}. It is concluded therefore that the novel type of approach as described leads to models of very high predictive power.

(© Wiley-VCH Verlag GmbH, 69451 Weinheim, Germany, 2002)

Introduction

Molecular mechanics has been established to be a highly efficient tool in understanding the conformational manifold of small organic molecules.[1,2] In coordination chemistry these methods should work as well, once the force field parameters describing the metal ligand interactions would be known. The fact, however, that there are many different metals along the periodic table and that all these metals may engage with the ligands in different geometries makes the molecular mechanics approach in general a cumbersome one.[3−5] Nevertheless different types of general force fields have been described which are in fact able to overcome many of these difficulties and are able to predict conformations of inorganic and organometallic compounds.[6,7] Such force fields are, however, limited in the accuracy with which they predict the energy differences between individual conformers. If, on the other hand, conformational pathways are at the focus of a molecular mechanics analysis and if the calculated energy differences are small and are to be compared to experimentally determined reaction enthalpies these generalised force fields do not reproduce energies to the desired and necessary accuracy.[8]

As an alternative to generalised force fields specific force fields may be developed for a specific class of compounds.[3−5] It may be hoped that such specific force fields might be able to reproduce not only the geometry but as well the relative energy of the conformational manifold in agreement with experimental data.[9,10] Such force fields, if developed in the traditional way, have been shown to correctly reproduce conformations while the energies of these conformations are still generally not reliable enough to compare small energy differences to experimental data. It is common practice to adjust force field parameters of a specific class of compound by hand such that a known structure is correctly reproduced and to optimise the parameters by trial-and-error on the basis of a few experimentally determined structures of the specific class of compounds analysed. Parameters thus obtained may be taken as such or may be used as a starting point for further optimisation. The optimisation procedures used in this case are local ones, i.e. they will lead to a locally optimised set of parameters which need not necessarily be the optimal solution of the global problem.

With this in mind optimisation procedures have been developed which − starting from a randomly selected point in parameter space − allow for a global search of the optimal

[a] Anorganisch-Chemisches Institut der Universität Heidelberg, Im Neuenheimer Feld 270, 69120, Germany
Fax: (internat.) + 49 (0)6221/545707
E-mail: g.huttner@indi.aci.uni-heidelberg.de
[†] August 18, 1947−April 26, 1998

set of parameters.[11−16] While optimisation procedures which will solve this type of problem with certainty within an finite amount of time are not available, optimisation by Genetic Algorithms has been found to be an efficient way around this problem in many situations.[17−19] It has in fact been shown that force fields derived by this strategy are well suited to predict structures as well as energy differences in agreement with experimental observations.[11−16] This kind of approach has been applied to analyse and predict the conformational properties of *tripod*-$Mo(CO)_3$ compounds [*tripod* = $RCH_2C(CH_2PR'_2)(CH_2PR''_2)(CH_2PR'''_2)$]. By this method it was possible to predict NOE-distances of compounds such as $CH_3C[CH_2P(R')(CH_2Ph)]_3Mo(CO)_3$ (R′ = Ph, 3,5-Xylyl) to within an rms of less than 0.3 Å with respect to the experimental values.[15] The same type of approach was used to predict the activation barriers of the conformational isomerisation of compounds $[CH_3C\{CH_2P(Ph)_2\}_{3-n}\{CH_2P(o\text{-Tol})_2\}_n]Mo(CO)_3$ (n = 1−3) to within less than 5 kJ·mol^{-1}.[16]

The quality of these results suggests that it might be worthwhile to apply a similar strategy to more complicated problems. 'More complicated' in this context means that there is a larger number of torsional degrees of freedom which cover a wide spread of torsion angles. In the *tripod* metal compounds analysed by now the chelate scaffolding of the bicyclo[2.2.0.]octane type is such that the individual six-membered chelate cycles are forced to adopt boat or twist conformations with any chair conformation excluded by the rigidity of the framework. In this sense the conformations of compounds of the type $[\{\kappa\text{-}PAr_2CH_2CH(OH)CH_2\text{-}\kappa\text{-}PAr'_2\}Rh\text{-}(\eta^4\text{-}COD)]^+PF_6^-$ are more complicated since the six-membered chelate cycles − which are not a part of a chelate cage − can adopt boat, twist or chair conformations.

Compounds of this type have been shown to be efficient precatalysts in the enantioselective hydrogenation of olefins.[20] The solid state structures of eleven members of this family of compounds are known[20] which are well suited as a basis to derive appropriate force field parameters by Genetic Algorithms. In addition, the solution structures of four of these compounds are known as well as the activation barriers for different types of conformational rearrangements.[8] With all these data given this class of compounds presents an ideal object for evaluating the power of the modelling approach as sketched above. In addition the problem is of some chemical interest since the conformational properties of six-membered diphosphane chelate cycles have not been analysed in detail, while, of course, it is just these properties which will control the stereochemical result of reactions mediated by chelate compounds containing these cycles.

Results and Discussion

The paper deals with the following problems:

"Definition of the Force Field"

− How to describe the forces which imply contributions by the metal?

"Optimisation of Force Field Parameters"

− How to optimise this description by Genetic Algorithms?

"Grid Search Analysis of 1−3"

− How to do a complete scan of the conformational hypersurface?

"Energy − Reaction Pathway"

− How to analyse conformational pathways and how to derive activation energies for these pathways?

"Force Field Model and Experimental Reality − Comparison of Results and Conclusion"

− How do the calculated results compare to the experimental ones?

The compounds **1**−**8** on which the analysis of these questions is based are shown in Figure 1. For some compounds δ and λ twist forms where found in one and the same crystal. In these cases the two crystallographically independent conformations have been dealt with as independent individual molecules.

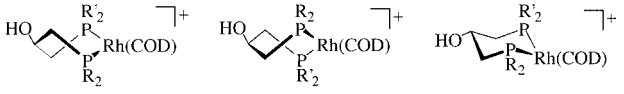

Compound	Structure	PR_2	PR'_2	X-ray		Chirality
1	**1a**	$PMes_2$	PPh_2	twist	δ	(S)
1	**1b**	$PMes_2$	PPh_2	twist	λ	(S)
2	**2a**	PPh_2	$P(o\text{-Tol})_2$	chair	OH-*eq*	(R)
3	**3a**	DBP	$P(o\text{-Tol})_2$	chair	OH-*eq*	(S)
4	**4a**	$PMes_2$	PEt_2	twist	δ	(S,R)
5	**5a**	$PMes_2$	$P(2\text{-MeOPh})_2$	twist	λ	(R)
5	**5b**	$PMes_2$	$P(2\text{-MeOPh})_2$	twist	δ	(R)
6	**6a**	$P(2\text{-MeOPh})_2$	PPh_2	twist	λ	(S)
6	**6b**	$P(2\text{-MeOPh})_2$	PPh_2	twist	δ	(S)
7	**7a**	$P(o\text{-Tol})_2$	PEt_2	chair	OH-*eq*	(S,R)
8	**8a**	PPh_2	PPh_2	chair	OH-*eq*	

Figure 1. Compounds **1**−**8**; the sequence in which the compounds are labelled is such that compounds **1**−**3** are the ones which are extensively analysed in this paper. For compounds **1**, **2**, **4**, **5** quantitative solution structures are available.[8] Qualitative NMR spectroscopic data for dynamic processes are available for **6**, **7**.[20] The numbering scheme follows this hierarchy.

Definition of the Force Field

Parameters describing interactions within the organic parts of the molecules were taken from the standard MM2* force field.[1,21,22] Parameters describing C−P−C angles

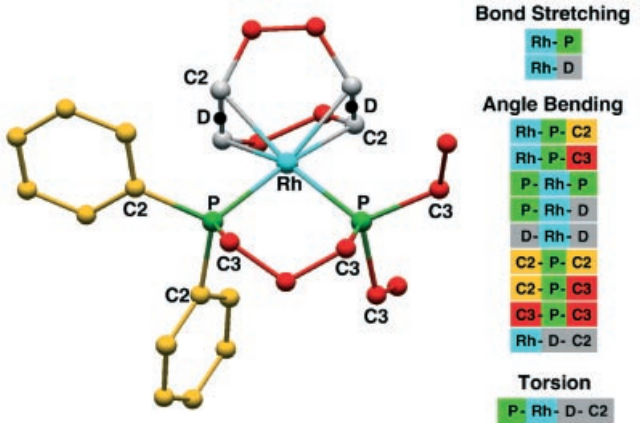

Figure 2. Illustration of the force field parameters which were refined; the colours refer to the individual atom types (C2: sp^2-carbon; C3: sp^3-carbon). The label D designates a dummy atom placed at the centre of a double bond of the COD ligand. Only the parameters which are listed in Figure 2 were allowed to refine.

(Figure 2) were defined as usual − they were however refined (see below). All parameters involving the rhodium atom were refined. Conventional descriptions were used to describe distances, angles and torsion angles (see Exp. Sect.).

Parameters involving parts of the COD coligand and the metal atom where defined as follows: dummy atoms were defined at the centre of each coordinated double bond (Figure 3). The distances between the dummy atoms and the rhodium centre (r_d, Figure 3) as well as the angles D−Rh−D (β, Figure 3) and D−Rh−P (γ, Figure 3) were described by conventional functionals (see Exp. Sect.). The angles enclosed by the rhodium centre, the dummy atoms and any of the two carbon atoms of the double bond adjacent to the dummy atom Rh−D−C2 (α, Figures 2 and 3) were as well modelled by the standard functional for valence angles (see Exp. Sect.). To define the rotational position of the π-ligands with respect to the rest of the molecule the rotation of the double bond around the axis Rh−D was defined by the torsion angle around this axis. The reference axis was defined as a Rh−P vector. Of the two Rh−P vectors the one was chosen whichever had the smaller D−Rh−P angle. The torsion angle (see Exp. Sect.) was defined with respect to one of the vectors D−C2 (Figures 2 and 3). The energy function for this angle (τ, Figure 3) was

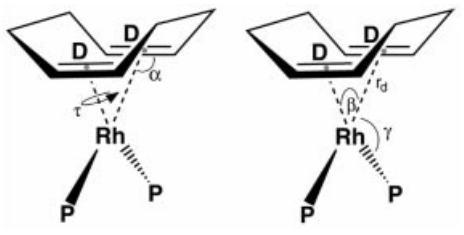

Figure 3. Definition of π bonds within the force field approach. Dummy atoms at the centre of the coordinated double bonds were used to define the parameters r_d, α, β, γ, and τ. The forces acting on the dummy atoms were distributed to the two carbon atoms of the respective double bonds. Half of the force acting upon D was assigned to each of these atoms.

chosen as $E(\tau) = k_{t2}\cdot[1 - \cos(2\tau)]$. τ values of ±90° correspond to an orientation of the double bond vertical to the coordination plane of the rhodium atom. These positions correspond to minima in the torsional potential function $E(\tau) = k_{t2}\cdot[1 - \cos(2\tau)]$ where the force constant k_{t2} has hence to be negative. τ values of ±90° correspond to the situation sketched in Figure 3 which is a minimum situation with cos(2τ) being −1. The forces on the dummy atoms have to be transferred to the carbon atoms of the double bonds to which they refer. The force field thus defined was incorporated in the body of the force field program YAMMP[23] (see Exp. Sect.).

This type of approach is similar to the one be taken by B. Bosnich and C. R. Landis et. al. for the force field description of coordinated Cp ligands.[24,25] Similar methods have been developed by van Gunsteren[26] for the force field description of proteins and by C. R. Landis et. al. for descriptions of different types of π-ligands.[27]

Optimisation of Force Field Parameters

In order to describe conformational behaviour by force field methods an algorithmic machinery is needed which correctly models the experimentally determined behaviour. Such a machinery has to be built up with appropriate functions and parameters. Once the functions are defined it is the parameters which have to be tuned. Tuning means to adapt the parameters such that the observed conformational properties of the molecule are correctly reproduced by the machinery. The conformational property chosen in most cases is the 'structure' of the molecule. Structures, however, are in general taken from crystallographic studies; this means that the molecule is embedded in a crystal and subject to external forces acting upon it from the neighbouring molecules. If force field parameters are fitted to reproduce such structures it is the solid state structures which they reproduce. Only if it is evident that these structures, even though determined in the solid state, are almost completely due to the inner molecular potential with vanishing contributions from the external forces, this approach will lead to a force field which models the inner molecular potential. If a large number of a family of crystal structures is known the question of whether these structures are by and large uninfluenced by crystal forces can be addressed by statistical analysis. In the first report on the use of Genetic Algorithms in the refinement of force field parameters which dealt with modelling the behaviour of *tripod*-$Mo(CO_3)$ compounds[14] statistical analysis by a variety of methods including Neural Network analysis had shown that these premises are met in this case.[11] Refinement of the force field parameters on the basis of solid state structures has been highly successful in this case.[14] In the present case there are too few individual structures available for a meaningful statistical test. A practical approach in this case is then to assume that the crystal structures are due to the inner molecular potentials, to refine the force field parameters on this basis and possibly to remove outliers if there are any. It is assumed in this case that structures which are less well reproduced than the average are influenced by

crystal forces acting on the molecules in the crystal lattice. This approach is taken in this paper.

Genetic Algorithms were applied to tune the force field parameters such that twelve crystallographically determined structures of the eight compounds (Figure 1) were reproduced to the best possible extent. A short explanation of how Genetic Algorithms work, may help to appreciate that the methodology is very simple indeed. The first thing to do is to make a guess for the numerical range which the individual parameters may possibly adopt. To give an example: it is known that the valence force constants can adopt values up to a maximum of 20 mdyn·Å^{-1} and, of course, that such force constants have to be greater than zero. In this case setting the range for this type of constant to $0 \leq k \leq 20$ covers all possible values. If it is known that the specific force constant k refers to a weak bond this range might be much smaller of course. Once the numerical range is determined it is divided in $2^{(n-1)}$ equally spaced intervals. The position of each specific interval may then be clearly defined by a binary number in the range $0 \leq 2^{n-1}$. The binary number may thus be taken as a representation of a numerical interval within the range allotted to the parameter. It may be decoded into the numerical value of this parameter with the resolution depending on the size of the interval.[28]

To start the optimisation process binary representations of the values of the individual parameters are generated stochastically. The binary representations of the individual parameters are combined in one binary string where the positions on the string clearly indicate to which parameter each part of the string belongs. A whole set of such parameter strings is generated; in the Genetic Algorithm idiom it is called a population (Figure 4). Each parameter string is decoded to produce the numerical values of the individual parameters. The parameters are fed into the force field program and the experimentally determined structures are subject to refinement. The quality of a given set of parameters is deduced by their capability to produce a set of refined structures in close agreement with the experimentally determined conformations. By some formalism this quality is expressed as a number. In the example given (Figure 4) a small number is meant to indicate a high quality and a large one to correspond to a low quality parameter set. The numerical values by which the sets are ranked are called the fitness values in the Genetic Algorithm idiom. For each individual within a given population this fitness is evaluated on the basis of all observations. With the problem at hand this means that for a given set of force field parameters each of the structures in the data base has to be optimised. This has to be done for all individuals of a population within each generation over and over again and thus is the really time consuming part within optimisations based on Genetic Algorithms. Optimisation itself is achieved by creating a next generation of parameter sets from the forgoing one such that the population of this next generation has a high probability to contain bit strings or parts of bit strings which had already been shown to produce high fitness values in the foregoing generation. This is achieved by making fit individuals produce offspring with higher probability than the less fit ones. Offspring is generated by exchanging parts of bit strings between the parents (Figure 4) that is by crossover. The idea behind this is that pieces of information (bit strings) which have already been found to be well adapted to solve the problem will accumulate from generation

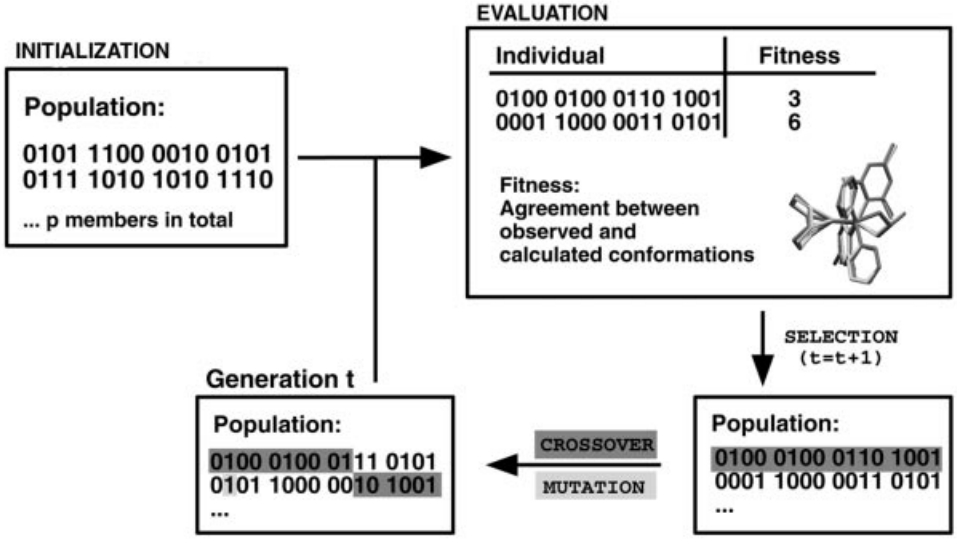

Figure 4. Refinement of the force field parameters by Genetic Algorithms. The parameters which are to be refined are encoded as binary strings. The sections within these strings refer to individual parameters. The values of these parameters are represented by the binary numbers within these sections. The first generation of such strings is generated at random. Each of these parameter strings is evaluated with respect to the quality with which it is capable of reproducing the structures of all compounds in the data basis by molecular mechanic calculations. The parameters which have a high 'fitness value' are preferentially selected to produce offspring by crossover and mutation. The next generation thus produced is subject to the same procedure of evaluation and offspring production. Iteration of this process leads to optimised parameters.

to generation such that the populations as a whole and their individual members will be more and more adapted to the problem from generation to generation. In order to avoid that the selection procedure leads to a suboptimal solution mutations are induced once in a while by inverting randomly selected bits (Figure 4).[29,30]

The optimisation by Genetic Algorithm (GA-optimisation) is generally an efficient optimisation strategy converging to optimal solutions also in those cases where traditional optimisation procedures fail.[31−33] A specific advantage of the underlined algorithmic scheme is that the time consuming step (evaluation of the fitness) may be performed independently on different processors, i.e. the algorithm is naturally parallel. With the problem at hand reasonable computing times can only be achieved if optimisations are performed on a parallel computer.

With the problem at hand GA-optimisation led to force field parameters, which when fed into the molecular mechanics program, were able to reproduce the observed structures. It was found that the agreement between calculated and observed structures was quite good for eleven members of this set (**1**−**8**) while one structure {**2b**: [{κ-PPh_2CH_2CH-$(OH)CH_2$-κ-P(*o*-Tol)$_2$}Rh-(η^4-COD)]$^+PF_6^-$} was less well reproduced. Analysis of the crystal structure indicated that the observed conformation might be biased by crystal forces and structure **2b** was therefor excluded from the data basis.[34] Refinement based on the optimisation of the eleven remaining structures led to satisfactory agreement for all the members of the set (Table 1 and Figure 5).

Table 1. RMS deviations of structures **1a**−**8a**

Structure[a]	RMS_{mm2_rms} [Å]	RMS_{mm2_int} [Å]
1a	0.343	0.368
1b	0.212	0.256
2a	0.384	0.441
3a	0.238	0.267
4a	0.357	0.249
5a	0.253	0.242
5b	0.286	0.284
6a	0.191	0.190
6b	0.195	0.187
7a	0.136	0.165
8a	0.196	0.284
average	0.254	0.267

[a] The column with the suffix mm2_rms was obtained on the basis of parameters calculated by using the RMS deviations between observed and calculated atom positions as the criteria to evaluate the fitness. The column labelled mm2_int refers to a parameter set which was obtained by basing the evaluation of fitness on the agreement between calculated and experimental values of a set of selected internal coordinates (optimised distances, angles, and torsion angles).

Expressed as the RMS deviation between observed and calculated atom positions the agreement is between 0.14 and 0.38 Å. Table 1 refers to two different procedures used for the evaluation of fitness during Genetic Algorithm refinement. The column with the suffix mm2_rms was obtained on the basis of parameters calculated by using the RMS deviations between observed and calculated atom positions as the criteria to evaluate the fitness. The column labelled mm2_int refers to a parameter set which was obtained by basing the evaluation of fitness on the agreement between calculated and experimental values of a set of selected internal coordinates (optimised distances, angles, and torsion angles). Independent of the criteria on which the evaluation of fitness was based, the refined parameter sets were able to reproduce the structures quite well. Figure 5 shows an overlay of observed and calculated conformations for an unbiased (cf. Table 1) selection of compounds.

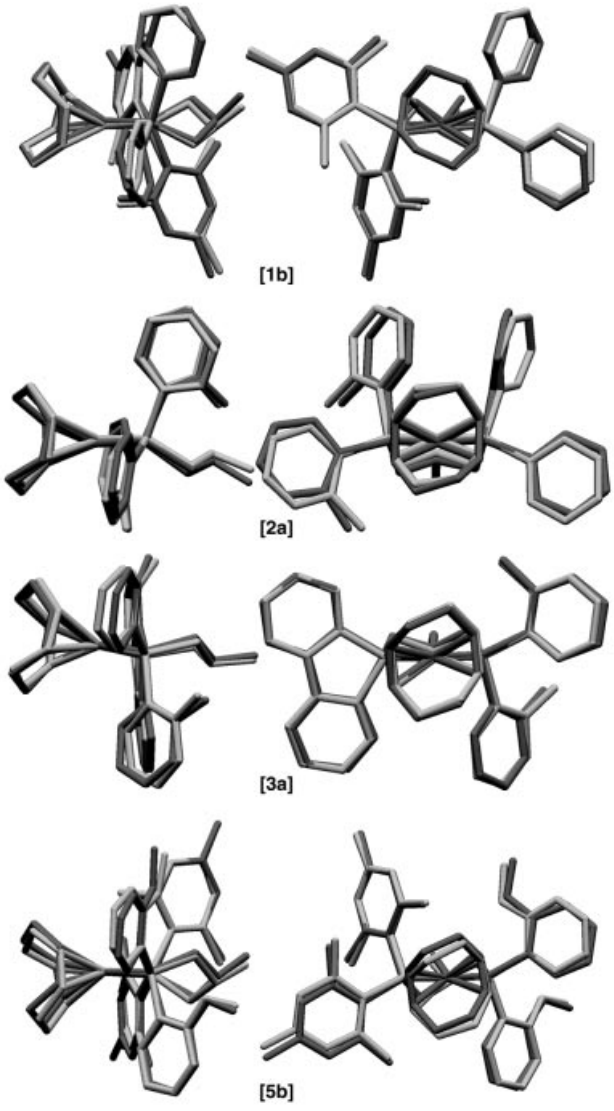

Figure 5. Illustration of the quality of agreement between calculated and observed conformations. From the compounds shown **2a** is the one with the lowest quality of reproduction (Table 1). The other compounds shown are of average quality.

Numerical values of force constants optimised by this approach have their meaning only as a whole: due to the interdependence of the internal coordinates which are used to describe the mechanical model within a force field program there is in general not just one optimal solution to the optimisation but there may be families of optimal solutions with quite different numerical values for the individual force

constants. When fed into a molecular modelling program as a whole these numerically different solutions will equally well reproduce the structures.

Table 2 shows the quality of agreement with respect to internal coordinates. The columns labelled average in Table 2 show that the average of the values for individual types of distances, angles and torsion angles taken over all structures are well reproduced by the two parameter sets. The force field mm2_int derived by minimising the discrepancy between observed and calculated values of internal coordinates is found to reproduce such internal coordinates (distances, angles, and torsion angles) somewhat better than the mm2_rms which minimises the discrepancy between atom positions (Table 2). The columns labelled rmsd represent the RMS deviation between calculated and observed values in each case. These deviations must be larger than the deviations between corresponding average values (Table 2) since in calculating the average positive and negative deviations may cancel each other while in calculating the RMS deviation (rmsd) they are accumulating independent of sign. From the numbers given in Table 2 it is seen for set mm2_rms that some valence angles are systematically too large or too small in comparison with the observed structures. Nevertheless valence angles are reproduced to an accuracy between 2° and 5°. Torsion angles do not appear to be biased. The accuracy with which they are reproduced is in the range of 3° and 8°. The accuracy of the force field is thus well within the range reported to be achievable by molecular modelling methods.[27,35,36]

Table 2. Agreement between calculated and experimental values of characteristic internal coordinates (distances [Å]; angles [°]

[a]	X-ray$_{av}$	mm2_rms$_{av}$	rmsd	mm2_int$_{av}$	rmsd
Rh−P	2.3	2.4	0.06	2.3	0.03
Rh−D	2.1	2.2	0.03	2.2	0.03
Rh−X			0.04		0.03
P−Rh−P	88.4	85.4	3.25	88.1	1.10
P−Rh−D	92.8	95.1	2.57	93.5	1.80
P−Rh−D	172.5	173.7	4.63	171.5	2.94
D−Rh−D	85.5	84.2	2.37	84.9	2.94
X−Rh−X			3.21		2.19
Rh−P−C3	114.0	116.2	2.90	114.2	1.86
Rh−P−C2	114.7	114.5	1.65	114.1	1.81
C2−P−C2	104.4	105.6	1.52	105.1	1.34
C2−P−C3	104.2	102.1	2.87	104.3	2.26
X−P−X			2.24		1.82
Rh−D−C2	85.5	84.2	2.37	84.9	2.94
P−Rh−D−C2	−93.6	−95.4	4.87	−94.1	2.57
Rh−P−C3−C3	−67.5	−67.6	4.00	−68.0	3.95
P−C3−C3−C3	−46.8	−44.7	7.95	−45.9	7.92
P−Rh−P−C3	−30.8	−31.5	4.02	−31.9	4.60

[a] The data in column X-ray$_{av}$ represent the average value of the corresponding internal coordinate over all eleven structures contained in the data basis. mm2_rms$_{av}$ and mm2_int$_{av}$ refer to the two sets of force field parameters reported in this paper. The numbers given under these column headers represent the mean of the corresponding internal coordinates for the calculated structures. The rms values given in each case represent the rms deviations for each class of internal coordinates as obtained by comparing calculated and experimentally observed values of each member of the corresponding set.

Grid Search Analysis of 1−3

A detailed analysis of the conformational space of molecules **1−3** is described in the following paragraphs. The analysis is based on the force field mm2_rms. To adequately scan the conformational space grids are defined as shown in Figure 6.

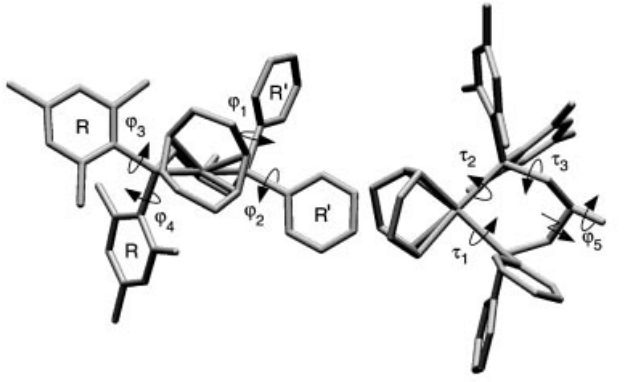

Compounds	PR_2	PR'_2		rotated fragments
1	$PMes_2$	PPh_2	τ_1	PR'_2CH_2
2	P(*o*–Tol)$_2$	PPh_2	τ_2	PR_2CH_2CHOH
3	DBP	P(*o*–Tol)$_2$	τ_3	CH_2CHOH

sense of positive rotation

ring closure bond

Figure 6. Conformational parameters of **1−3**. For a complete conformational search the actively driven conformational coordinates were chosen as shown. The four aryl rotations ($\varphi_1-\varphi_4$) were driven by using the rubberband protocol.[37] In order to relate the origin of the rotation to the coordination scaffolding the orientations where an aryl ring is parallel to the bisector of the P−Rh−P angle (vertical to the paper plane in the left hand side of the figure respectively horizontal in the right hand side of the figure) were defined as ±90°. The sense of rotation was taken as shown in the left hand diagram in Figure 6. By this definition an edge orientation is characterised by an φ value of ±90° while a face orientation corresponds to φ values of ±0°. The conformational coordinates ($\tau_1-\tau_3$) were as well actively driven using the ring closure bond protocol.[38] The rotational position of the OH group (φ_5) completes the coordinates of the eight dimensional conformational space.

The grid intervals for aryl rotations are set to the values in Table 3 upon detailed inspection of the experimentally determined structures of the relevant molecules. The resolutions were chosen such that any feasible rotational positions could be reached from the starting points. The conformations observed in the X-ray structures are selected as starting points in each case. To generate the starting conformations the 'rubberband' protocol was used which had already been found to be efficient with other compounds for which steric crowding did not allow for a direct rotation of their aryl groups.[37] The OH group was allowed to occupy the

Table 3. Definition and results of the grid search for compounds **1**−**3**

Compound	$\varphi_{1,2}$		$\varphi_{3,4}$		τ_{1-3}		φ_5		No. of starting geometries	No. of total minima	No. of minima in the range of $\Delta E \leq 50$ kJ·mol^{-1}
	range	step	range	step	range	step	range	step			
1	0°-180°	3	0°-180°	2	0°-360°	6	0°-360°	3	23328	91	82
2	0°-180°	2	0°-360°	3	0°-360°	6	0°-360°	3	23328	177	177
3	0°-360°	3	0°-360°	1	0°-360°	12	0°-360°	3	46656	92	92

three classical staggered positions. To construct chelate cycles with the appropriate torsion angles the 'ring closure' protocol was used.[38] Under this protocol the appropriate C−C bond is removed and reinstalled after adjusting the torsion angles to the selected values.

From the ten thousands of starting geometries (Table 3) force field minimisations lead to the same number of local minima, but many of them being the same. A comparison of these minimised structures leads to 91 independent minima for compound **1** and 92 of them in the case of **3**. For compound **2** there are 177 independent minima altogether reflecting the lower symmetry and the less strained situation in **2** as compared to the once in compounds **1** and **3**. From these local minima only a subset of 82, 177, and 92 is within a range of 50 kJ·mol^{-1} at or above the corresponding global minimum for compounds **1**−**3** in that sequence (Table 3).

To sort the conformations into classes with respect to the conformations adopted by their chelate cycles a Neural Network analysis of the Kohonen type was applied.[39] The six torsion angles characterising the conformations of the six-membered chelate cycles were used as the components of the input vectors. Self organisation of the 5 × 5 Kohonen network clearly revealed twelve individual classes in a two dimensional map.

The classes which lie within a energy window of 20 kJ·mol^{-1} are shown for **1** in Figure 7. It is seen that these classes conform to the standard classification of six-membered cycles. This means that the standard classification scheme is 'reinvented' by the Neural Network. If the different conformations are ranked according to the lowest energy calculated for the members of each specific class, the diagram as shown in Figure 7 results. It is satisfying to find that the λ and δ twist-boat conformations are at the lowest

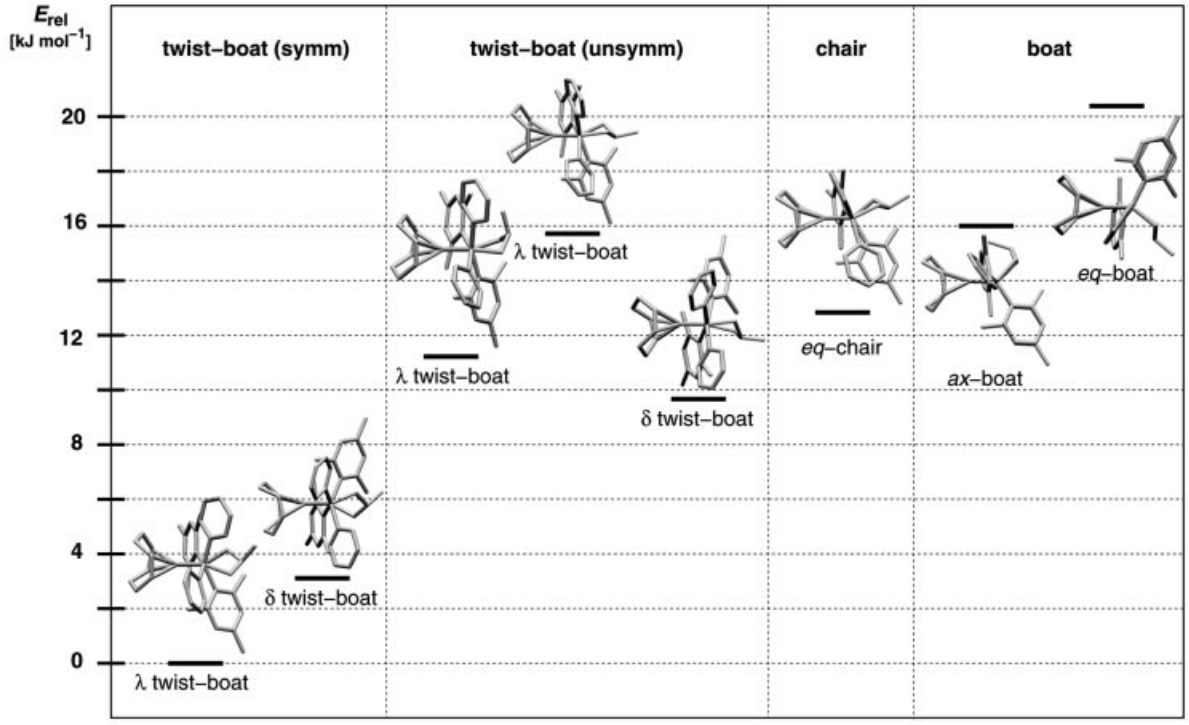

Figure 7. Classification of the conformations of the chelate cycle of **1**. The 91 independent local minima were sorted into the classes shown by Neural Network analysis. The energy scale refers to the lowest energy conformer in each class.

energy (Figure 7) since these are the conformations which are observed in the crystal of molecule **1**.

The same procedure when applied to the conformations which result as local energy minima from the analysis of **3** (Table 3) results in the diagram shown in Figure 8.

In this case the chair conformation − which almost exactly corresponds to the conformation of compound **3** in the solid state − has the lowest energy. It is however seen that other conformations are energetically almost equal to the one observed in the crystal such that the conformation

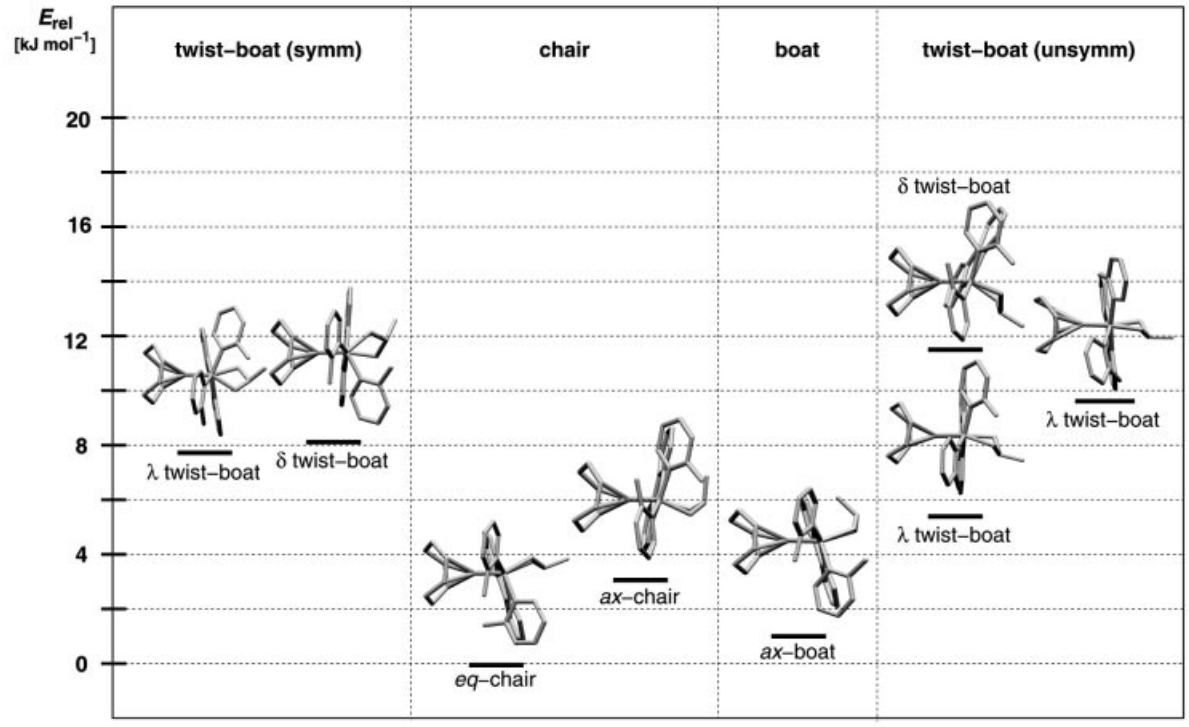

Figure 8. Classification of the conformations of the chelate cycle of **3**. The 92 independent local minima were sorted into the classes shown by Neural Network analysis. The energy scale refers to the lowest energy conformer in each class.

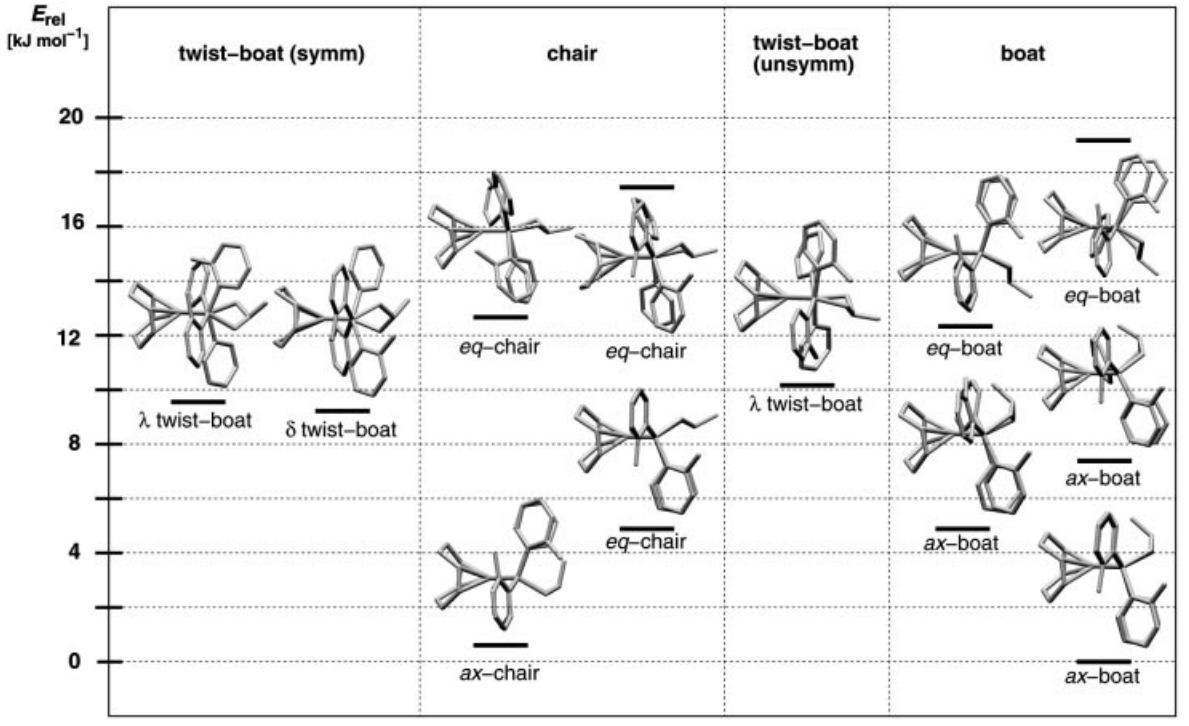

Figure 9. Classification of the conformations of the chelate cycle of **2**. The 177 independent local minima were sorted into the classes shown by Neural Network analysis. The energy scale refers to the lowest energy conformer in each class.

which should be found in the crystal cannot really be predicted. One would expect, however, that it should be one of the low energy molecular conformations which build up the crystal and it is in fact the one with the lowest calculated energy.

Figure 9 shows the same type of analysis for compound **2** where it is seen that the conformation observed in the crystal (chair, Figure 1) is amongst the conformations of the lowest energy of this compound but lies some 5 kJ·mol^{-1} above the global minimum.[40]

In comparing Figures 7−9 it is obvious that twist conformations are only preferred with **1** while **2** and **3** appear to prefer non-twisted conformations (chair or boat). Site differentiation by the two different PAr_2 groups is obviously largest for molecule **1** which prefers a twist conformation while the difference in the repulsive forces acting on the chelate cycle from the two different PAr_2 groups in **2** and **3** do not overcome the intrinsic preference of the more symmetric chair and boat conformations.

Energy − Reaction Pathway

With the approach taken in deriving force constants describing the potentials with respect to internal coordinates which involve the rhodium atom as a contributor there is no explicit reference to an energy scale (see paragraph Optimisation of Force Field Parameters). The reference is only implicit and the scale results by virtue of the scale intrinsic to the MM2* part of the force field. This part of the force field is thoroughly adapted to energy differences observed for organic molecules which means that it is capable of reproducing conformational pathways in organic chemistry not only with respect to structures but also with respect to relative energies. Since, with the molecules analysed, the interactions between their organic parts dominate it is expected that the force constants derived for the 'inorganic' part of the molecules by GA-optimisation will adapt to the major forces exerted by their organic part such that the scale of relative energies as calculated by the force field as a whole will be on scale with the observations. These expectations have been born out by similar analyses in related cases.[14−16] If the energies are on scale with the observations it must be possible to calculate conformationally relevant energies and to compare these with experimental values wherever available. The only molecule within the set studied for which experimental data relating to the relative stability of different conformers and to activation energies of conformational rearrangements are available is molecule **1**.[8] A more detailed analysis of the implications to be drawn from the force field calculations is therefore restricted to **1**.

An indication for the appropriateness of the energy scale is the finding (Figure 7) that the λ twist-boat conformation of **1** is calculated to be 3.1 kJ·mol^{-1} more stable than the δ twist-boat conformation. Experimentally it is observed that the energy difference between these conformers is $\Delta H =$ 3.4 kJ·mol^{-1} with the λ twist conformer being the more stable one.[8] The modelling approach hence predicts the correct sequence of relative stabilities and, even more, the calculated energy difference is in agreement with experiment.

NMR analysis shows that the conformational reaction pathway of the λ ⇄ δ interconversion of **1** is a complicated one.[8] It may or may not be accompanied by rotational rearrangements of the mesityl groups where on the other hand such mesityl rotations can only occur during λ ⇄ δ twist interchange.[8] If the force field approach is an appropriate one it should correctly predict this behaviour. To address this point contour maps were constructed in order to delineate the corresponding reaction path. To construct these maps with sufficient resolution with respect to the internal coordinates, which should best describe the pathway, grid points were calculated at a higher resolution (torsion angles $\tau_1-\tau_3$, rotational angles $\varphi_1-\varphi_4$, see Figure 6).

The diagrams (Figures 10−13, and 15) showing projections onto the τ_i/τ_j-planes ($i = 1-3$; $j = 2, 3$; $i \neq j$) were constructed in the following way: for any combination of the three τ-values (resolution in τ-space = 12°) the remaining coordinates ($\varphi_1-\varphi_5$) were allowed to refine in the same way as used in the global conformational search (see above). The lowest energy conformation from the stack of conformations thus obtained for each grid point was taken to represent the grid point in energy as well as in structure.

Figure 10 shows the isoenergy contour plot in a projection onto the τ_1/τ_3-plane. The λ and δ conformations which are the most stable conformations are shown on the left hand side of the diagram. A least energy pathway for the interconversion of these conformers along the τ_1/τ_3-plane is shown as a black line in the diagram. Individual conformations at the grid points corresponding to points along or close to this line are shown in sequence around the contour plot.

From this sequence of structural models it may be inferred that the rotation of the mesityl groups should occur at around $\tau_1 = 12°$; $\tau_3 = 24°$ (asterisk in the Figure 10) along the λ ⇄ δ interconversion pathway. It has already been stated that a whole stack of conformations has to be calculated for every grid point such that the one with the lowest energy can be chosen as a representative for each grid point. The conformations shown in Figure 10 are the ones having the lowest energy in each corresponding stack. For any conformation shown there is a pendant with an approximately opposite orientation of the mesityl groups, i.e. it is an orientation for which the aryl rotations ($\varphi_1-\varphi_4$ in Figure 6) are approximately equal in their absolute value but opposite in sign (compare $\mathbf{a_4}$ and $\mathbf{b_4}$ in Figure 10). The area around the point marked with an asterisk in Figure 10 is the one where the energy difference between these rotamers is the lowest one along the pathway i.e. less than 1 kJ·mol^{-1} against 10−80 kJ·mol^{-1} for the other grid points along the black line.

Figure 11 shows the isomerisation pathway in a projection onto the τ_1/τ_2- and τ_2/τ_3-planes. The values of the coordinates at which the concerted flip of the mesityl groups will occur are again (Figure 10) marked by an asterisk in each case.

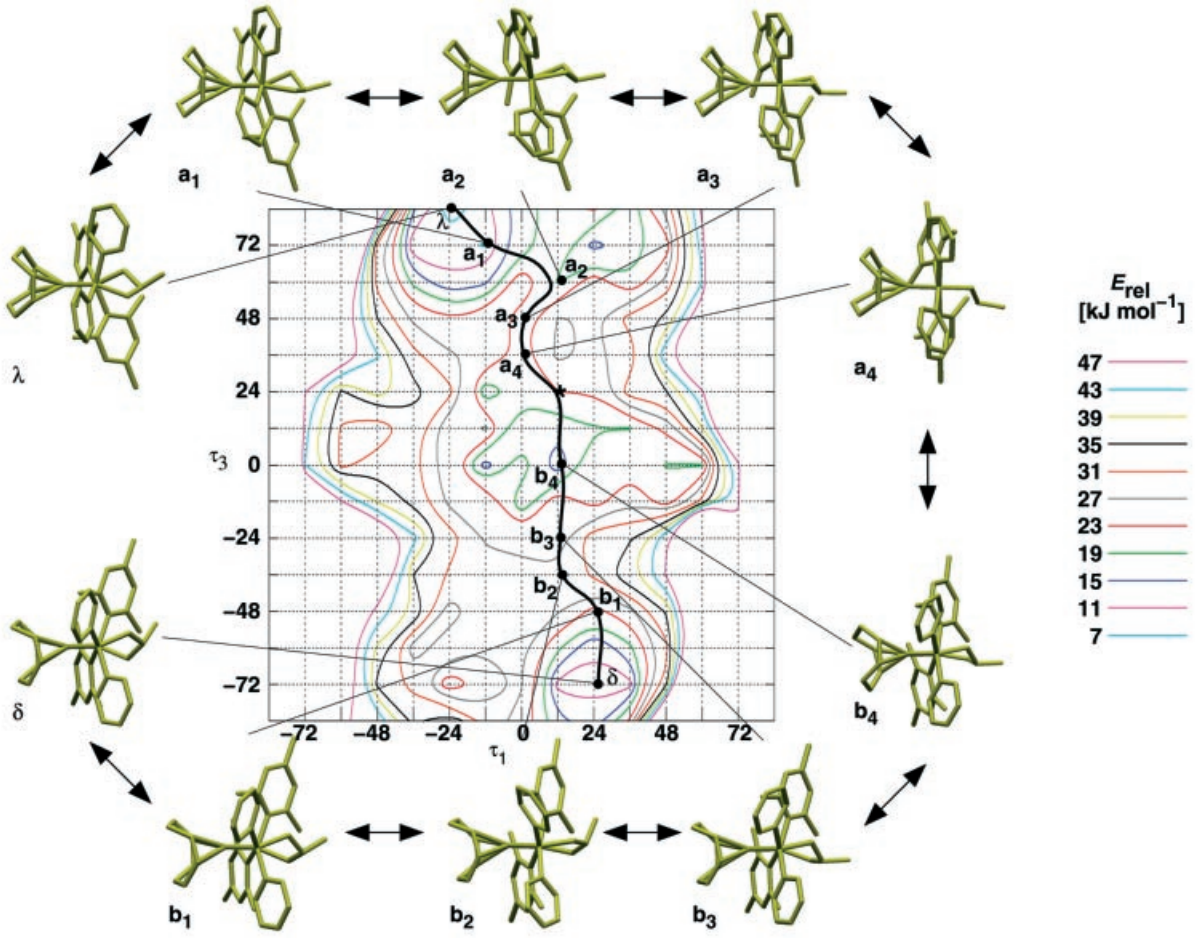

Figure 10. Projection of the energy hypersurface of **1** onto coordinates τ_1/τ_3, which characterise the conformation of the chelate cycle. To derive the contour plot the energy of the lowest energy conformation from each stack of conformations referring to each grid point was chosen as a representative. The reaction pathway (black line) was constructed such that it is a lowest energy route from the λ to the δ isomer. The conformations which characterise individual grid points are shown as molecular models around the contour plot. The conformations labelled **a** have an orientation of the aryl groups which corresponds in its sense to the one observed in the λ isomer. The conformations referenced by the label **b** have a different orientation which is similar to the one observed for the δ isomer. The region around the point marked with an asterisk is the one where the flip of the aryl rotation occurs.

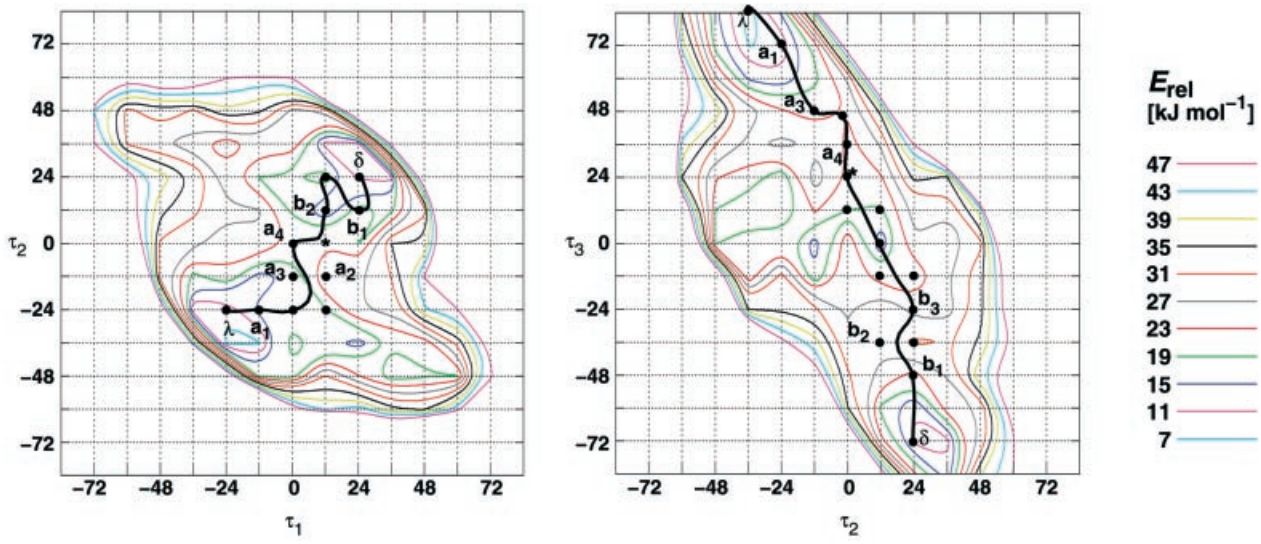

Figure 11. Projection of the energy hypersurface onto the τ_1/τ_2- and τ_2/τ_3-planes. The contour plots were constructed as described in the text and in the legend of Figure 10. The symbols **a**, **b**, λ, and δ refer to the conformations shown in Figure 10. The black lines indicate the projection of the reaction pathway for the $\lambda \rightleftarrows \delta$ isomerization. The asterisks pinpoint the region where the flip of the aryl rings occurs.

The reaction pathway, indicated by a black line in each case, corresponds to a smooth transition from one isomer into the other with all τ and φ values changing gradually along these curves. Only at the transition point marked by an asterisk there is a concerted flip of both mesityl groups by around 70° within a very short interval along the τ scale.

The kind of coupled rotation of the mesityl groups is evident from Figure 12 which shows the dependence of the energy on the rotational positions of the two mesityl groups. The diagram refers to the corresponding relative energies as calculated with τ_1, τ_2, and τ_3 fixed at 12°, 0°, and 24° respectively, i.e. at that point in τ-space (asterisk in Figures 10 and 11) which was found to induce the flip of the two mesityl groups.

It is found that the diagram shows pronounced minima at discrete positions which are labelled by **A** and **B**. The molecular models shown in Figure 12 illustrate the mutual arrangement of the mesityl groups. The conformation of the chelate cycle is the same in each case and corresponds to the specific triple of τ coordinates which was found to characterise the flip situation in τ space (asterisk in Figures 10 and 11). The energy minima labelled **A** correspond to a rotational position of the mesityl groups which is characteristic for the λ conformer. The labels **B** correspondingly refer to the rotational position of the mesityl groups as characteristic for the δ conformer. This means that all conformations labelled **A** will relax to the conformation of the λ isomer as soon as the τ values are allowed to refine. The conformations labelled **B** will correspondingly refine to the δ isomer upon relaxation of the constraints in τ space. Since the analysis of the τ-space diagrams (Figures 10 and 11) makes clear that any δ/λ transition and its reverse is necessarily accompanied by a concerted flip of the two mesityl groups the interpretation of Figure 12 is straightforward: A λ conformer (**A**) has two possibilities to change into a δ one. Starting from $\mathbf{A_1}$ as an example (Figure 12) there are two low energy pathways either to $\mathbf{B_1}$ or to $\mathbf{B_3}$. The rotational position of the mesityl groups corresponding to minima of type **B** is the one which corresponds to a δ isomer. This means that starting from the λ isomer ($\mathbf{A_1}$) a δ conformation can be reached on two ways: Either there will be a saddlepoint between $\mathbf{A_1}$ and $\mathbf{B_1}$ or a saddlepoint between $\mathbf{A_1}$ and $\mathbf{B_3}$. The barrier heights for these two types of transition are slightly different (Figure 12) while the energy of all the λ isomers (**A**) is necessarily the same but different from the energy of the δ isomers (**B**) which are again of equal energy for all members of the group. The only difference between energetically equal conformations such as $\mathbf{B_1}$ and $\mathbf{B_3}$ is then that the mesityl groups − even though they occupy fully equivalent positions in $\mathbf{B_1}$ and $\mathbf{B_3}$ as a whole − find themselves rotated by 180° on going from $\mathbf{B_1}$ to $\mathbf{B_3}$ (see colour coding of the conformations in Figure 12). The

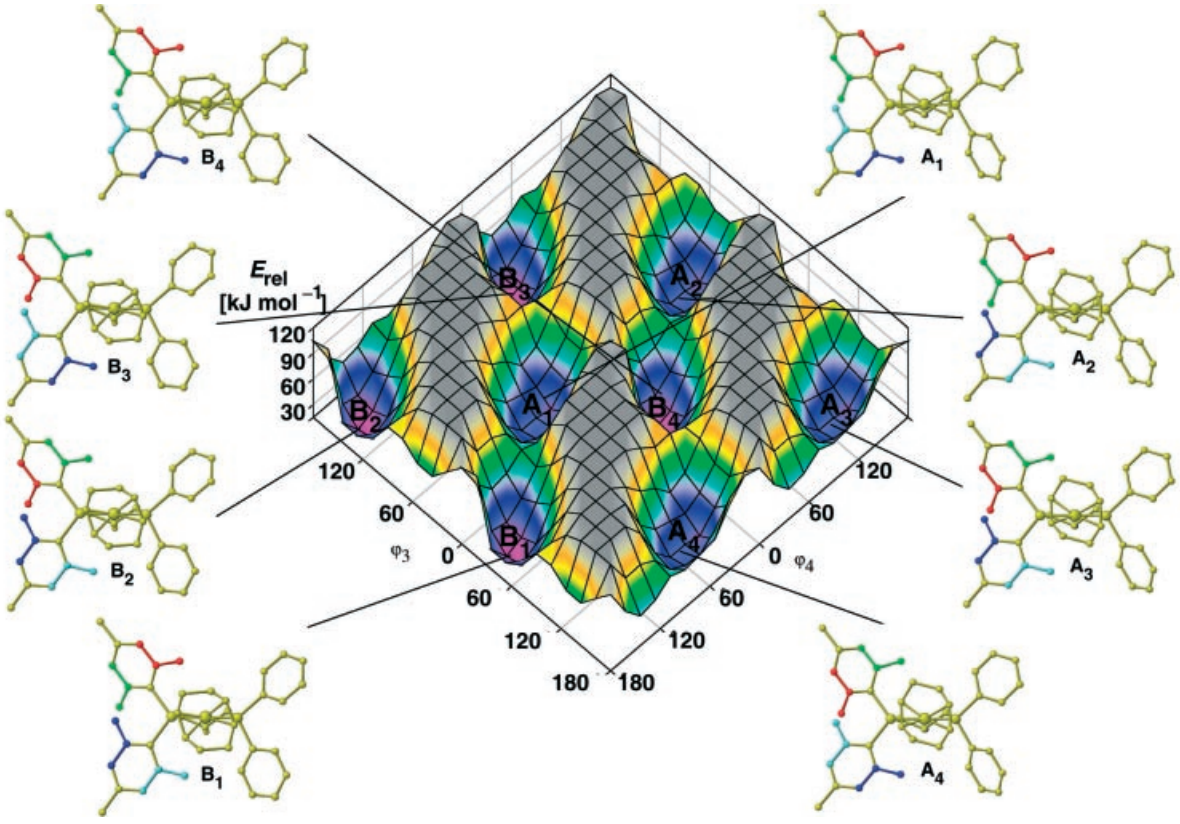

Figure 12. Energy diagram illustrating the pathways of rotational rearrangements of the $PMes_2$ entity of **1** during λ ⇄ δ isomerization. The translation symmetry of the graph is 180° in φ_3 and φ_4. The minima labelled **A** are characteristic for the λ isomer. The minima **B** likewise refer to the δ isomer. The molecular models $\mathbf{A_{1-4}}$ and $\mathbf{B_{1-4}}$ illustrate the rotational position of the mesityl groups for each of the eight minima shown. It is seen that the rotation of the mesityl groups at the $PMes_2$ entity is strictly coupled such that the groups have to rotate in mutually opposite sense.

conformations $\mathbf{B_1}$ and $\mathbf{B_3}$ are energetically fully equivalent; the ways however on which they are formed starting from $\mathbf{A_1}$ are different.

The energy diagram shown in Figure 12 has of course a translation period of 180°. The graph itself consists of four symmetrically independent unit cells. The fact that the mesi-

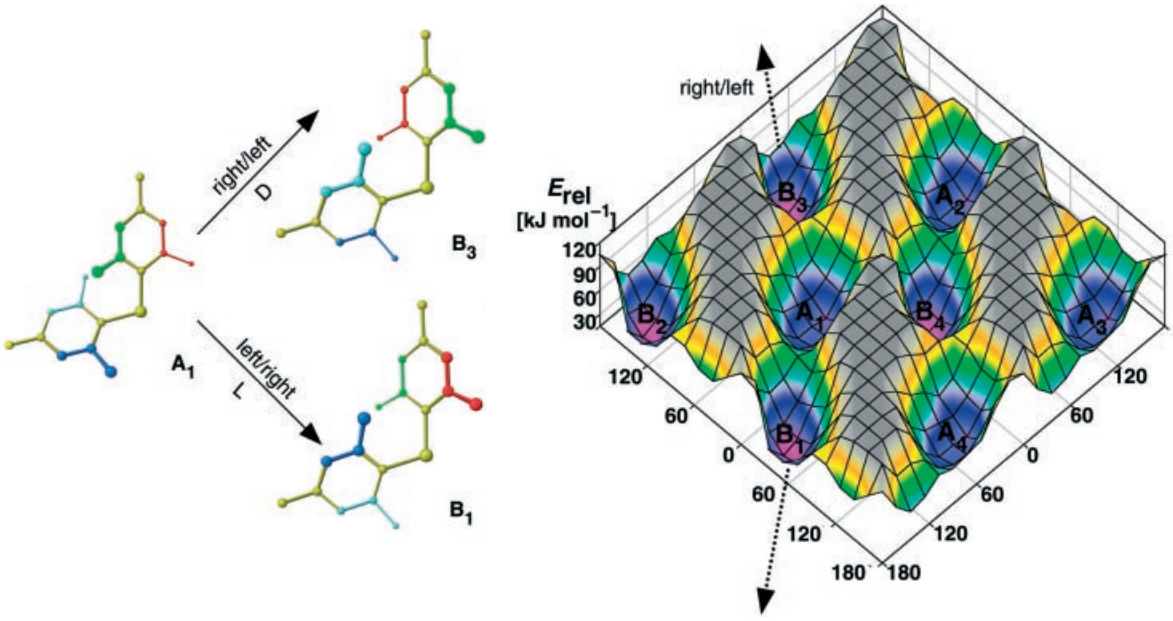

Figure 13. Illustration of the two energetically different pathways on which the $\lambda \rightleftarrows \delta$ isomerization of **1** may occur. The two pathways of $\lambda \rightleftarrows \delta$ isomerization are characterised by strictly coupled and countersense rotations of the mesityl groups at the $PMes_2$ entity. Depending on the sense of this coupled rotation different activation barriers have to be overcome. The two pathways labelled right/left (D) and left/right (L) are illustrated by molecular models.

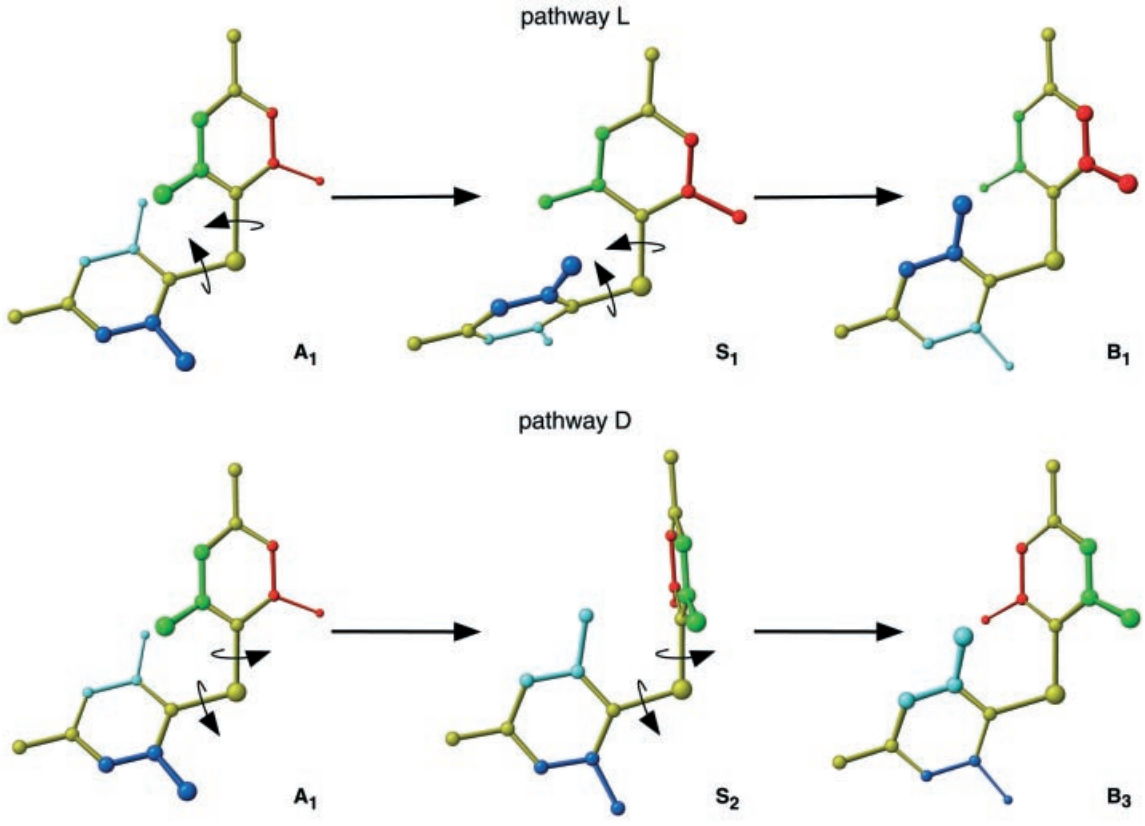

Figure 14. The one ring flip processes characterising the reorientation of the mesityl groups at the $PMes_2$ entity of **1** during $\lambda \rightleftarrows \delta$ isomerization. For the meaning of **A** and **B** see Figures 12 and 13. $\mathbf{S_1}$ and $\mathbf{S_2}$ correspond to the rotational positions of the mesityl groups at the saddlepoints (Figures 12 and 13).

tyl groups can only change their rotational positions as a strictly coupled pair is evident from Figure 12 as well. Only if the mesityl groups rotate in opposite sense the coupled rotation is allowed by low energy pathways. With the labelling scheme chosen $\mathbf{A_{(odd)}}$ can only interchange with $\mathbf{B_{(odd)}}$ and correspondingly $\mathbf{A_{(even)}}$ and $\mathbf{B_{(even)}}$ can interchange with each other. The corresponding reaction channels $\mathbf{B_1} \rightarrow \mathbf{A_1} \rightarrow \mathbf{B_3} \rightarrow \mathbf{A_3}$ are evident from Figure 12 where the minimum $\mathbf{A_3}$ is shown in a symmetrically equivalent position at the corner of the diagram (a phase shift in φ_3 by plus 180° will place $\mathbf{A_3}$ adjacent to $\mathbf{B_3}$). The channel $\mathbf{A_4} \rightarrow \mathbf{B_4} \rightarrow \mathbf{A_2} \rightarrow \mathbf{B_2}$ is likewise apparent in Figure 12 (a phase shift of −180° will place $\mathbf{B_2}$ adjacent to $\mathbf{A_2}$). A transition from a position on the pathway labelled by an uneven number subscript to any position on the pathway labelled by an even number subscript would correspond to either the rotation of just one mesityl group or to the coupled rotation of the two mesityl groups in the same rotational direction. Both possibilities are excluded by high potential barriers (grey barriers running vertical in Figure 12).

The rotational pathways taken by the mesityl groups upon $\lambda \rightleftarrows \delta$ isomerization are illustrated in Figure 13 in a different way. As an example the λ conformer $\mathbf{A_1}$ is taken as starting point. The mesityl groups labelled by φ_3 and φ_4 together with the phosphorus atom to which they are bonded are shown in a projection which keeps the $C_{ipso}-P-C_{ipso}$ fragment in the same orientation in each case (in the molecules themselves the pseudo-axial and pseudo-equatorial positions of the mesityl groups with respect to the coordination plane will exchange during the $\lambda \rightleftarrows \delta$ isomerization).

Following the pathway $\mathbf{A_1}$ to $\mathbf{B_3}$ (pathway D in Figure 12) the λ conformer transforms into the δ conformer such that φ_3 makes a clockwise rotation while φ_4 rotates in counterclock sense. This process needs a somewhat higher energy than the $\lambda \rightleftarrows \delta$ transformation from $\mathbf{A_1}$ to $\mathbf{B_1}$ (pathway L in Figure 13) which is accompanied by a counterclockwise rotation of φ_3 and a clockwise rotation of φ_4. These two pathways are labelled right/left for pathway D and left/right for pathway L respectively in Figure 13.

The two pathways L and D are illustrated in Figure 14 in yet another way. On the way from $\mathbf{A_1}$ to $\mathbf{B_1}$ (pathway L) the rotational arrangement corresponding to the saddlepoint (Figures 12 and 13) is the one shown ($\mathbf{S_1}$). The view taken in this Figure 14 is along the bisector of the P−Rh−P entity (Figure 6). The orientation is chosen such that one of the $P-C_{ipso}$ axes is vertical in each case in Figure 14.

The saddlepoint on the way from $\mathbf{A_1}$ to $\mathbf{B_3}$ (pathway D, Figures 12 and 13) is shown as well and labelled $\mathbf{S_2}$. It is

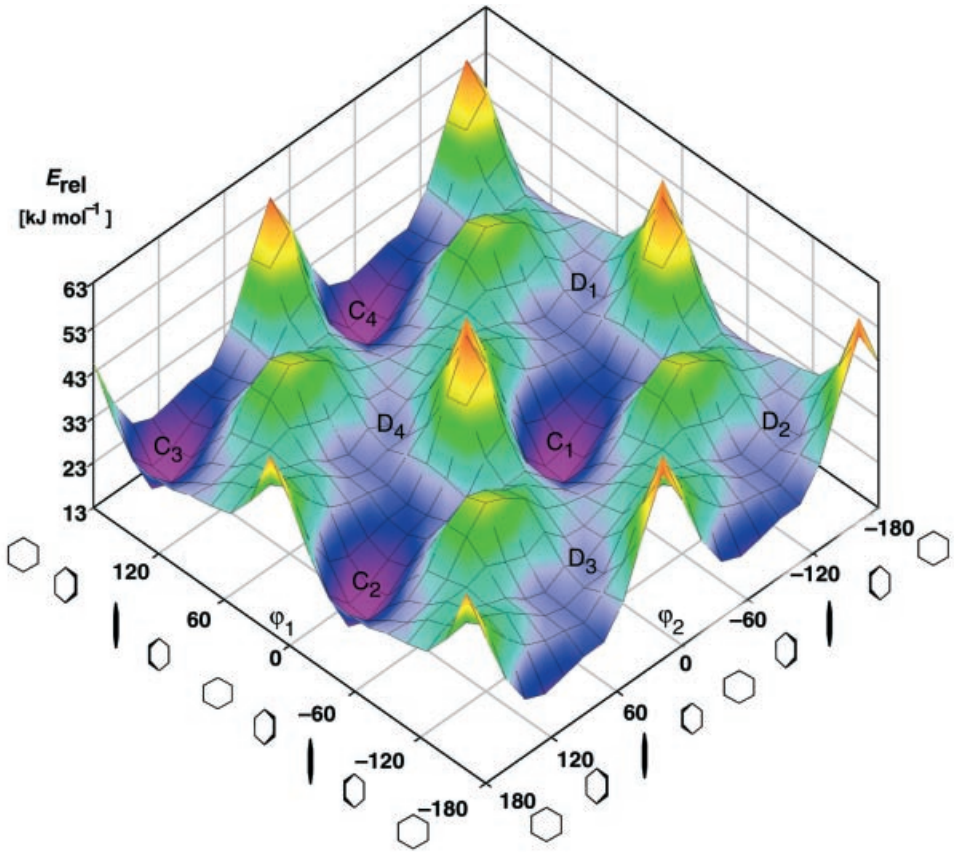

Figure 15. Energy diagram illustrating the ease of phenyl rotation at the PPh_2 group of **1**. The minima **C** are isoenergetic as are the flat minima **D**. The translation period of the graph is 180° in both axes. The energy scale is magnified with respect to the scale used in Figures 12 and 13. This larger magnification allows the illustration of the inherent asymmetry due to the chirality of **1**. The diagram is not symmetric with repect to the main diagonals (vertical in Figure 15).

seen that on both pathways the transition state corresponds to a situation where one of the aryl rings is almost vertical. The transitions thus correspond to a one ring flip process.[41]

The rotation of the phenyl groups at the PPh_2 entity is far less energy demanding than the rotation of the mesityl groups at the $PMes_2$ entity. The projection of the energy hypersurface onto the axes describing the rotation of the phenyl groups (φ_1, φ_2) is shown in Figure 15. This diagram is in principle analogous to the one shown in Figures 12 and 13. The energy scale and the energy profile are however quite different: In Figures 12 and 13 the barriers between the reaction channels (vertical reefs) are higher than 120 $kJ{\cdot}mol^{-1}$ (relative to the energy of the global minimum; Figures 12 and 13) and transition between different rotational positions is only energetically feasible along the two reaction channels.

The rotation of the phenyl groups on the other hand is far less restricted. The energy scale shown in Figure 15 is limited to 63 $kJ{\cdot}mol^{-1}$ with the highest barriers (orange) being covered within this range.

While a continuous reef separates the left hand and the right hand part of the Figures 12 and 13, in Figure 15 there are only isolated mountains and valleys between them. The positions of the minima **C** and **D** (Figure 15) are similar to the ones of **B** and **A** in Figures 12 and 13. This means that the low energy rotational positions of the aryl groups at the $PMes_2$ group and at the PPh_2 group are rather similar. There are however many energetically accessible pathways for concerted as well as for unconcerted phenyl rotations (Figure 15) while the mesityl groups can only rotate in a strictly concerted way (Figures 12 and 13). The barrier heights for the pathways reflecting the phenyl rotation are in the range of 12−15 $kJ{\cdot}mol^{-1}$ (Figure 15) while the barrier heights along the pathway of the strictly concerted rotation of the mesityl groups (pathways L and D, Figures 12 and 13) are in the range of 70−80 $kJ{\cdot}mol^{-1}$.

Force Field Model and Experimental Reality − Comparison of Results and Conclusion

The conformational behaviour of compounds **1**−**7** has been thoroughly analysed by NMR methods.[8] For compound **1** the quantitative details relating to the relative stability of its isomeric forms and to the pathways of isomerization and the activation enthalpy of this process are all available. It is found that the λ form of **1** is by 3.4 $kJ{\cdot}mol^{-1}$ more stable than its δ form.[8] Force field analysis calculates this energy difference as 3.1 $kJ{\cdot}mol^{-1}$ in almost exact numerical agreement (Figure 16). NMR exchange spectroscopy reveals that there are two different pathways for the isomerization of **1**.[8] Both pathways are characterised by a coupled rotation of the mesityl groups at the $PMes_2$ entity of **1**. The only difference between these two pathways is the opposite sense of this strictly coupled rotation.[8] The activation enthalpy for the enantiomerisation process as a whole is found to be $\Delta H^{\#}$ = 64.4 $kJ{\cdot}mol^{-1}$.[8] Force field calculations of **1** show that there are two pathways for λ ⇄ δ isomerization which comprise the strictly coupled countersense rotation of the mesityl groups at the $PMes_2$ entity and which differ only in the sense of rotation. The calculated activation enthalpy of the lower energy pathway is 69.1 $kJ{\cdot}mol^{-1}$, again in close nu-

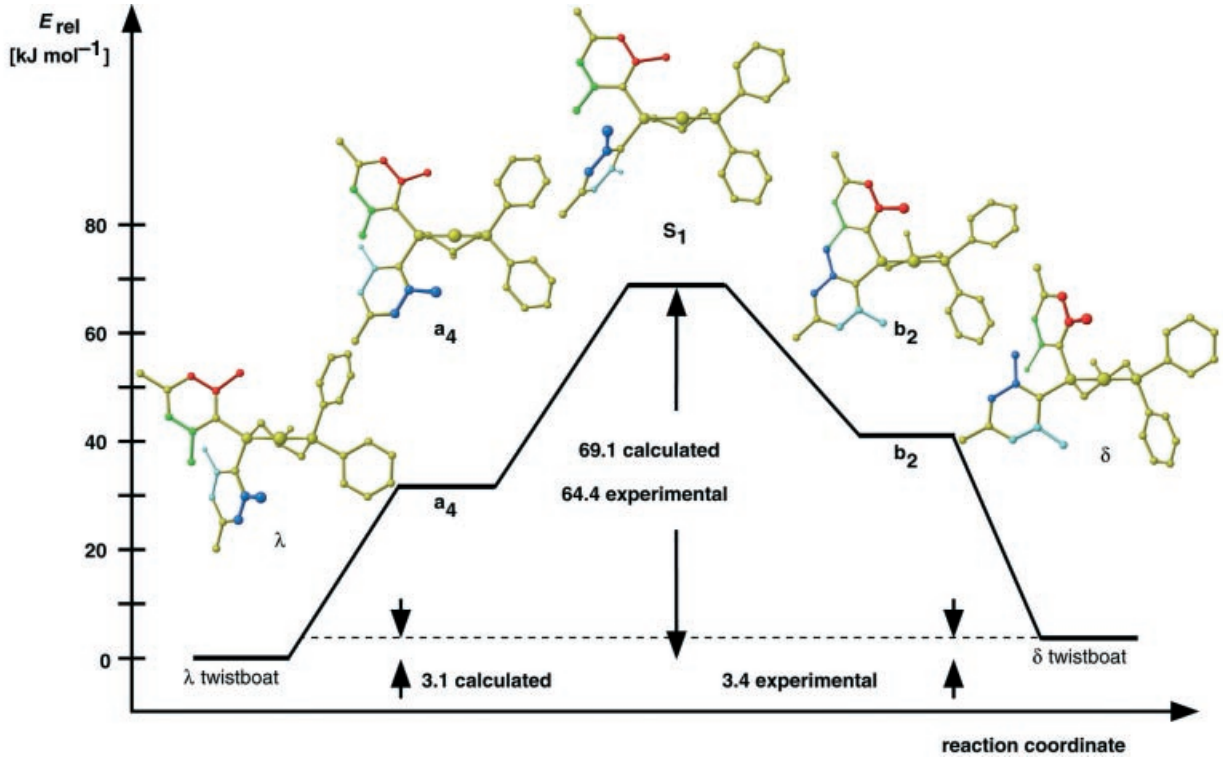

Figure 16. Comparison of experimental and calculated results for the λ ⇄ δ isomerization of **1**.

merical agreement with the experimental value (Figure 16). This type of quantitative and qualitative agreement between calculation and experiment lends quite some credit to the calculation procedures as reported. The force field calculations identify the conformation of the chelate ring at the saddlepoint as an unsymmetrical twist conformation. Starting from the λ isomer this transition state geometry is reached via a halfboat conformation (**a**$_4$ in Figure 16). Starting from the δ isomer a twist conformation (**b**$_2$ in Figure 16) is the intermediate.

It appears that the approach taken in deriving a force field model is a very promising one. The optimisation of the force field parameters on the basis of as many solid state structures as available for a class of compound had already been shown to lead to models of high predictive power.[14−16] The case studied here is the most complicated one of the ones analysed by this method so far and at the same time the one for which pathways and energies have been experimentally determined to the maximum possible extent.[8] It is highly satisfying to observe that the model is capable of predicting the types of conformational rearrangement processes as well as the energy differences associated with them.

Experimental Section

Force Field Calculations

The force field program used is based on the program set YAMMP[23] written by R. K. Z. Tan et al. in "C" which is available as a public domain source code.[42] The force field potentials were adapted to the units used in MacroModel MM2*.[21] Data transfer between MacroModel and YAMMP was accomplished by appropriate converters and YAMMP was embedded in a number of shells which make it available at different types of single processor machines (Pentium, SGI) and parallel computing systems (Parsytec GC, CRAY T3E).

The rms deviation between two structural models was calculated as the square root of the sum of the squares of the deviations between all n corresponding pairs of atoms divided by the square root of n (Hydrogen atoms were included in these calculations during GA optimisation). An overlay of the two structures was computed by a least-squares fitting procedure based on a program of D. Heisenberg[43] and implemented into YAMMP by K. Allinger.[14]

The following expressions were used for the potential energy:

Bond Length Deformation:

$$E(r) = 1/2\,k((r-r_0)^2 - (r-r_0)^3) \quad (1)$$

where r_0 represents the ideal bond length (minimum of the curve) and r represents the actual distance. This potential curve has a artificial maximum at large ($r-r_0$) values. For such large values only the quadratic term is used.

Valence Angle Deformation:

$$E(\alpha) = 1/2\,k((\alpha-\alpha_0)^2 + k'(\alpha-\alpha_0)^6) \quad (2)$$

α_0 and α have a similar meaning as r_0 and r above. The force constants k ank k' refer to the contributions of the harmonic and the unharmonic parts of the potential function to the energy.

Torsion Angle Deformation:

$$E(\tau) = k_{t1}(1+\cos\tau) + k_{t2}(1-\cos(2\tau)) + k_{t3}(1+\cos(3\tau)) \quad (3)$$

The variable τ describes the torsion angle. k_{t1}, k_{t2}, and k_{t3} are the force constants describing potential terms with twofold, fourfold and sixfold symmetry in this series.

π-Bonds: π-bonding was incorporated by defining a dummy atom D at the centre of the coordinated double bond (Figure 3). The position of the olefinic carbon atoms was then expressed as a function of r_d, α, β, γ, and τ (Figure 3). The terms needed in a molecular mechanics calculation are however of the type $\delta E/\delta x$ (x being any coordinate of any atom in real space) and not of the type $\delta E/\delta p$ (p being any internal coordinate). The potentials on the other hand are defined as $E = f(p)$ and it is necessary therefor to transform $\delta E/\delta p$ into $\delta E/\delta x$. This problem is solved for the standard set of conformational coordinates (distance, angle, torsion angle ...) in any standard molecular mechanics program. It is not incorporated, however, for parameters such as r_d, α, β, γ, and τ which were used to define a π bond (Figure 3). In principle the solution is given by differential calculus by $\delta E/\delta x = (\delta E/\delta p)\cdot(\delta p/\delta x)$. With the parameters r_d, α, β, γ, and τ the application of this rule is rather tedious. For this reason and since the corresponding expressions cannot be found in the literature the results are given here for the derivatives with respect to the x-coordinate in each case. The derivatives for the other coordinates are easily obtained from these expressions by cyclic permutation.

If a_x represents the x coordinate of the real atom (rhodium in Figure 3) and d_x the x coordinate of the dummy atom (D in Figure 3) the expression relating to r_d is:

$$\delta E/\delta d_x = -\delta E/\delta a_x = k\Delta r_d \cdot (a_x - d_x)/|r_d| \quad (4)$$

The term Δr_d means ($|\vec{r_0}| - |\vec{r}|$ where $|\vec{r}|$ is the distance r_d and $|\vec{r_0}|$ is the distance at the minimum of the potential function.

In order to derive the expressions relating to α, β, and γ (Figure 3) the following definition is used (Figure 17).

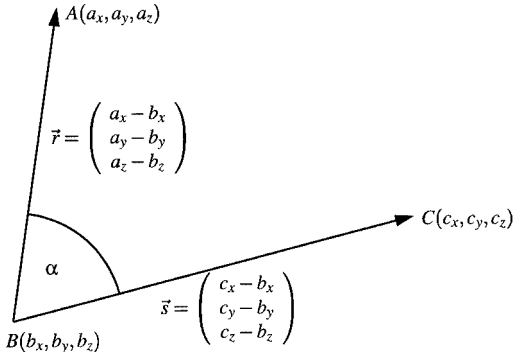

Figure 17. Definitions used in calculating derivatives with respect to angles.

If the potential function $E(\alpha) = {}^1/_2k\cdot[(\alpha - \alpha_0)^2 + k_{unh}\cdot(\alpha - \alpha_0)^6]$ is defined as above the derivatives with respect to the x coordinates of the points A, B, and C are:

$$\frac{\delta E(\alpha)}{\delta a_x} = k_{angle}\cdot\Delta\alpha\cdot\left(1+3\cdot k_{unh}\cdot(\Delta\alpha)^4\right)\cdot\frac{-1}{\sin\alpha} \cdot\frac{|\vec{r}|^2\cdot(c_x-b_x)-\vec{r}\cdot\vec{s}\cdot(a_x-b_x)}{|\vec{r}|^3\cdot|\vec{s}|}$$

$$\frac{\delta E(\alpha)}{\delta b_x} = k_{angle}\cdot\Delta\alpha\cdot\left(1+3\cdot k_{unh}\cdot(\Delta\alpha)^4\right)\cdot\frac{-1}{\sin\alpha} \cdot\frac{\vec{r}\cdot\vec{s}\cdot|\vec{s}|^2\cdot(a_z-b_x)-(a_x-2b_x+c_x)\cdot|\vec{r}|^2\cdot|\vec{s}|^2+\vec{r}\cdot\vec{s}\cdot|\vec{r}|^2\cdot(c_x-b_x)}{|\vec{r}|^3\cdot|\vec{s}|^3} \quad (5)$$

$$\frac{\delta E(\alpha)}{\delta c_x} = k_{angle}\cdot\Delta\alpha\cdot\left(1+3\cdot k_{unh}\cdot(\Delta\alpha)^4\right)\cdot\frac{-1}{\sin\alpha} \cdot\frac{|\vec{s}|^2\cdot(a_x-b_x)-\vec{r}\cdot\vec{s}\cdot(c_x-b_x)}{|\vec{r}|\cdot|\vec{s}|^3}$$

The term $\Delta\alpha$ means ($\alpha - \alpha_0$) in each case (see above).

For analysing $\delta E/\delta\tau$ (Figure 3) the definitions shown in Figure 18 are used.

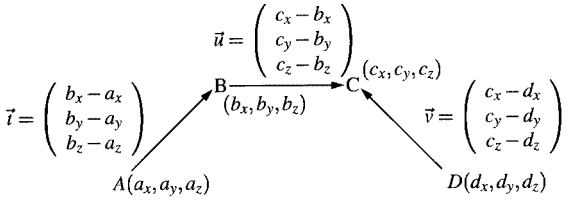

Figure 18. Definitions used in calculating derivatives with respect to torsion angles.

Two additional vectors are defined as:

$$\vec{r} = \vec{t}\times\vec{u} \text{ and } \vec{s} = \vec{u}\times\vec{v} \quad (6)$$

With a_x, b_x, c_x, and d_x being the x coordinates of the points A, B, C, and D in that sequence the following expressions result:

$$\frac{\delta E(\tau)}{\delta a_x} = \left(k_{t1}\cdot(1+\cos\tau)+k_{t2}\cdot(2\cos^2\tau-1)+k_{t3}\cdot(4\cos^3\tau-3\cos\tau)\right) \cdot\frac{|\vec{r}|\cdot|\vec{s}|\cdot(u_z s_y-u_y s_z)-\vec{r}\cdot\vec{s}\cdot\frac{|\vec{s}|}{|\vec{r}|}\cdot(r_y u_z-r_z u_y)}{|\vec{r}|^2\cdot|\vec{s}|^2}$$

$$\frac{\delta E(\tau)}{\delta b_x} = \left(k_{t1}\cdot(1+\cos\tau)+k_{t2}\cdot(2\cos^2\tau-1)+k_{t3}\cdot(4\cos^3\tau-3\cos\tau)\right) \cdot\left(\frac{|\vec{r}|\cdot|\vec{s}|\cdot(s_y(-t_z+u_z)+r_y v_z+s_z(-u_y+t_y)-r_z v_y)}{|\vec{r}|^2\cdot|\vec{s}|^2} -\frac{\vec{r}\cdot\vec{s}\cdot\left(\frac{|\vec{r}|}{|\vec{s}|}\cdot(r_y(u_z-t_z)+r_z(-u_y+t_y))+\frac{|\vec{r}|}{|\vec{s}|}\cdot(s_y v_z-s_z v_y)\right)}{|\vec{r}|^2\cdot|\vec{s}|^2}\right) \quad (7)$$

$$\frac{\delta E(\tau)}{\delta c_x} = \left(k_{t1}\cdot(1+\cos\tau)+k_{t2}\cdot(2\cos^2\tau-1)+k_{t3}\cdot(4\cos^3\tau-3\cos\tau)\right) \cdot\left(\frac{|\vec{r}|\cdot|\vec{s}|\cdot(r_y(-v_z+u_z)+s_y t_z+r_z(-u_y+v_y)-s_z t_y)}{|\vec{r}|^2\cdot|\vec{s}|^2} -\frac{\vec{r}\cdot\vec{s}\cdot\left(\frac{|\vec{r}|}{|\vec{s}|}(s_y(u_z-v_z)+s_z(v_y-u_y))+\frac{|\vec{r}|}{|\vec{s}|}\cdot(r_y t_z-r_z t_y)\right)}{|\vec{r}|^2\cdot|\vec{s}|^2}\right)$$

$$\frac{\delta E(\tau)}{\delta d_x} = k_{t1}\cdot(1+\cos\tau)+k_{t2}\cdot(2\cos^2\tau-1)+k_{t3}\cdot(4\cos^3\tau-3\cos\tau) \cdot\frac{|\vec{r}|\cdot|\vec{s}|\cdot(u_y r_z-u_y r_y)-\vec{r}\cdot\vec{s}\cdot\frac{|\vec{r}|}{|\vec{s}|}\cdot(s_z u_y-s_y u_z)}{|\vec{r}|^2\cdot|\vec{s}|^2}$$

Optimisation by GA

The procedures already explicitly described elsewhere[14] based on the use of the program GAPAO which itself uses functions of the

Table 4. Optimised force constants

(a) Bond Stretching[a]	parameter set mm2_rms r_0 [Å]	k_b [mdyn·Å^{-1}]	parameter set mm2_int r_0 [Å]	k_b [mdyn·Å^{-1}]
Rh−P	2.310	0.625	2.310	1.357*
Rh−D	2.140	1.000	2.140	1.267*
(b) Angle Bending	parameter set mm2_rms α_0 [°]	k_a [mdyn·rad^{-2}]	parameter set mm2_int α_0 [°]	k_a [mdyn·rad^{-2}]
P−Rh−P	88.6	0.600	93.0*	0.800*
P−Rh−D	93.5/175.8	0.500	93.5/175.8	0.047*
D−Rh−D	90.0	0.100	91.667*	0.500*
Rh−P−C3	118.133*	0.467*	117.067*	0.677*
Rh−P−C2	112.800*	0.967*	113.200*	0.633*
C2−P−C2	103.600*	1.200*	103.571*	0.700*
C2−P−C3	99.194*	0.867*	103.143*	0.533*
Rh−D−C2	90.000	0.250	90.000	1.000*
(c) Torsion	parameter set mm2_rms k_{t2} [kcal·mol^{-1}]	k_{t3} [kcal·mol^{-1}]	parameter set mm2_int k_{t2} [kcal·mol^{-1}]	k_{t3} [kcal·mol^{-1}]
P−Rh−D−C2	0.000*	0.000	−1.000*	0.000

[a] Parameter set mm2_rms was obtained by calculating the fitness on the basis of the distance between pairs of atoms, one atom belonging to the experimentally observed structure and the constitutionally equivalent atom belonging to the calculated structure. Parameter set mm2_int was obtained by evaluating the fitness on the basis of the internal coordinates as shown. Only parameters marked with an asterisk were refined. Harmonic potentials were used for the bond length deformation. The unharmonic term k_{unh} of the valence angle deformation (see text) was set at $k_{unh} = 0.754$ rad^{-4} throughout.

PGA-Genetic Algorithm Package[44] were applied. These functions are fully parallelised and are based on the Message Passing Interface Library[45] and thus GAPAO runs in single processor as well as in parallel processor environments.

The force constants as derived by optimisation on the basis of eleven structures are shown in Table 4.

Conformation Analysis

The procedure used was similar to the one described in detail elsewhere.[15] Two dimensional and pseudo-three dimensional contour plots were produced by using the program *SigmaPlot*.[46] Neural Network analyses were calculated and visualised by the program kmap.[47] The calculations were performed by using the modified program YAMMP as a minimizer and a shell around it which allowed to run the program on parallel processor environments. The standard program YAMMP was augmented by a part, written in "C", implementing a grid search algorithm. All calculations were performed on a Cray T3E.

Acknowledgments

Financial support by the German Science Foundation (DFG HU 151/24-1 and DFG HU 151/29-1), the Fonds der Chemischen Industrie and the Graduiertenkolleg "Selektivität in der organischen und metallorganischen Synthese und Katalyse" is gratefully acknowledged. The computations were made possible by grants of computing time at PARSYTEC (IWR Heidelberg) and CRAY [John von Neumann Institut (NIC)] parallel computing environments. We are indebted to J. Gasteiger, Erlangen, for the allowance to use the program kmap written by the Erlangen group.

[1] U. Burkert, N. L. Allinger, *Molecular Mechanics*, ACS monograph, Washington, **1992**.
[2] E. Juaristi, *Introduction to Stereochemistry & Conformational Analysis*, Wiley Interscience, **1991**.
[3] P. Comba, T. W. Hambley, Molecular Modelling of Inorganic Compounds, VCH Weinheim, **1995**.
[4] C. R. Landis, D. M. Root, T. Cleveland, in: *Reviews in Computational Chemistry*, Vol. 6 (Eds.: K. B. Lipkowitz, D. B. Boyd), VCH Publishers, Inc., New York, **1995**, 73−148.
[5] B. J. Hay, *Coord. Chem. Rev.* **1993**, *126*, 177−236.
[6] [6a] *Discover User Guide*, Versions 2.9.7 & 95.0/3.00, Biosym/MSI, **1995**. [6b] S. Barlow, A. L. Rohl, S. Shi, C. M. Freeman, D. O'Hare, *J. Am. Chem. Soc.* **1996**, *118*, 7578−7592. [6c] N. Jäger, U. Schilde, *Struct. Chem.* **1998**, *9*, 77−93.
[7] D. M. Root, C. R. Landis, T. Cleveland, *J. Am. Chem. Soc.* **1993**, *115*, 4201−4209.
[8] A paper presenting quantitative thermodynamic and kinetic data of the conformational rearrangements of diphosphane chelate compounds including **1** as deduced by NMR techniques is published aside: A. Frick, V. Schulz, G. Huttner, *Eur. J. Inorg. Chem.* **2002**, 3129−3147, following paper.
[9] T. W. Hambley, *J. Comput. Chem.* **1987**, *8*, 651−657.
[10] J. R. Gollogly, C. J. Hawkins, *Inorg. Chem.* **1972**, 156−161.
[11] S. Beyreuther, J. Hunger, G. Huttner, S. Mann, L. Zsolnai, *Chem. Ber.* **1996**, *129*, 745−757.
[12] G. Huttner, S. Beyreuther, J. Hunger, in: *Software-Entwicklung in der Chemie 10* (Ed.: J. Gasteiger), GDCH, Frankfurt am Main, **1996**, 201−207.
[13] J. Hunger, S. Beyreuther, G. Huttner, *Mol. Model.* **1996**, 2, 257−258.
[14] J. Hunger, S. Beyreuther, G. Huttner, K. Allinger, U. Radelof, L. Zsonai, *Eur. J. Inorg. Chem.* **1998**, 693−702.
[15] S. Beyreuther, J. Hunger, S. Cunskis, T. Diercks, A. Frick, E. Planker, G. Huttner, *Eur. J. Inorg. Chem.* **1998**, 1641−1653.
[16] S. Beyreuther, A. Frick, J. Hunger, G. Huttner, B. Antelmann, P. Schober, R. Soltek, *Eur. J. Inorg. Chem.* **2000**, 597−615.
[17] D. E. Goldberg, *Genetic Algorithms in Search, Research and Machine Learning*, Addison-Wesely, New York, **1989**.
[18] J. Devillers (Ed.), *Genetic Algorithms in Molecular Modelling*, Academic Press, San Diego, **1996**.
[19] R. Judson, in: *Reviews in Computational Chemistry*, Vol. 10 (Eds.: K. B. Lipkowitz, D. B. Boyd), VCH Publishers, Inc., New York, **1997**, 1−73.
[20] J. Karas, G. Huttner, K. Heinze, P. Rutsch, L. Zsnolnai, *Eur. J. Inorg. Chem.* **1999**, 405−420.
[21] The mm2 force field as implemented in MacroModel 5.0 (mm2*) has been used throughout (see: F. Mohamadi, N. G. J. Richards, W. C. Guida, R. Liskamp, M. Lipton, C. Caufield, G. Chang, T. Hendrickson, W. C. Still, *J. Comp. Chem.* **1990**, *11*, 440−467).
[22] N. L. Allinger, *J. Am. Chem. Soc.* **1977**, *99*, 8127−8134.
[23] R. K.-Z. Tan, S. C. Harvey, *J. Comp. Chem.* **1993**, *14*, 455−470.
[24] T. N. Doman, C. R. Landis, B. Bosnich, *J. Am. Chem. Soc.* **1992**, *114*, 7264−7272.
[25] B. Bosnich, *Chem. Soc. Rev.* **1994**, 387−395.
[26] W. F. van Gunsteren, R. Boelens, R. Kaptein, R. M. Scheek, E. R. P. Zuiderwig, *Molecular Dynamics and Protein Structure* (Ed.: J. Hermans), Polycrystal Book Service: West Springs, IL, **1985**, p. 92.
[27] V. S. Allured, C. M. Kelly, C. R. Landis, *J. Am. Chem. Soc.* **1991**, *113*, 12−20.
[28] The conventional binary code has the disadvantage that occasionaly more than one bit has to be changed in going from the binary representation of n to $n + 1$ (cf.: $n = 3$, code = 011; $n = 4$, code = 100). In applying Genetic Algorithms this would mean that it is more probable to change a 4 into a 5 (100; 101) than it is to change a 3 into a 4. 'Grey coding' avoids this problem by assigning a binary code such that only one bit has to be inverted in going from n to $n + 1$ throughout.
[29] J. H. Holland, *Adaption in Natural and Artifical Systems*, MIT Press, Cambridge, MA, **1992**.
[30] D. E. Goldberg, *Genetic Algorithms in Search, Research and Machine Learning*, Addison-Wesley, New York, **1989**.
[31] J. Devillers (Ed.), *Genetic Algorithms in Molecular Modelling*, Academic Press, San Diego, **1996**.
[32] R. Judson, in: *Reviews in Computational Chemistry, Vol. 10* (Eds.: K. B. Lipkowitz, D. B. Boyd), VCH Publishers, Inc. New York, **1997**, 1−73.
[33] D. Wienke, C. B. Lucasius, G. Kateman, *Anal. Chim. Acta* **1992**, *265*, 211−225.
[34] The structure contains one molecule CH_2Cl_2 and half a molecule Et_2O per formula unit. Both of these solvate molecules as well as PF_6^- counterions are disordered. Relatively short contacts between the hydroxy oxygen of the ligand and some of the fluorine substituents of the counterion PF_6^- (2.8 Å) and some of the chlorine atoms of the dichloromethane solvate (3.3 Å) indicate that the structure of the ligand might be biased by these contacts.
[35] B. P. Hay, *Coord. Chem. Rev.* **1993**, *126*, 177−236.
[36] P. Comba, *Coord. Chem. Rev.* **1993**, *123*, 1−48.
[37] J. S. Giovannetti, C. M. Kelly, C. R. Landis, *J. Am. Chem. Soc.* **1993**, *115*, 4040−4057.
[38] M. Lipton, W. C. Still, *J. Comp. Chem.* **1988**, *9(4)*, 343−355.
[39] T. Kohonen, *Self-Organization and Associative Memory*, 2nd. ed., Springer Verlag, Berlin **1988**.
[40] It is often observed that conformations found in the crystal do not correspond to the conformation of the global energy minimum but have conformations for which the calculated energies are some few kJ·mol^{-1} higher. In the example analysed crystal forces are weak throughout but obviously strong enough to overcome some few kJ·mol^{-1} (see ref[15]).
[41] [41a] D. A. V. Morton, A. G. Orpen, *J. Chem. Soc., Dalton*

Trans. **1992**, *4*, 641−653. [41b] K. Mislow, *Acc. Chem. Res.* **1976**, *9*, 26−33. [41c] H. B. Bürgi, *Acc. Chem. Res.* **1983**, *16*, 153−161. [41d] H. B. Bürgi, *Acta Crist, Sect. B.* **1988**, *44*, 445−448. [41e] S. Beyreuther, J. Hunger, G. Huttner, S. Mann, L. Zsolnai, *Chem. Ber.* **1996**, *129*, 745−757. [41f] S. Beyreuther, A. Frick, J. Hunger, G. Huttner, B. Antelmann, P. Schober, R. Soltek, *Eur. J. Inorg. Chem.* **2000**, 597−615.

[42] The program package YAMMP is available from: http://uracil.cmc.uab.edu/YammpWeb/

[43] D. Heisterberg, **1990**, unpublished results; the program is available from the software archive of the Computational Chemistry List (CCL) at http://ccl.ose.edu/chemistry.html

[44] D. Levine, Argonne National Laboratory, **1995**; the package is available at http://www.mcs.anl.gov/pgapack.html

[45] W. Gropp, E. Lusk, Argonne National Labratory, **1996** (available from http://www.mcs.anl.gov/mpi).

[46] *SigmaPlot for Windows Version 4.01*, Copyright 1986−1997, SPSS Inc.

[47] J. Zupan, J. Gasteiger, *J. Neural Networks in Chemistry*, VCH Weinheim, **1993**. The program kmap version 3.0 was kindly provided by J. Gasteiger, Erlangen.

Received Novemer 12, 2001
(publication delayed on the authors' request)
[I01451]

Interconversion of δ and λ Forms of Six-Membered Chelate Cycles − A Quantitative NMR Spectroscopic Study of (Diphosphane)rhodium Compounds

Axel Frick,[a] Volker Schulz,[a] and Gottfried Huttner*[a]

Prof. Dr. Matthias Drieß in recognition of his outstanding contributions to inorganic chemistry

Keywords: Conformational analysis / Diphosphanes / Rhodium / Kinetics / Thermodynamics

The stereochemical flexibility of six-membered chelate cycles containing phosphorus donor groups has not yet been analysed in detail. With a number of compounds of the type $[\{\kappa\text{-}PR_2CH_2CH(OH)CH_2\text{-}\kappa\text{-}PR'_2\}Rh(\eta^4\text{-}COD)]^+PF_6^-$ at hand, and since the solid state structures and the catalytic properties of these compounds are known, an ideal opportunity to study this topic was available. After assigning all of the important ^1H, ^{13}C, and ^{31}P NMR spectroscopic resonances by a combination of one- and two-dimensional NMR spectroscopic methods quantitative interpretation of the 2D NOESY/EXSY spectra was achieved for four compounds [PR_2 = $PMes_2$; PR'_2 = PPh_2 (**1**), DBP (**2**), PEt_2 (**3**), P(*o*-anisyl)$_2$ (**4**)]. It is found that the conformations that these compounds adopt in solution are similar to the ones observed for them in the solid state. The conformational ensemble in solution comprises λ twist and δ twist forms; λ and δ isomers are clearly differentiated by quantitative NOE-based structure analysis (distance geometry). Since the sense of chirality of the ligand is known, an absolute assignment of these conformations is possible. The equilibrium constants at 298 K for the δ ⇄ λ isomerisation of compounds **1**–**4** are not very different from one another, with reaction enthalpies ranging from −8 to −2 kJ mol^{-1} and the reaction entropies in the range of −10 to 8 J K^{-1} mol^{-1}. The activation barriers are again similar for **1**–**4** and lie at $\Delta H^{\neq} \approx 64$ kJ mol^{-1}. It is observed that the mesityl entities at the $PMes_2$ donor groups behave as coupled rotors with two rotational pathways open to them during the δ ⇄ λ interconversion while they are rotationally fixed in the λ and δ conformations themselves. Comparing the above results with the enantioselective discrimination found for the same compounds in hydrogenation experiments it becomes clear that there is no direct correlation between the preference of one twist form over the other in the precatalyst and its chiral performance.
(© Wiley-VCH Verlag GmbH, 69451 Weinheim, Germany, 2002)

Introduction

Enantiopure chelate ligands play an important role in metal-mediated enantioselective catalyses. Amongst chelate ligands which contain a saturated carbon chain as a linker between the donor groups, the ones forming five-membered cycles have been found to be most effective.[1] These cycles have only one torsional degree of freedom as soon as three valence angles and five distances are defined, such that their conformational behaviour may easily be controlled, e.g. DIPAMP.[2,3] If larger chelate cycles have been found to be effective in enantioselective catalyses they almost inevitably contain unsaturated parts such that the number of independent coordinates of torsional freedom is still low due to the fixed conformation at the double bonds, e.g. BINAP.[4] In some other cases where the conformation of the chelate cycle is almost inflexible, by the nature of the covalent framework, enantiodiscrimination ensues from the chirality of substituent groups at the chelate cycle, e.g. PHOX.[5] It is not astonishing therefore that chelate ligands containing a saturated three-carbon chain as a linker between the donor groups have not been studied much as coligands in enantioselective catalyses. The six-membered cycles derived from them have an additional degree of torsional freedom with respect to five-membered cycles, once the six distances and four valence angles are defined.[6] Nevertheless, it has been found that six-membered diphosphane chelate cycles may be quite efficient in enantioselective catalyses.[7,8] Transfer of the chiral information from the chelate metal template to the substrates must then occur via the chirally induced preference of one of the chiral conformations of the chelate cycle over the others. If six-membered chelate cycles are generally found to be inefficient in enantioselective catalyses the reason for this might well be that the diastereoselection of one ring conformation over the others is less efficient in six-membered cycles as compared to the one in five-membered ones. Since quantitative information about the conformational enantiomerisation of phos-

[a] Anorganisch-Chemisches Institut der Universität Heidelberg, Im Neuenheimer Feld 270, 69120, Germany
Fax: (internat.) + 49-(0)6221/545707
E-mail: g.huttner@indi.aci.uni-heidelberg.de
Supporting information for this article is available on the WWW under http://www.eurjic.org or from the author.

phorus-containing six-membered chelate cycles is still missing, it appeared worthwhile to study such conformational enantiomerisation processes in more detail. In this paper we report on an NMR analysis of several compounds of the type $[\{\kappa\text{-}PR_2CH_2CH(OH)CH_2\text{-}\kappa\text{-}PR'_2\}Rh(\eta^4\text{-}COD)]^+PF_6^-$ which results in precise estimates of the thermodynamic and kinetic parameters which control the conformational inversion of their six-membered chelate cycles.

Results

The syntheses and catalytic properties of compounds **1**−**7** (Figure 1) are described in the literature.[8] The solid state structures of these compounds are well known with the exception of the structures of **3** and **7**.[8]

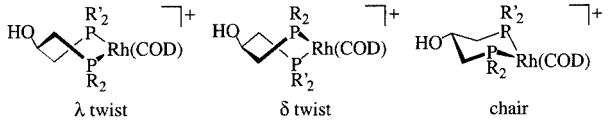

Compound	PR_2	PR'_2	X-ray		Chirality[b]
1	$PMes_2$	PPh_2	twist	λ,δ	(*S*)
2	DBP	$PMes_2$	twist	δ	(*R*)[c]
3	$PMes_2$	PEt_2	twist	λ,δ	(*S*,*R*)
4	$PMes_2$	P(2-MeOPh)$_2$	twist	λ,δ	(*R*)
5	P(2-MeOPh)$_2$	PPh_2	twist	λ,δ	(*S*)
6	PPh_2	P(*o*-Tol)$_2$	chair	OH-*eq*	(*R*)
7	P(*o*-Tol)$_2$	PEt_2	chair	OH-*eq*	(*S*,*R*)

Figure 1. Compounds **1**−**7**[a]
[a] The formulae indicate the constitution of compounds **1**−**7** as well as the three basic types of conformations (λ twist, δ twist, chair) which characterise the folding of the six-membered chelate cycle as found by X-ray analyses of crystals of the compounds. [b] The items in this column refer to the chirality of the ligand used for preparing the crystal material to which the X-ray data refer and from which the solutions for NMR spectroscopic analyses were prepared. [c] In the original paper[8] the sense of chirality of **2** was erroneously assigned as (*S*).

The structures of these latter two compounds have been determined for the racemates of compounds **3** and **7**.[9] The spread of substitution patterns in **1**−**7** and the fact that two conformational isomers are generally observed for these compounds in NMR studies[8] appeared to warrant a detailed NMR analysis of their conformational behaviour. Since, in addition, the solid state structures of the compounds are known, dissolving the crystals at low temperatures should produce solutions that contain the compounds in the same conformation as pertinent to the crystal. These conformations might well be metastable in solution at low temperatures and might thus help assign NMR signals to individual conformations. In the following paragraphs the procedures of complete assignment of all the relevant NMR signals of **1**−**4** will be described first (*Assignment of the NMR Spectra of **1**−**4***).

An EXSY analysis of the exchange processes between different ring conformations is described next (*Dynamic Exchange Processes*).

The information obtained by dissolving crystalline samples of **1**−**7** at low temperatures is given in the following paragraph (*Results from Dissolving Crystals of **1**−**7** at Low Temperatures*).

The last paragraph deals with the quantitative (distance geometry) NOE structure analysis of **1**−**4** (*Quantitative NMR Structure Analysis*).

Assignment of the NMR Spectra of 1−4

The general procedure of the assignment is given here for **1**. The procedures used for assigning the NMR resonances of **2**−**4** are, mutatis mutandis, the same. A view of the λ and δ conformations of **1** as found in the crystal[8] is shown in Figure 2.

The scheme adopted for referencing individual nuclei is shown in Figure 3.

The equilibrium between the λ and δ forms, that is observed in solution necessarily exchanges the positions that the substituents of the chelate ligand occupy with respect to the chelate cycle (Figure 4).

Thus, the mesityl group that is in a pseudo-axial position in the λ isomer (Figure 4, left) will be in a pseudo-equatorial position when the λ conformation transforms into the δ isomer. The same type of exchange occurs not only for the PR_2 groups, but also for the CH_2 protons of the chelate cycle (Figure 4). Referring to Figure 4 it is clear that the labelling scheme has been chosen, such as to identify the protons of the chelate cycle in the λ isomer by an unprimed number and refer to the same protons in the δ isomer by a primed number. The pseudo-axial or pseudo-equatorial position of these protons may always be extracted by inspecting Figure 4. If necessary, the atom identifier has been additionally labelled by the suffix *ax* or *eq* respectively.

A solution of **1** in CD_2Cl_2 contains two isomeric forms of **1** in a ratio of approximately 5:1, at 298 K. This had already been inferred from ^{31}P NMR spectroscopy.[8] The assignment of the individual nuclei of these two isomers is based on a combination of one- and two-dimensional NMR techniques including ^1H-^{31}P HMBC,[10] ^1H-^{13}C HSQC,[11] ^1H-^{13}C HMBC,[10] ^1H-^1H DQF-COSY,[12] and ^1H-^1H NOESY/EXSY.[13] DQF-COSY spectra at 298 K show the signals referring to the two isomers in an intensity ratio of 5:1 and allow one to clearly separate the data referring to one or the other isomer.

^1H-^{31}P HMBC spectra show that the mesityl groups are bonded to P1 (strong correlations to all of the protons of the mesityl groups). The protons H31,35 and H37,41 (Figure 3) are strongly correlated with P2 and must thus be the *ortho*-protons of the phenyl groups at the PPh_2 entity. Their correlations with the *meta*- and *para*-protons of the respective phenyl groups are evident from the COSY data (Table 3). The same type of correlation is found for the minor isomer.

The ^{13}C NMR signals of **1** were assigned by their ^1H-^{13}C correlations using ^1H-^{13}C HSQC and ^1H-^{13}C HMBC techniques. So far the assignment cannot differentiate be-

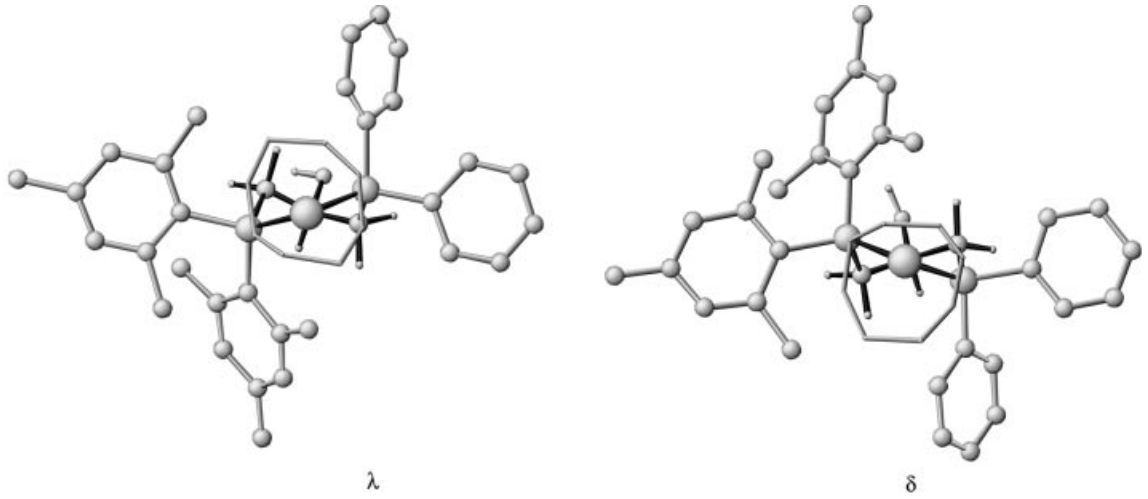

Figure 2. λ twist and δ twist isomers as found for independent constituents in the crystal of **1**; left-hand side: λ isomer; right-hand side: δ isomer; fFor the sake of clarity bonds to the carbon atoms of the COD ligands are not shown; hydrogen atoms are only shown for the chelate cycles

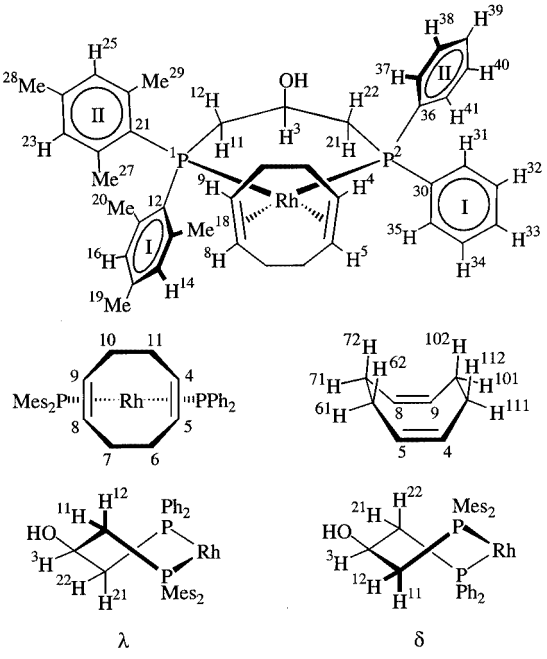

Figure 3. Labelling scheme used for **1**; the same numeric label as the hydrogen atoms to which they are bound, in general, designates the individual carbon atoms; carbon atoms belonging to the CH_2 groups of the COD ligand have labels which are numerically related to the labels used for the hydrogen atoms to which they are connected (e.g. C7−H71/H72, see figure); the carbon atoms of the three-carbon chain of the chelate ligand are numbered accordingly such that C1 binds to H11/H12, C2 to H21/H22, and C3 to H3; the labelling of the carbon atoms of the aryl groups is such that the carbon atoms have the same label as the respective protons; thus, C23 is bonded to H23, etc.; the carbon atoms are labelled with consecutive numbers around the cycles; the sense in which the numbers increase is evident from the labels assorted to the arene protons. The *ipso*-carbon atoms bonded to the phosphorus atoms have the lowest number in each case (C12, C21 for the mesityl groups; C30, C36 for the phenyl groups

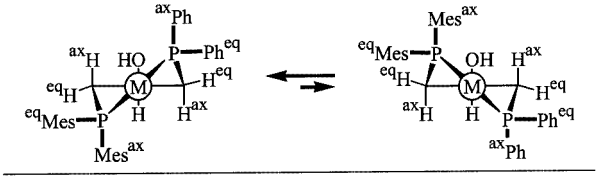

major isomer (λ)				minor isomer (δ)			
H^{eq}	H11	Mes^{eq}	H23–H29	H^{ax}	H11′	Mes^{ax}	H23′–H29′
H^{ax}	H12	Mes^{ax}	H14–H20	H^{eq}	H12′	Mes^{eq}	H14′–H20′
H^{eq}	H22	Ph^{eq}	H31–H35	H^{ax}	H22′	Ph^{ax}	H31′–H35′
H^{ax}	H21	Ph^{ax}	H37–H41	H^{eq}	H21′	Ph^{eq}	H37′–H41′

Figure 4. Labelling scheme for the two conformational isomers of **1**; the labelling scheme was chosen such that it refers to the identity of the specific atoms; this means that a proton that may occupy a pseudo-axial position in one isomer may find itself in a pseudo-equatorial position in the other one; the NMR spectroscopic signals referring to this specific proton will therefore find themselves at two distinctly different positions; throughout the paper the convention is adopted to assign unprimed numbers to the protons of the λ isomer and use primed numbers for the ones of the δ isomer. The pseudo-axial or pseudo-equatorial position of a proton, be it primed or unprimed, may be unequivocally inferred from the figure as given; for the ease of reading, the suffixes *ax* and *eq* are added to the labels wherever confusion might arise

tween e.g. nuclei in pseudo-axial and pseudo-equatorial groups, i.e. between different positions relative to the conformation of the chelate cycle. This differentiation is possible by NOE spectroscopy. Taking the λ and δ conformations observed for **1** in the crystal (Figure 2) as the ruler for distance based arguments the observed NOE cross-peaks can be consistently assigned.

The major isomer is found to correspond to the λ form of the chelate cycle (see below). The results are easily interpreted with respect to Figure 2 (left-hand side) which shows the structure of the λ isomer as found in the crystal. Referring to this figure the qualifiers left, right, top, and bottom make definite sense. The NOE analysis allows one to discriminate between the positions of individual groups with respect to these qualifiers. There are chains of contacts that link the top and bottom half of the molecule. A link on the rear side of the molecule (Figure 2, left) between the left-

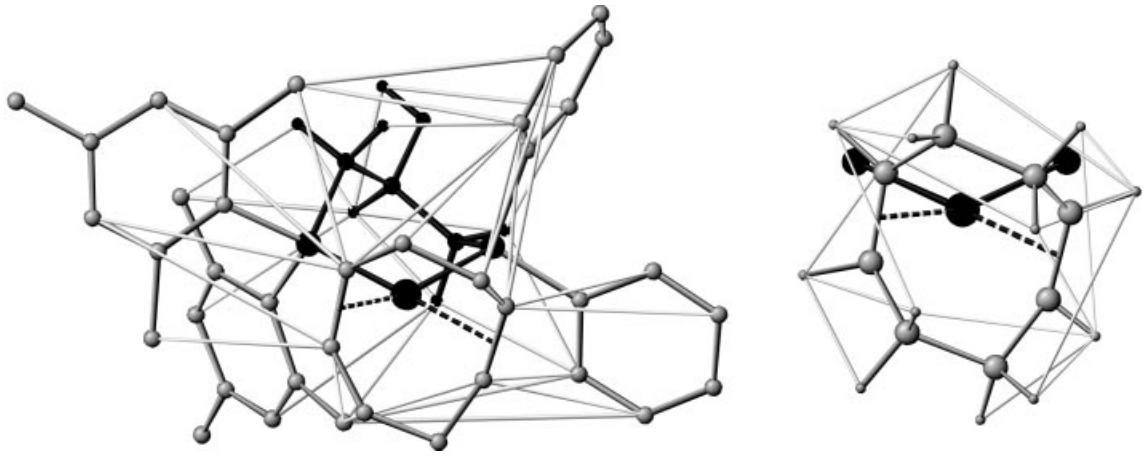

Figure 5. Scaffolding of NOE contacts characterising the λ twist conformer of **1**; NOE contacts are shown as light-grey shaded rods; right-hand side: conformationally relevant contacts within the COD coligand; left-hand side: contacts characterising the conformation of **1** as a whole (only a subset of observed contacts is shown; the full set is given in Table 8)

and the right-hand part of the molecule is formed by a number of contacts each of them involving the protons of the $CH_2-CH(OH)-CH_2$ linker (see above). On the front side of the molecule the left- and right-hand sides are also bridged by some interproton contacts (H18···H5, H18···H31,35; Figure 2 and 3). A tight scaffolding is therefore built up by the NOE contacts.

This scaffolding is shown in Figure 5 for the major isomer. The pertinent numeric information obtained by transforming NOE volume integrals into distances is given in Table 8. The NOE analysis of the minor isomer follows steps analogous to the ones used for the analysis of the major isomer. Due to the 1:5 ratio between the concentrations of the two isomers at the measuring temperature (298 K) a smaller number of contacts is observed. With the combination of methods described so far all the relevant ^1H-, ^{13}C-, and ^{31}P NMR signals of **1** can unequivocally be assigned (Table 3, 4, and 5). The details of the assignment of **1** are given in the Supporting Information.

Analogous procedures were used to assign individual nuclei in compounds **2**−**4**. The results pertaining to the assignment of **2**−**4** are shown in Table 5 and the Supporting Information.

Dynamic Exchange Processes

Dynamic exchange processes had already been found by variable-temperature 1D NMR spectroscopy for compounds of the type **1**−**7**.[8] To further elucidate these processes and to quantify activation barriers, 2D EXSY spectroscopy was applied to compounds **1**−**4**. Figure 6 shows parts of the 2D ^1H EXSY spectrum which characterises the dynamic exchange occurring for **1** in a CD_2Cl_2 solution at 298 K.

It is seen (Figure 6, left-hand side) that H3 exchanges with H3′; H11 is involved in a dynamic exchange process with H11′; H12 exchanges with H12′ and H22 is seen to exchange with H22′. It is clear from these observations that the shape of the chelate cycle switches between two conformations. With respect to the solid state structure of **1** which contains the λ and the δ isomers (Figure 2) the most

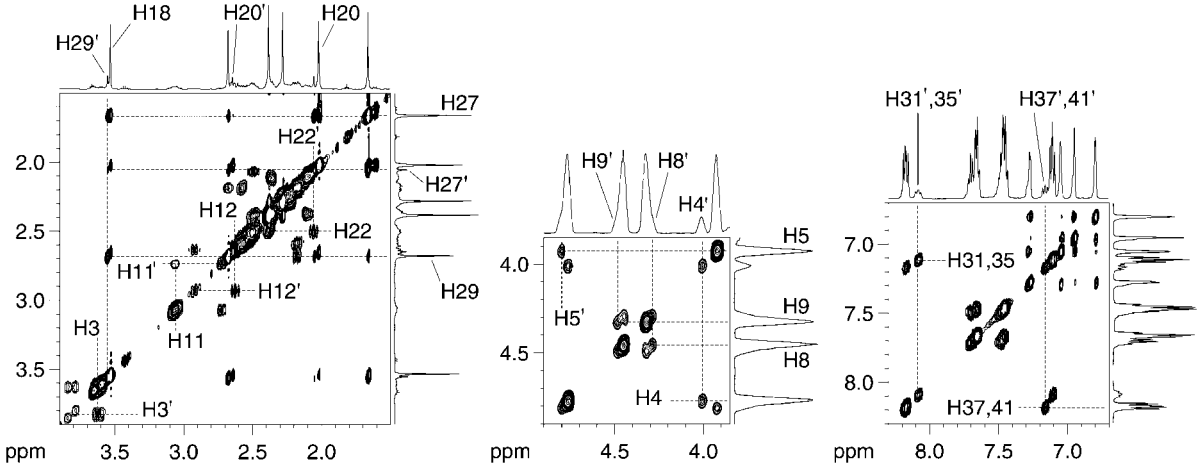

Figure 6. ^1H EXSY spectrum of **1** at 298 K; mixing time: 400 ms; all parts of the NOESY/EXSY spectrum of **1** are shown for which EXSY peaks can be observed; NOE peaks are suppressed in the figures shown

probable working hypothesis is to assume that the NMR observations pertain to the dynamic exchange between these two conformations (Figure 4). This hypothesis is proved by a series of further arguments including quantitative modelling of the conformations (see below). The part of the spectrum that characterises the dynamic behaviour of the COD coligand is shown in the center of Figure 6; H4 and H4′, as well as H5 and H5′, are in exchange with each other and so are H8/H8′ as well as H9/H9′. Exchange of the olefinic protons is hence only observed between protons at one and the same double bond. There is no cross-exchange between protons of the two different double bonds and any exchange process corresponding to a rotation of the COD coligand can therefore be ruled out. The observed process must then be due to an exchange of the surroundings of these olefinic protons such that, technically spoken, the COD coligand serves as a spectator ligand. Referring to Figure 2 it is seen that the position of the olefinic protons with respect to the PR_2 groups is just exchanged in the two isomers. In the course of the dynamic exchange between the two twist conformations (Figure 2) the substituents at the PR_2 groups must exchange their position with respect to their pseudo-axial or pseudo-equatorial positions. It is then expected that the phenyl *ortho*-protons H31,35 of one conformational isomer will exchange with the phenyl *ortho*-protons H31′,35′ of the other isomer (Figure 3 and 4). As Figure 6 (right-hand side) shows, this is in fact observed. The phenyl groups are free to rotate around their $P-C_{ipso}$ axes as is evident from the observation of just one signal for both *ortho*-protons of each of the phenyl groups. The mesityl groups on the other hand show well-separated sharp signals for each of their *ortho* and *meta* substituents in the one-dimensional ^1H NMR spectra. EXSY spectroscopy shows (Figure 6, left) that the exchange process includes an exchange of the mesityl groups as a whole. During this exchange process the mesityl groups are free to rotate since EXSY correlations are observed between H29′ and H29 as well as H27. The fact that each of the *ortho*-methyl groups at one mesityl group of one isomer is found to exchange with both of the *ortho*-methyl groups of the other mesityl residue in the other isomer, implies that at some stage of the isomerisation pathway the mesityl groups are free to rotate around their $P-C_{ipso}$ axes. As the corresponding exchange peaks are of different intensity, it follows that the probability of their rotation to either side is unequal. Some exchange is also observed between the *ortho*-methyl groups of the mesityl residues which is not accompanied by their switching between pseudo-axial and pseudo-equatorial positions, i.e. within one and the same isomer (Figure 6, left; H18/H20, H27′/H29′). This exchange process is again too slow to be apparent in the corresponding one-dimensional ^1H NMR spectra.

Quantitative analysis of the EXSY data (Exp. Sect.) reveals the dynamics of the system in quite some detail. The equilibrium $\delta \rightleftarrows \lambda$ has an equilibrium constant of $K = 4.7$ at 298 K. The rate constant determined for the conversion of the δ form into the λ form is $k_{\delta\rightarrow\lambda} = 1.8\ s^{-1}$, the reverse reaction shows $k_{\lambda\rightarrow\delta} = 0.4\ s^{-1}$ (Table 7). These rate constants have been derived from a whole series of ^1H-^1H EXSY experiments, with similar values stemming from ^{31}P-^{31}P EXSY spectra (see Exp. Sect.).

The transformation of the λ isomer into the δ isomer and the transformation of the δ isomer back into the λ isomer follows two different pathways with respect to the rotational motion of the mesityl groups. On both these pathways the mesityl groups are found to rotate in opposite directions around their $P-C_{ipso}$ axes. These motions are found to be strongly coupled (Figure 7).

Figure 7 illustrates the observed position of the respective methyl groups that ensues from the two different ways of $\lambda \rightleftarrows \delta$ transformation. The rotational pathway illustrated by the right-hand side of Figure 7 is deliberately assigned the label *D*. Pathway *D* refers to the clockwise rotation of the pseudo-equatorial mesityl group II around its $P-C_{ipso}$ axis that accompanies the $\lambda \rightleftarrows \delta$ transformation. EXSY analysis can of course not differentiate between a clockwise rotation of x degrees and a counter-clockwise rotation of $360 - x$ degrees. It can, however, clearly differentiate between the individual positions of the mesityl groups in the two isomers. The absolute positions are unequivocally established by NOE data and correspond to the ones shown in Figure 7. The left-hand side of Figure 7 illustrates the second pathway on which a $\lambda \rightleftarrows \delta$ isomerisation can occur. It is labelled *L* with respect to the counter-clockwise rotation of the pseudo-equatorial mesityl group II. EXSY data also demonstrate the strongly coupled and counter-sense rotation of the two mesityl groups on this second pathway. The probability of which pathway is taken is determined as $P_L = 0.8$ and $P_D = 0.2$ (the total probability that either of the two pathways will be taken during the transformation of the λ into the δ isomer ($\lambda \rightarrow \delta$) − and the reverse transformation ($\delta \rightarrow \lambda$) − is, of course, equal to 1). These probabilities are extracted from 2D ^1H EXSY measurements of the individual rate constants and are accurate to within 10% (Exp. Sect.).

Figure 8 illustrates the overall process. Starting from a λ isomer the two isoenergetic δ isomers, δ_L and δ_D, are formed. The only difference between these two forms is a 180° rotation of the mesityl groups around their $P-C_{ipso}$ axes.

The pathways shown in Figure 8 are illustrated with respect to the transformation of a λ into a δ isomer. During the back-transformation of a δ isomer into a λ one the same pathways are, of course, taken such that the δ_L as well as the δ_D isomer will again have the choice between two different pathways when transforming back into the λ conformation. The diagram in Figure 8 illustrates the reaction sequence $\lambda \rightarrow \delta \rightarrow \lambda$. The same arguments, as illustrated for this type of process, apply to the corresponding process starting from δ passing by λ and landing again at δ. In other words, if in the diagram every λ is replaced by a δ and every δ is replaced by a λ the corresponding probabilities remain unchanged. EXSY cross-peaks that refer to the pathways illustrated in Figure 8 are observed for $\lambda_{LD}/\lambda_{DL}$ as well as for the couple δ_{LD}/δ_{DL}. The two-step transformations from λ into λ_{LL} and λ_{DD} correspond to peaks on the diagonal and

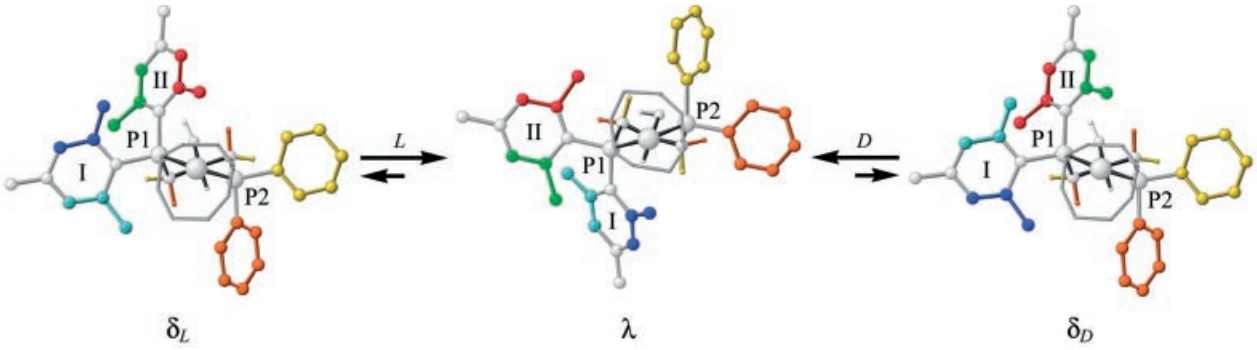

Figure 7. Coupling between λ ⇄ δ isomerisation and mesityl rotation; the rotation of the mesityl groups at a $PMes_2$ entity is strongly coupled; labels *L* and *D* for the pathways of the λ ⇄ δ isomerisation refer to the sense of this rotational process

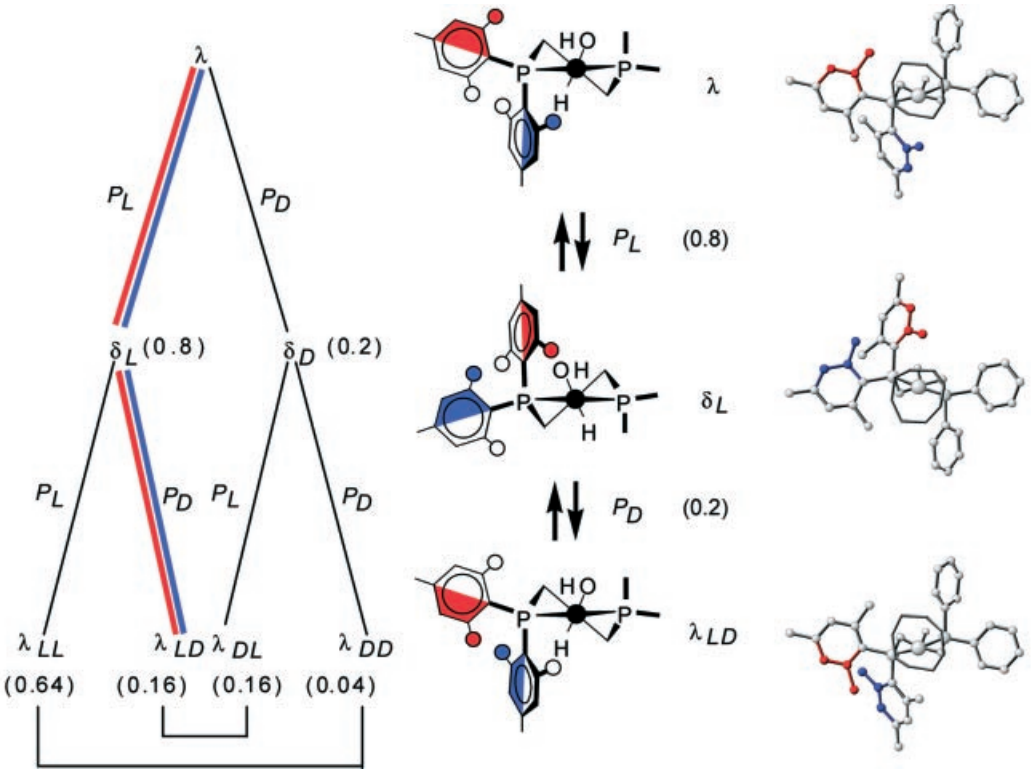

Figure 8. Probability of individual rotational motions of the mesityl groups during λ → δ/δ → λ isomerisation for **1**

are not seen directly. The fact that the couple $\lambda_{LD}/\lambda_{DL}$ can only ensue from λ by a sequence of two exchange steps is already clearly apparent from the time dependence of the corresponding 2D ^{1}H EXSY cross-peak intensity. If EXSY spectra are taken with different mixing times, single exchange processes are apparent by their nonzero slope at mixing time $\tau_m = 0$ s as well as by the linear dependence of the size of the corresponding integrals on mixing time over a range of short mixing times. Double exchange processes are, on the other hand, characterised by a zero slope at mixing time $\tau_m = 0$ s. The dependence of the corresponding integrals on time is close to parabolic instead of linear. The EXSY signals corresponding to the two-step processes $\lambda_{LD}/\lambda_{DL}$ and δ_{LD}/δ_{DL} show this parabolic dependence and zero slope at $\tau_m = 0$ s. The time dependence of the corresponding signals is correctly reproduced by the rate constants and reaction probabilities which were derived from the analysis of single-step processes (Table 7, Exp. Sect.).

With respect to the conformation of the $PMes_2$ group both pathways *D* and *L* involve a one-ring flip process.[14] This process is illustrated in Figure 9. The top half of this figure sketches the rotational reorientation undergone by the mesityl groups during a λ ⇄ δ isomerisation process following pathway *L* (major pathway). The bottom half correspondingly refers to pathway *D* (minor pathway). The diagrams show snapshots of these transformations. These snapshots have been obtained by a linear interpolation of the Rh−P−C_{ipso}−C_{ortho} torsion angles between their values in the λ and the δ isomers (X-ray structures taken as a basis). The graphs were obtained by orienting the $PMes_2$ group as a whole such that the pseudo-axial mesityl groups of the λ and δ isomers are close to vertical with the interme-

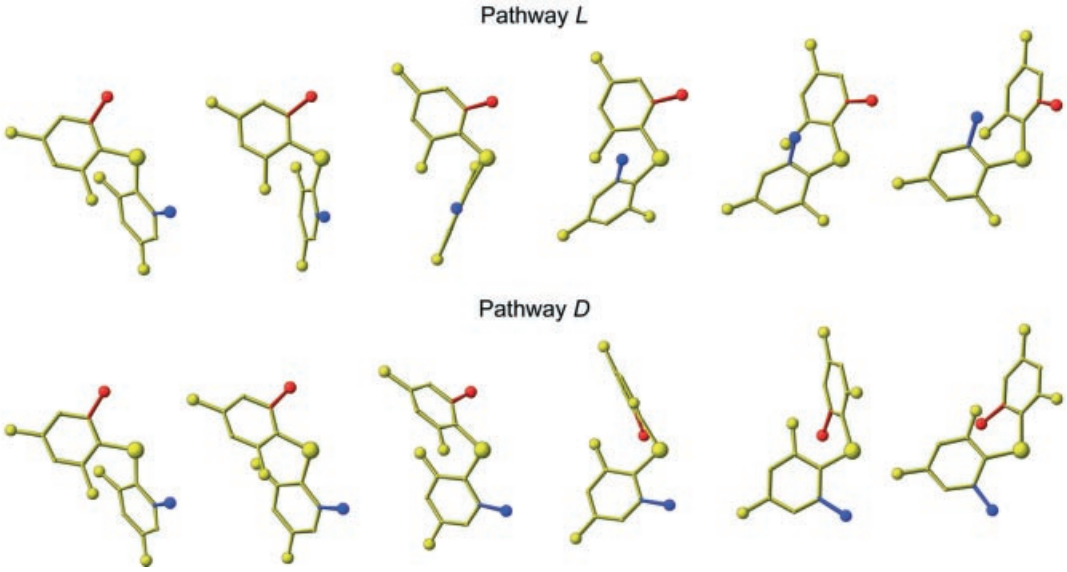

Figure 9. Illustration of the one-ring flip processes accompanying the λ ⇄ δ isomerisation for **1**; the labels *D* and *L* refer to the rotational pathways as illustrated in Figure 7

diate rotational positions again obtained by linear interpolation. The direction of view taken stays constant throughout Figure 9 and corresponds to a view along the pseudo-C_2 axis of the chelate framework. The sketches thus obtained are not to be taken as snapshots along the minimum energy pathway but they serve well to illustrate the fact that, whatever the real pathway looks like, it has to incorporate a one-ring flip process in each case.

The conformational isomerisation of **1** may thus be described as follows: δ and λ isomers interchange with one another with different rate constants (Table 7), with the λ isomer being the more stable one. The exchange process follows two different pathways with respect to the motion taken by the mesityl groups at the $PMes_2$ entity (Figure 9). There are two different types of motions both of which are such that the rotation of one mesityl group is strictly coupled to the rotation of the other mesityl group in each case (Figure 9). The barriers which correspond to these different pathways differ by approximately 4 kJ mol^{-1} at 298 K.

The same type of procedure as explicitly described for **1** was applied to compounds **2**−**4**. The corresponding data are given in the Exp. Sect. In the solid state **2** exists as just one conformational isomer [δ twist, (*R*) ligand; Figure 1].[15] For the purpose of further discussion, the argument is based on the (*S*) enantiomer of the ligand. The crystal structure of this isomer would of course correspond to the λ form (since the NMR experiments conducted are such that they do not differentiate between enantiomers in an absolute sense, this shift of reference frame has no further physical consequence; it is, however, indicated by the quest for a uniform illustration). NMR spectra show that two isomeric forms of **2** equilibrate with each other in solution. NMR structure analysis (see below, Exp. Sect.) proves that these two isomers are the λ and δ forms of the compound. At room temperature the λ isomer is the more stable one (K_{298} = 6.8). The activation barrier for the δ → λ transition amounts to $\Delta G^{\neq}_{298}$ = 68.1 kJ mol^{-1}; the barrier for the reverse transition is $\Delta G^{\neq}_{298}$ = 72.7 kJ mol^{-1} (Table 7). The process of δ ⇄ λ isomerisation is again coupled with a one-ring flip transition at the $PMes_2$ group. The process is as described for **1** and illustrated in Figure 7−9 for the case of **1**. The preference of one pathway over the other (*L* over *D*, Figure 7 and 8) is the same as observed for **1** with the relative probabilities of P_L and P_D amounting to 0.9 and 0.1.

The structure of compound **3** (Figure 1) has been determined for a crystal of the racemic compound.[9] In the solid state **3** exists as a 1:1 mixture of λ and δ forms. For the sake of a homogeneous description of the results, the arguments in this paper are based on the (*S*) enantiomer of the ligand; λ and δ isomers are clearly apparent in the NMR spectra of **3**. NMR structure analysis (see below and Exp. Sect.) shows that the λ isomer is the more stable one (K_{298} = 5.9). The barrier for the δ → λ transition is $\Delta G^{\neq}_{298}$ = 73.0 kJ mol^{-1}, and the barrier for the reverse process is $\Delta G^{\neq}_{298}$ = 77.4 kJ mol^{-1} (Table 7). As already observed for **1** and **2**, two different one-ring flip transitions are encountered along the isomerisation pathway. With respect to the illustrations given for **1** (Figure 7−9) the pathway labelled *L* is only slightly preferred over pathway *D* (P_L = 0.6, P_D = 0.4) in the case of **3**.

Compound **4** (Figure 1) exists as a 1:1 mixture of λ and δ isomers in the solid state.[8] The two isomers are also present in solution with a preference of 3:1 of the λ isomer over the δ isomer at 298 K. The activation barriers are $\Delta G^{\neq}_{298}$ = 71.6 kJ mol^{-1} for the δ → λ process and $\Delta G^{\neq}_{298}$ = 74.5 kJ mol^{-1} for the reverse transition (Table 7). With the ligand of **4** containing a $P(o\text{-anisyl})_2$ and a $P(mesityl)_2$ group different rotational orientations of the aryl groups at the PR_2 entities might in principle be apparent for both of the PR_2 groups. EXSY spectra indicate that there is also some exchange with respect to a rotation of the anisyl

groups. The corresponding EXSY peaks are an order of magnitude smaller than the ones referring to the analogous rotation of the mesityl groups. The smallness of the corresponding exchange peaks and their partial overlap with other signals excludes the quantitative analysis of this exchange. If these minor peaks are ignored and the exchange referring to the anisyl groups is correspondingly modelled as a two-site exchange process (Exp. Sect.) the resulting rate constants agree with the overall rates for the $\delta \rightleftarrows \lambda$ isomerisation process within the limits of error (Table 7). The individual probabilities for the pathways *L* and *D* are found to be $P_L = P_D = 0.5$.

Results from Dissolving Crystals of 1−7 at Low Temperatures

Crystals of **1**−**7** have been found to contain either just one conformational isomer (**2**: twist; **6**, **7**: chair) or two of them in equal amounts (**1**, **3**, **4**, **5**: λ, δ twist). If the activation barriers for the conformational isomerisation are high enough, dissolution of the crystals at low temperature should produce metastable solutions which would in the optimal case contain the conformational isomers in the same ratio as they are present in the crystals. This way an independent assignment of conformations could thus be possible. Another benefit of this type of experiment is that the rate constants of the processes as well as their dependence on temperature could be obtained in independent experiments. ^{31}P NMR spectroscopy was used as the experimental tool throughout.

As crystals of **1** contain a 1:1 mixture of λ and δ isomers, dissolution of these crystals at low temperatures is expected to produce a solution that contains the two isomers in a 1:1 ratio. The activation barriers for the $\delta \rightarrow \lambda$ and $\lambda \rightarrow \delta$ isomerisation have already been found to be above 70 kJ mol^{-1} (see above) such that at the lowest feasible temperature using CD_2Cl_2 as a solvent, isomerisation should be very slow. It is in fact observed that between 175 and 200 K the ratio with which the λ and δ isomers are contained in the solution is 1:1 [Figure 10; $\ln(c_\lambda/c_\delta) = 0$]. Above this temperature an increase of the concentration of one isomer over the other is observed. This increase upon warming the solution is observed in the temperature range between 200 and 230 K (Figure 10). From then on by rising the temperature further the isomer ratio follows an opposite trend. This behaviour is shown in Figure 10 in an $\ln(c_\lambda/c_\delta)$ vs. T^{-1} diagram.

The linear slope of the curve above 230 K indicates that an equilibrium between the two species is established at every measuring point. At the same time it is clear that the appearance of the sigmoidal curve as the temperature increases between 200 and 230 K relates to the fact that an equilibrium cannot be reached in this temperature interval within the time allotted to the experiment (ca. 3 h). The same conclusion is reached by cooling the solution from about 300 to 170 K. In the range of 300 to 230 K the slope of the $\ln(c_\lambda/c_\delta)$ vs. T^{-1} curve is linear, as was already found

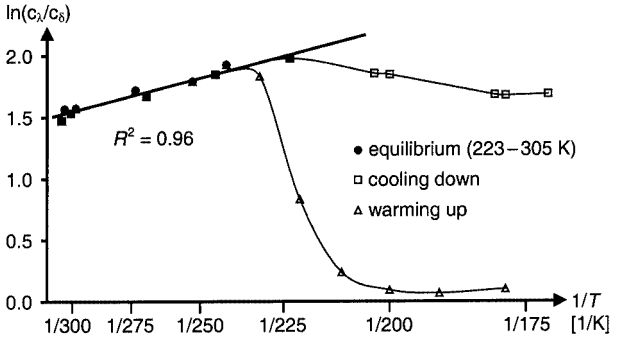

Figure 10. Isomeric ratio of **1**; the sigmoidal curve in the plot refers to ratios observed after dissolving crystals of **1** at low temperature and gradually warming these solutions (triangles); the points along the bold-face line correspond to experiments where thermal equilibrium has been reached; the open squares correspond to situations for which during cooling down equilibrium conditions could not be met; the abscissa is scaled as 1/*T*, the ordinate has a logarithmic scale

in the experiment where the temperature was increased from 230 to 300 K (Figure 10). From about 220 K on the measured ratios no longer follow the straight line but tend to level out at a value of $\ln(c_\lambda/c_\delta)$ of around 1.7 (c_λ/c_δ = 5.4). This behaviour must be due to the fact that at temperatures below 220 K equilibrium can no longer be achieved within the time given. From the slope of the straight line part of the diagram the ΔH and ΔS values relating to ΔG may be extracted; ΔS is found to be close to zero (ΔS = 1.7 J K^{-1} mol^{-1}) and ΔH amounts to −3.4 kJ mol^{-1} (Table 1).

Some information about the kinetics of the process is obtained by monitoring the time dependence of the concentration ratio c_λ/c_δ at low temperatures during the warming up experiment. From the equilibrium constant it is known that the rate constant of the forward process $\delta \rightarrow \lambda$ is about ten times larger than the rate constant referring to the back reaction. At low temperatures the mixture is far from equilibrium and the concentrations of both isomers are about equal. Evaluation of the time dependence of the c_λ/c_δ ratio at intervening temperatures leads to rate constants at these temperatures (see Exp. Sect.) such that the activation parameters for $\delta \rightleftarrows \lambda$ interconversion may be estimated (Table 1); $\delta \rightarrow \lambda$ isomerisation corresponds to $\Delta H^{\neq}$ = 60.5 kJ mol^{-1}, $\Delta S^{\neq} = -37$ J K^{-1} mol^{-1}, with the reverse reaction being characterised by $\Delta H^{\neq}$ = 64.4 kJ mol^{-1}, $\Delta S^{\neq} = -36$ J K^{-1} mol^{-1} (Table 1).

Similar experiments have been performed for compounds **2**−**7** (see Supporting Information) leading to estimates of thermodynamic and kinetic parameters as given in Table 1.

Quantitative NMR Spectroscopic Structure Analysis

While all NMR spectroscopic data show that compounds **1**−**7** exist as mixtures of two conformational isomers in solution, it is not clear from the beginning which conformation corresponds to which isomer. In the case of **2** the experiments referring to the dissolution of a crystalline

sample of **2** at low temperatures (see preceding paragraph) could decide between the λ and δ forms of this compound and an absolute assignment was thus possible.

As a general tool to assign definite conformations to the different isomers, distance geometry (DG) methods were applied to compounds **1**−**4**. Based on the ^{1}H NOE data (Table 8, Figure 5) restraints on interproton distances were defined in each case. The initial structural models were chosen as the λ and δ conformations, the structure of which is basically known from X-ray data. It was found that the results obtained were quite independent of whether those starting conformations were taken as the X-ray determined conformations themselves or as the appropriate conformations as modelled by the ESFF force field.[16] It was also found that when starting from a modelled chair conformation, which is quite improbable on the basis of the X-ray results, the final distance geometry determined conformations were the same as the ones reached from the other starting points. For the final calculations the X-ray determined models were used as the starting point. These calculations were performed for the major and for the minor isomer in each case. For each of the two conformational isomers observed in solution for compounds **1**−**4** both λ and δ twist conformations were chosen as the starting points.

For distance geometry refinement different strategies can be applied dependent on the amount of variation allowed to the NOE-derived restraints. With weak restraints, corresponding to a large amount of variation being permitted, λ and δ forms can interchange into one another. In order to discriminate between the two principle possibilities the resulting optimised conformations have to be sorted into λ and δ classes after refinement. The calculated NOE distances for these refined structures may then be compared with the experimental ones in order to decide whether λ or δ gives the better fit. Another strategy that was applied throughout for the calculations reported here consists of using strong NOE restraints, i.e. variations allowed only to within ±5% with respect to the NOE determined distances. With this strategy λ and δ forms cannot change into one another such that two sets of optimised structures are finally obtained, one exclusively containing conformations with a λ twist and the other one with only δ conformations. In the case of the major isomer it was observed for all compounds **1**−**4** that the rms values as calculated by the error function of the DG programme[17,18c,29a] were about one order of magnitude different for the two classes. The class relating to the lower rms values should then be the one to which the isomer belongs. Different types of qualifiers may be used to ascertain this decision (Exp. Sect.). All of them unequivocally lead to the same result, i.e. the λ isomer is the more stable one throughout (Exp. Sect., Table 8, 9). This result shows the power of distance geometry methods in assigning conformations. There is only one proton (H3;

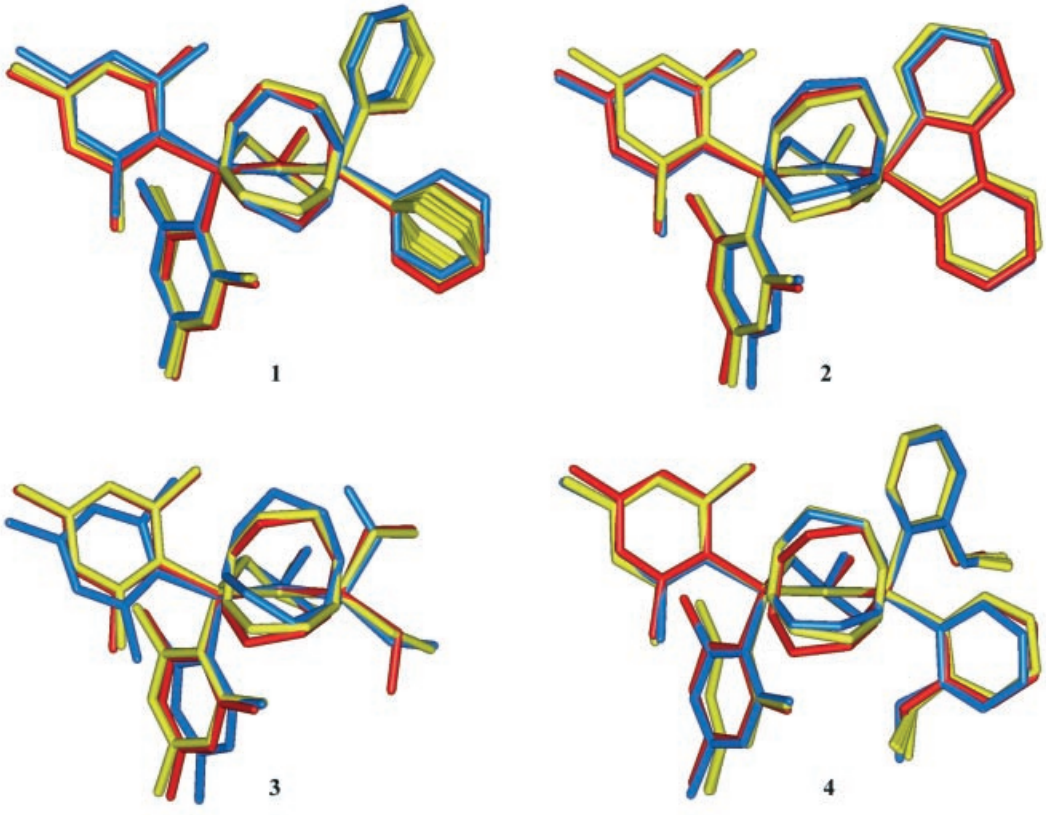

Figure 11. Overlay of the conformations of **1**−**4** (λ twist form) as inferred by different techniques; colour code: blue: X-ray structure; red: optimal single conformation as derived from force field refinement; yellow: DG-derived conformations

Figure 2 and 3 and 5), the proton at the chiral carbon atom, that directly pinpoints to λ and δ conformations. A sufficient number of NOE contacts involving H3 could be determined for each of the compounds **1**−**4** for the major isomer, and these contacts are most important in differentiating between λ and δ forms. For the minor isomer only a smaller number of contacts was experimentally accessible in each case. Nevertheless, applying the same procedure as described for the major isomer did not lead to any contradiction of the conclusive results obtained for the major isomer in each case. Whenever the major isomer was found to have a λ conformation, as was the case for each of the compounds **1**−**4**, the set of solutions obtained for the minor isomer by distance geometry refinement had a better fit for the models with δ conformation than for the ones with λ conformation (Exp. Sect., Table 9). This means that even with the small number of NOE contacts found for the minor isomer in each case, distance geometry methods are able to differentiate between λ and δ forms of the chelate cycle.

It is found throughout (Figure 11) that the average structure in solution conforms nicely to the structure in the solid state. This is shown in Figure 11 for all compounds **1**−**4** for the major isomer. The scatter of conformations as inferred from the results of DG runs is also shown in Figure 11.

It is seen that the only parts that are rotationally flexible to a higher or lesser degree, are the phenyl residues (**1**), the ethyl groups (**3**), and the methoxy groups (**4**). It is also seen that the conformations of **2** containing the DBP residue show no scatter at all. The graphs in Figure 11 also show a comparison with the structure of the least-energy model obtained in each case by force field refinement. Again, the difference between the solid state conformations and the force field calculated conformations is quite small in all cases; all three models, X-ray, DG refinement, and force field refinement are almost exactly congruent for **2** which means that due to steric repulsions and the fixed geometry of the DBP group this conformation finds itself in a minimum of the corresponding energy hypersurface which has steep ascents in all directions.

Discussion

An important result of this study is that it is found that structures determined by X-ray methods in the solid state and structures characterising the ensembles of molecules in solution are congruent within the limits of error. This gives much credit to the application of NMR spectroscopic structure analysis − which has been so successful in protein structure assignment[18] − also with small molecules. Even if the number of discriminative NOE contacts is much smaller in small molecules than it is in proteins (due to the fact that amino acids, which are far apart in a sequence,

Table 1. Thermodynamic and activation parameters for **1**−**7**

[a]		ΔH[b] [kJ mol^{-1}]	ΔS[b] [J K^{-1} mol^{-1}]	ΔG_{298} [b] [kJ mol^{-1}]	K_{298} [b]	$\Delta H^{\neq}$ [kJ mol^{-1}]	$\Delta S^{\neq}$ [J K^{-1} mol^{-1}]	$\Delta G^{\neq}_{298}$ [kJ mol^{-1}]
1	δ → λ λ → δ	−3.4(2)	1.7(9)	−3.9	4.7	60.5(20)[c] 64.4(18)[c]	−36.5(70)[c] −35.9(70)[c]	71.4[c] 75.1[c]
2	δ → λ λ → δ	−7.5(3)	−10.1(13)	−4.5	6.3	−	−	68.6 73.3
3	δ → λ λ → δ	−1.8(1)	8.4(5)	−4.3	5.7	65.8(12)[c] 67.4(11)[c]	−25.9(50) [c] −35.5(40) [c]	73.6[c] 78.0[c]
4	δ → λ λ → δ	−1.6(1)	4.2(4)	−2.8	3.1	−	−	72.1 75.0
5	A → B[d] B → A[d]	−0.5(1)	−0.6(4)	−0.3	1.2	53.2(15)[e] 53.7(15)[e]	5.0(60)[e] 5.6(60)[e]	51.7[e] 52.1[e]
6	A → B[d] B → A[d]	0.0(3)	3.8(13)	−1.2	1.6	41.4(10)[e] 41.4(10)[e]	−47.0(40)[e] −50.7(40)[e]	55.4[e] 56.5[e]
7	A → B[d] B → A[d]	−5.0(2)	−9.1(9)	−2.3	2.7	50.2(19)[e] 55.1(19)[e]	−31.1(70)[e] −22.1(70)[e]	59.4[e] 61.7[e]

[a] The estimated standard deviation in units of the least significant digit is given in parentheses. [b] The signs of the thermodynamic parameters refer to the process minor isomer ⇄ major isomer. [c] Values refer to Eyring plots which were based on the rate constants measured at higher temperatures by EXSY methods (Table 7) and rate constants determined under nonequilibrium conditions (**1**: T [K], $k_{\delta\rightarrow\lambda}$ [s^{-1}], $k_{\lambda\rightarrow\delta}$ [s^{-1}]: 221, 2.4·10^{-4}, 0.3·10^{-4}; 232, 1.8·10^{-3}, 0.3·10^{-3}; **3**: T [K], $k_{\delta\rightarrow\lambda}$ [s^{-1}], $k_{\lambda\rightarrow\delta}$ [s^{-1}]: 212, 1.3·10^{-5}, 0.2·10^{-5}; 224, 7.1·10^{-5}, 1.0·10^{-5}; 235, 5.2·10^{-4}, 0.8·10^{-4}). The $\Delta G^{\neq}_{298}$ values thus calculated are in close agreement to the ones determined from EXSY measurements alone. [d] A: minor isomer, B: major isomer; the exact geometry in solution has not been determined. For the solid state structures see Figure 1. [e] Activation parameters refer to Eyring plots based on rate constants determined by line shape analysis of ^{31}P NMR spectra.

may be in close contact to each other due to the folding of the proteins while constituents of a small molecule which are separated by a far smaller number of intervening atom−atom distances are rarely found to be in close contact to each other) this small number of contacts is still sufficient to determine the structure of small molecules as well.

The refinement of structural models as developed by DG methods has to make use of force field calculations. It appears that the general ESFF force field[16] is well parameterised for this purpose as seen by refining the X-ray derived models by these methods. Almost negligible changes of the conformations are observed in this case. It is also satisfying to note that the energy differences between the λ and δ isomers as calculated by the force field approach in each case are in the same order of magnitude as the ones which have been experimentally determined (Table 1). The calculated energy differences are $\Delta E = E_\lambda - E_\delta = 2.1$, -0.2, 6.1, and -2.5 kJ mol^{-1} in the series of compounds **1**−**4**. Comparison with the experimental ΔH values in Table 1, shows that the calculated values do not correctly predict which of the two forms is the more stable one nor do they rank the compounds correctly with respect to these energy differences. Since force field methods have been found to be quite appropriate for the calculation of such small energy differences in the stereochemistry of organic ring compounds[19] it is evident that it is not the force field method in itself which leads to wrong results in the case of **1**−**4** but that the parameterisation of these methods is not yet good enough for metal-containing compounds.

As far as the energy differences between the two conformers are concerned they are found to be in a small range for all compounds **1**−**7**. It is seen that the larger the steric discrimination between the two different PR_2 groups is [$PMes_2/PEt_2$ (**3**), $PMes_2/PPh_2$ (**1**), $PMes_2/P(o\text{-anisyl})_2$ (**4**)] the more the equilibrium will lie on the side of the λ twist form (Table 1). The λ twist form is even more preferred by **2** with its $PMes_2$ substituent on one side and a dibenzophospholyl group on the other side. The rigidity of the DBP residue obviously causes less interference within the molecule than even a PEt_2 group (Table 1). The almost 1:1 equilibrium between the two forms of **5** [$P(o\text{-anisyl})_2/PMes_2$] indicates that the steric influence of these two groups onto the chelate cycle is not greatly different. For compounds **6** and **7** [$P(o\text{-Tol})_2/PPh_2$ (**6**), $P(o\text{-Tol})_2/PEt_2$ (**7**)] the lesser steric demand of PEt_2 in comparison to PPh_2 again mirrors itself in the equilibrium constants with the equilibrium referring to **7** being more biased ($K = 2.7$) than the one referring to **6** ($K = 1.6$). Due to the differences in the entropic terms the ΔG_{298} values show a smaller difference amongst the series of compounds than do the ΔH values such that the equilibrium constants K_{298} are in the narrow range of 1.2−6.3.

Throughout the series of compounds **1**−**4** the λ isomer is the more stable one. The reason for this is intuitively clear from looking at the structural models (Figure 11) where it is seen that the C−O bond at the central carbon atom of the ligand is tilted such as to orient it away from the mesityl side of the compounds, i.e. away from the bulkier of the two PR_2 groups (Figure 11).

The activation barriers are higher than those normally found in saturated organic ring compounds (ca. 30 kJ mol^{-1} higher than in cyclohexane).[20] The activation entropies are definitely negative for the two compounds for which they could be determined (**1**, **3**). This indicates that sterically highly crowded situations are met along the transition pathway.

For all compounds **1**−**7** data about the efficiency in catalysing the enantioselective hydrogenation of (*Z*)-2-acetamidocinnamic acid are available.[8] No direct correlation between the reported *ee* values[8] and any of the thermodynamic and kinetic data reported in this paper is apparent. Thus, it has been found that compound **5** is the most enantiodiscriminating catalyst leading to *ee* values of the hydrogenation product of up to 85% *ee*[8] while the two isomers of this compound are present in a close to 1:1 ratio at the temperature of catalysis (298 K). Compounds **1** and **2** which show a strong predominance of the λ conformation (Table 1) produce *ee* values of only 40−60%.[8] Compound **6**, for which both conformations have equal enthalpies (Table 1) and for which the major/minor equilibrium is close to 1:1, yields the hydrogenation product with around 50% *ee*.[8] It is thus clear that the thermodynamic equilibrium of the λ and δ forms of the precatalyst has no direct bearing on the chirality of the transition state of the hydrogenation reaction. Table 1 and the data published on the catalytic activity of **1**−**7**[8] allow for the following hypothesis. Since both compounds **6** and **7** have a chair conformation in the solid state and are at the same time least efficient in enantiodiscrimination it appears probable that twist conformations are a prerequisite for an efficient enantioselective catalyst. Compounds **1**−**5** show twist conformations in their solid state structures. For compounds **1**−**4** the persistence of twist conformations in solution is proved in this paper. For compound **5** this persistence is not proven by NMR spectroscopic analysis but highly probable. Compound **5** is the most efficient enantioselective catalyst amongst compounds **1**−**5**. On the other hand **5** is a compound where the two forms (presumably λ and δ twist) are of almost equal stability (Table 1). A high degree of enantioselectivity as found for **5** can therefore not ensue from the predominance of one of the two chiral forms of **5** over the other. Enantiodiscrimination must then be due to an induced fit between the prochiral substrate and the chiral coordination scaffolding.[21] For this type of fit, as induced by the substrate, consisting of switching from λ to δ twist conformations or vice versa, it is seen from Table 1 that amongst the enantiodiscriminating catalysts **1**−**5** compound **5** is the one with the lowest activation barrier for this switching process. It may then be argued that a prerequisite for an efficient enantiodiscriminating catalyst is the intrinsic stability of its λ and δ twist forms as well as a low barrier for the transformation between these forms such that a prochiral substrate may easily induce the appropriate fit.

Conclusion

Compounds $[\{\kappa\text{-}PR_2CH_2CH(OH)CH_2\text{-}\kappa\text{-}PR'_2\}Rh(\eta^4\text{-}COD)]^+PF_6^-$ exist as λ and δ conformers when at least one of their PR_2 groups is a $PMes_2$ entity. As shown by quantitative NMR spectroscopic structure analysis their conformations in solution correspond to the conformations adopted by them in the solid state. From the two conformations the one which is preferred is that which keeps the central C−O bond of the chelate ligand away from the mesityl side. The experimentally determined difference between the enthalpy of the two isomers is found to lie within a few kJ mol^{-1} with ΔS values in the range of ± 10 J K^{-1} mol^{-1}. The free energies of activation for the conformational changes (δ → λ and λ → δ) are around 70 kJ mol^{-1}. Negative activation entropies indicate the steric strain along the reaction pathway. The mesityl groups at the $PMes_2$ entity behave as coupled rotors, their rotation is only possible in the transformation between λ and δ forms. Due to the chirality of the compounds the probabilities with which rotation in either sense will occur are not generally equal. The rotational pathways taken correspond to one-ring flip processes in each case. The precise thermodynamic data worked out in this paper may serve as criteria to evaluate force field models that describe the compounds in the sense of a mechanical molecular machine.[22]

Experimental Section

General Remarks: Bruker instruments of the type DPX200 operating at 200.13 (^{1}H), 81.014 MHz (^{31}P), DRX300 at 300.13 MHz (^{1}H), 75.468 (^{13}C), 121.495 MHz (^{31}P), and DRX500 at 500.13 (^{1}H), 125.758 (^{13}C), 202.456 MHz (^{31}P) were used throughout. Chemical shifts are given in ppm with respect to CD_2Cl_2 (^{1}H: δ = 5.32 ppm; ^{13}C: δ = 53.5 ppm) as internal standard. ^{31}P chemical shifts are expressed in ppm with respect to an aqueous solution of H_3PO_4 (85%) as external standard. All measurements were performed on samples dissolved in CD_2Cl_2 under argon in sealed NMR tubes. The dissolution of crystalline material at low temperature was performed as follows: NMR tubes were fixed to a vacuum line. The crystalline sample was introduced into the tube under argon and the tube was immersed into a liquid N_2 bath. CD_2Cl_2 was condensed onto it and the tube was sealed. The solid material (sample and CD_2Cl_2) was allowed to warm up to 160 K and transferred at this temperature into the NMR probehead. The temperature of the probehead was gradually increased until the shape of the ^{31}P NMR resonances showed that the sample had completely dissolved. The temperature was calibrated using [D_4]methanol (99.8%) and ethylene glycol samples.[23]

Measurement Techniques and Assignment: Standard pulse sequences were applied throughout. The acronyms given in Table 2 refer to the standard Bruker pulse sequence library. By a combination of 1D and 2D NMR spectroscopic experiments (Table 2) unequivocal assignment of the NMR resonances of the two isomers was possible for **1**−**4**. NMR spectroscopic data referring to **1** are shown in Table 3 and 4. NMR spectroscopic data for **2**−**4** are available as Supporting Information. For compounds **5**−**7** analysis was based on ^{31}P NMR spectra alone. The complete set of ^{31}P NMR spectroscopic assignments for **1**−**7** is given in Table 5. The peak volumes of 2D NMR spectra were measured by the volume integration algorithm supplied with the FELIX NMR spectroscopic processing software package.[24] 2D ^{1}H NOESY/EXSY data were collected with different mixing times (see Table 2) at 298 K throughout. For the purpose of quantitative interpretation of the ^{1}H NOE data the initial rate approximation was chosen.[25] The dependence of the peak volumes on mixing time was first analysed by the inspection of the corresponding graphs (Figure 12, right). Based on this inspection it was decided how many measuring points should be included for obtaining the slope in a linear fit. The peaks above and below the diagonal were analysed separately. Further evaluation was based on the one of the two graphs that showed the larger slope. In general the volume of the corresponding peaks above and below the diagonal were in good agreement (Figure 12, right).^{1}H EXSY peaks were evaluated by the same type of procedure (Figure 12, center), where the average of the volume integrals of the peaks above and below the diagonal, was used. To evaluate the rate constants the slope based on the values obtained for a mixing time of $\tau_m = 50$ ms was used throughout, since it was found that internal consistency of the rate data decreases if longer mixing times within the "linear" first part of the curve (Figure 12, center) are incorporated in calculating the slope. The volume integrals of the diagonal peaks showed the expected continuous decrease with increasing mixing time as seen from the curves in Figure 12 (left). A single exponential fit (solid line) is not completely appropriate especially at short mixing times. It was decided therefore to use the two integrals corresponding to the shortest and the next shortest mixing times (Figure 12, left) in a linear extrapolation in order to estimate the integral value at mixing time $\tau_m = 0$ s. 2D ^{31}P EXSY data were collected with mixing times of 100−600 ms at 298, 300, and 305 K. Volume integrals collected with mixing times of up to 400 ms were found to be far enough away from saturation such as to allow kinetic data to be extracted from them.

Coupling Constants: Since the experiments on **1**−**4** make it clear that the major isomer corresponds to the λ twist conformation of the chelate ring in each case and since the structure of the twist conformations is known from X-ray analysis as well as from modelling and NOE data, the torsion angles H−C−C−H, H−C−C−P

Table 2. Experimental details of the 2D NMR experiments for **1**−**4**

	DQF-COSY	^{1}H-^{31}P HMBC	^{1}H-^{13}C HSQC	^{1}H-^{13}C HMBC	^{1}H NOESY/EXSY	^{31}P EXSY
Pulse program[a]	cosygsmftp	inv4gslrnd	invietgssi	inv4gslplrnd	noesytp	noesydctp
TD (*F*2/*F*1)	4096/256	2048/128	2048/256	2048/256	4096/256	2048/128
NS	32	24	16	32	16	32
τ_m [ms]	−	25−180	−	60−80	50−800	100−600
D1 [s]	1.7	1.6	1.6	1.5	2.0	2.0

[a] The acronyms in this row refer to pulse programmes supplied under these names for the BRUKER Avance DPX/DRX series of instruments.

Table 3. ^{1}H NMR spectroscopic data of **1**

λ isomer[a] Major	δ(^{1}H)	Pattern ^{1}H	$^nJ_{H,H}$/($^nJ_{HP}$) [Hz]	δ isomer[a] Minor	δ(^{1}H)	Pattern ^{1}H	$^nJ_{H,H}$/($^nJ_{HP}$) [Hz]
H37,41$_{ax}$	8.16	ddd	7.1/(11.4/1.0)	H31′,35′$_{ax}$	8.08	dd	7.2/(10.3)
H39$_{ax}$	7.70	m	7.3/1.0	H33′$_{ax}$	7.69	ov	
H38,40$_{ax}$	7.64	m	8.0/1.1	H32′,34′$_{ax}$	7.66	ov	
H33$_{eq}$	7.49	m	7.1/(1.5)	H39′$_{eq}$	7.48	m	
H32,34$_{eq}$	7.44	m	7.6/(2.0)	H38′,40′$_{eq}$	7.46	ov	
H14$_{ax}$	7.26	br. d	(3.7)	H25′$_{ax}$	7.29	d	(3.7)
H31,35$_{eq}$	7.11	ddd	6.8/1.1/(9.5)	H37′,41′$_{eq}$	7.16	dd	7.3/(9.8)
H25$_{eq}$	7.04	br. s		H16′$_{eq}$	7.04	ov	
H16$_{ax}$	6.94	br. s		H23′$_{ax}$	6.96	s	
H23$_{eq}$	6.79	br. s		H14′$_{eq}$	6.79	ov	
H4	4.77	br. m	11.5/7.3	H5′	4.79	ov	12.5
H8	4.46	br. m	11.6/7.4/(4.1)	H9′	4.48	ov	15.0
H9	4.33	br. m	12.2/6.6	H8′	4.28	ov	15.0
H5	3.92	br. m	12.4/7.4/(4.1)	H4′	4.01	m	12.0/6.8
H3	3.63	m	10.6/6.0/(12.0)	H3′	3.82	m	8.2
H18$_{ax}$	3.52	s		H29′$_{ax}$	3.56	s	
H11$_{eq}$	3.07	dddd	13.7/5.6/2.3/(10.2)	H12′$_{eq}$	2.93	m	15.4/6.2
H29$_{eq}$	2.68	s		H20′$_{eq}$	2.64	s	
H12$_{ax}$	2.62	m	14.1/10.1	H11′$_{ax}$	2.73	dd	15.4/6.7
H111	2.58	m	14.2/6.8	H61′	2.55	ov	
H101	2.50	m		H71′	2.48	ov	
H22$_{eq}$	2.49	m	15.4/1.7	H21′$_{eq}$	2.67	ov	13.8/9.1
H19$_{ax}$	2.37	s		H28′$_{ax}$	2.38	ov	
H112	2.36	m	9.7/6.8	H62′	2.36	ov	
H71,72	2.33	m		H101′,102′	2.37	ov	
H28$_{eq}$	2.27	s		H19′$_{eq}$	2.27	ov	
H102	2.23	m	12.8/6.3	H72′	2.22	ov	
H21$_{ax}$	2.17	ddd	15.4/7.1/(1.8)	H22′$_{ax}$	2.05	ov	13.8/11.3
H61,62	2.13	m	16.4/10.6	H111′,112′	2.19	ov	
H20$_{ax}$	2.01	s		H27′$_{ax}$	2.05	s	
HO	1.74	d	4.7	HO′	1.43	d	8.8
H27$_{eq}$	1.66	s		H18′$_{eq}$	1.65	ov	

[a] Labels refer to Figures 3 and 4; measuring frequency: 500.13 MHz; temperature: 298 K; solvent: CD_2Cl_2; observed signal pattern abbreviations: s = singlet, d = doublet, t = triplet, m = multiplet, ov = overlapping signal, br. = broad.

and H−C−P−C can be calculated for both the λ twist and δ twist forms of each of the compounds **1**−**4**. The torsion angles allow the degree of ^3J coupling to be predicted in each case. Determination of the corresponding coupling constants is in part possible by 2D NMR spectroscopic experiments. Even in the case where a numerical value of an individual coupling constant cannot be obtained with sufficient accuracy, the relative degree of coupling may be inferred from the size of the corresponding volume integrals. If the observed degree of coupling is ranked as strong (*s*), medium (*m*) and weak (*w*) a comparison of the ranking derived from calculated torsion angles and the ranking derived from NMR spectroscopic experiments is possible. This type of comparison is shown in Table 6 for the λ twist isomer of **1** as an example. It is seen that on the basis of $^3J_{H,H}$ coupling the agreement between calculated and experimental degrees of coupling is definitely better for the values calculated for the λ twist isomer than for the ones derived from the geometry of the δ twist isomer. It is also seen that the $^3J_{HP}$ and $^3J_{HC}$ couplings do not differentiate between the two twist isomers. If on the other hand a chair conformation of the chelate cycle is chosen as the basis of comparison (Table 6) almost all of the experimental $^3J_{HX}$ couplings show a definite misfit. It is seen then that the $^3J_{HX}$ couplings strongly indicate that the solution structure of the major isomer of **1** adopts a twist conformation while only the $^3J_{H,H}$ couplings involving H3 (Figure 3) allow to differentiate between its λ twist and δ twist forms. The λ twist form that in fact corresponds to the conformation of the major isomer gives the best agreement, as expected. The same type of analysis, when performed for the minor isomer of **1,** shows a better fit for the δ twist isomer ($^3J_{H,H}$ coupling constants 6.2, 6.7, 11.3, 9.1 Hz in the sequence shown in Table 6, ranking of couplings: *m*, *m*, *s*, *m*). For compounds **2**−**4** the observed degree of $^3J_{HX}$ coupling is also in agreement with the conformations assigned to the individual isomers in each case (see Supporting Information).

Evaluation of Kinetic Data and Thermodynamic Parameters: The rate constants for the overall process of δ ⇄ λ isomerisation were evaluated by the method of exchange between two unequally populated sites.[26] In the case of the ^{31}P EXSY data this evaluation was based on the molar fraction approach.[26] For the ^{1}H EXSY data this approach as well as the evaluation using the integral values at zero mixing time were used, with only slight differences in the resulting rate constants which were found to be within the margins of error.

The protons of the mesityl groups are involved in a four-site exchange throughout. The mesityl groups are allowed to rotate only in connection with a δ ⇄ λ exchange; thus, in one exchange step a specified mesityl proton may exchange with two mesityl protons of the product; a consequent reverse reaction will then lead to an exchange with a proton of the mesityl group in the starting conformation. The rate data corresponding to these processes were evaluated by finding the solution to the four corresponding linear differential equations according to standard methods.[27] For the corresponding matrix operations MATHEMATICA[28] was used as the tool.

Table 4. $^{13}C\{^1H\}$ NMR spectroscopic data of **1**

λ isomer[a] Major	δ(^{13}C)	Pattern $^{13}C\{^1H\}$	$^nJ_{C,P}/(^nJ_{CRh})/[^1J_{CH}]$ [Hz]	δ isomer[a] Minor	δ(^{13}C)	Pattern $^{13}C\{^1H\}$	$^nJ_{C,P}/(^nJ_{CRh})$ [Hz]
$C17_{ax}$	144.33	d	(1.3)	$C22'_{ax}$	144.94	m	
$C15_{ax}$	142.83	d	2.0	$C24'_{ax}$	142.93	d	1.7
$C13_{ax}$	141.57	d	19.5	$C26'_{ax}$	141.35	ov	
$C22_{eq}$	141.49	d	7.0	$C13'_{eq}$	141.29	ov	
$C24_{eq}$	141.13	d	2.1	$C15'_{eq}$	141.00	ov	
$C26_{eq}$	140.12	d	9.5	$C17'_{eq}$	139.66	d	9.3
$C37,41_{ax}$	136.10	d	13.3	$C31',35'_{ax}$	135.35	d	11.9
$C39_{ax}$	133.06	d	2.1	$C33'_{ax}$	133.20	d	2.5
C30/C36	132.60	m	17.4/8.9	C30′/C36′	132.52	ov	
$C25_{eq}$	132.47	d	8.3	$C16'_{eq}$	132.28	ov	
C30/C36	132.27	d	18.2/9.7/(2.6)			ov	
$C23_{eq}$	132.14	d	7.5	$C14'_{eq}$	132.26	ov	
$C16_{ax}$	131.86	d	6.6	$C23'_{ax}$	131.96	ov	
$C14_{ax}$	131.81	d	8.7				
$C33_{eq}$	131.10	d	2.1	$C39'_{eq}$	131.29	d	1.7
$C31,35_{eq}$	130.40	d	8.3	$C37',41'_{eq}$	130.17	d	10.2
$C38,40_{ax}$	129.89	d	10.8	$C32',34'_{ax}$	129.86	m	
$C32,34_{eq}$	129.61	d	9.1	$C38',40'_{eq}$	129.68	m	
$C12_{ax}$	125.30	d	41.9	$C21'_{ax}$	125.42	d	36.5
$C21_{eq}$	124.65	d	37.7				
C9	106.83	dd	9.0	C8′	107.76	dd	7.2/(9.0)
C5	99.57	dd	7.3/(7.4)	C4′	99.12	ps. t	8.5/(7.0)
C4	94.89	ps. t	8.3/(7.4)	C5′	94.04	ps. t	8.1/(8.7)
C8	92.35	dd	11.2/(6.9)	C9′	93.04	dd	11.4/(6.7)
C3	65.68	d	3.7/1.7	C3′	65.87	m	6.4
C1	34.63	dd	27.2/20.9	C1′	33.13	dd	27.1/10.2
C10/C11	31.51	d	1.2	C6′/C7′	31.57	s	
C10/C11	31.17	s	1.7	C6′/C7′	31.21	ov	
C6/C7	30.72	m	2.5				
C2	30.57	m	25.3/10.0	C2′	30.64	ov	
C6/C7	30.39	m	4.2	C10′/C11′	30.47	ov	
$C18_{ax}$	27.02	dt	12.2/(2.6)/[125.0]	$C29'_{ax}$	26.77	m	10.2/(2.7)
$C29_{eq}$	25.64	d	5.9/[127.0]	$C20'_{eq}$	26.00	d	5.1
$C27_{eq}$	24.73	d	5.0/[128.0]				
$C20_{ax}$	22.44	d	3.3/[127.0]	$C20'_{ax}$	23.12	d	3.4
$C19_{ax}$	21.04	s	[127.0]	$C19'_{ax}$	21.06	s	
$C28_{eq}$	20.83	s	[127.0]	$C28'_{eq}$	20.80	s	

[a] Labels refer to Figures 3 and 4; measuring frequency: 125.758 MHz; temperature: 298 K; solvent: CD_2Cl_2; observed signal pattern abbreviations: s = singlet, d = doublet, t = triplet, m = multiplet, ov = overlapping signal, ps. = pseudo.

Table 5. $^{31}P\{^1H\}$ NMR spectroscopic data of **1**−**7**

[a]	R^1	R^2	T [K]		δ(P^1)	$^1J_{RhP1}$ [Hz]	δ(P^2)	$^1J_{RhP2}$ [Hz]	$^2J_{PP}$ [Hz]	Conformation[b]
1	Mes	Ph	299	major	−2.57	133.2	6.74	148.0	36.1	(*S*)-λ
				minor	−4.81	131.3	10.84	149.8	36.1	(*S*)-δ
2	Mes	DBP	299	major	−1.11	134.0	6.58	144.6	37.0	(*S*)-λ
				minor	−0.05	131.7	11.49	145.9	38.6	(*S*)-δ
3	Mes	Et	299	major	−3.29	136.2	2.56	141.2	35.7	(*S*)-λ
				minor	−2.39	134.8	7.23	140.5	36.0	(*S*)-δ
4	Mes	2-MeOPh	301	major	−3.79	134.1	8.26	148.0	33.8	(*R*)-λ
				minor	−6.99	132.7	12.03	150.3	33.8	(*R*)-δ
5	2-MeOPh	Ph	182	major	11.83	143.2	11.30	142.8	46.2	−
				minor	15.65	145.8	7.52	140.7	46.5	−
6	*o*-Tol	Ph	192	major	18.13	141.9	11.68	144.2	42.7	−
				minor	15.28	143.9	14.46	139.8	42.4	−
7	*o*-Tol	Et	224	major	24.73	141.1	7.25	138.2	42.3	−
				minor	20.61	141.2	11.08	136.7	41.4	−

[a] Measuring frequency: 202.456 MHz; solvent: CD_2Cl_2. [b] The configuration of the chelate ligand was chosen such as to make a homogeneous and consistent description of all the compounds **1**−**4** possible (see text).

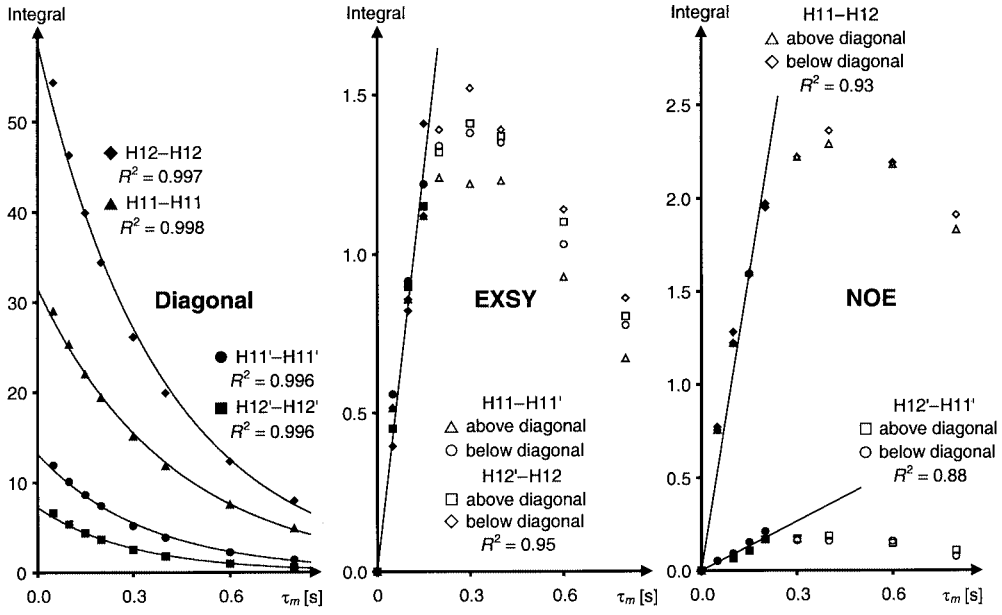

Figure 12. Characteristic time dependence of different types of peaks in 2D ^{1}H NOESY/EXSY experiments

Table 6. Comparison of the calculated and observed degrees of $^3J_{HX}$ coupling for the major isomer of **1**[a]

^{1}H DQF COSY	(*S*)-λ		(*S*)-δ				major	$^3J_{HH}$
Torsion	[°]	Torsion	[°]	λ	δ	chair	NMR	[Hz]
$H3_i-H11_{eq}$	−54	$H3'_i-H12'_{eq}$	−75	*m*	*w*	*w*	*m*	8.3
$H3_i-H12_{ax}$	−169	$H3'_i-H11'_{ax}$	39	*s*	*m*	*s*	*s*	10.9
$H3_i-H21_{ax}$	−24	$H3'_i-H22'_{ax}$	155	*m*	*m*	*s*	*m*	7.0
$H3_i-H22_{eq}$	91	$H3'_i-H21'_{eq}$	38	*w*	*m*	*w*	*w*	–
^{1}H,^{31}P-HMBC								
$H3_i-P1$	69	$H3'_i-P1'$	159	*m*	*m*	*m*	*w*	
$H3_i-P2$	−144	$H3'_i-P2'$	−86	*m*	*w*	*m*	*m*	
^{1}H,^{13}C-HMBC								
$H11_{eq}-C2$	−177	$H12'_{eq}-C2'$	167	*s*	*s*	*m*	*s*	
$H12_{ax}-C2$	69	$H11'_{ax}-C2'$	−79	*m*	*w*	*m*	*w*	
$H21_{ax}-C1$	100	$H22'_{ax}-C1'$	−88	*w*	*w*	*m*	*w*	
$H22_{eq}-C1$	−145	$H21'_{eq}-C1'$	−156	*m*	*m*	*m*	*s*	
$H11_{eq}-C12_{ax}$	78	$H12'_{eq}-C21'_{ax}$	−75	*w*	*w*	*m*	*w*	
$H11_{eq}-C21_{eq}$	−32	$H12'_{eq}-C12'_{eq}$	36	*m*	*m*	*m*	*m*	
$H12_{ax}-C12_{ax}$	−168	$H11'_{ax}-C21'_{ax}$	170	*s*	*s*	*s*	*m*	
$H12_{ax}-C21_{eq}$	84	$H11'_{ax}-C12'_{eq}$	−79	*w*	*w*	*m*	*w*	

[a] The degree of coupling is ranked as strong (*s*), medium (*m*) and weak (*w*). With respect to torsion angles the ranking is as follows: 0−14°, 165−180°: *s*; 15−74°, 105−164°: *m*; 75−104°: *w*.

The rate constants referring to the two individual pathways with respect to the mesityl rotation on which δ ⇄ λ exchange can occur must add to the rate constants of the overall process as determined by the analysis of the two-site exchange processes (Table 7). Within the margins of error this is in fact the case for all of the four-site exchange processes in compounds **1**−**4**. The rotational pathways which the mesityl groups take as a coupled pair in each case have been described as *L* and *D* (Figure 7−9). From the corresponding rate constants the probabilities with which these pathways are taken were calculated and are shown in Table 7. Rate constants for temperatures other than the ones listed in Table 7 were determined for two compounds by analysis of the behaviour of solutions of these compounds containing the isomers in nonequilibrium concentrations. These solutions were prepared by dissolving crystals of these compounds at low temperatures (see Figure 10). At certain temperatures during the warming up period (**1**: 221, 232 K; **3**: 212, 224, 235 K) the time dependence of the concentration ratio of the two isomers was measured at T = const. The time dependence of this ratio was evaluated by making use of the solution of the corresponding differential equations (see Supporting Information) which is Equation (1) (k: rate constant [s^{-1}]; t_x: time [s]; K: equilibrium constant; r_0: concentration ratio at t = 0 s; r_x: concentration ratio at $t = x$ s). From these k values at different temperatures $\Delta H^{\neq}$ and $\Delta S^{\neq}$ values, relating to the rate constants pertinent to compounds **1** and **3** were evaluated. From the temperature dependence of the equilibrium constants (Figure 10) the ΔH and ΔS values as shown in Table 1 were obtained.

$$-\frac{1}{(K+1)}\cdot\ln\frac{(r_0+1)\cdot(r_x-K)}{(r_x+1)\cdot(r_0-K)}=k\cdot t_x \qquad (1)$$

NMR Spectroscopic Structure Refinement: In order to transform NOE volume integrals into distances[25] some volume integrals referring to known distances had to be selected. The selection used (Table 8) was based on the inspection of the 2D NOE maps with the selection principle allowing only those volume integrals which were free from disturbance by other peaks to be incorporated. The resulting interproton distances for the major isomer of compound **1** as an example are shown in Table 8. These distances were used to define the distance matrix[29] on the basis of the known solid state structures of the compounds.[8,9] Distance geometry calculations were based on a model with λ conformation and another one with δ conformation in each case. From each of the two distance matrices one hundred conformations were allowed to evolve.

Table 7. Rate constants and activation energies for the δ → λ and λ → δ isomerisation of **1**−**4** as obtained from 2D EXSY data

			^{31}P EXSY			^{1}H EXSY					
	T [K]		k_{Twist} [s^{-1}]	$\Delta G^{\neq}$ [kJ mol^{-1}]	ΔG [kJ mol^{-1}]	k_{Twist}[a] [s^{-1}]	$\Delta G^{\neq}$ [kJ mol^{-1}]	ΔG [kJ mol^{-1}]	k_L[b] [s^{-1}]	k_D[b] [s^{-1}]	P_L/P_D[c]
1	299	δ → λ	2.17	71.2	−3.9	1.80(14)	71.7	−3.7	1.23(9)	0.31(3)	0.8:0.2
		λ → δ	0.45	75.1		0.41(4)	75.4		0.27(2)	0.06(1)	
	305	δ → λ	5.46	70.5	−3.7						
		λ → δ	1.25	74.2							
2	299	δ → λ	7.72	68.1	−4.6	6.10(39)	68.7	−4.7	6.64(16)	0.97(7)	0.9:0.1
		λ → δ	1.18	72.7		0.89(6)	73.4		0.99(2)	0.15(1)	
3	299	δ → λ	1.08	73.0	−4.4	0.70(7)	74.0	−4.4	0.60(6)	0.40(7)	0.6:0.4
		λ → δ	0.18	77.4		0.12(1)	78.4		0.10(1)	0.08(1)	
	301	δ → λ	1.18	73.3	−4.6						
		λ → δ	0.19	77.9							
4	299	δ → λ	1.83	71.6	−2.9	1.41(17)	72.3	−2.8	0.71(6)	0.92(7)	0.4:0.6
		λ → δ	0.58	74.5		0.45(5)	75.1		0.24(3)	0.30(2)	
	301	δ → λ	1.45	72.8	−2.7						
		λ → δ	0.49	75.5							

[a] The kinetic data presented in this column are the average of the corresponding rate constants as obtained by evaluating all EXSY peaks stemming from all the protons which show a two-site exchange excluding the ones of the mesityl groups (see table) which are engaged in a four-site exchange (see text). The numbers in parentheses give the estimated standard deviation in units of the least significant digit in each case. [b] Based on the estimated standard deviations of the rate constants a statistical test (student's test[32]) reveals that the values for k_L and k_D refer to two different distributions about different mean values within a confidence limit > 99.9% for compounds **1**−**3**. This means that there are in fact two different pathways *L* and *D* (Figures 7−9) of strongly coupled mesityl rotations. The estimated standard deviation in units of the least significant digit is given in parentheses. [c] P*L*, P*D* are the probabilities of pathways *L* and *D* (Figures 7−9) as inferred from k_L and k_D for each compound.

The initial restraints with respect to NOE-determined distances were set to an allowed variation of ±5% (major isomer) and ±10% (minor isomer) throughout. For those groups for which individual protons could not be assigned the "pseudoatom approach" was used.[30] Methyl groups, the three protons of which lead to one and the same signal, were modelled by a pseudoatom at the centre of the plane formed by the three hydrogen atoms. With respect to NOE distances, which involve these groups, the upper bounds of the corresponding distance intervals were increased by 1 Å. Phenyl groups which were found to be freely rotating (**1**) were described by replacing the pair of *ortho*-protons as well as the pair of *meta*-protons by corresponding pseudoatoms placed on the C_2 axis of the phenyl groups. The upper bound of NOE distances involving these protons was increased by 1.5 Å to 2.0 Å. Methylene protons (COD coligand for **1**−**4**, ethyl groups for **3**) for which the diastereotopic differentiation was found to be insufficient to resolve individual signals for each proton were modelled by a pseudoatom placed in the middle of these protons. The upper bound for NOE distances involving these protons was increased by 0.5 Å. These distance corrections for pseudoatoms as quoted were checked for their appropriateness by inspection of the starting models. The 2 × 100 conformations obtained by DG refinement were finally allowed to refine in the ESFF force field[16] with no NOE restraints imposed on them. Since many of the DG refined conformations relax into one and the same force field optimised conformation only a small number of different conformations remained from the 100 conformations in the starting set. These remaining conformations were found to be very similar to each other for the major isomer. Larger differences between these conformations occurred only with respect to dihedral angles involving methyl groups or phenyl *ortho* positions as the termini (**1**: phenyl; **3**: ethyl; **4**: OMe). For **2** with its DBP ligand constituent only one conformation remained since there are no rotational groups of this kind in this compounds. Only one type of orientation was found for the mesityl groups in each case. The conformation concerning the $PMes_2$ part of the compounds **1**−**4** was found to be roughly the same in each case (Figure 11). In order to decide whether the λ or the δ form was the one to give rise to the NOE data, the following procedure was adopted. The rms values as given by the DG program package which refer to a weighted sum of squares of different classes of distances[17] were taken as one of these criteria. It was found that for the major isomer these rms values were an order of magnitude smaller for the λ conformation than for the δ conformation, i.e. that the major isomer should be the λ one. The minor isomer must then be the δ one. The rms values obtained by DG runs on the minor isomer confirmed this expectation. The quality of agreement between the NOE distances calculated for the best DG structures and the NOE distances inferred from

Table 8. Comparison of calculated and measured distances of the λ isomer of **1**

No.	Atom	Pair[e]	NOE[a] d [Å]	X-ray[b] λ/δ d [Å]	DG[c] λ d [Å]	FF[d] λ d [Å]	No.	Atom	Pair[e]	NOE[a] d [Å]	X-ray[b] λ/δ d [Å]	DG[c] λ d [Å]	FF[d] λ d [Å]	No.	Atom	Pair[e]	NOE[a] d [Å]	X-ray[b] λ/δ d [Å]	DG[c] λ d [Å]	FF[d] λ d [Å]
1[f]	$H11_{eq}$	$H11_{ax}$	1.78	1.75/1.76	1.76	1.76	22	H3	$H11_{eq}$	2.41	2.52/2.53	2.46	2.38	45	$H31,35_{eq}$	$H21_{ax}$	2.22	2.49/2.44	2.61	2.31
2[f]	$H22_{eq}$	$H21_{ax}$	1.78	1.76/1.77	1.76	1.76	23	H3	$H21_{ax}$	2.29	2.27/3.03	2.32	2.30	46	$H31,35_{eq}$	$H22_{eq}$	2.99	3.24/3.14	1.75	2.82
3	H111	H112	2.07	1.75/1.74	1.77	1.76	24	H3	$H22_{eq}$	2.71	2.70/2.33	2.65	2.64	47	$H31,35_{eq}$	H4	2.32	2.89/2.67	1.83	2.39
4	$H31,35_{eq}$	$H32,34_{eq}$	2.12	2.41/2.41	2.44	2.45	25	H3	HO	2.15	2.24/2.81	2.51	2.84	48	$H31,35_{eq}$	H5	2.86	2.84/3.09	1.93	3.28
5	$H37,41_{ax}$	$H38,40_{ax}$	2.24	2.45/2.42	2.47	2.46	26	H3	$H16_{ax}$	3.79	3.86/6.00	3.89	4.03	49	$H31,35_{eq}$	$H18_{ax}$	2.48	2.23/2.15	3.90	2.32
							27	H3	$H20_{ax}$	2.24	2.69/3.97	2.35	2.56	50	$H32,34_{eq}$	H4	4.00	4.33/4.20	4.14	4.34
														51	$H32,34_{eq}$	H5	3.84	3.90/3.98	3.33	4.28
6	$H14_{ax}$	$H18_{ax}$	2.31	2.28/2.18	2.26	2.22	28	$H11_{eq}$	$H20_{ax}$	2.14	2.25/2.23	2.03	2.21	52	$H32,34_{eq}$	$H18_{ax}$	4.01	4.44/4.33	5.33	4.32
7	$H14_{ax}$	$H19_{ax}$	2.51	2.42/2.51	2.43	2.46	29	$H21_{ax}$	$H14_{ax}$	4.01	4.01/4.11	3.91	3.96	53	$H37,41_{ax}$	$H11_{ax}$	2.92	3.18/3.12	2.47	2.60
8	$H16_{ax}$	$H19_{ax}$	2.51	2.51/2.46	2.51	2.50	30	$H21_{ax}$	$H18_{ax}$	2.68	2.47/2.51	2.39	2.50	54	$H37,41_{ax}$	$H22_{eq}$	2.22	2.35/2.30	2.67	2.46
9	$H16_{ax}$	$H20_{ax}$	2.33	2.34/2.38	2.30	2.33								55	$H37,41_{ax}$	HO	3.07	3.69/5.04	4.17	2.86
10	$H23_{eq}$	$H27_{eq}$	2.23	2.40/2.35	2.40	2.30	31	H4	H101	3.28	3.63/3.66	3.43	3.40	56	$H37,41_{ax}$	H4	2.42	2.64/2.75	2.64	2.96
11	$H23_{eq}$	$H28_{eq}$	2.45	2.50/2.49	2.50	2.49	32	H5	$H18_{ax}$	2.90	2.96/3.04	3.04	2.88	57	$H37,41_{ax}$	H5	4.56	4.50/4.57	4.88	4.77
12	$H25_{eq}$	$H28_{eq}$	2.48	2.62/2.44	2.61	2.46	33	H5	H112	3.24	3.64/3.58	3.54	3.68	58	$H37,41_{ax}$	H9	3.59	3.62/3.71	3.42	3.74
13	$H25_{eq}$	$H29_{eq}$	2.23	2.33/2.44	2.30	2.28	34	H8	$H18_{ax}$	2.56	2.59/2.50	2.56	2.54	59	$H37,41_{ax}$	$H29_{eq}$	2.27	2.55/2.45	2.25	2.41
							35	H8	$H23_{eq}$	4.39	4.52/4.46	4.27	4.42	60	$H37,41_{ax}$	H102	4.64	3.95/4.10	4.30	4.38
							36	H8	$H27_{eq}$	2.22	2.21/2.12	2.48	2.25	61	$H37,41_{ax}$	H111	2.53	2.85/2.69	3.37	3.63
14	H4	H111	2.32	2.39/2.26	2.27	2.32	37	H9	$H23_{eq}$	4.67	4.82/4.85	4.82	4.83	62	$H38,40_{ax}$	H4	3.80	4.42/4.58	4.23	4.72
15	H4	H112	2.74	2.88/2.72	2.89	2.88	38	H9	$H25_{eq}$	3.72	4.13/4.15	3.88	4.00	63	$H38,40_{ax}$	$H29_{eq}$	3.40	3.97/3.94	3.74	3.90
16	H5	H61	2.23	2.23/2.23	2.09	2.29	39	H9	$H27_{eq}$	3.21	3.83/3.89	4.18	4.06	64	$H38,40_{ax}$	H111	3.57	3.95/3.98	4.24	4.93
17	H5	H62	2.79	2.47/2.56	2.61	2.53	40	H9	$H29_{eq}$	2.35	2.50/2.53	2.68	2.54					X-ray	DG	FF
18	H8	H71	2.38	2.23/2.29	2.23	2.32	41	H9	H72	3.26	3.58/3.56	3.55	3.65			rms[g]	[Å]	λ/δ	λ	λ
19	H8	H72	2.36	2.78/2.81	2.65	2.87	42	H9	H112	3.65	4.00/4.01	4.12	3.98			1−64		0.29/0.52	0.45	0.36
20	H9	H101	2.35	2.25/2.20	2.26	2.31	43	$H16_{ax}$	$H27_{eq}$	3.57	3.94/3.77	3.83	3.83			1−5		0.22/0.21	0.22	0.23
21	H9	H102	2.71	2.48/2.51	2.61	2.50	44	$H18_{ax}$	H71	2.68	3.20/2.96	3.03	3.11			6−21		0.17/0.16	0.13	0.16
																22−64		0.33/0.62	0.53	0.42
																22−27		0.20/1.23	0.16	0.33

[a] Distances as inferred from NOE measurements. [b] Distances referring to the λ isomer (correct) and those referring to the δ isomer (wrong!) in the solid state structure are given in that sequence separated by a slash. [c] Distances referring to the optimal model from DG refinement. [d] Distances referring to the optimal model from force field refinement. [e] The designators refer to Figures 3 and 4. [f] Contacts used as reference distances. [g] Root mean square (rms) deviations between distances obtained from NOE experiments and distances derived from model structures for selected sets of contacts.

measurement is shown as column DG in Table 8 for the λ isomer of **1**, which is the major isomer in this case as in the cases of **2**−**4**. This is shown in Table 8 for all of the 64 NOE contacts that could be measured for **1**-λ including those contacts that are fixed by the covalent framework. Contacts that may serve as reference contacts have the numbers 1−5 in Table 8. Contacts No. 1 and 2 were used in the transformation of NOE integrals into distances. The rms value relating to all NOE distances is 0.45 Å, the one relating to the potential reference distances is 0.22 Å as shown in Table 8. Distances No. 6−21 (Table 8) refer to 1−3 or 1−4 contacts which are, while being comparatively well fixed by the covalent framework, subject to variation on torsion angles and are therefore not so well suited as reference distances. The rms value for this group of distances is only 0.13 Å. For the comparison of distances involving methyl groups out of the three protons of such a group the one was chosen which had the shortest contact. This principle was also applied to make the proper choice between the two *ortho*- and *meta*-protons of the phenyl groups (Table 8). Contacts No. 22−64 will respond to the conformation, to a larger or lesser extent, due to the fact that there are quite a number of "long" distances above 3.5 Å which, by the nature of the experiment, are less well determined. The agreement is somewhat lower for this set of distances and is found to amount to an rms value of 0.53 Å. When the same type of comparison is made for the structural models derived by force field methods (column FF, Table 8) or from X-ray analysis of the λ isomer (column X-ray, Table 8) the overall agreement is good (Table 8 and rms values given in this table). This means that the average structure in solution is very close to the force field calculated minimum structure that is again very close to the structure determined by X-ray methods in the solid state. When the distances determined for the major isomer are compared with the ones calculated for the δ conformation (known from X-ray structure analysis) the agreement is worse for those classes of distances which contain distances that respond to conformational changes (of course not different for covalently fixed distances), i.e. for the group of all distances No. 1−64 and for the group of distances No. 22−64 (Table 8).

The most discriminating distances are found to be the ones radiating from H3 (Figure 3) as expected. The rms values based on this subset of distances (No. 22−27, Table 8), as calculated by comparison with the λ conformer and the δ conformer of the X-ray structure, are given in Table 8 and show that there can be no doubt about the fact that it is the λ form which corresponds to the conformation of the major isomer.

When the minor isomer of **1** is treated in the same way this same type of rms value is again maximally discriminating. It is found to be 0.31 Å for the correct assignment (δ) and 0.76 Å for the incorrect one (λ) (Table 9). This means that, even though, due to its low concentration, the NOE data for the minor isomer are less accurate and smaller in number, it is possible to discriminate between the two forms for the minor isomer. The same procedure, as explicitly described for **1**, was applied to compounds **2**−**4** leading to the result that, beyond doubt, the major isomer corresponds to the λ conformation in each case. The rms values with respect to the contacts radiating from H3 and referring to the differences between these distances as inferred from NOE measurements and the distances calculated either for the λ or the δ conformer of the X-ray structure, are collected in Table 9.[31] It is seen that these rms values are significantly different for the two assignments in all cases. The correct assignment is the one where the δ conformation is the one corresponding to the minor isomer and the λ conformation corresponds to the average structure of the major isomer. The agreement between the rms values as calculated on the basis of structural models derived from X-ray data or from DG refinement or also from force field refinement (Table 9 ROWSEP="YES") is found to be equally good for **2**−**4** as already observed for **1**.

Table 9. Discrimination between λ and δ isomers on the basis of rms values

[a]	No. of contacts	Major X-ray λ/δ	(λ) DG λ	FF λ	No. of contacts	Minor X-ray δ/λ	(δ) DG δ	FF δ
1	64	0.29/0.52	0.45	0.36	19	0.35/0.46	0.37	0.35
	6	0.20/1.23	0.16	0.33	3	0.31/0.76	0.25	0.33
2	73	0.39/0.75	0.38	0.36	14	0.39/0.41	0.33	0.36
	7	0.25/0.87	0.25	0.22	2	0.20/0.59	0.11	0.16
3	70	0.72/0.77	0.50	0.55	21	0.61/0.74	0.38	0.89
	6	0.10/1.04	0.14	0.09	5	0.22/0.79	0.05	0.37
4	60	0.36/0.50	0.33	0.44	27	0.25/0.30	0.17	0.36
	7	0.52/1.28	0.47	0.44	3	0.24/0.41	0.13	0.19

[a] Column headers have the same meaning as given in the footnote of Table 8. The first line refers to the corresponding rms values as calculated for the total of all the NOE contacts measured in this case, the second line refers only to those contacts which radiate from H3 in each case.

Acknowledgments

We are indebted to the German Science Foundation, SFB 247, HU 151/24-1, /29-1 and the Fonds der Chemischen Industrie for financial support. We are grateful to Prof. H. Friebolin for helpful discussions.

[1] [1a] M. Nógradi, *Stereoselective Synthesis*, 2nd ed., VCH, Weinheim, **1995**. [1b] H. Brunner, W. Zettlmeier, *Handbook of Enantioselective Catalysis with Transition Metal Compounds*, VCH, Weinheim, **1993**.

[2] [2a] B. D. Vineyard, W. S. Knowles, M. J. Sabacky, G. L. Bachmann, D. J. Weinkauff, *J. Am. Chem. Soc.* **1977**, *99*, 5946−5952. [2b] W. S. Knowles, M. J. Sabacky, B. D. Vineyard, D. J. Weinkauff, *J. Am. Chem. Soc.* **1975**, *97*, 2567−2568.

[3] [3a] J. M. Brown, D. Parker, *J. Chem. Soc., Chem. Commun.* **1980**, 342−344. [3b] W. C. Christopfel, B. D. Vineyard, *J. Am. Chem. Soc.* **1979**, *101*, 4406−4408.

[4] [4a] R. Noyori, M. Ohta, Y. Hsiao, M. Kitamura, T. Ohta, H. Takaya, *J. Am. Chem. Soc.* **1986**, *108*, 7117−7119. [4b] M. Kitamura, M. Tokunaga, R. Noyori, *J. Org. Chem.* **1992**, *57*, 4053−4054. [4c] B. Heiser, E. A. Broger, Y. Crameri, *Tetrahedron: Asymmetry* **1991**, *2*, 51−62.

[5] [5a] J. Sprinz, G. Helmchen, *Tetrahedron Lett.* **1993**, *34*, 1769−1772. [5b] P. von Matt, A. Pfaltz, *Angew. Chem.* **1993**, *105*, 614−615; *Angew. Chem. Int. Ed. Engl.* **1993**, *32*, 566−567. [5c] G. J. Dawson, C. G. Frost, J. M. J. Williams, S. J. Coote, *Tetrahedron Lett.* **1993**, *34*, 3149−3150. [5d] J. Sprinz, M. Kiefer, G. Helmchen, M. Reggelin, G. Huttner, O. Walter, L. Zsolnai, *Tetrahedron Lett.* **1994**, *35*, 1523−1526.

[6] [6a] J. D. Dunitz, J. Waser, *J. Am. Chem. Soc.* **1972**, *94*, 5645−5650. [6b] J. D. Dunitz, *Tetrahedron* **1972**, *28*, 5459−5467.

[7] [7a] P. A. McNeil, N. K. Roberts, B. Bosnich, *J. Am. Chem. Soc.* **1981**, *103*, 2273−2280. [7b] J. Bakos, I. Tóth, B. Heil, G. Szalontai, L. Párkányi, V. Fülöp, *J. Organomet. Chem.* **1989**, *370*, 263−276.

[8] J. Karas, G. Huttner, K. Heinze, P. Rutsch, L. Zsolnai, *Eur. J. Inorg. Chem.* **1999**, 405−420.

[9] CCDC-148008 (**3**) and -148009 (**7**) contain the supplementary crystallographic data for this paper. These data can be obtained free of charge at www.ccdc.cam.ac.uk/conts/retrieving.html or from the Cambridge Crystallographic Data Centre, 12, Union Road, Cambridge CB2 1EZ, UK [Fax: (internat.) + 44-1223/336-033; E-mail: deposit@ccdc.cam.ac.uk].

[10] A. Bax, M. F. Summers, *J. Am. Chem. Soc.* **1986**, *108*, 2093−2094.

[11] [11a] G. Bodenhausen, D. J. Ruben, *Chem. Phys. Lett.* **1980**, *69*, 185−188. [11b] L. E. Kay, P. Keifer, T. Saarinen, *J. Am. Chem. Soc.* **1992**, *114*, 10663−10665. [11c] A. G. Palmer III, J. Cavanagh, P. E. Wright, M. Rance, *J. Magn. Reson.* **1991**, *93*, 151−170. [11d] J. Schleucher, M. Schwendinger, M. Sattler, P. Schmidt, O. Schedletzky, S. J. Glaser, O. W. Sørensen, C. Griesinger, *J. Biomol. NMR* **1994**, *4*, 301−306.

[12] [12a] U. Piantini, O. W. Sørensen, R. R. Ernst, *J. Am. Chem. Soc.* **1982**, *104*, 6800−6801. [12b] M. Rance, O. W. Sørensen, G. Bodenhausen, G. Wagner, R. R. Ernst, K. Wüthrich, *Biochem. Biophys. Res. Commun.* **1983**, *117*, 479−485.

[13] J. Jeener, B. H. Meier, P. Bachmann, R. R. Ernst, *J. Chem. Phys.* **1979**, *71*, 4546−4563.

[14] [14a] D. A. V. Morton, A. G. Orpen, *J. Chem. Soc., Dalton Trans.* **1992**, *4*, 641−653. [14b] K. Mislow, *Acc. Chem. Res.* **1976**, *9*, 26−33. [14c] H. B. Bürgi, *Acc. Chem. Res.* **1983**, *16*, 153−161. [14d] H. B. Bürgi, *Acta Crystallogr., Sect. B* **1988**, *44*, 445−448. [14e] S. Beyreuther, J. Hunger, G. Huttner, S. Mann, L. Zsolnai, *Chem. Ber.* **1996**, *129*, 745−757. [14f] S. Beyreuther, A. Frick, J. Hunger, G. Huttner, B. Antelmann, P. Schober, R. Soltek, *Eur. J. Inorg. Chem.* **2000**, 597−615.

[15] In the original paper[8] the sense of chirality for **2** was erroneously assigned as (*S*).

[16] [16a] *Discover User Guide*, versions 2.9.7 & 95.0/3.00, Biosym/MSI, **1995**. [16b] S. Barlow, A. L. Rohl, S. Shi, C. M. Freeman, D. O'Hare, *J. Am. Chem. Soc.* **1996**, *118*, 7578−7592. [16c] N. Jäger, U. Schilde, *Struct. Chem.* **1998**, *9*, 77−93.

[17] *NMRchitect 98.0, DGII* program package, Molecular Simulations, Inc., 9685 Scranton Road, San Diego, CA 92121, **1998**.

[18] [18a] K. Wüthrich, *Science* **1989**, *243*, 45−50. [18b] K. Wüthrich, *Methods Enzymol.* **1989**, *177B*, 125−131. [18c] T. F. Havel, *Prog. Biophys. Mol. Biol.* **1991**, *45*, 43−78. [18d] M. P. Williamson, J. P. Waltho, *Chem. Soc. Rev.* **1992**, *21*, 227−236. [18e] J. M. Blaney, J. S. Dixon in *Reviews in Computational Chemistry*, vol. 5 (Eds.: K. P. Lipkowitz, D. B. Boyd), VCH Publishers, Inc., New York, **1996**, chapter 6.

[19] U. Burkert, N. L. Allinger, *Molecular Mechanics*, ACS monograph, Washington, **1989**.
[20] [20a] G. Binsch, *Top. Stereochem.* **1968**, *3*, 97−192. [20b] R. Bucourt, *Top. Stereochem.* **1974**, *8*, 159−224. [20c] G. M. Kellie, F. G. Riddell, *Top. Stereochem.* **1974**, *8*, 225−269.
[21] [21a] J. Halpern, D. P. Riley, A. S. C. Chan, J. J. Pluth, *J. Am. Chem. Soc.* **1977**, *99*, 8055−8057. [21b] A. S. C. Chan, J. Halpern, *J. Am. Chem. Soc.* **1980**, *102*, 838−840. [21c] P. S. Chua, N. K. Roberts, B. Bosnich, S. J. Okrasinski, J. Halpern, *J. Chem. Soc., Chem. Commun.* **1981**, 1278−1280. [21d] J. M. Brown, P. A. Chaloner, *Tetrahedron Lett.* **1978**, *21*, 1877−1880. [21e] C. R. Landis, J. Halpern, *J. Am. Chem. Soc.* **1987**, *109*, 1746−1754.
[22] A paper describing the force field model that precisely predicts the observed behaviour is published aside: V. Schulz, A. Frick, G. Huttner, *Eur. J. Inorg. Chem.* **2002**, 3111−3128, preceding paper.
[23] [23a] E. W. Hansen, *Anal. Chem.* **1985**, *57*, 2993−2994. [23b] A. L. Van Geet, *Anal. Chem.* **1970**, *42*, 679−680.
[24] *FELIX 98.0*, NMR processing package, Molecular Simulations, Inc., 9685 Scranton Road, San Diego, CA 92121, **1998**.
[25] B. A. Borgias, M. Gachin, D. Kerwood, T. L. James, *Progr. NMR Spectrosc.* **1990**, *22*, 83−100.
[26] C. L. Perrin, T. J. Dwyer, *Chem. Rev.* **1990**, *90*, 935−967.
[27] [27a] C. L. Perrin, R. K. Gipe, *J. Am. Chem. Soc.* **1984**, *106*, 4036−4038. [27b] R. Willem, M. Biesemans, K. Hallenga, G. Lippens, F. Malaisse-Lagae, W. J. Malaisse, *J. Biol. Chem.* **1992**, *267*, 210−217. [27c] R. Willem, *Prog. NMR Spectrosc.* **1987**, *20*, 1−94.
[28] Mathematica 4.0: S. Wolfram, *The Mathematica Book*, 3rd ed., Wolfram Media/Cambridge University Press, Cambridge, **1996**.
[29] [29a] G. M. Crippen, T. F. Havel, *Distance Geometry and Molecular Conformation*, Research Studies Press, Ltd., Somerset, England, **1988**. [29b]G. M. Crippen, *J. Comp. Phys.* **1977**, *24*, 96−107. [29c] G. M. Crippen, T. F. Havel, *Acta Crystallogr., Sect. A* **1978**, *34*, 282−284. [29d] I. D. Kuntz, J. F. Thomason, C. M. Oshiro, *Methods Enzymol.* **1989**, *177B*, 159−204. [29e] D. F. Mierke, M. Reggelin, *J. Org. Chem.* **1992**, *57*, 6365−6367. [29f] M. Reggelin, M. Köck, K. Conde-Frieboes, D. F. Mierke, *Angew. Chem.* **1994**, *106*, 822−824; *Angew. Chem. Int. Ed. Engl.* **1994**, *33*, 753−755. [29g] M. Köck, J. Junker, *J. Org. Chem.* **1997**, *62*, 8614−8615.
[30] M. Reggelin, H. Hoffmann, M. Köck, D. F. Mierke, *J. Am. Chem. Soc.* **1992**, *114*, 3272−3277.
[31] In the case of **2**, where only one twist conformation was observed in the crystal, the opposite one was constructed by inverting the structure and exchanging the positions of H3 and HO at the central carbon atom of the ligand.
[32] R. Zurmühl, *Praktische Mathematik*, 5th ed., Springer-Verlag, Berlin, Heidelberg, **1965**.

Received November 12, 2001
(publication delayed on the authors' request)
[I01452]

CH/π Interactions Implicated in the Crystal Structure of Transition Metal Compounds − A Database Study[‡]

Hiroko Suezawa,*[a] Takashi Yoshida,[a] Yoji Umezawa,[b] Sei Tsuboyama,[c] and Motohiro Nishio*[c]

Keywords: Hydrogen bonds / Noncovalent interactions / π interactions / Supramolecular chemistry

A statistical study was carried out to investigate the role of the CH/π interaction in the crystal structure of transition metal compounds. Thus, short CH/π distances were surveyed in crystal structures deposited in the Cambridge Structural Database. Among organometallic entries bearing C_6 or C_5 aromatic rings, a substantial part of the structures has been found to have intermolecular CH/π contacts shorter than the van der Waals distance. Further, in many structures short intramolecular CH/π contacts have been found. Interligand and intraligand CH/π interactions were also surveyed in coordination compounds bearing the typical ligands 1,10-phenanthroline, 2,2′-bipyridine, and 2,2′:6′,2′′-terpyridine, as well as triphenylphosphane complexes of ruthenium, rhenium, and rhodium. The results were discussed in the context of the CH/π interaction in controlling the crystal packing and the molecular structure of transition metal compounds. The compact structure with CH/π interactions is a general aspect in coordination and organometallic chemistry.
(© Wiley-VCH Verlag GmbH, 69451 Weinheim, Germany, 2002)

Introduction

Sigel and his co-workers studied the conformation of a number of ternary metal complexes with aromatic and aliphatic ligands such as M(bipy)(AA), M(phen)(AA)[1] and M(ATP)(AA)[2] [M = Cu^{2+} or Zn^{2+}, bipy = 2,2′-bipyridine, phen = 1,10-phenanthroline, ATP = adenosine triphosphate, AA = $RCH(NH_2)COOH$]. In every case, the alkyl group R (isopropyl, isobutyl, etc.) in AA was found to curl over the aromatic rings to form a folded rather than an extended conformation. A number of examples have been provided by these workers where, in complexes including nucleotides and amino acids as ligands, the structures displaying alkyl/arene as well as arene/arene interactions prevail in solution.[3] The results imply that an attractive interaction operates between these moieties.

Okawa first recognized the importance of CH/π interaction in the stereoselective formation of several metal complexes.[4] The relevance of the CH/π interaction[5] in coordination and organometallic chemistry has since been shown by a number of workers.[6] For instance, Brunner studied the crystal and solution structure of a series of ruthenium compounds with a cyclopentadienyl and/or benzene unit as ligand. One of the isomers in a half-sandwich complex, where a hydrogen atom of the η^5- or η^6-arene ligand points to an aromatic group in the neighboring ligand, has been shown to be more stable than the diastereoisomeric congener. They termed this the "β-phenyl effect",[7] and the phenomenon is now understood on the grounds of the CH/π hydrogen bond.[8] His finding has an obvious implication for the mechanism of enantioselective catalysis.[9]

The CH/π interaction is the weakest extreme of nonconventional hydrogen bonds[10] and is recognized to be the interaction between soft acids and soft bases,[11] in contrast to the ordinary hydrogen bond, that is the interaction between hard acids and hard bases. Though weak, the CH/π hydrogen bond plays significant roles in various fields of chemistry such as the conformation of molecules,[12] self-assembly[13] as well as chiral recognition.[14] The electronic substituent effect on the stereoselectivity of complex formation,[15] conformational equilibrium,[16] crystal packing,[17] and enantioselectivity[18] has demonstrated that the CH/π interaction is by no means merely a dispersion force. According to high-level ab initio calculations, the most important stabilization comes from the correlation energy.[19] The electrostatic interaction also contributes, but is a minor factor (ca. 20%)[20] in the CH/π interaction. Hence, the CH/π interaction is nonpolar and is effective in water unlike the conventional hydrogen bond and Coulomb force. This

[‡] CH/π Interactions − A comprehensive literature list for the CH/π interaction is available on the following website: http://www.tim.hi-ho.ne.jp/dionisio

[a] Instrumental Analysis Center, Yokohama National University, Hodogaya-ku, Yokohama 240-8501, Japan
E-mail: suezawa@ynu.ac.jp
[b] Institute of Microbial Chemistry, 3-14-23, Kamiosaki, Shinagawa-ku, Tokyo 141-0021, Japan
[c] CHPI Institute, 3-10-7 Narusedai, Machida-shi, Tokyo 194-0043, Japan
E-mail: dionisio@tim.hi-ho.ne.jp

point is of supreme importance when considering the role of CH/π interaction in biological environments. Evidence has in fact been presented for the ubiquity of CH/π bonds in the interaction involving protein[21,22] or DNA.[23]

CH/π interactions are often reported to occur in crystal packing[24] of organometallic compounds and in clathrates.[25] Braga and co-workers reported on a Cambridge Structural Database (CSD) study of organometallic entries including XH/π (X = O, N C) bonds and demonstrated the hydrogen bond character of these interactions.[26] Previously we showed, by analyzing structures in the CSD,[27] the prominence of CH/π interactions in the packing of organic crystals[28] and host/guest compounds.[29] To investigate the significance of the CH/π interaction in coordination and organometallic chemistry, we extended our approach to the crystal structure of transition metal compounds.

Method

The CSD version 5.21 and 5.22 (April and October 2001 release) were used. The 6- and 5-membered aromatic ring systems were chosen in view of their abundance in the database. The method of exploring CH/π interactions in the CSD was described in detail in our previous papers.[12a,28,29] For surveying CH/π interactions in compounds bearing an arene ring, several kinds of distance and angle parameters were defined to cover every possibility. This is necessary since a C−H group may interact in regions where the hydrogen atom is slightly offset out of the π-plane. Figure 1 illustrates the method for a six-membered arene ring. Nonbonding contacts were sought with appropriate cut-off values for the distance and angle parameters. Interatomic distances shorter than the sum of the van der Waals radii[30] were considered as relevant for the presence of CH/π interaction.[31] In practice, the software QUEST3D was used to find CH/π contacts within the above constraints.

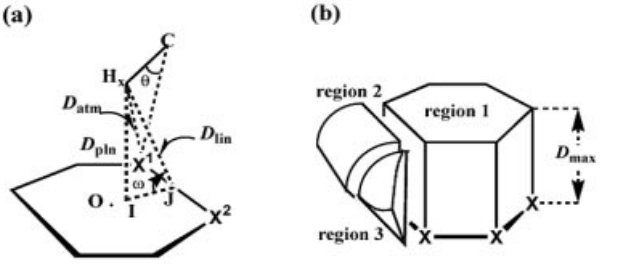

Figure 1. Method of surveying CH/π contacts with a 6-membered aromatic ring: (a) O: center of the plane; X^1 and X^2: nearest and second nearest sp^2 atoms, respectively, to H; ω: dihedral angle defined by X^1OX^2 and HX^1X^2 planes; θ: HCX^1; D_{pln}: H/π-plane distance (H/I); D_{atm}: interatomic distance (H/X^1); D_{lin}: distance between H and line X^1X^2 (H/J); (b) the program was run to search for H/π distances shorter than a cut-off value D_{max} in every region; $D_{pln} < D_{max}$, $\theta < 60°$, for the region just above the ring (region 1); $D_{lin} < D_{max}$, $\theta < 60°$, $90° < |\omega| < 130°$ for the region slightly offset from the ring (region 2); $D_{atm} < D_{max}$, $\theta < 60°$, $50° < \varphi < 90°$ for another possible region φ: HX^1I (region 3)

Results and Discussion

Intermolecular Interactions

First, coordinates determined by the neutron diffraction method were examined. Table 1 shows the results for entries bearing at least a C_6 aromatic group. The mean intermolecular CH/π distance D_{atm} increases to a larger value when the cut-off distance is longer. The proportion of hit entries, however, does not increase appreciably. The interatomic distance was then surveyed, separately, for sp^2- and sp^3-CH/π interactions. The aromatic CH groups interact with the π-system at a shorter distance than the alkyl groups.

Table 1. Intermolecular CH/π interactions in the crystal structure of organometallic compounds bearing a C_6 arene ring, determined by neutron diffraction (71 entries)

	Hit[a]	Ratio[b] (%)	D_{atm}/Å[c] (fragment)[d]
D_{max}			
3.05 Å	55	77	2.87 ± 0.13 (514)
sp^2-CH	35	49	2.86 ± 0.13 (226)
sp^3-CH	28	39	2.89 ± 0.12 (101)
3.20 Å	58	82	2.94 ± 0.17 (684)
3.50 Å	59	83	3.03 ± 0.23 (874)

[a] Number of entries with short CH/Ar contacts. [b] Proportion of hits. [c] Mean atomic distance. [d] Number of observations.

Intermolecular CH/π distances were then sought from the entire CSD (Table 2). Only error-free, nondisordered structures with $R < 10\%$ were accepted. Among 39570 organometallic entries with C_6 arene ring(s),[32] 28363 crystal structures (ca. 72%) have been found to have at least one CH/π distance shorter than 3.05 Å.[33] This proportion is a conservative estimate, since in the above 39570 entries, structures bearing no hydrogen coordinates are counted. The CH groups may also interact with nonbenzenoid π-systems such as heteroaromatics, cyclopentadienyl groups, or multiple bonds such as C≡C, C=O, etc. Further, the CH/π interaction may operate at a distance longer than 3.05 Å. D_{atm} shifted to a longer value for a larger D_{max} but the number of hits did not increase remarkably. Table 2 includes data obtained by surveying compounds with C_5 aromatic rings as the CH acceptor. D_{atm} is not appreciably distinct from the C_6 case; the results suggest that the π-donating property is not very different between these rings. The ratio of hits, on the other hand, is smaller in C_5 than in C_6 arenes. This probably reflects the smaller surface area of a cyclopentadienyl group than that of the C_6 aromatic compounds. Several database subsets were edited for 1st, 2nd, and 3rd row transition elements and surveyed. No appreciable difference has been noted between these subsets.

Figure 2 shows histograms recorded by surveying CH hydrogen atoms interacting with the C_6 aromatic ring. We see many distances shorter than the van der Waals distance. In Figure 3, positions of the hydrogen atoms are projected onto the C_6 π-plane.[34] It is remarkable that the C−H bond

Table 2. CH/π intermolecular contacts in the crystal of compounds containing transition metals (TR)

	DB[a]	Hit[b]	Ratio (%)[c]	D_{atm}/Å[d] (fragments)[e]
(a) C_6 aromatic ring as the CH acceptor				
D_{max} 3.05 Å				
All TR	39570	28363	72	2.90 ± 0.13 (> 10000)
1st row elements	15900	11361	71	2.90 ± 0.13 (> 10000)
2nd row	11366	8466	74	2.90 ± 0.13 (> 10000)
3rd row	9799	6846	70	2.90 ± 0.13 (> 10000)
D_{max} 3.20 Å	39570	29343	74	2.97 ± 0.16 (> 10000)
D_{max} 3.50 Å	39570	29922	76	3.08 ± 0.23 (> 10000)
(b) C_5 aromatic ring as the CH acceptor (D_{max} 3.05 Å)				
All TR	18198	8583	47	2.87 ± 0.13 (> 10000)
1st row elements	9496	4596	48	2.86 ± 0.14 (> 10000)
2nd row	7487	3579	48	2.87 ± 0.14 (8693)
3rd row	3946	1586	40	2.87 ± 0.14 (3302)

[a] Number of entries in the database subset. [b] Number of hits. [c] Proportion of hits. [d] Mean atomic distance. [e] Number of observations.

tends to point toward the center of the aromatic ring; this is consistent with our earlier experiences on organic crystals. Braga et al. also noticed the directionality of the XH/π-type interactions.

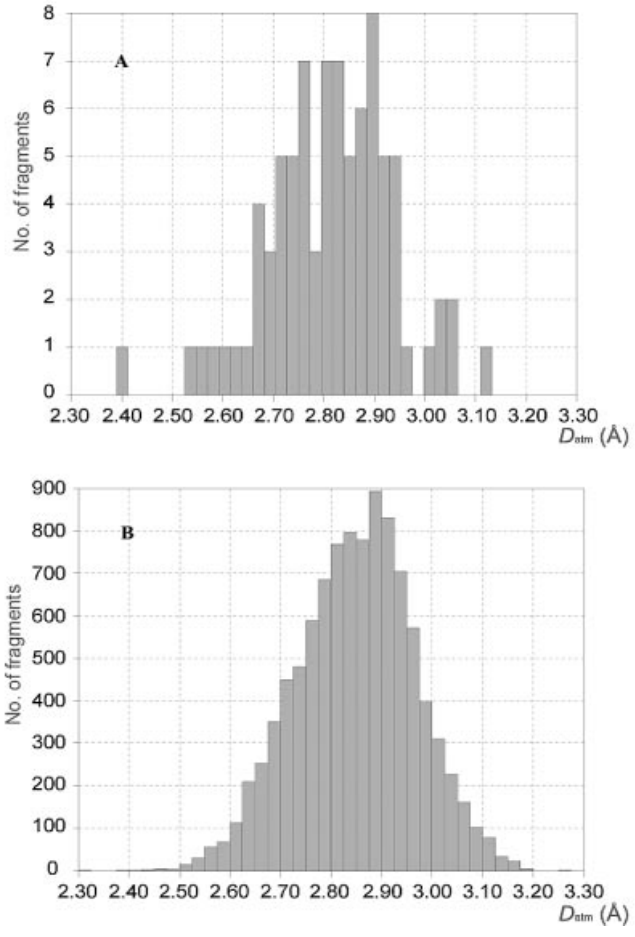

Figure 2. Histograms showing the distribution of CH/C-sp^2 interatomic distances in C_6 aromatic compounds; D_{max} 2.90 Å, region 1 (sp^2-CH); (a) neutron data; (b) X-ray data (VISTA version 2.0)

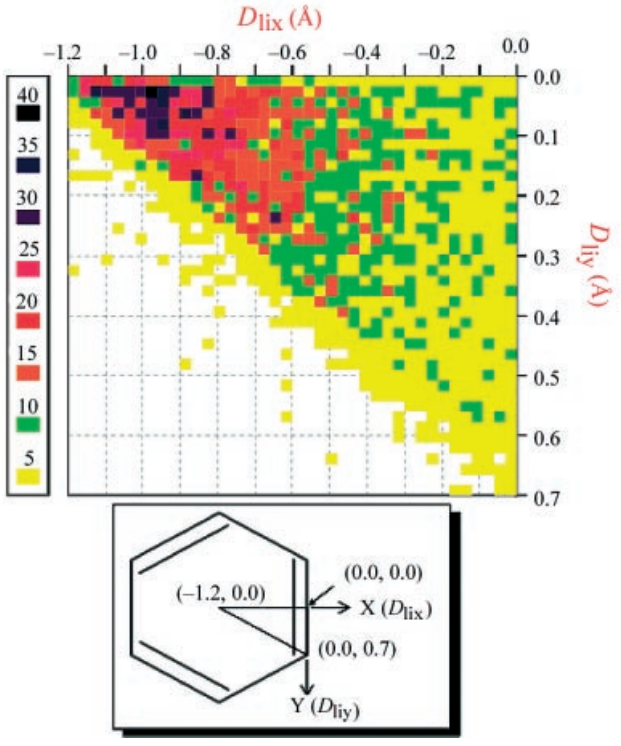

Figure 3. CH hydrogen atoms projected on the C_6 π-plane; only hydrogen atoms with D_{pln} < 2.90 Å are projected; region 1, sp^2-CH (VISTA version 2.0)

Table 3. Intramolecular CH/π interactions in the crystal structure of organometallic compounds bearing a C_6 arene ring, determined by neutron diffraction (71 entries)

	Hits[a]	Ratio (%)[b]	D_{atm}/Å[c] (fragment)[d]
N[e] = 4–999	48	67	2.70 ± 0.16 (311)
4–6	47	66	2.68 ± 0.15 (253)
7–9	23	32	2.79 ± 0.18 (54)
10	2	3	2.86, 3.06, 3.11, 3.06 Å

[a] Number of entries with short CH/Ar contacts. [b] Proportion of hits. [c] Mean atomic distance. [d] Number of observations. [e] Number of covalent bonds separating the hydrogen and carbon atoms.

Table 4. Intramolecular CH/π contacts in transition metal (TR) compounds (D_{max} 3.05 Å)

	DB[a]	Hit[b]	Ratio (%)[c]	D_{atm}/Å[d] (fragments)[e]
C_6 aromatic ring as the CH acceptor				
All TR elements	39570	20738	52	2.71 ± 0.17 (> 10000)
N[f] = 4−999				
4−6		18893	50	2.68 ± 0.16 (> 10000)
7−9		7985	39	2.83 ± 0.16 (> 10000)
10−12		2602	7	2.90 ± 0.14 (4747)
13−15		436	1	2.89 ± 0.14 (660)
> 16		60	< 0.2	2.89 ± 0.14 (86)
1st row elements	15900	7292	46	2.72 ± 0.17 (> 10000)
2nd row	11366	6890	61	2.71 ± 0.17 (> 10000)
3rd row	9799	5629	58	2.71 ± 0.17 (> 10000)
C_5 aromatic ring as the CH acceptor				
All TR elements	18198	1128	6	2.71 ± 0.19 (1845)
1st row	9496	871	9	2.70 ± 0.19 (1495)
2nd row	7487	386	5	2.70 ± 0.18 (610)
3rd row	3946	187	5	2.68 ± 0.18 (315)

[a] Number of entries in the database subset. [b] Number of hits. [c] Proportion of hits. [d] Mean atomic distance. [e] Number of observations. [f] Number of covalent bonds separating the hydrogen and carbon atoms.

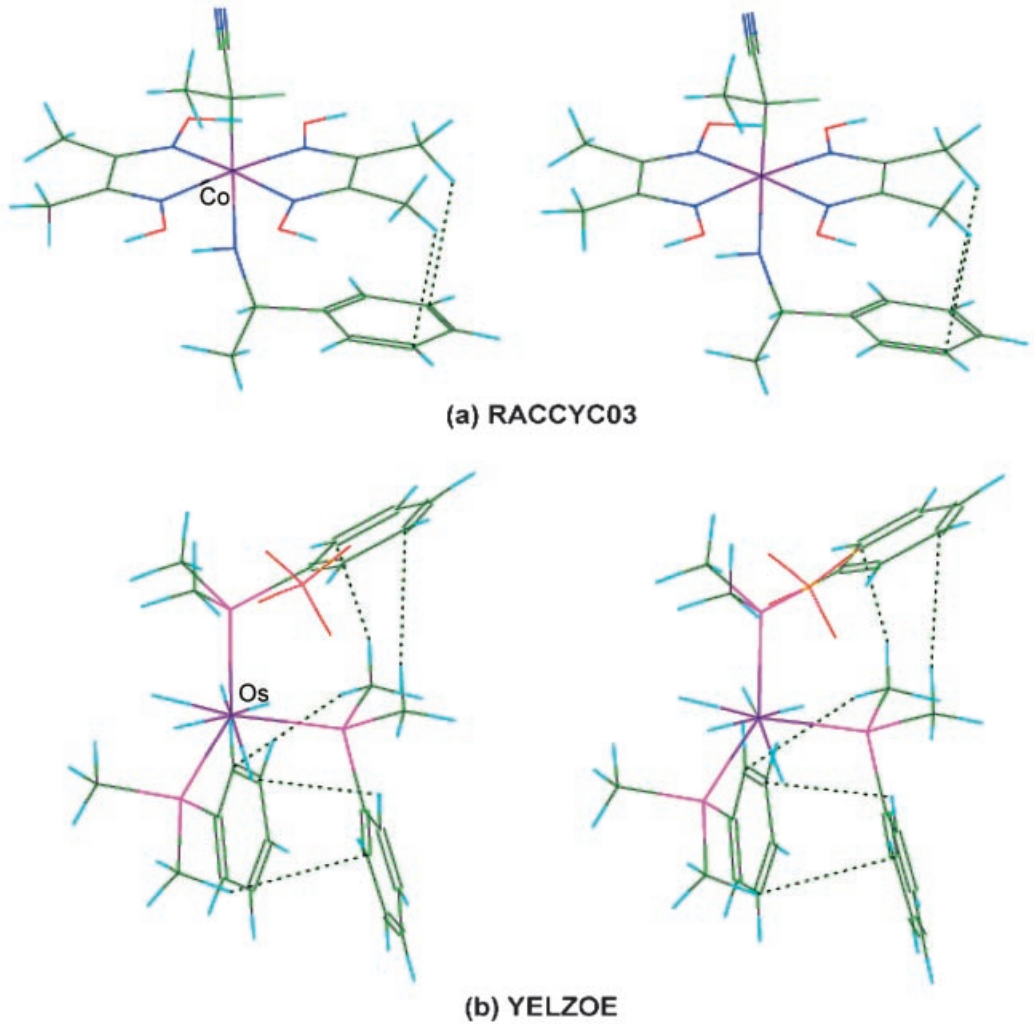

Figure 4. Intramolecular CH/π contacts disclosed in transition metal complexes (stereo view); dotted lines indicate CH/π contacts; purple: transition metal atom; (a) RACCYC03: [(*R*)-1-cyano-1-deuterioethyl][(*S*)-1-phenylethylamine]bis(dimethylglyoximato)cobalt(III); (b) YELZOE: Pentahydridotris[dimethyl(phenyl)phosphane]osmium tetrafluoroborate

Intramolecular Interactions

Table 3 gives the results obtained by examining intramolecular interactions; here the entries are limited to neutron diffraction data. We found that these structures have CH/π contacts both between and within the ligands.[35] Both the interligand and intraligand CH/π interactions seem to play an important part in controlling the shape of metal complexes.

Table 4 summarizes the results obtained by surveying the entire CSD. Among 39570 entries, 20738 crystal structures (ca. 52%) have been found to have at least one short CH/π intramolecular distance. Examples are given in Figure 4. Tables 3 and 4 show that the value of D_{atm} increases on going to a larger number of covalent bonds (N) separating the relevant H and C(sp^2) atom. The greater the value of N, the longer the CH/π interatomic distance. This is reasonable, since with a smaller N the position of CH is greatly restricted. The value of D_{atm} coalesces finally to that of the intermolecular interaction. Intramolecular interactions involving the C_5 aromatic ring as the CH acceptor are very scarce (ca. 6%). The exact reason remains unclear, but it may be pointed out that in these cyclopentadienyl compounds, ligands generally have few moieties that can make intramolecular contacts with the C_5 aromatic part.

Interactions Involved in Complexes with Certain Heteroaromatic Ligands

We then examined interactions among complexes bearing 1,10-phenanthroline, 2,2′-bipyridine, and 2,2′:6′,2′′-terpyridine as ligands. The importance of these ligands as supramolecular motives is well known.[36] In these surveys, six-membered heteroaromatic rings also acted as the CH acceptor. Table 5 lists the results. The proportion of hits in these complexes is lower than in the general cases reported in Table 4. This is probably because such nitrogen-containing flat ligands often form an offset π/π-stacked structure.[37,38] Representative examples are given in Figure 5. CH/π contacts are often found between an *ortho*-hydrogen atom of a pyridine moiety and an sp^2 atom of a nearby ring.

Interactions Involved in Complexes with Triphenylphosphane Ligands

Rhenium, rhodium, and ruthenium compounds bearing triphenylphosphane as ligands were also examined in view of their potent use as catalysts in the enantioselective reaction. Table 6 lists the results. The ratio of hits is considerably higher in these complexes than in the other cases. This certainly reflects the propensity of PPh_3 to form CH/π bonds within the ligand or with a nearby part of the complex. Figure 6 gives representative examples. Short contacts

Table 5. Intramolecular CH/π contacts in 1,10-phenanthroline, 2,2′-bipyridine, and 2,2′:6′,2′′-terpyridine complexes

Ligand	DB[a]	Hit[b]	Ratio (%)[c]	D_{atm}/Å[d] (fragment)[e]
Phenanthroline	789	314	40	2.79 ± 0.16 (1011)
Bipyridine	1479	592	40	2.70 ± 0.17 (2121)
Terpyridine	300	118	39	2.74 ± 0.17 (509)

[a] Number of entries in the database subset. [b] Number of hits. [c] Proportion of hits. [d] Mean atomic distance. [e] Number of observations.

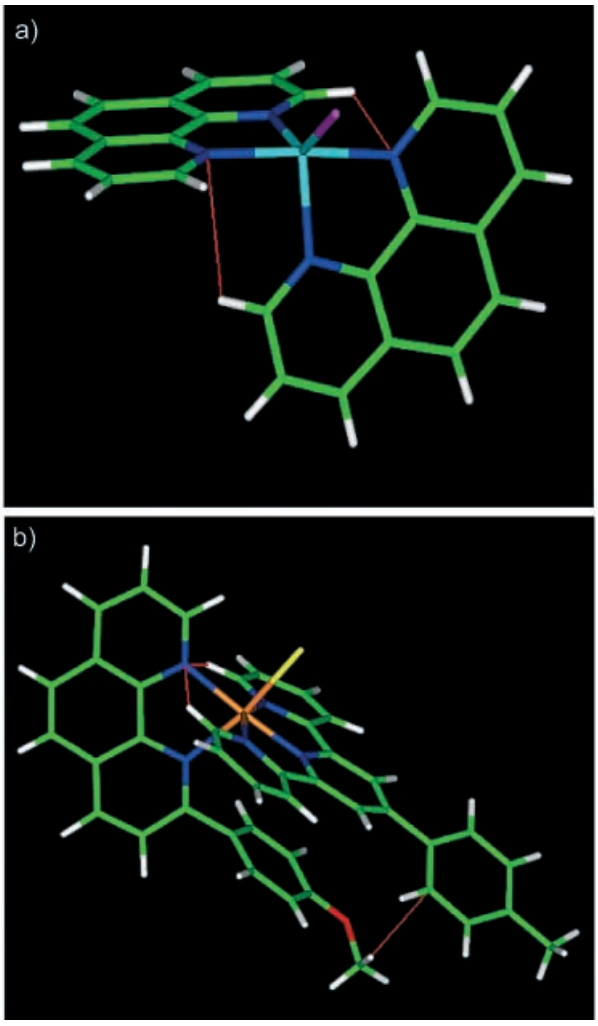

Figure 5. Interligand CH/π contacts disclosed in 1,10-phenanthroline complexes; red dotted lines indicate CH/π contacts; light blue: Cu; yellow: Cl; violet: I; orange: Ru; BASHIM: iodobis(1,10-phenanthroline)copper triiodide monoclinic polymorph; HOXLIP: chloro[4′-(*p*-tolyl)-2,2′:6′,2′′-terpyridine-*N*,*N*′,*N*′′][2-(*p*-anisyl)-1,10-phenanthroline-*N*,*N*′]ruthenium(II) hexafluorophosphate benzene solvate

Table 6. Intramolecular CH/π contacts in (triphenylphosphane)ruthenium, -rhenium, and -rhodium complexes

Metal	DB[a]	Hit[b]	Ratio (%)[c]	D_{atm}/Å[d] (fragment)[e]
Ruthenium	951	798	84	2.66 ± 0.17 (6144)
Rhenium	551	394	72	2.67 ± 0.16 (2857)
Rhodium	494	375	76	2.66 ± 0.16 (2667)

[a] Number of entries in the database subset. [b] Number of hits. [c] Proportion of hits. [d] Mean atomic distance. [e] Number of observations.

are found between CH groups of an alkyl chain as well as aromatic groups and a phenyl ring in the triphenylphosphane moiety. Dance and Scudder studied the interaction involved in both PPh_3 complexes [39] and Ph_4P^+ salts[40] in organometallic entries. They found many edge-to-face interactions and termed such a motif the "multiple phenyl embrace". These motifs seem to make the crystal structures compact and stable. Our suggestion is that this tight structure is achieved by a cooperative use of the aromatic CH/π interaction.[41]

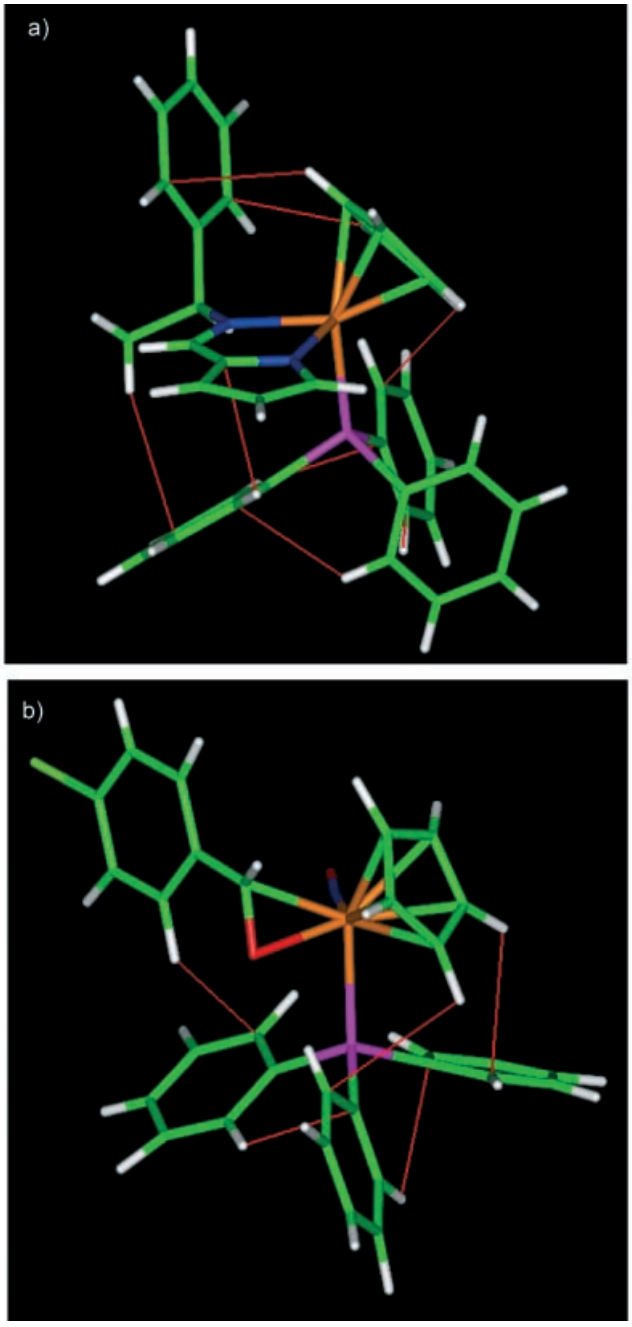

Figure 6. Intramolecular CH/π contacts disclosed in complexes bearing triphenylphosphane as a ligand; red dotted lines indicate interligand and intraligand CH/π contacts; orange: Ru or Re; violet: P; JUFQAC: η^5-cyclopentadienyl(triphenylphosphane){2-*N*-[(*S*)-1-phenylethyl]pyrrolecarbaldimine}ruthenium(II)]; ZAJSUY01: (η^5-cyclopentadienyl)nitrosyl-(η^2-*p*-chlorobenzaldehyde)(triphenylphosphane)rhenium hexafluorophosphate

Conclusion

To summarize, CH/π interactions are ubiquitously found in crystals of transition metal compounds. In other words, the CH/π-interacted crystal packing and the compact molecular structure are general aspects in coordination and organometallic chemistry. Janiak examined interactions involved in metal complexes with nitrogen-containing aromatic ligands[37] and found that the π/π-stacking[42] seldom occurs at a perfect parallel-stack geometry of the opposing parts. Nitrogen-containing flat ligands generally form an offset π/π-stacked structure. This is compatible with the present results that, for 1,10-phenanthroline complexes etc., aromatic CH/π interactions prevail but the ratio of hits is somewhat smaller than in the general cases. There are ample data in the literature demonstrating that the folded crystal conformation of metal compounds is maintained in solution.[43] The present statistical data suggest that these findings are not necessarily fortuitous, but exhibit a part of the general phenomenon. It is pertinent to point out in this regard that Taylor et al. presented unequivocal evidence by a CSD study that the so-called crystal packing forces do not provide systematic influence on molecular conformations.[44]

The enthalpy of one unit CH/π bond is certainly the smallest (around 1 kcal mol^{-1})[45] among the nonconventional hydrogen bonds. A notable feature of this molecular force, however, is that many CH groups can participate cooperatively in an interaction with π-bases. Besides, the CH/π interaction is entropically advantageous in that CH and π groups are generally arranged in a certain symmetric structure to make a persistent (stable and flexible) organization of molecules or molecular aggregates. We conclude that the concept of a CH/π hydrogen bond is vital in understanding various issues of chemistry and biochemistry of the transition metal compounds.

Acknowledgments

We thank Professor Helmut Sigel (University of Basle) for discussion and valuable comments.

[1] [1a] B. E. Fischer, H. Sigel, *J. Am. Chem. Soc.* **1980**, *102*, 2998−3008. [1b] G. Liang, R. Tribolet, H. Sigel, *Inorg. Chem.* **1988**, *27*, 2877−2887.
[2] H. Sigel, B. E. Fischer, E. Farkas, *Inorg. Chem.* **1983**, *22*, 925−934.
[3] [3a] H. Sigel, *Pure Appl. Chem.* **1989**, *61*, 923−932. [3b] H. Sigel, *Pure Appl. Chem.* **1998**, *70*, 969−976. [3c] O. Yamauchi, A. Odani, H. Masuda, H. Sigel, "Stacking interactions involving nucleotides and metal ion complexes", in *Metal Ions in Biological Systems* (Eds.: A. Sigel, H. Sigel), Marcel Dekker, Basle, **1996**, vol. 32, pp. 207−270 and references therein.
[4] [4a] H. Okawa, Y. Numata, A. Mio, S. Kida, *Bull. Chem. Soc. Jpn.* **1980**, *53*, 2248−2251. [4b] H. Okawa, K. Ueda, S. Kida,

Inorg. Chem. **1982**, *21*, 1594−1598. [4c] M. Nakamura, H. Okawa, T. Inazu, S. Kida, *Bull. Chem. Soc. Jpn.* **1982**, *55*, 2400−2403. [4d] M. Nakamura, H. Okawa, T. Ito, M. Kato, S. Kida, *Bull. Chem. Soc. Jpn.* **1987**, *60*, 539−543.

[5] M. Nishio, M. Hirota, Y. Umezawa, *The CH/π Interaction − Evidence, Nature, and Consequences*, Wiley-VCH, New York, **1998**.

[6] Review: [6a] H. Okawa, *Coord. Chem. Rev.* **1988**, *92*, 1−28. [6b] M. Nishio, M. Hirota, Y. Umezawa, *The CH/π Interaction. Evidence, Nature and Consequences*, Wiley-VCH, New York, **1998**, chapter 10.

[7] [7a] H. Brunner, *Angew. Chem.* **1983**, *95*, 921; *Angew. Chem. Int. Ed. Engl.* **1983**, *22*, 987−1012. [7b] H. Brunner, R. Oeschey, B. Nuber, *J. Chem. Soc., Dalton Trans.* **1996**, 1499−1508.

[8] H. Brunner, *Angew. Chem.* **1999**, *111*, 1248−1263; *Angew. Chem. Int. Ed.* **1999**, *38*, 1195−1208.

[9] [9a] H. Becker, P.-T. Hou, H. C. Kolb, S. Loren, P.-O. Norrby, K. B. Sharpless, *Tetrahedron Lett.* **1994**, *35*, 7315−7318. [9b] P. C. Cagle, O. Meyer, D. Vichard, K. Weickhardt, A. M. Arif, J. A. Gladysz, *Organometallics* **1996**, *15*, 194−204. [9c] R. W. Quan, Z. Li, E. N. Jacobsen, *J. Am. Chem. Soc.* **1996**, *118*, 8156−8157. [9d] T. Hashihayata, T. Punniyamurthy, R. Irie, T. Katsuki, M. Akita, Y. Morooka, *Tetrahedron* **1999**, *55*, 14599−14610. [9e] M. Yamakawa, H. Ito, R. Noyori, *J. Am. Chem. Soc.* **2000**, *122*, 1466−1478.

[10] G. R. Desiraju, T. Steiner, *The Weak Hydrogen Bond in Structural Chemistry and Biology*, Oxford University Press, Oxford, **1999**.

[11] M. Nishio, M. Hirota, *Tetrahedron* **1989**, *45*, 7201−7245.

[12] [12a] Y. Umezawa, S. Tsuboyama, H. Takahashi, J. Uzawa, M. Nishio, *Tetrahedron* **1999**, *55*, 10047−10056. [12b] S. Tsuzuki, H. Houjou, Y. Nagawa, K. Hiratani, *J. Chem. Soc., Perkin Trans. 2* **2001**, 1951−1955. [12c] M. Matsugi, M. Nojima, Y. Hagimoto, Y. Kita, *Tetrahedron Lett.* **2001**, *42*, 8039−8042. [12d] M. Kitamura, K. Nakano, T. Miki, M. Okada, R. Noyori, *J. Am. Chem. Soc.* **2001**, *123*, 8939−8950.

[13] [13a] S. J. Cantrill, J. A. Preece, J. F. Stoddart, Z.-H. Wang, A. J. P. White, D. J. Williams, *Tetrahedron* **2000**, *56*, 6675−6681. [13b] A. Arduini, G. Giorgi, A. Pochini, A. Secchi, F. Ugozzoli, *Tetrahedron* **2001**, *57*, 2411−2417.

[14] [14a] M. Akazome, Y. Ueno, H. Ooiso, K. Ogura, *J. Org. Chem.* **2000**, *65*, 68−76. [14b] K. Kinbara, Y. Harada, K. Saigo, *J. Chem. Soc., Perkin Trans. 2* **2000**, 1339−1348.

[15] M. Nakamura, H. Okawa, S. Kida, *Bull. Chem. Soc. Jpn.* **1985**, *58*, 3377−3378.

[16] H. Suezawa, T. Hashimoto, K. Tsuchinaga, T. Yoshida, T. Yuzuri, K. Sakakibara, M. Hirota, M. Nishio, *J. Chem. Soc., Perkin Trans. 2* **2000**, 1243−1249, and references cited therein.

[17] K. Kinbara, K. Oishi, Y. Harada, K. Saigo, *Tetrahedron* **2000**, *56*, 6651−6655.

[18] M. Yamakawa, I. Yamada, R. Noyori, *Angew. Chem. Int. Ed.* **2001**, *40*, 2818−2821.

[19] [19a] S. Sakaki, K. Kato, T. Miyazaki, Y. Musashi, K. Ohkubo, H. Ihara, C. Hirayama, *J. Chem. Soc., Faraday Trans.* **1993**, *89*, 659−664. [19b] S. Tsuzuki, K. Honda, T. Uchimaru, M. Mikami, K. Tanabe, *J. Am. Chem. Soc.* **2000**, *122*, 3746−3753.

[20] O. Takahashi, Y. Kohno, S. Iwasaki, K. Saito, M. Iwaoka, S. Tomoda, Y. Umezawa, S. Tsuboyama, M. Nishio, *Bull. Chem. Soc. Jpn.* **2001**, *74*, 2421−2430.

[21] Review: [21a] M. Nishio, Y. Umezawa, M. Hirota, Y. Takeuchi, *Tetrahedron* **1995**, *51*, 8665−8701. [21b] M. Nishio, M. Hirota, Y. Umezawa, *The CH/π Interaction. Evidence, Nature, and Consequences*, Wiley-VCH, New York, **1998**, chapter 11.

[22] Database studies: [22a] P. Chakrabarti, U. Samanta, *J. Mol. Biol.* **1995**, *251*, 9−14. [22b] M. Brandl, M. S. Weiss, A. Jabs, J. Shünel, R. Hilgenfeld, *J. Mol. Biol.* **2001**, *307*, 357−377. [22c] M. S. Weiss, M. Brandl, J. Shünel, D. Pal, R. Hilgenfeld, *Trends Biochem. Sci.* **2001**, *26*, 521−523.

[23] [23a] T. Nishinaka, Y. Ito, S. Yokoyama, T. Shibata, *Proc. Natl. Acad. Sci. USA* **1997**, *94*, 6623−6628. [23b] S.-H. Chou, Y.-Y. Tseng, *J. Mol. Biol.* **1999**, *285*, 41−48. [23c] Y. Umezawa, M. Nishio, *Bioorg. Med. Chem.* **2000**, *8*, 2643−2650. [23d] Y. Umezawa, M. Nishio, *Nucleic Acids Res.* **2002**, *30*, 2183−2192.

[24] [24a] T. Moriuchi, I. Ikeda, T. Hirao, *Organometallics* **1995**, *14*, 3578−3580. [24b] M. J. Hannon, C. L. Painting, N. W. Alcock, *Chem. Commun.* **1999**, 2023−2024. [24c] H. Takahashi, K. Kobayashi, M. Osawa, *Anal. Sci.* **2000**, *16*, 777−779. [24d] L. R. Hanton, K. Lee, *J. Chem. Soc., Dalton Trans.* **2000**, 1161−1166. [24e] V. Kulsomphob, G. C. Turpin, K.-C. Lam, C. Youngkin, W. Trakarnplruk, P. Carroll, A. Rheingold, R. D. Ernst, *J. Chem. Soc., Dalton Trans.* **2000**, 3086−3093. [24f] C.-Y. Su, B. S. Kang, C.-X. Du, Q.-C. Yang, T. C. W. Mak, *Inorg. Chem.* **2000**, *39*, 4843−4849. [24g] T. Mizutani, K. Wada, S. Kitagawa, *J. Org. Chem.* **2000**, *65*, 6097−6106. [24h] C. D. Abernethy, C. L. B. Macdonald, J. A. C. Clyburne, A. H. Cowley, *Chem. Commun.* **2001**, 61−62. [24i] S. Hartmann, R. F. Winter, T. Scheiring, M. Wanner, *J. Organomet. Chem.* **2001**, *637−639*, 240−250.

[25] [25a] T. E. Müller, D. M. P. Mingos, D. J. Williams, *J. Chem. Soc., Chem. Commun.* **1994**, 1787−1788. [25b] K. S. B. Hancock, J. W. Steed, *Chem. Commun.* **1998**, 1409−1410. [25c] T. Kusukawa, M. Fujita, *J. Am. Chem. Soc.* **1999**, *121*, 1397−1398. [25d] C. B. Smith, K. S. Wallwork, J. M. Weeks, M. A. Buntine, S. F. Lincoln, M. R. Taylor, K. P. Wainwright, *Inorg. Chem.* **1999**, *38*, 4986−4992. [25e] C. Janiak, S. Temizdemir, S. Dechert, W. Deck, F. Girgsdies, J. Heinze, M. J. Kolm, T. G. Scharmann, O. M. Zipffel, *Eur. J. Inorg. Chem.* **2000**, 1229−1241.

[26] D. Braga, F. Grepioni, E. Tedesco, *Organometallics* **1998**, *17*, 2669−2672. See also for a CSD survey on CH/π-interacted 6-membered chelate rings: G. A. Bogdanovic, A. Spasojevic-de Brie, S. D. Zaric, *Eur. J. Inorg. Chem.* **2002**, 1599−1602.

[27] F. H. Allen, *Acta Crystallogr., Sect. A* **1998**, *54*, 758−771.

[28] Y. Umezawa, S. Tsuboyama, K. Honda, J. Uzawa, M. Nishio, *Bull. Chem. Soc. Jpn.* **1998**, *71*, 1207−1213.

[29] [29a] H. Takahashi, S. Tsuboyama, Y. Umezawa, K. Honda, M. Nishio, *Tetrahedron* **2000**, *56*, 6185−6191. [29b] H. Suezawa, T. Yoshida, M. Hirota, H. Takahashi, Y. Umezawa, K. Honda, S. Tsuboyama, M. Nishio, *J. Chem. Soc., Perkin Trans. 2* **2001**, 2053−2058.

[30] L. Pauling, *The Nature of the Chemical Bonds*, Cornell University Press, Ithaca, New York, **1960**, p. 260.

[31] D_{max} 3.05 Å: 2.9 Å [(1.2 Å for C−H plus 1.7 Å for a half width of the aromatic ring) × 1.05] was used throughout the study unless otherwise noted; sp^2-C and -N atoms were not discriminated in the present survey. The C−H bond length and angle were normalized to standard values in the QUEST3D program, unless only coordinates from neutron studies are analyzed.

[32] The entries include metal complexes as well as organometallic compounds (screen −57 in the QUEST3D program) bearing at least one C_6 aromatic ring.

[33] In the hit entries, we note crystal structures of inorganic salts such as carbonylmetal complexes pairing with Ph_4P^+ as the counter ion.

[34] D_{max} 2.90 Å: Hydrogen atoms are limited to aromatic CH groups to minimize the chemical inhomogeneity.

[35] It is difficult in the present search to distinguish the intraligand and interligand CH/π interaction. Occurrence of intraligand interaction is not frequent, but we often note interactions within a ligand in certain ligands such as triphenylphosphane.

[36] I. Dance, M. Scudder, *J. Chem. Soc., Dalton Trans.* **1998**, 1341−1350.

[37] C. Janiak, *J. Chem. Soc., Dalton Trans.* **2000**, 3885−3896.

[38] V. Russell, M. Scudder, I. Dance, *J. Chem. Soc., Dalton Trans.* **2001**, 789−799.

[39] I. Dance, M. Scudder, *J. Chem. Soc., Chem. Commun.* **1995**, 1039−1040.

[40] I. Dance, M. Scudder, *J. Chem. Soc., Dalton Trans.* **1996**, 3755−3769.

[41] This type of interaction has been known and is often referred

to as the edge-to-face (or point-to-face, T-shape) π/π (or arene/arene, aromatic/aromatic) interaction.
[42] C. A. Hunter, *Chem. Soc. Rev.* **1994**, 101−109.
[43] [43a] H. M. Colquhoun, S. M. Doughty, J. F. Stoddart, A. M. Z. Slawin, D. J. Williams, *J. Chem. Soc., Dalton Trans.* **1986**, 1639−1652. [43b] S. K. Chowdhury, V. S. Joshi, A. G. Samuel, V. G. Puranik, S. S. Tavale, A. Sarkar, *Organometallics* **1994**, *13*, 4092−4096. [43c] K. Yamanari, T. Nozaki, A. Fuyuhiro, Y. Kushi, S. Kaizaki, *J. Chem. Soc., Dalton Trans.* **1996**, 2851−2856. [43d] K. Jitsukawa, K. Iwai, H. Masuda, H. Ogoshi, H. Einaga, *J. Chem. Soc., Dalton Trans.* **1997**, 3691−3698. [43e] H.-D. Hornung, K.-W. Klinkhammer, A. Schmidt, *Main Group Met. Chem.* **1997**, *20*, 157−167. [43f] A. Cavaglioni, R. Cini, *J. Chem. Soc., Dalton Trans.* **1997**, 1149−1158. [43g] C. Bellucci, R. Cini, *J. Inorg. Biochem.* **1999**, *76*, 243−250. [43h] M. Mizutani, S. Tomosue, H. Kinoshita, K. Jitsukawa, H. Masuda, H. Einaga, *Bull. Chem. Soc. Jpn.* **1999**, *72*, 981−988. [43i] N. Yoshida, K. Ichikawa, M. Shiro, *J. Chem. Soc., Perkin Trans. 2* **2000**, 17−26. [43j] T. Kawamoto, Y. Kushi, *J. Chem. Soc., Dalton Trans.* **2000**, 3022−3026.
[44] F. H. Allen, S. E. Harris, R. Taylor, *J. Comput.-Aided Mol. Des.* **1996**, *10*, 247−254. See also ref.[27]
[45] [45a] R. Ehama, A. Yokoo, M. Tsushima, T. Yuzuri, H. Suezawa, M. Hirota, *Bull. Chem. Soc. Jpn.* **1993**, *66*, 814−818. [45b] F. J. Carver, C. A. Hunter, E. M. Seward, *Chem. Commun.* **1998**, 775−776. [45c] E.-I. Kim, S. Paliwal, C. S. Wilcox, *J. Am. Chem. Soc.* **1998**, *120*, 11192−11193.

Received May 11, 2002
[I02249]

Reaction of $[(Cp_2TiCH_3)(THF)^+][BPh_4^-]$ with Tripeptide Derivatives: Formation of Cationic (Peptide)titanocene Complexes

Dirk Harmsen,[a] Gerhard Erker,*[a] Roland Fröhlich,[a][‡] and Gerald Kehr[a]

Keywords: Bioinorganic chemistry / Peptides / Metallocenes / Titanium / Cations

A series of Z- and Boc-protected tripeptide methyl esters [Z-/Boc-**5** to -**12**(pept)] was prepared using the amino acids glycine, alanine and valine. In both the alanine and the valine series a single glycine unit was introduced and its position inside the tripeptide framework was systematically varied. Reaction of these 16 tripeptide derivatives with the organometallic reagent $[Cp_2TiCH_3(THF)^+][BPh_4^-]$ (**13**) resulted in the formation of methyl(peptide)titanocene cation complexes that contained the strongly electrophilic $[Cp_2TiCH_3^+]$ cation moiety coordinated to a single carboxamide carbonyl oxygen atom. Mostly, the carbonyl oxygen atom of the central amino acid residue was specifically attached to yield the coordination products **5**–**12**(coord[7]). In a few specific cases, formation of the κO-adduct between the $[Cp_2TiCH_3^+]$ cation and the *N*-terminal amino acid moiety was also observed, especially in the cases of the *N*-terminal glycine derivatives. In one case we observed the migration of the $[Cp_2TiCH_3^+]$ group along the chain from the C4=O to the C7=O position. Subsequent thermally induced CH_4 elimination of the products **5**–**12**(coord) gave the cationic peptide chelate derivatives **5**–**12**(chel). These are characterized by the presence of a five-membered κ*O*,κ*N*-chelate with an anellated four-membered κ*N*,κ*O*-chelate. This is mostly centered around the central amino acid unit [products **5**–**12**(chel^B)], but in some cases the *N*-terminal amino acid, together with the *N*-terminal protective group, also forms this type of a stable peptide titanocene cation chelate complex [products **5**–**12**(chel^A)]. The selective formation of these series of (peptide)metallocene cation complexes was readily analyzed by means of their very characteristic ^1H and ^{13}C NMR spectra.
(© Wiley-VCH Verlag GmbH, 69451 Weinheim, Germany, 2002)

Introduction

Peptides represent interesting chiral ligand systems. Therefore, some of them have been used in organometallic chemistry and catalysis, although mostly such complexes derived from the middle or late transition metals are reported so far.[1−3] The usually rather oxophilic early metals, especially those of group 4 (and the f-elements), are not easily "tamed" to allow unrestricted bonding to the multifunctional oligopeptide frameworks. Some Cp group-4 metal complexes have found use in peptide synthesis.[4,5] A few (amino acid or peptide)cyclopentadienylzirconium complexes were previously described, and some catalytic features were reported;[6−10] *C*-terminal carboxylate-bonded amino acid derivatives were found useful in titanocene chemistry with regard to the development of novel antitumor pharmaceuticals.[11]

A cationic zirconocene complex of a dipeptide derivative (**2**) was first prepared by treatment of "Jordan's cation"[12] $[Cp_2ZrCH_3)(THF)^+][BPh_4^-]$ (**1a**) with the dipeptide isocyanate derivative. Addition of the $Zr-CH_3$ functionality to the *N*-terminal heterocumulene cleanly gave the $\kappa^2O,\kappa N$-chelate (dipeptide)zirconocene cation **2a** (see Scheme 1).[13] The typical metallatricyclic σ-framework of complex **2** was characterized by X-ray diffraction. The NMR spectroscopic analysis of **2** revealed typical spectroscopic features of this type of bonding, such as a strong shift of the $^{13}C4$ carbonyl resonance to larger δ values ($\Delta\delta \approx 8-10$ ppm) relative to the respective neutral noncoordinated peptides.[13] Treatment of the dipeptide derivative Boc-Ala-Val-OMe with **1** furnished the analogous zirconocene cation complex **3** (after loss of methane), that was characterized by an X-ray crystal structure analysis. It revealed the formation of a

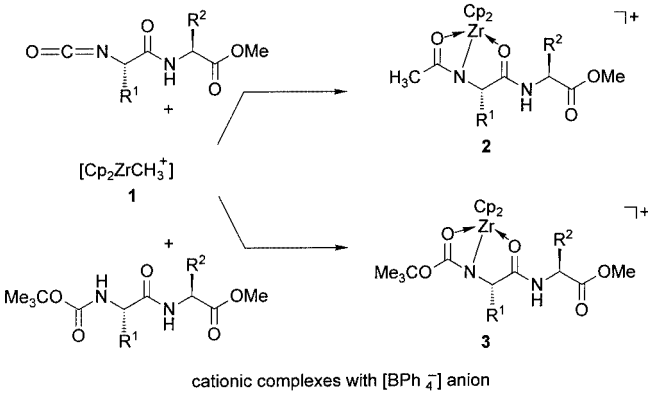

Scheme 1

[a] Organisch-Chemisches Institut der Universität Münster, Corrensstr. 40, 48149 Münster, Germany
[‡] X-ray crystal structure analyses.
Supporting information for this article is available on the WWW under http://www.eurjic.org or from the author.

metallatricyclic structure analogous to **2** (see Scheme 1), that again exhibits very typical ^1H and ^{13}C NMR features.[14]

A series of experiments using different di- and tripeptide systems revealed that $[Cp_2ZrCH_3^+]$ was in all the cases first attached to the C4 carbonyl oxygen atom under kinetic control, followed by migration of the metallocene unit along the chain. Subsequent intramolecular NH deprotonation with loss of CH_4 usually led to the formation of complex **4**(chel) (with a few exceptions), which is the thermodynamic product in the series investigated[14] (see Scheme 2).

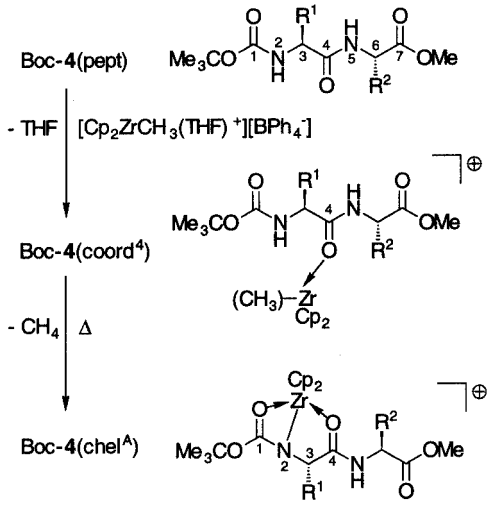

Scheme 2

We have now systematically examined the reaction of the titanium analog $[(Cp_2TiCH_3)(THF)^+][BPh_4^-]$[15] with peptides, employing two series of tripeptide derivatives (details see below), and found some similarities and some noteworthy differences in the formation of the cationic (peptide)titanocene complexes and in their chemical behavior.

Results and Discussion

Synthesis and Characterization of the Tripeptide Derivatives Employed in this Study

We have used two series of tripeptides in this study. The first involved a systematic combination of the natural amino acids glycine (Gly) and alanine (Ala) with a variation of the two *N*-terminal protecting groups benzyloxycarbonyl (Z)[16] and *tert*-butoxycarbonyl (Boc);[17] the *C*-terminal carboxylic acid was protected by a methyl ester group in each case. A single Gly amino acid was moved from the *N*-terminus through the center position to the *C*-terminus, and we used the corresponding $(Ala)_3$ systems for comparison. The Z-protected systems were prepared from the commercially available Z-dipeptide acids, to which the corresponding amino acid methyl esters were coupled using the IIDQ method.[18] The Boc-protected systems were synthesized in a similar way, although, the respective Boc-protected dipeptides were prepared by a variation using DCC.[19] In this way the eight tripeptide derivatives Z-**5**(pept) (= Z-Gly-Ala-Ala-OMe) to Boc-**8**(pept) (= Boc-Ala-Ala-Ala-OMe) were obtained[20] (for a compilation see Table 3).

The series of eight glycine- and valine-containing tripeptides Z-**9**(pept) (= Z-Gly-Val-Val-OMe) to Boc-**12**(pept) (= Boc-Val-Val-Val-OMe) were prepared analogously (for details see the Exp. Sect. and Table 3).

The ^1H and ^{13}C NMR chemical shifts of these 16 tripeptide derivatives were determined using 1D and 2D NMR spectroscopy. These data are presented in Table 4 in the Exp. Sect. It shows that the characteristic NMR features of the peptide backbones are largely independent of the protecting groups. Val and Ala building blocks give rise to characteristic alterations of the ^{13}C NMR chemical shifts at C3, C6, and C9. Glycine, of course, influences these δ values even more and also shows a small systematic decrease in the corresponding δ(C=O) values (see Table 4). The numbering scheme that we have used for characterization of the peptide backbones throughout this paper is depicted in Scheme 4.

Two of the tripeptide derivatives were characterized by X-ray diffraction. They belong to different structural types; Z-**5**(pept) (= Z-Gly-Ala-Ala-OMe) contains two independent molecules in the unit cell, that are only markedly different with regard to the conformational orientation of the phenyl group of the benzyloxycarbonyl protecting group at the *N*-terminus (see Figure 1). Compound Z-**5**(pept) shows no *intramolecular* hydrogen bonds, only *trans*-peptide linkages are found and all torsional angles ω (i.e. $C_\alpha-C_{(o)}-N-C_\alpha$) are close to 180°. However, this peptide derivative exhibits two types of *intermolecular* hydrogen bonds (between the carbonyl oxygen atom O2 and N2*−H of an adjacent molecule *and* between N8−H and C=O7*). This leads to the specific supramolecular peptide framework that is depicted in Figure 1.

Compound Z-**6**(pept) (i.e. Z-Ala-Gly-Ala-OMe) contains the amino acid glycine in the central position. Glycine allows for a fair amount of conformational flexibility inside the peptide chain. Compound Z-**6**(pept) is found to adopt a β-turn-type structure in the solid state (see Figure 2). It requires the involvement of four amino acid residues to complete the typical hydrogen-bonded β-turn ten-membered ring structure, that makes up the almost 180° turn of the peptide backbone structure.[21] In the tripeptide derivative Z-**6**(pept), the carbonyl group of the benzyloxycarbonyl protecting group Z at the *N*-terminus serves as a substitute for the missing fourth amino acid building block. The ten-membered ring in Z-**6**(pept) is then closed between N8−H and the Z-carbonyl oxygen atom C1=O2 (see Figure 2). The β-turn structure of Z-**6**(pept) in the solid state is characterized by the torsional angles φ_{i+1} (i.e. C1−N2−C3−C4) = −57.5(3)°, ψ_{i+1} (N2−C3−C4−N5) = 136.4(2)°, φ_{i+2} (C4−N5−C6−C7) = 71.3(3)°, and ψ_{i+2} (N5−C6−C7−N8) = 8.2(4)°. This is similar to the values for the most commonly observed βII-turn (ideal values: $\varphi_{i+1} = -60°$, $\psi_{i+1} = 120°$, $\varphi_{i+2} = 80°$, $\psi_{i+2} = 0°$).[22]

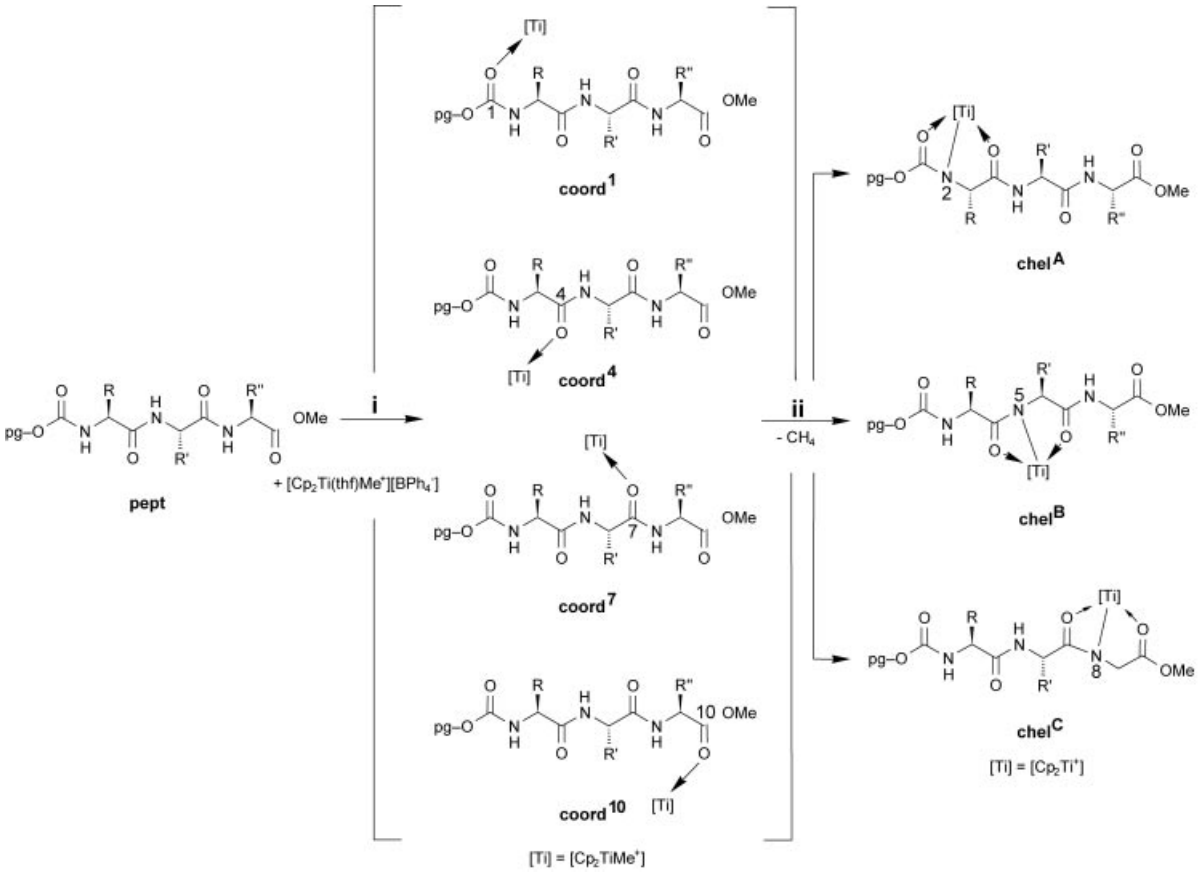

Scheme 3 . The series of possible primary and secondary products formed by the reaction between the tripeptide derivatives **5**−**12**(pept) with the $[Cp_2TiCH_3(THF)^+]$ salt **13**

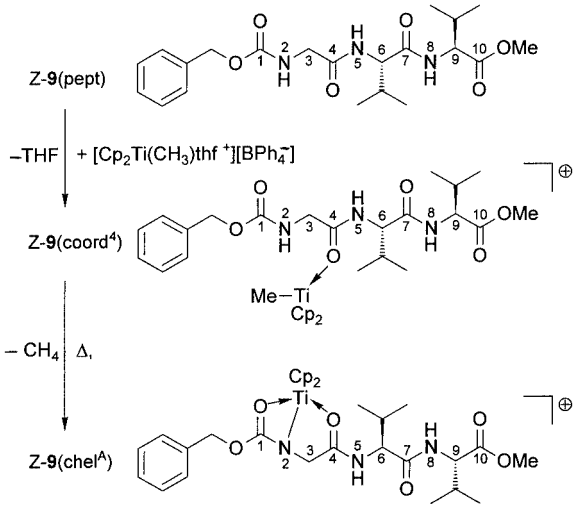

Scheme 4

Compound Z-**6**(pept) is characterized by the formation of two additional *intermolecular* hydrogen bonds, namely between N2−H2 and the carbonyl group C7*=O7* (N−H: 0.85 Å; H···O*: 2.04 Å; N−H···O angle: 164°) and between N5−H5 and C*4=O4* (N−H: 0.82 Å; H···O* 2.09 Å; angle 160°), in addition to the *intramolecular* N8−H8···O2 hydrogen bond. This results in the formation of a μ-H-bridged supramolecular structure of the tripeptide derivative Z-**6**(pept), as depicted in Figure 3.

The Cationic Titanocene Complexes

The *N*-protected tripeptide derivatives Z- and Boc-**5**(pept) to -**12**(pept) (see Table 3) were treated with the metallocene cation reagent $[Cp_2TiCH_3(THF)^+][B(C_6F_5)_4^-]$ (**13**).[15] Similarly, as previously observed for the related zirconocene system, the THF ligand is rapidly replaced at low temperature (< 0 °C). In contrast to the zirconium systems,[13,14] the resulting $[\kappa O\text{-}Cp_2Ti(CH)_3(peptide)^+]$ cation complexes are more stable. It usually required several hours at room temperature to allow for the subsequent methane elimination reaction to go to completion. Typically, reaction of the respective peptide derivative with reagent **13** was carried out at ca. −20 °C, and the resulting coordination products [**5**(coord) to **12**(coord)] were characterized by NMR spectroscopy at −5 °C. The samples were then kept overnight at room temperature to cleanly yield the final methane elimination products [**5**(chel) to **12**(chel)]. The latter compounds were all isolated and fully characterized.

The reaction of the protected tripeptides with **13** primarily proceeds by the replacement of the stabilizing THF ligand from the reactive oxophilic methyltitanocene cation, and coordination of the peptide through one of its carbonyl groups. In principle, this could result in the formation of

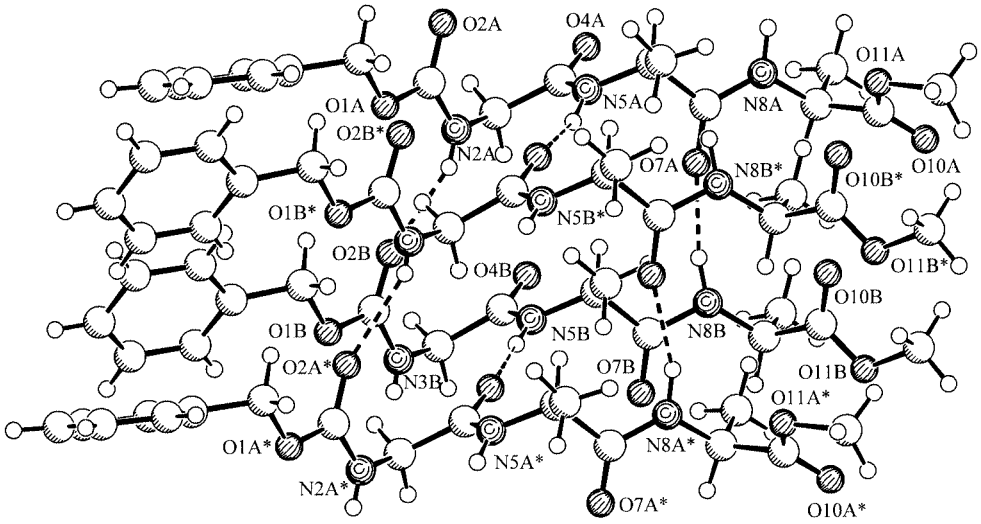

Figure 1. Molecular framework structure of Z-Gly-Ala-Ala-OMe [Z-**5**(pept)] in the solid state; the specific hydrogen bonding pattern between two pairs of Z-**5**(pept) molecules is depicted

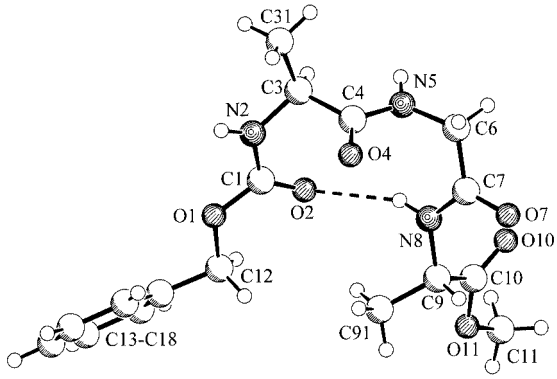

Figure 2. A view of the β-turn-like structure of compound Z-**6**(pept) in the crystal

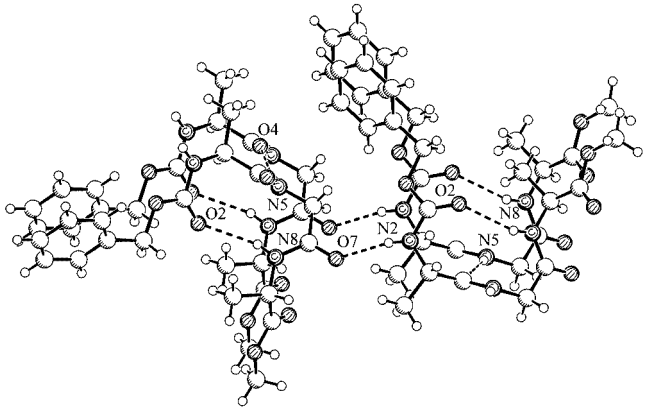

Figure 3. Supramolecular hydrogen-bridged network structure of Z-**6**(pept) in the solid state

four coordination products, which we will name e.g. Z-**5**(coord[1]), -**5**(coord[4]), -**5**(coord[7]), and -**5**(coord[10]), with the superscript denoting the atom number of the coordinating carbonyl group (see Scheme 3). Subsequent thermally induced methane elimination can then result in the formation of three different organometallic products, where the peptide ligand is bonded to the remaining titanocene unit in the typical chelate fashion. We will name these three products accordingly, e.g. Z-**5**(chel^{A}), -**5**(chel^{B}), and -**5**(chel^{C}). Here, the superscript denotes whether the chelate is formed by participation of the carbonyl-containing *N*-terminal protecting group (chel^{A}), the carbonyl group of the *C*-terminal ester (chel^{C}), or just the central peptide bonds (chel^{B}) (see Scheme 3).

The previously described detailed characterization of some of the zirconium complexes[13,14] enabled us to assign the structures of this large (and, as we will see, in some cases, quite complicated) series of (peptide)titanocene cation complexes. A rather simple example may serve as a demonstration. The peptide derivative Z-**9**(pept) (i.e. Z-Gly-Val-Val-OMe) reacts cleanly with **13** to give a single primary carbonyl coordination product, which is identified as Z-**9**(coord[4]).

The ^{13}C and, to a lesser extent, the ^{1}H NMR spectra reveal that in this case the [$Cp_2TiCH_3^+$] moiety is selectively coordinated to the C=O4 carbonyl oxygen. Very characteristically, the ^{13}C NMR resonance of the C4 carbonyl carbon atom is shifted by $\Delta\delta = +8.6$ ppm to a *larger* δ value [(Z-**9**(pept): δ = 169.6 (C4) vs. Z-**9**(coord[4]): δ = 178.2 (C4)]. In contrast, the other three carbonyl carbon chemical shifts are only marginally affected by [$Cp_2TiCH_3^+$] coordination. As expected, metallocene coordination to the C=O4 carbonyl group leads to some spectral changes for the atoms in the direct vicinity of this carbonyl group, most notably the anisotropy effects in the ^{1}H NMR spectra caused by the spatial vicinity of the aromatic Cp-ring systems.

Thus, the glycine 3-H/3-H′ ^{1}H NMR resonances shift to a lower δ value on complex formation, namely from δ = 3.90 ppm [(Z-**9**(pept)] to δ = 1.71 ppm [Z-**9**(coord[4])]. A similar effect is observed for the N2−H proton NMR resonance [δ = 5.92 ppm (pept) vs. δ = 4.23 ppm (coord[4])], and the rather remote C6−H signal [δ = 4.45 ppm (pept) vs. δ = 3.48 ppm (coord[4])], whereas the opposite effect is

observed for the N5−H resonance [δ = 7.05 ppm (pept), but δ = 7.48 ppm (coord[4])]. Coordination of the titanocene unit results in a diastereotopic splitting of the Cp resonances in **Z-9**(coord[4]) [δ = 6.19 ppm, 6.15 ppm (^{1}H)]. The methyl group at the titanium atom gives rise to a ^{1}H NMR singlet at δ = 1.14 ppm (^{13}C NMR resonance at δ = 52.0 ppm).

Overnight at room temperature, complex **Z-9**(coord[4]) looses 1 equiv. of methane to selectively form a single chelate (peptide)titanocene cation complex. The ^{1}H NMR spectrum shows that the *N2*-bound hydrogen atom is eliminated during this process. Its signal does not appear in the product spectrum and, consequently, we must assume that the [Cp_2Ti^+] unit is κ*N2*-bonded in the product. The overall coordination is likely to be κ^2(*O1*,*O4*),κ*N2*, i.e. the peptide is bound in a chelate fashion to the group-4 metal center, as had been previously demonstrated for the related zirconium systems. In the product **Z-9**(chel[A]), this specific type of bonding leads to very characteristic NMR features. The C4 ^{13}C NMR carbonyl resonance is shifted to larger δ values [δ = 175.3 ppm (chel[A])] relative to the parent peptide derivative [δ = 169.6 ppm (pept)], as is the C3 methylene carbon resonance [δ = 52.2 ppm (chel[A]) vs. δ = 44.8 ppm (pept)]. Remarkably, the κ*O*,κ*N* chelate moiety in this type of product typically leads to the observation of a slightly decreased ^{13}C NMR δ(C1=O) shift [(δ = 151.9 ppm (chel[A]) vs. δ = 156.9 ppm (coord[4]) vs. δ = 157.0 ppm (pept)], which probably results from an electronic compensation effect within the chelating κ*O*,κ*N* peptide anion moiety.[13,14] Of course, the Ti−methyl resonances are no longer observed in the spectra of **Z-9**(chel[A]), and the Cp_2Ti unit gives rise to resonances assigned to a pair of diastereotopic η^5-cyclopentadienide ligands [δ = 6.07 ppm and 6.00 ppm (^{1}H), δ = 118.8 ppm and 118.7 ppm (^{13}C NMR)].

In most other cases, the situation is more complicated than in the titanocene coordination chemistry of **Z-9**(pept). Often, other primary coordination products were obtained, sometimes mixtures of two compounds. In about half of the cases studied, mixtures of two final chelate products were obtained after subsequent methane elimination. In all these cases, the typical ^{1}H and, more importantly, ^{13}C NMR spectra allowed for a clear identification of the individual metal complexes in these mixtures. In the case of the primary [$Cp_2TiCH_3^+$] coordination products, the amino acid to which the metallocene residue was κ*O*-coordinated, could easily be identified, primarily by observing the typical marked downfield shift of the respective ^{13}C NMR carbonyl resonance. Eight examples in our series (for details see Table 2 and the Exp. Sect.) have the alkylmetallocene cation coordinated to the glycine residue on the **5**−**12**(coord) primary product stage. Their respective Gly(*C*=O) ^{13}C NMR chemical shifts are shifted to larger δ values by Δδ ≈ +8.6 and +10.6 (average: $\Delta\delta_{av}$ = +9.3). Similarly, $\Delta\delta_{av}$ = +11.4 for Ala(*C*=O) coordination (6 examples ranging from individual Δδ = +10.2 to +15.8), and $\Delta\delta_{av}$ = +10.4 for Val(*C*=O) coordination (6 individual examples with Δδ between +10.0 and +10.8). The NMR chemical shifts of the adjacent ^{1}H and ^{13}C nuclei are smaller; however, the Δδ ranges are similar to those described above for the selected example of complex **Z-9**(coord). For statistical details see Table 1 and Scheme 5.

Table 1. Individual and averaged ^{1}H and ^{13}C NMR Δδ values observed in the methyl(tripeptide)titanocene cation complexes **5**−**12**(coord) relative to the free peptide derivatives; the structural subunit is depicted in Scheme 5, substituent R followed by the number of individual examples is provided in parentheses

aa_1:	Gly (R = H, 8)	Ala (R = Me, 6)	Val (R = *i*Pr, 6)
N−*H*	−2.06 to −1.35 ∅ = −1.68	−1.18 to +1.35 ∅ = −0.60	−2.29 to −0.32 ∅ = −1.07
α-C*H*R	−2.19 to −1.67 ∅ = −1.87	−0.79 to −0.20 ∅ = −0.55	−0.69 to +0.16 ∅ = −0.28
α-*C*HR	−0.1 to +0.6 ∅ = +0.1	−0.4 to +1.5 ∅ = +1.0	−2.8 to +4.2 ∅ = +2.6
C=O	+8.6 to +10.6 ∅ = +9.3	+10.2 to +15.8 ∅ = +11.4	+10.0 to +10.8 ∅ = +10.4
aa_2:	Gly (R′ = H, 4)	Ala (R′ = Me, 8)	Val (R′ = *i*Pr, 8)
N−*H*	+0.76 to +1.83 ∅ = +1.18	+0.27 to +1.46 ∅ = +1.01	−1.03 to +1.81 ∅ = +0.58
α-C*H*R	−0.31 to −0.18 ∅ = −0.27	−0.96 to −0.49 ∅ = −0.70	−0.98 to +0.26 ∅ = −0.62
α-*C*HR	+0.9 to +1.4 ∅ = +1.2	−0.4 to +1.9 ∅ = +1.4	−0.4 to +2.8 ∅ = +1.4

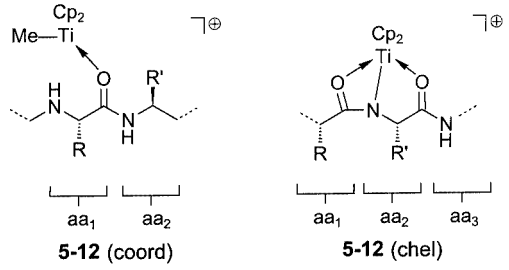

Scheme 5

Similarly, characteristic Δδ values are observed for the pairs of adjacent amino acid moieties that coordinate to the [Cp_2Ti^+] unit after CH_4 elimination in the products **5**−**12**(chel). In all cases strong Δδ effects are observed for the ^{13}C NMR resonances of the carbonyl group, *and* its adjacent α-carbon atom of the amino acid unit AS_2 (see Scheme 5) inside the five-membered chelate ring of the overall metallabicyclic structural subunits. The average ^{13}C NMR Δδ(*C*=O) values are about +5.7 ppm (see Table 2). The shielding effect is even larger for the α-*C*HR ^{13}C NMR resonance, with $\Delta\delta_{av}$ values between +9.0 and +10.3 ppm (see Table 2). The Δδ values of the *C*=O group in the anellated four-membered κ*O*,κ*N*-chelate is again much smaller because of the "carboxamide compensation effect". This is similar to that observed for the analogous zirconium complexes.[13,14]

With these characteristic NMR spectroscopic data it is possible to analyze the resulting product mixtures in a rather straightforward manner. The results are listed in Table 2. It can be seen that coordination of the intact

Table 2. Range of Δδ values for **5**−**12**(chel) relative to the free tripeptide derivatives **5**−**12**(pept); the structural subunit is depicted in Scheme 5, R and number of examples in parentheses

aa_1:	Gly (R = H, 2)	Ala (R = Me, 6)	Val (R = *i*Pr, 6)
α-C*H*R	−0.45, −0.35 ∅ = −0.40	−0.41 to −0.03 ∅ = −0.17	−0.46 to +0.20 ∅ = −0.22
α-*C*HR	−1.8, −1.4 ∅ = −1.6	−2.8 to +2.0 ∅ = −1.7	−2.4 to +0.2 ∅ = −1.6
C=O	+2.1 and +2.4 ∅ = +2.3	−1.3 to +1.4 ∅ = +0.7	+1.6 to +5.9 ∅ = +3.4
aa_2:	Gly (R′ = H, 7)	Ala (R′ = Me, 10)	Val (R′ = *i*Pr, 8)
α-C*H*R	−0.15 to +0.39 ∅ = +0.11	−0.16 to +0.58 ∅ = +0.33	+0.12 to +1.07 ∅ = +0.65
α-*C*HR	+7.4 to +10.1 ∅ = +9.0	+7.9 to +10.5 ∅ = +9.6	+8.7 to +12.3 ∅ = +10.3
C=O	+5.3 to +6.1 ∅ = +5.8	+5.2 to +6.4 ∅ = +5.6	+3.5 to +6.5 ∅ = +5.8

[$Cp_2TiCH_3^+$] cation to the amido carbonyl oxygen atom of the central amino acid building block of the tripeptide framework is favored in the majority of the cases. A single such product is formed in the cases of Z- and Boc-**6**, -**7**, -**8**, -**10**, and -**11**(coord^7). Deviations from this behavior are observed in the cases where the small glycine building block is located at the *N*-terminus of the tripeptide. Pure Z- and Boc-**9**(coord^4) adducts are formed in the PG-Gly-Val-Val-OMe series, and mixtures of the respective Z- and Boc-**5**(coord^4) and -**5**(coord^7) adducts are found in the PG-Gly-Ala-Ala-OMe cases (see Table 3).

The situation is similar for the final products obtained after subsequent thermally induced methane elimination, although in some cases it is slightly more complicated. Once again, it can be seen from Table 3 that coordination to the central section of the tripeptide framework is by far favored, i.e. the dominating products are Z- and Boc-**5**−**11**(chel^B), where the chelate structure is formed by the involvement of two adjacent amino acid moieties, without any participation of the carbonyl groups of the *N*-terminal protecting group nor the *C*-terminal ester. However, in many cases, mixtures of (chel^B) and (chel^A) (mostly minor) are found. Only in the extreme cases of Z- and Boc-Gly-Val-Val-OMe did we find the selective formation of the otherwise less favored **9**(chel^A) products that involve glycine and the RO−CO protective functionality in chelate bonding (see Table 3). The products (coord^1), (coord^{10}), or (chel^C) (see Scheme 3) were never observed in this series of experiments.

Methane elimination from the cationic primary coordination products [(coord)] is much slower in the case of the titanocene complexes than for the previously described zirconocene relatives. In one case, this has allowed for the observation of a rearrangement process at the stage of the formation of the κ*O*-[$Cp_2TiCH_3^+$] coordination products. The peptide Z-Val-Val-Val-OMe [Z-**12**(pept)] forms a 3:2 mixture of the two [$Cp_2TiCH_3^+$] coordination products Z-**12**(coord^4) and Z-**12**(coord^7). After 4 h at −5 °C, this changed to a ratio of Z-**12**(coord^4)/Z-**12**(coord^7) of 1:3. In the case of the Boc-protected system, Boc-**12**, the situation is even more pronounced. A Boc-**12**(coord^4)/Boc-**12**(coord^7) mixture of 4:1 is initially formed at −5 °C, that changed to a 1:3 ratio in favor of the generally thermodynamically favored internal coordination product after 4 h at −5 °C (see Scheme 6).

Table 3. A compilation of the products formed by the reaction of the tripeptide derivatives **5**−**12** with [$Cp_2TiCH_3^+$][BPh_4^-] (**13**)

Peptide (pept):	Coordination product (coord^4)/(coord^7)	Chelate product (chel^A)/(chel^B)
Alanine series:		
Z-Gly-Ala-Ala-OMe Z-**5**	2:1	−:1[a]
Boc-Gly-Ala-Ala-OMe Boc-**5**	3:1	1:2
Z-Ala-Gly-Ala-OMe Z-**6**	−:1	1:2
Boc-Ala-Gly-Ala-OMe Boc-**6**	−:1	1:2
Z-Ala-Ala-Gly-OMe Z-**7**	−:1	−:1
Boc-Ala-Ala-Gly-OMe Boc-**7**	−:1	1:2
Z-Ala-Ala-Ala-OMe Z-**8**	−:1	−:1
Boc-Ala-Ala-Ala-OMe Boc-**8**	−:1	3:2
Valine series:		
Z-Gly-Val-Val-OMe Z-**9**	1:−	1:−
Boc-Gly-Val-Val-OMe Boc-**9**	1:−	1:−
Z-Val-Gly-Val-OMe Z-**10**	−:1	−:1
Boc-Val-Gly-Val-OMe Boc-**10**	−:1	−:1
Z-Val-Val-Gly-OMe Z-**11**	−:1	2:3
Boc-Val-Val-Gly-OMe Boc-**11**	−:1	2:3
Z-Val-Val-Val-OMe Z-**12**[b]	3:2	1:1
Z-Val-Val-Val-OMe Z-**12**[c]	1:3	
Boc-Val-Val-Val-OMe Boc-**12**[b]	4:1	2:3
Boc-Val-Val-Val-OMe Boc-**12**[c]	1:3	

[a] −:1 denotes that only this specific single product is observed. [b] Initial ratio. [c] Ratio after rearrangement (4 h at −5 °C).

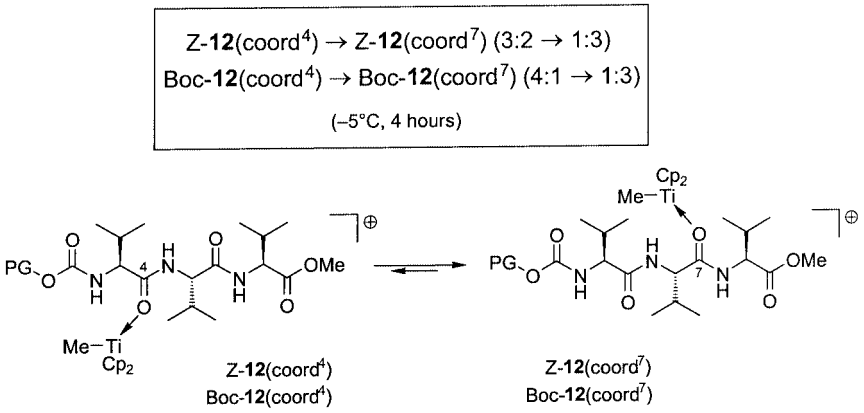

Scheme 6

Conclusions

We had previously shown that the "Jordan cation" $[Cp_2Zr(CH_3)(THF)^+]$[12] reacts with oligopeptide derivatives by displacement of THF and addition of the methylzirconocene cation to a peptide C=O moiety. Subsequently, rapid methane elimination was observed to yield the $[(peptide)Cp_2Zr^+]$ chelate complexes.[13,14] We have now shown that the reagent $[Cp_2Ti(CH_3)(THF)^+]$ reacts with Z- or Boc-protected tripeptide esters in a similar way; first, coordination to a peptide carbonyl oxygen atom is observed [(coord) product formation]; subsequently a thermally induced CH_4 elimination is observed to yield the respective (chel) products.

However, there are notable differences between the zirconocene- and titanocene-based reactions that make the latter more interesting and probably more important. The methylzirconocene cation reagent is much more reactive. Consequently, a dominating (coord^4) product formation was observed, followed by a rather rapid CH_4 elimination to predominately yield the chelate product that involved bonding of the C=O group of the respective alkoxycarbonyl protective group at the *N*-terminus of the peptide. In this respect, the Cp_2Zr^+-derived chemistry is not to be regarded as simple and typical peptide framework chemistry, but rather as a combination of general peptide and specific protective group chemistry.

This is significantly different in the Cp_2Ti^+ systems described here. We have predominately observed the formation of a purely peptide-derived internal chelate product (chel^B) that involves only a pair of adjacent amino acid moieties of the peptide framework. In a few cases, the (chel^A) product that involves bonding of the protective group is observed as a minor component of the product mixture. Only in cases where there is a significant difference in the steric bulk of the backbone units (see Table 3) was the (chel^A) product dominant. A similarly significant difference between the Cp_2Zr^+- and Cp_2Ti^+-derived systems is observed in the regioselectivity of the primary attack. In almost all cases, the internal coordination product (coord^7) was obtained at low temperature. Only in very few specific cases was (coord^4) product formation observed for titanium, in contrast to zirconium where this dominated. The Cp_2Ti^+ adducts are, in some cases, "just resistant enough" to allow a secondary rearrangement to be observed experimentally. The products Z-**12**(coord^4) and Boc-**12**(coord^4) seem to be formed under kinetic control, but then slowly rearrange to form their favored isomers Z-**12**(coord^7) and Boc-**12**(coord^7), respectively. For the first time it seems that we have observed the (intra- or intermolecular) migration of a group-4 metallocene cation derivative along an oligopeptide chain, with the metallocene actively searching for the best resting place available at the peptide backbone, before undergoing further reactions. We will see if this might serve as a first step towards the development of achieving the selective information transfer between a typical biomolecule chain and a catalytically active transition metal center.

Experimental Section

General: All reactions involving organometallic compounds were carried out under argon using a modified Schlenk technique or a glovebox. Melting points were determined with a differential scanning calorimeter TA-Instruments 2010 and the infrared spectra were recorded in KBr with a Nicolet 5 DXC FT IR spectrometer. A Perkin−Elmer polarimeter 241 was used to determine the optical rotations (25 °C; λ = 589 nm). Elemental analyses were performed with a Foss-Heraeus CHNO-Rapid apparatus. NMR spectra were recorded in CD_2Cl_2 at −5 °C with a 600 MHz Varian UNITYplus spectrometer. Chemical shifts (δ) are given in ppm, coupling constants (*J*) in Hz. Commercially available reagents were used as purchased. The reagents HCl·H-Gly-OMe,[23] HCl·H-Ala-OMe,[24] HCl·H-Val-OMe,[25] Boc-Gly-Ala-OH,[26] Boc-Gly-Val-OH,[27] Boc-Ala-Gly-OH,[28] Boc-Ala-Ala-OH,[29] Boc-Val-Gly-OH,[30] Boc-Val-Val-OH,[31] Z-Ala-Ala-OH,[32] and $[Cp_2TiCH_3(THF)^+][BPh_4^-]$ (**13**)[15] were prepared as described in the literature.

General Procedure of the Preparation of the Protected Tripeptides:[20c,33] Two separated ice-cooled solutions were prepared. In the first case triethylamine (0.69 mL, 506 mg, 5.00 mmol) was added to an ice-cooled solution of 20 mL of chloroform and the hydrochloride of the amino acid methyl ester (5.00 mmol). The second was prepared by adding IIDQ (1.52 g, 5.00 mmol) to the Boc- or Z-protected dipeptide (5.00 mmol) in 20 mL of chloroform while stirring. After stirring for 10 min at 0 °C, both solutions were com-

bined. The mixture was allowed to warm up to room temperature overnight. The reaction mixture was filtered and then extracted with 30 mL of aqueous 10% citric acid, 5% $NaHCO_3$ solution and water. The organic solution was dried with $MgSO_4$. The solvent was then removed in vacuo. Recrystallization of the crude product from ethyl acetate/cyclohexane (1:10) or purification by column chromatography gave the pure products. The characteristic NMR features of the 16 tripeptide derivatives prepared and used in this study are listed in Table 4.

Table 4. Selected ^1H and ^{13}C NMR spectroscopic data for the tripeptide derivatives **5**(pept) to **12**(pept)

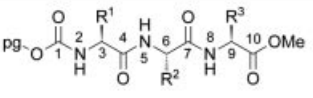

pg = $(C_6H_5)CH_2$–, $(CH_3)_3C$–

	1	2	3	4	5	6	7	8	9	10
Z-**5**(pept)		6.06	3.87		7.28	4.62		7.37	4.45	
ZGAAOMe	156.8		44.3	169.2		48.8	172.2		48.2	173.3
Boc-**5**(pept)		5.76	3.79		7.35	4.61		7.48	4.45	
BGAAOMe	156.2		44.0	169.7		48.7	172.3		48.2	173.3
Z-**6**(pept)		6.02	4.17		7.41	3.92		7.36	4.43	
ZAGAOMe	156.3		51.0	173.3		42.7	168.8		48.1	173.5
Boc-**6**(pept)		5.65	4.10		7.47	3.93		7.39	4.45	
BAGAOMe	155.9		50.7	173.8		42.8	169.1		48.3	173.5
Z-**7**(pept)		6.91	4.05		7.62	4.35		7.83	3.83	
ZAAGOMe	156.2		50.8	172.6		48.4	172.9		40.7	170.3
Boc-**7**(pept)		6.24	3.98		7.48	4.35		7.77	3.84	
BAAGOMe	155.8		50.5	172.9		48.4	172.9		40.8	170.3
Z-**8**(pept)		6.68	4.11		7.51	4.37		7.61	4.36	
ZAAAOMe	156.2		50.8	172.6		48.4	172.2		47.9	173.3
Boc-**8**(pept)		6.06	4.07		7.48	4.40		7.67	4.37	
BAAAOMe	155.6		50.3	172.9		48.5	172.3		48.0	173.3
Z-**9**(pept)		5.92	3.90		7.05	4.45		7.02	4.45	
ZGVVOMe	157.0		44.8	169.6		58.7	171.5		57.7	172.5
Boc-**9**(pept)		6.14	3.86		7.84	4.45		7.72	4.54	
BGVVOMe	156.2		43.9	170.0		57.3	172.6		58.5	172.2
Z-**10**(pept)		5.92	4.07		7.32	4.00		7.24	4.45	
ZVGVOMe	156.6		60.5	172.3		43.1	168.9		57.4	172.5
Boc-**10**(pept)		5.32	3.98		7.08	3.96		7.00	4.44	
BVGVOMe	156.0		60.0	172.4		43.1	168.9		57.4	172.5
Z-**11**(pept)		6.83	3.92		7.53	4.21		8.07	3.81	
ZVVGOMe	156.4		60.6	171.5		57.8	171.7		40.7	170.3
Boc-**11**(pept)		5.62	3.98		7.23	4.36		7.62	3.98	
BVVGOMe	156.2		60.4	172.1		58.2	171.8		41.0	170.2
Z-**12**(pept)		6.73	3.95		7.69	4.27		7.72	4.26	
ZVVVOMe	156.3		60.4	171.6		57.9	171.6		57.3	172.2
Boc-**12**(pept)		5.79	4.00		7.49	4.49		7.28	4.42	
BVVVOMe	156.0		60.1	172.3		57.1	171.7		58.7	172.4

[a] First line ^1H, second line $^{13}C\{^1H\}$ NMR spectroscopic data; the different amino acid fragments are illustrated by different colors: white (glycine or C1), light grey (alanine), dark grey (valine)

Representative Experimental Procedure of the Reaction of $[Cp_2TiCH_3(THF)^+][BPh_4^-]$ (13) with the Tripeptides (Monitored by NMR Spectroscopy): Equimolar amounts of **13** and the respective tripeptide derivative (ca. 20 mg, both in 0.5 mL CD_2Cl_2) were combined at −20 °C. After stirring for 10 min, the reaction mixture was decanted to a precooled NMR tube. The reaction was monitored by NMR spectroscopy at −5 °C and the resulting products identified. The reaction mixture was then stored for 12 h at room temperature to complete the formation of the chelate products. Only NMR spectroscopic data of the cations are listed below since the $[BPh_4^-]$ resonances are equivalent in all examples: ^1H NMR (tetraphenylborate): δ = 7.35 (m, 8 H, *ortho*-H), 7.06 (m, 8 H, *meta*-H), 6.92 (m, 4 H, *para*-H) ppm. ^{13}C NMR: δ = 164.6 (q, $^1J_{CB}$ = 49 Hz, C-*ipso*), 136.3 (C-*ortho*), 126.0 (C-*meta*), 122.1 (C-*para*) ppm. ^1H NMR (THF): δ = 3.70 (m, 4 H, α-H), 1.83 (m, 4 H, β-H). ^{13}C NMR: δ = 68.2 ppm (C-α), 26.0 (C-β).

General Procedure of the Preparation of the (Tripeptide)titanium Complexes: Reagent **13** (0.371 mmol), dissolved in 5 mL of CH_2Cl_2, was added to a solution of the respective tripeptide (0.371 mmol) in 5 mL of CH_2Cl_2 at −20 °C. The reaction mixture was allowed to warm to room temperature overnight. After removal of the solvent in vacuo, an orange-red residue was obtained. The solid was washed with 20 mL of pentane (2 ×), and dried under vacuum to yield the respective chelate (peptide)Ti cation complex. Only selected NMR spectra of the (coord)- and (chel)-type metal complexes are listed below. A complete compilation of data from the 1D and 2D NMR spectroscopic analysis is provided as Supporting Information.

Z-5(pept) (Z-Gly-Ala-Ala-OMe): Reaction of Z-Gly-Ala-OH (1.00 g, 3.57 mmol) with HCl·H-Ala-OMe (498 mg, 3.57 mmol) , triethylamine (0.50 mL, 3.57 mmol), IIDQ (1.08 g, 3.57 mmol) yielded 1.02 g (78%) of Z-**5**(pept). Single crystals were obtained by recrystallization from ethyl acetate. M.p. (DSC) 131 °C. $[\alpha]_D = -21$ (c = 1.0, CH_2Cl_2). IR (KBr): $\tilde{\nu}$ = 3321 (br. s, NH), 3063 (w), 2998 (w), 2953 (w), 1734 (vs, COO), 1692 (vs, CON), 1661 (vs, CON), 1530 (br. s), 1456 (m), 1344 (m), 1271 (br. s), 1150 (m), 1057 (m), 733 (m), 661 (w) cm^{-1}. $C_{17}H_{23}N_3O_6$ (365.4): calcd. C 55.88, H 6.34, N 11.50; found C 55.76, H 6.41, N 11.32.

X-ray Crystal Structure Analysis: Formula $C_{17}H_{23}N_3O_6$, M = 365.38, colorless crystal 0.45 × 0.20 × 0.05 mm, a = 6.135(1), b = 8.222(3), c = 18.418(3) Å, α = 84.94(2), β = 87.14(2), γ = 83.38(2)°, V = 918.5(4) $Å^3$, $\rho_{calcd.}$ = 1.321 g cm^{-3}, μ = 8.46 cm^{-1}, empirical absorption correction with ψ-scan data ($0.702 \leq T \leq 0.959$), Z = 2, triclinic, space group $P\bar{1}$ (no. 1), λ = 1.54178 Å, T = 223 K, ω/2θ scans, 4018 reflections collected ($\pm h$, $+k$, $\pm l$), [(sinθ)/λ] = 0.62 $Å^{-1}$, 4018 independent and 1688 observed reflections [$I \geq 2\,\sigma(I)$], 493 refined parameters, R = 0.057, wR^2 = 0.123, Flack parameter −0.2(4), max. residual electron density 0.24 (−0.21) e $Å^{-3}$, hydrogen atoms at the nitrogen atoms from difference Fourier calculations, others calculated and all refined as riding atoms.

Reaction of Z-5(pept) with 13

Z-5(coord^4)/Z-5(coord^7) = 2:1. Z-5(coord^4): ^1H NMR: δ = 7.55 (br., 1 H, 5-H), 7.37 [m, 5 H, 1-$OCH_2(C_6H_5)$], 6.46 (br. d, ^3J = 7.0 Hz, 1 H, 8-H), 6.20 and 6.17 (Cp-H and Cp′-H), 5.06 [AB, ^2J = 12.5 Hz, 2 H, 1-$OCH_2(C_6H_5)$], 4.44 (m, 1 H, 9-H), 4.34 (AB*X*, 1 H, 2-H), 3.73 (s, 3 H, 10-OCH_3), 3.66 (m, 1 H, 6-H), 1.98 (*AB*X, 2 H, 3-H and 3-H′), 1.42 (d, ^3J = 7.3 Hz, 3 H, 9-CH_3), 1.30 (d, ^3J = 7.2 Hz, 3 H, 6-CH_3), 1.12 (s, 3 H, Ti−CH_3) ppm. ^{13}C NMR: δ = 178.0 (C-4), 172.9 (C-10), 168.4 (C-7), 157.2 (C-1), 138.7 to 122.0 {1-$OCH_2(C_6H_5)$ and $[BPh_4]^-$}, 116.7 and 116.6 (C-Cp and C-Cp′), 67.7 [1-$OCH_2(C_6H_5)$], 52.9 (10-OCH_3), 52.3 (Ti−CH_3), 49.8 (C-9), 48.4 (C-6), 44.8 (C-3), 18.2 (6-CH_3), 17.6 (9-CH_3) ppm. **Z-5(coord^7):** ^1H NMR: δ = 8.63 (br. d, ^3J = 8.4 Hz, 1 H, 5-H), 7.37 [m, 5 H, 1-$OCH_2(C_6H_5)$], 6.08 (br., 1 H, 8-H, not visible), 6.27 and 6.26 (Cp-H and Cp′-H), 5.26 (AB*X*, 1 H, 2-H), 5.05 [AB, ^2J = 12.6 Hz, 2 H, 1-$OCH_2(C_6H_5)$], 3.83 (m, 1 H, 6-H), 3.78 (s, 3 H, 10-OCH_3), 3.66 (m, 1 H, 9-H), 3.38 (*AB*X, ^2J = 16.7 Hz, 2 H, 3-H and 3-H′), 1.44 (d, ^3J = 7.2 Hz, 3 H, 6-CH_3), 1.13 (s, 3 H, Ti−CH_3), 0.96 (d, ^3J = 7.3 Hz, 3 H, 9-CH_3) ppm. ^{13}C NMR: δ = 188.0 (C-7), 182.3 (C-10), 169.7 (C-4), 158.2 (C-1), 138.7−122.0 {1-$OCH_2(C_6H_5)$ and $[BPh_4]^-$}, 116.9 and 116.8 (C-Cp and C-Cp′), 67.8 [1-$OCH_2(C_6H_5)$], 53.3 (10-OCH_3), 51.7 (Ti−CH_3), 49.8 (C-9), 48.4 (C-6), 45.2 (C-3), 16.7 (9-CH_3), 15.9 (6-CH_3) ppm.

Product Z-5(chel^B): Reaction of Z-**5**(pept) (113 mg, $3.09 \cdot 10^{-4}$ mol) with **13** (181 mg, $3.09 \cdot 10^{-4}$ mol) yielded 248 mg (93%) of orange-red Z-**5**(chel^B). M.p. (DSC): 46 °C (dec.). $[\alpha]_D = -29$ (c = 1.0,

CH_2Cl_2). IR (KBr): $\tilde{\nu}$ = 3360 (br., NH), 3059 (w), 3034 (w), 1740 (m, COO), 1700 (s, CON), 1653 (s, CON), 1617 (vs, CON), 1521 (s), 1454 (s), 1261 (m), 1237 (m), 1153 (w), 1062 (w), 1030 (w), 824 (m), 735 (s), 706 (vs), 613 (w) cm^{-1}. ^1H NMR: δ = 7.37 [m, 5 H, 1-$OCH_2(C_6H_5)$], 7.68 (br., 1 H, 8-H), 6.09 and 6.07 (2 × s, 2 × 5 H, Cp-H and Cp′-H), 5.30 (AB*X*, 1 H, 2-H), 5.12 [AB, ^2J = 12.6 Hz, 2 H, 1-$OCH_2(C_6H_5)$], 4.46 (m, 1 H, 6-H), 4.26 (m, 1 H, 9-H), 3.78 (s, 3 H, 10-OCH_3), 3.42 (*AB*X, ^3J = 17.0 Hz, 2 H, 3-H and 3-H′), 1.42 (d, ^3J = 7.1 Hz, 3 H, 6-CH_3), 1.40 (d, ^3J = 7.3 Hz, 3 H, 9-CH_3) ppm. ^{13}C NMR: δ = 178.1 (C-7), 171.3 and 171.1 (C-4 and C-10), 156.8 (C-1), 138.8 to 122.2 {1-$OCH_2(C_6H_5)$ and $[BPh_4]^-$}, 118.5 and 118.2 (C-Cp and C-Cp′), 67.3 [1-$OCH_2(C_6H_5)$], 58.7 (C-6), 53.3 (10-OCH_3), 50.1 (C-9), 42.5 (C-3), 20.2 (6-CH_3), 17.0 (9-CH_3) ppm. $C_{51}H_{52}BN_3O_6Ti$ (861.7): calcd. C 71.09, H 6.08, N 4.88; found C 69.14, H 6.52, N 4.55.

Boc-5(pept) (Boc-Gly-Ala-Ala-OMe): Reaction of Boc-Gly-Ala-OH (1.68 g, 6.82 mmol) with HCl·H-Ala-OMe (952 mg, 6.82 mmol), triethylamine (0.95 mL, 6.82 mmol), and IIDQ (2.07 g, 6.82 mmol) yielded 1.51 g (67%) Boc-**5**(pept). R_f = 0.42 (ethyl acetate). M.p. (DSC): 117 °C. $[\alpha]_D$ = −25 (*c* = 1.0, CH_2Cl_2). IR (KBr): $\tilde{\nu}$ = 3286 (br. s, NH), 3085 (w), 2981 (m), 1748 (s, COO), 1716 (s, CON), 1650 (vs, CON), 1532 (br. s), 1453 (m), 1367 (m), 1285 (m), 1223 (s), 1169 (s), 1053 (m), 945 (m), 689 (w) cm^{-1}. $C_{14}H_{25}N_3O_6$ (331.4): calcd. C 50.75, H 7.60, N 12.68; found C 50.72, H 7.67, N 12.80.

Reaction of Boc-5(pept) with 13

Boc-5(coord^4)/Boc-5(coord^7) = 3:1. Boc-5(coord^4): ^1H NMR: δ = 7.75 (br. d, ^3J = 7.1 Hz, 1 H, 5-H), 6.53 (br. d, ^3J = 7.3 Hz, 1 H, 8-H), 6.20 and 6.19 (2 × s, 2 × 5 H, Cp-H and Cp′-H), 4.45 (m, 1 H, 9-H), 4.41 (AB*X*, 1 H, 2-H), 3.72 (s, 3 H, 10-OCH_3), 3.68 (m, 1 H, 6-H), 2.12 (*AB*X, ^2J = 18.4 Hz, 2 H, 3-H and 3-H′), 1.43 [s, 9 H, 1-$OC(CH_3)_3$], 1.41 (d, ^3J = 7.1 Hz, 3 H, 9-CH_3), 1.31 (d, ^3J = 7.2 Hz, 3 H, 6-CH_3), 1.13 (s, 3 H, Ti−CH_3) ppm. ^{13}C NMR: δ = 178.3 (C-4), 172.8 (C-10), 168.6 (C-7), 156.4 (C-1), 116.7 and 116.6 (C-Cp and C-Cp′), 81.7 [1-$OC(CH_3)_3$], 52.8 (10-OCH_3), 52.0 (Ti−CH_3), 50.0 (C-6), 48.8 (C-9), 44.6 (C-3), 28.0 [1-$OC(CH_3)_3$], 18.3 (6-CH_3), 17.6 (9-CH_3). **Boc-5(coord^7):** ^1H NMR: δ = 8.94 (br. d, ^3J = 8.4 Hz, 1 H, 8-H), 6.74 (br. d, ^3J = 7.9 Hz, 1 H, 5-H), 2 × 6.28 (2 × s, 2 × 5 H, Cp-H and Cp′-H), 5.09 (AB*X*, 1 H, 2-H), 4.41 (m, 1 H, 6-H), 3.85 (m, 1 H, 9-H), 3.79 (s, 3 H, 10-OCH_3), 3.41 (*AB*X, ^2J = 16.9 Hz, 2 H, 3-H and 3-H′), 1.43 [s, 9 H, 1-$OC(CH_3)_3$], 1.46 (d, ^3J = 7.3 Hz, 3 H, 9-CH_3), 1.34 (d, ^3J = 7.2 Hz, 3 H, 6-CH_3), 1.14 (s, 3 H, Ti−CH_3) ppm. ^{13}C NMR: δ = 182.6 (C-7), 172.3 (C-10), 169.8 (C-4), 156.7 (C-1), 116.9 and 116.8 (C-Cp and C-Cp′), 80.6 [1-$OC(CH_3)_3$], 52.7 (10-OCH_3), 51.6 (Ti−CH_3), 49.8 and 48.9 (C-6 and C-9), 45.0 (C-3), 28.1 [1-$OC(CH_3)_3$], 18.1 and 16.7 (6-CH_3 and 9-CH_3) ppm.

Products Boc-5(chel^A)/Boc-5(chel^B) = 1:2: Reaction of Boc-**5**(pept) (123 mg, $3.71 \cdot 10^{-4}$ mol) with **13** (217 mg, $3.09 \cdot 10^{-4}$ mol) yielded 289 mg (94%) of the orange isomeric mixture Boc-**5**(chel^A)/Boc-**5**(chel^B) = 1:2. M.p. (DSC): 77 °C (dec.). $[\alpha]_D$ = −69 (*c* = 0.65, CH_2Cl_2). IR (KBr): $\tilde{\nu}$ = 3369 (br., NH), 3055 (m), 2984 (m), 1746 (s, COO), 1695 (s, CON), 1614 (vs, CON), 1506 (s), 1450 (s), 1367 (w), 1250 (m), 1155 (s), 1030 (w), 826 (s), 735 (s), 706 (vs), 613 (m) cm^{-1}. $C_{48}H_{54}BN_3O_6Ti$ (827.7): calcd. C 69.66, H 6.58, N 5.08; found C 69.82, H 7.15, N 4.81. **Boc-5(chel^A):** ^1H NMR: δ = 7.76 (br., 1 H, 5-H), 7.11 (br., 1 H, 8-H), 6.11 and 6.07 (2 × s, 2 × 5 H, Cp-H and Cp′-H), 4.46 (m, 1 H, 9-H), 4.31 (m, 1 H, 6-H), 4.03 (AB, ^2J = 18.4 Hz, 2 H, 3-H and 3-H′), 3.80 (s, 3 H, 10-OCH_3), 1.54 [s, 9 H, 1-$OC(CH_3)_3$], 1.43 (d, ^3J = 7.2 Hz, 3 H, 6-CH_3), 1.36 (d, ^3J = 7.1 Hz, 3 H, 9-CH_3) ppm. ^{13}C NMR: δ = 175.8 (C-4), 171.5 (C-10), 169.8 (C-7), 153.3 (C-1), 118.4 and 118.3 (C-Cp and C-Cp′), 84.4 [1-$OC(CH_3)_3$], 52.9 (C-3), 52.7 (10-OCH_3), 50.5 (C-9), 48.6 (C-6), 28.9 [1-$OC(CH_3)_3$], 18.5, 18.2, 18.0 and 17.1 (6-CH_3 and 9-CH_3). **Boc-5(chel^B):** ^1H NMR: δ = 6.84 (br., 1 H, 8-H), 5.21 (AB*X*, 1 H, 2-H), 2 × 6.13 (2 × s, 2 × 5 H, Cp-H and Cp′-H), 4.71 (q, ^3J = 7.0 Hz, 1 H, 6-H), 4.46 (m, 1 H, 9-H), 3.72 (s, 3 H, 10-OCH_3), 3.44 (*AB*X, ^2J = 18.3 Hz, 2 H, 3-H and 3-H′), 1.50 (d, ^3J = 7.0 Hz, 3 H, 6-CH_3), 1.45 [s, 9 H, 1-$OC(CH_3)_3$], 1.36 (d, ^3J = 7.1 Hz, 3 H, 9-CH_3) ppm. ^{13}C NMR: δ = 178.7 (C-7), 172.1 (C-4), 170.1 (C-10), 156.6 (C-1), 118.5 and 118.1 (C-Cp and C-Cp′), 80.7 [1-$OC(CH_3)_3$], 59.2 (C-6), 52.8 (10-OCH_3), 51.2 (C-9), 42.6 (C-3), 28.4 [1-$OC(CH_3)_3$], 18.5, 18.2, 18.0 and 17.1 (6-CH_3 and 9-CH_3) ppm.

Z-6(pept) (Z-Ala-Gly-Ala-OMe): Reaction of Z-Ala-Gly-OH (1.50 g, 5.35 mmol) with HCl·H-Ala-OMe (747 mg, 5.35 mmol), triethylamine (0.75 mL, 5.35 mmol), and IIDQ (1.62 g, 5.35 mmol) yielded 1.62 g (83%) of Z-**6**(pept). M.p. (DSC): 131 °C. $[\alpha]_D$ = −5 (*c* = 1.0, CH_2Cl_2). IR (KBr): $\tilde{\nu}$ = 3355 (s, NH), 3307 (s, NH), 3352 (s, NH), 3049 (w), 1742 (s, COO), 1702 (s, CON), 1658 (vs, CON), 1549 (s), 1456 (m), 1313 (m), 1266 (s), 1236 (m), 1155 (m), 1039 (w), 659 (w) cm^{-1}. $C_{17}H_{23}N_3O_6$ (365.4): calcd. C 55.88, H 6.34, N 11.50; found C 56.03, H 6.45, N 11.67.

X-ray Crystal Structure Analysis: Formula $C_{17}H_{23}N_3O_6$, *M* = 365.38, colorless crystal 0.50 × 0.10 × 0.05 mm, *a* = 4.674(2), *b* = 16.520(2), *c* = 24.166(3) Å, *V* = 1866.0(9) $Å^3$, $\rho_{calcd.}$ = 1.301 g cm^{-3}, μ = 8.33 cm^{-1}, empirical absorption correction with ψ scan data (0.681 ≤ *T* ≤ 0.960), *Z* = 4, orthorhombic, space group $P2_12_12_1$ (no. 19), λ = 1.54178 Å, *T* = 223 K, ω/2θ scans, 2246 reflections collected (−*h*, +*k*, +*l*), [(sinθ)/λ] = 0.62 $Å^{-1}$, 2246 independent and 1764 observed reflections [$I \geq 2\,\sigma(I)$], 248 refined parameters, *R* = 0.038, wR^2 = 0.099, Flack parameter −0.4(4), max. residual electron density 0.19 (−0.21) e $Å^{-3}$, hydrogen atoms at the nitrogen atoms from difference Fourier calculations, others calculated and all refined as riding atoms.

Data sets were collected with an Enraf Nonius CAD4 diffractometer. Programs used: data collection EXPRESS (Nonius B.V., 1994), data reduction MolEN (K. Fair, Enraf−Nonius B.V., **1990**), structure solution SHELXS-97 (G. M. Sheldrick, *Acta Crystallogr.* **1990**, *A46*, 467−473), structure refinement SHELXL-97 (G. M. Sheldrick, Universität Göttingen, **1997**), graphics SCHAKAL (E. Keller, Universität Freiburg, **1997**). Crystallographic data (excluding structure factors) for the structures reported in this paper have been deposited with the Cambridge Crystallographic Data Centre as supplementary publication CCDC-184568 and -184569. Copies of the data can be obtained free of charge on application to CCDC, 12 Union Road, CambridgeCB2 1EZ, UK [Fax: (internat.) + 44-1223/336-033, E-mail: deposit@ccdc.cam.ac.uk].

Reaction of Z-6(pept) with 13. Z-6(coord^7): ^1H NMR: δ = 8.35 (br. d, ^3J = 8.4 Hz, 1 H, 8-H), 7.38 [m, 5 H, 1-$OCH_2(C_6H_5)$], 6.19 and 6.18 (Cp-H and Cp′-H), 5.40 (AB*X*, 1 H, 5-H), 5.27 (br. d, ^3J = 3.8 Hz, 1 H, 2-H), 5.10 [AB, ^2J = 12.5 Hz, 2 H, 1-$OCH_2(C_6H_5)$], 3.81 (s, 3 H, 10-OCH_3), 3.77 (m, 1 H, 9-H), 3.58 (m, 1 H, 3-H), 2.20 (*AB*X, ^2J = 17.9 Hz, 2 H, 6-H and 6-H′), 1.46 (d, ^3J = 7.3 Hz, 3 H, 9-CH_3), 1.24 (d, ^3J = 7.3 Hz, 3 H, 3-CH_3), 1.06 (s, 3 H, Ti−CH_3) ppm. ^{13}C NMR: δ = 178.1 (C-7), 172.5 (C-4), 170.2 (C-10), 157.1 (C-1), 138.9 to 122.3 {1-$OCH_2(C_6H_5)$ and $[BPh_4]^-$}, 116.7 and 116.5 (C-Cp and C-Cp′), 67.7 [1-$OCH_2(C_6H_5)$], 53.2 (10-OCH_3), 52.0 (Ti−CH_3), 51.3 (C-3), 49.8 (C-9), 42.8 (C-6), 16.4 (9-CH_3), 16.3 (6-CH_3) ppm.

Products Z-6(chel^A)/Z-6(chel^B) = 1:2: Reaction of Z-**6**(pept) (98 mg, $2.44 \cdot 10^{-4}$ mol) with **13** (142 mg, $2.44 \cdot 10^{-4}$ mol) yielded

204 mg (97%) of the orange isomeric mixture Z-**6**(chel^{A})/Z-**6**(chel^{B}) = 1:2. M.p. (DSC): 69 °C (dec.). $[\alpha]_D = -32$ (c = 1.0, CH_2Cl_2). IR (KBr): $\tilde{\nu}$ = 3348 (br., NH), 3056 (w), 3032 (w), 2983 (w), 1747 (s, COO), 1696 (s, CON), 1617 (s, CON), 1517 (s), 1453 (s), 1260 (m), 1026 (m), 820 (m), 734 (s), 705 (vs), 612 (m) cm^{-1}. $C_{51}H_{52}BN_3O_6Ti$ (861.7): calcd. C 71.09, H 6.08, N 4.88; found C 71.56, H 6.56, N 4.54. **Z-6(chel^{A}):** ^{1}H NMR: δ = 7.37 [m, 5 H, 1-OCH$_2$(C_6H_5)], 7.22 (br. d, ^3J = 7.5 Hz, 1 H, 8-H), 6.78 (ABX, 1 H, 5-H), 6.05 and 6.00 (2 × s, 2 × 5 H, Cp-H and Cp′-H), 5.09 [AB, ^2J = 12.1 Hz, 2 H, 1-OCH$_2$(C_6H_5)], 4.43 (m, 1 H, 9-H), 4.38 (m, 1 H, 3-H), 3.69 (s, 3 H, 10-OCH$_3$), 3.77 (ABX, 2 H, 6-H and 6-H′), 1.43 (d, ^3J = 7.2 Hz, 3 H, 9-CH$_3$), 1.32 (d, ^3J = 7.1 Hz, 3 H, 3-CH$_3$) ppm. ^{13}C NMR: δ = 178.9 (C-4), 173.8 (C-10), 169.5 (C-7), 156.9 (C-1), 138.8−122.2 {1-OCH$_2$(C_6H_5) and [BPh_4]$^-$}, 118.6 and 118.4 (C-Cp and C-Cp′), 67.4 [1-OCH$_2$(C_6H_5)], 58.9 (C-3), 52.7 (10-OCH$_3$), 52.1 (C-9), 43.4 (C-6), 17.4 and 17.2 (3-CH$_3$ and 9-CH$_3$). **Z-6(chel^{B}):** ^{1}H NMR: δ = 7.37 [m, 5 H, 1-OCH$_2$(C_6H_5)], 6.92 (br., 1 H, 8-H), 6.06 and 6.05 (2 × s, 2 × 5 H, Cp-H and Cp′-H), 5.47 (br., 1 H, 2-H), 5.14 [AB, ^2J = 12.2 Hz, 2 H, 1-OCH_2(C_6H_5)], 4.14 (m, 1 H, 3-H), 3.84 (AB, ^2J = 19.0 Hz, 2 H, 6-H and 6-H′), 3.81 (m, 1 H, 9-H), 3.77 (s, 3 H, 10-OCH_3), 1.37 (d, ^3J = 7.3 Hz, 3 H, 3-CH_3), 1.26 (d, ^3J = 7.3 Hz, 3 H, 9-CH_3) ppm. ^{13}C NMR: δ = 174.8 (C-7), 173.8 (C-4), 171.2 (C-10), 156.0 (C-1), 138.8−122.2 {1-OCH$_2$(C_6H_5) and [BPh_4]$^-$}, 118.6 and 118.5 (C-Cp and C-Cp′), 67.2 [1-OCH$_2$(C_6H_5)], 53.1 (10-OCH$_3$), 52.8 (C-6), 50.1 (C-9), 49.6 (C-3), 16.9 (9-CH$_3$), 15.3 (3-CH$_3$) ppm.

Boc-6(pept) (Boc-Ala-Gly-Ala-OMe): Reaction of Boc-Ala-Gly-OH (1.76 g, 7.13 mmol) with HCl·H-Ala-OMe (996 mg, 7.13 mmol), triethylamine (0.99 mL, 7.13 mmol), and IIDQ (2.16 g, 7.13 mmol) yielded 1.46 g (62%) of Boc-**6**(pept). R_f = 0.41 (ethyl acetate). M.p. (DSC): 219 °C. $[\alpha]_D = -7$ (c = 1.0, CH_2Cl_2). IR (KBr): $\tilde{\nu}$ = 3304 (br. s, NH), 2985 (w), 2939 (w), 1749 (s, COO), 1695 (vs, CON), 1652 (vs, CON), 1558 (s), 1456 (m), 1369 (w), 1325 (w), 1299 (m), 1280 (m), 1253 (s), 1167 (m), 1063 (w), 996 (w), 669 (w) cm^{-1}. $C_{14}H_{25}N_3O_6$ (331.4): calcd. C 50.75, H 7.60, N 12.68; found C 50.45, H 7.89, N 12.62.

Reaction of Boc-6(pept) with 13. Boc-6(coord^{7}): ^{1}H NMR: δ = 8.50 (br. d, ^3J = 7.4 Hz, 1 H, 8-H), 6.18 and 6.16 (2 × s, 2 × 5 H, Cp-H and Cp′-H), 5.75 (ABX, 1 H, 5-H), 5.00 (br. d, ^3J = 3.6 Hz, 1 H, 2-H), 3.79 (s, 3 H, 10-OCH_3), 3.78 (m, 1 H, 9-H), 3.56 (m, 1 H, 3-H), 2.10 (ABX, 2 H, 6-H and 6-H′), 1.48 [s, 9 H, 1-OC(CH_3)$_3$], 1.46 (d, ^3J = 7.2 Hz, 3 H, 9-CH_3), 1.25 (d, ^3J = 7.2 Hz, 3 H, 3-CH_3), 1.04 (s, 3 H, Ti−CH_3) ppm. ^{13}C NMR: δ = 178.4 (C-7), 172.5 (C-4), 170.1 (C-10), 157.0 (C-1), 116.7 and 116.5 (C-Cp and C-Cp′), 81.5 [1-OC(CH$_3$)$_3$], 53.1 (10-OCH$_3$), 51.4 (C-3), 51.3 (Ti−CH$_3$), 49.8 (C-9), 42.7 (C-6), 28.2 [1-OC(CH$_3$)$_3$], 2 × 16.4 (3-CH$_3$ and 9-CH$_3$).

Products Boc-6(chel^{A})/Boc-6(chel^{B}) = 1:2: Reaction of Boc-**6**(pept) (164 mg, 4.95·10^{-4} mol) with **13** (289 mg, 4.95·10^{-4} mol) gave 393 mg (96%) of the orange isomeric mixture Boc-**6**(chel^{A})/Boc-**6**(chel^{B}) = 1:2. M.p. (DSC): 81 °C (dec.). $[\alpha]_D = -23$ (c = 0.55, CH_2Cl_2). IR (KBr): $\tilde{\nu}$ = 3369 (br., NH), 3055 (w), 2984 (w), 1746 (m, COO), 1695 (s, CON), 1616 (vs, CON), 1580 (m), 1483 (s), 1450 (s), 1369 (w), 1261 (s), 1211 (m), 1157 (vs), 1101 (s), 1065 (s), 1016 (s), 824 (s), 735 (m), 706 (vs), 613 (w) cm^{-1}. $C_{48}H_{54}BN_3O_6Ti$ (827.7): calcd. C 69.66, H 6.58, N 5.08; found C 69.86, H 7.21, N 4.75. **Boc-6(chel^{A}):** ^{1}H NMR: δ = 7.23 (br., 1 H, 8-H), 5.98 (ABX, 1 H, 5-H), 6.09 and 6.08 (2 × s, 2 × 5 H, Cp-H and Cp′-H), 4.44 (m, 1 H, 9-H), 4.33 (q, ^3J = 6.9 Hz, 1 H, 3-H), 3.68 (s, 3 H, 10-OCH_3), 3.10 (ABX, ^2J = 16.8 Hz, 2 H, 6-H and 6-H′), 1.52 [s, 9 H, 1-OC(CH_3)$_3$], 1.44 (d, ^3J = 7.1 Hz, 3 H, 9-CH_3), 1.38 (d, ^3J = 7.2 Hz, 3 H, 3-CH_3) ppm. ^{13}C NMR: δ = 179.0 (C-4), 173.3 (C-10), 165.9 (C-7), 156.4 (C-1), 118.2 and 118.1 (C-Cp and C-Cp′), 83.9 [1-OC(CH$_3$)$_3$], 59.0 (C-3), 52.9 (10-OCH$_3$), 48.5 (C-9), 43.4 (C-6), 28.7 [1-OC(CH$_3$)$_3$], 18.3 (3-CH$_3$), 16.4 (9-CH$_3$) ppm. **Boc-6(chel^{B}):** ^{1}H NMR: δ = 6.63 (br., 1 H, 8-H), 6.10 and 6.07 (2 × s, 2 × 5 H, Cp-H and Cp′-H), 5.19 (br., 1 H, 2-H), 4.12 (m, 1 H, 9-H), 3.78 (AB, ^2J = 19.1 Hz, 2 H, 6-H and 6-H′), 3.75 (s, 3 H, 10-OCH_3), 3.69 (m, 1 H, 3-H), 1.47 [s, 9 H, 1-OC(CH_3)$_3$], 1.35 (d, ^3J = 7.2 Hz, 3 H, 9-CH_3), 1.22 (d, ^3J = 7.0 Hz, 3 H, 3-CH_3) ppm. ^{13}C NMR: δ = 174.9 (C-7), 172.5 (C-4), 171.2 (C-10), 155.5 (C-1), 2 × 118.3 (C-Cp and C-Cp′), 81.5 [1-OC(CH$_3$)$_3$], 53.1 (10-OCH$_3$), 52.7 (C-3), 52.2 (C-6), 49.8 (C-9), 28.2 [1-OC(CH$_3$)$_3$], 16.8 (9-CH$_3$), 15.2 (3-CH$_3$) ppm.

Z-7(pept) (Z-Ala-Ala-Gly-OMe):[34] Reaction of Z-Ala-Ala-OH (1.00 g, 3.40 mmol) with HCl·H-Gly-OMe (427 mg, 3.40 mmol), triethylamine (0.48 mL, 3.40 mmol), and IIDQ (1.04 g, 3.40 mmol) yielded 1.06 g (85%) of Z-**7**(pept). M.p. (DSC): 181 °C. $[\alpha]_D = -26$ (c = 0.5, CH_2Cl_2). IR (KBr): $\tilde{\nu}$ = 3285 (br. s, NH), 1749 (s, COO), 1686 (s, CON), 1638 (vs, CON), 1539 (s), 1455 (w), 1267 (m), 1243 (m), 1225 (s), 1051 (w), 698 (w) cm^{-1}. $C_{17}H_{23}N_3O_6$ (365.4): calcd. C 55.88, H 6.34, N 11.50; found C 55.89, H 6.45, N 11.46.

Reaction of Z-7(pept) with 13. Z-7(coord^{7}): ^{1}H NMR: δ = 8.59 (ABX, 1 H, 8-H), 7.37 [m, 5 H, 1-OCH$_2$(C_6H_5)], 6.44 (br., 1 H, 5-H), 2 × 6.25 (Cp-H and Cp′-H), 5.43 (br., 1 H, 2-H), 5.12 [AB, 2 H, 1-OCH_2(C_6H_5)], 3.91 (m, 1 H, 3-H), 3.80 (s, 3 H, 10-OCH_3), 3.76 (m, 1 H, 6-H), 3.52 (ABX, ^2J = 17.6 Hz, 2 H, 9-H and 9-H′), 1.30 (d, ^3J = 7.3 Hz, 3 H, 3-CH_3), 1.14 (s, 3 H, Ti−CH_3), 1.08 (d, ^3J = 7.3 Hz, 3 H, 6-CH_3) ppm. ^{13}C NMR: δ = 183.4 (C-7), 173.0 (C-4), 167.3 (C-10), 158.1 (C-1), 138.8 to 122.1 {1-OCH$_2$(C_6H_5) and [BPh_4]$^-$}, 116.9 and 116.8 (C-Cp and C-Cp′), 68.1 [1-OCH$_2$(C_6H_5)], 53.3 (10-OCH$_3$), 52.4 (C-3), 51.4 (Ti−CH$_3$), 49.9 (C6), 41.9 (C-9), 16.7 (3-CH$_3$), 16.1 (6-CH$_3$).

Product Z-7(chel^{B}): Reaction of Z-**7**(pept) (127 mg, 3.48·10^{-4} mol) with **13** (203 mg, 3.48·10^{-4} mol) yielded 227 mg (89%) of Z-**7**(chel^{B}). M.p. (DSC): 77 °C (dec.). $[\alpha]_D = -26$ (c = 1.0, CH_2Cl_2). IR (KBr): $\tilde{\nu}$ = 3292 (br., NH), 3056 (w), 2964 (w), 1748 (m, COO), 1686 (s, CON), 1640 (vs, CON), 1621 (m, CON), 1539 (m), 1437 (w), 1262 (vs), 1226 (s), 1153 (m), 1099 (vs), 1018 (vs), 802 (vs), 734 (m), 705 (s) cm^{-1}. ^{1}H NMR: δ = 7.36 [m, 5 H, 1-OCH$_2$(C_6H_5)], 6.06 and 5.98 (Cp-H and Cp′-H), 6.00 (ABX, 1 H, 8-H), 5.36 (br. d, ^3J = 5.8 Hz, 1 H, 2-H), 5.12 [AB, ^2J = 12.3 Hz, 2 H, 1-OCH_2(C_6H_5)], 4.70 (q, ^3J = 7.1 Hz, 1 H, 6-H), 3.94 (m, 1 H, 3-H), 3.73 (s, 3 H, 10-OCH_3), 3.31 (ABX, 2 H, 9-H and 9-H′), 1.32 (d, ^3J = 7.1 Hz, 3 H, 6-CH_3), 1.29 (d, ^3J = 7.1 Hz, 3 H, 3-CH_3) ppm. ^{13}C NMR: δ = 178.4 (C-7), 173.9 (C-4), 168.4 (C-10), 156.0 (C-1), 138.8−122.2 {1-OCH$_2$(C_6H_5) and [BPh_4]$^-$}, 118.4 and 118.0 (C-Cp and C-Cp′), 67.3 [1-OCH_2(C_6H_5)], 58.7 (C-6), 52.8 (10-OCH$_3$), 48.2 (C-3), 42.5 (C-9), 20.8 (6-CH$_3$), 16.1 (3-CH$_3$) ppm. $C_{51}H_{52}BN_3O_6Ti$ (861.7): calcd. C 71.09, H 6.08, N 4.88; found C 71.26, H 5.86, N 4.66.

Boc-7(pept) (Boc-Ala-Ala-Gly-OMe): Reaction of Boc-Ala-Ala-OH (1.31 g, 5.03 mmol) with HCl·H-Gly-OMe (6.27 mg, 5.03 mmol), triethylamine (0.70 mL, 5.03 mmol), and IIDQ (1.53 g, 5.03 mmol) yielded 1.18 g (71%) of Boc-**7**(pept). R_f = 0.39 (ethyl acetate/cyclohexane, 4:1). M.p. (DSC): 173 °C. $[\alpha]_D = -48$ (c = 0.5, CH_2Cl_2). IR (KBr): $\tilde{\nu}$ = 3312 (s, NH), 3278 (s, NH), 2980 (w), 1749 (s, COO), 1675 (s, CON), 1639 (vs, CON), 1520 (s), 1456 (m), 1261 (s), 1172 (m), 1054 (w), 668 (w) cm^{-1}. $C_{14}H_{25}N_3O_6$ (331.4): calcd. C 50.75, H 7.60, N 12.68; found C 50.22, H 7.61, N 12.61.

Reaction of Boc-7(pept) with 13: Boc-7(coord^{7}): ^{1}H NMR: δ = 9.02 (ABX, 1 H, 8-H), 6.53 (br. d, ^3J = 4.9 Hz, 1 H, 5-H), 6.26 and

6.25 (2 × s, 2 × 5 H, Cp-H and Cp′-H), 5.19 (br., 1 H, 2-H), 3.86 (m, 1 H, 3-H), 3.82 (m, 1 H, 6-H), 3.78 (s, 3 H, 10-OCH_3), 3.57 (*AB*X, ^2J = 17.3 Hz, 2 H, 9-H and 9-H′), 1.44 [s, 9 H, 1-OC(CH_3)$_3$], 1.29 (d, ^3J = 7.2 Hz, 3 H, 3-CH_3), 1.15 (s, 3 H, Ti−CH_3), 1.13 (d, ^3J = 7.3 Hz, 3 H, 6-CH_3) ppm. ^{13}C NMR: δ = 183.6 (C-7), 173.3 (C-4), 167.2 (C-10), 157.9 (C-1), 116.9 and 116.8 (C-Cp and C-Cp′), 82.4 [1-O*C*(CH$_3$)$_3$], 53.3 (10-O*C*H$_3$), 52.3 (C-3), 51.4 (Ti−*C*H$_3$), 49.7 (C-6), 41.9 (C-9), 28.1 [1-OC(*C*H$_3$)$_3$], 16.7 (3-*C*H$_3$), 16.3 (6-*C*H$_3$) ppm.

Products Boc-7(chel^A)/Boc-7(chel^B) = 1:2: Reaction of Boc-**7**(pept) (151 mg, 4.56·10^{-4} mol) with **13** (266 mg, 4.56·10^{-4} mol) yielded 347 mg (92%) of the isomeric mixture Boc-**7**(chel^A)/Boc-**7**(chel^B) = 1:2. M.p. (DSC): 68 °C (dec.). [α]$_D$ = −33 (*c* = 1.0, CH_2Cl_2). IR (KBr): ṽ = 3315 (s, NH), 3281 (m, NH), 2980 (w), 1765 (w, COO), 1747 (m, COO), 1676 (s, CON), 1641 (vs, CON), 1518 (s), 1456 (w), 1261 (s), 1168 (m), 1099 (vs), 1022 (s), 802 (s), 742 (w), 706 (m) cm^{-1}. $C_{48}H_{54}BN_3O_6Ti$ (827.7): calcd. C 69.66, H 6.58, N 5.08; found C 68.91, H 7.02, N 4.82. **Boc-7(chel^A):** ^{1}H NMR: δ = 7.55 (br., 1 H, 5-H), 6.13 and 6.12 (2 × s, 2 × 5 H, Cp-H and Cp′-H), 5.76 (ABX, 1 H, 8-H), 4.55 (q, ^3J = 6.9 Hz, 1 H, 3-H), 4.09 (m, 1 H, 6-H), 3.80 (ABX, ^2J = 18.2 Hz, 2 H, 9-H and 9-H′), 3.72 (s, 3 H, 10-OCH$_3$), 1.54 (d, ^3J = 7.1 Hz, 3 H, 3-CH$_3$), 1.53 [s, 9 H, 1-OC(CH$_3$)$_3$], 1.32 (d, ^3J = 7.0 Hz, 3 H, 6-CH$_3$) ppm. ^{13}C NMR: δ = 178.2 (C-4), 170.5 (C-7), 169.9 (C-10), 152.6 (C-1), 118.4 and 118.1 (C-Cp and C-Cp′), 84.2 [1-OC(CH$_3$)$_3$], 59.3 (C-3), 52.6 (10-OCH$_3$), 50.5 (C-6), 41.3 (C-9), 28.7 [1-OC(CH$_3$)$_3$], 18.8 (6-CH$_3$), 18.4 (3-CH$_3$) ppm. **Boc-7(chel^B):** ^{1}H NMR: δ = 6.10 and 6.09 (2 × s, 2 × 5 H, Cp-H and Cp′-H), 6.01 (AB*X*, 1 H, 8-H), 5.04 (br. d, ^3J = 5.8 Hz, 1 H, 2-H), 4.79 (q, ^3J = 7.1 Hz, 1 H, 6-H), 3.89 (m, 1 H, 3-H), 3.74 (s, 3 H, 10-OCH_3), 3.32 (*AB*X, 2 H, 9-H and 9-H′), 1.46 [s, 9 H, 1-OC(CH_3)$_3$], 1.35 (d, ^3J = 7.0 Hz, 3 H, 6-CH_3), 1.28 (d, ^3J = 7.1 Hz, 3 H, 3-CH_3) ppm. ^{13}C NMR: δ = 178.5 (C-7), 174.6 (C-4), 168.4 (C-10), 155.5 (C-1), 118.4 and 118.0 (C-Cp and C-Cp′), 80.6 [1-O*C*(CH$_3$)$_3$], 58.7 (C-6), 52.8 (10-O*C*H$_3$), 47.9 (C-3), 42.5 (C-9), 28.1 [1-OC(*C*H$_3$)$_3$], 20.9 (6-*C*H$_3$), 15.9 (3-*C*H$_3$) ppm.

Z-8(pept) (Z-Ala-Ala-Ala-OMe):[35] Reaction of Z-Ala-Ala-OH (1.00 g, 3.40 mmol) with HCl·H-Ala-OMe (474 mg, 3.40 mmol), triethylamine (0.47 mL, 3.40 mmol), and IIDQ (1.03 g, 3.40 mmol) yielded 0.92 g (71%) of Z-**8**(pept). M.p. (DSC): 174 °C. [α]$_D$ = −30 (*c* = 1.0, CH_2Cl_2). IR (KBr): ṽ = 3303 (s, NH), 3275 (s, NH), 3068 (w), 2984 (w), 1739 (s, COO), 1689 (s, CON), 1640 (vs, CON), 1542 (s), 1455 (w), 1331 (w), 1257 (s), 1231 (m), 1158 (w), 1052 (m), 697 (m) cm^{-1}. $C_{18}H_{25}N_3O_6$ (379.4): calcd. C 56.98, H 6.64, N 11.08; found C 57.00, H 6.80, N 10.92.

Reaction of Z-8(pept) with 13. Z-8(coord^7): ^{1}H NMR: δ = 8.78 (br. d, ^3J = 8.4 Hz, 1 H, 8-H), 7.38 [m, 5 H, 1-OCH$_2$(C$_6$*H*$_5$)], 6.36 (br. d, ^3J = 5.0 Hz, 1 H, 5-H), 2 × 6.27 (2 × s, 2 × 5 H, Cp-H and Cp′-H), 5.44 (br. d, 1 H, 2-H), 5.11 [AB, ^2J = 12.0 Hz, 2 H, 1-OC*H*$_2$(C$_6$H$_5$)], 3.95 (m, 1 H, 3-H), 3.86 (m, 1 H, 9-H), 3.81 (s, 3 H, 10-OCH_3), 3.80 (m, 1 H, 6-H), 1.45 (d, ^3J = 7.2 Hz, 3 H, 9-CH_3), 1.34 (d, ^3J = 7.1 Hz, 3 H, 3-CH_3), 1.15 (s, 3 H, Ti−CH_3), 1.01 (d, ^3J = 7.3 Hz, 3 H, 6-CH_3) ppm. ^{13}C NMR: δ = 182.4 (C-7), 172.5 (C-4), 170.0 (C-10), 158.0 (C-1), 136.0−122.0 {1-OCH$_2$(*C*$_6$H$_5$) and [BPh$_4$]$^-$}, 116.9 and 116.8 (C-Cp and C-Cp′), 68.0 [1-O*C*H$_2$(C$_6$H$_5$)], 53.3 (10-O*C*H$_3$), 52.5 (C-3), 51.7 (Ti−*C*H$_3$), 2 × 49.8 (C-6 and C-9), 17.0 (3-*C*H$_3$), 16.7 (9-*C*H$_3$), 16.0 (6-*C*H$_3$) ppm.

Product Z-8(chel^B): Reaction of Z-**8**(pept) (135 mg, 3.56·10^{-4} mol) with **13** (208 mg, 3.56·10^{-4} mol) yielded 293 mg (94%) of Z-**8**(chel^B). M.p. (DSC): 79 °C (dec.). [α]$_D$ = −59 (*c* = 1.0, CH_2Cl_2). IR (KBr): ṽ = 3357 (br., NH), 3055 (w), 2985 (w), 1743 (m, COO), 1660 (s, CON), 1616 (vs, CON), 1521 (m), 1481 (m), 1454 (s), 1237 (m), 1065 (m), 1018 (m), 825 (s), 734 (s), 705 (vs), 613 (m) cm^{-1}. ^{1}H NMR: δ = 7.45 (br. d, ^3J = 8.8 Hz, 1 H, 8-H), 7.37 [m, 5 H, 1-OCH$_2$(C$_6$*H*$_5$)], 6.09 and 6.01 (2 × s, 2 × 5 H, Cp-H and Cp′-H), 5.39 (br. d, ^3J = 6.3 Hz, 1 H, 2-H), 5.11 [AB, ^2J = 12.3 Hz, 2 H, 1-OC*H*$_2$(C$_6$H$_5$)], 4.91 (q, ^3J = 7.0 Hz, 1 H, 6-H), 4.30 (m, 1 H, 9-H), 3.94 (m, 1 H, 3-H), 3.79 (s, 3 H, 10-OCH_3), 1.51 (d, ^3J = 7.0 Hz, 3 H, 6-CH_3), 1.42 (d, ^3J = 7.3 Hz, 3 H, 9-CH_3), 1.31 (d, ^3J = 7.0 Hz, 3 H, 3-CH_3) ppm. ^{13}C NMR: δ = 178.0 (C-7), 173.9 (C-4), 171.4 (C-10), 156.1 (C-1), 138.8−122.1 {1-OCH$_2$(*C*$_6$H$_5$) and [BPh$_4$]$^-$}, 118.4 and 118.2 (C-Cp and C-Cp′), 67.3 [1-O*C*H$_2$(C$_6$H$_5$)], 58.9 (C-6), 53.3 (10-O*C*H$_3$), 50.2 (C-9), 48.3 (C-3), 21.0 (6-*C*H$_3$), 17.1 (9-*C*H$_3$), 15.9 (3-*C*H$_3$) ppm. $C_{52}H_{54}BN_3O_6Ti$ (875.7): calcd. C 71.32, H 6.22, N 4.80; found C 71.28, H 6.33, N 4.73.

Boc-8(pept) (Boc-Ala-Ala-Ala-OMe):[36] Reaction of Boc-Ala-Ala-OH (1.05 g, 4.03 mmol) with HCl·H-Ala-OMe (563 mg, 4.03 mmol), triethylamine (0.56 mL, 4.03 mmol), and IIDQ (1.22 g, 4.03 mmol) yielded 1.11 g (80%) of Boc-**8**(pept). M.p. (DSC): 185 °C. [α]$_D$ = −48 (*c* = 1.0, CH_2Cl_2). IR (KBr): ṽ = 3298 (s, NH), 3272 (s, NH), 2981 (m), 1744 (s, COO), 1709 (s, CON), 1692 (s, CON), 1675 (s, CON), 1638 (vs, CON), 1550 (s), 1524 (s), 1456 (m), 1365 (w), 1252 (m), 1218 (m), 1170 (m), 1052 (w), 703 (br. w) cm^{-1}. $C_{15}H_{27}N_3O_6$ (345.4): calcd. C 52.16, H 7.88, N 12.17; found C 52.84, H 7.87, N 12.07.

Reaction of Boc-8(pept) with 13: Boc-8(coord^7): ^{1}H NMR: δ = 9.07 (br. d, ^3J = 8.2 Hz, 1 H, 8-H), 6.40 (br. d, ^3J = 5.0 Hz, 1 H, 5-H), 2 × 6.29 (2 × s, 2 × 5 H, Cp-H and Cp′-H), 5.12 (br. d, ^3J = 2.2 Hz, 1 H, 2-H), 3.90 (m, 1 H, 3-H), 3.88 (m, 1 H, 9-H), 3.80 (s, 3 H, 10-OCH_3), 3.80 (m, 1 H, 6-H), 1.48 (d, ^3J = 7.3 Hz, 3 H, 9-CH_3), 1.45 [s, 9 H, 1-OC(CH_3)$_3$], 1.32 (d, ^3J = 7.3 Hz, 3 H, 3-CH_3), 1.14 (s, 3 H, Ti−CH_3), 1.32 (d, ^3J = 7.4 Hz, 3 H, 6-CH_3) ppm. ^{13}C NMR: δ = 182.7 (C-7), 172.6 (C-4), 169.9 (C-10), 157.6 (C-1), 116.9 and 116.8 (C-Cp and C-Cp′), 82.3 [1-O*C*(CH$_3$)$_3$], 53.3 (10-O*C*H$_3$), 52.2 (C-3), 51.7 (Ti−*C*H$_3$), 49.9 (C-9), 49.8 (C-6), 27.9 [1-OC(*C*H$_3$)$_3$], 16.9 (3-*C*H$_3$), 16.8 (9-*C*H$_3$), 16.4 (6-*C*H$_3$) ppm.

Products Boc-8(Chel^A)/Boc-8(Chel^B) = 3:2: Reaction of Boc-**8**(pept) (117 mg, 3.39·10^{-4} mol) with **13** (198 mg, 3.39·10^{-4} mol) yielded 251 mg (88%) of the isomeric mixture Boc-**8**(Chel^A)/Boc-**8**(Chel^B) = 3:2. M.p. (DSC): 68 °C (dec.). [α]$_D$ = −20 (*c* = 1.0, CH_2Cl_2). IR (KBr): ṽ = 3301 (br., NH), 3054 (w), 2981 (m), 1743 (m, COO), 1695 (s, CON), 1653 (vs, CON), 1617 (vs, CON), 1522 (s), 1480 (s), 1451 (s), 1262 (m), 1157 (m), 1066 (m), 1018 (s), 820 (s), 733 (m), 704 (vs) cm^{-1}. $C_{49}H_{56}BN_3O_6Ti$ (841.7): calcd. C 69.92, H 6.71, N 4.99; found C 71.07, H 7.45, N 4.55. **Boc-8(Chel^A):** ^{1}H NMR: δ = 7.39 (br., 1 H, 5-H), 6.10 and 6.07 (2 × s, 2 × 5 H, Cp-H and Cp′-H), 5.98 (br. d, ^3J = 7.2 Hz, 1 H, 8-H), 4.52 (q, ^3J = 6.9 Hz, 1 H, 3-H), 4.43 (m, 1 H, 9-H), 4.09 (m, 1 H, 6-H), 3.72 (s, 3 H, 10-OCH_3), 1.54 (d, ^3J = 7.3 Hz, 3 H, 3-CH_3), 1.52 [s, 9 H, 1-OC(CH_3)$_3$], 1.35 (d, ^3J = 8.0 Hz, 3 H, 6-CH_3), 1.35 (d, ^3J = 7.7 Hz, 3 H, 9-CH_3) ppm. ^{13}C NMR: δ = 178.1 (C-4), 172.8 (C-10), 169.7 (C-7), 152.7 (C-1), 118.4 and 118.1 (C-Cp and C-Cp′), 84.2 [1-O*C*(CH$_3$)$_3$], 59.3 (C-3), 52.9 (10-O*C*H$_3$), 50.4 (C-6), 48.7 (C-9), 28.7 [1-OC(*C*H$_3$)$_3$], 18.5 (3-*C*H$_3$), 19.2 and 17.9 (6-*C*H$_3$ and 9-*C*H$_3$) ppm. **Boc-8(Chel^B):** ^{1}H NMR: δ = 7.16 (br. d, ^3J = 8.8 Hz, 1 H, 8-H), 6.11 and 6.10 (2 × s, 2 × 5 H, Cp-H and Cp′-H), 4.98 (br. d, ^3J = 5.7 Hz, 1 H, 2-H), 4.98 (q, ^3J = 7.3 Hz, 1 H, 6-H), 4.30 (m, 1 H, 9-H), 3.88 (m, 1 H, 3-H), 3.79 (s, 3 H, 10-OCH_3), 1.52 (d, ^3J = 7.4 Hz, 3 H, 6-CH_3), 1.43 [s, 9 H, 1-OC(CH_3)$_3$], 1.42 (d, ^3J = 7.7 Hz, 3 H, 9-CH_3), 1.28 (d, ^3J = 8.0 Hz, 3 H, 3-CH_3) ppm. ^{13}C NMR: δ = 178.0 (C-7), 174.3 (C-4), 171.4 (C-10), 155.4

(C-1), 118.4 and 118.2 (C-Cp and C-Cp′), 80.6 [1-O*C*(CH_3)$_3$], 58.9 (C-6), 53.4 (10-O*C*H_3), 50.2 (C-9), 47.8 (C-3), 28.1 [1-OC(*C*H_3)$_3$], 21.1 (6-*C*H_3), 17.2 (9-*C*H_3), 15.8 (3-*C*H_3) ppm.

Z-9(pept) (Z-Gly-Val-Val-OMe):[37] Reaction of Z-Gly-Val-OH (1.00 g, 3.24 mmol) with HCl·H-Val-OMe (544 mg, 3.24 mmol), triethylamine (0.45 mL, 3.24 mmol), and IIDQ (984 mg, 3.24 mmol) yielded 0.91 g (67%) of Z-**9**(pept). M.p. (DSC): 143 °C. $[\alpha]_D = -12$ (c = 1.0, CH_2Cl_2). IR (KBr): $\tilde{\nu}$ = 3296 (br. s, NH), 2963 (m), 1748 (s, COO), 1692 (s, CON), 1643 (vs, CON), 1539 (s), 1393 (w), 1294 (m), 1248 (s), 1040 (w), 699 (m) cm^{-1}. $C_{21}H_{31}N_3O_6$ (421.5): calcd. C 59.84, H 7.41, N 9.97; found C 59.35, H 7.41, N 9.77.

Reaction of Z-9(pept) with 13. Z-9(coord^4): ^{1}H NMR: δ = 7.48 (br. d, ^3J = 9.2 Hz, 1 H, 5-H), 7.38 [m, 5 H, 1-OCH$_2$(C$_6$*H*$_5$)], 6.19 and 6.15 (2 × s, 2 × 5 H, Cp-H and Cp′-H), 6.13 (br. d, ^3J = 8.3 Hz, 1 H, 8-H), 5.07 [AB, ^2J = 12.5 Hz, 2 H, 1-OC*H*$_2$(C$_6$H$_5$)], 4.53 (dd, ^3J = 8.3, ^3J = 4.9 Hz, 1 H, 9-H), 4.23 (AB*X*, 1 H, 2-H), 3.75 (s, 3 H, 10-OC*H*$_3$), 3.48 (m, 1 H, 6-H), 2.24 [m, 1 H, 9-C*H*(CH$_3$)$_2$], 1.98 [m, 1 H, 6-C*H*(CH$_3$)$_2$], 1.71 (*AB*X, ^2J = 17.5 Hz, 2 H, 3-H and 3-H′), 1.14 (s, 3 H, Ti−C*H*$_3$), 0.99 and 0.95 [2 × d, 2 × ^3J = 7.1 Hz, 2 × 3 H, 9-CH(C*H*$_3$)(C*H*′$_3$)], 2 × 0.84 [2 × d, 2 × ^3J = 7.2 Hz, 2 × 3 H, 6-CH(C*H*$_3$)(C*H*′$_3$)] ppm. ^{13}C NMR: δ = 178.2 (C-4), 171.9 (C-10), 167.4 (C-7), 156.9 (C-1), 138.8−122.2 {1-OCH$_2$(*C*$_6$H$_5$) and [BPh$_4$]$^-$}, 2 × 116.7 (C-Cp and C-Cp′), 67.7 [1-O*C*H$_2$(C$_6$H$_5$)], 59.5 (C-6), 57.8 (C-9), 52.7 (10-O*C*H$_3$), 52.0 (Ti−*C*H$_3$), 44.9 (C-3), 31.7 [6-*C*H(CH$_3$)$_2$], 31.0 [9-*C*H(CH$_3$)$_2$], 19.0 and 17.9 [9-CH(*C*H$_3$)(*C*H′$_3$)], 18.4 and 17.6 [6-CH(*C*H$_3$)(*C*H′$_3$)] ppm.

Product Z-9(chel^A): Reaction of Z-**9**(pept) (143 mg, 3.39·10^{-4} mol) with **13** (198 mg, 3.39·10^{-4} mol) yielded 305 mg (98%) of Z-**9**(chel^A). M.p. (DSC): 63 °C (dec.). $[\alpha]_D = -23$ (c = 1.0, CH_2Cl_2). IR (KBr): $\tilde{\nu}$ = 3362 (br., NH), 3056 (w), 2963 (m), 1740 (s, COO), 1716 (s, CON), 1703 (s, CON), 1698 (s, CON), 1612 (vs, CON), 1501 (s), 1462 (s), 1268 (m), 1219 (m), 1024 (m), 824 (m), 734 (s), 705 (vs), 613 (w) cm^{-1}. ^{1}H NMR: δ = 8.17 (br., 1 H, 5-H), 7.40 [m, 5 H, 1-OCH$_2$(C$_6$*H*$_5$)], 6.26 (br. d, ^3J = 7.9 Hz, 1 H, 8-H), 6.07 and 6.00 (2 × s, 2 × 5 H, Cp-H and Cp′-H), 5.15 [AB, ^2J = 12.1 Hz, 2 H, 1-OC*H*$_2$(C$_6$H$_5$)], 4.45 (dd, ^3J = 7.9, ^3J = 4.8 Hz, 1 H, 9-H), 4.29 (AB, 2 H, 3-H and 3-H′), 4.25 (dd, ^3J = 8.5, ^3J = 5.9 Hz, 1 H, 6-H), 3.73 (s, 3 H, 10-OC*H*$_3$), 2.15 [m, 1 H, 9-C*H*(CH$_3$)$_2$], 2.09 [m, 1 H, 6-C*H*(CH$_3$)$_2$], 0.99 and 0.94 [2 × d, 2 × ^3J = 6.8 Hz, 2 × 3 H, 6-CH(C*H*$_3$)(C*H*′$_3$)], 2 × 0.92 [2 × d, 2 × ^3J = 6.8 Hz, 2 × 3 H, 9-CH(C*H*$_3$)(C*H*′$_3$)] ppm. ^{13}C NMR: δ = 175.3 (C-4), 171.8 (C-10), 169.4 (C-7), 151.9 (C-1), 138.8−122.0 {1-OCH$_2$(*C*$_6$H$_5$) and [BPh$_4$]$^-$}, 118.8 and 118.7 (C-Cp and C-Cp′), 68.2 [1-O*C*H$_2$(C$_6$H$_5$)], 60.0 (C-6), 58.0 (C-9), 52.7 (10-O*C*H$_3$), 52.5 (C-3), 32.1 [6-*C*H(CH$_3$)$_2$], 30.9 [9-*C*H(CH$_3$)$_2$], 19.1 and 18.9 [6-CH(*C*H$_3$)(*C*H′$_3$)], 18.0 and 17.8 [9-CH(*C*H$_3$)(*C*H′$_3$)] ppm. $C_{55}H_{60}BN_3O_6Ti$ (917.8): calcd. C 71.98, H 6.59, N 4.58; found C 71.77, H 6.91, N 4.30.

Boc-9(pept) (Boc-Gly-Val-Val-OMe):[14] Reaction of Boc-Gly-Val-OH (6.31 g, 23.0 mmol) with HCl·H-Val-OMe (3.86 g, 23.0 mmol), triethylamine (3.22 mL, 23.0 mmol), and IIDQ (6.98 g, 23.0 mmol) yielded 6.77 g (76%) of Boc-**9**(pept). R_f = 0.30 (ethyl acetate/cyclohexane, 2:1). M.p. (DSC): 215 °C. $[\alpha]_D = -11$ (c = 1.0, CH_2Cl_2). IR (KBr): $\tilde{\nu}$ = 3311 (s, NH), 2967 (m), 2936 (m), 2877 (w), 1747 (m, COO), 1723 (s, CON), 1648 (vs, CON), 1545 (s), 1367 (w), 1299 (m), 1162 (m) cm^{-1}. $C_{18}H_{33}N_3O_6$ (387.5): calcd. C 55.80, H 8.58, N 10.84; found C 55.36, H 8.60, N 10.52.

Reaction of Boc-9(pept) with 13. Boc-9(coord^4): ^{1}H NMR: δ = 7.57 (br., 1 H, 5-H), 6.20 and 6.13 (2 × s, 2 × 5 H, Cp-H and Cp′-H), 6.13 (br. d, ^3J = 4.9 Hz, 1 H, 8-H), 4.54 (dd, ^3J = 8.5, ^3J = 4.9 Hz, 1 H, 9-H), 4.14 (AB*X*, 1 H, 2-H), 3.74 (s, 3 H, 10-OC*H*$_3$), 3.48 (dd, ^3J = 8.8, ^3J = 5.1 Hz, 1 H, 6-H), 2.24 [m, 1 H, 9-C*H*(CH$_3$)$_2$], 1.97 [m, 1 H, 6-C*H*(CH$_3$)$_2$], 1.68 (*AB*X, 2 H, 3-H and 3-H′), 1.42 [s, 9 H, 1-OC(C*H*$_3$)$_3$], 1.13 (s, 3 H, Ti−C*H*$_3$), 0.98 and 0.94 [2 × d, 2 × ^3J = 7.2 Hz, 2 × 3 H, 9-CH(C*H*$_3$C*H*′$_3$)], 0.89 and 0.87 [2 × d, 2 × ^3J = 7.3 Hz, 2 × 3 H, 6-CH(C*H*$_3$C*H*′$_3$)] ppm. ^{13}C NMR: δ = 178.5 (C-4), 171.9 (C-10), 167.6 (C-7), 156.0 (C-1), 116.6 and 116.4 (C-Cp and C-Cp′), 81.5 [1-O*C*(CH$_3$)$_3$], 59.3 (C-6), 57.6 (C-9), 52.7 (10-O*C*H$_3$), 51.6 (Ti−*C*H$_3$), 44.7 (C-3), 32.0 [9-*C*H(CH$_3$)$_2$], 31.1 [6-*C*H(CH$_3$)$_2$], 25.7 [1-OC(*C*H$_3$)$_3$], 19.0, 18.4, 17.8 and 17.6 [6-CH(*C*H$_3$*C*H′$_3$) and 9-CH(*C*H$_3$*C*H′$_3$)] ppm.

Product Boc-9(chel^A): Reaction of Boc-**9**(pept) (102 mg, 2.63·10^{-4} mol) with **13** (154 mg, 2.63·10^{-4} mol) yielded 205 mg (88%) of Boc-**9**(chel^A). M.p. (DSC): 87 °C (dec.). $[\alpha]_D = -17$ (c = 1.0, CH_2Cl_2). IR (KBr): $\tilde{\nu}$ = 3357 (br., NH), 3056 (m), 2965 (s), 1741 (m, COO), 1661 (s, CON), 1616 (vs, CON), 1518 (s), 1496 (s), 1369 (w), 1262 (s), 1208 (w), 1153 (s), 1100 (m), 1018 (vs), 822 (s), 734 (m), 705 (vs), 613 (w) cm^{-1}. ^{1}H NMR: δ = 8.22 (br., 1 H, 5-H), 6.40 (br. d, ^3J = 8.2 Hz, 1 H, 8-H), 6.13 and 6.08 (2 × s, 2 × 5 H, Cp-H and Cp′-H), 4.49 (dd, ^3J = 8.2, ^3J = 4.8 Hz, 1 H, 9-H), 4.28 (dd, ^3J = 8.4, ^3J = 5.8 Hz, 1 H, 6-H), 4.25 (AB, 2 H, 3-H and 3-H′), 3.75 (s, 3 H, 10-OC*H*$_3$), 2.22 [m, 1 H, 9-C*H*(CH$_3$)$_2$], 2.10 [m, 1 H, 6-C*H*(CH$_3$)$_2$], 1.52 [s, 9 H, 1-OC(C*H*$_3$)$_3$], 1.01 and 0.97 [2 × d, 2 × ^3J = 7.7 Hz, 2 × 3 H, 6-CH(C*H*$_3$)(C*H*′$_3$)], 0.98 and 0.96 [2 × d, 2 × ^3J = 7.3 Hz, 2 × 3 H, 9-CH(C*H*$_3$)(C*H*′$_3$)] ppm. ^{13}C NMR: δ = 175.3 (C-4), 171.7 (C-10), 169.5 (C-7), 152.9 (C-1), 118.4 and 118.3 (C-Cp and C-Cp′), 84.3 [1-O*C*(CH$_3$)$_3$], 60.0 (C-6), 58.0 (C-9), 52.7 (C-3), 52.6 (10-O*C*H$_3$), 32.1 [9-*C*H(CH$_3$)$_2$], 31.0 [6-*C*H(CH$_3$)$_2$], 28.7 [1-OC(*C*H$_3$)$_3$], 19.1 and 17.9 [6-CH(*C*H$_3$)(*C*H′$_3$)], 19.0 and 18.0 [9-CH(*C*H$_3$)(*C*H′$_3$)] ppm. $C_{52}H_{62}BN_3O_6Ti$ (883.8): calcd. C 70.67, H 7.07, N 4.75; found C 70.57, H 7.41, N 4.50.

Z-10(pept) (Z-Val-Gly-Val-OMe): Reaction of Z-Val-Gly-OH (1.04 g, 3.37 mmol) with HCl·H-Val-OMe (566 mg, 3.37 mmol), triethylamine (0.47 mL, 3.37 mmol), and IIDQ (1.02 g, 3.37 mmol) yielded 1.15 g (81%) of Z-**10**(pept). R_f = 0.22 (ethyl acetate/cyclohexane, 3:1). M.p. (DSC): 128 °C. $[\alpha]_D = +4$ (c = 1.0, CH_2Cl_2). IR (KBr): $\tilde{\nu}$ = 3298 (br. s, NH), 2964 (m), 1742 (s, COO), 1693 (s, CON), 1644 (vs, CON), 1539 (s), 1393 (w), 1292 (m), 1246 (s), 1039 (w), 699 (m) cm^{-1}. $C_{21}H_{31}N_3O_6$ (421.5): calcd. C 59.84, H 7.41, N 9.97; found C 59.93, H 7.73, N 9.61.

Reaction of Z-10(pept) with 13. Z-10(coord^7): ^{1}H NMR: δ = 8.18 (br. d, ^3J = 9.2 Hz, 1 H, 8-H), 7.36 [m, 5 H, 1-OCH$_2$(C$_6$*H*$_5$)], 6.19 and 6.18 (2 × s, 2 × 5 H, Cp-H and Cp′-H), 5.26 (AB*X*, 1 H, 5-H), 5.20 (br., 1 H, 2-H), 5.11 [AB, ^2J = 12.1 Hz, 2 H, 1-OC*H*$_2$(C$_6$H$_5$)], 3.83 (s, 3 H, 10-OC*H*$_3$), 3.47 (m, 1 H, 9-H), 3.40 (dd, ^3J = 6.5, ^3J = 4.6 Hz, 1 H, 3-H), 2.28 (*AB*X, ^2J = 17.9 Hz, 2 H, 6-H and 6-H′), 2.15 [m, 1 H, 9-C*H*(CH$_3$)$_2$], 1.95 [m, 1 H, 3-C*H*(CH$_3$)$_2$], 1.13 (s, 3 H, Ti−C*H*$_3$), 0.93 and 0.90 [2 × d, 2 × ^3J = 7.2 Hz, 2 × 3 H, 3-CH(C*H*$_3$)(C*H*′$_3$)], 0.87 and 0.85 [2 × d, 2 × ^3J = 7.2 Hz, 2 × 3 H, 9-CH(C*H*$_3$)(C*H*′$_3$)] ppm. ^{13}C NMR: δ = 178.2 (C-7), 172.1 (C-4), 169.1 (C-10), 157.1 (C-1), 135.8−122.3 {1-OCH$_2$(*C*$_6$H$_5$) and [BPh$_4$]$^-$}, 116.6 and 116.5 (C-Cp and C-Cp′), 67.6 [1-O*C*H$_2$(C$_6$H$_5$)], 61.0 (C-3), 60.1 (C-9), 53.0 (10-O*C*H$_3$), 52.1 (Ti−*C*H$_3$), 43.1 (C-6), 30.0 [9-*C*H(CH$_3$)$_2$], 29.6 [3-*C*H(CH$_3$)$_2$], 19.4 and 18.7 [3-CH(*C*H$_3$)(*C*H′$_3$)], 18.5 and 18.3 [9-CH(*C*H$_3$)(*C*H′$_3$)] ppm.

Product: Z-10(chel^B): Reaction of Z-**10**(pept) (156 mg, 3.70·10^{-4} mol) with **13** (216 mg, 3.70·10^{-4} mol) yielded 326 mg (96%) of orange Z-**10**(chel^B). M.p. (DSC): 48 °C (dec.). $[\alpha]_D = -33$ (c = 1.0, CH_2Cl_2). IR (KBr): $\tilde{\nu}$ = 3360 (br., NH), 3055 (w),

2965 (m), 1741 (s, COO), 1718 (s, CON), 1701 (s, CON), 1696 (s, CON), 1617 (vs, CON), 1497 (s), 1465 (s), 1263 (m), 1220 (m), 1026 (m), 825 (m), 734 (s), 706 (vs), 613 (w) cm^{-1}. ^1H NMR: δ = 7.36 [m, 5 H, 1-OCH$_2$(C$_6$*H*$_5$)], 7.35 (br. d, ^3J = 8.1 Hz, 1 H, 8-H), 6.10 and 6.02 (2 × s, 2 × 5 H, Cp-H and Cp′-H), 5.41 (br. d, ^3J = 7.0 Hz, 1 H, 2-H), 5.11 [AB, ^2J = 12.2 Hz, 2 H, 1-OC*H*$_2$(C$_6$H$_5$)], 4.26 (m, ^3J = 8.1, ^3J = 5.4 Hz, 1 H, 9-H), 3.96 (AB, ^2J = 19.2 Hz, 2 H, 6-H and 6-H′), 3.74 (s, 3 H, 10-OC*H*$_3$), 3.64 (m, 1 H, 3-H), 2.15 [m, 1 H, 9-C*H*(CH$_3$)$_2$], 1.88 [m, 1 H, 3-C*H*(CH$_3$)$_2$], 0.98 and 0.96 [2 × d, 2 × ^3J = 7.3 Hz, 2 × 3 H, 3-CH(C*H*$_3$)(C*H*′$_3$)], 0.97 and 0.94 [2 × d, 2 × ^3J = 7.5 Hz, 2 × 3 H, 9-CH(C*H*$_3$)(C*H*′$_3$)] ppm. ^{13}C NMR: δ = 174.9 (C-7), 173.9 (C-4), 170.3 (C-10), 156.5 (C-1), 138.8−122.2 {1-OCH$_2$(*C*$_6$H$_5$) and [BPh$_4$]$^-$}, 118.3 and 118.2 (C-Cp and C-Cp′), 67.4 [1-O*C*H$_2$(C$_6$H$_5$)], 59.7 (C-9), 59.2 (C-3), 53.0 (10-O*C*H$_3$), 52.2 (C-6), 30.9 [9-*C*H(CH$_3$)$_2$], 29.0 [3-*C*H(CH$_3$)$_2$], 19.4 and 18.9 [3-CH(*C*H$_3$)(*C*H′$_3$)], 18.3 and 18.0 [9-CH(*C*H$_3$)(*C*H′$_3$)] ppm. $C_{55}H_{60}BN_3O_6Ti$ (917.8): calcd. C 71.98, H 6.59, N 4.58; found C 71.76, H 6.79, N 4.44.

Boc-10(pept) (Boc-Val-Gly-Val-OMe): Reaction of Boc-Val-Gly-OH (5.79 g, 21.1 mmol) with HCl·H-Val-OMe (3.54 g, 21.1 mmol), triethylamine (2.95 mL, 21.1 mmol), and IIDQ (6.40 g, 21.1 mmol) yielded 4.66 g (57%) of Boc-**10**(pept). R_f = 0.29 (ethyl acetate/cyclohexane, 2:1). M.p. (DSC): 226 °C. [α]$_D$ = −2 (*c* = 1.0, CH_2Cl_2). IR (KBr): ṽ = 3333 (br. m, NH), 2967 (m), 1747 (s, COO), 1693 (s, CON), 1648 (vs, CON), 1526 (s), 1392 (w), 1299 (m), 1172 (s), 1017 (w) cm^{-1}. $C_{18}H_{33}N_3O_6$ (387.5): calcd. C 55.80, H 8.58, N 10.84; found C 55.84, H 8.91, N 10.24.

Reaction of Boc-10(pept) with 13. Boc-10(coord^7): ^1H NMR: δ = 8.24 (br. d, ^3J = 9.1 Hz, 1 H, 8-H), 6.19 and 6.16 (2 × s, 2 × 5 H, Cp-H and Cp′-H), 5.60 (AB*X*, 1 H, 5-H), 4.90 (br. d, ^3J = 4.5 Hz, 1 H, 2-H), 3.80 (s, 3 H, 10-OC*H*$_3$), 3.46 (m, 1 H, 9-H), 3.42 (m, 1 H, 3-H), 2.19 (*AB*X, ^2J = 12.0 Hz, 2 H, 6-H and 6-H′), 2.15 [m, 1 H, 9-C*H*(CH$_3$)$_2$], 2.05 [m, 1 H, 3-C*H*(CH$_3$)$_2$], 1.48 [s, 9 H, 1-OC(C*H*$_3$)$_3$], 1.13 (s, 3 H, Ti−C*H*$_3$), 0.95 and 0.87 [2 × d, 2 × ^3J = 7.2 Hz, 2 × 3 H, 3-CH(C*H*$_3$C*H*′$_3$)], 0.89 and 0.88 [2 × d, 2 × ^3J = 7.2 Hz, 2 × 3 H, 9-CH(C*H*$_3$C*H*′$_3$)] ppm. ^{13}C NMR: δ = 178.4 (C-7), 171.8 (C-4), 168.9 (C-10), 156.8 (C-1), 116.7 and 116.5 (C-Cp and C-Cp′), 81.8 [1-O*C*(CH$_3$)$_3$], 60.3 (C-3), 60.0 (C-9), 52.8 (10-O*C*H$_3$), 51.9 (Ti−*C*H$_3$), 43.0 (C-6), 29.8 and 29.7 [3-*C*H(CH$_3$)$_2$ and 9-*C*H(CH$_3$)$_2$], 25.6 [1-OC(*C*H$_3$)$_3$], 19.5, 18.7, 18.5 and 17.8 [3-CH(*C*H$_3$*C*H′$_3$) and 9-CH(*C*H$_3$*C*H′$_3$)] ppm.

Product Boc-10(chel^B): Reaction of Boc-**10**(pept) (132 mg, 3.41·10^{-4} mol) with **13** (199 mg, 3.41·10^{-4} mol) yielded 268 mg (89%) of Boc-**10**(chel^B). M.p. (DSC): 85 °C (dec.). [α]$_D$ = −66 (*c* = 0.70, CH_2Cl_2). IR (KBr): ṽ = 3371 (br., NH), 3055 (w), 2966 (m), 1741 (m, COO), 1703 (s, CON), 1620 (vs, CON), 1481 (s), 1448 (w), 1369 (w), 1261 (m), 1154 (s), 1109 (m), 1017 (s), 823 (s), 734 (m), 706 (vs), 612 (w) cm^{-1}. ^1H NMR: δ = 7.02 (br. d, ^3J = 8.1 Hz, 1 H, 8-H), 6.12 and 6.09 (2 × s, 2 × 5 H, Cp-H and Cp′-H), 4.95 (br. d, ^3J = 6.8 Hz, 1 H, 2-H), 4.25 (dd, ^3J = 8.1, ^3J = 5.4 Hz, 1 H, 9-H), 3.98 (AB, ^2J = 18.9 Hz, 2 H, 6-H and 6-H′), 3.73 (s, 3 H, 10-OC*H*$_3$), 3.52 (dd, ^3J = 7.1, ^3J = 6.8 Hz, 1 H, 3-H), 2.15 [m, 1 H, 9-C*H*(CH$_3$)$_2$], 1.83 [m, 1 H, 3-C*H*(CH$_3$)$_2$], 1.45 [s, 9 H, 1-OC(C*H*$_3$)$_3$], 0.97 and 0.96 [2 × d, 2 × ^3J = 6.9 Hz, 2 × 3 H, 3-CH(C*H*$_3$)(C*H*′$_3$)], 0.97 and 0.94 [2 × d, 2 × ^3J = 7.5 Hz, 2 × 3 H, 9-CH(C*H*$_3$)(C*H*′$_3$)] ppm. ^{13}C NMR: δ = 174.9 (C-7), 174.6 (C-4), 170.2 (C-10), 156.0 (C-1), 118.4 and 118.3 (C-Cp and C-Cp′), 80.5 [1-O*C*(CH$_3$)$_3$], 59.7 (C-9), 58.6 (C-3), 53.0 (10-O*C*H$_3$), 52.2 (C-6), 30.9 [9-*C*H(CH$_3$)$_2$], 28.9 [3-*C*H(CH$_3$)$_2$], 28.2 [1-OC(*C*H$_3$)$_3$], 19.4 and 18.5 [3-CH(*C*H$_3$)(*C*H′$_3$)], 18.9 and 18.0 [9-CH(*C*H$_3$)(*C*H′$_3$)] ppm. $C_{52}H_{62}BN_3O_6Ti$ (883.8): calcd. C 70.67, H 7.07, N 4.75; found C 70.38, H 7.36, N 4.53.

Z-11(pept) (Z-Val-Val-Gly-OMe):[38] Reaction of Z-Val-Val-OH (0.99 g, 2.83 mmol) with HCl·H-Gly-OMe (352 mg, 2.83 mmol), triethylamine (0.40 mL, 2.83 mmol), and IIDQ (857 mg, 2.83 mmol) gave 0.99 g (83%) of Z-**11**(pept). M.p. (DSC): 190 °C. [α]$_D$ = −18 (*c* = 0.80, CH_2Cl_2). IR (KBr): ṽ = 3293 (br. s, NH), 2962 (m), 1755 (m, COO), 1693 (s, CON), 1641 (vs, CON), 1540 (s), 1393 (w), 1295 (m), 1247 (s), 1042 (m), 699 (s) cm^{-1}. $C_{21}H_{31}N_3O_6$ (421.5): calcd. C 59.84, H 7.41, N 9.97; found C 59.23, H 7.44, N 9.82.

Reaction of Z-11(pept) with 13. Z-11(coord^7): ^1H NMR: δ = 8.95 (AB*X*, 1 H, 8-H), 7.35 [m, 5 H, 1-OCH$_2$(C$_6$*H*$_5$)], 6.32 (br., 1 H, 5-H), 6.29 and 6.25 (2 × s, 2 × 5 H, Cp-H and Cp′-H), 5.38 (br., 1 H, 2-H), 5.11 [AB, ^2J = 12.0 Hz, 2 H, 1-OC*H*$_2$(C$_6$H$_5$)], 3.86 (m, 1 H, 3-H), 3.82 (s, 3 H, 10-OC*H*$_3$), 3.82 (m, 1 H, 6-H), 3.63 (*AB*X, ^2J = 17.6 Hz, 2 H, 9-H and 9-H′), 2.20 [m, 1 H, 3-C*H*(CH$_3$)$_2$], 1.83 [m, 1 H, 6-C*H*(CH$_3$)$_2$], 1.17 (s, 3 H, Ti−C*H*$_3$), 1.02 and 0.97 [2 × d, 2 × ^3J = 7.0 Hz, 2 × 3 H, 3-CH(C*H*$_3$)(C*H*′$_3$)], 0.92 and 0.74 [2 × d, 2 × ^3J = 6.9 Hz, 2 × 3 H, 6-CH(C*H*$_3$)(C*H*′$_3$)] ppm. ^{13}C NMR: δ = 182.5 (C-7), 171.6 (C-4), 164.5 (C-10), 158.9 (C-1), 138.8−122.0 {1-OCH$_2$(*C*$_6$H$_5$) and [BPh$_4$]$^-$}, 116.9 and 116.8 (C-Cp and C-Cp′), 68.5 [1-O*C*H$_2$(C$_6$H$_5$)], 62.5 (C-3), 58.5 (C-6), 53.4 (10-O*C*H$_3$), 51.5 (Ti−*C*H$_3$), 42.1 (C-9), 29.7 [3-*C*H(CH$_3$)$_2$], 28.7 [6-*C*H(CH$_3$)$_2$], 19.6 and 19.0 [6-CH(*C*H$_3$)(*C*H′$_3$)], 17.8 and 15.7 [3-CH(*C*H$_3$)(*C*H′$_3$)] ppm.

Products Z-11(chel^A)/Z-11(chel^B) = 2:3: Reaction of Z-**11**(pept) (122 mg, 2.89·10^{-4} mol) with **13** (169 mg, 2.89·10^{-4} mol) yielded 247 mg (93%) of the isomeric mixture Z-**11**(chel^A)/Z-**11**(chel^B) = 2:3. M.p. (DSC): 81 °C (dec.). [α]$_D$ = −32 (*c* = 0.70, CH_2Cl_2). IR (KBr): ṽ = 3368 (br., NH), 3055 (w), 2966 (w), 1751 (m, COO), 1713 (vs, CON), 1622 (vs, CON), 1580 (m), 1481 (s), 1439 (s), 1362 (m), 1261 (m), 1215 (m), 1096 (m), 1026 (s), 822 (s), 735 (vs), 706 (vs), 613 (w) cm^{-1}. $C_{55}H_{60}BN_3O_6Ti$ (917.8): calcd. C 71.98, H 6.59, N 4.58; found C 71.70, H 6.80, N 4.42. **Z-11(chel^A):** ^1H NMR: δ = 7.37 [m, 5 H, 1-OCH$_2$(C$_6$*H*$_5$)], 7.35 (br. d, ^3J = 9.7 Hz, 1 H, 5-H), 5.81 (AB*X*, 1 H, 8-H), 6.17 and 5.89 (2 × s, 2 × 5 H, Cp-H and Cp′-H), 5.19 [AB, ^2J = 12.1 Hz, 2 H, 1-OC*H*$_2$(C$_6$H$_5$)], 4.50 (d, ^3J = 2.8 Hz, 1 H, 3-H), 4.11 (dd, ^3J = 8.1, ^3J = 5.6 Hz, 1 H, 6-H), 3.81 (*AB*X, ^2J = 18.3 Hz, 2 H, 9-H and 9-H′), 3.71 (s, 3 H, 10-OC*H*$_3$), 2.34 [m, 1 H, 3-C*H*(CH$_3$)$_2$], 2.03 [m, 1 H, 6-C*H*(CH$_3$)$_2$], 1.14 and 1.09 [2 × d, 2 × ^3J = 6.9 Hz, 2 × 3 H, 3-CH(C*H*$_3$)(C*H*′$_3$)], 0.98 and 0.96 [2 × d, 2 × ^3J = 6.9 Hz, 2 × 3 H, 6-CH(C*H*$_3$)(C*H*′$_3$)] ppm. ^{13}C NMR: δ = 178.0 (C-4), 169.8 (C-7), 168.9 (C-10), 153.2 (C-1), 138.8−122.1 {1-OCH$_2$(*C*$_6$H$_5$) and [BPh$_4$]$^-$}, 119.4 and 117.8 (C-Cp and C-Cp′), 69.3 (C-3), 68.6 [1-O*C*H$_2$(C$_6$H$_5$)], 59.8 (C-6), 52.7 (10-O*C*H$_3$), 41.3 (C-9), 34.4 [3-*C*H(CH$_3$)$_2$], 31.4 [6-*C*H(CH$_3$)$_2$], 22.6−14.1 [3-CH(*C*H$_3$)(*C*H′$_3$) and 6-CH(*C*H$_3$)(*C*H′$_3$)] ppm. **Z-11(chel^B):** ^1H NMR: δ = 7.37 [m, 5 H, 1-OCH$_2$(C$_6$*H*$_5$)], 6.14 (AB*X*, 1 H, 8-H), 6.13 and 5.89 (2 × s, 2 × 5 H, Cp-H and Cp′-H), 5.64 (br., 1 H, 2-H), 5.12 (AB, ^2J = 12.1 Hz, 2 H, 1-OC*H*$_2$(C$_6$H$_5$)], 5.00 (d, ^3J = 3.1 Hz, 1 H, 6-H), 4.03 (m, 1 H, 3-H), 3.75 (s, 3 H, 10-OC*H*$_3$), 3.43 (*AB*X, ^2J = 18.0 Hz, 2 H, 9-H and 9-H′), 2.12 [m, 1 H, 6-C*H*(CH$_3$)$_2$], 2.03 [m, 1 H, 3-C*H*(CH$_3$)$_2$], 0.95 and 0.91 [2 × d, 2 × ^3J = 7.2 Hz, 2 × 3 H, 3-CH(C*H*$_3$)(C*H*′$_3$)] ppm. ^{13}C NMR: δ = 177.7 (C-7), 175.1 (C-4), 168.4 (C-10), 156.5 (C-1), 138.8−122.1 {1-OCH$_2$(*C*$_6$H$_5$) and [BPh$_4$]$^-$}, 118.5 and 117.8 (C-Cp and C-Cp′), 69.3 (C-6), 67.6 [1-O*C*H$_2$(C$_6$H$_5$)], 58.3 (C-3), 53.0 (10-O*C*H$_3$), 42.4 (C-9), 35.5 [6-*C*H(CH$_3$)$_2$], 29.2 [3-*C*H(CH$_3$)$_2$], 22.6−14.1 [3-CH(*C*H$_3$)(*C*H′$_3$) and 6-CH(*C*H$_3$)(*C*H′$_3$)] ppm.

Boc-11(pept) (Boc-Val-Val-Gly-OMe):[14] Reaction of Boc-Val-Val-OH (3.64 g, 11.5 mmol) with HCl·H-Gly-OMe (1.43 g, 11.5 mmol), triethylamine (1.60 mL, 11.5 mmol), and IIDQ (3.49 g, 11.5 mmol) yielded 3.16 g (71%) of Boc-**11**(pept). R_f = 0.43 (ethyl acetate/

cyclohexane, 3:1). M.p. (DSC): 176 °C. $[\alpha]_D = -35$ ($c = 1.0$, CH_2Cl_2). IR (KBr): $\tilde{\nu}$ = 3295 (s, NH), 2967 (s), 2933 (m), 1759 (m, COO), 1695 (s, CON), 1640 (vs, CON), 1554 (s), 1526 (s), 1393 (w), 1365 (m), 1209 (m), 1179 (m), 781 (s) cm^{-1}. ^1H NMR: δ = 7.62 (AB*X*, 1 H, 8-H), 7.23 (br. d, ^3J = 8.9 Hz, 1 H, 5-H), 5.62 (br. d, ^3J = 6.6 Hz, 1 H, 2-H), 4.36 (dd, ^3J = 8.9, ^3J = 6.8 Hz, 1 H, 6-H), 3.98 (*AB*X, 2 H, 9-H and 9-H′), 3.98 (m, 1 H, 3-H), 3.67 (s, 3 H, 10-OCH_3), 2.15 [m, 1 H, 6-C*H*(CH$_3$)$_2$], 2.05 [m, 1 H, 3-C*H*(CH$_3$)$_2$], 1.38 [s, 9 H, 1-OC(CH_3)$_3$], 0.95−0.94 [m, 4 × 3 H, 3-CH(CH_3C*H*′$_3$) and 6-CH(CH_3C*H*′$_3$)] ppm. ^{13}C NMR: δ = 172.1 (C-4), 171.8 (C-7), 170.2 (C-10), 156.2 (C-1), 79.9 [1-O*C*(CH$_3$)$_3$], 60.4 (C-3), 58.2 (C-6), 52.3 (10-O*C*H$_3$), 41.0 (C-9), 30.5 [3-*C*H(CH$_3$)$_2$], 30.4 [6-*C*H(CH$_3$)$_2$], 28.0 [1-OC(*C*H$_3$)$_3$], 19.1 and 19.0 [6-CH(*C*H$_3$C*H*′$_3$)], 17.9 and 17.6 [3-CH(*C*H$_3$C*H*′$_3$)] ppm. $C_{18}H_{33}N_3O_6$ (387.5): calcd. C 55.80, H 8.58, N 10.84; found C 55.81, H 8.61, N 10.63.

Reaction of Boc-11(pept) with 13. Boc-11(coord^7): ^1H NMR: δ = 9.45 (AB*X*, 1 H, 8-H), 6.49 (br. d, ^3J = 6.1 Hz, 1 H, 5-H), 6.27 and 6.23 (2 × s, 2 × 5 H, Cp-H and Cp′-H), 5.26 (br., 1 H, 2-H), 3.91 (m, 1 H, 6-H), 3.81 (m, 1 H, 3-H), 3.79 (s, 3 H, 10-OCH_3), 3.67 (*AB*X, ^2J = 19.6 Hz, 2 H, 9-H and 9-H′), 2.19 [m, 1 H, 6-C*H*(CH$_3$)$_2$], 1.93 [m, 1 H, 3-C*H*(CH$_3$)$_2$], 1.43 [s, 9 H, 1-OC(CH_3)$_3$], 1.18 (s, 3 H, Ti−CH_3), 1.03 and 0.99 [2 × d, 2 × ^3J = 7.0 Hz, 2 × 3 H, 3-CH(CH_3C*H*′$_3$)], 1.00 and 0.95 [2 × d, 2 × ^3J = 7.2 Hz, 2 × 3 H, 6-CH(CH_3C*H*′$_3$)] ppm. ^{13}C NMR: δ = 182.5 (C-7), 171.9 (C-4), 167.3 (C-10), 158.4 (C-1), 116.9 and 116.7 (C-Cp and C-Cp′), 82.7 [1-O*C*(CH$_3$)$_3$], 62.0 (C-3), 58.2 (C-6), 53.3 (10-O*C*H$_3$), 51.1 (Ti−*C*H$_3$), 41.9 (C-9), 29.5 [6-*C*H(CH$_3$)$_2$], 28.5 [3-*C*H(CH$_3$)$_2$], 27.9 [1-OC(*C*H$_3$)$_3$], 19.6, 18.9, 17.8 and 15.3 [3-CH(*C*H$_3$C*H*′$_3$) and 6-CH(*C*H$_3$C*H*′$_3$)] ppm.

Products Boc-11(chel^A)/Boc-11(chel^B) = 2:3: Reaction of Boc-**11**(pept) (149 mg, 3.85·10^{-4} mol) with **13** (225 mg, 3.85·10^{-4} mol) yielded 316 mg (93%) of the isomeric mixture Boc-**11**(chel^A)/Boc-**11**(chel^B) = 2:3. M.p. (DSC): 41 °C (dec.). $[\alpha]_D = -104$ (c = 0.90, CH_2Cl_2). IR (KBr): $\tilde{\nu}$ = 3375 (br., NH), 3056 (m), 2967 (s), 1751 (m, COO), 1662 (s, CON), 1607 (vs, CON), 1540 (s), 1481 (s), 1449 (s), 1369 (m), 1206 (w), 1152 (m), 1015 (w), 822 (m), 734 (s), 706 (vs), 613 (m) cm^{-1}. $C_{52}H_{62}BN_3O_6Ti$ (883.8): calcd. C 70.67, H 7.07, N 4.75; found C 71.18, H 8.10, N 4.23. **Boc-11(chel^A):** ^1H NMR: δ = 7.29 (br. d, ^3J = 8.2 Hz, 1 H, 5-H), 6.13 and 5.98 (2 × s, 2 × 5 H, Cp-H and Cp′-H), 5.76 (AB*X*, 1 H, 8-H), 5.05 (d, ^3J = 3.1 Hz, 1 H, 3-H), 4.12 (dd, ^3J = 8.2, ^3J = 5.6 Hz, 1 H, 6-H), 3.78 (*AB*X, ^2J = 18.0 Hz, 2 H, 9-H and 9-H′), 3.74 (s, 3 H, 10-OCH_3), 2.09 [m, 1 H, 3-C*H*(CH$_3$)$_2$], 2.03 [m, 1 H, 6-C*H*(CH$_3$)$_2$], 1.46 [s, 9 H, 1-OC(CH_3)$_3$], 1.18 and 1.12 [2 × d, 2 × ^3J = 7.4 Hz, 2 × 3 H, 3-CH(CH_3)(C*H*′$_3$)], 0.99 and 0.98 [2 × d, 2 × ^3J = 7.2 Hz, 2 × 3 H, 6-CH(CH_3)(C*H*′$_3$)] ppm. ^{13}C NMR: δ = 177.9 (C-4), 169.7 (C-10), 168.9 (C-7), 155.9 (C-1), 118.5 and 118.0 (C-Cp and C-Cp′), 84.8 [1-O*C*(CH$_3$)$_3$], 69.3 (C-3), 59.7 (C-6), 52.9 (10-O*C*H$_3$), 41.3 (C-9), 35.6 [3-*C*H(CH$_3$)$_2$], 31.5 [6-*C*H(CH$_3$)$_2$], 28.3 [1-OC(*C*H$_3$)$_3$], 19.7 and 17.6 [6-CH(*C*H$_3$)(*C*H′$_3$)], 19.5 and 17.8 [3-CH(*C*H$_3$)(*C*H′$_3$)] ppm. **Boc-11(chel^B):** ^1H NMR: δ = 6.18 and 6.07 (2 × s, 2 × 5 H, Cp-H and Cp′-H), 5.98 (AB*X*, 1 H, 8-H), 5.08 (br. d, ^3J = 7.3 Hz, 1 H, 2-H), 4.48 (d, ^3J = 3.0 Hz, 1 H, 6-H), 3.71 (s, 3 H, 10-OCH_3), 3.62 (dd, ^3J = 9.5, ^3J = 7.3 Hz, 1 H, 3-H), 3.35 (*AB*X, ^2J = 17.7 Hz, 2 H, 9-H and 9-H′), 2.29 [m, 1 H, 6-C*H*(CH$_3$)$_2$], 1.93 [m, 1 H, 3-C*H*(CH$_3$)$_2$], 1.54 [s, 9 H, 1-OC(CH_3)$_3$], 1.15 and 1.08 [2 × d, 2 × ^3J = 7.3 Hz, 2 × 3 H, 6-CH(CH_3)(C*H*′$_3$)], 1.06 and 0.99 [2 × d, 2 × ^3J = 7.2 Hz, 2 × 3 H, 3-CH(CH_3)(C*H*′$_3$)] ppm. ^{13}C NMR: δ = 178.1 (C-7), 175.6 (C-4), 168.3 (C-10), 154.1 (C-1), 119.1 and 117.5 (C-Cp and C-Cp′), 80.8 [1-O*C*(CH$_3$)$_3$], 69.3 (C-6), 58.0 (C-3), 52.6 (10-O*C*H$_3$), 42.4 (C-9), 34.6 (6-*C*H(CH$_3$)$_2$], 29.1 [3-*C*H(CH$_3$)$_2$], 28.6 [1-OC(*C*H$_3$)$_3$], 20.3 and 17.9 [6-CH(*C*H$_3$)(*C*H′$_3$)], 18.9 and 18.7 [3-CH(*C*H$_3$)(*C*H′$_3$)] ppm.

Z-12(pept) (Z-Val-Val-Val-OMe):[39] Reaction of Z-Val-Val-OH (1.00 g, 2.85 mmol) with HCl·H-Val-OMe (478 mg, 2.85 mmol), triethylamine (0.40 mL, 2.85 mmol), and IIDQ (866 mg, 2.85 mmol): Yield 1.12 g (85%) Z-**12**(pept). R_f = 0.24 (ethyl acetate/cyclohexane, 3:1). M.p. (DSC): 225 °C. $[\alpha]_D = -28$ (c = 1.0, CH_2Cl_2). IR (KBr): $\tilde{\nu}$ = 3290 (br. s, NH), 2963 (m), 1734 (m, COO), 1691 (s, CON), 1640 (vs, CON), 1539 (s), 1394 (w), 1294 (w), 1248 (m), 1041 (w), 699 (m) cm^{-1}. $C_{24}H_{37}N_3O_6$ (463.6): calcd. C 62.18, H 8.05, N 9.06; found C 61.67, H 8.06, N 8.85.

Reaction of Z-12(pept) with 13

Z-12(coord^4)/Z-12(coord^7) = 1:3. Z-12(coord^4): ^1H NMR: δ = 7.37 [m, 5 H, 1-OCH$_2$(C$_6H_5$)], 6.82 (br., 1 H, 8-H), 6.66 (br., 1 H, 5-H), 6.18 and 6.16 (2 × s, 2 × 5 H, Cp-H and Cp′-H), 5.83 (br., 1 H, 2-H), 4.84 [AB, ^2J = 12.4 Hz, 2 H, 1-OCH_2(C$_6H_5$)], 4.53 (dd, ^3J = 8.8, ^3J = 5.0 Hz, 1 H, 6-H), 4.44 (m, 1 H, 9-H), 4.11 (m, 1 H, 3-H), 3.70 (s, 3 H, 10-OCH_3), 2.18 [m, 1 H, 6-C*H*(CH$_3$)$_2$], 2.08 [m, 1 H, 3-C*H*(CH$_3$)$_2$], 2.03 [m, 1 H, 9-C*H*(CH$_3$)$_2$], 1.25 (s, 3 H, Ti−CH_3), 0.96−0.86 [3-CH(CH_3C*H*′$_3$), 6-CH(CH_3C*H*′$_3$) and 9-CH(CH_3C*H*′$_3$)] ppm. ^{13}C NMR: δ = 117.5 and 117.4 (C-Cp and C-Cp′), 71.4 [1-OCH$_2$(C$_6$H$_5$)], 60.9 (C-3), 58.9 (C-9), 57.5 (C-6), 54.7 (10-O*C*H$_3$), 52.5 (Ti−*C*H$_3$), 31.8, 31.2 and 30.4 [3-*C*H(CH$_3$)$_2$, 6-*C*H(CH$_3$)$_2$ and 9-*C*H(CH$_3$)$_2$], 19.1−17.4 [3-CH(*C*H$_3$C*H*′$_3$), 6-CH(*C*H$_3$C*H*′$_3$) and 9-CH(*C*H$_3$C*H*′$_3$)] ppm (C-1, C-4, C-7 and C-10 signals not observed). **Z-12(coord^7):** ^1H NMR: δ = 8.85 (br. d, ^3J = 9.4 Hz, 1 H, 8-H), 7.37 [m, 5 H, 1-OCH$_2$(C$_6H_5$)], 6.45 (br., 1 H, 2-H), 6.29 and 6.27 (2 × s, 2 × 5 H, Cp-H and Cp′-H), 5.40 (br., 1 H, 5-H), 5.11 [AB, ^2J = 10.8 Hz, 2 H, 1-OCH_2(C$_6H_5$)], 3.93 (m, 1 H, 6-H), 3.81 (s, 3 H, 10-OCH_3), 3.80 (m, 1 H, 3-H), 3.65 (dd, ^3J = 9.4, ^3J = 7.0 Hz, 1 H, 9-H), 2.30 [m, 1 H, 6-C*H*(CH$_3$)$_2$], 2.27 [m, 1 H, 9-C*H*(CH$_3$)$_2$], 1.85 [m, 1 H, 3-C*H*(CH$_3$)$_2$], 1.21 (s, 3 H, Ti−CH_3), 1.05 and 0.98 [2 × d, 2 × ^3J = 7.0 Hz, 2 × 3 H, 6-CH(CH_3C*H*′$_3$)], 0.96 and 0.95 [2 × d, 2 × ^3J = 7.1 Hz, 2 × 3 H, 9-CH(CH_3C*H*′$_3$)], 0.94 and 0.74 [2 × d, 2 × ^3J = 6.8 Hz, 2 × 3 H, 3-CH(CH_3C*H*′$_3$)] ppm. ^{13}C NMR: δ = 181.7 (C-7), 171.5 (C-4), 168.9 (C-10), 158.4 (C1), 138.8−121.9 {1-OCH$_2$(*C*$_6$H$_5$) and [BPh$_4$]$^-$}, 116.9 and 116.8 (C-Cp and C-Cp′), 68.2 [1-O*C*H$_2$(C$_6$H$_5$)], 62.1 (C-6), 60.1 (C-9), 59.1 (C-3), 53.2 (10-O*C*H$_3$), 51.9 (Ti−*C*H$_3$), 30.4 [9-*C*H(CH$_3$)$_2$], 29.6 [6-*C*H(CH$_3$)$_2$], 28.6 [3-*C*H(CH$_3$)$_2$], 19.6, 19.1, 19.1, 18.6, 17.4 and 16.4 [3-CH(*C*H$_3$C*H*′$_3$), 6-CH(*C*H$_3$C*H*′$_3$) and 9-CH(*C*H$_3$C*H*′$_3$)] ppm.

Products Z-12(chel^A)/Z-12(chel^B) = 1:1: Reaction of Z-**12**(pept) (164 mg, 3.54·10^{-4} mol) with **13** (207 mg, 3.54·10^{-4} mol) yielded 319 mg (94%) of the isomeric mixture Z-**12**(chel^A)/Z-**12**(chel^B) = 1:1. M.p. (DSC): 91 °C (dec.). $[\alpha]_D = -86$ (c = 0.60, CH_2Cl_2). IR (KBr): $\tilde{\nu}$ = 3369 (br., NH), 3055 (w), 2966 (s), 1740 (m, COO), 1715 (m, CON), 1651 (vs, CON), 1606 (s), 1580 (w), 1516 (m), 1481 (s), 1439 (m), 1263 (m), 1215 (w), 1096 (w), 1026 (m), 822 (m), 735 (s), 706 (vs), 613 (w) cm^{-1}. $C_{58}H_{66}N_3BO_6Ti$ (959.9): calcd. C 72.57, H 6.93, N 4.38; found C 71.59, H 6.72, N 4.35. **Z-12(chel^A):** ^1H NMR: δ = 7.76 (br., 1 H, 5-H), 7.36 [m, 5 H, 1-OCH$_2$(C$_6H_5$)], 6.31 (br., 1 H, 8-H), 6.16 and 6.15, 5.90 and 5.87 (each 2 × s, each 2 × 5 H, each Cp-H and Cp′-H), 5.19 [AB, ^2J = 12.2 Hz, 2 H, 1-OCH_2(C$_6H_5$)], 4.55 (dd, ^3J = 8.5, ^3J = 4.8 Hz, 1 H, 9-H), 4.52 (d, ^3J = 3.4 Hz, 1 H, 3-H), 4.20 (dd, ^3J = 9.3, ^3J = 6.7 Hz, 1 H, 6-H), 3.75 (s, 3 H, 10-OCH_3), 2.34 [m, 1 H, 3-C*H*(CH$_3$)$_2$], 2.21 [m, 1 H, 9-C*H*(CH$_3$)$_2$], 2.11 [m, 1 H, 6-C*H*(CH$_3$)$_2$], 1.11 and 1.04 [2 × d, 2 × ^3J = 7.2 Hz, 2 × 3 H, 3-CH(CH_3)(C*H*′$_3$)], 1.00 and 0.99 [2 × d, 2 × ^3J = 7.2 Hz, 2 × 3 H, 6-CH(CH_3)(C*H*′$_3$)], 0.93 and 0.91 [2 × d, 2 × ^3J = 7.4 Hz, 2 × 3 H, 9-CH(CH_3)(C*H*′$_3$)] ppm. ^{13}C

NMR: δ = 178.0 (C-4), 171.8 (C-10), 168.9 (C-7), 153.4 (C-1), 138.8−121.9 {1-OCH$_2$(C_6H$_5$) and [BPh$_4$]$^-$}, 119.2 and 118.8, 117.9 and 117.8 (each C-Cp and C-Cp′), 69.3 (C-3), 68.7 [1-O*C*H$_2$(C$_6$H$_5$)], 60.2 (C-6), 57.6 (C-9), 52.8 (10-O*C*H$_3$), 31.6 (6-*C*H(CH$_3$)$_2$], 31.0 [9-*C*H(CH$_3$)$_2$], 30.8 [3-*C*H(CH$_3$)$_2$], 21.4−17.2 [3-CH(*C*H$_3$)(*C*H′$_3$), 6-CH(*C*H$_3$)(*C*H′$_3$), 9-CH(*C*H$_3$)(*C*H′$_3$)] ppm. **Z-12(chel^B):** ^{1}H NMR: δ = 7.36 [m, 5 H, 1-OCH$_2$(C$_6$*H*$_5$)], 6.19 (br., 1 H, 2-H), 6.16 and 6.15, 5.90 and 5.87 (each 2 × s, each 2 × 5 H, Cp-H and Cp′-H of isomer A and B), 5.40 (br. d, ^3J = 7.4 Hz, 1 H, 8-H), 5.16 (br., 1 H, 6-H), 5.05 [AB, ^2J = 12.5 Hz, 2 H, 1-O*C*H$_2$(C$_6$H$_5$)], 4.15 (m, 1 H, 3-H), 3.82 (s, 3 H, 10-OC*H*$_3$), 3.67 (m, 1 H, 9-H), 2.33 [m, 1 H, 6-C*H*(CH$_3$)$_2$], 2.01 [m, 1 H, 3-C*H*(CH$_3$)$_2$], 1.98 [m, 1 H, 9-C*H*(CH$_3$)$_2$], 1.38 and 1.17 [2 × d, 2 × ^3J = 7.2 Hz, 2 × 3 H, 6-CH(C*H*$_3$)(C*H*′$_3$)], 1.06 and 1.00 [2 × d, 2 × ^3J = 7.2 Hz, 2 × 3 H, 9-CH(C*H*$_3$)(C*H*′$_3$)], 0.89 and 0.87 [2 × d, 2 × ^3J = 7.3 Hz, 2 × 3 H, 3-CH(C*H*$_3$)(C*H*′$_3$)] ppm. ^{13}C NMR: δ = 177.5 (C-4), 175.1 (C-7), 172.4 (C-10), 156.3 (C-1), 138.8−121.9 {1-OCH$_2$(C_6H$_5$) and [BPh$_4$]$^-$}, 119.2 and 118.8, 117.9 and 117.8 (each C-Cp and C-Cp′), 69.4 (C-6), 66.8 [1-O*C*H$_2$(C$_6$H$_5$)], 60.6 (C-3), 58.4 (C-9), 53.3 (10-O*C*H$_3$), 31.4 [3-*C*H(CH$_3$)$_2$], 31.2 [6-*C*H(CH$_3$)$_2$], 29.1 [9-*C*H(CH$_3$)$_2$], 21.4−17.2 [3-CH(*C*H$_3$)(*C*H′$_3$), 6-CH(*C*H$_3$)(*C*H′$_3$), 9-CH(*C*H$_3$)(*C*H′$_3$)] ppm.

Boc-12(pept) (Boc-Val-Val-Val-OMe):[40] Reaction of Boc-Val-Val-OH (1.00 g, 3.16 mmol) with HCl·H-Val-OMe (530 mg, 3.16 mmol), triethylamine (0.44 mL, 3.16 mmol), and IIDQ (959 mg, 3.16 mmol) yielded 3.16 g (71%) of Boc-**12**(pept). R_f = 0.36 (ethyl acetate/cyclohexane, 2:1). M.p. (DSC): 157 °C. [α]$_D$ = −36 (*c* = 1.0, CH$_2$Cl$_2$). IR (KBr): ṽ = 3290 (br. s, NH), 2966 (s), 1746 (m, COO), 1691 (s, CON), 1643 (vs, CON), 1550 (s), 1525 (s), 1392 (w), 1367 (w), 1299 (w), 1246 (m), 1019 (w) cm^{-1}. C$_{21}$H$_{39}$N$_3$O$_6$ (429.6): calcd. C 58.72, H 9.15, N 9.78; found C 59.21, H 9.14, N 9.68.

Reaction of Boc-12(pept) with 13

Boc-12(coord^4)/Boc-12(coord^7) = 1:3. Boc-12(coord^4): ^{1}H NMR: δ = 6.84 (br., 1 H, 8-H), 6.61 (br., 1 H, 5-H), 6.36 and 6.35 (2 × s, 2 × 5 H, Cp-H and Cp′-H), 5.47 (br. d, ^3J = 8.1 Hz, 1 H, 2-H), 4.55 (dd, ^3J = 8.8, ^3J = 5.0 Hz, 1 H, 6-H), 4.44 (dd, ^3J = 8.8, ^3J = 6.9 Hz, 1 H, 9-H), 4.03 (dd, ^3J = 8.1, ^3J = 4.8 Hz, 1 H, 3-H), 3.74 (s, 3 H, 10-OC*H*$_3$), 2.21 [m, 1 H, 6-C*H*(CH$_3$)$_2$], 2.12 [m, 1 H, 3-C*H*(CH$_3$)$_2$], 2.09 [m, 1 H, 9-C*H*(CH$_3$)$_2$], 1.38 [s, 9 H, 1-OC(C*H*$_3$)$_3$], 1.30 (s, 3 H, Ti−C*H*$_3$), 0.99 and 0.97 [2 × d, 2 × ^3J = 7.1 Hz, 2 × 3 H, 9-CH(C*H*$_3$C*H*′$_3$)], 0.95 and 0.87 [2 × d, 2 × ^3J = 7.2 Hz, 2 × 3 H, 3-CH(C*H*$_3$C*H*′$_3$)], 0.92 and 0.90 [2 × d, 2 × ^3J = 7.2 Hz, 2 × 3 H, 6-CH(C*H*$_3$C*H*′$_3$)] ppm. ^{13}C NMR: δ = 170.6 (C-10), 169.1 (C-7), 160.5 (C-1), 117.2 and 117.0 (C-Cp and C-Cp′), 89.1 [1-O*C*(CH$_3$)$_3$], 60.7 (C-3), 59.0 (C-9), 57.3 (C-6), 53.4 (10-O*C*H$_3$), 52.5 (Ti−*C*H$_3$), 32.1 [3-*C*H(CH$_3$)$_2$], 31.9 [9-*C*H(CH$_3$)$_2$], 31.2 [6-*C*H(CH$_3$)$_2$], 28.2 [1-OC(*C*H$_3$)$_3$], 19.7−16.2 [3-CH(*C*H$_3$C*H*′$_3$), 6-CH(*C*H$_3$C*H*′$_3$) and 9-CH(*C*H$_3$C*H*′$_3$)] ppm (C4 signal not observed). **Boc-12(coord^7):** ^{1}H NMR: δ = 9.09 (br. d, ^3J = 9.2 Hz, 1 H, 8-H), 6.54 (br. d, ^3J = 5.5 Hz, 1 H, 5-H), 6.31 and 6.29 (2 × s, 2 × 5 H, Cp-H and Cp′-H), 5.13 (br., 1 H, 2-H), 2 × 3.86 (m, 1 H, 3-H and 6-H), 3.83 (s, 3 H, 10-OC*H*$_3$), 3.64 (dd, ^3J = 9.2, ^3J = 7.7 Hz, 1 H, 9-H), 2.33 [m, 1 H, 3-C*H*(CH$_3$)$_2$ or 6-C*H*(CH$_3$)$_2$], 2.26 [m, 1 H, 9-C*H*(CH$_3$)$_2$], 1.93 [m, 1 H, 3-C*H*(CH$_3$)$_2$ or 6-C*H*(CH$_3$)$_2$], 1.47 [s, 9 H, 1-OC(C*H*$_3$)$_3$], 1.22 [s, 3 H, Ti−C*H*$_3$), 1.07 and 0.97 [2 × d, 2 × ^3J = 7.1 Hz, 2 × 3 H, 3-CH(C*H*$_3$C*H*′$_3$) or 6-CH(C*H*$_3$C*H*′$_3$)], 1.01 and 0.88 [2 × d, 2 × ^3J = 7.2 Hz, 2 × 3 H, 3-CH(C*H*$_3$C*H*′$_3$) or 6-CH(C*H*$_3$C*H*′$_3$)], 0.99 and 0.98 [2 × d, 2 × ^3J = 7.1 Hz, 2 × 3 H, 9-CH(C*H*$_3$C*H*′$_3$)] ppm. ^{13}C NMR: δ = 181.7 (C-7), 171.8 (C-4), 168.9 (C-10), 157.9 (C-1), 116.9 and 116.8 (C-Cp and C-Cp′), 82.2 [1-O*C*(CH$_3$)$_3$], 61.7 (C-3 or C-6), 60.5 (C-9), 59.1 (C-3 or C-6), 53.2 (10-O*C*H$_3$), 51.7 (Ti−*C*H$_3$), 30.3 [9-*C*H(CH$_3$)$_2$], 29.5 [3-*C*H(CH$_3$)$_2$ or 6-*C*H(CH$_3$)$_2$], 28.3 [3-*C*H(CH$_3$)$_2$ or 6-*C*H(CH$_3$)$_2$], 28.1 [1-OC(*C*H$_3$)$_3$], 19.7, 19.2, 19.1, 19.0, 17.3 and 16.2 [3-CH(*C*H$_3$C*H*′$_3$), 6-CH(*C*H$_3$C*H*′$_3$) and 9-CH(*C*H$_3$C*H*′$_3$)] ppm.

Products Boc-12(chel^A)/Boc-12(chel^B) = 2:3: Reaction of Boc-**12**(pept) (176 mg, 4.10·10^{-4} mol) with **13** (239 mg, 4.10·10^{-4} mol) yielded 364 mg (96%) of the isomeric mixture Boc-**12**(chel^A)/Boc-**12**(chel^B) = 2:3. M.p. (DSC): 59 °C (dec.). [α]$_D$ = −19 (*c* = 0.80, CH$_2$Cl$_2$). IR (KBr): ṽ = 3334 (br., NH), 3057 (w), 2966 (s), 1743 (m, COO), 1653 (vs, CON), 1507 (s), 1481 (s), 1456 (s), 1371 (w), 1260 (m), 1155 (s), 1017 (m), 816 (s), 734 (m), 705 (vs) cm^{-1}. C$_{55}$H$_{68}$BN$_3$O$_6$Ti (925.9): calcd. C 71.35, H 7.40, N 4.54; found C 70.45, H 7.64, N 4.52. **Boc-12(chel^A):** ^{1}H NMR: δ = 7.66 (br. d, ^3J = 8.5 Hz, 1 H, 5-H), 6.29 (br. d, ^3J = 7.1 Hz, 1 H, 8-H), 6.17 and 6.06, 6.17 and 6.01 (each 2 × s, each 2 × 5 H, each Cp-H and Cp′-H), 4.54 (dd, ^3J = 7.1, ^3J = 4.7 Hz, 1 H, 9-H), 4.50 (d, ^3J = 3.0 Hz, 1 H, 3-H), 4.21 (dd, ^3J = 8.5, ^3J = 6.5 Hz, 1 H, 6-H), 3.75 (s, 3 H, 10-OC*H*$_3$), 2.30 [m, 1 H, 3-C*H*(CH$_3$)$_2$], 2.22 [m, 1 H, 9-C*H*(CH$_3$)$_2$], 2.13 [m, 1 H, 6-C*H*(CH$_3$)$_2$], 1.53 [s, 9 H, 1-OC(C*H*$_3$)$_3$], 1.13 and 1.04 [2 × d, 2 × ^3J = 7.1 Hz, 2 × 3 H, 3-CH(C*H*$_3$)(C*H*′$_3$)], 1.03 and 1.02 [2 × d, 2 × ^3J = 7.4 Hz, 2 × 3 H, 6-CH(C*H*$_3$)(C*H*′$_3$)], 0.94 and 0.92 [2 × d, 2 × ^3J = 7.5 Hz, 2 × 3 H, 9-CH(C*H*$_3$)(C*H*′$_3$)] ppm. ^{13}C NMR: δ = 178.2 (C-4), 171.9 (C-10), 168.9 (C-7), 154.2 (C-1), 119.0 and 118.7, 117.9 and 117.6 (each C-Cp and C-Cp′), 84.9 [1-O*C*(CH$_3$)$_3$], 69.3 (C-3), 60.2 (C-6), 57.6 (C-9), 52.7 (10-O*C*H$_3$), 34.7 [3-*C*H(CH$_3$)$_2$], 31.2 [9-*C*H(CH$_3$)$_2$], 30.7 [6-*C*H(CH$_3$)$_2$], 28.7 [1-OC(*C*H$_3$)$_3$], 20.3−16.9 [3-CH(*C*H$_3$)(*C*H′$_3$), 6-CH(*C*H$_3$)(*C*H′$_3$), 9-CH(*C*H$_3$)(*C*H′$_3$)] ppm. **Boc-12(chel^B):** ^{1}H NMR: δ = 6.90 (br. d, ^3J = 8.2 Hz, 1 H, 8-H), 6.17 and 6.06, 6.17 and 6.01 (each 2 × s, each 2 × 5 H, Cp-H and Cp′-H both isomers), 5.18 (d, ^3J = 3.4 Hz, 1 H, 6-H), 5.09 (br. d, ^3J = 7.3 Hz, 1 H, 2-H), 4.42 (dd, ^3J = 8.2, ^3J = 4.7 Hz, 1 H, 9-H), 3.82 (s, 3 H, 10-OC*H*$_3$), 3.61 (dd, ^3J = 9.5, ^3J = 7.3 Hz, 1 H, 3-H), 2.34 [m, 1 H, 6-C*H*(CH$_3$)$_2$], 2.29 [m, 1 H, 9-C*H*(CH$_3$)$_2$], 1.95 [m, 1 H, 3-C*H*(CH$_3$)$_2$], 1.41 [s, 9 H, 1-OC(C*H*$_3$)$_3$], 1.41 and 1.18 [2 × d, 2 × ^3J = 7.6 Hz, 2 × 3 H, 6-CH(C*H*$_3$)(C*H*′$_3$)], 1.04 and 1.02 [2 × d, 2 × ^3J = 7.4 Hz, 2 × 3 H, 9-CH(C*H*$_3$)(C*H*′$_3$)], 1.06 and 1.00 [2 × d, 2 × ^3J = 7.3 Hz, 2 × 3 H, 3-CH(C*H*$_3$)(C*H*′$_3$)] ppm. ^{13}C NMR: δ = 177.6 (C-7), 175.8 (C-4), 172.4 (C-10), 155.9 (C-1), 119.0 and 118.7, 117.9 and 117.6 (each C-Cp and C-Cp′), 80.9 [1-O*C*(CH$_3$)$_3$], 69.4 (C-6), 59.5 (C-9), 58.0 (C-3), 53.3 (10-O*C*H$_3$), 35.9 [6-*C*H(CH$_3$)$_2$], 31.6 [9-*C*H(CH$_3$)$_2$], 29.1 [3-*C*H(CH$_3$)$_2$], 28.2 [1-OC(*C*H$_3$)$_3$], 20.3−16.9 [3-CH(*C*H$_3$)(*C*H′$_3$), 6-CH(*C*H$_3$)(*C*H′$_3$), 9-CH(*C*H$_3$)(*C*H′$_3$)] ppm.

Acknowledgments

Financial support from the Fonds der Chemischen Industrie and the Deutsche Forschungsgemeinschaft is gratefully acknowledged.

[1] [1a] Reviews: A. D. Ryabov, *Angew. Chem.* **1991**, *103*, 945, *Angew. Chem. Int. Ed. Engl.* **1991**, *30*, 931. [1b] Review: K. Severin, R. Bergs, W. Beck, *Angew. Chem.* **1998**, *110*, 1722; *Angew. Chem. Int. Ed.* **1998**, *37*, 1634.

[2] [2a] C. A. Krüger, K. W. Kuntz, C. D. Dzierba, W. G. Wirschun, J. D. Gleason, M. L. Snapper, A. H. Hoveyda, *J. Am. Chem. Soc.* **1999**, *121*, 4284. [2b] J. R. Porter, W. G. Wirschun, K. W. Kuntz, M. L. Snapper, A. H. Hoveyda, *J. Am. Chem. Soc.* **2000**, *122*, 2657. [2c] A. Berkessel, D. A. Hérault, *Angew. Chem.* **1999**, *111*, 99; *Angew. Chem. Int. Ed.* **1999**, *38*, 102.

[3] [3a] G. Jaouen, A. Vessières, I. S. Butler, *Acc. Chem. Res.* **1993**, *26*, 361. [3b] R. H. Fish, *Coord. Chem. Rev.* **1999**, *186*, 569. [3c] D. B. Grotjahn, *Coord. Chem. Rev.* **1999**, *192*, 1125. [3d] D. R.

van Staveren, T. Weyhermüller, N. Metzler-Nolte, *Organometallics* **2000**, *19*, 3730, and references cited therein.
[4] [4a] J. Recht, B. I. Cohen, A. S. Goldman, J. Kohn, *Tetrahedron Lett.* **1990**, *31*, 7281. [4b] K. Joshi, J. Bao, A. S. Goldman, J. Kohn, *J. Am. Chem. Soc.* **1992**, *114*, 6649. [4c] See also: K. Severin, W. Beck, G. Trojandt, K. Polborn, W. Steglich, *Angew. Chem.* **1995**, *107*, 1570; *Angew. Chem. Int. Ed. Engl.* **1995**, *34*, 1449.
[5] See for a comparison: W. Hoffmüller, M. Maurus, K. Severin, W. Beck, *Eur. J. Inorg. Chem.* **1998**, *729*, and references cited therein.
[6] M. Oberhoff, L. Duda, J. Karl, R. Mohr, G. Erker, R. Fröhlich, M. Grehl, *Organometallics* **1996**, *15*, 4005.
[7] D. Kunz, G. Erker, R. Fröhlich, G. Kehr, *Eur. J. Inorg. Chem.* **2000**, 409.
[8] For synthetically related group-4 metallocene chemistry see, e.g.: K. Klaß, L. Duda, N. Kleigrewe, G. Erker, R. Fröhlich, E. Wegelius, *Eur. J. Inorg. Chem.* **1999**, 11.
[9] See also: [9a] K. Klaß, R. Fröhlich, G. Erker, *J. Chem. Soc., Dalton Trans.* **1999**, 4457. [9b] D. Hüerländer, R. Fröhlich, G. Erker, *J. Chem. Soc., Dalton Trans.* **2002**, *7*, 1513.
[10] For related ferrocene-amino acid and -peptide chemistry see, e.g.: [10a] K. Schlögl, *Monatsh. Chem.* **1957**, *88*, 601. [10b] C. R. Hauser, J. K. Lindsay, *J. Org. Chem.* **1957**, *22*, 1246. [10c] H. Brunner, W. König, B. Nuber, *Tetrahedron: Asymmetry* **1993**, *4*, 699. [10d] B. Basu, S. K. Chattopadhyay, A. Ritzén, T. Frejd, *Tetrahedron: Asymmetry* **1997**, *8*, 1841. [10e] D. Freiesleben, K. Polborn, C. Robl, K. Sünkel, W. Beck, *Can. J. Chem.* **1995**, *73*, 1164. [10f] B. Kayser, J. Altman, H. Nöth, J. Knizek, W. Beck, *Eur. J. Inorg. Chem.* **1998**, 1791. [10g] H.-B. Kraatz, J. Lusztyk, G. D. Enright, *Inorg. Chem.* **1997**, *36*, 2400. [10h] H.-B. Kraatz, D. M. Leek, A. Houmam, G. D. Enright, J. Lusztyk, D. D. M. Wayner, *J. Organomet. Chem.* **1999**, *589*, 38. [10i] T. Moriuchi, A. Nomoto, K. Yoshida, T. Hirao, *J. Organomet. Chem.* **1999**, *589*, 50.
[11] [11a] T. M. Klapötke, H. Köpf, I. C. Tornieporth-Oetting, P. S. White, *Angew. Chem.* **1994**, *106*, 1587, *Angew. Chem. Int. Ed. Engl.* **1994**, *33*, 1518. [11b] T. M. Klapötke, H. Köpf, I. C. Tornieporth-Oetting, P. S. White, *Organometallics* **1994**, *13*, 3628. [11c] I. C. Tornieporth-Oetting, P. S. White, *Organometallics* **1995**, *14*, 1632. [11d] H. Sun, H. Li, R. A. Weir, P. J. Sadler, *Angew. Chem.* **1998**, *110*, 1622; *Angew. Chem. Int. Ed.* **1998**, *37*, 1577. [11e] M. Guo, P. J. Sadler, *J. Chem. Soc., Dalton Trans.* **2000**, 7. [11f] Review: P. Köpf-Meier, H. Köpf, *Chem. Rev.* **1987**, *87*, 1137.
[12] [12a] Review: R. F. Jordan, *Adv. Organomet. Chem.* **1991**, *32*, 325. [12b] Synthesis of the reagent **1a**: S. L. Borkowsky, R. F. Jordan, G. D. Hinch, *Organometallics* **1991**, *10*, 1268, and references cited therein.
[13] M. Oberhoff, G. Erker, R. Fröhlich, *Chem. Eur. J.* **1997**, *3*, 1521.
[14] J. Wonnemann, M. Oberhoff, G. Erker, R. Fröhlich, K. Bergander, *Eur. J. Inorg. Chem.* **1999**, 1111.
[15] [15a] Syntheses: R. Taube, L. Krukowka, *J. Organomet. Chem.* **1988**, *347*, C9. [15b] Preparation from $Cp_2TiMeCl$ with $Na^+BPh_4^-$: M. Bochmann, L. M. Wilson, *Organometallics* **1987**, *6*, 2556.
[16] M. Bergmann, L. Zervas, *Ber. Dtsch. Chem. Ges.* **1932**, *65*, 1192.
[17] L. A. Carpino, *J. Am. Chem. Soc.* **1957**, *79*, 98.
[18] Y. Kiso, H. Yajima, *J. Chem. Soc., Chem. Commun.* **1972**, 942.
[19] J. C. Sheehan, G. P. Hess, *J. Am. Chem. Soc.* **1955**, *77*, 1067.
[20] For general synthetic information about the methods employed for the preparation of the tripeptide derivatives used in this study see, e.g.: [20a] H.-D. Jakubke, *Peptide: Chemie und Biologie*, Spektrum, Akad. Verlag, Heidelberg, **1996**. [20b] E. Wünsch, *Methoden Org. Chem. (Houben-Weyl)*, **1974**, vol. 15/1 ("Synthese von Peptiden"). [20c] A. Bodanszky, M. Bodanszky, *The Practise of Peptide Chemistry*, 2nd ed., Springer-Verlag, Berlin, Heidelberg, **1994**.
[21] [21a] A. Lombardi, G. D'Auria, O. Maglio, F. Nastri, L. Quartara, C. Pedone, V. Pavone, *J. Am. Chem. Soc.* **1998**, *120*, 5879. [21b] S. R. Gilbertson, S. E. Collibee, A. Agarkov, *J. Am. Chem. Soc.* **2000**, *122*, 6522, and references cited therein.
[22] J.-S. Hu, A. Bax, *J. Am. Chem. Soc.* **1997**, *119*, 6360, and references cited therein.
[23] [23a] M. Brunner, W. Huber, *Helv. Chim. Acta* **1953**, *36*, 1109. [23b] P. Sørup, *Hoppe-Seyler's Z. Physiol. Chem.* **1977**, *358*, 99.
[24] [24a] A. L. Barker, G. S. Skinner, *J. Am. Chem. Soc.* **1924**, *46*, 403. [24b] W. Grassmann, E. Wünsch, A. Riedal, *Chem. Ber.* **1958**, *91*, 455. [24c] H. Zahn, H. Schüssler, *Justus Liebigs Ann. Chem.* **1961**, *641*, 176. [24d] M. Zaoral, J. Kolc, F. Korencki, V. P. Cereneckij, F. Šorun, *Coll. Czech. Chem. Commun.* **1967**, *32*, 843.
[25] [25a] R. L. M. Synge, *Biochem. J.* **1948**, *42*, 99. [25b] R. A. Boissonas, S. Guttmann, P.-A. Jaquenond, I.-P. Waller, *Helv. Chim. Acta* **1956**, *39*, 1421. [25c] R. Schwyzer, B. Iselin, H. Kappeler, B. Riniker, W. Rittel, H. Zuber, *Helv. Chim. Acta* **1958**, *41*, 1273.
[26] M. A. Barton, R. U. Lemieux, J. Y. Savoie, *J. Am. Chem. Soc.* **1973**, *95*, 4501.
[27] S. A. Miller, S. L. Griffiths, D. Seebach, *Helv. Chim. Acta* **1993**, *76*, 563.
[28] S. Gangwar, G. M. Pauletti, T. J. Siahaan, V. J. Stella, R. T. Borchardt, *J. Org. Chem.* **1997**, *62*, 1356.
[29] [29a] M. Narita, S.-I. Itsuno, M. Hirata, K. Masanori, K. Kusano, *Bull. Chem. Soc. Jpn.* **1980**, *53*, 1028. [29b] Y. Song, D. Niederer, P. M. Lane-Bell, L. K. P. Lam, S. Crawley, *J. Org. Chem.* **1994**, *59*, 5784.
[30] [30a] H. G. Bossler, D. Seebach, *Helv. Chim. Acta* **1994**, *77*, 1124. [30b] M. Eachlokhani-Niaraki, K. Yoshioka, H. Takahashi, F. Kato, M. Kondo, *J. Chem. Soc., Perkin Trans. 2* **1992**, *7*, 1187.
[31] A. Q. Lyons, L. D. Pettit, *J. Chem. Soc., Dalton Trans.* **1984**, 2305.
[32] H. Zahn, A. Meissner, *Justus Liebigs Ann. Chem.* **1960**, 132.
[33] [33a] J. R. Vaughan, R. L. Osato, *J. Am. Chem. Soc.* **1952**, *74*, 676. [33b] B. Belleau, G. Malek, *J. Am. Chem. Soc.* **1968**, *90*, 1651. [33c] Y. Kiso, H. Yajima, *J. Chem. Soc., Chem. Commun.* **1972**, 942.
[34] H. Gerlach, G. Haas, V. Prelog, *Helv. Chim. Acta* **1966**, *49*, 603.
[35] H. Brückner, G. Jung, *Liebigs Ann. Chem.* **1980**, 37.
[36] [36a] J. E. Shields, S. T. McDowell, J. Pavlos, G. R. Gray, *J. Am. Chem. Soc.* **1968**, *90*, 3549. [36b] D. L. Nguyen, J.-R. Dormoy, B. Castro, D. Prevot, *Tetrahedron* **1981**, *37*, 4229. [36c] C: Y. Ariyoshi, *Bull. Chem. Soc. Jpn.* **1985**, *58*, 1727. [36d] N. Voyer, B. Guerin, *Tetrahedron* **1994**, *50*, 989.
[37] [37a] T. Miyazawa, T. Donkai, T. Yamada, S. Kuwata, *Chem. Lett.* **1989**, 2125. [37b] F. Cavelier Frontin, F. Guendouz, R. Jacquier, J. Verducci, *Bull. Soc. Chim. Fr.* **1992**, *129*, 463.
[38] S. Tsuboi, K. Nakabayashi, Y. Matsumoto, N. Teno, Y. Tsuda, Y. Okada, Y. Nagamatsu, J. Yamamoto, *Chem. Pharm. Bull.* **1990**, *38*, 2369.
[39] [39a] J. E. Shields, S. T. McDowell, J. Pavlos, G. R. Gray, *J. Am. Chem. Soc.* **1968**, *90*, 3549. [39b] E. Vilkas, M. Vilkas, J. Sainton, *Tetrahedron Lett.* **1978**, *32*, 2933. [39c] K. Okada, Y. Kurosawa, S. Nagai, *Chem. Pharm. Bull.* **1979**, *27*, 2163. [39d] T. Miyazawa, T. Donkai, T. Yamada, S. Kuwata, *Chem. Lett.* **1989**, 2125−2128. [39e] C. Griehl, H. Eachschkeit, U. Schilken, A. Kolbe, *J. Chem. Soc., Perkin Trans. 2* **1990**, 47.
[40] [40a] L. Tomasic, A. Stefani, G. P. Lorenzi, *Helv. Chim. Acta* **1980**, *63*, 2000. [40b] Y. Ariyoshi, *Bull. Chem. Soc. Jpn.* **1985**, *58*, 1727.

Received May 7, 2002
[I02236]

$[Yb(THF)_3(C_5H_4PPh_2)_2W(CO)_4]\cdot 0.5THF$ and $^1_\infty[Yb(THF)(C_5H_4PPh_2)_2(\mu\text{-}OC)W(CO)_3]$: Two New Heterobimetallic Complexes Containing Yb^{II} and W^0

Klaus Müller-Buschbaum,*[a,b] Glen B. Deacon,[b] and Craig M. Forsyth[b]

Keywords: Heterometallic complexes / Ytterbium / Tungsten / Carbonyl ligands

The reaction of bis(diphenylphosphanylcyclopentadienyl)-ytterbium(II) with tungsten hexacarbonyl in tetrahydrofuran yields $[Yb(THF)_3(C_5H_4PPh_2)_2W(CO)_4]\cdot 0.5THF$ (**1**), whilst $[Yb(THF)(C_5H_4PPh_2)_2(\mu\text{-}OC)W(CO)_3]$ (**2**) is obtained from toluene. Complex **1** contains nine-coordinate bis(η^5-diphenylphosphanylcyclopentadienyl)tris(tetrahydrofuran)-ytterbium(II) units. Complex **2** has eight-coordinate ytterbium(II) with one carbonyl group showing an *iso*-carbonyl linkage to ytterbium (W–C≡O–Yb), thereby forming a structure of infinite chains. The $Yb(\eta^5\text{-}C_5H_4PPh_2)_2$ units in both **1** and **2** bind to tungsten through the phosphorus atoms giving an octahedral *cis*-$W(CO)_4P_2$ arrangements.
(© Wiley-VCH Verlag GmbH, 69451 Weinheim, Germany, 2002)

Introduction

Early lanthanoid-d-block bimetallic complexes such as $[Yb(THF)(C_5Me_5)_2Co(CO)_4]$[1] and $[Yb(C_5Me_5)_2Fe_3(CO)_{11}]$[2] involve the coordination of a transition metal carbonylate to the lanthanoid through a carbonyl oxygen. The introduction of the diphenylphosphanylcyclopentadienyl ligand ($CpPPh_2$) into organolanthanoid chemistry with $Yb(CpPPh_2)_2$ [3] enabled the preparation of the first lanthanoid-d-block bimetallic complex with the f-block element in the donor part of the molecule. Subsequently, other divalent[4–7] and trivalent[8–14] (diphenylphosphanylcyclopentadienyl)lanthanoid complexes have been prepared, including a Sm^{III} complex with four different ligands,[15] and a limited number of further bimetallics.[4,9,12] Crystallographically characterized derivatives are relatively scarce (see also the related $[Yb(THF)_2(C_4Me_4P)_2Ru(H)_2(PPh_3)_2]$[16]). $[Yb(THF)_2(CpPPh_2)_2Mo(CO)_4]\cdot THF$ and $[Yb(THF)(CpPPh_2)_2Mo(CO)_4]\cdot PhMe$ were prepared with carbonyls of Group 6 transition metals, and the latter was proposed to contain an *iso*-carbonyl–Yb linkage, although no crystal structures were determined.[4] By preparing the tungsten carbonyl analogs, we have succeeded in crystallizing the key complexes $[Yb(THF)_3(CpPPh_2)_2W(CO)_4]\cdot 0.5THF$ (**1**) and $[Yb(THF)(CpPPh_2)_2(\mu\text{-}OC)W(CO)_3]$ (**2**) whose structures illuminate the nature of the $Yb(CpPPh_2)_2$/Group 6 tetracarbonyl bimetallics.

[a] Institut für Anorganische Chemie, Universität zu Köln, Greinstrasse 6, 50939 Köln, Germany
E-mail: Klaus.Mueller-Buschbaum@Uni-Koeln.de
[b] School of Chemistry, Monash University, Victoria 3800, Australia

Results and Discussion

Reaction of $[Yb(THF)(CpPPh_2)_2]$[4] with $W(CO)_6$ in THF initially at room temperature and then at elevated temperatures yielded $[Yb(THF)_3(CpPPh_2)_2W(CO)_4]\cdot 0.5THF$ (**1**) [Equation (1)]. Single crystals were also obtained from the same solvent, and readily underwent decomposition when taken out of the mother liquor precluding opportunity for microanalysis.

$$[Yb(thf)(CpPPh_2)_2] + W(CO)_6 \xrightarrow{THF} [Yb(thf)_3(CpPPh_2)_2W(CO)_4]\cdot 0.5THF\ (\mathbf{1}) + 2\ CO \quad (1)$$

The infrared spectra of the product in Nujol and in THF show four ν(CO) absorptions consistent with a *cis*-$W(CO)_4$ moiety, with values quite similar to those (2010, 1900, 1880, 1845 cm^{-1})[4] for the proposed complex $[Yb(THF)_2(CpPPh_2)_2Mo(CO)_4]\cdot THF$ in Nujol. Although the complex is almost insoluble in toluene (see below) the spectrum of the light green solution shows ν(CO) absorptions similar to the values for the complex in THF, suggesting dissolution of some of the complex as unchanged **1**. The ^1H NMR spectrum in $[D_8]THF$ confirmed the presence of the diphenylphosphanylcyclopentadienyl ligand. A similar ^{31}P resonance was observed for **1** in $[D_8]THF$ and in C_6D_6 (sparing solubility at room temperature) consistent with the similar IR spectra for the compound in THF and toluene. As expected for a P–W coordination, a major shift of the ^{31}P resonance to higher frequencies (δ = 9–10 ppm) than the value for $[Yb(THF)_2(CpPPh_2)_2]$ (δ = −20.5 ppm[4]) is observed, although this change is not as marked as that seen upon coordination of the $Yb(CpPPh_2)_2$ ligand to $Ni(CO)_2$, $PtMe_2$, or $Mo(CO)_4$ (δ =

17−20 ppm).[4] Further evidence for P−W bonding comes from observation of W−P coupling (see Exp. Sect.) within the usual range for $^1J_{W,P}$.[17,18]

Complex **2** can be obtained as single crystals from the same reactants as **1** but by heating in toluene. Its identity was established as a Yb−O≡C−W-bridged complex [Equation (2)]. Although some **1** dissolves in toluene, the bulk gives dark colored insoluble $[Yb(THF)(CpPPh_2)_2(\mu\text{-}OC)W(CO)_3]$ (**2**) [Equation (3)].

$$[Yb(THF)(CpPPh_2)_2] + W(CO)_6 \xrightarrow{\text{toluene}} [Yb(THF)(CpPPh_2)_2(\mu\text{-}OC)W(CO)_3]\ (\mathbf{2}) + 2\ CO \quad (2)$$

$$[Yb(THF)_3(CpPPh_2)_2W(CO)_4]\cdot 0.5THF\ (\mathbf{1}) \xrightarrow{\text{toluene}} [Yb(THF)(CpPPh_2)_2(\mu\text{-}OC)W(CO)_3]\ (\mathbf{2}) + 2\ THF \quad (3)$$

The formation of **2** releases THF into toluene enabling the resulting solution to dissolve a little of **1** unchanged. The IR spectrum of solid **2** also displays four carbonyl absorptions indicative of a *cis*-$W(CO)_4$ arrangement. One of these bands (1758 cm^{-1}) is in the region for a bridging or *iso*-carbonyl group, and even lower than the corresponding value (1790 cm^{-1}) for the related molybdenum complex $[Yb(THF)(CpPPh_2)_2Mo(CO)_4]\cdot PhMe$.[4] Crystals of **2** are extremely unstable outside the mother liquor making a fast characterization by a low temperature X-ray determination necessary and precluding elemental analysis.

Although the compositions of **1** and **2** differ only in their THF content, the structures are very different. In complex **1** a formally nine-coordinate ytterbium atom is surrounded by three THF oxygen atoms and two η^5-bonded $CpPPh_2$ ligands, which chelate through the phosphorus atoms to a $W(CO)_4$ moiety in *cis* positions (Figure 1). The resulting nine-coordination is extremely unusual for $Ln^{II}(Cp')_2$-thf complexes which are normally eight-coordinate $[Ln(Cp')_2(THF)_2]$,[19−21] apart from $[Sm(ind)_2(THF)_3]$ (ind = indenyl).[22] It may be considered that **1** is more remarkable than the Sm^{II} complex[22] since the nine-coordinate ionic radius is 0.12 Å smaller for Yb^{2+} than Sm^{2+}.[23] It is possible that the electron-withdrawing effect of the $CpPPh_2$ ligands[24] more than compensates for the bulkiness of the PPh_2 substituent. The best-fit polyhedron[25] for the three oxygen donors and the centroids (cent) of the $CpPPh_2$ ligands around ytterbium is a distorted square-based pyramid with O(6) apical. The difference from a trigonal bipyramidal arrangement is best seen in the angle difference of a best-fit polyhedron calculation,[26] which is $\Delta = 14.4°$. For a trigonal bipyramidal arrangement the expected value would be 60° and 0° for an undistorted square-based pyramid. However, describing spherical phenomena such as Cp rings by single points representing the centroids of those rings has to be viewed cautiously. Tungsten shows a slightly distorted octahedron of two *cis* phosphorus and four carbon donor atoms.

In complex **2** each ytterbium is eight-coordinate and surrounded by two η^5-$CpPPh_2$ ligands, a THF oxygen and a carbonyl oxygen, with the two phosphorus atoms chelating

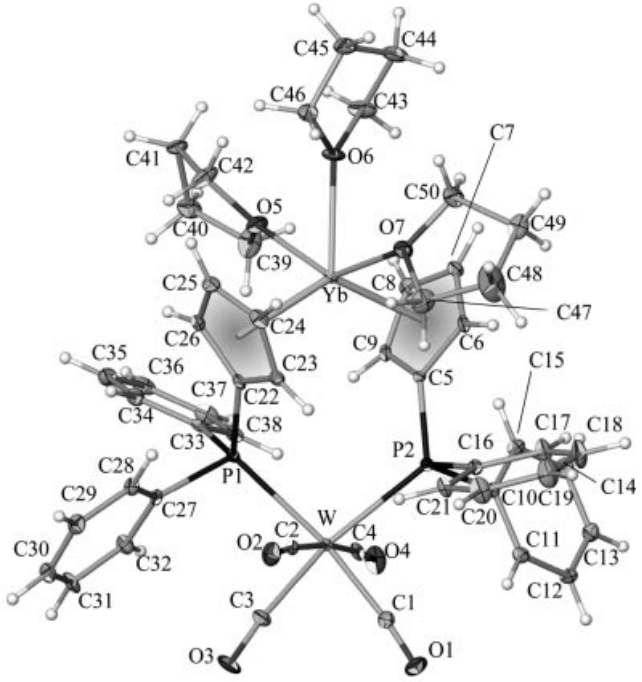

Figure 1. The molecular structure of $[Yb(THF)_3(CpPPh_2)_2W(CO)_4]\cdot 0.5THF$ (**1**); η^5-interactions between Yb and Cp are represented by bonds towards centroids of shaded Cp rings; the thermal ellipsoids here and in Figure 2 are scaled to a probability density of 50%

(*cis*) to a $W(CO)_4$ unit, one oxygen of which bridges to the adjacent ytterbium. The best-fit polyhedron[25] for the disparate oxygen donors and the $CpPPh_2$ centroids is a tetrahedron, whilst tungsten again shows a slightly distorted octahedral geometry (Figure 2). Only one other structure of a Ln−O≡C−W arrangement could be found in a search of the Cambridge Crystallographic Data Base, viz. $[Ce(Cp')_2(\mu\text{-}OC)_2W(CO)Cp]$ [$Cp' = C_5H_3(SiMe_3)_2$-1,3, $Cp = C_5H_5$],[27] although analogous molybdenum complexes are more numerous and include Mo−C≡O−Yb-bonded systems.[28−31]

Whilst complex **1** is molecular, complex **2** shows a one-dimensional chain structure running along [100] with neighbouring molecules connected via iso-carbonyl bridges (Figure 3). Complex **2** can therefore be described by the Niggli formula $^1_\infty[Yb(THF)(C_5H_4PPh_2)_2(\mu\text{-}OC)W(CO)_3]$.

Selected bond lengths and angles for **1** and **2** are given in Table 1. The average Yb−C distances (276 pm and 270 pm for **1** and **2** respectively) differ, as expected, for eight- and nine-coordinate Yb^{2+}.[23] In addition, the value for **2** corresponds to the average Yb−C bond length (271 pm) of eight-coordinate $[Yb(THF)_2(CpPPh_2)_2Z]\cdot thf$ {$Z = Ni(CO)_2$, $PtMe_2$}.[4] Although different methods for the calculation of ionic radii are present in the literature, subtraction of ionic radii from distances offers valuable data for comparison. Based on the values[23] for eight- and nine-coordinate Yb^{2+} the subtraction from[32,33] <Yb−C> distances gives a value of 156 pm, which is similar to values for analogous bimetallic complexes.[4] The attached $CpPPh_2$ ligands in **1** show a slight tilt associated with a difference in Yb−C distances of

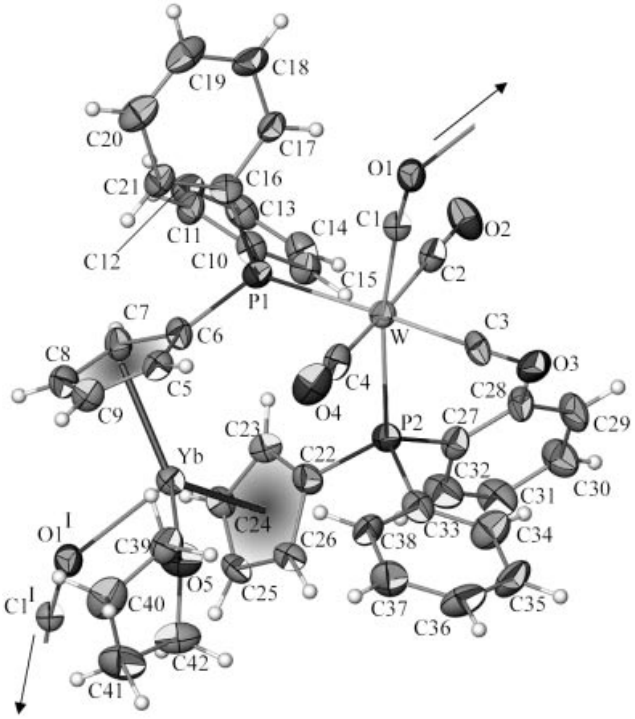

Figure 2. The molecular structure of $^{1}_{\infty}$[Yb(THF)($C_5H_4PPh_2$)$_2$(μ-OC)W(CO)$_3$] (**2**); η^5-interactions between Yb and Cp are represented by bonds towards centroids of shaded Cp rings; the *iso*-carbonyl-bridging to a neighbouring molecule is indicated by arrows

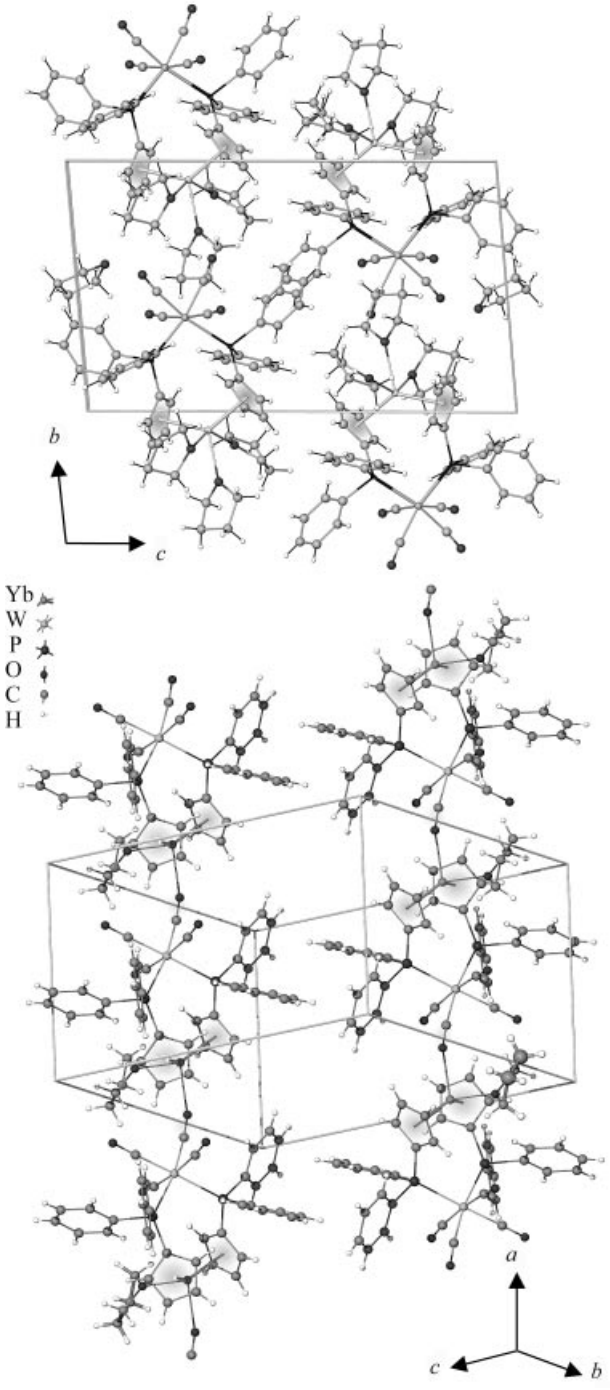

Figure 3. The crystal structures of [Yb(THF)$_3$($C_5H_4PPh_2$)$_2$-W(CO)$_4$]·0.5THF (**1**, above) and [Yb(THF)($C_5H_4PPh_2$)$_2$(μ-OC)W(CO)$_3$] (**2**, below); the unit cells are shown; whilst **1** is a packing of isolated molecules, **2** is a packing of infinite chains of molecules connected via *iso*-carbonyl bridges underlain in light grey

only 12 pm. Thus, there is no significant trend towards η^3-attachment, as subtraction of the ionic radius from the longest Yb−C distance gives a normal value[32,33] of 162 pm. The Ln−C distance variation is much less than that of [Er(η^5-CpPPh$_2$)$_3$(OPPh$_3$)].[7] The Yb−O(THF) distance of **2** corresponds well with those of [Yb(THF)$_2$(CpPPh$_2$)$_2$Ni(CO)$_2$] [242.4(4), 242.9(4) pm][4] and is marginally longer than <Yb−O> of the PtMe$_2$ analog (240 pm).[4] On the other hand the Yb−O distances of **1** show a wide variation. One is as short as that of eight-coordinate **2**, and two are much longer so that the average (253 pm) exceeds the value for **2** by more than the expected amount for the coordination number variation. As the shortest distance, Yb−O(6), is for the ligand that is apical in the Yb(cent)$_2$O$_3$ square pyramid (as best-fit polyhedron) whilst the other two THF ligands are *transoid* to each other, a *trans* influence may be invoked for the lengthening of Yb−O(5,7). Such influences are now well established in lanthanoid chemistry despite the ionic nature of the bonding.[34−37] Subtraction of an appropriate Yb^{2+} ionic radius from the Yb−O distances gives a value of 130 pm for **2**, which is at the short end of the range 134 ± 5 pm for ether complexes of organolanthanoids,[38] whilst the longer Yb−O distances of **1** give a value of 138−141 pm, which is at the higher end and greater than the expected ionic radius difference of about 6 pm due to the variation in coordination number. In contrast the shortest Yb−O distance of **1** gives a value of 124 pm, which is well below the normal range, reflecting the absence of any ligand *transoid* to oxygen. In addition, the CpPPh$_2$ ligand is electron withdrawing[24] and is known to cause bond-shortening upon attachment of coligands.[7] Unfortunately the precision of the [Sm(ind)$_2$(THF)$_3$] structure determination[22] is insufficient to be able to compare the Sm−O bond lengths with the present Yb−O bond lengths. Thus **1** provides currently unique data. The Yb−O(C) distances in **2** lie within the range 238−256 pm reported for recent *iso*-carbonyl-bonded ytterbium complexes[30,31,39−41] (cf. 225 pm for ytterbium(III) in two earlier structures[1,2]).

Table 1. Selected distances (pm) and angles(°) for $[Yb(THF)_3(CpPPh_2)_2W(CO)_4]\cdot 0.5THF$ (**1**) and $[Yb(THF)(CpPPh_2)_2(\mu\text{-}OC)W(CO)_3]$ (**2**); standard deviations are given in brackets

$[Yb(THF)_3(CpPPh_2)_2W(CO)_4]\cdot 0.5THF$ (**1**)			
Yb−C [range C(22−26)]	270.4(4)−282.2(4)	W−P(2)	256.3(1)
Yb−C [range C(5−9)]	271.6(4)−280.7(4)	W−P(1)	256.7(1)
Yb−C [average C(22−26)]	276.2(4)	W−C(3)	197.5(4)
Yb−C [average C(5−9)]	276.3(4)	W−C(1)	198.5(4)
Yb−O(6)	243.0(3)	W−C(4)	202.3(4)
Yb−O(5)	258.4(3)	W−C(2)	203.8(4)
Yb−O(7)	261.0(3)	P(1)−C(range)	180.7(4)−184.4(4)
Yb−W	534.0(2)	P(2)−C(range)	179.1(4)−185.1(4)
C−O (carbonyl, range)	114.6(5)−115.3(4)		
cent(1)−Yb-cent(2) [a]	130.1	P(1)−W−P(2)	98.31(3)
cent(1)−Yb−O(5)	99.0	P(1)−W−C(1)	91.1(2)
cent(1)−Yb−O(7)	95.0	P(1)−W−C(2)	101.9(2)
cent(1)−Yb−O(6)	117.1	P(2)−W−C(2)	83.0(2)
cent(2)−Yb−O(7) [b]	100.6	P(2)−W−C(3)	88.8(2)
cent(2)−Yb−O(5)	95.0	P(1)−W−C(4)	80.6(1)
cent(2)−Yb−O(6)	112.9	P(2)−W−C(4)	102.6(2)
O(5)−Yb−O(6)	73.30(9)	P(1)−W−C(3)	165.5(2)
O(5)−Yb−O(7)	144.47(8)	P(2)−W−C(2)	167.8(2)
O(6)−Yb−O(7)	71.24(9)	W−C(1)−O(1)	173.8(4)
C(2)−W−C(4)	174.1(2)	W−C(3)−O(3)	173.9(3)
		W−C(2)−O(2)	175.5(4)
$[Yb(THF)(CpPPh_2)_2(\mu\text{-}OC)\ W(CO)_3]$ (**2**)			
Yb−C [range C(5−9)]	268(2)−273(2)	W−P(1)	258.0(4)
Yb−C [range C(22−26)]	268(2)−273(2)	W−P(2)	259.4(4)
Yb−C [average C(5−9)]	270(2)	W−C(1)	199(1)
Yb−C [average C(22−26)]	270(2)	W−C(3)	201(2)
Yb−O(5)	244.1(9)	W−C(4)	203(2)
$Yb-O(1)^{I}$ [c]	248(1)	W−C(2)	204(2)
Yb−W	506.0(6)	P(1)−C(range)	181(2)−185(2)
$Yb^{II}-W$ [d]	525.5(6)	P(2)−C(range)	178(2)−188(2)
C−O(carbonyl, range)	113(2)−116(2)	O(1)−C(1)	113(2)
cent(1)−Yb-cent(2)	131.3	P(1)−W−P(2)	95.5(1)
$cent(1)-Yb-O(1)^{I}$ [c]	108.8	P(1)−W−C(1)	94.8(4)
cent(1)−Yb−O(5)	108.6	P(1)−W−C(2)	89.7(4)
$cent(2)-Yb-O(1)^{I}$ [c]	102.4	P(2)−W−C(2)	94.6(4)
cent(2)−Yb−O(5)	110.1	P(2)−W−C(3)	83.7(4)
$O(1)^{I}-Yb-O(5)$ [c]	85.8(3)	P(1)−W−C(4)	92.1(4)
C(2)−W−C(4)	173.0(5)	P(2)−W−C(4)	91.9(4)
W−C(2)−O(2)	173(2)	P(2)−W−C(1)	169.6(4)
W−C(3)−O(3)	178(2)	P(1)−W−C(3)	177.4(4)
$W-C(1)-O(1)-Yb^{II}$ [d]	143(2)	$Yb^{II}-O(1)-C(1)$ [d]	143.0(9)

[a] cent1 = centroid of the $CpPPh_2$ rings with the C atoms C(5)−C(9). [b] cent2 = centroid of the $CpPPh_2$ rings with the C atoms C(22)−C(26). [c] I: $x-1, y, z$. [d] II: $x+1, y, z$.

The coordination sphere around tungsten shows the expected features. Opening of the P−W−P angles of **1** and **2** by up to 12° from the normal value of 90° in response to the bulky substituents on phosphorus parallels a similar behavior in recently reported $WP_2(CO)_4$ complexes,[42−44] but is less than the 18.35° observed with bulky *cis*-PPh_2(*o*-Me-OC_6H_4) ligands.[42] On the other hand the W−P distances are close to those (256, 257 pm) with this bulky phosphane, and larger than those (247, 251 pm) of the less crowded [*cis*-$W(CO)_4(Ph_2PH)_2$].[43] Although the shorter W−C bonds in both **1** and **2** are located *trans* to phosphorus, consistent with a greater *trans* influence of CO than R_3P in W^0 complexes,[45] the differences are within a three esd range and hence are of limited significance. Coordination of the carbonyl group to Yb in **2** has no significant effect within error limits on the W−C bond lengths or W−C−O angles (Table 1), in contrast to $[Ce(Cp')_2(\mu\text{-}CO)_2WCp(CO)_2]$ [Cp′ = $C_5H_3(SiMe_3)_2$-1,3, Cp = C_5H_5] for which $W-C-O_{ter}$ is bent relative to near linear $W-C-O_{br}$.[27] The Yb−O−C angle is at the lower end for *iso*-carbonylytterbium complexes and is close to that of $[Yb(NCMe)_3(\mu\text{-}CO)_3Fe(CO)]_n$ (145.75°)[38] and quite different from the Ce−O−C angles (174.8, 154.4°) of $[Ce(Cp')_2(\mu\text{-}CO)_2WCp(CO)_2]$ [Cp′ = $C_5H_3(SiMe_3)_2$-1,3, Cp = C_5H_5].[27] Overall the W−C distances (bridging or terminal) of the cerium complex are much shorter than those of **1** and **2**,

consistent with a weaker trans influence of Cp than R_3P or CO in W^0 complexes.[45]

Conclusions

Observation of nine-coordinate ytterbium in $[Yb(THF)_3(CpPPh_2)_2W(CO)_4]\cdot 0.5THF$ (**1**) is a major surprise in view of the ubiquitous nature of eight-coordinate $[Yb(THF)_2(Cp')_2]$ complexes[19−21] and the presence of eight-coordinate Yb in $[Yb(THF)_2(CpPPh_2)_2PtMe_2]\cdot THF$ and $[Yb(THF)_2(CpPPh_2)_2Ni(CO)_2]$.[4] Accordingly, the proposal[4] that the analytically similar $[Yb(THF)_2(CpPPh_2)_2Mo(CO)_4]\cdot THF$ contains eight-coordinate $Yb(THF)_2(CpPPh_2)_2$ units may be questioned and it is likely that this complex also contains nine-coordinate $Yb(THF)_3(CpPPh_2)_2$ moieties. A single-crystal structure determination is therefore desirable. The only prior example of a nine-coordinate $[Ln(THF)_3(Cp')_2]$ complex, $[Sm(ind)_2(THF)_3]$,[22] is also unexpected given the bulky indenyl ligands, although lack of bond length data frustrates examination of possible slippage towards η^3 coordination

On the other hand, the structure of **2** with the *iso*-carbonyl−Yb linkage provides validation of the proposal of similar bonding in $[Yb(THF)(CpPPh_2)_2Mo(CO)_4]\cdot PhMe$ and indeed in $[Yb(THF)(CpPPh_2)_2Ni(CO)_2]$.[4] Accordingly, the structures of **1** and **2** are of strategic importance in understanding the behavior of $Yb(CpPPh_2)_2$ derived bimetallic complexes.

Experimental Section

All reactions were carried out under dry nitrogen using dry box and standard Schlenk techniques due to the air- and moisture-sensitivity of **1** and **2**. Solvents were dried by distillation from sodium wire/benzophenone. IR data (4000−650 cm^{-1}) were recorded either for Nujol mulls sandwiched between NaCl plates or as THF or PhMe solutions in a solution cell with AgBr plates using a Perkin−Elmer 1600 Fourier transform infrared spectrometer. NMR spectra were obtained on a Bruker AC300 instrument. ^{31}P spectra are referenced to external 85% H_3PO_4. Deuterated solvents were degassed and distilled from Na/K alloy prior to use. $W(CO)_6$ was purchased from Aldrich and used as received whilst $[Yb(THF)(CpPPh_2)_2]$ was prepared according to the literature procedure.[3]

$[Yb(THF)_3(CpPPh_2)_2W(CO)_4]\cdot 0.5THF$ (1): A Schlenk flask was charged with $W(CO)_6$ (1.2 mmol), $[Yb(THF)(CpPPh_2)_2]$ (0.7 mmol) and THF (40 mL) giving an intense dark red solution. The reaction mixture was stirred and heated to 60 °C for 48 h and then stirred for a further 48 h at room temperature. Hexane was added until a permanent precipitate formed. Upon heating, the solid re-dissolved and slow cooling to −20 °C gave dark red crystals of **1** and some colorless crystals of $W(CO)_6$. Subsequent warming to room temperature dissolved the colorless material and the remaining red crystals were collected by filtration and dried under vacuum at room temperature for 1 h to give a yield of 0.3 g (45%). Rapid decomposition outside the mother liquor, however, made it preferable to collect the product from solution. IR (Nujol): $\tilde{\nu}$ = 2005vs, 1894vs, 1872vs, 1849vs [all ν(CO)], 1570w, 1440s, 1204w, 1177m, 1153w, 1087m, 1045s, 1031s, 917w, 881m, 742m, 695m; (THF) ν(CO): 2015s, 1914s, 1893s, 1880sh, (PhMe) ν(CO) 2015s, 1917s, 1892s(br), 1868sh cm^{-1}. ^1H NMR (300 MHz, $[D_8]$THF): δ = 5.93 (br s, 4 H, β-C_5H_4), 6.17 (br s, 4 H, α-C_5H_4,), 7.37 [br s, 12 H, *m*-,*p*-*H*(Ph)], 7.59 [br s, 8 H, *o*-*H*(Ph)] ppm. $^{31}P\{^1H\}$ NMR (121.5 MHz, $[D_8]$THF): δ = 9.67 ($^1J_{W,P}$ = 237 Hz); (C_6D_6): 9.00 ($^1J_{W,P}$ = 232 Hz) ppm.

$[Yb(THF)(CpPPh_2)_2(\mu\text{-}OC)W(CO)_5]$ (2): (a) A glass ampoule was charged with $W(CO)_6$ (0.14 mmol), $[Yb(THF/DME)(CpPPh_2)_2]$ (0.14 mmol), and PhMe (1.5 mL) and then degassed and sealed under vacuum. Heating at 130 °C for 127 h gave a dark red solution. Upon cooling, very dark red crystals of **2** deposited, together with $W(CO)_6$ and some green crystals which disappeared on subsequent heating. Several of the dark red crystals were mounted for X-ray crystallography. The remaining material decomposed within hours in the inert drybox atmosphere also indicating instability outside the mother liquor.

(b) Red crystals of **1** were washed with successive amounts of PhMe (3 × 5 mL) until the washings were colorless. The remaining dark colored powder was dried under vacuum at room temperature for 1 h. IR (Nujol): $\tilde{\nu}$ = 2016vs, 1910vs, 1883vs [all $\nu(CO)_{ter}$], 1758vs [$\nu(CO)_{br}$], 1305w, 1177m, 1156w, 1085m, 1036s, 1027m, 894w, 756s, 737s, 694s, cm^{-1}.

X-ray Crystal Structure Determination: The data collection for single crystal X-ray determination of **1** was carried out on a κ-CCD diffractometer (Enraf Nonius), and the data collection for **2** on an IPDS-I diffractometer (STOE). Structure solution: SHELXS-86;[46] structure refinement: SHELXL-97.[47] Integrity of symmetry and geometry: PLATON.[48] All non-hydrogen atoms were refined anisotropically. Some hydrogen atoms of **1** were deduced from the Fourier map while most hydrogen atoms were placed in calculated positions and assigned to an isotropic displacement parameter of 1.2-times the size of the isotropic displacement parameter of the parent carbon atom. Two THF molecules of **1** show a split position of the carbon atom opposite to the oxygen atom of the THF rings in a ratio of about 2:1. In addition the free THF molecule is split by centers of symmetry.

Crystallographic Data for $C_{52}H_{56}O_{7.5}P_2WYb$ (1): Triclinic, $P\bar{1}$, Z = 2, T = 123(2) K, a = 1024.76(1) pm, b = 1255.72(1) pm, c = 2054.38(3) pm, α = 89.154(1)°, β = 75.803(1)°, γ = 68.069(1)°, V = 2368.7(5)·10^6 pm^3, μ = 45.1 cm^{-1}, Mo-K_α, 5.16 ≤ 2θ ≤ 56.56°, −13 ≤ h ≤ 13, −16 ≤ k ≤ 16, −24 ≤ l ≤ 27, F(000) = 1204, R_1 = 0.0340 for 9407 reflections [$I > 2\sigma(I)$], R_1 = 0.0482 and wR_2 = 0.0805 for 11547 unique reflections, GOOF on F^2 = 1.042.

Crystallographic Data for $C_{42}H_{36}O_5PWYb$ (2): Triclinic, $P\bar{1}$, Z = 2, T = 170(1) K, a = 1008.2(4) pm, b = 1195.0(5) pm, c = 1750.4(8) pm, α = 105.06(5)°, β = 97.98(5)°, γ = 106.18(5)°, V = 1904(2)·10^6 pm^3, μ = 55.9 cm^{-1}, Mo-K_α, 4.46 ≤ 2θ ≤ 50.0°, −11 ≤ h ≤ 11, −14 ≤ k ≤ 14, −20 ≤ l ≤ 20, F(000) = 1004, R_1 = 0.0564 for 3960 reflections [$I > 2\sigma(I)$], R_1 = 0.0868 and wR_2 = 0.1399 for 6299 unique reflections, GOOF on F^2 = 0.924. CCDC-177663 (**1**) and CCDC-177664 (**2**) contain the supplementary crystallographic data for this paper. These data can be obtained free of charge at www.ccdc.cam.ac.uk/conts/retrieving.html [or from the Cambridge Crystallographic Data Center, 12, Union Road, Cambridge CB2 1EZ, UK; Fax: (internat.) +44−1223/336−033; E-mail: deposit@ccdc.cam.ac.uk].

Acknowledgments

We are grateful to the Deutsche Forschungsgemeinschaft and the Australian Research Council for support.

[1] T. D. Tilley, R. A. Andersen, *J. Chem. Soc., Chem. Commun.* **1981**, 985−986.
[2] T. D. Tilley, R. A. Andersen, *J. Am. Chem. Soc.* **1982**, *104*, 1772−1774.
[3] G. B. Deacon, A. Dietrich, C. M. Forsyth, H. Schumann, *Angew. Chem. Int. Ed. Engl.* **1989**, *28*, 1370−1371.
[4] G. B. Deacon, C. M. Forsyth, W. C. Patalinghug, A. H. White, A. Dietrich, H. Schumann, *Aust. J. Chem.* **1992**, *45*, 567−582.
[5] G. Y. Lin, T. W. Wong, *J. Organomet. Chem.* **1996**, *523*, 93−98.
[6] G. Y. Lin, T. W. Wong, *J. Organomet. Chem.* **1995**, *495*, 203−208.
[7] G. B. Deacon, C. M. Forsyth, B. M. Gatehouse, A. Philosof, B. W. Skelton, A. H. White, P. A. White, *Aust. J. Chem.* **1997**, *50*, 959−970.
[8] G. B. Deacon, G. D. Fallon, C. M. Forsyth, *J. Organomet. Chem.* **1993**, *462*, 183−190.
[9] R. Broussier, G. Dolmas, P. Perron, B. Gautheron, J. L. Peterson, *J. Organomet. Chem.* **1995**, *511*, 185−192.
[10] G. B. Deacon, G. D. Fallon, B. M. Gatehouse, A. Rabinovich, B. W. Skelton, A. H. White, *J. Organomet. Chem.* **1995**, *501*, 23−30.
[11] H. Schumann, J. A. Meese-Merkschaftel, B. Gorella, F. H. Gorlitz, *J. Organomet. Chem.* **1992**, *428*, C27−C32.
[12] M. Visseaux, A. Dormond, M. M. Kibicki, C. Moise, *J. Organomet. Chem.* **1992**, *433*, 95−106.
[13] G. Y. Lin, T. W. Wong, *Polyhedron* **1995**, *14*, 3167.
[14] G. Y. Lin, T. W. Wong, *Polyhedron* **1994**, *13*, 3027.
[15] G. Lin, R. McDonald, J. Takats, *J. Organomet. Chem.* **2000**, *626*, 76−81.
[16] P. Desmurs, M. Visseaux, D. Baudry, A. Dormond, F. Nief, L. Ricard, *Organometallics* **1996**, *15*, 4178−4181.
[17] P*hosphorus-31 NMR Spectroscopy in Stereochemical Analysis-Organic Compounds and Metal Complexes* (Eds.: J. G. Verkade, L. D. Quin), VCH, Florida, **1987**.
[18] B. Granger, *Handbook of High Resolution Multinuclear NMR*, Wiley, New York, **1981**.
[19] *Organoderivatives of the Rare Earth Elements* (Eds.: M. N. Bochkarev, L. N. Zakharov, G. S. Kalinina), Kluwer, Dordrecht, **1995**.
[20] F. T. Edelmann, in *Comprehensive Organometallic Chemistry II*, Vol. 4 (Eds.: E. W. Abel, F. G. A. Stone, G. Wilkinson), Pergamon, Oxford, **1995**, p. Ch. 3.
[21] H. Schumann, J. A. Meese-Merkschaftel, L. Esser, *Chem. Rev.* **1995**, *95*, 865−986.
[22] W. J. Evans, T. S. Gummersheimer, T. J. Boyle, J. W. Ziller, *Organometallics* **1994**, *13*, 1281−1284.
[23] R. D. Shannon, *Acta Crystallogr., Sect. A* **1976**, *32*, 751−767.
[24] D. L. Du Bois, C. W. Eigenbrot, A. Miedaner, J. C. Smart, R. C. Haltiwanger, *Organometallics* **1986**, *5*, 1405−1411.
[25] M. Johnson, J. C. Taylor, C. W. Cox, *J. Appl. Crystallogr.* **1980**, *13*, 188.
[26] A. Schmuck, K. Seppelt, *Chem. Ber.* **1989**, *122*, 803−808.
[27] P. N. Hazin, J. C. Huffman, J. W. Bruno, *J. Chem. Soc., Chem. Commun.* **1988**, 1473−1474.
[28] A. A. Pasynskii, I. L. Eremenko, G. Z. Suleimanov, Y. A. Nuriev, I. P. Beletskaya, V. E. Shklover, Y. T. Struchkov, *J. Organomet. Chem.* **1984**, *266*, 45−52.
[29] G. Y. Lin, T. W. Wong, *J. Organomet. Chem.* **1996**, *522*, 271−275.
[30] Z. Hou, K. Aida, Y. Takagi, Y. Wakatsuki, *J. Organomet. Chem.* **1994**, *473*, 101−104.
[31] A. C. Hillier, A. Sella, M. R. J. Elsegood, *J. Chem. Soc., Dalton Trans.* **1998**, 3871−3874.
[32] K. N. Raymond, C. W. Eigenbrot, *Acc. Chem. Res.* **1980**, *13*, 276−286.
[33] S. C. Sockwell, T. P. Hanusa, *Inorg. Chem.* **1990**, *29*, 76−80.
[34] G. B. Deacon, B. M. Gatehouse, Q. Shen, G. Ward, E. R. T. Tiekink, *Polyhedron* **1993**, *12*, 1289−1294.
[35] J. E. Cosgriff, G. B. Deacon, B. M. Gatehouse, *Aust. J. Chem.* **1993**, *46*, 1881−1896.
[36] G. B. Deacon, T. Feng, B. W. Skelton, A. H. White, *Aust. J. Chem.* **1995**, *48*, 741−756.
[37] G. W. Rabe, C. S. Strissel, L. M. Liable-Sands, T. E. Concdino, A. L. Rheingold, *Inorg. Chem.* **1999**, *38*, 3446−3447.
[38] G. B. Deacon, P. I. MacKinnon, T. W. Hambley, J. C. Taylor, *J. Organomet. Chem.* **1983**, *259*, 91−97.
[39] H. Deng, S.-H. Chun, P. Floriani, P. J. G. Grandinetti, S. G. Shore, *Inorg. Chem.* **1996**, *35*, 389.
[40] D. Deng, X. Zheng, C. Qian, J. Sun, A. Dormond, D. Baudry, M. Visseaux, *J. Chem. Soc., Dalton Trans.* **1994**, 1665−1669.
[41] H. Deng, S.-H. Chun, P. Floriani, P. J. G. Grandinetti, S. G. Shore, *Inorg. Chem.* **1996**, *35*, 3891−3896.
[42] L. Hirsivaara, L. Guerricabeitia, M. Haukka, P. Suomalainen, R. H. Laitnen, T. A. Pakkanen, J. Pursianen, *Inorg. Chim. Acta* **2000**, *307*, 47−56.
[43] T. Campbell, A. M. Gibson, R. Hart, S. D. Orchard, S. J. A. Pope, G. Reid, *J. Organomet. Chem.* **1999**, *592*, 296−305.
[44] M. J. M. Vlaar, F. J. J. de Kanter, M. Schakel, M. Lutz, A. Spek, K. Lammertsma, *J. Organomet. Chem.* **2001**, *617*, 311−618.
[45] W. Buchner, W. A. Schenk, *Inorg. Chem.* **1984**, *23*, 132−137.
[46] G. M. Sheldrick, SHELXS-86, *Program for the resolution of crystal structures*; Göttingen **1986**.
[47] G. M. Sheldrick, SHELXL-97, *Program for the refinement of crystal structures*; Göttingen **1997**.
[48] A. L. Spek, PLATON-98, *A Multipurpose Crystallographic Tool*; Utrecht **1998**.

Received May 8, 2002
[I02239]

Variety in the Coordination Modes of the Ligand Hexakis(pyrazol-1-yl)benzene (Hpzb) to Pd^{II}, Pt^{II} and Cu^{I} Centres

Ana M. Guerrero,[a] Félix A. Jalón,*[a] Blanca R. Manzano,[a] Rosa M. Claramunt,[b] María Dolores Santa María,[b] Consuelo Escolástico,[b] José Elguero,[c] Ana M. Rodríguez,[d] Miguel A. Maestro,[e] and José Mahía[e]

Keywords: N ligands / Conformational analysis / Palladium / Platinum / Copper / Coordination chemistry

The structure and conformational analysis of eight complexes derived from hexakis(pyrazol-1-yl)benzene (hpzb) have been carried out by means of X-ray crystallography and NMR spectroscopy. The metallic fragments [$Pd(C_6F_5)_2$, [$Pd(\eta^3$-2-Me-$C_3H_4)]^+$, $PtCl_2$ and $Cu(PMe_3)^+$] coordinate with two adjacent pyrazole residues yielding complexes with one, two or three metallic centres. The crystal and molecular structures of [{$Pd(C_6F_5)_2$}$_2$(hpzb)], [{$Pd(\eta^3$-$C_4H_7)$}$_2$-(hpzb)]$(TfO)_2$, [{$Cu(PMe_3)$}$_2$(hpzb)]$(BF_4)_2$ and [{$Pd(\eta^3$-$C_4H_7)$}$_3$(hpzb)]$(TfO)_3$ have been determined. The structure of each of the complexes depends on the fact that the metal atoms, when two or three are present, prefer to be situated on opposite faces of the benzene ring. Evidence for restricted rotation of the uncoordinated pyrazolyl groups has been found for the free ligand and monometallic derivatives, while free rotation of these groups at room temperature has been observed for the dimetallic complexes. Furthermore, the derivative {[$Cu(PMe_3)]_2$(hpzb)}$(BF_4)_2$ and probably [{$Pd(\eta^3$-$C_4H_7)$}$_2$(hpzb)]$(TfO)_2$ exhibit metallotropy on the NMR time scale.
(© Wiley-VCH Verlag GmbH, 69451 Weinheim, Germany, 2002)

Introduction

The use of *N*-substituted pyrazoles as ligands is very common, with the three main types of derivatives being polypyrazolylborates (scorpionates), polypyrazolylmethanes **A** and polypyrazolylazines (pyridines, pyrimidines, *s*-triazines, etc.). On the other hand, polypyrazolylbenzenes have seldom been used if one excludes the (pyrazol-1-ylmethyl) derivatives **B** (“coelenterands”),[1−17] which have structures intermediate between pyrazolylalkanes and (pyrazol-1-yl)benzenes **C** (Scheme 1).

Only five ligands derived from **C** have been used in coordination chemistry: **D**,[18] **E**,[19] **F**,[20] **G** [21] and **H** [22−23] (Scheme 2). However, hexakis(pyrazol-1-yl)benzene (hpzb, **1**), which belongs to the “propellene” class of ligands that we have studied systematically,[24−29] has never previously been used.

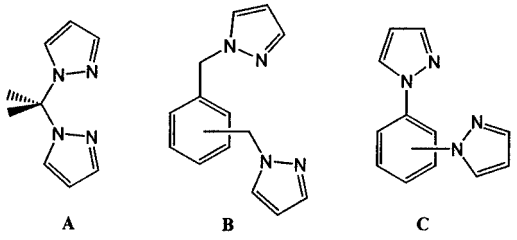

Scheme 1

In this paper, we will discuss the coordination chemistry of **1** (hpzb) to different metal atoms with two vacant coordination sites with special emphasis on its conformational aspects. Compound **1**, like other biphenyl-like compounds, has two rotational barriers: the planar barrier, due to steric effects, and the perpendicular one, due to the loss of conjugation. In propellenes the first barrier is much larger than the second one. Therefore, these compounds can be described as having the six azolyl residues librating about the perpendicular conformations, either (*P*) or (*M*) [plus (*P*) or minus (*M*) refers to the sense of rotation, clockwise or counterclockwise, with respect to a perpendicular orientation of the pyrazole and the benzene ring]. We are interested in determining whether in solution, not only in the free ligand but also in the complexes having non-coordinated pyrazolyl groups, free or restricted rotation of these rings exists. Concerning the metallic complexes we were also inter-

[a] Departamento de Química Inorgánica, Orgánica y Bioquímica, Universidad de Castilla-La Mancha, Facultad de Químicas, Avda. Camilo J. Cela, 10, 13071 Ciudad Real, Spain
Fax: (internat) + 34-926/295318
[b] Departamento de Química Orgánica y Biología, Facultad de Ciencias, UNED, Senda del Rey, 9, 28040 Madrid, Spain
[c] Instituto de Química Médica, CSIC, Juan de la Cierva, 3, 28006 Madrid, Spain
[d] Departamento de Química Inorgánica, Orgánica y Bioquímica, Universidad de Castilla-La Mancha, E. T. S. de Ingenieros Industriales, Avda. Camilo J. Cela, s/n, 13071 Ciudad Real, Spain
[e] Servicios Xerais de Apoio á Investigación, Universidad de A Coruña, Campus de A. Zapateira, 15071 A Coruña, Spain

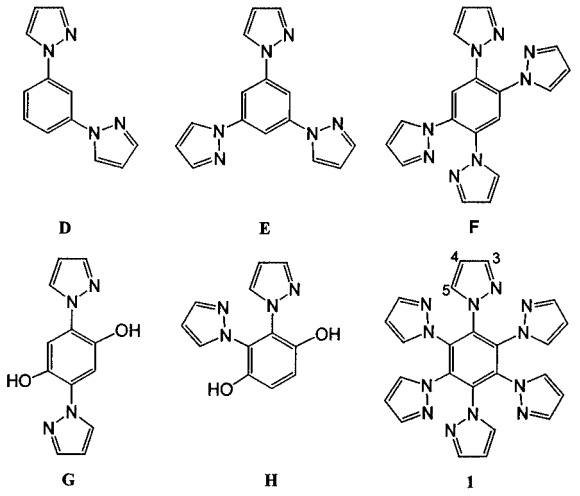

Scheme 2

ested in studying the following points: i) The number of metal atoms that is possible to introduce for each hpzb ligand. ii) The disposition of these metal atoms around the six pyrazolyl groups. For example, it was of interest to determine the possibility of having two or more metal atoms at the same side of the benzene plane or two metal atoms bonded to two contiguous pyrazolyl rings. It was foreseeable that the steric requirements of the metallic fragment considering the size and orientation of the ancillary ligands could play an important role in these two points. iii) The presence of fluxional behaviour due to metallotropic shifts and the factors that influence it. iv) Where possible, we also have an interest in analysing the solid-state structure. Interesting points concerning this aspect could be: similarity between complexes of different metals, cooperativity in the orientation of the pyrazolyl groups and correspondence between the solid-state and solution structures. We chose different fragments with late transition metals: $Pd(C_6F_5)_2$, $PtCl_2$, $[Pd(\eta^3\text{-}2\text{-}Me\text{-}C_3H_4)]^+$, and Cu^+/PMe_3. The first two examples with different metals and ancillary ligands of different size were supposed to exhibit a typical square-planar coordination. The allyl fragment had a different orientation of this group that could reduce the symmetry of the derivatives obtained increasing the number of possible isomers. The copper centre was chosen to analyse a case with a different metallic geometry (tetrahedral or trigonal-planar were open possibilities).

Results and Discussion

Conformational Analysis

Before describing the synthesis and characterisation of the new derivatives it would be useful to analyse the different isomers that could exist for the ligand and the mono-, di- and trinuclear complexes depending on the relative orientation of the metallic fragments and the uncoordinated pyrazolyl rings.

In derivative **1**, and according to our previous discussion, each pyrazol-1-yl group can adopt two perpendicular conformations depending on whether the N-2 lone pair is *up* (*u*, black dot) or *down* (*d*, white dot). This situation results in the eight isomers **Ia**−**Ih**, neglecting enantiomerism (**Ic** is chiral), which we have represented at the top of Scheme 3. The hpzb ligand exists in the solid state in two conformations (polymorphism) − *ududud* (**Ia**) and *udduud* (**Ic**).[25] According to AM1 and SAM calculations, these conformations have torsion angles close to 90°, with the most stable conformer being **Ia** followed, at about 9 kJ mol^{-1} higher, by **Ib**, **Ic** and **Id**, all of which have the same energy.[28]

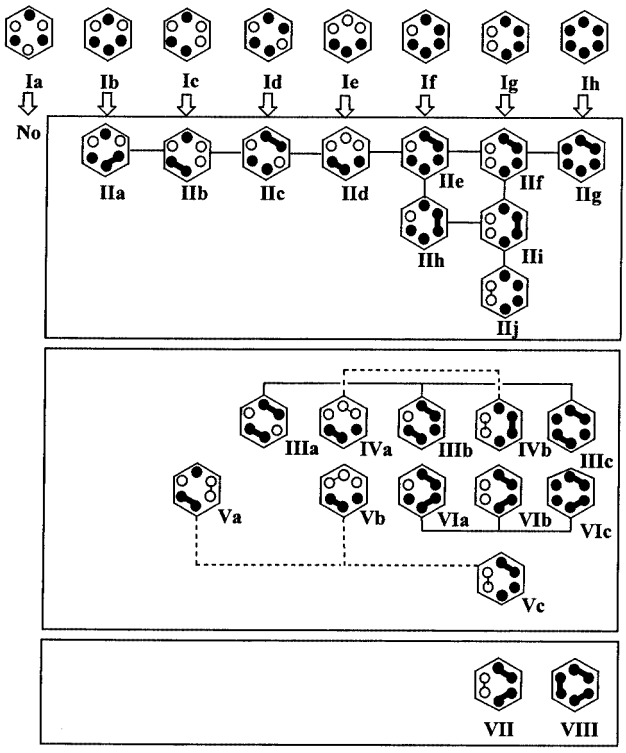

Scheme 3. Conformational description of ligand **1** and all possible mono- di- and trimetallic derivatives

The main difficulty concerning the conformation of **1** and its bidentate chelate complexes is to decide between a fixed *up-down* conformation and a free-rotating situation. If we represent a free-rotating pyrazole with a grey dot, we obtain the situation depicted in Scheme 4. In both Schemes we suppose that the metallic fragment does not reduce the symmetry of the complex. It should be noted, however, that free rotation does not signify that all conformations are equally populated. The classifications shown in Scheme 4 are only rigorously true when the *up* and *down* conformations have the same energy.

The formation of a bidentate chelate complex κ^2-*N*1*N*2-hpzb (**II**) is not possible for conformation **Ia** but is feasible for all the others, which are related by *u*/*d* rotations of the uncoordinated pyrazol-1-yl residues (ten conformers **IIa**−**IIj**). The formation of a second chelation could lead to four different isomers, **III**−**VI**, two with κ^4-*N*1*N*2,*N*4*N*5-

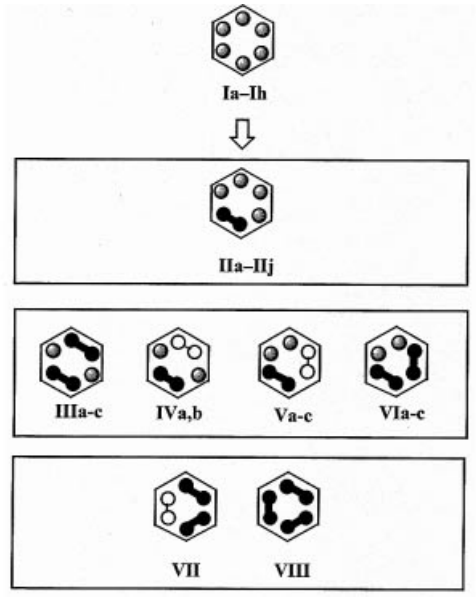

Scheme 4. Conformational description of ligand **1** and all possible mono-, di- and trimetallic derivatives assuming free rotation of the uncoordinated pyrazoles

hpzb coordination (three conformers **IIIa**−**IIIc** and two conformers **IVa**, **IVb**) and two with κ⁴-*N*1*N*2,*N*3*N*4-hpzb coordination (three conformers **Va**−**Vc** and three conformers **VIa**−**VIc**). Finally, the third and final chelation could lead to only two isomers κ⁶-*N*1*N*2,*N*3*N*4*N*5*N*6-hpzb (**VII** and **VIII**) without any rotational freedom (they are identical in Schemes 3 and 4).

Synthesis of Complexes

In order to follow the discussion more easily we have included the molecular structures of the new complexes in Scheme 5.

(a) Pd Complexes 2, 4, 5, 7 and 9

The reaction between hpzb and $[Pd(C_6F_5)_2(cod)]$ led to a mixture of three compounds whose relative proportions depended on the stoichiometry used:

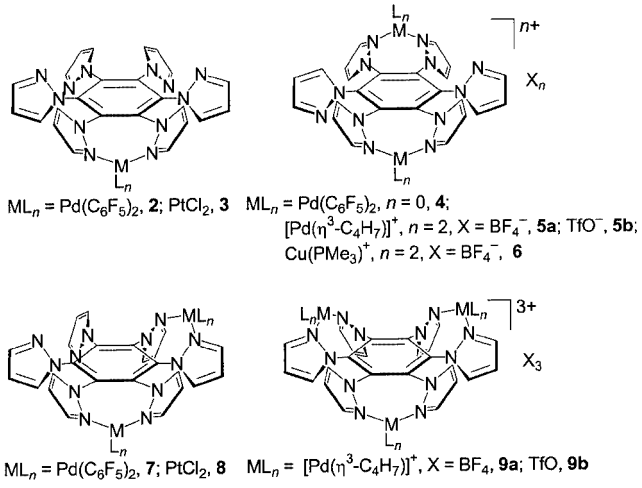

Scheme 5

1 hpzb + 0.5 $[Pd(C_6F_5)_2(cod)]$ → **2** + hpzb

1 hpzb + 1 or 2 $[Pd(C_6F_5)_2(cod)]$→ **2** + **4** + **7**

1 hpzb + 3 or 6 $[Pd(C_6F_5)_2(cod)]$ → **4** + **7**

When **4** and **7** are present in a reaction mixture, their relative ratio is near 50:50. The reaction corresponding to a 1:6 stoichiometry was only carried out in an NMR tube and the attempt to obtain a compound with three Pd centres (analogous to **9**) failed. In order to increase the yield of **2** we used a ratio of 1:0.5. Although **2** was the only metallic complex formed in this reaction we were not able to obtain it in a pure form because it was partially transformed into **4** and **7** in the crystallisation process. Compound **4** (previously separated by crystallisation) was dissolved in $(CD_3)_2CO$ and its ^1H NMR spectrum showed an approximately 50:50 mixture of **4** and **7**. This important result shows that structures of type κ⁴-*N*1*N*2,*N*4*N*5-hpzb (**IV**) and κ⁴-*N*1*N*2,*N*3*N*4-hpzb (**V**) rapidly equilibrate in solution.

On the other hand, the reactions with $[Pd(\eta^3\text{-}C_4H_7)(THF)_2]TfO$ or $[Pd(\eta^3\text{-}C_4H_7)(cod)]BF_4$ also depend on the proportions used. In the case of the reaction with $[Pd(\eta^3\text{-}C_4H_7)(cod)]BF_4$, the use of a 1:1 or 1:0.5 stoichiometry gives rise to a solid that could not be characterised as a pure product (see below for NMR in solution). Attempts to crystallise this solid failed. The elemental analyses of the crystallised sample were intermediate between those corresponding to mononuclear and dinuclear complexes.

On using 2 or 3 equiv. of the allyl derivatives, the only isolated metallic compound was **9**, which has three palladium centres (**9a** and **9b** differ only in the counteranion: BF_4^- for **9a** and TfO^- for **9b**).

1 hpbz + 2 $[Pd(\eta^3\text{-}C_4H_7)(cod)]BF_4$ → **9a** + hpzb

1 hpbz + 2 or 3 $[Pd(\eta^3\text{-}C_4H_7)(THF)_2]TfO$ → **9b** (+ hpzb)

The crystallisation of **9b** led not only to crystals of this trinuclear compound but also to a small amount of crystals of a complex of stoichiometry $[\{Pd(\eta^3\text{-}C_4H_7)\}_2(hpzb)](TfO)_2$ (**5b**).

(b) Pt Complexes 3 and 8

The different stoichiometries used correspond to two Equations:

hpzb + 0.5 or 1 $[PtCl_2(PhCN)_2]$ → **3** + **8** + hpzb

hpzb + 2 or 3 $[PtCl_2(PhCN)_2]$ → **8**

These reactions only reach completion after two weeks at room temperature. On using shorter reaction times the benzonitrile was not completely displaced from the Pt reagent and heating produced decomposition of Pt^{II} into Pt^0. Mono- and dimetallic derivatives can be separated by chromatography, with the mononuclear complex being eluted

first. We have verified that **8** does not dissociate into **3** and $PtCl_2$ in an acetone solution.

(c) Cu Complex 6

This compound was obtained according to the following Equation:

hpzb + 2 or 3 $[Cu(NCCH_3)_4](BF_4)$ + 2 or 3 $PMe_3 \rightarrow$ **6**

The same derivative was obtained when 2 equiv. of PMe_3 per Cu^+ were used.

The new derivatives are soluble in acetone, THF, chloroform and dichloromethane but are insoluble in pentane, hexane and diethyl ether.

Mass Spectrometry

The main information obtained by this technique concerns the number of metal centres in a given complex. Thus, the MAS-FAB$^+$ spectrum of **3** shows peaks at 740 $[M]^+$, 705 $[M - Cl]^+$, 638 $[M - pz - Cl]^+$, 602 $[M - pz - 2\ Cl]^+$ and 475 $[M - (PtCl_2)]^+$. The mixture of isomers **4** and **7** did not show the molecular ion peak, only fragments at 1188 $[M - C_6F_5]^+$, 1020 $[M - 2\ (C_6F_5)]^+$ and 513 $[M - pz - Pd - 4\ (C_6F_5)]^+$. Analogously, the most significant fragments in the case of **6** are 841 $[M - BF_4]^+$, 613 $[M - 2\ BF_4 - Cu(PMe_3)]^+$ and 537 $[M - 2\ BF_4 - Cu(PMe_3) - PMe_3]^+$, and for **8**, 1006 $[M]^+$, 933 $[M - 2\ Cl - H]^+$, 740 $[M - PtCl_2]^+$, 638 $[M - pz - Pt - 3\ Cl]^+$, 602 $[M - Pt - 4\ Cl]^+$ and 475 $[M - 2\ (PtCl_2)]^+$. The trinuclear complex **9b** presents a characteristic spectrum with peaks at 1257 $[M - TfO]^+$, 947 $[M - 2\ TfO - \{Pd(\eta^3\text{-}C_4H_7)\}]^+$ and 635 $[M - 3\ TfO - 2\ \{Pd(\eta^3\text{-}C_4H_7)\}]$.

X-ray Structural Characterisation of Complexes 4, 5b, 6 and 9b

A number of problems were encountered in the NMR spectroscopic study, including the difficulty in differentiating between the coordinated and noncoordinated pyrazoles. Hence, it is appropriate to discuss the crystallographic study first.

Crystallographic and selected structural data are compiled in Tables 1 and 2, respectively. ORTEP plots of the structures are shown in Figures 1−4. The bad quality of the crystals and the failure of obtaining new crystals made it impossible to obtain an adequate refinement for **5b**. However, the data indicate unambiguously the position of the two palladium fragments.

Pd or Cu atoms are in an approximately square- or trigonal-planar environment, respectively. The bite angle of hpzb for the Cu complex **6** is small (93.14°) for a trigonal-planar disposition, which indicates a marked difference in the angles of the coordination plane.

The molecular structures for complexes **4** (Figure 1), **5b** (Figure 2) and **6** (Figure 3) show the two metallic units in a coordination type **IV** (κ^4-*N*1*N*2,*N*4*N*5-hpzb) with one metal atom *up* and the other *down.* The existence, in these derivatives, of a crystallographic inversion centre in the geometric central point of the molecule ensures that the uncoordinated pyrazole rings are oppositely oriented with respect to the benzene plane (*up* and *down*). As a consequence, conformer **IVa** is the only one present in the solid state for

Table 1. Crystal data and structure refinement for **4**, **6** and **9b** ($R_1 = \Sigma||F_o| - |F_c||/\Sigma|F_o|$; $wR_2 = \{\Sigma\ [w(F_o^2 - F_c^2)^2]/\Sigma[w(F_o^2)^2]\}^{0.5}$)

	4	**6**	**9b**
Empirical formula	$C_{48}H_{18}F_{20}N_{12}Pd_2$	$C_{30}H_{36}B_2Cu_2F_8N_{12}P_2$	$C_{38}H_{40}F_9N_{12}O_9Pd_3S_3$
Formula mass	1355.54	927.35	1395.20
Temperature [K]	293(2)	173(2)	298(2)
Wavelength [Å]	0.71073	0.71073	0.71073
Crystal system	triclinic	monoclinic	orthorhombic
Space group	$P\bar{1}$	$P2_1/n$	*Pnma*
a [Å]	11.082(6)	11.5148(11)	28.404(5)
b [Å]	13.359(5)	13.2698(13)	17.494(3)
c [Å]	18.481(2)	13.4157(13)	11.498(2)
α [°]	71.55(1)	90	90
β [°]	80.58(2)	108.625(2)	90
γ [°]	72.32(4)	90	90
Volume [Å^3]	2465.9(16)	1942.6(3)	5713.5(19)
Z, calculated density [g/cm^3]	2, 1.826	2, 1.585	4, 1.622
Absorption coefficient [cm^{-1}]	0.856	1.257	1.129
F(000)	1324	940	2764
Crystal size [mm]	0.4 × 0.3 × 0.1	0.40 × 0.35 × 0.30	0.40 × 0.35 × 0.30
Limiting indices	$0 \le h \le 14$	$-15 \le h \le 15$	$-33 \le h \le 32$
	$-16 \le k \le 17$	$-17 \le k \le 17$	$-20 \le k \le 19$
	$-23 \le l \le 24$	$-17 \le l \le 12$	$-12 \le l \le 13$
Reflections collected/unique	11897/11897 [*R*(int) =0]	13692/4823 [*R*(int) = 0.0739]	29203/5048 [*R*(int) = 0.1567]
Data/restraints/parameters	11897/0/739	4823/0/325	5048/0/311
Goodness-of-fit on F^2	0.942	0.942	0.907
Final *R* indices [$I > 2\sigma(I)$]	*R*1 = 0.0421, *wR*2 = 0.0672	*R*1 = 0.0475, *wR*2 = 0.0864	*R*1 = 0.0886, *wR*2 = 0.2458
Largest diff. peak/hole [eÅ^{-3}]	0.758/−0.705	0.488/−0.437	1.42/−0.773

Table 2. Selected bond lengths [Å] and angles [°] for complexes **4**, **6** and **9b**

4

Pd(1)−C(41)	1.998(5)	C(41)−Pd(1)−N(11)	94.1(2)
Pd(1)−C(51)	1.983(5)	C(51)−Pd(1)−N(21)	94.3(2)
Pd(1)−N(11)	2.080(4)	C(41)−Pd(1)−N(21)	179.3(2)
Pd(1)−N(21)	2.089(4)	N(11)−Pd(1)−N(21)	85.2(1)
C(1)−C(2)	1.401(6)	C(3A)−C(1)−C(2)	119.3(4)
C(1)−N(31)	1.414(5)	C(3A)−C(1)−N(31)	120.4(4)
C(1)−C(3A)	1.390(6)	C(2)−C(1)−N(31)	120.2(4)
C(2)−C(3)	1.394(6)	C(3)−C(2)−C(1)	120.1(4)
C(2)−N(12)	1.414(5)	C(3)−C(2)−N(12)	120.4(4)
C(3)−N(22)	1.412(5)	C(1)−C(2)−N(12)	119.5(4)
C(51)−Pd(1)−C(41)	86.4(2)	C(1A)−C(3)−C(2)	120.5(4)
C(51)−Pd(1)−N(11)	177.1(2)	C(1A)−C(3)−N(22)	119.3(4)

6

Cu(1)−N(2)	2.004(2)	C(4)−C(5)	1.378(4)
Cu(1)−N(4)	2.044(3)	C(4)−C(6A)	1.396(4)
Cu(1)−P(1)	2.1756(9)	C(5)−C(6)	1.391(4)
C(4)−C(5)	1.378(4)	N(2)−Cu(1)−N(4)	93.14(9)
C(4)−C(6A)	1.396(4)	N(2)−Cu(1)−P(1)	143.62(7)
C(5)−C(6)	1.391(4)	N(4)−Cu(1)−P(1)	122.64(7)
N(1)−C(5)	1.426(3)	C(5)−C(4)−C(6A)	120.6(3)
N(3)−C(4)	1.422(4)	C(4)−C(5)−C(6)	119.8(2)
N(5)−N(6)	1.362(3)	C(5)−C(6)−C(4A)	119.6(3)

9b

Pd(1)−C(18)	2.15(2)	C(2)−C(3)	1.38(2)
Pd(1)−C(17)	2.13(2)	C(3)−C(3A)	1.42(2)
Pd(1)−C(16)	2.11(2)	C(1)−C(1A)	1.42(2)
Pd(1)−N(2)	2.12(1)	C(1)−C(2)	1.38(2)
Pd(1)−N(4)	2.12(1)	N(2)−Pd(1)−N(4)	89.9(4)
Pd(2)−C(13)	2.11(2)	N(6)−Pd(2)−N(6A)	88.4(7)
Pd(2)−C(14)	2.14(2)	C(2)−C(3)−C(3A)	119.2(6)
Pd(2)−N(6)	2.12(1)	C(2)−C(1)−C(1A)	119.0(6)
		C(1)−C(2)−C(3)	122(1)

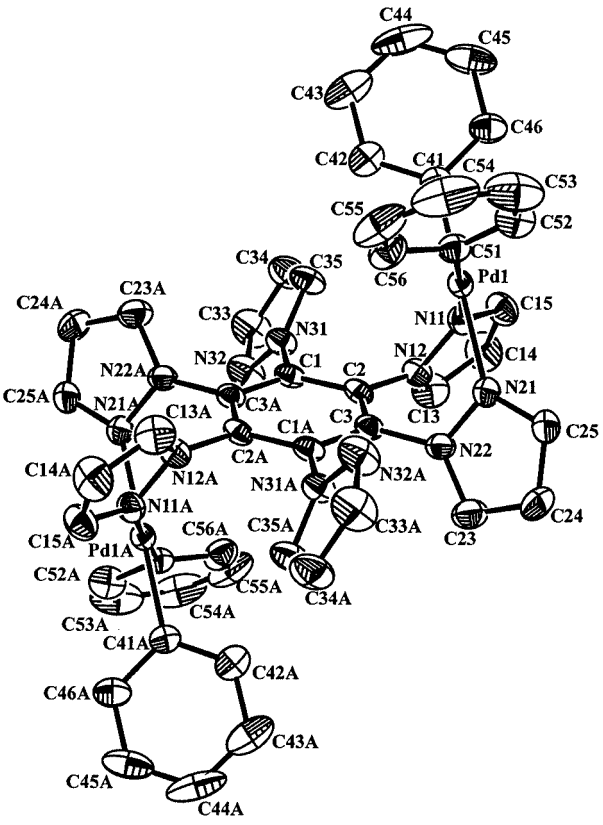

Figure 1. ORTEP view with atomic numbering of **4** (30% probability ellipsoids); the F atoms have been omitted for clarity

these dinuclear compounds. This is not the only similarity between the three structures: (i) Firstly, the uncoordinated pyrazole rings, which are in *para* positions with respect to one another, adopt a conformational orientation suitable for minimising the steric hindrance with the neighbouring rings, in such a way that the six pyrazole rings are distributed in two sets: three twisted (*P*) and three twisted (*M*). (ii) The dihedral planes of the pyrazole rings and the benzene rings are very similar (58−68°, Table 2), not only in **4** and **6** but also in one of the polymorphic forms of the free hpzb ligand.[25] (iii) The N−Pd−N bite angles do not differ greatly (84−93°). (iv) As a consequence of the two preceding statements the central cores, including the hpzb and the metallic centres, are practically superimposable for these three structures.

The structure of complex **4** (Figure 1) shows the two $Pd(C_6F_5)_2$ fragments oriented *up* and *down* in relation to the benzene ring and pointing in towards the core of the molecule. Considering this orientation and the considerable volume of this metallic fragment, it is very unlikely that three metallic units of this type could be coordinated with the same hpzb ligand and this hypothesis is in accordance with the experimental observations.

The trimetallic derivative $[\{Pd(\eta^3\text{-}C_4H_7)\}_3(hpzb)](TfO)_3$ (**9b**) (Figure 4) has a structure of type κ^6-*N*1*N*2,*N*3*N*4,*N*5*N*6-hpzb with two (allyl)palladium units on the opposite side to that of the third, with respect to the plane of the benzene ring (isomer type **VII**). The three methylallyl groups are oriented away from the molecule. This orientation, in conjunction with the considerably smaller volume of the (allyl)palladium unit with respect to the other groups used in this work, allows the coexistence of two vicinal metallic centres on the same side of the benzene ring. The small size of the crystals obtained precluded a final refinement of the structure, but a general overview of the backbone is possible. Bite and torsional angles of the pyrazole rings are in the range found for structures described previously. This structure is also preserved in solution (vide infra).

In summary, when more than one metal atom is present they prefer to be situated on opposite faces of the benzene ring. A reasonable extension to complexes **7** and **8** is that they adopt a **Va**, **Vb** or **Vc** disposition.

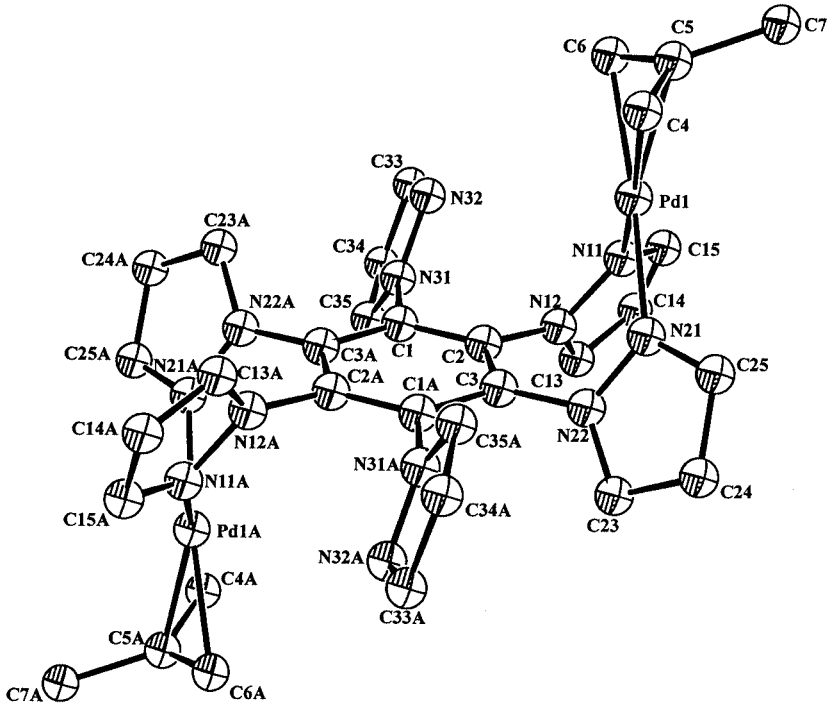

Figure 2. ORTEP view with atomic numbering of the cation of **5b** (30% probability ellipsoids)

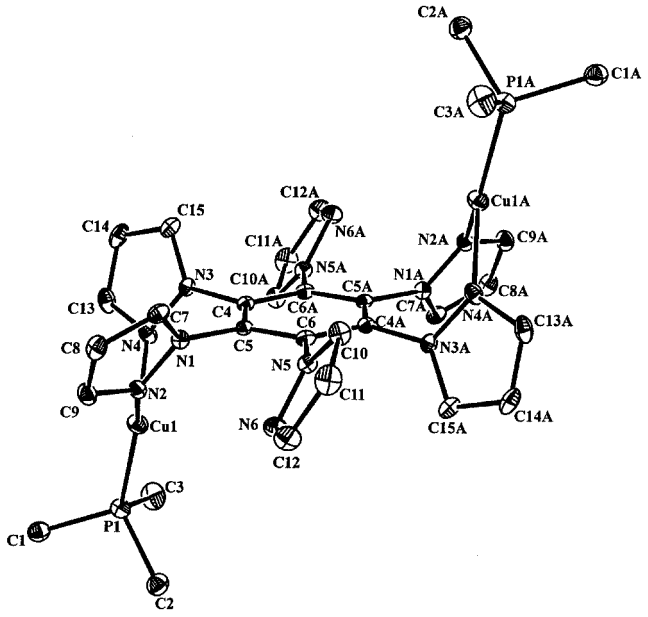

Figure 3. ORTEP view with atomic numbering of the cation of **6** (30% probability ellipsoids)

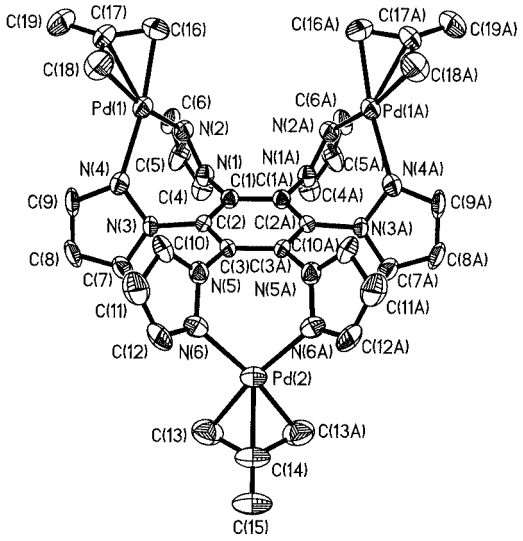

Figure 4. ORTEP view with atomic numbering of the cation of **9b** (30% probability ellipsoids)

NMR Spectroscopic Studies in Solution

Before a discussion on the NMR spectroscopic data is undertaken, it is useful to classify the different conformations of Schemes 3 and 4 according to their symmetry point groups and the expected number of different pyrazole rings (see Table 3). There is a one-to-one correspondence between the point group and the number of pyrazole rings with the exception of the C_s case where, depending on whether the symmetry plane lies between two *ortho*-pyrazole rings or through two *para*-pyrazole rings, the number of expected signals is 1:1:1 or 1:2:2:1, respectively.

Free Ligand hpzb (1)

This ligand can exist in the eight perpendicular conformations (**Ia**−**Ih**) shown in Scheme 3. When the ^{1}H NMR spectrum was recorded in $CDCl_3$ (4 mg/0.6 mL), signals of only one type of pyrazole ring could be observed (Table 4). This could correspond to the highly symmetric *ududud* (**Ia**) or *uuuuuu* (**Ih**) conformations or the average conformation

Table 3. Point groups and patterns of the signals in NMR spectra (see Schemes 3 and 4)

Conformation	Point group	No of pz rings	Conformation	Point group	No. of pz rings
Ia	D_{3d}	1	**Ia−Ih**	D_{6h}	1
Ib, If	C_s	1:2:2:1			
Ic	C_2	1:1:1			
Id	C_{2v}	1:2			
Ie	C_{2h}	1:2			
Ig	C_s	1:1:1			
Ih	C_{6v}	1			
IIa, IIb, IId, IIe, IIf, IIh	C_1	1:1:1:1:1:1	**IIa−IIj**	C_s	1:1:1
IIc, IIg, IIi, IIj	C_s	1:1:1			
IIIa, IIIc	C_{2v}	1:2	**IIIa−IIIc**	C_{2v}	1:2
IIIb	C_s	1:2:2:1			
IVa	C_i	1:1:1	**IVa/IVb**	C_{2h}	1:2
IVb	C_s	1:1:1			
Va, Vb	C_2	1:1:1	**Va−Vc**	C_2	1:1:1
Vc	C_1	1:1:1:1:1:1			
VIa	C_1	1:1:1:1:1:1	**VIa−VIc**	C_s	1:1:1
VIb, VIc	C_s	1:1:1			
VII	C_s	1:1:1	**VII**	C_s	1:1:1
VIII	C_{3v}	1	**VIII**	C_{3v}	1

Ia−Ih. Conformation **Ih** can be excluded on the basis of its very high energy.[25,28] The difficult problem remains in deciding between the static (except for librations) conformation **Ia** or the dynamic one **Ia−Ih**.

Table 4. ^{1}H NMR chemical shifts and ^{1}H-^{1}H coupling constants of the free ligand hpzb (**1**) (δ in ppm and *J* in Hz)

Solvent	Conformer	Intensity	3-H	4-H	5-H
$CDCl_3$	*ududud* (**Ia**)	1	7.41	6.12	7.25
			$^4J_{35}$ = 0.6	$^3J_{34}$ = 1.7	$^3J_{45}$ = 2.4
CD_3COCD_3	*ududud* (**Ia**)	1	7.32	6.11	7.43
			$^4J_{35}$ = 0.6	$^3J_{34}$ = 1.7	$^3J_{45}$ = 2.5
	uuduud (**Id**)	1	7.63	6.41	7.73
			$^4J_{35}$ = 0.6	$^3J_{34}$ = 1.8	$^3J_{45}$ = 2.5
		2	7.88	6.65	8.13
			$^4J_{35}$ = 0.6	$^3J_{34}$ = 1.8	$^3J_{45}$ = 2.5

When the spectrum of this compound was recorded in $(CD_3)_2CO$, in which the compound is rather insoluble, one or two isomers were observed depending on the concentration. In a very dilute solution (2 mg/0.6 mL) signals of only one kind of pyrazole ring was observed, as was the case in $CDCl_3$. However, in a more concentrated solution (saturated, i.e. about 6 mg/0.6 mL), two isomers were observed (the signals are narrow in all cases). The most abundant isomer (60%) corresponds to that already described above. The minor isomer (40%), however, has two kinds of pyrazole rings in a 1:2 ratio. First conclusion: the average **Ia−Ih** dynamic system shown in Scheme 4 can definitely be ruled out at room temperature on the NMR time-scale. A low-temperature ^{1}H NMR spectrum (193 K), in which signal splitting was not observed, also confirmed this statement. Consequently, the major isomer is **Ia** and the signals of the minor isomer, according to Table 3, should correspond either to conformer **Id** or **Ie**. Since the second conformer is much higher in energy,[25] we conclude that the minor isomer is the *uuduud* compound **Id**. It should be noted that this isomer has also been observed in a small amount in other hexakis(azol-1-yl)benzenes.[28]

The following discussion refers to the new complexes **2−9**.

(a) ^{1}H NMR Spectroscopy

The ^{1}H-^{1}H coupling constants, which are higher for 5-H/4-H than for 4-H/3-H, were used to differentiate the corresponding signals. In cases where different pyrazolyl groups were observed for a specific compound, COSY experiments allowed the signals belonging to the same pyrazole ring to be identified (Table 5).

For the mononuclear complexes **2** and **3**, three different types of pyrazole rings were evident, a situation in agreement with conformations **IIc**, **IIg**, **IIi** or **IIj** in Scheme 3 or with the dynamic situations **IIa−IIj** in Scheme 4 (see Table 3). In the low-temperature spectrum (193 K) of **2**, evidence for splitting of the signals was not observed. On extrapolating the result to **3**, we propose a static situation for both derivatives, similar to that found in the free ligand. If the orientation of two contiguous free pyrazolyl groups towards the same side of the benzene ring is considered less stable (see ref.[25] for energy calculations for the free ligand), **2** and **3** should have the structure of conformer **IIc**.

Three different situations have been found in the NMR spectra of the dinuclear compounds: (i) In complex **4** two kinds of pyrazole signals were observed in a ratio of two (coordinated) to one (noncoordinated). The existence of conformers **IIIa** or **IIIc** or the dynamic equilibria **IIIa/IIIb/IIIc** or **IVa/IVb** are consistent with the experimental data. However, according to the X-ray results the steric hindrance that will arise from the orientation of two $Pd(C_6F_5)_2$ fragments on the same side of the benzene ring allows us to rule out conformers of type **III** and, consequently, the equilibrium **IVa/IVb** is proposed. Moreover, the dynamic situ-

Table 5. ^{1}H NMR spectroscopic data for complexes **2**−**4** and **6**−**9**

Compd.[a]	3-H′	4-H′	5-H′	3-H"	4-H"	5-H"	3-H′"	4-H′"	5-H′"	Other groups		
2	7.44 d*	6.15 dd	7.14 d	7.42*d	6.21 dd	7.45 d	7.83 d	6.38 dd	7.75 d	−		
	J_{34} = 2.1		J_{45} = 2.7	J_{34} = 1.8		J_{45} = 2.8	J_{34} = 1.7		J_{45} = 2.7			
3	7.50 d	6.15 pt	7.68 d	7.37 d	6.25 pt	7.40 d	8.05 d	6.47 pt	7.66 d	−		
	J_{34} = 1.9		J_{45} = 2.6	J_{34} = 1.9		J_{45} = 2.5	J_{34} = 1.9		J_{45} = 2.9			
4	7.97 d	6.50m	7.75 d	7.99 d	6.50m	7.52	7.99 d	6.50 m	7.52	−		
	J_{34} = 2.1		J_{45} = 2.8	J_{34} = 2.1		J_{45} = 2.8	J_{34} = 2.1		J_{45} = 2.8			
6	7.66 d	6.46 pt	8.16 d	7.66 d	6.46 pt	8.16 d	7.66 d	6.46 pt	8.16 d	[1.42 br. s (PMe_3)]		
	J_{34} = 1.9		J_{45} = 2.9									
7	7.31 d	6.24 dd	6.94 d	7.47 d	6.28 dd	7.15 d	8.00 d	6.44 dd	7.13 d	−		
	J_{34} = 1.6		J_{45} = 2.4	J_{34} = 1.8		J_{45} = 2.4	J_{34} = 2.3		J_{45} = 2.8			
8	7.53 d	6.61 pt	7.23 d	8.10 d	6.52 pt	7.52 m[b]	8.15 d	6.38 pt	7.69 d	−		
	J_{34} = 1.9		J_{45} = 2.4	J_{34} = 2.5			J_{34} = 2.2		J_{45} = 2.9			
										η^3-C_4H_7 (2-Me-allyl)		
										CH_3	H_a	H_s
9b	8.15 d	6.60 pt	8.74 d	8.22 d	6.52m	8.02 d	8.11 d	6.52m	7.66 d	2.38 s (3 H)	3.91 br. s (2 H)	4.35 br. s (2 H)
	J_{34} = 2.1		J_{45} = 2.4	J_{34} = 1.9		J_{45} = 2.7	J_{34} = 2.1		J_{45} = 2.6	2.35 s (6 H)	3.70 br. s (4 H)	4.37 br. s (4 H)
9b[c]	8.36m	6.73 pt	8.77 d	8.48 d	6.68 pt	7.91 d	8.36 m	6.64 pt	7.66 m	2.31 br. s (9 H)	3.60 br. s (2 H)	4.38 br. s (6 H)
											3.71 br. s (2 H)	
											3.79 br. s (2 H)	
9a[d]	8.26 d	6.71 pt	8.48 d	8.37 d	6.63 pt	7.72 d	8.27 d	6.60 pt	7.48 d	2.35 s (6 H)	3.81 s (2 H)	4.32 s (2 H)
	J_{34} = 2.0		J_{45} = 2.6	J_{34} = 2.0		J_{45} = 3.0	J_{34} = 2.0		J_{45} = 2.8	2.38 s (3 H)	3.49 s (2 H)	4.36 s (2 H)
											3.66 s (2 H)	4.39 s (2 H)

[a] T = 293 K if not indicated; δ in ppm; J in Hz,; solvent = $(CD_3)_2CO$. See formula **1** in Scheme 2 for numbering. Unless specified, the signals are singlets; d = doublet, br. s = broad singlet, m = multiplet, pt = pseudotriplet. [b] Signal partially overlapped. [c] T = 183 K. [d] T = 213 K. The signals marked with * have not been unequivocally assigned to one specific pyrazole ring.

ation is confirmed by a low-temperature NMR spectrum (193 K). The resonances of the coordinated pyrazole rings are broad at 233 K and a splitting is finally observed at lower temperatures. Although the resonances of the noncoordinated pyrazole rings are less sensitive to temperature, the corresponding 5-H signal also broadens and splits at low temperature. (ii) In complexes **7** and **8** three different pyrazole rings in a 1:1:1 ratio are observed; two for each pair of coordinated pyrazole rings and a third for the noncoordinated system. If we again exclude conformers that have the two metallic fragments on the same side of the benzene plane (**VIb**, **VIc** and **VIa/VIb/VIc**) the possible conformers would be: **IVa**, **IVb**, **Va**, **Vb** or the equilibrium **Va/Vb/Vc** (see Table 3). In the case of complex **7**, conformers **IVa** and **IVb** are not possible because the equilibrium **IVa/IVb** is the only possibility for **4** and is observed separately from **7**. Splitting of some signals is observed in both derivatives at low temperature. Consequently, the equilibrium **Va/Vb/Vc** is proposed for **7** and **8** at room temperature. (iii) In **6**, other dynamic processes must operate in addition to pyrazolyl rotation. Only broad signals due to one type of pyrazole ring are observed, some of which remain broad even at 203 K. A metallotropic process by exchange of the metal atoms between the pyrazole rings must take place and averaged signals are observed.

For the solid obtained in the reaction between hpzb and $[Pd(\eta^3\text{-}C_4H_7)(cod)]BF_4$ (1:0.5 or 1:1 ratio), one broad signal for 4-H and two broad and overlapped signals for 3-H and 5-H are observed at room temperature. The spectrum at 323 K exhibits narrower signals and a very complex spectrum is observed at low temperature (193 K). We propose that a mixture of complex **5a** (analogous to **5b** with a BF_4^- anion), adopting some of the possible structural configurations, (**III**−**VI** of Scheme 3) and free hpzb are present in equilibrium at room temperature by a metallotropic process. The concomitant presence of a mononuclear complex cannot be excluded.

A particularly interesting case is that of complex **9**. Three kinds of pyrazole rings are observed in a 1:1:1 ratio. Although some signal overlap seems to occur in the allylic region, at low temperature three separate H_{anti} signals (1:1:1 ratio) are observed. It is necessary to consider that the methyl group of the 2-methylallyl group can point inside (*i*) or outside (*o*) the benzene ring. This reduction in symmetry of the (allyl)Pd fragment when compared with that of the previously described MX_n groups, makes the symmetry considerations in Table 3 not strictly applicable in this case. Scheme 6 shows representations of the isomers derived from structures **VII** (six isomers) and **VIII** (four isomers). The symmetry point group is indicated in each case. When the symmetry is C_{3v}, one type of pyrazole ring is expected, but six types would occur if the symmetry is C_1 and three if it is C_s. Consequently, the experimental data only fit with the conformers of C_s symmetry. Several NOE experiments were carried out at room temperature (**9a** and **9b**): upon irradiation of H_{anti} (*anti*) an NOE effect was observed with H_{syn} (*syn*) and when H_{syn} was irradiated the NOE effect was observed not only on H_{anti} but also on the three signals of 3-H (closer to H_{syn} than 5-H) (Scheme 7). This confirms the previous assignment of these pyrazolic protons but, more importantly, indicates that the three allyl groups have an outside orientation. Consequently, if we consider the con-

formers of C_s symmetry, only conformer **VII*ooo*** fits with the NOE data and we propose this structure for complex **9** in solution. The fact that interchange of the (allyl)palladium fragments between the pyrazolyl groups is not observed, in contrast to **5**, could be due to the absence of free pyrazolyl rings in this derivative.

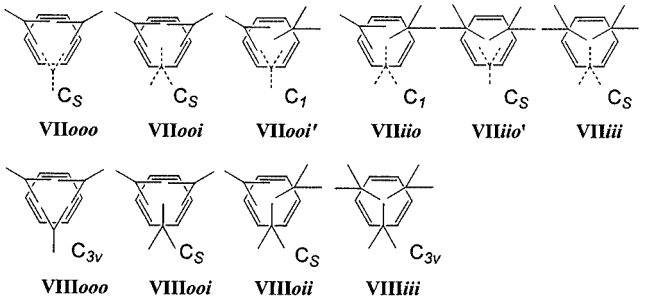

Scheme 6. Representation of the isomers corresponding to structures **VII** and **VIII**

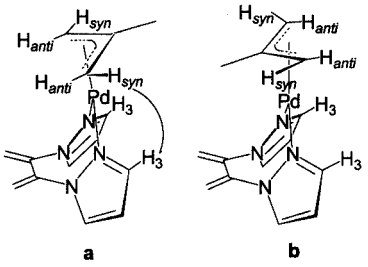

Scheme 7. **a** and **b** represent the outside and inside orientations, respectively, of the allyl group; only in **a** the NOE observed in compound **9** (indicated with an arrow between H_{syn} and 3-H of the pyrazolyl group is possible

Conclusions concerning the possible conformers in solution for complexes **2**−**9** are collected in Table 6. The conformation of the molecule in the solid state is also included in cases where it is known. The first conclusion is that structures found in the solid state are consistent with those in solution in the cases of complex **9** (one conformer) and with one of the possible conformations of **4**−**6**. A static behaviour has been found in the free ligand and the monometallic derivatives while in the dimetallic complexes free rotation of the uncoordinated pyrazolyl groups is observed at room temperature. A slowing down of this rotation is observed at low temperature. In derivatives **5** and **6** the occurrence of other fluxional processes has prevented the study of this phenomenon.

(b) ^{13}C NMR Spectroscopy

The most significant information from the data in Table 7 regards the number of different pyrazole rings observed that

Table 6. Conformation of complexes **2**−**9** in the solid state and in $(CD_3)_2CO$ solution

Compd.	Solid state		Solution		
	Class	Structure	Class	Structure rigid[a]	Structure free
2 (Pd)	**II**	**–**	**II**	***IIc*, IIg, IIi, IIj**	–
3 (Pt)	**II**	–	**II**	***IIc*, IIg, IIi, IIj**	**–**
4 (Pd)	**IV**	**IVa**	**IV**	–	**IVa/IVb**
5 (Pd)	**IV**	**IVa**	**IV**	[fluxional]	
6 (Cu)	**IV**	**IVa**	**IV**	[fluxional]	
7 (Pd)	–	–	**V**	–	**Va/Vb/Vc**
8 (Pt)	–	–	**IV, V**	–	**Va/Vb/Vc**
9 (Pd)	**VII**	**VII**	**VII**	**VII**	–

[a] Structure numbers in italics are considered to be the most stable.

Table 7. $^{13}C\{^1H\}$ NMR spectroscopic data for hpzb (**1**) ligand and complexes **2**−**4** and **6**−**9**

Compd.[a]	C-3′	C-4′	C-5′	Benzene	Other groups		
hpzb (**1**)[b]	141.5	107.2	132.3	136.6	–		
2	142.3	108.0	129.2	132.4	–		
	142.6	108.6	133.3	142.9			
	144.8	109.5	137.2	n.o.			
3	142.4	107.9	133.6	n.o.	–		
	144.0	110.1	134.4				
	147.0	111.8	138.1				
4	145.8[c]	111.6[c]	136.4[c]	n.o.	–		
	146.0	111.4	137.4				
6	143.4 br. s	108.7 br. s	134.5 br. s	137.7 br. s	[17.5 br. s, PMe_3]		
7	143.9	109.9	132.0	n.o.	–		
	144.4	110.6	132.7				
	146.8	112.4	135.8				
8	143.3	109.3	132.7	n.o.	–		
	146.4	111.2	137.2				
	146.7	112.5	137.8				
					η^3-C_4H_7 (2-Me-allyl)		
					−C=	CH_2	CH_3
9b	147.9	109.5	136.7	137.4	137.4	63.2[c]	23.3[c]
	147.9	110.7	138.4	137.7	137.8[c]	64.2	23.4
	148.2	111.0	140.3	138.1			

[a] T = 293 K; δ in ppm; solvent = $(CD_3)_2CO$. See formula **1** of Scheme 2 for numbering. [b] $CDCl_3$. [c] These peaks have an intensity twice that of the others. For **9b**, the $CF_3SO_3^-$ signal appears at δ = 121.7 (q, $^1J_{C,F}$ = 319 Hz) ppm.

Table 8. ^{19}F NMR chemical shifts (ppm from $CFCl_3$) and ^{19}F-^{19}F coupling constants (Hz) for **2**, **4** and **7** in $(CD_3)_2CO$

Compd.	F_{ortho}	F_{meta}	F_{para}
2	−119.8/−117 (br. m, 4 F)	−166.6 (br. m, 4 F)	−164.2 (t, 2 F) $^3J(F_p\text{-}F_m)$ = 18.3
4	−115.0 (d, 8 F) $^3J(F_o\text{-}F_m)$ = 30.5	−168.8 (m, 8 F)	−167.2 (t, 4 F) $^3J(F_p\text{-}F_m)$ = 18.3
7	−115.2 (d, 4 F) $^3J(F_o\text{-}F_m)$ = 30.6 −118.0 (d, 4 F) $^3J(F_o\text{-}F_m)$ = 30.5	−165.8 (br. m, 4 F) −166.4 (br. m, 4 F)	−163.3 (t, 2 F) $^3J(F_p\text{-}F_m)$ = 18.3 −163.9 (t, 2 F) $^3J(F_p\text{-}F_m)$ = 18.3

are in agreement with those presented in Table 5: **3** (1:1:1), **4** (1:2), **6** (fluxional behaviour), **7**, **8** and **9** (1:1:1).

(c) ^{19}F NMR Spectroscopy

In accordance with the expected symmetry, and as deduced from the number of F_{para} signals observed, one kind of C_6F_5 ring exists in compounds **2** and **4** and two kinds (1:1 ratio) in derivative **7**. These belong to C_6F_5 groups either close to the other metal centre or close to a noncoordinated pyrazole ring. The F_{ortho} or F_{meta} signals are broad in some cases, indicating a certain degree of restricted rotation (Table 8).

Conclusions

After the reaction of the ligand hpzb (**1**) with different metallic fragments {$[Pd(C_6F_5)_2]$, $[Pd(\eta^3\text{-}2\text{-}Me\text{-}C_3H_4)]^+$, $PtCl_2$ and $Cu(PMe_3)^+$} we have synthesised new mono-, di- and trinuclear derivatives. We have carried out an analysis of the complex energy hypersurface that these complexes present, reporting many examples which describe fairly well its multidimensional aspect. The incorporation of three metallic centres was only possible with the smaller group $[Pd(\eta^3\text{-}C_4H_7)]^+$, a clear indication of the influence of steric effects. We have found that the metallic fragments, when two or three are present, prefer to be situated on opposite faces of the benzene ring. As far as the fluxionality of the compounds is concerned, we observed two types of behaviour on the NMR spectroscopic time-scale: metallotropic processes and rotation of the uncoordinated pyrazolyl groups. The former process was found in the dimetallic derivatives **5** and **6** with (allyl)palladium and $Cu(PMe_3)$ fragments, respectively. The second process described was the free rotation of the uncoordinated pyrazolyl groups that was found in the rest of the dimetallic complexes (**4**, **7** and **8**) at room temperature, although the process slows down at low temperature. Restricted rotation was observed in the monometallic derivatives and the free ligand even at room temperature. For complex **9**, where all the pyrazole rings are involved in coordination to the metal centre, a fluxional process is not observed. Finally, on a much slower timescale, when the Pd^{II} derivative **4** was dissolved in $(CD_3)_2CO$ an approximately 50:50 mixture of **4** and **7** was obtained. This fact shows that structures of type κ^4-*N*1*N*2,*N*4*N*5-hpzb (**IV**) and κ^4-*N*1*N*2,*N*3*N*4-hpzb (**V**) equilibrate in solution (isomerism). The X-ray structure of three dimetallic derivatives (**4**, **5b** and **6**) and the trinuclear derivative **9b** was undertaken. All the structures with two metallic centres were of the type κ^4-*N*1*N*2,*N*4*N*5-hpzb (**IV**) and the central core (hpzh ligand and metal centre) was near superimposable. Cooperative rearrangement of the pyrazolyl rings to minimize the steric hindrance was found in these dinuclear derivatives. When allyl ligands were present, they had the methyl group pointing away from the molecule. In all cases, the structures determined in the solid state were in accordance with the situations found in solution.

Experimental Section

General Comments: All manipulations were carried out under dry oxygen-free nitrogen using standard Schlenk techniques. Solvents were distilled from the appropriate drying agents and degassed before use. The ligand hexakis(pyrazol-1-yl)benzene (hpzb, **1**) has been previously described.[25,27] $[Pd(C_6F_5)_2(cod)]$ (cod = 1,5-cyclooctadiene) was synthesised as described in the literature for similar complexes.[30] $[PtCl_2(PhCN)_2]$ was prepared according to Kharasch,[31] $[Pd(\eta^3\text{-}C_4H_7)(\mu\text{-}Cl)]_2$ according to Wilkinson [32] and $[Cu(CH_3CN)_4](BF_4)$ according to Kubas.[33] Elemental analyses were performed with a Perkin−Elmer 240 B microanalyser. IR spectra were recorded in Nujol mulls with a Perkin−Elmer 883 (4000−200 cm^{-1} range) spectrophotometer. ^1H, ^{13}C, and ^{19}F NMR spectra were recorded with a Varian Unity 300 spectrometer using, unless specified, $(CD_3)_2CO$ as solvent. Standard experimental conditions were employed.[34,35] Mass spectra (position of the peaks in Da) were recorded with a VG Autospec spectrometer (University of Zaragoza) using the FAB^+ technique and *m*-nitrobenzylic alcohol as matrix.

Preparation of Compounds

(a) $[Pd(C_6F_5)_2(hpzb)]$ (2) and $[\{Pd(C_6F_5)_2\}_2(hpzb)]$ (4 and 7): We have carried out the reaction using different metal/ligand stoichiometries (0.5, 1, 2 or 3). Different mixtures (white colour) of the three isomers were obtained accordingly with the results specified in the previous section. Here we report the experiment with a 1:3 stoichiometry. $Pd(C_6F_5)_2(cod)$ (242 mg, 0.42 mmol) was added to a solution of hpzb (70.0 mg, 0.14 mmol) in THF (20 mL). The mixture was stirred for 7 h. The solution was then concentrated to near dryness and pentane (10 mL) was added, a white solid precipitated that was filtered, washed with pentane to eliminate the cod and dried. Yield of **4** + **7**: 80% (155 mg). IR: $\tilde{\nu}$ = 1639−1627, 1510−1500, 1070−1054, 975−950, 798, 796 and 787 cm^{-1} (C_6F_5).

Although **2** was the only metallic complex (in a mixture with hpzb) formed in the reaction with a metal/ligand ratio of 0.5, we were not able to obtain it in a pure form because in the crystallisation process, it was partially transformed into **4** and **7**. Compound **7** was never isolated, only a mixture of **4** and **7** without **2** was obtained. **4 +7:** $C_{48}H_{18}F_{20}N_{12}Pd_2 \cdot 1/2C_4H_8O$ (1399.62): calcd. C 42.91, H 1.58, N 12.01; found C 43.13, H 1.53, N 11.75. From the mixture of the 1:3 reaction, a pure sample of **4** was obtained when preparing crystals for X-ray diffraction by diffusion with acetone/hexane.

(b) [($PtCl_2$)(hpzb)] (3) and [($PtCl_2$)$_2$(hpzb)] (8): 1 equiv. of $PtCl_2(PhCN)_2$ (74.6 mg, 0.16 mmol) under nitrogen was added to a solution of hpzb (75.0 mg, 0.16 mmol) in dry acetone (20 mL). The mixture was stirred at room temperature for 2 weeks. The solution was concentrated to near dryness and pentane (10 mL) was added, a yellow solid precipitated that was filtered, washed with pentane and dried. The mixture of **3** and **8** were separated by flash chromatography (silica gel; eluent: methanol) and a small amount of both derivatives was obtained. IR: $\tilde{\nu}$ = 347 cm^{-1} [ν(Pt−Cl)] for both complexes. **3**: $C_{24}H_{18}Cl_2N_{12}Pt$ (740.49): calcd. C 38.93, H 2.45, N 22.70; found C 38.79, H 2.37, N 22.60.

(c) [($PtCl_2$)$_2$(hpzb)] (8): The synthesis was carried out as described above, except that 2 equiv. of $PtCl_2(PhCN)_2$ {hpzb (37.9 mg), [$PtCl_2(PhCN)_2$] (75.5 mg)} were used. In this way a pure sample of **8** was obtained after washing the yellow precipitate with pentane. Yield: 86% (68.0 mg). $C_{24}H_{18}Cl_4N_{12}Pt_2$ (1006.48): calcd. C 29.63, H 1.80, N 16.61; found C 29.17, H 1.91, N 16.36. The use of a 1:3 stoichiometry again affords **8**.

(d) [{Pd(η^3-C_4H_7)}$_2$(hpzb)](X)$_2$ (5) and [{Pd(η^3-C_4H_7)}$_3$(hpzb)](X)$_3$ (9) [X = BF_4^- (a), TfO^- (b)]: We have carried out the reaction with different ligand/metal stoichiometries and using the solvate [Pd(η^3-C_4H_7)(THF)$_2$]TfO (TfO: triflate, trifluoromethylsulfonate) or the derivative [Pd(η^3-C_4H_7)(cod)]BF_4 as metallic precursors (see discussion of the results). Here we report on the experiment with a 1:3 stoichiometry and the solvate precursor. First, a solution of [Pd(η^3-C_4H_7)(THF)$_2$]TfO was prepared from [Pd(η^3-C_4H_7)(μ-Cl)]$_2$ (87.1 mg, 0.22 mmol) and AgTfO (113 mg, 0.44 mmol) in freshly distilled THF (20 mL). The mixture was stirred for 2 h and protected from light. The solution was filtered through Celite to eliminate AgCl. The addition to this solution of the ligand (70.0 mg, 0.15 mmol) produced a white precipitate and the suspension was stirred for 3 h. The solid was filtered and washed with diethyl ether. The solid was crystallised in acetone/pentane to obtain crystals of **9b**. IR: $\tilde{\nu}$ = 835 [ν(C−CH_3) of the allyl group], 1282, 1165, 1031, 767 and 638 cm^{-1} (TfO^- anion). Yield: 75% (155 mg). $C_{39}H_{39}F_9N_{12}O_9Pd_3S_3$ (1406.22): calcd. C 33.31, H 2.79, N 11.95; found C 33.01, H 2.08, N 11.53. When the crystallisation was carried out in acetonitrile/diethyl ether, crystals of [{Pd(η^3-C_4H_7)}$_2$(hpzb)](TfO)$_2$ (**5b**) were obtained.

(e) [{Cu(PMe_3)}$_2$(hpzb)](BF_4)$_2$ (6): PMe_3 (0.30 mmol, 0.30 mL, 1 M solution in toluene) was added to a solution of [Cu($NCCH_3$)$_4$](BF_4) (94.4 mg, 0.30 mmol) in dry acetone (30 mL). The colourless solution was stirred for 15 min, then hpzb (71.1 mg, 0.15 mmol) was added and the resulting pale yellow solution was stirred for 4 h, concentrated to dryness and washed with diethyl ether. A yellow solid was obtained. Yield: 81% (113 mg). $C_{30}H_{36}B_2Cu_2F_8N_{12}P_2$ (927.36): calcd. C 38.84, H 3.91, N 18.11; found C 38.22, H 4.02, N 18.07. IR: $\tilde{\nu}$ = 1084 and 520 cm^{-1} (BF_4 anion). The crystals for X-ray diffraction were obtained by crystallisation in dichloromethane/pentane.

X-ray Data Collection, Structure Determination, and Refinement of Complexes 4, 5b, 6 and 9b:[36] Crystal data and basic information about the data collection and structure refinement are listed in Table 1. The diffraction experiments were carried out with a CAD4-MACH3 diffractometer (**4** and **5b**) with ω-2θ scan technique to a maximum value of 56° and a Bruker Smart CCD based diffractometer (**6** and **9b**) by using graphite-monochromated Mo-K_α radiation with ψ-ω scan technique (**6** and **9b**). For **4**, the asymmetric unit comprises two half molecules, and for **5b** and **6,** one independent half molecule. Data were corrected for Lorentz and polarisation effects and absorption correction was made for **6** and **9b**. The structures were solved by direct methods (SHELXS)[37] and refined first isotropically by full-matrix least squares using SHELXL-97[38] program and then anisotropically by blocked full-matrix least squares for all the non-hydrogen atoms. The hydrogen atoms were included in calculated positions and refined "riding" on their parent carbon atoms.

Acknowledgments

We gratefully acknowledge financial support from the Dirección General de Enseñanza Superior e Investigaciones Científicas, DGES, Spain (Grant N. PB98-0315) and from the DGI/MCyT/ (project number BQU2000-0252).

[1] W.-K. Chang, S. C. Sheu, G.-H. Lee, Y. Wang, T.-I. Ho, Y.-C. Lin, *J. Chem. Soc., Dalton Trans.* **1993**, 687−694.
[2] W.-K. Chang, G.-H. Lee, Y. Wang, T.-I. Ho, Y. O. Su, Y.-C. Lin, *Inorg. Chim. Acta* **1994**, *223*, 139−144.
[3] C. M. Hartshorn, P. J. Steel, *Austr. J. Chem.* **1995**, *48*, 1587−1599.
[4] C. M. Hartshorn, P. J. Steel, *Angew. Chem. Int. Ed. Engl.* **1996**, *35*, 2655−2657; *Angew. Chem.* **1996**, *108*, 2818−2820.
[5] C. M. Hartshorn, P. J. Steel, *Chem. Commun.* **1997**, 541−542.
[6] C. M. Hartshorn, P. J. Steel, *Austr. J. Chem.* **1997**, *50*, 1195−1198.
[7] W.-K. Chang, G.-H. Lee, Y. Wang, Y. O. Su, T.-I. Ho, Y.-C. Lin, *J. Coord. Chem.* **1997**, *42*, 253−260.
[8] J. Chen, D. M. L. Goodgame, S. Menzer, D. J. Williams, *Polyhedron* **1997**, *16*, 1679−1687.
[9] J. S. Fleming, K. L. V. Mann, C.-A. Carraz, E. Psillakis, J. C. Jeffery, J. A. McCleverty, M. D. Ward, *Angew. Chem. Int. Ed.* **1998**, *37*, 1279−1281. *Angew. Chem.* **1998**, *110*, 1325−1328.
[10] J. S. Fleming, K. L. V. Mann, S. M. Couchman, J. C. Jeffery, J. A. McCleverty, M. D. Ward, *J. Chem. Soc., Dalton Trans.* **1998**, 2047−2052.
[11] C. M. Hartshorn, P. J. Steel, *Organometallics* **1998**, *17*, 3487−3496.
[12] B. Therrien, T. R. Ward, *Angew. Chem. Int. Ed.* **1999**, *38*, 405−408. *Angew. Chem.* **1999**, *111*, 418−421.
[13] J. Chin, C. Walsdorff, B. Stranix, J. Oh, H. J. Chung, S.-M. Park, K. Kim, *Angew. Chem. Int. Ed.* **1999**, *38*, 2756−2759. *Angew. Chem.* **1999**, *111*, 2923−2926.
[14] N. Fatin-Rouge, E. Toth, D. Perret, R. H. Backer, A. E. Merbach, J.-C. G. Bünzli, *J. Am. Chem. Soc.* **2000**, *122*, 10810−10820.
[15] C. M. Hartshorn, P. J. Steel, *Inorg. Chem. Commun.* **2000**, *3*, 476−481.
[16] A. J. Canty, J. Patel, B. W. Skelton, A. H. White, *J. Organomet. Chem.* **2000**, *607*, 194−202.
[17] H. P. Dijkstra, M. D. Meijer, J. Patel, R. Kreiter, G. P. M. van Klink, M. Lutz, A. L. Spek, A. J. Canty, G. van Koten, *Organometallics* **2001**, *20*, 3159−3168.
[18] A. J. Canty, R. T. Honeyman, B. W. Skelton, A. H. White, *J. Organomet. Chem.* **1990**, *389*, 277−288.
[19] M. Loi, M. W. Hosseini, A. Jouaiti, A. De Cian, J. Fischer, *Eur. J. Inorg. Chem.* **1999**, 1981−1985.
[20] A. Jouaiti, M. Loi, M. W. Hosseini, A. De Cian, *Chem. Commun.* **2000**, 2085−2086.

[21] P. Cornago, C. Escolástico, M. D. Santa María, R. M. Claramunt, D. Carmona, M. Esteban, L. A. Oro, C. Foces-Foces, A. L. Llamas-Saiz, J. Elguero, *J. Organomet. Chem.* **1994**, *467*, 293−301.
[22] [22a] T. E. Keyes, P. M. Jayaweera, J. J. McGarvey, J. G. Vos, *J. Chem. Soc., Dalton Trans.* **1997**, 1627−1632. [22b] T. E. Keyes, R. J. Forster, P. M. Jayaweera, C. G. Coates, J. J. McGarvey, J. G. Vos, *Inorg. Chem.* **1998**, *37*, 5925−5932.
[23] A. M. Bond, F. Marken, C. T. Williams, D. A. Beattie, T. E. Keyes, R. J. Forster, J. G. Vos, *J. Phys. Chem. B* **2000**, *104*, 1977−1983.
[24] C. Foces-Foces, A. L. Llamas-Saiz, R. M. Claramunt, N. Jagerovic, M. L. Jimeno, J. Elguero, *J. Chem. Soc., Perkin Trans. 2* **1995**, 1359−1371.
[25] C. Foces-Foces, A. L. Llamas-Saiz, C. Escolástico, R. M. Claramunt, J. Elguero, *J. Phys. Org. Chem.* **1996**, *9*, 137−144.
[26] C. Foces-Foces, C. Fernández-Castaño, R. M. Claramunt, C. Escolástico, J. Elguero, *J. Phys. Org. Chem.* **1996**, *9*, 717−727.
[27] C. Foces-Foces, A. L. Llamas-Saiz, C.C. Fernández-Castaño, R. M. Claramunt, C. Escolástico, J. L. Lavandera, M. D. Santa-María, M. L. Jimeno, J. Elguero, *J. Chem. Soc., Perkin Trans. 2* **1997**, 2173−2177.
[28] R. M. Claramunt, J. Elguero, C. Escolástico, C. Fernández-Castaño, C. Foces-Foces, A. L. Llamas-Sainz, M. D. Santa María, *Targets Heterocycl. Syst.* **1997**, *1*, 1−56.
[29] C. Foces-Foces, C. Fernández-Castaño, R. M. Claramunt, C. Escolástico, J. Elguero, *J. Incl. Phenom. Macrocycl. Chem.* **1999**, *33*, 169−189.
[30] P. Espinet, J. M. Martínez-de Ilarduya, C. Pérez-Briso, A. L. Casado, M. A. Alonso, *J. Organomet. Chem.* **1998**, *551*, 9−20.
[31] M. S. Kharasch, R. C. Sailer, F. R. Mayo, *J. Am. Chem. Soc.* **1938**, *60*, 882−887.
[32] W. T. Dent, R. Long, G. Wilkinson, *J. Chem. Soc.* **1964**, 1585−1588.
[33] G. J. Kubas, *Inorg. Synth.* **1979**, *19*, 90−92.
[34] F. Gómez-de la Torre, A. de la Hoz, F. A. Jalón, B. R. Manzano, A. Otero, A. M. Rodríguez, M. C. Rodríguez-Pérez, A. Echevarría, J. Elguero, *Inorg. Chem.* **1998**, *37*, 6606−6614.
[35] F. Gómez-de la Torre, A. de la Hoz, F. A. Jalón, B. R. Manzano, A. M. Rodríguez, J. Elguero, M. Martínez-Ripoll, *Inorg. Chem.* **2000**, *39*, 1152−1162.
[36] CCDC-185478 ([Pd $(C_6F_5)_2\}_2$(hpzb)], -185479 ([{Pd(η^3-2-Me-C_3H_4)}$_2$(hpzb)](TfO)$_2$], -185480 ({Cu(PMe_3)}$_2$(hpzb)](BF_4)$_2$ and -185481 ([{Pd(η^3-2-Me-C_3H_4)}$_3$(hpzb)](TfO)$_3$] contain the supplementary crystallographic data for this paper. These data can be obtained free of charge at www.ccdc.cam.ac.uk/conts/retrieving.html or from the Cambridge Crystallographic Data Centre, 12, Union Road, Cambridge CB2 1EZ, UK [Fax: (internat.) + 44-1223/336-033; E-mail: deposit@ccdc.cam.ac.uk].
[37] G. M. Sheldrick, *SHELXS-97*, University of Göttingen, Göttingen, Germany, **1990**.
[38] G. M. Sheldrick, *SHELXL-97, Program for the Refinement of Crystals Structures from Diffraction Data*, University of Göttingen, Göttingen,Germany, **1997**.

Received May 13, 2002
[I02252]

Synthesis, Microstructural Characterisation and Magnetic Study of Two New One-Dimensional Members of the $(A_3ZnMnO_6)_\alpha$ $(A_3Mn_3O_9)_\beta$ Homologous Series (A = Ba, Sr)

María Hernando,*[a] Khalid Boulahya,[a] Marina Parras,[a] and José M. González-Calbet[a]

Keywords: Electron diffraction / Electron microscopy / One-dimensional oxides / Magnetic properties / Twinned microstructure

Two new members of the $(A_3ZnMnO_6)_\alpha(A_3Mn_3O_9)_\beta$ one-dimensional homologous series have been synthesised with the compositions $Sr_4Mn_2ZnO_9$ and $Ba_5Mn_3ZnO_{12}$. Their structures can be described as a hexagonal array of infinite 1D-chain polyhedra, running parallel to the *c*-axis, formed by two face-sharing octahedra linked by one trigonal prism for $Sr_4Mn_2ZnO_9$, and one more octahedron between prisms for $Ba_5Mn_3ZnO_{12}$. Both oxides have a twinned microstructure as evidenced by SAED and HREM. $Sr_4Mn_2ZnO_9$ shows a pronounced antiferromagnetic character with a broad susceptibility maximum at 100 K due to short-range ordering. At low temperature, the susceptibility data suggest a transition to a 3D long-range ordering.

(© Wiley-VCH Verlag GmbH, 69451 Weinheim, Germany, 2002)

Introduction

The family of one-dimensional oxides structurally related to the 2H hexagonal perovskite ABO_3 [1] has been widely studied due to their striking magnetic properties. This structure and the K_4CdCl_6 [2] structural type define the two end-members of this 1D family. Both structures are formed by a hexagonal array of infinite chains of face-sharing polyhedra running parallel to the *c*-axis. In the 2H hexagonal type, $[BO_6]$ octahedra (O_h) constitute the polyhedra chains, whereas in K_4CdCl_6 ($A_3A'BO_6$) one $[BO_6]$ octahedron alternates with one $[A'O_6]$ trigonal prism (TP) in an ordered sequence. Between both structures, an unlimited number of one-dimensional related structures can be generated by varying the octahedron/trigonal-prism ratio.[3−6] There are several ways to describe the different members of this family. Among them, a very useful approach is to consider these structures as being formed by the ordered intergrowth of the structural units building up the two end-members. This building principle gives rise to the $(A_3A'BO_6)_\alpha(A_3B_3O_9)_\beta$ general formula, where α and β denote the number of $A_3A'BO_6$ and 2H-ABO_3 structural blocks, respectively, in each member.[7] A large number of oxides belonging to this family have already been reported. Usually, the A cation is an alkaline earth metal whereas the chemical nature of A′ and B is much wider since alkali, alkaline earth, transition, rare earth or main group metals can occupy such positions.

A wide range of magnetic properties are observed in these oxides. When both trigonal prism and octahedral sites contain magnetic cations, the system presents a 1D magnetic behaviour that can induce a 3D ordered state at low temperature.[8−10] However, this 1D character can be lost — a 3D character appearing — when diamagnetic cations separate the paramagnetic ones in the chain.[9,11] In this case, the superexchange pathways between such paramagnetic cations are not significantly shorter than those between metals located at different chains, hence the intrachain and interchain interactions are of comparable magnitude.

Up to now, only two phases have been stabilised in the A−Mn−Zn system (A = Ca and Ba), *viz.* Ca_3MnZnO_6 [9] and $Ba_6Mn_4ZnO_{15}$.[12] The former adopts the K_4CdCl_6 structure corresponding to the (α = 3 β = 0) member of the $(A_3A'BO_6)_\alpha(A_3B_3O_9)_\beta$ homologous series. The structure can be regarded as infinite 1D-chains, running along the *c*-axis, made up of alternate $[ZnO_6]$ face-sharing trigonal prisms and $[MnO_6]$ octahedra (Figure 1a). The magnetic cations are only located in the octahedral holes and, consequently, the $(Mn\text{-}Mn)_{intrachain}$ distances (5.3 Å) are similar to the $(Mn\text{-}Mn)_{interchain}$ distances (5.6 Å), giving rise to a 3D magnetic system.

$Ba_6Mn_4ZnO_{15}$,[12] which is isostructural to $Sr_6Co_5O_{15}$,[13] shows a different magnetic behaviour. This 1D-oxide corresponds to the (α = 3 β = 3) member of the above-mentioned homologous series. The chains are now made up of four face-sharing octahedra linked by one trigonal prism (Figure 1d). The cationic distribution in the different polyhedra is only partially ordered. Zn and Mn occupy the trigonal prismatic site in equal concentrations, with the re-

[a] Departamento de Química Inorgánica, Facultad de Químicas, Universidad Complutense
28040 Madrid, Spain
E-mail: jgcalbet@quim.ucm.es

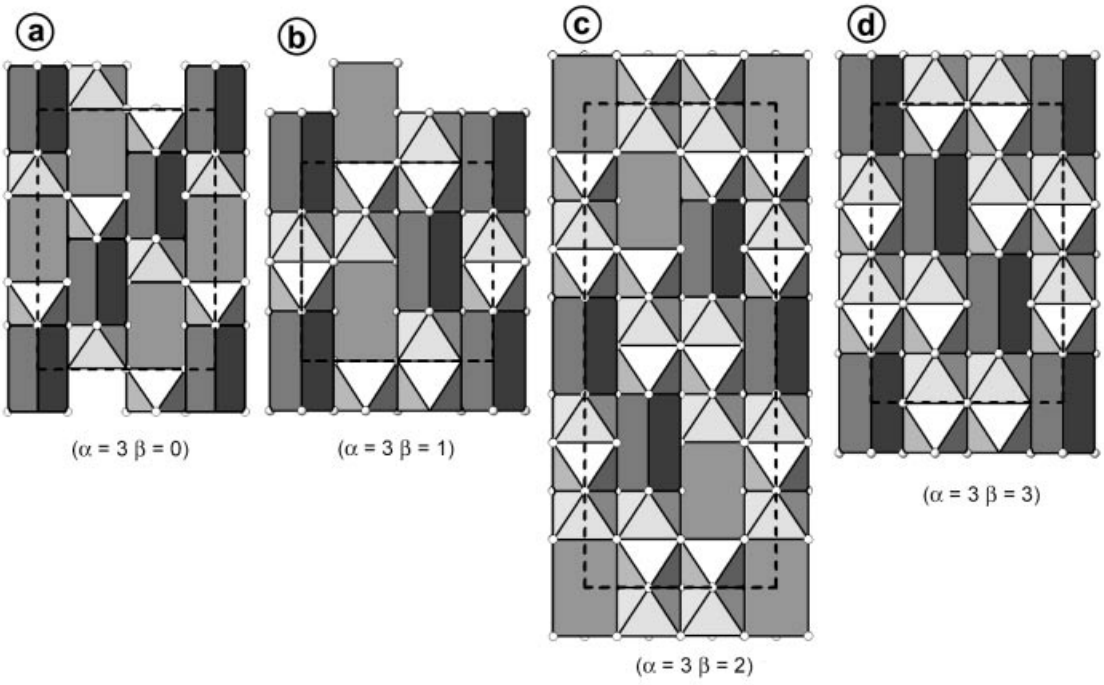

Figure 1. Schematic structures of Ca_3MnZnO_6 (a) and $Ba_6Mn_4ZnO_{15}$ (d), the ($\alpha = 3\,\beta = 0$) and ($\alpha = 3\,\beta = 3$) members of the $(A_3ZnMnO_6)_\alpha(A_3Mn_3O_9)_\beta$ homologous series; ideal structures correspond to intermediate phases of this series: the ($\alpha = 3\,\beta = 1$) (b) and the ($\alpha = 3\,\beta = 2$) (c) members; the unit cells are indicated by dotted lines

maining Zn and Mn distributed in the octahedral sites. A 1D magnetic ordering along the chains is observed due to antiferromagnetic interactions between Mn^{IV} ions. However, the presence of nonmagnetic Zn^{2+} cations in the octahedral environment suppresses the intrachain interaction between Mn atoms and, consequently, magnetic trimers, dimers and isolated $[Mn^{IV}O_6]$ octahedra are created. Uncompensated magnetic moments of the trimers and the isolated octahedra are responsible for the rise in the magnetic susceptibility at low temperature.

Between Ca_3MnZnO_6 ($\alpha = 3\,\beta = 0$) and $Ba_6Mn_4ZnO_{15}$ ($\alpha = 3\,\beta = 3$), two intermediate members can be envisaged. Actually, Figure 1b and 1c correspond to the ideal structures of the ($\alpha = 3\,\beta = 1$) and ($\alpha = 3\,\beta = 2$) terms of the above family. Therefore, in order to synthesise these novel 1D phases containing Mn as the only magnetic cation, we have explored the A−Mn−Zn−O system (A = Ba, Sr,) which has resulted in the stabilisation of $Sr_4Mn_2ZnO_9$ ($\alpha = 3\,\beta = 1$) as a single phase. Attempts to isolate the ($\alpha = 3\,\beta = 2$) term have been successful for the $Ba_5Mn_3ZnO_{12}$ composition although some impurities have been detected. Structurally, both phases can be regarded as a hexagonal array of infinite 1D-chains of face-sharing polyhedra running parallel to the crystallographic *c*-axis. In $Sr_4Mn_2ZnO_9$, two octahedra are linked by one trigonal prism, whereas in $Ba_5Mn_3ZnO_{12}$ one more octahedron is incorporated between the trigonal prisms in the polyhedra rows. The synthetic conditions, microstructural characterisation and magnetic properties are discussed.

Results and Discussion

Figure 2a shows the powder XRD pattern corresponding to $Sr_4Mn_2ZnO_9$. The whole pattern can be indexed on the basis of a trigonal unit cell (*P*321) with parameters $a = 0.9592(1)$ and $c = 0.7823(1)$ nm. On the other hand, the XRD pattern corresponding to $Ba_5Mn_3ZnO_{12}$ (Figure 2b), can be also indexed in a trigonal ($P\bar{3}c1$) unit cell with $a = 1.0060(1)$ and $c = 2.0812(1)$ nm. In fact, both patterns show the characteristic profile of one-dimensional oxides corresponding to the $(A_3A'BO_6)_\alpha(A_3B_3O_9)_\beta$ homologous series,[7] although some broad reflections are observed.

The SAED study sheds more light on the microstructural features of both compounds. For this purpose, it is helpful to consider these one-dimensional oxides as commensurate modulated superstructures of the 2H-hexagonal type. As we have previously reported, the superstructure direction can be expressed as $[\alpha+\beta\ \alpha+\beta\ i\ 2\alpha]^*_{2H}$ [7] and, thus, is related to the number of α and β blocks constituting every phase. The superstructure direction is determined from the $[1\bar{2}10]$ zone axis, which provides the most useful structural information.

$Sr_4Mn_2ZnO_9$

Figure 3a corresponds to the above-mentioned $[1\bar{2}10]$ zone axis of the $Sr_4Mn_2ZnO_9$ sample. All the observed crystals show the same features. The most intense spots correspond to hexagonal 2H planes (referred as sub-index 2H in the figure). The modulation direction, marked with an ar-

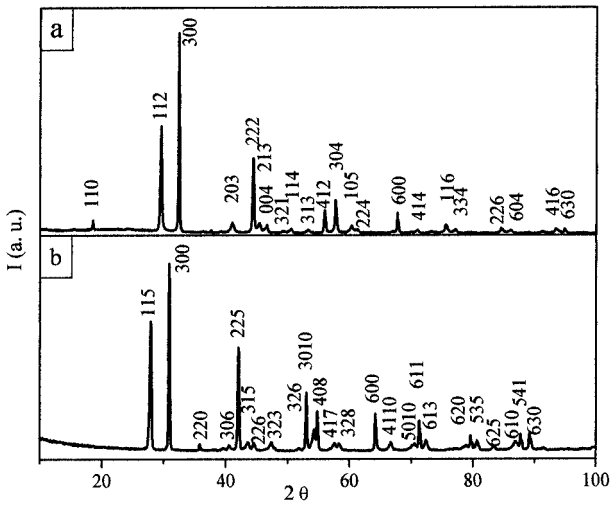

Figure 2. Powder XRD patterns of $Sr_4Mn_2ZnO_9$ (a) and $Ba_5Mn_3ZnO_{12}$ (b)

row, follows the reciprocal $[44\bar{8}6]^*_{2H}$ direction, according to the ($\alpha = 3$ $\beta = 1$) values. However, the features of this SAED pattern also indicate that the microstructure of this 1D-phase must be more complex than that shown by other isostructural oxides. Actually, if this reciprocal plane is compared to the same reciprocal net corresponding to the $(Sr_{0.5}Ca_{0.5})_4Co_3O_9$ isostructural oxide[14] (Figure 3b), some differences can be appreciated. Both SAED patterns present the same structural characteristics but the intensity distribution of the superstructure spots is clearly different. The modulated intensity of such spots, as observed in $(Sr_{0.5}Ca_{0.5})_4Co_3O_9$, is typical of this structure. Following the $[44\bar{8}6]^*_{2H}$ direction, the first-order satellite reflections are the most prominent ones, the intensity decreasing as the satellite order increases. On the contrary, in $Sr_4Mn_2ZnO_9$, such a modulation is not only noticeable along the $[44\bar{8}6]^*_{2H}$ direction but also at 90°, i.e., following the $[\bar{4}\bar{4}86]^*_{2H}$ direction. This feature could be due to twinning, as previously observed in isostructural $Sr_4CuIr_2O_9$.[15]

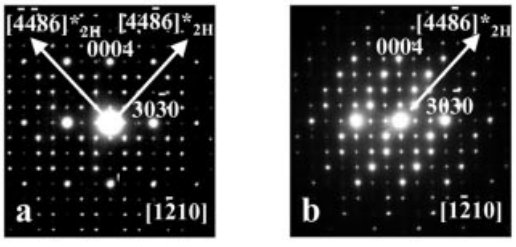

Figure 3. SAED patterns along the $[1\bar{2}10]$ zone axis of $Sr_4Mn_2ZnO_9$ (a) and $(Sr_{0.5}Ca_{0.5})_4Co_3O_9$ (b)

The multitwinned microstructure was confirmed by HREM. The image taken along the $[1\bar{2}10]$ zone axis is shown in Figure 4a. Several domains, tilted 90° to one another around the *c*-axis, are clearly evident. In each domain, d-spacings of 0.83 and 0.78 nm along the *a* and *c* axes, respectively, are observed and these correspond to d_{100} and d_{001} of the ($\alpha = 3$ $\beta = 1$) one-dimensional oxide. The contrast variation in each domain is also characteristic of this member of the series. This is clearly seen in the magnification of one of them (Figure 4b), where it can be observed that, following the *c*-axis, one bright dot alternates with two less-intense ones. We have previously reported that, in all these 1D oxides, the metal columns in the trigonal interstices and the Sr atoms are imaged as bright dots.[16] Therefore, the contrast sequence in this experimental image is as expected for the ...O_hO_hTP... polyhedral sequence in the 1D-chains. The calculated image (inset of Figure 4b) shows a good fit with the experimental one for $\Delta t = 6$ nm and $\Delta f = -65$ nm. It is worth mentioning that the domains are quite narrow, not exceeding approx. 2−3 nm along one direction. The small size of the domains is responsible for the broad reflections observed in the XRD pattern. In addition, the HREM image shows that the twins are coherent since no relative displacement is observed at the twin boundaries. This is outlined in Figure 5 and illustrated in the inset, where a schematic model of two domains of the ($\alpha = 3$ $\beta = 1$) structure meet at the (0001) twin plane. It can be appreciated that both domains are rotated 180° to one another around the twin plane.

The optical Fourier transforms corresponding to domains A and B (Figure 4a) are depicted in Figure 4c and Figure 4d, respectively. In domain A, the superstructure direction follows the $[44\bar{8}6]^*_{2H}$ reciprocal direction, while in domain B, tilted 90° with regard to the former, the satellite reflections are located along the $[\bar{4}\bar{4}86]^*_{2H}$ direction. In both domains, the intensity distribution of the spots is as expected for a modulated superstructure. The juxtaposition of both patterns (Figure 4e) corresponds to the experimental SAED shown in Figure 3a.

In the [0001]* reciprocal plane (Figure 6a) the reflections are distributed in a hexagonal array corresponding to a lattice parameter close to 0.9 nm. All the reflections are visible according to the trigonal *P*321 space group. The corresponding HREM (Figure 6b) also shows the presence of domains tilted by 60°, which are related to the previous twinning. Actually, in this image domains at 60° can be seen around the twin plane ($11\bar{2}0$); this is probably due to a mismatch between the chains.

$Ba_5Mn_3ZnO_{12}$

The SAED study of the title sample shows that it is not a single phase. It is worth noting that, in these 1D-phases, the most intense diffraction maxima are those corresponding to the 2H-subcell and, thus, they appear at very close d-spacings. This fact makes it difficult to detect small amounts of other members of the series that might be present as impurity phases in very small proportion by XRD. However, the SAED study reveals that, although almost all crystals correspond to the expected ($\alpha = 3$ $\beta = 2$) member of this series, a small fraction, presenting the structural features of the ($\alpha = 3$ $\beta = 3$) member, is also detected; such a

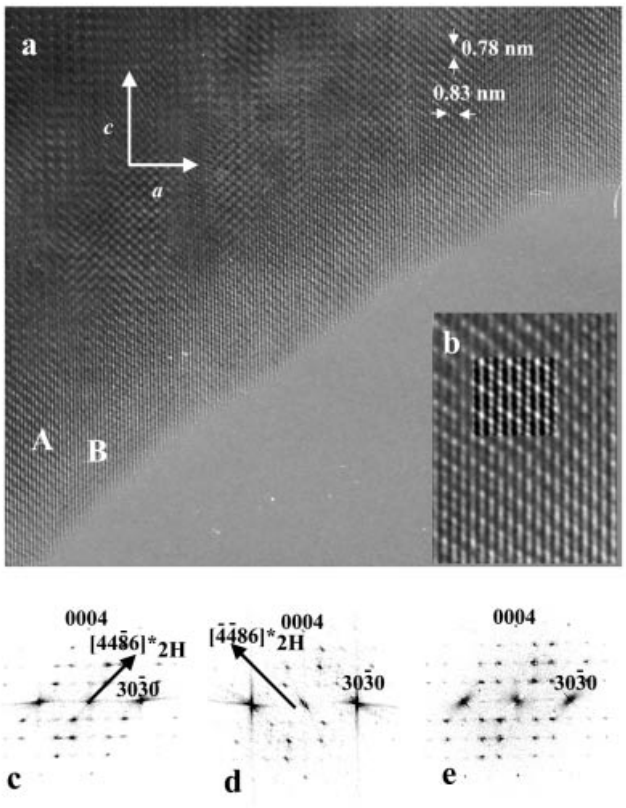

Figure 4. (a) HREM of $Sr_4Mn_2ZnO_9$ along [1$\bar{2}$10]; a twinned microstructure is clearly seen; (b) magnification of one of the microdomains shown in Figure 4a; the calculated image is shown in the inset; optical Fourier transforms (FT) corresponding to domains marked with A (c) and B (d) in Figure 4a; (e) FT corresponding to the juxtaposition of both A and B domains

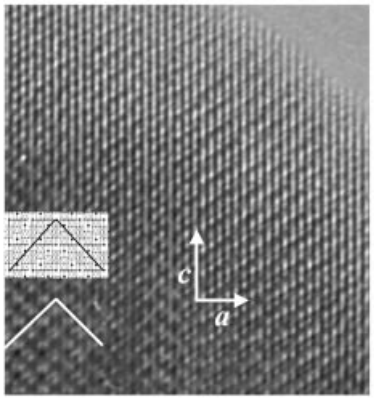

Figure 5. A magnification of the HREM image along [1$\bar{2}$10] showing a coherent twin structure; the twin boundary is labelled; a schematic model illustrating the twin boundary between two (α = 3 β = 1) domains is shown in the inset

member corresponds to the previously reported $Ba_6Mn_4ZnO_{15}$.[12] In spite of this, the majority of the phase corresponds to the new (α = 3 β = 2) member of the series and, therefore, we have performed the microstructural study of this phase.

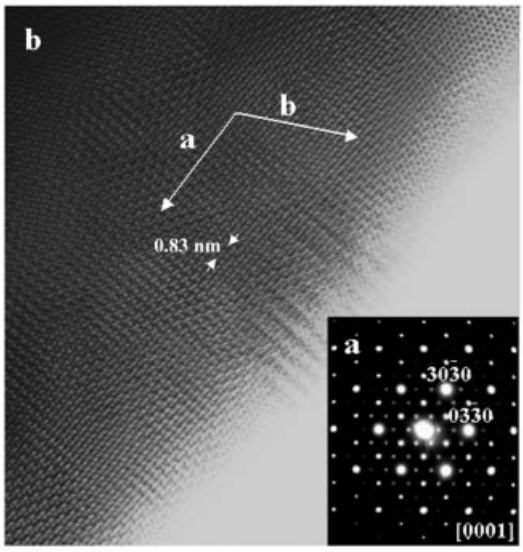

Figure 6. (a) SAED pattern corresponding to $Sr_4Mn_2ZnO_9$ along [0001]; (b) corresponding HREM image

The SAED pattern along the [1$\bar{2}$10] zone axis of the majority phase is shown in Figure 7a. EDS analysis performed on these crystals is in agreement with the nominal cationic ratio. The structural features of this pattern are those corresponding to the (α = 3 β = 2) member. Actually, only the 00l, $l = 2n$ reflections are visible ($P\bar{3}c1$ space group) and the modulation direction follows the $[55i6]^*_{2H}$ reciprocal axis. Once again, the intensity distribution of the spots suggests a twinned microstructure. As can be seen, satellite reflections appear not only along the $[55i6]^*_{2H}$ direction, as expected for this structure, but also along $[\bar{5}\bar{5}i6]^*_{2H}$ in a similar manner to that observed for $Sr_4Mn_2ZnO_9$. The presence of domains, tilted nearly 90° to each other, is clearly visible in the HREM taken along the [1$\bar{2}$10] direction (Figure 7b). Each domain shows the characteristic image of this (α = 3 β = 2) member and the calculated image (inset) is in agreement with the experimental one for Δt = 3.5 nm and Δf = −70 nm. The twin plane follows the [0001] direction, as in the previous case, but the domain size is much larger.

Taken together the SAED and HREM results indicate that both 1D oxides present a twinned microstructure. In order to establish if such a feature is a general characteristic of all Zn−Mn 1D oxides, we also studied oxide $Ba_6Mn_4ZnO_{15}$,[12] i.e., the (α = 3 β = 3) member of the series, by means of SAED and HREM. This oxide incorporates one more octahedron between the trigonal prisms than the previous $Ba_5Mn_3ZnO_{12}$ phase. The unit cell has rhombohedral symmetry ($R32$) with parameters a = 1.004 and c = 1.283 nm. The corresponding SAED pattern along [1$\bar{2}$10] is shown in Figure 8a. The superstructure spots appear not only along the $[66i6]_{2H}$ direction but also along the $[\bar{6}\bar{6}i6]_{2H}$ reciprocal direction and, consequently, a pseudotrigonal symmetry results. Once again, this is related to the presence of twinning as evidenced in the HREM along the

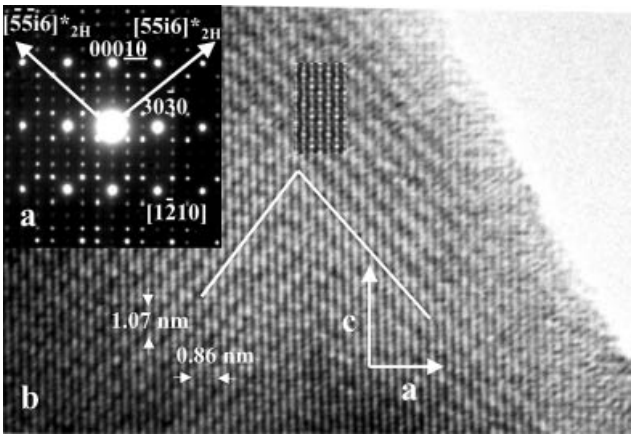

Figure 7. (a) SAED pattern corresponding to $Ba_5Mn_3ZnO_{12}$ along [1$\bar{2}$10]; (b) corresponding HREM image

same zone (Figure 8b). All the crystals checked exhibit the same features.

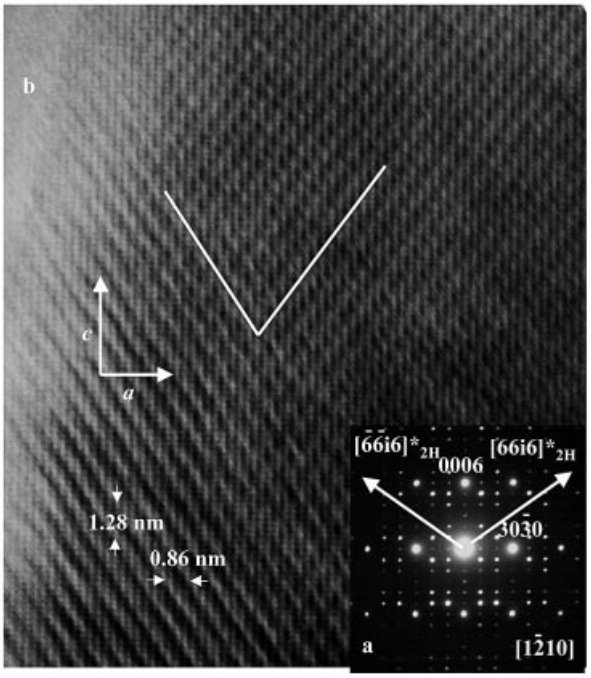

Figure 8. (a) SAED pattern corresponding to $Ba_6Mn_4ZnO_{15}$ along the [1$\bar{2}$10] zone axis; (b) corresponding HREM image; a twin plane is outlined

The stabilisation of one-dimensional oxides in the A−Mn−O system is a new example of the flexibility of the oxygen polyhedra chain in accommodating metal cations of very different size. The small size of Mn^{4+} (r_i = 0.53 Å) when compared with Zn^{2+} (r_i = 0.74 Å)[17] should give rise to a regular distribution of both transition metals in such a way that Zn would occupy the TP sites while Mn would be located in the octahedral ones. This is the case for Ca_3ZnMnO_6,[9] where [MnO_6] octahedra and [ZnO_6] trigonal prisms form a 1D chain with no sign of disorder between the metals over the two different sites. However, when the number of octahedra between trigonal prisms increases, it seems that both transition metals can be accommodated in the same oxygen environment. Neutron diffraction data on $Ba_6Mn_4ZnO_{15}$ [12] indicate that Mn^{4+} and Zn^{2+} ions are distributed in equal concentration in the trigonal prismatic polyhedra; consequently, Zn must also located in the octahedral sites.

The origin of the twinning cannot be easily determined, although it could be related to the cationic disorder in the structure. In this sense, it is worth noting that the presence of twinning related to cationic disorder has been previously reported in Sr_3CuPtO_6.[18] This compound crystallises in a distorted monoclinic structure (*C*2/*c*) closely related to the trigonal unit cell corresponding to the (α = 3 β = 0) member of this 1D homologous series. In this oxide, in which the single crystal X-ray diffraction data indicate that some disorder between Cu and Pt cations could exist, all crystals appear heavily twinned. Moreover, it is also noticeable that Ca_3ZnMnO_6,[9] in which an ordered distribution of Zn (into the TP sites) and Mn (into the O_h ones) is achieved, is the only 1D Zn/Mn-containing oxide that does not present a twinning microstructure. Figure 9 shows the SAED pattern corresponding to Ca_3ZnMnO_6 along the [1$\bar{2}$10] zone axis. A threefold superstructure is visible along the $[33i6]_{2H}$ reciprocal direction, corresponding to the (α = 3 β = 0) member of the series. The lack of superstructure maxima along the $[\bar{3}\bar{3}i6]_{2H}$ direction indicates that this is an untwinned compound. Although we do not have direct evidence of the cationic distribution in the new reported phases, it seems plausible to assume that increasing the number of octahedra between the trigonal prisms could facilitate the interchange between cations, giving rise to some cationic disorder. Such a disorder could be accompanied by local structural deformations which introduce some structural strain that is compensated by twin formation, as observed by HREM. The structural foundation of this observation will be further studied by neutron diffraction.

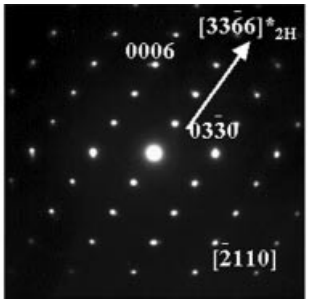

Figure 9. SAED pattern corresponding to Ca_3MnZnO_6 along [1$\bar{2}$10].

On the other hand, when the micrographs corresponding to $Ba_6Mn_4ZnO_{15}$ (Figure 8b), $Ba_5Mn_3ZnO_{12}$ (Figure 7b) and $Sr_4Mn_2ZnO_9$ (Figure 4a) are compared, it can be appreciated that the domain size decreases as the TP/O_h ratio increases. Actually, the highest concentration of twin planes is attained when the number of polyhedra per row and unit cell is lower. This feature seems to indicate that the struc-

tural strains are more pronounced when the Zn^{2+} ions can be distributed over a smaller number of octahedral sites. In addition, the smaller size of Sr^{2+}, in comparison to the Ba^{2+} cations, generates polyhedral sites of smaller volume, which increase the structural strain originating from the incorporation of Zn into the octahedral holes, thus supporting the small domain size in $Sr_4Mn_2ZnO_9$.

Magnetic Properties

The temperature dependence of the magnetic susceptibility corresponding to the single phase $Sr_4Mn_2ZnO_9$ measured at $H = 1000$ Oe is depicted in Figure 10a. The ZFC and FC data overlap in the temperature range measured and show a broad maximum at a temperature close to 100 K. At lower temperature (below 40 K), a sharp increase of the susceptibility is observed. The susceptibility curve cannot be fitted by a Curie−Weiss law over any temperature range.

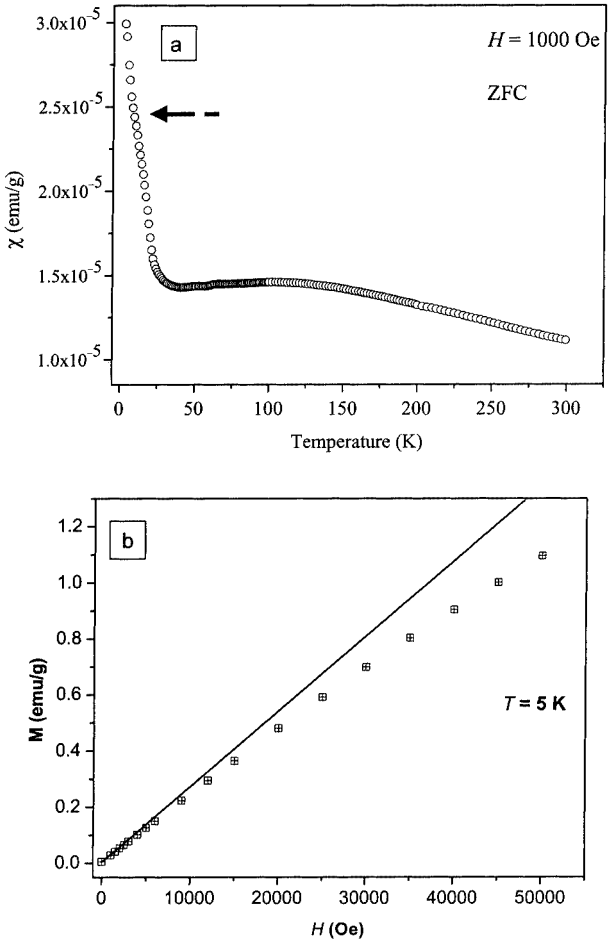

Figure 10. (a) Temperature dependence of the magnetic susceptibility of $Sr_4Mn_2ZnO_9$ at H = 1000 Oe; (b) magnetisation vs. applied field at 5 K; a nonlinear magnetisation field dependence is clearly observed

The magnetic behaviour of this 1D oxide is quite similar to that observed in $Ba_6Mn_4ZnO_{15}$,[12] although, in this case, the broad maximum is shifted to lower temperatures (50 K). The presence of such a maximum is characteristic of a 1D magnetic behaviour and it represents the onset of the 1D ordering along the chains. Such an ordering corresponds to antiferromagnetic interactions between Mn^{4+} in the chain, and therefore low magnetic susceptibility values are obtained in the measured temperature range. The increase of the number of octahedra between prisms seems to result in a weakening of the intrachain interactions and, consequently, the broad maximum is shifted to lower temperatures.

On the other hand, as can be observed in Figure 10a, the susceptibility passes through a local minimum and increases below 40 K. This rise of the magnetic susceptibility has also been observed in $Ba_6Mn_4ZnO_{15}$ and is associated with the presence of uncompensated magnetic moments that result from the irregular distribution of Mn^{4+} and Zn^{2+} in the polyhedra chains. Thus, these results agree with the presence of cationic disorder in the polyhedra chains in this new phase.

Unlike $Ba_6Mn_4ZnO_{15}$,[12] in which the 3D ordering is not observed in the magnetic susceptibility, the susceptibility curve corresponding to $Sr_4Mn_2ZnO_9$ shows a very small inflexion (marked in Figure 10a with an arrow) at about 7 K. This feature can be associated with a transition from 1D to 3D magnetic ordering. This weak interchain interaction is confirmed by slight nonlinear magnetisation-field dependence (Figure 10b). This different behaviour could be a consequence of the smaller interchain distance in the Sr compound due to their smaller size compared to Ba oxides.

It is worth recalling that a similar 1D-3D transition has previously been reported in Ca_3MnNiO_6.[9] The temperature-dependence susceptibility curve for this oxide is analogous to that corresponding to $Sr_4Mn_2ZnO_9$. Actually, a broad peak at around 100 K, attributed to a 1D antiferromagnetic ordering, and a small inflexion at 20 K, associated with a 3D ordering, are observed. This long range (3D) ordering has been confirmed by a neutron diffraction study.

Experimental Section

Polycrystalline $Sr_4Mn_2ZnO_9$ and $Ba_5Mn_3ZnO_{12}$ were synthesised by the ceramic procedure by heating stoichiometric amounts of ACO_3 (A = Sr, Ba; Aldrich, 99.9+%), $MnCO_3$ (Aldrich, 99.9+%) and ZnO (Aldrich, 99.99%) in air. The former was treated at 875 °C for five days and the latter at 1050 °C for six days with intermediate grindings. In both cases the products were quenched to room temperature.

The average cationic composition was determined by ICP while the local composition in every crystal was established by X-ray Energy Dispersive Spectroscopy (EDS). For this purpose, a JEOL 2000 FX electron microscope equipped with a OXFORD ISIS 300-analyser system was employed. Chemical compositions are consistent with the nominal ones.

Powder X-ray diffraction (XRD) patterns were collected with Cu-K_α radiation at room temperature on a PHILIPS X′PERT diffractometer equipped with a graphite monochromator.

Selected-area electron diffraction (SAED) was carried out using a JEOL 2000FX electron microscope fitted with a double-tilting

goniometer stage (±45°). High resolution electron microscopy (HREM) was performed on a JEOL 4000EX electron microscope fitted with a double-tilting goniometer stage (±25°). Simulated HREM images were calculated by the multislice method using the MacTempas software package.

Magnetic susceptibility was measured with a SQUID magnetometer in a temperature range from 5 to 300 K, under a maximum applied magnetic field of 5 T.

Acknowledgments

Financial support through research project MAT2001-1440 (CICYT, Spain) is acknowledged.

[1] J. J. Lander, *Acta Crystallogr.* **1951**, *4*, 148−156.
[2] G. Bergerhoff, O. Schmitz-Dumont, *Z. Anorg. Allg. Chem.* **1956**, *284*, 10−14.
[3] J. Darriet, M. A. Subramanian, *J. Mater. Chem.* **1995**, *6*, 543−552.
[4] P. D. Battle, G. R. Blake, J. Darriet, J. G. Gore, F. Weill, *J. Mater. Chem.* **1997**, *7*, 1559−1564.
[5] M. Evain, F. Boucher, O. Gourdon, V. Petricok, M. Dusek, P. Bezdicka, *Chem. Mater.* **1998**, *10*, 3068−3076.
[6] M. Zakhour-Nakhl, J. B. Claridge, J. Darriet, F. Weill, H. C. zur Loye, J. Pérez-Mato, *J. Am. Chem.* Soc. **2000**, *122*, 1618−1623.
[7] K. Boulahya, M. Parras, J. M. González-Calbet, *Chem. Mater.* **2000**, *12*, 25−32.
[8] S. Aasland, H. Fjellvåg, B. C. Hauback, *Solid State Commun.* **1997**, *3*, 187−192.
[9] S. Kawasaki, M. Takano, T. Inami, *J. Solid State Chem.* **1999**, *145*, 302−308.
[10] S. Niitaka, H. Kageyama, M. Kato, K. Yoshimura, K. Kosuge, *J. Solid State Chem.* **1999**, *146*, 137−143.
[11] J. Darriet, F. Grasset, P. D. Battle, *Mater. Res. Bull.* **1997**, *32*, 139−150.
[12] E. J. Cussen, J. F. Vente, P. D. Battle, *J. Am. Chem. Soc.* **1999**, *121*, 3958−3967.
[13] W. T. A. Harrison, S. L. Hegwood, A. J. Jacobson, *J. Chem. Soc., Chem. Commun.* **1995**, 1953−1954.
[14] K. Boulahya, M. Parras, J. M. González-Calbet, *J. Solid State Chem.* **1999**, *145*, 116−127.
[15] P. D. Battle, G. Blake, J. Sloan, J. F. Vente, *J. Solid State Chem.* **1998**, *136*, 103−114.
[16] K. Boulahya, M. Parras, J. M. González-Calbet, *J. Solid State Chem.* **1999**, *142*, 419−427.
[17] R. D. Shannon, *Acta Crystallogr., Sect. A* **1976**, *32*, 751−767.
[18] J. L. Hodeau, H. Y. Tu, P. Bordet, T. Fournier, P. Strobel, M. Marezio, *Acta Crystallogr., Sect. B* **1992**, *48*, 1−11.

Received April 21, 2002
[I02210]

Preparation and Electrochemical Properties of Polynuclear Organometallic Complexes Derived from Ferrocene-Containing Bidentate Ligands

Ryo Horikoshi,[a] Tomoyuki Mochida,*[a] Reiko Torigoe,[a] and Yasuhiro Yamamoto[a]

Keywords: Bridging ligands / Cyclic voltammetry / Ruthenium / Rhodium / Iridium / Metallocenes

The reaction of the ferrocene-containing bridging ligands 1,1′-bis(4-pyridylthio)ferrocene (**1**), 1′,1‴-bis(4-pyridylthio)biferrocene (**2**), and 1′,1‴-bis(diphenylphosphanyl)biferrocene (**3**), with the chloro-bridged dinuclear complexes $[(p\text{-cymene})RuCl(\mu\text{-}Cl)]_2$ and $[Cp^*MCl(\mu\text{-}Cl)]_2$ (M = Rh, Ir) affords trinuclear and tetranuclear metal complexes in good yields: $[\{(p\text{-cymene})RuCl(\mu\text{-}Cl)\}_2(\mu\text{-}L)]$ (**4**: L = **1**; **7**: L = **2**; **10**: L = **3**), $[\{Cp^*MCl(\mu\text{-}Cl)\}_2(\mu\text{-}L)]$ (**5**: L = **1**, M = Rh; **6**: L = **1**, M = Ir, **8**: L = **2**, M = Rh; **9**: L = **2**, M = Ir; **11**: L = **3**, M = Rh; **12**: L = **3**, M = Ir). The molecular structures of **3** and **5** have been determined by X-ray structure analysis. These complexes show quasi-reversible redox processes of the bridging ligands as well as irreversible redox processes of the terminal metal ions. Reaction of $[\{Cp^*MCl(\mu\text{-}Cl)\}_2(\mu\text{-}\mathbf{1})]$ with $AgPF_6$ affords $[\{(Cp^*M)_4(\mu\text{-}Cl)_4\}(\mu\text{-}\mathbf{1})_2](PF_6)_4$ (**13**: M = Rh, **14**: M = Ir), which are chloro-bridged polynuclear complexes.

Introduction

Metal-containing supramolecules and coordination polymers have attracted much interest in recent years, and a variety of supramolecular compounds have been prepared by the spontaneous self-assembly of metal ions and spacer ligands.[1−10] Recently it has been shown that supramolecular architectures can be constructed in a stepwise manner, using organometallic compounds.[11−16] Molecular squares and boxes have been synthesized by combining bidentate ligands, which have organometallic building blocks containing octahedral metals of Ru,[11,12] Rh[13,14] or Ir[15,16], with arene, cyclopentadienyl or pentamethylcyclopentadienyl (Cp*) groups.

The redox activities of ferrocene and biferrocene derivatives are well documented,[17] and we have recently synthesized redox-active bridging ligands containing ferrocene and have characterized their coordination polymers.[18] The syntheses of organometallic polynuclear compounds of Ru, Rh, and Ir with ferrocene- and biferrocene-based bidentate ligands are reported here. These compounds may be useful as redox-active building blocks for supramolecules showing multi-step redox properties. This paper describes the preparation and electrochemical properties of a series of tri- and tetranuclear organometallic complexes containing bidentate ligands of 1,1′-bis(4-pyridylthio)ferrocene (**1**), 1′,1‴-bis(4-pyridylthio)biferrocene (**2**), and 1′,1‴-bis(diphenylphosphanyl)biferrocene (**3**), as shown in Scheme 1: $[\{(p\text{-cymene})RuCl(\mu\text{-}Cl)\}_2(\mu\text{-}L)]$ (**4**: L = **1**; **7**: L = **2; 10**: L = **3**), $[\{Cp^*MCl(\mu\text{-}Cl)\}_2(\mu\text{-}L)]$ (**5**: L = **1**, M = Rh; **6**: L = 1, M = Ir, **8**: L = **2**, M = Rh; **9**: L = **2**, M = Ir; **11**: L = **3**, M = Rh; **12**: L = **3**, M = Ir). Coupling reactions of the trinuclear complexes were also investigated; treatment of **5** or **6** with $AgPF_6$ afforded $[\{(Cp^*M)_4(\mu\text{-}Cl)_4\}(\mu\text{-}\mathbf{1})_2](PF_6)_4$ (**13**: M = Rh, **14**: M = Ir), which are chloro-bridged polynuclear complexes.

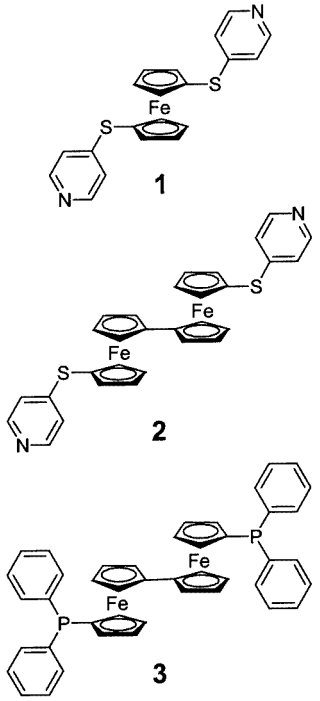

Scheme 1. Ferrocene-based bridging ligands: 1,1′-bis(4-pyridylthio)-ferrocene (**1**), 1′,1‴-bis(4-pyridylthio)biferrocene (**2**), and 1′,1‴-bis(diphenylphosphanyl)biferrocene (**3**)

[a] Department of Chemistry, Faculty of Science, Toho University, Miyama, Funabashi, Chiba 274−8510, Japan
Fax: (internat.) +81-47/472-4406
E-mail: mochida@chem.sci.toho-u.ac.jp

 © 2002 WILEY-VCH Verlag GmbH & Co. KGaA, 69451 Weinheim 1434−1948/02/1212−3197 $ 20.00+.50/0

Results and Discussion

Preparation and Properties of the Bridging Ligands 1, 2, and 3

The bidentate ligands 1,1′-bis(4-pyridylthio)ferrocene (**1**), 1′,1‴-bis(4-pyridylthio)biferrocene (**2**), and 1′,1‴-bis(diphenylphosphanyl)biferrocene (**3**) were chosen so as to generate bridged polynuclear complexes, rather than chelate ones. The ligand **1** was synthesized as reported previously,[18] and **2** and **3** were synthesized from dilithiobiferrocene. The ligand **3** is a biferrocene analogue of 1,1′-bis(diphenylphosphanyl)ferrocene (dppf), although dppf mostly forms chelate complexes.[17,19−23] The molecular structure of **3** has been characterized by X-ray crystallography. An ORTEP[24] view of the compound is shown in Figure 1 along with the numbering scheme. The molecule sits on a crystallographic inversion centre and the phosphorus atoms are arranged in opposite directions, demonstrating the versatility of this ligand as a bidentate. The distances from the iron atom to the Cp planes are approximately 1.64 Å, which is typical for neutral ferrocene. The bond lengths and angles around the phosphorus atom are similar to those found in dppf.[25]

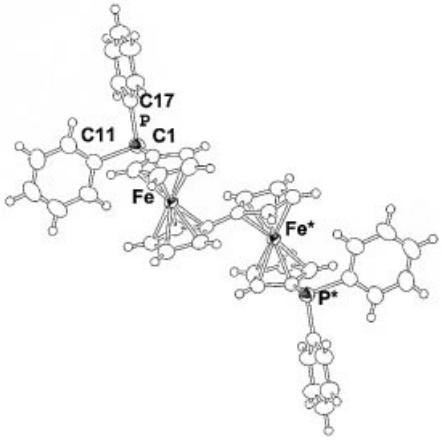

Figure 1. An ORTEP drawing of the molecular structure **3** with the atom numbering scheme; displacement ellipsoids are shown at the 50% probability level; selected bond lengths (Å) and angles (°): P(1)−C(1) 1.815(3), P(1)−C(11) 1.847(2), P(1)−C(17) 1.836(2), C(1)−P(1)−C(11) 99.4(1), C(1)−P(1)−C(17) 102.1(1), C(11)−P(1)−C(17) 101.2(1)

The redox properties of **2** and **3** were investigated by cyclic voltammetry. Complex **2** shows two quasi-reversible redox waves of the biferrocenyl moiety at $E_{1/2}$ = 0.14 V and 0.37 V (vs. $FeCp_2/FeCp_2^+$), exhibiting slight positive shifts relative to biferrocene, due to the electron-withdrawing effect of the pyridinethio moieties. The complex **3** exhibits several complicated redox waves; these could not be analyzed, although peaks corresponding to the oxidations of the biferrocene moiety were identified at $E_{1/2}$ = 0.03 V and 0.40 V (vs. $FeCp_2/FeCp_2^+$). The redox behaviour might be analogous to that of dppf,[26] in which oxidation is accompanied by reactions such as intermolecular coupling of the phosphorus groups, giving rise to complicated behaviour.

Preparation and Characterization of the Polynuclear Complexes

Reactions of the ferrocene-containing ligands **1**−**3** with the chloro-bridged dinuclear complexes [(*p*-cymene)RuCl(μ-Cl)]$_2$ and [Cp*MCl(μ-Cl)]$_2$ (M = Rh, Ir) produced tri- and tetranuclear metal complexes **4**−**12**, in good yields. Satisfactory analytical data were obtained for all products. The NMR spectroscopic and elemental analysis data confirm the 2:1 molar ratio of the organometallic moieties and the bridging ligands. These compounds are air-stable and are soluble in common polar organic solvents.

The trinuclear molecular structure of **5** was confirmed by X-ray structure analysis. An ORTEP view of the trinuclear complex is shown in Figure 2, along with the numbering scheme. The coordination environment of the rhodium atom is pseudooctahedral, with N(1)−Rh(1)−Cl(1), N(1)−Rh(1)−Cl(2), N(2)−Rh(2)−Cl(3), N(2)−Rh(2)−Cl(4) angles of 88.7(3), 87.0(2), 89.1(3), and 86.8(3) °, respectively, and Rh(1)−N(1) and Rh(2)−N(2) distances of 2.117(8) and 2.127(9) Å, respectively. The cyclopentadienyl rings are located ca. 1.77 Å away from the rhodium atom. The conformation of the two ferrocenyl rings is synclinal (eclipsed) with an S···S separation of ca. 4.26 Å. The ferrocenyl rings are planar and located 1.65 Å away from the iron atom.

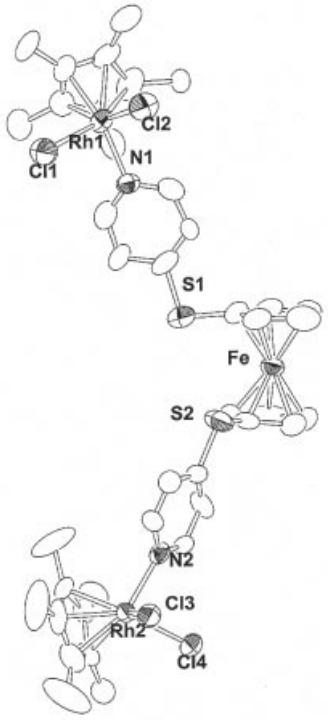

Figure 2. An ORTEP drawing of the molecular structure **5** with the atom numbering scheme; displacement ellipsoids are shown at the 50% probability level; selected bond lengths (Å) and angles (°): Rh(1)−N(1) 2.117(8), Rh(2)−N(2) 2.127(9), S(1)−C(1) 1.743(13), S(1)−C(11) 1.782(11), S(2)−C(6) 1.711(13), S(2)−C(16) 1.766(11), C(1)−S(1)−C(11) 103.5(6), C(6)−S(2)−C(16) 104.6(6)

The ^{1}H NMR spectra of the pyridine-ligated complexes **4**−**9** show two doublets at around δ(H_α) = 8.6 and δ(H_β) =

6.8 ppm, which are assigned to the metal-coordinated pyridine ring protons. The chemical shifts of the pyridyl α-protons are shifted downfield by 0.3−0.4 ppm relative to those of the free ligands of **1** [$\delta(H_\alpha)$ = 8.31, $\delta(H_\beta)$ = 6.89 ppm][18] and **2** [$\delta(H_\alpha)$ = 8.24, $\delta(H_\beta)$ = 6.83 ppm]. The NMR spectroscopic signals of the ferrocenyl protons in complexes **4**−**10** are observed at almost identical positions to those of the corresponding free ligands **1**−**3**. The signals of the ferrocenyl protons in **11** and **12** are very broad at room temperature, and become sharper when the temperature is lowered to −60 °C.

The ^{31}P NMR spectroscopic signals of the phosphane-ligated complexes **10**−**12** are observed at δ = 18.99, 22.33 and −8.53 ppm, respectively, and show significant low-field shifts relative to the free ligand **3**. The chemical shifts have reasonable values for metal-coordinated phosphorus atoms.[27−29]

Self-coupling reactions of the trinuclear complexes **5** or **6** were performed by treating these complexes with $AgPF_6$. The yields were low — 27% and 16% for **13** and **14**, respectively — and recovery of the starting materials was mainly observed, with no significant side products. Based on the spectroscopic data, elemental analysis data, and the 18-electron rule, these products are considered to be chloro-bridged polynuclear complexes. Infrared spectra of the products exhibit characteristic P−F stretching vibrations at 1112, 848 and 558 cm^{-1}, showing the presence of the PF_6^- anion. The ^1H NMR spectroscopic signals of the Cp* protons are observed at higher fields than those of the precursors **5** and **6**, which may be a consequence of changes in the electron density on the metal centres. The ^1H NMR spectroscopic signals of the bridging moieties are observed at slightly lower fields than the precursors. Although we could not determine the crystal structures of **13** and **14**, we speculate that these complexes are most likely to have dimeric structures, i.e. n = 2 in Scheme 2, because of their close resemblance to the tetranuclear chloro-bridged complexes of $[\{Cp^*M(\mu\text{-}Cl)\}_4L_2]X_4$ (M = Rh, Ir).[13,14] The present complexes are soluble in common organic solvents such as dichloromethane, acetonitrile, and methanol, suggesting that they are oligomers and not coordination polymers.[18]

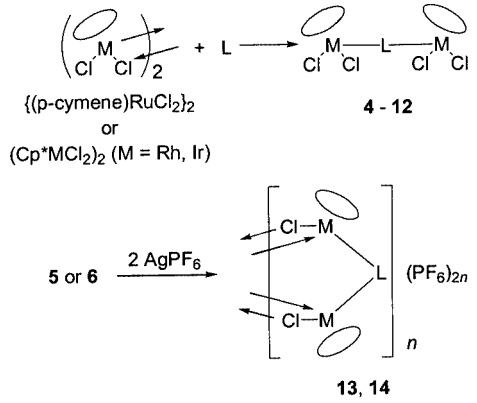

Scheme 2. General reaction scheme

Electrochemical Properties of the Trinuclear and Tetranuclear Complexes

The redox properties of complexes **4**−**10** were investigated by cyclic voltammetry. Figure 3 and 4 show the cyclic voltammograms in dichloromethane solutions. The redox potentials are listed in Table 1. Cyclic voltammetry studies on complex **4** revealed that there are two oxidation waves at 0.50 and 0.93 V (vs. $FeCp_2/FeCp_2^+$), and one reduction wave at 0.34 V. The redox waves around 0.4 V are assigned to the redox processes of the ferrocene moiety, and the oxidation wave at 0.93V is assigned to that of the Ru^{II} to Ru^{III} process.

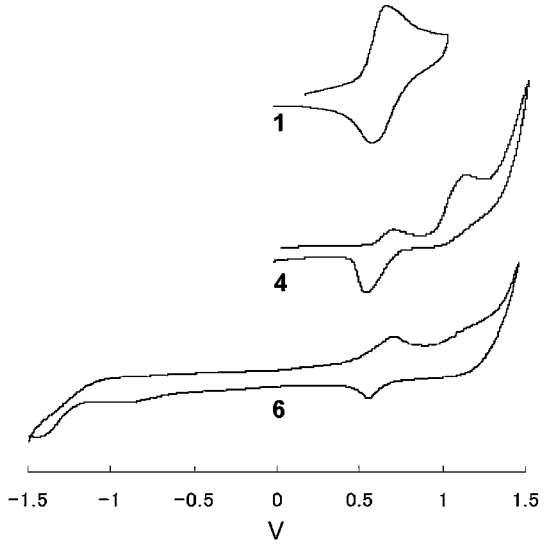

Figure 3. Cyclic voltammograms (vs. Ag/Ag^+) of **1**, **4** and **6**

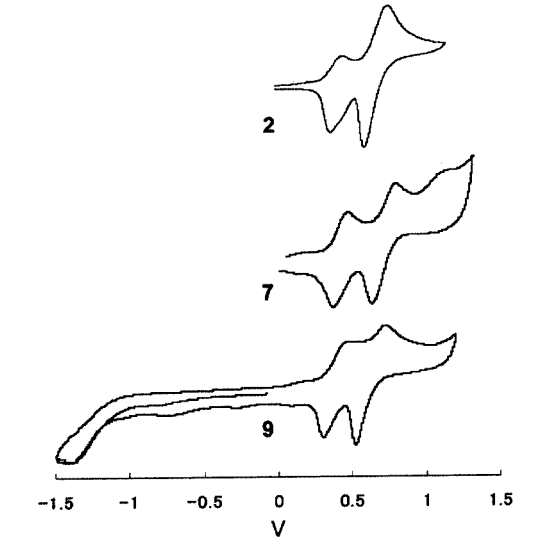

Figure 4. Cyclic voltammograms (vs. Ag/Ag^+) of **2**, **7** and **9**

The cyclic voltammogram of complex **5** exhibits an irreversible reduction wave of the Rh^{III} state at −1.60 V, and a quasi-reversible redox wave of the bridging ligand at $E_{1/2}$ = 0.45 V. Similarly, the cyclic voltammogram of the iridium

Table 1. Redox potentials (in V vs. $FeCp_2/FeCp_2^+$)

Compound	E_{pc} (Rh, Ir)	E_{pc} E_{pa} (1st ferrocene)		E_{pc} E_{pa} (2nd ferrocene)		E_{pa} (Ru)
1		0.38	0.48			
2		0.11	0.17	0.30	0.44	
3		–	0.03[a]	0.21 [a]	0.55	
4		0.34	0.50			0.93
5	−1.60	0.35	0.52			
6	−1.54	0.41	0.57			
7		0.13	0.22	0.36	0.51	0.84
8	−1.64	0.09	0.27	0.25	0.50	
9	−1.64	0.10	0.28	0.34	0.54	
10		–	0.02	–	0.30	0.73

[a] Several unresolved redox waves were also present

complex **6** exhibits an irreversible reduction wave of the metal ion at −1.54 V, and a quasi-reversible redox wave of the bridging ligand at $E_{1/2} = 0.47$ V. It seems that the redox potentials of the ferrocene moiety roughly increase in the order $E_{1/2}$ (**1**) < $E_{1/2}$ (**5**: M = Rh) < $E_{1/2}$ (**6**: M = Ir). This tendency is consistent with the stronger electron-withdrawing nature of the Ir complex than that of the Rh complex.

The biferrocene-containing ruthenium complex **7** shows two quasi-reversible and one irreversible oxidation wave. The reversible ones [$E_{1/2}(1) = 0.17$ V, $E_{1/2}(2) = 0.44$ V] are assigned to the redox processes of the biferrocene moiety, and the irreversible one ($E_{pa} = 0.84$ V) to that of the ruthenium ion. The rhodium and iridium complexes of **8** and **9** show two quasi-reversible and one irreversible reduction wave on scanning from 0 to −1.5 V. It seems that the redox potentials of the biferrocene moiety roughly increase in the order $E_{1/2}$ (**2**) < $E_{1/2}$ (**8**: M = Rh) < $E_{1/2}$ (**9**: M = Ir), showing a similar tendency to the derivatives of **1**. Since the redox spectra of the terminal metal ions exhibit only one wave in **4**−**9**, it follows that interactions between the terminal metal ions through the bridging ligand are negligible.

The diphenylphosphanyl-coordinated complexes **10**−**12** show highly complicated redox behaviours compared with the pyridine-coordinated complexes **4**−**9**. The redox behaviour of complex **10** is slightly clearer than that of its precursor **3**; three oxidation processes for the biferrocene moiety and the Ru^{II} centre can be discerned, although these are irreversible. It is conceivable that the addition of the end-capping groups prevents chemical reactions such as intermolecular coupling,[26] which complicate the redox processes of **3**. The first oxidation process of the biferrocene moiety in **10** is quasi-reversible on scanning from 0 to 0.15 V, although both the first and the second waves become irreversible on scanning from 0 to 0.40 V. In complexes **4**−**9**, the redox processes of the ferrocene moiety are only slightly affected by the coordination of the metal ions. This is probably because the sulfur bridge terminates the conjugation between the ferrocene moiety and the pyridyl group. By contrast, coordination of the metal ions to the phosphorus atom in **3** leads to significant interaction between the metal ions and the ferrocene moieties, which could complicate the redox behaviour of **10**−**12**.

Experimental Section

General Remarks: All reactions were carried out by Schlenk techniques under nitrogen. Reagent grade solvents were dried, distilled, and stored under a nitrogen atmosphere. The starting complexes [(*p*-cymene)RuCl(μ-Cl)]$_2$ [30] and [Cp*MCl(μ-Cl)]$_2$ (M = Rh, Ir),[31,32] and the bridging ligand **1**[18] were prepared by a published procedure.

Elemental analyses were performed using a Yanagimoto C−H−N recorder (MT-3) and Elementar Vario EL. Infrared spectra were recorded on a JASCO FT-IR 230 spectrometer as KBr pellets in the 4000−400 cm^{-1} range. NMR spectra were recorded on a JEOL JNM-ECL-400 spectrometer. Chemical shifts are cited relative to $SiMe_4$ (^1H) and 85% H_3PO_4 (^{31}P). Cyclic voltammograms were obtained with an ALS/chi electrochemical-analyzer, model 600A. The working electrode was a glassy disk electrode with an Ag/Ag^+ reference electrode. NBu_4ClO_4 and CH_2Cl_2 were used as the supporting electrolyte and solvent, respectively.

Synthesis of 1′,1‴-Bis(4-pyridylthio)biferrocene (2): A THF solution (10 mL) of 4,4′-dipyridyl disulfide (660 mg, 3 mmol) was added dropwise to a suspension of dilithiobiferrocene, prepared from dibromobiferrocene (528 mg, 1 mmol), in THF (30 mL) at −80 °C for 4 h, and left to stir at room temperature for 4 h. The resulting brown solution was filtered, the solvent evaporated, and the orange residue dissolved in chloroform. Concentration of the solution to ca. 10 mL and addition of diethyl ether gave **2** as an orange solid. Further purification was achieved by recrystallization from chloroform/acetonitrile (1:1 v/v) as an orange solid that was obtained in a yield of 53% (312 mg). $C_{30}H_{24}Fe_2N_2S_2$ (588.36): calcd. C 61.20, H 4.11, N 4.76; found C 60.91, H 4.12, N 4.56. ^1H NMR (400 MHz, $CDCl_3$, 25 °C): δ = 4.16 (m, 4 H), 4.26 (m, 4 H), 4.34 (m, 4 H), 4.51 (m, 4 H), 6.83 (m, 4 H), 8.24 (m, 4 H) ppm. IR (KBr): $\tilde{\nu}$ = 3094 cm^{-1} (m), 1575 (s), 1479 (m), 1409 (m), 802 (m), 705 (s), 494 (m), 418 (m).

Synthesis of 1′,1‴-Bis(diphenylphosphanyl)biferrocene (3): The procedure was similar to that described for the preparation of **2**, except that diphenylphosphanyl chloride (0.54 mL, 3 mmol) was used instead of 4,4′-dipyridyl disulfide. The product **3** was obtained in 68% (502 mg) yield. Crystals suitable for X-ray measurements were grown by slow diffusion of diethyl ether into a solution of **3** in chloroform at ambient temperature. $C_{44}H_{36}Fe_2P_2$ (738.41): calcd. C 71.56, H 4.91; found C 71.47, H 4.91. ^1H NMR (400 MHz, $CDCl_3$, 25 °C): δ = 3.87 (m, 4 H), 4.01 (m, 4 H), 4.11 (m, 4 H), 4.18 (m, 4 H), 7.37−7.27 (m, 20 H) ppm. ^{31}P NMR (160 MHz, $CDCl_3$, 25 °C): δ = −16.09 ppm. IR (KBr): $\tilde{\nu}$ = 3053 cm^{-1} (m), 1477 (m), 1433 (s), 1159 (m), 1033 (m), 836 (m), 829 (m), 805 (m), 742 (s), 697 (s), 495 (s), 419 (s).

Synthesis of [{(*p*-cymene)RuCl(μ-Cl)}$_2$(μ-1)] (4): A dichloromethane solution (10 mL) of 1,1′-bis(4-pyridylthio)ferrocene (20 mg, 0.05 mmol) was added to a solution of [(*p*-cymene)RuCl(μ-Cl)]$_2$ (31 mg, 0.05 mmol) in dichloromethane (5 mL), and the mixture was stirred for 5 h at room temperature. The resulting orange solution was evaporated to dryness and the red residue recrystallized from dichloromethane/diethyl ether (1:1 v/v). The orange solid of **4** was obtained in a yield of 74% (38 mg). $C_{40}H_{44}Cl_4FeN_2Ru_2S_2$ (1016.73): calcd. C 47.25, H 4.36, N 2.76; found C 46.95, H 4.42, N 2.85. ^1H NMR (400 MHz, $CDCl_3$, 25 °C): δ = 1.29 (d, 12 H),

2.10 (s, 6 H), 2.97 (sept, $J_{H,H}$ = 7.0 Hz, 2 H), 4.47 (m, 4 H), 4.58 (m, 4 H), 5.19 (d, $J_{H,H}$ = 3.0 Hz, 4 H), 5.41 (d, $J_{H,H}$ = 3.0 Hz, 4 H), 6.86 (m, 4 H), 8.66 (m, 4 H) ppm. IR (KBr): $\tilde{\nu}$ = 3045 cm^{-1} (m), 2965 (m), 2872 (m), 1594 (s), 1481 (m), 1417 (m), 1219 (m), 1110 (m), 1061 (m), 815 (m), 724 (m), 514 (m), 418 (m).

Synthesis of [{Cp*RhCl(μ-Cl)}$_2$(μ-1)]·CH_2Cl_2 (5): The procedure was similar to that described for the preparation of **4**, except that [Cp*RhCl(μ-Cl)]$_2$ (31 mg, 0.05 mmol) was used instead of [(*p*-cymene)RuCl(μ-Cl)]$_2$. The orange solid of **5** was obtained in a yield of 95% (47 mg). ^{1}H NMR (400 MHz, $CDCl_3$, 25 °C): δ = 1.57 (s, 30 H), 4.47(m, 4 H), 4.58 (m, 4 H), 6.92 (m, 4 H), 8.62 (m, 4 H) ppm. $C_{41}H_{48}Cl_6FeN_2Rh_2S_2$ (1107.35): calcd. C 44.47, H 4.27, N 2.53; found C 44.4, H 4.5, N 2.5. ^{1}H NMR (400 MHz, [D$_6$]DMSO, 25 °C): δ = 1.66 (s, 30 H), 4.61 (m, 4 H), 4.66 (m, 4 H), 6.93 (m, 4 H), 8.31 (m, 4 H) ppm. IR (KBr): $\tilde{\nu}$ = 1636 cm^{-1} (m), 1592 (s), 1479 (m), 1417 (m), 1375 (m), 1216 (m), 1109 (m), 1062 (m), 1025 (m), 896 (m), 817 (m), 726 (m), 504 (m), 419 (s).

Synthesis of [{Cp*IrCl(μ-Cl)}$_2$(μ-1)] (6): The procedure was similar to that described for the preparation of **4**, except that [Cp*IrCl(μ-Cl)]$_2$ (39 mg, 0.05 mmol) was used instead of [(*p*-cymene)RuCl(μ-Cl)]$_2$. The yellow solid of **6** was obtained in a yield of 87% (51 mg). $C_{40}H_{46}Cl_4FeIr_2N_2S_2$ (1201.04): calcd. C 40.00, H 3.86, N 2.33; found C 39.73, H 3.89, N 2.20. ^{1}H NMR (400 MHz, $CDCl_3$, 25 °C): δ = 1.56 (s, 30 H), 4.49 (m, 4 H), 4.58 (m, 4 H), 6.88 (d, $J_{H,H}$ = 3.4 Hz, 4 H), 8.61 (d, $J_{H,H}$ = 3.2 Hz, 4 H) ppm. ^{1}H NMR (400 MHz, [D$_6$]DMSO, 25 °C): δ = 1.63 (s, 30 H) 4.61 (m, 4 H), 4.67 (m, 4 H), 6.95 (m, 4 H), 8.31 (m, 4 H) ppm. IR (KBr): $\tilde{\nu}$ = 2917 cm^{-1} (m), 1636 (m), 1595 (s), 1478 (m), 1419 (m), 1380 (m), 1215 (m), 1111 (m), 1061 (m), 1029 (m), 896 (m), 816 (m), 728 (m).

Synthesis of [(*p*-cymene)RuCl(μ-Cl)}$_2$(μ-2)](7): The procedure was similar to that described for the preparation of **4**, except that **2** (30 mg, 0.05 mmol) was used instead of **1**. The orange solid of **7** was obtained in a yield of 52% (31 mg). $C_{50}H_{52}Cl_4Fe_2N_2Ru_2S_2$ (1200.75): calcd. C 50.00, H 4.37, N 2.33; found C 49.71, H 4.46, N 2.44. ^{1}H NMR (400 MHz, $CDCl_3$, 25 °C): δ = 1.27 (d, 12 H), 2.07 (s, 6 H), 2.95 (sept, $J_{H,H}$ = 7.0 Hz, 2 H), 4.12 (m, 4 H), 4.27 (m, 4 H), 4.35 (m, 4 H), 4.49 (m, 4 H), 5.14 (d, $J_{H,H}$ = 3.0 Hz, 4 H), 5.36 (d, $J_{H,H}$ = 3.0 Hz, 4 H), 6.80 (m, 4 H), 8.58 (m, 4 H) ppm. IR (KBr): $\tilde{\nu}$ = 3085 cm^{-1} (w), 3037 (w), 2961 (w), 2870 (w), 1593 (s), 1480 (m), 1418 (m), 1111 (m), 1059 (m), 1026 (m), 890 (m), 816 (m), 725 (m), 500 (m), 419 (m).

Synthesis of [Cp*RhCl(μ-Cl)}$_2$(μ-2)]·CH_2Cl_2 (8): The procedure was similar to that described for the preparation of **5**, except that **2** (30 mg, 0.05 mmol) was used instead of **1**. The orange solid of **8** was obtained in a yield of 52% (32 mg). $C_{51}H_{56}Cl_6Fe_2N_2Rh_2S_2$ (1291.37): calcd. C 47.43, H 4.37, N 2.17; found C 47.6, H 4.5, N 2.1. ^{1}H NMR (400 MHz, $CDCl_3$, 25 °C): δ = 1.54 (s, 30 H), 4.12 (m, 4 H), 4.27 (m, 4 H), 4.35 (m, 4 H), 4.50 (m, 4 H), 6.86 (m, 4 H), 8.55 (m, 4 H) ppm. IR (KBr): $\tilde{\nu}$ = 2870 cm^{-1} (w), 1636 (m), 1592 (s), 1478 (m), 1417 (m), 1374 (m), 1215 (m), 1165 (m), 1109 (m), 1061 (m), 1024 (m), 890 (m), 817 (m), 725 (m), 499 (m).

Synthesis of [{Cp*IrCl(μ-Cl)}$_2$(μ-2)]·$(CH_2Cl_2)_{1.5}$ (9): The procedure was similar to that described for the preparation of **6**, except that **2** (30 mg, 0.05 mmol) was used instead of **1**. The yellow solid of **9** was obtained in a yield of 67% (46 mg). $C_{51.5}H_{57}Cl_3Fe_2Ir_2N_2S_2$ (1370.65): calcd. C 40.90, H 3.80, N 1.85; found C 41.20, H 3.89, N 1.72. ^{1}H NMR (400 MHz, $CDCl_3$, 25 °C): δ = 1.54 (s, 30 H), 4.14 (m, 4 H), 4.28 (m, 4 H), 4.36 (m, 4 H), 4.51 (m, 4 H), 6.82 (m, 4 H), 8.58 (m, 4 H) ppm. IR (KBr): $\tilde{\nu}$ = 3075 cm^{-1} (w), 2913 (w), 1595 (s), 1479 (m), 1420 (m), 1377 (m), 1215 (m), 1167 (m), 1111 (m), 1062 (m), 1031 (m), 891 (m), 822 (m), 727 (m), 500 (m).

Synthesis of [{(*p*-cymene)RuCl(μ-Cl)}$_2$(μ-3)]·CH_2Cl_2 (10): The procedure was similar to that described for the preparation of **4**, except that **3** (37 mg, 0.05 mmol) was used instead of **1**. The orange solid of **10** was obtained in a yield of 45% (32 mg). $C_{65}H_{66}Cl_6Fe_2P_2Ru_2$ (1435.73): calcd. C 54.37, H 4.63; found C 54.63, H 4.71. ^{1}H NMR (400 MHz, $CDCl_3$, 25 °C): δ = 0.96 (d, 12 H), 1.75 (s, 6 H), 2.52 (sept, $J_{H,H}$ = 7.0 Hz, 2 H), 3.61 (m, 4 H), 3.89 (m, 4 H), 4.00 (m, 4 H), 4.30 (m, 4 H), 5.07 (s, 8 H), 7.43−7.37 (m, 12 H), 7.85−7.80 (m, 8 H) ppm. ^{31}P NMR (160 MHz, $CDCl_3$, 25 °C): δ = 18.99 ppm. IR (KBr): $\tilde{\nu}$ = 3044 cm^{-1} (w), 2958 (w), 2868 (w), 1482 (m), 1437 (s), 1384 (m), 1159 (m), 1095 (m), 1032 (s), 825 (s), 742 (s), 694 (s), 540 (m), 517 (s), 472 (s), 450 (s).

Synthesis of [{Cp*RhCl(μ-Cl)}$_2$(μ-3)]·$(CH_2Cl_2)_{0.5}$ (11): The procedure was similar to that described for the preparation of **5**, except that **3** (37 mg, 0.05 mmol) was used instead of **1**. The orange solid of **11** was obtained in a yield of 79% (54 mg). $C_{64.5}H_{67}Cl_5Fe_2P_2Rh_2$ (1398.95): calcd. C 55.38, H 4.83; found C 55.8, H 5.0. ^{1}H NMR (400 MHz, $CDCl_3$, −60 °C): δ = 1.27 (s, 30 H), 3.93−3.70 (m, 4 H), 4.28−4.02 (m, 8 H), 4.50 (m, 4 H), 7.55−7.30 (m, 12 H), 8.10−7.82 (m, 8 H) ppm. ^{31}P NMR (160 MHz, $CDCl_3$, 25 °C): δ = 22.33 (d) ppm. IR (KBr): $\tilde{\nu}$ = 2359 cm^{-1} (w), 1483 (m), 1434 (s), 1373 (m), 1305 (m), 1192 (m), 1159 (m), 1113 (m), 1094 (m), 1023 (m), 834 (m), 748 (m), 697 (m), 540 (s), 479 (m).

Synthesis of [{Cp*IrCl(μ-Cl)}$_2$(μ-3)] (12): The procedure was similar to that described for the preparation of **6**, except that **3** (37 mg, 0.05 mmol) was used instead of **1**. The orange solid of **12** was obtained in a yield of 71% (54 mg). $C_{64}H_{66}Cl_4Fe_2Ir_2P_2$ (1535.12): calcd. C 50.07, H 4.33; found C 49.8, H 4.3. ^{1}H NMR (400 MHz, $CDCl_3$, −60 °C): δ = 1.25 (s, 30 H), 3.82−3.75 (m, 4 H), 4.20−3.90 (m, 8 H), 4.60−4.25 (m, 4 H), 7.50−7.20 (m, 12 H), 8.10−7.70 (m, 8 H) ppm. ^{31}P NMR (160 MHz, $CDCl_3$, 25 °C): δ = −8.53 (s) ppm. IR (KBr): $\tilde{\nu}$ = 3072 cm^{-1} (w), 2912 (w), 1636 (m), 1435 (s), 1374 (m), 1159 (m), 1098 (m), 1085 (m), 1030 (m), 836 (m), 749 (m), 697 (m), 545 (s), 518 (m), 476 (m).

Synthesis of [{(Cp*Rh)$_4$(μ-Cl)$_4$}(μ-1)$_2$](PF$_6$)$_4$·CH_2Cl_2 (13): A diethyl ether solution (30 mL) of $AgPF_6$ (26 mg, 0.1 mmol) was added to a solution of **5** (52 mg, 0.05 mmol) in dichloromethane (30 mL), and the mixture was stirred for 12 h at room temperature. The resulting orange solution was filtered, the solvents evaporated to dryness and the red residue recrystallized from dichloromethane/diethyl ether (1:1 v/v). The orange solid of **13** was obtained in a yield of 27% (21 mg). $C_{81}H_{94}Cl_6F_{24}Fe_2N_4P_4Rh_4S_4$ (2567.81): calcd. C 37.89, H 3.69, N 2.18; found C 38.08, H 3.34, N 2.02. ^{1}H NMR (400 MHz, [D$_6$]DMSO, 25 °C): δ = 1.54 (s, 60 H), 4.72 (m, 8 H), 4.76 (m, 8 H), 7.31 (m, 8 H), 8.36 (m, 8 H) ppm. IR (KBr): $\tilde{\nu}$ = 1596 cm^{-1} (s), 1482 (m), 1422 (m), 1377 (m), 1112 (m), 1062 (m), 1023 (m), 844 (s).

Synthesis of [{(Cp*Ir)$_4$(μ-Cl)$_4$}(μ-1)$_2$](PF$_6$)$_4$ (14): The procedure was similar to that described for the preparation of **13**, except that **6** (61 mg, 0.05 mmol) was used instead of **5**. The yellow solid of **14** was obtained in a yield of 16% (16 mg). $C_{80}H_{92}Cl_4F_{24}Fe_2Ir_4N_4P_4S_4$ (2840.14): calcd. C 33.83, H 3.26, N 1.97; found C 33.44, H 3.00, N 2.18. ^{1}H NMR (400 MHz, [D$_6$]DMSO, 25 °C): δ = 1.55 (s, 60 H), 4.73 (m, 8 H), 4.77 (m, 8 H), 7.31 (m, 8 H), 8.43 (m, 8 H) ppm. IR (KBr): $\tilde{\nu}$ = 1598 cm^{-1} (s), 1483 (m), 1458 (m), 1425 (m), 1387 (m), 1230 (m), 1140 (m), 1115 (m), 1061 (m), 1031 (m), 848 (s).

X-ray Crystallographic Study: Crystals of compound **3** or **5** were mounted on a glass fibre and transferred to the diffractometer. The X-ray data were collected with a Rigaku AFC-5S four-circle diffractometer (**3**) or a Rigaku Mercury CCD diffractometer (**5**) using graphite-monochromated Mo-K_α radiation. Crystal data, data col-

Table 2. Crystal data and structure refinement of **3** and **5**

	3	**5**
Empirical formula	$C_{44}H_{36}Fe_2P_2$	$C_{41}H_{48}Cl_6FeN_2Rh_2S_2$
Molecular weight	738.41	1107.34
Temperature [K]	296	296
Radiation used (λ [Å])	Mo-K_α (0.71069)	Mo-K_α (0.71069)
Crystal description	prismatic, orange	prismatic, orange
Crystal size [mm]	0.8×0.6×0.1	0.15×0.1×0.1
Crystal system	triclinic	monoclinic
Space group	$P\bar{1}$ (No. 2)	$P2_1/c$ (No. 14)
a [Å]	9.000(3)	16.776(3)
b [Å]	9.144(3)	11.883(2)
c [Å]	14.061(3)	26.952(4)
α [°]	110.91(2)	
β [°]	59.43(2)	110.127(7)
γ [°]	117.46(3)	
V [Å^3]	872.6(5)	5044.5(12)
$2\theta_{max}$ [°]	55.0	55.0
Z	1	4
F(000)	382	2232
$\rho_{calcd.}$ [g·cm^{-3}]	1.405	1.458
μ [mm^{-1}]	9.54	13.57
Total reflections	4250	24822
Unique reflections	4246	10881
R (int)	0.027	0.087
$R1$, $wR2$ [$I > 3\sigma(I)$][a]	0.0439, 0.1122	0.089, 0.177
Goodness-of-fit on F^2	1.546	0.87
Max./min. el. dens. [e Å^{-3}]	0.70/ −0.43	1.56/ −0.75

[a] $R1 = \Sigma||F_0| - |F_c||/\Sigma|F_0|$; $wR2 = [\Sigma w(F_0^2 - F_c^2)^2/\Sigma w(F_0^2)^2]^{1/2}$.

lection parameters, and analysis statistics for **3** and **5** are listed in Table 2. All calculations were performed using the teXsan crystallographic software package.[33] The structures were solved by direct methods (SIR 92[34] and SHELX-97[35]) and expanded using Fourier techniques. The non-hydrogen atoms were refined anisotropically, and absorption correction was applied. The hydrogen atoms were inserted at the calculated positions and allowed to ride on their respective parent atoms.

CCDC-181949 (**3**) and CCDC-184341 (**5**) contain the supplementary crystallographic data for this paper. These data can be obtained free of charge at www.ccdc.cam.ac.uk/conts/retrieving.html [or from the Cambridge Crystallographic Data Centre, 12, Union Road, Cambridge CB2 1EZ, UK; Fax: (internat.) +44-1223/336-033; E-mail: deposit@ccdc.cam.ac.uk].

Acknowledgments

We are grateful to Prof. Tadashi Sugawara and Dr. Michio M. Matsushita (The University of Tokyo) for help with X-ray measurements. We thank Mr. Jouji Seta (Toho University) for help with ^{31}P NMR spectroscopy measurements. We also thank Prof. Hiroshi Moriyama (Toho University) for his assistance and Ms. Yumiko Sato (Toho University) the for elemental analyses. We are indebted to Mr. Masaru Nakama (WarpStream Ltd., Tokyo) for the Web-DB computer system.

[1] R. Robson, B. F. Abrahams, S. R. Batten, R. W. Gable, B. F. Hoskins, J. Liu, *Supramolecular Architecture, ACS Symp. Ser.* **1992**, *499*, 256−263.
[2] *Comprehensive Supramolecular Chemistry* (Eds: J.-M. Lehn, J. L. Atwood, J. E. D. Davies, D. D. MacNicol, F. Vogtle), Pergamon Press, Oxford **1995**, vol. *1−11*.
[3] P. L. Stang, B. Olenyuk, *Acc. Chem. Res.* **1997**, *30*, 502−518.
[4] M. Fujita, K. Ogura, *Coord. Chem. Rev.* **1996**, *148*, 249−264.
[5] B. Olenyuk, A. Fechtenkotter, P. J. Stang, *J. Chem. Soc., Dalton Trans.* **1998**, 1707−1728.
[6] B. Moulton, M.J. Zaworotko, *Chem. Rev.* **2001**, *101*, 1629−1658.
[7] M. J. Zaworotko, *Chem. Commun.* **2001**, 1−9.
[8] P. J. Hagrman, D. Harman, J. Zubieta, *Angew. Chem.* **1999**, *111*, 2798−2848; *Angew. Chem. Int. Ed.* **1999**, *38*, 2639−2684.
[9] S. R. Batten, *CrystEngComm.* **2001**, *18*, 1−7.
[10] G. F. Swiegers, T. J. Malefertse, *Chem. Eur. J.* **2001**, *7*, 3637−3643.
[11] P. J. Fagan, M. D. Ward, J. C. Calabrese, *J. Am. Chem. Soc.* **1989**, *111*, 1698−1719.
[12] Y. Yamamoto, H. Nakamura, J.-F. Ma, *J. Organomet. Chem.* **2001**, *640*, 10−30.
[13] Y. Yamamoto, H. Suzuki, N. Tajima, K. Tatsumi, *Chem. Eur. J.* **2002**, *8*, 372−379.
[14] H. Suzuki, N. Tajima, K. Tatsumi, Y. Yamamoto, *Chem. Commun.* **2000**, 1801−1802.
[15] H. Amouri, C. Guyard-Duhayon, J. Vaissermann, M. N. Rager, *Inorg. Chem.* **2002**, *41*, 1397−1403.
[16] H. Amouri, M. N. Rager, F. Cagnol, J. Vaissermann, *Angew. Chem.* **2001**, *113*, 3748−3750; *Angew. Chem. Int. Ed.* **2001**, *40*, 3636−3638.
[17] A. Togni, T. Hayashi, *Ferrocenes − Homogeneous Catalysis, Organic Synthesis and Material Science*, VCH, Weinheim **1995**.
[18] R. Horikoshi, T. Mochida, H. Moriyama, *Inorg. Chem.* **2001**, *41*, 3017−3024.
[19] S. Onaka, Y. Katsukawa, M. Shiotsuka, O. Kanegawa, M. Yamashita, *Inorg. Chim. Acta* **2001**, *312*, 100−110.
[20] J.-F. Ma, Y. Yamamoto, *Inorg. Chim. Acta* **2000**, *299*, 164−171.
[21] J.-F. Ma, Y. Yamamoto, *J. Organomet. Chem.* **1999**, *574*, 148−154.
[22] P. M. N. Low, Z.-Y. Zhang, T. C. W. Mak, T. S. A. Hor, *J. Organomet. Chem.* **1997**, *539*, 45−51.

[23] J.-F. Ma, Y. Yamamoto, *J. Organomet. Chem.* **1997**, *545−546*, 577−559.
[24] C. K. Johnson, ORTEP, Report ORNL-5138, Oak Ridge National Laboratory, Oak Ridge, TN, **1976**.
[25] U. Casellato, D. Ajo, G. Valle, B. Corain, B. Longato, R. Graziani, *J. Crystallogr. Spectrosc. Res.* **1988**, *18*, 583−590.
[26] G. Pilloni, B. Longato, B. Corain, *J. Organomet. Chem.* **1991**, *420*, 57−65.
[27] F. Canales, M. C. Gimeno, A. Laguna, P. G. Jones, *J. Am. Chem. Soc.* **1996**, *118*, 4839−4845.
[28] M.C. Gimeno, P.G. Jones, A. Laguna, C. Sarroca, *J. Chem. Soc., Dalton Trans.* **1995**, 1473−1481.
[29] F. Canales, M. C. Gimeno, P. G. Jones, A. Laguna, C. Sarroca, *Inorg. Chem.* **1997**, *36*, 5206−5211.
[30] M. A. Bennett, T.-N. Huang, T. W. Matheson, A. K. Smith, *Inorg. Synth.* **1982**, *21*, 74−78.
[31] J. W. Kang, K. Moseley, P. M. Maitlis, *J. Am. Chem. Soc.* **1969**, *91*, 5971−5977.
[32] Y. Yamamoto, K. Kawasaki, S. Nishimura, *J. Organomet. Chem.* **1999**, *587*, 49−57.
[33] teXsan: Crystal Structure Analysis Package, Molecular Structure Corporation, The Woodlands, TX, **1985** and **1999**.
[34] A. Altomare, M. C. Burla, M. Camalli, M. Cascarano, C. Giacovazzo, A. Guagliardi, G. Polidori, *J. Appl. Crystallogr.* **1994**, *27*, 435.
[35] G. M. Sheldrick, *SHELX-97: Program for the Solution of Crystal Structures*, University of Göttingen, Germany, **1997**.

Received April 23, 2002
[I02211]

Reactivity of a Triruthenium Ynenyl Cluster Complex with Diynes: Cluster-Mediated Combination of up to Three Substituted Butadiyne Molecules into a Carbon-Rich Hydrocarbyl Ligand

Javier A. Cabeza,*[a] Ignacio del Río,[a] Marta Moreno,[a] Santiago García-Granda,[b] Mónica Pérez-Priede,[b] and Víctor Riera[a]

Keywords: Ruthenium / Clusters / Alkynes / C-C bond formation / N ligands

The triruthenium ynenyl cluster complex $[Ru_3(\mu_3\text{-}\eta^2\text{-apyr})(\mu\text{-}\eta^3\text{-MeCH=CC}\equiv\text{CMe})(\mu\text{-CO})_2(CO)_6]$ (**2**; Hapyr = 2-aminopyrimidine) has been prepared in two steps from $[Ru_3(CO)_{12}]$, 2-aminopyrimidine and 2,4-hexadiyne. Its reactivity with two conjugated diynes has been studied. With 2,4-hexadiyne, it affords $[Ru_3(\mu_3\text{-}\eta^2\text{-apyr})\{\mu\text{-}\eta^5\text{-MeC}\equiv\text{CC=CMeC(=CHMe)-C}\equiv\text{CMe}\}(\mu\text{-CO})_2(CO)_5]$ (**3**), which contains a diynedienyl ligand that arises from the coupling of 2,4-hexadiyne with the hex-2-yn-4-en-4-yl ligand of **2**, whereas the reaction of complex **2** with diphenylbutadiyne gives $[Ru_3(\mu_3\text{-}\eta^2\text{-apyr})\{\mu_3\text{-}\eta^7\text{-PhC}\equiv\text{CC=CPhCMe=CC(=CHMe)C(C}\equiv\text{CPh)=CPh}\}(\mu\text{-CO})(CO)_6]$ (**4**). Complex **4** contains an unprecedented diynetetraentriyl ligand that arises from the coupling of two diphenylbutadiyne molecules with the hex-2-yn-4-en-4-yl ligand of **2**.

(© Wiley-VCH Verlag GmbH, 69451 Weinheim, Germany, 2002)

Introduction

In previous studies, it was observed that 2-amidopyridine-bridged hydrido triruthenium carbonyl complexes[1] activate alkynes, rendering derivatives of the type $[Ru_3(\mu_3\text{-}\eta^2\text{-apy})(\mu\text{-}\eta^2\text{-alkenyl})(\mu\text{-CO})_2(CO)_6]$ (apy = 2-amidopyridine-type ligand).[2,3] These alkenyl derivatives have been recognized as catalytic precursors for the hydrogenation,[4,5] dimerization,[6] polymerisation[6] and hydroformylation[7] of selected alkynes.

The natural evolution of these investigations led us to study the reactivity of apy-bridged hydrido triruthenium complexes with diynes. In this field, we have already reported that the complex $[Ru_3(\mu\text{-H})(\mu_3\text{-}\eta^2\text{-ampy})(CO)_9]$ (Hampy = 2-amino-6-methylpyridine) reacts with diphenylbutadiyne and 1,6-diphenoxy-2,4-hexadiyne to give ynenyl complexes of the type $[Ru_3(\mu_3\text{-}\eta^2\text{-ampy})(\mu\text{-}\eta^3\text{-RCH=CC}\equiv\text{CR})(\mu\text{-CO})_2(CO)_6]$ (R = Ph, CH_2OPh). These ynenyl compounds are prone to react with alkynes and diynes to give interesting coupling products, including η^5-cyclopentadienyl and η^5-ruthenacyclopentadienyl derivatives.[8] However, the analogous ynenyl complex derived from $[Ru_3(\mu\text{-H})(\mu_3\text{-}\eta^2\text{-ampy})(CO)_9]$ and 2,4-hexadiyne could not be isolated and, therefore, its reactivity could not be studied.[9]

We report herein that the use of 2-aminopyrimidine (Hapyr) as a ligand precursor, instead of 2-amino-6-methylpyridine, leads to the isolation of a trinuclear ynenyl derivative of 2,4-hexadiyne, $[Ru_3(\mu_3\text{-}\eta^2\text{-apyr})(\mu\text{-}\eta^3\text{-MeCH=CC}\equiv\text{CMe})(\mu\text{-CO})_2(CO)_6]$, and allows the study of the reactivity of the latter complex with diynes. We also report that a product of one of these reactions contains an unprecedented hydrocarbyl ligand that arises from the coupling of three diyne molecules.

Results and Discussion

Synthesis of Compounds 1 and 2

The reaction of $[Ru_3(CO)_{12}]$ with 2-aminopyrimidine in THF at reflux temperature leads to the trinuclear derivative $[Ru_3(\mu\text{-H})(\mu_3\text{-}\eta^2\text{-apyr})(CO)_9]$ (**1**) (Scheme 1). The compound was characterised by its mass spectrum, which shows the molecular ion, and by its IR and NMR spectra, which are similar to those of $[Ru_3(\mu\text{-H})(\mu_3\text{-}\eta^2\text{-ampy})(CO)_9]$.[10] Thus, the behaviour of 2-aminopyrimidine in its reaction with $[Ru_3(CO)_{12}]$ is similar to that of 2-aminopyridines.

The thermal reaction (refluxing THF) of 2,4-hexadiyne with compound **1**, in a 1:1 mol ratio, leads to a mixture of compounds from which the major product, the ynenyl derivative $[Ru_3(\mu_3\text{-}\eta^2\text{-apyr})(\mu\text{-}\eta^3\text{-MeCH=CC}\equiv\text{CMe})(\mu\text{-CO})_2(CO)_6]$ (**2**) (Scheme 1), could be separated by TLC.

[a] Departamento de Química Orgánica e Inorgánica, Instituto de Química Organometálica "Enrique Moles", Universidad de Oviedo-CSIC,
33071 Oviedo, Spain
Fax: (internat.) + 34-985/103446
E-mail: jac@sauron.quimica.uniovi.es
URL: http://www12.uniovi.es/investigacion/jac/
[b] Departamento de Química Física y Analítica, Universidad de Oviedo,
33071 Oviedo, Spain

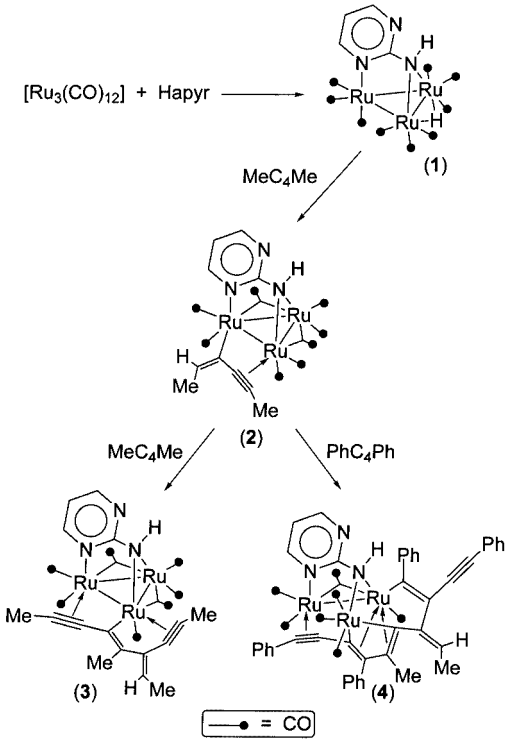

Scheme 1

The mass spectrum of **2** shows the corresponding molecular ion. Its IR spectrum indicates the presence of bridging CO ligands. The ^{1}H NMR spectrum also confirms the insertion of the original diyne into a Ru−hydride bond of **1** to give an ynenyl ligand. The multiplicity of the signal of this hydrogen atom in **2** (quadruplet, J = 6.5 Hz) indicates that it is adjacent to a methyl group. The structure depicted for this compound in Scheme 1, which shows a bridging three-electron donor hex-2-yn-4-en-4-yl ligand, is also supported by the similarity of its spectroscopic data with those of the compounds [$Ru_3(\mu_3$-η^2-ampy)(μ-η^3-RCH=CC≡CR)(μ-CO)$_2$(CO)$_6$] (R = Ph, CH_2OPh), the structures of which have been determined by X-ray diffraction methods.[8]

We have recently reported that the isolation of the 2-amido-6-methylpyridine derivative [$Ru_3(\mu_3$-η^2-ampy)(μ-η^3-MeCH=CC≡CMe)(μ-CO)$_2$(CO)$_6$] could not be achieved. Although this complex was spectroscopically detected in the reaction of [$Ru_3(\mu$-H)(μ_3-η^2-ampy)(CO)$_9$] with 2,4-hexadiyne, mixtures of inseparable products were always obtained, regardless of the ratio of the reactants.[9] This prevented the study of its derivative chemistry. As desired, the slightly different polarity of analogous ampy and apyr derivatives allows the successful TLC separation of complex **2**.

Considering the asymmetry of each triple bond of hexa-2,4-diyne, the insertion of one of its triple bonds into a Ru−H bond of **1** could lead to two different products. As occurred with [$Ru_3(\mu$-H)(μ_3-η^2-ampy)(CO)$_9$],[9] the reaction is selective in the sense that only the insertion product containing a hex-2-yn-4-en-4-yl ligand, (compound **2**) is formed. The alternative product would have a hex-2-yn-4-en-5-yl ligand. This selectivity has also been observed previously for the reaction of compound **1** with 1,6-diphenoxy-2,4-hexadiyne,[8] but not with diphenylbutadiyne.[9,11] A mechanistic proposal accounting for the formation of compounds similar to **2** from conjugated diynes and hydrido trinuclear clusters has been reported.[8]

Apart from the above-mentioned ynenyl compounds derived from [$Ru_3(\mu$-H)(μ_3-η^2-ampy)(CO)$_9$],[8] only a few more ynenyl derivatives have heretofore been reported as products of reactions of carbonylruthenium clusters with diynes, i.e. the compounds [$Ru_2(\mu$-N=CPh$_2$)(μ-η^2-CH$_2$=CCH$_2$C≡CSiMe$_3$)(CO)$_6$],[12] [$Ru_3(\mu_3$-η^2-pyNMe)(μ-η^3-PhCH=CC≡CPh)(μ-CO)$_2$(CO)$_6$],[11] and [$Ru_4(\mu$-η^2-dmpz)(μ_4-η^4-MeCH=CC≡CMe)(μ-CO)(CO)$_{10}$] (Hdmpz = 3,5-dimethylpyrazole).[13] The cluster complex [Ru_3{μ-NS(O)MePh}(μ-η^3-PhCH=CC≡CPh)(CO)$_9$] also contains an ynenyl ligand, but in this case the ligand arises from an alkynyl−vinylidene coupling.[14]

Reactions of Compound 2 with Diynes

Treatment of compound **2** with 2,4-hexadiyne in THF at reflux temperature leads to [$Ru_3(\mu_3$-η^2-apyr){μ-η^5-MeC≡CC=CMeC(=CHMe)C≡CMe}(μ-CO)$_2$(CO)$_5$] (**3**) in quantitative yield (Scheme 1). Its analytical and spectroscopic data, although indicating the presence of the apyr ligand, the existence of bridging and terminal CO ligands, and the incorporation of the new 2,4-hexadiyne molecule, did not reveal its molecular structure, which was determined by X-ray diffraction.

Figure 1 shows a view of compound **3**. A selection of bond lengths is given in Table 1. The new ligand, which can be described as a 5-methyl-6-(ethylidene)nona-2,7-diyn-4-en-4-yl ligand, behaves as a five-electron donor. It spans the longest edge of the metal triangle [Ru(1)−Ru(3): 2.8874(9) Å], and is attached to Ru(1) through a C≡C triple bond (two-electron π-type interaction) and to Ru(3) through the remaining C≡C triple bond (two-electron π-type interac-

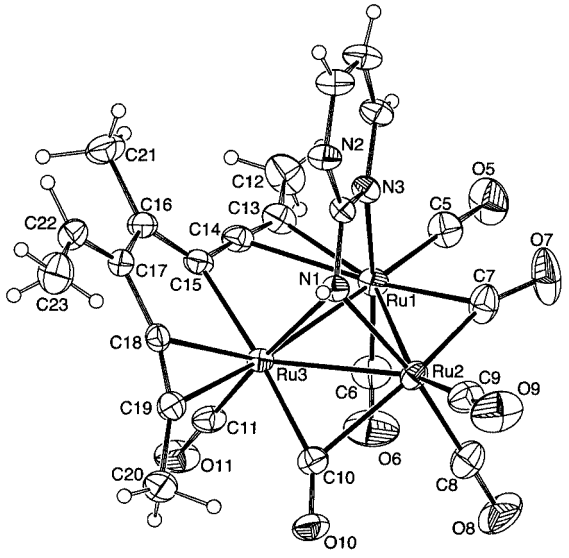

Figure 1. Molecular structure of compound **3**; thermal ellipsoids are drawn at a 40% probability level

tion) and the C(15) carbon atom (one-electron σ-type interaction). The remaining edges of the metal triangle are shorter [Ru(1)−Ru(2): 2.7846(9) Å, Ru(2)−Ru(3): 2.6662(8) Å], and each one is asymmetrically bridged by a CO ligand. The apyr ligand caps the Ru_3 triangle, and is attached to the Ru(2)−Ru(3) edge through the exocyclic N(1) atom and to the Ru(1) atom through the heterocyclic N(3) atom. The cluster shell is completed with five terminal CO ligands. Thus, the compound is a closed-shell 48-electron cluster. Overall, the structure resembles that of the related ampy derivative, which contains an analogous diynedienyl ligand.[9]

Table 1. Selected Interatomic Distances [Å] in Compound **3**

Ru(1)−Ru(2)	2.7846(9)	Ru(1)-Ru(3)	2.8874(9)
Ru(2)−Ru(3)	2.6662(8)	Ru(1)−N(3)	2.147(3)
Ru(2)−N(1)	2.156(3)	Ru(3)−N(1)	2.186(3)
Ru(1)−C(5)	1.903(4)	Ru(1)−C(6)	1.862(4)
Ru(1)−C(7)	2.249(4)	Ru(1)−C(13)	2.245(4)
Ru(1)−C(14)	2.434(4)	Ru(2)−C(7)	1.965(4)
Ru(2)−C(8)	1.863(4)	Ru(2)−C(9)	1.895(4)
Ru(2)−C(10)	2.235(4)	Ru(3)−C(10)	2.024(4)
Ru(3)−C(11)	1.839(3)	Ru(3)−C(15)	2.117(3)
Ru(3)−C(18)	2.268(3)	Ru(3)−C(19)	2.388(3)
C(5)−O(5)	1.134(5)	C(6)−O(6)	1.143(5)
C(7)−O(7)	1.157(5)	C(8)−O(8)	1.154(5)
C(9)−O(9)	1.122(5)	C(10)−O(10)	1.154(4)
C(11)−O(11)	1.148(5)	C(12)−C(13)	1.475(6)
C(13)−C(14)	1.242(5)	C(14)−C(15)	1.377(5)
C(15)−C(16)	1.345(5)	C(16)−C(17)	1.463(5)
C(16)−C(21)	1.497(5)	C(17)−C(18)	1.437(5)
C(17)−C(22)	1.342(5)	C(18)−C(19)	1.222(5)
C(19)−C(20)	1.470(5)	C(22)−C(23)	1.481(8)

The reaction of complex **2** with one equivalent of diphenylbutadiyne, in THF at reflux temperature, led only to intractable mixtures. However, the use of a 1:2 ratio of the reactants led to a mixture of compounds from which the trinuclear derivative [$Ru_3(\mu_3$-η^2-apyr){μ_3-η^7-PhC≡CC=CPhCMe=CC(=CHMe)C(C≡CPh)=CPh}(μ-CO)$(CO)_6$] (**4**) could be separated by TLC. X-ray diffraction was necessary to determine its structure, since its analytical and spectroscopic data, although suggesting the incorporation of two diphenylbutadiyne molecules to complex **2**, did not allow a structural assignment.

Figure 2 shows a view of compound **4**. A selection of bond lengths is given in Table 2. While the Ru(1)−Ru(3) distance [2.8341(5) Å] corresponds to a metal−metal bond, the Ru(1)−Ru(2) and Ru(2)−Ru(3) distances [4.0288(5) Å and 3.0929(5) Å respectively] are too long to be assigned to Ru−Ru bonds. The new ligand spans the two long Ru−Ru edges and is attached to Ru(1) through a C≡C triple bond (two-electron π-type interaction). It is involved in a ruthenacyclopentadiene fragment with Ru(2), to which it is bonded through the carbon atoms C(18) and C(24) (two one-electron σ-type interactions). It also binds to Ru(3) through both double bonds of the ruthenacyclopentadiene fragment (two two-electron π-type interactions) and the C(12) carbon atom (one-electron σ-type interaction). This hydrocarbyl ligand, which can be systematically named as a 1,4,9-triphenyl-5-methyl-7-ethyliden-8-(phenylethynyl)nona-1-yn-3,5,8-trien-3,6,9-triyl ligand, behaves as a nine-electron donor. The apyr ligand is attached to the Ru(2) and Ru(3) atoms through the exocyclic N(1) atom and to Ru(1) through the heterocyclic N(3) atom. The Ru(1)−Ru(3) edge is asymmetrically bridged by a CO ligand. The complex shell is completed with six terminal CO ligands. Thus, the compound is a 52-electron species.

Although a few hydrocarbyl ligands resulting from the coupling of two diyne molecules at metal cluster cores have

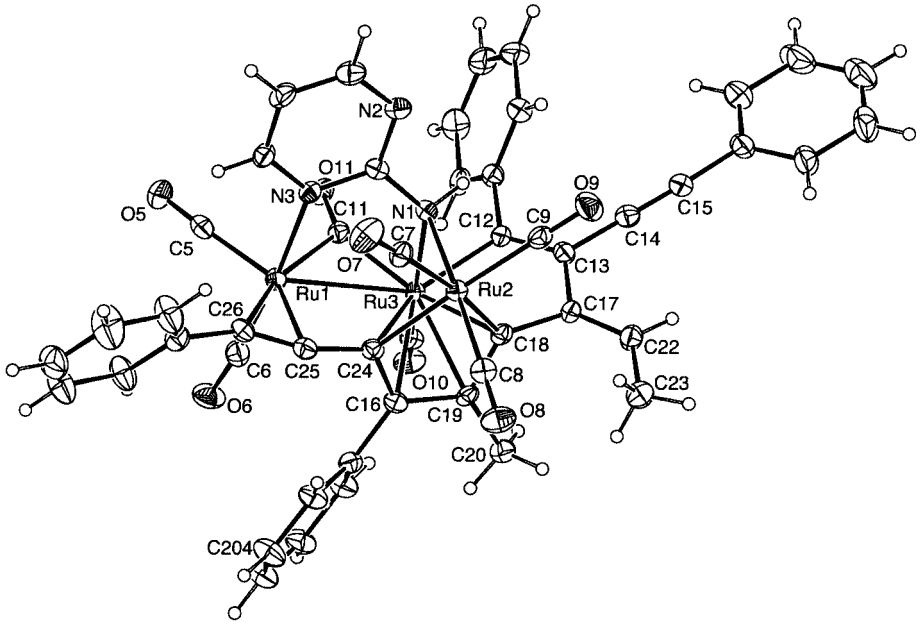

Figure 2. Molecular structure of compound **4**; thermal ellipsoids are drawn at a 40% probability level

Table 2. Selected interatomic distances [Å] in compound **4**

Ru(1)−Ru(2)	4.0288(5)	Ru(1)−Ru(3)	2.8341(5)
Ru(2)−Ru(3)	3.0929(5)	Ru(1)−N(3)	2.161(4)
Ru(2)−N(1)	2.170(4)	Ru(3)−N(1)	2.232(4)
Ru(1)−C(5)	1.875(6)	Ru(1)−C(6)	1.889(6)
Ru(1)−C(11)	2.226(5)	Ru(1)−C(25)	2.263(5)
Ru(1)−C(26)	2.253(5)	Ru(2)−C(7)	1.974(6)
Ru(2)−C(8)	1.892(6)	Ru(2)−C(9)	1.956(5)
Ru(2)−C(18)	2.133(5)	Ru(2)−C(24)	2.125(5)
Ru(3)−C(10)	1.853(5)	Ru(3)−C(11)	1.995(5)
Ru(3)−C(12)	2.106(4)	Ru(3)−C(16)	2.457(5)
Ru(3)−C(18)	2.227(5)	Ru(3)−C(19)	2.372(5)
Ru(3)−C(24)	2.547(5)	C(5)−O(5)	1.131(7)
C(6)−O(6)	1.139(7)	C(7)−O(7)	1.127(7)
C(8)−O(8)	1.129(7)	C(9)−O(9)	1.138(6)
C(10)−O(10)	1.138(6)	C(11)−O(11)	1.176(6)
C(12)−C(13)	1.356(7)	C(13)−C(14)	1.439(7)
C(13)−C(17)	1.483(7)	C(14)−C(15)	1.199(9)
C(16)−C(19)	1.438(7)	C(16)−C(24)	1.448(7)
C(17)−C(18)	1.489(6)	C(17)−C(22)	1.326(7)
C(18)−C(19)	1.404(7)	C(19)−C(20)	1.517(7)
C(22)−C(23)	1.489(8)	C(24)−C(25)	1.399(7)
C(25)−C(26)	1.258(7)		

been reported,[8,9,15] complex **4** is the first example of a hydrocarbyl ligand resulting from the coupling of three diyne molecules.

The compounds $[Ru_3(\mu_3\text{-}\eta^2\text{-ampy})(\mu\text{-}\eta^3\text{-RCH=CC}\equiv\text{CR})(\mu\text{-CO})_2(CO)_6]$ (R = Ph, CH_2OPh), structurally analogous to **2**, are the only ynenyl derivatives whose reactivity with alkynes and diynes has been studied. They systematically give trinuclear products containing η^5-ruthenacyclopentadienyl fragments which arise from the coupling of the coordinated ynenyl ligands with a C≡C triple bond of the new reagent (alkyne or diyne).[8] It is noteworthy that the reactions of **2** with 2,4-hexadiyne and diphenylbutadiyne do not give related products, but instead give compounds **3** and **4**. At this stage, it seems that this different reactivity is not due to steric reasons, but it is not yet clear whether it may be caused by the different substituents of the ynenyl ligands, the different capping *N*-donor ligands or a combination of both.

We also studied the reactions of **2** with some monoalkynes, but complex mixtures, from which we could not isolate and characterise any product, were formed in all cases.

Experimental Section

General Remarks: Solvents were dried over sodium diphenyl ketyl (THF, hydrocarbons) or calcium hydride (dichloromethane) and distilled under nitrogen prior to use. The reactions were carried out under nitrogen, using Schlenk and vacuum line techniques, and were routinely monitored by solution IR spectroscopy (carbonyl stretching region) and by spot TLC (silica gel). All reagents were purchased as analytically pure samples. IR: Perkin−Elmer Paragon 1000 FT spectrometer. NMR: Bruker AC-200, AC-300 or DPX-300 spectrometers, room temperature, $SiMe_4$ as internal standard. Microanalyses were obtained from the University of Oviedo's Analytical Service. FAB-MS were obtained from the University of Santiago de Compostela's Mass Spectroscopic Service; data given refer to the most abundant molecular ion isotopomer.

$[Ru_3(\mu\text{-H})(\mu_3\text{-}\eta^2\text{-apyr})(CO)_9]$ (1): A mixture of $[Ru_3(CO)_{12}]$ (300 mg, 0.468 mmol) and 2-aminopyrimidine (71 mg, 0.749 mmol) in THF (50 mL) was stirred at reflux temperature for 90 min. After concentration under reduced pressure to approximately 2 mL, the solution was applied to the top of a chromatography column (10 × 2 cm) packed with activity I neutral alumina in hexane. Hexane/dichloromethane (1:1) eluted two bands. The first, yellow, contained some $[Ru_4H_4(CO)_{12}]$ product (IR identification). The second band, yellow-orange, afforded compound **2** after solvent removal (150 mg, 48%). $C_{13}H_5N_3O_9Ru_3$ (650.44): calcd. C 24.01, H 0.77, N 6.46; found C 23.85, H 0.76, N 6.38. FAB-MS: *m*/*z* = 652 [M^+]. IR (CH_2Cl_2): ν(CO) = 2084 (m), 2054 (s), 2030 (vs), 1998 (s), 1964 (m) cm^{-1}. ^1H NMR ($CDCl_3$): δ = 8.42 (dd, *J* = 5.1, 2.4 Hz, 1 H), 8.20 (dd, *J* = 5.1, 2.4 Hz, 1 H), 6.76 (t, *J* = 5.1 Hz, 1 H), 4.55 (br. s, 1 H), −11.31 (s, 1 H) ppm.

$[Ru_3(\mu_3\text{-}\eta^2\text{-apyr})(\mu\text{-}\eta^3\text{-MeCH=CC}\equiv\text{CMe})(\mu\text{-CO})_2(CO)_6]$ (2): A solution of complex **1** (150 mg, 0.230 mmol) and 2,4-hexadiyne (20 mg, 0.256 mmol) in THF (20 mL) was stirred at reflux temperature for 60 min. The colour changed from yellow to red. After concentration under reduced pressure to approximately 2 mL the solution was applied to preparative silica gel TLC plates. Repeated elution with hexane/dichloromethane (3:1) allowed the separation of two bands. The second band, orange, contained a small amount of compound **3** (9 mg, 5%). The first band, orange, gave compound **2** (51 mg, 30%) upon extraction with dichloromethane. $C_{18}H_{11}N_3O_8Ru_3$ (700.54): calcd. C 30.86, H 1.58, N 6.00; found C 30.91, H 1.63, N 5.84. FAB-MS: *m*/*z* = 702 [M^+]. IR (CH_2Cl_2): ν(CO) = 2064 (s), 2030 (vs), 2022 (vs), 1994 (s), 1969 (w), 1873 (w), 1820 (m) cm^{-1}. ^1H NMR ($CDCl_3$): δ = 8.00 (m, 2 H), 6.50 (t, *J* = 5.4 Hz, 1 H), 6.43 (q, *J* = 6.5 Hz, 1 H), 4.05 (br. s, 1 H), 2.94 (s, 3 H), 2.45 (d, *J* = 6.5 Hz, 3 H) ppm.

$[Ru_3(\mu_3\text{-}\eta^2\text{-apyr})\{\mu\text{-}\eta^5\text{-MeC}\equiv\text{CC=CMeC(=CHMe)C}\equiv\text{CMe}\}(\mu\text{-CO})_2(CO)_5]$ (3): A solution of complex **2** (15 mg, 0.021 mmol) and 2,4-hexadiyne (2 mg, 0.025 mmol) in THF (10 mL) was stirred at reflux temperature for 60 min. The original yellow colour of the solution darkened slightly. The solvent was removed under reduced pressure and the residue was washed with hexane (2 mL) to give compound **3** (14 mg, 89%) as a yellow-orange solid. $C_{23}H_{17}N_3O_7Ru_3$ (750.65): calcd. C 36.80, H 2.28, N 5.60; found C 36.76, H 2.12, N 5.59. FAB-MS: *m*/*z* = 752 [M^+]. IR (CH_2Cl_2): ν(CO) = 2064 (vs), 2012 (s), 1980 (s), 1955 (w), 1876 (w), 1815 (m) cm^{-1}. ^1H NMR ($CDCl_3$): δ = 7.92 (dd, *J* = 4.3, 2.1 Hz, 1 H), 7.73 (dd, *J* = 5.5, 2.1 Hz, 1 H), 6.36 (dd, *J* = 5.5, 4.3 Hz, 1 H), 6.09 (q, *J* = 7.6 Hz, 1 H), 4.22 (br. s, 1 H), 3.12 (s, 3 H), 2.84 (s, 3 H), 2.15 (s, 3 H), 2.11 (d, *J* = 7.6 Hz, 3 H) ppm.

$[Ru_3(\mu_3\text{-}\eta^2\text{-apyr})\{\mu_3\text{-}\eta^7\text{-PhC}\equiv\text{CC=CPhCMe=CC(=CHMe)-C(C}\equiv\text{CPh)=CPh}\}(\mu\text{-CO})(CO)_6]$ (4): A solution of complex **2** (45 mg, 0.064 mmol) and diphenylbutadiyne (29 mg, 0.143 mmol) in THF (30 mL) was stirred at reflux temperature for 150 min. The colour changed from yellow to brown. After concentration under reduced pressure to approximately 2 mL, the solution was applied to preparative silica gel TLC plates. Multiple elution with hexane/dichloromethane (2:1) allowed the isolation of compound **4** (10 mg, 15%) from the major band, orange, upon extraction with dichloromethane. $C_{49}H_{31}N_3O_7Ru_3$ (1077.05): calcd. C 54.64, H 2.90, N 3.90; found C 54.34, H 2.80, N 3.77. FAB-MS: *m*/*z* = 1023 [M^+ − 2CO]. IR (CH_2Cl_2): ν(CO) = 2092 (s), 2029 (vs), 2013 (m), 1963 (m), 1809 (m) cm^{-1}. ^1H NMR ($CDCl_3$): δ = 8.05 (d, *J* = 7.4 Hz, 1 H), 7.95 (dd, *J* = 4.4, 2.5 Hz, 1 H), 7.82 (dd, *J* = 5.4, 2.5 Hz, 1

Table 3. Relevant Crystal and Refinement Data for Compounds **3** and **4**

Compound	**3**	**4**
Formula	$C_{23}H_{17}N_3O_7Ru_3$	$C_{49}H_{31}N_3O_7Ru_3$
Molecular weight	750.61	1076.98
Crystal system	monoclinic	triclinic
Space group	$P2_1/n$	$P\bar{1}$
a [Å]	11.019(3)	9.7568(7)
b [Å]	13.125(5)	14.7937(6)
c [Å]	18.308(5)	16.0347(7)
α [°]	90	106.385(2)
β [°]	104.67(4)	101.442(4)
γ [°]	90	101.120(4)
V [Å^3]	2561.5(14)	2098.7(2)
Z	4	2
F(000)	1456	1068
$D_{calcd.}$ [g cm^{-3}]	1.946	1.704
λ (radiation) [Å]	0.71073 (Mo-K_α)	1.54184 (Cu-K_α)
Crystal size [mm^3]	0.45 × 0.36 × 0.23	0.15 × 0.10 × 0.05
T [K]	293(2)	200(2)
μ [mm^{-1}]	1.793	9.108
Min./max. *h, k, l*	0/13, 0/16, −22/21	−11/11, −17/17, −18/19
Measured reflns	5287	11222
Unique reflns	5020	7858
Reflns with [$I > 2\sigma(I)$]	4385	6826
Parameters	393	563
GoF on F^2	1.147	1.158
R_1 [on F, $I > 2\sigma(I)$]	0.0253	0.0394
wR_2 (on F^2, all data)	0.0716	0.1276
Min., max. Δρ, [e Å^{-3}]	−0.651, 0.528	−0.862, 0.983

H), 7.6−7.1 (m, 19 H), 6.48 (q, J = 7.4 Hz, 1 H), 6.28 (dd, J = 5.4, 4.4 Hz, 1 H), 4.01 (br. s, 1 H), 2.29 (s, 3 H), 2.18 (d, J = 7.4 Hz, 3 H) ppm.

X-ray Crystallographic Studies: Selected crystal and refinement data are given in Table 3. Crystals of compound **3** were obtained by slow diffusion of pentane into a solution of the complex in dichloromethane. Crystals of **4** were obtained by slow diffusion of pentane vapor into a solution of the complex in 1,2-dichloroethane. Diffraction data were obtained on Nonius CAD4 (**3**) and KappaCCD (**4**) diffractometers. Absorption corrections were applied using DIFABS[16] (for **3**) or XABS2[17] (for **4**). Maximum and minimum transmission factors 0.631 and 0.480 (for **3**) and 0.131 and 0.062 (for **4**). The structures were solved by Patterson interpretation using DIRDIF-96.[18] Isotropic and full-matrix anisotropic least-squares refinements were carried out using SHELXL-97.[19] All non H-atoms were refined anisotropically. All the hydrogen atoms of **3** were found and refined. For **4**, the NH hydrogen atom was located and its position was refined, while the remaining hydrogen atom positions were calculated and refined riding in their parent atoms. The molecular plots were made with the EUCLID program package.[20] The WINGX program system[21] was used throughout the structure determinations.

CCDC-185400 (**3**) and CCDC-185401 (**4**) contain the supplementary crystallographic data for this paper. These data can be obtained free of charge at www.ccdc.cam.ac.uk/conts/retrieving.html [or from the Cambridge Crystallographic Data Centre, 12, Union Road, Cambridge CB2 1EZ, UK; Fax: (internat.) +44-1223/336-033; E-mail: deposit@ccdc.cam.ac.uk].

Acknowledgments

This work has been supported by the Spanish DGESIC (grants PB98-1555 to J.A.C. and BQU2000-0219 to S.G.-G.). M. M. thanks the Spanish Ministry of Education for a predoctoral fellowship (FPI program).

[1] For a recent review of the reactivity of 2-amidopyridine-bridged triruthenium carbonyl clusters complexes, see: J. A. Cabeza, *Eur. J. Inorg. Chem.* **2002**, 1559−1570.
[2] N. Lugan, F. Laurent, G. Lavigne, T. P. Newcomb, E. W. Liimata, J. J. Bonnet, *J. Am. Chem. Soc.* **1990**, *112*, 8607−8609.
[3] J. A. Cabeza, J. M. Fernández-Colinas, A. Llamazares, V. Riera, S. García-Granda, J. F. van der Maelen, *Organometallics* **1994**, *13*, 4352−4359 and references therein.
[4] J. A. Cabeza, in *Metal Clusters in Chemistry* (Eds.: P. Braunstein, L. A. Oro, P. R. Raithby), Wiley-VCH, Weinheim, **1999**, p.715.
[5] For a review on alkyne hydrogenation mediated by 2-amidopyridine-bridged triruthenium carbonyl cluster complexes, see: J. A. Cabeza, J. M. Fernández-Colinas, A. Llamazares, *Synlett* **1995**, 579−586.
[6] P. Nombel, N. Lugan, F. Mulla, G. Lavigne, *Organometallics* **1994**, *13*, 4673−4675.
[7] P. Nombel, N. Lugan, B. Donnadieu, G. Lavigne, *Organometallics* **1999**, *18*, 187−196.
[8] J. A. Cabeza, I. del Río, S. García-Granda, G. Lavigne, N. Lugan, M. Moreno, P. Nombel, M. Pérez-Priede, V. Riera, A. Rodríguez, M. Suárez, J. F. van der Maelen, *Chem. Eur. J.* **2001**, *7*, 2370−2381.
[9] J. A. Cabeza, I. del Río, S. García-Granda, M. Moreno, V. Riera, *Organometallics* **2001**, *20*, 4973−4976.

[10] P. L. Andreu, J. A. Cabeza, V. Riera, Y. Jeannin, D. Miguel, *J. Chem. Soc., Dalton Trans.* **1990**, 2201−2206.

[11] Unpublished results cited in: [11a] G. Lavigne, B. Bonneval, in *Catalysis by Di- and Polynuclear Metal Cluster Complexes* (Eds.: R. D. Adams, F. A. Cotton), Wiley-VCH, New York, **1998**, p. 39. [11b] G. Lavigne, *Eur. J. Inorg. Chem.* **1999**, 917−930. [11c] P. Nombel, PhD Thesis, Université Paul Sabatier, Toulouse, **1996**.

[12] J. A. Cabeza, F. Grepioni, M. Moreno, V. Riera, *Organometallics* **2000**, *19*, 5424−5430.

[13] J. A. Cabeza, M. Moreno, V. Riera, M. J. Rosales, *Inorg. Chem. Commun.* **2001**, *4*, 57−59.

[14] V. Ferrand, C. Gambs, N. Derrien, C. Bolm, H. Stoeckli-Evans, G. Süss-Fink, *J. Organomet. Chem.* **1997**, *549*, 275−282.

[15] [15a] C. S.-W. Lau, W.-T. Wong, *J. Chem. Soc., Dalton Trans.* **1999**, 2511−2519. [15b] M. I. Bruce, B. W. Skelton, A. H. White, N. N. Zaitseva, *Inorg. Chem. Commun.* **1998**, *1*, 134−136. [15c] M. I. Bruce, N. N. Zaitseva, B. W. Skelton, A. H. White, *Aust. J. Chem.* **1998**, *51*, 165−168. [15d] M. I. Bruce, N. N. Zaitseva, B. W. Skelton, A. H. White, *Russ. Chem. Bull.* **1998**, *47*, 983−987. [15e] M. I. Bruce, N. N. Zaitseva, B. W. Skelton, A. H. White, *J. Organomet. Chem.* **1997**, *536−537*, 93−107. [15f] M. I. Bruce, N. N. Zaitseva, B. W. Skelton, A. H. White, *Inorg. Chim. Acta* **1996**, *250*, 129−138. [15g] M. I. Bruce, B. W. Skelton, A. H. White, N. N. Zaitseva, *J. Organomet. Chem.* **1998**, *558*, 197−207. [15h] S. P. Tunik, E. V. Grachova, V. R. Denisov, G. L. Starova, A. B. Nikol'skii, F. M. Dolgushin, A. I. Yanovsky, Y. T. Struchkov, *J. Organomet. Chem.* **1997**, *536−537*, 339−343. [15i] C. J. Adams, M. I. Bruce, B. W. Skelton, A. H. White, *J. Organomet. Chem.* **1999**, *589*, 213−221.

[16] N. Walker, D. Stuart, *Acta Crystallogr., Sect. A* **1983**, *39*, 158.

[17] S. Parkin, B. Moezzi, H. Hope, *J. Appl. Cryst.* **1995**, *28*, 53−56.

[18] P. T. Beurskens, G. Beurskens, W. P. Bosman, R. de Gelder, S. García-Granda, R. O. Gould, R. Israël, J. M. M. Smits, *The DIRDIF-96 Program System*, Crystallography Laboratory, University of Nijmegen, The Netherlands, **1996**.

[19] G. M. Sheldrick, *SHELXL-97, version 97−2*, University of Göttingen, Germany, **1997**.

[20] A. L. Spek, *The EUCLID Package*, in *Computational Crystallography* (Ed.: D. Sayre), Clarendon Press, London, **1982**, p. 528.

[21] L. J. Farrugia, *J. Appl. Cryst.* **1999**, *32*, 837−838.

Received May 10, 2002
[I02244]

Formation and Structure of the Novel Heptanuclear Lead(II) Oxo Cluster $[Pb_7(\mu_3\text{-}O)(\mu_4\text{-}O)(\mu_3\text{-}OMe)_4(\mu_2\text{-}I)_4]I_2$ with an Unprecedented Cage Structure

Yu-Jun Shi,[a] Yan Xu,[a] Xue-Tai Chen,*[a] Ziling Xue,[b] and Xiao-Zeng You*[a]

Keywords: Lead / Cluster compounds / Alkoxides / Oxo ligands / Crystal structure

A novel lead(II) cluster $[Pb_7(\mu_3\text{-}O)(\mu_4\text{-}O)(\mu_3\text{-}OMe)_4(\mu_2\text{-}I)_4]I_2$ (**1**) has been isolated from the reaction mixture of PbI_2 and pyrazine in DMF/MeOH solvent with a reasonable yield (46%). The X-ray crystallography shows that **1** exhibits a novel unprecedented cage structure with centered μ_3-O and μ_4-O atoms and four different coordination environments of lead atoms. It is the first structurally characterized example of a lead compound containing bridging oxo, methoxide and iodide ligands. Compound **1** crystallizes in the tetragonal space group $P42_1m$, $a = b = 11.7768(13)$, $c = 9.8606(16)$ Å, $Z = 2$, $V = 1367.6(3)$ Å^3.

(© Wiley-VCH Verlag GmbH, 69451 Weinheim, Germany, 2002)

Introduction

Lead(II) alkoxides and oxo alkoxides have been extensively studied for their uses as molecular precursors to lead-containing metal oxide materials via chemical routes such as MOCVD and sol-gel processes.[1] There has been much research interest focused on the synthesis and spectroscopic characterization of lead alkoxide and oxoalkoxide complexes. However, only a limited number of crystal structures have been reported for lead alkoxides and oxoalkoxides. These include oxygen-free, monomeric, trimeric, and one-dimensional $Pb(OR)_2$ (R = 2,6-di-*tert*-butyl-4-methylphenyl,[2] *t*Bu,[3] *i*Pr,[3] and CH_2CH_2OMe[3]), and two oxygen-centered, regular polyhedral clusters $[Pb_4(\mu_4\text{-}O)(OSiPh_3)_6]$[4] and $[Pb_6(\mu_3\text{-}O)_4(\mu_3\text{-}O\textit{i}Pr)_4]$.[5] Sita and coworkers[6] recently reported a novel lead(II) oxoalkoxide cluster $[Pb_7(\mu_3\text{-}O)(\mu_4\text{-}O)(\mu_2\text{-}OSiMe_3)_{10}]$ containing $Pb_4(\mu_4\text{-}O)$ and $Pb_3(\mu_3\text{-}O)$ units. Obviously the structures of lead alkoxides are highly dependent on the R groups and the method of preparation.

We have recently become interested in the construction of supramolecular structures using PbX_2 as the building blocks and have reported a novel 2-D coordination polymer $[PbI_2(4,4'\text{-bpy})]$ from the reaction of 4,4-bipyridine and PbI_2 in DMF/MeOH.[7] We intended to extend this chemistry from 4,4-bipyridine to pyrazine with the expectation of preparing a similar PbI_2 complex containing pyrazine ligands. We were surprised that the mixture of PbI_2 and pyrazine in MeOH/DMF gave a cluster complex $[Pb_7(\mu_3\text{-}O)(\mu_4\text{-}O)(\mu_3\text{-}OMe)_4(\mu_2\text{-}I)_4]I_2$ (**1**) reproducibly in 46% isolated yield, which contains bridging oxo, methoxide and iodide ligands. Lead(II) dimethoxide has been reported previously, although it was only poorly characterized due to its low solubility and air- and moisture-sensitivity.[8] To the best of our knowledge, there have been no lead oxomethoxide complexes reported in the literature. Herein we report the preparation of the unusual heptanuclear lead oxo cluster **1** and its unprecedented cage structure.

Results and Discussion

The syntheses of **1** and our previously reported cluster are summarized in Scheme 1, indicating how different products can be isolated by varying the ligand from 4,4-bipyridine to pyrazine. The formation of **1** can be rationalized as follows. As the basicity of pyrazine is greater than that of 4,4′-bipyridine, pyrazine could act as a stronger proton acceptor than 4,4-bipyridine in abstracting the proton of MeOH and H_2O and enhance coordination between lead(II) and the oxo and methoxide ligands. The low solubility of **1** might also favor its isolation from solution. A nitrogen-containing heterocyclic ligand plays a similar role in the preparation of transition metal clusters, for example $[Fe_{13}O_4F_{24}(OMe)_{12}]^{5-}$,[9] which was isolated from $FeF_3{\cdot}3H_2O$ and pyridine in MeOH.

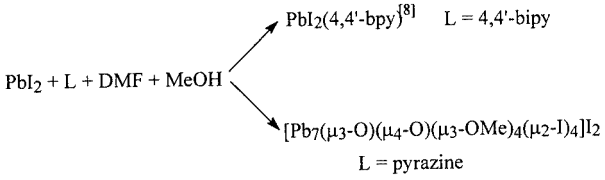

Scheme 1

[a] State Key Laboratory of Coordination Chemistry, Coordination Chemistry Institute, Nanjing University, Nanjing 210093, China
E-mail: xtchen@netra.nju.edu.cn
[b] Department of Chemistry, The University of Tennessee, Knoxville, Tennessee 37996-1600, USA

Compound **1** is insoluble in common organic solvents, which prevents its characterization in solution. The crystal structure of **1** was determined by X-ray crystallography. A labeled ORTEP diagram of the cluster cation of **1** is shown in Figure 1 and bond lengths and bond angles are listed in Table 1. The structure of the cluster **1** exhibits C_{2v} symmetry with a C_2 axis through Pb(3), O(3) and O(1). There are four symmetrically different sets of lead atoms which vary in the type and number of coordinated ligands. The pyramidal Pb(2) and Pb(2A) are three-coordinate with one μ_4-O and two μ_3-OMe ligands, while Pb(1) and Pb(1A) are in an inverted square-pyramidal configuration surrounded by one μ_4-O, one μ_3-O, and two μ_3-OMe ligands. More interesting is the mixed coordination environment around Pb(4) and Pb(4A), and Pb(3). Pb(4) and Pb(4A) are coordinated by two μ_3-OMe and two iodide ligands, and the unique Pb(3) is in an inverted square pyramidal I_4O environment. The coordination spheres of all four Pb atoms in **1** are strongly distorted as a result of the presence of the stereochemically active $6s^2$ lone-pair electrons on the Pb^{II} cations. The Pb−O bond lengths fall into three different categories depending on the environments of the O atoms. The mean bond lengths of Pb-(μ_3-O), Pb-(μ_4-O), and Pb−OMe are 2.20(3), 2.28(2), 2.439(17) Å, respectively. The Pb−I bond lengths of 3.198(2)−3.302(3) Å are normal.[10−12] *The cage structure of **1** can also be viewed as being built-up from a Pb_4(μ_4-O) unit bonded to Pb(4), Pb(4A) and Pb(3) through four μ_3-OMe groups, a μ_3-O and four iodide atoms. The μ_4-O(1) atom tetrahedrally bridges Pb(2), Pb(2A), Pb(1), and Pb(1A). The planar μ_3-O is surrounded by Pb(1), Pb(1A) and Pb(3). A similar three-coordinate planar configuration has been observed in the lead(II) thiolate cluster $[Pb_5O(SR_F)_8]\cdot 2C_7H_8$ [R_F = 2,4,6-trsi(trifluromethylphenyl)].[13]

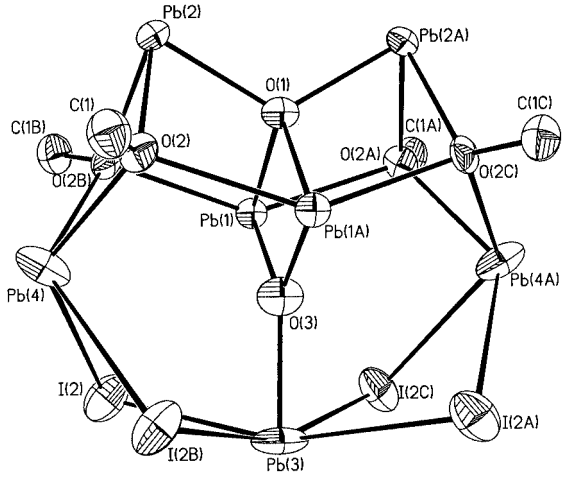

Figure 1. The ORTEP diagram of cluster cation of **1**

The Pb^{II} atoms of the cluster cation are involved in weak interactions with the anion I^- as shown in Figure 2, where each I^- anion links three cationic clusters to form an extensive three-dimensional supramolecular assembly through the six weak interactions [I(1)···Pb(1a)(1 − *y*, *x* − 1, 1 − *z*), 3.63(2); I(1)···Pb(2), 3.68(2); I(1)···Pb(2a) (*y*, 1 − *x*, 1 − *z*), 3.49(2); I(1)···Pb(2b) (1 − y, −1 + *x*, 1 − *z*), 3.49(2); I(1)···Pb(3a) (*y*, 1 − *x*, 1 − *z*), 4.01(2) and I(1)···Pb(4), 3.48(2) Å].

Table 1. Crystal data and structure refinement for **1**

Empirical formula	$C_4H_{12}I_6O_6Pb_7$
Formula mass	2367.94
Temperature (K)	293(2)
Wavelength (Å)	0.71073
Crystal system, space group	Tetragonal, $P42_1m$
Unit cell dimensions	a = 11.7768(13) Å, α =90° b = 11.7768(13) Å, β = 90° c = 9.8606(16) Å, γ = 90°
Volume (Å^3)	1367.6(3)
Z	2
Calculated density (Mg/m^3)	5.750
Absorption coefficient (mm^{-1})	49.712
F(000)	1952
Crystal size (mm)	0.011 × 0.009 × 0.009
θ range for data collection (°)	2.07 to 26.02
Limiting indices	$-14 \le h \le 7$, $-14 \le k < 14$, $-12 \le l \le 12$
Reflections collected	9808
Independent reflections	837 (R_{int} = 0.0684)
Absorption correction	Empirical
Max. and min. transmission	0.639 and 0.590
Refinement method	Full-matrix least-squares on F^2
Data/restraints/parameters	837/24/65
Goodness-of-fit on F^2	1.062
Final R indices [$I > 2\sigma(I)$]	R_1 = 0.0420, wR_2 =0.1008
Largest diff. peak and hole (e·Å^{-3})	2.824 and −2.724

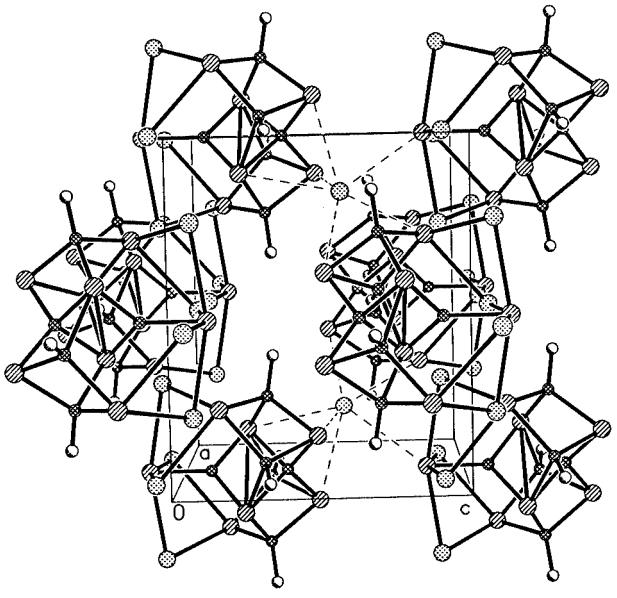

Figure 2. The cell packing of the crystal structure of **1** showing the weak interactions

Conclusions

In summary, a novel heptanuclear lead(II) cluster **1** has been isolated and characterized by X-ray crystallography.

Table 2. Bond lengths [Å] and angles [°] for **1** (symmetry transformations used to generate equivalent atoms: A: $-x + 2$, $-y + 1$, z; B: $y + 1/2$, $x - 1/2$, z; C: $-y + 3/2$, $-x + 3/2$, z)

Pb(1)−O(3)	2.22(2)	Pb(3)−I(2)	3.198(2)
Pb(1)−O(1)	2.34(2)	Pb(3)−I(2B)	3.198(2)
Pb(1)−O(2A)	2.565(17)	Pb(4)−O(2B)	2.417(18)
Pb(1)−O(2B)	2.565(17)	Pb(4)−O(2)	2.417(18)
Pb(1)−Pb(1A)	3.632(3)	Pb(4)−I(2B)	3.302(3)
Pb(2)−O(1)	2.240(16)	Pb(4)−I(2)	3.302(3)
Pb(2)−O(2)	2.336(17)	O(1)−Pb(2A)	2.240(16)
Pb(2)−O(2B)	2.336(16)	O(1)−Pb(1A)	2.34(2)
Pb(3)−O(3)	2.16(4)	O(2)−C(1)	1.48(3)
Pb(3)−I(2C)	3.198(2)	O(2)−Pb(1A)	2.565(17)
Pb(3)−I(2A)	3.198(2)	O(3)−Pb(1A)	2.22(2)
O(3)−Pb(1)−O(1)	74.2(10)	O(2)−Pb(4)−I(2B)	81.7(4)
O(3)−Pb(1)−O(2A)	93.2(5)	O(2B)−Pb(4)−I(2)	81.7(4)
O(1)−Pb(1)−O(2A)	71.7(4)	O(2)−Pb(4)−I(2)	129.3(4)
O(3)−Pb(1)−O(2B)	93.2(5)	I(2B)−Pb(4)−I(2)	82.44(9)
O(1)−Pb(1)−O(2B)	71.7(4)	Pb(3)−I(2)−Pb(4)	85.90(7)
O(2A)−Pb(1)−O(2B)	139.4(7)	Pb(2)−O(1)−Pb(2A)	120.3(14)
O(1)−Pb(2)−O(2)	77.9(7)	Pb(2)−O(1)−Pb(1A)	108.28(16)
O(1)−Pb(2)−O(2B)	77.9(7)	Pb(2A)−O(1)−Pb(1A)	108.28(16)
O(2)−Pb(2)−O(2B)	75.4(9)	Pb(2A)−O(1)−Pb(1)	108.28(16)
O(3)−Pb(3)−I(2C)	80.78(5)	Pb(2)−O(1)−Pb(1)	108.28(16)
O(3)−Pb(3)−I(2A)	80.78(5)	Pb(1A)−O(1)−Pb(1)	101.8(12)
I(2C)−Pb(3)−I(2A)	85.75(8)	C(1)−O(2)−Pb(2)	122.9(15)
O(3)−Pb(3)−I(2)	80.78(5)	Pb(2)−O(2)−Pb(4)	103.5(7)
I(2C)−Pb(3)−I(2)	91.31(9)	C(1)−O(2)−Pb(1A)	107.1(15)
I(2A)−Pb(3)−I(2)	161.57(10)	Pb(2)−O(2)−Pb(1A)	98.4(6)
O(3)−Pb(3)−I(2B)	80.78(5)	Pb(4)−O(2)−Pb(1A)	109.1(6)
I(2C)−Pb(3)−I(2B)	161.57(10)	C(1)−O(2)−Pb(4)	114.2(15)
I(2A)−Pb(3)−I(2B)	91.31(9)	Pb(3)−O(3)−Pb(1)	125.1(7)
I(2)−Pb(3)−I(2B)	85.75(8)	Pb(3)−O(3)−Pb(1A)	125.1(7)
O(2B)−Pb(4)−O(2)	72.4(8)	Pb(1)−O(3)−Pb(1A)	109.8(15)
O(2B)−Pb(4)−I(2B)	129.3(4)		

The isolation of **1** implies that a suitable choice of base and alkoxide ligand could lead to the formation of novel mixed-coordinate lead clusters.

Experimental Section

Materials and Methods: All chemicals are commercially available and were used without further purification, except PbI_2, which was prepared by the reaction of PbO with HI 35%. C, H and N analyses were carried on a Perkin−Elmer 240C elemental analyzer. IR spectra were recorded on a Bruker Optik Gmbh spectrophotometer (range: 400−4000 cm^{-1}) as KBr pellets.

Preparation of 1: Single crystals of **1** were grown at room temperature by using a layered solution approach. The bottom solution layer, contained within a long straight tube, consisted of PbI_2 (0.239 g, 0.5 mmol) dissolved in DMF. A mixed-solvent layer of methanol/DMF (1:1) was carefully placed on top of the PbI_2 solution using a syringe. Finally, pyrazine (a stoichiometric quantity relative to the PbI_2) dissolved in methanol was added to the top of the buffer. As the layers slowly mixed, well-formed crystals of **1** appeared that were suitable for X-ray single-crystal analysis. Yield 77.8 mg, 46% (based on PbI_2). $C_4H_{12}I_6O_6Pb_7$ (2368.0): calcd. C, 2.03, H 0.51; found C 2.22, H 0.63. IR (KBr): $\tilde{\nu}$ = 603.86 cm^{-1} (vs), 682.04 (m), 750.83 (w), 838.09 (w), 1401.10 (s), 1608.43 (m).

X-ray Crystallographic Analysis: X-ray data were collected at 293 K on a Bruker Apex CCD diffractometer equipped with graphite-monochromated Mo-K_α radiation (λ = 0.7103Å) by using the $\theta/2\theta$ scan mode. An empirical absorption correction was applied to the data, and structure solution and refinement on F^2 were done. The structures were solved by direct methods by using SHELXS 97[14] and refined by full-matrix least-squares calculation on F^2 with SHELXL 97.[15] All non-hydrogen atoms were refined anisotropically, whereas the hydrogen atoms were generated geometrically. Crystal data, data collection parameters, and refinement statistics for **1** are listed in Table 1. Relevant bond lengths and bond angles for **1** are collected in Table 2.

CCDC-184695 contains the supplementary crystallographic data for this paper. These data can be obtained free of charge at www.ccdc.cam.ac.uk/conts/retrieving.html [or from the Cambridge Crystallographic Data Center, 12, Union Road, Cambridge CB2 1EZ, UK; fax: (internat.) +44-1223/336-033; E-mail: deposit@ccdc.cam.ac.uk].

Acknowledgments

This work was supported by Major State Basic Research Development Program (Grant No. G2000077500), Overseas Outstanding Young Scholar Fund from the National Natural Science Foundation of China (No. 20028101) and Natural Science Grant of Jiangsu Province (BK, 99032).

[1] [1a] K. G. Caulton, L. G. Hubert-Pfalzgraf, *Chem. Rev.* **1990**, *90*, 969−995. [1b] D. C. Bradley, *Chem. Rev.* **1989**, *89*, 1317−1322. [1c] D. J. Teff, J. C. Huffman, K. G. Caulton, *J. Am. Chem. Soc.* **1996**, *118*, 4030−4035.
[2] B. Cetinkaya, I. Gümrükcü, M. F. Lappert, J. L. Atwood, R.

D. Rogers, M. J. Zaworotko, *J. Am. Chem. Soc.* **1980**, *102*, 2088−2089.
[3] S. C. Goel, M. Y. Chian, W. E. Buhro, *Inorg. Chem.* **1990**, *29*, 4640−4646.
[4] C. Gaffney, P. G. Harrison, T. J. King, *J. Chem. Soc., Chem. Commun.* **1980**, 1251−1252.
[5] A. I. Yanovskii, N. Y. Turova, E. P. Turevskaya, Y. T. Struchkov, *Koord. Khim.* **1982**, *8*, 153−156.
[6] C. S. Weinert, I. A. Guzei, A. L. Rheingold, L. R. Sita, *Organometallics* **1998**, *17*, 498−500.
[7] Y. J. Shi, Y. Xu, Y. Zhang, B. Huang, D. R. Zhu, C. M. Jin, H. G. Zhu, Z. Yu, X. T. Chen, X. Z. You, *Chem. Lett.* **2001**, 678−679.
[8] [8a] E. Amberger, R. Hönigschmid-Grossich, *Chem. Ber.* **1965**, *98*, 3795−3803. [8b] R. J. Puddephatt, G. H. Thistlethwaite, *J. Chem. Soc., Dalton Trans.* **1972**, 570−572.
[9] A. Bino, M. Ardon, D. Lee, B. Spingler, S. L. Lippard, *J. Am. Chem. Soc.* **2002**, *124*, 4578−4579.
[10] V. N. Kokozay, A. V. Sienkiewicz, *Polyhedron* **1995**, *14*, 1547−1551.
[11] H. Krautscheid, C. Lode, F. Vielsack, H. Vollmer, *J. Chem. Soc., Dalton Trans.* **2001**, 1099−1104.
[12] Z. Tang, A. M. Guloy, *J. Am. Chem. Soc.* **1999**, *121*, 452−453.
[13] F. T. Edelmann, J-K. F. Buijink, S. A. Brooker, R. Herbst-Irmer, U. Kilimann, F. M. Bohnen, *Inorg. Chem.* **2000**, *39*, 6134−6135.
[14] G. M. Sheldrick, SHELXS 97, *Program for crystal structure determinations*, Univeristy of Göttingen, **1997**.
[15] G. M. Sheldrick, SHELXL 97, *Program for crystal structure determinations*, Univeristy of Göttingen, **1997**.

Received July 8, 2002
[I02375]

Structure, Properties and Cytostatic Activity of Triorganotin (Aminoaryl)carboxylates

Florian P. Pruchnik,*[a] Małgorzata Bańbuła,[a] Zbigniew Ciunik,[a] Henryk Chojnacki,[b] Małgorzata Latocha,[c] Barbara Skop,[c] Tadeusz Wilczok,[c] Adam Opolski,[d] Joanna Wietrzyk,[d] and Anna Nasulewicz[d]

Keywords: Tin / Cytostatic agents / Antitumor activity / O ligands

The properties of vinyltin and phenyltin complexes $[Sn(CH=CH_2)_3\{\mu\text{-}OOCC_6H_3(NH_2)_2\text{-}3,4\}]_n$ (**1**), $[Sn(C_6H_5)_3\{OOCC_6H_3(NH_2)_2\text{-}3,4\}]$ (**2**), $[Sn(C_6H_5)_3\{OOC\text{-}2\text{-}C_6H_4N{=}NC_6H_4N(CH_3)_2\text{-}4\}]$ (**3**) and $[Sn(CH=CH_2)_3\{OOC\text{-}2\text{-}C_6H_4N{=}NC_6H_4N(CH_3)_2\text{-}4\}]$ (**4**) have been investigated. The structures of complexes **1**, **2**, and **3**, have been determined by X-ray crystallography. Compound **1** is a distorted trigonal-bipyramidal complex and compounds **2** and **3** adopt a distorted tetrahedral structure. Complex **1** is a single-strand polymer with a bridging 3,4-diaminobenzoato ligand coordinating via the O(1) atom of the carboxylato group and the nitrogen atom of the *para*-amino group. The oxygen and nitrogen atoms occupy the axial coordination sites. The Sn(1)–N(2A) bond is weak. In complexes **2** and **3** the carboxylato ligands are strongly coordinated to the central atom via one oxygen atom, and the Sn(1)–O(2) distances are considerably longer. Weak interactions of the central atom with the amino group in complex **1**, and with the O(2) atoms in complexes **2** and **3**, as well as the hydrogen bonds, stabilize the crystal structure. The complexes are effective cytostatic agents.
(© Wiley-VCH Verlag GmbH, 69451 Weinheim, Germany, 2002)

Introduction

Coordination and organometallic compounds belong to the very important group of antitumor agents.[1,2] Many platinum complexes and other transition metal compounds, as well as organometallic compounds of the main group metals show high cytostatic activity. A number of organotin compounds have been shown to be active against various types of cancers. A series of organotin dipeptide compounds and a number of diorganotin halides containing amino ligands $[SnR_2X_2L_2]$ have displayed modest antitumor activity.[3,4] Many di-*n*-butyl-, tri-*n*-butyl-, and triphenyltin hydroxycarboxylates, oxycarboxylates, and fluorocarboxylates display interesting antitumor activities.[5−15] However, only few tin carboxylates with amino groups have been investigated. These complexes comprise pyridinocarboxylato and aminosalicylato organotin compounds.[5] Here, we report on the synthesis, properties, structure, and in vitro cytostatic activity of trivinyltin and triphenyltin complexes with 3,4-diaminobenzoate and 2-[4-(dimethylamino)phenylazo]benzoate.

Results and Discussion

The complexes $[Sn(CH=CH_2)_3\{\mu\text{-}OOCC_6H_3(NH_2)_2\text{-}3,4\}]_n$ (**1**), $[Sn(C_6H_5)_3\{OOCC_6H_3(NH_2)_2\text{-}3,4\}]$ (**2**), $[Sn(C_6H_5)_3\{OOC\text{-}2\text{-}C_6H_4N{=}NC_6H_4N(CH_3)_2\text{-}4\}]$ (**3**) and $[Sn(CH=CH_2)_3\{OOC\text{-}2\text{-}C_6H_4N{=}NC_6H_4N(CH_3)_2\text{-}4\}]$ (**4**) are soluble in ethanol, methanol, acetone, chloroform, dichloromethane, and in other polar organic solvents, and are slightly soluble in aqueous ethanol (50%). The vinyl complexes **1** and **4** have been obtained by the reactions of $SnO(CH=CH_2)_2$ and the appropriate acid in ethanol, while complexes **2** and **3** have been prepared by the reactions of $SnO(C_6H_5)_2$ or $\{Sn(C_6H_5)_3\}_2O$ with the acids. Thus, in the reactions of $SnO(CH=CH_2)_2$ and $SnO(C_6H_5)_2$ with the acids, the vinyl or phenyl groups are transferred. Other products obtained were SnO(R)(OOCR′), $Sn(OH)_2R(OOCR')$ and similar monoorganotin(IV) compounds, however, these compounds were not pure enough.

[a] Faculty of Chemistry, University of Wrocław,
ul. Joliot-Curie 14, 50-383 Wrocław, Poland
[b] Institute of Physical and Theoretical Chemistry, Wrocław University of Technology,
Wyb. Wyspiańskiego 27, 50-370 Wrocław, Poland
[c] Department of Molecular Biology, Biochemistry and Biopharmacy, Medical University of Silesia,
41-200 Sosnowiec, ul. Narcyzów 1, Poland
[d] Institute of Immunology and Experimental Therapy, Polish Academy of Sciences,
Wrocław, Poland

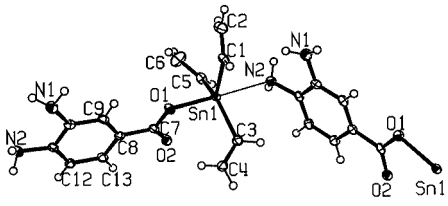

Figure 1. $[Sn(CH{=}CH_2)_3\{\mu\text{-}OOCC_6H_3(NH_2)_2\text{-}3,4\}]_n$

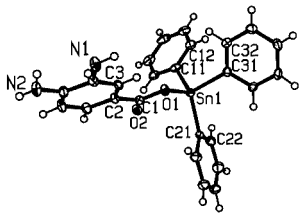

Figure 2. $[Sn(C_6H_5)_3\{OOCC_6H_3(NH_2)_2\text{-}3,4\}]$

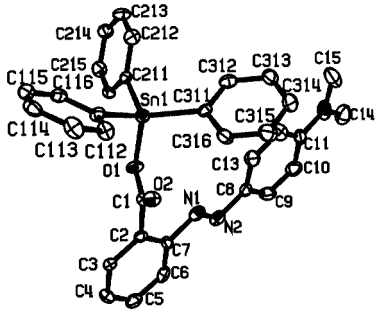

Figure 3. $[Sn(C_6H_5)_3\{OOC\text{-}2\text{-}C_6H_4N{=}NO_6H_4N(CH_3)_2\text{-}4\}]$

Table 1. Bond lengths [Å] and angles [°] for complex **1**

Sn(1)−C(3)	2.118(3)	C(3)−Sn(1)−C(1)	113.18(12)
Sn(1)−C(5)	2.120(3)	C(5)−Sn(1)−C(1)	112.63(12)
Sn(1)−C(1)	2.135(3)	C(3)−Sn(1)−O(1)	96.01(10)
Sn(1)−O(1)	2.1353(19)	C(5)−Sn(1)−O(1)	98.73(10)
Sn(1)−O(2)	2.955(3)	C(1)−Sn(1)−O(1)	92.61(10)
Sn(1)−N(2i)	2.685(3)	C(3)−Sn(1)−N(2i)	84.69(10)
O(1)−C(7)	1.310(3)	C(5)−Sn(1)−N(2i)	80.05(10)
O(2)−C(7)	1.240(4)	C(1)−Sn(1)−N(2i)	88.04(10)
C(3)−Sn(1)−C(5)	130.87(12)	O(1)−Sn(1)−N(2i)	178.76(7)

Table 2. Bond lengths [Å] and angles [°] for complex **2**

Sn(1)−O(1)	2.069(2)	O(1)−Sn(1)−C(11)	112.05(12)
Sn(1)−C(11)	2.121(3)	O(1)−Sn(1)−C(21)	109.64(12)
Sn(1)−C(21)	2.128(3)	C(11)−Sn(1)−C(21)	119.14(13)
Sn(1)−C(31)	2.146(3)	O(1)−Sn(1)−C(31)	95.72(11)
Sn(1)−O(2)	2.680(3)	C(11)−Sn(1)−C(31)	108.51(13)
O(1)−C(1)	1.320(4)	C(21)−Sn(1)−C(31)	109.21(13)
O(2)−C(1)	1.241(4)	O(2)−Sn(1)−C(31)	149.18(13)

The structures of complexes **1**, **2** and **3** are shown in Figures 1, 2, and 3, and selected bond lengths and angles are given in Tables 1, 2, and 3, the lengths and angles of the hydrogen bonds in the solid compounds in Tables 4, 5, and 6, and the crystallographic data in Table 8. Compound $[Sn(CH{=}CH_2)_3\{OOCC_6H_3(NH_2)_2\text{-}3,4\}]$ (**1**) is a distorted trigonal-bipyramidal complex, it consists of three vinyl ligands and a bridging 3,4-diaminobenzoato ligand, which is coordinated via one oxygen atom and the nitrogen atom of the *para*-amino group. The monodentate coordination of the carboxylate group is reflected in the short Sn(1)−O(1) bond [2.1353(19) Å] and the different C(7)−(O1) and C(7)−O(2) distances of 1.310(3) and 1.240(4) Å, respectively. The Sn−O(2) bond [2.955(3) Å] is much longer than the Sn−O(1) bond [2.1353(19) Å], thus the interaction of the O(2) atom with the central atom is very weak. The fifth

Table 3. Bond lengths [Å] and angles [°] for complex **3**

Sn(1)−O(1)	2.054(2)	O(1)−Sn(1)−C(311)	108.23(12)
Sn(1)−O(2)	2.827(2)	O(1)−Sn(1)−C(111)	109.32(12)
Sn(1)−C(311)	2.117(4)	C(311)−Sn(1)−C(111)	118.20(15)
Sn(1)−C(111)	2.121(4)	O(1)−Sn(1)−C(211)	95.81(12)
Sn(1)−C(211)	2.126(4)	C(311)−Sn(1)−C(211)	112.61(14)
O(1)−C(1)	1.314(4)	C(111)−Sn(1)−C(211)	110.29(14)
O(2)−C(1)	1.219(4)	C(1)−O(1)−Sn(1)	110.1(2)

Table 4. Lengths [Å] and angles [°] of the hydrogen bonds in solid compound **1**

D−H···A[a]	D−H	H···A	D···A	D−H···A
N(2)−H(4N)···O(2)^{i}	0.90(4)	2.06(4)	2.956(3)	170(3)
N(2)−H(3N)···C(2)^{ii}	0.84(3)	3.08(3)	3.712(4)	134(3)
N(1)−H(1N)···X1A (C1/C2)^{iii}	0.88(4)	2.63	3.50	170
N(1)−H(2N)···X1B (C3/C4)^{iv}	0.89(4)	2.94	3.53	125

[a] Symmetry transformations used to generate equivalent atoms: i: $-x + 1/2, y - 1/2, -z + 1/2$; ii: $-x, y - 1, -z + 1/2$; iii: $x, -y, z - 1/2$; iv: $-x, y, -z + 1/2$.

Table 5. Lengths [Å] and angles [°] of the hydrogen bonds in solid compound **2**

D−H···A[a]	D−H	H···A	D···A	D−H···A
N(1)−H(2N)···N(2)^{ii}	0.87	2.40	3.181(5)	150.5
N(2)−H(3N)···O(2)^{iii}	0.92	2.08	2.979(4)	165.7

[a] Symmetry transformations used to generate equivalent atoms: i: $-x, -y - 1, -z$; ii: $-x, -y, -z$; iii: $-x, y - 1/2, -z + 1/2$.

Table 6. Lengths [Å] and angles [°] of weak C−H···π hydrogen bonds in solid complex **3**

C−H···Ph[a]	H···Ph	Offset	C−H···Ph
C(13)−H(13)···Ph5	3.07	0.91	134
C(3)−H(3)···Ph4^{i}	2.54	0	155
C(213)−H(213)···Ph3^{ii}	3.07	1.04	144
C(315)−H(315)···Ph1^{iii}	2.63	0.32	168

[a] Ph1 is defined by C(2), C(3), C(4), C(5), C(6), and C(7) atoms; Ph3 by C(111), C(112), ..., C(116) atoms; Ph4 by C(211), C(212), ..., C(216) atoms; Ph5 by C(311), C(312), ..., C(316) atoms. Symmetry code superscript: (none) x, y, z; (i) $x + 1, y, z$; (ii) $x - 1, y, z$; (iii) $x, y - 1, z$.

coordination site is occupied by the N(2A) atom of a neighboring molecule (Figure 1). Thus, complex **1** is a single-strand polymer in the solid state. The Sn(1)−N(2A) distance is 2.685(3) Å and the O(1)−Sn(1)−N(2A) angle is 178.76(7)°. The angles C(1)−Sn(1)−C(3) [113.18(12)°] and C(1)−Sn(1)−C(5) [112.63(12)°] are considerably smaller, and the C(3)−Sn(1)−C(5) angle [130.87(12)°] is substantially larger than those expected for a regular trigonal bipyramid. A relatively strong Sn(1)−N(2A) bonding interaction is important for the stabilization of the crystal structure of complex **1**. The crystal structure is also stabilized by the relatively strong hydrogen bond N(2)−H(4N)···O(2)(i) and the weaker hydrogen bonds N(2)−H(3N)···C(2)(ii), N(1)−H(1N)···X1A(C1/C2)(iii), and N(1)−H(2N)···X1B-(C3/C4)(iv) (Table 4). In complex **2**, the central atom has a distorted tetrahedral geometry, with the Sn(1)−O(1) bond length of 2.069(2) Å, the Sn(1)−C bond lengths of 2.121(3)−2.146(3) Å, and the considerably longer Sn(1)−O(2) distance of 2.680(3) Å. The C(11)−Sn(1)−C(31) and C(21)−Sn(1)−C(31) angles are 108.51(13) and 109.21(13)°, respectively, and the C(11)−Sn(1)−C(21) angle is 119.14(13)°. The interaction of the oxygen atom O(2) with the central atom Sn(1) is relatively strong in comparison with analogous interactions in complex **1**. The O(2)−Sn(1)−C(31) angle is 149.18(13)°, while the O(2)−Sn(1)−C(11) and O(2)−Sn(1)−C(21) angles are 84.67(13) and 86.38(13)°, respectively. The structure of complex **2** is similar to that of $[Sn(C_6H_5)_3(OOCC_6H_5)]$, in which the O(2)−Sn distance is 2.674(3) Å.[7,16] The crystal structure of the complex **2** is stabilized not only by the Sn(1)−O(2) interaction, but also by intermolecular hydrogen bonds, namely, N(1)−H(2N)···N(2)(ii) and N(2)−H(3N)···O(2)(iii) (Table 5). Complex **3** has a molecular structure similar to that of compound **2**, with the Sn(1)−O(1) bond length of 2.054(2) Å, Sn(1)−C bond lengths of 2.117(4)−2.126(4) Å and Sn(1)−O(2) bond length of 2.827(3) Å. Thus, in this compound the interaction between the Sn(1) and O(2) atoms is weaker than in complex **2**. However, the crystal structure of compound **3** is also stabilized by weak C−H···Ph intermolecular and intramolecular hydrogen bonds (Table 6), as well as by intermolecular stacking interactions between parallel C(2)−C(7) and C(8)(i)−C(13)(i) phenyl rings of the two neighboring molecules. The distance between these rings is 2.49 Å and the offset is 1.42 Å. There are three intermolecular and one intramolecular C(13)−H(13)···Ph5 (C311,C312, ..., C316 ring) hydrogen bonds (Table 6). Two bonds with short distances between the hydrogen donor atom and the phenyl centroid (Ph1 and Ph4) have a short offset, which is defined as the distance from the ring centroid to the projection of the H-atom position on the plane of the ring.[17] These bonds are also more linear than long hydrogen bonds. Intermolecular hydrogen bonds link all the molecules located along the [100] and [010] directions in the crystal. Short lattice vectors ***a*** and ***b***, relative to ***c***, suggest that analyzed weak hydrogen bonds control the growth of the crystals. The same was observed earlier in the case of other compounds.[18]

Infrared spectra of all investigated complexes are consistent with X-ray data for compounds **1**, **2**, and **3**. The presence of $\nu_{as}(COO)$ and $\nu_s(COO)$ in the ranges 1600−1614 cm^{-1}, and 1334−1368 cm^{-1}, respectively, and therefore the large $\Delta\nu = \nu^{as}_{COO} - \nu^{s}_{COO}$ values are consistent with the presence of the asymmetrically coordinated carboxylato group in complexes **1**, **2**, **3**, and **4**. The ν(SnC) bands for the vinyl compounds (**1** and **4**) are observed in the range 496−542 cm^{-1}, and are similar to the values in other vinyl−Sn^{IV} compounds.[19] The substituent-sensitive r-modes for the phenyl groups were observed at 620 cm^{-1} and 588 cm^{-1} for complex **2**, and 636 cm^{-1}, 610 cm^{-1}, and 590 cm^{-1} for compound **3**, and the y-modes at 452 cm^{-1} and 442 cm^{-1} for **2**, and 457 cm^{-1} and 444 cm^{-1} for **3**. These values agree well with the data for $Sn(C_6H_5)_4$.[19]

The ^1H chemical shift ranges for the trivinyl, triphenyl moieties and the carboxylato ligands were deduced from resonance intensities and $^nJ(^1H\text{-}^1H)$ coupling constants. Both chemical shifts and coupling constants for complexes **1**−**4** agree well with the data found for $[Sn(C_6H_5)_3(OOCC_6H_5)]$,[7] $[Sn(C_6H_5)_3(OOCC_6H_4NH_2)]$, and other triphenyltin(IV) compounds,[20,21] $[Sn(CH{=}CH_2)_2X_2]$ and $[Sn(CH{=}CH_2)_3X]$,[22−24] and with the spectra of 3,4-diaminobenzoic and 2-[(4-dimethylamino)phenylazo]benzoic acid and their metal salts. The first-order spectra of the vinyl ligands of the $[Sn(CH{=}CH_2)_3(OOCR)]$ complexes **1** and **4** consist of three quadruplets with $^{119/117}Sn$ satellites. The chemical shifts of H^7, H^8, and H^9 and the $^3J(H^7H^9)$, $^3J(H^7H^8)$, and $^2J(H^8H^9)$ coupling constants in chloroform solution are slightly higher than those found for $[Sn(CH{=}CH_2)_3X]$ (X = Cl, Br, I). It has been found that the ^1H chemical shifts and the $^nJ(^1H\text{-}^1H)$ coupling constants of the vinyltin halides depend on the electronegativity of the halide.[22] Thus, deshielding of H^1, H^2, and H^3 and a slight increase in the $^nJ(^1H\text{-}^1H)$ coupling constants are caused by the higher electronegativity of the RCOO ligand in comparison with that of the ligands Cl, Br, and I. The chemical shift differences $[\delta(H^7) - \delta(H^8)]$ for complexes **1** and **4** are also greater because of the higher electronegativity of the carboxylato ligand. These differences increase in more polar solvents. They are equal to δ = 0.24 ppm in $CDCl_3$ and 0.36 ppm in $(CD_3)_2CO$ and $(CD_3)_2SO$. The ^{119}Sn chemical shifts are higher for four-coordinate compounds than for the five-coordinate complexes. The values of $\delta(^{119}Sn)$ in the latter are shifted upfield over a wide range.[20−22,24] The ^{119}Sn chemical shifts for compounds **1** and **4** in acetone are δ = −167.9 and −168.9 ppm, respectively. They are lower than the chemical shift for $Sn(CH{=}CH_2)_4$ (δ = −157.4 ppm),[24] and greater than for $[Sn(CH{=}CH_2)_2(OOCPh)_2]$ in $CDCl_3$ (δ = −317.7 ppm).[23] The value of the $^1J(^{119/117}Sn\text{-}^{13}C^7)$ coupling constant for complex **4** in chloroform is 600.2/574.9 Hz and is similar to that found for complex $[Sn(CH{=}CH_2)_3Cl]$ in $CDCl_3$ (594.7/568.2 Hz). Thus, the ^1H, ^{13}C, and ^{119}Sn NMR spectra indicate that complexes **1** and **4** in chloroform solution are tetrahedral molecules, and that the coordination of acetone, methanol or dimethyl sulfoxide with tin compounds is rather weak. The formation of weak adducts of complexes **2** and **3** with

polar solvents is also confirmed by the ^{13}C and ^{119}Sn NMR spectra. The $^{1}J(^{119}Sn\text{-}^{13}C)$ coupling constants for tetrahedral $SnPh_3X$ (X = Cl, RCOO, etc.) complexes in chloroform solution are in the range 550−650 Hz, while for five-coordinate complexes, they are often in the range 770−850 Hz. The $^{2}J(^{119}Sn\text{-}^{13}C)$ coupling constants do not depend on the coordination number of tin and have values of 47.6−50.0 Hz, and the $^{3}J(^{119}Sn\text{-}^{13}C)$ and $^{4}J(^{119}Sn\text{-}^{13}C)$ coupling constants are slightly greater for five-coordinate compounds than for four-coordinate complexes and are in the range 63−73 Hz and 12.7−14.6 Hz, respectively.[20−22,24] Small differences between five-coordinate and four-coordinate triphenyltin(IV) compounds were found in the values of the chemical shifts $\delta(^{13}C^{i})$ of the carbon atoms in the *ipso*-positions of the phenyl groups. The values of the $\delta(^{13}C^{i})$ for the five-coordinate complexes are shifted downfield from those of four-coordinate tin compounds by several ppm.[20] The ^{13}C chemical shifts and $^{n}J(^{119}Sn\text{-}^{13}C)$ coupling constants for complexes **2** and **3** in chloroform are in the range characteristic of tetrahedral triphenyltin compounds since $\delta(^{13}C^{i})$ = 138.88 ppm and $^{1}J(^{119/117}Sn\text{-}^{13}C^{i})$ = 651.0/621.8 Hz for the *ipso*-carbon atoms of complex **2**, and $\delta(^{13}C^{i})$ = 138.48 ppm and $^{1}J(^{119/117}Sn\text{-}^{13}C^{i})$ = 644.6/618.5 Hz for those of compound **3**. The chemical shift $\delta(^{13}C^{i})$ is slightly higher in more polar solvents, thus for complex **2** in $(CD_3)_2CO$ a value of δ = 140.69 ppm is observed and for compound **3** in CD_3OD, a value of δ = 140.12 ppm is observed. The values of $\delta(^{119}Sn)$ in $CDCl_3$ for **2** and **3** are δ = −118.9 and −108.6 ppm, and are similar to those found for complexes $[SnPh_3(OOCC_6H_4NH_2\text{-}4)]$ and $[SnPh_3(OOCC_6H_4NH_2\text{-}2)]$ (δ = −122.6 and −116.8 ppm).[20] The $\delta(^{119}Sn)$ values for complex **2** in acetone (δ = −123.1 ppm) is ca. 4 ppm greater than that in chloroform. These data also confirm the formation of weak adducts of compounds **2** and **3** with polar solvents.

The molecular and electronic structures of a single molecule of $[Sn(CH{=}CH_2)_3(OOCC_6H_3(NH_2)_2\text{-}3,4)]$ with C_1 symmetry has been studied by both semiempirical and nonempirical ab initio methods. The quantum chemical calculations were performed using the PM3 of the MOPAC2000 package,[25] and the GAUSSIAN-98 computer program.[26]

The geometry optimization in the first case was performed at the PM3 level and in the second case within the 3-21G basis set and MP2 formalism. The evaluated Sn−O1 bond length with PM3 is found to be 2.019 Å and the Sn···O2 distance 2.685 Å. The respective ab initio results are 2.071 Å and 2.609 Å, whereas the relevant crystallographic values are 2.1353(19) Å and 2.955(2) Å, respectively. This discrepancy results from the formation of the weak Sn(1)−N(2A) bond and the distorted trigonal-bipyramidal coordination of the tin atom in the solid state. In complex **2**, in which the Sn−N bond in the solid state is not formed, the Sn(1)−O(1) bond [2.069(2) Å] and the Sn(1)−O(2) bond [2.680(3) Å] are very similar to those calculated with semiempirical and ab initio methods. Thus, these methods can most likely be applied for the calculations of the interactions of Sn^{IV} compounds with nucleotides and other molecules important for the explanation of the biological activity of tin compounds. The theoretical dipole moment is 1.543 D, the ionization energy is 8.572 eV, and the heat of formations is estimated to be 9.98 kJ/mol.

Complexes **1**, **2**, **3**, and **4** belong to the efficient cytostatic agents (Table 7). Compound **2** is very active against HCV29T cells (ID_{50} = 0.0072 μmol/dm^3). The activity of the compounds against the HCV29T cell line decreases in the order **2** > **1** > **3** > **4**. It is worth noting that the complexes are also very active in ethanol solution. Cytostatic activity of complexes **1** and **2** against the A549 and CACO-2 lines is relatively high, although lower than that against HCV29T cells. Thus, these compounds are promising cytostatic agents against some tumor lines in vitro.

Conclusion

Investigations of the structures of the complexes $[Sn(CH{=}CH_2)_3\{\mu\text{-}OOCC_6H_3(NH_2)_2\text{-}3,4\}]_n$ (**1**), $[Sn(C_6H_5)_3\{OOCC_6H_3(NH_2)_2\text{-}3,4\}]$ (**2**), and $[Sn(C_6H_5)_3\{OOC\text{-}2\text{-}C_6H_4N{=}NC_6H_4N(CH_3)_2\text{-}4\}]$ (**3**) reveal that the coordination of the central atom in complex **1** is distorted trigonal-bipyramidal, and in complexes **2** and **3** distorted tetrahedral. Complex **1** is a regular single-strand polymer. The vinyl

Table 7. Inhibition doses ID_{50} of complexes **1**−**4**

Compound	Cancer HCV29T		A549		CACO	
	ID_{50} [μmol/dm^3]	Solvent	ID_{50} [μmol/dm^3]	Solvent	ID_{50} [μmol/dm^3]	Solvent
1	1.36	MeOH	20.0	EtOH	12.0	EtOH
2	0.0072	MeOH	0.90	EtOH	i.	EtOH
	0.058	EtOH				
3	3.40	DMSO	n. d.[a]		n. d.	
	0.53	EtOH				
4	7.05	DMSO	n. d.		n. d.	
	1.28	EtOH				
$HOOCC_6H_4N{=}NC_6H_4NMe_2\text{-}4$	20.16	DMSO	i.	H_2O	i.	EtOH
	84.29	EtOH				
$HOOCC_6H_3(NH_2)_2\text{-}3,4$	i.	EtOH	i.	EtOH	i.	H_2O

[a] n.d.: activity was not determined; i.: inactive.

ligands are coordinated in the equatorial positions and the bridging 3,4-diaminobenzoato ligands occupy the axial coordination sites, and form a strong Sn−O bond and a weak Sn−N bond with the *para*-amino group, the Sn(1)−O(1) and Sn(1)−N(2A) distances are 2.1353(19) and 2.685(3) Å, respectively. In complexes **2** and **3**, the carboxylato ligand is strongly coordinated to the central atom via one oxygen atom and the Sn(1)−O(2) distances are considerably longer. However, these weak interactions, as well as the N−H···O, N−H···C, N−H···N hydrogen bonds, and in the case of complex **3** the C−H···Ph hydrogen bonds, stabilize the crystal structure of these complexes. The crystal structure of complex **3** is additionally stabilized by the intermolecular stacking interaction between parallel C(2)−C(7) and C(8)(i)−C(13)(i) phenyl rings of the 2-[4-(dimethylamino)-phenylazo]benzoato ligand of two neighboring molecules. The IR and NMR spectra reveal that the structure of complex **4** is analogous to that of the complexes **2** and **3**. The molecular and electronic structure of a single molecule of complex **1** [$Sn(CH=CH_2)_3(OOCC_6H_3(NH_2)_2$-3,4)], calculated both with semiempirical and ab initio methods, reveal that coordination about the tin atom is similar to that in complex **2**. Thus, the relatively long Sn(1)−O(1) bond in complex **1**, relative to that in compounds **2** and **3**, results from the weak interaction between the Sn atom and the N atom of the *para*-amino group of the 3,4-diaminobenzoato ligand. The complexes are effective cytostatic agents against HCV29T, A549 and CACO-2 tumor lines.

Experimental Section

Materials and Methods

Compounds: 3,4-diaminobezoic acid was obtained from Aldrich, 2-[4-(dimethylamino)phenylazo]benzoic acid from POCH (Poland), diphenyltin dichloride and divinyltin dichloride from Strem and used without further purification. Diphenyltin oxide, triphenyltin oxide, and divinyltin oxide were prepared from diphenyltin dichloride, triphenyltin chloride, and divinyltin dichloride with sodium hydroxide in aqueous ethanol solution. Syntheses were carried out under nitrogen. Infrared spectra (KBr pellets) were recorded with a Bruker IFS 113v, and ^{1}H NMR spectra were recorded with a Bruker AMX 300 and a Bruker Avance 500. C,H,N analyses were performed with a Perkin−Elmer 2400 CHN analyzer, and Sn was determined using ICP-AES with an ARL 3410.

Synthesis of Complexes

$[Sn(CH=CH_2)_3\{OOCC_6H_3(NH_2)_2$-3,4$\}]$ (1): A suspension of $Sn(CH=CH_2)_2O$ (0.75 g, 3.95 mmol) and $HOOCC_6H_3(NH_2)_2$ (0.60 g, 3.95 mmol) in ethanol (10 mL) was refluxed with stirring for 5 h. The dark-brown solid was filtered and the filtrate was concentrated to dryness. The dry residue was extracted with chloroform. The light beige solid was filtered. The filtrate was concentrated and the obtained solid was crystallized from hot toluene. The light brown product $[Sn(CH=CH_2)_3\{OOCC_6H_3(NH_2)_2$-3,4$\}]$ (**1**) was filtered and washed with cold toluene. Yield 0.32 g (46%). $C_{13}H_{16}N_2O_2Sn$ (350.95): C 44.49, H 4.59, N 7.98, Sn 33.82; found: C 44.06, H 4.50, N 7.65, Sn 33.43. Single crystals were grown by concentration of a toluene solution of the compound. IR (KBr, cm^{-1}): $\tilde{\nu}$ = 3412 s (ν_{NH2}), 3348 s (ν_{NH2}), 3048 w (ν_{CH}), 2984 w (ν_{CH}), 2940 w (ν_{CH}), 1614 vs (ν_{COO}), 1599 s ($\nu_{C=C}$), 1590 s, 1584 s, 1570 s, 1556 vs (ν_{COO}), 1520 s, 1442 m, 1396 s, 1362 vs (ν_{COO}), 1332 vs(ν_{COO}),1304 vs, 1248 vs, 1152 m, 1096 w, 1004 s, 956 s, 904 w, 820 m, 784 s, 648 m, 588 m, 542 m (ν_{SnC}), 498 m (ν_{SnC}), 451 m, 389 m. ^{1}H NMR ($CDCl_3$, ppm): δ = 7.50 [dd, $^3J(H^5H^6)$ = 8.1, $^4J(H^2H^6)$ = 1.8 Hz, H^6], 7.43 (d, H^2), 6.65 [d, H^5], 6.59 [dd, $^3J(H^7H^8)$ = 13.5, $^3J(H^7H^9)$ = 20.4, $^2J(^{119/117}SnH^7)$ = 125.9/120.4 Hz, H^7], 6.32 [dd, $^2J(H^8H^9)$ = 2.6, $^3J(^{119/117}SnH^8)$ = 236.2/226.0 Hz, H^8], 5.96 [dd, $^3J(^{119/117}SnH^9)$ = 115.9/110.9 Hz, H^9], 3.47, 3.69 (2s, H^3, H^4). ^{1}H NMR [$(CD_3)_2CO$, ppm]: δ = 7.60 [dd, $^3J(H^5H^6)$ = 8.3, $^4J(H^2H^6)$ = 1.9 Hz, H^6], 7.20 (d, H^2), 6.74 (d, H^5), 6.62 [dd, $^3J(H^7H^8)$ = 13.6, $^3J(H^7H^9)$ = 20.4, $^2J(^{119/117}SnH^7)$ = 129.0/122.9 Hz, H^7], 6.26 [dd, $^2J(H^8H^9)$ = 2.9, $^3J(^{119/117}SnH^8)$ = 239.5/228.2 Hz, H^8], 6.01 [dd, $^3J(^{119/117}SnH^9)$ = 114.9/109.9 Hz, H^9], 3.47, 3.69 (H^3, H^4). ^{119}Sn NMR [$(CD_3)_2CO$, ppm]: δ = −167.9.

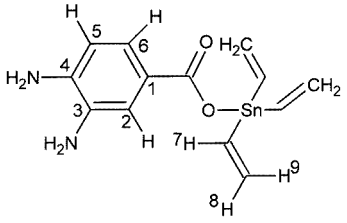

$[Sn(C_6H_5)_3\{OOCC_6H_3(NH_2)_2$-3,4$\}]\cdot 0.5C_6H_5CH_3$ (2). Method a: A mixture of $Sn(C_6H_5)_2O$ (0.58 g, 2.01 mmol) and $HOOCC_6H_3(NH_2)_2$ (0.31 g, 2.03 mmol) in toluene/ethanol (3:1) (10 mL) was refluxed with stirring for 4 h. The light brown solid was filtered. The yellow filtrate was slowly concentrated giving yellow crystals of complex **2**. The solid was washed with cold ethanol and dried in vacuo. Yield 0.32 g (56%). $C_{28,5}H_{26}N_2O_2Sn$ (547.24): C 62.55, H 4.79, N 5.12, Sn 21.69; found C 62.50, H 4.85, N 5.40, Sn 22.02. Single crystals for X-ray investigations were prepared by slow concentration of a toluene/ethanol solution of the complex. **Method b:** A mixture of $\{Sn(C_6H_5)_3\}_2O$ (0.716 g, 1.0 mmol) and $HOOCC_6H_3(NH_2)_2$ (0.31 g, 2.03 mmol) in ethanol (15 mL) was refluxed with stirring for 0.3 h. The red-brown solution was filtered. The filtrate was concentrated, giving a yellow polycrystalline precipitate of complex **2**. The solid was recrystallized from toluene and washed with cold ethanol and dried in vacuo. Yield 0.652 g (65%). IR (KBr, cm^{-1}): $\tilde{\nu}$ = 3408 s (ν_{NH2}), 3320 s (ν_{NH2}), 3295 w (ν_{NH2}), 3250 w (ν_{NH2}), 3200 w (ν_{NH2}), 3075 w (ν_{CH}), 3070 w (ν_{CH}), 3064 w (ν_{CH}), 1632 s (δ_{NH2}), 1600 vs (ν_{COO}), 1572 vs, (ν_{COO}), 1518 s, 1480 s, 1446 w 1430 vs, 1368 vs (ν_{COO}), 1334 vs (ν_{COO}),1300 vs, 1246 vs, 1192 w, 1152 s, 1112 w, 1076 s, 1060 w, 1024 w, 956 vw, 898 w, 836 m, 778 s, 732 vs, 700 vs, 658 s, 620 w (r-mode SnC), 588 w (r-mode SnC), 512 m, 468 w, 452 m (y-mode SnC), 442 s (y-mode SnC), 402 m. $C_{28,5}H_{26}N_2O_2Sn$ (547.24): C 62.55, H 4.79, N 5.12, Sn 21.69; found C 62.40, H 4.65, N 5.30, Sn 21.92. ^{1}H NMR ($CDCl_3$, ppm): δ = 7.78−7.84 [m, $^3J(^1H$-$^{119/117}Sn)$ = 63.6 Hz, H^o], 7.60 [dd, $^3J(H^5H^6)$ = 8.1, $^4J(H^2H^6)$ = 1.8 Hz, H^6], 7.50 (d, H^2), 7.43−7.49 (m, $H^{m,p}$), 7.29 [H^m(toluene)], 7.19 [$H^{o,p}$(toluene)], 6.63 (d, H^5), 3.38, 3.69 (2s, $H^{3,4}$), 2.37 [s, CH_3(toluene)]. ^{13}C NMR ($CDCl_3$, ppm): δ = 173.34 (COO), 140.39 (C^4) 138.88 , [$^1J(^{13}C$-$^{119/117}Sn)$ = 651.0/621.8 Hz, C^i], 136.88 [$^2J(^{13}C$-$^{119/117}Sn)$ = 48.0 Hz, C^o], 133.20 (C^3), 129.93 [$^4J(^{13}C$-$^{119/117}Sn)$ = 13.0 Hz, C^p], 128.78 [$^3J(^{13}C$-$^{119/117}Sn)$ = 62.7 Hz, C^m], 124.49 (C^6), 120.91 (C^1), 119.46 (C^2), 114.73 (C^5); toluene: 137.82 (C^i), 128.99 (C^o), 128.19 (C^m), 125.26 (C^p), 21.41 (CH_3). ^{13}C NMR [$(CD_3)_2CO$, ppm]: δ = 172.14 (COO), 141.79 (C^4), 140.69 (C^i), 137.65 [$^2J(^{13}C$-$^{119/117}Sn)$ = 47.5 Hz, C^o], 134.61 (C^3), 130.61 [$^4J(^{13}C$-$^{119/117}Sn)$ = 13.2 Hz, C^p], 129.50 [$^3J(^{13}C$-$^{119/117}Sn)$ = 64.4 Hz,C^m], 123.57 (C^6), 119.71 (C^1),

118.43 (C^2), 114.24 (C^5); toluene: 129.73 (C^o), 129.01 (C^m) 126.09 (C^p), 21.43 (CH_3). ^{119}Sn NMR ($CDCl_3$, ppm): δ = −118.9, [$(CD_3)_2CO$, ppm]: δ = −123.1.

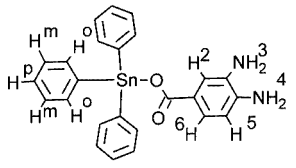

[$Sn(C_6H_5)_3${OOC-2-C_6H_4N=$NC_6H_4N(CH_3)_2$-4}] (3). Method a: A mixture of $Sn(C_6H_5)_2O$ (0.58 g, 2.01 mmol) and 2-[4-(dimethylamino)phenylazo]benzoic acid [$HOOCC_6H_4N$=$NC_6H_4N(CH_3)_2$-4] (0.58 g, 2.01 mmol) in ethanol (15 mL) was refluxed with stirring for 4 h. The red solid was filtered. The red filtrate was slowly concentrated, giving red crystals of complex **3**. The solid was washed with cold hexane and dried in vacuo. Yield 0.32 g (50%). $C_{33}H_{29}N_3O_2Sn$ [$Sn(C_6H_5)_3${OOC-2-C_6H_4N=$NC_6H_4N(CH_3)_2$-4}] (618.33): C 64.10, H 4.73, N 6.80, Sn 19.20; found C 64.80, H 4.95, N 7.15, Sn 18.85. **Method b:** A mixture of $\{Sn(C_6H_5)_3\}_2O$ (0.716 g, 1.0 mmol) and) and 2-[(4-dimethylamino)phenylazo]benzoic acid [$HOOCC_6H_4N$=$NC_6H_4N(CH_3)_2$-4] (0.54 g, 2.01 mmol) in ethanol (15 mL) was refluxed with stirring for 0.3 h. The red solution was filtered. The red filtrate was slowly concentrated, giving a red product. The solid was washed with cold hexane and dried in vacuo. Yield 0.841 g (68%). $C_{33}H_{29}N_3O_2Sn$ [$Sn(C_6H_5)_3${OOC−2-C_6H_4N=$NC_6H_4N(CH_3)_2$-4}] (618.33): C 64.10, H 4.73, N 6.80, Sn 19.20; found C 64.40, H 4.85, N 7.04, Sn 18.94. IR (KBr, cm^{-1}): $\tilde{\nu}$ = 3068 w (ν_{CH}), 3048 w, 3020 vw, 1640 m, 1600 vs (ν^{as}_{COOH}), 1560 w, 1520 s, 1480 m, 1442 w, 1432 m, 1416 w, 1406 m, 1366 vs (ν^{s}_{COOH}), 1340 s (ν^{s}_{COOH}), 1312 m, 1276 w, 1250 w, 1232 w, 1190 vw, 1144 vs, 1088 w, 1076 w, 1020 vw, 996 wm, 944 m, 860,w, 820 ms, 784 w, 760 m, 746 w, 736 s, 726 s, 696 s, 676 w 636 w (r-mode SnC), 610 vw (r-mode SnC), 590 vw (r-mode SnC), 570 vw, 546 m, 510 wvw, 494 vw, 464 w, 457 m (y-mode SnC), 444 m (y-mode SnC), 390 w. ^1H NMR (CD_3OD, ppm): δ = 7.78−7.86 [m, $^3J(^1H$-$^{119/117}Sn)$ = 63 Hz, H^o], 7.62 [d, $^3J(H^{2'}H^{3'})$ = 9.1 Hz, $H^{2'}$ + $H^{6'}$], 7.48−7.59 (m, H^3 + H^6), 7.30−7.46 (m, H^4 + H^5 + H^m + H^p), 6.71 [d, $^3J(H^{5'}H^{6'})$ = 9.1 Hz, $H^{3'}$ + $H^{5'}$], 3.08 (s, CH_3). ^{13}C NMR ($CDCl_3$, ppm): δ = 174.47 (COO), 152.88 (C^2), 152.43 ($C^{4'}$), 143.89 ($C^{1'}$), 138.48 [$^1J(^{13}C$-$^{119/117}Sn)$ = 644.6/618.5 Hz, C^i], 136.99 [$^2J(^{13}C$-$^{119/117}Sn)$ = 48.0 Hz, C^o], 131.50 (C^1, C^4), 130.31 (C^6), 129.91 [$^4J(^{13}C$-$^{119/117}Sn)$ = 13.0 Hz, C^p], 128.76 [$^3J(^{13}C$-$^{119/117}Sn)$ = 63.5 Hz, C^m], 128.06 (C^5), 125.48 ($C^{2'}$, $C^{6'}$), 118.36 (C^3), 111.36 ($C^{3'}$, $C^{5'}$), 40.25 (NCH_3). ^{13}C NMR (CD_3OD, ppm): δ = 173.25 (COO), 154.45 (C^2), 152.54 ($C^{4'}$), 144.76 ($C^{1'}$), 140.12 (C^i), 137.76 [$^2J(^{13}C$-$^{119/117}Sn)$ = 48.1 Hz, C^o], 132.57 (C^1), 131.62 (C^4), 130.36 (C^p), 130.05 (C^6), 129.58 (C^m), 129.11 (C^5), 126.62 ($C^{2'}$, $C^{6'}$), 118.23 (C^3), 112.63 ($C^{3'}$, $C^{5'}$), 40.45 (NCH_3). ^{119}Sn NMR ($CDCl_3$, ppm): δ = −108.6.

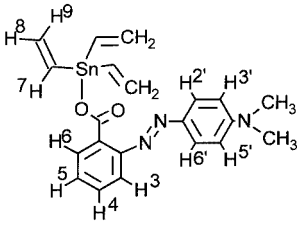

[$Sn(CH$=$CH_2)_3${OOC-2-C_6H_4N=$NC_6H_4N(CH_3)_2$-4}] (4): A mixture of $Sn(CH$=$CH_2)_2O$ (0,38 g, 2.0 mmol) and 2-[4-(dimethylamino)phenylazo]benzoic acid $HOOCC_6H_4N$=$NC_6H_4N(CH_3)_2$-4 (0.54 g, 2.0 mmol) in ethanol (15 mL) was refluxed with stirring for 4 h. The red solid was filtered. The red filtrate was concentrated, giving a red solid that was crystallized from a hot dioxane/toluene mixture (1:4, v/v). Red needles of complex **4** were separated and washed with diethyl ether and dried in vacuo. Yield 0.22 g (47%). $C_{21}H_{23}N_3O_2Sn$ [$Sn(CH$=$CH_2)_3${OOC-2-C_6H_4N=$NC_6H_4N(CH_3)_2$-4}] (468.15): C 53.88, H 4.95, N 8.98, Sn 25.36; found C 53.40, H 4.65, N 9.05, Sn 24.69. IR (KBr, cm^{-1}): $\tilde{\nu}$ = 3070 vw (ν_{CH}), 3065 vw (ν_{CH}), 3040 vw (ν_{CH}), 2980 w (ν_{CH}), 2936 w (ν_{CH}), 2860 vw (ν_{CH}), 2800 vw (ν_{CH}), 1602 vs (ν^{as}_{COO}), 1560 ms, 1546 ms, 1526 s, 1482 m 1465 w, 1452 vw, 1442 wm, 1420 ms, 1400 s, 1366 vs (ν^{s}_{COO}), 1338 w, 1312 s,1276 ms, 1248 w, 1230 m1196 vw, 1148 vs, 1112 ms, 1092 m, 1060 w, 1040 vw, 998 m, 944 ms, 880 vw, 860 vw, 830 w, 820 s, 790 vw, 766 ms, 747 vw, 730 w, 688 w672 wm, 636 wm, 618 vw, 580 w, 544 s, 520 wm (ν_{SnC}), 496 m (ν_{SnC}), 426 vw, 416 w, 390 w, 385 w. ^1H NMR ($CDCl_3$, ppm): δ = 7.81 [d, $^3J(H^{2'}H^{3'})$ = 8.9 Hz, $H^{2'}$ + $H^{6'}$], 7.27−7.67 (m, H^3 + H^4 + H^5 + H^6), 6.73 (d, $H^{3'}$ + $H^{5'}$), 6.56 [dd, $^3J(H^7H^8)$ = 13.5, $^3J(H^7H^9)$ = 20.2, $^2J(^{119/117}SnH^7)$ = 128.2/125.6 Hz, H^7], 6.32 [dd, $^2J(H^8H^9)$ = 2.5, $^3J(^{119/117}SnH^8)$ = 236.6/225.2 Hz, H^8], 5.95 [dd, $^3J(^{119/117}SnH^9)$ = 114.2/109.2 Hz, H^9], 3.14 (s, CH_3). ^1H NMR [$(CD_3)_2CO$, ppm]: δ = 7.83 [d, $^3J(H^{2'}H^{3'})$ = 8.9 Hz, $H^{2'}$ + $H^{6'}$], 7.35−7.65 (m, H^3 + H^4 + H^5 + H^6), 6.83 (d, $H^{3'}$ + $H^{5'}$), 6.59 [dd, $^3J(H^7H^8)$ = 13.6, $^3J(H^7H^9)$ = 20.4 Hz, H^7], 6.23 [dd, $^2J(H^8H^9)$ = 3.0 Hz, H^8], 5.99 (dd, H^9), 3.11 (s, CH_3). ^1H NMR [$(CD_3)_2SO$, ppm]: δ = 7.73 [d, $^3J(H^{2'}H^{3'})$ = 8.9 Hz,$H^{2'}$ + $H^{6'}$], 7.33−7.50 (m, H^3 + H^4 + H^5 + H^6), 6.79 (d, $H^{3'}$ + $H^{5'}$), 6.50 [dd, $^3J(H^7H^8)$ = 13.3, $^3J(H^7H^9)$ = 20.2, $^2J(^{119/117}SnH^7)$ = 132.1/127.4 Hz, H^7], 6.14 [dd, $^2J(H^8H^9)$ = 3.1 Hz, $^3J(^{119/117}SnH^8)$ = 244.5/234.2 Hz, H^8], 5.92 [dd, $^3J(^{119/117}SnH^9)$ = 122.2/116.0 Hz, H^9], 3.05 (s, CH_3). ^{13}C NMR ($CDCl_3$, ppm): δ = 173.53 (COO), 152.38 (C^2), 151.28 ($C^{4'}$), 143.95 ($C^{1'}$), 137.79 (C^8), 135.95 [$^1J(^{13}C$-$^{119/117}Sn)$ = 600.2/574.9 Hz, C^7], 133.58 (C^1), 130.62 (C^4), 129.22 (C^6), 128.26 (C^5), 125.60 ($C^{2'}$, $C^{6'}$), 116.68 (C^3), 111.26 ($C^{3'}$, $C^{5'}$), 40.29 (NCH_3). ^{119}Sn NMR [$(CD_3)_2CO$, ppm]: δ = −168.9.

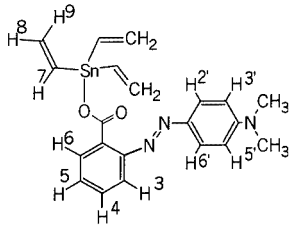

X-ray Crystallographic Study: All measurements were performed at low temperature using an Oxford Cryosystem device with a Kuma KM4CCD κ-axis diffractometer with graphite-monochromated Mo-K_α radiation (Table 8). The crystal was positioned at 65 mm from the CCD camera. 612 frames were measured at 0.75Θ intervals with a counting time of 20 s. Accurate cell parameters were determined and refined by least-squares fit of the strongest reflections. The data were corrected for Lorentz and polarization effects. No absorption correction was applied. Data reduction and analysis were carried out with the Oxford Diffraction, Poland (formerly Kuma Diffraction Wrocław, Poland), programs. The structure was solved by direct methods (program SHELXS-97[27]) and refined by the full-matrix least-squares method on all F^2 data using the SHELXL-97[28] programs. Non-hydrogen atoms were refined with anisotropic vibrational parameters; hydrogen atoms were included from the geometry of the molecules and Δρ maps and were refined with isotropic vibrational parameters. CCDC-176692, -176693, and -176694 contain the supplementary crystallographic data for this paper. These data can be obtained free of charge at www.ccdc.cam.ac.uk/conts/retrieving.html or from the Cambridge

Table 8. Crystal data and structure refinement for complexes [Sn(CH=CH$_2$)$_3${OOCC$_6$H$_3$(NH$_2$)$_2$-3,4}] (**1**), [Sn(C$_6$H$_5$)$_3${OOCC$_6$H$_3$(NH$_2$)$_2$-3,4}]·0.5C$_6$H$_5$CH$_3$ (**2**·0.5C$_6$H$_5$CH$_3$), and [Sn(C$_6$H$_5$)$_3${OOC-2-C$_6$H$_4$N=NC$_6$H$_4$N(CH3)$_2$-4}] (**3**)

	1	**2**·0.5C$_6$H$_5$CH$_3$	**3**
Empirical formula	$C_{13}H_{16}N_2O_2Sn$	$C_{25}H_{22}N_2O_2Sn{\cdot}0.5C_6H_5CH_3$	$C_{33}H_{29}N_3O_2Sn$
Formula mass	350.97	547.20	618.28
T [K]	100(2)	100(2)	100(2)
λ [Å]	0.71073	0.71073	0.71073
Crystal system	monoclinic	monoclinic	triclinic
Space group	$C2/c$	$P2_1/c$	$P\bar{1}$
a [Å]	20.137(3)	15.4320(19)	7.958(2)
b [Å]	8.0714(15)	9.3788(12)	8.719(2)
c [Å]	19.020(3)	17.510(2)	21.162(4)
α [°]	90	90	88.20(3)
β [°]	117.04(3)	102.291(10)	87.58(3)
γ [°]	90	90	76.72(3)
V [Å^3]	2753.4(8)	2476.3(5)	1427.4(6)
Z	8	4	2
$D_{calcd.}$ [Mg·m^{-3}]	1.693	1.468	1.438
μ [mm^{-1}]	1.852	1.059	0.929
F(000)	1392	1108	628
Crystal size [mm]	0.15 × 0.15 × 0.12	0.14 × 0.12 × 0.08	0.15 × 0.10 × 0.10
Diffractometer	Kuma KM4CCD	Kuma KM4CCD	Kuma KM4CCD
θ range [°]	3.31−28.42	3.47−28.41	3.21−28.44
Ranges of h,k,l	−26/26, −10/6, −25/25	−19/20, −12/12, −23/14	−10/6, −11/11, −28/28
Reflections collected	8935	15971	9924
Independent reflections (R_{int})	3151(0.0436)	5788(0.0268)	6270(0.0584)
Data/parameters	3151/227	5788/355	6270/469
GOF(F^2)	1.079	1.078	0.910
Final R_1/wR_2 ind.($I > 2\sigma_I$)	0.0313/0.0777	0.0389/0.0981	0.0453/0.0568
Largest difference peak/hole [e· Å^{-3}]	1.568/−1.412	1.982/−1.852	0.616/−0.585

Crystallographic Data Centre, 12, Union Road, Cambridge CB2 1EZ, UK [Fax: (internat.) + 44-1223/336-033; E-mail: deposit@ccdc.cam.ac.uk].

Cytostatic Activity in vitro: Human cell lines HCV29T, A549 (lung adenocarcinoma) and CACO-2 were used for the proliferation assay. The experiments were repeated in triplicate for each tested Sn compound concentration. Statistical significance was tested using Student's t-test ($p < 0.05$ was considered statistically significant). The in vitro tests against all cell lines were performed as described previously.[29−31] The results of cytotoxic activity in vitro were expressed as ID_{50} − the dose of compound that inhibits proliferation rate of the tumor cells by 50% as compared with untreated control cells.

Acknowledgments

The authors are grateful to KBN (Committee of Scientific Research) for support of this work (grant no. 3T09A 064 16).

[1] E. Wong, C. M. Giandomenico, *Chem. Rev.* **1999**, *99*, 2451.
[2] M. J. Clarke, F. Zhu, D. R. Frasca, *Chem. Rev.* **1999**, *99*, 2511.
[3] F. Huber, R. Barbieri, in: *Metal Complexes in Cancer Chemotherapy* (Ed.: B. Keppler), VCH, Weiheim, New York, **1993**, p. 351.
[4] M. Nath, S. Pokharia, R. Yadav, *Coord. Chem. Rev.* **2001**, *215*, 99.
[5] M. Gielen, *Coord. Chem. Rev.* **1996**, *151*, 41.
[6] M. Gielen, M. Biesemans, D. de Vos, R. Willem, *J. Inorg. Biochem.* **2000**, *79*, 139, and references therein.
[7] R. Willem, A. Bouhdid, B. Mahieu, L. Ghys, M. Biesemans, E. R. T. Tieking, D. de Vos, M. Gielen, *J. Organomet. Chem.* **1997**, *531*, 151.
[8] M. Gielen, A. Bouhdid, F. Kayser, M. Biesemans, D. de Vos, B. Mahieu, R. Willem, *Appl. Organomet. Chem.* **1995**, *9*, 251.
[9] J. Tao, W. Xiao, Q. Yang, *J. Organomet. Chem.* **1997**, *531*, 223.
[10] J. J. Bonire, S. P. Fricker, *J. Inorg. Biochem.* **2001**, *83*, 217.
[11] D. de Vos, R. Willem, M. Gielen, K. E. van Wingerden, K. Nooter, *Met.-Based Drugs* **1998**, *5*, 179.
[12] M. Kemmer, M. Gielen, M. Biesemans, D. de Vos, R. Willem, *Met.-Based Drugs* **1998**, *5*, 189.
[13] J. Li, Y. Ma, R. Liu, J. Li, *Appl. Organomet. Chem.* **2001**, *15*, 227.
[14] E. R. T. Tiekink, M. Gielen, A. Bouhdid, R. Willem, V. I. Bregadze, L. V. Ermanson, S. A. Glazun, *Met.-Based Drugs* **1997**, *4*, 75.
[15] M. Gielen, K. Handlir, M. Hollein, D. de Vos, *Met.-Based Drugs* **2000**, *7*, 233.
[16] E. R. T. Tiekink, *Appl. Organomet. Chem.* **1991**, *5*, 1.
[17] Z. Ciunik, G. R. Desiraju, *Chem. Commun.* **2001**, 703−704].
[18] Z. Ciunik, S. Jarosz, *J. Mol. Struct.* **1998**, *442*, 115.
[19] E. Maslowsky, *Vibrational Spectra of Organometallic Compounds*, J. Wiley, New York, **1977**.
[20] J. Holeček, M. Nádvornik, K. Handliř, A. Lyčka, *J. Organomet. Chem.* **1983**, *241*, 177.
[21] A. Lyčka, J. Holeček, M. Nádvornik, K. Handliř, *J. Organomet. Chem.* **1985**, *280*, 323.
[22] E. Vincent, L. Verdonck, l. Naessens, G. P. van der Kelen, *J. Organomet. Chem.* **1984**, *277*, 235.
[23] J. Holeček, K. Handliř, M. Nádvornik, S. M. Teleb, A. Lyčka, *J. Organomet. Chem.* **1988**, *339*, 61.
[24] B. Wrackmeyer, *Annu. Rep. NMR Spectrosc.* **1999**, *38*, 203.
[25] *MOPAC2000*, Version 1.06, Fujitsu Limited, **1999**.
[26] M. J. Frisch, G. W. Trucks, H. B. Schlegel, G. E. Scuseria, M. A. Robb, J. R. Cheeseman, V. G. Zakrzewski, J. A. Montgomery, Jr., R. E. Stratmann, J. C. Burant, S. Dapprich, J. M. Millam, A. D. Daniels, K. N. Kudin, M. C. Strain, O. Farkas, J.

Tomasi, V. Barone, M. Cossi, R. Cammi, B. Mennucci, C. Pomelli, C. Adamo, S. Clifford, J. Ochterski, G. A. Petersson, P. Y. Ayala, Q. Cui, K. Morokuma, D. K. Malick, A. D. Rabuck, K. Raghavachari, J. B. Foresman, J. Cioslowski, J. V. Ortiz, A. G. Baboul, B. B. Stefanov, G. Liu, A. Liashenko, P. Piskorz, I. Komaromi, R. Gompers, R. L. Martin, D. J. Fox, T. Keith, M. A. Al-Laham, C. Y. Peng, A. Nanayakkara, M. Challacombe, P. M. W. Gill, B. Johnson, W. Chen, M. W. Wong, J. L. Andres, C. Gonzales, M. Head-Gordon, E. S. Replogle, J. A. Pople, *Gaussian 98, Revision A.9*, Gaussian, Inc., Pittsburgh, PA, **1998**.

[27] G. M. Sheldrick, *SHELXS-97, Program for solution of crystal structures*, University of Göttingen, **1997**.

[28] G. M. Sheldrick, *SHELXL-97, Program for crystal structure refinement*, University of Göttingen, **1997**.

[29] F. P. Pruchnik, D. Duś, *J. Inorg. Biochem.* **1996**, *61*, 55.

[30] F. P. Pruchnik, R. Starosta, Z. Ciunik, A. Opolski, J. Wietrzyk, E. Wojdat, D. Duś, *Can. J. Chem.* **2001**, *79*, 868.

[31] F. P. Pruchnik, M. Bańbuła, Z. Ciunik, H. Chojnacki, B. Skop, M. Latocha, T. Wilczok, *J. Inorg. Biochem.* **2002**, *90*, 149.

Received December 20, 2001
[I02523]

Experimental and Computational Study on a Variety of Structural Motifs and Coordination Modes in Aluminium Complexes of Di(2-pyridyl)amides and -phosphanides

Matthias Pfeiffer,[a] Alexander Murso,[a] Lepakshaiah Mahalakshmi,[a] Damien Moigno,[b] Wolfgang Kiefer,[b] and Dietmar Stalke*[a]

Keywords: Aluminium / Computational chemistry / Conformation analysis / N ligands / P ligands

The $(2\text{-Py})_2N^-$ ligand shows much more conformational freedom than the $(2\text{-Py})_2P^-$ anion in aluminium coordination. The two isomers $[Al\{(NPy)Py\}_3]$ (**1a**) and $[Al\{(NPy)Py\}_2(Py_2N)]$ (**1b**) were isolated, the former containing exclusively *cis-trans* ligands, and the latter *cis-trans* ligands together with a *trans-trans* ligand. The energy differences in the noncoordinated anions $(2\text{-Py})_2E^-$ (E = N, P) were determined by computational methods to be low in the amide. While the N→Al donor bond energy is appreciable (96 kJ/mol), that of the P→Al donor bond is much lower (45 kJ/mol). This explains why the P-analogous donor-acceptor complex to $Et_2Al(2\text{-Py})_2N{\rightarrow}AlEt_3$ could never be isolated. The P-centred systems are much better π-donors to soft metals than σ-donors to hard metals.

(© Wiley-VCH Verlag GmbH, 69451 Weinheim, Germany, 2002)

Introduction

Since the historic discovery of Ziegler−Natta catalysts for polymerisation reactions, the industrial importance of organoaluminium compounds has expanded into several other fields, including applications as ceramic precursors, as volatile organometallic precursors for semiconducting materials in electronic industry, and as selective reagents in organic synthesis.[1] Furthermore, current knowledge of the important role of cationic group-13 complexes in catalytic chemistry has resulted in a resurgence of interest in the field of catalytic chemistry.[2] On the other hand, interest in aluminium amide chemistry is due to the potential for the preparation of aluminium nitride thin films.[3] The aluminium nitride can adopt a great variety of structural motifs, oligomerisation through the bridging amido nitrogen atom normally being observed.[4] Suitable tuning of steric factors, however, can prevent such oligomerisation, resulting in monomeric aluminium complexes, as reported by several research groups[5] ($[Al\{N(SiMe_3)_2\}_3]$[5a] and $[AlH_2\{N\text{-}CMe_2CH_2)_2CH_2\}(NMe_3)]$[5b]). Heteroaromatic substituted amides capable of intramolecular side arm donation were found to be able to give rise to several different coordination modes.[6] The presence of diverse donor groups integrated in the ligand periphery can provide electronic and steric stabilisation to the aluminium atom.[5c,5d] During our study on the reactivity and coordination behaviour of 2-pyridyl-based ligand systems[6] − 2-pyridyl derivatives of methane,[7] amines,[8,9] phosphanes,[9,10] arsanes,[10b] phosphanylamines,[11,12a] iminophosphoranes[11,12] and aminoiminophosphoranes[11] − we have isolated several aluminium complexes. The structural variety and large number of coordination modes possible in the case of pyridylamide-based systems[8,9,13] prompted us to carry out a detailed structure and bonding study of dipyridylamide-based aluminium complexes. This paper deals with both crystallographic and theoretical investigations into the structures of some of the aluminium complexes isolated in this group.

Results and Discussion

Syntheses and Crystal Structure of $[Al\{(NPy)Py\}_3]$ (1a) and $[Al\{(NPy)\ Py\}_2\ (Py_2N)]$ (1b)

$LiAlH_4$ is extensively used as a reagent in organic chemistry.[14a,14b] Nöth et al. described the reaction of secondary aliphatic amines with $LiAlH_4$,[14c] we reported the isolation of the intermediate product obtained in the reaction between $(Me_3Si)_2NH$ and $LiAlH_4$ in 1992,[14d] and analogous reactions between $LiAlH_4$ and primary and secondary aromatic amines were reported by Roesky et al. in 1997.[14e] In continuation of our research into the reactivity of $LiAlH_4$ we investigated its reaction behaviour with $(2\text{-Py})_2NH$.

In a reaction similar to that reported by Raston et al.,[13e] treatment of $(2\text{-Py})_2NH$ with $LiAlH_4$ in Et_2O, replacement

[a] Institut für Anorganische Chemie der Universität Würzburg, Am Hubland, 97074 Würzburg, Germany
Fax: (internat.) + 49-(0)931/888-4619
E-mail: dstalke@chemie.uni-wuerzburg.de
[b] Institut für Physikalische Chemie der Universität Würzburg, Am Hubland, 97074 Würzburg, Germany

Supporting information for this article is available on the WWW under http://www.eurjic.org or from the author.

of the solvent by pyridine, subsequent filtration of the undissolved material, and cooling of the solution to 0 °C gives the aluminium triamide [Al{(NPy)Py}$_3$] (**1a**). However, a significantly higher yield of **1a** is obtained on treatment of (2-Py)$_2$NH with Et$_3$Al in Et$_2$O at −78 °C. Stirring for 2 d at room temperature and storage of the resulting solution at −40 °C give crystals of **1a** in 90% yield (Scheme 1). Raston et al.[13e] observed dynamic behaviour of **1a** in solution, as a consequence of which they were unable to distinguish the coordinated and uncoordinated nitrogen atoms of the pyridyl rings in NMR experiments. This dynamic behaviour can be explained by the rearrangement process associated with the ligands, confirmed by the isolation of the isomer **1b** in our studies. In this work, however, eight signals in the ^{1}H NMR and ten signals in the ^{13}C NMR could, as expected, be detected in the solid state structure for the coordinated and the uncoordinated pyridyl rings.

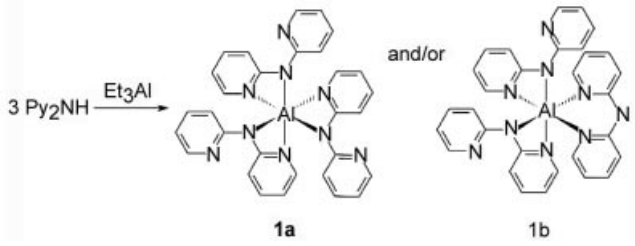

Scheme 1. Synthesis of [Al{(NPy)Py}$_3$] (**1a**) and [Al{(NPy)Py}$_2$-(Py$_2$N)] (**1b**)

Figure 1 shows the molecular structure of **1a**. The geometric features correspond to data obtained from crystals grown after the reaction between (2-Py)$_2$NH and LiAlH$_4$. Three uncoordinated pyridine molecules are present in the asymmetric unit of **1a**. The aluminium amide was isolated several times under different reaction conditions and from various solvents, with the same structural data being obtained in each case. The details show that **1a** incorporates various lattice solvents in different amounts, either as [Al{(NPy)Py}$_3$] + 3PyH (**1a**), [Al{(NPy)Py}$_3$] + thf (space group $P\bar{1}$) or solvent-free [Al{(NPy)Py}$_3$] (space group $P2_1/n$).

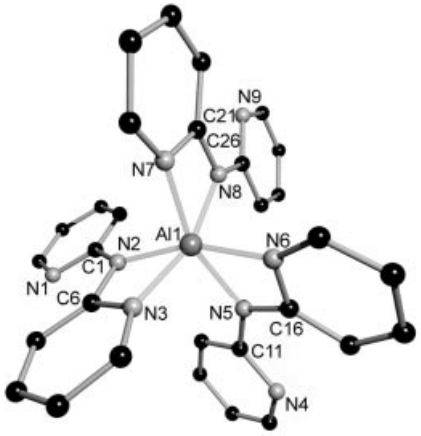

Figure 1. Structure of [Al{(NPy)Py}$_3$] (**1a**) in the solid state; the three pyridine molecules in the lattice have been omitted for clarity

In the solid state, **1a** is a monomer. Each of the three Py$_2$N$^-$ ligands in **1a** adopts a *cis-trans* conformation and exhibits a chelating coordination mode to the aluminium atom. Each Py$_2$N$^-$ ligand coordinates to the metal atom through one pyridyl nitrogen atom and the bridging nitrogen atom of the ligand. The geometry around the aluminium atom is distorted octahedral [N−Al−N angles 66.7(7)−160.37(7)°; Table 1]. The average bond length of 197.3(2) pm for Al1−N(bridge) is slightly shorter than the average bond length of 200.6(2) pm for Al1−N(pyridyl). Both distances, however, are considerably longer than the amidic Al−N single-bond length of 178 pm found in tricoordinate aluminium amide systems such as [Al{N(SiMe$_3$)$_2$}$_3$],[5a] which is due to the higher coordination number of six found in **1a**. On the other hand, the bond lengths are on average 7 pm shorter than in a purely dative Al←N(PyH) bond, with a length of 206 pm in [(PyH)$_3$AlCl$_3$][5e] or 205.7 pm in [Me$_3$Al(Py$_3$P)].[6,10]

The Py$_2$N$^-$ anion in [Al{(NPy)Py}$_3$] (**1a**) coordinates to the metal atom in a *cis-trans* conformation, as previously found in [Me$_2$Tl{(NPy)Py}]$_n$ (see Scheme 2).[8] The Py$_2$N$^-$ ligand is nearly planar, as the angle between the two pyridyl ring planes is only 9° on average, leaving the bridging nitrogen atom sp^2-hybridised. The aluminium atom is displaced at an average distance of 7.5 pm out of the plane of the coordinating rings. NMR spectroscopic studies show that the structure in solution emulates that in the solid state. The ^{1}H NMR spectrum obtained in C$_6$D$_6$ shows the expected eight signals in the aromatic region, while the ^{13}C NMR spectrum displays ten resonances. Dynamic behaviour was not detected at room temperature.

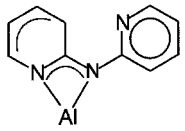

Scheme 2. Mesomeric structure of Py$_2$N$^-$ in [Al{(NPy)Py}$_3$] (**1a**)

Slow evaporation of the deuterated NMR solvent from a sample of **1a** at room temperature resulted in the recrystallisation of a aluminiumtris[di(2-pyridyl)]amide that turned out to be a different conformational isomer [Al{(NPy)Py}$_2$(Py$_2$N)] (**1b**). This isomer contains two C$_6$D$_6$ molecules in the asymmetric unit rather than the three pyridine molecules in **1a**.

In the solid state, **1b** is found to be a monomer similar to **1a**. The three Py$_2$N$^-$ ligands chelate the aluminium atom and the metal centre exists in a distorted octahedrally coordinated polyhedron [N−Al−N angles vary from 64.69(17) to 167.8(2)°]. However, one of the Py$_2$N$^-$ ligands in [Al{(NPy)Py}$_2$(Py$_2$N)] (**1b**) now adopts a *trans-trans* conformation and coordinates to the aluminium atom through both pyridyl nitrogen atoms, leaving one bridging nitrogen atom uncoordinated (Figure 2, Table 2). The bond parameters of the *cis-trans* ligand containing N1 to N3 indicate a bonding situation similar to that of the Py$_2$N$^-$ ligands in **1a**.

Table 1. Selected average bond lengths [pm] and angles [°] in [Al{(NPy)Py}$_3$] (**1a**); the tabulated structural parameters correspond to the average values for the di(2-pyridyl)amide ligand according to the numbering scheme

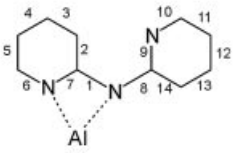

Al1−N(bridge)	197.3(2)	Al1−N(pyridyl)	200.6(2)	1	137.3(2)
2	139.9(3)	3	137.6(3)	4	137.5(3)
5	137.0(3)	6	133.7(2)	7	136.1(2)
8	138.6(3)	9	134.1(2)	10	134.4(2)
11	136.8(2)	12	138.3(3)	13	137.1(2)
14	140.2(3)	N(coord. pyridyl)···N(bridge)	218.6		
N(noncoord. pyridyl)···N(bridge)	236.2				
N2−Al1−N6	158.10(7)	N8−Al1−N3	160.37(7)	N5−Al1−N7	156.81(7)
N2−Al1−N5	103.46(7)	N8−Al1−N2	104.92(7)	N5−Al1−N8	106.24(7)
N(pyridyl)−Al1−N(bridge)	66.7(7)	C(*ipso*)−N(bridge)−C(*ipso*)	124.8(2)		

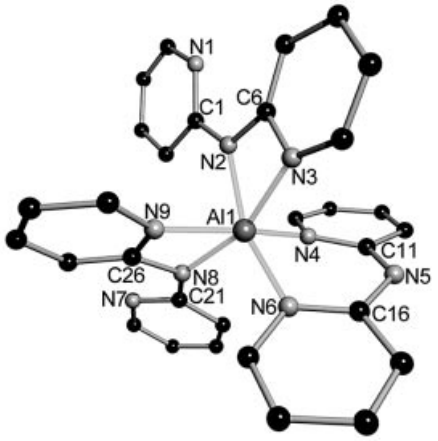

Figure 2. Structure of [Al{(NPy)Py}$_2$(Py$_2$N)] (**1b**) in the solid state; the two C_6D_6 molecules in the lattice have been omitted for clarity

The situation in the second *cis-trans* ligand, between the atoms from N7 to N9, is quite different from that in **1a**. The variance of the two Al−N bonds is larger [Al1−N8 197.0(5) and Al1−N9 202.5(4) pm]. This indicates a greater accumulation of charge density at the bridged nitrogen atom N8, which is further supported by the angle defined by the best planes between the two pyridyl rings. This large angle of 17.7°, in contrast to the average 9° in **1a** and 7.2° in the previous ligand (N1 to N3) in **1b**, points to more pronounced sp^3 hybridisation at the bridging nitrogen atom N8. The aluminium atom is found at a distance of 31.5 pm out of the heteroallyl system plane, in contrast to the analogous distance of just 7.5 pm in **1a**.

Similarly, the *trans-trans* conformation of the Py$_2$N$^-$ ligand in [Al{(NPy)Py}$_2$(Py$_2$N)] (**1b**) shows another structural feature different to that found in [Me$_2$Al(Py$_2$N)] (Scheme 3).[8] Although both ligands show similar coordination to the metal atom, with the N−C bond lengths in [Me$_2$Al(Py$_2$N)] indicating a symmetric charge distribution over both pyridyl rings, they are unsymmetrical in **1b**. This can be seen in all the N(bridge)−C(*ipso*), C(*ipso*)−N(pyridyl) and Al−N bond lengths. Regardless of the fact that both pyridyl rings take part in the metal coordination, the greater part of the electron density is accumulated in only one of them (C11−C15 and N4). This results in shorter Al1−N4 [196.9(4) compared to 200.9(5) pm for Al1−N6] and N5−C11 bonds [134.2(7) in comparison to 139.3(7) pm for N5−C16]. In solution, **1b** converts into the conformational isomer **1a**, and so no difference is observed in the spectroscopic data. Conformer **1b** seems to be energetically disfavoured in comparison to **1a**, but can be crystallised under the conditions described in the Exp. Sect.

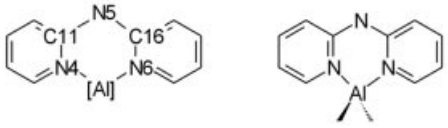

Scheme 3. The *trans-trans* conformation of Py$_2$NH$^-$ in [Al{(NPy)Py}$_2$(Py$_2$N)] (**1b**) and [Me$_2$Al(Py$_2$N)]

Syntheses and Crystal Structure of [(PyH)$_2$AlCl$_2${(NPy)Py}] (2)

A solution of di(2-pyridyl)amine and aluminium trichloride, when treated with *n*-butyllithium and allowed to warm to room temperature, gives [(PyH)$_2$AlCl$_2${(NPy)Py}] (**2**) (Scheme 4). Colourless crystals of **2** were isolated after 4 d at 0 °C. The crystals were found to decompose at 50 °C.

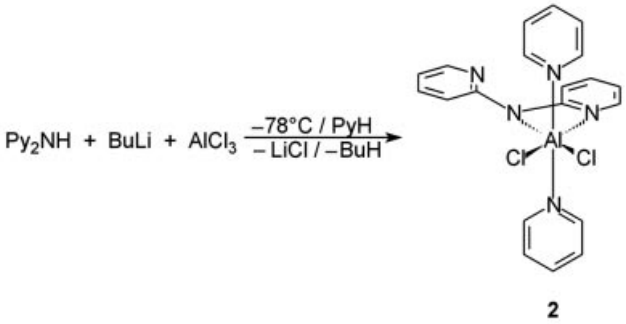

Scheme 4. Synthesis of [(PyH)$_2$AlCl$_2${(NPy)Py}] (**2**)

Table 2. Selected bond lengths [pm] and angles [°] in [Al{(NPy)Py}$_2$(Py$_2$N)] (**1b**)

Al1−N2	201.9(4)	Al1−N3	203.1(5)	Al1−N4	196.9(4)	
Al1−N6	200.9(5)	Al1−N8	197.0(5)	Al1−N9	202.5(4)	
N2−C1	137.4(6)	C1−C2	144.2(8)	C2−C3	140.8(8)	
C3−C4	135.5(9)	C4−C5	132.3(10)	C5−N1	133.8(8)	
N1−C1	135.1(6)	N2−C6	135.4(6)	C6−C7	139.4(7)	
C7−C8	143.6(9)	C8−C9	139.9(8)	C9−C10	133.0(8)	
C10−N3	131.4(7)	N3−−C6	136.5(6)	N5−C11	134.2(7)	
C11−C12	144.3(8)	C12−C13	134.8(8)	C13−C14	137.1(9)	
C14−C15	133.9(9)	C15−N4	133.2(7)	N4−C11	137.3(7)	
N5−C16	139.3(7)	C16−C17	137.5(7)	C17−C18	135.8(8)	
C19−C20	135.8(8)	C20−N6	137.2(6)	N6−C16	135.5(7)	
N8−C21	135.4(7)	C21−C22	139.8(7)	C22−C23	137.1(7)	137.1(7)
C23−C24	136.7(9)	C24−C25	135.2(9)	C25−N7	135.5(8)	
N7−C21	136.1(7)	N8−C26	139.4(7)	C26−C27	137.9(8)	
C27−C28	140.0(8)	C29−C30	138.8(8)	C30−N9	133.8(7)	
N9−C26	133.4(7)					
N2···N3	216.7	N4···N6	276.6	N8···N9	219.6	
N2−Al1−N3	64.69(17)	N4−Al1−N6	88.10(19)	N8−Al1−N9	66.68(19)	
N2−Al1−N6	156.48(19)	N4−Al1−N9	167.8(2)	N8−Al1−N3	160.34(19)	
N2−Al1−N9	88.20(16)	N4−Al1−N2	90.87(17)	N8−Al1−N4	101.7(2)	
C1−N2−C6	124.9(4)	C11−N5−C16	125.1(5)	C21−N8−C26	127.2(5)	

Compound **2** exists as a monomer in the solid state (Figure 3). Di(2-pyridyl)amide coordinates to the aluminium atom through one of the pyridyl ring nitrogen atoms and the bridging central nitrogen atom. The coordination sphere is completed by the coordination of two chloro ligands and the nitrogen atoms of two pyridine molecules to give a distorted octahedral geometry around the aluminium centre (N5−Al1−N4 174.4°, Cl1−Al1−Cl2 137.5°, N2−Al1−N3 65.9°). Because of the absence of steric strain the two pyridyl rings are coplanar.

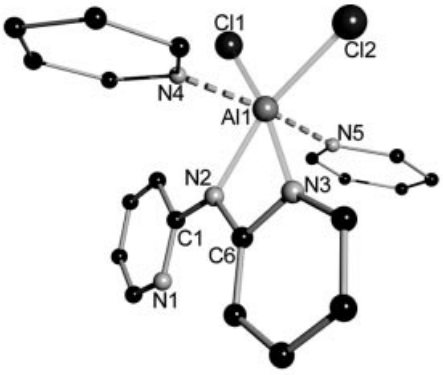

Figure 3. Structure of [(PyH)$_2$AlCl$_2${(NPy)Py}] (**2**) in the solid state

The di(2-pyridyl)amide ligand in **2** adopts a *cis-trans* conformation, as in the cases of **1a** and [Me$_2$Tl{(NPy)Py}]$_n$ [8] (Figure 3, Table 3). The distance between the coordinated central nitrogen atom and the pyridyl nitrogen atom is 218.1 pm. In the octahedral coordination sphere, the aluminium atom lies nearly in the plane of the di(2-pyridyl)amide ligand (7.6° angle between the pyridyl ring planes) in the Al1−Cl1−Cl2 plane. This is the first example of *cis-trans* coordination of the monoanionic di(2-pyridyl)amide in a monomeric metal complex. As in **1a** and **1b**, the *cis*−*cis* conformation is precluded due to the greater $N_{ring}\cdots N_{ring}$ distance, while in a hypothetical planar *trans-trans* conformation there would be steric interaction between the hydrogen atoms of the ring and the chlorine atoms, due to their closer proximity. Hence, by adopting the *cis-trans* conformation, the system avoids such disadvantageous steric factors (Scheme 5). Because of the coordination through the central nitrogen atom N2 and through the pyridyl nitrogen atom N3 of the di(2-pyridyl)amide, different electronic situations exist in the pyridyl rings. The distances from the bridging nitrogen atom N2 to the *ipso*-carbon atoms (N2−C1 139.3 and N2−C6 136.8 pm) deviate significantly in the same way as seen for the $C_{ipso}-N_{ring}$ distance (C6−N3 136.8 and C1−N1 134.2 pm). The N2−C6 bonding exhibits a more pronounced double bond character, in contrast to N2−C1. Furthermore, C6−N3 is shorter than C1−N1. The charge of the anionic ligand is predominantly localised at the N3 nitrogen atom of the coordinated pyridyl ring (Scheme 6).

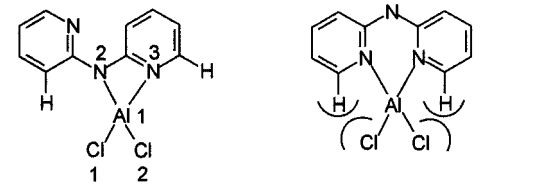

cis-trans conformation in **2** hypothetical *trans-trans* arrangement

Scheme 5. View of [(PyH)$_2$AlCl$_2${(NPy)Py}] (**2**) along the $N_{PyH}-Al-N_{PyH}$ axis (left) and the precluded *trans-trans* arrangement (right)

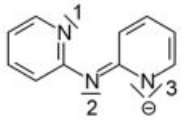

Scheme 6. The mesomeric structures of the di(2-pyridyl)amide ligand in [(PyH)$_2$AlCl$_2${(NPy)Py}] (**2**)

Table 3. Selected bond lengths [pm] and angles [°] in $[(PyH)_2AlCl_2\{(NPy)Py\}]$ (**2**)

Al1−Cl1	223.7(2)	Al1−N3	198.4(3)	Al1−N2	202.7(3)
Al1−Cl2	226.2(1)	Al1−N4	205.9(3)	Al1−N5	207.7(3)
C1−C2	139.9(5)	C2−C3	138.0(5)	C3−C4	137.4(6)
C4−C5	137.0(6)	C5−N1	134.7(5)	N1−C1	134.2(5)
C1−N2	139.3(4)	N2−C6	136.8(5)	C6−C7	139.9(5)
C7−C8	136.6(5)	C8−C9	138.7(6)	C9−C10	135.5(6)
C10−N3	133.8(5)	N3−C6	136.8(4)	N4−C11	135.2(4)
N4−C15	133.9(5)	N5−C16	134.5(5)	N5−C20	134.5(5)
Cl1−Al1−Cl2	137.5(1)	N5−Al1−N4	174.3(1)	N5−Al1−N3	88.8(1)
N2−Al1−N3	65.9(1)	N5−Al1−Cl1	91.5(1)	N4−Al1−N2	87.5(1)
N2−Al1−Cl1	104.6(1)	N5−Al1−Cl2	92.8(1)	N4−Al1−N3	87.9(1)
N2−Al1−Cl2	159.5(1)	N4−Al1−Cl1	91.1(1)	N1−C2−N2	119.4(4)
N3−Al1−Cl1	170.4(1)	N4−Al1−Cl2	92.0(1)	N2−C6−N3	105.8(3)
N3−Al1−Cl2	93.6(1)	N5−Al1−N2	86.9(1)	C2−C1−N2	118.7(4)
				C7−C6−N2	135.4(4)

The aluminium−nitrogen and aluminium−chloride distances in **2** can be compared with those in the following compounds: $[Cl_2Al(PyH)_4][AlCl_4]$ (Al−N 206, Al−Cl 227 pm),[5e] $Cl_3Al(PyH)_3$ (Al−N 206, Al−Cl 227 pm),[5e] and $Cl_2Al(bpy)_2$ (Al−N 203, Al−Cl 225 pm).[5f] The Al1−N4 (205.9 pm) and Al1−N5 (207.7 pm) bond lengths in the donating pyridine molecules correspond to the dative aluminium−nitrogen bonding in $[Cl_2Al(PyH)_4][AlCl_4]$[5e] and $[Cl_3Al(PyH)_3]$,[5f] each with an Al−N distance of 206 pm. The aluminium−nitrogen bonds in the monoanionic di(2-pyridyl)amide ligands are substantially shorter. Because of the higher charge density at the pyridyl ring nitrogen atom N3, the Al1−N3 bond length (198.4 pm) is shorter than the Al1−N2 bond length (202.7 pm).

Both aluminium−chloride bond lengths lie in the range expected for Al−Cl bond lengths (226 pm). However, Al1−Cl1 (223.7 pm) is shorter than Al1−Cl2 (226.2 pm). The different Al−N distances result from the difference in the dipole moment parallel to Al1−N3 and Al1−N2. Thus, the Al−Cl bond length is likewise different. As a compensation for these differences a shortening of the Al1−Cl1 bond and a lengthening of the Al1−Cl2 bond results.

The ^1H and the ^{13}C NMR spectra at room temperature do not resolve the magnetic and chemical differences of the pyridyl substituents. Because of the overlap of the signals in the ^1H NMR spectrum, no exact assignment could be made. Eight signals are observed in the ^{13}C NMR spectrum of **2**; three correspond to the pyridine molecules and four to the di(2-pyridyl)amide ligand [δ = 116.6 (C5), 117.7 (C3), 123.6 (C_{para}), 139.7 (C_{meta}), 141.5 (C4), 142.7 (C_{ortho}), 144.1 (C6), 152.8 (C2) ppm]. NMR experiments conducted at −60°C show no further splitting of the signal pattern.

Comparison of Structural Parameters for Compounds 1a, 1b and 2

Structural comparison of the various complexes shows that the Py_2N^- ligand is flexible enough, depending on the electronic and steric demand, to suit different coordination modes, giving rise to a variety of metal complexes. Scheme 7 illustrates the different possible coordination modes for the dipyridyl amide ligand. Furthermore, the negative charge density at the bridging nitrogen atom of the Py_2N^- ligand is more or less delocalised over the pyridyl ring. The degree of delocalisation and density accumulation depends on the coordinated metal atom, the degree of aggregation and the conformation of the ligand. This has a distinct effect on the geometrical parameters of the ligand, accounting for the significant perturbation of the aromatic ring systems.

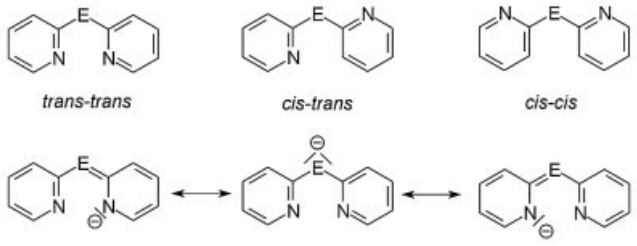

Scheme 7. The different possible coordination modes of the di(2-pyridyl)amide and -phosphanide ligand (top) and the mesomeric structures for the ligand in the *trans-trans* coordination mode (bottom)

Table 4 gives an overview of the structural parameters of the Py_2N^- ligand for compounds **1a**, **1b** and **2**, in comparison with PyH (**A**),[17] $(2\text{-Py})_2NH$ (**B**),[15] $[Me_2Al(Py_2N)]$ (**C**),[8] $[Et_2Al(2\text{-}Py_2N)AlEt_3]$ (**D**),[9] Py_2PH (**E**),[9] $[Me_2Al(Py_2P)]$ (**F**)[10a][10b] and $[Et_2Al(Py_2P)]$ (**G**).[9] The structural parameters shown in Table 4 follow the ordering scheme shown in the Figure. Three different kinds of polymorphs are known for the $(2\text{-Py})_2NH$ molecule; a hydrogen-bridging dimer exists in the orthorhombic[18a] and triclinic[18b] polymorphs, while on the other hand, the hydrogen bridging produces a tetramer in the case of the monoclinic[9] polymorph. Distinct and strong differences exist in the torsion angles (the angle β between the pyridyl planes) of the various polymorphs found in $(2\text{-Py})_2NH$. The angles are 73, 40 and 0° in the triclinic, orthorhombic and monoclinic forms, respectively. However, the bond lengths in the different polymorphs are identical. The free electron pair in neutral $(2\text{-Py})_2NH$ is also partly delocalised over the pyridyl ring. The bridging nitrogen atom has sp^2 character. Assessment of the electronic structure in di(2-pyridyl)amide li-

Table 4. Comparison of the structural parameters of the di(2-pyridyl)amide ligands in compounds **1a**, **1b** and **2** with PyH **(A)**,[17] Py_2NH **(B)**,[15] $[Me_2Al(Py_2N)]$ **(C)**,[8] $[Et_2Al(2\text{-}Py_2N)AlEt_3]$ **(D)**,[9] Py_2PH **(E)**,[9] $[Me_2Al(Py_2P)]$ **(F)**[10a,10b] and $[Et_2Al(Py_2P)]$ **(G)**[9]

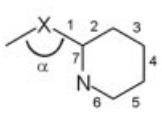

α = C(*ipso*)–N(bridge)–C(*ipso*)
β = angle between the two pyridyl ring planes
X = N, P

[a]	Aggr.	Conf.	1	2	3	4	5	6	7	α	β
A				139.4	139.2	139.2	139.4	133.8	133.8		
B	dimer, tetramer	*cis-trans*	138.0	139.5	137.0	137.0	136.5	134.0	133.5	131.1	
C	monomer	*trans-trans*	134.3	142.1	135.3	139.5	135.5	136.6	136.6	125.5	10.4
D	monomer	*trans-trans*	138.8	139.5	136.2	139.5	135.2	136.7	138.6	122.4	10.4
E		*cis-trans*	186.6	141.1	140.0	140.3	140.3	134.8	135.1	102.6	
F	monomer	*trans-trans*	178.4	141.5	136.2	139.8	135.8	136.2	136.8	106.6	25.0
G	monomer	*trans-trans*	177.8	142.0	135.8	139.0	135.5	136.6	136.8	107.4	17.0
1a	monomer	*cis (c)-*	137.2	139.9	137.6	137.5	137.0	133.7	136.1	124.8	9.0
		trans (nc)	138.6	140.2	137.1	138.3	136.8	134.4	134.1		
1b	monomer	*cis (c)-*	137.2	138.8	140.9	138.7	136.3	132.9	135.1		21.3
		trans (nc)	136.9	141.7	138.8	136.5	134.4	134.7	135.5	125.2	7/18.6
		trans (c)	136.4	141.3	135.4	139.2	135.0	135.6	136.2	125.9	
2	monomer	*cis (c)-*	136.8	139.9	136.6	138.7	135.5	133.8	136.8	123.8	8.2
		trans (nc)	139.3	139.9	138.0	137.4	137.0	134.7	134.2		

[a] The bond lengths correspond to average values for compounds with more than one equivalent pyridyl ring; (c) = coordinated pyridyl ring; (nc) = non-coordinated pyridyl ring; for compound **E** the data correspond to the optimised geometry obtained from DFT calculations with BPW91/6-31+G*, standard bond lengths[16]: N−C 147 pm, N=C 129 pm, C−C 154 pm, C=C 134 pm, P−C 185 pm, P=C 161 pm,[22] N−C 147 pm, N=C 129 pm, C−C 154 pm, C=C 134 pm.

gands in various metal complexes is possible by comparison with $(2\text{-}Py)_2NH$.

Theoretical Studies of the $(2\text{-}Py)_2P^-$ and $(2\text{-}Py)_2N^-$ Anions

To obtain deeper insights [e.g., the energetic differences between the conformers and the quantification of an Al−N(amide) versus Al←N(donor) bond energy contribution in the light of the related $(2\text{-}Py)_2P^-$ phosphanide system] into these structures, we performed DFT calculations. Coordination modes with the *cis-cis*, *cis-trans* and *trans-trans* conformers are documented for both $(2\text{-}Py)_2E^-$ anions (E = N, P).[7,10] Although the bridging nitrogen atom in $Et_2Al(2\text{-}Py)_2N$ might be employed in an additional N→Al donor bond towards $AlEt_3$ to give the adduct $Et_3Al{\leftarrow}N(2\text{-}Py)AlEt_2$, Lewis acid/base pairing was precluded with the related phosphanide $Et_2Al(2\text{-}Py)_2P$.[9] However, the di(2-pyridyl)phosphanide ligand shows a metal-dependent coordination response and is involved in a highly unusual σ/π interaction with the soft metal caesium.[10c] The phosphorus atom in the anion is sufficiently Lewis basic to bridge two soft organometallic iron centres. In this context, the different conformers of $(2\text{-}Py)_2N^-$ and $(2\text{-}Py)_2P^-$ were analysed by DFT calculations (Figure 4).

As anticipated, the *cis-trans* conformers of both $(2\text{-}Py)_2E^-$ anions are more stable than the *trans-trans* and *cis-cis* conformers. The twisted *trans-trans* conformer of Py_2N^- is only 1.4 kJ/mol more stable than the twisted *cis-cis* form (each av. dihedral angle 52°), while the twisted *cis-cis* form of the Py_2P^- anion (each av. dihedral angle 42°) is significantly more stable than the twisted *trans-trans* form (11.42 kJ/mol, Figure 4). This allows full conjugation throughout the heteroallylic system and intramolecular $N^{\delta-}\cdots{}^{\delta+}H(C)$ hydrogen bonding. While the N(bridge)−C(*ipso*) distances from the calculated anions match those in the experimental contact ion pairs **1a**, **1b** and **2** almost exactly, the P(bridge)−C(*ipso*) distances seem to be marginally too long (compare Tables 1−3 and 5). While the C−E−C angle in the amides is widened to values considerably larger than 120°, it is much sharper in the phosphanides, and smaller even than the value expected for an sp^3-hybridised phosphorus atom. Both features match the experimentally found values in the contact ion pairs. Closer examination of the bond lengths reveals partially localised double bonds in the pyridyl rings at the 3- and 5-positions. The small energetic differences between the *trans-trans* and the *cis-trans* conformers − 7.4 kJ/mol for the Py_2N^- and 23.2 kJ/mol for the Py_2P^- anion − can easily be overcompensated by metal coordination.

Theoretical Studies of the E→Al Donor Bond (E = N, P)

The next challenge was to determine the E→Al donor-acceptor bond energies in the experimentally verified complex $Et_2Al(2\text{-}Py)_2NAlEt_3$ and the model compounds $Me_2Al(2\text{-}Py)_2N{\rightarrow}AlMe_3$ and $Me_2Al(2\text{-}Py)_2P{\rightarrow}AlMe_3$, since $Et_2Al(2\text{-}Py)_2P$ does not form the adduct $Et_2Al(2\text{-}Py)_2P{\rightarrow}AlEt_3$ with a second equivalent of $AlEt_3$. One difference between the Lewis-type donor-acceptor bond and a covalent bond is that dissociation of the former yields two

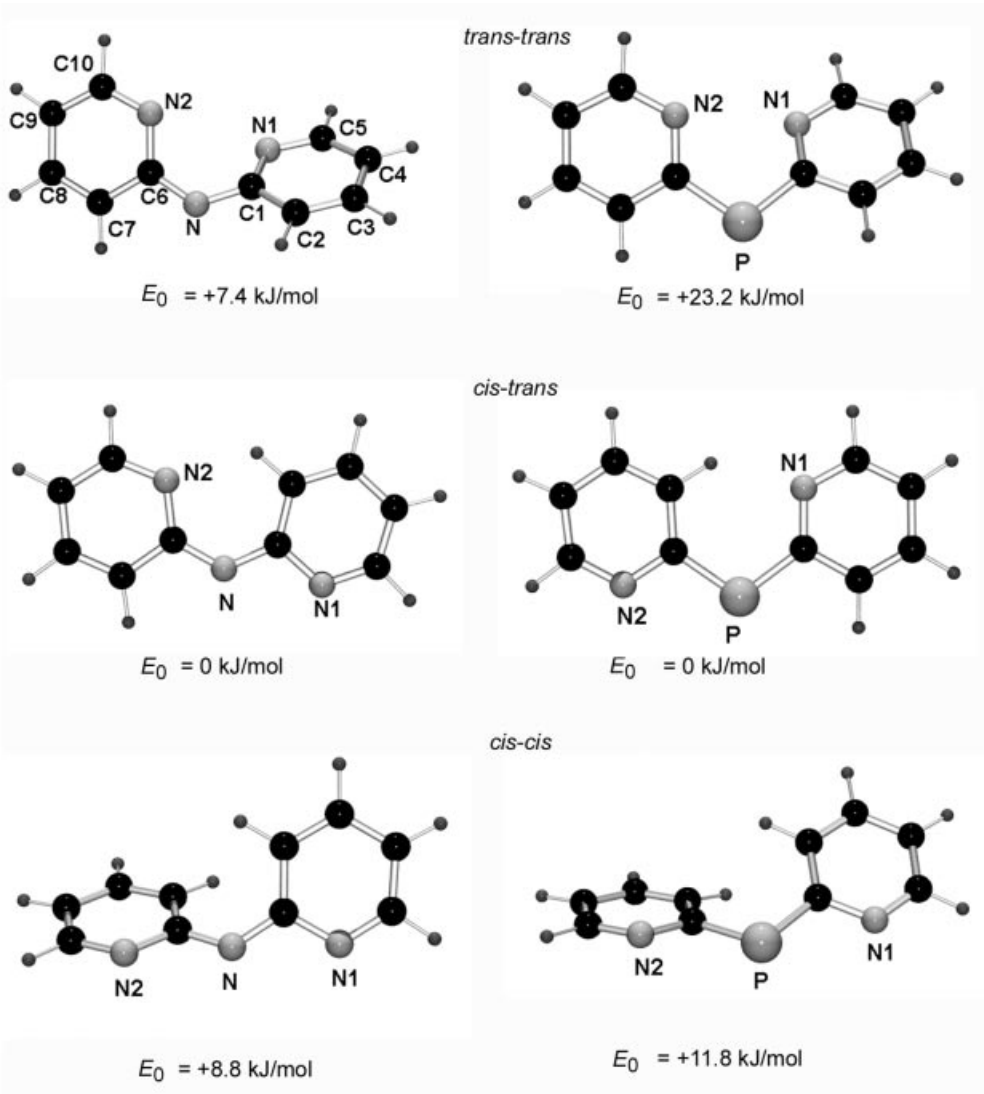

Figure 4. Optimised geometries for the different conformers of the free $(2\text{-Py})_2N^-$ and $(2\text{-Py})_2P^-$ anions by the BPW91/6-31+G(d) method

Table 5. Selected calculated bond lengths [pm] and angles [°] for the free $(2\text{-Py})_2N^-$ and $(2\text{-Py})_2P^-$ anions at the BPW91/6-31+G(d) level of theory

	$(2\text{-Py})_2N^-$			$(2\text{-Py})_2P^-$		
	trans-trans	*cis-trans*	*cis-cis*	*trans-trans*	*cis-trans*	*cis-cis*
E−C1	135.4	136.2	135.1	182.1	182.0	182.2
C1−C2	144.2	144.3	144.6	143.5	143.1	143.4
C2−C3	138.9	139.4	139.0	139.2	139.5	139.2
C3−C4	141.4	140.9	141.3	141.3	141.1	141.2
C4−C5	140.6	140.7	140.6	140.6	140.7	140.6
C5−N1	134.1	133.8	134.0	134.2	134.0	134.1
N1−C1	138.1	138.7	138.5	137.2	138.0	138.2
N1···N2	301.6			308.2		
E−C6	135.4	135.3	135.1	182.1	181.8	182.2
C6−C7	144.2	144.7	144.6	143.5	144.0	143.4
C7−C8	138.9	138.6	139.0	139.2	138.8	139.2
C8−C9	141.4	141.8	141.3	141.3	141.8	141.2
C9−C10	140.6	140.1	140.6	140.6	140.1	140.6
C10−N2	134.1	134.5	134.0	134.2	134.6	134.1
N2−C6	138.1	138.8	138.5	137.2	137.9	138.2
C1−E−C6	124.5	126.5	123.9	107.0	108.4	105.0

closed-shell fragments with an electron lone-pair donor and an electron-pair acceptor, while the latter gives two open-shell fragments.[19] Another difference is that the bond length of a covalent bond would not usually change much in different aggregation states, while donor-acceptor bonds frequently show larger interatomic distances in the gas phase than in the solid state. As we wanted to investigate the above-mentioned donor-acceptor complexes by theoretical methods, we first tested them by employing the molecular structures of the complexes $Me_3N{\rightarrow}AlMe_3$ and $Me_3P{\rightarrow}AlMe_3$, which have already been determined structurally in the gas phase.[20] Their donor-acceptor bond dissociation energies were determined experimentally. The theoretical parameters calculated at the CBS-4, MP2/6-31+G(d) and BPW91/6-31+G(d) levels of theory were evaluated and compared to the experimental values obtained by Haaland. As expected, the most powerful computational methods CBS-4M and MP2/6-31+G(d) gave the best match with the experimentally ascertained structures and energies. The BPW91/6-31+G(d) method calculates the N→Al and P→Al donor-acceptor bond lengths as being

slightly too long, and the resulting bond dissociation energies are too low (Figure 5).

To force the central donating atom into the sp^2 hybridisation of an amide or phosphanide we performed calculations for $H_2C{=}(Me)N{\rightarrow}AlMe_3$ and $H_2C{=}(Me)P{\rightarrow}AlMe_3$, since these models should be more consistent with $Me_2Al(2\text{-}Py)_2N{\rightarrow}AlMe_3$ and $Me_2Al(2\text{-}Py)_2P{\rightarrow}AlMe_3$. In contrast to the shortening of the Al−N bond, by 1 and 5 pm, the P−Al interatomic distances surprisingly lengthened by 5 and 10 pm by the MP2 and BPW91/6-31+G(d) methods, respectively. Furthermore, the calculated bond dissociation energies at the most reliable MP2 level of theory were determined in these cases to be 95.7 and 44.9 kJ/mol for $H_2C{=}(Me)N{\rightarrow}AlMe_3$ and $H_2C{=}(Me)P{\rightarrow}AlMe_3$, respectively (Figure 5). Consequently, the sp^2 hybridisation of the heteroatom and the coupling of the charge to the substituents has a strong effect on the dissociation enthalpy of the E→Al bond, and particularly in the phosphanide adduct. While the energy is only decreased by a factor of one fifth in the amide adduct, it is halved in the phosphanide adduct. In addition, the "hard" aluminium atom prefers the "hard" nitrogen donor rather than the "soft" phosphane function. Population analysis schemes, such as Natural Population Analysis,[21] assign most pronounced negative partial charges to the ring nitrogen atoms in $Me_2Al(2\text{-}Py)_2N$ and $Me_2Al(2\text{-}Py)_2P$. In the latter, the divalent P^{III} centre even shows a partial positive charge. (Scheme 8).

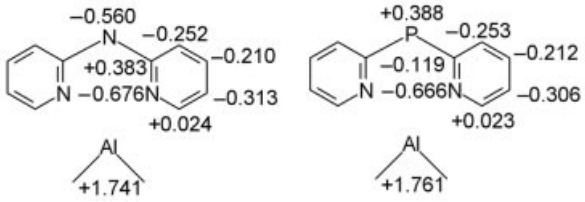

Scheme 8. Calculated natural charges in $[e]^-$ for the complexes $Me_2Al(2\text{-}Py)_2N$ and $Me_2Al(2\text{-}Py)_2P$, determined by natural population analysis

The s and p_π populations of the atomic orbitals of the bridging phosphorus and nitrogen atoms are significantly different. The 3s orbital in the phosphorus atom is more highly populated than the 2s orbital of the nitrogen atom, while the charge density in the p orbitals of the phosphorus atom is depleted relative to the bridging nitrogen atom.

Since this suggests the formation of a metal−nitrogen bond rather than a metal−phosphorus bond, we became interested in quantitatively evaluating the E→Al bond energies in the model compounds $Me_2Al(2\text{-}Py)_2N{\rightarrow}AlMe_3$ and $Me_2Al(2\text{-}Py)_2P{\rightarrow}AlMe_3$. Selected bond lengths and angles for these compounds are reported in Table 6, in comparison

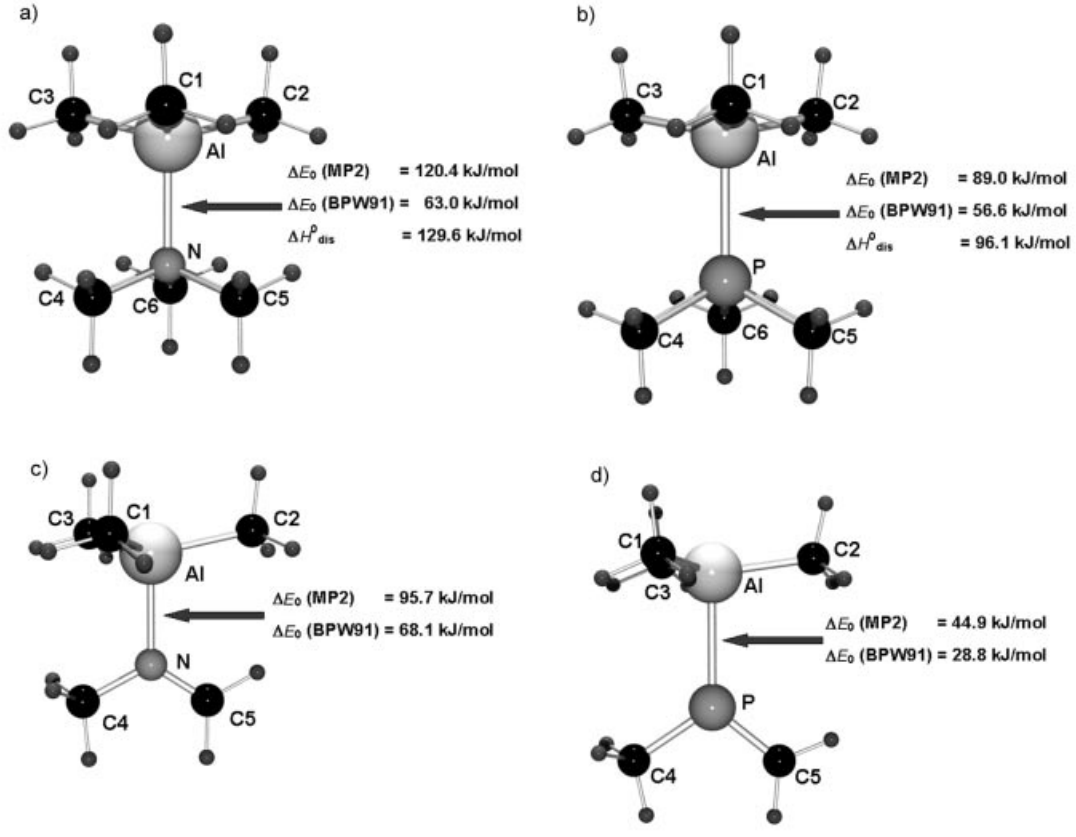

Figure 5. Optimised geometries for the adducts $Me_3N{\rightarrow}AlMe_3$ (a), $Me_3P{\rightarrow}AlMe_3$ (b), $H_2C{=}(Me)N{\rightarrow}AlMe_3$ (c) and $H_2C{=}(Me)P{\rightarrow}AlMe_3$ (d), with the related E→Al donor bond energies

Table 6. Selected calculated bond lengths [pm] and angles [°] of $Me_2Al(2\text{-}Py)_2N{\rightarrow}AlMe_3$ and $Me_2Al(2\text{-}Py)_2P{\rightarrow}AlMe_3$ in comparison to the experimentally ascertained data for $Et_2Al(2\text{-}Py)_2N{\rightarrow}AlEt_3$

	E = N		**E = P**
	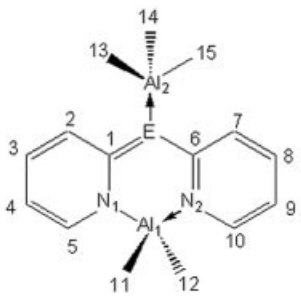		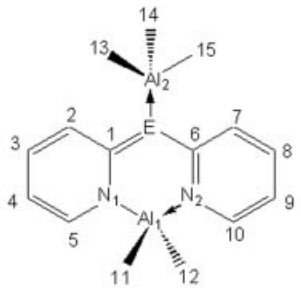
	BPW91/6-31+G(d)	Expt.	BPW91/6-31+G(d)
E−C1/E−C6	137.8	138.3(4)/139.2(5)	180.4
E−Al2	212.9	201.0(3)	266.0
C1−C2/C6−C7	142.5	137.2(6)/140.7(5)	143.0
C2−C3/C7−C8	138.6	137.0(5)/135.5(5)	138.6
C3−C4/C8−C9	141.3	139.5(5)	141.7
C4−C5/C9−C10	138.4	134.0(5)/136.7(5)	138.5
C5−N1/C10−N2	136.7	138.0(5)/135.4(4)	136.8
N1−C1/N2−C6	137.7	138.0(5)/136.2(5)	138.5
N1−Al1/N2−Al1	197.8	191.1(1)/193.3(3)	197.4
C1−E−Al2	118.0	117.4(2)	112.0
C1−E−C6	123.3	122.4(3)	102.2
E−Al2−C13	106.6	109.04(14)	106.2
E−Al2−C15	103.8	105.24(14)	102.8
Al1−E−Al2	139.1		151.3
C11−Al1−C12	121.6	122.7(2)	120.2
N1−Al1−N2	90.1	91.57(14)	97.1

to the experimentally determined values for the complex $Et_2Al(2\text{-}Py)_2N{\rightarrow}AlEt_3$. Because of the coordination of the additional $AlMe_3$ fragment by the bridging nitrogen atom, the $Me_2Al(2\text{-}Py)_2N$ moiety adopts an accentuated butterfly conformation analogous to that of $Me_2Al(2\text{-}Py)_2P$. Furthermore, the heteroatom in the bridging position seems to become a pseudo-sp^3-hybridised centre, giving rise to a displacement of the $AlMe_3$ fragment from the plane containing the N1, E and N2 atoms. Surprisingly, comparison between the model compounds $Me_2Al(2\text{-}Py)_2N{\rightarrow}AlMe_3$ and $Me_2Al(2\text{-}Py)_2P{\rightarrow}AlMe_3$ reveals a different position of the $AlMe_3$ fragment relative to the second aluminium atom of the $Me_2Al(2\text{-}Py)_2E$ butterfly moiety. While both metal atoms are located on the same side in the nitrogen complex, they are positioned on opposite sides in the phosphorus complex (Figure 6).

The experimentally determined Al2→N bond length of 201.0(3) pm in $Et_2Al(2\text{-}Py)_2NAlEt_3$ is significantly longer than a covalent bond and about 5 pm shorter than a pure dative bond.[9] The calculated Al2→N bond length of 212.9 pm in the model complex $Me_2Al(2\text{-}Py)_2N{\rightarrow}AlMe_3$ is much longer, possibly due to the gas-phase nature of the simulation.

The calculated E→Al bond energies at the MP2/6-31+G(d) level for the complexes $Me_3E{\rightarrow}AlMe_3$ (E = N, P) differ from the experimentally determined values only by less than 10 kJ/mol. Consequently, a single-point calculation at the MP2 level of theory was performed for the $Me_2Al(2\text{-}Py)_2N{\rightarrow}AlMe_3$ and $Me_2Al(2\text{-}Py)_2P{\rightarrow}AlMe_3$ complexes. The fully optimised geometry from the BPW91/6−31+G(d) calculations was employed. The calculated bond dissociation energy for the complex $Me_2Al(2\text{-}Py)_2N{\rightarrow}AlMe_3$ (125.4 kJ/mol) is very close to the experimentally determined value for $Me_3N{\rightarrow}AlMe_3$ (129.6 kJ/mol), but the donor-acceptor bond energy of 75.4 kJ/mol in $Me_2Al(2\text{-}Py)_2P{\rightarrow}AlMe_3$ is considerably lower (by 20.7 kJ/mol) than the experimentally determined value for $Me_3P{\rightarrow}AlMe_3$ (96.1 kJ/mol).

In summary, all di(2-pyridyl)amides and -phosphanides coordinate the R_2Al^+ fragment through at least one ring nitrogen atom. This in itself suggests that the charge density in the anions is coupled into the rings and accumulated at the ring nitrogen atoms. The Lewis basicity of the central nitrogen atom in $Me_2Al(2\text{-}Py)_2N$ is still high enough to coordinate a second equivalent of $AlEt_3$ to form the Lewis acid/base adduct $Et_2Al(2\text{-}Py)_2N{\rightarrow}AlEt_3$. All these findings confirm the formation of metal nitrogen rather than of metal−phosphorus bonds even in reaction pathways, as established by Budzelaar for reactions between (2-pyridyl)-phosphanes and methyllithium.[22] The theoretical results presented show that while the bridging nitrogen atom in the amides (E = N) is still a typical Lewis base, the situation in

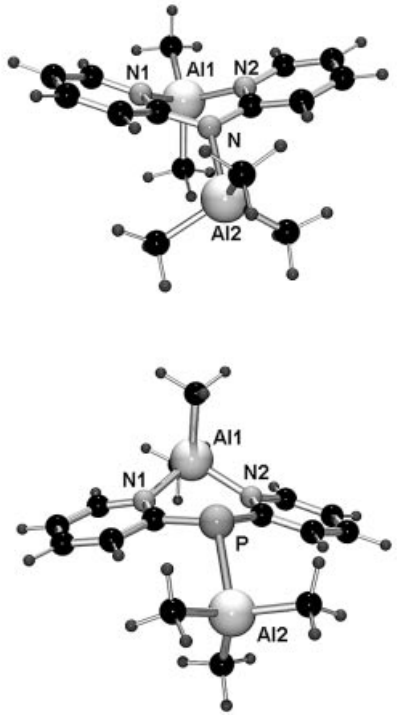

Figure 6. BPW91/6-31+G*-optimised geometries of $Me_2Al(2\text{-}Py)_2N{\rightarrow}AlMe_3$ (top) and $Me_2Al(2\text{-}Py)_2P{\rightarrow}AlMe_3$ (bottom)

the corresponding phosphanides (E = P) is different. Here, nearly all the charge density couples into the pyridyl rings, leaving the central phosphorus atom attractive only for soft metals, in the form of a π-acid-type of coordinating centre to reinforce the otherwise poor phosphorus donor bond energy, shown in the P−N−C allylic coordination to the soft Cs atom.[10c]

Conclusion

The competition between the amidic bridging nitrogen atom and the pyridyl nitrogen atoms for the charge density in Py_2N^- provides for greater conformational variety than in the analogous Py_2E^- systems (E = CH,[7a,7b] P,[10a,10b] As[10b]). The former system shows considerable Lewis basicity at the bridging nitrogen atom, while the charge density at the bridging phosphorus atom is depleted and coupled into the rings. The small energy differences of about 8 kJ/mol between the *cis-trans*, *trans-trans* and *cis-cis* conformers in the Py_2N^- anion can easily be overcome by various crystallisation techniques from different solvents at different temperatures (**1a** from pyridine at 0 °C or from diethyl ether at −40 °C, **1b** from C_6D_6 at room temperature). The 23 kJ/mol by which the *trans-trans* conformer in Py_2P^- is disfavoured against the *cis-trans* form can easily be compensated for by coordination to the hard organometallic Me_2Al^+ fragment. The energy gained from the E→Al donor bonds, in which the charge density at E = N or P can be delocalised to an adjacent carbon atom, is only half the amount with phosphorus than with nitrogen. Hence, the P-centred systems are much better π-donors to soft metals than σ-donors to hard metals. We found computational methods extremely helpful for interpreting the coordination behaviour of di(2-pyridyl)amides and -phosphanides.

Experimental Section

General Remarks: All manipulations were performed under dry N_2 with Schlenk techniques or under argon in a glove box. All solvents were dried with Na/K alloy and distilled prior to use. NMR spectra were obtained in C_6D_6 or $CDCl_3$ as solvent, with $SiMe_4$ or H_3PO_4 as external reference, with a Bruker AMX 250 MHz spectrometer. Mass spectra were recorded with a Finnigan Mat 8230 or Varian Mat CH5 spectrometer. Elemental analyses were performed by the Analytisches Laboratorium, Universität Würzburg.

$[Al\{(NPy)Py\}_3]$ (1a) and/or $[Al\{(NPy)Py\}_2(Py_2N)]$ (1b)

1a. Method a: A solution of Py_2NH (4.00 g, 23.3 mmol) in Et_2O (20 mL) was added dropwise to a suspension of $LiAlH_4$ (220 mg, 5.8 mmol) in Et_2O (20 mL), cooled to 0 °C. After the mixture had been stirred at room temp. for 2 d, the diethyl ether was replaced by PyH (20 mL). The reaction mixture was filtered through Celite to remove the undissolved solids, and the clear solution was allowed to stand at 0 °C. After 1 d, crystals of **1a** suitable for single-crystal X-ray diffraction were isolated. For analytic and spectroscopic analysis the crystals were washed twice with hexane (10 mL) and dried under vacuum. Yield: 1.03 g (50%). **Method b:** Py_2NH (2 g, 11.6 mmol) in Et_2O (25 mL) was cooled to −78 °C. Et_3Al (5.95 mL of 15% solution in hexane, 3.83 mmol) was added dropwise to the cooled mixture, which was allowed to gradually attain room temp. Stirring at room temp. was continued for 2 d. Crystals of **1a** suitable for X-ray diffraction study were isolated from the reaction mixture stored at −40°C. For analytical and spectroscopic analysis the crystals were washed twice with hexane (10 mL each time) and dried under vacuum. Yield: 1.85 g (90%). Decomposition point: 83 °C; The ^1H and ^{13}C NMR spectra show different resonance peaks for the coordinated pyridyl ring and noncoordinated pyridyl rings. An unambiguous assignment of all the resonances was not possible. ^1H NMR (C_6D_6): δ = 6.13 (dd, $^3J_{H\text{-}H}$ = 6.2, $^3J_{H\text{-}H}$ = 6.3, 1 H), 6.45 (s_{br}, 1 H,) 7.01 (s_{br}, 2 H, 5-H, 5-H′, 4-H and 4′-H), 7.26 (d, $^3J_{H\text{-}H}$ = 6.6, 1 H,), 7.77 (s_{br}, 1 H), 7.83 (s_{br}, 1 H), 8.12 (s_{br}, 1 H, 3-H, 3′-H, 6-H and 6′-H) ppm. ^{13}C NMR (C_6D_6): δ = 112.0 (s), 113.7 (s), 114.5 (s), 116.3 (s, C-5, C-5′, C-4 and C-4′), 137.5 (s), 138.2 (s), 139.0 (s), 148.1 (s, C-3, C-3′, C-6 and C-6′), 154.1 (s), 160.8 (s, C-2 and C-2′) ppm. EI-MS: *m/z* (%) = 170.1 (100) [Py_2N], 78.1 (24.9) [Py]. $C_{30}H_{24}AlN_9$ (537.56): calcd. C 67.1, H 4.50, N 23.5; found C 65.7, H 4.70, N 23.1.

1b: Compound **1a** was dissolved in C_6D_6 for spectroscopic studies. Reducing the volume of the solution slowly gives rise to crystals of the isomer **1b**. In solution, **1b** converts into **1a**, and hence the spectroscopic data are identical.

$[(PyH)_2AlCl_2\{(NPy)Py\}]$ (2): A mixture of di(2-pyridyl)amine (0.50 g, 2.90 mmol) and aluminium trichloride (0.39 g, 2.90 mmol) in pyridine (30 mL) was cooled to −40 °C. An equimolar quantity of *n*-butyllithium (1.90 mL of a 1.6 M solution in *n*-hexane) was added dropwise to this mixture, which was gradually allowed to attain room temp. by standing overnight. Stirring of the resulting clear solution at room temp. was continued for 2 d. Needle-shaped, colourless crystals suitable for single-crystal diffraction studies were isolated from the solution after 4 d at 0 °C. After removal of the mother liquor, the crystals were further washed several times with hexane (10 mL) and vacuum-dried for analytic and spectroscopic

studies. Yield: 0.87 g (70.2%). Decomposition point: 50 °C. ^{1}H NMR ($CDCl_3$): δ = 7.04−8.70 (m, 18 H, Py-H) ppm. ^{13}C NMR ($CDCl_3$): δ = 116.6 (s, C-5), 117.7 (s, C-3), 126.6 (s, C_{para}), 139.7 (s, C_{meta}), 141.5 (s, C-4), 142.7 (s, C_{ortho}), 144.1 (s, C-6), 152.8 (s, C-2) ppm. EI-MS: *m*/*z* (%) = 170.1 (12.8) [Py_2N], 119.1 (0.10) [(AlPyN)], 105.1 (0.12) [(AlPy)], 79.1 (100) [PyH]. $C_{20}H_{18}AlCl_2N_5$ (426.28): calcd. C 56.4, H 4.26, N 16.43; found C 54.7, H 4.53, N 15.84.

Crystal Structure Determination: Crystallographic details pertaining to data collection and refinement are presented in Table 7. The data for **1a** and **2** were collected with an Enraf−Nonius CAD4 four-circle diffractometer, and the data for **1b** with a Stoe-IPDS single-circle diffractometer with graphite-monochromated Mo-K_α radiation (λ = 71.073 pm). All data were collected at low temperatures, using oil-coated shock-cooled crystals.[23] After determination and refinement of the cell parameters for **1a** and **2**, the intensity of the reflections was detected by the background-peak-background method.[24] All reflections were collected by the 2θ/ω-scan method for **1a** and **2**, while in the case of **1b** the reflections were detected by the φ-scan mode with stepwise rotation of every 1°. All structures were solved by direct methods by use of the SHELXS-97 program for compounds **1a** and **1b** and SHELXS-96 for **2**.[25a] Refinement of the structures was performed by full-matrix, least-squares methods against F^2 with SHELXL-97[25b] (for **1a** and **1b**) and SHELXL-96[25c] (for **2**). All non-hydrogen atoms were refined with anisotropic displacement parameters. Hydrogen atoms were assigned ideal positions and refined isotropically with a riding model with U_{iso} constrained to 1.2 times of U_{eq} of the parent atom. Structure refinement: Compound **1a** crystallises in the centrosymmetric triclinic space group $P\bar{1}$. The [Al{(NPy)Py}$_3$] (**1a**) molecule shows almost threefold symmetry. In the asymmetric unit, three non-coordinated pyridine molecules are present as solvent from crystallisation. They are not disordered and do not give rise to any hydrogen-bonding pattern. Single-crystal data for compound **1a** in this conformation were obtained in different solvents. Compound **1a** has also been reported by another research group.[13e] The different forms show varying cell parameters, and a comparison of these parameters is listed in the Supporting Information. Compound **1b**, which is a conformational isomer of **1a**, crystallises in the centrosymmetric monoclinic space group $P2_1/c$. Two noncoordinated C_6D_6 solvent molecules are present in the asymmetric unit. The donating pyridine molecules in compound **2** were refined with ADP and distance restraints. Selected bond lengths and angles are summarised in Tables 1−3. The CCDC numbers listed in Table 7 contain the supplementary crystallographic data for this paper. These data can be obtained free of charge at www.ccdc.cam.ac.uk/conts/retrieving.html or from the Cambridge Crystallographic Data Centre, 12, Union Road, Cambridge CB2 1EZ, UK [Fax: (internat.) + 44-1223/336-033; E-mail: deposit@ccdc.cam.ac.uk].

Computational Details: The calculations were carried out with the GAUSSIAN98 program package.[26] For the evaluation of the donor-acceptor bond energies of the complexes $Et_2Al(2\text{-}Py)_2N\rightarrow AlEt_3$ and $Et_2Al(2\text{-}Py)_2P\rightarrow AlEt_3$, calculations at the BPW91,[27] MP2[28] and CBS-4[29] levels of theory were carried out. The 6-31+G(d) basis set was used for the calculations.[30] Because of the

Table 7. Crystallographic data for **1a**, **1b** and **2**

	1a	**1b**	**2**
Empirical formula	$C_{30}H_{24}AlN_9+3C_5H_4N$	$C_{30}H_{24}AlN_9+2C_6D_6$	$C_{20}H_{18}AlCl_2N_5+3C_5H_5N$
CCDC-	180594	180595	180596
Formula mass	774.86	693.78	663.0
Crystal size [mm]	0.2 × 0.3 × 0.5	0.2 × 0.2 × 0.4	0.5 × 0.5 × 0.6
T [K]	173(2)	173(2)	153(2)
Space group	$P\bar{1}$	$P2_1/c$	$P2_1/n$
Crystal system	triclinic	monoclinic	monoclinic
a [pm]	1073.3(3)	969.97(19)	869.4(1)
b [pm]	1387.3(3)	1976.0(4)	2062.5(2)
c [pm]	1425.5(4)	1893.3(4)	1830.3(1)
α [°]	109.556(13)	90	90
β [°]	98.84(2)	105.32(2)	93.723(10)
γ [°]	93.67(2)	90	90
V [nm^3]	1.9612(5)	3.5982(12)	3.2747(4)
Z	2	4	4
ρ_c [Mg m^{-3}]	1.312	1.281	1.346
μ_c [mm^{-1}]	0.103	0.101	0.264
F(000)	812	1456	1384
2θ range [°]	6−50	5−47	6−50
No. of reflns. measd.	7483	14288	11156
No. unique reflns.	6885	4984	4608
No. of restraints	0	0	25
No. of parameters	523	469	415
*R*1[a] [$I > 2\sigma(I)$]	0.043	0.091	0.053
*wR*2[b] (all data)	0.100	0.262	0.101
g_1/g_2 [c]	0.043/0.528	0.157/2.401	0.035/0.543
Largest diff. peak/hole [e·nm^{-3}]	190/−278	1936/−483	502/−252

[a] $R1 = \frac{\sum \left||F_o|-|F_c|\right|}{\sum |F_o|}$ [b] $wR2 = \sqrt{\frac{w(F_o^2-F_c^2)^2}{w(F_o^2)^2}}$ [c] $w = \frac{1}{\sigma^2(F_o^2)+(g_1P)^2+g_2P}; P = \frac{(\max(F_o^2,0)+2F_c^2)}{3}$

relatively large size of the bipyridyl complexes, the geometries were fully optimised at the BPW91/6-31+G(d) level and used to compute vibrational harmonic wavenumbers and zero-point corrections. In order to obtain more reliable total energies and bond energies, MP2/6-31+G(d) energy calculations were also performed with the BPW91/6-31+G(d)-optimised geometries, and this type of calculation is designated by the standard notation MP2/6-31+G(d)//BPW91/6-31+G(d).

Acknowledgments

The authors thank the Deutsche Forschungsgemeinschaft (especially the SFB 347, Teilprojekte C2 and D4), the Fonds der Chemischen Industrie and Bruker Nonius, Karlsruhe, for financial support.

[1] J. J. Eisch, in "Aluminium" (Eds.: E. W. Abel, F. G. A. Stone, G. Wilkinson) *Comprehensive Organometallic Chemistry II*, Elsevier, Oxford, UK, **1995**, vol. 1, chapter 10, p. 431 and vol. 11, chapter 6, p. 277.

[2] [2a] D. A. Atwood, *Coord. Chem. Rev.* **1998**, *176*, 407−430. [2b] N. Emig, H. Nguyen, H. Krautscheid, R. Reau, J. B. Cazaux, G. Bertrand, *Organometallics* **1998**, *17*, 3599−3608. [2c] M. Bochmann, D. M. Dawson, *Angew. Chem. Int. Ed. Engl.* **1996**, *35*, 2226−2228; *Angew. Chem.* **1996**, *108*, 2371−2373.

[3] [3a] J. D. Bolt, F. N. Tebbe, *Adv. Ceram.* **1989**, *26*, 69−76. [3b] A. C. Jones, *J. Cryst. Growth* **1993**, *129*, 728−773. [3c] C. Jones, G. A. Koutsantonis, C. L. Raston, *Polyhedron* **1993**, *12*, 1829−1848. [3d] J. Pinkas, T. Wang, R. A. Jacobson, J. G. Verkade, *Inorg. Chem.* **1994**, *33*, 4202−4210. [3e] C. L. Watkins, L. K. Krannich, S. J. Schauer, *Inorg. Chem.* **1995**, *34*, 6228−6230 and references therein. [3f] H. Sussek, O. Stark, A. Devi, H. Pritzkow, R. A. Fischer, *J. Organomet. Chem.* **2000**, *602*, 29−36. [3g] D. C. Bertolet, J. W. Rogers Jr., *Chem. Mater.* **1993**, *5*, 391−395.

[4] [4a] M. F. Lappert, P. P. Power, A. R. Sanger, R. C. Srivastava, *Metal and Metalloid Amides*, E. Horwood, Chichester, **1980**, and references therein. [4b] A. J. Downs, *Chemistry of Aluminium, Gallium, Indium and Thallium*, 1st ed., Blackie, Glasgow, **1993**.

[5] [5a] G. M. Sheldrick, W. S. Sheldrick, *J. Chem. Soc. A* **1969**, 2279−2282. [5b] J. L. Atwood, G. A. Koutsantonis, F. C. Lee, C. L. Raston, *J. Chem. Soc., Chem. Commun.* **1994**, 91−92. [5c] J. T. Leman, J. Braddock-Wilking, A. J. Coolong, A. R. Barron, *Inorg. Chem.* **1993**, *32*, 4324−4336. [5d] J. L. Atwood, S. M. Lawrence, C. L. Raston, *J. Chem. Soc., Chem. Commun.* **1994**, 73−74. [5e] P. Pullmann, K. Hensen, J. W. Bats, *Z. Naturforsch., Teil B* **1982**, *37*, 1312−1315. [5f] P. L. Bellavance, E. R. Corey, J. Y. Corey, G. W. Hey, *Inorg. Chem.* **1977**, *16*, 462−467. [5g] W. Zheng, C. N. Moesch-Zanetti, T. Blunck, H. W. Roesky, M. Noltemeyer, H. -G. Schmidt, *Organometallics* **2001**, *20*, 3299−3303. [5h] N. J. Hardman, C. Cui, H. W. Roesky, W. H. Fink, P. P. Power, *Angew. Chem. Int. Ed.* **2001**, *40*, 2172−2176; *Angew. Chem.* **2001**, *113*, 2230−2232. [5i] C. Cui, H. W. Roesky, H-G. Schmidt, M. Noltemeyer, H. Hao, F. Cimpoesu, *Angew. Chem. Int. Ed.* **2000**, *39*, 4274−4276; *Angew. Chem.* **2000**, *112*, 4444−4446.

[6] T. Kottke, D. Stalke, *Chem. Ber./Recueil* **1997**, *130*, 1365−1374.

[7] [7a] H. Gornitzka, D. Stalke, *Organometallics* **1994**, *13*, 4398−4405. [7b] H. Gornitzka, D. Stalke, *Angew. Chem.* **1994**, *106*, 695−698; *Angew. Chem. Int. Ed. Engl.* **1994**, *33*, 693−695. [7c] U. Pieper, D. Stalke, *Organometallics* **1993**, *12*, 1201−1206. [7d] H. Gornitzka, C. Hemmert, G. Bertrand, M. Pfeiffer, D. Stalke, *Organometallics* **2000**, *19*, 112−114.

[8] H. Gornitzka, D. Stalke, *Eur. J. Inorg. Chem.* **1998**, 311−317.

[9] [9a] M. Pfeiffer, F. Baier, T. Stey, D. Leusser, D. Stalke, B. Engels, D. Moigno, W. Kiefer, *J. Mol. Model.* **2000**, *6*, 299−311. [9b] M. Pfeiffer, F. Baier, T. Stey, D. Leusser, D. Stalke, B. Engels, D. Moigno, W. Kiefer, in *Highlights in Computational Chemistry* (Ed.: T. Clark), Springer-Verlag, Berlin, Heidelberg, **2001**. [9c] L. Mahalakshmi, D. Stalke, in *Structure and Bonding*, vol. 103, 86−115 (Eds.: H. W. Roesky, D. A. Atwood), Springer-Verlag, Berlin, Heidelberg, **2002**.

[10] [10a] A. Steiner, D. Stalke, *J. Chem. Soc., Chem. Commun.* **1993**, 444−446. [10b] A. Steiner, D. Stalke, *Organometallics* **1995**, *14*, 2422−2429. [10c] M. Pfeiffer, T. Stey, H. Jehle, B. Klüpfel, W. Malisch, V. Chandrasekhar, D. Stalke, *Chem. Commun.* **2001**, 337−338.

[11] S. Wingerter, M. Pfeiffer, A. Murso, C. Lustig, T. Stey, V. Chandrasekhar, D. Stalke, *J. Am. Chem. Soc.* **2001**, *123*, 1381−1388.

[12] [12a] S. Wingerter, M. Pfeiffer, F. Baier, T. Stey, D. Stalke, *Z. Anorg. Allg. Chem.* **2000**, *626*, 1121−1130. [12b] S. Wingerter, H. Gornitzka, G. Bertrand, D. Stalke, *Eur. J. Inorg. Chem.* **1999**, *1*, 173−178. [12c] S. Wingerter, H. Gornitzka, R. Bertermann, S. K. Pandey, J. Rocha, D. Stalke, *Organometallics* **2000**, *19*, 3890−3894. [12d] S. Wingerter, M. Pfeiffer, T. Stey, M. Bolboaca, W. Kiefer, V. Chandrasekhar, D. Stalke, *Organometallics* **2001**, *20*, 2730−2735. [12e] A. Steiner, D. Stalke, *Angew. Chem.* **1995**, *107*, 1908−1910; *Angew. Chem. Int. Ed. Engl.* **1995**, *34*, 1752−1755.

[13] [13a] S. Wang, *Coord. Chem. Rev.* **2001**, *215*, 79−98. [13b] J. Ashenhurst, L. Brancaleon, S. Gao, W. Liu, H. Schmider, S. Wang, G. Wu, Q. G. Wu, *Organometallics* **1998**, *17*, 5334−5341. [13c] W. Liu, A. Hassan, S. Wang, *Organometallics* **1997**, *16*, 4257−4259. [13d] X.-M. Wang, H.-S. Sun, X.-Z. You, X. -Y. Huang, *Polyhedron* **1996**, *15*, 3543−3546. [13e] L. M. Engelhardt, M. G. Gardiner, C. Jones, C. P. Junk, L. C. Raston, A. H. White, *J. Chem. Soc., Dalton Trans.* **1996**, 3053−3057.

[14] [14a] A. E. Finholt, A. C. Bond, H. I. Schlesinger, *J. Am. Chem. Soc.* **1947**, *69*, 1199−1203. [14b] E. Wiberg, E. Amberger, *Hydrides of the Elements of the Main Groups 1−4*, Elsevier, Amsterdam, **1971**, p. 285. [14c] G. Liniti, H. Nöth, P. Rahm, *Z. Naturforsch., Teil B* **1988**, *43*, 53−60. [14d] A. Heine, D. Stalke, *Angew. Chem.* **1992**, *104*, 941−942; *Angew. Chem. Int. Ed. Engl.* **1992**, *31*, 854−855. [14e] M. L. Montero, H. Wessel, H. W. Roesky, M. Teichert, I. Usón, *Angew. Chem.* **1997**, *109*, 644−647; *Angew. Chem. Int. Ed. Engl.* **1997**, *36*, 629−631.

[15] [15a] J. E. Johnson, R. A. Jacobson, *Acta Crystallogr., Sect. B* **1973**, *29*, 1669−1674. [15b] G. J. Pyrka, A. A. Pinkerton, *Acta Crystallogr., Sect. C* **1992**, *48*, 91−94. [15c] H. Schödel, C. Näther, H. Bock, F. Butenschön, *Acta Crystallogr. Sect.* **1996**, *52*, 842−853.

[16] P. Rademacher, *Strukturen Organischer Moleküle*, VCH, Weinheim, **1987**.

[17] T. Eicher, S. Hauptmann, *Chemie der Heterocyclen*, VCH, Weinheim, **1995**.

[18] [18a] S. Aduldecha, B. Hathaway, *J. Chem. Soc., Dalton Trans.* **1991**, 993−998. [18b] F. A. Cotton, L. M. Daniels, C. A. Murillo, I. Pascual, *J. Am. Chem. Soc.* **1997**, *119*, 10223−10224.

[19] [19a] A. Haaland, *Angew. Chem.* **1989**, *101*, 1017−1032; *Angew. Chem. Int. Ed. Engl.* **1989**, *28*, 992−1017. [19b] V. Jonas, G. Frenking, M. T. Reetz, *J. Am. Chem. Soc.* **1994**, *116*, 8741−8753.

[20] [20a] A. Almenningen, L. Fernholt, A. Haaland, J. Weidlein, *J. Organomet. Chem.* **1978**, *145*, 109−119. [20b] G. A. Andersen, F. R. Forgaard, A. Haaland, *Acta Chem. Scand.* **1972**, *26*, 1947−1949.

[21] A. E. Reed, R. B. Weinstock, F. Weinhold, *J. Chem. Phys.* **1985**, *82*, 735−746.

[22] [22a] P. H. M. Budzelaar, *J. Org. Chem.* **1998**, *63*, 1131−1137. [22b] G. Talarico, V. Barone, P. H. M. Budzelaar, C. Adamo, *J. Phys. Chem.* **2001**, *105*, 9014−9023.·

[23] [23a] D. Stalke, *Chem. Soc. Rev.* **1998**, *27*, 171−178. [23b] T. Kottke, R. J. Lagow, D. Stalke, *J. Appl. Crystallogr.* **1996**, *29*, 465−468. [23c] T. Kottke, D. Stalke, *J. Appl. Crystallogr.* **1993**, *26*, 615−619.

[24] Enraf−Nonius, CAD4 diffractometer program, **1989**.

[25] [25a] G. M. Sheldrick, *Acta Crystallogr., Sect. A* **1990**, *46*,

467−473. [25b] G. M. Sheldrick, *SHELXL-97, Program for crystal structure refinement*, Göttingen **1997**. [25c] G. M. Sheldrick, *SHELXL-96, Program for crystal structure refinement*, Universität Göttingen, **1996**.

[26] M. J. Frisch, G. W. Trucks, H. B. Schlegel, G. E. Scuseria, M. A. Robb, J. R. Cheeseman, V. G. Zakrzewski, J. A. Montgomery, R. E. Stratmann, J. C. Burant, S. Dapprich, J. M. Millam, A. D. Daniels, K. N. Kudin, M. C. Strain, O. Farkas, J. Tomasi, V. Barone, M. Cossi, R. Cammi, B. Mennucci, C. Pomelli, C. Adamo, S. Clifford, J. Ochterski, G. A. Petersson, P. Y. Ayala, Q. Cui, K. Morokuma, D. K. Malick, A. D. Rabuck, K. Raghavachari, J. B. Foresman, J. Cioslowski, J. V. Ortiz, B. B. Stefanov, G. Liu, A. Liashenko, P. Piskorz, I. Komaromi, R. Gomperts, R. L. Martin, D. J. Fox, T. Keith, M. A. Al-Laham, C. Y. Peng, A. Nanayakkara, C. Gonzalez, M. Challacombe, P. M. W. Gill, B. G. Johnson, W. Chen, M. W. Wong, J. L. Andres, M. Head-Gordon, E. S. Replogle, J. A. Pople, *GAUSSIAN98*, Revision A.7, Gaussian, Inc., Pittsburgh, PA, **1998**.

[27] [27a] A. D. Becke, *Phys. Rev.* **1988**, *A38*, 3098−3100. [27b] J. P. Perdew, Y. Wang, *Phys. Rev.* **1992**, *B45*, 13244−13249. [27c] J. P. Perdew, K. Burke, Y. Wang, *Phys. Rev.* **1996**, *B54*, 16533−16539.

[28] C. Møller, M. S. Plesset, *Phys. Rev.* **1934**, *14*, 618−622.

[29] J. W. Ochterski, G. A. Petersson, J. A. Montgomery, *J. Chem. Phys.* **1996**, *104*, 2598−2619.

[30] [30a] R. Ditchfield, W. J. Hehre, J. A. Pople, *J. Chem. Phys.* **1971**, *54*, 724−728. [30b] W. J. Hehre, R. Ditchfield, J. A. Pople, *J. Chem. Phys.* **1972**, *56*, 2257−2261. [30c] P. C. Hariharan, J. A. Pople, *Mol. Phys.* **1974**, *27*, 209−214. [30d] M. S. Gordon, *Chem. Phys. Lett.* **1980**, *76*, 163−168. [30e] P. C. Hariharan, J. A. Pople, *Theor. Chim. Acta* **1973**, *28*, 213−222. [30f] T. Clark, J. Chandrasekhar, G. W. Spitznagel, P. v. R. Schleyer, *J. Comp. Chem.* **1983**, *4*, 294−301.

Received March 5, 2002
[I02115]

Si−H-Functionalized Ferriodisiloxanes: Synthesis from the Ferriodimethylsilanols $C_5R_5(OC)_2Fe-SiMe_2OH$ (R = H, Me) and Photoinduced Transformation into μ_2-Disiloxanediyl-Bridged Dinuclear Iron Complexes[‡]

Wolfgang Malisch,*[a] Marco Hofmann,[a] Günter Kaupp,[a] Harald Käb,[a] and Joachim Reising[a]

Keywords: Iron / Metallacycles / Oxidative addition / Silicon / Siloxanes

Hydrolysis of the ferriochlorosilanes $C_5R_5(OC)_2Fe–SiMe_2Cl$ [R = H (**1a**), Me (**1b**)] in the presence of Et_3N yields the corresponding ferriosilanols $C_5R_5(OC)_2Fe–SiMe_2(OH)$ (**2a** and **2b**). In addition, **2b** is also obtained by oxo-functionalization of $C_5Me_5(OC)_2Fe–SiMe_2H$ (**3**) with dimethyldioxirane. The ferriosilanol **2a** can be converted into the ferriodisiloxanes $Cp(OC)_2Fe–SiMe_2OSiR_3$ [R_3Si = $Me_2(H)Si$ (**5a**), $pTol_2(H)Si$ (**5b**), Me_3Si (**5c**) and *p*Tol(Me)(H)Si (**5d**)] by condensation with the chloro(organo)silanes R_3SiCl (**4a**–**d**). Irradiation of **5a** and **5b** results in CO elimination, followed by dimerization to give the cyclic 1,5-diferratetrasiloxanes $[\mu_2\text{-}SiMe_2OSi(R)_2]_2[Fe(H)(CO)Cp]_2$ [R = Me (**6a**) and *p*Tol (**6b**)]. Compounds **2b** and **6b** have been characterized by single-crystal X-ray structure determination.
(© Wiley-VCH Verlag GmbH, 69451 Weinheim, Germany, 2002)

Introduction

Transition metal substituted silicon compounds have attracted great attention in recent years, especially with regard to the effect of the metal component on the reactivity of the silicon unit.[2−5] In the context of our systematic studies on the reactivity of functionalized silicon−transition metal complexes[6−13] we have shown that metallosilanols with a direct M−Si bond of the general type $L_nM-Si(R)_{3-n}(OH)_n$ (n = 1−3)[14−30] are characterized by remarkably high stability towards self-condensation, due to the electron-releasing effect of the metal fragment. This property has permitted the isolation of a number of transition metal substituted silanols,[14−26] mainly of the chromium and iron groups, including examples with stereogenic metal and silicon atoms[26] and even of metallosilanediols[27,28] and -silanetriols.[29,30]

The reactivity of this special class of silanols has so far not been explored in detail. However, preliminary studies showed facile condensation with chlorosilanes as an efficient route to metallosiloxanes.[22−24,26−30] In particular, those bearing an SiH function at the γ-silicon atom offer high synthetic potential in terms of the oxidative addition of the SiH unit to electronically unsaturated metal centres to provide access to Si−O−Si-bridged dinuclear metal complexes.[27]

This was strong motivation to perform the synthesis of novel metallosilanols, especially with the well-known iron fragments $C_5R_5(OC)_2Fe$ (R = H, Me), and condensation reactions to afford the corresponding disiloxanes. Furthermore, the SiH-functional derivatives were used for photoinduced transformation, providing novel eight-membered cyclic dimetallasiloxanes.

Results and Discussion

Access to the ferriodimethylsilanols **2a** and **2b**, the precursors for synthesis of the ferriodisiloxanes, is given by two procedures − hydrolysis of chloroferriosilanes[14,18] and oxo-functionalization of ferriosilanes.[16,20]

Hydrolysis of the chloroferriodimethylsilanes **1a** and **1b** in diethyl ether in the presence of the auxiliary base Et_3N at room temperature afforded the metallated silanols **2a** and **2b** in good yields [89% (**2a**), 70% (**2b**)] [Equation (1), route a]. The C_5Me_5-substituted complex **1b** undergoes ligand exchange (48 h) significantly more slowly than the Cp compound **1a**. This difference can be associated with the reduced electrophilicity of the silicon atom, deriving from the greater electron-releasing effect of the permethylated Cp ring. Controlled Cl/OH exchange can be performed without an auxiliary base, as demonstrated for **2a**, indicating that the Fe−Si bonds in both **1a** and **2a**, in contrast to those in

[‡] Synthesis and Reactivity of Silicon Transition Metal Complexes, 51. Metallo-Silanols and Metallo-Siloxanes, 23. Part 50/22: Ref.[1]

[a] Institut für Anorganische Chemie der Universität Würzburg, Am Hubland, 97074 Würzburg, Germany
Fax: (internat.) + 49-931/888-4618
E-mail: Wolfgang.Malisch@mail.uni-wuerzburg.de

trialkylferriosilanes, are resistant towards cleavage with HCl.

In addition, the C_5Me_5-substituted ferriosilanol **2b** was obtained by oxygenation of the corresponding ferriodimethylsilane **3** with dimethyldioxirane [Equation (1), route b]. This method gave shorter reaction times and a more convenient workup procedure than the hydrolysis route. However, the yield was significantly lower (36%), presumably due to oxidation of the transition metal centre.[31]

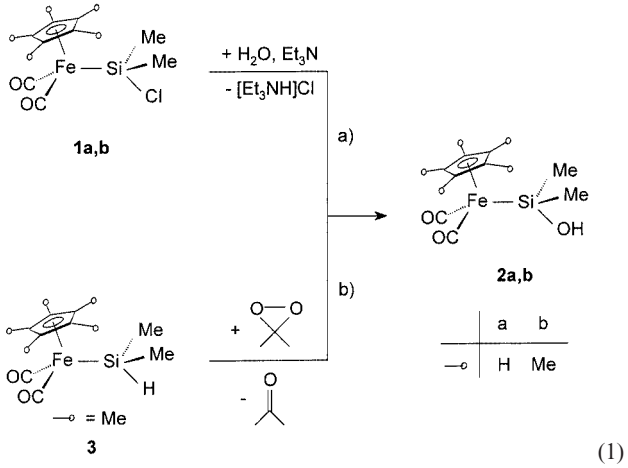

(1)

The ferriodimethylsilanols **2a** and **2b** were obtained as slightly air-sensitive, pale yellow solids, showing good solubility in all kinds of organic solvents. Compounds **2a** and **2b** did not undergo self-condensation at room temperature even in the presence of Et_3N.

In order to gain an insight into the solid-state structure of the ferriodimethylsilanols **2a** and **2b**, especially with respect to hydrogen-bonded aggregation, an X-ray structure determination of **2b** was performed. Two molecules were found in the asymmetric unit (Figure 1). For the central iron atom a pseudo-octahedral coordination sphere is indicated by the ligand−iron−ligand angles, which are close to 90°. A larger angle exists between the carbonyl carbon atoms [98.3(3)°], while those between the CO ligands and the silicon atom are diminished [83.1(2)°/84.1(2)° and 83.9(2)°/84.0(2)°]. Newman projection along the Fe−Si bond reveals a staggered conformation of the substituents, with one of the methyl groups *trans* to the C_5Me_5 ring and the OH group consequently occupying the space between the C_5Me_5 ring and one carbonyl ligand. The Fe−Si distances [2.313(2) Å and 2.319(2) Å] lie within the range observed in known iron−silicon compounds.[32,33] The Si−O bond lengths [1.676(9) Å and 1.653(6) Å] are slightly greater than those in organosilanols,[34] indicating some electronic saturation of the silicon atom by the transition metal component. The silicon atoms show a distorted tetrahedral coordination with reduced angles between the methyl and hydroxy substituents [104.8(3)−106.2(4)°] and enlarged ones to the metal component [111.6(4)−115.5(3)°]. Triorganosilanols often show interesting hydrogen-bonded superstructures, forming chains,[35,36] tetramers[37] or dimers,[38−40] depending on the steric demand of the organic substituents. A few examples show that, as far as the formation of hydrogen bonds is concerned, the transition metal components show an effect analogous to that of organic substituents, the difference being that the acidity of the OH hydrogen atom is reduced and the basicity of the oxygen atom is increased.[16,22] Compound **2b**, because of the bulkiness of the metal component, prefers hydrogen-bonded "dimerization", indicated by an oxygen−oxygen distance of 2.889 Å. This arrangement is similar to that found in $C_5Me_5(OC)_2Ru-Si(o\text{Tol})_2OH$.[22]

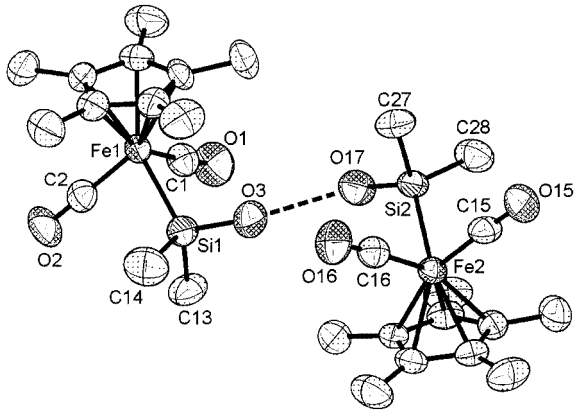

Figure 1. ORTEP Plot of **2b** (O···O bond is dashed); selected bond lengths [Å], angles [°] and torsion angles [°]: Fe1−C1 1.731(8), Fe1−C2 1.755(7), Fe1−Si1 2.313(2), O3−Si1 1.676(9), Si1−C14 1.864(7), Si1−C13 1.871(7), Fe2−C15 1.732(7), Fe2−C16 1.743(8), Fe2−Si2 2.319(2), Si2−O17 1.653(6), Si2−C28 1.864(7), Si2−C27 1.894(7); C1−Fe1−C2 98.3(3), C1−Fe1−Si1 83.1(2), C2−Fe1−Si1 84.1(2), O3−Si1−C14 105.2(5), O3−Si1−C13 106.2(4), C14−Si1−C13 104.9(4), O3−Si1−Fe1 111.6(4), C16−Fe2−C15 98.3(3), C15−Fe2−Si2 83.9(2), C16−Fe2−Si2 84.0(2), O17−Si2−C28 105.1(3), O17−Si2−C27 106.0(3), C28−Si2−C27 104.8(3), O17−Si2−Fe2 113.5(2), C28−Si2−Fe2 113.8(2), C27−Si2−Fe2 112.8(2); C1−Fe1−Si1−O3 74.0(4), C2−Fe1−Si1−O3 173.1(4), C15−Fe2−Si2−O17 −177.0(3), C16−Fe2−Si2−O17 −77.9(3)

Due to their high stabilities with respect to self-condensation, the ferriosilanols **2a** and **2b** are excellent starting materials for further reactions. Among these, condensation with chlorosilanes is of special interest for investigation of the transition metal effect on the Si−O−Si bonding system and the γ-silicon atom of the resulting ferriodisiloxanes. Treatment of **2a** with the chloro(organo)silanes **4a**−**d** in Et_2O in the presence of the auxiliary base Et_3N at room temperature afforded the ferriodisiloxanes **5a**−**d** [34% (**5c**) to 95% (**5b**) yield] after 1−12 h, these compounds being isolated as pale yellow (**5c**) or orange (**5a**, **5b**, **5d**) oils displaying high solubility in benzene and *n*-pentane [Equation (2)].

Compounds **5a** and **5d** were also obtained in the absence of triethylamine, but the reaction rate was significantly lower [70% (**5a**)/10% (**5d**) conversion after 7 d].

Comparison of the spectroscopic data of the ferriosilanol **2a** and of the ferriosiloxanes **5a**−**d** shows no significant effect concerning the $\nu(CO)_{sym}$ and $\nu(CO)_{asym}$ frequencies of the CO ligands, while for the ^{29}Si NMR resonance a high-field shift for the iron-bound silicon atom from δ = 66.05 ppm (**2a**) to δ = 58.73 (**5a**), 61.45 (**5b**) or 59.97 ppm (**5d**) is

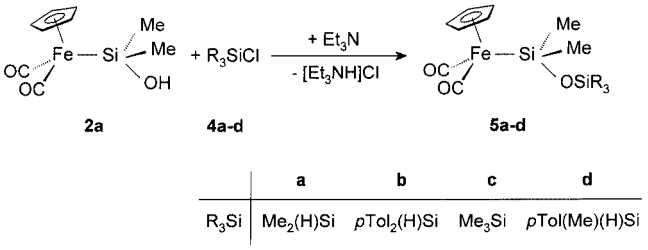

(2)

found. The $\tilde{\nu}$(SiH) absorptions of **5a**, **5b** and **5d** (2123−2112 cm^{-1}) lie in the normal range of Si−H functional organosilanes or organosiloxanes, showing that the "transition metal effect" on the silicon atom in the γ-position is negligible. This finding implies that for these systems the known reactivity behaviour of Si−H-functional silanes − photoinduced oxidative addition of SiH functions to coordinatively unsaturated metal centres, for example, resulting in the formation of M(H)−Si units − may be expected.[5] Indeed, irradiation of **5a** and **5b** with UV light in cyclohexane for 7 h/20 h resulted in controlled CO elimination, followed by Si−H addition to the iron atom. The resulting eight-membered cyclic ferriodisiloxanes **6a** and **6b** were obtained as white (**6a**) and beige (**6b**) solids in 19% (**6a**) and 10% (**6b**) yields [Equation (3)].

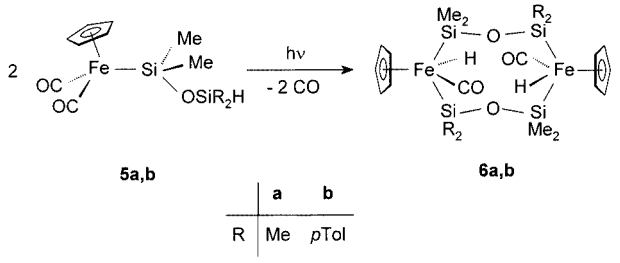

(3)

The structures of **6a** and **6b** were confirmed by the Fe−H resonance in the ^{1}H NMR at δ = −13.31 (**6a**)/−12.54 ppm (**6b**), with ^2J(HFeSi) coupling constants of 23.6 (**6a**)/24.0 Hz (**6b**) excluding agostic FeHSi interaction.[5] In addition, the ^{29}Si{^{1}H} NMR spectra show singlets at δ = 45.11 (**6a**) and 46.71 (**6b**) ppm, indicating chemical equivalence of the methyl-substituted silicon atoms.

Intramolecular cyclization to the four-membered *cyclo*-ferradisiloxanes Cp(OC)(H)Fe-($SiMe_2OSiR_2$-κ^2-Si)[41−45] can be ruled out, as shown by the X-ray structure determination of **6b**. This type of siloxane is obviously disfavoured, due to high ring strain.

Figure 2 shows that **6b** can be regarded as deriving from the well-known cyclic organotetrasiloxanes by replacement of the oxygen atoms in the 1- and 5-positions with the isolobal iron fragment Cp(OC)(H)Fe.[46]

The Fe−Si bond lengths of 2.339(1) Å (Fe1−Si1) and 2.311(1) Å (Fe1−Si2) show the expected decrease on going from the methyl- to the tolyl-substituted metal−silicon unit

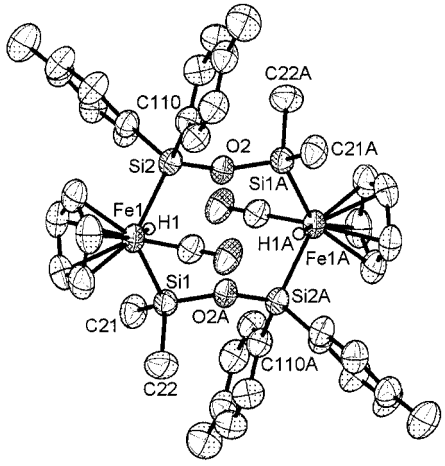

Figure 2. ORTEP Plot of **6b**; selected bond lengths [Å], angles [°] and torsion angles [°]: Fe1−Si1 2.339(1), Fe1−Si2 2.311(1), Fe1−H1 1.4644(5), Si1−O2A 1.636(2), Si2−O2 1.635(2), Si1−C21 1.868(4), Si2−C110 1.891(3); Si1−Fe1−Si2 109.43(4), Si2−Fe1−H1 55.88(3), Si1−Fe1−H1 62.03(3), C1−Fe1−H1 102.4(2), Si2−O2−Si1A 153.6(1), Fe1−Si1−O2A 110.81(9); Fe1−Si2−O2 111.75(9), Fe1−Si1−C21 116.0(2), C21−Si1−C22 107.5(3), Fe1−Si2−C110 114.4(1), Fe1−Si2−O2−Si1A −128.18(8), H1−Fe1−Si2−O2 −51.09(8), Si1−Fe1−Si2−O2 −18.29(7)

and lie within the range of known bis(silyl)iron complexes.[47,48] The Si−O distances [1.636 (Si1) and 1.635 Å (Si2)] are significantly shorter than those in four-membered *cyclo*-metalladisiloxanes {e.g., $(Ph_3P)_2$(OC)(H)Ir($SiMe_2O$-$SiMe_2$-κ^2-Si) [*d*(Si−O) = 1.690/1.678 Å][44] or (dppe)Pt(Si-Me_2OSiMe_2-κ^2-Si) [*d*(Si−O) = 1.693/1.689 Å][49]} and imply a partial double bond character for the Si−O bond.[50−55] The value of 153.6(1)° for the Si−O−Si angle is similar to that in cyclic organotetrasiloxanes.[32] The iron atoms show a pseudo-square-pyramidal arrangement, with the Cp ligand in the apical position and the two Si atoms at the tetragonal base arranged *trans* to each other [Si1−Fe1−Si2 109.43(4)°] as well as the CO and H ligands [C1−Fe1−H1 102.4(2)°]. The silicon atoms show distorted tetrahedral coordination with different Fe−Si−C angles depending on the nature of the organic ligand [114.4(1)/111.3(1)° Fe−Si−C(*p*Tol); 116.0(2)/109.2(2)° Fe−Si−C(Me)], with the Fe−Si−C(Me) angles showing stronger deviation from the ideal value.

For $(R_2SiO)_4$ rings a variety of conformations (C_i chair, C_2 boat, S_4 boat) has been found in the solid state,[32] with $(t Bu_2SiOSiMe_2O)_2$ representing an exception, due to the planarity of the ring.[56] The eight-membered $Fe_2Si_4O_2$ arrangement of **6b** adopts a chair conformation with both metal components bent in opposite directions out of the plane defined by the four silicon atoms (Figure 3). An identical situation holds for the oxygen atoms.

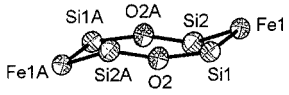

Figure 3. Chair conformation of the eight-membered ring of **6b**

Conclusions

The γ-SiH-functionalized ferriodisiloxanes presented in this paper proved to be synthetically valuable precursors for the simple synthesis of Si−O−Si-bridged homodinuclear iron complexes. Further investigation is currently being directed towards heteronuclear derivatives with metal complexes characterized by a high tendency towards oxidative addition of SiH functions, such as Pt or Ir. Another aspect concerns the introduction of hydroxy groups at the γ-silicon atom, giving access to metallosiloxanols. These compounds are of special interest for further condensation to afford transition metal fragment substituted oligosiloxanes. We regard these species as model compounds for catalytic systems immobilized on a silica surface.

Experimental Section

General Remarks: All reactions were performed under purified nitrogen. Solvents were dried by conventional procedures, distilled and saturated with N_2 prior to use. ^1H, $^{13}C\{^1H\}$ and $^{29}Si\{^1H\}$ NMR spectra were recorded with Jeol FX 90Q, Bruker AC 200 and Bruker AMX 400 spectrometers; $\delta(^{29}Si)$ chemical shifts are measured relative to external Me_4Si; $\delta(^1H)/(^{13}C)$ are reported downfield from Me_4Si, referenced to the residual proton signal (^1H) or natural-abundance carbon signal of C_6D_6 (^{13}C). Infrared spectra were recorded with a Perkin−Elmer 283 grating spectrometer. The solutions were measured in NaCl cells of 0.1 mm path length with a resolution of about 2 cm^{-1}. Melting points: differential thermal analysis (Du Pont 9000 Thermal Analysis System). Literature procedures were employed to synthesize $Cp(OC)_2Fe-SiMe_2Cl$ (**1a**)[57] and dimethyldioxirane.[58] $Me_2Si(H)Cl$ (**4a**), Me_3SiCl (**4c**), Et_3N and 18-crown-6 were obtained commercially and were distilled prior to use.

1. Chloro[dicarbonyl(η^5-pentamethylcyclopentadienyl)ferrio]dimethylsilane (1b): Me_2SiCl_2 (1680 mg, 13.03 mmol) was added to a suspension of $Na[Fe(CO)_2C_5Me_5]$ (880 mg, 3.26 mmol) in 50 mL of cyclohexane and the mixture was vigorously stirred for 40 h at room temperature. After filtration, the solvent was removed in vacuo, the red residue was extracted three times with 10 mL of *n*-pentane, and **1b** crystallized at −78 °C. Yield 410 mg (37%). Orange, microcrystalline powder. M.p. 96 °C. ^1H NMR (60 MHz, [D$_6$]benzene): δ = 1.60 [s, 15 H, $(H_3C)_5C_5$], 0.97 ppm (s, 6 H, H_3CSi). IR (*n*-pentane): $\tilde{\nu}$ = 1993 cm^{-1} (vs), 1941 (vs) [ν(CO)]. $C_{14}H_{21}ClFeO_2Si$ (340.74): calcd. C 49.35, H 6.23, Cl 10.40; found C 49.07, H 5.91, Cl 10.60.

2. [Dicarbonyl(η^5-pentamethylcyclopentadienyl)ferrio]dimethylsilane (3): The preparation was as described under 1., from $Na[Fe(CO)_2C_5Me_5]$ (700 mg, 2.59 mmol) and $Me_2Si(H)Cl$ (735 mg, 7.77 mmol) in 100 mL of cyclohexane (20 h). Further purification of **3** was performed by sublimation at 83−85 °C (10^{-2} Torr). Yield 420 mg (53%). Yellow, microcrystalline powder. M.p. 43 °C. ^1H NMR (60 MHz, [D$_6$]benzene): δ = 4.72 [sept, ^3J(HSiCH) = 3.6 Hz, 1 H, HSi], 1.50 [s, 15 H $(H_3C)_5C_5$], 0.62 ppm [d, ^3J(HCSiH) = 3.6 Hz, 6 H, $(H_3C)_2Si$]. $^{13}C\{^1H\}$ NMR (50 MHz, [D$_6$]benzene): δ = 217.27 (s, CO), 94.57 [s, $C_5(CH_3)_5$], 9.45 [s, $(CH_3)_5C_5$], 2.79 ppm [s, $(CH_3)_2Si$]. $^{29}Si\{^1H\}$ NMR (18 MHz, [D$_6$]benzene): δ = 28.36 ppm (s). IR (cyclohexane): $\tilde{\nu}$ = 2043 cm^{-1} [w, ν(SiH)], 1984 (vs), 1931 (vs) [ν(CO)]. $C_{14}H_{22}FeO_2Si$ (306.3): calcd. C 54.90, H 7.24; found C 54.72, H 6.95. MS (30 °C): *m*/*z* (%) = 306 (3) [M$^+$], 278 (36) [M − CO$^+$], 248 (26) [$C_5Me_5(CO)Fe$ − SiH$^+$], 191 (100) [$C_5Me_5Fe^+$].

3. [Dicarbonyl(η^5-cyclopentadienyl)ferrio]dimethylsilanol (2a): $Cp(OC)_2Fe-SiMe_2Cl$ (**1a**, 256 mg, 0.96 mmol), dissolved in 25 mL of Et_2O, was treated with Et_3N (144 mg, 1.44 mmol) and H_2O (100 mg, 5.55 mmol). After 45 min of stirring at room temperature, the precipitate of $[Et_3NH]Cl$ was separated, the orange solution was concentrated to dryness, and the resulting ferriosilanol was washed five times with 2 mL of *n*-pentane and dried in vacuo. Yield 215 mg (89%). Light yellow, microcrystalline powder. M.p. 45 °C (decomp.). ^1H NMR (200 MHz, [D$_6$]benzene): δ = 4.27 (s, 5 H, H_5C_5), 1.77 (br. s, 1 H, HO), 0.70 ppm (s, 6 H, H_3C). $^{29}Si\{^1H\}$ NMR (18 MHz, [D$_6$]benzene): δ = 66.05 ppm (s). IR (cyclohexane): $\tilde{\nu}$ = 3690 cm^{-1} [br, w, ν(OH)], 1998 (s), 1947 (vs) [ν(CO)]. $C_9H_{12}FeO_3Si$ (252.13): calcd. C 42.88, H 4.80; found C 42.14, H 4.79.

4. Synthesis of 2a in the Absence of an Auxiliary Base: H_2O (1000 mg, 55.6 mmol) was added to a solution of $Cp(OC)_2Fe-SiMe_2Cl$ (**1a**, 270 mg, 1.00 mmol) in Et_2O (20 mL). After 2 h of stirring at room temperature, the organic layer was separated and concentrated in vacuo. The resulting **2a** was washed twice with 2 mL of *n*-pentane and dried in vacuo. Yield 242 mg (96%).

5. [Dicarbonyl(η^5-pentamethylcyclopentadienyl)ferrio]dimethylsilanol (2b): The preparation was as described under 3., from $C_5Me_5(OC)_2Fe-SiMe_2Cl$ (**1b**, 235 mg, 0.69 mmol), H_2O (12 mg, 0.69 mmol) and Et_3N (730 mg, 7.2 mmol) (48 h). Yield 155 mg (70%). Yellow microcrystalline powder. M.p. 72 °C (decomp.). ^1H NMR (400 MHz, [D$_6$]benzene): δ = 1.55 [s, 15 H, $(H_3C)_5C_5$], 1.02 (s, 1 H, HO), 0.67 ppm [s, 6 H, $(H_3C)_2Si$]. $^{13}C\{^1H\}$ NMR (101 MHz, [D$_6$]benzene): δ = 217.62 (s, CO), 95.13 [s, $C_5(CH_3)_5$], 9.96 [s, $(CH_3)_2Si$], 9.80 ppm [s, $(CH_3)_5C_5$]. $^{29}Si\{^1H\}$ NMR (80 MHz, [D$_6$]benzene): δ = 66.83 ppm (s). IR (toluene): $\tilde{\nu}$ = 3629 cm^{-1} [w, br, ν(OH)], 1979 (vs), 1922 (vs) [ν(CO)]. $C_{14}H_{22}FeO_3Si$ (322.26): calcd. C 52.18, H 6.88; found C 52.63, H 7.15.

6. Synthesis of 2b by Oxygenation of $C_5Me_5(OC)_2Fe-SiMe_2H$ (3) with Dimethyldioxirane: A solution of dimethyldioxirane in acetone (0.10 M, 10 mL) was added dropwise at −78 °C to a solution of $C_5Me_5(OC)_2Fe-SiMe_2H$ (**3**, 265 mg, 0.87 mmol) in 20 mL of toluene. After 1 h of stirring, the mixture was allowed to warm to room temperature and the solvent was evaporated in vacuo. The orange residue was extracted with 10 mL of *n*-pentane, and **2b** crystallized at −78 °C. Yield 100 mg (36%).

7. Chlorobis(4-methylphenyl)silane (4b): A Grignard solution, freshly prepared from Mg (2.43 g, 0.1 mol) and 4-bromotoluene (1.71 g, 0.1 mol) in 50 mL of diethyl ether, was added dropwise over 1 h to a cooled solution (0 °C) of $HSiCl_3$ (6.77 g, 0.05 mol) in 100 mL of Et_2O. After the mixture had been stirred for 1 h at room temperature, the precipitate was filtered off and the resulting dark brown, oily residue was fractionally distilled. Yield 12.69 g (51%). Colourless liquid. B.p. 105−107 °C/0.01 Torr. ^1H NMR (60 MHz, [D$_6$]benzene): δ = 7.53 [d, $^3J_{HCCH}$ = 8.0 Hz, 4 H, H-3/5 of H_4C_6], 6.97 [d, $^3J_{HCCH}$ = 8.0 Hz, 4 H, H-2/6 of H_4C_6], 5.90 (s, 1 H, HSi), 1.92 ppm (s, 6 H, H_3C). IR (cyclohexane): $\tilde{\nu}$ = 2159 cm^{-1} [s, ν(SiH)].

8. 1-[Dicarbonyl(η^5-cyclopentadienyl)ferrio]-1,1,3,3-tetramethyldisiloxane (5a)

a) From $Cp(OC)_2Fe-SiMe_2OH$ (2a), $Me_2Si(H)Cl$ (4a) and Et_3N: A solution of $Cp(OC)_2Fe-SiMe_2OH$ (**2a**, 224 mg, 0.89 mmol) in 20 mL of Et_2O was treated with Et_3N (101 mg, 1.00 mmol) and $Me_2Si(H)Cl$ (**4a**, 308 mg, 2.84 mmol). After the mixture had been stirred for 1 h at room temperature, the precipitate of $[Et_3NH]Cl$

was filtered off and all volatiles were removed in vacuo. The red oily residue was extracted with 3 mL of *n*-pentane, the solvent was removed, and **5a** was dried in vacuo. Yield 218 mg (79%).

b) From $Cp(OC)_2Fe-SiMe_2OH$ (2a), NaH and $Me_2Si(H)Cl$ (4a): A cooled solution (−78 °C) of $Cp(OC)_2Fe-SiMe_2OH$ (**2a**, 100 mg, 0.40 mmol) in 10 mL of toluene was treated with NaH (10 mg, 0.40 mmol) and 18-crown-6 (10 mg) and stirred for 30 min. After addition of $Me_2Si(H)Cl$ (**4a**, 47 mg, 0.50 mmol) the mixture was allowed to warm to room temperature and stirred for another 10 min. After filtration through a Celite pad, the solvent was removed and **5a** was washed at −78 °C with 3 mL of *n*-pentane and dried in vacuo. Yield 104 mg (84%). Orange oil. M.p. −37 °C. ^{1}H NMR (400.1 MHz, [D$_6$]benzene): δ = 5.04 [sept, ^3J(HSiCH) = 2.7, $^1J_{SiH}$ = 202.0 Hz, 1 H, HSi], 4.12 (s, 5 H, H_5C_5), 0.63 (s, 6 H, H_3CSiFe), 0.23 ppm [d, ^3J(HSiCH) = 2.7 Hz, 6 H, H_3CSiH]. ^{29}Si{^{1}H} NMR (79.5 MHz, [D$_6$]benzene): δ = 58.73 (s, SiFe), −8.27 ppm (s, SiH). IR (*n*-pentane): $\tilde{\nu}$ = 2117 cm^{-1} [w, ν(SiH)], 1998 (s), 1957 (vs) [ν(CO)]. $C_{11}H_{18}FeO_3Si_2$ (310.28): calcd. C 42.58, H 5.85; found C 42.29, H 5.82.

9. 1-[Dicarbonyl(η^5-cyclopentadienyl)ferrio]-1,1-dimethyl-3,3-bis(4-methylphenyl)disiloxane (5b): The preparation was as described under 8a., from $Cp(OC)_2Fe-SiMe_2OH$ (**2a**, 699 mg, 2.77 mmol), Et_3N (722 mg, 7.14 mmol) and $(p\text{Tol})_2Si(H)Cl$ (**4b**, 1026 mg, 4.16 mmol) in 60 mL of diethyl ether (5 h). Yield 1214 mg (95%). Orange oil. M.p. −20 °C. ^{1}H NMR (400.1 MHz, [D$_6$]benzene): δ = 7.69 [d, $^3J_{HCCH}$ = 6.8 Hz, 2 H, H-3/H-5 of H_4C_6], 7.07 [d, $^3J_{HCCH}$ = 6.8 Hz, 2 H, H-2/H-6 of H_4C_6], 5.87 [s, $^1J_{SiH}$ = 211.3 Hz, 1 H, HSi], 4.13 (s, 5 H, H_5C_5), 2.11 (s, 6 H, $H_3CC_6H_4$), 0.71 ppm (s, 6 H, H_3CSi). ^{13}C{^{1}H} NMR (100.6 MHz, [D$_6$]benzene): δ = 215.42 (s, CO), 140.00 (s, C-1 of C_6H_4), 134.76 (s, C-3/C-5 of C_6H_4), 133.48 (s, C-4 of C_6H_4), 129.11 (s, C-2/C-6 of C_6H_4), 83.64 (s, C_5H_5), 21.52 (s, $CH_3C_6H_4$), 11.08 ppm (s, CH_3Si). ^{29}Si{^{1}H} NMR (79.5 MHz, [D$_6$]benzene): δ = 61.45 (s, SiFe), −22.76 ppm [s, Si(*p*Tol)$_2$H]. IR (*n*-pentane): $\tilde{\nu}$ = 2123 cm^{-1} [w, ν(SiH)], 2000 (vs), 1949 (vs) [ν(CO)], 1252 [vw, ν(SiCH$_3$)], 1042 [m, br, ν_{as}(-SiOSi)], 597 [s, ν_s(SiOSi)]. $C_{23}H_{26}FeO_3Si_2$ (462.474): calcd. C 59.73, H 5.67; found C 59.84, H 5.80.

10. 1-[Dicarbonyl(η^5-cyclopentadienyl)ferrio]-1,1,3,3,3-pentamethyldisiloxane (5c): The preparation was as described under 8a., from $Cp(OC)_2Fe-SiMe_2OH$ (**2a**, 366 mg, 1.43 mmol), Et_3N (211 mg, 2.09 mmol) and Me_3SiCl (**4c**, 244 mg, 2.25 mmol) in 15 mL of Et_2O (12 h). Further purification of **5c** was performed by distillation at 50 °C (10^{-4} Torr). Yield 153 mg (34%). Pale yellow oil. M.p. −32 °C. ^{1}H NMR (60 MHz, [D$_6$]benzene): δ = 4.21 (s, 5 H, H_5C_5), 0.63 [s, 6 H, $(H_3C)_2SiFe$], 0.19 ppm [s, 9 H, $(H_3C)_3Si$]. ^{29}Si{^{1}H} NMR (79.5 MHz, [D$_6$]benzene): δ = 55.50 (s, SiFe), 5.44 ppm (s, $SiMe_3$). IR (benzene): $\tilde{\nu}$ = 1994 cm^{-1} (vs), 1936 (vs) [ν(CO)]. $C_{12}H_{20}FeO_3Si_2$ (324.31): calcd. C 44.44, H 6.22; found C 44.90, H 5.77. MS: *m*/*z* = 324 [M$^+$].

11. 1-[Dicarbonyl(η^5-cyclopentadienyl)ferrio]-1,1,3-trimethyl-3-(4-methylphenyl)disiloxane (5d): The preparation was as described under 8a., from $Cp(OC)_2Fe-SiMe_2OH$ (**2a**, 302 mg, 1.20 mmol), Et_3N (203 mg, 2.01 mmol) and *p*Tol(Me)Si(H)Cl (**4d**, 420 mg, 2.46 mmol) in 20 mL of Et_2O (1 h). Further purification of **5d** was performed by column chromatography (20 × 2 cm, Al_2O_3, activity IV, cyclohexane). Yield 270 mg (70%). Orange oil. M.p. 4 °C. ^{1}H NMR (60 MHz, [D$_6$]benzene): δ = 7.64 [d, $^3J_{HCCH}$ = 8.5 Hz, 2 H, H-3/5 of H_4C_6], 7.12 [d, $^3J_{HCCH}$ = 8.5 Hz, 2 H, H-2/6 of H_4C_6], 5.47 [q, ^3J(HSiCH) = 2.8, $^1J_{SiH}$ = 207.0 Hz, 1 H, HSi], 4.08 (s, 5 H, H_5C_5), 2.10 (s, 3 H, $H_3CC_6H_4$), 0.68, 0.67 (2 s, 6 H, H_3CSiFe), 0.49 ppm [d, ^3J(HSiCH) = 2.8 Hz, 3 H, H_3CSiH]. ^{13}C{^{1}H} NMR (50 MHz, [D$_6$]benzene): δ = 215.49 (s, CO), 139.75 (s, C-1 of C_6H_4), 134.98 (s, C-4 of C_6H_4), 133.91 (s, C-2/6 of C_6H_4), 129.06 (s, C-3/5 of C_6H_4), 83.55 (s, C_5H_5), 21.48 (s, $CH_3C_6H_4$), 11.03 (s, CH_3SiFe), 1.02 ppm (s, CH_3SiH). ^{29}Si{^{1}H} NMR (18 MHz, [D$_6$]benzene): δ = 59.97 (s, SiFe), −15.39 ppm (s, SiH). IR (cyclohexane): $\tilde{\nu}$ = 2112 cm^{-1} [w, ν(SiH)], 1999 (s), 1947 (vs) [ν(CO)]. $C_{17}H_{22}FeO_3Si_2$ (386.38): calcd. C 52.85, H 5.74; found C 52.17, H 5.78.

12. Treatment of $Cp(OC)_2Fe-SiMe_2OH$ (2a) with $Me_2Si(H)Cl$ (4a) or *p*Tol(Me)Si(H)Cl (4d) in the Absence of an Auxiliary Base: A solution of $Cp(OC)_2Fe-SiMe_2OH$ (**2a**, 151 mg, 0.60 mmol) and either $Me_2Si(H)Cl$ (**4a**, 300 mg, 3.17 mmol) or *p*Tol(Me)Si(H)Cl (**4d**, 258 mg, 1.51 mmol) in 15 mL of Et_2O was stirred at room temperature. After 7 d, conversion into **5a/5d** was 70%/10% complete.

13. Bis(μ-1,1,3,3-tetramethyldisiloxane-1,3-diyl)bis[carbonyl(η^5-cyclopentadienyl)hydridoiron(IV)] (6a): A solution of $Cp(OC)_2Fe-SiMe_2OSiMe_2H$ (**5a**, 581 mg, 1.87 mmol) in 40 mL of cyclohexane was irradiated with UV light (quartz lamp TQ 718, 700 W, Hanau) for 7 h. After removal of the solvent in vacuo, the residue was purified by column chromatography (20 × 1 cm, silica gel, 0.063−0.2 mm, 20 °C, cyclohexane/benzene, 2:1). The eluate from the yellow zone was concentrated to dryness, the residue was stirred with 2 mL of ice-cold *n*-pentane, and the precipitate of **6a** separated and dried in vacuo. Yield: 100 mg (19%). White microcrystalline powder. M.p. 126 °C (decomp.). ^{1}H NMR (60 MHz, [D$_6$]benzene): δ = 3.94 (s, 10 H, H_5C_5), 0.80 (s, 12 H, H_3C), 0.65 (s, 12 H, H_3C), −13.31 ppm [s, ^2J(HFeSi) = 23.6 Hz, 2 H, HFe]. ^{13}C{^{1}H} NMR (50 MHz, [D$_6$]benzene): δ = 212.98 (s, CO), 82.46 (s, C_5H_5), 13.37 (s, CH_3), 12.97 ppm (s, CH_3). ^{29}Si{^{1}H} NMR (18 MHz, [D$_6$]benzene): δ = 45.31 ppm (s). IR (cyclohexane): $\tilde{\nu}$ = 1955 cm^{-1} [vs, ν(CO)], 1257 (m), 1247 (m) [ν(SiCH$_3$)], 1070 (s), 1065 (m, sh) [ν_{as}(-SiOSi)], 576 (m), 565 (m) [ν_s(SiOSi)]. $C_{20}H_{36}Fe_2O_4Si_4$ (564.542): calcd. C 42.55, H 6.43; found C 42.24, H 6.50.

14. Bis[μ-1,1-dimethyl-3,3-bis(4-methylphenyl)disiloxane-1,3-diyl]-bis[carbonyl(η^5-cyclopentadienyl)hydridoiron(IV)] (6b): The preparation was as described under 13., from $Cp(OC)_2Fe-SiMe_2OSi(p\text{Tol})_2H$ (**5b**, 998 mg, 2.16 mmol) in 40 mL of cyclohexane (20 h). Crystallization of **6b** occurred at −78 °C in *n*-pentane. Yield: 90 mg (10%). Beige, microcrystalline powder. M.p. 179 °C (decomp.). ^{1}H NMR (60 MHz, [D$_6$]benzene): δ = 8.01, 7.90 [2 d, $^3J_{HCCH}$ = 7.7/7.6 Hz, 8 H, H-3/H-5 of H_4C_6], 7.25, 7.19 [2 d, $^3J_{HCCH}$ = 7.6/7.7 Hz, 8 H, H-2/H-6 of H_4C_6], 3.93 (s, 10 H, H_5C_5), 2.26, 2.19 (2 s, 12 H, $H_3CC_6H_4$), 0.70, 0.63 (2 s, 12 H, H_3C), −12.54 ppm [s, ^2J(HFeSi) = 24.0 Hz, 2 H, HFe]. ^{13}C{^{1}H} NMR (50 MHz, [D$_6$]benzene): δ = 213.17 (s, CO), 142.97, 142.22 (2 s, C-1 of C_6H_4), 138.14, 138.03 (2 s, C-4 of C_6H_4), 135.38, 134.61 (2 s, C-3/C-5 of C_6H_4), 128.72, 128.37 (2 s, C-2/C-6 of C_6H_4), 83.99 (s, C_5H_5), 21.47, 21.43 (2 s, $CH_3C_6H_4$), 13.57, 13.17 ppm (2 s, CH_3Si). ^{29}Si{^{1}H} NMR (18 MHz, [D$_6$]benzene): δ = 46.71 ppm [s, $Si(CH_3)_2$], Si(*p*Tol)$_2$ signal not detected. IR (cyclohexane): $\tilde{\nu}$ = 1956 cm^{-1} (vs), 1945 (m, sh) [ν(CO)], 1258 [m, br, ν(SiCH$_3$)], 1051 (s, br), 1020 (m, br) [ν_{as}(SiOSi)], 574 (m), 565 (w) [ν_s(SiOSi)]. $C_{44}H_{52}Fe_2O_6Si_2$ (868.929): calcd. C 60.82, H 6.03; found C 60.85, H 5.88.

15. X-ray Crystal Structure Determination of 2b: Colourless crystals of **2b** suitable for X-ray diffraction were grown by slow diffusion of *n*-pentane into a benzene solution of **2b** at room temperature. Crystal data: $C_{28}H_{44}Fe_2O_6Si_2$, *M* = 644.52, monoclinic, space group $P2_1$ (no. 5), *a* = 9.042(10) Å, *b* = 13.941(5) Å, *c* = 13.125(9) Å, β = 104.14(4)°, *V* = 1604.2(22) Å^3, *Z* = 4, $d_{calcd.}$ = 1.334

g·cm^{-3}, CAD4 diffractometer (Enraf−Nonius), radiation type: Mo-K_α, wavelength: λ = 0.71073 Å, graphite monochromator, crystal size: 0.19 × 0.10 × 0.07 mm, temperature: 293 K, ω/Θ-scan, scale range: 1.60° < Θ < 22.50°, $F(000)$ = 680, total reflections: 2373, independent reflections: 2211 with $I > 2.0\sigma(I)$, absorption coefficient: μ = 1.018 mm^{-1}, empirical absorption correction ($T_{min.}/T_{max.}$ = 0.8779/0.9978), structure solution: SHELXS-86[59] by direct methods, structure refinement: SHELXL-93[60] (369 parameters), R_1 = 0.0293, wR_2 = 0.0683. The positions of the OH hydrogen atoms were located and isotropically refined, while the remaining hydrogen atoms were geometrically positioned and subsequently refined with a riding model. CCDC-158196 contains the supplementary crystallographic data for this compound. These data can be obtained free of charge at www.ccdc.cam.ac.uk/conts/retrieving.html or from the Cambridge Crystallographic Data Centre, 12, Union Road, Cambridge CB2 1EZ, UK [Fax: (internat.) + 44-1223/336-033; E-mail: deposit@ccdc.cam.ac.uk].

16. X-ray Crystal Structure Determination of 6b: Pale yellow crystals of **6b** suitable for X-ray diffraction were grown by slow diffusion of *n*-pentane into a toluene solution of **6b** at −35 °C. Crystal data: $C_{26}H_{31}FeO_2Si_2$, M = 487.54, triclinic, space group: $P\bar{1}$ (no. 2), a = 8.882(3) Å, b = 9.241(6) Å, c = 15.243(9) Å, α = 87.423(12)°, β = 79.07(2)°, γ = 86.49(2)°, V = 1225.5(11) Å^3, Z = 2, $d_{calcd.}$ = 1.321 g·cm^{-3}, CAD4 diffractometer (Enraf−Nonius), radiation type: Mo-K_α, wavelength: λ = 0.71073 Å, graphite monochromator, crystal size: 0.50 × 0.40 × 0.20 mm, temperature: 293 K, ω/Θ-scan, scale range: 2.20° < Θ < 26.91°, $F(000)$ = 514, total reflections: 5545, independent reflections: 4314 with $I > 2\sigma(I)$, absorption coefficient: μ = 0.735 mm^{-1}, empirical absorption correction (T_{min}/T_{max} = 0.9433/0.9965), structure solution: SHELXS-86[59] by direct methods, structure refinement: SHELXL-93[60] (371 parameter), R_1 = 0.0405, wR_2 = 0.1189. The positions of all hydrogen atoms except those of the *p*Tol methyl groups were located and isotropically refined, while the remaining hydrogen atoms were geometrically positioned and subsequently refined with a riding model. In addition, one toluene molecule with a disordered CH_3 group was found in the unit cell. CCDC-158197 contains the supplementary crystallographic data for this compound. These data can be obtained free of charge at www.ccdc.cam.ac.uk/conts/retrieving.html or from the Cambridge Crystallographic Data Centre, 12, Union Road, Cambridge CB2 1EZ, UK [Fax: (internat.) + 44-1223/336-033; E-mail: deposit@ccdc.cam.ac.uk].

Acknowledgments

We gratefully acknowledge financial support from the Deutsche Forschungsgemeinschaft (Schwerpunktprogramm "Spezifische Phänomene in der Siliciumchemie") as well as from the Fonds der Chemischen Industrie.

[1] W. Malisch, M. Vögler, D. Schumacher, M. Nieger, *Organometallics*, **2002**, *21*, 2891−2897.
[2] B. J. Aylett, *Adv, Inorg. Chem. Radiochem.* **1982**, *25*, 1−133.
[3] T. D. Tilley in *The Chemistry of Organic Silicon Compounds* (Eds.: S. Patai, Z. Rappoport), J. Wiley & Sons Ltd., New York, **1989**, chapter 24.
[4] J. Y. Corey, *J. Organomet. Chem.* **1986**, *313*, 1−140.
[5] J. Y. Corey, J. Braddock-Wilking, *Chem. Rev.* **1999**, *99*, 175−292.
[6] W. Malisch, M. Kuhn, *Chem. Ber.* **1974**, *107*, 2835−2851.
[7] W. Malisch, *Chem. Ber.* **1974**, *107*, 3835−3849.
[8] W. Malisch, W. Ries, *Chem. Ber.* **1979**, *112*, 1304−1315.
[9] S. Schmitzer, U. Weis, H. Käb, W. Buchner, W. Malisch, T. Polzer, U. Posset, W. Kiefer, *Inorg. Chem.* **1993**, *32*, 303−309.
[10] W. Malisch, R. Lankat, S. Schmitzer, R. Pikl, U. Posset, W. Kiefer, *Organometallics* **1995**, *14*, 5622−5627.
[11] W. Malisch, S. Möller, O. Fey, H.-U. Wekel, R. Pikl, U. Posset, W. Kiefer, *J. Organomet. Chem.* **1996**, *507*, 117−124.
[12] W. Malisch, R. Lankat, W. Seelbach, J. Reising, M. Noltemeyer, R. Pikl, U. Posset, W. Kiefer, *Chem. Ber.* **1995**, *128*, 1109−1115.
[13] W. Malisch, H. Jehle, S. Möller, G. Thum, J. Reising, A. Gbureck, V. Nagel, C. Fickert, W. Kiefer, M. Nieger, *Eur. J. Inorg. Chem.* **1999**, 1597−1605.
[14] C. S. Cundy, M. F. Lappert, C. K. Yuen, *J. Chem. Soc., Dalton Trans.* **1978**, 427−433.
[15] L. S. Chang, M. P. Johnson, M. J. Fink, *Organometallics* **1991**, *10*, 1219−1221.
[16] W. Adam, U. Azzena, F. Prechtl, K. Hindahl, W. Malisch, *Chem. Ber.* **1992**, *125*, 1409−1411.
[17] H. Handwerker, C. Leis, R. Probst, P. Bissinger, A. Grohmann, P. Kiprof, E. Herdtweck, J. Bluemel, N. Auner, C. Zybill, *Organometallics* **1993**, *12*, 2162−2176.
[18] W. Malisch, S. Schmitzer, G. Kaupp, K. Hindahl, H. Käb, U. Wachtler, in *Organosilicon Chemistry: From Molecules to Materials*, vol. 1 (Eds.: N. Auner, J. Weis), VCH, Weinheim, **1994**, p. 185.
[19] W. Malisch, S. Schmitzer, R. Lankat, M. Neumayer, F. Prechtl, W. Adam, *Chem. Ber.* **1995**, *128*, 1251−1255.
[20] W. Malisch, K. Hindahl, H. Käb, J. Reising, W. Adam, F. Prechtl, *Chem. Ber.* **1995**, *128*, 963−965.
[21] R. Goikhman, M. Aizenberg, H.-B. Kraatz, D. Milstein, *J. Am. Chem. Soc.* **1995**, *117*, 5865−5866.
[22] S. Möller, O. Fey, W. Malisch, W. Seelbach, *J. Organomet. Chem.* **1996**, *507*, 239−244.
[23] W. Malisch, S. Möller, R. Lankat, J. Reising, S. Schmitzer, O. Fey, in *Organosilicon Chemistry II: From Molecules to Materials* (Eds.: N. Auner, J. Weis), VCH, Weinheim, **1996**, p. 575.
[24] W. Malisch, H. Jehle, C. Mitchel, W. Adam, *J. Organomet. Chem.* **1998**, *566*, 259−262.
[25] S. H. A. Petri, D. Eikenberg, B. Neumann, H.-G. Stammler, P. Jutzi, *Organometallics* **1999**, *18*, 2615−2618.
[26] W. Malisch, M. Neumayer, O. Fey, W. Adam, R. Schuhmann, *Chem. Ber.* **1995**, *128*, 1257−1260.
[27] W. Malisch, R. Lankat, O. Fey, J. Reising, S. Schmitzer, *J. Chem. Soc., Chem. Commun.* **1995**, 1917−1919.
[28] W. Malisch, H. Jehle, S. Möller, C. S. Möller, W. Adam, *Eur. J. Inorg. Chem.* **1998**, 1585−1587.
[29] C. E. F. Rickard, W. R. Roper, D. M. Salter, L. J. Wright, *J. Am. Chem. Soc.* **1992**, *114*, 9682−9683.
[30] W. Malisch, R. Lankat, S. Schmitzer, J. Reising, *Inorg. Chem.* **1995**, *34*, 5701−5702.
[31] S. Wolowiec, J. K. Kochi, *Inorg. Chem.* **1991**, *30*, 1215−1221.
[32] W. S. Sheldrick, in *The Chemistry of Organic Silicon Compounds*, part 1 (Eds.: S. Patai, Z. Rappoport), J. Wiley & Sons Ltd., New York, **1989**, chapter 3.
[33] H. Kobayashi, K. Ueno, H. Ogino, *Organometallics* **1995**, *14*, 5490−5492.
[34] P. D. Lickiss, *Adv. Inorg. Chem.* **1995**, *42*, 147−262.
[35] M. Haque, W. Horne, S. E. Cremer, C. S. Blankenship, *J. Chem. Soc., Perkin Trans. 2* **1983**, 395−398.
[36] J. D. Buynak, J. B. Strickland, G. W. Lamb, D. Khasnis, S. Modi, D. Williams, H. Zhang, *J. Org. Chem.* **1991**, *56*, 7076−7083.
[37] H. Puff, K. Braun, H. Reuter, *J. Organomet. Chem.* **1991**, *409*, 119−129.
[38] A. Rengstl, U. Schubert, *Chem. Ber.* **1980**, *113*, 278−288.
[39] Z. H. Aiube, N. H. Buttrus, C. Eaborn, P. B. Hitchcock, J. A. Zora, *J. Organomet. Chem.* **1985**, *292*, 177−188.

[40] A. I. Al-Mansour, S. S. Al-Juaid, C. Eaborn, P. B. Hitchcock, *J. Organomet. Chem.* **1994**, *480*, 139−143.
[41] M. D. Curtis, J. Greene, *J. Am. Chem. Soc.* **1978**, *100*, 6362−6367.
[42] M. D. Curtis, P. S. Epstein, *Adv. Organomet. Chem.* **1981**, *19*, 213−255.
[43] J. Greene, M. D. Curtis, *J. Am. Chem. Soc.* **1977**, *99*, 5176−5177.
[44] M. D. Curtis, J. Greene, W. M. Butler, *J. Organomet. Chem.* **1978**, *164*, 371−380.
[45] W. A. Gustavson, P. S. Epstein, M. D. Curtis, *J. Organomet. Chem.* **1982**, *238*, 87−97.
[46] R. Hoffmann, *Angew. Chem.* **1982**, *94*, 725−739; *Angew. Chem. Int. Ed. Engl.* **1982**, *21*, 711−725.
[47] L. Manojlovic−Muir, K. W. Muir, J. A. Ibers, *Inorg. Chem.* **1970**, *9*, 447−452.
[48] R. A. Smith, M. J. Bennett, *Acta Crystallogr., Sect. B* **1977**, *33*, 1118−1122.
[49] E. K. Pham, R. West, *Organometallics* **1990**, *9*, 1517−1523.
[50] T. J. Barton, R. West, *J. Chem. Educ.* **1980**, *57*, 165−169, and cited references.
[51] S. Shambayati, J. F. Blake, S. G. Wierschke, W. L. Jorgensen, S. L. Schreiber, *J. Am. Chem. Soc.* **1990**, *112*, 697−703, and cited references.
[52] H. Bock, *Angew. Chem.* **1989**, *101*, 1659−1682; *Angew. Chem. Int. Ed. Engl.* **1989**, *28*, 1627−1650.
[53] H.-D. Höltje, T. Busch, *Dtsch. Apoth. Ztg.* **1986**, *38*, 2007−2011.
[54] R. A. Jackson, *J. Organomet. Chem.* **1979**, *166*, 17−19.
[55] M. D. Healy, A. R. Barron, *J. Organomet. Chem.* **1990**, *381*, 165−172.
[56] E. Egert, M. Haase, U. Klingebiel, C. Lensch, D. M. Schmidt, G. M. Sheldrick, *J. Organomet. Chem.* **1986**, *315*, 19−25.
[57] W. Malisch, M. Kuhn, *Chem. Ber.* **1974**, *107*, 979−995.
[58] W. Adam, J. Bialas, L. Hadajiarapoglou, *Chem. Ber.* **1991**, *124*, 2377.
[59] G. M. Sheldrick, *SHELXS-86, Program for crystal structure solution*, University of Göttingen, **1986**.
[60] G. M. Sheldrick, *SHELXL-93, Program for crystal structure refinement*, University of Göttingen, **1993**.

Received March 15, 2002
[I02132]

Synthesis, Structural Characterization and Reactivity of the (Ferriomethyl)silanols $C_5R_5(OC)_2Fe-CH_2-SiMe(R')OH$ (R = H, Me; R′ = Me, Ph)[‡]

Wolfgang Malisch,*[a] Marco Hofmann,[a] Martin Nieger,[b] Wolfgang W. Schöller,[c] and Andreas Sundermann[c]

Keywords: Silicon / Iron / Oxygenation / (Metalloalkyl)silanols / Density functional calculations

The novel (ferriomethyl)-substituted silanols $C_5R_5(OC)_2Fe–CH_2–SiMe(R')OH$ [R = H, R′ = Me (**4a**), Ph (**4b**); R = Me, R′ = Me (**4c**)] are obtained by hydrolysis of the chloro(ferriomethyl)silanes $C_5R_5(OC)_2Fe–CH_2–SiMe(R')Cl$ [R = H, R′ = Me (**3a**), Ph (**3b**); R = Me, R′ = Me (**3c**)] in the presence of Et_3N. Another access to this class of compounds is offered by the oxygenation of Si–H-functional (ferriomethyl)silanes with dimethyldioxirane, as shown for **4a** by the oxo-functionalization of the (ferriomethyl)silane $Cp(OC)_2Fe–CH_2–SiMe_2H$ (**3d**). **4a–c** have been characterized spectroscopically and by X-ray structure analyses showing the formation of tube- or chain-like arrangements in the solid state caused by hydrogen bonding. In addition, the bonding situation in the related (ferriomethyl)silanol $Cp(OC)_2Fe–CH_2–SiH_2OH$ has been analyzed on the basis of density functional calculations. **4a** shows self-condensation to give the 1,3-bis(ferriomethyl)disiloxane $[Cp(OC)_2Fe–CH_2–SiMe_2]_2O$ (**5**), which is also obtained by the reaction of **4a** with **3a**. Analogous treatment of **4a** with the chloro(organo)silanes R(R′)Si(Me)Cl (R = H, R′ = Me, *p*-Tol; R = R′ = Me) yields the monometalated disiloxanes $Cp(OC)_2Fe–CH_2–Si(Me)_2OSi(Me)(R)R'$ [R = H, R′ = Me (**6a**), *p*-Tol (**6b**); R = R′ = Me (**6c**)].

(© Wiley-VCH Verlag GmbH, 69451 Weinheim, Germany, 2002)

Introduction

Transition metal substituted siloxanes represent attractive model compounds for catalytically active transition metal complexes anchored on silica surfaces.[2–5] They offer an opportunity to determine the reaction mechanisms of heterogeneous catalyzed reactions on a molecular level in order to improve the selectivity, activity and lifetime of a heterogeneous catalyst. As a consequence many of those model compounds have been synthesized in the last few years often starting from stable organosilanetriols[6–10] or incompletely condensed silsesquioxanes[11–18] which can react with various metal complexes resulting in the formation of metallosiloxanes with the structural unit $L_nM-O-Si$, i.e. a silanolate ligand sphere around the transition metal centre.

Another approach to transition metal substituted siloxanes involves the synthesis of metallosilanols of the general type $L_nM-Si(R)_{3-n}(OH)_n$ (n = 1–3)[19–34] and their extensive condensation with chlorosilanes giving access to metallosiloxanes with a direct metal–silicon bond. In this context, metallosilanols containing the metal fragments $C_5R_5(OC)_2(Me_3P)M$ (M = Mo, W; R = H, Me),[19–24] $C_5R_5(OC)_2M$ (M = Fe, Ru; R = H, Me),[23–27] $(Ph_3P)_2(OC)(Cl)Os$,[28] $(OC)_5Cr$,[29] (dcpe)(Ph)Pt,[30] $(Et_3P)_2(Cl)(H)Ir$[33] and $Cp_2(H)Mo$[34] have been realized. Due to the strong electron-releasing effect of the metal fragment the acidity of the Si–OH proton and the tendency towards self-condensation are strongly decreased. This situation offers the possibility of isolating metal derivatives with an $Si(OH)_3$ unit,[20,28] which are synthetically useful for the generation of well-defined metallosiloxanes by controlled co-condensation processes.

In recent years, two routes – hydrolysis of chloro(metallo)silanes in the presence of an auxiliary base[23–25] and oxo-functionalization of hydrido(metallo)silanes with the mild oxidizing agent dimethyldioxirane[31,32,35–37] – proved to be most efficient for the generation of metallosilanols. The electrophilic oxygen insertion is especially productive for metallosilanes with electron-rich Si–H bonds provided by metal fragments with high donor capacity. For these sys-

[‡] Synthesis and Reactivity of Silicon Transition Metal Complexes, 52. Metallosilanols and Metallosiloxanes, 24. Part 51/23: Ref.[1]

[a] Institut für Anorganische Chemie der Universität Würzburg, Am Hubland, 97074 Würzburg, Germany
Fax: (internat.) + 49-(0)931/888-4618
E-mail: Wolfgang.Malisch@mail.uni-wuerzburg.de
[b] Institut für Anorganische Chemie der Universität Bonn, Gerhard-Domagk-Straße 1, 53121 Bonn, Germany
[c] Fakultät für Chemie der Universität Bielefeld, Postfach 100131, 33501 Bielefeld, Germany
E-mail: Wolfgang.Schoeller@uni-bielefeld.de

tems the hydrolysis of the analogous chloro(metallo)silanes fails since the electrophilicity of the silicon atom is too weak.

Our interest has now turned to silanols having the Si−OH moiety separated from the metal fragment by a methylene group in order to check the "transition metal effect" on silanol units that are not directly bound to the transition metal atom. The spacer group should also help to suppress undesirable decomposition reactions involving "β-hydrogen abstraction" from the Si−OH group, observed for ferriosilanols of the type $Cp(OC)_2Fe-Si(R)(R')OH$ (R, R′ = alkyl, aryl).[38]

Although the Me_3SiCH_2 ligand has found wide application in transition metal chemistry due to its inertness with respect to β-hydride abstraction,[39−41] only a few examples exist in the literature with a silylmethyl ligand having one or more functional groups at the silicon atom.[42−52] These compounds have been used as precursors in the synthesis of silene transition metal complexes, which were originally proposed by Pannell[42] as intermediates in the β-elimination reaction of $Cp(OC)_2Fe-CH_2-SiMe_2H$ and were spectroscopically observed by Wrighton et al. by low-temperature near-UV photolysis of $C_5R_5(OC)_3W-CH_2-SiMe_2H$ (R = H, Me)[46] and $C_5Me_5(OC)_2Fe-CH_2-SiMe_2H$.[47] The chloro-functional (silylmethyl)tungsten complex $Cp_2W(Cl)-CH_2-SiMe_2Cl$ has been used by Berry et al. to generate a stable silene transition metal complex by reductive dechlorination with magnesium.[48]

No attempts so far have been made to generate or isolate any (metallomethyl)-substituted silanols from these silicon-functional complexes. Here we report on the synthesis of the first (ferriomethyl)-substituted silanols bearing a methylene group between the silanol and the iron fragment.

Results and Discussion

Synthesis of Si−Cl- and Si−H-Functional (Ferriomethyl)silanes (3a−d)

The chloro-functional (ferriomethyl)silanes $C_5R_5(OC)_2Fe-CH_2-SiMe(R')Cl$ [R = H, R′ = Me (**3a**), Ph (**3b**); R = Me, R′ = Me (**3c**)] are obtained by nucleophilic metallation of the organosilanes $ClCH_2SiMe(R')Cl$ [R′ = Me (**2a**); Ph (**2b**)] with the sodium ferrates $Na[Fe(CO)_2C_5R_5]$ [R = H (**1a**), Me (**1b**)] in THF or cyclohexane after reaction periods of 16−36 h at room temperature (Scheme 1).[53] The heterogeneous method using cyclohexane as a solvent proved to be advantageous over the homogeneous one using THF because of the formation of considerable amounts of undesirable by-products in the latter case.

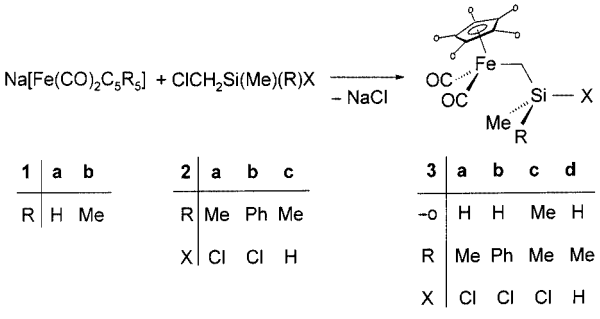

Scheme 1. Synthesis of the (ferriomethyl)silanes **3a−d**

In the synthesis of **3a**,**b** metallation of **2a**,**b** occurs primarily at the silicon atom. The initially formed ferriosilanes $Cp(OC)_2Fe-SiMe(R')(CH_2Cl)$ [R′ = Me (**3a′**), Ph (**3b′**)] can be subsequently converted into the chloro(ferriomethyl)-silanes **3a**,**b** by thermal rearrangement at 120 °C. In the case of **3a** this rearrangement is nearly quantitative after 1 h,[44,45] whereas in the other case a mixture of the two isomers is produced after heating for 3 h (**3b**/**3b′** ≈ 80:20), from which **3b** can be separated by crystallization at −78 °C from *n*-pentane. Prolonged heating and a higher temperature lead to extensive decomposition of **3b**.

In the metallation of **2a** with the pentamethylcyclopentadienyl-substituted ferrate **1b** no isomer of **3c** is detected; **3c** is obtained directly at room temperature after appropriate workup in a moderate yield of 33% due to the formation of considerable amounts of $C_5Me_5(OC)_2Fe-Cl$, which are removed by repeated fractional crystallization at −20 °C.

The Si−H-functional (ferriomethyl)silane **3d** is obtained analogously by nucleophilic metallation of $ClCH_2SiMe_2H$ (**2c**) with **1a** in THF.[42,43]

Synthesis of (Ferriomethyl)silanols (4a−c)

The (ferriomethyl)silanol $Cp(OC)_2Fe-CH_2-SiMe_2OH$ (**4a**) is available by hydrolysis of **3a** in diethyl ether in the presence of the auxiliary base Et_3N. It can be isolated after 2 h at room temperature in 89% yield (Scheme 2, route a). A second approach to **4a** involves oxygenation of **3d** with dimethyldioxirane in acetone after 2 h (−78 °C to room temp.) in 67% yield (Scheme 2, route b). The oxygenation route guarantees a more convenient workup procedure but proved to be inferior to the hydrolysis route with respect to the lower yield of the resulting silanol **4a**, presumably due to oxidative decomposition reactions at the metal fragment.

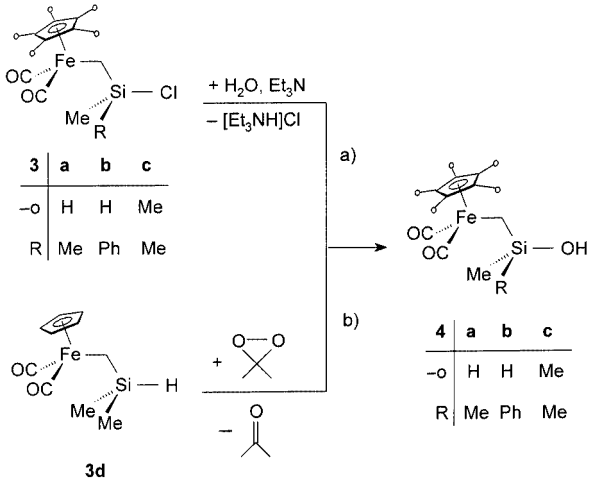

Scheme 2. Synthesis of the (ferriomethyl)silanols **4a−c** by hydrolysis or oxygenation

For the synthesis of the (ferriomethyl)silanols $C_5R_5(OC)_2Fe-CH_2-Si(Me)(R')OH$ [R = H, R′ = Ph (**4b**); R = Me, R′ = Me (**4c**)] only the hydrolysis route (Scheme 2, route a) has been applied; **4b**,**c** can be isolated after reaction periods of 4 h at room temperature in the presence of Et_3N in yields of 74% (**4b**) and 40% (**4c**), respectively.

The (ferriomethyl)silanols **4a**−**c** are obtained as slightly air-sensitive yellow-brown waxy solids [m.p. 38 °C (**4a**), to 89 °C (**4c**)], which show good solubility in diethyl ether and aromatic solvents like benzene and toluene and are rather soluble even in aliphatic solvents like *n*-pentane. They are characterized in the IR spectrum by the OH stretching band at $\tilde{\nu}$ = 3698 cm^{-1} (**4a**), 3682 cm^{-1} (**4b**) and 3703 cm^{-1} (**4c**) (*n*-pentane solution), and in the ^1H NMR spectrum (C_6D_6) by a broad signal for the hydroxy proton at δ = 0.95 (**4a**), 1.28 (**4b**) and 0.92 (**4c**) ppm. The characteristic upfield signal of the CH_2 protons is detected at δ = −0.42 (**4a**) and −0.62 (**4c**) ppm. In the case of **4b**, the asymmetric silicon atom leads to diastereotopic CH_2 protons which are detected as pair of doublets at δ = −0.09 and −0.38 ppm. In the ^{13}C NMR spectra the signals for the CH_2 group are observed between δ = −12.4 (**4c**) and −24.5 (**4b**) ppm. The chemical shifts in the ^{29}Si NMR spectra [δ = 21.8 (**4a**), 11.7 (**4b**), 21.1 (**4c**) ppm] reveal a decreased influence of the transition metal fragment on the silicon atom in the β-position. For example, in the case of **4a**, the signal is shifted by approximately 44 ppm to a higher field compared with its counterpart $Cp(OC)_2Fe-SiMe_2OH$ (δ = 66.1 ppm)[1] without a methylene bridge.

X-ray Analyses of 4a−c

Final evidence for the structural assignments of **4a**−**c** is given by single-crystal X-ray structure determinations (Figures 1−3). In the case of **4a**, two crystallographically independent molecules have been found in the asymmetric unit.

The crystal structures of **4a**−**c** reveal a pseudo-octahedral coordination sphere at the iron atom, indicated by the ligand−iron−ligand angles close to 90°. The largest one is in all cases found between the carbonyl carbon atoms lying between 97.52(9)° (**4c**) and 93.15(7)° (**4a**), while the angles between the methylene carbon atom and the CO ligands are slightly smaller [92.00(8)° (**4c**), to 85.94(7)° (**4a**)].

The conformation along the iron−methylene bond reveals a distorted staggered pseudo-ethane arrangement. In the case of **4a**,**b** the SiR_3 substituent adopts a nearly "*anti*" position to one of the CO groups [C2−Fe1−C8−Si1 164.21(11)/150.30(11)° (**4a**), −161.32(11)° (**4b**)] and is positioned between the cyclopentadienyl and the other carbonyl ligand, but as the dihedral angles indicate in the case of **4a**, that a major difference exists concerning the orientation in the two different molecules of the asymmetric unit (see also below).

Looking at **4c**, the silanol group is positioned between the two carbonyl ligands [C1B−Fe1−C11−Si1 41.70(12)°; C1A−Fe1−C11−Si1 −55.91(12)°] in a mutually "*anti*" position to the pentamethylcyclopentadienyl group, which is in sharp contrast to **4a**,**b** and probably a consequence of the higher steric demand of the C_5Me_5 ligand.

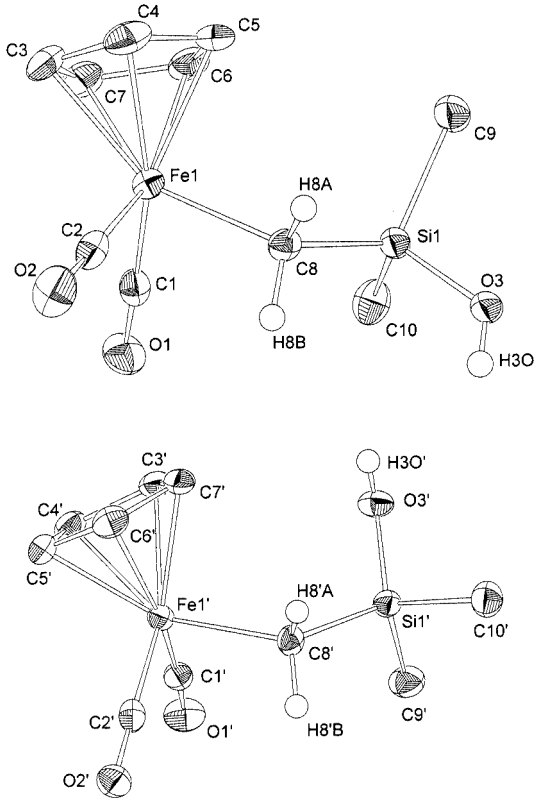

Figure 1. ORTEP view of $Cp(OC)_2Fe-CH_2-SiMe_2OH$ (**4a**), showing the two crystallographically independent molecules; hydrogen atoms have been omitted for clarity (except for those at C8 and O3); selected bond lengths [Å] and angles [°]: Fe1−Cp(Z) 1.728(2)/1.730(2), Fe1−C8 2.0896(16)/2.0863(17), C8−Si1 1.8451(17)/1.8508(16), Si1−O3 1.6599(13)/1.6558(13), Si1−C10 1.8596(19)/1.8686(19), Si1−C9 1.8668(17)/1.8508(18); C1−Fe1−C2 93.61(8)/93.15(7), C1−Fe1−C8 89.38(8)/92.32(8), C2−Fe1−C8 87.20(7)/85.94(7), Cp(Z)−Fe1−C1 126.8(2)/126.3(2), Cp(Z)−Fe1−C2 125.1(1)/126.5(1), Cp(Z)−Fe1−C8 123.4(1)/121.6(1), Fe1−C8−Si1 120.36(8)/120.51(8), C8−Si1−O3 108.41(7)/114.90(7), C9−Si1−O3 102.63(7)/104.03(8); selected torsion angles [°]: Fe1−C8−Si1−O3 −174.24(8)/40.09(12), C1−Fe1−C8−Si1 70.57(11)/57.31(11), Fe1−C8−Si1−C9 71.72(12)/−77.92(12)

The lengths of the iron−methylene bonds lie in a close range between 2.0931(18) (**4b**) and 2.0775(16) Å (**4c**) and are similar to other $C_5R_5(OC)_2Fe-CR_3$ complexes bearing an sp^3-carbon atom at the iron atom.[54−56]

The Fe−C−Si bond angle is in all cases wider than the tetrahedral angle and is up to 124.89(9)° for **4c**, which is in agreement with a higher s-character of the carbon orbital interactions with the more electropositive iron and silicon atoms according to Bent's rule,[57,58] but also shows the higher steric demand of the iron and silanol groups in comparison to the H atoms at the methylene carbon atom. This finding parallels that for the complexes $Cp(OC)(Ph_3P)Fe-CH_2-SiMe_3$ [Fe−C−Si 122.8(2)°],[59] $Cp(OC)_2Fe-CH_2-SiMe_2-SiMe_2-Fe(CO)_2Cp$ [Fe−C−Si 123.4(2)°][60] and *meso*-$[Cp(OC)_2Fe-CH_2-Si(Me)(Ph)]_2$ [Fe−C−Si 120.5(1)°][61] which, to the best of our know-

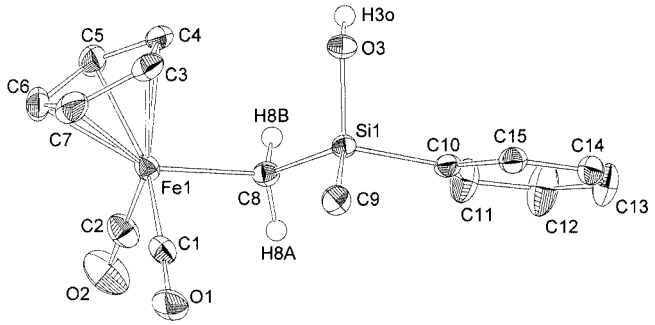

Figure 2. ORTEP view of $Cp(OC)_2Fe-CH_2-Si(Me)(Ph)OH$ (**4b**); hydrogen atoms have been omitted for clarity (except for those at C8 and O3); selected bond lengths [Å] and angles [°]: Fe1−Cp(Z) 1.734(1), Fe1−C8 2.0931(18), C8−Si1 1.8464(18), Si1−O3 1.6645(13), Si1−C9 1.8598(18), Si1−C10 1.8825(19); C1−Fe1−C2 93.38(9), C1−Fe1−C8 90.98(8), C2−Fe1−C8 86.42(8), Cp(Z)−Fe1−C1 126.2(1), Cp(Z)−Fe1−C2 126.2(1), Cp(Z)−Fe1−C8 122.4(1), Fe1−C8−Si1 116.14(9), C8−Si1−O3 112.18(7), C9−Si1−O3 104.72(8), C8−Si1−C9 114.89(8), O3−Si1−C10 105.80(7); selected torsion angles [°]: Fe1−C8−Si1−O3 −67.89(10), Fe1−C8−Si1−C10 173.59(8), C1−Fe1−C8−Si1 −68.00(10), Fe1−C8−Si1−C9 51.55(12)

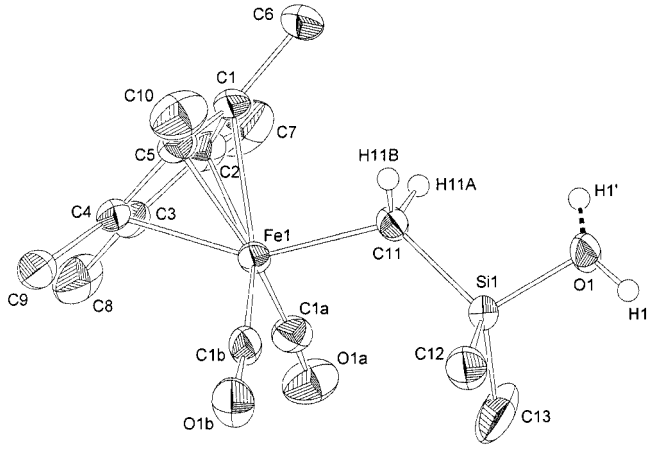

Figure 3. ORTEP view of $C_5Me_5(OC)_2Fe-CH_2-SiMe_2OH$ (**4c**); hydrogen atoms have been omitted for clarity (except for those at C11 and O1); selected bond lengths [Å] and angles [°]: Fe1−C_5Me_5(Z) 1.759(2), Fe1−C11 2.0775(16), C11−Si1 1.8477(17), Si1−O1 1.6589(12), Si1−C12 1.859(2), Si1−C13 1.865(2); C1B−Fe1−C1B 97.52(9), C1B−Fe1−C11 92.17(7), C1A−Fe1−C11 92.00(8), C_5Me_5(Z)−Fe1−C1A 122.2(1), C_5Me_5(Z)−Fe1−C1B 124.1(1), C_5Me_5(Z)−Fe1−C11 120.7(1), Fe1−C11−Si1 124.89(9), C11−Si1−O1 106.66(7), C12−Si1−O1 106.39(8), C11−Si1−C12 113.72(9), O1−Si1−C13 107.53(10), C11−Si1−C13 114.29(10), C12−Si1−C13 107.78(13); selected torsion angles [°]: C1B−Fe1−C11−Si1 41.70(12), C1A−Fe1−C11−Si1 −55.91(12), Fe1−C11−Si1−O1 169.61(10), Fe1−C11−Si1−C12 −73.43(13), Fe1−C11−Si1−C13 50.93(16)

ledge, are the only other structurally characterized compounds with a $CpL_2Fe-CH_2-SiR_3$ (L = CO, PPh_3) moiety.

The Si−O bond lengths with values between 1.6645(13) (**4b**) and 1.6558(13) Å (**4a**) are nearly identical and lie within the range of other organo- and metallo-substituted silanols.[19−34,62−65] The silicon atom shows in all cases a distorted tetrahedral arrangement of substituents with the expected smaller angle between the OH and CH_3 group[57,58] [106.39(8) (**4c**) to 102.63(7)° (**4a**)] and enlarged ones to the methylene carbon atom [114.89(8) (**4b**) to 114.29(10)° (**4c**)].

Looking at the arrangement of the substituents along the methylene−silicon bond, in the case of **4b** there is a nearly ideal "*anti*" arrangement of the iron fragment and the phenyl group, with a small deviation of only about 6° [Fe1−C8−Si1−C10 173.59(8)°], whereas in the case of **4c** the hydroxy group adopts the "*anti*" position to the iron fragment [Fe1−C11−Si1−O1 169.61(10)°] with a deviation of about 10°.

The situation in the case of **4a** is a bit more complex. The two different molecules are characterized by a nearly ideal "*anti*" position of the iron atom and the hydroxy group [Fe1−C8−Si1−O3 −174.24(8)] in the one case and a "*gauche*" position of these ligands with a more significant deviation from ideal conformation of about 20° [Fe1−C8−Si1−O3 40.09(12)°] in the other. This situation is clearly a consequence of the formation of a polymeric arrangement of the molecular subunits based on hydrogen bonding (see also below).

Triorganosilanols often show interesting hydrogen-bonded superstructures, the pattern of which depends on the nature of the organic substituents.[65] In contrast to the structures of other diorgano(metallo)silanols L_nM-SiR_2OH, which prefer hydrogen-bonded "dimerization", e.g. $C_5Me_5(OC)_2Fe-SiMe_2OH$[1] and $C_5Me_5(OC)_2Ru-Si(o\text{-Tol})_2OH$,[26] in the case of the (ferriomethyl)silanols **4a**,**b** strong intermolecular OH···O bridges lead to the formation of discrete tetrameric units in the solid state, indicated by O···O distances of 2.7320(16)/2.7410(17) (**4a**) and 2.6965(17) Å (**4b**). This arrangement is similar to that found for Ph_3SiOH.[62]

Looking at **4a**, the tetramers consist of the two types of staggered conformers, concerning the C8−Si bond (see above). They are formed by an alternating arrangement of

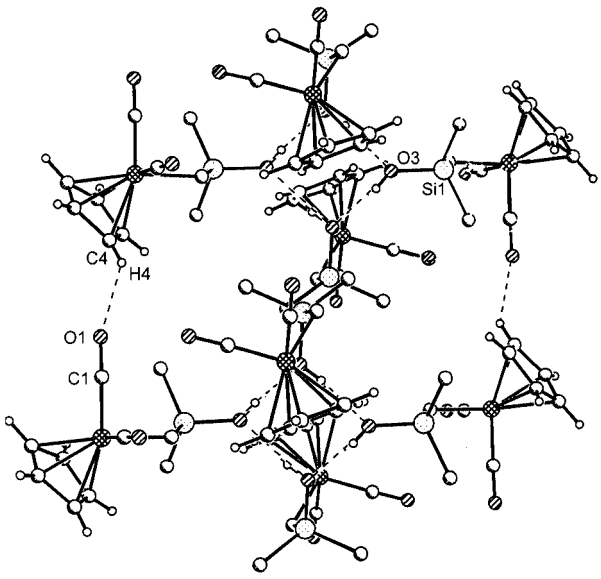

Figure 4. Ladder-type connection of **4a** between the "*anti*" conformers of neighboring tetramers via CH···OC bridges

the "*anti*" and "*gauche*" conformers and exhibit a centre of symmetry.

The tetrameric units are connected to each other in a ladder-type fashion by weak CH···OC interactions of the Cp and one CO ligand [C4···O1 3.358(3) Å] between two "*anti*" conformers of neighbouring units, as depicted in Figure 4. This kind of hydrogen bonding, although very rare, has recently been found by Braga et al. in the structures of $[Cp(CO)_2Fe]_2$ and $Cp_2Fe_2(CO)_2(\mu\text{-}CO)(\mu\text{-}CHMe)$.[66,67]

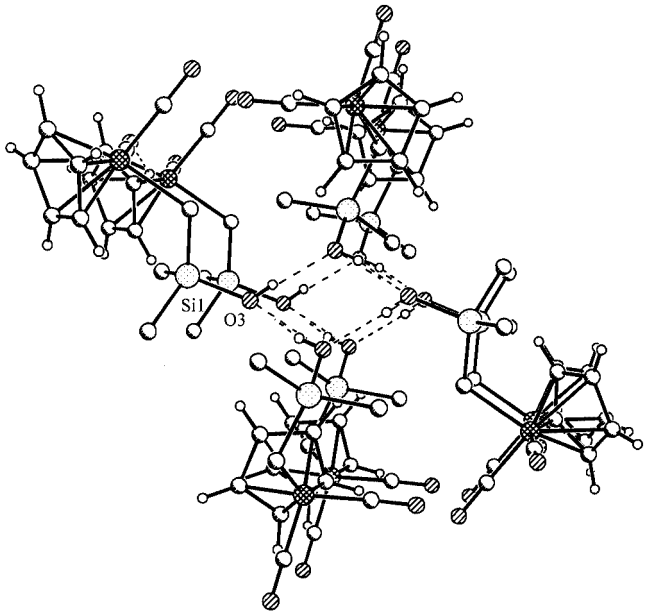

Figure 5. View inside the tube-like arrangement of the tetrameric units of **4a**

The tetrameric units are stacked on top of each other in the same way, resulting in a tube-like arrangement of the Si−OH moieties, which can be seen from Figure 5. The tubes can be considered as hydrophilic channels inside a lipophilic shape of the remaining (ferriomethyl) fragments. Between atoms of different tubes there are no or only marginal interactions, indicated by C···O distances of more than 3.70 Å.

In the case of **4b**, the situation is similar, but in contrast to **4a** there are no conformational isomers in the crystal structure, but two pairs of enantiomers which form the tetramer. The enantiomers are linked in an alternate fashion by hydrogen bonding to produce the centrosymmetric tetra-

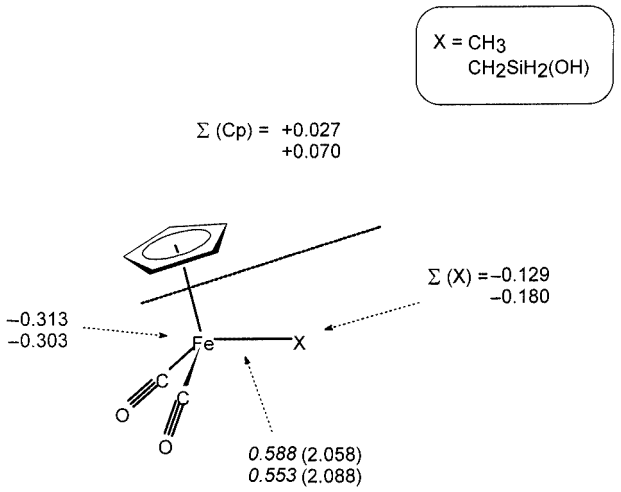

Figure 9. Population analysis of $Cp(OC)_2Fe-X$ (X = CH_3, CH_2SiH_2OH), NBO charges and Wiberg bond indices (in italics); in parentheses are Fe−X equilibrium distances

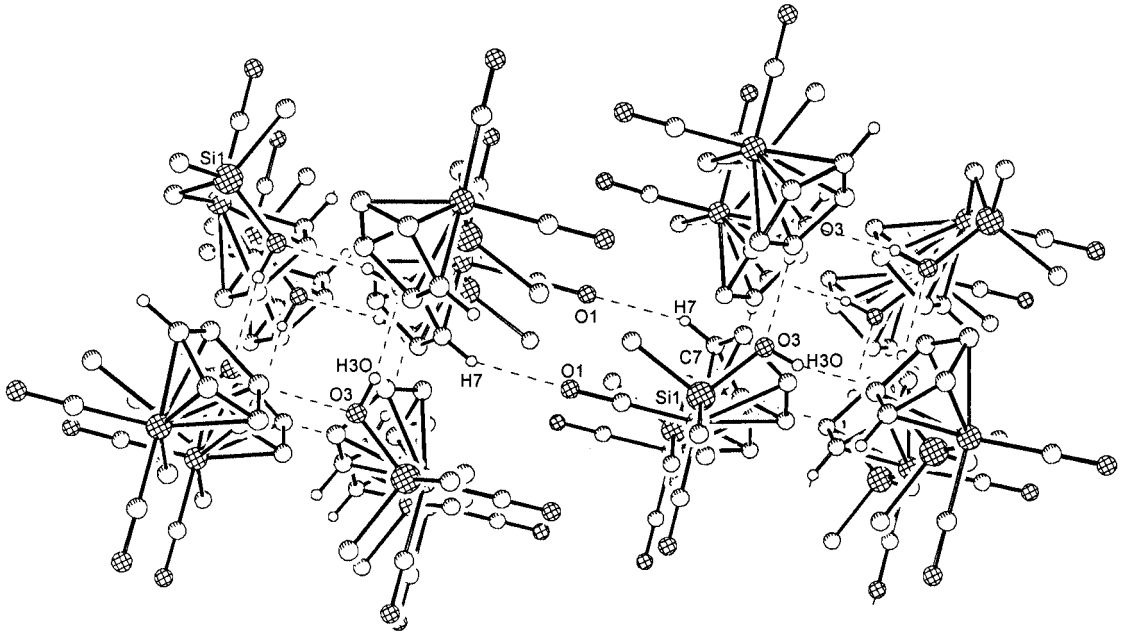

Figure 6. View inside the tube-like arrangement of the tetrameric units of **4b** with connection of the tubes via CH···OC bridges; hydrogen atoms (except for those involved in hydrogen bonding) as well as the phenyl carbon atoms (except for the *ipso* carbon atom) have been omitted for clarity

mer. Like **4a**, the tetramers are stacked on top of each other to produce a tube-like arrangement (Figure 6). These tubes are linked by weak CH···OC interactions of the Cp and one CO ligand of two enantiomers with the same configuration of neighboring tubes [C7···O1 3.406(2) Å].

The situation for the (ferriomethyl)silanol **4c** is somehow different. The molecules are connected by OH···O bridges giving rise to the formation of an infinite chain structure. This arrangement is a result of a "flip mechanism" of the disordered Si−OH proton[68] which guarantees the linkage of the molecules in two directions (intermolecular O···O distance 2.751/2.789 Å). This connection via hydrogen bonding is repeated in an infinite fashion to result in the formation of a linear chain structure, as depicted in Figure 7.

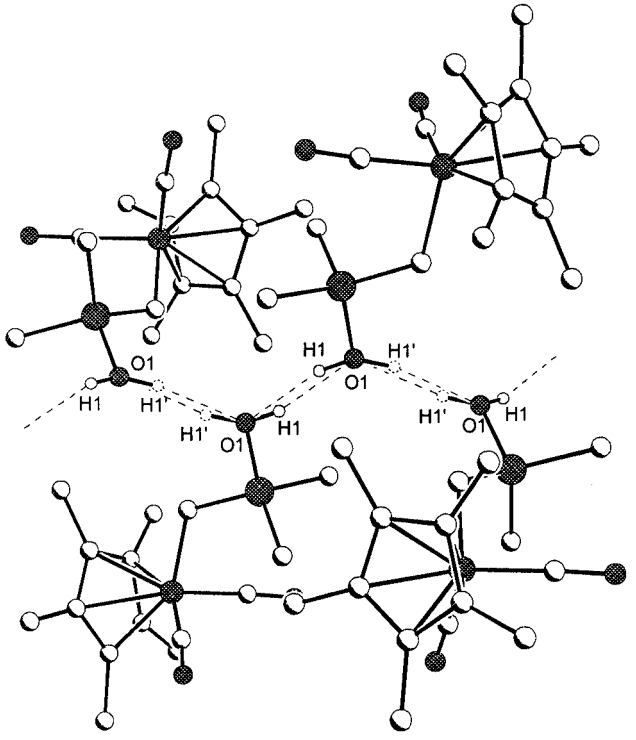

Figure 7. Chain structure of **4c** via OH···O bridges of the disordered SiOH proton

These chains interact by weak CH···OC contacts of the C_5Me_5 and one CO ligand with intermolecular C···O distances lying between 3.409(2) and 3.632(3) Å (Figure 8).

DFT Calculations

In order to analyze the bonding situation in the (ferriomethyl)silanol **4a** in more detail, we performed density functional calculations[69] on the model compounds $Cp(OC)_2Fe-X$ (X = CH_3, CH_2SiH_2OH). Plots of their equilibrium structures, determined at BP86/SBK(d) level,[70−73] are shown in Figure 9, together with the results of a natural bond orbital population analysis (NBO).[74]

The bonding parameters for X = CH_2SiH_2OH are in agreement with the X-ray investigation on **4a** (Fe−C: computed 2.088 Å, experimental 2.089 Å). The calculations also predict a widened valent angle at the carbon atom [X = $CH_2SiH_2(OH)$: Fe−C−Si = 115.7°], in agreement with the expectations from Bent's rule.[57,58] It is of interest to analyze the electron density distributions within the calculated structures. The substituent X (CH_3, CH_2SiH_2OH) is only weakly bound to the metal atom (Wiberg bond index for Fe−C 0.59 vs. 0.55), as compared with a stronger coordination of the carbonyl units (bond index 0.89 vs. 0.90). Interestingly, the iron atom accumulates negative charge, although the overall metal fragment releases electron density to X. The electron-withdrawing effect of X (−I) is more strongly pronounced for X = CH_2SiH_2OH than for X = CH_3.

Condensation Behavior of 4a

Although **4a** can be stored at −20 °C for several months without any self-condensation, at room temperature, this process slowly starts even in the solid state, leading to the 1,3-bis(ferriomethyl)disiloxane **5**.[43] The disiloxane formation also occurs in solution, which was proven by monitoring a C_6D_6 solution by NMR spectroscopy. In this case, **5** is formed in 33% yield after 30 d.

The disiloxane **5** is additionally obtained by the reaction of **4a** with the chloro(ferriomethyl)silane **3a** in diethyl ether in the presence of the auxiliary base Et_3N after a reaction period of 3 d at room temperature (Scheme 3).

Disiloxanes with only one iron fragment are available in the same manner using the chlorosilanes R(R′)Si(Me)Cl (R = H, R′ = Me, *p*-Tol; R = R′ = Me) (Scheme 4). The (ferriomethyl)-substituted disiloxanes **5** and **6a**−**c** are obtained in good yields of 76−85% as orange-brown (**5**) and yellow-brown oils (**6a**−**c**), respectively, which can be stored under nitrogen at room temperature for several months without decomposition.

The dinuclear disiloxane **5** shows a characteristic upfield shift of δ = 9 ppm in the ^{29}Si NMR spectrum compared to the silanol **4a** [δ = 12.8 (**5**) versus 21.8 (**4a**) ppm], which finds its counterpart in the resonances of triorganosilanols and the corresponding disiloxanes.[75]

In accordance with this finding, the ^{29}Si NMR resonances of the β-Si atom of **6a**−**c** are observed at δ = 15.9 (**6a**), 17.0 (**6b**) and 13.8 (**6c**) ppm. The Si−H-functionalized disiloxanes **6a**,**b** offer the possibility of further functionalization. In this context, experiments to effect Si−H/Si−OH transformation are under investigation, as well as oxidative addition reactions to electronically unsaturated metal fragments.

Conclusion

The results of this paper demonstrate that (ferriomethyl)-substituted silanols are accessible either by Cl/OH exchange at the silicon atom of chloro(ferriomethyl)silanes or by oxygen insertion into the Si−H bond of the corresponding (ferriomethyl)silanes. They show interesting structural features, like aggregation to tetramers and the formation of tube- or

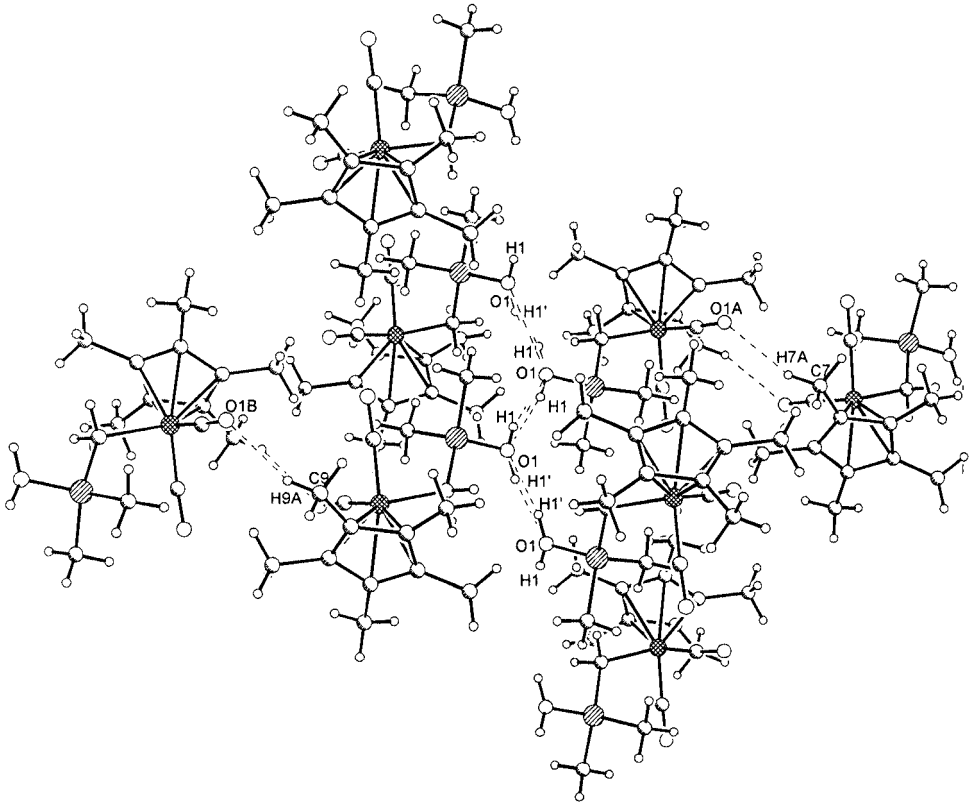

Figure 8. Connection of the chains of **4c** via CH···OC interactions

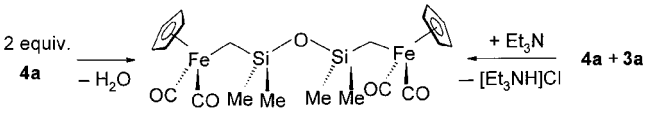

5

Scheme 3. Synthesis of the 1,3-bis(ferriomethyl)disiloxane **5**

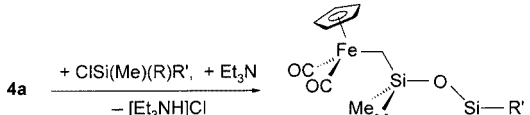

6	a	b	c
R	H	H	Me
R'	Me	*p*-Tol	Me

Scheme 4. Synthesis of the (ferriomethyl)disiloxanes **6a**–**c**

chain-like arrangements, which is a consequence of intermolecular hydrogen bonding.

The stability of this type of metal fragment substituted silanols with respect to self-condensation is reduced, compared with the ferriosilanols $C_5R_5(OC)_2Fe-SiMe_2OH$ (R = H, Me)[1] bearing the Si–OH unit directly at the transition metal atom. As a consequence, the silanol **4a** undergoes condensation to a disiloxane, which is well known from triorganosilanols. Apart from that, these compounds are ideal precursors to perform controlled reactions with chlorosilanes to generate novel transition metal containing siloxanes.

Current work deals with the generation of (ferriomethyl)-substituted silanediols and silanetriols in order to check the capability of these species to create metal-substituted oligo- or polysiloxanes by controlled self-condensation reactions.

Experimental Section

General Remarks: All operations were performed under purified and dried nitrogen using Schlenk-type techniques. Solvents were dried according to conventional procedures, distilled and saturated with N_2 prior to use. NMR: Jeol Lambda 300 (300.4 MHz, 75.5 MHz, and 59.6 MHz for ^1H, ^{13}C, and ^{29}Si, respectively). [D_6]Benzene as a solvent: δ_H = 7.15 ppm, δ_C = 128.0 ppm; for ^{29}Si rel. to TMS external. IR: Perkin–Elmer 283 grating spectrometer. Melting points: differential thermo analysis (Du Pont 9000 Thermal Analysis System). Elemental analyses were performed in the laboratories of the Institut für Anorganische Chemie der Universität Würzburg. Starting materials were prepared according to literature procedures: $Na[Fe(CO)_2Cp]$,[76] $Na[Fe(CO)_2C_5Me_5]$,[77] $ClCH_2Si(Me)(Ph)Cl$,[78] $Cp(OC)_2Fe-CH_2-SiMe_2H$,[43] $Cp(OC)_2Fe-CH_2-SiMe_2Cl$,[45] $ClSi(Me)(p\text{-Tol})H$[79] and dimethyldioxirane.[37] $ClCH_2SiMe_2Cl$, $ClSiMe_2H$ and $ClSiMe_3$ were purchased commercially and distilled prior to use.

1. Chloro{[dicarbonyl(η^5-cyclopentadienyl)ferrio]methyl}methyl(phenyl)silane (3b): A stirred suspension of $Na[Fe(CO)_2Cp]$ (**1a**)

(1329 mg, 6.65 mmol) in cyclohexane (40 mL) was treated with $ClCH_2Si(Me)(Ph)Cl$ (**2b**) (2157 mg, 10.51 mmol) and stirred for 36 h at room temperature in the dark. The reaction mixture was filtered through a Celite pad and the filtrate concentrated in vacuo. Excess **2b** was distilled off at 90 °C (10^{-2} Torr) and the remaining dark brown oil was heated to 120 °C for 3 h. After cooling to room temperature, the mixture was suspended in *n*-pentane (20 mL) and filtered off from insoluble decomposition products through a Celite pad. The filtrate was reduced to a volume of 8 mL and **3b** was crystallized at −78 °C and dried in vacuo. Yield: 1093 mg (47%). Orange-brown, waxy solid. M.p. 55 °C. ^{1}H NMR: δ = 7.69 (m, 2 H, H_5C_6Si), 7.20 (m, 3 H, H_5C_6Si), 3.97 (s, 5 H, H_5C_5), 0.75 (s, 3 H, H_3C), −0.02 (d, $^2J_{H,H}$ = 12.9 Hz, 1 H, H_2C), −0.05 ppm (d, $^2J_{H,H}$ = 12.9 Hz, 1 H, H_2C). $^{13}C\{^1H\}$ NMR: δ = 216.99 (s, CO), 216.96 (s, CO), 139.7 (s, C-1 of C_6H_5), 133.7 (s, C-2, C-6 of C_6H_5), 129.9 (s, C-4 of C_6H_5), 128.2 (s, C-3, C-5 of C_6H_5), 84.8 (s, C_5H_5), 3.3 (s, CH_3), −24.9 (s, CH_2) ppm. $^{29}Si\{^1H\}$ NMR: δ = 27.9 (s) ppm. IR (*n*-pentane): $\tilde{\nu}$ = 1999 (s, CO), 1962 cm^{-1} (vs, CO). $C_{15}H_{15}ClFeO_2Si$ (346.75): calcd. C 51.97, H 4.36; found C 51.60, H 4.64.

2. Chloro{[dicarbonyl(η^5-pentamethylcyclopentadienyl)ferrio]methyl}dimethylsilane (3c): A stirred suspension of $Na[Fe(CO)_2C_5Me_5]$ (**1b**) (1315 mg, 4.87 mmol) in cyclohexane (40 mL) was treated with $ClCH_2SiMe_2Cl$ (**2a**) (1087 mg, 7.60 mmol) and stirred for 20 h at room temperature in the dark. The reaction mixture was filtered through a Celite pad and the filtrate concentrated in vacuo. The orange-red residue was treated with *n*-pentane (15 mL) and stored at −20 °C overnight to crystallize the by-products $[C_5Me_5(OC)_2Fe]_2$ and $C_5Me_5(OC)_2FeCl$. The supernatant liquid was separated and the volume reduced in vacuo to 10 mL. Remaining $C_5Me_5(OC)_2FeCl$ was crystallized at −20 °C and filtered off. The filtrate was reduced in vacuo to 5 mL and **3c** was crystallized at −78 °C, washed twice with *n*-pentane (each 1 mL) at this temperature and dried in vacuo. Yield: 571 mg (33%). Orange-brown, waxy solid. M.p. 60 °C (decomp.). ^{1}H NMR: δ = 1.25 [s, 15 H, $(H_3C)_5C_5$], 0.66 (s, 6 H, H_3CSi), −0.43 (s, 2 H, H_2C) ppm. $^{13}C\{^1H\}$ NMR: δ = 219.5 (s, CO), 95.7 [s, $C_5(CH_3)_5$], 9.1 [s, $(CH_3)_5C_5$], 4.7 (s, CH_3Si), −12.0 (s, CH_2) ppm. ^{29}Si NMR: δ = 35.5 (non, $^2J_{Si,H}$ = 6.7 Hz) ppm. IR (cyclohexane): $\tilde{\nu}$ = 1983 (s, CO), 1931 cm^{-1} (vs, CO). $C_{15}H_{23}ClFeO_2Si$ (354.75): calcd. C 50.79, H 6.53; found C 50.51, H 6.30.

3. {[Dicarbonyl(η^5-cyclopentadienyl)ferrio]methyl}dimethylsilanol (4a). a) Hydrolysis of $Cp(OC)_2FeCH_2SiMe_2Cl$ (3a) in the Presence of Et_3N: A stirred solution of **3a** (237 mg, 0.83 mmol) in Et_2O (30 mL) was treated with Et_3N (730 mg, 7.21 mmol) and H_2O (100 mg, 5.55 mmol). After addition, stirring was continued for 2 h at room temperature. Precipitated $[Et_3NH]Cl$ and excess H_2O were removed by filtration through Na_2SO_4. The filtrate was concentrated in vacuo, leaving yellow-brown oily **4a**, which was crystallized from *n*-pentane (3 mL) at −78 °C and dried in vacuo. Yield: 197 mg (89%). **b) Oxygenation of $Cp(OC)_2FeCH_2SiMe_2H$ (3d) with Dimethyldioxirane:** A stirred solution of **3d** (238 mg, 0.95 mmol) in acetone (10 mL) was treated dropwise at −78 °C with a solution of dimethyldioxirane (1.22 mmol,16 mL, 0.076 M) in acetone. After addition, the reaction mixture was stirred for 1 h at this temperature and an additional 1 h at room temperature. All volatiles were removed in vacuo, leaving brown oily **4a**, which was crystallized from *n*-pentane (3 mL) at −78 °C and dried in vacuo. Yield: 170 mg (67%). Yellow-brown, waxy solid. M.p. 38 °C. ^{1}H NMR: δ = 4.24 (s, 5 H, H_5C_5), 0.95 (br. s, 1 H, HO), 0.23 (s, 6 H, H_3C), −0.42 (s, 2 H, H_2C) ppm. $^{13}C\{^1H\}$ NMR: δ = 218.0 (s, CO), 84.8 (s, C_5H_5), 3.2 (s, CH_3), −23.1 (s, CH_2) ppm. $^{29}Si\{^1H\}$ NMR: δ = 21.8 (s) ppm. IR (*n*-pentane): $\tilde{\nu}$ = 3698 (w, OH), 2000 (s, CO), 1959 cm^{-1} (vs, CO). $C_{10}H_{14}FeO_3Si$ (266.15): calcd. C 45.13, H 5.30; found C 45.11, H 5.21.

4. {[Dicarbonyl(η^5-cyclopentadienyl)ferrio]methyl}methyl(phenyl)silanol (4b): According to 3.a) obtained from **3b** (352 mg, 1.02 mmol), Et_3N (219 mg, 2.16 mmol) and H_2O (100 mg, 5.56 mmol) in Et_2O (20 mL) after 4 h at room temperature. Yield: 247 mg (74%). Yellow-orange, crystalline solid. M.p. 60 °C. ^{1}H NMR: δ = 7.63 (m, 2 H, H_5C_6Si), 7.26 (m, 3 H, H_5C_6Si), 4.18 (s, 5 H, H_5C_5), 1.28 (br. s, 1 H, HO), 0.44 (s, 3 H, H_3CSi), −0.09 (d, $^2J_{H,H}$ = 12.8 Hz, 1 H, H_2C), −0.38 (d, $^2J_{H,H}$ = 12.8 Hz, 1 H, H_2C) ppm. $^{13}C\{^1H\}$ NMR: δ = 217.8 (s, CO), 217.6 (s, CO), 142.9 (s, C-1 of C_6H_5), 133.5 (s, C-2, C-6 of C_6H_5), 129.1 (s, C-3, C-5 of C_6H_5), 128.0 (s, C-4 of C_6H_5), 84.8 (s, C_5H_5), 1.8 (s, CH_3), −24.9 (s, CH_2) ppm. $^{29}Si\{^1H\}$ NMR: δ = 11.7 (s) ppm. IR (*n*-pentane): $\tilde{\nu}$ = 3682 (w, br, OH), 1995 (s, CO), 1952 cm^{-1} (vs, CO). $C_{15}H_{16}FeO_3Si$ (328.23): calcd. C 54.89, H 4.91; found C 54.60, H 5.06.

5. {[Dicarbonyl(η^5-pentamethylcyclopentadienyl)ferrio]methyl}dimethylsilanol (4c): According to 3.a) obtained from **3c** (126 mg, 0.36 mmol), Et_3N (365 mg, 3.60 mmol) and H_2O (200 mg, 11.1 mmol) in Et_2O (20 mL) after 4 h at room temperature. Precipitated $[Et_3NH]Cl$ and excess H_2O were removed by filtration through Na_2SO_4. The filtrate was concentrated in vacuo and treated with *n*-pentane (5 mL). The by-products $C_5Me_5(OC)_2FeCl$ and $[C_5Me_5(OC)_2Fe]_2$ were crystallized at 0 °C and separated by filtration through a Celite pad. The filtrate was reduced to 2 mL and **6c** was crystallized at −78 °C and dried in vacuo. Yield: 48 mg (40%). Yellow-orange solid. M.p. 89 °C (decomp.). ^{1}H NMR: δ = 1.35 [s, 15 H, $(H_3C)_5C_5$], 0.92 (br. s, 1 H, HO), 0.40 (s, 6 H, H_3CSi), −0.62 (s, 2 H, H_2C) ppm. $^{13}C\{^1H\}$ NMR: δ = 220.1 (s, CO), 95.2 [s, $C_5(CH_3)_5$], 9.2 [s, $(CH_3)_5C_5$], 3.2 (s, CH_3Si), −12.4 (s, CH_2) ppm. $^{29}Si\{^1H\}$ NMR: δ = 21.1 (s) ppm. IR (*n*-pentane): $\tilde{\nu}$ = 3703 (w, OH), 1988 (s, CO), 1936 cm^{-1} (vs, CO). $C_{15}H_{24}FeO_3Si$ (336.29): calcd. C 53.57, H 7.19; found C 53.82, H 7.05.

6. 1,3-Bis{[dicarbonyl(η^5-cyclopentadienyl)ferrio]methyl}-1,1,3,3-tetramethyldisiloxane (5). a) Self Condensation of $Cp(OC)_2FeCH_2SiMe_2OH$ (4a): In an NMR sample tube **4a** (20 mg, 0.08 mmol) was dissolved in C_6D_6 (0.6 mL). After 30 d at room temperature, **5** was formed in 33% yield as determined by ^{1}H NMR spectroscopy. **b) Reaction of $Cp(OC)_2FeCH_2SiMe_2OH$ (4a) with $Cp(OC)_2FeCH_2SiMe_2Cl$ (3a): 3a** (103 mg, 0.48 mmol) in Et_2O (20 mL) was added dropwise to a stirred solution of **4a** (108 mg, 0.41 mmol) in Et_2O (20 mL). After stirring for 3 d in the dark at room temperature, all volatiles were removed in vacuo. The residue was suspended in *n*-pentane (15 mL) and filtered through a Celite pad. The volume of the filtrate was reduced in vacuo to 3 mL and **5** crystallized at −78 °C. Solid **5** melts upon warming to room temperature. Yield: 163 mg (77%). Orange-brown oil. ^{1}H NMR: δ = 4.24 (s, 10 H, H_5C_5), 0.36 (s, 12 H, H_3C), −0.25 (s, 4 H, H_2C) ppm. $^{13}C\{^1H\}$ NMR: δ = 218.0 (s, CO), 84.9 (s, C_5H_5), 4.0 (s, CH_3), −22.4 (s, CH_2) ppm. $^{29}Si\{^1H\}$ NMR: δ = 12.8 (s) ppm. IR (*n*-pentane): $\tilde{\nu}$ = 2003 (s, CO), 1961 cm^{-1} (vs, CO). $C_{20}H_{26}Fe_2O_5Si_2$ (514.29): calcd. C 46.71, H 5.09; found C 46.37, H 5.32.

7. 1-{[Dicarbonyl(η^5-cyclopentadienyl)ferrio]methyl}-1,1,3,3-tetramethyldisiloxane (6a): According to 6.b) obtained from **4a** (866 mg, 3.26 mmol), Et_3N (1186 mg, 11.50 mmol) and $Me_2Si(H)Cl$ (694 mg, 10.26 mmol) in Et_2O (60 mL) after stirring in the dark at room temperature for 12 h. The residue was suspended in *n*-pentane (40 mL) and filtered through a Celite pad. The filtrate was concentrated in vacuo, leaving **6a**. Yield: 900 mg (85%). Yellow-

brown oil. ^{1}H NMR: δ = 5.05 (sept, $^3J_{H,H}$ = 2.4, $^1J_{H,Si}$ = 201.6 Hz, 1 H, HSi), 4.19 (s, 5 H, H_5C_5), 0.28 [s, 6 H, $(H_3C)_2SiCH_2$], 0.22 [d, $^3J_{H,H}$ = 2.4 Hz, 6 H, $(H_3C)_2SiH$], −0.39 (s, 2 H, H_2C) ppm. $^{13}C\{^1H\}$ NMR: δ = 217.9 (s, CO), 84.8 (s, C_5H_5), 3.4 [s, $(CH_3)_2SiCH_2$], 1.2 [s, $(CH_3)_2SiH$], −23.0 (s, CH_2) ppm. $^{29}Si\{^1H\}$ NMR: δ = 15.9 (s, $SiCH_2Fe$), −8.0 (s, SiH) ppm. IR (*n*-pentane): $\tilde{\nu}$ = 2116 (w, br, SiH), 2003 (s, CO), 1961 cm^{-1} (vs, CO). $C_{12}H_{20}FeO_3Si_2$ (324.30): calcd. C 44.44, H 6.21; found C 44.09, H 6.21.

8. 1-{[Dicarbonyl(η^5-cyclopentadienyl)ferrio]methyl}-1,1,3-trimethyl-3-(*p*-tolyl)disiloxane (6b): According to 7. obtained from **4a** (296 mg, 1.11 mmol), Et_3N (219 mg, 2.16 mmol) and (*p*-Tol)(Me)(H)SiCl (189 mg, 1.11 mmol) in Et_2O (40 mL) after stirring for 24 h in the dark at room temperature. After workup the crude product was dried for 6 h at 5 × 10^{-5} Torr. Yield: 338 mg (76%). Brown oil. ^{1}H NMR: δ = 7.63 (d, $^3J_{H,H}$ = 7.4 Hz, 2 H, H_4C_6), 7.08 (d, $^3J_{H,H}$ = 7.4 Hz, 2 H, H_4C_6), 5.47 (q, $^3J_{H,H}$ = 2.8, $^1J_{H,Si}$ = 206.4 Hz, 1 H, HSi), 4.16 (s, 5 H, H_5C_5), 2.10 (s, 3 H, $H_3CC_6H_4$), 0.47 (d, $^3J_{H,H}$ = 2.8 Hz, 3 H, H_3CSiH), 0.31 [s, 6 H, $(H_3C)_2SiCH_2$], −0.35 (s, 2 H, H_2C) ppm. $^{13}C\{^1H\}$ NMR: δ = 217.8 (s, CO), 139.8 (s, C-1 of C_6H_4), 135.0 (s, C-4 of C_6H_4), 134.0 (s, C-2, C-6 of C_6H_4), 129.1 (s, C-3, C-5 of C_6H_4), 84.8 (s, C_5H_5), 21.5 (s, $CH_3C_6H_4$), 3.5 [s, $(CH_3)_2SiCH_2$], 0.1 (s, CH_3SiH), −23.1 (s, CH_2) ppm. ^{29}Si NMR: δ = 17.0 (m, $SiCH_2Fe$), −14.6 (dsext, $^1J_{Si,H}$ = 206.4, $^2J_{Si,H}$ = 6.4 Hz, SiH) ppm. IR (*n*-pentane): $\tilde{\nu}$ = 2119 (w, br, SiH), 2002 (s, CO), 1960 cm^{-1} (vs, CO). $C_{18}H_{24}FeO_3Si_2$ (400.41): calcd. C 53.99, H 6.04; found C 54.00, H 5.97.

9. 3-{[Dicarbonyl(η^5-cyclopentadienyl)ferrio]methyl}-1,1,1,3,3-pentamethyldisiloxane (6c): According to 7. obtained from **4a** (213 mg, 0.80 mmol), Et_3N (219 mg, 2.16 mmol) and Me_3SiCl (257 mg, 2.37 mmol) in Et_2O (30 mL) after stirring for 24 h in the dark at room temperature. Yield: 204 mg (79%). Yellow-brown oil. ^{1}H NMR: δ = 4.21 (s, 5 H, H_5C_5), 0.28 [s, 6 H, $(H_3C)_2Si$], 0.18 [s, 9 H, $(H_3C)_3Si$], −0.36 (s, 2 H, H_2C) ppm. $^{13}C\{^1H\}$ NMR: δ = 217.9 (s, CO), 84.9 (s, C_5H_5), 3.8 [s, $(CH_3)_2Si$], 2.3 [s, $(CH_3)_3Si$], −22.5 (s, CH_2) ppm. ^{29}Si NMR: δ = 13.8 (m, $SiCH_2Fe$), 6.2 [dec, $^2J_{Si,H}$ = 7.0 Hz, $Si(CH_3)_3$] ppm. IR (Et_2O): $\tilde{\nu}$ = 2000 (vs, CO), 1953 cm^{-1} (vs, CO). $C_{13}H_{22}FeO_3Si_2$ (338.33): calcd. C 46.15, H 6.55; found C 46.80, H 6.63.

X-ray Crystal Structure Analyses of 4a−c: Table 1 contains details of the structures. The intensities were measured with a Nonius-Kappa CCD diffractometer (Mo-K_α radiation, λ = 0.71073 Å, graphite monochromator) at T = −150 °C. The structures were solved by direct methods (Patterson methods)[80] (SHELXS-97) and refined by least-squares methods based on F^2 with all measured reflections (SHELXL-97) (full-matrix least-squares on F^2,[81]). Non-hydrogen atoms were refined anisotropically, H atoms localized by difference electron density and refined using a "riding" model [H(O) free]. An empirical absorption correction was applied. CCDC-115086 (**4a**), -148145 (**4b**) and -156552 (**4c**) contain the supplementary crystallographic data for this paper. These data can be obtained free of charge at www.ccdc.cam.ac.uk/conts/retrieving.html or from the Cambridge Crystallographic Data Centre, 12 Union Road, Cambridge CB2 1EZ, UK [Fax: (internat.) + 44-1223/336-033; E-mail: deposit@ccdc.cam.ac.uk].

Acknowledgments

We gratefully acknowledge financial support from the Deutsche Forschungsgemeinschaft (Schwerpunktprogramm "Spezifische Phänomene in der Siliciumchemie") as well as from the Fonds der Chemischen Industrie. M. N. wants to thank the DAAD for financial support.

Table 1. Data for the crystal structure analyses

	4a	**4b**	**4c**
Empirical formula	$C_{10}H_{14}FeO_3Si$	$C_{15}H_{16}FeO_3Si$	$C_{15}H_{24}FeO_3Si$
Formula mass	266.15	328.22	336.28
Crystal system	triclinic	tetragonal	monoclinic
Space group	$P\bar{1}$ (no. 2)	$I4_1/a$ (no. 88)	$C2/c$ (no. 15)
Unit cell			
a [Å]	8.0351(4)	22.0578(10)	27.2245(2)
b [Å]	11.4028(4)	22.0578(10)	13.8293(1)
c [Å]	13.9508(6)	12.4151(6)	9.3090(1)
α [°]	75.637(2)	90	90
β [°]	79.190(2)	90	101.394(1)
γ [°]	76.894(2)	90	90
Volume [Å^3]	1194.27(9)	6040.5(5)	3435.73(5)
Z	4	16	8
Calcd. density [g/cm^3]	1.480	1.444	1.300
μ [mm^{-1}]	1.347	1.081	0.951
F(000)	552	2720	1424
Crystal size [mm]	0.30 × 0.25 × 0.09	0.40 × 0.35 × 0.30	0.35 × 0.20 × 0.10
θ range [°]	2.85/28.30	1.85/26.35	1.66/25.00
Index ranges (h, k, l)	$-10 \le h \le 9$ $-14 \le k \le 14$ $-17 \le l \le 14$	$-27 \le h \le 27$ $-25 \le k \le 25$ $-12 \le l \le 15$	$-32 \le h \le 32$ $-16 \le k \le 16$ $-11 \le l \le 11$
No. of reflections	11445	13115	34665
No. of unique reflections	5413	3035	3020
Parameters, restraints	277, 4	184, 1	186, 0
$R1$ [$I > 2\sigma_I$]	0.0275	0.0299	0.0255
$wR2$	0.0678	0.0664	0.0690
T [K]	123(2)	123(2)	123(2)
Max. residual electron density [e/Å^3]	0.367/−0.353	0.220/−0.304	0.282/−0.268

[1] W. Malisch, M. Hofmann, G. Kaupp, H. Käb, J. Reising, *Eur. J. Inorg. Chem.* **2002**, 3235−3241, preceding paper.
[2] P. Panster, S. Wieland in *Applied Homogeneous Catalysis with Organometallic Compounds* (Eds.: B. Cornils, W. A. Herrmann), VCH, Weinheim, **1996**, p. 605.
[3] Y. Iwasawa, *Tailored Metal Catalysts*, Reidel, Dordrecht, **1986**.
[4] F. R. Hartley, *Supported Metal Complexes*, Reidel, Dordrecht, **1985**.
[5] Y. I. Yermakov, B. N. Kuznetsov, V. A. Zakharov, *Catalysis by Supported Complexes*, Elsevier, Amsterdam, **1981**.
[6] R. Siefken, M. Teichert, D. Chakraborty, H. W. Roesky, *Organometallics* **1999**, *18*, 2321−2325.
[7] P. Jutzi, M. Schneider, H.-G. Stammler, B. Neumann, *Organometallics* **1997**, *16*, 5377−5380.
[8] R. Murugavel, V. Chandrasekhar, H. W. Roesky, *Acc. Chem. Res.* **1996**, *29*, 183−189.
[9] N. Winkhofer, A. Voigt, H. Dorn, H. W. Roesky, A. Steiner, D. Stalke, A. Reller, *Angew. Chem.* **1994**, *106*, 1414−1416; *Angew. Chem. Int. Ed. Engl.* **1994**, *33*, 1352−1354.
[10] N. Winkhofer, H. W. Roesky, M. Noltemeyer, W. T. Robinson, *Angew. Chem.* **1992**, *104*, 670−671; *Angew. Chem. Int. Ed. Engl.* **1992**, *31*, 599−601.
[11] H. C. L. Abbenhuis, *Chem. Eur. J.* **2000**, *6*, 25−32.
[12] F. J. Feher, T. A. Budzichowski, *Polyhedron* **1995**, *14*, 3239−3253.
[13] H. C. L. Abbenhuis, S. Krijnen, R. A. van Santen, *Chem. Commun.* **1997**, 331−332.
[14] F. J. Feher, F. Nguyen, D. Soulivong, J. W. Ziller, *Chem. Commun.* **1999**, 1705−1706.
[15] F. J. Feher, R. Terroba, R.-Z. Jin, *Chem. Commun.* **1999**, 2513−2514.
[16] G. Calzaferri, *Nachr. Chem. Tech. Lab.* **1992**, *40*, 1106−1114.
[17] F. T. Edelmann, *Angew. Chem.* **1992**, *104*, 600−601; *Angew. Chem. Int. Ed. Engl.* **1992**, *31*, 586−587.
[18] W. A. Herrmann, R. Anwander, V. Dufaud, W. Scherer, *Angew. Chem.* **1994**, *106*, 1338−1340; *Angew. Chem. Int. Ed. Engl.* **1994**, *33*, 1285−1286.
[19] W. Malisch, H. Jehle, C. Mitchel, W. Adam, *J. Organomet. Chem.* **1998**, *566*, 259−262.
[20] W. Malisch, R. Lankat, S. Schmitzer, J. Reising, *Inorg. Chem.* **1995**, *34*, 5701−5702.
[21] W. Malisch, R. Lankat, O. Fey, J. Reising, S. Schmitzer, *J. Chem. Soc., Chem. Commun.* **1995**, 1917−1919.
[22] W. Malisch, S. Schmitzer, R. Lankat, M. Neumayer, F. Prechtl, W. Adam, *Chem. Ber.* **1995**, *128*, 1251−1255.
[23] W. Malisch, S. Möller, R. Lankat, J. Reising, S. Schmitzer, O. Fey, in *Organosilicon Chemistry II: From Molecules to Materials* (Eds.: N. Auner, J. Weis), VCH, Weinheim, **1996**, p. 575.
[24] W. Malisch, S. Schmitzer, G. Kaupp, K. Hindahl, H. Käb, U. Wachtler, in *Organosilicon Chemistry: From Molecules to Materials*, vol. 1 (Eds.: N. Auner, J. Weis), VCH, Weinheim, **1994**, p. 185.
[25] W. Malisch, H. Jehle, S. Möller, C.-S. Möller, W. Adam, *Eur. J. Inorg. Chem.* **1998**, 1585−1587.
[26] S. Möller, O. Fey, W. Malisch, W. Seelbach, *J. Organomet. Chem.* **1996**, *507*, 239−244.
[27] C. S. Cundy, M. F. Lappert, C. K. Yuen, *J. Chem. Soc., Dalton Trans.* **1978**, 427−433.
[28] C. E. F. Rickard, W. R. Roper, D. M. Salter, L. J. Wright, *J. Am. Chem. Soc.* **1992**, *114*, 9682−9683.
[29] H. Handwerker, C. Leis, R. Probst, P. Bissinger, A. Grohmann, P. Kiprof, E. Herdtweck, J. Bluemel, N. Auner, C. Zybill, *Organometallics* **1993**, *12*, 2162−2176.
[30] L. S. Chang, M. P. Johnson, M. J. Fink, *Organometallics* **1991**, *10*, 1219−1221.
[31] W. Adam, U. Azzena, F. Prechtl, K. Hindahl, W. Malisch, *Chem. Ber.* **1992**, *125*, 1409−1411.
[32] W. Malisch, K. Hindahl, H. Käb, J. Reising, W. Adam, F. Prechtl, *Chem. Ber.* **1995**, *128*, 963−965.
[33] R. Goikhman, M. Aizenberg, H.-B. Kraatz, D. Milstein, *J. Am. Chem. Soc.* **1995**, *117*, 5865−5866.
[34] S. H. A. Petri, D. Eikenberg, B. Neumann, H.-G. Stammler, P. Jutzi, *Organometallics* **1999**, *18*, 2615−2618.
[35] W. Adam, R. Mello, R. Curci, *Angew. Chem.* **1990**, *102*, 916−917; *Angew. Chem. Int. Ed. Engl.* **1990**, *29*, 890−891.
[36] W. Adam, A. K. Smerz, *Bull. Soc. Chim. Belg.* **1996**, *105*, 581−599.
[37] W. Adam, J. Bialas, L. Hadajiarapolou, *Chem. Ber.* **1991**, *124*, 2377.
[38] W. Malisch, M. Hofmann, M. Vögler, H. Jehle, D. Schumacher, unpublished results.
[39] W. Mowat, G. Wilkinson, *J. Chem. Soc., Dalton Trans.* **1973**, 1120−1124.
[40] P. J. Davidson, M. F. Lappert, R. Pearce, *Acc. Chem. Res.* **1974**, *7*, 209−217.
[41] R. R. Schrock, G. W. Parshall, *Chem. Rev.* **1976**, *76*, 243−268.
[42] K. H. Pannell, *J. Organomet. Chem.* **1970**, *21*, P17−P18.
[43] J. E. Bulkowski, N. D. Miro, D. Sepelak, C. H. Van Dyke, *J. Organomet. Chem.* **1975**, *101*, 267−277.
[44] C. Windus, S. Sujishi, W. P. Giering, *J. Am. Chem. Soc.* **1974**, *96*, 1951−1952.
[45] C. Windus, S. Sujishi, W. P. Giering, *J. Organomet. Chem.* **1975**, *101*, 279−293.
[46] C. Lewis, M. S. Wrighton, *J. Am. Chem. Soc.* **1983**, *105*, 7768−7770.
[47] C. L. Randolph, M. S. Wrighton, *Organometallics* **1987**, *6*, 365−371.
[48] T. S. Koloski, P. J. Carroll, D. H. Berry, *J. Am. Chem. Soc.* **1990**, *112*, 6405−6406.
[49] J. E. Bulkowski, R. Stacy, C. H. Van Dyke, *J. Organomet. Chem.* **1975**, *87*, 137−143.
[50] K. Itoh, T. Fukahori, *J. Organomet. Chem.* **1988**, *349*, 227−234.
[51] A. D. Horton, A. G. Orpen, *Organometallics* **1992**, *11*, 1193−1201.
[52] M. Enders, J. Fink, V. Maillant, H. Pritzkow, *Z. Anorg. Allg. Chem.* **2001**, *627*, 2281−2288.
[53] **3a** was first synthesized by Giering et al.[44,45]
[54] L. Pope, P. Sommerville, M. Laing, *J. Organomet. Chem.* **1976**, *112*, 309−324.
[55] G.-H. Lee, S.-M. Peng, S.-F. Lush, D. Mu, R.-S. Liu, *Organometallics* **1988**, *7*, 1155−1161.
[56] M. Akita, A. Kondoh, Y. Moro-oka, *J. Chem. Soc., Dalton Trans.* **1989**, 1083−1087.
[57] H. A. Bent, *Chem. Rev.* **1961**, *61*, 275−311.
[58] R. L. Scholl, G. E. Maciel, W. K. Musker, *J. Am. Chem. Soc.* **1972**, *94*, 6376−6385.
[59] S. G. Davies, I. M. Dordor-Hedgecock, K. H. Sutton, M. Whittaker, *J. Am. Chem. Soc.* **1987**, *109*, 5711−5719.
[60] K. H. Pannell, T. Kobayashi, F. Cervantes-Lee, Y. Zhang, *Organometallics* **2000**, *19*, 1−3.
[61] Y. Zhang, F. Cervantes-Lee, K. H. Pannell, *J. Am. Chem. Soc.* **2000**, *122*, 8327−8328.
[62] H. Puff, K. Braun, H. Reuter, *J. Organomet. Chem.* **1991**, *409*, 119−129.
[63] Z. H. Aiube, N. H. Buttrus, C. Eaborn, P. B. Hitchcock, J. A. Zora, *J. Organomet. Chem.* **1985**, *292*, 177−188.
[64] P. D. Lickiss, N. L. Clipston, D. W. H. Rankin, H. E. Robertson, *J. Mol. Struct.* **1995**, *344*, 111−116.
[65] P. D. Lickiss, *Adv. Inorg. Chem.* **1995**, *42*, 147−262.
[66] D. Braga, F. Grepioni, K. Biradha, V. R. Pedireddi, G. R. Desiraju, *J. Am. Chem. Soc.* **1995**, *117*, 3156−3166.
[67] D. Braga, F. Grepioni, *Acc. Chem. Res.* **1997**, *30*, 81−87.
[68] The difference electron density determination [after refinement taking H(C) into account, which was also localized by difference electron density determination and refined using a riding model] shows two difference peaks in a reasonable O−H distance, also with reasonable intermolecular H−O distances forming hydrogen bonds (to Si−OH in two different molecules).

There is a significant gap between those two peaks and the remaining peaks in the difference density map. Using HFIX 87, HFIX 147 and HTAB in the SHELXL-97 refinement two possible H(O) positions, very close to the low localized density peaks, are indicated. This all suggests a disorder (50:50) of the Si−OH group with "flipping" hydrogen bond pattern. In addition, data are collected at 123 K and the quality is "not so bad", which even improves the possibility of localization of disordered H atoms.

[69] All quantum chemical calculations were performed with the Gaussian set of programs. M. J. Frisch, G. W. Trucks, H. B. Schlege, G. E. Scuseria, M. A. Robb, J. R. Cheeseman, V. G. Zakrzewski, J. A. Montgomery, R. E. Stratmann, J. C. Burant, S. Dapprich, J. M. Millam, A. D. Daniels, K. N. Kudin, M. C. Strain, O. Farkas, J. Tomasi, V. Barone, M. Cossi, R. Cammi, B. Mennucci, C. Pomelli, C. Adamo, S. Clifford, J. Ochterski, G. A. Petersson, P. Y. Ayala, Q. Cui, K. Morokuma, D. K. Malick, A. D. Rabuck, K. Raghavachari, J. B. Foresman, J. Cioslowski, J. V. Ortiz, B. B. Stefanov, G. Liu, A. Liashenko, P. Piskorz, I. Komaromi, R. Gomperts, R. L. Martin, D. J. Fox, T. Keith, M. A. Al-Laham, C. Y. Peng, A. Nanyakkara, C. Gonzalez, M. Challacombe, P. M. W. Gill, B. G. Johnson, W. Chen, M. W. Wong, J. L. Andres, M. Head-Gordon, E. S. Replogle, J. A. Pople, *Gaussian 98* (Revision A.1), Gaussian Inc., Pittsburgh PA, **1998**.

[70] Basis set SBK(d): W. J. Stevens, H. Basch, M. Krauss, *J. Chem. Phys.* **1984**, *81*, 6026−6033.

[71] W. J. Stevens, M. Krauss, H. Basch, P. Jasien, *Can. J. Chem.* **1992**, *70*, 612−630.

[72] T. Cundari, W. J. Stevens, *J. Chem. Phys.* **1993**, *98*, 5555−5565. The d-orbital exponents for the polarization functions are: Si 0.395, C. 0.800, O. 0.800.

[73] Gradient-corrected density functional of Perdew: J. P. Perdew, *Phys. Rev.* **1986**, *B33*, 8822−8824.

[74] A. E. Reed, L. A. Curtiss, F. Weinhold, *Chem. Rev.* **1988**, *88*, 899−926. E. D. Glendening, A. E. Reed, J. E. Carpenter, F. Weinhold, *NBO*, version 3.1.

[75] H. Marsmann, in *NMR − Basic Principles and Progress*, vol. 17 (Eds.: P. Diehl, E. Fluck, R. Kosfeld), Springer-Verlag, Berlin, Heidelberg, New York, **1981**, p. 151.

[76] T. S. Piper, G. Wilkinson, *J. Inorg. Nucl. Chem.* **1956**, *3*, 104−124.

[77] T. Blackmore, M. I. Bruce, F. G. A. Stone, *J. Chem. Soc. A* **1968**, 2158−2162.

[78] N. Auner, J. Grobe, *J. Organomet. Chem.* **1980**, *188*, 151−177.

[79] A. Kunai, E. Toyoda, T. Kawakami, M. Ishikawa, *Organometallics* **1992**, *11*, 2899−2903.

[80] *SHELXS-97:* G. M. Sheldrick, *Acta Crystallogr., Sect. A* **1990**, *46*, 467−473.

[81] G. M. Sheldrick, *SHELXL-97*, University of Göttingen, **1997**.

Received March 15, 2002
[I02131]

Stable $Rh_2(MTPA)_4$ Phosphane Adducts − The First Example of *P*-Chirality Recognition by ^{103}Rh NMR Spectroscopy

Damian Magiera,[a] Wolfgang Baumann,[b] Ivan S. Podkorytov,[c] Jan Omelanczuk,[d] and Helmut Duddeck*[a]

Keywords: Phosphanes / Rhodium / NMR spectroscopy / Chirality / Chiral discrimination

The optimal parameters for ^{31}P-detected ^{103}Rh HMQC NMR spectroscopy of AMX spin systems (A = ^{31}P; M and X = ^{103}Rh) have been derived and applied to adducts of $Rh_2[(R)\text{-MTPA}]_4$ with PPh_3 (**1**) and a chiral phosphane (**2**). It is shown that all nuclei (^1H, ^{13}C, ^{31}P, and ^{103}Rh) reflect the diastereomerism of the latter complex.
(© Wiley-VCH Verlag GmbH, 69451 Weinheim, Germany, 2002)

Introduction

In a series of papers[1] we have studied the potential of the dirhodium complex $Rh_2[(R)\text{-MTPA}]_4$ (**Rh***; MTPA-H = methoxytrifluoromethylphenylacetic acid, Mosher's acid) as a chiral solvating agent for the chiral recognition of various chiral monofunctional ligands **L**, i.e. for the determination of enantiomeric ratios.[2] We have shown that our "dirhodium method" is particularly suitable for soft-base functionalities where the classical method of chiral lanthanide-shift reagents (CLSR)[3] usually fails. Typically, **Rh*** and **L** form kinetically labile adducts so that only averaged NMR signals can be observed (in analogy to the CLSR method) for the **L** molecules in equilibria as depicted in Scheme 1.

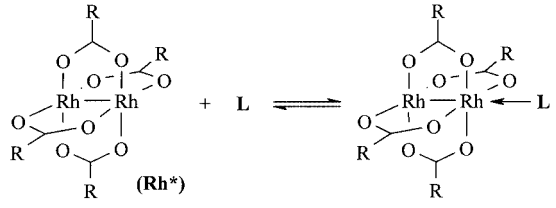

Scheme 1. Structure of $Rh_2[(R)\text{-MTPA}]_4$ (**Rh***) and schematic representation of adduct formation with a ligand **L**

[a] Hannover University, Institute of Organic Chemistry, Schneiderberg 1B, 30167 Hannover, Germany
Fax: (internat.) +49-(0)511/762-4616
E-mail: duddeck@mbox.oci.uni-hannover.de
[b] Institute of Organic Catalysis Research at Rostock University, Buchbinderstr. 5−6, 18055 Rostock, Germany
[c] S. V. Lebedev Central Synthetic Rubber Research Institute, Gapsalskaya 1, St. Petersburg 198035, Russia
[d] Centre of Molecular and Macromolecular Studies, Polish Academy of Sciences, Department of Organic Sulfur Compounds, 90−363 Łódź, Sienkiewicza 112, Poland

Although the ^{103}Rh nucleus has some advantageous properties (spin 1/2 and 100% natural abundance), it is not easy to monitor by direct ^{103}Rh NMR measurement because of its low receptivity (18% of that of ^{13}C) and rather long spin-lattice relaxation times.[4−6] So far, only one study has reported the ^{103}Rh chemical shift for the bis(trimethylphosphite) adduct of dirhodium tetraacetate (δ = 6694 ppm).[7] In our dirhodium system, however, any direct ^{103}Rh NMR spectroscopy is impossible due to the relatively low solubility of **Rh*** in $CDCl_3$.

Results and Discussion

Very recently, we reported the "dirhodium method" as the first to discriminate enantiomeric phosphane sulfides ($R_3P{=}S$) in a direct way; as for any other previously studied ligand,[1] the adducts (Scheme 1) are kinetically unstable.[8] However, when we later turned to phosphanes (R_3P) as ligands we were surprised to find that phosphane adducts are kinetically stable, i.e., the lifetimes of these adducts are long with respect to the NMR timescale. Thus, for the first time we were able to see the [**Rh***←phosphane] adducts in the ambient temperature ^{31}P NMR spectra without any averaging; the ^{31}P signals are doublets of doublets due to one- and two-bond ^{103}Rh couplings (adducts with **1**, see Scheme 2 and Table 1 and Table 2). In the case of chiral phosphanes, such as **2**, a further doubling of the signal is caused by diastereomeric dispersion.

For the first time in our dirhodium project, this offers the possibility of indirect ^{103}Rh observation by ^{31}P-detected ^{103}Rh HMQC NMR experiments. Experiments of this kind — or analogous ^1H-detected ^{103}Rh HMQC — have not been described very frequently as they require special equipment.[5,6,9] Furthermore, it was thought that if more

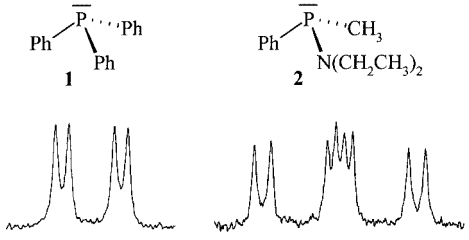

Scheme 2. Structures of the phosphanes **1** and **2** (**2** as racemate) and the respective ^{31}P signals; for the $^{103}Rh,^{31}P$ coupling constants in **1** and **2** and for the dispersion Δν in **2** see Tables 1 and 2

Table 1. ^{1}H, ^{13}C, ^{31}P, and ^{103}Rh chemical shifts (δ, in ppm), coupling constants $^{n}J(^{31}P,X)$ of free PPh_3 (**1**) and of the adduct **Rh*←1** (1:1 molar ratio of the components), adduct formation shifts (Δδ, in ppm); in $CDCl_3$

X		Free ligand δ	Free ligand $^{n}J(^{31}P,X)$	Ligand in the adduct δ	Ligand in the adduct $^{n}J(^{31}P,X)$	Δδ
^{1}H	*ortho*	7.35	n.d.[a]	7.59	$^{3}J = 10.7$	≈ 0.3
	meta	to	n.d.	≈7.23	n.d.	−0.1 to 0
	para	7.28	n.d.	7.42	$^{5}J = 0-2$	≈ 0.1
^{13}C	*ipso*	137.3	$^{1}J = 10.8$	130.2	$^{1}J = 33.4$	−7.1
	ortho	133.7	$^{2}J = 19.4$	134.4	$^{2}J = 10.6$	−2.6
	meta	128.5	$^{3}J = 7.0$	128.9	$^{3}J = 9.8$	0.2
	para	128.7	$^{4}J \leq 1$	130.6	$^{4}J \leq 3$	1.9
^{31}P		−4.2		−35.3	$^{1}J_{RhP} = 96.1$ $^{2}J_{RhP} = 23.3$	−31.1
^{103}Rh	(1)			6963		
	(2)			7455		

[a] n.d.: not determined due to signal overlap or signal complexity.

Table 2. ^{1}H, ^{13}C, ^{31}P, and ^{103}Rh chemical shifts (δ), coupling constants $^{n}J(^{31}P,X)$ of free *rac*-Ph-P(CH_3)-N(CH_2-CH_3)$_2$ (**2**) and of the adduct **Rh*←2** (1:1 molar ratio of the components), adduct formation shifts (Δδ, in ppm), and dispersion effects (Δν, in Hz, at 11.74 Tesla); in $CDCl_3$

X		Free ligand[a] δ	Free ligand[a] $^{n}J(^{31}P,X)$	Ligand in the adduct[a] δ	Ligand in the adduct[a] $^{n}J(^{31}P,X)$	Δδ	Δν
^{1}H	P-CH_3	1.489	$^{2}J = 5.6$	1.985	$^{2}J = 9.7$	0.50	1.7
	N-CH_2	3.023	$^{3}J = 9.7$	3.301	$^{3}J = 9.2$	0.28	< 1
		2.999		3.282			
	N-CH_2-CH_3	1.078	$^{4}J \leq 0.5$	1.084	$^{4}J \leq 0.5$	0.006	< 1
	ortho	7.370	$^{3}J \approx 10$	7.789	$^{3}J \approx 9$	0.42	≈ 9
				7.773		0.40	
	meta	7.322	$^{4}J \approx 2$	7.23	n.d.[b]	n.d.	n.d.
	para	7.226	$^{5}J < 1$	7.353	$^{5}J \approx 1$	0.16	≈ 1
^{13}C	P-CH_3	14.1	^{1}J =18.2	11.6	$^{1}J = 17.8$	−2.5	72.6
				11.1	$^{1}J = 15.6$	−3.0	
	N-CH_2	43.7	$^{2}J = 14.6$	41.8	$^{2}J = 2-3$	−1.9	28.4
				41.6	$^{2}J = 2-3$	−2.1	
	N-CH_2-CH_3	15.2	$^{3}J = 3.1$	14.5	$^{3}J = 3.1$	−0.7	18.2
				14.4	$^{3}J = 3.1$	−0.8	
	ipso	144.5	$^{1}J = 14.6$	134.6	$^{1}J = 34.8$	9.9	25.9
				134.4	$^{1}J = 36.7$	10.1	
	ortho	129.5	$^{2}J = 16.1$	131.3	$^{2}J = 10.3$	1.8	0.9
				131.2	$^{2}J = 10.3$	1.7	
	meta	128.0	$^{3}J = 4.1$	128.3	$^{3}J = 9.6$	0.3	5.2
				128.3	$^{3}J = 9.4$	0.3	
	para	127.2	$^{4}J = 1.0$	130.0	$^{4}J = 2.4$	2.8	2.5
				130.0	$^{4}J = 2.6$	2.8	
^{31}P		49.9		11.5	$^{1}J_{RhP} = 106.2$ $^{2}J_{RhP} = 21.5$	−38.4	89.1[c]
				11.0	$^{1}J_{RhP} = 106.2$ $^{2}J_{RhP} = 23.0$	−38.9	
^{103}Rh	(1)	–		6949, 6963			182[c]
	(2)	–		7153			9[c]

[a] Dispersions at MTPA-OCH_3: ^{1}H: δ = 2.99 and 2.97 ppm, Δν = 12.1 Hz; ^{13}C: δ = 54.6_0 and 54.5_6 ppm, Δν = 4.0 Hz. [b] n.d.: not determined due to signal overlap or signal complexity. [c] At 9.4 Tesla.

than one such insensitive nucleus (e.g., ^{103}Rh) is coupled to the sensitive detection nucleus (^{1}H or ^{31}P), triple-quantum effects may modulate the intensities and even the positions of the cross-peaks because all of the involved nuclei are ubiquitous (100% natural abundance) and rules valid for simple AX spin systems might not be applicable.[10,11] Therefore, we first had to explore the correct parameters in the HMQC experiment for our first-order AMX spin system (A = ^{31}P; M and X = ^{103}Rh). This is described in the Appendix.

^{31}P-Detected ^{103}Rh HMQC NMR Spectroscopy

Despite the low solubility of the complexes, we succeeded in obtaining ^{103}Rh correlation signals by ^{31}P-detected HMQC spectroscopy (Figure 1 and 2). The choice of the transfer delay d_2 according to Equations (7) and (8) (see Appendix) allows the discrimination and selection of signals originating from Rh(1) or Rh(2). Using the coupling constants $^{n}J(^{103}Rh,^{31}P)$ for the complex [Rh(2)−Rh(1)←**1**] (Figure 1), we obtained a first maximum for Rh(1) at d_2 = 5 ms, $f_1(0.005) = 0.940$, while Rh(2) cannot be observed: $f_2(0.005) = 0.024$. The reverse situation occurs at d_2 = 21 ms, $f_1(0.021) = 0.002$, $f_2(0.021) = 0.990$, thus only a correlation signal for Rh(2) is observable. These predictions were verified experimentally. As exemplified in Figure 1, the choice of other delays allows the simultaneous observation

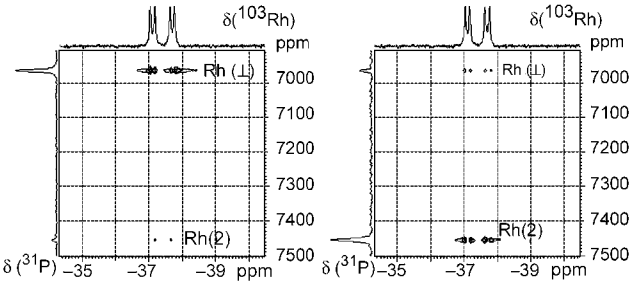

Figure 1. $^{31}P,^{103}Rh\{^{1}H\}$ HMQC NMR spectra of [**Rh*←1**] at ca. 298 K, magnitude representation.; left: transfer delay d_2 = 2.6 ms, selection of Rh(1): $f_1(0.0026) = 0.692$, $f_2(0.0026) = 0.125$; right: transfer delay d_2 = 11.6 ms, selection of Rh(2): $f_1(0.0116) = -0.234$, $f_2(0.0116) = -0.671$; calculated from J_1 = 95.5, J_2 = 21.7 Hz

of both signals, although with a somewhat reduced intensity.

In the F_2 dimension (^{31}P), the signals appear as doublets of doublets, split by the coupling constants $^{1}J(^{103}Rh,^{31}P)$ and $^{2}J(^{103}Rh,^{31}P)$, as expected. An additional splitting of ca 10 Hz is observed in the F_1 dimension (^{103}Rh), provided

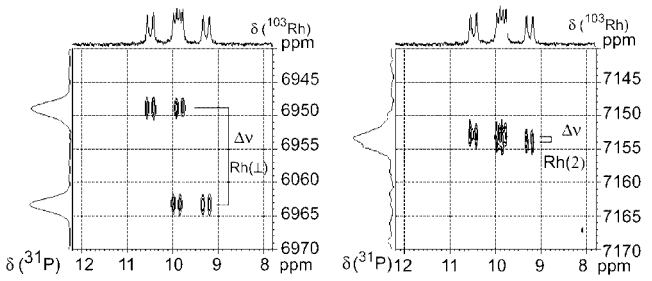

Figure 2. Sections of ^{31}P,^{103}Rh{^{1}H} HMQC NMR spectra of [**Rh*←2**] at ca. 298 K; digital resolution in F_1 is 2.9 Hz per point; top: transfer delay d_2 = 4.5 ms, selection of Rh(1): $f_1(0.0045) = 0.95$, $f_2(0.0045) = 0.02$; bottom: transfer delay d_2 = 19.0 ms, selection of Rh(2): $f_1(0.019) = -0.001$, $f_2(0.019) = 0.967$; calculated from J_1 = 105.2, J_2 = 22.0 Hz

the digital resolution is sufficient. We attribute this to the homonuclear coupling $^{1}J(^{103}Rh,^{103}Rh)$ which is to be regarded as a "passive coupling" with respect to the ^{31}P,^{103}Rh spin pair under observation and should show up in F_1. For the related symmetric phosphite adduct $[Rh_2(\mu\text{-}OAc)_4][P(OMe)_3]_2$ this coupling was determined to be 8 Hz.[7] Another origin for this splitting is unlikely as the protons are decoupled and a coupling to the fluorine atoms is not observable: the ^{19}F{^{1}H} NMR signal of (**Rh*←1**) is a singlet at δ = −72 ppm with a half-width of 3 Hz (including 1 Hz line broadening by exponential multiplication).

^{1}H, ^{13}C, ^{31}P, and ^{103}Rh NMR Parameters of 1 and 2 and Chiral Recognition

All chemical shifts and coupling constants of the phosphanes **1** and **2**, as free ligands and as their adducts with **Rh***, are listed in Table 1 and Table 2. In addition, the complexation shifts [Δδ = δ(adduct) − δ(free)] are given, and Table 2 shows the dispersion effects Δν (in Hz), which are the signal splittings due to the existence of two diastereomeric complexes. Dispersion values are field-dependent and refer to B_0 = 11.74 Tesla corresponding to 500 MHz ^{1}H (except for the ^{103}Rh values: B_0 = 9.4 Tesla, see Scheme 3).

Strong complexation shifts Δδ are observed for the phosphorus atom and for carbons nearby, and numerous ^{31}P,^{1}H and ^{31}P,^{13}C coupling constants are changed significantly as well, up to threefold or down to one half. This is clearly

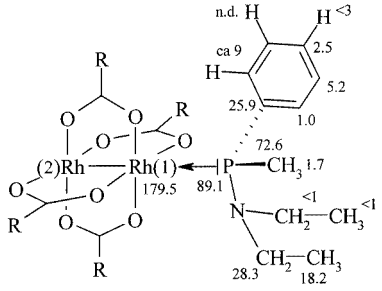

Scheme 3. Diastereomerism dispersions (Δν, in Hz) of **Rh*←2**, in $CDCl_3$ at 11.74 Tesla (^{103}Rh at 9.4 Tesla); R = MTPA; the two ethyl groups are not diastereotopic due to rapid interchange by nitrogen inversion; in contrast, the hydrogen atoms of the CH_2 groups are diastereotopic

a consequence of the above-mentioned strong interaction between the phosphanes and the rhodium atoms they are ligated to. Even a deshielding of 3.2 ppm for the *para*-carbon in **2** and one of 1.9 ppm for **1** can be noticed indicating that the inductive effect of the phosphorus atom on the benzene system is severely changed by adduct formation.

As can be seen in Scheme 3, strong dispersions appear at the phosphorus and the carbon atoms of **2**. Thus, enough nuclei exist for a safe, direct determination of the enantiomeric ratio of the phosphane (chiral recognition). Interestingly, the ^{1}H atoms in the phosphane do not show well-resolved signals in these phosphanes, except for the P-CH_3 signal — although this nucleus is generally favourable for chiral recognition — and measurements of further nuclei are often not required.[1,8] Currently, we are investigating a great variety of further chiral phosphanes to see whether or not this is a general rule.

It should be noted that dispersions of **Rh*** signals can be observed in the phosphane adducts with **2** as well, namely those of the ^{1}H and the ^{13}C signal of the methoxy group in the MTPA ligands (^{1}H: δ = 2.99 and 2.97 ppm, Δν = 12.1 Hz; ^{13}C: $\delta = 54.6_0$ and 54.5_6 ppm, Δν = 4.0 Hz). This is another proof for the fact that the adducts **Rh*←1** and **Rh*←2** are kinetically stable. If the complexes were kinetically unstable (as usually occurs for ligands other than phosphanes), only one time-averaged signal each would be visible.

As mentioned above, ^{103}Rh NMR spectroscopy is not straightforward. Only a few reports seem to exist approaching stereochemical problems by ^{103}Rh NMR spectroscopy, all on mononuclear complexes. They cover studies on catalytically active species, for example on diastereomeric enamide complexes,[12] on the stereoselectivity of the hydrogen addition to them,[13] or on the relation between δ(^{103}Rh) and changes in the ligand sphere affecting catalytic activity.[9f,9j]

In our study, the rhodium atoms reflect the diastereomerism of the **Rh*←2** adducts (Figure 2). The directly attached rhodium atom [Rh(1)] shows a large chemical shift difference of 14 ppm for the two diastereomeric complexes, corresponding to a dispersion (Δν) of 182 Hz whereas, expectedly, the remote one [Rh(2)] is much less sensitive; the correlation peaks can show a slight dispersion of 9 Hz, whereas the ^{103}Rh signal in the F_1 projection cannot resolve it (Figure 2, right). This proves the sensitivity of the rhodium nuclei in the chiral recognition experiment. Further molecular systems are currently under investigation in our laboratory.

Conclusion

For the first time, a methodology was derived for observing ^{103}Rh resonances in dirhodium-phosphane adducts (AMX spin systems) based on ^{31}P-detected ^{103}Rh HMQC NMR spectroscopy. It is shown that not only ^{31}P and ^{13}C but also ^{103}Rh signals reflect the stereochemistry of the complexes with chiral phosphanes with great sensitivity.

Experimental Section

Compounds: The synthesis of **Rh*** has been described before.[1a] Triphenylphosphane (**1**) is commercially available. *N*,*N*-Diethylamino-(methyl)(phenyl)phosphane (**2**) was synthesized according to a known procedure: Bis(*N*,*N*-diethylamino)phenylphosphane [$PhP(NEt_2)_2$], prepared from dichloro(phenyl)phosphane and diethylamine,[14] was reacted with dichlorophenylphosphane as described[15] (although without solvent) to produce *N*,*N*-diethylamino-(chloro)(phenyl)phosphane [$PhP(NEt_2)Cl$]. This compound was converted into **2** by reaction with MeLi in diethyl ether according to the procedure described by Nöth et al.[16] Yield 74%.

NMR Spectroscopy: ^1H (500.1 MHz), ^{13}C (125.8 MHz), and ^{31}P NMR measurements (202.4 MHz) of the free ligands **1** and **2** in the absence and presence of **Rh*** were performed on a Bruker DRX-500 spectrometer equipped with a broad-band probe head. Solutions were about 0.05−0.06 M in $CDCl_3$. Standards were internal tetramethylsilane ($\delta = 0$) for ^1H and ^{13}C, and external aqueous H_3PO_4 (85%) ($\delta = 0$) for ^{31}P. Digital resolutions were 0.27 Hz/point in the ^1H, 0.48 Hz/point in the ^{13}C and 0.43 Hz/point in the ^{31}P NMR spectra. ^{19}F NMR (235.4 MHz) of [**Rh***←**1**] was measured on a Bruker AC 250 spectrometer with the shift referenced against CCl_3F.

Typically, the samples were prepared by mixing 48.6 mg of **Rh*** (0.043 mmol) and a molar equivalent of **1** in 0.75 mL $CDCl_3$; 7 μL (1 drop) of [D_6]acetone were added to increase the solubility of **Rh***.[1e,8]

The unequivocal signal assignments in the ^1H and ^{13}C NMR spectra of **1** and **2** were assisted by H,H COSY, and ^1H-detected ^{13}C HMQC and HMBC NMR experiments using standard Bruker software. In cases where signal splittings due to ^{31}P-coupling had to be differentiated from dispersion effects (Δν), spectra were recorded at different B_0 (9.40 and 11.74 Tesla). (Δν values are field-dependent, coupling constants are not.)

^{103}Rh NMR spectroscopy was carried out on a Bruker ARX 400 spectrometer, equipped with a commercial triple-resonance probe, by "inverse detection" with ^{31}P as the sensitive nucleus. The standard four-pulse HMQC sequence with continuous proton decoupling was applied,[17,18] the choice of the transfer delay (d_2) was according to criteria described in the text. The chemical shifts were referenced against Ξ (^{103}Rh) = 3.16 MHz.[19] The samples of both complexes had a tetramethylsilane proton frequency of 400.130010 MHz, leading to a rhodium reference frequency, $\delta(^{103}Rh) = 0$, of 12.644108 MHz. Each experiment was performed *at least* twice with a variation of the rhodium offset and the t_1 increment to ensure that the signals in the F_1 dimension (^{103}Rh) are not folded. The digital resolution in this direction was better than 0.5 ppm in the final spectra that were recorded for shift determination. Rhodium shifts were reproducible to within ±2 ppm; we attribute observed variations to slight temperature changes (rhodium shifts have a pronounced temperature coefficient[9e][19b]). Although the data were acquired with TPPI phase cycling, a proper phasing of the signals was not always possible (regardless of whether an additional refocusing delay of duration d_2 was inserted between the last HF pulse and the data acquisition or not), hence some spectra presented in this paper are in the magnitude mode.

For a given spin system, the effect of varying experimental parameters on the HMQC spectra was tested by simulation with the NMR-SIM program (Bruker Rheinstetten). In all cases, results were as predicted by Equations (1)−(9) (see Appendix), and they were compatible with the experimental results.

APPENDIX

Signal Intensities and Multiple-Quantum Coherences in HMQC Spectroscopy of First-Order AMX Spin Systems (A = ^{31}P; M and X = ^{103}Rh): The following discussion holds for the standard four-pulse HMQC experiment, $\pi/2(^{31}P) - d_2 - \pi/2(^{103}Rh) - d_0/2 - \pi(^{31}P) - d_0/2 - \pi/2(^{103}Rh) -$ acquisition[17] in its simple as well as in its phase-sensitive (TPPI) version. The behaviour of the three-spin system ^{31}P-$^{103}Rh(1)$-$^{103}Rh(2)$ with $J[P,Rh(1)] = J_1$ and $J[P,Rh(2)] = J_2$ under the influence of this sequence can be described as follows. At the beginning of the evolution period d_0, just after the first $\pi/2(^{103}Rh)$ pulse ($t = d_2$), the state of the three-spin system is given by the density operator:

$$\sigma = (0Rh) + (1Rh_1) + (1Rh_2) + (2Rh) \quad (1)$$

where

$$(0Rh) = P(\pi/2)f_0(d_2) \quad (2)$$

$$(1Rh_1) = -2P(0)Rh_1(\pi/2)f_1(d_2) \quad (3)$$

$$(1Rh_2) = -2P(0)Rh_2(\pi/2)f_2(d_2) \quad (4)$$

$$(2Rh) = -4P(\pi/2)Rh_1(\pi/2)Rh_2(\pi/2)f_{12}(d_2) \quad (5)$$

with

$$f_0(t) = \cos(\pi J_1 t)\cos(\pi J_2 t) \quad (6)$$

$$f_1(t) = \sin(\pi J_1 t)\cos(\pi J_2 t) \quad (7)$$

$$f_2(t) = \cos(\pi J_1 t)\sin(\pi J_2 t) \quad (8)$$

$$f_{12}(t) = \sin(\pi J_1 t)\sin(\pi J_2 t) \quad (9)$$

The ^{31}P chemical shift frequency is set to zero in these equations, and the notation follows that given in ref.:[11] $P(\varphi)$ and $Rh_i(\varphi)$ denote the phosphorus and rhodium, Rh(i), spin operators for arbitrary phase φ. The zero- and two-spin rhodium coherences ($0Rh$) and ($2Rh$) are suppressed by complete phase cycling. The single-rhodium terms ($1Rh_1$) and ($1Rh_2$) produce the desired 2D peaks at true rhodium chemical shifts in the F_1 dimension. The magnitude of these correlation signals is defined by the trigonometric factors $f_1(t)$ and $f_2(t)$, see Equations (7) and (8) and Scheme 3. It is important to note that the extreme points of $f_1(t)$ and $f_2(t)$ do not coincide with the extreme points of $\sin(\pi J_1 t)$ and $\sin(\pi J_2 t)$. They cannot be deduced from the equation $d_2 = (2J)^{-1}$, as is normal for HMQC, as this might lead to complete lack of signal intensity in unfavourable cases (see Scheme 4)! A homonuclear coupling between the rhodium atoms would lead to a splitting along F_1 by J(Rh,Rh) solely of the ($1Rh$) correlation signals. This has been tested by simulation (see Exp. Sect.).

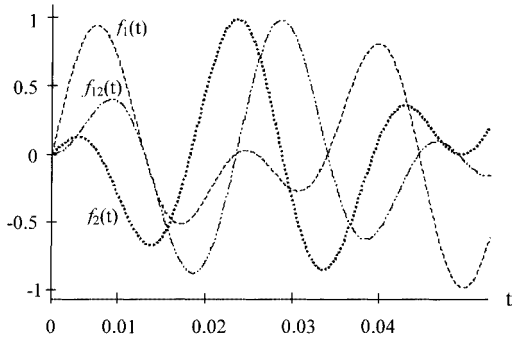

Scheme 4. Time dependence of the trigonometric factors $f_n(t)$ [Equations (7)−(9)] in a three-spin system ^{31}P-^{103}Rh-^{103}Rh, calculated for $J_1 = 95.5$ Hz and $J_2 = 21.6$ Hz (values applicable for [**Rh***←**1**])

Acknowledgments

This work has been performed within the project "Biologically Active Natural Products: Synthetic Diversity" (Department of Chemistry, Hannover University) and was supported by the Deutsche Forschungsgemeinschaft and the German Academic Exchange Service (DAAD). J. O. is grateful to the Alexander-von-Humboldt foundation for a fellowship.

[1] [1a] K. Wypchlo, H. Duddeck, *Tetrahedron: Asymmetry* **1994**, *5*, 27. [1b] K. Wypchlo, H. Duddeck, *Chirality* **1997**, *9*, 601. [1c] S. Hameed, R. Ahmad, H. Duddeck, *Heteroatom Chem.* **1998**, *9*, 471. [1d] S. Hameed, R. Ahmad, H. Duddeck, *Magn. Reson. Chem.* **1998**, *36*, S47. [1e] C. Meyer, H. Duddeck, *Magn. Reson. Chem.* **2000**, *38*, 29; see also: C. Meyer, PhD thesis, Hannover University, **1999**.

[2] It has been shown that enantiomeric purities of aromatic functionalities can be determined by ^{31}P NMR spectroscopy using a mononuclear bdpp-containing rhodium complex: J. M. Buriak, J. A. Osborn, *J. Chem. Soc., Chem. Commun.* **1995**, 689.

[3] [3a] G. R. Sullivan, *Top. Stereochem.* **1978**, *10*, 287. [3b] P. L. Rinaldi, *Progr. NMR Spectrosc.* **1983**, *15*, 291. [3c] D. Parker, *Chem. Rev.* **1991**, *91*, 1441.

[4] C. Brevard, P. Granger, *Handbook of High Resolution Multinuclear NMR*, John Wiley & Sons, Toronto **1981**, p. 158.

[5] B. E. Mann, in *Transition Metal Nuclear Magnetic Resonance* (Ed.: P. S. Pregosin), Elsevier Science Publishers, Amsterdam **1991**, p. 177ff.

[6] W. v. Philipsborn, *Chem. Soc. Rev.* **1999**, *28*, 95.

[7] E. B. Boyar, S. D. Robinson, *Inorg. Chim. Acta* **1982**, *64*, L193.

[8] S. Rockitt, H. Duddeck, J. Omelanczuk, *Chirality* **2001**, *13*, 214.

[9] Some examples: [9a] C. Brevard, R. Schimpf, *J. Magn. Reson.* **1982**, *47*, 528. [9b] C. J. Elsevier, J. M. Ernsting, W. G. J. de Lange, *J. Chem. Soc., Chem. Commun.* **1989**, 585. [9c] J. M. Ernsting, C. J. Elsevier, W. G. J. de Lange, K. Timmer, *Magn. Reson. Chem.* **1991**, *29*, S118. [9d] C. J. Elsevier, B. Kowall, H. Kragten, *Inorg. Chem.* **1995**, *34*, 4836. [9e] L. Carlton, *Magn. Reson. Chem.* **1997**, *35*, 153. [9f] K. Angermund, W. Baumann, E. Dinjus, R. Fornika, H. Görls, M. Kessler, C. Krüger, W. Leitner, F. Lutz, *Chem. Eur. J.* **1997**, *3*, 755. [9g] N. Feiken, P. Pregosin, G. Trabesinger, *Organometallics* **1998**, *17*, 4510. [9h] J. G. Donkervoort, M. Bühl, J. M. Ernsting, C. J. Elsevier, *Eur. J. Inorg. Chem.* **1999**, 27. [9i] M. Bühl, W. Baumann, R. Kadyrov, A. Börner, *Helv. Chim. Acta* **1999**, *82*, 811. [9j] W. Leitner, M. Bühl, R. Fornika, C. Six, W. Baumann, E. Dinjus, M. Kessler, C. Krüger, A. Rufińska, *Organometallics* **1999**, *18*, 1196.

[10] [10a] D. Nanz, W. von Philipsborn, *J. Magn. Reson.* **1991**, *92*, 560. [10b] H. Rüegger, D. Moskau, *Magn. Reson. Chem.* **1991**, *29*, S11.

[11] B. T. Heaton, J. A. Iggo, I. S. Podkorytov, D. J. Smawfield, S. P. Tunik, R. Whyman, *J. Chem. Soc., Dalton Trans.* **1999**, 1917.

[12] T. Ohkuma, R. Noyori, *Chemtracts: Org. Chem.* **1993**, *6*, 325.

[13] B. R. Bender, M. Koller, D. Nanz, W. von Philipsborn, *J. Am. Chem. Soc.* **1993**, *115*, 5889.

[14] G. Ewart, D. S. Payne, A. L. Porte, A. P. Lane (in part), *J. Chem. Soc.* **1962**, 3984.

[15] N. A. Andreev, O. N. Grishina, *Zh. Obshch. Khim.* **1979**, *49*, 2230, engl. Transl. 1959.

[16] H. Nöth, H.-J. Vetter, *Chem. Ber.* **1963**, *96*, 1109.

[17] A. Bax, R. H. Griffey, B. L. Hawkins, *J. Magn. Reson.* **1983**, *55*, 301.

[18] [18a] R. Benn, C. Brevard, *J. Am. Chem. Soc.* **1986**, *108*, 5622. [18b] R. Benn, A. Rufińska, *Magn. Reson. Chem.* **1988**, *26*, 895.

[19] [19a] R. G. Kidd, R. J. Goodfellow, in *NMR and the Periodic Table* (Eds.: R. K. Harris, B. E. Mann), Academic Press, London **1978**, Chap. 8. [19b] R. J. Goodfellow, in *Multinuclear NMR* (Ed.: J. Mason), Plenum Press, New York **1987**, chapter 20.

Received April 22, 2002
[I02208]

Synthesis, Characterisation and Reactivity towards Pd^{II} and Pt^{II} of *ortho*-, *meta*- and *para*-Xylyl-Based Phosphorus-Containing Macrocycles

Lluis Escriche,*[a] José Antonio Muñoz,[a] Raikko Kivekäs,[b] Reijo Sillampää,[c] and Jaume Casabó[a]

Keywords: Macrocycles / Palladium, Platinum / S ligands / Phosphanes

The new *meta*- and *para*-xylyl-based phosphadithiamacrocycles 6-phenyl-6-phospha-3,9-dithiabicyclo[9,3,1]pentadeca-1(15),12,14-triene (L2) and 6-phenyl-6-phospha-3,9-dithiabicyclo[9,2,2]pentadeca-1(13),12,14-triene (L3) have been synthesised and characterised. The reactivity of these ligands and the previously described *ortho*-xylyl macrocycle 6-phenyl-6-phospha-3,9-dithiabicyclo[9,4,0]pentadeca-1(11),12,14-triene (L1) with $[PdCl_2(cod)]$ and $K_2[PtCl_4]$ has been studied. $[MCl_2(L)]$ complexes have been obtained and characterised by NMR spectroscopy. X-ray structural analyses have been carried out in the case of $[PdCl_2L2]\cdot CH_3CN$ (**2·CH$_3$CN**) and $[PdCl_2L3]$ (**3**). In both compounds the Pd^{II} ion adopts a slightly distorted square-planar coordination defined by one *S*-thioether, the P-phosphane atoms of the ligand and two chlorine atoms, which are oriented in a mutual *cis* position, whereas the second *S*-thioether atom of the ligand remains uncoordinated. According to the spectroscopic data, the same coordination mode is found for the Pt^{II} complexes.

(© Wiley-VCH Verlag GmbH, 69451 Weinheim, Germany, 2002)

Introduction

The synthesis and chemical properties of phosphamacrocycles are less developed and studied than those of their oxygen or nitrogen equivalents.[1] This is partially due to the air-sensitivity of the reagents used in their preparations and problems in isolating the final products, especially in the case of homoleptic polyphosphamacrocycles,[2] which are usually obtained by template methods.[3] Phosphathiamacrocycles are more accessible as free ligands and several examples can be found in the literature.[4−6] Generally, the interest in asymmetric phosphorus-sulfur donor ligands, which has recently been reviewed,[7] is focused mainly towards their ability to act as hemilabile ligands and their potential use in catalytic processes.[8] Other interesting possibilities are found when these P−S donor systems are integrated in macrocyclic systems, such as the documented ability of their phosphoryl[9,10] and thiophosphoryl[11] derivatives to interact selectively with ionic species, thus acting as chemical sensors for anions.

As part of our work in this field, we report here the synthesis of the new xylyl-based phosphadithiamacrocycles 6-phenyl-6-phospha-3,9-dithiabicyclo[9,3,1]pentadeca-1(15),12,14-triene (L2) and 6-phenyl-6-phospha-3,9-dithiabicyclo[9,2,2]pentadeca-1(13),12,14-triene (L3), and the reactions of these compounds and the previously described 6-phenyl-6-phospha-3,9-dithiabicyclo[9,4,0]pentadeca-1(11),12,14-triene (L1),[12] with $[PdCl_2(cod)]$ and $K_2[PtCl_4]$.

Results and Discussion

The ligands L2 an L3 were obtained by reaction of 3-phenyl-3-phosphapenta-1,5-dithiolate (generated in situ)

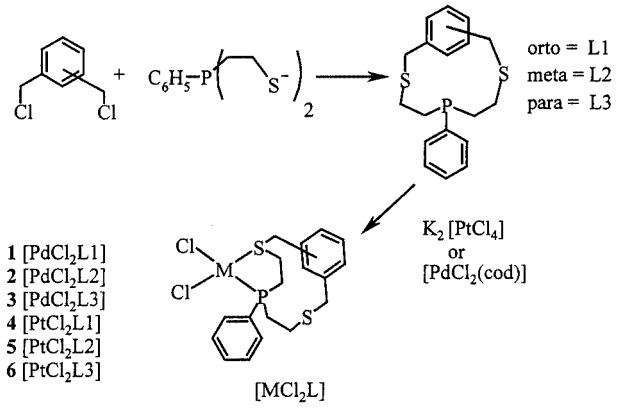

Scheme 1

[a] Departament de Química, Universitat Autònoma de Barcelona
08193 Bellaterra, Barcelona, Spain
Fax: (internat.) + 34-93/581-2497
E-mail: lluis.escriche@uab.es
[b] Department of Chemistry, University of Helsinki, Finland,
P. O. Box 55, 00014 Helsinki, Finland
[c] Department of Chemistry, University of Jyväskylä,
40351 Jyväskylä, Finland

and the appropriate α,α′-dichloro-xylene (Scheme 1) in similar conditions to those described for the synthesis of L1.[12] The yields of L2 and L3 (17% and 15%, respectively) were lower than that reported for L1 (23%), which reflects the steric hindrance imposed by the *meta* and *para* substitution of the xylyl unit to obtain the [1+1] macrocyclic compound.

The $^{31}P\{^1H\}$ NMR spectra of L2 and L3 show singlet at δ = −23.7 and −27.2 ppm, respectively, corresponding to the intraannular phosphorus atom. These values are similar to that previously reported for the ligand L1 (δ = −21.4 ppm)[12] and other similar phosphorus-containing macrocycles.[13,24] As can be seen, there is a small, but systematic, high-field shift of the P-resonances through the *ortho*, *meta* and *para* sequence, which probably reflects the increasing interaction between the aromatic π-system of the xylene ring and the phosphorus nucleus as a consequence of the different structural requirements in this series of macrocycles.

The ^1H NMR spectra of both macrocycles exhibit a complex pattern due to the high inversion energy barrier of the phosphane group,[14] which makes the geminal methylene protons non-equivalent. In both cases the aromatic protons of the phenyl rings appear as a complex multiplet between δ = 7 and 7.5 ppm, whereas the -S−CH_2-Ar methylene protons appear as a doublet of doublets (AB system) centred at δ = 3.74 and 3.80 ppm for L2 and L3, respectively. The two remaining methylene groups give four groups of complex signals between δ = 1.0 and 2.4 ppm. This reflects a coupling between all four protons and the phosphorus atom defining an ABMNX system similar to that found in the L1 ligand[12] and in other related phosphorous-containing macrocyclic molecules,[15,24] which makes the assignment of these signals difficult

The $^{13}C\{^1H\}$ NMR spectra of L2 and L3 are similar and only show one signal for each different carbon atom in the molecule, split in some cases by P−C coupling. The -S−C−Ar carbon atoms appear as a sharp singlet at δ = 35.0 and 36.6 ppm for L2 and L3, respectively, whereas the -S−C−C−P carbon atoms appear as a doublet of doublets centred at δ = 26.0 ($J_{P,C}$ = 20.3 Hz) and 26.9 ppm ($J_{P,C}$ = 22.2 Hz) for L2, and δ = 25.5 ($J_{P,C}$ = 18.7 Hz) and 28.6 ppm ($J_{P,C}$ = 16.4 Hz) for L3. According to literature data for the P−C(13) coupling constants[16] and the observed chemical shift of similar phosphane-containing ligands,[12,17,24] we assigned the first and second doublets to the carbon atoms located in the α- and β-positions, respectively, with respect to the phosphorus atom.

The Pd^{II} complexes $[PdCl_2L1]$ (**1**), $[PdCl_2L2]\cdot CH_3CN$ (**2·CH$_3$CN**) and $[PdCl_2L3]$ (**3**) were obtained by reaction of equimolar amounts of $[PdCl_2(cod)]$ dissolved in methanol (**1**) or acetonitrile (**2**, **3**) and a dichloromethane solution of the corresponding ligand (Scheme 1).

The compound **1** containing the *o*-xylyl based macrocycle L1 was obtained as an amorphous yellow material highly insoluble in all tested solvents and no additional measurements could be done. However, compounds **2** and **3** are sufficiently soluble in acetonitrile to allow their slow crystallisation from the reaction mixture if large quantities of solvent are used in the synthesis. These complexes are also sufficiently soluble in DMSO to record their NMR spectra.

The $^{31}P\{^1H\}$ NMR spectra of **2** and **3** only show one signal each at δ = 73.7 and 69.3 ppm, respectively, which suggests the presence of a unique species in solution. The positions of these resonances are similar to those found in other *cis*-$[PdCl_2L]$ complexes where L is a macrocyclic[18] or open-chain ligand[19] containing a phosphane-thioether donor-set of atoms coordinated to the Pd atom forming a five-membered chelate ring. It is well-known that chelating phosphanes in a five-membered ring are deshielded (by about 25−35 ppm) in the ^{31}P NMR spectrum, whereas in a six-membered ring they are shielded (by about 5−15 ppm), relative to related nonchelating ligands.[5,20]

The ^1H NMR spectra of both compounds are significantly more complex than those of the corresponding ligands, especially between δ = 0.3 and 3.5 ppm where the number of broad signals seems to indicate that all eight -S−CH_2−CH_2−P- protons become nonequivalent. The region between δ = 3.7 and 5.0 ppm, where the -S−CH_2−Ph-methylene proton resonances appear, is more informative regarding the coordinating behaviour of these macrocycles. Complex **2** shows two pairs of doublets in this area, indicating the presence of four nonequivalent protons (Figure 1b). The first high-field pair of doublets has an average position (δ = 3.87 ppm) similar to that found in the free ligand (δ = 3.74 ppm), and the same coupling constant ($J_{H,H}$ = 13.8 Hz), although the chemical shift difference between the centre of gravity of both doublets increases from 0.08 ppm in L2 to 0.18 ppm in **2** (Figure 1a). The second pair of doublets ($J_{H,H}$ = 13.8 Hz) is centred at δ = 4.51 ppm with a Δδ value of 0.59 ppm. This situation is similar for **3**, although a more complex spectrum is obtained. This is a result of the small difference in the chemical shift of three of the four doublets, which appear between δ = 3.84 and 4.02 ppm. To clarify this situation we performed a simulation of the above-mentioned spectra. Figure 1d and 1c show the experimental spectrum and the spectrum fitted with the gNMR simulation software,[21] respectively, for **3** in this region. The coincidence between them permits the calculation of the values of δ and the coupling constants for both pairs of doublets, which are centred at δ = 4.22 ppm (Δδ = 0.59 ppm, $J_{H,H}$ = 12.4 Hz) and δ = 3.97 ppm (Δδ = 0.06 ppm, $J_{H,H}$ = 11.7 Hz). As observed for **2**, the position and the appearance of the first high-field pair of doublets of **3** is similar to that found in free L3 (δ = 3.81 ppm, Δδ = 0.07 ppm). These data indicate a loss of symmetry in ligands L2 and L3 when they coordinate to the Pd^{II} ion, making the two -S−CH_2-Ph methylene groups nonequivalent. The fact that one of these CH_2 groups appears centred at a similar chemical shift to the free ligand in both complexes, whereas the other, more deshielded, shows a significant increase in the Δδ value between the two geminal protons suggests that only one of the *S*-thioether atoms is involved in coordination to the Pd^{II} atom. The structural information provided by the NMR spectra of **2** and **3** indicates that the behaviour of L2 and L3 as ligands with the Pd^{II} cation implies the simultaneous coordination of

one *S*-thioether and the P-phosphane atoms, forming a five-membered chelate ring and leaving the remaining *S*-thioether atom uncoordinated.

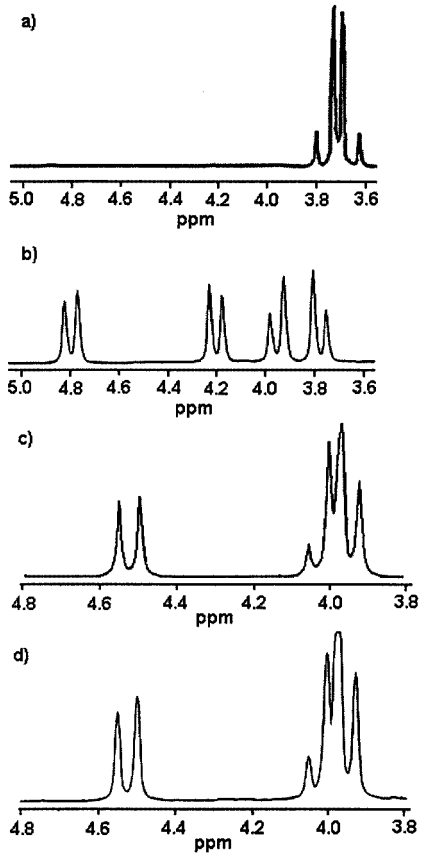

Figure 1. ^{1}H NMR spectra showing the -S−CH_2-Ar proton signals corresponding to: (a) the free ligand L2, (b) complex **2·CH_3CN**, (c) the simulation obtained with the gNMR software for **3** and (d) the complex **3**

The Pt^{II} complexes [$PtCl_2$L1] (**4**), [$PtCl_2$L2] (**5**) and [$PtCl_2$L3] (**6**) were obtained in a similar manner to that described for the Pd^{II} complexes using nitromethane solutions of $K_2[PtCl_4]$ as starting material. These complexes are significantly less soluble than their Pd^{II} equivalents. The $^{31}P\{^1H\}$ NMR spectra of **5** and **6** show a singlet, with satellites corresponding to the ^{195}Pt-^{31}P coupling, at δ = 46.4 ppm ($J_{Pt,P}$ = 3583 Hz) and δ = 41.2 ppm ($J_{Pt,P}$ = 3674 Hz), respectively. These values are similar to those found in related [*cis*-$PtCl_2$(P−S)] complexes where the P−S ligand forms a five-membered chelate ring.[18−20,22] The ^{1}H NMR spectra of both compounds show the same pattern as those recorded for **2** and **3**. Taking these data into account, it can be concluded that the platinum complexes **5** and **6** are isostructural with the Pd complexes **2** and **3**.

The X-ray diffraction analysis of **2·CH_3CN** and **3** confirms these structural deductions. The ORTEP diagrams for **2** and **3** are shown in Figure 2 and 3, respectively. Crystallographic data for both structures are listed in Table 1, and selected bond lengths and angles are summarised in Table 2. The coordination geometry around the Pd atom in both complexes is a slightly distorted square-plane defined by one *S*-thioether, the P-phosphane atoms of the ligand and two chlorine atoms, which are oriented in a mutual *cis* position. The distortion from ideal geometry around the Pd metal ions is evidenced by the P−Pd−S1 angles [87.44(5)° and 87.79(6)° for **2·CH_3CN** and **3** respectively]; this distortion can be attributed to the bite angle of the chelating ligand. In both complexes, the two Pd−Cl distances [2.3851(12) Å and 2.3118(14) Å for **2**, 2.3874(18) Å and 2.3094(18) Å for **3**] differ significantly. The Pd−Cl distance *trans* to the phosphorus atom is larger, reflecting the stronger *trans* effect of the phosphorus ligand atom relative to sulfur. The values of these Pd−Cl distances and the Pd−P and Pd−S distances lie in the same range as those found in related *cis*-[$PdCl_2$L] compounds, where L is a *P,S*-chelating ligand.[18,19,23] An interesting feature of the L3 ligand skeleton in **3** is the marked distortion observed around the *para*-substituted xylene ring as seen by the significant displacement of the methylene carbon atoms C1 and C8 out of the plane defined by the aromatic ring [0.32(1) Å and 0.40 (1) Å, respectively]. This fact reflects the steric constraint imposed on this ligand by the *P,S*-chelate ring

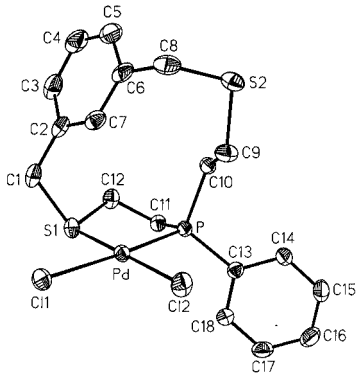

Figure 2. Perspective view of the complex unit of **2·CH_3CN** showing 30% displacement ellipsoids; hydrogen atoms are omitted for clarity

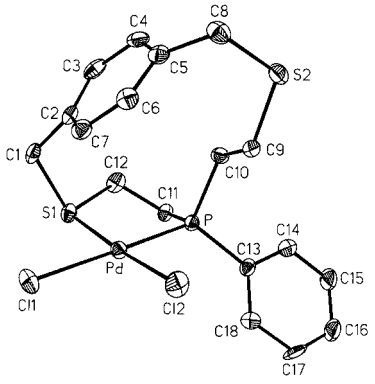

Figure 3. Perspective view of **3** showing 30% displacement ellipsoids; hydrogen atoms are omitted for clarity

formation, which forces the xylene unit to interact with the aliphatic chain.

Table 1. Crystallographic data for **2** and **3**

	2·CH$_3$CN	**3**
Chemical formula	$C_{20}H_{24}Cl_2NPPdS_2$	$C_{18}H_{21}Cl_2PPdS_2$
M	550.79	509.74
Crystal colour	Yellow	Yellow
Crystal dimensions/mm	0.26 × 0.22 × 0.18	0.20 × 0.14 × 0.06
Crystal system	Monoclinic	Monoclinic
Space group	$P2_1/c$ (No. 14)	$C2/c$ (no.15)
a (Å)	8.256(2)	20.100(4)
b (Å)	27.222(4)	13.289(2)
c (Å)	10.884(2)	15.582(2)
β (°)	112.005(14)	108.953(11)
U (Å^3)	2267.9(8)	3936.4(11)
Z	4	8
T (°C)	23	21
λ (Å)	0.71069	0.71069
D_c (g·cm^{-3})	1.613	1.720
μ (cm^{-1})	13.15	15.06
*R*1[a]	0.0363	0.0427
wR [b]	0.0706	0.0766

[a] $R1 = \Sigma||F_o| - |F_c||/\Sigma|F_o|$ (observed reflections). [b] $wR2 = [\Sigma w(|F_o^2| - |F_c^2|)^2/\Sigma w|F_o^2|^2]^{1/2}$ (observed reflections).

Table 2. Selected bond lengths (Å) and angles for compounds **2** and **3**

	2·CH$_3$CN	**3**
Pd−P	2.2182(12)	2.2248(18)
Pd−S(1)	2.2654(13)	2.2959(17)
Pd−Cl(1)	2.3851(12)	2.3874(18)
Pd−Cl(2)	2.3118(14)	2.3094(18)
S(1)−C(1)	1.836(5)	1.845(6)
S(1)−C(12)	1.827(4)	1.835(7)
S(2)−C(8)	1.819(5)	1.829(7)
S(2)−C(9)	1.810(4)	1.816(6)
P−C(10)	1.826(4)	1.827(6)
P−C(11)	1.828(4)	1.838(6)
P−C(13)	1.804(4)	1.814(6)
C(1)−C(2)	1.492(7)	1.522(9)
C(8)−C(Ar)*[a]	1.506(7)	1.494(9)
P−Pd−S(1)	87.44(5)	87.79(6)
P−Pd−Cl(2)	90.64(5)	91.75(7)
S(1)−Pd−Cl(2)	177.29(5)	175.19(8)
P−Pd−Cl(1)	174.85(5)	174.82(7)
S(1)−Pd−Cl(1)	87.43(5)	87.37(6)
Cl(2)−Pd−Cl(1)	94.50(5)	93.22(7)
C(12)−S(1)−C(1)	102.8(2)	102.1(3)
C(12)−S(1)−Pd	106.94(15)	105.7(2)
C(1)−S(1)−Pd	106.12(16)	104.9(2)
C(9)−S(2)−C(8)	101.0(2)	105.1(3)
C(13)−P−C(10)	109.4(2)	107.0(3)
C(13)−P−C(11)	107.4(2)	104.9(3)
C(10)−P−C(11)	104.6(2)	103.7(3)
C(13)−P−Pd	116.35(15)	120.5(2)
C(10)−P−Pd	112.43(14)	113.9(2)
C(11)−P−Pd	105.81(14)	105.1(2)
C(10)−C(9)−S(2)	113.2(3)	113.5(5)
C(9)−C(10)−P	115.5(3)	115.9(5)
C(12)−C(11)−P	110.1(3)	109.6(4)
C1(11)−C1(12)−S(1)	108.6(3)	109.5(4)

[a] C(Ar) = C(6) for **2·CH$_3$CN** and C(5) for **3**.

Conclusion

X-ray diffraction analysis of compounds **2·CH$_3$CN** and **3** shows an exocyclic coordination to Pd^{II} by these phosphorus- and sulfur-containing *meta*- and *para*-xylyl-based macrocyclic ligands. This coordination involves only one sulfur atom of the ligand and the P-phosphane unit. The coordination sphere is completed by two chlorine atoms. A comparative experimental and theoretical study of the ^{1}H, ^{13}C{^{1}H} and ^{31}P{^{1}H} NMR spectra of compounds **2**, **3**, **5** and **6**, especially in the region in which the proton methylene resonances of the -S−CH$_2$-Ph unit appear, allowed us to assign the same coordination mode to the corresponding Pt^{II} compounds. The insolubility of **1** and **4** prevents further structural characterisation, but the similarity observed between the related ligands L2 and L3 in their coordinating behaviour permits us to extend it to the *o*-xylyl-based ligand L1.

Experimental Section

General Remarks: All syntheses were carried out using standard Schlenk techniques under a dry dinitrogen atmosphere. The solvents were dried by conventional methods and distilled under dinitrogen before use. Dilithium 3-phenyl-3-phosphapenta-1,5-dithiolate[24] and 6-phenyl-6-phospha-3,9-dithiabicyclo[9,4,0]pentadeca-1(11),12,14-triene (L1)[12] were prepared according literature procedures. Elemental analyses were performed using a Carlo Erba EA-1108 instrument in the Chemical Analysis Service of the Universitat Autònoma de Barcelona. All NMR spectra were run by the NMR Service of the Universitat Autònoma de Barcelona. ^{1}H and ^{13}C{^{1}H} NMR spectra were recorded using a Bruker 400 MHz AM instrument and the ^{31}P{^{1}H} NMR spectra were recorded using a Bruker 250 MHz AC instrument with chemical shifts given in ppm relative to 85% H_3PO_4. COSY and HETCOR ^{1}H-^{13}C experiments were made in order to assign the ^{1}H and ^{13}C spectra by using general standard parameters. Mass spectra were recorded using a HP298S GC/MS system.

6-Phenyl-6-phospha-3,9-dithiabicyclo[9,3,1]pentadeca-1(15),12,14-triene (L2): A solution of dilithium 3-phenyl-3-phosphapenta-1,5-dithiolate in THF (100 mL, 0.18 M) and a solution of α,α′-dichloro-*m*-xylene (3.13 g, 18 mmol) in THF (100 mL) were added simultaneously to THF (500 mL) over a period of five hours at room temperature under a dinitrogen atmosphere. The resulting mixture was then stirred for a further 48 h. The THF was removed under vacuum and the resulting oily yellow residue was treated with diethyl ether (150 mL). The LiCl precipitate was filtered off and the filtrate was evaporated to a final volume of 5 mL and chromatographed over neutral Al_2O_3. The fraction eluting with toluene/CH_2Cl_2 (1:1) was collected and evaporated to obtain L2 as a colourless oil. Yield 1.02 g, 17%. $C_{18}H_{21}PS_2$ (332.5): calcd. C 65.04, H 6.37, S 19.26; found C 64.9, H 6.2, S 19.1. ^{1}H NMR (400 MHz, $CDCl_3$): δ = 1.66−1.84 (m, 4 H, -S−C*H*$_2$−CH$_2$-), 2.08−2.42 (m, 4 H, -S−CH$_2$−C*H*$_2$−P-), 3.71 (d, $J_{H,H}$ = 13.1 Hz, 2 H, -S−C*H*$_2$-Ph), 3.77 (d, $J_{H,H}$ = 13.1 Hz, 2 H, -S−C*H*$_2$-Ph), 7.07−7.45 (m, 9 H, Ar) ppm. ^{13}C{^{1}H} NMR (100 MHz, $CDCl_3$): δ = 26.0 (d, $J_{P,C}$ = 20.3 Hz, S−CH$_2$-*C*H$_2$−P-), 26.9 (d, $J_{P,C}$ = 22.2 Hz, −S-*C*H$_2$−CH$_2$−P-), 35.1 (-S-*C*H$_2$-Ph), 127.8 (-CH$_2$-*Ph*−CH$_2$-), 128.2 (s, P-Ph), 128.3 (d, $J_{P,C}$ = 7.4 Hz, P-Ph), 130.3 (-CH$_2$-*Ph*−CH$_2$-), 130.5 (-CH$_2$-*Ph*−CH$_2$-), 131.4 (d, $J_{P,C}$ = 16.6 Hz, P-Ph), 136.7 (d,

$J_{P,C}$ = 12.9 Hz, P-Ph), 137.3 (-CH_2-*Ph*−CH_2-) ppm. $^{31}P\{^1H\}$ NMR (101 MHz, $CDCl_3$): δ = −23.7 ppm. MS: (EI): *m*/*z* = 332 [M^+].

6-Phenyl-6-phospha-3,9-dithiabicyclo[9,2,2]pentadeca-1(13),12,14-triene (L3): The compound was prepared by the same procedure as for L2 using α,α′-dichloro-*p*-xylene (3.13 g, 18 mmol). Yield 0.89 g, 15%. $C_{18}H_{21}PS_2$ (332.5): calcd. C 65.04, H 6.37, S 19.26; found C 65.1, H 6.3, S 19.0. ^1H NMR (400 MHz, $CDCl_3$): δ = 0.98−1.42 (m, 4 H, -S−C*H*$_2$−CH_2-), 2.32 (m, 4 H, -S−CH_2−C*H*$_2$−P-), 3.77 (d, $J_{H,H}$ = 13.1 Hz, 2 H, -S−C*H*$_2$-Ph), 3.84 (d, $J_{H,H}$ = 13.1 Hz, 2 H, -S−C*H*$_2$-Ph), 7.12−7.45 (m, 9 H, Ar) ppm. $^{13}C\{^1H\}$ NMR (100 MHz, $CDCl_3$): δ = 25.5 (d, $J_{P,C}$ = 18.7 Hz, S−CH_2-*C*H_2−P-), 28.7 (d, $J_{P,C}$ = 16.4 Hz, -S-*C*H_2−CH_2−P-), 36.6 (-S-*C*H_2-Ph), 128.2 (d, $J_{P,C}$ = 4.7 Hz, P-Ph), 128.4 (s, P-Ph), 130.4 (-CH_2-*Ph*−CH_2-), 131.8 (d, $J_{P,C}$ = 18.7 Hz, P-Ph), 136.6 (-CH_2-*Ph*−CH_2-), 136.9 (d, $J_{P,C}$ = 16.4 Hz, P-Ph) ppm. $^{31}P\{^1H\}$ NMR (101 MHz, $CDCl_3$): δ = −27.2. MS (EI): *m*/*z* = 332 [M^+].

[$PdCl_2$L1] (1): A solution of L1 (50 mg, 0.15 mmol) in dichloromethane (5 mL) was slowly added to a solution of [$PdCl_2$(cod)] (43 mg, 0.15 mmol) in methanol (10 mL). The yellow complex obtained was filtered off, washed with diethyl ether and vacuum dried. Yield 0.057 g, 74%. $C_{18}H_{21}Cl_2PPdS_2$ (509.8): calcd. C 42.53, H 4.17, S 12.59; found C 42.3, H 4.1, S 12.3.

[$PdCl_2$L2]·CH_3CN (2·CH_3CN): A solution of L2 (230 mg, 0.69 mmol) in dichloromethane (3 mL) was slowly added to a solution of [$PdCl_2$(cod)] (198 mg, 0.69 mmol) in acetonitrile (200 mL). The resulting mixture was refluxed for 48 h and cooled down slowly to room temperature. A yellow crystalline material suitable for X-ray diffraction analysis was filtered off, washed with diethyl ether and vacuum dried. Yield 0.266 g, 70%. $C_{20}H_{24}Cl_2NPPdS_2$ (562.9): calcd. C 43.72, H 4.41, N 2.55, S 11.65; found C 43.6, H 4.3, N 2.5, S 11.5. ^1H NMR [400 MHz, $(CD_3)_2SO$]: δ = 0.95−3.44 (m, 8 H, -S−C*H*$_2$−C*H*$_2$−P), 3.78 (d, $J_{H,H}$ = 13.8 Hz, 1 H, −S−C*H*$_2$-Ph), 3.96 (d, $J_{H,H}$ = 13.8 Hz, 1 H, −S−C*H*$_2$-Ph), 4.21 (d, $J_{H,H}$ = 13.1 Hz, 1 H, -S−C*H*$_2$-Ph), 4.80 (d, $J_{H,H}$ = 13.1 Hz, 1 H, −S−C*H*$_2$-Ph), 7.26−8.43 (m, 9 H, Ar) ppm. $^{13}C\{^1H\}$ NMR [100 MHz, $(CD_3)_2SO$]: δ = 24.6 (d, $J_{P,C}$ = 24.0 Hz, S-*C*H_2−CH_2-), 27.9 (s, -CH_2-*C*H_2−P-), 28.1 (s, -CH_2-*C*H_2−P-), 33.7 (d, $J_{P,C}$ = 33.3 Hz, S-*C*H_2−CH_2-), 38.6 (s, -S-*C*H_2-Ph), 40.7 (s, -S-*C*H_2-Ph), 127.1, 128.5, 128.6, 129.3, 129.9, 131.1, 131.9 132.3, 132.4, 133.26, 142.1 (Ar) ppm. $^{31}P\{^1H\}$ NMR [101 MHz, $(CD_3)_2SO$]: δ = 73.7 ppm.

[$PdCl_2$L3] (3): This compound was prepared by the same procedure as for **2** using L3 as ligand. Yield 0.270 g, 70%. $C_{18}H_{21}Cl_2PPdS_2$ (509.8): calcd. C 42.53, H 4.17, S 12.59; found C 42.2, H 4.0, S 12.4. ^1H NMR [400 MHz, $(CD_3)_2SO$]: δ = 0.33−3.25 (m, 8 H, -S−C*H*$_2$−C*H*$_2$−P), 3.84 (d, $J_{H,H}$ = 11.7 Hz, 1 H, -S−C*H*$_2$−Ph), 3.95 (d, $J_{H,H}$ = 12.4 Hz, 1 H, -S−C*H*$_2$−Ph), 4.02 (d, $J_{H,H}$ = 11.7 Hz, 1 H, -S−C*H*$_2$−Ph), 4.51 (d, $J_{H,H}$ = 12.4 Hz, 1 H, -S−C*H*$_2$-Ph), 7.32−8.75 (m, 9 H, Ar) ppm. $^{13}C\{^1H\}$ NMR [100 MHz, $(CD_3)_2SO$]: δ = 23.9 (s, -CH_2-*C*H_2−P), 26.5 (d, $J_{P,C}$ = 16.6 Hz, -S-*C*H_2−CH_2-), 28.9 (s, -CH_2-*C*H_2−P-), 34.8 (s, -S-*C*H_2-Ph), 36.1 (d, $J_{P,C}$ = 33.3 Hz, -S-*C*H_2−CH_2-), 42.1 (s, -S-*C*H_2-Ph), 127.3, 128.23, 128.55, 128.6, 130.9, 131.4, 131.8, 131.9, 132.29, 132.5, 132.8, 135.8, 137.8 (Ar) ppm. $^{31}P\{^1H\}$ NMR [101 MHz, $(CD_3)_2SO$]: δ = 69.3 ppm.

[$PtCl_2$L1] (4): A solution of L1 (100 mg, 0.30 mmol) in dichloromethane (2 mL) was slowly added to a solution of $K_2[PtCl_4]$ (125 mg, 0.30 mmol) in nitromethane (100 mL) and the resulting mixture was refluxed for 3 h. A white precipitate of **4** mixed with KCl appeared which was filtered off, washed with water (50 mL) and diethyl ether (50 mL) and vacuum dried. Yield 0.173 g, 96%. $C_{18}H_{21}Cl_2PPdS_2$ (509.8): calcd. C 36.18, H 3.55, S 10.71; found C 35.9, H 3.5, S 10.6.

[$PtCl_2$L2] (5): A solution of L2 (190 mg, 0.57 mmol) in dichloromethane (2 mL) was slowly added to a solution of $K_2[PtCl_4]$ (237 mg, 0.57 mmol) in nitromethane (100 mL) and the resulting mixture was refluxed for 48 h. The solvent was then removed under vacuum and the residue treated with dichloromethane (100 mL). The KCl precipitate was filtered off and the remaining solution was then evaporated to a final volume of 50 mL. A microcrystalline solid appeared, which was filtered off and recrystallised from acetonitrile. Yield 0.240 g, 70%. $C_{18}H_{21}Cl_2PPdS_2$ (509.8): calcd. C 36.18, H 3.55, S 10.71; found C 36.0, H 3.5, S 10.7. ^1H NMR [400 MHz, $(CD_3)_2SO$]: δ = 0.71−3.53 (m, 8 H, -S−C*H*$_2$−C*H*$_2$−P), 3.74 (d, $J_{H,H}$ = 13.4 Hz, 1 H, -S−C*H*$_2$-Ph), 3.90 (d, $J_{H,H}$ = 13.4 Hz, 1 H, -S−C*H*$_2$-Ph), 4.35 (d, $J_{H,H}$ = 13.4 Hz, 1 H, -S−C*H*$_2$-Ph), 4.75 (d, $J_{H,H}$ = 13.4 Hz, 1 H, -S−C*H*$_2$-Ph), 7.22−8.43 (m, 9 H, Ar) ppm. $^{13}C\{^1H\}$ NMR [100 MHz, $(CD_3)_2SO$]: δ = 23.2 (d, $J_{P,C}$ = 23.1 Hz, -S-*C*H_2−CH_2-), 26.5 (s, -CH_2-*C*H_2−P), 28.1 (s, -CH_2-*C*H_2−P-), 31.5 (d, $J_{P,C}$ = 38.8 Hz, S-*C*H_2−CH_2-), 37.5 (s, -S-*C*H_2-Ph), 38.8 (s, -S-*C*H_2-Ph), 125.3, 127.34, 127.52, 128.1, 128.5, 128.6, 130.3, 130.7, 130.8, 131.2, 131.37, 131.43, 140.7 (Ar) ppm. $^{31}P\{^1H\}$ NMR [101 MHz, $(CD_3)_2SO$]: δ = 46.4 (t, $J_{Pt,C}$ = 3583 Hz).

[$PtCl_2$L3] (6): This compound was prepared by the same procedure as for **5** using L3 as ligand. Yield 0.233 g, 68%. $C_{18}H_{21}Cl_2PPdS_2$ (509.8): calcd. C 36.18, H 3.55, S 10.71; found C 36.0, H 3.2, S 10.6. ^1H NMR [400 MHz, $(CD_3)_2SO$]: δ = 0.43−3.07 (m, 8 H, -S−C*H*$_2$−C*H*$_2$−P), 3.85−4.71 (m, 4 H, -S−C*H*$_2$-Ph), 7.28−8.48 (m, 9 H, Ar) ppm. $^{31}P\{^1H\}$ NMR [101 MHz, $(CD_3)_2SO$]: δ = 41.2 ppm (t, $J_{Pt,C}$ = 3674 Hz) ppm.

X-ray Crystallographic Study: Single-crystal data collections for compounds **2·CH_3CN** and **3** were performed at ambient temperature on a Rigaku AFC5S diffractometer using graphite-monochromatised Mo-K_α radiation. The unit cell parameters for both compounds were determined by least-squares refinement of 25 carefully centred reflections. Both sets of data obtained were corrected for Lorentz and polarisation effects, and for dispersion. Corrections for empirical absorption (ψ scan) were also applied. A total of 4267 and 3566 reflections giving 3980 and 3462 unique reflections (R_{int} = 0.0199 and 0.0257) were collected by ω/2θ scan mode ($2\theta_{max}$ = 50°) for **2·CH_3CN** and **3**, respectively.

Both structures were solved by direct methods by using the SHELXS-86 program[25] and least-squares refinements were performed using the SHELX-97 program system.[26] For both complexes non-hydrogen atoms were refined with anisotropic displacement parameters. Hydrogen atoms were included in the calculations at the fixed distances from their host atoms and treated as riding atoms using the SHELX-97 default parameters.

CCDC-193056 (**2·CH_3CN**) and -193057 (**3**) contain the supplementary crystallographic data for this paper. These data can be obtained free of charge at www.ccdc.cam.ac.uk/conts/retrieving.html [or from the Cambridge Crystallographic Data Centre, 12, Union Road, Cambridge CB2 1EZ, UK; Fax: (internat.) +44-1223/336-033; E-mail: deposit@ccdc.cam.ac.uk].

Acknowledgments

We acknowledge with thanks the financial assistance of Comisión Interministerial de Ciencia y Tecnología (C.I.C.Y.T.) of the Spanish Government provided by the project BQU2000−0233.

[1] A. M. Caminade, J. P. Majoral, *Chem. Rev.* **1994**, *94*, 1183−1213.
[2] T. Lebbe, P. Machnitzki, O. Stelzer, W. S. Sheldrick, *Tetrahedron* **2000**, *56*, 157−164; S. J. Coles, P. G. Edwards, J. S. Fleming, M. B. Hursthouse, S. S. Liyanage, *Chem. Commun.* **1996**, 293−294.
[3] P. G. Edwards, M. L. Whatton, R. Haigh, *Organometallics* **2000**, *19*, 2652−2654 and references therein.
[4] M. Ciampolini, *Pure Appl. Chem.* **1986**, *58*, 1429−1436 and references therein.
[5] E. P. Kyba, R. E. Davis, M. A. Fox, C. N. Clubb, S. T. Liu, G. A. Reitz, V. J. Scheuler, R. P. Kashyap, *Inorg. Chem.* **1987**, *26*, 1647−1658 and references therein.
[6] P. J. Blower, A. V. Chadwick, J. C. Jeffery, G. E. D. Mullen, A. K. Powell, S. N. Salek, R. J. Smith, M. J. Went, *Inorg. Chim. Acta* **1999**, *294*, 170−178; J. A. Muñoz, L. Escriche, J. Casabó, C. Pérez-Jiménez, R. Kivekäs, R. Sillanpää, *Inorg. Chem.* **1997**, *36*, 947−949; P. J. Blower, J. C. Jeffery, J. R. Miller, S. N. Salek, D. Schmaljohann, R. J. Smith, M. J. Went, *Inorg. Chem.* **1997**, *36*, 1578; N. R. Champness, C. S. Frampton, G. Reid, D. A. Tocher, *J. Chem. Soc., Dalton Trans.* **1994**, 3031−3037; R. J. Smith, A. K. Powell, N. Barnard, J. R. Dilworth, P. J. Blower, *J. Chem. Soc., Chem. Commun.* **1993**, 54−56; P. B. Savage, S. K. Holmgren, J. M. Desper, S. H. Gellman; *Pure Appl. Chem.* **1993**, *65*, 461−463; T. L. Jones, A. C. Willis, S. B. Wild, *Inorg. Chem.* **1992**, *31*, 1411−1416.
[7] J. R. Dilworth, N. Wheatley, *Coord. Chem. Rev.* **2000**, *199*, 89−158.
[8] C. S. Slone, D. A. Weinberger, C. A. Mirkin, *Prog. Inorg. Chem.* **1999**, *48*, 233−350.
[9] P. B. Savage, S. K. Holmgren, S. H. Gellman, *J. Am. Chem. Soc.* **1994**, *116*, 4069−4070.
[10] J. Casabó, L. Escriche, C. Pérez- Jiménez, J. A. Muñoz, F. Teixidor, J. Baucells, A. Errachid, *Anal. Chim. Acta* **1996**, *320*, 63−68.
[11] E. I. Sinyavskaya, *Koord. Khim.* **1986**, *12*, 1155−1177; E. N. Tsvetkov, A. N. Bovin, V. K. Syundyukova, *Russ. Chem. Rev.* **1988**, 776−827; R. M. Izatt, K. Pawlak, J. S. Bradshaw, R. L. Bruening, *Chem. Rev.* **1991**, *91*, 1721−1785.
[12] R. Kivekäs, J. A. Muñoz, L. Escriche, J. Casabó, R. Sillanpää, *Acta Crystallogr., Sect. C* **1997**, *53*, 126−128.
[13] E. P. Kyba, A. M. John, S. B. Brown, C. W. Hudson, M. S. McPhaul, A. Harding, K. Larsen, S. Niedzwiecki, R. E. Davis, *J. Am. Chem. Soc.* **1980**, *102*, 139−147; E. P. Kyba, S. S. P. Chou, *J. Am. Chem. Soc.* **1980**, *102*, 7012−7014.
[14] R. D. Baechler, K. Mislow, *J. Am. Chem. Soc.* **1970**, *92*, 3090−3093.
[15] R. Boese, R. Boetzel, G. Hägele, *Magn. Reson. Chem.* **1994**, *32*, 409−414.
[16] L. M. Green, D. W. Meek, *Polyhedron* **1990**, *9*, 35−45; *Phosphorus-31 NMR Spectral Properties in Compounds. Characterization and Structural Analysis* (Eds.: J. G. Verkade, L. D. Quin), VCH, New York, **1994**.
[17] L. D. Quin, J. H. Somers, *J. Org. Chem.* **1972**, *37*, 1217−1222; S. O. Grim, W. L. Briggs, R. C. Barth, C. A. Tolman, J. P. Jesson, *Inorg. Chem.* **1974**, *13*, 1095−1100; G. D. McDonell, K. D. Berlin, J. R. Baker, S. E. Ealick, D. Van der Helm, K. L. Marsi, *J. Am. Chem. Soc.* **1978**, *100*, 4535−4540.
[18] P. H. Leung, A. Liu, K. F. Mok, A. J. P. White, D. J. Williams, *J. Chem. Soc., Dalton Trans.* **1999**, 1277−1282.
[19] E. Hauptman, P. J. Fagan, W. Marshall, *Organometallics* **1999**, *18*, 2061−2073.
[20] P. E. Garrou, *Chem. Rev.* **1981**, *81*, 229−266.
[21] IvorySoft Scientific Software; g NMR Version 3.6 for Windows.
[22] L. V. Andreasen, O. Simonsen, O. Wenberg, *Inorg. Chim. Acta* **1999**, *295*, 153−163.
[23] [23a] K. Aurivillius, G.-I. Bertinsson, *Acta Crystallogr., Sect. B* **1981**, *37*, 2073−2076. [23b] S.-T. Liu, C.-L. Tsao, M.-C. Cheng, S.-M. Peng, *Polyhedron* **1990**, *9*, 2579−2584. [23c] L.-F. Zhang, J. Yang, D.-J. Huang, *Sci. China, Ser. B (Engl.)* **1993**, *36*, 513−525. [23d] A. S. Abu-Surrah, K. Lappalainen, M. Klinga, M. Leskelä, H. A. Hodali, B. Rieger, *Acta Crystallogr., Sect. C* **1999**, *55*, 188−190.
[24] J. A. Muñoz, L. Escriche, J. Casabó, C. Pérez-Jiménez, R. Kivekäs, R. Sillanpää, *Inorg. Chim. Acta* **1997**, *257*, 99−104.
[25] G. M. Sheldrick, *SHELXS-86, Program for Crystal Structure Solution*, University of Göttingen, Germany, 1986.
[26] G. M. Sheldrick, *SHELX-97, Program for Crystal Structure Refinement*, University of Göttingen, Germany, **1997**.

Received May 3, 2002
[I02220]

A Novel Chiral Silver(I) Complex from the Reaction of Thiazolidinethione with AgOAc

Min Shi,*[a] Jian-Kang Jiang,[a] and Gui-Ling Zhao[a]

Keywords: Silver / Cluster compounds / S ligands / Structure elucidation

A novel chiral silver(I) complex was successfully synthesized from the reaction of chiral (*S*)-4-isopropylthiazolidine-2-thione ligand (**1**) with AgOAc in dichloromethane in the presence of Et_3N and DMAP at room temperature. Its unique crystal structure was unambiguously disclosed by X-ray analysis. The six silver atoms and six (*S*)-4-isopropylthiazolidine-2-thione ligands present in the complex are connected through the S and N atoms to form a cluster containing a silver octahedron with six faces of the octahedron capped by ligands.
(© Wiley-VCH Verlag GmbH, 69451 Weinheim, Germany, 2002)

Introduction

Historically, the chemistry of metal-sulfur-nitrogen cluster complexes has been a very active field for organometallic chemists because of the novelty and versatility of the structures and reactivities of such clusters, as well as their potential applications as models for the active site in nonheme proteins such as the ferredoxins.[1] In addition, many cluster complexes bearing chiral ligands can be used as catalysts in asymmetric reactions.[2] Recently, during our investigations on the utilization of thiazolidine-2-thione as a chiral auxiliary, we found that the nitrogen atom and sulfur atom of the thiocarbonyl group of thiazolidine-2-thione can readily coordinate to a metal center to afford the corresponding chiral metal complex. In particular, with AgOAc as the metal source we found that a very unusual chiral metal cluster was formed under very mild reaction conditions. This novel cluster has a silver octahedron with six faces of the octahedron capped by chiral ligands. Herein, we wish to report the synthesis and crystal structure of this novel chiral Ag^I cluster complex.

Results and Discussion

The chiral ligand (*S*)-4-isopropylthiazolidine-2-thione (**1**) was prepared according to a literature procedure.[3] The reaction of **1** with AgOAc gave a novel Ag^I complex **2** in the presence of Et_3N and DMAP in dichloromethane under very mild reaction conditions (Scheme 1). The structure of **2** was established by spectroscopic data and microanalysis.

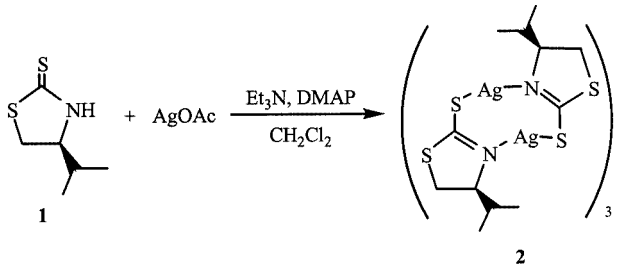

Scheme 1

We believe that the formation of **2** is caused by the fact that (*S*)-4-isopropylthiazolidine-2-thione (**1**) is in equilibrium with its tautomer **1′**, which reacts directly with AgOAc to give the corresponding Ag^I complex **2** (Scheme 2).[4] In order to clarify the crystal structure of **2** by X-ray analysis, we recrystallized **2** from dichloromethane and petroleum ether (1:5) to obtain a yellowish single crystal of **2** in which one molecule of CH_2Cl_2 was included (see the microanalysis data of **2** in the Exp. Section). The crystal structure is shown in Figure 1. Selected bond lengths and bond angles are shown in Table 1 and the crystal data of **2** are summarized in Table 2.

The chiral Ag^I complex **2** is an air- and moisture-stable solid which crystallizes in the space group *P*2(1)3. Six (*S*)-4-isopropylthiazolidine-2-thione (**1**) ligands and six Ag^I atoms form a cluster possessing a silver octahedron with six faces of the octahedron capped by ligands that alternate in

Scheme 2

[a] State Key Laboratory of Organometallic Chemistry, Shanghai Institute of Organic Chemistry,
Chinese Academy of Sciences. 354 Fenglin Lu, Shanghai 200032, China
Fax: (internat.) + 86-21/6416-6128
E-mail: Mshi@pub.sioc.ac.cn

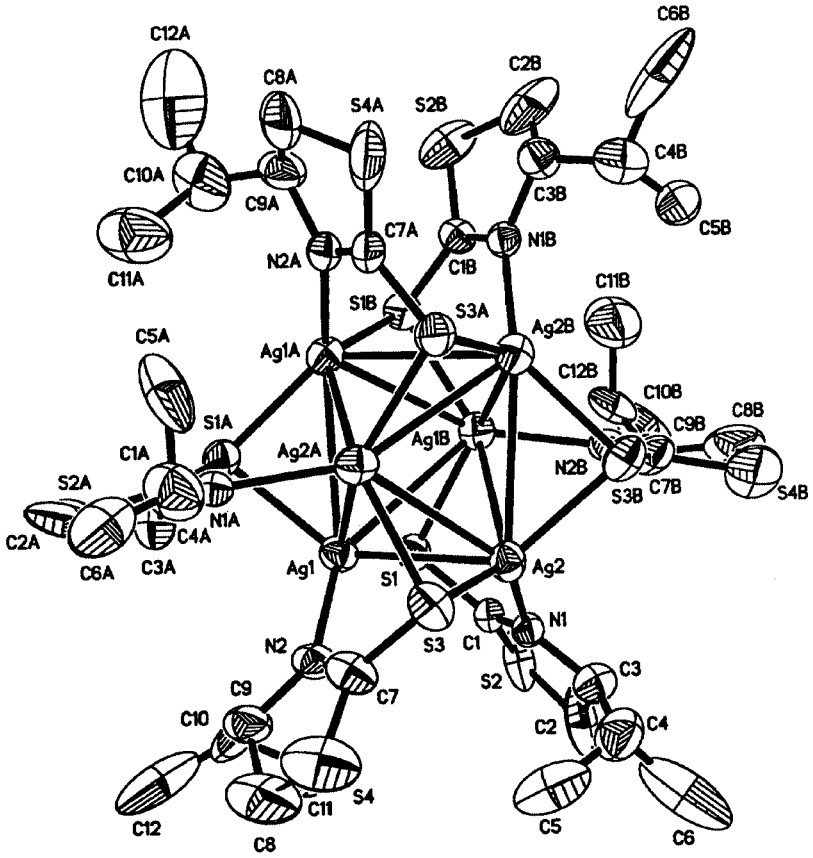

Figure 1. The X-ray crystal structure of **2**

Table 1. Selected bond lengths [Å] and angles [deg] for **2**

Ag(1)−N(2)	2.250(5)	Ag(1)−S(1)	2.4511(16)
Ag(1)−S(1)#1	2.5117(17)	Ag(1)−Ag(2)	2.9812(6)
Ag(1)−Ag(2)#1	3.2076(6)	Ag(1)−Ag(1)#2	3.3260(8)
Ag(1)−Ag(1)#1	3.3260(8)	Ag(2)−N(1)	2.261(5)
Ag(2)−S(3)	2.4582(18)	Ag(2)−S(3)#2	2.5139(19)
Ag(2)−Ag(1)#2	3.2076(6)	S(1)−Ag(1)#2	2.5117(17)
N(2)−Ag(1)−S(1)	128.03(14)	N(1)−Ag(2)−S(3)	129.07(13)
N(2)−Ag(1)−S(1)#1	108.60(13)	N(1)−Ag(2)−S(3)#2	108.65(12)
S(1)−Ag(1)−S(1)#1	116.67(8)	S(3)−Ag(2)−S(3)#2	116.77(9)
N(2)−Ag(1)−Ag(2)	83.41(15)	N(1)−Ag(2)−Ag(1)	83.63(12)
S(1)−Ag(1)−Ag(2)	80.93(4)	S(3)−Ag(2)−Ag(1)	80.46(4)
S(1)#1−Ag(1)−Ag(2)	136.62(4)	S(3)#2−Ag(2)−Ag(1)	134.88(5)
N(2)−Ag(1)−Ag(2)#1	78.21(14)	N(1)−Ag(2)−Ag(1)#2	78.05(13)
S(1)−Ag(1)−Ag(2)#1	135.74(4)	S(3)−Ag(2)−Ag(1)#2	133.90(4)
S(1)#1−Ag(1)−Ag(2)#1	75.60(4)	S(3)#2−Ag(2)−Ag(1)#2	75.24(4)
Ag(2)−Ag(1)−Ag(2)#1	66.131(19)	Ag(1)−Ag(2)−Ag(1)#2	64.898(19)
N(2)−Ag(1)−Ag(1)#2	144.19(15)	C(1)−S(1)−Ag(1)	105.9(2)
S(1)−Ag(1)−Ag(1)#2	48.70(4)	C(1)−S(1)−Ag(1)#2	98.75(19)
S(1)#1−Ag(1)−Ag(1)#2	99.77(4)	Ag(1)−S(1)−Ag(1)#2	84.15(5)
Ag(2)−Ag(1)−Ag(1)#2	60.844(17)	C(7)−S(3)−Ag(2)	104.5(2)
Ag(2)#1−Ag(1)−Ag(1)#2	88.441(13)	C(7)−S(3)−Ag(2)#1	99.7(2)
N(2)−Ag(1)−Ag(1)#1	128.88(13)	Ag(2)-S(3)−Ag(2)#1	85.71(6)
S(1)−Ag(1)−Ag(1)#1	101.09(4)	C(1)−N(1)−Ag(2)	122.3(4)
S(1)#1−Ag(1)−Ag(1)#1	47.15(4)	C(3)−N(1)−Ag(2)	124.9(4)
Ag(2)−Ag(1)−Ag(1)#1	92.372(15)	C(7)−N(2)−Ag(1)	122.5(5)
Ag(2)#1−Ag(1)−Ag(1)#1	54.258(15)	C(9)−N(2)−Ag(1)	125.5(5)
Ag(1)#2−Ag(1)−Ag(1)#1	60.0		

Table 2. Crystal data and structure refinement of **2**

Empirical formula	$C_{37}H_{62}Ag_6Cl_2N_6S_{12}$
Formula weight	1693.77
Temperature	293(2) K
Crystal system	cubic
Lattice type	primitive
a [Å]	18.2009(4)
b [Å]	18.2009(4)
c [Å]	18.2009(4)
α	90°
β	90°
γ	90°
V [Å^3]	6029.5(2)
Space group	*P*2(1)3
Z	4
$D_{calcd.}$ [g/cm^3]	1.866
F(000)	3336
θ range for data collection	1.58 to 28.31°
Reflections collected/unique	37226/4896 [*R*(int) = 0.0947]
Completeness to θ = 28.32	98.2%
Absorption correction	Sadabs
Max. and min. transmission	1.0000 and 0.7809
Refinement method	full-matrix least-squares on F^2
Data/restraints/parameters	4896/2/222
Goodness-of-fit on F^2	0.738
Final *R* indices [$I > \sigma(I)$]	$R_1 = 0.0329$, $wR_2 = 0.0655$
R indices (all data)	$R_1 = 0.0801$, $wR_2 = 0.0688$
Absolute structure parameter	−0.02(4)
Extinction coefficient	0.000 085(18)
Largest diff. peak and hole [e·Å^{-3}]	0.609 and −0.386

their orientation (Figure 1): two adjacent ligands take an anti-parallel direction using their S and N atoms to coordinate to the Ag center forming the Ag/S,N core network. Each Ag atom is coordinated by two sulfur atoms with bond lengths of 2.4527(16) and 2.5121(16) Å and a nitrogen atom with a bond length of 2.247(5) Å. In addition, the Ag^I-Ag^I distances are 2.9811(6), 3.2071(6), 3.3269(8), and 3.2071(6) Å. This distance is within the sum of the van der Waals radii of Ag of 3.44 Å (Ag = 1.72 Å[5]). The six silver atoms and six sulfur atoms present in complex **2** are connected with S and N atoms with the bond angles shown in Table 2. The Ag/S,N core forms a six-silver network. Two faces located at opposite sites of the cluster **2** are open. Based on a powder XRD analysis of the **2** obtained directly from the solvent after column chromatography (Figure 2) and of a single crystal of **2** obtained after recrystallization from dichloromethane and petroleum ether (1:5) (Figure 3), we can conclude that both samples are essentially the same. It is impossible to form by-products such as clusters of different nuclearity or coordination polymers from solution.

Compared to the metal-metal distances in the open-shell metallic silver in cluster **2** as well as to the rather underestimated sum of van der Waals radii (Ag−Ag = 3.44), we believe that a closed-shell d^{10}-d^{10} metallophilic interaction (argentophilic interaction) may exist in the above clusters[6] as the Ag−Ag distance is close to the upper van der Waals limit.[7] Assignment of these metal-metal contacts to crystal packing forces is unwarranted since the M−M vectors have a specific directionality. In addition, the M−M interactions do not seen to be dictated by ligand-packing effects. No π-

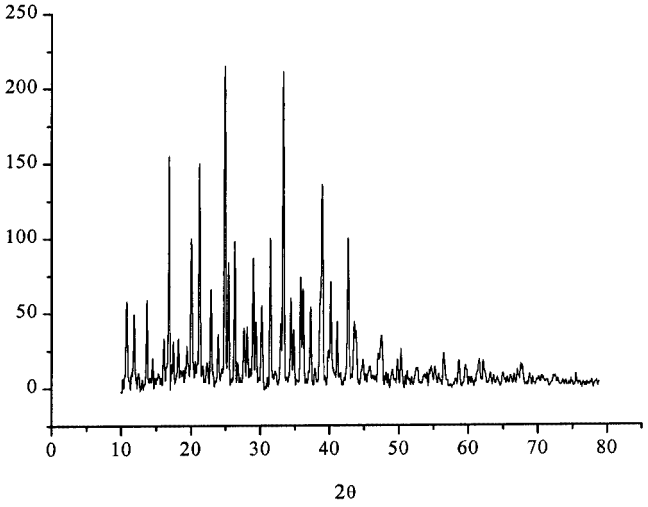

Figure 2. The powder XRD spectrum of **2** obtained directly by column chromatography

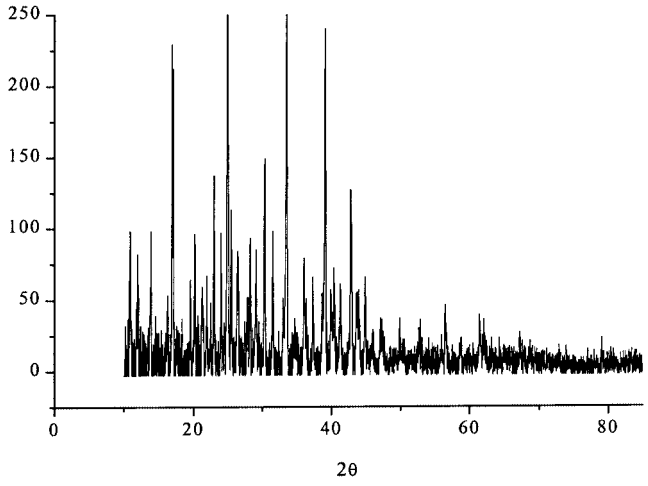

Figure 3. The powder XRD spectrum of **2** obtained after recrystallization

stacking or hydrogen-bonding interactions are apparent in the crystal structures of **2**.

It should be emphasized here that when using the simplest thiazolidine-2-thione **3** as the substrate under the same reaction conditions, no reaction occurred (Scheme 3). We believe that this may be due to the fact that the tautomer of **3** is very unstable and the equilibrium between **3** and its tautomer lies almost completely in the direction of **3**.

Yamamoto and co-workers have reported many catalytic enantioselective reactions using chiral phosphane ligand·Ag^I complexes as the catalyst, although they did not disclose the nature of the active species.[8] Therefore, we also

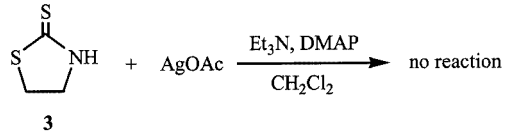

Scheme 3

tried to use this novel chiral cluster in some catalytic asymmetric reactions. Unfortunately we found that these reactions are very sluggish. We are now looking for suitable reaction conditions for these catalytic asymmetric reactions.

In conclusion, we have isolated a novel Ag^I/S,N metal cluster from the reaction of (*S*)-4-isopropylthiazolidine-2-thione (**1**) with AgOAc and determined its structure by X-ray analysis. This result also confirms that silver(I) can easily form an unexpected polymeric metal cluster with an S,N ligand. Such a chiral metal cluster should be very interesting in the synthesis of novel metal complexes for asymmetric catalysis. Work in this direction is currently in progress.

Experimental Section

Melting points were obtained with a Yanagimoto micro melting point apparatus and are uncorrected. Optical rotations were determined in a solution of $CHCl_3$ or methanol at 20 °C by using a Perkin−Elmer-241 MC digital polarimeter; $[\alpha]_D$ values are given in units of 10^{-1} deg·cm^2·g^{-1}. ^{1}H NMR spectra were determined for solutions in $CDCl_3$ with tetramethylsilane (TMS) as internal standard on a Bruker AMX-300 spectrometer; *J* values are in Hz. IR spectra were determined on a Perkin−Elmer 983 spectrometer. Mass spectra were recorded with an HP-5989 instrument. All solid compounds reported in this paper gave satisfactory CHN microanalyses. The chiral starting materials (*S*)-4-isopropylthiazolidine-2-thione (**1**) and thiazolidine-2-thione (**3**) were prepared according to literature procedures.[3]

(*S*)-4-Isopropylthiazolidine-2-thione (1): Yield 300 mg, 96%; mp: 66−67 °C; $[\alpha]_D^{20}$ = −35.4 (*c* = 0.96, $CHCl_3$). ^{1}H NMR ($CDCl_3$, 300 MHz, TMS): δ = 1.0 (d, *J* = 7.2 Hz, 3 H, CH_3), 1.03 (d, *J* = 7.2 Hz, 3 H, CH_3), 1.96 (quintet, *J* = 7.2 Hz, 1 H, CH), 3.33 (dd, *J* = 11.2, 8.5 Hz, 1 H, CH), 3.52 (dd, *J* = 11.2, 5.5 Hz, 1 H, CH), 4.0−4.10 (m, 1 H, CH), 7.62 (s, 1 H, NH) ppm. The physical data and ^{1}H NMR spectroscopic data are consistent with those reported in the literature.[3c]

Thiazolidine-2-thione (3): Yield 450 mg, 95%. ^{1}H NMR ($CDCl_3$, 300 MHz, TMS): δ = 3.58 (t, J = 7.6 Hz, 2 H, CH_2), 4.01 (t, J = 7.6 Hz, 2 H, CH_2), 8.27 (s, 1 H, NH) ppm. The physical data and ^{1}H NMR spectroscopic data are consistent with those reported in the literature.[3c]

Preparation of Chiral Silver(i) Complex 2: (*S*)-4-isopropylthiazolidine-2-thione (**1**) (65 mg, 0.5 mmol), AgOAc (84 mg, 0.5 mmol) and DMAP (6.0 mg, 0.05 mmol) were added to a Schlenk tube under argon atmosphere. CH_2Cl_2 (5.0 mL) and Et_3N (61 mg, 0.6 mmol) were added successively and the reaction mixture was stirred at room temperature for 24 h. After filtration, the filtrate was washed with water (10 mL) and the organic layer was dried with anhydrous $MgSO_4$. The solvent was removed under reduced pressure and the residue was purified by silica gel column chromatography (length: 20 cm, φ: 2 cm) to give the complex **2** as a yellowish solid (eluent: EtOAc/petroleum ether, 1:4). 120 mg, 83%; m.p. 158−160 °C (dec.); $[\alpha]_D^{20}$ = +251 (*c* = 0.11, $CHCl_3$). IR (KBr): $\tilde{\nu}$ = 1265, 1421, 1541 cm^{-1}. ^{1}H NMR ($CDCl_3$, 300 MHz, TMS): δ = 0.94 (d, *J* = 6.7 Hz, 3 H, CH_3), 0.97 (d, *J* = 6.7 Hz, 3 H, CH_3), 2.22−2.40 (m, 1 H, CH), 3.30 (d, *J* = 9.7 Hz, 2 H, CH_2), 4.20−4.32 (m, 1 H, CH) ppm. ESI-MS: *m/z* = 1259 [M^+] (acetone/acetonitrile, 2:1) $C_{36}H_{60}Ag_2N_6S_{12}\cdot CH_2Cl_2$ (1693.77): calcd. C 26.24, H 3.69, N 4.96; found C 26.45, H 3.64, N 4.94.

X-ray Crystallography: A suitable crystal was mounted on the top of a glass capillary. Crystal data and details of data collection and structure refinement are given in Table 2. Data were collected on a CCD area detector with graphite-monochromated Mo-K_α radiation (λ= 0.71073 Å) using the ω-2θ technique at 20 °C. A total of 4896 unique reflections was collected. The data were collected for Lorentz polarization effects. The structure was solved by direct methods and expanded using Fourier techniques. The non-hydrogen atoms were refined anisotropically by full-matrix least-squares. All hydrogen atoms were included in their calculated positions. All calculations were performed using the SHELXS-97 (Sheldrick, 1990) crystallographic software package. Final *R* and R_w values were 0.0329 and 0.0655. CCDC-177953 contains the supplementary crystallographic data for this paper. These data can be obtained free of charge at www.ccdc.cam.ac.uk/conts/retrieving.html [or from the Cambridge Crystallographic Data Centre, 12, Union Road, Cambridge CB2 1EZ, UK; Fax: (internat.) +44-1223/336-033; E-mail: deposit@ccdc.cam.ac.uk].

Acknowledgments

We thank the Inoue Photochirogenesis Project for chemical reagents, the State Key Project of Basic Research (Project 973) (No. G2000048007) and the National Natural Science Foundation of China (20025206) for financial support.

[1] For comprehensive reviews, see: [1a] R. D. Adams, M. Tsai, *J. Cluster Sci.* **1979**, *1*, 249−267. [1b] L. Marko', B. Marko'-Monostory, in *The Organic Chemistry of Iron* (Eds.: E. A. K. von Gustorf, F.-W. Grevels, I. Fischer); Academic Press: New York, **1981**; p. 283. [1c] H. Ogino, S. Inomata, H. Tobita, *Chem. Rev.* **1998**, *98*, 2093−2121.

[2] *Catalytic Asymmetric Synthesis* (Ed.: I. Ojima); VCH Publishers: Cambridge, **1993**.

[3] [3a] C. Agami, F. Couty, B. Prince, O. Vehier, *Tetrahedron Lett.* **1993**, *34*, 7061−7062. [3b] I. Ryu, S. Murai, N. Sonoda, *J. Org. Chem.* **1986**, *51*, 2391−2393. [3c] D. Delaunay, L. Toupet, M. L. Corre, *J. Org. Chem.* **1995**, *60*, 6604−6607.

[4] S. Jasmin, D. R. Dalton, *J. Heterocycl. Chem.* **1994**, *31*, 1079−1081.

[5] A. Bondi, *J. Phys. Chem.* **1964**, *68*, 441−451.

[6] For closed-shell d^{10}-d^{10} interaction in inorganic chemistry see: P. Pyykko, *Chem. Rev.* **1997**, *97*, 597−636.

[7] For ligand-unsupported metal-metal (M = Cu, Ag) interactions see: [7a] K. Singh, J. R. Long, P. Stavropoulos, *J. Am. Chem. Soc.* **1997**, *119*, 2942−2943. [7b] C.-M. Che, M.-C. Tse, M. C. W. Chan, K. K. Cheung, D. L. Phillips, K.-H. Leung, *J. Am. Chem. Soc.* **2000**, *122*, 2464−2468.

[8] [8a] A. Yanagisawa, H. Nakashima, A. Ishiba, H. Yamamoto, *J. Am. Chem. Soc.* **1996**, *118*, 4723−4724. [8b] A. Yanagisawa, Y. Nakatsuka, H. Nakashima, H. Yamamoto, *Synlett* **1997**, 933−934. [8c] A. Yanagisawa, A. Ishiba, H. Nakashima, H. Yamamoto, *Synlett* **1997**, 88−90. [8d] A. Yanagisawa, Y. Nakatsuka, K. Asakawa, H. Kageyama, H. Yamamoto, *Synlett* **2001**, 69−72. [8e] M. Shi, W.-S. Sui, *Tetrahedron: Asymmetry* **2000**, *11*, 773−779.

Received May 24, 2002
[I02288]

Cyclic and Polycyclic Gallium-Antimony Compounds: Synthesis and Crystal Structures of $[GaCl(PnPr_2Ph)(SbSiiPr_3)]_2$ and $[(GaCl)_4(SbSiiPr_3)_4(PnPr_2Ph)_2]$

Carsten von Hänisch,*[a] Petra Scheer,[a] and Birgit Rolli[a]

Keywords: Gallium / Antimony / Polycycles / Heterocycles / Semiconductors

The reaction of $[(DME)LiE(SiMe_3)_2]$ (E = As, Sb) with iPr_3SiCl in DME yields the mixed silylated compounds $iPr_3SiE(SiMe_3)_2$ (**1**: E = As, **2**: E = Sb). Compounds **1** and **2** were characterised by multinuclear NMR spectroscopy and mass spectrometry. The antimony compound **2** reacts with $[GaCl_3PnPr_2Ph]$ to give the cyclic compound $[GaCl(PnPr_2Ph)(SbSiiPr_3)]_2$ (**3**). The polycyclic Ga-Sb compound $[(GaCl)_4(SbSiiPr_3)_4(PnPr_2Ph)_2]$ (**4**) can be obtained from a solution of **3** in benzene. The central structural motif of **3** is a folded Ga_2Sb_2 four-membered ring. Compound **4** consists of a ladder-like Ga_4Sb_4 unit and is the first polycyclic Ga-Sb compound described. Compounds **3** and **4** were characterised by single crystal X-ray diffraction. The thermal decomposition of both compounds results in the formation of the binary phase GaSb.

Introduction

In the last few years different groups have reported the synthesis of four- and six-membered Ga-Sb ring compounds of the general formula $[R_2GaSbR'_2]_n$ (R = alkyl, chloride; R′ = alkyl, silyl; n = 2, 3).[1] In these compounds the Ga and Sb atoms have the coordination number four. Cyclic compounds with lower coordinated Ga and/or Sb atoms or polycyclic molecules are unknown so far. In contrast, several cyclic or polycyclic gallium phosphorus or gallium arsenic compounds with low-coordinate Ga and P/As atoms have been described.[2,3] We obtained the cyclic and polycyclic Ga-Sb compounds $[GaCl(PnPr_2Ph)(SbSiiPr_3)]_2$ (**3**) and $[(GaCl)_4(SbSiiPr_3)_4(PnPr_2Ph)_2]$ (**4**) from the reaction of the mixed silylated antimony compound $iPr_3SiSb(SiMe_3)_2$ (**2**) with the gallium chloride phosphane complex $[GaCl_3PnPr_2Ph]$. The structure of compounds **3** and **4** was determined by X-ray crystal structure analysis.[4]

Results and Discussion

The reaction of $[(DME)LiE(SiMe_3)_2]_2$ (E = As, Sb) with iPr_3SiCl in DME at 0 °C yields the mixed silylated compounds $iPr_3SiE(SiMe_3)_2$ (**1**: E = As, **2**: E = Sb). These compounds are highly viscous liquids which solidify to a glass-like solid when cooled to −78 °C. Both compounds were characterised by multinuclear NMR spectroscopy and mass spectrometry. Whereas the arsenic compound **1** shows no reaction towards gallium chloride phosphane complexes the antimony compound **2** reacts with the phosphane complex $[GaCl_3PnPr_2Ph]$ in diisopropyl ether to give the cyclic compound **3** as illustrated in Equation (1). Compound **3** can be obtained in crystalline form by cooling the reaction mixture to 6 °C.

$$2\,[GaCl_3{\cdot}PnPr_2Ph] + 2\,iPr_3SiSb(SiMe_3)_2 \rightarrow [GaCl(PnPr_2Ph)(SbSiiPr_3)]_2\,(\mathbf{3}) + 4\,Me_3SiCl \quad (1)$$

Compound **3** crystallises with an orthorhombic unit cell containing four molecules in the space group $Pna2_1$, and has been refined as an inversion twin (Figure 1). The central structural motif is a folded Ga_2Sb_2 four-membered ring in which the Sb atoms are trigonal pyramidally coordinated by two Ga atoms and one $SiiPr_3$ group. The gallium centres have a distorted tetrahedral geometry consisting of a chloride atom, a $PnPr_2Ph$ ligand and the two Sb atoms. Due to the mutual repulsion of the sterically demanding $PnPr_2Ph$ and $SiiPr_3$ groups they are orientated on different sides of the ring. The shape of **3** is therefore similar to the recently described gallium phosphorus and gallium arsenic compounds $[GaCl(PtBu_2Me)(ESiMe_3)]_2$ (E = P, As).[2b] The clear folding of the ring — the Sb−Ga−Sb planes have an angle of 139.0° to each other — is caused by the lower coordination number at the Sb atoms and by the *cis* orientation of the sterically demanding $SiiPr_3$ and $PnPr_2Ph$ groups. The Ga−Sb bonds in **3** are 264.1 pm on average and therefore shorter than in the Ga−Sb ring compounds with coordination number four at the gallium and the antimony atoms (267−277 pm) mentioned above. This shortening can be explained by the lower coordination number of the Sb atoms and the purely covalent character of the Ga−Sb bonds in **3**. A Ga−Sb bond length of 264.8(1) pm, however, can be observed in the acyclic compound $[LGaEt_2{-}Sb(SiMe_3)_2]$ [L = 4-(dimethylamino)pyridine], also featuring coordination number three at the anti-

[a] Institut für Nanotechnologie, Forschungszentrum Karlsruhe
Postfach 3640, 76021 Karlsruhe, Germany
Fax: (internat.) +49-(0)7247/826-368
E-Mail: carsten.vonhaenisch@int.fzk.de

 © 2002 WILEY-VCH Verlag GmbH & Co. KGaA, 69451 Weinheim 1434−1948/02/1212−3268 $ 20.00+.50/0 *Eur. J. Inorg. Chem.* **2002**, 3268−3271

mony and four at the gallium atom.[5] The endocyclic angles in **3** are 98.7° at the gallium and 75.2° at the antimony atoms. The Ga−Cl bonds are, on average, 225.2 pm long, and the exocyclic dative P−Ga bond is 244.2 pm long. Compound **3** is stable in the mother liquor but decomposes over a period of two weeks time with release of the phosphane ligands and the formation of a brown residue when isolated.

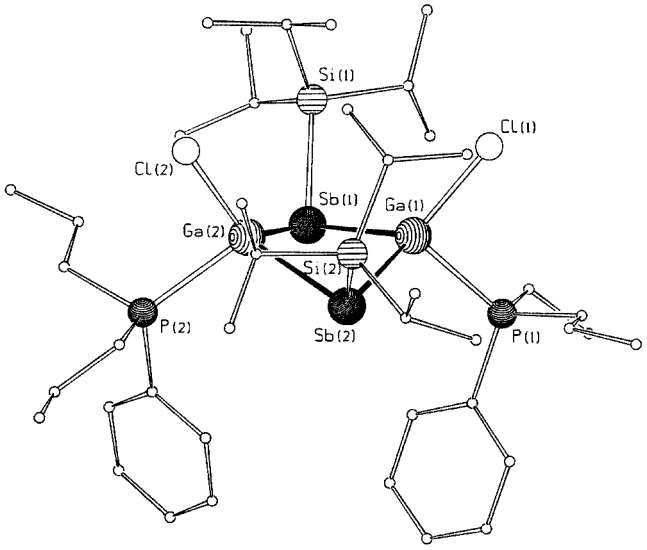

Figure 1. Molecular structure of **3**; selected bond lengths (pm) and bond angles (°): Ga(1)−Sb(1) 264.1(1), Ga(1)−Sb(2) 265.1 (1), Ga(2)−Sb(1) 263.5 (1), Ga(2)−Sb(2) 263.6(1), Ga(1)−Cl(1) 224.8(2), Ga(1)−P(1) 244.8(2), Ga(2)−Cl(2) 225.6(2), Ga(2)−P(2) 243.6(2), Sb(1)−Si(1) 258.1(2), Sb(2)−Si(2) 258.2(2); Ga(1)−Sb(1)−Ga(2) 75.3(1), Ga(1)−Sb(2)−Ga(2) 75.1(1), Sb(1)−Ga(1)−Sb(2) 98.4(1), Sb(1)−Ga(2)−Sb(2) 99.0(1), Cl(1)−Ga(1)−P(1) 93.7(1), Cl(2)−Ga(2)−P(2) 92.3(1), Si(1)−Sb(1)−Ga(1) 107.5(1), Si(1)−Sb(1)−Ga(2) 116.0(1), Si(2)−Sb(2)−Ga(1) 117.1(1), Si(2)−Sb(2)−Ga(2) 105.9(1)

Red crystals with the composition $[(GaCl)_4(SbSi\text{-}i Pr_3)_4(P n Pr_2Ph)_2]$ (**4**) · 2 C_6H_6 were obtained from a solution of **3** in benzene over a period of three days. Obviously compound **3** undergoes a condensation reaction to give **4** and two free phosphane molecules [Equation (2)].

$$2\,[GaCl(P n Pr_2Ph)(SbSi i Pr_3)]_2 \rightarrow [(GaCl)_4(SbSi i Pr_3)_4(P n Pr_2Ph)_2]\,(\mathbf{4}) + 2\,P n Pr_2Ph \quad (2)$$

The molecular structure of **4** (Figure 2), which contains an inversion centre, consists of a central planar Ga_2Sb_2 four-membered ring in which the silyl groups and the Cl atoms are *trans* orientated. Two slightly folded Ga_2Sb_2 rings with an all *cis* orientation of the silyl groups and the Cl atoms are connected to the central ring on opposite sides. These three Ga_2Sb_2 rings are not coplanar, instead the three moieties form a chair-like structure. A similar structure has been observed for the aluminium-phosphorus compound $[(AlCl)_4(PR)_4(OEt_2)_2]$ (R = Si*i*Pr$_3$, Si*i*Pr$_2$Me) which was recently obtained by reaction of $AlCl_3$ with Li_2PR in diethyl ether.[6]

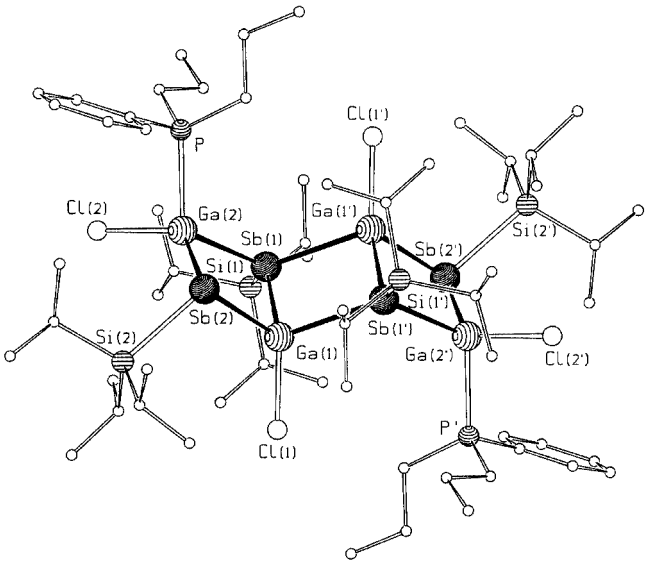

Figure 2. Molecular structure of **4**; selected bond lengths (pm) and bond angles (°): Ga(1)−Sb(1) 271.7(1), Ga(1)−Sb(1′) 269.1(1), Ga(1)−Sb(2) 264.4(1), Ga(2)−Sb(1) 266.2(1) Ga(2)−Sb(2) 261.8(1), Ga(1)−Cl(1) 222.5(2), Ga(2)−Cl(2) 222.9(2), Ga(2)−P: 242.9(2), Sb(1)−Si(1) 258.9(2), Sb(2)−Si(2) 259.1(2); Ga(1)−Sb(1)−Ga(2) 80.4(1), Ga(1)−Sb(1)−Ga(1′) 86.3(1), Ga(1′)−Sb(1)−Ga(2) 117.7(1), Ga(1)−Sb(2)−Ga(2) 82.6(1), Sb(1)−Ga(1)−Sb(2) 97. 0(1), Sb(1)−Ga(1)−Sb(1′) 93.7(1), Sb(1′)−Ga(1)−Sb(2) 110.9(1), Sb(1)−Ga(2)−Sb(2) 99.0(1), Cl(2)−Ga(2)−P 93.3(1)

The coordination sphere of the outer Ga atoms [Ga(2) and Ga(2′)] in **4** is completed by the phosphane ligands, so that all Ga atoms have coordination number four. The Sb atoms in **4** have two different coordination numbers: the Sb atoms of the central ring [Sb(1) and Sb(1′)] have a coordination number of four, whereas the outer Sb atoms are trigonal pyramidal coordinated. The Ga−Sb bond lengths in **4** vary greatly. In the central ring they are 269.1(1) to 271.7(1) pm long, whereas the Ga(1)−Sb(2) and the Ga(2)−Sb(1) bond lengths are 264.4(1) and 266.2(1) pm, respectively. The shortest Ga−Sb bond known so far can be observed between Ga(2) and Sb(2) [261.8(1) pm].

The UV/Vis spectrum of the yellow compound **3** shows a first absorption maxima at 425 nm. The red compound **4** reveals the first absorption maxima at 450 nm. In the IR spectra of both compounds the typical peaks of the P*n*Pr$_2$Ph ligands and the Si*i*Pr$_3$ groups are observed.

Thermogravimetric analysis of compound **3** under vacuum shows a one-step decomposition in the temperature range of 110 to 160 °C. The on-line mass spectra of the cleavage products shows the phosphane ligands and the silyl groups. The overall mass loss is 70.0% (calculated for the formation of GaSb: 66.9%). Powder X-ray diffraction measurements of the grey residue obtained display only the reflections of cubic GaSb. From element analyses the carbon content of the residue was determined to be 1.5(5)%. Analogous thermogravimetric experiments on **4** show a two-step decomposition. In a first step, between 75 and 120 °C, the cleavage of the crystal solvent can be observed (mass

loss: calcd. 7.5%, observed 7.1%). At 180 °C all volatile constituents have been eliminated and the formation of cubic GaSb occurs.

Experimental Section

All manipulations were performed with rigorous exclusion of oxygen and moisture using a Schlenk line and nitrogen atmosphere. Solvents were dried and freshly distilled before use. $[(DME)LiE(SiMe_3)_2]_2$ was prepared according to a literature procedure.[7] $GaCl_3$ (99.99%) and iPr$_3$SiCl (97%) were obtained from Aldrich and used as received.

iPr$_3$SiAs(SiMe$_3$)$_2$ (1): A mixture of iPr$_3$SiCl (12.1 g) in DME (20 mL) was added to a solution of $[(DME)LiAs(SiMe_3)_2]_2$ (20 g, 63 mmol) in DME (200 mL) over a period of two hours at 0 °C. Subsequently the reaction mixture was stirred for an additional 16 hours at room temperature and then filtered. All volatile components were then removed under vacuum and the resulting residue was fractionally distilled to give **1** as a highly viscous liquid at 90−100 °C and 10^{-3} mbar. Yield: 15.5 g (65%). ^{1}H NMR (C_6D_6): δ = 0.52 (s, 18 H, SiMe$_3$), 1.29 (m, 21 H, SiiPr$_3$) ppm. ^{13}C{^{1}H} NMR (C_6D_6): δ = 5.7 (s, SiMe$_3$), 15.8 [s, CH(CH$_3$)$_2$], 20.3 [s, CH(CH$_3$)$_2$] ppm. ^{29}Si{^{1}H} NMR (C_6D_6): δ = 2.4 (s, SiMe$_3$), 25.0 (s, SiiPr$_3$) ppm. MS (EI, 70 eV): m/z (%) = 378 (30) [M$^+$], 363 (0.5) [M$^+$ − Me], 335 (1) [M$^+$ − iPr], 293 (0.7) [M$^+$ − iPr, − CH$_2$CHCH$_3$], 251 (0.7) [M$^+$ − 2iPr − CH$_2$CHCH$_3$], 206 (22) [M$^+$ − Me − SiiPr$_3$], 157 (18) [SiiPr$_3$], 73 (100) [SiMe$_3$].

iPr$_3$SiSb(SiMe$_3$)$_2$ (2): A mixture of iPr$_3$SiCl (10.5 g) in DME (20 mL) was added to a solution of $[(DME)LiSb(SiMe_3)_2]_2$ (20 g, 55 mmol) in DME (200 mL) over a period of two hours at 0 °C. Subsequently the reaction mixture was stirred for an additional 16 hours at room temperature and then filtered. All volatile components were removed under vacuum and the resulting residue was fractionally distilled to give **2** as a highly viscous liquid at 110−120 °C and 10^{-3} mbar. Yield: 13.5 g (58%). ^{1}H NMR (C_6D_6): δ = 0.58 (s, 18 H, SiMe$_3$), 1.27 (m, 21 H, SiiPr$_3$) ppm. ^{13}C{^{1}H} NMR (C_6D_6): δ = 6.0 (s, SiMe$_3$), 15.4 [s, CH(CH$_3$)$_2$], 20.6 [s, CH(CH$_3$)$_2$] ppm. ^{29}Si{^{1}H} NMR (C_6D_6): δ = −10.2 (s, SiMe$_3$), 27.1 (s, SiiPr$_3$) ppm. MS (EI, 70 eV): m/z (%) = 424 (4) [M$^+$], 409 (0.4) [M$^+$ − Me], 252 (5) [M$^+$ − Me − SiiPr$_3$], 157 (30) [SiiPr$_3$], 73 (100) [SiMe$_3$].

3: PnPr$_2$Ph (0.94 g, 4.88 mmol) was added to a solution of $GaCl_3$ (0.43 g, 2.44 mmol) in 30 mL of iPr$_2$O. After stirring for one hour iPr$_3$SiSb(SiMe$_3$)$_2$ (1.04 g, 2.44 mmol) was added. The reaction mixture was then stirred for an additional 24 hours. Subsequently the resulting red solution was filtered to remove small amounts of insoluble residues and the volume was reduced to 10 mL under vacuum. After addition of 5 mL heptane and cooling to 6 °C yellow crystals of **3** formed over a period of two days. Yield: 0.59 g (42%). $C_{42}H_{80}Cl_2Ga_2P_2Sb_2Si_2$ (1157.02): calcd. C 43.60, H 6.97; found C 43.16, H 6.98. ^{31}P{^{1}H} NMR (C_6D_6/PnPr$_2$Ph): δ = −30.5 (s) ppm. IR (KBr): $\tilde{\nu}$ = 3077(w), 3049(w), 2960(s), 2937(vs), 2860(vs), 1983(vw), 1959(vw), 1906(vw), 1806(vw), 1758(vw), 1484(m), 1463(vs), 1437(vs), 1407(m), 1380(m), 1364(w), 1358(w), 1226(m), 1105(w), 1068(s), 1027(m), 995(vs), 918(m), 882(s), 842(w), 828(m), 770(w), 746(vs), 693(s), 658(vs), 634(s), 557(vs), 503(m), 489(w), 459(s), 393(w) cm^{-1}. UV/Vis (suspension in mineral oil): λ_{max} = 425 nm (sh), 370 (sh), 260, 220.

4: Compound **3** (0.2 g) was dissolved in 2 mL benzene and stirred for two hours at room temperature. Subsequently the solution was cooled to 6 °C. After three days red crystals of **4** formed from this solution. Yield: 0.1 g (54%). $C_{60}H_{122}Cl_4Ga_4P_2Sb_4Si_4 \cdot 2\ C_6H_6$ (2081.77): calcd. C 41.54, H 6.49; found C 41.38, H 6.96. ^{31}P{^{1}H} NMR (C_6D_6): δ = −20.2 (s) ppm. IR (KBr): $\tilde{\nu}$ = 3087(vw), 3059(w), 3033(vw), 2960(s), 2939(vs), 2862(vs), 1959(vw), 1859(w), 1816(vw), 1459(vs), 1437(s), 1413(w), 1384(m), 1365(w), 1292(w), 1224(m), 1105(w), 1083(m), 1069(m), 1020(s), 993(s), 918(m), 878(vs), 846(w), 802(w), 740(m), 690(m), 693(s), 658(m), 639(s), 564(s), 520(w), 494(vs), 458(m) cm^{-1}. UV/Vis (suspension in mineral oil): λ_{max} = 450 nm, 380 (sh), 300.

Acknowledgments

This research was supported by a grant from the G.I.F., the German-Israeli Foundation for Scientific Research and Development. We thank Dr. P. Kramkowski for his valuable help with the manuscript.

[1] [1a] S. Schulz, *Coord. Chem. Rev.* **2001**, *215*, 1−37. [1b] A. Kuczkowski, S. Schulz, M. Nieger, P. Saarenketo, *Organometallics* **2001**, *20*, 2000−2006. [1c] E. E. Foos, R. J. Louet, R. L. Wells, A. L. Rheingold, L. M. Liable-Sands, *J. Organomet. Chem.* **1999**, *582*, 45−52. [1d] S. Schulz, M. Nieger, *J. Organomet. Chem.* **1998**, *570*, 275−278. [1e] R. L. Wells, E. E. Foos, P. S. White, A. L. Rheingold, L. M. Liable-Sands, *Organometallics* **1997**, *16*, 4771−4775. [1f] A. H. Cowley, R. A. Jones, C. M. Nunn, D. L. Westmoreland, *Chem. Mater.* **1990**, *2*, 221−222. [1g] A. H. Cowley, R. A. Jones, K. B. Kidd, C. M. Nunn, D. L. Westmoreland, *J. Organomet. Chem.* **1988**, *341*, C1−C5.

[2] [2a] C. von Hänisch, O. Hampe, *Angew. Chem.* **2002**, *114*, 2198−2200; *Angew. Chem. Int. Ed.* **2002**, *41*, 2095−2097. [2b] C. von Hänisch, *Z. Anorg. Allg. Chem.* **2001**, *627*, 68−72. [2c] D. A. Atwood, A. H. Cowley, R. A. Jones, M. A. Mardones, *J. Am. Chem. Soc.* **1991**, *113*, 7050−7052. [2d] H. Hope, D. C. Pestana, P. P. Power, *Angew. Chem.* **1991**, *103*, 726−727; *Angew. Chem. Int. Ed. Engl.* **1991**, *30*, 691−692. [2e] A. H. Cowley, R. A. Jones, M. A. Mardones, J. Ruiz, J. L. Atwood, S. G. Bott, *Angew. Chem.* **1990**, *102*, 1169−1171; *Angew. Chem. Int. Ed. Engl.* **1990**, *29*, 1150−1152.

[3] [3a] A. Dashti-Mommertz, B. Neumüller, *Z. Anorg. Allg. Chem.* **1999**, *625*, 954−960. [3b] W. Uhl, M. Benter, *Chem. Commun.* **1999**, 771−772. [3c] M. Driess, S. Kuntz, K. Merz, H. Pritzkow, *Chem. Eur. J.* **1998**, *4*, 1628−1632. [3d] K. Niedick, B. Neumüller, *Chem. Ber.* **1994**, *127*, 67−71. [3e] R. L. Wells, A. P. Purdy, A. T. McPhail, C. G. Pitt, *J. Chem. Soc., Chem. Commun.* **1986**, 487−488.

[4] STOE-IPDS2, graphite monochromator, Mo-K_α radiation, λ = 0.71073 Å. **3**: a = 2070.9(4), b = 1201.7(2), c = 2125.6(4) pm, α = β = γ = 90°, V = 5290.0(2) × 10^6 pm^3; orthorhombic, $Pna2_1$, Flack parameter. 0.609, Z = 4, ρ_{ber} = 1.453 g/cm^3, μ(Mo-K_α) = 2.251 mm^{-1}, T = 200 K, $2\Theta_{max}$ = 52°; 12172 reflections measured, 7798 independent reflections, (R_{int} = 0.0287), 7035 independent reflections with $F_o > 4\sigma(F_o)$. The structure was solved by direct methods and refined by full-matrix least-squares techniques against F^2, 470 parameters (Ga, Sb, Si, P, Cl, C refined anisotropically, H atoms calculated at ideal positions), $R1$ = 0.0312, $wR2$ = 0.0856 (all data), residual electron density: 0.618 e/Å^3. **4**·2C$_6$H$_6$: a = 1386.4(3), b = 2006.5(4), c = 1679.2(3) pm, α = 90°, β = 97.12(3)°, γ = 90°, V = 4634.9(16) × 10^6 pm^3; monoclinic, $P2_1/n$, Z = 2, ρ_{ber} = 1.492 g/cm^3, μ(Mo-K_α) = 2.527 mm^{-1}, T = 200 K, $2\Theta_{max}$ = 52°; 16486 reflections measured, 8252 independent reflections, (R_{int} = 0.0754), 5909 independent reflections with $F_o > 4\sigma(F_o)$. The structure was solved by direct methods and refined by full-matrix least-squares techniques against F^2, 406 parameters

(Ga, Sb, Si, P, Cl, C refined anisotropically, H atoms calculated at ideal positions), $R1 = 0.0475$, $wR2 = 0.1126$ (all data), residual electron density: 1.365 e/Å^3. CCDC-187743 (**3**) and CCDC-187744 (**4**) contain the supplementary crystallographic data for this paper. These data can be obtained free of charge at www.ccdc.cam.ac.uk/conts/retrieving.html [or from the Cambridge Crystallographic Data Centre, 12, Union Road, Cambridge CB2 1EZ, UK; Fax: (internat.) +44-1223/336-033; E-mail: deposit@ccdc.cam.ac.uk].

[5] F. Thomas, S. Schulz, M. Nieger, *Eur. J. Inorg. Chem.* **2001**, 161−166.
[6] C. von Hänisch, F. Weigend, *Z. Anorg. Allg. Chem.* **2002**, *628*, 389−393.
[7] [7a] G. Becker, A. Münch, C. Witthauer, *Z. Anorg. Allg. Chem.* **1982**, *492*, 15−27. [7b] G. Becker, C. Witthauer, *Z. Anorg. Allg. Chem.* **1982**, *492*, 29−36.

Received June 25, 2002
[I02343]

Synthesis and Structure of the Decanuclear Gold(I) Cluster Cation $[Au_8(AuCl)_2\{\mu_3\text{-}P(t\text{Bu})\}_2\{\mu\text{-}P(t\text{Bu})=C(NMe_2)_2\}_6]^{4+}$ with Bridging Phosphaalkene and Phosphanediide Ligands

Lothar Weber,*[a] Ulrich Lassahn,[a] Hans-Georg Stammler,[a] Beate Neumann,[a] and Konstantin Karaghiosoff[b]

Keywords: Cluster compounds / Gold / Phosphaalkenes / Phosphinidenes

Reaction of the inversely polarized phosphaalkene HP=C(NMe$_2$)$_2$ (**1**) with [AuCl(PPh$_3$)] (**2a**) in a molar ratio of 2:1 in THF led to the formation of complex [Au{HP=C(NMe$_2$)$_2$}$_2$]Cl (**3**) as a pale yellow solid. In contrast to this, treatment of **2a** with two molar equivalents of *t*BuP=C(NMe$_2$)$_2$ (**4**) afforded a mixture of [Au{P(*t*Bu)=C(NMe$_2$)$_2$}$_2$]$^+$Cl$^-$ (**5**) and [{(Me$_2$N)$_2$C=(*t*Bu)PAu}$_2$(μ-Cl)]$^+$Cl$^-$ (**6**). In CH_2Cl_2 solution this mixture was slowly converted into the novel decanuclear complex $[Au_8(AuCl)_2\{\mu_3\text{-}P(t\text{Bu})\}_2\{\mu\text{-}P(t\text{Bu})=C(NMe_2)_2\}_6]^{4+}(Cl^-)_4$ (**7**) featuring six edge-bridging phosphaalkene ligands and two μ_3-*tert*-butylphosphanediide ligands. In solution the cluster **7** shows a high order $^{31}P\{^1H\}$ NMR spectrum of the $[AB_2C]_2$ type. According to the X-ray structural analysis the Au_{10} framework may be described as a slightly puckered ladder constructed of three quadrangles. The central Au_4 parallelogram is capped on both faces by a pair of [*t*BuPAuCl] units.
(© Wiley-VCH Verlag GmbH, 69451 Weinheim, Germany, 2002)

Introduction

The chemistry of multinuclear complexes has been studied by several research groups for academic reasons as well as for potential industrial applications.[1] In contrast to a wide variety of chalcogen-bridged gold complexes,[2] gold clusters with phosphorus-containing ligands in bridging positions are rare. Cluster cations with "naked" phosphorus atoms are $[P(AuL)_4]^+$,[4] $[P(AuL)_5]^{2+}$,[5] $[P(Au_5L_6)]^{2+}$,[6] $[P(AuL)_6]^{3+}$,[7] $[Au\{P(AuL)_4\}_2]^{3+}$.[3] In $[arylP(AuL)_3]^+$ [5a,8] and $[arylP(AuL)_4]^{2+}$ [8] phosphinidene ligands are bridging the Au atoms and the terminal ligands (L) are tertiary phosphanes. The chemistry of gold(I) phosphanides is also poorly developed. Apart from polymeric $[\{Au(\mu\text{-}PR_2)\}_n]$ (R = phenyl, substituted phenyl, ethyl, or *n*-octyl),[9] structurally characterized dinuclear complex anions $[(AuX)_2(\mu\text{-}PPh_2)]^-$ (X = Cl, Br, I)[10,11] are known. Laguna et al. have recently reported the synthesis of dinuclear Au^{III} complexes $[\{Au(C_6F_6)_3\}_2(\mu\text{-}PPh_2)]^-$, $[Au_2(C_6F_5)_4(\mu\text{-}PPh_2)_2)]$[13] as well as the trinuclear $Au^{III}-Au^{I}$ phosphanido-bridged derivatives $[\{(C_6F_5)_3Au(\mu\text{-}PPh_2)\}_2Au]^-$,[14] $[\{C_6F_5Au(\mu\text{-}PPh_2)\}_2Au(C_6F_5)_2]^-$,[15] $[\{(Ph_3P)Au(\mu\text{-}PPh_2)\}_2Au(C_6F_5)_2]^+$ [15] and the tetranuclear complex $[\{Au(C_6F_5)_2(\mu\text{-}PPh_2)_2Au\}_2]$.[15] Structurally characterized polynuclear ($n > 4$) and homometallic μ-phosphanido clusters of gold are without precedent to the best of our knowledge.

C-Amino-substituted phosphaalkenes $R'P=C(NR_2)_2$ are zwitterions in which the negatively charged phosphanide unit is stabilized by an adjacent carbenium center[16,17] (Scheme 1).

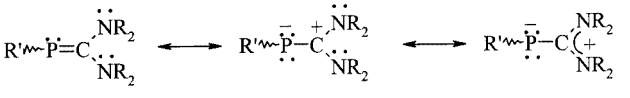

Scheme 1. Limiting formulae of amino-substituted phosphaalkenes

In the context of the present work, the question as to whether phosphaalkenes with an inverse distribution of π-electron density can function as bridging ligands in polynuclear gold complexes was intriguing.

Results and Discussion

The reaction of the gold complexes [Au(Cl)L] (**2**) (**a**: L = PPh_3, **b**: tetrahydrothiophene (THT), **c**: CO) with two molar equivalents of phosphaalkene **1** in THF at ambient temperature leads to the precipitation of the yellow mononuclear complex **3** (Scheme 2).

[a] Fakultät für Chemie der Universität Bielefeld
Universitätsstraße 25, 33615 Bielefeld, Germany
Fax: (internat.) +49-(0)521/106-6146
E-mail: lothar.weber@uni-bielefeld.de
[b] Department Chemie der Universität München
Butenandtstraße 5-13 (Haus D), 81377 München, Germany
E-Mail: klk@cup.uni-muenchen.de

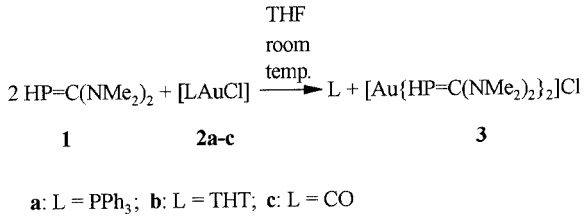

Scheme 2. Reaction of $HP{=}C(NMe_2)_2$ with [LAuCl]

Compound **3** is readily soluble in dichloromethane. The ^{31}P NMR signal in the proton-coupled spectrum of **3** at $\delta = -90$ ppm (d, $^1J_{P,H} = 219$ Hz) is shifted to higher field with respect to the free ligand **1** ($\delta = -73$ ppm, d, $^1J_{P,H} = 156$ Hz). A peak at $m/z = 461$ in the electrospray-ionization mass spectrum (ESI-MS) is assigned to the cation of **3**. The reaction of **2** with the more bulky and more basic phosphaalkene tBuP=C(NMe$_2$)$_2$ (**4**) under analogous conditions produces an amorphous green-yellow precipitate, which according to an ESI mass spectrum contains the complex cations **5** (m/z =573) and **6** (m/z =805) (Scheme 3).

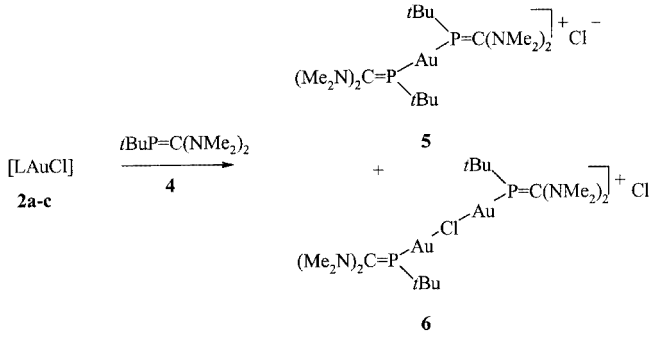

Scheme 3. Reaction of tBuP=C(NMe$_2$)$_2$ with [LAuCl]

The $^{31}P\{^1H\}$ NMR spectrum of the mixture displays a broad signal at $\delta = 37$ ppm, which again is considerably shielded with respect to the free ligand ($\delta = 81$ ppm). In the ^1H NMR spectrum of the same sample, broad singlets at $\delta = 3.62$ and 1.42 ppm are attributed to the protons of the dimethylamino functions and the *tert*-butyl groups. In free **4** the corresponding resonances are observed at $\delta =$ 2.83 and 1.19 ppm. Thus ligand exchange between cations **5** and **6** in solution is obvious. Attempted separation of these salts on a preparative scale was unsuccessful. Also, attempts to separate the components by crystallization from dichloromethane led to the complete transformation of **5** and **6** into the yellow salt **7** with a decanuclear complex cation (Scheme 4). The cation $[(Me_2N)_2CCl]^+$ was formed by an unprecedented nucleophilic cleavage of a P=C double bond by a chloride. This cation was identified from its $^{13}C\{^1H\}$ NMR spectrum, where singlets at $\delta = 44.5$ and 157.9 ppm appeared (ref.:[18] $\delta = 45$ and 159 ppm). The same transformation of **5** and **6** was observed when using acetonitrile as a solvent.

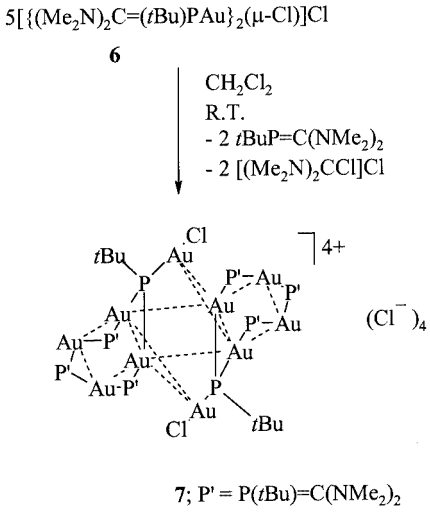

Scheme 4. Formation of **7** from **6** (idealized)

Compound **7** is readily soluble in acetonitrile and water but only moderately soluble in dichloromethane.

In the $^{31}P\{^1H\}$ NMR spectrum of cluster **7** three groups of signals are observed at $\delta = 42.2$, 34.0, and 20.3 ppm with a relative intensity of 2:1:1 respectively.. The pattern of the signals indicates the presence of an $[AB_2C]_2$ spin system. This is also consistent with the symmetry of the compound as derived from the X-ray diffraction study. The signal at $\delta = 34.0$ ppm shows only four lines and, in a first approximation, may be regarded as the A-part of an AB_2 spectrum, implying that the A nucleus is only coupling with the B nuclei (but not with the B′ nuclei). Thus, the signal at $\delta =$ 34.0 ppm is assigned unambiguously to the peripheral phosphorus atoms P_A and $P_{A'}$ in Figure 1.

The signal at $\delta = 42.2$ ppm with the highest intensity is attributed to P_B; consequently, the resonance at $\delta =$ 20.3 ppm is caused by P_C. The interaction between both AB_2C parts occurs exclusively through the coupling between the nuclei P_C and $P_{C'}$ and causes the splitting of the higher order signals of P_B and P_C. Within the AB_2C parts $^2J_{PP}$ couplings are observed, whereas between both AB_2C halves of the cation a $^3J_{PP}$ coupling is present, which is also reflected by the different signs of the coupling constants. The relative signs result from the iterative fitting of the spectrum assuming positive values for the two-bond P-P couplings. The relatively large $^2J_{PP}$ coupling constants agree with a trans-arrangement of the coupling P atoms.

The fourfold positive charge of the cation is compensated for by four chloride ions. Accordingly, the ESI mass spectrum features a peak at m/z =836.0, indicating a mass of 3344 Dalton for the cation $[C_{62}H_{144}Au_{10}Cl_2N_{12}P_8]^{4+}$; this peak shows the correct isotopic pattern.

X-ray Structural Analysis of 7·14CH$_2$Cl$_2$

Bright yellow single crystals of **7** as a solvate with 14 molecules of CH_2Cl_2 were grown over two weeks from a solution of **7** in dichloromethane layered with *n*-hexane at 4 °C. The X-ray structural analysis (Figure 2) shows a cation

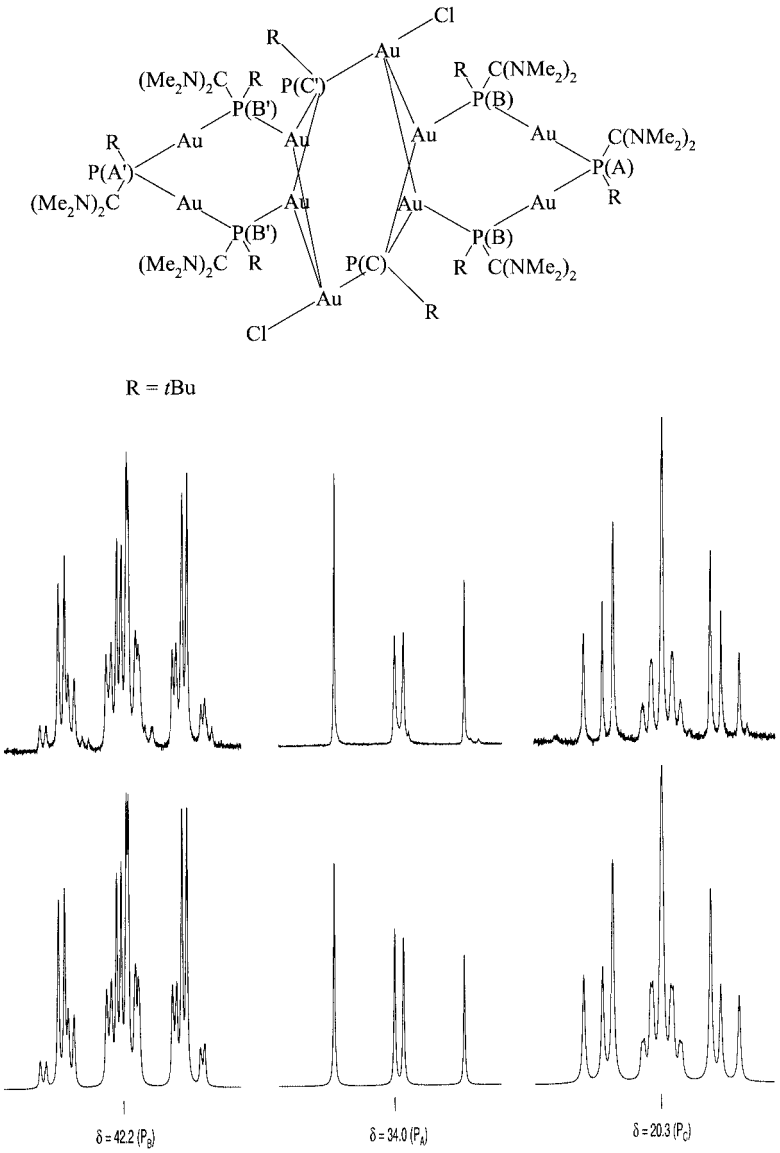

Figure 1. Observed and simulated $^{31}P\{^{1}H\}$ NMR spectrum of **7**

containing ten gold atoms. Eight atoms [Au(1) to Au(4) and Au(1a) to Au(4a)] form a puckered ladder made up of three quadrangles [Au(1)−Au(2)−Au(3) = 158.22(2)°, Au(2)−Au(3)−Au(4) = 159.43(2)°].

The central quadrangle — a parallelogram defined by the atoms Au(2), Au(2a), Au(3), and Au(3a) — is capped on both faces by a [*t*BuPAuCl] entity, which leads to the triangles Au(2),Au(3a),P(2a); Au(2a),Au(3),P(2); Au(2),Au(3a),Au(5a); and Au(2a),Au(3),Au(5). The center of this parallelogram is located on a crystallographic center of inversion. In pairs, the three edges of both peripheral quadrangles Au(1)−Au(4a), Au(1a)−Au(4), Au(1)−Au(2), Au(1a)−Au(2a), Au(3)−Au(4), and Au(3a)−Au(4a) are bridged by six phosphaalkene ligands via their P atoms. The Au−Au distances vary from 3.030(1) Å [Au(2a)−Au(5), Au(2)−Au(5a)] to 3.426(1) Å [Au(1)−Au(4a), Au(1a)−Au(4)] and have to be regarded as weak aurophilic contacts. The Au(5)−P(2a) and Au(5a)−P(2) bond lengths within the [P(*t*Bu)AuCl] units [2.272(4) Å] are similar to the Au−P distances in $[(Ph_3PAu)_6C]^{2+}$ [2.269(1)−2.274(1) Å][19] but they are significantly shorter than the Au−P contacts to the μ-phosphaalkene ligands [2.306(4)−2.324(3) Å]. The Au−P−Au valence angles at the P atoms of the phosphaalkene bridges vary from 90.9(1)° at P(3) to 91.6(1)° at P(1), and to 95.7(1)° at P(4). They are significantly compressed in comparison to the ideal tetrahedral angle. The same holds for the Au(2a)−P(2)−Au(3) angle, which is 92.7(1)°. In contrast to this the Au(3)−P(2)−Au(5a) [119.7(2)°] and Au(2a)−P(2)−Au(5a) [116.4(2)°] angles are significantly widened. The P−Au−P angles at the atoms Au(1) and Au(4) average 170.5° — close to linearity. Similarly the P(2a)−Au(5)−Cl(1) angle is 173.8(1)°. The Au−Cl bond lengths in **7** [2.332(4) Å] exceed those in [tBu$_3$PAuCl] [2.28(6) Å][20] and [Au(CO)Cl] [2.2261(5) Å].[21] The

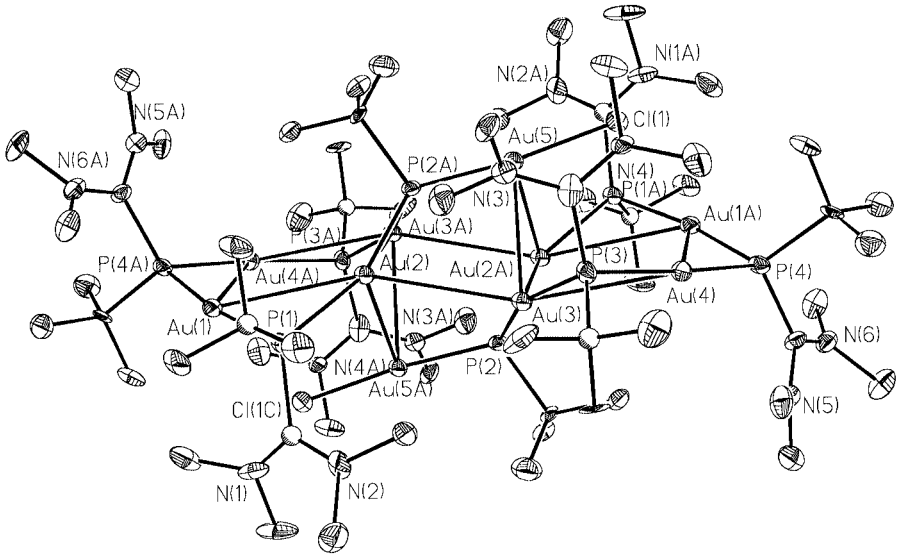

Figure 2. Structure of the cation of **7** in the crystal; selected bond lengths [Å] and angles [°]: Au(1)−Au(2) 3.323(1), Au(2)−Au(3) 3.285(1), Au(3)−Au(4) 3.303(1), Au(4)−Au(1a) 3.426(1), Au(2)−Au(3a) 3.372(1), Au(2)−Au(5a) 3.030(1), Au(3)−Au(5) 3.102(1), Au(1)−P(1) 2.313(4), Au(2)−P(1) 2.322(3), Au(3)−P(3) 2.324(4), Au(4)−P(3) 2.310(4), Au(4)−P(4) 2.316(4), Au(1a)−P(4) 2.306(4), Au(2)−P(2a) 2.332(3), Au(3a)−P(2a) 2.330(3), Au(5)−P(2a) 2.272(4), Au(5)−Cl(1) 2.332(4); Au(4a)−Au(1)−Au(2) 89.31(2), Au(1)−Au(2)−Au(3a) 90.34(2), Au(2)−Au(3a)−Au(4a) 90.59(2), Au(3a)−Au(4a)−Au(1) 89.74(2), Au(2)−Au(3)−Au(2a) 87.51(2), Au(3)−Au(2)−Au(3a) 92.49(2), Au(2a)−Au(5)−Au(3) 66.71(2), Au(5)−Au(3)−Au(2a) 55.62(2), Au(3)−Au(2a)−Au(5) 57.67(2), Au(1)−P(1)−Au(2) 91.60(13), Au(3)−P(3)−Au(4) 90.91(13), Au(1)−P(4a)−Au(4a) 95.67(14), Au(2)−P(2a)−Au(3a) 92.66(12), Au(2)−P(2a)−Au(5) 116.41(16), Au(3a)−P(2a)−Au(5) 119.72(15). P(2a)−Au(5)−Cl(1) 173.77(12), P(4a)−Au(1)−P(1) 170.60(12), P(4)−Au(4)−P(3) 170.41(14)

P=C double bond of precursor **4** {C−P in **1**: 1.740(1) Å[22]} is elongated to single bond length upon incorporation into the cluster cation **7** [1.849(16)−1.877(14) Å]. A similar bond length [1.8751(17) Å] was observed after the ligation of $[Tp^*(CO)_2Mo{\equiv}C-P{=}C(NMe_2)_2]$ to two [AuCl] units to give $[Tp^*(CO)_2Mo{\equiv}C-P(AuCl)_2C(NMe_2)_2]$ {Tp^*= $HB(3,5\text{-}Me_2pz)_3$}.[17] The three-coordinate carbon atoms of the phosphaalkenes remain planar. π-Conjugation to the N-atoms of the dimethylamino groups results in short $C(sp^2)-N(sp^2)$ bonds [1.292(18)−1.358(19) Å] with respect to the standard value for a C−N single bond (1.45 Å).[22] The formation of cluster **7** is remarkable for several reasons:

1) It is the first polynuclear gold compound with bridging phosphaalkene ligands.

2) The degradation of a phosphaalkene to a tBuP^{2-} ligand and a chloroformamidinium ion by chloride ions in the coordination sphere of a metal is without precedent.

3) The structural architecture is new for Au_{10} derivatives.

The metal frameworks in $[Au(AuNCO)(AuPPh_3)_8]Cl$[23] and $[Au(AuCl)(AuPPh_3)_8]^+$ [24] are derived from a square antiprism with a gold atom in the center of the cage. One square-face of the anti-prism is capped by the AuNCO or the AuCl moiety. The cluster $[Au_{10}(C_6F_5)_4(PPh_3)_5]$ is of toroidal geometry,[25] whereas the Au_{10} skeleton of $[PtAu_{10}\{Ph_2P(CH_2)_3PPh_2\}_5](NO_3)_2$ [26] and $[Pt(AuPEt_3)_{10}](BPh_4)_2$ [27] are segments of an icosahedron. In the cation $[Au_{10}Se_4(dppm)_4]^{2+}$ [dppm = $(Ph_2P)_2CH_2$], eight Au atoms form an irregular puckered octagon with two additional Au atoms in the center.[27] The Au_{10} skeleton of $[Au_{10}(AsPh)_4(PhAsSiMe_3)_2(PnPr_3)_6]$ can be described as an edge-shared bioctahedron, the four vertices of which are linked by pairs.[28] The cation $[Au_{10}Se_4(dppf)_4]^{2+}$ (dppf = 1,1′-diphenylphosphanylferrocene) consists of two [Au{Se(Au_2dppf)}] subunits, which are combined via aurophilic interactions.[2k] The structure of the cation $[Au_{10}\{\mu\text{-}Ph_2PN(nPr)PPh_2\}_4(\mu\text{-}S)_4]^{2+}$ is similar to a propeller.[2h]

Experimental Section

General: All manipulations were performed under dry argon. Organic solvents were rigorously dried with an appropriate drying agent and freshly distilled before use. The following compounds were prepared as described in the literature: $[AuCl(PPh_3)]$ (**2a**),[29] [AuCl(THT)],[30] [AuCl(CO)],[31] $HP{=}C(NMe_2)_2$ [32] (**1**), tBuP= $C(NMe_2)_2$ [33] (**4**). IR spectra: Bruker FTIR Vector 22, Bruker FTIR IFS66. ^1H, ^{13}C, ^{31}P NMR spectra: Bruker Avance DRX 500 (^1H: 500.13 MHz, ^{13}C: 125.76 MHz, ^{31}P: 202.46 MHz); references: $SiMe_4$ (^1H, ^{13}C), 85% H_3PO_4 (^{31}P). For solution and simulation of the ^{31}P NMR spectrum of **7** the PERCH program package[34] was used. 754 of the 890 allowed transitions were assigned to experimentally observed lines. The simulation converged at an RMS value of 0.95. MS: Esquire 3000/Tune-ESI.MS

$[Au\{HP{=}C(NMe_2)_2\}_2]Cl$ (3): A solution of $[AuCl(PPh_3)]$ (**2a**) (0.30 g, 0.6 mmol) in 10 mL of tetrahydrofuran (THF) was treated at ambient temperature with of $HP{=}C(NMe_2)_2$ (**1**; 0.15 g, 1.15 mmol). After stirring for 2 h the light yellow slurry was filtered, the solid washed with THF (3 × 10 mL), and dried in vacuo to give 0.26 g (85%) of **3**. IR (KBr): $\tilde{\nu}$ = 2949w cm^{-1}, 2328m [ν(PH)], 1558s, 1507w, 1465m, 1410m, 1385s, 1286m, 1173m, 1109m, 919m. ^1H NMR (CD_2Cl_2): δ = 3.27(s, 24 H, NMe_2), 3.71(d, $^1J_{P,H}$=219 Hz, PH) ppm. $^{13}C\{^1H\}$ NMR (CD_2Cl_2): δ =

44.5 (br. s, NCH_3), 197.6 (d, $^1J_{P,C}$=56 Hz, P=CN_2) ppm. MS-ESI: *m*/*z* = 461.1 [Au{HP=$C(NMe_2)_2$}]$^+$. $C_{10}H_{26}AuClN_4P_2$ (496.71): calcd. C 24.18, H 5.28, N 11.28; found C 24.34, H 5.00, N 10.94.

$[Au_8(AuCl)_2\{\mu_3\text{-}P(t\text{Bu})\}_2\{\mu\text{-}P(t\text{Bu})\text{=}C(NMe_2)_2\}_6]^{4+}(Cl^-)_4$ (7): Neat *t*BuP=$C(NMe_2)_2$ (**4**) (0.75 g, 3.98 mmol) was added to a solution of [AuCl(PPh_3)] (**2a**) (1.00 g, 2.02 mmol) in THF (50 mL) at 20 °C. The resulting yellow slurry was stirred for 1 h and then filtered. The isolated solid was washed with THF (2 × 5 mL) and dried in vacuo to give 0.95 g of a mixture of **5** and **6**. ^{1}H NMR (CD_2Cl_2): δ = 1.42 (s, 9n H, *t*Bu), 3.62 (s, 12n H, NMe_2) ppm. $^{31}P\{^1H\}$ NMR (CD_2Cl_2): δ = 37 (s, br) ppm. MS-ESI: *m*/*z* (%) = 805.1 (19) [$Au_2Cl\{t\text{BuP=}C(NMe_2)_2\}_2$]$^+$, 573.2 (100) [Au{*t*BuP=$C(NMe_2)_2\}_2$]$^+$. A sample of this mixture (0.85 g) was dissolved in dichloromethane (40 mL) and then *n*-hexane was added dropwise until a slight cloudiness of the liquid phase persisted. Stirring at 20 °C was continued for three days before the solution was concentrated to about 25% of its volume resulting in the separation of **7** as a yellow powder. The mother liquor was syringed off and the residue was dried to yield 0.58 g (82% yield with respect to **2a**) of **7**. ^{1}H NMR (CD_3CN): δ = 1.34, 1.37, 1.41 (3s, 72 H, *t*Bu), 3.28 (s, 12 H, NMe_2), 3.66 (br. s, 48 H, NMe_2), 4.29 (s, 12 H, NMe_2) ppm. $^{31}P\{^1H\}$ NMR (CD_3CN): $(AB_2C)_2$-type spectrum: δ(A) = 34.0 (P4, P4a), δ(B) = 42.2 (P1, P1a, P3, P3a), δ(C) = 20.3 (P2, P2a) ppm; $^2J_{AB} = {}^2J_{A'B'}$ = 221.6, $^2J_{BC} = {}^2J_{B'C'}$ = 197.4, $^3J_{BC'} = {}^3J_{B'C}$ = −3.6, $^3J_{CC'}$ = −94.5 Hz. MS-ESI: *m*/*z* = 836.0 [$Au_8(AuCl)_2(t\text{BuP})_2\{t\text{BuP=}C(NMe_2)_2\}_6$]$^{4+}$. The salt is solvated with varying amounts of dichloromethane. Samples isolated from acetonitrile crystallize with three molecules of CH_3CN as shown by ^{1}H NMR spectroscopy. $C_{62}H_{144}Au_{10}Cl_6N_{12}P_8\cdot 3CH_3CN$ (3611.26): calcd. C 22.62, H 4.27, N 5.82; found C 22.78, H 4.54, N. 5.81.

X-ray Structural Analysis of $7\cdot 14CH_2Cl_2$: Yellow single crystals of $7\cdot 14CH_2Cl_2$ were grown from a CH_2Cl_2/*n*-hexane solution at +4 °C over 2 weeks; 0.29 × 0.28 × 0.20 mm^3, *T* = 100 K, Nonius Kappa CCD, Mo-K_α (graphite monochromator, λ = 0.71073 Å), empirical formula $[C_{62}H_{144}Au_{10}Cl_2N_{12}P_8]Cl_4\cdot 14CH_2Cl_2$, monoclinic space group $P2_1/n$; unit cell dimensions *a* = 13.1890(1) Å, *b* = 16.627(2) Å, *c* = 33.4040(3) Å, β = 95.2320(5)°; *V* = 7294.76(12) Å^3, d_{calcd} = 2.129 g/cm^{-3}, *Z* = 2; μ = 10.762 mm^{-1}; range for data collection: 2.9 < θ < 25.0°; index ranges: −15 ≤ *h* ≤ 15, −18 ≤ *k* ≤ 19, −39 ≤ *l* ≤ 39; reflections collected 88813; unique reflections 12561 (R_{int} = 0.098); parameters 661; absorption correction: multi-scan min/max transmission 0.2221/0.1464; Program used: SHELXL-97; structure refinement: full-matrix least-squares on F^2, wR_{F^2} = 0.1405 (all data), R_F = 0.059, wR_F = 0.1314 based on 9916 unique reflections with $I > 2\sigma(I)$. GOOF(F^2) = 1.098; maximum residual electron density 4.099 e·Å^{-3}, 1.01 Å nearby Au(3). Disorder of Cl(4) on two positions (48:52), disorder of Cl(11) on two positions (65:35). CCDC-183582 (**7**) contains the supplementary crystallographic data for this paper. These data can be obtained free of charge at www.ccdc.cam.ac.uk/conts/retrieving.html or from the Cambridge Crystallographic Data Center, 12 Union Road, Cambridge CB2/1EZ, UK; Fax: (internat.)+44−1223/336-033; E-mail: deposit@ccdc.cam.ac.uk.

Acknowledgments

This work was generously supported by the Deutsche Forschungsgemeinschaft, the Fonds der Chemischen Industrie and the Degussa AG, Hanau, Germany.

[1] *Clusters and Colloids. From Theory to Applications* (Ed.: G. Schmid), VCH, Weinheim, **1994**.
[2] μ-O: [2a] K. Angermaier, H. Schmidbaur, *Inorg. Chem.* **1994**, *33*, 2069−2070. [2b] H. Schmidbaur, S. Hofreiter, M. Paul, *Nature* **1995**, *377*, 503−504. [2c] A. N. Nesmeyanov, E. G. Perevalova, Y. T. Struchkov, M. Y. Antipin, K. I. Grandberg, V. P. Dyadchenko, *J. Organomet. Chem.* **1980**, *201*, 343−349. μ-S: [2d] F. Canales, M. C. Gimeno, P. G. Jones, A. Laguna, *Angew. Chem.* **1994**, *106*, 811−812; *Angew. Chem. Int. Ed. Engl.* **1994**, *33*, 769−770. [2e] P. G. Jones, G.-M. Sheldrick, H. Hädicke, *Acta Crystallogr., Sect. B* **1980**, *36*, 2777−2779. [2f] P. G. Jones, C. Lensch, G.-M. Sheldrick, *Z. Naturforsch., Teil B* **1982**, *37*, 141−143. [2g] G. Marbach, J. Strähle, *Angew. Chem.* **1984**, *96*, 695−696; *Angew. Chem. Int. Ed. Engl.* **1984**, *23*, 715−716. [2h] V. W.-W. Yam, E. C.-C. Cheng, Z.-Y. Zhou, *Angew. Chem.* **2000**, *112*, 1749−1751; *Angew. Chem. Int. Ed.* **2000**, *39*, 1683−1685. [2i] V. W.-W. Yam, E. C.-C. Cheng, N. Zhu, *Angew. Chem.* **2001**, *113*, 1813−1815; *Angew. Chem. Int. Ed.* **2001**, *40*, 1763−1765. μ-Se: [2j] C. Lensch, P. G. Jones, G.-M. Sheldrick, *Z. Naturforsch., Teil B* **1982**, *37*, 944−949. [2k] S. Canales, O. Crespo, M. C. Gimeno, P. G. Jones, A. Laguna, *Chem. Commun.* **1999**, 679−680. [2l] S. Canales, O. Crespo, M. C. Gimeno, D. G. Jones, A. Laguna, F. Mendizabal, *Organometallics* **2000**, *19*, 4985−4994. [2m] D. Fenske, T. Langetepe, M. M. Kappes, O. Hampe, P. Weis, *Angew. Chem.* **2000**, *112*, 1925−1928, *Angew. Chem. Int. Ed.* **2000**, *39*, 1857−1860.
[3] Review: H. Schmidbaur, *Chem. Soc. Rev.* **1995**, 391−400.
[4] E. Zeller, H. Beruda, H. Schmidbaur, *Chem. Ber.* **1993**, *126*, 2033−2036.
[5] [5a] H. Schmidbaur, G. Weidenhiller, O. Steigelmann, *Angew. Chem.* **1991**, *103*, 442−444; *Angew. Chem. Int. Ed. Engl.* **1991**, *30*, 433−436. [5b] R. E. Bachman, H. Schmidbaur, *Inorg. Chem.* **1996**, *35*, 1399−1401.
[6] H. Beruda, E. Zeller, H. Schmidbaur, *Chem. Ber.* **1993**, *126*, 2037−2040.
[7] E. Zeller, H. Schmidbaur, *J. Chem. Soc., Chem. Commun.* **1993**, 69−70.
[8] [8a] H. Schmidbaur, E. Zeller, G. Weidenhiller, O. Steigelmann, H. Beruda, *Inorg. Chem.* **1992**, *31*, 2370−2376. [8b] E. Zeller, H. Beruda, J. Riede, H. Schmidbaur, *Inorg. Chem.* **1993**, *32*, 3068−3071. [8c] H. Schmidbaur, E. Zeller, J. Ohshita, *Inorg. Chem.* **1993**, 4524−4526.
[9] R. J. Puddephatt, P. J. Thompson, *J. Organomet. Chem.* **1976**, *117*, 395−403.
[10] D. B. Dyson, R. V. Parish, C. A. Mc Auliffe, R. G. Pritchard, R. Fields, B. Beagley, *J. Chem. Soc., Dalton Trans.* **1989**, 907−914.
[11] J. Vicente, M. T. Chicote, P. G. Jones, *Inorg. Chem.* **1993**, *32*, 4960−4964.
[12] R. G. Pritchard, D. B. Dyson, R. V. Parish, C. A. Mc Auliffe, B. Beagley, *J. Chem. Soc., Chem. Commun.* **1987**, 371−372.
[13] M. C. Blanco, E. J. Fernandez, A. K. Fischer, P. G. Jones, A. Laguna, M. E. Olmos, M. D. Villacampa, *Inorg. Chem. Commun.* **2000**, *3*, 163−165.
[14] M. C. Blanco, E. J. Fernandez, P. G. Jones, A. Laguna, J. M. Lopez de Luzuriaga, M. E. Olmos, M. D. Villacampa, *Angew. Chem.* **1998**, *110*, 3199−3201; *Angew. Chem. Int. Ed.* **1998**, *37*, 3042−3044.
[15] M. C. Blanco, E. J. Fernandez, J. M. Lopez de Luzuriaga, M. E. Olmos, O. Crespo, M. C. Gimeno, A. Laguna, P. G. Jones, *Chem. Eur. J.* **2000**, *6*, 4116−4123.
[16] Review: L. Weber, *Eur. J. Inorg. Chem.* **2000**, 2425−2441.
[17] L. Weber, G. Dembeck, P. Lönnecke, H.-G. Stammler, B. Neumann, *Organometallics* **2001**, *20*, 2288−2293.
[18] H. O. Kalinowski, S. Berger, S. Braun, *^{13}C NMR-Spektroskopie*, Thieme, Stuttgart, New York, **1984**, 371.
[19] F. P. Gabbai, A. Schier, J. Riede, H. Schmidbaur, *Chem. Ber./Recl.* **1997**, *130*, 111−113.
[20] H. Schmidbaur, B. Brachthäuser, O. Steigelmann, H. Beruda, *Chem. Ber.* **1992**, *125*, 2705−2710.

[21] P. G. Jones, *Z. Naturforsch., Teil B* **1982**, *37*, 823−824.
[22] A. N. Chernega, A. V. Ruban, V. D. Romanenko, L. N. Markovskii, A. A. Korkin, M. Y. Antipin, Y. T. Struchkov, *Heteroatom Chem.* **1991**, *2*, 229−241.
[23] J. Pethe, J. Strähle, *Z. Naturforsch., Teil B* **1999**, *54*, 381−384.
[24] J. Pethe, C. Maichle-Mössmer, J. Strähle, *Z. Anorg. Allg. Chem.* **1998**, *624*, 1207−1210.
[25] A. Laguna, M. Laguna, M. C. Gimeno, P. G. Jones, *Organometallics* **1992**, *11*, 2759−2760.
[26] D. A. Krogstad, V. G. Young, Jr., L. H. Pignolet, *Inorg. Chem. Acta* **1997**, *264*, 19−32.
[27] D. A. Krogstad, W. V. Konze, L. H. Pignolet, *Inorg. Chem.* **1996**, *35*, 6763−6771.
[28] D. Fenske, F. Simon, *Z. Anorg. Allg. Chem.* **1996**, *622*, 45−52.
[29] W. P. Fehlhammer, W. A. Herrmann, K. Öfele, in *Handbuch der Präparativen Anorganischen Chemie* Vol. 3 (Ed.: G. Brauer), Enke Stuttgart **1981**, p. 2019
[30] R. Uson, A. Laguna, M. Laguna, *Inorg. Synth.* **1989**, *26*, 85−91.
[31] W. P. Fehlhammer, W. A. Herrmann, K. Öfele, in *Handbuch der Präparativen Anorganischen Chemie* Vol. 3 (Ed.: G. Brauer), Enke Stuttgart **1981**, p. 1965−1966.
[32] M. I. Povolotskii, V. V. Negrebetskii, V. D. Romanenko, V. I. Ivanchenko, T. V. Sarina, L. N. Markovskii, *Zh. Obshch. Khim.* **1990**, *60*, 2238−2244; *Chem. Abstr.* **1991**, *115*, 8934w.
[33] L. Weber, M. Meyer, H.-G. Stammler, B. Neumann, *Chem. Eur. J.* **2001**, *7*, 5401−5408.
[34] R. Laatikainen, M. Niemitz, U. Weber, T. Sundelin, T. Hassinen, J. Vepsäläinen, *J. Magn. Reson. A* **1996**, *120*, 1.

Received July 25, 2002
[I02418]

Hydrogenperoxo-[(bztpen)Fe(OOH)]$^{2+}$ and Its Deprotonation Product Peroxo-[(bztpen)Fe(O_2)]$^{+}$, Studied by EPR and Mössbauer Spectroscopy − Implications for the Electronic Structures of Peroxo Model Complexes

Olivier Horner,*[a] Claudine Jeandey,[a] Jean-Louis Oddou,[a] Pierre Bonville,[b] Christine J. McKenzie,[c] and Jean-Marc Latour[a]

Dedicated to the memory of Prof. William E. Hatfield

Keywords: EPR spectroscopy / Iron / Mössbauer spectroscopy / Peroxo ligands

The purple hydrogenperoxo species [Fe(bztpen)(OOH)]$^{2+}$ (**1**) can be generated in methanol solution by treatment of [Fe(bztpen)Cl]$^{3+}$ with a large excess of hydrogen peroxide [A. Hazell, C. J. McKenzie, L. P. Nielsen, S. Schindler, M. Weitzer, *J. Chem. Soc., Dalton Trans.* **2002**, 310–317]. Addition of 30 equivalents of triethylamine to a solution of [Fe(bztpen)(OOH)]$^{2+}$ gives the [Fe(bztpen)(O_2)]$^{+}$ (**2**) species, in which it has been proposed that the peroxo ligand is coordinated in the η^2 mode. We have synthesized both 100% ^{57}Fe-enriched non-heme Fe^{III} peroxo species and studied them by EPR and Mössbauer spectroscopy. Species **1** displays a typical S = 1/2 low-spin ferric EPR spectrum, the g values of which have been analysed in terms of the Griffith model [J. S. Griffith, *Proc. R. Soc. London, A* **1956**, *234*, 23–36]. We have thus obtained insight into the electronic structure of **1**. The EPR spectrum of **2** is characteristic of a high-spin Fe^{III} species in a nearly axial ligand field. We have determined all Mössbauer parameters for both complexes by a numerical treatment of applied field Mössbauer data. Species **1** exhibits an isomer shift $\delta_{/Fe}$ = 0.16 mm/s and a quadrupole splitting ΔE_Q = −2.08 mm/s (T = 4.2 K). In the case of **2**, we obtain an isomer shift $\delta_{/Fe}$ = 0.63 mm/s and a quadrupole splitting ΔE_Q = 1.12 mm/s (T = 4.2 K). These values are close to those published very recently by Bill et al. for [Fe(trispicMeen)(OOH)]$^{2+}$ (**3**) and [Fe(trispicMeen)(η^2–OO)]$^{+}$ (**4**) species, where bztpen and trispicMeen ligands differ by a noncoordinating group [A. J. Simaan, F. Banse, J.-J. Girerd, K. Wieghardt, E. Bill, *Inorg. Chem.* **2001**, *40*, 6538–6540]. We have also used the extension of the Griffith model developed by Lang et al. for Mössbauer spectroscopy [W. T. Oosterhuis, G. Lang, *Phys. Rev.* **1969**, *178*, 439–456] to evaluate the ^{57}Fe hyperfine tensor of **1** and reproduce the experimental data. On comparison with the Mössbauer data available for η^2-peroxo Fe^{III} complexes, our Mössbauer study of **2** agrees well with a high-spin Fe^{III} side-on peroxo complex. Very characteristic $\delta_{/Fe}$ and ΔE_Q ranges for hydrogenperoxo and side-on peroxo Fe^{III} species are now available, which should aid in the detection of comparable species formed in biological systems.

(© Wiley-VCH Verlag GmbH, 69451 Weinheim, Germany, 2002)

Introduction

There is currently great interest in non-heme peroxo species, since they are suspected to be key intermediates in several enzymatic or metabolic processes.[1] Detailed spectroscopic characterizations of peroxo species for diiron enzymes such as ribonucleotide reductase and methane monooxygenase are available in the literature.[1b] Where non-heme mononuclear peroxo intermediates are concerned, a well known example is the antitumor drug bleomycin: when this protein is exposed to dioxygen, a transient activated form involved in DNA-cleaving activity is formed. This has been demonstrated to be a hydrogenperoxo FeOOH species.[2] Peroxo species have also been proposed for mononuclear, non-heme, Fe-based superoxide dismutase[3] and more recently, from pulsed radiolysis studies, for the product of superoxide reductase reaction with superoxide.[4] In the recent past, several non-heme mononuclear peroxo model complexes, generated in solution, have been described in the literature.[5] Raman spectroscopy has been fruitful for gaining insight into the peroxo ligand binding mode; hydrogenperoxo and side-on (η^2) peroxo coordination geometries have been characterized.[5i] These two species have very different reactivities. Hydrogenperoxo species

[a] Laboratoire de Physicochimie des Métaux en Biologie, FRE CEA/CNRS/UJF 2427, Département de Réponse et Dynamique Cellulaires CEA/Grenoble,
38054 Grenoble Cedex 9, France
Fax: (internat.) +33−(0)438785090
E-mail: horner@cea.fr
[b] Service de Physique de l'Etat Condensé, Département de Recherche sur l'Etat Condensé, les Atomes et les Molécules, CEA/Saclay,
91191 Gif-sur-Yvette Cedex, France
[c] Department of Chemistry, University of Southern Denmark, Odense Campus,
5230 Odense M, Denmark
Supporting information for this article is available on the WWW under http://www.eurjic.org or from the author.

are believed to intervene in oxidation and hydroxylation reactions of substrates, and are likely to operate by the cleavage of the activated O−O bond to generate a catalytically active high-valent iron intermediate. In contrast, the O−O bond in a side-on peroxo complex is not activated for direct cleavage and the species is relatively stable, but can react as a nucleophile towards protonation, probably to produce highly reactive species.[6] No η^2-FeO_2 peroxo species has yet been characterized by Mössbauer spectroscopy in biological systems. A well known example of an η^2-FeO_2 peroxo model complex is $[Fe(edta)(O_2)]^{3-}$, which has been studied by many spectroscopic techniques,[6] including a recently detailed Mössbauer spectroscopy study.[7]

Indeed, Mössbauer spectroscopy is particularly well adapted for the study of iron compounds.[8] Nevertheless, few Mössbauer data for non-heme peroxide species are currently available in the literature.[7,9] We therefore decided to study the hydrogenperoxo complex $[^{57}Fe(bztpen)(OOH)]^{2+}$ (**1**) and its deprotonation product $[^{57}Fe(bztpen)(O_2)]^{2+}$ (**2**) [bztpen stands for *N*-benzyl-*N*,*N*′,*N*′-tris(2-pyridylmethyl)-ethane-1,2-diamine[10]] by Mössbauer spectroscopy. The two complexes **1** and **2** can be interchanged by a protonation-deprotonation sequence as shown in Scheme 1.

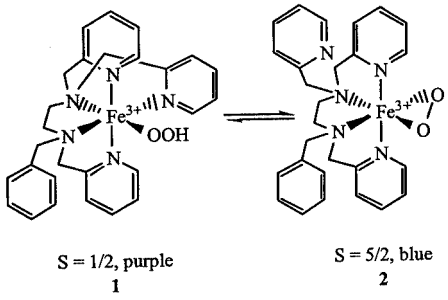

Scheme 1

While this work was nearing completion, Bill et al. published a detailed Mössbauer study of non-heme Fe^{III} hydrogenperoxo $[Fe(trispicMeen)(OOH)]^{2+}$ (**3**) and η^2-peroxo $[Fe(trispicMeen)(O_2)]^{+}$ (**4**) complexes [trispicMeen stands for *N*-methyl-*N*,*N*′,*N*′-tris(2-pyridylmethyl)ethane-1,2-diamine].[9b]

In this article we report the complete Mössbauer spectroscopy study of complexes **1** and **2**. The characteristic Mössbauer parameters obtained for each compound are in full agreement with Bill's results[9b] and give clear Mössbauer signatures for both non-heme mononuclear hydrogenperoxo and side-on peroxo species. This should aid in the detection of comparable species formed in biological systems.

Results

The ligand bztpen was prepared as described previously.[10] For the synthesis of $[^{57}Fe(bztpen)Cl](ClO_4)_2$, $^{57}FeCl_3{\cdot}6H_2O$ was used as a starting compound. Addition of $NaClO_4{\cdot}H_2O$ resulted in the immediate precipitation of the complex $[^{57}Fe(bztpen)Cl](ClO_4)_2$. The purple hydrogenperoxo complex **1** was generated in solution by treatment of $[^{57}Fe(bztpen)Cl]^{2+}$ with a large excess of hydrogen peroxide. Addition of 30 equivalents of triethylamine to this solution gave **2**, in which it has been proposed that the peroxo ligand is coordinated in the η^2 mode.[10] Both species were studied in detail by EPR and Mössbauer spectroscopy as described below.

EPR Spectroscopy

The hydrogenperoxo species **1** was studied by X-band EPR spectroscopy at low temperature. Figure 1 shows the EPR spectrum of **1** in methanol at $T = 6.3$ K; it is typical of a $S = 1/2$ low-spin Fe^{III} species, with g values observed at $g_{max} = 2.22$, $g_{inter} = 2.18$ and $g_{min} = 1.97$.

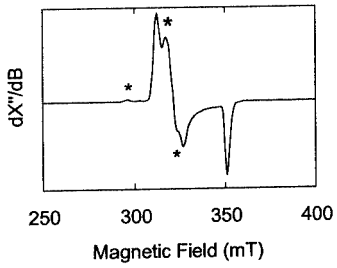

Figure 1. X-band EPR spectrum of **1** in methanol. EPR conditions : temperature 6.3 K, microwave frequency 9.678 GHz, power 2 mW, modulation 1.0 mT/100 kHz. The asterisks denote the components of a minor amount of $[^{57}Fe^{III}(bztpen)(OCH_3)]^{2+}$.

The stars in Figure 1 denote the components of the EPR signal arising from a minor amount (less than 1%) of a precursor species, which corresponds to the low-spin $[Fe^{III}(bztpen)(OCH_3)]^{2+}$.[10]

The 4.2 K X-band EPR spectrum of **2**, shown in Figure 2, exhibits signals at $g = 7.6$ and $g = 5.8$ and a broad unresolved signal in the $g = 4.5$ region.

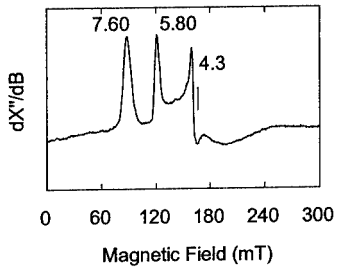

Figure 2. X-band EPR spectrum of **2** in methanol. EPR conditions: temperature 6.3 K, microwave frequency 9.678 GHz, power 20 mW, modulation 1.0 mT/100 kHz.

In addition, an EPR signal arising from a high-spin Fe^{III} contaminant in a rhombic ligand field is seen at $g = 4.3$, but the EPR signal of **1** has completely disappeared, indicating its quantitative transformation upon addition of triethylamine (data not shown). The spectrum of **2** is characteristic of a $S = 5/2$ Fe^{III} complex in a nearly axial ligand field and was analyzed by the rhombogram method.[11] For an $S = 5/2$ spin multiplet, observation of resonances at $g =$

Table 1. Mössbauer parameters for **1** and **2** at $T = 4.2$ K; published spin Hamiltonian parameters for non-heme Fe^{III} peroxo complexes with nitrogen ligands are also given for purposes of comparison; for **1**, with $g_x = -2.18$, $g_y = 2.22$ and $g_z = -1.97$, $A_x = 4.30$ T, $A_y = 6.26$ T and $A_z = 42.26$ T are obtained in the fitting procedure (n.a.: not available)

Compound	**1**	**3**	$[Fe(N_4P_y)(OOH)]^{2+}$	**2**	**4**	$[Fe(N_4P_y)(O_2)]^{+}$	$[Fe(edta)(O_2)]^{3-}$
Spin	1/2	1/2	1/2	5/2	5/2	5/2	5/2
D (cm^{-1})				−0.90	−1.7	n.a.	−1.0
E/D				0.08	0.08	n.a.	0.21
g_x	2.18	2.12	2.16	2.0	2.0	2.0	2.0
g_y	2.22	2.19	2.11	2.0	2.0	2.0	2.0
g_z	1.97	1.95	1.98	2.0	2.0	2.0	2.0
$A_x/g_n\beta_n$ (T)	−4.31	7.77	−6.63	−20.3	−22.71	−21.5	−23.1
$A_y/g_n\beta_n$ (T)	6.62	−3.65	4.45	−22.4	−22.09	−21.6	−21.4
$A_z/g_n\beta_n$ (T)	−42.26	−41.09	−38.42	−20.3	−20.40	−20.3	−20.8
ΔE_Q (mm/s)	−2.07	−2.01	1.62	+1.12	+1.37	n.a.	+0.72
η	0.26	0.4	n.a.	0.0	0.98	n.a.	0.4
$\delta_{/Fe}$ (mm/s)	+0.17	+0.19	+0.17	+0.63	+0.64	+0.61	+0.65
Euler angles	α = 64°	α = 43°	n.a.			n.a.	
reference	this work	[9b]	[9a]	this work	[9b]	[9a]	[7]

7.6, 5.8 and 4.5 is consistent with E/D ≈ 0.08. In particular, the signal at $g = 7.6$ arises from the $M_s = \pm 1/2$ Kramers doublet and the signal at $g = 5.8$ arises from the $M_s = \pm 3/2$ Kramers doublet. The temperature dependence of these signals is consistent with the $M_s = \pm 1/2$ doublet being the highest in energy (Supporting Information; see also footnote on the first page of this article). Consequently, the zero-field splitting parameter D must be negative for **2**, as for $[Fe(edta)O_2]^{3-}$ and **4** (Table 1).

Mössbauer Spectroscopy

The hydrogenperoxo complex **1** was studied by Mössbauer spectroscopy at low temperature in one low and two high magnetic fields applied parallel to the propagation direction of the Mössbauer γ-rays. Figure 3 shows Mössbauer spectra of **1** at $T = 4.2$ K ($H = 50$ mT, $H = 3$T) and $T = 10$ K ($H = 7$ T).

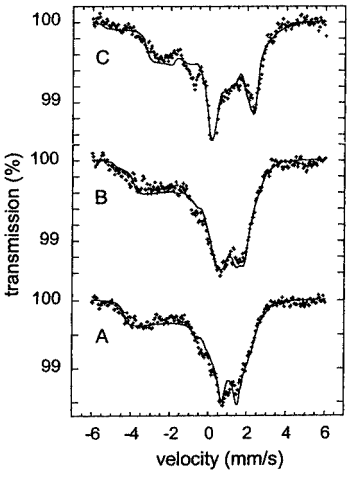

Figure 3. Mössbauer spectra in **1** in methanol. The experimental spectra taken at $T = 4.2$ K in an applied parallel field of 50 mT (A) and 3 T (B) and at $T = 10$ K in an applied parallel field of 7.0 T (C), were fitted (solid curves) with the parameters set of Table 1.

The rather featureless spectra obtained can be fitted simultaneously in the slow relaxation limit within the spin Hamiltonian formalism using a unique set of parameters. We were not fully able to reproduce the shape of the feature at velocity of about −1 mm/s in the 7 T spectrum (Figure 3, curve C). No high-spin Fe^{III} impurity was detected on a higher velocity scale (data not shown). The minor amount of precursor species $[Fe^{III}(bztpen)(OCH_3)]^{2+}$ discernible in the EPR spectrum of **1** was not taken into account in the Mössbauer fitting data. The g-values were taken as positive and fixed to the values obtained by EPR spectroscopy, with $g_x = 2.18$, $g_y = 2.22$ and $g_z = 1.97$ (vide infra). This is not a restriction, as a Mössbauer spectrum is only sensitive to the sign of the products $A_i \cdot g_i$, $i = x, y, z$[12] The Mössbauer parameters obtained from the fit are listed in Table 1.

At $T = 4.2$ K, complex **1** exhibits an isomer shift $\delta_{/Fe} = 0.17$ mm/s. This parameter, which is typical for a low-spin Fe^{III} complex, is similar to those published for hydrogenperoxo complexes with nitrogen ligands (Table 1). The quadrupole splitting $\Delta E_Q = -2.07$ mm/s is large and negative, and the asymmetry parameter $\eta = 0.26$ is low. Our fit was improved by introducing an Euler angle $\alpha = 64°$ between the [A] and [V] tensors. This means that the [A], [g] and [V] tensors share the same principal z axis. These experimentally ascertained values are close to those obtained for **3**[9b] and for the hydroperoxo complex $[Fe(N_4Py)(OOH)]^{2+}$, where N_4Py stands for *N*-[bis(2-pyridyl)methyl]-*N*,*N*-bis(2-pyridylmethyl)amine.[9a]

Complex **2** was studied by Mössbauer spectroscopy at low temperature in one small and one high magnetic field applied parallel to the propagation direction of the Mössbauer γ-rays. Figure 4 shows the Mössbauer spectra obtained at $H = 50$ mT ($T = 4.2$ K and 10 K) and at $H = 7$ T ($T = 4.2$ K).

These spectra were simultaneously fitted at the slow relaxation limit within the spin Hamiltonian formalism using a unique set of parameters. The Mössbauer parameters ob-

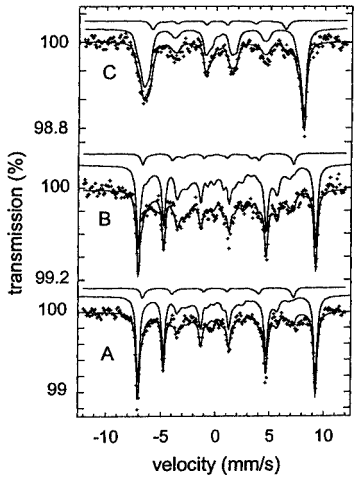

Figure 4. Mössbauer spectra in **2** in methanol. The experimental spectra taken at $T = 4.2$ K (A) and $T = 10$ K (B) in an applied parallel field of 50 mT, and at $T = 4.2$ K in an applied parallel field of 7.0 T (C), were fitted (solid curves) with the parameters set of Table 1. A Fe^{III} impurity (9.4 %) is also present. The solid curves located above the experimental spectrum show the contribution of both species (dashed lines).

tained from the fit are given in Table 1. The spectra of **2** are superimposed by the sextuplet spectra of a minor (9.4%) high-spin Fe^{III} component ($D = +2.9$ cm^{-1}, $E/D = 0.33$, $g = 2.0$, $[A]/g_n\beta_n = -18.0$ T), probably a degradation product of the peroxo complex.

At $T = 4.2$ K under a small applied field ($H = 50$ mT), complex **2** exhibits a sextuplet Mössbauer spectrum. The internal field can be evaluated from its overall splitting and is about 54 T. This is typical for a high-spin Fe^{III} complex. The axial zero-field parameter D is found to be of the order of -1 cm^{-1}, and is close to the D values already published for $[Fe(edta)(O_2)]^{3-}$ and for **4** (Table 1). For $E/D = 0.08$ (zero-field splitting parameter $D < 0$), the lower Kramers doublet $M_s = \pm 5/2$ is uniaxial (it has an easy axis of magnetization along z) and yields a sextuplet Mössbauer spectrum.[13] At $T = 4.2$ K, the levels of population of the upper doublets are much smaller than that of the ground doublet. Therefore, the observed Mössbauer spectrum at $T = 4.2$ K is attributed to the $M_s = \pm 5/2$ doublet and measures the V_{zz} component of the electric field gradient tensor [V]. It can be seen from the experimental spectrum that V_{zz} is positive, as the inner transitions are shifted to the left of the spectrum, and so ΔE_Q is positive for **2**.[13] A Mössbauer spectrum of **2** recorded at higher temperature should give an insight into the other components of the electric field gradient V_{xx} and V_{yy} and allow the asymmetry parameter $\eta = (V_{xx} - V_{yy})/V_{zz}$ to be determined.[7,13] The spectrum recorded at $T = 10$ K and $H = 50$ mT is shown in Figure 4, part B: several additional features appear as the contributions of the middle and upper Kramers doublets (which are not uniaxial) increase. By simultaneous fitting of the three experimental spectra, a value of $\eta = 0$ and a large positive quadrupole splitting $\Delta E_Q = +1.12$ mm/s were determined for **2**. A large isomer shift value $\delta_{/Fe} = 0.63$ mm/s is obtained for this high-spin Fe^{III} complex. The hyperfine coupling tensor of **2** is negative ($A_{av}/g_n\beta_n = -21$ T) because of the main contribution of the Fermi contact term and slightly anisotropic, as for $[Fe(edta)(O_2)]^{3-}$, **4** and the η^2-peroxo complex $[Fe(N_4Py)(O_2)]^+$ (Table 1).

Discussion

The theoretical model developed by Griffith[14] and adapted by Taylor[15] is commonly used to evaluate the tetragonal and rhombic field parameters Δ/λ and V/λ, respectively (where λ is the spin-orbit coupling constant), of low-spin ferric complexes from their g-values determined by EPR spectroscopy. Such a calculation assumes a symmetry not lower than rhombic, a condition not always met, as discussed below for **1**. Therefore, in this model the electronic [g] tensor, the magnetic hyperfine [A] tensor and the electric field gradient [V] tensor are assumed to have a common axis system.[12] Moreover, the orbital reduction factor k is taken to be equal to 1.[14] Following the proposal of Girerd et al. for **3**, the product $g_x.g_y.g_z$ is taken to be positive (with $g_x = -2.18$, $g_y = 2.22$, $g_z = -1.97$),[5] as initially shown by Burger et al.[16] We selected the system of axes described by Taylor, such that $|V| < (2/3)|\Delta|$, where the three real coefficients a, b and c of the ground Kramers doublet are given by the following Equations:[15]

$$\begin{aligned} a &= (g_z + g_y)[8(g_z + g_y - g_x)]^{-1/2} \\ b &= (g_z - g_y)[(g_z + g_y - g_x)]^{-1/2} \\ c &= (g_y - g_x)[(g_z + g_y - g_x)]^{-1/2} \end{aligned} \quad (1)$$

From the experimental g values, we obtain: $a = 0.0567$, $b = 0.0476$ and $c = 0.9979$, which in turn give the field parameters $\Delta/\lambda = -10.10$ and $V/\lambda = 1.85$.[5g,5i,15] This set of values implies that the unpaired electron is located in an orbital with a predominant d_{xy} character, which is strongly destabilized by an antibonding interaction with the π^* orbital of the OOH ligand.[5g,5i] The field parameters of **1** are close to those obtained by Girerd et al. for the hydrogenperoxo complex **3** involving a nitrogen ligand with a similar coordinating environment.[5g,5i] These results agree with a $(d_{xz})^2(d_{yz})^2(d_{xy})^1$ low-spin Fe^{III} electronic configuration, which gives a large negative V_{zz} value (and a large negative ΔE_Q) and a small asymmetry parameter, as found experimentally (Table 1).

By use of the extension of the Griffith model developed by Lang et al. for Mössbauer spectroscopy, one can evaluate the ^{57}Fe hyperfine tensor; the hyperfine tensor values are given by:[17]

$$A_x = -P[-4bc - (1 + \kappa)(a^2 - b^2 - c^2) + 3/7(a^2 - 3b^2 - 3c^2 + 2ab + 2ac)]$$

$$A_y = -P[4ac - (1 + \kappa)(a^2 - b^2 + c^2) + 3/7(3a^2 - b^2 + 3c^2 - 2ab - 2bc)]$$

$$A_z = -P[4ab - (1 + \kappa)(a^2 + b^2 - c^2) + 3/7(3a^2 + 3b^2 - c^2 - 2ac - 2bc)]$$

where a, b and c are given by Equation (1), κ is a parameter characterizing the isotropic contact contribution ($\kappa =$

0.35 for low-spin ferric heme proteins) and P is a scaling factor accounting for the radial distribution of the valence electrons of the Fe^{III} ion ($P/g_n\beta_n \approx -62$ T for low-spin ferric heme proteins).[18] It was possible to reproduce the anisotropic experimental [A] tensor by choosing $\kappa = 0.35$ and $P/g_n\beta_n = -50.3$ T.

[A]/$g_n\beta_n$ (−3.92; 6.09; 42.15) was obtained ($A_{iso}/g_n\beta_n$ = 14.8 T). The low value obtained for P indicates higher covalency for the low-spin iron ion in **1** than for low-spin ferric ions in heme proteins and activated bleomycin.[16]

It is worth noting that different approaches are used in the literature to deal with the signs of the g-values to be employed within the Griffith model. In the case of "activated bleomycin" $Fe^{III}OOH$, Solomon et al. concluded that the three g-values should be taken to be positive.[19] Indeed, they argued that other signs of the g-values would produce crystal field parameters V and Δ that would not allow the experimentally determined higher-energy intra-t_{2g} transition to be reproduced ($E_{exp} \approx 3800$ cm^{-1}). They used an axis system in which the z-axis (which corresponds to the y-axis in this paper) was taken along the Fe−hydrogenperoxo bond. On the other hand, different signs ($g_x = -2.17$; $g_y = 2.26$; $g_z = -1.94$) were obtained by Girerd et al.[5i] for "activated bleomycin" under the same assumption as made by Scholes et al.[20] that $g_xg_yg_z$ is positive. Moreover, upon using the crystal field parameters determined from the latter g-values, one obtains a higher-energy intra-t_{2g} transition at 3900 cm^{-1} (using a covalently reduced spin-orbit coupling constant[19] of 380 cm^{-1} for Fe^{III}). This value is very close to that of 3950 cm^{-1} predicted from field parameters with g_x, g_y and g_z taken to be all positive,[19] and not in contradiction with the near IR MCD results. To probe this point further, we carried out simultaneous fitting of the Mössbauer data for **1** with g_x, g_y and g_z all positive, z being along the Fe−hydrogenperoxo bond. Identical fits were obtained, but with Mössbauer parameters expressed in the new coordinate system.

As noted by Münck et al.[18b] and reemphasized in the case of **3** by Bill et al.,[9b] the Griffith-Taylor model might not be fully valid when the symmetry is less than rhombic. It can be seen in the EPR spectrum of **1** (Figure 1) that the $g_z = 1.97$ resonance does not exhibit any ^{57}Fe magnetic hyperfine splitting. On the other hand, a large component of the hyperfine coupling tensor along the z-axis of the [A] proper axis system is determined experimentally. These conflicting observations can be reconciled if the principal axis frames of the [A] and [g] tensors of **1** are rotated relative to each other. Such a case has already been observed for the low-spin Fe^{III} centre in the active nitrile hydratase.[18b]

Finally, it must be noted that the isomer shift and the quadrupole splitting of **1** are within the range observed for hydrogenperoxo Fe^{III} complexes ($\delta_{/Fe} = 0.16-0.19$ mm/s and a large and negative $\Delta E_Q \approx -2.0$ mm/s at $T = 4.2$ K). These parameters match those of activated bleomycin ($\delta_{/Fe} = 0.16$ mm/s and $\Delta E_Q = -2.96$ mm/s at T = 4.2 K),[16] substantiating the proposition that **1** is a relevant model for these biological hydroperoxo non-heme iron species.

The isomer shift value $\delta_{/Fe} = 0.63$ mm/s obtained for **2** is large for a high-spin Fe^{III} complex but is located in the 0.61−0.65 mm/s range that characterizes high-spin Fe^{III}-η^2O_2 complexes, as shown in Table 1. The side-on peroxo complexes in Table 1 are also characterized by positive ΔE_Q values in the 0.72−1.37 mm/s range ($T = 4.2$ K). Isomer shifts above 0.60 mm/s up to 0.68 mm/s have also been reported in the literature for dinuclear Fe^{III} peroxo complexes, which generally exhibit ΔE_Q values greater than 1.50 mm/s, although some exceptions exist.[22] An isomer shift $\delta_{/Fe}$ = 0.67 mm/s ($T = 4.2$ K) has also been reported for the high-spin porphyrin Fe^{III} η^2-O_2 complex $[Fe(OEP)(O_2)]^-$ (OEP stands for the octaethylporphyrin dianion ligand).[23] In addition, a large quadrupole splitting is observed for **2**, as for the series of side-on peroxo complexes in Table 1. This specific feature is probably due to the 3d anisotropy introduced by the η^2-FeO_2 binding mode, as suggested by theoretical calculations.[24]

Conclusion

The Mössbauer parameters obtained for **1** and **2** in this study agree with the proposal of McKenzie et al. that **1** is a hydrogenperoxo complex and **2** an η^2-peroxo Fe^{III} complex.[10] The coordination number of Fe^{III} in **2** (7 or 6) still remains unknown, the latter being obtained with the decoordination of a picolyl arm of bztpen; the isolation and crystallization of such a species would be useful.

Table 1 shows that non-heme hydrogenperoxo and side-on peroxo Fe^{III} complexes exhibit very characteristic and unambiguous isomer shift values, and $\delta_{/Fe}$ and ΔE_Q ranges are now available for both types of mononuclear peroxo complexes. In particular, no confusion is possible between a mononuclear Fe^{III} species of biological interest with nitrogen/oxygen or sulfur ligands and a mononuclear Fe^{III}-η_2O_2 species. This should make the Mössbauer identification of such species possible in biological systems.

In addition, the Mössbauer parameters obtained here reemphasize both the peculiarity of peroxo Fe^{III} derivatives among ferric complexes and their similarity with their nitrosyl analogues. Indeed, η_2-O_2 iron complexes and $[FeNO]^7$ ($S = 3/2$) species display high isomer shifts, and theoretical descriptions show in both cases that the metal-ligand bond involves a strong σ bonding and a weak additional Π interaction.[24,25]

Experimental Section

EPR spectra were recorded on a Bruker EMX spectrometer. For low-temperature studies, an Oxford Instruments continuous-flow helium cryostat and a temperature control system were used.

All Mössbauer measurements were performed with a constant acceleration spectrometer calibrated with hematite, and isomer shifts are reported relative to an Fe metal standard at room temperature. Variable-temperature experiments were carried out with the sample placed in the tail section of a variable-temperature cryostat. The

temperature of the sample was regulated to within 0.2 K with a conventional PID system. The samples for Mössbauer spectroscopy contained ≈ 4 mM ^{57}Fe in a 200 μL nylon cell. The Mössbauer spectra were analysed with the WMOSS (WEB Research, Edina, MN) software package. For the analysis, the Hamiltonian **H** describing the system is used:

$$\mathbf{H} = D[\mathbf{S}_z^2 - (1/3)S(S+1) + (E/D)(\mathbf{S}_x^2 - \mathbf{S}_y^2)] + \beta_e \cdot \mathbf{S} \cdot [g] \cdot \mathbf{B} + \langle \mathbf{S} \rangle \cdot [A] \cdot \mathbf{I} - g_n \beta_n \mathbf{B} \cdot \mathbf{I} + \mathbf{H_Q}$$

where D and E are the axial and rhombic zero field splitting parameters, respectively, β_e the electronic Bohr magneton, [g] the electronic g-tensor, $\langle \mathbf{S} \rangle$ the appropriately taken spin expectation value, [A] the magnetic hyperfine tensor, g_n the nuclear g-factor, β_n the nuclear Bohr magneton and $\mathbf{H_Q}$ the quadrupolar interaction Hamiltonian.

Synthesis of [^{57}Fe(bztpen)Cl](ClO$_4$)$_2$ and of Complexes 1 and 2

Caution: Although no problems were encountered in the preparation of the perchlorate salts, care should be taken when handling such potentially hazardous compounds.

The ligand bztpen was synthesized as previously described.[10] The $^{57}FeCl_3 \cdot 6H_2O$ starting compound was obtained as recently published.[7] Methanol was purchased from Prolabo, $NaClO_4$ from Sigma, hydrogen peroxide and triethylamine from Aldrich, and all were used without further purification. For the synthesis of [^{57}Fe(bztpen)Cl](ClO$_4$)$_2$, $^{57}FeCl_3 \cdot 6H_2O$ (53.2 mg, 0.197 mmol) in dry methanol (1 mL) was added to a solution of bztpen (83.3 mg, 0.197 mmol) in 2 mL of dry methanol. A yellow precipitate formed immediately and redissolved spontaneously after 2 minutes. Addition of $NaClO_4$ (72.6 mg, 0.591 mmol) resulted in precipitation of a yellow product, which was isolated by filtration. Treatment of this yellow compound, dissolved in dry methanol, with hydrogen peroxide (30%, 300 equivalents) generated the purple species **1**. Addition of triethylamine (99%, 30 equivalents) produced a blue solution of **2**.

Acknowledgments

N. Genand-Riondet (CEA/Saclay) is thanked for recording Mössbauer experiments and helping in the design of Mössbauer cells for the in-field experiments.

[1] [1a] L. Que, R. Y. Ho, *Chem. Rev.* **1996**, *96*, 2607−2624. [1b] E. I. Solomon, T. C. Brunold, M. I. Davis, J. N. Kemsley, S.-K. Lee, N. Lehnert, F. Neese, A. J. Skulan, Y.-S. Yang, J. Zhou, *Chem. Rev.* **2000**, *100*, 235−349. [1c] M. Costas, K. Chen, L. Que, Jr., *Coord. Chem. Rev.* **2000**, 200−202, 517−544.

[2] [2a] J. W. Sam, X.-J. Tang, J. Peisach, *J. Am. Chem. Soc.* **1994**, *116*, 5250−5256. [2b] R. J. Guajardo, J. D. Tan, P. K. Mascharak, *Inorg. Chem.* **1994**, *33*, 2838−2840.

[3] [3a] C. Bull, J. A. Fee, *J. Am. Chem. Soc.* **1985**, *107*, 3295−3304. [3b] D. M. Dooley, J. L. Karas, T. F. Jones, C. E. Coté, S. B. Smith, *Inorg. Chem.* **1986**, *25*, 4761−4766.

[4] [4a] M. Lombard, C. Houée-Levin, D. Touati, M. Fontecave, V. Nivière, *Biochemistry* **2001**, *16*, 5032−5040. [4b] M. D. Clay, F. E. Jenney, Jr., P. L. Hagedoorn, G. N. George, M. W. W. Adams, M. K. Johnson, *J. Am. Chem. Soc.* **2002**, *124*, 788−805.

[5] [5a] I. Bernal, I. M. Jensen, K. B. Jensen, C. J. McKenzie, H. Toftlund, J. P. Tuchagues, *J. Chem. Soc., Dalton Trans.* **1995**, 3667−3675. [5b] C. Kim, K. Chen, J. Kim, L. Que, Jr., *J. Am. Chem. Soc.* **1997**, *119*, 5964−5965. [5c] M. Lubben, A. Meetsma, E. C. Wilkinson, B. Feringa, L. Que, Jr., *Angew. Chem. Int. Ed. Engl.* **1995**, *34*, 2048− 2051. [5d] Y. Zhang, T. E. Elgren, Y. Dong, L. Que, Jr., *J. Am. Chem. Soc.* **1993**, *115*, 811−813. [5e] K. B. Jensen, C. J. McKenzie, L. P. Nielsen, J. Z. Pedersen, H. M. Svendsen, *Chem. Commun.* **1999**, 1313−1314. [5f] A. J. Simaan, F. Banse, P. Mialane, A. Boussac, S. Un, T. Kargar-Grisel, G. Bouchoux, J.-J. Girerd, *Eur. J. Inorg. Chem.* **1999**, 993−996. [5g] A. J. Simaan, S. Döpner, F. Banse, S. Bourcier, G. Bouchoux, A. Boussac, P. Hildebrandt, J.-J. Girerd, *Eur. J. Inorg. Chem.* **2000**, 1627−1633. [5h] A. Hazell, C. J. McKenzie, L. P. Nielsen, S. Schindler, M. Weitzer, *J. Chem. Soc., Dalton Trans.* **2002**, 310−317. [5i] J.-J. Girerd, F. Banse, A. J. Simaan, *Struture and Bonding*, Springer-Verlag, New York, **2000**, 97, 145−177.

[6] F. Neese, E. I. Solomon, *J. Am. Chem. Soc.* **1998**, *120*, 12829−12848.

[7] O. Horner, C. Jeandey, J.-L. Oddou, P. Bonville, J.-M. Latour, *Eur. J. Inorg. Chem.* **2002**, 1186−1189.

[8] [8a] P. Gütlich, R. Link, A. Trautwein, Mössbauer Spectroscopy and Transition Metal Chemistry, Springer-Verlag, Berlin, **1979**. [8b] V. Schünemann, H. Winkler, *Rep. Prog. Phys.* **2000**, *63*, 263−353.

[9] [9a] V. Vrajmasu, E. Münck, R. Ho, L. Que, Jr., G. Roefles, B. L. Feringa, *J. Inorg. Biochem.* **2001**, *86*, 472. [9b] A. J. Simaan, F. Banse, J.-J. Girerd, K. Wieghardt, E. Bill, *Inorg. Chem.* **2001**, *40*, 6538−6540.

[10] A. Hazell, C. J. McKenzie, L. P. Nielsen, S. Schindler, M. Weitzer, *J. Chem. Soc., Dalton Trans.* **2002**, 310−317.

[11] H. H. Wickman, P. M. Klein, D. A. Shirley, *Phys. Rev.* **1966**, *152*, 345−357.

[12] B. H. Huynh, M. H. Emptage, E. Münck, *Biochim. Biophy. Acta* **1978**, *534*, 295−306.

[13] E. Münck in *Physical Methods in Bioinorganic Chemistry − Spectroscopy and Magnetism* (Ed.: L. Que, Jr.), University Science Books, **2000**, chapter 6.

[14] J. S. Griffith, *Proc. R. Soc. London, A* **1956**, *234*, 23−36.

[15] C. P. S. Taylor, *Biochim. Biophys. Acta* **1977**, *491*, 137−149.

[16] R. M. Burger, T. A. Kent, S. B. Horwitz, E. Munck, J. Peisach, *J. Biol. Chem.* **1983**, *258*, 1559−1564.

[17] W. T. Oosterhuis, G. Lang, *Phys. Rev.* **1969**, *178*, 439−456.

[18] [18a] G. Lang, *Q. Rev. Biophys.* **1970**, *3*, 1−60. [18b] V.-C. Popescu, E. Münck, B. G. Fox, Y. Sannakis, J. G. Cummings, I. M. Turner, Jr., M. J. Nelson, *Biochemistry* **2001**, *40*, 7984−7991.

[19] F. Neese, J. M. Zaleski, K. L. Zaleski, E. I. Solomon, *J. Am. Chem. Soc.* **2000**, *122*, 11703−11724.

[20] A. Veselov, H. Sun, A. Sienkiewicz, H. Taylor, R. M. Burger, C. P. Sholes, *J. Am. Chem. Soc.* **1995**, *117*, 7508−7512.

[21] J. W. Sam, X.-Jun Tang, J. Peisach, *J. Am. Chem. Soc.* **1994**, *116*, 5250−5256.

[22] C. Hauser, T. Glaser, E. Bill, T. Weyermüller, K. Wieghardt, *J. Am. Chem. Soc.* **2000**, *122*, 4352−4365.

[23] J. A. Broadwater, C. Achim, E. Münck, B. G. Fox, *Biochemistry* **1999**, *38*, 12197−12204 and references therein.

[24] J. N. Burstyn, J. A. Roe, A. R. Miksztal, B. A. Shaevitz, G. Lang, J. S. Valentine, *J. Am. Chem. Soc.* **1988**, *110*, 1382−1388.

[25] F. Neese, E. I. Solomon, *J. Am. Chem. Soc.* **1998**, *120*, 12829−12848.

[26] C. A. Brown, M. A. Pavlosky, T. E. Westre, Y. Zhang, B. Hedman, K. O. Hodgson, E. I. Solomon, *J. Am. Chem. Soc.* **1995**, *117*, 715−732.

Received March 22, 2002
[I02154]

Syntheses of Zinc Complexes with Multidentate Nitrogen Ligands: New Catalysts for Aldol Reactions

Tamis Darbre,*[a] Christian Dubs,[a] Eduard Rusanov,[b] and Helen Stoeckli-Evans[b]

Keywords: Aldol reaction / Catalysis / N ligands / N,O ligands / Zinc

The ligands 2,6-bis{[(pyrid-2-ylmethyl)amino]methyl}-pyridine with an N_5 pattern and (6-{[(pyrid-2-ylmethyl)amino]methyl}pyrid-2-yl)methanol with an N_3O pattern were synthesized. Zn^{II} complexes of the two ligands could be obtained, and the single-crystal X-ray structure of (2,6-bis{[(pyrid-2-ylmethyl)amino]methyl}pyridine)zinc chloride showed Zn coordination to all five nitrogen atoms. The strong complexation of 2,6-bis{[(pyrid-2-ylmethyl)-amino]methyl}pyridine and (6-{[(pyrid-2-ylmethyl)amino]-methyl}pyrid-2-yl)methanol with Zn^{II} were demonstrated by ^1H NMR spectroscopic studies and electrospray mass spectrometry. The coupling of 2-hydroxyacetophenone and benzaldehyde was studied in the presence of the prepared Zn complexes, and it was shown that the coupling product was obtained at room temperature in up to 60% yield with 7.5 mol % of the zinc catalyst. The present complexes mimic the active site of the zinc-dependent class II aldolases, where Zn^{II} is coordinated to three nitrogen atoms.
(© Wiley-VCH Verlag GmbH, 69451 Weinheim, Germany, 2002)

Introduction

The aldol reaction is of central importance for construction of C−C bonds in organic chemistry.[1] It is therefore not surprising that several catalysts and reagents have been developed in order to achieve efficient condensation with high diastereomeric and enantiomeric selectivity.[2] Furthermore, due to its importance for organic synthesis, the asymmetric aldol reaction has become, without doubt, one of the most important topics in modern catalytic synthesis.

From the several methods available for the aldol reaction, the direct condensation of an aldehyde with a ketone[3] is a most attractive approach since it does not require the isolation of preformed enolates.[4] Therefore, the development of new catalysts for the direct condensation is a field of considerable importance.

In nature, aldol reactions also constitute an important reaction class that is mediated by aldolases, ubiquitous enzymes that catalyze among other reactions, the reversible aldol cleavage of fructose-1,6-bis(phosphate) (FBP) in glycolysis. Aldolases are divided into two distinct classes according to their enzymatic mechanism. Whereas the class I aldolases form a Schiff base intermediate between the e-amino group of a lysine residue and the carbonyl carbon atom of the substrate, class II aldolases are zinc-dependent.[5] Three histidine side chains and a carboxylate group of a glutamic acid are coordinated to the Zn^{II} ion in class II fuculose 1-phosphate aldolase produced by *E. coli*.[6] Upon substrate binding, the carboxylate group dissociates from the Zn^{II} reaction center and moves away, providing space for the hydroxy ketone to bind to the Zn^{II} ion and at the same time deprotonating the carbon atom in the α-position to the carbonyl group. The resulting enediolate is proposed to be stabilized through binding to the zinc ion and to act as a nucleophile (Figure 1).[6]

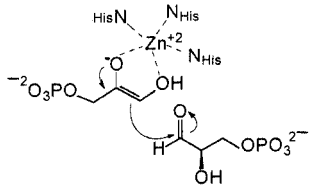

Figure 1. Proposed mechanism for the aldol reaction catalyzed by type II aldolase[6]

Although it has been demonstrated that Zn^{II} salts catalyze the aldol condensation,[7] Zn complexes with nitrogen ligands have not been explored much as catalysts for aldol reactions. In a structural model for aldolases, a modified tris(pyrazolyl)borate ligand[8] was used to mimic the three nitrogen atoms in the enzyme's active site. A model with four nitrogen atoms and a carbonyl group bound to the zinc ion has also been developed.[9] Proline has been used as an asymmetric catalyst,[10,11] and some early work has shown that the Zn^{II} ion coordinated to pyridine and bi- and ter(pyridine)s can catalyze the reaction of aldehydes and ketones to give unsaturated ketones.[12]

Chiral dinuclear Zn complexes with chiral binol as ligand as well as other oxygen-containing ligands have been re-

[a] Department of Chemistry and Biochemistry, University of Bern,
Freiestrasse 3, 3012, Switzerland
[b] Institute of Chemistry, University of Neuchâtel,
Avenue de Bellevaux 51, 2007 Neuchatel, Switzerland

cently reported to catalyze asymmetric aldol reactions.[13−18]

Inspired by the Zn^{II} coordination site in the active site of the class II aldolases, we have prepared ligands containing nitrogen-binding sites in order to develop novel catalysts for the aldol reaction.

Here we report on the efficient synthesis of ligands containing nitrogen as binding sites (N_5 and N_3O), the synthesis of new Zn^{II} complexes where the zinc center is coordinated to nitrogen atoms, and our first results on the activity of the new zinc complexes as catalysts for the condensation of benzaldehyde and 2-hydroxyacetophenone.

Results and Discussion

The syntheses of the ligands with N_5 and N_3O coordination sites (**6** and **9**) are shown in Scheme 1. Synthesis of tosylamine **3** was achieved by treatment of 2-(aminomethyl)-pyridine with NaOH and tosyl choride in a two-phase system (H_2O/diethyl ether) in 89% yield.[19] Coupling of **3** with 2,6-bis(bromomethyl)pyridine (**4**), also in a two-phase system and nBu_4NBr as a phase-transfer catalyst, gave product **5**, which could be isolated after chromatography in 86% yield. The tosyl group was removed by heating the tosylate **5** with concentrated sulfuric acid to yield the ligand **6** in 94% yield. The three-step synthesis gives **6** in an overall yield of 72%. There are two reports in the literature of compounds related to **6**; in the first the tetraammonium salt of **6** is prepared by a different procedure,[20] and in the second G. Newkome et al.[19] report the synthesis of **6** in 28% yield. The latter authors describe the product obtained as an unstable oil whereas we isolated **6** as a brownish, stable solid.

For the synthesis of the new ligand **9**, the tosylamine **3** was alkylated with [6-(bromomethyl)pyrid-2-yl]methanol (**7**) in the presence of K_2CO_3 in acetonitrile to give **8** in 74% yield. The latter was deprotected in the same way as **5** to give **9** in 76% yield (Scheme 1).

The ligands **6** and **9** became readily available in a few steps and high yields by the syntheses developed here.

Complexation of 6 and 9 with Zn Salts

Having the two ligands **6** and **9** at hand, we have prepared a series of Zn^{II} complexes to test their ability to act as catalysts for aldol reactions. Thus, ligand **6** was refluxed with $ZnCl_2$, $Zn(CH_3COO)_2{\cdot}2H_2O$ or $Zn(ClO_4)_2{\cdot}6H_2O$ in a 1:1 ration in MeOH to give the corresponding complexes **1a**, **1b** and **1c** in 64%, 82% and 81% yield, respectively. All three complexes could be identified by their ^1H and ^{13}C NMR spectra, and ESI-MS. The ^1H NMR spectrum in CD_3OD of **1a**, **1b**, **1c** showed shifts of the signals for the pyridine hydrogen atoms as well as for the two methylene groups [the signals of the $pyCH_2N$ methylene groups appear at δ = 3.97 ppm (8 H) for the ligand **6** and at δ = 4.28 ppm (4 H) and δ = 4.39 ppm (4 H) for the acetate complex **1b**]. The ESI-MS data showed for the three complexes, **1a**, **1b** and **1c**, peaks at *m*/*z* = 382, 384, 386, that can be assigned to [**6** − H^+ + Zn^{II}], with relative intensities of 100:59:41 for **1a**, 100:61:38 for **1b** and 100:59:41 for **1c**, in good agreement with the calculated intensities of 100:60:42 for the three zinc isotopes. Furthermore, the peaks for [**6** + Zn^{II} + Cl^-] at *m*/*z* = 418, 420 and 422 are also observed for **1a**, as well as the peaks for the [**6** + Zn^{II} + CH_3COO^-] at *m*/*z* = 442,444 and 446 and for the [**6** + Zn^{II} + ClO_4^-] at *m*/*z* = 482, 484 and 486 for **1b** and **1c**, respectively. The free ligand **6**, however, could not be detected in the ESI-MS.

Insight into the geometry of the complexes and the binding mode of the zinc atom with the ligand **6** was obtained by single-crystal X-ray analysis. The reaction of **6** with $ZnCl_2$ gave two pseudo-polymorphs, **1a**·CH_3OH solvate and **1a**·$2H_2O$. Here the Zn^{II} ion is coordinated to the five

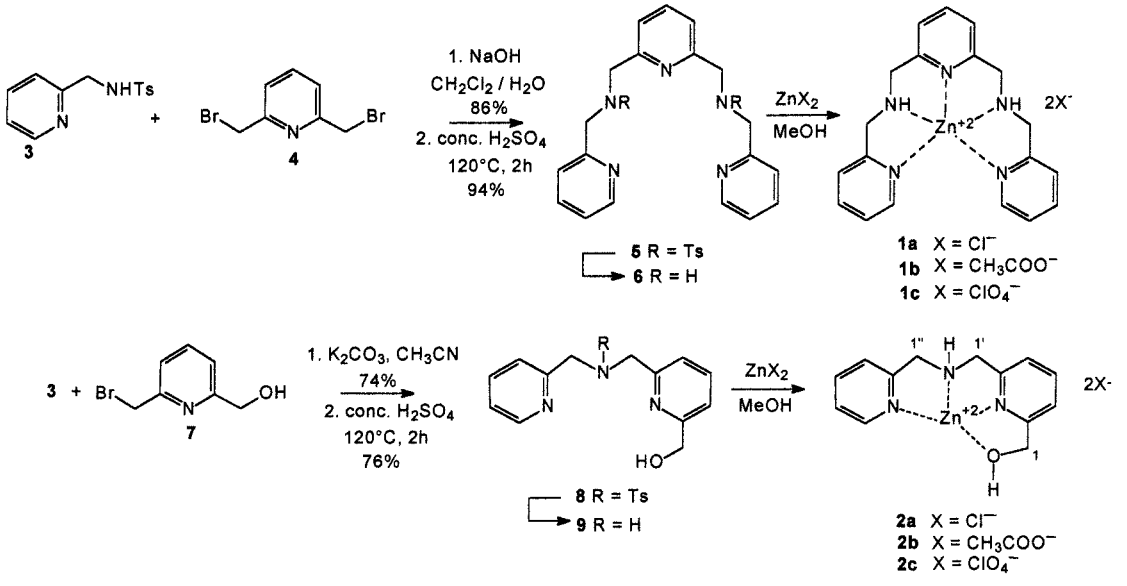

Scheme 1

nitrogen atoms of the ligand and to a chloride anion, producing complexes with pseudo-C_2 symmetry (for example, see Figure 2). The zinc atoms and the pyridine rings of the side chain are almost co-planar. The amine N atoms, N2 and N4, are displaced above this plane towards the central pyridine ring. The reaction of **6** with $Zn(ClO_4)_2$ gave **1c**, in which the metal ion is pentacoordinate, with all five nitrogen atoms coordinated to the metal (Figure 3). Due to the lack of a sixth ligand, the two pyridine rings are bent downwards, but the complex retains the pseudo-C_2 symmetry. The bond angles N1−Zn−N3 and N3−Zn−N5 have an average value of 128.3° relative to 89.3° for the two hexacoordinate **1a** complexes. The zinc−N bond lengths in **1c** are notably shorter than those observed in complexes **1a**·CH_3OH and **1a**·$2H_2O$. These differences are particularly important for the central Zn−N(pyridine) distance (ca. 0.1 Å) and the outer Zn−N(pyridine) distances (ca. 0.15 Å). Selected bond lengths and angles for the three structures are given in Table 1.

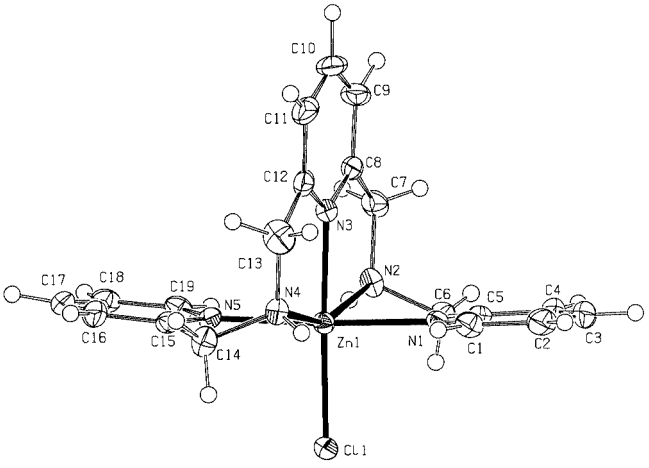

Figure 2. Perspective view of cation **1a**·CH_3OH solvate, showing the crystallographic numbering scheme, and thermal ellipsoids at 50% probability; the Cl^- anion and the CH_3OH solvent molecule have been omitted for clarity

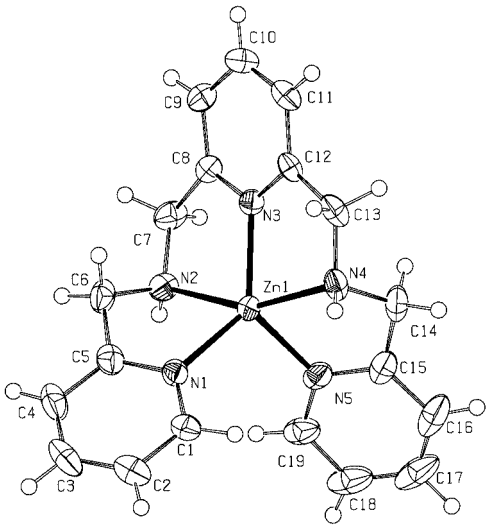

Figure 3. Perspective view of cation **1c**, showing the crystallographic numbering scheme, and thermal ellipsoids at 50% probability; the ClO_4^- anions have been omitted for clarity

Table 1. Selected bond lengths [Å] and angles [°] for complexes **1a**·CH_3OH solvate, **1a**·$2H_2O$ and **1c**

	1a·CH_3OH	**1a**·$2H_2O$	**1c**
Zn−N1	2.199(3)	2.214(2)	2.051(2)
Zn−N2	2.221(3)	2.200(2)	2.174(2)
Zn−N3	2.12183)	2.121(2)	2.029(2)
Zn−N4	2.200(3)	2.212(2)	2.179(2)
Zn−N5	2.190(3)	2.154(2)	2.027(2)
Zn−Cl1	2.376(1)	2.383(1)	
N1−Zn−N2	77.71(10)	77.81(7)	81.07(10)
N1−Zn−N3	86.73(11)	88.26(6)	128.98(9)
N1−Zn−N4	101.02(11)	101.38(7)	114.16(9)
N1−Zn−N5	176.87(11)	179.36(7)	103.44(10)
N2−Zn−N3	77.18(12)	77.74(7)	78.64(9)
N2−Zn−N4	154.44(12)	155.26(7)	157.32(01)
N2−Zn−N5	101.44(10)	102.82(7)	111.89(10)
N3−Zn−N4	77.26(11)	77.52(7)	78.69(10)
N3−Zn−N5	90.14(11)	91.87(6)	127.55(9)
N4−Zn−N5	78.41(11)	78.03(7)	81.95(10)
Cl1−Zn−N1	91.18(8)	89.08(5)	
Cl1−Zn−N2	101.32(9)	101.73(5)	
Cl1−Zn−N3	177.64(8)	177.34(5)	
Cl1−Zn−N4	104.24(9)	102.99(5)	
Cl1−Zn−N5	91.95(8)	90.79(5)	

Complexes **2a**, **2b** and **2c** were obtained by refluxing the zinc salts and **9** in a 1:1 ratio in methanol. Partial evaporation of the solvent and addition of diethyl ether gave [(6-{[(pyrid-2-ylmethyl)amino]methyl}pyrid-2-yl)methanol]zinc dichloride (**2a**), [(6-{[(pyrid-2-ylmethyl)amino]methyl}-pyrid-2-yl)methanol]zinc diacetate (**2b**) and [(6-{[(pyrid-2-ylmethyl)amino]methyl}pyrid-2-yl)methanol]zinc diperchlorate (**2c**) as white solids (Scheme 1), in 41, 62 and 66% yields, respectively.

The complexes **2a**, **2b**, **2c** were characterized by ^1H and ^{13}C NMR spectroscopy, and ESI-MS. The ^1H NMR spectrum in [D_4]methanol of **9**, **2b** and **2c** are shown in Figure 4. In general, we can see that for the three methylene groups a strong downfield shift is observed upon complexation, whereas the aromatic protons are less influenced by the Zn coordination. For ligand **9**, three signals for the 6 H atoms in the positions 1, 1′ and 1′′ (see numbering in Scheme 1) can be seen; a singlet at δ = 4.72 ppm (2 H1), and two close singlets (δ = 3.95 and 3.96 ppm) corresponding to four protons (2 H1′ and 2 H1′′). After complexation, five signals appeared for the same six hydrogen atoms and the two H1, two H1′ and two H1′′ atoms, became nonequivalent. We observe two broad signal at δ = 5.05 and 4.97 ppm for the two H1 atoms, a broad signal at δ = 4.54 ppm for two hydrogen atoms (1 H1′ and 1 H1′′) and two broad doublets at δ = 4.16 and 3.82 ppm for the remaining two hydrogen atoms (1 H1′ and 1 H1′′). For **2c** the signals are well defined.

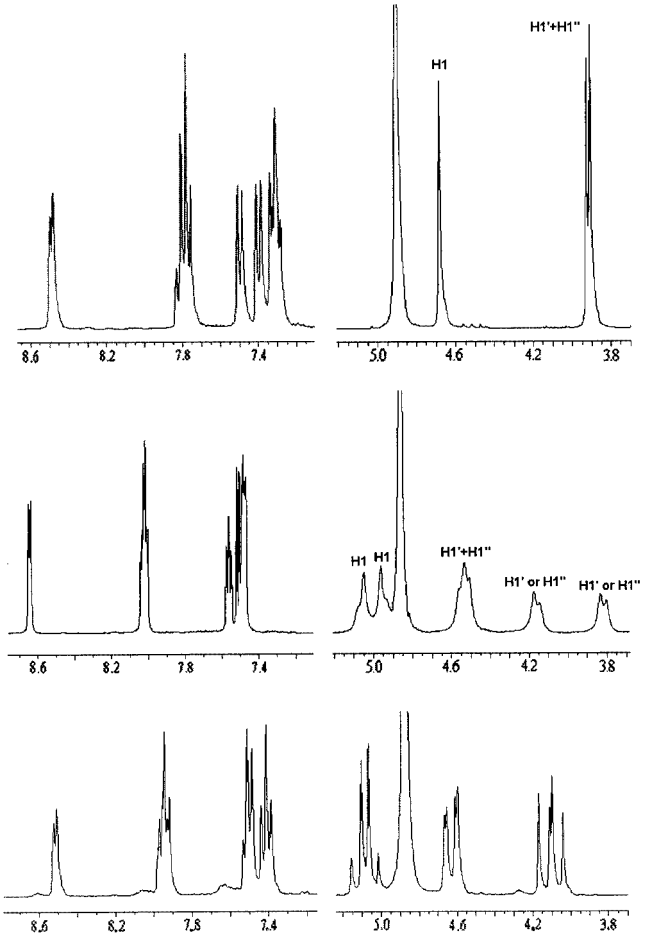

Figure 4. Top: ^{1}H NMR in CD_3OD of ligand **9**; center: ^{1}H NMR spectrum, in CD_3OD, of complex **2b**; bottom: ^{1}H NMR spectrum in CD_3OD of complex **2c**; the aromatic region and the methylene groups are shown (in ppm)

The assignment of the hydrogen signals in the ^{1}H NMR spectrum of complex **2b** was determined by a ^{1}H-^{1}H COSY measurement.

The electrospray mass spectra of **2a**, **2b** and **2c** show the peaks corresponding to [**9** − H^+ + Zn^{II}] at m/z = 292, 294 and 296 in the expected relative intensities, consistent with the structure shown in Scheme 1. The peaks corresponding to [**9** − H^+ + Zn^{II} + Cl^-] for **2a** and [**9** − H^+ + Zn^{II} + CH_3COO^-] for **2b** are also present. Similar to the complexes of **6**, the peak corresponding to the free ligand **9** is not observed in the ESI-MS.

The structures for the complexes **2a**, **2b**, **2c** in Scheme 1 indicate a protonated hydroxy group, although deprotonation cannot be excluded. The presence of a hydroxy group was inferred by the fact that the ^{1}H NMR spectrum of the acetate complex **2b** showed six protons for two acetate anions, indicating the presence of two counter-anions in **2b**.

The acetates **1b** and **2b** proved to be soluble in a variety of organic solvents, an important property for efficient catalysis of organic reactions. The acetate anion can also act as a base to deprotonate a ketone in the aldol reaction. Therefore, the preliminary reactivity studies described below were conducted with the acetates.

Reactivity Studies

In order to explore the ability of the new zinc complexes to act as catalysts for aldol reactions, the zinc-catalyzed reaction of benzaldehyde (**10**) with 2-hydroxyacetophenone (**11**) to give 1,3-diphenylpropan-1-one (**12**) was investigated (Scheme 2).

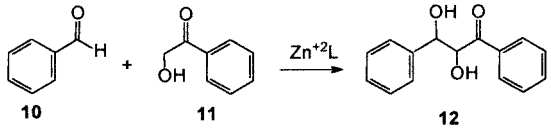

Scheme 2

The results are summarized in Tables 2−4. The aldol product **12** was formed when a mixture of 1.0 equiv. of benzaldehyde (**10**) and 1.5 equiv. of 2-hydroxyacetophenone (**11**) reacted in the presence of 7.5 mol % of either **6** or **9** and 7.5 mol % of zinc acetate.[21] The reaction took place in THF but also in a protic solvent, methanol, and the yields improved with addition of 0.5 equiv. of triethylamine. The ligand **9** was the more efficient of the two ligands studied, giving the addition product in 53% in methanol and 56% in THF. The conversion was higher when diethylzinc was added to **9** (62%, Entry 7, Table 3). The preformed complexes **1b** and **2b** could also catalyze the aldol reaction; **2b** gave the higher yield (59%) of **12**. We have also observed that an excess of benzaldehyde or 2-hydroxyacetophenone can lead to better yields (51−52%) when **1b** is the catalyst (Entries 4 and 7 in Table 4). The *syn*/*anti* ratio of **12**, determined by ^{1}H NMR spectroscopy for the reactions shown in the tables, was 1:1 for all the experiments with exception of Entry 4 inTable 3 (1.5:1 *syn*/*anti* ratio) and Entry 5 in Table 3 (3:1 *syn*/*anti* ratio).

Table 2. Aldol reaction using the ligands **6** and **9** and zinc salts as catalysts in MeOH (in all experiments, 0.5 mmol of benzaldehyde, 0.75 mmol of 2-hydroxyacetophenone and 0.05 mmol of catalyst were used; **12** was obtained as a 1:1 *syn*/*anti* mixture and the yields and diastereomeric ratios were determined by ^{1}H NMR spectroscopy; Py: pyridine; Im: imidazole; Et_3N: triethylamine)

Entry	Catalyst (7.5 mol %)	Additives	Yield of **12** (%)
1	**6**		0
2	**6**, $Zn(Ac)_2$		37
3	**6**, $Zn(CH_3COO)_2$	0.25 mmol Et_3N	45
4	**6**, $Zn(CH_3COO)_2$	0.25 mmol py	24
5	**6**, $Zn(CH_3COO)_2$	0.25 mmol Im	17
6	**9**		0
7	**9**, $Zn(CH_3COO)_2$		38
8	**9**, $Zn(CH_3COO)_2$	0.25 mmol Et_3N	53
9	**9**, $Zn(CH_3COO)_2$	Na_2SO_4	35

Table 3. Aldol reaction using the ligands **6** and **9** and zinc salts as catalysts in THF (in all experiments, 0.5 mmol of benzaldehyde, 0.75 mmol of 2-hydroxyacetophenone and 0.05 mmol of catalyst were used; **12** was obtained as a 1:1 syn/*anti* ratio and the yields and diastereomeric ratios were determined by ^{1}H NMR spectroscopy; Py: pyridine; Et_3N: triethylamine; MS: molecular sieves

Entry	Catalyst (7.5 mol %)	Additives	Yield of **12** (%)
1	**6**, $Zn(CH_3COO)_2$		40
2	**6**, $Zn(CH_3COO)_2$	MS	40
3	**6**, $Zn(CH_3COO)_2$	0.25 mmol Et_3N, MS	50
4	**6**, $Zn(CH_3COO)_2$	0.25 mmol py, MS	48
5	**9**,$Zn(CH_3COO)_2$	MS	38
6	**9**,$Zn(CH_3COO)_2$	0.25 mmol Et_3N, MS	56
7	**9**, $Zn(Et)_2$		62

Table 4. Aldol reaction using the complexes **1b** and **2b** as catalysts (Entries 1−9 in THF; Entries 10, 11 in MeOH)

Entry	Catalyst (7.5 mol %)	Additives	Yield of **12** (%)
1[a]	1b	MS	40
2[a]	1b	0.25 mmol Et_3N, MS	48
3[a]]	1b	0.25 mmol py, MS	38
4[b]	**1b**	MS	51[c]
5[b]	**1b**	0.25 mmol Et_3N, MS	39[d]
6[e]	**1b**	MS	45
7[e]	**1b**	0.25 mmol Et_3N, MS	52
8[a]	2b	MS	41
9[a]	**2b**	0.25 mmol Et_3N, MS	59
10[a]	2b		29
11[a]	**2b**	Na_2SO_4	23

[a] 0.5 mmol benzaldehyde, 0.75 mmol 2-hydroxyacetophenone. [b] 1 mmol benzaldehyde, 0.25 mmol 2-hydroxyacetophenone. [c] 1.5:1 *syn*/*anti*. [d] 3:1 *syn*/*anti*. The yields and diastereomeric ratios were determined by ^{1}H NMR spectroscopy. MS: molecular sieves. Py: pyridine; Et_3N: triethylamine. [e] 0.25 mmol benzaldehyde, 0.75 mmol 2-hydroxyacetophenone. In all experiments 0.05 mmol of catalyst was used. **12** was obtained as a 1:1 *syn*/*anti* ratio with the exception of footnotes [c] and [d].

Further studies of the catalytic system developed with other substrates and screening for reaction conditions that will lead to improved yields are now under way.

Conclusions

In a search for new Zn^{II} complexes that can act as catalysts for aldol reactions, we have prepared novel zinc complexes with N_5 and N_3O coordination. For that, the ligands **6** and **9** were synthesized in a few steps with high yields. The complexes prepared catalyze the reaction of hydroxyacetophenone and benzaldehyde to give 2,3-diphenylpropan-1-one in yields of 60% when **9** plus diethylzinc or the preformed zinc complex **2b** were the catalysts.

Experimental Section

General Remarks: All reactions were carried out, unless mentioned, in open flasks, without exclusion of O_2 or H_2O. Technical solvents were distilled prior to use. Chemicals were purchased from commercial suppliers (FLUKA and Aldrich) and, unless otherwise stated, used without further purification. Acetonitrile was refluxed under nitrogen for 2 h in the presence of CaH_2, distilled and kept over molecular sieves. Column chromatography (CC): silica gel 60 from FLUKA; thin layer chromatography (TLC): silica gel plates Alugram® Sil G/UV254; visualization was made with a UV lamp (λ = 254 nm) or with 10% ninhydrin solution in 90% ethanol. NMR spectra: Bruker AC-300 spectrometer, 300 MHz for ^{1}H and 75 MHz for ^{13}C. Chemical shifts δ are given in ppm and were calibrated against the deuterated solvent. The multiplicity of the ^{13}C NMR peaks were determined by ^{13}C NMR DEPT spectra and the expected chemical shifts; the *J* values are in Hz. Mass spectra were provided by the Service of Mass Spectrometry of the Department of Chemistry and Biochemistry in Bern. Infrared spectroscopy was performed with a Perkin-Elmer 1600 series FTIR spectrometer. Frequencies $\tilde{\nu}$ are given in cm^{-1} (s strong, m medium, w weak).

Caution: Perchlorates are potentially explosive and should be handled with the necessary precautions.[22]

2-[(Tosylamino)methyl]pyridine (3): Prepared as described.[19] Tosyl chloride (14.12 g, 74 mmol) in diethyl ether (14 mL) was added to a mixture of 2-(aminomethyl)pyridine (8 g, 74 mmol) and NaOH (4.4 g, 110 mmol) in water (20 mL). The two-phase reaction mixture was stirred in a closed flask for 18 h. The ether was then evaporated and the pH of the aqueous phase adjusted to 7 with 1 M HCl solution. The precipitated white solid was filtered, dried and dissolved in ethanol. The ethanol was evaporated to yield **3** as a white solid (17.36 g, 89% yield). ^{1}H NMR ($CDCl_3$): δ = 2.39 (s, 3 H, CH_3Ts), 4.24 (d, *J* = 5.49, 2 H, NCH_2Py), 5.90 (br. t, 1 H, NH), 7.14−7.19 (m, 2 H, 3-pyH and 5-pyH), 7.23−7.26 (m, 2 H, 3-phH), 7.61 (ddd, 1 H, 4-pyH), 7.74 (d, *J* = 7.7, 12 H, 2-phH), 8.45 (d, *J* = 4.77, 1 H, 6-pyH) ppm. ^{13}C NMR ($CDCl_3$): δ = 22.17 (q), 48.05 (t), 122.65 (d), 123.29 (d), 127.91 (d), 130.8 (d), 137.52 (d), 144.04 (q), 149.57 (d), 155.47 (q) ppm.

2,6-Bis(bromomethyl)pyridine (4) and [6-(Bromomethyl)pyrid-2-yl]-methanol (7): 2,6-bis(hydroxymethyl)pyridine (2 g,14.4 mmol) was heated for 15 h in 48% HBr solution (20 mL). The solution was cooled with an ice bath and 10 M NaOH was added until pH = 12 was reached. After extraction with ether (3 × 60 mL), the ether phase was dried with $MgSO_4$, filtered and the ether evaporated to give a white solid. The products were separated by column chromatography (diethyl ether/hexane, 3:7) to give two fractions. Fraction A: **4** (1.94 g, yield 51%) as white needle-like crystals. R_f = 0.4 (diethyl ether/hexane, 3:7). ^{1}H NMR ($CDCl_3$): δ = 4.55 (s, 4 H, CH_2Py), 7.39 (d, *J* = 7.74 Hz, 2 H, 3-pyH), 7.72 (ap. t, *J* = 7.73 Hz, 1 H, 4-pyH) ppm. ^{13}C NMR ($CDCl_3$): δ = 33.45 (t), 122.79 (d), 138.11 (d), 156.73 (s) ppm. Fraction B: **7** (720 mg, yield 24%) as white needle-like crystals. R_f = 0.05 (diethyl ether/hexane, 3:7). ^{1}H NMR ($CDCl_3$): δ =3.66 (br. s, 1 H, OH), 4.56 (s, 2 H, OCH_2py), 4.77 (s, 2 H, $BrCH_2$py), 7.18 (d, *J* = 7.7 Hz, 1 H,), 7.36 (d, *J* = 7.5 Hz, 2 H), 7.61 (app t, *J* = 7.7 Hz, 1 H, 4-pyH) ppm. By adding more HBr after 15 h and refluxing for a longer time, the yield of **4** could be increased to 69%. By stopping the reaction immediately after all the 2,6-bis(hydroxymethyl)pyridine had disappeared on the TLC the yield of **7** could be increased to 37%.

2,6-Bis{[(pyrid-2-ylmethyl)(tosyl)amino]methyl}pyridine (5): $n$$Bu_4NBr$ (6.48 g) and KOH (80 g) in water (240 mL) was added to 2-[(tosylamino)methyl]pyridine (**3**) (8 g, 30.4 mmol) in dichloromethane (800 mL). The reaction mixture was heated to reflux and 2,6-bis(bromomethyl)pyridine (**4**) (4 g, 15.2 mmol) in dichloromethane was added at once. The reaction mixture was refluxed for 14 h. The

two phases were separated and the dichloromethane was evaporated to leave a brown oil. Column chromatography (hexane/ethyl acetate, 1:1 with 1% triethylamine) yielded **5** as a brown viscous oil (8.25 g, yield 86%). R_f = 0.1 (hexane/ethyl acetate, 1:1). ^{1}H NMR ($CDCl_3$): δ = 2.39 (s, 3 H, $TsCH_3$), 4.36 (s, 4 H, $pyCH_2$), 4.49 (s, 4 H, $pyCH_2$), 7.05−7.09 (m, 4 H,3,5-pyH), 7.23 (d, J = 8.1 Hz, 4 H, phH), 7.31 (d, J = 7.92 Hz, 2 H, 3,5-pyH), 7.36 (ap. t, J = 7.71 Hz, 1 H, 4-pyH), 7.53 (ddd, J = 7.63, J = 1.6 Hz, 2 H, 4-pyH), 7.65 (d, J = 8.2 Hz, 4 H, phH), 8.34 (d, J = 4.2 Hz, 2 H, 6-pyH) ppm. ^{13}C NMR ($CDCl_3$): δ = 22.16 (q), 54.31 (t), 54.56 (t), 121.83 (d), 123.02 (d), 123.36 (d), 128.06 (d), 130.24 (d), 137.26 (d), 137.61 (d), 144.03 (s), 149.44 (d), 156.42 (s), 157.14 (s) ppm.

2,6-Bis{[(pyrid-2-ylmethyl)amino]methyl}pyridine (6): **5** (7.6 g, 12.1 mmol) was dissolved in 98% H_2SO_4 (10 mL) and heated to 120 °C for 3 h. The liquid turned black. The solution was poured into a brine/NaOH solution (20 mL) and the pH of the solution was adjusted to 12 with an NaOH solution The aqueous solution was extracted with dichloromethane (4 × 100 mL). The organic phase was dried with $MgSO_4$, filtered and the dichloromethane evaporated to give **6** as a brown solid (3.65 g, yield 94%). ^{1}H NMR ($CDCl_3$): δ = 2.32 (s, 2 H, NH), 3.96 and 3.98 (2s, 8 H, CH_2py), 7.13−7.15 (m, 2 H, pyH), 7.21 (d, J = 7.71, 2 H, pyH), 7.35 (d, J = 7.71 Hz, 2 H, 3,5-pyH), 7.57−7.66 (m, 3 H, 4-pyH), 8.54 (d, J = 4.8 Hz, 2 H, 6-pyH) ppm. ^{13}C NMR ($CDCl_3$): δ = 55.31 (t) 55.44 (t), 121.15 (d), 122.63 (d), 123.01 (d), 137.15 (d), 137.59 (d), 149.96 (d), 159.70 (s), 160.31 (s) ppm. IR ($CHCl_3$): ṽ = 3425 s, 1604 m, 1215 s, 742 s, 668 s cm^{-1}. MS: m/z (%) = 319 (1.6) [M$^+$], 241 (2.6), 227 (3.0), 213 (71), 107 (88), 93 (100). FAB (DTT/DTE): m/z = 320 [M + 1]. HRMS: calculated for $C_{19}H_{21}N_5$ 319.179696, found 319.179690.

[6-{[(Pyrid-2-ylmethyl)(tosyl)amino]methyl}pyrid-2-yl]methanol (8): A mixture of **3** (1.9 g, 7.2 mmol), **7** (1.5 g, 7.2 mmol) and K_2CO_3 (2.7 g) in acetonitrile (140 mL) was refluxed for 6 h. The precipitate was collected by vacuum filtration and washed with acetonitrile. The acetonitrile was evaporated to give an orange oil. Chromatography using a gradient (ethyl acetate/hexane/triethylamine, 1000:100:1 to ethyl acetate/methanol/triethylamine, 1000:100:1) gave **8** as a colorless viscous oil (2.05 g, yield 74%). R_f = 0.62 (ethyl acetate/methanol, 25:2). ^{1}H NMR ($CDCl_3$): δ =2.42 (s, 3 H, CH_3Ts), 4.54−4.56 (3 s, 6 H, CH_2py), 6.98 (d, J = 7.8 Hz, 1 H, 3-pyH), 7.06−7.10 (m, 1 H, 5-pyH), 7.16 (d, J = 7.35 Hz, 1 H, 5-pyH), 7.27 (d, J = 7.71 Hz, 2 H, phH), 7.35 (d, J = 8.1 Hz, 1 H, 3,5-pyH), 7.48- 7.58 (m, 2 H, 4-pyH), 7.70 (d, J = 8.34 Hz, 2 H, phH), 8.33 (d, J = 4.77 Hz, 1 H, 6-pyH) ppm. ^{13}C NMR ($CDCl_3$): δ = 22.17 (q), 54.01 (t), 54.61 (t), 64.40 (t), 119.65 (d), 122.03 (d), 123.04 (d), 123.44 (d), 127.98 (d), 130.30 (d), 137.20 (d), 137.31 (s), 137.79 (d), 144.15 (s), 149.57 (d), 155.70 (s), 157.12 (s), 159.99 (s) ppm. IR ($CHCl_3$): ṽ = 3018 m, 1597 s, 1576 s, 1339 s, 1159 s, 1091 m, 756 s, 668 m cm^{-1}. MS: m/z (%) = 207 (11), 162 (27), 155 (30), 134 (33), 105 (30), 91 (52), 69 (69), 57 (100). FAB-NBA: m/z = 384 [M + 1]. High resolution LSIMS: calculated for $C_{20}H_{22}N_3O_3S$ 384.138189; found 384.13812.

[6-{[(Pyrid-2-ylmethyl)amino]methyl}pyrid-2-yl]methanol (9): The tosylate **8** (2.0 g, 5.2 mmol) was dissolved in 98% H_2SO_4 (10 mL) and heated to 120 °C for 3 h. The liquid turned black. The solution was poured into a brine/NaOH solution (20 mL), and the pH was adjusted to 12 with NaOH solution. The water phase was extracted with dichloromethane (4 × 100 mL). The organic phase was dried with $MgSO_4$, filtered and the dichloromethane evaporated to give **9** as an oil with a slight orange color (0.91 g, yield 76%). ^{1}H NMR ($CDCl_3$): δ = 3.15 (br. s, 2 H, OH + NH), 3.95 and 3.96 (2 s, 4 H, CH_2py), 4.72 (s, 2 H, $pyCH_2O$), 7.10 (d, J = 7.71 Hz, 1 H, 3-pyH), 7.14−7.18 (m, 1 H, 5-pyH), 7.23 (d, J = 7.71 Hz, 1 H, 3-pyH), 7.33 (d, J = 7.7 Hz, 1 H, 5-pyH), 7.59−7.66 (m, 2 H, 4-pyH), 8.55 (d, J = 4.05 Hz, 1 H, 6-pyH) ppm. ^{1}H NMR(CD_3OD): δ = 3.91 and 3.93 (2 s, 4 H), 4.69 (s, 2 H), 7.25−7.34 (m, 2 H), 7.40 (d, J = 7.74 Hz, 1 H), 7.50 (d, J = 7.71 Hz, 1 H), 7.72−7.85 (m, 2 H), 8.49 (d, J = 4.02 Hz, 1 H) ppm. ^{13}C NMR ($CDCl_3$): δ = 54.97 (t), 55.24 (t), 64.68 (t), 119.34 (d), 121.44 (d), 122.74 (d), 123.08 (d), 137.23 (d), 137.81 (d), 149.98 (d), 159.02 (s), 159.37 (s), 159.99 (s) ppm. IR ($CHCl_3$): ṽ = 3016 w, 1595 m, 1576 m, 1216 s, 754 s, 668 m cm^{-1}. FAB-NBA: m/z = 230 [M + 1]. High resolution ESI-TOF-MS: calculated for $C_{13}H_{16}N_3O$: 230.1293; found 230.1288.

(2,6-Bis{[(pyrid-2-ylmethyl)amino]methyl}pyridine)zinc Dichloride (1a): 2,6-bis{[(pyrid-2-ylmethyl)amino]methyl}pyridine (**6**) (200 mg, 0.63 mmol) and $ZnCl_2$ (85 mg, 0.63 mmol) were dissolved in methanol (15 mL) and chloroform (3 mL). The solution was refluxed for 3 h. The methanol was reduced to 3 mL, and complex **1a** could be obtained as crystals (183 mg; yield 64%) by gradually adding (day by day 0.3−0.5 mL) diethyl ether. ^{13}C NMR ($CDCl_3$): δ = 52.29 (t), 54.28 (t), 123.32 (d), 125.49 (d), 125.97 (d), 142.01 (d), 142.64 (d) 148.83 (d), 155.32 (s), 157.87 (s) ppm. IR: ṽ = 3462 s, 3196 s, 1653 w, 1627 w, 1603 s, 1586 m, 1434 s, 1097 m, 915 m, 781 m, 771 s, 760 s cm^{-1}. ESI-MS: m/z (%) = 382 (86) [**6**-H$^+$ + ^{64}Zn], 384 (51) [**6**-H$^+$ + ^{66}Zn], 386 (35) [**6**-H$^+$ + ^{68}Zn], 418 (100) [**6** + ^{64}Zn + ^{35}C] , 420 (92) [**6** + ^{64}Zn+ ^{37}Cl, **6** + ^{66}Zn+ ^{35}Cl], 422 (65) [**6** + ^{66}Zn + ^{37}Cl, **6** + ^{68}Zn + ^{35}Cl]. High resolution ESI-TOF-MS: $C_{19}H_{20}N_5Zn$ calcd. 382.1010, found 382.1005; $C_{19}H_{20}ClN_5Zn$ calcd. 418.0776; found 418.0742. For X-ray structure see X-ray section.

(2,6-Bis{[(pyrid-2-ylmethyl)amino]methyl}pyridine)zinc Diacetate (1b): **6** (150 mg, 0.5 mmol) and $Zn(CH_3COO)_2$ (108 mg, 0.5 mmol) were dissolved in methanol (5 mL). After refluxing for 3 h, the methanol was evaporated to leave the **1b** complex as a brown viscous oil (200 mg, yield 82%). The complex was soluble in various organic solvents (THF, acetonitrile, dichloromethane and methanol). ^{1}H NMR (MeOD): δ = 1.83 (s, $COOCH_3$, 6 H), 4.28 and 4.39 (2 br. s, 8 H, CH_2py), 7.34−7.43 (m, 4 H, pyH), 7.54 (d, J = 7.71 Hz, 2 H, pyH), 7.87−7.99 (m, 3 H, pyH), 8.49 (d, J = 3.66 Hz, 2 H, 6-pyH) ppm. ^{13}C NMR (CD_3OD): δ = 23.46 (q), 52.54 (t), 54.14 (t), 122.91 (d), 124.95 (d), 125.30 (d), 140.95 (d), 141.81 (d), 148.87 (d), 155.68 (s), 157.62 (s) ppm. IR: ṽ = 3447 s, 1653 m, 1560 s, 1419 m, 1215 w, 770 s cm^{-1}. FAB MS (matrix: 3-NBA): m/z (%) = 382 (100) [**6**-H$^+$ + ^{64}Zn], 384 (61) [**6**-H$^+$ + ^{66}Zn], 386 (38) [**6**-H$^+$ + ^{68}Zn], 442 (34) [**6** + ^{64}Zn + CH_3COO^-], 444 (19) [**6** + ^{66}Zn + CH_3COO^-], 446 (12) [**6** + ^{68}Zn + CH_3COO^-]. HR ESI-TOF-MS: $C_{19}H_{20}N_5Zn$ calcd. 382.1010, found 382.1027; $C_{21}H_{24}N_5O_2Zn$ calcd. 442.1221, found 442.1226.

(2,6-Bis{[(pyrid-2-ylmethyl)amino]methyl}pyridine)zinc Diperchlorate (1c): **6** (150 mg, 0.5 mmol) and $Zn(ClO_4)_2$ (175 mg, 0.5 mmol) were dissolved in methanol (4 mL) The solution was refluxed for 3 h. By addition of the $Zn(ClO_4)_2$ a white solid immediately precipitated. The methanol was evaporated to leave **1c** as a white solid (235 mg, yield 81%). The solid was dissolved in acetonitrile and upon slow evaporation crystals were obtained. ^{1}H NMR (DMSO): δ = 4.10 (br. s, 4 H, CH_2py), 4.57 (br. d, 4 H, CH_2py), 5.77 (br. t, N−H, 2 H), 7.43 (d, J = 7.71 Hz, 2 H, 5-pyH), 7.58 (t, J = 6.26 Hz, 2 H, 3-pyH), 7.66 (d, J = 7.71 Hz, 2 H, 3,5-pyH), 7.97 (t, J = 7.73 Hz, 1 H, 4-pyH), 8.10 (dd, J = 7.71, J = 1.47 Hz, 2 H, 6-pyH) ppm. ^{13}C NMR (CD_3OD): δ =60.84 (t), 62.47 (t), 131.26 (d), 133.70 (d), 133.94 (d), 150.27 (d), 150.55 (d), 157.00 (d), 163.09 (s), 165.96 (s) ppm. IR ($CHCl_3$): ṽ = 3500 s, 1610 s, 1450 s, 1100 s, 770 s, 620 s cm^{-1}. ESI-MS: m/z (%) = 382 (22) [**6**-H$^+$ + ^{64}Zn], 384 (13) [**6**-H$^+$ + ^{66}Zn], 386 (9) [**6**-H$^+$ + ^{68}Zn], 482 (100) [**6** +

$^{64}Zn+ {}^{35}ClO_4$], 484 (95) [**6** + ^{64}Zn + $^{37}ClO_4$, **6** + ^{66}Zn + $^{35}ClO_4$, 486 (63) [**6** + ^{66}Zn + $^{37}ClO_4$, **6** + ^{68}Zn + $^{35}ClO_4$]. HR ESI-TOF-MS: $C_{19}H_{21}N_5O_4ClZn$ calcd. 482.0573, found 482.0586; $C_{19}H_{20}N_5Zn$ calcd. 382.1010, found 382.1035.

(6-{[(Pyrid-2-ylmethyl)amino]methyl}pyrid-2-yl]methanol)zinc Chloride (2a): 9 (150 mg, 0.66 mmol) and $Zn(Cl)_2$ (89 mg, 0.66 mmol) were dissolved in methanol (15 mL) and refluxed for 1 h. The methanol was reduced to 3−4 mL and by addition of diethyl ether **2a** precipitated as a white amorphous solid (98 mg, 41%). Recrystallization from ethanol/dichloromethane gave crystals that were too small to perform X-ray analysis. ^1H NMR (CD_3OD): δ = 3.77 (br. d, 1 H, CH_2py), 4.23 (br. d, 1 H, CH_2py), 4.45−4.66 (br. m, 2 H, CH_2py), 5.05 (br. d, 2 H, $pyCH_2O$), 7.51−7.66 (m, 4 H, 3,5-pyH), 8.09 (dd, *J* = 7.80, *J* = 5.31 Hz, 2 H, 4-pyH), 8.61 (d, *J* = 5.3 Hz, 1 H, 6-pyH) ppm. ^{13}C NMR (CD_3OD): δ = 51.69 (t), 52.85 (t), 61.86 (t), 122.28 (d), 123.86 (d), 124.94 (d), 126.04 (d), 142.34 (d), 142.60 (d), 148.79 (d), 155.81 (s), 157.69 (s), 158.10 (s) ppm. IR ($CHCl_3$): $\tilde{\nu}$ = 3414 s, 3223 s, 2908 m, 1604 s, 1575 m, 1465 m, 1452 m, 1444 m, 1285 w, 1063 s, 1012 s, 802 m, 767 s, 644 w cm^{-1}. ESI-MS: *m*/*z* (%) = 292 (100) [**9**-H^+ + ^{64}Zn], 294 (57) [**9**-H^+ + ^{66}Zn], 296 (38) [**9**-H^+ + ^{68}Zn], 328 (24) [**9** + ^{64}Zn + $^{35}Cl^-$], 330 (21) [**9** + ^{64}Zn+ $^{37}Cl^-$, **9** + ^{66}Zn+ $^{35}Cl^-$], 332 (14) [**9** + ^{66}Zn+ $^{37}Cl^-$, **9** + ^{68}Zn+ $^{35}Cl^-$]. HR ESI-TOF-MS: $C_{13}H_{14}N_3OZn$ calcd. 292.0428, found 292.0429; $C_{13}H_{15}ClN_3OZn$ calcd. 328.0195, found 328.0214.

[(6-{[(Pyrid-2-ylmethyl)amino]methyl}pyrid-2-yl)methanol)]zinc Acetate (2b): 9 (150 mg, 0.66 mmol) and $Zn(CH_3COO)_2$ (143 mg, 0.66 mmol) in methanol (15 mL) were refluxed for 1 h. The methanol was reduced to 3−4 mL and the complex precipitated by addition of diethyl ether to give **2b** as a white amorphous solid (168 mg, 62% yield). ^1H NMR (MeOD): δ = 1.93 (s, $COOCH_3$, 6 H), 3.82 (br. d, 1 H, CH_2py), 4.16 (br. d, 1 H, CH_2py), 4.47−4.60 (br. m, 2 H, CH_2py), 5.01 (br. d, 2 H, $pyCH_2O$), 7.43−7.58 (m, 4 H, 3,5-pyH), 7.97−8.06 (m, 2 H, 4-pyH), 8.64 (d, *J* = 4.77, 1 H, 6-pyH) ppm. ^{13}C NMR (MeOD): δ = 22.98 (q), 52.09 (t), 52.78 (t), 62.64 (t), 121.87 (d), 123.20 (d), 124.56 (d), 125.63 (d), 141.78 (d), 142.00 (d), 148.97 (d), 155.68 (s), 157.97 (s), 159.03 (s), 180.89 (s) ppm. IR ($CHCl_3$): $\tilde{\nu}$ = 3406 m, 2924 w, 1606 s, 1385 s, 1080 m, 1014 m, 668 w cm^{-1}. ESI-MS: *m*/*z* (%) = 292 (100) [**9**-H^+ + ^{64}Zn], 294 (55) [**9**-H^+ + ^{66}Zn], 296 (33) [**9**-H^+ + ^{68}Zn]. HR ESI-MS-TOF: $C_{13}H_{14}N_3OZn$ calcd. 292.0428, found 292.0438.

[(6-{[(Pyrid-2-ylmethyl)amino]methyl}pyrid-2-yl)methanol]zinc Perchlorate (2c): 9 (400 mg, 1.74 mmol) and $Zn(ClO_4)_2·6H_2O$ (650 mg, 1.74 mmol) in methanol (25 mL) were refluxed for 1 h. The methanol was reduced to 3−4 mL and the complex precipitated by addition of diethyl ether to give **2b** as a white amorphous solid (565 mg, 66% yield). ^1H NMR (CD_3OD): δ = 4.04−4.17 (2 d, 2 H, CH_2py), 4.50−4.70 (2 d, 2 H, CH_2py), 5.00−5.16 (2 d, 2 H, $pyCH_2O$), 7.40−7.53 (m, 4 H, 3,5-pyH), 7.92−8.00 (m, 2 H, 4-pyH), 8.51 (d, 1 H, 6-pyH) ppm. ^{13}C NMR (CD_3OD): δ = 53.99 (t), 54.70 (t), 61.40 (t), 121.78 (d), 123.28 (d), 125.23 (d), 125.85 (d), 141.60 (d), 142.04 (d), 148.04 (d), 154.49 (s), 155.18 (s), 156.70 (s) ppm. IR: $\tilde{\nu}$ = 3331 s, 2739 s, 2330 w, 2023 w, 1615 s, 1486 s, 1109 s, 658 s cm^{-1}. ESI-MS: *m*/*z* (%) = 292 (100) [**9**-H^+ + ^{64}Zn], 294 (58) [**9**-H^+ + ^{66}Zn], 296 (37) [**9**-H^+ + ^{68}Zn]. HR ESI-TOF-MS: $C_{13}H_{14}N_3OZn$ calcd. 292.0428, found 292.0418.

X-ray Crystallography: Intensity data for crystals of **1a**·CH_3OH solvate (0.25 × 0.15 × 0.15mm), **1a**·$2H_2O$ (0.25 × 0.18 × 0.15 mm), and **1c** (0.40 × 0.35 × 0.35 mm), were collected at 153 K with a Stoe Image Plate Diffraction System[23] using Mo-K_α graphite-monochromated radiation. Image plate distance 70 mm, φ oscillation scans 0−180° or 0−200°, step Δφ = 1.2°, 1.5° and 2°, respectively. 2θ range 3.27−52.1°, $d_{max.}-d_{min.}$ = 12.45−0.81 Å. The structures were solved by direct methods using the program SHELXS-97.[24] Refinement and all further calculations were carried out using SHELXL-97.[25] The H atoms were located from difference maps and refined isotropically. In **1a**·CH_3OH, the solvent H atoms were included in calculated positions and treated as riding atoms using SHELXL default parameters. The non-H atoms were refined anisotropically, using weighted full-matrix least squares on F^2. The molecular structure and crystallographic numbering schemes are illustrated in the PLATON[26] figures. Further crystallographic data are summarized in Table 5. CCDC-183956 (**1a**·CH_3OH), -183957 (**1a**·$2H_2O$) and -183958 (**1c**) contain the supplementary crystallographic data for this paper. These data can be obtained free of charge at www.ccdc.cam.ac.uk/conts/retrieving.html or from the Cambridge Crystallographic Data Centre, 12, Union Road, Cam-

Table 5. Crystallographic data for complexes **1a**·CH_3OH, **1a**·$2H_2O$, and **1c**

	1a·CH_3OH	**1a**·$2H_2O$	**1c**
Empirical formula	$C_{19}H_{20}Cl_2N_5Zn·CH_3OH$	$C_{19}H_{20}Cl_2N_5Zn·2H_2O$	$C_{19}H_{21}N_5Zn·(ClO_4)_2$
Formula mass [g mol^{-1}]	487.72	491.71	583.68
a [Å]	8.9211(6)	9.0366(7)	13.4064(13)
b [Å]	9.2475(6)	16.1489(14)	14.3351(14)
c [Å]	26.2005(14)	15.2881(11)	12.2712(11)
α [°]	90	90	90
β [°]	95.58(1)	97.34(10)	102.01(1)
γ [°]	90	90	90
V [$Å^3$]	2154.6(2)	2212.7(3)	2306.7(4)
Z	4	4	4
Space group	$P2_1/c$	$P2_1/c$	$P2_1/c$
T [K]	153(2)	153(2)	153(2)
$\rho_{calcd.}$ [g cm^{-1}]	1.504	1.476	1.681
λ [Å]	0.71073	0.71073	0.71073
μ [mm^{-1}]	1.409	1.376	1.354
*R*1[a] (obsd. data)	0.0381	0.0261	0.0329
*wR*2[b] (obsd. data)	0.0764	0.0537	0.0761

[a] $R1 = \Sigma||F_o| - |F_c||/\Sigma|F_o|$. [b] $wR2 = [\Sigma w(|F_o^2| - |F_c^2|)^2/\Sigma wF_o^4]^{1/2}$.

bridge CB2 1EZ, UK [Fax: (internat.) + 44-1223/336-033; E-mail: deposit@ccdc.cam.ac.uk].

Reactivity Tests: All reactivity tests were performed using the 12 place Carousel Reaction Station with Reflux Heads from Radleys Discovery Technologies (RR98030) or the Cooled Carousel Reaction Station from Radleys Discovery Technologies (RR99900). All the reactions were performed under nitrogen at room temperature in 5 mL of solvent. For more details refer to the result section. The benzaldehyde was distilled prior to use and 2-hydroxyacetophenone was purified on a silica gel column (hexane/ethyl acetate, 1:1). Procedure A (Entry 7, Table 2): diethylzinc (46 μL, 1.1 M) in toluene was added to ligand **9** (11.5 mg, 0.0.05 mmol) in dry THF (5 mL). After 10 min, benzaldehyde (53 mg, 0.5 mmol), and hydroxyacetophenone (90 mg, 0.66 mmol) were added, and the reaction mixture was stirred under N_2 for 48 h. The solvent was evaporated and the products analyzed by ^{1}H NMR spectroscopy. The coupling product **12** was formed in 62% yield. The ^{1}H NMR spectroscopic yields were determined by the ratio of the areas of the following peaks: benzaldehyde (δ = 10.03 ppm, 1 H), 2-hydroxyacetophenone (δ = 4.90 ppm, 2 H) and the four doublets corresponding to the two diastereomers of **12** (*anti*: δ = 5.41 ppm, 1 H and δ = 5.08 ppm, 1 H; *syn*: δ = 5.24 ppm, 1 H and δ = 4.95 ppm, 1 H).[27] Procedure B: Benzaldehyde (53 mg, 0.5 mmol), 2-hydroxyacetophenone (90 mg, 0.66 mmol), **2b** (20.1 mg, 0.049 mmol) and 35 μL of triethylamine in dry methanol (5 mL) were stirred at room temperature under N_2 for 48 h. The reaction mixture was analyzed as described above to give 59% of product **12**.

[1] *Comprehensive Organic Synthesis*, vol. 2 (Eds.: B. M. Trost, I. Fleming, C. H. Heathcock), Pergamon, Oxford, **1991**.

[2] For review articles and references: [2a] C.-H. Wong, T. Machajewski, *Angew. Chem.* **2000**, *112*, 1406 −1430; *Angew. Chem. Int. Ed.* **2000**, *39*, 1352−1374. [2b] C. Palomo, M. Oiarbide, J. M. Garcia, *Chem. Eur. J.* **2002**, *8*, 36−34. [2c] S. Takayama, G. McGarvey, C.-H. Wong, *Chem. Soc. Rev.* **1997**, *26*, 407−414.

[3] [3a] Y. M. A. Yamada, N. Yoshikawa, H. Sasai, M. Shibasaki, *Angew. Chem. Int. Ed. Engl.* **1997**, *36*, 1871−1873; *Angew. Chem.* **1997**, *109*, 1942−1944. [3b] Y. M. A. Yamada, A. Shibasaki, *Tetrahedron Lett.* **1998**, *39*, 5561−5564. [3c] N. Yoshikawa, Y. M. A. Yamada, J. Das, H. Sasai, M. Shibasaki, *J. Am. Chem. Soc.* **1999**, *121*, 4168−4178.

[4] [4a] S. E. Denmark, R. A. Stavenger, *J. Org. Chem.* **1998**, *63*, 9524−9527. [4b] S. E. Denmark, R. A. Stavenger, *Acc. Chem. Res.* **2000**, *33*, 432−440. [4c] S. E. Denmark, R. A. Stavenger, *J. Am. Chem. Soc.* **2000**, *122*, 8837−8847.

[5] D. Veot, J. G. Veot, Biochemistry, John Wiley & Sons, Inc., Weinheim, **1990**.

[6] [6a] G. Schulz, M. Dreyer, *J. Mol. Biol.* **1996**, *259*, 458−466. [6b] B. S. Szwergold, K. Ugurbil, T. R. Brown, *Arch. Biochem. Biophys.* **1995**, *317*, 244−252. [6c] N. S. Blom, S. Tétreault, R. Coulombe, J. Sygusch, *Nat. Struct. Biol.* **1996**, *3*, 856−862.

[7] [7a] L. Liu, S.H. Chen, Y. L Wang, Z. X. Yang, *Chin. Chem. Lett.* **2000**, *6*, 485−488. [7b] M. Iwata, S. Emoto, *Chem. Lett.* **1974**, 959−960. [7c] Y. Zhang, W. Xu, *Synth. Commun.* **1989**, *19*, 1291−1296.

[8] H. Vahrenkamp, I. Brasack, K. Weis, M. Ruf, *Inorg. Chim. Acta* **1996**, *250*, 271−281.

[9] E. Kimura, T. Gotoh, T. Koike, M. Shiro, *J. Am. Chem. Soc.* **1999**, *121*, 1267−1274.

[10] B. List, R. A. Lerner, C. F. Barbas, III, *J. Am. Chem. Soc.* **2000**, *122*, 2395−2396.

[11] W. Notz, B. List, *J. Am. Chem. Soc.* **2000**, *122*, 7386−7387.

[12] K. Watanabe, K. Irie, *Bull. Chem. Soc. Jpn.* **1980**, *53*, 1366−1371; K. Watanabe, Y. Yamada, K. Goto, *Bull. Chem. Soc. Jpn.* **1985**, *58*, 1401−1406.

[13] M. Shibasaki, T. Suzui, T. Ohshima, G. Moll, S. Matsunaga, N. Kumagai, N. Yoshikawa, *J. Am. Chem. Soc.* **2001**, *123*, 2466−2467.

[14] M. Shibasaki, T. Ohshima, N. Yoshikawa, S. Matsunaga, N. Kumagai, *Org. Lett.* **2001**, *3*, 1539−1542.

[15] M. Shibasaki, N. Yoshikawa, *Tetrahedron* **2001**, *57*, 2569−2579.

[16] B. Trost, H. Ito, *J. Am. Chem. Soc.* **2000**, *122*, 12003−12004.

[17] B. Trost, H. Ito, E. Silcoff, *J. Am. Chem. Soc.* **2001**, *123*, 3367−2268.

[18] B. Trost, H. Ito, E. Silcoff, *Org. Lett.* **2001**, *3*, 2497−2500.

[19] G. R. Newkome, V. K. Gupta, F. R. Fronczek, S. Pappalardo, *Inorg. Chem.* **1984**, *23*, 2400−2408.

[20] D. W. Gruenwedel, *Inorg. Chem.* **1968**, *7*, 495−501.

[21] The condensation is also catalyzed by $Zn(OAc)_2$ and other zinc salts under the conditions described. The yields were, however, lower than the ones obtained in the presence of the ligands.

[22] W. C. J. Wolsey, *J. Chem. Educ.* **1973**, *50*, A335−A336.

[23] Stoe & Cie, *IPDS Software*, Stoe & Cie GmbH, Darmstadt, Germany, **2000**.

[24] *SHELXS-97, Program for Crystal Structure Determination:* G. M. Sheldrick, *Acta Crystallogr., Sect. A* **1990**, *46*, 467−473.

[25] G. Sheldrick, *SHELXL-97*, Universität Göttingen, Göttingen, Germany, **1999**.

[26] *PLATON/PLUTON* (version 1999): A. L. Spek, *Acta Crystallogr., Sect. A* **1990**, *46*, C-34.

[27] For the ^{1}H NMR characterization of **12**, see: O. Porta, A. Clerici, *J. Org. Chem.* **1989**, *54*, 3872−3878.

Received April 25, 2002
[I02226]

Synthesis, Crystal Structures, and Magnetic Properties of Two New 1D Copper(II) Coordination Polymers Containing Fumarate(−2) and Chelating N,N′-Donor as Ligands

Sudipta Dalai,[a] Partha Sarathi Mukherjee,[a] Guillaume Rogez,[b] Talal Mallah,*[b] Michael G. B. Drew,[c] and Nirmalendu Ray Chaudhuri*[a]

Keywords: Coordination polymers / Copper / Magnetic properties / N ligands

Two new polynuclear complexes of Cu^{II}, $[Cu_2(fum)(\mu\text{-}OH)(bpy)_2(H_2O)](NO_3)\cdot 2H_2O$ (**1**) (fum = fumarate dianion, bpy = 2,2′-bipyridine) and $[Cu(fum)(tmen)]\cdot 2H_2O$ (**2**) (tmen = *N*,*N*,*N*′,*N*′-tetramethylethane-1,2-diamine), have been synthesized and structurally characterized by X-ray crystallography. Complex **1**, $C_{24}H_{27}Cu_2N_5O_{12}$, crystallizes in a triclinic system, space group $P\bar{1}$, with a = 10.168(14), b = 11.347(14), c = 14.74(2) Å, and Z = 2; complex **2**, $C_{10}H_{22}CuN_2O_6$, crystallizes in an orthorhombic system, space group *Pbca*, with a = 14.701(19), b = 14.899(19), c = 26.90(3) Å, and Z = 16. Compound **1** is an alternating chain compound, with alternate repetition of bis(monodentate) (μ_2) and bis(bidentate) (μ_4) bridging modes of fumarate, showing ferromagnetic interaction between Cu^{II} ions through hydroxo bridges with a Cu–O–Cu angle of 108.5°. Compound **2** is a linear 1D zig-zag polymer. There are two copper(II) ions with equivalent coordination and geometry in the asymmetric unit, each of them bonded to a bidentate tmen ligand and to two different fumarate moieties. Magnetic susceptibility data were measured in the 300–2 K temperature range. The magnetic data for **1** were fitted by use of a ferromagnetic/antiferromagnetic alternating S = 1/2 chain system and show the following results: J_F = +5.4 cm^{-1}, J_{AF} = −0.25 cm^{-1}, g = 1.96. The susceptibility data of **2** were fitted by use of the Bonner–Fisher expression for antiferromagnetically coupled S = 1/2 local spins, giving the parameters J = −1.81 cm^{-1}, g = 2.03.

Introduction

The chemistry of metal complexes containing paramagnetic metal ions and exhibiting extended structures is at the forefront of modern research, due to these compounds' potential applications in molecular magnetism.[1−4] The most useful strategy by which to construct such extended systems is to employ appropriate bridging ligands capable of binding metal centers through direct bond formation, promoting magnetic interactions. Di- and polycarboxylates are good candidates as bridging ligands for the construction of such extended systems. Previous reports have revealed that dicarboxylic acids can coordinate to metal centers either in the chelating bis(bidentate) mode or as bridging bis(monodentate) ligands.[5−7] Although the use of various dicarboxylic acids to form bridges between paramagnetic metal centers has been extensively studied with terephthalate, malonate, oxalate, maleate, etc.,[8−12a] systems with fumarate as bridging ligand are much fewer in number,[12b] due to their poor solubilities in all common organic solvents. Our current attention to the use of fumarate dianion as an organic coupler with which to obtain polymetallic complexes[1,4,13,14] is due to its versatile coordination mode (Scheme 1). We have recently reported a few fumarate-bridged Cu^{II} and Ni^{II} systems.[13,14] Here we report the synthesis and structural characterization of two different kinds of copper(II) fumarate systems that make use of N-donor ligands − 2,2′-bipyridine (bpy) and *N*,*N*,*N*′,*N*′-tetramethylethane-1,2-diamine (tmen) − as blocking ligands. Both were magnetically characterized, interestingly showing different kinds of magnetic behavior. Complex **1** is a chain of $[Cu_2(fum)(\mu\text{-}OH)(bpy)_2(H_2O)](NO_3)\cdot 2H_2O$ (fum = fumarate dianion, bpy = 2,2′-bipyridine) with alternate repetition of bis(monodentate) (μ_2) and bis(bidentate) (μ_4) fumarate bridging modes. It represents the first molecular system with both bis(monodentate) and bis(bidentate) bridging fumarate. Magnetic studies show the existence of ferromagnetic exchange coupling between the Cu^{II} ions through the hydroxo bridge. To the best of our knowledge, this is the first report of a ferromagnetic interaction between Cu^{II} ions through a hydroxo bridge with a Cu−O−Cu angle as large

[a] Department of Inorganic Chemistry,
Indian Association for the Cultivation of Science,
Jadavpur, Kolkata 700032, India
Fax: (internat.) + 91-33/473-2805
E-mail: icnrc@mahendra.iacs.res.in
[b] Laboratoire de Chimie Inorganique, UMR CNRS 8613,
Universite de Paris-Sud,
91405 Orsay, France
[c] Department of Chemistry, University of Reading,
Whiteknights, Reading RG6 6AD, UK

 © 2002 WILEY-VCH Verlag GmbH & Co. KGaA, 69451 Weinheim 1434−1948/02/1212−3292 $ 20.00+.50/0 *Eur. J. Inorg. Chem.* **2002**, 3292−3297

as 108.5°. Complex **2** is a one-dimensional zig-zag polymer of composition $[Cu(fum)(tmen)]\cdot 2H_2O$. Here, fumarate coordinates in bis(monodentate) bridging fashion, and a weak antiferromagnetic interaction (300−2 K) is observed between the two Cu^{II} centers. The attainment of magnetic ordering generally requires the organization of transition metal centers into three-dimensional networks, but reduced dimensionalities (one- and two-dimensional) are preferable for development of the necessary theoretical models required for better interpretation of the magnetic properties of three-dimensional coordination polymers. In this context, one-dimensional systems (such as complexes **1** and **2**) are being thoroughly investigated from both experimental and theoretical viewpoints.

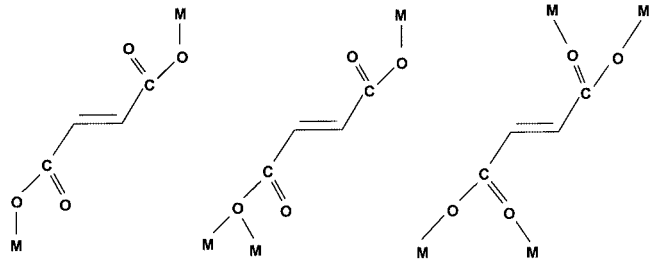

Scheme 1

Results and Discussion

Description of the Structures

$[Cu_2(fum)(\mu\text{-}OH)(bpy)_2(H_2O)]\ (NO_3)\cdot 2H_2O$ (1)

This complex is a one-dimensional polymeric chain made up of dinuclear (bpy)CuOHCu(bpy) units linked together by fumarate anions. The fumarate ligand adopts two bridging coordination modes through the chain, bis(monodentate) and bis(bidentate) (Figure 1). The two Cu^{II} ions in the asymmetric unit are in square-pyramidal environments each with one additional weak bond (shown as dotted line in Figure 1) to complete the octahedron. Thus, Cu(1) is bonded to the bridging hydroxide O(1) at 1.921(5) and to the two nitrogen atoms of the bipyridine ligand at 2.005(5) and 2.030(4) Å. It is also bonded to O(31) [at 2.026(5) Å] and O(41) [at 2.196(5) Å] from bridging fumarate ligands, the latter being the axial position. The second axial site is completed with a weak interaction to O(33) [2.800(2) Å]. The Cu(2) atom is bonded to the bridging hydroxide ion at 1.926(5) Å, to two nitrogen atoms of the bipyridine ligand at 2.010(5) and 2.027(6) Å, to an oxygen atom belonging to the bridging fumarate ligand at 1.940(4) Å, and to a water molecule at 2.420(6) Å in the axial position. The sixth coordination site is completed with a weak bond to a fumarate ligand oxygen atom O(31) at 2.720(2) Å. The Cu···Cu distance in complex **1** is 3.1212 Å. The

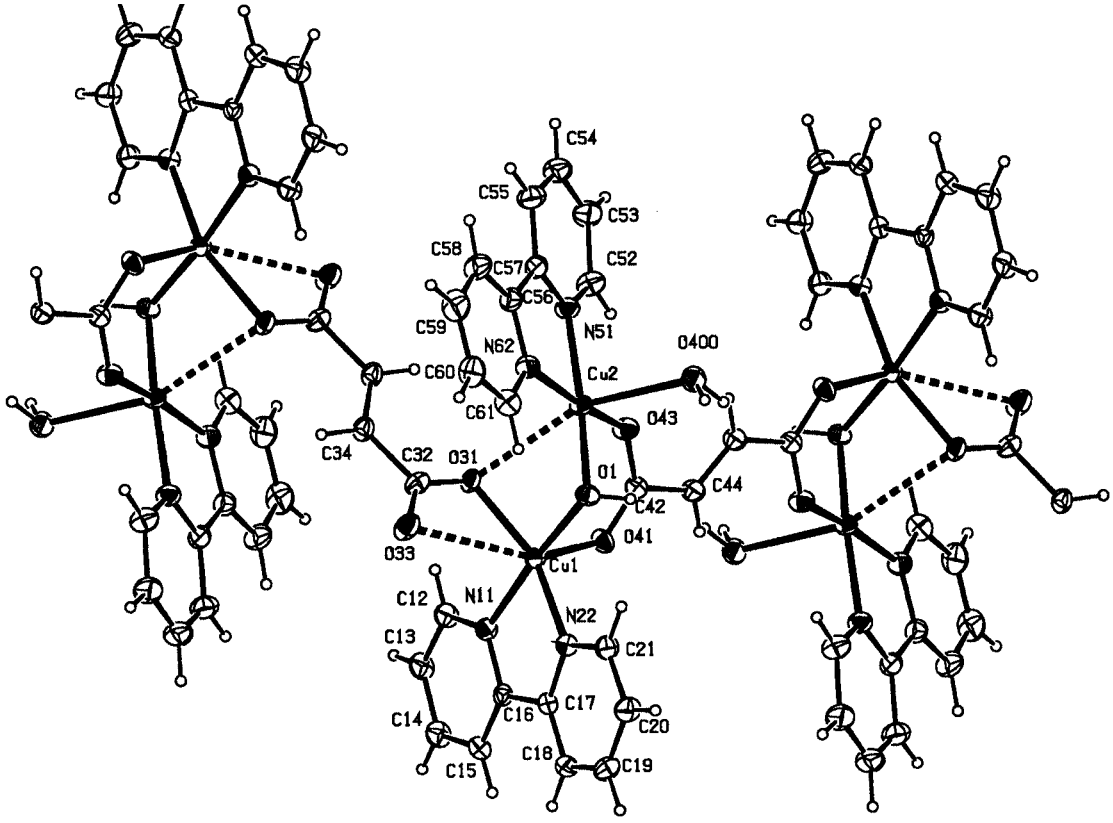

Figure 1. The polymeric structure of **1** at 20% probability; weak bonds in the metal coordination spheres are shown as dotted lines; the nitrate anion and the lattice water molecules in the asymmetric unit are not shown

structure is stabilized by an extensive hydrogen bond network with the water molecules and nitrate anion. The alternate repetition of the bidentate and tetradentate bridging modes of the fumarate makes the compound unique.

[Cu(fum)(tmen)]·2H$_2$O (2)

The structure of **2** is shown in Figure 2, together with its atom numbering scheme. In this complex the copper atoms are each in a four-coordinate square-planar environment, the asymmetric unit possessing two metal atoms. Each has equivalent coordination and geometry and each is part of a self-contained quasi-one-dimensional zig-zag polymer (Figure 3). Each metal ion is bonded to a bidentate tmen ligand and to two different fumarate ligands. The ligands are centrosymmetric. The carboxylate groups can be considered to be monodentate, with distances of 1.985(4)/2.015(4) and 2.001(4)/1.987(4) Å in the two coordination spheres, but the other oxygen atoms are weakly bonded at distances ranging from 2.450(5) to 2.592(5) Å, and could be considered to complete a distorted octahedral coordination sphere. The Cu···Cu distances in complex **2** are Cu−Cu (interchain) 7.3526 Å and Cu−Cu (intrachain) 9.0421 Å.

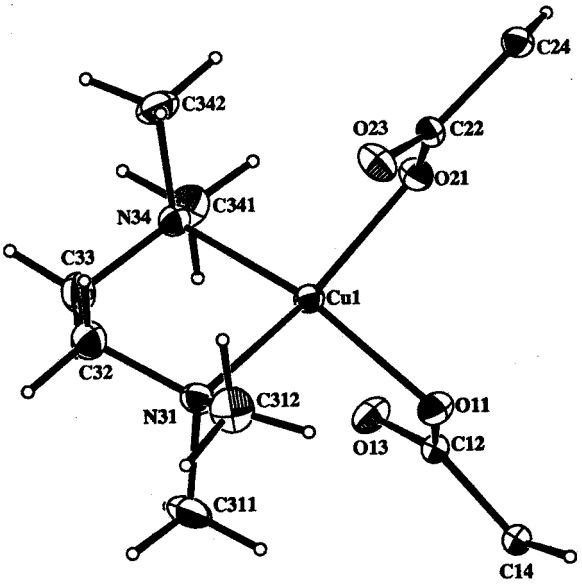

Figure 2. The coordination sphere of Cu^{II} in complex **2**; the ellipsoids are at 15% probability

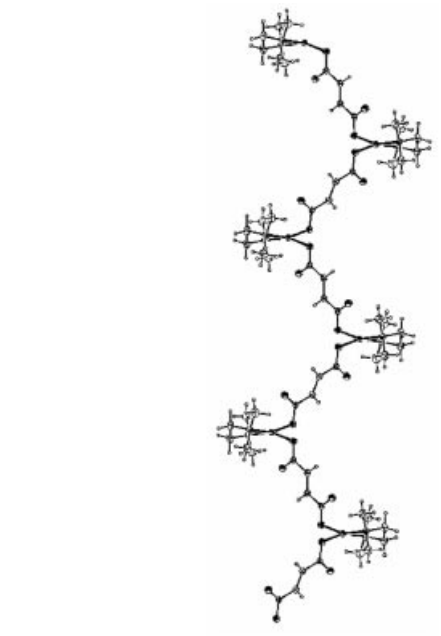

Figure 3. View of the zig-zag chain for complex **2**

Magnetic Results

Variable-temperature magnetic susceptibility data for complexes **1** and **2** were collected in the 300−2 K temperature range with a SQUID magnetometer. For complex **1**, the $\chi_M T$ value at room temperature corresponds to what is expected for isolated $S = 1/2$ spins (0.73 cm^{3}mol^{-1}K, $g = 1.96$). On cooling down, $\chi_M T$ increases, reaches a maximum of 0.83 cm^{3}mol^{-1}K at $T = 4$ K, and then rapidly decreases (Figure 4). This behavior can be explained by the existence of a ferromagnetic interaction between the Cu^{II} ions within the hydroxo- and carboxylato-bridged dinuclear unit and a much weaker antiferromagnetic interaction between the dinuclear units through the fumarate bridges. The magnetic data were therefore fitted by use of a ferromagnetic/antiferromagnetic alternating[15−16] $S = 1/2$ chain system and gave the following results: $J_F = +5.4$ cm^{-1}, $J_{AF} = -0.25$ cm^{-1}, $g = 1.96$, and an agreement factor $R = 6{\cdot}10^{-6}$. The ferromagnetic exchange coupling between the Cu^{II} ions is surprising because of the presence of a hydroxo bridge with a Cu−O−Cu angle of 108.5°. The presence of a carboxylato bridge within the dinuclear unit might produce a counter-complementarity between the two bridges, which could explain the ferromagnetic interaction. However, this cannot reasonably be operative since the oxygen atom O(41) of the bridging carboxylate group linked to Cu(1) is in an apical

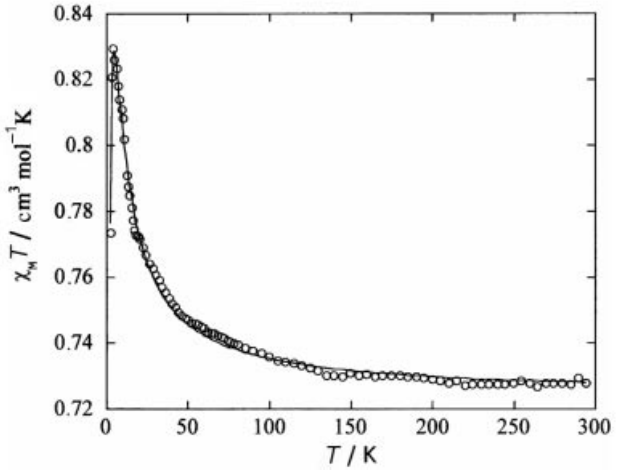

Figure 4. Plot of $\chi_M T$ versus T for complex **1**; the solid line shows the best fit obtained

position and the carboxylate bridge does not participate much in the magnetic coupling. In order to understand the experimentally observed ferromagnetic interaction, we carried out semiempirical calculations on the dinuclear unit.[17] The results show that the two single electrons are described by molecular orbitals (Schemes 2 and 3) mainly localized on each copper atom.[18]

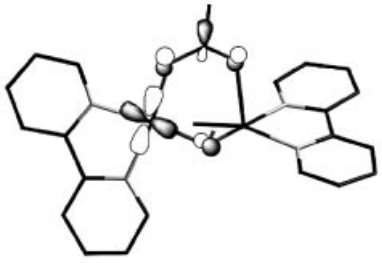

Scheme 2

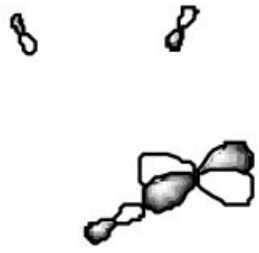

Scheme 3

From a structural viewpoint, complex **2** is a homogeneous chain of Cu^{II} with fumarate bridging. The geometry of each Cu^{II} is distorted octahedral. A plot of $\chi_M T$ against T is given in Figure 5, and shows a gradual decrease in $\chi_M T$ value with decreasing temperature, revealing the existence of antiferromagnetic interaction within the chain. The temperature dependence of the susceptibility data was analyzed by use of the Bonner−Fisher expression for antiferromagnetically coupled $S = 1/2$ spins.[19]

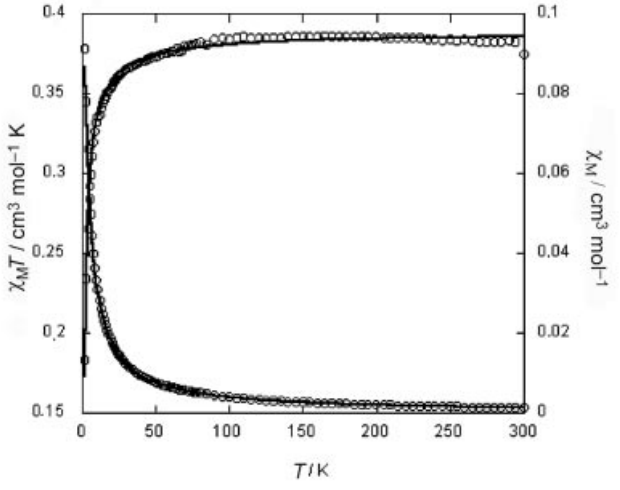

Figure 5. Plot of $\chi_M T$ versus T for complex **2** with solid lines showing the best fit obtained

The Hamiltonian for the isotropic interaction between nearest neighbor ions is

$$H = -J\sum_{i=1}^{n-1} S_i \cdot S_{i+1}$$

and according to Bonner and Fisher[20] the molar susceptibility is given by

$$\chi = \frac{Ng^2\beta^2(0.25 + 0.074975x + 0.075235x^2)}{kT(1 + 0.9931x + 0.172135x^2 + 0.757825x^3)}$$

where $x = |J|/kT$ and J is the exchange coupling parameter describing the magnetic interaction between any two nearest-neighbor $S = 1/2$ spins. The results of the best fit (Figure 5) are $J = -1.81\text{cm}^{-1}$, $g = 2.03$, and $R = 2.9\cdot10^{-5}$ (R is the agreement factor defined as $R = [(\chi_M)_{obsd.} - (\chi_M)_{calcd.}]^2/[(\chi_M)_{obsd.}]^2$). The very low J value is obviously due to a long-range superexchange pathway and this result agrees with previously reported results.[1e,4]

Conclusion

Fumarate(−2) has been employed as a bridging ligand, because of its potential for the construction of coordination polymers with different structures and its possible combination with bidentate bridging (and not chelating) N,N′-donors, as in previous work by our group.[1e,4] We present here the synthesis, single-crystal X-ray structure, and magnetic behavior of two fumarate-bridged Cu^{II} complexes. Complex **1** is a one-dimensional polymeric chain made up of dinuclear (bpy)CuOHCu(bpy) units linked together by fumarate anions. The fumarate ion adopts two coordination bridging modes through the chain, bis(monodentate) and bis(bidentate). The magnetic data were thus fitted by use of a ferromagnetic/antiferromagnetic alternating $S = 1/2$ chain system, with the result $J_F = +5.4\ \text{cm}^{-1}$, $J_{AF} = -0.25\ \text{cm}^{-1}$, $g = 1.96$, and an agreement factor $R = 6\cdot10^{-6}$. The ferromagnetic exchange coupling between the Cu^{II} ions is unusual because of the presence of a hydroxo bridge with a Cu−O−Cu angle of 108.5°. Compound **2** is a 1D zig-zag chain of Cu^{II} in which the fumarate ion binds in a bis(monodentate) fashion and the diamine is a blocking ligand. Fitting of the temperature-dependent susceptibility data (300−2 K) by use of the Bonner−Fisher equation gives $J = -1.81\ \text{cm}^{-1}$.

Experimental Section

Synthesis

$[Cu_2(fum)(\mu\text{-}OH)(bpy)_2(H_2O)](NO_3)\cdot2H_2O$ (1): $Cu(NO_3)_2\cdot3H_2O$ (1 mmol) dissolved in water/methanol (50:50) solution (15 mL) was mixed with 2,2′-bipyridine (1 mmol). A water/methanol (50:50) solution (10 mL) of fumaric acid (1 mmol) and triethylamine (2 mmol) was added, and the mixture was heated under reflux for 1 h at 80 °C. A sky-blue solid separated, and this remained insoluble in all common organic solvents. It was dissolved in a minimum amount of dilute (4 N) ammonia and allowed to crystallize. After

a week, suitable green single crystals of X-ray diffraction quality were obtained. Yield ca. 60%. $C_{24}H_{27}Cu_2N_5O_{12}$ (704.59): calcd. C 40.8, H 3.8, N 9.9; found C 40.9, H 3.6, N 9.8.

[Cu (fum)(tmen)]·2H$_2$O (2): A methanolic solution (10 mL) of $Cu(NO_3)_2·3H_2O$ (1 mmol) and tmen (1 mmol) was added dropwise, with constant stirring, to a water/methanol (50:50) solution (10 mL) of fumaric acid (1 mmol) and triethylamine (2 mmol). Suitable blue single crystals of X-ray diffraction quality were obtained after a week on keeping the resulting blue solution in a refrigerator. Yield ca. 65%. $C_{10}H_{22}CuN_2O_6$ (329.81): calcd. C 36.5, H 6.4, N 8.6; found C 36.3. H 6.6, N 8.4.

Crystallographic Data Collection and Refinement: Intensity data were collected with Mo-K_α radiation by use of the MAR research Image Plate System. The crystals were positioned at 70 mm from the Image Plate. 100 frames were measured at 2° intervals with a counting time of 2 min. Data analysis was carried out with the XDS program.[21] The structures were solved by direct methods with the SHELX-86 program.[22] In both structures, the non-hydrogen atoms were refined with anisotropic thermal parameters. The hydrogen atoms bonded to carbon atoms were included in geometric positions and given thermal parameters equivalent to 1.2 times those of the atom to which they were attached. The structures were refined on F^2 by use of SHELXL-93.[23]. Selected bond lengths and angles are given in Table 1 (complex **1**) and Table 2 (complex **2**). Selected crystallographic data are summarized in Table 3 and hydrogen bonds of complex **1** are shown in Table 4. CCDC-165333 and -185540 for complexes **1** and **2**, respectively, contain the supplementary crystallographic data for this paper. These data can be obtained free of charge at www.ccdc.cam.ac.uk/conts/retrieving.html or from the Cambridge Crystallographic Data Centre, 12 Union Road, Cambridge, CB2 1EZ, UK [Fax: (internat.) + 44-1223/336-033; E-mail: deposit@ccdc.cam.ac.uk].

Table 1. Selected bond lengths [Å] and bond angles [°] in complex **1**

Cu(1)−O(1)	1.921(5)	Cu(1)−O(31)	2.026(5)
Cu(1)−O(41)	2.196(5)	Cu(1)−N(11)	2.005(5)
Cu(2)−O(1)	1.926(5)	Cu(2)−O(43)	1.940(4)
Cu(2)−O(400)	2.420(6)	Cu(2)−N(51)	2.027(6)
Cu(2)−N(62)	2.010(5)	O(1)−Cu(1)−O(31)	89.60(18)
O(1)−Cu(1)−O(41)	91.19(17)	O(1)−Cu(1)−N(11)	175.44(18)
O(1)−Cu(1)−N(22)	96.23(19)	O(31)−Cu(1)−O(41)	93.87(16)
O(31)−Cu(1)−N(11)	94.77(18)	O(31)−Cu(1)−N(22)	157.27(16)
O(41)−Cu(1)−N(11)	87.24(18)	O(41)−Cu(1)−N(22)	107.90(17)
O(400)−Cu(2)−N(51)	92.90(20)	O(400)−Cu(2)−N(62)	96.05(19)
N(51)−Cu(2)−N(62)	80.30(20)		

Table 2. Selected bond lengths [Å] in complex **2**

Cu(1)−O(21)	1.985(4)	Cu(2)−O(48)	1.987(4)
Cu(1)−O(11)	2.015(4)	Cu(2)−O(41)	2.001(4)
Cu(1)−N(34)	2.034(5)	Cu(2)−N(51)	2.040(5)
Cu(1)−N(31)	2.036(5)	Cu(2)−N(54)	2.041(4)
Cu(1)−O(23)	2.592(5)	Cu(2)−O(43)	2.533(5)
Cu(1)−O(13)	2.450(5)	Cu(2)−O(47)	2.546(5)

Table 3. Crystal data and structure determination for complexes **1** and **2**

	1	**2**
Empirical formula	$C_{24}H_{27}Cu_2N_5O_{12}$	$C_{10}H_{22}CuN_2O_6$
Formula mass	704.59	329.81
Space group	$P\bar{1}$	*Pbca*
a [Å]	10.168(14)	14.701(19)
b [Å]	11.347(14)	14.899(19)
c [Å]	14.74(2)	26.90(3)
α, β, γ [°]	109.936(10), 93.334(10), 113.470(10)	90, 90, 90
V [Å^3]	1428	5892(13)
Z	2	16
T [°C]	20	20
λ(Mo-K_α) [Å]	0.71073	0.71073
$\rho_{calcd.}$ [g cm^{-1}]	1.633	1.469
μ(Mo-K_α) [mm^{-1}]	1.6	1.5
R[a]	0.0621	0.0588
$R_w{}^2$ [b]	0.1803	0.1696

[a] $R = \|\|F_o| - |F_c\|\|/|F_o|$. [b] $Rw = [\{w(F_o^2 - F_c^2)^2\}/\{w(F_o^2)^2\}]^{1/2}$.

Table 4. Hydrogen bonds [Å, °] for complex **1**

D−H···A	D−H	H···A	D···A	D−H···A
O400−H401···O101	0.91(2)	2.00(3)	2.895(8)	165(7)
O400−H401···O103	0.91(2)	2.56(6)	3.260(9)	134(6)
O400−H402···O402	0.89(6)	1.88(7)	2.754(10)	166(8)
O402−H421···O102	0.97(10)	1.96(10)	2.892(11)	161(9)
O402−H422···O403	0.84(10)	1.96(11)	2.771(12)	163(10)
O403−H431···O33	0.92(7)	1.97(6)	2.805(8)	150(7)
O403−H432···O401	0.90(8)	1.97(8)	2.808(10)	154(7)

Physical Measurements: Elemental analyses (carbon, hydrogen, and nitrogen) were performed with a Perkin−Elmer 240C elemental analyzer. The magnetic measurements were carried out on polycrystalline samples with a SQUID magnetometer working in the 300−2 K temperature range. Diamagnetic corrections were estimated from Pascal's Tables.

Acknowledgments

The authors are grateful to the Council of Scientific and Industrial Research (New Delhi) for financial support (NRC). M. G. B. Drew thanks the EPSRC and the University of Reading for funds for the Image Plate System.

[1] [1a] O. Kahn, *Acc. Chem. Res.* **2000**, *33*, 647. [1b] A. Escuer, R. Vicente, J. Ribas, X. Solans, *Inorg. Chem.* **1995**, *34*, 1793. [1c] J. Ribas, M. Monfort, C. Diaz, C. Bastos, X. Solans, *Inorg. Chem.* **1994**, *33*, 484. [1d] A. Escuer, R. Vicente, M. A. S. Goher, F. A. Mautner, *Inorg. Chem.* **1996**, *35*, 6386. [1e] P. S. Mukherjee, S. Dalai, G. Mostafa, E. Zangrando, T-H. Lu, G. Rogez, T. Mallah, N. Ray Chaudhuri, *Chem. Commun.* **2001**, 1346.
[2] P. S. Mukherjee, S. Dalai, E. Zangrando, F. Lloret, N. Ray Chaudhuri, *Chem. Commun.* **2001**, 1444.
[3] T. K. Maji, P. S. Mukherjee, G. Mostafa, T. Mallah, J. Cano-Boquera, N. Ray Chaudhuri, *Chem. Commun.* **2001**, 1012.
[4] S. Dalai, P. S. Mukherjee, E. Zangrando, F. Lloret, N. Ray Chaudhuri, *J. Chem. Soc., Dalton Trans.* **2002**, 822.
[5] J. Cano, G. DeMunno, J. L. Sanj, R. Ruiz, J. Faus, F. Lloret, M. Julve, A. Caneschi, *J. Chem. Soc., Dalton Trans.* **1997**, 1915.
[6] K. S. Burger, P. Chaudhuri, K. Weighardt, B. Nuber, *Chem. Eur. J.* **1995**, *1*, 583.
[7] E. Bakalbassis, P. Bergarat, O. Kahn, S. Jeannin, Y. Jeannin, Y. Dromzee, M. Guillot, *Inorg. Chem.* **1992**, *31*, 625.
[8] L. Deakin, M. A. Arif, J. S. Miller, *Inorg. Chem.* **1999**, *38*, 5072.

[9] J. J. Girerd, O. Kahn, M. Verdaguer, *Inorg. Chem.* **1980**, *19*, 274.
[10] M. Julve, M. Verdaguer, A. Gleizes, M. Philoche- Lavisalles, O. Kahn, *Inorg. Chem.* **1984**, *23*, 3808.
[11] M. Julve, J. Faus, M. Verdaguer, A. Gleizes, *J. Am. Chem. Soc.* **1984**, *106*, 3808.
[12] [12a] A. E. Tapper, E. J. Billo, J. A. Gollen, *Inorg. Chim. Acta* **1993**, *210*, 71. [12b] Y. Y. Wang, X. Wang, Q. Z. Shi, Y. C. Gao, *Transition Met. Chem.* **2002**, *27*, 481.
[13] P. S. Mukherjee, T. K. Maji, G. Mostafa, J. Ribas, M. S. El Fallah, N. Ray Chaudhuri, *Inorg. Chem.* **2001**, *40*, 928.
[14] S. Konar, P. S. Mukherjee, F. Lloret, E. Zangrando, N. Ray Chaudhuri, *Angew. Chem. Int. Ed.* **2002**, *41*, 1561.
[15] J. J. Borras-Almer, E. Coronado, J. Curely, R. George, J. C. Gianduzzo, *Inorg. Chem.* **1994**, *33*, 5171.
[16] J. W. Hall, W. E. Marsh, R. R. Weller, W. E. Hatfield, *Inorg. Chem.* **1981**, *20*, 1033.
[17] A *Mac Spartan* version was used to perform semiempirical PM3 calculations on the triplet state of a dinuclear hydroxo-bridged unit, in which the fumarate bridges were substituted by acetate.
[18] The calculations show, as expected, that the molecular orbital localized on Cu1 makes almost no contribution to the bridging carboxylate belonging to the fumarate.
[19] J. C. Bonner, M. E. Fischer, *Phys. Rev. A* **1964**, *135*, 640.
[20] W. E. Estes, D. P. Havel, W. E. Hatfield, D. Hodgson, *Inorg. Chem.* **1978**, *17*, 1415.
[21] W. Kabsch, *J. Appl. Crystallogr.* **1988**, *21*, 916.
[22] *SHELX-86:* G. M. Sheldrick, *Acta Crystallogr., Sect. A* **1990**, *46*, 467.
[23] G. M. Sheldrick, *SHELXL, Program for Crystal Structure Refinement*, University of Göttingen, Germany. **1993**.

Received June 3, 2002
[I02291]

The Effect of HCl on the Copper(II) Chloride/Pyridine/Water System: Synthesis, Properties and Crystal Structure of $[(pyH)_2CuCl_4]$ and $[(pyH)_2Cu_3Cl_8(H_2O)_2]_n$

Mátyás Czugler,[a] László Kótai,*[a] Bojja Sreedhar,*[b] Antal Rockenbauer,[a] István Gács,[a] and Sándor Holly[a]

Keywords: Copper / IR spectroscopy / EPR spectroscopy / Hydrogen bonds

Bis(pyridinium) tetrachlorocuprate monomer **1** and bis(pyridinium) octachlorodiaquatricuprate polymer **2** were synthesized and their crystal structures were determined. Both complexes contain pyridinium cations with bifurcated H-bridges. These H-bridges stabilize the monomeric structure of the tetrachlorocuprate anion together with the steric demand of the relatively large pyridinium ions in the crystal lattice of **1**. Conversely, at the lower pyridinium ion:copper(II) ratio of **2**, the bifurcated hydrogen bonds reduce the electron density on the chloride ions in such a way that the electron repulsion decreases and coordination spheres with more ligand interactions develop. Obviously, water may be a successful competitor for ligand sites in **2** as well. The octahedral and square-pyramidal structural units condense into polymeric chains which are stabilized by the interchain hydrogen bond networks of the water molecules. The structure motif of SP-5-[*OC-6-SP-5-SP-5*]-OC-6 (–$CuCl_5$-[$CuCl_4(OH_2)_2$-$CuCl_5$-$CuCl_5$]-$CuCl_4(OH_2)_2$-) were observed in **2**, and the two neighboring square-pyramidal units were found to be localized in a *transoid* position. The IR and ESR spectroscopical characterization of complexes was also performed.

Introduction

Due to their structural variety, modes of coordination and application in chemical and material sciences[1–4] a great deal of attention has been paid to the study of copper(II) halide complexes. The plasticity of the coordination sphere of the copper cations and the bridge-forming ability of the halide anions can lead to a variety of crystalline architectures with different coordination numbers, geometries and nuclearities.[2] The copper(II) ion in these complexes exhibits normal coordination as well as semi-coordination. In the latter case, the bond lengths are 0.3–1.0 Å longer. The coordination numbers may vary from four to six (with typically distorted geometries). The building species form chains of edge-sharing monomers with halide bridges between the neighboring copper(II) ions. The coordination spheres of the copper atoms in these chains are frequently supplemented with other ligands.

Pyridinium salts of chlorocuprate anions are of special interest both from a theoretical and a practical point of view. This is attributed to the fact that protonation of the pyridine ring decreases its coordination ability, and hydrogen-bond-forming properties of the N–H hydrogen atom introduces additional structure-building possibilities, hence pyridinium cations are capable of stabilizing MX_4^{2-} layer-type structures.[3]

Although the structure and properties of several chlorocuprate(II) compounds of substituted pyridine bases have been documented,[4] no X-ray crystal structure of unsubstituted pyridinium chlorocuprate(II) compounds has yet been reported. In this paper the synthesis, properties and crystal structures of monomeric bis(pyridinium) tetrachlorocuprate(II) (**1**) and polymeric bis(pyridinium) octachlorodiaquatricuprate(II) dihydrate (**2**) are reported.

Results and Discussion

Synthesis of Pyridinium Chlorocuprates

The protonation of pyridine ligand led to the formation of complexes **1** and **2**. The key to the formation of these two compounds in the $CuCl_2/C_5H_5N/HCl/H_2O$ system in the presence of excess hydrochloric acid lies in the distribution of the pyridinium cations between chlorocuprate anions. One of the chlorocuprate compounds may contain one copper(II) ion, while the other may have three copper(II) ions. Thus, formation of equimolar amounts of **1** and **2** is possible due to the 1:1 pyridine:copper molar ratio in the polymeric $[CuCl_2(py)]_n$ starting material. Decreasing the amount of HCl in the reaction leads to an increase in the

[a] Chemical Research Center, Hungarian Academy of Sciences, 1025, Budapest, Pusztaszeri u. 59–67, Hungary
E-mail: kotail@chemres.hu
[b] Inorganic Chemistry Division, Indian Institute of Chemical Technology
Hyderabad 500 007, India

 © 2002 WILEY-VCH Verlag GmbH & Co. KGaA, 69451 Weinheim 1434–1948/02/1212–3298 $ 20.00+.50/0 *Eur. J. Inorg. Chem.* **2002**, 3298–3304

amount of **2** formed and to a decrease in the amount of **1**. The increased yield of **2** can be attributed to an incomplete release of pyridine from the $[CuCl_2(py)]_n$ polymer, since the neutral pyridine ligand may form other compounds with $CuCl_2$.[5,9] This way, the molar ratio of pyridinium ion:copper(II) can be lower than 1:1 and formation of the 2:3 pyridinium complex **2** becomes possible. Consequently, complex **1**, which has a pyH:Cu(II) stoichiometry of 2:1, can form in only a small amount.

In order to check the polymer complex, we reproduced some earlier experiments.[5] The reaction of copper(II) chloride and pyridine hydrochloride in a molar ratio of 3:2 in conc. HCl led to the precipitation of **2**, and only a small amount of **1** was formed. If a stoichiometric amount of HCl was used for the reaction only the $[CuCl_2(py)]_n$ polymer was obtained.[5] Further addition of HCl, however, led to the dissolution of the $[CuCl_2(py)]_n$ polymer and the complexes mentioned above could be obtained.

ESR Spectral Characterization of Pyridinium Chlorocuprate Complexes

The ESR spectra of both compounds were recorded at 77 K and 300 K. No significant effect of the temperature on the signal positions and splittings could be observed.

The tetrachlorocuprate anion in **1** gives a single broad ESR signal at $g = 2.209$. The lack of anisotropy can be explained either by a dynamic Jahn−Teller effect or by strong spin-exchange between centers that are randomly distorted by the static Jahn−Teller interaction. The temperature-independent line-width makes the latter mechanism more likely. The large *g*-factor suggests anionic ligand-to-metal bonds.

Complex **2** has a broad anisotropic ESR signal at $g_{zz} = 2.49$ and $g_{xx} = g_{yy} = 2.126$. The large *g*-factors indicate ionic bonds, the order of *g*-factors reveals a $d_x^2 - {}_y^2$ ground state for the $3d^9$ electron configuration. This ground state is compatible with square-planar or square-pyramidal coordination. Magnetic interactions between neighboring Cu^{II} centers should be strong, since no hyperfine splitting is observed. Presumably the dipolar interactions dominate over the exchange interactions, since the bonds are not covalent.

IR Spectroscopic Investigations of 1 and 2

In order to assign the internal vibrations, it was presumed that the proton acts as a complex-forming ligand and the pyridinium ion is a quasi-metallic complex of the pyridine and the hydrogen ion wherein the central pseudo-metallic hydrogen atom can also interact with other atoms. In the IR spectra of both compounds we could identify the IR-active bands of the pyridine ring as well as the stretching vibrations of the N−H bond. The positions of the assigned vibrations were compared with the vibrations of non-complexed free pyridine base and with the vibrations of pyridine-coordinated $MCl_2(py)_2$ complexes.[10]

The values of the coordination-sensitive stretchings of pyridine were found to be up to 640 and 440 cm^{-1}, respectively; these values are similar to the values of transition metal complexes.[10] Based on the band shifts, the binding force of the proton in these compounds is very similar to the binding force of copper(II) to the pyridine in $[CuCl_2(py)_2]$. This strong coordination ability of the H^+ to the pyridine nitrogen atom may induce the formation of a pyridinium salt instead of an HCl complex of the pyridine-coordinated copper(II) chloride complexes as has been assumed previously.[5] Owing to the similar binding ability of H^+ and Cu^{2+} to the pyridine N-atom, however, the formation of N-coordinated Cu-chloro complexes or pyridinium-chlorocuprate complexes depends strongly on the HCl concentration of the $CuCl_2$/pyridine/HCl/H_2O system.

The coordination of the proton to the pyridine N atom generally causes higher band-shifts of the ring-atoms than in the metal complexes. The IR spectra of **1** and **2** are very similar, the position of the C−H out-of plane and in-plane stretchings and ring-stretchings or breathing bands show almost the same frequencies in both spectra. Characteristic bands of the pyridinium ion ($\tilde{\nu}$ = 1540, 1327, 1295 and 1250 cm^{-1}) can be seen in both spectra, although the degree of degeneracy is lower in **2** due to the more complicated multidendate hydrogen-bonding network structure. Symmetric N−H stretchings are lowered from 3200 cm^{-1} to 2850 cm^{-1} due to the presence of well-defined hydrogen bonds.[11] The OH vibrations in **2** give well-defined bands at $\tilde{\nu}$ = 3300 and 3400 cm^{-1}.

The γ(NH) band at around 900 cm^{-1} is very sensitive to the presence of hydrogen bonds. There is one band in compound **1** at 905 cm^{-1}, and an irregular triplet is present at 875, 900 and 905 cm^{-1} in the spectrum of **2**. This also indicates the presence of characteristic hydrogen bonds. The strength of the hydrogen bonds of **1** and **2** is similar to the strength of the N−H···Br bond in [pyNH]Br.[11]

The bands of the Cu−Cl and Cu−O vibrations fall outside the detection limit of our IR spectrometer (400 cm^{-1}). The broad Cu−N bands between 400 and 440 cm^{-1}could not be observed in the IR spectra of either compound. The narrow band at 405 cm^{-1} is a characteristic pyridine-ring vibration.[10]

X-ray Crystal structures of 1 and 2

The structural chemistry of chlorocuprate(II) salts was studied recently.[1−4] In tetrachlorocuprate(II) compounds the Cu−Cl distances vary between 2.205 Å and 2.265 Å and the *trans*-Cl bond angles vary from 104.5 to 180° (i.e. between the limiting values of tetrahedral and square-planar geometry). In **1** (Figure 1 and Table 1) the Cu−Cl(3) bond is slightly shorter [2.233(1) Å] than the Cu−Cl(2) bond [2.251(1) Å, Table 2]. Both chloride ions take part in the network of the hydrogen bonds (Table 2), and form a bifurcated bridge to the cationic proton of the pyridinium ion. The crystal structure of compound **1** is composed of discrete $CuCl_4^{2-}$ polyhedra and isolated pyridinium cat-

ions. The copper atom sits on a crystallographic twofold axis.

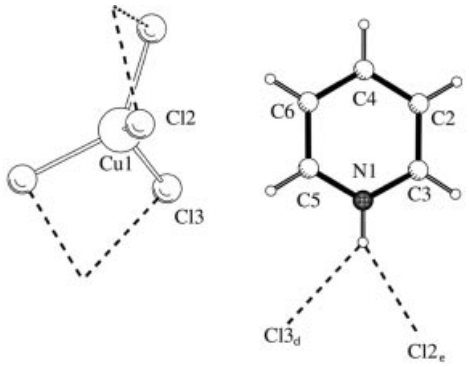

Figure 1. Molecular structure of bis(pyridinium) tetrachlorocuprate(II) (**1**) with atomic numbering and hydrogen-bond contacts indicated in broken lines

The Cl−Cu−Cl bond angles in **1** vary between 97.83(2) and 132.05(2)° showing a geometry intermediate between square planar and tetrahedral coordination. The 0.695 packing coefficient of **1** indicates close packing. The mean plane of the chloride anions lies perpendicular to the *b* crystallographic axis, and the pyridinium ions lie almost perpendicular to the Cu−Cl(2) vector. These data together with the crystal packing (Figure 2) show the basic forces directing crystal growth. Packing appears as separate columns of cations and anions. The cations are oriented so as to minimize electrostatic repulsion between identical charges and simultaneously maximize attraction between opposite ones. The steric demand of the pyridinium cations neighbouring to each tetrachlorocuprate(II) anion, their hydrogen bonds and the shielding as a joint effect isolates the tetrachlorocuprate anions in the monomeric form. Since the nearest non-covalent Cu−Cu and the shortest Cl···Cl distances are both longer than the sum of the respective van der Waals radii, there is no visible interaction between the tetrachlorocuprate(II) anions.

Table 2. Coordination geometry and normalized hydrogen bonding data (Å, °) with their esd's for non-hydrogen atoms in (**1**)

M−X	M−X(Å)	X−M−X	X−M−X(°)[a]
Cu1−Cl3	2.2327(6)	Cl3−Cu1−$Cl3_i$ [b]	101.82(2)
		Cl2−Cu1−$Cl2_i$	100.53(2)
Cu1−Cl2	2.2505(6)	Cl2−Cu1−$Cl3_i$	97.83(2)
		Cl2−Cu1−Cl3	132.05(2)
Donor···H···Acceptor	D−H (Å)	H···A	D-H···A (°)
N(1)···H(1)···$Cl(3)_{ii}$ [c]	1.009	2.604	133.1
N(1)···H(1)···$Cl(2)_{iii}$ [d]	1.009	2.386	141.4

[a] Only non-redundant angles are shown. [b] *i* = 1 − *x*, *y*, 1/2 − *z*. [c] *ii* = 1 − *x*, −*y*, −*z*. [d] *iii* = *x*, −*y*, −1/2 + *z*.

The structure of **2** shows a very distinct pattern (Figure 3). The tetrachlorocuprate anions polymerize with the formation of a condensed Cl-bridged chain-structure by complementing the coordination sphere with water. The building block of the crystal may be described as an endless concatenation of edge-sharing five-coordinate square-pyramidal (MX_4Y type *SP*) and hexacoordinate octahedral (MX_4Y_2 type *OC*) metal centers. The *SP*-[*OC*-*SP*-*SP*]-*OC* sequence is repeated throughout the crystallographic trans-

Table 1. Crystal data and details of the structure determination for **1** and **2**

	1	**2**
Empirical formula	$(C_5H_5NH)_2[CuCl_4]$	$(C_5H_5NH)_2[Cu_3Cl_8(H_2O)_2]$
Molecular weight	365.57	670.47
Crystal system	Monoclinic	Monoclinic
Space group	*C*2/*c* (No.15)	$P2_1/c$ (No. 14)
a [Å]	7.980(1)	7.889(1)
b [Å]	13.818(1)	14.145(1)
c [Å]	13.523(1)	9.914(1)
β [°]	94.81(1)	99.20(1)
V [Å^3]	1485.9(2)	1092.1(2)
Z	4	2
D(calc) [Mg/m^3]	1.634	2.039
μ (Mo-K_α) [mm^{-1}]	2.2	3.9
Crystal Size [mm]	0.25 × 0.30 × 0.40	0.15 × 0.25 × 0.50
Temperature (K)	295	295
Radiation λ [Å, Mo-K_α]	0.7107	0.7107
Θ min.-max. [°]	3.0, 35.0	2.5, 34.9
Data set *h*, *k*, *l* (min, max)	−12→12; −22→22; −21→21	−12→12; −22→8; 0→15
Total, Unique data, $R_{(int)}$	6900, 3254, 0.023	5143, 4769, 0.025
Observed data [$I > 2.0\sigma(I)$]	1725	3033
N_{ref}, N_{par}	3254, 84	4769, 116
R_1, *wR*2, *S*	0.0385, 0.1018, 0.93	0.0562, 0.1439, 0.94
Max. and av. shift/error	0.01, 0.00	0.01, 0.00
Min. and max. resid. dens. [e/Å^3]	−0.47, 0.71	−1.95, 1.85

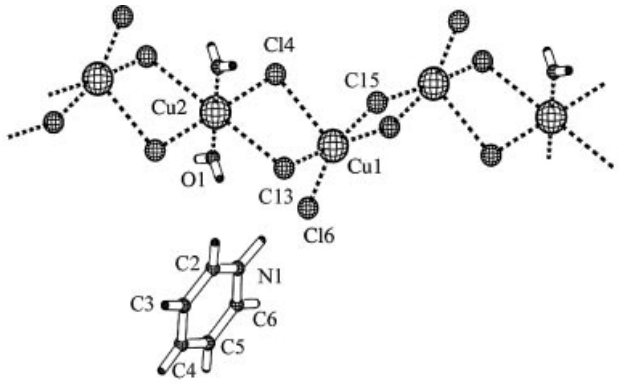

Figure 2. Packing motif in bis(pyridinium) tetrachlorocuprate(II) (**1**); hydrogen bonds are shown by broken lines

lation along the *c* axis. The *OC*-*SP* link occurs through the edge sharing of the axial ligands of both the *SP* and the *OC* polyhedra. Consequently, edge-sharing occurs between the connected *SP*-*SP* polyhedra through the equatorial positions. The coordination geometry of the two independent Cu^{II} ions forming the asymmetric unit is different not only in their ligating relationships but also in the water that coordinates solely to the hexacoordinate Cu^{II}. Pentacoordinate Cu(1) binds only to chlorides. This latter polyhedron has approximately equal and ideal equatorial distances ranging from 2.267(1) Å to 2.313(1) Å, while the axial distance is longer [2.675(1) Å], due to a Jahn−Teller effect. The shape of the coordination polyhedron is intermediate but relatively close to a square-pyramid conformation (τ descriptor[12] is 0.20). The value of 85.2% of the Berry pseudorotation from the trigonal bipyramid form to the *SP* one is also in agreement with this conclusion. The pyridinium cation behaves as if it would replace a missing sixth coordination site opposite the true ligand, the axial Cl(4) chloride ion. The SP-coordinated polyhedron is capped from this second axial ligand position (see Figure 3). The other metal [Cu(2)] has an apparently more regular coordination. Symmetry dependence makes the polyhedron more symmetric on the one hand, and distorted from the coordination distances on the other (Table 3). The long axial distance occupied by Cl(3) [2.874(1) Å] is the longest observed here, while the water has a rather short equatorial distance. The other equatorial distance pair [2.279(1) Å] maintained by the Cl(4) is in agreement with the expected value of approx. 2.3 Å. The alternating Cu(1)···Cu(1)···Cu(2)···Cu(1) metal centers are displaced by 3.597(1) Å−3.411(1) Å−3.597(1) Å from each other. The polymeric chains running in the *c* direction at $x = 0$ and $x = 1/2$ are crosslinked by hydrogen bonds (Table 3, Figure 4). Both edge-sharing anions of the hexacoordinate metal are involved in four acceptor interactions, while the pentacoordinated one assumes five acceptor interactions, four of which are common to the hexacoordinated one. One of the three chloride anions [Cl(5)] does not take part in any hydrogen bonds as it is shielded in the central edge-sharing between the two neighboring *SP* polyhedra. Three of these six H-bridges are of the weaker C−H···Cl type. Interestingly, these three bridges also serve as cross-links between the two *ortho*- and the *para*-positioned hydrogen atoms of the pyridinium cations. Analogously to **1** the cationic proton of the pyridinium ion appears in the bifurcated hydrogen bridge.

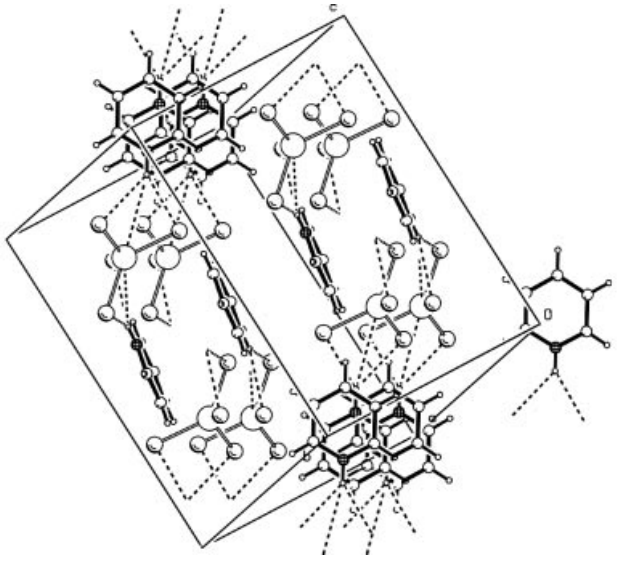

Figure 3. Crystal structure of bis(pyridinium) octachlorodiaquatricuprate(II) (**2**); only the atoms forming the asymmetric unit are numbered; polymeric contacts are shown by broken lines

The dielectric role of both ligand types (pyridinium and water molecules) in insulating the octahedral and square-pyramidal copper coordination centers is such that they effectively and simultaneously shield and compensate for opposite charges. Since the hydrogen bond network removes the charges of the chloride ions, the anion may relax back towards the square-planar geometry favored by crystal-field effects.[10] Other factors may have an influence on the size and nature of the distortions of the octahedral units of the CuX_4Y_2 octahedra, for instance the Jahn−Teller distortion and the difference between the donor strength of the axial water ligands and the equatorial chloro-bridges may be the main reasons for the tetragonal distortion of the OC-6 units in **2**.[13,14] The 0.732 packing coefficient of **2** indicates fairly close packing in the crystal.

Conclusions

Based on the results of the chemical analysis, the IR, the Raman and the ESR spectroscopic studies and the single crystal investigations, the structure of water-soluble compounds formed in the $CuCl_2$/pyridine/HCl/H_2O system has been determined. The two compounds, namely bis(pyridinium) tetrachlorocuprate monomer **1** and bis(pyridinium) octachlorodiaquatricuprate polymer **2** are formed in an obviously pH-dependent manner. The effect of steric and electronic supplements in building the structural units can be

Table 3. Coordination geometry and normalized hydrogen-bonding data (Å, °) with their esd's for non-hydrogen atoms in (**2**) a) coordination geometry (Å, °)

M−X	M−X/Y (Å)	X−M−Y	X−M−Y (°)[a]
		Cl3−Cu1−Cl4	88.98(3)
		Cl3−Cu1−Cl5	91.29(3)
Cu1−Cl3	2.2672(8)	Cl3−Cu1−Cl6	91.46(3)
Cu1−Cl4	2.6748(9)	Cl3−Cu1−$Cl5_i$ [b]	172.84(4)
Cu1−Cl5	2.3128(9)	Cl4−Cu1−Cl5	98.77(3)
Cu1−Cl6	2.2934(8)	Cl4−Cu1−Cl6	100.35(3)
Cu1−$Cl5_i$	2.2937(9)	Cl4−Cu1−$Cl5_i$	97.33(3)
		Cl5−Cu1−Cl6	160.72(3)
		Cl5−Cu1−$Cl5_i$	84.45(3)
		$Cl5_i$−Cu1−Cl6	90.71(3)
		Cl3−Cu2−Cl4	84.00(3)
		Cl3−Cu2−O1	93.76(7)
		Cl3−Cu2−$Cl4_{ii}$ [c]	96.00(3)
Cu2−Cl3	2.8735(8)	Cl3−Cu2−$O1_{ii}$	86.24(7)
Cu2−Cl4	2.2788(8)	$Cl3_{ii}$−Cu2−Cl4	96.00(3)
Cu2−O1	1.978(2)	Cl4−Cu2−O1	88.87(6)
		Cl4−Cu2−$O1_{ii}$	91.13(6)
Donor···H···Acceptor	D-H (Å)	H···A	D-H···A (°)
N(1)···H(1N)···Cl(3)	1.009	2.399	134.8
N(1)···H(1N)···Cl(6)	1.009	2.495	140.6
O(1)···H(1O)···$Cl(6)_{iii}$ [d]	0.980	2.717	109.4
C(2)···H(2)···$Cl(3)_{iv}$ [e]	1.083	2.644	134.5
C(4)···H(4)···$Cl(4)_v$ [f]	1.083	2.640	145.5
C(6)···H(6)···$Cl(4)_{vi}$ [g]	1.083	2.631	154.5

[a] Only non-redundant and symmetry-unconstrained angles are shown. Constrained angles (such as Cl3−Cu2−$Cl3_{ii}$ = 180, Cl4−Cu2−$Cl4_{ii}$ = 180 and O1−Cu2−$O1_{ii}$ = 180) are not given explicitly. [b] $i = -x, 1-y, -z$. [c] $ii = -x, 1-y, 1-z$. [d] $iii = x, 1/2-y, 1/2+z$. [e] $iv = 1-x, 1-y, 1-z$. [f] $v = 1+x, 1/2-y, 1/2+z$. [g] $vi = -x, -1/2+y, 1/2-z$.

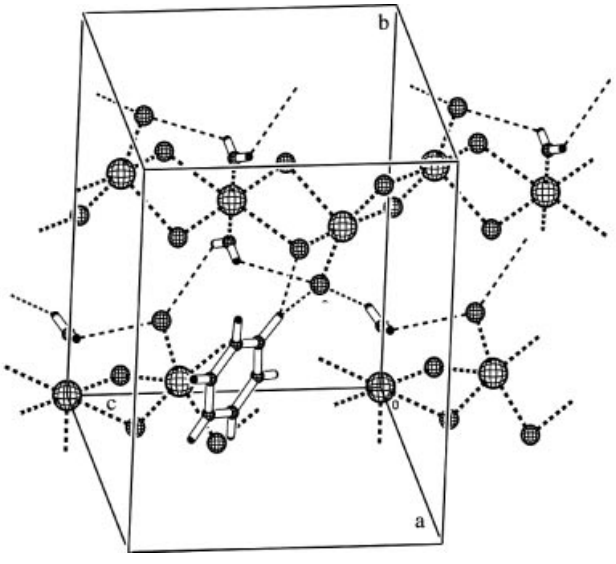

Figure 4. Packing viewed down c^* in bis(pyridinium) octachlorodiaquatricuprate(II) (**2**), with hydrogen bonds indicated by broken lines

rationalized on the basis of their crystal structures. Both complexes contain pyridinium cations in bifurcated H-bridges. As the HCl concentration increases the coordinating ability of the pyridine-nitrogen decreases due to protonation, with a concomitant enhancement of the H-bond formation ability. These H-bridges stabilize the monomeric structure of the tetrachlorocuprate anion together with the steric demand of the relatively large pyridinium ions in the crystal lattice of **1**. Conversely, at the lower pyridinium ion:copper(II) ratio of **2**, the bifurcated hydrogen bonds reduce the electron density on the chloride ions in such a way that the electron repulsion decreases and coordination spheres with more ligand interactions develop. Obviously, water may be a successful competitor for ligand sites in **2** as well. The octahedral and square-pyramidal structural units condense into the polymeric chains, which are stabilized by the interchain hydrogen bond networks of the water molecules. In **2** the two neighboring pyramidal units are localized in the *transoid* positions. To the best of our knowledge the SP-5-[*OC-6-SP-5-SP-5*]-OC-6 -$CuCl_5$-[$CuCl_4(OH_2)_2$-$CuCl_5$-$CuCl_5$]-$CuCl_4(OH_2)_2$- structural motif observed in **2** has not been detected yet.

Experimental Section

General: Analytical grade $CuCl_2 \cdot 2H_2O$, conc. HCl (35% by wt.) and pyridine (99.8%, anhydrous) were purchased from Aldrich. Anhydrous copper(II) chloride (13.5 g, 0.1 mol) obtained by thermal treatment of $CuCl_2 \cdot 2H_2O$ at 150 °C in a dry HCl stream was mixed

with equimolar amount of pyridine (0.1 mol, 8 mL) in dry acetone. The blue solution formed was refluxed for 3 h.[5] The gray precipitate formed was filtered off, then dissolved in 500 mL of conc. hydrochloric acid. From the solution obtained nearly equal amounts of compound **1** (green prisms or brownish microcrystals) and compound **2** (yellow plates) crystallized concurrently.

The carbon, hydrogen and nitrogen contents of compounds **1** and **2** were determined with a Fisons CHN 1018S elemental analyser. The chloride content was determined by argentometric microtitration using a chloride-selective electrode, and the copper content was determined by an ICP spectrometer (Atomscan 25, Thermo Jarrel Ash).

Results of the elemental analysis: **1**: $(C_5H_5NH)_2[CuCl_4]$ (365.57): calcd. C 32.85, H 3.30, N 7.66, Cl 38.79, Cu 17.38; found C 33.49, H 3.35, N 7.68, Cl 41.11, Cu 17.68. **2**: $(C_5H_5NH)_2[Cu_3Cl_8(H_2O)_2]$ (670.47); calcd. C 17.91, H 2.40, N 4.18, Cl 42.30, Cu 28.43; found C 17.98, H 2.41, N 4.18, Cl 42.21, Cu 28.18.

Diffraction-quality single crystals of **1** and **2** were obtained by slow crystallization from the hydrochloric acid solution. For the diffraction measurements the single crystals (**1** and **2**) were placed into glass capillaries. The single-crystal X-ray diffraction data were recorded by means of an Enraf−Nonius CAD4 diffractometer (graphite monochromator; Mo-K_α radiation, $\lambda = 0.71070$ Å) at 295(2) K in the range of $2.95 < \theta < 34.96°$ for **1** and $2.53 < \theta < 34.94°$ for **2** using $\omega/2\theta$ scans. The intensities of three standard reflections were monitored regularly in both cases. In order to establish the final structure models, the initial structures obtained by direct methods were refined by standard procedures (anisotropic full-matrix least-squares refinement on F^2 for all non-hydrogen atoms, riding H atoms except the N−H ones which were found in difference electron-density maps).[6] Figures and geometry analyses were done by means of PLATON.[7]

Cell parameters were determined by least-squares of the setting angles of 25 standard reflections (**1**: $8.67 \leq \theta \leq 17.3°$; **2**: $15.34 \leq \theta \leq 16.70°$). In the case of **1**, the intensities of the standard reflections remained constant within experimental error throughout the data collection. A total of 6900 reflections were collected of which 3254 were unique [R(int) = 0.0226, $R(\sigma) = 0.0415$]; the intensities of 1725 reflections were greater than $2\sigma(I)$. Completeness to $2\theta = 100\%$. No absorption correction was applied. Final model yielded $R_1 = 0.0385$ and $wR^2 = 0.0915$ for 1725 [$I > 2\sigma(I)$] and $R_1 = 0.0869$ and $wR^2 = 0.1018$ for all 3254 intensity data (goodness-of-fit = 0.925; the maximum and mean shift/esd 0.008 and 0.001). The maximum and minimum residual electron density in the final difference map was 0.706 and −0.474 e·Å^{-3}.

In the case of **2** the intensities of the standard reflections indicated a crystal decay of 4% (the data were corrected for decay). A total of 5143 reflections were collected of which 4769 were unique [R(int) = 0.0249, $R(\sigma) = 0.0370$]; the intensities of 3033 reflections were greater than $2\sigma(I)$. Completeness to $2\theta = 99.7\%$. An empirical (psi scan)[8] absorption correction was applied to the data (the minimum and maximum transmission factors were 0.6767 and 1.000). Final model gave $R_1 = 0.056$ and $wR^2 = 0.134$ for 3033 [$I > 2\sigma(I)$] and $R_1 = 0.088$ and $wR2 = 0.144$ for all 4769 intensity data [goodness-of-fit = 0.942; the maximum and mean shift/esd 0.009 and 0.002; extinction coefficient 0.027(2)]. The maximum and minimum residual electron density in the final difference map was 1.851 and −1.954 e·Å^{-3}. The crystallographic data and refinement results for **1** and **2** are collected in Table 1.

CCDC-192665 (**1**) and -192666 (**2**) contains the supplementary crystallographic data for this paper. These data can be obtained free of charge at www.ccdc.cam.ac.uk/conts/retrieving.html [or from the Cambridge Crystallographic Data Centre, 12, Union Road, Cambridge CB2 1EZ, UK; fax: (internat.) +44−1223/336−033; E-mail: deposit@ccdc.cam.ac.uk].

Infrared spectra were recorded by the diffuse reflectance method in KBr. Measurements were carried out between 4000−400 cm^{-1} by means of a Nicolet 170SX FT-IR spectrometer with a resolution of 1 cm^{-1}. ESR spectra were recorded by a JEOL JES-FE/3X ESR spectrometer (upgraded for data acquisition with an IBM PC Pentium I), in the X microwave band with 100 kHz field modulation. Manganese(II)-doped magnesium oxide powder was used as a standard for calibration of the g-values.

Acknowledgments

MC and AR thank the Hungarian Research Fund for support for these investigations (grant Nos. T025910 and T032929).

[1] R. D. Willet, *Coord. Chem. Rev.* **1991**, *109*, 181−205; D. W. Smith, *Coord. Chem. Rev.* **1976**, *21*, 93−158.
[2] B. J. Hathaway, *Structure and Bonding (Berlin)* **1984**, *57*, 55−118.
[3] R. D. Willett, H. Place, M. Middleton, *J. Am. Chem. Soc.* **1988**, *110*, 8639−8650.
[4] T. J. Coffey, C. P. Landee, W. T. Robinson, M. M. Turnbull, M. Winn, F. M. Woodward, *Inorg. Chim. Acta* **2000**, *303*, 54−60; K. Halverson, C. Patterson, R. D. Willet, *Acta Crystallogr.* **1990**, *B46*, 508−519; M. Bagieu-Beucher, R. Masse, D. T. Qui, *Z. Anorg. Allgem. Chem.* **1991**, *606*, 59−71; M. R. Bond, H. Place, Z. Wang, R. D. Willett, Y. L. Liu, T. E. Grigereit, J. E. Drumheller, G. F. Tuthill, *Inorg. Chem.* **1995**, *34*, 3134−3141; M. R. Bond, R. D. Willett, *Inorg. Chem.* **1989**, *28*, 3267−3269; M. R. Bond, R. D. Willett, G. V. Rubenacker, *Inorg. Chem.* **1990**, *29*, 2713−2720; K. E. Halvorson, T. Grigereit, R. D. Willett, *Inorg. Chem.* **1987**, *26*, 1716−1720; A. J. Blake, N. R. Champness, P. A. Cooke, J. E. B. Nicholson, *Acta Crystallogr.,* **1999**, *C55*, 1422−1425; J. H. Russell, S. C. Wallwork, *Acta Crystallogr.* **1969**, *B25*, 1691−1695; P. Murray-Rust, *Acta Crystallogr.* **1975**, *B31*, 1771−1772; H. Place, R. D. Willet, *Acta Crystallogr.* **1987**, *C43*, 1497−1500; M. R. Bond, R. D. Willett, *Acta Crystallogr.* **1987**, *C43*, 2304−2309; R. D. Willet, *Acta Crystallogr.* **1995**, *C51*, 1517−1519; M. Bukowska-Strzyzewska, A. Tosik, *Polish J. Chem.* **1979**, *53*, 2423−2428; S. P. Narula, S. Kaur, S. K. Sharma, D. Povey, *J. Cryst. Spect. Res.* **1992**, *22*, 139−143; J. T. Blanchette, R. D. Willett, *Inorg. Chem.* **1988**, *27*, 843−849; U. Geiser, R. M. Gaura, R. D. Willett, D. X. West, *Inorg. Chem.* **1986**, *25*, 4203−4212; G. S. Long, M. Wei, R. D. Willett, *Inorg. Chem.* **1997**, *36*, 3102−3107; T. E. Grigereit, B. L. Ramakrishna, H. Place, R. D. Willett, G. C. Pellacani, T. Manfredini, L. Menabue, A. Bonamartini-Corradi, L. P. Battaglia, *Inorg. Chem.* **1987**, *26*, 2235−2243.
[5] V. V. Udovenko, E. M. Osipova, *Zh. Obshch. Khim.* **1952**, *22*, 2095−2097.
[6] G. M. Sheldrick, (**1997**) SHELXS-97 *Program for Crystal Structure Solution*, University of Göttingen, Germany; G. M. Sheldrick, SHELXL-97 *Program for Crystal Structure Refinement*, University of Göttingen, Germany.
[7] A. L. Spek, *Acta Crystallogr., Sect. A* **1990**, *46*, C34.
[8] J. Reibenspies, (1989) DATCOR program for empirical absorp-

tion correction, Texas A & M University, College Station, Tx, USA.
[9] H. Remy, G. Laves, *Ber. Deutsch. Chem. Gess.* **1933**, *66*, 401−407; C. Renz, *Z. Anorg. Allg. Chem.* **1903**, *36*, 110; W. Libus, I. Uruska, *Inorg. Chem.* **1966**, *5*, 256−264; R. S. Vakhidov, *Izv. Vuzov. Vysshik. Ucheb. Zav. Khim. Khim. Tekhnol.* **1995**, *38*, 64−69; (*Chem. Abstr.* **1996**, *124*, 187847). W. Libus, S. K. Hoffmann, M. Kluczkowski, H. Twardowska, *Inorg. Chem.* **1980**, *19*, 1625−1632.
[10] J. Hu, G. Cheng, T. Ji, G. Wang, *Guangpuxue Yu Guangpu Fenxi (Spectroscopy and Spectral Analysis)* **1994**, *14*, 15−18; N. S. Gill, R. S. Nyholm, G. A. Barclay, T. I. Christie, P. J. Pauling, *J. Inorg. Nucl. Chem.* **1961**, *18*, 88−97.
[11] N. S. Gill, R. H. Nuttall, D. E. Scaife, D. W. A. Sharp, *J. Inorg. Nucl. Chem.* **1961**, *18*, 79−87; R. Foglizzo, A. Novak, *J. Chim. Phys.* **1969**, *66*, 1539−1550; R. Foglizzo, A. Novak, *J. Chem. Phys.* **1969**, *50*, 5366−5373.
[12] A. W. Addison, T. N. Rao, J. Reedijk, J. van Rijn, G. C. Verschoor, *J. Chem. Soc., Dalton Trans.* **1984**, 1349−1356; E. L. Muetterties, L. J. Guggenberger, *J. Am. Chem. Soc.* **1974**, *96*, 1748−1756.
[13] M. A. Hitchman, *Comments Inorg. Chem.* **1994**, *15*, 197−254.
[14] M. Atanasov, S. Angelov, D. Reinen, *Bulg. Chem. Commun.* **1992**, *25*, 26−38.

Received April 9, 2002
[I02183]

Steric Control of Cyclometallation Reactions in Schiff-Base Complexes of Cobalt(I) Containing an Anchoring Diphenylphosphanyl Group

Hans-Friedrich Klein,*[a] Robert Beck,[a] Ulrich Flörke,[b] and Hans-Jürgen Haupt[b]

Keywords: Cyclometallation / Cobalt / P ligands / Schiff bases / Regioselectivity

2-(Diphenylphosphanyl)alkyliminobenzaldehydes (2-$Ph_2PC_6H_4CHNR$) react with $[CoCH_3(PMe_3)_4]$ forming five-membered metallacycles in complexes [(2-$Ph_2PC_6H_4CNR$-*C,P*)$Co(PMe_3)_3$] [**1**: R = C_2H_5, **2**: R = $CH(CH_3)_2$, **3**: R = *cyclo*-C_6H_{11}] while the *ortho*-metallation pathway is selectively followed in the formation of [{2-$Ph_2PC_6H_3(CHNR)$-C^1,*P*}$Co(PMe_3)_3$] [**4**: R = $C(CH_3)_3$]. The presence of a four-membered cobaltocycle in the molecular structure of **4** was confirmed by X-ray analysis. Carbonylation of **2** and **3** gives the monocarbonyl derivatives [(2-$Ph_2PC_6H_4CNR$-*C,P*)Co(CO)$(PMe_3)_2$] [**5**: R = $CH(CH_3)_2$, **6**: R = *cyclo*-C_6H_{11}] while **4** undergoes ring expansion by insertion forming [{2-$Ph_2PC_6H_3(CHNR)CO$-*C,P*}$Co(CO)(PMe_3)_2$] [**7**: R = $C(CH_3)_3$]. Monosubstitution occurs under 1 bar of ethene giving the π-ethene complexes [(2-$Ph_2PC_6H_4CNR$-*C,P*)$Co(C_2H_4)(PMe_3)_2$] [**8**: R = $CH(CH_3)_2$, **9**: R = *cyclo*-C_6H_{11}] and [{2-$Ph_2PC_6H_3(CHNR)$-C^1,*P*}$Co(C_2H_4)(PMe_3)_2$] [**10**: R = $C(CH_3)_3$]. The molecular structure of **9** shows an equatorial π-ethene ligand. Iodomethane oxidizes **2** and **3** to afford the cobalt(II) complexes [(2-$Ph_2PC_6H_4CNR$-*C,P*)$CoI(PMe_3)_2$] [**11**: R = $CH(CH_3)_2$, **12**: R = *cyclo*-C_6H_{11}] and oxidatively adds to **4** to give *mer-trans*-[{2-$Ph_2PC_6H_3(CHNR)$-C^1,*P*}$CoI(CH_3)(PMe_3)_2$] [**13**: R = $C(CH_3)_3$].

(© Wiley-VCH Verlag GmbH, 69451 Weinheim, Germany, 2002)

Introduction

Methylnickel complexes have been shown to activate the CHO function of 2-diphenylphosphanylbenzaldehyde forming acylnickel compounds.[1]

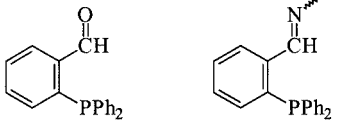

A **B**

We have recently described cobalt(I) complexes containing soft/hard P,N-chelating ligands,[2] where the introduction of an imino ligand function increases the softness of the N-donor. The isoelectronic relationship between 2-diphenylphosphanyl benzaldehyde **A** and its Schiff base derivatives **B** raises the possibility of a cyclometallation route to iminoacyl metal complexes. The coordination modes of iminoacyl complexes, which depend on the number of metal valence electrons and steric limitations, show an active participation of the neighbouring N-donor whenever needed.

Therefore, in Schiff-base complexes of transition metal ions six-membered rings are the dominant structural features, and complexes of the chelating ligands **B** are no exception, as shown by the few reported examples of complexes of these ligands with cobalt,[3] molybdenum,[4] rhodium,[5] and iridium.[6] Preferred coordination of the N-donor would appear to prevent an attack of the metal at the C−H bond which would explain the scarcity of iminoacyl metal complexes arising from C−H activation.[7] However, in cyclometallation reactions with $[CoMe(PMe_3)_4]$ there is evidence for steric control being dominant.[8] Consequently we have studied the effect of a bulky N-substituent in our investigation of the prechelate species **B**.

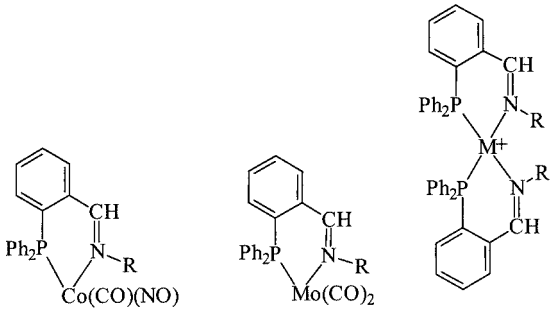

R = alkyl M = Rh, Ir

[a] Eduard-Zintl-Institut für Anorganische und Physikalische Chemie der Technischen Universität Darmstadt, Petersenstrasse 18, 64285 Darmstadt, Germany
[b] Anorganische und Analytische Chemie der Universität Paderborn, Warburger Straße, 33098 Paderborn, Germany

Results and Discussion

Metallation Reactions

An iminoacyl side-chain containing an N-donor function and an activated C−H bond was attached to one of the six *ortho*-positions of triphenylphosphane to give the Schiff-base compounds 2-(diphenylphosphanyl)alkyliminobenzaldehyde. Reaction with [$CoMe(PMe_3)_4$] proceeded at −70 °C in THF [Equation (1)] and afforded the C-metallated complexes **1**−**3**.

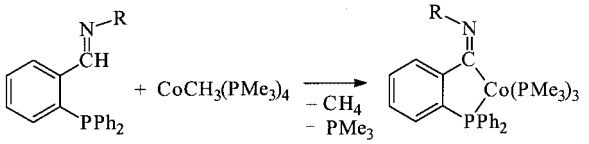

(1)

	1	2	3
R	C_2H_5	$CH(CH_3)_2$	*cyclo*-C_6H_{11}

Black quadrangular crystals of **1** and **2** were obtained from pentane solution while **3** formed dark brown scales. Decomposition was noticed above 109−113 °C under argon. The ν(C=N) absorptions in the IR spectra are shifted bathochromically (by about 100 cm^{-1}) with respect to those of the free ligands upon metallation. The ^{31}P NMR spectra of **1**−**3** show little variation in the dominant signals. A large low-field shift of the PPh_2 resonances is compatible only with five-membered cobaltocycles, and two doublets of doublets for one axial and two equatorial P-donor atoms with almost identical $J_{P,P}$ values indicate a tbp-coordinated cobalt in **1**−**3**. Only in the spectrum of **1** (Figure 1) are all the resonances accompanied by those of an isomer (12%) with quite different coupling constants.

Angular distortions of the tbp geometry can be expected in a configuration [(*E*)-alkyliminoacyl] where the ethyl substituent is sterically accommodated within the ligand sphere. Therefore the larger substituents in **2** and **3** are exclusively arranged in the opposite *Z*-configuration.

At first glance 2-diphenylphosphanyl-*tert*-butylbenzimide appeared to react similarly as evolution of a gas was observed at −70 °C. The reaction mixture became a slightly deeper red colour than **1**−**3**, and eventually dark red rhombic crystals of **4** were obtained from pentane. However, upon metallation there is almost no shift in the infrared absorption of the C=N band (1626 cm^{-1}), and in the ^1H NMR spectrum a singlet resonance (δ = 7.95 ppm) clearly represents an aldimine proton. The ^{31}P NMR spectrum shows a pattern of resonances well-known from *ortho*-metallated complexes,[8] strongly suggesting a regioselective cyclometallation reaction [Equation (2)].

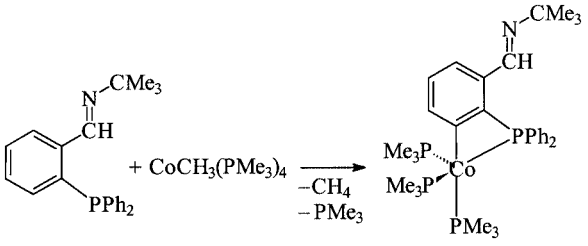

(2)

4

The presence of a four-membered cobaltocycle in **4** was confirmed by elucidation of the molecular structure (Figure 2).

The cobalt atom occupies the central position of a trigonal bipyramid with an axial C1 atom and a PMe_3 group

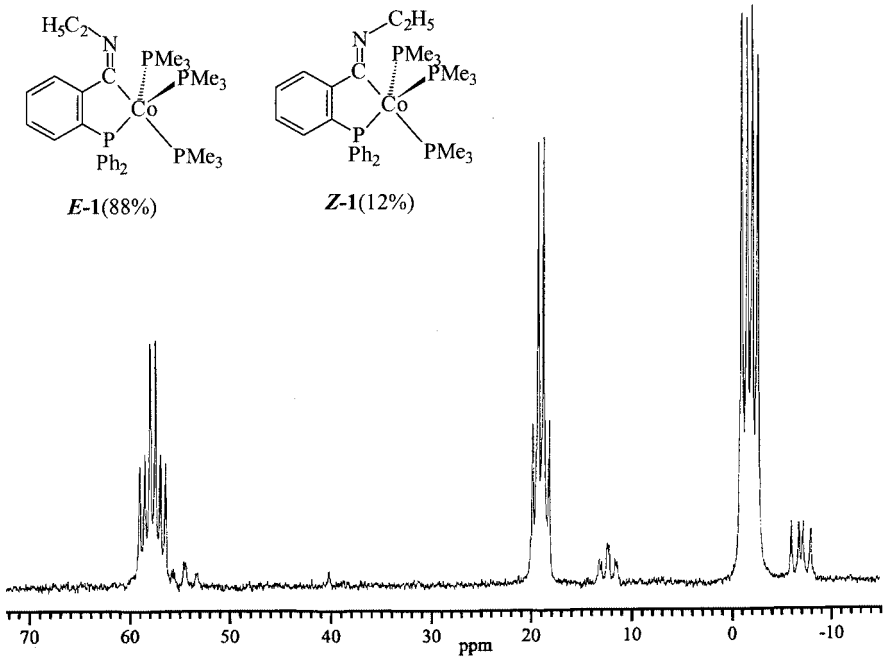

E-**1**(88%) *Z*-**1**(12%)

Figure 1. ^{31}P NMR spectrum of **1** (81 MHz, [D_8]THF, 203 K)

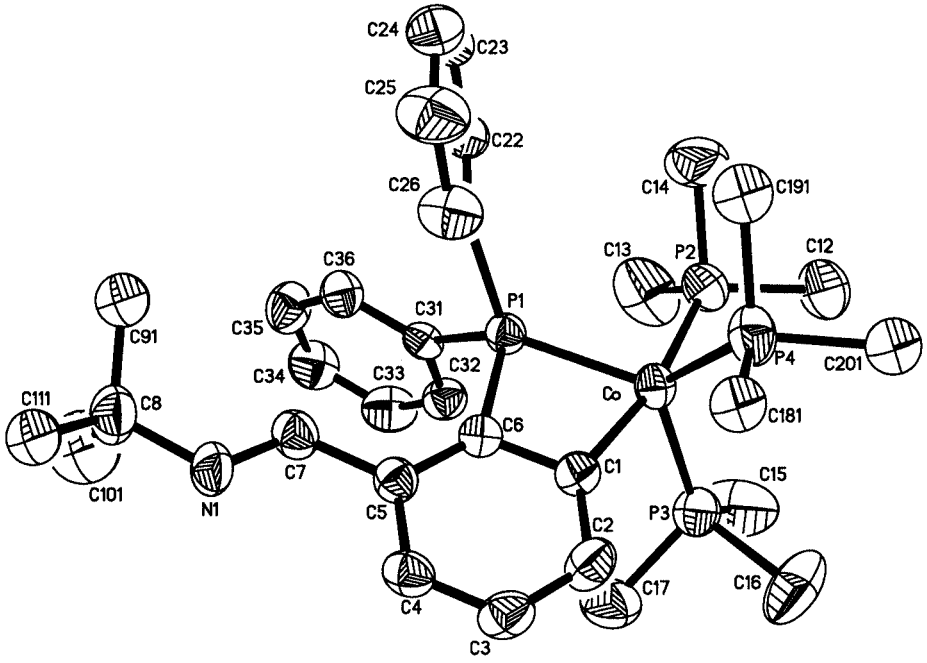

Figure 2. Molecular structure of **4**, only one position of disordered *t*Bu and PMe_3 groups shown (ORTEP plot with hydrogen atoms omitted); selected bond lengths [Å] and angles [°]: Co−C1 1.977(4), Co−P1 2.2075(12), Co−P2 2.1997(15), Co−P3 2.1836(14), Co−P4 2.1821(15), P1−C6 1.802(4), C1−C6 1.403(5); C1−Co−P1 71.09(12), C1−Co−P2 167.82(12), C1−Co−P3 87.92(12), C1−Co−P4 90.78(12), P1−Co−P2 97.11(5), P1−Co−P3 124.02(5), P1−Co−P4 113.76(5), P2−Co−P3 96.66(6), P2−Co−P4 96.96(6), P3−Co−P4 117.93(6)

(P2). A planar [C,P] metallacycle (sum of internal angles = 360°) spans the axial and equatorial positions with a narrow bite-angle [C1−Co−P1 = 71.09(12)°]. Except for one of the equatorial PMe_3 groups (P4), which shows rotational disorder, the Co−C, Co−P, and P−C bond lengths are close to the average of reported values in arylcobalt compounds. The bond lengths and angles resemble those found in the unsubstituted parent compound.[8]

The bulky CMe_3 substituent appears to prevent a close approach of the CH=N group to the cobalt and causes complete switching of the metallation reaction onto the selective *ortho*-pathway where the four *ortho* positions of the PPh_2 group are not involved.[2]

Reactions with Carbon Monoxide

An experimental distinction between four- and five-membered cobaltocycles was achieved by placing solutions of **2**−**4** under a pressure of 1 bar CO at 20 °C. While the iminoacyl complexes **2** and **3** undergo monosubstitution [Equation (3)], compound **4** takes up two equivalents of CO and undergoes a ring expansion [Equation (4)].

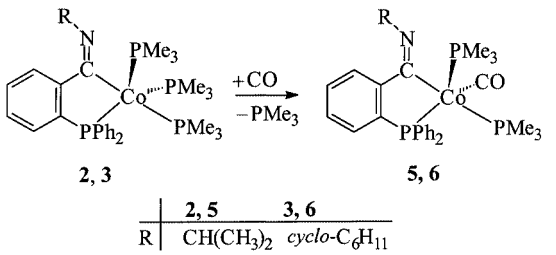

(3)

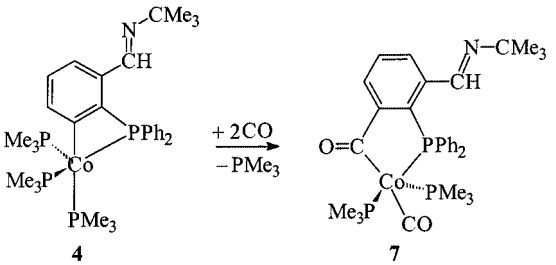

(4)

The iminoacyl(carbonyl)cobalt complexes **5** and **6** are yellow solids that can be handled in air for several hours and under argon are thermally stable up to 165 °C. They are insoluble in pentane or diethyl ether and show moderate solubility in THF. Their IR spectra display characteristic bands around 1876 cm^{-1} for terminal carbonyl ligands and around 1539 cm^{-1} for exocyclic C=N groups; these are hypsochromically shifted by about 18 cm^{-1} with respect to **2** and **3**. The ^{31}P NMR spectra show three resonances as doublets of doublets which are compatible with trimethylphosphane in axial and equatorial positions and an equatorial CO ligand.

The acyl(carbonyl)cobalt complex **7** is soluble in pentane or diethyl ether. In the IR spectrum the acyl and carbonyl groups are represented by new bands that fall precisely in the positions expected for a tbp molecular configuration with axial acyl and CO ligands.[2] The NMR spectroscopic data confirm this configuration in solution, and isomers with equatorial CO ligands are not detected.

Reactions with Ethene

Red-brown solutions of **2** or **3** under 1 bar C_2H_4 turned orange red within 5 min indicating that a reaction had taken place [Equation (5)].

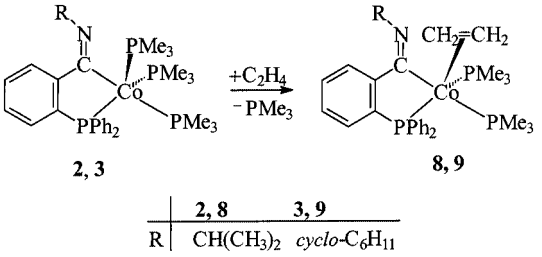

2, 3 **8, 9** (5)

R	2, 8	3, 9
	$CH(CH_3)_2$	*cyclo*-C_6H_{11}

Short orange rods of **8** or orange rhombs of **9** were obtained from pentane that release ethene while decomposing above 93 °C under argon. The ^{31}P NMR spectra consist of three doublets of doublets with $J_{P,P}$ coupling constants of between 24 and 36 Hz, indicating P-nuclei of trimethylphosphanes in axial and equatorial positions leaving an equatorial position free for coordination of the ethene ligand.

In the crystal **9** has a molecular structure showing the expected configuration (Figure 3).

A cobalt atom in the centre of a trigonal bipyramid is coordinated to an equatorial ethene and two trimethylphosphanes in axial and equatorial positions. A five-membered metallacycle spans the C-axial and P-equatorial positions with a C7−Co−P1 bite angle of 79.11(9)° and considerable bending (sum of internal angles = 520.7° as compared with 540° for a planar arrangement). The side-on coordinated ethene shows the expected increase of 5 pm in the C8−C9 bond relative to free ethene. The Co−C1 and Co−P bond lengths fall in the typical range reported for arylcobalt complexes.

When compared with the isoelectronic (2-diphenylphosphanyl)benzoyl complex derived from the prechelate system **A**, in which cobalt fails to coordinate ethene, the iminoacyl group places enough electron density on the metal centre to support olefin binding. As was observed earlier a four-membered cobaltocycle induces weaker olefin coordination.[2] Compound **4** forms a π-ethene compound **10** [Equation (6)] only after thermal pretreatment.

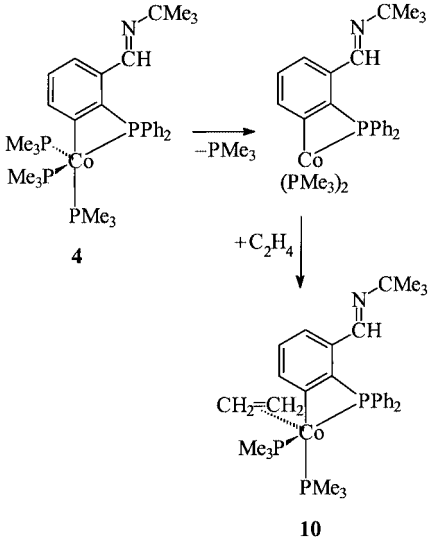

4 **10** (6)

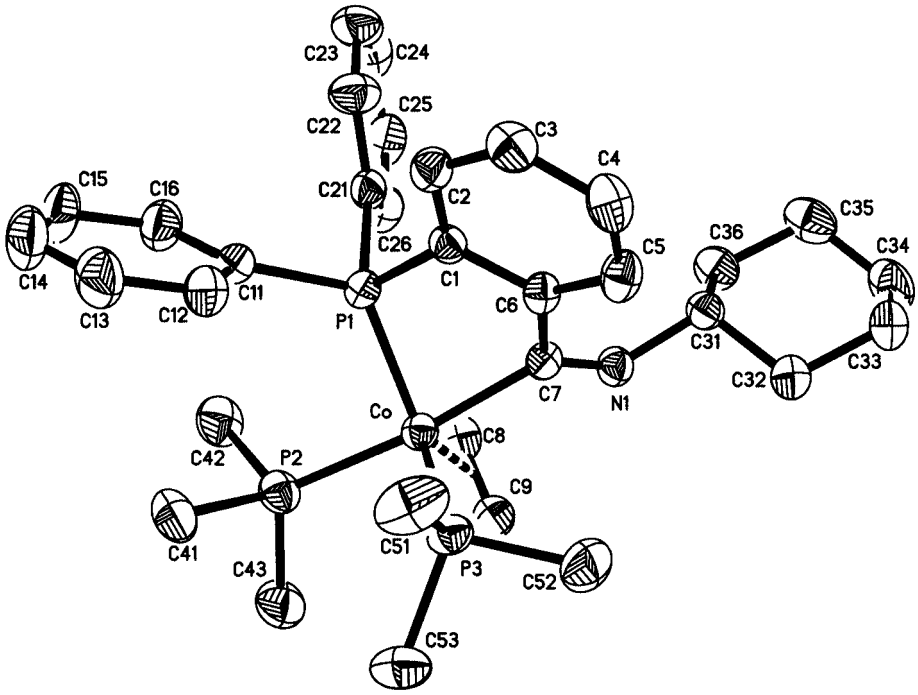

Figure 3. Molecular structure of **9** (ORTEP plot with hydrogen atoms omitted); selected bond lengths [Å] and angles [°]: Co−C7 2.014(3), Co−C8 2.055(3), Co−C9 2.046(3), Co−P1 2.1748(10), Co−P2 2.2232(12), Co−P3 2.1985(11), P1−C1 1.803(3), C1−C6 1.401(4), C6−C7 1.507(4), C8−C9 1.397(5); C7−Co−P1 79.11(9), C7−Co−P2 173.14(9), C7−Co−P3 87.17(9), P1−Co−P2 95.40(4), P1−Co−P3 113.32(4), P2−Co−P3 98.84(4), Co−C7−C6 114.3(2), C1−C6−C7 114.3(3), C6−C1−P1 110.4(2)

The orange crystals of **10** are readily soluble in diethyl ether or pentane. Before melting under argon at 105−107 °C with decomposition they turn red brown. This behaviour indicates a tetracoordinate intermediate which, however, could not be isolated as an analytically pure compound. The spectroscopic data of **10** are in agreement with an overall replacement reaction of one equatorial trimethylphosphane ligand by ethene.

Reactions with Iodomethane

Complexes **2** and **3** react with two molar equivalents of iodomethane in tetrahydrofuran [Equation (7)] to form the iodocobalt(II) complexes **11** and **12** with formal loss of a methyl group.

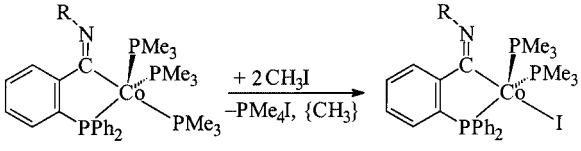

2, 3 **11, 12** (7)

	2, 11	3, 12
R	$CH(CH_3)_2$	*cyclo*-C_6H_{11}

Dark brown crystals with a magnetic moment of 1.98 were obtained. A diamagnetic cobalt(III) intermediate as described earlier[2] could not be isolated from reactions in less polar diethyl ether or pentane solvents.

This particular reactivity has been observed with type **A** systems where structural proof of a tbp molecular structure was obtained with acyl and iodo groups in axial positions.[1] On the basis of their mutual *trans*-influences a *trans*-arrangement of the iminoacyl and iodo ligands would suggest itself also for **11** and **12**.

Under otherwise similar conditions **4** oxidatively adds iodomethane with substitution and quaternization of a trimethylphosphane ligand [Equation (8)].The dark red crystals of **13** melt at 117−119 °C with decomposition and with no indication of the formation of a paramagnetic iodocobalt(II) complex as an intermediate. Solutions in THF slowly decompose at 273 K, but at 203 K the ^{31}P NMR spectroscopic data confirm a *mer-trans* arrangement of the six ligand functions.

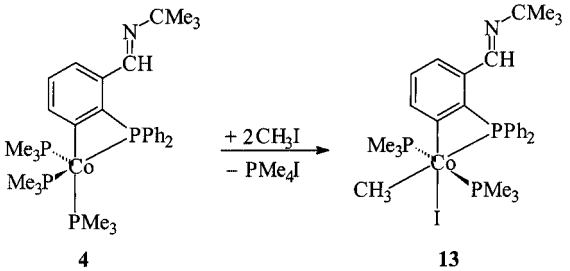

4 **13** (8)

The steric influence of the alkylimino group in **13** does not affect the coordination sphere of cobalt, therefore the stereoselective oxidative *cis*-addition proceeds with retention of the metallacycle, as with other ring substituents.[1] As the iminoacyl group remains uncoordinated, it retains an *E*-configuration.

Experimental Section

General Procedures and Materials: All air-sensitive and volatile materials were handled using standard vacuum techniques and were kept under argon. Microanalyses: Kolbe Microanalytical Laboratory, Mülheim/Ruhr, Germany. Melting points/decomposition temperatures: Sealed capillaries, uncorrected values. Chemicals (Merck/Schuchardt) were used as purchased. Literature methods were followed in the preparation of 2-(diphenylphosphanyl)-benzaldehyde,[9,10] 2-(diphenylphosphanyl)-*N*-alkyliminobenzaldehyde,[5,11] and $[CoMe(PMe_3)_4]$.[12] IR: Nujol mulls between KBr discs, Bruker spectrophotometer type FRA 106. ^1H and ^{13}C NMR spectra (300 MHz and 75 MHz, respectively) were recorded with a Bruker ARX-300 spectrometer, ^{31}P NMR spectra (81 MHz) with a Bruker AM-200 instrument. ^{13}C and ^{31}P resonances were obtained with broad-band proton decoupling. Magnetic susceptibility data were obtained by the Faraday method using a Cahn D 200 torsion balance (Bruker) at 1.5 Tesla.

[(*E,Z*)-2-(Diphenylphosphanyl)-*N*-ethylbenzimino-*C,P*]tris-(trimethylphosphane)cobalt(I) (1): 2-(Diphenylphosphanyl)-*N*-ethylbenzimide (377 mg, 1.18 mmol) in 30 mL of THF was combined at −70 °C with $[CoMe(PMe_3)_4]$ (450 mg, 1.18 mmol) in 80 mL of THF. During warm-up evolution of gas was noticed and the mixture became red brown. The mixture was kept at 20 °C for 18 h. The volatiles were then removed in vacuo, and the solid residue was extracted with two 70 mL portions of pentane. The solution was cooled to −27 °C to afford dark crystals of **1**. Yield 322 mg (45%); m.p. 109−111 °C (dec.). IR (Nujol): $\tilde{\nu}$ = 1542 cm^{-1} (C=N). ^1H NMR (300 MHz, $[D_8]$THF, 296 K): δ = 0.89 (br. s, 9 H, PCH_3), 1.18 (br. s, 18 H, PCH_3), 1.29 (t, ^3J = 6.9 Hz, 3 H, CH_3), 3.65 (q, ^3J = 6.9 Hz, 2 H, CH_2), 6.90 (t, ^3J = 7.2 Hz, 1 H, CH), 7.01 (t, ^3J = 7.3 Hz, 1 H, CH), 7.18−7.29 (m, 8 H, CH), 7.47−7.53 (m, 4 H, CH) ppm. ^{13}C NMR (75.4 MHz, $[D_8]$THF, 296 K): δ = 17.9 (s, CH_3), 23.0 (m, PCH_3), 24.8 (m, PCH_3), 50.5 (s, CH_2), 123.4 (d, $^2J_{P,C}$ = 17.8 Hz, CH), 125.8, 126.2 (s, CH), 128.1 (d, $^2J_{P,C}$ = 7.2 Hz, CH), (s, CH), 131.1 (s, CH), 133.8 (d, $^2J_{P,C}$ = 12.2 Hz, CH), 142.2 (s, C) ppm. ^{31}P NMR (81 MHz, $[D_8]$THF, 203 K): *E*-**1** (88%) δ = −1 (dd, $^2J_{P,P}$ = 84 and 44 Hz, 2 P, PCH_3), 18 (dd, $^2J_{P,P}$ = 45 and 44 Hz, 1 P, PCH_3), 57 (dt, $^2J_{P,P}$ = 84 and 45 Hz, 1 P, PPh_2); *Z*-**1** (12%) δ = −6 (dd, $^2J_{P,P}$ = 95 and 63 Hz, 2 P, PCH_3), 12 (dt, $^2J_{P,P}$ = 63 and 15 Hz, 1 P, PCH_3), 56 (dt, $^2J_{P,P}$ = 95 and 15 Hz, 1 P, PPh_2) ppm. $C_{30}H_{46}CoNP_4$ (603.2): calcd. C 59.70, H 7.68, N 2.32, P 20.53; found C 59.85, H 7.60, N 2.35, P 20.52.

[(*Z*)-2-(Diphenylphosphanyl)-*N*-isopropylbenzimino-*C,P*]tris-(trimethylphosphane)cobalt(I) (2): 2-(Diphenylphosphanyl)-*N*-isopropylbenzimide (622 mg, 1.87 mmol) was combined with $[CoMe(PMe_3)_4]$ (710 mg, 1.87 mmol) as described above to afford dark red crystals of **2**. Yield 683 mg (59%); m.p. 109−111 °C (dec.). IR (Nujol): $\tilde{\nu}$ = 1520 cm^{-1} (C=N). ^1H NMR (300 MHz, $[D_8]$THF, 296 K): δ = 0.99 (d, $^2J_{P,H}$ = 6.1 Hz, 9 H, PCH_3), 1.29 (d, ^3J = 5.9 Hz, 6 H, CH_3), 1.12 (br. s, 18 H, PCH_3), 4.20 (septet, ^3J = 5.9 Hz, 1 H, CH), 3.65 (q, ^3J = 6.9 Hz, 2 H, CH_2), 6.88 (dt, ^3J = 5.9, ^4J = 1.5 Hz, 1 H, CH), 6.98 (dt, ^3J = 5.9, ^4J = 1.5 Hz, 1 H, CH), 7.08 (m, 2 H, CH), 7.20−7.22 (m, 6 H, CH), 7.77−7.84 (m, 4 H, CH) ppm. ^{13}C NMR (75.4 MHz, $[D_8]$THF, 296 K): δ = 21.4 (m, PCH_3), 23.9 (s, CH_3), 53.5 (s, CMe_2), 120.4 (d, $^1J_{P,C}$ = 17.2 Hz, CH), 123.6, 123.9 (s, CH), 126.2 (d, $^3J_{P,C}$ = 7.2 Hz, CH), 128.6 (s, C), 132.1 (d, $^2J_{P,C}$ = 11.8 Hz, CH) ppm. ^{31}P NMR (81 MHz,

[D$_8$]THF, 203 K): δ = −4 (dd, $^2J_{P,P}$ = 79 and 45 Hz, 2 P, PCH_3), 17 (dd, $^2J_{P,P}$ = 45 and 44 Hz, 1 P, PCH_3), 55 (dt, $^2J_{P,P}$ = 79 and 44 Hz, 1 P, PPh_2) ppm. $C_{31}H_{48}CoNP_4$ (617.2): calcd. C 60.29, H 7.83, N 2.27, P 20.06; found C 59.95, H 7.40, N 2.26, P 20.43.

[(*E*)-2-(Diphenylphosphanyl)-*N*-cyclohexylbenzimino-*C,P*]tris-(trimethylphosphane)cobalt(I) (3): 2-(Diphenylphosphanyl)-*N*-cyclohexylbenzimide (790 mg, 2.08 mmol) was combined with [CoMe(PMe$_3$)$_4$] (775 mg, 2.08 mmol) as described above to afford dark red crystals of **3**. Yield 1070 mg (78%); m.p. 113−115 °C (dec.). IR (Nujol): $\tilde{\nu}$ = 1527 cm^{-1} (C=N). ^{1}H NMR (300 MHz, [D$_8$]THF, 296 K): δ = 0.98 (br. s, 9 H, PCH_3), 1.18 (br. s, 18 H, PCH_3), 1.34−1.84 (m, 10 H, CH_2), 3.90 (m, 1 H, CH), 6.90 (t, ^3J = 7.1 Hz, 1 H, CH), 7.00 (t, ^3J = 7.0 Hz, 1 H, CH), 7.05 (m, 2 H, CH), 7.21−7.31 (m, 6 H, CH), 7.61−7.95 (m, 4 H, CH) ppm. ^{13}C NMR (75.4 MHz, [D$_8$]THF, 296 K): δ = 21.4 (m, PCH_3), 23.2, 25.2, 30.9, 34.3 (s, CH_2), 60.2 (s, NCH), 120.6 (d, $^1J_{P,C}$ = 17.3 Hz, CH), 123.6, 124.0 (s, CH), 126.3 (d, $^3J_{P,C}$ = 7.1 Hz, CH), 127.3 (d, $^2J_{P,C}$ = 12.2 Hz, CH), 128.8, 130.9 (s, C), 131.1 (d, $^2J_{P,C}$ = 9.5 Hz, CH), 132.1 (d, $^2J_{P,C}$ = 11.9 Hz, CH) ppm. ^{31}P NMR (81 MHz, [D$_8$]THF, 203 K): δ = −4 (dd, $^2J_{P,P}$ = 80 and 44 Hz, 2 P, PCH_3), 16 (dd, $^2J_{P,P}$ = 45 and 44 Hz, 1 P, PCH_3), 56 (dt, $^2J_{P,P}$ = 80 and 45 Hz, 1 P, PPh_2) ppm. $C_{34}H_{52}CoNP_4$ (657.2): calcd. C 62.10, H 7.97, N 2.13, P 18.84; found C 62.22, H 7.41, N 2.10, P 19.09.

[(*E*)-2-(Diphenylphosphanyl)-*N*-*tert*-butylbenzimide-*C^1,P*]tris-(trimethylphosphane)cobalt(I) (4): 2-(Diphenylphosphanyl)-*tert*-butylbenzimide (530 mg, 1.50 mmol) in 50 mL of THF was combined at −70 °C with [CoMe(PMe$_3$)$_4$] (570 mg, 1.50 mmol) in 50 mL of THF and a gas evolved. After 16 h at 20 °C all volatiles were removed from the mixture in vacuo, and the solid residue was extracted with 80 mL of pentane. From the solution 250 mg of dark red rhombic crystals were obtained which proved suitable for X-ray diffraction. Upon cooling to −27 °C a second fraction of **4** was collected and combined with the first. Yield 790 mg (83%); m.p. 114−116 °C (dec.). IR (Nujol): $\tilde{\nu}$ = 1625 cm^{-1} (C=N). ^{1}H NMR (300 MHz, [D$_8$]THF, 296 K): δ = 0.91 (s, 9 H, CH_3), 1.11 (d, $^2J_{P,H}$ = 6.4 Hz, 9 H, PCH_3), 1.28 (t′, $|^2J_{P,H} + {}^4J_{P,H}|$ = 4.7 Hz, 18 H, PCH_3), 6.70 (t, ^3J = 7.4 Hz, 1 H, CH), 6.90 (m, 1 H, CH), 7.13 (d, ^3J = 7.0 Hz, 1 H, CH), 7.25−7.30 (m, 6 H, CH), 7.74−7.82 (m, 4 H, CH), 7.95 (s, 1 H, NCH) ppm. ^{13}C NMR (75.4 MHz, [D$_8$]THF, 296 K): δ = 21.7−22.9 (m, PCH_3), 27.3 (s, CH_3), 55.6 (s, CMe_3), 115.4 (s, CH), 126.5 (d, $^3J_{P,C}$ = 7.8 Hz, CH), 126.8, 127.5 (s, CH), 131.7 (d, $^2J_{P,C}$ = 12.9 Hz, CH), 138.0, 138.6 (s, C), 152.2 (d, $^2J_{P,C}$ = 6.9 Hz, NCH) ppm. ^{31}P NMR (81 MHz, [D$_8$]THF, 233 K): δ = −28 (dt, $^2J_{P,P}$ = 90 and 71 Hz, 1 P, PPh_2), −3 (dd, $^2J_{P,P}$ = 90 and 48 Hz, 2 P, PCH_3), 21 (dt, $^2J_{P,P}$ = 71 and 48 Hz, 1 P, PCH_3) ppm. $C_{32}H_{50}CoNP_4$ (631.2): calcd. C 60.86, H 7.98, N 2.22, P 19.62; found C 60.55, H 7.98, N 2.21, P 19.98.

[(*E*)-2-(Diphenylphosphanyl)-*N*-isopropylbenzimino-*C,P*]carbonylbis-(trimethylphosphane)cobalt(I) (5): A sample of **2** (430 mg, 0.69 mmol) in 70 mL of diethyl ether was kept stirring under 1 bar of CO for 30 min to form a light yellow precipitate. The volatiles were then removed in vacuo, and the solid residue of **5** was washed with 20 mL of cold diethyl ether and dried in vacuo. Yield 368 mg (93%); m.p. 185−187 °C (dec.). IR (Nujol): $\tilde{\nu}$ = 1874 cm^{-1} (C≡O), 1538 cm^{-1} (C=N). ^{1}H NMR (300 MHz, [D$_8$]THF, 296 K): δ = 1.05 (br. s, 18 H, PCH_3), 1.30 (m, 6 H, CH_3), 4.30 (m, 1 H, NCH), 7.09 (m, 2 H, CH), 7.29−7.31 (m, 8 H, CH), 7.43−7.58 (m, 2 H, CH), 8.22−8.28 (m, 2 H, CH) ppm. ^{13}C NMR (75.4 MHz, [D$_8$]THF, 296 K): δ = 19.9 (m, PCH_3), 23.1 (s, CH_3), 8.5 (s, NCH), 127.5 (d, $^2J_{P,C}$ = 16.5 Hz, CH), 128.2 (d, $^2J_{P,C}$ = 15.9 Hz, CH), 129.1 (d, $^2J_{P,C}$ = 7.0 Hz, CH), 143.1 (m, C) ppm. ^{31}P NMR (81 MHz, [D$_8$]THF, 203 K): δ = −4 (dd, $^2J_{P,P}$ = 63 and 53 Hz, 1 P, PCH_3), 21 (dd, $^2J_{P,P}$ = 53 and 36 Hz, 1 P, PCH_3), 68 (dd, $^2J_{P,P}$ = 63 and 36 Hz, 1 P, PPh_2) ppm. $C_{29}H_{39}CoNOP_3$ (569.2): calcd. C 61.16, H 6.90, N 2.46, P 16.32; found C 60.97, H 6.87, N 2.45, P 16.20.

[(*E*)-2-(Diphenylphosphanyl)-*N*-cyclohexylbenzimino-*C,P*]-carbonylbis(trimethylphosphane)cobalt(I) (6): Carbonylation of **3** (510 mg, 0.77 mmol) in 50 mL of diethyl ether was carried out as in the preparation of **5** to afford **6** as a yellow solid. Yield 449 mg (95%); m.p. 165−167 °C (dec.). IR (Nujol): $\tilde{\nu}$ = 1880 cm^{-1} (C≡O), 1540 cm^{-1} (C=N). ^{1}H NMR (300 MHz, [D$_8$]THF, 296 K): δ = 1.04 (br. s, 18 H, PCH_3), 1.26−1.86 (m, 10 H, CH_2), 3.99 (m, 1 H, NCH), 7.04 (m, 2 H, CH), 7.29−7.31 (m, 8 H, CH), 7.41−7.43 (m, 2 H, CH), 8.00−8.03 (m, 2 H, CH) ppm. ^{13}C NMR (75.4 MHz, [D$_8$]THF, 296 K): δ = 21.9 (m, PCH_3), 24.7, 25.2, 26.8, 34.5 (s, CH_2), 68.8 (s, NCH), 125.5 (d, $^2J_{P,C}$ = 16.5 Hz, CH), 128.2 (d, $^3J_{P,C}$ = 3.9 Hz, CH), 128.7 (s, CH), 129.1 (d, $^2J_{P,C}$ = 7.1 Hz, CH), 133.8 (m, C) ppm. ^{31}P NMR (81 MHz, [D$_8$]THF, 203 K): δ = −4 (dd, $^2J_{P,P}$ = 61 and 54 Hz, 1 P, PCH_3), 21 (dd, $^2J_{P,P}$ = 54 and 39 Hz, 1 P, PCH_3), 69 (dd, $^2J_{P,P}$ = 61 and 39 Hz, 1 P, PPh_2) ppm. $C_{32}H_{43}CoNOP_3$ (609.2): calcd. C 63.05, H 7.11, N 2.30, P 15.24; found C 61.62, H 6.35, N 2.06, P 16.49. (Crystals of the analytical sample contained ca. 3% of trimethylphosphane oxide.)

[(*E*)-2-(Diphenylphosphanyl)benzoyl-3-*N*-*tert*-butylimidomethyl-*C,P*]carbonylbis(trimethylphosphane)cobalt(I) (7): A sample of **4** (520 mg, 0.82 mmol) in 70 mL of diethyl ether was kept stirring under 1 bar of CO for 1 h during which time the colour of the mixture turned from red brown to orange. The volatiles were removed in vacuo, and the solid residue was extracted with two 50 mL portions of pentane. Crystallization at −27 °C afforded dark red rhombs of **7**. Yield 380 mg (75%); m.p. 123−125 °C (dec.). IR (Nujol): $\tilde{\nu}$ = 1906 cm^{-1} (C≡O), 1630 cm^{-1} (C=N), 1540 cm^{-1} (C=O). ^{1}H NMR (300 MHz, [D$_8$]THF, 296 K): δ = 0.76 (s, 9 H, CH_3), 1.04 (t′, $|^2J_{P,H} + {}^4J_{P,H}|$ = 7.3 Hz, 18 H, PCH_3], 7.28−7.34 (m, 6 H, CH), 7.46 (dt, ^3J = 7.6, ^4J = 2.6 Hz, 1 H, CH), 7.54 (dd, ^3J = 6.4, ^4J = 1.6 Hz, 1 H, CH) ppm. ^{13}C NMR (75.4 MHz, [D$_8$]THF, 296 K): δ = 17.9 (m, PCH_3), 27.8 (s, CH_3), 56.1 (s, CMe_3), 68.8 (s, NCH), 125.5 (d, $^2J_{P,C}$ = 20.5 Hz, CH), 126.8 (s, CH), 127.3 (d, $^3J_{P,C}$ = 8.8 Hz, CH), 129.8 (d, $^2J_{P,C}$ = 11.4 Hz, CH), 137.1 (s, C), 138.5 (d, $^1J_{P,C}$ = 30.7 Hz, CH), 139.7 (d, $^2J_{P,C}$ = 23.9 Hz, CH), 153.3 (s, C), 159.1 (s, NCH) ppm. ^{31}P NMR (81 MHz, [D$_8$]THF, 233 K): δ = 9 (d, $^2J_{P,P}$ = 79 Hz, 1 P, PCH_3), 79 (t, $^2J_{P,P}$ = 79 Hz, 1 P, PPh_2) ppm. $C_{31}H_{41}CoNO_2P_3$ (611.2): calcd. C 60.89, H 6.76, N 2.29, P 15.20; found C 61.03, H 7.52, N 2.28, P 14.85.

[(*E*)-2-(Diphenylphosphanyl)-*N*-isopropylbenzimino-*C,P*]ethenebis-(trimethylphosphane)cobalt(I) (8): A sample of **2** (650 mg, 1.05 mmol) in 50 mL of diethyl ether was kept stirring under 1 bar of C_2H_4 for 30 min to form an orange solution. The volatiles were removed in vacuo, and the solid residue was extracted with two 50 mL portions of pentane. Crystallization at −27 °C afforded orange crystals of **8**. Yield 365 mg (61%); m.p. 105−107 °C (dec.). IR (Nujol): $\tilde{\nu}$ = 1541 cm^{-1} (C=N). ^{1}H NMR (300 MHz, [D$_8$]THF, 296 K): δ = 0.69 (d, $^2J_{P,H}$ = 6.2 Hz, 9 H, PCH_3), 1.02 (d, ^3J = 5.9 Hz, 6 H, CH_3), 1.10 (d, $^2J_{P,H}$ = 6.1 Hz, 9 H, PCH_3), 1.67 (m, 2 H, CCH_2), 2.25 (m, 2 H, CCH_2), 3.98 (septet, $^2J_{P,H}$ = 6.2 Hz, 1 H, NCH), 6.79 (dd, ^3J = 5.7, ^4J = 1.4 Hz, 1 H, CH), 6.93 (dd, ^3J = 7.5, ^4J = 1.4 Hz, 1 H, CH), 7.03 (m, 1 H, CH), 7.26−7.30 (m, 6 H, CH), 7.74−7.83 (m, 4 H, CH) ppm. ^{13}C NMR (75.4 MHz, [D$_8$]THF, 296 K): δ = 17.5 (d, $^1J_{P,C}$ = 13.3 Hz, PCH_3), 21.1 (d, $^1J_{P,C}$ = 23.0 Hz, PCH_3), 23.9 (s, CH_3), 48.2 (d, $^2J_{P,C}$ = 20.4 Hz, CCH_2), 52.1 (d, $^2J_{P,C}$ = 13.9 Hz, CCH_2), 54.1 (s, NCH), 122.5 (d, $^2J_{P,C}$ = 15.2 Hz, CH), 126.8 (s, CH), 127.9−134.0 (s, CH), 134.9

(d, $^2J_{P,C}$ = 12.1 Hz, CH), 138.3 (m, CH), 139.2 (d, $^2J_{P,C}$ = 9.6 Hz, CH), 140.2 (d, $^1J_{P,C}$ = 22.4 Hz, CH) ppm. ^{31}P NMR (81 MHz, [D$_8$]THF, 203 K): δ = 8 (dd, $^2J_{P,P}$ = 30 and 26 Hz, 1 P, PCH_3), 16 (dd, $^2J_{P,P}$ = 30 and 36 Hz, 1 P, PCH_3), 67 (dd, $^2J_{P,P}$ = 36 and 26 Hz, 1 P, PPh_2) ppm. $C_{30}H_{43}CoNP_3$ (569.2): calcd. C 63.27, H 7.61, N 2.46, P 16.32; found C 63.40, H 7.80, N 2.41, P 15.80.

[(*E*)-2-(Diphenylphosphanyl)-*N*-cyclohexylbenzimino-*C,P*]ethenebis(trimethylphosphane)cobalt(I) (9): A sample of **3** (680 mg, 1.03 mmol) in 50 mL of pentane was kept stirring under 1 bar of C_2H_4 for 20 min to form a yellow solid. The supernatant solution was decanted and kept at −4 °C to afford yellow crystals of **9**. The solid was recrystallised from pentane. Combined yields 460 mg (73%); m.p. 93−95 °C (dec.). IR (Nujol): $\tilde{\nu}$ = 1557 cm^{-1} (C=N). ^{1}H NMR (300 MHz, [D$_8$]THF, 296 K): δ = 0.66 (d, $^2J_{P,H}$ = 6.3 Hz, 9 H, PCH_3), 1.07 (d, ^3J = 6.1 Hz, 9 H, PCH_3), 1.24−1.99 (m, 10 H, CH_2), 1.80 (m, 2 H, CCH_2), 2.19 (m, 2 H, CCH_2), 3.41 (septet, $^3J_{P,H}$ = 3.8 Hz, 1 H, NCH), 6.83 (dd, ^3J = 5.5, ^4J = 1.5 Hz, 1 H, CH), 7.00 (dt, ^3J = 7.3, ^4J = 1.5 Hz, 1 H, CH), 7.26−7.30 (m, 6 H, CH), 7.34 (dt, ^3J = 5.2, ^4J = 0.9 Hz, 1 H, CH), 7.44 (ddd, ^3J = 5.7, 5.0, ^4J = 1.1 Hz, 2 H, CH), 7.98 (ddd, ^3J = 9.5, ^4J = 1.9, 1.5 Hz, 2 H, CH) ppm. ^{13}C NMR (75.4 MHz, [D$_8$]THF, 296 K): δ = 18.0 (d, $^1J_{P,C}$ = 13.2 Hz, PCH_3), 20.6 (d, $^1J_{P,C}$ = 22.8 Hz, PCH_3), 24.9, 25.2, 27.2, 35.2, 36.0 (s, CH_2), 48.3 (d, $^2J_{P,C}$ = 18.4 Hz, CCH_2), 51.5 (d, $^2J_{P,C}$ = 11.3 Hz, CCH_2), 60.3 (s, NCH), 122.5 (d, $^3J_{P,C}$ = 16.0 Hz, CH), 125.1 (d, $^4J_{P,C}$ = 4.4 Hz, CH), 126.8 (s, CH), 128.0 (d, $^3J_{P,C}$ = 8.7 Hz, CH), 128.5 (d, $^3J_{P,C}$ = 7.6 Hz, CH), 129.1 (d, $^3J_{P,C}$ = 8.6 Hz, CH), 134.5 (d, $^2J_{P,C}$ = 10.1 Hz, CH), 134.9 (d, $^2J_{P,C}$ = 12.1 Hz, CH), 138.8 (d, $^2J_{P,C}$ = 9.8 Hz, CH), 139.2 (d, $^2J_{P,C}$ = 9.6 Hz, CH), 141.1 (d, $^1J_{P,C}$ = 22.8 Hz, C], 146.7 (d, $^1J_{P,C}$ = 44.9 Hz, C), 156.4 (dd, $^1J_{P,C}$ = 43.5, $^2J_{P,C}$ = 10.4 Hz, NC) ppm. ^{31}P NMR (81 MHz, [D$_8$]THF, 203 K): δ = 7 (dd, $^2J_{P,P}$ = 30 and 24 Hz, 1 P, PCH_3), 16 (dd, $^2J_{P,P}$ = 30 and 36 Hz, 1 P, PCH_3), 66 (dd, $^2J_{P,P}$ = 36 and 24 Hz, 1 P, PPh_2) ppm. $C_{33}H_{47}CoNP_3$ (609.2): calcd. C 65.02, H 7.77, N 2.30, P 15.24; found C 64.79, H 7.39, N 2.22, P 15.30.

[(*E*)-2-(Diphenylphosphanyl)-*N*-*tert*-butylbenzimide-*C^1,P*]ethenebis(trimethylphosphane)cobalt(I) (10): A sample of **4** (640 mg, 1.01 mmol) was kept at 100 °C in vacuo for 5 h. After cooling 30 mL of diethyl ether was condensed upon the red brown solid, and at 20 °C the solution was kept stirring under 1 bar of ethene for 1 h. The volatiles were removed in vacuo, and the solid residue was extracted with two 30 mL portions of pentane. Crystallization at −4 °C afforded orange crystals of **10**. Yield 236 mg (40%); m.p. 105−107 °C (dec.). IR (Nujol): $\tilde{\nu}$ = 1633 cm^{-1} (C=N). ^{1}H NMR (300 MHz, [D$_8$]THF, 296 K): δ = 0.82 (s, 9 H, CH_3), 0.90 (d, $^2J_{P,H}$ = 6.3 Hz, 9 H, PCH_3), 1.05 (d, ^3J = 6.2 Hz, 9 H, PCH_3), 1.61 (m, 2 H, CCH_2), 1.80 (m, 2 H, CCH_2), 5.99 (m, 1 H, CH), 6.44 (m, 1 H, CH), 6.75 (dt, ^3J = 7.5, ^4J = 2.0 Hz, 1 H, CH), 7.17−7.19 (m, 3 H, CH), 7.29 (s, 1 H, NCH), 7.34−7.36 (m, 3 H, CH), 7.71−7.77 (m, 2 H, CH), 7.92−7.98 (m, 2 H, CH) ppm. ^{13}C NMR (75.4 MHz, [D$_8$]THF, 296 K): δ = 16.8 (d, $^1J_{P,C}$ = 17.9 Hz, PCH_3), 19.1 (d, $^1J_{P,C}$ = 17.9 Hz, PCH_3), 24.9 (s, CH_3), 25.2 (s, CMe_3), 33.2 (m, CCH_2), 35.3 (m, CCH_2), 109.5 (s, CH), 125.8 (d, $^2J_{P,C}$ = 15.6 Hz, C), 126.6 (d, $^3J_{P,C}$ = 7.9 Hz, CH), 126.8 (d, $^2J_{P,C}$ = 8.4 Hz, CH), 127.2, 128.8 (s, CH), 132.1 (d, $^2J_{P,C}$ = 12.3 Hz, CH), 132.9 (d, $^2J_{P,C}$ = 12.6 Hz, CH), 169.1 (s, NCH) ppm. ^{31}P NMR (81 MHz, [D$_8$]THF, 203 K): δ = −21 (dd, $^2J_{P,P}$ = 51 and 47 Hz, 1 P, PPh_2), 9 (dd, $^2J_{P,P}$ = 47 and 32 Hz, 1 P, PCH_3), 17 (dd, $^2J_{P,P}$ = 32 and 51 Hz, 1 P, PCH_3) ppm. $C_{31}H_{45}CoNP_3$ (583.2): calcd. C 63.81, H 7.77, N 2.40, P 15.92; found C 63.46, H 7.30, N 2.36, P 16.48.

[(*E*)-2-(Diphenylphosphanyl)-*N*-isopropylbenzimino-*C,P*]iodobis(trimethylphosphane)cobalt(II) (11): A sample of **2** (850 mg, 1.37 mmol) in 50 mL of THF at −70 °C was combined with iodomethane (488 mg, 3.44 mmol). After 3 h at 20 °C an off-white solid of tetramethylphosphonium iodide (IR) was filtered off, and the filtrate was evaporated to dryness. Extraction with three 80 mL portions of diethyl ether and cooling to 4 °C afforded dark brown platelets of **11**. Yield 440 mg (48%); m.p. 130−132 °C (dec.). IR (Nujol): $\tilde{\nu}$ = 1554 cm^{-1} (C=N). Magnetic moment: μ_{eff} = 1.98 μ_B. $C_{28}H_{39}CoINP_3$ (668.1): calcd. C 50.32, H 5.88, N 2.10, P 13.90; found C 50.56, H 6.58, N 2.02, P 13.88.

[(*E*)-2-(Diphenylphosphanyl)-*N*-cyclohexylbenzimino-*C,P*]iodobis(trimethylphosphane)cobalt(II) (12): A sample of **3** (790 mg, 1.20 mmol) in 80 mL of THF at −70 °C was combined with iodomethane (375 mg, 2.64 mmol). After 3 h at 20 °C workup proceeded as in the preparation of **11** to afford dark brown platelets of **12**. Yield 505 mg (63%); m.p. 128−134 °C (dec.). IR (Nujol): $\tilde{\nu}$ = 1547 cm^{-1} (C=N). Magnetic moment: μ_{eff} = 1.98 μ_B. $C_{31}H_{43}CoINP_3$ (708.1): calcd. C 52.56, H 6.12, N 1.98, P 13.12; found C 52.60, H 5.74, N 1.98, P 12.58.

***mer-trans*-[(*E*)-2-(Diphenylphosphanyl)-*N*-*tert*-butylbenzimide-*C^1,P*]iodo(methyl)bis(trimethylphosphane)cobalt(III) (13):** A sample of **4** (920 mg, 1.45 mmol) in 50 mL of diethyl ether at −70 °C was combined with excess iodomethane (455 mg, 3.20 mmol). After 1 h at 20 °C the solution became red. An off-white solid of tetramethylphosphonium iodide was filtered off, and the solution at 4 °C afforded red crystals of **13**. Yield 518 mg (51%); m.p. 117−119 °C (dec.). IR (Nujol): $\tilde{\nu}$ = 1633 cm^{-1} (C=N). ^{1}H NMR (300 MHz, [D$_8$]THF, 296 K): δ = 0.54 (m, 3 H, $CoCH_3$), 0.80 (s, 9 H, CCH_3), 1.04 (br. s, 18 H, PCH_3), 7.51−7.56 (m, 6 H, CH), 7.74−7.79 (m, 4 H, CH), 8.20 (s, 1 H, NCH) ppm. ^{13}C NMR (75.4 MHz, [D$_8$]THF,

Table 1. Crystal data for compounds **4** and **9**

	4	**9**
Empirical formula	$C_{32}H_{50}CoNP_4$	$C_{33}H_{47}CoNP_3$
Molecular mass	631.5	609.6
Crystal size [mm]	0.48 × 0.42 × 0.30	0.52 × 0.30 × 0.26
Crystal system	monoclinic	monoclinic
Space group	$P2_1/n$	$P2_1/c$
a [Å]	13.950(2)	14.930(4)
b [Å]	18.288(6)	12.674(3)
c [Å]	14.056(3)	18.584(4)
β [°]	102.18(1)	112.04(2)
V [Å^3]	3505.2(15)	3259.5(14)
Z	4	4
$D_{calcd.}$ [g/cm^3]	1.197	1.242
μ(Mo-K_α) [mm^{-1}]	0.693	0.696
Temperature [K]	293(2)	293(2)
Data coll. range [°]	4.4 ≤ 2Θ ≤ 50	5.5 ≤ 2Θ ≤ 55
h	−16 ≤ h ≤ 0	−1 ≤ h ≤ 14
k	0 ≤ k ≤ 21	−16 ≤ k ≤ 1
l	−16 ≤ l ≤ 16	−24 ≤ l ≤ 22
No. reflect. measured	6439	8014
No. unique data	6171 [R_{int} = 0.0310]	6551 [R_{int} = 0.0205]
Parameters	394	356
GoF on F^2	0.982	1.045
$R1$ [$I \geq 2\sigma(I)$]	0.0536	0.0419
$wR2$ (all data)	0.1215	0.1094

296 K): δ = 16.9 (m, PCH_3), 28.2 (s, CH_3), 56.6 (s, CMe_3), 121.5 (d, $^2J_{P,C}$ = 11.5 Hz, C), 126.5 (s, CH), 128.4 (s, CH), 129.6 (d, $^2J_{P,C}$ = 11.4 Hz, CH), 137.1 (s, C), 138.2 (s, C), 139.5 (m, C), 160.1 (s, NCH) ppm. ^{31}P NMR (81 MHz, [D_8]THF, 203 K): δ = −34 (t, $^2J_{P,P}$ = 25 Hz, 1 P, PPh_2), 11 (d, $^2J_{P,P}$ = 25 Hz, 2 P, PCH_3) ppm. $C_{30}H_{44}CoINP_3$ (697.1): calcd. C 51.66, H 6.36, N 2.10, P 13.32; found C 51.65, H 6.52, N 1.98, P 13.26.

Crystal Structure Analyses: Crystal data are presented in Table 1. Data collection: Complex **4**: A crystal was sealed under argon in a glass capillary and mounted on a Bruker AXS P4 diffractometer. Reflections were collected (ω-scans) using graphite monochromated Mo-K_α radiation; a Lorentz polarisation and an absorption correction based on psi-scans were applied. The structure was solved by direct and conventional Fourier methods. All non-hydrogen atoms were treated anisotropically, hydrogen atoms were treated with a riding model in idealised positions. The *t*Bu group as well as the P(4)Me_3 group are disordered over four positions along the N(1)−C(8) axis and the Co(1)−P(4) axis, respectively. These positions were refined with split models. Resulting site occupation factors for the 4 *t*Bu positions are 0.24(2), 0.24(2), 0.34(3), and 0.18(2); site occupation factors for the 4 PMe_3 positions are 0.26(2), 0.13(1), 0.36(2), and 0.25(2). Complex **9**: Crystal mounting, data collection, structure solution, and refinement as for **4**.

CCDC-184403 (**4**) and CCDC-184404 (**9**) contain the supplementary crystallographic data for this paper. These data can be obtained free of charge at www.ccdc.cam.ac.uk/conts/retrieving.html [or from the Cambridge Crystallographic Data Centre, 12, Union Road, Cambridge CB2 1EZ, UK; Fax: (internat.) +44−1223/336−033; E-mail: deposit@ccdc.cam.ac.uk].

Acknowledgments

Financial support of this work by Fonds der Chemischen Industrie is gratefully acknowledged.

[1] H.-F. Klein, U. Lemke, M. Lemke, A. Brand, *Organometallics* **1998**, *17*, 4196−4201.
[2] H.-F. Klein, R. Beck, U. Flörke, H.-J. Haupt, *Eur. J. Inorg. Chem.* **2002**, in press.
[3] H. Brunner, P. Faustmann, A. Dieth, B. Nuber, *J. Organomet. Chem.* **1997**, *542*, 255−283.
[4] T. B. Rauchfuss, *J. Organomet. Chem.* **1978**, *162*, C19−C22.
[5] C. A. Ghilardi, S. Midollini, S. Moneti, A. Orlandini, G. Scappacci, *J. Chem. Soc., Dalton Trans.* **1992**, 3371−3376.
[6] P. Barbaro, C. Bianchini, F. Laschi, S. Midollini, S. Moneti, G. Scappacci, *Inorg. Chem.* **1994**, *33*, 1622−1630.
[7] J. Ko, W. C. Joo, Y. K. Kong, *Bull. Korean Chem. Soc.* **1986**, *7*, 338 −341.
[8] H.-F. Klein, S. Schneider, M. He, U. Flörke, H.-J. Haupt, *Eur. J. Inorg. Chem.* **2000**, 2295−2301.
[9] G. P. Schiemenz, A. Kaack, *Justus Liebigs Ann. Chem.* **1973**, 1480−1493.
[10] J. E. Hoots, T. B. Rauchfuss, D. A. Wrobleski, *Inorg. Synth.* **1982**, *21*, 175−179.
[11] P. Wehman, H. M. A. van Donge, A. Hagos, P. C. J. Kamer, P. W. N. M. van Leeuwen, *J. Organomet. Chem.* **1997**, *535*, 183−193.
[12] H.-F. Klein, H. H. Karsch, *Chem. Ber.* **1975**, *108*, 944−954.
[13] F. H. Carré, C. Chuit, R. J. P. Corriu, W. E. Douglas, D. M. H. Guy, C. Reyé, *Eur. J. Inorg. Chem.* **2000**, 647−653.
[14] T. Bartik, T. Himmler, H.-G. Schulte, K. Seevogel, *J. Organomet. Chem.* **1984**, *272*, 29−41.
[15] M. A. Bennett, W. R. Kneen, R. S. Nyholm, *J. Organomet. Chem.* **1971**, *25*, 293−303.

Received June 27, 2002
[I02353]

Helical 1D Coordination Polymers − Structure and Magnetic Properties of *catena*-Poly[chloro(μ-({2-[(hydroxyimino)methyl]phenoxy}acetato-*N*,*O*,*O*,O′)copper(II)]

Sergiu Shova,*[a] Ghenadie Novitchi,[b] Maria Gdaniec,[c] Andrea Caneschi,[d] Dante Gatteschi,[d] Ludmila Korobchenko,[e] Violeta K. Voronkova,[e] Yurii A. Simonov,[a] and Constantin Turta[f]

Keywords: Copper / EPR spectroscopy / Magnetic properties / N ligands / O Ligands

A new compound $[CuHLCl]_n$, where H_2L is the product of the condensation reaction between 2-formylphenoxyacetic acid and hydroxylamine, has been synthesized and its crystal structure determined. The copper(II) atom is in an O_3NCl coordination environment and the helical chains of the complex are formed by square-pyramidal copper(II) ions bridged by *anti-anti* carboxylate ligands in basal-apical positions. The chloride ion acts as monodentate ligand and is involved in intramolecular hydrogen bonding to the oxime group. The results of magnetic susceptibility and EPR measurements performed on the polycrystalline sample over a wide temperature range are presented. The magnetic susceptibility data have been fitted by use of the linear chain model and $J = -2.5$ cm^{-1} as the value of antiferromagnetic interaction. The value of the exchange exceeds the Zeeman energy difference for two adjacent magnetically nonequivalent copper centers, and signals of these centers are averaged out. The temperature dependence of the EPR spectra shows increases in the linewidth and the shifts of the signals as the temperature decreases, indicating a short-range-order effect in the chain. Shifts of the EPR signals in the Q-band were discovered for the orientations perpendicular to the chain direction as the temperature decreased below 10 K. The nature of this shift is discussed.
(© Wiley-VCH Verlag GmbH, 69451 Weinheim, Germany, 2002)

Introduction

The quasi-one-dimensional magnetic systems of transition metal ions (metallopolymers) are of particular interest for physicists and chemists because of their special properties resulting from the nature of the magnetic ions. On the other hand, one-dimensional polymeric helical motifs are also attracting increased attention in supramolecular chemistry,[1−4] which certainly originates from the observed importance of these motifs in biological systems and enantioselective catalysis.[5−7]

This paper reports the synthesis, crystal structure, and magnetic properties of an anhydrous copper(II) complex existing in crystals in the form of a helical polymeric chain of formula $[Cu(HL)Cl]_n$, where H_2L is the product of the condensation reaction between 2-formylphenoxyacetic acid and hydroxylamine. There is currently renewed interest in copper(II) complexes with carboxylic ligands[8−13] because carboxylic groups can exhibit several different coordination modes to the central atom, giving rise to compounds with ferromagnetic or antiferromagnetic properties[14,15] depending on the copper magnetic orbitals involved in bonding and the coordination mode of the carboxylic group. Studies of structure and magnetic exchange interactions in this type of compounds are aimed at understanding of the structural and chemical features determined by the magnitude and sign of the exchange interaction.

[a] Institute of Applied Physics, Academy of Sciences of Moldova, Moldavian State University
Mateevicistr. 60, Chisinau, MD 2009 Moldova
[b] Faculty of Chemistry, State University of Moldova, MD2009 Chisinau, Moldova
[c] Faculty of Chemistry, A. Mickiewicz University, 60-780 Poznan, Poland
[d] Department of Chemistry, University of Florence, 50019 Florence, Italy
[e] Zavoisky Physical-Technical Institute of the Russian Academy of Sciences, 42009 Kazan, Russia
[f] Institute of Chemistry, Academy of Sciences of Moldova, MD2028 Chisinau, Moldova

Results and Discussion

Synthesis

The template synthesis of the copper(II) coordination compound was carried out according to Scheme 1.

Copper(II) chloride and acetate were used for the reaction, but the yield was less when the acetate was used instead of the chloride. The compound [Cu(HL)Cl] was also formed when copper(II) chloride reacted directly with the oxime.

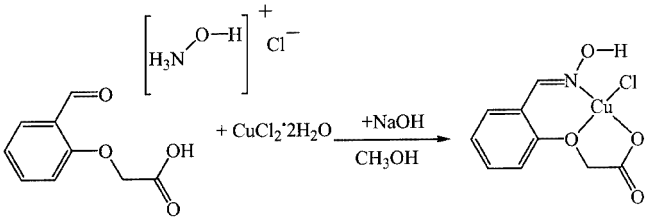

Scheme 1

IR Spectra

The IR spectrum of $[Cu(HL)Cl]_n$ does not contain absorption bands attributable to the vibration of the aldehyde group of 2-formylphenoxyacetic acid [ν(CH=O): $\tilde{\nu}$ = 1754, 1712 cm^{-1}], but it does show the vibration bands of the coordinated imino group [ν(C=N): $\tilde{\nu}$ = 1604 cm^{-1}], indicating that the template reaction is accompanied by condensation between 2-formylphenoxyacetic acid and hydroxylamine.[16] In addition, the IR spectrum of the complex shows the characteristic absorption bands of the carboxyl group of the formylphenoxyacetic fragment [$\nu_{as}(COO^-)$: $\tilde{\nu}$ = 1570 cm^{-1}; $\nu_s(COO^-)$: $\tilde{\nu}$ = 1414cm^{-1}], which were assigned according to ref.[17] The 156 cm^{-1} difference in the wavenumbers of the absorption bands $\nu_{as}(COO^-)$ and $\nu_s(COO^-)$ suggests the bidentate bridge mode of coordination. The shift of the $\nu_s(C-O-C)$ absorption band (1164 cm^{-1}) of the ether group by 52 cm^{-1} in the lower wavenumber range and of the $\nu_{as}(C-O-C)$ band (1244 cm^{-1}) by 4 cm^{-1} in the higher wavenumber range (relative to their counterparts in 2-formylphenoxyacetic acid) confirm the participation of the ether oxygen atom in coordination. The presence of the absorption band of the stretching frequency ν(OH) at $\tilde{\nu}$ = 3100−3300 cm^{-1} testifies to the presence of the protonated aldoxime group.

Structure

The crystal of the complex $[Cu(HL)Cl]_n$ consists of infinite helical chains directed along the *b* axis. Two antiparallel enantiomorphic helices in the crystal are shown in Figure 1, together with the atom-labeling scheme. The monomeric units of the $[Cu(HL)Cl]_n$ chain are sequentially bridged by *anti-anti* carboxylate groups. The monodeprotonated HL^- anion acts as a tridentate ligand towards one copper(II) ion and as a monodentate ligand towards another copper(II) center. The copper(II) ions each exist in distorted square-pyramidal coordination with the O_3NCl atom-donor set. The basal coordination sites are occupied by three donor atoms of the ligand [Cu−O(1) 2.089(3), Cu−O(2) 1.908(3) and Cu−N(1) 1.966(3) Å] and the chlorine atom [Cu−Cl 2.245(1) Å], whereas the carboxylate O(3) atom of the ligand from the adjacent monomeric unit along the chain resides in the apical position [Cu−O(3)′ 2.189(3) Å]. Thus, each *anti-anti* carboxylate group is located in the basal-apical positions of the coordination polyhedra and bridges two copper(II) ions. The Cu atom is displaced by 0.208 Å from the OONCl plane toward the axially coordinated O(3)′ atom. The distance between the nearest Cu atoms along the chain, 5.845 Å, is longer than those observed in similar helical chains but with the *syn-anti* carboxylate coordination mode.[12] The H-atom of the oxime group is involved in intramolecular hydrogen bonding [O(4)···Cl 3.058 Å, H···Cl 2.34 Å, OHCl 150°], closing a five-membered ring. No intermolecular hydrogen bonds are formed in this crystal; however, there is some overlap of the aromatic rings belonging to adjacent helical chains, with the distances between the ring atoms being in the 3.22−3.62 Å range, suggesting that π-π interactions may be of some importance in stabilizing this crystal structure (Figure 1). In the lattice, right- and left-handed helices alternate, resulting in an optically inactive racemic crystal, spontaneous resolution of two isomers being rare.[11,12]

Magnetic Susceptibility

The temperature dependence of the magnetic susceptibility and χT is presented in Figure 2. The value of χT (see a in Figure 2) decreases as the temperature decreases, indicating antiferromagnetic behavior. The Hamiltonian appropriate for a Heisenberg linear chain of S = 1/2 spins is given by Equation (1).

$$H = J\Sigma S_i \cdot S_{i+1} \quad (1)$$

The experimental data for the variation of susceptibility with temperature can be satisfactorily fitted into the analytic expression introduced to represent the Bonner−Fisher model[18] for a uniformly spaced Heisenberg chain of spins with S = 1/2 [Equation (2)].[19]

$$\chi = \left(Ng^2\beta^2/kT\right)\left\{\frac{0.25 + 0.074975x + 0.075235x^2}{1.0 + 0.9931x + 0.172135x^2 + 0.757825x^3}\right\} \quad x = |J/kT| \text{ with.} \quad (2)$$

The solid line in Figure 2 (part b) is the curve calculated according to Equation (2) with J = 2.5 cm^{-1}, g = 2.15. It shows good agreement between experimental data and calculated $\chi(T)$. Although the decrease in $\chi(T)$ in the temperature range studied is not observed experimentally, the measured values of $\chi(T)$ in the low-temperature range (inset in part b of Figure 2) would allow the presence of the maximum in this range. We considered the one-dimensional model, neglecting the interaction between the chains, as the distances between the paramagnetic copper centers in adjacent chains (R = 9.50 Å) exceed the intrachain copper distance (R = 5.85 Å) and there are no channels for indirect exchange between neighboring chains. Hence the antiferromagnetic interaction is produced only inside the chains.

It should be noted that the given data are in good agreement with a model chain of equally spaced copper(II) ions. In fact, the bridging fragments between the copper complexes in the chains coincide completely, although the chain is built up of magnetically nonequivalent copper centers: square-pyramidal copper(II) polyhedra $CuClNO_3$ are rotated with respect to each other along the direction of the chain. This chain structure results in a small value for the

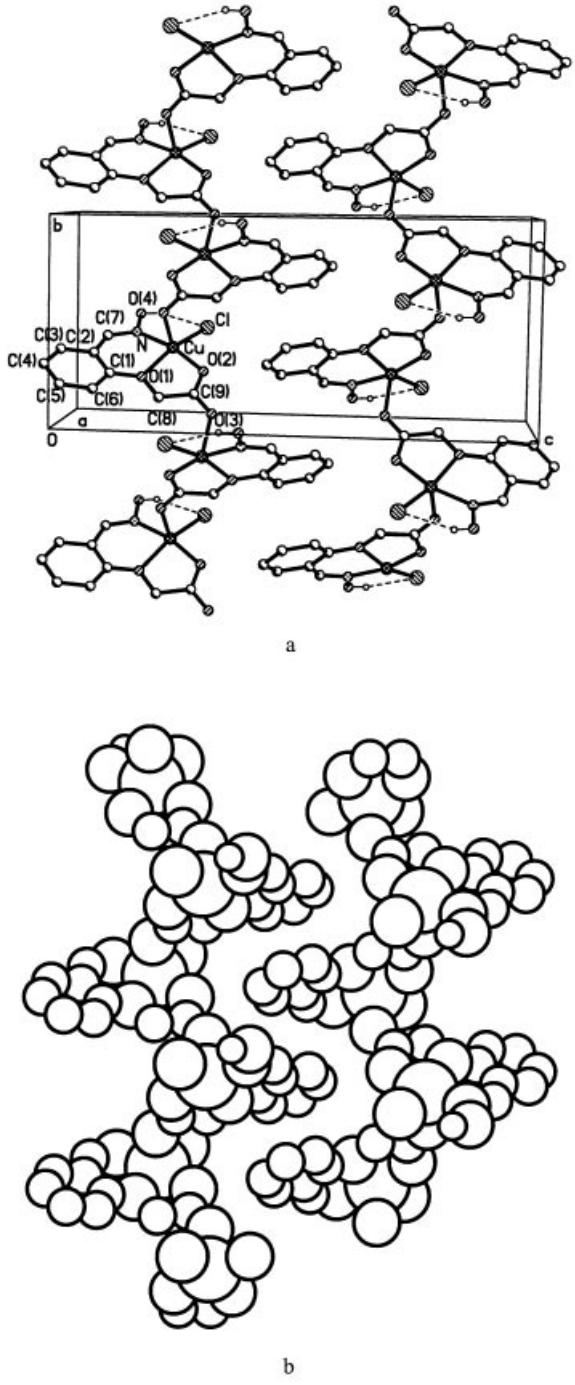

Figure 1. Crystal structure of $[Cu(HL)Cl]_n$: ball-and-stick model showing atom labelling (a); space-filling diagram of two adjacent enantiomorphic helices (b)

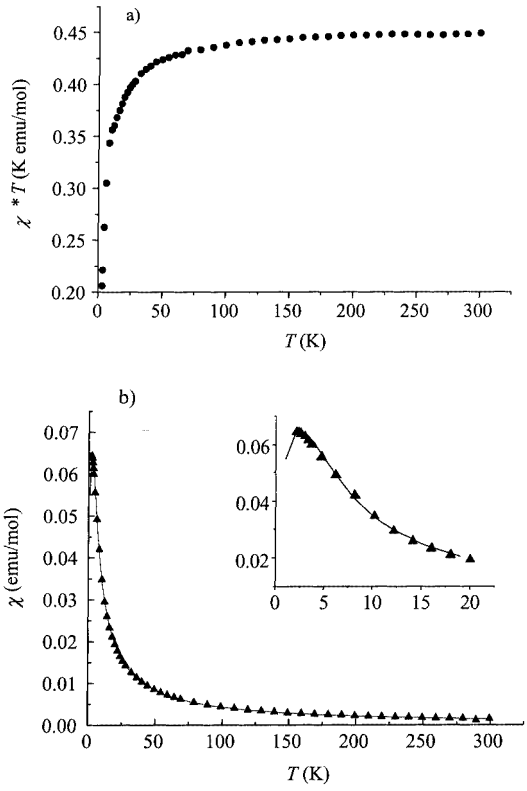

Figure 2. Temperature dependence of the experimental values of χT (a) and measured (black triangles) and calculated (solid line) of the values $\chi(T)$ (b); the inset presents the low-temperature range of $\chi(T)$ on a larger scale

antiferromagnetic interaction between the copper centers in the chains.

The value of the isotropic exchange interaction is determined by the overlap integral between ground-state orbitals, which for an indirect exchange is produced through intermediate orbitals of bridging ligands (the ground state of a square-pyramidal copper complex is the $d_{x^2-y^2}$ orbital). A weak antiferromagnetic coupling is justified by the small overlap of the magnetic orbitals according to the Goodenough−Kanamori rule.[20−22]

EPR Investigation

EPR spectra of the polycrystalline sample are shown in Figures 3 and 4. The spectrum is typical for the state $S = 1/2$ with the rhombic symmetry of the $\{g\}$ tensor. The temperature dependence of the spectra at the Q-band indicates the change of the values of the {g} tensor: $g_1 = 2.239 \pm 0.002$, $g_2 = 2.159 \pm 0.002$, $g_3 = 2.060 \pm 0.002$ at $T = 293$ K; $g_1 = 2.236 \pm 0.002$, $g_2 = 2.129 \pm 0.002$, $g_3 = 2.044 \pm 0.002$ at $T = 4.2$K.

The X-band anisotropy of the spectra is not resolved completely, but computer analysis of the spectra has allowed the temperature dependence of the g factor anisotropy and linewidths to be estimated. The temperature dependence of the linewidth for the high-field signal (Figure 5) shows that the appreciable changes are already detectable at $T = 10$ K and that the effect increases as the temperature decreases.

As we have already noted, the principal axes of g tensors of the neighboring copper ions are rotated with respect to each other. As the exchange interaction exceeds the difference of Zeeman energies for two magnetically inequivalent molecules, collapse of the lines occurs and for this spectrum the temperature dependence of the g tensor is detectable due to the merging effect. In principle, the temperature de-

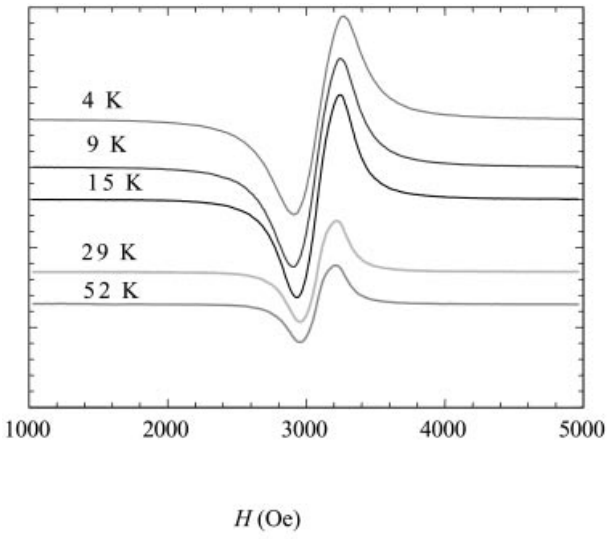

Figure 3. Temperature dependence of the EPR spectra of the polycrystalline sample of $[Cu(HL)Cl]_n$ at the *X*-band

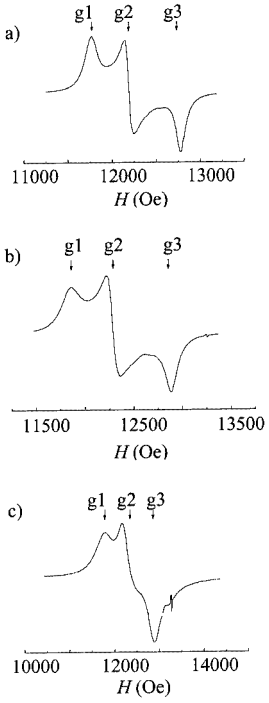

Figure 4. The EPR spectra at the *Q*-band at 298 K (a), 77 K (b), 4.2 K (c)

pendence of the positions of the signals may be due to small structural changes and to short-range order effects in the chain. Consider the correlation between observed g_1, g_2, g_3 components and molecular $\{g\}$ tensors. On the assumption of the axial symmetry of the molecular *g* tensor ($g_\parallel$, $g_\perp$) the resulting components of the *g* tensor are given by Equation (3).[23]

$$g_3 = g_\perp$$
$$g_1 = (g_\parallel^2 \cos^2\gamma + g_\perp^2 \sin^2\gamma)^{1/2} \quad (3)$$
$$g_2 = (g_\parallel^2 \sin^2\gamma + g_\perp^2 \cos^2\gamma)^{1/2}$$

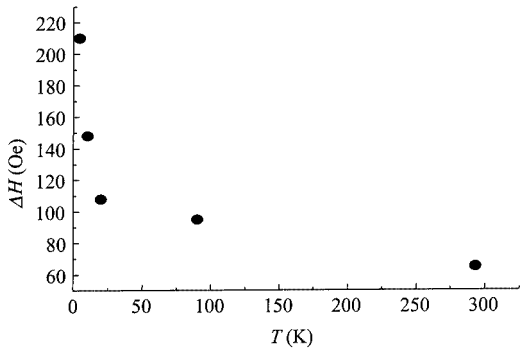

Figure 5. The temperature dependence of the linewidth of the high-field signal at the *X*-band

The 2γ term is the angle between the g_z directions of two neighboring complexes. It might be expected that this angle should be equal to the angle between the directions of the apical Cu−O bonds of two consecutive copper positions. According to Equation (3), for $\gamma \approx 36°$ and typical values of $g_\parallel$ and $g_\perp$ for the square-pyramidal copper complexes it would be expected that the change in the g_2 value due to possible small structural changes with temperature should not exceed the change of the g_1 value. However, the g_1 value is practically independent of the temperature and the supposition about the temperature dependence of the *g* value due to the availability of the short-range order effect is preferable. Analysis of the expressions of Equation (3) indicates that the g_1 component corresponds to the orientation of the magnetic field along the chain and the $g_{2,3}$ components are perpendicular to the chain direction.

The temperature dependence of the EPR spectra unequivocally shows that the linewidth for all orientations increases as the temperature decreases, and that the *g* factors shift for orientations perpendicular to the direction of the chain. No shift of the signal relative to the direction of the magnetic field along the direction of the chain is observed. The effects of the increase in the linewidth and the shifts of the signals for quasi-one-dimensional systems as the temperature approaches the value of the exchange interaction inside a chain have previously been explained in terms of the availability of the short-range order and the presence of the preferable direction for antiferromagnetic or ferromagnetic ordering due to the anisotropy of the interaction.[24−26] Changes of different signs were observed for the g factor, depending on the direction of a magnetic field: parallel or perpendicular to the direction of the chain. These experimental data are satisfactorily described by the assumption that the anisotropy of the interaction has a dipole-dipole character.

The $[Cu(HL)Cl]_n$ crystal provides an example of a new type of behavior of magnetic properties close to the temperature $T \approx J$. The change in behavior is probably connected with the change of the nature of the anisotropy of the interaction. For $[Cu(HL)Cl]_n$, the distance between the copper centers in a chain (R = 5.85 Å), allows us to assume that the main role is played by the anisotropy of the exchange interaction, including the antisymmetric interaction. For

the orientations of the magnetic field in the plane perpendicular to the direction of the chain, as the temperature decreases in the range $T \approx J$, the EPR signals shift to higher fields.

In principle, interaction between copper ions of adjacent chains in the plane perpendicular to the direction of the chains could give a similar effect. Because of the absence of the channels for such indirect exchange between copper ions of neighboring chains, however, this supposition is improbable. Measurements on single crystals would be necessary for more detailed investigation, because the spectrum of the polycrystalline sample contains only the signals corresponding to appropriate orientations of the magnetic field along the principal axes of the *g* tensor.

Experimental Section

Synthesis of [Cu(HL)Cl]$_n$: 2-Formylphenoxyacetic acid (0.9 g, 0.005 mol) was added to $CuCl_2 \cdot 2H_2O$ (0.85 g, 0.005 mol) in methanol (20 mL). A mixture of hydroxylamine−hydrochloride (0.35 g, 0.005mol) and NaOH (0.4 g, 0.01 mol) in methanol (25 mL) was then added, with stirring, to the resulting solution. The obtained solution was heated in a water bath at 50 °C for 30 min. The dark blue crystals, precipitating after cooling, were filtered, washed with cold methanol, and dried in air. Yield: 1.025 g, 70%. $C_9H_8ClCuNO_4$ (293): calcd. C 36.86, H 2.73, Cl 12.12, Cu 21.67, N 4.78; found C 36.93, H 2.76, Cl 12.09, Cu 21.78, N 4.80.

IR Spectra: These were recorded as oil suspensions with a Specorde M-80 spectrometer in the 4000−400 cm^{-1} range.

X-ray Crystal Structure Analysis: The crystal used for measurements was a prism of approximate dimensions 0.4 × 0.4 × 0.2 mm. The crystal was a non-mesohedral twin with the twin matrix [1 0 0 0 −1 0 −0.5 0 −1]. The data were collected with a Kuma Diffraction KM4 diffractometer by use of graphite-monochromatized Cu-K_α radiation. Lattice parameters were obtained from the least-squares refinement of 27 reflections with 16° ≤ 2θ ≤ 70°. The intensities were measured by the ω/2θ scan technique up to $2\theta_{max}$ = 129.6°. The intensities of three reflections were checked every 100 measurements to monitor instrument and crystal stability. Their intensity variation was within 3%. The structure was solved by direct methods with SHELXS-86[27] and refined by full-matrix, least squares on F^2 with SHELXL-93.[28] Instruction HKLF5 from SHELXL-93 was used for the refinement, because half of all the reflections belonged to both twin domains while the second half belonged to one domain. The non-hydrogen atoms were refined by the least-squares method in the anisotropic approximation. The positions of H atoms bonded to C atoms were calculated by assuming C−H distances of 0.96 Å. Positional parameters of the oxime H atom were obtained from difference Fourier syntheses and verified by the hydrogen bond geometric parameters. Isotropic displacement parameters of H atoms were fixed at 1.2 × U_{eq} for the relevant C and O atoms. The main crystallographic parameters and structure refinement details are summarized in Table 1, bond lengths and angles in Table 2. CCDC-182198 contains the supplementary crystallographic data for this paper. These data can be obtained free of charge at www.ccdc.cam.ac.uk/conts/retrieving.html or from the Cambridge Crystallographic Data Centre, 12 Union Road, Cambridge CB2 1EZ, UK [Fax: (internat.) + 44-1223/336-033; E-mail: deposit@ccdc.cam.ac.uk].

EPR and Magnetic Measurements: The measurements were carried out on the polycrystalline sample of [Cu(HL)Cl]$_n$. The static magnetic susceptibility was measured over the 2−300 K temperature range. The data were corrected for a diamagnetic contribution by use of Pascal constants.[29] The magnetization vs. *B* was recorded

Table 1. Crystal data for [Cu(HL)Cl]$_n$

Empirical formula	$C_9H_8ClCuNO_4$
M	293.15
Temperature [K]	293(2)
Wavelength [Å]	1.54178
Space group	$P2_1/c$
a [Å]	6.5090(10)
b [Å]	8.311(2)
c [Å]	18.923(4)
β [°]	94.98(3)
V [Å^3]	1019.8(4)
Z	4
$\rho_{calcd.}$ [Mg/m^3]	1.909
μ_{Mo} [mm^{-1}]	5.457
F(000)	588
Crystal size [mm]	0.4 × 0.4 × 0.2
θ range [°]	4.69−64.82
Index ranges	$-7 \le h \le 7$, $-9 \le k \le 9$, $-22 \le l \le 22$
Number of reflections:	
measured	2772
unique	1811 [$R_{(int)}$ = 0.048]
Number of refined parameters	147
GOOF for F^2	1.130
R factor [$I > 2\sigma(I)$]	R_1 = 0.0648, wR_2 = 0.1608
R factor (all data)	R_1 = 0.0670, wR_2 = 0.1621
$\Delta\rho_{max}$, $\Delta\rho_{min}$ [e Å^3]	1.413, −1.213

Table 2. Selected bond lengths [Å] and angles [°]; symmetry transformations: (′): $-x, y + 1/2, -z + 1/2$; (′′): $-x, y - 1/2, -z + 1/2$

Cu−O(2)	1.908(3)	N−C(7)	1.293(6)
Cu−N	1.966(3)	C(1)−C(6)	1.372(6)
Cu−O(1)	2.089(3)	C(1)−C(2)	1.417(6)
Cu−O(3)′	2.189(3)	C(2)−C(3)	1.406(6)
Cu−Cl	2.245(1)	C(2)−C(7)	1.424(6)
O(1)−C(1)	1.374(5)	C(3)−C(4)	1.381(7)
O(1)−C(8)	1.452(5)	C(4)−C(5)	1.364(7)
O(2)−C(9)	1.274(5)	C(5)−C(6)	1.391(6)
O(3)−C(9)	1.223(5)	C(8)−C(9)	1.505(5)
O(4)−N	1.391(5)		
O(2)−Cu−N	167.0(1)	O(4)−N−Cu	120.9(3)
O(2)−Cu−O(1)	81.9(1)	C(6)−C(1)−O(1)	123.0(4)
N−Cu−O(1)	87.5(1)	C(6)−C(1)−C(2)	120.2(4)
O(2)−Cu−O(3)′	96.9(1)	O(1)−C(1)−C(2)	116.8(4)
N−Cu−O(3)	89.6(1)	C(3)−C(2)−C(1)	117.2(4)
O(1)−Cu−O(3)′	85.0(1)	C(3)−C(2)−C(7)	115.8(4)
O(2)−Cu−Cl	93.6(1)	C(1)−C(2)−C(7)	127.0(4)
N−Cu−Cl	94.9(1)	C(4)−C(3)−C(2)	121.8(4)
O(1)−Cu−Cl	165.42(9)	C(5)−C(4)−C(3)	119.7(4)
O(3)′−Cu−Cl	109.36(9)	C(4)−C(5)−C(6)	120.3(4)
C(1)−O(1)−C(8)	117.1(3)	C(1)−C(6)−C(5)	120.8(4)
C(1)−O(1)−Cu	128.8(2)	N−C(7)−C(2)	127.2(4)
C(8)−O(1)−Cu	110.6(2)	O(1)−C(8)−C(9)	109.3(3)
C(9)−O(2)−Cu	118.3(2)	O(3)−C(9)−O(2)	123.9(3)
C(9)−O(3)−Cu′′	131.5(3)	O(3)−C(9)−C(8)	117.5(4)
C(7)−N−O(4)	111.1(3)	O(2)−C(9)−C(8)	118.6(3)
C(7)−N−Cu	127.8(3)		

at 2.5 and 4.5 K. EPR spectra were recorded at the *X*-band in the temperature range from room temperature to 4 K and at the *Q*-band at T = 298, 77, 4.2 K.

Acknowledgments

We acknowledge INTAS financial support, Projects 2000-00565, and the Russian Foundation for Basic Research, Project 01-03-32270.

[1] C. Piguet, G. Bernardinelli, G. Hopfgarther, *Chem. Rev.* **1997**, *97*, 2005−2062.
[2] J.-M. Lehn, *Supramolecular Chemistry: Concept and Perspectives*, VCH, Weinheim, **1995**.
[3] J. W. Steed, J. L. Atwood, *Supramolecular Chemistry*, John Wiley and Sons, Ltd. Chichester, New York, **2000**.
[4] L. Plasseraud, H. Maid, F. Hampel, R. W. Saalfrank, *Chem. Eur. J.* **2001**, *7*, 4007−4011.
[5] E. J. Corey, C. L. Cymin, M. C. Noe, *Tetrahedron Lett.* **1994**, *35*, 69−72.
[6] K. Maruoka, N. Murase, H. Yamamoto, *J. Org. Chem.* **1993**, *58*, 2938−2939.
[7] L. Stryer, *Biochemistry*, W. H. Freeman and Co., New York, **1988**.
[8] E. Colacio, J. M. Dominguez-Vera, J. P. Costes, R. Kivekas, J. P. Laurent, J. Ruiz, M. Sundberg, *Inorg. Chem.* **1992**, *31*, 774−778 and references therein.
[9] L. S Long, S. P. Yang, Y. X. Tong, Z. W. Mao, X. M. Chen, L. N. Ji, *J. Chem. Soc., Dalton Trans.* **1999**, 1999−2004.
[10] R. W. Saalfrank, H. Maid, F. Hampel, K. Peters, *Eur. J. Inorg. Chem.* **1999**, 1859−1867 and references therein.
[11] K. K. Nanda, A. W. Addison, E. Sinn, L. K. Thompson, *Inorg. Chem.* **1996**, *35*, 5966−5967.
[12] E. Colacio, M. Ghazi, R. Kivekas, J. M. Moreno, *Inorg. Chem.* **2000**, *39*, 2882−2890.
[13] R. L. Carlin, K. Kopinga, O. Kahn, M. Verdaguer, *Inorg. Chem.* **1986**, *25*, 1786−1789.
[14] B. S. Tsukerblat, M. I. Belinskii, *Magnetochemistry and spectroscopy of exchange clusters*, Iz. "Stiinta" (in Russ.), Kishinev, **1983**.
[15] V. T. Kalinicov, Yu. V. Rakitin, *Introduction to magnetochemistry − The static magnetic susceptibility method in chemistry*, Iz. "Nauka" (Russ.), Moscow, **1980**.
[16] S. Shova, G. Novitski, M. Gdaniec, Yu. A. Simonov, K. Turte, *Russ. J. Inorg. Chem.* **2000**, *45*, 1193−1200.
[17] K. Nakamoto, *Infrared and Raman Spectra of Inorganic Compounds*, New York, Wiley, **1988**.
[18] J. C. Bonner, M. E. Fisher, *Phys. Rev.* **1964**, *A135*, 640−658.
[19] W. E. Hatfield, *J. Appl. Phys.* **1981**, *52*, 1985−1990.
[20] J. B. Goodenough, *Phys. Rev.* **1955**, *100*, 564−573.
[21] J. B. Goodenough, *J. Phys. Chem. Solids* **1958**, *6*, 287−297.
[22] J. Kanamori, *J. Phys. Chem. Solids* **1959**, *10*, 87−98.
[23] B. J. Hathaway, D. E. Billing, *Coordin, Chem. Rev.* **1970**, *5*, 143−207.
[24] A. Bencini, D. Gatteschi, *Electron Paramagnetic Resonance of Exchange Coupled Systems*, Springer Verlag, Berlin, **1990**.
[25] K. Nagata, Yu. Tazuke, *J. Phys. Soc. Jpn.* **1972**, *32*, 337−345.
[26] K. Nagata, Yu. Tazuke, K. Tsushima, *J. Phys. Soc. Jpn.* **1972**, *32*, 1486−1492.
[27] SHELX86: G. M. Sheldrick, *Acta Crystallogr., Sect. A* **1990**, *46*, 467−473.
[28] G. M. Sheldrick, *SHELXL-93, Program for the refinement of crystal structure*, University of Göttingen, Germany, **1993**.
[29] E. König, G. König, *Magnetic Properties of Coordination and Organometallic Transition Metal Compounds* (Eds: K. H. Hellwege, A. M. Hellwege), Springer-Verlag, Berlin, **1976.**

Received March 22, 2002
[I02152]

Synthesis of New Pd^{II} Complexes Containing Thioether−Pyrazole Hemilabile Ligands − Structural Analysis by ^1H and ^{13}C NMR Spectroscopy and Crystal Structures of $[PdCl_2(bddo)]$ and $[Pd(bddo)](BF_4)_2$ [bddo = 1,8-Bis(3,5-dimethyl-1-pyrazolyl)-3,6-dithiaoctane]

Jordi García-Antón,[a] Josefina Pons,*[a] Xavier Solans,[b] Mercè Font-Bardia,[b] and Josep Ros*[a]

Keywords: Hemilabile ligands / N ligands / Palladium / S ligands

Treatment of the ligands 1,6-bis(3,5-dimethyl-1-pyrazolyl)-2,5-dithiahexane (bddh), 1,7-bis(3,5-dimethyl-1-pyrazolyl)-2,6-dithiaheptane (bddhp), 1,8-bis(3,5-dimethyl-1-pyrazolyl)-3,6-dithiaoctane (bddo) and 1,9-bis(3,5-dimethyl-1-pyrazolyl)-3,7-dithianonane (bddn) with $[PdCl_2(CH_3CN)_2]$ produces $[PdCl_2(L)]$ or $[Pd_2Cl_4(L)]$ complexes, depending on the stoichiometry. Treatment of the complexes $[PdCl_2(bddo)]$ and $[PdCl_2(bddn)]$ with $AgBF_4$ gives $[Pd(bddo)](BF_4)_2$ and $[Pd(bddn)](BF_4)_2$. These Pd^{II} complexes have been characterised by elemental analyses, conductivity measurements, IR and ^1H and ^{13}C NMR spectroscopy where possible. The X-ray structures of the complexes $[PdCl_2(bddo)]$ and $[Pd(bddo)](BF_4)_2$ have been determined. In $[PdCl_2(bddo)]$ the thioether–pyrazole ligand is coordinated through the azine nitrogen atoms to the metal atom, which completes its coordination with two chloride ions in a *trans* disposition. In $[Pd(bddo)](BF_4)_2$ the metal atom is tetracoordinated by the two thioether sulfur atoms and the two azine nitrogen atoms of the pyrazole rings. Complexes $[PdCl_2(bddo)]$ and $[PdCl_2(bddn)]$ were obtained again when the complexes $[Pd(bddo)](BF_4)_2$ and $[Pd(bddn)](BF_4)_2$ were heated under reflux in a solution of Et_4NCl in CH_2Cl_2/MeOH (1:1).
(© Wiley-VCH Verlag GmbH, 69451 Weinheim, Germany, 2002)

Introduction

The chemistry of hemilabile ligands has been widely studied in recent years.[1] The term ''hemilabile ligand'', introduced in 1979 by Jeffrey and Rauchfuss,[2] refers to polydentate chelates containing at least two types of bonding groups displaying different properties in substitution reactions (one labile and one inert). Thus, one group bonds strongly to a metal centre and the other group is weakly bonded and easily displaced by coordinating ligands. This makes them very attractive for catalytic purposes.

In recent years, we have studied and reported on the properties of hemilabile ligands based on the pyrazolyl group and on some other groups, containing N,[3] P[4] or O[5] atoms. This article is the initial part of a study of ligands containing pyrazolyl and thioether groups.

The literature describes the use of low molecular mass coordination compounds (with cations such as Ni^{II}, Cu^{I}, Cu^{II}, Co^{II}, Zn^{II}, Cd^{II} and Ag^{I}) with ligands of this kind for the modelling of metalloprotein-active centres in the bioinorganic field.[6−9] Our goal is to extend these studies to include the potential hemilabile capability of ligands that coordinate Pd^{II}.

Here we report the synthesis of the ligand 1,7-bis(3,5-dimethyl-1-pyrazolyl)-2,6-dithiaheptane (bddhp). We have also studied the reactivity towards Pd^{II} of the previously described ligands 1,6-bis(3,5-dimethyl-1-pyrazolyl)-2,5-dithiahexane (bddh),[6] 1,8-bis(3,5-dimethyl-1-pyrazolyl)-3,6-dithiaoctane (bddo)[7] and 1,9-bis(3,5-dimethyl-1-pyrazolyl)-3,7-dithianonane (bddn)[8] (Scheme 1). We have isolated the following complexes: $[PdCl_2L]$ with L = bddh (**1**), L = bddhp (**2**), L = bddo (**3**) and L = bddn (**4**), and $[Pd_2Cl_4L]$ with L = bddhp (**5**), L = bddo (**6**) and L = bddn (**7**). Treatment of **3** and **4** with $AgBF_4$ affords $[Pd(bddo)](BF_4)_2$ (**8**) and $[Pd(bddn)](BF_4)_2$ (**9**). NMR studies and the X-ray crystal structures of **3** and **8** are also presented.

Results and Discussion

The pyrazole ligands bddh, bddo and bddn were synthesised as described in the literature.[6−8] The bddh ligand was further purified by chromatography (silica gel 60) with methanol/dichloromethane (1:9) as eluent; bddo and bddn were purified by extraction ($CHCl_3$/H_2O/NaOH).

[a] Departament de Química, Facultat de Ciències, Universitat Autònoma de Barcelona,
08193 Bellaterra-Cerdanyola, Barcelona, Spain
Fax: (internat.) + 34-93/581-3101
E-mail: Josefina.Pons@uab.es
[b] Cristal·lografia, Mineralogia i Dipòsits Minerals, Universitat de Barcelona,
Martí i Franquès s/n, 08028 Barcelona, Spain

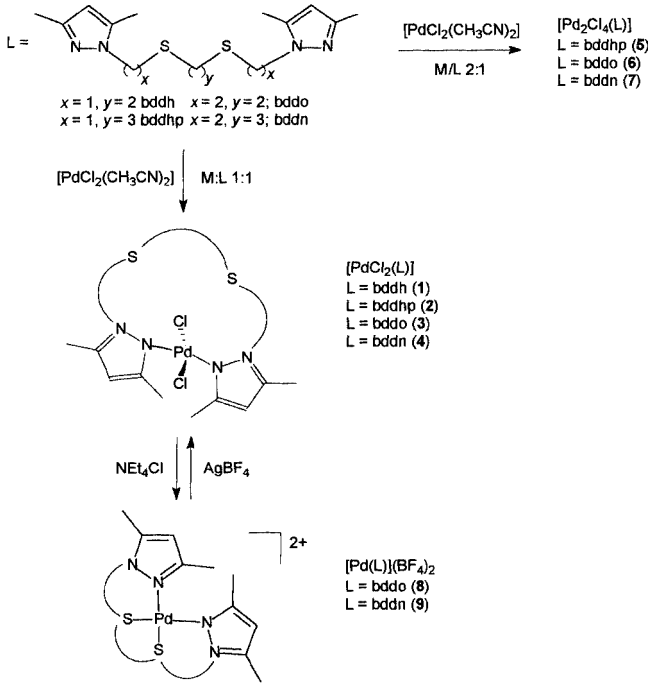

Scheme 1

Ligand bddhp, not previously reported in the literature, was prepared by a synthetic route similar to that used for the ligand bddh.[6a] Treatment of 2-(hydroxymethyl)-3,5-dimethylpyrazole with thionyl chloride gave 2-(chloromethyl)-3,5-pyrazolium chloride. This compound, on treatment with 1,3-propanedithiol in the presence of sodium hydroxide, yielded the desired product. The ligand bddhp was characterised by elemental analysis, mass spectrometry and IR, ^{1}H and ^{13}C NMR spectroscopy.

Complexes $[PdCl_2L]$ [L = bddh (**1**), bddhp (**2**), bddo (**3**) and bddn (**4**)] were obtained by treatment of the corresponding ligand either with $[PdCl_2(CH_3CN)_2]$ or with [PdCl$_2$(COD)] in a 1:1 M/L ratio. Complexes $[Pd_2Cl_4L]$ [L = bddhp (**5**), bddo (**6**) and bddn (**7**)] were obtained by use of a 2:1 M/L ratio.

Treatment of **3** and **4** with $AgBF_4$ gave compounds of formula $[PdL](BF_4)_2$ [L = bddo (**8**) and bddn (**9**)]. In contrast, use of the same reaction conditions with complexes **1** and **2** gave decomposition products. When complexes **8** and **9** were heated under reflux in a solution of Et_4NCl in CH_2Cl_2/MeOH (1:1) for 24 h, complexes **3** and **4** were obtained again.

The elemental analyses of products **5**, **6** and **7** are consistent with the formulas $[Pd_2Cl_4L]$. The low solubilities of the complexes were sufficient for their conductivity and ^{1}H NMR spectra to be measured, but their ^{13}C NMR spectra could not be recorded.

Conductivity values in acetonitrile for complexes **1**−**4**, and in DMSO for complexes **5**−**7**, are in agreement with non-electrolyte natures (Table 4). Conductivity values in methanol for complexes **8** and **9** are in agreement with 2:1 electrolytes. The reported values for 10^{-3} M solutions of non-electrolyte complexes are lower than 120 $\Omega^{-1}cm^2mol^{-1}$ or 50 $\Omega^{-1}cm^2mol^{-1}$ in acetonitrile or DMSO, respectively, while the range of conductivity values for 10^{-3} M solutions of 2:1 electrolyte compounds in methanol is between 160 and 220 $\Omega^{-1}cm^2mol^{-1}$.[10]

The IR spectra of all complexes are similar to those of the ligands, the most characteristic bands being those attributable to the pyrazolyl group: ν(C=C) and ν(C=N) between 1564−1554 cm^{-1} and $\delta(C-H)_{oop}$ between 820 and 778 cm^{-1}. The ν(B−F) band at 1061 cm^{-1} is characteristic for **8** and **9**.[11]

The IR spectra of the complexes in the 500−100 cm^{-1} region were also studied. Complexes $[PdCl_2L]$ (**1**−**4**) show two well-defined bands corresponding to ν(Pd−Cl) at 340−326 cm^{-1} and ν(Pd−N) at 473−448 cm^{-1}. For the $[Pd_2Cl_4L]$ complexes **5**−**7**, three bands can be observed. One of these can be assigned to ν(Pd−N) at 459−452 cm^{-1}. The number and energy of the other two bands are consistent with the presence of terminal (366−360 cm^{-1}) and bridging (335−299 cm^{-1}) Pd−Cl bonds. For complexes **8** and **9** the ν(Pd−N) and ν(Pd−S) bands can be attributed to the signals appearing between 461−456 and 238−247 cm^{-1}, respectively.[12]

NMR Experiments

The ^{1}H and ^{13}C NMR spectra of complexes **1**−**4**, **8** and **9** show the signals of coordinated ligands. NMR spectroscopic data are shown in the Exp. Sect. NMR spectra of compounds **3**, **4**, **8** and **9** were studied in more detail.

Study of the S−CH$_2$−CH$_2$−N fragment (in **3** and **4**) as an AA′XX′ system gave a set of coupling constants for each compound. These constants were consistent with the simulated spectra for compounds **3** and **4**, obtained with the aid of the *g* NMR program.[13] All these results are reported in Table 1. Figure 1 shows the experimentally determined and simulated spectra for **3**.

Table 1. ^{1}H NMR results: chemical shifts (ppm) and ^{1}H,^{1}H coupling constants (Hz) for **3** and **4** in $CDCl_3$

Compound	**3**	**4**
δ(CH$_2$) (6)	4.93	4.89
δ(CH$_2$) (7)	3.08	3.14
^2J(6a,6b)	−12.28	−12.87
^2J(7a,7b)	−12.28	−14.32
^3J(6a,7a) = ^3J(6b,7b), ^3J(6a,7b) = ^3J(6b,7a)	4.81, 13.01	4.87, 12.39

The Karplus equation cannot be used directly to calculate the dihedral angle between adjacent hydrogen atoms if the ethylenic fragments are α-substituted by heteroatoms (O, S, NR). In such cases, coupling constants are dependent on the electronegativity of the α-heteroatom substituent as well as on the dihedral angle.[14] Here, we have used a program based on the Karplus equation but which takes account of the electronegativity of the fragments connected

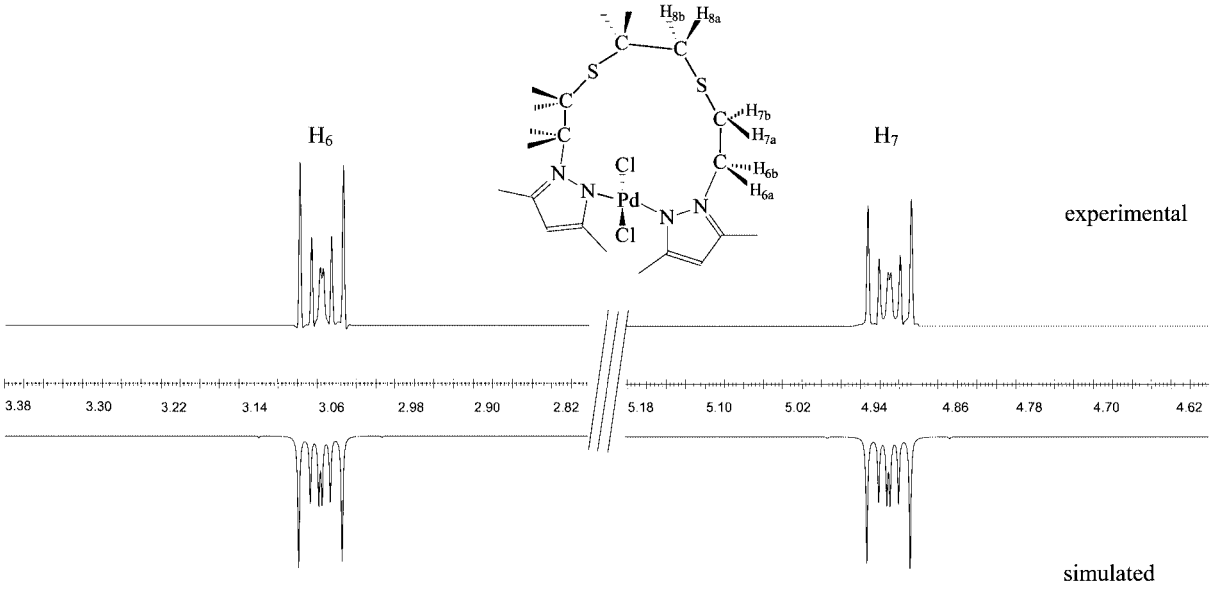

Figure 1. The 400-MHz ^1H NMR and the simulated *g* NMR spectra for the NCH_2CH_2S fragment of $[PdCl_2(bddo)]$ (**3**)

to the two carbon atoms involved.[15] Although this program was designed for organic molecules, in our case it works correctly when our ligands are coordinated to Pd^{II}. By use of this program, the dihedral angles corresponding to the observed adjacent coupling constants ($^3J_{6a,7a}$ = 4.81 and 4.87 Hz for **3** and **4**, respectively) are 51° and 52° for **3** and **4**, respectively. These values are in both cases consistent with an *anti* conformation (Figure 2).

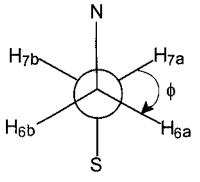

$[PdCl_2(bddo)]$ $\phi = 52°$
$[PdCl_2(bddn)]$ $\phi = 51°$

Figure 2. Dihedral angles for the NCH_2CH_2S fragment of $[PdCl_2(bddo)]$ (**3**)

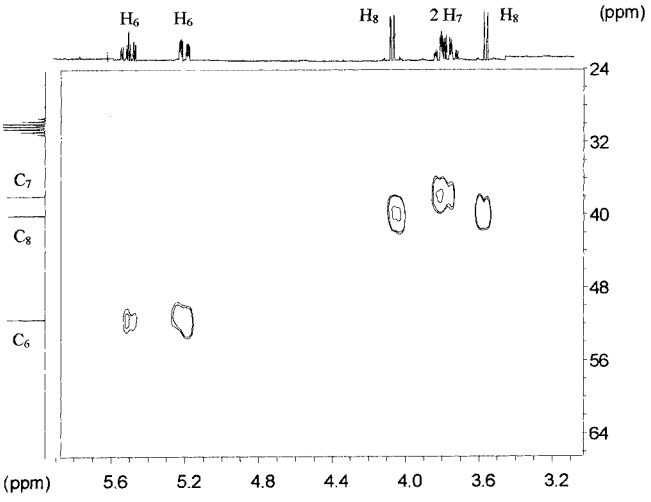

Figure 3. The 250-MHz 2D HMQC spectrum of $[Pd(bddo)](BF_4)_2$ (**8**)

The two different chains $[S-(CH_2)_2-N$ and $S-(CH_2)_x-S$; x = 2 for **8** and x = 3 for **9**] were studied separately. HMQC spectra were used to assign the signals of protons H_6, H_7 and H_8 for **8** and H_6, H_7, H_8 and H_9 for **9** (Figure 3). Simulated ^1H NMR spectra of both chains were obtained by use of the *g* NMR program.[13] The coupling constants are reported in Table 2.

Because of the symmetry of **8**, the two CH_2 units in the $S-CH_2-CH_2-S$ fragment are equivalent. The two protons of each CH_2, though, are diastereotopic and can be assigned to the two doublets found at δ = 3.52 and 4.04 ppm. The signal of H_8 for the $S-(CH_2)_3-S$ chain in compound **9** is superposed on that of H_7 and could not be further studied.

Table 2. ^1H NMR results: chemical shifts (ppm) and $^1H,^1H$ coupling constants (Hz) for **8** and **9** in $[D_6]$acetone

Compound	**8**	**9**
δ(H) (6*R*), δ(H) (6*S*)	5.19, 5.50	5.23, 5.58
δ(H) (7*S*), δ(H) (7*R*)	3.72, 3.78	3.52, 3.92
δ(H) (8*R*), δ(H) (8*S*)	3.52, 4.04	3.53
δ(H) (9*R*), δ(H) (9*S*)	−	2.70
^2J(6*R*,6*S*)	−13.56	−8.80
^2J(7*R*,7*S*)	−13.70	−4.40
^3J(6*R*,7*R*), ^3J(6*S*,7*S*),	2.11, 3.17,	2.92, 10.28,
^3J(6*R*,7*S*), ^3J(6*S*,7*R*)	3.84, 12.45	15.24, 15.52
^2J(8*R*,8*S*)	−8.04	−

For complexes **8** and **9**, the two protons of each CH_2 group in the $S-CH_2-CH_2-N$ chain are diastereotopic, thus giving rise to four groups of signals, each attributable to a single hydrogen atom. This happens because of the rigid conformation of the ligand when it is complexed. In this way, each group of signals can be assigned as a double double doublet. In **8**, the two signals of lower δ value appear partially superimposed. Figure 4 shows the experimental and the simulated spectra for **8**.

Crystal Structure of [$PdCl_2$(bddo)] (3)

The structure of **3** (Figure 5) consists of discrete [$PdCl_2$(bddo)] units. The palladium atom is coordinated by two pyrazole nitrogen and two chlorine atoms in a distorted square-planar geometry. The tetrahedral distortion can be observed in the mean separation [±0.174(3)] of the atoms coordinated to the Pd atom in relation to the mean plane. Tetrahedral distortion of the square-planar geometry can

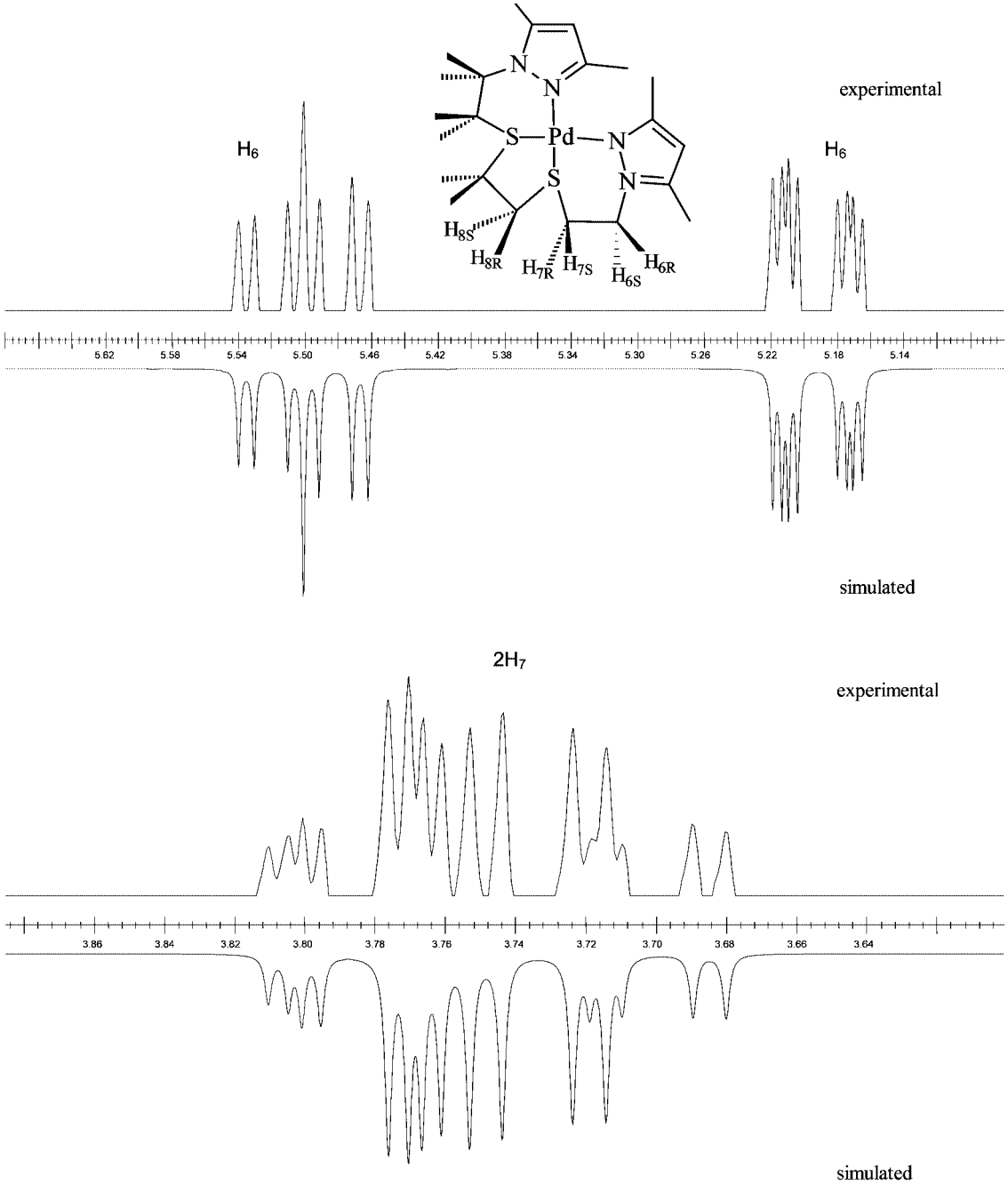

Figure 4. The 400-MHz ^1H NMR and the simulated *g* NMR spectra for the H_6 and H_7 protons of the NCH_2CH_2S fragment of [Pd(bddo)]$(BF_4)_2$ (**8**)

also be observed in the angles Cl(1)−Pd−Cl(2) and N(1)−Pd−N(3), of 172.47(4) and 168.65(9)°, respectively. The dihedral angle between the planes N(1)−Pd−Cl(1) and N(3)−Pd−Cl(2) is 13.5(1)°.

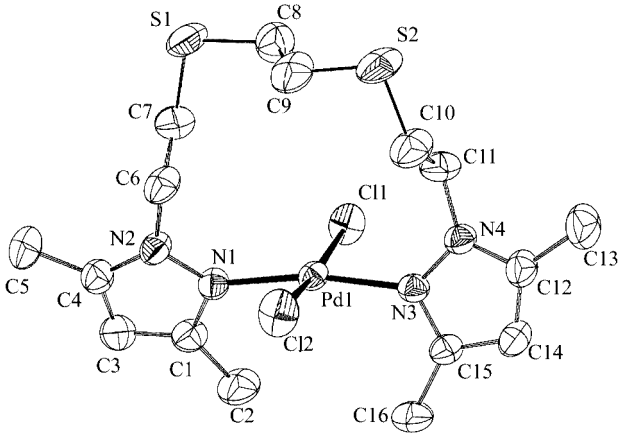

Figure 5. ORTEP drawing of $[PdCl_2(bddo)]$ (**3**, 273 K determination) showing all non-hydrogen atoms and the atom-numbering scheme; 50% probability amplitude displacement ellipsoids are shown

The pyrazolyl groups are *trans* to each other. The PdN_2Cl_2 core (containing pyrazole nitrogen atoms and terminal chloride ions) is found in 11 complexes described in the literature (seven of the complexes found had *trans* geometry and five were *cis*).[16] Both the Pd−N and the Pd−Cl bond lengths in **3** are of the same order as those found in the literature.[17] The palladium atom does not interact with the sulfur atoms, the Pd−S distances being 5.02(8) and 5.16(8) Å, respectively. The SCH_2CH_2S bridging segment is disordered in the crystal.

The structure of **3** is similar to that found for the complex $[CuCl_2(bddo)]$,[7b] but the copper complex shows greater distortion of the square-planar geometry. This can be observed in the dihedral angle between the planes N(1)−Cu−Cl(1) and N(3)−Cu−Cl(2), which is 27°. Table 3 lists some selected bond lengths and angles for this complex.

Table 3. Selected bond lengths (Å) and angles (°) for **3** and **8**, with estimated standard deviations (e.s.d.) in parentheses

3		**8**	
Pd(1)−N(1)	2.027(3)	Pd(1)−N(1)	2.027(4)
Pd(1)−N(3)	2.017(3)	Pd(1)−N(4)	2.030(4)
Pd(1)−Cl(1)	2.292(1)	Pd(1)−S(1)	2.246(1)
Pd(1)−Cl(2)	2.287(1)	Pd(1)−S(2)	2.247(1)
N(1)−Pd(1)−Cl(1)	90.98(9)	N(1)−Pd(1)−N(4)	97.4(2)
N(1)−Pd(1)−Cl(2)	90.03(9)	N(1)−Pd(1)−S(2)	86.2(1)
N(3)−Pd(1)−Cl(1)	91.38 (9)	N(4)−Pd(1)−S(1)	86.8(1)
N(3)−Pd(1)−Cl(2)	89.08(9)	S(1)−Pd(1)−S(2)	89.78(6)
N(1)−Pd(1)−N(3)	168.65(9)	N(1)−Pd(1)−S(1)	175.4(1)
Cl(1)−Pd(1)−Cl(2)	172.47(4)	N(4)−Pd(1)−S(2)	175.2(1)

Crystal Structure of $[Pd(bddo)](BF_4)_2 \cdot H_2O$ (8)

The structure of **8** (Figure 6) consists of cationic units of $[Pd(bddo)]^{2+}$, BF_4^- anions and solvent molecules (H_2O). Two nitrogen atoms of the pyrazolyl groups and two thioether groups coordinate the palladium atom in a slightly distorted square-planar geometry. The pyrazolyl groups are *cis* to each other. The tetrahedral distortion of the square-planar geometry can be observed in the mean separation of the atoms linked to Pd from the mean plane, which is ±0.050(3) Å. The dihedral angle between the planes N(1)−Pd−N(4) and S(1)−Pd−S(2) is 3.79(9)°. Some selected bond lengths and bond angles for this complex are listed in Table 3.

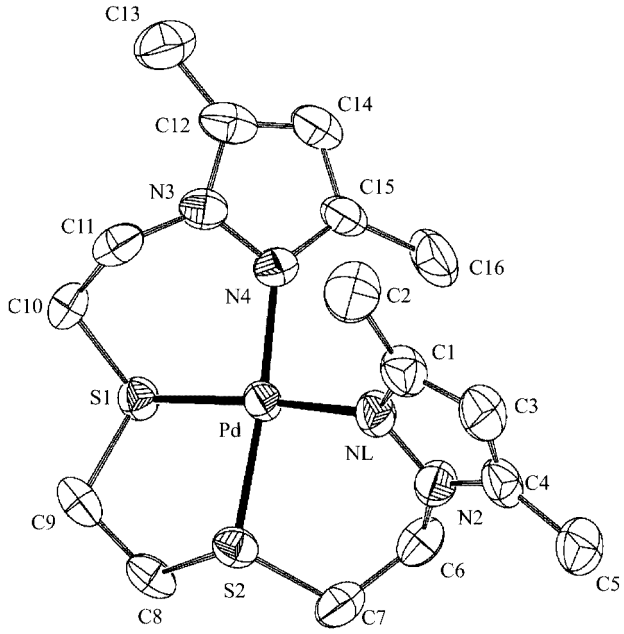

Figure 6. ORTEP drawing of $[Pd(bddo)](BF_4)_2$ (**8**, 273 K determination) showing all non-hydrogen atoms and the atom-numbering scheme; 50% probability amplitude displacement ellipsoids are shown

The PdN_2S_2 core (N in aromatic amine and S thioether) is found in five complexes in the literature.[18] The Pd−N and Pd−S distances in complex **8** are of the same order as those found in the literature for this kind of complexes.[17]

Ligand bddo acts as a tetradentate chelate and forms two Pd−N−N−C−C−S six-membered rings and one Pd−S−C−C−S five-membered ring. All of these have half-chair configurations. For the six-membered rings the N(4)−Pd−S(1) and N(1)−Pd−S(2) bite angles are 86.8(1) and 86.2(1)°, respectively. For the five-membered ring, the S(1)−Pd−S(2) bite angle is 89.75(6)°. These bite angles are similar to those reported in the literature for $[Pd(pdto)](ClO_4)_2$ [pdto = 1,8-bis(2-pyridyl)-3,6-dithiaoctane] (N−Pd−S bite angles are 86.9 and 87.2° and the S−Pd−S bite angle is 89.4°).[18d] This is the only compound with a PdN_2S_2 core similar to that presented in this paper, with two six-membered rings and one five-membered ring.

The half-chair distortions in the six-membered rings are ΔC_S(Pd) = 10.9(4)° and 17.0(4)° and ΔC_S[S(1)−C(10)] = 11.95(5)°, ΔC_S[S(2)−C(7)] = 14.0(6)° for Pd−S(1)−C(10)−C(11)−N(3)−N(4) and Pd−S(2)−C(7)−C(6)−N(2)−N(1), respectively.

Conclusion

We have shown that thioether−pyrazole N_2S_2 ligands can coordinate Pd^{II} centres in different ways. Treatment of $[PdCl_2(CH_3CN)_2]$ with these ligands gave complexes in which the Pd^{II} centre is bonded to two pyrazole rings and two chloride ions in a *trans* disposition. Abstraction of the chloride components in **3** and **4** with $AgBF_4$ gave complexes **8** and **9** with the $Pd^{II}N_2S_2$ core. These kinds of complexes were not obtained with bddh and bddhp ligands, probably because of the imposed geometry of the hypothetical PdNNCS metallacycle, which would induce steric hindrance between the methyl groups of the pyrazole rings. The Cl_2N_2 and N_2S_2 coordination modes of Pd^{II} can be interconverted. Thus, if **8** and **9** are heated under reflux in solutions with Et_4NCl, **3** and **4** are formed again. This reactivity is confirmation of the hemilabile behaviour of these thioether−pyrazole ligands in the complexation of Pd^{II}.

Experimental Section

Generals Remarks: Preparations were performed by use of conventional vacuum line and Schlenk techniques. All reagents were commercial grade materials and were used without further purification. Acetonitrile and dichloromethane were dried and distilled by standard methods and deoxygenated in the vacuum line in advance. Samples of $[PdCl_2(CH_3CN)_2]$[19] and $[PdCl_2(COD)]$[20] were prepared as described in the literature. 1,6-Bis(3,5-dimethyl-1-pyrazolyl)-2,5-dithiahexane (bddh),[6a] 1,8-bis(3,5-dimethyl-1-pyrazolyl)-3,6-dithiaoctane (bddo)[7a] and 1,9-bis(3,5-dimethyl-1-pyrazolyl)-3,7-dithianonane (bddn)[8] were prepared according to the published methods. Analyses (C, H, N, S) were performed in our analytical laboratory with a Carlo Erba CHNS EA-1108 instrument. Conductivity measurements were performed at room temperature in 10^{-3} M acetonitrile, DMSO or methanol solutions, with the aid of a Crison micro CM 2200 conductimeter. Infrared spectra were recorded as KBr pellets or polyethylene mulls under nitrogen over the 4000−100 cm^{-1} range. The ^1H, $^{13}C\{^1H\}$ NMR and HMQC spectra were obtained either with Bruker 250-MHz or 400-MHz instruments. Chemical shifts (δ) were determined relative to internal TMS and are given in ppm. Mass spectra were obtained with an HP 5989A apparatus.

1,7-Bis(3,5-dimethyl-1-pyrazolyl)-2,6-dithiaheptane (bddhp): 2-(Chloromethyl)-3,5-pyrazolium chloride[6a] (720 mg, 3.98 mmol) and 1,3-propanedithiol (0.20 mL, 1.97 mmol) were dissolved in dry DMF (6 mL) and the mixture was then heated to 90 °C. After the mixture had been maintained at this temperature for 15 min, sodium hydroxide (500 mg, 12.1 mmol), dissolved in water (7 mL), was added dropwise. Heating was stopped; after 15 min, additional water (7 mL) was added. After cooling to room temperature, the reaction mixture was extracted four times with $CHCl_3$ (15 mL). The collected organic layers were dried with anhydrous sodium sulfate and removed under vacuum. The product was purified by chromatography (silica gel 60) with methanol/dichloromethane (1:9) as eluent to give a white solid. Yield: 0.46 g (72%). M.p. 30−32 °C. IR (NaCl, cm^{-1}): $\tilde{\nu}$ = 2918 [ν(C−H)$_{al}$], 1558 [ν(C=C), ν(C=N)], 1455 [$\delta(CH_3)_{as}$], 1378 [$\delta(CH_3)_s$], 779 [δ(C−H)$_{oop}$]. ^1H NMR (250 MHz, $CDCl_3$ solution): δ = 1.76 (q, ^3J = 7 Hz, 2 H, $CH_2-CH_2-CH_2$), 2.22 (s, 6 H, *Me*), 2.31 (s, 6 H, *Me*), 2.67 (t, ^3J = 7 Hz, 4 H, $S-CH_2-CH_2$), 5.05 (s, 4 H, pz-CH_2−S), 5.86 (s, 2 H, pz-CH) ppm. $^{13}C\{^1H\}$ NMR ($CDCl_3$ solution, 63 MHz): δ = 11.6 (*Me*), 13.9 (*Me*), 29.4 ($CH_2-CH_2-CH_2$), 30.3 (S-CH_2-CH_2), 50.3 (pz-CH_2−S), 106.9 (pz-CH), 139.4 (pz-C), 148.1 (pz-C) ppm. MS (CI, NH_3): *m*/*z* (%) = 325 (100) [MH^+]. $C_{15}H_{24}N_4S_2$ (324): calcd. C 55.52, H 7.45, N 17.27, S 19.76; found C 55.21, H 7.25, N 16.96, S 19.71.

Synthesis of the Pd^{II} Complexes

Complexes $[PdCl_2L]$ with L = bddh (1), bddhp (2), bddo (3) and bddn (4): A solution of $[PdCl_2(CH_3CN)_2]$ or $[PdCl_2(COD)]$ (0.36 mmol) in dichloromethane (30 mL) was added to a solution of the appropriate ligand (0.36 mmol) in dichloromethane (10 mL). After the mixture had been stirred for 12 h, most of the solvent was removed under vacuum. Diethyl ether was then added to induce precipitation. The resulting precipitate was then filtered and washed with diethyl ether, yielding the desired compound.

Complex 1: IR (KBr, cm^{-1}): $\tilde{\nu}$ = 2951 [ν(C−H)$_{al}$], 1562 [ν(C=C), ν(C=N)], 1462 [$\delta(CH_3)_{as}$], 1380 [$\delta(CH_3)_s$], 778 [δ (C−H)$_{oop}$]. IR (polyethylene, cm^{-1}): $\tilde{\nu}$ = 459 [ν(Pd−N)$_{as}$], 326 [ν(Pd−Cl)]. ^1H NMR (400 MHz, $CDCl_3$ solution): δ = 2.35 (s, 6 H, *Me*), 2.85 (s, 6 H, *Me*), 3.96 (s, 4 H, $S-CH_2-CH_2-S$), 5.96 (s, 2 H, pz-CH), 5.98 (s, 4 H, pz-CH_2−S) ppm. $^{13}C\{^1H\}$ NMR (100 MHz, $CDCl_3$ solution): δ = 12.5 (*Me*), 16.3 (*Me*), 31.6 ($S-CH_2-CH_2-S$), 48.8 (pz-CH_2−S), 108.9 (pz-CH), 144.8, 152.5 (pz-C) ppm.

Complex 2: IR (KBr, cm^{-1}): $\tilde{\nu}$ =3130 [ν(C−H)$_{ar}$], 2923 [ν(C−H)$_{al}$], 1559 [ν(C=C), ν(C=N)], 1464 [$\delta(CH_3)_{as}$], 1381 [$\delta(CH_3)_s$], 800 [δ(C−H)$_{oop}$]. IR (polyethylene, cm^{-1}): $\tilde{\nu}$ = 448 [ν(Pd−N)$_{as}$], 338 [ν(Pd−Cl)]. ^1H NMR (400 MHz, $CDCl_3$ solution): δ = 2.38 (s, 6 H, *Me*), 3.01 (s, 6 H, *Me*), 3.13 (m, 2 H, $CH_2-CH_2-CH_2$), 3.22 (m, 4 H, $S-CH_2-CH_2$), 5.84 (s, 4 H, pz-CH_2−S), 6.02 (s, 2 H, pz-CH) ppm. $^{13}C\{^1H\}$ NMR (100 MHz, $CDCl_3$ solution): δ = 12.7 (*Me*), 16.4 (*Me*), 27.2 ($CH_2-CH_2-CH_2$), 31.4 ($S-CH_2-CH_2$), 48.3 (pz-CH_2−S), 109.7 (pz-CH), 144.6, 151.4 (pz-C) ppm.

Complex 3: IR (KBr, cm^{-1}): $\tilde{\nu}$ = 3129 [ν(C−H)$_{ar}$], 2918 [ν(C−H)$_{al}$], 1557 [ν(C=C), ν(C=N)], 1469 [$\delta(CH_3)_{as}$], 1393 [$\delta(CH_3)_s$], 820 [δ(C−H)$_{oop}$]. IR (polyethylene, cm^{-1}): $\tilde{\nu}$ = 453 [ν(Pd−N)$_{as}$], 340 [ν(Pd−Cl)]. ^1H NMR (400 MHz, $CDCl_3$ solution): δ = 2.28 (s, 6 H, *Me*), 2.95 (s, 6 H, *Me*), 3.08 (m, 4 H, CH_2-CH_2−S), 3.20 (s, 4 H, $S-CH_2-CH_2$−S), 4.93(m, 4 H, pz-CH_2-CH_2), 5.94 (s, 2 H, pz-CH) ppm. $^{13}C\{^1H\}$ NMR (100 MHz, $CDCl_3$ solution): δ = 12.1 (*Me*), 15.5 (*Me*), 30.8 (S-CH_2-CH_2−S), 34.0 (CH_2-CH_2−S), 51.1 (pz-CH_2-CH_2), 108.8 (pz-CH), 142.9, 150.6 (pz-C) ppm.

Complex 4: IR (KBr, cm^{-1}): $\tilde{\nu}$ = 3126 [ν(C−H)$_{ar}$], 2917 [ν(C−H)$_{al}$], 1554 [ν(C=C), ν(C=N)], 1469 [$\delta(CH_3)_{as}$], 1390 [$\delta(CH_3)_s$], 789 [δ(C−H)$_{oop}$]. IR (polyethylene, cm^{-1}): $\tilde{\nu}$ = 473 [ν(Pd−N)$_{as}$], 335 [ν(Pd-Cl)]. ^1H NMR (400 MHz, $CDCl_3$ solution): δ = 2.28 (s, 6 H, *Me*), 2.97 (s, 6 H, *Me*), 1.72 (q, 2 H, $CH_2-CH_2-CH_2$), 2.84 (t, 4 H, $CH_2-CH_2-CH_2$), 3.14 (m, 4 H, CH_2-CH_2−S), 4.89 (m, 4 H, pz-CH_2-CH_2), 5.94 (s, 2 H, pz-CH) ppm. $^{13}C\{^1H\}$ NMR (100 MHz, $CDCl_3$ solution): δ = 12.1 (*Me*), 15.6 (*Me*), 29.5, 29.6, 30.6 (pz-CH_2-CH_2−S, $CH_2-CH_2-CH_2$, $CH_2-CH_2-CH_2$), 50.7 (pz-CH_2-CH_2), 108.8 (pz-CH), 143.1, 150.9 (pz-C) ppm.

Complexes $[Pd_2Cl_4L]$ with L = bddhp (5), bddo (6) and bddn (7): A solution of $[PdCl_2(CH_3CN)_2]$ (0.36 mmol) in dichloromethane

(30 mL) was added to a solution of the appropriate ligand (0.18 mmol) in dichloromethane (10 mL). After the mixture had been stirred for 12 h, a precipitate had formed. This precipitate was filtered off, washed with diethyl ether and dried under vacuum, yielding the desired compound. No Pd^{II} complex of this stoichiometry with bddh as ligand could be isolated.

Complex 5: IR (KBr, cm^{-1}): $\tilde{\nu}$ = 3129 [ν(C−H)$_{ar}$], 2967 [ν(C−H)$_{al}$], 1564 [ν(C=C)], 1463 [ν(C=N), $\delta(CH_3)_{as}$], 1392 [$\delta(CH_3)_s$], 808 [δ(C−H)$_{oop}$]. IR (polyethylene, cm^{-1}): $\tilde{\nu}$ = 452 [ν(Pd−N)$_{as}$], 366 [ν(Pd−Cl)], 335 [ν_B(Pd−Cl)]. ^{1}H NMR (400 MHz, [D$_6$]DMSO solution): δ = 2.16 (s, 6 H, *Me*), 2.34 (s, 6 H, *Me*), 2.69 (br, 2 H, $CH_2-CH_2-CH_2$), 2.97 (br, 4 H, $S-CH_2-CH_2$), 5.67 (br, 4 H, pz-CH_2−S), 5.97 (s, 2 H, pz-CH).

Complex 6: IR (KBr, cm^{-1}): 3120 [ν(C−H)$_{ar}$], 2967 [ν(C−H)$_{al}$, ν(C=C)], 1554 [ν(C=N)], 1467 [$\delta(CH_3)_{as}$], 1395 [$\delta(CH_3)_s$], 797 [δ(C−H)$_{oop}$]. IR (polyethylene, cm^{-1}): 456 [ν(Pd−N)$_{as}$], 367 [ν(Pd−Cl)], 322 [ν_B(Pd−Cl)]. ^{1}H NMR (400 MHz, [D$_6$]DMSO solution): δ = 2.36 (s, 6 H, *Me*), 2.43 (s, 6 H, *Me*), 2.79 (br, 4 H, CH_2-CH_2−S), 4.23 (br, 4 H, S−CH_2-CH_2−S), 4.92 (br, 4 H, pz-CH_2-CH_2), 6.19 (s, 2 H, pz-CH) ppm.

Complex 7: IR (KBr, cm^{-1}): $\tilde{\nu}$ = 3126 [ν(C−H)$_{ar}$], 2958 [ν(C−H)$_{al}$], 1560 [ν(C=C), ν(C=N)], 1470 [$\delta(CH_3)_{as}$], 1400 [$\delta(CH_3)_s$]. IR (polyethylene, cm^{-1}): $\tilde{\nu}$ = 459 [ν(Pd−N)$_{as}$], 360 [ν(Pd−Cl)], 319 [ν_B(Pd−Cl)]. ^{1}H NMR (400 MHz, [D$_6$]DMSO solution): δ = 2.25 (s, 6 H, *Me*), 2.80 (s, 6 H, *Me*), 2.05 (br, 2 H, $CH_2-CH_2-CH_2$), 2.42 (br, 4 H, $CH_2-CH_2-CH_2$), 4.50 (br, 4 H, CH_2-CH_2−S), 4.90 (br, 4 H, pz-CH_2-CH_2), 6.20 (s, 2 H, pz-CH) ppm.

Complexes [Pd(bddo)](BF$_4$)$_2$·H$_2$O (8) and [Pd(bddn)](BF$_4$)$_2$ (9): A solution of $AgBF_4$ (0.86 mmol) was added dropwise with vigorous stirring to a solution of [PdCl$_2$(L)] (L = bddo or bddn, 0.43 mmol) in dichloromethane (10 mL) and methanol (10 mL). The reaction was carried out in the dark to prevent reduction of Ag^I to Ag^0. After 5 min, stirring was stopped, and AgCl was filtered off. When the volume of the resultant solution had been reduced to roughly 5 mL, the product precipitated as a yellow solid. This solid was filtered and washed with dichloromethane.

Complex 8: IR (KBr, cm^{-1}): $\tilde{\nu}$ = 3141 [ν(C−H)$_{ar}$], 2956 [ν(C−H)$_{al}$], 1553 [ν(C=C), ν(C=N)], 1470 [$\delta(CH_3)_{as}$], 1395 [$\delta(CH_3)_s$], 1061 [ν(B−F)], 791 [δ(C−H)$_{oop}$]. IR (polyethylene, cm^{-1}): $\tilde{\nu}$ = 461 [ν(Pd−N)$_{as}$], 238 [ν(Pd−S)]. ^{1}H NMR (400 MHz, [D$_6$]acetone): δ = 1.99 (s, 6 H, *Me*), 2.52 (s, 6 H, *Me*), 3.72/ 3.78/ 5.19/ 5.50 (pz-CH_2-CH_2), 6.26 (s, 2 H, pz-CH) ppm. ^{13}C{^{1}H} NMR (100 MHz, [D$_6$]acetone): δ = 11.9 (*Me*), 13.3 (*Me*), 31.4 (S−CH_2-CH_2), 48.3 (pz-CH_2-CH_2−S), 109.0 (pz-CH), 147.0, 152.1 (pz-C) ppm.

Complex 9: IR (KBr, cm^{-1}): $\tilde{\nu}$ = 3129 [ν(C−H)$_{ar}$], 2985−2928 [ν(C−H)$_{al}$], 1549 [ν(C=C), ν(C=N)], 1472 [$\delta(CH_3)_{as}$], 1393 [$\delta(CH_3)_s$], 1061 [ν(B−F)], 810 [δ(C−H)$_{oop}$]. IR (polyethylene, cm^{-1}): $\tilde{\nu}$ = 456 [ν(Pd−N)$_{as}$], 247 [ν(Pd−S)]. ^{1}H NMR (400 MHz, [D$_6$]acetone): δ = 1.85 (s, 6 H, *Me*), 2.52 (s, 6 H, *Me*), 3.52/3.92/ 5.23/5.58 (pz-CH_2-CH_2), 6.24 (s, 2 H, pz-CH) ppm. ^{13}C{^{1}H} NMR (100 MHz, [D$_6$]acetone): δ = 11.3 (*Me*), 12.7 (*Me*), 22.8 ($CH_2-CH_2-CH_2$), 31.2 (pz-CH_2-CH_2), 36.4 ($CH_2-CH_2-CH_2$), 49.9 (pz-CH_2-CH_2), 108.9 (pz-CH), 146.1, 152.1 (pz-C) ppm.

Tables 1 and 2 show coupling constants for complexes **3**, **4**, **8** and **9**; Table 4 shows other analytical and physical data for all complexes.

X-ray Crystallographic Study: Crystals of compounds **3** and **8** suitable for X-ray diffraction experiments were obtained by crystallisation from CH_2Cl_2 and MeOH, respectively. The data for **3** were collected with an Enraf−Nonius CAD$_4$ four-circle diffractometer, by the Ω/2θ scan technique. The data for **8** were collected with an MAR345 diffractometer with an image plate detector, by the φ-scan technique. Both crystals were subjected to graphite-monochromated Mo-K_α radiation. The structures were solved by direct methods with the SHELXS 97 computer program[21] and refined by full-matrix, least squares with the SHELXL 97 program.[22] All hydrogen atoms were computed and refined by use of a riding model. The final *R* (on *F*) factor and ω*R* (on F^2) values, as well as the numbers of parameters refined and other details concerning the refinement of the crystal structure are presented in Table 5. CCDC-185048 (**3**) and -185049 (**8**) contain the supplementary crystallographic data for this paper. These data can be obtained free of charge at www.ccdc.cam.ac.uk/conts/retrieving.html or from the Cambridge Crystallographic Data Centre, 12 Union Road, Cam-

Table 4. Physical and analytical data for complexes **1**−**9**

Compound	Yield (%)	Analysis[a] N	C	H	S	Conductivity (Ω^{-1} cm^2 mol^{-1})
[PdCl$_2$(bddh)] (**1**)	77	(11.49)	(34.47)	(4.55)	(13.15)	80[b]
		11.27	34.35	4.43	13.40	
[PdCl$_2$(bddhp)] (**2**)	74	(11.16)	(35.90	(4.82)	(12.78)	89[b]
		10.88	35.85	4.69	13.07	
[PdCl$_2$(bddo)] (**3**)	96	(10.86)	(37.25	(5.08)	(12.43)	96[b]
		10.98	37.03	5.33	12.57	
[PdCl$_2$(bddn)] (**4**)	98	(10.57)	(38.53	(5.33)	(12.10)	74[b]
		10.32	38.36	5.34	12.47	
[Pd$_2$Cl$_4$(bddhp)] (**5**)	80	(8.25)	(26.53)	(3.56)	(9.44)	27[c]
		8.05	26.42	3.33	9.25	
[Pd$_2$Cl$_4$(bddo)] (**6**)	87	(8.08)	(27.72)	(3.78)	(9.25)	29[c]
		7.81	27.49	3.88	9.59	
[Pd$_2$Cl$_4$(bddn)] (**7**)	83	(7.92)	(28.87)	(3.99)	(9.07)	23[c]
		7.58	28.72	3.95	8.86	
[Pd(bddo)](BF$_4$)$_2$ ·H$_2$O (**8**)	89	(8.80)	(30.19)	(4.43)	(10.07)	163[d]
		8.61	30.03	4.36	10.39	
[Pd(bddn)](BF$_4$)$_2$ (**9**)	90	(8.86)	(32.28)	(4.46)	(10.14)	175[d]
		8.69	31.89	4.36	10.02	

[a] Calculated analytical values are given in parentheses. [b] 10^{-3} M in acetonitrile. [c] 10^{-3} M in DMSO. [d] 10^{-3} M in MeOH.

Table 5. Crystallographic data for crystal structures **3** and **8**

Compound	**3**	**8**
Empirical formula	$C_{16}H_{26}Cl_2N_4PdS_2$	$C_{16}H_{28}B_2F_8N_4OPdS_2$
Formula mass [g·mol^{-1}]	515.83	636.56
Temperature [K]	293(2)	293(2)
Crystal system	monoclinic	orthorhombic
Space group	$P2_1/n$	Pbca
Unit cell dimensions		
a [Å]	8.821(8)	14.219(1)
b [Å]	28.22(1)	16.493(1)
c [Å]	9.305(2)	20.834(1)
β [°]	112.62(3)	90
Volume [Å^3]	2138(2)	4885.9(5)
Z	4	8
$D_{calcd.}$ [g cm^{-3}]	1.602	1.736
μ [mm^{-1}]	1.320	1.009
F(000)	1048	2576
Crystal size [mm]	0.1 × 0.1 × 0.2	0.1 × 0.1 × 0.2
θ range [°]	2.48 to 29.99	2.13 to 25.01
Reflections collected: total, independent, R_{int}	6539, 6168, 0.0578	17711, 3987, 0.0438
Data/restraints/parameters	6118/0/263	3987/0/295
a[a]	0.0285	0.0829
Final $R1$, $wR2$	0.0313, 0.0631	0.0398, 0.1259
$R1$ (all data), $wR2$	0.0946, 0.0762	0.0657, 0.1343
Residual electron density [e·Å^{-3}]	+0.433, −0.426	+0.694, −0.709

[a] The function minimised was $\Sigma w(|F_o|)^2 - |F_c|^2)^2$, where $w = [\sigma^2(I) + (aP)^2]^{-1}$, and $P = (|F_o|^2 + 2|F_c|^2)/3$.

bridge CB2 1EZ, UK [Fax: (internat.) + 44-1223/336-033; E-mail: deposit@ccdc.cam.ac.uk].

Acknowledgments

Support by the Ministerio de Educación y Cultura of Spain (Project BQU2000-0238 and grant to J. G.) is gratefully acknowledged.

[1] [1a] A. Bader, E. Lindner, *Coord. Chem. Rev.* **1991**, *108*, 27. [1b] C. S. Slone, D. A. Weinberger, C. A. Mirkin, *Prog. Inorg. Chem.* **1999**, *48*, 233.
[2] [2a] J. C. Jeffrey, and T. B. Rauchfuss, *Inorg. Chem.* **1979**, *18*, 2658. [2b] S. Borns, R. Kadyrov, D. Heller, W. Baumann, A. Spannenberg, R. Kempe, J. Holz, A. Börner, *Eur. J. Inorg. Chem.* **1998**, 1291. [2c] P. Jutzi, T. Redeker, *Eur. J. Inorg. Chem.* **1998**, 663. [2d] I. Moldes, E. de la Encarnación, J. Ros, A. Álvarez-Larena, J. F. Piniella, *J. Orgonomet. Chem.* **1998**, *556*, 165.
[3] [3a] R. Mathieu, G. Esquius, N. Lugan, J. Pons, J. Ros, *Eur. J. Inorg. Chem.* **2001**, 2683. [3b] G. Esquius, J. Pons, R. Yáñez, J. Ros, *J. Organomet. Chem.* **2001**, *619*, 14. [3c] G. Esquius, J. Pons, R. Yáñez, J. Ros, X. Solans, M. Font-Bardía, *J. Organomet. Chem.* **2000**, *605*, 226. [3d] G. Esquius, J. Pons, R. Yáñez, J. Ros, X. Solans, M. Font-Bardía, *Acta Crystallogr.* **2002**, *C58*, 133.
[4] R. Tribó, J. Pons, R. Yáñez, J. F. Piniella, A. Álvarez-Larena, J. Ros, *Inorg. Chem. Commun.* **2000**, *3*, 545.
[5] A. Boixassa, J. Pons, A. Virgili, X. Solans, M. Font-Bardía, J. Ros, *Inorg. Chim. Acta*, accepted.
[6] [6a] W. G. Haanstra, W. L. Driessen, J. Reedijk, R. Fröhlich, B. Krebs, *Inorg. Chim. Acta* **1991**, *185*, 175. [6b] W. G. Haanstra, W. L. Driessen, R. A. G. de Graaff, J. Reedijk, Y. F. Wang, C. H. Stam, *Inorg. Chim. Acta* **1991**, *186*, 215.
[7] [7a] W. G. Haanstra, W. L. Driessen, J. Reedijk, U. Turpeinen, R. Hämäläinen, *J. Chem. Soc., Dalton Trans.* **1989**, 2309. [7b] W. G. Haanstra, W. A. J. W. van der Donk, W.L. Driessen, J. Reedijk, J. S. Wood, M. G. B. Drew, *J. Chem. Soc., Dalton Trans.* **1990**, 3123.
[8] W. G. Haanstra, W. A. J. W. van der Donk, W. L. Driessen, J. Reedijk, M. G. B. Drew, J. S. Wood, *Inorg. Chim. Acta* **1990**, *176*, 299.
[9] [9a] W. G. Haanstra, W. L. Driessen, M. van Roon, A. L. E. Stoffels, J. Reedijk, *J. Chem. Soc., Dalton Trans.* **1992**, 481. [9b] R. Burth, H. Vahrenkamp, *Inorg. Chim. Acta* **1998**, *282*, 193. [9c] P. Gosh, M. Wood, J. B. Bonano, T. Hascall, G. Parkin, *Polyhedron* **1999**, *18*, 107.
[10] [10a] W. J. Geary, *Coord, Chem. Rev.* **1971**, *7*, 81. [10b] L. K. Thompson, F. L. Lee, E. J. Gabe, *Inorg. Chem.* **1988**, *27*, 39.
[11] [11a] E. Pretsch, T. Clerc, J. Seibl, W. Simon, *Tables of Determination of Organic Compounds. ^{13}C NMR, ^{1}H NMR, IR, MS, UV\Vis, Chemical Laboratory Practice*, Springer-Verlag, Berlin, Germany, **1989**. [11b] D. H. Williams, I. Fleming, *Spectroscopic Methods in Organic Chemistry*, McGraw-Hill, London, UK, **1995**.
[12] [12a] R. J. H. Clark, G. Natile, U. Belluco, L. Cattalini, C. Filippin, *J. Chem. Soc. A* **1970**, 659. [12b] K. Nakamoto, *Infrared and Raman Spectra of Inorganic and Coordination Compounds*, John Wiley and Sons, New York, USA, **1986**.
[13] P. H. M. Budzelaar, *g NMR ver. 4.0*, IvorySoft, Cherwell Scientific, Oxford, UK, **1997**.
[14] [14a] J. Elguero, A. Fruchier, *An. Quim.* **1974**, *70*, 141. [14b] I. Akorta, J. Elguero, A. Fruchier, D. J. Macquarrie, A. Virgili, *J. Organomet. Chem.* **2001**, *625*, 148.
[15] C. M. Cerda-García-Rojas, L. G. Zepeda, P. Joseph-Nathan, *Tetrahedron Comput. Methodol.* **1990**, *3*, 113.
[16] [16a] V. M. Agre, N. P. Kozlova, V. K. Trunov, L. G. Makarevich, O. V. Ivanov, *Koord. Khim.* **1979**, *5*, 1406. [16b] V. M. Agre, N. P. Kozlova, V. K. Trunov, V. M. Oziomko, E. S. Zaitseva, *Koord. Khim.* **1980**, *6*, 948. [16c] V. I. Sokol, M. A. Porai-Koshits, T. O. Vardosanidze, V. N. Voropaev, E. S. Dominina, G. G. Skvortsova, *Koord. Khim.* **1983**, *9*, 539. [16d] A. A. Watson, D.

A. House, P. J. Steel, *J. Organomet. Chem.* **1986**, *311*, 387. [16e] G. Minghetti, M. A. Cinellu, A. L. Bandini, G. Banditelli, F. Demartin, M. Manassero, *J. Organomet. Chem.* **1986**, *315*, 387. [16f] C. Cheng, J. Lain, Y. Wu, S. Wang, *Acta Crystallogr.* **1990**, *C46*, 208. [16g] A. Chandrasekaran, S. S. Krishnamurthy, M. Nethaji, *Inorg. Chem.* **1993**, *32*, 6102. [16h] A. T. Baker, J. K. Crass, M. Maniska, D. C. Craig, *Inorg. Chim. Acta* **1995**, *230*, 225. [16i] C. M. Hartshorn, P. J. Steel, *Chem. Commun.* **1997**, 541. [16j] S. Tsuji, D. C. Swenson, R. F. Jordan, *Organometallics* **1999**, *18*, 4758.

[17] F. H. Allen, O. Kennard, *Chem. Des. Autom. News* **1993**, *8*, 31.

[18] [18a] H. Nikol, H. Bürgi, K. I. Hardcastle, H. B. Grey, *Inorg. Chem.* **1995**, *34*, 6319. [18b] A. J. Blake, Y. V. Roberts, M. Schröeder, *J. Chem. Soc., Dalton Trans.* **1996**, 1885. [18c] F. Contu, F. Demartin, F. A. Devillanova, A. Garau, F. Isaia, V. Lippolis, A. Salis, G. Verani, *J. Chem. Soc., Dalton Trans.* **1997**, 4401. [18d] S. V. Kolotilov, E. A. Goreshnik, V. V. Pavlishuk, K. B. Yatsimirskii, *Zh. Neorg. Khim.* **2000**, *45*, 967.

[19] S. Komiya, *Synthesis of Organometallic Compounds: A Practical Guide*, John Wiley and Sons, New York, USA, **1997**.

[20] F. A. Cotton, *Inorg. Synth.* **1972**, *13*, 52.

[21] G. M. Sheldrick, *Acta Crystallogr.* **1990**, *A46*, 467.

[22] G. M. Sheldrick, *SHELXS 97, SHELXL 97, CIFTAB − Program for Crystal Structure Analysis (Release 97−2)*, Institut für Anorganische Chemie der Universität, Tammanstraße 4, 3400 Göttingen, Germany, **1998**.

Received June 5, 2002
[I02296]

Formation and Characterization of Zwitterionic Stereoisomers from the Reaction of $B(C_6F_5)_3$ and NEt_2Ph: (*E*)- and (*Z*)-[$EtPhN^+=CHCH_2$-$B^-(C_6F_5)_3$]

Nicolas Millot,[a] Catherine C. Santini,*[a] Bernard Fenet,[b] and Jean Marie Basset[a]

Keywords: Boranes / Aniline / Zwitterions / NMR spectroscopy

The stoichiometric reaction of $B(C_6F_5)_3$ and NEt_2Ph **I**, at room temperature, in an aromatic solvent, has been investigated by 1D and 2D NMR spectroscopy (^1H, ^{11}B,^{13}C, ^{15}N and ^{19}F). No $Et_2PhN{\cdot}B(C_6F_5)_3$ adduct was observed. An equilibrium between free $B(C_6F_5)_3$, NEt_2Ph, $[HB(C_6F_5)_3]^-(HNEt_2Ph)^+$ and two zwitterionic stereoisomers (*E*)- and (Z)-[$EtPhN^+=CH$-CH_2-$B^-(C_6F_5)_3$] (30%) in an *E*/*Z* ratio of 3:2 was observed. Whatever the protic reagent Z-OH [Z = H, $SiPh_3$, (c-$C_5H_9)_7O_{12}Si_8$, or silanol group of silica], all the equilibria involved in solutions of **I** are quantitatively displaced towards the ionic form $[Z\text{-}O\text{-}B(C_6F_5)_3]^-(HNEt_2Ph)^+$. In the case of dimethylaniline, besides free $B(C_6F_5)_3$ and Me_2NPh, the 1:1 adduct $(C_6F_5)_3B{\cdot}NMe_2Ph$ and an iminium salt $[PhCH_3N=CH_2]^+[HB(C_6F_5)_3]^-$ have been identified.
(© Wiley-VCH Verlag GmbH, 69451 Weinheim, Germany, 2002)

Introduction

In homogeneous metallocene-based olefin polymerization catalysis, ammonium salts are known to activate neutral alkyl precursors into highly active metallocenium cations by irreversible protonolysis. These salts are generally composed of a tertiary ammonium cation $[HNR_2R']^+$ (R = Me, Et; R′ = Ph, Et) and various non-coordinating anions such as metallacarboranes[1] or borates.[2−6] From the latter, the non-coordinating character of pentafluorophenylborates {$[XB(C_6F_5)_3]$, X = -C_6F_5,[7] -OH,[8] -OR,[9] (c-$C_5H_9)_7O_{12}Si_8$ [10]}, and their resistance towards anion decomposition, even though pentafluorophenylborates are far less stable towards decomposition when X = OR,[11] have allowed the successful enhancement of the activity of metallocenium catalysts.[12]

$$Cp_2ZrMe_2 + [HNR_2R']^+[B(C_6F_5)_4]^- \rightarrow [Cp_2ZrMe]^+[B(C_6F_5)_4]^- + MeH + NR_2R'$$

Interestingly, despite the fact that anilines are commonly used with tris(pentafluorophenyl)borane $[B(C_6F_5)_3]$ in the preparation of heterogeneous cocatalysts for olefin polymerization,[13−16] no reports exist on the Lewis acid/base reactivity of such compounds in solution and the possible formation of aniline·$B(C_6F_5)_3$ adducts. Like boron trihalides,[17,18] the strong Lewis acid $B(C_6F_5)_3$ is known to form stable adducts with amines or pyridines.[19]

We report in this paper the results obtained by multinuclear 1D and 2D NMR spectroscopy (^1H, ^{11}B, ^{13}C, ^{15}N, ^{19}F) on stoichiometric solutions of $B(C_6F_5)_3$ and NR_2Ph (R = Et, Me).

Results and Discussion

The addition of one equivalent of NEt_2Ph to $B(C_6F_5)_3$ in aromatic solvents led instantaneously to a pink coloration of the solution **I**. The ^{11}B NMR spectrum of **I** shows three resonance at δ = −13.7, −23.6 and 60 ppm indicating the presence of at least three different species in the reaction mixture. In order to determine their structure, a study was performed using multinuclear ^1H, ^{11}B, ^{13}C, ^{15}N and ^{19}F NMR spectroscopy.

In the ^1H NMR spectrum of solution **I** (Figure 1), the major peaks at δ = 0.82 (CH_3), 2.8 (CH_2) and 6.5−7 ppm

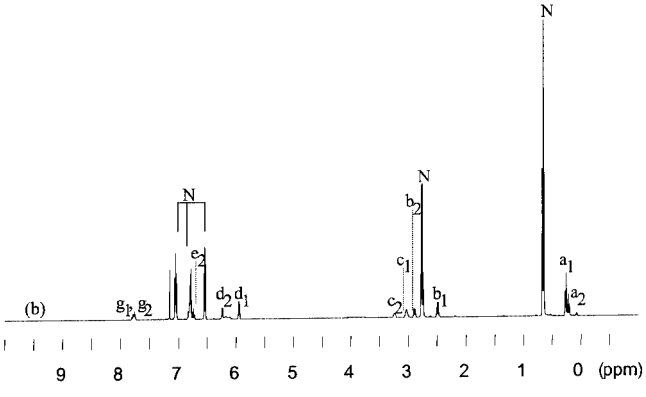

Figure 1. ^1H NMR spectrum (500 MHz, 25 °C, C_6D_6) of solution **I**; N indicates peaks due to free Et_2NPh

[a] Laboratoire de Chimie Organométallique de Surface, UMR 9986 CNRS − ESCPE Lyon,
43, bd du 11 Novembre 1918, 69626 Villeurbanne Cedex France
[b] Centre de RMN, UMR 5012 UCB Lyon 1 − ESCPE Lyon,
43 bd du 11 Novembre 1918, 69626 Villeurbanne Cedex France

(aromatic protons) are characteristic of the free amine in solution. Additional peaks appear in the region of methyl (a_1, a_2), methylene (b_1, b_2; c_1, c_2) and aromatic (d_1, d_2, e_2) protons. Two deshielded overlapping triplets (g_1, g_2) and a very broad signal are also observed at $\delta = 7.8$ and 3.9 ppm, respectively. The intensities of these peaks, relative to those of the free amine, do not exceed 30%, and are sensitive to the concentration of the solution, suggesting the existence of an equilibrium or equilibria between NEt_2Ph and other species in solution. In all experiments, a ratio of 3:2 is observed for the areas of the peaks x_1/x_2 (x = a−g).

In the 2D-COSY NMR spectrum of **I** (Figure 2) the triplets a_1 and a_2 are correlated to the quadruplets b_1 and b_2, respectively, supporting the fact that two different -$CH_{2\text{-}b}$-$CH_{3\text{-}a}$ fragments are present. A correlation is also detected between (c_1, c_2) and (g_1, g_2), indicating that the H_g protons are coupled to the -$CH_{2\text{-}c}$-X fragments (Figure 2a). Analysis of the aromatic proton region of the spectrum (Figure 2b) shows the presence of two types of non-equivalent phenyl groups (in a d_1/d_2 ratio of 3:2). At lower levels, a weak correlation can be detected between the (b_1, b_2) quadruplets and the (g_1, g_2) triplets.

The solution ^{13}C NMR spectrum of **I** (Figure 3) shows the characteristic peaks for the methyl ($\delta = 11.4$ ppm), methylene ($\delta = 49.4$ ppm) and aromatic carbons ($\delta = 116-142$ ppm) of diethylaniline, as well as doublets representative of the pentafluorophenyl carbons ($\delta = 138-149$ ppm) of $B(C_6F_5)_3$. As in the ^1H NMR spectrum, two sets of additional peaks appear in the ^{13}C NMR spectrum of **I** for each methyl, methylene and aromatic carbon atom. Two new peaks are also present near $\delta = 190$ ppm that can be attributed to a C=Y group, where Y is an electron-withdrawing center (O, N).

The upfield shift of the methyl and *ipso* carbons, as well as the downfield shifts of the methylene, *ortho* and *para* carbons of the diethylaniline (see Exp. Sect.) could indicate a protonation[20,21] or a weakly coordinative interaction between NEt_2Ph and $B(C_6F_5)_3$, as described for other boron-aniline complexes.[17]

More accurate structural information on the species present in **I** can be obtained by a ^1H-^{13}C HSQC NMR experiment (Figure 4). The carbons of the methyl (a_1, a_2) and methylene (b_1, b_2) groups of the two -$CH_{2\text{-}b}$-$CH_{3\text{-}a}$ fragments can be assigned. The two broad methylene protons (c_1, c_2) are correlated to a broad carbon resonance at $\delta = 34.5$ ppm, suggesting the proximity of a boron atom. The aromatic resonances associated with the *ortho* (d_1, d_2), *meta* (e_1, e_2) and *para* (f_1, f_2) hydrogen atoms confirm the presence of two distinct phenyl groups in addition to the phenyl ring of the free aniline (Figure 4b). The two most deshielded carbons ($\delta = 190$ ppm) exhibit a correlation with the triplets (g_1, g_2, $\delta = 8$ ppm), supporting the presence of an H_g-C=Y group (Y = O, N). In accordance with the results obtained by ^1H-^1H COSY NMR experiments, the ^1H-^{13}C HSQC NMR experiment confirms the existence of two different -$CH_{2\text{-}b}$-$CH_{3\text{-}a}$, phenyl and H_g-(C=Y)-$CH_{2\text{-}c}$-X fragments.

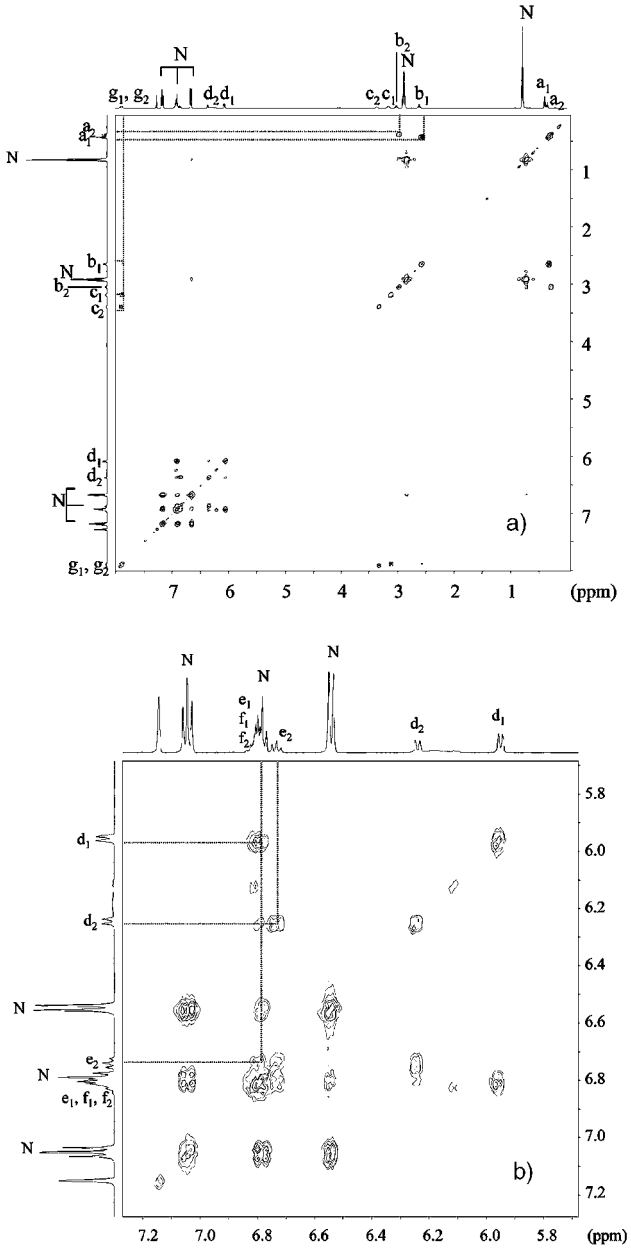

Figure 2. a) ^1H-^1H COSY NMR spectrum (500 MHz, 25 °C, C_6D_6) of solution **I**; b) expanded [$\delta = 7.2-5.7$ ppm] region

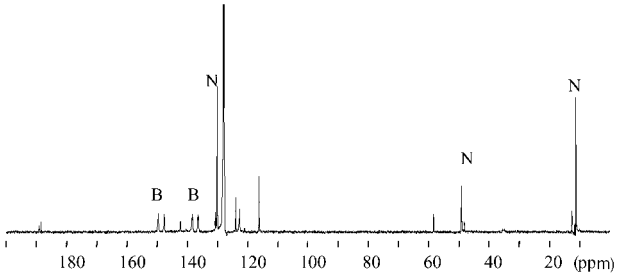

Figure 3. ^{13}C NMR spectrum (500 MHz, 25 °C, C_6D_6) of solution **I**; N and B indicate peaks due to free Et_2NPh and $B(C_6F_5)_3$, respectively

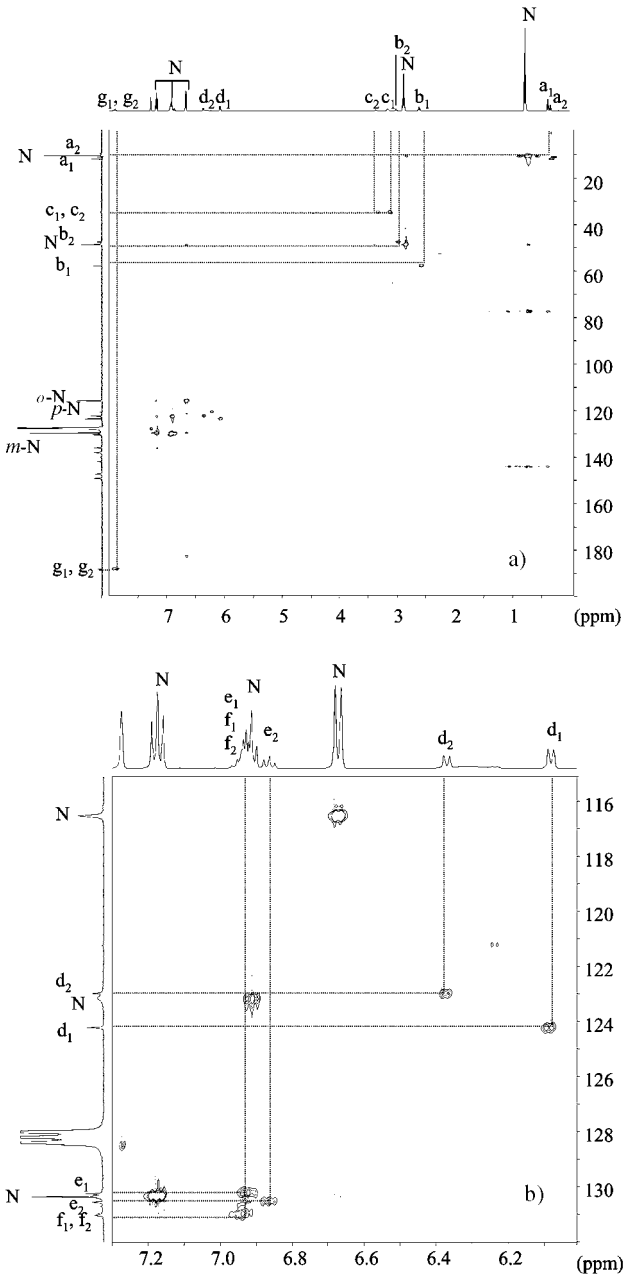

Figure 4. a) ^{1}H-^{13}C HSQC NMR spectrum (500 MHz, 25 °C, C_6D_6) of solution **I**; b) expanded [δ = 7.3−6.0/δ = 132−115 ppm] region

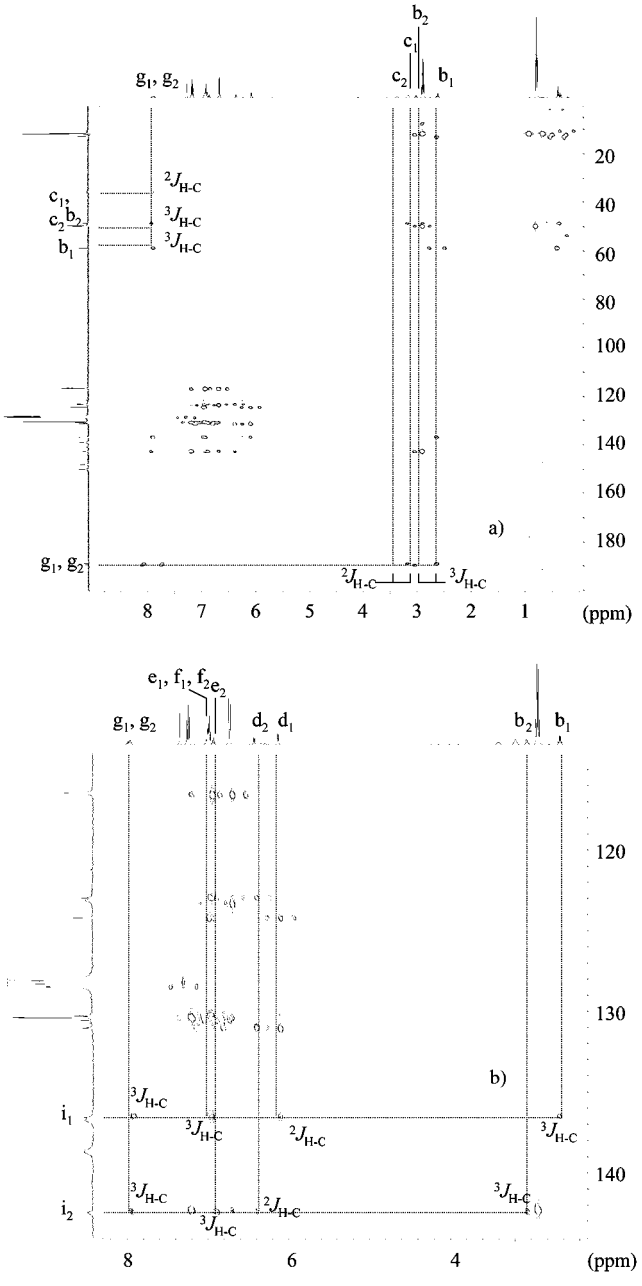

Figure 5. a) ^{1}H-^{13}C HMBC NMR spectrum (500 MHz, 25 °C, C_6D_6) of solution **I**; b) expanded [δ = 8.3−2.3/δ = 144 to −114 ppm] region

The ^{1}H-^{13}C HMBC NMR experiments on **I** (Figure 5) allow the *ipso* carbons of the two distinct phenyl rings to be assigned (Figure 5b), and show their couplings with the methylene protons (b_1, b_2 − $^{3}J_{C\text{-}H}$), with the deshielded triplets (g_1, g_2 − $^{3}J_{C\text{-}H}$), and with aromatic *meta* (e_1, e_2 − $^{3}J_{C\text{-}H}$) and *ortho* (d_1, d_2 − $^{2}J_{C\text{-}H}$) hydrogens. The coupling between the deshielded triplets (g_1, g_2 − $^{3}J_{C\text{-}H}$) and methylene protons (b_1, b_2 − $^{3}J_{C\text{-}H}$) and, (c_1, c_2 − $^{2}J_{C\text{-}H}$) is also evident (Figure 5a).

The ^{11}B NMR spectrum of **I** on a 300 MHz spectrometer shows two sharp peaks at δ = −13.7 and −23.6 ppm, characteristic of tetracoordinate anionic boron centers[22] and a broad resonance at δ = 60 ppm assigned to free $B(C_6F)_3$ [23−25] (Figure 6). No resonance characteristic of a $(C_6F_5)_3B{\cdot}NEt_2Ph$ adduct is observed in the region between 0 and −5 ppm.[22] The resonance at δ = −23.6 ppm is unambiguously assigned to $[HB(C_6F_5)_3]^-$ due to the observed ^{11}B-^{1}H coupling constant ($^{1}J_{B\text{-}H}$ = 77.5 Hz[22,26]). This assignment is consistent with the presence of a broad signal at δ = 3.9 ppm characteristic of the hydride[27] in the ^{1}H NMR spectrum of **I**. The third resonance at δ = −13.7 ppm is assigned by comparison to related

systems[8,28–30] to a $[R\text{-}B(C_6F_5)_3]^-$ fragment (where R is an alkyl group with an sp^3 carbon bound to boron). The ^{11}B NMR spectrum of **I** on a 500 MHz spectrometer shows that there are two signals at $\delta = -13.1$ (B_2) and -13.5 ppm (B_1) in an approximate B_2/B_1 ratio of 2:5 (Figure 6). This indicates the presence of two types of anionic boron compound in which the boron atoms are located in very similar environments.

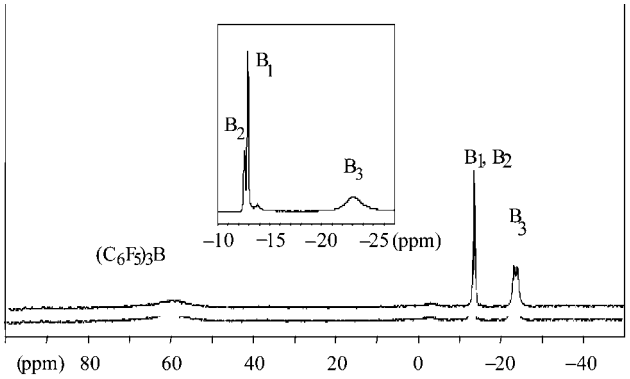

Figure 6. ^{11}B NMR spectrum (500 MHz, 25 °C, C_6D_6) of solution **I**

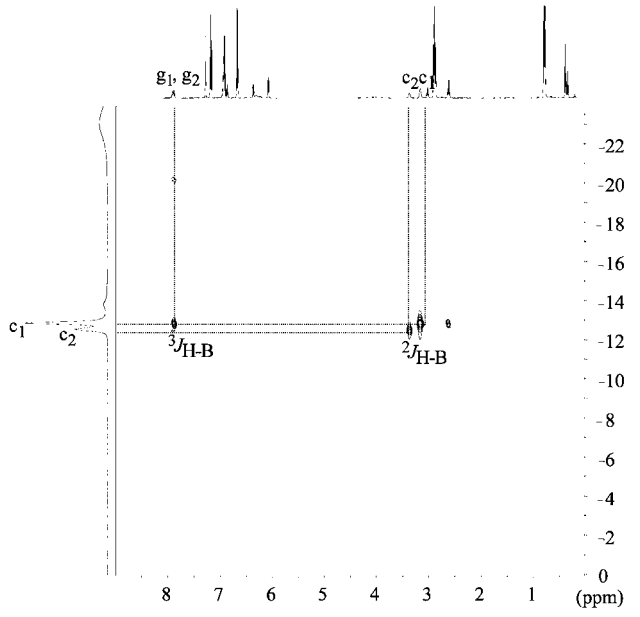

Figure 7. ^1H-^{11}B NMR HMBC NMR spectrum (500 MHz, 25 °C, C_6D_6) of solution **I**

^1H-^{11}B HMBC NMR experiments show a $^2J_{B\text{-}H}$ coupling between the $[R\text{-}B(C_6F_5)_3]^-$ boron atoms and the (c_1, c_2) protons (Figure 7). In spite of the short T_2 of the quadrupolar ^{11}B nucleus, ^1H-^{11}B HMBC experiments were attempted to confirm the linkage of the $\text{-}CH_2\text{-}B(C_6F_5)_3$. The quality of the 2D matrix was surprisingly good and allowed us to attribute the broad resonances c_1 and c_2 in the ^1H ($\delta c_1 = 3.15$, $\delta c_2 = 3.45$ ppm) and ^{13}C NMR spectra ($\delta c_1, c_2 = 34.5$ ppm) to be attributed to the $\text{-}CH_2\text{-}B(C_6F_5)_3$ moieties.[30–32] A $^3J_{B\text{-}H}$ coupling of the $[\text{-}CH_2\text{-}B(C_6F_5)_3]^-$ boron atoms with the (g_1, g_2) protons is an additional proof for the structure of $H\text{-}(C{=}X)\text{-}CH_2\text{-}B(C_6F_5)_3$. Furthermore, a third coupling is observed between the major boron resonance B_1 and the methylene protons b_1, while there is no correlation between B_2 and the methylene protons b_2.

^1H-^{15}N HMBC NMR experiments indicate that three different nitrogen resonances are present at $\delta = 74$, 209.5 and 210.2 ppm (Figure 8 and 9). The major peak at $\delta = 74$ ppm (N) corresponds to the nitrogen atom of NEt_2Ph. The resonances at $\delta = 209.5$ for (N_1) and $\delta = 210.2$ ppm (N_2) are characteristic of an sp^2-hybridized nitrogen atom, such as an iminium center.[22] Correlations are observed between these peaks and the methyl (a_1, a_2 – $^3J_{N\text{-}H}$), the methylene (b_1, b_2 – $^2J_{N\text{-}H}$; c_1, c_2 – $^3J_{N\text{-}H}$), the *ortho* (d_1, d_2 – $^3J_{N\text{-}H}$) and imino (g_1, g_2 – $^2J_{N\text{-}H}$) protons, indicating the existence of two types of iminium center in slightly different environments, as observed in the ^{11}B NMR spectrum.

The ^{19}F NMR spectrum of **I** reveals a complex pattern of non-equivalent pentafluorophenyl groups at ambient temperature, three types of pentafluorophenyl ligand (**a**, **b**, **c**) bound to anionic boron centers are present[32] (Table 1). No pentafluorobenzene is formed in solution.

Thus, multinuclear NMR studies indicate that in solutions containing equimolar amounts of $B(C_6F_5)_3 + NEt_2Ph$ (**I**) at ambient temperature, several species are present: $B(C_6F_5)_3$, NEt_2Ph, $[HB(C_6F_5)_3]^-(HNEt_2Ph)^+$ and two new species (A_1, A_2 in Scheme 1) in a constant A_1/A_2 ratio of 3:2. In none of the experiments is formation of the $(C_6F_5)_3B{\cdot}NEt_2Ph$ adduct observed. The zwitterionic stereoisomeric species A_1 (*E* isomer) and A_2 (*Z* isomer) come closest to explaining the 2D NMR experimental data.

In the ^1H-^{11}B HMBC NMR spectra, the long range coupling between the boron resonance B_1 and the methylene protons b_1 is only possible for the *trans*-isomer A_1 (*E* isomer) in a particular conformation. According to the relative intensities of the peaks associated with A_1 in the ^1H, ^{11}B and ^{15}N NMR spectra, this result definitively proves that A_1 (*E* isomer) is the major species, as expected on the basis of steric considerations.

Multinuclear NMR studies performed on **I** at ambient temperature enable the other boron species, besides unchanged $B(C_6F_5)_3$, to be identified as $[HB(C_6F_5)_3]^-$ and the two stereoisomers A_1 and A_2 of $[RCH_2\text{-}B(C_6F_5)_3]^-$. The formation of the $[HB(C_6F_5)_3]^-$ anion can be explained by a reversible abstraction of the α-hydrogen from NEt_2Ph by $B(C_6F_5)_3$ affording the iminium cations (B) (reaction 1 in Scheme 2). This hydride abstraction by $B(C_6F_5)_3$ could be facilitated by conjugation with the lone pair of the nitrogen atom, and has already been reported for organic substrates[33] and for organometallic complexes.[26,27] However, there is no evidence for the presence of the iminium cations (B) in solution. It is likely that, in the presence of NEt_2Ph, the iminium salt (B) initially formed is rapidly converted into enamine (C) and an anilinium salt (reaction 2, Scheme 2). The conversion of tertiary iminium salts into enamines in presence of a base is well documented.[34] At this stage, an electrophilic addition of $B(C_6F_5)_3$ to the enamine intermediate yields the zwitterions (A_1, A_2) (reaction

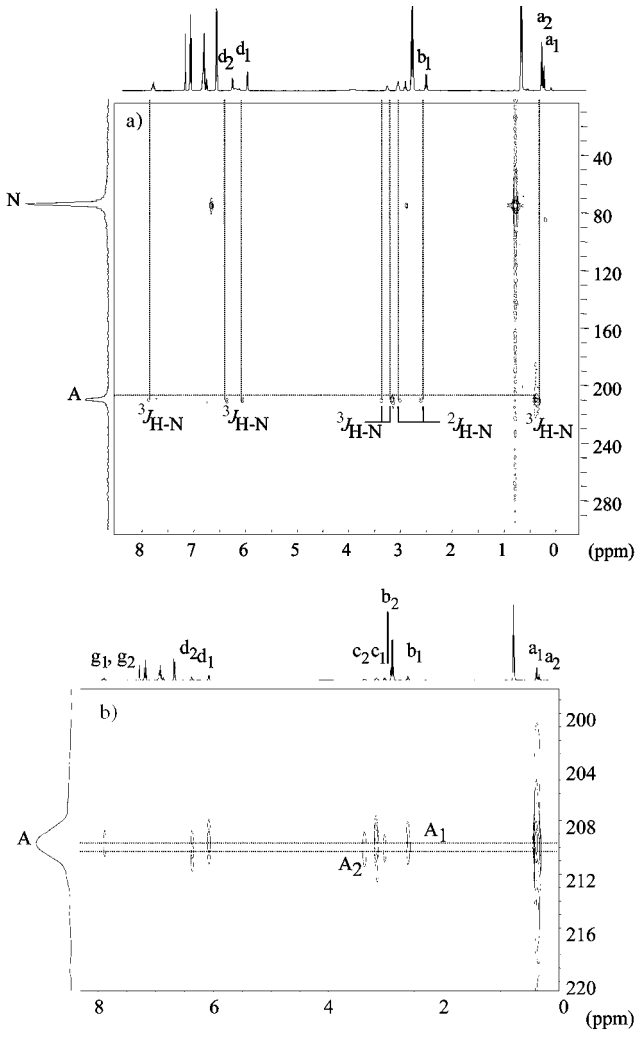

Figure 8. a) ^1H-^{15}N NMR HMBC NMR spectrum (500 MHz, 25 °C, C_6D_6) of solution **I**; b) expanded [δ = 199−220 ppm] region

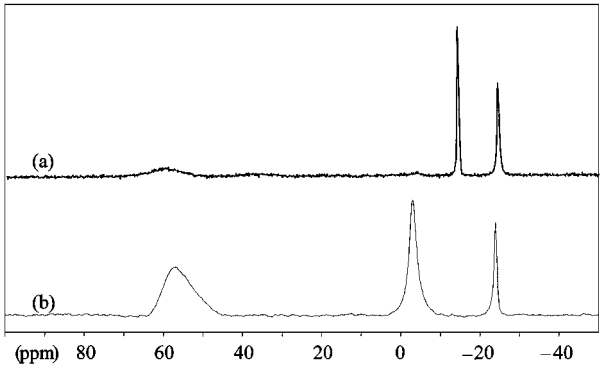

Figure 9. ^{11}B NMR spectrum (300 MHz, 25 °C, C_6D_6) of: a) solution **I**; b) solution $\mathbf{I_{Me}}$

3, Scheme 2), as already reported for other Lewis acids such as $GeCl_4$, $SnCl_4$,[35] and $TiCl_4$.[36,37]

The involvement of the iminium ion (B) as an intermediate is demonstrated by using dimethylaniline as a base instead of diethylaniline. The reaction of equimolar amounts of $B(C_6F_5)_3$ and NMe_2Ph in concentrated [D_6]benzene solution was monitored by ^{11}B NMR spectroscopy at room temperature. The spectra of the pale pink solution of $\mathbf{I_{Me}}$ show the presence of a sharp peak at δ = −24 ppm characteristic of the $[HB(C_6F_5)_3]^-$ anion. This indicates the formation of the iminium (B_{Me}) by α-hydrogen abstraction with $B(C_6F_5)_3$ (reaction 5, Scheme 3). It should be noted that there is also a peak at δ = −3 ppm which is assigned to the Lewis acid-base complex $(C_6F_5)_3B{\cdot}NMe_2Ph$ (**V**). The fact that no peak characteristic of zwitterions A_1 and A_2 is present at δ = −13 ppm proves that electrophilic addition of $B(C_6F_5)_3$ does not proceed for dimethylaniline. This can be rationally explained by the fact that formation of an enamine intermediate is not possible in the case of dimethylaniline. Thus, the reaction pathway is stopped at the stage of the formation of the ternary iminium salt (B_{Me}).

The overall equilibria observed in solutions **I** and $\mathbf{I_{Me}}$ are summarized in reaction 4 (Scheme 2) and reaction 6 (Scheme 3) respectively. It should be noted that in the ^{11}B NMR spectrum of **I** (Figure 9) the intensity ratio of 1:0.9 between the two sharp peaks at δ = −13.7 and −23.6 ppm, that is $[CH_2\text{-}B(C_6F_5)_3]^-/[HB(C_6F_5)_3]^-$, is in good agreement with the stoichiometry expected from reaction 4 in Scheme 2. However, in all cases, the reaction of R-OH compounds [R = H, Ph_3Si, (c-$C_5H_9)_7O_{12}Si_8$ or silanol group of silica] with [$B(C_6F_5)_3$ + NEt_2Ph] solutions leads quantitatively to the formation of $[RO\text{-}B(C_6F_5)_3]^-(HNEt_2Ph)^+$ confirming that all equilibria involved in solutions of **I** are displaced towards the ionic form $[RO\text{-}B(C_6F_5)_3]^-(HNEt_2Ph)^+$ in the presence of protic compounds.[39]

Table 1. ^{19}F NMR chemical shifts of C_6F_5 ligands in **I**

Attribution	Chemical shifts[a]			$\Delta(\delta_{m,p})$
	o-C_6F_5	p-C_6F_5	m-C_6F_5	
$B(C_6F_5)_3$ [b]	−128.7	−141.7	−160.0	18.3
a[b]	−132.6	−158.6	−164.8	6.2
b[b]	−132.2	−159.5	−164.3	4.8
c[b]	−133.5	−161.2	−165.4	4.2

[a] δ in ppm. [b] At 25 °C in C_6D_6.

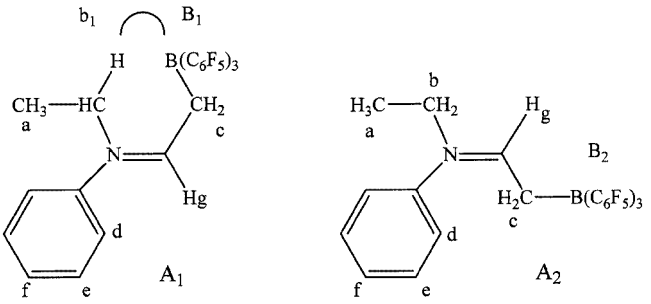

Scheme 1. Structure of the two stereoisomers (A_1) and (A_2) present in solution **I**

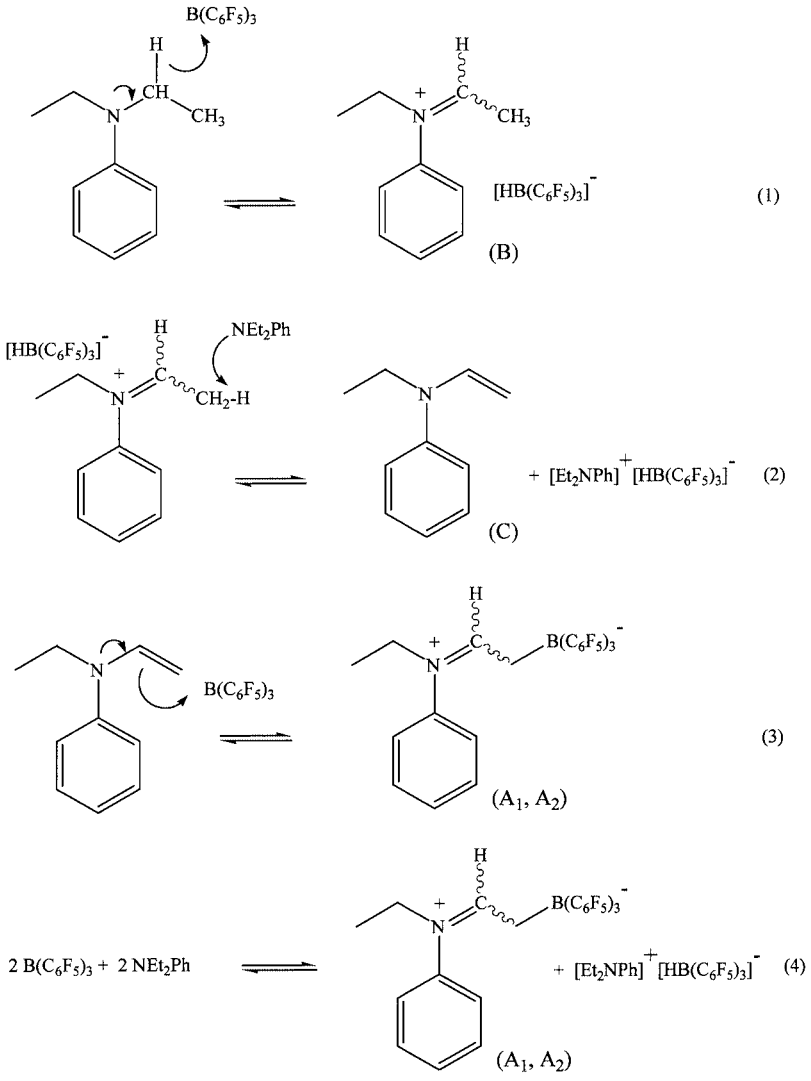

Scheme 2. Proposed mechanism to explain the formation of stereoisomers (A_1) and (A_2)

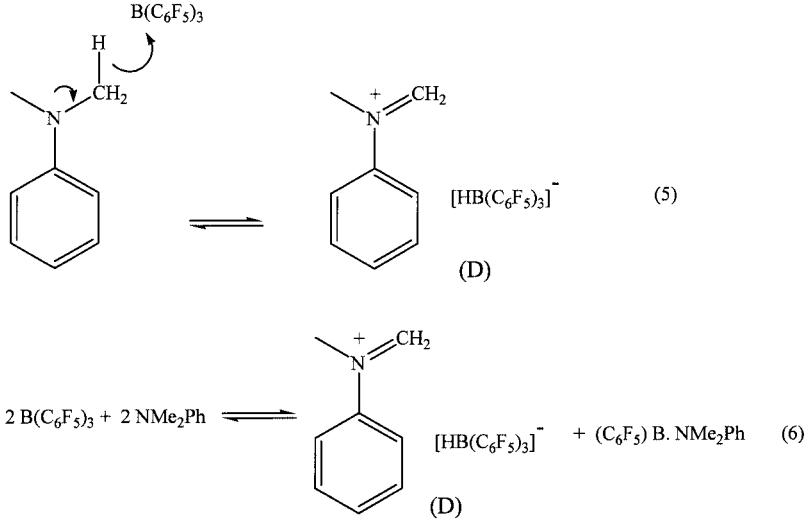

Scheme 3. Structure of the compounds of the reaction of $B(C_6F_5)_3$ and Me_2NPh, solution $\mathbf{I_{Me}}$

Conclusion

The presence of several species in equilibrium in a solution of $(C_6F_5)_3B$ and R_2NPh (1: 1) has been established by several NMR experiments. In the case of dimethylaniline, besides free $B(C_6F_5)_3$ and Me_2NPh, the 1:1 adduct $(C_6F_5)_3B{\cdot}NMe_2Ph$ and an iminium salt $[PhCH_3N{=}CH_2]^+[HB(C_6F_5)_3]^-$ have been identified. With diethylaniline, 40% of the products were unchanged $(C_6F_5)_3B$ and Et_2NPh, 30% were the iminium salt $[HB(C_6F_5)_3]^-(HNEt_2Ph)^+$, and the remaining 30% were converted into the zwitterionic stereoisomers (*E*)- and (*Z*)-$[PhEtN^+{=}CH\text{-}CH_2B^-(C_6F_5)_3]$ in a 3:2 ratio. In the presence of a protic compound this equilibrium is totally displaced towards the ionic form $[RO\text{-}B(C_6F_5)_3]^-[HNEt_2Ph]^+$.

Experimental Section

All operations were carried out under an argon atmosphere using glovebox (Jacomex or MBraun) or vacuum-line techniques. Toluene and pentane were distilled under argon from Na/K alloy, degassed and stored under argon over Na (toluene) or 3 Å molecular sieves (pentane). C_6D_6 (SDS − 99.6%) and CD_2Cl_2 (SDS − 99.6%) were degassed by three "freeze-pump-thaw" cycles and dried over freshly regenerated 3 Å molecular sieves. NEt_2Ph (Aldrich Chemicals, 98%) and NMe_2Ph (Aldrich Chemicals, 99%) were dried over KOH, distilled under vacuum and used immediately. $B(C_6F_5)_3$ (Merck Chemicals, > 97%) was dried using Me_3SiCl,[38] purified by vacuum sublimation and controlled by ^{19}F NMR spectroscopy before use. The NMR spectra were recorded with Bruker AC 200 MHz (^{19}F), AC 300 MHz (^1H, ^{13}C), DRX 300 MHz (^{11}B) and DRX 500 MHz (^1H, ^{13}C, ^{11}B, ^{15}N 2D NMR) spectrometers. Chemical shifts are reported in ppm and referenced to residual solvent resonances (C_6D_6: δ = 7.15 ppm for ^1H, δ = 128 ppm for ^{13}C; CD_2Cl_2: δ = 5.32 ppm for ^1H, δ = 53.8 ppm for ^{13}C), or external standards (^{19}F: $CFCl_3$; ^{11}B: $BF_3{\cdot}OEt_2$; ^{15}N: *N*,*N*-dimethylformamide).

2D COSY experiments were acquired with the standard Bruker COSYgp experiment and processed in absolute mode. 2D HSQC experiment were acquired with the standard Bruker inviegts experiment and processed in phases mode. 2D HMBC experiment were acquired with the standard Bruker inv4gplrnd and processed in absolute mode, as shown in Table 2.

Table 2. Standard parameters for the 2D NMR experiments

	^1H-^{13}C	^1H-^{15}N	^1H-^{11}B
D6	50ms	100 ms	25 ms
Gradients	20−20−10	70−30−50	60−20−6567
Row data size	4096 × 1024	4096 × 256	2048 × 512

Reactions of Equimolar Amounts of $[B(C_6F_5)_3{+}NEt_2Ph]$ (I) and $[B(C_6F_5)_3{+}NMe_2Ph]$ (I_{Me})

Preparation of I: In an NMR tube, $B(C_6F_5)_3$ (75 mg, 0.15 mmol) was dissolved in 0.4 mL of C_6D_6. NEt_2Ph (23.3 μL, 0.15 mmol) was then added with a syringe to give a pink solution after agitation.

NEt_2Ph: ^1H NMR (C_6D_6): δ = 7.17 (dd, $^3J_{H\text{-}H}$ = 7.9 Hz, 2 H, *m*-C_6H_5), 6.9 (t, $^3J_{H\text{-}H}$ = 7.2 Hz, 1 H, *p*-C_6H_5), 6.66 (d, $^3J_{H\text{-}H}$ = 8.2 Hz, 2 H, *o*-C_6H_5), 2.80 (q, $^3J_{H\text{-}H}$ = 7.1 Hz, 4 H, CH_2), 0.82 (t, $^3J_{H\text{-}H}$ = 7.1 Hz, 6 H, CH_3) ppm. ^{13}C NMR: δ = 142.4 (s, *i*-C_6H_5), 130.3 (s, *m*-C_6H_5), 123.1 (br. s, *p*-C_6H_5), 116.4 (s, *o*-C_6H_5), 49.4 (s, CH_2), 11.4 (s, CH_3) ppm. ^{15}N NMR: δ = 71 (s, NEt_2Ph) ppm.

$B(C_6F_5)_3$: ^{11}B NMR: δ = 59 (br. s, $B(C_6F_5)_3$] ppm. ^{13}C NMR: δ = 148.8 (d, $^1J_{C\text{-}F}$ = 243 Hz, *o*-C_6F_5), 141.5 (d, $^1J_{C\text{-}F}$ = 230 Hz, *p*-C_6F_5), 137.7 (d, $^1J_{C\text{-}F}$ = 247 Hz, *m*-C_6F_5) ppm. ^{19}F NMR: δ = −128.6 (br. s, 6 F, *o*-C_6F_5), −141.7 (br. s, 3 F, *p*-C_6F_5), −160.0 (br. s, 6 F, *m*-C_6F_5) ppm.

[A_1, (*E*)-isomer]: ^1H NMR (20%): δ = 7.88 (t, $^3J_{H\text{-}H}$ = 7.9 Hz, 1 H, H-C=N), 6.92 (m, *m*- and *p*-C_6H_5), 6.17 (d, $^3J_{H\text{-}H}$ = 7.2 Hz, 2 H, *o*-C_6H_5), 3.15 (br. m, 2 H, CH_2-B), 2.60 (q, $^3J_{H\text{-}H}$ = 7.25 Hz, 2 H, CH_2), 0.40 (t, $^3J_{H\text{-}H}$ = 7.2 Hz, 3 H, CH_3) ppm. ^{11}B NMR: δ = −12.9 (s, [-CH_2-$B(C_6F_5)_3]^-$) ppm. ^{13}C NMR: δ = 188.6 (s, C=N), 136.5 (s, i-C_6H_5), 131 (s, *m*-C_6H_5), 130.2 (s, *p*-C_6H_5), 124.2 (s, *o*-C_6H_5), 58.5 (s, CH_2), 34.5 (br, CH_2-B), 12.7 (s, CH_3) ppm; C_6F_5 signals not resolved. ^{15}N NMR: δ = 209.5 (s, $EtPhN^+{=}CH$-) ppm. ^{19}F NMR: δ = −132.6 (d, $^3J_{F\text{-}F}$ = 19 Hz, 6 F, *o*-C_6F_5), −158.6 (br. s, 3 F, *p*-C_6F_5), −164.8 (br. s, 6 F, *m*-C_6F_5) ppm.

[A_2, (*Z*)-isomer]: ^1H NMR (10%): δ = 7.91 (t, $^3J_{H\text{-}H}$ = 8.5 Hz, 1 H, H-C=N), 6.92 (m, *m*-C_6H_5), 6.85 (t, $^3J_{H\text{-}H}$ = 7.7 Hz, 1 H, *p*-C_6H_5), 6.36 (d, $^3J_{H\text{-}H}$ = 7.9 Hz, 2 H, *o*-C_6H_5), 3.45 (br.m, 2 H, CH_2-B), 3.10 (q, $^3J_{H\text{-}H}$ = 7.4 Hz, 2 H, CH_2), 0.35 (t, $^3J_{H\text{-}H}$ = 7.2 Hz, 3 H, CH_3) ppm. ^{11}B NMR: δ = −12.6 (s, [-CH_2-$B(C_6F_5)_3]^-$) ppm. ^{13}C NMR: δ = 189.2 (s, C=N), 142.4 (s, *i*-C_6H_5), 130.9 (s, *m*-C_6H_5), 130.5 (s, *p*-C_6H_5), 122.9 (s, *o*-C_6H_5), 48.3 (s, CH_2), 34.5 (br, CH_2-B), 11.8 (s, CH_3) ppm; C_6F_5 signals not resolved. ^{19}F NMR: δ = −132.6 (d, $^3J_{F\text{-}F}$ = 19 Hz, 6 F, *o*-C_6F_5), −158.6 (br. s, 3 F, *p*-C_6F_5), −164.8 (br. s, 6 F, *m*-C_6F_5) ppm. ^{15}N NMR: δ = 210.2 (s, $EtPhN^+{=}CH$-) ppm.

$[HB(C_6F_5)_3]^-$: ^1H NMR: δ = 3.90 (br, 1 H) ppm. ^{11}B NMR: δ = −23.6 (d, $^1J_{B\text{-}H}$ = 77.5 Hz) ppm. ^{19}F NMR: δ = −132.2 (d, $^3J_{F\text{-}F}$ = 22 Hz, 6 F, *o*-C_6F_5), −159.5 (t, $^3J_{F\text{-}F}$ = 22 Hz, 3 F, *p*-C_6F_5), −164.3 (m, 6 F, *m*-C_6F_5) ppm; δ = −133.5 (br. m, 6 F, *o*-C_6F_5), −161.2 (br. m, 3 F, *p*-C_6F_5), −165.4 (br. m, 6 F, *m*-C_6F_5) ppm.

Preparation of I_{Me}: In an NMR tube, $B(C_6F_5)_3$ (97 mg, 0.19 mmol) was dissolved in 0.4 mL of C_6D_6. NMe_2Ph (24 μL, 0.19 mmol) was then added with a syringe to give a pale pink solution.

NMe_2Ph: ^1H NMR: δ = 7.31 (dd, $^3J_{H\text{-}H}$ = 7.0 Hz, 2 H, *m*-C_6H_5), 6.88 (t, $^3J_{H\text{-}H}$ = 7.0 Hz, 1 H, *p*-C_6H_5), 6.72 (d, $^3J_{H\text{-}H}$ = 8.5 Hz, 2 H, *o*-C_6H_5), 2.62 (s, 3 H, CH_3) ppm. ^{15}N NMR: δ = 43.7 (s, NMe_2Ph) ppm.

$(C_6F_5)_3B{\cdot}NMe_2Ph$: ^1H NMR: δ = 7.17 (d, $^3J_{H\text{-}H}$ = 8.5 Hz, 2 H, *o*-C_6H_5), 6.8 (t, $^3J_{H\text{-}H}$ = 8.2 Hz, 1 H, *p*-C_6H_5), 6.67 (t, $^3J_{H\text{-}H}$ = 8.4 Hz, 2 H, *m*-C_6H_5), 2.55 (s, 6 H, CH_3) ppm. ^{11}B NMR: δ = −2.9 (s, $(C_6F_5)_3B$-NMe_2Ph) ppm. ^{15}N NMR: δ = 52.3 [s, $(C_6F_5)_3B$-NMe_2Ph] ppm. ^{19}F NMR: δ = −132.7 (d, $^3J_{F\text{-}F}$ = 20 Hz, 6 F, *o*-C_6F_5), −159.1 (t, $^3J_{F\text{-}F}$ = 20 Hz, 3 F, *p*-C_6F_5), −165.4 (m, 6 F, *m*-C_6F_5) ppm.

$[PhMe(N{=}CH_2)]^+[HB(C_6F_5)_3]^-$: ^{11}B NMR: δ = −23.9 (s, $[HB(C_6F_5)_3]^-$) ppm. ^{19}F NMR: δ = −132.1 (d, $^3J_{F\text{-}F}$ = 22 Hz, 6 F, *o*-C_6F_5), −159.7 (t, $^3J_{F\text{-}F}$ = 22 Hz, 3 F, *p*-C_6F_5), −164.4 (m, 6 F, *p*-C_6F_5); δ = −133.3 (br. m, 6 F, *o*-C_6F_5), −161.6 (br. m, 3 F, *p*-C_6F_5), −165.4 (br. m, 6 F, *m*-C_6F_5) ppm.

Acknowledgments

We thank Dr. R. Andersen, Pr. M. Ciufolini and Pr. A. Smith for fruitful discussions. We are also grateful to CNRS and ESCPE Lyon for financial support, and to the French Ministry for Education and Research for a fellowship (N. M.).

[1] G. G. Hlatky, R. R. Eckman, H. W. Turner, *Organometallics* **1992**, *11*, 1413−1416.
[2] Z. Lin, J. F. Le Marechal, M. Sabat, T. J. Marks, *J. Am. Chem. Soc.* **1987**, *109*, 4127−4129.
[3] H. W. Turner, *EP 0277004*; Exxon Chemicals, **1988**.
[4] G. G. Hlatky, H. W. Turner, R. R. Eckman, *J. Am. Chem. Soc.* **1989**, *111*, 2728−2729.
[5] M. Bochmann, A. J. Jaggar, J. C. Nicholls, *Angew. Chem. Int. Ed. Engl.* **1990**, *29*, 780−782.
[6] A. D. Horton, A. G. Orpen, *Organometallics* **1991**, *10*, 3910−3918.
[7] X. Yang, C. L. Stern, T. J. Marks, *Organometallics* **1991**, *10*, 840−842.
[8] A. R. Siedle, R. A. Newmark, W. M. Lamanna, J. C. Huffman, *Organometallics* **1993**, *12*, 1491−1492.
[9] A. R. Siedle, W. M. Lamanna, R. A. Newmark, *Makromol. Chem. Macromol. Symp.* **1993**, *66*, 215−224.
[10] R. Duchateau, R. A. Van Santen, G. P. A. Yap, *Organometallics* **2000**, *19*, 809−816.
[11] A. Metcalfe, D. I. Kreller, J. T. Hoon Kim, N. J. Taylor, J. F. Corrigan, S. Collins, *Organometallics* **2002**, *21*, 1719−1726.
[12] W. E. Piers, T. Chivers, *Chem. Soc. Rev.* **1997**, *26*, 345−354.
[13] J. Walzer, J.Flexer, *US Patent 5,643,847*; Exxon Chemicals, **1997**.
[14] D. G. Ward, E. M. Carnahan, *U.S. Patent*; W. R. Grace and Co: United States, US 5,939,347 1999.
[15] S. J. Lancaster, S. M. O′Hara, M. Bochmann, *Metallorganic Catalysts for Synthesis and Polymerization* (Ed.: W. Kaminsky), Springer, **1999**.
[16] M. Bochmann, G. J. Pindado, S. J. Lancaster, *J. Mol. Cat.* **1999**, *146*, 179−190.
[17] A. Fox, J. S. Hartman, R. E. Humphries, *J. Chem. Soc., Dalton Trans.* **1982**, 1275−1283.
[18] E. J. McLauchlan, E. F. Mooney, *Spectrochimica Acta* **1967**, *23A*, 1227−1230.
[19] A. G. Massey, A. J. Park, F. G. A. Stone, *Proc. Chem. Soc.* **1963**, 212; A. G. Massey, A. J. Park, *J. Organomet. Chem.* **1964**, *2*, 245−250; M. J. G. Lesley, A. Woodward, N. J. Taylor, T. B. Marder, I. Cazenobe, I. Ledoux, J. Zyss, A. Thornton, D. W. Bruce, A. K. Kakkar, *Chem. Mater.*, **1998**, *10*, 1355−1365; D. R. Neithamer, *US Pat. 5.721.183*, Dow Chemical, **1998**.
[20] G. L. Nelson, G. C. Levy, J. D. Cargioli, *J. Am. Chem. Soc.* **1972**, *94*, 3089−3094.
[21] J. E. Sarneski, H. L. Surprenant, F. K. Molen, C. N. Reilley, *Anal. Chem.* **1975**, *47*, 2116−2124.
[22] J. D. Kennedy, *Multinuclear NMR* (Ed.: J. Mason), Plenum Press: New York, 1987; pp 221−258.
[23] D. C. Bradley, I. S. Harding, A. D. Keefe, M. Motevalli, D. H. Zheng, *J. Chem. Soc., Dalton Trans.* **1996**, 3931−3936.
[24] L. H. Doerrer, M. L. H. Green, *J. Chem. Soc., Dalton Trans.* **1999**, 4325−4329.
[25] J. Tian, S. Wang, Y. Feng, J. Li, S. Collins, *J. Mol. Cat.* **1999**, *144*, 137−150.
[26] F. C. Liu, J. Liu, E. A. Meyers, S. G. Shore, *J. Am. Chem. Soc.* **2000**, *122*, 6106−6107.
[27] X. Yang, C. L. Stern, T. J. Marks, *Angew. Chem. Int. Ed. Engl.* **1992**, *31*, 1375−1377.
[28] X. Yang, T. J. Marks, *J. Am. Chem. Soc.* **1991**, *113*, 3623−3625.
[29] G. S. Hill, L. Manojlovic-Muir, K. W. Muir, R. J. Puddephatt, *Organometallics* **1997**, *16*, 525−530.
[30] S. Döring, G. Erker, R. Fröhlich, O. Meyer, K. Bergander, *Organometallics* **1998**, *17*, 2183−2187.
[31] C. Pellecchia, A. Immirzi, A. Grassi, A. Zambelli, *Organometallics* **1993**, *12*, 4473−4478.
[32] [32a] A. D. Horton, J. de With, *Organometallics* **1997**, *16*, 5424−5436. [32b] A. D. Horton, J. de With, A. J. van der Linden, H. van de Weg, *Organometallics* **1996**, *15*, 2672−2674.
[33] D. J. Parks, J. M. Blackwell, W. Piers, *J. Org. Chem.* **2000**, *65*, 3090−3098.
[34] L. W. Haynes, A. G. Cook, *Enamines: synthesis, structures and reactions* (Ed.: A. G. Cook), Marcel Dekker: NY, **1988**.
[35] H. Weingarten, J. S. Wager, *J. Chem. Soc., Chem. Commun.* **1970**, 854.
[36] P. Bharathi, M. Periasamy, *Org. Lett.* **1999**, *1*, 857−859.
[37] M. Periasamy, K. N. Jayakumar, P. Bharathi, *Chem. Commun.* **2001**, 1728−1729.
[38] L. W. M. Lee, W. E. Piers, M. Parvez, S. J. Rettig, V. G. Young, *Organometallics* **1999**, *18*, 3904−3912.
[39] N. Millot, A. Cox, C. C. Santini, Y. Molard, J.-M. Basset, *Chem. Eur. J.* **2002**, *8*, 1438−1442.

Received June 21, 2002
[I02333]

Metallation of Unactivated Methyl Groups − Platinum(II) Derivatives with 6-Alkyl-2,2′-bipyridines

Antonio Zucca,*[a] Sergio Stoccoro,[a] Maria Agostina Cinellu,[a] Giovanni Minghetti,[a] Mario Manassero,[b] and Mirella Sansoni[b]

Keywords: Platinum / N ligands / Cyclometallation

The reaction of $K_2[PtCl_4]$ with three 6-alkyl-2,2′-bipyridines HL, ($N_2C_{10}H_7R$; R = CH_2Me, HL^{et}; $CHMe_2$, HL^{ip}; CH_2CMe_3, HL^{np}) affords five- and six-membered cyclometallated complexes [Pt(L)Cl] where L is a terdentate *N,N,C* anionic ligand which originates from HL through direct activation of a C(sp^3)–H bond. In the case of HL^{ip}, metallation generates a stereogenic carbon atom β to the metal. Complex **5**, [$Pt(L^{np})Cl$], having an uncommon six-membered ring containing a Pt–C(sp^3) bond, was studied in depth in solution, by means of 1- and 2- dimensional NMR spectroscopy, and in the solid state by X-ray diffraction. Differences are observed in the behaviour of these ligands: thus with HL^{et} an adduct, [$Pt(HL^{et})Cl_2$], was also isolated and its structure was determined by X-ray diffraction. In the metallated species, the fourth ligand, Cl, can easily be substituted by neutral or anionic ligands (CO, PPh_3, CN^-). The metallated species react with potentially bidentate ligands L′–L′′ [$Ph_2PCH_2PPh_2$ (dppm), $Ph_2P(CH_2)_2PPh_2$ (dppe), $Ph_2P(CH_2)_2AsPh_2$ (dppae)] to give, with different Pt:L ratios, mononuclear [Pt(L)(L′–L′′)]$^+$ or dinuclear [(L)Pt(μ–L′–L′′)Pt(L)]$^{++}$ cationic species. In the second case an uncommon unsupported L′–L′′ bridge is present. The cyclometallated species are stable in air and moisture, and the *N,N,C* system is rather robust.

(© Wiley-VCH Verlag GmbH, 69451 Weinheim, Germany, 2002)

Introduction

Cyclometallated compounds, in particular those derived from nitrogen ligands, have attracted considerable interest as a consequence of the wide range of their potential applications in many areas including organic synthesis,[1] homogeneous catalysis[2] (even asymmetric), photochemistry[3], and the design of new metallomesogens[4], sensors[5] and antitumour drugs.[6]

In recent years, in addition to the classical bidentate N,C systems, attention has also been devoted towards potentially terdentate-bound anionic ligands able to coordinate through different sets of donor atoms (e.g. *N,N,C*,[7] *N,C,N*,[8] *C,N,C*[9]). The sequence of coordinating atoms, the size of the metallacycles and the type of metallated carbon atom can be tuned to obtain complexes with different properties.

Although cyclometallation reactions, especially those concerning metals of the platinum group, have been extensively studied, the factors that control the process are not completely understood. Whereas for Pd^{II} the most common mechanism is electrophilic, in the case of Pt^{II} both electrophilic and nucleophilic behaviour has been ascertained.[10] The reaction, besides the obvious electronic and steric factors, seems to be affected by a number of factors: we have shown in previous papers that even subtle differences in the substituents of the ligands can drive the cyclometallation reactions towards unpredictable results.[7a]

In general, nitrogen donor ligands show a strong tendency to form five-membered rings, although a few six-membered rings are known. The great majority of papers in this field concern C(sp^2)−H bond activation, in spite of the present interest in activation of alkyl groups. Only few cyclometallated species containing nitrogen ligands and C(sp^3)−Pt bonds are known and, to the best of our knowledge, only two six-membered cyclometallated species with a Pt−C(sp^3) bond have been described,[11] but none of them derives from a true C−H activation.

Here we describe a series of platinum(II) complexes containing terdentate bound anionic ligands with an *N,N,C*(sp^3) sequence of donor atoms obtained by the direct activation of a methyl group of 6-alkyl-2,2′-bipyridines. The substituents on the bipyridines have been chosen in order to compare five and six-membered rings. In addition, one of the ligands (HL^{ip}, $N_2C_{10}H_7CHMe_2$–6), is potentially able to give a stereogenic carbon atom directly by metallation.

Depending on the ligand and the reaction conditions both adducts [$Pt(HL)Cl_2$] and five- or six-membered cyclo-

[a] Dipartimento di Chimica, Università di Sassari,
Via Vienna 2, 07100 Sassari, Italy
Fax: (internat.) +39−079/229559
E-mail: zucca@uniss.it
[b] Centro CNR,
Dipartimento di Chimica Strutturale e Stereochimica Inorganica, Università di Milano
Via Venezian 21, 20133 Milano, Italy
E-mail: m.manassero@csmtbo.mi.cnr.it

metallated species, [Pt(L)Cl], can be obtained from $K_2[PtCl_4]$. The chloride ligand in the metallated species has been found to be rather substitution labile, so that its replacement by anionic or neutral ligands as CN^-, CO or PPh_3 has been studied. We also report on the reaction with the potentially chelating ligands L′−L′′ [$Ph_2PCH_2PPh_2$ (dppm), $Ph_2P(CH_2)_2PPh_2$ (dppe), $Ph_2P(CH_2)_2AsPh_2$ (dppae)] with 1:1 and 2:1 Pt/L′−L′′ molar ratios.

The behaviour of $[PtCl_4]^{2-}$ is compared with that of $[PdCl_4]^{2-}$, which is previously described.[7a]

Results and Discussion

The ligands 6-ethyl-2,2′-bipyridine (HL^{et}), 6-isopropyl-2,2′-bipyridine (HL^{ip}) and 6-neopentyl-2,2′-bipyridine (HL^{np}) were obtained as previously described.[12]

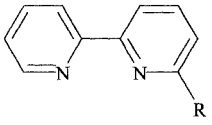

R	
CH_2CH_3	HL^{et}
$CH(CH_3)_2$	HL^{ip}
$CH_2C(CH_3)_3$	HL^{np}

The activation of one C(sp^3)−H bond was achieved with HL^{ip} and HL^{np}, in high yields (ca. 90%), by reacting the ligand with $K_2[PtCl_4]$ in aqueous HCl under refluxing conditions. In the case of HL^{et} the metallation, possibly owing to the presence of only one methyl group, is more difficult and a mixture of the metallated complex [Pt(L^{et})Cl] (**2**) and the adduct [Pt(HL^{et})Cl_2] (**1**), is obtained. We recently reported[7a] that the analogous reactions of these ligands with $Na_2[PdCl_4]$ give only the adducts [Pd(HL)Cl_2]: C−H activation however can be easily obtained from [Pd($OAc)_2$]. A peculiar behaviour is observed with a forth ligand HL^{tb} (R = $C(CH_3)_3$]: activation of a methyl group by reaction with $[PdCl_4]^{2-}$ occurs even at room temperature, whereas refluxing conditions are needed with $[PtCl_4]^{2-}$.

The adduct [Pt(HL^{et})Cl_2], **1**, can also be synthesised from *cis*-[Pt($DMSO)_2Cl_2$] (see the Exp. Sect.) in fairly good yields. The ^{1}H NMR spectrum (see Table 1) shows all the expected resonances: in particular the 6′-H and the CH_2 protons are strongly deshielded with respect to the free ligand ($\Delta\delta$ = 0.95 and 0.83 ppm, respectively) as is often observed when a chlorine atom is coordinated in their proximity. In addition the 6′-H is strongly coupled to platinum ($^3J_{Pt\text{-}H}$ = 40 Hz), providing evidence for the coordination of the nitrogen atom of the unsubstituted pyridine ring. Complex **1** was characterised in the solid state by X-ray diffraction.

The structure consists of the packing of [Pt(HL^{et})Cl_2] molecules with no unusual van der Waals contacts. There are two crystallographically independent molecules, A and B, in the asymmetric unit. Selected bond lengths and angles for the two molecules are reported in Table 4. An ORTEP view of molecule A is shown in Figure 1. The platinum atom displays a square-planar coordination with a slight square-pyramidal distortion. The displacement of the metal atom from the best plane of atoms Cl(1), Cl(2), N(1), and N(2) is 0.090(1) Å in molecule A and 0.111(1) Å in molecule B. Corresponding bond lengths and angles in the two molecules are all very similar (see Table 4). The Pt−Cl(1) and Pt−Cl(2) distances, (average 2.298 and 2.284 Å, respectively) are both in good agreement with the Pt−Cl bond length, 2.299(2) Å, found in [PtCl(Me)(HL^{et})], compound **19**.[13] The Pt−N(2) distance, average 2.050 Å, is longer than the Pt−N(1) one, average 1.996 Å, and the Cl(1)−Pt−N(2) angle, average 100.5°, is much larger than the Cl(2)−Pt−N(1) angle, average 92.7°. Both effects are probably due to the steric hindrance of the ethyl substituent on atom C(10). An even larger Cl−Pt−N(2) angle, 103.1(1)°, had been found in **19**. It must be observed that in compound **19** a clear intramolecular hydrogen bond was found between a CH_2 hydrogen atom and the Cl ligand (Cl···H 2.28 Å, C(11)−H···Cl angle 160.4°, see ref.[13]). There is no such hydrogen bond in either of the two present independent molecules, which exhibit different conformations of the ethyl substituent, with a shortest Cl(1)···H distance of 2.52 Å and a C(11)−H···Cl(1) angle of 126.6° in molecule B.

Metallated Compounds

From $K_2[PtCl_4]$ the metallated compounds [Pt(L^{ip})Cl] (**3**) and [Pt(L^{np})Cl] (**5**) have been obtained in pure form, whereas isolation of complex **2** requires separation from adduct **1** by column chromatography. The synthesis of complex **4** has been previously reported.[7b]

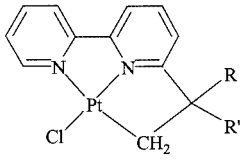

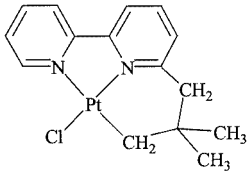

2 R = R′ = H

3 R = H, R′ = CH_3

4 R = R′ = CH_3

5

Metallation entails a C(sp^3)−H activation to give a five-membered cycle in the case of compounds **2**, **3** and **4**, and a less common six-membered ring in the case of complex **5.** To the best of our knowledge this is the first six-membered cyclometallated species of platinum(II) with nitrogen donors originating directly from an unactivated C(sp^3)−H bond: two precedent reports involved a benzylic C−H bond[11a] and an acidic C−H group in the presence of alkali.[11b]

The metallated species were fully characterised by analytical and spectroscopic methods. In particular NMR spectroscopy (^{1}H and ^{13}C{^{1}H}) gives evidence for a methylenic

Table 1. Proton NMR spectroscopic data[a]

		CH_3	CH_2-Pt	CH_2-C, CH_2-P/As	CH	H(6′)	other aromatics
$Pt(HL^{et})Cl_2$	**1**	1.43 (t, 3 H) (7.5)		3.73 (q, 2 H) (7.5)		9.65 (dd, 1 H) [40]	7.4−8.2 (m, 6 H)
$Pt(L^{et})Cl$	**2**		2.96 (t, 2 H) (6.4)[85]	3.92 (t, 2 H) (6.4) [31]		9.23 (ddd, 1 H) [10]	7.4−8.35 (m, 6 H)
$Pt(L^{ip})Cl$	**3**	1.46 (d, 3 H) (7.2)	2.66 (dd 1 H) (12.0, 5.6) [89] 3.07 (dd 1 H) (12.0, 7.5) [79]		3.45 (m, 1 H)	9.21 (ddd, 1 H) [12]	7.25−8.25 (m, 6 H)
$Pt(L^{np})Cl$	**5**	1.09 (s, 6 H)	2.43 (s, 2 H) [87]	2.82 (s, 2 H)		9.56 (ddd, 1 H) 10]	7.28−8.10 (m, 6 H)
$[Pt(L^{ip})(CN)$	**6**	1.42 (d, 3 H) (7.1)	2.57 (dd, 1 H) (12.9, 5.5) [78] 3.01 (dd, 1 H) (12.9, 7.2) [64]		3.54 (m, 1 H)	9.08 (dd, 1 H) [15]	7.40−8.18 (m, 6 H)
$[Pt(L^{ip})(CO)][BF_4]$	**7**	1.54 (d, 3 H) (7.0)	2.83 (dd,1 H) (12.2, 5.6) [66] 3.25 (dd, 1 H) (12.2, 6.6) [52]		3.88 (m, 1 H)	8.85 (ddd, 1 H) [15]	7.68−8.55 (m, 6 H)
$[Pt(L^{np})(CO)][BF_4]$	**8**	1.17 (s, 6 H)	2.50 (s, 2 H) [52]	3.14 (s, 2 H)		8.76 (dd, 1 H) [n.r]	7.58−8.82 (m, 6 H)
$[Pt(L^{et})(PPh_3)][BF_4]$	**9**		2.21 (td, 2 H) (6.2) [71]{2.7}	3.97 (t, 2 H) (6.2) [35]		[c]	7.14−8.71 (m, 7 H)
$[Pt(L^{ip})(PPh_3)][BF_4]$	**10**	1.43 (d, 3 H) (7.1)	2.08 (ddd, 1 H) (12.4, 6.8){3.4}[n.r.] 2.24 (ddd, 1 H) (12.4, 5.6){2.2}[n.r.]		3.52 (m, 1 H)	[c]	7.14−8.69 (m, 22 H)
$[Pt(L^{np})(PPh_3)][BF_4]$	**11**	0.86 (s, 6 H)	1.60 (d, 2 H) {7.1} [67]	2.91 (s, 2 H)		[c]	6.94−8.72 (m, 22 H)
$[Pt_2(L^{np})_2(\mu\text{-dppm})][BF_4]_2$	**12**	0.93 (s, 12 H)	1.52 (d, 4 H) {6.5} [60]	2.65 (s, 4 H) (bipy) 3.71 (t, 2 H) {12.2} (dppm)		[c]	6.97−8.35 (m, 34 H)
$[Pt_2(L^{ip})_2(\mu\text{-dppe})][BF_4]_2$	**13**	1.33 (d, 6 H) (7.2)	2.12 (m, 2 H) 2.28 (m, 2 H)	2.81 (m, 4 H)	3.53 (m, 2 H)	[c]	7.24−8.42 (m, 34 H)
$[Pt_2(L^{np})_2(\mu\text{-dppe})][BF_4]_2$	**14**	0.81 (s, 12 H)	1.61 (d, H) [60] {ca 5.0}	2.94 (s, 4 H) (bipy) 2.72 (m, 4 H) (dppe)		[c]	6.94−8.42 (m, 34 H)
$[Pt_2(L^{np})_2(\mu\text{-dppae})][BF_4]_2$	**15**[b]	0.87 (s, 6 H) 0.88 (s, 6 H)	1.73 (d, 2 H) {6.9} [ca 65] 1.84 (s, 2 H) [ca 65][d]	2.97 (s, 2 H) (bipy) 2.99 (s, 2 H) (bipy) 2.73 (m, 4 H) (dppae)		[c]	6.96−8.42 (m, 34 H)
$[Pt(L^{np})(dppm)][BF_4]$	**16**	0.85 s, 6H	1.69 (d, 2 H) {7.3} [65]	2.84 (s, 2 H) (bipy) 3.43 d {10.5} [49] 2H (dppm)		[c]	6.97−8.56 (m, 27 H)
$[Pt(L^{np})(dppe)][BF_4]$	**17**	0.31 (s, 3 H) 0.76 (s, 3 H)	1.18−2.84 (m, 8 H)[d]			[c]	6.43−8.19 (m, 27 H)
$[Pt(L^{np})(dppae)][BF_4]$	**18**	0.91 (s 6 H)	1.79 (d, 2 H) {6.8} [62]	2.96 (s, 2 H) (bipy) 2.25 (m, 2 H) (dppae) 2.42 (m, 2 H) (dppae)		[c]	6.92−8.64 (m, 27 H)

[a] Room temperature, solvent $CDCl_3$, chemical shifts in ppm from internal $SiMe_4$, coupling constants in, $J_{Pt,H}$ in square brackets, $J_{P,H}$ in braces; n.r. = not resolved. [b] Solvent: CD_2Cl_2. [c] In all the phosphane complexes the 6′-H is strongly shielded. [d] Complex pattern from δ = 1.18 to 2.84 ppm, due CH_2-Pt, CH_2 (dppe), CH_2(bipy), 8 H.

group strongly coupled to the metal ($^2J_{Pt,H}$ = 80−90, $^1J_{Pt,C}$ = 668−743 Hz, see Table 1 and 2).

In complexes **2−5** the signals of the 6′-H protons are strongly deshielded and coupled to the metal ($^3J_{Pt,H}$ = ca. 10 Hz). In the series of palladium(II) and platinum(II) *N,N,C* cyclometallated compounds derived from 6-substituted 2,2′-bipyridines[7a−7g] (see Scheme 1) the chemical shifts of 6′-H appear to be strongly dependent on the nature of the metal and of the fourth ligand as well as on the size of the metallated cycle.

Coordinated halides exert a strong deshielding effect. At variance, the chemical shifts are not remarkably affected by the nature of the carbon atom, $C(sp^3)$ or $C(sp^2)$, bonded to the metal.

For platinum(II) compounds, in the case of 5,5 fused rings, values of ca. δ = 9.20 ppm are typical, whereas for 5,6 fused rings more deshielded resonances (ca. 9.60 ppm) are usually observed. In the analogous palladium species the same trend is observed, but all the signals are less deshielded (ca. 0.4 ppm) than in the corresponding platinum

Table 2. ^{13}C NMR spectroscopic data (room temperature, $CDCl_3$, chemical shifts in ppm from TMS, coupling constants in Hz, $J_{Pt,C}$ in square brackets

	[Pt(L^{et})Cl], **2**	[Pt(L^{ip})Cl], **3**	[Pt(L^{np})Cl], **5**	[Pt(L^{ip})(CO)][BF_4], **7**
CH_2−Pt	- 1.2 [743]	10.1 [736]	18.2 [668]	16.2 [567]
CH_3		21.8 [44]	29.6 [28]	22.4 [39]
CH_2	44.0		55.5 [68]	
CH		49.3 [10]		49.4 [5]
C			32.2 [28]	
C3, C3′	127.7, 124.1 [51]	127.3, 124.2 [59]	120.2 [33], 121.3	129.8 [15], 125.3 [14]
C5, C5′	123.4 [11], 119.8 [35]	121.8 [12], 119.7 [36]	128.7 [45], 126.8	125.1 [47], 122.1 [25]
C4, C4′	138.5, 135.6	138.1, 135.4	136.6 (C4) 137.8 (C4′)	143.5, 142.3
C2, C2′		156.2, 152.6	157.6, 154.6	
C6		172.5	164.2	
C6′	147.9 [19]	147.8 [19]	148.0 [25]	152.3 [30]

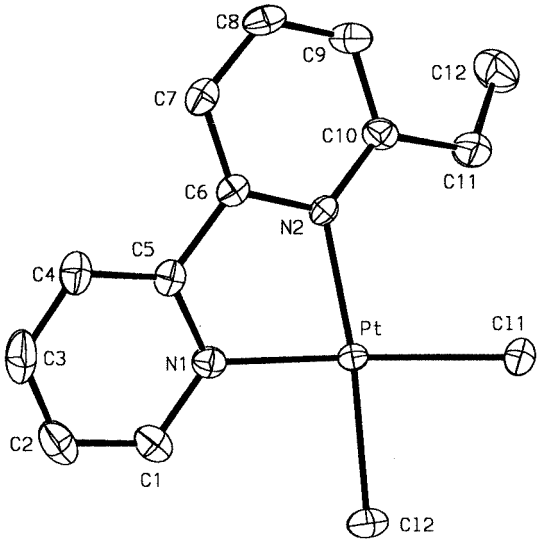

Figure 1. ORTEP view of molecule A in compound **1**; thermal ellipsoids are drawn at the 30% probability level

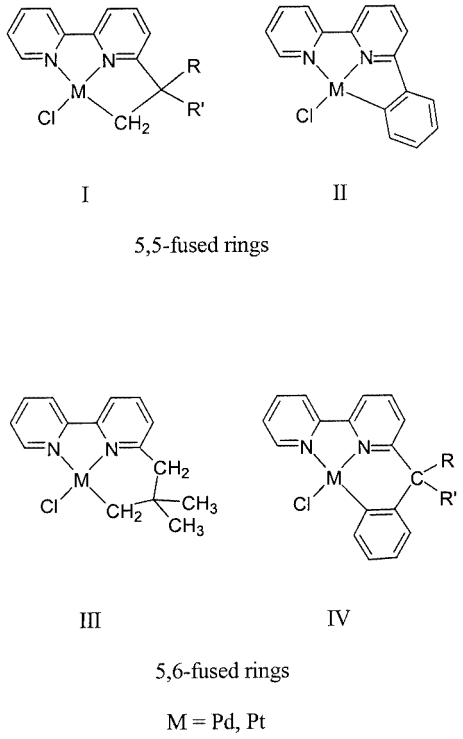

Scheme 1

complexes. Similar trends have also been recently observed for analogous gold(III) cationic species $[Au(N,N,C)Cl]^+$ [7g] for which, however, less experimental data are available.

The $^{13}C\{^1H\}$ spectra of **2**−**5** deserve comments: the chemical shifts of the CH_2−Pt resonances depend mainly on the degree of substitution on the carbon β to the metal, irrespective of the cycle [e.g. Pt−CH_2−$C(CH_3)_2$−, ca. 18−19 ppm (**4** and **5**), Pt−CH_2−$CH(CH_3)$−, ca. δ = 10 ppm (**3**), and Pt−CH_2−CH_2-, −1.2 ppm (**2**)] reflecting only electronic effects. At variance, the $^1J_{Pt,C}$ values are higher for the five-membered rings (ca 740 Hz, **2**−**4**) than for the six-membered one (668 Hz in **5**).

In the analogous palladium compounds the CH_2−Pd resonances are shifted downfield (e.g. Pd(L^{tb})Cl, δ = 32.8 ppm; Pd(L^{np})Cl, δ = 34.9 ppm).[7a]

In the case of compound **5**, taking into account the rarity of six-membered cyclometallated rings containing C(sp^3)−Pt bonds, complete assignment of ^1H and ^{13}C signals was accomplished by 2D NMR studies (COSY and HETCOR experiments, see experimental). The coupling constants $J_{Pt,C}$ in the inner pyridine ring are much larger than those of the outer one [e.g.: ^3J(Pt−C(3) = 33 Hz, ^3J(Pt−C(3′)] not observed, ^4J(Pt−C(4) = 45 Hz, ^4J(Pt−C(4′) not observed] indicating that the pyridine involved in the cyclometallation is more tightly bonded than the other one, in agreement with the X-ray data.

The crystal structure of **5**·$CHCl_3$ consists of the packing of [Pt(L^{np})Cl] and $CHCl_3$ molecules in a 1:1 molar ratio with no unusual van der Waals contacts. Selected bond parameters are listed in Table 5. An ORTEP view of **5** is shown in Figure 2. The Pt atom is in a square-planar coordination with a very slight square-pyramidal distortion. It is displaced by only 0.026(1) Å from the best plane of atoms Cl(1), N(1), N(2), and C(13). A comparison can be made between compound **5** and the corresponding Pd derivative,

Table 3. ^{31}P NMR spectroscopic data (room temperature, solvent $CDCl_3$, chemical shifts in ppm downfield from external 85% H_3PO_4)

		solvent	δ	$^1J_{Pt,P}$ /Hz	$J_{P,P}$ /Hz	$^3J_{Pt,P}$ /Hz
$[Pt(L^{et})(PPh_3)][BF_4]$	**9**		20.27	4038		
$[Pt(L^{ip})(PPh_3)][BF_4]$	**10**		20.36	4066		
$[Pt(L^{np})(PPh_3)][BF_4]$	**11**		22.59	4453		
$[Pt_2(L^{np})_2(\mu\text{-dppm})][BF_4]_2$	**12**	CD_2Cl_2	8.86	4581		32
$[Pt_2(L^{ip})_2(\mu\text{-dppe})][BF_4]_2$	**13**	CD_2Cl_2	14.49	4020	52	
$[Pt_2(L^{np})_2(\mu\text{-dppe})][BF_4]_2$	**14**	CD_2Cl_2	15.28	4412	52	
$[Pt_2(L^{np})_2(\mu\text{-dppae})][BF_4]_2$	**15**	CD_2Cl_2	15.14	4414		
$[Pt(L^{np})(dppm)][BF_4]$	**16**		7.69	4421	83	
			−25.09			94
$[Pt(L^{np})(dppe)][BF_4]$	**17**		44.84	1912		
			32.37	4138		
$[Pt(L^{np})(dppae)][BF_4]$	**18**		15.22	4382		

Table 4. Selected bond lengths (Å) and angles (°) with e.s.d.s in parentheses for compound **1**

	molecule A	molecule B
Pt−Cl(1)	2.295(2)	2.300(2)
Pt−Cl(2)	2.286(2)	2.282(2)
Pt−N(1)	1.998(6)	1.994(5)
Pt−N(2)	2.045(5)	2.054(5)
Cl(1)−Pt−Cl(2)	84.9(1)	87.1(2)
Cl(1)−Pt−N(1)	170.8(2)	170.9(2)
Cl(1)−Pt−N(2)	101.3(2)	99.7(2)
Cl(2)−Pt−N(1)	93.0(2)	92.4(2)
Cl(2)−Pt−N(2)	173.6(2)	172.5(2)
N(1)−Pt−N(2)	80.6(2)	80.3(2)

Table 5. Selected bond lengths (Å) and angles (°) with e.s.d.s in parentheses for compound **5**

Pt−Cl(1)	2.309(1)	Pt−N(1)	2.116(3)
Pt−N(2)	2.020(3)	Pt−C(13)	2.040(4)
Cl(1)−Pt−N(1)	95.5(1)	Cl(1)−Pt−N(2)	175.0(1)
Cl(1)−Pt−C(13)	88.1(1)	N(1)−Pt−N(2)	79.8(1)
N(1)−Pt−C(13)	176.1(1)	N(2)−Pt−C(13)	96.7(1)

[PdL^{np}Cl], compound **20**.[7a] The Pt−Cl, Pt−N(1), and Pt−N(2) distances, 2.309(1), 2.116(3), and 2.020(3) Å, respectively, are slightly shorter than the corresponding ones involving palladium, 2.314(1), 2.138(2), and 2.046(2) Å, respectively. This is in keeping with the recent observation that platinum is slightly smaller than palladium.[7a,14] On the contrary, the Pt−C(13) bond, 2.040(4) Å, is slightly longer than the Pd−C(13) one, 2.022(3) Å. As pointed out in ref.[7a], this can be due to the different packing forces in the two nonisomorphous crystals. The conformation of the Pd−N(2)−C(10)−C(11)−C(12)−C(13) six-membered ring is irregular, as previously found in **20**, ref.[7a]. Atoms Pt, N(2), C(10), and C(13) are approximately planar (maximum distances from their best plane are +0.033(3) Å for N(2) and −0.023(4) Å for C(10)], with atoms C(11) and C(12) lying at −0.336(4) and +0.471(4) Å from this best plane.

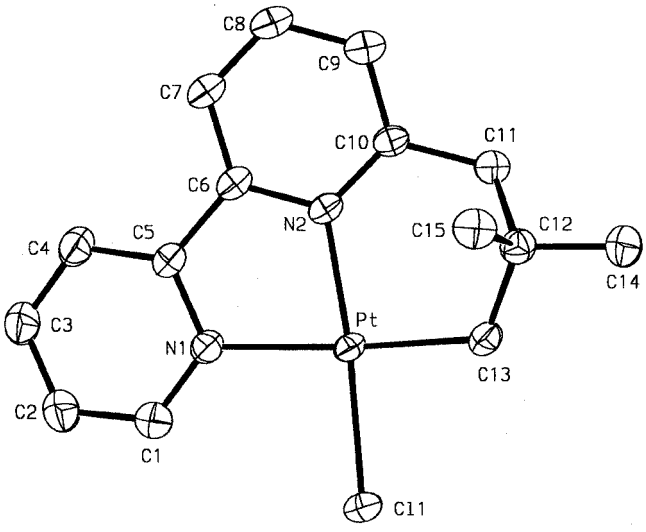

Figure 2. ORTEP view of compound **5**. Thermal ellipsoids as in Figure 1.

In the case of compound **3**, the activation of the methyl group directly generates a stereogenic carbon atom β to the metal atom, a result still rare,[7a] even if not unprecedented. In agreement, the ^1H NMR spectrum shows two diastereotopic hydrogens α to the metal atom (δ_A = 2.66, dd; δ_B = 3.07, dd).

Reactivity of the Metallated Species

In contrast with the behaviour of the analogous cyclometallated species containing Pt−C(sp^2) bonds,[7d] displacement of the chloride ligand in complexes **2**−**5** is easily accomplished in mild conditions by both neutral (e.g. CO, PPh_3) and anionic ligands (e.g. CN^-)

Derivatives **7**−**12** were obtained in good yields in the presence of $[BF_4]^-$ and characterised by analytical and spectroscopic methods. In particular the carbonyl derivatives [Pt(L)CO][BF_4], **7** and **8**, show strong IR absorptions in the region around 2100 cm^{-1} [$\tilde{\nu}_{max}$ (cm^{-1}) = 2107, **7**; 2100, **8**)].

In the ^1H and $^{13}C\{^1H\}$ NMR spectra of **7**, the $^2J_{Pt\text{-}H}$ and $^1J_{Pt\text{-}C}$ values relevant to the metallated methylene group are small ($J_{Pt,H}$ = 66 and 52 Hz; $J_{Pt\text{-}C}$ = 567 Hz) in comparison with those of the chloride species **5** (J = 89, 79 and 736 Hz, respectively), as previously observed when a strong π acceptor ligand is *cis* to the metal−carbon bond.[7b]

Compounds **9−11**, $[Pt(L)(PPh_3)][BF_4]$, can be obtained both with a Pt/P 1:1 or 1:2 molar ratio, showing that the terdentate *N,N,C* system is rather robust. The ^{31}P NMR spectra (see Table 3) are in agreement with a phosphorus *trans* to a nitrogen atom: the $^1J_{Pt,P}$ values in the five-membered compounds **9** and **10**, as well as in $[Pt(L^{tb})(PPh_3)][BF_4]$,[7b] are in the range 4000−4100 Hz, whereas in the six-membered species **11** a greater value, 4453 Hz is found. Similar values (4400−4471 Hz) have been observed in the case of the *N,N,C*(sp^2) six-membered compounds derived from substituted benzylbipyridines[7d] (see Scheme 1, compounds of type IV, M = Pt).

The reactivity of compound **5** with the potentially bidentate ligands L′−L′′ ($Ph_2P(CH_2)PPh_2$, dppm, $Ph_2P(CH_2)_2PPh_2$, dppe, and $Ph_2P(CH_2)_2AsPh_2$, dppae) was studied with the aim of establishing whether square-planar (mono- or dinuclear) or five-coordinated complexes were formed.

The reaction was investigated both with a 1:1 and a 2:1 Pt/L′−L′′ molar ratio: in the first case mononuclear cationic species of the general formula $[Pt(L)(L'-L'')]^+$ were formed, whereas dinuclear species containing a not so common unsupported L′−L′′ bridging unit were isolated in the second case.

The dinuclear species $[(L)Pt(\mu\text{-}L'-L'')Pt(L)]^{2+}$, **12−15**, were characterised mainly on the basis of ^1H and $^{31}P\{^1H\}$ NMR spectroscopy. In particular the $^{31}P\{^1H\}$ NMR spectra of **12−15** deserve comments: the chemical shifts rule out a chelating behaviour of the ligands L′−L′′ and support a bridging coordination.[15] In the analysis of the ^{31}P NMR spectra, due to the presence of ^{31}P (100% natural abundance) and ^{195}Pt (33.8% natural abundance) nuclei, four isotopomers have to be considered.

I	$Pt_A\text{-}P_A \frown P_B\text{-}Pt_B$	43.8%
II	$^{195}Pt_A\text{-}P_A \frown P_B\text{-}Pt_B$	22.4%
III	$Pt_A\text{-}P_A \frown P_B\text{-}^{195}Pt_B$	22.4%
IV	$^{195}Pt_A\text{-}P_A \frown P_B\text{-}^{195}Pt_B$	11.4%

In symmetric species, such as **12** and **14**, the ^{31}P NMR spectra should consist of a singlet due to isotopomer I located in the centre of a satellite system. If the complex pattern due to IV is ignored owing to its low natural abundance, the satellite system is governed by species II−III, which in symmetric species, are equivalent. Isotopomers II and III give rise to an ABX spin system (X = ^{195}Pt) and the ^{31}P spectrum can be described as being formed by two AB subspectra.[16] Two different situations are shown by the dppm and dppe bridging systems, respectively: in the former case no $^2J_{P\text{-}P}$ has been resolved, but a $^3J_{Pt\text{-}P}$ (32 Hz) is observed, whereas in the latter case a $^3J_{P\text{-}P}$ = 52 Hz is present but the $^4J_{Pt,P}$ is negligible. The reaction with dppe has also been carried out on complex **3**, $[Pt(L^{ip})Cl]$: in this case, due to the presence of a couple of stereogenic centres two diastereomers are expected, and this is reflected by the complex pattern of the ^1H NMR spectrum,. It is also worth noting that in these dinuclear complexes the $^1J_{Pt,P}$ is very different in the six- and five-membered species ($^1J_{Pt,P}$ = 4020 Hz, **13**, and $^1J_{Pt,P}$ = 4412 Hz, **14**). Compound **15**, $[(L^{np})Pt(\mu\text{-dppae})Pt(L^{np})][BF_4]_2$, at variance with compounds **12−14**, is no longer symmetric so that resonances relevant to two different bipy units are present in the ^1H NMR spectrum (Table 1).

When the reaction is carried out with a Pt/L′−L′′ 1:1 molar ratio at least three different species should be considered: a pentacoordinated, (A), and two square-planar compounds (B and C).

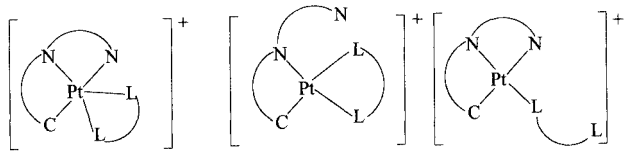

A B C

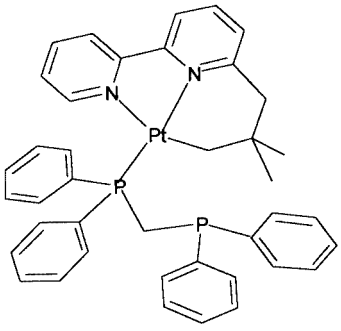

16

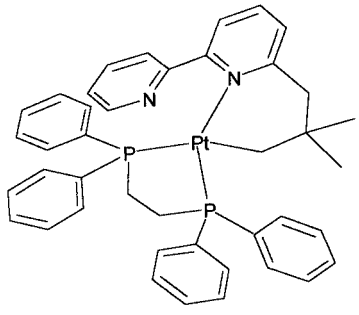

17

In the case of dppm a type C species, **16**, is formed as indicated, inter alia, by the $^{31}P\{^1H\}$ NMR spectrum which shows two different signals, corresponding to a coordinated (δ = 7.69 ppm, doublet, $^1J_{Pt,P}$ = 4421, $^2J_{P,P}$ = 83 Hz), and to an uncoordinated phosphorus atom (δ = −25.9 ppm doublet, $^3J_{Pt,P}$ = 94, $^2J_{P,P}$ = 83 Hz). The ^1H NMR spectrum, as expected, is almost coincident with that of $[Pt(L^{np})(PPh_3)]^+$ (e.g. CH_2−Pt, δ = 1.60 ppm, **11**; 1.69, **16**). At variance, with dppe a type-B complex is obtained, **17**: in the $^{31}P\{^1H\}$ NMR spectrum two sets of signals, centred at δ = 44.84 ppm ($^1J_{Pt\text{-}P}$ = 1912 Hz) and 32.37 ppm, ($^1J_{Pt\text{-}P}$ = 4138 Hz), are consistent with phosphorus atoms *trans* to a carbon and a nitrogen nucleus, respectively. The ^1H NMR spectrum is complex, which is likely due to the crowded environment, all the protons of the four CH_2 groups are not equivalent anymore.

The nature of complex **17** has been confirmed by the resolution of the structure.

The crystal consists of the packing of $[Pt(L^{np})(dppe)]^+$ cations, $[BF_4]^-$ anions and CH_2Cl_2 molecules in the molar ratio 1:1:1 with no unusual van der Waals contacts. Principal bond parameters are listed in Table 6. An ORTEP view of the cation is shown in Figure 3. The Pt atom displays a square-planar coordination with a slight tetrahedral distortion, with maximum distances from the best plane of −0.084(2) and +0.1035(3) Å for atoms C(13) and N(2), respectively. The Pt−P(1) distance, 2.314(1) Å, is markedly longer than the Pt−P(2) one, 2.209(1) Å, because of the strong *trans* influence of the C(13) alkyl atom. Also the Pt−C(13), 2.115(3) Å, and Pt−N(2), 2.127(2) Å, bond lengths are elongated by the *trans* influence of atoms P(1) and P(2), respectively. The Pt−N(2)−C(10)−C(11)−C(12)−C(13) ring is in a boat conformation, with atoms N(2), C(11), C(12), and C(13) approximately planar [maximum distances from their best plane are −0.068(2) Å for N(2) and +0.074(3) Å for C(10)] and atoms Pt and C(11) lying at −1.289(1) and −0.615(3) Å from the best plane, respectively. The P(1)−Pt−N(2) angle, 100.9(1)°, is larger than the P(2)−Pt−C(13) one, 92.4(1)°, probably as a result of the steric hindrance of the noncoordinated pyridine ring. The two pyridine rings are planar and form a dihedral angle of 29.2(2)°.

Table 6. Selected bond lengths (Å) and angles (°) with e.s.d.s in parentheses for cation **17**

Pt−P(1)	2.314(1)	Pt−P(2)	2.209(1)
Pt−N(2)	2.127(2)	Pt−C(13)	2.115(3)
P(1)−Pt−P(2)	85.5(1)	P(1)−Pt−N(2)	100.9(1)
P(1)−Pt−C(13)	173.5(1)	P(2)−Pt−N(2)	173.0(1)
P(2)−Pt−C(13)	92.4(1)	N(2)−Pt−C(13)	81.6(1)

The spectroscopic evidences for **18**, $[Pt(L^{np})(dppae)][BF_4]$, indicate a monodentate P coordination of dppae, as for dppm, so that the *N,N,C* coordination environment is retained. The $^{31}P\{^1H\}$ NMR resonance at δ = 15.22 ppm, is indicative of a nonchelating behaviour of dppae and the $^1J_{Pt,P}$ = 4382 Hz is typical for a P nucleus *trans* to a pyridinic nitrogen atom. In the ^1H NMR spectrum the signals of the pyridine rings as well as those of the CH_2−Pt groups are almost superimposable to those of compounds **11** and **16**, providing further evidence for the terdentate behaviour of the *N,N,C* ligand. In crowded species such as **16**−**18**, it is reasonable to deem that either the different size or the coordinating ability of the As atom with respect to P can direct the reaction towards a different outcome.

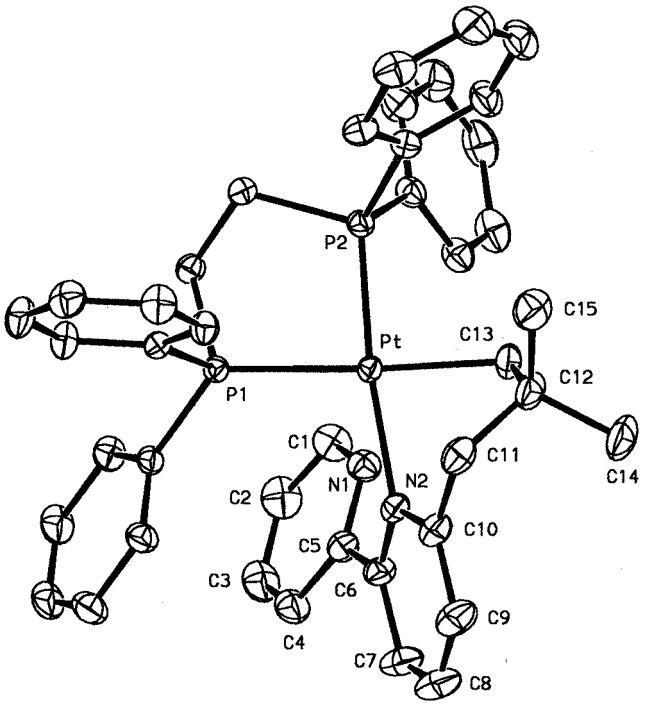

Figure 3. ORTEP view of compound **17**; thermal ellipsoids as in Figure 1

Conclusions

In this paper we have shown that organoplatinum(II) compounds containing an *N,N,C*(sp^3) terdentate ligand are readily formed from $K_2[PtCl_4]$ through a direct C(sp^3)−H bond activation of an unactivated aliphatic chain. Among the species obtained, $[Pt(L^{np})Cl]$, having a rare six-membered cyclometallated N,C(sp^3) cycle, and $[Pt(L^{ip})Cl]$, where a stereogenic centre has been directly formed through metallation, are of particular interest. The ligands studied have different reactivities: with HL^{et} the metallation can be achieved with difficulty and an adduct species, which can be regarded as an intermediate in the cyclometallation, has been isolated in the solid state and studied by X-ray diffraction. Also the structure of $[Pt(L^{np})Cl]$ has been solved, allowing comparisons to be made with the analogous Pd^{II} six-membered N,C(sp^3) metallacyle. NMR spectroscopic data seem to indicate that in the six-membered $[Pt(N,N,C)L]^{n+}$ species (L = neutral, n = 1; or anionic ligand, n = 0) the Pt−C bond is weaker and the Pt−L (L = PR_3) bond is stronger than in the five-membered ones, as indicated by $^1J_{Pt,C}$ in **2**−**5** and by $^1J_{Pt,P}$ in **9**−**18**.

In the course of the study on the reactivity of these species the chloride ligand has been shown to be rather labile whereas the *N*,*N*,*C* system is rather robust. The chloride ligand can easily be removed by anionic and neutral ligands: in the case of neutral bidentate ligands both mono- and binuclear species can be obtained. Only in one case (with dppe) has the external nitrogen atom of the terdentate *N*,*N*,*C* ligand been displaced from the metal to give a crowded $[Pt(N,C)(P,P)]^+$ compound whose structure has been resolved in the solid state.

All the new species are remarkably stable towards air and moisture, even in solution, and so all the reactions can be performed in air.

Experimental Section

The ligands HL were prepared according to literature methods.[12] $K_2[PtCl_4]$ (43.035% Pt) was obtained from Engelhard S.r.l. and $[(DMSO)_2PtCl_2]$ was synthesised as described in ref[17]. All the solvents were purified before use according to standard methods.[18] Elemental analyses were performed with a Perkin−Elmer Elemental Analyser 240B by Mr. A. Canu (Dipartimento di Chimica, Università di Sassari). Conductivities were measured with a Philips PW 9505 conductimeter. Infrared Spectra were recorded with a Perkin−Elmer 983 using Nujol mulls. ^1H, $^{13}C\{^1H\}$ and $^{31}P\{^1H\}$ NMR spectra were recorded with a Varian VXR 300 spectrometer operating at 299.9, 75.4 and 121.4 MHz respectively, and are collected in Table 1−3.

Chemical shifts are given in ppm relative to internal TMS (^1H, ^{13}C) and external 85% H_3PO_4 (^{31}P). The 2D experiments were performed by means of standard pulse sequences.

The mass spectrometric measurements were performed on a VG 7070EQ instrument, equipped with a PDP 11−250 J data system and operating under positive ion fast atom bombardment (FAB) conditions with 3-nitrobenzyl alcohol as supporting matrix.

Preparations

$[Pt(HL^{et})Cl_2]$ (1): a) *cis*-$[(DMSO)_2PtCl_2]$ (215 mg, 0.51 mmol) was added to a solution of HL^{et} (92 mg, 0.50 mmol) in $CHCl_3$ (50 mL). The yellow solution was stirred for 36 h, then evaporated to dryness. The resulting solid was crystallised from CH_2Cl_2/Et_2O to give the analytical sample as a yellow solid. Yield 85% (191 mg). The reaction can also be carried out in other solvents (e.g. EtOH).

b) $K_2[PtCl_4]$ (43.035% Pt, 1.297 g, 2.86 mmol) was dissolved in H_2O (30 mL) and filtered. HL^{et} (523.7 mg, 2.85 mmol) and of 2 M HCl (5 mL) were added to the solution. The mixture was stirred at room temperature until the solution became colourless. The precipitate that formed was filtered, washed with H_2O, EtOH and Et_2O and recrystallised from CH_2Cl_2/Et_2O to give the analytical sample. Yield 30% (384 mg). M.p. 220 °C. $C_{12}H_{12}Cl_2N_2Pt$ (450.2): calcd. C 32.01; H 2.69; N 6.22 ; found C 31.97; H 2.65; N 6.11%. IR (Nujol): $\tilde{\nu}$ = 1600 s 1558 w, 1375 s, 335 w cm^{-1}.

$[Pt(L^{et})Cl]$ (2): HL^{et} (184 mg, 1.00 mmol) and 2 M HCl (3.5 mL) were added to an aqueous solution (30 mL) containing $K_2[PtCl_4]$ (1.00 mmol) in water. The mixture was heated in a water bath for 1 d: the precipitate that formed was filtered, washed with water, EtOH and Et_2O and recrystallised from CH_2Cl_2/Et_2O. The crude obtained (362 mg) was a mixture ca. 1:1 of compounds **1** and **2** (NMR criterion). The products were separated by column chromatography on silica gel, using a mixture of CH_2Cl_2/acetone 20:1 as eluent. Complex **2** was obtained with a 30% yield. M.p. 258−260 °C (dec). $C_{12}H_{11}ClN_2Pt$ (413.8): calcd. C 34.83, H 2.68, N 6.77; found C 35.44, H 2.80, N 6.50%. IR (Nujol): $\tilde{\nu}$ = 1597 s 1556 w, 328 s cm^{-1}. FAB^+: *m*/*z* = 413 $[M^+]$, 378 [M − Cl], 791 $[M_2-Cl]$.

$[Pt(L)Cl]$ ($L = L^{ip}$, 3; $L = L^{np}$, 5): HL (1.00 mmol) and 2 M HCl (3.0 mL) were added to an aqueous solution (30 mL) containing K_2PtCl_4 (1.00 mmol). The mixture was heated in a water bath until a colourless solution was obtained and an orange precipitate formed. The suspension was filtered off, washed with water, ethanol and diethyl ether and recrystallised from CH_2Cl_2/Et_2O

3: Yield 91% (389 mg), m.p. 245 °C. $C_{13}H_{13}ClN_2Pt$ (427.8): calcd. C 36.50, H 3.06, N 6.55; found C 36.50, H 3.05, N 6.25%. IR (Nujol): $\tilde{\nu}$ = 1596 s, 1552 w, 332 s cm^{-1}. FAB^+: *m*/*z* = 427 $[M^+]$, 392 [M − Cl], 819$[M_2-Cl]$.

5: Yield 90% (410 mg), m.p.: 233 °C (dec). $C_{15}H_{17}ClN_2Pt$ (455.8) calcd. C 39.52, H 3.76, N 6.15; found C 39.27, H 3.84, N 6.04%. IR (Nujol): $\tilde{\nu}$ = 1600 s, 1564 w, 328 s cm^{-1}. FAB^+: *m*/*z* = 455 $[M^+]$.

$[Pt(L^{ip})(CN)]$ (6): Complex **3** (175 mg, 0.41 mmol) was added to a methanolic solution (25 mL) of KCN (27 mg, 0.41 mmol) whilst stirring. The mixture was stirred for 1 day, then evaporated to dryness and the solid residue recrystallised from CH_2Cl_2/Et_2O to give the analytical sample as a yellow solid. Yield 56% (96 mg), m.p. 115 °C. $C_{14}H_{13}N_3Pt$ (418.3) calcd. C 40.19, H 3.13, N 10.04; found C 39.67, H 3.06, N 9.62%. IR (Nujol): $\tilde{\nu}$ = 2105 m, 1595 s, 1557 w cm^{-1}.

$[Pt(L)(CO)]$ $[BF_4]$ ($L = L^{ip}$, 7; $L = L^{np}$, 8): $NaBF_4$ (121 mg, 1.00 mmol) was added to a solution of the relevant [Pt(L)Cl] (0.25 mmol) in acetone (20 mL) whilst stirring and carbon monoxide, at atmospheric pressure, was bubbled through the solution. After 6 h the solvent was evaporated to dryness and the solid residue was crystallised from CH_2Cl_2/Et_2O.

7 Yield 70% (89 mg), m.p.: 235 °C. Λ_M ($5\cdot10^{-4}$ M, acetone) = 138 ohm^{-1} cm^2 mol^{-1}. $C_{14}H_{13}BF_4N_2OPt$ (507.2): calcd. C 33.16, H 2.58, N 5.52; found C 33.28, H 2.60, N 5.30%. IR (Nujol): $\tilde{\nu}$ = 2107 s 1598 s 1563 s 1050 b. FAB^+: *m*/*z* = 420 $[M^+]$, 392 [M − CO].

8: Yield: 76% (102 mg), m.p.182−184 °C. Λ_M (5.10^{-4} M, acetone) = 157 ohm^{-1} cm^2 mol^{-1}. $C_{16}H_{17}BF_4N_2OPt$ (535.2): calcd. C 35.91, H 3.20, N 5.23; found C 35.40, H 3.06, N 5.11%. IR (Nujol): $\tilde{\nu}$ = 2100 s, 1600 s, 1560 w, 1050 s cm^{-1}.

$[Pt(L)(PPh_3)][BF_4]$ ($L = L^{et}$, 9; $L = L^{ip}$, 10; $L = L^{np}$, 11): PPh_3 (0.22 mmol) and $NaBF_4$ (100 mg, 0.900 mmol) were added to a solution of the relevant [Pt(L)Cl] (0.20 mmol) in acetone (30 mL) whilst stirring. The mixture was stirred at room temperature, then evaporated to dryness and crystallised from CH_2Cl_2/Et_2O.

9: Yield 90% (131 mg), m.p. 253 °C. Λ_M ($5\cdot10^{-4}$ M acetone) = 150 ohm^{-1} cm^2 mol^{-1}. $C_{30}H_{26}BF_4N_2PPt$ (727.4): calcd. C 49.54, H 3.60, N 3.85; found C 48.93, H 3.55, N 3.71%. FAB^+: *m*/*z* = 640 $[M^+]$, 378 $[M - PPh_3]$.

10: Yield 76% (113 mg), m.p. 275 °C. Λ_M ($5\cdot10^{-4}$ M, acetone) = 130 ohm^{-1} cm^2 mol^{-1}. $C_{31}H_{28}BF_4N_2PPt$ (741.4): calcd. C 50.22, H 3.81, N 3.78; found C 50.34, H 3.91, N 3.63%. IR (Nujol): $\tilde{\nu}$ = 1598 s, 1564 w, 1102 s, 1050br, s. FAB^+: *m*/*z* = 654 $[M^+]$ 392 $[M - PPh_3]$.

11: Yield: 77% (118 mg), m.p. 263 °C. Λ_M ($5\cdot10^{-4}$ M, acetone) = 150 ohm^{-1} cm^2 mol^{-1}. $C_{33}H_{32}BF_4N_2PPt$ (769.5): calcd. C 51.51,

H 4.19, N 3.64%; found C 51.26, H 4.09, N 3.65%. IR (Nujol): $\tilde{\nu}$ = 1602 s, 1568 w, 1050 s, 540 w. FAB$^+$: *m*/*z* = 682 [M$^+$].

[Pt$_2$(L^{np})$_2$(μ-dppm)] [BF$_4$]$_2$ (12): A mixture containing **5** (42 mg, 0.092 mmol), dppm (17.4 mg, 0.046 mmol) and NaBF$_4$ (43 mg) in acetone (30 mL) was stirred at room temperature for 4 days, then evaporated to dryness and recrystallised from CH_2Cl_2/Et_2O, to give the analytical sample as a yellow solid. Yield: 59% (34 mg), m.p 168 °C (dec.). Λ_M (5 10^{-4} M, acetone) = 260 ohm^{-1} cm^2 mol^{-1}. $C_{55}H_{56}B_2F_8N_4P_2Pt_2{\cdot}0.5CH_2Cl_2$ (1441.2): calcd. C 46.25, H 3.99, N 3.89 ; found C 46.37, H 4.03, N 3.96%. IR (Nujol): $\tilde{\nu}$ = 2100 s, 1600 s, 1560 w, 1050 br s cm^{-1}. FAB$^+$: *m*/*z* = 1224 [M$^+$], 1311 [M$^+$ + BF$_4$].

[Pt$_2$(L)$_2$(μ-dppe)] [BF$_4$]$_2$ (L = L^{ip}, 13; L = L^{np}, 14): dppe (0.20 mmol) and NaBF$_4$ (150 mg) were added to a suspension of the relevant [Pt(L)Cl] (0.40 mmol) in acetone (25 mL) whilst stirring. The mixture was stirred for a few hours, then evaporated to dryness and crystallised by CH_2Cl_2/Et_2O to give the analytical sample.

13: Yield 75% (203 mg); m.p. 280 °C. Λ_M (5.10^{-4} M, acetone) = 202 ohm^{-1} cm^2 mol^{-1}. $C_{52}H_{50}B_2F_8N_4PPt_2$ (1356.7): calcd. C 46.04, H 3.71, N 4.13; found C 45.74, H 3.74, N 4.01%. (IR (Nujol): $\tilde{\nu}$ = 1598 s 1564 w, 1050 broad cm^{-1}.

14: (yellow) Yield 93% (279 mg); m.p. 184 °C (dec). Λ_M (5 10^{-4} M, acetone) = 248 ohm^{-1} cm^2 mol^{-1}. $C_{56}H_{58}B_2F_8N_4P_2Pt_2{\cdot}CH_2Cl_2$ (1497.7): calcd. C 45.71, H 4.04, N 3.74 ; found C 46.26, H 4.18, N 3.71%. IR (Nujol): $\tilde{\nu}$ = 1602 s, 1569 w, 1050 br s cm^{-1}.

[Pt$_2$(L^{np})$_2$(μ-dppae)] [BF$_4$]$_2$ (15): A mixture containing **5** (39 mg, 0.085 mmol), dppae (18.8 mg, 0.0425 mmol) and NaBF$_4$ (50 mg) in acetone (30 mL) was stirred at room temperature for 1 day, then evaporated to dryness and crystallised from CH_2Cl_2/Et_2O, to give the analytical sample as a yellow solid. Yield 80% (51 mg), m.p. 250−255 °C. $C_{56}H_{58}AsB_2F_8N_4Pt_2P{\cdot}0.5CH_2Cl_2$ (1499.2): calcd. C 45.26, H 3.97, N 3.74; found C 45.02, H 3.98, N 3.68%.

[Pt(L^{np})(L′−L′′)][BF$_4$] (L′−L′′ = dppm, 16, L′−L′′ = dppe, 17, L′−L′′ = dppae, 18): NaBF$_4$ (120 mg) was added to an acetone solution (30 mL) of **5** (103 mg, 0.25 mmol) and L′−L′′ (0.25 mmol) whilst stirring. The mixture was stirred for 4 h, then evaporated to dryness. The solid obtained was crystallised from CH_2Cl_2/Et_2O to give the analytical sample as a yellow solid.

L′−L′′ = dppm, **16**, pale-yellow. Yield: 90% (201 mg); m.p. 238−240 °C. $C_{40}H_{39}BF_4N_2P_2Pt$ (891.6): calcd. C 53.88, H 4.41, N 3.14; found C 53.40, H 4.53, N 3.07%.

L′−L′′ = dppe, **17**, yellow. Yield: 88% (199 mg). M.p. 182−5 °C (dec). Λ_M (5 10^{-4} M, acetone) = 133 ohm^{-1} cm^2 mol^{-1}. $C_{41}H_{41}BF_4N_2P_2Pt$ (905.6): calcd. C 54.38, H 4.56, N 3.09; found C 54.42, H 4.56, N 3.11%. IR (Nujol): $\tilde{\nu}$ = 1600, 1580 w, 1050 s, 540 s cm^{-1}.

Table 7. Crystallographic experimental details

Compound	**1**	**5**·$CHCl_3$	**17**[BF_4]·CH_2Cl_2
Formula	$C_{12}H_{12}Cl_2N_2Pt$	$C_{16}H_{18}Cl_4N_2Pt$	$C_{42}H_{43}BCl_2F_4N_2P_2Pt$
M	450.24	575.24	990.57
Colour	yellow	yellow-orange	pale yellow
Crystal system	monoclinic	triclinic	triclinic
Space group	$P2_1/c$ (no. 14)	$P\bar{1}$ (no. 2)	$P\bar{1}$ (no. 2)
a/Å	14.909(2)	9.209(1)	11.969(1)
b/Å	9.503(1)	10.813(1)	13.307(1)
c/Å	17.732(2)	10.980(1)	13.659(1)
α/°	90	78.77(1)	75.97(1)
β/°	99.87(2)	65.60(1)	83.35(1)
γ/°	90	82.07(1)	89.67(1)
V/Å^3	2511.2(6)	974.6(2)	2095.8(3)
Z	8	2	2
F(000)	1680	548	984
T/K	296	296	296
D_c/g cm^{-3}	2.38	1.96	1.57
Crystal dimensions (mm)	0.33 × 0.45 × 0.50	0.16 × 0.27 × 0.44	0.13 × 0.30 × 0.44
μ (Mo-K_α)/cm^{-1}	117.0	78.3	36.3
Min. and max.transmiss. factors	0.81−1.00	0.88−1.00	0.59−1.00
Scan mode	ω	ω	ω
ω-scan width/°	1.20 + 0.35 tan θ		
Frame width/°		0.30	0.30
Time per frame/s		20	20
No. of frames		2450	2450
Detector/sample distance/cm		5.00	5.00
θ-range/°	3−27	3−26	3−26
Reciprocal space explored	quadrant	full sphere	full sphere
Measured reflections (total, independent)	5444, 5444	12214, 4798	32505, 12183
R_{int}		0.029	0.026
Unique observed reflections with $I>3\sigma(I)$	4239	3965	10764
Final *R* and *R′*[a]	0.030, 0.037	0.023, 0.028	0.024, 0.033
No. of variables	308	209	496
Goodness of fit[b]	1.40	0.94	1.19

[a] $R = [\Sigma(|F_o - k|F_c||)/\Sigma F_o]$, $R' = [\Sigma w(F_o - k|F_c|)^2/\Sigma w F_o^2]^{1/2}$. [b] $[\Sigma w(F_o - k|F_c|)^2/(N_o - N_v)]^{1/2}$, where $w = 1/[\sigma(F_o)]^2$, $\sigma(F_o) = [\sigma^2(F_o^2) + (0.04F_o^2)^2]^{1/2}/2F_o$, N_o is the number of observations, N_v the number of variables.

L′−L′′ = dppae, **18**, yellow. Yield: 84% (199 mg), m.p. 205−213 °C (dec). Λ_M (5 10^{-4} M, acetone) = 147 ohm^{-1}cm^{2}mol^{-1}. $C_{41}H_{41}AsBF_4N_2PPt$ (949.6): calcd. C 51.86, H 4.35, N 2.95; found C 51.47, H 4.39, N 2.97%. IR (Nujol): $\tilde{\nu}$ = 1600 s, 1560 w, 1050 br, 530 s cm^{-1}.

X-ray Data Collection and Structure Determination: Crystal data and other experimental details are summarised in Table 7. The diffraction experiment concerning **1** was carried out on an Enraf−Nonius CAD-4 diffractometer at room temperature using Mo-K_α radiation (λ = 0.71073 Å) with a graphite crystal monochromator in the incident beam. A periodic monitoring of three standard reflections did not reveal any crystal decay. The diffracted intensities were corrected for Lorentz, polarisation, and absorption effects (empirical correction).[19]

The diffraction experiments concerning **5**·$CHCl_3$ and **17**[BF_4]·CH_2Cl_2 were carried out on a Bruker SMART CCD area-detector diffractometer at room temperature using Mo-K_α radiation (λ = 0.71073 Å) with a graphite crystal monochromator in the incident beam. Cell parameters and orientation matrix were obtained from the least-squares refinement of 69 reflections (for **5**·$CHCl_3$) and of 148 reflections (for **17**[BF_4]·CH_2Cl_2) measured in three different sets of 15 frames each, in the range $3 < \theta < 23°$. At the end of data collections the first 50 frames, containing 171 and 362 reflections (for **5**·$CHCl_3$ and **17**[BF_4]·CH_2Cl_2, respectively) were recollected to have a monitoring of crystal decay, which was not observed, so that no time-decay correction was needed. The collected frames were processed with the software SAINT,[20] and an empirical absorption correction was applied (SADABS[21]) to the collected reflections. Scattering factors and anomalous dispersion corrections were taken from ref.[22].

The calculations were performed on a Pentium III PC using the Personal Structure Determination Package[23] and the physical constants tabulated therein.

The structures were solved by Patterson and Fourier methods and refined by full-matrix least-squares, minimising the function $\Sigma\omega(F_o - k|F_c|)$ (refinement on *F*). In compound **17**[BF_4]·CH_2Cl_2 three fluorine atoms of the BF_4^- anion are disordered. Anisotropic thermal factors were refined for all the non-hydrogen atoms. Hydrogen atoms were placed in their ideal positions (C−H: 0.97 Å, B: 1.10 times that of the carbon atom to which they are attached) and not refined . The final Fourier maps showed maximum residuals of 1.34(19) e/Å^3 at 0.87 Å from Pt_A (in compound **1**), 1.22(11) e/Å^3 at 0.96 Å from Pt (in compound **5**·$CHCl_3$), and of 1.18(9) e/Å^3 at 0.83 Å from Pt (in compound **17**[BF_4]·CH_2Cl_2). The atomic coordinates of the structure models have been deposited with the Cambridge Data File.

CCDC-181834 (**1**), -181835 (**5**·$CHCl_3$) and -181836 (**17**-[BF_4]·CH_2Cl_2) contain the supplementary crystallographic data for this paper. These data can be obtained free of charge at www.ccdc.cam.ac.uk/conts/retrieving.html [or from the Cambridge Crystallographic Data Centre, 12, Union Road, Cambridge CB2 1EZ, UK; Fax: (internat.) +44-1223/336-033; E-mail: deposit@ccdc.cam.ac.uk].

Acknowledgments

Financial support from Università di Sassari is gratefully acknowledged.

[1] A. D. Ryabov, *Synthesis* **1985**, 233.
[2] [2a] D. M. Grove, G. van Koten and A. H. M. Verschuuren, *J. Mol. Catal.* **1988**, *45*, 169−174. [2b] M. Camargo, P. Dani, J. Dupont, R. F. De Souza, M. Pfeffer, I. Tkatchenko, *J. Mol. Catal.* **1996**, *109*, 127.
[3] [3a] Y. Wakatsuki, H. Yamazaki, P. A. Grutsch, M. Southanam, M. Kutal, *J. Am. Chem. Soc.* **1985**, *107*, 8153. [3b] C. Cornioley-Deuschel, T. Ward, A. von Zelewsky, *Helv. Chim. Acta* **1988**, *71*, 130. [3c] M. Maestri, D. Sandrini, V. Balzani, A. von Zelewsky, P. Jolliet, *Helv. Chim. Acta* **1988**, *71*, 134. [3d] R. Schwartz, G. Gliemann, P. Jolliet, A. von Zelevsky, *Inorg. Chem.* **1989**, *28*, 742. [3e] C. A. Craig, R. Watts, *Inorg. Chem.* **1989**, *28*, 309.
[4] [4a] D. P. Lydon, J. P. Rourke, *Chem. Commun.* **1997**, 1741−1742 and references therein. [4b] P. Espinet, M. A. Esteruelas, L. A. Oro, J. L. Serrano, E. Sola, *Coord. Chem. Rev.* **1992**, *117*, 215.
[5] M. Albrecht, M. Lutz, A. M. M. Schreurs, E. T. H. Lutz, A. L. Spek, G. van Koten, *J. Chem. Soc., Dalton Trans.* **2000**, 3797−3805.
[6] [6a] G. Marcon, S. Carotti, M. Colonnello, L. Messori, E. Mini, P. Orioli, T. Mazzei, M. Cinellu, G. Minghetti, *J. Med. Chem.* **2002**, *45*, 1672−1677. [6b] C. Navarro-Ranninger, I. Lopez-Solera, J. M. Perez, J. R. Masaguer, C. Alonso, *Appl. Organomet. Chem.* **1993**, *7*, 57.
[7] e. g. [7a] A. Zucca, M. A. Cinellu, M. V. Pinna, S. Stoccoro, G. Minghetti, M. Manassero, M. Sansoni, *Organometallics* **2000**, *19*, 4295−4304. [7b] G. Minghetti, M. A. Cinellu, S. Stoccoro, A. Zucca, M. Manassero, *J. Chem. Soc., Dalton Trans.* **1995**, 777−781. [7c] G. Minghetti, M. A. Cinellu, G. Chelucci, S. Gladiali, F. Demartin, M. Manassero, *J. Organomet. Chem.* **1986**, *307*, 107. [7d] G. Sanna, G. Minghetti, A. Zucca, M. I. Pilo, R. Seeber, F. Laschi, *Inorg. Chim. Acta* **2000**, *305*, 189−205. [7e] E. C. Constable, R. P. G. Henney, T. A. Leese, T. A. Tocher, *J. Chem. Soc., Chem. Commun.* **1990**, 513. [7f] E. C. Constable, R. P. G. Henney, T. A. Leese, T. A. Tocher, *J. Chem. Soc., Dalton Trans.* **1990**, 443. [7g] M. A. Cinellu, A. Zucca, S. Stoccoro, G. Minghetti, M. Manassero, M. Sansoni, *J. Chem. Soc., Dalton Trans.* **1996**, 4217−4225. [7h] M. A. Cinellu, G. Minghetti, M. V. Pinna, S. Stoccoro, A. Zucca, M. Manassero, *Chem. Commun.* **1998**, 2397−2398. [7i] S. W. Lai, M. C. W. Chan, K. K. Cheung, C. M. Che, *Organometallics* **1999**, *18*, 3327. [7j] A. Zucca, S. Stoccoro, M. A. Cinellu, G. Minghetti, M. Manassero, *J. Chem. Soc., Dalton Trans.* **1999**, 3431. [7k] F. Neve, A. Crispini, S. Campagna, S. Serroni, *Inorg. Chem.* **1999**, *38*, 2250. [7l] G. Garcìa-Herbosa, A. Munoz, D. Miguel, S. Garcìa-Granda, *Organometallics* **1994**, *13*, 1775−1780. [7m] M. Crespo, C. Grande, A. Klein, *J. Chem. Soc., Dalton Trans.* **1999**, 1629−1637. [7n] C. Anderson, M. Crespo, M. Font-Bardìa, A. Klein, X. Solans, *J. Organomet. Chem.* **2000**, *601*, 22−33. [7o] A. Fernández, P. Urìaa, J. J. Fernández, M. López-Torres, A. Suárez, D. Vázquez-García, M. T. Pereira, J. M. Vila, *J. Organomet. Chem.* **2001**, *620*, 8−19. [7p] J. M. Vila, M. Gayoso, M. T. Pereira, M. Lopez Torres, J. J. Fernandez, A. Fernandez, J. M. Ortigueira, *J. Organomet. Chem.* **1997**, *532*, 171. [7q] M. Crespo, M. Font-Bardìa, S. Pérez, X. Solans, *J. Organomet. Chem.* **2002**, *642*, 171−178. [7r] P. L. Alsters, P. F. Engel, M. P. Hogerheide, M. Copijn, A. L. Spek, G. van Koten, *Organometallics* **1993**, *12*, 1831−1844.
[8] e. g. [8a] P. Steenwinkel, R. A Gossage,; G. van Koten, *Chem. Eur. J.* **1998**, *4*, 759. [8b] A. W. Kleij, H. Kleijn, J. T. B. H. Jastrzebski, A. L. Spek, G. van Koten, *Organometallics* **1999**, *18*, 277. [8c] P. Steenwinkel, R. A. Gossage, T. Maunula, D. M. Grove, G. van Koten, *Chem. Eur. J.* **1998**, *4*, 763. [8d] M. Albrecht, P. Dani, M. Lutz, A. L. Spek, G. van Koten, *J. Am. Chem. Soc.* **2000**, *122*, 11822−11833. [8e] M.-C. Lagunas, R. A. Gossage, A. L. Spek, G. van Koten, *Organometallics* **1998**, *17*, 731−741. [8f] G. van Koten, J. Terhijeden, J. A. M. van Beek, I. C. M. Wehman-Ooyevaar, F. Muller, C. H. Stam, *Organometallics* **1990**, *9*, 903−912. [8g] M. Schmülling, D. M. Grove, G. van Koten, R. van Eldik, N. Veldman, A. L. Spek, *Organometallics* **1996**, *15*, 1384−1391. [8h] D. J. Cardenas, A. M. Echavarren, M. C. Ramirez de Arellano, *Organometallics* **1999**, *18*, 3337. [8i] M. H. P. Rietveld, D. M. Grove, G. van Koten, *New. J. Chem.* **1997**, *21*, 751. [8j] A. J. Canty, N. J. Minchin, B. W. Skelton, A. H. White, *J. Chem. Soc., Dalton Trans.* **1987**, 1477. [8k] A. J. Canty, J. Patel,

B. W. Skelton, A. H. White, *J. Organomet. Chem.* **2000**, *607*, 194.

[9] e. g. [9a] G. W. V. Cave, F. P. Fanizzi, R. J. Deeth, W. Errington, J. P. Rourke, *Organometallics* **2000**, *19*, 1355. [9b] G. W. V. Cave, N. W. Alcock, J. P. Rourke, *Organometallics* **1999**, *18*, 1801. [9c] W. Lu, M. C. W. Chan, K. K. Cheung, C. M. Che, *Organometallics* **2001**, *12*, 2477. [9d] C. Cornioley-Deutschel, T. Ward, A. von Zelewsky, *Helv. Chim. Acta* **1988**, *71*, 130. [9e] G. R. Newkome, T. Kawato, D. K. Kohli, W. E. Puckett, B. D. Olivier, G. Chiari, F. R. Fronczek, W. A. Deutsch, *J. Am. Chem. Soc.* **1981**, *103*, 3423. [9f] K. H. Wong, K. K. Cheung, M. C. W. Chan, C. M. Che, *Organometallics* **1998**, *17*, 3505. [9g] C. P. Newman, G. W. V. Cave, M. Wong, W. Errington, N. W. Alcock, J. P. Rourke, *J. Chem. Soc., Dalton Trans.* **2001**, 2678−2682.

[10] A. D. Ryabov, *Chem. Rev.* **1990**, *90*, 403−424.

[11] [11a] L. Calligaro, R. A. Michelin, P. Uguagliati, *Inorg. Chim. Acta* **1983**, *76*, L83. [11b] G. R. Newkome, K. J. Theriot, F. R. Fronczek, B. Villar, *Organometallics* **1989**, *8*, 2513.

[12] [12a] U. Azzena, G. Chelucci, G. Delogu, S. Gladiali, M. Marchetti, F. Soccolini, C. Botteghi, *Gazz. Chim. Ital.* **1986**, *116*, 307. [12b] C. Botteghi, G. Chelucci, G. Chessa, G. Delogu, S. Gladiali, F. Soccolini, *J. Organomet. Chem.* **1986**, *304*, 217.

[13] A. Doppiu, M. A. Cinellu, G. Minghetti, S. Stoccoro, A. Zucca, M. Manassero, M. Sansoni, *Eur. J. Inorg. Chem.* **2000**, 2555−2563.

[14] K. Herbst, B. Rink, L. Dahlenburg, M. Brorson, *Organometallics* **2001**, *20*, 3655−3660.

[15] P. S. Pregosin, R. W. Kunz, *^{31}P and ^{13}C* NMR of Transition Metal Phosphane Complexes, Springer-Verlag, Berlin, **1979**.

[16] J. B. Benson, E. A. Keiter, R. L. Keiter, *J. Organomet. Chem.* **1995**, *495*, 77−81.

[17] R. Romeo, L. Monsù Scolaro, *Inorg. Synth.* **1998**, *32*, 153.

[18] *Vogel's Textbook of Practical Organic Chemistry*, fifth edition, Longman Scientific and Technical Ed., Harlow, **1989**.

[19] A. C. T. North, D. C. Phillips, F. S. Mathews, *Acta Crystallogr., Sect. A* **1968**, *24*, 351.

[20] SAINT, *Reference manual*, Siemens Energy and Automation, Madison, WI, **1994− 1996**.

[21] G. M. Sheldrick, SADABS, Empirical Absorption Correction Program, University of Gottingen, **1997**.

[22] *International Tables for X-ray Crystallography*, Vol.4, Kynoch Press, Birmingham, 1974.

[23] [23a] B. A. Frenz, *Comput. Phys.* **1988**, *2*, 42. [23b] B. A. Frenz, *Crystallographic Computing 5*, Oxford University Press: Oxford, U. K., **1991**; chapter 11, p. 126 .

Received April 2, 2002
[I02173]

Synthesis, Magnetochemistry, and Spectroscopy of Heterometallic Trinuclear Basic Trifluoroacetates $[Fe_2M(\mu_3\text{-}O)(CF_3COO)_6(H_2O)_3]\cdot H_2O$ (M = Mn, Co, Ni)

Konstantin S. Gavrilenko,[a] Attila Vértes,[b] Gyorgy Vanko,[b] Laszlo F. Kiss,[c] Anthony W. Addison,*[d] Thomas Weyhermüller,[e] and Vitaly V. Pavlishchuk*[a]

Keywords: Heterometallic complexes / Carboxylate ligands / Magnetic properties / Iron / Manganese / Cobalt / Nickel / Trinuclear complexes

Three new μ_3-oxo(trifluoroacetato) complexes $[Fe_2^{III}M^{II}(\mu_3\text{-}O)(CF_3COO)_6(H_2O)_3]\cdot H_2O$ [M = Mn (**1**), Co (**2**), Ni (**3**)] have been prepared. Compounds **1** and **2** crystallize in the monoclinic space groups *C*2/*c* [*a* = 22.002(5), *b* = 13.647(3), *c* = 24.767(4) Å, β = 98.23(3)°] and *C*2/*m* [*a* = 21.426(4), *b* = 15.100(2), *c* = 14.815(3) Å, β = 117.99(2)°], respectively. The coordination spheres of the metal ions are essentially octahedral, with the Fe–O distances [1.870(5) Å] falling in the usual range for these systems. Magnetochemical studies reveal the presence of antiferromagnetic exchange in the isosceles triangular skeletons of the polynuclear species. Application of the isotropic spin Hamiltonian $H = -2J_{FeM}[S_{Fe1}S_M + S_MS_{Fe2}] - 2J_{FeFe}[S_{Fe1}S_{Fe2}]$ gives the fitting parameters: $g_{Fe} = g_{Mn} = 2.00$, $J_{Fe\text{-}Fe} = -56.50(7)$ and $J_{Fe\text{-}Mn} = -16.23(4)$ cm^{-1} (**1**), $g_{mol} = 2.09(1)$, $J_{Fe\text{-}Fe} = -42.8(3.5)$ cm^{-1}, $J_{Fe\text{-}Co} = -17.8(1.4)$ cm^{-1} (**2**) and $g_{Fe} = 2.00$, $g_{Ni} = 2.215(2)$, $J_{Fe\text{-}Fe} = -45.60(1)$ and $J_{Fe\text{-}Ni} = -16.96(2)$ cm^{-1} (**3**). A Mössbauer investigation confirms that no electron transfer from Mn^{II} or Co^{II} to Fe^{III} occurs during the syntheses of these complexes.

(© Wiley-VCH Verlag GmbH, 69451 Weinheim, Germany, 2002)

Introduction

Polynuclear carboxylates of the 3d transition metals have been attracting renewed interest because of their intramolecular magnetic exchange interactions[1,2] and their application as simple models of oligonuclear active sites in metalloproteins.[3−6] Particular attention is being paid to polynuclear complexes behaving as single-molecular magnets.[7−9] Trinuclear (carboxylato)(oxo) complexes are also found within supramolecular arrays of higher nuclearity, and thus are of interest as building blocks ("*molecular Legos*™") with regard to modern magnetic materials.[10,11]

[a] L.V. Pisarzhevskii Institute of Physical Chemistry of the National Academy of Sciences of the Ukraine,
prospekt Nauki 31, 03039 Kiev, Ukraine
Fax: (internat.) + 38-044/265-6216
E-mail: pavlisvv@phyche.freenet.kiev.ua
[b] Research Group for Nuclear Techniques in Structural Chemistry of the Hungarian Academy of Sciences at Eötvös University of Budapest
Pf. 32, 1518 Budapest 112, Hungary
Fax: (internat.) + 36-1/209-0602
E-mail: vertesa@ludens.elte.hu
[c] Research Institute for Solid State Physics and Optics
P. O. Box 49, 1121 Budapest, Hungary
Fax: (internat.) + 36-1/395-9278
E-mail: kiss@power.szfki.kfki.hu
[d] Department of Chemistry, Drexel University,
Philadelphia, PA 19104, U.S.A.
Fax: (internat.) + 1-215/895-1265
E-mail: addisona@drexel.edu
[e] Max-Planck Institut für Strahlenchemie,
Stiftstraße 34−36, 45470 Mülheim, Germany
Fax: (internat.) + 49-208/306-3951
E-mail: weyherm@mpi-muelheim.mpg.de

The first heterometallic trinuclear acetates of tripositive iron and chromium $[X_2^{III}Z^{III}(\mu_3\text{-}O)(CH_3COO)_6(H_2O)_3]^+$ (where X_2Z = Fe_2Cr, Cr_2Fe)[12] and of mixed-valence metals $[Fe_2^{III}M^{II}(\mu_3\text{-}O)(CH_3COO)_6(H_2O)_3]$ (where M = Co, Mn, Ni, Zn)[13] were synthesized by Weiland. Difficulties in the synthesis and in the interpretation of the physicochemical properties of these heterometallic trinuclear carboxylates discouraged their extensive investigation.[14] Nonetheless, the consequences of straightforward variations in their structures, such as substitution of the acetate group by other functionalised carboxylates, appear to be fundamental in the development of new materials derived from them. This class of compounds is also active with respect to alkane activation, the catalytic activity being dependent on the carboxylate and metal identities.[15,16]

Thus, it is attractive to combine this property of superacidity and catalytic activity of trinuclear (carboxylato)(μ_3-oxo) complexes using strong acids such as trifluoroacetic acid as the ligand source. We present here the syntheses, structures and investigation of the spectroscopic and magnetic behaviour of the trinuclear heterometallic basic trifluoroacetates $[Fe_2^{III}M^{II}(\mu_3\text{-}O)(CF_3COO)_6(H_2O)_3]$ (M = Mn, Co, Ni).

Results and Discussion

Synthesis

The heteronuclear basic trifluoroacetates $[Fe_2^{III}M^{II}(\mu_3\text{-}O)(CF_3COO)_6(H_2O)_3]\cdot H_2O$ [M = Mn (**1**), Co (**2**), Ni (**3**)]

were synthesized by metathesis reaction between trifluoroacetate and the acetate trimers. The reactions proceeded smoothly in aqueous trifluoroacetic acid as the solvent without any destruction of the oxo-bridged trinuclear skeleton of the Mn, Co, or Ni complexes, despite the substantial acidity of trifluoroacetic acid [Equation (1)].

$$[Fe_2^{III}M^{II}(\mu_3\text{-}O)(CH_3COO)_6(H_2O)_3]\cdot 3H_2O + 6\,CF_3COOH \rightarrow [Fe_2^{III}M^{II}(\mu_3\text{-}O)(CF_3COO)_6(H_2O)_3]\cdot H_2O + 6\,CH_3COOH + 2\,H_2O \quad (1)$$

Similar metathesis reactions have also been applied successfully to higher-nuclearity carboxylates.[17] All the trifluoroacetate compounds are readily soluble in water and a variety of organic solvents, so that growing single crystals of **1**−**3** by concentration, vapour diffusion or liquid diffusion was limited to certain solvent combinations, as reflected by the compositions of the crystals described below.

Description of Structures

Molecular structures of $[Fe_2Mn(\mu_3\text{-}O)(CF_3COO)_6(H_2O)_3]\cdot 2MeNO_2\cdot H_2O$ (**1′**) and $[Fe_2Co(\mu_3\text{-}O)(CF_3COO)_6(H_2O)_3]\cdot 3Me_2CO\cdot 1/2Mes$ (**2′**) were examined under cryogenic conditions (100 K). An ORTEP diagram of $[Fe_2Co(\mu_3\text{-}O)(CF_3COO)_6(H_2O)_3]$ is presented in Figure 1. The principal lattice matrices of the complexes are listed in Table 6, while bond lengths and angles of **2′** are presented in Table 1.

$[Fe_2Co(\mu_3\text{-}O)(CF_3COO)_6(H_2O)_3]\cdot 3Me_2CO\cdot 1/2Mes$ (Mes = 1,3,5-trimethylbenzene) (2′)

The monoclinic unit cell of the complex contains 4 molecules of the trinuclear complex, 12 molecules of acetone, and 2 molecules of mesitylene. In the crystal structure of **2′**, all the trinuclear molecules are located in parallel layers of sequence *ABAB*. Hence the molecules of the third layer occupy positions precisely above those of the first layer. The absence of interlayer trimer−trimer cohesion forces (e.g. through the lack of any intertrimer hydrogen bonds) allows the solvent molecules to readily penetrate and occupy the interlayer volume. The interstices between trinuclear species are occupied by molecules of acetone and mesitylene, the aromatic ring planes of mesitylene being perpendicular to the trimetal planes. The *R* factor (0.0857) for this structure is somewhat raised by the disorder in the trifluoromethyl groups, as well as in the mesitylene (lying on the C_2 axes) and acetone molecules (lying on the symmetry planes).

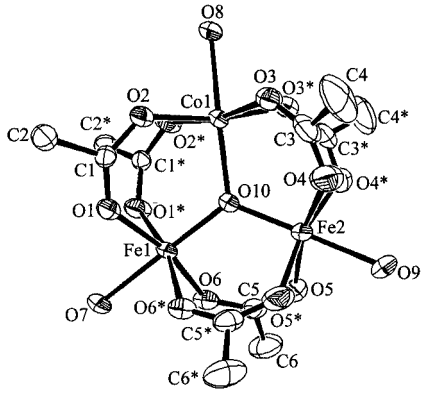

Figure 1. ORTEP plot of the structure of the skeleton of complex **1′**; thermal ellipsoids are shown at the 20% level for clarity; H and F atoms are omitted for clarity of presentation

Table 1. Selected distances and angles in $[Fe_2Co(\mu_3\text{-}O)(CF_3COO)_6(H_2O)_3]\cdot 3Me_2CO\cdot 1/2Mes$

Distances [Å]			
Fe1−Fe2	3.26(1)	Fe2−O4	2.030(4)
Fe1−Co	3.33(1)	Fe2−O4*[a]	2.030(4)
Fe2−Co	3.33(1)	Fe2−O5	2.049(4)
Fe1−O10	1.873(5)	Fe2−O5*	2.049(4)
Fe1−O1	2.028(6)	Fe2−O9	2.079(5)
Fe1−O1*	2.028(6)	Co−O10	1.993(5)
Fe1−O6	2.076(6)	Co−O2	2.069(4)
Fe1−O6*	2.076(6)	Co−O2*	2.069(4)
Fe1−O7	2.080(7)	Co−O3*	2.078(4)
Fe2−O10	1.867(5)	Co−O3	2.078(4)
		Co−O8	2.076(6)
Angles [°]			
Fe1−O10−Fe2	121.5(3)	O4*−Fe2−O5*	88.6(2)
Fe1−O10−Co	119.1(3)	O4−Fe2−O5*	166.7(2)
Fe2−O10−Co	119.4(3)	O4−Fe2−O9	83.6(2)
O10−Fe1−O1	96.6(2)	O4*−Fe2−O5	166.7(2)
O10−Fe1−O1*	96.6(2)	O4−Fe2−O5	88.6(2)
O10−Fe1−O6	95.8(2)	O4*−Fe2−O9	83.6(2)
O10−Fe1−O6*	95.8(2)	O5*−Fe2−O5	90.6(2)
O10−Fe1−O7	178.8(3)	O5−Fe2−O9	83.2(2)
O1−Fe1−O1*	91.1(4)	O5*−Fe2−O9	83.2(2)
O1*−Fe1−O6*	89.3(2)	O10−Co1−O2	94.3(2)
O1−Fe1−O6*	167.5(2)	O10−Co1−O2*	94.3(2)
O1*−Fe1−O7	84.3(2)	O10−Co1−O8	178.1(2)
O1*−Fe1−O6	167.5(2)	O10−Co1−O3	95.4(2)
O1−Fe1−O6	89.3(2)	O10−Co1−O3*	95.4(2)
O1−Fe1−O7	84.3(2)	O2−Co1−O2*	90.0(2)
O6*−Fe1−O6	87.6(3)	O2*−Co1−O8	84.4(2)
O6−Fe1−O7	83.3(2)	O2*−Co1−O3*	91.7(2)
O6*−Fe1−O7	83.3(2)	O2−Co1−O3*	170.0(2)
O10−Fe2−O4	97.2(2)	O2−Co1−O8	84.4(2)
O10−Fe2−O4*	97.2(2)	O2*−Co1−O3	170.0(2)
O10−Fe2−O5	96.1(2)	O2−Co1−O3	91.7(2)
O10−Fe2−O5*	96.1(2)	O8−Co1−O3	85.9(2)
O10−Fe2−O9	178.9(2)	O8−Co1−O3*	85.9(2)
O4−Fe2−O4*	89.1(3)	O3*−Co1−O3	84.9(3)

[a] The positions of the atoms with an asterisk are defined by the appropriate symmetry operations. The standard deviations are reported in parentheses.

The molecular structure of the complex is based on an isosceles triangular Fe_2Co fragment, with a μ_3-bridging oxide oxygen atom μ_3-O(O10) at the centre of the triangle made up by two iron(III) atoms and a cobalt(II) atom. Six μ-trifluoroacetate anions also join the metal atoms through carboxylate oxygen atoms (O_c), reinforcing the triangular framework: in each case the carboxylate groups have a μ-O,O′ coordination. The oxygen donor atoms of the water molecules bring the coordination number of each metal 3d-ion to 6, so that each Fe^{3+} and Co^{2+} ion manifests a distorted octahedral environment of oxygen atoms. The coplanarity of the μ_3-oxygen atom with the triangle of the

metal ions shows that it is an sp^2-hybridised oxide ion, removing the ambiguity associated with a possible μ_3-OH^- bridge. The average μ_3-O−Fe distance of 1.870(5) Å is typical for $Fe^{3+}-O^{2-}$ bonds in trinuclear (carboxylato)(μ_3-oxo) complexes.[18] Comparison of this value with corresponding distances in $[Fe^{III}_2Fe^{II}(\mu_3\text{-}O)(CH_3COO)_6(4\text{-Et-py})_3]$ (μ_3-O−Fe^{2+} 2.01 Å, μ_3-O−Fe^{3+}, 1.86 Å at 163 K)[19] favours the assumption that the oxidation state of the iron atoms in **2** remains +3. If the μ_3-O^{2-} ionic radius is taken as 1.22 Å,[20] the ionic radius of Fe^{3+} can be estimated to be 0.64 Å, somewhat smaller than the value reported at room temperature (0.78 Å[20]). The μ_3-O−Co distance [1.993(5) Å] is greater than μ_3-O−Fe, due to the larger ionic radius of Co^{2+}.[20] For each Fe^{3+} ion, three sets of values of the Fe−O bond lengths are found: short μ_3-O−Fe distances (1.87 Å), two intermediate Fe−O_c distances (2.03 Å for Fe−O1 and Fe1−O1*), and three longer Fe−O_c and Fe−OH_2 bonds (ranging from 2.05 Å for Fe2−O5 and Fe2−O5*, to 2.08 Å for Fe1−O7 and Fe2−O9, where O_c are oxygen atoms of the carboxylate bridges). For the Co^{2+} ion, the differences between the Co−O_c bond lengths [2.069(4) and 2.078(4) Å] are less significant than the corresponding bond lengths in analogous trinuclear acetato complexes. This can be rationalised by a weaker donor power of the trifluoroacetate ion (due to the inductive effect of the CF_3− group) in comparison with the acetate group. All the M−OH_2 bond lengths are 2.08 Å.

In the acetato complex $[Fe_2Co(\mu_3\text{-}O)(CH_3COO)_6(H_2O)_3]\cdot 2H_2O$, which crystallises in a monoclinic system ($Z = 8$),[21] disorder causes the metal atoms to appear to be arranged at the corners of an equilateral triangle, hence concealing the identities of the individual Fe^{3+} and Co^{2+} ions. In the present trifluoroacetate case, the observed C_{2v} symmetry of the trimetal unit allows the distinction between Fe^{3+} and Co^{2+} to be made.

$[Fe_2Mn(\mu_3\text{-}O)(CF_3COO)_6(H_2O)_3]\cdot 2MeNO_2\cdot H_2O$ (**1′**)

This complex also crystallises in a monoclinic space group. The parallel layers of trinuclear species are arranged in an *ABCDEABCDE* sequence. The overall *R* factor for the structure is quite large because of substantial disordering of the trifluoromethyl groups and solvent molecules. However, the trinuclear skeleton is confirmed and certain details are clearly apparent. The structure of **1′** is not identical to that of **2′**, the trimetal moiety forms a slightly distorted isosceles triangle: [Fe1−Mn 3.328(2) Å; Fe2−Mn 3.368(2) Å; Fe−Fe 3.273(2) Å]. The coordination spheres of the metal ions are essentially octahedral, with the Fe−μ_3-O distances in the typical range for these systems: the μ_3-O−Fe bond lengths (1.86 and 1.87 Å for atoms Fe1 and Fe2, respectively) differ slightly from the corresponding values in **2′**, while a similar effect is seen for the Fe−OH_2 bond (2.10 and 2.06 Å for Fe1 and Fe2, respectively). The Fe−O_c distances vary from 2.01 to 2.07 Å, similar Fe−O_c distances have been found in analogous compounds.[22] Meanwhile, the μ_3-O−Mn (2.02 Å), Mn−O_c and Mn−OH_2 distances (2.11−2.15 Å) are in a range consistent with the persistence of Mn^{2+} under the conditions of synthesis. In consonance with this, the Mössbauer spectrum of this compound (vide infra) testifies to the presence of iron(III) rather than iron(II) in **1′**.

Mass Spectra

FAB mass spectra clearly indicate the trinuclear nature of complexes **1**−**3**, as well as the persistence of the $Fe_2M^{II}(\mu_3\text{-}O)$ skeletons. Although ions such as $[Fe_2M^{II}(\mu_3\text{-}O)(CF_3COO)_6(H_2O)_2]^+$ or $[Fe_2M^{II}(\mu_3\text{-}O)(CF_3COO)_5]^+$ are not immediately apparent, intense peaks associated with partially solvated $[Fe_2M^{II}(\mu_3\text{-}O)(CF_3COO)_5(H_2O)_2]^+$ cations are present in each case (Table 2). The spectra also display fragmentation patterns corresponding to consecutive loss of trifluoroacetate groups and water molecules. The relative intensities suggest a greater lability for trifluoroacetate than for water.

Table 2. FAB-MS data for the complexes $[Fe_2M(\mu_3\text{-}O)(CF_3COO)_6(H_2O)_3]\cdot H_2O$ (M = Mn, Co, Ni)

Ion composition	*m/z*		
	Mn	Co	Ni
$[Fe_2M(\mu_3\text{-}O)(CF_3COO)_5(H_2O)_2]^+$	787	791	790
$[Fe_2M(\mu_3\text{-}O)(CF_3COO)_5]^+$	748	752	–
$[Fe_2M(\mu_3\text{-}O)(CF_3COO)_4(H_2O)_2]^+$	674	678	677
$[Fe_2M(\mu_3\text{-}O)(CF_3COO)_4]^+$	635	639	638
$[Fe_2M(\mu_3\text{-}O)(CF_3COO)_3(H_2O)]^+$	541	545	544
$[Fe_2M(\mu_3\text{-}O)(CF_3COO)_3]^+$	522	526	525
$[Fe_2M(\mu_3\text{-}O)(CF_3COO)_2(H_2O)_2]^+$	447	451	450
$[Fe_2M(\mu_3\text{-}O)(CF_3COO)_2(H_2O)]^+$	428	432	431
$[Fe_2M(\mu_3\text{-}O)(CF_3COO)(H_2O)_2]^+$	334	338	337

IR Spectra

The IR absorption bands for **1**−**3** (Table 3) are consistent with those reported in the literature for the acetate analogues[22,23] and are similarly assigned: $\nu(COO^-)_s$ and $\nu(COO^-)_{as}$ in **1**−**3** are shifted to a lower energy by 40−50 cm^{-1} relative to the trinuclear basic acetates,[22] indicating

Table 3. IR data for trinuclear carboxylates [cm^{-1}]

Complex	$\nu(M_3O)_{as}$	$\nu(COO^-)_s$	$\nu(COO^-)_{as}$	$\Delta\nu$[a]
$[Fe_2Mn(\mu_3\text{-}O)(CF_3COO)_6(H_2O)_3]\cdot H_2O$	622	1470	1640	170
$[Fe_2Co(\mu_3\text{-}O)(CF_3COO)_6(H_2O)_3]\cdot H_2O$	627	1475	1630	155
$[Fe_2Ni(\mu_3\text{-}O)(CF_3COO)_6(H_2O)_3]\cdot H_2O$	630	1475	1645	170

[a] $\Delta\nu = \nu(COO^-)as - \nu(COO^-)s$.

that the replacement of the CH_3 radical by the more powerfully electron-accepting CF_3 moiety weakens the metal$-O_c$ force constant.

The splitting of the symmetric and asymmetric valence vibrations ($\Delta\nu$, Table 3) signals bidentate bridging carboxylate groups around the $Fe_2M(\mu_3\text{-}O)$ fragment,[12] while the bands at 600−650 cm^{-1} are assigned to vibrations of the $Fe_2M(\mu_3\text{-}O)$ skeleton.

Electronic Spectra

The electronic spectra of **1**−**3** (Table 4) are similar to those reported for other trinuclear basic carboxylates containing iron(III),[22] and are useful in revealing the spin states of the metal ions. At longer wavelengths, absorbance bands are observed which are characteristic of d−d transitions from the $^6A_{1g}$ ground state of a distorted octahedral high-spin Fe^{3+} ion. For instance, the band at 17500 cm^{-1} is assigned to the $^6A_{1g}\rightarrow{}^4A_{2g}$ d−d transition, the intensity of which is enhanced due to the influence of exchange interactions[24] inside the trinuclear moiety. The remaining Fe^{3+} d−d transitions are obscured by intense absorbance bands near 29000 and 22000 cm^{-1} (ε = 1500−3000 $dm^3\cdot mol^{-3}\cdot cm^{-1}$) associated with the ligand-to-metal charge-transfer transitions which are characteristic of such iron(III) systems.[25,26] The electronic spectrum of $[Fe_2Ni(\mu_3\text{-}O)(CF_3COO)_6(H_2O)_3]\cdot H_2O$ (**3**) exhibits an absorbance band at 13580 cm^{-1} (Table 4). The position and intensity of this band are consistent with a $^3A_{2g}\rightarrow{}^3T_{2g}$ assignment for an octahedral Ni^{2+} chromophore.[25] The intensity of this band in **3** is slightly enhanced relative to similar bands in mononuclear Ni^{2+} complexes, which is likely to be related to the exchange interactions in the $Fe_2Ni^{2+}(\mu_3\text{-}O)$ moiety.[24] Literature data for various other basic carboxylates[22,24] also confirm that the exchange interactions are generally orders of magnitude less than the differences amongst the term energies of the individual ions.

Table 4. UV/VIS spectra of the trinuclear complexes in acetonitrile solution

Complex	λ_{max} [cm^{-1}] (ε[a] [L cm^{-1} mol^{-1}])
$[Fe_2Mn(\mu_3\text{-}O)(CF_3COO)_6(H_2O)_3]\cdot H_2O$	29200 (3970), 25640 (540) sh, 21490 (223), 17420 (103) sh
$[Fe_2Co(\mu_3\text{-}O)(CF_3COO)_6(H_2O)_3]\cdot H_2O$	29600 (3655), 22330 (1356), 17400 (368)
$[Fe_2Ni(\mu_3\text{-}O)(CF_3COO)_6(H_2O)_3]\cdot H_2O$	28640 (2450), 17600 (309), 13580 (36)

[a] Molar extinction coefficient in parentheses.

Magnetic Studies

Temperature dependencies of the magnetic susceptibilities of complexes **1**−**3** were measured in the 5−300 K range.

Complex $[Fe_2Mn(\mu_3\text{-}O)(CF_3COO)_6(H_2O)_3]\cdot H_2O$ (1)

With decreasing temperature, $\chi_M T$ (in $cm^3\cdot K\cdot mol^{-1}$, where χ_M is per mol of trimer) decreased smoothly from 4.51 at 300 K to 3.19 at 5 K (Figure 2). The observed $\chi_M T$ value for this complex, even at room temperature, is significantly lower than the expected spin-only $\chi_M T$ value (13.125 $cm^3\cdot K\cdot mol^{-1}$) for a non-interacting $g = 2$ high-spin set of one manganese(II) and two iron(III) ions. This clearly indicates strong antiferromagnetic coupling within the Fe_2Mn framework. In general, two high-spin iron(III) ions with $S = 5/2$ and one manganese(II) ion with $S = 5/2$ can couple to give a total molecular spin (S_T) ranging from 1/2 to 15/2. Magnetic data were analysed according to the exchange Hamiltonian [Equation (2)], and the coupling pathways are presented in Scheme 1.

$$H = -2J_{FeM}[S_{Fe1}S_M + S_MS_{Fe2}] - 2J_{FeFe}[S_{Fe1}S_{Fe2}] \quad (2)$$

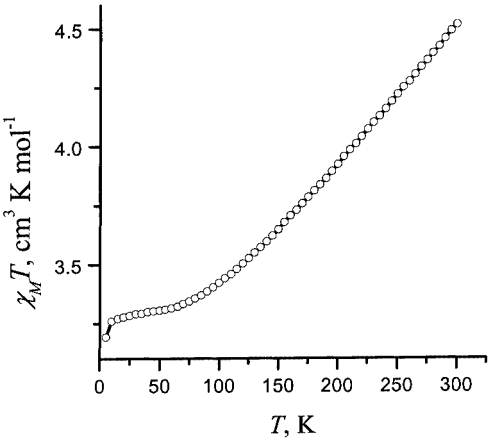

Figure 2. Temperature dependence of the magnetic susceptibility of **1**, plotted as χT vs. T; the solid line is the least-squares fit

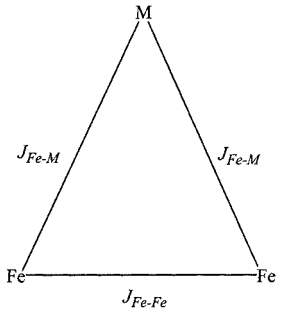

Scheme 1. Magnetic exchange pathways in the trinuclear core

The zero-field energy levels for the Fe_2M complexes were calculated according to Equation (3),[5] where $S_{Fe} = 5/2$; S_M is the spin of M^{II} (5/2 for Mn^{II}, 3/2 for Co^{II}, and 2/2 for Ni^{II}); $S^* = S_{Fe} + S_{Fe}$; $S_T = S^* + S_M$ according to Kambe's notation.[27]

$$E(S_T, S^*) = J_{FeM}[2S_{Fe}(S_{Fe} + 1) - S_T(S_T + 1)] + J_{FeFe}[S_T(S_T + 1) + S_M(S_M + 1) - S^*(S^* + 1)] \quad (3)$$

Within this approach, S^* ranges integrally from 0 to 5, so that for instance, when $S^* = 1$, S_T for the Co^{II}-containing molecule may take values of 1/2, 3/2, or 5/2. Substitution

of the eigenvalues for the spin-states derived from the above exchange Hamiltonian into the van Vleck equation results in an expression for the $\chi_M T$ values for the Fe_2Mn complex [Equation (4)], where $a = -25J_{Fe\text{-}Mn} - 12.5J_{Fe\text{-}Fe}$; $b = -10J_{Fe\text{-}Mn} - 12.5J_{Fe\text{-}Fe}$; $c = 3J_{Fe\text{-}Mn} - 12.5J_{Fe\text{-}Fe}$; $d = 14J_{Fe\text{-}Mn} - 12.5J_{Fe\text{-}Fe}$; $e = 23J_{Fe\text{-}Mn} - 12.5J_{Fe\text{-}Fe}$; $f = 30J_{Fe\text{-}Mn} - 12.5J_{Fe\text{-}Fe}$; $\gamma = -20J_{Fe\text{-}Mn} - 2.5J_{Fe\text{-}Fe}$; $h = -7J_{Fe\text{-}Mn} - 2.5J_{Fe\text{-}Fe}$; $\omega = 4J_{Fe\text{-}Mn} - 2.5J_{Fe\text{-}Fe}$; $j = 13J_{Fe\text{-}Mn} - 2.5J_{Fe\text{-}Fe}$; $\kappa = 20J_{Fe\text{-}Mn} - 2.5J_{Fe\text{-}Fe}$; $l = 25J_{Fe\text{-}Mn} - 2.5J_{Fe\text{-}Fe}$; $m = -15J_{Fe\text{-}Mn} + 5.5J_{Fe\text{-}Fe}$; $n = -4J_{Fe\text{-}Mn} + 5.5J_{Fe\text{-}Fe}$; $o = 5J_{Fe\text{-}Mn} + 5.5J_{Fe\text{-}Fe}$; $p = 12J_{Fe\text{-}Mn} + 5.5J_{Fe\text{-}Fe}$; $q = 17J_{Fe\text{-}Mn} + 5.5J_{Fe\text{-}Fe}$; $r = 20J_{Fe\text{-}Mn} + 5.5J_{Fe\text{-}Fe}$; $s = -10J_{Fe\text{-}Mn} + 11.5\ J_{Fe\text{-}Fe}$; $t = -J_{Fe\text{-}Mn} + 11.5J_{Fe\text{-}Fe}$; $u = 6J_{Fe\text{-}Mn} + 11.5J_{Fe\text{-}Fe}$; $v = 11J_{Fe\text{-}Mn} + 11.5J_{Fe\text{-}Fe}$; $w = 14J_{Fe\text{-}Mn} + 11.5J_{Fe\text{-}Fe}$; $x = -5J_{Fe\text{-}Mn} + 15.5J_{Fe\text{-}Fe}$; $y = 2J_{Fe\text{-}Mn} + 15.5J_{Fe\text{-}Fe}$; $z = -7J_{Fe\text{-}Mn} + 15.5J_{Fe\text{-}Fe}$; $\varphi = 17.5J_{Fe\text{-}Fe}$.

$$\chi_M T = (Ng^2\beta^2/3k)(1020e^{-a/kT} + 682.5e^{-b/kT} + 429e^{-c/kT} + 247.5e^{-d/kT} + 126e^{-e/kT} + 52.5e^{-f/kT} + 682.5e^{-\gamma/kT} + 429e^{-h/kT} + 247.5e^{-\omega/kT} + 126e^{-j/kT} + 52.5e^{-\kappa/kT} + 15e^{-l/kT} + 429e^{-m/kT} + 247.5e^{-n/kT} + 126e^{-o/kT} + 52.5e^{-p/kT} + 15e^{-q/kT} + 1.5e^{-r/kT} + 247.5e^{-s/kT} + 126e^{-t/kT} + 52.5e^{-u/kT} + 15e^{-v/kT} + 1.5e^{-w/kT} + 126e^{-x/kT} + 52.5e^{-y/kT} + 15e^{-z/kT} + 52.5e^{-\varphi/kT})/(16e^{-a/kT} + 14e^{-b/kT} + 12e^{-c/kT} + 10e^{-d/kT} + 8e^{-e/kT} + 6e^{-f/kT} + 14e^{-\gamma/kT} + 12e^{-h/kT} + 10e^{-\omega/kT} + 8e^{-j/kT} + 6e^{-\kappa/kT} + 4e^{-l/kT} + 12e^{-m/kT} + 10e^{-n/kT} + 8e^{-o/kT} + 6e^{-p/kT} + 4e^{-q/kT} + 2e^{-r/kT} + 10e^{-s/kT} + 8e^{-t/kT} + 6e^{-u/kT} + 4e^{-v/kT} + 2e^{-w/kT} + 8e^{-x/kT} + 6e^{-y/kT} + 4e^{-z/kT} + 6e^{-\varphi/kT}) \quad (4)$$

Despite the deviation of this complex from an exact isosceles triangle, a satisfactory fit was achieved using two J parameters. The best fit was obtained with fixed values of $g_{Fe} = g_{Mn} = 2.00$, giving $J_{Fe\text{-}Fe} = -56.50(7)$ and $J_{Fe\text{-}Mn} = -16.23(4)$ cm^{-1} [$R^2 = 1.85\cdot10^{-5}$ where $R^2 = \Sigma(\chi_{obs}-\chi_{calc})^2/\Sigma\chi^2_{obs}$]. An energy diagram (Figure 3) for the spin states of **1** reveals that the ground state is a quadruplet (S_T, S^*) = (3/2, 1), with a low-lying sextuplet (5/2, 0) 0.61 cm^{-1} above it. The experimental $\chi_M T$ value at 5 K (3.19) is intermediate between the calculated values for these two spin-states: 1.88 cm^3·K·mol^{-1} for a quadruplet and 4.38 cm^3·K·mol^{-1} for a sextuplet ground state, and the $\chi_M T$ data thus betoken Boltzmann distribution over these two states. Previously, Blake et al. reported that $S_T = 3/2$ is the ground state for $[Fe_2Mn(\mu_3\text{-}O)(CH_3COO)_6(py)_3]\cdot0.7py$.[24]

Complex $[Fe_2Co(\mu_3\text{-}O)(CF_3COO)_6(H_2O)_3]\cdot H_2O$ (2)

In general, the magnetic properties of **2** resembled those of the manganese analogue (Figure 4). On cooling, $\chi_M T$ for this complex decreased from 4.76 cm^3·K·mol^{-1} at 300 K to 2.00 at 5 K (Figure 4). The observed χ_MT value at room temperature is less than one half of the spin-only χ_MT value (10.61 cm^3·K·mol^{-1}) for a non-interacting FeCoFe ion set. Again, this directly testifies for the existence of strong antiferromagnetic coupling within the Fe_2Co framework. Two high-spin irons(III) ions and one high-spin ($S = 3/2$) cobalt(II) ion can couple to give spins ranging from $S_T = 1/2$ to $S_T = 13/2$. The experimental data were fitted according to the isotropic spin-Hamiltonian [Equation (2)] to give Equation (5), where $a = -15J_{Fe\text{-}Co} - 12.5J_{Fe\text{-}Fe}$; $b = -2J_{Fe\text{-}Co} - 12.5J_{Fe\text{-}Fe}$; $c = 9J_{Fe\text{-}Co} - 12.5J_{Fe\text{-}Fe}$; $d = 18J_{Fe\text{-}Co} - 12.5J_{Fe\text{-}Fe}$; $e = -12J_{Fe\text{-}Co} - 2.5J_{Fe\text{-}Fe}$; $f = -J_{Fe\text{-}Co} - 2.5J_{Fe\text{-}Fe}$; $\gamma = 8J_{Fe\text{-}Co} - 2.5J_{Fe\text{-}Fe}$; $h = 15J_{Fe\text{-}Co} - 2.5J_{Fe\text{-}Fe}$; $\omega = -9J_{Fe\text{-}Co} + 5.5J_{Fe\text{-}Fe}$; $j = 5.5J_{Fe\text{-}Fe}$; $\kappa = 7J_{Fe\text{-}Co} + 5.5J_{Fe\text{-}Fe}$; $l = 12J_{Fe\text{-}Co} + 5.5\ J_{Fe\text{-}Fe}$; $m = -6\ J_{Fe\text{-}Co} + 11.5J_{Fe\text{-}Fe}$; $n = J_{Fe\text{-}Co} + 11.5J_{Fe\text{-}Fe}$; $o = 6J_{Fe\text{-}Co} + 11.5J_{Fe\text{-}Fe}$; $p = 9J_{Fe\text{-}Co} + 11.5J_{Fe\text{-}Fe}$; $q = -3J_{Fe\text{-}Co} + 15.5J_{Fe\text{-}Fe}$; $r = 2J_{Fe\text{-}Co} + 15.5J_{Fe\text{-}Fe}$; $s = 5J_{Fe\text{-}Co} + 15.5J_{Fe\text{-}Fe}$; $t = 17.5J_{Fe\text{-}Fe}$.

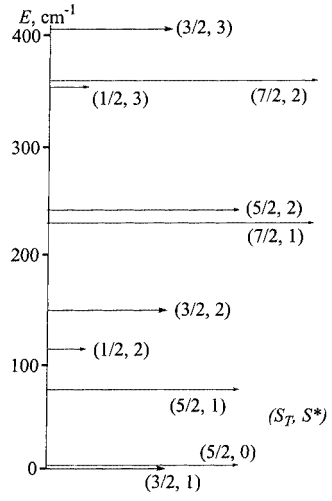

Figure 3. Energy diagram for low-lying spin levels of **1**

$$S_T = [(Ng_{mol}^2\beta^2/3k)(682.5e^{-a/kT} + 429e^{-b/kT} + 247.5e^{-c/kT} + 126e^{-d/kT} + 429e^{-e/kT} + 247.5e^{-f/kT} + 126e^{-\gamma/kT} + 52.5e^{-h/kT} + 247.5e^{-\omega/kT} + 126e^{-j/kT} + 52.5e^{-\kappa/kT} + 15e^{-l/kT} + 126e^{-m/kT} + 52.5e^{-n/kT} + 15e^{-o/kT} + 1.5e^{-p/kT} + 52.5e^{-q/kT} + 15e^{-r/kT} + 1.5e^{-s/kT} + 15e^{-t/kT})/(14e^{-a/kT} + 12e^{-b/kT} + 10e^{-c/kT} + 8e^{-d/kT} + 12e^{-e/kT} + 10e^{-f/kT} + 8e^{-g/kT} + 6e^{-h/kT} + 10e^{-\omega/kT} + 8e^{-j/kT} + 6e^{-\kappa'/kT} + 4e^{-l/kT} + 8e^{-m/kT} + 6e^{-n/kT} + 4e^{-o/kT} + 2e^{-p/kT} + 6e^{-q/kT} + 4e^{-r/kT} + 2e^{-s/kT} + 4e^{-t/kT})](1 - \rho) + S(S+1)(Ng^2\beta^2/3k)\rho + TIP \quad (5)$$

Here, ρ is the fraction of a mononuclear ferric paramagnetic ($S = 5/2$) impurity, and g_{mol} is for the trinuclear complex.

The best fit was obtained with $g_{mol} = 2.09(1)$; $J_{Fe\text{-}Fe} = -42.8(3.5)$ cm^{-1}; $J_{Fe\text{-}Co} = -17.8(1.4)$ cm^{-1}; $\rho = 0.031(5)$ and $TIP = 0$ ($R^2 = 6.17\cdot10^{-6}$). Fixing g_{Fe} at 2.00 gave $g_{Co} = 2.27$ according to $3g_{mol} = (2\ g_{Fe} + g_{Co})$. The associated spin ladder energy diagram reveals a (1/2, 1) ground state with a (3/2, 0) state 3.2 cm^{-1} above it (Figure 5). These states are well-separated from the second excited state (3/2, 1), which is 50 cm^{-1} above them.

Complex $[Fe_2Ni(\mu_3\text{-}O)(CF_3COO)_6(H_2O)_3]\cdot H_2O$ (3)

For this complex, the $\chi_M T$ value monotonically decreased from 3.03 cm^3·K·mol^{-1} at 300 K to about 1.15

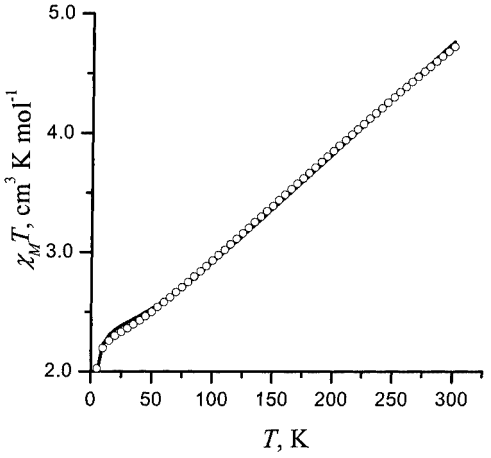

Figure 4. Temperature dependence of the magnetic susceptibility of **2**, plotted as χT vs. T; the solid line is the least-squares fit

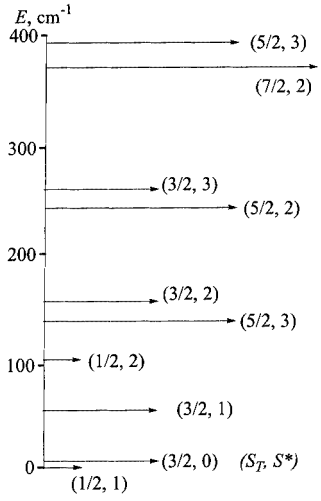

Figure 5. Energy diagram for low-lying spin levels of **2**

cm^3·K·mol^{-1} at 32 K, and after passing through a broad minimum at 50−20 K, increased somewhat again as T approached 5 K Figure 6). Comparison with the calculated spin-only $\chi_M T$ value (9.73 cm^3·K·mol^{-1}) for non-interacting ions again indicates strong antiferromagnetic exchange within the trimetallic species. Two high-spin S = 5/2 iron(III) ions and one high-spin S = 1 nickel(II) ion can couple to give S_T values ranging from 0 to 12/2. Magnetic data were fitted in agreement with the exchange Hamiltonian [Equation (2)] and the expression for $\chi_M T$ [Equation (6)], where $a = -10J_{Fe\text{-}Ni} - 12.5J_{Fe\text{-}Fe}$; $b = 2J_{Fe\text{-}Ni} - 12.5J_{Fe\text{-}Fe}$; $c = 12J_{Fe\text{-}Ni} - 12.5J_{Fe\text{-}Fe}$; $d = {}_{Fe\text{-}Ni} - 2.5J_{Fe\text{-}Fe}$; $e = 2J_{Fe\text{-}Ni} - 2.5J_{Fe\text{-}Fe}$; $f = 10J_{Fe\text{-}Ni} - 2.5J_{Fe\text{-}Fe}$; $\gamma = -6J_{Fe\text{-}Ni} + 5.5J_{Fe\text{-}Fe}$; $h = 2J_{Fe\text{-}Ni} + 5.5J_{Fe\text{-}Fe}$; $\omega = 8J_{Fe\text{-}Ni} + 5.5J_{Fe\text{-}Fe}$; $j = -4J_{Fe\text{-}Ni} + 11.5J_{Fe\text{-}Fe}$; $\kappa = 2J_{Fe\text{-}Ni} + 11.5J_{Fe\text{-}Fe}$; $l = 6J_{Fe\text{-}Ni} + 11.5J_{Fe\text{-}Fe}$; $m = -2J_{Fe\text{-}Ni} + 15J_{Fe\text{-}Fe}$; $n = 2J_{Fe\text{-}Ni} + 15.5J_{Fe\text{-}Fe}$; $o = 4J_{Fe\text{-}Ni} + 15.5J_{Fe\text{-}Fe}$; $p = 17.5J_{Fe\text{-}Fe}$.

$$\chi_M T = (Ng_{mol}^2\beta^2/3k)\cdot(546e^{-a/kT} + 330e^{-b/kT} + 180e^{-c/kT} + 330e^{-d/kT} + 180e^{-e/kT} + 84e^{-f/kT} + 180e^{-\gamma/kT} + 84e^{-h/kT} + 30e^{-\omega/kT} + 84e^{-j/kT} + 30e^{-\kappa/kT} + 6e^{-l/kT} + 30e^{-m/kT} + 6e^{-n/kT} + 6e^{-p/kT})/(13e^{-a/kT} + 11e^{-b/kT} + 9e^{-c/kT} + 7e^{-d/kT} + 11e^{-e/kT} + 9e^{-f/kT} + 7e^{-\gamma/kT} + 5e^{-h/kT} + 9e^{-\omega/kT} + 7e^{-j/kT} + 5e^{-\kappa/kT} + 3e^{-l/kT} + 7e^{-m/kT} + 5e^{-n/kT} + 3e^{-o/kT} + e^{-p/kT}) \quad (6)$$

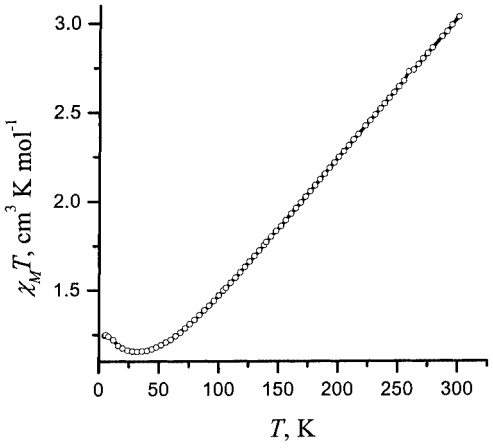

Figure 6. Temperature-dependence of the magnetic susceptibility of **3**, plotted as χT vs. T; the solid line is the least-squares fit

The best fit was obtained with a fixed g_{Fe} value of 2.00 and g_{Ni} = 2.215(2); $J_{Fe\text{-}Fe}$ = −45.60(1) and $J_{Fe\text{-}Ni}$ = −16.96(2) cm^{-1} ($R^2 = 8.54\cdot10^{-5}$). The unexpected shape of the $\chi_M T$ vs. T curve can be clarified from the associated energy diagram for the spin-states (Figure 7). This reveals a (1, 0) ground state, succeeded by the first two excited states (0, 1) and (1, 1), so that there is a diamagnetic state between the two lowest-lying triplet states. When the temperature is decreased, the singlet first excited state becomes populated and the higher states with $S_T \geq 1$ become less populated, reducing $\chi_M T$. However, a further decrease in temperature depopulates this singlet level, in favour of the triplet ground state, so that the reduction in the $\chi_M T$ value with decreasing temperature is thus arrested and reversed.

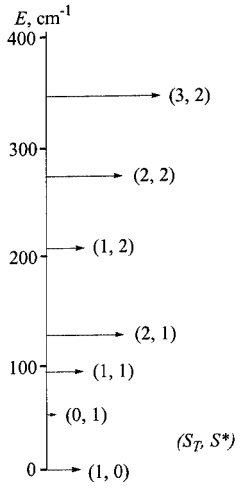

Figure 7. Energy diagram for low-lying spin levels of **3**

When comparing the magnetochemical characteristics of **1**−**3**, one notes that $J_{Fe\text{-}M}$ (M = M^{II}) is insensitive to the identity of M^{II}, whereas the $J_{Fe\text{-}Fe}$ values are affected by the nature of the third metal ion in the triangular skeleton. These results are in agreement with observations by Blake et al.[24] that $J_{Fe\text{-}Fe}$ increases significantly in Fe_2M^{II} relative to that in similar trinuclear (carboxylato)(oxo)iron(III) complexes. It is noteworthy that trinuclear pivalate complexes[28] also show significant antiferromagnetic exchange.

Mößbauer Spectra

The electronic properties of complexes **1**−**3** were examined by ^{57}Fe Mößbauer spectroscopy at 80 and 300 K (Figure 8, Table 5). Each of the spectra display one quadrupole-split doublet. The values of the isomer shifts (IS, δ) and quadrupole splittings (QS) for **1**−**3** are close to those reported previously for similar heterometallic trinuclear complexes,[29] and correspond to a high-spin iron(III) ion. Second-order Doppler effects (an increase in the isomer shift at cryogenic temperature[30]) and Goldanskii−Karyagin anisotropy[30] (manifested by the different relative intensities of the two peaks of the doublet at higher temperatures) are minor, but detectable in the spectra. The data indicate that there is no occurrence of any intermetallic redox process during or subsequent to the synthesis − i.e. there is no electron transfer from M^{2+} (especially from the more readily oxidizable Co^{2+} and Mn^{2+}) to Fe^{3+}. However, the isomer shifts in **1**−**3** are smaller than in some other[31] heterotrinuclear complexes (Table 5), which may be accounted for by the electron-withdrawing nature of the CF_3 group; the decreased donor ability of the carboxylate group thus reduces the electron density in the 3d subshell.[30] Similar effects have been reported for other homopolynuclear iron(III) species.[32,33] The relatively high quadrupole splitting in **1**−**3** also reflects the significant electron-density transfer from the iron(III) centre to the trifluroacetate anion. Previous work[22,31] indicates that quadrupole splitting increases with Fe^{III}−carboxylate bond ionicity.

The Mössbauer results reveal no spin-spin interactions which would be indicative of the exchange coupling that is so compellingly suggested by the magnetic susceptometry.

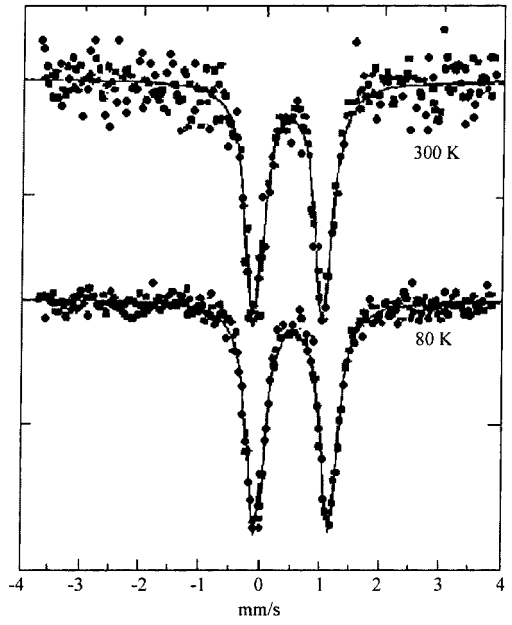

Figure 8. ^{57}Fe Mössbauer spectrum of **1**; the solid line is the least-squares fit; isomer shifts are referred to α-iron at room temperature

The relatively high J values alone lead to the expectation that a "coupled" spectrum might be observed at 80 K. However, similar apparently paradoxical results have been reported by Rentschler and co-workers,[28] who pointed out that they are a consequence of the difference in the experimental time scales of the phenomena on which the two types of measurements are based; the magnetic exchange occurs on a timescale that is too fast to be detected by ^{57}Fe Mößbauer spectroscopy.

Conclusion

Three new heterometallic trinuclear basic trifluoroacetates $[Fe_2M^{II}(\mu_3\text{-}O)(CF_3COO)_6(H_2O)_3]\cdot H_2O$ (M = Mn, Co, Ni) have been prepared. The crystal structures of two complexes were obtained at 100 K. FAB-MS data, IR and UV/

Table 5. Mössbauer spectroscopic parameters of complexes **1**−**3**

Complex	T [K]	IS [Mm/s]	QS [mm/s]	I_1/I_2
$[Fe_2Mn(\mu_3\text{-}O)(CF_3COO)_6(H_2O)_3]\cdot H_2O$	80	0.55	1.38	1.02(6)
	300	0.44	1.22	1.10(6)
$[Fe_2Co(\mu_3\text{-}O)(CF_3COO)_6(H_2O)_3]\cdot H_2O$	80	0.54	1.17	0.89(6)
	300	0.39	0.90	0.91(6)
$[Fe_2Ni(\mu_3\text{-}O)(CF_3COO)_6(H_2O)_3]\cdot H_2O$	80	0.53	1.23	1.01(6)
	300	0.43	1.15	1.05(6)
$[Fe_2^{III}Fe^{II}(\mu_3\text{-}O)(CF_3COO)_6(H_2O)_3]\cdot CF_3COOH$[a]	80	1.51	2.38	Fe^{II}
		0.61	0.97	Fe^{III}
	300	0.75	1.05	−
$[Fe_3(\mu_3\text{-}O)(CH_3COO)_6(H_2O)_3]Cl\cdot 5H_2O$[b]	80	0.71	0.61	−
	30	0.58	0.55	−

[a] K. I. Turte, S. A. Bobkova, R. A. Stukan, *Zh. Neorg. Khimii* **1982**, *27*, 954−960. [b] G. J. Long, W. T. Robinson, W. P. Tappmeyer, D. L. Bridges, *J. Chem. Soc., Dalton. Trans.* **1973**, 573−578.

Vis spectra, along with magnetochemical and Mössbauer studies were interpreted in terms of the trinuclear nature of the compounds. The complexes exhibit substantial intramolecular antiferromagnetic exchange. The absence of any iron(II) centre, as proved by the Mössbauer investigation, showed that no electron transfer from Mn^{II} or Co^{II} to Fe^{III} occurred in these complexes. Increased values of quadrupole splittings are a result of the electron-withdrawing abilities of the CF_3- group in the trifluoroacetate anions.

Experimental Section

General: Reagents and solvents (UkrReaKhim and Merck) were generally used as received. The precursory acetate complexes $[Fe_2^{III}M^{II}(\mu_3\text{-}O)(CH_3COO)_6(H_2O)_3]\cdot 3H_2O$ (M = Mn, Co, Ni) were prepared as described elsewhere.[24]

$[Fe^{III}_2M^{II}(\mu_3\text{-}O)(CF_3COO)_6(H_2O)_3]\cdot H_2O$ (M = Mn, Co, Ni): The initial acetato complex $[Fe_2^{III}M^{II}(\mu_3\text{-}O)(CH_3COO)_6(H_2O)_3]\cdot 3H_2O$ (1.3 g, ca. 2 mmol) was dissolved in aqueous trifluoroacetic acid (15 mL of a 60% solution), and the resulting solution was refluxed for 1 h. After cooling, the reaction mixture was diluted with an equal volume of acetone. Slow concentration of the reaction mixture at room temperature over several days resulted in the formation of red-brown crystals, which were filtered, washed with cold water and dried in vacuo with KOH. Yield: 60−80%.

$[Fe^{III}_2Co(\mu_3\text{-}O)(CF_3COO)_6(H_2O)_3]\cdot H_2O$: $C_{12}H_8CoF_{18}Fe_2O_{17}$ (936.77): calcd. C 15.4, H 0.85, Co 6.30, Fe 11.9; found C 15.3, H 0.83, Co 6.42, Fe 11.6. Yield 1.43 g (75%).

$[Fe^{III}_2Ni(\mu_3\text{-}O)(CF_3COO)_6(H_2O)_3]\cdot H_2O$: $C_{12}H_8F_{18}Fe_2NiO_{17}$ (936.54): calcd. C 15.4, H 0.86, Ni 6.27, Fe 12.0; found C 15.3, H 0.80, Ni 6.40, Fe 11.7. Yield 1.38 g (72%).

$[Fe^{III}_2Mn(\mu_3\text{-}O)(CF_3COO)_6(H_2O)_3]\cdot H_2O$: $C_{12}H_8F_{18}Fe_2MnO_{17}$ (932.76): calcd. C 15.4, H 0.86, Mn 5.89, Fe 12.0; found C 15.4, H 0.88, Mn 5.80, Fe 12.1. Yield 1.26 g (66%).

Physical Measurements: Electronic absorption spectra were recorded with a Carl-Zeiss-Jena Specord-M40 spectrophotometer, IR spectra with a Carl-Zeiss-Jena Specord-75. C,H,N contents were determined using a Carlo Erba 1106 microanalyzer. Mass spectra were obtained with a VG-ZABHF instrument, using 2-nitrobenzyl alcohol as the matrix for the FAB mode. The temperature and field dependencies of the magnetic susceptibilities were measured with an MPMS-5S SQUID magnetometer, Pascal's diamagnetic corrections were applied according to a standard text.[2] Magnetisation experiments were performed at 5 and 300 K. Möβbauer spectra were measured in the transmission mode on conventional spectrometers, a temperature-controlled Leybold cryostat was used for low-temperature spectra. A $3\cdot10^9$ Bq $^{57}Co(Rh)$ sample was used as the γ-ray source, while isomer shifts were referred to α-iron at room temperature. Spectra were deconvoluted using the MossWin program.[34]

X-ray Crystallographic Study: Crystals suitable for crystallography were grown from CH_3NO_2/mesitylene (for the Mn complex) or from $CH_3NO_2/(CH_3)_2CO$/mesitylene layering (for the cobalt complex). A dark red single crystal of **2′** was coated with perfluoropolyether, picked up with a glass fibre and immediately mounted in the cold nitrogen stream to prevent loss of solvent. Intensity data were collected with a Siemens SMART diffractometer at 100 K using graphite-monochromated Mo-K_α radiation (λ= 0.71073 Å). Final cell constants were obtained from a least-squares fit of 4419 reflections. Data collection was performed by hemisphere runs taking frames at 0.3°. A semiempirical absorption correction using the program SADABS[35] was performed on the data set of **2**. Crystallographic data are listed in Table 6. The Siemens SHELXTL1 software package was used for solution, refinement and artwork of the structure. The structure was readily solved by direct methods and difference Fourier techniques. All non-hydrogen atoms except atoms in disordered parts were refined anisotropically and hydrogen atoms were placed at calculated positions and refined as riding atoms with isotropic displacement parameters. Split atom models were used to account for the disorder of the CF_3COO groups and a mesitylene solvent molecule lying on the crystallographic mirror plane. The C−F and F−F distances of the CF_3 groups were re-

Table 6. Crystal data and structure refinement details

	1′	**2′**
Empirical formula	$C_{16}H_{14}N_2O_{21}F_{18}Fe_2Mn$	$C_{25.5}H_{30}O_{19}F_{18}Fe_2Co$
Formula mass	1078.89	1153.13
Crystal system	monoclinic	monoclinic
Space group	*C*2/*c*	*C*2/*m*
a [Å]	22.002(5)[a]	21.426(4)
b [Å]	13.647(3)	15.100(2)
c [Å]	24.767(4)	14.815(3)
β [°]	98.23(3)	117.99(2)
V [Å^3]	7359.9(2)	4232.50(13)
Z	8	4
$\rho_{calcd.}$ [g cm^{-3}]	1.241	1.810
T [K]	100(2)	100
μ [mm^{-1}] (Mo-K_α)	1.16	1.214
Number of reflections collected	11349	8847
Number of independent reflections	6424	3622
Number of parameters	457	346
R_{int}	0.0739	0.0541
R1 (all data)	0.1316	0.0874
wR(F^2) (all data)	0.3665	0.1822

The standard deviations are reported in parentheses.

strained to be equal within errors, and equal displacement parameters were used for the split fluorine atoms. Crystallographic data (excluding structure factors) for the structures reported in this paper have been deposited with the Cambridge Crystallographic Data Centre as supplementary publication no. CCDC-176586. Copies of the data can be obtained free of charge on application to CCDC, 12 Union Road, Cambridge CB21EZ, UK [Fax: 44-1223/336-033; E-mail: deposit@ccdc.cam.ac.uk].

Acknowledgments

V. V. P. acknowledges support from the DAAD foundation and the Max-Planck-Institut für Strahlenchemie. This work was also supported by the Hungarian Science Foundation OTKA No. T034839. A. W. A. thanks Drexel University for support.

[1] *Molecule-based Magnetic Materials* (Eds.: M. M. Turnbull, T. Sugimoto, L. K. Thompson), ACS Symposium Series, USA, **1996**, p. 341.
[2] O. Kahn, *Molecular Magnetism*, VCH Publishers Inc., New York, USA, **1993**, p. 225.
[3] C. M. Davis, A. C. Royer, J. B. Vincent, *Inorg. Chem.* **1997**, *36*, 5316−5320.
[4] M. Fontecave, S. Ménage, C. Doboe-Toia, *Coord. Chem. Rev.* **1998**, *187−188*, 1555−1572.
[5] J. D. Bois, T. J. Mizoguchi, S. J. Lippard, *Coord. Chem. Rev.* **2000**, *200−202*, 443−485.
[6] W.E. Ruettinger, G.C. Dismukes, *Inorg. Chem.* **2000**, *39*, 1021−1027.
[7] D. Gatteschi, R. Sessoli, A. Cornia, *Chem. Commun.* **2000**, 725−732.
[8] V. V. Pavlishchuk, *Teor. Eksp. Khim.* **1997**, *33*, 341−361.
[9] D. Gatteschi, A. Caneschi, R. Sessoli, A. Cornia, *Chem. Soc. Rev.* **1996**, *25*, 101−109.
[10] S. Asirvatham, M. A. Khan, K.M. Nicholas, *Inorg. Chem.* **2000**, *39*, 2006−2007.
[11] H. J. Appley, H.-L. Tsai, N. De Vries, K. Folting, G. Christou, D. N. Hendrickson, *J. Am. Chem. Soc.* **1995**, *117*, 301−317.
[12] R. F. Weinland, E. Gussmann, *Ber. Dtsch. Chem. Ges.* **1909**, *42*, 2997−3005.
[13] R. F. Weinland, H. Holtmeier, *Z. Anorg. Chem.* **1928**, *173*, 49−61.
[14] J. B. Vincent, *Inorg. Chem.* **1994**, *33*, 5604−5606.
[15] S. A. Chavan, D. Srinavas, P. Ratnasamy, *Chem. Commun.* **2001**, 1124−1125.
[16] *Activation and Functionalization of Alkanes* (Ed.: C. L. Hill), John Wiley and Sons, Inc., New York, **1989**, p. 341.
[17] A. R. Schake, H.-L. Tsai, R.J. Webb, K. Folting, G. Christou, D. N. Hendrickson, *Inorg. Chem.* **1994**, *33*, 6020−6022.
[18] S. G. Shova, I. G. Kadelnik, M. Gdanec, Yu. A. Simonov, T. K. Zhovmir, V. M. Meriacre, G. Filotti, K. I. Turte, *Zh. Strukt. Khim.* **1998**, *39*, 917−933.
[19] S. M. Oh, D. N. Hendrickson, K. L. Hassett, R. E. Davis, *J. Am. Chem. Soc.* **1985**, *107*, 8009−8018.
[20] R. D. Shannon, *Acta Crystallogr., Sect. A* **1976**, *32*, 751−755.
[21] T. Sato, F. Ambe, *Acta Crystallogr., Sect. C* **1996**, *52*, 3005−3007.
[22] R. D. Cannon, R. P. White, *Prog. Inorg. Chem.* **1988**, *36*, 195−298.
[23] M. M. Mansurov, O. V. Semenova, S. S. Sokhibov, *Zh. Neorg. Khim. (Russ. Ed.)* **1991**, *36*, 2810−2815.
[24] A. B. Blake, A. Yavari, W. E. Hatfield, C. N. Sethulekshmi, *J. Chem. Soc., Dalton Trans.* **1985**, 2509−2520.
[25] A. B. P. Lever, *Inorganic Electronic Spectroscopy*, 2nd ed., Elsevier, New York, **1984**, p. 334.
[26] C. Fernandes, E. Stadler, V. Drago, C. G. da Cunha, I. N. Kuwabara, *Spectrochim. Acta* **1996**, *A52*, 1815−1821.
[27] C. Kambe, *J. Phys. Soc. Jpn.* **1950**, *5*, 48−55.
[28] E. Rentschler, K. Wieghardt, G. Timko, N. Gerbeleu, *213th National ACS Meeting*, San Francisco, **1997**, INOR 501.
[29] M. K. Johnson, R. D. Cannon, D. B. Powell, *Spectrochim. Acta* **1982**, *38A*, 307−315.
[30] A. Vértes, L. Korecz, K. Burger, *Mössbauer Spectroscopy*, Elsevier, Amsterdam, **1979**.
[31] S. K. Abdulaev, O. A. Nasonova, K. I. Yakubov, K. I. Turte, V. V. Zelentsov, R. A. Stukan, *Zh. Neorg. Khim. (Russ. Ed.)* **1988**, *33*, 1765−1770.
[32] T. Sato, F. Ambe, K. Endo, M. Katada, H. Maeda, T. Nakamoto, H. Sano, *J. Am. Chem. Soc.* **1996**, *118*, 3450−3458.
[33] B. D. Rumbold, G. V. H. Wilson, *J. Phys. Chem. Solids* **1973**, *34*, 1887−1891.
[34] Z. Klencsár, E. Kuzmann, A. Vértes, *J. Radioanal. Nucl. Chem.* **1996**, *A210*, 105.
[35] *SHELXTL*, version 5, Siemens Analytical X-ray Instruments, Inc., Göttingen, **1994**.

Received February 11, 2002
[I02071]

Hydrothermal Syntheses, Structures, and Properties of First Examples of Lanthanide(III) 2,3-Pyrazinedicarboxylates with Three-Dimensional Framework

Xiang-Jun Zheng,[a] Lin-Pei Jin,*[a] and Shao-Zhe Lu[b]

Keywords: Hydrothermal synthesis / Lanthanides / Coordination polymer / N ligands / O ligands

Lanthanide 2,3-pyrazinedicarboxylate complexes with three-dimensional frameworks, $[Ln_2(pzdc)_3(H_2O)]_x \cdot 2xH_2O$ [Ln = Pr (**2**), Nd (**3**), and Eu (**4**)], were obtained by hydrothermal reactions of 2,3-pyrazinedicarboxylic acid (H_2pzdc) and the lanthanide(III) chlorides, while $[La_2(pzdc)_3(H_2O)]_x \cdot 2xH_2O$ (**1**) was obtained by hydro(solvo)thermal reaction of $LaCl_3 \cdot 7H_2O$ and 2,3-pyrazinedicarboxylic acid. They are isomorphous and exhibit complicated 3-D structures based on $[Ln_2(pzdc)_3(H_2O)]$ building blocks. In the asymmetric unit, the two Ln^{3+} ions are both nine-coordinate, but with different coordination environments. The ligand pzdc coordinates to the central Ln^{3+} ions in a tetradentate, hexadentate, or heptadentate manner. Utilizing the characteristic of Eu^{3+} ion to act as a conformational probe, we determined the high-resolution spectra of **4**, which show that there are two Eu^{3+} ion sites in the coordination polymer. This is also in agreement with the results of the X-ray single-crystal diffraction study. It was concluded that there are two La^{3+}, two Pr^{3+} and two Nd^{3+} ion sites in polymers **1**, **2**, and **3**, respectively. The thermogravimetric analyses of these complexes show that all coordinated and uncoordinated water molecules were lost at the first weight loss above 240 °C.
(© Wiley-VCH Verlag GmbH & Co. KGaA, 69451 Weinheim, Germany, 2002)

Introduction

The field of coordination polymers has undergone an explosive growth since numerous one-, two-, and three-dimensional structures have been obtained.[1−8] Much attention in this area has been focussed on coordination polymers with multifunctional ligands as the presence of different functional groups allows for the incorporation of interesting properties into the resulting coordination networks. Such polymeric structures are generally neutral, which simplifies the ability to control their structures and increases the chances of obtaining porous solids.[6] 2,3-Pyrazinedicarboxylic acid is a commonly used multifunctional ligand. Its complexes with d-block transition metals have been synthesized and their structures have been obtained.[9−16] However, the lanthanide complexes of this ligand are relatively unexplored. Up to now, no structural characterization of the lanthanide complexes of 2,3-pyrazinedicarboxylic acid has been reported. In light of the fact that lanthanide and d-block transition metal ions differ in their coordination number, pzdc may coordinate with them in a different manner, resulting in a characteristic structure. As these complexes have potential applications as new materials, we synthesized the lanthanide coordination polymers of pzdc by hydrothermal and hydro(solvo)thermal syntheses. Here, we report on their crystal structures and their properties.

[a] Department of Chemistry, Beijing Normal University, Beijing 100875, P. R. China
Fax: (internat.) + 86-10/62200567
E-mail: lpjin@bnu.edu.cn
[b] Laboratory of Excited States Processes, Chinese Academy of Sciences, Changchun Institute of Optics, Fine Mechanics and Physics, Chinese Academy of Sciences, Changchun 130021, P. R. China

Results and Discussion

Crystal Structures

The three coordination polymers are isomorphous. Only the structure of **4** will be described in detail. The asymmetric unit of **4** consists of two europium(III) ions, three 2,3-pyrazinedicarboxylate groups, one coordinated water and two lattice water molecules (Figure 1). There are three coordination modes for the three bridging 2,3-pyrazinedicarboxylate groups, as shown in Scheme 1. The three pyrazine rings are orientated differently in the crystal. The dihedral angles between the pyrazine rings are 70.8, 76.3, and 14.4°, owing to the steric effects in the formation of lanthanide coordination polymers. Although Eu1 and Eu2 are both nine-coordinate, the coordination environments around them are different. A hexadentate and a tetradentate pzdc ligand coordinate to Eu1 in a bidentate chelating mode through a nitrogen atom N(2A) of the pyrazinyl group and an oxygen atom O(4A) of an adjacent carboxylate group, and through N(3) and O(5).

In addition, Eu1 is coordinated to two oxygen atoms [O(1), O(2)] from a μ_2,η^3-carboxylate group of a hexadent-

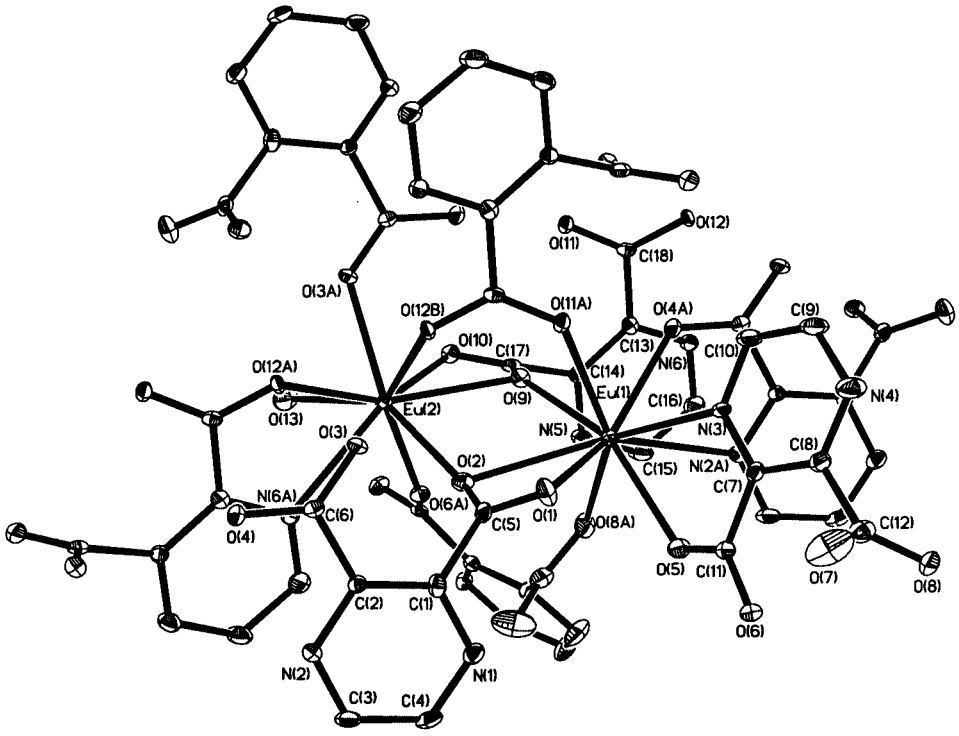

Figure 1. Coordination environment of complex **4**; the asymmetric unit and the related coordination atoms are labeled; lattice water molecules and all hydrogen atoms are omitted for clarity; thermal ellipsoids are shown at the 30% probability level

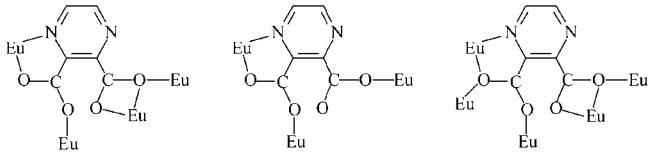

Scheme 1. The coordination modes of the pzdc ligand in complex **4**

ate pzdc ligand, one oxygen atom [O(8A)] from the carboxylate group of a tetradentate ligand, one oxygen atom [O(11A)] from the μ_2,η^2-carboxylate group of a heptadentate pzdc ligand and one oxygen atom [O(9)] from the μ_2,η^3-carboxylate group of another heptadentate pzdc ligand. Compared with Eu1, there is only one heptadentate pzdc ligand that is coordinated to Eu2 through one nitrogen atom [N(6A)] of pyrazinyl group and one carboxylate oxygen atom [O(12A)]. Eu2 is also coordinated to two oxygen atoms [O(9), O(10)] of a carboxylate group from a heptadentate pzdc ligand, four oxygen atoms[O(2), O(3A), O(6A), O(12B)] from the carboxylate groups of two hexadentate, one tetradentate, and another heptadentate pzdc ligands. An oxygen atom [O(13)] from a water molecule coordinates to Eu2 to complete the coordination number of nine. Altogether, there are six pzdc ligands bound to every Eu^{3+} ion. Eu1 is coordinated to two tetradentate, two hexadentate, and two heptadentate pzdc ligands, while Eu2 is coordinated to two hexadentate, one tetradentate, and three heptadentate pzdc ligands, as well as a water molecule. However, their modes of coordination differ, as mentioned above.

The framework structure of **4** is constructed from an $Eu_2(pzdc)_3H_2O$ unit. Firstly, two hexadentate and two heptadentate pzdc ligands link two dieuropium building units to form a parallelogram, the four vertices of which are occupied by four Eu^{3+} ions (Figure 2). The two heptadentate pzdc ligands are located above and below the plane of the parallelogram and link the four Eu^{3+} ions, resulting in a "cage-like" motif. The distances between Eu1 and Eu2, and Eu1 and Eu2B are 4.08 Å and 6.04 Å, respectively, and that between Eu2 and Eu2B is 4.22 Å. Four tetradentate pzdc ligands then link every parallelogram with four adja-

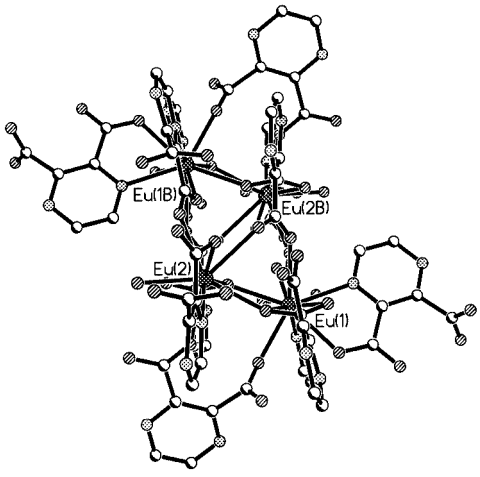

Figure 2. Perspective view of the parallelogram motif along the *a* axis formed by linking two dieuropium building blocks of **4** through tetradentate and hexadentate pzdc ligands

cent parallelograms which are orientated in a different manner. The parallelograms extend infinitely on the plane (100). Simultaneously, along the *a* axis, the parallelograms are linked by the hexadentate and heptadentate pzdc ligands forming a pillar of parallelograms, as shown in Figure 3. Thus, a complicated three-dimensional architecture is built with many cavities along the *a* axis.

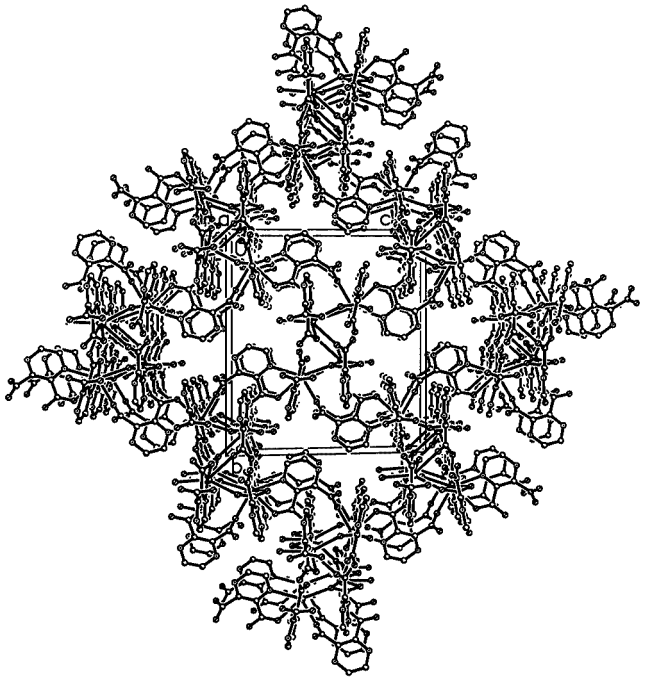

Figure 3. 3-D framework of **4** viewed along the *a* axis; all hydrogen atoms and uncoordinated water molecules are omitted for clarity

Although we have not determined the crystal structure of **3**, we can conclude that **3** has the same 3-D structure as complexes **1**, **2**, and **4** since they have the same components based on elemental analyses; furthermore, complexes **1**, **2**, and **4** are isomorphous and Nd is situated between La, Pr, and Eu in the lanthanide series. The pzdc ligands in **1**, **2**, and **3** have the same bridging modes, as shown in Scheme 1. In the reported binary d-block transition metal complexes with pzdc, there are four bridging modes for pzdc, as shown in Scheme 2. In $[M(pzdc)(H_2O)_2]_x{\cdot}2xH_2O$ (M = Co, Ni, Cu),[16] $[Co(pzdc)(H_2O)_2]_x$[17] and $[Cu(pzdc){\cdot}HCl]_x$,[13] the pzdc ligands bridge the metal ions through 1,4-diazine links that are supported by forming chelates to both metal ions, as depicted in Scheme 2 (a).

In $[M(pzdc)(H_2O)_2]_x{\cdot}2xH_2O$ (M = Fe,[9] M = Mn[15]) and $[Zn(pzdc){\cdot}3H_2O]_x$,[18] the pzdc ligands chelate to a metal ion in one chain and bridge two metal ions in the second chain by O−C−O links of a second carboxylate group of the same pzdc ligand, as shown in Scheme 2 (b). While in $[M(pzdc)(H_2O)_3]_x{\cdot}xH_2O$ (M = Zn,[19] M = Cd[15]), the pzdc ligand links one metal ion forming a chelate and bridges another metal ion with a second carboxylate group in a monodentate fashion, as depicted in Scheme 2 (c). In $[NH_4]_x[Ag(pzdc)]_x$,[14] besides one Ag^+ ion coordinated by one nitrogen atom of 1,4-diazine, two carboxylate groups of pzdc coordinate to one Ag^+ ion in a monodentate fashion, as seen in Scheme 2 (d). Generally speaking, in the above reported d-block transition metal complexes, the pzdc ligand adopts only one bridging mode in every complex. While in the title complexes, pzdc adopts three bridging modes in every complex, and its bridging mode is much more complicated than those in the d-block transition metal complexes (see Scheme 1). This can be attributed to the larger radii and greater positive charge of the Ln^{III} ions, and hence the large coordination number and different coordination modes required by the lanthanide ions.

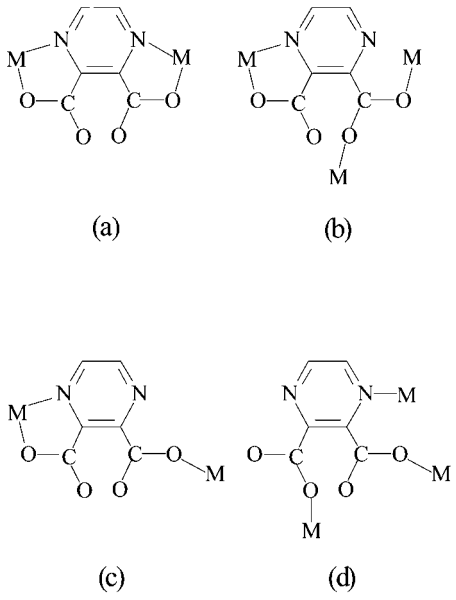

Scheme 2. Coordination modes of the pzdc ligand in the reported binary d-block transition metal complexes

In addition, two types of hydrogen bonds exist in the crystal. A hydrogen bond forms between the lattice water molecules, and another between the coordinated water molecule and the lattice water molecule. These hydrogen bonds stabilize the crystal.

Photophysical Properties of $[Eu_2(pzdc)_3(H_2O)_x]{\cdot}2xH_2O$

Figure 4 illustrates the high-resolution emission spectrum of **4** excited at 355 nm at 77 K, corresponding to the $^5D_0 \rightarrow {}^7F_J$ ($J = 0-4$) transitions. From Figure 4 it can be seen that the intensity ratio of $^5D_0 \rightarrow {}^7F_2/{}^5D_0 \rightarrow {}^7F_1$ is 3.2, which indicates that the Eu^{III} ions are not in an inversion center. The number of components of the $^5D_0 \rightarrow {}^7F_1$ transition indicates the presence of more than one chemically different Eu^{III} ion sites. The intensity of the $^5D_0 \rightarrow {}^7F_0$ transition is relatively weak and the emission band is not symmetrical. The non-homogeneous broadening of the $^5D_0 \rightarrow {}^7F_0$ emission band arises from the site to site variation in the local field acting on the ions, and has consequently been studied by selective excitation techniques.

Among the transitions from the lowest emission state $^5D_0$ to the ground state ^7F_J ($J = 0-6$), the $^5D_0 \rightarrow {}^7F_2$ transition

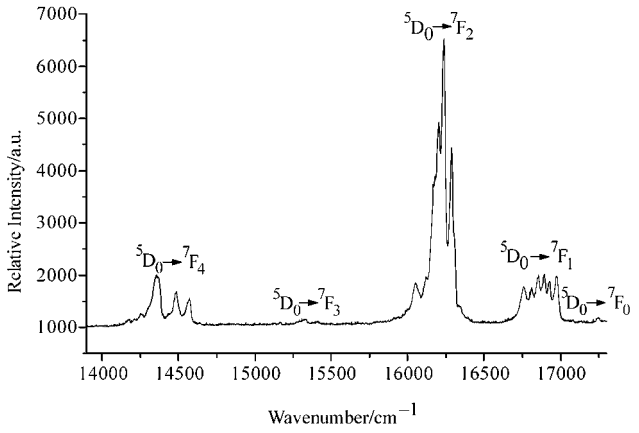

Figure 4. Emission spectrum of **4** corresponding to the $^5D_0 \rightarrow {}^7F_J$ ($J = 0-4$) transitions at 77 K, $\lambda_{exc} = 355$ nm

is the electronic dipole transition which is hypersensitive, and is greatly affected by the coordination environment. On the other hand, the $^5D_0 \rightarrow {}^7F_1$ transition is the magnetic dipole transition and is much less sensitive to the coordination environment. Therefore, the time-resolved spectra of complex **4** in the range of 16500−15900 cm^{-1} (corresponding to $^5D_0 \rightarrow {}^7F_2$ transition) were recorded and are shown in Figure 5. From Figure 5 it can be seen that the relative intensity of the emission peaks change. With a time delay, the peaks marked with "a" decay sharply relative to those marked with "b", which indicates that they arise from the Eu^{III} ion sites with different life-times. However, the less-developed bands show that it is difficult to obtain the exact life-time of each Eu^{III} ion site because they have slightly different chemical environments. Therefore, they may be simultaneously excited, or there may be an energy transfer between the Eu^{III} ion sites when excited, resulting in averaged life-times.

The excitation spectra of **4** (Figure 6) were recorded at 77 K, the analyzing wavenumbers were 16178, 16195, 16216, and 16304cm^{-1}. There are two main peaks located at 579.52 nm and 579.75 nm in every spectrum, which indicates that there are two Eu^{III} ion sites in the complex. This is in agreement with the results of the X-ray single-crystal diffraction study. It is worth noting that the excitation peaks are not narrow enough, and this is possibly a result of the slightly different chemical environments of the Eu^{III} ions in coordination polymers.

Thermogravimetric Analyses

Thermogravimetric analyses of the four complexes were carried out to examine their thermal stabilities. The data of the thermogravimetric analyses for **1**−**4** are listed in Table 1. All four complexes undergo loss of their coordinated and uncoordinated water molecules at the first weight loss.

Their dehydration temperatures range from 240 to 310 °C. They began to decompose beyond 430 °C. Looking at **1** as an example, the TGA curve shows that the first weight

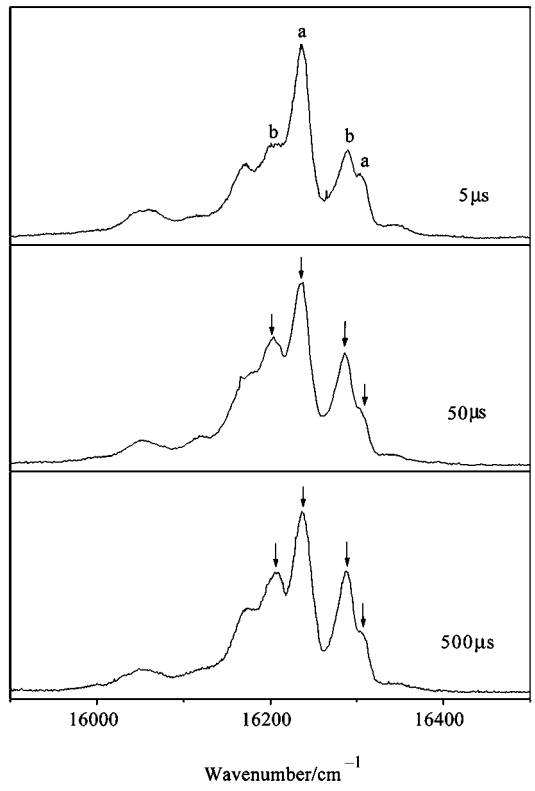

Figure 5. Time-resolved spectra of **4** at 77 K in the range of 16500−15900cm^{-1}; delay times: 5, 50, 500 μs; $\lambda_{exc} = 355$ nm

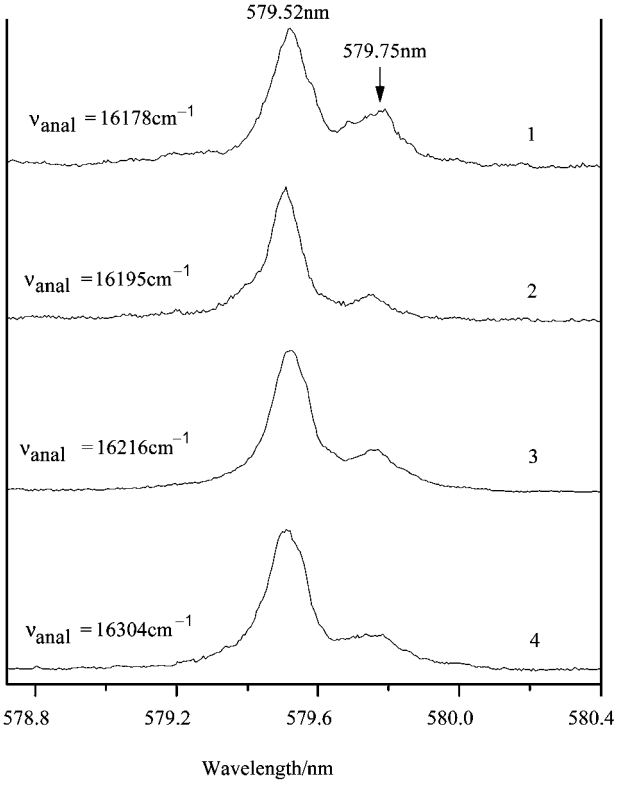

Figure 6. Excitation spectra of **4** at 77 K; analyzing wavenumber: 16178 cm^{-1} (1), 16195 cm^{-1} (2), 16216 cm^{-1} (3), and 16304 cm^{-1} (4)

Table 1. Thermogravimetric analyses of **1**−**4**

	1	**2**	**3**	**4**
Dehydration temperature [°C]	242.3−277.2	259.5−294.7	263.7−293.1	276.2−309.7
Loss of water:				
Calculated [%]	6.5	6.5	6.4	6.3
Found [%]	6.2	6.4	6.2	5.8
Further decomposition temperature [°C]	443	429.7	432.2	421.2

loss of 6.2%,which occurs between 242.3 and 277.2 °C corresponds to the loss of two uncoordinated water molecules and one coordinated water molecule (calculated: 6.5%). Further decomposition of **1** occurs above 443 °C (see Table 1).

Conclusion

Complexes **1**−**4** exhibit the same 3-D structures because they are isomorphous. The pzdc ligands in the complexes all adopt tetradentate, hexadentate and heptadentate bridging modes. By utilizing the characteristic of Eu^{3+} to act as a conformational probe, two Eu^{3+} ion sites have been observed in the coordination polymer **4**. In the coordination polymers, the La^{3+}, Pr^{3+}, and Nd^{3+} ions may have similar coordination environments to that of Eu^{3+}. Therefore, a conclusion could be reached that in polymers **1**, **2**, and **3**, there are two La^{3+} ion sites, two Pr^{3+} ion sites, and two Nd^{3+} ion sites, respectively. The four complexes are relatively stable. They all lose their coordinated and lattice water molecules at the first weight loss, above 240 °C.

Experimental Section

General: $LaCl_3{\cdot}7H_2O$, $NdCl_3{\cdot}6H_2O$, and $EuCl_3{\cdot}6H_2O$ were prepared by dissolving their oxides in concentrated hydrochloric acid and the solvents were evaporated to dryness. The stock solution of $PrCl_3$ was prepared by dissolving Pr_6O_{11} in concentrated hydrochloric acid and diluted to 0.49 mol/L. All the other reagents were commercially available and used without further purification. Elemental analyses were performed with an Elementar Vario EL analyzer. The IR spectra were recorded with a Nicolet Avatar 360 FT-IR spectrometer using the KBr pellet technique. Thermogravimetric analyses were performed with a ZRY-2P Thermal Analyzer.

$[La_2(pzdc)_3(H_2O)]_x{\cdot}2xH_2O$ (1): A solution of $LaCl_3{\cdot}7H_2O$ (0.111 g, 0.3 mmol), 2,3-pyrazinedicarboxylic acid (0.077 g, 0.45 mmol), H_2O (6.0 mL), ethanol (1 mL), and aqueous NaOH (1.6 mL, 1.04 mmol) was sealed in a 25-mL stainless steel reactor with Teflon liner and heated at 190 °C for 96 h. Colorless crystals of **1** were obtained in a 72.3% yield (0.09 g). $C_{18}H_{12}La_2N_6O_{15}$ (830.16): calcd. C 26.04, H 1.46, N 10.12; found C 25.64, H 1.08, N 9.73. IR data (KBr pellet, $\tilde{\nu}$ [cm^{-1}]): 3501 m, 1618s, 1558 s,1448 s, 1366 s, 1119 s, 895 m, 837 m, 443 m.

$[Pr_2(pzdc)_3(H_2O)]_x{\cdot}2xH_2O$ (2): An aqueous solution of $PrCl_3$ (0.61 mL, 0.3 mmol), 2,3-pyrazinedicarboxylic acid (0.077 g, 0.45 mmol), H_2O (6.5 mL), and aqueous NaOH (1.6 mL, 1.04 mmol) was sealed in a 25-mL stainless steel reactor with Teflon liner and heated at 190 °C for 62 h. Green crystals of **2** were obtained in a 79.9% yield (0.1 g). $C_{18}H_{12}Pr_2N_6O_{15}$ (834.16): calcd. C 25.92, H 1.45, N 10.07; found C 25.79, H 1.02, N 9.84. IR data (KBr pellet, $\tilde{\nu}$ [cm^{-1}]): 3492 m, 1619 s, 1558 s, 1447 s, 1366 s, 1120 s, 891 m, 843 m, 837 m, 444 m.

$[Nd_2(pzdc)_3(H_2O)]_x{\cdot}2xH_2O$ (3): A solution of $NdCl_3{\cdot}6H_2O$ (0.108 g, 0.3 mmol), 2,3-pyrazinedicarboxylic acid (0.077 g, 0.45 mmol), H_2O (7 mL), and aqueous NaOH (1.46 mL, 0.95 mmol) was sealed in a 25-mL stainless steel reactor with Teflon liner and heated at 190 °C for 62 h. Purple crystals of **3** were obtained in a 79.2% yield (0.1 g). $C_{18}H_{12}Nd_2N_6O_{15}$ (840.76): calcd. C 25.71, H 1.44, N 10.00; found C 25.39, H 1.12, N 9.84. IR data (KBr pellet, $\tilde{\nu}$ [cm^{-1}]): 3492 m, 1621 s, 1558 s, 1448 s, 1366 s, 1120 s, 891 m, 837 m, 445 m.

$[Eu_2(pzdc)_3(H_2O)]_x{\cdot}2xH_2O$ (4): A solution of $EuCl_3{\cdot}6H_2O$ (0.11 g, 0.3 mmol), 2,3-pyrazinedicarboxylic acid (0.077 g, 0.45 mmol), H_2O (8.4 mL), and aqueous NaOH (1.4 mL, 0.91 mmol) was sealed in a 25-mL stainless steel reactor with Teflon liner and heated at 190 °C for 88 h. Colorless crystals of **4** were obtained in a 77.8% yield (0.1 g). $C_{18}H_{12}Eu_2N_6O_{15}$ (856.26): calcd. C 25.25, H 1.41, N 9.81; found C 24.78, H 1.10, N 9.43. IR data (KBr pellet, $\tilde{\nu}$ [cm^{-1}]): 3486 m, 1627 s, 1561 s, 1449 s, 1368 s, 1122 s, 898 m, 845 m, 838 m, 449 m.

Measurement of the High-Resolution Luminescence Spectra: The excitation light source was a YAG:Nd laser that emits at 1.064 μm, and the excitation wavelength was 355 nm. The sample was placed in a Dewar bottle and cooled with liquid nitrogen. The fluorescence emitted was collected at right angles through a Spex 1403 monochromator with a photomultiplier tube, then averaged with a Boxcar integrator and finally the data were transferred to a computer.

X-ray Data Collections and Structure Determinations: The X-ray single-crystal data collections for complexes **1**, **2**, and **4** were performed with a Bruker Smart 1000 CCD diffractometer, using graphite-monochromated Mo-K_α radiation (λ = 0.71073 Å). Semi-empirical absorption corrections were applied using the SADABS program. The structures were solved by direct methods and refined by full-matrix least squares on F^2 using the SHELXTL-97 program.[16] All non-hydrogen atoms were refined with anisotropic displacement parameters. The hydrogen atoms were generated geometrically and treated by a mixture of independent and constrained refinements. Experimental details for X-ray data collection of **1**, **2**,

Table 2. Crystal data for **1**, **2**, and **4**

	1	**2**	**4**
Empirical formula	$C_{18}H_{12}La_2N_6O_{15}$	$C_{18}H_{12}Pr_2N_6O_{15}$	$C_{18}H_{12}Eu_2N_6O_{15}$
Formula mass	830.16	834.16	856.26
Crystal system	monoclinic	monoclinic	monoclinic
Space group	$P2_1/c$	$P2_1/c$	$P2_1/c$
a [Å]	9.004(3)	8.945(2)	8.853(3)
b [Å]	17.001(5)	16.924(5)	16.771(5)
c [Å]	15.599(5)	15.482(4)	15.302(4)
α [°]	90	90	90
β [°]	101.739(5)	101.291(5)	100.823(5)
γ [°]	90	90	90
V [Å^3]	2337.9(12)	2298.3(11)	2231.5(11)
Z	4	4	4
T [K]	293(2)	293(2)	293(2)
$\rho_{calcd.}$ [g/cm^3]	2.358	2.411	2.549
μ [mm^{-1}]]	3.699	4.285	5.668
R_1 [a]	0.0221	0.0317	0.0246
wR_2 [a]	0.0489	0.0581	0.0552

[a] The values were calculated for data with [$I > 2\sigma(I)$].

Table 3. Selected bond lengths [Å] and bond angles[°] for complex **1**

La(1)−O(6)$^{\#1}$ [a]	2.447(3)	O(13)−La(1)−O(12)$^{\#4}$	126.69(10)	O(8)$^{\#1}$−La(2)−O(10)$^{\#5}$	145.27(9)
La(1)−O(2)$^{\#2}$	2.497(3)	O(3)$^{\#3}$−La(1)−O(12)$^{\#4}$	70.95(8)	O(5)−La(2)−O(10)$^{\#5}$	129.77(9)
La(1)−O(13)	2.528(3)	O(9)−La(1)−O(12)$^{\#4}$	144.24(8)	O(12)$^{\#4}$−La(2)−O(10)$^{\#5}$	69.61(9)
La(1)−O(3)$^{\#3}$	2.530(3)	O(6)$^{\#1}$−La(1)−O(9)$^{\#5}$	139.15(8)	O(1)−La(2)−O(10)$^{\#5}$	69.78(9)
La(1)−O(9)	2.566(3)	O(2)$^{\#2}$−La(1)−O(9)$^{\#5}$	69.31(9)	O(8)$^{\#1}$−La(2)−O(4)$^{\#3}$	102.66(11)
La(1)−O(12)$^{\#4}$	2.589(3)	O(13)−La(1)−O(9)$^{\#5}$	138.98(9)	O(5)−La(2)−O(4)$^{\#3}$	66.27(9)
La(1)−O(9)$^{\#5}$	2.648(3)	O(3)$^{\#3}$−La(1)−O(9)$^{\#5}$	68.86(9)	O(12)$^{\#4}$−La(2)−O(4)$^{\#3}$	114.09(9)
La(1)−O(11)$^{\#4}$	2.726(3)	O(9)−La(1)−O(9)$^{\#5}$	66.88(9)	O(1)−La(2)−O(4)$^{\#3}$	142.06(9)
La(1)−N(5)	2.767(3)	O(12)$^{\#4}$−La(1)−O(9)$^{\#5}$	77.48(8)	O(10)$^{\#5}$−La(2)−O(4)$^{\#3}$	78.62(9)
La(2)−O(8)$^{\#1}$	2.392(3)	O(6)$^{\#1}$−La(1)−O(11)$^{\#4}$	69.37(8)	O(8)$^{\#1}$−La(2)−N(3)	136.73(10)
La(2)−O(5)	2.501(3)	O(2)$^{\#2}$−La(1)−O(11)$^{\#4}$	79.78(8)	O(5)−La(2)−N(3)	61.28(9)
La(2)−O(12)$^{\#4}$	2.509(3)	O(13)−La(1)−O(11)$^{\#4}$	77.92(10)	O(12)$^{\#4}$−La(2)−N(3)	141.04(9)
La(2)−O(1)	2.510(3)	O(3)$^{\#3}$−La(1)−O(11)$^{\#4}$	115.06(8)	O(1)−La(2)−N(3)	74.80(10)
La(2)−O(10)$^{\#5}$	2.568(3)	O(9)−La(1)−O(11)$^{\#4}$	150.41(8)	O(10)$^{\#5}$−La(2)−N(3)	77.91(9)
La(2)−O(4)$^{\#3}$	2.619(3)	O(12)$^{\#4}$−La(1)−O(11)$^{\#4}$	49.10(8)	O(4)$^{\#3}$−La(2)−N(3)	78.58(10)
La(2)−N(3)	2.706(3)	O(9)$^{\#5}$−La(1)−O(11)$^{\#4}$	112.43(8)	O(8)$^{\#1}$−La(2)−O(3)$^{\#3}$	76.21(9)
La(2)−O(3)$^{\#3}$	2.725(3)	O(6)$^{\#1}$−La(1)−N(5)	72.03(9)	O(5)−La(2)−O(3)$^{\#3}$	100.80(8)
La(2)−N(1)	2.737(3)	O(2)$^{\#2}$−La(1)−N(5)	121.73(9)	O(12)$^{\#4}$−La(2)−O(3)$^{\#3}$	69.03(8)
O(6)$^{\#1}$−La(1)−O(2)$^{\#2}$	144.24(9)	O(13)−La(1)−N(5)	70.18(10)	O(1)−La(2)−O(3)$^{\#3}$	138.33(8)
O(6)$^{\#1}$−La(1)−O(13)	81.87(10)	O(3)$^{\#3}$−La(1)−N(5)	78.37(9)	O(10)$^{\#5}$−La(2)−O(3)$^{\#3}$	79.43(8)
O(2)$^{\#2}$−La(1)−O(13)	74.20(10)	O(9)−La(1)−N(5)	60.07(9)	O(4)$^{\#3}$−La(2)−O(3)$^{\#3}$	48.91(9)
O(6)$^{\#1}$−La(1)−O(3)$^{\#3}$	73.84(9)	O(12)$^{\#4}$−La(1)−N(5)	139.96(9)	N(3)−La(2)−O(3)$^{\#3}$	125.84(9)
O(2)$^{\#2}$−La(1)−O(3)$^{\#3}$	138.13(9)	O(9)$^{\#5}$−La(1)−N(5)	114.77(9)	O(8)$^{\#1}$−La(2)−N(1)	73.98(10)
O(13)−La(1)−O(3)$^{\#3}$	144.93(9)	O(11)$^{\#4}$−La(1)−N(5)	132.53(9)	O(5)−La(2)−N(1)	70.87(9)
O(6)$^{\#1}$−La(1)−O(9)	132.00(8)	O(8)$^{\#1}$−La(2)−O(5)	79.40(10)	O(12)$^{\#4}$−La(2)−N(1)	107.49(9)
O(2)$^{\#2}$−La(1)−O(9)	72.38(9)	O(8)$^{\#1}$−La(2)−O(12)$^{\#4}$	78.70(10)	O(1)−La(2)−N(1)	60.74(9)
O(13)−La(1)−O(9)	84.93(10)	O(5)−La(2)−O(12)$^{\#4}$	157.53(8)	O(10)$^{\#5}$−La(2)−N(1)	128.51(9)
O(3)$^{\#3}$−La(1)−O(9)	92.76(8)	O(8)$^{\#1}$−La(2)−O(1)	115.26(11)	O(4)$^{\#3}$−La(2)−N(1)	136.79(10)
O(6)$^{\#1}$−La(1)−O(12)$^{\#4}$	75.11(8)	O(5)−La(2)−O(1)	120.36(9)	N(3)−La(2)−N(1)	76.49(10)
O(2)$^{\#2}$−La(1)−O(12)$^{\#4}$	98.31(9)	O(12)$^{\#4}$−La(2)−O(1)	74.21(9)	O(3)$^{\#3}$−La(2)−N(1)	150.04(9)

[a] Symmetry operation: $^{\#1}$ $x, -y + 1/2, z + 1/2$; $^{\#2}$ $-x + 1, -y, -z + 1$; $^{\#3}$ $x - 1, y, z$; $^{\#4}$ $x + 1, y, z$; $^{\#5}$ $-x, -y, -z + 1$; $^{\#6}$ $x, -y + 1/2, z - 1/2$.

and **4** are presented in Table 2, while selected bond lengths, and angles for **1**, **2**, and **4** are listed in Tables 3, 4, and 5, respectively. CCDC-186337, -186338, and -186339 contain the supplementary crystallographic data for this paper. These data can be obtained free of charge at www.ccdc.cam.ac.uk/conts/retrieving.html or from the Cambridge Crystallographic Data Centre, 12, Union Road, Cambridge CB2 1EZ, UK [Fax: (internat.) + 44-1223/336-033; E-mail: deposit@ccdc.cam.ac.uk].

Table 4. Selected bond lengths [Å] and bond angles[°] for complex **2**

Pr(1)−O(11)	2.409(4)	O(13)−Pr(1)−O(7)	126.86(14)	O(10)−Pr(2)−O(6)$^{\#1}$ [a]	146.22(15)
Pr(1)−O(3)$^{\#1}$	2.458(4)	O(2)$^{\#2}$−Pr(1)−O(7)	70.70(13)	O(7)−Pr(2)−O(6)$^{\#1}$	70.36(13)
Pr(1)−O(13)	2.490(5)	O(5)$^{\#2}$−Pr(1)−O(7)	143.75(13)	O(12)$^{\#3}$−Pr(2)−O(6)$^{\#1}$	129.63(14)
Pr(1)−O(2)$^{\#2}$	2.501(4)	O(11)−Pr(1)−O(5)$^{\#1}$	140.26(14)	O(4)−Pr(2)−O(6)$^{\#1}$	68.85(13)
Pr(1)−O(5)$^{\#2}$	2.526(4)	O(3)$^{\#1}$−Pr(1)−O(5)$^{\#1}$	69.34(13)	O(10)−Pr(2)−O(1)$^{\#2}$	103.22(15)
Pr(1)−O(7)	2.542(4)	O(13)−Pr(1)−O(5)$^{\#1}$	138.78(14)	O(7)−Pr(2)−O(1)$^{\#2}$	113.68(13)
Pr(1)−O(5)$^{\#1}$	2.605(4)	O(2)$^{\#2}$−Pr(1)−O(5)$^{\#1}$	69.28(13)	O(12)$^{\#3}$−Pr(2)−O(1)$^{\#2}$	66.35(14)
Pr(1)−O(8)	2.707(4)	O(5)$^{\#2}$−Pr(1)−O(5)$^{\#1}$	66.36(15)	O(4)−Pr(2)−O(1)$^{\#2}$	140.85(14)
Pr(1)−N(3)$^{\#2}$	2.726(5)	O(7)−Pr(1)−O(5)$^{\#1}$	77.47(12)	O(6)$^{\#1}$−Pr(2)−O(1)$^{\#2}$	77.57(14)
Pr(2)−O(10)	2.348(4)	O(11)−Pr(1)−O(8)	69.07(13)	O(10)−Pr(2)−N(6)$^{\#3}$	136.73(15)
Pr(2)−O(7)	2.469(4)	O(3)$^{\#1}$−Pr(1)−O(8)	78.14(12)	O(7)−Pr(2)−N(6)$^{\#3}$	141.24(14)
Pr(2)−O(12)$^{\#3}$	2.471(4)	O(13)−Pr(1)−O(8)	77.46(14)	O(12)$^{\#3}$−Pr(2)−N(6)$^{\#3}$	62.35(14)
Pr(2)−O(4)	2.476(4)	O(2)$^{\#2}$−Pr(1)−O(8)	115.40(13)	O(4)−Pr(2)−N(6)$^{\#3}$	75.64(14)
Pr(2)−O(6)$^{\#1}$	2.532(4)	O(5)$^{\#2}$−Pr(1)−O(8)	149.30(13)	O(6)$^{\#1}$−Pr(2)−N(6)$^{\#3}$	76.90(14)
Pr(2)−O(1)$^{\#2}$	2.583(4)	O(7)−Pr(1)−O(8)	49.76(13)	O(1)$^{\#2}$−Pr(2)−N(6)$^{\#3}$	77.70(14)
Pr(2)−N(6)$^{\#3}$	2.654(5)	O(5)$^{\#1}$−Pr(1)−O(8)	112.58(12)	O(10)−Pr(2)−N(1)	74.62(16)
Pr(2)−N(1)	2.691(5)	O(11)−Pr(1)−N(3)$^{\#2}$	72.07(14)	O(7)−Pr(2)−N(1)	108.26(14)
Pr(2)−O(2)$^{\#2}$	2.694(4)	O(3)$^{\#1}$−Pr(1)−N(3)$^{\#2}$	123.40(14)	O(12)$^{\#3}$−Pr(2)−N(1)	71.10(14)
O(11)−Pr(1)−O(3)$^{\#1}$	142.48(14)	O(13)−Pr(1)−N(3)$^{\#2}$	70.88(15)	O(4)−Pr(2)−N(1)	61.65(14)
O(11)−Pr(1)−O(13)	80.96(15)	O(2)$^{\#2}$−Pr(1)−N(3)$^{\#2}$	77.67(14)	O(6)$^{\#1}$−Pr(2)−N(1)	127.91(14)
O(3)$^{\#1}$−Pr(1)−O(13)	74.42(15)	O(5)$^{\#2}$−Pr(1)−N(3)$^{\#2}$	60.83(13)	O(1)$^{\#2}$−Pr(2)−N(1)	136.77(15)
O(11)−Pr(1)−O(2)$^{\#2}$	74.57(14)	O(7)−Pr(1)−N(3)$^{\#2}$	139.44(13)	N(6)$^{\#3}$−Pr(2)−N(1)	76.28(15)
O(3)$^{\#1}$−Pr(1)−O(2)$^{\#2}$	138.48(14)	O(5)$^{\#1}$−Pr(1)−N(3)$^{\#2}$	114.36(13)	O(10)−Pr(2)−O(2)$^{\#2}$	75.49(14)
O(13)−Pr(1)−O(2)$^{\#2}$	144.81(14)	O(8)−Pr(1)−N(3)$^{\#2}$	132.80(13)	O(7)−Pr(2)−O(2)$^{\#2}$	68.64(13)
O(11)−Pr(1)−O(5)$^{\#2}$	132.88(13)	O(10)−Pr(2)−O(7)	78.91(15)	O(12)$^{\#3}$−Pr(2)−O(2)$^{\#2}$	99.68(13)
O(3)$^{\#1}$−Pr(1)−O(5)$^{\#2}$	72.96(13)	O(10)−Pr(2)−O(12)$^{\#3}$	78.21(15)	O(4)−Pr(2)−O(2)$^{\#2}$	137.50(13)
O(13)−Pr(1)−O(5)$^{\#2}$	84.94(15)	O(7)−Pr(2)−O(12)$^{\#3}$	156.35(13)	O(6)$^{\#1}$−Pr(2)−O(2)$^{\#2}$	80.45(13)
O(2)$^{\#2}$−Pr(1)−O(5)$^{\#2}$	93.41(13)	O(10)−Pr(2)−O(4)	115.85(15)	O(1)$^{\#2}$−Pr(2)−O(2)$^{\#2}$	49.50(14)
O(11)−Pr(1)−O(7)	75.48(13)	O(7)−Pr(2)−O(4)	73.64(13)	N(6)$^{\#3}$−Pr(2)−O(2)$^{\#2}$	125.85(14)
O(3)$^{\#1}$−Pr(1)−O(7)	97.16(13)	O(12)$^{\#3}$−Pr(2)−O(4)	122.42(14)	N(1)−Pr(2)−O(2)$^{\#2}$	149.93(14)

[a] Symmetry operation: $^{\#1}-x, -y, -z+1$; $^{\#2}x-1, y, z$; $^{\#3}x, -y+1/2, z-1/2$; $^{\#4}x+1, y, z$; $^{\#5}x, -y+1/2, z+1/2$.

Table 5. Selected bond lengths [Å] and bond angles[°] for complex **4**

Eu(1)−O(8)$^{\#1}$ [a]	2.295(4)	O(4)$^{\#2}$−Eu(1)−O(1)	140.23(12)	O(6)$^{\#1}$−Eu(2)−O(12)$^{\#5}$	134.29(11)
Eu(1)−O(9)	2.405(3)	O(5)−Eu(1)−O(1)	66.28(12)	O(3)$^{\#4}$−Eu(2)−O(12)$^{\#5}$	73.11(11)
Eu(1)−O(4)$^{\#2}$	2.420(3)	O(11)$^{\#3}$−Eu(1)−O(1)	76.91(12)	O(13)−Eu(2)−O(12)$^{\#5}$	84.29(12)
Eu(1)−O(5)	2.431(3)	O(8)$^{\#1}$−Eu(1)−N(3)	136.85(13)	O(2)−Eu(2)−O(12)$^{\#5}$	94.83(11)
Eu(1)−O(11)$^{\#3}$	2.460(3)	O(9)−Eu(1)−N(3)	141.65(12)	O(6)$^{\#1}$−Eu(2)−O(9)	76.14(11)
Eu(1)−O(1)	2.538(3)	O(4)$^{\#2}$−Eu(1)−N(3)	76.43(12)	O(3)$^{\#4}$−Eu(2)−O(9)	95.33(11)
Eu(1)−N(3)	2.585(4)	O(5)−Eu(1)−N(3)	63.83(12)	O(13)−Eu(2)−O(9)	127.02(12)
Eu(1)−N(2)$^{\#2}$	2.635(4)	O(11)$^{\#3}$−Eu(1)−N(3)	76.31(12)	O(2)−Eu(2)−O(9)	70.65(11)
Eu(1)−O(2)	2.653(3)	O(1)−Eu(1)−N(3)	77.23(12)	O(12)$^{\#5}$−Eu(2)−O(9)	143.38(11)
Eu(2)−O(6)$^{\#1}$	2.347(3)	O(8)$^{\#1}$−Eu(1)−N(2)$^{\#2}$	74.53(13)	O(6)$^{\#1}$−Eu(2)−O(12)$^{\#3}$	141.86(11)
Eu(2)−O(3)$^{\#4}$	2.396(3)	O(9)−Eu(1)−N(2)$^{\#2}$	108.56(11)	O(3)$^{\#4}$−Eu(2)−O(12)$^{\#3}$	69.46(11)
Eu(2)−O(13)	2.419(4)	O(4)$^{\#2}$−Eu(1)−N(2)$^{\#2}$	62.74(12)	O(13)−Eu(2)−O(12)$^{\#3}$	138.38(12)
Eu(2)−O(2)	2.424(3)	O(5)−Eu(1)−N(2)$^{\#2}$	71.42(12)	O(2)−Eu(2)−O(12)$^{\#3}$	69.40(11)
Eu(2)−O(12)$^{\#5}$	2.458(3)	O(11)$^{\#3}$−Eu(1)−N(2)$^{\#2}$	128.02(12)	O(12)$^{\#5}$−Eu(2)−O(12)$^{\#3}$	65.61(11)
Eu(2)−O(9)	2.476(3)	O(1)−Eu(1)−N(2)$^{\#2}$	136.74(12)	O(9)−Eu(2)−O(12)$^{\#3}$	77.77(10)
Eu(2)−O(12)$^{\#3}$	2.563(3)	N(3)−Eu(1)−N(2)$^{\#2}$	76.49(13)	O(6)$^{\#1}$−Eu(2)−N(6)$^{\#5}$	72.05(12)
Eu(2)−N(6)$^{\#5}$	2.664(4)	O(8)$^{\#1}$−Eu(1)−O(2)	74.88(12)	O(3)$^{\#4}$−Eu(2)−N(6)$^{\#5}$	125.67(12)
Eu(2)−O(10)	2.687(3)	O(9)−Eu(1)−O(2)	67.94(10)	O(13)−Eu(2)−N(6)$^{\#5}$	71.58(13)
O(8)$^{\#1}$−Eu(1)−O(9)	78.58(12)	O(4)$^{\#2}$−Eu(1)−O(2)	136.41(11)	O(2)−Eu(2)−N(6)$^{\#5}$	76.99(12)
O(8)$^{\#1}$−Eu(1)−O(4)$^{\#2}$	115.96(13)	O(5)−Eu(1)−O(2)	98.65(11)	O(12)$^{\#5}$−Eu(2)−N(6)$^{\#5}$	62.27(12)
O(9)−Eu(1)−O(4)$^{\#2}$	73.14(11)	O(11)$^{\#3}$−Eu(1)−O(2)	81.03(11)	O(9)−Eu(2)−N(6)$^{\#5}$	138.99(12)
O(8)$^{\#1}$−Eu(1)−O(5)	76.94(12)	O(1)−Eu(1)−O(2)	50.23(11)	O(12)$^{\#3}$−Eu(2)−N(6)$^{\#5}$	113.62(11)
O(9)−Eu(1)−O(5)	154.50(11)	N(3)−Eu(1)−O(2)	126.25(11)	O(6)$^{\#1}$−Eu(2)−O(10)	68.59(11)
O(4)$^{\#2}$−Eu(1)−O(5)	124.69(11)	N(2)$^{\#2}$−Eu(1)−O(2)	149.25(12)	O(3)$^{\#4}$−Eu(2)−O(10)	75.93(11)
O(8)$^{\#1}$−Eu(1)−O(11)$^{\#3}$	146.65(12)	O(6)$^{\#1}$−Eu(2)−O(3)$^{\#4}$	140.14(11)	O(13)−Eu(2)−O(10)	76.65(12)
O(9)−Eu(1)−O(11)$^{\#3}$	71.11(11)	O(6)$^{\#1}$−Eu(2)−O(13)	79.75(12)	O(2)−Eu(2)−O(10)	116.26(11)
O(4)$^{\#2}$−Eu(1)−O(11)$^{\#3}$	68.26(11)	O(3)$^{\#4}$−Eu(2)−O(13)	74.83(12)	O(12)$^{\#5}$−Eu(2)−O(10)	146.93(11)
O(5)−Eu(1)−O(11)$^{\#3}$	130.04(11)	O(6)$^{\#1}$−Eu(2)−O(2)	75.95(11)	O(9)−Eu(2)−O(10)	50.73(10)
O(8)$^{\#1}$−Eu(1)−O(1)	103.65(13)	O(3)$^{\#4}$−Eu(2)−O(2)	138.47(12)	O(12)$^{\#3}$−Eu(2)−O(10)	113.39(10)
O(9)−Eu(1)−O(1)	113.42(11)	O(13)−Eu(2)−O(2)	144.87(12)	N(6)$^{\#5}$−Eu(2)−O(10)	132.77(11)

[a] Symmetry operation: $^{\#1}x, -y+1/2, z-1/2$; $^{\#2}x-1, y, z$; $^{\#3}-x, -y, -z$; $^{\#4}-x+1, -y, -z$; $^{\#5}x+1, y, z$; $^{\#6}x, -y+1/2, z+1/2$.

Acknowledgments

This work is supported by the National Natural Science Foundation of China (29971005 and 20071004) and the State Key Project of Fundamental Research (G1998061308)

[1] M. J. Zaworotko, *Chem. Soc. Rev.* **1994**, 283−288.
[2] S. R. Batten, R. Robson, *Angew. Chem. Int. Ed.* **1998**, *37*, 1461−1494.
[3] P. J. Hagrman, D. Hagrman, J. Zubieta, *Angew. Chem. Int. Ed.* **1999**, *38*, 2638−2684.
[4] M. Munakata, L. P. Wu, T. Kuroda-Soda, *Adv. Inorg. Chem.* **1999**, *46*, 173−304.
[5] H. J. Chen, Z. W. Mao, S. Gao, X. M. Chen, *Chem. Commun.* **2001**, 2320−2321.
[6] P. Ayyappan, O. R. Evans, W. B. Lin, *Inorg. Chem.* **2001**, *40*, 4627−4632.
[7] M. Eddaoudi, J. Kim, N. Rosi, D. Vodak, J. Wachter, M. O'keeffe, O. M. Yaghi, *Science* **2002**, *295*, 469−472.
[8] Z. Shi, S. H. Feng, Y. Sun, J. Hua, *Inorg. Chem.* **2001**, *40*, 5312−5313.
[9] S. Gao, B. Q. Ma, T. Yi, Z. M. Wang, C. S. Liao, C. H. Yan, G. X. Xu, *Chem. Lett.* **1999**, 773−774.
[10] J. Z. Zou, Z. Xu, W. Chen, K. M. Lo, X. Z. You, *Polyhedron* **1999**, *18*, 1507−1512.
[11] M. Wenkin, M. Devillers, B. Tinant, J. P. Declercq, *Inorg. Chim. Acta* **1997**, *258*, 113−118.
[12] F. Jaber, F. Charbonnier, R. Faure, *J. Chem. Crystallogr.* **1994**, *24*, 681−684.
[13] C. J. O'Connor, C. L. Klein, R. J. Majeste, L. M. Trefonas, *Inorg. Chem.* **1982**, *21*, 64−67.
[14] G. Smith, A. N. Reddy, K. A. Byriel, C. H. L. Kennard, *J. Chem. Soc., Dalton Trans.* **1995**, 3565−3570.
[15] L. Mao, S. J. Rettig, R. C. Thompson, J. Trotter, S. H. Xia, *Can. J. Chem.* **1996**, *74*, 2413−2423.
[16] L. Mao, S. J. Rettig, R. C. Thompson, J. Trotter, S. H. Xia, *Can. J. Chem.* **1996**, *74*, 433−444.
[17] G. M. Sheldrick, *SHELXTL-97, Program for the refinement of Crystal Structures*, University of Göttingen, Germany, **1997**.
[18] P. Richard, D. T. Qui, E. F. Bertaut, *Acta Crystallogr., Sect. B* **1973**, *29*, 111.
[19] P. Richard, D. T. Qui, E. F. Bertaut, *Acta Crystallogr., Sect. B* **1974**, *30*, 628.
[20] H. Ptasiewicz-Bak, J. Leciejewicz, *Pol. J. Chem.* **1999**, *73*, 1887−1894.

Received May 11, 2002
[I02272]